ChemComm
FEATURE ARTICLE

Organometallic and related metal-containing dendrimers

Meredith A. Hearshaw and John R. Moss*†

Department of Chemistry, University of Cape Town, Private Bag, Rondebosch 7701, South Africa. E-mail: jrm@psipsy.uct.ac.za

Received (in Cambridge, UK) 12th May 1998, Accepted 8th July 1998

Reports of the synthesis of new dendrimers containing organometallic fragments have increased dramatically over the past few years and examples of dendrimers containing many different metals are now known. This article highlights some of the the ways in which transition metals and their ligand systems have been incorporated into the growing number of dendrimers. Some structural details and properties of metal-containing dendrimers are described, and their applications are also discussed. The cover illustration shows Table Mountain, South Africa and a fourth generation ruthenium dendritic wedge.

Introduction

Nature has the ability to manipulate and control the structures of molecules in three dimensions. The rising demand for materials with improved and novel properties has now changed the emphasis in polymer research to new classes of materials with highly controlled molecular architectures.[1,2] New families of highly branched three-dimensional molecules, termed dendrimers, arborals or starburst polymers, have recently been prepared and have sparked great interest. Several review articles have appeared recently.[1] One of the driving forces in the study of these highly branched macromolecules has been the anticipation that these new materials will have fundamentally different properties when compared to more traditional linear polymers. While the majority of dendrimers prepared so far have been purely organic in nature, there is growing interest in the synthesis of dendrimers containing transition metals. The metal centres can be incorporated at the core, throughout the structure, or at the periphery of a dendrimer and may give compounds with novel or unusual properties. Such compounds are new materials and may have important applications, including uses as molecular devices, as antennas for harvesting light or as catalysts. Exploration of the synthesis, properties, structures and applications of these new materials is both challenging and exciting. Over the past six years, we have developed a methodology for synthesizing dendrimers containing covalent metal–carbon sigma bonds. To date, we have concentrated on compounds containing Ru–C and Fe–C bonds but we are currently investigating the synthesis of many other organometallic systems. In the following pages, we describe some of our work along with that of others in the field. Dendrimers are discussed according to the mode of bonding between the metal and dendrimer.

John R. Moss was born in Aberdeen, Scotland. He obtained his BSc (Hons) degree in 1965 and completed his PhD (1968) with B. L. Shaw, both at Leeds University, England. After post-doctoral fellowships with W. A. G. Graham in Canada and F. G. A. Stone at Bristol, he joined Rhodes University, South Africa in 1973 as a lecturer. In 1979, he moved to the University of Cape Town, where he is now Jamison Professor of Inorganic Chemistry and Head of the Department of Chemistry. His research interests are in the synthesis of new organotransition metal compounds and their applications as catalysts, new materials and medicines.

Meredith A. Hearshaw (née Timme) was born in Cape Town, South Africa and obtained her BSc (Hons) degree in 1993 in the First Class. She is currently completing her PhD degree on the synthesis, structure and chemistry of organometallic dendrimers under the supervision of Professors John Moss and Mino Caira at the University of Cape Town.

Dendrimers with M–C σ bonds

The first transition metal alkyl compound was prepared by Pope and Peachey in 1907[3] and today alkyl compounds of nearly every transition metal are known.[4] A driving force for this development has been in part due to the important applications of the alkyl species in catalytic reactions of industrial importance, for example titanium and zirconium catalysts for the polymerization of alkenes, as well as cobalt and rhodium catalysts in hydroformylation and hydrogenation reactions.[5] Our research group has worked on transition metal alkyl and functionalized alkyl compounds for many years.[4] From our studies on haloalkyl compounds,[6] we have developed methods for the preparation of organometallic dendrimers containing metal–carbon sigma bonds.[7] We applied the convergent methodology developed by Hawker and Fréchet[2] and used 3,5-dihydroxybenzyl alcohol as the monomer unit.[7] The advantage of using the convergent approach is that it allows for precise control over the number and placement of functional groups at the surface of the final dendrimer. The reactions are carried out in a stepwise fashion and the dendritic wedges were isolated, purified and characterized after each step. Since the products are all highly soluble, in spite of the large number of metals present, the reactions could be monitored by NMR spectroscopy, so that defects in branching of the wedges could be detected prior to complexation with a core molecule. Our first attempts to build dendrimers were with functionalized iron complexes of the type $Cp(CO)_2Fe(CH_2)_3Br$.[6] Although the reaction with 3,5-dihydroxybenzyl alcohol yielded the expected binulcear complex (see Scheme 1), conversion of the benzyl alcohol to the benzyl bromide gave a low yield, which we attributed to the instability of the iron-alkyl bond of the benzyl bromide. Iron dendrimers containing Cp (Cp = η^5-C_5H_5) acyl and Cp* (Cp* = η^5-C_5Me_5) monomer units have since been prepared and will be reported in further publications.[8]

We explored the reactions of $Cp(CO)_2RuR$ derivatives, *e.g.* $Cp(CO)_2Ru(CH_2)_5Ru(CO)_2Cp$ or $Cp(CO)_2RuR$ (R = alkyl) with PPh_3 and showed that no reaction occurred in refluxing THF over 25 h, forcing conditions (refluxing xylene, 140 °C) being necessary to get the reaction to go at all.[9] This suggested to us that the ligand system around the metal in these $Cp(CO)_2RuR$ derivatives was both thermodynamically stable and kinetically relatively inert. It was for this reason that we turned our attention to building up organometallic dendrimers with ruthenium–carbon sigma bonds. Thus, the reaction of 3,5-dihydroxybenzyl alcohol with $Cp(CO)_2Ru(CH_2)_3Br$ was investigated and we obtained the expected benzyl alcohol (see Scheme 1). This and higher generation dendritic wedges could

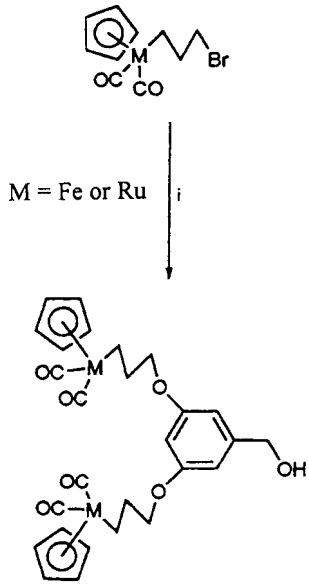

Scheme 1 *Reagents and conditions:* i, 3,5-dihydroxybenzyl alcohol, K_2CO_3, 18-crown-6, reflux, acetone, 48 h.

be converted to the corresponding benzyl bromides in good yield (see Scheme 2).[7] These ruthenium-based dendritic wedges

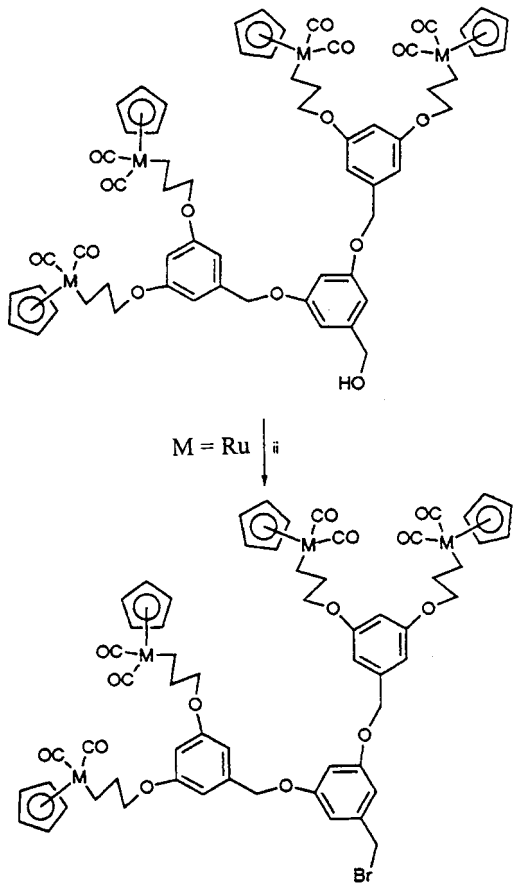

Scheme 2 *Reagents and conditions:* ii, CBr_4, PPh_3, room temp., 20 min.

were sufficiently stable to withstand the vigorous conditions required for their synthesis and thus it was possible to build up large dendritic wedges, and organometallic dendrimers, containing Ru–C sigma bonds. For these ruthenium complexes, the reactions of the organometallic wedges behaved similarly to the analogous organic reactions, although the yields tended to be slightly lower. The ruthenium dendrimers described above are highly soluble in common polar organic solvents and have been characterized by conventional spectroscopic (NMR, IR, MS) and analytical techniques.[7] Since the first publication in 1993, our group has made organometallic dendrimers of high purity up to the fourth generation containing 48 metal atoms and with a molecular mass of over 18 000.[7]

We have thus shown that with the correct choice of metal and ligand system, it is possible to build up very large organometallic molecules. We are currently working on dendrimers of a range of other metals, including those containing iron, cobalt, rhenium, chromium and tungsten, as well as investigating the properties and applications of some of these dendrimers.[10]

It has been shown that oxidative addition of primary alkyl or benzyl halides, RX to $[PtMe_2(NN)]$ gives $[PtXMe_2R(NN)]$ (where NN represents a diimine ligand such as 2,2′-bipyridine) and these complexes can be prepared in essentially quantitative yields.[11] The oxidative addition reactions occur in high yield but the ability to grow large oligomers is limited since the solubility decreases with chain length. This strategy was adapted to prepare star-shaped multinuclear organoplatinum complexes.[12] The oxidative addition reactions occur with a colour change from orange–red of platinum(II) to the pale yellow of platinum(IV) and hence the reactions were easily monitored by visible spectroscopy.[12] The reaction cycles were repeated until NMR spectroscopy showed that the products contained defects. The limit to growth appears to occur after formation of the Pt_{14} dendrimer, shown in Fig. 1. Growth

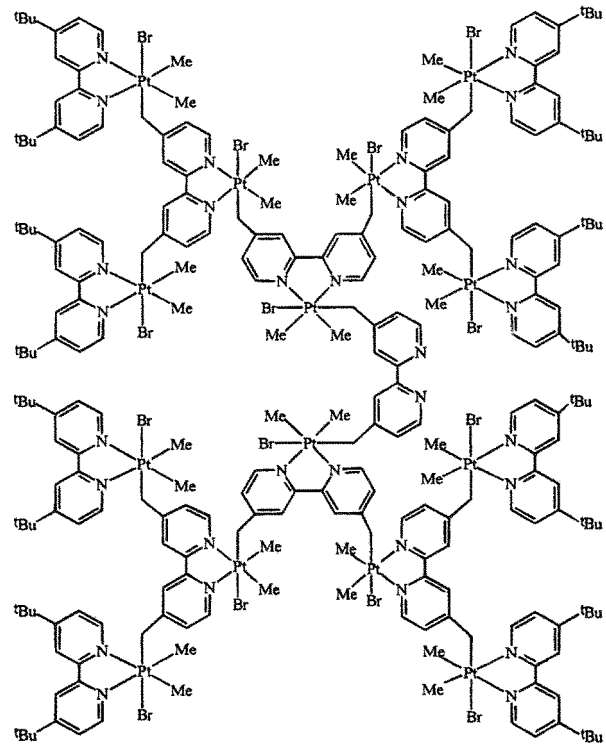

Fig. 1 The pale yellow Pt_{14} dendrimer.[11] Reprinted with permission from *Organometallics*, 1996, **15**, 43, copyright (1996) American Chemical Society.

beyond this to give the Pt_{30} dendrimer failed.[11] The limit to growth can be understood in terms of steric hindrance. The synthesis of larger platinum dendrimers was achieved by modification of the ligand. The key reagent for this work is the tetrafunctional core, 1,2,4,5-tetrakis(bromomethyl)benzene which could react with four organoplatinum(II) centres by oxidative addition of the C–Br bonds. In this approach, larger fragments are built first and then coupled to a polyfunctional core.[12] The solubility of the complexes was enhanced by the addition of the *tert*-butyl groups and the solubility of the products was found to increase with increased branching.

Recent work of the Puddephatt group has focussed on multinuclear organopalladium complexes and heterobimetallic palladium–platinum complexes. The authors wanted to see if

the oxidative addition reactions used previously could be employed. They found that incorporation of palladium in the structures is limited by the tendency of organopalladium(IV) complexes to undergo reductive elimination or alkyl halide transfer reactions. Some model complexes have been sucessfully synthesized.[13]

A sucessful route to multinuclear platinum complexes involves oxidative addition of an alkyl halide to platinum(II) providing the branching step, while ligand substitution by the bipyridine group provides a means of regenerating a reactive platinum(II) centre for the next growth cycle.[13]

Dendrimers with M–C π bonds

Ferrocene-based dendrimers

The majority of iron dendrimers reported to date have involved ferrocene derivatives. Perhaps the most obvious reason for this is that ferrocene chemistry is well established and documented and the compounds are stable. The construction of well defined dendrimers possessing redox-active organometallic units linked together in close proximity, so that there can be electronic communication between the metal sites in the dendritic structure, is a challenging target.[14] The dendrimer shown in Fig. 2 is the first example of an organometallic molecule to display

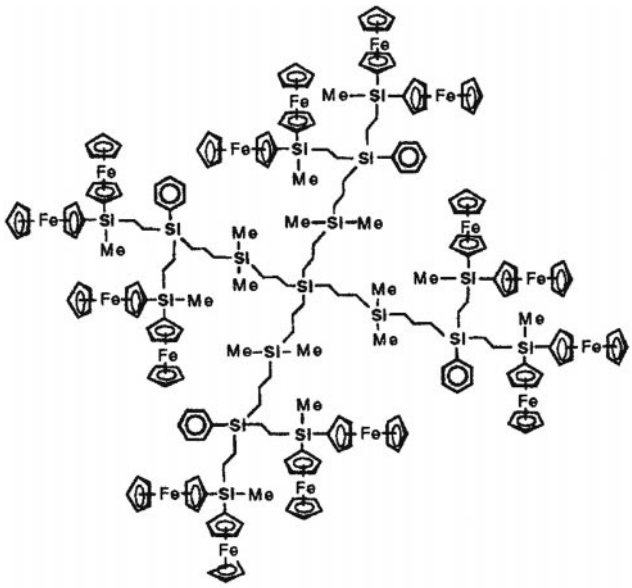

Fig. 2 A second generation silicon based dendrimer with ferrocenyl surface groups.[14] Reprinted with permission from *J. Am. Chem. Soc.*, 1997, **119**, 7613, copyright (1997) American Chemical Society.

electronic interaction between the transition metal atoms in the dendritic structure.[14]

Polymers containing ferrocene units are useful as redox catalysts for the modification of electrodes, and as biosensors.[15] $[FeCp(arene)]^+$ can serve as an excellent starting core for dendrimers since polyalkylation, polyallylation and polybenzylation of polymethyl arenes leads to various topologies.[15] The reaction of $[FeCp(C_6Me_6)]PF_6$ with excess base and an alkyl halide results in selective hexasubstitution [eqn. (1)].

$$[FeCp(C_6Me_6)]PF_6 \xrightarrow[RI\ (R\ =\ ferrocenylalkyl)]{KOR'\ (R'\ =\ H,\ Bu^t)} [FeCp\{C_6(CH_2R)_6\}]PF_6 \quad (1)$$

Cyclic voltammetry experiments showed that all six ferrocene units are electrochemically equivalent. The central cationic unit showed no influence on the oxidation process as the six outer ferrocene groups were oxidized at the same potential. The $CpFe^+$-induced hexaferrocenylalkylation of C_6Me_6 opens the route to isolable mixed-valence star-shaped molecules with independent redox centres and leads to a fully reversible six-electron redox system which may be useful for multielectron redox catalysis.[15] The multinuclear compounds have dendritic cores with organometallic surface groups.

One may also think of dendrimers as multisite guests for chemical interactions of any nature due to the regular placement of repeating residues on the dendrimer surface.[16] Ferrocenyl-functionalized amino dendrimers have been shown to include well known molecular hosts, specifically the cyclodextrins. The dendrimer serves as a three-dimensional template to organize the cyclodextrin receptors at the periphery of the dendritic structure, giving rise to large supramolecular assemblies.[16] The number of ferrocene units that can be included by the bulky cyclodextrin host is limited by the steric congestion on the surface of the dendrimer.

Fig. 3 shows the first heterometallic dendrimer containing

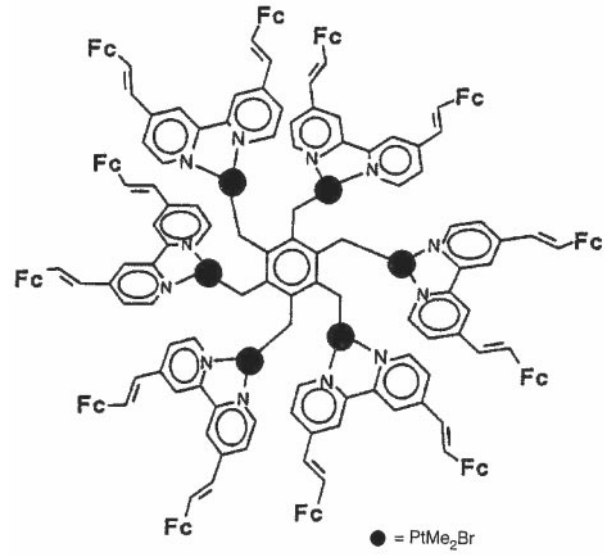

Fig. 3 A heterometallic dendrimer containing six platinum and twelve ferrocenyl centres.[17] Reprinted with permission from *Inorg. Chem.*, 1997, **36**, 2314, copyright (1997) American Chemical Society.

different transition metals in different layers.[17] This dendrimer features platinum(IV) units arranged in a concentric fashion around a central organic unit, with ferrocenyl groups as the surface functional groups. In this approach, dendritic arms containing one platinum and two ferrocenyl moieties were built first and then attached to a polyfunctional core *via* a convergent synthesis (Fig. 3).[17] The inclusion of redox-active centres into the dendrimers allows their composition to be determined by cyclic voltammetry. This alternative method of characterization may prove useful for other redox-active dendrimers.

Until recently, molecular recognition using dendrimer-based sensors was unknown. Some amido-ferrocenyl dendrimers have been synthesized and have been shown to be excellent redox sensors for the recognition of small inorganic anions such as Cl^-, NO_3^- and HSO_4^- (Fig. 4).[18] Cyclic voltamograms of these ferrocenyl dendrimers all show a single anodic reversible wave, indicating that all the iron(II)/iron(III) redox centres are independent and equivalent.[18] The dendrimers ability to sense and recognize the anions by cyclic voltammetry as the dendritic generation increases was found to be maximum for the generation (18 ferrocene groups) preceeding steric surface saturation (36 ferrocene groups). As the dendritic generation becomes higher, the ferrocenyl termini of the different dendritic branches become closer to one another, making the surface hole for the penetration of the anion smaller. Since the anions are small, the greatest effect and selectivity is found for the highest generation that is soluble because it forms the best open cavities. In comparison, endoreceptors also favour anion inclusion with open cavities where size compatibility is important.[18]

One potential role for a dendrimer is as an encapsulating shell around small molecules within it, or around the core of the

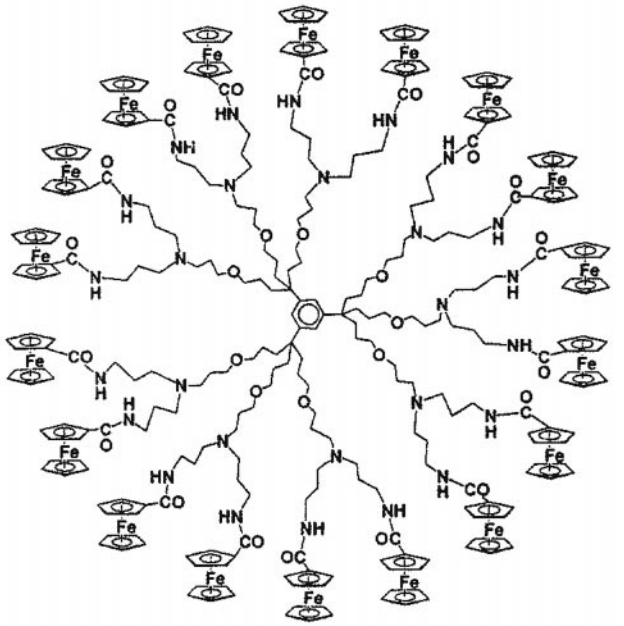

Fig. 4 An amidoferrocenyl dendrimer which acts as a redox sensor for the recognition of small inorganic anions.[18] Reprinted with permission from *J. Am. Chem. Soc*., 1997, **119**, 2588, copyright (1997) American Chemical Society.

dendrimer itself. Dendritic encapsulation offers a means of preventing facile electron transfer between closely spaced molecules which would result in loss of stored information.[19] One such application is as a molecular switch, in which an electroactive group can be held alternately in one of two binary states (corresponding to 'on' or 'off').[19] A third generation dendrimer with an electroactive core is shown in Fig. 5. The

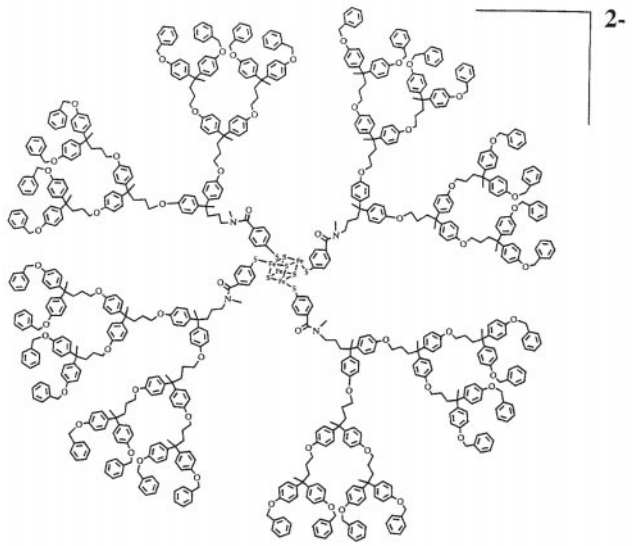

Fig. 5 An electroactive third generation encapsulated dendrimer.[19] Reprinted with permission from *Adv. Mater*., 1997, **9**, 1117, copyright (1997) Wiley-VCH.

core of one such dendrimer is an $Fe_4S_4(SR)_4^{2-}$ unit such as that found in some iron–sulfur proteins and is capable of existing in two stable redox states. Cyclic voltammetry experiments showed that as the number of branches in the dendrimer ligands around this core increased, the kinetic facility of electron transfer to and from the core decreased.[19]

From the number of ferrocene-containing dendrimers synthesized, it is evident that the ferrocene group is useful in the construction of dendrimers. The dendrimers prepared can be relatively easily characterized and their properties investigated by electrochemical methods.

Metal arene complexation

π-Complexation of transition metals to terminal arene ligands is another method of dendrimer modification. First and second generation organosilicon dendrimers have been prepared with aromatic rings on the periphery.[20] These surface-located arene rings were then π-coordinated to $Cr(CO)_3$ groups to give a new family of organometallic dendritic macromolecules containing η^6-arene coordinated $Cr(CO)_3$ groups at the periphery of the organosilicon dendritic cores; the tetranuclear compound is shown in Fig. 6. Attempts to prepare the octachromium

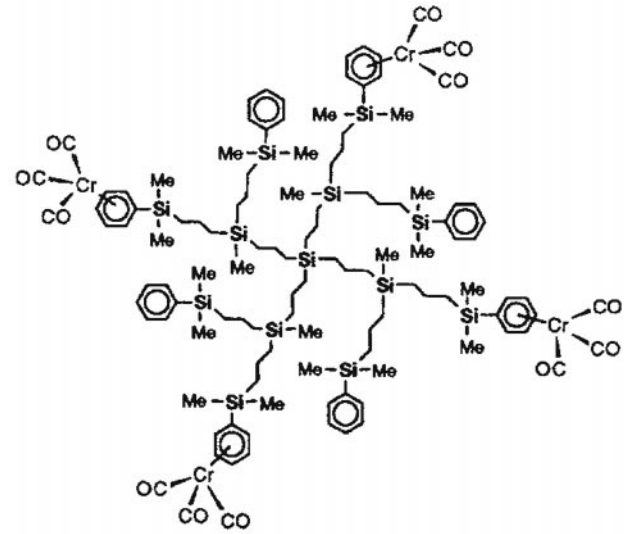

Fig. 6 The tetranuclear $Cr(CO)_3$ dendrimer.[20] Reprinted from *J. Organomet. Chem.*, 1996, **509**, 109, copyright (1996), with permission from Elsevier Science.

macromolecules failed probably due to the forcing reaction conditions which caused decomposition. The silicon dendrimers were prepared following a divergent approach which involved hydrosilylation and allylation as a means of growth.[20] These authors anticipate that the ability of the transition metals to π-complex to the peripheral aromatic rings of the novel silicon-based dendrimers should also be possible and will provide increased versatility for the design and synthesis of new families of dendritic macromolecules with different organo-transition metal groups.[20]

Dendrimers with tertiary phosphine ligands

Chemical functionality can be used as a means to control the 'placement' of the metal atom. Tertiary phosphines are known to bind to almost all transition metals of the periodic table.[21] It is thus not surprising to find a number of papers where a variety of metals, including palladium, rhodium and iridium, have been included in dendrimers *via* coordination of the metal to the surface phosphines. Thus, phosphorus-containing dendrimers up to the tenth generation and posessing either aldehyde groups or P–Cl bonds on the surfaces have been synthesized.[22] These terminal functions were reacted in order to anchor diphosphino groups on the surface of the dendrimer. The ability of the higher generation dendrimers to act as ligands towards palladium, platinum and rhodium complexes was then investigated. It was found that the end groups $\{-CH{=}NN(CH_2PPh_2)_2\}$ remained available for complexation with the metals and these new dendrimers may be of use as catalysts.[22]

Similarly, reactions of phosphorus dendrimers with ruthenium polyhydrides were investigated.[23] The new dendrimers have characteristic spectroscopic properties, in particular their ^{31}P and ^{1}H NMR spectra. Preliminary catalytic tests indicate good activity of these compounds for ketone hydrogenation.[23] The excellent coordinating ability of phosphorus to transition metals has been used to synthesize many novel organometallic

dendrimers and a number of these examples are discussed in the 'Dendrimers as catalysts' section.

Dendrimers with nitrogen donor ligands

Coordination centres in every layer

Dendrimers with coordination centres in every layer were constructed using transition metal coordination complexes as building blocks for branching or bridging to yield polynuclear compounds which behave as supramolecular systems.[24] The synthetic procedure is based on a protection/deprotection procedure in which a complex with free chelating sites is used as a ligand, and those with labile ligands play the role of metals ('complexes-as-ligands/complexes-as-metals' synthetic strategy).[25] This procedure allows the construction of large polynuclear metal complexes *via* metal–ligand coordination bonds. One of the advantages of this approach is that it is possible to introduce the desired building blocks at each stage of the synthesis. Dendrimers containing units of different chemical nature can exhibit valuable properties with specific functions, *e.g*. gradients for photoinduced directional energy and electron transfer, and sites for multi-electron transfer catalysis (see Fig. 7).[25]

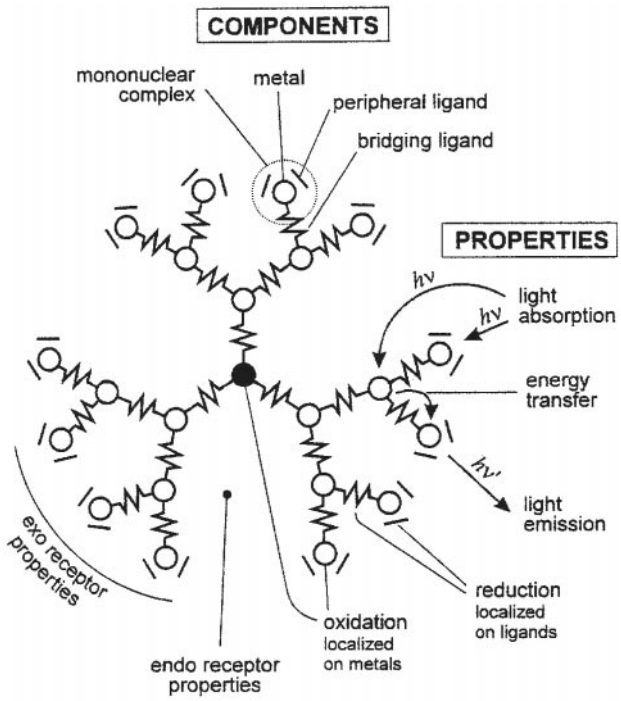

Fig. 7 Schematic representation of a luminescent and redox-active docosanuclear dendrimer with some of the properties indicated.[25] Reprinted with permission from *J. Mater. Chem*., 1997, **7**, 1227, copyright (1997) The Royal Society of Chemistry.

Because of their remarkable photophysical and electrochemical properties, ruthenium(II)– and osmium(II)–polypyridine complexes[25,26] are ideal components to synthesize luminescent and redox-active oligonuclear species where energy and electron transfer can be driven by light.[26] A great number of compounds have been synthesized using the 2,3- and 2,5-bis(2-pyridyl)pyrazine (2,3- and 2,5-dpp) bridging ligands, and the 2,2′-bipyridine (bpy) and 2,2′-biquinoline (biq) terminal ligands.[26]

The complexes studied contain several chromophoric units in addition to a large number of redox-active centres. Studies carried out on these complexes show the oxidation behaviour to exhibit a selectivity based on the nature of the metal ion and its position in the supramolecular array, thus offering a means of fingerprinting the compounds. Because of the presence of both interacting and non-interacting redox centres, these complexes are good candidates for multielectron-transfer catalysts.[26] The dendrimers reported also display luminescence in solution at room temperature.[25]

2,2′:6′,2″-Terpyridine as a ligand

The coordination of appropriate organic molecules containing multiple metal-binding sites to metal ions provides a versatile alternative to carbon–carbon or carbon–heteroatom bond formation for the construction of dendrimers.[27,28] 2,2′:6′,2″-Terpyridine (terpy), has been reported by a number of authors as a successful connecting ligand to combine preconstructed metal–ligand fragments.[29] Such connectivity permitted the analysis of the final product by electrochemical methods. It had previously been shown that benzylic halides react smoothly with the triruthenium nucleophile, [(terpy)Ru(botpy)Ru(botpy)Ru(HOtpy)][PF_6]$_6$, [botpy = bis(4′-(2,2′:6′,2″-terpyridinyl) ether, HOtpy = 2,2′:6′,2″-terpyridin-4′(1′*H*)-one].The reaction of 1 equiv. of hexakis(bromomethyl) benzene with 6 equiv. of [(terpy)Ru(botpy)Ru(botpy)Ru(HOtpy)][PF_6]$_6$ gave the octadecaruthenium complex (Fig 8).[27] MALDI TOF mass spectrometry provided a convenient and rapid method for the determination of the nuclearity.[27]

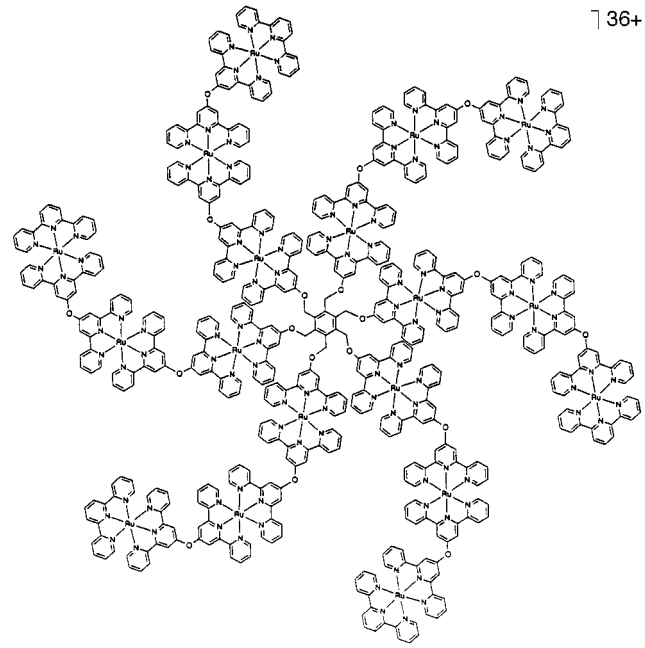

Fig. 8 An octadecaruthenium metallodendrimer.[27] Reprinted from *Inorg. Chim. Acta*, 1996, **252**, 9, copyright (1996), with permission from Elsevier Science.

The construction of this new type of double-tiered metallodendrimer illustrates the importance of stepwise construction by means of controlled metal complexation.[29] This approach also provides versatile methodology for the synthesis of specifically assembled metallodendrimers and related polymers using a combination of the convergent and divergent approaches.[29]

Pincer-type complexes

There is considerable interest in the synthesis of well defined structures of nanometer dimensions.[30] Nanostructures can be developed in an efficient way through non-covalent interactions, *e.g*. H-bonds as opposed to covalent bonds which require multistep syntheses.[30] The early work was carried out using building blocks containing kinetically inert SCS Pd-pincer complexes, coupled *via* branched spacers. The complexes are labile when the fourth ligand is nitrile but not chloride. The coordination of the nitrile ligand to coordinatively unsaturated palladium centres was exploited to assemble the dendrimer building blocks *via* non-covalent interactions. Changing from SCS to PCP ligands made it possible to introduce a variety of transition metals.[31] Ligands derived from the coupling of 3,5-bis[(diphenylphosphino)methyl]phenoxy

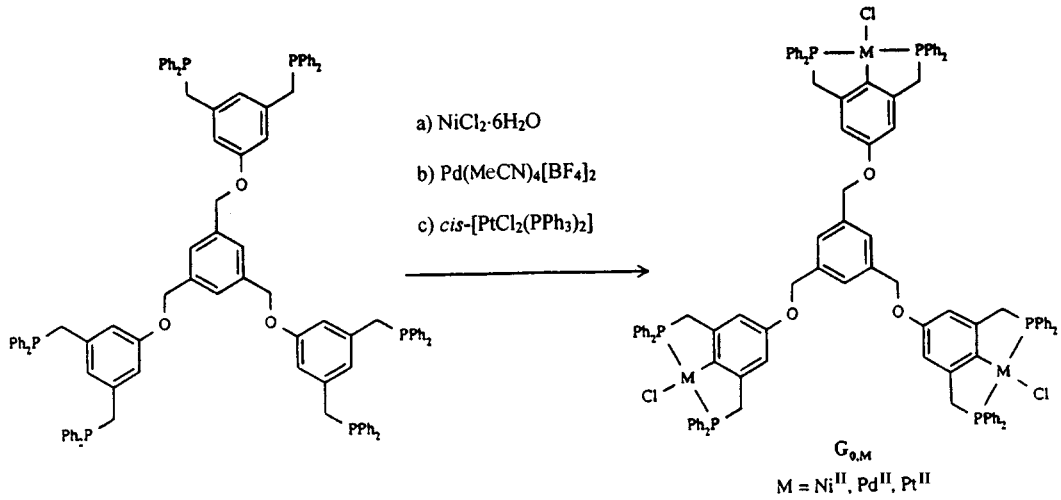

Scheme 3 Reprinted with permission from *Organometallics*, 1997, **16**, 4287, copyright (1997) American Chemical Society.

groups to bi- and tri-functional spacers have been cyclometalated with $[Pd(MeCN)_4][BF_4]_2$, *cis*-$[PtCl_2(PPh_3)_2]$ or $NiCl_2 \cdot 6H_2O$ and the resulting cationic complexes converted to neutral complexes. These resulting pincer complexes were then used as building blocks for the controlled assembly of homo- and hetero-multinuclear dendrimers (see Scheme 3).[31] ^{31}P NMR spectroscopy was successfully used as a diagnostic tool for the assembly process as the chemical shift values are very sensitive towards small changes in the microenvironment around the metal centre.

Polynuclear gold(I) complexes

Very little is known about the surface coordinating properties of dendrimers.[32] A few papers on surface-complexing properties of polynuclear gold(I) complexes have been reported[32,33] Dendritic polyamines have been functionalized with terminal diphenylphosphino groups which are ideal for surface complexation of transition metals in low oxidation states and a tailor made 'spacer' bearing a group suitable for coupling.[32] A fourth generation polynuclear gold(I) complex with 32 terminal chloro(diphenylphosphino)gold(I) groups is shown in Fig. 9.[32]

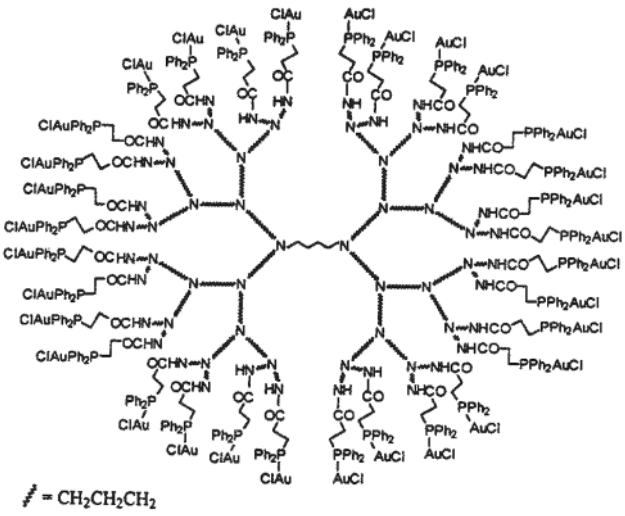

Fig. 9 A polynuclear gold(I) complex with 32 terminal chloro(diphenylphosphino)gold(I) groups.[32] Reprinted with permission from *Inorg. Chem.*, 1996, **35**, 637, copyright (1996) American Chemical Society.

X-Ray crystallography was carried out on the smaller mono- and di-nuclear gold(I) complexes. Intermolecular NH···O hydrogen bonds direct the aggregation of the molecules in the solid state to give chainlike structures. These multinuclear gold(I) complexes[32] represent a new type of metal-containing polymer with a well defined, probably spherical structure and having dendrimer molecules as supporting matrices. They have potential applications in catalysis, biochemical diagnostics and imaging.[32]

Seventh generation phosphorus-containing dendrimers containing reactive functional groups also allowed the complexation of gold derivatives.[33] These appear to be the largest polyphosphine complexes ever prepared, with 3072 $CH_2PPh_2(AuCl)$ end groups.[33]

Main group dendrimers

Much attention has been focussed on main-group-element-based dendrimers, in particular on those based on silicon because of their optical properties and importance in surface functionalization.[34] We will only mention here the recently prepared germanium/silicon dendrimers[35] in this article. The most direct method of preparation would have involved sucessive alkenylations and hydrogermylations, starting with $GeCl_4$. However allylic germanium derivatives are very sensitive to electrophilic reagents. To avoid difficulties associated with undesirable by-products and to diminish the steric strain resulting from the accumulation of branched chains, six-membered ω-ethylenic chains, which are more stable than α- or β-ethylenic chains, were used. Bis(dimethylphenylgermyl)-(methyl) silyllithium was used as the building agent. Using this method, second generation dendrimers having a molecular weight of 5590 were synthesized.[35] Very recently, some dendritic molecules with alternating silicon and germanium atoms along the dendritic backbone, including the molecular structure of a first-generation hybrid permethylated dendrimer, have also been reported.[34]

Structural details and properties of dendrimers

There has been much controversy over the exact shape of dendrimers in solution and many conflicting results have been obtained. The first attempts to calculate dendritic structures were by de Gennes and Hervet.[36] They showed the chain ends to be on the periphery and found a density minimum at the core and a density maximum at the surface. In contrast, Lescanec and Muthukumar allowed the inward folding of chain ends in their calculations which resulted in a density maximum between the dense core and the periphery.[37] Other solution studies showed dendrimers to have low intrinsic viscosities that decreased as the molecular weight increased. They concluded that dendrimers posess globular shapes and lack intermolecular entanglements.[38]

Monte Carlo calculations by Mansfield and Klushin found the chain ends to be distributed throughout the structure, and in close proximity to the core and revealed a density maximum between the centre of mass and the periphery.[39]

Our investigations of Fréchet type poly(benzylphenyl ether) dendrimers functionalized with arene tricarbonylchromium(0)

groups showed a transition from an extended to a globular structure as the generation number increased.[40] Solvent accessible surface calculations showed more backfolding to occur as the dendrimer became larger. Although the chain ends were found in all regions of the dendrimer to some extent, most were still located on the periphery of the molecule or in a solvent accessible area for those dendrimers studied. Recent rotational-echo double-resonance NMR experimnets by Wooley *et al.* used experimental constraints on molecular dynamics simulations for the prediction of dendritic structure.[41]

Generally speaking, lower generation dendrimers tend to exist in relatively open forms, but as sucessive layers are added, dendrimers adopt a spherical three-dimensional structure. Solution state properties of dendrimers are generally consistent with a globular shape with the chain ends accessible to the surface, but the precise shape and chain end locations remain uncertain.

Applications of dendrimers as catalysts

One of the most important and exciting uses of dendrimers is expected to be in the field of catalysis. There is great scope for the development of new materials that combine the advantages and minimise the disadvantages associated with heterogeneous and homogeneous catalysts.[42] One approach to such materials is to anchor homogeneous catalysts to polymer supports. Such polysiloxane polymers containing a catalytically active nickel(II) centre have been prepared.[43] However, the disadvantages encountered when anchoring catalytically active metal sites to polymers include the difficulty of accurate control of the number and location of these sites.[42] An ideal polymeric catalyst should be a soluble, multifunctional macromolecule, favouring configurations in which all active sites would be exposed towards the reaction mixture so that they are easily accessible to migrating reactants. Owing to their expected spherical nature, dendritic catalysts are expected to retain the benefits of homogeneous catalysts, such as faster kinetics and accessibility of metal sites but should be easily recoverable from a product-containing solution because of their large size. Ultrafiltration techniques could be used as a means of separation.

The most well known example of a dendrimer used as a catalyst was published in 1994.[42] Zero and first generation polysilane dendrimers were functionalized with diamino arylnickel(II) complexes on their periphery, the metal centre being fixed by a metal–carbon sigma bond to the ligand system (Fig. 10). These dendrimers have been successfully used as homogeneous catalysts for the Kharasch addition of polyhalogenoalkanes to an alkenic C═C double bond. Under mild reaction conditions (room temperature, CH_2Cl_2 as solvent) using methyl methacrylate as substrate and CCl_4 as reagent, the catalytic activity of these zero and first generation dendrimers, as shown by kinetic data, is 20 and 30 % respectively less than the monomeric compound.[42] Molecular models of these dendrimers such as that in Fig. 10, show the nickel sites to be well separated from one another at the end of long flexible branches and consequently the accessibility of the catalytically active nickel centres should be similar to the monomeric model compounds synthesized previously. All the characteristics found for the monomeric model are retained in the dendrimer catalyst system. These new dendrimers represent nanoscopic catalysts with physical characteristics such as size, solubility and dispersity of catalytic sites that are very precisely defined, so affording these molecules advantageous properties for physical separation and catalyst recycling.[42]

The excellent coordinating ability of phosphines has been used to prepare novel organometallic dendrimers. It has previously been shown that mononuclear [Pd(triphosphine)(MeCN)][BF_4]$_2$ complexes will catalyse the electrochemical reduction of CO_2 to CO.[44] The presence of a triphosphine ligand in these catalysts suggests that dendrimers containing this unit may also catalyse the reduction. Two approaches have been used to synthesize such dendrimers, the first involving sequential addition of diethyl vinylphosphonate to primary phosphines

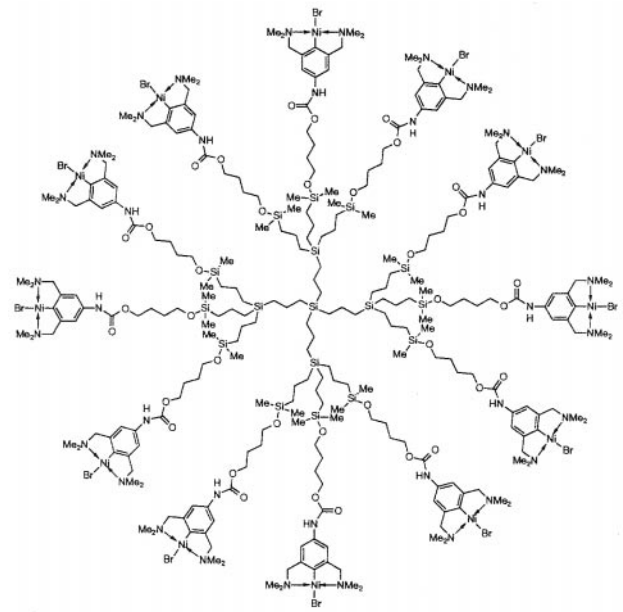

Fig. 10 Schematic structure of the first generation poylsilane dendrimer functionalized with catalytically active diamino arylnickel(II) complexes on the periphery.[42] reprinted with permission from *Nature*, 1994, **372**, 659, copyright (1994) Macmillan Magazines Ltd.

followed by reduction with lithium aluminium hydride; the second approach using the addition of bis[(diethylphosphino)ethyl]phosphine to tetravinylsilane. Small dendrimers containing 12 or 15 phosphorus atoms metallated with [Pd(MeCN)$_4$][BF_4]$_2$ have now been shown to exhibit catalytic activity for the electrochemical reduction of CO_2. These results demonstrate the feasibility of performing catalytic reactions using metallated organophosphine dendrimers.[44]

Dendritic diphosphines synthesized from polyamino dendrimers by double phosphinomethylation of each of the primary amino end-groups provides the possibility of specific complexation with a variety of transition metals including iridium, palladium and rhodium (Fig. 11).[45] The metal-containing

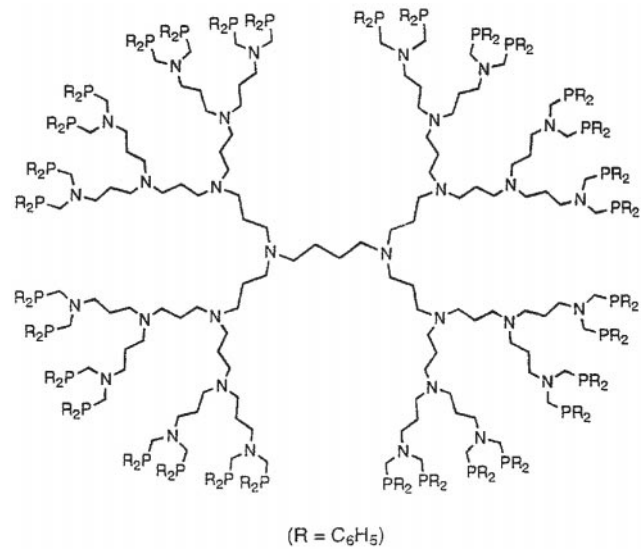

Fig. 11 The phosphinomethylated dendrimer with sixteen bidentate ligands on the outer surface provides the possibility of complexation with many transition metals.[39] Reprinted with permission from *Angew. Chem., Int. Ed. Engl.*, 1997, **36**, 1526, copyright (1997) Wiley-VCH.

dendrimers were successfully used to catalyse the Heck reaction of bromobenzene and styrene to form stilbene. The reaction mixture was analysed by gas chromatography.[45] In previous examples of catalysis with dendritic metal complexes, the catalytic activity was shown to be slightly or significantly lower than that of the corresponding monomeric parent compounds.

This system, however, showed a significantly higher activity, which is attributable to the higher thermal stability of the dendritic complexes. The strategy developed here for the synthesis of dendritic diphosphines opens up a general method for preparing transition metal-containing dendrimers for use in catalysis.[45]

Most of the optically active chelating phosphines used in enantioselective transition metal catalysis involve a chiral skeleton bearing two diphenylphosphino groups.[46] The chiral information is transferred from the ligand to the catalytically active centre *via* the arrangement of the phenyl rings of the diphenylphosphino groups.[46] Owing to the limited size of the diphenylphosphino groups, the idea of using larger phosphines represents a promising new approach.[46] The expanded phosphines should contain a chelate skeleton, *e.g.* the PCH_2CH_2P grouping, and several layers of branching units built up with optically active groups attached to the phosphorus atoms.[46] Owing to the space-filling nature of the expanded ligands, the chiral information should be forced towards the pocket of the catalyst, in which the enantioselective reaction takes place. Because the catalytic reaction takes place at the core of the dendrimer, the system resembles the prosthetic group of an enzyme. For this reason, these molecules have been termed 'dendrizymes'.

Conclusions and future developments

An exciting future is forseen for dendrimers, and transition-metal-containing dendrimers in particular. Already the rapidly growing increase in the number of publications is an indication that dendrimers represent a new and important class of compounds. It has been demonstrated in the examples above that it is possible to synthesize mono- and multi-metallic molecules with desirable characteristics and properties by careful choice of metal and ligand systems. Little work on the solid-state structures of dendrimers has thus far been carried out, presumably because of the difficulty of crystallising them. For this reason, molecular modelling is expected to play a key role in providing some of the answers concerning structures and also properties. Dendrimer research has already shifted from a purely synthetic orientation towards investigating the novel properties and exploring the potential applications of these molecules, in particular catalysis. Already we have seen their novel applications as encapsulation reagents, artificial gene-transfer materials, as building blocks for the self-assembly of larger nanostructures and in chiral recognition. Important applications will likely emerge in the next few years in a diversity of fields. New synthetic methods will continue to be important until dendrimers can be produced cheaply and easily on an industrial scale.

Only time will unveil the full range of applications of these large and beautiful molecules.

Acknowledgements

We thank the University of Cape Town, the Foundation for Research Development and Polifin Ltd for support, and Dr Alan Hutton for many valuable comments.

Notes and references

1 D. A. Tomalia, H. M. Brothers II, L. T. Piehler and Y. Hsu, *Polym. Mater. Sci. Eng*., 1995, **73**, 75; N. Ardoin and D. Astruc, *Bull. Soc. Chim. Fr*., 1995, **132**, 875 and references therein; F. Zeng and S. Zimmerman, *Chem. Rev*., 1997, **97**, 1681 and references therein.
2 C. J. Hawker and J. M. J. Fréchet, *J. Am. Chem. Soc*., 1990, **112**, 7638; K. L. Wooley, C. J. Hawker and J. M. J. Fréchet, *J. Chem. Soc., Perkin Trans. 1*, 1991, 1059.
3 W. J. Pope and S. J. Peachey, *Proc. Chem. Soc*., 1907, **23**, 86.
4 J. R. Moss, *Trends Organomet. Chem.*, 1994, **1**, 211 and references therein; *Comprehensive Organometallic Chemistry*, ed. E. W. Abel, F. G. A. Stone and G. Wilkinson, Pergamon, New York, Series I (1982) and II (1995).
5 B. C. Gates, *Catalytic Chemistry*, Wiley, New York, 1992.
6 H. B. Friedrich and J. R. Moss, *Adv. Organomet. Chem*., ed. F. G. A. Stone and R. West, Academic Press, London, 1991, vol. 33, p. 235.
7 Y.-H. Liao and J. R. Moss, *Organometallics*, 1996, **15**, 4307; 1995, **14**, 2130; *J. Chem. Soc., Chem. Commun*., 1993, 1774.
8 M. A. Hearshaw, J. R. Moss, W. McLean and M. R. Caira, unpublished work.
9 R. George, J.-A. M. Andersen and J. R. Moss, *J. Organomet. Chem*., 1995, **505**, 131.
10 M. A. Hearshaw, J. R. Moss, F. Waggie, S. J. Hughes, X. Yin, R. Zeng and I. Mavunkal, unpublished work.
11 S. Achar, J. J. Vittal and R. J. Puddephatt, *Organometallics*, 1996, **15**, 43.
12 S. Achar and R. J. Puddephatt, *Organometallics*, 1995, **14**, 1681, *Angew. Chem., Int. Ed. Engl.*,1994, **33**, 847.
13 G.-X. Liu and R. J. Puddephatt, *Organometallics*, 1996, **15**, 5257, *Inorg. Chim. Acta*, 1996, **251**, 319.
14 I. Cuadrado, C. Casado, B. Alonso, M. Morán, J. Losada and V. Belsky, *J. Am. Chem. Soc.*, 1997, **119**, 7613; B. Alonso, M. Morán, C. M. Casado, F. Lobete, J. Losada and I. Cuadrado, *Chem. Mater*., 1995, **7**, 1440.
15 J.-L. Fillaut, J. Linares and D. Astruc, *Angew. Chem., Int. Ed. Engl.*, 1994, **33**, 2460; J.-L. Fillaut and D. Astruc, *J. Chem. Soc., Chem. Commun*., 1993, 1320; F. Moulines, L. Djakovitch, R. Boese, B. Gloaguen, W. Thiel, J.-L. Fillaut, M-H. Delville and D. Astruc, *Angew. Chem., Int. Ed. Engl*., 1993, **32**, 1075.
16 R. Castro, I. Cuadrado, B. Alonso, C. M. Casado, M. Morán and A. E. Kaifer, *J. Am. Chem. Soc*., 1997, **119**, 5760.
17 S. Achar, C. E. Immoos, M. G. Hill and V. J. Catalano, *Inorg. Chem*., 1997, **36**, 2314.
18 C. Valério, J.-L. Fillaut, J. Ruiz, J. Guittard, J-C. Blais and D. Astruc, *J. Am. Chem. Soc*., 1997, **119**, 2588.
19 C. Gorman, *Adv. Mater*., 1997, **9**, 1117.
20 F. Lobete, I. Cuadrado, C. M. Casado, B. Alonso, M. Morán and J. Losada, *J. Organomet. Chem*., 1996, **509**, 109.
21 *Transition Metal Complexes of Phosphorus, Arsenic and Antimony Ligands*, ed. C. A. McAuliffe, Macmillan, London, 1973.
22 M. Bardaji, M. Kustos, A.-M. Caminade, J.-P. Majoral and B. Chaudret, *Organometallics*, 1997, **16**, 403.
23 M. Bardaji, A.-M. Caminade, J.-P. Majoral and B. Chaudret, *Organometallics*, 1997, **16**, 3489.
24 S. Serroni, G. Denti, S. Campagna, A. Juris, M. Ciano and V. Balzani, *Angew. Chem., Int. Ed. Engl*, 1992, **31**, 1493.
25 S. Serroni, A. Juris, M. Venturi, S. Campagna, I. R. Resino, G. Denti, A. Credi and V. Balzani, *J. Mater. Chem*., 1997, **7**, 1227.
26 G. Denti, S. Campagna, S. Serroni, M. Ciano and V. Balzani, *J. Am. Chem. Soc*., 1992, **114**, 2944.
27 E. Constable and P. Harverson, *Inorg. Chim. Acta*, 1996, **252**, 9.
28 E. Constable, *Chem. Commun*., 1997, 1073.
29 G. Newkome and E. He, *J. Mater. Chem*, 1997, **7,** 1237; G. R. Newkome, F. Cardullo, E. C. Constable, C. N. Moorefield and A. M. W. Cargill Thompson, *J. Chem. Soc., Chem. Commun*., 1993, 925.
30 W. T. S. Huck, F. C. J. M. van Veggel and D. N. Reinhoudt, *Angew. Chem., Int. Ed. Engl.*,1996, **35**, 1213.
31 W. T. S. Huck, B. Snellink-Ruel, F. C. J. M. van Veggel and D. N. Reinhoudt, *Organometallics*, 1997, **16**, 4287.
32 P. Lange, A. Schier and H. Schmidbaur, *Inorg. Chem*., 1996, **35**, 637; *Inorg. Chim. Acta*, 1995, **235**, 263.
33 M. Slany, M. Bardají, M.-J. Cassanove, A.-M. Caminade, J.-P. Majoral and B. Chaudret, *J. Am. Chem. Soc*., 1995, **117**, 9764.
34 M. Nanjo and A. Sekiguchi, *Organometallics*, 1998, **17**, 492.
35 V. P. Huc, P. Boussaguet and P. Mazerolles, *J. Organomet. Chem*., 1996, **521**, 253.
36 P. G. de Gennes and H. Hervet, *Phys.: Lett.*, 1983, **44**, L351.
37 R. L. Lescanec and M. Muthukumar, *Macromolecules*, 1990, **23**, 2280.
38 T. H. Mourey, S. R. Turner, M. Rubinstein, J. M. J. Fréchet, C. J. Hawker and K. L. Wooley, *Macromolecules*, 1992, **25**, 2401.
39 M. L. Mansfield and L. I. Klushin, *Macromolecules*, 1993, **26**, 4262.
40 K. J. Naidoo, S. J. Hughes and J. R. Moss, *Macromolecules*, in press.
41 K. L. Wooley, C. A. Klug, K. Tasaki and J. Schaefer, *J. Am. Chem. Soc*., 1997, **119**, 53.
42 J. W. J. Knapen, A. W. van der Made, J. C. de Wilde, P. W. N. M. van Leeuwen, P. Wijkens, D. M. Grove and G. van Koten, *Nature*, 1994, **372**, 659.
43 L. A. van de Kuil, D. M. Grove, J. W. Zwikker, L. W. Jenneskens, W. Drenth and G. van Koten, *Chem. Mater*., 1994, **6**, 1675.
44 A. Miedaner, C. J. Curtis, R. M. Barkley and D. L. DuBois, *Inorg. Chem*., 1994, **33**, 5482 and references therein.
45 M. T. Reetz, G. Lohmer and R. Schwickardi, *Angew. Chem., Int. Ed. Engl*, 1997, **36**, 1526.
46 H. Brunner, *J. Organomet. Chem*., 1995, **500**, 39.

Paper 8/03535K

Steroidal guanidinium receptors for the enantioselective recognition of *N*-acyl α-amino acids

Anthony P. Davis* and Laurence J. Lawless

Department of Chemistry, Trinity College, Dublin 2, Ireland. E-mail: adavis@tcd.ie

Received (in Liverpool, UK) 23rd October 1998, Accepted 9th November 1998

Guanidinium cations 4 and 5 extract *N*-acetyl α-amino acids into $CHCl_3$ from an aqueous medium with enantiomeric excesses of up to 80%.

Enantioselective recognition is of continuing interest in supramolecular chemistry,[1] especially where relevant to the large-scale resolution of racemates. Enantioselective phase transfer is particularly attractive, raising the possibility of 'catalytic' resolutions based on the transport of substrates through otherwise impermeable barriers.[2] Carboxylates/carboxylic acids are suitable targets for this approach, because of their ability to partition between aqueous and organic phases. Amino acids, and their *N*-acyl derivatives, are attractive substrates because of their biological significance and practical importance.[3]

Herein we describe a new strategy for the enantioselective extraction of chiral carboxylates from aqueous into organic media, and its realisation in the form of receptors which show significant enantiodiscrimination in the case of *N*-acetyl α-amino acids. In common with previous work on carbohydrate[4] and anion recognition,[5] our design exploits cholic acid **1** as a starting material. The secondary hydroxy groups in **1** can be independently modified to give differentiated, co-directed substituents as in **2**.[6] Groups A–C are spaced so as to allow, in

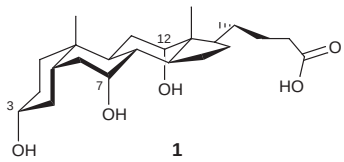

1

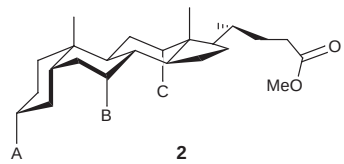

2

a typical case, cooperative effects on a substrate with minimum interference from intramolecular interactions. The design is suggestive of 'three-point contact', as required for the classical model of enantioselective recognition.[7]

For carboxylate extraction, it is useful that one of groups A–C should form a specific, electroneutral complex with the anionic centre. To serve this purpose we have chosen the guanidinium unit **3**, capable of binding carboxylates as shown.[8] Of the possible variations on our general theme, we report the synthesis and properties of two initial examples; the bis-phenylcarbamate **4** and its asymmetrically-substituted relative **5**. Receptor **4** was accessible from 3α-azide **6**[9] as shown in Scheme 1, while receptor **5** was prepared *via* a longer sequence with alcohol **7** as the penultimate intermediate.

As anticipated, solutions of **4**·Cl^- and **5**·Cl^- in $CHCl_3$ were capable of extracting carboxylic acids from neutral or basic aqueous solutions, presumably through exchange of carboxylate for chloride. In the case of *N*-acetyl α-amino acids the ^1H NMR spectra of the complexed substrates were enantiomer-

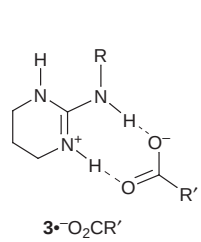

3•$^-O_2CR'$

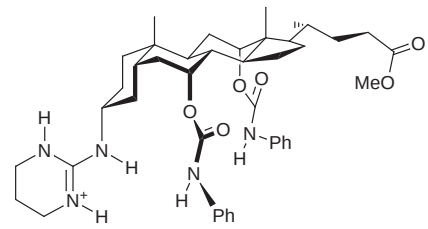

4

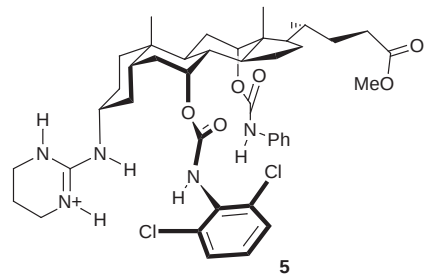

5

dependent, allowing the determination of enantioselectivities, as well as extraction efficiencies, by simple integration. The results are shown in Table 1. Extraction efficiencies were moderate to good for substrates with non-polar side-chains, although neither receptor was effective with the polar asparagine derivative. Receptor **4** proved remarkably consistent in its

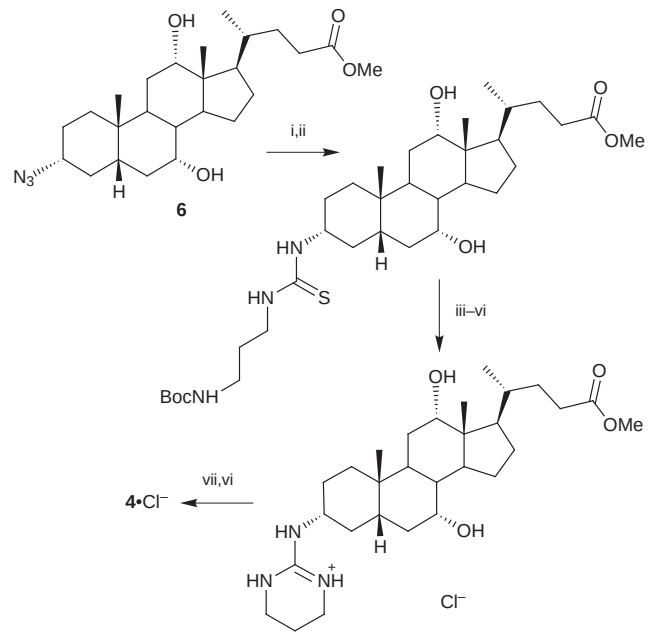

Scheme 1 *Reagents and conditions*: i, Zn dust, AcOH, room temp., 24 h; ii, $SCN(CH_2)_3NHBoc$, Pr^i_2NEt, dry CH_2Cl_2, room temp., 72 h; iii, MeI, MeOH, reflux; iv, TFA, CH_2Cl_2, room temp.; v, Pr^i_2NEt, MeOH, room temp., 24 h; vi, aq. NaOH then aq. HCl; vii, PhNCO, conc. aq. HCl (cat.), CH_2ClCH_2Cl, reflux, 72 h.

Table 1 Extractions by **4**·Cl⁻ and **5**·Cl⁻ of racemic *N*-acetyl α-amino acids from aqueous buffer (pH 7.4) into $CHCl_3$[a]

	Receptor **4**		Receptor **5**	
Substrate	Extraction efficiency (mol%)[b]	Enantio-selectivity (L:D)[c]	Extraction efficiency (mol%)[b]	Enantio-selectivity (L:D)[c]
N-Ac-alanine	52	7:1	76	6:1
N-Ac-phenylalanine	87	7:1	93	9:1
N-Ac-tryptophan	83	7:1	92	6:1
N-Ac-valine	71	7:1	89	9:1
N-Ac-*tert*-leucine	[d]	[d]	82	5:2
N-Ac-methionine	[d]	[d]	93	9:1
N-Ac-proline	[d]	[d]	74	4:1
N-Ac-asparagine	0	—	0	—

[a] Solutions of receptor in $CHCl_3$ (6 mM, 1 ml), and substrate in phosphate buffer (7–8 mM, 5 ml), were stirred vigorously for 2 h. The organic phases were isolated, dried by passage through hydrophobic filter paper, then evaporated. The residues were dissolved in $CDCl_3$ (0.6 ml) and analysed by ^{1}H NMR spectroscopy. [b] Determined by ^{1}H NMR integration of substrate α-C*H* and N*H vs*. 7/12β-*H* of receptor. [c] Determined by ^{1}H NMR integration of α-C*H* and N*H* signals for enantiomers of substrates. Assignments confirmed through control experiments with enantiopure substrates. [d] Not determined.

ability to differentiate between enantiomers, irrespective of side-chain bulk. Receptor **5** showed generally higher extraction abilities, possibly due to the greater acidity of the dichlorophenylcarbamoyl NH, and was more sensitive to side-chain structure. Perhaps surprisingly, the substrate with the most sterically hindered asymmetric centre (*N*-Ac-*tert*-leucine) gave the lowest selectivity.

^{1}H NMR spectroscopy and molecular modelling combined to suggest plausible models for the binding geometries. A Monte Carlo Molecular Mechanics (MCMM) search† on the complex between **5** and *N*-acetyl-L-valinate **8** yielded the configuration shown in Fig. 1. The carboxylate accepts H-bonds from the 7-carbamoyl and two guanidinium NH groups, while the acetyl oxygen is bound to the 12-carbamoyl NH. In support of this structure, the receptor carbamate and 2 of the 3 guanidinium N*H* signals moved downfield on complex formation, while a weak

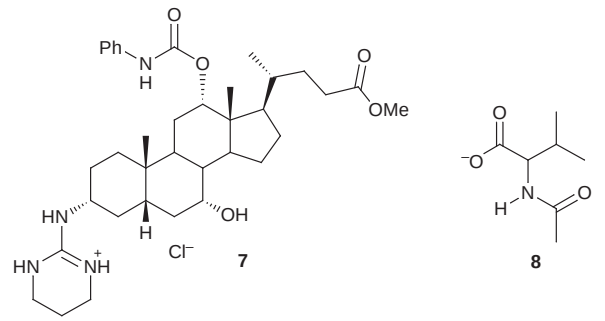

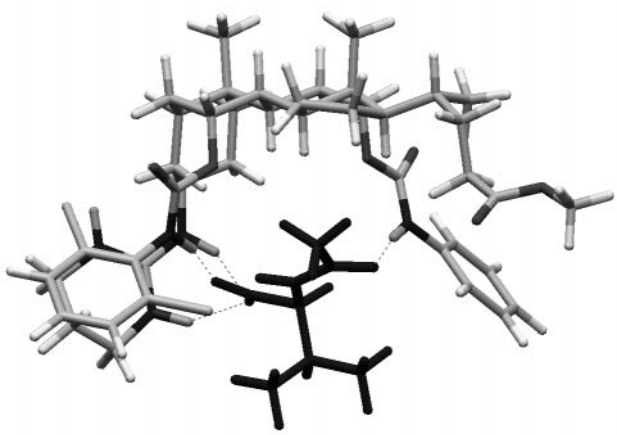

Fig. 1 Structure of **5** + L-**8** (black) derived from computer-based molecular modelling. Intermolecular hydrogen bonds are shown as broken lines.

intermolecular NOE was observed from the α-C*H* in L-**8** to the *ortho* protons of **5**-NH*Ph* (consistent with Fig. 1, allowing for some rotational freedom about the N–Ph bond‡). A similar MCMM search† on **5** + D-**8** yielded a higher-energy structure in which the acetyl O···HN interaction is missing, the 12-carbamoyl NH forming a fourth (apparently strained) hydrogen bond to the carboxylate.

Viewed as forerunners of an extended family of receptors, **4** and **5** show encouraging levels of enantioselectivity. Many variants are within easy reach, a majority with much greater differentiation between the three substituents. We hope to report examples with improved performance in the foreseeable future.

Financial support for this work was provided by Forbairt, the Irish Science and Technology Agency, Schering Plough (Avondale) Ltd., and the EU Training and Mobility for Researchers programme. We are grateful to Peter Ashton (University of Birmingham) for mass spectra, Dr John O'Brien for non-routine NMR experiments, and Freedom Chemical Diamalt GmbH for generous gifts of cholic acid.

Notes and references

† Calculations employed MacroModel V5.5 (ref. 10), the Amber* force field, $CHCl_3$ GB/SA solvation, and 5000 steps of MCMM. Six and three separate searches were conducted for the L and D substrates respectively, all from widely differing starting geometries and all yielding essentially similar final structures.

‡ Rotation about N–Ph allows an *ortho* proton to make van der Waals contact with the substrate α-CH.

1 T. H. Webb and C. S. Wilcox, *Chem. Soc Rev*., 1993, **22**, 383.
2 M. Newcomb, J. L. Toner, R. C. Hegelson and D. J. Cram, *J. Am. Chem. Soc*., 1979, **111**, 6294.
3 Enantioselective extraction/transport of amino acids or *N*-acyl amino acids : (*a*) J. L. Sessler and A. Andrievsky, *Chem. Eur. J*., 1998, **4**, 159; (*b*) N. Voyer and B. Guerin, *Chem. Commun*., 1997, 2329; (*c*) J. Y. Zheng, K. Konishi and T. Aida, *Tetrahedron*, 1997, **53**, 9115; (*d*) K. Konishi, K. Yahara, H. Toshishige, T. Aida and S. Inoue, *J. Am. Chem. Soc*., 1994, **116**, 1337; (*e*) A. Metzger, K. Gloe, H. Stephan and F. P. Schmidtchen, *J. Org. Chem*., 1996, **61**, 2051; (*f*) H. Tsukube, J. Uenishi, T. Kanatani, H. Itoh and O. Yonemitsu, *Chem. Commun*., 1996, 477; (*g*) G. J. Pernia, J. D. Kilburn and M. Rowley, *J. Chem. Soc., Chem. Commun*., 1995, 305; (*h*) A. Galán, D. Andreu, A. M. Echavarren, P. Prados and J. de Mendoza, *J. Am. Chem. Soc*., 1992, **114**, 1511; (*i*) J. de Mendoza and F. Gago, in *Computational approaches in supramolecular chemistry*, ed. G. Wipff, Kluwer Academic Publishers, 1994, p. 79. Ref. 3(*a*) serves as a leading reference to amino acid recognition in general.
4 A. P. Davis, *Chem. Soc. Rev*., 1993, **22**, 243; A. P. Davis, R. P. Bonar-Law and J. K. M. Sanders, in *Comprehensive Supramolecular Chemistry*, ed. Y. Murakami, Pergamon, Oxford, 1996, vol. 4 (*Supramolecular Reactivity and Transport*: *Bioorganic Systems*), p. 257.
5 A. P. Davis, J. F. Gilmer and J. J. Perry, *Angew. Chem., Int. Ed. Engl*., 1996, **35**, 1312; A. P. Davis, J. J. Perry and R. P. Williams, *J. Am. Chem. Soc*., 1997, **119**, 1793.
6 Podand-type receptors derived from the bile acids have been reported by other groups. See for example: R. Boyce, G. Li, H. P. Nestler, T. Suenaga and W. C. Still, *J. Am. Chem. Soc*., 1994, **116**, 7955; Y. A. Cheng, T. Suenaga and W. C. Still, *J. Am. Chem. Soc*., 1996, **118**, 1813; L. J. D'Souza and U. Maitra, *J. Org. Chem*., 1996, **61**, 9494. However, none of these systems possesses three differentiated α-substituents as implied for **2**.
7 C. Dalgliesh, *J. Chem. Soc*., 1952, 3940.
8 The analogous five-membered ring has been widely used in carboxylate and phosphate receptors. For examples, see: E. Fan, S. A. V. Arman, S. Kincaid and A. D. Hamilton, *J. Am. Chem. Soc*., 1993, **115**, 369; M. S. Muche and M. W. Göbel, *Angew. Chem., Int. Ed. Engl*., 1996, **35**, 2126; A. Metzger, V. M. Lynch and E. V. Anslyn, *Angew. Chem., Int. Ed. Engl*., 1997, **36**, 862. The six-membered **3** was chosen for the present work because of its greater stability and lipophilicity, and because it was expected to hold a substrate closer to the α-face of the steroid.
9 For a two-step synthesis of **6** from methyl cholate, see: A. P. Davis, S. Dresen and L. J. Lawless, *Tetrahedron Lett*., 1997, **38**, 4305.
10 F. Mohamadi, N. G. J. Richards, W. C. Guida, R. Liskamp, C. Caufield, G. Chang, T. Hendrickson and W. C. Still, *J. Comput. Chem*., 1990, **11**, 440.

Communication 8/08245F

Enantioselective conjugate addition of diethylzinc to enones catalyzed by a copper complex of chiral aryl diphosphite

Ming Yan, Li-Wei Yang, Kwok-Yin Wong and Albert S. C. Chan*

Union Laboratory of Asymmetric Synthesis and Department of Applied Biology and Chemical Technology, The Hong Kong Polytechnic University, Hong Kong, China. E-mail: bcachan@polyu.edu.hk

Received (in Cambridge, UK) 15th October 1998, Accepted 16th November 1998

The 1,4-conjugate addition of diethylzinc to cyclohex-2-enone and cyclopent-2-enone catalyzed by a copper complex of a chiral aryl diphosphite gave the desired products with 90.2 and 76.6% ee respectively.

The enantioselective conjugate addition of chiral organometallic reagents to enones is an attractive method for C–C bond formation. A number of successful methods for stereoselective 1,4-addition based on chiral auxiliaries or stoichiometric organometallic reagents have been developed, but a highly enantioselective catalytic version is still rare.[1] Ni^{II} and Co^{II} catalysts containing chiral amino alcohol ligands are of substantial interest, but they show enantioselectivity only for acyclic enones.[2] The copper complexes of chiral phosphites,[3] phosphorus amidites,[4] phosphines,[5] thiols[6] and aminophosphines[7] have been used in the catalytic conjugate addition of Et_2Zn or Grignard reagents to enones with low to moderate enantioselectivity. Recently several chiral phosphorus amidites[8] and phosphite oxazolines[9] have been used in the copper-catalyzed conjugate addition of dialkylzinc to cyclohex-2-enone with excellent enantioselectivity. These ligands shared a common feature of a bridging of binaphthol with a chiral amine through a phosphorus center. The active catalyst in the reaction has been proposed by Feringa *et al*. to be an alkyl–Cu^{I} species coordinated with two ligand molecules.[8] The C_2-symmetric bidentate ligands in these reactions are of substantial interest.[4a] Here we report the catalytic conjugate addition of Et_2Zn to enones using a C_2-symmetric chiral aryl diphosphite–$Cu(OTf)_2$ complex with good enantioselectivity and high catalytic activity.

Optically pure aryl diphosphite (*S*,*S*,*S*)-**1** was prepared by the reaction of the (*S*)-chlorophosphite **2** and (*S*)-binaphthol in the presence of Et_3N (Scheme 1). The crude product was easily purified by recrystallization in CH_2Cl_2–EtOH. The structure of the compound was supported by elemental analysis and spectral data.[10]

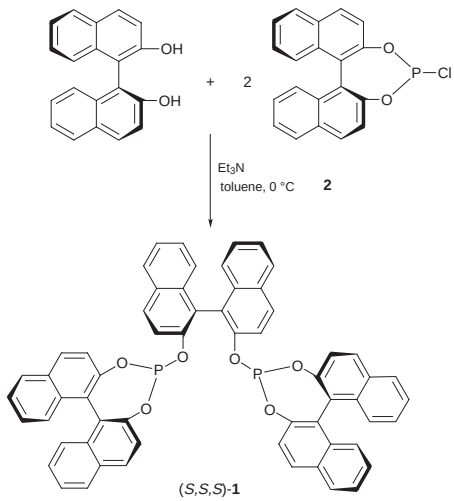

Scheme 1

In 1991 Pringle *et al*. reported the synthesis of (*R*,*R*,*R*)-**1** from trichlorophosphine and (*R*)-binaphthol. A Ni^0 complex of (*R*,*R*,*R*)-**1** was used in the hydrocyanation of norbornene, giving a product with 38% ee.[11] It is noticeable that the structure of **1** is entirely based on chiral binaphthol. (*S*,*S*,*S*)-**1** is fairly stable to oxygen in the solid state but is somewhat air- and moisture-sensitive in solution.

The addition of Et_2Zn to cyclohex-2-enone **3b** was used as a model (Scheme 2). The effects of reaction temperature, solvent and the ratio of (*S*,*S*,*S*)-**1** to $Cu(OTf)_2$ were investigated and the results are summarized in Table 1. In most cases complete conversion and good enantioselectivity were obtained. No 1,2-addition product was detected by GC analysis. The reaction was strongly dependent on the choice of solvents. The best solvent was found to be toluene (90.2% ee, 100% conversion). Coordinative solvents such as THF and MeCN gave substantially lower conversion rates and enantioselectivities (22.4% conversion, 72.2% ee and 6.5% conversion, 0% ee, respectively). The use of 2 equiv. (*S*,*S*,*S*)-**1** increased the enantioselectivity from 83.2 to 90.2% ee (entry 2 *vs*. entry 3). Further increase of the ratio of (*S*,*S*,*S*)-**1** to $Cu(OTf)_2$ decreased the catalytic activity (entry 1). When less than 1 equiv. (*S*,*S*,*S*)-**1** was used, the enantioselectivity decreased but the catalytic activity was still high (entry 4). The optimum reaction temperature was found to be *ca*. 0 °C. When the reaction temperature decreased to −40 °C, the reaction became sluggish and far less enantioselective (entry 8). Although the use of a low catalyst:substrate ratio was rather ineffective, it is of interest to note that increasing the concentration of the catalyst lowered the enantioselectivity (entries 9–11). The preliminary results revealed that a catalyst concentration of 0.0008–0.0012 M was optimum. The copper complexes at different concentrations may form different catalytic species. Similar results had been reported by Feringa *et al*.[4a] When EtMgCl was used in place of Et_2Zn only racemic **4b** was obtained as the major product and small amounts of 1,2-addition product were observed (entry 12).

The ^{31}P NMR spectrum of the catalyst solution (L:Cu = 2:1, toluene-d_8) showed two peaks at δ 231.6 and 149.0. The peak at δ 149.0 corresponded to free (*S*,*S*,*S*)-**1** and the low field peak at δ 231.6 is expected to be (*S*,*S*,*S*)-**1**–$Cu(OTf)_2$. When excess Et_2Zn was added at room temperature, the peak at δ 231.6 disappeared quickly and a new peak at δ 124.0 was observed. This new species may be postulated to be an Et–Cu^{I} complex containing a molecule of (*S*,*S*,*S*)-**1**. The electron-rich nature of Et–Cu^{I} caused the significant ^{31}P NMR shift. Coordinative solvents such as THF or MeCN competed with the enone substrates for the coordinating site of the Cu^{I} catalyst and

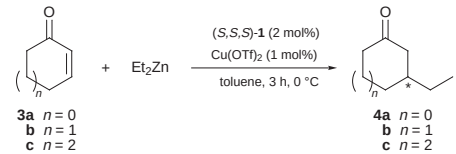

Scheme 2

Table 1 Enantioselective 1,4-addition of diethylzinc to cyclohex-2-enone **3b** catalyzed by (*S*,*S*,*S*)-**1**–$Cu(OTf)_2$[a]

Entry	$Cu(OTf)_2$/**3b**	**1**/$Cu(OTf)_2$	*T*/°C	Conversion (%)[b]	Ee (%)[b]	Configuration[c]
1	0.01	4	0	81.7	88.3	*S*
2	0.01	2	0	100 (92.0[d])	90.2	*S*
3	0.01	1	0	100	83.2	*S*
4	0.01	0.5	0	100	79.1	*S*
5	0.01	2	40	100	70.9	*S*
6	0.01	2	20	100	87.7	*S*
7	0.01	2	−20	100	84.6	*S*
8	0.01	2	−40	24.1	39.4	*S*
9	0.001	2	0	54.5	67.5	*S*
10	0.05	2	0	100	57.1	*S*
11	0.2	2	0	100	45.2	*S*
12[e]	0.01	2	−78	100[f]	0	—

[a] 1.5 equiv. of diethylzinc was used and the reactions were carried out in toluene for 3 h. [b] The conversions and ee values were determined by GC with a Chiraldex A-TA column (30 m × 0.25 mm); no 1,2-addition product was observed. [c] The absolute cofiguration was determined by optical rotation (ref. 12). [d] Isolated yield. [e] Ethylmagnesium chloride was used. [f] A small amount of 1,2-addition product was observed.

decreased the rate of reaction as well as the enantioselectivity.

The Cu^{II} complex of (*S*,*S*,*S*)-**1** was also tested in the conjugate addition of diethylzinc to cyclopent-2-enone **3a**, cyclohept-2-enone **3c** and chalcone **5**, and the results are summarized in Table 2. Up to now the catalytic conjugate addition of organometallic reagents to **3a** has been relatively unsuccessful.[4c,8,9] With the (*S*,*S*,*S*)-**1**–$Cu(OTf)_2$ catalyst system, the conjugate addition of Et_2Zn to **3a** gave a good yield of the desired product with 76.6% ee (entry 1). To the best of our knowledge, this enantioselectivity was the best one so far obtained for this reaction. Interestingly the absolute configuration of the product was opposite to that from the conjugate addition to **3b**. The reversal of enantiofacial selectivity for **3a** was also observed previously by Rossiter *et al*.[13] The conjugate addition of Et_2Zn to **3c** gave a lower conversion rate and enantioselectivity than the reaction with **3b** and **3a** (entry 2, Scheme 2).

Table 2 The addition of diethylzinc to enones **3a**,**c** and **5** catalyzed by (*S*,*S*,*S*)-**1**–$Cu(OTf)_2$

Entry	Substrate	Solvent	*T*/°C	Conversion (%)[a]	Ee (%)[a]	Configuration
1	**3a**	Toluene	0	100 (71.3[b])	76.6	*R*[c]
2	**3c**	Toluene	0	40.0	56.0	nd[d]
3	**5**	Toluene	0	45	9.3	*R*[e]
4	**5**	THF	0	62	16.5	*R*

[a] The ee value of **4a** and the conversion were determined by GC with a Chiraldex A-TA Column (30 m × 0.25 mm). The ee value of **4c** and the conversion were determined by GC with a Chrompack CP-Chirasil-Dex CB (25 m × 0.25 mm). The ee value of **6** and the conversion were determined by HPLC with a Diacel-OD column. [b] Isolated yield. [c] The absolute configuration was determined by optical rotation (ref. 14). [d] Not determined. [e] Comparison of the retention time of **6** in HPLC with known data (ref. 9).

The conjugate addition of Et_2Zn to chalcone gave **6** with poor enantioselectivity and low conversion (entries 3 and 4, and Scheme 3). The high specificity of the matching of substrate and catalyst had been found in many other catalyst systems.[2c,8,9]

The chiral match of the three binaphthol rings is very important for efficient enantiocontrol. (*S*,*R*,*S*)-**1** was prepared and used for the addition of Et_2Zn to **3b** using the optimum reaction conditions [1 mol% $Cu(OTf)_2$, 2 mol% (*S*,*R*,*S*)-**1**, 0 °C, toluene]. Compound **4b** was obtained with only 30.6% ee (*S*).

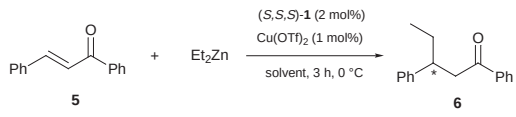

Scheme 3

We thank the Hong Kong Polytechnic University and the Hong Kong Research Grants Council (Project number PolyU34/96P) for financial support of this study.

Notes and references

1 Reviews: R. Noyori, *Asymmetric Catalysis in Organic Synthesis*, VCH, New York, 1993; P. Prelmutter, *Conjugate Addition Reactions in Organic Synthesis*, Pergamon, Oxford, 1992; *Advanced Asymmetric Synthesis*, ed. G. R. Stephenson, Chapman & Hall, London, 1996; *Advances in Catalytic Processes*, ed. M. P. Doyle, JAI Press, Greemwich, Connecticut, 1995, vol. 1; B. E. Rossiter and H. M. Swingle, *Chem. Rev*., 1992, **92**, 771; N. Krause, *Angew. Chem*., *Int. Ed*., 1998, **37**, 283.

2 (*a*) C. L. Gibson, *Tetrahedron*: *Asymmetry*, 1996, **7**, 3357; (*b*) A. H. M. de Vries and B. L. Feringa, *Tetrahedron*: *Asymmetry*, 1997, **8**, 1377; (*c*) A. H. M. de Vries, R. Imbos and B. L. Feringa, *Tetrahedron*: *Asymmetry*, 1997, **8**, 1467; (*d*) Recently Ni^{II} catalysts containing chiral diphosphine ligands were used in asymmetric addition of Grignard reagents to unsaturated cyclic acetals with moderate enantioselectivity: see E. Gomez-Bengoa, N. M. Heron, M. T. Didiuk, C. A. Lachaco and A. H. Hoveyda, *J. Am. Chem. Soc*., 1998, **120**, 7649.

3 A. Alexakis, J. Vastra, J. Burton and P. Mangency, *Tetrahedron*: *Asymmetry*, 1997, **8**, 3193.

4 (*a*) A. H. M. de vries, A. Meetsma and B. L. Feringa, *Angew. Chem*., *Int. Ed. Engl*., 1996, **35**, 2374; (*b*) F. Y. Zhang and A. S. C. Chan, *Tetrahedron*: *Asymmetry*, 1998, **9**, 1179; (*c*) E. Keller, J. Maurer, R. Naasz, T. Schader, A. Meetsma and B. L. Feringa, *Tetrahedron*: *Asymmetry*, 1998, **9**, 2409.

5 A. Alexakis, J. Burton, J. Vastra and P. Mangency, *Tetrahedron*: *Asymmetry*, 1997, **8**, 3987.

6 D. Seebach, G. Jaeschke, A. Pichota and L. Audergon, *Helv. Chim. Acta*., 1997, **80**, 2515.

7 T. Mori, K. Kosaka, Y. Nakagawa, Y. Nagaoka and K. Tomioka, *Tetrahedron*: *Asymmetry*, 1998, **9**, 3175

8 B. L. Feringa, M. Pineschi, L. A. Arnold, R. Imbos and A. H. M. de Vries, *Angew. Chem*., *Int. Ed. Engl*., 1997, **36**, 2620.

9 A. K. H. Knobel, I. H. Escher and A. Pfaltz, *Synlett*, 1997, 1429.

10 *Selected data* for (*S*,*S*,*S*)-**1** containing 0.5EtOH (solvent of crystallization): Calc. for $C_{60}H_{36}O_6P_2{\cdot}0.5C_2H_6O$: C, 78.12; H, 4.16%. Found: C, 78.13; H, 4.16%; $\delta_P(CDCl_3)$ 145.7; $\delta_H(CDCl_3$, 400MHz) 7.97 (d, *J* 8.8, 2H), 7.90 (d, *J* 8.0, 2H), 7.82 (dd, J_1 8.0, J_2 8.8, 4H), 7.73 (d, *J* 8.0, 2H), 7.52 (d, *J* 8.8, 2H), 7.37 (m, 8H), 7.16–7.31 (m, 14H), 6.53 (d, *J* 8.8, 2H), 3.72 (q, *J* 6.8, 1H), 2.36 (s, 0.5H), 1.24 (t, *J* 6.8, 1.5H); $\delta_C(CDCl_3)$ 147.2, 147.0, 146.5, 134.2, 132.7, 132.2, 131.4, 131.0, 130.8, 130.2, 130.0, 129.5, 128.3, 128.2, 128.1, 126.9, 126.8, 126.2, 126.0, 125.8, 125.1, 124.9, 124.6, 124.2, 122.4, 121.8, 121.7, 121.1; *m/z* (ESI) 915 (M^+ + 1, 100%); Mp 196–198 °C (decomp.); $[\alpha]_D^{20}$ +346.6 (*c* 1.085, THF) [a rather different $[\alpha]_D^{20}$ value was reported by Pringle *et al*. (ref. 11)].

11 M. J. Baker and P. G. Pringle, *J. Chem. Soc*., *Chem. Commun*., 1991, 1292.

12 G. H. Posner and L. L. Frye, *Isr. J. Chem*., 1984, **24**, 88.

13 B. E. Rossiter, M. Eguchi, G. B. Miao, N. M. Swingle, A. E. Hernandez, D. Vickers, E. Fluckiger, R. G. Patterson and K. V. Reddy, *Tetrahedron*, 1993, **49**, 965.

14 R. K. Dieter and M. Tokles, *J. Am. Chem. Soc*., 1987, **109**, 2040.

Communication 8/07997H

Substituted siloxysilanes and the structure of oligomeric liquid crystals

Georg H. Mehl* and John W. Goodby

Department of Chemistry, The Faculty of Science and the Environment, The University of Hull, Hull, UK HU6 7RX. E-mail: G.H.Mehl@chem.hull.ac.uk; J.W.Goodby@chem.hull.ac.uk

Received (in Cambridge, UK) 28th September 1998, Accepted 6th November 1998

The sequential addition of 4-cyanobiphenyl moieties to a silyl core unit results in a modification of the molecular shape of the molecules from rod-like to cross-shaped. The variation of molecular size and shape determines the nature (interdigitated SmAd or monolayer SmAl) and the stability range of the liquid-crystalline phases of these materials.

The research into branched and hyper-branched systems has focused mainly on synthesis of 'number generation' and less attention has been paid to the influence of the sequential introduction of sub-molecular systems into supermolecular structures.[1,2]

In order to understand this influence it is necessary to investigate the properties of the submolecular blocks and to examine how the stepwise introduction of those units into each generation of the supramolecular scaffolding affects the properties of the system.

This allows for the examination of the relationships and interplay between discrete molecular and polymeric systems and between the submolecular units, the polymeric framework, and the topology of their interconnections.

The above relationships are of importance to low molar mass, oligomeric and polymeric liquid-crystalline systems where there is constant debate concerning the identities, dynamics and topologies of mesogenic groups, spacer chains and polymer backbones in complex macromolecular systems. These relationships are of particular importance in determining viscoelastic and rheological properties. For example, it has been shown that defined or discrete oligomeric materials can exhibit properties usually associated with polymers, whilst still retaining the fluidity and viscosity of low molar mass liquid crystals.

In order to investigate these relationshps a series of model materials was synthesised, consisting of molecules where the number of mesogenic groups attached to a central silane core was sequentially increased in number from one to four. In addition the associated solid state behaviour of each of the materials was investigated. In this systematic study we prepared and investigated a family of branched supermolecules that were designed to have a controllable number of 4-cyanobiphenyl mesogenic submolecular units attached to a central silane core. The materials were conveniently prepared *via* a synthetic route based on combining a 4'-ω-alkenyl-4-cyanobiphenyl with an (oligo)vinylsilane moiety.

Initially, 4'-(10-undecenyl)-4-cyanobiphenyl was treated with a tenfold excess of 1,3-dihydro-1,1,3,3-tetramethylsiloxane in a hydrosylation reaction that was carried out in toluene at room temperature using Karstedt's catalyst (Pt–divinyl-tetramethylsiloxane in xylene), thereby yielding [4-cyano-4′-{11-[3-hydro-1,1,3,3-tetramethyldisiloxy]undecanyloxy}biphenyl] **1**.[3–5] The target materials **2**–**5** were obtained under similar reaction conditions, but by using an excess of **1** relative to the number of reactive vinyl groups in the silane cores (alkylvinylsilanes) to which the mesogenic submolecular units were to be attached. In each case, isolation of the product (**2**–**5**, Fig. 1) was achieved by column chromatography over silica gel using a mixture of hexane–dichloromethane (6 : 1) as the eluent. The absence of peaks in the vicinity of 2.0 ppm in the ^{1}H NMR spectra was indicative (within experimental error) of complete α-addition of the vinyl groups to the hydridosilicone core unit. The ^{29}Si NMR spectra revealed the shift of the signal of the hydridosiloxane group at 10.0 ppm to values of 7.08 to 7.43 ppm after conversion (the exact value measured being somewhat dependent on the structure of the core). The signal for the silicon bonded to four alkyl groups was found to shift from 3.04 to 6.88 ppm with the concomitant increase in the number of mesogenic substituents from one to four. These results were matched by high resolution ^{1}H NMR spectra, which is not usually the case for oligomeric materials.

Calorimetric studies reveal that all of the materials exhibit liquid crystal phases. The values for the transition temperatures and the associated enthalpies and entropies for the second heating cycles of each compound are listed in Table 1. Thermal polarised light transmission microscopy reveals that as each material is cooled from the isotropic liquid into the liquid crystal state, homeotropic and focal-conic defect textures are formed. The combination of homeotropy with the hyperbolic and elliptical lines of optical discontinuity associated with focal-

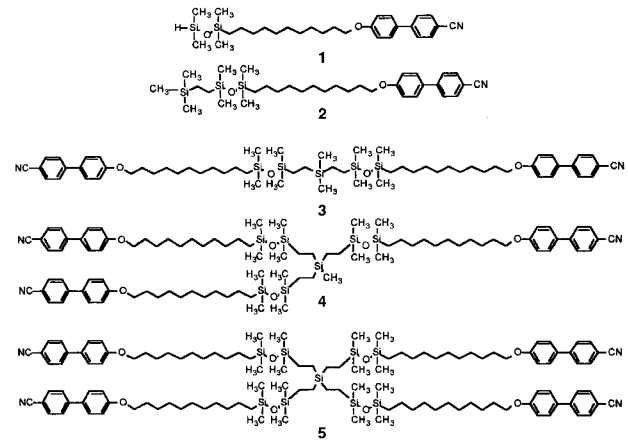

Fig. 1 Structure of the liquid-crystalline materials **1**–**5**.

Table 1 The transition temperatures (°C) and enthalpy and entropy data (ΔH/J g^{-1}, ΔC_p/J g^{-1} K^{-1}) obtained for compounds **2**–**4**. Cr_1, Cr_2, Cr_3 and Cr_4 are crystal or soft crystal phases.

Compound	T_g/°C (ΔC_p/J g^{-1} K^{-1})	Transition temperature/°C and enthalpies (ΔH/J g^{-1})	$\Delta S_{mol}/R$	$(\Delta S_{mol}R)/n$
2	—	Cr 27.3 (57.6) SmA 50.6 (4.14) Iso Liq	0.90	0.90
3	—	Cr 30.8 (30.89) SmA 76.0 (7.53) Iso Liq	2.79	1.40
4	−28.5 (0.19)	Cr_1 − 19.6 (−6.51) Cr_2 20.3 (4.25) Cr_3 22.4 (−2.58) Cr_4 35.0 (14.54) SmA 89.1 (4.89) Iso Liq	2.55	0.85
5	−22.3 (0.42)	Cr_1 −10.2 (−13.05) Cr_2 27.2 (10.17) Cr_3 29.2 (−12.48) Cr_4 50.8 (27.48) SmA 97.9 (7.77) Iso Liq	5.20	1.30

conic defects is diagnostic for the presence of a smectic A phase. Mechanical shearing of the specimens in the microscope shows that the smectic A phase flows easily and has a relatively low viscosity. In addition, only a short time is required for the focal-conic defect pattern to form on cooling from the isotropic liquid, indicating that the compounds have rheological properties more in common with low molar mass materials than with oligomers or polymers.

Increasing the number of branches carrying mesogenic groups from one to four results in the isotropization temperature being increased from 50.6 °C for compound **2** to 97.9 °C for **5** indicating an increasing stability of the liquid crystal properties as a function of the number of mesogenic units. Interestingly, if the values of the reduced molar entropy ($\Delta S_{mol}/R$) are used as a measure of the degree of ordering within the liquid crystal phase at the isotropization temperature an alternating odd–even effect is manifested. The middle members, **3** and **4**, exhibit roughly similar values of 2.79 and 2.55 placing them between those of the terminal members of the series, *i.e.* 0.90 for **2** and 5.20 for **5**. Taking into account the number of mesogenic moieties per molecule [$(\Delta S_{mol}/R)/n$] reveals an odd–even effect. The odd members of the series have reduced molar entropies between 0.8 and 0.9, and the even substituted materials have values between 1.3 and 1.4 per mesogenic side-chain. This result is in line with the concept of having a higher degree of ordering in the liquid-crystalline state for the even members of the series. This can be attributed to the higher degree of molecular symmetry of the even members. The higher degree of symmetry helps in the intra- and inter-molecular packing of the mesogenic subunits or arms, which in turn aids the organization and packing of the supermolecules within the layers of the smectic phase. Moreover, the occurrence of glass transitions for materials **4** and **5**, with an increase in their vitrification temperatures from −28.6 to −22.3 °C as the series is ascended, suggests that there is a higher degree of polymeric character associated with the materials as the number of mesogenic units is increased.

The structure of the smectic A phase exhibited by the materials was investigated further using X-ray diffraction. High flux synchrotron radiation was used in order to perform temperature scans at a rate of 2 °C min^{-1} for fibre samples in Lindemann tubes. The diffraction patterns were found to be typical of the smectic A phase. The results for the *d*-spacings (*d*) for compounds **2**–**5**, as a function of the reduced temperature ($T - T_{iso}$) from the isotropization point (T_{iso}), are shown in Fig. 2. For all of the materials a reduction in the *d*-spacing was observed as the isotropization point was approached. The members with a higher degree of substitution were found to have smaller *d*-spacing than the mono- or di-substituted materials. These results agree with earlier findings for other liquid-crystalline oligosiloxanes.[5–7]

The comparison of the calculated lengths (*l*) of the simulated structures of **2**–**5** (Cerius^2, 3.0 from MSI) with the corresponding layer spacing (*d*) gives *d*/*l* values of 1.6 for **2** and between

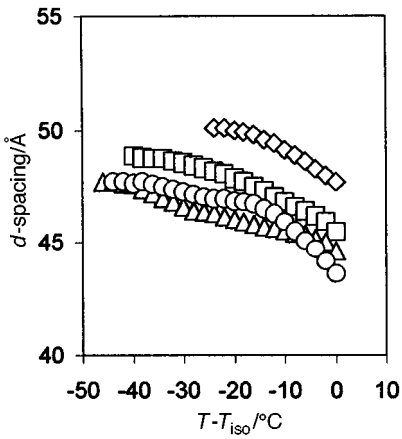

Fig. 2 *d*-Spacings for compounds **2**–**5** plotted against the reduced temperature $T_{Iso} - T$; (◇) **2**, (□) **3**, (△) **4**, (○) **5**.

Table 2 *d*-Spacings determined by X-ray diffracton and calculated lengths for compounds **2**–**5**

Compound	Calc. length *l*/Å	d_{max}/l	*d*-Spacing (max)/Å	*d*-Spacing (T_{Iso-10})/Å
2	30.8	1.63	50.1	48.8
3	48.4	0.98	48.8	46.6
4	49.6	0.96	47.7	45.6
5	50.9	0.94	47.7	45.6

0.9 and 1.0 for compounds **3**–**5**, Table 2. The result for compound **2** fits with an interdigitated bilayer structure for the smectic A phase, thereby classifying the phase as smectic A_d. Interdigitation takes place *via* overlap of the aromatic regions of the dimeric molecules in adjacent lamellae. The decrease in the *d*-spacing with rising temperature for compounds **2** can then be attributed either to increased disordering of the molecules or increased overlap of the molecules. The *d*/*l* values of 0.9–1.0 for the higher homologues indicate the occurrence of a different phase structure for the smectic A phase. One possibility is that the supermolecules in their fully extended conformational structures are arranged in disordered monolayers as in a conventional smectic A_1 phase. As each molecule possesses silyl and aromatic moieties, when these molecular subunits pack together they can do so *via* internal microphase separation. Thus for a microphase separated structure an object molecule can provide mesogenic units to potential aromatic layers above and below a layer containing the silyl core units. Thus, the results are consistent with a structure where the silicone cores are located in the central regions of the layers and where some overlap of the terminal cyanobiphenyl groups occurs between layers.[5,6] This classifies the high temperture smectic phase for the materials **3**–**5** as smectic A with respect to the silane core and quasi-smectic A bilayer for the mesogenic units.

For this series the results indicate that as the number of mesogenic groups is increased the temperature range of the liquid crystal state increases. The ordering of the molecules within the structure of the mesophase tends to be higher for the members of the series that have an even number of mesogenic subunits attached to the central silicon atom. This may be due to symmetry considerations allowing for better packing of the molecules. As the mesogenic count per silyl core is increased so the mesogenic arms have less freedom of movement, and therefore certain molecular topologies become favoured, this in turn affects the physico-chemical properties.

We wish to thank the EPSRC for financial support. We are also grateful to Dr B. U. Komanschek of Daresbury Research Laboratories for technical support at DARL Station 8.2 (Non-Crystalline Diffraction). We acknowledge Dr D. Ewing and Mrs B. Worthington for providing spectroscopic analyses.

Notes and references

1 G. R. Newkome, C. N. Moorefield and F. Vögtle, in *Dendritic Molecules*, Verlag Chemie, Weinheim, 1996.
2 K. Lorenz, D. Hölter, B. Stühn, R. Mühlhaupt and H. Frey, *Adv. Mater.*, 1996, **8**, 414; D. Seyferth, D. Y. Son, A. L. Rheingold and R. L. Ostrander, *Organometallics*, 1994, **13**, 2682; S. A. Ponomarenko, E. A. Rebrov, A. Y. Bobrovsky, N. I. Boiko, A. M. Muzafarov and V. P. Shibaev, *Liq. Cryst.*, 1996, **21**, 1.
3 M. A. Hampenius, R. G. H. Lammertink and G. J. Vansco, *Macromolecules*, 1997, **30**, 266.
4 B. D. Karstedt, General Electrics, US Pat. 3814730, 1974.
5 G. H. Mehl and J. W. Goodby, *Chem. Ber.*, 1996, **129**, 521 and references therein; *Angew. Chem., Int. Ed. Engl.*, 1996, **35**, 2641 and references therein.
6 M. Ibn-Elhaj, H. J. Coles, D. Gouillon and A. Skoulios, *J. Phys. II (Paris)*, 1993, **3**, 1807.
7 W. Bras, G. E. Derbyshire, D. Bogg, J. Cooke, M. J. Elwell, B. U. Komanschek, S. Naylor and A. J. Ryan, *Science*, 1995, **267**, 996; W. Folkhard, W. Geercken, E. Knoerzer, E. Mosler, H. Nemetschek-Gansler, T. Nemetschek and M. H. J. Koch, *J. Mol. Biol.*, 1987, **193**, 405.
8 B. J. Ostrovskij, *Liq. Cryst.*, 1993, **14**, 131.

Communication 8/07549B

An efficient dye-sensitized photoelectrochemical solar cell made from oxides of tin and zinc

K. Tennakone,* G. R. R. A. Kumara, I. R. M. Kottegoda and V. P. S. Perera

Institute of Fundamental Studies, Hantana Road, Kandy, Sri Lanka. E-mail: ifs@ifs.ac.lk

Received (in Cambridge, UK) 1st September 1998, Accepted 19th November 1998

A photoelectrochemical solar cell made from a porous film consisting of a mixture of tin (IV) and zinc oxides sensitized with a ruthenium bipyridyl complex suppresses recombination of the photogenerated electrons and dye cations, generating a short-circuit photocurrent of *ca*. 22.8 mA cm^{-2} and an open-circuit voltage of *ca*. 670 mV in direct sunlight (900 W m^{-2}) with an efficiency *ca*. 8 %.

Dye-sensitized (DS) photoelectrochemical cells (PECs) based on nanoporous films of TiO_2 are gaining much attention as promising solar energy conversion devices.[1–6] Although dye-sensitization can be achieved with porous films of high band-gap semiconductors other than TiO_2, DS PECs as efficient as the Gratzel's cell have not been fabricated earlier using other materials. We have succeeded in constructing a DS PEC from porous films of tin(IV) oxide containing *ca*. 53% zinc oxide. The cell generates an I_{sc} of *ca*. 22.8 mA cm^{-2} and V_{oc} of *ca.* 670 mV at 900 W m^{-2} in direct sunlight. The energy conversion efficiency of *ca*. 8% at this intensity is increased to *ca*. 15 % in diffuse daylight (100 W m^{-2}) as a consequence of the increase of the fill factor from 0.5 to 0.6. Both oxides (Sn and Zn) are essential for functioning of the cell. The enhanced values of I_{sc} and V_{oc} are explained as resulting from the high probability of transfer of an electron by an excited dye molecule adsorbed at a SnO_2 crystallite to a ZnO crystallite and subsequent relaxation to the conduction band (CB) of another SnO_2 crystallite attached to the original ZnO crystallite. This process leads to efficient spatial separation of photogenerated charges (D^+ and e^-), suppressing recombinations.

Porous films consisting of SnO_2 and ZnO were prepared by the following method. A colloidal 15% aqueous solution of SnO_2 of crystallite size of *ca*. 0.015 μm. (1.5 ml), acetic acid (0.1 ml) and ZnO of crystallite size of *ca.* 2 μm (0.3 g, prepared by thermal decomposition of zinc oxalate) were ground in an agate mortar, mixed with 20 ml of methanol and agitated ultrasonically for 30 min. The solution was sprayed onto a fluorine doped conducting tin oxide (CTO) glass plate (1.25 × 1.5 cm, sheet resistance *ca*. 10 Ω □$^{-1}$) heated to 150 °C until a layer of thickness *ca*. 8–10 μm was deposited and sintered at 500 °C in air for 35 min (sintering completely removes organic compounds in the solution). The sintered film was coated with the dye {*cis*-dithiocyanato [*N*-bis(2,2′-bipyridyl-4-4′-dicarboxylic acid)]ruthenium(II)} by boiling the plate in the dye solution (2 × 10^{-4} M in ethanol) for 3 min. A lightly platinized CTO glass plate, used as the counter electrode was kept in contact with the dyed film and the edges are sealed after introducing the electrolyte (0.5 M KI + 0.03 M I_2 in acetonitrile containing 10% ethylene glycol). The construction of the cell is schematically depicted in the inset of Fig. 1.

The *I*–*V* characteristics of the cell in direct sunlight (900 W m^{-2}) and diffuse daylight presented in Fig. 1 correspond to efficiencies of 8 and 15%, respectively. In direct sunlight, the efficiency is comparable to that of the Gratzel's cell based on TiO_2. However, at lower intensities (diffuse daylight) the efficiency of the present system appears to exceed that of Gratzel's cell. When the film is 100 % SnO_2, the maximum values of I_{sc} and V_{oc} obtained are *ca*. 2.5 mA cm^{-2} and *ca.* 335 mV respectively. Introduction of even a small quantity of ZnO increases both I_{sc} and V_{oc} significantly. The optimum values of I_{sc} and V_{oc} are reached when ZnO% is *ca*. 53%, a further increase of ZnO decreases I_{sc} and V_{oc} and for a cell made from 100% ZnO, I_{sc} = *ca*. 4 mA cm^2 and V_{oc} = *ca*. 540 mV. As SnO_2 particles have much smaller dimensions compared to ZnO (r_{ZnO}/r_{SnO_2} = *ca*. 133). The surface area of SnO_2 film ($S = 3w/\rho r$, where w = weight of the oxide, ρ = density, r = radius of the particle) is *ca*. 107 times the ZnO surface when the ZnO% corresponds to the optimum. Consequently, the light absorption occurs mostly at the dye coated SnO_2. The above observation is also supported by the photocurrent action spectra of cells made with composite SnO_2/ZnO films and those of SnO_2 and ZnO. The peaks of the action spectra of SnO_2 and SnO_2/ZnO systems were observed at almost the same position (*ca*. 539 nm), whereas a pure ZnO cell showed a peak at *ca*. 528 nm, indicating that in the composite system photocurrent originates mostly *via* sensitization of SnO_2. Furthermore ZnO adsorbs the Ru-complex, very feebly compared to SnO_2.

The mechanism of photocurrent generation which can explain the observations is as follows: in the composite film the larger ZnO particles are surrounded by SnO_2 particles (Fig. 2). An excited dye molecule on a SnO_2 particle could inject an electron to the CB of SnO_2 as in normal dye-sensitization of a semiconductor. However, as the excited level of the dye is above the CB of ZnO (Fig. 2) the energetic electron (*i.e.* the 'hot carrier' which has not relaxed to the CB of the SnO_2 particle) could also be driven to the CB of a ZnO particle in its vicinity, traversing across several SnO_2 particles. This enables a significant number of dye coated SnO_2 particles to participate in

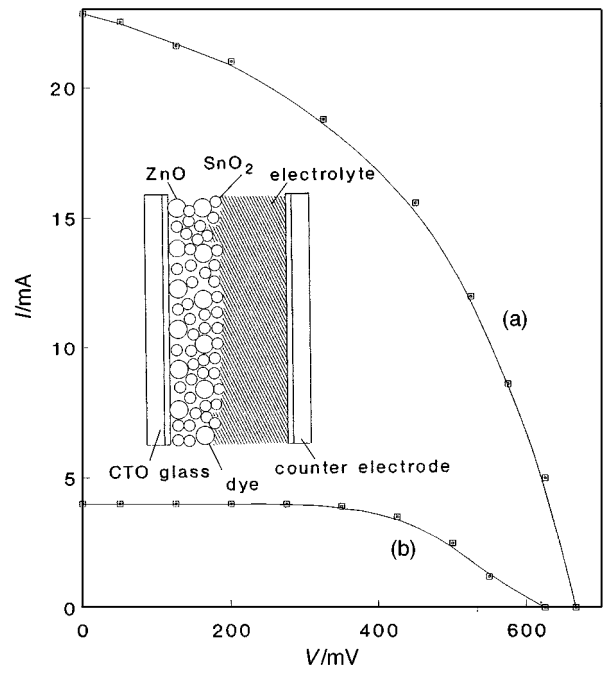

Fig. 1 *I*–*V* characteristics of the cell in (a) direct sunlight (900 W m^{-2}, measurements conducted for 1030–1130 h) and (b) diffuse daylight (100 W m^{-2}). Inset: construction of the cell.

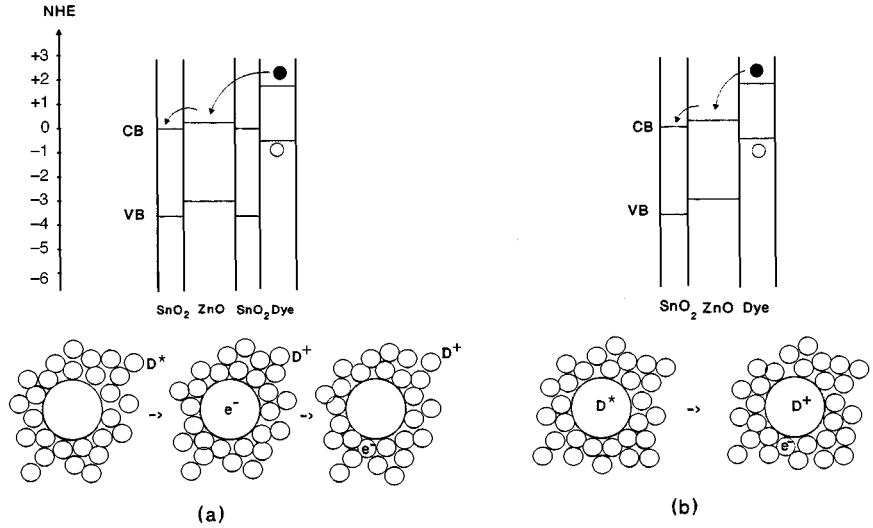

Fig. 2 An energy level diagram (NHE = normal hydrogen electrode) and a schematic diagram illustrating the transfer of an electron by an excited dye molecule (a) adsorbed at the surface of a SnO_2 particle to the CB of a ZnO particle in the vicinity and to the CB of another SnO_2 particle and (b) adsorbed at the surface of a ZnO particle to the CB of the ZnO particle and then to the CB of a SnO_2 particle.

the above electron injection process. The transfer of the electron into the CB of ZnO which is at a higher level in comparison to the CB of SnO_2 generates a V_{oc} greater than that of a cell comprising of 100% SnO_2. Subsequently the electron excited to the CB of ZnO is transferred to the CB of a SnO_2 particle in contact with the ZnO particle. As a result photogenerated negative and positive charges (D^+ and e^-) are widely separated by a ZnO barrier and the recombination is suppressed. An energy level diagram and a schematic diagram illustrating interparticle charge transfer are presented in the Fig. 2(a). The electrons separated from the dye cations are taken to CTO back contact *via* interconnection of SnO_2 particles. In DS PECs of the Gratzel type, the recombination of the photogenerated electron with the dye cation is one of the principal factors that limits the photocurrent quantum efficiency[7–10] and to some extent the V_{oc}. In the present system recombinations of this nature are largely suppressed due to rapid movement of the electron to a distance comparable to the size of the ZnO particle. This is supported by the observation that if ZnO particles of size comparable to that of SnO_2 particles are used the enhancement of I_{sc} and V_{oc} is not significant. As explained earlier, the contribution to the photocurrent from sensitization of ZnO is less effective compared to that from SnO_2. However, even this process suppresses recombinations, because the electron injected to the CB of ZnO from the excited dye molecule is immediately transferred to a SnO_2 particle in contact with ZnO [Fig. 2(b)]. Although the I_{sc} and V_{oc} of the cell are quite high, the efficiency at higher intensities are low because of the lower fill factor at higher intensities (*i.e.* 0.6 at 100 W m^{-2} and 0.5 at 900 W m^{-2}). This is the general behavior of DS PECs based on nanoporous semiconductor films. A possible cause is recombination (D^+ and e^-) across voids (where CTO surface is exposed to the electrolyte) in the film. When the surface density of voids is high, the fill factor is found to decrease. The cell remained stable during the few days of operation. Apart from fluctuations, I_{sc} and V_{oc} did not show any signs of decay.

Notes and references

1 A. J. McEvoy and M. Gratzel, *Sol. Energy Mater. Sol. Cells*, 1994, **32**, 221.
2 B. O. Regan and M. Gratzel, *Nature*, 1991, **353**, 737.
3 A. Mills and S. L. Hunte, *J. Photochem. Photobiol.*, 1997, **108**, 1.
4 G. Smestad, C. Bignozi and R. Argazzi, *Sol. Energy Mater. Sol. Cells*, 1994, **32**, 259.
5 M. K. Nazeerudin, A. Kay, I. Rodicio, R. Humphry Baker, E. Miller, P. Liska, N. Vlachopoulus and M. Gratzel, *J. Am. Chem. Soc.*, 1993, **115**, 6382.
6 A. Hagfeldt and M. Gratzel, *Chem. Rev.*, 1995, **95**, 45.
7 H. Lu, J. N. Prieskorn and J. T. Hupp, *J. Am. Chem. Soc.*, 1993, **115**, 4927.
8 B. O. Regan, B. Moser, M. Anderson and M. Gratzel, *J. Phys. Chem.*, 1990, **94**, 8720.
9 G. Hodes, I. D. J. Howell and L. McPeter, *J. Electrochem. Soc.*, 1992, **139**, 3136.
10 P. V. Kamat and B. Patrick, in *Electrochemistry in Colloids and Dispersions*, ed. R. A. Mackay and J. Teseter, VCH Publishers, New York, 1992.

Communication 8/06801A

Binuclear tin and germanium calix[4]arenes

Brian G. McBurnett and Alan H. Cowley*

Department of Chemistry and Biochemistry, The University of Texas at Austin, Austin, Texas 78712, USA. E-mail: cowley@mail.utexas.edu

Received (in Columbia, MO, USA) 6th September 1998, Accepted 17th November 1998

Ditin(II) and digermanium(II) calix[4]arenes, [Bu^{t}calix]M_2 (1, M = Sn; 2, M = Ge) have been prepared by treatment of [Bu^{t}calix]H_4 with $M(NR_2)$ (R = Me or Me_3Si); the reaction of [Bu^{t}calix]Li_4 with $SnCl_4$ affords the mixed valence ditin derivative [Bu^{t}calix]Sn_2Cl_2 3.

Calixarenes offer the prospect of serving as oxo-matrices for the construction of poly-Lewis acid or poly-Lewis base assemblies. Although there is considerable current interest in this field,[1] relatively little information is available regarding main group calixarene chemistry, particularly for systems that feature more than one main group element in the lower rim. Such poly-functionalized derivatives are limited to alkali metals,[2] aluminium,[3] gallium,[3c] silicon,[4] and phosphorus.[2,4a,5,6] We report the synthesis and X-ray crystal structures of (i) the first binuclear tin(II) calixarene, (ii) the first binuclear germanium(II) calixarene, and (iii) a calixarene that features both a tin(II) and a tin(IV) centre.[7]

The reaction of [Bu^{t}calix]H_4 with $Sn(NMe_2)_2$ took place in toluene solution at ambient temperature and afforded a 78% yield of colorless, crystalline [Bu^{t}calix]Sn_2 **1**.† The HRMS (CI) for **1** exhibited a parent peak corresponding to the composition $C_{44}H_{52}O_4Sn_2$ and an isotopic distribution consistent with the presence of two tin atoms. The ^{1}H NMR spectrum of **1** revealed the presence of two pairs of *para*-Bu^{t}ArO moieties and the ^{119}Sn NMR spectrum consisted of a single peak at δ 23.0.

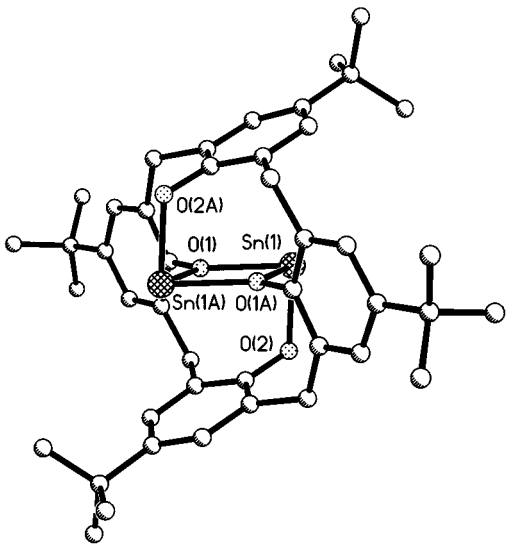

Fig. 1 Molecular structure of **1** showing the atom numbering scheme. Selected bond distances (Å) and angles (°) for **1** (the corresponding values for **2** are shown in parentheses) Sn(1)–O(1) 2.193(2) [Ge(1)–O(1) 1.997(6)], Sn(1)–O(1A) 2.169(2) [Ge(1)–O(1A) 1.991(6)], Sn(1)–O(2) 2.054(2) [Ge(1)–O(2) 1.844(6)]; O(1)–Sn(1)–O(1A) 68.22(11) [O(1)–Ge(1)–O(1A) 71.9(2)], Sn(1)–O(1)–Sn(1A) 117.78(11) [Ge(1)–O(1)–Ge(1A) 108.1(2)], O(1)–Sn(1)–O(2) 86.02(9) [O(1)–Ge(1)–O(2) 91.0(3)], O(2)–Sn(1)–O(1A) 85.78(9) [O(2)–Ge(1)–O(1A) 92.2(2)]. Because there are two half molecules in the asymmetric unit, there are two independent molecules for both **1** and **2**. The metrical parameters for these pairs of independent molecules do not differ greatly and only one such molecule is shown in either case.

Further characterisation necessitated an X-ray crystal structure determination.‡ The solid state (Fig. 1) consists of individual molecules of **1** and CH_2Cl_2; there are no unusually short intermolecular contacts. The central structural feature of **1**, which resides on a centre of symmetry, is an Sn_2O_2 parallelogram. The bond angles at tin [68.2(1)°] and oxygen [111.8(1)°] within the Sn_2O_2 kernel deviate significantly from 90° and the two Sn–O bonds differ in length by *ca.* 0.2 Å. Each tin atom is bonded to a third oxygen and this bond distance [Sn(1)–O(2)] is *ca.* 0.1 Å shorter than those in the Sn_2O_2 parallelogram. The O–Sn–O bond angles of the SnO_3 moiety are remarkably acute as shown in the graphical abstract (sum of O–Sn–O bond angles = 240.02°). The structure of **1** can be considered to arise *via* the dimerisation of two otherwise coordinatively unsaturated $(ArO)_2Sn$ units as shown below (**A**). As a consequence of the

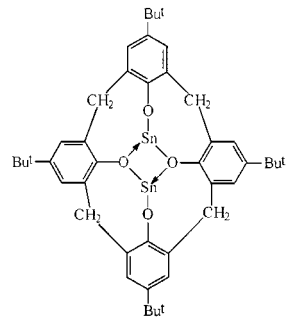

A

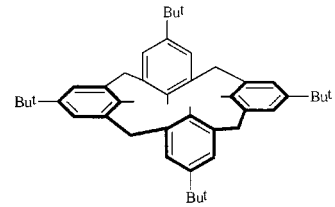

B

formation of two donor–acceptor bonds, the conformation of the calix[4]arene changes from bowl-shaped to that of a flattened partial cone (**B**).

The digermanium derivative [Bu^{t}calix]Ge_2 **2** was prepared in an analogous fashion† in 26% yield by treatment of [Bu^{t}calix]H_4 with $Ge[N(SiMe_3)_2]_2$. The virtually identical ^{1}H NMR data for **1** and **2** implied similar structures for both compounds. Confirmation was provided by X-ray analysis (Fig. 1).‡ Comparable trends are evident in the metrical parameters for **1** and **2**, namely within the central Ge_2O_2 moiety the bond angle at germanium [71.9(2)°] is smaller than that at oxygen [108.1(2)°] and the bond distance of the exterior oxygen [O(2)] is shorter than those within the ring. However, in the case of **2**, the intra-annular bond distances are the same within experimental error.

The reaction of [Bu^{t}calix]Li_4 with $SnCl_4$ in diethyl ether solution afforded a ditin derivative of composition [Bu^{t}calix]Sn_2Cl_2 **3** in 45% yield.† The observation of two peaks in the ^{119}Sn NMR spectrum† indicated that the tin atoms are present in distinctly different environments. By means of X-ray crystallography,‡ it was established that the molecular structure involves a flattened cone or boat-type conformation in which the tin atoms occupy *exo* and *endo* positions (Fig. 2). The hexacoordinate *exo* tin atom adopts a distorted octahedral geometry, being bonded to O(1), O(2), O(3), O(4), Cl(1) and Cl(2). Two of these interactions, O(1) and O(3), can be regarded as donor–acceptor bonds hence Sn(1) is in the +4 oxidation state. As expected, the Sn(1)–O(1) and Sn(1)–O(3) bond distances [av. 2.126(6) Å] are longer than the Sn(1)–O(2) or

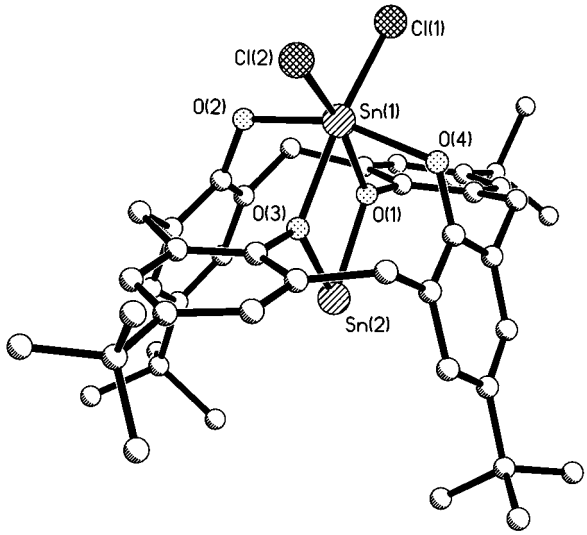

Fig. 2 Molecular structure of **3** showing the atom numbering scheme. Selected bond distances (Å) and angles (°): Sn(1)–Cl(1) 2.340(3), Sn(1)–Cl(2) 2.349(3), Sn(1)–O(1) 2.124(6), Sn(2)–O(1) 2.118(6), Sn(2)–O(3) 2.089(6), Sn(1)–O(3) 2.128(6), Sn(1)–O(2) 2.044(7), Sn(1)–O(4) 2.079(7); Cl(1)–Sn(1)–Cl(2) 100.7(1), O(1)–Sn(1)–O(3) 72.0(2), Sn(1)–O(1)–Sn(2) 107.0(3), O(1)–Sn(2)–O(3) 72.9(2), Sn(2)–O(3)–Sn(1) 107.9(3), O(2)–Sn(1)–O(4) 160.1(3).

Sn(1)–O(4) distances [av. 2.061(7) Å]. There is considerable departure from the ideal octahedral angles at Sn(1) due to the demands of the ligand system. Thus the angles O(2)–Sn(1)–O(4) [160.1(3)°] and O(1)–Sn(1)–O(3) [72.0(2)°] are unusually small whilst the Cl(1)–Sn(1)–Cl(2) bond angle is enlarged commensurately [100.7(1)°]. The *endo* tin atom, Sn(2), is two-coordinate and thus in the +2 oxidation state. The Sn(2) geometry is V-shaped with an O(1)–Sn(2)–O(3) bond angle of 72.9(2)°.

We thank the National Science Foundation and the Robert A. Welch Foundation for financial support.

Notes and references

† *Experimental procedures*: **1**: a solution of 4.2 mmol (0.87 g) of $Sn(NMe_2)_2$ in 30 mL of toluene was added *via* cannula to a toluene suspension of 2.1 mmol (1.37 g) of *p-tert*-butylcalix[4]arene at room temperature. Following the complete addition of $Sn(NMe_2)_2$, the solution turned clear and, after 15 min, a white precipitate formed. The reaction mixture was allowed to stir overnight and the toluene was removed *in vacuo*. The remaining white solid was washed with hexane (3 × 50 mL) and redissolved in 60 mL of CH_2Cl_2. The solution was filtered and stored for two days at −20 °C resulting in the formation of colorless X-ray quality crystals (1.45 g, 78% yield). ^{1}H NMR (300 MHz, $CDCl_3$) δ 7.22 (s, 4H, Ar), 7.19 (s, 4H, Ar), 4.46 (d, 4H, CH_2), 3.64 (d, 4H, CH_2), 1.40 (s, 18H, Bu^t), 1.25 (s, 18H, Bu^t); MS (CI) *m/z* (M^+) 877; HRMS (CI) *m/z* calc. for $C_{44}H_{53}O_4Sn_2$: 877.197873, found 877.196806 (M^+).

2: this colorless, crystalline compound was prepared in 26% yield using the procedure described for **1**. ^{1}H NMR (300 MHz, $CDCl_3$) δ 7.23 (s, 4H, Ar), 7.20 (s, 4H, Ar), 4.45 (d, 4H, CH_2), 3.63 (d, 4H, CH_2), 1.40 (s, 18H, Bu^t), 1.26 (s, 18H, Bu^t); MS (CI) *m/z* (M^+) 789; HRMS (CI) *m/z* calc. for $C_{44}H_{53}O_4Ge_2$: 785.242885, found 785.242345.

3: A diethyl ether solution of 4.0 mmol (2.50 g) of *p-tert*-butylcalix[4]arene was treated with a 1.6 M solution of *n*-BuLi (16.0 mmol, 10.0 mL) at room temperature and the resulting orange slurry and was stirred for 2 h. Neat $SnCl_4$ (0.5 mL, 4.0 mmol) was added *via* syringe to the suspension whereupon the colour changed from orange to dark red. The reaction mixture was allowed to stir overnight, following which the solvent and volatiles were removed *in vacuo*. The residual red solid was redissolved in 50 mL of toluene. The solution was filtered and stored for two weeks at −20 °C resulting in the formation of colorless X-ray quality crystals (1.68 g, 45% yield). ^{1}H NMR (300 MHz, $CDCl_3$) δ 7.36 (s, 4H, Ar), 7.26 (s, 4H, Ar), 4.47 (d, 4H, CH_2), 3.61 (d, 4H, CH_2), 1.49 (s, 18H, Bu^t), 1.19 (s, 18H, Bu^t); ^{119}SnNMR (111.85 MHz, $CDCl_3$) δ 215.5, −51.6; MS (CI) *m/z* (M^+) 877; HRMS (CI) *m/z* calc. for $C_{44}H_{52}Cl_2O_4Sn_2$: 946.127753, found 946.127928 (M^+).

‡ *Crystal data*: **1**: $C_{44}H_{52}O_4Sn_2{\cdot}2CH_2Cl_2$, M = 1052.09, triclinic, space group $P\bar{1}$, a = 12.903(2), b = 14.1920(10), c = 14.236(2) Å, α = 91.72(1), β = 109.35(1), γ = 111.12(1)°, U = 2261.1(5) Å^3, Z = 2, D_c = 1.545 g cm^{-3}, T = 163(2) K, μ = 1.382 mm^{-1}, wR_2 = 0.0983 (8997 independent reflections), R = 0.0351 [$I > 2\sigma(I)$]. There is residual electron density near the tin atom.

2: $C_{44}H_{52}Ge_2O_4{\cdot}3.5CH_2Cl_2$, M = 1087.28, triclinic, space group $P\bar{1}$, a = 13.201(2), b = 14.188(2), c = 15.212(2) Å; α = 84.63(1), β = 73.46(1), γ = 64.98(1)°, U = 2473.8(6) Å^3, Z = 2, D_c = 1.460 g cm^{-1}, T = 183(2) K, μ = 1.635 mm^{-1}, wR_2 = 0.2629 (9687 independent reflections), R = 0.0860 [$I > 2\sigma(I)$].

3: $C_{44}H_{52}Cl_2O_4Sn_2{\cdot}2.5C_7H_8$, M = 1183.47, monoclinic, space group $P2_1/c$, a = 19.286(4), b = 12.008(2), c = 23.956(4) Å, β = 96.26(2)°, U = 5515(2) Å^3, Z = 4, D_c = 1.425 g cm^{-3}, T = 183(2) K, μ = 1.049 mm^{-1}, wR_2 = 0.2666 (8717 independent reflections), R = 0.0981 [$I > 2\sigma(I)$]. CCDC 182/1091. See http://www.rsc.org/suppdata/cc/1999/17/ for crystallographic files in cif format.

1 C. D. Gutsche, *Calixarenes*, RSC, Cambridge, 1989; *Calixarenes. A Versatile Class of Macrocyclic Compounds*, ed. J. Vincens and V. Böhmer, Kluwer Academic Publishers, Dordrecht, 1991; D. M. Roundhill, *Prog. Inorg. Chem.*, 1995, **43**, 533.
2 C. Floriani, D. Jacoby, A. Chiesi-Villa and C. Guastini, *Angew. Chem., Int. Ed. Engl.*, 1989, **28**, 1376; D. M. Roundhill, E. Georgiev and A. Yordanov, *J. Inclusion Phenom.*, 1994, **19**, 101.
3 (*a*) J. L. Atwood, S. G. Bott, C. Jones and C. L. Raston, *J. Chem. Soc., Chem. Commun.*, 1992, 1349; (*b*) V. C. Gibson, C. Redshaw, W. Clegg and M. R. J. Elsegood, *Polyhedron*, 1997, **16**, 4385; (*c*) J. L. Atwood, M. G. Gardiner, C. Jones, C. L. Raston, B. W. Skelton and A. H. White, *Chem. Commun.*, 1996, 2487.
4 (*a*) I. Neda, H.-J. Plinta, R. Sonnenburg, A. Fischer, P. G. Jones and R. Schmutzler, *Chem. Ber.*, 1995, **128**, 267; (*b*) V. Bohmer, *Angew. Chem., Int. Ed. Engl.*, 1995, **34**, 713.
5 C. Loeber, D. Matt, P. Briard and D. Grandjean, *J. Chem. Soc., Dalton Trans.*, 1996, 513; M. Stolmàr, C. Floriani, A. Chiesi-Villa and C. Rizzoli, *Inorg. Chem.*, 1997, **36**, 1694.
6 W. Xu, J. J. Vittal and R. J. Puddephatt, *J. Am. Chem. Soc.*, 1995, **117**, 8362.
7 For a recent report of mononuclear germanium and tin calixarene derivatives, see T. Hascall, A. L. Rheingold, I. Guzei and G. Parkin, *Chem. Commun.*, 1998, 101.

Communication 8/07167E

Combining four different model nucleobases (uracil, adenine, guanine, cytosine) *via* metal binding and H bond formation in a single compound

Roland K. O. Sigel, Susan M. Thompson,† Eva Freisinger and Bernhard Lippert*

Fachbereich Chemie, Universität Dortmund, D-44221 Dortmund, Germany. E-mail: Lippert@pop.uni-dortmund.de

Received (in Basel, Switzerland) 21st September 1998, Accepted 9th November 1998

A cyclic arrangement of the four model nucleobases 1-methyluracilate (mura), 9-ethyladenine (eade), 9-ethylguanine (Hegua) and 1-methylcytosine (mcyt), held together by two metal entities [*trans*-$(NH_3)_2Pt^{II}$ and *trans*-$(MeNH_2)_2Pt^{II}$] and multiple H bond interactions, is presented.

Complementary and likewise non-complementary nucleobases can be cross-linked by suitable (usually linear or *trans*-square-planar) metal ions to give 'metal-modified' base pairs,[1,2] triples,[2] or quartets.[3] If combined with H bond formation, many variants are possible.[4] Here we report on an example of a nucleobase quartet which combines models of all four RNA bases uracil (U), adenine (A), guanine (G) and cytosine (C) in a single compound. In {*trans*,*trans*-[$(NH_3)_2$Pt(mura-N^3)(eade-N^7,N^1)Pt$(MeNH_2)_2$(Hegua-N^7)•mcyt]}$_2$[mcyt•Hmcyt][ClO_4]$_{4.5}$-[NO_3]$_{2.5}$•8.7H_2O **5** (Fig. 1) the four bases are joined *via* two linear metal entities and multiple H-bonding interactions. These include a Watson–Crick pair between Hegua and mcyt, which is reinforced by a fourth H-bond between the second amino proton of mcyt and a carbonyl oxygen atom of mura. In addition there is hemiprotonated 1-methylcytosine [mcyt•Hmcyt]$^+$ present in the lattice, displaying the well-known[5] threefold H bonding scheme.

The title compound was prepared in a stepwise fashion from *trans*-[$(NH_3)_2$Pt(mura-N^3)Cl] **1** as outlined in Scheme 1. Intermediates **2**–**4** have been isolated.‡ The title compound **5** was crystallized from an aqueous solution of **4** (20 mg, 0.0167 mmol dissolved in 3 mL of water), to which an excess of mcyt (6.27 mg, 0.05 mmol) had been added, with the pH adjusted to 5.3 with HNO_3. Colourless crystals of **5** suitable for X-ray crystallography§ were obtained upon slow evaporation of the solvent at 22 °C.

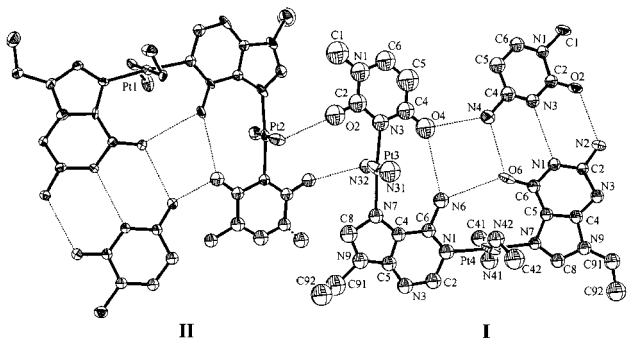

Fig. 1 View from the top of the two crystallographically independent cations **I** and **II** in **5**. The ellipsoids are drawn at 30% probability.

Compound **5** crystallizes with two crystallographically independent cations (**I**, **II**) in the asymmetric unit, which display two slightly different quartets. In the first one (**I**), the four bases give, despite moderate dihedral angles between each other, the picture of an essentially coplanar base quartet. In contrast, in cation **II** the guanine, cytosine entity on one hand, and the uracil, adenine entity on the other are markedly propeller-twisted about the Hegua-N^7–Pt^1–eade-N^1 bonds, thereby making in particular the two pyrimidine bases markedly non-coplanar (Table 1). This feature is reminiscent of the situation with an open base quartet consisting of four purine bases (A_2, G_2) and three metal ions (Pt^{II}).[3] In the present case (**II**) disorder (60 : 40) of the uracil base about the Pt^2–N^3-mura bond facilitates this feature: If, as is the case in the predominant rotamer, O^2 of mura participates in H bonding within the quartet, the CH_3 group of mura is pointing toward mcyt, thereby causing repulsion between C^5H (mcyt) and CH_3 (mura). Another effect is stacking of the guanine nucleobases of two cations **II** (3.2 Å, symmetry operation $-x + 2$, $-y + 1$, $-z + 2$).

As expected from relative orientations of the three platinated bases, exocyclic groups are involved in weak H bonding interactions (Table 1). Geometries of the Watson–Crick pairs in **I** and **II** are normal.[6] **I** and **II** are joined by two additional H bonds between NH_3 groups of Pt^2 and Pt^3 as well as O^2 and O^4/O^2 of mura ligands (Fig. 1).

We have previously observed[7] that Pt–N vectors in diplatinated adenine bases are close to perpendicular, and found that in mixed di- or tri-nuclear purine complexes this feature is likewise confirmed.[1–3] As evident from the data of **5**, addition of the pyrimidine base mura causes a marked deviation toward smaller angles. For example, in **I** this angle is 84.4(7)° and in **II** it is even smaller, 80.7(5)°. Considering the relatively large errors in nucleobase angles, it is not possible to relate this fact to a unique structural feature, *e.g.* variations in external ring angles at the sites of metal coordination.

In conclusion, a compound (**5**) has been prepared which combines four different model RNA nucleobases in a single compound. It displays simultaneously a metal-modified Hoogsteen pairing scheme (A, U), a metal-modified mispair (A, G), and a Watson–Crick pair (G, C). In principle, a corresponding quartet containing the DNA bases G, C, A and T (T = thymine) of type **II** is feasible. The (nearly) coplanar arrangement of the three metalated nucleobases in **5** contrasts that of a compound with three different bases (G, A, C) combined in a mononuclear complex, with the nucleobases arranged mutually perpendicu-

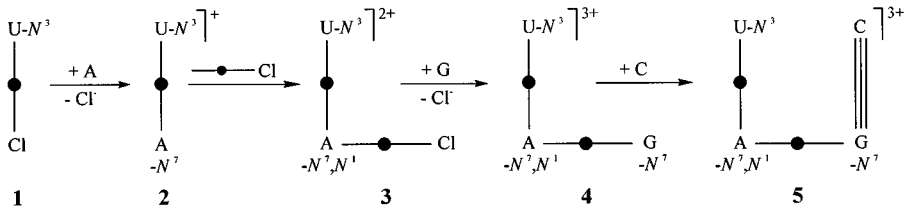

Scheme 1

Table 1 Selected dihedral angles (°) and H-bonding distances (Å) in the two independent cations **I** and **II** in **5**

	I	II
U/A	17.9(10)	6.1(5)
A/G	14.0(7)	11.6(3)
G/C	14.7(9)	14.0(6)
C/U	5.9(9)	26.1(7)
O^6(G)···N^6(A)	3.18(3)	3.21(2)
N^6(A)···O^4(U)	3.31(4)	—
N^6(A)···O^4/O^2(U)	—	3.09(2)
O^4(U)···N^4(C)	2.82(4)	—
O^4/O^2(U)···N^4(C)	—	3.15(2)
N^2(G)···O^2(C)	2.80(2)	2.83(2)
N^1(G)···N^3(C)	2.95(3)	2.89(2)
O^6(G)···N^4(C)	2.86(3)	2.89(2)
N^7(G)–N^1(A)/Pt^3–N^7(A)	84.4(7)	—
N^7(G)–N^1(A)/Pt^2–N^7(A)	—	80.7(5)

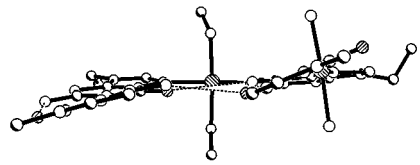

I

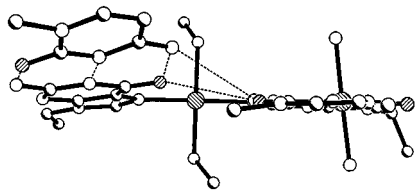

II

Fig. 2 View from the side of the two crystallographically independent cations **I** and **II** in **5**.

lar.[8] Considering the ever increasing number of RNA tertiary structures,[9] **5** represents a unique example of an interplay between nucleobases, metal ions and H bonds. Preliminary solution studies indicate clearly that H bonding between the metalated G base and the C model nucleobase is not only taking place in the solid state but also in solution.

The authors wish to thank the following institutions for support of this work: Deutsche Forschungsgemeinschaft (DFG), Fonds der Chemischen Industrie (FCI), the Swiss National Science Foundation and the Swiss Federal Office for Education and Science (TMR fellowship to R. K. O. S.; No. 83EU-046320), and the European Socrates exchange program (S. M. T.).

Notes and references

† Exchange student from University College London, Department of Chemistry, 20 Gordon Street, London, UK WC1H 0AJ.

‡{*trans*,*trans*-[$(NH_3)_2$Pt(mura-N^3)(eade-N^7,N^1)Pt$(MeNH_2)_2$(Hegua-N^7)•mcyt]}$_2$ [mcyt•Hmcyt][ClO_4]$_{4.5}$[NO_3]$_{2.5}$•8.7H_2O **5** was synthesized as follows: compounds **1** and **2** have been synthesized according to ref. 1, where 1-methylthymine was used instead of mura. The yields were 68% for *trans*-[$(NH_3)_2$Pt(mura-N^3)Cl] **1** and 63% for *trans*-[$(NH_3)_2$Pt(mura-N^3)(eade-N^7)]NO_3 **2**.

To a 20 mM aqueous solution of **2**, 1.2 equiv. of *trans*-[$(MeNH_2)_2PtCl_2$] were added and stirred for 36 h at 45 °C. Precipitated excess of *trans*-[$(MeNH_2)_2PtCl_2$] was filtered off and the solution concentrated at room temperature to 3 mL. After addition of 4 equiv. of $NaClO_4$ and cooling at 4 °C for 24 h, *trans*,*trans*-[$(NH_3)_2$Pt(mura-N^3)(eade-N^7,N^1)Pt$(MeNH_2)_2$Cl]-[ClO_4]$_2$•3 H_2O (**3**) could be isolated as a white powder in 61% yield. Anal. Calc. for $C_{14}H_{30}N_{11}O_{10}Cl_3Pt_2$: C, 15.8; H, 3.4; N, 14.5. Found: C, 15.8; H, 3.2; N, 14.5 %.

To a 8 mM aqueous solution of **3**, 0.95 equiv. of $AgNO_3$ were added and stirred at 40 °C in the dark overnight. After removal of AgCl, 1.2 equiv. of Hegua were added and the solution (pH 4.0, HNO_3) stirred at 40 °C for 36 h. The solution (pH 7.1, NaOH) was slowly concentrated at room temperature and precipitated excess of Hegua removed. The residue was recrystallized from water to give **4** in its hemideprotonated form {*trans*,*trans*-[$(NH_3)_2$Pt(mura-N^3)(eade-N^7,N^1)Pt$(MeNH_2)_2$($H_{0.5}$egua)]-[ClO_4]$_{2.5}$•1.25 H_2O}$_2$ in 28% yield. Anal. calc. for $C_{42}H_{77}N_{32}O_{26}Cl_5Pt_4$: C, 20.6; H, 3.4; N, 18.3. Found: C, 20.7; H, 3.4; N, 18.5%.

To a 5 mM aqueous solution of **4** (pH 5.3, HNO_3), 3 equiv. of mcyt were added and the solution evaporated to dryness at room temperature, which gave yellow crystals of **5** suitable for X-ray crystallography.

§ *Crystal data* for **5**: $C_{62}H_{122.4}O_{44.2}N_{46.5}Cl_{4.5}Pt_4$, M_r = 3166.55, triclinic, space group $P\bar{1}$, a = 15.004(3), b = 17.795(4), c = 21.662(4) Å, α = 97.81(3), β = 103.21(3), γ = 92.16(3)°, U = 5564.2(20) Å^3, Z = 2, D_c = 1.890 g cm^{-3}, μ(Mo-Kα) = 5.226 mm^{-1}, T = 126(2) K, Enraf–Nonius–KappaCCD[10] with graphite monochromator, ω-scans, 10 299 independent reflections, R_{int} = 0.043, structure solved by standard Patterson methods[11] and refined by full matrix least squares on F^2 using SHELXL-93.[12] Only a few non hydrogen atoms were refined anisotropically, because of the poor reflection to parameter ratio. Hydrogens were placed at calculated positions and no further refined. The methyl group of the uracil molecule of cation **II** is disordered over two positions (occupancy factors 0.6 and 0.4) and also the oxygens of three perchlorate anions and some of the water molecules show disorder. Another half occupied perchlorate anion shares the same position with a 25% occupied nitrate anion. 981 refined parameters gave R_1 = 0.0670 and wR_2 = 0.1697 for 6896 reflections with $I \geq 2\sigma(I)$ and R_1 = 0.1062 and wR_2 = 0.1947 for all data, minimum and maximum features in the difference Fourier map were −2.786 and 2.479 e Å^{-3} (near Pt). CCDC 182/1087. See http://www.rsc.org/suppdata/cc/1999/19/ for crystallographic files in .cif format.

1 O. Krizanovic, M. Sabat, R. Beyerle-Pfnür and B. Lippert, *J. Am. Chem. Soc.*, 1993, **115**, 5538.
2 A. Schreiber, M. S. Lüth, A. Erxleben, E. C. Fusch and B. Lippert, *J. Am. Chem. Soc.*, 1996, **118**, 4124; S. Metzger, A. Erxleben and B. Lippert, *J. Biol. Inorg. Chem.*, 1997, **2**, 256; M. S. Lüth, E. Freisinger, F. Glahé, J. Müller and B. Lippert, *Inorg. Chem.*, 1998, **37**, 3195.
3 M. S. Lüth, E. Freisinger, F. Glahé and B. Lippert, *Inorg. Chem.*, 1998, **37**, 5044.
4 B. Lippert, *J. Chem. Soc., Dalton Trans.*, 1997, 3971 and references therein; C. Meiser, E. Freisinger and B. Lippert, *J. Chem. Soc., Dalton Trans.*, 1998, 2059; R. K. O. Sigel, E. Freisinger and B. Lippert, *Chem. Commun.*, 1998, 219; R. K. O. Sigel, E. Freisinger, S. Metzger and B. Lippert, *J. Am. Chem. Soc.*, in press.
5 M. Rossi, J. P. Caradonna, L. G. Marzilli and A. T. Kistenmacher, *Adv. Mol. Relax. Interact Process*, 1979, **15**, 103.
6 E. J. O'Brien, *J. Mol. Biol.*, 1963, **7**, 107.
7 A. Schreiber, E. C. Hillgeris, A. Erxleben and B. Lippert, *Z. Naturforsch., Teil B*, 1993, **48**, 1603; S. Jaworski, S. Menzer, B. Lippert and M. Sabat, *Inorg. Chim. Acta*, 1993, **205**, 31.
8 A. Hegmans, M. Sabat, I. Baxter, E. Freisinger and B. Lippert, *Inorg. Chem.*, 1998, **37**, 4921.
9 J. H. Cate, A. R. Gooding, E. Podell, E. Zhou, B. L. Golden, A. A. Szewczak, C. E. Kundrot, T. R. Cech and J. A. Doudna, *Science*, 1996, **273**, 1696 and references therein.
10 NONIUS BV, KappaCCD package, Röntgenweg 1, P.O.Box 811, 2600 AV Delft, Netherlands; Z. Otwinowsky and W. Minor, *Processing of X-ray Diffraction Data Collected in Oscillation Mode*, *Methods in Enzymology*, ed., C. W. Carter, Jr. and R. M. Sweet, Academic Press, 1996, **276**, 307.
11 G. M. Sheldrick, *Acta Crystallogr., Sect. A*, 1990, **46**, 467.
12 G. M. Sheldrick, SHELXL-93, Program for crystal structure refinement, University of Göttingen, Germany, 1993.

Communication 8/07322H

Sensing and amplification of oligonucleotide-DNA interactions by means of impedance spectroscopy: a route to a Tay–Sachs sensor

Amos Bardea, Fernando Patolsky, Arie Dagan and Itamar Willner*

Institute of Chemistry, The Hebrew University of Jerusalem, Jerusalem 91904, Israel. E-mail: willnea@vms.huji.ac.il

Received (in Cambridge, UK) 27th October 1998, Accepted 19th November 1998

A three-component oligonucleotide/DNA layered assembly on a Au-electrode acts as a specific biosensor for the analysis of the Tay–Sachs mutant by means of Faradaic impedance spectroscopy.

The development of DNA-sensor devices attracts substantial recent research efforts directed to gene analyses, detection of genetic disorders, tissue matching, and forensic applications.[1,2] Significant progress was accomplished recently with the assembly of biochips for the optical detection of DNA.[3] Electronic transduction of the formation of oligonucleotide–DNA complexes could reveal a significant advance in DNA analysis as it could provide quantitative information on the analyte interactions with the sensing interface.[4] The development of a DNA-sensor requires the assembly of the sensing interface on a transducer element for the appropriate electronic transduction of the analyte recognition process, and simultaneously, the tailoring of a specific and selective sensing interface. Electrochemical DNA sensors based on the electrostatic attraction or intercalation of transition metal complexes,[5,6] *e.g.*, $Co(bpy)_3^{3+}$, or dyes such as acridine or Hoechst 33258 were reported. Control of the gate interface potential of field effect transistors, FET, was employed to identify the formation of ds-DNA complexes.[7] Recently, microgravimetric quartz-crystal-microbalance, QCM, analyses were applied to sense oligonucleotide–protein[8] or oligonucleotide–DNA[9] complexes. The sensitivity of these DNA sensors is, however, low, and the specificity of the sensing interfaces needs further studies.

Impedance spectroscopy is an effective method to probe the interfacial properties (capacitance, electron transfer resistance) of modified electrodes.[10] Impedance transduction of the formation of antigen–antibody[11] or biotin–avidin[12] complexes at electrode supports was reported. The assembly of the negatively-charged oligonucleotides and specifically double-stranded (ds) oligonucleotide complexes onto electrode supports is anticipated to control the double-layer potential at the electrode surfaces. As a result, the Faradaic impedance responses of the electrode in the presence of a charged solution-solubilized redox probe, are expected to be controlled upon the formation of a double-stranded DNA oligonucleotide complex at the electrode support. Here we wish to report on the specific, sensitive and confirmative analysis of DNA using Faradaic impedance spectroscopy. As a model system we employ the Tay–Sachs (TS)[13] oligonucleotide mutant that could eventually lead to a TS-sensor device.

The 13-mer oligonucleotide **1** includes a 12-base sequence that is complementary to a part of the TS mutant **2**.[14] In addition, **1** includes a five-base thiophosphate-T tag for its assembly onto a Au-electrode.[15] A Au-electrode was interacted with **1** (50 μM, 10 h) resulting in the assembly of the sensing interface on the gold support, Scheme 1. The resulting **1**-functionalized electrode was interacted with the TS-mutant (30 ng mL^{-1}; 30 min treatment). Fig. 1 shows the impedance features presented as Nyquist plots (Z_{im} *vs.* Z_{re}) of the bare Au-electrode, curve (a), the **1**-functionalized electrode, curve (b), and the functionalized electrode after treatment with the complementary mutant, **2**, curve (c) in the presence of $[Fe(CN)_6]^{3-/4-}$ as the redox probe. Significant differences in the impedance spectra are observed upon the stepwise formation of the ds-oligonucleotide–**2**

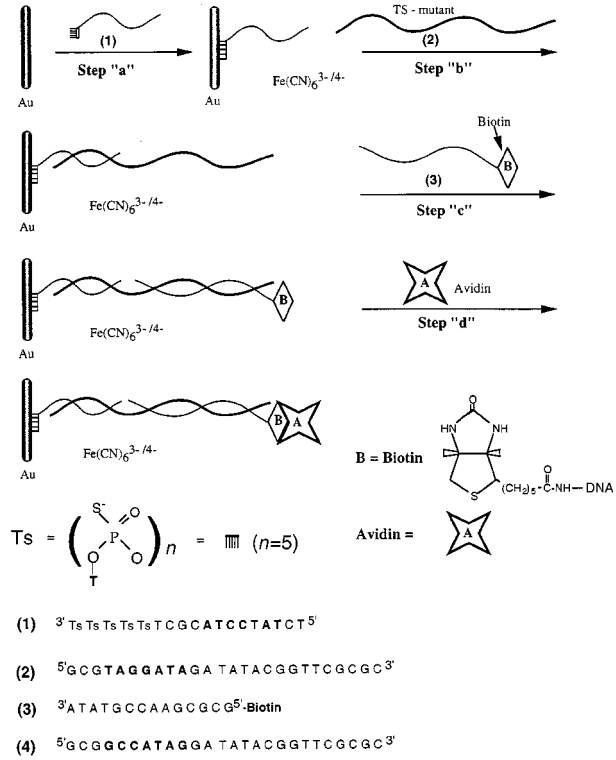

Scheme 1 Model system for sensing and amplified impedance analysis of a Tay–Sachs oligonucleotide.

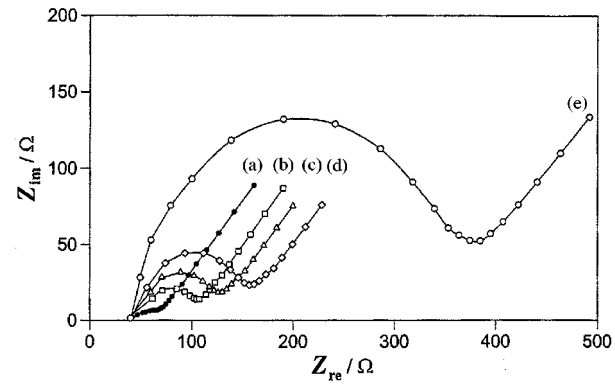

Fig. 1 Nyquist-diagram (Z_{im} *vs.* Z_{re}) for the Faradaic impedance measurements of a Au-electrode in the presence of 10 mM $[Fe(CN)_6]^{3-/4-}$ (1 : 1-mixture): (a) bare electrode, (b) **1**-functionalized electrode, (c) **1**-functionalized electrode after 30 min of incubation with **2**, (30 ng mL^{-1}) in SSC buffer (SSC = 15 mM Na citrate and 150 mM NaCl) , (d) ds-oligonucleotide complex with **2** after 30 min of incubation with **3** (40 ng mL^{-1}) in SSC buffer, (e) after 10 min of incubation with avidin (5 ng mL^{-1}) in phosphate buffer solution, pH = 7.1, 0.1 M. The impedance spectra were recorded within the frequency range 0.1 Hz–50 kHz at the formal potential of the $[Fe(CN)_6]^{3-/4-}$ redox couple. The amplitude of the alternate voltage was 5 mV.

complex. The impedance spectra follow the theoretical shapes and include a semicircle portion, observed at higher frequencies, that corresponds to the electron-transfer limited process, followed by a linear part characteristic of the lower frequency attributable to a diffusionally limited electron transfer. The respective semicircle diameters (obtained by extrapolation of the semicircles to lower frequencies on the Z_{re}-axis) correspond to the electron transfer resistances, R_{et}, at the electrode surface. The electron-transfer resistance, R_{et}, for the bare Au-electrode is *ca.* 60 Ω and it increases to *ca.* 80 Ω and *ca.* 105 Ω upon functionalization of the surface with **1** and formation of the ds-oligonucleotide complex with **2**. This is consistent with the fact that the negatively charged interface, formed upon the assembly of **1** on the electrode, repels the negatively charged redox probe. This introduces a barrier for interfacial electron transfer and an increase in the electron-transfer resistance. Formation of the ds-oligonucleotide complex with **2** enhances the double-layer potential at the electrode interface. This results in a further repulsion of the redox-probe and an increase in the electron transfer resistance at the electrode [*cf.* Fig. 1 (c)].

Although the impedance spectra change upon interaction of **2** with the oligonucleotide sensing interface reflects the hybridization process and the formation of the ds-complex with the analyte DNA, one would like to *confirm* and *amplify* the formation of the ds-complex at the sensor interface. Towards these goals the resulting ds-oligonucleotide interface was interacted with the biotinylated oligonucleotide, **3**, Scheme 1. The latter oligonucleotide is complementary to the residual sequence of the analyte DNA, and hence could be used as an oligonucleotide probe for the primary formation of the ds-DNA complex. Fig. 1(d), shows the impedance spectrum of the ds-DNA-functionalized electrode upon interaction with **3** and using $[Fe(CN)_6]^{3-/4-}$ as redox-probe. An increase in the electron transfer resistance to $R_{et} \approx 134$ Ω is observed, consistent with the formation of an additional negatively charged ds-assembly. Provided the system exhibits specificity, the latter process is observed only if the primary ds-system is formed with the sensing interface. Thus, the interaction of the modified surface with **3** provides a confirmation test for the formation of the primary ds-oligonucleotide assembly. As the secondary oligonucleotide is labeled by biotin, the subsequent reaction of the oligonucleotide-monolayer superstructure with avidin is anticipated to insulate the interfacial electron transfer due to the hydrophobic insulation of the interface. Fig. 1(e), shows the impedance spectrum of the layered ds-oligonucleotide superstructure after interaction with avidin. A substantial increase in the diameter of the semicircle is observed, implying a high electron transfer resistance, $R_{et} \approx 340$ Ω. This originates from the formation of the hydrophobic biotin–avidin complex at the electrode surface, a process that introduces a barrier for the interfacial electron transfer. Through the hydrophobic biotin–avidin complex, the latter process amplifies the initial formation of ds-oligonucleotide superstructure. The increase in the electron transfer resistance upon formation of the initial ds-oligonucleotide complex is controlled by the concentration of the analyte in the sample (and the time of interaction of the sensing interface and the sample). We were able to easily sense oligonucleotide concentrations corresponding to 3.5×10^{-12} mol mL^{-1} using this method (incubation time, 30 min). The incubation time of the sensing interface with the analyte **2** controls the loading of the electrode by the ds-assembly. The content of the ds-oligonucleotide/DNA on the electrode then controls the subsequent interfacial electron transfer resistance upon the association of **3** and avidin. The experimental incubation time, 30 min, represents an optimized parameter. Shorter incubation times perturbed the sensitivity of the system, whereas longer incubation times slightly enhanced the observed interfacial electron transfer resistance.

Several control experiments were performed to reveal the selectivity of the sensing interface. Treatment of the **1**-functionalized electrode with the biotin-labeled oligonucleotide **3** and then with avidin but without interaction of the electrode with **2**, does not lead to any noticeable changes in the impedance spectra. Thus, the sequence of changes in the impedance spectra is only stimulated if the primary analyte **2** is bound to the sensing interface. Also, the impedance responses of the sensing electrode upon interaction with oligonucleotide **4** were examined following the identical sequence of analysis. Oligonucleotide **4** includes the normal gene sequence in which the 7-base mutation shown in **2** leads to the TS-genetic disorder. No noticeable changes occur in the impedance spectrum of the **1**-functionalized electrode upon interaction with **4** or subsequent treatment of the electrode with **3** or avidin. Thus, the **1**-functionalized electrode reveals high selectivity for the detection of the TS-mutant, and the normal gene is effectively discriminated by the sensing interface. The results also indicate that the sensing interface is not affected by the non-specific binding of proteins.

In conclusion, we have demonstrated a novel sensitive method for the electronic transduction of DNA-complexes using Faradaic impedance spectroscopy. The method provides a means to sense the analyte–DNA complex, to confirm the analysis process using a biotin-labeled oligonucleotide probe, and to amplify the sensing process by the biotin–avidin complex at the sensing interface. The method reveals high specificity and selectivity. This originates from the fact that the primary sensing interface consists of an oligonucleotide that includes a limited number of bases capable of forming a single helix with the complementary analyte. Thus, any perturbation will be identified by the sensing interface. Although a detailed stability of the sensing electrode has not yet been performed, it appears that the sensing interface is stable for at least several days upon storage at 4 °C in a dry state. The examination of this biosensor assembly for the analysis of other oligonucleotides, *e.g.* c-DNA or t-RNA, is underway in our laboratory.

This research is supported by the Szold Foundation, The Hebrew University of Jerusalem.

Notes and references

1 M. Yang, M. E. McGovern and M. Thompson, *Anal. Chim. Acta*, 1997, **346**, 259.
2 P. G. Righetti and C. Gelfi, *Electrophoresis*, 1997, **18**, 1709.
3 A. C. Pease, D. Solas, E. J. Sullivan, M. T. Cronin C. P. Holmes and S. P. A. Fodor, *Proc. Natl. Acad. Sci. USA*, 1994, **91**, 5022.
4 J. Wang, E. Palecek, P. E. Nielsen, G. Rivas, X. Cai, H. Shiraishi, N. Dontha, D. Luo and P. A. M. Farias, *J. Am. Chem. Soc.*, 1996, **118**, 7667.
5 A. J. Bard and M. T. Carter, *J. Am. Chem. Soc.*, 1987, **109**, 7528; A. J. Bard and M. Rodriguez, *Anal. Chem.*, 1990, **62**, 2658.
6 K. M. Millan and S. R. Mikkelsen, *Anal. Chem.*, 1993, **65**, 2317; K. Hashimoto, K. Ito and Y. Ishimori, *Anal. Chem.*, 1994, **66**, 3830.
7 J. C. Van Kernhof, P. Bergveld and R. B. M. Schasfoort, *Biosens. Bioelectron.*, 1995, **10**, 269; E. Souteyrand, J. P. Cloarec, J. R. Martin, C. Wilson, I. Lawrence, S. Mikkelsen and M. F. Lawrence, *J. Phys. Chem. B*, 1997, **101**, 2980.
8 K. Niikura, K. Nagata and Y. Okahata, *Chem. Lett.*, 1996, 863.
9 K. Ito, K. Hashimoto and Y. Ishimori, *Anal. Chim. Acta*, 1996, **327**, 29; F. Caruso, E. Rodda and D. Furlong, *Anal. Chem.*, 1997, **69**, 2043.
10 C. Gabrielli, *Use and Application of Electrochemical Impedance Techniques*, Farnborough 1990.
11 M. Knichel, P. Heiduschka, W. Beck, G. Jung and W. Göpel, *Sens. Actuators B*, 1995, **28**, 85; J. Rickert, W.Göpel, W. Beck, G. Jung and P. Heiduschka,. *Biosens. Bioelectron.*, 1996, **11**, 757.
12 D. Athey, M. Ball, C. J. McNeil and R. D. Armstromg, *Electroanalysis*, 1995, **7**, 270.
13 R. A. Gravel, J. T. R. Clarke, M. M. Kaback, D. Mahuran, K. Sandhoff and K. Suzuki in *The Metabolic and Molecular Basis of Inherited Disease*, ed. C. R. Scriver, A. L. Beaudet, W. S. Sly and D. Valle, McGraw Hill, New York, 1995, vol. 2, pp. 2839–2879.
14 R. Myerowitz and F. C. Costigan, *J. Biol. Chem.*, 1988, **263,** 18 587.
15 A. Bardea, A. Dagan, I. Ben-Dov, B. Amit and I. Willner, *Chem. Commun.*, 1998, 839.

Communication 8/08319C

Synthesis and characterization of a new mixed-metal oxide framework material composed of vanadium oxide clusters: X-ray crystal structure of $(N_2H_5)_2[Zn_3V^{IV}_{12}V^{V}_{6}O_{42}(SO_4)(H_2O)_{12}]\cdot 24H_2O$

M. Ishaque Khan,*[a] Elizabeth Yohannes[a] and Douglas Powell[b]

[a] *Department of Biological, Chemical and Physical Sciences, Illinois Institute of Technology, Chicago, IL 60616, USA. E-mail: chemkhan@charlie.cns.iit.edu*

[b] *Department of Chemistry, University of Wisconsin, Madison, WI 53706, USA*

Received (in Bloomington, IN, USA) 25th September, 1998, Accepted 20th November 1998

The reaction of a slurry of V_2O_5 with $LiOH\cdot H_2O$ and hydrazinium sulfate gives a dark colored solution that upon treatment with $ZnSO_4\cdot 7H_2O$ yields the novel framework material $(N_2H_5)_2[Zn_3V^{IV}_{12}V^{V}_{6}O_{42}(SO_4)(H_2O)_{12}]\cdot 24H_2O$, composed of three-dimensional arrays of the mixed-valence $\{V_{18}O_{42}(SO_4)\}$ clusters interlinked *via* $\{Zn(H_2O)_4\}$ bridging groups, containing tunnels occupied by exchangeable cations and water molecules.

Polyoxovanadates constitute an important subclass of metal oxide clusters with an exceptional capacity to form mixed-valence compounds that exhibit rich electronic and magnetic properties and have relevance to catalysis, geochemical and biochemical processes, and in materials science.[1] Well characterized clusters containing four to 34 vanadium atoms – many with mixed-valence and coupled V^{IV}-centers, ranging from closed cages and spherical shells to basket, bowl, barrel, and belt shaped open structures are known.[2] Strikingly, their structures are related to, and in principle derived from, the appropriate V_2O_5 sheet fragments.[2] Given the significance of transition metal oxide surfaces[3] and proven roles of polyoxometalate clusters in catalysis,[4] it is conceivably rewarding to attempt to design and prepare transition metal oxide based materials (*e.g.* novel surfaces and zeolitic and layered solids) with desired and controllable properties by assembling metal oxide clusters of appropriate attributes. Through this communication we describe the synthesis and characterization of a novel framework material, composed of well defined vanadium oxide clusters, prepared under mild synthetic conditions.

The reaction of a stirring slurry of V_2O_5 (2.5 mmol) in water (25 mL) at 84–86 °C with $LiOH\cdot H_2O$ (5 mmol) and hydrazinium sulfate (2.5 mmol) gave a dark colored solution that upon treatment with $ZnSO_4\cdot 7H_2O$ (1.25 mmol) yielded prism-shaped dark crystals of $(N_2H_5)_2[Zn_3V^{IV}_{12}V^{V}_{6}O_{42}(SO_4)(H_2O)_{12}]\cdot 24H_2O$, **1**, in 12 h at room temperature in 65% yield (based on V). Besides the H_2O and hydrazine absorption bands, the IR spectrum (KBr Pellet) of **1** exhibits features at 1135m $\nu(SO_4)$], 989s [$\nu(V–O_{terminal})$] and 704m and 631m cm^{-1} [$\nu(V–(\mu_3\text{-}O)$].

The extended highly symmetrical structure of **1**,[5] shown in Fig. 1, consists of three-dimensional arrays of $\{V_{18}O_{42}(SO_4)\}$ clusters each one connected to six other neighboring units *via* $\{Zn(H_2O)_4\}$ bridging groups. The building block units in the structure of **1**, shown in Fig. 2, consist of $\{V_{18}O_{42}(SO_4)\}$ clusters formed from the $\{V_{18}O_{42}\}$ shell[6] encapsulating a tetrahedral $\{SO_4\}^{2-}$ moiety with disordered oxygen atoms. The host shell, constructed from $18\{VO_5\}$ square pyramids sharing edges through 24 μ_3-oxygen atoms, behaves as a container for the $\{SO_4\}^{2-}$ group which is not an integral part of the shell. The guest $\{SO_4\}^{2-}$ group with normal S–O distances (1.472 Å) rattles inside the host shell. The square pyramidal geometry around each vanadium (V1) in twelve of the $18\{VO_5\}$ groups is defined by a terminal oxo group (O2) and four μ_3-oxygens (O1) of the shell. The geometry around vanadium (V2) in the remaining $6\{VO_5\}$ units is defined by four basal μ_3-oxo groups (O1) and an apical μ-oxygen (O3) which in turn is linearly bonded to the zinc(II) center of one of the six $\{Zn(H_2O)_4\}$ bridges, forming $\{V(2)–O(3)–Zn(H_2O)_4–O(3)–V(2)\}$ bonds, that link $\{V_{18}O_{42}(SO_4)\}$ clusters. The octahedral geometry around each zinc(II) is completed by four oxygen atoms (O4) from the aqua ligands, each one disordered over two positions, and two *trans*-μ-oxo (O3) groups.

The Zn(1)–O(4) distance (2.063 Å) and the bond valence sum (BVS)[7] value (0.36) identify O(4) oxygen as H_2O. This conclusion and the result of the manganometric titration of V^{IV} sites (12 V^{IV} per formula unit) requires two units of negative charge per $[Zn_3V^{IV}_{12}V^{V}_{6}O_{42}(SO_4)(H_2O)_{12}]$ unit which is balanced by the two $N_2H_5^+$ -hydrazinium cations. The cations and lattice waters (with disordered hydrogens) occupy the rectangular tunnels, defined by $\{V_{18}O_{42}(SO_4)\}$ and $\{Zn(H_2O)_4\}$ units, in the structure (Fig. 1). The cations are readily exchangeable by other cations (NH_4^+, Na^+, K^+, *etc.*) without noticeable change in the framework structure.

This report presents a new synthetic solid with three-dimensional structure composed of well defined vanadium oxide clusters held together without incorporating conventional ligands[8] in its structure. This underlines the potential of polyoxometalates in the design and development of well

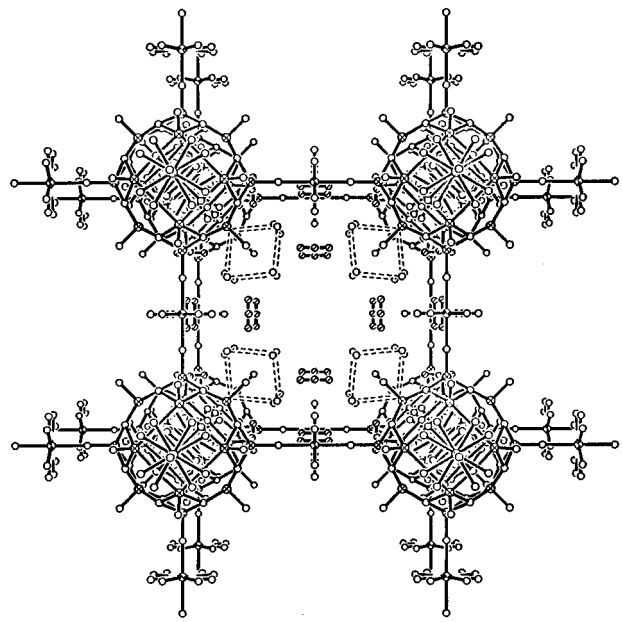

Fig. 1 View of the extended structure of $(N_2H_5)_2[Zn_3V^{IV}_{12}V^{V}_{6}O_{42}(SO_4)(H_2O)_{12}]\cdot 24H_2O$ showing interpenetrating nets of $\{V_{18}O_{42}(SO_4)\}$ clusters interconnected through $\{Zn(H_2O)_4\}$ bridging groups, and rectangular channels occupied by the hydrogen bonded water molecules (open circles) and hydrazinium ions (striped circles). Hydrogen atoms and the central cluster in the unit cell are not shown.

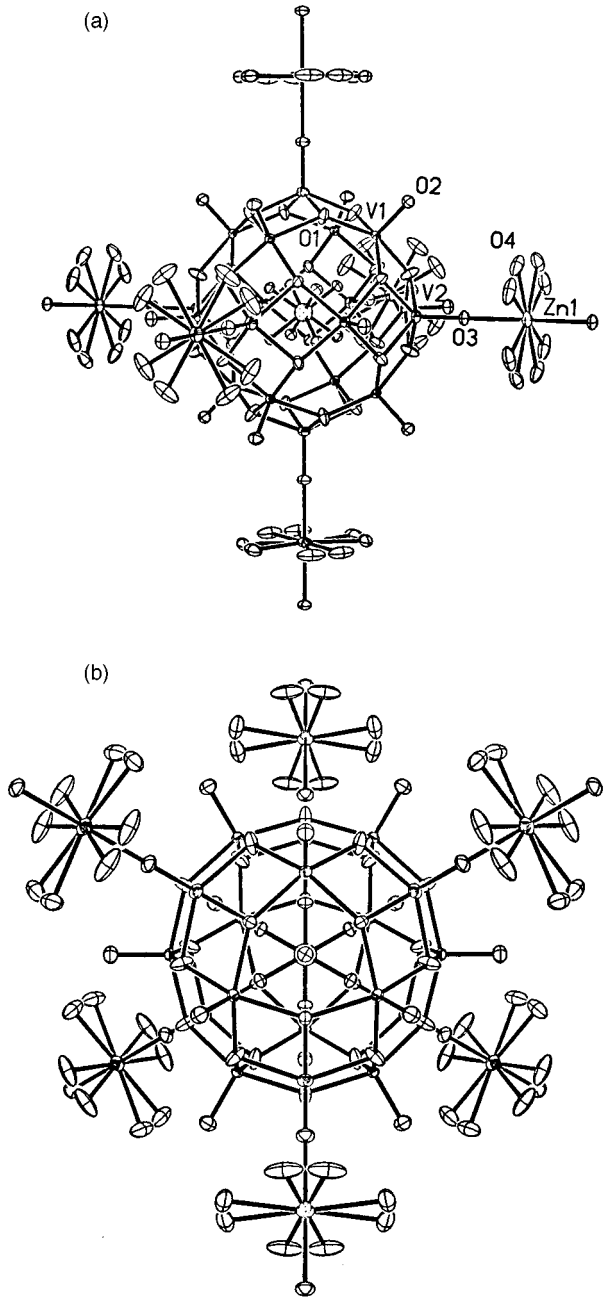

Fig. 2 (a) The building block units in the crystal structure of $(N_2H_5)_2[Zn_3V^{IV}{}_{12}V^{V}{}_6O_{42}(SO_4)(H_2O)_{12}]\cdot 24H_2O$ showing the atom labeling scheme in the asymmetric unit. (b) A view of the building unit along the threefold axis (hydrazinium ions and water molecules are omitted). Key: central circle with regular dot pattern represnts sulfur atom (S1); Atoms bonded to S1 represent O5 atoms. Displacement ellipsoids are drawn at the 50% probability level. Selected bond lengths (Å): V(1)–O(2) 1.588, V(1)–O(1) 1.9515, V(2)–O(3) 1.634, V(2)–O(1) 1.953, Zn(1)–O(4)(H_2) 2.063, Zn(1)–O(3) 2.122, S(1)–O(5) 1.472, V(1)–V(2) 2.9441 Å.

characterizable solids whose properties could possibly be correlated with their constituent units. Besides their possible catalytic, ion exchange and sorbtive properties, currently under investigation in our labs, synthetic solids, like **1,** composed essentially of metal oxide fragments may provide a model for understanding the chemical transformations catalyzed by metal oxide surfaces.[9]

This work was supported by Illinois Institute of Technology.

Notes and references

1 M. T. Pope and A. Müller, *Angew. Chem., Int. Ed. Engl*., 1991, **30**, 34; *Polyoxometalates: From Platonic Solids To Anti-Retroviral Activity*; ed. M. T. Pope and A. Müller, Kluwer Academic, Dordrecht, 1994; A. Müller, F. Peters, M. T. Pope and D. Gatteschi, *Chem. Rev.*, 1998, **98**, 239; M. T. Pope, *Heteropoly and Isopoly Oxometalates*, Springer, Berlin, 1983; A. Müller, *Nature*, 1991, **352**, 115.

2 W. G. Klemperer, T. A. Marquart and O. M. Yaghi, *Angew. Chem., Int. Ed. Engl*., 1992, **31**, 49.

3 I. M. Campbell, *Catalysis at Surfaces*, Chapman and Hall, London, 1988; H. Kung, *Transition Metal Oxides: Surface Chemistry and Catalysis*, Elsevier, New York, 1989; R. K. Grasselli and J. D. Burrington, *Adv. Catal*., 1981, **30**, 133; J. M. Thomas, *Angew Chem., Int. Ed. Engl*., 1988, **27,** 1673.

4 N. Mizuno and M. Misono, *Chem. Rev.*, 1998, **98**, 199; I. V. Kozhevnikov, *Chem. Rev*., 1998, **98**, 171; C. L. Hill, *Coord. Chem. Rev.*, 1995, **143**, 407; Y. Izumi, K. Urabe and M. Onaka, *Zeolite, Clay, and Heteropoly Acid in Organic Reactions*, VCH, Weinheim, 1992; M. Pohl, D. K. Lyon, N. Mizuno, K. Nomiya and R. G. Finke, *Inorg. Chem*., 1995, **34**, 1413.

5 Crystal data for $H_{82}N_4O_{82}SV_{18}Zn_3$ **1**: cubic space group $Im\bar{3}m$ (no. 229), a = 15.4973(11), V = 3721.9(5) Å^3, Z = 2, D_c = 2.316 Mg m^{-3}, μ(Mo-Kα) = 3.251 mm^{-1}. The data were collected at 133 K using a Siemens P4/CCD diffractometer (graphite monochromatized Mo-K_α radiation; λ = 0.71073 Å) and ψ-scan frames. Of the 3364 reflections ($2.63 \leqslant \theta \leqslant 29.11°$), 512 unique reflections were used to solve the structure by direct methods (SHELXTL Version 5) and refine it on F^2 by full-matrix least-squares techniques. At convergence, R1 = 0.0430 [$I > 2\sigma(I)$] and the goodness-of-fit on F^2 is 1.271. CCDC 18271096.

6 G. K. Johnson and E. O. Schlemper, *J. Am. Chem. Soc.*, 1978, **100**, 3645; A. Müller, J. Doring, H. Boegge and E. Krickemeyer, *Chimia*, 1988, **42**, 300; A. Müller, R. Sessoli, E. Krickemeyer, H. Bögge, J. Meyer, D. Gatteschi, L. Pardi, J. Westphal, K. Hovemeier, R. Rohlfing, J. Doring, F. Hellweg, C. Beugholt and M. Schmidtmann, *Inorg. Chem.*, 1997, **36**, 5239.

7 I. D. Brown, in *Structure and Bonding in Crystals*, ed. M. O'Keefe and A. Navrotsky, Academic Press, New York, 1981, vol. 2, p.1.

8 For a report on one- and two-dimensional solids containing vanadium oxide units linked *via* organometallic moities see: J. R. D. DeBord, R. C. Haushalter, L. M. Meyer, D. J. Rose, P. J. Zaf and J. Zubieta, *Inorg. Chim. Acta*, 1997, **256**, 165. Chains of mixed-metal addenda Keggins are reported in: Jose. R. Galan-Mascaros, C. Gimenez-Saiz, S. Triki, C. Gomez-Garcia, E. Coronado and L. Ouahab, *Angew. Chem., Int. Ed. Engl*., 1995, **34**, 1460. For a report on a layered and a framework material composed of paratungstate units joined by {CoO_6} groups see: I. Loose, M. Bösing, R. Klein, B. Krebs, R. Schulz and B. Scharbert, *Inorg. Chim. Acta*, 1997, **263**, 99.

9 K. Isobe and A. Yagasaki, *Acc. Chem. Res*., 1993, **26**, 524.

Communication 8/07503D

ChemComm

Arene hydrogenation in a room-temperature ionic liquid using a ruthenium cluster catalyst

Paul J. Dyson,[a] David J. Ellis,[b] David G. Parker[c] and Thomas Welton[b]

[a] *Department of Chemistry, The University of York, Heslington, York, UK YO10 5DD. E-mail: pjd14@york.ac.uk*
[b] *Department of Chemistry, Imperial College of Science, Technology and Medicine, South Kensington, London, UK SW7 2AY. E-mail: t.welton@ic.ac.uk*
[c] *ICI Group R & T Affairs, PO Box 90, Wilton Centre, Middlesbrough, Cleveland, UK TS90 8JE*

Received (in Cambridge, UK) 24th September 1998, Accepted 13th November 1998

The air and moisture stable system [bmim][BF_4]–[$Ru_4(\eta^6$-$C_6H_6)_4$][BF_4] {[bmim]$^+$ = 1-butyl-3-methylimidazolium cation} presents a novel medium for conducting hydrogenations of arenes; the environmental problems associated with related aqueous–organic biphasic regimes are eliminated.

The heterogenisation of homogenous catalysts is rapidly becoming an important area of chemistry.[1] It is hoped that the advantages of both homogeneous (greater efficiency, all metal centres being involved in the process) and heterogeneous (ease of catalyst separation, greater selectivity) catalysts can be combined in one system. One increasingly attractive route to greater catalyst separation exploits the use of biphasic liquid reaction systems.[2,3] Not surprisingly, aqueous–organic biphasic systems have emerged as an important class of catalysts and have found several industrial applications.[4] However, the method is not without problems; it precludes the use of water sensitive catalysts and reagents and, from an environmental perspective, trace amounts of organic compounds in water are notoriously difficult to remove.

An alternative system that will allow the use of water sensitive reagents and catalysts and solves some of the containment problems associated with aqueous–organic systems is that based on biphasic ionic liquid–organic systems. The development of a variety of air and moisture stable ionic liquids in recent years has lead to their deployment in a number of processes.[4] Building on our previous results with the chloroaluminate(III) ionic liquids,[5] we have been investigating the [bmim][BF_4] ionic liquid {[bmim]$^+$ = 1-butyl-3-methylimidazolium cation}, which has received some attention as a solvent for the hydrogenation of olefins using Wilkinson's and related catalysts.[6] Whilst these catalysts are moderately effective they are deactivated by trace quantities of chloride ions remaining in the ionic liquid from its preparation.

The hydrogenation of arenes is an important industrial process, particularly for the generation of cleaner diesel fuels,[7] and is dominated by the use of heterogeneous catalysts. In an attempt to develop biphasic methodologies for the hydrogenation of arenes we describe herein the use of a [bmim][BF_4]–organic system. Many catalysts, especially neutral species, are not soluble in [bmim][BF_4] and therefore careful choice of catalyst is required. Ionic inorganic and organometallic compounds tend to be highly soluble in [bmim][BF_4] and for this reason we chose to investigate the cluster, [$H_4Ru_4(\eta^6$-arene)][BF_4]$_2$, which proved to be both soluble and stable. Clusters of this type were first reported by Maitlis and coworkers[8] and then later by Süss–Fink and coworkers who went on to fully characterise these intriguing electronically unsaturated cluster cations.[9] Süss-Fink and coworkers then went on to show that they could be used as catalyst precursors for the hydrogenation of fumeric acid and arenes under aqueous–organic biphasic conditions.[9–11] This provides an ideal opportunity to compare the two systems directly. Table 1 lists a number of biphasic hydrogenation reactions of arenes employing the [bmim][BF_4] ionic liquid and water with [$H_4Ru_4(\eta^6$-$C_6H_6)_4$][BF_4]$_2$ as the catalyst precursor.†

The turnover frequencies obtained in the ionic liquid and aqueous regimes are similar. This would suggest that the active catalytic species is the same in both systems. It has been clearly shown that [$H_4Ru_4(\eta^6$-$C_6H_6)_4]^{2+}$ can oxidatively add hydrogen to give [$H_6Ru_4(\eta^6$-$C_6H_6)_4]^{2+}$, which is the hydrogenating species.[10] This contrasts with many cluster-based catalyst precursors that are believed to fragment into mononuclear species during reaction.[12] Few other effective hydrogenation catalysts are known and most of these cannot be used in biphasic processes and they tend to be air and moisture sensitive.[11,13] The turnover frequencies compare well to other homogeneous arene hydrogenation systems, such as [$(\eta^6$-$C_6Me_6)_2Ru_2(\mu$-Cl)]Cl_2 which will hydrogenate benzene at 50 °C and 50 atm with a catalytic turnover of 246 mol mol^{-1} h^{-1}.[14] However, the main advantage of the ionic liquid–organic system arises from the ease of separation of the catalyst from the starting material/product stream and the subsequent purification of the solvent, allowing different compounds to be hydrogenated without contamination. The aqueous phase in a biphasic hydrogenation processes cannot be used for different arenes or returned to the environment without expensive treatment to remove trace quantities of organic compounds. Since the [bmim][BF_4] ionic liquid has no vapour pressure, organic compounds (and water) may be removed by merely placing the liquid under a high vacuum. Using this technique we have been able to repeatedly use the same batch of ionic liquid for the catalytic hydrogenation of several different arenes.

We are currently investigating the hydrogenation of functionalized arenes and heteroaromatics using a series of ionic clusters in the full range of available ionic liquids.

Table 1 Biphasic hydrogenation reactions of arenes in the [bmim][BF_4] ionic liquid and water with [$H_4Ru_4(\eta^6$-$C_6H_6)_4$][BF_4]$_2$ as the catalyst precursor

Substrate	Reaction system	Reaction conditions	Conversion (%)	Catalytic turnover[a]/ mol mol^{-1} h^{-1}
Benzene	Ionic liquid	60 atm H_2, 90 °C, 2.5 h	91	364
	Water	60 atm H_2, 90 °C, 2.5 h	88	352
Toluene	Ionic liquid	60 atm H_2, 90 °C, 3 h	72	240
	Water	60 atm H_2, 90 °C, 3 h	78	261
Cumene	Ionic liquid	60 atm H_2, 90 °C, 2.5 h	34	136
	Water	60 atm H_2, 90 °C, 2.5 h	31	124

[a] Catalytic turnover is calculated on the assumption that the tetraruthenium catalyst does not break down into monoruthenium fragments which is entirely consistent with the data.

We would like to thank to thank The Royal Society for a University Research Fellowship and ICI (Wilton) for financial support (D. J. E.).

Notes and references

† The ionic liquid [bmim][BF_4] was prepared using the literature method.[6] [$H_4Ru_4(\eta\text{-}C_6H_6)$][$BF_4$]$_2$ is very soluble and stable in this ionic liquid and is readily characterised in the ionic liquid using ^{1}H NMR spectroscopy which revealed and spectrum similar to that in conventional solvents.

Hydrogenations were carried using a Parr stainless steel autoclave (300 ml) fitted with either a glass or PTFE liner. The catalyst [$H_4Ru_4(\eta^6\text{-}C_6H_6)$][$BF_4$]$_2$ was added together with the required amount of [bmim][BF_4] ionic liquid. The autoclave was then sealed and purged with hydrogen gas (99.9995% purity) and the appropriate reaction pressure was then set at room temperature. The autoclave was then sealed and heated to the required reaction temperature and stirred for the time period required. After reaction the contents were then separated into organic and ionic liquid phases and the products analysed by ^{1}H NMR spectroscopy and GC. The only products observed were the perhydrogenated cycloalkanes, there was no evidence for the formation of partially hydrogenated products or polymeric by-products.

1 J. H. Clark and D. J. Macquarrie, *Chem. Commun*., 1998, 853.
2 *Aqueous-Phase Organometallic Catalysis, Concepts and Applications*, ed. B. Cornils and W. A. Herrmann, Wiley–VCH, Weinheim, 1998.
3 P. J. Dyson, D. J. Ellis and T. Welton, *Platinum Met. Rev*., in press.
4 Y. Chauvin, L. Mussmann and H. Olivier, *Angew. Chem., Int. Ed. Engl.*, 1995, **34**, 2698.
5 P. J. Dyson, M. C. Grossel, N. Srinivasan, T. Vine, T. Welton, D. J. Williams, A. J. P. White and T. Zigras, *J. Chem. Soc., Dalton Trans.*, 1997, 3465.
6 P. A. Z. Suarez, J. E. L. Dullis, S. Einloft, R. F. de Souza and J. Dupont, *Polyhedron*, 1996, **15**, 1217.
7 A. Stanislaus and B. H. Cooper, *Catal. Rev.-Sci. Eng*., 1994, **36**, 73.
8 J. A. Cabeza, A. Nutton, B. E. Mann, C. Brevard and P. M. Maitlis, *Inorg. Chim. Acta*, 1986, **115**, L47.
9 G. Meister, G. Rheinwald, H. Stoecki-Evans and G. Süss-Fink, *J. Chem. Soc., Dalton Trans.*, 1994, 3215.
10 L. Plasseraud and G. Süss-Fink, *J. Organomet. Chem*., 1997, **539**, 163.
11 E. G. Fidalgo, L. Plasseraud and G. Süss-Fink, *J. Mol. Catal. A*, 1998, **132**, 5.
12 B. F. G. Johnson, *Transition metal clusters*, Wiley, Chichester, 1980.
13 I. P. Rothwell, *Chem. Commun*., 1997, 1331 and references therein.
14 M. A. Bennett, T.-N. Huang and T. W. Turney, *J. Chem. Soc., Chem. Commun.*, 1979, 312.

Communication 8/07447J

Neutral highly branched metallomacromolecules: incorporation of a (2,2′:6′,2″-terpyridine)ruthenium(II) complex without external counterions

George R. Newkome,* Enfei He, Luis A. Godínez and Gregory R. Baker

Center for Molecular Design and Recognition, Department of Chemistry, University of South Florida, 4202 E. Fowler Ave., Tampa, FL 33620-5250, USA.

Received (in Corvallis, OR, USA) 17th August 1998, Accepted 18th November 1998

Neutral dendritic metallomacromolecules possessing four bis-terpyridine Ru^{II} linking sites with internal counter ions have been prepared and their electrochemical properties have been studied.

The assembly of highly branched metallomacromolecules has been reported, and they have been shown to possess interesting magnetic, electronic, electrochemical, photooptical and catalytic properties.[1] To the best of our knowledge, these assemblies all utilize external counter ions, *e.g.* Cl^-, BF_4^-, PF_6^-. We herein report the construction of two tiers of overall neutral, dendritic metallomacromolecules, **1** and **2**, which incorporate (2,2′:6′,2″-terpyridine)ruthenium(II) ([< Ru >]) complexes with internally counter balanced charges. The use of four [< Ru >] linkages generated a supramolecular construct of precise description, based on the structural analysis of its components, and the eight internal carboxylate ions balance the charges of these Ru^{II} centers.

The core construct **10** was prepared from $EtNO_2$ with 2 equiv. of *tert*-butyl acrylate in liquid NH_3 affording (95%) di-*tert*-butyl 4-nitro-4-methylheptane-1,7-dioate **3**, which was converted (96%) to amine **4** by Raney Nickel reduction (Scheme 1).[2] Treatment of **4** with nitroisophthalic acid monochloride **5**[3] gave (58%) monocarboxylic acid **6**. Subsequent DCC coupling[4] of **6** with 5-aminopentyl 4′-(2,2′:6′,2″-terpyridinyl) ether[5] **7** generated **8** (92%), which was reduced[6] with 10% Pd-C and ammonium formate to afford the desired monomer **9** (90%). Treatment of **9** (4 equiv.) with a tetraacyl chloride core in the presence of Et_3N gave **10** (67%) possessing eight easily hydrolyzed *tert*-butyl ester moieties. All components were characterized by ^1H NMR, ^{13}C NMR, IR and elemental analyses, and ESI-MS.

4′-Chloro-2,2′:6′,2″-terpyridine **11**[7] was heated with PrOH and powdered KOH in DMSO[5] to give (93%) propyl 4′-(2,2′:6′,2″-terpyridinyl) ether **12**, which was refluxed with $RuCl_3·3H_2O$ in EtOH to afford (89%) the unbranched **13** (Scheme 2). The surface branching, amine **15**[8] was coupled with 4-[4′-oxa-(2,2′:6′,2″-terpyridinyl)]butanoic acid[5] **16** to afford **17** (86%), which was similarly transformed (84%) with $RuCl_3·3H_2O$ to give appendage **18** (Scheme 3). Both **13** and **18** were used without further purification due to their extremely low solubility in most organic solvents; fortunately, their purity was confirmed by elemental analyses and the analyses of the resultant assemblies.

Core **10** (1 equiv.) was refluxed with 4 equiv. of either **13** or **18** in EtOH in the presence of 4-ethylmorpholine, as reducing agent, to assemble **19** (93%) or **21** (96%), respectively (Scheme 4). Although **13** and **18** possessed limited initial solubility, they dissolved upon addition of the reducing agent to give the characteristic deep-red color of the [< Ru >] complex. After

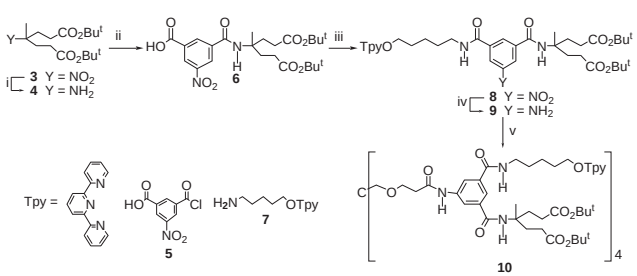

Scheme 1 *Reagents and conditions*: i, Raney nickel, H_2, 4 atm., 12 h, 25 °C; ii, **5**, Et_3N, THF, 12 h, −5 °C; iii, **7**, DCC, 1-HOBT, DMF, 24 h, 25 °C; vi, 10% Pd on C, HCO_2NH_4, MeOH, 30 min, 50 °C; v, Et_3N, $C[CH_2OCH_2CH_2COCl]_4$, THF, 12 h, 25 °C.

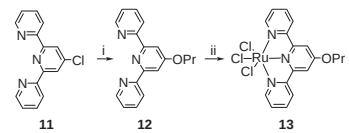

Scheme 2 *Reagents and conditions*: i, PrOH, KOH, DMSO, 24 h, 60 °C; ii, $RuCl_3·3H_2O$, Et_3OH, 4 h, reflux.

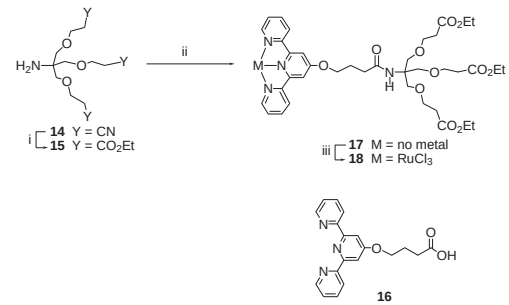

Scheme 3 *Reagents and conditions*: i, HCl, EtOH, 6 h, reflux; ii, **16**, DCC, 1-HOBT, DMF, 24 h, 25 °C; iii, $RuCl_3·3H_2O$, EtOH, 6 h, reflux.

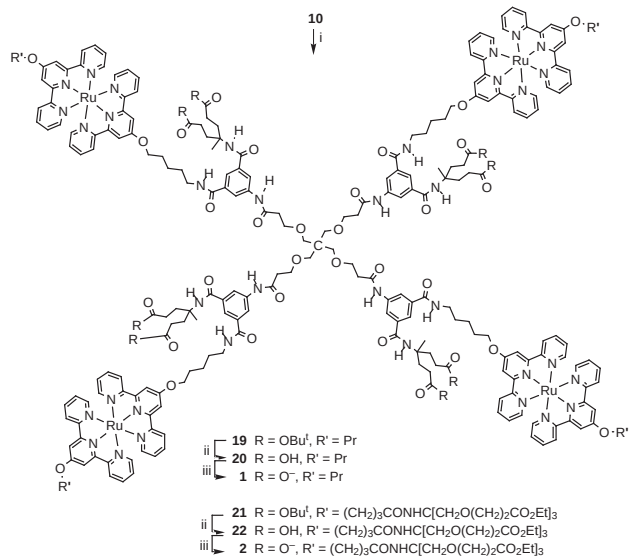

Scheme 4 *Reagents and conditions*: i, **13 (→19)** or **18 (→21)** (4 equiv.), 4-ethylmorpholine, EtOH, 6 h, reflux; ii, HCO_2H, 6 h, 25 °C; iii, KOH, H_2O–MeOH, dialysis, 24 h, 25 °C.

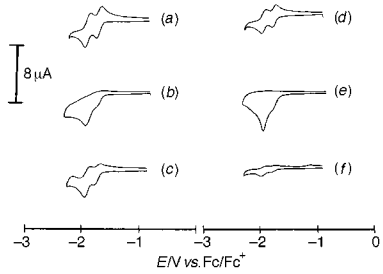

Fig. 1 CV responses for 1.0 mM solutions of (*a*) **21**, (*b*) **22**, (*c*) **2**, (*d*) **19**, (*e*) **20**, and (*f*) **1** (the smaller current observed was due to the limited solubility of **1** that presented in DMF) in Et_4NBF_4 (0.1 M) in DMF at 25 °C; scan rate 200 mV s^{-1}.

dialysis, the desired constructs were supported by the significant downfield shift (^{13}C NMR) of all terpyridine carbons. The *tert*-butyl groups were removed from **19** or **21** by treatment with formic acid,[9] affording complexes **20** (98%) or **22** (97%), respectively. The characteristic downfield shift of ^{13}C NMR ($\Delta\delta$ = 4 ppm) of the carbonyl carbon supports the transformation; the retention of the external alkyl ester moieties was evidenced by the presence of the ethyl signals. Final neutral complexes **1** (92%) or **2** (97%) were formed by addition of a slight excess of KOH into a H_2O–MeOH solution of **20** or **22**. After dialysis, the desired neutral complexes **1** and **2** were analyzed (0.00% of Cl), and only one downfield shift ($\Delta\delta$ = 3.4 ppm for **1** and 4.2 ppm for **2**) for the internal acid carbonyl carbon supports the formation of the carboxylate carbon centers. The UV–VIS spectra of the macromolecules possessing the four [< Ru >] linkages are analogous to related systems.[5,10] All the intermediate molecules and final complexes exhibit correct molecular weights. MALDI-TOF mass spectra of **19** and **21** exhibited low sensitivity and broad signals with all attempted matrices.

Electrochemical experiments with these metallodendrimers gave further insight to their electrocatalytic potential. Fig. 1(*a*) shows the two reversible waves that characterize the cathodic CV response of the two terpyridine ligands of **21**[11]. After internal deprotection of the *tert*-butyl groups, the presence of the carboxylic acid moieties in **22** results in a merging of the two redox waves and the virtual disappearance of the corresponding anodic signal [Fig. 1(*b*)]. Based on previous studies of the electrochemical reduction of pyridine and its derivatives,[12] the observed irreversibility is due to an electrochemical–chemical reaction in which a proton from the vicinal carboxylic acid group quenches the aromatic anion radical resulting in a probable 1,4-reduction of one of the pyridine rings of each terpyridine ligand. This explanation is further supported by CV experiments with neutral dendrimer **2**; as seen in Fig. 1(*c*), the lack of neighboring acidic protons, readily available in **22**, results in the recovery of the typical 'two wave' reversible response of the terpyridine ligands.

CV experiments on the first tier dendrimer series **19**, **20** and **1** showed similar voltammetric responses to those discussed above. By careful inspection of Table 1, however, the second tier assemblies **21** and **2** show slightly larger ΔE_p values than those corresponding to the first tier series **19** and **1**. This observation is in perfect agreement with previous reports[13] and has been attributed to the slower electron transfer kinetics that characterizes molecules featuring bulkier dendritic structures around their electroactive sites.

Table 1 CV data for **1**, **2**, **19**–**22**

Compound	Terpyridines		Ru^{III}/Ru^{II}
	$E_{1/2}$/V (ΔE_p/V)[a]	$E_{1/2}$/V (ΔE_p/V)[a]	$E_{1/2}$/V (ΔE_p/V)[a]
19	−1.945 (0.082)	−1.759 (0.068)	0.627 (0.073)
20	I[b]	I[b]	0.629 (0.057)
1	−1.950 (0.072)	−1.788 (0.077)	0.624 (0.059)
21	−1.950 (0.086)	−1.751 (0.088)	0.640 (0.100)
22	I[c]	I[c]	0.627 (0.097)
2	−1.935 (0.102)	−1.767 (0.106)	0.634 (0.089)

[a] *E*/V *vs.* Fe/Fe^+. Same conditions as those described in Fig. 1. [b] Irreversible cathodic peak at −1.945 V. [c] Irreversible cathodic peak at −1.968 V.

In summary, we have constructed $[< Ru >]_4$ dendrimers possessing an overall neutral charge. The loss of external counterions in these metallomacromolecules had a marginal effect on their spectra, as well as stability and physical properties. However, the solubilities of these neutral species decreased in polar solvents, such as MeOH and H_2O. Complexes **19–22** are all slightly soluble in H_2O, whereas, **1** and **2** are insoluble in H_2O. The neutral metallodendrimers have internally balanced carboxylates, which are weaker counter ions than most others like Cl^-, NO_3^- and PF_6^-. Thus, addition of inorganic salts to these neutral species allows convenient interchange between external counter ions. Notably, **1** and **2** are not soluble in DMF, but quickly go into solution upon addition of salts like BF_4^- or PF_6^-. Another important aspect is that these neutral metallomacromolecules were more easily ionized (*i.e.* lower laser power) and gave stronger signals in MALDI-TOF mass spectrometry in comparison to the *tert*-butyl and acid metallodendrimers possessing external Cl^- or PF_6^- counter ions. The observed intramolecular proton transfer during the redox process stands to give insight into the potential chemistry within such macromolecular constructs.

We gratefully acknowledge support of this work from the National Science Foundation (DMR-96-22609; BIR-95-12208) and the Army Research Office (DAAH04-95-1-0373; DAAH04-96-1-0306).

Notes and references

† All new compounds exhibited satisfactory spectral, elemental and mass data.

‡ *Selected data* for **1**: $C_{233}H_{240}N_{36}O_{40}Ru_4$; *M* = 4589.0; mp > 230 °C (decomp.); Found: C, 60.61; H, 5.45; N, 10.23; Cl, 0.00; requires: C, 60.98; H, 5.27; N, 10.99; Cl, 0.00%; *m/z* (MALDI-TOF, IAA matrix) 4590 [M + H^+].

For **2**: $C_{313}H_{372}N_{40}O_{80}Ru_4$; *M* = 6378.9; mp > 210 °C (decomp.); Found: C, 58.49; H, 5.86; N, 8.71; Cl, 0.00; requires: C, 58.94; H, 5.88; N, 8.78; Cl, 0.00%; *m/z* (MALDI-TOF, IAA matrix) 6381 [M + H^+].

1 For recent reviews see: G. R. Newkome, C. N. Moorefield and F. Vögtle, *Dendritic Molecules*: *Concepts*, *Syntheses*, *Perspectives*, VCH, Weinheim, 1996; V. Balzani, S. Campagna, G. Denti, A. Juris, S. Serroni and M. Venturi, *Acc. Chem. Res*., 1998, **31**, 26; H.-F. Chow, T. K. K. Mong, M. F. Nongrum and C.-W. Wan, *Tetrahedron*, 1998, **54**, 8543; V. V. Narayanan and G. R. Newkome, *Top. Curr. Chem*., 1998, 19; P. L. Boulas, M. Gómez-Kaifer and L. Echegoyen, *Angew. Chem., Int. Ed*., 1998, **37**, 216; C. Gorman, *Adv. Mater*., 1998, **10**, 295; A. Matthews, A. N. Shipway and J. F. Stoddart, *Prog. Polym. Sci*., 1998, **23**, 1; E. C. Constable, *Chem. Commun*., 1997, 1973.
2 G. R. Newkome and C. D. Weis, *Org. Prep. Proced. Int*., 1996, **28**, 485.
3 K. Landsteiner and J. Van Der Scheer, *J. Exp. Med*., 1938, **67**, 709.
4 J. Klausner and B. Bodansky, *Synthesis*, 1972, 453.
5 G. R. Newkome and E. He, *J. Mater. Chem*., 1997, **7**, 1237.
6 S. Ram and R. E. Ehrenkaufer, *Tetrahedron Lett*., 1984, **25**, 3415.
7 E. C. Constable and M. D. Ward, *J. Chem. Soc., Dalton Trans*., 1996, **28**, 485.
8 G. R. Newkome and X. Lin, *Macromolecules*, 1991, **24**, 1443.
9 S. Chandrasekaran, A. F. Kluge and J. A. Edwards, *J. Org. Chem*., 1977, **42**, 3972.
10 G. R. Newkome, E. He and L. A. Godínez, *Macromolecules*, 1998, **31**, 4382.
11 G. R. Newkome, R. Güther, C. N. Moorefield, F. Cardullo, L. Echegoyen, E. Pérez-Cordero and H. Luftmann, *Angew. Chem., Int. Ed. Engl*., 1995, **34**, 2023.
12 A. P. Tomilov, S. G. Mairanovskii, M. Y. Fioshin and V. A. Smirnov, *Electrochemistry of Organic Compounds*, Wiley, NY, 1972.
13 P. J. Dandlilker, F. Diederich, J.-P. Gisselbrecht, A. Louati and M. Gross, *Angew. Chem., Int. Ed. Engl*., 1995, **34**, 2725; C. B. Gorman, B. L. Parkhurst, W. Y. Su and K.-Y. Chen, *J. Am. Chem. Soc*., 1997, **119**, 1141.

Communication 8/06509H

Bis[1,2]dithiolo[3,4-*b*][4′,3′-*e*][1,4]thiazine-3,5-dione, a planar 1,4-thiazine

Carlos F. Marcos,[a] Oleg A. Rakitin,[b] Charles W. Rees,[c] Tomás Torroba,[a] Andrew J. P. White[c] and David J. Williams[c]

[a] *Departamento de Química Orgánica, Facultad de Veterinaria, Universidad de Extremadura, 10071 Cáceres, Spain. E-mail: ttorroba@unex.es*
[b] *N. D. Zelinsky Institute of Organic Chemistry, Academy of Sciences, Leninsky Prospect, 47, 117913 Moscow, Russia*
[c] *Department of Chemistry, Imperial College of Science, Technology and Medicine, London, UK SW7 2AY*

Received (in Liverpool, UK) 21st October 1998, Accepted 17th November 1998

***N*-Benzyldiisopropylamine 1 and S_2Cl_2 give the *N*-benzylbisdithiolothiazine 2, shown by X-ray crystallography to have the typically folded tricyclic structure; 2 is debenzylated by H_2SO_4 to give the title compound 4 which atypically has a rare near-planar 1,4-thiazine ring, gives a blue anion in solution and does not extrude sulfur thermally.**

Sulfur–nitrogen heterocycles with a high proportion of heteroatoms are of theoretical and, when reasonable syntheses are available, practical interest in the chemistry of new materials. We have shown that Hünig's base and related diisopropylamines are fully sulfurated in both isopropyl groups by S_2Cl_2 in one-pot reactions to yield bis[1,2]dithiolo[3,4-*b*:4′,3′*e*]-[1,4]thiazines (*cf.* **2**, **3**)[1–4] and bis[1,2]dithiolo[4,3-*b*:3′,4′*d*]-pyrroles (*cf.* **6**, **8**),[2,4] new families of stable fully unsaturated heterocycles which are revealing a rich chemistry.

The *N*-unsubstituted parent ring systems would be particularly interesting from the structural point of view, and as intermediates in the preparation of *N*-substituted derivatives. Unfortunately these key compounds could not be prepared directly from Pr^i_2NH since this is decomposed by S_2Cl_2. Presumably the first step in the tertiary amine–S_2Cl_2 reaction is oxidation of an isopropyl group to give an iminium ion[5] which reacts further with S_2Cl_2 to form the 1,2-dithiole ring and ultimately the tricyclic system. Readily removable groups on nitrogen, such as acetyl and cyano, which would destabilise the iminium ion suppress the reaction with S_2Cl_2.[4]

We therefore treated *N*-benzyldiisopropylamine[6] **1** with S_2Cl_2 (10 equiv.) and 1,4-diazabicyclo[2.2.2]octane (DABCO) (9 equiv.) in 1,2-dichloroethane for 3 d at room temperature. Formic acid (20 equiv.) was then added and the mixture heated under reflux for 1.5 h, since this treatment gives cleaner reactions by facilitating conversion of the 3-chlorodithiolium salts into dithiole-3-ones. Products **2**† [orange crystals, mp 200–202 °C (21%)] and **3**† [orange solid, mp 209–210 °C (7%)] were obtained after chromatography (Scheme 1).

Structure **2** was confirmed by X-ray crystallography‡ which shows the molecule (Fig. 1) to have a scorpion-like conformation very similar to the *N*-ethyl analogue,[4] the benzyl ring being folded back and partially overlaying the thiazine ring (Fig. 1). The molecule has crystallographic C_s symmetry about a plane passing through S(8), N(4), C(9), C(10) and C(13). The fold angle about the N···S axis of the thiazine ring is 32°,*cf.* 34° in the *N*-ethyl analogue. The pattern of bonding in the thiazine and dithiole ring systems does not differ significantly from that observed in the *N*-ethyl analogue. The molecules pack to form corrugated sheets (Fig. 2) dominated by strong intermolecular O···S interactions [3.02 Å]. There are no intersheet interactions of note.

Treatment of a dilute solution of the *N*-benzyl compound **2** in CH_2Cl_2 with concentrated H_2SO_4 at 5–10 °C for 5 min gave the debenzylated compound **4**† (orange–red crystals, mp 222–224 °C) in quantitative yield. All its properties, including a broad *N*–H absorption at 3474 cm^{-1} and one carbonyl absorption at 1640 cm^{-1} are in agreement with the parent bis[1,2]dithiolo[3,4-*b*:4′,3′-*e*][1,4]thiazine-3,5-dione structure **4**. X-Ray analysis of the N–H species **4** shows that removal of the *N*-benzyl substituent results in a dramatic flattening of the molecule, the non-hydrogen atoms being co-planar to within

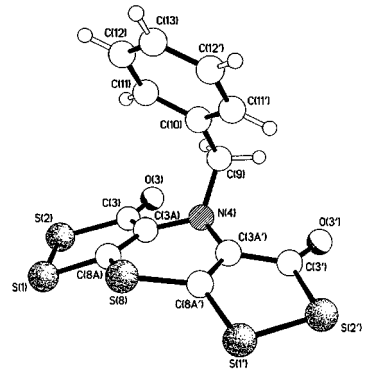

Fig. 1 The molecular structure of **2**. The geometry at N(4) is pyramidal, with the nitrogen atom lying 0.24 Å out of the plane of its substituents.

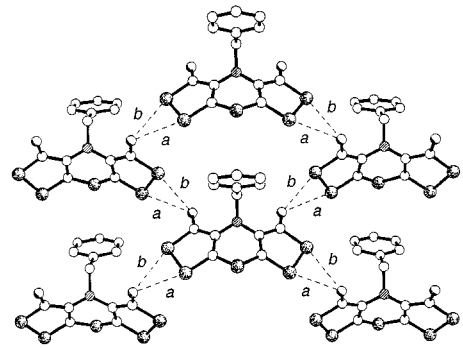

Fig. 2 Part of one of the corrugated sheets of molecules present in the crystals of **2**. The intermolecular O···S contacts (*a*) and (*b*) are both 3.02 Å.

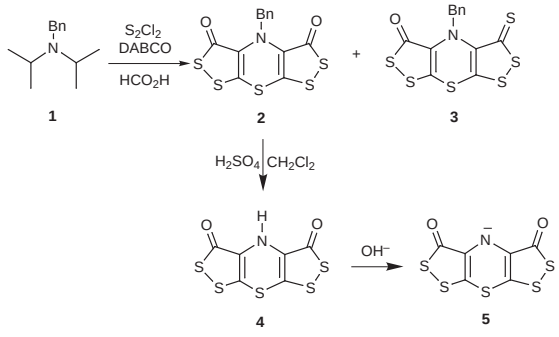

Scheme 1

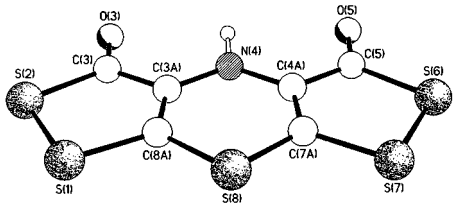

Fig. **3** The molecular structure of **4**.

0.11 Å with only a 5° fold about the thiazine N···S vector (Fig. 3)§ compared to greater than 30° for its *N*-alkyl derivatives and 27° for dibenzo-1,4-thiazine (phenothiazine).[7] The only significant change in the pattern of bonding, compared with **2**, is a small decrease in the C(3A)–N(4) distance and a slight increase in the C(8A)–S(8) bond length. The molecules pack as alternating bi-directional π–π stacked tapes, the planes of adjacent stacks being inclined by 89° (Fig. 4). The tapes are produced by head-to-tail linking of molecules *via* pairs of O···S interactions [3.08 and 3.09 Å], and orthogonal tapes by similar strength O···S, and weaker S···S, interactions [3.15 and 3.54 Å respectively]. The *N*–H hydrogen atom is not involved in any significant intermolecular interactions, possibly because of its steric congestion.

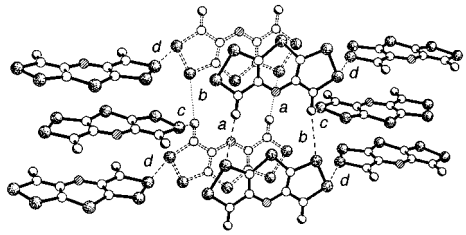

Fig. **4** Part of the array of orthogonally oriented p-stacked tapes present in the crystals of **4**, the mean interplanar separation being *ca*. 3.4 Å. The intermolecular O···S and S···S contacts are (*a*) 3.09, (*b*) 3.08, (*c*) 3.15 and (*d*) 3.54 Å.

The *N*-H compound **4** readily formed purple solutions of the lithium or sodium salt **5** by reaction with LiHMDS or NaH in THF from which a hygroscopic deep purple solid could be isolated by evaporation. Compound **4**, with a UV spectrum of λ_{max} = 310 nm, ε = 8860 in THF, gave a blue solution in aq. 0.1 M NaOH with λ_{max} = 600 nm, ε = 8000. The aqueous alkaline solution was stable for a few days, and the blue spot formed by immersion of TLC plates in aq. NaOH provides a good method of detection of **4**.

Compound **4** and its sodium salt **5** either did not react with common electrophiles such as BnCl, BzCl, MeI and TMSCl under standard conditions or gave unstable products which reverted to **4** during isolation. In striking contrast with its *N*-alkyl derivatives,[2,4] **4** did not extrude sulfur on heating in chlorobenzene for 6 h or in 1,2-dichlorobenzene for 2 h. The expected product **9** (below) was made alternatively. Attempted thiation of **4** with Lawesson's reagent in refluxing THF gave an unstable product that decomposed on work-up; debenzylation of the oxothione **3** by sulfuric acid also gave an unstable product, and we have not yet succeeded in preparing thiocarbonyl derivatives of the parent structure **4**.

Treatment of **1** with S_2Cl_2 (10 equiv) and DABCO (10 equiv) in chlorobenzene for 3 d at room temperature followed by heating under reflux for 2 h gave the pyrrole **6**† [black crystals, mp 223–224 °C (13%)] (Scheme 2) formed by selective sulfur extrusion from the intermediate 1,4-thiazine.[2,4]

The pyrrole **6** was not debenzylated by the sulfuric acid treatment that is so successful with the thiazine **2**. Treatment of **6** in THF at 0 °C for 15 min with excess of ethoxycarbonyl nitrile oxide **7** generated *in situ* from ethyl chlorooximidoacetate and Et_3N[4] readily gave the corresponding dioxo derivative **8** [yellow crystals, mp 211–213 °C (decomp.) (86%)], a structure supported by all its analytical and spectroscopic properties (Scheme 2). The sulfuric acid treatment of **8** in

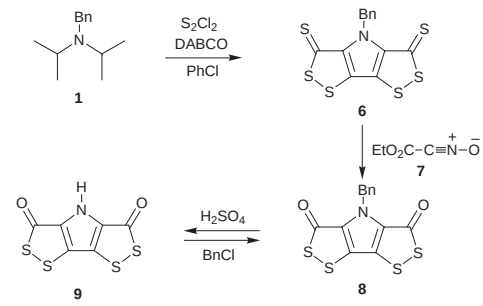

Scheme 2

CH_2Cl_2 at room temperature overnight did now give the debenzylated compound **9** as yellow crystals [mp 267–268 °C (decomp.) (58%)]. The structure of **9** is based upon spectroscopic data and its almost quantitative reconversion to the *N*-benzyl compound **8** with Bu^{t}OK and BnCl in DMF (Scheme 2). Unexceptionally, **9** did not give a coloured solution in 0.1 M aq. NaOH.

Thus the parent bisdithiolopyrrole **9** and bisdithiolo-1,4-thiazine **4** have been prepared in very short sequences from **1**. Whilst the properties of the former are entirely normal, the thiazine **4** is abnormal in that it is almost planar, it readily gives a highly coloured anion which is inert to substitution on nitrogen, and it does not extrude the thiazine sulfur atom on heating. It is not yet clear how these unusual properties, which appear to indicate enhanced electronic delocalisation and stabilisation, result from simply replacing an *N*-alkyl group by hydrogen, nor why the analogous compounds with one or two thiocarbonyl groups should be unstable.

We gratefully acknowledge financial support from the Dirección General de Enseñanza Superior of Spain (DGES Project ref. PB96-0101), the NATO Linkage Grant 970596, MDL Information Systems (UK) Ltd, and an RSC Journals Grant to O. A. R., and we thank the Wolfson Foundation for establishing the Wolfson Centre for Organic Chemistry in Medical Science at Imperial College.

Notes and references

† The structures of all new compounds are based upon IR, MS, HRMS, ^{1}H and ^{13}C NMR and elemental analysis.

‡ *Crystal data* for **2**: $C_{13}H_7NO_2S_5$, M = 369.5, orthorhombic, *Pnma* (no. 62), a = 11.573(3), b = 16.113(1), c = 8.064(1) Å, V = 1503.7(4) Å^3, Z = 4 (the molecule has crystallographic C_s symmetry), D_c = 1.632 g cm^{-3}, μ(Cu-Kα) = 71.3 cm^{-1}, F(000) = 752, T = 293 K; orange hexagonal prisms 0.58 × 0.43 × 0.40 mm. For **4**: $C_6HNO_2S_5$, M = 279.4, monoclinic, $C2/c$ (no. 15), a = 11.323(1), b = 8.071(1), c = 20.066(2) Å, β = 104.49(1)°, V = 1775.4(3) Å^3, Z = 8, D_c = 2.090 g cm^{-3}, μ(Mo-Kα) = 12.7 cm^{-1}, F(000) = 1120, T = 203 K; orange–red blocky needles 0.73 × 0.22 × 0.17 mm. 1232 (2601) Independent reflections were measured on Siemens P4/PC diffractometers using ω-scans for **2** (**4**) respectively. The structures were solved by direct methods and all of the non-hydrogen atoms were refined anisotropically using full-matrix least-squares based on F^2 with absorption corrected data to give R_1 = 0.036 (0.037), wR_2 = 0.093 (0.078) for 1118 (2063) independent observed reflections [$|F_o| > 4\sigma(|F_o|)$, $2\theta \leqslant 124°$ (60°)] and 104 (131) parameters for **2** (**4**) respectively. CCDC 182/1095.

§ In the thiazine ring the C and N atoms are coplanar to within 0.01 Å with the S atom lying 0.11 Å and the H atom 0.20 Å out of this plane.

1 C. F. Marcos, C. Polo, O. A. Rakitin, C. W. Rees and T. Torroba, *Angew. Chem*., 1997, **109**, 283; *Angew. Chem., Int. Ed. Engl*., 1997, **36**, 281.
2 C. F. Marcos, C. Polo, O. A. Rakitin, C. W. Rees and T. Torroba, *Chem. Commun*., 1997, 879.
3 C. F. Marcos, O. A. Rakitin, C. W. Rees, L. I. Souvorova, T. Torroba, A. J. P. White and D. J. Williams, *Chem. Commun*., 1998, 453.
4 C. W. Rees, A. J. P. White, D. J. Williams, O. A. Rakitin, C. F. Marcos, C. Polo and T. Torroba, *J. Org. Chem*., 1998, **63**, 2189.
5 For related examples, see: S. L. Schreiber, *Tetrahedron Lett*., 1980, **21**, 1027; T. Netscher and P. Bohrer, *Tetrahedron Lett*., 1996, **37**, 8359.
6 N. C. Deno and R. E. Fruit, *J. Am. Chem Soc*., 1968, **90**, 3502.
7 J. D. Bell, J. F. Blount, O. V. Briscoe and H. C. Freeman, *J. Chem. Soc., Chem. Commun*., 1968, 1656.

Communication 8/08192A

Tributyltin radical-induced addition–carbocyclization on chiral perhydro-1,3-benzoxazines: a facile entry to enantiopure tin-containing auxiliaries

Celia Andrés, Juan Pablo Duque-Soladana and Rafael Pedrosa*

Departamento de Química Orgánica, Facultad de Ciencias, Universidad de Valladolid, Dr. Mergelina s/n. 47011 - Valladolid, Spain. E-mail: pedrosa@qo.uva.es

Received (in Liverpool, UK) 6th October 1998, Accepted 17th November 1998

***N*-Acryloylperhydro-1,3-benzoxazines 1a,b undergo stereoselective addition–carbocyclization when reacted with Bu_3SnH, leading to stannylated lactamic rings that can be transformed into enantiopure pyrrolidines.**

The design and synthesis of optically active alkylstannanes is currently considered a challenge in both organic and organometallic chemistry.[1] Activated non-racemic stannanes have been used in a variety of reactions which include allylation of aldehydes catalysed by Lewis acids,[2] tin–lithium exchange,[3] palladium cross-coupling[4] and cyclopropanation;[5] however, the number of examples reported to date is small.

Except for the ready accessibility of chiral α-heterosubstituted stannanes,[6] there is a lack of general methods for preparation of non-racemic organotin compounds and therefore chirality transfer from another reagent is generally preferred.[2,7]

The carbon–tin bond is easily activated in the neighbourhood of a functional group.[8] In this context α-alkoxystannanes and allyltin compounds are suitable substrates for metal exchange[9] and nucleophilic addition reactions[2] respectively. On the other hand the nature of the alkyl substituents at the Sn atom is sometimes crucial since large substituents causes diminished reactivity.

As part of a project on stereoselective radical cyclizations in perhydrobenzo-1,3-benzoxazines[10] we focused our attention on the preparation of alkylstannanes attached to a perhydrobenzoxazine chiral auxiliary. This new type of structure plays a highly versatile role in synthesis since it behaves as a source of organometallic species as well as a classical organic auxiliary.[11]

Encouraged by the stereoselectivity of intramolecular radical cyclizations, the synthesis of organotin compounds was tested *via* addition–cyclization of acrylamides[10] **1a**,**b** with Bu_3SnH, a less toxic and volatile reagent than trimethyltin derivatives[12] (Scheme 1).

Treatment of **1a** with commercial Bu_3SnH in the presence of AIBN as initiator was performed under different conditions as summarized on Table 1. Attempts to use the Stork method (Bu_3SnCl + $NaCNBH_3$)[13] or palladium catalysis [$Pd(PPh_3)_3$][14] failed. The best chemical yield corresponded to a short heating of a mixture of Bu_3SnH, AIBN and the acrylamide in refluxing benzene (entry 3), or alternatively, without solvent at 80–90 °C (entry 4). This one is an extremely rapid, violent reaction and it is not recommended for preparative purposes. Slow addition of reagent (entry 1) or ultraviolet irradiation at room temperature (entry 2) causes a decrease in the chemical yield although a slight improvement in the diastereomeric ratio is observed at that temperature.

The four diastereomeric stannylated lactams **2a**–**5a**† were separated by flash chromatography and their stereochemistry was determined by NOESY experiments. Interestingly, although two stereocenters were created, addition–cyclization on acrylamide **1b** under thermal conditions (entries 5, 6) led to a mixture of only two diastereomers (**2b** and **3b**) which are epimers at the α-lactamic carbon. It is worth noting in both cases that major cyclization products **2a**,**b** showed a C-2/C-3 *trans* relationship at the newly created stereocenters. This result is contrary to that predicted by the Beckwith radical model[15] and no satisfactory reasons have been ascertained to date.[16]

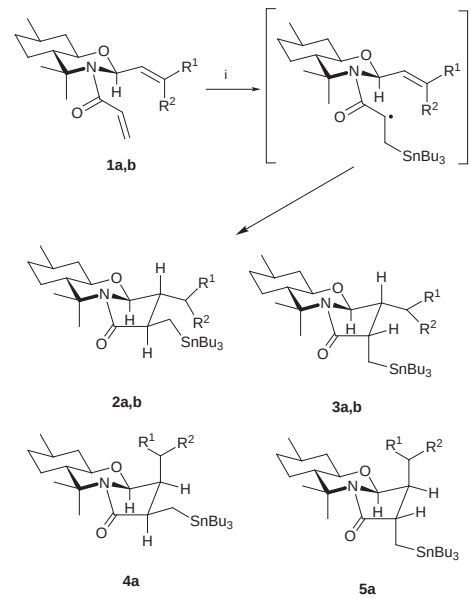

Scheme 1 *Reagents and conditions*: i, Bu_3SnH (1.2 equiv.), AIBN (5–10 equiv.), 80–90 °C (see Table 1).

Table 1 Radical addition-cyclization of acrylamides **1a**,**b**

						Products (%)				
Entry	R^1	R^2	Solvent	*T*/°C	*t*/min	**2**	**3**	**4**	**5**	Yield (%)
1	Ph	H	PhH	80	720	**2a** (59)	**3a** (21)	**4a** (16)	**5a** (4)	76
2	Ph	H	PhH	25	900	**2a** (65)	**3a** (22)	**4a** (9)	**5a** (4)	48
3	Ph	H	PhH	80	30	**2a** (59)	**3a** (21)	**4a** (16)	**5a** (4)	99
4	Ph	H	–	90	5	**2a** (56)	**3a** (22)	**4a** (16)	**5a** (6)	99
5	Me	Me	PhH	80	30	**2b** (68)	**3b** (32)			98
6	Me	Me	–	90	5	**2b** (68)	**3b** (32)			99

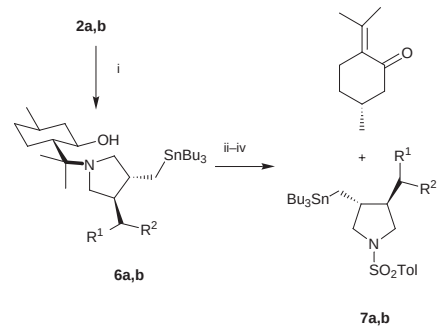

Scheme 2 *Reagents and conditions*: i, $LiAlH_4$ (5 equiv.), $AlCl_3$ (2 equiv.), THF, 0 °C, 5 min; ii, PCC (4 equiv.), CH_2Cl_2, 1 h; iii, KOH (2.5 M)–THF–MeOH (1:2:1), 2 h; iv, TsCl (2 equiv.), $Pr^1{}_2NEt$ (4 equiv.), CH_2Cl_2, 24 h.

Preliminary MO calculations (UHF/PM3) performed in our system suggested that the major lactams **2a**,**b** arise from biased conformations in which allylic 1,3-strain controls the olefinic appendage and a planar *Z* isomer is preferred for the intermediate amide radical. As a consequence, late transition states or thermodynamic equilibration can be discarded as explanations for the *trans* selectivity of such processes.

Once isolated, the major diastereomeric lactams **2a**,**b** were transformed quantitatively into the stannylated menthol derivatives **6a**,**b** by reduction with $LiAlH_4$ at 0 °C in THF. Sequential PCC oxidation of **6a**,**b** followed by treatment with methanolic KOH[17] of the intermediate amino ketone led to enantiopure stannylated pyrrolidines **7a**,**b** isolated as tosylates, although in modest overall yield (34 and 44% respectively) (Scheme 2).

On the other hand, it was interesting to explore the reactivity at the metal center and the possibility of easy destannylation. To this end, after isolation by flash chromatography, pure diastereomers **2b** and **3b** obtained in the reaction of **1b** with Bu_3SnH were subjected to Sn–Ti exchange[18] to generate the corresponding titanium homoenolates by reaction with $TiCl_4$ in CH_2Cl_2 at 0 °C (Scheme 3). This kind of metal homoenolates has been described for alkyl propionates but, to the best of our knowledge, no examples concerning lactams are known.

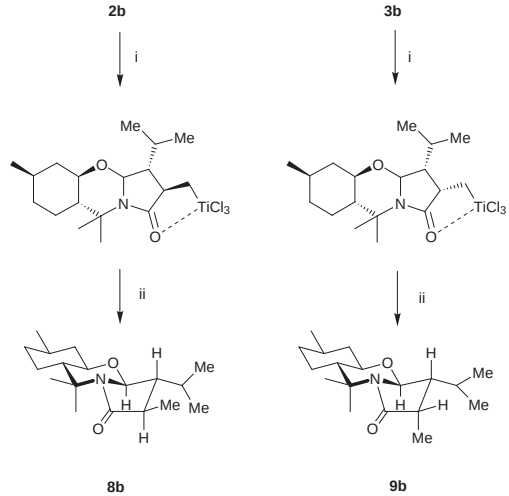

Scheme 3 *Reagents and conditions*: i, $TiCl_4$ (1.3 equiv.), CH_2Cl_2, 0 °C, 10 h; ii, SiO_2, CH_2Cl_2 or HCl, H_2O.

The titanium intermediates were transformed into enantiopure lactams **8b** and **9b** respectively by hydrolytic cleavage of the metal–carbon bond with silica gel or aq. HCl. It is noteworthy that the *trans* relationship of the substituent at the lactam coincides with the stereochemistry of the starting stannylated compounds, indicating that the metal interchange does not affect the configuration at the α-carbon in the lactamic ring. The reactivity of these titanium homoenolates with other electrophiles is currently being examined and the results will be published in due course.

We thank Spanish DGES for financial support (project PB95-707). One of us (J. P. D.-S.) also thanks the Spanish Ministerio de Educación y Ciencia for a fellowship (FPU program).

Notes and references

† *Selected data* for **2a**: $[\alpha]_D{}^{23}$ −9.38 (*c* 1.20 $CHCl_3$); δ_H(300 MHz, $CDCl_3$) 0.80 (m, 6H), 0.90 (t, 12 H), 0.95 (d, 3H), 1.12 (s, 3H), 1.20–1.35 (m, 8H), 1.35–1.50 (m, 8H), 1.70 (s, 3H), 1.72 (m, 2H), 1.94 (m, 2H), 2.10–2.20 (m, 1H), 2.71 (dd, 1H, *J* 7.9, 13.6), 2.98 (dd, 1H, *J* 5.9, *J* 13.6), 3.31 (dt, 1H, *J* 4.2, 10.6), 4.53 (d, 1H, *J* 6.2), 7.1–7.3 (m, 5H); δ_C(75.5 MHz, $CDCl_3$) 10.0, 11.2, 13.7, 18.3, 22.0, 23.9, 25.4, 27.4, 29.1, 31.1, 34.5, 37.4, 41.0, 45.0, 49.5, 49.8, 56.0, 76.0, 87.7, 126.2, 128.3, 129.2, 138.8, 175.2. For **2b**: $[\alpha]_D{}^{23}$ −5.38 (*c* 1.0 CH_2Cl_2); δ_H(300 MHz, $CDCl_3$) 0.80–1.00 (m, 26H), 1.13 (s, 3H), 1.20–1.35 (m, 9H), 1.35–1.55 (m, 10H), 1.67 (s, 3H), 1.72 (m, 2H), 1.95 (m, 1H), 2.15 (m, 1H), 3.34 (dt, 1H, *J* 4.1, 10.6), 4.54 (d, 1H, *J* 6.9); δ_C(75.5 MHz, $CDCl_3$) 10.0, 13.6, 13.7, 18.5, 19.9, 20.7, 21.9, 23.9, 25.3, 27.4, 29.2, 30.0, 31.2, 34.4, 41.2, 43.4, 49.7, 56.6, 76.6, 86.9, 175.3. For **7a**: $[\alpha]_D{}^{23}$ +36.9 (*c* 1.06 CH_2Cl_2); δ_H (300 MHz, $CDCl_3$) 0.52 (dd, 1H, *J* 10.0, 13.1), 0.75–1.00 (m, 7H), 0.89 (t, 9H, *J* 7.2), 1.20–1.35 (m, 6H), 1.35–1.50 (m, 6H), 1.7–1.9 (m, 2H), 2.30 (dd, 1H, *J* 9.1, 13.7), 2.42 (s, 3H), 2.71 (dd, 1H, *J* 8.7, 9.5), 2.80 (dd, 1H, *J* 4.2, 13.7), 2.95 (dd, 1H, *J* 8.0, 10.0), 3.30 (dd, 1H, *J* 6.8, 10.0), 3.50 (dd, 1H, *J* 6.7, 9.5), 7.05 (d, 2H, *J* 8.2), 7.20–7.40 (m, 5H), 7.65 (d, 2H, *J* 8.2); δ_C(75.5 MHz, $CDCl_3$) 9.2, 11.0, 13.7, 21.5, 27.3, 29.1, 37.9, 42.6, 49.6, 52.8, 55.7, 126.2, 127.4, 128.4, 128.6, 129.5, 133.7, 139.5, 143.2. For **7b**: $[\alpha]_D{}^{23}$ +33.3 (*c* 1.56 CH_2Cl_2); δ_H(300 MHz, $CDCl_3$) 0.51 (dd, 1H, *J* 10.5, 13.2), 0.74 (d, 3H, *J* 6.9), 0.80 (d, 3H, *J* 8.0), 0.85–1.00 (m, 6H), 0.89 (t, 9H, *J* 7.1), 1.20–1.35 (m, 8H), 1.35–1.50 (m, 6H), 1.69 (octuplet, 1H, *J* 6.8), 1.8–2.0 (m, 1H), 2.43 (s, 3H), 2.60 (t, 1H. *J* 9.2), 3.01 (dd, 1H, *J* 8.9, 9.7), 3.28 (dd, 1H, *J* 8.3, 9.7), 3.44 (dd, 1H, *J* 7.2, 9.2), 7.32 (d, 2H, *J* 8.0); 7.70 (d, 2H, *J* 8.0); δ_C(75.5 MHz, $CDCl_3$) 9.2, 11.6, 13.6, 17.3, 21.4, 21.7, 27.3, 27.5, 29.1, 39.7, 49.2, 53.9, 56.1, 127.5, 129.5, 133.4, 143.2.

1 For general reviews on organotin chemistry see: A. G. Davies, in *Comprehensive Organometallic Chemistry*, ed. G. Wilkinson, F. G. Stone and E. W. Abel, Pergamon, London, 1982; A. G. Davies and P. J. Smith, in *Comprehensive Organometallic Chemistry II*, ed. G. Wilkinson, F. G. Stone and E. W. Abel, Pergamon, London, 1995; W. P. Neuman, *Synthesis*, 1987, 665.
2 Y. Yamamoto and N. Asao, *Chem. Rev*., 1993, **93**, 2207.
3 I. Coldham, S. Holman and M. M. S. Lang-Anderson, *J. Chem. Soc*., *Perkin Trans. 1*, 1997, 1481.
4 J. Ye, R. K. Bhatt, J. R. Falck, *J. Am. Chem. Soc*., 1994, **116**, 1; T. N. Mitchel, *Synthesis*, 1992, 803.
5 S. Hanessian, U. Reinhold and G. Gentile, *Angew. Chem*., *Int. Ed. Engl*., 1997, **36**, 1881.
6 P. C.-M. Chan and J. M. Chang, *J. Org. Chem*., 1988, **53**, 5586; J. A. Marshall, G. S. Wellmaker and B. W. Gung, *J. Am. Chem. Soc*., 1991, **113**, 647; J.-C. Cintrat, E. Blart, J.-L. Parrain and J.-P. Quintard, *Tetrahedron*, 1998, **53**, 7615.
7 J. San Filippo, Jr. and J. Silbermann, *J. Am. Chem. Soc*., 1982, **104**, 2831; M. Nishida, A. Nishida and N. Kawahara, *J. Org. Chem*., 1996, **61**, 3574.
8 T. Sato, *Synthesis*, 1990, 259.
9 W. C. Still, *J. Am. Chem. Soc*., 1978, **100**, 1481.
10 C. Andrés, J. P. Duque-Soladana, J. M. Iglesias and R. Pedrosa, *Tetrahedron Lett*., 1996, **37**, 9085; C. Andrés, J. P. Duque-Soladana, J. M. Iglesias and R. Pedrosa, *Synlett*, 1997, 1391.
11 A. Alberola, M. A. Alvarez, C. Andrés, A. González and R. Pedrosa, *Synthesis* 1990, 153; A. Alberola, C. Andrés and R. Pedrosa, *Synlett*, 1990, 763; C. Andrés, G. Maestro, J. Nieto, R. Pedrosa, S. García-Granda and E. Pérez-Carreño, *Tetrahedron Lett*., 1997, **38**, 1463.
12 P. J. Smith, *Toxicological Data on Organotin*, ITRI Pub. 538, International Research Institute, UK, 1997.
13 G. Stork and P. M. Sher, *J. Am. Chem. Soc*., 1986, **108**, 303; A. Srikrishna, S. Nagaraju and G. V. R. Sharma, *J. Chem. Soc*., *Chem. Commun*., 1993, 285.
14 M.-J. Wu, C.-L. Fu, T.-H. Duh and J.-Y. Yeh, *Synthesis*, 1996, 462.
15 A. L. J. Beckwith and C. H. Schiesser, *Tetrahedron*, 1985, **41**, 3925; D. C. Spellmeyer and K. N. Houk, *J. Org. Chem*., 1987, **52**, 959.
16 S. Hanessian, U. Reinhold and S. Ninkovic, *Tetrahedron Lett*., 1996, **37**, 8967.
17 C. Andrés, J. Nieto, R. Pedrosa and M. Vicente, *J. Org. Chem*., in the press.
18 E. Nakamura and I. Kuwajima, *J. Am. Chem. Soc*., 1983, **105**, 651; R. Goswami, *J. Org. Chem*., 1985, **50**, 5907.

Communication 8/07773H

The stereochemistry of a retro-carbolithiation reaction

Reinhard W. Hoffmann and Ralf Koberstein

Fachbereich Chemie der Philipps-Universität Marburg, Hans-Meerwein-Strasse, 35032 Marburg, Germany. E-mail: rwho@ps1515.chemie.uni-marburg.de

Received (in Liverpool, UK) 29th October 1998, Accepted 17th November 1998

Ring-opening of the cyclopropylmethyl lithium compound 7 to give the α-duryl thio-substituted alkyllithium compound 8 proceeds in a stereochemically defined manner at the lithium-bearing stereocentre.

The stereochemical course of reactions in which organolithium compounds are generated may reveal fundamental details of organolithium chemistry. For instance, tin–lithium exchange to generate alkyllithium compounds has been found to proceed with retention of configuration.[1–3] The carbolithiation of vinyl sulfides has been shown to proceed in a non-stereospecific manner.[4] Here we would like to address the stereochemistry of a retro-carbolithiation reaction, the ring-opening of cyclopropylmethyl lithium compounds. The prototype of this rearrangement (**1**→**2**) was shown by Lansbury[5] to proceed at −70 °C with a half life of 53 min in Et_2O (Scheme 1).

The related ring-opening of **3** should create a chiral organolithium compound **4**. This would allow the determination of the stereochemistry in the generation of the new carbon–lithium bond, provided that the resulting organolithium compound **4** is configurationally stable and the regioselectivity of the ring opening is such as to generate compound **4** and not the isomer **5**. We surmised that both conditions would be met when X is a durylthio group. α-Durylthio alkyllithium compounds are configurationally stable at −110 °C[4] and stabilization of the negative charge by a sulfur substituent should direct the ring opening of **3** to give **4**. There remains, however, the necessity to effect the ring opening at −110 °C. We surmised that breaking of the carbon–lithium bond in **3** would be rate determining. Therefore, a delocalized allylic system at the migration origin should facilitate this process. This led us to investigate the ring-opening of the lithium compound **7**, generated by a low temperature selenium–lithium exchange reaction.[6]

The seleno ether **6** of 90% ee (determined by Mosher ester analysis of the precursor **14**) was treated with Bu^{t}Li at −107 °C in THF in a two-compartment low temperature reaction vessel (Scheme 2).[7] The organolithium compound **7** formed in this manner immediately underwent ring opening, since quenching with (−)-menthyl(dimethyl)tin bromide **9**[2,8] after 30 min led to the tin compounds **10a** and **10b** in a 9:1 *E/Z* ratio (67% yield). ^{119}Sn NMR analysis revealed that the major *E*-isomer was formed with 76% diastereomeric excess. Quenching after 10 or 60 min, or quenching with the enantiomeric reagent *ent*-**9**, generated the tin compounds with a constant de in the range of 76–82%. This shows that the organolithium compound **8** is configurationally stable under the conditions applied, and that quenching of **8** with **9** is not complicated by kinetic resolution.

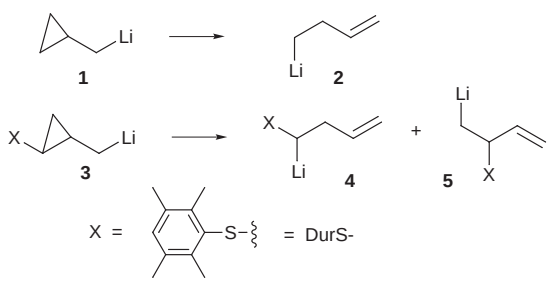

Scheme 1

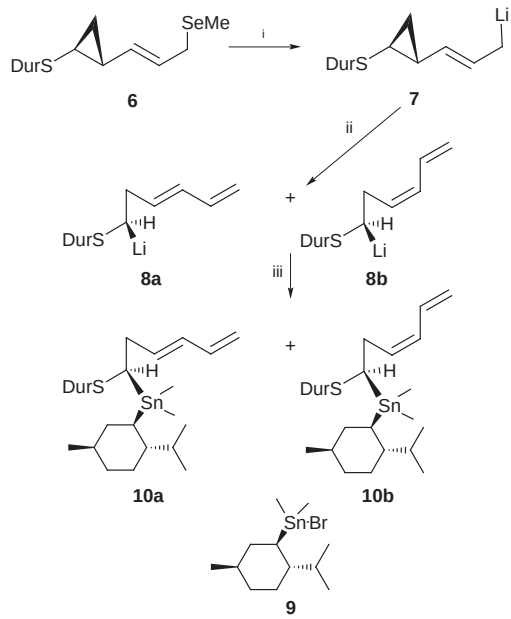

Scheme 2 *Reagents and conditions*: i, Bu^{t}Li, THF, −107 °C; ii, −107 °C, 30 min; iii, **9**.

In order to determine the stereochemistry of the ring opening process, pre-cooled MeI was added to the organolithium compound **8** after 30 min at −107 °C (Scheme 3). This resulted in 88% of a 88:12 *E/Z* mixture of the hexadienyl thioether **11**. Hydrogenation of the mixture provided uniform dextrorotatory 2-durylthiopentane **12**. The optical purity and the absolute configuration of **12** was determined with the aid of a sample prepared from (*S*)-heptan-2-ol.

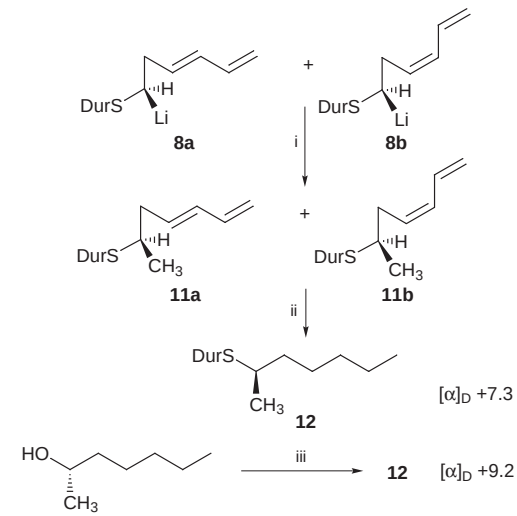

Scheme 3 *Reagents and conditions*: i, MeI; ii, H_2, $(Ph_3P)_3RhCl$; iii, MsCl, pyridine; iv, DurSLi.

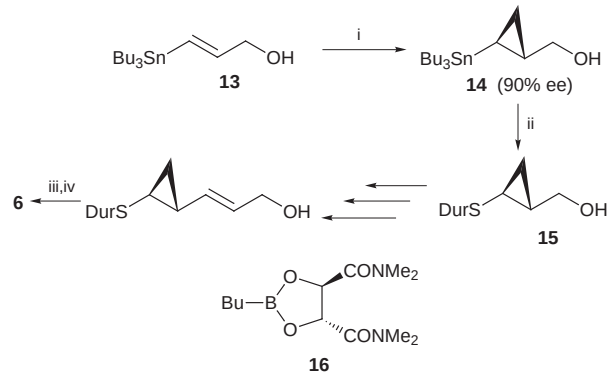

Scheme 4 *Reagents and conditions*: i, **16**, $Zn(CH_2I)_2$·DME; ii, Bu^nLi, $(DurS)_2$; iii, Bu^nLi, TsCl; iv, MeSeLi.

The optical purity of **12** (*ca*. 80% o.p.) corresponds to the de values of the tin compounds **10** and shows that the ring opening of **7** to give **8** proceeds with at most 10% loss of enantiomeric composition. The minor loss in enantiomeric purity of **8** during its generation at −107 °C from **7** should be associated with the ring opening process of **7**.[9]

Knowledge of the absolute configuration of the starting material **6** and that of the product **11** shows that the overall transformation proceeds with retention of configuration at the sulfur-bearing carbon atom. There is, however, some element of uncertainty regarding the stereochemistry of the individual steps. It is generally accepted[10] that the methylation of 'low reactive' sp^3-hybridized organolithium compounds by MeI proceeds with retention of configuration. If this applies also to the transformation of **8** into **11** it follows that the ring opening of **7** to give **8** proceeds with predominant retention of configuration at the lithium-bearing carbon atom.

The synthesis of the starting material **6** relied on the asymmetric cyclopropanation developed by Charette.[11] Cyclopropanation of **13** should furnish the cyclopropane **14** of the absolute configuration shown (Scheme 4). The latter was then converted to **15** and on to the selenoether **6** in a series of standard transformations (Swern oxidation, Horner olefination, DIBAL-H reduction).

We are grateful to the Deutsche Forschungsgemeinschaft (SFB 260) and the Fonds der Chemischen Industrie for support of this study.

Notes and references

1 W. C. Still and C. Sreekumar, *J. Am. Chem. Soc*., 1980, **102**, 1201; J. S. Sawyer, A. Kucerovy, T. L. Macdonald and G. J. McGarvey, *J. Am. Chem. Soc*., 1988, **110**, 842; H. J. Reich, J. P. Borst, M. B. Coplien, and N. H. Phillips, *J. Am. Chem. Soc*., 1992, **114**, 6577.
2 F. Hammerschmidt, A. Hanninger and H. Völlenkle, *Chem. Eur. J*., 1997, **3**, 1728.
3 For an exception and for leading references, see: J. Clayden and J. H. Pink, *Tetrahedron Lett*., 1997, **38**, 2565.
4 R. W. Hoffmann, R. Koberstein, B. Remacle and A. Krief, *Chem. Commun*., 1997, 2189.
5 P. T. Lansbury, V. A. Pattison, W. A. Clement and J. D. Sidler, *J. Am. Chem. Soc*., 1964, **86**, 2247; *cf*. also. A. B. Charette and J. Naud, *Tetrahedron Lett*., 1998, **39**, 7259.
6 H. Gilman and R. L. Bebb, *J. Am. Chem. Soc*., 1939, **61**, 109; H. Gilman and F. J. Webb, *J. Am. Chem. Soc*., 1949, **71**, 4062; D. Seebach and N. Peleties, *Angew. Chem*., 1969, **81**, 465; *Angew. Chem., Int. Ed. Engl*., 1969, **8**, 450; M. Clarembeau and A. Krief., *Tetrahedron Lett*., 1984, **25**, 3629.
7 H. C. Stiasny and R. W. Hoffmann, *Chem. Eur. J*., 1995, 619.
8 H. Schumann and B. C. Wassermann, *J. Organomet. Chem*., 1989, 365, C1.
9 Electrophilic ring opening of cyclopropanes both with retention and inversion of configuration has precedent: D. H. Gibson and C. H. DePuy, *Chem. Rev*., 1974, **74**, 605.
10 D. Hoppe and T. Hense, *Angew. Chem*., 1997, **109**, 2376; *Angew. Chem., Int. Ed. Engl*., 1997, **36**, 2282; for an exception see: R. E. Gawley and Q. Zhang, *J. Org. Chem*., 1995, **60**, 5763.
11 A. B. Charette, S. Prescott and C. Brochu, *J. Org. Chem*., 1995, **60**, 1081.

Communication 8/08410F

ChemComm

Aldol polymerization as a novel polyaddition based on Mukaiyama aldol reaction and its application to the synthesis of optically active polymer

Kenichi Komura, Shinichi Itsuno* and Koichi Ito

Department of Materials Science, Toyohashi University of Technology, Toyohashi, 441-8580 Japan.
E-mail: itsuno@tutms.tut.ac.jp

Received (in Cambridge, UK) 28th October 1998, Accepted 12th November 1998

Repetitive Mukaiyama aldol reaction between bis(silyl ketene acetal) and dialdehyde proceeded in the presence of Lewis acid to afford poly(hydroxy ester).

The Mukaiyama aldol reaction is one of the most powerful tools for the construction of new C–C bonds in organic synthesis.[1–4] In spite of high reactivity and the subtle possibilities of side reactions in a number of aldol reactions under controlled reaction conditions, polymer synthesis utilizing this excellent reaction has not been studied extensively. Aldol-GTP (Aldol - Group Transfer Polymerization)[5,6] is the only exception, which is based on repetitive aldol reaction. Monomers for the aldol-GTP are however limited to trialkylsilyl vinyl ethers,[7,8] which give silylated poly(vinyl alcohol)s. In the Mukaiyama aldol reaction, Lewis acid activates or catalyses the reactions of silyl enolates or silyl ketene acetals with carbonyl compounds to give β-hydroxycarbonyl derivatives in excellent yield. If the same reaction occurs with the combination of bis(silyl enol ether)s and dialdehyde, this would be one of the most suitable ways for the preparation of poly(β-hydroxycarbonyl)s in a polyaddition manner. We found that bis(silyl ketene acetal)s reacted with dialdehydes in the presence of Lewis acid to afford poly-(hydroxy ester)s. Here we report a polyaddition between bis(silyl ketene acetal) and dialdehyde, which we propose to term 'aldol polymerization'. Asymmetric aldol reactions have also been studied extensively.[9] Several efficient chiral catalysts were designed for the aldol reaction. Thus, it should be possible to prepare optically active polymers if a chiral catalyst is employed in the aldol polymerization. Asymmetric aldol polymerization was also examined.

In the first place, we attempted to prepare bis(trimethylsilyl-ketene acetal) **2** as a monomer for aldol polymerization using LDA/Me_3SiOTf (Scheme 1).[10] However the monomer **2** was contaminated with a small amount of the monoketene acetal after distillation of the product, since trimethylsilylketene acetal is susceptible to hydrolysis. Monomers for polyaddition reactions always require high purity in order to obtain high molecular weight polymers. In stead of trimethylsilylketene acetal, the preparation of triethylsilyl derivatives **4** was then examined. In the literature it was reported that aldol reaction of triethylsilylketene acetals with aldehyde smoothly occurred to afford the aldol products in high yield.[11,12] We found that the hydrosilylation method shown in Scheme 2 was suitable for the preparation of **4**. Hydrosilylation of bismethacrylate **3** with triethylsilane in the presence of a rhodium catalyst afforded **4** in good yield.[13,14] More importantly, the higher stability of the triethylsilylketene acetal made it possible to use normal silica gel column chromatography for its purification. It is also possible to purify this monomer by simple distillation. As a model reaction of polyaddition, the monomer **4** was allowed to react with 2 equiv. of benzaldehyde in the presence of $TiCl_4$. Aldol reaction between **4** and benzaldehyde occurred smoothly at −78 °C to give the corresponding aldol in good isolated yield. This result encouraged us to apply the reaction to the polymer synthesis. Terephthalaldehyde **6** was chosen as the comonomer in this polymerization (Scheme 3). Results for the aldol polymerization are shown in Table 1. Since aldol reactions of silylketene acetal with aldehyde using $TiCl_4$ were reported to give excellent yields at −78 °C,[15] the polymerization was carried out at this temperature. Without Lewis acid, no reaction was detected between **4** and **6**. When neat $TiCl_4$ was added to the monomer solution in CH_2Cl_2, resulting in a heterogeneous system, the reaction afforded a polymer insoluble in common organic solvents (run 1). Addition of a 1.0 M CH_2Cl_2 solution of $TiCl_4$ to the mixture of **4** and **6** at −78 °C initiated the aldol polymerization to give the desired aldol polymer which was isolated after precipitation into MeOH–H_2O (7:3). During isolation of the polymer **7a**, a small number of the triethylsilyl ether groups in the polymer were converted to hydroxy groups (**7b**). Although this polymeric silyl ether is quite resistant towards dilute hydrochloric acid, the use of TBAF in THF led to the complete cleavage of the Si–O bonds to give poly(hydroxy ester) **7b**. The structure of the obtained polymer **7** was supported by spectroscopic analyses. The molecular weight of **7** was measured by GPC (THF as an eluent) using polystyrene calibration curves. The use of $ZnBr_2$ as Lewis acid resulted in a high yield of the polymer at room temperature (run 3). Mukaiyama aldol reaction is normally activated by stoichiometric amounts of Lewis acid, whereas catalytic activity of rare earth metal triflates has recently been reported in the same reaction.[16,17] We have found that catalytic amount of triflates such as $Yb(OTf)_3$ and $Sc(OTf)_3$ were effective for the aldol polymerization to give the polymer. In the case of $Sc(OTf)_3$, the temperature should be kept below 0 °C during its addition into the monomer solution (run 6), otherwise insoluble polymer was yielded as the main product (run 5). As another novel dialdehyde monomer for the aldol polymerization, we prepared **8**, which has somewhat better solubility than **6**. As can be seen in the polymerization of **4** with **6**, addition of a 1.0 M CH_2Cl_2

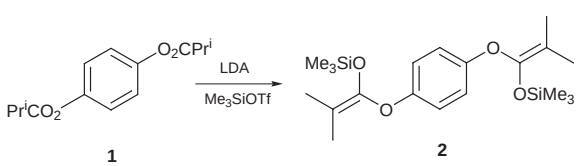

1 **2**

Scheme 1

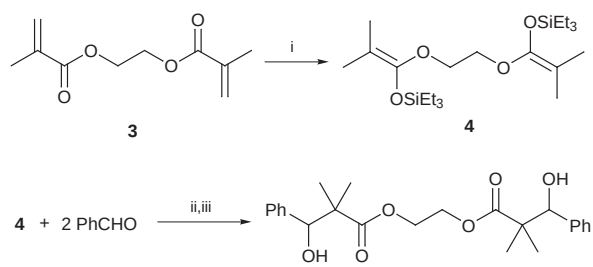

3 **4** **5**

Scheme 2 *Reagents and conditions*: i, Et_3SiH, $(Ph_3P)_3RhCl$, $CHCl_3$, 60 °C, 1 min, 80%; ii, $TiCl_4$, CH_2Cl_2, −78 °C, 4 h, 80%; iii, TBAF, THF, room temp., 94%.

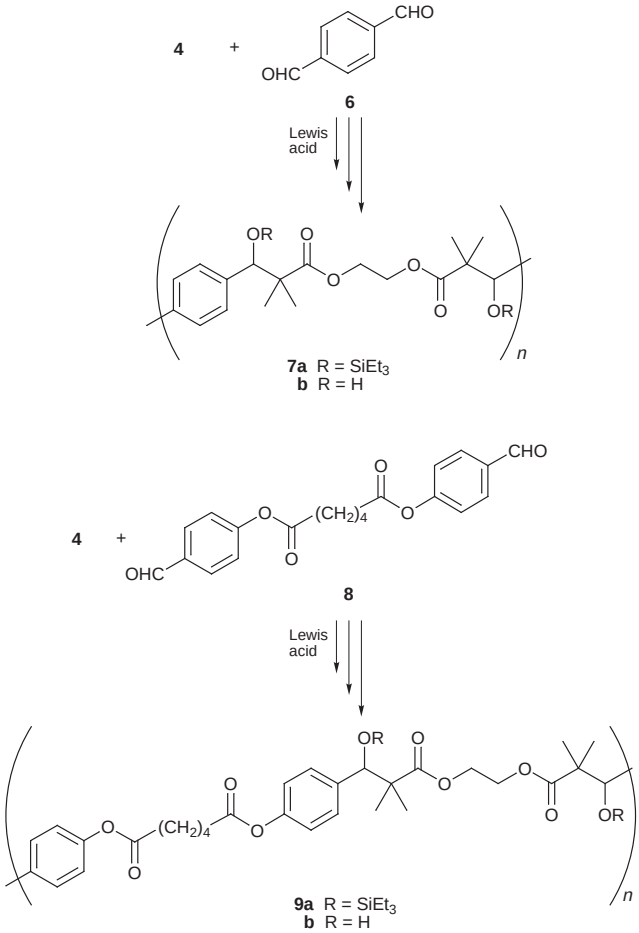

Scheme 3

solution of $TiCl_4$ to the mixture of **4** and **8** at −78 °C also yielded the desired aldol polymer **9a**. A catalytic amount of $Yb(OTf)_3$ or $Sc(OTf)_3$ as a Lewis acid catalyst also made it possible to synthesize the aldol polymer **9** having high molecular weight (runs 9 and 10). The structure of **9a** was confirmed by NMR and IR analysis.

The use of chiral Lewis acids for enantioselective aldol reactions has recently received great attention.[9] One of the efficient chiral catalyst for the asymmetric Mukaiyama aldol

Table 1 Aldol polymerization of bis(silyl ketene acetal) **4** with dialdehyde in CH_2Cl_2

Run	Dialdehyde	Lewis acid (equiv.)	T/°C	t/h	Yield (%)[a]	M_n[b]	M_w/M_n[b]
1	**6**	$TiCl_4$[c] (2.0)	−78	4	86	—[d]	—[d]
2	**6**	$TiCl_4$[e] (2.0)	−78	4	21	1500	1.60
3	**6**	$ZnBr_2$ (2.0)	20	48	84	2800	2.21
4	**6**	$Yb(OTf)_3$ (0.2)	20	72	17	2200	1.60
5	**6**	$Sc(OTf)_3$ (0.1)	20	72	21	—[d]	—[d]
6	**6**	$Sc(OTf)_3$ (0.1)	−5 to 20	72	40	3800	3.89
7	**8**	$TiCl_4$[e] (2.0)	−78	4	29	2700	3.27
8	**8**	$ZnBr_2$ (2.0)	20	48	47	1800	3.41
9	**8**	$Yb(OTf)_3$ (0.2)	20	72	15	11300	7.32
10	**8**	$Sc(OTf)_3$ (0.1)	−5 to 20	72	50	55700	2.38
11	**8**	**10** (1.0)	−78	4	62	1900	2.38

[a] Isolated yield after purification by reprecipitation. [b] Obtained by GPC calibrated by polystyrene standards using THF as an eluent. [c] Neat reagent was used. [d] Insoluble in common organic solvents. [e] 1.0 M solution in CH_2Cl_2.

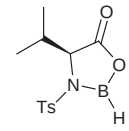

10

reaction is chiral *N*-sulfonyloxazaborolidinone **10** reported by Kiyooka.[18,19] For example, benzaldehyde activated with chiral Lewis acid **10** reacted with silylketene acetal to afford the corresponding *R*-aldol product in high yield with high enantiopurity (up to 94% ee).[19] We applied this chiral catalyst for the aldol polymerization of **4** with **8**. The asymmetric polymerization was performed at −78 °C, since undesired reduction of the ester group with the hydride of **10** might take place after aldol reaction at higher temperature, which destroys the polymer main chain. Although relatively low molecular weight polymer was obtained at −78 °C, the produced polymer showed optical activity.[20] To the best of our knowledge, this is the first example of the synthesis of optically active polymer from prochiral monomer using repetitive asymmetric aldol reaction.

In summary, we have found that Mukaiyama aldol reaction could be successfully utilized for the polyaddition of bis(silylketene acetal)s with dialdehydes. Polymers having a unique main chain structure consisting of poly(hydroxy ester)s were prepared readily by this polymerization. Catalytic amounts of rare earth metal triflates such as $Yb(OTf)_3$ and $Sc(OTf)_3$ are effective for the polyaddition to give polymers with high molecular weights. It is also possible to prepare optically active polymers using chirally-modified Lewis acid catalyst.

We thank Professor T. Nakai (Tokyo Institute of Technology) for suggestions and encouragement. This work was partially supported by a Grant-in-Aid for Scientific Research in Priority Areas from the Ministry of Education, Science, Sports, and Culture, Japan (Monbusho).

Notes and references

1 T. Mukaiyama, *Org. React.*, 1982, **28**, 203.
2 T. Mukaiyama and S. Kobayashi, *Org. React.*, 1994, **46**, 1.
3 T. Mukaiyama, *Aldrichim. Acta*, 1996, **29**, 59.
4 S. G. Nelson, *Tetrahedron*: *Asymmetry*, 1998, **9**, 357.
5 F. P. Boettcher, *Makromol. Chem., Macromol. Symp.*, 1988, **13/14**, 193.
6 T. Aida, in *Catalysis in Precision Polymerization*, ed. S. Kobayashi, Wiley, Chichester, 1997, p. 323.
7 T. Hirabayashi, T. Kawasaki and K. Yokota, *Polym. J.*, 1990, **22**, 287.
8 D. Y. Sogah and O. W. Webster, *Macromolecules*, 1986, **19**, 1775.
9 S. G. Nelson, *Tetrahedron*: *Asymmetry*, 1998, **9**, 357.
10 H. Emde, D. Domsch, H. Feger, U. Frick, A. Götz, H. H. Hergott, K. Hofmann, W. Kober, K. Krägeloh, T. Oesterle, W. Steppan, W. West and G. Simchen, *Synthesis*, 1982, 1.
11 J. Chen and J. Otera, *Synlett*, 1997, 29.
12 J. Otera and J. Chen, *Synlett*, 1996, 321.
13 E. Yoshii, Y. Kobayashi, T. Koizumi and T. Oribe, *Chem. Pharm. Bull.*, 1974, **22**, 2767.
14 I. Ojima and M Kumagai, *J. Organomet. Chem.*, 1976, **111**, 43.
15 K. Saigo, M. Osaki and T. Mukaiyama, *Chem. Lett.*, 1975, 989.
16 S. Kobayashi, I. Hachiya, H. Ishitani and M. Araki, *Synlett*, 1993, 472.
17 S. Kobayashi, *Synlett*, 1994, 689.
18 S. Kiyooka, *J. Synth. Org. Chem. Jpn.*, 1997, **55**, 313.
19 S. Kiyooka, Y. Kaneko, M. Komura, H. Matsuo and M. Nakano, *J. Org. Chem.*, 1991, **56**, 2276.
20 $[\Phi]_D$ −54.3 (*c* 1.52, $CHCl_3$).

Communication 8/08357F

ChemComm

Heterogeneously catalysed cleavage of carbon–carbon double bonds with hydrogen peroxide using calcined heteropolyacids on oxide supports

Christopher D. Brooks, Ling-chu Huang, Moya McCarron and Robert A. W. Johnstone*

Department of Chemistry, University of Liverpool, Liverpool, UK L69 3BX. E-mail: rj05@liverpool.ac.uk

Received (in Cambridge, UK) 27th July 1998, Accepted 13th November 1998

Reaction of an alkene with aqueous hydrogen peroxide and a catalytic quantity of a heteropolyacid adsorbed onto magnesium, aluminium or zinc oxide leads to complete, rapid cleavage of the alkene to give carbonyl compounds.

Oxidative cleavage of alkenes to ketones, aldehydes or carboxylic acids is useful synthetically. Reagents for effecting this reaction include ozone and lead tetraacetate, although the latter often gives only small yields of cleavage products.[1] Alkenes are often cleaved indirectly through intentional or incidental prior formation of 1,2-diols, followed by further oxidation. There are many reagents for effecting this last cleavage, as with sodium bismuthate, osmium tetroxide, chromium compounds, permanganates and ruthenium oxides.[1] All of these reactions are carried out in homogeneous solution and are generally stoichiometric, or they use expensive oxidants to recycle precious metal catalysts. Here, oxidative cleavage of alkenes has been attained through the use of heterogeneous calcined heteropolyacid catalysts supported on zinc, magnesium or aluminium oxide, with hydrogen peroxide as a cheap, environmentally benign oxidant.

Heteropolyacids are easy to prepare from readily available tungstates, molybdates and phosphates and are soluble in organic solvents.[2] Those based on molybdenum and/or tungsten have been used as catalysts for effecting epoxidation of alkenes[3] and for ring-opening of epoxides.[4] Small yields (5–7%) of adipic acid have been reported during homogeneous conversion of cyclohexene to its *trans*-1,2-diol.[3a] Similar homogeneous oxidation of cyclopentene gave a fair to modest yield of glutaraldehyde.[3c] In homogeneous two-phase transfer systems, 12-tungstophosphoric acid and hydrogen peroxide have been reported to give epoxides and 1,2-diols from alkenes. On extended reaction, some complete cleavage of alkene was observed.[3b]

In the present work, 12-molybdophosphoric (PMA), 12-tungstophosphoric (PWA) or 6-molybdo-6-tungstophosphoric acid (PMWA) were deposited onto aluminium, zinc or magnesium oxide or hydroxide and then calcined to give heterogeneous catalysts. The alkenes shown in Table 1 were oxidatively cleaved to give acids, ketones or keto acids in high yields. In the presence of aqueous hydrogen peroxide and 2-methylpropan-2-ol as solvent, these catalysts gave very poor and often only fleeting yields of epoxides and 1,2-diols, unlike analogous oxidations reported for homogeneous heteropolyacid systems, from which high yields of epoxide can be obtained.[3] As revealed by gas chromatographic monitoring of the reactions, the initial alkene disappeared completely from the reaction medium, but final percentage yields of oxidation products such as epoxides and 1,2-diols did not remotely match the percentage disappearance of starting material. Although the formation of 1,2-diols suggested that epoxides were being formed and were then being ring-opened solvolytically, no significant amounts of 1,2-diols were found at the end of reaction when all the alkene had disappeared. However, when MeOH was used as solvent, considerable quantities of 1-hydroxy-2-methoxy derivatives were found; such solvolysis products are typical of ring-opening of epoxides by nucleophilic solvents. Unlike the 1,2-diols, the 1-hydroxy-2-alkoxy compounds appear to be stable towards cleavage under the present reaction conditions and can form significant proportions of the final reaction product. In the poorly nucleophilic solvent, 2-methylpropan-2-ol, no 1-hydroxy-2-butoxy derivatives were found and the very small quantities of 1,2-diol observed as intermediate products presumably arose from water in the hydrogen peroxide. Although in MeOH, yields of 1-hydroxy-2-methoxy derivatives reached a steady value towards the end of reaction, any 1,2-diols produced at the same time first increased in amount during the early stages of reaction and then decreased to zero towards the end. For example, during oxidation of cyclohexene with a PWA catalyst, maximum intermediate yields of some 7% epoxide and 15% cyclohexane-1,2-diol were observed during the course of oxidation, in which 100% of the alkene was converted to other products; at the end of reaction almost all of the epoxide and 1,2-diol had disappeared. Work-up of this reaction mixture for non-volatile components showed that the alkene double bond had been completely cleaved to give adipic acid in high yield and selectivity (Table 1), which had not been observed by GC monitoring. Other alkenes behaved similarly (Table 1). It is clear that these supported heteropolyacids (or their anions on the supporting oxides and hydroxides) split alkenes efficiently so as to give complete double-bond cleavage (Scheme 1). Any

Table 1 Oxidative cleavage of alkenes with supported heteropolyacids and hydrogen peroxide

Alkene	Heteropolyacid[a]	*t*/h[b]	Product (% yield)
2,3-Dimethyl-2-butene	PMWA:Mg:C:150/0.5	8	acetone[c] (91)
Cyclohexene	PMA:Al:C:150/0.5	24	adipic acid[d] (90)
1-Methylcyclohexene	PWA:Al:C:150/0.5	24	6-ketoheptanoic acid[d] (96)
Oct-1-ene	PMWA:Mg:C:150/0.5	4	heptanoic acid[d] (100)
Cyclooctene	PMWA:Al:A:150/0.5	10	epoxide[e]
Styrene	PWA:Al:C:500/4	24	benzoic acid (90)
trans-Stilbene	PWA:Al:C:500/4	24	benzoic acid (92)
trans-Stilbene	PWA:Al:C:500/4	24	*f*

[a] See text for code. [b] All reactions were carried out at 60 °C in 2-methylpropan-2-ol as solvent, except for entry *f*. [c] Isolated as its 2,4-dinitrophenylhydrazone. [d] Isolated and identified by comparison with authentic material for mp, ^{1}H NMR and mass spectrum. [e] The epoxide of cyclooctanone is well-known for its resistance to nucleophilic attack. In this instance, after about 50% conversion of alkene, its epoxide was isolated in 30% yield along with some suberic acid (7% yield). [f] This example is included to show the effect of MeOH as solvent. The bulk of the product consisted of equal amounts of the enantiomeric pair of 1-hydroxy-2-methoxy-1,2-diphenylethanes, together with surprisingly only a little of the *meso* derivative.

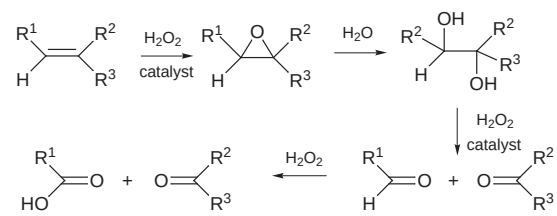

Scheme 1

final oxidation of aldehyde to carboxylic acid may or may not be catalysed.

Where the carbonyl formed on cleavage is an aldehyde, further oxidation to carboxylic acid ensues rapidly, since intermediate aldehydes are rarely observed, one such exception occurring in the oxidation of styrene. The oxidation of aldehydes to acids by hydrogen peroxide is known.[5] 1-Hydroxy-2-methoxy derivatives appear not to be oxidised further in these systems. For this reason, for optimum cleavage yields, either 2-methylpropan-2-ol or MeCN were used as solvent (Table 1).

For all oxidations, a blank reaction was carried out by omitting the catalyst from the reaction mixture. No oxidation was observed. To verify that leakage of catalyst from heterogeneously-supported materials to give homogeneous catalysts was not significant, parallel experiments were carried out by first refluxing the catalyst with the reaction mixture minus hydrogen peroxide and then filtering the mixture. The filtrate was used without more catalyst to determine its ability to effect oxidation of an alkene and the residue was used likewise. In all cases, the degree of oxidation observed with the filtrate as catalyst was very small but the solid residual catalysts were as efficient as the initial one. Finally, the longevity of the catalysts was examined by using the same catalyst for several successive oxidations. Generally, by the fourth cycle, the catalyst had lost most of its potency.

The catalysts were prepared in several ways to examine changes in their effectiveness with their pre-treatments. In some cases, the heteropolyacids were deposited onto preformed oxides (method A) or hydroxides (method B) but, in others, the catalyst was co-precipitated during formation of the hydroxide (method C). In all cases, the resulting solids were dried to 80 °C *in vacuo* and then calcined at either 150 or 500 °C. The catalysts are distinguished by a code. Thus, (PMA:Al:A:500/4) means 12-molybdophosphoric acid deposited onto aluminium oxide by method A and calcined at 500 °C for 4 h. Not all catalysts were equally effective for cleavage of alkenes. Generally, catalysts prepared by method B gave either inferior or no better yields than the corresponding catalysts prepared by method A or C.

In a typical catalyst preparation, 6-molybdo-6-tungstophosphoric acid (19.5 g)[6] in water (20 ml) was added to an approximately equal weight of freshly prepared and washed aluminium hydroxide, prepared from aluminium ammonium sulfate and sodium hydroxide; the mixture was stirred for 1 h. Excess of water was removed by centrifugation and the residue was washed with distilled water (3 × 20 ml). The solid product was dried at 80 °C *in vacuo* (20 mmHg) until its weight remained constant (about 2 days). The dried product was calcined by heating it either at 150° for 30 min or 500 °C for 4 h to give 45.3 g of the required catalyst, PMWA:Al:C:150/0.5.

In a typical oxidation, 1-methylcyclohexene (1.00 g; 10 mmol), dodecane (0.1 g, used as internal GC standard), hydrogen peroxide (70% w/w; 3–4 equiv. to alkene) and the catalyst (PWA:Al:C:150/0.5; 0.5 g) in 2-methylpropan-2-ol (25 ml) were stirred together at 60 °C. The progress of reaction was monitored by GC and the concentration of hydrogen peroxide was assessed with test strips (Merck). After complete conversion of the alkene or after a maximum of 24 h, the reaction was cooled, the catalyst filtered off and the filtrate was evaporated to dryness. The residue was distilled to give 6-oxoheptanoic acid, mp 33–34° (lit.,[7] 34–35 °C), identified by ^{1}H NMR spectroscopy and mass spectrometry. The other alkenes were reacted similarly and the products were isolated (see Table 1).

The authors thank the Eschenmoser Trust (L.-c. H.) and Rentokil Initial (C. D. B.) for financial assistance.

Notes and references

1 For general discussions of alkene cleavage see, J. March, *Advanced Organic Chemistry*, Wiley, New York, 1992, pp. 1177–1182; P. M. Henry and G. L. Lange, in *The Chemistry of Functional Groups, Suppl. A, Part I*, ed, S. Patai, Wiley, New York, 1977, pp. 965–1098; M. Hudlicky, *Oxidation of Organic Compounds*, ACS Monograph, ACS, Washington, 1990, pp. 77–84.
2 Y. Izumi, K. Urabe and M. Onaka, *Zeolite, Clay and Heteropolyacids*, Kondasha, Tokyo, 1992, p. 163.
3 (*a*) M. Schwegler, M. Floor and H. van Bekkum, *Tetrahedron Lett*., 1988, **29**, 823; (*b*) Y. Ishii, K. Yamakawaki, T. Ura, H. Yamada and M. Ogawa, *J. Org. Chem*., 1988, **53**, 3587; (*c*) H. Furukawa, T. Nakamura, H. Inagaki, E. Nishikawa, C. Imai and M. Misono, *Chem. Lett*., 1988, 877.
4 Y. Uzumi and K. Hayashi, *Chem. Lett*., 1980, 789.
5 C. W. Smith and R. T. Holm, *J.Org.Chem*., 1957, **22**, 746.
6 M. Misono, N. Mizuno, K. Katamura, A. Kisai, Y. Konishi, K. Sakata, T. Okuhara and Y. Yoneda, *Bull. Chem. Soc. Jpn*., 1982, **55**, 400.
7 J. R. Schaeffer and A. O. Snoddy, *Org. Synth*., 1963, **Coll**. **Vol**. **4**, 9.

Communication 8/05831H

Enantioselective reduction of ketones with triethoxysilane catalyzed by chiral bis-oxazoline titanium complexes

Marco Bandini, Pier Giorgio Cozzi,* Lucia Negro and Achille Umani-Ronchi*

Dipartimento Chimico 'G. Ciamician', Università di Bologna, Via Selmi 2, 40126 Bologna, Italy. E-mail: umani@ciam.unibo.it; pgcozzi@ciam.unibo.it

Received (in Liverpool, UK) 7th September 1998, Accepted 17th November 1998

Chiral bis-oxazoline titanium complexes [Ti(BOX)$_2$X$_2$] prepared from C_2 chiral bis-oxazolines, BuLi and titanium salts, catalyze the enantiosective reduction of ketones in the presence of triethoxysilane.

Enantioselective reduction of ketones is an important and widely utilized methodology for the preparation of key intermediates for the synthesis of drugs and biologically active compounds.[1] Corey's oxazaborolidine and related compounds play a decisive role in these chirotechnologies.[2] Recently, Buchwald has demonstrated that chiral titanium metallocenes are able to catalyze the enantioselective hydrosilylation of ketones and imines with high ees.[3] For these reactions enantiomerically pure titanocene complexes should be available. Although a new methodology to prepare the chiral C_2 metallocene complexes in high diastereomeric ratios was recently reported,[4] a resolution process is still needed to access the enantiomerically pure metal complex.[5] Based on a different strategy, *i.e*. replacing chiral metallocene with more accessible, easily prepared, chiral metal complexes, we have explored the possibility of using chiral bis-oxazolines[6] as ligands in coordinating group 4 metals and to employ the corresponding complexes in asymmetric catalysis (Fig. 1). To the best of our knowledge, until now the use of early transition metals with C_2 chiral bis-oxazolines in asymmetric catalysis has never been reported.[7]

Herein, we present a novel method for the enantioselective titanium-catalyzed hydrosilylation of ketones and α-halo ketones. The procedure involves the treatment of C_2 chiral bis-oxazolines (BOX **1–7**) with BuLi followed by the addition of a titanium salt.[8] Since the titanium complex was prepared *in situ* using a 2:1 molar ratio between the methylene bis-oxazoline and a titanium salt, we suggest that the BOX–titanium complex could have an octahedral structure (Fig. 1, M = Ti; X = Cl, F, OPr^i).[9] These new BOX–titanium complexes were treated with (EtO)$_3$SiH leading to a catalytic system for the hydrosilylation of ketones and α-halo ketones. It is noteworthy that no particular activation is necessary for the preparation of the active catalytic species. Various silyl hydrides such as Cl$_3$SiH, (EtO)$_3$SiH, Ph$_3$SiH, PhSiH$_3$ and poly(methylhydrosiloxane) were tested for asymmetric reduction catalyzed by the BOX–titanium complex. However, in general, (EtO)$_3$SiH gave better results. Initially we investigated the reaction of acetophenone with (EtO)$_3$SiH using various titanium salts and oxazolines (Scheme 1). As reported in Table 1 the best results were obtained using 3–5 mol% of the catalyst prepared from

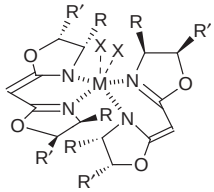

M = Ti, Zr, Hf ; X = F, Cl, Br, OR, NR$_2$

Fig. 1 Hypothetic structure of M(BOX)$_2$X$_2$.

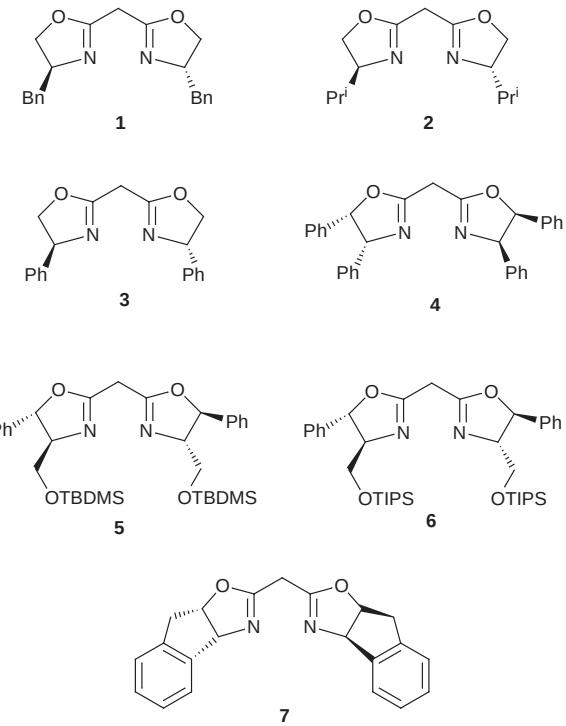

commercially available TiF$_4$ and oxazoline **4** as ligand. The hydrosilylation proceeded at room temperature, affording in 48 h the (*S*)-1-phenylethan-1-ol[3a] in 86% yield and 61% ee. The ee obtained in the asymmetric reaction seems to depend on the steric hindrance of the BOX ligand (entries 4,9 and 10). THF was the most suitable solvent with respect to both enantioselectivities and chemical yields. In the process of optimizing catalytic conditions with a variety of titanium salts, we found that TiF$_4$ was more effective in preparing the soluble orange–yellow BOX–titanium complexes. On the other hand, TiCl$_4$(THF)$_2$ gave insoluble complexes and we occasionally observed a definite change in the color of the reaction to blue, indicative of the presence of a Ti^{III} species.[10]

Since TiF$_4$, bis(oxazoline) **4** and (EtO)$_3$SiH afforded the best results,† the catalyst system reported in Scheme 2 was successfully applied to the asymmetric reduction of branched aromatic ketones and α-halo ketones.[11] From the data in Table 2, it is evident that the enantioselectivity is independent of the

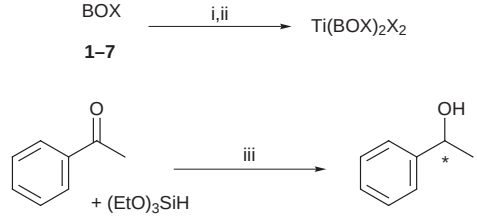

Scheme 1 *Reagents and conditions*: i, BuLi, THF; ii, TiX$_4$, THF; iii, Ti(BOX)$_2$X$_2$ (3-8 mol%), room temp.

Table 1 Enantioselective reduction of acetophenone catalyzed by Titanium-BOX complex[a]

Entry	BOX	TiX_4 (mol%)	Yield (%)	Ee[b] (%)
1	**1**	$TiCl_4(THF)_2$ (4)	60	30 (*R*)
2[c]	**1**	$TiCl_4(THF)_2$ (3)	60	50 (*R*)
3[c]	**3**	$TiCl_4(THF)_2$ (4)	20	23 (*R*)
4	**1**	$TiCl_2(OPr^i)_2$ (15)	87	18 (*S*)
5	**4**	$TiCl_2(OPr^i)_2$ (4)	85	51 (*S*)
6	**7**	$TiCl_2(OPr^i)_2$ (3)	13	64 (*S*)
7	**4**	TiF_4 (5)	86	61 (*S*)
8[d]	**4**	TiF_4 (4)	28	72 (*S*)
9	**5**	TiF_4 (5)	30	56 (*S*)
10	**6**	TiF_4 (5)	18	51 (*S*)

[a] Reaction conditions as in Scheme 1. All the reactions were performed by employing 4 equiv. of $(EtO)_3SiH$ as the reducing agent. The reactions were stirred at room temperature for 2–3 d. [b] The ee was evaluated by GC analysis with a chiral cyclodextrin Megadex column. [c] The reaction was effected in the presence of molecular sieves 4 Å (1 g. for 1 mol of ketone). [d] The reaction was performed in Et_2O.

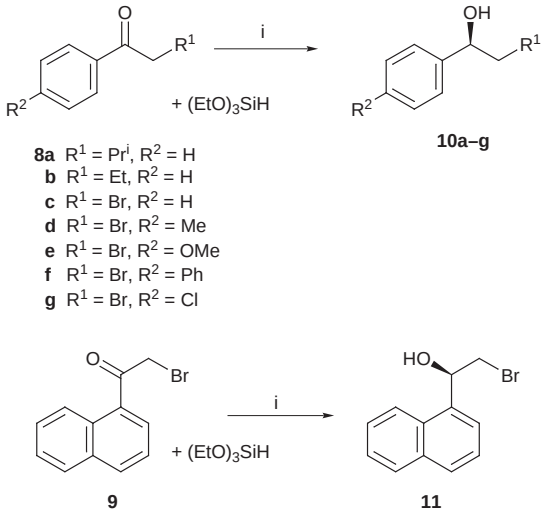

Scheme 2 *Reagents and conditions*: i, **4** (8 mol%), room temp., 80–120 h.

Table **2** Enantioselective reduction of ketones and α-halo ketones catalyzed by titanium–BOX complexes[a]

Entry	Ligand	Ketone	Alcohol	Yield (%)[b]	Ee (%)[c]
1	**4**	**8a**	**10a**	61	85 (*S*)
2	**4**	**8c**	**10c**	60	84 (*R*)
3	**4**	**8d**	**10d**	61	83 (*R*)
4	**4**	**9**	**11**	64	84 (*R*)
5	**4**	**8e**	**10e**	53	80 (*R*)
6	**4**	**8f**	**10f**	50	78 (*R*)
7	**4**	**8b**	**10b**	58	75 (*S*)[d]
8	**4**	**8g**	**10g**	50	65 (*R*)

[a] All the reactions were performed as reported in the experimental procedure. [b] Isolated yield after chromatographic purification. [c] The ee was determined by GC analysis on Megadex cyclodextrin chiral column. The configurations of **10a**,**c** were assigned by comparison of the $[\alpha]_D$ values reported in the literature. In the other cases, the absolute configuration was assigned by analogy. [d] The ee was determined on the silylated alcohol.

nature of the ketone, showing generality from aromatic substituted ketones to α-halo ketones.[12] The excellent enantioselectivity and the satisfactory yields observed in these reactions, accompanied by the simple protocol and the commercial availability of the ligands and reagents, make this procedure useful for the preparation of optically active epoxides and α-amino alcohols.[1]

Bis(oxazoline) ligands are able to replace Britzinger's C_2 metallocenes in these reductions, suggesting that other early transition metal-mediated reactions can be successfully catalyzed by early transition metals and appropriate BOX ligands. At the present time we can only speculate about the mechanism of this reaction. In particular, we are unable to definitively demonstrate that the reduction is due to the formation of an active titanium(III)[3a,b] or titanium(IV) species,[14] or if other mechanisms are involved.[15] In conclusion, we have developed a new methodology for the enantioselective reduction of ketones based on chiral titanium bis(oxazoline) complexes.

We thank the MURST (Rome) (National Project 'Stereoselezione in Sintesi Organica. Metodologie ed Applicazioni') and Bologna University (funds for selected research topics) for the financial support of this research.

Notes and references

† Typical experimental procedure: A solution of **4** (0.044 g, 0.097 mmol) in anhydrous THF (1.5 ml) was cooled to −78 °C and then BuLi (0.064 ml, 1.5 M in hexane) was added under nitrogen. The resulting pale yellow solution was stirred for 5 min at −78 °C and then warmed to 0 °C for 15 min. To this yellow solution TiF_4 was added (0.006 g, 0.048 mmol) all at once and the mixture was vigorously stirred until complete dissolution of the salt. The resulting solution was stirred for 60 min at room temperature and then $(EtO)_3SiH$ (0.240 ml, 1.2 mmol) and **8e** (0.14 ml, 0.605 mmol) were added. The mixture was stirred for 96 h at room temperature. The reaction mixture was diluted with AcOEt (5 ml) and then carefully made basic (pH 12) by the addition of aq. NaOH (1 M). The solution was stirred at room temperature until a white precipitate was formed. The solid was separated by filtration and the organic phase was collected. The aqueous phase was then extracted with AcOEt (2 × 3 ml). The organic layers were combined, dried over anhydrous Na_2SO_4, then concentrated under reduced pressure to give a yellow oil which was purified by column chromatography on silica gel (pentane–Et_2O, 9:1) (53%).

1 R. Hett, C. H. Senanayake and S. Wald, *Tetrahedron Lett*., 1998, **39**, 1705 and references cited therein.
2 *Catalytic Asymmetric Synthesis*, Ed. I. Ojima, VCH, New York, 1993; R. Noyori, *Asymmetric Catalysis In Organic Synthesis*, Wiley, New York, 1994; R. A. Sheldon, *Chirotechnology*, Marcel Dekker, New York, 1993.
3 (*a*) M. B. Carter, B. Schiøtt, A. Gutiérrez and S.L. Buchwald, *J. Am. Chem. Soc*., 1994, **116**, 11667; (*b*) X. Verdaguer, U. E. W. Lange, M. T. Reding and S. L. Buchwald, *J. Am. Chem. Soc*., 1996, **118**, 6784; X. Verdaguer, U. E. W. Lange and S. L. Buchwald, *Angew. Chem*., 1998, **110**, 1174; *Angew. Chem., Int. Ed*., 1998, **37**, 1103. For the use of other chiral ansa-titanocenes see also: S. Xin and J. F. Harrod, *Can. J. Chem*., 1995, **73**, 999; R. L. Halterman, T. M. Ramsey and Z. Chen, *J. Org. Chem*., 1994, **59**, 2642.
4 G. M. Diamond, R. F. Jordan and J. L. Petersen, *J. Am. Chem. Soc*., 1996, **118**, 8024.
5 B. Chin and S. L. Buchwald, *J. Org. Chem*., 1996, **61**, 5650.
6 For a recent and comprehensive review see: A. K. Ghosh, P. Mathivanan and J. Cappiello, *Tetrahedron*: *Asymmetry*, 1998, **9**, 1.
7 Singh has reported the preparation of various titanium(IV)–bis(oxazoline) complexes, but not their use. The structures of the BOX–Ti complexes, prepared in toluene with a 1:1 ligand to titanium reagent ratio, have been proposed to adopt a trigonal bipyramidal geometry in which two nitrogen atoms of the BOX ligand occupy equatorial sites. The author described such complexes as not quite stable: R. P. Singh, *Synth. React. Inorg. Met.-Org. Chem*. 1997, **27**, 155.
8 M. Nakamura, M. Arai and E. Nakamura, *J. Am. Chem. Soc*., 1995, **117**, 1179; M, Nakamura, A. Hirai and E. Nakamura, *J. Am. Chem. Soc*., 1996, **118**, 8489; S. Hanessian and R.-Y. Yang, *Tetrahedron Lett*., 1996, **37**, 8997.
9 The crystal structures of octahedral titanium(III) and titanium(IV) hydroxyphenyloxazoline complexes have been reported: P. G. Cozzi, C. Floriani, A. Chiesi-Villa and C. Rizzoli, *Inorg. Chem*. 1995, **34**, 2921.
10 In these cases, only racemic alcohol was obtained. Reduction of titanium depending on the ligand is well known problem in metallocene chemistry.
11 Aliphatic, non-branched aromatic and cyclic ketones were reduced with our titanium catalyst in lower ees. For example, the reduction of octan-2-one and indan-2-one afforded the corresponding alcohols in 65% yield, 20% ee and 70% yield, 29% ee, respectively.
12 The absolute configurations of **10a** [ref. 3(*a*)] and **10c** (ref. 13) were determined by comparison with the $[\alpha]_D$ values reported in the literature. The absolute configurations of **10b** and the other halo ketones were assigned by analogy.
13 S. Itsuno, M. Nakano, K. Miyazaki, H. Masuda, K. Ito, A. Irao and S. Nakahama, *J. Chem. Soc*., *Perkin Trans. 1*, 1985, 2039.
14 T. Nakai, M. Mori and H. Imma, *Synlett*., 1996, 1229.
15 D. J. Parks and W. E. Piers, *J. Am. Chem. Soc*., 1996, **118**, 9440.

Communication 8/07028H

New entry for asymmetric deoxyazasugar synthesis: syntheses of deoxymannojirimycin, deoxyaltrojirimycin and deoxygalactostatin

Koji Asano, Toshikazu Hakogi, Seiji Iwama and Shigeo Katsumura*

School of Science, Kwansei Gakuin University, Uegahara, Nishinomiya 662-8501, Japan.
E-mail: katumura@kwansei.ac.jp

Received (in Cambridge, UK) 28th September 1998, Accepted 9th November 1998

Deoxyazasugars such as deoxymannojirimycin, deoxyaltrojirimycin and deoxygalactostatin were stereoselectively synthesized starting from (*R*)-(+)-4-methoxycarbonyloxazolidinone *via* a bicyclic oxazolidinylpiperidine as a common synthetic intermediate.

Recently, polyhydroxylated piperidine alkaloids have received much attention due to their importance as glycosidase inhibitors.[1] Among them, deoxymannojirimycin **1** isolated from *Lonchocarpus* sp.,[2] deoxyaltrojirimycin **2**[3] and deoxygalactostatin **3**[4] can be regarded as deoxyazasugars based on their structural relationship to deoxysugars. Deoxy compound **1** is a moderate inhibitor of α-mannosidases and a good inhibitor of mammalian α-fucosidase, compound **2** is known as an analogue of **1** and is named in the relation with altrose, and compound **3** is a potent inhibitor of galactosidase. Because of the significant biological activities of these compounds as well as their characteristic structure, a number of synthetic efforts have been reported.[5]†

We previously developed both enantiomers of 4-methoxycarbonyloxazolidinone **4** as a chiral building block for the synthesis of natural amino alcohols, and realized the stereoselective syntheses of both γ-hydroxy-β-amino alcohols[6] and sphingolipids.[7] As part of our continuing interest in the synthetic utility of **4**, we have applied this methodology to the synthesis of deoxyazasugars. As a new flexible deoxyazasugar synthesis, we now report the stereoselective asymmetric syntheses of deoxymannojirimycin **1**, deoxyaltrojirimycin **2** and deoxygalactostatin **3** from common intermediate **9**.

Synthesis of deoxymannojirimycin **1** *via* the common intermediate **9** is shown in Scheme 1. Reaction of (*R*)-(+)-ester **4** with the lithium anion of propargyl alcohol silyl ether at −100 °C in THF gave ketone **5** [mp 31.0–32.0 °C; $[\alpha]_D^{23}$ +32.2 (*c* 0.88, $CHCl_3$)]. The successful stereoselective reduction of the ketone to produce the desired *anti* alcohol **6** was achieved with diisobutylaluminium 2,6-di-*tert*-butyl-4-methylphenoxide in 92% yield; the *anti*:*syn* selectivity was 11:1 by ^{1}H NMR analysis. Reduction with $NaBH_4$ and L-Selectride® gave a 5:3 and 1:2 mixture of *anti*- and *syn*-derivatives, respectively, and triisobutylaluminium reduction showed 9:1 selectivity. The obtained stereoselectivity can be understood by considering the reaction intermediates as shown in Fig. 1. In the case of diisobutylaluminium 2,6-di-*tert*-butyl-4-methylphenoxide reduction, two possible conformers **A** and **B** in the transition state were considered based on an intramolecular fashion of this reagent. Compared to intermediate **A**, intermediate **B** is disfavored due to steric interactions between the bulky aluminium reagent and the methylene group of the oxazolidinone ring, and hence this reaction resulted in high *anti*-selectivity. On the other hand, conformers **C** and **D** were anticipated in sodium borohydride and L-Selectride® reduction. There was considered to be no significant difference in steric interactions between these conformers due to the intermolecular fashion of the hydride attack of these reagents, and they resulted in poor selectivity, despite the fact that the L-Selectride® is sterically more demanding than $NaBH_4$.

With *anti*-alcohol **6** in hand, our attention turned to the construction of the bicyclic oxazolidinylpiperidine. Reduction of **6** along with its stereoisomer with Lindlar catalyst produced *cis*-allyl alcohol **7**,‡ which was isolated, then treated with sodium in liquid ammonia followed by acid to give the corresponding diol. Unfortunately, cyclization attempts utilizing the obtained diol *via* the tosylate of the primary alcohol were unsuccessful. The secondary hydroxy group of **7** was then protected with a TBDMS group, and the terminal silyl group was selectively removed by treatment with aq. HF in MeCN to give allyl alcohol **8**.[9] The cyclization proceeded successfully upon treatment of **8** with MsCl followed by NaH to produce

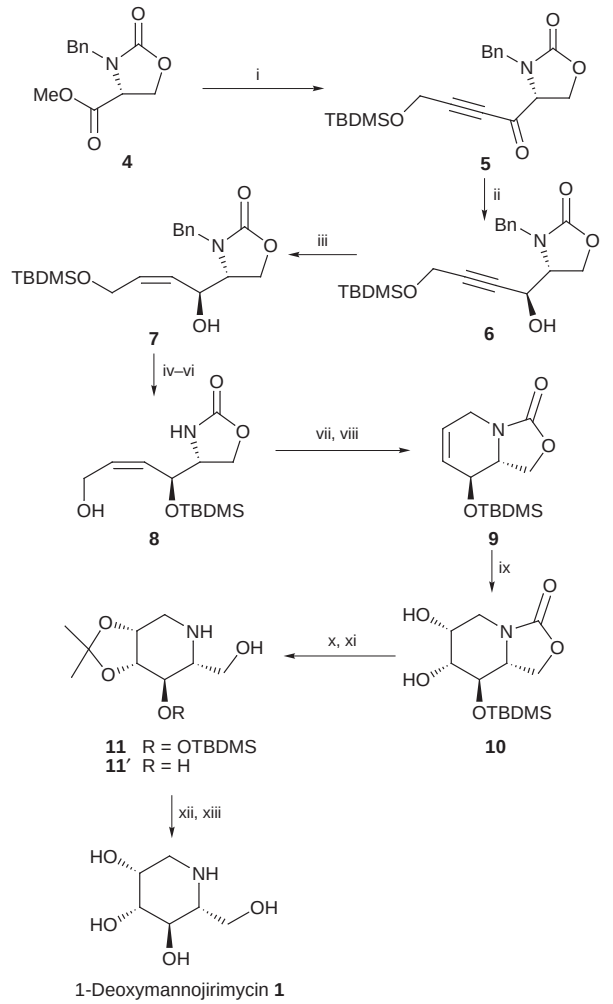

Scheme 1 *Reagents and conditions*: i, $TBDMSOCH_2C{\equiv}CLi$, THF, −100 °C (82%); ii, diisobutylaluminium 2,6-di-*tert*-butyl-4-methylphenoxide, toluene, 0 °C (92%); iii, Lindlar catalyst, H_2, MeOH (90%); iv, Na, liquid NH_3, −78 °C; v, TBDMSCl, imidazole, DMF (67% for 2 steps), vi, 55% aq. HF, MeCN, −20 °C (98%); vii, MsCl, Et_3N, DMAP, DMF; viii, NaH, DMF, 0 °C (80% for 2 steps); ix, OsO_4, NMO, Bu^tOH, H_2O (86%); x, $Me_2C(OMe)_2$, PPTS, acetone (92%); xi, 6 M aq. NaOH, dioxane, reflux, 24 h (71%); xii, conc. HCl, MeOH, reflux, 4 h (quant.); xiii, basic ion-exchange resin.

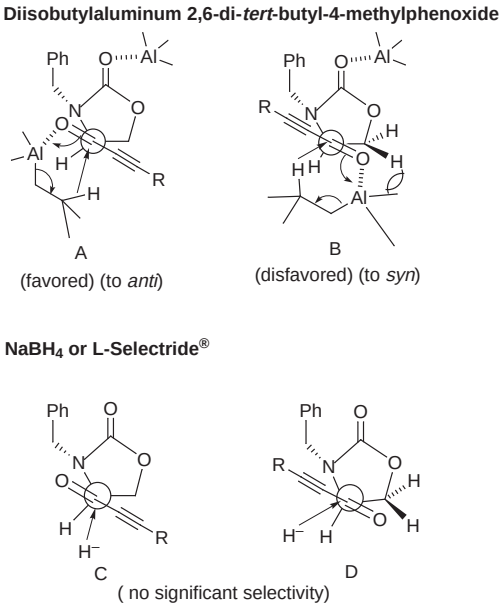

Fig. 1

bicyclic oxazolidinylpiperidine **9**§. This compound was used as the common intermediate for the present deoxyazasugar synthesis. Oxidation of **9** with OsO_4 yielded diol **10** as the sole product, the stereochemistry of which was assumed to be *anti* to the neighbouring siloxy group at this stage. Acetonide formation followed by cleavage of the oxazolidinone ring with aq. NaOH in dioxane gave a mixture of monosilyl ether **11** and diol **11′**. Upon treatment of the mixture with acid, deoxymannojirimycin **1** was quantitatively obtained after purification with basic ion-exchange resin.¶

Next is the synthesis of deoxyaltrojirimycin **2** (Scheme 2). Epoxidation of bicyclic compound **9** after removal of the silyl group gave epoxy alcohol **12**, which was treated with BF_3–Et_2O in acetone to produce acetonide **13** [mp 123.0–124.0 °C; $[\alpha]_D^{22}$ +49.9 (*c* 0.48, $CHCl_3$)] resulting from diaxial opening of the epoxide ring. Synthesis of **2** from **13** was achieved by the same procedures as those in the deoxymannojirimycin synthesis (6 M aq. NaOH, conc. HCl; 85% for two steps).¶

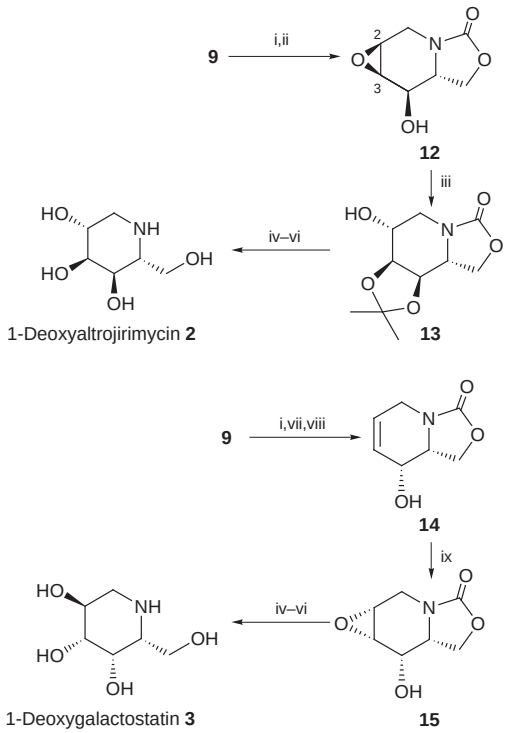

Scheme 2 *Reagents and conditions*: i, TBAF, THF (98%); ii, MCPBA, CH_2Cl_2 (78%); iii, BF_3–OEt_2, acetone, 0 °C (70%); iv, 6 M aq. NaOH, dioxane, reflux, 24 h; v, conc. HCl, MeOH, reflux, 4 h (85% for 2 steps); vi, basic ion-exchange resin; vii, PDC, 4 Å molecular sieves, CH_2Cl_2 (73%); viii, L-Selectride®, $CeCl_3$, THF (77%); ix, MCPBA, $CHCl_3$, 3 d (65%).

The synthetic strategy for deoxyaltrojirimycin was applied to the synthesis of deoxygalactostatin **3** (Scheme 2), which is not a natural product but was synthesized as an analogue of deoxygalactose. Oxidation of **9** with PDC after removal of the silyl group gave the corresponding ketone. Reduction of the ketone obtained with L-Selectride® in the presence of cerium chloride produced *syn* alcohol **14** with a high degree of stereoselectivity (20:1 by ^{1}H NMR analysis; 77%). Although epoxidation of **14** with MCPBA was very slow (room temp., 3 days, $CHCl_3$), we obtained the desired α-oriented epoxide **15** in 65% conversion yield. The synthesis of deoxygalactostatin **3** was achieved from **15** by the same procedure employed in the synthesis of deoxyaltrojirimycin. Thus, formation of acetonide (52%), hydrolysis of oxazolidinone (67%), and then acid treatment (quant.) yielded deoxygalactostatin **3**.¶

In conclusion, 4-methoxycarbonyloxazolidinone **4** has been proved to be a versatile chiral building block for the syntheses of deoxyazasugars *via* bicyclic oxazolidinylpiperidine **9** as a common synthetic intermediate.

This work was supported by a Grant-in-Aid for Scientific Research from Monbusho (No.09480145). S. I. is grateful to the Japan Promotion of Science for a postdoctoral fellowship.

Notes and references

† Recently, Cinfolini and co-workers described an elegant synthesis of deoxyazasugars *via* the aza-Achmatowicz reaction: M. A. Cinfolini, C. Y. W. Hermann, Q. Dong, T. Shimizu, S. Swaminathan and N. Xi, *Synlett*, 1998, 105.

‡ *Selected data* for **7**: mp 83.0–84.0 °C; $[\alpha]_D^{24}$ −23.9 (*c* 0.19, $CHCl_3$); ν(KBr)/cm^{-1} 3262, 1778, 1119; δ_H(400 MHz, $CDCl_3$) 0.067 (3H, s), 0.073 (3H, s), 0.90 (9H, s), 3.10 (1H, br s), 3.61–3.65 (1H, a pair of ddd, *J* 2.9, 6.1, 9.0), 4.26 (5H, m), 4.58 (1H, br d, *J* 6.1), 4.82 (1H, d, *J* 15.1), 5.37 (1H, ddt, *J* 1.7, 7.3, 11.5), 5.72 (1H, m), 7.34 (5H, m).

§ *Selected data* for **9**: mp 92.5–93.0 °C; $[\alpha]_D^{23}$ +26.0 (*c* 1.00, $CHCl_3$); ν(KBr)/cm^{-1} 2953, 1786, 1630; δ_H(400 MHz, $CDCl_3$) 0.11 (3H, s), 0.13 (3H, s), 0.90 (9H, s), 3.51 (1H, ddd, *J* 4.2, 8.1, 8.1), 3.65 (1H, m), 4.09 (1H, m), 4.15 (1H, m), 4.22 (1H, dd, *J* 4.2, 8.9), 4.51 (1H, dd, *J* 8.1, 8.9), 5.72 (2H, s); δ_C(100 MHz, $CDCl_3$) −4.68, −4.20, 17.86, 25.61, 40.82, 56.42, 67.21, 68.37, 123.83, 130.48, 157.24.

¶ *Selected data* for **1**: mp 186.0–186.5 °C; $[\alpha]_D^{27}$ −35.7 (*c* 0.07, MeOH) [lit.,[5a] mp 183–185 °C; $[\alpha]_D^{20}$ −36.2 (*c* 0.342, MeOH)]. For **2**: $[\alpha]_D^{23}$ +16.3 (*c* 0.8, H_2O) [lit. (of enantiomer),[3b] $[\alpha]_D^{20}$ −14.5(*c* 0.7, $CHCl_3$)]. For **3**: $[\alpha]_D^{27}$ +40.3 (*c* 0.38, H_2O) [lit.,[5c] $[\alpha]^{25}_D$ +44.6(*c* 1.1, H_2O)].

1 E. W. Baxter and A. B. Reitz, *J. Org. Chem.*, 1994, **59**, 3175; F. M. Platt, G. R. Neises, R. A. Dwek and T. D. Butters, *J. Biol. Chem.*, 1994, **269**, 8362 and references cited therein.
2 L. E. Fellows, E. A. Bell, D. G. Lynn, F. J. Pilkiewcz, I. Miura and K. Nakanishi, *J. Chem. Soc., Chem. Commun.*, 1979, 977.
3 (*a*) X. Yi-Ming and Z. Wei-Shan, *J. Chem. Soc., Perkin Trans. 1*, 1997, 741; (*b*) R. Grandel and U. Kazmaier, *Tetrahedron Lett.*, 1997, **38**, 8009.
4 Y. Miyake and M. Ebata, *J. Antibiol.*, 1987, **40**, 122; Y. Miyake and M. Ebata, *Agric. Biol. Chem.*, 1988, **52**, 153.
5 Deoxymannojirimycin: (*a*) K. H. Yong, Y. J. Yoon and S. G. Lee, *J. Chem. Soc., Perkin Trans. 1*, 1994, 2621; (*b*) X.-D. Wu, S.-K. Khim, X. Zhang, E. M. Cederstrom and P. S. Mariano, *J. Org. Chem.*, 1998, **63**, 841 and references cited therein. Deoxyaltrojirimycin: see ref. 3. Deoxygalactostatin: (*c*) P. L. Barili, G. Berti, G. Catelani, F. D'Andrea, F. D. Rensis and L. Puccioni, *Tetrahedron*, 1997, **53**, 3407; (*d*) J. P. Shilvock and G. W. J. Fleet, *Synlett*, 1998, 554 and references cited therein.
6 S. Katsumura, N. Yamamoto, M. Morita and Q. Han, *Tetrahedron: Asymmetry*, 1994, **5**, 161 and references cited therein.
7 S. Katsumura, Y. Yamamoto, E. Fukuda and S. Iwama, *Chem. Lett.*, 1995, 393; M. Murakami, S. Iwama, S. Fujii, K. Ikeda and S. Katsumura, *Bioorg. Med. Chem. Lett.*, 1997, **7**, 1725.
8 S. Iguchi, H. Nakai, M. Hayashi and H. Yamamoto, *J. Org. Chem.*, 1979, **44**, 1363.
9 S. J. Danishefsky, D. M. Armistead, F. E. Wincott, H. G. Selnick and R. Hungate, *J. Am. Chem. Soc.*, 1989, **111**, 2967.

Communication 8/07532H

Monomer emission from pyrene adsorbed in surfactant-intercalated graphite oxide

Yoshiaki Matsuo,* Kazuya Hatase and Yosohiro Sugie

Department of Applied Chemistry, Faculty of Engineering, Himeji Institute of Technology, 2167 Shosha, Himeji, Hyogo, 671-2201, Japan. E-mail: matsuo@chem.eng.himeji-tech.ac.jp

Received (in Cambridge, UK) 28th September 1998, Accepted 13th November 1998

Monomer emission from pyrene highly concentrated in octadecyltrimethylammonium ion-intercalated graphite oxide has been observed.

Organoammonium ion-intercalated layered materials have attracted much attention because of their interesting structure, absorption of harmful molecules or photoactive ones and application as catalysts. Studies on these materials have been well summarized recently by Ogawa and Kuroda.[1] Among these studies, interesting results on fluorescence, thermal properties or photo-isomerization have been reported by immobilizing photochromic molecules such as pyrene,[2,3] azobenzene,[4,5] spiropirane,[6] *etc*., in the two dimensional space of intercalation compounds. On the other hand, we have found that graphite oxide (GO) which is classified as a covalent type of graphite intercalation compound allows formation of intercalation compounds with alkyltrimethylammonium ions and the maximum content of surfactant in the layer is very large compared with that of clays and covers a wide range.[7] Such intercalation compounds of GO are easily dispersed in chloroform, which can lead to further intercalation of aromatic molecules by casting the solution containing both the intercalation compound and guest molecules. These facts suggest that it is possible to control the adsorption state of photochromic molecules in the two dimensional space of surfactant-intercalated GO over a wide range by changing the size of the spacing between the alkyl chains of surfactant.

In this study, we chose pyrene as a probe photochromic molecule in order to characterize the surfactant-intercalated GO as a new host material for photochromic molecules. The aggregation state of pyrene was analyzed by using X-ray diffraction and fluorescence spectra as was used for the characterization of pyrene in montmollironite.[2,3]

Graphite oxide ($C_8O_{3.5}H_{2.8}$) was obtained from natural graphite powder by a modified Staudenmaier method.[8,9] Oxidation of graphite was carried out for 2 days. Intercalation of octadecyltrimethylammonium ion ($C_{18}H_{37}Me_3N^+$; $C_{18}3C_1N$) and dimethyldioctadecyl ammonium ion [$(C_{18}H_{37})_2Me_2N^+$; $2C_{18}2C_1N$] was performed by adding an aqueous solution of surfactants to a colloidal solution of GO.[7] The repeat distance along the *c*-axis (I_c) of surfactant of $C_{18}3C_1N$- and $2C_{18}2C_1N$-intercalated GO as hosts of pyrene were 3.25 and 3.11 nm, respectively. The contents of surfactant in GO were 0.33 and 0.23 mol per 100 g of GO in these intercalation compounds when calculated from weight uptake data. These values are very large when compared with those of clay minerals. The samples obtained in this study were highly soluble in chloroform. Intercalation of pyrene was performed by casting from $CHCl_3$ solution (5 ml) containing the intercalation compound (10 mg) and pyrene (2.5, 3.3 or 5.0 mg) on a quartz substrate. X-Ray diffraction was performed on a Rigaku Rint-2100 diffractometer. Absorption and luminescence spectra were recorded on a Hitachi U-3000 spectrometer and JASCO FP-777 spectrofluorometer at an excitation wavelength of 330 nm, respectively.

Casting of a $CHCl_3$ solution containing surfactant-intercalated GO and pyrene gave slightly brownish transparent films for all the samples. Fig. 1 shows the X-ray diffraction patterns of the cast films of PY-$C_{18}3C_1N$-GO, PY-$2C_{18}2C_1N$-GO, $C_{18}3C_1N$-GO and $2C_{18}2C_1N$-GO, together with that of pristine GO. In both cases, the I_c values of surfactant-intercalated GO increased to about 3.8 nm after the addition of pyrene, indicating the intercalation of pyrene into the surfactant-intercalated GO materials. These I_c values were similar to those observed for pyrene-$C_{18}3C_1N$- or pyrene-$2C_{18}2C_1N$-montmorillonites.[2] They were almost constant regardless of the amount of added pyrene. When the weight ratio of surfactant-intercalated GO to pyrene was $> 1:0.5$, a diffraction peak at $2\theta = 10.3°$ appeared in the diffractogram of both PY-$C_{18}3C_1N$-GO and PY-$2C_{18}2C_1N$-GO, probably due to saturation of pyrene in the interlayer spacing of the intercalation compounds and crystallization of excess pyrene at the surface of the samples. The molar ratios of pyrene : $C_{18}3C_1N$ and pyrene : $2C_{18}2C_1N$ are *ca.* 1 : 1 and 2 : 1, respectively, when pyrene is saturated in the layers of the intercalation compounds. In other words, saturation of pyrene occurred when the ratio of pyrene : octadecyl group was *ca.* 1 : 1.

Fig. 2 shows the UV absorption spectra of cast films of PY-$C_{18}3C_1N$-GO, PY-$2C_{18}2C_1$-GO, a pyrene film and an ethanolic solution of pyrene. In the absorption spectra of cast films of intercalation compounds containing pyrene, absorption bands due to π–π^* transitions of pyrene were observed at 340, 324, 312, 275, 264, 243 and 235 nm. For pyrene in ethanolic solution, absorption bands were observed at 334, 318, 305, 272, 261, 240 and 230 nm. The red shift (*ca.* 5 nm) of absorption bands indicated that pyrene in GO interlayers is present in a more polar environment than in ethanolic solution.

Fig. 3 shows the fluorescence spectra of PY-$C_{18}3C_1N$-GO, PY-$2C_{18}2C_1$-GO, an ethanolic solution of pyrene and crystalline pyrene. It is well known that the emission bands observed at *ca.* 390 and 450 nm arise from pyrene monomer and eximer,

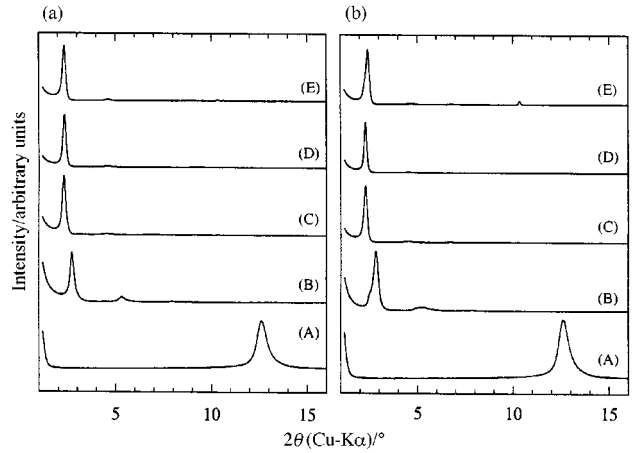

Fig. 1 (a) X-Ray diffraction patterns of (A) GO, and cast films of (B) $C_{18}3C_1N$-GO and of PY-$C_{18}3C_1N$-GO with $C_{18}3C_1N$-GO : pyrene ratios; (C) 1 : 0.25, (D) 1 : 0.33 and (E) 1 : 0.5. (b) X-Ray diffraction patterns of (A) GO, and cast films of (B) $2C_{18}2C_1N$-GO and of PY-$2C_{18}2C_1N$-GO with $2C_{18}2C_1N$-GO : pyrene ratios; (C) 1 : 0.25, (D) 1 : 0.33 and (E) 1 : 0.5.

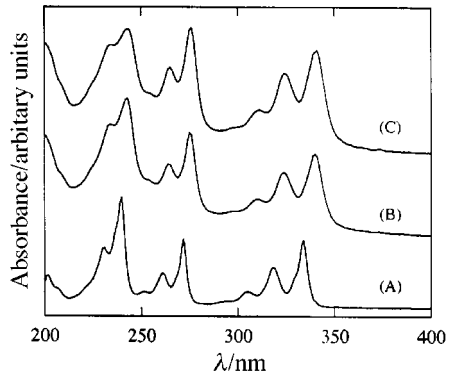

Fig. 2 The absorption spectra of (A) an ethanolic solution of pyrene, (B) PY-$C_{18}3C_1$N-GO with a $C_{18}3C_1$N-GO : pyrene ratio of 1 : 0.25 and (C) PY-$2C_{18}2C_1$N-GO with a $2C_{18}2C_1$N-GO : pyrene ratio of 1 : 0.25.

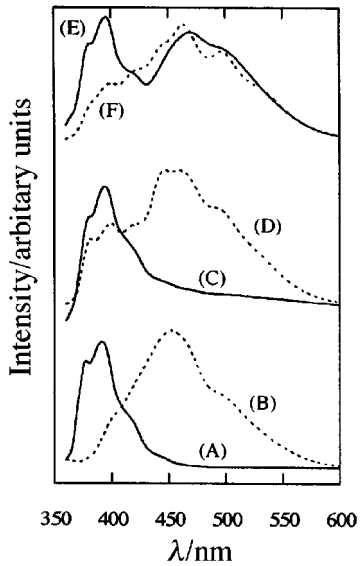

Fig. 3 The emission spectra of (A) crystalline pyrene, (B) an ethanolic solution of pyrene, and of PY-$C_{18}3C_1$N-GO with $C_{18}3C_1$N-GO : pyrene ratios of (C) 1 : 0.25 and (D) 1 : 0.33 and PY-$2C_{18}2C_1$N-GO with $2C_{18}2C_1$N-GO : pyrene ratios of (E) 1 : 0.25 and (F) 1 : 0.33.

respectively. The emission from the monomer is usually observed only in highly dilute solutions as shown in Fig. 3(A). However, in the spectra of intercalation compounds with very high pyrene content, this line was observed clearly and its relative intensity increased when the loaded amount of pyrene was decreased. Moreover, it is noteworthy that almost no emission from the eximer was observed for PY-$C_{18}3C_1$N-GO (1 : 0.25), indicating that pyrene molecules in the layer are almost completely separated from each other by alkyl chains of surfactants. This would be because the high content of surfactant in the layer of GO makes the size of single pyrene molecules suitable to occupy the space present between alkyl chains of the surfactant. On the other hand, for PY-$2C_{18}2C_1$-GO, eximer emission was preferably observed even when the pyrene content was similar to that of PY-$C_{18}3C_1$N-GO showing monomer emission. Similar results on the change of aggregation state of pyrene were reported for montmorillonite based compounds;[2] however, in the latter case, the ratio of pyrene to surfactant chain was rather lower, at most 1 : 0.36, and eximer emission was observed to a considerable extent. The difference of emission spectra of the two intercalation compounds would be due to the difference of the size of the sites for pyrene adsorption.

Finally, we would like to emphasize that these surfactant-intercalated graphite oxides are suitable host materials for including photochromic molecules in separated sites at a very high concentration. It would be possible to control their aggregation over a wide range by changing the size of the spaces between the alkyl chains of the surfactants.

The authors are grateful to Dr Kazushige Yamana of the Himeji Institute of Technology for his assistance in UV–VIS and fluorescence measurements, and for fruitful discussions.

Notes and references

1 M. Ogawa and K. Kuroda, *Bull. Chem. Soc. Jpn.*, 1997, **70**, 2593.
2 M. Ogawa, T. Aono, K. Kuroda and C. Kato, *Langmuir*, 1993, **9**, 1529.
3 M. Ogawa, T. Igarashi and K. Kuroda, *Chem. Mater.*, 1998, **10**, 1382.
4 M. Ogawa, H. Kimura, K. Muroda and C. Kato, *Clay Sci.*, 1996, **10**, 57.
5 M. Ogawa, M. Hama and K. Kuroda, *Clay Miner.*, in press.
6 T. Seki and K. Ichimura, *Macromolecules*, 1990, **23**, 31.
7 Y. Matsuo, T. Niwa and Y. Sugie, *Carbon*, in press.
8 L. Staudenmaier, *Ber. Dtsch. Chem. Ges.*, 1898, **31**, 1484.
9 T. Nakajima and Y. Matsuo, *Carbon*, 1994, **32**, 469.

Communication 8/07550F

ChemComm

Efficient site-specific cleavage of RNA using a terpyridine–copper(II) complex joined to a 2′-*O*-methyloligonucleotide by a non-flexible linker

Hideo Inoue,* Takako Furukawa, Masaki Shimizu, Takashi Tamura, Miwa Matsui and Eiko Ohtsuka

Graduate School of Pharmaceutical Sciences, Hokkaido University, Kita-12, Nishi-6, Kita-ku, Sapporo 060-0812, Japan. E-mail: inoue@pharm.hokudai.ac.jp

Received (in Cambridge, UK) 3rd November 1998, Accepted 17th November 1998

A terpyridine–Cu(II) complex conjugated to an antisense 2′-*O*-methyloligonucleotide at the 5′-end cleaved RNA predominantly at the site opposite the 5′-end in moderate yield, but the cleavage yield increased by more than two-fold when a 2′-*O*-methyloligonucleotide was allowed to bind to the single-stranded region of the RNA-antisense complex.

Recently, chemical agents that cleave RNA site-specifically without enzymatic assistance have been developed.[1] This is potentially important in antisense chemotherapy because cleavage of a specific mRNA will lead to loss of its function.[2] These agents can also be useful for studies on structure–function relationships of native RNAs.[3] One relatively active class of RNA cleavers is metal complexes covalently linked to oligonucleotides; the cleavage mechanism may involve transphosphorylation promoted by the metal. Complexes, such as terpyridine–Cu(II),[4,5] macrocyclic terpyridine derivative–Ln(III),[6,7] texaphyrin–Ln(III),[8,9] and iminodiacetate–Ln(III),[10] have been attached by a flexible linker to DNA oligomers for sequence-specific recognition. Here, we describe a new RNA cleaver with an alternative arrangement, consisting of a 2′-*O*-methyl RNA oligomer, as an efficient RNA hybridization probe,[3,11] and a terpyridine–Cu(II) complex directly attached to the 5′-end of the 2′-*O*-methyloligomer. We also demonstrate RNA cleavage by the cleaver in the presence of a cleavage facilitator.

For oligonucleotide synthesis, 5′-*O*-terpyridyl 3′-phosphoramidite derivatives of 2′-deoxyadenosine **1a** and 2′-*O*-methyladenosine **1b** were prepared, using standard methods for all steps (Scheme 1). The synthetic route involving *O*-terpyridylation[12] is easy and applicable to the other nucleosides. The two building units **5a**,**b** were used for the preparation of 5′-end-modified 2′-*O*-methyloligonucleotides.

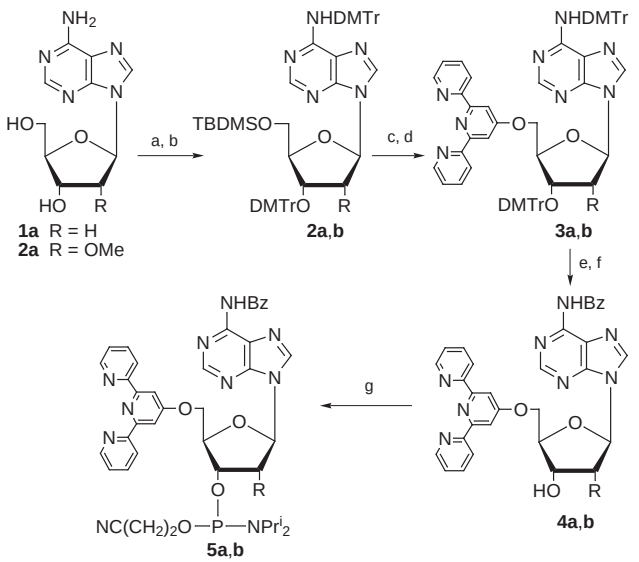

Scheme 1 *Reagents and conditions*: for **5b** (all reactions were carried out at room temperature). a, TBDMSCl (1.2 equiv.), imidazole (2.4 equiv.), DMF, 1.5 h, 77%; b, DMTrCl (2.6 equiv.), pyridine, 23 h, 77%; c, Bu_4NF (1.2 equiv.), THF, 30 min, 99%; d, 4′-chloro-2,2′ : 6′,2″-terpyridine (1.2 equiv.), KOH, DMSO, 44 h, 90%; e, 80% $MeCO_2H$ aq, 4 h, 100%; f, successive steps: i, TMSCl (3 equiv.), pyridine, 30 min; ii, BzCl (5 equiv.), 3.5 h; iii, H_2O, 5 min; iv, 28% NH_3 aq, 30 min, 64% (overall); g, 2-cyanoethyl diisopropylchlorophosphoramidite (1.2 equiv.), diisopropylethylamine (3 equiv.), CH_2Cl_2, 50 min, 50%. DMTr = 4,4′-dimethoxytrityl.

Cleavage reactions of RNA oligomers with the terpyridine–Cu(II)-oligomer conjugates were carried out with the 5′[^{32}P]-end-labeled RNA target in a buffer at 45 °C for 20 h. Representative examples of an analysis of the cleavage products and all results are indicated in Figs. 1 and 2, respectively. Cleavage of the RNA 24-mer (R24) with the 5′-*O*-Cu(II)–terpyridyl-2′-deoxyadenosine-linked 12-mer (dA*12) occurred predominantly between U12–U13, in which U12 is positioned at the end of the 12-mer recognition region [Figs. 1 and 2(a)].† The extent of specific cleavage was 18% after 20 h [Fig. 2(c)]. Minor cleavage occurred at U13–U14 in *ca.* 1% yield. For the corresponding 5′-*O*-Cu(II)–terpyridyl-2′-*O*-methyladenosine-conjugate (Am*12), similar cleavage results were obtained. An RNA 21-mer with no sequence similarity to R24 was also specifically cleaved by a dA*-13-mer at a predetermined site, 5′U–A3′ (26% yield, data not shown).

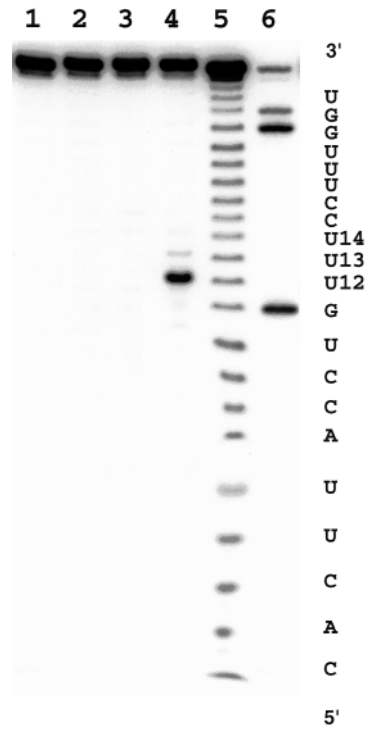

Fig. 1 Autoradiogram of products from the reaction of the labeled target R24 with the agent dA*12 after 20% denaturing polyacrylamide gel electrophoresis. The reaction was carried out for 20 h at 45 °C in a total volume of 10 μl containing: 0.1 M $NaClO_4$, 20 mM HEPES (pH 7.5), 0.1 μM RNA, 1 μM agent, and 1 μM $CuCl_2$. Lane 1: R24; lane 2: R24 + free terpyridine–Cu(II) complex + control 12-mer without terpyridine moiety; lane 3: R24 + dA*12 + EDTA (10 mM); lane 4: R24 + dA*12; lanes 5 and 6: bicarbonate and ribonuclease T1 sequencing reactions, respectively.

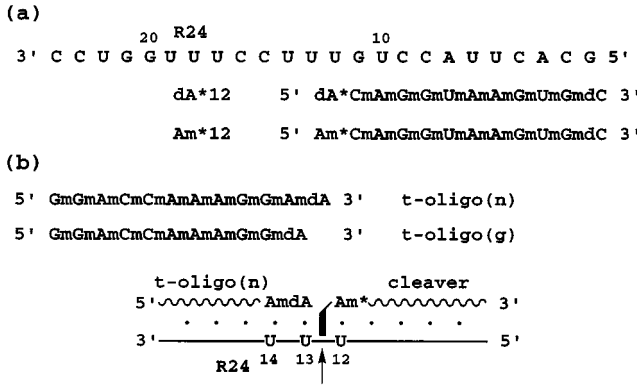

reactions	yields of cleavage between U12-U13	
	dA*12	Am*12
without t-oligo	18%	21%
with t-oligo(n)	27%	48%
with t-oligo(g)	17%	24%
(minor cleavage[a]	3%	6%)

Fig. 2 (a) Sequences of the RNA substrate and terpyridine–Cu(II)-linked oligomer agents. Nm refers to a 2′-*O*-methylnucleoside residue, and the asterisk indicates the site of the linked terpyridine moiety. (b) Sequences of the tandem 2′-*O*-methyloligomers, and schematic representation of RNA cleavage by the use of Am*12 and the t-oligo(n) (the arrow shows the cleavage site). The terpyridine–Cu(II) moiety is indicated as a black rectangle. All 2′-*O*-methyloligomers used in this study had a 2′-deoxynucleoside residue at the 3′-end. (c) Yields of site-specific cleavage of R24 by agents with or without tandem oligonucleotides.
[a] The minor cleavage site is U13–U14 site, and other reactions also gave this cleavage, but in yields of less than 1%.

For induction of RNA cleavage, the terpyridine–Cu(II) complex attached to the non-flexible linker should be close to the RNA strand. To explore the spatial orientation of the terpyridine moiety in the oligonucleotide hybrid, we prepared a terpyridine-linked duplex with a self-complementary sequence (dA*CmAmGmCmUmGmUm) and examined its melting temperature [conditions: 0.1 M $NaClO_4$, 10 mM Na phosphate (pH 7.5), 10 μM oligonucleotides, 12 μM $CuCl_2$]. It was found that the T_m value (72 °C) was very high, as compared with that (52 °C) for the control duplex without terpyridine moieties in the presence of 12 μM $CuCl_2$. These results may mean that the terpyridine moiety interacts with the end of the hybrid in an end-capping manner [Fig. 2(b)].[13]

To explore efficient RNA cleavage, which may be affected by the environment around the terpyridine–Cu(II) moiety in the RNA–agent hybrid, we carried out the RNA cleavage reaction in the presence of a 2′-*O*-methyl RNA complementary to the RNA single strand region adjacent to the terpyridyl conjugated 12-mer. The adjacent oligonucleotide was positioned in two ways: first, to provide a nick, and second a gap at the terpyridine site. In each reaction, with or without the tandem oligonucleotide [t-oligo(n) or t-oligo(g), Fig. 2(b)], Am*12 was more effective than dA*12 [Fig. 2(c)]. The cleavage efficiency for the reaction with the gapped tandem sequences was similar to that for the reaction without the additional oligonucleotide, but the cleavage site-specificity was lower. On the other hand, the reactions using the nicked tandem sequences increased the cleavage efficiency. Moreover, when Am*12 instead of dA*12 was used, the cleavage yield was 48%.‡ The spatial orientation of the terpyridine moiety probably became more suitable for RNA cleavage by the presence of the nick-forming tandem sequences and the 2-*O*-methylribose linker.

The present RNA cleaver has the metal complex at the end of the 2′-*O*-methyloligonucleotide. On the other hand, RNA cleaving metal complexes that were attached within DNA oligomers have been reported.[4,5,7,9] Some of the agents were designed to remain in a local region (such as a bulge) containing the cleavage site loose[14] while hybridized with the target RNA. This kind of agent is expected to be developed into an artificial ribonuclease that acts with catalytic turnover. Our findings, including the results on the nick-containing RNA hybrid, provide valuable information for the design of catalysts and the creation of more efficient cleavers.

We thank Prof. Donald E. Bergstrom (Purdue University) for critical reading of the manuscript. This work was supported in part by a Grant-in-Aid from the Ministry of Education, Science, Sports and Culture of Japan.

Notes and references

† For the reaction, the agent and $CuCl_2$ were directly added to the RNA solution. The addition after premixing both compounds gave similar results for the cleavage. We have used 10 molar equivalents of the terpyridine–Cu(II) agent and found that 2 molar equivalents were sufficient for the reaction. The use of such small amounts of cleavage agents has not been reported.

‡ Recently Daniher and Bashkin reported RNA cleavage using a terpyridine–Cu(II) complex attached to a flexible linker on an abasic site analog within DNA oligomers.[5] Our cleavage yield using the 2′-*O*-methyl facilitator and our data for the site-specificity of the RNA cleavage seem to be comparable with the reported data.

1 B. N. Trawick, A. T. Daniher and J. K. Bashkin, *Chem. Rev.*, 1998, **98**, 939.
2 A. D. MesMaeker, R. Häner, P. Martin and H. E. Moser, *Acc. Chem. Res.*, 1995, **28**, 366.
3 Y. Hayase, H. Inoue and E. Ohtsuka, *Biochemistry*, 1990, **29**, 8793.
4 J. K. Bashkin, E. I. Frolova and U. Sampath, *J. Am. Chem. Soc.*, 1994, **116**, 5981.
5 A. T. Daniher and J. K. Bashkin, *Chem. Commun.*, 1998, 1077.
6 J. Hall, D. Hüsken, U. Pieles, H. E. Moser and R. Häner, *Chem. Biol.*, 1994, **1**, 185.
7 J. Hall, D. Hüsken and R. Häner, *Nucleic Acids Res.*, 1996, **24**, 3522.
8 D. Magda, R. A. Miller, J. L. Sessler and B. L. Iverson, *J. Am. Chem. Soc.*, 1994, **116**, 7439.
9 D. Magda, M. Wright, S. Crofts, A. Lin and J. L. Sessler, *J. Am. Chem. Soc.*, 1997, **119**, 6947.
10 K. Matsumura, M. Endo and M. Komiyama, *J. Chem. Soc., Chem. Commun.*, 1994, 2019.
11 H. Inoue, Y. Hayase, A. Imura, S. Iwai, K. Miura and E. Ohtsuka, *Nucleic Acids Res.*, 1987, **15**, 6131.
12 G. R. Newkome, R. Güther, C. N. Moorefield, F. Cardullo, L. Echegoyen, E. Pérez-Cordero and H. Luftmann, *Angew. Chem., Int. Ed. Engl.*, 1995, **34**, 2023.
13 K. M. Guckian, B. A. Schweitzer, R. X.-F. Ren, C. J. Sheils, P. L. Paris, D. C. Tahmassebi and E. T. Kool, *J. Am. Chem. Soc.*, 1996, **118**, 8182.
14 K. A. Kolasa, J. R. Morrow and A. P. Sharma, *Inorg. Chem.*, 1993, **32**, 3983.

Communication 8/08522F

Novel conversion of perfluoro(2,6-dimethyl-1-azacyclohexene) to 3,3,4,4,5-pentafluoro-2,6-diphenyl-2,6-bis(trifluoromethyl)-1-azabicyclo[3.1.0]hexane

R. Eric Banks,* Mohamed K. Besheesh, Nicholas J. Lawrence,* Robin G. Pritchard and David J. Tovell

Chemistry Department, UMIST, PO Box 88, Manchester, UK M60 1QD. E-mail: n.lawrence@umist.ac.uk

Received (in Liverpool, UK) 2nd October 1998, Accepted 17th November 1998

Unexpectedly, treatment of perfluoro(2,6-dimethyl-1-azacyclohexene) with 2 equiv. of PhLi in cyclohexane–Et_2O at −50 to 40 °C gives a good yield (72%) of (±)-3,3,4,4,5-pentafluoro-2,6-diphenyl-2,6-bis(trifluoromethyl)-1-azabicyclo-[3.1.0]hexane 1; the nitranion implicated in this novel conversion can be trapped with sulfuric acid, giving 2,2,4,4,5,5-hexafluoro-2(e),6(e)-diphenyl-2(a),6(a)-bis(trifluoromethyl)piperidine 5.

1-Azabicyclo[3.1.0]hexanes are not new: synthesis of the parent compound was reported in the mid-1960s,[1,2] and synthetic studies on its derivatives[3] gained impetus in the late 1980s owing to the isolation of the azinomycin antitumour antibiotics[4] which possess this ring system. Surprisingly, however, no fluorinated derivatives appear to have been described heretofore.

The polyfluorinated species **1** disclosed here was obtained serendipitously during research into the electronic and steric influences of α-substituents on the effectiveness and modes of action of 3,3,4,4,5,5-hexafluoro-*N*-fluoropiperidines, *e.g.* **3**, as selective electrophilic fluorinating agents, the ultimate objective being to develop chiral analogues of perfluoro-*N*-fluoropiperidine, the prototypical 'F^+' delivery agent of the N–F class.[5] The synthesis strategy being used centres on nucleophilic attack on perfluoro-(2,6-dimethyl-1-azacyclohexene) **2**.[6] This worked well (Scheme 1) when MeLi was used as the nucleophilic reagent: acidic work-up of the reaction mixture gave the expected N–H compound **4**† in 63% yield, and this was converted smoothly to 3,3,4,4,5,5-hexafluoro-2(a),6(a)-dimethyl-2(e),6(e)-bis(trifluoromethyl)-*N*-fluoropiperidine **3** (82% yield) on treatment with F_2 in cold $CFCl_3$ containing anhydrous KF. The stereochemistry of this new N–F compound was established beyond doubt by X-ray analysis,[7] hence the geometry of its N–H precursor **4** follows.

By contrast, similar treatment of the perfluoro imine **2** with PhLi [in c-C_6H_{12}–Et_2O (7:3) at −25 °C] gave a complex product from which, after careful addition of aqueous H_2SO_4 at −50 °C followed by flash chromatography, were isolated samples of (±)-3,3,4,4,5-pentafluoro-2,6-diphenyl-2,6-bis(trifluoromethyl)-1-azabicyclo[3.1.0]hexane **1** and 3,3,4,4,5,5-hexafluoro-2(e),6(e)-diphenyl-2(a),6(a)-bis(trifluoromethyl)-piperidine **5** in 4 and 28% yield, respectively. The structures of these products were established unambiguously by X-ray analysis (Fig. 1).‡ The *cis* disposition of the CF_3 substituents in each compound, coupled with the subsequent discovery that the yield of the azabicycloheptane **1** can be increased to 72% simply by not quenching the presumptive nitranion **6** formed from **2** and PhLi, but gradually raising the temperature of the reaction mixture to about 40 °C, prompts us to favour the reaction mechanism shown in Scheme 2. The ease of ring contraction presumably stems from the considerable relief of 1,3-diaxial $CF_3\cdots CF_3$ repulsions in the monocyclic moiety, the distance between the carbon centres of the trifluoromethyl substituents in the azabicyclohexane **1** being 33% greater than in the piperidine **5**; this belief is supported by our failure to convert the lithium salt of the diequatorial $(CF_3)_2$ analogue **4** of **5** to an

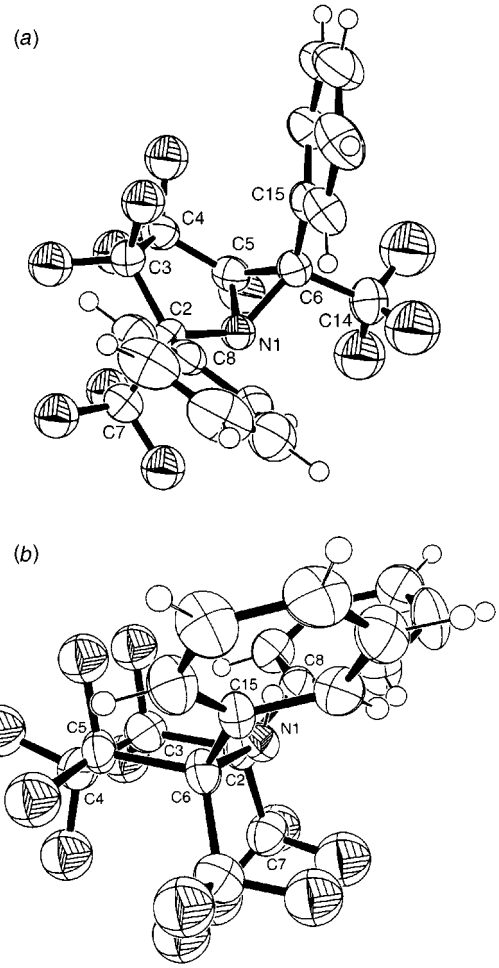

Fig. 1 ORTEP diagrams of (*a*) azabicycloheptane **1** and (*b*) piperidine **5** with 50% thermal ellipsoids.

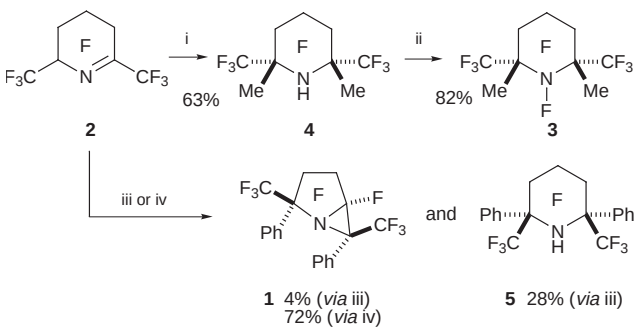

Scheme 1 *Reagents and conditions*: i, MeLi (2 equiv.), Et_2O, −78 °C, then aq. H_2SO_4; ii, F_2–N_2 (*ca.* 1:9 v/v), KF, $CFCl_3$, −30 °C; iii, PhLi (2 equiv.), c-C_6H_{12}–Et_2O (7:3), −25 °C, then aq. H_2SO_4, − 50 °C; iv, PhLi (2 equiv.), c-C_6H_{12}–Et_2O (7:3), −25 °C, then 40 °C.

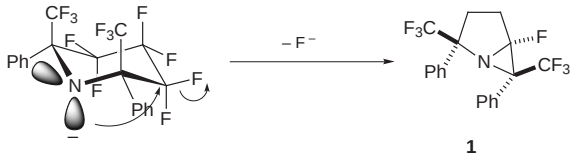

1

Scheme 2

azabicyclo[3.1.0]hexane in boiling Et_2O. Interestingly, the conversion **5**→**1** finds something of a parallel in the preparation of (5*S*)-1-azabicyclo[3.1.0]heptane in abysmal yield *via* basification of the sulfuric acid ester derived from 3-hydroxypiperidine.[2]

Notes and references

† All new compounds (**1**, **3**–**5**) possessed consistent NMR parameters (^{1}H, ^{13}C, and ^{19}F); good elemental analyses (C, H, F, and N) were obtained for **1**, **3** and **5** except that the F value for **1** was low.

‡ *Crystal data* for **1**: $C_{19}H_{10}F_{11}N$, M = 461.28, monoclinic, a = 10.217(2), b = 8.6426(10), c = 21.054(3) Å, β = 101.22(2)°, U = 1823.5(5) Å^3, T = 293(2) K, space group $P2_1/c$ (no. 14), monochromated Mo-Kα radiation, λ = 0.71069 Å, Z = 4, D_c = 1.680 Mg m^{-3}, F(000) = 920, colourless plates, dimensions 0.40 × 0.35 × 0.25 mm, μ(Mo-Kα) = 0.178 mm^{-1}, Rigagku AFC6S diffractometer, ω–2θ scan, 4 < 2θ < 50°, 3378 reflections measured, 3197 unique reflections. The structure was solved by direct methods and refined by full-matrix least-squares (SHELX 97). All non-hydrogen atoms were refined anisotropically; hydrogens were constrained to chemically reasonable positions. The final cycle of least-squares refinement (for 320 parameters) converged with $wR2$ = 0.1057 (for all data) and $R1$ = 0.0389 (for 1926 reflections [I > 2σ(I)]). Selected bond distances: C(7)–(14), 4.76(1); C(5)–N, 1.436; C(6)–N, 1.499; C(5)–(6), 1.485 Å. Selected bond angles: C(5)–N–(6), 60.75; C(5)–C(6)–N, 57.51; C(6)–(5)–N, 61.74°.

For **5**: $C_{19}H_{11}F_{12}N$, M = 481.29, orthorhombic, a = 27.339(2), b = 8.3850(10), c = 15.593(2) Å, U = 3574.5(7) Å^3, T = 203(2) K, space group *Pbcn* (No. 60), monochromated Mo-Kα radiation, λ = 0.71069 Å, Z = 8, D_c = 1.789 Mg m^{-3}, F(000) = 1920, colourless needles, dimensions 0.40 × 0.25 × 0.15 mm, μ(Mo-Kα) = 0.193 mm^{-1}, Nonius Mach3 diffractometer, ω–2θ scan, 4 < 2θ < 50°, 3129 reflections measured, 3129 unique reflections. The structure was solved by direct methods and refined by full-matrix least-squares (SHELX 97). All non-hydrogen atoms were refined anisotropically; hydrogens were constrained to chemically reasonable positions. The final cycle of least-squares refinement (for 333 parameters) converged with $wR2$ = 0.0808 (for all data) and $R1$ = 0.0355 (for 2295 reflections [I > 2σ(I)]). Selected bond distances: C(2)–N, 1.464(3); C(2)–C(3), 1.549(3); C(2)–C(7), 1.554(3); C(2)–C(8), 1.540(3); C(3)–C(4), 1.531(3); C(4)–C(5), 1.533(3); C(4)–F, 1.339(3); C(5)–C(6), 1.547(3); C(6)–N, 1.460(3); C(6)–C(14), 1.551(3); C(6)–C(15), 1.554(3); C(7)–F, 1.321(3); C(8)=C(9), 1.387(3); C(14)–F, 1.322(3) Å. Selected bond angles: C(2)–N–C(6), 128.05(18); N–C(2)–C(8), 106.77(17); N–C(2)–C(7), 112.03(17); N–C(2)–C(3), 109.38(17); C(4)–C(3)–C(2), 116.25(18); C(5)–C(4)–C(3), 112.99(18); C(4)–C(5)–C(6), 115.88 (18); N–C(6)–C(5), 109.67(17)°. CCDC 182/1092. This data is available as two .cif files from the RSC web site, see: http://www.rsc.org/suppdata/cc/1999/47

1 A. L. Logothetis, *J. Am. Chem. Soc*., 1965, **87**, 749.
2 P. G. Gassman and A. Fentiman, *J. Org. Chem*., 1967, **32**, 2388.
3 For example, see D. St. C. Black and J. E. Doyle, *Aust. J. Chem*., 1978, **31**, 2247; E. Breuer and S. Zbaida, *J. Org. Chem*., 1977, **42**, 1904; J. Mulzer, R. Becker and E. Brunner, *J. Am. Chem. Soc*., 1989, **111**, 7500; E. J. Moran, J. E. Tellew, Z. Zhao and R. W. Armstrong, *J. Org. Chem*., 1993, **58**, 7848.
4 S. Ishizaki, M. Ohtsuka, K. Irinoda, K. Kukita, K. Nagaoka and T. Nakashima, *J. Antibiot*., 1987, **40**, 60.
5 R. E. Banks and G.E. Williamson, *Chem. Ind* (*London*), 1964, 1864; R. E. Banks, V. Murtagh and E. Tsiliopoulos, *J. Fluorine Chem*., 1991, **52**, 389; R. E. Banks and V. Murtagh, *Encyclopedia of Reagents for Organic Synthesis*, ed. L. A. Paquette, Wiley, New York, 1995, **6**, 3942.
6 R. E. Banks, M. G. Barlow and M. Nickkho-Amiry, *J. Fluorine Chem*., 1979, **14**, 383.
7 D. J. Tovell, Ph.D. Thesis, UMIST, 1997; R. E. Banks, M. K. Besheesh, N. J. Lawrence, R. G. Pritchard and D. J. Tovell, publication in preparation.

Communication 8/07673A

Phase-transfer catalyzed asymmetric Darzens reaction of cyclic α-chloro ketones

Shigeru Arai,*[a] Yoshiki Shirai,[a] Toshimasa Ishida[b] and Takayuki Shioiri*[a]

[a] *Faculty of Pharmaceutical Sciences, Nagoya City University, Tanabe-dori, Mizuho-ku, Nagoya 467-8603, Japan. E-mail: shioiri@phar.nagoya-cu.ac.jp*

[b] *Osaka University of Pharmaceutical Sciences, 4-20-1 Nasahara, Takatsuki, Osaka 569-1041, Japan*

Received (in Cambridge, UK) 8th August 1998, Accepted 28th October 1998

Catalytic asymmetric Darzens reaction using cyclic α-chloro ketones promoted by chiral quaternary ammonium salts as a phase-transfer catalyst proceeded smoothly under mild reaction conditions to afford the desired products with reasonable enantioselectivities at room temperature.

The Darzens reaction, which allows the generatation of new stereocenters with complete diastereocontrol, is one of the most powerful methodologies for the synthesis of α,β-epoxy carbonyl and related compounds, and therefore has been recognized as one of the most significant C–C bond forming processes in synthetic organic chemistry. Although many trials have been performed aimed at developing an asymmetric equivalent in recent decades, many of them require a stoichiometric amount of chiral source[1] and few examples which proceed catalytically are known.[2] We have previously reported an effective catalytic asymmetric Darzens reaction promoted by a chiral quaternary ammonium salt acting as a phase-transfer catalyst (PTC).[3a] According to this procedure, the desired products were obtained with reasonable enantioselectivities in a stereoselective fashion under mild reaction conditions. Here we report recent results for a new system utilizing cyclic α-chloro ketones in the catalytic asymmetric Darzens reaction.

At the outset, we investigated the reaction of the easily prepared cyclic α-chloro ketones **1**[4] as the carbon nucleophile with various aldehydes **2** in the presence of a catalytic amount of the commercially available chiral quaternary ammonium salt PTC **A**, derived from cinchonine under mild reaction conditions. In this system, chiral quaternary carbons which are commonly considered to be difficult to create *via* direct carbon–carbon bond forming reactions, can be formed by the use of α-substituted chloro ketones. The reaction of isobutyraldehyde **2a** with α-chloro ketone **1a** *via* the use of a stoichiometric amount of LiOH in the presence of chiral PTC **A** (10 mol%) in Bu_2O proceeded smoothly to give the desired epoxide **3aa** in good yield at room temperature. The diastereoselectivity of the reaction was perfect and its enantioselectivity was found to be 69% ee *via* HPLC analysis,[5] as shown in Table 1. Next, we attempted to use as PTCs other easily prepared quaternary salts derived from cinchonine involving *O*-protected or substituted benzyl moieties. In spite of our efforts, higher enantioselectivities were not realized in the formation of **3aa** *via* use of a catalytic amount of these analogous PTCs.[6] Although the role of the 4-trifluoromethyl group on the phenyl ring is not clear in this asymmetric induction at present, we believe that the electron-deficiency of the phenyl group in the PTC skeleton plays an important role because the 4-methylated PTC, which is sterically equivalent to the 4-trifluoromethylated derivative (PTC **A**), afforded **3aa** with 0% ee. Also the unsuccessful results obtained by use of the hydroxy-protected PTC in this reaction system support the possibility that the hydrogen bonding, based upon the hydroxy group, between a catalyst and a substrate is a significant interaction in the asymmetric induction, similar to the known related reaction systems.[7] Herein, we have found that 4-trifluoromethylated quaternary salt PTC **A** derived from cinchonine appears to act as an efficient PTC in asymmetric Darzens reactions utilizing cyclic ketones.[8] Encouraged by this result, other aliphatic aldehydes such as **2be** were applied using similar reaction conditions with **1a**, revealing that the reaction with **1** proceeded smoothly to give the corresponding coupling adducts **3**. In particular, treatment of **1a** with **2d** or **2e** afforded the corresponding compounds **3ad** or **3ae** in good yield with 84 and 86% ee, respectively (entries 4 and 5). The reaction of other substrates such as **1b** with aldehydes **2b** or **2e** also gave the corresponding products with moderate ee (entries 6 and 7). The relative configurations of the coupling adducts were determined by both X-ray crystallographic analysis† using the coupling product **3ba** obtained from **1b** with **2a** and comparison of ^{1}H NMR analyses. The ORTEP figure shown in Fig. 1 reveals that it was the *trans* isomer, and other analogous products were determined

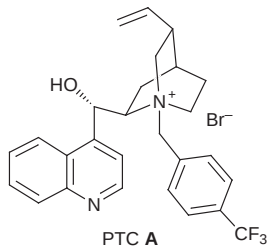

PTC **A**

Table 1 Catalytic asymmetric Darzens reaction under PTC conditions

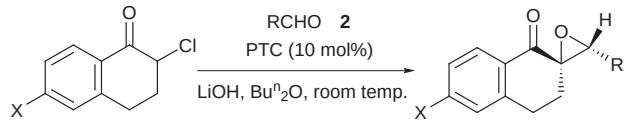

1a X = H
b X = OMe

3

Entry	Ketone	Aldehyde	*t*/h	Product	Yield (%)	Ee (%)
1	**1a**	2a R = Pr^i	61	**3aa**	99	69
2	**1a**	2b R = Bu^i	63	**3ab**	86	74
3	**1a**	2c R = *c*-Hex	62	**3ac**	80	69
4	**1a**	2d R = Et_2CH	252	**3ad**	67	84
5	**1a**	2e R = Bu$^tCH_2$	84	**3ae**	86	86[a]
6	**1b**	2b R = Bu^i	48	**3bb**	65	50
7	**1b**	2e R = Bu$^tCH_2$	63	**3be**	90	75

[a] 85% de.

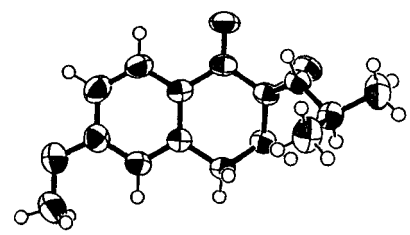

Fig. 1

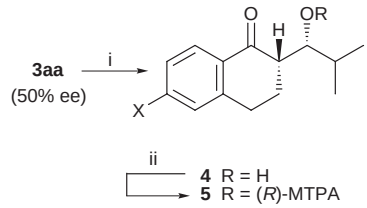

Scheme 1 *Reagents and conditions*: i, SmI_2, 53%; ii, (*R*)-MTPACl, 85%.

by comparison of the coupling constants observed in their ^{1}H NMR spectra. To the best of our knowledge, this is the first example of the preparation of α,β-epoxy ketones *via* catalytic asymmetric Darzens reaction with more than 80% ee.

The absolute configuration of the coupling product **3aa** was determined by transformation to the corresponding (*R*)-MTPA ester. As shown Scheme 1, **3aa** (50% ee) was treated with SmI_2[9] in THF–MeOH to afford the corresponding β-hydroxy ketone **4** [$[\alpha]_D^{28}$ −13.8 (*c* 2.7, $CHCl_3$)] as a sole product without racemization, as shown by the HPLC analysis. The stereochemistry of **4** was determined as *syn* by comparison with the literature data.[10] The following esterification afforded **5** in 85% yield. Application of the product **5** to the Mosher method[11] revealed that **5** has the β*R* configuration.

In conclusion, we have demonstrated both the catalytic asymmetric Darzens reaction under PTC conditions utilizing cyclic α-chloro ketones and enantiocontrol for the formation of the quaternary carbons *via* direct C–C bond formation. This methodology is effective for producing α,β-epoxy ketones involving a chiral quaternary carbon in optically active form.

One of the authors (S. A.) is grateful to the Ciba-Geigy Foundation (Japan) for the Promotion of Science for their financial support. This work was also supported by Grants-in-Aid from the Ministry of Education, Science, Sports and Culture of Japan, and the Ohara Award in Synthetic Organic Chemistry (S. A.), Japan.

Notes and references

† *Crystal data* for **3ba**: $C_{15}H_{18}O_3$, M = 246.31, colourless prismatic crystal, 0.80 × 0.20 × 0.60 mm, monoclinic, $P2_1/a$, a = 9.919(4), b = 12.587(5), c = 11.624(5) Å, β = 112.71(3)°, V = 1338.8(9) Å^3, T = 293 K, Z = 4, μ(Cu-Kα) = 6.80 cm^{-1}, 2441 reflections measured, 2294 independent reflections, 1878 reflections observed, R = 0.052, Rw = 0.211. CCDC 182/1075. The crystallographic data is available as a .cif file at http://www.rsc.org/suppdata/cc/1999/49

1 K. Ohkata, J. Kimura, Y. Shinohara, R. Takagi and Y. Hiraga, *Chem. Commun*., 1996, 2411; T. Takahashi, M. Maruoka, M. Capo and K. Koga, *Chem. Pharm. Bull*., 1995, **43**, 1821.
2 J. C. Hummelen and H. Wynberg, *Tetrahedron Lett*., 1978, 1089; S. Colonna, R. Fornasier and U. Pfeiffer, *J. Chem. Soc*., *Perkin Trans. 1*, 1978, 8; R. Annunziata, S. Banfi and S. Colonna, *Tetrahedron Lett*., 1985, **26**, 2471; Y. Masaki and M. Shi, *J. Chem. Res*. (*S*), 1995, 40; P. Bako. A. Szollosy and L. Toke, *Synlett*, 1997, 291.
3 (*a*) S. Arai and T. Shioiri, *Tetrahedron Lett*., 1998, **39**, 2145. We have succeeded in the development of other useful PTC-catalyzed reactions; see (*b*) S. Arai, S. Hamaguchi and T. Shioiri, *Tetrahedron Lett*., 1998, **39**, 2997; (*c*) S. Arai, H. Tsuge and T. Shioiri, *Tetrahedron Lett*., 1998, **39**, 7563.
4 D. Masilamani and M. M. Rogic, *J. Org. Chem*., 1981, **46**, 4486.
5 Use of α-bromo ketones as substrate instead of chloro ketones gave **3aa** with significantly lower enantio- and diastereo-selectivities.
6 Easily prepared PTCs substituted at the 4-position on the phenyl ring with other electron-withdrawing groups such as NO_2 or CN, and electron-donating groups such as MeO or alkyl groups, gave **3aa** with lower ee (4-NO_2, 5% ee; 4-CN, 6% ee; 4-OMe, 0% ee; 4-Bu^t, 5% ee). The PTC involving both a methyl-protected hydroxy group and a 4-trifluoromethylbenzyl unit afforded **3aa** as racemate. Other types of PTC including 2- or 3-substituted benzyl moieties also gave **3aa** with lower ee [3-CF_3, 3% ee; 2,4-$(CF_3)_2$, 17% ee].
7 K. B. Lipkowitz, M. W. Cavanaugh, B. Baker and M. J. O'Donnell, *J. Org. Chem*., 1991, **56**, 5181; D. L. Hughes, U.-H. Dolling, K. M. Ryan, E. F. Schoenewaldt and E. J. Grabowski, *J. Org. Chem*., 1987, **52**, 4745; M. Masui, A. Ando and T. Shioiri, *Tetrahedron Lett*., 1988, **29**, 2835.
8 A typical procedure for the catalytic asymmetric Darzens reaction is as follows: To a suspension of **1a** (53.0 mg, 0.3 mmol), PTC **A** (16.0 mg, 0.03 mmol) and aldehyde **2a** (0.06 ml, 0.6 mmol) in Bu_2O (1.5 ml) was added LiOH (28.4 mg, 1.2 mmol) at room temperature. After the mixture had been stirred for 45 h, more **2a** (0.06 ml, 0.6 mmol) was added, the mixture was stirred for an additional 16 h and the reaction mixture was quenched with 1 M HCl (3.0 ml), extracted with Et_2O (15 ml × 3), washed with brine and dried over Na_2SO_4. Removal of the solvent followed by flash column chromatography (silica gel, hexane–Et_2O, 5:1) gave the desired coupling adduct **3aa** as a colorless oil (64.2 mg, 99%, 69% ee): $[\alpha]_D^{25}$ +55 (*c* 2.1, $CHCl_3$). Ees were determined by HPLC analysis by use of DAICEL CHIRALCEL OD+OD, hexane–Pr^{i}OH, 20:1, retention time, 16.9 (major) and 18.6 min (minor).
9 G. A. Molander, *Chem. Rev*., 1992, **92**, 29 and references cited therein.
10 M. Hojo, H. Harada, H. Itoh and A. Hosomi, *J. Am. Chem. Soc*., 1997, **119**, 5459.
11 J. A. Dale and H. S. Mosher, *J. Am. Chem. Soc*., 1973, **95**, 512.

Communication 8/08321E

ChemComm

A method for the synthesis of high quality large crystal MCM-41

Robert Mokaya,* Wuzong Zhou* and William Jones

Department of Chemistry, University of Cambridge, Lensfield Road, Cambridge, UK CB2 1EW.
E-mail: rm140@cus.cam.ac.uk; wz100@cus.cam.ac.uk

Received (in Bath, UK) 23rd September 1998, Accepted 26th November 1998

Preparation of large crystal MCM-41 has been achieved by using calcined small crystallite MCM-41 as seeds in a multistage synthesis method. The possible formation mechanism is discussed. We believe that the newly discovered method is particularly important in making high quality thin films of mesoporous materials.

Following the discovery of the M41S family of ordered silica materials,[1,2] considerable attention has been focused on tailoring their pore structures.[3–6] For example, the diameter of hexagonally packed one-dimensional channels in MCM-41 can be tailored from 15 to over 100 Å[2–6] by a variety of methods which include using templating surfactant molecules with different alkyl chain lengths,[2] adding auxiliary organic molecules (which are solubilised in the hydrophobic region of the templating aggregates thus increasing micellar size)[2] or hydrothermal restructuring in the mother liquor over longer crystallization time or at higher reaction temperature.[3–6] The pore size uniformity or long range structural ordering can also be improved by careful choice and control of synthesis conditions.[7,8] However, there are very few reports on the control or increase in crystal size of MCM-41 despite the fact that crystal size is crucial to the fabrication and use of this material in thin film applications (such as in separation membranes) and in making molecular wires.[9] This is not surprising because, compared to the three-dimensional MCM-48, the formation of large crystals of MCM-41 would be difficult due to the one-dimensional channel structure which is subject to bending and fracture. Here we report on a new synthetic approach which involves the use of calcined MCM-41 as the seeds for further synthesis. The resulting material (herein referred to as secondary MCM-41) shows significantly improved long range structural ordering and a marked increase in crystal size.

The parent MCM-41 material (herein referred to as the primary MCM-41) was prepared following a normal procedure.† For secondary synthesis a synthetic gel of the same molar ratio was assembled except that the primary MCM-41 was used as 'silica source' instead of the fumed silica. The experimental procedures were exactly the same as described for the primary synthesis.† The MCM-41 yield, based on silica recovery, was *ca.* 60% for the primary synthesis and > 90% for the secondary synthesis.

The powder X-ray diffraction (XRD) patterns obtained from the calcined primary and secondary MCM-41 are shown in Fig 1. The pattern of the primary MCM-41 is typical of a well ordered specimen and shows an intense (100) diffraction peak and three higher order (110), (200) and (210) peaks. The pattern of the secondary MCM-41 shows an increase in the intensity of the (100) peak along with an increase in intensity and improvement in the resolution of the higher order peaks. In addition we were able to observe the (300) peak and a diffuse (220, 310) peak; these peaks are seldom observed even in the 'best' quality MCM-41 reported previously.[8] The presence of these higher order peaks indicates an improvement in long range ordering while the increase in peak intensities and associated reduction in full width at half maxima (FWHM) is a reflection of larger scattering domain (or crystal) size. The secondary synthesis does not however have any significant effect on the d_{100} spacing of the calcined samples. We note that doubling the primary synthesis time from 48 hours to 96 hours results in an increase in d_{100} spacing and a decrease in long range ordering with no apparent change in crystal size. Preliminary porosity data indicate that the surface area and pore volume of the secondary MCM-41 are slightly lower than those of the primary MCM-41. The average pore diameter (APD) is also lower for the secondary MCM-41. The lower APD taken together with the unchanging basal spacing is an indication that secondary synthesis results in a material with thicker pore walls. Thicker pore walls are expected to impart greater thermal and hydrothermal stability; indeed we have found that the secondary MCM-41 is relatively more stable to refluxing in boiling water compared to the primary material.

Transmission electron microscopic (TEM) images and selected area electron diffraction (SAED) patterns of the samples were obtained from a Jeol JEM-200CX electron microscope. The crystal size of the primary MCM-41 is in the range 400–600 Å range and no crystallites larger than 1000 Å were observed. This is similar to other normal MCM-41 specimens presented in previous reports.[10] On the other hand, the crystal size of the secondary MCM-41 is from 4000 to 8000 Å and crystallites smaller than 1000 Å were never observed. A typical TEM image together with a corresponding SAED pattern is shown in Fig. 2. It is clearly demonstrated that the secondary synthesis results in an increase in the crystal size of MCM-41 and crystallinity of the specimen has been significantly improved as indicated by

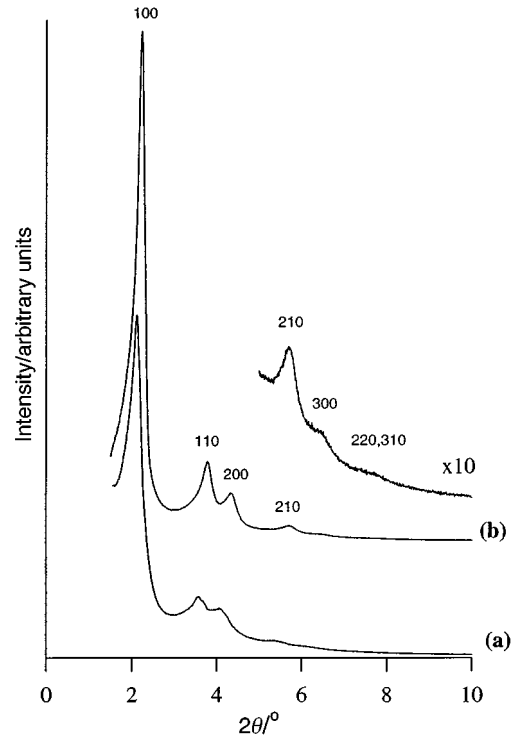

Fig. 1 Powder XRD patterns of calcined (a) primary MCM-41 and (b) secondary MCM-41.

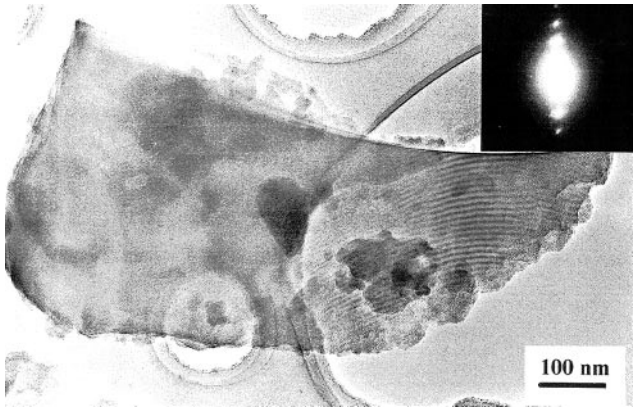

Fig. 2 TEM image and corresponding SAED pattern of a large crystal of MCM-41.

SAED patterns where four or more pairs of diffraction spots appear along the [100] direction, while only one or two pairs can been seen from the primary MCM-41 crystallites.

Thermogravimetric analysis (TGA) of the as-synthesized samples indicate that the amount of template occluded by the secondary MCM-41 is *ca.* 18% lower than in the primary MCM-41. This indicates that less amine is required during the secondary synthesis which would be the case if the primary MCM-41 (which is the silica source) remains largely intact with its crystallites acting as seeds or starting points for further MCM-41 formation. In this scenario the real source of silicate ions for crystal enlargement is amorphous silica which is usually part of any MCM-41 yield.

The extension of the MCM-41 framework is preceded by the dissolution (which is made possible by the presence of OH^- ions from TMAOH) of the 'silica source'.[11] The OH ions are used up during the dissolution and therefore the extent to which the concentration of OH ions (or pH) reduces during the crystallization period is a measure of the amount of dissolution.[11] For the primary synthesis we observed a decrease in pH from 12.4 to 11.5 after ageing for 20 hours at room temperature and a further decrease to 10.7 after heating at 150 °C for 48 hours. In contrast the gel for secondary synthesis had a pH of 11.5 which remained largely unaffected by aging at room temperature and reduced only slightly to 11.2 after heating for 48 hours at 150 °C. We attribute this smaller reduction in pH to the fact that there was much less dissolution during the secondary synthesis. In other words, if the MCM-41 particulates had dissolved extensively (to the same extent as the dissolution of fumed silica during the primary synthesis) we would have observed a larger pH decrease similar to that observed for the primary synthesis. These results along with the higher silica recovery are a strong indication that the primary MCM-41 is preserved during the secondary synthesis and that the slight decrease in pH is due to the dissolution of amorphous silica phase.

The TGA of the as-synthesized primary and secondary samples also indicated that the weight loss attributable to dehydroxylation of silanol groups (between 350 and 800 °C)[3,12] was 35% less for the secondary sample. This is a clear indication that the as-synthesized secondary MCM-41 is at a much higher level of silicate polymerization compared to its primary precursor and agrees with our suggestion that the primary MCM-41 remains largely intact during the secondary synthesis. This is further supported by our observation that on calcination the basal spacing of the primary MCM-41 reduced by 8.0% compared to a reduction of 2.5% for the secondary MCM-41. It is generally accepted that a higher extent of contraction is an indication of a less polymerized or cross-linked framework which therefore undergoes greater dehydroxylation.[11] Indeed ^{29}Si MAS NMR of the as-synthesized samples indicates that the Q4/Q3 ratio is higher for the secondary MCM-41.

According to a recent report,[13] during the preparation of MCM-41, the cylindrical surfactant and the silica aggregates are simultaneously formed. The silicate ions enter the particles from the surface perpendicular to the *c* axis of the aggregates and the molecules of the surfactant must enter along the aggregate cylinders until the density of the surfactant approaches its maximum value. In the present work, when the calcined MCM-41 crystallites were used as seeds during the secondary synthesis, it is possible that the template molecules attach themselves at the mouth of the pore channels of the primary MCM-41 and encourage crystal growth parallel to the channels and, consequently, growth of larger crystals becomes possible. This method can be applied in future preparation of large single crystals and high quality thin films of MCM-41.

R. M. acknowledges the EPSRC for an Advanced Fellowship.

Notes and references

† *Preparative procedure of the primary MCM-41*: tetramethylammonium hydroxide (TMAOH) and cetyltrimethyammonium bromide (CTAB) were dissolved in distilled water by stirring at 35 °C. The silica source, fumed silica (Sigma), was added to the solution under stirring for 1 hour. After further stirring for 1 hour the resulting synthetic gel of composition SiO_2 : 0.25 CTAB : 0.2 TMAOH : 40 H_2O was left to age for 20 hours at room temperature following which the mixture was transferred to a teflon-lined autoclave and heated at 150 °C for 48 hours. The solid product was obtained by filtration, washed with distilled water, dried in air at room temperature and calcined at 550 °C for 8 hours.

1 C. T. Kresge, M. E. Leonowicz, W. J. Roth, J. C. Vartuli and J. S. Beck, *Nature*, 1992, **359**, 710.
2 J. S. Beck and J. C. Vartuli, W. J. Roth, M. E. Leonowizc, C. T. Kresge, K. D. Schmitt, C. T.-W. Chu, D. H. Olson, E. W. Shepard, S. B. McCullen, J. B. Higgins and J. L. Schlenker, *J. Am. Chem. Soc.*, 1992, **114**, 10834.
3 D. Khushalani, A. Kuperman, G. A. Ozin, K. Tanaka, J. Garces, M. M. Olken and N. Coombs, *Adv. Mater.*, 1995, **7**, 842.
4 C.-F. Cheng, W. Zhou and J. Klinowski, *Chem. Phys. Lett.*, 1996, **263**, 247.
5 A. Corma, Q. Kan, M. T. Navarro, J. Perez-Pariente and F. Rey, *Chem. Mater.*, 1997, **9**, 2123.
6 A. Sayari, P. Liu, M. Kruk and M. Jaroniec, *Chem. Mater.*, 1997, **9**, 2499.
7 R. Ryoo and J. M. Kim, *J. Chem. Soc., Chem. Commun.*, 1995, 711.
8 K. J. Elder and J. W. White, *Chem. Mater.*, 1997, **9**, 1226.
9 C. G. Wu and T. Bein, *Science*, 1994, **264**, 1757.
10 Z. Luan, C. Cheng, W. Zhou and J. Klinowski, *J. Phys. Chem.*, 1995, **99**, 1018.
11 C.-F. Cheng, D. H. Park and J. Klinowski, *J. Chem. Soc., Faraday Trans.*, 1997, **93**, 193.
12 P. T. Tanev and T. J. Pinnavaia, *Chem. Mater.*, 1996, **8**, 2068.
13 W. Zhou and J. Klinowski, *Chem. Phys. Lett.*, 1998, **292**, 207.

Communication 8/07402J

Conversion of propane into butanes catalyzed by sulfated zirconia mixed with Pt/ZrO_2

Makoto Hino[a] and Kazushi Arata*[b]

[a] *Hakodate Technical College, Tokura-cho, Hakodate 042-8501, Japan*
[b] *Department of Science, Hokkaido University of Education, Hachiman-cho, Hakodate 040-8567, Japan. E-mail: karata@hak.hokkyodai.ac.jp*

Received (in Cambridge, UK) 21st September 1998, Accepted 17th November 1998

An active catalyst for the conversion of propane into butanes is obtained by mechanically mixing sulfated ZrO_2 and Pt/ZrO_2.

Among conversion of light alkanes by cracking, coupling, or isomerization in heterogeneous catalytic sytems much attention has been focused on the coupling of methane, but the catalytic systems still require high temperatures to obtain satisfactory activity and selectivity.[1] Sulfated zirconia and related catalysts have received attention because of their high activities for butane isomerization.[2,3] Cheung and Gates tested Fe–Mn-promoted sulfated ZrO_2 for conversions of ethane and propane, but conversions were low, being only 0.6% for the highest propane conversion observed at 300 °C.[4–6] We have demonstrated that impregnation of sulfated ZrO_2 with noble metals such as Pt and Ir leads to pronounced activity for butane conversion, the Pt concentration being 7–8 wt%; the catalyst with Pt showed highest activity for the reaction.[7,8] These noble metal-added sulfated zirconias were applied to propane, but the conversions were still low. However, the conversion was found to be promoted by simply mechanically mixing Pt-supported zirconia (Pt/ZrO_2) with sulfated zirconia (SO_4/ZrO_2).

SO_4/ZrO_2 and 0.5 wt% Pt/ZrO_2 catalysts were prepared as described elsewhere.[3,8,9] The thus-prepared catalysts, 0.3 g SO_4/ZrO_2 and 0.3 g Pt/ZrO_2, were mixed well by kneading with a mortar and pestle. Other catalysts of sulfated Al_2O_3, TiO_2, and Fe_2O_3, together with WO_3/ZrO_2, were prepared as described elsewhere.[9]

Reactions of propane were carried out in a microcatalytic pulse reactor as described elsewhere.[8] The catalyst was heated at 300 °C for 1 h in an He flow before reaction. A slightly continual gain of conversion was observed with pulse number, and thus conversions were calculated on the basis of mol fraction as the average of the 6th–10th pulse values.

Table 1 Activities of the catalysts for the reaction of propane

Catalyst	*T*/°C	Conversion (%)	Products (%) C_1	C_2	C_4	C_5
SO_4/ZrO_2	200	0.1	Tr[a]	Tr	0.1	0
$Pt–SO_4/ZrO_2$[b]	200	0.2	0	Tr	0.2	0
$Pt–SO_4/ZrO_2$[c]	250	0.3	Tr	0.2	0.1	0
$SO_4/ZrO_2–Pt/ZrO_2$	200	3.2	Tr	0.2	3.0	Tr
$SO_4/ZrO_2–Pt/ZrO_2$[d]	200	4.2	0.1	0.7	3.4	Tr
$SO_4/ZrO_2–Pt/ZrO_2$[e]	200	4.6	0.3	1.2	3.1	0
$SO_4/ZrO_2–Pt/ZrO_2$	225	6.1	0.3	1.6	4.1	0.1
$SO_4/ZrO_2–Pt/ZrO_2$	250	10.6	1.8	4.9	3.8	0.1
$SO_4/Al_2O_3–Pt/ZrO_2$	250	8.4	2.1	6.3	Tr	0
$SO_4/TiO_2–Pt/ZrO_2$	250	8.9	2.4	6.4	0.1	0
$SO_4/Fe_2O_3–Pt/ZrO_2$	250	13.3	3.9	9.4	0	0
$WO_3/ZrO_2–Pt/ZrO_2$	250	14.0	3.3	10.7	0	0
$SO_4/ZrO_2–Pt/ZrO_2$[f]	250	5.8	5.5	0.3[g]	0	0
SO_4/ZrO_2-Pt/ZrO_2[f]	300	16.3	16.2	0.1[g]	0	0

[a] Trace. [b,c] Prepared by sulfation of zirconia gel followed by platinization and calcination ([b] 0.5, [c] 2 wt% Pt). [d,e] Reaction with [d] 0.6 or [e] 1.2 g of 0.5% Pt/ZrO_2 and 0.3 g of SO_4/ZrO_2. [f] Reaction of ethane. [g] Yield of C_3.

The reaction of propane (C_3) was carried out at 200 °C and 20 ml min^{-1} of He carrier over 0.3 g of SO_4/ZrO_2, but the conversion was only 0.1%. The addition of platinum (0.5 or 2 wt%), $Pt-SO_4/ZrO_2$ (0.3 g), was ineffective even at 250 °C as shown in Table 1. The addition of Pt was, however, effective when Pt/ZrO_2 was mechanically mixed with SO_4/ZrO_2. A mixture of 0.3 g of SO_4/ZrO_2 and 0.3 g of 0.5 wt% Pt/ZrO_2, where the Pt quantity was equivalent to that in 0.3 g of 0.5 wt% $Pt-SO_4/ZrO_2$, gave 3.2% conversion. The major product was butanes (C_4); trace amounts of pentanes (C_5) were observed in addition to ethane (C_2) and methane (C_1). Dehydrogenated materials were not observed, though ethylene and propylene were formed over Fe–Mn-sulfated ZrO_2.[5,6]

The catalysts were then examined in butane; the Pt co-impregnated catalyst, $Pt–SO_4/ZrO_2$[c] in Table 1, gave 48% conversion for the first pulse at 80 °C (catalyst amount: 0.1 g), while the mixture of SO_4/ZrO_2 and Pt/ZrO_2 only gave 8% conversion. Thus, the catalyst which is effective for butane is not efficient for propane and *vice versa*.

The effect of mixing was examined further at temperatures of 225 and 250 °C; the yields of C_4 were $\approx$4% with higher conversions of C_3, but showing lower selectivity for the formation of C_4 (Table 1). In terms of preparation temperature of the catalysts the highest activity was observed upon calcination at 600 °C for SO_4/ZrO_2 and 750°C for Pt/ZrO_2.

The effect of modifying the proportion of platinum in the catalyst was studied. Catalysts with 0.6 and 1.2 g of Pt/ZrO_2 showed 4.2 and 4.6% propane conversion at 200 °C, with 3.4 and 3.1% C_4 yields, respectively. This indicates that the effect of concentration of platinum is relatively small. In terms of isomers of C_4 the selectivity for isobutane was 60–65% in each case.

The effect of mixing of Pt/ZrO_2 for the reaction of propane was examined for other sulfated metal oxides, Al_2O_3, TiO_2, and Fe_2O_3 in addition to WO_3/ZrO_2, the acidities of which are lower relative to SO_4/ZrO_2.[3] These materials showed a noticeable effect upon mixing for the conversion reaction of butane to isobutane.[9,10] Remarkable conversions of C_3 over these substances mixed with Pt/ZrO_2 were obtained at 250 °C, but the yield of C_4 was low, at most 0.1%. Thus, high superacidity is needed to form C_4 products.

XPS experiments were carried out in order to elucidate the surface properties of Pt/ZrO_2. The binding energy of Pt 4f was 72.6 eV, which was far from that of the metallic state (71.7 eV), but close to that of cationic Pt species.[11]

The formation of higher molecular weight alkanes is brought about by catalysis of the cracking ability in addition to the protonation of propane by a superacid to form a carbonium ion.[5] This behavior was also shown by the formation of propane from ethane in the present system, although the yield was low (Table 1).

Notes and references

1 E. N. Voskresenskaya, V. G. Roguleva and A. G. Anshits, *Catal. Rev.-Sci. Eng.*, 1995, **37**, 101.
2 X. Song and A. Sayari, *Catal. Rev.-Sci. Eng.*, 1996, **38**, 329.

3 K. Arata, *Appl. Catal. A*, 1996, **146**, 3.
4 T.-K. Cheung and B. C. Gates, *Chem. Commun.*, 1996, 1937.
5 T.-K. Cheung, F. C. Lange and B. C. Gates, *Catal. Lett.*, 1995, **34**, 351.
6 T.-K. Cheung, F. C. Lange and B. C. Gates, *J. Catal.*, 1996, **159**, 99.
7 M. Hino and K. Arata, *Catal. Lett.*, 1995, **30**, 25.
8 M. Hino and K. Arata, *J. Chem. Soc. Chem. Commun.*, 1995, 789.
9 M. Hino and K. Arata, *Appl. Catal. A*, 1998, **173**, 121.
10 M. Hino and K. Arata, *Appl. Catal.*. A, 1998, **169**, 151.
11 A. Sayari and A. Dicko, *J. Catal.*, 1994, **145**, 561.

Communication 8/07316C

Aggregation/deaggregation processes in vanadium(II) carboxylate chemistry

Peter J. Bonitatebus, Jr. and William H. Armstrong*

Department of Chemistry, Merkert Chemistry Center, Boston College, Chestnut Hill, MA 02167-3860, USA. E-mail: william.armstrong@bc.edu

Received (in Bloomington, IN, USA) 3rd August 1998, Accepted 26th October 1998

Reactions of potassium tris(3,5-dimethylpyrazolyl)borate ($KTpb^{Me_2}$) with the low-valent mixed-metal complex $[(thf)_3V(\mu\text{-}Cl)(\mu\text{-}tfa)_2V(thf)_3][ZnCl_3(thf)]$ resulted first in $ZnCl^+$ abstraction and tetramer formation, then in asymmetric binuclear product formation through ligand substitution.

Our efforts in developing the chemistry of low-valent vanadium in an anionic oxygen ligand donor environment,[1–4] including that of vanadium(II) carboxylate coordination chemistry,[1] stems from the reported reducing and oxophilic character of these types of V^{II} complexes in both protic and aprotic media. For example, α,ω-dicarboxylic acids have been shown to promote the reaction between N_2 and vanadium(II) to yield N_2H_4 in the presence of hydroxide *via* by a proposed carboxylato-bridged V^{II} aggregate.[5] These reported conditions are mild, aqueous and heterogeneous in nature. Studies in organic, aprotic media of the interaction of V^{II} and trifluoroacetate (tfa) by Cotton *et al.* in an attempt to synthesize a multiply-bonded metal species, '$V{\equiv}V^{4+}$', resulted instead in the isolation of an oxidized oxo-centered triangular core, $[V_3(\mu_3\text{-}O)(\mu\text{-}tfa)_6(thf)_3]$ **1**.[6,7] Carboxyl group O-atom abstraction was postulated as the source of the (μ_3-O) atom in **1**, a conclusion based on the high oxophilicity of V^{II}. Although this latter report presented results of a synthetic strategy directed toward a '$V{\equiv}V^{4+}$' compound, it also served as an initial effort to homogenize and probe the original interesting N_2-fixing system.[5] Later efforts in our laboratory, under rigorously anaerobic and dry conditions using a similar preparation to that reported for **1**, demonstrated the existence and relative thermal stablility of a V^{II} carboxylate dimer, $[(thf)_3V(\mu\text{-}Cl)(\mu\text{-}tfa)_2V(thf)_3][ZnCl_3(thf)]$, **2** (Scheme 1), isolated as a highly air- and moisture-sensitive compound in good crystalline yield.[1] Herein we describe our continued effort and interest in vanadium(II) carboxylate coordination chemistry by reporting on the synthesis, structure and some properties of a novel binuclear carboxylate complex along with its tetrameric precursor—an unprecedented example of vanadium(II) isolated at this nuclearity. These new 'zinc-free' and halide-bridged multinuclear V^{II} compounds represent an important advance in probing the N_2-fixing system of Folkesson and Larsson by serving as starting materials for reactions with hydroxide or alkoxide ligands. Alkoxide donors, in conjunction with carboxylato-bridged V^{II} aggregates, are conceivably required for efficient homogeneous small molecule multielectron reduction, as were hydroxide ions in the original heterogeneous V^{II} carboxylate N_2-fixing system.[5]

Treating green-purple **2** (0.22 mmol scale) with one equivalent of potassium tris(3,5-dimethylpyrazolyl)borate ($KTpb^{Me_2}$) in 15 mL of THF (Scheme 1) and stirring overnight gave deposition of a white precipitate (KCl) which was removed by filtration. Layering the resulting blue-green filtrate with 3–5 mL of pentane and allowing it to stand for 12 h at 0 °C discharged another colorless solid, but in crystalline form, which was filtered off and identified by X-ray crystallography to be $[Zn(Tpb^{Me_2})Cl]$, **3**.† Layering and cooling the filtrate again completed the isolation of crystalline sky-blue $[V_4(\mu_3\text{-}Cl)_2(\mu\text{-}Cl)_2(\mu\text{-}tfa)_4(thf)_6]$ **4** (Fig. 1).‡ Apparently, this reaction involves scavenging the Zn^{II} of **2** as $[Zn(Tpb^{Me_2})Cl]$, **3**, using $KTpb^{Me_2}$, with concomitant KCl formation and chloride ion liberation. This freed Cl drives the cationic core of **2** to dimerize assembling a $[V_4tfa_4]^{4+}$ aggregate, compound **4**.§

The crystal structure of **4** (Fig. 1) revealed a tetramer with crystallographically imposed inversion symmetry.† Selected dimensions, listed in Fig. 1, show V–O_{thf} and V–O_{tfa} bond lengths (av. 2.139, av. 2.101 Å, respectively) to be in good agreement with those of **2** (av. 2.140, av. 2.091 Å, respectively).[1] The apical (μ_3) chloride distances in **4** (av. 2.506 Å) are only slightly shorter than similar bonds seen for the *triangulo*-trinuclear species $[V_3(\mu_3\text{-}Cl)_2(\mu\text{-}Cl)_3]^+$ (av. 2.519 Å).[8] The V···V separations in **4** (4.169, 3.637, 3.351 Å) vary within a relatively large range (0.818 Å) as a consequence of the different numbers and types of bridging groups between vanadium centers. The angle made by V(1)–Cl(1)–V(2) is also significantly widened [112.81(4)°] compared with the V–Cl–V

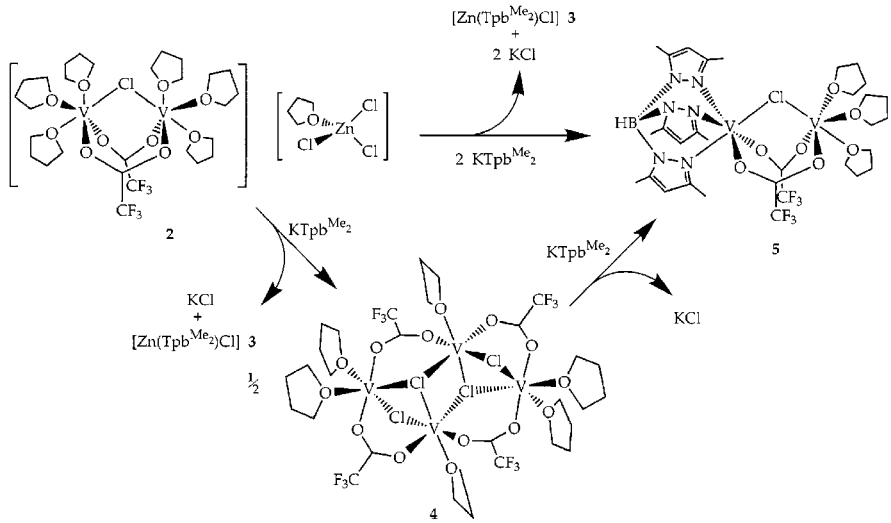

Scheme 1 Synthesis of carboxylato-bridged vanadium(II) aggregates.

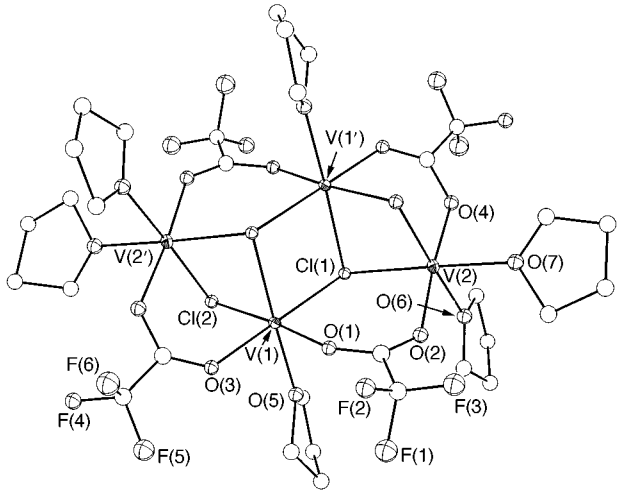

Fig. 1 Structure of **4** (hydrogen atoms are omitted for clarity). Selected bond distances (Å) and angles (°) are: V(1)–Cl(1) 2.515(1), V(1)–Cl(2) 2.481(1), V(2)–Cl(1) 2.489(1), V(1)–O(1) 2.109(3), V(2)–O(2) 2.090(3), V(1)–O(5) 2.129(3), V(2)–O(7) 2.140(4), V(1)–V(2) 4.169, V(1)–V(1′) 3.637, V(2)–V(1′) 3.351; V(1)–Cl(1)–V(2) 112.81(4), V(1)–Cl(1)–V(1′) 92.59(4), V(1)–Cl(2)–V(2′) 85.20(4), O(7)–V(2)–O(6) 86.4(2), O(1)–V(1)–Cl(2) 175.86(9), O(3)–V(1)–Cl(1) 179.90(9).

angle of **2** [100.3(1)°].[1] Compound **4** is the first example of an isolated vanadium(II) tetramer, and is resembled closest in terms of vanadium–ligand core connectivity and oxidation state by the methoxide-containing V_4^{10+} catecholato-bridged aggregate of Shilov and coworkers, the only structure reported to date from their vanadium-based N_2-fixing system.[9]

The aggregation of **2** → **4** invites a question regarding the outcome of a reaction involving **4** with one more equivalent of $KTpb^{Me_2}$. Reaction of **4** with $KTpb^{Me_2}$ in THF [or treatment of **2** with two equivalents (0.45 mmol scale) of $KTpb^{Me_2}$, Scheme 1] develops a light-brown solution from which KCl precipitates after 12 h of stirring. Filtration, pentane layering, and cooling overnight produced the neutral, asymmetric dimer $[(Tpb^{Me_2})V(\mu\text{-Cl})(\mu\text{-tfa})_2V(thf)_3]$, compound **5** (Fig. 2), in crystalline form.‡ Evidently this reaction converts the $[V_4tfa_4]^{4+}$ aggregate back to a $[V_2tfa_2]^{2+}$ core.§

The structure of **5** (Fig. 2), the first asymmetric $V_2^{II,II}$ dimer reported to date, consists of two V^{II} ions bridged by one chloride and two trifluoroacetate groups and coordinated terminally by a Tpb^{Me_2} group on one side and by THF molecules on the other.† The $V–O_{tfa}$ (av.) and V–Cl bond lengths are slightly different for each vanadium [V(1): 2.118, 2.507; V(2): 2.092, 2.456 Å respectively] reflecting the asymmetry in the molecule. These differences affect the V···V separation [3.868(1) Å] and the V–Cl–V angle [102.40(6)°] which are longer and wider as compared to **2** [3.796(2) Å, 100.3(1)°].[1]

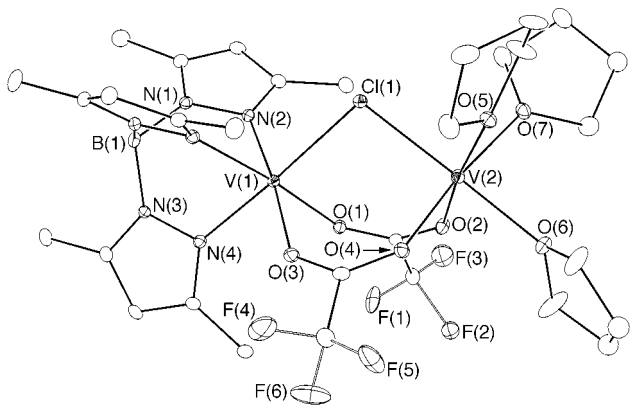

Fig. 2 Structure of **5** (hydrogen atoms are omitted for clarity). Selected bond distances (Å) and angles (°) are: V(1)–Cl(1) 2.507(2), V(2)–Cl(1) 2.456(2), V(1)–O(3) 2.122(4), V(2)–O(4) 2.091(4), V(1)–N(4) 2.150(5), V(2)–O(6) 2.152(4), V(1)–V(2) 3.868(1); V(1)–Cl(1)–V(2) 102.40(6), O(3)–V(1)–N(2) 174.7(2), O(4)–V(2)–O(7) 172.8(2).

Use of the Tpb^{Me_2-} ligand in reactions with **2**, has resulted in a doubling of the number of known bridged V^{II} carboxylates in the literature[1,10] and has encouraged aggregation/deaggregation behavior in vanadium(II) carboxylate chemistry. The first examples of a tetrameric and an asymmetrical dimeric V^{II} species were unveiled. We are currently examining the reaction chemistry of the carboxylato-bridged aggregate **4**, as a halide-rich and 'zinc-free' starting material, especially with alkoxides in the presence of reducible small molecules. Also, the use of $KTpb^{Me_2}$ for scavenging inner-sphere charge-sharing Zn^{II} ions present in other potentially reactive low-valent mixed-metal V–Zn alkoxide compounds synthesized recently in our laboratory,[11] is currently under investigation. Application of this unusual synthetic avenue, along with directed reactivity at the solvated face of **5**, will be reported elsewhere.

Notes and references

† *Crystal data* for **3**: $C_{15}H_{22}N_6B_1Cl_1Zn_1$, M = 398.01, a = 13.087(2), b = 8.054(1), c = 17.313(4) Å, V = 1824.9(6) Å^3, T = 183(2) K, μ = 1.499 mm^{-1}, orthorhombic, $Pmc2_1$, Z = 2, 2064 reflections total, R indices of R_1 = 3.85% and wR_2 = 10.45% for $I > 2\sigma(I)$. For **4**: $C_{32}H_{48}O_{14}F_{12}Cl_4V_4$, M = 1230.23, a = 12.9139(1), b = 12.6158(2), c = 16.3596(2) Å, β = 111.048(1)°, V = 2487.46(5) Å^3, T = 183(2) K, monoclinic, $P2_1/c$, Z = 2, 14099 reflections total, 5403 unique. A semi-empirical absorption correction from ψ-scans was applied (μ = 1.044 mm^{-1}). The structure was solved using anisotropic thermal parameters for all non-hydrogen atoms and a model including 2-fold rotational disorder for both the four THF carbons of O(7) and the two CF_3 groups, to values of R_1 = 6.75% and wR_2 = 16.37% for $I > 2\sigma(I)$. Final difference map features were within 0.672 and −0.541 e Å^{-3}. For **5**·THF: $C_{31}H_{46}N_6O_7B_1F_6Cl_1V_2\cdot C_4H_8O_1$, M = 948.93, a = 12.1724(1), b = 18.4139(3), c = 19.207 Å, β = 92.799(1)°, V = 4299.92(8) Å^3, T = 183(2) K, monoclinic, $P2_1/n$, Z = 4, 16,507 reflections total, 5547 unique. A semi-empirical absorption correction from ψ-scans was applied (μ = 0.573 mm^{-1}). The structure was solved using anisotropic thermal parameters for all non-hydrogen atoms and a model including 2-fold rotational disorder for both CF_3 groups and a THF solvate to values of R_1 = 6.77% and wR_2 = 13.90% for $I > 2\sigma(I)$. Final difference map features were within 0.416 and −0.303 e Å^{-3}. CCDC 182/1071.

‡ **4**: Anal. (calc.) C 31.34 (31.24), H 4.21 (3.93), N 0.00 (0.02)%; 45% yield. **5**: Anal. (calc.) C 43.42 (42.46), H 5.52 (5.29), N 9.21 (9.58)%; 47% yield. Analyses of non-crystalline samples often suggested inadequate removal of **3**.

§ *Selected spectroscopic data* for **4**: EPR [THF (77K), X-band] g = 2 (br), with a small absorbance at g = 3.9; IR (Nujol, cm^{-1}) 1698 (ν_{OCO} asym), 1575 (ν_{OCO} sym). Given the similarity in EPR spectra of **4** and **2** it is possible **4** may be dissociating in solution, to exist perhaps as the chloride salt, $[(thf)_3V(\mu\text{-Cl})(\mu\text{-tfa})_2V(thf)_3][Cl]$. For **5**: EPR [THF (77K), X-band] g = 2 (br, superimposed 8-line), with a small absorbance at g = 4; IR (Nujol, cm^{-1}) 2521 (ν_{BH}), 1709 (ν_{OCO} asym), 1545 (ν_{OCO} sym).

1 L. Gelmini and W. H. Armstrong, *J. Chem. Soc., Chem. Commun.*, 1989, 1904.
2 P. J. Bonitatebus, Jr., S. K. Mandal and W. H. Armstrong, *Chem. Commun.*, 1998, 939.
3 W. C. A. Wilisch, M. J. Scott and W. H. Armstrong, *Inorg. Chem.*, 1988, **27**, 4333.
4 M. J. Scott, W. C. A. Wilisch and W. H. Armstrong, *J. Am. Chem. Soc.*, 1990, **112**, 2429.
5 B. Folkesson and R. Larsson, *Acta Chem. Scand., Ser. A*, 1979, **33**, 347.
6 F. A. Cotton, M. W. Extine, L. R. Falvello, D. B. Lewis, G. E. Lewis and C. A. Murillo, *Inorg. Chem.*, 1986, **25**, 3505.
7 F. A. Cotton, G. E. Lewis and G. N. Mott, *Inorg. Chem.*, 1982, **21**, 3127 and 3316.
8 P. B. Hitchcock, D. L. Hughes, L. F. Larkworthy, G. J. Leigh, C. J. Marmion and J. R. Sanders, *J. Chem. Soc., Dalton Trans.*, 1997, 1127.
9 N. P. Luneva, S. A. Mironova, A. E. Shilov, M. Y. Antipin and Y. T. Struchkov, *Angew. Chem.*, 1993, **105**, 1240.
10 J. J. H. Edema, S. Hao, S. Gambarotta and C. Bensimon, *Inorg. Chem.*, 1991, **30**, 2584.
11 J. A. Davis, P. J. Bonitatebus, Jr., C. P. Davie and W. H. Armstrong, manuscript in preparation.

Communication 8/06105J

PFG NMR study of the transport properties of A-type zeolite membranes

Wilfried Heink,[a] Jörg Kärger,[a] Tim Naylor[b] and Ulf Winkler[a]

[a] *Universität Leipzig, Fakultät für Physik und Geowissenschaften, Linnéstr. 5, 04103 Leipzig, Germany. E-mail: kaerger@physik.uni-leipzig.de*

[b] *Smart Chemical Company Ltd., Unit 5, Blatchford Road, Horsham, West Sussex, UK RH13 5QR*

Received (in Cambridge, UK) 5th October 1998, Accepted 25th November 1998

The transport properties of an A-type zeolite membrane are traced by monitoring the diffusion paths of ethane and propane from *ca*. 300 nm up to 10 μm; over distances < 1 μm, the diffusivities are found to be comparable with those in a mono-crystal, while for large displacements by a factor of two to three smaller diffusivities were observed.

Offering a number of most exciting technological advantages in catalysis and gas separation, microporous membranes have become an attractive subject of applied research. Owing to their thermal and chemical stability, among them the inorganic membranes have attained special attention.

Zeolite membranes have recently been made available on a commercial basis and have been shown to be capable of achieving very high levels of separation along with very high permeate fluxes for a range of binary mixtures, for example water removal from methanol, ethanol and isopropyl alcohol.[1] The particular materials used in this study were pieces of membranes that were fragmented during handling. From scanning electron micrographs, these pieces appeared to be crystallite agglomerates with diameters of tens to hundreds of micrometers, where the crystallite diameters were of the order of micrometers.

The membranes were prepared from homogeneous solution with a composition given by the molar ratio 5 SiO_2 : Al_2O_3 : 55.12 Na_2O : 1004.66 H_2O. An aluminate solution was prepared by dissolving small pieces of aluminium wire (Aldrich, 2.4 g) in aqueous NaOH (86.56 g Analytical grade NaOH pellets in 362.46 g distilled water) over a 48 h period. A sodium silicate solution was prepared by dissolving NaOH pellets (80 g) in distilled water (340.4 g) then adding an aqueous silicate solution (BDH, 25.5% SiO_2, 7.5% Na_2O, 40.82 g) with vigorous stirring. After at least 15 min of stirring, the pre-heated aluminate solution was added, and the stirring continued for 5 min. The resultant solution was transferred to a preheated container for membrane preparation. Free-standing samples of zeolite membrane were prepared by placing the above solution in a sealed Teflon container which was placed in an oven at 50 °C for 48 h. The container was removed from the oven, drained and the zeolite film that lightly adhered to the container walls was throughly rinsed with distilled water until the rinsings were pH neutral. Samples of the membrane detached themselves during this procedure and were collected and dried at 70 °C overnight. The material was ion exchanged to the Ca-form by soaking it in 0.1 M $Ca(NO_3)_2$ overnight followed by thorough rinsing in doubly distilled, deionised water. The material was oven-dried at 120 °C for 24 h.

The pulsed field gradient (PFG) NMR method is a bulk technique, which allows the determination of the probability distribution of molecular displacements within the sample.[2,3] The displacements, which may be resolved by this technique are in the range of micrometers, with observation times of typically milliseconds.

For the preparation of the PFG NMR samples, the zeolite material was filled into glass tubes of 7.5 mm o.d. and activated by heating at a rate of 10 K h^{-1} under continuous pumping up to a final temperature of 400 °C, where it was kept for 10 h. After cooling to room temperature the probe molecules (the 'diffusants') were introduced by chilling from a calibrated gas volume with a set pressure. The amount adsorbed was afterwards checked by measuring the intensity of the NMR signal.

The diffusion measurements have been carried out by means of the home-built PFG NMR spectrometer FEGRIS 400 at a proton resonance frequency of 400 MHz with magnetic field gradient amplitudes up to 24 T m^{-1}.[3,4] The attenuation of the

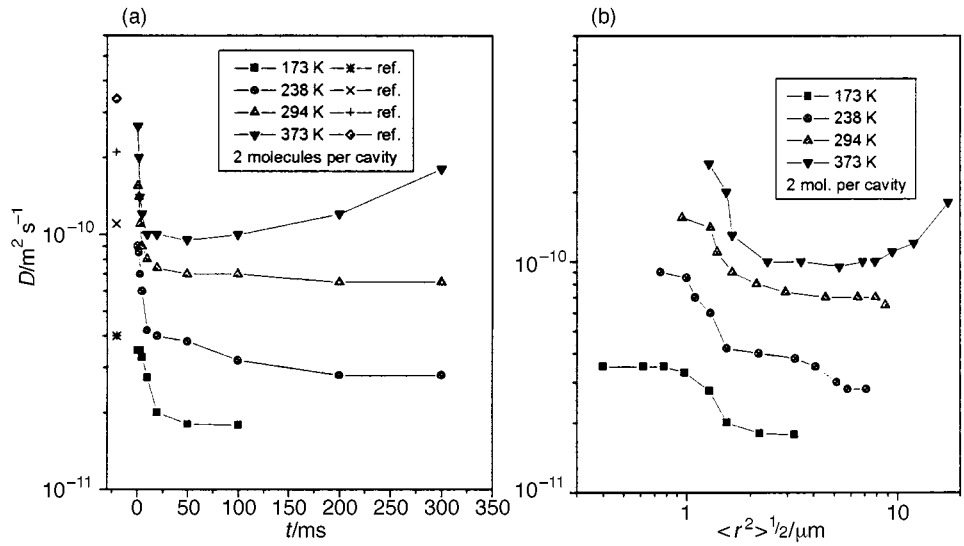

Fig. 1 (a) Ethane diffusivity in NaCaA membrane as a function of the observation time at different temperatures; ref.: results of previous PFG NMR studies with crystalline zeolite NaCaA. (b) Ethane diffusivities in NaCaA membrane as a function of the root mean square displacement at different temperatures.

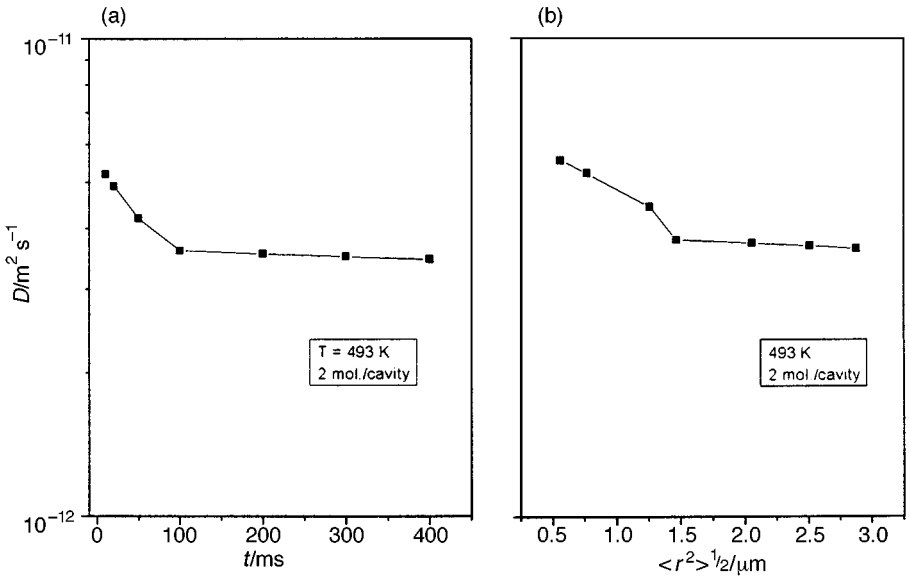

Fig. 2 (a) Propane diffusivity in NaCaA membrane: (a) as a function of the observation time and (b) as a function of the root mean square displacement.

NMR signal (the 'spin echo') *versus* the squared gradient amplitude was essentially found to follow a monoexponential decay, as to be expected for normal diffusion in a quasihomogeneous medium. The effective diffusivity was determined by comparing the signal decay with that of a standard [water, D = (2.04 ± 0.08) × 10^{-9} m^2 s^{-1} at 20 °C].[5] It is defined as the ratio

$$D = \langle r^2(t) \rangle / 6t \quad (1)$$

between the mean square displacement and the observation time.

Fig. 1(a) shows the dependence of the ethane diffusivity in the zeolite membrane at a loading of two molecules per cavity for different temperatures. For comparison, the diffusivity data of previous PFG NMR studies[6] with ethane in NaCaA zeolite crystallites are also included. It appears that these data are in reasonably good agreement with the results of the present study for sufficiently short observation times. The information provided by these studies becomes more obvious in the representation of the diffusivities *versus* the covered displacements [Fig. 1(b)]. There is a pronounced decay for displacements around 1 μm, which should be attributed to transport resistances, most likely situated at the interfaces between the individual crystallites. For shorter displacements, the majority of the diffusants do not interfer with these barriers; one is able to trace the true intracrystalline diffusion. For larger displacements, the molecules repeatedly have to overcome these transport resistances. This leads to a slight reduction of the diffusivity. The enhancement observed in the high-temperature case for displacements > *ca.* 10 μm may be associated with the occurence of long-range diffusion, when more and more molecules are able to get out of the zeolite bulk phase, either through cracks in the material or through the outer surface of the membrane particles.

As a consequence of the substantially lower mobility, propane in NaCaA offers much poorer measuring conditions. The most reliable measurements for this system have therefore been carried out at 493 K, the highest temperature accessible with our device. Fig. 2(a) and (b) represent the corresponding diffusivity data. Similarly as with ethane, for molecular displacements < *ca.* 1 μm, there is an increase in the diffusivities, which should be a consequence of unrestricted diffusion for displacements sufficiently small in comparison with the crystallite radii. It should be mentioned that previously measured diffusivities of propane in NaCaA zeolite crystallites under the same measuring conditions revealed slightly lower values (2.5 × 10^{-12} m^2 s^{-1}).[6] It is possible that the difference to the value which in the present studies is assumed to be the true intracrystallite one, is caused by slight differences in the degree of calcium exchange. Such differences should be much more significant for propane than for ethane having a smaller critical diameter.

To our knowledge, in these investigations, for the first time transition resistances between the individual crystalline compartments in nanoporous membranes have been probed microscopically. For the considered probe molecules (ethane, propane) a notable transport resistance was observed, which, however, was found to be much smaller than the surface resistance on isolated NaCaA type crystallites.[7] Further experimental evidence is required to decide whether the observed behaviour is a general feature of polycrystalline membranes.

Financial support by the European Community (Joule JOE3-CT95-0018) and Deutsche Forschungsgemeinschaft (SFB 294) is gratefully acknowledged.

Notes and references

1 T. Naylor, Poster presentation by The Smart Chemical Company Ltd, ICOM96 Japan, 1996.
2 J. Kärger and D. H. Ruthven, *Diffusion in Zeolites and Other Microporous Solids*, Wiley, New York, 1992.
3 W. Heink, J. Kärger and H. Pfeifer, *J. Chem. Soc., Chem. Commun.*, 1990, **20**, 1454.
4 J. Kärger, N.-K. Bär, W. Heink, H. Pfeifer and G. Seiffert, *Z. Naturforsch., Teil A*, 1995, **50**, 186.
5 H. Weingärtner, *Z. Phys. Chem. Neue Folge*, 1982, **132**, 129.
6 W. Heink, J. Kärger, H. Pfeifer, K. P. Datema and A. K. Nowak, *J. Chem. Soc., Faraday Trans.*, 1992, **88**, 3505.
7 J. Kärger, H. Pfeifer, R. Richter, H. Fürtig, W. Roscher and R. Seidel, *AIChE J.*, 1988, **34**, 1185.

Communication 8/07733I

Quinuclidine *N*-oxide: a potential replacement for HMPA

Ian A. O'Neil,*[a] Justine Y. Q. Lai[b] and Duncan Wynn[a]

[a] *Robert Robinson Laboratories, Department of Chemistry, University of Liverpool, Crown St, Liverpool, UK L69 7ZD. E-mail: ion@liv.ac.uk*

[b] *Rhone Poulenc Rorer, Rainham Rd South, Dagenham, Essex, UK RM10 7XS*

Received (in Cambridge, UK) 10th November 1998, Accepted 17th November 1998

The use of quinuclidine *N*-oxide as a replacement for HMPA is described.

There are numerous significant and important reactions in organic synthesis which require the addition of hexamethylphosphoric triamide (HMPA) to render them viable.[1] HMPA is a dipolar aprotic compound with a superb ability to form cation–ligand complexes and it can enhance the rates of a wide variety of main group organometallic reactions. In addition, it can also influence the regio- and stereo-chemistry of key reactions such as enolate formation. Other reactions in which HMPA can enhance reactivity include carbanion formation, carbanion reactivity, carbanion regioselectivity (1,2 *vs*. 1,4 addition), ylide reactivity and anion reactivity. In essence, it is thought that HMPA acts as a metal binding agent, disrupting the aggregation states that enolates normally exist in.[2]

HMPA is a listed mutagen and as such does not find widespread use either in industry or academia. Several other substances, such as 1,3-dimethyl-3,4,5,6-tetrahydropyrimidin-2(1*H*)-one (DMPU) have been used as replacements but all have their limitations.[3] An amine oxide bears the same type of charge distribution as a phosphine oxide, but the dipole moment is much larger. Therefore an amine oxide would be expected to behave in a similar fashion to a reagent such as HMPA. The major problem lies with the instability of most amine oxides towards strong bases, azomethine ylide formation being the most common pathway.[4]

As a consequence of our previous work with amine oxides,[5] we have carried out preliminary studies using quinuclidine *N*-oxide (QNO) as a replacement for HMPA, since it is an amine oxide that is known to be stable in strongly basic conditions. Indeed, it can be deprotonated with Bu^{t}Li and the corresponding anion can be reacted with aldehydes and ketones.[6] This amine oxide is stable because elimination of lithium oxide would lead to a bridgehead iminium ion (anti-Bredt) (Scheme 1).

We chose to study four key reactions in which HMPA is known to play a vital role and we have investigated the effect of replacing the HMPA by quinuclidine *N*-oxide. The reactions examined were enolate alkylation,[7] 1,4 *vs*. 1,2 addition,[8] diastereoselective nitroaldol reactions[9] and epoxide opening.[10] Quinuclidine *N*-oxide has been prepared by the oxidation of quinuclidine with 30% H_2O_2 in MeOH.[11] However, we routinely use MCPBA as the oxidant as it is more convenient on a laboratory scale.[12] The product can be purified by chromatography on silica gel. The product is dried under vacuum over P_2O_5. It is a hygroscopic solid and needs to be stored under vacuum over P_2O_5. The quinuclidine nucleus is ideal since it is a rigid structure amenable to rapid modification. In addition, a number of functionalised derivatives can be readily made, some in chiral form.[13]

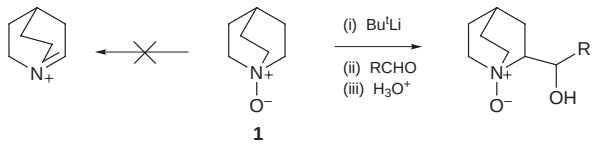

1

Scheme 1

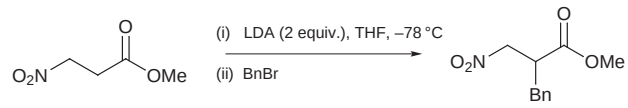

2 **3**

Additive (equiv.)	Yield (%)
0	8
HMPA (5.2)	85
DMPU (10)	85
QNO (1.4)	37
QNO (3.0)	47
QNO (5.0)	78

Scheme 2

Our investigations started with the alkylation of the dianion of methyl 3-nitropropionate, a reaction that is known to require 5 equiv. of HMPA to proceed in good yield. It was found that with just 3 equiv. of QNO the required product was isolated in a reasonable 47%, and the use of 5 equiv. gave a yield comparable to that with HMPA (Scheme 2).

We next examined the regioselectivity of addition of 2-lithiodithiane to cyclohex-2-en-1-one. In the absence of HMPA the predominant mode of addition is 1,2. When 1 equiv. of HMPA is added the 1,4 addition product becomes the major one.[8] Addition of QNO switched the reaction to give the 1,4 addition product with good selectivity (Scheme 3). Indeed, it was considerably more selective than the use of DMPU.

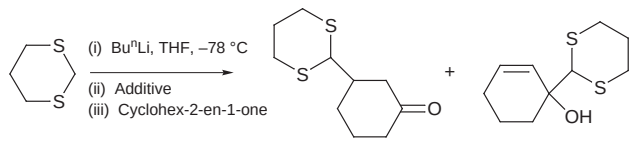

4 **5** **6**

Additive (equiv.)	Yield (%)	Yield (%)
—	8	92
HMPA (1)	88	12
HMPA (2)	95	5
DMPU (2)	82	18
QNO (1)	88	12
QNO (2)	90	10

Scheme 3

We then studied the addition of the dianion of 1-nitropropane to benzaldehyde. This gives the nitroaldol products as a mixture of diastereoisomers. In the presence of HMPA, the *syn* diastereoisomer is the major product.[9] The addition of 1.5 equiv. of QNO was also found to promote formation of the *syn* diastereoisomer giving a 4:1 mixture of diastereoisomers in 62%. The addition of more QNO did not appear to improve the selectivity (Scheme 4).

Finally, Denmark and co-workers have recently reported the use of HMPA and $SiCl_4$ to cleave epoxides to give chlorohydrins.[10] With a chiral phosphinamide, the ring opening of *meso* epoxides gave enantiomerically enriched chlorohydrins. It was gratifying to find that QNO mediated the ring opening of cyclohexene oxide to give the chlorohydrin in a yield identical

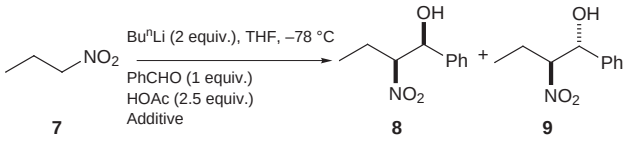

7 **8** **9**

Aditive (equiv.)	Yield (%)	Yield (%)
HMPA (5)	90	10
QNO (1.5)	81	19
QNO (3)	79	21

Scheme 4

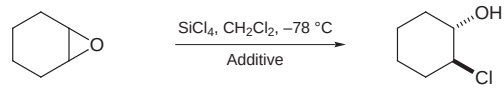

10 **11**

Additive (equiv.)	Yield (%)
HMPA (0.1)	89
QNO (0.1)	89

Scheme 5

to that obtained using HMPA. In the absence of QNO the chlorohydrin was isolated in low yield (Scheme 5).

Significantly, QNO was found to be negative in the bacterial reverse mutation test conducted on *Salmonella typhimurium* TA98, TA100 and TA102 in the presence or absence of metabolic activation. Additionally it was also found to be negative in the test to evaluate its potential to induce micronuclei in Chinese hamster ovary cells using the cytokinesis block method in the presence or absence of metabolic activation.

In summary, we have shown that quinuclidine *N*-oxide can act as a replacement for HMPA in a range of reactions.[14] We are currently exploring other reactions known to require HMPA, and synthesising second generation quinuclidine *N*-oxides which are chiral and bear additional metal binding sites for enhanced reactivity and solubility. Their properties, applications and use in a range of asymmetric transformations will be reported shortly.

We would like to thank the EPSRC for a studentship (to D. W.). I. O. N. would like to thank the James Black Foundation for their continued financial support and Cambridge Combinatorial for a generous unrestricted research grant.

Notes and references

1 R. R. Dykstra, *Encyclopedia of Organic Reagents*, ed. L. Paquette, 1995, vol. 4, p. 2668.
2 D. Seebach, *Angew. Chem., Int Ed. Engl*., 1988, **27**, 1624.
3 T. Mukhopadhyay and D. Seebach, *Helv. Chim. Acta*., 1982, **65**, 385.
4 R. Beugelmans, L. Benadjila-Iguertsira and G. Roussi, *J. Chem. Soc., Chem. Commun*., 1982, 544; G. Roussi and J. Zhang, *Tetrahedron*, 1991, **47**, 5161.
5 I. A. O'Neil, N. D. Miller, J. Peake, J. V. Barkley, C. M. R. Low and S. B. Kalindjian, *Synlett*, 1993, 515; I. A. O'Neil, N. D. Miller, J. V. Barkley, C. M. R. Low and S. B. Kalindjian, *Synlett*, 1995, 617 and 619; I. A. O'Neil, C. D. Turner and S. B. Kalindjian, *Synlett*, 1997, 777; I. A. O'Neil and A. J. Potter, *Tetrahedron Lett*., 1997, **38**, 5731; I. A. O'Neil and A. J. Potter, *Chem. Commun*., 1998, 1487.
6 D. H. R. Barton, R. Beuglmans and R. N. Young, *Nouv. J. Chim*., 1978, **2**, 363.
7 D. Seebach, R. Henning and T. Mukhopadhyay, *Chem. Ber*., 1982, **115**, 1705.
8 C. A. Brown and A. Yamaichi, *J. Chem. Soc., Chem. Commun*., 1979, 101.
9 F. Lehr, J. Gonnermann and D. Seebach, *Helv. Chim. Acta*., 1979, **62**, 2259.
10 S. E. Denmark, P. A Barsanti, K. T. Wong and R. A. Stavenger, *J. Org. Chem*., 1998, **63**, 2428; S. E. Denmark, D. M. Coe, N. E. Pratt and B. D. Griedel, *J. Org. Chem*., 1994, **59**, 6161.
11 S. Srinivas and K. G. Taylor, *J. Org. Chem*., 1990, **55**, 1779; H. C. Kolb, P. G. Andersson and K. B. Sharpless, *J. Am. Chem. Soc*., 1994, **116**, 1278.
12 J. C. Craig and K. K. Purushothaman, *J. Org. Chem*., 1970, **35**, 1721.
13 K. A. Bairamov, A. G. Douglass and P. Kaszynski, *Syn. Commun*., 1998, **28**, 527; M. Langlois, C. Meyer and J. L. Soulier, *Syn. Commun*., 1992, **22**, 1895.
14 Alkylation of methyl 3-nitropropanoate: A solution of diisopropylamine (0.9 ml, 0.63 mmol) and quinuclidine *N*-oxide (1.78 g, 14 mmol) in dry THF (40 ml) was cooled to −78 °C. To this solution was added BuLi (4.0 ml, 1.6 M in hexane, 0.63 mmol). The solution was stirred for 30 min, then methyl 3-nitropropanoate (0.37 g, 2.8 mmol) was added. After stirring for 60 min benzyl bromide (0.4 ml, 0.35 mmol) was added. The solution was stirred for 5 h. Acetic acid (1.0 ml, 2.8 mmol) was added followed by distilled water (5.0 ml). The solution was warmed to room temperature and water (50 ml) was added. Diethyl ether (50 ml) was added, the organic layer separated and the aqueous layer extracted with diethyl ether (3 × 50 ml). The combined organic layers were washed with water (100 ml), and dried over $MgSO_4$. The solvent was removed *in vacuo*. The crude reaction mixture was purified by flash chromatography over silica gel eluting with EtOAC–light petroleum (bp 40–60 °C), 1 : 9 to give the desired product (0.48 g, 78%). The aqueous layer contains the quinuclidine *N*-oxide.

Communication 8/08779B

Imidodiphosphinate ligands as antenna units in luminescent lanthanide complexes

Steven W. Magennis,[a] Simon Parsons,[a] Anne Corval,[b] J. Derek Woollins[c] and Zoe Pikramenou*[a]

[a] *Department of Chemistry, The University of Edinburgh, King's Buildings, West Mains Road, Edinburgh, UK EH9 3JJ. E-mail: z.pikramenou@ed.ac.uk*
[b] *Laboratoire de Spectrométrie Physique, Université Joseph Fourier, BP 87 38402, Saint Martin d'Hères Cedex, France*
[c] *Department of Chemistry, Loughborough University, Loughborough, Leics., UK LE11 3TU*

Received (in Basel, Switzerland) 16th October 1998, Accepted 24th November 1998

Imidodiphosphinate ligands form a hydrophobic shell around terbium and europium ions leading to long-lived, highly luminescent complexes.

The design of miniature 'antenna' systems based on lanthanides for collecting light and converting it to a different frequency has important applications in the development of photonic devices and sensors.[1] Europium and terbium ions are attractive luminescent centers due to their visible, long-lived emission. A breakthrough in lanthanide chemistry came with the design of cryptand ligands that encapsulate the lanthanide ion, protecting it from coordinating solvent molecules that quench its emission. [2] When the arms of the cryptand are light-harvesting units they act as an antenna for collecting light and transferring the energy to the lanthanide.[1,3] Research efforts have focused on the development of ligand systems for lanthanides based on podand-type structures,[3,4] calixarenes[5] or helicates.[6] We are interested in the development of neutral lanthanide complexes with ligands that completely encapsulate the ion forming a hydrophobic shell around the metal ion. Rather than using a highly designed cryptate ligand we aim to use simple lanthanide complexation principles to govern the formation of such species. In order to achieve this, we need strong binding sites that coordinate to the lanthanide and bulky aromatic units that are 'independent/remote' from the binding site and which form the hydrophobic shell. By using remote light-harvesters (rather than harvesters that are themselves the binding units, *e.g.* polypyridines) we can optimize the ion emission by choosing the best sensitizer, aromatic unit, for the ion; this is important as it is rare to find systems that are ideal both for europium and terbium emission. While remote harvesting units have previously been successfully employed in macrocyclic supramolecular structures to enhance the lanthanide emission,[7,8] using lanthanide complexation principles should allow less synthetically challenging open chain ligands to be used.

We have chosen tetraphenyl imidodiphosphinate (tpip) as an ideal ligand with which to test our design.[9] The imidodiphosphinate binding site can chelate to the lanthanide and does not contain any O–H, C–H or N–H bonds in the binding site that can contribute to the quenching of the lanthanide emission.[10] Attached to each of these binding units are four phenyl groups that (i) play the role of remote light-harvesting units and (ii) form a hydrophobic shell around the ion. We wish now to report our studies on the europium and terbium complexes of tpip which demonstrate that the ligands act as light-collector units forming a hydrophobic shell around the ion resulting in highly luminescent europium and terbium complexes. The chemistry contrasts with the analogous lanthanide β-diketonates where the binding site is surrounded by two rather than four aryl units and short lifetimes result from lack of protection of the lanthanide from the water (which limits their applications as sensors or biolabels). [11]

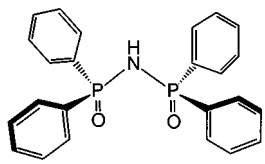

Htpip

Reaction of K(tpip) with $EuCl_3$ or $TbCl_3$, in 3:1 molar ratio, leads to the formation of the neutral complexes $[Eu(tpip)_3]$ and $[Tb(tpip)_3]$, respectively. The complexes have been fully characterized and analysed by spectroscopic methods.† X-Ray quality crystals of $[Tb(tpip)_3]$ were obtained by slow evaporation from chloroform. The crystal structure (Fig. 1)‡ shows that the twelve phenyl groups surround the lanthanide ion, forming a hydrophobic cage leading to a six-coordinate terbium ion. Two molecules in the unit cell which are different in the symmetry around terbium are observed; **1** being a distorted octahedron and **2** trigonal prismatic. Edge-to-face π stacking is present in both structures with C–H to centroid distance of *ca.* 3.0 Å of two phenyl groups in different ligands. Although there is no water coordinated to terbium, in contrast with the praseodymium crystal structure, there is a short van der Waals contact, observed only in **2**, between the terbium ion and a water molecule situated at the top of the trigonal prism with a Tb–O distance of 3.85 Å (expected van der Waals 4.08 Å). The $[Eu(tpip)_3]$ crystal structure is similar to the terbium one with three molecules in the unit cell, in two of which the symmetry around europium is trigonal prismatic and the other one is a

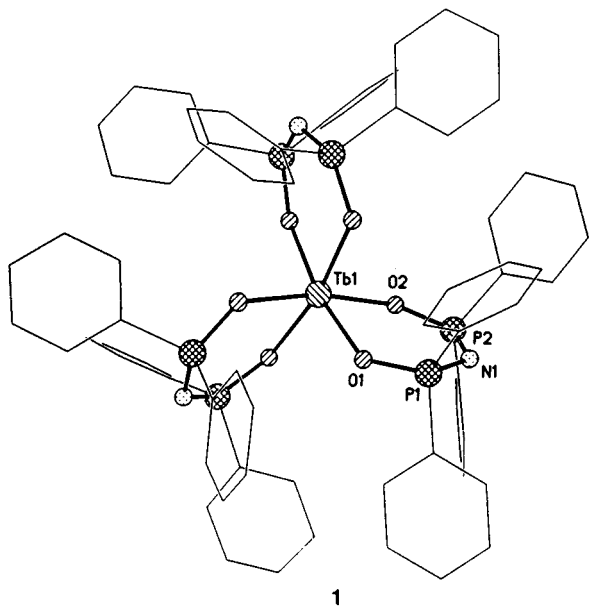

1

Fig. 1 Crystal structure of $[Tb(tpip)_3]$.

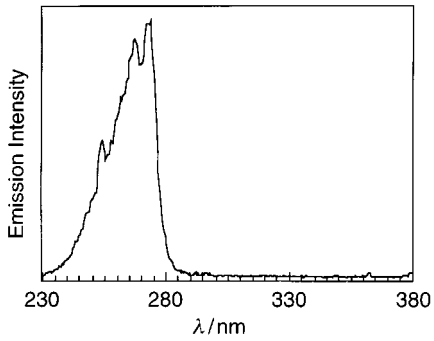

Fig. 2 Excitation spectrum of $[Eu(tpip)_3]$ in $CHCl_3$, λ_{em} = 620 nm.

distorted octahedron. The short water van der Waals distance is again observed only in the trigonal prismatic molecules. The low coordination numbers of europium and terbium are attributed to the bulkiness of the ligands, with the twelve phenyl groups forming a cage around the ion.

Upon excitation at 273 nm (ε = 5,000 $dm^3\ mol^{-1}\ cm^{-1}$) the $[Eu(tpip)_3]$ and $[Tb(tpip)_3]$ complexes exhibit strong emission, red and green respectively, characteristic of the ion. The excitation spectra of the complexes show a band centered at 270 nm, characteristic of the absorption of the ligand confirming that the emission of the complex is due to energy transfer from the ligand to the lanthanide luminescent center (Fig. 2).

Both europium and terbium complexes exhibit long lifetimes in solution compared with previously reported antenna complexes where lifetimes are optimized either for europium or for terbium. The emission lifetimes were found to be 1.8 ms for $[Eu(tpip)_3]$ and 2.8 ms for $[Tb(tpip)_3]$ in dry acetonitrile. Although there is no evidence of water coordination in the crystal structure, addition of water in the acetonitrile solution of $[Tb(tpip)_3]$ and $[Eu(tpip)_3]$ leads to shortening of the emission lifetime by 25 and 43%, respectively. The shortening in the lifetime indicates some involvement of the water molecules in the coordination sphere of the lanthanide. It may be attributed to a twist of the complex conformation in solution to fit the water molecule and agrees with the observed short water van der Waals contacts. The larger effect of water quenching in europium complexes has been well documented.[12]

The quantum yields of the complexes were measured in dry acetonitrile and determined using the method established by Haas and Stein, using $[Ru(bipy)_3]Cl_2$ (Φ = 0.028 in water) and quinine sulfate (Φ = 0.546 in 0.5 M H_2SO_4) as standards for the europium and terbium complex, respectively, taking into account the different excitation wavelength correction.[13] The values obtained are 1.3% for $[Eu(tpip)_3]$ and 20% for $[Tb(tpip)_3]$. We postulate that the quenching of the europium emission *via* an LMCT state is not as effective as in the case of calixarene complexes where the quantum yields of the europium and terbium complexes can differ by more than three orders of magnitude.[5] Further photophysical experiments are currently underway to obtain more information about the mechanism of the energy transfer. The lack of any back energy transfer processes observed when bipyridine ligands are employed in terbium complexes leads to a high quantum yield for terbium.

We have introduced the imidodiphosphinate ligands as successful 'antenna' ligands for sensitizing both europium and terbium emission. The crystal structures of the complexes show unusual six-coordinate lanthanide ions where the ligands form a hydrophobic cage around the ion. We are currently further investigating the formation of these encapsulated lanthanide complexes based on these design principles.

This work was supported by EPSRC (S. W. M.) and Novartis Fellowship Trust.

Notes and references

† *Selected spectroscopic data* $[Tb(tpip)_3]$: ^1H NMR (360 MHz, $CDCl_3$, 25 °C, TMS) δ 7.97 (24H, Ar), 7.35 (12H, *p*-Ar), 6.28 (24H, Ar); $^{31}P\{^1H\}$ NMR (146 MHz, $CDCl_3$, 25 °C, 85% H_3PO_4) δ 200.7(s); MS (FAB^+ in *m*-NBA) *m/z* 1408 (MH^+), 991 (M^+ − tpip). $[Eu(tpip)_3]$: ^1H NMR (360 MHz, $CDCl_3$, 25 °C, TMS) δ 7.48–7.54 (m, 24H, *o*-Ar), 7.21 [t, ^3J (HH) 7.4 Hz, 12H, *p*-Ar], 6.95–6.99 (m, 24H, *m*-Ar); $^{31}P\{^1H\}$ NMR (146 MHz, $CDCl_3$, 25 °C, 85% H_3PO_4) δ 37.7(s); MS (FAB^+ in *m*-NBA) *m/z* 1400 (MH^+), 983 (M^+ − tpip). The ^{31}P and ^1H NMR spectra at low temperature in deuterated dichloromethane or acetone reveal only one solution species which contains only one ligand environment. The lifetime measurements are monoexponential. The paramagnetic shifts on ^{31}P confirm the metal coordination. From these observations, we can conclude that (i) there is only one solution species (ii) all three ligands are in identical environments (iii) the ligand is bound to the metal centre. We believe that the only formulation that satisfies all these requirements is $[ML_3]$ similar to that observed in the solid state.

‡ *Crystal data* $[Tb(tpip)_3]\cdot 0.7\underline{5}\ H_2O$: $C_{72}H_{61.50}TbN_3O_{6.75}P_6$, M = 1421.48, rhombohedral, space group $R3$, Z = 12, a = 23.372(4), c = 42.956(8) Å, U = 20320(6) $Å^3$, T = 220 K, μ = 1.240 mm^{-1}, final R = 0.0624 [based on F and 5674 data with $F > 4\sigma(F)$], wR_2 = 0.1744 (based on F^2 and all 7979 unique data used in refinement) for 535 parameters. The structure was solved by direct methods (SIR 92) and refined by full-matrix least-squares procedures on F^2 (SHELXL-97).[14]

$[Eu(tpip)_3]\cdot\underline{0}.67H_2O$: $C_{72}H_{61.33}EuN_3O_{6.67}P_6$, M = 1411.75, trigonal, space group $P3$, Z = 6, a = 23.418(2), c = 21.185(3) Å, U = 10061.4(19) $Å^3$, T = 220 K, μ = 1.13 mm^{-1}; final R = 0.0426 and R_w = 0.0418 [both based on 8591 out of 11861 unique data with $F > 4\sigma(F)$], for 800 parameters. The structure was solved by Patterson methods (DIRDIF) and refined by full-matrix least-squares procedures on F (CRYSTALS).[15] CCDC 182/1097. See http://www.rsc.org/suppdata/cc/1999/61/ for crystallographic files in .cif format.

1 V. Balzani and F. Scandola, *Supramolecular Photochemistry*, Ellis Horwood, Chichester, UK, 1991; A. P. de Silva, H. Q. Nimal Gunaratne, T. Gunnlaugsson, A. J. M. Huxley, C. P. McCoy, J. T. Rademacher and T. E. Rice, *Chem. Rev.*, 1997, **97**, 1515; T. Gunnlaugsson and D. Parker, *Chem. Commun*., 1998, 511.
2 J.-M. Lehn, *Angew. Chem., Int. Ed. Engl.*, 1988, **27**, 89; *Supramolecular Chemistry*, VCH, Weinheim, 1995.
3 N. Sabbatini, M. Guardigli and J.-M. Lehn, *Coord. Chem. Rev*., 1993, **123**, 201 and references therein.
4 M. P. Lowe, P. Caravan, S. J. Rettig and C. Orvig, *Inorg. Chem*., 1998, **37**, 1637; G. Ulrich, M. Hissler, R. Ziessel, I. Manet, G. Sarti and N. Sabbatini, *New J. Chem*., 1997, **21**, 147; D. A. Bardwell, J. C. Jeffery, P. L. Jones, J. A. McCleverty, E. Psillakis, Z. Reeves and M. D. Ward, *J. Chem. Soc., Dalton Trans*., 1997, 2079.
5 L. J. Charbonnière, C. Balsiger, K. J. Schenk and J.-C. G. Bünzli, *J. Chem. Soc., Dalton Trans*., 1998, 505; M. P. Oude Wolbers, F. C. J. M. van Veggel, R. H. M. Heeringa, J. W. Hofstraat, F. A. J. Geurts, G. J. van Hummel, S. Harkema and D. N. Reinhoudt, *Liebigs Ann./Recueil*, 1997, 2587; G. Ulrich, R. Ziessel, I. Manet, M. Guardigli, N. Sabbatini, F. Fraternali and G. Wipff, *Chem. Eur. J*., 1997, **3**, 1815; N. Sabbatini, M. Guardigli, A. Mecati, V. Balzani, R. Ungaro, E. Ghidini, A. Casnati and A. Pochini, *J. Chem. Soc., Chem. Commun.*, 1990, 878.
6 C. Piguet, G. Bernardinelli and G. Hopfgartner, *Chem. Rev*., 1997, **97**, 2005.
7 S. Aime, M. Botta, R. S. Dickins, C. L. Maupin, D. Parker, J. P. Riehl and J. A. G. Williams, *J. Chem. Soc., Dalton Trans*., 1998, 881; P. R. Selvin, J. Jancarik, M. Li and L.-W. Hung, *Inorg. Chem.*, 1996, **35**, 700; N. Sato and S. Shinkai, *J. Chem. Soc., Perkin Trans. 2*, 1993, 621.
8 M. A. Mortellaro and D. G. Nocera, *J. Am. Chem. Soc*., 1996, **118**, 7414; Z. Pikramenou, J-a Yu, A. Ponce and D. G. Nocera, *Coord. Chem. Rev.* 1994, **132**, 181; Z. Pikramenou and D. G. Nocera, *Inorg. Chem*., 1992, **31**, 532.
9 Some lanthanide complexes of tpip have previously been prepared as NMR shift reagents: N. Platzer, H. Rudler, C. Alvarez, L. Barkaoui, B. Denise, N. Goasdoué, M.-N. Rager, J. Vaissermann and J.-C. Daran, *Bull. Soc. Chim. Fr*., 1995, **132**, 95; I. Rodriguez, C. Alvarez, J. Gomez-Lara, R. A. Toscano, N. Platzer, C. Mulheim and H. Rudler, *J. Chem. Soc., Chem. Commun*., 1987, 1502.
10 Y. Haas and G. Stein, *J. Phys. Chem.*, 1972, **76**, 1093. D. Parker and J. A. G. Williams, *J. Chem. Soc., Dalton Trans.*, 1996, 3613.
11 The presence of a C–H bond in the binding site of the diketonates is further detrimental to the lifetimes of these complexes. For a general reference see: G. E. Buono-Cuore, H. Li and B. Marciniak, *Coord. Chem. Rev.*, 1990, **99**, 55.
12 W. DeW. Horrocks, Jr. and D. R. Sudnick, *Acc. Chem. Res*., 1981, **14**, 384.
13 Y. Haas and G. Stein, *J. Phys. Chem.*, 1971, **75**, 3668.
14 G. M. Sheldrick, SHELXL-97, Siemens Analytical X-ray, 1995.
15 D. J. Watkin, C. K. Pront, J. R. Carruthus and P. W. Betteridge, CRYSTALS, University of Oxford, 1996.

Communication 8/08046A

Isolation of the reactive intermediate in palladium-catalysed coupling of secondary phosphine–boranes with aryl halides

Annie-Claude Gaumont,[a] Michael B. Hursthouse,[b] Simon J. Coles[b] and John M. Brown[a]

[a] *Dyson Perrins Laboratory, South Parks Road, Oxford, UK OX1 3QY. E-mail: bjm@ermine.ox.ac.uk*
[b] *Department of Chemistry, University of Wales, Cardiff, UK CF1 3TB*

Received (in Cambridge, UK) 8th October 1998, Accepted 5th November 1998

$Ph_2PH{\cdot}BH_3$ is converted into its K salt with $KOSiMe_3$ in THF, and the anion reacts with (dppp)Pd(Ph)I to produce the complexed secondary phosphine–borane which decomposes to $PPh_3{\cdot}BH_3$ at −10 °C; the C_6F_5 analogue has been crystallographically characterised.

The ability of palladium complexes to effect catalysed σ-bond couplings has been extended significantly in recent years with some emphasis on the formation of C–heteroatom bonds.[1] Formation of C–P bonds has been achieved by the Pd-catalysed reaction of secondary phosphine oxides $R_2P(H)O$ with aryl triflates;[2] if the phosphine rather than the phosphine oxide is desired then either Ni or Pd catalysis with R_2PH as the nucleophile may be effective.[3] Less success has been achieved with secondary phosphine boranes, although the coupling reaction with ArI has been demonstrated.[4]

Following Imamoto's work,[4] satisfactory conditions were established for the catalytic synthesis of triarylphosphine–boranes, *e.g.* $Ar_3P{\cdot}BH_3$ **1a–d** from ArI, but less cleanly from aryl triflates (Scheme 1). An important observation was that the

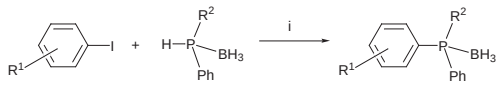

	R^1	R^2
1a	H	Ph
b	*p*-MeO	Ph
c	*o*-F	Ph
d	H	*o*-An

Scheme 1 *Reagents and conditions*: i, $dppfPdCl_2$ (5 mol%), K_2CO_3 (2 equiv.), MeCN, (for **1a**) room temp., 24 h, 92%; (for **1b**) room temp., 18 h, 89%; (for **1c**) 50 °C, 48 h, 74%; (for **1d**) 30 °C, 24 h, 90%.

reaction took place at ambient temperature or below (0 °C). Monitoring by ^{31}P NMR demonstrated that after completion of the reaction, only (dppf)Pd(Ar)I **2** was present when an excess of ArI was used.[5] Initial attempts at defining intermediates in the catalytic reaction were unsuccessful. When complex **2** (Ar = Ph) was generated *in situ* from either the corresponding $(dppf)PdC_8H_8$ complex[6] or $(dppf)Pd(CH_2{=}CHCO_2Me)$[7] rapid reaction with $K^+Ph_2P{\cdot}BH_3^-$ (optimally generated from the secondary phosphine–borane and $KOSiMe_3$; quantitative by NMR spectroscopy) was observed at −70 °C in THF (Scheme 2). The product $Ph_3P{\cdot}BH_3$ could be characterised in

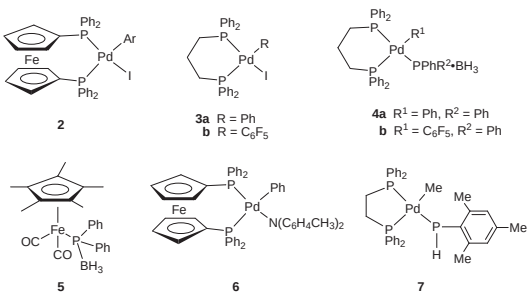

2 **3a** R = Ph, **b** R = C_6F_5 **4a** R^1 = Ph, R^2 = Ph **b** R^1 = C_6F_5, R^2 = Ph

5 **6** **7**

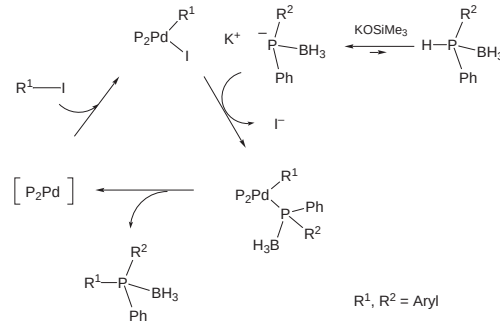

Scheme 2

the solution above −30 °C, but intermediates were too ill-defined to characterise. Hence our attention shifted to the corresponding dppp complexes, known[5,8] to react more slowly than their dppf analogues in the reductive elimination step as a consequence of the smaller chelate bite angle.

Addition of $KOSiMe_3$ to an equimolar mixture of complex **3a** and $Ph_2PH{\cdot}BH_3$ in THF at −70 °C led to an immediate and quantitative change to a single new species whose distinctive ^{31}P NMR spectrum is shown in Fig. 1, revealing the *trans*-relationship of (P1–Pd–P3–B). This is consistent with the structure **4a**, whose spectrum persisted up to 0 °C. At that temperature it decomposed (half-life *ca.* 30 min.) giving rise only to $Ph_3P{\cdot}BH_3$ and an unidentified Pd product; when reaction was carried out in the presence of an excess of PhI, species **3a** was regenerated. The same type of transformation was shown to occur with other secondary phosphine–boranes and other PdArI complexes, as indicated. With more electron-withdrawing aryl groups in Ar–Pd, the elimination step was slower.

The linkage between the stoichiometric and catalytic reactions was strengthened by experiments where the breakdown of adduct **4a**, which led quantitatively to the formation of $Ph_3P{\cdot}BH_3$ **1a**, was followed by ^{31}P NMR (Fig. 2). An identical reaction was carried out with a four-fold excess of both the

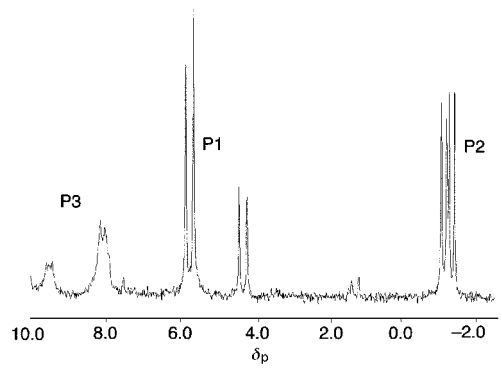

Fig. 1 The ^{31}P NMR spectrum of complex **4b** in THF solution at −50 °C, taken directly after mixing of precursors at −70 °C. Assignments: δ 9.0 (P3, J_{P2P3} 31 Hz), 5.2 (P1, J_{P1P3} 297, J_{P1P2} 43 Hz), −1.35 (P2). On standing at or above 0 °C the reductive elimination product grows in at *ca.* δ 1.

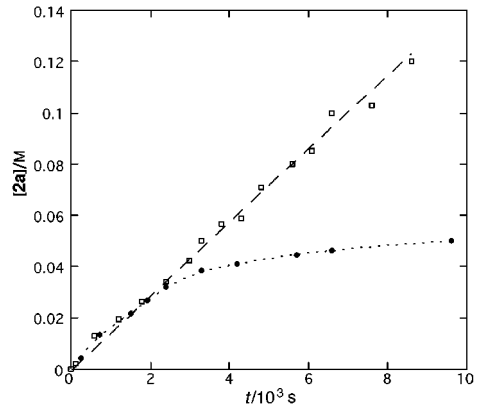

Fig. 2 (●) Stoichiometric formation of borane **1a** from breakdown of complex **4a**, 0.0532 M in THF at 0 °C, reaction followed by loss of **4a** in the ^{31}P NMR spectrum, dotted line is smoothed curve. (□) Catalytic turnover of a mixture of PhI and $KPh_2P{\cdot}BH_3$ (both 0.213 M) in THF at 0 °C in the presence of complex **3a** (0.0532 M), followed by the appearance of borane **1a**. The dashed line is the predicted rate of turnover based on the rate-constant 2.9×10^{-4} s^{-1} derived for the stoichiometric process above.

anion and PhI, and catalytic turnover was followed by the appearance of **2a**. Within experimental error, the rate of catalytic turnover is defined by the rate of the reductive elimination step. This provides firm support for the mechanism suggested in Scheme 2. A correlation between reductive elimination and catalytic turnover has been observed for the C–C bond forming step in the breakdown of (dppf)Pd(Ph)Me.[5]

In the extreme case of **3b**, the intermediate complex **4b** was formed cleanly at −70 °C but was stable in solution at ambient temperature for a significant period of time (half-life *ca*. 96 h) and could be isolated by filtration through silica and precipitation. The isolated material gives rise to phosphine–borane **2e** on redissolution and prolonged standing, accompanied by some decomposition to the phosphine oxide. In characterisation of complex **4b**, we observed an unusual [M − 1] cation peak in the electrospray mass spectrum† which will be the subject of further investigation; such behaviour has previously been observed in the mass spectra of amine–boranes.[9] Recrystallisation (CH_2Cl_2, Et_2O) gave blocks suitable for X-ray analysis.‡ The structure is shown in Fig. 3 and demonstrates a slightly distorted square planar arrangement with the Pd–P bond of the

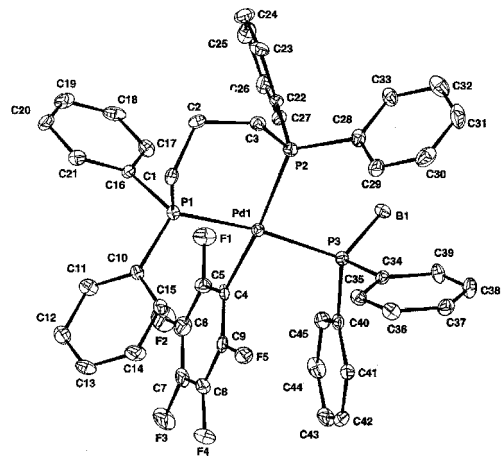

Fig. 3 The X-ray crystal structure of complex **4b**. Selected bond lengths and angles: Pd(1)–P(1) 2.337(2), Pd(1)–P(2) 2.334(2), Pd(1)–P(3) 2.375(2), Pd(1)–C(4) 2.053(6), P(3)–B(1) 1.925(6); C(4)–Pd(1)–P(2) 170.4(2), C(4)–Pd(1)–P(1) 87.6(2), P(2)–Pd(1)–P(1) 90.84(6), C(4)–Pd(1)–P(3) 88.0(2), P(2)–Pd(1)–P(3) 94.35(6), P(1)–Pd(1)–P(3) 173.09(6) B(1)–P(3)–Pd(1) 119.4(2).

phosphine borane only slightly longer than Pd–P bonds in the chelate (0.237 *vs*. 0.233 nm). The only previous example of a simple η^1-coordinated phosphine–borane structure is that of complex **5**, which is a stable isolable material.[10]

These experiments indicate that the catalytic cycle for phosphinylation of aryl iodides with secondary phosphine–boranes is very simple, and the true reactive intermediate is amenable to characterisation. Unlike the corresponding intermediate **6** observed in catalytic amination,[11] it reacts rapidly below ambient temperature and very likely does not involve prior chelate dissociation. Studies of the reductive elimination of neutral Pd phosphido complex **7** and analogous (dppe)Pd η^1-Ar η^1-(PPh_2) complexes have been carried out by Glueck and co-workers,[12] who generated these intermediates by deprotonation of cationic phosphine complexes.

Future work will be directed towards stereochemical control of the P–Pd addition step with a view to applications in the asymmetric synthesis of arylphosphines.

We thank CNRS for granting leave of absence to A-C. G., EPSRC and NATO for support and Johnson-Matthey for loans of Pd salts. We greatly appreciate an open exchange of information with Professor David Glueck (Dartmouth).

Notes and references

† *Selected data* for **4b**: $\delta_P(CD_2Cl_2$, 202 MHz) 14.3 (P3, $J_{1,3}$ 296), 1.95 (P1, $J_{1,2}$ 49.5, $J_{1,3}$ 296) −1.2 (P2, $J_{2,1}$ 49.5, $J_{2,3}$ 34); $\delta_B(CD_2Cl_2$, 80 MHz) −33.2 (br s); $\delta_F(CD_2Cl_2$, 235 MHz) −164.3 (m), −163.4 (m), −114.8 (m); $\delta_H(CD_2Cl_2$, 500MHz) 1.90 (m, CH_2) , 2.35 (m, CH_2P) , 2.55 (m, CH_2P) , 6.95, 7.04, 7.2, 7.24, 7.3, 7.4 (H_{ar}); $\delta_C(CD_2Cl_2$, 125 MHz) 18.1 (CH_2), 23.6 (CH_2P), 27.3 (CH_2P), 126.9 (Ar), 127.4 (Ar), 127.8 (Ar), 129.3 (Ar), 130.2 (Ar), 130.9 (Ar), 132.3 (Ar), 132.9 (Ar), 133.8 (Ar), 138.5 (Ar); *m/z* (ES, +30 V) 883.02 ([M − 1]$^+$, 100%), 717.06 ([M − C_6F_5]$^+$, 70%), 703.03 ([M − C_6F_5 − BH_3]$^+$, 68%).

‡ *Crystal data* for $C_{45}H_{39}BF_5P_3Pd{\cdot}0.5CH_2Cl_2$ M_r = 927.35, monoclinic, space group $P2_1/c$, a = 11.481(2), b = 27.923(6), c = 14.005(3) Å, β = 107.15(3)°, U = 4290(2) Å^3, Z = 4, D_c = 1.436 g cm^{-3}, μ = 0.660 mm^{-1}, F(000) 1884, T = 150(2) K, Crystal size 0.18 × 0.14 × 0.10 mm, 6219 independent reflections, 15833 collected. Refinement method: full-matrix least-squares on F^2, Goodness-of-fit on F^2 = 0.877, Final R indices [$I > 2\sigma(I)$] R_1 = 0.0424, ωR_2 = 0.0951. CCDC 182/1086.

1 R. A. Widenhoefer and S. L. Buchwald, *J. Am. Chem. Soc*., 1998, **120**, 6504; B. C. Hamann and J. F. Hartwig, *J. Am. Chem. Soc*., 1998, **120**, 3694; D. Baranano, G. Mann and J. F. Hartwig, *Curr. Org. Chem*., 1997, **1**, 287; S. Wagaw, R. A. Rennels and S. L. Buchwald, *J. Am. Chem. Soc*.,1997,**119**, 8451 and earlier papers from these groups.

2 L. Kurz, G. Lee, D. Morgans, M. J. Waldyke and T. Ward, *Tetrahedron Lett*., 1990, **31**, 6321; J. M. Brown and H. Doucet, *Tetrahedron: Asymmetry*, 1997, **8**, 3775 .

3 D. W. Cai, J. F. Payack, D. R. Bender, D. L. Hughes, T. R. Verhoeven and P. J. Reider, *J. Org. Chem*., 1994, **59**, 7180; D. J. Ager, M. B. East, A. Eisenstadt and S. A. Laneman, *Chem. Commun*., 1997, 2359; G. Martorell, X. Garcias, M. Janura and J. M. Saa, *J. Org. Chem*., 1998, **63**, 3463.

4 T. Imamoto, T. Oshiki, T. Onozawa, M. Matsuo, T. Hikosaka and M. Yanagawa, *Heteroatom Chem*., 1992, **3**, 799; T. Imamoto, M. Matsuo, T. Nonomura, K. Kishikawa and M. Yanagawa, *Heteroatom Chem*., 1993, **4**, 475; T. Imamoto, T. Yoshizawa, K. Hirose, Y. Wada, H. Masuda, K. Yamaguchi and H. Seki, *Heteroatom Chem*., 1995, **6**, 99.

5 J. M. Brown and P. J. Guiry, *Inorg. Chim. Acta*, 1994, **220**, 249.

6 J. M. Brown and N. A. Cooley, *Organometallics*, 1990, **9**, 343; F. Schager, K. J. Haack, R. Mynott, A. Rufinska and K. R. Porschke, *Organometallics*, 1998, **17**, 807.

7 A. Jutand, K. K. Hii, M. Thornton-Pett and J. M. Brown, unpublished work.

8 M. Kranenburg, P. Kamer and P. Van Leeuwen, *Eur. J. Inorg. Chem*. 1998, 155; J. E. Marcone and K. C. Moloy, *J. Am. Chem. Soc*., 1998, **120**, 8527.

9 Z. Polivka, V. Kubelka, N. Holubova and M. Ferles, *Collect. Czech. Chem. Commun*., 1970, **35**, 1131.

10 W. Angerer, W. S. Sheldrick and W. Malisch, *Chem. Ber*. 1985, **118**, 1261; see also: D. Dou, G. L. Wood, E. N. Duesler, R. T. Paine and H. Noth, *Inorg. Chem*., 1992, **31**, 1695; D. A. Hoic, W. M. Davis and G. C. Fu, *J. Am. Chem. Soc*., 1996, **118**, 8176.

11 M. S. Driver and J. F. Hartwig, *J. Am. Chem. Soc*., 1997, **119**, 8232.

12 D. K. Wicht, I. V. Kourkine, B. M. Lew, J. M. Nthenge and D. S. Glueck, *J. Am. Chem. Soc*., 1997, **119**, 5039; M. D. Zhuravel, R. D. Sweeder and D. S. Glueck, to be published; see D. K. Wicht, S. N. Paisner, B. M. Lew, D. S. Glueck, G. Yap, L. M. LiableSands, A. L. Rheingold, C. M. Haar and S. P. Nolan, *Organometallics*, 1998, **17**, 652 for related platinum chemistry.

Communication 8/07830K

Modulating the pH-dependent redox potential of a flavin analog *via* incorporation into a self-assembled monolayer on gold

Suk-Wah Tam-Chang,* James Mason, Isaac Iverson, Ki-Oh Hwang and Christa Leonard

Department of Chemistry, University of Nevada, Reno, Nevada 89557, USA. E-mail: tchang@chem.unr.edu

Received (in Columbia, MO, USA) 10th August 1998, Accepted 19th November 1998

We report the first example of modifying the pH-dependent electrochemical properties of a flavin analog on gold by changing the pK_a value of its N^1 proton.

Flavoenzymes are important electron shuttles in a wide range of biological redox reactions.[1] The redox potential of flavin (the redox active moiety of flavoenzymes) varies by at least 600 mV, as governed by binding in different apoproteins. Non-covalent interactions (including π-stacking,[2] hydrophobic effects, hydrogen bonding, and electrostatic interactions)[3] between flavin and apoproteins play important roles; however, it is difficult to examine the effects of individual interactions in complex biological systems. A fundamental understanding of environmental effects on the flavin redox potential can be expected to provide insight into biological mechanisms for tuning the redox potential of flavoenzymes. In addition, control over its redox activity may increase selectivity of electrocatalysis in synthetic devices.[4] Monolayers prepared from alkanethiols or disulfides with electroactive derivatives[5] are commonly used for studying environmental effects on electron-transfer kinetics.[6] The present work presents novel self-assembled monolayer (SAM) formation based on an alkanethiolate derivatized flavin analog[7] and the modulation of its redox properties *via* incorporation into SAMs.

Disulfide **1** was synthesized according to the procedure outlined in Scheme 1.[8] SAMs containing isoalloxazine (the heterocyclic ring system of flavin) were prepared by immersing a gold coated (500 Å) silicon wafer in an acetonitrile solution of **1** and were characterized by cyclic voltammetry (Fig. 1). Flavin and its analogs undergo two reversible one-electron reduction steps with overlapping potentials in aqueous buffer solutions (Scheme 2).[9] The surface coverage was calculated to be *ca.* 5×10^{-10} mol cm^{-2} by integrating the area under the oxidation or reduction peak. This surface coverage coincides with a densely packed film of the flavin based on modeling the molecular area expected for a flavin unit. The pH-dependent formal potential (E^0) of the bound isoalloxazine moiety was determined from the mean value of the cathodic and anodic peak potentials. Upon changing from acidic to basic conditions, the full-widths at half maxima of the peaks increase. This change may be indicative of structural heterogeneity or differences in the rates of electron transfer for the two electron transfer steps (Fig. 1).

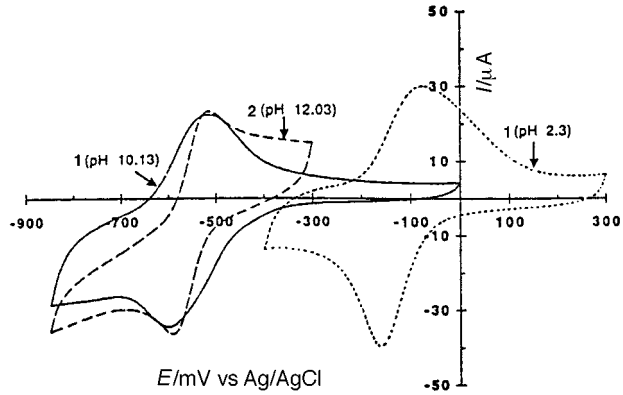

Fig. 1 Cyclic voltammogram (steady state cycle) of (a) (·····) a SAM from **1** in an aqueous buffer solution of pH 2.3, (b) (——) a SAM from **1** in an aqueous buffer solution of pH 10.13, and (c) (- - - - -) **2** (1 mM) in an aqueous buffer solution of pH 12.03. A bare gold working electrode is used in the determination of E^0 of **2**. Scan rates are 0.1 V s^{-1}.

To examine the importance of microenvironment on the one-electron processes of Scheme 2, we compared the pH dependent redox potential of flavin analog **2** in solution (shown in Scheme 2) with that of immobilized isoalloxazine. As shown in Fig. 2, the formal potential of **2** dissolved in solution is linearly related to pH, with a slope of −0.057 V (pH unit)$^{-1}$ up to pH 6.7. After this inflection point the redox processes of **2** remain reversible (Fig. 1); however, the slope changes to −0.027 V (pH unit)$^{-1}$ at higher pH values;[10] The pH at the inflection point is the pK_a of the N^1-proton in the reduced form.[9–11] A pK_a value of 6.7 for the N^1-proton in the reduced form of **2** and the decrease in slope are consistent with those reported for mononucleotide (FMN) and flavin adenine dinucleotides (FAD).[9,12] In contrast, the slope of the E^0–pH plot for the monolayer of **1** is uniform until pH ≈ 10

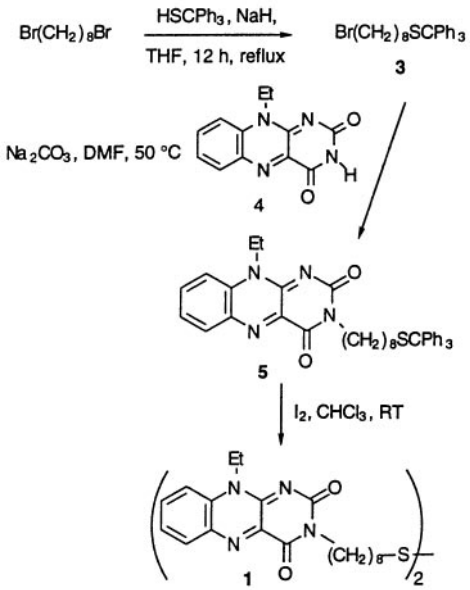

Scheme 1

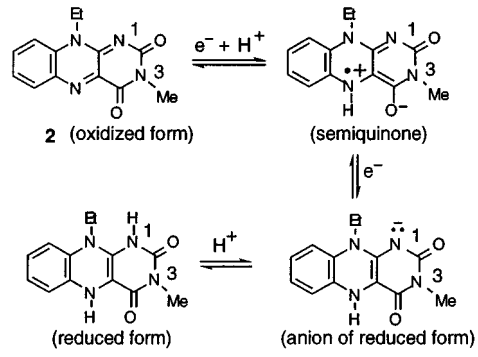

Scheme 2

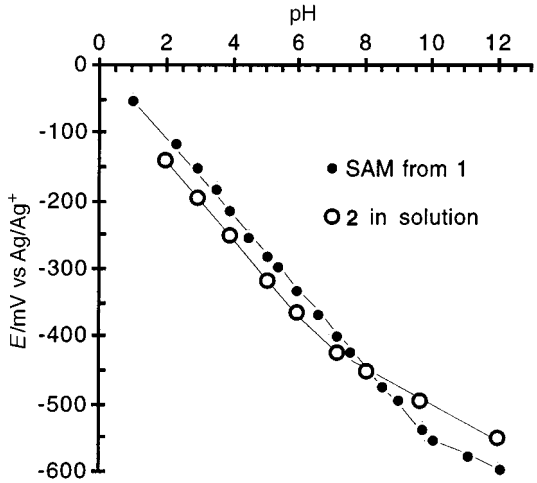

Fig. 2 The pH dependence of redox potential (E^0) of isoalloxazine of **1** in SAM compared with **2** (1 mM) dissolved in aqueous buffer solution.

(Fig. 2). The intersection point of the linear portions yields a pK_a value of 9.7. This dramatic increase in the pK_a value indicates that the microenviroment of the N^1-proton in SAM is less polar than the aqueous solution. These results are in line with the observations of Whitesides and coworkers who demonstrated by contact angle measurements increased pK_a values of acidic groups of ω-mercaptoalkanecarboxylic and phosphonic acids upon incorporation into monolayers.[13] They proposed that a low interfacial dielectric constant and/or electrostatic interactions cause the unfavorable formation of negatively charged species in a closely packed monolayer compared with that in water.[13]

We prepared mixed monolayers from unsymmetrical disulfide **6** and dodecyl disulfide or octyl disulfide thereby reducing the surface coverage of the isoalloxazine moiety to

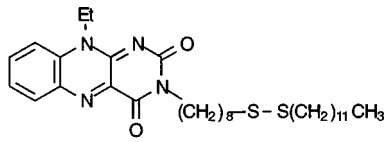

6

about 10% of that in the monolayer from **1**.[14] This reduction of charge/charge repulsion at the interface did not lower the pK_a value of the N^1-proton. In addition, the change in alkyl chain length of the mixed SAM in which N^1-proton is embedded did not influence its pK_a value. These results suggest that the low dielectric constant of the underlying alkyl chains may be the predominant factor influencing the dissociation constant.

In summary, our work demonstrates that the pH-dependent electrochemical properties of the isoalloxazine moiety can be modified *via* incorporation into SAMs, as well as the known mechanisms such as selective H-bonding and π-stacking.

This research was supported by the National Science Foundation (CHE-9510344) and the NSF EPSCOR cooperative agreement OSR-9353227 (WISE Program). C. C. Leonard acknowledges support from the REU Program, UNR. We appreciate the helpful suggestions of the reviewers.

Notes and references

1 C. Walsh, *Enzymatic Reaction Mechanisms*, W. H. Freeman and Company, New York, 1979; P. Hemmerich, C. Veeger and H. C. S. Wood, *Angew. Chem., Int. Ed. Engl.*, 1965, **4**, 671.

2 Elegant models have been designed to quantify the effects of π-stacking on flavin redox chemistry in aprotic solvents: A. Niemz, J. Imbriglio and V. M. Rotello, *J. Am. Chem. Soc.*, 1997, **119**, 887; E. C. Breinlinger, A. Niemz and V. M. Rotello, *J. Am. Chem. Soc.*, 1995, **117**, 5379; E. C. Breinlinger and V. M. Rotello, *J. Am. Chem. Soc.*, 1997, **119**, 1165.

3 B. J. Stockman, T. E. Richardson and R. P. Swenson, *Biochemistry*, 1994, **33**, 15 298; R. P. Swenson and G. D. Krey, *Biochemistry*, 1994, **33**, 8505; F. C. Chang and R. P. Swenson, *Biochemistry*, 1997, **36**, 9013; M. Inoue, Y. Okudo, I. Ishida and M. Nakagaki, *Arch. Biochem. Biophys.*, 1983, **227**, 52.

4 S. Fukuzumi, K. Tanii and T. Tanaka, *Chem. Commun.*, 1989, 816; S. W. Tam, L. Jimenez and F. Diederich, *J. Am. Chem. Soc.*, 1992, **114**, 1503; M. Ishikawa, H. Okimoto, M. Masayuki and Y. Matsuda, *Chem. Lett.*, 1996, 953.

5 C. E. D. Chidsey, C. R. Bertozzi, T. M. Putvinski and A. M. Mujsce, *J. Am. Chem. Soc.*, 1990, **112**, 4301; N. L. Abbott and G. M. Whitesides, *Langmuir*, 1994, **10**, 1493; D. M. Collard and M. A. Fox, *Langmuir*, 1991, **71**, 1192.

6 H. C. D. Long and D. A. Buttry, *Langmuir*, 1992, **8**, 2491; S. E. Creager and G. K. Rowe, *Anal. Chim. Acta*, 1991, **246**, 233; H. O. Finklea and D. D. Hanshew, *J. Am. Chem. Soc.*, 1992, **114**, 3173.

7 For flavin analogs immobilized on gold *via* other linkers, see: S. Sakamoto, H. Aoyagi, N. Nakashima and H. Mihara, *J. Chem. Soc., Perkin Trans. 2*, 1996, 2319; B. Mallik and D. Gani, *J. Electroanal. Chem.*, 1992, **326**, 37.

8 Disulfide is used instead of the analogous thiol due to the thiol's vulnerability to oxidation by the flavin moiety.

9 B. Janik and P. J. Elving, *Chem. Rev.*, 1968, **68**, 295.

10 The theoretical value for the slope of each linear segment of the E^0–pH curve is 0.059 *p*/*n* at 25 °C (where *p* and *n* are the numbers of protons and electrons involved respectively) P. J. Elving, *Pure Appl. Chem.*, 1963, **7**, 423.

11 For the methods and theory in determining pK_a values from E^0–pH plots, see: W. M. Clark, *Oxidation–Reduction Potentials of Organic Systems*, Williams and Wilkin Co., Baltimore, 1960, pp. 118.

12 W. M. Clark, *Oxidation–Reduction Potentials of Organic Systems*, Williams and Wilkin Co., Baltimore, 1960, p. 439.

13 C. D. Bain, G. M. Whitesides, *Langmuir*, 1989, **5**, 1370; T. R. Lee, R. I. Carey, H. A. Biebuyck and G. M. Whitesides, *Langmuir*, 1994, **10**, 741.

14 In addition to the decrease in peak areas, the full-widths at half maxima and the separation between the anodic and cathodic peaks (*ca.* 70 mV) in the mixed SAMs are smaller than those of the SAM from **1**.

Communication 8/06315J

CdS nanoparticle-modified electrodes for photoelectrochemical studies

Stephanie Drouard, Stephen G. Hickey and D. Jason Riley*

School of Chemistry, University of Bristol, Cantock's Close, Bristol, UK BS8 1TS. E-mail: Jason.Riley@bristol.ac.uk

Received (in Exeter, UK) 4th November 1998, Accepted 1st December 1998

A novel method of preparing CdS nanoparticle-modified electrodes is described and a relationship between CdS particle size and the photoelectrochemical properties of such electrodes demonstrated.

Nanocrystalline semiconductors exhibit a wide range of novel chemical and physical properties.[1] Hence research on nanocrystalline semiconductors is developing into a large interdisciplinary field. The properties of nanocrystalline particles differ from those of bulk materials for two reasons. First, the high surface area to volume ratio results in there being almost as many atoms at the surface as in the crystalline lattice. Secondly, the electronic bands are split into discrete energy levels as a result of the three-dimensional confinement of charge carriers. This quantum confinement of charge results in an increase in band gap with decreasing particle size. Indeed determination of the band edge allows the calculation of the particle size.[2] Investigations of how the interesting properties of nanoparticles may be exploited in optoelectronic devices,[3] photovoltaic[4] and clean technology applications[5] are being performed in many laboratories.

CdS is the material of choice when studying quantum confinement effects since methods of controlling the size of CdS nanoparticles are well established.[6–8] The study of charge transfer in nanoparticle systems is an active area of research. Electron exchange in colloidal CdS solutions has been extensively studied using photoelectrochemical[9] and radiolysis techniques.[10] However, if the novel properties of CdS nanoparticles are to be exploited in optoelectronic devices, methods of electrically addressing the particles directly are required. This communication is concerned with the preparation and characterisation of electrodes modified with sub-monolayers of nanoparticles; it is demonstrated that such electrodes allow the optoelectronic properties of the nanoparticles to be probed. In previous studies[11–15] of CdS coated surfaces the nanoparticles have been prepared in inverse micelles and deposited on to gold surfaces using dithiols as molecular anchors. Fourier transform IR spectroscopy,[12] UV–VIS spectroscopy,[13] X-ray photoelectron spectroscopy,[14] scanning tunnelling microscopy[15] and limited electrochemical studies have been performed on such electrodes. In this communication a novel method of preparing CdS nanoparticle modified electrodes is described and initial investigations of the optoelectronic properties of the CdS nanoparticles reported. The method of preparation is considerably simpler than that reported previously and allows deposition of CdS on to optically transparent electrodes; this facilitates studies of the optoelectronic properties of the particles. To illustrate that the CdS nanoparticles at the modified electrode surface may be addressed photoelectrochemically the photocurrent spectra are reported.

The strategy employed in the preparation of the CdS nanoparticle modified electrodes is detailed schematically in Fig. 1. The method is essentially a three-step process. First a tin oxide electrode surface is functionalised[16] using established methods. Then CdS nanoparticles are grown and grafted on to the functional groups.

The tin oxide electrodes were first cleaned in a Piranha bath at 70 °C and then placed in a solution of 3 mol dm^{-3} potassium hydroxide for *ca.* 2 h, in order to activate the surface. The electrode surface was then silanised by immersion in a 1 : 10 (3-mercaptopropyl)trimethoxysilane (MPTMS): methanol solution. The resultant surface possessed pendent thiol groups to which the CdS nanoparticles could be anchored.

The CdS colloidal nanoparticles were prepared in non-aqueous solution using a method first reported by Fischer and Henglein.[7] CdS was formed by bubbling H_2S, (2×10^{-4} mol dm^{-3}), into a 1×10^{-3} mol dm^{-3} $Cd(ClO_4)_2$ THF solution. The resultant colloids were strerically stabilised by addition of hexanethiol to the THF. It has been shown that the CdS nanoparticle size may be controlled by varying the hexanethiol concentration.

Initial attempts to attach the CdS nanoparticles to the functionalised surface involved the immersion of the electrodes in a solution containing CdS nanoparticles. This strategy proved unsuccessful; it has been reported[7] that stabiliser exchange is not possible with colloids prepared by this procedure. Hence, to obtain the CdS nanoparticle electrodes the functionalised tin oxide surfaces were immersed in the THF solution during colloid formation, in order that the surface-colloid bonds are formed as nanoparticle growth proceeds. The size of the particles was controlled by varying the hexane thiol concentration, solutions containing 0.400, 8.57×10^{-3} and 5.275×10^{-3} mol dm^{-3} of the stabiliser were studied. After rigorous washing the photoelectrochemical properties of the electrodes were investigated.

Prior to photoelectrochemical investigations of the modified electrodes the UV–VIS adsorption spectra of the parent

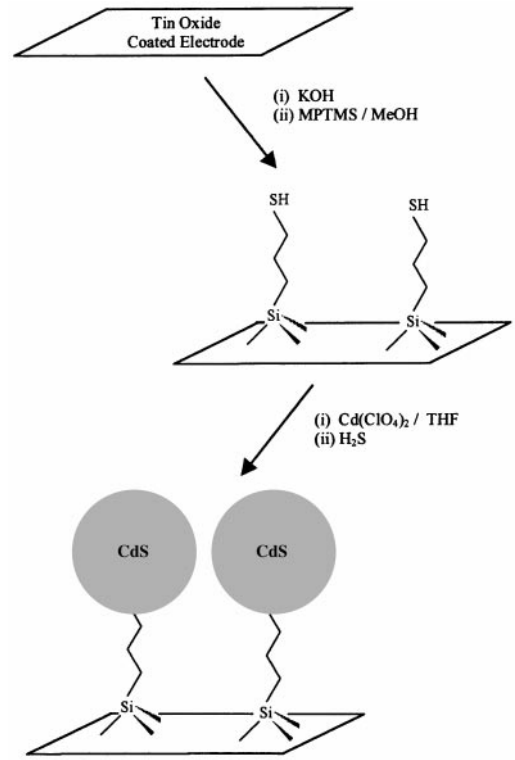

Fig. 1 A schematic of the method employed for the preparation of the CdS nanoparticle modified electrodes [MPTMS = (3-mercaptopropyl)trimethoxysilane].

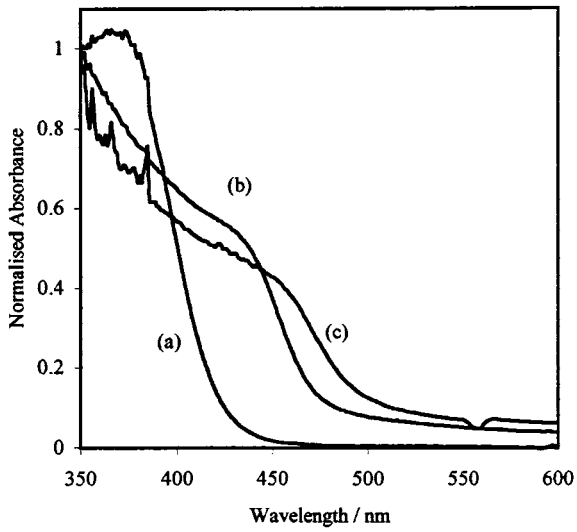

Fig. 2 Normalised UV–VIS absorbance spectra of CdS colloidal suspensions. The suspensions were prepared using varying concentrations of hexanethiol: (a) 0.400, (b) 8.57×10^{-3} and (c) 5.275×10^{-3} mol dm^{-3}.

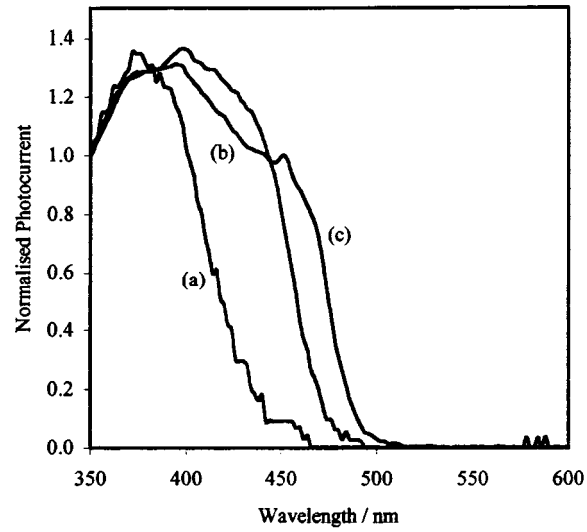

Fig. 3 Normalised photocurrent spectra of CdS nanoparticle modified electrodes. The electrodes were prepared using varying concentrations of hexanethiol: (a) 0.400, (b) 8.57×10^{-3} and (c) 5.275×10^{-3} mol dm^{-3}.

colloidal suspensions were recorded. The spectra for the suspensions prepared using the three different hexanethiol concentrations are shown in Fig. 2. It is apparent that by controlling the stabiliser concentration it is possible to change the band gap of the CdS nanoparticles formed in the solution phase. The sizes of the nanoparticles were determined from band-edge measurements. It was found that hexanethiol concentrations of 0.400, 8.57×10^{-3} and 5.275×10^{-3} mol dm^{-3} result in CdS nanoparticles in the colloidal suspension of 2, 4 and 10 nm diameter, respectively. More detailed studies of the influence of hexanethiol concentration on nanoparticle size in colloidal suspensions have been published.[7]

It was necessary to determine the band gap of the nanoparticles formed at the electrode interface in order to verify that they were of the same size as those formed in the solution phase. Unfortunately it was not possible to record the UV–VIS adsorption spectra for the modified electrodes as the CdS particles were present in sub-monolayer quantities. Hence, the optical properties of the CdS nanoparticles at the modified electrode surfaces were characterised using the more sensitive technique of photocurrent spectroscopy. All electrochemical experiments were performed at 0.2 V *vs.* Ag|AgCl| 3 mol dm^{-3} NaCl in a 1.0 mol dm^{-3} aqueous Na_2SO_3 solution buffered at pH 12. The photocurrent spectra were recorded using chopped monochromatic light and a lock-in amplifier. Photocurrent spectra for modified electrodes prepared using the three different hexanethiol concentrations are shown in Fig. 3. The excellent agreement between the UV–VIS spectra and the photocurrent spectra indicates that the particles deposited on the electrode surfaces were of the same size as those in the parent suspension.

In conclusion, a method of preparing optically transparent electrodes modified with sub-monolayers of CdS nanoparticles has been developed. Further, it has been shown that the size of the CdS nanoparticles on the surface can be controlled by varying the hexanethiol concentration. The photocurrent experiments demonstrate that the physical properties of the CdS nanoparticles at the surface can be addressed using photoelectrochemical techniques. Intensity-modulated photocurrent spectroscopy studies of the effect of quantum confinement on the kinetics of charge transfer from photoexcited CdS nanoparticles are presently in progress.

Notes and references

1 H. Weller, *Angew. Chem., Int. Ed. Engl.*, 1993, **32**, 41.
2 L. Brus, *J. Phys. Chem.*, 1986, **90**, 2555.
3 A. Loni, A. J. Simons, T. I. Cox, P. D. J. Calcott and L. T. Canham, *Electron. Lett.*, 1995, **31**, 1288.
4 B. O'Regan and M. Grätzel, *Nature*, 1991, **353**, 739.
5 W. Y. Lin and K. Rajeshwar, *J. Electrochem. Soc.*, 1997, **144**, 2751.
6 A. Chemseddine and H. Weller, *Ber. Bunsenges. Phys. Chem.*, 1993, **97**, 636.
7 C. H. Fischer and A. Henglein, *J. Phys. Chem.*, 1989, **93**, 5578.
8 C. B. Murray, D. J. Norris and M. G. Bawendi, *J. Am. Chem. Soc.*, 1993, **115**, 8706.
9 W. J. Albery, P. N. Bartlett and J. D. Porter, *J. Electrochem. Soc.*, 1984, **131**, 2892.
10 S. Baral, A. Fojtik, H. Weller and A. Henglein, *J. Am. Chem. Soc.*, 1986, **108**, 375.
11 V. L. Colvin, A. N. Goldstein and A. P. Alvisatos, *J. Am. Chem. Soc.*, 1992, **114**, 5221.
12 T. Nakanishi, B. Ohtani, K. Uosaki, *J. Phys. Chem. B.*, 1998, **102**, 1571.
13 K. Hu, M. Brust and A. J. Bard, *Chem. Mater.*, 1998, **10**, 1160.
14 T. Nkanishi, B. Ohtani, K. Shimazu and K. Uosaki, *Chem. Phys. Lett.*, 1997, **278**, 233.
15 S. Ogawa, F. F. Fan and A. J. Bard, *J. Phys. Chem.*, 1995, **99**, 11182.
16 K. R. Brown, A. P. Fox and M. J. Natan, *J. Am. Chem. Soc.*, 1996, **118**, 1154.

Communication 8/08572B

Selective adsorption of Hg^{2+} by thiol-functionalized nanoporous silica

Jennifer Brown,[a] Louis Mercier*[a] and Thomas J. Pinnavaia[b]

[a] *Department of Chemistry and Biochemistry, Laurentian University, Sudbury, Ontario, Canada P3E 2C6. E-mail: lmercien@nickel.laurentian.ca*

[b] *Department of Chemistry and Center for Fundamental Materials Research, Michigan State University, East Lansing, Michigan 48824, USA*

Received (in Cambridge, UK) 16th September 1998, Accepted 30th November 1998

Thiol-functionalized nanostructured silicas with uniform porosities exhibit selective complexation affinity for Hg^{2+}, while other metal ions (Cd^{2+}, Pb^{2+}, Zn^{2+}, Co^{3+}, Fe^{3+}, Cu^{2+} and Ni^{2+}) have little or no binding ability with the adsorbents.

Effective metal ion adsorbents have been prepared by the immobilization of thiol ligands onto the surface of various substrates, including silica gel,[1,2] clays,[3,4] polymers[5] and, most recently, mesoporous silica.[6–8] The effectiveness of such materials in binding metal ions has been attributed to the complexation chemistry between the ligand and the metal, the specificity of a particular ligand towards target metal ions being the result of a conventional acid–base interaction between the two. Although some of these thiol-functionalized adsorbents can exhibit specific interactions with soft Lewis acids (such as Hg^{2+}, Cd^{2+}, Pb^{2+} and Ag^{+}),[1–4] the selectivities of these materials are usually unremarkable because many metals have the ability to bind with thiol ligands. In this study, we have prepared a series of nanostructured thiol-functionalized silica adsorbents with uniform porosity[9–11] and investigated their affinity for heavy metal ion binding.

Nanostructured adsorbents with variable loadings of thiol groups were prepared by stirring tetraethoxysilane (TEOS) and 3-mercaptopropyltrimethoxysilane (MPTMS) in 0.116 M *n*-octylamine solutions at room temperature [the molar composition of each mixture was 0.22 surfactant : $(1 - X)$/100 TEOS : X/100 MPTMS, where $X = 0$, 2.3, 4.5, 6.9 and 9.0]. After aging for 24 h, the resulting powders were filtered, air dried and washed by Soxhlet extraction over ethanol for 24 h. The materials were labeled as HMS ($X = 0$) and MP-HMS-X, where X represents the percentage of silicon atoms in the synthesis mixture present as MPTMS.

The physical and chemical properties of the functionalized silicas, shown in Table 1, were determined using X-ray diffraction (XRD), N_2 sorptometry and ^{29}Si MAS NMR. The single-reflection XRD powder patterns denoted disordered wormhole structures, with d_{100} values ranging from 2.9–3.4 nm. The N_2 adsorption isotherms showed that the adsorbents had very high surface areas and narrow Horvath–Kawazoe pore size distributions in the micropore range (< 2.0 nm). All of these characteristics are indicative of neutral–surfactant-assembled nanostructured silica frameworks with uniform porosities.[12–14]

Table 1 Physicochemical characteristics of the thiol-functionalized nanoporous adsorbents

Adsorbent	Lattice spacing/ nm	Surface area/ $m^2\ g^{-1}$	Pore diameter/ nm	SH content/ mmol g^{-1}	Hg^{2+} adsorption capacity/ mmol g^{-1}
HMS	3.15	1408	1.95	0	0
MP-HMS-2.3	3.13	1221	1.75	0.35	0.19
MP-HMS-4.5	2.96	1331	1.65	0.68	0.28
MP-HMS-6.9	3.13	1087	1.51	1.0	0.46
MP-HMS-9.0	3.34	1063	1.48	1.3	0.59

Resonances at δ −65 in the ^{29}Si MAS NMR spectra of the adsorbents demonstrated the incorporation of MPTMS within the material frameworks. By comparing the relative integral intensities of the MPTMS signals with respect to the total signal intensity,[9,11] we deduced that the amount of thiol groups incorporated in the materials (Table 1) corresponded within experimental uncertainty to the stoichiometry of the synthesis mixture. Consequently, the surface areas and pore sizes of the materials systematically decrease as a result of the increased coverage of thiol groups on the surface of the pore channels (Table 1). No evidence of thiol group oxidation was found in the materials, as evidenced by the detection of S–H stretching bands in their FTIR spectra (2580 cm^{-1}), and the presence of symmetric signals at δ −27 in their ^{13}C NMR spectra (characteristic of R–CH_2–SH functions[7,9]).

The uptake of metal ions by the adsorbents were determined by titrating aqueous metal ion solutions into a slurry of each adsorbent, stirring for 24 h, and analyzing the supernatant solution for metal ion content using flame AAS (cold-vapour AAS for Hg). This process was repeated until no significant metal ion uptake by the materials was observed. Thus, each adsorbent was tested for their ability to adsorb Hg^{2+}, Cd^{2+}, Pb^{2+} and Zn^{2+} from independent homoionic solutions at neutral pH. The adsorbents exhibited little or no affinity for these metals, with the exception of Hg^{2+}. The very efficient binding of Hg^{2+} ions reduced the metal concentrations to negligible levels (< 10 ppb) until saturation was reached [Fig. 1(a)]. The Hg^{2+} adsorption capacities of the materials systematically increased in proportion to the thiol group content in the materials [up to

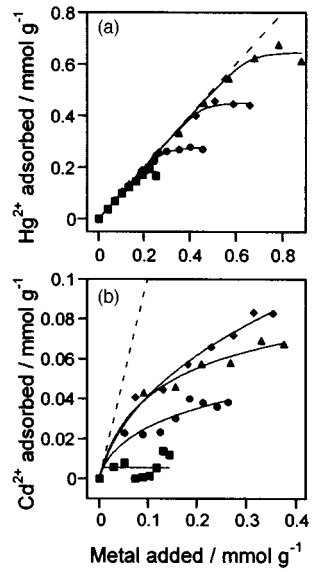

Fig. 1 Homoionic (a) Hg^{2+} and (b) Cd^{2+} uptake curves for MP-HMS-X adsorbents [$X = 2.3$(■), 4.5(●), 6.9(◆) and 9.0(▲)]. The x-axis denotes the total amount of metal added to the system per unit mass of adsorbent. The dashed lines are the unity slopes representing the theoretical total uptake of metal ions.

0.65 mmol g^{-1}, Fig. 1(a)]. Approximately one half of the incorporated thiol groups in each adsorbent is accessible for Hg^{2+} binding (Table 1). The constricted nature of the microporous channels most likely controls access of Hg^{2+} ions to the adsorbents' binding sites.[8,9] Multidentate SH binding with the Hg^{2+} ions may also contribute to the high S:Hg stoichiometry. Of the other metals studied, only Cd^{2+} demonstrated some interaction with the adsorbents [Fig. 1(b)]. As in the case of Hg^{2+}, a correlation between the thiol group content in the adsorbents and the Cd^{2+} loading is denoted, but saturation of the binding sites is reached at very low levels [$<<0.1$ mmol g^{-1}, Fig. 1(b)]. Significant residual concentrations of Cd^{2+} remained in the treated solutions, even at low metal concentrations [Fig. 1(b)]. The adsorbents thus demonstrate considerably weaker affinity for Cd^{2+} than for Hg^{2+}.

By the uptake process described above, the adsorbents were also used to treat a mixed metal solution containing nearly equimolar amounts of Cd^{2+}, Pb^{2+}, Zn^{2+}, Hg^{2+}, Co^{3+}, Fe^{3+}, Cu^{2+} and Ni^{2+}. The uptake of Hg^{2+} from this mixed metal ion solution was virtually identical to the uptake observed for the homoionic solutions [Fig. 1(a)]. Negligible adsorption of the other metals was observed. This demonstrates the remarkable selectivity of the nanoporous adsorbents for Hg^{2+} binding.

That Hg^{2+} ions exhibit high binding affinity towards the immobilized thiol groups is not unexpected. What is unique for the nanostructured adsorbents, however, is their extreme lack of affinity towards other d^{10} metal ions (Cd^{2+}, Zn^{2+} and Pb^{2+}) which usually bind strongly with these ligands (especially in the absence of other competing ions), as observed previously for thiol-functionalized silica gel[1] and montmorillonite.[3] We propose that, while Hg^{2+} has the ability to bind with the thiol groups lining the framework pore channels of the nanoporous adsorbents (representing the bulk of the adsorbent binding sites), the other metal ions are unable to bind to intraframework, complexing only with the comparatively low number of thiol groups present at the external surface of the adsorbent particles.

By comparing these results with those of other sorption studies on similar materials,[1–3] we infer that the uniform porosity of the nanostructured adsorbents is ultimately responsible for their selective adsorption behaviour. The inability of Cd^{2+}, Zn^{2+} and Pb^{2+} to bind to the thiol groups in the adsorbent pore channels may tentatively be explained by the thermodynamic inability of these ions to coordinate within the confined spaces of the pore channels. Using thermodynamic data tables[15] and the model reaction $H_2S + M^{2+} \longrightarrow MS + 2H^+$ to represent the metal ion binding process, we estimate the ΔG^0 value for the reaction in which M = Hg was calculated as -181.6 kJ mol^{-1}, while the free energies of the reactions in which M = Cu, Cd, Pb, Ni and Fe were -85.7, -45.3, -40.9, -0.5 and 11.9 kJ mol^{-1}, respectively. We postulate that the restricted volumes of the channels reduce the ΔS^0 values of the above reactions, resulting in positive (non-spontaneous) ΔG^0 values for most of the intraframework metal–ligand reactions. Only in the reaction with Hg^{2+} is the change in enthalpy (ΔH^0) sufficiently negative to overcome this unfavourable entropy effect and maintain reaction spontaneity. Further investigations are currently underway to verify this hypothesis and to better elucidate the factors involved in metal-ion binding to nanoporous adsorbents.

We acknowledge the Natural Science and Engineering Research Council (Canada), the Laurentian University Research Fund, the National Science Foundation (USA) and the National Institute of Environmental Health and Safety (USA) for financial support.

Notes and references

1 M. Volkan, D. Y. Ataman and A. G. Howard, *Analyst*, 1987, **112**, 1409.
2 E. F. S. Vieira, J. de A. Simoni and C. Airoldi, *J. Mater. Chem.*, 1997, **7**, 2249.
3 L. Mercier and C. Detellier, *Environ. Sci. Technol.*, 1995, **29**, 1318.
4 N. L. Dias Filho, Y. Gushikem and W. L. Polito, *Anal. Chim. Acta*, 1995, **306**, 167.
5 C. Kantipuly, S. Katragadda, A. Chow and H. D. Gesser, *Talanta*, 1990, **37**, 491.
6 L. Mercier and T. J. Pinnavaia, *Adv. Mater.*, 1997, **9**, 500.
7 X. Feng, G. E. Fryxell, L.-Q. Wang, A. Y. Kim, J. Liu and K. M. Kemner, *Science*, 1997, **276**, 923.
8 L. Mercier and T. J. Pinnavaia, *Environ. Sci. Technol.*, 1998, **32**, 2749.
9 M. H. Lim, C. F. Blanford and A. Stein, *Chem. Mater.*, 1998, **10**, 467.
10 W. M. Van Rhijn, D. E. DeVos, B. F. Sels, W. D. Bossaert and P. A. Jacobs, *Chem. Commun.*, 1998, 317.
11 R. Richer and L. Mercier, *Chem. Commun.*, 1998, 1775.
12 P. T. Tanev and T. J. Pinnavaia, *Science*, 1995, **267**, 865.
13 S. A. Bagshaw, E. Prouzet and T. J. Pinnavaia, *Science*, 1995, **269**, 1242.
14 D. J. Macquarrie, *Chem. Commun.*, **1996**, 1961.
15 *CRC Handbook of Chemistry and Physics*, 77th edn., CRC Press: London, 1996.

Communication 8/07249C

Selective catalytic reduction of NO by ammonia over Fe-ZSM-5 catalysts

Ai-Zeng Ma† and W. Grünert*

Lehrstuhl für Technische Chemie, Ruhr-Universität Bochum, D-44 780 Bochum, Germany.
E-mail: w.gruenert@techem.ruhr-uni-bochum.de

Received (in Bath, UK) 21st September 1998, Accepted 9th November 1998

In the selective catalytic reduction (SCR) of NO by ammonia, over-exchanged Fe-ZSM-5 prepared by sublimation of $FeCl_3$ into H-ZSM-5, shows superior catalytic activity and stability in a wide temperature range; its activity is promoted by the presence of water in the feed while SO_2 is a weak poison at low but a promoter at high temperatures; its remarkable durability towards H_2O and SO_2 makes this zeolite catalyst a potential choice in Denox applications for stationary sources and heavy Diesel engines with ammonia or urea reductants.

In the selective catalytic reduction (SCR) of nitrogen oxides, metal-exchanged MFI-type zeolites, in particular Cu-ZSM-5, have received much attention due to their ability to catalyze the SCR not only by hydrocarbons,[1–3] but also by ammonia.[4] The insufficient stability of these catalysts has so far prevented their practical application in flue-gas abatement devices. Faced with the tail-gases of combustion engines containing high amounts of water, and often also SO_2, they suffer structural changes leading to deactivation. For the use of hydrocarbon reductants, water is also known as a reversible poison while it has been reported to promote the SCR activity with the reductant ammonia.[4]

In view of these problems, the recent discovery of the remarkable stability of over-exchanged Fe-ZSM-5 in the SCR of NO with isobutane[5] has been considered a breakthrough in flue-gas catalysis research. Further progress has to cope with a reproducibility problem in the preparation of these materials[6] and with the fact that the reductant isobutane that provides the highest reaction rates with these catalysts is impractical for any commercial purpose. We report here a superior catalytic performance of over-exchanged Fe-ZSM-5 in the SCR of nitrogen oxides with ammonia. The catalyst provides excellent activity and selectivity over a wide temperature range. It is promoted by water and, in certain temperature ranges, also by SO_2 (with or without water) and does not suffer any deactivation from these feed components on a time scale of 10–15 h.

The Fe-ZSM-5 was prepared on the basis of a Na-ZSM-5 (Si/Al ≈ 14, Chemiewerk Bad Köstritz, Germany). Iron was introduced by a modified sublimation technique derived from a route described in ref. 7 (sublimation of $FeCl_3$ vapour into the H-form of the zeolite under vacuum). Subsequently, the catalyst was calcined in air at 823 K without any washing step. Elemental analysis showed that this preparation provides an Fe/Al ratio of 1 : 1, which is a formal exchange degree of 300%. The sample will be, therefore, denoted as Fe-ZSM-5-14-300 indicating the Si/Al ratio and the formal exchange degree by the last two figures. A Cu-ZSM-5-14-220 prepared by the conventional ion-exchange method described by Iwamoto *et al.*[8] was also obtained from the same Na-ZSM-5 for use as a reference material.

The SCR of NO by ammonia was carried out in a microcatalytic flow reactor. A calibrated mass spectrometer and a combined non-dispersive IR/UV detector were employed to analyse the reaction product. The feed gas contained 1000 ppm NO, 1000 ppm NH_3, and 2% O_2 (balance He) and was loaded by 2.5% H_2O and/or 200 ppm SO_2 in the poisoning experiments. Under standard reaction conditions, 260 ml min^{-1} of this mixture were fed over 35 mg of catalyst, which results in a space velocity of 304 000 h^{-1}.

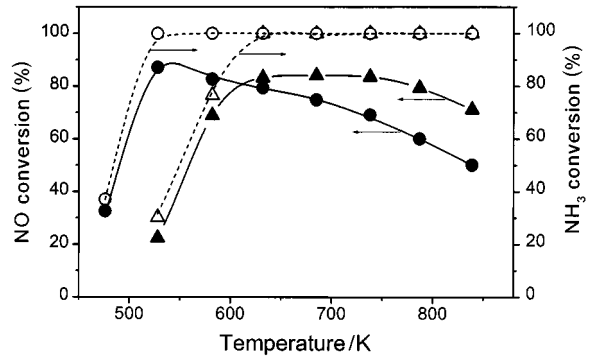

Fig. 1 Selective catalytic reduction of NO by NH_3 with over-exchanged Fe-ZSM-5 and comparison with over-exchanged Cu-ZSM-5. Dry condition: 1000 ppm NO, 1000 ppm NH_3, 2% O_2, balance He; 304 000 h^{-1}, (▲, △) Fe-ZSM-5-14-300, (○, ●) Cu-ZSM-5-14-220, filled symbols, NO conversion, open symbols, NH_3 conversion.

Fig. 1 shows the conversions of NO and NH_3 at different reaction temperatures over Fe-ZSM-5-14-300 and Cu-ZSM-5-14-220. Cu-ZSM-5 is very active for the SCR with ammonia, and the conversions obtained with our preparation are at all temperatures well above those reported in the literature for a somewhat lower space velocity.[4] Fe-ZSM-5-14-300 provides the same conversions as Cu-ZSM-5-14-220 proving inferior only in the low-temperature region (≤573 K). Over this catalyst, the temperature window for high NO conversion is significantly wider than over the Cu catalyst: NO conversions >75% can be held between 573 and 823 K. The ammonia conversion is close to the NO conversion below 423 K, but is 100% at all temperatures above, which makes ammonia slip rather unlikely with such catalysts. Remarkably, the only oxidation product is nitrogen, neither NO_2 nor N_2O formation were detected in the whole temperature range. With Cu-ZSM-5-14-220, ammonia oxidation becomes significant already at 523 K, and since the NO conversion decreases steadily with increasing temperature, the copper catalyst is inferior in the ammonia utilization at almost all temperatures.

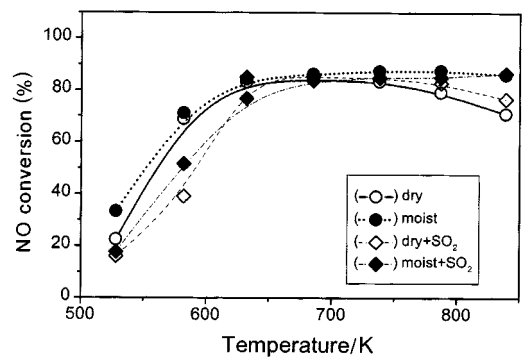

Fig. 2 Influence of water and sulfur dioxide on the NO conversion over Fe-ZSM-5-14-300. Space velocity, 304 000 h^{-1}, dry condition: 1000 ppm NO, 1000 ppm NH_3, 2% O_2, balance He. Moist condition: as dry, with 2.5% H_2O added, '+SO_2', with 200 ppm SO_2 added.

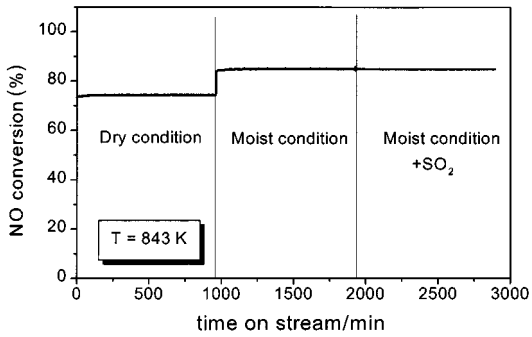

Fig. 3 Durability of Fe-ZSM-5-14-300 under the influence of water and SO_2: dry condition; moist condition; moist condition + SO_2 as in Fig. 2.

The impact of H_2O and/or SO_2 on the NO conversion over Fe-ZSM-5-14-300 is shown in Fig. 2. It is evident that SO_2 exerts a poisoning influence at low temperature both in dry and in moist feed. Remarkably, this effect is reversed at higher temperature: Above 700 K, the NO conversion is always higher with SO_2 present. On the other hand, water promotes the activity at all temperatures over our Fe-ZSM-5, which is similar to the behaviour found with Cu-ZSM-5.[4,9] This is most favourable at the upper end of the temperature range where an NO conversion of 85% (at *ca*. 300 000 h^{-1}) may be held up to a reaction temperature of 850 K in a moist feed stream.

The durability of Fe-ZSM-5-14-300 in various feed mixtures was tested at 840 K (Fig. 3). Under dry conditions, a slight increase of the NO conversion (by *ca*. 3% in 15 h) can be noted. Upon addition of 2.5% H_2O to the feed, a sudden increment in the NO conversion of *ca*. 10% is achieved. Addition of SO_2 into the wet feed does not lead to further changes. No deactivation of the catalyst is observed either in 15 h time-on-stream in moist feed or under the simultaneous action of H_2O and SO_2. It should be noted that such conditions would cause severe deactivation with the Cu-ZSM-5 system.[3]

The preparation of the Fe-ZSM-5 catalyst is critical also for its application to the SCR with ammonia. An Fe-ZSM-5 catalysts obtained by conventional aqueous exchange, which resulted in a formal exchange degree of < 100%, was inferior to Fe-ZSM-5-14-300.[9] In a recent paper,[10] Fe-ZSM-5 prepared by aqueous exchange with subsequent precipitation provided NO conversions below 50%, with considerable N_2O formation at lower temperatures, at a space velocity of only 180 000 h^{-1}. Notably, in the SCR of NO by isobutane, our Fe-ZSM-5-14-300 sample could not compete with Cu-ZSM-5-14-220, and the NO conversions achieved[9] were much lower than those reported by Feng and Hall.[5] In addition, the air calcination step in the catalyst preparation (*vide supra*), which proved deleterious for the SCR with isobutane[9] in accordance with the literature,[6] had a slightly deactivating effect only in the low-temperature range but did not did not affect the peak conversion with ammonia.[9] This implies that the active sites required by the two reactions may be different.

In conclusion, over-exchanged Fe-ZSM-5 prepared by a sublimation technique shows highly promising catalytic performance in the SCR of NO by ammonia. Studies concerning the structure of the active sites in this catalyst and about its behaviour with respect to the oxidation of SO_2 are under way.

We acknowledge financial support from the Research Institute of Petroleum Processing, Beijing, China

Note and references

† On leave from Research Institute of Petroleum Processing, Beijing 100083, China.

1 W. Held, A. König, T. Richter and L. Puppe, *SAE-Pap.*, 1990, 900496.
2 M. Iwamoto, H. Yahiro, S. Shundo, Y. Yu-u and N. Mizuno, *Shokubai*, 1990, **32**, 430.
3 M. Shelef, *Chem. Rev.*, 1995, **95**, 209.
4 J. A. Sullivan, J. Cunningham, M. A. Morris and K. Keneavey, *Appl. Catal. B*, 1995, **7**, 137.
5 X. Feng and W. K. Hall, *Catal. Lett.*, 1996, **41**, 45.
6 W. K. Hall, X. Feng, J. Dumesic and R. Watwe, *Catal. Lett.*, 1998, **52**, 13.
7 H.-Y. Chen and W. M. H. Sachtler, *Catal. Today*, 1998, **42**, 73.
8 M. Iwamoto, H. Yahiro, Y. Mine and S. Kagawa, *Chem. Lett.*, 1989, 213.
9 A.-Z. Ma, F. Heinrich and W. Grünert, to be published.
10 A. V. Salker, B. Maurer and W. Weisweiler, *Chem.-Ing.-Technol.*, 1998, **70**, 566.

Communication 8/07490I

One-pot synthesis of new liquid crystalline indeno heterocyclic materials

Lidia S. Konstantinova,[a] Oleg A. Rakitin,[a] Charles W. Rees,[b] Ljudmila I. Souvorova,[a] Tomás Torroba,[c] Andrew J. P. White[b] and David J. Williams[b]

[a] *N. D. Zelinsky Institute of Organic Chemistry, Academy of Sciences, Leninsky Prospect, 47, 117913 Moscow, Russia*

[b] *Department of Chemistry, Imperial College of Science, Technology and Medicine, London, UK SW7 2AY*

[c] *Departamento de Química Orgánica, Facultad de Veterinaria, Universidad de Extremadura, 10071 Cáceres, Spain*

Received (in Liverpool, UK) 8th October 1998, Accepted 18th November 1998

Disulfur dichloride converts 1-(dicyanomethylene)indane 3 into the methyleneindene 4 and the red indeno-1,2-thiazine 5; it also converts inden-3-ylacetic acid 7 into methyleneindenes 8 and 9, dithiolone 10 and the deep purple thiophenone 11; upon melting crystals of 4 and 11 are strongly birefringent and 5 exhibits thermochromicity; mechanisms are outlined for the novel transformations and X-ray crystal structures for 5 and 10 are analysed.

During a search for materials with both novel and useful electronic and optical properties we discovered a simple route to some heterocyclic pseudoazulenes[1] which constitute a new class of discotic liquid crystals where the mesophases are not supported by long aliphatic chains or by H-bonding.[2] The new discotic mesomorphism appears to arise from interactions of central aromatic structures with polarised chlorine, sulfur and cyano groups. In a continuation of this work disulfur dichloride, S_2Cl_2, is shown to react with simple organic substrates to provide new members of this family of molecules which exhibit liquid crystalline behaviour.

We have shown, for example, that S_2Cl_2, NCS and Hünig's base in THF converted 1-(cyanomethyl)cyclopentene **1** into the dark blue trichlorocyclopenta[*c*][1,2]dithiole **2**, crystals of which showed strong birefringence upon melting on a hot stage polarising microscope.[1] We have now selected related indeneacetonitrile and indeneacetic acid derivatives for reaction with the same reagents.

When 1-(dicyanomethylene)indane **3**[3] was treated with 5 equiv. each of S_2Cl_2, Hünig's base and NCS in THF at 0 °C for 3 d and then heated at reflux for 5 h, chromatography gave 2,3-dichloro-1-(dicyanomethylene)indene **4** (90%) as orange crystals, mp 133–135° and then 163–165 °C, and 3,9-dichloroindeno[1,2-*e*][1,2]thiazine **5** (9%) as red crystals, mp 206–208 °C (Scheme 1). The structures of both products followed from their analytical and spectroscopic data and structure **5** was confirmed by X-ray crystallography (Fig. 1).† The ring systems are co-planar to within 0.02 Å with Cl(3) and Cl(9) lying 0.07 and 0.02 Å out of this plane, respectively. The molecules pack to produce slightly distorted close-packed hexagonal sheet arrays, the shortest intermolecular contacts being between the cyano nitrogen atom in one molecule and Cl(3) in a centrosymmetrically related counterpart and *vice versa* (3.18 Å) and between Cl(9) in one molecule and S(1) in the next (3.51 Å) about an independent inversion centre. Adjacent sheets are π-stacked (3.45 Å separation) with the thiazine rings in one sheet overlaying the C_5 rings of another and *vice versa*.

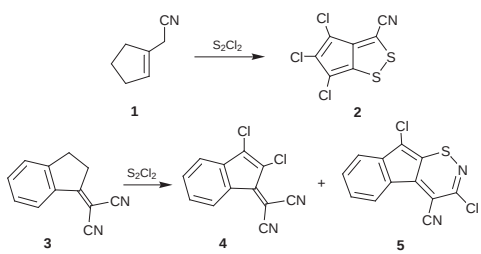

Scheme 1

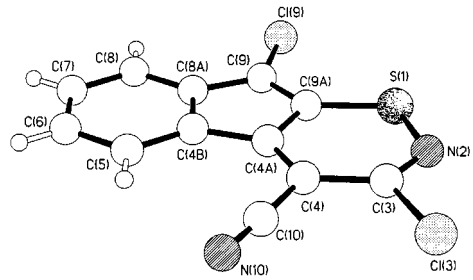

Fig. 1 The molecular structure of **5**.

The dichloroindene **4** presumably arises by extensive chlorination and dehydrochlorination, which we have observed in other S_2Cl_2 reactions.[1,4,5] Upon melting on a hot stage polarising microscope, compound **4** exhibited strong birefringence indicative of liquid crystallinity, whilst the indenothiazine **5** showed reversible thermal transitions from red to blue crystals and gave a blue molten phase. Compound **5** also gave blue solutions in common organic solvents, with λ_{max} = 653 nm, ε = 946 in CH_2Cl_2.

A possible pathway, initiated by addition of S_2Cl_2 to a nitrile bond,[6] for the conversion of dicyanide **3** into thiazine **5** is outlined in Scheme 2.

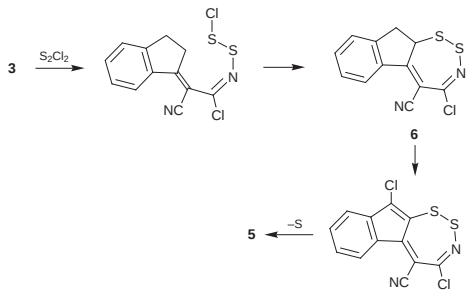

Scheme 2

Inden-3-ylacetic acid **7**[7] was similarly treated with S_2Cl_2, Hünig's base and NCS in THF, $CHCl_3$, or $(CH_2Cl)_2$ to give four products (Scheme 3) in varying yields: the yellow tetra-

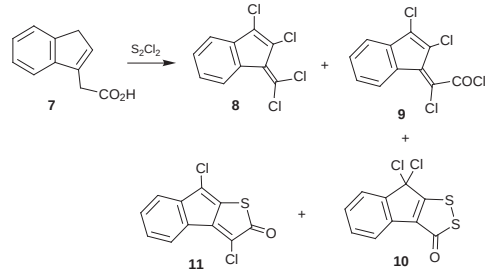

Scheme 3

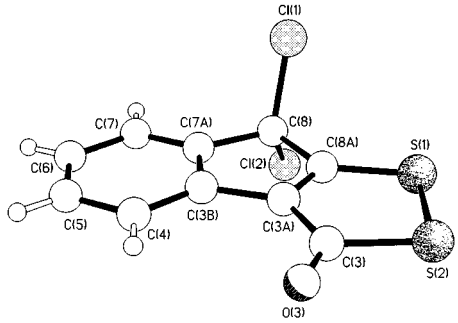

Fig. **2** The molecular structure of **10**.

chloroindene **8**, mp 80–83 °C, in up to 32% yield, the deep yellow acid chloride **9**, mp 96–98 °C (33%) and two unexpected sulfur heterocyclic compounds **10**, mp 97–98 °C (yellow, 51%) and **11**, mp 88–90 °C and then 124–125 °C (deep purple, 37%); combined yields were up to 85%. Structures **8–11** are based on analytical and spectroscopic data, and structure **10** was confirmed as 8,8-dichloro-3,8-dihydroindeno[2,3-*c*][1,2]dithiol-3-one by X-ray crystallography (Fig. 2).† The crystals contain two independent molecules each with very similar geometries, the fused ring systems being co-planar to within 0.09 Å in one and to within 0.04 Å in the other. The out of plane distortions are a consequence of a slight folding (6° in one molecule and 3° in the other) about an axis passing through C(8) and bisecting the C(3A)–C(3B) bond. Pairs of independent molecules are arranged to form essentially co-planar tetrads, interlinked *via* strong O···S interactions[8] [Fig. 3(*a*)–(*d*)] ranging between 2.88 and 3.14 Å. Both the benzo and dithiolo rings are involved in π–π stacking with their symmetry equivalent neighbours.

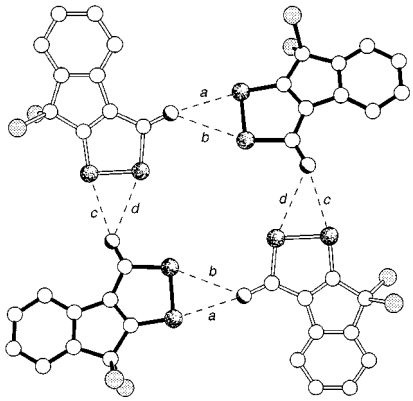

Fig. **3** One of the near co-planar tetrads present in the crystals of **10**. The intermolecular O···S contacts are (*a*) 2.91, (*b*) 3.14, (*c*) 2.88 and (*d*) 3.10 Å. The closed and open bonds serve to distinguish between the two crystallographically independent molecules present in the asymmetric unit.

The highly delocalised 3,8-dichloro-2*H*-indeno[2,1-*b*]thiophen-2-one structure **11** is tentatively assigned to the purple product; this retains the carbon connectivity of the starting material **7**, now fully unsaturated and substituted. Encouragingly, compound **11** also showed birefringence on melting on a hot stage polarising microscope.

Routes to the dithiolone **10** and thiophenone **11** from **7** can be envisaged (Schemes 4 and 5). The former is based upon the propensity of the reagents to form 1,2-dithioles with activated allylic substrates, accompanied by extensive chlorination–dehydrochlorination.[4,5,9] The latter, in a new type of S_2Cl_2 reaction, is based on the rare conversion of acids into acid chlorides by S_2Cl_2.[10] An intermediate in this transformation *e.g.* **12**, could be diverted by cyclisation, ultimately to form **11**.

Thus we have shown that some very simple indenes are readily converted by S_2Cl_2 directly into new liquid crystalline and thermochromic materials.

We gratefully acknowledge financial support from the Dirección General de Enseñanza Superior of Spain (DGES Project ref. PB96-0101), the Consejería de Educación de la Junta de Extremadura y Fondo Social Europeo (ref. PRI97C123), the Royal Society, the NATO Linkage Grant 970596, an RSC Journals Grant to O. A. R. and the Wolfson Foundation for establishing the Centre for Organic Chemistry in Medical Science at Imperial College.

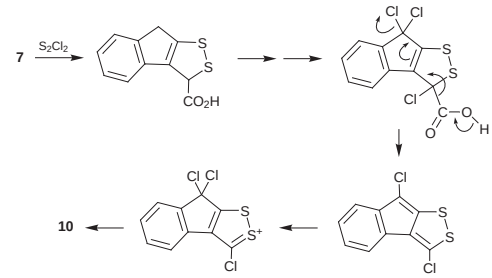

Scheme 4

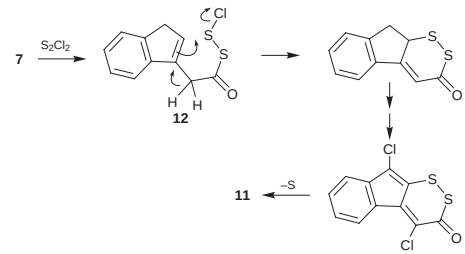

Scheme 5

Notes and references

† *Crystal data* for **5**: $C_{12}H_4N_2SCl_2$, M = 279.1, triclinic, $P\bar{1}$ (no. 2), a = 7.619(1), b = 8.392(2), c = 9.946(2) Å, α = 65.28(1), β = 75.81(1), γ = 84.17(2)°, V = 560.0(2) Å^3, Z = 2, D_c = 1.655 g cm^{-3}, μ(Cu-Kα) =_67.4 cm^{-1}, F(000) = 280. For **10**: $C_{10}H_4OS_2Cl_2$, M = 275.2, triclinic, $P1$ (no. 2), a = 8.837(2), b = 10.787(1), c = 12.986(1) Å, α = 68.09(1), β = 75.10(1), γ = 87.02(1)°, V = 1108.4(3) Å^3, Z = 4 (there are two crystallographically independent molecules in the asymmetric unit), D_c = 1.649 g cm^{-3}, μ(Mo-Kα) = 9.27 cm^{-1}, F(000) = 552. 1696 (3819) independent reflections were measured on Siemens P4/PC diffractometers with Cu-Kα (Mo-Kα) radiation using θ–2θ (ω) scans for **5** (**10**) respectively. The structures were solved by direct methods and all of the non-hydrogen atoms were refined anisotropically using full-matrix least-squares based on F^2 with absorption corrected data to give R_1 = 0.039 (0.038), wR_2 = 0.106 (0.090) for 1548 (3143) independent observed reflections [$|F_o| > 4\sigma(|F_o|)$, $2\theta \leqslant 128°$ (50°)] and 155 (272) parameters for **5** (**10**) respectively. CCDC 182/1098.

1 O. A. Rakitin, C. W. Rees and T. Torroba, *Chem. Commun*., 1996, 427; O. A. Rakitin, C. W. Rees, D. J. Williams and T. Torroba, *J. Org. Chem*., 1996, **61**, 9178.
2 J. Barberá, O. A. Rakitin, M. B. Ros and T. Torroba, *Angew. Chem., Int. Ed. Engl*., 1998, **37**, 296.
3 D. M. W. Anderson, F. Bell and J. L. Duncan, *J. Chem. Soc*. 1961, 4705.
4 M. J. Plater, C. W. Rees, D. G. Roe and T. Torroba, *J. Chem. Soc., Perkin Trans 1*, 1993, 769.
5 C. W. Rees, A. J. P. White, D. J. Williams, O. A. Rakitin, C. F. Marcos, C. Polo and T. Torroba, *J. Org. Chem*., 1998, **63**, 2189.
6 D. Martinetz, *Z. Chem*., 1980, **20**, 332.
7 M. H. Tankard and J. S. Whitehurst, *J. Chem. Soc., Perkin Trans. 1*, 1973, 615.
8 For a recent discussion of such interactions, see Y. Nagao, T. Hirata, S. Goto, S. Sano, A. Kakehi, K. Iizuka and M. Shiro, *J. Am. Chem. Soc*., 1998, **120**, 3104.
9 C. F. Marcos, C. Polo, O. A. Rakitin, C. W. Rees and T. Torroba, *Angew. Chem., Int. Ed. Engl*., 1997, **36**, 281.
10 Y. Takada, T. Matsuda and G. Inoue, *Jap Pat*. 12,123/1968 (*Chem. Abstr*., 1969, **70**, 19819); A. E. Lippman USP 3,636,102 (*Chem. Abstr*., 1972, **76**, 72049); T. Matsuda, K. Yokota and Y. Takata, *Hokkaido Daigaku Kogakubu Kenkyu Hokoku*, 1978, **87**, 151 (*Chem. Abstr*., 1979, **90**, 6055).

Communication 8/07885H

Effect of a cobalt(II) complex on the radical reaction of vinyl type sulfides. A 'radico-catalysis'

Masaru Tada,* Tomohiro Uetake and Yoshinobu Hanaoka

Department of Chemistry, the Advanced Research Center for Science and Engineering, and Materials Research Laboratory for Bioscience and Photonics, Waseda University, Shinjuku, Tokyo 169-8555, Japan.
E-mail: mtada@mn.waseda.ac.jp

Received (in Cambridge, UK) 4th November 1998, Accepted 27th November 1998

Vinyl type sulfides show increased radicophilicity at the β-position *via* the coordination to a cobalt(II) complex, and hence the balance between Smiles rearrangement and an *ortho*-substitution, in vinyl type sulfides having an intramolecular alkyl radical, is lost to favor the latter reaction.

Acid and base catalysis generates a 'paired electron hole' [eqn. (1)] and a 'paired electron pool' [eqn. (2)], respectively. Likewise radical catalysis can be defined as the generation of 'unpaired electron density' at the reaction center [eqn. (3)].

Acid catalysis: RX + Acid ⟶ $R^{\delta+}$---X---$Acid^{\delta-}$ (1)
Base catalysis: RX + Base ⟶ $R^{\delta-}$---X---$Base^{\delta+}$ (2)
Radico-catalysis: RX + •(Rad) ⟶ $R^{\delta\bullet}$---X---$Rad^{\delta\bullet}$ (3)

We have demonstrated that a cobalt(II) complex, cobaloxime(II),[1]† accelerates the radical substitutions on the sulfur of a thioester group [eqn. (4)][2] and the radical 1,2-rearrangement of a thioester group [eqn. (5)].[2,3] Caddick *et al*.,[4] Aldabbagh and

$$Me\bullet + RCOSAr \xrightarrow{[Co^{II}]L} MeSAr + RCO\bullet \quad (4)$$

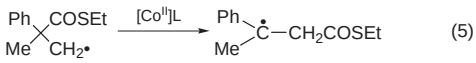

(5)

Bowman,[5] and Tada *et al*.[6] showed the usefulness of the sulfur function in the radical annelation on indole and benzimidazole systems, in which the intramolecular alkyl radicals attack the *ipso*-position to yield indoleno or benzimidazoleno carbocycles by the extrusion of the sulfur function. We have suggested the effect of cobaloxime(II) in the radical annelation of 2-phenylthioindole *via* an intramolecular *N*-alkyl radical.[6]

Here we report another type of radico-catalysis by cobaloxime(II) in the radical annelation of benzothiophene and uracil derivatives. Coordination of a vinyl type sulfide to cobalt(II) generates an unpaired electron (spin) density on the sulfur, which can delocalize to the β-position of the vinyl group as shown in Fig 1. The coordination has been proven *via* an EPR

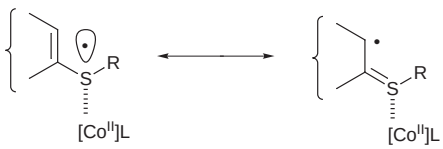

Fig. 1 Resonance expression of spin delocalization in a sulfur–cobalt(II) complex.

study by us[7] and characterized by back donation from cobalt(II) to sulfur. The bonding force of this back donation makes the unstable two-centered three electron bond feasible.

Homolysis of triphenyltin cobaloxime produces a triphenyltin radical and cobaloxime(II) [eqn. (6)] but the former dissipates *via* reaction with a halide to leave an organo radical [eqn. (7)]. Thus the organo radical and cobaloxime(II) coexist in the reaction system and associate by the coordinative interaction discussed above [eqn. (8)]. The interaction of the vinyl type

$Ph_3Sn[Co]L \longrightarrow Ph_3Sn\bullet + [Co^{II}]L$ (6)
$RBr + \bullet SnPh_3 \longrightarrow R\bullet + Ph_3SnBr$ (7)
$R\bullet + [CO^{II}]L \longrightarrow (R\bullet)\text{---}[CO^{II}]L$ (8)

sulfide and the cobalt(II) species may increase the radicophilicity of the vinyl moiety.

Thus 3-(benzothiophen-2-ylthio)-2,2-dimethylpropyl bromide **1** was treated with triphenyltin cobaloxime under heating and the products **3** and **5** were obtained as shown in Scheme 1. The thermolysis gives the cobaloxime(II) radical and the intermediate radical **A** which interact with each other by the coordination discussed above to give radical **B** and thus product **3** (Scheme 2).

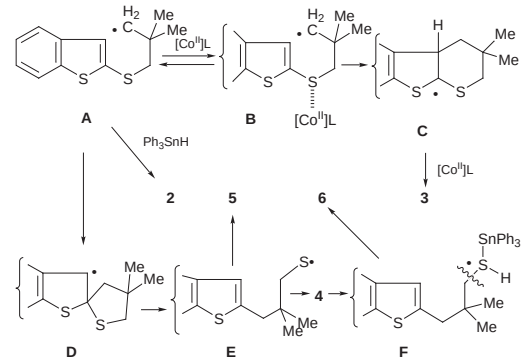

Scheme 2

Treatment of bromide **1** with Ph_3SnH–AIBN gave the products **4** and **6** after Smiles rearrangement by an addition–elimination mechanism (**A**→**D**→**E** in Scheme 2)[8] and the reduction product **2**. Thus the cobaloxime(II) in the reaction system evidently accelerates the radical attack on the 3-position of benzothiophene and *ortho*-substitution becomes competitive with the radical Smiles rearrangement.[8–10] On the other hand, in

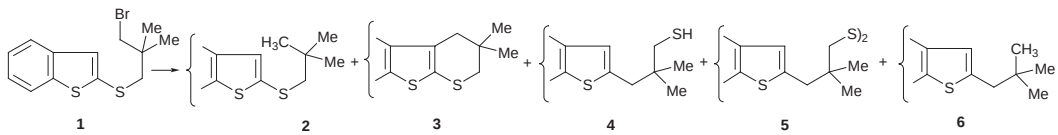

	2	3	4	5	6
$Ph_3Sn[Co]L$ / 130 °C‡	—	17%	—	70%	—
Ph_3SnH–AIBN / 80 °C§	11%	—	71%	—	14%

Scheme 1

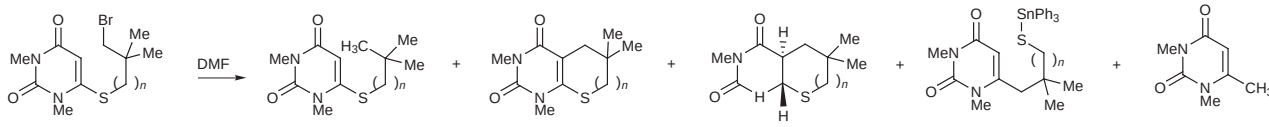

	7	8	9	10	11	12
n = 1 Ph_3Sn[Co]L‡	—	—	73%	—	—	—
n = 1 Ph_3SnH–AIBN§	—	—	—	38%	45%	8%
n = 2 Ph_3Sn[Co]L‡	28%	47%	—	—	—	—
n = 2 Ph_3SnH–AIBN§	82%	—	—	—	—	—

Scheme 3

addition to product **2**, only the products of Smiles rearrangement were obtained without cobaloxime(II). The formation of the product **6** is accounted for by radical substitution on sulfur through the radical intermediate **F**. A reasonable mechanism for formation of these products is shown in Scheme 2.

Next we tested the effect of cobaloxime(II) on the radical from *n*-(1,3-dimethyluracil-5-ylthio)-2,2-dimethylalkyl bromide **7** and a similar acceleration effect was observed for the *ortho*-substitution, as shown in Scheme 3. Bromide **7** (*n* = 1) gave the substitution product **9** in the presence of cobaloxime(II) whereas the reaction with Ph_3SnH gave the addition product **10** and the products **11** and **12** formed *via* Smiles rearrangement (Scheme 4).

Both Smiles rearrangement *via* a six-membered intermediate (**J**) (*n* = 2) and *ortho*-addition *via* a seven-membered intermediate (**I**) (*n* = 2) are slow and the only product from the reaction of Ph_3SnH and bromide **7** (*n* = 2) is the direct reduction product. The reaction with triphenyltin cobaloxime, however, gave the *ortho*-substitution product **9** (*n* = 2) as a major product, however the intramolecular radical addition is still slow and hydrogen abstraction form the solvent to give product **8** (*n* = 2) is the dominant process. A reasonable mechanism for formation of **8**–**12** is illustrated in Scheme 4. The intermediate radical **I** (*n* = 1) which gives **10** (*n* = 1) is formed even without cobaloxime(II), although with lower efficiency, while radical **I** (*n* = 2) which gives **9** (*n* = 2) is formed only with the assistance by cobaloxime(II). The intermediates **I** (*n* = 1,2) give products **9** (*n* = 1,2) with hydrogen elimination by cobaloxime(II) and the product **10** (*n* = 1) *via* hydrogen abstraction from the tin hydride. Products **11** and **12** derive from the intermadiate **L** (*n* = 1) *via* hydrogen elimination [route (a)] and the fragmentation process [route (b)], respectively, after Smiles rearrangement (Scheme 4).

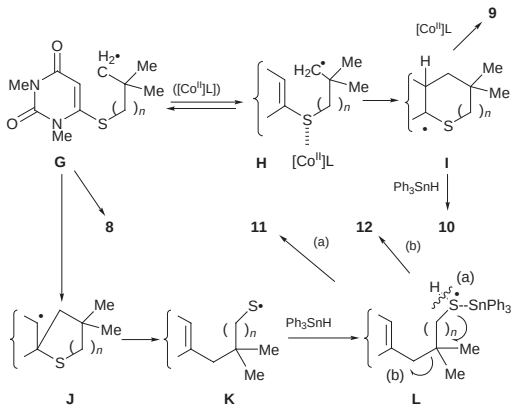

Scheme 4

All the experimental results shown here suggest an acceleration effect of cobalt(II) species on the radical attack of an alkyl radical on a vinyl type sulfide. Thus the coordination of a vinyl sulfide to a paramagnetic cobalt(II) complex generates a spin density at the β-position and makes the β-position more radicophilic. We propose a term 'radico-catalysis' for this effect even though the reaction is stoichiometric and not 'catalytic' in the correct sense.

Experimental details and structural assignments of the products will be reported in a full paper.

The present work was supported by Waseda University and the Ministry of Education, Culture, and Sports of Japan through an Annual Project Program and a Grant-in-Aid for Scientific Research, respectively

Notes and references

† Cobaloxime(II) is bis(dimethylglyoximato)(4-*tert*-butylpyridine)cobalt(II) and denoted here by [Co^{II}]L.

‡ *Reaction conditions*: **1** or **7** (0.1 mmol), Ph_3Sn[Co]L (0.3 mmol), DMF (5.0 ml), 130 °C, 24 h.

§ *Reaction conditions*: **1** or **7** (0.1 mmol), Ph_3SnH (0.2 mmol), AIBN (0.1 mmol), benzene (40 ml), 80 °C, 4 h.

1 Review on cobaloxime: J. Halpern, *B_{12}*, ed. D. Dolphin, Wiley, New York, 1981, vol. 1, ch. 14; D. Dodd and M. D. Johnson, *J. Organomet. Chem*., 1973, **52**, 1; G. N. Schrauzer, *Angew. Chem*., *Int. Ed. Engl*., 1976, **15**, 417; N. B. Pahor, F. Forcolin, L. Randaccio, L. G. Marzilli, M. F. Summers and P. J. Toscano, *Coord. Chem. Rev*., 1985, **63**, 1.

2 M. Tada, K. Inoue and K. Sugaweara, *Chem. Lett*., 1985, 1821; M. Tada, T. Yoshihara and K. Sugano, *J. Chem. Soc*., *Perkin Trans. 1*, 1995, 1941.

3 M. Tada. K. Inoue, K. Sugawara and M. Okabe, *Chem. Lett*., 1986, 703; M. Tada, T. Nakamura and M. Matsumoto, *J. Am. Chem. Soc*., 1988, **110**, 4697.

4 S. Caddick, K. Aboutyab and R. I. West, *Synlett*, 1993, 231; *J. Chem. Soc*., *Chem. Commun*., 1995, 1353; S. Caddick, K. Aboutyab, K. Jenkins and R. I. West, *J. Chem. Soc*., *Perkin Trans. 1*, 1996, 675; K. Aboutyab, S. Caddick, K, Jenkins, S. Joshi and S. Khan, *Tetrahedron*, 1996, **52**, 11329; S. Caddick, C. L. Shering and S. N. Wadman, *Tetrahedron Lett*., 1997, **38**, 6249.

5 F. Aldabbagh and W. R. Bowman, *Tetrahedron Lett*., 1997, **38**, 3793.

6 T. Uetake, M. Nishikawa and M. Tada, *J. Chem. Soc*., *Perkin Trans 1*, 1997, 3591.

7 M. Tada and R. Shino, *J. Inorg. Biochem*., 1991, **44**, 89.

8 D. C. Harrowven, *Tetrahedron Lett*., 1993, **34**, 5653.

9 L. Benati, L. Capella, P. C. Montevecchi and P. Spagnolo, *J. Org. Chem*., 1994, **59**, 2818; 1995, **60**, 7941; L. Capella, P. C. Montevecchi and D. Nanvi, *J. Org. Chem*., 1994, **59**, 3368; L. Capella, P. C. Montevecchi and M. L. Navacchia, *J. Org. Chem*., 1995, **60**, 7424; P. C. Montevecchi and M. L. Navacchia, *J. Org. Chem*., 1998, **63**, 537.

10 E. Lee, H-S. Whang and C. K. Chung, *Tetrahedron Lett*., 1995, **36**, 913.

Communication 8/08576E

Facile synthesis of amino-functionalised ferrocenes and vanadocenes

Sam Bradley, Patrick C. McGowan,* Karrie A. Oughton, Mark Thornton-Pett and Mark E. Walsh

School of Chemistry, University of Leeds, UK LS2 9JT. E-mail: p.c.mcgowan@chem.leeds.ac.uk

Received (in Cambridge, UK) 6th November 1998, Accepted 27th November 1998

We report a general and high yielding route to the synthesis of late and early metallocenes; reported is an amino-functionalised vanadocene which is an unusual example of a 1,1-substituted vanadocene outside of a group 14 substituted derivative.

The importance of metallocenes has been documented recently with potential applications in several areas of chemistry.[1,2] There has been a considerable amount of research done with functionalised ferrocenes, and besides potential therapeutic activity,[3] other useful functions with these types of molecules have been their ability to recognise neutral molecules,[4] as well as cations and anions.[5] Multidentate functionalised ferrocenes have also been prepared where there are more than two donor heteroatoms.[6] These, like many bis-functionalised ferrocenes, start with ferrocene as the starting material and quite often there are many steps to arrive at the end product. For example, there has been a report of one primary alkylaminoferrocene synthesised in small amounts, but this takes four steps starting from ferrocene.[7] Whilst it is relatively facile to make the mono-functionalised aminoferrocene, it is somewhat more difficult to make the bis-functionalised analogues. The main problem about preparing bis-1,1-aminoferrocenes is the poor yield of the substitution of the second ring.

Conversely, research into vanadocene chemistry has been remarkably low. This is unfortunate given the potential anti-tumour properties of such complexes,[8] but one of the main problems is the highly sensitive nature of these compounds.[2] With both of these criteria in mind, this paper presents a general, convenient and efficient method of synthesising bis-functionalised ferrocenes and vanadocenes from the parent substituted cyclopentadienyl analogue and the appropriate metal halide. We have deliberately chosen a late and an early metal derivative to show the general nature of the methodology.

A high yielding route to synthesise and isolate the pure amino-functionalised sodium cyclopentadienide salt routinely on a scale of 15–20 g has been developed.[9] Using this method, we can methodically and easily vary the length of the spacer group between the cyclopentadienyl group and the amino group; the substituents attached to the nitrogen atom can also be modified. This paper describes the high yielding route to different bis-1,1-amino-ferrocenes and -vanadocenes which have different spacer groups and end groups. Yields have been typically 65–80%.

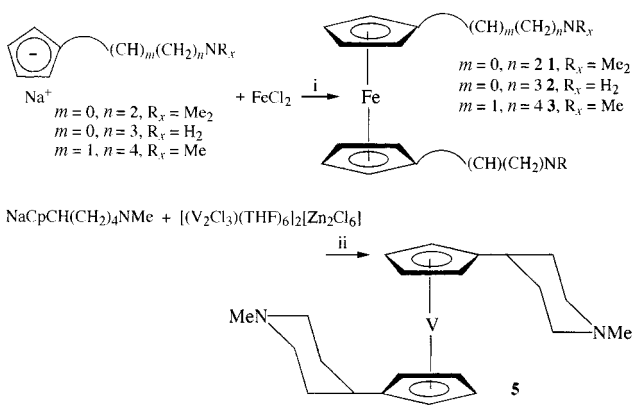

Scheme 1 Reagents and conditions: i, THF, 65–76%; ii, THF, 72%.

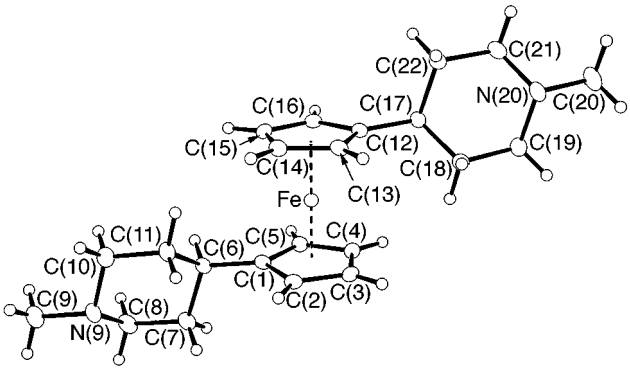

Fig. 1 X-Ray structure of ferrocene **3**.

Reaction of 2 equivalents of $NaCp(CH_2)_2NMe_2$ with $FeCl_2$ yields $Fe[Cp(CH_2)_2NMe_2]_2$ **1** in 76% yield as an analytically pure yellow–orange oil (Scheme 1).† Using this versatile and facile method, we can produce primary alkylaminoferrocenes as well. As already mentioned, these compounds are notoriously difficult to synthesise by other means[7] and to our knowledge $Fe[Cp(CH_2)_3NH_2]_2$ **2** is only the second example of this type. It is synthesised by readily available starting materials such as $FeCl_2$ and 2 equivalents of $NaCp(CH_2)_3NH_2$ and has the advantage that it is high yielding and is one step. Decreasing the flexible nature of the substituted arm has a profound effect on the ferrocene in that we can isolate an orange solid $Fe[CpCH(CH_2)_4NMe]_2$ **3** as opposed to the oils obtained for **1** and **2**.‡ The molecular structure§ of **3** can be seen in Fig. 1 and the steric encumbrance of the piperidyl groups is evident as they lie *trans* to each other.

Complex **1** reacts with equivalents of MeI to afford the ferrocene salt $Fe[Cp(CH_2)_2NMe_3]_2^{2+}2[I]^-$ **4** (Scheme 2) which was recrystallised from methanol. **4** crystallises as a yellow microcrystalline analytically pure material which was characterised by ^1H and ^{13}C spectroscopy and again occurs in high yield, 75%. It is methanol and water soluble and air stable. Alternative entry into this class of compound has been achieved by a three step synthesis from ferrocene to yield ferrocene-1,1′-diylbis(methyltrimethylammonium iodide).[10]

The functionalised sodium cyclopentadienide salts can also be used to prepare early metal metallocenes. The only heteroatom ring substituted vanadocenes that we are aware of are $(C_5H_4EMe_3)_2V$ (E = Si, Ge, Sn).[11] Thus, outside of the group 14 ring substituted vanadocenes, we report here an unusual fully characterised example of a 1,1-substituted

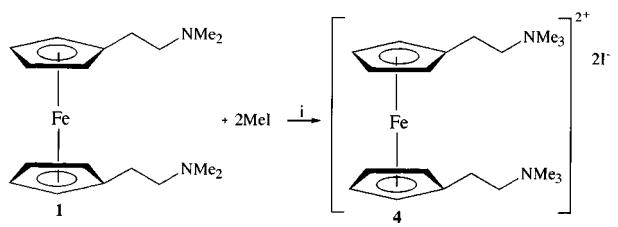

Scheme 2 Reagents and conditions: i, Et_2O, 75%.

vanadocene. This has been synthesised using the starting material $[(THF)_3V(\mu\text{-}Cl)_3V(THF)_3]_2[Zn_2Cl_6]$[12] and $NaCpCH(CH_2)_4NMe$ to yield compound **5** in 72% yield. This highly air and water sensitive paramagnetic material is deep purple in colour and difficult to characterise. The X-ray crystal structure§ has been determined and is isomorphous with **3**. We are currently carrying out oxidation reactions of this and other analogues of amino-substituted vanadocenes.[13] It is important to note that, for both the vanadocene and ferrocene analogues highlighted in this paper, we have had no need to use chromatographic techniques and they have been synthesised as analytically pure compounds.

We have also embarked on a strategy of synthesising ligands where there would be more chance of the nitrogen moiety interacting with a metal centre. Therefore we synthesised the ligand **6**. During the course of this work the preparation of the ligand **6** and the thallium salt and the reactivity with group IV transition metals have been reported.[14] We have used our methodology to isolate the sodium salt **7** from the reaction of **6** with NaH giving the new compound **7** which is air and water sensitive. This has been characterised by ^1H and ^{13}C NMR. Like previously reported compounds[9] this compound undergoes exchange with the deuterated solvent (CD_3CN) where the protons from the ring exchange with the deuterons of the solvent.

$$\underset{\mathbf{6}}{C_5H_5CH_2C_6H_4N} + NaH \xrightarrow{THF} \underset{\mathbf{7}}{NaCpCH_2C_6H_4N}$$

In summary, we feel that the generality of our procedures will allow the isolation and tailoring of many types of amino-substituted metallocenes in high yields starting from the sodium salts of the substituted cyclopentadiene and a transition metal halide salt. We have proved this by the isolation of amino-functionalised ferrocenes; especially significant is the isolation of the primary alkylaminoferrocenes. We have also found an effective route into amino-functionalised vanadocenes, which have been synthesised and fully characterised for the first time.

Notes and references

† All compounds were characterised by CHN analyses, ^1H, ^{13}C NMR and FAB mass spectrometry.

‡ A typical procedure is as follows: to a solution of $FeCl_2$ (1 g, 0.0078 mol) in THF (30 ml) was added two equivalents of $NaCpCH(CH_2)_4NMe$ (2.9 g, 0.0176 mol). An orange colour was observed. After several hours the THF was removed under vacuum, and the residues extracted twice with toluene (20 ml) and then dried under vacuum. The product was recrystallised from toluene. Yield = 1.9 g, 67%.

§ Crystal data for **3**: $C_{22}H_{32}FeN_2$, 380.35, triclinic, space group $P\bar{1}$, a = 7.1259(5), b = 10.7296(10), c = 13.4298(11) Å, α = 103.584(8), β = 96.905(7), γ = 101.691(8)°, V = 962.08(13) Å^3, Z = 2, D_c = 1.313 Mg m^{-3}. 3780 unique reflections collected (Stoe STADI4 diffractometer, Mo-Kα, 150 K) of which 3678 were observed [$F^2 > 2.0\sigma F^2$]. Solved by direct methods (SHELXS-97) and refined by full-matrix least squares (SHELXL-97) on F^2 of all unique data to R_1 = 0.0248 (observed data), wR = 0.0695 (all data), S = 1.093. For **5**: $C_{22}H_{32}VN_2$, 375.44, triclinic, space group $P\bar{1}$, a = 7.6238(2), b = 10.4591(3), c = 13.8715(2) Å, α = 102.695(2), β = 98.438(2), γ = 101.3270(12)°, V = 1036.97(4) Å^3, Z = 2, D_c = 1.202 Mg m^{-3}. 12278 reflections collected (Nonius KappaCCD diffractometer, Mo-Kα, 190 K) of which 4434 were unique and 3629 were observed [$F^2 > 2.0\sigma F^2$]. Structure solution and refinement as above, R_1 = 0.0339 (observed data), wR = 0.0996 (all data), S = 1.095. CCDC 182/1099. See http://www.rsc.org/suppdata/cc/1999/77/, for crystallographic files in .cif format.

1 *Ferrocenes: homogeneous catalysis, organic synthesis, materials science*, ed. A. Togni and R. L. Hayashi, VCH, Weinheim, 1995.
2 *Metallocenes*, A. Togni and R. L. Halterman, Wiley-VCH, 1998.
3 C. Price, M. Aslanoglu, C. J. Isaac, M. R. J. Elsegood, W. Clegg and B. R. Horrocks, *J. Chem. Soc., Dalton Trans.*, 1996, 4115.
4 J. D. Carr, L. Lambert, D. E. Hibbs, M. B.Hursthouse, K. M. A. Malik and J. H. R. Tucker, *Chem. Commun.*, 1997, 1649.
5 P. D. Beer, *Acc. Chem. Res.*, 1998, **31**, 71.
6 N. J. Long, J. Martin, A. J. P. White and D. J. Williams, *J. Chem. Soc., Dalton Trans.*, 1997, 3083.
7 M. Herberhold and M. Ellinger, *Organometallic Synthesis, Vol. 3*, ed. R. B. King and J. J. Eisch, Elsevier, 1986.
8 P. Köpf-Maier and H. Köpf, *Z. Naturforsch. Teil B*, 1979, **34**, 805.
9 P. C. McGowan, C. E. Hart, B. Donnadieu and R. Poilblanc, *J. Organomet. Chem.*, 1997, **528**, 191.
10 C. Glidewell, B. J. L. Royles and D. M. Smith, *J. Organomet. Chem.*, 1997, **527**, 259.
11 F. H. Köhler and W. A. Geike, *J. Organomet. Chem.*, 1987, **328**, 35.
12 C. Floriani and V. Mange, *Inorganic Synthesis*, ed. R. J. Angelici, John Wiley and Sons, 1990.
13 S. Bradley and P. C. McGowan, unpublished work.
14 M. S. Blais, J. C. W. Chien and M. D. Rausch, *Organometallics*, 1998, **17**, 3775.

Communication 8/08685K

What is the mechanism of phosphoryl transfer in protein kinases? A hybrid quantum mechanical/molecular mechanical study

Jason C. Hart, David W. Sheppard, Ian H. Hillier* and Neil A. Burton

Department of Chemistry, University of Manchester, Manchester, UK M13 9PL. E-mail: ian.hillier@man.ac.uk

Received (in Cambridge, UK) 17th November 1998, Accepted 20th November 1998

Hybrid QM/MM studies suggest that the conserved aspartate in protein kinases is not protonated during the phosphoryl transfer reaction, and thus does not act as a general base.

Protein kinase enzymes are critical to the regulation of cellular signalling pathways and changes in their activity has been linked to several diseases including cancer and diabetes. These enzymes phosphorylate serine (Ser), threonine (Thr) and tyrosine (Tyr) residues at target proteins *via* transfer of the γ-phosphate of adenosine triphosphate (ATP). Around 2000 different protein kinase enzymes are predicted from the human genome[1] and structural data suggest that a conserved catalytic core is present in all such enzymes.[2] A conserved phosphoryl transfer mechanism is predicted with the regions of the protein outside the catalytic core influencing substrate specificity.

A conserved aspartate (Asp) residue is present in the active site which has been widely proposed to act as a general base during the phosphorylation reaction,[3] which involves nucleophilic attack of Ser at the γ-phosphate centre. It has been suggested that the role of Asp is to deprotonate Ser, providing a more powerful nucleophile to achieve phosphate hydrolysis leading to the products shown in Fig. 1(*b*). On the other hand, recent experimental data on serine[4] and tyrosine[5] kinases have questioned whether Asp is basic enough to remove the proton from Ser (compare solution pK_a of 4 and 14 for Asp and Ser, respectively) or Tyr residues. An alternative role is proposed of aligning the OH group before reaction[4] with proton transfer to Asp occurring after the O–P bond is formed.

In an attempt to elucidate the mechanism of phosphoryl transfer in this important class of enzymes we here describe hybrid quantum mechanical (QM)/molecular mechanical (MM) calculations of the potential energy surface associated with this reaction. Such studies have been helpful in the study of the reactions in a variety of enzymes.[6–11] We employ our hybrid QM/MM code[11] which couples the QM code GAUSSIAN 94[12] with the MM code AMBER 4.0[13] to perform the calculations.

We utilised the crystal structure of cAMP dependent kinase (cAPK) complexed with ATP and a peptide inhibitor,[14] building a model of the native system by replacing the alanine residue of the inhibitor with Ser. Energy minimisation of this new residue, keeping the remainder of the active site fixed, was carried out using AMBER. This structure was used as a starting point for subsequent QM/MM calculations with the QM part of the structure consisting of the 46 atoms shown in Fig. 2. The QM region contains the Ser substrate, the conserved Asp and a lysine (Lys) residue (although our conclusions are not altered if Lys is modelled by MM), the triphosphate group and the two Mg ions which coordinate the triphosphate. The bulk of the enzyme and the non-reacting parts of the peptide and ATP substrates were kept fixed during the modelling of the reaction and were represented by around 6200 MM atoms including crystallographic waters. We chose to use the PM3[15] Hamiltonian in the QM calculations due to its success in modelling phosphoryl transfer reactions.[16]

The reaction products resulting from proton transfer from Ser to Asp along with nucleophilic attack at phosphorus leading to ADP and a phosphorylated serine (pSer) dianion [Fig. 1(*b*)] were found to be higher in energy than the reactant structure [Fig. 1(*a*)] by 36 kcal mol^{-1}. However, an alternative product [Fig. 1(*c*)] involving an ionised Asp and a pSer monoanion were found to be lower in energy than the reactants by 24 kcal mol^{-1}. Our computational scheme allows the various contributions to the large energy difference (60 kcal mol^{-1}) between structures in Fig. 1(*b*) and (*c*) to be identified. In the absence of Lys-154 and the rest of the enzyme, the two structures have essentially the same energy in spite of the bulk pK_as favouring the structure in Fig. 1(*c*). This is due to the stabilisation of the phosphate dianion by the magnesium ions. However, interaction with the bulk of the enzyme leads to the preferential stabilisation of the structure in Fig. 1(*c*), with Lys-154 contributing ~20 kcal mol^{-1}. Thus, as a number of authors[17] have emphasised, it is the

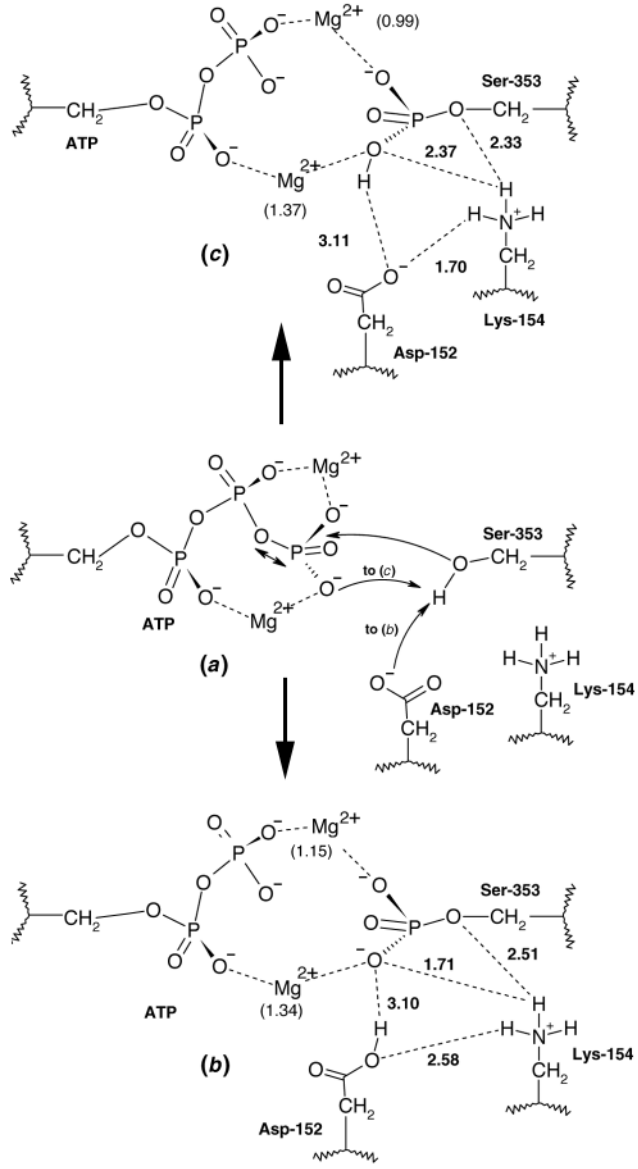

Fig. 1 Alternative mechanisms of phosphoryl transfer in protein kinase, with optimised structures (Å) and, in parenthesis, atomic charges.

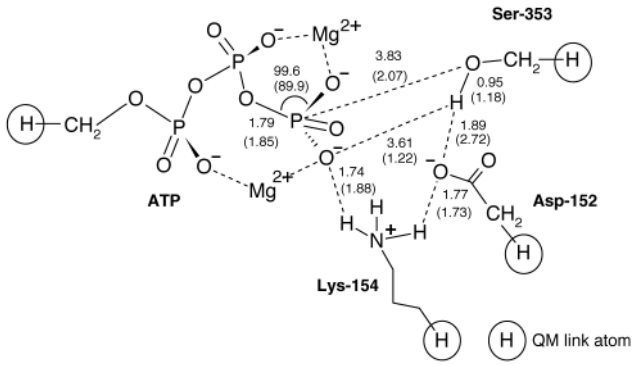

Fig. 2 Optimised reactant, and in parenthesis, transition state geometry (Å) in cAMP dependent kinase.

local electrostatic microenvironment that is important in determining the effective pK_as of the residues, rather than the bulk values (6.3[18] and 4.0[19] for pSer and Asp respectively).

In view of this result we have modelled the potential energy surface for the reaction which involves proton transfer from Ser to a terminal oxygen of ATP and nucleophilic attack at the phosphorus atom of ATP leading to the structure shown in Fig. 1(*c*) without the formation of a high energy serine anion intermediate. The properly characterised transition state (Fig. 2, imaginary frequency 2064*i* cm^{-1}) involves a concerted cleavage of the Ser O–H and P–O(bridge) bonds and formation of H–O(P) and P–O(Ser) bonds, and has a barrier of 39 kcal mol^{-1}. The alternative mechanism involving transfer of the proton from Ser to Asp either before or after O–P bond formation leads to a neutral Asp residue [Fig. 1(*b*)] and has higher barriers in the region of 45–50 kcal mol^{-1}, as well as leading to the higher energy product.

Thus although our calculations at the PM3 level are only semi-quantitative they do suggest that the role of the Asp residue may not be as a general base, but rather to stabilise protonated pSer in the active site [Fig. 1(*c*)]. Such stabilisation by protonation is often observed when two charged groups are in close proximity[20] and the position of a proton between Asp and Glu residues in a protein has been established by high resolution crystallography.[21] The relative pK_a values of pSer and Asp in model systems would suggest that protonation of pSer will be favoured in line with our computational results. A similar mechanism may also be involved in other enzyme catalysed phosphoryl transfer reactions, such as those involving protein tyrosine phosphatases, where a conserved Asp residue is found and is considered to be a general acid.[22] Here protonation of the phosphate terminal oxygen rather than Asp may occur in the reactants. Thus possible enzyme mechanisms other than those in which the Asp is a general acid or base should be considered in these important and widely occurring classes of enzymes.

We thank the EPSRC for support of this work.

Notes and references

1 T. Hunter, *Biochem. Soc. Trans.*, 1996, **24**, 307.
2 D. Bossemeyer, *FEBS Lett.*, 1995, **369**, 57.
3 A. S. Mildvan, *Proteins: Struct., Funct., Genet.*, 1997, **29**, 401.
4 J. Zhou and J. A. Adams, *Biochemistry*, 1997, **36**, 2977.
5 K. Kim and P. A. Cole, *J. Am. Chem. Soc.*, 1997, **119**, 11 096.
6 A. Warshel and M. Levitt, *J. Mol. Biol.*, 1976, **103**, 227.
7 M. J. Field, P. A. Bash and M. Karplus, *J. Comput. Chem.*, 1990, **11**, 700.
8 J. Aqvist and A. Washel, *Chem. Rev.*, 1993, **93**, 2523.
9 U. C. Singh and P. A. Kollman, *J. Comput. Chem.*, 1986, **7**, 718.
10 B. Waszkowycz, I. H. Hillier, N. Gensmantel and D. W. Payling, *J. Chem. Soc., Perkin Trans. 2*, 1991, 225.
11 M. J. Harrison, N. A. Burton and I. H. Hillier, *J. Am. Chem. Soc.*, 1997, **119**, 12 285.
12 M. J. Frisch, G. W. Trucks, H. B. Schlegel, P. M. W. Gill, B. G. Johnson, M. A. Robb, J. R. Cheeseman, T. A. Keith, G. A. Petersson, J. A. Montgomery, K. Raghavachari, M. A. Al-Laham, V. G. Zakrzewski, J. V. Ortiz, J. B. Foresman, J. Cioslowski, B. B. Stefanov, A. Nanayakkara, M. Challacombe, C. Y. Peng, P. Y. Ayala, W. Chen, M. W. Wong, J. L. Andres, E. S. Replogle, R. Gomperts, R. L. Martin, D. J. Fox, J. S. Binkley, D. J. Defrees, J. Baker, J. P. Stewart, M. Head-Gordon, C. Gonzalez and J. A. Pople, GAUSSIAN94, Gaussian Inc., Pittsburgh PA, 1995.
13 D. A. Pearlman, D. A. Case, J. C. Caldwell, G. L. Seibel, U. C. Singh, P. Weiner and P. A. Kollman, AMBER 4.0, University of California, San Francisco, 1994.
14 D. R. Knighton, J. Zheng, L. F. Ten Eyck, N.-H. Xuong, S. S. Taylor and J. M. Sowadski, *Science*, 1991, **253**, 414.
15 J. J. P. Stewart, *J. Comput. Chem.*, 1989, **10**, 209.
16 J. Wilkie and D. Gani, *J. Chem. Soc., Perkin Trans. 2*, 1996, 783.
17 A. Warshel and J. Aqvist, *Annu. Rev. Biophys. Biophys. Chem.*, 1991, **20**, 267; P. A. Frey, *Science*, 1995, **269**, 104.
18 D. J. Graves and S. Luo, *Biochem. Biophys. Res. Commun.*, 1994, **205**, 618.
19 A. Fersht, *Enzyme Structure and Mechanism*, W. H. Freeman, New York, 1985.
20 T. Bugg, *An Introduction to Enzyme and Coenzyme Chemistry*, Blackwell Science, Oxford, 1997.
21 J. R. Helliwell, *Nat. Struct. Biol.*, 1997, **4**, 874.
22 Z.-Y. Zhang, *Crit. Rev. Biochem. Mol. Biol.*, 1998, **33**, 1.

Communication 8/08955H

A non-hydrolytic route to organically-modified silica

John Hay,*[a] David Porter[b] and Hema Raval[a]

[a] *Department of Chemistry, School of Physical Sciences, University of Surrey, Guildford, UK GU2 5XH. E-mail: j.hay@surrey.ac.uk*

[b] *SMC, DERA, Farnborough, Hampshire, UK GU14 0LX*

Received (in Bath, UK) 21st September 1998, Accepted 26th November 1998

A versatile route to organic–inorganic hybrid nanocomposite materials is described, where organically modified silicon halides and alkoxides are reacted together in a solvent-free non-hydrolytic sol–gel process.

The combination of organic species and inorganic minerals and networks has attracted much interest in recent years for a number of reasons,[1–4] including the development of next generation passive (*e.g.* semi-structural[5]) and active (*e.g.* electronic[6]) materials. Much work has focused on the preparation of sol–gel hybrids, such as the combination of inorganic oxides (particularly silica) with polymers[4,5,7] and the organic modification of silica ('Ormosils') starting from alkylalkoxysilanes.[8–10] All of these methods use the well established hydrolytic route to the oxide. In recent years, the group of Corriu[11–13] and others including ourselves[14,15] have reported the synthesis of inorganic oxides *via* a non-hydrolytic sol–gel route which involves the reaction of a 'metal' halide with an oxygen donor such as an alkoxide, an ether, an alcohol, *etc.* One advantage of this approach is that it can avoid the use of solvents and their associated drawbacks. In addition, residual silanol groups in the product should be substantially reduced because of the different mechanism involved. The method has been extended to the formation of copolysiloxanes[16] and erbium doped methyl-modified silicates.[17] To the best of our knowledge, there have been no reports to date of the extension of this method to the preparation of hybrid Ormosils with a variety of organic groups.

Here, we describe the synthesis of organic–inorganic hybrids using the non-hydrolytic sol–gel method starting from organically modified precursors. Silica hybrids are particularly accessible by this route since the necessary precursors such as alkylalkoxysilanes and alkylchlorosilanes are in many cases commercially available. Related hybrids such as those based on alumina suffer from the serious drawback of the high, sometimes pyrophoric, reactivity of the metal–alkyl bonds. The silica hybrids are represented by the general equations shown below:

$$RSiCl_3 + 0.75Si(OR')_4 \rightarrow [RSi_{1.75}O_3]_n + 3R'Cl \quad (1)$$

$$RSiCl_3 + RSi(OR')_3 \rightarrow [R_2Si_2O_3]_n + 3R'Cl \quad (2)$$

The use of a single organically-modified precursor [eqn. (1)] leads to an Ormosil with only one type of organic modifying group. If both precursors are organically modified [eqn. (2)], the resulting hybrid can contain two different types of organic modification. The organic groups can be alkyl (groups of varying length from methyl to decyl have been used), vinyl or aryl. In a typical experiment, the hexyl-modified silica was formed by reacting hexyltrichlorosilane (5.62 g, 26 mmol) with tetraethylorthosilicate (TEOS) (4.00 g, 19 mmol) in the presence of iron(III) chloride catalyst (0.071 g, 0.73%) under nitrogen. The material gelled within 1–2 days at 35 °C. The resulting solid (containing a colourless liquid) was subjected to Soxhlet extraction using diethyl ether for three days, yielding a white, semi-transparent waxy product (3.92 g, 84%). Elemental analysis gave: C, 39.9; H, 8.1 (Calc. C, 39.5; H 7.2%). The organic content calculated from the elemental analysis is 48.0%, in good agreement with the theoretical value of 46.7%. Thermogravimetric (TG) analysis in nitrogen at a heating rate of 10 K min^{-1} from 40 to 900 °C showed a weight loss of 47%, in excellent agreement with the theoretical organic content. The diffuse reflectance IR spectrum showed C–H stretching vibrations at 2860–2970 cm^{-1}, an $SiCH_2$ deformation band at 1400–1420 cm^{-1} and various Si–O–Si vibrations between 480 and 1210 cm^{-1}. Preliminary BET surface area analysis gave values well below 1 m^2 g^{-1} for the total surface area, but isotherms are complex and are the subject of further work.

Gelation could normally be accomplished at temperatures of 90 °C or below using iron(III) chloride as catalyst.[14] Gel times at 90 °C typically range from a few minutes to several hours depending on the nature of the organic modification. For long alkyl chains and phenyl groups, gel times were longer for the organically-modified systems than for pure silica because of the combined effects of reduction of the concentration of reacting groups and steric hindrance by the bulky organic groups. The presence of short alkyl chains such as methyl and ethyl in the halide precursor had little effect on gel times, the effect of reduced functionality presumably being counterbalanced by the electron-donating capacity of the alkyl groups increasing the reactivity of the silicon halide. This effect is particularly marked in the case of vinyl-modified systems, where use of vinyltrichlorosilane in place of silicon(IV) chloride could reduce the gel times by an order of magnitude. The non-hydrolytic approach therefore provides a rapid route to the Ormosils.

The non-hydrolytic route produces a volatile by-product, in this case an alkyl, aryl or vinyl chloride, hence the liquid produced in the above experiment. The by-product and any unreacted starting materials are easily separated from the product by Soxhlet extraction. In the case of vinyl-substituted silica, and perhaps also the aryl-substituted materials, a possible side reaction is electrophilic attack of 'R^+' (a possible intermediate in the non-hydrolytic reaction[11]) on the double bond leading in the vinyl case to addition of RCl across the double bond. IR and solid state ^{13}C CPMAS NMR spectroscopy show the presence of unreacted vinyl group and suggest that any side reaction is insignificant. The double bond vibrations are clearly visible in the IR spectrum at 1610, 1000 and 960 cm^{-1}, while the ^{13}C NMR spectrum (Fig. 1) shows intense vinyl carbon resonances at δ 130.4 and 137.0. The existence of an Si–C bond is indicated by an IR absorption at *ca.* 1400 cm^{-1} and a large peak in the ^{29}Si CPMAS NMR spectrum at δ −79.8

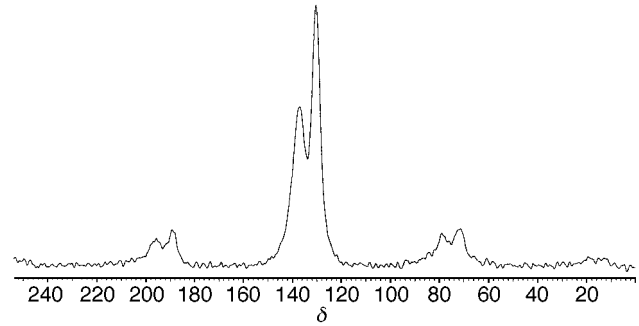

Fig. 1 ^{13}C NMR spectrum of vinyl-substituted silica.

consistent with the presence of the T^3 species.[18] Peaks due to T^2 [R–Si$(OSi)_2$(OR)] (δ −71.2), Q^3 and Q^4 species are also present as expected.

In general, TG analysis to 900 °C showed weight losses in good agreement with the theoretical organic content of the hybrids since all organic material is expected to volatilise by this temperature. The physical nature of the hybrids varies according to the type of organic modification with short alkyl chains leading to solid Ormosils, while those containing longer alkyl chains (C_8–C_{10}) are rubbery in appearance. DSC, however, shows no obvious glass transitions from −70 to 200 °C.

Molecular modelling using the Cerius² software package (Molecular Simulations Inc.) suggests that hybrids such as hexyl-modified silica could form a layered structure, but we have no experimental evidence to support this prediction. Future work is planned using extended X-ray absorption fine structure (EXAFS) to attempt to clarify this. None of the hybrids shows any evidence for crystallinity or other structural ordering by X-ray diffraction (XRD). Potential packing problems in the system may inhibit formation of an ordered structure. The synthesis of the hexyl-modified silica was carried out at a lower temperature and a longer reaction time than usual to try to facilitate ordering of the organic and inorganic components of the hybrid; however, XRD provides no evidence for such ordering.

Surface area analysis of these hybrids is complex. BET nitrogen adsorption isotherms and mercury porosimetry suggest the hybrids have low surface area, but further work is in progress to characterise these materials more fully.

Current work is aimed at characterising the properties of these hybrids more fully and assessing their use as precursors to new microporous silicas. Preliminary results show that removal of the organic component at elevated temperatures can lead to microporous silicas with surface areas above 150 $m^2\ g^{-1}$.

The authors thank EPSRC and the Defence, Evaluation and Research Agency (DERA) for the award of a CASE studentship (to H. R.). We also thank DERA for undertaking XRD analysis, the University of Durham for provision of solid state ^{13}C and ^{29}Si NMR services and Quantachrome for mercury porosimetry work. This work was carried out as part of Technology Group 4 (Materials and Structures) of the MOD Corporate Research Programme.

Notes and references

1 D. Avnir, *Acc. Chem. Res.*, 1995, **28**, 328.
2 A. H. Heuer, D. J. Fink, V. J. Laraia, J. L. Arias, P. D. Calvert, K. Kendall, G. L. Messing, J. Blackwell, P. C. Rieke, D. H. Thompson, A. P. Wheeler, A. Veis and A. I. Caplan, *Science*, 1992, **255**, 1098.
3 P. M. Calvert, in *Biomimetic Materials Chemistry*, ed. S. Mann, VCH, New York, 1996, ch. 11.
4 B. M. Novak, *Adv. Mater.*, 1993, **5**, 422.
5 J. E. Mark, *Polym. Eng. Sci.*, 1996, **36**, 2905.
6 Y. Wei, J.-M. Yeh, D. Jin, X. Jia, J. Wang, G.-W. Jang, C. Chen and R. W. Gumbs, *Chem. Mater.*, 1995, **7**, 969.
7 L. Mascia, *Trends Polym. Sci.*, 1995, **3**, 61.
8 D. A. Loy and K. J. Shea, *Chem. Rev.*, 1995, **95**, 1431.
9 D. L. Ou and A. B. Seddon, *J. Non-Cryst. Solids*, 1997, **210**, 187.
10 D. L. Ou and A. B. Seddon, *J. Sol–Gel Sci. Tech.*, 1997, **8**, 139.
11 S. Acosta, P. Arnal, R. J. P. Corriu, D. Leclercq, P. H. Mutin and A. Vioux, *Mater. Res. Soc. Symp. Proc.*, 1994, **346**, 43.
12 R. J. P. Corriu, D. Leclercq, P. Lefèvre, P. H. Mutin and A. Vioux, *J. Non-Cryst. Solids*, 1992, **146**, 301.
13 R. J. P. Corriu, D. Leclercq, P. Lefèvre, P. H. Mutin and A. Vioux, *J. Sol–Gel Sci. Tech.*, 1997, **8**, 89.
14 J. N. Hay and H. M. Raval, *J. Mater. Chem.*, 1998, **8**, 1233.
15 J. N. Hay and H. M. Raval, *J. Sol–Gel Sci. Tech.*, in press.
16 R. J. P. Corriu, D. Leclercq, P. H. Mutin, H. Samson and A. Vioux, *J. Organomet. Chem.*, 1994, **466**, 43.
17 S.-K. Yuh, E. P. Bescher, F. Babonneau and J. D. Mackenzie, *Mater. Res. Soc. Symp. Proc.*, 1994, **346**, 803.
18 T. Jermouni, M. Smaihi and N. Hovnanian, *J. Mater. Chem.*, 1995, **5**, 1203.

Communication 8/07491G

‘Molecular Chinese blinds’: self-organization of tetranitrato lanthanide complexes into open, chiral hydrogen bonded networks

C. V. Krishnamohan Sharma and Robin D. Rogers*

Department of Chemistry, The University of Alabama, Tuscaloosa, AL 35487, USA. E-mail: RDRogers@Bama.ua.edu

Received (in Columbia, MO, USA) 20th July 1998, Accepted 3rd July 1998

Lanthanide ions, with their unique electronic properties, rich stereochemistry, and consistent structural patterns offer a novel approach to the design of polar/chiral networks.

In recent years a wide variety of networks have been designed using the two major branches of crystal engineering (*i.e.* organic solids and inorganic coordination polymers), yet the rational design of polar/chiral networks continues to be an elusive and challenging goal for crystal engineers.[1–5] The difficulty results from synthetic strategies which rely upon the propagation of molecular symmetry into crystalline symmetry through rigid directional forces (hydrogen bonds and/or metal-coordination bonds), because such symmetry driven open networks tend to crystallize in *centrosymmetric* space groups.[3,6] However, using lanthanides, one can easily induce dissymmetry at metal centers simply by coordination with suitable ligand(s) which may thus result in controllable 1D, 2D, or 3D chiral networks with the aid of complementary hydrogen bonding functional groups.

In order to explore the role of lanthanide metal complexes in the context of crystal engineering, we have synthesized lanthanum nitrate metal complexes of 1,2-bis(4-pyridyl)ethane (bpe). $La(NO_3)_3{\cdot}6H_2O$ (0.433 g, 1 mmol) was reacted with bpe (0.368 g, 2 mmol) in EtOH (25 mL) and heated until both the reactants were completely dissolved. Crystals of **1**, $[bpeH]^+[La(NO_3)_4(OH_2)(bpe)]^-$, were obtained within 2–3 days. Complex **1** is also formed when $La(NO_3)_3$ and bpe are reacted in 1:2 or 1:3 molar ratios in 3:1 solvent mixtures of MeCN–MeOH.[7]†

Compound **1** crystallizes in the chiral space group $C222_1$.‡ The lanthanum cations are 11-coordinate, complexed with four bidentate nitrate anions, two bridging bpe ligands, and one water molecule resulting in an anionic 1D coordination polymer. The two protons of the water molecule along with oxygen atoms of adjacent nitrate anions constitute complementary divergent hydrogen bonding recognition sites on the backbone of the 1D coordination polymer (Fig. 1).

The hydrogen bonded nature of the 1D polymers [H···O, O···O, O-H···O; 2.155(3), 2.818(3) Å, 135.7(2)°] leads to the formation of a pleated-sheet structure with unusual cavities (Fig. 2). Each of these cavities is threaded by two linear 1D hydrogen bonded chains of the monoprotonated $bpeH^+$ molecules (N···N, 2.664(3) Å) resulting in an unprecedented polypseudo-rotaxane-type architecture.[8] To the best of our knowledge, this is the first structure to be reported with these unique 2D threading/interweaving structural features, *i.e.* threaded pleated-sheets, or a ‘chinese blinds’ structure. Also, formation of **1** under different experimental conditions, sug-

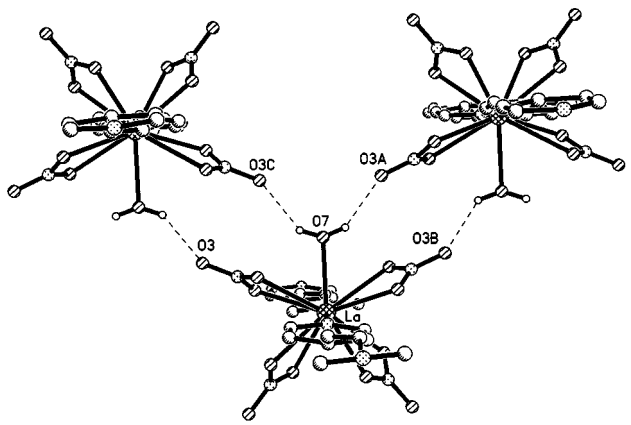

Fig. 1 Hydrogen bonded self-assembly of $[La(NO_3)_4(OH_2O)(bpe)]^-$ anions in **1**. The 1D coordination polymers run perpendicular to plane of the paper.

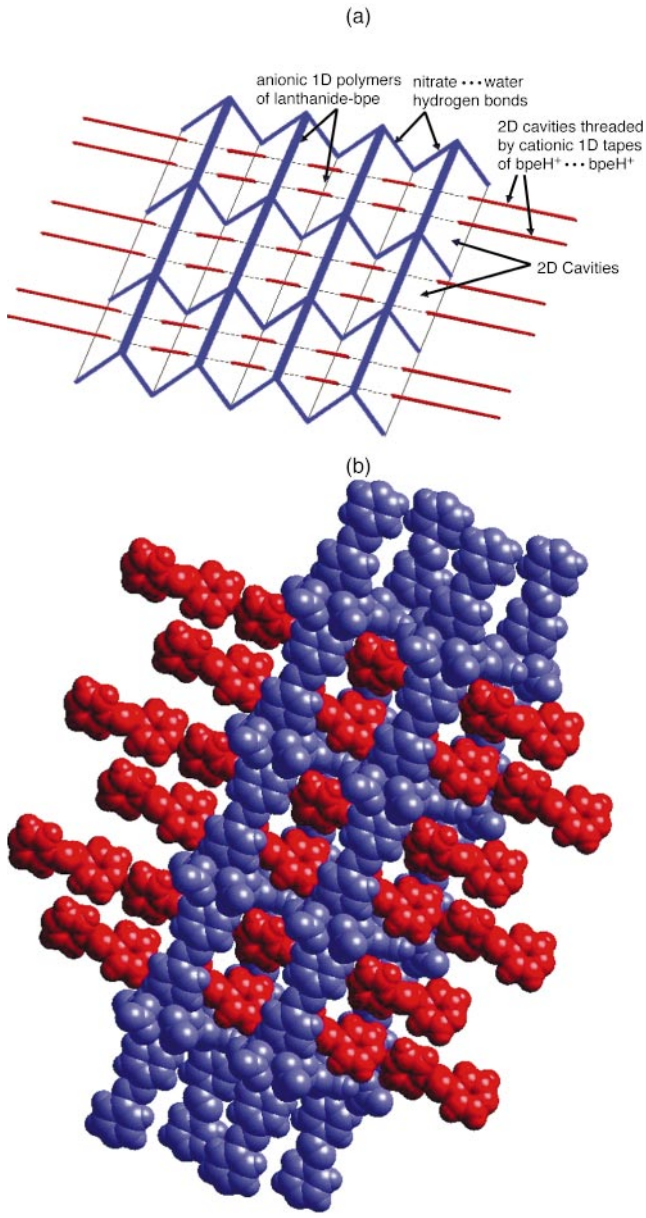

Fig. 2 Schematic (a) and space-filling (b) representations of a single sheet of **1** with the chiral 2D pleated-sheet of $[La(NO_3)_4(OH_2)(bpe)]^-$ (blue) threaded by 1D linear chains of $bpeH^+{\cdots}bpeH^+$ (red).

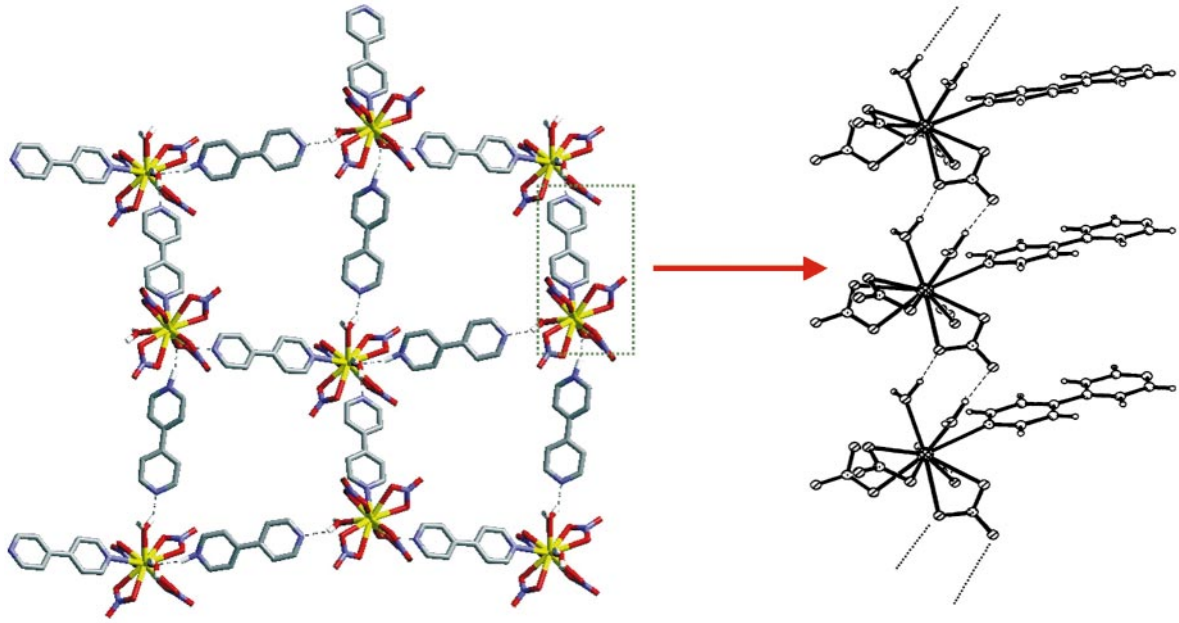

Fig. 3 A portion of the chiral, open 3D grids formed by **2a** resulting from hydrogen bonding between the complex anion, $[La(NO_3)_4(OH_2)_2(bipy)]^-$, and cation, $bipyH^+$. Two such independent networks interpenetrate.[9] The square grids are locked into place by hydrogen bonding between NO_3^- and H_2O groups in the third dimension.

gests strong complementary interactions among the various building blocks associated in the self-organization. Further, the nitro groups that are not part of the hydrogen bonding network interdigitate with neighboring 2D pleated-sheets through off-set stacking for efficient close packing.

The interesting open, chiral networks in **1** prompted us to carefully examine the 20 (many of them isostructural) $Ln(NO_3)_3$ complexes in the Cambridge Structural Database (April 1997 release) with the more rigid 4,4′-bipyridine (bipy). These complexes may be classified into three structurally distinct series: neutral hydrogen bonded cocrystals, metal–ligand coordination complexes, and organic cation–inorganic anion pairs. Two different isostructural series are particularly important to the crystal engineer in the design of open, chiral networks, each crystallizing in the chiral space group $P2_12_12_1$: the charged coordination complexes $[bipyH]^+[Ln(NO_3)_4(OH_2)_2(bipy)]^-$ (Ln = La, Ce, Pr, Nd: **2a-d**) and the neutral, hydrogen bonded cocrystals $[Ln(NO_3)_3(OH_2)_3]\cdot 2bipy\cdot H_2O$ (Ln = Nd, Pr: **3a**,**b**). In the former series complementary hydrogen bonding of the complex anions and $bipyH^+$ results in a well defined infinite chiral 3D open architecture (Fig. 3) that undergoes self-interpenetration.[9] The latter complexes form hydrogen bonded layered structures where bipy molecules function as pillars between the layers.[10]

We have synthesized further examples of **2** and **3** to determine the commonality of this approach. $La(NO_3)_3\cdot 6H_2O$ (0.433 g, 1 mmol) was reacted with 4,4′-bipyridyl (0.312 g, 2 mmol) in MeOH (15 mL) and single crystals of $[bipyH]^+[La(NO_3)_4(OH_2)_2(bipy)]^-$ **2a**, were obtained over a period of two weeks. The neutral hydrogen bonded crystals of $[La(NO_3)_3(OH_2)_3]\cdot 2bipy\cdot H_2O$ **3c**, were obtained when $La(NO_3)_3$ and bipy were reacted in 1:2 molar ratio in a solution mixture of xylene and MeOH.§

The crystal structures of **1**-**3** suggest a simple and efficient way to design chiral crystals with predictable networks and further suggest that lanthanides form exotic supramolecular networks which are of importance not only for their aesthetic appeal, but also for their potential use in the design of functional solids. Lanthanides, with their interesting electronic, spectral, and magnetic properties coupled with their availability, propensity to form isostructural complexes, and range in ionic radii are thus, attractive targets for exploring such structure–function correlations.

Notes and references

† The complexation properties of $Ln(NO_3)_3$ with softer N-donor ligands (*e.g.* 4,4′-bipyridyl) are sensitive to the solvent of crystallization. Any slight variations in nature of the solvent, acidity, basicity, or solvent:water ratio leads to drastic changes in the complex formed.

‡ *Crystal data* for **1**, M = 774.4, orthorhombic, space group $C222_1$, a = 14.9977(2), b = 16.3302(1), c = 11.8663(2) Å, V = 2906.24(6) Å^3, D_c = 1.770 Mg m^{-3} for Z = 4. 3369 unique absorption corrected reflections measured at 173 K with a Siemens CCD area detector diffractometer ($4 < \theta < 56°$), on convergence gave final values of R = 0.019, R_w = 0.046. The sp^3 C atoms of the bpe ligand coordinated to the lanthanide exhibit ± *gauche* disorder. CCDC 182/1081

§ Complexes **2a** and **3c** crystallize in the orthorhombic space group $P2_12_12_1$. The unit cell parameters of **2a** have been reported previously at room temperature,[7] while **3c** is a new member of the complex **3** series. We have crystallographically characterized both **2a** and **3c** at −100 °C utilizing a Siemens CCD area detector diffractometer with molybdenum radiation: **2a**: a = 7.2658(4), b = 18.5137(11), c = 19.9204(12) Å. **3c**: a = 7.1228(3), b = 16.1694(6), c = 24.7284(10) Å. CCDC 182/1081

1 G. R. Desiraju, *Angew. Chem., Int. Ed. Engl.*, 1995, **34**, 2311.
2 M. J. Zaworotko, *Chem. Soc. Rev.*, 1994, **23**, 283.
3 P. Brunet, M. Simard and J. D. Wuest, *J. Am. Chem. Soc.*, 1997, **119**, 2737; G. B. Gardner, D. Venkataraman, J. S. Moore and S. Lee, *Nature*, 1995, **374**, 792; O. M. Yaghi, G. Li and H. Li, *Nature*, 1995, **378**, 703.
4 C. Janiak, *Angew. Chem. Int. Ed. Engl.*, 1997, **36**, 1431; P. Ball, *Nature*, 1996, **381**, 648.
5 L. R. MacGillivray and J. L. Atwood, *Nature*, 1997, **389**, 469.
6 C. V. K. Sharma and M. J. Zaworotko, *Chem. Commun.*, 1996, 2655; O. J. Ermer, *J. Am. Chem. Soc.*, 1988, **110**, 3747.
7 T. J. R. Weakley, *Inorg. Chim. Acta*, 1982, **63**, 161; M. Fréchette, I. R. Butler, R. Hynes and C. Detellier, *Inorg. Chem.*, 1992, **31**, 1650.
8 D. B. Amabilino, J. F. Stoddart and D. J. Williams, *Chem. Mater.*, 1994, **6**, 1159.
9 K. T. Al-Rasoul and T. J. R. Weakley, *Inorg. Chim. Acta*, 1982, **60**, 191; M. Bukowska-Strzyzewska and A. Tosik, *Inorg. Chim. Acta*, 1978, **30**, 189.
10 K. T. Al-Rasoul and M. G. B. Drew, *Acta Crystallogr., Sect. C*, 1987, **43**, 2081.

Communication 8/05752D

Carbon allotropes of dumbbell structure: C_{121} and C_{122}

N. Dragoe,*[ab]† S. Tanibayashi,[a] K. Nakahara,[a] S. Nakao,[a] H. Shimotani,[a] L. Xiao,[a] K. Kitazawa,[ab] Y. Achiba,[c] K. Kikuchi[c] and K. Nojima[d]

[a] *Department of Applied Chemistry, University of Tokyo, Tokyo 113-8656, Japan. E-mail: tdragoe@hongo.ecc.u-tokyo.ac.jp*
[b] *Japan Science and Technology Corporation, CREST, Japan*
[c] *Department of Chemistry, Tokyo Metropolitan University, Tokyo 192-0003, Japan*
[d] *JEOL Ltd., Tokyo 196-8558, Japan*

Received (in Cambridge, UK) 13th November 1998, Accepted 19th November 1998

The synthesis, isolation and preliminary characterization of all-carbon [60]fullerene dimers C_{121} and C_{122} are reported.

We here report data concerning the synthesis and preliminary characterization of all-carbon fullerene derivatives C_{121} **1**, a new dumbbell-like dimer, and C_{122} **2**. The existence of these molecules was first suggested by Osterodt and Vogtle,[1] and Strongin *et al*.[2] recently succeeded in the synthesis of C_{122}. C_{121} and C_{122} were previously detected in the mass spectra of $C_{60}CBr_2$,[3] $C_{60}CH_2$[1] and $C_{60}(CO_2Et)_2$.[4]

Recently we succeeded in the synthesis, separation and characterization of **1** and **2**. The synthesis was based on the reaction described in Scheme 1. Typically, 50 mg of $C_{60}CBr_2$ and 250 mg of C_{60} were mixed and gently ground. The powder was then heated in an argon atmosphere (flow 50 ml min^{-1}) up to 450 °C at a rate of 5 K min^{-1} and subsequently cooled to room temperature. The resulting black powder was soluble in CS_2 and *o*-dichlorobenzene, giving a red–brown solution (the same product could be obtained by using $C_{60}CHCO_2Et$ instead of $C_{60}CBr_2$, and a higher temperature, *i.e*. 550 °C). The product was a mixture of unreacted C_{60} and other phases, as detected by gel permeation chromatography, GPC (toluene, 340 nm detection, 12 ml min^{-1}). The GPC peak at 1320 ml was collected‡ and found to contain **1** and **2** as major and minor phases, respectively. The yield in **1** was about 10% and it increased slightly with an increase in the $C_{60}/C_{60}CBr_2$ ratio. The amount of **2** decreased when increasing the $C_{60}/C_{60}CBr_2$ ratio; the formation of **2** could be suppressed when using a large excess of C_{60} (more than ten-fold) but in this case the separation of the dimer product from the mixture was more difficult. The separation between C_{60}, **1** and **2** was made by GPC in recycling mode. In Fig. 1 a GPC experiment for the mixture of **1** and **2** is shown. After 24 h the separation between the two peaks was large enough to allow the collection of pure samples of C_{121} and C_{122}. The GPC elution volume for **1** was smaller than for C_{60} or $C_{60}CBr_2$ and similar to that of **2**, indicating that their molecular volumes are roughly the same but higher than those of C_{60} or $C_{60}CBr_2$. The laser desorption and ionization time of flight (LDI TOF) mass spectrum§ of **1** is presented in Fig. 2. The peak at *m/z* 1452.9, with a characteristic isotopic pattern, was assigned to C_{121} (negative ionization, calculated *m/z* 1453.3). A small C_{122} peak was also observed in the mass spectrum of C_{121}. This is probably due to the association of C_{61} clusters under the mass spectroscopy conditions, since the C_{122} peak increased with the laser power. The LDI TOF mass spectrum of **2** presented an intense peak for C_{122} (*m/z* 1465.4, calc. *m/z* 1465.3) but no C_{121} peak, irrespective of the laser power (Fig. 3).

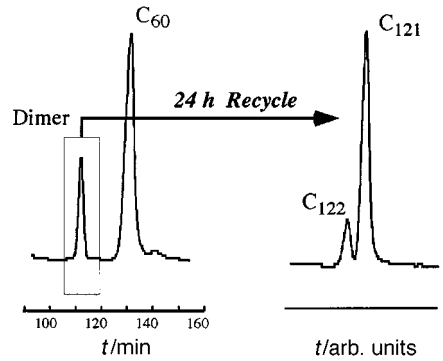

Fig. 1 GPC experiments for the separation of C_{121}.

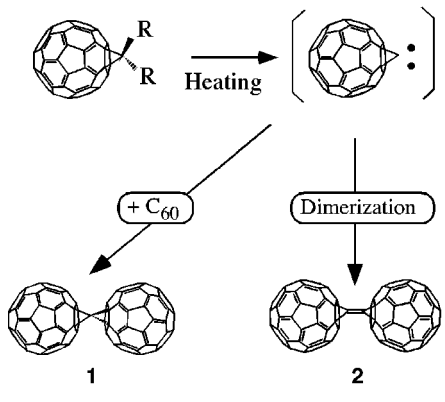

Scheme 1

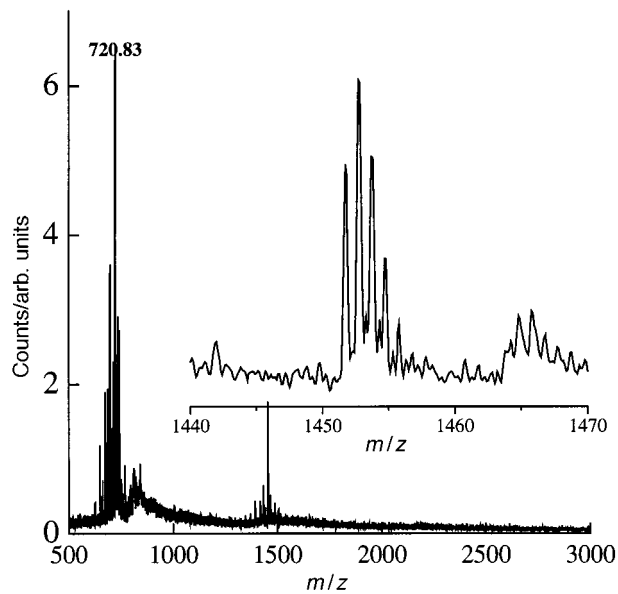

Fig. 2 LDI-TOF MS of C_{121}; inset is a detail of the dimer peak, reflector mode, negative ionization.

† Permanent address: Department of Physical Chemistry, Faculty of Chemistry, University of Bucharest, Romania.

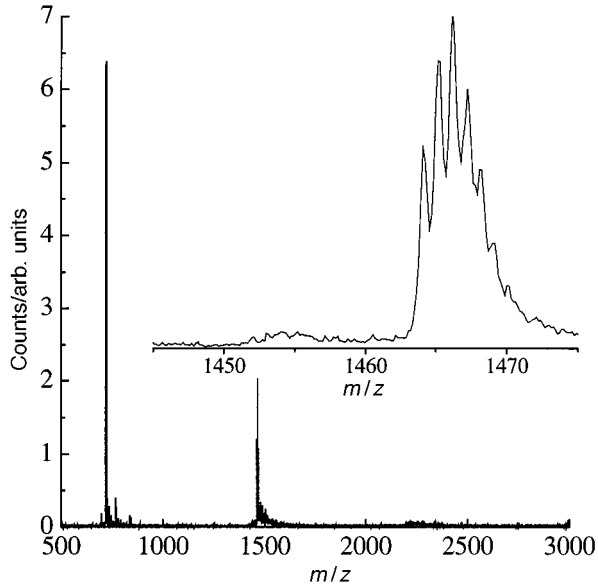

Fig. 3 LDI-TOF MS of C_{122}; inset is a detail of the dimer peak, linear mode, negative ionization.

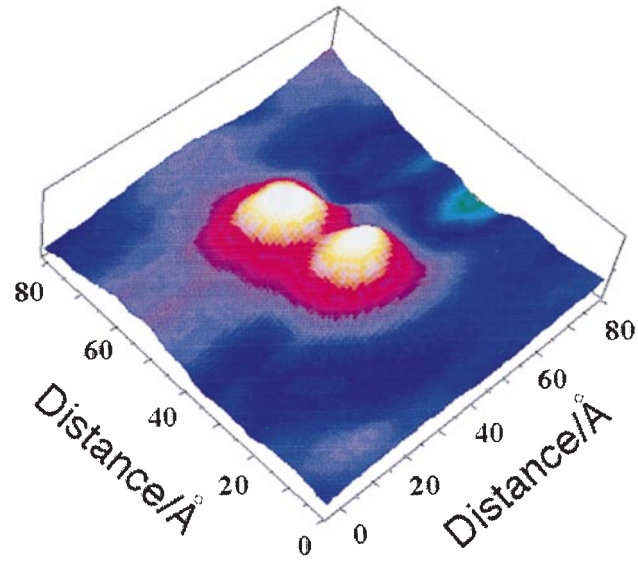

Fig. 4 An STM image of C_{122} deposited on graphite (sample voltage −0.5 V, current 0.5 nA, 80 K, ultra-high vacuum).

The UV–VIS spectra¶ of **1** and **2** showed peaks at 430 and 700 nm, usually observed for 1,2-dihydrofullerenes. IR spectroscopy‖ measurements revealed the presence of the C_{60} cage and some additional peaks due to the lower symmetry of **1** and **2** relative to C_{60}. In the spectra of **1**, a peak appearing at 1022.4 cm^{-1} was assigned to a cyclopropane skeletal stretch,[5] expected at 1017–1025 cm^{-1}.

So far, we have been unable to obtain a ^{13}C NMR spectrum of **2**, either because of its low solubility or the presence of impurities or other isomers in the sample. The ^{13}C NMR spectrum** of **1** was also rather difficult to obtain, due to the low C_{121} solubility and a low relaxation rate for the carbon nuclei. Sixteen low signal-to-noise lines were observed between δ 140–148 (16 lines expected in this region for a C_{2v} symmetry C_{121} molecule), in agreement with the high symmetry of this dimer. Three additional lines were sometimes observed in the cluster at δ 142, possibly related to either the presence of C_{122} or other impurities in the sample. A small upfield resonance at δ 67.7 could be assigned to the four sp^3 fullerene cyclopropane carbons. This value suggests a 6:6 closed connection to the fullerene core,†† in agreement with the proposed carbene attack mechanism (for an extensive discussion of ^{13}C NMR in fullerene derivatives, see ref. 6 and the references cited therein). The bridge between the two fullerenes could not be identified beyond doubt; its intensity should be eight times smaller than most of the fullerene cage carbons. We tentatively assign a δ 48.8 resonance to the carbon bridge.

We also performed scanning tunnelling microscopy (STM) measurements on samples of **1** and **2** deposited on graphite. Fig. 4 shows an image of **2**; the size of the dimer is in agreement with that expected. STM images of **1** were similar to that of **2**, also showing dumbbell-like structures.

The LDI TOF mass spectrum of C_{121} showed extensive fragmentation around *m/z* 1452 and 720 as well as the presence of both odd- and even-numbered carbon clusters. These peaks are likely to be the result of the addition/loss of C_2 units to/from C_{121} in the mass spectrometer. The even-numbered carbon clusters were produced by aggregation of C_{61} and subsequent loss/addition of C_2 units. Whether the detected odd-numbered carbon clusters are stable or only transient species in the mass spectrometer still remains an open question. However, these results suggest that either weakly bound or spirane-like clusters are formed under the mass spectrometry conditions without the coalescence of the fullerene spheres. The elimination of C_2 units in the mass spectra of fullerene derivatives does not seem to require the formation of closed clusters, since it takes place for both even- and odd-numbered carbon clusters. Further studies on the laser-induced decomposition of odd-numbered carbon clusters should give an insight into the formation mechanism of fullerene molecules.

In conclusion, we succeeded in the synthesis and isolation of all-carbon fullerene dimers C_{121} and C_{122}. The dumbbell-like structure of these dimers is supported by ^{13}C NMR, IR, UV–VIS, mass and STM measurements.

We thank Professor K. Saigo, Dr M. Hayashi and Dr K. Kinbara, University of Tokyo, for help provided during this work. The authors acknowledge support from the Japan Science and Technology Corporation (JST-CREST).

Notes and references

‡ With GPC Jaigel 1H40-2H40 preparative columns, the elution volumes of C_{60} and $C_{60}CBr_2$ are 1580 and 1500 ml, respectively.

§ Maldi TOF mass spectroscopy was performed with a JMS Voyager Elite instrument (337 nm laser) in linear and reflector modes in both positive and negative ionization. Either dithranol or α-cyano 4-hydroxycinnamic acid was used as the matrix. The instrument calibration was performed with neurotensin, $[MH^+]$ = 1672.91 amu. LDI TOF mass spectroscopy was performed with a Perseptive Biosystems Voyager instrument.

¶ UV–VIS spectra of **1** and **2** were measured in CS_2 and *o*-dichlorobenzene: λ_{max}/nm 430 and 700.

‖ *Selected data* for **1**: ν_{max}(KBr)/cm^{-1} 1462, 1359, 1260, 1190, 1083, 1022, 801, 763, 736, 573, 525, 416. For **2**: ν_{max}(KBr)/cm^{-1} 1380, 1321, 1180, 1186, 1015, 920, 785, 602, 585, 571, 531, 526, 418.

** *Selected data* for **1**: δ_C 147.88, 147.54, 146.7, 146.43, 146.09, 145.55, 145.49, 144.8, 142.85, 142.59, 142.51, 142.42, 142.31, 141.3, 140.85, 140.1, 67.7. ^{13}C NMR spectra were measured using a JEOL 270 instrument, 67.7 MHz in CS_2 and 1,2-dichlorobenzene-d_4 or benzene-d_4 for field/frequency lock.

†† *i.e.* at the connections between two hexagons on the fullerene core.

1 J. Osterodt and F. Vogtle, *Chem. Commun*., 1996, 547.
2 T. S .Fabre, W. L. Treleaven, T. D. McCarley, C. L. Newton, R. M. Landry, M. C. Saraiva and R. M. Strongin, *J. Org. Chem*., 1998, **63**, 3522.
3 T. Ishida, T. Furudate, T. Nogami, M. Kubota, T. Hirano and M. Ohashi, *Fullerene Sci. Technol*., 1995, **3**, 399.
4 R. D. Beck, P. Weis, A. Hirsch and I. Lamparth, *J. Phys. Chem*., 1994, **98**, 9683.
5 C. N. R. Rao, *Chemical Applications of IR Spectroscopy*, Academic Press, New York, 1963, p. 125.
6 L. Isaacs, A. Wehrsig and F. Diederich, *Helv. Chim. Acta*, 1993, **76**, 1231.

Communication 8/08874H

ChemComm

One-pot incorporation of titanium catalytic sites into mesoporous true liquid crystal templated (TLCT) silica

Maria E. Raimondi,[a] Leonardo Marchese,*[b] Enrica Gianotti,[b] Thomas Maschmeyer,[c] John M. Seddon*[a] and Salvatore Coluccia[b]

[a] *Department of Chemistry, Imperial College, London, UK SW7 2AY. E-mail: j.seddon@ic.ac.uk*
[b] *Dipartimento di Chimica IFM, Università di Torino, Via P. Giuria 7, I-10125 Torino, Italy*
[c] *Davy Faraday Research Laboratory, The Royal Institution of G.B., 21 Albemarle Street, London, UK WX1 4BS*

Received (in Bath, UK) 20th August 1998, Accepted 26th November 1998

A one-pot synthesis procedure is described for the production of catalytically active titanium-incorporated mesoporous silica; the nature and accessibility of Ti(IV) sites derived from two different Ti sources was elucidated by means of catalytic tests, UV–VIS and photoluminescence spectroscopy.

Titanosilicates are of great interest for various catalytic applications.[1] TS-1, a microporous titanium silicate containing catalytically active tetrahedral Ti(IV) sites, was first synthesised by Taramasso *et al.*[2] and was found to catalyse a wide range of low-temperature oxidations with hydrogen peroxide. In 1994, Corma *et al.*[3] and Pannavaia and coworkers[4] published their work on introducing titanium into the silica framework of MCM-41, and since then a considerable number of papers have been written dealing with various aspects of Ti-incorporated MCM-41, reviewed by Maschmeyer.[5] These materials can be prepared in principally two ways: (i) Grafting titanium species to the mesopore surfaces *via* a post-synthetic procedure[6] and (ii) substituting Ti into the silica framework by adding a titanium alkoxide precursor to the MCM-41 synthesis gel.[3,4]

Here, we describe a novel 'one-pot' method for the synthesis of titanium-incorporated mesoporous silica *via* a true liquid crystal templating (TLCT) process.[7] The advantage of this method over those previously described for Ti-MCM–41 is that no post-synthetic, and potentially damaging, treatment of the mesoporous silicates is required, and the disordered side products often associated with classical MCM-41 formation are avoided. Two types of titanium precursor were used for comparison: titanium cyclopentadienyl dichloride (Aldrich) and Tilcom TAA (Tioxide Specialities Ltd). Tilcom TAA consists of a 75 wt% solution of diisopropoxy bis(pentane-2,4-dionato)titanium(IV), or titanium acetylacetonate, in isopropanol. The titanium content of Tilcom TAA is 9.9 wt%. The precursors were dissolved directly in the synthesis gel consisting of a 1 : 1 : 2.1 weight ratio of octaethylene glycol monododecyl ether ($C_{12}EO_8$, Fluka), 10^{-2} M HCl and tetramethoxysilane (TMOS, Aldrich), respectively. For 1.5 g of surfactant template, 0.06 g of titanocene dichloride or 150 μl of Tilcom TAA were added.

The hexagonal mesoporous product formed overnight, under constant vacuum (to remove the methanol TMOS hydrolysis by-product), at room temperature. The deep orange colour of the titanocene-doped as-synthesised material suggested that the titanocene complex remained unhydrolysed throughout the synthesis (hydrolysis products would have been light orange/yellow). It is also supposed that owing to the hydrophobic nature of the cyclopentadienyl ligands, the transition metal was located primarily in the central hydrocarbon regions of the polyoxyethylene (POE) cylindrical micelles (Scheme 1), *i.e.* on the internal surfaces of the mesopores once the materials were calcined. The POE micelles therefore protected the complex from the aqueous regions of the synthesis mixture, pointing to a potentially general method for mesopore functionalisation.

We propose that due to the high solubility of Tilcom TAA in the aqueous regions of the liquid crystalline synthesis gel, a large proportion of the titanium sites in the final calcined products were buried in the silica framework (Scheme 1). Calcination of the materials at 500 °C produced silicate structures consisting of hexagonal arrays of long channels of *ca.* 25 Å diameter (as determined by TEM and N_2 adsorption measurements with BJH calculation). The hexagonal symmetry of the materials was confirmed by polarising microscopy (characteristic optical texture under crossed polarisers) and small-angle X-ray diffraction. After calcination at 500 °C, the hexagonal structure remained intact (seen by X-ray diffraction), but the location of the titanium species remained to be determined. The Ti contents in the calcined materials were calculated from the initial gel compositions, assuming complete hydrolysis and condensation to SiO_2, and complete removal of the organic template by calcination. Assuming all of the titanium species remained implanted in the mesoporous structures after calcination, the titanium metal loading for the products were 0.92 wt% for the titanocene-doped material (Ti[CP]) and 1.18 wt% for the Tilcom TAA-doped product (Ti[ACAC]). The amount of titanocene dichloride lost during the calcination process by evaporation/sublimation is not actually known; this would of course affect the Ti content in the calcined material.

Catalytic tests (data not shown) on Ti[CP] showed that it was both active in the epoxidation of octene using *tert*-butylhydroperoxide (TBHP) as the source of oxygen,[8] and in the peroxidative bromination of phenol red (phenolsulfonephthalein) to tetrabromophenol blue (3′,3″,5′,5″-tetrabromophenolsufonephthalein).[9] No catalytic tests were done on Ti[ACAC], only on the calcined Ti[CP], as this appeared to be the most promising material from the spectroscopic studies. The epoxidation reaction was carried out at 80 °C under an inert argon atmosphere, and the reaction mixture consisted of 0.15 mol oct-1-ene, 0.0075 mol mesitylene, 0.0075 mol TBHP and 0.265 g Ti[CP] catalyst. Samples were taken from the reaction mixture at regular intervals and the reaction products were quantified by GC analysis. Octene was in large excess and acted as the solvent as well as reactant, mesitylene was the standard

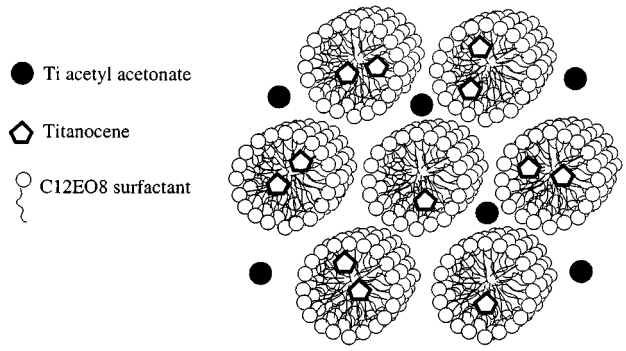

Scheme 1 Representation of the assumed locations of the titanium precursors, Ti acetyl acetonate and titanocene dichloride within the hexagonal liquid crystal phase.

for GC analysis. The reaction rate calculated after the first hour of reaction was 84 mol epoxide per mole Ti per hour; this value was comparable (within 30%) with the reaction rates obtained for grafted Ti–MCM-41 materials[6] in a previous study. Our catalytic test results show that the material is active in the epoxidation of octene, with high selectivity for the epoxide (no other octene oxidation products were observed). The activity of the catalyst suggests that isolated tetrahedral Ti(IV) species were present.[1,5]

The peroxidative bromination test gave a qualitative indication of the catalytic activity of the catalyst, and the formation of bromophenol blue from phenol red was monitored by UV–VIS spectroscopy.† Our Ti[CP] catalyst again had slightly lower but comparable catalytic activity to the TiMCM materials described in the literature.[9]

The diffuse reflectance UV–VIS spectrum for calcined Ti[CP] had an intense maximum absorbance centred at 220 nm (Fig. 1). The electronic transition responsible for this absorption band in the UV diffuse reflectance spectrum is a ligand to metal charge transfer (LMCT) transition from oxygen to tetrahedral Ti(IV).[10–16] There were additionally two further much less intense absorption peaks at 330 and 460 nm, which may have been due to degradation products of the cyclopentadienyl ligands of the titanocene precursor.[17] Calcined Ti[ACAC] produced a somewhat different UV–VIS absorption spectrum from Ti[CP]. The maximum absorption peak had a similar intensity to that for Ti[CP], but was displaced to 240 nm and was somewhat broadened with respect to the Ti[CP] absorption band. The displacement of the main adsorption peak to longer wavelength for the framework-substituted Ti[ACAC] product was likely to be due to a somewhat different chemical environment for the tetrahedrally coordinated Ti atoms in the structure. The fact that the band was broadened with respect to the Ti[CP] material suggested that there was a greater number of chemically differing Ti sites within the Ti[ACAC] structure, absorbing at different wavelengths.

In the case of isolated tetrahedral Ti(IV) sites, photoluminescence is due to the reverse LMCT process to that

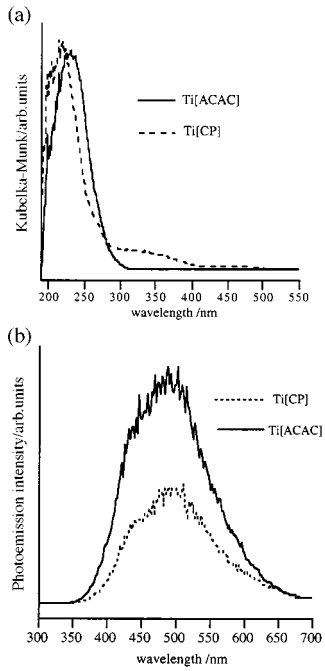

Fig. 1 (a) UV–VIS diffuse reflectance spectra recorded using a Perkin Elmer spectrometer equipped with an integrating sphere attachment. The absorbance output from the instrument was converted using the Kubelka-Munk algorithm. (b) Photoluminescence spectra recorded at 77 K (λ_{ex} = 250 nm) using a SPEX FLUOROLOG-2 1680 spectrometer. For all UV–VIS spectroscopy measurements samples were ground to fine powders and inserted into quartz cells purpose-made for *in situ* thermal treatments. Samples were pre-oxidised and spectroscopy measurements were conducted under strict exclusion of air.

responsible for the UV diffuse reflectance absorption.[10,11,18] The photoemission spectra for materials containing tetrahedral coordination Ti(IV) sites contain features in the range 400–600 nm. Photoluminescence spectra obtained for the Ti[CP] and Ti[ACAC] samples at 77 K were characterised by two main emission maxima at 440 and 490 nm. Both these emission bands had a maximum excitation at 250 nm. In agreement with the diffuse reflectance spectra, the excitation band for the Ti-[ACAC] material was broader than for Ti[CP].

The major difference between the photoemission spectra for Ti[CP] and Ti[ACAC], both reoxidised and degased in the same way, was that the Ti[ACAC] emission bands were 2–3 times more intense than the Ti[CP] bands. Adsorption of oxygen onto the Ti-doped samples only partially quenched the photoemission signals, though somewhat more for the Ti[CP] sample than for the Ti[ACAC] sample. This suggested that more of the Ti(IV) sites in the Ti[ACAC] sample were inaccessible (*e.g.* situated within the silica framework) to the oxygen than in Ti[CP].[17] These results agree substantially with what could be predicted from the partitioning behaviour of the titanium precursor in the original synthesis gels.

Our results have shown that a one-pot TLCT synthesis procedure can be used to introduce catalytically active sites into mesoporous silica. The accessibility of the Ti(IV) sites to external gaseous probe molecules (oxygen in the case of our photoluminescence studies) has been found to depend on the hydrophobic or hydrophilic nature of the titanium precursor used in the synthesis gel. We propose that this method for producing metal-incorporated mesoporous materials may be generalised to many other species of catalytic interest.

M. E. R. thanks the EPSRC for a PhD Studentship; guidance from Dr M. Attfield for the epoxidation test and helpful discussions with Dr G. Martra are gratefully acknowledged.

Notes and references

† The reaction solution consisted of 0.1 mM phenol red, 0.05 M KBr, 5 mM H_2O_2 and 0.05 M Hepes buffer (pH ≈ 6.5); 0.16 g of finely ground Ti[CP] catalyst was added to this. The samples were continuously shaken throughout the tests using an electrical flask shaker (moderate speed), and at regular intervals decanted samples were taken for spectroscopic analysis.

1 B. Notari, *Adv. Catal.*, 1996, **41**, 252.
2 M. Taramasso, G. Perego and B. Notari, *US Pat.* 4410501, 1983.
3 A. Corma, M. T. Navarro and J. P. Pariente, *J. Chem. Soc., Chem. Commun.*, 1994, 147.
4 P. T. Tanev, M. Chibwe and T. J. Pinnavaia, *Nature*, 1994, **368**, 321.
5 T. Maschmeyer, *Curr. Opin. Solid State Mater. Sci.*, 1998, **3**, 71.
6 T. Maschmeyer, F. Rey, G. Sankar and J. M. Thomas, *Nature*, 1995, **378**, 159.
7 G. S. Attard, J. C. Glyde and C. G. Göltner, *Nature*, 1995, **378**, 366.
8 M. Crocker, R. H. M. Herold and A. G. Orpen, *Chem. Commun.*, 1997, 2411.
9 J. V. Walker, M. Morey, H. Carlsson, A. Davidson, G. D. Stucky and A. Butler, *J. Am. Chem. Soc.*, 1997, **119**, 6921.
10 L. Marchese, E. Gianotti, T. Maschmeyer, G. Martra, S. Coluccia and J. M. Thomas, *Nuovo Cimento Soc. Ital. Fis. D–Condens. Matter At. Mol. Chem. Phys. Fluids Plasmas Biophys.*, 1997, **19**, 1707.
11 L. Marchese, T. Maschmeyer, E. Gianotti, S. Coluccia and J. M. Thomas, *J. Phys. Chem. B*, 1997, **101**, 8836.
12 R. J. Davis and Z. F. Liu, *Chem. Mater.*, 1997, **9**, 2311.
13 S. Bordiga, S. Coluccia, C. Lamberti, L. Marchese, A. Zecchina, F. Boscherini, F. Buffa, F. Genoni, G. Leofanti, G. Petrini and G. Vlaic, *J. Phys. Chem.*, 1994, **98**, 4125.
14 J. Klaas, G. SchulzEkloff and N. I. Jaeger, *J. Phys. Chem. B*, 1997, **101**, 1305.
15 S. Klein, B. M. Weckhuysen, J. A. Martens, W. F. Maier and P. A. Jacobs, *J. Catal.*, 1996, **163**, 489.
19 L. Lenoc, D. Trong On, S. Solomykina, B. Echchahed, F. Beland, C. Cartier dit Moulin and L. Bonneviot, *Stud. Surf. Sci. Catal.*, 1996, **101**, 611.
20 M. E. Raimondi, E. Gianotti, L. Marchese, G. Martra, T. Maschmeyer, J. M. Seddon and S. Coluccia, in preparation.
21 H. Yamashita, Y. Ichihashi, M. Anpo, M. Hashimoto, C. Louis and M. Che, *J. Phys. Chem.*, 1996, **100**, 16041.

Communication 8/06700G

A novel parachute-shaped C_{60}–porphyrin dyad

Peng Cheng, Stephen R. Wilson and David I. Schuster*

Department of Chemistry, New York University, 100 Washington Square East, New York, NY 10003, USA. E-mail: david.schuster@nyu.edu

Received (in Corvallis. OR, USA) 14th September 1998, Accepted 23rd November 1998

A novel covalently linked C_{60}–porphyrin dyad has been prepared by cyclopropanation of C_{60} with a strapped porphyrin malonate; its fluorescence spectrum shows strong quenching of the porphyrin singlet excited state by the attached C_{60}.

Photosynthetic model systems rely on spatially organized units with suitable photochemical and electronic properties. Recently much attention has been focused on using C_{60} as the electron acceptor in donor–acceptor systems due to its unique shape and redox properties.[1–3] To continue a project aimed at studying interactions between two chromophores in covalently linked C_{60}–porphyrin dyads with flexible and rigid tethers,[3] we became interested in the synthesis of a novel parachute-shaped dyad in which the two π-systems are forced into a face-to-face arrangement.

We synthesized a key intermediate porphyrin **4** using a strapped porphyrin strategy[4] in order to avoid tedious chromatographic separation of two *ortho*-linked atropisomers (Scheme 1). Esterification of 2-(3-hydroxypropyl)benzaldehyde with malonyl dichloride gave compound **2**. Condensation of the dialdehyde with 4 equiv. of benzyl 3,4-diethylpyrrole-2-carboxylate[5] gave compound **3**. Hydrogenation of **3** followed by reaction with methyl orthoformate catalyzed by trichloroacetic acid led to strapped porphyrin **4**, which was separated in 12% yield by flash column chromatography (silica gel, CH_2Cl_2–MeOH 20:1). The porphyrin malonate was then attached to C_{60} *via* Bingel cyclopropanation[6] accomplished by the action of CBr_4 and DBU.[7] The dyad **5**† was isolated in 25% yield by preparative TLC (silica gel, CH_2Cl_2–MeOH 25:1).

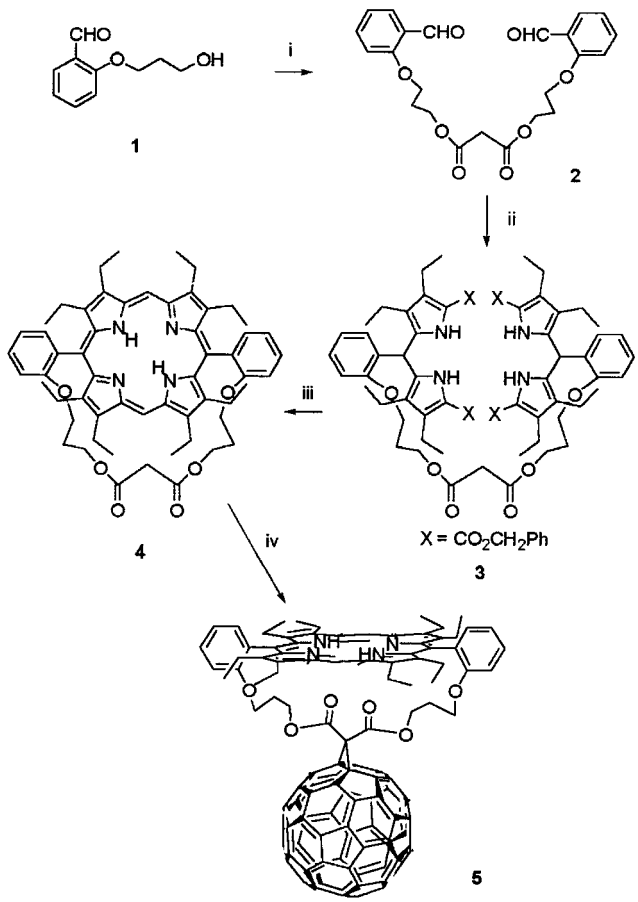

Scheme 1 *Reagents and conditions*: i, malonyl dichloride, Et_3N, CH_2Cl_2, 0 °C; ii, benzyl 3,4-diethylpyrrole-2-carboxylate, HCl, EtOH, reflux, 5 h; iii, H_2, 10% Pd/C, Et_3N, THF, room temp., 5 h, then $CH(OCH_3)_3$, Cl_3CCO_2H, CH_2Cl_2, room temp., 48 h; iv, C_{60}, CBr_4, DBU, toluene, room temp.

The structure of dyad **5** was confirmed by spectral data including ^{1}H MMR, ^{13}C NMR, ^{3}He NMR, UV–VIS and MALDI-TOF mass spectra.‡ The ^{1}H NMR spectrum in $CDCl_3$ exhibits the expected features with correct integration ratios, which is similar to the spectrum of porphyrin **4** except for the disappearance of the two protons on the methylene carbon between the two carbonyl groups. The ^{13}C NMR spectrum of **5** shows eight of the nine resonances for the sp^3 carbon atoms, 24 of the 28 resonances in the region δ 97.0–160.0 arising from the sp^2 carbon atoms of the C_{60} moiety and the porphyrin, as well as a resonance (δ 161.53) for the malonate carbonyl groups, clearly demonstrating that dyad **5** has C_{2v} symmetry. Interestingly, the dyad made from ^{3}He@C_{60} shows a peak at δ −8.5 relative to ^{3}He gas *via* ^{3}He NMR spectroscopy, whereas typical methano-1,2-dihydrofullerenes-C_{60} like **6** have a ^{3}He NMR

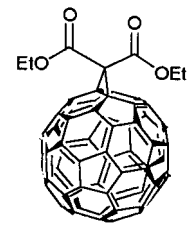

6

resonance at δ −8.1.[8] The upfield shift is attributable to the shielding effect of the porphyrin ring current. Calculations indicate that the average distance between the center of the four pyrrole N atoms and the center of the two sp^3 carbons on the C_{60} is 6.4 Å in the CVFF minimized structure (InsightII 97.2, Discover 3). The two tethers make the system relatively rigid.

The UV–VIS spectrum of **5** displays strong absorption bands due to both the porphyrin and fullerene moieties. Fig. 1 shows the UV–VIS spectrum of **5** together with that of porphyrin **4** and **6** for comparison. Since the porphyrin dominates the visible region whereas C_{60} dominates the UV region, the electronic spectrum of **5** is a virtual superimposition of the two independent chromophores present in the molecule, indicating no appreciable ground state interaction between the two π-systems.

In CH_2Cl_2, porphyrin **4** displays fluorescence maxima at 635 and 698 nm (Fig. 2). The dyad **5**, excited at 580 nm, shows an emission spectrum with characteristic features of the porphyrin. However, the porphyrin emission is efficiently quenched by the attached C_{60} by a factor of 40. It remains to be clarified from time-dependent measurements whether the quenching of the

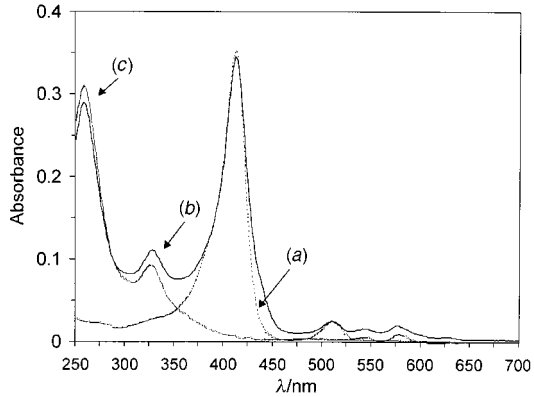

Fig. 1 UV–VIS spectra of (*a*) **4**, (*b*) **5** and (*c*) **6** in CH_2Cl_2 (2.5×10^{-6} mol dm^{-3}).

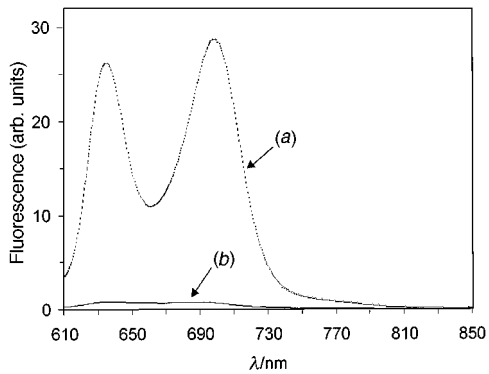

Fig. 2 Fluorescence spectra of (*a*) **4** and (b) **5** in CH_2Cl_2 (2.5×10^{-6} mol dm^{-3})

porphyrin fluorescence results from photoinduced energy transfer and/or electron transfer.

We thank Dr Anthony Khong (Yale University) for the ^{3}He NMR measurement. Financial support of this research by the US National Science Foundation is gratefully acknowledged. We also thank Andreas Hirsch (Erlangen) and François Diederich (ETH, Zürich) for communication prior to publication of independent synthesis of rigid C_{60}–porphyrin cyclophanes.[2]

Notes and references

† Detailed procedures for the synthesis and spectroscopic data of **4** and **5** will be reported elsewhere.

‡ *Selected data* for **5**: δ_H(200 MHz, $CDCl_3$, 25 °C) 10.33 (2H,s), 8.57 (2H, d), 7.80 (2H, t), 7.46 (2H, t), 7.13 (2H, d), 4.09 (8H, q), 3.80 (4H, t), 3.18 (4H, m), 2.72 (4H, m), 2.16 (4H, t), 1.97 (12H, t), 1.22 (12H, t), 1.11 (4H, m), −1.90 (2H, br s); δ_C(75 MHz, $CDCl_3$, 25 °C) 161.53,159.83, 145.44, 145.06, 144.98, 144.90, 144.53, 144.39, 144.29, 143.58, 142.85, 142.75, 142.67, 141.95, 141.61, 141.09, 140.62, 138.06, 134.03, 131.75, 130.45, 120.21, 113.46, 112.83, 97.27, 65.01, 63.37, 32.35, 27.89, 20.78, 19.91, 18.47, 17.48; δ_{He}(500 MHz, 1-methylnaphthalene–CD_2Cl_2) −6.5 (^{3}He@C_{60}), −8.5 (^{3}He@ **5**); λ_{max}(CH_2Cl_2)/nm (ε/dm^3 mol^{-1} cm^{-1}) 259 (115600), 328 (44400), 412 (138000), 510 (10000), 544 (6400), 577 (7600); fluorescence (λ_{exc} = 580 nm) λ_{max}(CH_2Cl_2)/nm 698, 635; *m/z* (MALDI-TOF) 1622.3 (M + H$^+$), calc. 1622.8 (M + H$^+$).

1 For examples, see P. A. Liddell, J. P. Sumida, A. N. Macpherson, L. Noss, G. R. Seely, K. N. Clark, A. L. Moore, T. A. Moore and D. Gust, *Photochem. Photobiol*., 1994, **60**, 537; H. Imahori, K. Hagiwara, T. Akiyama, S. Taniguchi, T. Okada and Y. Sakata, *Chem. Lett*., 1995, 265; T. Drovetskaya, C. A. Reed and P. Boyd, *Tetrahedron Lett*., 1995, **36**, 7971; M. G. Ranasinghe, A. M. Oliver, D. F. Rothenfluh, A. Salek and M. N. Paddon-Row, *Tetrahedron Lett*., 1996, **37**, 4797; H. Imahori, K. Yamada, M. Hasegawa, S. Taniguchi, T. Okada and Y. Sakata, *Angew, Chem., Int. Ed. Engl*., 1997, **36**, 2626; D. Carbonera, M. Di Valentin, C. Corvaja, G. Agostini, G. Giacometti, P. A. Liddell, D. Kuciauskas, A. L. Moore, T. A. Moore and D. Gust, *J. Am. Chem. Soc*., 1998, **120**, 4398; E. Dietel, A. Hirsch, J. Zhou and A. Rieker, *J. Chem. Soc., Perkin Trans. 2*, 1998, 1357.

2 E. Dietel, A. Hirsch, E. Eichhorn, A. Rieker, S. Hackbarth and B. Roder, *Chem. Commun*., 1998, 1981; J.-P. Bourgeois, F. Diederich, L. Echegoyen and J.-F. Nierengarten, *Helv. Chim. Acta*, 1998, **81**, 1835.

3 P. S. Baran, R. R. Monaco, A. U. Khan, S. R. Wilson and D. I. Schuster, *J. Am. Chem. Soc*., 1997, **119**, 8363; I. G. Safanov, P. S. Baran and D. I. Schuster, *Tetrahedron Lett*., 1997, **38**, 8133; R. Fong II, D. I. Schuster, H. Mi, S. R. Wilson and A. U. Khan, *Proc. Electrochem. Soc*., 1998, **98**, 262.

4 J. E. Baldwin, M. J. Crossley, T. Klose, E. A. O'Rear III and M. K. Peters, *Tetrahedron*, 1982, **38**, 27

5 T. D. Lash, J. R. Bellettini, J. A. Bastian and K. B. Couch, *Synthesis*, 1994, 170.

6 C. Bingel, *Chem. Ber*., 1993, **126**, 1957

7 X. Camps and A. Hirsch, *J. Chem. Soc., Perkin Trans. 1*, 1997, 1595

8 R. J. Cross, H. A. Jiménez-Vázquez, Q. Lu, M. Saunders, D. I. Schuster, S. R. Wilson and H. Zhao, *J. Am. Chem. Soc*., 1996, **118**, 11 454

Communication 8/07214K

Temperature-controlled selectivity of isomeric guest inclusion: enclathration and release of xylenes by 1,1′-binaphthyl-2,2′-dicarboxylic acid

Kayrat Beketov,[a] Edwin Weber,*[a] Jürgen Seidel,[b] Kurt Köhnke,[b] Kabul Makhkamov[c] and Bakhtiyar Ibragimov[c]

[a] *Institut für Organische Chemie der Technischen Universität Bergakademie Freiberg, Leipziger Str. 29, D-09596 Freiberg/Sachsen, Germany. E-mail: weber@tu-freiberg.de*
[b] *Institut für Physikalische Chemie der Technischen Universität Bergakademie Freiberg, Leipziger Str. 29, D-09596 Freiberg/Sachsen, Germany*
[c] *Institute of Bioorganic Chemistry, Uzbekistan Academy of Sciences, H. Abdullaev Str. 83, Tashkent 700143, Uzbekistan*

Received (in Liverpool, UK) 7th October 1998, Accepted 26th November 1998

Selectivity of enclathration and desolvation of xylene isomers by a dicarboxylic host depends on temperature.

Selective inclusion of guest species during crystallization is becoming of increasing importance in both the chemical and pharmaceutical industries, thus giving rise to the study of this phenomenon.[1,2] Recently, 1,1′-binaphthyl-2,2′-dicarboxylic acid (BNDA) was reported as a new clathrate host, and was found to exhibit clathrate formation selectivity for guests containing hydroxy groups.[3] However, a dependence of this selectivity upon the thermodynamic conditions of crystallization, such as that described here for the inclusion of xylene isomers, has not been discussed before.

Crystallization of BNDA from xylene isomers at room temperature gives three different channel-type clathrates.† In these crystals the BNDA molecules are incorporated into infinite zigzag chains created by H-bonded carboxylic group dimers. In the BNDA/*m*-xylene clathrate [Fig. 1(*a*)] these chains run along the *c*-axis and stack parallel to the *ac* plane in a 'face-to-face' mode, while in the BNDA/*p*-xylene clathrate [Fig. 1(*b*)] the chains are displaced by 1.5 Å along the *c*-axis. There are two BNDA molecules in the asymmetric part of the unit cell of the BNDA/*o*-xylene clathrate [Fig. 1(*c*)] which form zigzag chains in the [011] direction. Owing to the packing of these chains, two different channels are formed in the crystal.

In addition, simultaneous differential scanning calorimetric (DSC) and thermogravimetric (TG)‡ investigations of the thermal decomposition of these clathrates have been performed (Fig. 2). The release of the guest molecules during a linear temperature scan occurs in the temperature intervals 50–100 °C and 100–120 °C for the BNDA clathrates of *o*- and *p*-xylene, respectively. The observed mass losses correspond to the results of the X-ray structure analysis. Heats of clathrate decomposition have been calculated from the DSC curves to be 58 ± 1 and 49 ± 2 kJ mol^{-1} for the *p*- and *o*-xylene clathrates, respectively. These values are considerably higher than the heat of evaporation of xylenes (36 kJ mol^{-1}), suggesting specific stabilizing interactions in the clathrate crystals. The *m*-xylene clathrate of BNDA, however, causes problems in the TG-DSC because of its high instability; during sample preparation for an experiment the crystals lost *ca*. 30% of the included *m*-xylene molecules. Therefore, the determined host–guest ratio does not exactly correspond to the X-ray data. Nevertheless, based on the mass loss during the TG-DSC experiment a heat of decomposition of *ca*. 30 ± 5 kJ mol^{-1} has been estimated. The lower precision is caused by the uncertainty of the DSC baseline due to the sample instability. Taking into account this limited accuracy the heat of decomposition of the BNDA/*m*-xylene clathrate is much lower than the values determined for the stable BNDA clathrates and compares to the heat of evaporation of xylene.

The decomposed products obtained by vacuum desolvation (0.5 mbar, 8 h) of the BNDA clathrates at different temperatures were also characterized by X-ray powder diffraction.§ The BNDA clathrates with *m*- and *o*-xylene can be decomposed to

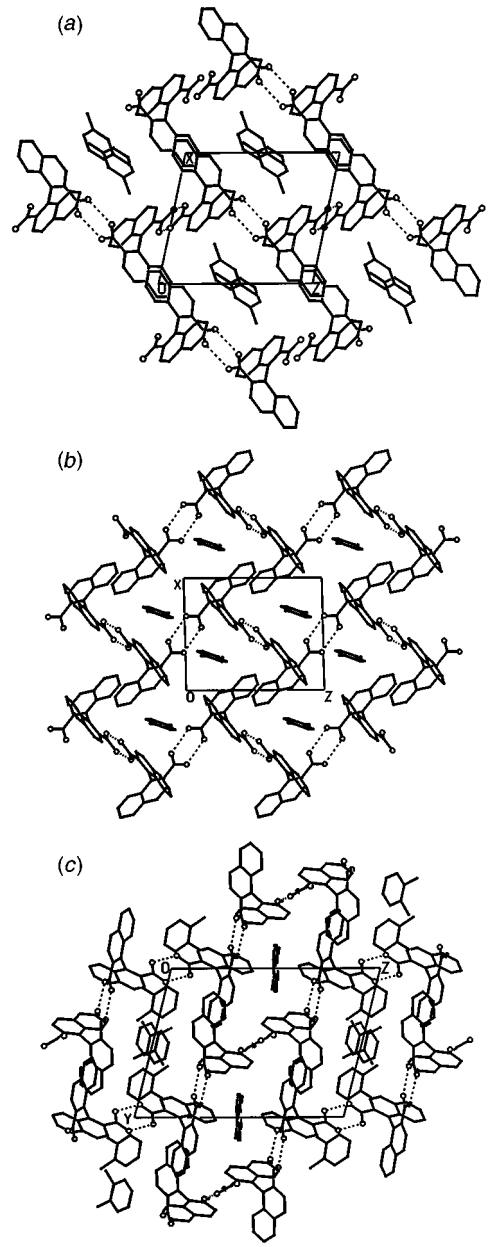

Fig. 1 Packing structures of the clathrates between BNDA and (*a*) *m*-xylene, (*b*) *p*-xylene and (*c*) *o*-xylene.

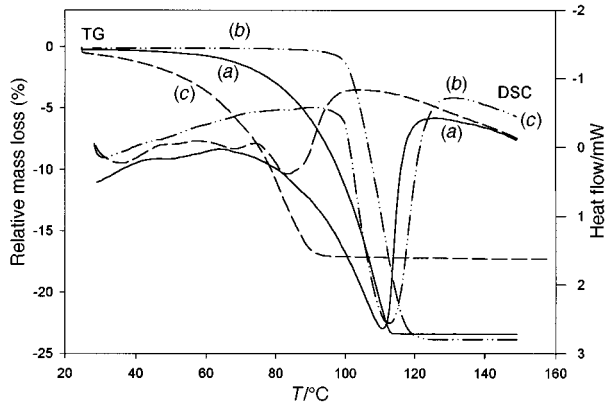

Fig. 2 Thermal degradations of (*a*) BNDA/*o*-xylene, (*b*) BNDA/*p*-xylene and (*c*) BNDA/m-xylene clathrates.

yield a desolvated phase **P1** of BNDA at 50 °C while the desolvation of the BNDA/*p*-xylene clathrate at higher temperature (100 °C) gives only a guest free phase **P2**. Recently, a crystal structure of the orthorhombic phase **P2** has been reported,[4] whereas single crystals of the triclinic phase **P1** have only now been obtained at 80 °C from an equimolar mixture of xylene isomers and its crystal structure has been determined.† The measured diffraction patterns of the desolvated samples correspond to theoretical diffractograms calculated from the appropriate structure data.

The different stabilities of the BNDA/xylene clathrates outlined above suggest a probable enclathration selectivity for the different xylene isomers, which prompted us to study the formation of BNDA clathrates from an equimolar mixture of the three xylene isomers. X-Ray diffraction and TG-DSC techniques were used to identify the obtained crystals. The crystallization temperature was varied within over −10 to +80 °C. If the crystallization temperature is between −10 and +10 °C a stable BNDA/*p*-xylene clathrate was found. Around room temperature a mixture of crystals of BNDA/*p*- and *o*-xylene clathrates was formed. TG-DSC curves of this crystal mixture are presented in Fig. 3 showing the two phases as distinctive steps. At +40 and +60 °C crystals of the BNDA/*o*-xylene clathrate were obtained, and crystals of the triclinic phase **P1** were formed at +80 °C. However, crystallization of the *m*-xylene clathrate from the mixed solution did not occur.

Thus, formation of clathrates or guest free host compounds and enclathration selectivity for a given host may be controlled by varying the crystallization temperature. These findings can be applied to purification and separation problems of isomeric mixtures or for the preparation of compounds of interest in

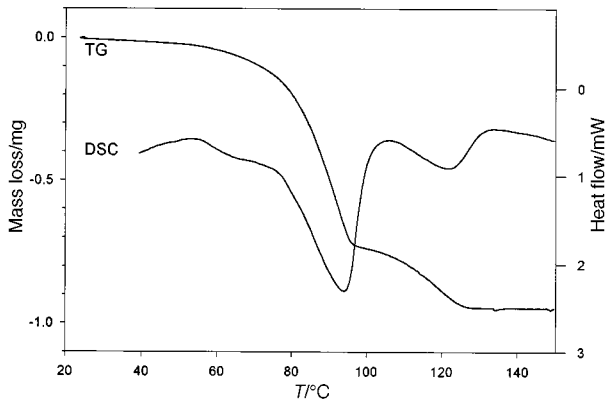

Fig. 3 Thermal degradation of the mixture of BNDA/*o*- and *p*-xylene crystals obtained at room temperature from a solution of an equimolar mixture of the three xylene isomers.

different crystal forms having different stability, composition, solubility *etc*.

K. B. thanks the Alexander von Humboldt-Stiftung for a scholarship. E. W. thanks the Deutsche Forschungsgemeinschaft (DFG) and the Fonds der Chemischen Industrie for financial support. This work is part of the Graduate School Program (GRK 208) of the TU Bergakademie Freiberg supported by the DFG.

Notes and references

† *Crystal data*: intensity data were collected at room temperature on a Syntex $P2_1$ diffractometer using Cu-Kα radiation (λ = 1.54178 Å) for the BNDA/*m*-xylene crystal and on an Enraf-Nonius CAD-4 diffractometer using Mo-Kα radiation (λ = 0.71073 Å) for the other three crystals.

BNDA/*o*-xylene: $C_{60}H_{48}O_8$, M = 896.98, triclinic, $P\bar{1}$, a = 10.843(2), b = 12.954(3), c = 17.599(4) Å, α = 103.64(3), β = 94.69(3), γ = 92.39(2)°, V = 2389.4(9) Å^3, Z = 2, D_c = 1.180 g cm^{-3}, μ(Mo-Kα) = 0.080 mm^{-1}, F(000) = 892, crystal size 0.2 × 0.35 × 0.45 mm, 10244 independent reflections. Final R = 0.0876 for 4648 reflections with $I > 2\sigma(I)$ and $wR2$ = 0.3288 for all data.

BNDA/*m*-xylene: $C_{30}H_{24}O_4$, M = 448.49, triclinic, $P\bar{1}$, a = 10.117(2), b = 10.556(2), c = 11.864(3) Å, α = 77.19(3), β = 77.81(3), γ = 86.63(2)°, V = 1207.5(5) Å^3, Z = 2, D_c = 1.233 g cm^{-3}, μ(Cu-Kα) = 0.651 mm^{-1}, F(000) = 472, crystal size 0.2 × 0.4 × 0.5 mm, 3400 independent reflections. Final R = 0.0544 for 2470 reflections with $I > 2\sigma(I)$ and $wR2$ = 0.1477 for all data.

BNDA/*p*-xylene: $C_{30}H_{24}O_4$, M = 448.49, triclinic, $P\bar{1}$, a = 10.117(2), b = 10.520(1), c = 11.913(1) Å, α = 83.48(1), β = 89.27(1), γ = 72.64(2)°, V = 1202.0(3) Å^3, Z = 2, D_c = 1.239 g cm^{-3}, μ(Mo-Kα) = 0.082 mm^{-1}, F(000) = 472, crystal size 0.35 × 0.5 × 0.5 mm, 5228 independent reflections. Final R = 0.0486 for 3938 reflections with $I > 2\sigma(I)$ and $wR2$ = 0.1493 for all data.

Polymorph **P1** of BNDA: $C_{44}H_{28}O_8$, M = 684.66, triclinic, $P\bar{1}$, a = 9.932(2), b = 11.320(2), c = 15.733(3) Å, α = 81.75(3), β = 80.57(3), γ = 89.34(3)°, V = 1726.8(6) Å^3, Z = 2, D_c = 1.317 g cm^{-3}, μ(Mo-Kα) = 0.091 mm^{-1}, F(000) = 712, crystal size 0.1 × 0.3 × 0.5 mm, 7529 independent reflections. Final R = 0.0624 for 3528 reflections with $I > 2\sigma(I)$ and $wR2$ = 0.2227 for all data.

The structures were solved by direct methods using the program SHELXS-86. The refinement of the structures against all $|F^2|$ data was carried out by the program SHELXL-93 with anisotropic displacement parameters for non-hydrogen atoms, and isotropic parameters for the guest molecules in the BNDA/*o*-xylene complex and the disordered O atoms in the polymorph **P1**. The H-atoms of all structures were placed at the calculated positions. CCDC 182/1100.

‡ *Thermal analysis*: The thermal decomposition of the different clathrate phases was studied by means of a simultaneous TG-DSC 111 system (Seteram, France) using open aluminium crucibles, sample weights of *ca*. 4 mg, a linear heating rate of 5 K min^{-1} and argon at 1 l h^{-1} as purge gas for all measurements. Crystals of an average size of 0.5–1 mm were taken from the mother liquor, quickly dried on filter paper and transferred into the crucible for immediate weighing and performance of the TG-DSC experiments

§ *X-Ray powder diffaction analysis*: Experiments were performed using a horizontal goniometer HZG 4 (Präzisionsmechanik Freiberg, Germany) and Cu-Kα radiation.

1 T. Kobayashi, S. Isoda and K. Kubono, in *Comprehensive Supramolecular Chemistry*, vol. 6 (*Solid-state Supramolecular Chemistry-Crystal Engeneering*), ed. J. L. Atwood, J. E. D. Davies, D. D. MacNicol and F. Vögtle, Elsevier, Oxford, 1996, p. 399; M. R. Caira and L. R. Nassimbeni, in *Comprehensive Supramolecular Chemistry*, vol. 6 (*Solid-state Supramolecular Chemistry-Crystal Engeneering*), ed. J. L. Atwood, J. E. D. Davies, D. D. MacNicol and F. Vögtle, Elsevier, Oxford, 1996, p. 825; E. Weber, in *Kirk-Othmer Encycopedia of. Chemical Thechnology*, 4th edn., vol. 14, ed. J. L. Kroschwitz, Wiley, New York, 1995, p. 122.

2 M. R. Caira, L. R. Nassimbeni and J. L. Scott, *J. Chem. Soc., Chem. Commun*., 1993, 612.

3 E. Weber, I. Csöregh, B. Stensland and M. Czugler, *J. Am. Chem. Soc*., 1984, **106**, 3297.

4 B. Ibragimov, K. Beketov, K. Makhkamov and E. Weber, *J. Chem. Soc., Perkin Trans. 2*, 1997, 1349.

Communication 8/07803C

Novel discotic mesogen: synthesis and liquid crystalline behavior of TAAB (tetrabenzo[*b,f,j,n*][1,5,9,13]tetraazacyclohexadecine) derivatives with long alkoxy chains†

Seok Ho Kang,[a] Miok Kim,[a] Hyung-Kun Lee,[a] Yoon-Sok Kang,[b] Wang-Cheol Zin[b] and Kimoon Kim*[a]

[a] National Research Initiative Center for Smart Supramolecules, Department of Chemistry, and [b] Department of Materials Science and Engineering, Pohang University of Science and Technology, San 31, Hyojadong, Pohang 790-784, South Korea. E-mail: kkim@postech.ac.kr

Received (in Cambridge, UK) 9th November 1998, Accepted 27th November 1998

The self-condensation of 3,4-dialkoxy-2-aminobenzaldehyde (alkoxy = *n*-$C_8H_{17}O$, *n*-$C_{10}H_{21}O$ and *n*-$C_{12}H_{25}O$) in the presence of HBF_4 gives the tetrafluoroborate salt of diprotonated octaalkoxy-TAAB which exhibits a hexagonal columnar mesophase over a wide range of temperatures including room temperature.

Discotic liquid crystals are well-known examples of supramolecular assemblies based on self-organization.[1] The columnar arrangement of disk-like mesogens such as triphenylenes, porphyrins and phthalocyanines is a promising architecture for anisotropic materials with potential applications such as one-dimensional conductors,[2] photoconductors,[3] molecular wires and fibers,[4] light emitting diodes[5] and photovoltaic cells.[6]

We are interested in studying new discotic mesogens.[7] Among the potential discotic mesogens we chose to examine was the macrocyclic compound tetrabenzo[*b,f,j,n*][1,5,9,13]-tetraazacyclohexadecine (TAAB). Metal complexes of TAAB (**A**), which have been known for over three decades, are synthesized by the self-condensation reaction of *o*-aminobenzaldehyde in the presence of metal ions (Scheme 1).[8] Without metal ion templates, however, the self-condensation reaction produces various polycyclic compounds including the eight-membered ring macrocyclic compound 4b,5,15,16-tetrahydrodibenzo[3,4:7,8][1,5]diazocino[2,1-*b*:6,5-*b*]diquinazoline-11,22-diium ion (**B**)‡ (Scheme 1).[9] In fact, no metal-free TAAB derivatives have been reported until now. Furthermore, no liquid crystalline compound having a TAAB core is known. Herein we describe the first successful synthesis of metal-free TAAB derivatives having long alkoxy substituents on the phenyl rings and their liquid crystalline behavior.

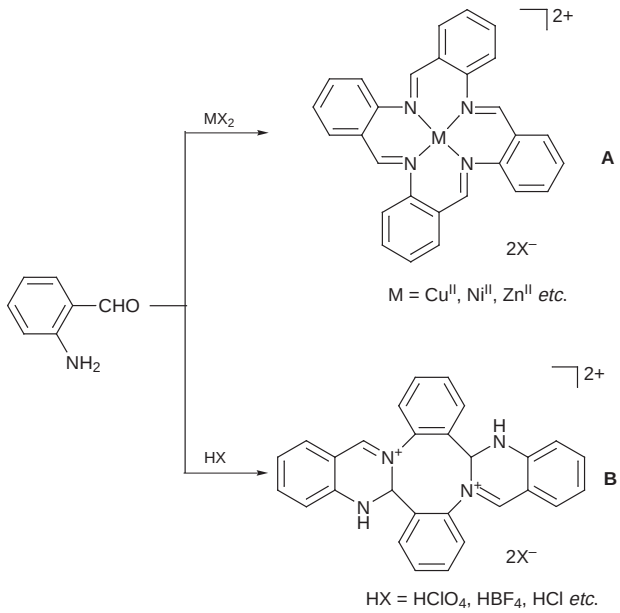

Scheme 1

The synthesis of metal free, octaalkoxy-TAAB compounds **5a–c** is shown in Scheme 2. 3,4-Dihydroxybenzaldehyde **1** was alkylated with alkyl bromide (alkyl = *n*-octyl, *n*-decyl and *n*-dodecyl) and subsequently converted into the corresponding 2-nitrobenzaldehyde by nitration. The key step for the synthesis of TAAB derivatives is the reduction of the 3,4-dialkoxy-2-nitrobenzaldehyde **3**. The proper choice of reducing agent is crucial because these reduction reactions are undoubtedly complicated by competing inter- and intra-molecular condensation reactions. Attempts to reduce **3** with previously-used reducing agents such as titanium(III) chloride and ferrous sulfate gave none of the desired product, while sodium sulfide gave only a 10% yield. However, the 3,4-dialkoxy-2-aminobenzaldehyde **4** could be prepared by hydrogenation of **3** with H_2 and Pd/C in 60–83% yield. In contrast to 2-aminobenzaldehyde, the dialkoxyaminobenzaldehydes are stable at room temperature; their stability increases with increasing alkyl chain length.

The self-condensation of **4** using HBF_4 in refluxing EtOH gives the tetrafluoroborate salt of diprotonated octaalkoxy-TAAB (**5a–c**) in 14–21% yield. The products have been characterized by NMR, UV–VIS, IR and mass spectroscopy and gave satisfactory elemental analyses.§ Their simple ^1H and ^{13}C NMR spectral patterns are consistent with the 16-membered

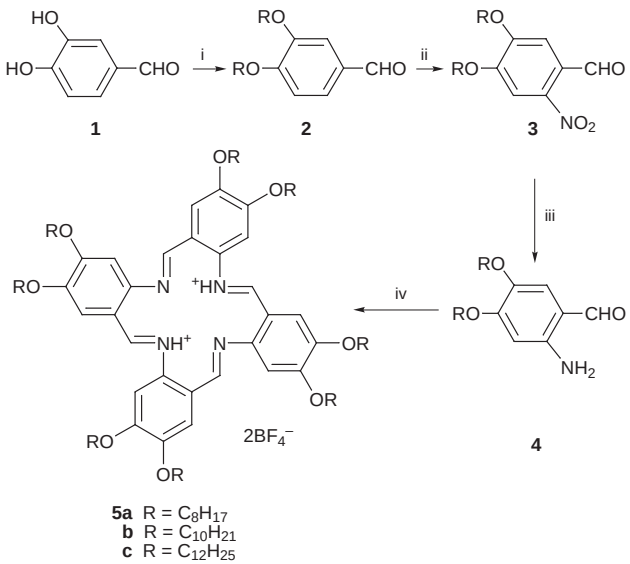

Scheme 2 *Reagents and conditions*; i, RBr, K_2CO_3, acetone; ii, HNO_3, $NaNO_2$, CH_2Cl_2; iii, H_2, Pd/C (10%), CH_2Cl_2, room temp.; iv, HBF_4, EtOH, reflux.

† Synthetic and spectroscopic data for **2–5** and a photograph of the texture of **5c** under a polarizing microscope at 70 °C is available from the RSC web site, see: http://www.rsc.org/suppdata/cc/1999/93

Table 1 Phase behavior of **5a–c**[a]

Compound	Transition	*T*/°C	ΔH/J g^{-1}	Lattice constant/Å
5a	K–D_{hd}	−4.3	2.17	25.46
	D_{hd}–I	271[b]		
5b	K–D_{hd}	2.8	5.23	27.69
	D_{hd}–I	263[b]		
5c	K–D_{hd}	22.5	22.64	29.62
	D_{hd}–I	249[b]		

[a] Transition temperatures and enthalpies were determined by DSC (scan rate 10 °C min^{-1}). K, crystalline phase; D_{hd}, hexagonal columnar phase; I, isotropic phase. [b] Transition observed only by polarizing microscopy.

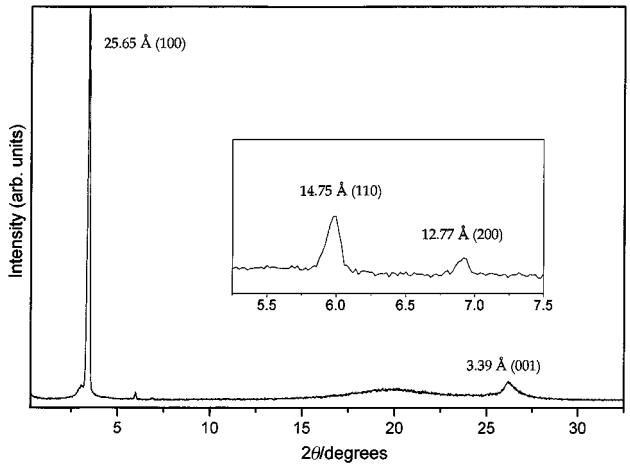

Fig. 1 X-Ray diffraction pattern of **5c** taken at room temperature.

TAAB core being in a diprotonated form. This is in sharp contrast to the fact that the self-condensation of simple 2-aminobenzaldehyde under the same conditions yields **B** having an eight-membered ring core (Scheme 1). This is the first example of the self-condensation reaction of an *o*-amino-benzaldehyde without metal ion templates leading to the formation of the 16-membered macrocyclic TAAB core. The electron-donating alkoxy substituents appear to stabilize the diprotonated TAAB core in **5**.

The diprotonated TAAB derivatives **5a–c** show mesomorphic behavior over a wide range of temperatures as revealed by differential scanning calorimetry (DSC), polarizing microscopy and X-ray diffraction measurements (Table 1). For example, **5c** shows a columnar mesophase at room temperature and transforms into an isotropic liquid at 249 °C. These transitions are not observed by DSC due to the low isotropic transition enthalpy, but are observed by polarizing microscopy. In optical microscopy a pseudo-focal conic texture is observed, which is typical for columnar mesophases. The compound starts decomposing just above the clearing point.

In order to clarify the mesomorphism of these compounds, we performed X-ray diffraction experiments at room temperature. The X-ray diffraction pattern (Fig 1) of the mesophase of **5c** shows a set of sharp reflections in the small-angle region which correspond to reciprocal spacings in a ratio of $1:\sqrt{3}:\sqrt{4}$. These peaks were assigned to the (100), (110) and (200) reflections from a hexagonal arrangement with a lattice constant a = 29.62 Å. In the wide-angle region, X-ray diffraction measurement also shows two broad and diffuse rings. The first one corresponds to a spacing of 4–5 Å, which is related to the liquid-like correlation between the molten aliphatic chains. The second ring at 3.39 Å is presumably related to the periodic stacking of the macrocyclic subunits within the columns. A molecular mechanical calculation suggests that the diprotonated TAAB core has a saddle-shaped conformation similar to those for metal complexes of unsubstituted TAAB reported earlier.[8b] The saddle-shaped macrocycles are stacked along the column with a mean interplanar distance of 3.39 Å. The columns are in turn arranged in a two-dimensional hexagonal array.

In summary, we synthesized novel discotic liquid crystals containing the macrocyclic TAAB core. The key to the successful synthesis of the stable diprotonated TAAB core is the introduction of electron–donating alkoxy substituents. The long alkoxy chains stabilize not only the precursor 3,4-dialkoxy-2-aminobenzaldehyde but also the diprotonated TAAB core formed by self-condensation of the precursor. These macrocyclic compounds exhibit hexagonal columnar mesophases over a wide range of temperatures including room temperature, demonstrating that the saddle-shaped macrocyclic core may be successfully used as a new discotic mesogen. These novel liquid crystalline materials may have interesting physical properties which are currently under investigation. The successful syntheses of the metal-free TAABs open up new possibilities for synthesizing a variety of metal complexes using these compounds as ligands. We are also working along this line.

This work was supported by the Creative Research Initiative Program (the Korean Ministry of Science and Technology). The X-ray diffraction measurements were performed at the Pohang Accelerator Laboratory (Beamline 3C2). We thank Mr Woo Sung Jeon for molecular mechanical calculations and Professor G. V. Smith for helpful suggestions in preparation of the manuscript.

Notes and references

‡ Old literature (ref. 8,9) refers to compound **B** as (TAAB)$(HBF_4)_2$ or $[(TAAB)H_2][BF_4]$, but these abbreviations are misleading because the macrocycle core **B** is different from that of **A**.

§ All the compounds have been fully characterized by ^{1}H NMR, UV–VIS, IR and mass spectroscopy and gave satisfactory elemental analyses. *Selected data* for **5c**: $\delta_H(CDCl_3$, 300 MHz) 0.87 (t, 24H, CH_3), 1.44 [m, 144H, $(CH_2)_9$], 1.73 (m, 16H, CH_2), 3.83 (q, 16H, OCH_2), 6.42 (s, 4H, Ar), 6.58 (s, 4H, Ar), 7.96 (s, 4H, N=CH); $\delta_C(CDCl_3$, 75 MHz) 14.51, 23.13, 24.91, 26.56, 29.75, 29.89, 30.24, 30.33, 32.40, 69.39, 69.66, 99.92, 117.70, 119.87, 124.68, 138.44, 149.29, 154.71, 157.56; ν_{max}(KBr)/cm^{-1} 1635 (C=C), 1555 (C=N); *m/z* (FAB) 1887.7 ($M + H^+ - 2HBF_4$); Calc. for $C_{124}H_{214}N_4O_8B_2F_8$: C, 72.21; H, 10.46; N, 2.72. Found: C, 71.97; H, 10.32; N, 2.84.

1 S. Chandrasekar, in *Advances in Liquid Crystals*, ed. G. H. Brown, Academic Press, New York, vol. 5, 1982; C. Destrade, P. Foucher, H. Gasparoux, N-H. Tinh, A. M. Levelut and J. Malthete, *Mol. Cryst. Liq. Cryst.*, 1984, **106**, 121; S. Chandrasekar, *Liq. Cryst.*, 1993, **14**. 3.
2 N. Boden, R. Bissell, J. Clements and B. Movaghar, *Liq. Crystal. Today*, 1996, **6**, 1.
3 J. Simmerer, B. Glusen, W. Paulus, A. Kettner, P. Schuhmacher, D. Adam, K. H. Etzbach, K. Siemensmeyer, J. H. Wendorff, H. Ringsdorf and D. Haarer, *Adv. Mater.*, 1996, **8**, 815.
4 C. F. van Nostrum and R. J. M. Nolte, *Chem. Commun.*, 1996, 2385; E. J. Osburn, A. Schmidt, L. K. Chau, S. Y. Chen, P. Smolenyak, N. R. Armstrong and D. F. O'Brian, *Adv. Mater.*, 1996, **8**, 926.
5 T. Christ, B. Glusen, A. Greiner, A. Kettner, R. Sander, V. Stumpflen, V. Tsukruk and J. H. Wendorff, *Adv. Mater.*, 1997, **9**, 48.
6 C.-Y. Liu, H.-L. Pan, M. A. Fox and A. J. Bard, *Science*, 1993, **261**, 897.
7 S. J. Kim, S. H. Kang, K.-M. Park, H. Kim, W.-C. Zin, M.-G. Choi and K. Kim, *Chem. Mater.*, 1998, **10**, 1889.
8 (*a*) J. S. Skuratowicz, I. L. Madden and D. H. Busch, *Inorg. Chem.*, 1977, **16**, 1721; (*b*) A. J. Jircitano, R. I. Sheldon and K. B. Mertes, *J. Am. Chem. Soc.*, 1983, **105**, 3022.
9 F. Seidel and W. Dick, *Ber. Dtsch. Chem. Ges.*, 1927, **60**, 2018; J. D. Goddard and T. Norris, *Inorg. Nucl. Chem. Lett.*, 1978, **14**, 211; P. G. Owston and L. S. Shaw, *Acta Crystallogr.*, 1988, **B44**, 39.

Communication 8/08739C

A most user-friendly protocol for ring closing metathesis reactions

Alois Fürstner* and Lutz Ackermann

Max-Planck-Institut für Kohlenforschung, D-45470 Mülheim/Ruhr, Germany.
E-mail: fuerstner@mpi-muelheim.mpg.de

Received (in Cambridge, UK) 10th November 1998, Accepted 25th November 1998

Ring closing metathesis reactions (RCM) can be conveniently achieved in a photo-assisted manner simply by heating a solution of the diene substrate, catalytic amounts of commercially available [(*p*-cymene)$RuCl_2$]$_2$ 4 and PCy_3 in CH_2Cl_2 under neon light.

The advent of well-defined ruthenium-based metathesis pre-catalysts has triggered an explosive growth of interest in this transformation in both the organic and polymer chemists' communities.[1] Among them, the ruthenium carbene complexes **1** (R′ = Ph, $CH{=}CPh_2$) developed by Grubbs *et al*. set the standards in the field.[2] These reagents turned out to be very efficient and highly tolerant pre-catalysts for all kinds of metathesis reactions and have therefore found numerous applications in the synthesis of complex target molecules and the preparation of speciality polymers.[1,3]

Although the rapidly increasing demand has led to the development of considerably improved methods for the preparation of **1**,[4,5] the recent literature also documents a search for alternative metathesis initiators of comparable performance and improved accessibility. In this context, we have introduced the cationic, 18-electron ruthenium allenylidene species **2** as a

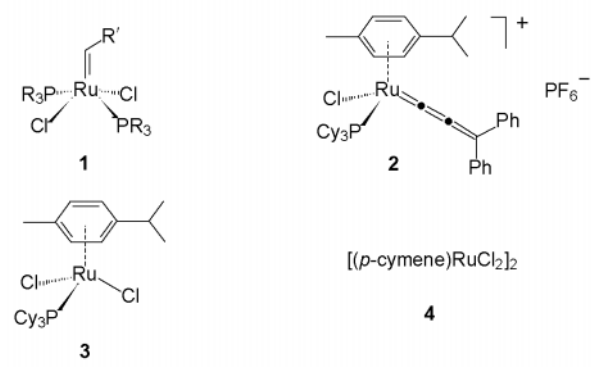

versatile pre-catalyst for various ring closing metathesis (RCM) reactions.[6] This compound is easily prepared by cleaving the chloride bridges of commercially available [(*p*-cymene)$RuCl_2$]$_2$ **4** with PCy_3, followed by treatment of the resulting monomer **3** with 1,1-diphenylprop-2-ynyl alcohol in the presence of $NaPF_6$. Other groups have reported alternative methods for activating compound **3**: thus, Noels *et al*. found that this complex converts into an efficient catalyst for ring opening metathesis polymeri-

Table 1 Neon light driven RCM using [(*p*-cymene)$RuCl_2$]$_2$ **4** (2.5 mol%) + PCy_3 (5.5 mol%) in CH_2Cl_2 as an *in situ* catalyst mixture

Entry	Substrate	Product	Yield (%)	Ref.
1	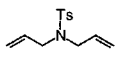		90	6
2			90[a,b]	
3	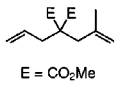 E = CO_2Me		86	12
4	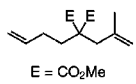 E = CO_2Me		87	12
5	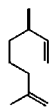		82[b]	
6	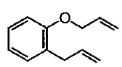		78	
7	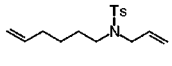		77	6
8	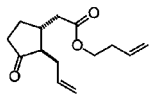	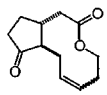	65[c]	13
9	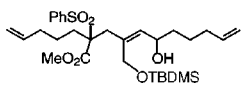	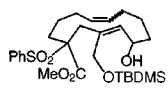	68[d]	14
10	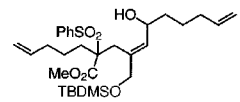	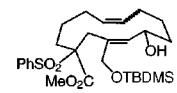	70[c]	14
11	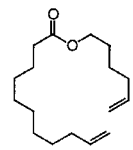	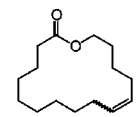	80	15
12	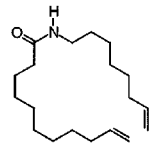	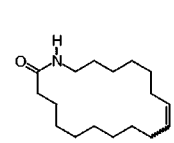	75	15
13	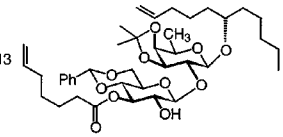	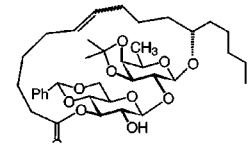	70[c]	16
14	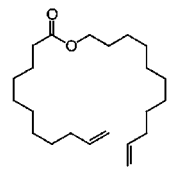	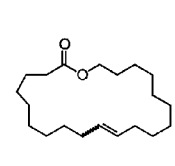	72	15

[a] Using (*p*-cymene)$Ru(PCy_3)Cl_2$ **3** (2.5 mol%) as the pre-catalyst instead of the *in situ* mixture. [b] GC yield. [c] Using [(*p*-cymene)$RuCl_2$]$_2$ (5 mol%) + PCy_3 (11 mol%). [d] Using [(*p*-cymene)$RuCl_2$]$_2$ (15 mol%) + PCy_3 (30 mol%).

zations (ROMP) upon treatment with diazo alkanes,[7] whereas Hafner *et al*. initiated ROMP reactions with **3** after exposure to UV light (200 W Hg lamp).[8] These latter procedures, however, either require hazardous additives or special photochemical equipment and have not yet been applied to RCM.

We now report an even more convenient method for the activation of this key compound. Thus, heating a solution of a diene in the presence of catalytic amounts of **3** or, preferably, a mixture of commercially available $[(p\text{-cymene})RuCl_2]_2$ **4** and PCy_3 effects a clean and very efficient cyclization of the substrate, provided that the reactions are exposed to neon light or strong daylight.† Several aspects of this method are noteworthy:

(i) Light emitted by neon tubes commonly used for the lighting of laboratories is sufficient.

(ii) The reactions are performed in standard laboratory glassware (DURAN®) which absorbs 50% of UV light with λ = 300 nm and more than 95% of UV light with $\lambda \leqslant 285$ nm.[9]

(iii) Control experiments carried out in the dark clearly prove the photochemical effect on the rate of reaction.[10]

(iv) Refluxing CH_2Cl_2 turned out to be the best solvent.[11]

(v) Under these photo-assisted conditions, the reactions proceed very cleanly and reproducibly and neither activation by hazardous diazo alkanes nor any special photochemical devices or equipment is necessary.

(vi) Although the rate of reaction is slower than that obverved with Grubbs carbenes, the isolated yields are good to excellent and comparable to those obtained with **1** in all RCM experiments carried out so far. Note that a slow initiation is a disadvantage in polymerization reactions, whereas it is of minor importance for RCM.

(vii) As can be seen from the examples compiled in Table 1, this new procedure tolerates a wide range of functional groups in the substrates, including esters, amides, ketones, ethers, silyl ethers, acetals, glycosides, sulfones, sulfonamides, and even unprotected secondary hydroxy groups.

(viii) This new procedure applies to all ring sizes including medium-sized and macrocyclic ones. Furthermore it allows the preparation of even trisubstituted olefins in the five- and six-membered ring series as shown in entries 3–5 of Table 1.[12]

Finally—and most importantly—we would like to stress that this new protocol is distinguished by a hitherto unrivaled 'low tech' nature. It requires only commercially available reagents, avoids the (multi-step) preparation of peculiar complexes as well as the use of hazardous additives and needs no special equipment whatsoever; importantly, however, its efficiency and scope favorably compare with all current alternatives described in the literature. Therefore we believe that this extremely simple, yet highly productive methodology may help to increase the popularity of RCM even further and should find many applications in advanced organic synthesis.

Studies to elucidate the mechanism of the photochemical activation step on a molecular level are underway and will be reported in due course.

Notes and references

† *Representative procedure*: A solution of *N*,*N*-bis(allyl)toluene-*p*-sulfonamide (1.00 g, 3.99 mmol), $[(p\text{-cymene})RuCl_2]_2$ **4** (61 mg, 0.1 mmol) and PCy_3 (62 mg, 0.22 mmol) in CH_2Cl_2 (40 ml) was refluxed under Ar for 16 h in a well-illuminated hood. The solvent was removed *in vacuo* and the residue was purified by flash chromatography on silica using hexane–EtOAc (10:1) as eluent. This affords *N*-tosyl-2,5-dihydro-1*H*-pyrrole as colorless crystals (799 mg, 90%), mp 123-124 °C; δ_H(300 MHz, $CDCl_3$) 7.70 (d, *J* 8, 2H), 7.29 (d, *J* 8, 2H), 5.63 (s, 2H), 4.10 (s, 4H), 2.41 (s, 3H); δ_C(75 MHz, $CDCl_3$) 143.8, 134.7, 130.1, 127.8, 125.8, 55.2, 21.9; *m/z* 223 (35, $[M^+]$), 155 (32), 91 (77), 68 (100), 41 (24).

1 For reviews see: R. H. Grubbs and S. Chang, *Tetrahedron*, 1998, **54**, 4413; A. Fürstner, *Top. Organomet. Chem*., 1998, **1**, 37; S. K. Armstrong, *J. Chem. Soc., Perkin Trans. 1*, 1998, 371; M. Schuster and S. Blechert, *Angew. Chem., Int. Ed. Engl*., 1997, **36**, 2036; A. Fürstner, *Top. Catal*., 1997, **4**, 285; K. J. Ivin and J. C. Mol, *Olefin Metathesis and Metathesis Polymerization*, Academic Press, New York, 1997.

2 S. T. Nguyen, R. H. Grubbs and J. W. Ziller, *J. Am. Chem. Soc*., 1993, **115**, 9858; S. T. Nguyen, L. K. Johnson, R. H. Grubbs and J. W. Ziller, *J. Am. Chem. Soc*., 1992, **114**, 3974; P. Schwab, R. H. Grubbs and J. W. Ziller, *J. Am. Chem. Soc*., 1996, **118**, 100.

3 For recent reviews on applications in polymer chemistry see: D. Tindall, J. H. Pawlow and K. B. Wagener, *Top. Organomet. Chem*., 1998, **1**, 180; L. L. Kiessling and L. E. Strong, *Top. Organomet. Chem*. 1998, **1**, 196 and references cited therein.

4 J. Wolf, W. Stüer, C. Grünwald, H. Werner, P. Schwab and M. Schulz, *Angew. Chem*., 1998, **110**, 1165; T. R. Belderrain and R. H. Grubbs, *Organometallics*, 1997, **16**, 4001; T. E. Wilhelm, T. R. Belderrain, S. N. Brown and R. H. Grubbs, *Organometallics*, 1997, **16**, 3867.

5 For structural modifications of **1** see: S. Chang, L. Jones, C. Wang, L. M. Henling and R. H. Grubbs, *Organometallics*, 1998, **17**, 3460; E. L. Dias and R. H. Grubbs, *Organometallics*, 1998, **17**, 2758; T. Weskamp, W. C. Schattenmann, M. Spiegler and W. A. Herrmann, *Angew. Chem*., 1998, **110**, 2631.

6 A. Fürstner, M. Picquet, C. Bruneau and P. H. Dixneuf, *Chem. Commun*., 1998, 1315. This complex also responds to *hν*, *cf*. M. Picquet, C. Bruneau and P. H. Dixneuf, *Chem. Commun*., 1998, 2249.

7 A. Demonceau, A. W. Stumpf, E. Saive and A. F. Noels, *Macromolecules*, 1997, **30**, 3127; A. W. Stumpf, E. Saive, A. Demonceau and A. F. Noels, *J. Chem. Soc., Chem. Commun*., 1995, 1127; A. Demonceau, A. F. Noels, E. Saive and A. J. Hubert, *J. Mol. Catal*., 1992, **76**, 123.

8 A. Hafner, A. Mühlebach and P. A. van der Schaaf, *Angew. Chem*., 1997, **109**, 2213.

9 Constant irradiation of the reaction mixture with a UV emitting quartz lamp dipped into the solution at room temperature is inappropriate, leaving 98% of the substrate unchanged after 16 h reaction time.

10 Reaction of *N*,*N*-bis(allyl)toluene-*p*-sulfonamide in refluxing CH_2Cl_2 with **4** (2.5 mol%) and PCy_3 (5.5 mol%) in the dark shows that 92% of the substrate (GC) is unchanged after 16 h. Note that after this period of time, the photoassisted reaction is quantitative.†

11 RCM can also be carried out in toluene at 80 °C; in this medium, however, the reactions tend to be less selective as shown by the following prototype experiment:

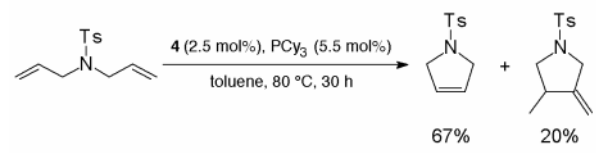

12 For an in-depth study on the effect of substitution on RCM see: T. A. Kirkland and R. H. Grubbs, *J. Org. Chem*., 1997, **62**, 7310.

13 A. Fürstner and T. Müller, *Synlett*, 1997, 1010.

14 A. Fürstner, T. Gastner and H. Weintritt, *J. Org. Chem.*, in the press.

15 A. Fürstner and K. Langemann, *J. Org. Chem*., 1996, **61**, 3942; A. Fürstner and K. Langemann, *Synthesis*, 1997, 792; A. Fürstner and K. Langemann, *J. Am. Chem. Soc*., 1997, **119**, 9130.

16 A. Fürstner and T. Müller, *J. Org. Chem*., 1998, **63**, 424.

Communication 8/08810A

Vapor-phase transport synthesis of ZnAPO-34 molecular sieve

Lixiong Zhang and George R. Gavalas*

Chemical Engineering 210-41, California Institute of Technology, Pasadena, CA 91125, USA.
E-mail: gavalas@cheme.caltech.edu

Received (in Bloomington, IN, USA) 3rd September, 1998, Revised manuscript received 19th November 1998, Accepted 20th November 1998

ZnAPO-34 molecular sieve can be synthesized by the vapor-phase transport technique using triethylamine as a structure-directing agent.

Aluminium phosphate molecular sieves (AlPO-n) are crystalline framework structures formed from alternating AlO_4 and PO_4 tetrahedra.[1,2] Their pore sizes and adsorption properties are similar to those of zeolites but their framework is electrically neutral. By substitution of divalent ions of metals like Co or Zn for part of the aluminium ions, the framework acquires negative charges balanced by acidic protons possessing acidic catalytic activity.[3]

Since the first report on AlPO preparation,[1] interest in these materials has increased because of their potential as adsorbents, catalysts or catalyst supports[4,5] and, more recently, as membranes for gas separations.[6] The attractive properties of AlPOs that distinguish them from zeolites are their generally higher thermal stability and easier incorporation of metals in the framework.[1,4]

Zeolites and AlPOs are conventionally prepared by hydrothermal synthesis,[7] but zeolites can be prepared by other techniques as well, such as solvothermal synthesis[8] and vapor-phase transport (VPT).[9–11] The VPT technique involves crystallization of dry gel in a vapor phase containing organic template and water, and has certain advantages over other methods including minimum use of expensive organic template, elimination of the need to separate products from mother liquid, and production of molecular sieve coatings on various substrates.

Since 1990 when Xu *et al.*[9] first synthesized ZSM-5 by exposure of dry amorphous aluminosilicate gels in a vapor of ethylenediamine, triethylamine (Et_3N) and water, zeolites, such as ANA, FER, MOR and CHA, have been synthesized by several groups by VPT.[10,11] However, the VPT technique has not been applied so far to aluminophosphate molecular sieves. The purpose of this communication is to report synthesis of ZnAPO-34 molecular sieve by the vapor-phase transport technique.

Hydrothermal synthesis of ZnAPO-34 is normally carried out using tetraethylammonium hydroxide (TEAOH) as a structure-directing agent (SDA).[12] However, because TEAOH is non-volatile, we carried out the VPT synthesis using Et_3N as the SDA. Before attempting VPT synthesis we verified that normal hydrothermal synthesis of ZnAPO-34 using Et_3N is feasible. The hydrogel for the hydrothermal synthesis was the same as reported in literature[12] except that Et_3N was used instead of TEAOH. The product was characterized by XRD and SEM and, as shown in Fig. 1(a), it has the same cubic morphology as that prepared using TEAOH.[12] Analysis of the powder XRD pattern shown in Fig. 2(a) verified the that the product was ZnAPO-34 and the unit cell constants calculated were a = 13.746, b = 13.746, c = 14.730 Å (trigonal system, hexagonal axes) in agreement with those reported previously.[13]

VPT synthesis of ZnAPO-34 using Et_3N as organic template was carried out next. Dry gels for this synthesis were prepared by adding the specified quantities of zinc acetate, aluminium isopropoxide, and phosphoric acid into water successively. The system was stirred vigorously at room temperature to a homogeneous mixture each time prior to the addition of the next component. The resulting mixture was dried either at room temperature or at 90 °C overnight. VPT syntheses of ZnAPO-34 were conducted in a 23ml Teflon-lined stainless steel autoclave.

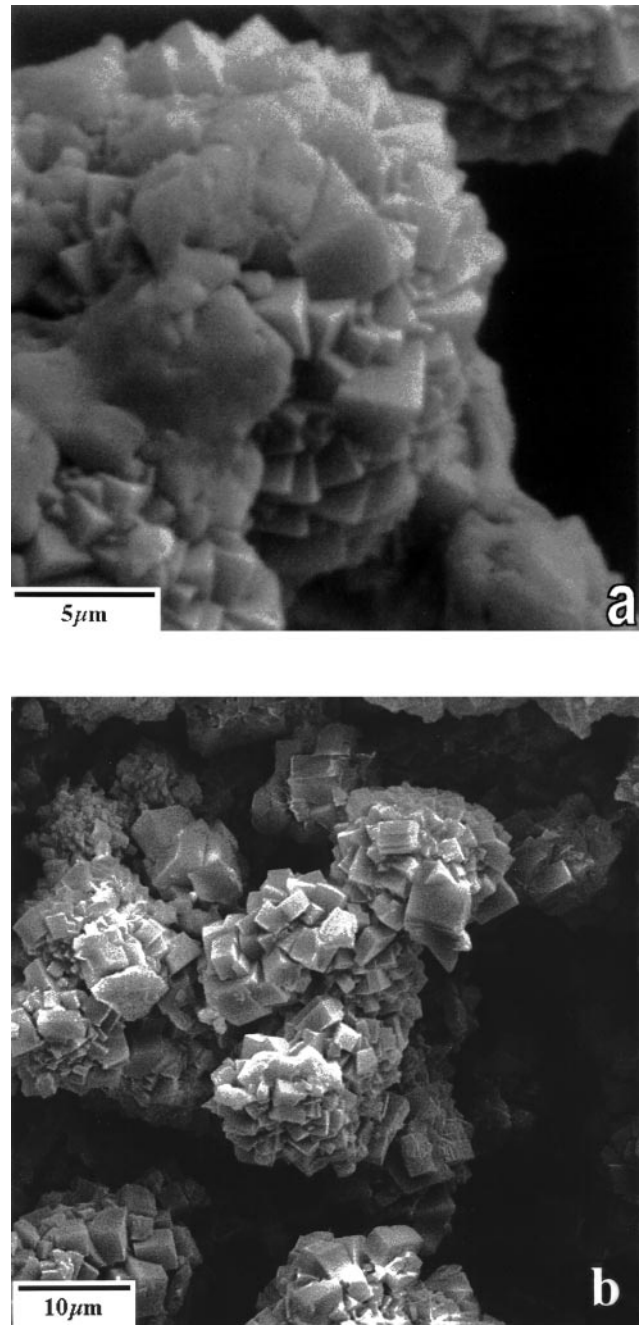

Fig. 1 Scanning electron micrograms of (a) product prepared by hydrothermal synthesis using Et_3N as a structure-directing agent; (b) product prepared by the VPT technique.

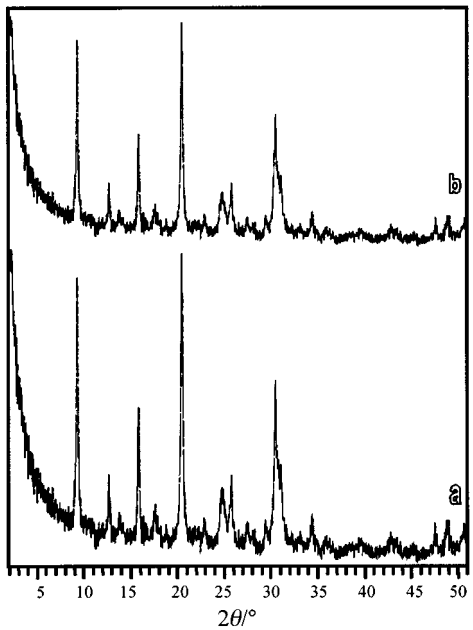

Fig. 2 XRD patterns of (a) product prepared by hydrothermal synthesis using Et_3N as a structure-directing agent; (b) product prepared by the VPT technique.

About 6 ml of a mixture of Et_3N and water was poured into the bottom of the autoclave. The dry gel was placed on a Teflon plate, which was installed in the autoclave above the liquid level. The autoclave was placed into a convection oven preheated to 170 °C and maintained at that temperature for 24 h. The autoclave was subsequently quenched in tap water and the products were washed, dried and characterized by SEM and XRD.

Table 1 lists the synthesis composition and resulting products. In the first set of experiments, the dry gel was prepared using the composition $0.4ZnO:0.8Al_2O_3:1P_2O_5:75H_2O$. Fig. 1(b) shows that the morphology of the resulting product is the same as that of Fig. 1(a). The XRD pattern of the product shown in Fig. 2(b) is also identical to that of Fig. 2(a).

Table 1 Experimental conditions and results.

Entry	Composition for synthesis of amorphous gel	Liquid phase	Result by XRD
1	$0.4ZnO:0.8Al_2O_3:1P_2O_5:75H_2O$[a]	$2Et_3N:150H_2O$	ZnAPO-34
2	$0.4ZnO:0.8Al_2O_3:1P_2O_5:150H_2O$[a]	$2Et_3N:150H_2O$	ZnAPO-34
3	$0.4ZnO:0.8Al_2O_3:1P_2O_5:150H_2O$[b]	$2Et_3N:150H_2O$	ZnAPO-34
4	$0.4ZnO:0.8Al_2O_3:1P_2O_5:150H_2O$[b]	$99Et_3N:1H_2O$	ZnAPO-34
5	$0.4ZnO:0.8Al_2O_3:1P_2O_5:150H_2O$[b]	$2Et_3N$:150EtOH	Amorphous
6	$0.4ZnO:0.8Al_2O_3:1P_2O_5:300H_2O$[b]	$2Et_3N:150H_2O$	ZnAPO-34
7	$0.4ZnO:0.8Al_2O_3:1P_2O_5$:150EtOH[b]	$2Et_3N:150H_2O$	Amorphous
8	$0.4SiO_2:0.8Al_2O_3:1P_2O_5:150H_2O$[b]	$2Et_3N:150H_2O$	SAPO-34

[a] Gel was dried at ambient temperature. [b] Gel was dried at 90 °C.

The other preparations listed in Table 1 involved the following variations. Some gels were prepared with different amounts of water or were dried at 90 °C. In one preparation the liquid phase contained 99% Et_3N. In another it contained Et_3N and ethanol instead of water. Finally in one experiment the gel was prepared with ethanol instead of water. As shown in Table 1, the VPT synthesis product was always ZnAPO-34 as long as the gel was initially prepared using water and the liquid placed at the bottom of the autoclave contained water. Even 1% water contained in sample 4 was evidently sufficient. However, if the gel was prepared using ethanol or if the liquid introduced into the autoclave was an ethanol–Et_3N mixture, the product was amorphous. Entry 8 in Table 1 shows that SAPO-34 can also be prepared using VPT method with Et_3N as the structure-directing agent.

Funding of this work by Elf Atochem, North America, Inc. is greatly appreciated. We thank Ms Lin Luo for analyzing the XRD patterns.

Notes and references

1 S. T. Wilson, B. M. Lok, C. A. Messina, T. R. Cannan and E. M. Flanigen, *J. Am. Chem . Soc.*, 1982, **104**, 1146.
2 R. Szostak, *Molecular Sieves*, van Nostrand Reinhold, New York, pp. 254–281.
3 Z. Zhao and R. Zhao, *Zeolites*, 1993, **13**, 634.
4 J. Das, S. P. Lohokare and D. K. Chakrabarty, *Indian J. Chem., Sect. A*, 1992, **31**, 742.
5 S. T. Wilson, B. M. Lok, C. A. Messina and E. M. Flanigen, in *Proc. 6th Int. Zeol. Conf.*, ed. D. Olson and A. Bisio, Butterworth, London, 1984, pp. 97–109.
6 J. C. Poshusta, T. A. Vu, J. L. Falconer and R. D. Noble, *Proc. Int. Workshop on Zeolitic Membranes and Films*, Gifu, Japan, June 28–30, 1998, pp. 9–12.
7 M. E. Davis and R. L. Lobo, *Chem. Mater*., 1992, **4**, 756.
8 D. M. Bibby and M. P. Dole, *Nature*, 1985, 317.
9 W. Xu, J. Dong, J. Li and F. Wu, *J. Chem. Soc., Chem. Commun*., 1990, 755.
10 M. H. Kim, H.X. Li and M. E. Davis, *Microporous Mater*., 1993, **1**, 191.
11 M. Matsukata, N. Nishiyama and K. Ueyama, *Microporous Mater*., 1993, **1**, 219.
12 N. N. Tusar, V. Kaucic, S. Geremia and G. Vlaic, *Zeolites*, 1995, **15**, 708.
13 A. Tuel, I. Arcon, N. N. Tusar, A. Meden and V. Kausic, *Microporous Mater*., 1996, **7**, 271.

Communication 8/09399G

Atom transfer polymerisation of methyl methacrylate mediated by solid supported copper catalysts

David M. Haddleton,* Dax Kukulj and Arnaud P. Radigue

Department of Chemistry, University of Warwick, Coventry, UK CV4 7AL. Fax: +44 (0)1203 524112. E-mail: d.m.haddleton@warwick.ac.uk

Received (in Cambridge, UK) 27th October 1998, Accepted 27th November 1998

Atom transfer polymerisation of methyl methacrylate can be effected using solid supported copper(I) pyridylmethanimine catalysts which facilitate easy removal and reuse of the catalyst.

Controlled polymerisation of vinyl monomers, such as methacrylates, acrylates and styrene, is of continuing interest for the synthesis of polymers of specific composition and structure.[1] Controlled, or living, free-radical systems are attracting increasing attention as processes which are tolerant to protic species in the medium, *e.g.* from solvents, monomers, impurities, *etc.* Transition metal mediated living radical polymerisation, or atom transfer polymerisation, has been developed by Matyjaszewski[2–4] and Sawamoto,[5,6] utilising Cu(I)X/bipyiridines (X = Cl, Br) and $Ru_2Cl_2(PPh_3)_3$, respectively.[7] In our laboratories we have been developing catalysts based on Cu(I)X and alkylpyridylmethanimine Schiff base ligands.[8–12] The attraction of these catalysts is that the Schiff base ligands are simple to synthesise and allow scope to vary the catalyst properties (*e.g.* redox potential, solubility) by varying the appropriate substituent groups.

Typical [monomer] : [catalyst] ratios are 100 : 1 with stoichiometric amounts of initiator and catalyst, in order for acceptable rates of polymerisation. A potential solution to this problem is the use of supported catalysts. Inorganic supported catalysts, *e.g.* silica, have found widespread use in the polymerisation of olefins.[13] The extension of this approach to the use of functionalised inert poly(styrene) as supports for vanadium ethylene polymerisation catalysts has also been recently described.[14] This recent work prompts us to report our own work where we have been utilising supported catalysts for living radical polymerisation reactions; to the best of our knowledge this is the first example of the use of inert poly(styrene) supports for a non-co-ordination type polymerisation.

We describe herein polymerisation of MMA mediated by Cu(I)Br supported Schiff base complexes (prepared from both primary amine functionalised silica gel and cross-linked poly(styrene) resins) *via* an atom transfer polymerisation process. In order to evaluate the potential of supported catalysts for atom transfer polymerisation, four different solid supports were tried in combination with CuBr. In the first two examples, the ligand was covalently attached to the solid support, either primary amino-functionalised silica gel (SiO_2) or amino-functional cross-linked poly(styrene) beads (PS), Scheme 1. In the second and third examples, free ligand was used in conjunction with primary amine-functionalised and non-functionalised silica gel. The reactions were performed with 33 vol. % MMA in toluene solution with ethyl-2-bromoisobutyrate as the initiator.

Addition of CuBr to ligated silica produces a dark brown–orange free flowing powder, Scheme 1.† Atom transfer polymerisation of methyl methacrylate proceeds effectively at 90 °C, reaching 70.4% conversion with a number average molecular mass, M_n, of 15 500 after 300 min, reaction 1 in Table 1.† The polydispersity index, PDI, remains approximately 1.5 throughout the reaction which is slightly broader than observed in conventional homogeneous atom transfer polymerisation

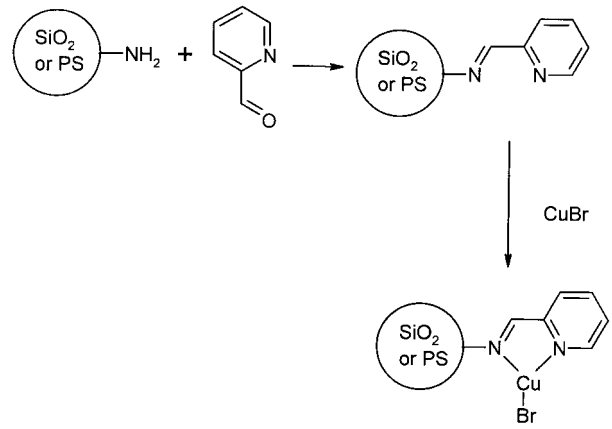

Scheme 1

(typically ≈1.2[9,12]) but is lower than that obtained for conventional free-radical polymerisation and suggests that the reaction is proceeding by reversible activation of the C–Br ω-terminus of the growing polymer chain, as in conventional atom transfer polymerisation. As conversion increases, M_n also increases but is significantly higher than that predicted and suggests an inefficient initiation process. The reaction mixture remained a deep red–brown colour throughout the polymerisation. Once agitation was ceased the supported catalyst settled to the bottom of the flask leaving a colourless solution which was easily separated from the catalyst.

To demonstrate the living character of the polymerisation, a regrowth experiment was performed. Firstly, MMA was

Table 1 Molecular weight and conversion data for poly(methyl methacrylate) produced using atom transfer polymerisation with various supported CuBr catalysts

Reaction	Time/min	Conv.(%)	M_n^{theor} [a]	M_n [b]	PDI [b]
1A[c]	60	33.4	3340	12 300	1.59
1B	120	47.3	7730	13 600	1.57
1C	180	56.9	5690	15 200	1.50
1D	240	62.9	6290	15 100	1.53
1E	300	70.4	7040	15 500	1.55
2A[d]	60	36.7	3670	8670	1.54
2B	120	49.4	4940	10 200	1.51
2C	180	60.1	6010	11 100	1.53
2D	240	68.6	6860	11 700	1.51
2E	300	75.2	7520	11 700	1.56
3A[e]	60	55.3	5530	8630	1.40
3B	135	75.0	7500	9770	1.40
3C	180	81.0	8100	10 400	1.39
3D	285	86.6	8660	10 700	1.40
4A[f]	30	34.7	3470	10 100	1.32
4B	80	70.7	7070	13 400	1.32
4C	120	84.1	8410	14 600	1.33
4D	180	95.1	9510	15 700	1.34

[a] Theoretical M_n. [b] Determined using SEC against poly(MMA) standards. [c] Pyridylmethanimine ligand covalently bound to silica gel particles.† [d] Pyridylmethanimine ligand covalently bound to cross-linked poly(styrene) beads.† [e] Physically adsorbed catalyst on silica gel.‡ [f] Physically adsorbed catalyst on amino-functionalised silica gel.‡

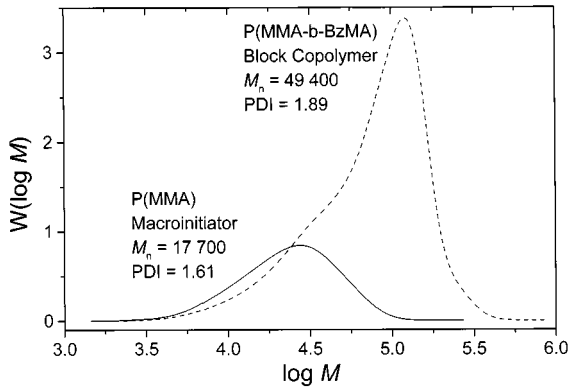

Fig. 1 Molecular weight distributions for the reinitiation of P(MMA) with benzyl methacrylate (BzMA) showing that the majority of chains are still active. Peak areas scaled for conversion.

polymerised under similar conditions to reaction 1, yielding a polymer of M_n = 17 700 and PDI = 1.61. This polymer was then isolated by precipitation into hexanes and used as a macroinitiator in homogenous atom transfer polymerisation to polymerise benzyl methacrylate (BzMA), yielding a block copolymer of M_n = 49 400 and PDI = 1.89. Fig. 1 shows the molecular weight distributions of both the macroinitiator and the final block copolymer. The increase in molecular weight suggests formation of block copolymer. Broadening on the low molecular weight side indicates that some termination has occurred removing active end-groups thus reducing re-initiation efficiency.

The solid supported catalyst was used in several subsequent reactions, Fig. 2. The initial polymerisation was performed under similar conditions to reaction 1, except three times as much silica supported ligand was used in order to achieve a higher rate of reaction. Reuse of the catalyst was achieved by the addition of MMA, toluene and initiator (no additional CuBr or ligand) to the washed supported catalyst. The second use of catalyst leads to polymer in high conversion on leaving overnight. This was repeated three additional times giving a total of five uses of the same solid supported catalyst over a five day period, Fig. 2. Care was taken to keep the catalyst under nitrogen at all stages to avoid degradation from exposure to oxygen. It is apparent that the catalyst is effective for each reuse; however, activity is reduced as observed by the decrease in the rate of polymerisation. The reduction in catalytic activity may be due to several reasons: (i) some loss of the supported catalyst when removing the polymer solution and subsequent washing, (ii) oxidation of the Cu(I) to Cu(II) during the reaction, and (iii) degradation due to side reactions compounded over several uses. The polydispersity indices for this series of polymers are higher than observed in reaction 1 ($\approx$2 *vs.* $\approx$1.5) and seem to be due to the higher concentration of solid supported ligand leading to an increased reaction rate which in turn leads to a higher concentration of free radicals in solution and thus a higher amount of termination due to radical–radical reactions.

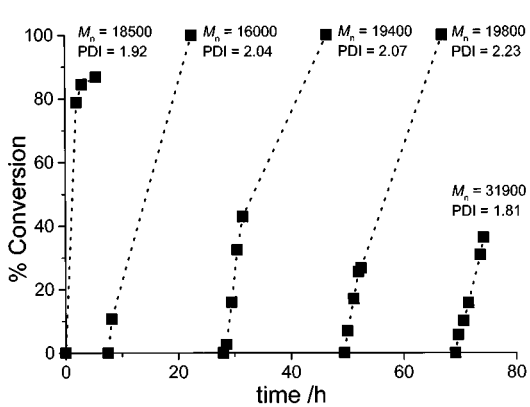

Fig. 2 Conversion *vs.* time for the four monomer additions in reaction 1.

Catalyst derived from pyridylmethanimine ligand covalently bound to cross-linked poly(styrene) beads, reaction 2, Table 1,† performs similarly to that on silica. Atom transfer polymerisation of MMA with this catalysts gives 75.2% conversion with a number average molecular mass, M_n, of 11 700 after 300 min. Again, M_n increases only slightly with conversion (but is higher than predicted), the polydispersity indices are similar, $\approx$1.5, and the catalyst settles to the bottom of the flask when stirring is ceased leaving a colourless solution. The rates of polymerisation for reactions 1 and 2 are very similar.

In addition to using catalysts covalently bound to the support, silica gel and amino functionalised silica gel (reactions 3 and 4, respectively‡) were added to a conventional atom transfer polymerisation to physically adsorb the catalyst, Table 1. Both of these reactions give lower polydispersity indices, $\approx$1.4 for silica and $\approx$1.3 for amino-functional silica, than the covalently bound catalysts of reactions 1 and 2. Indeed, the polydispersities are comparable to those of homogenous atom transfer polymerisation. After allowing the support to settle, a slight yellow colour remained in the solution due to some free catalyst/ligand.

In summary, solid supported atom transfer polymerisation catalysts promote effective polymerisation of methyl methacrylate. This allows the facile removal of the catalyst and also reuse of the catalyst in subsequent reactions. It is also possible to use the polymers produced to reinitiate polymerisation and produce block copolymers.

We would like to thank the EPSRC (D. K. GR/L10314) and Elf-Atochem (A. P. R.) for funding of this work.

Notes and references

† The supported catalyst was prepared by adding pyridine-2-carbaldehyde (0.714 g) to amine functionalised silica gel (3.00 g, 1.05×10^{-3} mol NH_2 g^{-1}) (or amino functional cross-linked poly(styrene) beads, 2.8×10^{-3} mol NH_2 g^{-1}) in 50 mL of dry toluene and refluxed for 5 h. The suspension was allowed to settle and the solvent was decanted off. Take up of the aldehyde on the support was monitored by NMR and UV of the residual pyridine-2-carbaldehyde in the solution against internal standards. To the support (0.967 g) was added MMA (10.0 mL), toluene (20.0 mL) and ethyl-2-bromoisobutyrate (0.137 mL) and the mixture degassed by three freeze–pump–thaw cycles followed by the addition of CuBr (0.134 g). Supported copper concentration was monitored by ICP analysis. The mixture was then placed in an oil bath at 90 °C. At the end of the reaction the reaction flask was removed from the oil bath and the insolubles allowed to settle (approximately 30 min due to the viscosity of the solution). The clear solution was removed *via* cannula.

‡ A solution of toluene (20 mL), MMA (10 mL), ethyl-2-bromoisobutyrate (0.137 mL) and *N*-(*n*-pentyl)-2-pyridylmethanimine (0.342 g) and silica gel (1.02 g) (or amine functionalised silica gel) and CuBr (0.134 g) was added and the flask placed in an oil bath at 90 °C.

1 T. P. Davis, D. M. Haddleton and S. N. Richards, *J. Macromol. Sci., Rev. Macromol. Chem. Phys. C*, 1994, **34**, 243.
2 K. Matyjaszewski, *Macromolecules*, 1998, **31**, 4701.
3 J. S. Wang and K. Matyjaszewski, *Macromolecules*, 1995, **28**, 7901.
4 J.-S. Wang and K. Matyjaszewski, *J. Am. Chem. Soc.*, 1995, **117**, 5614.
5 M. Kato, M. Kamigaito, M. Sawamoto and T. Higashimura, *Macromolecules*, 1995, **28**, 1721.
6 J. Ueda, M. Matsuyama, M. Kamigaito and M. Sawamoto, *Macromolecules*, 1998, **31**, 557.
7 B. Giese, *Radicals in Organic Synthesis: Formation of Carbon–Carbon Bonds*, Pergamon, 1988.
8 D. M. Haddleton, C. B. Jasieczek, M. J. Hannon and A. J. Shooter, *Macromolecules*, 1997, **30**, 2190.
9 D. M. Haddleton, C. Waterson, P. J. Derrick, C. Jasieczek and A. J. Shooter, *Chem. Commun.*, 1997, 683.
10 D. M. Haddleton, A. M. Heming, D. Kukulj, D. J. Duncalf and A. J. Shooter, *Macromolecules*, 1998, **31**, 2016.
11 D. M. Haddleton, A. J. Clark, D. J. Duncalf, A. H. Heming, D. Kukulj and A. J. Shooter, *J. Mater. Chem.*, 1998, **8**, 1525.
12 D. M. Haddleton, D. Kukulj, D. J. Duncalf, A. H. Heming and A. J. Shooter, *Macromolecules*, 1998, **31**, 5201.
13 M. P. McDaniel, *Adv. Catal.*, 1985, **33**, 47.
14 M. C. W. Chan, K. C. Chew, C. I. Dalby, V. C. Gibson, A. Kohlmann, I. R. Little and W. Reed, *Chem. Commun.*, 1998, 1673.

Communication 8/08308H

Facile C≡C bond cleavage of polyynediyldiiron complexes, Fp*–(C≡C)$_n$–Fp* [Fp* = Fe(η^5-C$_5$Me$_5$)(CO)$_2$; n = 3, 4], with Fe$_2$(CO)$_9$ leading to bis(μ$_3$-alkylidyne) complexes, Fp*–C≡C-μ$_3$-C–Fe$_3$(CO)$_9$–μ$_3$-C–(C≡C)$_{n-2}$–Fp*

Munetaka Akita,* Aizoh Sakurai and Yoshihiko Moro-oka*

Research Laboratory of Resources Utilization, Tokyo Institute of Technology, 4259 Nagatsuta, Midori-ku, Yokohama 226-8503, Japan. E-mail: makita@res.titech.ac.jp

Received (in Cambridge, UK) 9th November, Accepted 3rd December 1998

Reaction of the polyynediyldiiron complexes, Fp*–(C≡C)$_n$–Fp* [Fp* = Fe(η^5-C$_5$Me$_5$)(CO)$_2$; n = 3, 4], with Fe$_2$(CO)$_9$ at room temperature results in C≡C bond cleavage to give the bis(μ$_3$-alkylidyne) complexes, Fp*–C≡C-μ$_3$-C–Fe$_3$(CO)$_9$–μ$_3$-C–(C≡C)$_{n-2}$–Fp*, a trinuclear cluster complex sandwiched by the two conjugated (C≡C)$_x$–Fe systems.

Carbon–carbon bond cleavage reaction on transition metal species has for a long time been an intriguing subject in the field of organotransition metal chemistry[1] since such studies should provide new strategies for activation and functionalization of hydrocarbons. C(sp)–C(sp) (C≡C) bond cleavage and coupling reactions on polynuclear systems have had several precedents over the last three decades and the group 9 metal systems [M(η$_5$-C$_5$R$_5$): M = Co, Rh, Ir] have been studied most extensively.[2] Previously reported C≡C cleavage reactions, however, require vigorous reaction conditions such as pyrolytic reactions. During the course of the synthetic study of polynuclear C$_{2n}$ complexes (2n = 2, 4, 6, 8) derived from the corresponding polyynediyldiiron complexes, Fp*–(C≡C)$_n$–Fp* **1** [Fp* = Fe(η^5-C$_5$Me$_5$)(CO)$_2$],[3] we observed C≡C bond cleavage reaction of **1** under very mild reaction conditions.

Reaction of the octatetraynediyldiiron complex **1a** with Fe$_2$(CO)$_9$ in CH$_2$Cl$_2$ (or THF, benzene) for 7 h at ambient temperature afforded orange complex **2a** (18% yield)† as a single product after removal of insoluble materials by filtration [eqn. (1)]. Complex **2a** was also obtained by reaction with

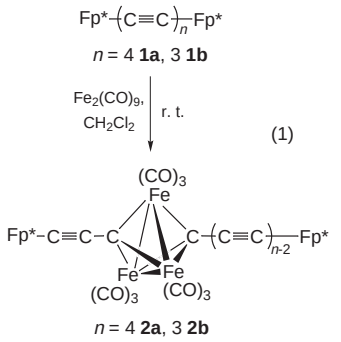

Fe$_3$(CO)$_{12}$. The ^{1}H NMR spectrum of **2a** contains two Cp* signals indicating an unsymmetrical structure and only η^1-CO ligands are detected by IR. The most characteristic spectroscopic feature of **2a** is the highly deshielded quaternary carbon signals [δ_C (CDCl$_3$) 270.1, 289.6], which suggest formation of a complex bearing two μ$_3$-alkylidyne functional groups, *i.e.* a C≡C bond in the C$_8$ linkage is cleaved by the action of the iron carbonyls. The C≡C bond cleavage position is definitely confirmed to be the inner C3≡C4 bond as revealed by X-ray crystallography [Fig. 1(a)].‡ The (μ$_3$-C)$_2$Fe$_3$(CO)$_9$ unit adopts a typical bicapped μ3-alkylidyne structure as indicated by its structural parameters: (i) the Fe$_3$ moiety is virtually an equilateral triangle with Fe–Fe separations of Fe31–Fe41 2.498(2), Fe31–Fe51 2.514(2), Fe41–Fe51 2.518(2) Å; (ii) the μ$_3$-alkylidyne carbon atoms are located almost equidistant from the three iron centers [Fe–μ$_3$-C: C3–Fe31: 1.955(5), C3–Fe41 1.981(8), C3–Fe51 1.972(8), C4–Fe31 1.962(9), C4–Fe41 1.962(7), C4–Fe51 1.942(5) Å]. These parameters are comparable to those of previously reported μ$_3$-alkylidyne triiron cluster compounds.[4] The acetylenic moiety is essentially linear and clear bond alternation is observed: [Fe11-C1 1.900(6), C1≡C2 1.228(9), C2–C3 1.389(9), C4–C5 1.39(1), C5≡C6 1.21(1), C6–C7 1.38(1), C7≡C8 1.19(1), C8–Fe21 1.904(7) Å; C–C–C(or Fe11,21) 173.9–179.1(8)°]. The absence of **2b** (see below) in the reaction mixture indicates that the present C≡C cleavage reaction involves an intramolecular process.

C≡C cleavage was also observed for an analogue, the hexatriynediyl complex **1b** (10% yield)[5] [eqn. (1)]. Spectroscopic and crystallographic analyses of the product **2b**† reveal cleavage between the central C3≡C4 bond, and the structural parameters for the Fe–C≡C–(μ$_3$–C)Fe$_3$(μ$_3$–C)–C≡C–Fe moiety [Fe–Fe 2.503–2.538(4), C–Fe$_3$ 1.92–2.00(1) Å, Fe1–C1 1.87(1), C1≡C2 1.26(1), C2–C3 1.38(1), C4–C5 1.37(1), C5≡C6 1.23(1), C6–Fe2 1.88(1) Å; C–C–C(or Fe1,2) 172–176(1)°] are similar to those of **2a**.

The present C≡C cleavage reaction of **1a**,**b** is in sharp contrast to the results of the reactions of the lower congeners, the butadiynediyl (**1c**: n = 2) and ethynediyl complexes (**1d**: n = 1), which afford other types of products (**4**–**6**)[3b] The C≡C units

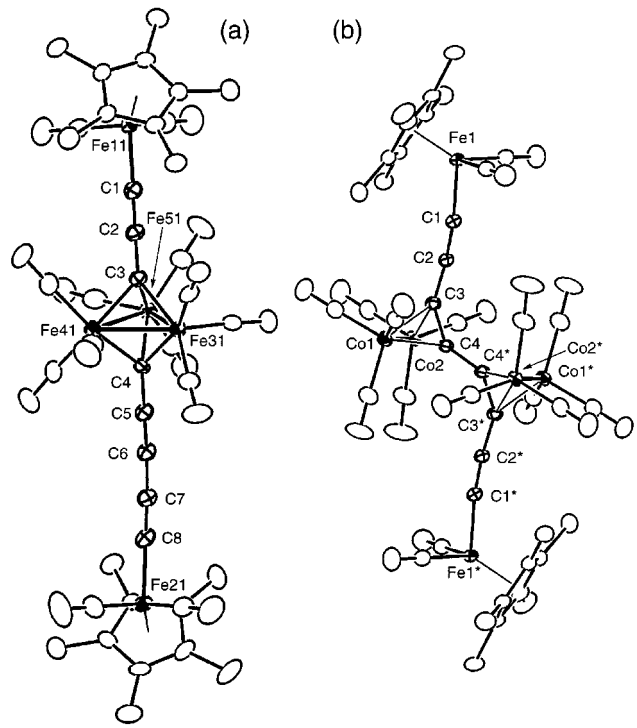

Fig. 1 Molecular structures of **2a** (molecule 1: A-series) (a) and **7** (b) drawn at the 30% probability level.

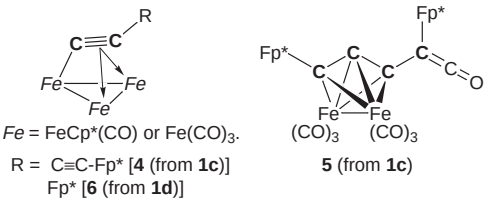

Fe = FeCp*(CO) or Fe(CO)$_3$.

R = C≡C-Fp* [**4** (from **1c**)]
Fp* [**6** (from **1d**)]

5 (from **1c**)

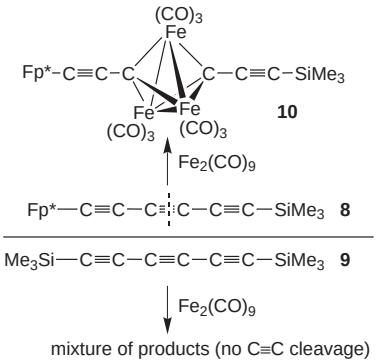

Scheme 1

in **1c**,**d** are directly bonded to the iron atoms, and their formation mechanism should involve reaction of the C≡C moiety with a diironcarbonyl species, $Fe_2(CO)_x$, followed by interaction with either of the adjacent atoms, Fe or C, associated with decarbonylation (M–M bond formation) and/or CO-migration.[6] In contrast, **1a**,**b** contain two kinds of C≡C functional groups; one directly bonded to the Fp* group and the other sandwiched by the two C≡C groups. Because the latter can avoid steric repulsion with the bulky Fp* group, the ironcarbonyl species would first interact with the central C≡C moiety to induce the cleavage reaction. In accord with this consideration, reaction of **1a** with $Co_2(CO)_8$ gave adduct **7** with tetrahedral C_2Co_2 cores (55% yield),§ where the central C≡C bonds interact with the dicobalt species [Fig. 1(b)].

In order to examine the effect of the substituents at the C_x termini, C_6-silyl derivatives (the precursors for **1b**),[5] Fp*–C≡C–$SiMe_3$ **8** and Me_3Si–(C≡C)–$SiMe_3$ **9**, were subjected to reaction with $Fe_2(CO)_9$ (Scheme 1). The reaction of **8** resulted in C≡C cleavage at the C3≡C4 bond to give the bis-μ_3-alkylidyne complex **10** (22% yield)§ analogous to **2**, whereas **9** gave a mixture of products, which did not show any ^{13}C NMR resonances > δ250 indicating absence of C≡C cleavage. Thus at least one Fp* substitution at the C_x termini is crucial for C≡C bond cleavage. The details of the mechanism of C≡C cleavage, however, is not clear at present. Interaction with diironcarbonyl species would give an adduct with a tetrahedral C_2Fe_2 core[7] analogous to the structure of **7** and subsequent addition of a third iron atom would induce C≡C bond cleavage and formation of an Fe_3 triangle. Electron-donating groups such as Fp* may stabilize the electron-deficient intermediate, which should be formed prior to C≡C cleavage.[2e]

Thus the present study reveals the possibility of C≡C bond cleavage of a polyyne linkage under very mild conditions. The obtained bis(μ_3-alkylidyne) complexes **2** belong to a new class of compounds, where the trinuclear cluster core containing d electrons is sandwiched by two π-conjugated $(C{\equiv}C)_x$–M systems. Interaction of M–$(C{\equiv}C)_n$–M′ with various metal species is now under further study and results will be reported in due course.

We are grateful to the Ministry of Education, Science, Sports, and Culture of the Japanese Government and the Ishikawa Foundation for Carbon Science and Technology for financial support of this research.

Notes and references

† *Selected spectroscopic data*: **2a**: ν(C≡C) 2095, 2068, ν(CO) 2037, 2011, 1981 cm^{-1} (CH_2Cl_2); δ_H($CDCl_3$) 1.91, 1.95 (Cp* × 2); δ_C($CDCl_3$) 83.8, 96.6, 116.5, 143.4, 144.4, 172.1, 270.1, 289.6 (C_8). **2b**: ν(CO) 2037, 2028, 2002, 1992, 1979 cm^{-1}; δ_H 1.94 (Cp*); δ_C 141.4, 163.2, 281.6 (C_6). **7**: ν(C≡C) 2092, ν(CO) 2073, 2053, 2014, 1973 cm-1; δ_H 1.84 (Cp*); δ_C 87.7, 93.7, 109.0, 135.0 (C_8). **10**: ν(CO) 2041, 2015, 1983 cm^{-1}; δ_H 1.96 (Cp*), 0.37 ($SiMe_3$); δ_C 122.7, 127.8, 144.3, 269.9, 296.9 (C_6: one of the C_6 signals could not be located).

‡ X-Ray diffraction measurements were made on a Rigaku RAXIS IV imaging plate area detector with graphite-monochromated Mo-Kα radiation. The triiron cluster moieties in **2a**,**b** and **10** were found to be disordered with respect to the C≡C–C···C–C≡C axis and refined taking into account minor components. *Crystal data*: for **2a**: $C_{41}H_{30}O_{13}Fe_5$, M = 1009.9, T = −60 °C, triclinic, space group $P\bar{1}$, a = 15.287(5), b = 24.814(3), c = 13.540(3), α = 102.56(2)°, β = 115.10(3)°, γ = 102.68(2)°, V = 4247(2) Å^3, Z = 4, D_c = 1.58 g cm^{-3}, μ = 17.3 cm^{-1}, R(R_w) = 0.062 (0.084) for 10185 unique data with $I > 3\sigma(I)$ and 1357 parameters. The unit cell contained two independent molecules. For **2b**: $C_{39}H_{30}O_{13}Fe_5$, M = 985.9, T = −60 °C, monoclinic, space group $P2_1/n$, a = 13.520(4), b = 38.03(1), c = 8.136(2) Å, β = 91.67(2)°, V = 4181(1) Å^3, Z = 4, D_c = 1.57 g cm^{-3}, μ = 17.5 cm^{-1}, R(R_w) = 0.079 (0.086) for 3614 unique data with $I > 3\sigma(I)$ and 551 parameters. For **7**: $C_{44}H_{30}O_{16}Fe_2Co_4$, M = 1162.1, T = −60 °C, monoclinic, space group $P2_1/c$, a = 8.890(4), b = 18.890(5), c = 14.10(2) Å, β = 99.22(5)°, V = 2337(2) Å^3, Z = 2, D_c = 1.65 g cm^{-3}, μ = 20.6 cm^{-1}, R(R_w) = 0.047 (0.060) for 4035 unique data with $I > 3\sigma(I)$ and 358 parameters. For **10**: $C_{30}H_{24}O_{11}SiFe_5$, M = 812.0, T = −60 °C, monoclinic, space group $P2_1/n$, a = 11.929(3), b = 14.071(2), c = 21.55(1) Å, β = 99.691(3)°, V = 3564(1) Å^3[l], Z = 4, D_c = 1.51 g cm^{-3}, μ = 16.8 cm^{-1}, R(R_w) = 0.080 (0.100) for 4041 unique data with $I > 3\sigma(I)$ and 532 parameters. CCDC 182/1103.

§ Complexes **7** and **10** were characterized by X-ray crystallography.‡ *Selected structural parameters*: for **7**: Fe1–C1 1.898(3), C1–C2 1.219(4), C3–C4 1.362(4), C4–C4* 1.408(6), Co1–Co2: 2.4696(8), Co–C 1.953–1.984(4) Å, Fe1–C1–C2 173.2(3), C1–C2–C3 173.7(3), C2–C3–C4 144.1(3), C3–C4–C4* 141.6(3)°. For **10**: Fe2–Fe3 2.507(3), Fe2–Fe4 2.501(3), Fe3–Fe4 2.504(3), C3–Fe2 1.978(7), C3–Fe3 1.936(8), C3–Fe4 1.991(7), C4–Fe2 1.966(8), C4-Fe3: 1.949(8), C4-Fe4: 1.929(8), Fe1-C1 1.890(6) , C1≡C2 1.236(9), C2–C3 1.376(9), C4–C5 1.39(1), C5≡C6 1.22(1), C6–Si1 1.829(9) Å; C–C–C(or Fe1,2) 171.1–178.8(9)°.

1 B. Rybtchinski, A. Vigalok, Y. Ben-David and D. Milstein, *J. Am. Chem. Soc.*, 1996, **118**, 12406; H. Suzuki, Y. Takaya and T. Takemori, *J. Am. Chem. Soc.*, 1994, **116**, 10779 and references therein.

2 Co: (*a*) R. B. King and C. A. Harmon, *Inorg. Chem.*, 1976, **15**, 879; (*b*) H. Yamazaki, Y. Wakatsuki and K. Aoki, *Chem. Lett.*, 1979, 1041; (*c*) J. R. Fritch and K. P. C. Vollhardt, *Angew. Chem., Int. Ed. Engl.*, 1980, **19**, 559; (*d*) N. T. Allison, J. R. Fritch, K. P. C. Vollhardt and E. C. Walborsky, *J. Am. Chem. Soc.*, 1983, **105**, 1384. Rh: (*e*) A. D. Clauss, J. R. Shapley, C. N. Winlker and R. Hoffmann, *Organometallics*, 1984, **3**, 619; Fe: (*f*) D. Nuel, F. Dahan and R. Mathieu, *Organometallics*, 1985, **4**, 1436; (*g*) J. A. Hriljac and D. F. Shriver, *J. Am. Chem. Soc.*, 1987, **109**, 6010; (*h*) E. Cabrera, J. C. Daran and Y. Jeannin, *J. Chem. Soc., Chem. Commun.*, 1988, 607.

3 (*a*) M. Akita, M.-C. Chung, A. Sakurai, S. Sugimoto, M. Terada, M. Tanaka and Y. Moro-oka, *Organometallics*, 1997, **16**, 4882; (*b*) M. Akita, M.-C. Chung, M. Terada, M. Miyauti, M. Tanaka and Y. Moro-oka, *J. Organomet. Chem.*, 1998, **565**, 49; (*c*) M. Akita and Y. Moro-oka, *Bull. Chem. Soc. Jpn.*, 1995, **68**, 420; (*d*) See also references cited in references 3(a) and (b).

4 M. Akita, in *Comprehensive Organometallic Chemistry II*, ed. E. W. Abel, F. G. A. Stone and G. Wilkinson, Pergamon Press, Oxford, 1995, vol. 7, ch. 4.

5 Complex **1b** was prepared by Cu-catalyzed coupling between Fp*–C_6H and Fp*–Cl analogous to the synthesis of **1a**.[3a] A. Sakurai, M. Akita and Y. Moro-oka, to be reported.

6 The interaction of the attached diiron part with the Fe atom σ-bonded to the C_{2n} group leads to the stable trinuclear μ-acetylide cluster structure (**4**, **6**) and, in the formation of **5**, the interaction with the adjacent carbon atom (C3) would leave the carbene carbon atom (C4), which may be stabilized by interaction with the Fp*-group at the other terminus and finally couples with CO to give the ketene structure.[3b]

7 F. A. Cotton, J. D. Jamerson and B. R. Shults, *J. Am. Chem. Soc.*, 1976, **98**, 1774.

Communication 8/08712A

ChemComm

Excellent performance of lithium doped sulfated zirconia in oxidative dehydrogenation of ethane

Shaobin Wang, K. Murata, T. Hayakawa, S. Hamakawa and K. Suzuki

National Institute of Materials and Chemical Research, Tsukuba, Ibaraki 305-8565, Japan.
E-mail: swang@nimc.go.jp

Received (in Cambridge, UK) 6th November 1998, Accepted 23rd November 1998

Sulfated zirconia doped with lithium catalysts are found to be effective for the oxidative dehydrogenation of ethane to ethylene, giving 98% ethane conversion and 70% selectivity towards ethylene as well as 68% ethylene yield at 650 °C.

The selective oxidation of alkanes into their corresponding olefins has been of great interest in recent years. Ethane is an abundant component in natural gas, however, it receives the least attention due to the existing thermal cracking process. Conversion of ethane into ethylene by oxidative dehydrogenation (ODH) has several advantages and been studied over several oxide-based catalysts. Catalysts containing vanadium, molybdate and lithium are found to be effective for this reaction. However, most of these systems are based on alumina, silica, titania and magnesia.[1–4] Little work has concentrated on zirconia, in particular, sulfated zirconia based catalysts. Sulfated zirconia as a super acid solid is known as a very active catalyst for the conversion of small hydrocarbons.[5,6] One of the authors has discovered the excellent performance of Li-doped sulfated zirconia in the oxidative coupling of methane (OCM).[7] The oxidative coupling of methane to C_2-hydrocarbons is inevitably accompanied by the concurrent conversion of ethane to ethylene. Here we report the results of sulfated zirconia based catalysts for the oxidative dehydrogenation of ethane into ethylene.

The zirconia sample was prepared by two steps.[7] The resultant ZrO_2 was then used to prepare sulfated zirconia (SZ) by wetness impregnation using ammonium sulfate, and then calcined at 700 °C for 3 h with a corresponding anion content of 6 wt%. After this, zirconia samples were impregnated with lithium chloride, and calcined at 700 °C for 3 h. The loading of lithium was varied between 2 and 8 wt%. A series of Li-doped sulfacted zirconia (SZ) catalysts were also prepared using different Li precursor compounds at 5 wt% Li content by wetness impregnation as described above. The catalytic tests were carried out in a fixed-bed vertical-flow reactor constructed from a high-purity alumina tube (id = 6 mm) packed with 1.0 g catalyst samples and 2 g quartz sand and mounted inside a tube furnace. The feed, consisting of 10% ethane, 10% oxygen and 80% nitrogen, was introduced into the reactor at a flow rate of 60 ml min^{-1}. The reactants and products were analysed using a gas chromatography (GC-8A) equipped with a Porapak Q column using flame ionisation detector (FID) for hydrocarbons and a 5Å molecular sieve column for CO, CO_2, CH_4, O_2, N_2, and H_2 using thermal conductivity detector (TCD). Before catalyst testing, an empty tube loaded with only quartz sand was evaluated for the oxidative dehydrogenation of ethane under various conditions. It is found that the homogeneous contribution was negligible since ethane conversion was < 2% at 650 °C.

Table 1 presents the performance of ethane ODH over supports (ZrO_2 and SZ) and LiCl-based catalysts with 3.5 wt% Li as well as Li_2ZrO_3 catalyst. It is found that the main products of ethane oxidative dehydrogenation are C_2H_4, CO and CO_2 with lower amounts of other products such as CH_4, EtOH, and C_3H_6. Ethane conversion increases with the increasing temperature over all catalysts, however, ethylene selectivity exhibits varying patterns with temperature depending on catalyst. For zirconia, sulfated zirconia and Li/ZrO_2, ethylene selectivity increases with temperature.

However, a decreasing trend of ethylene selectivity is observed on Li/SZ at 600–650 °C. Li_2ZrO_3 shows similar ethylene selectivity at the same temperature range. For zirconia and sulfated zirconia, ethane conversions are > 60% with ethylene selectivity of *ca.* 30% at 650 °C. However, sulfated zirconia exhibits slightly higher catalytic activity and selectivity towards ethylene. Doped lithium chloride on supports remarkably improves ethane conversion and selectivity to

Table 1 Catalytic behavior of ethane ODH over zirconia-based catalysts at 650 °C

			Conversion (%)		Selectivity (%)				Yield (%)
Catalyst	S_{BET}/m^2 g^{-1}	*T*/°C	C_2H_6	O_2	C_2H_4	CO	CO_2	CH_4	C_2H_4
Quartz sand		600	0.2	0.01	97.8			2.2	0.20
		620	0.4	0.4	98.0			2.0	0.39
		650	2.0	2.4	97.7			2.3	1.95
ZrO_2	21.2	600	51.6	100	10.8	24.5	64.4	0.3	5.6
		620	55.4	100	15.0	24.0	60.2	0.8	8.3
		650	65.9	100	29.2	19.2	49.2	1.7	19.2
SZ	72.5	600	42.3	69.7	16.6	38.6	42.6	2.2	7.0
		620	53.8	86.3	18.0	35.6	43.9	2.5	9.6
		650	70.4	100	30.8	18.8	47.3	3.1	21.7
LiCl/ZrO_2	4.6	600	48.8	69.9	54.6	7.3	33.7	0.6	26.6
		620	66.5	83.0	58.3	6.0	28.4	0.8	38.8
		650	87.2	95.3	60.1	9.3	21.8	1.4	52.4
LiCl/SZ	2.0	600	62.4	50.2	82.5	5.4	8.5	0.5	51.5
		620	83.7	69.5	79.5	6.4	10.1	0.6	66.5
		650	97.6	96.3	69.8	11.9	14.3	1.7	68.1
Li_2ZrO_3	< 1	600	5.9	6.0	85.7	13.8	0	0.5	5.0
		620	8.3	8.2	86.4	12.9	0	0.7	7.2
		650	20.3	15.1	83.3	8.0	8.0	0.7	16.9

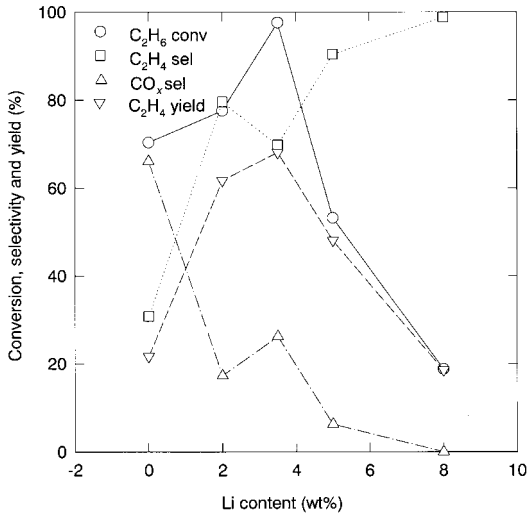

Fig. 1 Effect of Li content in the LiCl/SZ system on catalytic activity.

ethylene. For $LiCl/ZrO_2$, ethane conversion is enhanced to 87% and ethylene selectivity is increased to > 60%. Similarly, ethane conversion and ethylene selectivity over LiCl/SZ are also significantly improved with 70% selectivity at 98% conversion, giving 68% ethylene yield. LiCl/SZ also exhibits higher ethylene selectivity than Li/ZrO_2, suggesting that sulfation of zirconia modifies the surface properties and could promote ethylene selectivity. It has been found that Li/SZ shows better catalytic performance than Li/ZrO_2 in OCM reaction.[7] Another catalyst, Li_2ZrO_3, shows the lowest catalytic activity, but the highest ethylene selectivity and the ethylene yield is lower than that over the two supports (ZrO_2 and SZ). Several researchers have reported that Li-doped catalysts are much more selective to ethylene in ethane ODH because of the increase of in number of active sites for dehydrogenation.[9,10]

Conway and Lunsford[8] found that 5 g Li^+–MgO–Cl^- could produce a C_2H_6 conversion of 75–79% at a C_2H_4 selectivity of 70% with 58% ethylene yield at 650 °C under a flow rate of 60 ml min^{-1}. Ji *et al.*[9] also obtained 60% ethane conversion with 75% ethylene selectivity, giving 45% ethylene yield over Li/La/CaO catalysts at 650 °C. Therefore, the values obtained in this work are much better than the above results.

From Table 1, it can be seen that the catalytic activity is not dependent on the surface area. XRD measurements indicate that two phases (monoclinic and tetragonal ZrO_2) coexist in sulfated zirconia while monoclinic ZrO_2 with a trace of tetragonal ZrO_2 is present in ZrO_2. Li/ZrO_2 and Li/SZ catalysts consist of monoclinic ZrO_2 and a fraction of Li_2ZrO_3 crystallites. The peak intensities for Li_2ZrO_3 are higher for Li/SZ, suggesting that a larger amount of Li_2ZrO_3 is present in Li/SZ. Therefore, it is deduced that the synergistic effect of multiphases in the catalyst are responsible for the catalytic activity and selectivity. For Li doped catalyst, chlorine present in catalyst can also play an important role for the higher selectivity over these catalysts. Some researches have revealed that chlorine can promote the decomposition of ethyl radicals to ethylene.[10,11] Further work on catalyst surface characterisation is in progress to elucidate the active sites for the reaction.

The effect of lithium precursor ($LiNO_3$, LiCl, LiF and Li_2CO_3) in sulfated zirconia systems on the catalytic conversion, ethylene selectivity and yield was also studied. It is found that $LiNO_3$ and LiCl doped SZ catalysts exhibit higher ethane conversions, but that $LiNO_3$/SZ shows the lowest ethylene selectivity. The other three lithium doped SZ catalysts show similar ethylene selectivity. In terms of ethylene yields, LiCl doped sulfated zirconia catalyst generally gives the highest values; the overall order is: LiCl/SZ > $LiNO_3$/SZ > LiF/SZ > Li_2CO_3/SZ.

It is also found that lithium content affects the catalyst performance. The dependence of activity, selectivity and yield of LiCl/SZ catalysts with different lithium content at 650 °C is shown in Fig. 1. It can be seen that ethylene selectivity is enhanced over all Li-doped SZ catalysts. However, the ethane conversion and ethylene yield depend on lithium content. A maximum value can be attained over 3.5 wt% Li/SZ.

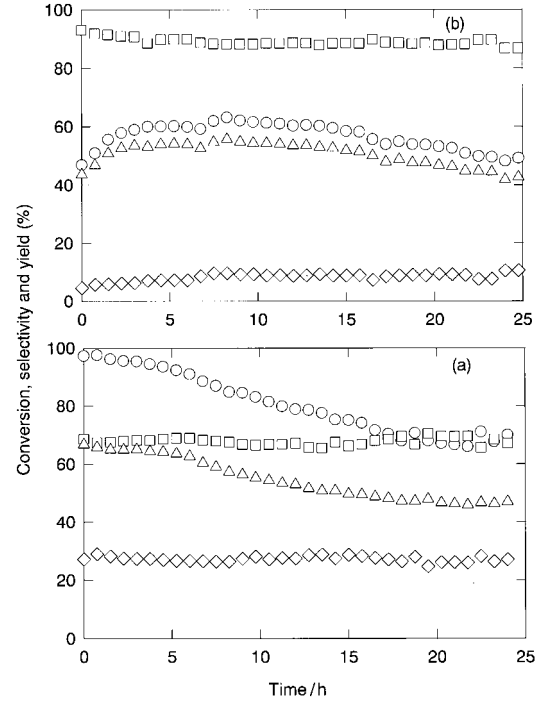

Fig. 2 Catalytic activity of ethane ODH as a function of time over LiCl/SZ at 650 °C.

Fig. 2 shows the catalytic performance of 3.5 wt% LiCl/SZ and 5 wt% LiCl/SZ catalysts at 650 °C in terms of reaction time. One can see that the two catalysts show different stability behaviour. For 3.5 wt% LiCl/SZ ethane conversion and ethene yield decrease gradually over 15 h and then remains nearly unchanged thereafter. Ethane conversion and ethene yields are reduced from 98 and 68% to 70 and 46%, respectively. Ethene and CO_x selectivities stay at the same level during 24 h of testing. The ethane conversion and ethene yield over 5 wt% LiCl/SZ increases in the first 10 h and then decreases, however, the deactivation rates are much slower than those of 3.5 wt% LiCl/SZ. After 25 h testing, ethane conversion and ethene yield are 50 and 42%, respectively. Like the behavior of 3.5 wt% LiCl/SZ, ethene and CO_x selectivities show no alteration. Investigations on 2 wt% LiCl/SZ and 8 wt% LiCl/SZ reveal that 2 wt% LiCl/SZ shows similar catalytic behaviour as 3.5 wt% LiCl/SZ while 8 wt% LiCl/SZ presents the same characteristics as that of 5 wt% LiCl/SZ. All these results seem to suggest that LiCl loading on catalysts is a crucial factor influencing the catalyst performance. Too high a LiCl content with result in a decrease in activity.

In summary, sulfation of zirconia promotes selectivity towards ethylene in the oxidative dehydrogenation of ethane. LiCl-doped SZ exhibits not only a high ethane conversion but also high selectivity towards ethylene and also high stability.

Notes and references

1 H. H. Kung and M. C. Kun, *Appl. Catal.*, 1997, **157**, 105.
2 T. Blasco and J. M. Lopez-Nieto, *Appl. Catal.*, 1997, **157**, 117.
3 E. A.Mamedov and V. Cortes-Corberan, *Appl. Catal.*, 1995, **127**, 1.
4 F. Cavani and F. Trifiro, *Catal. Today*, 1995, **24**, 307.
5 X. Song and A. Sayari, *Catal. Rev.*, 1996, **38**, 329.
6 T.-K. Cheung and B. C. Gates, *J. Catal.*, 1997, **168**, 522.
7 K. Murata, T. Hayakawa and K. Fujita, *Chem. Commun.*, 1997, 221.
8 S. J. Conway and J. H. Lunsford, *J. Catal.*, 1991, **131**, 513.
9 L. Ji, J. Liu, X. Chen and M. Li, *Catal. Lett.*, 1996, **39**, 247.
10 R. Burch, E. M. Crabb, G. D. Squire and S. C. Tsang, *Catal. Lett.*, 1989, **2**, 249.
11 D. Wang, M. P. Rosynek and J. H. Lunsford, *J. Catal.*, 1995, **151**, 155.

Communication 8/08708C

Photochromic flavylium compounds as multistate/multifunction molecular-level systems

Fernando Pina,[a] Mauro Maestri[b] and Vincenzo Balzani[b]†

[a] *Departamento de Química, Centro de Química Fina e Biotecnologia, Universidade Nova de Lisboa, 2825 Monte de Caparica Portugal*

[b] *Dipartimento di Chimica 'G. Ciamician', Università di Bologna, 40126 Bologna, Italy*

Received (in Cambridge, UK) 16th July 1998, Accepted 3rd August 1998

Synthetic flavylium compounds can exist in several forms (*multistate*) that can be interconverted by more than one type of external stimulus (*multifunctional*). The intricate network of their reactions, when examined from the view point of 'molecular-level devices', reveals very interesting properties.

Introduction

Great effort is currently being devoted to the design of molecular-level switching devices and, more generally, to the chemistry of signal generation, transfer, conversion, storage, and detection (semiochemistry).[1] By reducing the switching elements to molecular size, the memory density of computers could be increased by several orders of magnitude and the power input decreased very significantly.[2] Apart from future applications for information processing at the molecular level,[3] the study of compounds capable of existing in different forms that can be interconverted by external stimuli is a topic of great fundamental interest.[1–9] Molecules that can exist in two forms which are interconvertible by an external input are rather common. Typical examples of such bistable systems are the so-called photochromic compounds, where the input causing the switching between the two species is light.[10] Systems capable of existing in more than two forms (*multistate*) that can be interconverted by more than one type of external stimulus (*multifunctional*) are less common.[11,12] Such multistate/multifunctional systems can behave as complex logic devices and can therefore play the role of models for an initial understanding of the chemical basis of important biological processes.

Fernando Pina has been Professor of Chemistry at the Faculdade de Ciências e Tecnologia, Universidade Nova de Lisboa, since 1985, and coordinator of its photochemistry research unit. He is editor of Rev. Port. Quim. *His research interests are focused on the areas of supramolecular chemistry, proton-transfer, chemosensors and molecular-level devices.*

Mauro Maestri has been Professor of Chemistry at the University of Bologna since 1983. His research interests are mainly devoted to photochemistry, photophysics, electron-transfer processes, supramolecular chemistry and molecular-level devices.

Vincenzo Balzani has been Professor of Chemistry at the University of Bologna since 1972. He was Director of the FRAE-CNR Institute of Bologna (1977–1988) and Chairman of the European Photochemistry Association (1988–1992). He has obtained several awards, including the Ziegler–Natta Lectureship of the German Chemical Society (1993) and the Centenary Lectureship of the Royal Chemical Society UK (1995–1996). His research interests include photochemistry, photophysics, electron-transfer processes, supramolecular chemistry, and molecular-level devices.

Like anthocyanins,[13] which are one of the most important sources of colour in flowers and fruits, synthetic flavylium salts in aqueous solutions undergo various structural transformations[14–17] that can be driven by pH changes and, particularly in the flavylium salts, also by light excitation. Such transformations are often accompanied by quite dramatic colour changes or colour disappearance. In the last few years we have investigated in a systematic way the thermal and photochemical reactions of several synthetic flavylium salts.[18–23] The main purpose of our studies has been to emphasize the multistate/multifunctional character of the chemistry of these compounds and, more generally, to show that examination of complex chemical systems from the view points of 'molecular-level devices' and 'molecular level logic functions' may reveal very interesting aspects and may be useful to introduce new concepts in the field of chemical research.

Nature of the species involved

The basic scheme for the discussion of the structural transformations of flavylium-type compounds is that shown in Scheme 1.[14–17] As we will see below, other forms may also be involved, depending on the nature of the substituents in the 4-, 7-, and 4′-positions. The flavylium cation $\mathbf{AH^+}$, which is the stable form in strongly acid solution, can be easily prepared by acid condensation of salicylaldehyde and acetophenone derivatives, as well as by other routes.[24] In moderately acidic or neutral solution, the thermodynamically stable form is the neutral *trans*-2-hydroxychalcone species **Ct**, which is formed from $\mathbf{AH^+}$ through the two intermediate compounds **B2** and **Cc**. **B2** is a hemiacetal species, obtained by hydration of the flavilyium cation, and **Cc** is a *cis*-2-hydroxychalcone, formed from the hemiacetal **B2** through a tautomeric process. The interesting feature of these systems is that the $\mathbf{AH^+}$ and **B2** forms can be reversibly interconverted by pH changes,[14–17] whereas **Cc** and **Ct** can be interconverted by photoexcitation.[18–23,25–28] Since the **B2** and **Cc** forms are in tautomeric equilibrium, it follows that pH and light stimulations can be used to cause interconversion of the four fundamental forms (Scheme 1). Furthermore, the $\mathbf{AH^+}$ form exhibits acid properties not only in the 2-, but also in the 4-position, to give the **B4** basic species. In their turn, **Cc** and **Ct** can undergo deprotonation to give the respective $\mathbf{Cc^-}$ and $\mathbf{Ct^-}$ monoanions which, being *cis*/*trans* isomers, can in principle be interconverted by light excitation. As we will see later, depending on the nature of the substituents, other acid/base equilibria and *cis*/*trans* couples may be present. It is therefore clear that in these systems pH changes coupled with light excitation may cause very intricate series of chemical reactions, with dramatic changes in the absorption spectra (*i.e.* in the colour of the system). A further interesting aspect is that some of the species exhibit fluorescence; this is not only another analytical 'handle' to control the

behaviour of the system, but also a very interesting signal for the purpose of information processing.

Several works concerning the thermodynamic as well as the kinetic aspects of the thermal reactions of flavylium-type compounds have long since been reported in literature,[13–17] whereas the photochemical and photophysical aspects have been examined more recently.[14–23,28] As we shall see below, pH jump, temperature jump, and flash photolysis experiments allow the measurement of the rate constants of some of the reactions involved, and steady state titration experiments (by using UV–VIS and NMR techniques) allow the measurement of equilibrium constants. In order to illustrate the complex reaction network of these systems, we will now focus on the behaviour of the 4′-methoxyflavylium ion[19] (Scheme 1; $R^4 = R^7 = H$, $R^{4'} = OCH_3$).

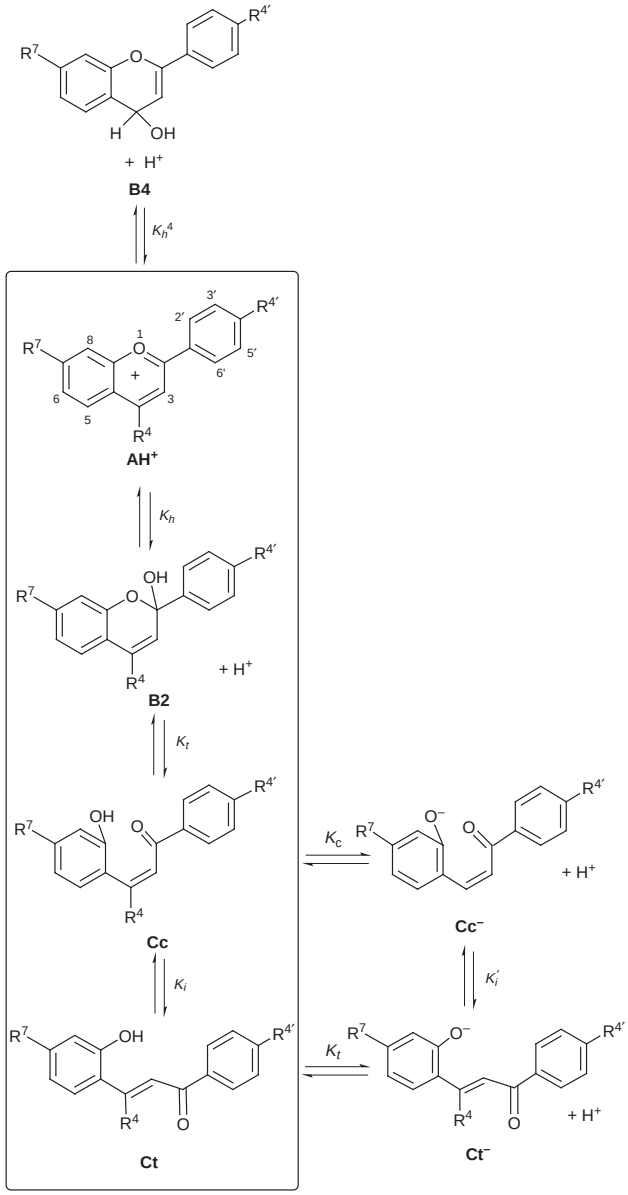

Scheme 1 Structural transformations of the flavylium-type compounds. Only the most important forms are shown.

Thermal reactions of the 4′-methoxyflavylium ion

A very careful spectral and kinetic investigation of the transformations undergone by the 4′-methoxyflavylium ion was originally performed by McClelland and Gedge.[16] By using the pH jump technique, they found that seven different species are involved, as transient or equilibrium compounds, depending on the experimental conditions (Scheme 1). The absorption spectra of the strongly colored 4′-methoxyflavylium ion **AH**$^+$ (λ_{max} = 435 nm, ε = 42000 M^{-1} cm^{-1}), the colorless *trans*-4′-methoxychalcone **Ct** (λ_{max} = 350 nm, ε = 18000 M^{-1} cm^{-1}), and the **B2** and **Cc** mixture are shown in Fig. 1.

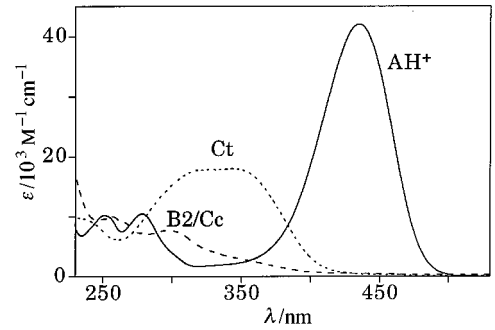

Fig. 1 Absorption spectra in aqueous solution at 25 °C of the 4′-methoxyflavylium compound: **AH**$^+$ at pH 1.0, **Ct** at pH 4.0 and **B2**/**Cc** mixture at pH 7.0. Reprinted with permission from ref. 19.

The molar fraction distribution[16,27a] of the various species in aqueous solution at 25 °C as a function of pH, obtained from the equilibrium constants (*vide infra*), is shown in Fig. 2. The

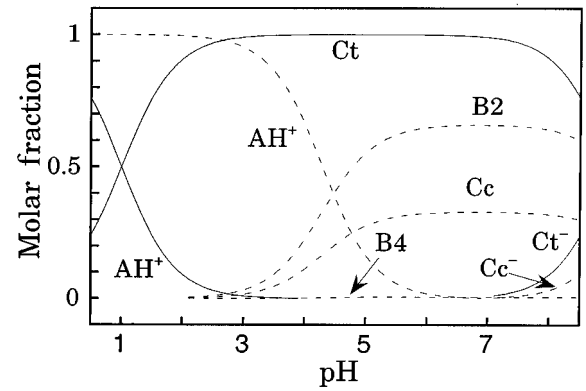

Fig. 2 Molar fraction distribution in aqueous solution at 25 °C as a function of pH for the 4′-methoxyflavylium compound. Solid lines refer to the species obtained at the thermodynamic equilibrium. Dashed lines refer to species obtained bringing **AH**$^+$ solutions from pH 1 to higher pH values by the pH jump technique or by exciting **Ct** solutions by flashed light. Such species reach a pseudo-equilibrium on the second time scale and then undergo a very slow thermal reaction to **Ct**. Reprinted with permission from ref. 19.

thermodynamically stable form in the pH range 2–8 is the *trans*-4′-methoxychalcone, **Ct**, which, at higher pH, is transformed into its anion, **Ct**$^-$ (Fig. 2, solid lines). In strongly acidic solutions, **AH**$^+$ becomes thermodynamically stable; however, **Ct** cannot be converted to **AH**$^+$ because of the very large activation barrier which involves isomerization of **Ct** to the intermediate compound **Cc** (Scheme 1). Furthermore, a solution of **AH**$^+$ is almost indefinitely stable at room temperature below pH 3, since under such conditions a very large kinetic barrier prevents conversion of **AH**$^+$ to the thermodynamically stable **Ct** form *via* the hydrated (pseudobase) species **B2** and the **Cc** isomer (Scheme 1). At higher pH, however, **AH**$^+$ is very reactive.[16] For example, starting from an aqueous solution of **AH**$^+$ at 25 °C and pH 1, a pH jump to pH 4.29 leads within a few seconds to a pseudo-equilibrium consisting of 50% **AH**$^+$, 33.2% **B2**, 0.3% **B4**, and 16.5% **Cc** (Fig. 2, dashed lines). A much slower reaction follows (half-life 19.7 h), resulting in complete conversion to the thermodynamically stable form **Ct**.

At pH 8, **AH**$^+$ reacts mainly with solvent water[16] (half-life 0.44 s) to produce 64% **B4**, 24% **B2**, and 12% **Cc**, the last two being in equilibrium with each other (half-life of the equilibration, 7×10^{-5} s). This is followed by another fast reaction (half-life 66 s) in which **B4**, a product of kinetic control of the initial neutralization of **AH**$^+$, is converted *via* **AH**$^+$ to **B2** and **Cc**,

yielding a pseudo-equilibrated mixture of 66.3% **B2**, 33.1% **Cc**, and 0.6% **B4** (Fig. 2, dashed lines). A much slower reaction (half-life 9.9 h) then occurs, resulting in complete conversion to **Ct**.

Photochemical behaviour of the 4′-methoxyflavylium ion

As described above, in the pH range 2–8 the colorless *trans*-4′-methoxychalcone **Ct** is the thermodynamically stable species and therefore it is the final product of the transformations of the strongly colored 4′-methoxyflavylium ion $\mathbf{AH^+}$. Even at pH 1, when $\mathbf{AH^+}$ is the thermally stable species, **Ct** can be kinetically stable because of the high energy barrier of its transformation to **Cc**. **Ct**, however, can be converted into $\mathbf{AH^+}$ by a photochemical reaction.[19] As expected from the thermal behavior of the system, the photoreaction causes a transient or an almost permanent effect depending on temperature and pH of the irradiated solution.

Continuous irradiation[19]

Continuous irradiation of 2.3×10^{-5} M aqueous solutions of **Ct** at pH 1.0 with 365 nm light causes strong spectral changes, with five isosbestic points and formation of a very intense band in the visible region with maximum at 435 nm [Fig. 3(*a*)]. Analysis of

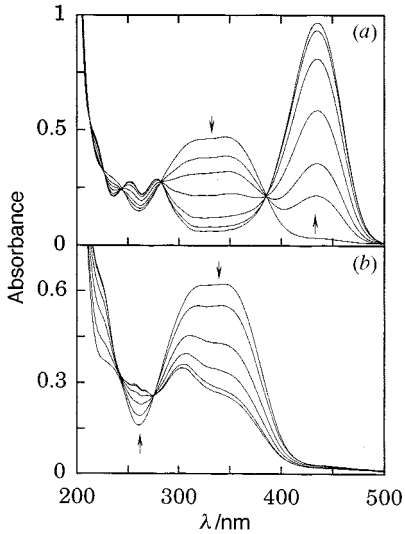

Fig. 3 Spectral changes caused by continuous irradiation of an aqueous solution of the **Ct** form of 4′-methoxyflavylium ion with 365 nm light: (*a*) pH 1.0, [**Ct**] = 2.5×10^{-5} M; the curves correspond to the following irradiation times: 0, 0.5, 1, 2, 4, 7 and 12 min. (*b*) pH 7.0, [**Ct**] = 3.2×10^{-5} M; the curves correspond to the following irradiation times: 0, 0.25, 1.5, 3, 6 and 10 min. Reprinted with permission from ref. 19.

the spectral changes shows that the photoreaction converts **Ct** into $\mathbf{AH^+}$, without formation of sizeable amounts of other products. The quantum yield of the photoreaction is 0.04, independent of the presence of dioxygen in solution. At pH 1.0, no back reaction takes place and irradiation with 434 nm light, corresponding to the maximum of the absorption band of $\mathbf{AH^+}$ (Fig. 1), does not cause any effect.

When irradiation of **Ct** is carried out at pH 4.0, the quantum yield of the photoreaction leading from **Ct** to $\mathbf{AH^+}$ does not change, but the expected thermal back reaction of $\mathbf{AH^+}$ to **Ct** is observed. The rate of the back reaction increases with temperature (activation energy 93 kJ mol^{-1} at pH 4.0). Irradiation at pH 7.0 causes the spectral changes shown in Fig. 3(*b*). At this pH the disappearance of **Ct** does not cause any increase of absorbance in the visible spectral region, showing that $\mathbf{AH^+}$ is not formed. Furthermore, the back reaction is very fast so that complete disappearance of **Ct** cannot be observed. This is in full agreement with the expectations based on the data shown in Fig. 2, which indicate that at pH 7.0 the pseudo-equilibrated mixture of products is constituted essentially by the open **Cc** and closed **B2** *cis* forms. Their absorption spectrum, as is always the case for aromatic derivatives of ethylene,[29] is less intense and slightly blue-shifted compared to the spectrum of the *trans* form (Fig. 1). Under such conditions, irradiation of the mixture with 313 nm light causes the reverse *cis* → *trans* photoisomerization reaction with an apparent quantum yield of *ca*. 0.5 (based on the total light absorbed by **Cc** and **B2**).

Interestingly, **Ct** and $\mathbf{AH^+}$ exhibit intense fluorescence bands with λ_{max} at 430 and 530 nm, respectively.[19] The fluorescence lifetime is shorter than 1 ns in both cases. It is worth noting that the occurrence of the above-described thermal and photochemical reactions can also be followed by fluorescence measurements.

Pulsed irradiation[19]

Flash photolysis is a powerful technique for investigating the kinetics of conversion of the various forms of flavylium ions.[27c] Even using a simple flash-photolysis apparatus with a time resolution of *ca.* 0.2 s it is possible to obtain kinetic data that can complement and/or replace those obtainable by the pH jump technique.

Flash excitation[19] of a 6.0×10^{-5} M aqueous solutions of **Ct** at 25 °C and pH 3.0 or 7.0 causes a bleaching in the 300–400 nm region that can be assigned to the disappearance of **Ct**. At pH 3, a strong increase in absorbance in the 400–500 nm region is observed, as expected for the formation of $\mathbf{AH^+}$. The absorbance *vs.* time traces show that **Ct** disappears within the time scale of the flash, but its disappearance does not lead directly to $\mathbf{AH^+}$. One or more intermediate products are formed (**Cc** and **B2** according to Scheme 1), which then convert completely to $\mathbf{AH^+}$ in a few seconds. At pH 7.0, the decrease of absorbance in the 300–400 nm region, corresponding to the disappearance of **Ct**, is not accompanied by an increase in absorbance in the visible region because in neutral solution $\mathbf{AH^+}$ is not stable and the main products of the photoreaction are **B2** and **Cc** (Fig. 2). None of the thermal and photochemical processes observed are affected by the presence of oxygen in the solution and the degree of reversibility of the system is satisfactory.[19]

In conclusion, the photochemical behaviour is in very good agreement with the behaviour observed by pH jump experiments. Although **Cc** is obviously the primary product of flash excitation, the observed species and their survival time (from seconds to years) before going back to the thermodynamically stable form **Ct** depend on temperature and pH.

Flavylium ions with OH substituents

In flavylium compounds that carry an OH substituent in the 4′- and/or 7-positions other forms, not present in the above discussed 4′-methoxyflavylium compound, can be obtained because of the deprotonation of the OH group, as illustrated in Scheme 2 for the 4′-hydroxyflavylium ion.[21] The new species are the quinoidal base **A**, obtained by simple deprotonation of the $\mathbf{AH^+}$ flavylium cation, and the dianionic $\mathbf{Cc^{2-}}$ and $\mathbf{Ct^{2-}}$ forms, obtained by second deprotonation of **Cc** and **Ct**. The roles played by these forms depend on the specific compound and pH conditions. For example, in the case of 4′-hydroxyflavilium ion the $\mathbf{Ct^{2-}}$ species exhibits fluorescence and the $\mathbf{Cc^{2-}}$ one undergoes photoisomerization to $\mathbf{Ct^{2-}}$ (*vide infra*).[21] Interestingly, for the 4-methyl-7-hydroxy- and 4′,7-dihydroxyflavylium compounds both the $\mathbf{AH^+}$ cation and the **A** quinoidal base exhibit fluorescence. Moreover, in the former compound, for which only two forms ($\mathbf{AH^+}$ and **A**) are observed, the pK_a of the ground state (4.4) is higher than the apparent pK_a of the excited state (0.7) and a very efficient adiabatic excited state proton transfer reaction (yield = 0.95) transforms $\mathbf{AH^{+*}}$ into **A***. These results show that 4-methyl-7-hydroxyflavylium

behaves as a four-level system and suggests that it could be used, in principle, to obtain a laser effect.[20]

Energy level diagrams

As discussed above for the 4′-methoxyflavylium compound, pH jump, temperature jump, and flash photolysis experiments allow the measurement of the rate constants of some of the reactions involved, and steady state titration experiments (by using UV–VIS and NMR techniques) allow the measurement of equilibrium constants. The values obtained for the most important processes of four flavylium compounds are gathered in Table 1.

From an operative viewpoint, the complex equilibria involving the species present at moderately acid pH (Scheme 2) can be described in terms of a single acid–base equilibrium between the acid species **AH**$^+$ and a conjugated base '**CB**' having a concentration equal to the sum of the concentrations of the species **A**, **B4**, **B2**, **Cc** and **Ct** [eqn. (1)],

$$\mathbf{AH}^+ \overset{K_a'}{\rightleftharpoons} \text{'}\mathbf{CB}\text{'} + H^+ \qquad (1)$$

where $K_a' = K_a + K_h + K_h 4 + K_h K_t + K_h K_t K_i$. The equilibrium constant of such an overall process is also given in Table 1. By using the data shown in Table 1, an energy level diagram can be constructed for each compound. Simplified versions of such diagrams (*e.g.* Fig. 4) can then be used to illustrate the behaviour of the various compounds[18–23] and to discuss the effect of the substituents.[22]

An intuitive way to describe the interconversion processes in flavylium-type compounds is their description using an hydraulic analogy.[22] Using such an analogy, the behaviour of an aqueous solution of flavylium ions upon a pH jump from 1.0 to 4.2 can be schematically represented as in Fig. 5. In the case of 4′-hydroxyflavylium, **Cc** converts very slowly to **Ct** and thus **B2** and **Cc** accumulate, whereas for 4′,7-dihydroxyflavylium and 7-hydroxyflavylium **Cc** converts very rapidly to **Ct** so that **Cc** and **B** disappear as soon as they are formed.

The hydraulic analogy can also be used to illustrate the photochemical behaviour of these compounds, the light playing the role of a pump. The scheme shown in Fig. 6 is appropriate for 4′-hydroxyflavylium.[22]

Properties of the network of chemical processes

As mentioned in the introduction, molecular or supramolecular systems capable of existing in different forms (*multistate*) that can be interconverted by different external stimuli (*multifunctional*) are interesting for both basic and application reasons. As we have seen above, the flavylium compounds can be interconverted into a number of different transient and stable forms using two different inputs, namely light or changes in pH. Several interesting aspects emerge when the resulting networks of chemical processes are analyzed in terms of 'molecular-level devices' and 'molecular level logic functions'. To illustrate these aspects, we will discuss the case of the 4′-hydroxyflavilylium compound (Scheme 1, $R^4 = R^7 = H$ and $R^{4'} = OH$; Fig. 4). For the sake of simplicity, in the following discussion the **A**, **B4** and **B2** transient species have been neglected since in the compound under examination they are always in rapid equilibrium with either **AH**$^+$ or **Cc**.

A write-lock-read-unlock-erase cycle

It is well known that photochromic systems represent potential molecular-level memory devices.[10–12] A number of problems, however, must be solved for practical applications. A most challenging one is to find systems with multiple storage and non-destructive readout capacity, *i.e.* the record can be erased when necessary, but is not destroyed by the readout. The 4′-hydroxyflavylium ion[21] (as well as the 4′-methoxyflavilium ion)[19] can be taken as the basis for an optical memory system with multiple storage and non-destructive readout capacity through a *write-lock-read-unlock-erase* cycle. This behavior can be described making reference to Figs. 4 and 7:

(i) At pH 4–7, the stable or kinetically inert (depending on pH) colorless **Ct** species can be photochemically converted (365 nm light) into the thermodynamically unstable, but relatively inert, **Cc** form (*write*).
(ii) Using a second stimulus (addition of acid), **Cc** can be converted into the kinetically inert or thermodynamically stable (depending on pH) **AH**$^+$ form (*lock*); if the initial pH is 1, the **Cc** species autolocks as **AH**$^+$.
(iii) The **AH**$^+$ species is photochemically inactive and shows an absorption spectrum clearly distinct from that of **Ct**, so that it can be optically detected (*read*).
(iv) Upon addition of base, **AH**$^+$ can be reconverted into **Cc** (*unlock*).
(v) **Cc** can be reconverted to the initial **Ct** form by a thermal or a photochemical reaction (*erase*).

Reading without writing in a write-lock-read-unlock-erase cycle

A generally overlooked difficulty with photochromic systems is that the starting form (**Ct** in the above discussion) is the photoreactive one, so that it cannot be read by absorption spectroscopy without writing. With the 4′-hydroxyflavylium ion, this difficulty can be overcome starting from **AH**$^+$, which is the thermodynamically stable form at pH 1 (Figs. 4 and 8).[21] Since this form is not photosensitive, it can be read by light excitation (*i.e.* by recording its absorption spectrum) without writing. Then it can be unlocked by a pH jump to 12 which yields the metastable $\mathbf{Cc}^{2-}$ form. At this stage, one can write the optical information obtaining the stable (locked) $\mathbf{Ct}^{2-}$ form that can then be read. When necessary, the information stored into

Table 1 Thermodynamic and kinetic constants for the structural transformations of some synthetic flavilium compounds[a]

	Flavylium ion			
Parameter	7-OH[b]	4′,7-$(OH)_2$[c]	4′-OH[d]	4′-OMe[e]
K_a'	2.0×10^{-3}	8.9×10^{-4}	1.26×10^{-2} [f]	8.0×10^{-2}
K_a	2.8×10^{-4}	1.0×10^{-4}	3.16×10^{-6}	
K_h	8.0×10^{-6}	1.4×10^{-6}	3.6×10^{-6}	3.4×10^{-5}
K_t	—	—	1	0.50
K_i	5.0×10^{2}	1.4×10^{3}	3.5×10^{3}	*ca.* 10^2
k_h/s^{-1}	0.48	1.8×10^{-2}	8.9×10^{-2}	0.47
$k_{-h}/s^{-1}\ M^{-1}$	3×10^{4} [g]	1.3×10^{4} [g]	2.5×10^{4} [g]	1.38×10^{4}
k_i/s^{-1}	0.57 [g]	0.26 [g]	3.7×10^{-5}	5.8×10^{-5}
k_{-i}/s^{-1}	8.3×10^{-4}	1.8×10^{-4}	$< 10^{-7}$	$< 10^{-6}$

[a] Measured by means of pH jump techniques at 25 °C, unless otherwise noted. [b] Ref. 22. [c] Ref. 18. [d] Refs. 17 and 21. [e] Refs. 16 and 19. [f] At 60 °C. [g] Measured by flash photolysis.

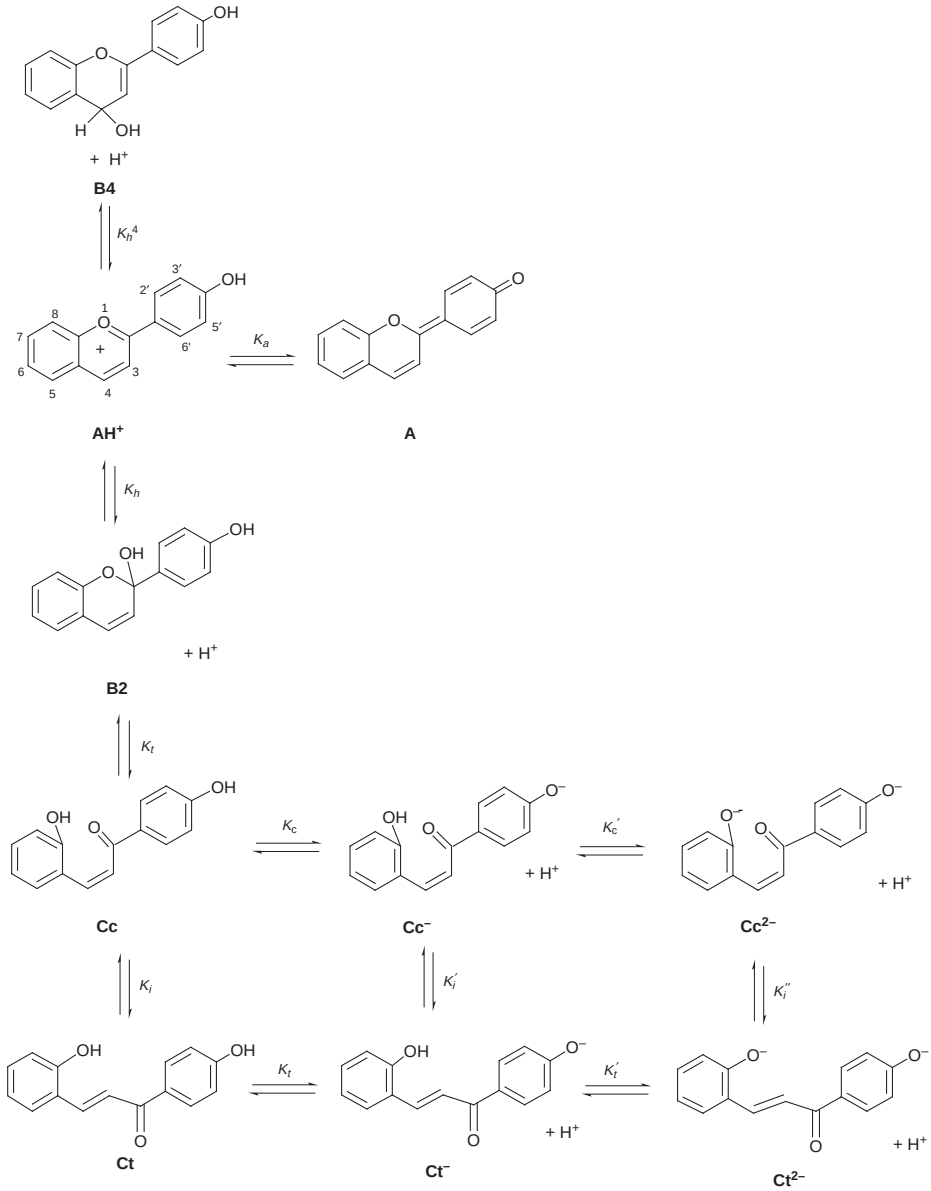

Scheme 2 Structural transformations of the 4′-hydroxyflavylium compound.

Ct²⁻ can be unlocked by a pH jump yielding **Ct** and can then be erased by light excitation. The same performance can be obtained starting from **Ct²⁻**.

Permanent and temporary memories

In our brain there are shallow and deep memory forms.[30] The network of processes interconverting the various species of the 4′-hydroxyflavylium ion allows the presence of different levels of memory.[21] Once the permanent (deep) **AH⁺** form of memory has been obtained (*write* and *lock*, Fig. 9), a jump to pH 12 leads to the formation of a temporary (shallow) memory state, **Cc²⁻**, whose spontaneous slow erasure to give the deep **Ct²⁻** memory can be accelerated by light. Reset can then be accomplished by a back pH jump to pH 4.

Oscillating absorbance patterns

Another feature of the 4′-hydroxyflavylium ion should be emphasized.[21] Starting from **AH⁺**, alternation of pH jump and light excitation causes oscillation patterns of absorbance at different wavelengths, as shown in Fig. 10. Such patterns may be interesting for signal generation purposes.

Logic operations

From a logic viewpoint,[6,7,9,31] simple (bistable) photochromic systems perform YES/NO functions. Multistate/multifunctional molecular-level systems can be taken as bases for more complex logic operations. Chemical systems capable to perform AND,[31] OR,[31] XOR,[32] and XNOR[33]logic operations at the molecular level have been recently reported. With the 4′-hydroxyflavylium compound, light excitation and pH jumps can be taken as inputs, and absorbance or fluorescence as outputs. Starting from the non-emitting **Ct** species, and taking the emission of **AH⁺** at 515 nm as output signal, a jump to pH 1 alone or light excitation alone are not able to generate the output, whereas when these two imputs are applied in series, the output is obtained (AND logic function).[21]

Multiple reaction patterns

It can be interesting to observe that in the network of processes of the 4′-hydroxyflavylium compound some species are interconnected by multiple reaction patterns.[21] For example, in order to go from **AH⁺** to **Ct** three different routes can be chosen (Fig. 11). (i) A jump to pH 12 with formation of **Cc²⁻**, followed by excitation with 313 nm light to obtain **Ct²⁻**, and a jump to pH 6. (ii) A jump to pH 6 to form **Cc**; at this stage, one can choose between two sub-routes, *i.e.* (iia) light excitation with 313 nm

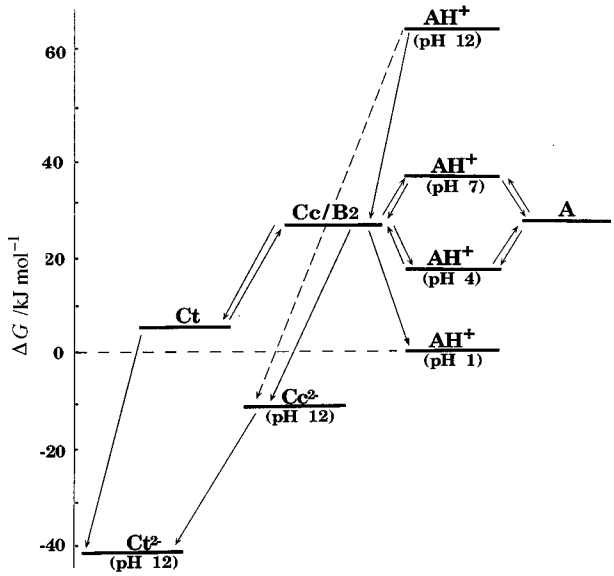

Fig. 4 Energy level diagram for the species involved in the pH jump and flash-photolysis experiments carried out on the 4′-hydroxyflavylium compound. pH values are indicated in brackets. For the sake of simplicity the species **Cc** and **B2** are represented by the same energy level. The ratio between the concentrations of **Cc** and **B2** is *ca.* 1. Reprinted with permission from ref. 21.

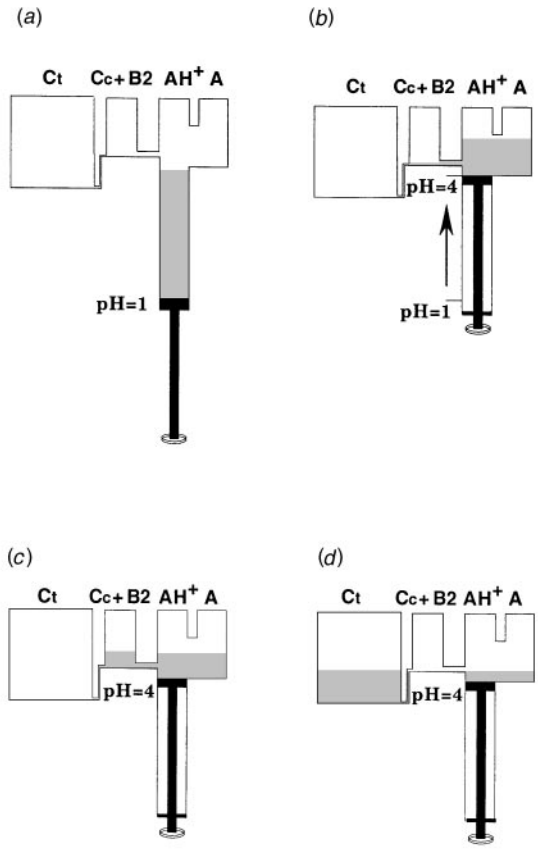

Fig. 5 Hydraulic analogy for a pH jump from pH 1.0 to 4.0: (*a*) the system is equilibrated at pH 1.0; (*b*) the system has been taken to pH 4.0; the pH jump has an effect comparable to raising the piston and the figure represents the situation immediately after the proton transfer process; (*c*) when the *cis*→*trans* isomerization is very slow it is possible to obtain an intermediate (pseudo-equilibrium) state involving the species **AH**$^+$, **A**, **B2** and **Cc**; (*d*) thermodynamic equilibrium at pH 4.0. Reprinted with permission from ref. 22.

light, or (iib) a jump to pH 12 to merge into the preceeding path which goes *via* **Cc**$^{2-}$ and **Ct**$^{2-}$. Once **Ct** has been obtained, one can go back to **AH**$^+$ by two different routes: (iii) light excitation at 365 nm to obtain **Cc** and subsequent jump to pH 1, or, *vice versa*, (iv) a jump to pH 1 and subsequent light excitation at 365 nm. Interestingly, in some cases, *i.e.* starting from **Ct** at pH 6, one obtains the same result (**AH**$^+$) regardless of the order in which light excitation (365 nm) and the pH jump (pH 1) are applied. In other cases, however, this is not true. For example (not shown in Fig. 11), starting from **AH**$^+$ at pH 1, light excitation followed by a pH jump to pH 12 leads to **Cc**$^{2-}$,

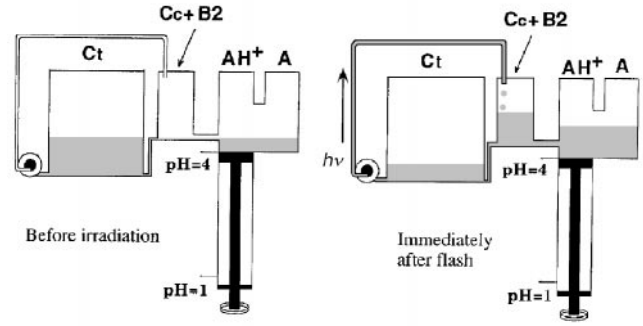

Fig. 6 Hydraulic analogy for the photochemical reaction of **Ct**. Light behaves like a pump that increases (in a transient mode as represented, or in steady state) the quantity of liquid in the reservoir **Cc**. Reprinted with permission from ref. 22.

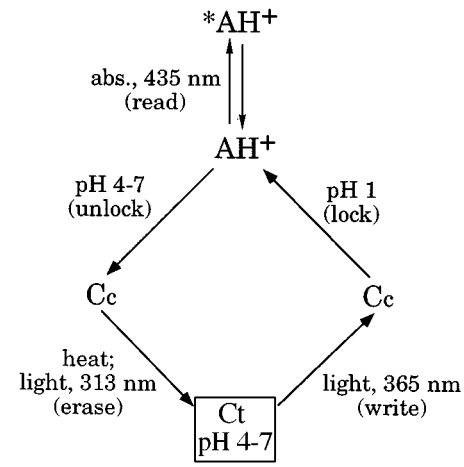

Fig. 7 Write-lock-read-unlock-erase cycle starting from the **Ct** form of the 4′-hydroxyflavylium compound. Reprinted with permission from ref. 21.

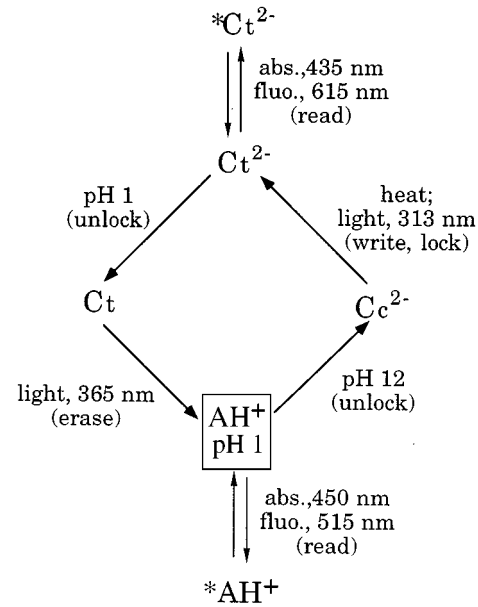

Fig. 8 Read-write-lock-read-unlock-erase cycle starting from the **AH**$^+$ form of the 4′-hydroxyflavylium compound. Reprinted with permission from ref. 21.

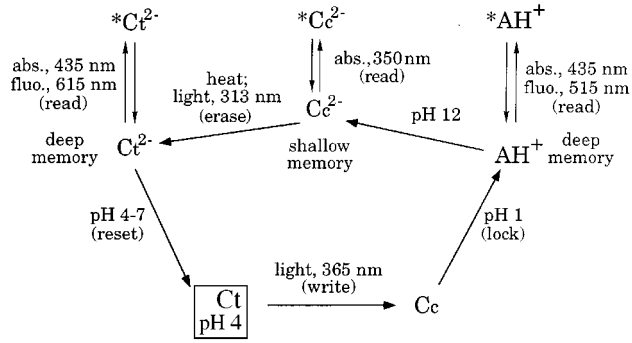

Fig. 9 A write-lock-read-unlock-erase cycle with two memory levels based on the 4′-hydroxyflavylium compound. Reprinted with permission from ref. 21.

whereas when the two inputs are applied in the reverse order one gets $\mathbf{Ct^{2-}}$. Since $\mathbf{Cc^{2-}}$ and $\mathbf{Ct^{2-}}$ exhibit very different spectroscopic properties (*e.g.* $\mathbf{Ct^{2-}}$ exhibits fluorescence whereas $\mathbf{Cc^{2-}}$ does not), from the state of the systems after the two inputs one can establish in which sequence the two inputs have been applied.

Color-tap effect

Because of the competition between the pH dependent rate of the reaction leading from the uncoloured **Cc** form to the colored $\mathbf{AH^+}$ and **A** species and the pH independent back *cis* → *trans* isomerization, the amount of colored species formed upon light excitation depends on the pH of the solution. In other words, the pH of the solution plays the role of a tap for the color intensity generated by light excitation.[22] This also means that this system can be viewed as a light-switchable pH indicator. In the case of 4′,7-dihydroxyflavylium the color-tap effect is larger than for 7-hydroxyflavylium.

Conclusions

Synthetic flavylium compounds can exist in several forms (*multistate*) that can be interconverted by more than one type of external stimulus (*multifunctional*). The intricate network of their reactions, when examined from the view points of 'molecular-level devices' and 'molecular level logic functions', reveal that these systems exhibit very interesting properties.

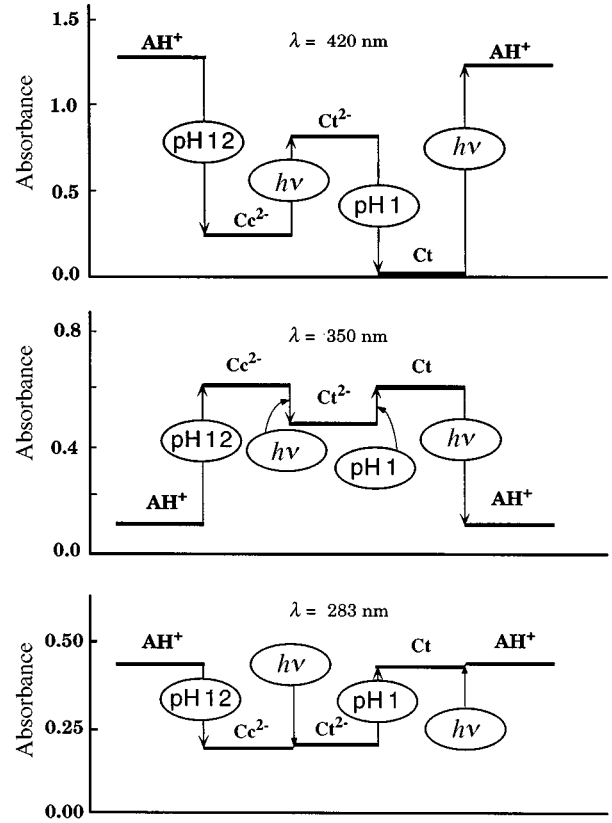

Fig. 10 Absorbance oscillations caused by alternate pH jump and light excitation on a 3.3×10^{-5} M aqueous solution starting from the $\mathbf{AH^+}$ form of the 4′-hydroxyflavylium compound at pH 1. Reprinted with permission from ref. 21.

In our brain, neurons store, exchange, and retrieve information *via* extremely complicated chemical processes. Synthetic multistate/multifunctional systems may play the role of models to begin understanding the chemical basis of complex biological processes. It is not at all clear whether 'wet' artificial systems can find real applications, for example in molecular-scale computers.[34] However, the study of molecular or supramolecular species capable of existing in different forms that can be interconverted by external stimuli is a topic of great interest since it introduces new concepts into the field of chemistry and

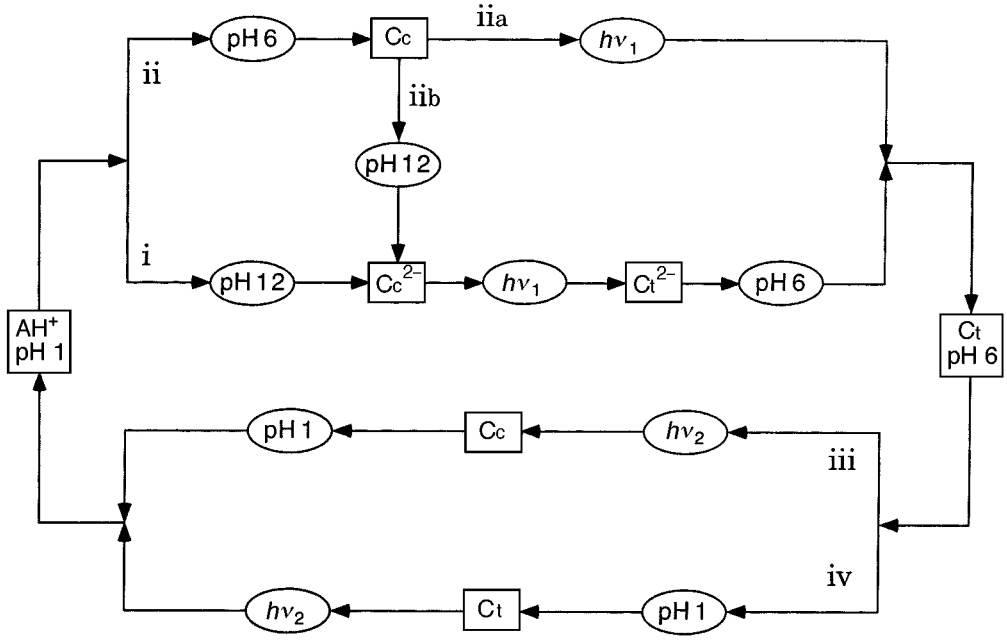

Fig. 11 The network of processes caused by pH jumps and light excitations interconnecting the $\mathbf{AH^+}$ and **Ct** forms of the 4′-hydroxyflavylium compound. Reprinted with permission from ref. 21.

stimulates the ingenuity of research workers engaged in the 'bottom up' approach to nanotechnology.

Acknowledgments

This work was supported in Portugal by Programa Plurianual CQFB and in Italy by MURST (Supramolecular Devices project) and the University of Bologna (Funds for Selected Research Topics). F. P. is grateful for a grant from JNICT (Portugal)/CNR Bologna (Italy).

Notes and References

† E-mail: vbalzani@ciam.unibo.it

1 J.-M. Lehn, *Supramolecular Chemistry: Concepts and Perspectives*, VCH, Weinheim, 1995.
2 *Molecular Electronic Devices*, ed. F. L. Carter, R. E. Siatkowsky and H. Woltjien, Elsevier, Amsterdam, 1988; K. E. Drexler, *Nanosystems: Molecular Machinery, Manufacturing, and Computation*, Wiley, New York, 1992; T. Thompson, *Byte*, 1996, 45.
3 D. Rouvray, *Chem. Br.*, 1998, **34**(2), 26.
4 V. Balzani and F. Scandola, *Supramolecular Photochemistry*, Ellis Horwood, Chichester, 1991.
5 L. B. Feringa, W. F. Jager and B. de Lange, *Tetrahedron* 1993, **49,** 8267.
6 A. P. de Silva and C. P. McCoy, *Chem. Ind.*, 1994, 992.
7 A. P. de Silva, H. Q. N. Gunaratne, T. Gunnlaugsson, A. J. M. Huxley, C. P. McCoy, J. T. Rademacher and T. E. Rice, *Chem. Rev.*, 1997, **97,** 1515.
8 V. Balzani and F. Scandola, in *Comprehensive Supramolecular Chemistry*, ed. D. N. Reinhoudt, Pergamon, Oxford, England, 1996, vol. 10, p. 687.
9 V. Balzani, A. Credi and F. Scandola, *Chim. Ind. (Milan)*, 1997, **79**, 751.
10 *Photochromism—Molecules and Systems*, ed. H. Dürr and H. Bouas-Laurent, Elsevier, Amsterdam, 1990.
11 For seminal examples concerning photochromic systems, see: (*a*) J. Daub, J. Salbeck, T. Knöchel, C. Fischer, H. Kunkely and K. M. Rapp, *Angew Chem., Int. Ed. Engl.*, 1989, **28**, 1494; (*b*) T. Iyoda, T. Saika, K. Honda and T. Shimidzu, *Tetrahedron Lett.*, 1989, **30**, 5429; (*c*) J. Daub, C. Fischer, J. Salbeck and K. Ulrich, *Adv. Mater.*, 1990, **8**, 366; (*d*) Y. Yokoyama, T. Ymamane and Y. Kurita, *J. Chem. Soc., Chem. Commun.*, 1991, 1722; (*e*) K. Uchida and M. Irie, *J. Am. Chem. Soc.*, 1993, **115**, 6442; (*f*) M. Irie, *Mol. Cryst. Liq. Cryst.*, 1993, **227**, 263; (*g*) M. Irie, O. Miyatake, K. Uchida, T. Eriguchi, *J. Am. Chem. Soc.*, 1994, **116**, 9894; (*h*) M. J. Preigh, F.-T. Lin, K. Z. Ismail and S. G. Weber, *J. Chem. Soc., Chem. Commun.*, 1995, 2091; (*i*) S. H. Kawai, S. L. Gilat, R. Posinet and J.-M. Lehn, *Chem. Eur. J.*, 1995, **1**, 285; (*j*) G. M. Tsivgoulis and J.-M. Lehn, *Chem. Eur. J.*, 1996, **2**, 1399; (*k*) M. Inouye, K. Akamatsu and H. Nakazumi, *J. Am. Chem. Soc.*, 1997, **119**, 9160.
12 For multiplexing optical systems based on mixtures of photochromic compounds, see: G. M. Tsivgoulis and J.-M. Lehn, *Adv. Mater.*, 1991, **9**, 627.
13 R. Brouillard, in *The Flavonoids, Advances in Research*, ed. J. Harborne, Chapman and Hall, London, 1988, p. 525; R. Brouillard, in *Anthocyanins as food colors*, ed. P. Markakis, Academic Press, New York, 1982, ch. 1.
14 R. Brouillard and J. E. Dubois, *J. Am. Chem. Soc.*, 1997, **99**, 1359.
15 R. Brouillard and J. Delaporte, *J. Am. Chem. Soc.*, 1997, **99**, 8461.
16 R. A. McClelland and S. Gedge, *J. Am. Chem. Soc.*, 1980, **102**, 5838.
17 R. A. McClelland and G. H. McGall, *J. Org. Chem.*, 1982, **47,** 3730.
18 F. Pina, M. J. Melo, L. Flamigni, R. Ballardini and M. Maestri, *New. J. Chem.*, 1997, **21**, 969.
19 F. Pina, M. J. Melo, M. Maestri, R. Ballardini and V. Balzani, *J. Am. Chem. Soc.*, 1997, **119**, 5556.
20 F Pina, M. J. Melo, M. H. Santos, J. C. Lima, I. Abreu, R. Ballardini and M. Maestri, *New J. Chem.*, 1998, in the press.
21 F. Pina, A. Roque, M. J. Melo, M. Maestri, L. Belladelli and V. Balzani, *Chem. Eur. J.*, 1998, **4**, 1184.
22 F. Pina, M. J. Melo, A. J. Parola, M. Maestri and V. Balzani, *Chem. Eur. J.*, 1998, in the press.
23 F. Pina, *J. Chem. Soc., Faraday Trans.*, 1998, **94**, 2109.
24 C. Michaelis and R. Wizinger, *Helv. Chim. Acta*, 1951, **34**, 1761; A. W. Johnson and R. R. Melhuish, *J. Chem. Soc.*, 1947, 346; C. Bullow and H. Wagner, *Ber. Dtsch. Chem. Ges.*, 1901, **34**, 1782.
25 W. von Sperling, F. C. Werner and H. Kuhn, *Ber. Bunsenges. Phys. Chem.*, 1966, **70**, 530.
26 G. Haucke, P. Czerney, C. Igney and H. Hartmann, *Ber. Bunsenges. Phys. Chem.*, 1989, **93**, 805; G. Haucke, P. Czerney, D. Steen, W. Rettig and H. Hartmann, *Ber. Bunsenges. Phys. Chem.*, 1993, **97**, 561.
27 (*a*) P. Figueiredo, J. C. Lima, H. Santos, M.-C. Wigand, R. Brouillard and F. Pina, *J. Am. Chem. Soc.*, 1994, **116**, 1249; (*b*) F. Pina, L. Benedito, M. J. Melo, A. J. Parola and M. A. Bernardo, *J. Chem. Soc. Faraday Trans.*, 1996, **92**, 1693; (*c*) M. Maestri, R. Ballardini, F. Pina and M. J. Melo, *J. Chem. Educ.*, 1997, **74**, 1314.
28 R. Matsushima, H. Mizuno, H. Itoh, *J. Photochem. Photobiol. A*, 1995, **89**,251; R. Matsushima, H. Mizuno and A. Kajiura, *Bull Chem. Soc. Jpn.*, 1994 , **67,** 1762; R. Matsushima and M. Suzuki, *Bull Chem. Soc. Jpn.*, 1992, **65**, 39.
29 J. Saltiel and Y.-P. Sun, in *Photochromism-Molecules and Systems*, ed. H. Dürr and H. Bouas-Laurent, Elsevier, Amsterdam, 1990, ch. 3.
30 H. Eichenbaum, *Science* ,1997, **277**, 330. For an example of an artificial system showing deep and shallow memory forms, see ref. 11(*b*).
31 A. P. de Silva, H. Q. N. Gunaratne and C. P. McCoy, *Nature*, 1993, **364**, 42.
32 A. Credi, V. Balzani, S. J. Langford and J. F. Stoddart, *J. Am. Chem. Soc.*, 1997, **119**, 2679.
33 M. Asakawa, P. R. Ashton, V. Balzani, A. Credi, G. Mattersteig, O. A. Matthews, M. Montalti, N. Spencer, J. F. Stoddart and M. Venturi, *Chem. Eur. J.*, 1997, **3**, 1992.
34 P. Ball and L. Garvin, *Nature*, 1992, **355**, 761; D. Bradley, *Science*, 1993, **259**, 890.

8/05522J

Evidence for zirconocene dications in Kaminsky type catalysts

Malcolm L. H. Green and Jörg Saßmannshausen

Inorganic Chemistry Laboratory, South Parks Road, Oxford, UK OX1 3QR. E-mail: malcolm.green@icl.ox.ac.uk

Received (in Cambridge, UK) 22nd October 1998, Accepted 25th November 1998

Low temperature NMR studies indicate that the dicationic salts $[Zr(\eta\text{-}C_5H_4CMe_2C_6H_4Me\text{-}p)_2]^{2+}[MeB(C_6F_5)_3]^-{}_2$ and $[Zr(\eta\text{-}C_5H_4CMe_2Ph)_2]^{2+}$ $[MeB(C_6F_5)_3]_2^-$ are formed when the neutral compounds $[Zr(\eta\text{-}C_5H_4CMe_2Ph)_2Me_2]$ and $[Zr(\eta\text{-}C_5H_4CMe_2C_6H_4Me\text{-}p)_2Me_2]$ and $[Zr(\eta\text{-}C_5H_4CMe_2Ph)_2Me_2]$ are treated with 2 equivalents of $B(C_6F_5)_3$.

Cationic zirconocene complexes are of great interest as catalysts for hydrogenation,[1] isomerisation[2] and especially olefin polymerisation reactions.[3–8] The donor free 14-electron $[Zr(\eta\text{-}C_5H_5)_2R]^+$ cation is believed to be an active species in Ziegler–Natta type olefin polymerisation. However, they are extremely reactive and not isolable. The corresponding 16-electron donor stabilised cations of the type $[Zr(\eta\text{-}C_5H_5)_2R(L)]^+$ or the 18-electron cations $[Zr(\eta\text{-}C_5H_5)_2R(L)_2]^+$ are known where the donor ligands are nitriles, cyclic ethers[9–16] or tertiaryphosphines.[17]

Recently, we described the reactions of the compounds $[Zr(\eta\text{-}C_5H_5)(\eta\text{-}C_5H_4CMe_2Ph)Me_2]$ **1**, $[Zr(\eta\text{-}C_5H_5)(\eta\text{-}C_5H_4CMe_2C_6H_4Me\text{-}p)Me_2]$ **2**, $[Zr(\eta\text{-}C_5H_4CMe_2Ph)_2Me_2]$ **3**, and $[Zr(\eta\text{-}C_5H_4CMe_2C_6H_4Me\text{-}p)_2Me_2]$ **4** with the Lewis acid $B(C_6F_5)_3$ which gave monocations, *e.g.* $[Zr(\eta\text{-}C_5H_5)(\eta\text{-}C_5H_4CMe_2Ph)Me_2]^+[MeB(C_6F_5)_3]^-$. The NMR evidence indicated there was intramolecular phenyl coordination to the cationic zirconium centre.[18] These complexes may be regarded as models of solvated cationic zirconocene species presumed to be present in toluene solutions of Kaminsky type olefin polymerisation catalysts.

Metallocene dications $[M(\eta\text{-}C_5H_5)_2L_2]^{2+}X^-{}_2$ have been reported,[19–22] (M = Ti, Zr; L = H_2O or MeCN; X = $CF_3SO_4^-$ ClO_4^-, BPh_4^-) and notably recent work by Erker and coworkers (**A**).[17]

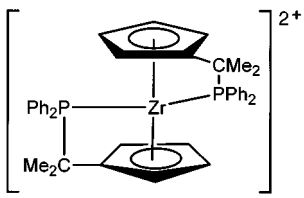

A

Here we report evidence for the formation of dicationic zirconocenes stabilised by metal-arene interactions.

The previously described[18] compounds $[Zr(\eta\text{-}C_5H_4CMe_2Ph)_2Me_2]$ **3** and $[Zr(\eta\text{-}C_5H_4CMe_2C_6H_4Me\text{-}p)_2Me_2]$ **4** were treated with 2 equivalents of $B(C_6F_5)_3$ in CD_2Cl_2. The reactions were monitored by NMR spectroscopy. At −60 °C the reaction of **4** proceeds cleanly to give a single product, which the NMR data below clearly indicate is the salt $[Zr(\eta\text{-}C_5H_4CMe_2C_6H_4Me\text{-}p)_2]^{2+}[MeB(C_6F_5)_3]_2^-$ **5**.

The NMR spectroscopic evidence supporting the structure proposed for **5** is:

(i) A broad signal at δ 0.40 in the ^{1}H NMR spectrum and a corresponding broad signal at δ 9.58 in the ^{13}C NMR spectrum which can be assigned to the separate $[MeB(C_6F_5)_3]^-$ anion.[23] This observation is further strengthened by the chemical shift difference $\Delta\delta(m,p\text{-F})$ between the *m*- and *p*-^{19}F of the anion.[24] Values of $\Delta\delta(m,p\text{-F})$ between 3 and 6 ppm indicate coordination of the anion to the zirconium centre whilst values < 3 ppm indicate non coordination of the anion. The observed value of $\Delta\delta$ 2.8 ppm corresponds to a solvent-separated ion pair.

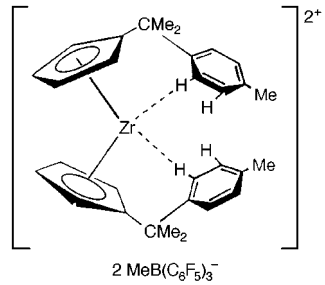

5

(ii) The absence of a Zr*Me* signal in ^{1}H and ^{13}C NMR together with the integration of the $[MeB(C_6F_5)_3]^-$ anion (6H) indicates the abstraction of *two* rather than *one* methide group from the metal.

(iii) Unlike the reaction product of **4** with *one* equivalent of $B(C_6F_5)_3$ [18] the dication **5** possesses a C_2 axis, which renders the two phenyl groups and the two cyclopentadienyl ligands equivalent. Therefore only four signals for the phenyl group and four signals for the cyclopentadienyl ligand are observed in the ^{1}H NMR spectrum. Furthermore, unlike the reaction product of **4** with 1 equivalent of $B(C_6F_5)_3$, the signals for the cyclopentadienyl hydrogens are *sharp*, as seen in Fig. 1 showing the ^{1}H NMR spectrum of the reaction product of **4** with 1 equivalent of $B(C_6F_5)_3$ and Fig. 2, the spectrum of the dication **5** formed with 2 equivalents of $B(C_6F_5)_3$.

(iv) One of the proton signals of each of the cyclopentadienyl ligands of **5** is significantly shifted *upfield* (δ 3.70) which can be explained by the magnetic anisotropy of the phenyl group. In contrast to the ^{1}H NMR spectrum of the reaction product of $[Zr(\eta\text{-}C_5H_5)(C_5H_4CMe_2C_6H_4Me\text{-}p)Me_2]$ **2** and 1 equivalent of $B(C_6F_5)_3$, where one of the cyclopentadienyl hydrogen signals is shifted *downfield* (δ 6.94), due to a *deshielding* effect of the phenyl ring,

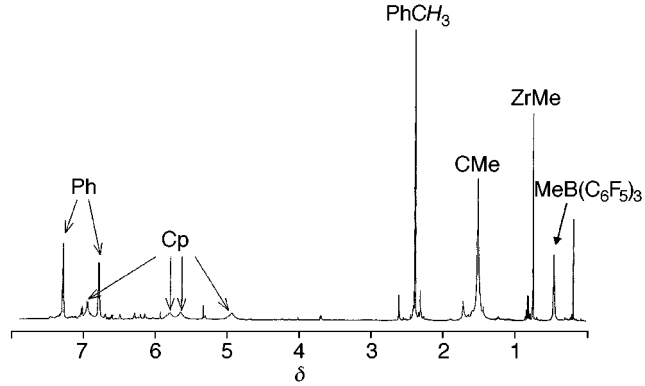

Fig. 1 ^{1}H NMR spectrum of **4** with 1 equivalent of $B(C_6F_5)_3$ at −60 °C.

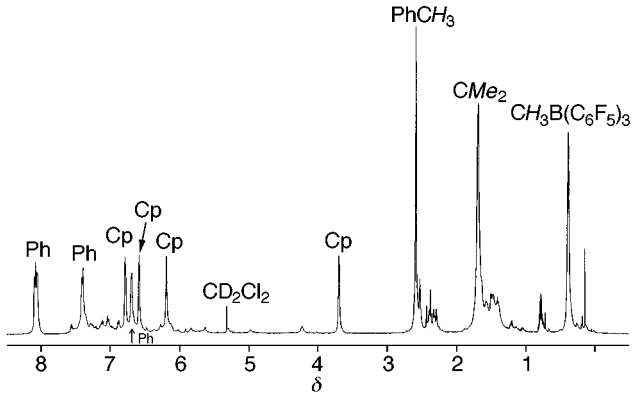

Fig. 2 ^{1}H NMR spectrum of **4** with 2 equivalents of $B(C_6F_5)_3$ at −60 °C.

here the phenyl ring is located slightly differently probably due to the more sterically crowded environment around the zirconium metal and the cyclopentadienyl hydrogen encounters a *shielding* effect. Interesting is the corresponding ^{13}C signal, which is observed at δ 128.43 (assignment *via* CH correlation spectroscopy).

(v) Similar to the ^{1}H NMR of the reaction product of **2** with 1 equivalent $B(C_6F_5)_3$, one of the phenyl hydrogen signals is shifted *upfield* to δ 6.69 (*cf.* Fig. 2). This can be assigned to a hydrogen coordinated, or close to, to the zirconium centre. Similar observations of upfield shifts of coordinated phenyl-hydrogen have been made before,[25] notably by Horton *et al.*[26]

(vi) Warming the sample of **5** to −40 °C changes the NMR spectra giving new peaks which are identical to the previously described monocation $[Zr(\eta\text{-}(C_5H_4CMe_2C_6H_4Me\text{-}p)_2Me]^+[MeB(C_6F_5)_3]^-$ [18] and the presence of excess $B(C_6F_5)_3$ also appears in the ^{19}F NMR spectrum. This reaction is reversible and on re-cooling the sample to −60 °C the original spectrum is restored. Further warming above −40 °C increases the amount of the monocation, however some decomposition products are also observed.

The reaction between $[Zr(\eta\text{-}C_5H_4CMe_2Ph)_2Me_2]$ **3** and 2 equivalents of $B(C_6F_5)_3$ also gives a product with similar properties to **5**. However it is less soluble than **5** and this restricts investigations at −60 °C. Nonetheless the data are fully consistent with the proposed formulation of the product $[Zr(\eta\text{-}C_5H_4CMe_2Ph)_2]^{2+}$ $[MeB(C_6F_5)_3]^-{}_2$ **6**. Crystals of **6** were not suitable for X-ray crystallography due to twinning. The NMR data for the compounds **5** and **6** are available as supplementary data (see http://www.rsc.org/suppdata/cc/1999/115).

In conclusion the reaction of **3** and **4** with 2 equivalents of $B(C_6F_5)_3$ leads to the formation of dicationic complexes **5** and **6**. These complexes have been characterised by NMR spectroscopy and elemental analysis. The dications of **5** and **6** can be viewed as a model for the cationic species $[Zr(\eta\text{-}C_5H_5)_2(solvent)_2]^{2+}$ and these may well be present in aromatic solutions of Kaminsky-type zirconocene olefin polymerisation catalysts systems.

We would like to thank Dr L. H. Doerrer and Dr D. Häußinger for helpful discussions.

Notes and references

1 Y. Qian, G. Li and Y. Huang, *J. Mol. Catal.*, 1989, **54**, L19.
2 Y. Qian, J. Lu and W. Xu, *J. Mol. Catal.*, 1986, **34**, 31.
3 M. Bochmann, *J. Chem. Soc., Dalton Trans.*, 1996, 225.
4 P. C. Möhring, N. Vlachakis, N. E. Grimmer and N. J. Coville, *J. Organomet. Chem.*, 1994, **483**, 159.
5 T. Ushioda, M. L. H. Green, J. Haggitt and X. Yan, *J. Organomet. Chem.*,1996, **518**, 155.
6 W. Kaminsky and M. Arndt, *Adv. Polym. Sci.*, 1995, **127**, 144.
7 H.-H. Brintzinger, D. Fischer, R. Mülhlhaupt, B. Rieger and R. Waymouth, *Angew. Chem.*, 1995, **107**, 1255; *Angew. Chem., Int. Ed. Engl.*, 1995, **34**, 1143.
8 M. Aulbach and F. Küber, *Chem. Z*, 1994, **28**, 197.
9 R. F. Jordan, C. S. Bajgur, R. Willet and B. Scott, *J. Am. Chem. Soc.*, 1986, **108**, 7410.
10 R. F. Jordan, R. E. LaPointe, C. S. Bajgur, S. F. Echols and R. Willet, *J. Am. Chem. Soc.*, 1987, **109**, 4111.
11 R. F. Jordan, R. E. LaPointe, N. C. Baenzinger and G. D. Hinch, *Organometallics*, 1990, **9**, 1539.
12 J. J. W. Eshuis, Y. Y. Tan, A. Meetsma and J. H. Teuben, *Organometallics*, 1992, **11**, 362.
13 J. J. W. Eshuis, Y. Y. Tan, A. Meetsma and J. H. Teuben, *J. Mol. Catal.*, 1990, **62**, 277.
14 D. M. Amorose, R. P. Lee and J. L. Petersen, *Organometallics*, 1991, **10**, 2191.
15 Y. W. Alelyunas, R. F. Jordan, S. F. Echols, S. L. Borkowsky and P. K. Bradley, *Organometallics*, 1991, **10**, 1406.
16 S. L. Borkowsky, R. F. Jordan and G. D. Hinch, *Organometallics*, 1991, **10**, 1268.
17 B. E. Bosch, G. Erker, R. Fröhlich and O. Meyer, *Organometallics*, 1997, **16**, 5449.
18 L. H. Doerrer, D. Häußinger, M. L. H. Green and J. Saßmannshausen, *J. Chem. Soc., Dalton Trans.*, submitted.
19 Zirconium: L = H_2O, X = $CF_3SO_4^-$, CLO_4^-: W. Lasser and U. Thewalt, *J. Organomet. Chem.*, 1986, **311**, 69; L = H_2O, X = $CF_3SO_4^-$: U. Thewalt and W. Lasser, *J. Organomet. Chem.*, 1984, **276**, 341; L = CH_3CN, X = BPh_4^-: R. F. Jordan and S. F. Echols, *Inorg. Chem.*, 1987, **26**, 383.
20 P. N. Billinger, P. P. K. Claire, H. Collins and G. R. Willey, *Inorg. Chim. Acta*, 1988, **149**, 63.
21 Titanium: L = THF, X = $Co(CO)_4$: J. S. Merola, K.S. Campo, R. A. Gentile and M. A. Modrick, *Inorg. Chim. Acta*, 1989, **165**, 87; L = THF; X = AsF_6: P. Gowik and T. Klapötke, *J. Organomet. Chem.*, 1989, **372**, 33; L = THF, MeCN; X = AsF_6:T. Klapötke, *Polyhedron*, 1989, **8**, 311; L = bipy, X = $CF_3SO_4^-$: U. Thewalt and K. Berhalter, *J. Organomet. Chem.*, 1986, **302**, 193; U. Thewalt and H.-P. Klein, *J. Organomet. Chem.*, 1980, **194**, 297; B. Honold and U. Thewalt *J. Organomet. Chem.*, 1986, **316**, 291; K. Berhalter and U. Thewalt, *J. Organomet. Chem.*, 1987, **322**, 123.
22 For Diels–Alder reactions: T. K. Hollis, N. P. Robinson and B. Bosnich, *J. Am. Chem. Soc.*, 1992, **114**, 5464.
23 D. J. Gillis, M. J. Tudoret and M. C. Baird, *J. Am. Chem. Soc.*, 1993, **115**, 2543.
24 A. D. Horton, J. deWith, J. v. d. Linden and H. v. d. Weg, *Organometallics*, 1996, **15**, 2672.
25 G. G. Hlatky, H. W. Turner and R. R. Eckman, *J. Am. Chem. Soc.*, 1989, **111**, 2728.
26 A. D. Horton and J. H. G. Frijns, *Angew. Chem., Int. Ed. Engl.*, 1991, **30**, 1152.

Communication 8/08197B

The first total synthesis of (±)-pallescensin B

Wen-Cheng Liu and Chun-Chen Liao*

Department of Chemistry, National Tsing Hua University, Hsinchu, Taiwan 300. E-mail: ccliao@faculty.nthu.edu.tw

Received (in Cambridge, UK) 9th November 1998, Accepted 20th November 1998

The first total synthesis of the title compound has been accomplished using an intramolecular Diels–Alder reaction of a masked *o*-benzoquinone, anionic [1,3]-rearrangement of a vinylbicyclo[2.2.2]octenol and intramolecular hetero-Michael addition of a hydroxy enone as the key steps.

Pallescensins are a group of furanosesquiterpenoids isolated from the marine sponge *Disidea pallescens* by Cimino *et al*.[1] The common feature of these terpenoids is that they all contain a furan moiety; however they have carbon skeletons of varying complexity. Among the pallescensins, pallescensin B **1** presents the most complex architecture, with a unique bicyclo[4.2.2]decane system fused to a furan moiety. Interestingly, bicyclo[4.2.2]decane skeletons are relatively rare among natural products, the only other known example being nakafuran-8 **2**.[2]

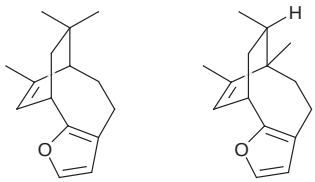

1 **2**

The synthesis of the bicyclo[4.2.2]decane skeleton poses a considerable challenge. Although a few methods exist for their synthesis,[2,3] they lack versatility and provide the desired skeleton only after several steps. Despite the long sequence of reactions it requires, Uyehara's approach to this skelecton is noteworthy.[2] Quite recently, we have developed a novel and efficient four-step methodology starting from 2-methoxyphenols, *via* anionic [1,3]-rearrangement of vinylbicyclo[2.2.2]-octenol derivatives as the key step, for the stereocontrolled synthesis of functionalized bicyclo[4.2.2]decenones (Scheme 1).[4] We herein report the first total synthesis of (±)-**1** clearly expressing the utility of the aforementioned methodology.

It was planned to use compound **10** as the key intermediate to achieve the synthesis of **1**, as we expected compound **9** to undergo anionic [1,3]-rearrangement. Synthesis of compound **10** was accomplished as shown in Scheme 2. Accordingly, the

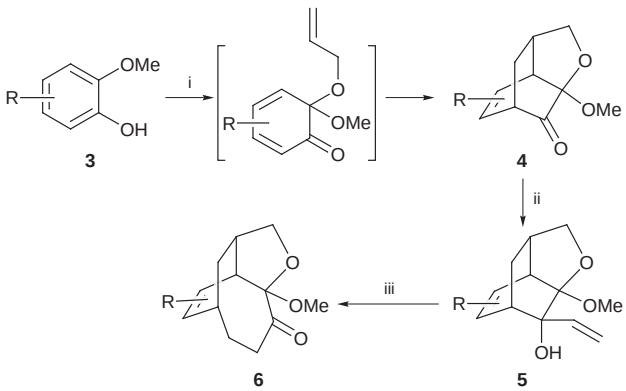

Scheme 1 *Reagents and conditions*: i, allyl alcohol, $PhI(OAc)_2$, CH_2Cl_2; ii, CH_2=CHMgBr; iii, KH, 18-crown-6.

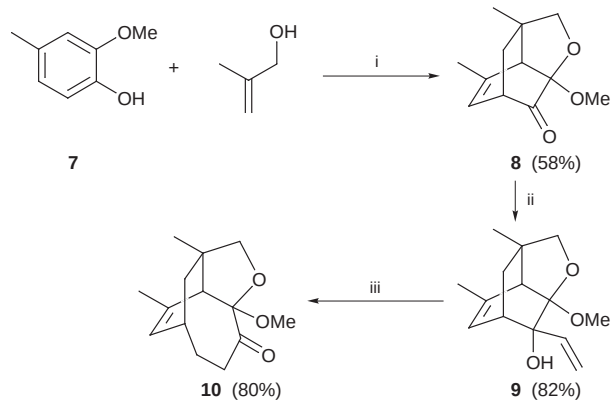

Scheme 2 *Reagents and conditions*: i, $PhI(OAc)_2$, $NaHCO_3$, 55–60 °C; ii, CH_2=CHMgBr, $ZnBr_2$, −78 °C to room temp.; iii, KH, 18-crown-6, 1,4-dioxane, reflux.

requisite bicyclo[2.2.2]octenone derivative **8** was prepared from 2-methoxy-4-methylphenol **7** in 58% yield, following a procedure developed in our laboratory for the synthesis of similar compounds.[5] Stereoselective addition of vinylmagnesium bromide to compound **8** in the presence of zinc bromide at −78 °C afforded **9** in 82% yield as the only discernible product. Subsequent anionic [1,3]-rearrangement of **9** proceeded smoothly to provide **10** in 80% yield (Scheme 2).

With compound **10** in hand, the stage is set for the construction of the furan ring, which was accomplished *via* seven synthetic steps, as shown in Scheme 3. The required two-carbon unit was introduced *via* alkylation of **10** using 1-bromo-2-(2-tetrahydropyranyloxy)ethane in the presence of KH at 0 °C in THF to obtain compound **11** in 89% yield as a 1:1 mixture of diastereomers. Then compound **11** was converted into the corresponding enone **12** using Saegusa's procedure[6] in two steps and in about 78% yield. The removal of the THP group was achieved *via* transacetalization with Pr^{i}OH catalyzed by PPTS to obtain the alcohol **13** as a single product. Intra-

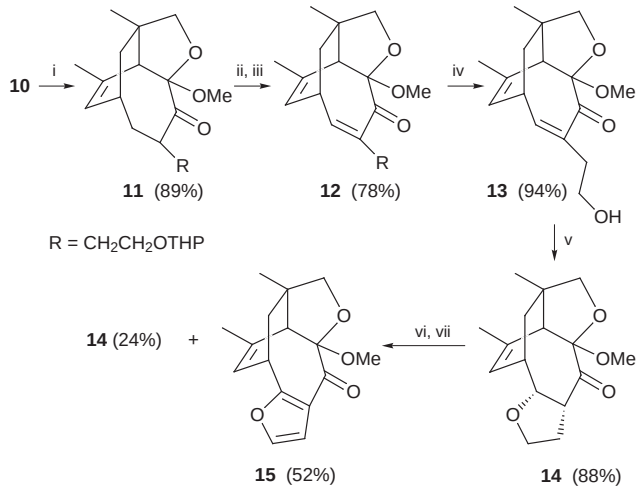

Scheme 3 *Reagents and conditions*: i, RBr, KH, THF, 0 °C; ii, KH, TMSCl; iii, $Pd(OAc)_2$, MeCN; iv, Pr^{i}OH, PPTS, 55 °C; v, NaOH, MeOH, 80 °C; vi, KH, TMSCl; vii, DDQ, benzene, reflux.

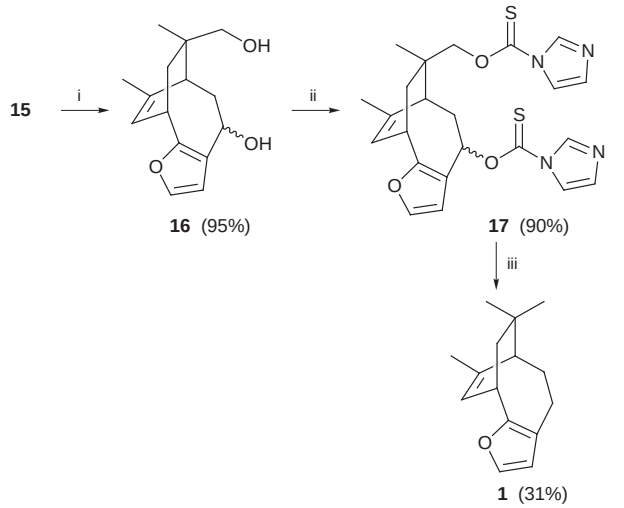

Scheme 4 *Reagents and conditions*: i, SmI_2, MeOH, THF; ii, 1,1′-thiocarbonyldiimidazole, $ClCH_2CH_2Cl$, reflux; iii, Bu_3SnH, AIBN, toluene, reflux.

molecular Michael addition of **13** by treatment with 6 M aq. NaOH in MeOH at 80 °C furnished the tetrahydrofuran **14** as a single stereoisomer in 88% yield. The assigned stereochemistry of compound **14** was based on NOE experiments. Aromatization of **14** was accomplished *via* treatment of its silyl enol ether (KH, TMSCl) with DDQ in refluxing benzene to obtain the desired compound **15** in 52% yield, along with 24% of **14** (Scheme 3).

With construction of the complete carbon framework of **1** accomplished, the remaining task was to deoxygenate **15**. Towards this end, reduction of **15** with SmI_2 in the presence of MeOH was carried out first to obtain the diols **16** as a mixture of epimers,[7] which were converted then into a mixture of the corresponding bis-thiocarbamates **17** in 90% yield. The last hurdle to target compound **1** was passed by means of reduction of **17** with tin hydride initiated by AIBN in refluxing toluene (Scheme 4).[8] The structure of **1** was unambiguously established by its IR, ^1H and ^{13}C NMR, low and high resolution mass spectral data.[9] The UV, ^1H NMR and mass spectral data of synthetic (±)-**1** were found to be essentially identical with those reported by Cimino *et al*. for the natural product.[1]

Thus the synthesis of (±)-**1** was accomplished in 13 steps from readily available starting materials. In conclusion, the synthesis of (±)-**1** described here clearly exhibits the versatility of our methodology for the construction of the bicyclo[4.2.2]-decane skeleton and also confirms the structural assignments of the natural product.

The authors thank the National Science Council of the Republic of China for the financial support of this research work. We also thank Dr P. Dharma Rao for helpful discussions.

Notes and references

1 G. Cimino, S. De Stefano, A. Guerriero and L. Minale, *Tetrahedron Lett*., 1975, 1417, 1421 and 1425.
2 T. Uyehara, M. Sugimoto, I. Suzuki and Y. Yamamoto, *J. Chem. Soc., Chem. Commun*., 1989, 1841; T. Uyehara, M. Sugimoto, I. Suzuki and Y. Yamamoto, *J. Chem. Soc., Perkin Trans. 1*, 1992, 1785.
3 Y. Sakai, K. Terashima, Y. Tobe and Y. Odaira, *Bull. Chem. Soc. Jpn*., 1981, **54**, 2229; A. Gambacorta, S. Turchetta and S. Stefanelli, *Tetrahedron Lett*., 1991, **32**, 6805.
4 T.-H. Lee, C.-C. Liao and W.-C. Liu, *Tetrahedron Lett*., 1996, **37**, 5897.
5 C.-S. Chu, T.-H. Lee and C.-C. Liao, *Synlett*, 1994, 635.
6 Y. Ito, T. Hirao and T. Saegusa, *J. Org. Chem*., 1978, **43**, 1011.
7 C.-S. Chu, C.-C. Liao and P. D. Rao, *Chem. Commun*., 1996, 1537.
8 D. H. R. Barton and S. W. McCombie, *J. Chem. Soc., Perkin Trans. 1*, 1975, 1574; S. A. Boyd, R. A. Mantei, C.-N. Hsiao and W. R. Baker, *J. Org. Chem*., 1991, **56**, 438.
9 *Selected data* for synthetic **1**: ν_{max}(neat)/cm^{-1} 2922 (s), 1505 (m), 1439 (m); δ_H(400MHz, $CDCl_3$) 7.07 (d, *J* 1.6, 1H), 6.03 (d, *J* 1.6, 1H), 5.81 (dq, *J* 6.9, 1.2, 1H), 3.43 (ddd, *J* 6.9, 6.6, 2.4, 1H), 2.36–2.28 (m, 1H), 2.21–2.04 (m, 3H), 1.92–1.84 (m, 1H), 1.60–1.53 (m, 2H), 1.79 (d, *J* 1.2, 3H), 0.91 (s, 3H), 0.77 (s, 3H); δ_C(100 MHz, $CDCl_3$) 153.2 (C), 141.2 (C), 138.0 (CH), 120.7 (CH), 118.1 (C), 113.5 (CH), 50.1 (CH), 43.8 (CH_2), 36.7 (CH_3), 33.8 (CH), 33.5 (C), 30.5 (CH_2), 29.9 (CH_3), 23.6 (CH_3), 22.0 (CH_2); *m/z* (70 eV) 216 (M^+); HRMS (EI): Calc. for $C_{15}H_{20}O$: 216.1514; found : 216.1504.

Communication 8/08714H

Synthesis of an unsymmetrical bis-lexitropsin-1,2,9,9a–tetrahydrocyclopropa[*c*]benzo[*e*]indol-4-one (CBI) conjugate

Guofeng Jia, Hirokazu Iida and J. William Lown*

Department of Chemistry, University of Alberta, Edmonton, AB, Canada T6G 2G2.
E-mail: annabella.wiseman@ualberta.ca

Received (in Corvallis, OR, USA) 8th October 1998, Accepted 23rd November 1998

A practical synthesis of a novel bis-functionalized precursor of 1,2,9,9a-tetrahydrocyclopropa[*c*]benzo[*e*]indol-4-one (CBI) is described; the first unsymmetrical bis-lexitropsin–CBI precursor conjugate was thereby synthesized.

CC-1065, an antitumor antibiotic isolated from the culture of *Streptomyces zelensis*,[1] is one of the most potent cytotoxic agents ever discovered and has a wide spectrum of activity against tumor cells *in vitro* and *in vivo* as well as against microbial organisms.[2] However, CC-1065 cannot be used in humans because it was found that it caused delayed death in experimental animals.[3] In the search for compounds with better antitumor selectivity and DNA sequence specific binding

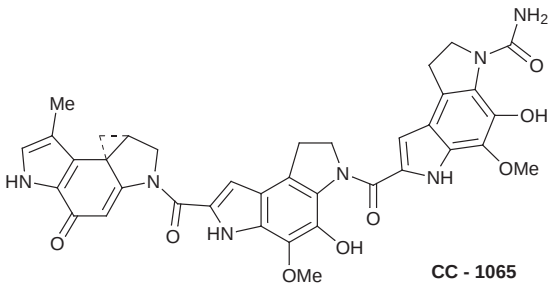

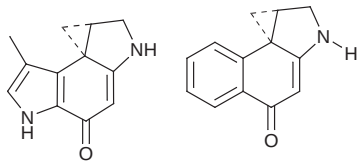

properties, many CC-1065 analogs have been synthesized in attempts to avoid the undesired side effects while retaining its potency against tumor cells.[4] As a successful example of modification of 1,2,8,8a-tetrahydro-7-methylcyclopropa[*c*]-pyrrolo[3,2-*e*]indol-4-one (CPI), the DNA alkylating moiety of CC-1065, Boger first reported that the simplified moiety, 1,2,9,9a-tetrahydrocyclopropa[*c*]benzo[*e*]indol-4-one (CBI), and its analogs were more stable and more potent than the CPI counterparts.[5]

In our group, attempts have been made to link CPI with lexitropsins, the well-established DNA minor groove binders. It was found that some optimized CPI–lexitropsin conjugates exhibit up to 10000 times higher potency than CC-1065 against KB human cancer cells.[3] Molecular modeling studies predicted that a CBI moiety bearing a lexitropsin carrier on both sides should be more firmly bound to its DNA target sequence and might therefore show enhanced potency. This strategy is designed to exploit binding-driven bonding of the alkylating moiety. We have already reported the synthesis of conjugates of CBI bearing two identical lexitropsins which containing pyrrole units.[6] Studies on lexitropsins or information reading molecules show that replacement of pyrrole units by imidazoles in lexitropsins may cause a change in the base site recognition from AT to GC in minor groove of B-DNA.[7] In order to permit targeting of mixed DNA sequences and to thereby investigate the effects of DNA sequence selective ability, we herein

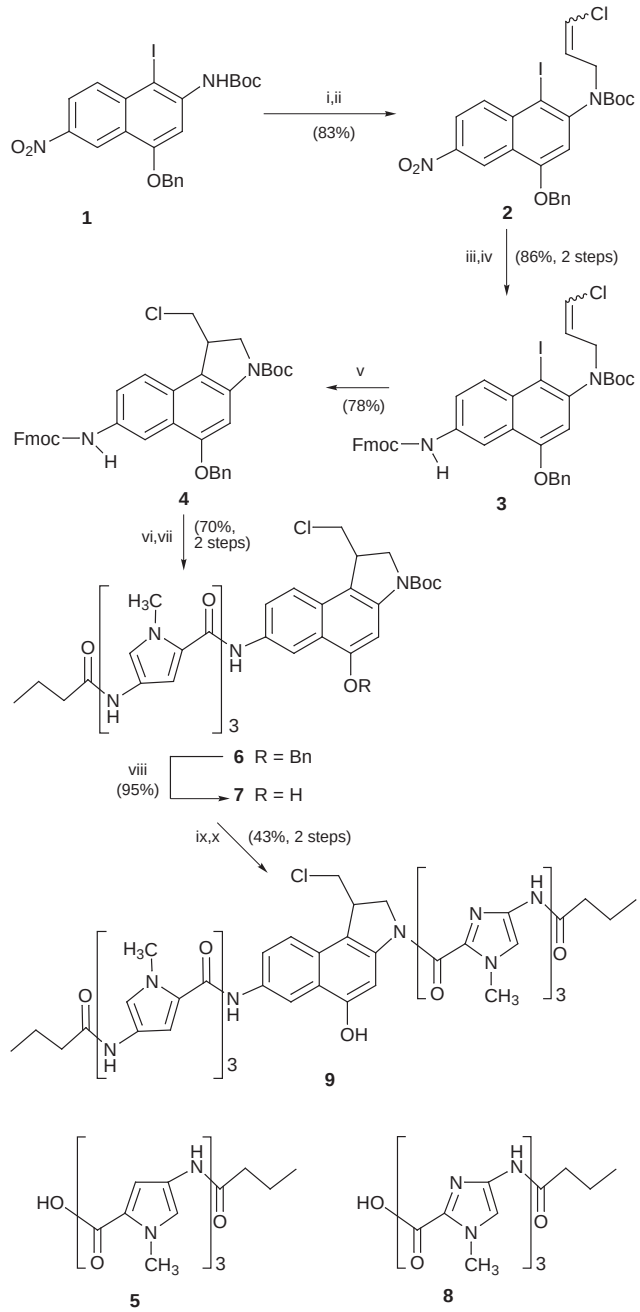

Scheme 1 *Reagents and conditions*: i, NaH; ii, ClCH=CHCH$_2$Cl, Bu$_4$NI; iii, hydrazine hydrate, FeCl$_3$, C; iv, FmocCl, Et$_3$N; v, Bu$_3$SnH, AIBN; vi, TBAF; vii, **5**; viii, HCO$_2$NH$_4$, Pd/C; ix, HCl; x; **8**.

describe the synthesis of an unsymmetrical bis-lexitropsin–CBI conjugate, which contains two different lexitropsins. In our previous work,[6] the CBI moiety was obtained by an *in situ* primary radical trap with TEMPO. Here, the CBI moiety was synthesized by using a more concise and shorter route which was recently developed by Patel and co-workers.[8]

Deprotonation of carbamate **1**[6] using NaH, followed by alkylation of the resulting anion with 1,3-dichloropropene in the presence of the phase transfer catalyst Bu_4NI gave an mixture of *Z* and *E* isomers of vinyl chloride **2**. Selective reduction of the nitro group of **2** using hydrazine,[9] followed by protection of the amino group, provided **3**, the desired precursor for the intramolecular aryl radical cyclization on to a tethered vinyl chloride.[8] A deoxygenated solution of **3** in dry benzene was heated at reflux for 15 h in the presence of 2 equiv. of Bu_3SnH and a catalytic amount of AIBN to give the fully protected bifunctionalized CBI prodrug form, racemic **4**.† Although not investigated in detail, no reaction occurred when nitro compound **2** was treated under the same conditions as amine **3**.

Detachment[10] of the Fmoc group from **4**, followed by coupling with polypyrrole carboxamide **5**[11] using HOBt and EDCI as the coupling agents[11b,c] afforded the hybrid **6**. Hydrogenolysis[8a] of **6** served to remove the benzyl ether almost quantitatively and provided **7**. Acid-mediated deprotection of **7**, followed by coupling with polyimidazole carboxamide **8**[11] using EDCI provided the final bis-lexitropsin–CBI precursor conjugate **9**‡ in fair yield.

In summary, we have described a synthesis of the bis-functionalized CBI precursor containing two different protective groups and obtained the corresponding unsymmetrical bis-lexitropsin conjugate. Results on the DNA sequence preferences and biological evaluation will be reported in due course.

We are grateful for a research grant (to J. W. L.) from the Natural Sciences and Engineering Research Council of Canada.

Notes and references

† *Selected data* for **4**: δ_H(360 MHz, acetone-d_6) 9.02 (s, NH), 8.38 (s, 1H, C6-H), 7.88–7.30 (m, 16H, Ar-H), 5.30 (s, 2H, $PhCH_2O$), 4.50 (d, 2H, *J* 6.9, CH_2 in Fmoc), 4.30 (t, 1H, *J* 6.9, CH in Fmoc), 4.22–4.05 (m, 3H, C1-H, C2-H), 4.01 (dd, 1H, *J* 3.1, 11.1, C*H*HCl), 3.70 (dd, 1H, *J* 8.4,11.0, CH*H*Cl), 1.58 (s, 9H, Boc-H); Calc. for $C_{40}H_{37}N_2O_5Cl$: C, 72.66; H, 5.64; N, 4.24. Found C, 72.55; H, 5.74; N, 4.20%.

‡ *Selected data* for **9**: δ_H(360 MHz, DMSO-d_6) 10.35 (s, 1H), 10.30 (s, 1H), 10.18 (s, 1H), 9.90 (s, 1H), 9.86 (s, 1H), 9.75 (s, 1H), 9.62 (s,1H), 9.59 (s, 1H), 8.55 (d, 1H, *J* 2.0, C6-H), 7.97 (s, 1H, C4-H), 7.86 (dd, 1H, *J* 2.0, 7.5, C8-H), 7.74 (d, 1H, *J* 7.5, C9-H), 7.64 (s, 1H, Im-H), 7.60 (s, 1H, Im-H), 7.51 (s, 1H, Im-H), 3.31 (d, 1H, *J* 1.5, Py-H), 7.24 (d, 1H, *J* 1.5, Py-H), 7.21 (d, 1H, *J* 1.5, Py-H), 7.16 (d, 1H, *J* 1.5, Py-H), 7.07 (d, 1H, *J* 1.5, Py-H), 6.88 (d, 1H, *J* 1.5, Py-H), 4.7–3.6 (m, 23H, NCH_3, $ClCH_2$, C1-H, C2-H), 2.28 (t, 2H, J 7.3, $COCH_2$), 2.20 (t, 2H, *J* 7.4, $COCH_2$), 1.63–1.53 (m, 4H, $COCH_2CH_2$), 0.91–0.86 (m, 6H, $COCH_2CH_2CH_3$); Calc. for $C_{54}H_{58}N_{17}O_9Cl$: C, 57.15; N, 21.17. Found C, 57.06; N, 20.97%.

1 L. J. Hanka, A. Dietz, S. A. Gerpheide, S. L. Kuentzel and D. G. Martin, *J. Antibiot.*, 1978, **31**, 1211.
2 B. K. Bhuyan, K. A. Newell, S. L. Crampton and D. D. Von Hoff, *Cancer Res.*, 1982, **42**, 3532.
3 H. Iida and J. W. Lown, *Recent Res. Dev. Synth. Org. Chem.*, 1998, **1**, 17 and references cited therein.
4 D. L. Boger and R. S. Coleman, *J. Am. Chem. Soc*, 1988, **110**, 4796; C. H. Lin, D. Sun and L. H. Hurley, *Chem. Res. Toxicol.*, 1991, **4**, 21; M. A. Mitchell, R. C. Kelly, N. A. Wicnienski, N. T. Hatzenbuhler, M. G. Williams, G. L. Petzold, J. L. Slightom and D. R. Siemieniak, *J. Am. Chem. Soc.*, 1991, **113**, 8994; R. C. Kelly, I. Gebhard, N. Wicknienski, P. A. Aristoff, P. D. Johnson and D. G. Martin, *J. Am. Chem. Soc.*, 1987, **109**, 6837; D. L. Boger and D. S. Johnson, *Angew. Chem., Int. Ed. Engl.*, 1996, **35**, 1439.
5 D. L. Boger, T. Ishizaki, R. J. Wysocki, Jr., S. A. Munk, P. A. Kitos and O. Suntornwat, *J. Am. Chem. Soc.*, 1989, **111**, 6461; D. L. Boger and T. Ishizaki, *J. Org. Chem.*, 1990, **55**, 5823; D. L. Boger, W. Yun and B. R. Teegarden, *J. Org. Chem.*, 1992, **57**, 2873; D. L. Boger, P. Mesini and C. M. Tarby, *J. Am. Chem. Soc.*, 1994, **116**, 6461; D. L. Boger and J. A. McKie, *J. Org. Chem.*, 1995, **60**, 1271; P. A. Aristoff and P. D. Johnson, *J. Org. Chem.*, 1992, **57**, 6234; K. J. Drost and M. P. Cava, *J. Org. Chem.*, 1991, **56**, 2240.
6 G. Jia, H. Iida and J. W. Lown, *Heterocycl. Commun.*, 1998, in the press.
7 K. E. Rao and J. W. Lown, *Trends Org. Chem.*, 1992, **3**, 141 and references cited therein.
8 (*a*) V. F. Patel, S. L. Andis, J. K. Enkema, D. A. Johnson, J. H. Kennedy, F. Mohamadi, R. M. Schultz, D. J. Soose and M. M. Spees, *J. Org. Chem.*, 1997, **62**, 8868; (*b*) D. L. Boger, C. W. Boyce, R. M. Garbaccio and M. Searcey, *Tetrahedron Lett.*, 1998, **39**, 2227.
9 D. L. J. Clive, A. G. Angoh and S. M. Bennett, *J. Org. Chem.*, 1987, **52**, 1339.
10 M. Ueki and M. Amemiya, *Tetrahedron Lett.*, 1987, **28**, 6617.
11 (*a*) E. Nishiwaki, S. Tanaka, H. Lee and M. Shibuya, *Heterocycles*, 1988, **27**, 1945; (*b*) L. Huang, J. C. Quada, Jr. and J. W. Lown, *Bioconjugate Chem.*, 1995, **6**, 21; (*c*) R. Zhao, N. H. Al-Said, D. L. Sternbach and J. W. Lown, *J. Med. Chem.*, 1997, **40**, 216.

Communication 8/07884J

Trimethylsilylation of ordered and disordered titanosilicates: improvements in epoxidation with aqueous H_2O_2 from micro- to meso-pores and beyond†

Michael B. D'Amore* and Stephan Schwarz*

DuPont Central Research and Development, Experimental Station, Wilmington, DE 19880-0262, USA. E-mail: michael.b.damore@usa.dupont.com.stephan.schwarz@usa.dupont.com

Received (in Bloomington, IN, USA) 3rd August 1998, Revised manuscript received 19th November 1998, Accepted 20th November 1998

A novel method for trimethylsylilation of micro- and mesoporous titanosilcates using BSTFA [N,O-bis(trimethylsilyl-)trifluoroacetamide] renders Ti-MCM-41 and SiO_2/TiO_2 aerogels active for olefin epoxidation with aqueous H_2O_2, and even improves the activity of TS-1.

The importance of hydrophobicity for titanosilicate catalyzed oxidation reactions with aqueous H_2O_2 has been the subject of much recent research. The hydrophobicity of the interior pores of titanosilicalite (TS-1) and Al-free Ti-beta renders them active for aqueous H_2O_2 oxidation of alkanes and alkenes.[1,2] By comparison, Al containing Ti-beta is less efficient, mainly because of framework Al induced hydrophilicity.[3] Because of their mesoporous nature (25–100 Å pores) Ti-MCM types[4,5] would be useful as oxidation catalysts for larger, higher value molecules. However, Corma and coworkers[5] observed that because of its hydrophilic nature, Ti-MCM-41 was much less effective for oxidation with aqueous H_2O_2 than even Al-Ti-beta. Therefore it is not surprising that efforts to render Ti-MCM's hydrophobic and hence, more active, were undertaken: Tatsumi *et al*.[6] trimethylsilylated Ti-MCM-41 and Ti-MCM-48 using trimethylsilyl chloride and hexamethyldisiloxane and observed increased oxidation activity.[4] Amorphous silica/titanias with even wider pores present opportunity for further increasing the range of oxidation substrates. Recently non-catalytic and hydrophilic amorphous silica/titanias have been made hydrophobic and catalytic by substituting alkoxy groups in the silica precursors with alkyl or phenyl groups during the sol–gel synthesis.[7,8]

Herein we report a simple and effective technique for trimethylsilylation of microporous crystalline TS-1, mesoporous Ti-MCM-41(Ti-MCM), and SiO_2/TiO_2 aerogels (Ti-Agel). The resultant materials are hydrophobic and have enhanced activity for olefin epoxidation with aqueous H_2O_2.

TS-1 was synthesized by the method of Thangaraj and Sivasanker.[9] Corma's method[5] for the preparation of Ti-MCM-41 was modified by using a single precursor for titanium and silicon: Gelest diethoxysiloxane–ethyltitanate copolymer (no. in Gelest catalogue = PSITI-019), $[(EtO)_2SiO][(EtO)_2TiO]$, Si : Ti ≈ 15. The general method for the preparation of aerogel catalysts was that of Dutoit *et al*.,[10] with acetylacetone-modified titanium isopropoxide. The sol–gel was continuously extracted with supercritical CO_2 at 40 °C at 24.2 MPa for 5 h. The resulting fluffy yellow powder was calcined at 400 °C for 1 h in N_2 followed by 600 °C for 5 h in air.

A typical procedure for the trimethylsilylation of catalysts is as follows: a mixture of *N,O*-bis(trimethylsilyl)trifluoroacetamide [$CF_3COSiMe_3)_3$]=$NSiMe_3$ or BSTFA] (1.0 g) and toluene (8 g) was added to the catalyst (0.5 g). The mixture was stirred for 2 h at room temperature, filtered, and the solids washed with toluene and air dried. The dried materials' hydrophobicity was evidenced by their floating on water. In addition, using a TGA method derived from Anderson and Klinowski[17] we obtained the following hydrophobicities (mg water adsorbed silylated/mg water adsorbed non-silylated at 50 °C) for TS-1, Ti-MCM, and TiAgel respectively: 1.04, 0.41, 0.68. As expected, the ratio for trimethylsilylated TS-1 was near unity because trimethylsilylation is not expected to affect the interior pore system. However, for the mesoporous materials the ratio is less than unity consistent with trimethylsilylation of the accessible surface. Other trimethylsilylating agents such as trimethylsilyl chloride and hexamethydisilazane were also used successfully. However, these required more severe conditions and, in the case of the chloride, resulted in loss of Ti from the aerogels. While BSTFA has been used to derivatize organics and end group cap chromatographic columns,[11] there is no reference to using it to modify catalysts. Characterization data for the catalysts are given in Table 1.

BSTFA treatment of TS-1 introduces IR bands consistent with trimethylsilylation. Because of the strong asymmetric stretch of the silicate lattice at *ca*. 1225–1230 cm^{-1}, we are unable to detect the diagnostic symmetric methyl deformation in the 1250–1260 cm^{-1} region.[12] We do see the antisymmetric methyl deformation at *ca*. 1400 cm^{-1}, as well as bands at *ca*. 725 and 700 cm^{-1} that may be assigned to the antisymmetric Si–C and the symmetric Si–C stretching modes, respectively.

Table 1 Characterization data for TS-1, Ti-MCM and Ti-Agel[a]

$$CF_3C(OSiMe_3)=NSiMe_3 + 2\ [O_3Si–OH]_s \rightarrow CF_3CONH_2 + 2\ [O_3Si–O–SiMe_3]_s$$

Sample name	XRD[b]	IR[c]/cm^{-1}	I_{960}/I_{1090}	A_1, A_2 (UV–VIS/nm)	A_1/A_2 (UV–VIS/nm)	Si/Ti ICP	N_2 adsorption SA	PV	APD
TS-1	MFI	962	0.10	215, 258[d]	1.34	26	485	0.11	52
TS-1-syl	MFI	972	0.05	207, 260	1.45	—	453	0.14	74
Ti-MCM	MCM-41	960	0.37	216, 268	0.97	8[e]	810	0.12	27
Ti-MCM-syl	—	950	0.23	214, 269	0.99	—	727	0.14	24
Ti-Agel	Amorphous	959	0.34	214, 255	1.21	12	493	1.50	148
Ti-Agel-syl	—	955	0.32	214, 260	1.15	—	318	1.33	166

[a] Elemental analysis by inductively coupled plasma spectroscopy (ICP): MCM: Ti-MCM-41, Ti-Agel: SiO_2/TiO_2 Aerogel, syl: trimethylsilylated I_{960}: assumed to be ν(Si–O–Ti):[10] I_{1090}: ν(Si–O–Si).[10] A_1: absorbance of band due to isolated Ti. A_2: absorbance of band due to $(Ti–O)_n$ oligomers. SA: BET N_2 surface area/$m^2\ g^{-1}$. PV: BJH N_2 pore volume ml g^{-1}. APD: BJH N_2 av. pore diameter/Å. [b] No TiO_2 phases observed by XRD in any of the samples. [c] Position of 960 band, KBr pellet technique. [d] Si/Ti charged = 15. [e] Shoulder at ≈320 nm indicates anatase.

Bands near 1680 and 1750 cm^{-1} are assigned to the amide group of trifluoroacetamide (the silylation byproduct) and residual BSTFA, respectively. The IR spectrum of Ti-Agel is very similar to that of Ti-MCM, which is to be expected since the latter is composed of amorphous walls. For both Ti-MCM and Ti-Agel, silylation added bands to the IR spectra that can be attributed to $SiMe_3$ groups, especially the very distinctive band at 1250–1260 cm^{-1}, and the CH_3 rocking modes at *ca*. 840 and 755 cm^{-1}.[12]

The IR band at *ca*. 960 cm^{-1} (the 960 band) has been attributed to Si–O–Ti bonds as a fingerprint for tetrahedral Ti substitution in silicate lattices,[10] or to Si–OH groups.[13, 14] We hypothesize that for our TS-1 loss of silanol groups after trimethylsilylation results in a decrease in the 960 band intensity. The intensity of the 960 band of Ti-MCM decreased on silylation, in agreement with Tatsumi *et al*.[6] However, the 960 band of Ti-Agel decreases only slightly upon trimethylsilylation, consistent with a smaller fraction of silanols available to the silylating agent compared to MCM. Based upon the pronounced hydrophobic nature of the silylated material these must be the ones which confer hydrophilicity to the base aerogel.

Analysis of the UV–VIS data[15] for all of the base materials indicates the presence of isolated Ti and oligomeric $(Ti–O)_n$ species; in addition, TS-1 and Ti-MCM are contaminated by anatase. The non-isolated Ti-species may have a detrimental effect on the epoxidation reaction, since they have been reported to decompose H_2O_2 homolytically.[16] Ti-isolation, as measured roughly by the ratio of the absorbance of band due to isolated Ti to the band due to $(Ti–O)_n$ oligomers, (A_1/A_2), is better for Ti-Agel compared with Ti-MCM. This may be ascribed to the acac modification performed on the Ti-precursor for Ti-Agel, which slows down the condensation rate of the hydrolyzed Ti species.[10] The effect of trimethylsilylation on the UV–VIS spectra of the samples is not great, indicating that the silylation procedure probably did not result in reaction with the isolated Ti sites or H_2O_2 destroying sites.

N_2 adsorption measurements on Ti-MCM confirmed that surface area and pore size decrease on trimethylsilylation.[6] Our Ti-MCM contains microporosity, probably related to the titania or silica/titania impurities resulting from the high Ti-concentration in the synthesis gel. For Ti-Agel, trimethylsilylation decreases surface area and mesopore volume as expected. Because of limitations in the N_2 adsorption techniques, the effect of trimethylsilylation on the microporosity of TS-1 could not be determined.

Trimethylsilylation of the available surfaces of TS-1, Ti-MCM, and Ti-Agel increased the efficiency of olefin epoxidation reactions with dilute aqueous hydrogen peroxide (Table 2). Especially striking were the results with Ti-MCM and the aerogels where epoxidation yields were dramatically increased after the treatment. Rendering the catalyst surfaces hydrophobic has either improved access of the olefin to the active sites or has diminished the inhibitory effect of water.[1] Either scenario should result in increased catalytic activity.

In the case of the TS-1 the improved activity after trimethylsilylation may be attributed to better wetting of the microcrystallite surface with the olefin. While it is possible that the increase in activity is related to loss of oligomeric $(Ti-O)_n$ H_2O_2 decomposition sites after trimethylsilylation, lack of changes in the UV–VIS and the probably very low concentration of reaction sites for silylation argue against this.

It is important to note that the trimethylsilylation technique described in this communication results in nearly equivalent epoxidation activity for any of the titanosilicates studied, the only requirement being the presence of isolated, tetrahedral Ti sites. Especially striking is the treatment of normally inert aerogel; we believe this to be the first report of *post synthesis* activation of this material. In addition the expectation of epoxidizing molecules too large to fit in the pores of TS-1 has been realized for the Ti-aerogel after the silylation treatment. *cis*-Cyclooctene is epoxidized readily by Ti-Agel-syl compared to almost no reaction with either TS-1 or TS-1-syl.

In summary we have demonstrated a general method for significantly increasing the activity of titanosilicate oxidation catalysts using aqueous hydrogen peroxide by rendering their surfaces hydrophobic by treatment with the trimethylsilylating agent BSTFA.

Table 2 Effect of trimethylsilylation on the epoxidation activity of Ti-Agel, Ti-MCM, and TS-1 titanosilicates[a]

Catalyst	$\%H_2O_2$	Olefin[b]	Epoxide yield[c]
Ti-Agel	10	1-Oct	0.2
Ti-Agel	10	COT	0.5
Ti-Agel-syl	10	1-Oct	6
Ti-Agel-syl	10	COT	32
Ti-MCM	3	1-Oct	0.5
Ti-MCM-syl	3	1-Oct	23.6
TS-1	10	1-Oct	2.4
TS-1	10	COT	0
TS-1-syl	10	1-Oct	12.9
TS-1-syl	10	COT	0.5

[a] *Reaction conditions*: olefin (3 ml), aq. H_2O_2 (1 ml), catalyst (50–100 mg)[d] stirred at room temperature for 24 h. [b] 1-Oct: oct-1-ene, COT: *cis*-cyclooctene. [c] Yield of the corresponding epoxide was based on initial H_2O_2 concentration. The only significant byproduct with oct-1-ene was octan-1-al (5–10%); with cyclooctene no byproducts were observed. [d] 100 mg with Ti-Agel and TS-1, 50 mg with Ti-MCM.

Notes and references

† Contribution number 7801.

1 C. B. Khouw, C. B. Dartt, J. A. Labinger and M. E. Davis, *J. Catal*., 1994, **149**, 195.
2 T. Blasco, M. A. Camblor, A. Corma, P. Esteve, J. M. Guil, A. Martinez, J. A. Perdigon-Melon and S. Valencia, *J. Phys. Chem. B*, 1998, **102**, 75.
3 A. Corma, P. Esteve and A. Martinez, *J. Catal*., 1996, **161**, 11.
4 J. S. Beck, J. C. Vartuli, W. J. Roth, M. E. Leonowicz, C. T. Kresge, K. D. Schmitt, C. T.-W. Chu, D. H. Olson, E. W. Sheppard, S. B. McCullen, J. B. Higgins and J. L. Schlenker, *J. Am. Chem. Soc*., 1992, **114**, 10 834.
5 T. Blasco, A. Corma, M. T. Navarro and J. Perez Pariente, *J. Catal*., 1995, **156,** 65.
6 T. Tatsumi, K. A. Koyano and N. Igarashi, *Chem. Commun*., 1998, 325.
7 H. Kochkar and F. Figueras, *J. Catal*., 1997, **171**, 420.
8 S. Klein and W. F. Maier, *Angew. Chem., Int. Ed. Engl*., 1996, **35,** 2230.
9 A. Thangaraj and S. Sivasanker, *J. Chem. Soc., Chem. Commun*.,1992, 123.
10 D. C. M. Dutoit, M. Schneider and A. Baiker, *J. Catal*., 1995, **153**, 165.
11 K. D. McMurtrey, *J. Liq. Chromatogr*., 1988, **11**, 3375; M. G. Horning, E. A. Boucher, and A. M. Moss, *J. Gas Chromatogr*., 1967, **5**, 297.
12 L. J. Bellamy, *The infrared spectra of complex molecules vol. 2: Advances in infrared group frequencies*, Chapman and Hall, New York, 2nd edn., 1980.
13 F. Boccuzzi, S. Coluccia, G. Ghiotti, C. Morterra and A. Zecchina, *J. Phys. Chem*., 1978, **82**, 1298.
14 M. Decottignies, J. Phalippou and J. Zarzycki, *J. Mater. Sci*., 1978, **13**, 2605.
15 T. Blasco, M. A. Camblor, A. Corma and J. Perez-Pariente, *J. Am. Chem. Soc*., 1993, **115,** 11 806.
16 M. G. Clerici and P. Ingallina, *J. Catal*., 1993, **140**, 71.
17 M. W. Anderson and J. J. Klinowski, *J. Chem. Soc., Faraday Trans. 1*, 1986, **82**, 1449.

Communication 8/09396B

ChemComm

Syntheses and structures of quinuclidine-stabilized four- and five-coordinate mono- and di-chlorogallane

Bing Luo, Victor G. Young, Jr. and Wayne L. Gladfelter*

Department of Chemistry, University of Minnesota, Minneapolis MN 55455, USA. E-mail: gladfelt@chem.umn.edu

Received (in Columbia, MO, USA) 10th September 1998, Accepted 18th November 1998

Hydride/chloride redistribution reactions provided high yields of $GaCl_2H$(quin) I, $GaCl_2H(quin)_2$ II, $GaClH_2$(quin) III and $GaClH_2(quin)_2$ IV(quin = quinuclidine) and structural characterization of compounds II and IV authenticate the unusual five-coordinate geometry for gallium hydride complexes.

Organogallium compounds are used extensively to prepare solid state materials such as GaN.[1] In metal organic chemical vapor deposition (MOCVD) processes, for instance, the high volatility, long shelf-life and chemical reactivity of compounds such as $GaMe_3$ have made them especially attractive molecular precursors. One of the drawbacks of organogallium compounds is the presence of direct Ga–C bonds that can lead to unwanted incorporation of carbon into the solid state product. In sensitive opto-electronic devices such as lasers, even trace quantities of carbon can seriously degrade performance.[2] Replacement of the carbon-based ligands with hydrides appears as an attractive alternative but suffers from the lower stability and more difficult syntheses of the compounds. We report in this paper the preparation and structure of mono- and di-chlorogallanes stabilized by quinuclidine. Strong donors, including trimethylamine,[3,4] quinuclidine[5] and tricyclohexylphosphine,[6] stabilize GaH_3, which in the absence of the donor exists as Ga_2H_6 and decomposes above −30 °C.[7] The presence of chloro ligands offers attractive synthetic routes to molecules that can be used as single source precursors in CVD processes.

Unstabilized mono- and di-chlorogallane have been synthesized by the reaction of $GaCl_3$ with trimethylsilane[8,9] and have been stabilized by direct reaction with donors. Chloride/hydride exchange has proven to be successful for the syntheses of other substituted gallanes,[10,11] and the following alternative routes bypass the need to prepare and purify $[GaClH_2]_2$ and $[GaCl_2H]_2$. All reactions were conducted under an atmosphere of prepurified nitrogen. A diethyl ether (20 mL) solution of $GaCl_3$ (0.957 g, 5.44 mmol) was added to a stirred, 30 mL ether solution of GaH_3(quin) (quin = quinuclidine) (0.500 g, 2.72 mmol) at room temperature over a period of 1 h. The resulting mixture was stirred at room temperature for an additional 6 h, at which point an additional equivalent of quinuclidine (5.44 mmol) dissolved in ether was added. This delayed addition of quinuclidine facilitated the ligand redistribution reaction [eqn. (1)], which presumably required an available coordination site

$$2\ GaCl_3 + GaH_3(quin) + 2\ quin \rightarrow 3\ GaCl_2H(quin) \quad (1)$$

on the gallium. The reaction mixture was stirred for another 14 h, then filtered. Upon concentration and storage at −15 °C, the colorless filtrate yielded 1.65 g (80% yield) of crystalline $GaCl_2H$(quin) **I**.[12] Compound **I** decomposed without melting at 92 °C. Chemical ionization mass spectrometry revealed the presence of an intense parent ion (plus one) at *m/z* 252. A strong ν_{GaH} (KBr pellet) was observed in **I** at 1946 cm^{-1}; however, no hydride resonance was observed in ^1H NMR spectrum. Compound **I** was also prepared in 25% yield by addition of quinuclidine to an ether suspension comprised of 4 equiv. of LiH and 1 equiv. of $[NH_4][GaCl_4]$.

Reaction of **I** with one equivalent of quinuclidine at room temperature in ether produced the bis(quinuclidine) adduct in high yield. Needle-like crystals of $GaCl_2H(quin)_2$ **II**,[13] were stable up to 174 °C and appeared to decompose gradually above this temperature. Coordination of the second ligand shifted the ν_{GaH} to 1882 cm^{-1}. While AlH_3 and related aluminium hydrides form many five-coordinate structures, this is uncommon in gallium hydride chemistry where the only reported examples of five-coordinate hydrido complexes of gallium contain chelating ligands.[14–17]

Crystalline monochlorogallane derivative, $GaClH_2$(quin) **III**, was synthesized in 81% yield by the related ligand redistribution reaction shown in eqn. (2).

$$GaCl_2H(quin) + GaH_3(quin) \rightarrow 2\ GaClH_2(quin) \quad (2)$$

Following addition of an ether solution of GaH_3(quin) to an ether solution of **I**, the reaction mixture was refluxed for 40 h. After filtration and concentration, crystals of **III**[18] were isolated upon cooling the solution to −15 °C. The ν_{GaH} (KBr) was lowered to 1892 cm^{-1}, characteristic of replacing one of the electronegative chloro ligands in **I** with a hydride. In addition to resonances from the quinuclidine ligand, the ^1H NMR spectrum (in C_6D_6) displayed a broad resonance at δ 5.14 assignable to the GaH_2 unit.

Reaction of **III** with excess quinuclidine in refluxing ether followed by crystallization at −15 °C formed the five-coordinate complex, $GaH_2Cl(quin)_2$ **IV**.[19] Batches of crystalline **IV** typically exhibited three absorptions (1891s, 1852m and 1817w cm^{-1}) in the Ga–H stretching region of the IR spectrum (KBr). Given the symmetry of the compound (*vide infra*), we expect only two absorptions and suggest that the crystals were mixtures of **III** and **IV**. Thus, only the peaks at 1852 and 1817 cm^{-1} are assigned to **IV**. These are similar to the values of 1854 and 1837 cm^{-1} reported for $GaH_2[2,6\text{-}(Me_2NCH_2)_2C_6H_3]$.[16] This interpretation was consistent with the elemental analytical data that were always closer to the values calculated for **III**.

Compounds **I**, **II** and **IV** were characterized using single crystal X-ray crystallography. Each molecule of **I** sits on a crystallographic mirror plane that passes through Ga(1), N(1) and H(1) in addition to three of the quinuclidine carbons (Fig. 1).[20] The hydride ligand was located, and its position and isotropic thermal parameters were refined. The basic arrangement of the four ligands is that of a slightly distorted tetrahedron where the angles listed in the figure caption show that the larger, heavy atom ligands are splayed back away from the hydride.

Despite the observation that bulk samples of **IV** were contaminated with **III**, a suitable single crystal was selected for study. The five-coordinate complex **IV**, sits on a crystallographic twofold axis collinear with the Ga(1)–Cl(1) bond (Fig. 2).[20] The structure is close to a perfect trigonal bipyramid bearing the quinuclidine ligands in the axial positions. The only significant deviation is an enlarged H(1)–Ga(1)–H(1C) angle of 127(2)°. The corresponding Cl(1) Ga(1)–H(1) angles are diminished to 116.9(9)°; a pattern consistent with Bent's rule.[21] Comparing the bond distances of **I** and **IV**, we find an increase for all of the heavy atoms for **IV** appropriate for the increase in coordination number. The Ga–H distances, however, decrease from 1.66(5) Å in **I** to 1.51(2) Å in **IV**.

The structure of the five-coordinate dichlorogallane **II**, was also trigonal bipyramidal; however, the hydride was not located (Fig. 3).[20] As in the structure of **IV**, small angular deviations from the ideal geometry were observed and were consistent

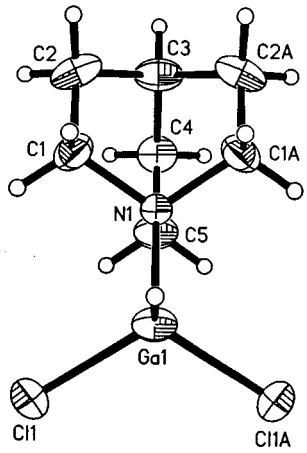

Fig. 1 Structure of **I** showing 50% thermal ellipsoids. Selected bond distances (Å) and angles (°): Ga(1)–N(1) 2.017(3), Ga(1)–H(1) 1.66(5), Ga(1)–Cl(1) 2.185(1); N(1)–Ga(1)–Cl(1) 103.40(6), Cl(1)–Ca(1)–Cl(1A) 108.24(6), N(1)–Ga(1)–H(1) 110(2), Cl(1)–Ga(1)–H(1), 115.2(8).

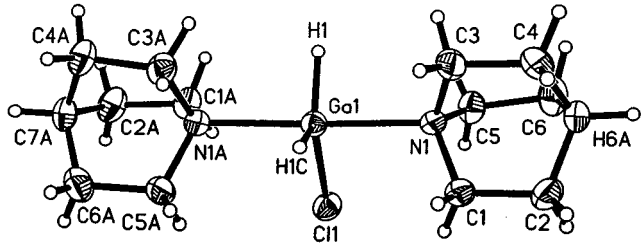

Fig. 2 Structure of **IV** showing 50% thermal ellipsoids. Selected bond distances (Å) and angles (°): Ga(1)–N(1) 2.259(2), Ga(1)–H(1) 1.51(2), Ga(1)–Cl(1) 2.2653(8); N(1)–Ga(1)–N(1A) 178.25(9), N(1)–Ga(1)–Cl(1) 90.88(4), N(1A)–Ga(1)–H(1), 89.1(9), N(1)–Ga(1)–H(1) 90.1(9), Cl(1)–Ga(1)–H(1) 116.6(9), H(1)–Ga(1)–H(1C) 127(2).

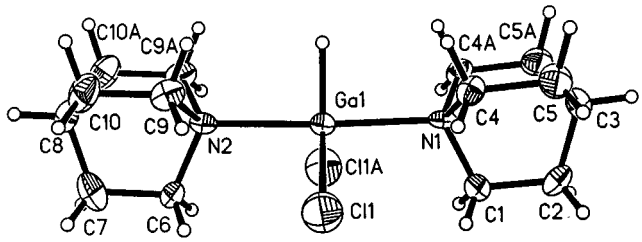

Fig. 3 Structure of **II** showing 50% thermal ellipsoids and the idealized position of the hydride ligand. Selected bond distances (Å) and angles (°): Ga(1)–N(1) 2.254(8), Ga(1)–N(2) 2.232(8), Ga(1)–Cl(1) 2.246(2); N(1)–Ga(1)–N(2) 177.2(3), Cl(1)–Ga(1)–Cl(1A) 113.0(2), Cl(1)–Ga(1)–N(1) 91.0(1), Cl(1)–Ga(1)–N(2) 90.5(1).

with Bent's rule. The crystallographically independent Ga–N distances [2.254(8) and 2.232(8) Å] were similar the value found in **IV** [2.259(2) Å].

All attempts to prepare the five-coordinate trichlorogallium complex, $GaCl_3(quin)_2$, were unsuccessful and always resulted in nearly quantitative isolation of $GaCl_3(quin)$ **V**.[22] It is intriguing that the five-coordinate geometry is only stable enough relative to the four-coordinate structure to allow isolation with the mixed H/Cl ligand complexes. While replacing hydrides with chlorides will increase the Lewis acidity, it will also increase the steric repulsion. Our results suggest that the maximum stability is achieved in **IV** where two chlorides and one hydride are present. Quinuclidine does not differ qualitatively from other donors, rather the combination of improved donor strength and smaller cone angle causes a quantitative shift in the appropriate equilibria that stabilize the five-coordinate products.

This research was supported by a grant from the National Science Foundation (CHE-9616501).

Notes and references

1 D. A. Neumayer and J. G. Ekerdt, *Chem. Mater.*, 1996, **8**, 9.
2 R. L. Moon and Y.-M. Houng, in *Organometallic Vapor Phase Epitaxy of III–V Materials*, ed. M. L. Hitchman and K. F. Jensen, London, 1993.
3 D. F. Shriver and R. W. Parry, *Inorg. Chem.*, 1963, **2**, 1039.
4 D. F. Shriver and C. E. Nordman, *Inorg. Chem.*, 1963, **2**, 1298.
5 J. L. Atwood, S. G. Bott, F. M. Elms, C. Jones and C. L. Raston, *Inorg. Chem.*, 1991, **30**, 3792.
6 J. L. Atwood, K. D. Robinson, F. R. Bennett, F. M. Elms, G. A. Koutsantonis, C. L. Raston and D. J. Young, *Inorg. Chem.*, 1992, **31**, 2674.
7 C. R. Pulham, A. J. Downs, M. J. Goode, D. W. H. Rankin and H. E. Robertson, *J. Am. Chem. Soc.*, 1991, **113**, 5149.
8 H. Schmidbaur, W. Findeiss and E. Gast, *Angew. Chem.*, 1965, **77**, 170.
9 M. J. Goode, A. J. Downs, C. R. Pulham, D. W. H. Rankin and H. E. Robertson, *J. Chem. Soc., Chem. Commun.*, 1988, 768.
10 N. N. Greenwood and A. Storr, *J. Chem. Soc.*, 1965, 3426.
11 F. M. Elms, G. A. Koutsantonis and C. L. Raston, *J. Chem. Soc., Chem. Commun.*, 1995, 1669.
12 Compound **I**: ^{1}H NMR (300 MHz, C_6D_6, 25 °C); δ 0.76 (6H, m, CH_2), 0.95 (1H, m, CH), 2.53 (6H, t, NCH_2). Anal. Calc. for $C_7H_{14}Cl_2GaN$: C, 33.26; H, 5.58; N, 5.54. Found: C, 32.28; H, 5.98; N, 5.45%.
13 Compound **II**: ^{1}H NMR (300 MHz, C_6D_6, 25 °C): δ 0.99 (6H, m, CH_2), 1.22 (1H, m, CH), 2.64 (6H, t, NCH_2). Anal. Calc. for $C_{14}H_{27}Cl_2GaN_2$: C, 46.19; H, 7.48; N, 7.70. Found: C, 45.80; H, 7.72; N, 7.62%.
14 S. J. Rettig, A. Storr and J. Trotter, *Can. J. Chem.*, 1974, **52**, 2206.
15 S. J. Rettig, A. Storr and J. Trotter, *Can. J. Chem.*, 1975, **53**, 58.
16 A. H. Cowley, F. P. Gabbaï, D. A. Atwood, C. J. Carrano, L. M. Mokry and M. R. Bond, *J. Am. Chem. Soc.*, 1994, **116**, 1559.
17 J. L. Atwood, S. G. Bott, C. Jones and C. L. Raston, *Inorg. Chem.*, 1991, **30**, 4868.
18 Compound **III**: mp: 89 °C, (decomp.). ^{1}H NMR (300 MHz, C_6D_6, 25 °C): δ 0.82 (6H, m, CH_2), 1.04 (1H, m, CH), 2.49 (6H, t, NCH_2), 5.14 (2H, br s, GaH_2). Anal. Calc. for $C_7H_{15}ClGaN$: C, 38.50; H, 6.92; N, 6.41. Found: C, 38.27; H, 7.11; N, 6.30%.
19 Compound **IV**: MS (CI): 329.1 (11.8%, $[(C_7H_{13}N)_2GaClH_3]^+$), 293.2 (15.7%, $[(C_7H_{13}N)_2GaH_2]^+$), 216.0 (16.0%, $[C_7H_{13}NGaClH_2]^+$), 182.0 (19.9%, $C_7H_{13}NGaH_2]^+$), 112.1 (100%, $[C_7H_{13}NH]^+$).
20 *Crystal data*: **I**: $C_7H_{14}Cl_2GaN$, M = 252.81, orthorhombic, space group *Pbcm*, a = 6.0102(2), b = 15.8808(3), c = 10.7925 (3) Å, V = 1030.11(5) Å^3, T = 173(2) K, Z = 4, μ = 3.132 mm^{-1}, 6030 reflections collected, 962 independent reflections, 853 with $I > 2\sigma(I)$, R_1 = 0.0338, wR_2 = 0.0802.
IV: $C_{14}H_{28}ClGaN_2$, M = 329.56, orthorhombic, space group *Pbcn*, a = 10.9098(2), b = 12.0848(2), c = 12.3099(3) Å, V = 1622.97(6) Å^3, T = 173(2) K, Z = 4, μ = 1.847 mm^{-1}, 8527 reflections collected, 1433 independent reflections, 1202 with $I > 2\sigma(I)$, R_1 = 0.0296, wR_2 = 0.0606.
II: $C_{14}H_{23}Cl_2GaN_2$, M = 359.96, orthorhombic, space group *Pmn2*$_1$, a = 10.2217(6), b = 12.2916(7), c = 6.4620(4) Å, V = 811.89(8) Å^3, T = 173(2) K, Z = 2, μ = 2.013 mm^{-1}, 4661 reflections collected, 1458 independent reflections, 1321 with $I > 2\sigma(I)$, R_1 = 0.0529, wR_2 = 0.1365. CCDC 182/1093. See http://www.rsc.org/suppdata/cc/1999/123/ for crystallographic files in .cif format.
21 H. A. Bent, *Chem. Rev.*, 1961, **61**, 275.
22 Compound **V**: mp 239–245 °C. ^{1}H NMR (300 MHz, C_6D_6, 25 °C): δ 0.66 (m, 6H, CH_2), 0.89 (m, 1H, CH), 2.62 (t, 6H, NCH_2). Anal. Calc. for $C_7H_{13}NGaCl_3$: C, 29.27; H, 4.56; N, 4.88. Found: C, 29.48; H, 4.98; N, 4.81%.

Communication 8/07169A

The template synthesis and X-ray crystal structure of the first dinuclear lanthanide(III) iminophenolate cryptate

Fernando Avecilla,[a] Andrés de Blas,*[a] Rufina Bastida,[b] David E. Fenton,[c] José Mahía,[d] Alejandro Macías,[b] Carlos Platas,[a] Adolfo Rodríguez[b] and Teresa Rodríguez-Blas*[a]

[a] *Dpto. Q. Fundamental e Industrial, Universidade da Coruña, Campus da Zapateira s/n 15071 La Coruña, Spain. E-mail: mayter@udc.es*
[b] *Dpto. Q. Inorgánica, Universidad de Santiago, Avda. de las Ciencias s/n 15706, Santiago de Compostela, Spain*
[c] *Chemistry Department, The University, Sheffield, UK S3 7HF*
[d] *Servicios Xerais de Apoio á Investigación, Universidade da Coruña, Spain*

Received (in Basel, Switzerland) 23rd September 1998, Accepted 18th November 1998

Lanthanide ions act as templates in the formation of dinuclear Ln(III) complexes with a cryptand ligand bearing three phenolate groups; the presence of both lanthanide ions into the cavity of the cryptand was confirmed by X-ray structure analysis and spectroscopic data.

Encapsulating ligands can enhance some interesting properties that make complexes of the lanthanide(III) ions valuable for the development of different technological applications such as the selective extraction of metals, NMR shift and relaxation reagents, contrast-enhancing agents in magnetic resonance imaging and fluoroimmunoassay agents.[1] In particular, current interest in binuclear lanthanide complexes arises from their potential value in studying the nature and application of lanthanide metal–metal compounds in lasers[2] and phosphors,[3] the molecular recognition processes which govern lanthanide(III) cation pairing events[4] and their application in novel tunable photonic devices.[5]

Although a dinuclear europium(III) cryptate, synthesised by reaction of a europium salt with a preformed macrotricyclic tetralactam containing 1,10-phenanthroline units, has been reported without structural details[6] no examples, to date, of dinuclear lanthanide cryptates derived from iminophenolato-cryptands have appeared. This is surprising as several examples of homo- and hetero-polynuclear complexes of lanthanides with macrocycles have been described in the literature.[7–9] Here we report the first examples of dinuclear lanthanide complexes of an iminophenolate cryptand together with the crystal structure of a dilutetium(III) complex.

Metal-templated reactions between triethylammonium 2,6-diformyl-4-methylphenolate and tris(2-aminoethyl)amine in the presence of hydrated lanthanide nitrates (Ln = Gd–Lu) in a 3:2:2 mole ratio in absolute ethanol for *ca.* 12 h yield orange solids of formula $[Ln_2L(NO_3)_2][NO_3]\cdot xH_2O\cdot y$EtOH† where L is the anionic cyptand shown in Scheme 1. Their FAB mass spectra display intense peaks corresponding to fragments $[Ln_2L(NO_3)_2]^+$ and $[Ln(L+H)]^+$, confirming the presence of the macrobicycle in the complex. It is found that in all cases the former peak is clearly more intense than the latter, particularly in case of Tb, Ho, Tm and Lu for which the peak due to $[Ln_2L(NO_3)_2]^+$ appears with 100% base peak intensity.

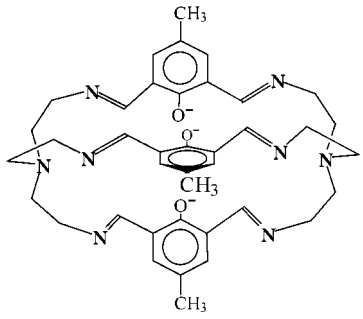

Scheme 1 Anionic cryptand L.

Slow evaporation of ethanolic solutions of the lutetium cryptate gave orange crystals of X-ray quality. The structural analysis of this complex‡ confirmed the presence of two metal ions in the cavity of the anionic Schiff-base macrobicycle receptor. The crystals contain the cation $[Lu_2L(NO_3)_2]^+$, an independent nitrate anion and highly disordered molecules of ethanol and water. Fig. 1 illustrates the structure of the cation. Both lutetium(III) ions have crystallographically identical coordination environments; each is bound to one bridgehead nitrogen atom, three imino-nitrogen atoms, and to the three μ-phenolate oxygen atoms. Eight coordination is completed by one oxygen of a monodentate nitrate ion and the coordination polyhedron can be best described as distorted dodecahedron. The Lu–azomethine nitrogen distances are in the range 2.359–2.445 Å, similar and even shorter than those found in literature.[11] A strong interaction between Lu and the phenolate oxygens is shown by the short distance between them that falls in the range 2.286–2.363 Å. Only two X-ray crystal structures

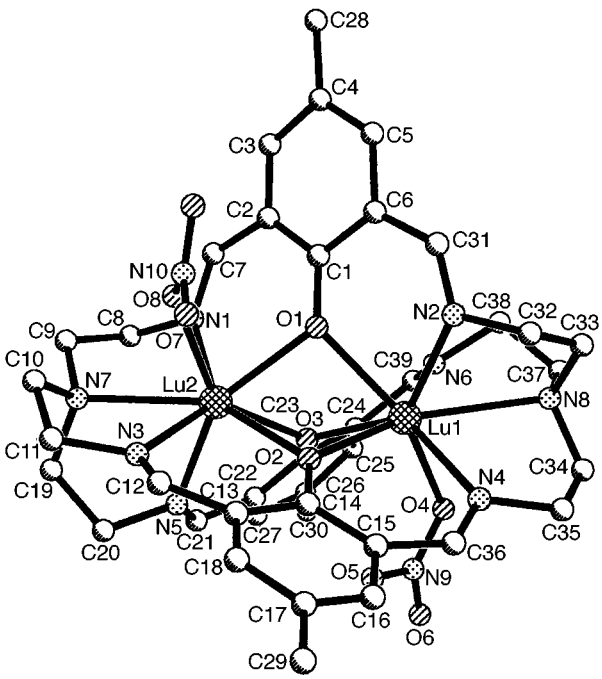

Fig. 1 Crystal structure of $[Lu_2L(NO_3)_2]^+$; hydrogen atoms are omitted for simplicity. Selected bond lengths (Å): Lu(1)–O(3) 2.288(8), Lu(1)–O(2) 2.347(8), Lu(1)–O(1) 2.316(9), Lu(1)–N(6) 2.359(11), Lu(1)–O(4) 2.372(9), Lu(1)–N(4) 2.421(12), Lu(1)–N(2) 2.445(10), Lu(1)–N(8) 2.675(9), Lu(2)–O(1) 2.286(8), Lu(2)–O(7) 2.329(10), Lu(2)–O(3) 2.329(8), Lu(2)–O(2) 2.363(8), Lu(2)–N(1) 2.363(11), Lu(2)–N(5) 2.420(12), Lu(2)–N(3) 2.414(13), Lu(2)–N(7) 2.609(10).

of binuclear lutetium complexes with macrocycles have been reported.[9] In both cases the macrocycle receptors are calixarenes. The distance between the lutetium ions encapsulated into the cryptate we present here is 3.447(1) Å. This is considerably shorter than those reported in the literature (3.56 and 3.68 Å).[9]

The cryptand adopts a conformation resembling a triple helix twisting around a pseudo C_3-axis which runs through the two bridgehead nitrogen atoms. Both metal ions are deviated from this axis; nevertheless, the deviation is so slight that the symmetry of the cryptate can also be described as threefold. The angles between the phenolate ring planes are 69.9, 76.2 and 79.9°, while the distances between each two phenolate oxygens are O(1)···O(2) 2.73 Å, O(1)···O(3) 2.53 Å and O(2)···O(3) 2.80 Å. The distance between the bridgehead nitrogens is 8.65 Å, longer than that found for mononuclear lanthanide cryptates (8.36 Å)[12] with the protonated macrobicycle L, but shorter than that of $[Cd_2L]^{3+}$ (9.01 Å).[13] This shows that the cryptand can expand or contract to fit the metal size or to accommodate two metal ions inside the cavity.

That the dinuclear structure is retained in solution is evidenced by the proton NMR spectrum run in $(CD_3)_2SO$. The spectrum of the related mononuclear lutetium complex[12] shows two signals for the azomethine hydrogens [δ 8.87 (d), 8.43 (s)], the latter is ascribed to the coordinated azomethines and the former arises as a consequence of proton transfer from the phenolic groups to the non-coordinated azomethines.[12,14–16] There is also a very broad signal centered on δ 12.50 which may be assigned to the O···HN$^+$ protons and signals due to the aromatic hydrogens [δ 7.73 (d, J = 1), 7.59 (d, J = 1 Hz)], ethylene bridges [δ 3.82 (3H), 3.68 (3H), 3.59 (3H), 3.27 (3H), 3.08 (3H), 2.94 (3H), 2.81 (6H)] and the methyl groups [δ 2.27 (s)]. The proton NMR spectrum of the dilutetium cryptate is simpler in the low field region and agrees with an effective C_3 symmetry in solution. As expected, the very broad signal due to the phenolic protons presented in the mononuclear complex spectrum does not appear in that of the binuclear complex. Likewise, the two signals due to the azomethine hydrogens and the signals due to the aromatic protons became now in one signal for each type [δ 8.45 (s), 7.57 (s), respectively]. A complicated group of very broad signals [δ 2–4 (m)] due to the ethylene bridges are present indicating that the protons bonded to the same carbon atom are non-equivalent. The signal of the methyl groups [δ 2.29 (s)] is also observed.

Mononuclear lanthanide(III) cryptates derived from ligands closely related to L (the *para*-substituent on the phenol being *t*-Bu, CH_3O or Cl) have been prepared by transmetallation of the appropriate sodium cryptates.[14–17] Attempts to introduce a second lanthanide ion cation have been unsuccessful, and it has been stated that this is probably due to the high coordination numbers and large radii of the lanthanides.[15]

In order to design cryptand receptors for more than one lanthanide(III) ion certain key features must be kept in mind: the high coordination numbers preferred by these cations, their large ionic radii and their high charge. In this respect the influence of the lanthanide contraction would suggest that accommodation of two cations from the second half of the series would be preferred. To be useful for dinuclear reception the ligands must have a large receptor cavity comprised of an adequate number of suitably disposed donor atoms. The anionic cryptand L possesses these features together with three phenolic groups which can serve as endogenous anionic groups capable of providing bridges between the lanthanide(III) ions so helping to overcome the electrical repulsions that would otherwise occur between two tripositive ions placed in close proximity. Previously we have described the lanthanide-assisted synthesis of Schiff-base macrobicycles as mononuclear lanthanide cryptates.[12] In the present work we have extended the application of this metal template method to assemble homodinuclear lanthanide(III) cryptates so providing the first opportunity to study the properties of two lanthanide ions held in close proximity and isolated from interaction with the solvent.

We thank the Xunta de Galicia (XUGA20903B96) for financial support and Dr Miguel Maestro for his help in X-ray crystal structure details. C. P. also acknowledges Xunta de Galicia for a postgraduate fellowship.

Notes and references

† $[Gd_2L][NO_3]_3{\cdot}H_2O{\cdot}EtOH$: yield: 30%. Found: C, 39.8; H, 4.3; N, 12.4. $C_{41}H_{53}N_{11}O_{14}Gd_2$ requires C, 39.6; H, 4.1; 12.8%. $[Tb_2L][NO_3]_3{\cdot}H_2O{\cdot}EtOH$: yield: 35%. Found: C, 39.7; H, 4.3; N, 12.4. $C_{41}H_{53}N_{11}O_{14}Tb_2$ requires C, 39.7; H, 4.3; N, 12.5%. $[Dy_2L][NO_3]_3{\cdot}H_2O{\cdot}EtOH$: yield: 15%. Found: C, 39.9; H, 4.3; N, 12.3. $C_{41}H_{53}N_{11}O_{14}Dy_2$ requires C, 39.6; H, 4.4; N, 12.4%. $[Ho_2L][NO_3]_3{\cdot}H_2O{\cdot}EtOH$: yield: 20%. Found: C, 39.3; H, 4.3; N, 12.3. $C_{41}H_{53}N_{11}O_{14}Ho_2$ requires C, 39.8; H, 4.4; N, 12.8%. $[Tm_2L][NO_3]_3{\cdot}4H_2O$: yield: 30 %. Found: C, 36.9; H, 4.2; N, 12.1. $C_{39}H_{53}N_{11}O_{16}Tm_2$ requires C, 36.3; H, 4.0; N, 12.3%. $[Yb_2L][NO_3]_3{\cdot}2H_2O{\cdot}EtOH$: yield: 15%. Found: C, 38.2; H, 4.3; N, 12.0. $C_{41}H_{55}N_{11}O_{15}Yb_2$ requires C, 38.3; H, 4.3; N, 12.0%. $[Lu_2L][NO_3]_3{\cdot}2H_2O{\cdot}EtOH$: yield: 15%. Found: C, 38.1; H, 4.3; N, 11.9. $C_{41}H_{55}N_{11}O_{15}Lu_2$ requires C, 38.5; H, 4.3; N, 12.1%.

‡ *Crystal data*: $[Lu_2C_{39}H_{45}N_8O_3(NO_3)_3]{\cdot}CH_3CH_2OH{\cdot}2.5H_2O$, $Lu_2C_{41}H_{56}N_{11}O_{15.5}$, M = 1300.92; orange block, 0.35 × 0.20 × 0.10 mm, tetragonal, space group $P4_12_12$, a = 17.7057 (2), b = 17.7057 (2), c = 29.0649 (5) Å, V = 9111.6 (2) Å^3, Z = 8; D_c = 1.881 Mg m^{-3}, μ = 4.392 mm^{-1}. Using Mo-Kα radiation (λ = 0.71073 Å) at 173 K, a total of 42911 reflections was collected, of which 5957 were independent. Owing to crystal nature and diffraction capabilities, only data to 2θ = 45° were used for crystal refinement. Refinement converged with R_1 = 0.0429, wR_2 = 0.0974 for $I > 2\sigma(I)$ and R_1 = 0.0595, wR_2 = 0.1090 for all data. CCDC 182/1101.

1 N. Sabbatini, M. Guardigli and J.-M. Lehn, *Coord. Chem. Rev.*, 1993, **123**, 201; V. Alexander, *Chem. Rev.*, 1995, **95**, 273.
2 L. F. Johnson and H. J. Guggeinheim, *Appl. Phys. Lett.*, 1971**,** **19**, 44; S. A. Pollack and D. B. Chang, *J. Appl. Phys.*, 1988, **64**, 2885.
3 G. Blasse and G. Bril, *Philips Tech. Rev.*, 1970, **31**, 303; H. S. Killian, F. P. Van Herwijnen and G. Blasse, *J. Solid State Chem.*, 1988, **74**, 39.
4 K. D. Matthews, R. A. Fairman, A. Johnson, K. V. N. Spence, I. A. Kahwa, G. L. McPherson and H. Robotham, *J. Chem. Soc., Dalton Trans.*, 1993, 1719.
5 J. P. Desvergne, F. Fages, H. Bouas-Laurent and P. Marsau, *Pure Appl. Chem.*, 1992, **64**, 1231.
6 B. Cathala, L. Cazaux, C. Picard and P. Tisnés, *Tetrahedron Lett.*, 1994, **35**, 1863.
7 I. A. Kahwa, J. Selbin, T. C. Y. Hsieh and R. A. Lane, *Inorg. Chim. Acta*, 1986, **118**, 179; I. A. Kahwa, S. Folkes, D. J. Williams, S. V. Ley, C. A. O'Mahoney and G. L. McPherson, *J. Chem. Soc., Chem. Commun.*, 1989, 1531; P. Guerriero, P. A. Vigato, J.-C. G. Bunzli and E. Moret, *J. Chem. Soc., Dalton Trans.*, 1990, 647; K. D. Matthews, I. A. Kahwa and D. J. Williams, *Inorg. Chem.*, 1994, **33**, 1382.
8 R. Ziessel, M. Maestri, L. Prodi, V. Balzani and A. V. Dorsselaer, *Inorg. Chem.*, 1993, **32**, 1237; C. H. Aspinall, J. Black, I. Dodd, M. M. Harding and S. J. Winkley, *J. Chem. Soc., Dalton Trans.*, 1993, 709.
9 J. M. Harrowfield, M. I. Odgen and A. H. White, *Aust. J. Chem.*, 1991, **44**, 1249, 1237.
10 B. M. Furphy, J. M. Harrowfield, D. L. Kepert, B. W. Skelton, A. H. White and F. R. Wilner, *Inorg. Chem.*, 1987**,** **26**, 4231; J. H. Harrowfield, M. Y. Odgen, A. H. White and F. R. Wilner, *Aust. J. Chem.*, 1989, **42**, 949.
11 P. P. K. Claire, C. J. Jones, K. W. Chiu, J. R. Thornback and M. McPartlin, *Polyhedron*, 1992, **11**, 499.
12 F. Avecilla, R. Bastida, A. de Blas, D. E. Fenton, A. Macías, A. Rodríguez, T. Rodriguez-Blas, S. García-Granda and R. Corzo-Suárez, *J. Chem. Soc., Dalton Trans.*, 1997, 409.
13 M. G. B. Drew, O. W. Howarth, B. G. Morgan and J. Nelson, *J. Chem. Soc., Dalton Trans.*, 1994, 3149.
14 M. G. B. Drew, O. W. Howarth, C. J. Harding N. Martin and J. Nelson, *J. Chem. Soc., Chem. Commun.*, 1995, 903.
15 S.-Y. Hu, Q. Huang, B. Wu, W-J. Zhang and X.-T. Wu, *J. Chem. Soc., Dalton Trans.*, 1996, 3883.
16 S.-Y. Yu, Q.-M. Wang, B. Wu, X.-T. Wu, H.-M. Hu, L.-F. Wang and A.-X. Wu. *Polyhedron*, 1997, **16**, 321.
17 C.-J. Feng, Q.-H. Luo, C.-Y. Duan, M.-C. Shen and Y.-J. Lau, *J. Chem. Soc., Dalton Trans.*, 1998, 1377.

Communication 8/07435F

ChemComm

Designing enzymatic resolution of amines

Shuichi Takayama, Shelly T. Lee, Shang-Cheng Hung and Chi-Huey Wong*

Department of Chemistry and the Skaggs Institute for Chemical Biology, The Scripps Research Institute, 10550 North Torrey Pines Road, La Jolla, CA 92037, USA. E-mail: wong@scripps.edu

Received (in Corvallis, OR, USA) 15th October 1998, Accepted 23rd November 1998

A new strategy, utilizing IR and mass spectrometry, has been developed to design appropriate reagents and reaction conditions for enantioselective enzymatic protection of amines with readily removable protecting groups.

Stereoselective enzymatic acylation of alcohols *via* transesterification in organic solvents has become a useful strategy in enzymatic synthesis.[1] This method has been further improved to eliminate the problems of reversible reactions and product inhibition by using irreversible acyl donors,[2,3] and among these reagents enol esters have proven to be the most useful.[3] Much less developed, however, is the enzymatic protection of amines,[4] as two major problems are often encountered: (i) amines are much more nucleophilic than alcohols and react non-enzymatically with the esters commonly used in the enzymatic acylation of alcohols, and (ii) unlike esters, which can be readily cleaved under basic conditions, once amines are acylated, harsh conditions are often required to liberate the free amine.

We have systematically investigated a number of potentially useful amine protecting reagents and their reactivities and conditions in order to develop a general strategy for the selection of appropriate protecting reagents. To tackle the first problem, the reactivities of a number of amine protecting reagents were studied by comparing, with TLC, the amount of spontaneous background reaction with an amine in a non-reaction-suppressing (toluene) or reaction-suppressing solvent (3-methylpentan-3-ol),[4d,i,j] and by measuring the IR absorption maxima of the carbonyl groups [ν(C=O)]. The ν(C=O) values reflect the C=O bond length and correlate with the reactivity of carbonyl compounds; the larger the wavenumber, the shorter the C=O bond, and the more reactive the carbonyl group (Fig. 1).[5] The correlation between the IR absorption maxima and the reactivity is most accurate for comparing compounds with similar structures, but can also be useful for estimating the reactivity of dissimilar esters and carbonates.

As seen in Fig. 1, amine protecting reagents can be categorized into three categories depending on their reactivity with amines of interest: (*a*) reagents that react spontaneously with amines; (*b*) reagents that spontaneously react with amines but can be suppressed under special conditions; (*c*) reagents that do not react spontaneously with amines. Based on our experience, reagents in category (*a*) are not useful for selective enzymatic protection of amines. Reagents in category (*b*) may be useful under conditions that suppress spontaneous reactions (high dilution and/or use of a reaction-suppressing solvent such as 3-methylpentan-3-ol[4i,j]). Reagents in category (*c*) are perhaps the most useful and can be used under any condition compatible with the enzyme, so the use of high concentrations of reactants is not a problem and in many cases is actually beneficial for the reaction. Since reagents in category (*b*) do not have good leaving groups, they are poor reagents for protecting alcohols, and in fact can be used to selectively protect amines in the presence of hydroxy groups (Table 1, entry 6). In contrast, some of the reagents in categories (*a*) and (*b*) possess good leaving groups and are thus useful for the protection of alcohols and amino alcohols (*e.g.* **7**–**9**).

To solve the second problem of liberating free amines, we then selected reagents that will give readily removable amine protecting groups.[6] These exercises allowed us to quickly identify several novel (*e.g.* **6**, **8**, **11**), and some known (*e.g.* **9**,[4i] **10**[4e]) enzymatic amine protecting reagents, along with suitable reaction conditions for their use.

Benzylisopropenyl carbonate **8** is also a mildly activated reagent that gives benzyl carbamates under spontaneous reaction suppressing conditions. Dibenzyl carbonate **11** is a less reactive version of reagent **8** and useful for amine resolution when used under highly concentrated reaction conditions.

Previous attempts to use **11** in amine resolutions have been unsuccessful,[4e,7] perhaps due to poor design of reaction conditions.

Allyl pent-4-enoate **6** is a less reactive version of **9** and can be used under highly concentrated conditions whereas reagent **9** requires use of spontaneous reaction-suppressing conditions.

Representative new examples of using these protecting reagents/reaction conditions for enzymatic resolution of amines, including the pharmaceutically important 1-amino-indane,[4j] are shown in Table 1. Reagents **6**, **10** and **11** are especially useful, given that they are readily available, that the

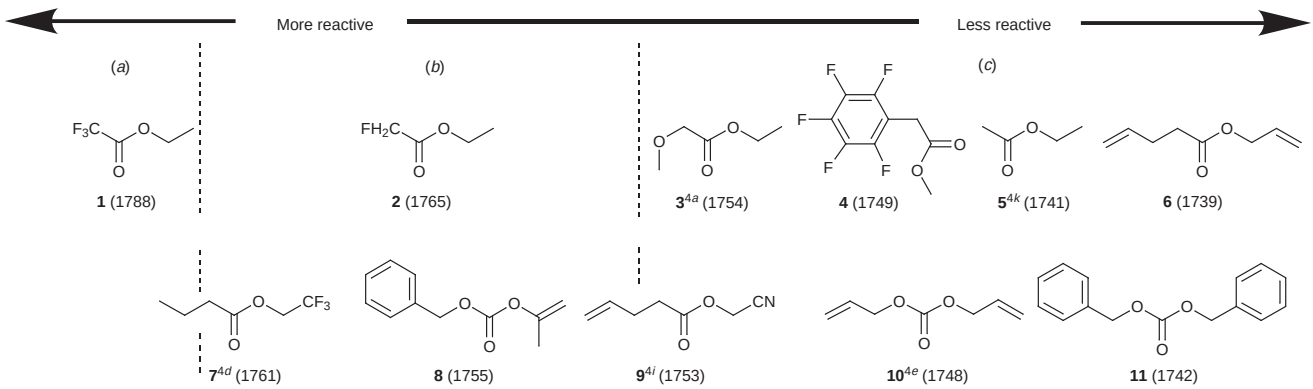

Fig. 1 Reactivity of protecting reagents and their usefulness in enzymatic protection: (*a*) too reactive, (*b*) useful under spontaneous reaction suppressing conditions and (*c*) useful under reaction promoting conditions. The number in parenthesis is IR absorption maxima for the carbonyl group.

Table 1 Examples of amine resolution using the newly designed amine protecting reagents and reaction conditions†

Entry	Product	Reagent	Conditions[a]	Yield (%)[b]	Ee (%)	$[\alpha]_D^{24}$[c]
1	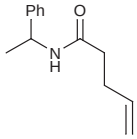	**6**	A	43	(*R*) 99%	+98 (0.73)
2	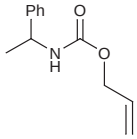	**10**	A	46	(*R*) 83%	+48 (0.74)
3		**11**	A	33	(*R*) 99%	+44 (0.59)
4		**8**	B	34	(*R*) 86%	+38 (0.85)
5	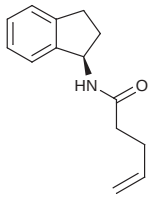	**6**	A	46	(*R*) 99%	+56 (0.89)
6	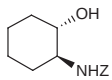	**11**	A	36	(*S*,*S*) 82%	+1.8 (0.80)
7	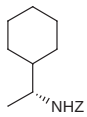	**11**	A	41	(*R*) 81%	–2.8 (0.47)
8	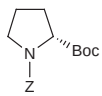	**11**	A	19	(*R*) 57%	+19 (0.70)

[a] A: toluene (high concentration), *Candida antarctica* lipase (CAL); B: hexane (dilute), CAL. [a] Isolated yield. [b] In 10^{-1} deg cm^2 g^{-1}.[c] Concentration (*c*) in $CHCl_3$ shown in parenthesis.

reaction conditions are simple and user friendly (does not even require a pH meter), and that they give amides and carbamates that are widely utilized as amine protecting groups.[6]

Finally, since the efficiency of enzymatic reactions may not correlate with chemical reactivity, quantitative mass spectrometry[8] has been used to compare reagents **6** and **11** for their efficiency in *Candida antarctica* lipase catalyzed protection of amines. The amount of protected amine, formed in an enzymatic reaction containing equimolar amounts of protecting reagents **6** and **11** but with a limiting amount of amine, was measured by directly injecting a quenched reaction mixture into a mass spectrometer and comparing the peak intensities of the products to those of internal standards.‡ Compound **6** was found to be approximately five times as efficient as **11** in enzymatic amine protection. Thus, the chemical reactivity of a reagent determined by its IR absorption combined with a rapid assessment of its enzymatic reactivity using mass spectrometry illustrated in this study provides a new effective strategy for the development of new protecting reagents and conditions for efficient enzymatic amine resolutions. We have used **6** and **11** for enantioselective enzymatic transformation of more than 50 amines so far and work is in progress to further expand the scope of their application.

We thank Dr J. Wu and Professor G. Siuzdak for mass spectral analysis, and the NIH (GM 44154) for financial support.

Notes and references

† Condition A: Amine (0.94 mmol), toluene (230 μl), protecting reagent (1.69 mmol), molecular sieves 4 Å powder (114 mg) and *Candida antarctica* lipase (20 mg) was stirred for 48–70 h at 24 °C. The mixture was directly chromatographed (SiO_2; hexanes–Et_2O, 3:1) to give the products. The ees were determined by HPLC (Chiralpak AD or Chiralcel OD-H).

Condition B: (±)-Methylbenzylamine (168 mg, 1.39 mmol), hexane (10 ml), **8** (197 mg, 1.03 mmol), molecular sieves 4 Å powder (920 mg), and *Candida antarctica* lipase (240 mg, Sigma) was stirred for 60 h at 24 °C. The reaction was filtered through Celite, the filtrate was diluted with Et_2O, washed (dilute HCl; brine), dried ($MgSO_4$) and concentrated *in vacuo*. The residue was chromatographed (SiO_2; hexanes–Et_2O, 4:1) to give the product (120 mg, 34%).

‡ Measurement of reaction efficiency using mass spectrometry: (*R*)-α,4-Dimethylbenzylamine (35 mg, 0.29 mmol), **6** (80 mg, 0.57 mmol), **11** (138 mg, 0.57 mmol), toluene (3 ml) molecular sieves 4A (300 mg), and *Candida antarctica* lipase (20 mg) was stirred for 24 h at room temperature. After filtering through Celite, a portion of the filtrate (5 μl) was mixed with an internal standard (10 μl of a 1:1 solution of **14**:**12**), and injected directly into a PE SCIEX API100 electrospray mass spectrometer in the positive ionization mode. The relative amount of products formed was determined by the peak intensity ratio of the $[M + H^+]$ peaks (218/204 = 14.5) of the pent-4-enamides and the $[M + Na^+]$ peaks (292/278 = 3.14) of the benzyl carbamates (14.5:3.14 = 4.6:1).

1 A. M. Klibanov, *Acc. Chem. Res*., 1990, **23**, 114.
2 Y.-F. Wang, J. J. Lalonde, M. Momongan, D. E. Bergbreiter and C.-H. Wong, *J. Am. Chem. Soc*., 1988, **110**, 7200; H. M. Sweers, C.-H. Wong, *J. Am. Chem. Soc*., 1986, **108**, 6421; J. M. Fang and C.-H. Wong, *Synlett*, 1994, **6**, 393; M. Degueil-Castaing, B. DeJeso, S. Drouillard and B. Maillard, *Tetrahedron Lett*., 1987, **28**, 953; J. B. West, J. Scholten, N. J. Stolowich, J. L. Hogg, A. I. Scott and C.-H. Wong, *J. Am. Chem. Soc*., 1988, **110**, 3709; A. Ghogare and G. S. Kumar, *J. Chem. Soc*., *Chem. Commun*., 1989, 1533; V. Gotor and R. Pulido, *J. Chem. Soc*., *Perkin Trans. 1*, 1991, 491; M. Pozo, R. Puliddo and V. Gortor, *Tetrahedron*, 1992, **48**, 6477; G. Kretzsdchmar and M. Schudok, *Tetrahedron Lett*., 1997, **38**, 387.
3 A. Zaks and D. R. Dodds, *Drug Discovery Today*, 1997, **2**, 513; K. Faber, *Biotransformations in Organic Chemistry*, Springer, Heidelberg, 1995; C.-H. Wong and G. M. Whitesides, *Enzymes in Synthetic Organic Chemistry*, Pergamon, Oxford, 1994.
4 (*a*) F. Balkenhohl, K. Ditrich, B. Hauer and W. Ladner, *J. Prakt. Chem*., 1997, **339**, 381; (*b*) V. Gotor, E. Menendez, Z. Moulougui and A. Gasset, *J. Chem. Soc*., *Chem. Commun*., 1993, 2453; (*c*) V. Gotor, *Tetrahedron*, 1993, **49**, 4321; (*d*) H. Kitaguchi, P. A. Fitspatrick, J. E. Huber and A. M. Klibanov, *J. Am. Chem. Soc*., 1989, **111**, 3094; (*e*) B. Orsat, P. B. Alper, W. J. Moree, C.-P. Mak and C.-H. Wong, *J. Am. Chem. Soc*., 1996, **118**, 712; (*f*) M. Pozo and V. Gotor, *Tetrahedron*, 1993, **49**, 10725; (*g*) M. Pozo, V. Gotor, *Tetrahedron*, 1993, **49**, 4321; (*h*) S. Puertas, F. Robelledo, V. Gotor, *Tetrahedron*, 1995, **51**, 1495; (*i*) S. Takayama, W. J. Moree and C.-H. Wong, *Tetrahedron Lett*., 1996, **35**, 6287; (*j*) A. L. Gutman, E. Meyer, E. Kalerin, F. Polyak and J. Sterling, *Biotechnol. Bioeng*., 1992, **40**, 760; (*k*) K.-E. Jaeger, K. Liebeton, A. Zonta, K. Schimossek and M. T. Reetz, *Appl. Microbiol. Biotechnol*., 1996, **46**, 99; (*l*) S. Fernandez, R. Brieva, F. Rebolledo and V. Gotor, *J. Chem. Soc*., *Chem. Commun*., 1992, 2885; (*m*) E. Schoffers, A. Golebiowski and C. R. Johnson, *Tetrahedron*, 1996, **52**, 3769; (*n*) M. Pozo, R. Pulido and V. Gotor, *Tetrahedron*, 1992, **48**, 6477.
5 For *v* values, see: R. M. Silverstein, G. C. Bassler and T. C. Morrill, *Spectrometric Identification of Organic Compounds*, Wiley, New York, 1991.
6 T. W. Greene and P. G. M. Wuts, *Protective Groups in Organic Synthesis*, Wiley, New York, 1991; R. Madsen, C. Roberts and B. Fraser-Reid, *J. Org. Chem*., 1995, **60**, 7920.
7 A. Maestro, C. Astorga and V. Gotor, *Tetrahedron*: *Asymmetry*, 1997, **8**, 3153.
8 S. Takayama, R. Martin, J. Wu, K. Laslo, G. Siuzdak and C.-H. Wong, *J. Am. Chem. Soc*., 1997, **119**, 8146; J. Wu, S. Takayama, C.-H. Wong and G. Siuzdak, *Chem. Biol*., 1997, **4**, 653.

Communication 8/08028C

Synthesis of a key intermediate for corossolin using hydrolytic kinetic resolution of epoxides

Qian Yu, Yikang Wu, Li-Jun Xia, Min-Hua Tang and Yu-Lin Wu*

State Key Laboratory of Bio-organic and Natural Products Chemistry, Shanghai Institute of Organic Chemistry, Chinese Academy of Sciences, Shanghai 200032, China. E-mail: ylwu@pub.sioc.ac.cn

Received (in Cambridge, UK) 16th November 1998, Accepted 4th December 1998

A convergent synthesis of the key intermediate for corossolin has been achieved using hydrolytic resolution of epoxides as the key step, which extends the scope of the applicable substrates for hydrolytic kinetic resolution to cover multifunctionalized large molecules.

Annonaceous acetogenins (AAs) are a relatively new class of natural products, which have been isolated from the tropical and subtropical plants of the *Annonaceae* family. They are characterized by one or more tetrahydrofuran rings, together with a terminal α,β-unsaturated γ-lactone on a 35- or 37-carbon chain. A majority of these compounds exhibit[1] high cytotoxicity and immunomodulating activities, which make these compounds potential parasiticidal, insecticidal, and above all, powerful tumoricidal agents.

As part of our research on the synthesis[2] of annonaceous acetogenins, we performed first a total synthesis[2c] of the

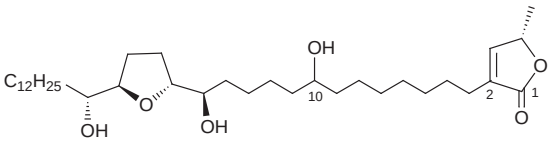

(10*RS*)-epimer mixture of corossolin **1**,[3] and later of both[4] 10-epimers, in an effort to establish the configuration at C-10 of natural corossolin, which was not given in the original structural determination. In our latter work, both epimers of the epoxide fragment were constructed through the chiron approach. Herein we report a more convenient synthesis of the (10*R*)-epoxide **7**, the key intermediate of natural (10*R*)-corossolin, using Jacobsen's hydrolytic kinetic resolution (HKR)[5] to resolve the terminal epoxides as the key step.

The HKR method uses readily accessible cobalt-based chiral salen complexes as catalyst and water as the only reagent to afford chiral epoxides and diols of high ee in excellent yields. These advantages have made it a very attractive asymmetric synthetic tool. However, up to now HRK has *only* been applied to the resolution of simple[6] epoxides of small molecular weight such as styrene oxide, or monofunctional unbranched alkyl-substituted[7] epoxides. In the present work, we pushed the limits further, extending the scope of the applicable substrates to cover multifunctionalized large molecules when developing a facile access to the key intermediate[4] in our previous synthesis of AA.

The substrate for the HKR, the 'racemic' epoxide, was prepared as shown in Scheme 1. Starting from the commercially available methyl undec-10-enoate, the alcohol **2** was prepared in 80% yield by aldol condensation with the aldehyde derived from ethyl L-lactate employing our previous[2b,c] procedure. Conversion of **2** to the acetate ester **3** was achieved in 91% yield. Treatment of **3** with 10% aq. H_2SO_4 in THF removed the THP protecting group and the newly unmasked hydroxy group underwent an intramolecular ester exchange reaction to give lactone **4** in 83% yield. Subsequent epoxidation of **4** with MCPBA gave **5**, which on β-elimination using DBU gave the unsaturated lactone **6** in high yield. The two diastereomers of **6** could not be differentiated on silica gel, presumably due to the large distance between the two stereogenic centers.

The HKR was performed with (*R*,*R*)-salen–Co(OAc) complex (0.5 mol%) and H_2O (0.55 equiv.) to yield epoxide **7** (46%) and diol **8** (38%). The diol **8** could be recycled[4] to **7** in 52% yield, or to the diastereoisomer of **7** in 82% yield. Due to the difficulty in separating chiral epoxide **7** from the salen catalyst, the measurement of its diastereoisomeric excess was performed on **9** and **10**, which were derived in 78% and 85% yields from **7** and **6**, respectively, by reaction with lithium trimethylsilylacetylide. The diastereoisomeric purity of **9** was 99.0% as shown by HPLC (OJ column, 95:5 of hexane–Pr^{i}OH) with the C-10 epimer mixture compound **10** as reference. This is in excellent agreement with the result of optical rotation measurements (+15.1 and +15.3 for **9** and the authentic[4] sample from the chiron approach, respectively). The diastereoisomer of **7** can also be prepared from the (*S*, *S*)-salen–Co(OAc) complex using HKR of **6**.

In conclusion, with HKR of terminal epoxides as the key step, we have developed a short and efficient synthesis (six steps from methyl undec-10-enoate with the overall yield > 24.3%

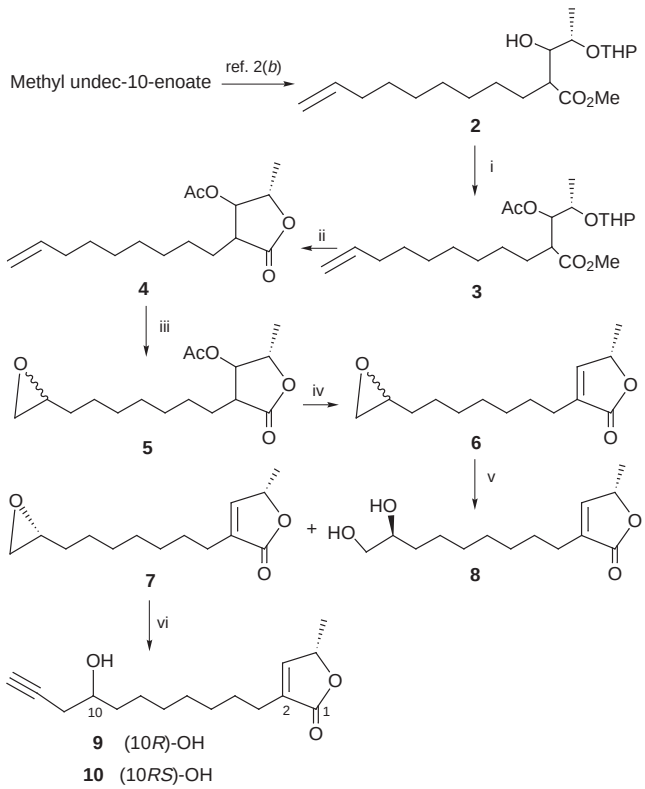

Scheme 1 *Regents and conditions*: i, Ac_2O, Py, (91%); ii, 10% H_2SO_4, THF, (83%); iii, MCPBA, CH_2Cl_2, (91%); iv, DBU, THF, 2 h, (96%); v, (*R*,*R*)-salen–Co(OAc) (0.5 mol%), dist. H_2O, 40 h, (46% for **7**, 38% for **8**); vi, Bu^{n}Li, trimethylsilylacetylene, $BF_3{\cdot}OEt_2$, −78 °C, (78% and 85%, respectively, 99.0% de).

without taking into consideration the recycled **7** from **8**) of a key intermediate of (10*R*)-corossolin. The present approach is simpler than and therefore superior to the chiral pool method, in which the starting materials are (2*R*)-2,3-*O*-isopropylideneglyceral and azelic acid monoethyl ester (requiring a total of nine steps with 13.4% overall yield[4]), or (2*S*)-1,2-*O*-isopropylidenebutane-1,2,4-triol [derived[5] from (*S*)-malic acid] and a substituted γ-lactone prepared by White's method[9] (in eight steps[8] with 15.1% overall yield for a similar compound). It should be noted that the present approach also provides a facile access to other[10] annonaceous acetogenins with a C-10 hydroxy group.

We thank the State Committee of Science and Technology of China, Chinese academy of Sciences (KJ-952-S1-503) and the National Natural Science Foundation of China (29472070, 29790126) for financial support.

Notes and references

1 J. K. Rupprecht, Y. H. Hui and J. L. McLaughlin, *J. Nat. Prod*., 1990, **53**, 237; X. P. Fang, M. J. Rieser, Z. M. Gu and J. L. McLaughlin, *Phytochem. Anal*., 1993, **4**, 27; L. Zeng, Q. Ye, N. H. Oberlies, G. E. Shi, Z. M. Gu, K. He and J. L. Mclaughlin, *Nat. Prod. Rep*., 1996, 275; A. Cave, B. Figadere, A. Laurens and D. Cortes, *Prog. Chem. Org. Nat. Prod*., 1997, **70**, 81.

2 (*a*) Z. J. Yao, Y. B. Zhang and Y. L. Wu, *Acta Chim. Sin*., 1992, **50**, 901; (*b*) Z. J. Yao and Y. L. Wu, *Tetrahedron Lett*., 1994, **35**, 157; (*c*) Z. J. Yao and Y. L. Wu, *J. Org. Chem*., 1995, **60**, 1170; (*d*) Z. J. Yao and Y. L. Wu, *Youji Huaxue*, 1995, **15**, 120; (*e*) Z. J. Yao, Q. Yu and Y. L. Wu, *Synth. Commun*., 1996, **19**, 3613.

3 D. Cortes, S. L. Myint, A. Laurens, R. Hocquemiller, M. Leboeuf and A. Cave, *Can. J. Chem*., 1991, **69**, 8.

4 Q. Yu, Z. J. Yao, X. G. Chen and Y. L. Wu, unpublished work.

5 M. Tokunaga, J. F. Larrow, F. Kakiuchi and E. N. Jacobsen, *Science*, 1997, **277**, 936.

6 S. E. Schaus, J. Brånalt and E. N. Jacobsen, *J. Org. Chem*., 1998, **63**, 4876.

7 P. S. Stavle, M. J. Lamoreaux, J. F. Berry and R. D. Gandour, *Tetrahedron*: *Asymmetry*, 1998, **9**, 1843.

8 H. Makabe, H. Tanimoto, A. Tanaka and T. Oritani, *Heterocycles*, 1996, **43**, 2229.

9 J. D. White, T. C. Somers and G. N. Reddy, *J. Org. Chem*., 1992, **57**, 4991.

10 G. X. Zhao, L. R. Miesbauer, D. L. Smith and J. L. McLaughlin, *J. Med. Chem*., 1994, **37**, 1971; G. X. Zhao, Z. M. Gu, L. Zeng, Z. F. Chao, J. F. Koslowski, K. V. Wood and J. L. McLaughlin, *Tetrahedron*, 1995, **51**, 7149; F. Alali, L. Zeng, Y. Zhang, Q. Ye, D. C. Hopp, J. L. Schwedler and J. L. McLaughlin, *Bioorg. Med. Chem*., 1997, **3**, 549.

Communication 8/08923J

Chiral bis(oxazolinyl)phenylrhodium(III) complexes as Lewis acid catalysts for enantioselective allylation of aldehydes

Yukihiro Motoyama, Hiroki Narusawa and Hisao Nishiyama*

School of Materials Science, Toyohashi University of Technology, Tempaku-cho, Toyohashi, Aichi 441-8580, Japan. E-mail: hnishi@tutms.tut.ac.jp

Received (in Cambridge, UK) 5th October 1998, Accepted 4th November 1998

The reaction of (Phebox)$SnMe_3$ 1 [PheboxH = 2,6-bis(oxazolinyl)benzene] and [(*c*-octene)RhCl]$_2$ in the presence of CCl_4 provided air-stable and water-tolerant (Phebox)$RhCl_2(H_2O)$ complexes 2 which acted as asymmetric catalysts for the enantioselective allylation of aldehydes in up to 80% ee.

The development of chiral Lewis acid catalysts, particularly for carbon–carbon bond forming reactions, is one of the most challenging and formidable endeavors in organic synthesis.[1] Among various carbon–carbon bond forming reactions, asymmetric allylation of carbonyl compounds is a valuable means of constructing chiral functionalized structures, and therefore many chiral allylmetal reagents have been designed and synthesised.[2] Although numerous reactions using a stoichiometric amount of chiral allylmetal reagents have been reported,[3] there are only a few reports of catalytic processes using chiral Lewis acid complexes, including chiral (acyloxy)borane (CAB) complex and allylsilanes[4] or allylstannanes,[5] binaphthol-derived chiral titanium complexes and allylstannanes[6] or allylsilanes,[7] and BINAP-derived chiral silver complexes and allylstannanes.[8] The key to success in developing a new chiral Lewis acid catalyst is the choice of the central metal and the design of the chiral ligands. Traditional Lewis acids, such as boron, aluminium, titanium and tin, are extremely moisture-sensitive, and are known to form oligomers in solution. Furthermore, chiral complexes are almost always generated *in situ*, so there are a variety of species having different Lewis acid activity and enantioselectivity. On the other hand, transition metal complexes are generally insensitive to water and form a single well-defined species.[9,10] Here we report a catalytic enantioselective allylation reaction of aldehydes with allyltributylstannane catalyzed by new air-stable and water-tolerant rhodium(III) complexes **2** bearing a 2,6-bis(oxazolinyl)phenyl group (Phebox) as chiral ligands.[11] The Phebox ligand bonds *via* a central carbon–metal covalent bond and both of the oxazoline rings.

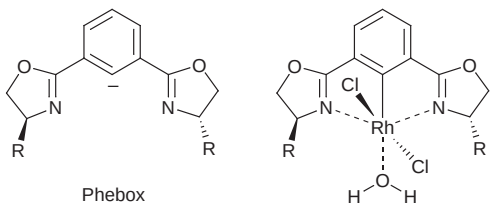

The (Phebox)$RhCl_2(H_2O)$ complexes **2**† were easily synthesized by the transmetalation reaction of [(*c*-octene)$_2$RhCl]$_2$ and (Phebox)$SnMe_3$ **1** in CH_2Cl_2 followed by treatment with CCl_4.‡ These complexes are air-stable enough to be purified by silica gel chromatography (Scheme 1).

The optimized allylation reaction conditions employed benzaldehyde and allyltributylstannane§ in the presence of 5 mol% of the (*S*,*S*)-(Phebox)$RhCl_2(H_2O)$ complex **2** as a chiral catalyst (Scheme 2). The absolute configuration of the allylated product was determined to be *S* by comparison of its optical rotation value with literature data.[3e] The rate of this allylation reaction was strongly dependent on the solvent: the allylation reaction proceeded smoothly in CH_2Cl_2, but when using THF or an aromatic solvent such as benzene or toluene, the reaction rates were remarkably slow although the enantioselectivities was almost the same (entries 1–4). In the presence of 4 Å molecular sieves this catalytic reaction was accelerated while the enantiomeric excess of the product **3** was not changed (Table 1, entries 4 *vs*. 5). The selectivity did not improve when the reaction temperature was lowered to 0 °C (entries 5 *vs*. 6). The substituent on the oxazoline rings had a significant effect on the chemical yields and ees (entries 5, 7–9). Notably, the enantioselectivity reaching 61% ee using Bn-Phebox-derived complex **2c**. It is worth noting that the complex **2** can be recovered almost quantitatively from the reaction medium by silica gel chromatography, and the recovered complex **2** catalyses the reaction with almost the same catalytic activity and enantioselectivity (entries 5 *vs*. 10).

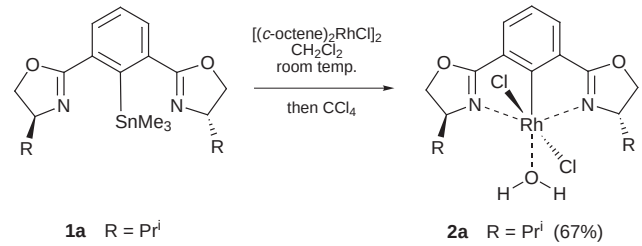

Scheme 1

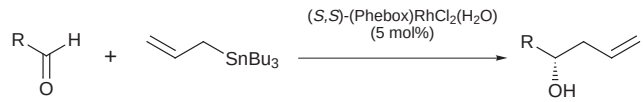

Scheme 2

Table 1 Asymmetric catalytic allylation of benzaldehyde catalyzed with Phebox–Rh^{III} complexes **2**[a]

Entry	Catalyst	Solvent	*T*/°C	*t*/h	Yield (%)	Ee (%)[b]
1	**2a**	toluene	room temp.	24	23	45
2	**2a**	benzene	room temp.	24	64	45
3	**2a**	THF	room temp.	24	66	52
4	**2a**	CH_2Cl_2	room temp.	7	79	52
5[c]	**2a**	CH_2Cl_2	room temp.	7	88	51
6[c]	**2a**	CH_2Cl_2	0	24	46	49
7[c]	**2b**	CH_2Cl_2	room temp.	7	42	6
8[c]	**2c**	CH_2Cl_2	room temp.	7	88	61
9[c]	**2d**	CH_2Cl_2	room temp.	7	43	46
10[c,d]	**2a**	CH_2Cl_2	room temp.	7	88	49

[a] All reactions were carried out using 0.5 mmol of benzaldehyde, 0.75 mmol of allyltin and 0.025 mmol of chiral catalyst **2** in 2 ml of solvent. [b] Determined by chiral HPLC analysis using Daicel CHIRALCEL OD. [c] In the presence of 4 Å molecular sieves (250 mg). [d] Recovered catalyst was used.

Table 2 Asymmetric catalytic allylation of aldehydes catalyzed with Phebox–Rh^{III} complex **2c**[a]

Entry	Aldehyde	Yield (%)	Ee (%)[b]	Configuration[c]	Ref
1	4-BrC_6H_4CHO	94	43[d]	*S*[e]	8(*a*)
2	PhCHO	88	61[f]	*S*	3(*e*)
3	4-MeOC_6H_4CHO	99	80	*S*	3(*n*)
4	2-MeC_6H_4CHO	98	53[g]	*S*[e]	8(*a*)
5	2-furyl-CHO	94	58[d]	*S*[e]	8(*a*)
6	PhCH_2CH_2CHO	84	63	*R*	3(*n*)
7	(*E*)-PhCH=CHCHO	98	77	*S*	3(*e*)

[a] All reactions were carried out using 0.5 mmol of aldehyde, 0.75 mmol of allyltributyltin and 0.025 mmol of chiral catalyst **2c** in 2 ml of CH_2Cl_2 in the presence of 4 Å molecular sieves (250 mg) at room temperature for 7 h. [b] Determined by chiral HPLC analysis using Daicel CHIRALCEL OD-H. [c] Assignment by comparison of the sign of optically rotation with reported value. [d] Determined by chiral HPLC analysis using Daicel CHIRALCEL OJ. [e] By analogy to the other case that is known unambiguously. [f] Determined by chiral HPLC analysis using Daicel CHIRALCEL OD. [g] Determined by chiral HPLC analysis using Daicel CHIRALPAK AD.

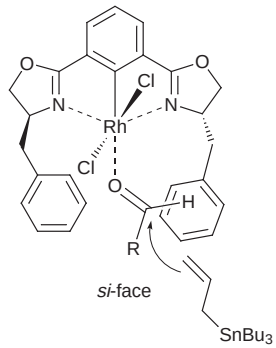

Fig. 1

Table 2 summarizes the results obtained for the allylation reaction of a variety of aldehydes catalysed with the complex **2c**. The characteristic features of the results are as follows: (i) an electron-donating substituents at the *para*-position of benzaldehyde increases the enantioselectivity; (ii) a methyl group at the *ortho*-position of benzaldehyde decreases the selectivity; (iii) all reactions result in high yields and comparable enantioselectivities with both aromatic and aliphatic aldehydes; (iv) in the reaction with enals, 1,2-addition reaction occurs exclusively; (v) in all of the cases, allyltributylstannane attacks to the *si*-face of the aldehyde's C=O plane.

A transition state that accounts for the observed stereoselectivities is shown in Fig. 1. The allylstannane approaches the carbonyl *si*-face because the *re*-face is shielded by the substituent on the oxazoline ring of the Phebox ligand.

In summary, we have demonstrated the effectiveness of Phebox–Rh^{III} complexes as chiral transition metal Lewis acid catalysts for the enantioselective addition of allyltributylstannane to aldehydes. Application of these complexes to other asymmetric reactions is now under investigation.

This work was partly supported by a Grant-in-Aid for Scientific Research from the Ministry of Education, Science and Culture, Japan.

Notes and references

† We previously reported the synthesis of **2a** by the transmetalation of $RhCl_3(H_2O)_3$ and **1a** in 47% yield (see ref 12). However, the chemical yield of Ph-Phebox-derived **2b** is very low (16%) by this method.

‡ We have already reported that the (dMe-Pybox)RhCl complex prepared from the dMe-Pybox and $[(c\text{-octene})_2RhCl]_2$ readily reacted with alkyl chlorides to form Rh^{III} species *via* an oxidative addition reaction, see ref. 13(*a*). And recently, Vrieze reported the same oxidative addition of carbon–chloride bonds to rhodium(I) complexes containing terdentate nitrogen ligands $[2,6\text{-}(CR^1{=}NR^2)_2C_2H_3N]$, see ref. 13(*b*).

§ Other substituted allylstannane reagents gave lower yields and enantioselectivities when catalyzed by **2a**: allyltrimethylstannane (48%, 35% ee), allyltriphenylstannane (7%, 27% ee).

1 Reviews: R. Noyori, *Asymmetric Catalysis in Organic Synthesis*, Wiley, New York, 1994; B. Bosnich, *Asymmetric Catalysis*, Martinus Nijhoff, Dordrecht, The Netherlands, 1986.

2 Reviews: W. R. Roush, in *Comprehensive Organic Synthesis*, ed. B. M. Trost, I. Fleming and C. H. Heathcock, Pergamon, Oxford, 1991, vol. 2, p. 1; Y. Yamamoto and N. Asao, *Chem. Rev*., 1993, **93**, 2207; T. Bach, *Angew. Chem., Int. Ed. Engl*., 1994, **33**, 417; A. H. Hoveyda and J. P. Morken, *Angew. Chem., Int. Ed. Engl*., 1996, **35**, 1262.

3 Allylboranes: (*a*) H. C. Brown and P. K. Jadhav, *J. Am. Chem. Soc*., 1983, **105**, 2092; (*b*) R. P. Short and S. Masamune, *J. Am. Chem. Soc*., 1989, **111**, 1892; (*c*) U. S. Racherla and H. C. Brown, *J. Org. Chem*., 1991, **56**, 401; Allylboronates: (*d*) T. Herold and R. W. Hoffmann, *Angew. Chem., Int. Ed. Engl*., 1978, **17**, 768; (*e*) R. W. Hoffmann and T. Herold, *Chem. Ber*., 1981, **114**, 375; (f) W. R. Roush, A. E. Walts and L. K. Hoong, *J. Am. Chem. Soc*., 1985, **107**, 8186; (*g*) W. R. Roush and L. Banfi, *J. Am. Chem. Soc*., 1988, **110**, 3979; (*h*) W. R. Roush, L. K. Hoong, M. A. J. Palmer and J. C. Park, *J. Org. Chem*., 1990, **55**, 4109; (*i*) M. T. Reetz and T. Zierke, *Chem. Ind*., 1988, 663; Allylboradiazolidines: (*j*) E. J. Corey, C.-M. Yu and S. S. Kim, *J. Am. Chem. Soc*., 1989, **111**, 5495; Allyltitanates: (*k*) M. Riediker and R. O. Duthaler, *Angew. Chem., Int. Ed. Engl*., 1989, **28**, 494; (*l*) B. Schmidt and D. Seebach, *Angew. Chem., Int. Ed. Engl*., 1991, **30**, 99; (*m*) A. Hafner, R. O. Duthaler, R. Marti, G. Rihs, P. Rothe-Streit and F. Schwarzenbach, *J. Am. Chem. Soc*., 1992, **114**, 2321; Allylaluminium derivatives: (*n*) N. Minowa and T. Mukaiyama, *Bull. Chem. Soc. Jpn*., 1987, **60**, 3697; Allylstannans: (*o*) J. Otera, Y. Kawasaki, H. Mizuno and Y. Shimizu, *Chem. Lett*., 1983, 1529; (*p*) J. Otera, Y. Yoshinaga, T. Yamaji, T. Yoshioka and Y. Kawasaki, *Organometallics*, 1985, **4**, 1213; (*q*) G. P. Boldrini, E. Tagliavini, C. Trombini and A. Umani-Ronchi, *J. Chem. Soc., Chem. Commun*., 1986, 685; (*r*) G. P. Boldrini, L. Lodi, E. Tagliavini, C. Tarasco, C. Trombini and A. Umani-Ronchi, *J. Org. Chem*., 1987, **52**, 5447; (*s*) C. Boga, D. Savoia, E. Tagliavini, C. Trombini and A. Umani-Ronchi, *J. Organomet. Chem*., 1988, **353**, 177; Allylchromium complexes: (*t*) K. Sugimoto, S. Aoyagi and C. Kibayashi, *J. Org. Chem*., 1997, **62**, 2322.

4 K. Furuta, M. Mouri and H. Yamamoto, *Synlett*, 1991, 561; K. Ishihara, M. Mouri, Q. Gao, T. Maruyama, K. Furuta and H. Yamamoto, *J. Am. Chem. Soc*., 1993, **115**, 11490.

5 J. A. Marshall and Y. Tang, *Synlett*, 1992, 653; J. A. Marshall and M. R. Palovich, *J. Org. Chem*., 1998, **63**, 4381.

6 S. Aoki, K. Mikami, M. Terada and T. Nakai, *Tetrahedron*, 1993, **49**, 1783; A. L. Costa, M. G. Piazza, E. Tagliavini, C. Trombini and A. Umani-Ronchi, *J. Am. Chem. Soc*., 1993, **115**, 7001; G. E. Keck and D. Krishnamurthy, *J. Org. Chem*., 1993, **58**, 6543; G. E. Keck, K. H. Tarbet and L. S. Geraci, *J. Am. Chem. Soc*., 1993, **115**, 8467; G. E. Keck and L. S. Geraci, *Tetrahedron Lett*., 1993, **34**, 7827; S. Weigand and R. Rrückner, *Chem. Eur. J*., 1996, **2**, 1077.

7 D. R. Gauthier, Jr. and E. M. Carreira, *Angew. Chem., Int. Ed. Engl*., 1996, **35**, 2363.

8 (*a*) A. Yanagisawa, H. Nakashima, A. Ishiba and H. Yamamoto, *J. Am. Chem. Soc*., 1996, **118**, 4723; (*b*) A. Yanagisawa, A. Ishiba, H. Nakashima and H. Yamamoto, *Synlett*, 1997, 88.

9 H. Nishiyama and Y. Motoyama, in *Lewis Acid Chemistry*: *A Practical Approach*, ed. H. Yamamoto, OUP, UK, 1998, ch. 13; W. Odenkirk, A. L. Rheingold and B. Bosnich, *J. Am. Chem. Soc*., 1992, **114**, 6392; T, K. Hollis, W. Odenkirk, N. P. Robinson, J. Whelan and B. Bosnich, *Tetrahedron*, 1993, **49**, 5415.

10 Recent representative papers; chiral iron complex: E. P. Kündich, B. Bourdin and G. Bernardinelli, *Angew. Chem., Int. Ed. Engl*., 1994, **33**, 1856; Chiral ruthenium complex: D. L. Davies, J. Fawcett, S. A. Garratt and D. R. Russell, *Chem. Commun*., 1997, 1351; Chiral rhodium complex: A. J. Davenport, D. L. Davies, J. Fawcett, S. A. Garratt, L. Lad and D. R. Russell, *Chem. Commun*., 1997, 2347; Chiral nickel complex: S. Kanemasa, Y. Oderaotoshi, H. Yamamoto, J. Tanaka, E. Wada and D. P. Carran, *J. Org. Chem*., 1997, **62**, 6454; S. Kanemasa, Y. Oderaotoshi, S. Sakaguchi, H. Yamamoto, J. Tanaka, E. Wada and D. P. Carran, *J. Am. Chem. Soc*., 1998, **120**, 3074.

11 S. E. Denmark, R. A. Stavenger, A.-M. Faucher and J. P. Edwards, *J. Org. Chem*., 1997, **62**, 3375; M. A. Stark and C. J. Richards, *Tetrahedron Lett*., 1997, **38**, 5881.

12 Y. Motoyama, N. Makihara, Y. Mikami, K. Aoki and H. Nishiyama, *Chem. Lett*., 1997, 951.

13 (*a*) H. Nishiyama, M. Horihata, T. Hirai, S. Wakamatsu and K. Itoh, *Organometallics*, 1991, **10**, 2706; (*b*) H. F. Haarman, J. M. Ernsting, M. Kranenburg, H. Kooijman, N. Veldman and K. Vrieze, *Organometallics*, 1997, **16**, 887.

Communication 8/07716I

Total synthesis of (+)-pramanicin and stereochemical elucidation of the natural product

Anthony G. M. Barrett,*[a] John Head,[b] Marie L. Smith[a] and Nicholas S. Stock[a]

[a] *Department of Chemistry, Imperial College of Science, Technology and Medicine, South Kensington, London, UK SW7 2AY. E-mail: m.stow@ic.ac.uk*

[b] *Celltech Therapeutics, 216 Bath Rd, Slough, Berkshire, UK SL1 4EN*

Received (in Liverpool, UK) 14th October 1998, Accepted 27th November 1998

Total synthesis of (+)-pramanicin is achieved through a 'one pot' Michael addition of an aminosilyl zincate species to an α,β-unsaturated lactam and quenching of the resultant enolate with an α,β-unsaturated γ,δ-epoxy aldehyde.

(−)-Pramanicin **1**, recently isolated from a fungus belonging to the *Stagonospora* species, contains a highly functionalised γ-lactam-based head group with a functionalised lipophilic side chain.[1] The isolated compound shows antifungal activity towards various fungal pathogens including *Candida albicans*, *Candida parapsilosis* and *Cryptococcus neoformans*. The latter micro-organism is responsible for meningitis infection in AIDS patients and therefore pramanicin **1** poses an interesting target for synthesis. Recently, Harrison and co-workers have elucidated the biosynthesis of pramanicin and showed that the carbon skeleton derives from eight acetate units and a serine residue.[2]† Herein we report the total synthesis of (+)-pramanicin **9** which unequivocally establishes the full relative and absolute stereochemistry of the natural product.

Retrosynthetically, pramanicin can be divided into two fragments, the suitably protected lactam **2** derived from L-glutamic acid and the side chain epoxy aldehyde **3**.‡ We envisaged that these two components could be joined *via* the addition of a silyl entity (masked hydroxy group) in a conjugate fashion to **2** and trapping of the resultant enolate with the aldehyde **3**. The addition of this silyl group should occur in an *anti* fashion to the TBDMS protected hydroxymethyl pendant, thus establishing the correct stereochemistry of the secondary alcohol following Tamao oxidation[4] (Scheme 1).

Thus, reaction of lactam **2**§ with a 1:1 mixture of (diethylamino)diphenylsilyllithium and diethylzinc at −78 °C and trapping of the resulting enolate with the aldehyde **3** followed by ethanolysis of the sensitive silylamine furnished compound **4** (60%). This reaction clearly establishes the complete carbon backbone of pramanicin with a readily oxidisable alkoxysilyl appendage. Confirmation of the stereochemical outcome of the silyl zincate addition has been made *via* addition of the phenyldimethylsilyl[5] group to lactam **2** under identical conditions and removal of the protecting groups to afford **11** for single crystal X-ray analysis¶ (Scheme 2).

Oxidation of the β-hydroxy lactam **4** to the corresponding diketone **5** could only be accomplished using Dess–Martin periodinane as oxidant. Chromium based reagents led to extensive decomposition and no reaction was observed using manganese dioxide. The diketone **5** proved to be unstable to prolonged exposure to air and to chromatography thus preclud-

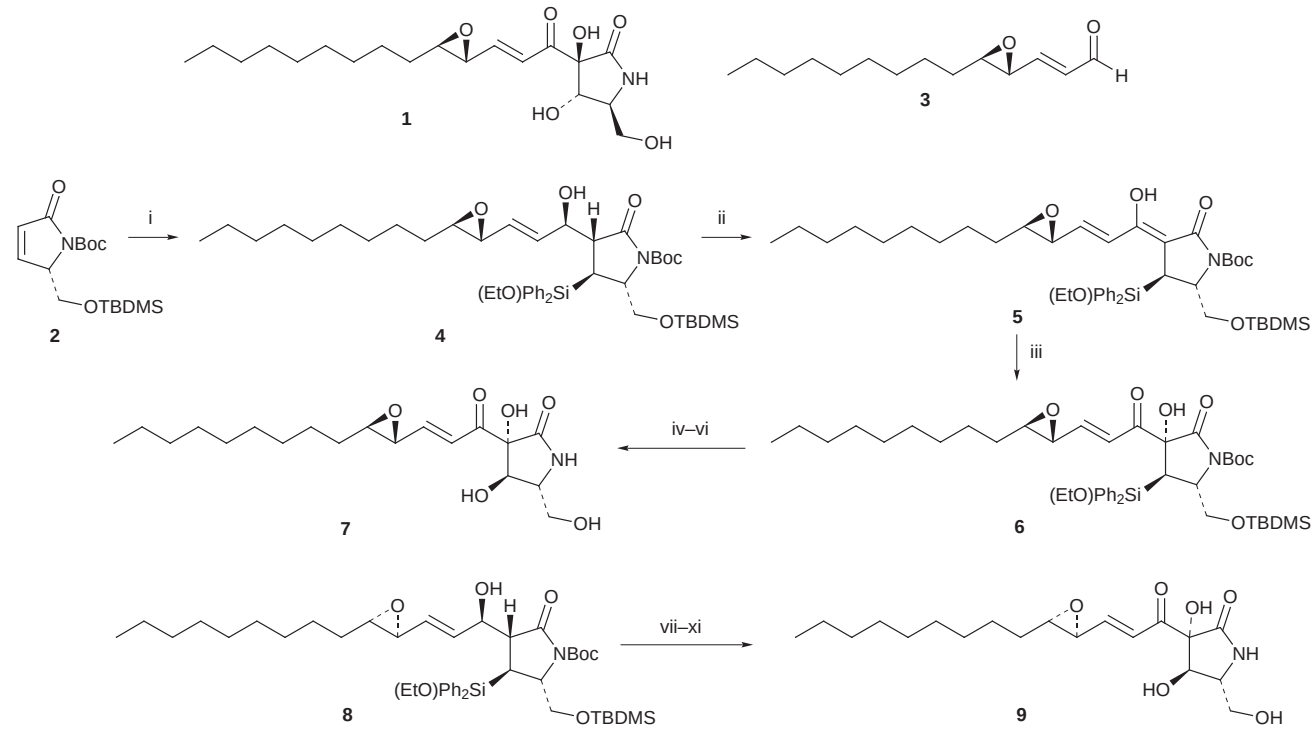

Scheme 1 *Reagents and conditions*: i, $(Et_2N)Ph_2SiLi$, Et_2Zn, −78 °C, then **3**, THF, −78 °C, then EtOH, NH_4Cl, 24 h, 60%; ii, Dess–Martin periodinane, CH_2Cl_2, 0 to 25 °C; iii, dimethyldioxirane, $Ni(acac)_2$ (cat.), acetone, H_2O, 0 °C, 60% from **4**; iv, MCPBA (3 equiv.), KHF_2 (2.5 equiv.), DMF, 0 °C, 53%; v, SiO_2,45 °C, 0.1 mmHg, 84%; vi, H_2SiF_6 (20–25% aq.), THF, 0 to 25 °C, 53%; vii, Dess–Martin periodinane, CH_2Cl_2, 0 to 25 °C; viii, dimethyldioxirane, $Ni(acac)_2$ (cat.), acetone, H_2O, 0 °C, 59% from **8**; ix, MCPBA (3 equiv.), KHF_2 (2.5 equiv.), DMF, 0 °C, 70%; x, TFA, CH_2Cl_2, 0 to 25 °C, 78%; xi, H_2SiF_6 (20–25% aq.), THF, 0 to 25 °C, 55%.

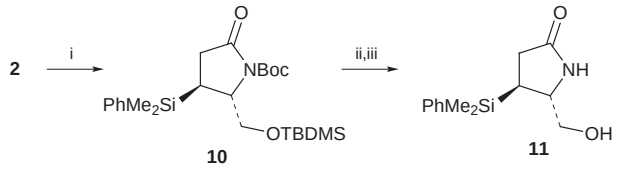

Scheme 2 *Reagents and conditions*: i, $PhMe_2SiLi$, Et_2Zn, THF, −78 °C, 99%; ii, TBAF, THF, 80%; iii, TFA, CH_2Cl_2, 85%.

ing its purification. Therefore immediate oxidation of the diketone unit with dimethyldioxirane and a nickel(II) acetylacetonate[6] catalyst gave hydroxy dione **6** as a single diastereoisomer in excellent overall yield (60%). The ethoxy(diphenyl)silyl group blocked the top face of the diketone directing reaction to the opposite face and thus setting the configuration of the tertiary alcohol as required. Tamao oxidation of silane **6** proceeded smoothly at low temperature with MCPBA as oxidant to produce the secondary alcohol with retention of configuration as desired. The use of peracetic acid or hydrogen peroxide as alternative oxidants gave only intractable mixtures of products. Removal of the Boc group *via* thermolysis on silica under vacuum[7] followed by deprotection of the TBDMS moiety using fluorosilicic acid[8] furnished compound **7** (Scheme 1). Comparison of **7** with authentic pramanicin by NMR analysis revealed very slight differences in the chemical shift of the protons associated with the alkene and the epoxide ring system. Alternatively, synthesis of diastereoisomer **8** using *ent*-**3** as the enolate quench (62%) and elaboration as before yielded isomer **9**. This diastereoisomer **9** was identical by ^1H and ^{13}C NMR spectroscopy with authentic pramanicin (see Fig. 1). Whilst the Merck group[1] established the relative stereochemistry of the γ-lactam ring of the natural

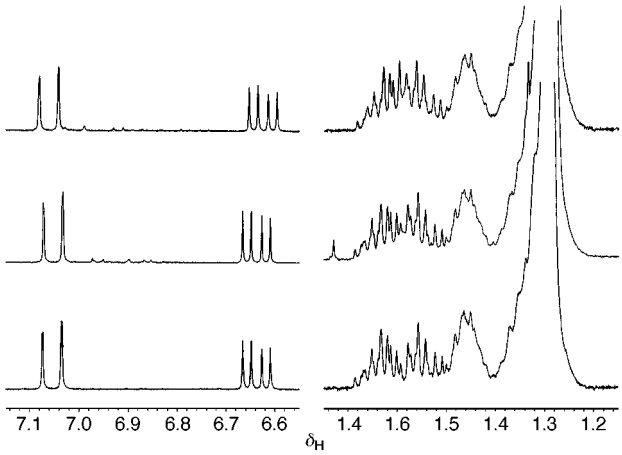

Fig. 1 ^1H NMR (400 MHz, $CDCl_3$) spectra showing olefinic resonance's (left) and protons α to epoxide ($\delta \sim 1.6$, right); top: diastereoisomer **7**; middle: diastereoisomer **9**; bottom: authentic pramanicin.

product and that the side chain epoxide was *trans*, they did not establish the stereochemistry of the side chain relative to the lactam entity. In their paper, pramanicin was depicted (arbitrarily) as *ent*-**7**. This work clearly establishes the relative stereochemistry to be as in isomer **9**. However, the optical rotation of isomer **9** ($[\alpha]_D^{25}$ +28.8, *c* 0.21 in MeOH) is of opposite sign to that reported for authentic pramanicin ($[\alpha]_D^{25}$ −31.5, *c* 0.21 in MeOH) and thus indicates the absolute stereochemistry of pramanicin to be that of **1**.‖

We thank Dr R. E. Schwartz at the Merck Research Laboratories for the generous donation of authentic pramanicin, GlaxoWellcome Research Ltd. for the endowment (to A. G. M. B.), the Wolfson Foundation for establishing the Wolfson Centre for Organic Chemistry in Medical Science at Imperial College, the Royal Society for a Dorothy Hodgkin Fellowship (to M. L. S.), Celltech Therapeutics for their financial support (to N. S. S.) and the EPSRC.

Notes and references

† Harrison and co-workers have also published a biomimetic synthesis of the fatty acid side chain of pramanicin in racemic form; see ref. 3.

‡ Aldehyde **3** was prepared from (*E*)-dodec-2-enol *via* Sharpless asymmetric epoxidation, oxidation to the aldehyde using Dess–Martin periodinane, Horner–Emmons homologation under standard conditions and reduction of the α,β-unsaturated ester using DIBAL-H followed by oxidation to give aldehyde **3**, again employing Dess–Martin periodinane as oxidant (55% overall)

§ Lactam **2** was prepared from pyroglutamic acid methyl ester *via* $NaBH_4$ reduction to the alcohol, protection of the alcohol as the TBDMS ether and Boc protection of the amide under standard conditions. α-Selenation employing LDA and phenylselenyl bromide followed by *syn* elimination using hydrogen peroxide and pyridine afforded lactam **2** (46% overall).

¶ Full details of the X-ray crystallographic studies on lactam **11** will be reported elsewhere.

‖ Note added at proof: Harrison and co-workers have recently determined the absolute stereochemisty of the lactam entity of pramanicin from biosynthetic considerations; see ref. 9.

1 R. E. Schwartz, G. L. Helms, E. A. Bolessa, K. E. Wilson, R. A. Giacobbe, J. S. Tkacz, G. F. Bills, J. M. Liesch, D. L. Zink, J. E. Curotto, B. Pramanik and J. C. Onishi, *Tetrahedron*, 1994, **50**, 1675.
2 P. H. M. Harrison, D. W. Hughes and R. W. Riddoch, *Chem. Commun.*, 1998, 273.
3 C. Cow, D. Valentini and P. Harrison, *Can. J. Chem.*, 1997, **75**, 884.
4 K. Tamao, N. Ishida, T. Tanaka and M. Kumada, *Organometallics*, 1983, **2**, 1694. For a review on the oxidation of the carbon–silicon bond see G. R. Jones and Y. Landais, *Tetrahedron*, 1996, **52**, 7599.
5 I. Fleming, R. Henning, D. C. Parker, H. E. Plaut and P. E. J. Sanderson, *J. Chem. Soc., Perkin Trans. 1*, 1995, 317.
6 W. Adam and A. K. Smerz, *Tetrahedron*, 1996, **52**, 5799.
7 T. Apelqvist and D. Wensbo, *Tetrahedron Lett.*, 1996, **37**, 1471
8 A. S. Pilcher and P. DeShong, *J. Org. Chem.*, 1993, **58**, 5130.
9 P. Duspara, S. I. Jenkins, D. W. Hughes and P. H. M. Harrison, *Chem. Commun.*, 1998, 2643.

Communication 8/07988I

O-Neophyl-type 1,2-phenyl rearrangement initiated by electron transfer: development of kinetic probes of dissociative electron transfer

Robert L. Donkers, Joseph Tse and Mark S. Workentin*

Department of Chemistry, The University of Western Ontario, London, ON, Canada N6A 5B7. E-mail: mworkent@julian.uwo.ca

Received (in Corvallis, OR, USA) 7th October 1998, Accepted 18th November 1998

The first example of an O-neophyl-type rearrangement in a distonic radical anion was found in the electron transfer induced dissociative reduction of 9,10-diphenyl-9,10-epidioxyanthracene.

Electron transfer (ET) to endoperoxides and peroxides results in the cleavage of the weak oxygen–oxygen (O–O) bond.[1–5] This process proceeds in peroxides and endoperoxides generally by a dissociative ET mechanism,[1–6] in which ET and O–O bond fragmentation are concerted [eqn. (1) or (2)]. Only in the case of

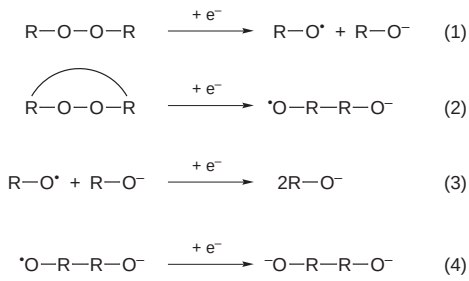

tert-butyl-*p*-cyanoperbenzoate is there evidence for a transition to a stepwise mechanism with formation of the intermediate radical anion.[5] Such mechanistic studies are important because electron transfer processes of peroxides and endoperoxides play a key role in their activity in chemical and biological systems.[7,8] For example, Fe^{II}-promoted ET reduction of the O–O bond in the antimalarial endoperoxide artemisinin and its semi-synthetic derivatives has recently been shown to be the key step in its antimalarial activity.[9,10] In the cases studied to date using direct electrochemical methods, the alkoxy radical fragment produced in the dissociative reduction (R–O· for acyclic peroxides or ·O–R–R–O⁻ for endoperoxides) is reduced in a second ET [eqn. (3) or (4)]; *i.e*. no reactivity resulting from the alkoxyl radical fragment is observed.[1–5] Since the initial O–O bond reduction is dissociative, the alkoxyl radical fragment is generated at the electrode that is at a potential more negative than the reduction potential of the R–O· fragment. Therefore, the alkoxyl radical is reduced spontaneously because of the large driving force. Here we report the first observed[11] reactivity from the alkoxyl radical in the ·O–R–R–O⁻ distonic radical anion formed in a heterogenous dissociative ET, namely a 1,2-phenyl migration (O-neophyl rearrangement). This O-neophyl-type rearrangement of a phenyl group to the alkoxyl radical fragment occurs in the distonic radical anion formed by electrochemical single ET to the O–O bond in the endoperoxide 9,10-diphenyl-9,10-epidioxyanthracene (**DPA-O_2**). In addition to being the first example of this type of reaction, this rearrangement occurs at the expense of the reduction of the alkoxyl radical portion of the distonic radical anion [eqn. (4)]. This suggests that systems such as these can be developed as kinetic probes of the rate of the second heterogeneous ET [eqn. (3) and (4)].

Electrochemical reduction of **DPA-O_2** was investigated in MeCN and DMF solutions containing 0.1 M tetraethylammonium perchlorate (TEAP) using cyclic voltammetry (CV).[12] In MeCN, **DPA-O_2** is reduced with a peak potential (E_p) of −1.12 V *vs*. SCE at a scan rate (v) of 0.1 V s^{-1} and the E_p shifts to more negative potentials with increasing scan rate. The irreversible reduction wave is very broad, with a peak width ($E_p - E_{p/2}$) of 148 mV (at 0.1 V s^{-1}) and α values[13] of 0.32, 0.27, 0.23 and 0.21 at 0.1, 1, 5 and 10 V s^{-1}. These voltammetric characteristics are consistent with the reduction of **DPA-O_2** being dissociative.[6] A representative cyclic voltammogram is shown in Fig. 1(*a*). Following the dissociative reduction wave there is a second reversible redox couple at a more negative potential. The reduction wave of this couple[14*a*] is not well-defined until the potential is scanned to more negative values. This feature and the reversibility of this 1 F mol^{-1} process[14*b*] are illustrated in Fig. 1(*b*). This reversible reduction at −1.804 V *vs*. SCE was identified as 9-phenoxy-10-phenylanthracene (**PPA**) by product isolation and characterization, and by its standard reduction potential ($E°$). The amount of **PPA** formed in the CV experiment depends on the scan rate and the time the potential is held at values more negative than *ca*. −1.9 V. Based on peak current measurements (i_p) the formation of **PPA** is quantitative on the cyclic voltammetry timescale at very slow scan rates and when the potential is held at the negative potentials.[15] Also observed in the CV on the return cycle are two weak oxidation waves; these disappear on addition of a weak acid (see Fig. 1) and are assigned to electrogenerated basic intermediates. In no case was there evidence for direct reduction of the distonic radical anion leading to the corresponding 9,10-diol, **DPA-$(OH)_2$** (Path **A** in Scheme 1), contrary to that observed in all other peroxide/endoperoxide systems studied to date.[1–5]

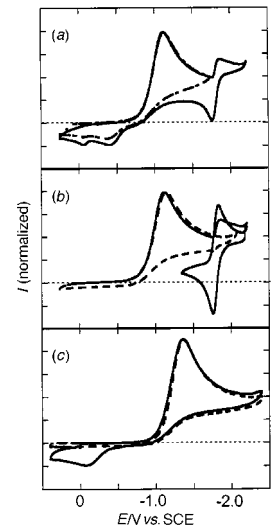

Fig. 1 (*a*) Cyclic voltammogram showing the reduction of a 2 mM solution of **DPA-O_2** in 0.1 M TEAP/MeCN at 0.2 V s^{-1}. (*b*) CV as in (*a*) where the potential was held at the negative potential limit for 30 s prior to the positive scan. The CV shown in the dashed line is that measured after the addition of 5 equiv. of 2,2,2-trifluorethanol. (*c*) Cyclic voltammogram showing the reduction of a 2.8 mM solution of **DMA-O_2** in 0.1 M TEAP/MeCN at 0.1 V s^{-1} both in the presence (solid line) and the absence (dashed line) of 2,2,2-trifluoroethanol.

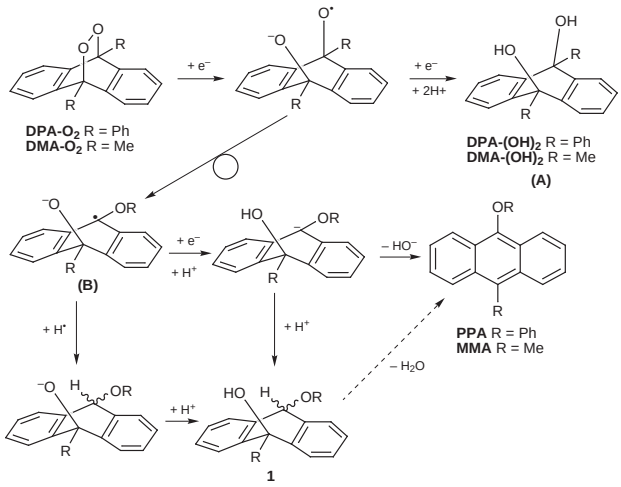

Scheme 1

In contrast, reduction of 9,10-dimethyl-9,10-epidioxyanthracene (**DMA-O_2**) generates the corresponding 9,10-diol [**DMA-$(OH)_2$**] quantitatively *via* a two-electron (2 F mol^{-1}) reduction (Path **A** in Scheme 1). No evidence for 9-methoxy-10-methylanthracene (**MMA**) was found. Other voltammetric characteristics are similar to **DPA-O_2**: E_p = −1.35 V *vs*. SCE at 0.1 V s^{-1}, a peak width ($E_p - E_{p/2}$) of 153 mV (at 0.1 V s^{-1}) yielding α values of 0.31, 0.27 and 0.25 at 0.1, 1 and 10 V s^{-1}. Since this is a two electron process the shift of E_p to more negative potentials by 113 mV/(log ν) gives an average α value of 0.25.

We rationalize formation of **PPA** in the reduction of **DPA-O_2** by an O-neophyl-type rearrangement from the initially formed distonic radical anion (path **B** in Scheme 1); specifically the distonic radical anion undergoes a 1,2-phenyl migration to the alkoxyl radical center to generate the carbon-centered radical intermediate. At the potential where **DPA-O_2** is reduced (E_p = −1.12 V *vs*. SCE) the resulting diarylphenoxymethyl radical is not expected to be reduced.[16] This intermediate can be reduced at more negative potentials and eventually lead to **PPA** *via* aromatization with loss of OH^-. This result is consistent with the CV results and was verified by the constant potential electrolysis studies. Electrolysis at −1.2 V does not result in formation of **PPA**; instead it generates *via* a 1 F mol^{-1} process a product that forms **PPA** quantitatively after work-up of the electrolysis mixture. However, if the electrolysis is performed at more negative potentials (−1.6 V) **PPA** is formed quantitatively consuming 2 F mol^{-1}. Likewise if the electrolyses are performed in the presence of a weak acid like 2,2,2-trifluorethanol or acetanilide, **PPA** is not the initial product, but it is the only product isolated after work-up. We suggest that in these latter experiments **1** is formed by trapping the intermediate formed after the O-neophyl rearrangement. No **DPA-$(OH)_2$**, which is stable to the work-up conditions, is isolated.

The O-neophyl rearrangement occurs exclusively; no diol, which would be generated on reduction corresponding to eqn. (4), is observed. Thus, the rearrangement must occur with a rate faster than the rate of the heterogeneous ET reduction of the alkoxyl radical formed on the dissociative reduction. The reduction potential of $Ph_3C–O^{\cdot}$ ($E°_{Ph_3CO^{\cdot}/Ph_3CO^-}$) is −0.03 V *vs*. SCE;[4] thus the driving force for reduction of the alkoxyl radical at −1.2 V is favorable by at least 23 kcal mol^{-1}. By analogy to the rate constant reported by Falvey *et al*. for the rearrangement of the triphenylmethoxyl radical to α-phenoxydiphenylmethyl radical we expect the O-neophyl rearrangement to be occurring with a rate constant in the order of 5×10^{10} s^{-1} or greater.[17] Thus, the rate of the second ET cannot compete with the O-neophyl rearrangement. This puts an upper timescale by which to compare the rate of the second heterogenous ET. Similar O-neophyl rearrangements were not reported during the electrochemical reduction of $Ph_3CO–OCPh_3$ or $Ph_3CO–OBu^t$,[4] suggesting that there may be a stereoelectronic effect on the rearrangement in the **DPA-O_2** system.

In the reduction of **DMA-O_2** the corresponding 1,2-methyl shift or β-scission does not compete with reduction of the distonic radical anion. Although the β-scission reaction is not known for $Ph_2MeCO^{\cdot}$ the rate constant of the 1,2-methyl shift rate is estimated to be 4.4×10^6 s^{-1}.[17] This provides a lower rate limit to compare the second heterogenous ET.

Observation of this O-neophyl rearrangement in the reduction of **DPA-O_2** may provide a method to quantify the partitioning ratio (if any) between the charge and spin in the distonic radical anions formed on reduction of unsymmetrically substituted endoperoxides (for example, 9-methyl-10-phenyl-9,10-epidioxyanthracene). Studies of this type are currently in progress. Also in progress are studies addressing the generality of this type of rearrangement on the reduction of other polycyclic aromatic endoperoxides and other aryl substituted endoperoxides, in an attempt to provide 'clock' reactions for secondary reduction of distonic radical anions (and its implications on the theory of dissociative ET).

This work is supported financially by NSERC and UWO.

Notes and references

1 M. S. Workentin and R. L. Donkers, *J. Am. Chem. Soc*., 1998, **120**, 2664; R. L. Donkers and M. S. Workentin, manuscript in preparation.
2 R. L. Donkers and M. S. Workentin, *J. Phys. Chem. B,* 1998, **102**, 4061.
3 M. S. Workentin, F. Maran and D. D. M. Wayner, *J. Am. Chem. Soc*., 1995, **117**, 2120.
4 S. Antonello, M. Musumeci, D. D. M. Wayner and F. Maran, *J. Am. Chem. Soc*., 1997,**119**, 9541.
5 S. Antonello and F. Maran, *J. Am. Chem. Soc*., 1997, **119**, 12595.
6 J.-M. Savéant, in *Advances in Electron Transfer Chemistry*, ed. P. S. Mariano, 1994, vol. 4, pp. 53–116 and references cited therein.
7 *Organic Peroxides*, ed. W. Ando, Wiley, Chichester, England, 1992.
8 *Active Oxygen in Chemistry*, *Search Series Vol. 2*, ed. C. S. Foote, J. S. Valentine, A. Greenberg and J. F. Lieban, Blackie, New York, 1995; *Active Oxygen in Biochemistry*, *Search Series Vol. 3*, ed. C. S. Foote, J. S. Valentine, A. Greenberg and J. F. Lieban, Blackie, New York, 1995.
9 W.-M. Wu, Y. Wu, Y.-L. Wu, Z.-J. Yao, C.-M. Xhou, Y. Li and F. Shan, *J. Am. Chem. Soc*., 1998, **120**, 3316.
10 G. H. Posner, S. B. Park, L. González, D. Wang, J. N. Cumming, D. Klinedinst, T. A. Shapiro and M. D. Bachi, *J. Am. Chem. Soc*., 1996, **118**, 3537; J. N. Cumming, D. Wang, S. B. Park, T. A. Shapiro and G. H. Posner, *J. Med. Chem*., 1998, **41**, 952 and references therein; A. Robert and B. Meunier, *Chem. Soc. Rev*., 1998, **27**, 273.
11 The reduction of 9,10-dihydro-9,10-epidioxyanthracene was reported in the paired electrosynthesis of anthracene and oxygen on the femtolitre scale: C. Amatore and A. R. Brown, *J. Am. Chem. Soc*., 1996, **118**, 1482.
12 Electrochemical experiments were performed using standard equipment and electrodes as described in ref. 1. All potentials were calibrated internally to ferrocene ($E°_{Fc^+/Fc}$ is 0.449 and 0.475 *vs*. SCE in MeCN and DMF, respectively). Data in DMF is similar and will be reported in the full account of this work.
13 The transfer coefficient (or symmetry factor) α is defined as $\partial\Delta G^{\ddagger}/\partial\Delta G°$, where $\Delta G^{\ddagger}$ is the free energy of activation and $\Delta G°$ is the free energy of the ET.
14 (*a*) The reduction of **DPA-O_2** is a 1 F mol^{-1} process except under the conditions indicated later. Full details including simulations will be reported separately. (*b*) Determined by comparison of the peak current (i_p) of PPA formed in an electrolysis with that measured with a known concentration of an authentic sample of **PPA**.
15 At higher scan rates the amount of **PPA** formed in the CV is less than quantitative; its presence by CV is absent at scan rates higher than 75 V s^{-1}. In product studies the amount of product derived from the O-neophyl rearrangement is always quantitative. This may be due to a rate limiting aromatization.
16 The reduction potential of the triphenylmethyl radical is at least −1.2V *vs*. SCE and that of tritolylmethyl radical is −1.36 V *vs*. SCE (S. Bank, C. Ehrlich and J. A. Zubieta, *J. Org. Chem*., 1979, **44**, 1454).
17 D. E. Falvey, B. S. Khambatta and G. B. Schuster, *J. Phys. Chem*., 1990, **94**, 1056.

Communication 8/07795I

ChemComm

New 1,4,7-triazacyclononane-based functional analogues of the Fe/Cu active site of cytochrome *c* oxidase: structure, spectroscopy and electrocatalytic reduction of oxygen

James P. Collman,* Reinhold Schwenninger, Miroslav Rapta, Martin Bröring and Lei Fu

Department of Chemistry, Stanford University, Stanford, CA 94305, USA. E-mail: jpc@chem.stanford.edu

Two new covalently linked functional model compounds for the Fe_{a3}/Cu_B active sites of heme-copper oxidases have been prepared and characterized by novel synthetic methodologies; the X-ray structure of the Zn form and the electrocatalytic reduction of O_2 by the Fe/Cu forms are reported.

Cytochrome *c* oxidase (C*c*O) is a membrane-bound metalloenzyme which catalyzes the $4e^-$, $4H^+$ reduction of O_2 to H_2O.[1] Toxic intermediates such as H_2O_2 and HO_2^- are not released during this exergonic reaction. The energy produced by the O_2 reduction is coupled to proton translocation, contributing to the protomotive force which drives conversion of ADP to ATP.[2] Recent X-ray structures of bacterial[3] and mammalian[4] forms of this enzyme have initiated increased activity among biomimetic chemists.[5] There are several unresolved issues concerning the mechanism of O_2 reduction at the heme a_3/Cu_B bimetallic center: (a) the role of the Cu_B and Tyr residue in O_2 binding and activation, (b) the nature of the peroxy-intermediate, and (c) the possible involvement of an imidazole ligand in the proton pumping mechanism.[1,6]

The construction of covalently-linked functional model compounds which closely resemble the Fe_{a3}/Cu_B active site is an important part of the effort to resolve these issues. We have previously reported the synthesis and catalytic activity of two such model compounds prepared by a congruent multiple Michael addition methodology.[7] Of these, the 1,4,7-triazacyclononane- (TACN) 'capped' Co/Cu and *N*,*N*′,*N*″-tribenzyltris(aminoethyl)amine- (TBTren) 'capped' Fe/Cu complexes have shown $4e^-$, $4H^+$ electrocatalytic reduction of O_2 to H_2O at physiological pH. Prompted by these encouraging results we have developed a more flexible synthetic strategy[8] and prepared two new TACN-capped porphyrins, **1** and **2** (Scheme 1), with different covalently attached axial ligands.

Herein, we describe a new methodology for the selective incorporation of Zn(II) or Fe(II) into these new ligands. We present ^{1}H NMR analysis of the free base, Zn(II), Fe(II), Zn(II)/Cu(I), and Fe(II)/Cu(I) forms as a useful tool for partial elucidation of the conformations of these complexes in solution. Furthermore, we report the crystal structure of the pyridine-tailed Zn(II) complex—the first structural characterization within this family of compounds. Finally we present preliminary results on the electrocatalytic reduction of O_2 to H_2O by these new Fe/Cu model compounds.

Porphyrinato–Zn(II) complexes **3a** and **4a** are diamagnetic, redox-inactive analogues of the porphyrinato–Fe(II) complexes. These are easily prepared by reaction of the free base with an excess of zinc acetate, followed by basic-alumina filtration using a solvent saturated with NH_3(g). Selective introduction of Fe(II) into the porphyrin is achieved by the reaction of the free base porphyrin with excess $FeBr_2$ without using external base, followed by basic-alumina filtration.[9] Final Zn(II)/Cu(I) and Fe(II)/Cu(I) complexes **5** and **6** are prepared by the reaction of the appropriate porphyrinato complex with copper(I) triflate.[10]

The ^{1}H NMR spectra of **2** and its Zn(II) complex **4a** are compared in Fig. 1. The desired $\alpha_3\beta$ symmetry of the porphyrin

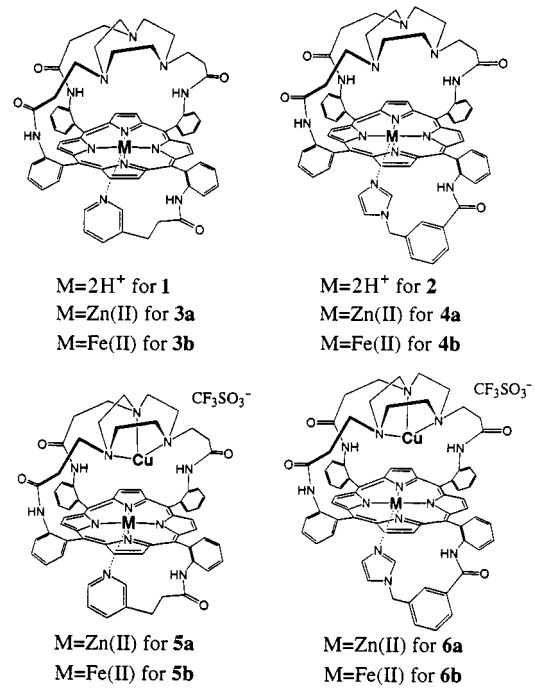

Scheme 1

core can be deduced from the pattern of β-pyrrolic and phenyl resonances.[11] The broad, upfield-shifted CH_2 resonances of the TACN ligand confirm the flexible structure of the cap as well as its location above the porphyrin ring. Introduction of Zn(II) into the porphyrin results in significant upfield shifts for the axial ligand resonances: signals *ortho* to the coordinated nitrogen are shifted by > 3.5 ppm, reflecting the close proximity to the porphyrin ring. The two *ortho* proton resonances of the axial base in the Fe(II)CO forms[9] are at higher field than in the Zn(II)

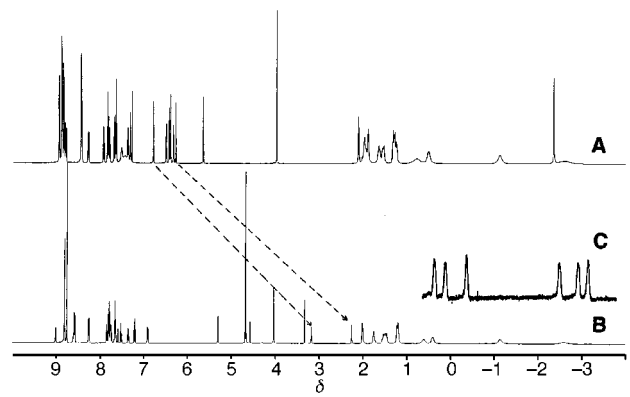

Fig. 1 ^{1}H NMR spectra ($CDCl_3$) of the free base porphyrin **2** (spectrum A) and its Zn(II) complex **4a** (spectrum B). Dashed lines illustrate upfield shifts for the axial ligand resonances in complex **4a**. Trace C shows sharpening of the TACN cap resonances in Zn(II)/Cu(I) complex **6a**.

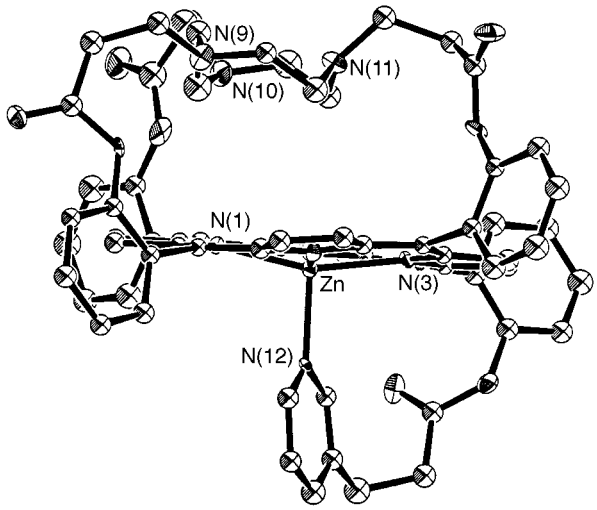

Fig. 2 Thermal ellipsoid plot of the molecular structure of **3a**. Selected bond lengths (Å) and bond angles (°): Zn–N(1) 2.064(9), Zn–N(2) 2.075(8), Zn–N(3) 2.095(8), Zn–N(4) 2.095(8), Zn–N(12) 2.109(9); N(1)–Zn–N(2) 88.1(3), N(1)–Zn–N(3) 159.0(4), N(1)–Zn–N(12) 100.4(4), N(2)–Zn–N(3) 89.2(3), N(2)–Zn–N(4) 160.2(4), N(2)–Zn–N(12) 101.9(3), N(3)–Zn–N(4) 87.5(3), N(3)–Zn–N(12) 100.5(4), N(4)–Zn–N(12).

complexes, which is consistent with stronger coordination of the axial ligand to Fe(II). The high-field portion of the spectrum for the Zn(II)/Cu(I) complex **6a** (Fig. 1, trace C) shows a significant sharpening of the TACN cap resonances, consistent with a single conformation in solution.

The geometry of the empty-cap porphyrinato–Zn(II) complex **3a** was further eluciated by single crystal X-ray diffraction.[12] The thermal-ellipsoid plot is shown in Fig. 2 with key bond distances and bond angles. The zinc atom shows an expected distorted square-pyramidal geometry with the four porphyrin nitrogens in equatorial positions [average Zn–N distance of 2.074(9) Å] and a pyridine ligand occupying an apical position [Zn–N_{pyr} distance of 2.109(9) Å]. The Zn atom is displaced 0.37 Å from the porphyrin plane, which shows a moderate degree of ruffling similar to those of related Zn and Fe porphyrin complexes.[13] The TACN cap is in a chair conformation which is probably preferred for efficient crystal packing. This conformation must change upon coordination of Cu(I) in order to achieve effective binding to all three nitrogen ligands. Other bond distances and bond angles are similar to those of the related compounds and will be analyzed in detail elsewhere.

In their reduced forms, Fe(II)/Cu(I) complexes **5b** and **6b** show UV–VIS spectra identical to those of the Fe(II)–porphyrinato precursors.[9] On the other hand, incorporation of Cu(I) (as the triflate salt) has a significant effect on the complexes' reactivities toward O_2, as well as their solubilities in organic solvents. Reversible binding of O_2 to the emtpy-cap Fe(II) complexes becomes irreversible with the FeCu complexes, resulting in the formation of an apparent peroxo–Fe(III) (O_2^{2-}) Cu(II) intermediate [λ_{max} 422 nm (Soret)]. In dry toluene or acetononitrile a 'peroxo-signature' around 800 cm^{-1} can be detected by IR spectroscopy. Addition of protic solvent (*e.g.* methanol) or exposure to the atmosphere results in complete disappearance of this vibrational mode, indicating a fast decomposition of the peroxo-species in the presence of protons.

The electrocatalytic reduction of O_2 by these Fe/Cu complexes have been studied by rotating graphite disc–platinum ring voltammetry.[14] Both new complexes show predominantly $4e^-$ reduction of O_2 to H_2O, with a negligible production of peroxide, as determined by the comparison of the ring and disc currents. The half-wave potential for the electroreduction of O_2 is 45 mV more positive for the imidazole-tailed complex **6b** in comparison with the pyridine-tailed complex **5b**. These results show that our new Fe/Cu complexes are functional models of the C*c*CO Fe_{a3}/Cu_B active site, and together with our related studies,[7] represent a prime example of fine-tuning their catalytic properties by small structural changes in the porphyrin ligand. We consider these new robust, capsule-like Fe/Cu complexes to be ideal model compounds for solution catalytic studies and for the isolation and structural characterization of various forms of the cytochrome *c* oxidase Fe_{a3}/Cu_B active site.

We thank the NIH (grant 5R37 GM-17880-26) and the NSF (grant CHE9123187-A2) for financial support. We thank Dr Tapan K. Lae for his assistance with X-ray crystallography.

Notes and references

1 S. Ferguson-Miller and G. T. Babcock, *Chem. Rev.*, 1996, **96**, 2889.
2 M. Wikström, *Nature*, 1977, **266**, 271.
3 S. Iwata, C. Ostermeier, B. Ludwig and H. Michel, *Nature*, 1995, **376**, 660.
4 T. Tsukihara, H. Aoyama, E. Yamashita, T. Tomizaki, H. Yamaguchi, K. Sinzawa-Itoh, R. Nakashima, R. Yaono and S. Yoshikawa, *Science*, 1995, **269**, 1069; T. Tsukihara, H. Aoyama, E. Yamashita, T. Tomizaki, H. Yamaguchi, K. Shinzawa-Itoh, R. Nakashima, R. Yaono and S. Yoshikawa, *Science*, 1996, **272**, 1136.
5 For Fe/Cu complexes with a covalently attached Cu binding site see: V. Bulach, D. Mandon and R. Weiss, *Angew. Chem., Int. Ed. Engl.*, 1991, **5**, 572; T. Sasaki and Y. Naruta, *Chem. Lett.*, 1995, 650; J. O. Baeg and R. H. Holm, *Chem. Commun.*, 1998, 571; T. Sasaki, N. Nakamura and Y. Naruta, *Chem. Lett.*, 1998, 351; F. Tani, Y. Matsumoto, Y. Tachi, T. Sasaki and Y. Naruta, *Chem. Commun.*, 1998, 1731.
6 T. Kitagawa and T. Ogura, *Prog. Inorg. Chem.*, 1997, **45**, 431; A. Sucheta, K. E. Georgiadis and Ó Einarsdóttir, *Biochemistry*, 1997, **36**, 554; S. Yoshikawa, *Curr. Opin. Struct. Biol.*, 1997, **7**, 574; S. Yoshikawa, K. Shinzawa-Itoh, R. Nakashima, R. Yaono, E. Yamashita, N. Inoue, M. Yao, M. Fei, C. P. Libeu, T. Mizushima, H. Yamaguchi, T. Tomizaki and T. Tsukihara, *Science*, 1998, **280**, 1723.
7 J. P. Collman, L. Fu, P. C. Herrmann and X. Zhang, *Science*, 1997, **275**, 949; J. P. Collman, *Inorg. Chem.*, 1997, **36**, 5145; J. P. Collman, L. Fu, P. C. Herrmann, Z. Wang, M. Rapta, M. Bröring, R. Schwenninger and B. Boitrel, *Angew. Chem.*, 1998, in press.
8 J. P. Collman, M. Bröring, L. Fu, M. Rapta, R. Schwenninger and A. Straumanis, *J. Org. Chem.*, 1998, **63**, 8082; J. P. Collman, M. Bröring, L. Fu, M. Rapta and R. Schwenninger, *J. Org. Chem.*, 1998, **63**, 8084.
9 Iron(II)–porphyrin **3b**: MS(LSIMS$^+$): *m/z* 1152.3 (MH^+) for $C_{67}H_{60}N_{12}O_4Fe$. UV–VIS (MeCN): λ_{max} 445 (Soret), 565 nm. ^{1}H NMR ($CDCl_3$): δ 48–54 (four broad peaks characteristic of β-pyrrolic protons on a paramagnetic five-coordinate iron (S = 2) porphyrin with $\alpha_3\beta$ symmetry. ^{1}H NMR ($CDCl_3$ under CO atmosphere, axial ligand resonances only): δ 6.15(d, 1H), 5.22(m, 1H), 1.52(d, 1H), 1.37(s, 1H).
Iron(II)–porphyrin **4b**: MS(LSIMS$^+$): *m/z* 1204.3 (MH^+) for $C_{70}H_{61}N_{13}O_4Fe$. UV–VIS (MeCN): λ_{max} 444 (Soret), 566 nm. ^{1}H NMR ($CDCl_3$): δ 48–54 (m, see above); ^{1}H NMR ($CDCl_3$ under CO atmosphere, axial ligand resonances only): δ 7.24(d, 1H), 6.95(m, 1H), 6.62(d, 1H), 4.68(s, 1H), 3.62(s, 2H), 3.37(s, 1H), 2.05(s, 1H), 2.31(s, 1H). Full analysis by 1D and 2D ^{1}H NMR spectroscopy of Zn(II) and Fe(II) complexes **3** and **4** will be published elsewhere.
10 MS (LSIMS$^+$): *m/z* 1224.9 (MH^+) for $C_{68}H_{60}N_{12}O_4ZnCu$ (for Zn/Cu complex **5a**); *m/z* 1274.1 for $C_{70}H_{61}N_{13}O_4ZnCu$ (for Zn/Cu complex **6a**); *m/z* 1217.2 (MH^+) for $C_{68}H_{60}N_{12}O_4FeCu$ (for Fe/Cu complex **5b**); *m/z* 1266.3 for $C_{70}H_{61}N_{13}O_4FeCu$ (for Fe/Cu complex **6b**). The spectra match the calculated isotope distributions exactly.
11 Y. Sun, E. A. Martell and M. Tsutsui, *J. Heterocycl. Chem.*, 1986, **23**, 561.
12 *Crystal data*: $ZnC_{67}H_{60}N_{12}O_4{\cdot}3CHCl_3$, M = 1520.80, triclinic, space group $P\bar{1}$, a = 13.3435(8), b = 13.5214(8), c = 20.850(1) Å, α = 103.096(1), β = 91.287(1), γ = 111.723(1)°, V = 3380.1(3) Å^3, Z = 2, D_c = 1.494 g cm^{-3}, T = −146 °C, μ = 0.779 mm^{-1}, $R(R_w)$ = 0.098(0.112). All C atoms have been refined isotopically. CCDC 182/1090. See http://www.rsc.org/suppdata/cc/1999/137/ for crystallographic files in .cif format.
13 J. P. Collman, P. C. Herrmann, L. Fu, T. A. Eberspacher, M. Eubanks, B. Boitrel, P. Hayoz, X. Zhang, J. I. Brauman and V. W. Day, *J. Am. Chem. Soc.*, 1997, **119**, 3481 and references therein.
14 (*a*) T. Geiger and F. C. Anson, *J. Am. Chem. Soc.*, 1981, **103**, 7489; (*b*) J. Koutecky and V. G. Levich, *Zh. Fiz. Khim.*, 1956, **17**, 203; (*c*) Half-wave potentials (*vs.* SSCE) for the reduction of O_2 in air-saturated phosphate buffer (pH = 7) at a graphite disk electrode coated with catalyst and rotated at 200 rpm are −95 and −50 mV for **5b** and **6b**, respectively. Number of electrons involved in the reduction of O_2 as estimated from the slopes of Koutecky–Levich plots[14b] are n_{app} = 3.89 for **5b** and n_{app} = 3.92 for **6b**.

Communication 8/07598K

Functional transformation of aldehydes and ketones *via* homolytic induced decomposition of unsaturated peroxy acetals and peroxy ketals

L. Moutet, D. Bonafoux, M. Degueil-Castaing and B. Maillard*

Laboratoire de Chimie Organique et Organométallique, associé au CNRS UMR 5802, Université Bordeaux 1, F-33405 Talence-Cedex, France. E-mail: b.maillard@lcoo.u-bordeaux.fr

Received (in Cambridge, UK) 30th October 1998, Accepted 23rd November 1998

Induced decomposition of unsaturated peroxy acetals prepared from trimethyl orthoformate, dodecanal or 2-methylundecanal and 2,3-dimethyl-2-hydroperoxybut-3-ene, in the presence of ethyl iodoacetate, CCl_4 or dodecanethiol, allowed respectively their iodo-, chloro- and hydrodecarbonylation with yields of over 70%; the same reaction applied to the monoperoxy ketal or diperoxy ketal of cyclohexanone in the presence of ethyl iodoacetate resulted in its functional transformation in methyl 6-iodohexanoate or 1,5-diiodopentane with respective yields of 65 and 40%.

In the last decades, reactions involving free radicals have been increasingly used[1] in synthesis for the creation of carbon–carbon and carbon–heteroatom bonds. Another important field of interest for free radical reactions is the functional transformations one, pioneered by Barton and his group[2] with the development of the chemistry related to *O*-acyl thiohydroxamates. This allows the reductive decarboxylation of an acid or its decarboxylative transformation into a halide, sulfone, nitrile, alcohol *etc*. This methodology is based on a free radical chain reaction, in which the decarboxylation step is the classical generation of an alkyl radical from an acyloxy one.

In the last few years, our attention turned to the reactivity of unsaturated peroxy acetals and peroxy ketals, *via* polymer chemistry,[3] since it was shown that their corresponding alkoxy radicals undergo a very rapid β-scission reaction[4] to generate an alkyl radical. Thus, the homolytic induced decomposition of unsaturated peroxy acetals and peroxy ketals, derived from the ethyl 2-(1-hydroperoxyethyl)propenoate, was applied for the preparation of glycidic esters[5] (Scheme 1, path **A**). As this method of producing glycidic esters requires the preparation of a specific unsaturated peroxy derivative for each application, we developed a more general method[6] using ethyl 2-[1-(1-methoxy-1-methylethylperoxy)ethyl]propenoate (Scheme 1, path **B**, R = R′ = Me). In the light of these results and taking into account the fact that no general method for the decarbonylative functionalization of aldehydes has been described,[7] we decided to approach these transformations using the induced decomposition of unsaturated peroxy acetals. Indeed, applying the type of methodology that we have just described (Scheme 1, path **B**, R′ = H), it appeared possible to generate an alkyl iodide from the aldehyde, as it could be obtained from the hemiacetal *via* Suarez's method.[8]

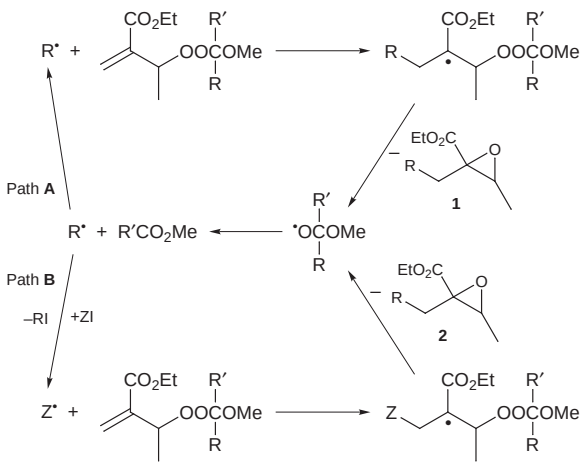

Scheme 1

The decomposition of benzoyl peroxide in a cyclohexane solution of peroxy acetal, obtained from dodecanal, in the presence of a stoichiometric amount of ethyl iodoacetate (relative ratios 0.1:5:1:1.1) afforded the desired 1-iodoundecane (Scheme 1, path **B**, R = $C_{11}H_{23}$, R′ = H) in a 60% yield. In order to check the general character of this reaction, ethyl iodoacetate was replaced by CCl_4: 1-chloroundecane was obtained but with a much lower yield than the corresponding iodide, even when operating in neat perhalogeno solvent (25%). Moreover, in addition to the expected epoxide **2** (Z = CCl_3), the formation of epoxide **1** (R = $C_{11}H_{23}$) with a 46% yield was observed, showing that competition occurred for the alkyl radical between chlorine atom abstraction and addition to the activated double bond of the peroxy acetal. Thus, in order to achieve an effective decarbonylative functionalization of the aldehyde, it appears that the double bond of the peroxy acetal should not be too reactive towards the produced alkyl radical, but very reactive towards the radical $Z^{\cdot}$, formed in the atom transfer with ZX.

Allylic hydroperoxides, possessing a terminal double bond with no electron-withdrawing substituent on it, appeared to be attractive candidates as starting materials for the synthesis of the desired unsaturated peroxy acetals. The easy preparation of allylic hydroperoxides by reaction of singlet oxygen with alkenes[9] prompted us to test the ones produced from the photooxygenation of 2,3-dimethylbut-2-ene (2,3-dimethyl-2-hydro-peroxybut-3-ene), 2-methylbut-2-ene (a mixture of 2-methyl-2-hydroperoxybut-3-ene and 3-methyl-2-hydroperoxybut-3-ene) and 6,7,7-trimethylbicyclo[3.1.1]hept-5-ene (7,7-dimethyl-5-hydroperoxy-6-methylenebicyclo[3.1.1]heptane). The thermolysis of benzoyl peroxide in mixtures of the corresponding peroxy acetals of dodecanal and CCl_4 (relative molar ratios: 0.1:1:5) afforded the 1-chloroundecane in 72, 62 and 42% yield, respectively. These results led us to replace ethyl 2-(1-hydroperoxyethyl)propenoate with 2,3-dimethyl-2-hydroperoxybut-3-ene. The general method for achieving decarbonylative functionalization of the aldehyde is summarized in Scheme 2.

Having determined the appropriate nature of the unsaturated peroxide, it was necessary to optimize the temperature of the reaction. Indeed, in addition to the expected 1-chloroundecane, methyl dodecanoate was obtained (with a yield of about 5% relative to the peroxy ketal). The formation of this compound could be attributed to the disproportionation, in the solvent cage, of the oxyl radicals formed by the spontaneous decomposition of the unsaturated peroxy acetal.[10] Performing the same reaction at room temperature with initiation by BEt_3–O_2 (a BEt_3 solution in hexane was added slowly to the mixture of the other reactants prepared under air, the needle of the syringe being in the liquid) confirmed this origin since no methyl dodecanoate was detected under these conditions and 1-chloro-

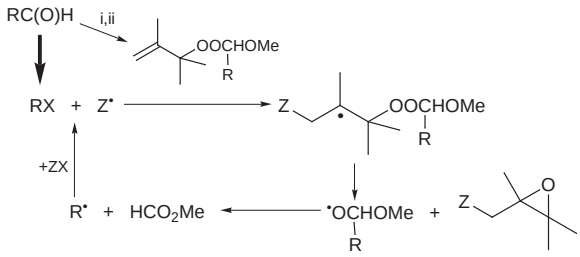

Scheme 2 *Reagents and conditions*: i, $HC(OMe)_3$, TsOH; ii, 2,3-dimethyl-2-hydroperoxybut-3-ene, TsOH.

undecane was obtained with a yield of 86% relative to the starting aldehyde. The iododecarbonylation of dodecanal realized using the same conditions (ethyl iodoacetate–peroxyacetal–cyclohexane: 1.1:1:5; BEt_3–O_2; room temperature) led to 1-iodoundecane with a yield of 75% relative to aldehyde.

The halodecarbonylation of 2-methylundecanal confirmed the general character of this approach since 2-chloroundecane and 2-iodoundecane were also isolated with yields of about 75%.[11] Peroxy acetals formed from aldehydes bearing a tertiary alkyl group have not been studied as a consequence of their lower stability.[12] Moreover, since the decarbonylation of the corresponding acyl radical is a much faster process[13] than that for the one bearing primary and secondary alkyl groups, there is less synthetic need for the setting of such a reaction.

In order to identify possible extensions of this induced decomposition of unsaturated peroxy acetals we decided, on the first hand, to perform the same reaction with both aldehyde derivatives, replacing ethyl iodoacetate by dodecanethiol to achieve the reductive decarbonylations. In each case, undecane was obtained with a yield of about 75%. Thus, this reaction appears to be an attractive alternative, under less drastic conditions, to the direct one designed from the aldehyde by Berman *et al.*[14]

On the other hand, the efficiency of this reaction prompted us to check a possible extension of this methodology to ketones. We therefore tried to achieve the iododeacylation of cyclohexanone. The peroxy ketal was prepared by addition of the hydroperoxide to 1-methoxycyclohexene, with acid catalysis by TsOH, since the reaction of the hydroperoxide with the corresponding acetal leads to a mixture of monoperoxy ketal and diperoxy ketal. The addition of BEt_3 to a non-degassed solution of ethyl iodoacetate and 1-(1,1,2-trimethylprop-2-enylperoxy)-1-methoxycyclohexane in cyclohexane, under the conditions previously described, afforded the desired methyl 6-iodohexanoate (65%) (Scheme 3, Y = Me). The homolytic induced decomposition of cyclohexanone diperoxy ketal, obtained from the corresponding acetal, under the same conditions, but using 2.2 equiv. of ethyl iodoacetate, produced 1,5-diiodopentane in a 40% yield (Scheme 3, Y = CH_2=$CMeCMe_2O$).

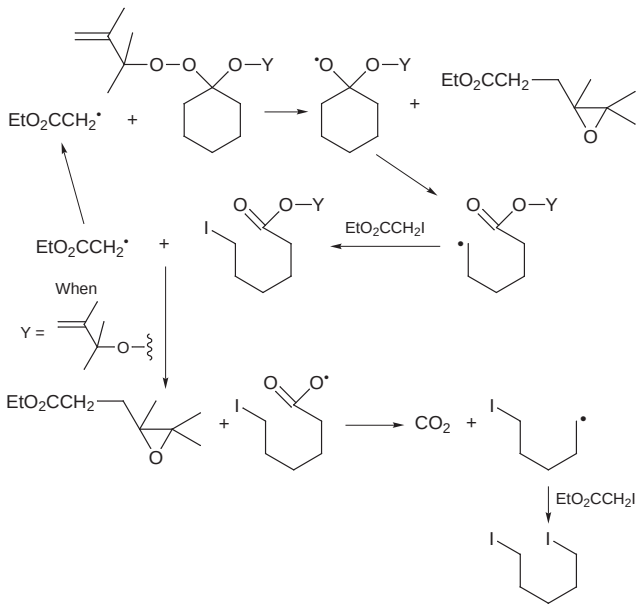

Scheme 3

In conclusion, homolytic induced decomposition of unsaturated peroxy acetals and mono- and di-peroxyketals appears to be a promising way of achieving decarbonylative functionalization of aldehydes and deacylative functionalization of ketones. The search for new X–Z molecules able to generate other useful transformations is in progress in our laboratory.

Notes and references

1 B. Giese, *Free Radicals in Organic Synthesis*: *Formation of Carbon-Carbon Bonds*, Pergamon Press, New York, 1986; M. Ramaiah, *Tetrahedron*, 1987, **43**, 3541; D. P. Curran, *Synthesis*, 1988, 417 and 489; C. P Jasperse, D. P. Curran and J. L. Feuig, *Chem. Rev*., 1991, **91**, 1237; D. P. Curran, in *Comprehensive Organic Synthesis*, ed. B. M. Trost and I. Fleming, Pergamon, Oxford, 1991, vol. 4.

2 D. Crich, *Aldrichim. Acta*, 1987, **20**, 35; D. Crich and L. Quintero, *Chem. Rev*., 1989, **89**, 1413; D. H. R. Barton, *Tetrahedron*, 1992, **48**, 2529; W. B. Motherwell and D. Crich, *Free Radical Chain Reactions in Organic Synthesis*, Academic Press, London, 1992.

3 L. L. T. Vertommen, J. Meijer and B. Maillard, *Int. Pat.*, 1992, WO 92/0953.

4 M. Degueil-Castaing and B. Maillard, unpublished results.

5 D. Colombani and B. Maillard, *J. Chem. Soc*., *Chem. Commun*., 1994, 1259; *J. Org. Chem*.,1994, **59**, 4765.

6 F. Ramon, M. Degueil-Castaing and B. Maillard, *J. Org. Chem*., 1996, **61**, 2071.

7 *Comprehensive Organic Functional Groups Transformation*, ed. A. R. Katritsky, O. Meth-Cohn and C. W. Rees, Pergamon, 1995.

8 P. Armas, C. G. Francisco and E. Suarez, *Angew. Chem., Int. Ed. Engl*., 1992, **31**, 772; P. Armas, C. G. Francisco, E. Suarez, *J. Am. Chem. Soc*., 1993, **115**, 8865.

9 A. P. Schaap, *Singlet Molecular Oxygen, Benchmark Papers in Organic Chemistry Series, vol. 5*, Dowden, Hutchinson and Ross, Stroudsburg, 1976; H. H. Wasserman, R. W. Murray, *Singlet Oxygen*, Academic Press, New York, 1979; A. A. Frimer, *Singlet Oxygen*, CRC Press, Boca Raton, 1985, vol. 2,.

10 C. Helgorsky, A. Saux, M. Degueil-Castaing and B. Maillard, *Tetrahedron*, 1996, **52**, 8263 and cited references.

11 Reaction of the aldehyde with trimethyl orthoformate in presence of TsOH yielded, after elimination of methyl formate and excess orthoformate, the raw acetal. Addition of 2,3-dimethyl-2-hydroperoxybut-3-ene (ref. 6) to the acetal, with continuous distillation of MeOH under vacuum (ref. 5), produced the peroxy acetal. After elimination of TsOH by washing the ethereal solution with sodium carbonate and water, followed by drying over magnesium sulfate, the solvent was removed under vacuum. BEt_3 in hexane was added to a solution of the peroxy acetal and the required atom transfer agent in the reaction solvent (cyclohexane, $CHCl_3$ or CCl_4) until total disappearance of the peroxy acetal as determined by ^1H NMR spectroscopy. After elimination of the solvent and the low boiling reaction products, the expected product was separated by column chromatography (SiO_2).

12 C. Helgorsky, M. Bevilacqua, M. Degueil-Castaing and B. Maillard, *Thermochim. Acta*, 1996, **289**, 55.

13 C. Chatgilialoglu, C. Ferreri, M. Lucarini, P. Pedrielli and G. F. Pedulli, *Organometallics*, 1995, **14**, 2672.

14 J. D. Berman, J. H. Stanley, W. V. Sherman and S. G. Cohen, *J. Am. Chem. Soc*., 1963, **85**, 4010.

Communication 8/08418A

Stereoselectivity in the double reductive alkylation of pyrroles: synthesis of *cis*-3,4-disubstituted pyrrolidines

Timothy J. Donohoe,*[a] Rakesh R. Harji[a] and Rick P. C. Cousins[b]

[a] *Department of Chemistry, The University of Manchester, Oxford Road, Manchester, UK M13 9PL. E-mail: t.j.donohoe@man.ac.uk*

[b] *GlaxoWellcome Research and Development, Medicines Research Centre, Gunnels Wood Road, Stevenage, UK SG1 2NY*

Received (in Liverpool, UK) 23 November 1998, Accepted 26th November 1998

The preparation and Birch reduction of a 1,3,4-tri-substituted pyrrole is described: the heterocycle is loaded with electron-withdrawing groups and undergoes a double reductive alkylation reaction to yield *cis*-3,4-disubstituted pyrrolidines.

The Birch reduction is a particularly useful synthetic reaction capable of transforming aromatic substrates into partially unsaturated products.[1] We have recently investigated and developed the partial reduction of heterocycles and found that Birch reductive alkylation of electron-deficient pyrroles takes place readily (Scheme 1).[2] For example, the transformation of pyrroles **1** and **2** into either 2- or 3-pyrroline isomers is a high yielding process that enables introduction of an alkyl group adjacent to the activating ester.[3–5] In each case, we believe that addition of electrons to the pyrrole forms a dianion which deprotonates ammonia to furnish an enolate; this reacts with an external electrophile to produce the observed products.

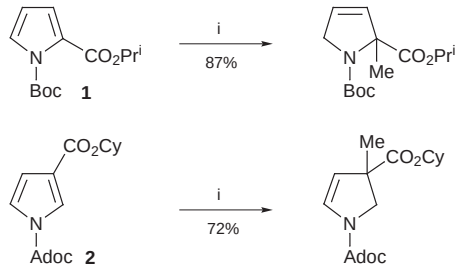

Scheme 1 *Reagents and conditions*: i, Na (3 equiv.), NH_3/THF, then MeI (excess), −78 °C.

Recently we have attempted to expand this work by using more highly-substituted pyrroles as substrates for the Birch reduction. In these cases diastereoisomeric products can be formed and we now present data that shows a high level of stereochemical control is possible. In addition, we also describe a *double* reductive alkylation reaction whereby two alkyl groups can be introduced onto the heterocycle in one step.

Studies began with the preparation of electron-deficient pyrrole **3** using standard methodology (Scheme 2). Reaction of $TsCH_2NC$,[6] $KOBu^t$ and diethyl fumarate gave a 3,4-disubstituted pyrrole which was protected, on nitrogen, as a adamantyloxycarbonyl (Adoc) derivative using adamantyl fluoroformate (45% overall yield from diethyl fumarate).

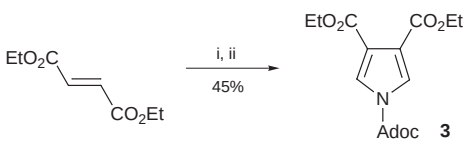

Scheme 2 *Reagents and conditions*: i, $TsCH_2NC$, Bu^tOK, THF; ii, Adoc-F, MeCN, Et_3N.

Subjection of pyrrole **3** to reductive alkylation conditions (6 equiv. Li in NH_3) is described in Scheme 3. We routinely add $(MeOCH_2CH_2)_2NH$ (10 equiv.) to Birch reductions as this amine appears to 'mop-up' lithium amide formed during the reaction and reduces the presence of undesirable by-products.[5]† Isoprene 'quenches' excess electrons in the reaction after reduction is complete (addition of isoprene caused the reaction to turn from deep blue to yellow—this colour was dissipated upon addition of an alkyl halide). The first reaction was quenched with MeI and produced a single product in good yield. We identified the pyrrolidine **4** (R = Me) from ^{1}H NMR spectroscopic data (Table 1).‡ We were then able to repeat the reaction and quench with a variety of electrophiles to generate compounds **5**–**7** in good yields (Table 1). In every case ^{1}H NMR spectroscopy showed that an alkyl group had been introduced α to each of the two esters, and also revealed the presence of the four protons adjacent to the pyrrolidine nitrogen.

Unfortunately, the NMR spectra of **4**–**7** did not allow us to assign relative stereochemistry and this was subsequently proved by conversion to the corresponding quarternary ammonium salts *via* a two step sequence (Scheme 3). Assignment of *cis* relative stereochemistry to compounds **4**–**7** would mean that the two *N*-methyl groups on (*meso*) salts **8**–**11** are diastereotopic, and could therefore resonate at different chemical shifts. On the other hand, *trans* stereochemistry would make the *N*-methyl groups of **8**–**11** (now C_2 symmetrical) homotopic and they would therefore have identical chemical shifts. Gratifyingly, salts **8**–**11** each displayed two (3H) singlets in the ^{1}H NMR spectrum,‡ thus allowing us to assign with confidence the stereochemistry of **4**–**7** as shown (Table 2).

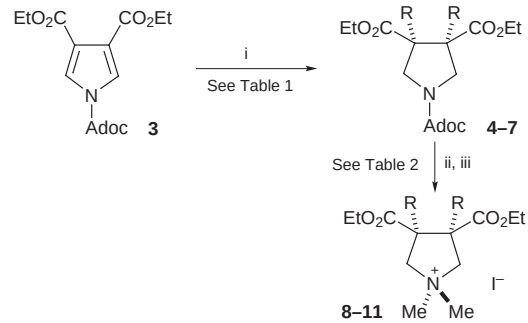

Scheme 3 *Reagents and conditions*: i, Li (6 equiv.), NH_3, THF, $(MeOCH_2CH_2)_2NH$, −78 °C, then isoprene (3 drops), then RI (excess); ii, TFA, CH_2Cl_2; iii, MeI, $KHCO_3$, MeOH.

Table 1 Birch reduction of **5**

Entry	RX	*cis*/*trans*	Yield (%)	Compound
1	MeI	⩾20:1	77	**4**
2	EtI	⩾10:1	82	**5**
3	Bu^iI	⩾10:1	79	**6**
4	Allyl-I	⩾10:1	70	**7**

Table 2 Quaternary ammonium salts

Entry	R	δ_H(NMe) ($CDCl_3$)	Yield (%)	Compound
1	Me	3.52, 3.77	52	**8**
2	Et	3.67, 3.81	61	**9**
3	Bu^i	3.69, 3.77[a]	55	**10**
4	Allyl	3.65, 3.83	58	**11**

[a] NMR run in acetone-d_6.

Compounds **4**–**7** were formed with high levels of stereoselectivity; such ratios were formulated by examination of the NMR spectra of the crude reaction mixtures. As far as the formation of **4** is concerned we were able to prepare an authentic sample of the *trans* isomer by another route and (in comparison with this standard) could not observe the *trans* isomer in the crude reduction reaction. Although each of the other cases was assigned ⩾10:1 selectivity without comparison to a standard, we believe this is a conservative estimate. Not only were the Birch reduced products **5**–**7** free from detectable impurities but also the amines formed by Adoc deprotection and the salts **8**–**11** appeared as single isomers by NMR spectroscopy.

We noticed that the alkylation step of the Birch reduction proceeded at different rates with the electrophiles that were used. Not surprisingly, reaction with Bu^{i}I was much slower than reaction with MeI. Using this information we developed a protocol for the sequential dialkylation of the pyrrole with two different electrophiles (Scheme 4). So, reaction of **3** with

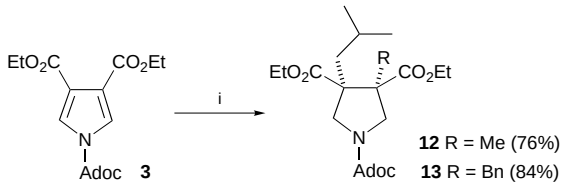

Scheme 4 *Reagents and conditions*: i, Li (6 equiv.), NH_3, THF, $(MeOCH_2CH_2)_2NH$, −78 °C, then isoprene (3 drops), then Bu^{i}I (excess) , then RX (excess).

lithium metal as before but quenching with excess Bu^{i}I and then (after 2 min) excess MeI (or BnBr) enabled the synthesis of **12** and **13** in good yields. In both cases the reaction gave a single product as judged by ^{1}H NMR spectroscopy. Further proof of the identity of **12** was obtained by conversion to **14** under standard conditions (**14** appeared as one isomer) and subsequent NOE studies (Fig. 1). The NOE experiment described shows that **14** is the *cis* isomer. With all of this evidence for *cis* stereoselectivity in the dialkylation reaction, compound **13** was assigned as *cis* by analogy.

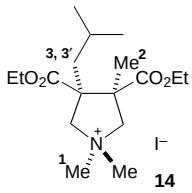

14

Irradiate	Percent NOE observed 1	2	3	3'
1	X	1	0	3
2	1	X	4	5
3	1	4	X	9
3'	3	6	8	X

Fig. 1 NOE studies on **14**

In terms of mechanism, we suggest that **3** accepts two electrons and forms dianion **A** (Fig. 2). Dianion **A** is then basic enough to deprotonate ammonia and form enolate **B**. Presumably, the presence of an ester group at C-4 means that the C-4,5 alkene in **B** is susceptible to further reduction by addition of two electrons and protonation at C-5 (by ammonia) to give **C**,[7] which is then alkylated twice. Presumably, the relative stereochemistry is determined by the facial selectivity of the second alkylation step (reaction of **D**) and it is surprising that such high levels of control are observed. Additional experiments show that both potassium and sodium metals give identical selectivity to lithium, thus dampening arguments based on chelation. However, we have preliminary results which show that, remarkably, the ammonia solvent is essential in order to achieve high stereoselectivity. We cannot comment on the exact role of the ammonia at this point, but note that Schultz has previously observed a similar relationship between solvent and the stereoselectivity displayed by enolates generated in the Birch reduction.[8]

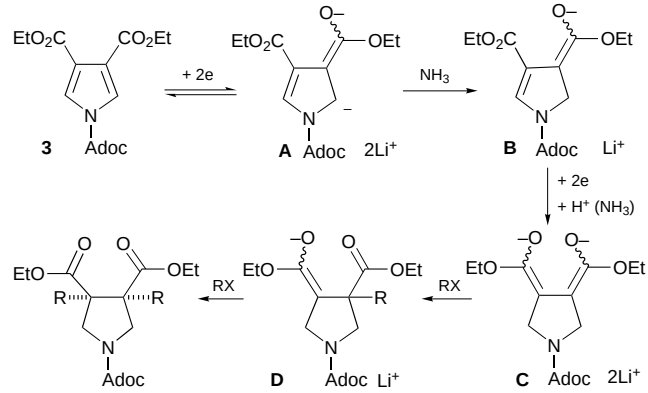

Fig. 2

We believe this type of reaction will be of use in both natural product synthesis and medicinal chemistry and that, as this reaction results in the formation of two adjacent quarternary chiral centres with control of relative stereochemistry, it is worthy of further study.

We wish to thank GlaxoWellcome (CASE award to R. R. H.) and Zeneca Pharmaceuticals (Strategic Research Fund) for financial support.

Notes and references

† We assume that $(MeOCH_2CH_2)_2NH$ is acidic enough to become deprotonated by lithium amide. Presumably, the anion derived from the amine additive is chelated and is a relatively unreactive species compared to lithium amide itself. We also note that $(MeOCH_2CH_2)_2NH$ is not acidic enough to protonate any enolate formed in the reaction, hence allowing us to add 10 equiv. without complication.

‡ *Selected data for* **4**: δ_H(140 °C, 1,2-$Cl_2C_6H_4$) 4.28 (2H, AB, CH_2N), 4.24 (4H, q, *J* 7.5, CH_2O), 3.38 (2H, AB, CH_2N), 2.32 (6H, br s, Adoc), 2.22 (3H, br s, Adoc), 1.75 (6H, br s, Adoc), 1.50 (6H, s, CH_3), 1.33 (6H, t, *J* 7.5 , CH_3CH$_2$); HRMS (CI): $C_{23}H_{35}NO_6$ requies 422.2542, found 422.2534. For **8**: δ_H($CDCl_3$) 4.40 (AB, 2H, CH_2N), 4.20–4.08 (4H, m, CH_2O), 4.05 (2H, AB, CH_2N), 3.77 (3H, s, NCH_3), 3.52 (3H, s, NCH_3), 1.58 (s, 6H, CH_3), 1.23 (6H, t, *J* 7.1, CH_3CH$_2$); Calc. for $C_{14}H_{26}NO_4I$: C, 42.12; H, 6.56; N, 3.51. Found C, 42.39; H, 6.40; N, 3.40%.

1 L. N. Mander, in *Comprehensive Organic Synthesis*, ed. B. M. Trost and I. Fleming, Pergamon, New York, 1991, vol. 8; P. W. Rabideau and Z. Marcinow, *Org. React*., 1992, **42**, 1; P. W. Rabideau, *Tetrahedron*, 1989, **45**, 1579.
2 T. J. Donohoe, R. Garg and C. A. Stevenson, *Tetrahedron*: *Asymmetry*, 1996, **7**, 317.
3 T. J. Donohoe and P. M. Guyo, *J. Org. Chem*., 1996, **61**, 7664.
4 T. J. Donohoe, P. M. Guyo, R. L. Beddoes and M. Helliwell, *J. Chem Soc*., *Perkin Trans. 1*, 1998, 667.
5 T. J. Donohoe, P. M. Guyo, R. R. Harji, M. Helliwell and R. P. C. Cousins, *Tetrahedron Lett*., 1998, **39**, 3075.
6 A. M. van Leusen, H. Siderius, B. E. Hoogenboom and D. van Leusen, *Tetrahedron Lett*., 1972, 5337; D. P. Arnold, L. J. Nitschinsk, C. H. L. Kennard and G. Smith, *Aust. J. Chem*., 1991, **44**, 323.
7 S. Li, X. Fang, Z. Wang, Y. Yang and Y. Li, *Synth. Commun*., 1993, **23**, 2051; A. G. Schultz, M. Macielag, D. E. Podhorez, J. C. Suhadolnik and R. K. Kullnig, *J. Org. Chem*., 1988, 53, 2456.
8 See A. G. Schultz, M. Macielag, P. Sundararaman, A. G. Taveras and M. Welch, *J. Am. Chem. Soc*., 1988, **110**, 7228.

Communication 8/09193E

Total synthesis of sulfur-containing pyrroloiminoquinone marine product, (±)-makaluvamine F using hypervalent iodine(III)-induced reactions

Yasuyuki Kita,* Masahiro Egi and Hirofumi Tohma

Graduate School of Pharmaceutical Sciences, Osaka University, 1-6 Yamada-oka, Suita, Osaka 565-0871, Japan. E-mail: kita@phs.osaka-u.ac.jp

Received (in Cambridge, UK) 9th November 1998, Accepted 20th November 1998

The first total synthesis of potent cytotoxic makaluvamine F 1, a sulfur-containing pyrroloiminoquinone marine product, has been accomplished using hypervalent iodine(III)-induced reactions.

The makaluvamines,[1] a new family of marine alkaloids, were isolated from the Fijian sponge *Zyzzya cf. marsailis* (A–F) and the Indonesian sponge *Histodermella* sp. (G). Among them,

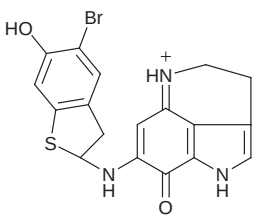

makaluvamine F **1**

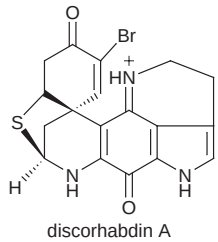

discorhabdin A (prianosin A)

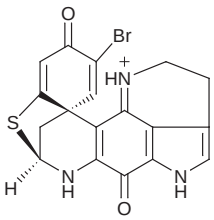

discorhabdin B

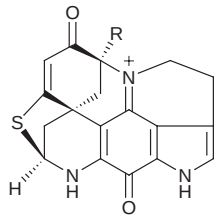

discorhabdin D (prianosin D) (R = H)
prianosin C (R = OH)

makaluvamine F **1** exhibits the most potent biological activity [*e.g.* cytotoxicity towards the human colon tumor cell-line HCT-116 (IC_{50} = 0.17 μM) and inhibition of topoisomerase II][1,2] and has an α-aminodihydrobenzothiophene skeleton which is a labile *N*,*S*-acetal structure present in all sulfur-containing discorhabdins.[3] Synthetic studies towards makaluvamines and discorhabdins have been carried out by several groups.[4] We have also reported the total synthesis of discorhabdin C (Scheme 1)[5] and a facile and efficient synthesis of pyrroloiminoquinone derivatives **2** using the hypervalent iodine(III) reagent, phenyliodine(III) bis(trifluoroacetate) (PIFA) (Scheme 2).[6] However, in most cases these efforts have been

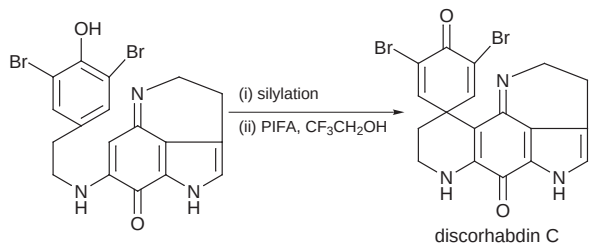

Scheme 1

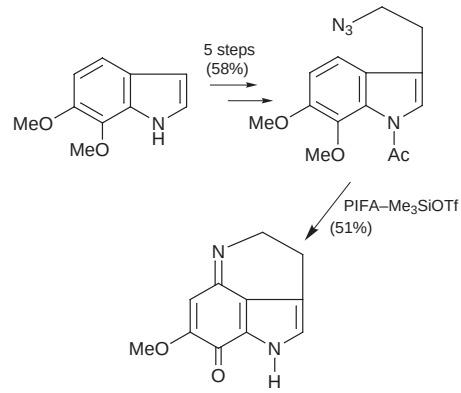

Scheme 2

devoted only towards the preparation of the pyrroloiminoquinone and spirodienone units.

To the best of our knowledge, the total syntheses of sulfur-containing discorhabdins and **1** have not yet been reported, in spite of their potent cytotoxicity and their unique structure. This is probably due to the difficulty of construction of the labile and highly strained *N*,*S*-acetal skeletons. We report herein the first total synthesis of potent cytotoxic makaluvamine F **1** using hypervalent iodine(III)-induced reactions. Our synthetic strategy for the total synthesis of **1** involves a final coupling reaction between **2** and 2-aminodihydrobenzothiophene derivative **3**.

In order to construct **3** bearing the *N*,*S*-acetal skeleton, it was first essential to develop an efficient route for the synthesis of the starting dihydrobenzothiophene bearing a hydroxy group. In our previous report, various dihydrobenzothiophenes were prepared from phenol ethers bearing an alkyl sulfide sidechain *via* intramolecular cyclization using PIFA–BF_3·Et_2O followed by treatment with aq. $MeNH_2$ without yielding any sulfoxides (Scheme 3).[7] Using this method, 6-benzyloxy-5-bromodihydrobenzothiophene **4** was synthesized effectively.

Next, we attempted to introduce the azido group at the 2-position of **4**. Subsequent to the first report by Böhme and Morf,[8] acyclic α-azido sulfides have generally been synthesized stepwise, *via* halogenation followed by azidation of sulfides,[9] or *via* thioketals.[10] On the other hand, α-azidation of dihy-

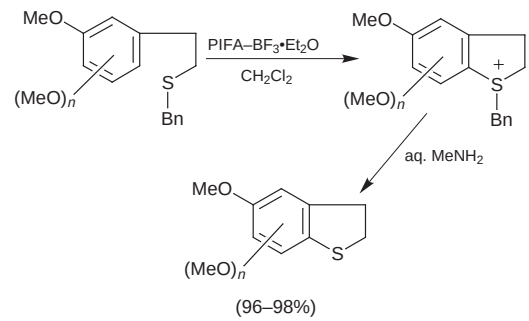

Scheme 3

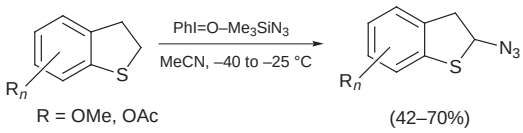

Scheme 4

drobenzothiophenes has never been reported, probably due to readily occurring side reactions such as aromatization, sulfoxide formation, benzylic oxidation and α-oxidation of the sulfur atom under oxidative conditions. We examined the known stepwise methods to obtain α-azidodihydrobenzothiophene. However, the aromatization occurred exclusively to give benzothiophene derivatives in the initial halogenation step.

Very recently, we developed a novel and direct α-azidation of dihydrobenzothiophenes using a combination of PhI=O and Me_3SiN_3 (Scheme 4).[11] However, the azidation of **4** gave only a trace amount of the expected α-azido compound. This is because there appears to be a large number of reactive sites on phenol ether **4** toward the hypervalent iodine-induced azidation. Hence, we then performed the azidation after debenzylation followed by acetylation of **4** to give the corresponding α-azido compound **5** in 46% yield. After hydrolytic deprotection of the 6-acetoxy group, 2-azido-5-bromo-6-hydroxy-dihydrobenzothiophene **6** was finally obtained. The route to **6** from commercially available methyl (4-hydroxyphenyl)acetate is outlined in Scheme 5.

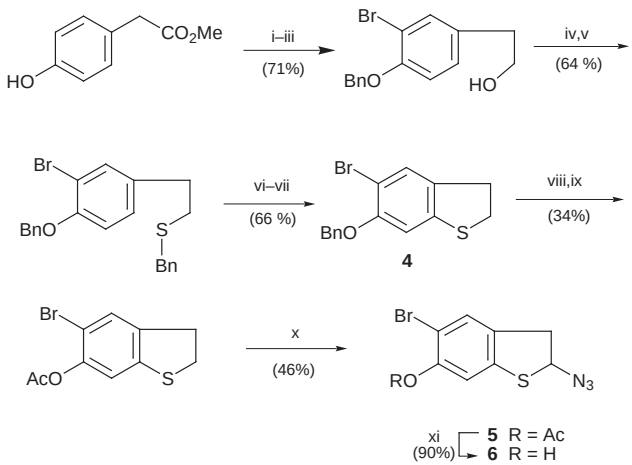

Scheme 5 *Reagents and conditions*: i, Br_2, AcOH; ii, BnBr, K_2CO_3, EtOH; iii, $LiAlH_4$, THF; iv, I_2, PPh_3, imidazole, PhMe; v, AcSBn, NaOH, MeOH; vi, PIFA–BF_3·OEt_2; vii, aq. $MeNH_2$; viii, BF_3·OEt_2, EtSH; ix, Ac_2O, NaOAc, aq. NaOH; x, PhI=O–Me_3SiN_3, MeCN, −40 to −25 °C; xi, 5% NaOH, MeOH.

Sequential attempts to transform the azido group to the amino group by catalytic hydrogenation or other reductive methods under non-acidic conditions proved unsatisfactory (*i.e.* 2-amino-5-bromo-6-hydroxydihydrobenzothiophene **3** was found to be quite labile under basic conditions). Furthermore, Wittig-type reactions between the phosphine imine prepared from **6** and several quinones were also unsuccessful. Finally, we found that the catalytic hydrogenation of **6** using 10% Pd-C in the presence of 4 equiv. of TFA resulted in complete reduction to give **3** as a TFA salt in quantitative yield without any side reactions. The final coupling reaction in MeOH between both synthetic precursors, **3** (TFA salt) and **2**, proceeded in 86% yield

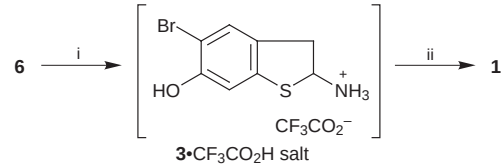

Scheme 6 *Reagents and conditions*: i, H_2, 10% Pd-C, EtOH–TFA; ii, **2**, MeOH, room temp.

to give the TFA salt of **1**, whose spectral data were identical to those previously reported[1] (Scheme 6).

In conclusion, the first total synthesis of (±)–makaluvamine F has been achieved *via* a facile construction of the labile *N*,*S*-acetal skeleton by a combination of hypervalent iodine oxidation reactions. Synthetic studies towards more complicated sulfur-containing discorhabdins and their analogs are now underway.

Notes and references

1 D. C. Radisky, E. S. Radisky, L. R. Barrows, B. R. Copp, R. A. Kramer and C. M. Ireland, *J. Am. Chem. Soc*., 1993, **115**, 1632.

2 L. R. Barrows, D. C. Radisky, B. R. Copp, D. S. Swaffar, R. A. Kramer, R. L. Warters and C. M. Ireland, *Anti-Cancer Drug Des*., 1993, **8**, 333.

3 J.-F. Cheng, Y. Ohizumi, M. R. Wälchli, H. Nakamura, Y. Hirata, T. Sasaki and J. Kobayashi, *J. Org. Chem*., 1988, **53**, 4621; H. H. Sun, S. Sakemi, N. Burres and P. McCarthy, *J. Org. Chem*., 1990, **55**, 4964; J. W. Blunt, M. H. G. Munro, C. N. Battershill, B. R. Copp, J. D. McCombs, N. B. Perry, M. R. Prinsep and A. M. Thompson, *New J. Chem*., 1990, **14**, 761; J. Kobayashi, J.-F. Cheng, S. Yamamura and M. Ishibashi, *Tetrahedron Lett*., 1991, **32**, 1227 and references cited therein; T. F. Molinski, *Chem. Rev*., 1993, **93**, 1825; B. R. Copp, K. F. Fulton, N. B. Perry, J. W. Blunt and M. H. G. Munro, *J. Org. Chem*., 1994, **59**, 8233; A. Yang, B. J. Baker, J. Grimwade, A. Leonard and J. B. McClintock, *J. Nat. Prod*., 1995, **58**, 1596.

4 Y. Kita, T. Yakura, H. Tohma, K. Kikuchi and Y. Tamura, *Tetrahedron Lett*., 1989, **30**, 1119; H. J. Knölker and K. Hartmann, *Synlett*, 1991, 428; S. Hamabuchi, H. Hamada and M. Somei, *Heterocycles*, 1991, **32**, 443; S. Nishiyama, J.-F. Cheng, X. L. Tao and S. Yamamura, *Tetrahedron Lett*., 1991, **32**, 4151; T. Izawa, S. Nishiyama and S. Yamamura, *Tetrahedron*, 1994, **50**, 13593; J. D. White, K. M. Yager and T. Yakura, *J. Am. Chem. Soc*., 1994, **116**, 1831; E. V. Sadanandan, S. K. Pillai, M. V. Lakshmikantham, A. D. Billimoria, J. S. Culpepper and M. P. Cava, *J. Org. Chem*., 1995, **60**, 1800; D. Roberts, M. Alvarez and J. A. Joule, *Tetrahedron Lett*., 1996, **37**, 1509; R. Zhao and J. W. Lown, *Synth. Commun*., 1997, **27**, 2103; D. Roberts, J. A. Joule, M. A. Bros and M. Alvarez, *J. Org. Chem*., 1997, **62**, 568; M. Makosza, J. Stalewski and O. S. Maslennikova, *Synthesis*, 1997, 1131; M. Iwao, O. Motoi, T. Fukuda and F. Ishibashi, *Tetrahedron*, 1998, **54**, 8999; G. A. Kraus and N. Selvakumar, *Synlett*, 1998, 845.

5 Y. Kita, H. Tohma, M. Inagaki, K. Hatanaka and T. Yakura, *J. Am. Chem. Soc*., 1992, **114**, 2175.

6 Y. Kita, M. Egi, A. Okajima, M. Ohtsubo, T. Takada and H. Tohma, *Chem. Commun*., 1996, 1491; Y. Kita, H. Watanabe, M. Egi, T. Saiki, Y. Fukuoka and H. Tohma, *J. Chem. Soc*., *Perkin Trans. 1*, 1998, 635.

7 Y. Kita, M. Egi, M. Ohtsubo, T. Saiki, T. Takada and H. Tohma, *Chem. Commun*., 1996, 2225.

8 H. Böhme and D. Morf, *Chem. Ber*., 1957, **90**, 446.

9 H. Böhme and F. Ziegler, *Liebigs Ann. Chem*., 1974, 734; I. W. J. Still, W. L. Brown, R. J. Colville and G. W. Kutney, *Can. J. Chem*., 1984, **62**, 586.

10 B. M. Trost, M. Vaultier and M. L. Santiago, *J. Am. Chem. Soc*., 1980, **102**, 7929.

11 H. Tohma, M. Egi, M. Ohtsubo, H. Watanabe, S. Takizawa and Y. Kita, *Chem. Commun*., 1998, 173.

Communication 8/08715F

Photochemical C–H bond activation of the diruthenium bridging methylene complex, $Cp_2Ru_2(\mu\text{-}CH_2)_2(CO)_2$: insertion of norbornadienes into the methylene C–H bond and unprecedented intramolecular H–D exchange between the two methylene units

Munetaka Akita,* Sadahiro Nakanishi, Hideki Musashi and Yoshihiko Moro-oka*

Research Laboratory of Resources Utilization, Tokyo Institute of Technology, 4259 Nagatsuta, Midori-ku, Yokohama 226-8503, Japan. E-mail: makita@res.titech.ac.jp

Received (in Cambridge, UK) 30th October 1998, Accepted 16th November 1998

Two photochemical reactions of the diruthenium bis-μ-methylene complex $(\eta^5\text{-}C_5H_5)_2Ru_2(\mu\text{-}CH_2)_2(CO)_2$ are described: (i) insertion reaction of norbornadiene into the methylene C–H bonds leading to $(\eta^5\text{-}C_5H_5)_2Ru_2(\mu\text{-}CHR')_2(CO)_2$ (R′ = 5-*exo*-norbornenyl) and (ii) H exchange between the two methylene units, involve μ-methylidyne intermediates generated *via* C–H bond activation of the μ-methylene ligand.

C1 species (CH_x) are pivotal intermediates in surface catalyzed reactions, such as catalytic conversion of CO and hydrocarbons,[1] and organometallic compounds containing the CH_x ligands have been studied extensively as model compounds for surface-bound species.[2] Although C–C coupling of C1 species is a key step of the carbon chain propagation during the catalytic processes, only a limited number of successful C–C coupling reactions of bridging hydrocarbyl complexes, in particular, μ-CH_2 complexes, have been reported so far, and most of the C–C coupling processes involve coordination of an unsaturated C–C bond (or alkylidene species) to the metal vacant site followed by insertion into the M–μ-CR_x bond.[3,4d] During the course of our studies of the photochemical reactions of the diruthenium di-μ-methylene complex $Cp_2Ru_2(\mu\text{-}CH_2)_2(CO)_2$ **1a**,[4] we found an unusual C–C coupling reaction at the bridging methylene carbon atom and unprecedented H exchange between the two methylene carbon atoms, which should involve μ-methylidyne species as a key intermediate.

Irradiation of a THF solution of the di-μ-methylene complex **1a**[4a] in the presence of an excess of norbornadiene (nbd) for 5 h gave a yellow isomeric mixture of products (**2a**; 89% yield) after TLC separation (Scheme 1). The significant change in the ^{1}H NMR signals of the μ-CH_x part compared to **1a** [(i) intensity: 2H (from 4H); (ii) ^3J = 11.7 Hz for μ-CH (from ^2J = 0.6 Hz for μ-CH_2)]† suggested the occurrence of a C–C coupling reaction at the μ-methylene carbon atom. The molecular structure of the η^5-C_5H_4Me derivative (**2a′**) was determined by X-ray crystallography,‡ which revealed (i) insertion of the C=C bond in nbd into the C–H bonds of both of the μ-methylene ligands, and (ii) C–C coupling from the less sterically congested *exo*-side of nbd. Reaction of the μ-methylene-μ-ethylidene complex **1b** resulted in exclusive insertion into the μ-methylene part to give the 1:1 adduct **3b**, as indicated by a similar change in the μ-CH_2 signals and the unchanged μ-$CHCH_3$ pattern.† Furthermore, the photochemical C–C coupling reaction was also observed for the cyclohexyl isocyanide complex **1c**, while the dppe derivative **1d** remained unreacted.§ We also attempted the C–C coupling of **1a** with a variety of unsaturated hydrocarbons such as 2- or 7-substituted nbd, norbornene, cyclohexa-1,4-diene, butadiene, quadricyclene, ethyl acrylate and 1,1-diphenylethylene. However, only a few 2-substituted nbds (Me and Me_3Si derivatives) afforded 1:1 adducts **3** (R = H); the others did not give any C–C coupling product.[5]

For elucidation of the reaction mechanism, a labeling experiment using **1a**-d_4 [(μ-$CD_2)_2$] was carried out and the distribution of the deuterium atoms was determined by ^{1}H and ^{13}C NMR, as illustrated in Scheme 2. The D distribution over the moiety originating from the C=C bond in nbd clearly indicated that the C–C coupling process was not a simple insertion reaction into the C–D bonds, but consisted of a multistep reaction sequence. The result may be interpreted in terms of a μ-methylidyne intermediate **4** as summarized in Scheme 2. Possible candidates for **4** are the decarbonylated μ-methylidyne species $Cp_2Ru_2(\mu\text{-}CH)(H)(\mu\text{-}CH_2)(CO)$ **4′**, suggested by the H–D exchange reaction (see below)[6] and the radical species **4″**, generated by H abstraction. Addition of **4′** or **4″** to the π-

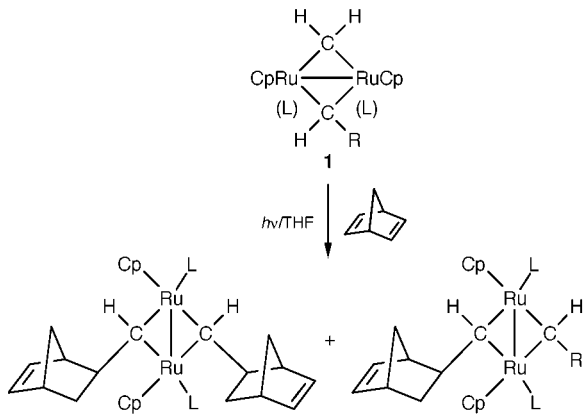

	R	L	products
1a	H	CO	**2a** (89 %)
1a'	H	CO	**2a'** (80 %)
1b	CH_3	CO	**3b** (38 %)
1c	H	CNCy	**2c** (23 %)
1d	H	dppe	–

(**1a'**, **2a'**: η^5-$C_5H_4CH_3$ derivatives)

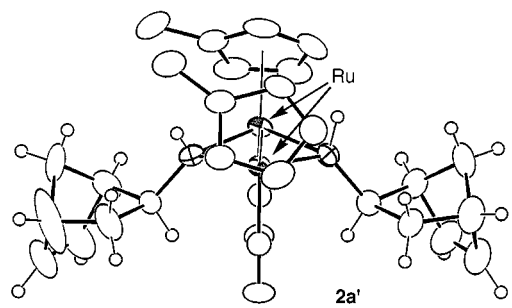

Scheme 1

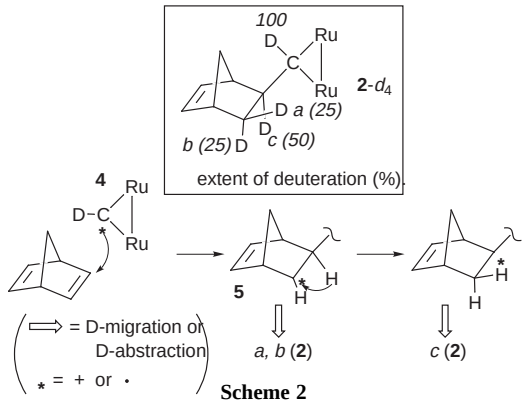

Scheme 2

electrons of nbd should form intermediate **5**. Direct H recombination gives **2**-d_4 deuterated at either of sites *a* or *b*, whereas a 1,2-H shift finally leads to deuteration at the site *c*, and the driving force for the 1,2-H migration should be formation of the tertiary cation (or radical), which is more stable than the secondary one (**5**). Subsequently, the C–C coupling reaction will be completed by either intramolecular H(D) migration (**4′**) or intermolecular H(D) abstraction [**4″**: from **2**-d_2 (radical chain reaction)]. Although the mechanism involving H migration can account for the D distribution, the reaction is not retarded by addition of cation and radical quenchers (*e.g.* MeOH and hydroquinones, respectively) and intermediate **4** cannot be trapped by diphenylethylene and ethyl acrylate (cation and radical trapping agents).

In order to obtain further information on the properties of the μ-methylene complexes, a benzene-d_6 solution of the labeled compound $Cp_2Ru_2(\mu\text{-}CH_2)(\mu\text{-}{}^*CD_2)({}^*CO)_2$ (**1a**-*CD_2; *C = *ca*. 30% ^{13}C-enriched) was subjected to irradiation *in the absence of nbd* (Scheme 3). As a result, the intensity of the quintet μ-*CD_2 signals of **1a**-*CD_2 [δ_C 107.4 (*cis* isomer), 108.8 (*trans* isomer)] diminished and instead there appeared the triplet (*cis*-**1a**-*CDH: δ_C 107.7) and then the singlet signals (*cis*-**1a**-*CH_2: δ_C 108.8) as shown in Fig. 1.¶ An equilibrated mixture of the isotopomers was obtained after 40 h irradiation. The spectral changes unequivocally indicates that the hydrogen atoms attached to the two methylene carbon atoms exchange with each other. Similar isomerization was also observed for $Cp_2Ru_2(\mu\text{-}CD_2)(\mu\text{-}CHCH_3)(CO)_2$ **1b**-d_2, which was converted

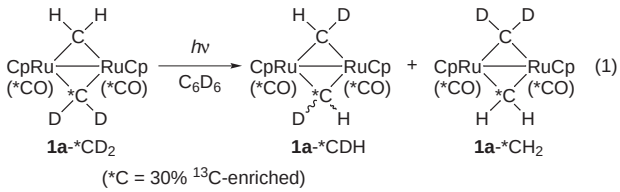

Scheme 3

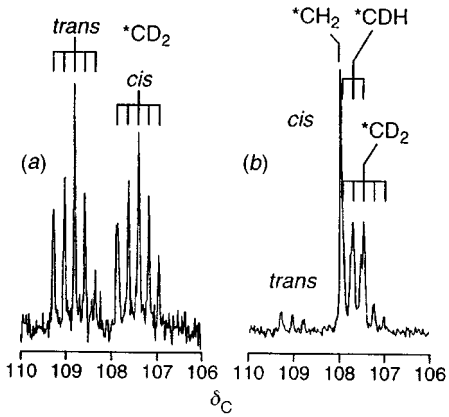

Fig. 1 ^{1}H decoupled ^{13}C NMR spectra of **1a**-*CD_2:expanded views of the μ-CH_2 region (*a*) before and (*b*) after irradiation for 40 h.

to $Cp_2Ru_2(\mu\text{-}CDH)(\mu\text{-}CDCH_3)(CO)_2$. A plausible intermediate for the exchange reaction of **1a** is the μ-methylidyne species $Cp_2Ru_2(\mu\text{-}CH)(\mu\text{-}CH_2)(H)(CO)$ **4′** formed by decarbonylation followed by H migration from the bridging carbon atom to the ruthenium center; the H–D exchange reaction would be completed by a 1,3-H(D) shift, reversed H(D) migration and CO recombination.

In summary, we have reported the two photochemical C–H bond cleavage reactions of the bridging alkylidene complexes **1**; the present work reveals a new type of functionalization of bridging alkylidene complexes by way of μ-alkylidyne intermediates. In addition, combined with our previous results of the $CH_3\leftrightarrow CH_2$–H[4b] and $CH_2\leftrightarrow$CH–H interconversions[4c] on diruthenium systems, our results suggest the occurrence of analogous interconversions of CH_x species (x = 1–3) on a catalyst surface.

We are grateful to the Ministry of Education, Science, Sports, and Culture of the Japanese Government for financial support of this research.

Notes and references

† *Selected data* for **2a**: $\delta_H(C_6D_6)$ 9.26 (d, *J* 11.7, μ-CH), 6.40, 6.15 (m, =CH), 4.71, 4.67 (Cp_2); $\nu(CH_2Cl_2)/cm^{-1}$ 1946, 1913 (CO). For **2b**: $\delta_H(C_6D_6)$ 9.60 (d, *J* 7.3, μ-C*H*CH_3), 9.25 (q, $^3J_{HH}$ 11.7, μ-CH), 6.42, 6.16 (m, =CH), 4.62, 4.60 (Cp_2), 3.10 (d, $^3J_{HH}$ 11.7, $CHCH_3$); $\nu(CH_2Cl_2)/cm^{-1}$ 1949, 1914 (CO). For **6**: $\delta_H(C_6D_6)$ 10.03 (d, $^3J_{HH}$ 11.2, μ-CH), 4.70 (Cp_2); $\nu(CH_2Cl_2)/cm^{-1}$ 1974, 1934, 1779 (CO).

‡ X-Ray diffraction measurements were made on a Rigaku RAXIS IV imaging plate area detector with graphite-monochromated Mo-Kα radiation. The structure was solved by using the SHELXL-93 least-squares program (refined on F^2) linked to the teXsan crystal structure analysis package. *Crystal data* for **2a′**: $C_{30}H_{34}O_2Ru_2$, M = 628.7, T = −60 °C, orthorhombic, space group *Pbca*, a = 17.621(2), b = 18.267(2), c = 16.085(4) Å, V = 1552(1) Å^3, Z = 8, D_c = 1.61 g cm^{-3}, μ = 11.92 cm^{-1}, R_1 = 0.072 for the 4828 data with $F_o > 4\sigma(F_o)$ and 317 parameters. CCDC 182/1094.

§ Similar reaction of the mono-μ-methylene complex, $Cp_2Ru_2(\mu\text{-}CH_2)(CO)_3$, also resulted in C–C coupling to give $Cp_2Ru_2(\mu$-CH-nortricyclyl$)(CO)_3$ **6**.

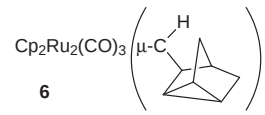

¶ Irradiation of **1a** initially brought about the *trans*-to-*cis* isomerization (within 1 h) as can be seen from the spectral change. Similar isomerization is usually observed for the related $Cp_2M_2(\mu\text{-}X)_2(CO)_2$ systems (M = Ru, Fe) (ref. 7).

1 G. A. Somorjai, *Introduction to Surface Chemistry and Catalysis*; Wiley Interscience, New York, 1994.
2 Reviews for μ-alkylidene complexes: (*a*) W. A. Herrmann, *Adv. Organomet. Chem*., 1982, **20**, 159; (*b*) S. A. R. Knox, *J. Organomet. Chem*., 1990, **400**, 255.
3 J. A. K. Howard, S. A. R. Knox, N. J. Terrill and M. I. Yates, *J. Chem. Soc., Chem. Commun*., 1989, 640; M. J. Fildes, S. A. R. Knox, A. G. Orpen, M. L. Turner and M. I. Yates, *J. Chem. Soc., Chem. Commun*., 1989, 1681. See also references cited in ref. 2(*b*).
4 (*a*) M. Akita, R. Hua, T. Oku and Y. Moro-oka, *Organometallics*, 1996, **15**, 2548; (*b*) M. Akita, R. Hua, T. Oku, M. Tanaka and Y. Moro-oka, *Organometallics*, 1996, **15**, 4162; (*c*) M. Akita, R. Hua, S. Nakanishi , M. Tanaka and Y. Moro-oka, *Organometallics*, 1997, **16**, 5572; (*d*) M. Akita, R. Hua, S. A. R. Knox, Y. Moro-oka, S. Nakanishi and M. I. Yates, *J. Organomet. Chem*., 1998, **567**, 71.
5 M. Akita, S. Nakanishi and Y. Moro-oka, to be reported.
6 D. L. Davies, B. P. Gracy, V. Guerchais, S. A. R. Knox and A. G. Orpen, *J. Chem. Soc., Chem. Commun*., 1984, 841; N. Connelly, N. J. Forrow, B. P. Gracey, S. A. R. Knox and A. G. Orpen, *J. Chem. Soc., Chem. Commun*., 1985, 14; C. P. Casey, P. J. Fagan and W. H. Miles, *J. Am. Chem. Soc*., 1982, **104**, 1134; C. P. Casey and P. J. Fagan, *J. Am. Chem. Soc*., 1982, **104**, 4950; C. P. Casey, P. J. Fagan, W. H. Miles and S. R. Marder, *J. Mol. Catal*., 1983, **21**, 173.
7 H. Ogino and H. Tobita, *Adv. Organomet. Chem*., 1998, **42**, 223 and references cited therein.

Communication 8/08411D

Phosphorus octaethyltetraphenylporphyrins [(oetpp)P(Me)(X)]PF_6 (X = Me, OH, F) having saddle (X = Me) or ruffled (X = OH, F) conformations

Akihiro Yamamoto, Wataru Satoh, Yohsuke Yamamoto* and Kin-ya Akiba*

Department of Chemistry, Faculty of Science, Hiroshima University, 1-3-1 Kagamiyama, Higashi-Hiroshima 739-8526, Japan. E-mail: akiba@sci.hiroshima-u.ac.jp

Received (in Cambridge, UK) 5th October 1998, Accepted 8th December 1998

X-Ray crystallographic structures of [(oetpp)P(Me)(X)]PF_6 revealed that the axial ligand (X) plays a major role in changing the conformation of the porphyrin core from saddle (X = Me) to ruffled (X = OH and F).

There has been considerable interest in the conformations of metalloporphyrins since they have a profound influence on the physicochemical properties of the macrocycle such as redox potential and electron transfer rates, and therefore its reactivity in a protein.[1] The interest has prompted the synthesis of many substituted porphyrins in which deformations (mainly saddle type deformation) from planarity are induced by crowding of substituents at the periphery of the macrocycle.[2] There is now a considerable body of information describing the structural and spectroscopic properties of highly non-planar octaalkyltetraphenylporphyrins bearing transition metals[3] which show saddle conformations. Although those bearing main group elements have not been reported, phosphorus octaalkyltetraphenylporphyrins are interesting because phosphorus has been the smallest atom which can occupy the center of a porphyrin ring. Recent report on X-ray crystallographic structures of $[(oep)P(X)(Y)]^+Z^-$ revealed essentially ruffled conformations in order to accommodate the small phosphorus atom. The electronegativities of the axial ligands (X and Y) played a major role in determining the deformation, for example, $[(oep)P(Me)_2]PF_6$ showed a planar conformation.[4] Here we report the synthesis and X-ray structures of phosphorus octaethyltetraphenylporphyrins, [(oetpp)P(Me)(X)]PF_6 (X = OH **2**, Me **3**, F **4**), which showed strong effects of the axial ligands on the conformations, *i.e.*, a saddle conformation was observed in $[(oetpp)P(Me)_2]PF_6$ (**3**-PF_6) but ruffled ones were observed in [(oetpp)P(Me)(OH)]ClO_4 (**2**-ClO_4) and [(oetpp)P-(Me)(F)]PF_6 (**4**-PF_6).

The reaction of oetppLi_2 **1** with $MePCl_2$ was carried out under dichloromethane reflux for 12 h. After removal of the solvent and excess of $MePCl_2$, the residue was subjected to neutral alumina column chromatography (CH_2Cl_2) to give [(oetpp)P(Me)(OH)]Cl (**2**-Cl) (Scheme 1). After counter anion exchange **2**-ClO_4 was obtained pure for elemental analysis.

The hydroxy group of **2**-Cl was substituted by a methyl group by the reaction of **2**-Cl with phosphorus trichloride followed by treatment with an excess of trimethylaluminium in dichloromethane to yield $[(oetpp)P(Me)_2]PF_6$ (**3**-PF_6) in 79% yield after counter anion exchange according to the method recently reported by us for group 15 element porphyrins.[5] [(oetpp)P-(Me)(F)]PF_6 (**4**-PF_6) was obtained in 61 % yield by the reaction of **2**-PF_6 with phosphorus trichloride (Scheme 1).[6]

Crystals of **2**-ClO_4, **3**-PF_6 and **4**-PF_6 suitable for X-ray analysis were grown from dichloromethane–*n*-hexane. The crystallographic analyses of **3**-PF_6 and **4**-PF_6 are not of good quality owing to extensive disorder of the counter anion (PF_6^-) and dichloromethane as a solvent in **4**-PF_6, but the structures of the porphyrin core could be definitely determined. Figs. 1–3 show ORTEP drawings of **2**-ClO_4, **3**-PF_6 and **4**-PF_6 (counter anions and dichloromethane in **4**-PF_6 are omitted for clarity). The crystal structure of **3**-PF_6 exhibits a distorted saddle conformation which is characterized by large displacements of $C_{pyrrole\text{-}\beta}$ atoms from the mean plane of the core. By contrast, the

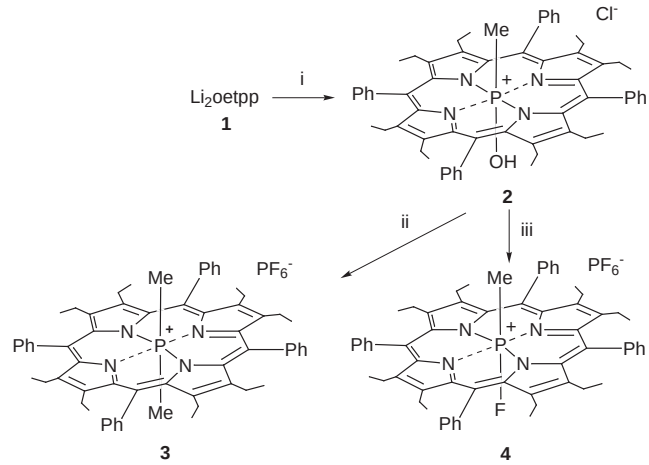

Scheme 1 *Reagents and conditions*: i, $MePCl_2$, CH_2Cl_2, reflux, 12 h; ii, PCl_3, CH_2Cl_2, reflux, 3 h, then $AlMe_3$ in hexane, CH_2Cl_2, room temp., 12 h; iii, KPF_6; then PCl_3, CH_2Cl_2, room temp., 12 h.

crystal structures of **2**-ClO_4 and **4**-PF_6 exhibit ruffled conformations which are characterized by significant C_{meso} displacements from the core and twist of the pyrrole rings so that the β carbons lie above and below the core plane. **4**-PF_6 is more distorted than **2**-ClO_4 as is evident from the average displacement of the C_{meso} atoms from the mean plane of the molecule (**4**-PF_6, 1.20 Å; **2**-ClO_4, 1.07 Å).

The results can be explained based on the conclusions found for [(oep)P(X)(Y)]Z.[4] The introduction of the electronegative axial substituents [X = OH **2** and X = F **4** in (oetpp)P(Me)(X)] reduces the size of the central phosphorus atom and the average P–N bond distances become shorter [1.94(1) Å in **3**-PF_6 (X = Me), 1.849(4) Å in **2**-ClO_4 (X = OH) and 1.810(8) Å in **4**-PF_6 (X = F)], and leads to the ruffled conformation becoming preferable in **2**-ClO_4 and **4**-PF_6 in order to accommodate the

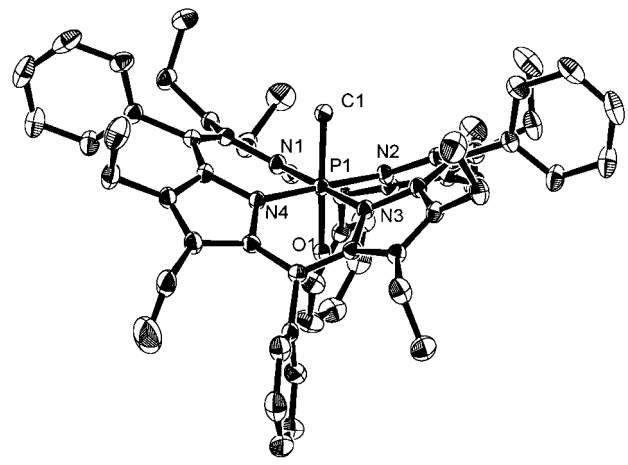

Fig. 1 Molecular structure of **2**-ClO_4. Selected bond lengths (Å): P–C1 1.854(4), P–O1 1.657(3), P–N1 1.838(4), P–N2 1.850(4), P–N3 1.845(4), P–N4 1.861(4).

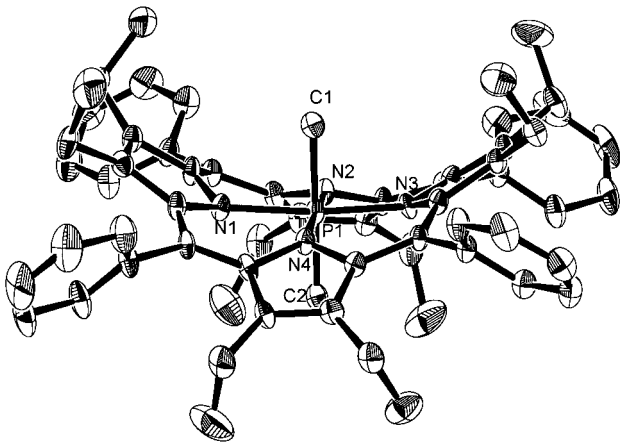

Fig. 2 Molecular structure of **3**-PF_6. Selected bond lengths (Å): P–C1 1.85(1), P–C2 1.82(1), P–N1 1.949(9), P–N2 1.94(1), P–N3 1.918(9), P–N4 1.95(1).

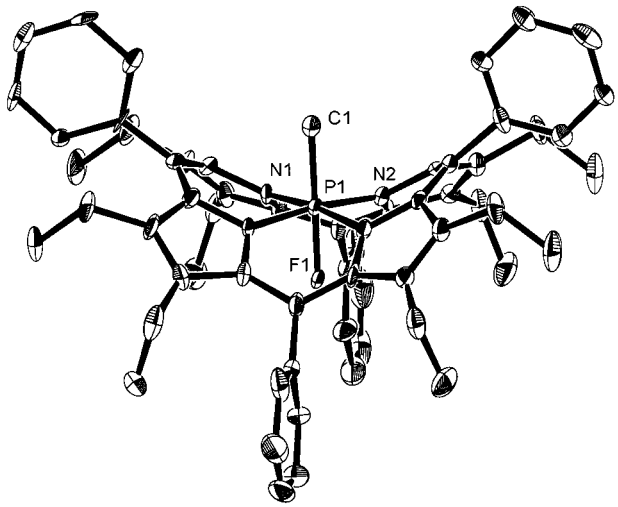

Fig. 3 Molecular structure of **4**-PF_6. Selected bond lengths (Å): P–C1 1.83(2), P–F 1.648(9), P–N1 1.827(8), P–N2 1.793(8).

smaller phosphorus atom. Although metal size dependence of the degree of deformation of saddle conformations has already been investigated for transition metals,[3] such large electronic effects of the axial ligands to change the fundamental conformations have never been observed. The structures of **2**-ClO_4 and **4**-PF_6 are the first examples for metallooctaalkyltetraphenylporphyrins showng ruffled conformations.

It is interesting that the Q(0,0) band of ruffled **2** (627 nm) and **4** (622 nm) are siginificantly blue shifted in the UV–VIS in comparison with that of **3** (667 nm) and free base octaethyltetraphenylporphyrin (686 nm) with saddle conformation.[2] Since such a large shift has not been observed in the [(oep)P(Me)(Y)]Z series, the shift can be ascribed to the difference of core conformations. In order to rationalize the results further structural and spectroscopic studies are now in progress.

Notes and references

† Compounds, **2**-ClO_4, **3**-PF_6 and **4**-PF_6 gave satisfactory C, H, N elemental analyses. *Spectroscopic data*: **2**-ClO_4; ^{1}H NMR ($CDCl_3$) δ −4.48 (d, 3H, *J* 14 Hz), 0.85 (t, 24H, *J* 7 Hz), 2.9–3.0 (br m, 16H), 7.48 (t, 8H, *J* 7 Hz), 7.58 (t, 4H, *J* 7 Hz), 7.68 (d, 8H, *J* 7 Hz). ^{31}P NMR ($CDCl_3$) δ −206.4. UV–VIS (CH_2Cl_2) λ_{max} (log ε) 375 (3.48), 447 (5.34), 579 (3.93), 627(3.49). **3**-PF_6; ^{1}H NMR ($CDCl_3$) δ −5.05 (d, 6 H, *J* 16 Hz), 0.64 (t, 24 H, *J* 7 Hz), 2.73 (q, 16 H, *J* 7 Hz), 7.69 (t, 8 H, *J* 7 Hz), 7.77 (t, 4 H, *J* 7 Hz), 8.01 (d, 8 H, *J* 7 Hz). ^{31}P NMR ($CDCl_3$) δ −195.3 (s), −143.9 (spt, *J* 715 Hz). UV–VIS (CH_2Cl_2) λ_{max} (log ε) 391 (4.87), 467 (5.49), 596 (4.06), 667(4.34). **4**-PF_6; ^{1}H NMR ($CDCl_3$) δ −4.14 (d, 3 H, *J* 12 Hz), 0.85 (t, 24 H, *J* 7 Hz), 2.7–3.3 (br m, 16 H), 7.54 (t, 8 H, *J* 7 Hz), 7.6–7.7 (br t, 4 H), 7.62 (d, 8 H, *J* 7 Hz). ^{31}P NMR ($CDCl_3$) δ −203.1 (d, *J* 730 Hz), −143.8 (spt, *J* 715 Hz). UV–VIS (CH_2Cl_2) λ_{max} (log ε) 443 (5.37), 481 (3.96), 575 (4.13), 622 (3.83).

‡ *Crystal data*: **2**-$ClO_4 \cdot CH_2Cl_2$: $C_{62}H_{66}N_4O_5Cl_3P$, *M* = 1084.5, orthorhombic, space group $P2_12_12_1$, *a* = 17.30(1), *b* = 20.64(3), *c* = 15.196(6) Å, *U* = 5426(6) Å^3, *Z* = 4, D_c = 1.22 g cm^{-3}, *T* = 297 K.

4-$PF_6 \cdot CH_2Cl_2$: $C_{61}H_{63}N_4F_7Cl_2P_2$, *M* = 1118.0, monoclinic, space group $P2_1/m$, *a* = 11.560(2), *b* = 25.797(5), *c* = 11.533(2) Å, β = 107.01(1)deg, *U* = 3288.8(9) Å^3, *Z* = 2, D_c = 1.13 g cm^{-3}, *T* = 297 K.

Both data sets were collected on a Mac Science DIP2030 imaging plate equipped with graphite-monochromated Mo-Kα radiation (λ = 0.710 73 Å). Unit cell parameters were determined by autoindexing several images in each data set separately with program DENZO.[7] For each data set, rotation images were collected in 6° increments with a total rotation of 180° about ϕ. Data were processed by using SCALEPACK.[7] The structure was solved using the teXsan (Rigaku) system and refined by full-matrix least squares. Final *R*1 = 0.052 (R_w = 0.048) for 5580 observed reflections (676 parameters) with $I > 3\sigma(I)$ in **2**-$ClO_4 \cdot CH_2Cl_2$, and *R*1 = 0.134 (R_w = 0.150) for 2530 observed reflections (392 parameters) with $I > 4\sigma(I)$ in **4**-$PF_6 \cdot CH_2Cl_2$.

3-PF_6: $C_{63}H_{68}N_4F_6Cl_2P_2$, *M* = 1128.1, triclinic, space group $P\bar{1}$, *a* = 13.303(3), *b* = 13.911(5), *c* = 17.602(3) Å, α = 73.49(2), β = 69.76(1), γ = 71.46(2)°, *U* = 2841(1) Å^3, *Z* = 2, D_c = 1.32 g cm^{-3}, *T* = 297 K. Crystal data for the product were collected on a Mac Science MXC-3 diffractometer and irradiated with graphite-monochromated Cu-Kα radiation (λ = 1.5418 Å). The structure was solved using the teXsan (Rigaku) system and refined by full-matrix least squares. Final *R*1 = 0.105 (R_w = 0.122) for 4308 observed reflections (663 parameters) with $I > 5\sigma(I)$. CCDC 182/1107. See http://www.rsc.org/suppdata/cc/1999/147/ for crystallographgic files in .cif format.

1 For reviews: M. O. Senge, *J. Photochem. Photobiol. B: Biol*., 1992, **16**, 3; W. R. Scheidt and C. A. Reed, *Chem. Rev*., 1981, **81**, 543; M. Ravikanth and T. K. Chandrashekar, *Struct. Bonding (Berlin)*, 1995, **82**, 105.

2 For recent reports: K. M. Barkigia, M. D. Berber, J. Fajer, C. J. Medforth, M. W. Renner and K. M. Smith, *J. Am. Chem. Soc.*, 1990, **112**, 8851; S. A. Sibilia, S. Hu, C. Piffat, D. Malamed and T. G. Spiro, *Inorg. Chem.*, 1997, **36**, 1013; K. M. Kadish, E. Van Caemelbecke, F. D'Souza, C. J. Medforth, K. M. Smith, A. Tabard and R. Guilard, *Inorg. Chem.*, 1995, **34**, 2984.

3 L. D. Sparks, C. J. Medforth, M.-S. Park, J. R. Chamberlain, M. R. Ondrias, M. O. Senge, K. M. Smith and J. A. Shelnutt, *J. Am. Chem. Soc.*, 1993, **115**, 581; K. M. Barkigia, M. W. Renner, L. R. Furenlid, C. J. Medforth, K. M. Smith and J. Fajer, *J. Am. Chem. Soc*., 1993, **115**, 3627.

4 Y. Yamamoto, R. Nadano, M. Itagaki and K.-y. Akiba, *J. Am. Chem. Soc.*, 1995, **117**, 8287.

5 K.-y. Akiba, Y. Onzuka, M. Itagaki, H. Hirota and Y. Yamamoto, *Organometallics*, 1994, **13**, 2800. W. Satoh, R. Nadano, Y. Yamamoto and K.-y. Akiba, *Chem. Commun.*, 1996, 2451; W. Satoh, R. Nadano, G. Yamamoto, Y. Yamamoto and K.-y. Akiba, *Organometallics*, 1997, **16**, 3664.

6 For similar fluoride transfer: K. M. Kadish, M. Autret, Z. Ou, K.-y. Akiba, S. Masumoto, R. Wada and Y. Yamamoto, *Inorg. Chem.*, 1996, **35**, 5564.

7 Z. Otwinowski, University of Texas, Southwestern Medical Center. The program is available from Mac Science Co.

Communication 8/09601E

Reversible changes in the redox behaviour of a $Ce_{0.68}Zr_{0.32}O_2$ mixed oxide: effect of alternating the re-oxidation temperature after reduction at 1223 K

Richard T. Baker,[a] Serafin Bernal,*[a] Ginesa Blanco,[a] Ana M. Cordón,[a], José M. Pintado,[a] José M. Rodríguez-Izquierdo,[a] Fabienne Fally[b] and Vincent Perrichon[b]

[a] *Departamento de Ciencia de los Materiales, Ingeniería Metalúrgica y Química Inorgánica, Facultad de Ciencias, Universidad de Cádiz, Apartado 40, Puerto Real, Cádiz, Spain. Fax: +34-956-834924. E-mail: cezirencat@uca.es*

[b] *Laboratoire d'Application de la Chimie à l'Environnement (LACE), UMR 5634, CNRS-UCB Lyon1, 43 Bd. du 11 Novembre 1918, F-69622 Villeurbanne Cedex, France*

Received (in Cambridge, UK) 22nd October 1998, Accepted 8th December 1998

The redox behaviour of a $Ce_{0.68}Zr_{0.32}O_2$ mixed oxide is reversibly modified by alternating high temperature (1223 K) reduction with either mild (823 K) or high temperature (1223 K) re-oxidation treatments.

Ceria/zirconia mixed oxides constitute a real alternative to pure ceria in advanced three way catalyst (TWC) formulations.[1,2] It has been shown that the incorporation of zirconium into the ceria lattice improves its textural stability[3,4] and redox behaviour.[5–7] The Ce/Zr mixed oxides also show enhanced OSC (oxygen storage capacity)[8] which has been interpreted as due to the occurrence of bulk reduction at moderate temperatures.[9] This would also explain the remarkably high OSC values they exhibit even when heavily sintered.[10] Moreover, in spite of the inherent loss of surface area, the high temperature ageing treatments under reducing conditions may actually improve their reducibility and OSC properties.[7] This behaviour contrasts with the severe deterioration of redox properties always observed for pure ceria on ageing.[11,12] Recent studies which directly compare the reduction behaviour of Ce/Zr mixed oxides with that of pure CeO_2 clearly demonstrate this point.[7,10]

We report on the strong influence of the re-oxidation conditions on the redox behaviour of $Ce_{0.68}Zr_{0.32}O_2$ previously reduced at high temperature. Alternate mild (823 K) and high temperature (1223 K) re-oxidation treatments, after reduction at 1223 K in each case, result in very different, but reversible, redox behaviours. The mild re-oxidation leads to enhanced oxide reducibility whereas subsequent high temperature re-oxidation induces the opposite effect: severe loss of reducibility. This behaviour can be reproduced in a cyclic manner, demonstrating the reversibility of this effect.

The starting Ce/Zr oxide, hereafter denoted LS, had a BET surface area of 23 $m^2\ g^{-1}$ and was prepared by coprecipitation, calcination and then prolonged ageing (140 h) in wet synthetic air at 1173 K.

Fig. 1 shows the TPR-MS (temperature programmed reduction-mass spectrometry) traces for H_2O (*m/z*: 18) evolution recorded when a series of the above-mentioned redox treatments were applied successively. The TPR experimental conditions were: amount of sample: 200 mg; H_2(5%)–Ar flow rate: 60 $cm^3\ min^{-1}$; heating rate: 10 $K\ min^{-1}$; top limit temperature: 1223 K; heating time at 1223 K: 2 h. Before running any of the TPR–MS experiments, the oxide sample was routinely oxidised either under mild (MO) or high temperature (HTO) conditions. The MO treatment consisted of: heating from 298 to 823 K in flowing O_2(5%)/He at 10 $K\ min^{-1}$ followed by a 1 h isothermal step at 823 K, cooling to 473 K, also under flowing O_2(5%)–He, and finally cooling to 298 K in a flow of He. The HTO treatment is similar to the MO, the only difference being that the top limit re-oxidation temperature was 1223 K. As confirmed by the magnetic balance data, both MO and HTO protocols ensure the full oxidation of the sample. Likewise, our magnetic balance and TPD studies confirm that the final cooling step from 473 to 298 K, in flowing He, does not induce any significant reduction of the oxide. However, it allows us to avoid any possible contribution to the TPR–MS traces from chemisorbed oxygen species. TPD–MS results also show that both MO and HTO re-oxidation treatments lead to heavily dehydroxylated oxide samples. In summary, the reported TPR–MS traces should be interpreted as due only to the sample reduction with inherent creation of oxygen vacancies.

The high temperature reduction treatment consisted of heating the MO pre-treated LS oxide under flowing H_2 (60 $cm^3\ min^{-1}$) from 298 up to 1223 K (heating rate: 10 $K\ min^{-1}$), followed by a dwell at 1223 K for 5 h, evacuation at 1223 K (1 h) in a flow of He, cooling to 298 K also in flowing He, and a further MO re-oxidation treatment. The resulting oxide sample will be hereafter referred to as SR.

Traces (a) and (b) in Fig. 1 present the TPR–MS diagrams recorded for the LS and SR samples respectively. Compared

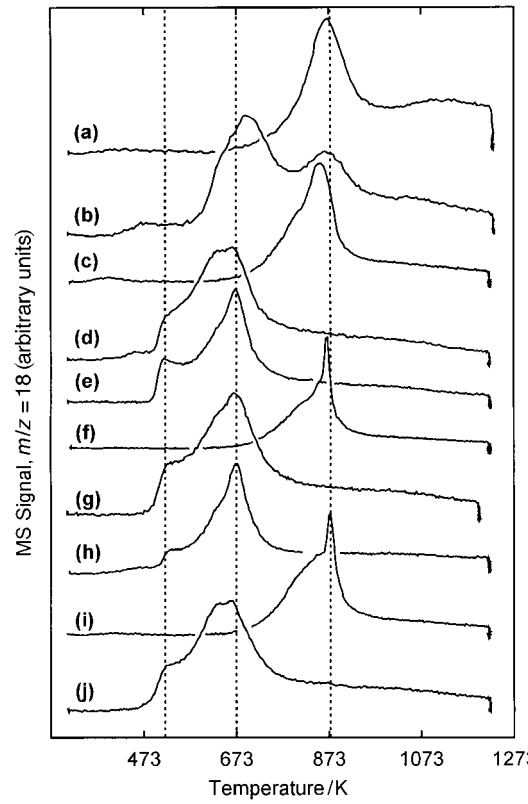

Fig. 1 Influence of the pre-treatment conditions on the reducibility of a Ce/Zr mixed oxide (CZ-68/32-LS). TPR–MS traces corresponding to the sample pre-treated as follows: (a) fresh oxide sample, (b) SR pre-treatment, (c) HTO, (d) MO, (e) MO, (f) HTO, (g) MO, (h) MO, (i) HTO, (j) MO. Experiments (b)–(f) were recorded successively on the same oxide sample. For details of the SR, HTO and MO treatments, see text.

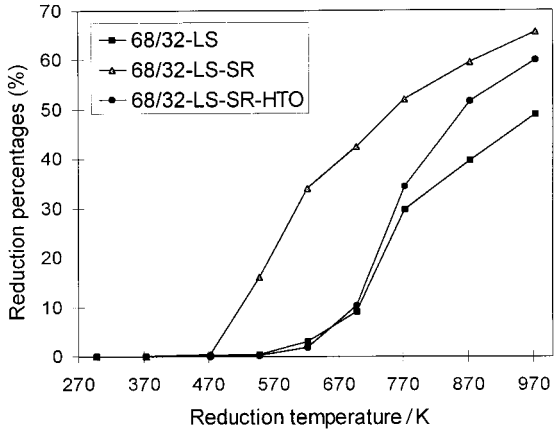

Fig. 2 Reduction percentage of $Ce_{0.68}Zr_{0.32}O_2$ obtained from the magnetic susceptibility measurements and expressed as $Ce^{3+}/(Ce^{3+} + Ce^{4+})$ as a function of the reduction temperature [1 h at each temperature under H_2(5%)–He flow].

with the LS oxide, the reducibility of the SR sample is significantly enhanced. The Faraday microbalance has proved to be particularly useful in characterising the redox behaviour of ceria based catalytic materials.[11–14] As in pure ceria, the reduction of Ce/Zr mixed oxides transforms diamagnetic Ce^{4+} cations into paramagnetic Ce^{3+} species. Thus, the evolution of the magnetic susceptibility as a function of the step by step reduction treatment provides direct information about the changing redox state of the oxide. In Fig. 2, the evolution of the reduction percentage expressed as $Ce^{3+}/(Ce^{3+} + Ce^{4+})$ clearly confirms the improved reducibility of the SR sample.

The oxide resulting from the TPR experiment in Fig. 1(b) was further re-oxidised at high temperature by following the HTO protocol. The resulting sample is referred to as SR-HTO. The corresponding TPR–MS diagram is shown in Fig. 1(c). Compared with Fig. 1(b), the main reduction peak in Fig. 1(c) is strongly shifted upwards in temperature, implying a considerable deterioration of sample reducibility. This is also seen in the magnetic balance results reported in Fig. 2.

Fig. 1(d)–(j) show the evolution of the redox properties of the oxide during the series of successive TPR–MS/Re-oxidation (MO or HTO) treatments. When the sample resulting from the TPR–MS experiment shown in Fig. 1(c), is re-oxidised by following the MO protocol, the subsequent TPR–MS diagram [Fig. 1(d)] shows a 200 K shift in the reduction peak towards lower temperatures. By repeating the MO and TPR–MS routine, a trace [Fig. 1(e)] very close to the previous one was obtained. By contrast, the TPR–MS reduction peaks are then shifted upwards again [Fig. 1(f)] by applying the HTO re-oxidation procedure to this sample. The last four TPR–MS diagrams [Fig. 1(g)–(j)] allow us to confirm that this behaviour is fully reversible. No change of the BET surface area was observed throughout the whole series of experiments.

The above results prompted us to investigate the effect of an intermediate re-oxidation temperature (923 K). Fig. 3(b) shows the corresponding TPR–MS trace. The diagrams recorded after re-oxidation at 823 K (a) and 1223 K (c) are also included for comparison. We can conclude that the choice of the re-oxidation conditions may critically modify the redox properties of the oxide. Fig. 3 shows that a moderate increase of the re-oxidation temperature, from 823 to 923 K, has a strong influence on the reducibility of the oxide.

In conclusion, these results may help towards a better understanding of the behaviour of this family of TWC redox materials. Our results suggest the convenience of performing specific studies aimed at establishing the effect of the ageing treatments under real TWC operation conditions on the redox behaviour of these mixed oxides. Finally, our observations are also relevant for comparative purposes: the pre-treatment conditions appear to play an important role in determining the redox behaviour of the resulting oxides. Consequently, the pre-treatment routine should be carefully controlled when comparative evaluations of Ce/Zr mixed oxides are to be made.

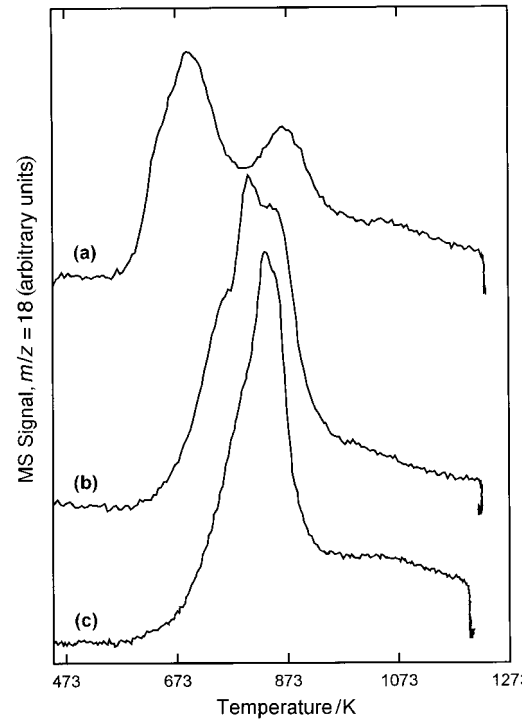

Fig. 3 Influence of the oxidising pre-treatment on the reducibility of a Ce/Zr mixed oxide (CZ-68/32-LS). TPR–MS traces corresponding to: (a) SR sample (MO pre-oxidation protocol); (b) SR sample further heated under O_2(5%)–He at 923 K (experimental pre-oxidation protocol similar to the MO and HTO procedures); (c) SR sample further submitted to the HTO treatment.

This work has received financial support from the TMR Program of the EU (CEZIRENCAT Project, Contract No.: ERB-FMRX-CT-96-0060), the CICYT (Project: MAT96-0931), the DGICYT (Project PB95-1257) and the Junta de Andalucía.

Notes and references

1 M. Ozawa, M. Kimura and A. Isogai, *J. Alloys Compd.*, 1993, **193**, 73.
2 J. P. Cuif, G. Blanchard, O. Touret, A. Seigneurin, M. Marczi and E. Quéméré, Society of Automotive Engineers paper 970463 (1997).
3 M. Pijolat, M. Prin, M. Soustelle, O. Touret and P. Nortier, *J. Chem. Soc., Faraday Trans.*, 1995, **91**, 3941.
4 J. P. Cuif, G. Blanchard, O. Touret, M. Marczi and E. Quéméré, SAE paper 961906 (1996).
5 A. Trovarelli, F. Zamar, J. Llorca, C. Leitenburg, G. Dolcetti and J. T. Kiss, *J. Catal.*, 1997, **169**, 490.
6 S. Otsuka-Yao, H. Morikawa, N. Izu and K. Okuda, *J. Jpn. Inst. Met.*, 1995, **59**, 1237.
7 P. Fornasiero, G. Balducci, R. Di Monte, J. Kaspar, V. Sergo, G. Gubitosa, A. Ferrero and M. Graziani, *J. Catal.*, 1996, **164**, 173.
8 P. Fornasiero, R. Di Monte, G. Ranga Rao, J. Kaspar, S. Meriani, A. Trovarelli and M. Graziani, *J. Catal.*, 1995, **151**, 168.
9 P. Vidmar, P. Fornasiero, J. Kaspar, G. Gubitosa and M. Graziani, *J. Catal.*, 1997, **171**, 160.
10 G. Balducci, P. Fornasiero, R. Di Monte, J. Kaspar, S. Meriani and M. Graziani, *Catal. Lett.*, 1995, **33**, 193.
11 V. Perrichon, A. Laachir, G. Bergeret, R. Fréty, L. Tournayan and O. Touret, *J. Chem. Soc., Faraday Trans.*, 1994, **90**, 773.
12 A. Laachir, V. Perrichon, A. Badri, L. Lamotte, E. Catherine, J. C. Lavalley, J. El Fallah, L. Hilaire, F. Le Normand, E. Quéméré, G. N. Sauvion and O. Touret, *J. Chem. Soc., Faraday Trans., 1991,* **87**, 1601.
13 S. Bernal, J. J. Calvino, G. A. Cifredo, J. M. Rodríguez-Izquierdo, V. Perrichon and A. Laachir, *J. Catal.*, 1992, **137**, 1.
14 S. Bernal, J. J. Calvino, G. A. Cifredo, A. Laachir, V. Perrichon and J. M. Herrmann, *Langmuir*, 1994, **10**, 717.

Communication 8/08203K

Preparation and synthetic applications of α-fluorovinylphosphonium salts

Takeshi Hanamoto,* Yasuhide Kiguchi, Keiko Shindo, Miki Matsuoka and Michio Kondo

Department of Chemistry, Saga University, Honjyo-machi, Saga 840-8502, Japan.
E-mail: hanamoto@cc.saga-u.ac.jp

Received (in Cambridge, UK) 13th October 1998, Accepted 7th December 1998

α-Fluorovinylphosphonium salts 3 and 4 were synthesized and underwent Michael addition followed by Wittig olefination to give the corresponding monofluoroethylene compounds in good yields.

The replacement of a hydrogen atom by a fluorine atom often causes large changes in the biological activity of organic compounds, and the preparation of such fluorinated compounds has recently received much attention in the fields of medical and agricultural chemicals.[1] Although some methods for the direct exchange of the hydrogen by the fluorine are well-accepted, special techniques and equipment are required.[2] Thus, the development of versatile fluorinated building blocks has become a significant task in this field.[3] We have considered the title compounds as promising candidates for a monofluorinated building block which would be stable and easy to handle. As vinyltriphenylphosphonium bromide (Schweizer reagent) exhibits excellent performance,[4] we would expect similar reactivity for the title compound. This report describes the first preparation and reaction of the α-fluorovinylphosphonium salts as useful reagents for introducing a monofluoroethylene moiety into carbonyl compounds.[5]

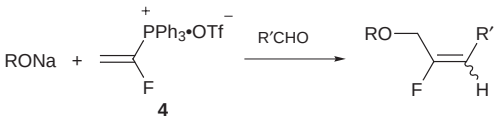

Our synthetic route for the preparation of the α-fluorovinylphosphonium salts **3** or **4** is depicted in Scheme 1. Initially, we examined the convenient preparation of α-fluorovinyldiphenylphosphine **2** as a precursor for the salts. Since it is well-documented that nucleophilic addition followed by elimination of the fluoride for producing 1,1-difluoroethylene derivatives is facile,[6] it was therefore anticipated that the reaction of lithium diphenylphosphide[7] and 1,1-difluoroethylene **1** should afford the facile preparation of the phosphine **2**. The modest yield we encountered when conducting the reaction in THF–toluene at −78 °C led us to controlling the reaction temperature. When the reaction was conducted over the temperature range of −60 to −40 °C, the yield improved to 86%. However, if the reaction temperature exceeded −40 °C, undesirable 1,1-bis(diphenylphosphinyl)ethylene was produced as a by-product.

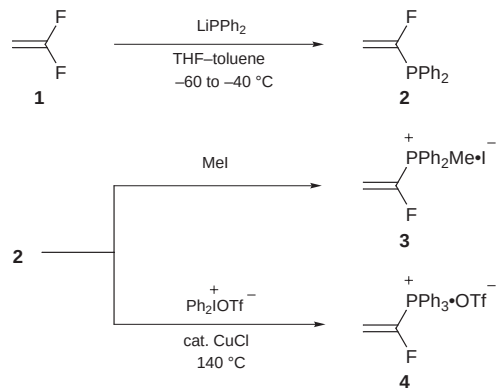

Scheme 1

Table 1 Reaction of α-fluorovinylphosphonium salts with variuos aldehydes

Entry	R	R′	Yield (%)[a]	*E*:*Z*[b]
1[c]	Me	Ph	43	52:48
2	Me	Ph	63	40:60
3[c]	Et	Ph	52	53:47
4	Et	Ph	75	43:57
5	Et	4-$MeOC_6H_4$	80	35:65
6	Et	4-PhC_6H_4	70	47:53
7	Et	4-NCC_6H_4	69	52:48
8	Et	2-naphthyl	77	41:59
9	Et	(*E*)-PhCH=CH	82	37:63
10	Et	$PhCH_2CH_2$	trace	—

[a] Isolated yield. [b] Determined by capillary GC–MS analysis. [c] Salt **3** was used in place of **4**.

Quaternization of the phosphine **2** with MeI proceeded smoothly to give the α-fluorovinyldiphenylmethylphosphonium iodide **3** in 91% yield; however, reaction of **2** with aryl halides or aryl triflates did not take place under various conditions. Kitamura and co-workers have described the direct S-arylation of benzo[*b*]thiophenes to produce the 1-arylbenzo[*b*]thiophenium salt.[8] This prompted us to use the diaryliodonium salts for P-arylation of the phosphine **2** instead of S-arylation of the sulfides. After many unsuccessful experiments, the α-fluorovinyltriphenylphosphonium triflate **4** was finally obtained by the reaction of diphenyliodonium triflate in the presence of CuCl in 1,1,2,2-tetrachloroethane at 140 °C in 82% yield.† We believe that this P-arylation method provides a new route for the synthesis of the aryl phosphonium salts.

The β-ethoxy-α-fluoroethyltriphenylphosphonium ylide, generated *via* the addition of an ethoxide anion to **4** in ethanol at room temperature, reacted with benzaldehyde to provide 1-benzylidene-1-fluoro-2-ethoxyethane as a 43:57 mixture of the *E* and *Z* isomers in 75% yield (Table 1, entry 4).‡ The *E*:*Z* ratio was determined by capillary GC–MS analysis. The geometrical isomers were characterized from their NMR spectra. The coupling constants with fluorine showed a value of 20 Hz for the *E* isomer and 39 Hz for the *Z* isomer. The effects of the reaction conditions on these relative *E*:*Z* ratios have not been studied. Some selected data are shown in Table 1. The reactivity of salt **4** was much higher than that of salt **3** (compare the yields in entries 1 *vs*. 2 and 3 *vs*. 4). Although aromatic aldehydes and an α,β-unsaturated aldehyde gave good results, the aliphatic aldehyde gave poor results. Studies on the synthesis of a variety of monofluorinated heterocyclic ring systems are now in progress in our laboratory.

This work was supported by the Mitsubishiyuka Foundation, the Yamanouchi Foundation, and a Grant-in-Aid for Scientific Research (10650836) from the Ministry of Education, Science, and Culture, Japan.

Notes and references

† Preparation of **2**: To a solution of lithium wire (0.54 g, 83.8 mmol) in 40 ml of THF was added diphenylchlorophosphine (6.0 ml, 33.4 mmol) at

room temperature under argon. The solution was stirred for 3 h and followed by the addition of 40 ml of toluene. After stirring for an additional 1 h, the solution was cooled to −60 °C. At this temperature, argon was replaced with 1,1-difluoroethylene. The mixture was gradually warmed to −40 °C and quenched with sat. NH_4Cl solution. After the usual workup, the residue was chromatographed on silica gel (hexane–EtOAc 100:1) to give the desired product (6.3 g, 86%): ν(neat)/cm^{-1} 3056, 1622, 1482, 1435, 1153, 1095, 1027, 997, 916, 885, 742 and 694; δ_H($CDCl_3$) 4.97 (1H, ddd, *J* 2.9, 6.3, 50.8), 5.39 (1H, ddd, *J* 2.9, 21.0, 23.4), 7.25–7.80 (m, 10 H); HRMS: 230.0661(M^+); Calc. for $C_{14}H_{12}FP$: C, 73.04; H, 5.25. Found: C, 72.96; H, 5.28%.

Preparation of **4**: A mixture of α-fluorovinyldiphenylphosphine **2** (1.47 g, 6.4 mmol), diphenyliodonium triflate (3.30 g, 7.7 mmol), copper(I) chloride (63.3 mg, 0.64 mmol), a catalytic amount of Cu wire (30 mg) and 4 Å molecular sieves (0.5 g) in 1,1,2,2-tetrachloroethane (1.5 ml) was heated at 140 °C for 30 min under argon. After cooling the reaction mixture to room temperature, it was chromatographed on silica gel (CH_2Cl_2 then CH_2Cl_2–acetone 2:1) to give the desired product (2.41g, 82%). Further purification for the combustion analysis was conducted by recrystallization from Bu^tOH–Et_2O: mp 101.2–101.7 °C; ν(KBr)/cm^{-1} 3137, 3062, 3007, 1632, 1588, 1581, 1486, 1482, 1441, 1370, 1257, 1227, 1172, 1152, 1114, 1029, 995, 935, 913, 760, 736, 709, 689 and 641; δ_H($CDCl_3$) 5.79 (1H, ddd, *J* 6.4, 7.3, 49.3), 6.49 (1H, ddd, *J* 6.4, 21.5, 29.8), 7.7–8.0 (m, 15 H); *m/z* (FAB) 307 (M^+ − OTf); Calc. for $C_{21}H_{17}F_4O_3PS$: C, 55.27; H, 3.75. Found: C, 55.08; H, 3.67%.

‡ *General procedure*: To a solution of NaH (1.2 equiv.) in EtOH (5 ml) under Ar was added α-fluorovinyltriphenylphosphonium triflate (0.5 mmol) at room temperature. The resulting solution was stirred for 10 min, benzaldehyde (1.2 equiv.) was added to the solution, and the reaction mixture was stirred for 16 h. After the usual workup, column chromatography (silica gel, hexane–EtOAc 30:1) of the residue afforded 27.7 mg of (*E*)-1-benzylidene-2-ethoxy-1-fluoroethane and 39.1 mg of (*Z*)-1-benzylidene-2-ethoxy-1-fluoroethane (total 75% yield). (*E*)-isomer: ν(neat)/cm^{-1} 2978, 2924, 2873, 1685, 1598, 1489, 1447, 1380, 1261, 1143, 1098, 997, 883, 750, 699 and 630; δ_H($CDCl_3$) 1.25 (3H, t, *J* 6.84), 3.58 (2H, q, *J* 6.83), 4.18 (2H, d, *J* 22.95), 6.45 (1H, d, *J* 20.02), 7.24–7.38 (5H, m); *m/z* 180 (30, M^+), 151 (46), 135 (60), 133 (56), 115 (80), 109 (100), 104 (30); Calc. for $C_{11}H_{13}FO$: C, 73.31; H, 7.27. Found: C, 73.54; H, 7.44%. (*Z*)-isomer: ν(neat)/cm^{-1} 3025, 2978, 2865, 1695, 1598, 1496, 1450, 1351, 1099, 880, 755 and 694; δ_H($CDCl_3$) 1.27 (3H, t, *J* 6.83), 3.60 (2H, q, *J* 6.83), 4.12 (2H, d, *J* 15.14), 5.76 (1H, d, *J* 38.57), 7.21–7.53 (5H, m); *m/z* 180 (52, M^+), 151 (52), 135 (76), 133 (62), 115 (90), 109 (100); Calc. for $C_{11}H_{13}FO$: C, 73.31; H, 7.27. Found: C, 73.44; H, 7.35%.

1 J. T. Welch, *Tetrahedron*, 1987, **43**, 3123; M. Schlosser, *Tetrahedron*, 1978, **34**, 3; *Biomedical Aspects of Fluorine Chemistry*, ed. R. Filler and Y. Kobayashi, Kodansha, Tokyo, 1982.

2 S. T. Purrington, B. S. Kagan and T. B. Patrick, *Chem. Rev*., 1986, **86**, 997

3 J. R. McCarthy, E. W. Huber, T-B. Le, F. M. Laskovics and D. P. Matthews, *Tetrahedron*, 1996, **52**, 45; T. Ernet and G. Haufe, *Tetrahedron Lett*., 1996, **37**, 7251; S. A. Fontana, C. R. Davis, Y-B. He and D. J. Burton, *Tetrahedron*, 1996, **52**, 37; P. J. Crowley, J. M. Percy and K. Stansfield, *Tetrahedron Lett*., 1996, **37**, 8233 and references cited therein.

4 E. E. Schweizer, L. D. Smucker and R. J. Votral, *J. Org. Chem*., 1966, **31**, 467 and references cited therein.

5 The synthesis of α-fluorovinylphosphonates has been reported. G. M. Blackburn and M. J. Parratt, *J. Chem. Soc., Perkin Trans. 1*, 1986, 1417; G. M. Blackburn and M. J. Parratt, *J. Chem. Soc., Chem. Commun*., 1982, 1270.

6 H. F. Koch and A. J. Kielbania, Jr, *J. Am. Chem. Soc*., 1970, **92**, 729.

7 E. J. Corey and M. A. Tius, *Tetrahedron Lett*., 1980, **21**, 3535.

8 T. Kitamura, M. Yamane, B-X. Zhang and Y. Fujiwara, *Bull. Chem. Soc. Jpn*., 1998, **71**, 1215; T. Kitamura, M. Yamane, R. Furuki, H. Taniguchi and M. Shiro, *Chem. Lett*., 1993, 1703.

Communication 8/07933A

Hydrogen bonded assemblies of a cyclic trimeric hydroxy gallium(III) derivative: $[\{Me_2Ga(\mu\text{-}OH)\}_3{\cdot}3H_2O]_2{\cdot}$18-crown-6

Paul D. Croucher, Alexander Drljaca, Stavroula Papadopoulos and Colin L. Raston*

Department of Chemistry, Monash University, Clayton, Melbourne, Victoria 3168 Australia.
E-mail: c.raston@sci.monash.edu.au

Received (in Columbia, MO, USA) 5th October 1998, Accepted 8th December 1998

Addition of hydrolysed trimethylgallium to an excess of 18-crown-6 in water affords an alkyl μ-hydroxo bridged Ga(III) trimer in solution (pH *ca.* 6) and the solid, isolated as the hydrogen bonded assembled supermolecule $[\{Me_2Ga(\mu\text{-}OH)\}_3{\cdot}3H_2O]_2{\cdot}$18-crown-6.

The oxidation and reaction of group 13 alkyl compounds with water is often extremely exothermic and under controlled conditions it is possible to isolate some metal oxide/hydroxide intermediate compounds *en route* to complete hydrolysis to the alkane and metal hydroxides.[1] These compounds have provided information about the hydrolysis reactions and certain derivatives have also been found to function as co-catalysts in the Ziegler–Natta polymerisation of olefins.[2] The oxide, hydroxide and mixed oxide–hydroxide chemistry of aluminium, and also indium, has been extensively studied.[3] In contrast, there have been relatively few studies concerning analogous gallium chemistry.[3–11] The first organogallium–oxo compound reported $[Bu^tGa(\mu_3\text{-}O)]_9$ was characterised by mass spectrometry and NMR spectroscopy,[12] soon followed by the synthesis and structural authentication of the only known cyclic trimeric hydroxy derivative of gallium, $[Bu^t_2Ga(\mu\text{-}OH)]_3$.[5] This compound was originally identified as an impurity formed during the synthesis of $[Bu^t_2Ga(\mu\text{-}PH_2)]_3$.[13] More recently, the structural characterisation of the largest galloxane hydroxide isolated thus far, $[Ga_{12}Bu^t_{12}(\mu_3\text{-}O)_8(\mu\text{-}O)_2(\mu\text{-}OH)_4]$, has been described.[4] Further studies on the stabilization and structural characterisation of controlled hydrolysis products of $[Ga(2,4,6\text{-}Me_3C_6H_3)_3]$ by deprotonation reactions involving alkyllithium reagents have also been reported.[14]

In addressing the difficulties associated with isolating the intermediates formed during the hydrolysis of substitutionally labile alkyl metal compounds from aqueous solution we use a crown ether to promote supramolecular complexation and crystallisation. A similar technique has been used to crystalise a known dinuclear aqua cation formed during the hydrolytic polymerisation of Cr(III).[15] In the present study we show that using this supramolecular self assembly approach results in the formation of a new alkyl μ-hydroxo bridged Ga(III) trimer, $[\{Me_2Ga(\mu\text{-}OH\}_3{\cdot}3H_2O]_2{\cdot}$18-crown-6, which has been characterised in solution and in the solid state.

Addition of an aqueous solution of hydrolysed trimethylgallium to 2 equiv. of 18-crown-6 in water at room temperature (pH of the mixture *ca.* 6) results in the formation of colorless crystals of $[\{Me_2Ga(\mu\text{-}OH)\}_3{\cdot}3H_2O]_2{\cdot}$18-crown-6 (Fig. 1)† suitable for X-ray crystallography. It is noteworthy that the product yield is enhanced by increasing the concentration of 18-crown-6 relative to hydrolysed Me_3Ga in the reaction mixture; molar ratios for 18-crown-6: hydrolysed Me_3Ga of 2 : 1, 1 : 1 and 0.5 : 1 afford the trimer in 70, 40 and 20% yield respectively. The ^{1}H NMR spectrum of the complex in acetone exhibits a singlet at $\delta -0.45$, assigned to the Me_2Ga units, a less intense singlet at δ 4.46, assigned to the GaOH protons, and a singlet at δ 3.59 assigned to the ethylene groups of the 18-crown-6. The integration, 6 : 1 : 4 respectively, is consistent with the proposed formulation. In acetone hydrogen bonding interactions (Fig. 2) between GaOH groups and solvent are likely and in this context we note that in chloroform the singlet for GaOH shifts to δ 1.43. The trimeric complex was found to be insoluble in hexane and water which contrasts with previous findings for the *tert*-butyl analogue $[Bu^t_2Ga(\mu\text{-}OH)]_3$.[6]

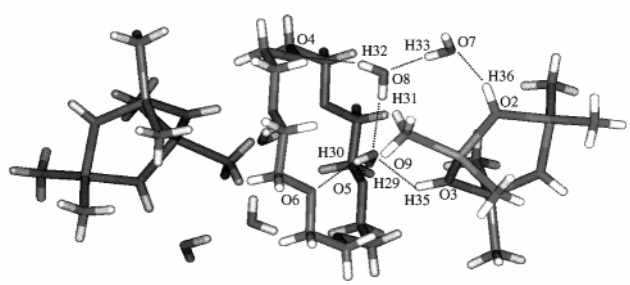

Fig. 1 The molecular structure of $[\{Me_2Ga(\mu\text{-}OH)\}_3{\cdot}3H_2O]_2{\cdot}$18-crown-6.

The variable-temperature ^{1}H NMR spectra of the complex show shifts in the singlet due to GaOH from δ 4.4 (+30 °C) to a doublet (2 : 1) at 5.2 (−60 °C) which may be due to the hydrogen bonding interactions of two of the three possible bridging OH groups with water molecules hydrogen bonded to the crown ether (Fig. 1). This change was not observed in the variable-temperature ^{1}H NMR spectra of $[Bu^t_2Ga(\mu\text{-}OH)]_3$[6] and is consistent with the presence of the crown ether complex in solution. Addition of D_2O to the complex in acetone results in the spontaneous disappearance of the O–H signal, indicating very fast proton exchange on the bridging OH groups. By comparison the OH signal for $[Bu^t_2Ga(\mu\text{-}OH)]_3$ in D_2O disappeared slowly over 120 h (slow proton exchange).[6] This is to be expected since terminal methyl groups sterically crowd the bridging OH groups less thus providing greater access to the bulk solvent (for exchange) than *tert*-butyl groups on the same gallium trimer.

The ^{13}C{^{1}H} NMR spectrum at 20 °C contains two singlets at δ 11.04 and 71.40 due to 18-crown-6 and Me_2Ga groups, respectively. The positive ion electrospray mass spectrum (ESMS) confirmed the trimeric nature of the complex in the gas phase {$[Me_2Ga(OH)]_3$ = 350.1 u}. IR spectroscopic data confirm the presence of the O–H and C–O (18-crown-6) groups (ν_{O-H} 3420 cm^{-1}, ν_{C-O} 1110 cm^{-1}).

The compound crystallises in the space group $P\bar{1}$ with the asymmetric unit comprised of one $[GaMe_2(OH)]_3$ cluster and half a crown ether molecule, bound together by a chain of three hydrogen bonded water molecules (Fig. 1).‡ Crystallographic symmetry places one cluster on each side of the crown ether

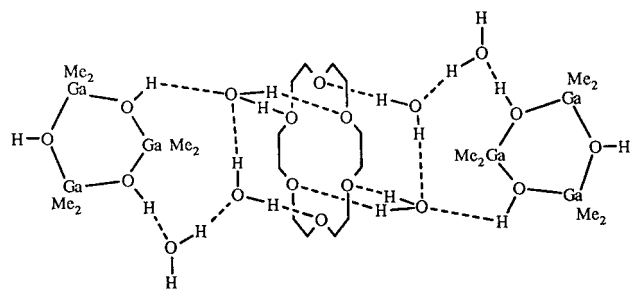

Fig. 2

Table 1 Hydrogen bonding distances (Å) and angles (°) in the supermolecule

A	H	B	A···B	A–H	H···B	A–H···B
O(2)	H(36)	O(7)	2.693(3)	0.950(2)	1.940(3)	134.5(2)
O(3)	H(35)	O(9)	2.824(4)	0.950(2)	2.104(3)	131.5(2)
O(7)	H(33)	O(8)	2.687(5)	0.85(4)	1.84(5)	173(4)
O(7)	H(34)	O(2)	2.887(4)	0.86(6)	2.07(6)	158(5)
O(8)	H(31)	O(9)	2.767(5)	0.80(5)	2.00(5)	163(5)
O(8)	H(32)	O(4)	2.834(4)	0.75(4)	2.11(4)	164(4)
O(9)	H(29)	O(5)	2.882(4)	0.91	1.98	177.1
O(9)	H(30)	O(6)	2.816(5)	0.66	2.16	170.9

molecule which is arranged with adjacent oxygen atoms alternating between pointing towards one of the gallium clusters and to its symmetry relative, *i.e.* three up and three down. Two water molecules hydrogen-bond with each face of the crown, the first bridging two crown ether oxygens, O···O 2.88(1) and 2.82(1) Å, while the second bridges the first water molecule O···O 2.68(1) Å and the remaining crown ether oxygen O···O 2.83(1) Å. The hydrogen bonding sphere of the first water molecule is completed by a hydrogen bond to one of the hydroxy groups from the gallium cluster O···O 2.82(1) Å while a third water molecule connects the second water molecule and the gallium cluster *via* hydrogen bonding to a second hydroxy of the cluster O···O 2.69(1) Å. Hydrogen bonding distances and angles in the supermolecule are shown in Table 1.

In conclusion we have shown the supramolecular hydrogen bonded self assembly of a novel cyclic trimeric hydroxy gallium(III) derivative with 18-crown-6 [{$Me_2Ga(\mu$-$OH)\}_3\cdot 3H_2O$]·18-crown-6. Evidence for the presence of the supermolecule was obtained from both solid state and solution studies. Furthermore, X-ray crystallographic data showed that in the solid state each supermolecule exists as a discrete unit comprising of two gallium trimer clusters hydrogen bonded through six lattice water molecules to a central crown ether. We are currently investigating using this approach to crystallise other group 13 alkyl hydroxy compounds from aqueous solution.

This work was supported by the Australian Research Council.

Notes and references

† Synthesis and characterisation of [{$Me_2Ga(\mu$-$OH)\}_3\cdot 3H_2O]_2$·18-crown-6: Me_3Ga (1 ml) was added to distilled water (30 ml) in an extremely exothermic reaction (**CAUTION!**) Aliquots of this solution were taken and added to aqueous solutions of 18-crown-6 such that the ratio of 18-crown-6 to hydrolysed Me_3Ga was 2 : 1 at pH *ca.* 6. This resulted in the formation of colorless crystals over a period of a week. Yield: 70% with respect to Ga. Mp 64–66 °C. Insoluble in hexane and water; soluble in acetone and chloroform. IR (KBr disk): 3420m br, 2956m, 2912m, 1637w, 1473vw, 1353w, 1253vw, 1202w, 1109s, 962m, 838vw, 802vw, 734m, 583m, 532m cm^{-1}. ^1H NMR [300.07 MHz, 20 °C, $(CD_3)_2CO$] δ −0.45 [s, 18H, $(Me_2Ga)_3$], 3.59 (s, 24H, 18-crown-6), 4.46 {s, 3H, $[Ga(OH)]_3$}. ^1H NMR (200.13 MHz, 20 °C, CD_3Cl) δ −0.34 [s, 18H, $(Me_2Ga)_3$]), 1.43 {s, 3H, $[Ga(OH)]_3$}, 3.68 (s, 24H, 18-crown-6). $^{13}C\{^1H\}$ NMR (75.45 MHz, 20 °C, $(CD_3)_2CO$] δ 11.04 (s, 18-crown-6), 71.40 [s, $(Me_2Ga)_3$]. ESMS (MI, Me_2CO), *m*/*z* 480.1 {$[Me_2Ga(OH)]_3\cdot Me_2CO\cdot 4H_2O$}, 408.1 {$[Me_2Ga$-$(OH)]_3\cdot Me_2CO$}, 363.2 ($Me_2Ga$·18-crown-6), 350.1 {$[Me_2Ga$-$(OH)]_3$}. Anal. Calc. for $[Ga_3O_9C_{12}H_{39}]_2$: C, 26.84; H, 7.27. Found: C, 2701; H, 7.40%.

‡ Data collected on an Enraf Nonius CCD diffractometer at 123 K using graphite-monochromated Mo-Kα radiation (λ = 0.71013 Å) were corrected for Lorenzian and polarisation but not absorption. The structure was solved using TEXSAN. All non-hydrogen atoms were refined using a full-matrix least-squares refinement against *F*. All hydrogen atoms, other than those attached to water molecules, were included at calculated positions with a riding model. Those hydrogen atoms attached to water molecules were included by the detection of electron density between heteroatoms situated at hydrogen-bonded distances *i.e.* < 2.9 Å and refined. *Crystal data*. $C_{23}H_{78}O_{18}Ga_6$. M_r = 1073.18, triclinic, space group $P\bar{1}$, a = 8.9725(3), b = 11.3120(3), c = 12.8986(5) Å, α = 77.522(1), β = 75.876(1), γ = 67.686(6)°, U = 1163.35(6) $Å^3$, Z = 2, μ = (Mo-Kα) = 8.935 mm^{-1}, 3139 reflections, 242 parameters, R_1 = 0.0309, wR = 0.0338. CCDC 182/1106. See http://www.rsc.org/suppdata/cc/1999/153/ for crystallographic files in .cif format.

1 M. B. Power, W. M. Cleaver, A. W. Apblett, A. R. Barron and J. W. Ziller, *Polyhedron*, 1992, **11**, 477.
2 S. Pasynkiewicz, *Polyhedron*, 1990, **9**, 429.
3 A. R. Barron, *Comments Inorg. Chem.*, 1993, **14**, 123.
4 C. C. Landry, C. J. Harlan, S. G. Bott and A. R. Barron, *Angew. Chem., Int. Ed. Engl.*, 1995, **34**, 1201.
5 M. B. Power, W. M. Cleaver, A. W. Apblett, A. R. Barron and J. W. Ziller, *Polyhedron*, 1992, **11**, 477.
6 A. D. Atwood, A. H. Cowley, P. R. Harris, R. A. Jones, S. U. Koschmieder and C. M. Nunn, *Organometallics*, 1993, **12**, 24.
7 A. A. Naiini, V. Young, H. Han, M. Akinc and J. G. Verkade, *Inorg. Chem.*, 1993, **32**, 3781.
8 M. E. Kenney and A. W. Laubengayer, *J. Am. Chem. Soc.*, 1954, **74**, 4839; G. S. Smith and J. L. Hoard, *J. Am. Chem. Soc.*, 1959, **81**, 3907.
9 R. D. Schluter, H. S. Isom, A. H. Cowley, D. A. Atwood, R. A. Jones, F. Olbrich, S. Corbelin and R. J. Lagow, *Organometallics*, 1994, **13**, 4058.
10 J. Storre, T. Belgardt, H. W. Roesky and D. Stalke, *Angew. Chem., Int. Ed. Engl.*, 1994, **33**, 1244.
11 C. Schnitter, H. W. Roesky, T. Albers, H.-G. Schmidt, C. Ropken, E. Parisini and G. M. Scheldrick, *Chem. Eur. J.*, 1997, **3**, 1783.
12 M. B. Power, J. W. Ziller and A. R. Barron, *Organometallics*, 1992, **11**, 2783.
13 A. H. Cowley, P. R. Harris, R. A. Jones and C. M. Nunn, *Organometallics*, 1991, **10**, 652.
14 J. Storre, C. Schnitter, H. W. Roesky, H.-G. Schmidt, M. Noltemeyer, R. Fleischer and D. Stalke, *J. Am. Chem. Soc.*, 1997, **119**, 7505.
15 A. Drljaca, D. C. R. Hockless, B. Moubaraki, K. S. Murray and L. Spiccia, *Inorg. Chem.*, 1997, **36**, 1988.

Communication 8/07995A

A new method of intercalation by anion exchange in layered double hydroxides

Eduardo L. Crepaldi, Paulo C. Pavan and João B. Valim*

Department of Chemistry, Faculdade de Filosofia, Ciências e Letras de Ribeirão Preto, Universidade de São Paulo, Av. dos Bandeirantes 3900, CEP.: 14.040-901, Ribeirão Preto, SP Brazil. E-mail: jobvalim@usp.br

Received (in Cambridge, UK) 4th November 1998, Accepted 1st December 1998

A new anion exchange method of intercalation in layered double hydroxides (LDHs), based on the formation and organic phase extraction of a salt between dodecylsulfate anions and a cationic surfactant (CTA), is described which is shown to be a very fast and efficient way to obtain a wide variety of LDH-intercalated organic and inorganic anions, using the precursor Zn(II)–Cr(III)–dodecylsulfate LDH.

Layered double hydroxides (LDHs), or the so-called hydrotalcite-like compounds, can be represented by the general formula $[M^{II}_{1-x}M^{III}_x(OH)_2](A^{m-})_{x/m}\cdot nH_2O$. The structure of this kind of compound, based on the stacking of positively charged layers with hydrated anions in the interlamellar domain, confers relatively high mobility on these anions.[1–3]

Direct synthesis of LDHs can be conducted by various methods, *e.g.* coprecipitation,[1,2] the salt–oxide method,[2,3] hydrothermal synthesis,[1] as well as less studied methods.[4,5] However, there are some indirect methods based on the use of LDH precursors prepared by direct synthesis in order to obtain a new different compound. Indirect synthesis can traditionally be conducted using three main techniques: (i) direct anion exchange, using an LDH intercalated with chloride (sometimes nitrate or perchlorate) as the precursor;[2,3,6] (ii) anion exchange by elimination of the precursor interlamellar species (usually carbonate or terephthalate) susceptible to acid attack;[7–9] and (iii) regeneration of the material obtained by the calcination of an LDH intercalated with carbonate (eventually others), in a solution containing the anion of interest.[1,10–12]

In this work a new method of anion exchange in a surfactant-intercalated LDH is described. The mechanism involved is based on the formation of a salt between an anionic surfactant (sulfated or sulfonated) and a cationic one (*e.g. N*-cetyl-*N*,*N*,*N*-trimethylammonium bromide, CTAB, or benzyldimethylalkylammonium chloride, BAC).[13] The salt is then removed from the aqueous medium into an organic phase such as dichloromethane, chloroform, di- and tri-chloroethanes or hexane.

The LDH precursor used in this method should contain an anionic surfactant (in this work dodecylsulfate, DS, was used) in the interlayer domain. The precursor was synthesised by the coprecipitation method at constant pH (7.0 ± 0.2), with a Zn : Cr ratio of 3 : 1.[2] This one-step synthesis is very easy to perform. The product obtained is well-crystallised without further treatments, as can be seen from the powder X-ray diffraction (PXRD) pattern of this precursor in Fig. 1a (Siemens X-ray diffractometer D5005, Cu-K_α = 1.5406 Å). This fact can be attributed to the self organisation of DS anions in the interlamellar domain, promoted by interactions between the hydrophobic chains. The obtained basal spacing is very close to those reported in the literature.[8] The high crystallinity of the precursor is very important for the synthesis of LDHs by indirect methods since the crystallinity of the product is directly related to that of the precursor.[1,9,12]

The anion exchange was carried out by adding 20 mL of a 0.15 M CTAB solution to an aqueous mixture containing 20 g of a suspension of the precursor (approximately 1.3 g of Zn–Cr–DS–LDH), 50 mL of the solution of the anion of interest containing an excess of the amount necessary for a quantitative exchange and the organic phase (30 mL of chloroform was used). The surfactant anion was removed from the interlayer domain by the formation of the salt with the cationic surfactant, which migrates to the organic phase favouring the concomitant intercalation of the anion of interest. The formation of this salt and its migration to the organic phase are fast and so is the anion exchange process. The surfactant salt is insoluble (or only sparingly soluble) in the aqueous phase, so its migration to the organic medium enhances the efficiency of the process by displacing the equilibrium to the surfactant salt formation. A schematic illustration of the process is shown in Fig. 2. The contact time was 30 minutes, after which the material obtained was washed three times with chloroform, once with acetone and twice with water, and separated by centrifugation. The materials obtained were dried under vacuum. No pH control was carried out, except in the case of polyoxometalate, where the pH was adjusted to 5.0 in order to obtain the decavanadate species.[14]

To test this method a great variety of anions, including chloride, carbonate, some carboxylates, decavanadate and a tetrasulfonated phthalocyanine, were used to displace the DS anion. The occurrence of anion exchange without the addition of the cationic surfactant was tested using the carbonate anion to substitute the DS anion. The choice of carbonate anion to test the exchange without the addition of CTAB was made due to its high stability when intercalated, compared with the other anions used. The occurrence of the exchange starting from the dried precursor was also checked.

The presence of bromide anions (CTAB counter ion) in the obtained materials was also tested using a model 9635 ionplus series bromide electrode from Orion Res. Inc.

The PXRD patterns of the samples obtained by anion exchange are shown in Fig. 1. A well-organised hydrotalcite-

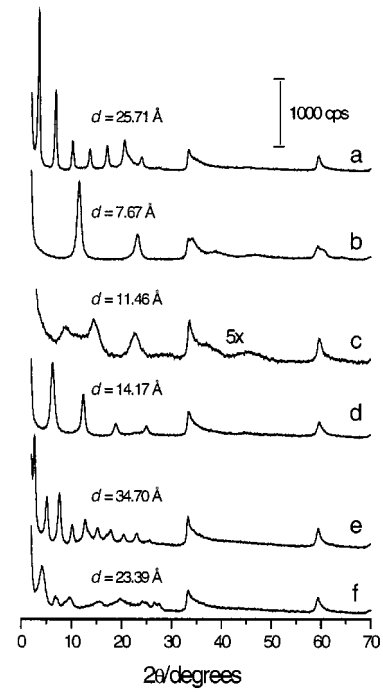

Fig. 1 PXRD patterns for the prepared samples: (a) DS-intercalated LDH precursor; and LDH anion-exchanged by (b) carbonate; (c) decavanadate; (d) terephthalate; (e) cholate; and (f) copper(II) phthalocyaninetetrasulfonate.

like compound with a basal spacing close to reported data[3] was obtained (see Fig. 1b) by the exchange of dodecylsulfate by carbonate anions (using the precursor suspension). Similar results were obtained when the precursor was dried and re-suspended (particles were dispersed by brief sonication, for less than 1 min). The exchange of DS with chloride anion (data not shown, d = 7.78 Å) presented similar results to those obtained for carbonate anion. Without the addition of CTAB, the anion exchange of DS with carbonate did not occur. Even when the contact time was increased to 24 h, the resulting PXRD pattern was very close to that obtained from the precursor.

Based on these results, it is possible to conclude that the presence of CTAB in the medium is necessary to promote anion exchange. The extraction of the salt formed between the cationic and anionic surfactants into the organic phase should enhance the exchange process, making it faster and more efficient. The exchange process by this method is not affected if the precursor is dried before use. This is a very important observation, since the literature reports that drying the precursor can hinder the anion exchange when using both methods, the one based on chloride (or nitrate or perchlorate) containing precursors[2,6] and the one based on the acidification of carbonate (or terephthalate) containing precursors.[7–9]

The PXRD pattern for decavanadate anion exchange is shown in Fig. 1c. The low crystallinity obtained is characteristic of LDHs intercalated with decavanadate, and the basal spacing obtained is close to reported data.[8,9] The intercalation of carboxylate anions also presented good results, as can be seen in Fig. 1d and e for terephthalate and cholate respectively. High structural organisation is again observed, as well as phase purity. Similar results were obtained for the naphthoate anion (data not shown, d = 20.54 Å). Note that, even though cholate is considered to be a surfactant, the exchange occurs successfully, emphasising the fact that the formation of the water-insoluble salt is characteristic of sulfated and sulfonated surfactants. Furthermore, the cholate anion was successfully intercalated with a basal spacing (34.70 Å) greater than that obtained for the DS anion, showing that it is possible to expand the interlayer spacing by this anion exchange method. The basal spacing obtained for the naphthoate intercalate is close to reported data,[10] and indicates that this anion was intercalated as a bilayer in the interlayer domain.

The intercalation of the phthalocyanine anion showed a material with crystallinity and basal spacing (see Fig. 1f) comparable with those reported for a similar compound.[12] In this case it is also important to note that the negative charge of this anion is derived from sulfonate groups, although no salt formation was observed between this macrocycle anion and CTA. This was demonstrated by the observation that the chloroform phase collected at the end of the preparation process did not show the characteristic blue colour of this anion.

A quantity of the anionic–cationic surfactant salt was prepared separately in order to take its PXRD pattern, which showed very intense and sharp peaks (data not shown). These peaks were not observed in the solid PXRD patterns, but were observed in the PXRD pattern of the residue from the evaporation of the organic phase used in the anion exchange. Chemical analysis showed the presence of a small amount of sulfur in some samples, which is probably due to high affinity adsorption of DS anions with LDHs.[15]

The analysis of bromide in the materials obtained showed a concentration in the range 0.15 to 0.22% (in mass). This amount of bromide anions can be assigned to both adsorbed and intercalated bromide. However, if we consider that all this bromide is intercalated, neutralising the layer charges, we will obtain a relation of only 1.0 to 1.5% of substitution by bromide anions.

Based on these results, we conclude that through this method it is possible to obtain a wide variety of organic or inorganic anions intercalated in LDHs in a simple manner. The synthesis of a precursor containing DS anions is required, but this can be carried out very easily. Moreover, this method presents great versatility: (i) it can be applied within a large range of pH values, depending only on the pH range supported by the substituting anion and by the LDH; (ii) the anion exchange is very fast and efficient; (iii) the maintenance of the precursor in a suspension is not necessary; and (iv) the formation of the water-insoluble salt with an ammonium quaternary surfactant is specific for sulfated and sulfonated surfactants.

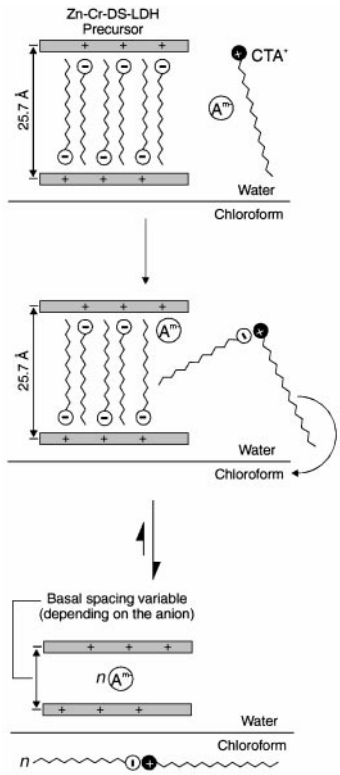

Fig. 2 Schematic representation of the proposed mechanism.

We thank the Brazilian agencies: FAPESP (95/5752-0, 95/3735-1, 96/6030-1 and 96/12373-9), CNPq/PADCT and CAPES for financial support.

Notes and references

1 W. T. Reichle, *Solid State Ionics*, 1986, **22**, 135.
2 A. de Roy, C. Forano, K. El Malki and J. P. Besse, in *Synthesis of Microporous Materials*, ed. M. L. Occelli and H. E. Robson, Van Nostrand Reinhold, New York, 1992, vol. II, p. 108.
3 M. Lal and A. T. Howe, *J. Solid State Chem*., 1981, **39**, 368.
4 T. Lopez, P. Bosch, E. Ramos, R. Gomez, O. Novaro, D. Acosta and F. Figueras, *Langmuir*, 1996, **12**, 189.
5 L. Indira, M. Dixit and P. V. Kamath, *J. Power Sources*, 1994, **52**, 93.
6 M. Tsuji, G. Mao and Y. Tamaura, *Clays Clay Miner*., 1992, **40**, 742.
7 D. L. Bish, *Bull. Minéral*., 1980, **103**, 170.
8 M. A. Drezdzon, *Inorg. Chem*., 1988, **27**, 4628.
9 F. Kooli, V. Rives and M. A. Ulibarri, *Inorg. Chem*., 1995, **34**, 5114.
10 W. Kagunya, M. Chibwe and W. Jones, *Mol. Cryst. Liq. Cryst*., 1994, **244**, 155.
11 F. Kooli, C. Depège, A. Ennaqadi, A. de Roy and J. P. Besse, *Clays Clay Miner*., 1997, **45**, 92.
12 L. Ukrainczyk, M. Chibwe, T. J. Pinnavaia and S. A. Boyd, *J. Phys. Chem*., 1994, **98**, 2668.
13 E. Heinerth, in *Surfactant Science Series*, ed. J. Cross, Marcel Dekker Inc., New York, 1977, vol. 8, p. 221.
14 M. T. Pope, *Heteropoly and Isopoly Oxometalates*, Springer-Verlag, Heidelberg, 1983.
15 P. C. Pavan, G. A. Gomes and J. B. Valim, *Microporous Mater*., 1998, **21**, 659.

Communication 8/08567F

Self-assembly of free-base tetrapyridylporphyrin units by metal ion coordination

Long Pan,[a] Bruce C. Noll[b] and Xiaotai Wang*[a]

[a] *Department of Chemistry, University of Colorado at Denver, Campus Box 194, PO Box 173364, Denver, CO 80217, USA. E-mail: xwang@carbon.cudenver.edu*

[b] *Department of Chemistry and Biochemistry, University of Colorado at Boulder, Boulder, CO 80309, USA*

Received (in Columbia, MO, USA) 16th September 1998, Accepted 8th December 1998

The first free-base *meso*-tetraarylporphyrin coordination polymer is assembled from *meso*-tetrapyridylporphyrin and $HgBr_2$ *via* 4-connected peripheral ligation, and it possesses a novel one-dimensional structural motif with large inter-porphyrin cavities.

There has been recent research interest in crystal engineering supramolecular architectures assembled from metal ions and polydentate ligands by coordinate covalent bonding.[1] Functionalized *meso*-tetraarylporphyrin ligands have been employed to ligate metal ions using the donor atoms (*e.g.* N) on the four *meso*-aryl substituents.[2] Incorporation of such tetraarylporphyrin units into supramolecular oligomers or polymers *via* peripheral ligation is attractive for several reasons. Tetraarylporphyrin molecules are robust, rigid and highly symmetrical and thus serve as desirable, slab-like building blocks for synthesizing microporous materials with large cavities and channels that have potential catalytic activity.[3] Supramolecular systems containing multiporphyrin units have applications as biomimetic models for the study of energy/electron transfer processes in photosynthesis.[4–7] Understanding such processes is fundamental for developing molecule-based opto-electronic materials.[8]

However, investigations of the aforementioned *meso*-tetraarylporphyrin coordination polymers are still lacking in scope. To our knowledge, only three infinite network structures have been reported by Robson and coworkers,[2] which contain metalloporphyrin units connected by additional metal ions *via* all four *meso*-peripheral functions on each metalloporphyrin molecule. Also noteworthy are the structures of several coordination polymers obtained by recrystallization of Zn- or Cu-*meso*-tetraarylporphyrins from certain organic solvents without additional metal ions.[9] In these materials, it is the ligation of two of the functionalized aryls on each metalloporphyrin molecule to the metal centers of two adjacent metalloporphyrins that forms the infinite structures. Although several groups have described the use of free-base *meso*-tetrapyridylporphyrin in assembling porphyrin oligomers,[6,10] no *coordination polymers* built upon free-base *meso*-tetraarylporphyrin units have been reported in the literature. We are interested in exploring self-assembly of free-base *meso*-tetraarylporphyrin building blocks and metal ions of various coordination environments. Our strategy involves using functionalized *meso*-aryl groups to ligate metal ions. These porphyrins are readily available commercially or synthetically.[9b] The use of unmetallated porphyrins avoids the possible ligation of the metal center in the cavity of one metalloporphyrin molecule to the periphery of another metalloporphyrin molecule. Such additional linkages could complicate the design and engineering of solid state structures. In this communication, we report the synthesis and X-ray crystal structure of a novel one-dimensional infinite polymer in which free-base *meso*-tetrapyridylporphyrin (hereafter H_2TPyP) units are interconnected by mercury(II) centers *via* peripheral pyridyl ligation.

Under ambient conditions, a methanol solution (50 mL) of $HgBr_2$ (0.111 mg, 0.31 mmol) was added to a chloroform solution (50 mL) of H_2TPyP (0.047 mg, 0.076 mmol), leading to the precipitation of a purple, microcrystalline solid. This solid was isolated by filtration, washed thoroughly with methanol and then chloroform, and dried under vacuum for 12 h to give 0.071 g of product (70% yield based on H_2TPyP). As shown in the IR spectra (KBr), the pyridine ring vibrational band of H_2TPyP (1629 cm^{-1}) is significantly shifted to 1600 cm^{-1} upon pyridyl N-coordination to mercury. A combustion analysis (for C, H and N) of the product supports an empirical formula of $Hg(H_2TPyP)_{0.5}Br_2$ ($C_{20}H_{13}N_4Br_2Hg$)† that is further confirmed by single crystal X-ray analysis (see below). This material is insoluble in common solvents. Moreover, it is air- and moisture-stable, exhibiting no sign of decomposition or degradation in the EA and IR analyses after being exposed in air for weeks. The air and moisture stability of $Hg(H_2TPyP)_{0.5}Br_2$ is as expected for Hg(II) complexes with pyridine-type ligands.[11]

Crystals suitable for single crystal X-ray analysis were obtained by layering a dilute methanol solution of $HgBr_2$ (0.01 M, 4 mL) over a dilute chloroform solution of H_2TPyP (0.0025 M, 4 mL). Platelike red–purple crystals were formed as the solvate of empirical formula $Hg(H_2TPyP)_{0.5}Br_2{\cdot}CHCl_3$ as revealed by X-ray crystallography.‡ The infinite solid state structure may be viewed as composed of the building-block unit $Hg_2(H_2TPyP)Br_4{\cdot}2CHCl_3$ shown in Fig. 1. In the extended one-dimensional motif shown in Fig. 2, the Hg(II) center is ligated to two bromides and two pyridyl nitrogens, thereby adopting a distorted tetrahedral geometry. This is a rare example of a crystallographically characterized tetrahedral mercury(II)–

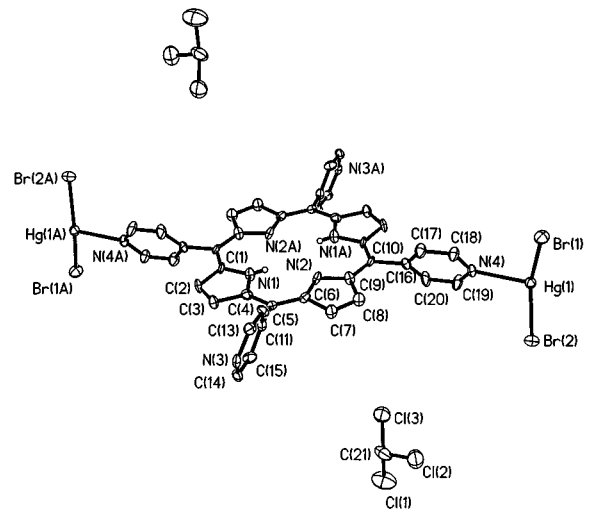

Fig. 1 Molecular structure of the building-block unit $Hg_2(H_2TPyP)Br_4{\cdot}2CHCl_3$, with all hydrogen atoms omitted except the two in the porphyrin cavity. Atoms labeled with A are related to atoms without this letter by an inversion symmetry operation.

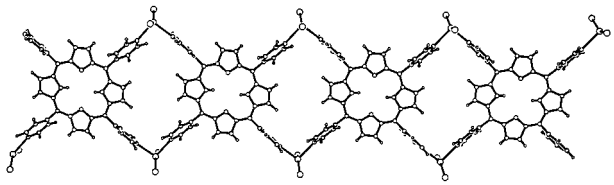

Fig. 2 View of the extended one-dimensional motif in $Hg(H_2TPyP)_{0.5}Br_2{\cdot}CHCl_3$. H_2TPyP molecules are bridged by $HgBr_2$ moieties through pyridyl ligation, forming interporphyrin cavities. Solvent molecules ($CHCl_3$) are not shown.

nitrogen complex of general formula HgL_2X_2, where L = pyridine or its derivatives and X = halide.[11] In addition, the four pyridyl rings are twisted with respect to the plane of the parent porphyrin ring. The N(3)- and N(3A)-containing pyridyl rings each form a dihedral angle with the porphyrin ring at 73.2°. The corresponding dihedral angles for N(4)- and N(4A)-containing pyridyl rings are 67.8° each. The Hg(1)–Br(1) and Hg(1)–Br(2) bond distances are 2.4671(10) and 2.4770(10) Å respectively; the average of 2.472 Å is close to the average shortest Hg–Br distance (2.48 Å) in $HgBr_2$.[12] The Hg–N distances range from 2.482(6) to 2.410(6) Å.

The one-dimensional structural motif shown in Fig. 2 is unprecedented in porphyrin- or metalloporphyrin-based *coordination polymers*. In this framework $HgBr_2$ moieties act as linkers to bridge the H_2TPyP molecules with each Hg(II) center connecting two pyridyls from adjacent porphyrins. This results in relatively large interporphyrin cavities in the extended chain. The size of the cavity is measured by the Hg···Hg distance (14.2 Å) and the shortest distance between the two *meso*-carbons of two adjacent porphyrins (9.72 Å). Inside the cavity, the distances between the van der Waals surfaces are estimated at 8.4 Å between the diagonal pyridyls and 3.7 Å between the β-hydrogens of the two adjacent porphyrin molecules. The two neighboring porphyrin ring planes within a chain are parallel but are canted by *ca.* 1.60 Å. Solvent ($CHCl_3$) molecules (not shown) partially fill the interchain space, and they are not included in the interporphyrin cavities. When removed from the mother liquor, crystals of $Hg(H_2TPyP)_{0.5}Br_2{\cdot}CHCl_3$ lose $CHCl_3$ and collapse rapidly, showing no sharp peaks in X-ray powder diffraction patterns. The resultant solid does not absorb CH_2Cl_2, $CHCl_3$, CH_3OH or benzene to form inclusion compounds. It seems that crystallinity of the one-dimensional $Hg(H_2TPyP)_{0.5}Br_2{\cdot}CHCl_3$ cannot be sustained after loss of interchain space-filling solvent of crystallization. Networks of higher dimensionalities may be required for porphyrin coordination polymers to function like porous materials.

Currently, we are studying the physical properties of $Hg(H_2TPyP)_{0.5}Br_2$ using a combination of photoacoustic, reflection UV–VIS and fluorescent spectrometries. Additionally, we are examining different metal ions as potential linkers to assemble porphyrin coordination polymers of higher dimensionalities, including 2-D sheets and 3-D networks.

The authors gratefully acknowledge support for this work from the University of Colorado at Denver in the forms of startup funding and Junior Faculty Development Awards (X. W.).

Notes and references

† Calc. (found) for $C_{20}H_{13}N_4Br_2Hg$: C, 35.87 (36.15); H, 1.96 (2.08); N, 8.37 (8.31)%.

‡ *Crystal data* for $Hg(H_2TPyP)_{0.5}Br_2{\cdot}CHCl_3$: M = 1578.24, space group $P\bar{1}$, a = 9.507(3), b = 11.641(2), c = 12.732(4) Å, α = 73.418(9), β = 80.316(16), γ = 66.294(7)°, U = 1234.2(6) Å^3, Z = 1, D_c = 2.123 Mg m^{-3}, $F(000)$ = 738, λ(Mo-Kα) = 0.71073 Å, crystal size = 0.11 × 0.05 × 0.02 mm, 16409 reflections collected on a Siemens SMART CCD diffractometer at 171 K, 6489 independent reflections, final $R1$ = 0.0548 for 4487 reflections with $I > 2\sigma(I)$, $wR2$ = 0.0831, GOF = 1.032. The structure was solved by using Patterson heavy atom method. CCDC 182/1104. See http://www.rsc.org/suppdata/cc/1999/157/ for crystallographic files in .cif format.

1 M. J. Zaworotko, *Chem. Soc. Rev.*, 1994, **23**, 283; D. Philp and J. F. Stoddart, *Angew. Chem., Int. Ed. Eng.*, 1996, **35**, 1154.
2 B. F. Abrahams, B. F. Hoskins and R. Robson, *J. Am. Chem. Soc.*, 1991, **113**, 3606; B. F. Abrahams, B. F. Hoskins, D. M. Michail and R. Robson, *Nature*, 1994, **369**, 727.
3 S. L. Suib, *Chem. Rev.*, 1993, **93**, 803.
4 V. S.-Y. Lin, S. G. DiMagno and M. J. Therien, *Science*, 1994, **264**, 1105.
5 H. Yuan, L. Thomas and K. L. Woo, *Inorg. Chem.*, 1996, **35**, 2808.
6 S. Anderson, H. L. Anderson, A. Bashall, M. McPartlin and J. K. M. Sanders, *Angew. Chem., Int. Ed. Engl.*, 1995, **34**, 1096.
7 C. A. Hunger and R. K. Hyde, *Angew. Chem., Int. Ed. Engl.*, 1996, **35**, 1936.
8 T. J. Marks, *Angew. Chem., Int. Ed. Eng.*, 1990, **29**, 857.
9 (*a*) H. Krupitsky, Z. Stein, I. Golderberg and C. E. Strouse, *J. Inclusion Phenom.*, 1994, **18**, 177; (*b*) R. K. Kumar, S. Balasubramanian and I. Golderberg, *Inorg. Chem.*, 1998, **37**, 541.
10 N. Kariya, T. Imamura and Y. Sasaki, *Inorg. Chem.*, 1997, **36**, 833.
11 P. A. W. Dean, *Prog. Inorg. Chem.*, 1978, **24**, 109.
12 H. Braekken, *Z. Kristallogr.*, 1932, **81**, 152.

Communication 8/07242F

Pyrazolyl[(methylthio)methyl]borates: hybrid ligands providing nitrogen and sulfur donors

Show-Jen Chiou, Pinghua Ge, Charles G. Riordan,* Louise M. Liable-Sands and Arnold L. Rheingold

Department of Chemistry and Biochemistry, University of Delaware, Newark, DE 19716, USA. E-mail: Riordan@udel.edu

Received (in Bloomington, IN, USA) 19th October 1998, Accepted 4th December 1998

Two new borate ligands, $PhB(CH_2SCH_3)_2(pz)^-$ ($\mathbf{1}^-$) and $Ph_2B(CH_2SCH_3)(pz)^-$ ($\mathbf{2}^-$) (pz = 1-pyrazolyl), have been prepared to provide mixed donor sets, 'NS_2' and 'NS', respectively, to transition metal ions.

Metalloenzyme catalytic sites often contain coordination spheres that consist of a mixture of nitrogen and sulfur ligands in the forms of histidine, cysteine and methionine residues. Representative examples include the zinc sites in liver alcohol dehydrogenase[1] and methionine synthase,[2] the nickel sites in carbon monoxide dehydrogenase/acetyl coenzyme A synthase[3] and cobalt- and iron-containing nitrile hydratases.[4] A fundamental understanding of the chemical transformations performed by these enzymes would be advanced by the preparation of synthetic representations of these sites. To this end, we have designed and prepared a new series of borate ligands that contain nitrogen and sulfur donors. This first report highlights the preparation, and spectroscopic and structural characterization of representative metal ion derivatives of a tridentate 'NS_2' ligand ($\mathbf{1}^-$) and a bidentate 'NS' ligand ($\mathbf{2}^-$). Face-capping 'N_xS_y' chelate complexes derived from borates have been reported recently by Parkin and co-workers.[5] However, our contribution combines the synthetic flexibility of pyrazolyls and thioethers into a versatile ligand class wherein steric and electronic properties may be intimately tuned by judicious choice of substituents at the 3-pyrazolyl position *and* on sulfur.[6,7] While the ligands may be viewed as hybrids of Trofimenko's hydridotris(pyrazolyl)borates, Tp^-,[8] and our phenyltris((alkylthio)methyl)borates, $PhTt^-$,[9] we find that the metal complexes possess properties not predicted from such a simplified extrapolation.

The synthesis of ligands $\mathbf{1}^-$ and $\mathbf{2}^-$ proceeded smoothly using the one-pot, stepwise protocol outlined in Scheme 1. Using the appropriate borane, the thioether substituent(s) was/were added first followed by the pyrazolyl group. The ligands were isolated cleanly by precipitation from water as either the Tl^+ or N^+Bu_4 salts in moderate to good yield. The metal complexes were prepared *via* metathesis from the appropriate metal halide (Scheme 1). For example, synthesis of *cis*–$[\mathbf{1}]_2Ni$ proceeds in 60% yield from the reaction of 2 equiv. of $[NBu_4]\mathbf{1}$ and $NiCl_2{\cdot}6H_2O$ in methanol. Recrystallization from CH_2Cl_2–Et_2O yielded purple blocks. Analytical and combustion data† were consistent with the indicated formula that was corroborated by X-ray diffraction analysis.‡ The molecular structure of *cis*–$[\mathbf{1}]_2Ni$ is depicted in Fig. 1 with selected metric parameters given in the caption. The coordination geometry is octahedral with four sulfur and two nitrogen donors. The most noteworthy and unexpected feature of the structure is the *cis* configuration. The Ni–N bond lengths of 2.063(2) and 2.053(2) Å are similar to those in the all-nitrogen analogue containing two different Tp^- ligands, $[Tp^{3\text{-}i\text{Pr},4\text{-}Br}][Tp^{3,5\text{-}Me2}]Ni$, 2.05–2.16 Å.[10] The four Ni–S distances are all similar averaging to 2.47 Å. This value matches that in the S_6 derivative, $[PhTt]_2Ni$, 2.433 Å.[9] The *trans* influence of pyrazolyl and thioether donors is similar in this case as evidenced by experimentally indistinguishable Ni–S distances for sulfur *trans* to nitrogen *vs*. sulfur *trans* to sulfur. Consistent with little-to-no preference for *cis vs. trans* structures in NiS_4N_2 complexes are the *trans* structures of $[([9]aneS_2N)_2Ni]^{2+}$ and $[([10]aneS_2N)_2Ni]^{2+}$ in which nine- and ten-membered macrocycles, respectively, are the chelating ligands.[11] The macrocycles differ from $\mathbf{1}^-$ in that secondary amines are the nitrogen donors rather than pyrazoles. Analogous derivatives of Fe(II) and Co(II) have been prepared. Spectroscopic data are consistent with exclusive production of *cis*–$[\mathbf{1}]_2Fe$ and *cis*–$[\mathbf{1}]_2Co$.† *cis*–$[\mathbf{1}]_2Fe$ appears to be a spin-crossover complex with a room temperature magnetic moment of 4.1 μ_B. *cis*–$[\mathbf{1}]_2Co$ is high spin with a magnetic moment of 4.1μ_B, close to the spin-only value. For comparison, in the all sulfur analogs, $[PhTt]_2Fe$ exhibits spin-crossover behavior and $[PhTt]_2Co$ is low-spin.[10] Complete details will be reported elsewhere.[12]

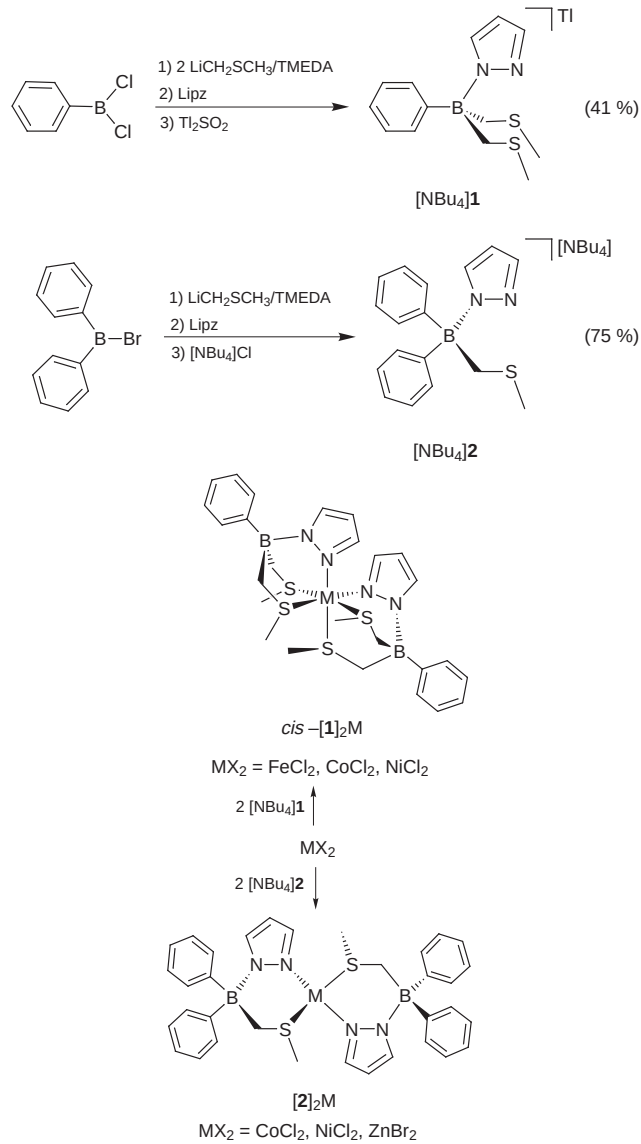

Scheme 1

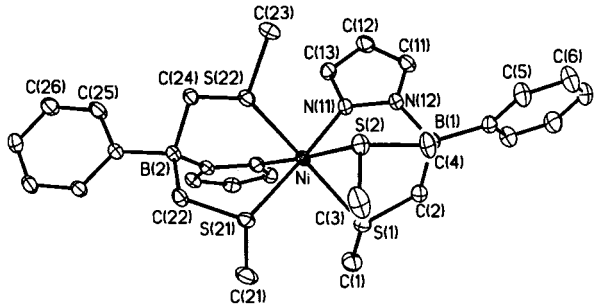

Fig. 1 (a) Thermal ellipsoid plot of *cis*-[**1**]$_2$Ni at 30% probability level showing the atom labeling scheme. The hydrogen atoms are omitted for clarity. Selected bond distances (Å) and bond angles (°): Ni–N(11) 2.053(2), Ni–N(31) 2.067(2), Ni–S(1) 2.4678(8), Ni–S(2) 2.4545(7), Ni–S(21) 2.4859(6), Ni–S(22) 2.4620(7), S(1)–Ni–S(2) 82.92(3), S(1)–Ni–N(11) 92.27(6), S(2)–Ni–N(11) 86.46(6), N(11)–Ni–N(31) 92.99(8), N(11)–Ni–S(21) 176.87(6), S(1)–Ni–S(22) 161.22(3).

Four coordinate complexes [**2**]$_2$M, (M = Ni, Co and Zn), have been prepared in 70–80% yield from the bidentate ligand, **2**$^-$, (Scheme 1).† The molecular structure of pink [**2**]$_2$Co has been determined (Fig. 2).‡ The geometry is tetrahedral with two sulfur and two nitrogen donors. The solution magnetic moment, 4.0 μ_B, is consistent with three unpaired electrons. While this represents the first crystallographically determined structure of Co(II) with two nitrogen and two *thioether* sulfur ligands, there are molecular precedents that contain two nitrogen and two thiolate donors.[13] The ligand bond angle of 100.11(1)° (N–Co–S) is larger than that of the bis[(methylthio)methyl] chelate, Ph_2Bt^- [86.31(1)°], reflecting the sp^2 hybridization of the pyrazolyl nitrogens.[14] Each six-membered chelate ring is in the twist-boat conformation. [**2**]$_2$Co and the isostructural Zn complex, [**2**]$_2$Zn, are chiral possessing C_2 point symmetry. Consistent with C_2 symmetry, the ^{1}H NMR spectrum of [**2**]$_2$Zn contains well resolved methylene resonances for the diastereotopic protons.† Although the phenyl substituents on boron are also expected to be magnetically inequivalent, their resonances are not well separated and appear as broad features. [**2**]$_2$Ni is square planar based on its NMR (diamagnetic) and electronic spectra. Interpretation of the proton NMR spectrum of [**2**]$_2$Ni, displaying signals qualitatively analogous to those observed for [**2**]$_2$Zn, specifically diastereotopic methylene and broad aryl resonances, is consistent with a single isomer in solution. To date, crystallographic data collected on [**2**]$_2$Ni has not yielded a chemically reasonable solution. Consequently, the identity of the single isomer, *cis* or *trans*, remains unknown. Given the disposition of ligand substituents in [**1**]$_2$Ni, it is attractive to propose that the single isomer is *cis*-[**2**]$_2$Ni. This geometry provides the favorable electronic configuration of placing the strong σ-donor nitrogen ligands *trans* to the thioethers. Efforts to improve the quality of the crystals for X-ray analysis continue. Additionally, we aim to distinguish the isomeric form of [**2**]$_2$Ni in solution using molecular dipole moment measurements.

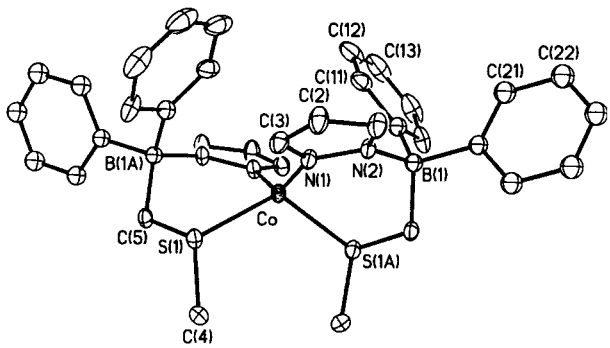

Fig. 2 (a) Thermal ellipsoid plot of [**2**]2Co•2C_6H_{14} at 30% probability level showing the atom labeling scheme. The hydrogen atoms and solvent molecules are omitted for clarity. Selected bond distances (Å) and bond angles (°): Co–S(1) 2.362(1), Co–N(1) 1.957(3), S(1)–Co–N(1) 101.1(1), S(1)–Co–S(1A) 117.67(7), S(1)–Co–N(1A) 100.1(1), S(1A)–Co–N(1) 100.1(1).

Research in progress is directed toward utilizing the new donor sets as supporting ligands for the preparation of synthetic analogues for the zinc sites in methionine synthase, cobalt-containing nitrile hydratase and the nickel sites in CO dehydrogenase.

We thank the Petroleum Research Fund administered by the ACS for partial support of this research (30627-AC3). C. G. R. thanks National Science Foundation for a National Young Investigator Award (CHE-9896001). We are grateful to Dr S. Trofimenko for helpful discussions.

Footnotes and references

† Spectroscopic and analytical data for new compounds are consistent with the proposed structures.

‡ *Crystal data* for $C_{26}H_{36}B_2N_4NiS_4$ (*cis*-[**1**]$_2$Ni): M = 613.2, triclinic, space group $P\bar{1}$, a = 7.9656(1), b = 12.7601(2), c = 15.6007(2) Å, α = 79.9636(7), β = 82.8552(8), γ = 74.3877(2)°, V = 1498.78(5) Å^3, Z = 2, T = 198(2) K, μ = 0.949 mm^{-1}, $R(F)$ = 0.0416 for 5045 observed independent reflections ($4 \leqslant 2\theta \leqslant 57°$). For $C_{34}H_{34}B_2CoN_4S_2$ ([**2**]$_2$Co)•2C_6H_{14}: M = 817.7, monoclinic, space group $C2/c$, a = 22.1546(7), b = 10.1634(3), c = 21.7947(6) Å, β = 117.423(1)°, V = 4356.0(3) Å^3, Z = 4, T = 198(2) K, μ = 0.527 mm^{-1}, $R(F)$ = 0.0659 for 2714 observed independent reflections ($4 \leqslant 2\theta \leqslant 57°$). There are two molecules of *n*-hexane co-crystallized in the asymmetric unit. Based on a preliminary structure of minimum quality, [**2**]$_2$Zn is isostructural with [**2**]$_2$Co: monoclinic, space group $P2_1/c$, a = 12.4085(2), b = 36.8532(15), c = 14.5336(6) Å, β = 96.1980(8)°, V = 6607.2(8) Å^3, Z = 8, T = 198(2) K. CCDC 182/1114.

1 W. N. Lipscomb and N. Sträter *Chem. Rev.*, 1996, **96**, 2375.
2 J. C. González, K. Peariso, J. E. Penner-Hahn and R. G. Matthews, *Biochemistry*, 1996, **35**, 12 228; C. W. Goulding and R. G. Matthews, *Biochemistry*, 1997, **36**, 15 749.
3 S. W. Ragsdale and M. Kumar, *Chem. Rev.*, 1996, **96**, 2515; S. W. Ragsdale and C. G. Riordan, *J. Biol. Inorg. Chem.*, 1996, **1**, 489.
4 Recent structures of the Fe NHases have shown the two N donors are amides from the peptide backbone: W. Huang, J. Jia, J. Cummings, M. Nelson, G. Schneider and Y. Lindqvist, *Structure*, 1997, **5**, 691; S. Nagashima, M. Nakasako, N. Dohmae, M. Tsujimura, K. Takio, M. Odaka, M. Yohda, N. Kamiya and I. Endo, *Nature Struct. Biol.*, 1998, **5**, 347; M. J. Nelson, H. Jin, I. M. Turner Jr., G. Grove, R. C. Scarrow, B. A. Brennan and L. Que, *J. Am. Chem. Soc.*, 1991, **113**, 7072; B. A. Brennan, G. Alms, M. J. Nelson, L. T. Durney and R. C. Scarrow, *J. Am. Chem. Soc.*, 1996, **118**, 9194.
5 C. Kimblin, T. Hascall and G. Parkin, *Inorg. Chem.*, 1997, **36**, 5680; P. Ghosh and G. Parkin, *Chem. Commun.*, 1998, 413.
6 J. C. Calabrese, S. Trofimenko and J. S. Thompson, *J. Chem. Soc., Chem. Commun.*, 1986, 1122.
7 C. Ohrenberg, C. G. Riordan, L. Liable-Sands and A. L. Rheingold, *Coord. Chem. Rev.*, 1998, **174**, 301; P. Schebler, C. G. Riordan, I. Guzei and A. L. Rheingold, *Inorg. Chem.*, 1998, **37**, 4754.
8 S. Trofimenko, *Chem. Rev.*, 1993, **93**, 943.
9 C. Ohrenberg, P. Ge, P. Schebler, C. G. Riordan, G. P. A. Yap and A. L. Rheingold, *Inorg. Chem.*, 1996, **35**, 749.
10 M. D. Olson, S. J. Rettig, A. Storr and S. Trofimenko, *Acta Crystallogr. Sect. C*, 1991, **47**, 1544.
11 A. McAuley and S. Subramanian, *Inorg. Chem.*, 1990, **29**, 2830; S. Chandrasekhar and A. McAuley, *Inorg. Chem.*, 1992, **31**, 2234; J. P. Danks, N. R. Champness and M. Schröder, *Coord. Chem. Rev.*, 1998, **174**, 417.
12 S. Chiou and C. G. Riordan, unpublished work.
13 D. Mastropaolo, J. A. Thich, J. A. Potenza and H. J. Schugar, *J. Am. Chem. Soc.*, 1977, **99**, 424; D. T. Corwin Jr., R. Fikar and S. A. Koch, *Inorg. Chem.*, 1987, **26**, 3079; D. T. Corwin Jr., E. S. Gruff and S. A. Koch, *J. Chem. Soc., Chem. Commun.*, 1987, 966.
14 P. Ge, C. G. Riordan, G. P. A. Yap and A. L. Rheingold, *Inorg. Chem.*, 1996, **35**, 5408.

Communication 8/08199I

Synthesis and study of an acridine substituted Tröger's base: preferential binding of the (–)-isomer to B-DNA

Arnaud Tatibouët, Martine Demeunynck,* Chantal Andraud, André Collet and Jean Lhomme

[a] *LEDSS, UMR CNRS 5616, Université Joseph Fourier, BP53, Grenoble cedex, 38041 France*
[b] *UMR CNRS 117, École Normale Supérieure de Lyon, Stéréochimie et Interactions Moléculaires, Lyon cedex 07, 69364 France*

Received (in Cambridge, UK) 11th November, 1998, Accepted 10th December 1998

The acridine substituted Tröger's base 4 was prepared, resolved and the (−)-(7*R*,17*R*) enantiomer was shown to bind preferentially to calf-thymus B-DNA.

The development of molecular probes to study local conformations in DNA is of major interest; until now, only chiral metal complexes have been studied for enantioselective recognition of DNA conformations.[1] We report herein that combining the geometry and chirality of Tröger's base[2] (methanodibenzo-

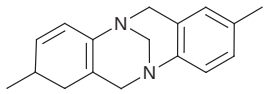

Tröger's Base **1**

[1,5]diazocine) **1** with the DNA binding properties of acridines[3] leads to a new family of C_2-chiral DNA binding molecules, such as **4**. The geometry of the Tröger's base unit gives the molecules a helix shape which can be similar or opposite to the helicity of DNA (Fig. 1). A preliminary molecular modelling study[4] suggested that the binding of such probes to DNA should be enantioselective.

Compound **4** was prepared in two steps from monoacetylated proflavine **2** (Scheme 1).[5] Condensation of **2** with formaldehyde in TFA[6,7] gave the diacetamido derivative (±)-**3** (76%). Treatment of **3** under basic conditions (EtOH, NaOH) cleaved the two acetamido groups without affecting the methanodiazocine bridge, to give (±)-**4** (90%). The structure of **4** was supported by detailed 2D ^{1}H NMR studies.[8]

Resolution of (±)-**4** was achieved by crystallisation of its dibenzoyltartrate salts; (+)-**4** showed = $[\alpha]_D^{20}$ +4650 (*c* 9 × 10^{-3}, 95% EtOH). The enantiomeric excess (ee) was close to 80% (NMR).† Similarly, (+)-dibenzoyltartaric acid gave (−)-**4**. The circular dichroism (CD) spectra of both enantiomers are shown in Fig. 2.

The presence of the primary amino functions on the acridine rings of **4** turned out to be of major importance in the design of a molecule binding selectively to DNA. Solubility in water is considerably increased as compared to the parent unsubstituted molecule.[6] More important, the basicity is much higher (pK_a 5.5 and 6.8 *cf.* 3.2 for **1**)[9] and protonation occurs on the acridine ring nitrogens and not on the nitrogens of **1** (UV–VIS data). This protects **4** from racemization as is usually observed in acidic media for Tröger's base (such as **1**).[10] Indeed compound **4** did not racemize in 0.1 M HCl in DMF (20 °C, 40 days).

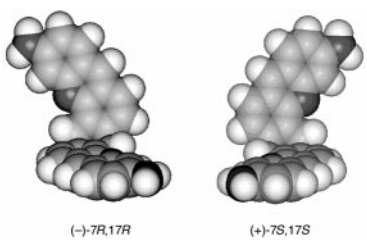

Fig. 1 Molecular modelling representation of the two enantiomers of **4**.

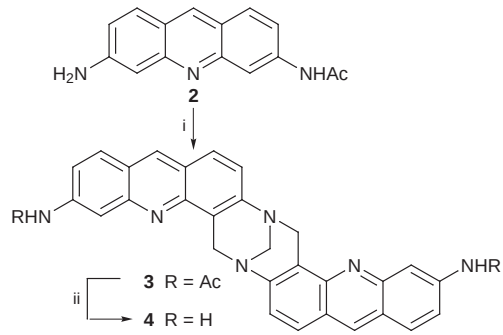

Scheme 1 *Reagents and conditions*: i, HCHO (1.5 equiv.), TFA, room temp., 4 h; EtOH–NaOH (10 M) (3 : 1), 85 °C, 6 h.

The absolute configuration of the enantiomers was assigned as follows. Enantiomer (+)-**4** displays a broad positive band of weak intensity at low energy (380–470 nm, $\Delta\varepsilon$ +26 M^{-1} cm^{-1}), and a strong bisignate system at high energy with maxima at 290 ($\Delta\varepsilon$ +218 M^{-1} cm^{-1}) and 250 nm ($\Delta\varepsilon$ −163 M^{-1} cm^{-1}). The low energy CD band corresponds to a broad UV absorption at 350–450 nm, whereas the bisignate pattern is centred on a strong UV band at 272 nm (ε 101400 M^{-1} cm^{-1}). There is evidence that each component of the bisignate system comprises at least two mutually overlapping bands. Given the two-fold symmetry of **4** and the nature of its chromophore, we assume that the bisignate pattern is due to the exciton coupling[11] of some long-axis polarised transitions of the aminoacridine units. Based on simple geometric arguments, we expect that in **4** the symmetric (*A*) coupling and the antisymmetric (*B*) coupling of these transitions in the two acridine units are polarised along the C_2 axis and perpendicularly to that axis, respectively. This picture together with the further assumption that the *A* coupling is at higher energy than the *B* coupling[12] leads us to assign the (*S*,*S*) configuration to (+)-**4**.

In the past, application of the exciton chirality method to **1** itself has lead to a wrong assignment of its absolute configuration,[13] because the direction of polarisation of the considered transitions have not been correctly established. For this reason we found it desirable to verify the consistency of our

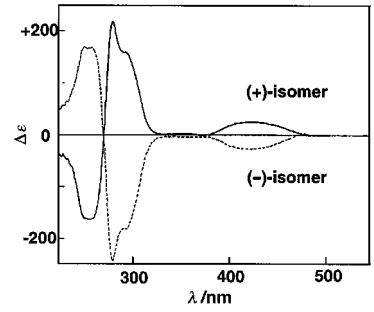

Fig. 2 Circular dichroism spectra of (+)-**4** (solid line) and (−)-**4** (dotted line) in ethanol (10^{-4} M). For (+)-**4**: $[\alpha]_D^{20}$ +4200 (*c* 1.6 × 10^{-3}, ethanol) and for (−)-**4**: $[\alpha]_D^{20}$ −4800 (*c* 1.5 × 10^{-3}, ethanol).

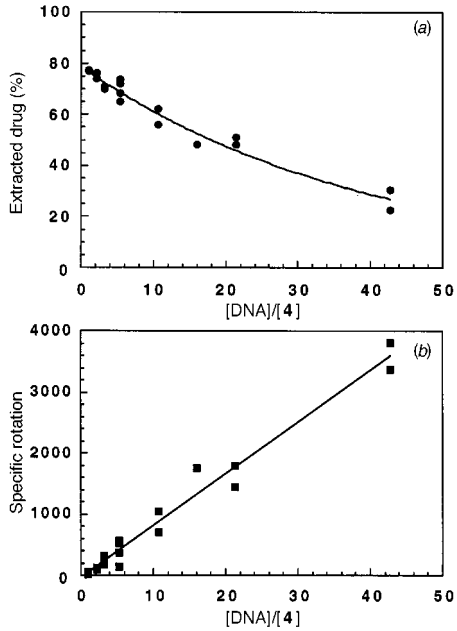

Fig. 3 (*a*) Percent of **4** extracted in butanol as a function of DNA(bp) : **4** ratio. The concentration was calculated from the absorbance measured at 390 nm (ε = 18 800 M^{-1} cm^{-1} in butanol); (*b*) Optical activity of the butanol layer as a function of the DNA(bp) : **4** ratio. The specific rotation ($[\alpha]_D^{20}$) was recorded in 95% ethanol, the concentration being calculated from the absorbance at 390 nm (ε = 20 000 M^{-1} cm^{-1} in 95% ethanol).

assumptions regarding the exciton mechanism in **4**. This was done by semi-empirical calculations[14] of the electronic transitions in **4** and in the corresponding monomeric fragment. The calculated absorption spectrum of the monomer shows two strong transitions at 325 and 310 nm, which are polarised along the long axis. The corresponding transition levels in the dimer are each split into two levels which are almost degenerate and orthogonally polarised (314/314 nm and 283/282 nm); in each pair, one of the components is parallel and the other perpendicular to the C_2 axis. These features are in line with the exciton mechanism and account for the splitting of each component of the bisignate couplet in the experimental CD spectrum.

The UV–VIS spectrum of (±)-**4** was recorded in the presence of increasing concentrations of calf thymus DNA in phosphate buffered solutions (pH 7). Large changes of the spectrum were observed, characterised by the appearance of a new broad band centred at 467 nm, whose intensity increased when the DNA to drug ratio *r* was increased in the range 0–10. These experiments demonstrate that **4** interacts with DNA. The variations observed in the presence of increasing amounts of DNA are similar to those occurring when the spectrum of **4** was recorded at acidic pHs. The simplest interpretation is that the interaction with DNA is accompanied by protonation of the two acridines. The existence of acidic domains surrounding the DNA molecule has already been proposed by Lamm *et al.*[15] Comparison of the CD spectra of **4** in the presence of calf thymus DNA and in 3 M HCl solution leads to the same conclusion.

Liquid–liquid partition[16] of (±)-**4** between an aqueous solution of DNA and butanol revealed that the binding of **4** to calf thymus DNA is enantioselective. Solutions containing various ratios of (±)-**4** and calf thymus DNA in phosphate buffered aqueous solution (pH 7) were mixed with butanol, in which **4** is soluble and DNA is not. After vigorous stirring, the two phases were separated and analysed by CD spectroscopy. The butanol layers gave spectra showing a broad positive band centred at 420 nm, similar to that of the (+)-enantiomer recorded independently under the same conditions. The intensity of this band increased with the DNA : **4** ratio *r*. The spectra of the aqueous phases were similar to those of solutions of (−)-**4** added to various concentrations of calf thymus DNA in phosphate buffer (pH 7). These results indicate that (+)-**4** and (−)-**4** distribute differently between the DNA-containing aqueous phase and butanol, and that (−)-**4** preferentially associates to calf thymus DNA. The enantioselectivity was evaluated by determining the quantities and ees of **4** extracted in the butanol layer (from the UV absorbance and rotation, respectively). The results are reported in Fig. 3(*a*) and 3(*b*) for DNA : drug ratios *r* varying in the range 1–40. As expected, when the DNA : **4** ratio increased, the quantity of **4** extracted in the butanol phase decreased, while the corresponding ee increased (*e.g.* 30% ee when 50% of **4** was extracted and 70% ee when only 20% of **4** was extracted).

The 7*R*,17*R* configuration of (−)-**4** is consistent with the best fit of this enantiomer to right-handed B-DNA,[17] either through intercalation or by interaction in the groove. Work is in progress to determine the mode of interaction.

Notes and references

† All new compounds have been fully characterised by UV–VIS spectroscopy, FAB MS, ^{1}H NMR and elemental analysis.

1 B. Norden, P. Lincoln, B. Akerman and E. Tuite, in *Metal Ions in Biological Systems*, eds. A. Sigel and H. Sigel, Marcel Dekker, New York, 1996, vol. 33, ch. 7, pp. 205–252; C. M. Dupureur and J. K. Barton, *Inorg. Chem.*, 1997, **36**, 33 and references cited therein; S. Satyanarayana, J. C. Dabrowiak and J. B. Chaires, *Biochemistry*, 1993, **32**, 2573; A. D. Baker, R. J. Morgan and T. C. Strekas, *J. Am. Chem. Soc.*, 1991, **113**, 1411.

2 For a review on Tröger's base, see: F. Vögtle, *Fascinating Molecules in Organic Chemistry*, J. Wiley, New York, 1992, pp. 237–249.

3 R. B. Silverman, *The organic chemistry of drug design and drug action*, Academic Press, San Diego, 1992, pp. 239–241.

4 Y. Coppel, Ce. Coulombeau, C. Coulombeau, J. Lhomme, M.-L Dheu-Andries and P. Vatton, *J. Biomol. Struct. Dyn.*, 1995, **12**, 637.

5 A. Wardani and J. Lhomme, *Tetrahedron Lett.*, 1993, **34**, 6411.

6 A. Tatibouët, M. Demeunynck, H. Salez, R. Arnaud, J. Lhomme and C. Courseille, *Bull. Soc. Chim. Fr.*, 1997, **134**, 495.

7 H. Salez, A. Wardani, M. Demeunynck, A. Tatibouët and J. Lhomme, *Tetrahedron Lett.*, 1995, **36**, 1271; A. Tatibouët, M. Demeunynck and J. Lhomme, *Synth. Commun.*, 1996, **26**, 4375.

8 M. Demeunynck, C. Fontaine and J. Lhomme, *Magn. Reson. Chem.*, 1998, in the press.

9 B. M. Wepster, *Recl. Trav. Chim. Pays. Bas.*, 1953,**72**, 661.

10 A. Greenberg, N. Molinaro and M. Lang, *J. Org. Chem.*, 1984, **49**, 1127.

11 N. Harada and K. Nakanishi, *Circular Dichroic Spectroscopy*, University Science Books, Mill Valley, California, 1983. See also: K. Nakanishi, N. Berova and R. W. Woody, *Circular Dichroism, Principles and Applications*, VCH, Weinhem, 1994

12 This situation, which prevails in the exciton coupling of most C_2 systems, is supported in this specific case by examination of Dreiding models.

13 S. F. Mason, G. W. Vane, K. Schofield, R. J. Wells and J. S. Whitehust, *J. Chem. Soc. (B)*, 1967, 553; S. H. Wilen, J. Z. Qi and P. G. Williard, *J. Org. Chem.*, 1991, **56**, 485.

14 The absorption wavelengths and the transition moments were calculated by means of a CNDO/S program parametrized to reproduce the properties of the molecules in solution: C. Andraud, T. Brotin, C. Garcia, F. Pellé, P. Goldner, B. Bigot and A. Collet, *J. Am. Chem. Soc.*, 1994, **116**, 2094; T. Brotin, C. Andraud, I. Ledoux, S. Brasselet, J. Zyss, M. Perrin, A. Thozet and A. Collet, *Chem. Mater.*, 1996, **8**, 890.

15 G. Lamm and G. Pack, *Proc. Natl. Acad. Sci. U.S.A.*, 1990, **87**, 9033.

16 S. S. Peacock, D. M. Walba, F. C. A. Gaeta, R. C. Helgeson and D. J. Cram, *J. Am. Chem. Soc.*, 1980, **102**, 2043.

17 Right-handed twist is also observed for other DNA intercalating drugs such as anthracyclines; for a review, see: J. W. Lown, *Chem. Soc. Rev.*, 1993, 165.

Communication 8/08822E

A small supramolecular system which emulates the unidirectional, path-selective photoinduced electron transfer (PET) of the bacterial photosynthetic reaction centre (PRC)

A. Prasanna de Silva and Terence E. Rice

School of Chemistry, Queen's University, Belfast, Northern Ireland, UK BT9 5AG. E-mail: a.desilva@qub.ac.uk

Received (in Cambridge, UK) 23rd November 1998, Accepted 4th December 1998

The singlet excited state of the 4-aminonaphthalimide fluorophore in 1a and 1b directs electron transfer from intramolecular but external amine groups along only one of two available paths.

The availability of high-resolution X-ray structural information concerning the engines of photosynthesis, such as the bacterial reaction centres[1] and the antenna complexes,[2] challenges chemists to emulate their functions.[3] One of the most enigmatic aspects of PRC function is the unidirectional, path-selective electron transfer from the photoexcited porphyrin special pair to a quinone moiety along the L-branch rather than the symmetry-related M-branch. The path-selectivity in the PRC was established by picosecond transient absorption signatures which distinguished between the nearly identical bacterichlorophyll stations along the two possible electron paths.[4] In the present instance, we use pH-dependent steady-state fluorescence spectroscopy to distinguish between the two possible PET paths in a small supramolecular system[5] by means of the acid–base characteristics of two rather similar amine PET donors. As an additional point of interest, unidirectionality is much sought after in several research areas of photoscience and molecular electronics.[6] We now provide a simple basis for unidirectionality in PET processes.

Many aminoalkyl substituted fluorophores show weak fluorescence in basic solution owing to rapid PET from the amine unit to the fluorophore. Protonation of the amine arrests this PET process and causes a sharp fluorescence recovery.[7] We use the fluorescent 4-aminonaphthalimide chromophore[8] as the core of our system **1** since its photogenerated molecular-scale

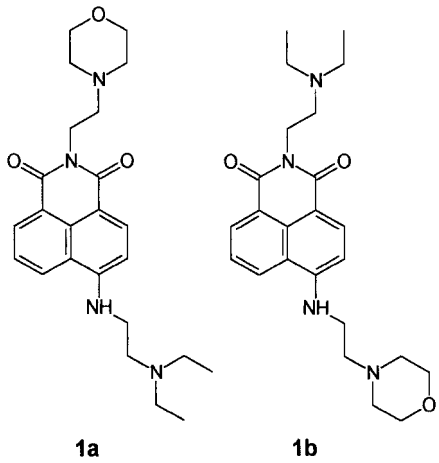

1a **1b**

electric field can be used to control electron transfer rates.[9] Two nearly identical PET paths are provided for the fluorophore to choose from, in the form of two dialkylaminoethyl sidechains only differing in their dialkyl substituents. Such a choice of PET paths is also available to the porphyrin special pair in the PRC. The thermodynamic driving force for PET is equal in **1a** and **1b** for any given amine receptor. **1a** and **1b** are isomers which differ only in the placement of one oxygen and two hydrogen atoms at the termini. So the major difference between **1a** and **1b** regarding PET is the relative orientation of the photogenerated electric field of the 4-aminonaphthalimide excited state towards a given amine receptor. Supramolecular systems composed of a fluorophore flanked by two dissimilar receptors are also useful as selective sensors[10] and as AND logic gates.[11] Synthesis of **1a** and **1b**† is easily achieved in two steps (Scheme 1) starting from commercially available materials.

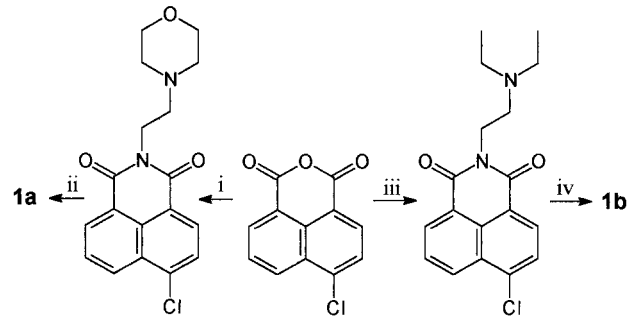

Scheme 1 *Reagents* i, 2-(morpholino)ethylamine, PhMe; ii, 2-(diethylamino)ethylamine; iii, 2-(diethylamino)ethylamine, PhMe; iv, 2-(morpholino)ethylamine.

The electronic absorption and fluorescence emission spectra of **1a** and **1b** are measured as a function of pH. The absorption spectra show variations across some pH ranges. These absorbance (A) changes are analyzed according to eqn. (1)[12] and the pK_a values obtained are given in Table 1. The variations in fluorescence emission spectra are largely confined to changes in the quantum yield (ϕ_{Flu}). These are plotted in Fig. 1 and analyzed according to eqn. (2).[13]

Table 1 Optical and acid–base parameters of **1a** and **1b**[a]

	1a	**1b**
$\lambda_{Abs\ pH\ =\ 3.0}$/nm (log ε)[b]	432 (4.19)	433 (4.21)
$\lambda_{Abs\ pH\ =\ 7.0}$/nm (log ε)[b]	432 (4.19)	452 (4.23)
$\lambda_{Abs\ pH\ =\ 10.8}$/nm (log ε)[b]	450 (4.20)	452 (4.23)
$\lambda_{Isosbestic}$	439	437
pK_a (morpholinoethyl)[c]	—[d]	5.8
pK_a (diethylaminoethyl)[c]	8.6	—[d]
λ_{Flu}/nm[e]	526	524
$\phi_{Flu\ pH\ =\ 3.0}$	0.53	0.52
$\phi_{Flu\ pH\ =\ 7.0}$	0.66	0.062
$\phi_{Flu\ pH\ =\ 10.8}$	0.030	0.070
$FE_{pH\ =\ 3.0/pH\ =\ 7.0}$[f]	0.81	8.4
$FE_{pH\ =\ 7.0/pH\ =\ 10.8}$[f]	21	0.83
pK_a' (morpholinoethyl)[g]	5.8	5.7
pK_a' (diethylaminoethyl)[g]	8.7	9.1

[a] 10^{-5} M **1a** or **1b** in aerated H_2O–MeOH (1 : 1, v/v). Fluorescence emission spectra are obtained by excitation at the isosbestic wavelength. [b] Extinction coefficient ε in units of dm^3 mol^{-1} cm^{-1}. [c] *via* Absorbance measurements. [d] Absorbance change is not large enough to permit analysis according to eqn. (1). [e] Value changes little with pH. [f] Fluorescence enhancement factor due to protonation in the specified pH range. [g] *via* Fluorescence measurements.

$$\log[(A_{max} - A)/(A - A_{min})] = pH - pK_a \quad (1)$$

$$\log[(\phi_{Flu\,max} - \phi_{Flu})/(\phi_{Flu} - \phi_{Flu\,min})] = pH - pK_a' \quad (2)$$

Considering **1a**, we find there is only one clear sigmoidal step corresponding to proton-triggered fluorescence recovery as expected of a PET system. The fluorescence is enhanced by an order of magnitude. The corresponding pK_a' value (8.7) clearly belongs to the strongly basic diethylaminoethyl unit attached to the 4-amino position. There is a smaller sigmoidal step corresponding to weak fluorescence quenching due to protonation. This is due to the formation of an intramolecular hydrogen bond between the protonated amine and the imide carbonyl oxygen.[14] The corresponding pK_a' value (5.8) can be easily assigned to the morpholinoethyl unit attached to the imide position. We note that the two dialkylamino groups are held far enough apart by the rigid chromophore in **1a** (and **1b**) to prevent mutual perturbation of pK_a values.

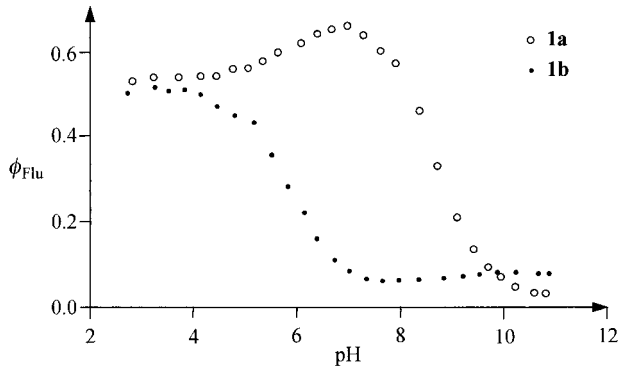

Fig. 1 Fluorescence quantum yields of **1a** and **1b** as a function of pH.

System **1b** shows the fluorescent PET switch behaviour with emission enhancement due to protonation of the morpholinoethyl unit connected to the 4-amino position. The dominant sigmoidal step has pK_a' = 5.7. The minor sigmoidal step has pK_a' = 9.1 which can be associated with the diethylaminoethyl group on the imide position. The slight fluorescence quenching seen upon protonation is again due to the intramolecular hydrogen bonding discussed above for **1a**.

The above analysis shows that in each case the electron transfer originates from the dialkylamino unit attached to the 4-amino position irrespective of the difference in PET driving force for the two alkylamino moieties. In the case of **1b** it is particularly remarkable that the PET path of apparently smaller PET driving force is selected by the supramolecular system. The morpholino unit is clearly a poorer PET donor than the diethylamino group when used in conjunction with porphyrin fluorophores for instance.[15] The PET path selection by the supramolecular system shows the remarkable marshalling efficiency of the excited state dipole of the 4-aminonaphthalimide fluorophore.[9] Unidirectional PET (but not path selectivity) has also been arranged with the ground state dipole of α-helical oligopeptides.[16] Taken together, these results demonstrate the capability of local electric fields to direct electron traffic. It is interesting that local electric fields due to the protein matrix of the PRC are among the possible causes advanced for the path-selectivity of PET.[17]

In conclusion, the simple technique of pH-dependent fluorescence is combined with the carefully designed, but structurally simple supramolecular systems **1a** and **1b** in order to emulate the one-way electron transfer seen within the PRC.

We thank EPSRC, DENI and Dr H. Q. Nimal Gunaratne for support and help.

Notes and references

† **1a**: Found: C, 68.2; H, 7.4; N, 13.1. $C_{24}H_{32}N_4O_3$ requires: C, 67.9; H, 7.6; N, 13.2%. ^{1}H NMR δ 1.09 (t, 6H, CH_3CH$_2$N), 2.63 (t, 4H, NCH_2CH$_2$O), 2.68 (q, 4H, CH$_3$CH_2N), 2.71 (t, 2H, CH_2NCH$_2$CH$_2$O), 2.90 (t, 2H, NCH_2CH$_2$NH), 3.41 (t, 2H, NCH$_2$CH_2NH), 3.71 (t, 4H, NCH$_2$CH_2O), 4.39 (t, 2H, CH_2CH$_2$NCH$_2$CH$_2$O), 6.53 (br s, 1H, NH), 6.67–8.61 (m, 5H, ArH); *m/z*(%) 425 (M^+, 14), 312(63), 100(52), 86(100); **1b**; Found: C, 68.2; H, 7.8; N, 13.3. $C_{24}H_{32}N_4O_3$ requires: C, 67.9; H, 7.6; N, 13.2%. ^{1}H NMR δ 1.13 (t, 6H, CH_3CH$_2$N), 2.58 (t, 4H, NCH_2CH$_2$O), 2.69 (q, 4H, CH$_3$CH_2N), 2.72 (t, 2H, NCH_2CH$_2$NH), 2.84 (t, 2H, CH$_3$CH$_2$NCH_2), 3.44 (t, 2H, NCH$_2$CH_2NH), 3.79 (t, 4H, NCH$_2$CH_2O), 4.29 (br t, 2H, CH_2CH$_2$NCH$_2$CH$_3$), 6.29 (br s, 1H, NH), 6.66–8.60 (m, 5H, ArH); *m.z*(%) 425 (M^+, 13), 326(17), 100(77), 86(100).

1 J. Deisenhofer, O. Epp, K. Miki, R. Huber and H. Michel, *J. Mol. Biol.*, 1984, **180**, 385; H. Michel, O. Epp and J. Deisenhofer, *EMBO J.*, 1986, **5**, 2445.

2 G. McDermott, S. M. Prince, A. A. Freer, A. M. Hawthornthwaite-Lawless, M. Z. Papiz, R. J. Cogdell and N. W. Isaacs, *Nature*, 1995, **374**, 517.

3 M. R. Wasielewski, *Chem. Rev.*, 1992, **92**, 435; A. Harriman and J.-P. Sauvage, *Chem. Soc. Rev.*, 1996, **25**, 41; C. A. Hunter and R. K. Hyde, *Angew. Chem., Int. Ed. Engl.*, 1996, **35**, 1936; C. A. Hunter and R. J. Shannon, *Chem. Commun.*, 1996, 1361.

4 C. Kirmaier, D. Holten and W. W. Parson, *Biochim. Biophys. Acta*, 1985, **810**, 33; C. Kirmaier, D. Holten and W. W. Parson, *Biochim. Biophys. Acta*, 1985, **810**, 49; M. Bixon, J. Jortner, M. E. Michel-Beyerle and A. Ogrodnik, *Biochim. Biophys. Acta*, 1989, **977**, 273.

5 V. Balzani and F. Scandola, *Supramolecular Photochemistry*, Ellis-Horwood, Chichester, 1991; R. A. Bissell, A. P. de Silver, H. Q. N. Gunaratne, P. L. M. Lynch, G. E. M. Maguire and K. R. A. S. Sandanayake, *Chem. Soc. Rev.*, 1992, **21**, 187; J.-M. Lehn, *Supramolecular Chemistry*, VCH, Weinheim, 1995.

6 M. A. Fox, *Acc. Chem. Res.*, 1992, **25**, 569; A. Sucheta, B. A. C. Ackrell, B. Cochran and F. Armstrong, *Nature*, 1992, **356**, 361; A. S. Martin and J. R. Sambles, *Nanotechnology*, 1996, **7**, 401.

7 R. A. Bissell, A. P. de Silva, H. Q. N. Gunaratne, P. L. M. Lynch, G. E. M. Maguire, C. P. McCoy and K. R. A. S. Sandanayake, *Top. Curr. Chem.*, 1993, **168**, 223; *Chemosensors for Ion and Molecule Recognition*, ed. J.-P. Desvergne and A. W. Czarnik, Kluwer, Dordrecht, 1997; A. P. de Silva, H. Q. N. Gunaratne, T. Gunnlaugsson, A. J. M. Huxley, C. P. McCoy, J. T. Rademacher and T. R. Rice, *Chem. Rev.*, 1997, **97**, 1515.

8 W. J. Ni, J. H. Su, K. C. Chen and H. Tian, *Chem. Lett.*, 1997, 101; K. A. Mitchell, R. G. Brown, D. Yuan, S. C. Chang, R. E. Utecht and D. E. Lewis, *J. Photochem. Photobiol.: A. Chem.*, 1998, **118**, 157; I. Grabchev, *Dyes Pigm*, 1998, **38**, 219; F. Cosnard and V. Wintgens, *Tetrahedron Lett.*, 1998, **39**, 2752; A. P. de Silva, H. Q. N. Gunaratne and T. Gunnlaugsson, *Tetrahedron Lett.*, 1998, **39**, 5077.

9 A. P. de Silva, H. Q. N. Gunaratne, J.-L. Habib-Jiwan, C. P. McCoy, T. E. Rice and J.-P. Soumillion, *Angew. Chem., Int. Ed. Engl.*, 1995, **34**, 1728; S. R. Greenfield, W. A. Svec, D. Gosztola and M. R. Wasielewski, *J. Am. Chem. Soc.*, 1996, **118**, 6767; S. N. Smirnov, C. L. Braun, S. R. Greenfield, W. A. Svec and M. R. Wasielewski, *J. Phys. Chem.*, 1996, **100**, 12 329; S. R. Greenfield, W. A. Svec, D. Gosztola and M. R. Wasielewski, *New J. Chem.*, 1996, **20**, 815.

10 A. P. de Silva, H. Q. N. Gunaratne, C. McVeigh, G. E. M. Maguire, P. R. S. Maxwell and E. O'Hanlon, *Chem. Commun.*, 1996, 2191; C. R. Cooper and T. D. James, *Chem. Commun.*, 1997, 1419.

11 A. P. de Silva, H. Q. N. Gunaratne and C. P. McCoy, *J. Am. Chem. Soc.*, 1997, **119**, 7891. *cf.*, A. P. de Silva, H. Q. N. Gunaratne and C. P. McCoy, *Nature*, 1993, **364**, 42.

12 K. Connors, *Binding Constants: The Measurement of Molecular Complex Stability*, Wiley, New York, 1987.

13 R. A. Bissell, E. Calle, A. P. de Silva, S. A. de Silva, H. Q. N. Gunaratne, J. L. Habib-Jiwan, S. L. A. Peiris, R. A. D. D. Rupasinghe, T. K. S. D. Samarasinghe, K. R. A. S. Sandanayake and J.-P. Soumillon, *J. Chem. Soc., Perkin Trans. 2*, 1992, 1559.

14 A. Pardo, E. Martin, J. M. L. Poyato, J. J. Camacho, M. F. Brana and J. M. Castellano, *J. Photochem. Photobiol.: A. Chem.*, 1987, **41**, 69.

15 R. Grigg and W. D. J. A. Norbert, *J. Chem. Soc., Chem. Commun.*, 1992, 1298.

16 A. Knorr, E. Galoppini and M. A. Fox, *J. Phys. Org. Chem.*, 1997, **10**, 484; M. A. Fox and E. Galoppini, *J. Am. Chem. Soc.*, 1997, **119**, 5277.

17 M. R. Gunner, A. Nicholls and B. Honig, *J. Phys. Chem.*, 1996, **100**, 4277.

Communication 8/09119F

A novel open-framework zinc phosphate with intersecting helical channels

S. Neeraj, Srinivasan Natarajan and C. N. R. Rao*

Chemistry and Physics of Materials Unit, Jawaharlal Nehru Centre for Advanced Scientific Research, Jakkur P.O., PO Box 6436, Bangalore 560 064, India. E-mail: cnrrao@jncasr.ac.in

Received (in Cambridge, UK) 16th November 1998, Accepted 9th December 1998

A new open-framework zinc phosphate, possessing two interpenetrating 8-membered helical channels, has been synthesized under mild hydrothermal conditions.

Materials required for enantioselective separation and synthesis are becoming increasingly important in recent years.[1] For example, it is known that chiral rhodium complexes supported on a zeolite matrix give rise to asymmetric hydrogenation of *N*-acyldehydrophenylalanine derivatives with an enantioselectivity of > 95%.[2] In this context, it is desirable to have materials which are chiral or possess helical channels. There have been some efforts to make chiral solids which could also be shape-selective. Zeolite-β (polymorph A) is chiral with a 4-fold screw axis but it has not been possible to synthesize this material in a pure form.[3] Chiral open-framework phosphates have been prepared in the presence of chiral metal complexes and structure-directing agents.[4,5] Recently, a chiral tin(II) phosphate has been prepared using an achiral template, and both the enantiometers of this material have been isolated and characterized.[6] A helical metal borophosphate with the helix running along the 6_1 screw axis has also been reported.[7] Very recently, Gier *et al*.[8] have reported chiral zinc and beryllium arsenates with three-dimensional helical structure containing two independent crosslinked helical channels. We have been able to isolate a new chiral zinc phosphate formed under hydrothermal conditions in the presence of an achiral structure-directing amine, diethylenetriamine. Here we report the synthesis and structure of a chiral zinc phosphate, $[NH_3(CH_2)_2NH_2(CH_2)_2NH_3]^{3+}[Zn_4(PO_4)_3(HPO_4)]^{3-}\cdot H_2O$, **1**.

Compound **1** was synthesized hydrothermally using diethylenetriamine (DETA) as the structure-directing agent[9] and characterized by single crystal X-ray diffraction using the Siemens SMART system.[10] The asymmetric unit contains 32 non-hydrogen atoms and the atomic coordinates are given as supplementary data (see http://www.rsc.org/suppdata/cc/1999/165). The structure is built from the networking of ZnO_4, PO_4 and HPO_4 tetrahedral units. The vertex linkage between these units creates an anionic framework of formula $[Zn_4(PO_4)_3(HPO_4)]^{3-}$ and charge compensation is achieved by the protonated amine $[NH_3(CH_2)_2NH_2(CH_2)_2NH_3]^{3+}$. The structure has one water molecule in the channels formed by the networking of the various units.

The most interesting aspect of this Zn phosphate is that it crystallizes in a polar space group $P2_1$. The entire framework of **1**, can be considered to be built from the networking of three-, four-, six- and eight-membered rings. The three- and four-membered rings are connected together, edge wise, forming one-dimensional helical columns along the *b* axis as shown in Fig. 1 which shows how these columns are interconnected *via* the HPO_4 group forming an eight-membered channel system along the *a* axis. This eight-membered channel along the *a* axis is connected to another eight-membered channel along the *b* axis, forming a helical interconnected one-diemsional channel system within which the amine and water molecules are situated. Fig. 2 shows the connectivity between the ZnO_4 and PO_4 moieties that creates the other eight-membered channel system along the *b* axis. Thus, **1** possesses an interpenetrating eight-membered channel system. There is a strong hydrogen bonded interaction between the framework and the structure-directing amine providing structural stability. The framework density[11] (number of tetrahedral framework atoms in 1000 Å^3) for this material is 16.7, indicating a degree of openness comparable to aluminophosphate moecular sieves such as AlPO-12[11] and AlPO-16.[11]

A few comments on the structural parameters of **I** would be in order. Of the sixteen oxygens in the asymmetric unit, one

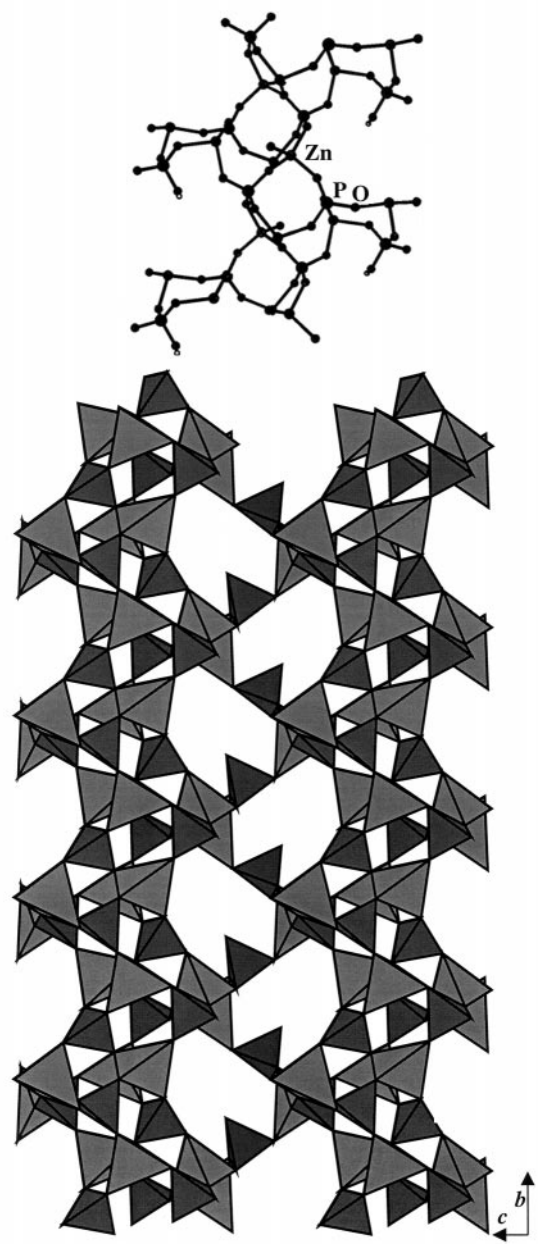

Fig. 1 Structure of $[NH_3(CH_2)_2NH_2(CH_2)_2NH_3]^{3+}[Zn_4(PO_4)_3(HPO_4)]^{3-}\cdot H_2O$ showing the eight-membered cavities (channels) along the *100* direction and the helical channels. Amine and water molecules are omitted for clarity. The connectivity in the one-dimensional columns is also shown.

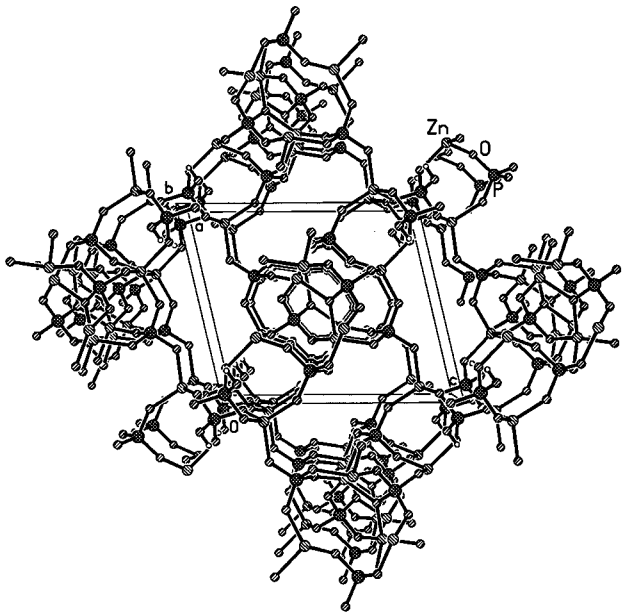

Fig. 2 Structure of $[NH_3(CH_2)_2NH_2(CH_2)_2NH_3]^{3+}[Zn_4(PO_4)_3(HPO_4)]^{3-}\cdot H_2O$ showing the eight-membered channels along the *010* direction. Amine and water molecules are not shown.

makes a trigonal connection with two Zn atoms and one P atom forming a three-membered ring and one is a terminal oxygen while the remainder of the oxygens form Zn–O–P linkages. The P–O bond distances are in the range 1.502–1.581 Å (av. 1.537 Å) and the bond angles are in the range 104.8–114.5° (av. 109.5°), in agreement with those observed previously in such materials. The P–O distance of 1.581 Å [P(3)–O(16)] indicates protonation leading to the formation of the HPO_4 unit. The Zn atoms are all connected with P through oxygens, with the Zn–O distances in the range 1.890–2.004 Å (av. 1.954 Å). The O–Zn–O bond angles are in the range 94.5–120.6° (av. 109.4°). The longest Zn–O distance and the largest O–Zn–O angle are found for oxygens involved in three-coordination.

References

1 A. Baiker, *Curr. Opin. Solid State Mater. Sci*., 1998, **3**, 86.
2 A. Corma, M. Iglesias, C. del Pina and F. Sanchez, *J. Chem. Soc., Chem. Commun*., 1991, 1235; *Organomet. Chem*., 1992, **431**, 233.
3 J. M. Newsam, M. M. J. Treacy, W. T. Koetsier and C. B. de Gruyter, *Proc. R. Soc. London, Sect A*, 1998, **420**, 375.
4 K. Morgan, G. Gainsford and N. Milestone, *J. Chem. Soc., Chem. Commun*., 1995, 425; D. A. Bruce, A. P. Wilkinson, M. G. White and J. A. Bertrand, *J. Solid State Chem*., 1996, **125**, 228.
5 H.-M. Lin and K.-H. Lii, *Inorg. Chem*., 1998, **37**, 4220.
6 S. Ayyappan, X. Bu, A. K. Cheetham and C. N. R. Rao, *Chem. Mater*., 1998, **10**, 3308.
7 R. Kniep, H. G. Will, I. Boy and C. Röhr, *Angew. Chem., Int. Ed. Engl*., 1997, **36**, 1013.
8 T. E. Gier, X. Bu, P. Feng and G. D. Stucky, *Nature*, 1998, **395**, 154.
9 0.407 g of ZnO was dispersed in 9 ml of water and 0.365 g of HCl and 0.98 g of 85 wt% of H_3PO_4 were added to the mixture and stirred for 10 min. To this mixture 0.516 g of diethylenetriamine (DETA) was added and the mixture homogenized, transferred into a Parr pressure bomb and heated initially at 150 °C for 5 days which resulted in the formation of a large number of needles. The final composition of the mixture was $ZnO : 2H_3PO_4 : 2HCl : DETA : 80H_2O$.
10 *Crystal data* for **1**: $[NH_3(CH_2)_2NH_2(CH_2)_2NH_3]^{3+}[Zn_4(PO_4)_3(HPO_4)]^{3-}\cdot H_2O$, M = 766.6(1), monoclinic, space group = $P2_1$ (no. 4), a = 10.021(4), b = 8.286(3), c = 11.856(7) Å, β = 103.13(1)°, V = 958.7(7) Å^3, Z = 9, D_c = 2.655 g cm^{-3}, μ(Mo-Ka) = 5.37 mm^{-1}, Mo-Kα radiation, λ = 0.71073 Å, 1.76 < θ < 23.26°. Data collection was performed using a Siemens SMART-CCD diffractometer. A total of 4056 data were collected and were merged to give 2565 unique reflections of which 2217 were considered to be observed [$I > 2\sigma(I)$]. The structure was solved and refined using SHELXTL-PLUS package of program against $|F^2|$. Final R = 0.054, R_w = 0.13, S (goodness of fit) = 0.838 were obtained for all the data and 289 parameters. The final Fourier map had a minimum and maximum of −0.880 and 0.897 e Å^{-3}, respectively. CCDC 182/1109
11 *Atlas of zeolite structure types* ed. W. H. Meier, D. H. Olson and Ch. Baerlocher, Elsevier, Boston, MA, 1996.

Communication 8/08899C

Synthesis of optically pure threonine-containing dipeptides by regio- and stereo-controlled ring expansion of aziridine-2-imide derivatives

Giuliana Cardillo,* Luca Gentilucci and Alessandra Tolomelli

Dipartimento di Chimica 'G. Ciamician', Università di Bologna and C.S.F.M, via Selmi 2, 40126 Bologna, Italy. E-mail: Cardillo@ciam.unibo.it

Received (in Liverpool, UK) 8th September 1998, Accepted 3rd December 1998

The regio- and stereo-selective ring expansion of chiral *N*-(α-amino acyl)aziridine-2-imides to oxazolines and subsequent ring opening to optically pure threonine-containing dipeptides with the desired stereochemistry is described.

β-Hydroxy α-amino acids are structural units present in a large number of naturally occurring biologically active compounds.[1] For instance, hexadepsipeptide antibiotic azinothricin,[2] depsipeptides variapeptin and citropeptin,[3] and the macrocyclic lactone antiobiotic lysobactin[4] contain in their sequence several β-hydroxy-α-amino acids linked together.

The importance of these amino acids has stimulated the development of numerous methods for their stereoselective synthesis.[5] Nevertheless a conceptually new strategy for the preparation of non-proteogenic α-amino acid derivatives starting from suitable heterocyclic compounds has been recently investigated for direct use in peptide coupling reactions. Ring-opening coupling reactions of enantiomerically pure 3-hydroxy β-lactams with various (*S*)-amino acid esters to give the corresponding dipeptides have been described by Ojima *et al*.,[6] while access to non-proteogenic peptide fragments of lysobactin from chiral azetidin-2-ones has been recently reported by Palomo *et al*.[7]

We describe here a new and efficient strategy for the synthesis of threonine-containing dipeptides starting from enantiomerically pure aziridine-2-imides *via* a ring expansion to oxazolines[8] that occurs in a regio- and stereo-controlled manner.[9]

Thus the enantiopure aziridine (2′*R*, 3′*S*)-**1**[10] was treated with *N*-acetylleucine and DCC in CH_2Cl_2–MeCN giving compound **2a** in 95% yield, which spontaneously converted into oxazoline-4-imide **3a** (Scheme 1), obtained in quantitative yield and purified by flash chromatography. Hydrolysis of **3a** performed with TsOH in MeOH–H_2O gave dipeptide **4a** in almost quantitative yield. The *trans* configuration of aziridine **2a** was retained in **3a** as shown by the oxazoline coupling constant value of H4 and H5 ($J_{H4–H5}$ = 4.7 Hz; lit.,[11] J_{trans} = 4–7 Hz). The regiochemistry of the aziridine ring expansion was easily established by ^{1}H NMR analysis of **3a** and confirmed by ^{1}H NMR decoupling experiments on **4a**.

In a similar way, **2b** was obtained by treatment of **1** with *N*-Boc-phenylalanine and DCC. The ring expansion of **2b** was promoted by $BF_3{\cdot}Et_2O$ in the presence of trace water and afforded at once the (*S*)-Phe-(2′*R*, 3′*S*)-Thr derivative **4b**, which is immediately treated with Ac_2O to give **5**.[12] Under these acidic conditions, fast ring opening of oxazoline **3b** to **4b** was observed, **3b** being detected in only trace amounts in the ^{1}H NMR spectrum of the crude reaction mixture.

These results show that (2*R*, 3*S*)-threonine can be easily introduced in a polypeptide sequence. The design and synthesis of modified peptides offers opportunities for drug preparation. Among the modifications designed to obtain higher biological activity and greater resistance to enzymatic hydrolysis, the substitution of non-proteinogenic amino acids in a polypeptide sequence is of current interest.

In order to prepare the (2*S*, 3*R*)-threonine-containing dipeptide, the *trans* aziridine **6**[10] was treated with *N*-Boc-phenylalanine and DCC to give **7**. The ring expansion was performed under the conditions reported for **2b** and compound **8** was finally isolated in good yield after acetylation. The ^{1}H NMR and ^{13}C NMR spectra confirmed the structure (Scheme 2).

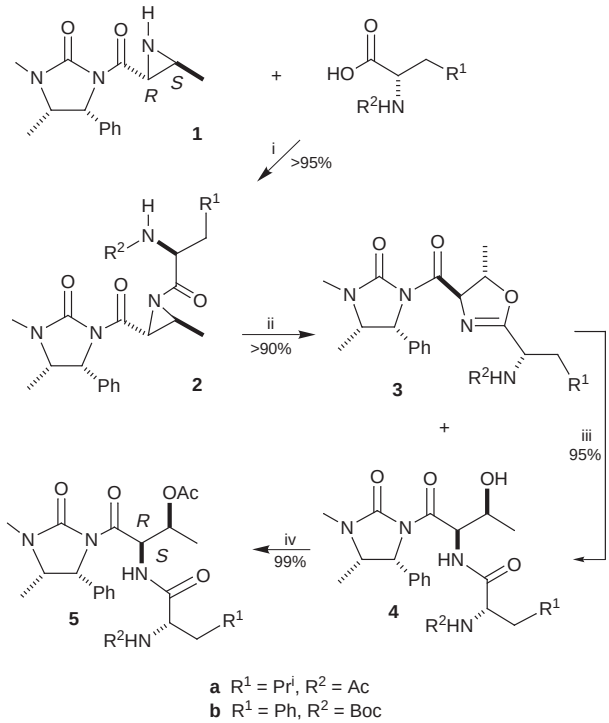

Scheme 1 *Reagents and conditions*: i, DCC (1.1 equiv.), CH_2Cl_2–MeCN, 12 h, room temp.; ii, $BF_3{\cdot}Et_2O$ (1 equiv.), CH_2Cl_2, room temp.; iii, TsOH (1.1 equiv.), MeOH–H_2O, room temp.; iv, Ac_2O (1.2 equiv.), pyridine (1.2 equiv.), CH_2Cl_2, 2 h, room temp.

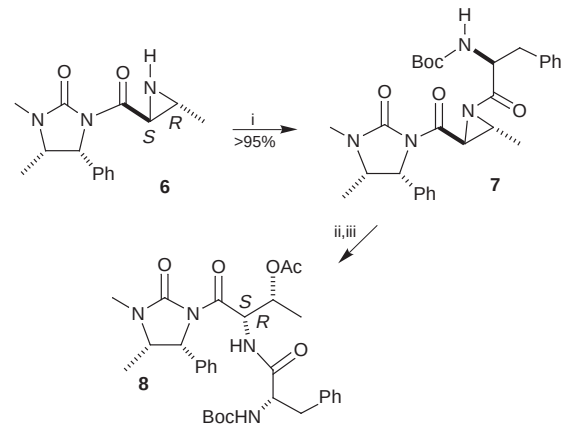

Scheme 2 *Reagents and conditions*: i, DCC (1.1 equiv.), CH_2Cl_2–MeCN, 12 h, room temp.; ii, $BF_3{\cdot}Et_2O$ (1 equiv.), CH_2Cl_2, room temp.; iii, Ac_2O (1.2 equiv.), pyridine (1.2 equiv.), CH_2Cl_2, 2 h, room temp.

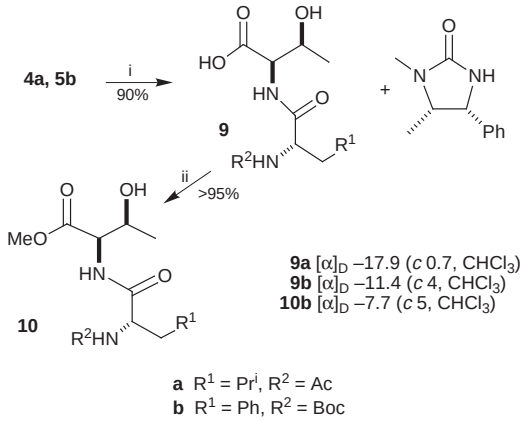

Scheme 3 *Reagents and conditions*: i, LiOH (3 equiv.), H_2O_2 (4 equiv.), THF–H_2O, 2 h, 0 °C; ii, CH_2N_2.

Finally, to obtain the free dipeptide, **4a** was submitted to non-destructive removal of the chiral auxiliary under Evans' conditions,[13] by means of LiOOH in THF–H_2O (Scheme 3). After 2 h the *N*-acetyl-(*S*)-Leu-(2*R*, 3*S*)-Thr dipeptide **9a** was recovered in good yield. Longer reaction times should be avoided; indeed, after 6 h the reaction mixture contained 10% of epimerized product.

On the basis of these results, **5b** was hydrolysed over 2 h giving without any epimerization the *N*-Boc-(*S*)-Phe-(2*R*, 3*S*)-Thr dipeptide **9b**,[14] which was essentially pure after work-up according to analysis of the crude reaction mixture. Compound **9b** was converted by means of CH_2N_2 into the corresponding methyl ester **10b**.[15]

In order to confirm the stereochemistry of the aziridine ring expansion *via* an S_Ni mechanism for **2** and **7**, an authentic sample of dipeptide **8b** was prepared from commercially available (2*R*, 3*S*)-threonine and (*S*)-phenylalanine (Scheme 4).

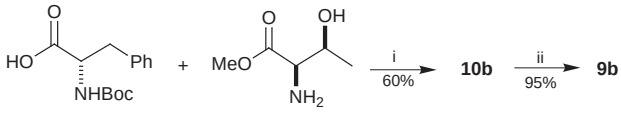

Scheme 4 *Reagents and conditions*: i, DCC (1.1 equiv.), CH_2Cl_2–MeCN, 12 h, room temp.; ii, LiOH (2 equiv.), H_2O_2 (3 equiv.), THF–H_2O, 1 h, 0 °C.

The (2*R*, 3*S*)-threonine methyl ester and *N*-Boc-(*S*)-phenylalanine were coupled with DCC in CH_2Cl_2–MeCN and the desired dipeptide derivative was obtained in satisfactory yield. This compound was treated with LiOOH in THF–H_2O[13] and afforded the corresponding carboxylic acid. Both **9b** and **10b** showed ^{1}H NMR and ^{13}C NMR spectra which were identical, and optical rotation values which were comparable, with the authentic samples.

In conclusion, we have reported a new method that permits the synthesis of β-hydroxy α-amino acids coupled with other α-amino acids, starting from aziridine derivatives. Furthermore, due to the observed retention of configuration in the ring expansion of the starting aziridine, the stereochemistry of the final dipeptide can be fixed by using the appropriate starting material.

We thank the University of Bologna for funds for selected research topics.

Notes and references

1 A. Saeed and D. W. Young, *Tetrahedron*, 1992, **48**, 2507 and references cited therein; R. B. Herbert, B. Wilkinson, G. J. Ellames and K. E. Kunec, *J. Chem. Soc., Chem. Commun*., 1993, 205.

2 H. Maehr, C. M. Liu, N. J. Pelleroni, J. Smallheer, L. Todaro, T. H. Williams and J. F. Blount, *J. Antibiot*., 1986, **39**, 17.

3 M. Nakagawa, Y. Hayakawa, K. Furihata and H. Seto, *J. Antibiot*., 1990, **43**, 477.

4 J. O'Sullivan, J. E. McCullough, A. A. Tymiak, D. R. Kirsch, W. H. Trejo and P. A. Principe, *J. Antibiot*., 1988, **41**, 1740; T. Kato, H. Hinoo, Y. Tervi, J. Kikuchi and J. Shoji, *J. Antibiot*., 1988, **41**, 719.

5 H. Shao and M. Goodman, *J. Org. Chem*., 1996, **61**, 2582; Williams, Z. Zhang, F. Shao, P. J. Carroll and M. Joulliè, *Tetrahedron*, 1996, **52**, 11673 and references cited therein; K. J. Hale, S. Manaviazar and V. M. Delisser, *Tetrahedron*, 1994, **50**, 9181; S. Kanemasa, T. Mori and A. Tatsukawa, *Tetrahedron Lett*., 1993, **34**, 8293; T. Sanuzaka, T. Nagamitsu, H. Tanaka, S. Omura, P. A. Sprengler and A. B. Smith, *Tetrahedron Lett*., 1993, **34**, 4447; E. J. Corey, D.-H. Lee and S. Choi, *Tetrahedron Lett*., 1992, **33**, 6735.

6 I. Ojima, C. M. Sun and Y. H. Park, *J. Org. Chem*., 1994, **59**, 1249; I. Ojima, H. Wang, T. Wang and E. W. Ng, *Tetrahedron Lett*., 1998, **39**, 923.

7 C. Palomo, J. M. Aizpurua, I. Gamboa, B. Odriozola, E. Maneiro, J. I. Miranda and R. Urchegui, *Chem. Commun*., 1996, 161; C. Palomo, I. Gamboa, B. Odriozola and A. K. Linden, *Tetrahedron Lett*., 1997, **38**, 3093.

8 I. J. Burnstein, P. E. Fanta and B. S. Green, *J. Org. Chem*. 1970, **35**, 4084; T. A. Foglia, L. M. Gregory and G. Maerkel, *J. Org. Chem*., 1970, **35**, 3779; C. U. Pittman and S. P. McManus *J. Org. Chem*., 1970, **35**, 1187; D. Haidukewych and A. I. Meyers, *Tetrahedron Lett*., 1972, **30**, 3031; S. G. Bates and M. A. Varelas, *Can. J. Chem*., 1980, **58**, 2562; J. Legters, L. Thijs and B. Zwanenburg, *Recl. Trav. Chim. Pays-Bas*, 1992, **111**, 16.

9 K. Hory, T. Nishiguchi and A. Nabeja, *J. Org. Chem*., 1997, **62**, 3081; G. Cardillo, L. Gentilucci, A. Tolomelli and C. Tomasini, *Tetrahedron Lett*., 1997, **38**, 6953.

10 G. Cardillo, S. Casolari, L. Gentilucci and C. Tomasini, *Angew. Chem., Int. Ed. Engl*., 1996, **35**, 1848; A. Bongini, G. Cardillo, L Gentilucci and C. Tomasini, *J. Org. Chem*., 1997, **62**, 9148.

11 S. H. Pines, M. A. Kozlowski and S. Karady, *J. Org. Chem*., 1969, **34**, 1621; D.-M. Gou, Y.-C. Liu and C.-S. Chen, *J. Org. Chem*., 1993, **58**, 1287.

12 *Selected data* for **5**: δ_H($CDCl_3$) 0.80 (d, *J* 6.7, 3H, CH_3CHCHPh), 1.20 (d, *J* 6.5, 3H, CH_3CHOAc), 1.32 (s, 9H, But), 1.95 (s, 3H, COCH_3), 2.88 (s, 3H, NCH_3), 2.95–3.18 (m, 2H, CH_2Ph), 4.00 (dq, *J* 6.7, 8.4, 1H, CH_3C*H*CHPh), 4.34–4.50 (m, 1H, C*H*CH_2Ph), 4.88 (d, *J* 6.0, 1H, *H*NBoc), 5.05 (d, *J* 8.4, 1H, CH_3CHC*H*Ph), 5.50 (dq, *J* 1.3, 6.5, C*H*OAc), 6.08 (dd, *J* 1.3, 9.5, 1H, C*H*CHOAc), 6.65 (d, *J* 9.5, 1H, *H*NCHCH), 7.02–7.46 (m, 10H, ArH); δ_C($CDCl_3$) 14.7, 20.8, 24.9, 25.6, 28.2, 33.9, 49.1, 54.3, 55.5, 59.9, 70.4, 77.8, 126.9, 128.2, 128.6, 129.2, 136.2, 136.3, 155.0, 155.4, 168.5, 170.5, 171.2.

13 J. R. Gage and D. A. Evans, *Org. Synth*., 1989, **68**, 83.

14 *Selected data* for **9b**: ν_{max}/cm^{-1} 3300 br, 3050, 1720, 1700, 1660; δ_H($CDCl_3$) 0.93 (d, *J* 6.0, CH_3), 1.35 (s, 9H, But), 2.85–3.20 (m, 2H, CH_2Ph), 4.20–4.40 (m, 1H, C*H*OH), 4.40–4.67 (m, 2H, C*H*CHOH + C*H*CH_2Ph), 5.40 (d, *J* 6.0, 1H, *H*NBoc), 6.00–6.40 (m, 3H, OH + *H*NCHCH + CO_2H), 7.10–7.40 (m, 5H, ArH); δ_C($CDCl_3$) 19.3, 28.2, 38.9, 55.7, 57.4, 67.6, 80.1, 127.0, 128.6, 129.3, 136.4, 156.3, 172.2, 173.4; [α]D −11.4 (*c* 4, $CHCl_3$).

15 *Selected data* for **10b**: ν_{max}/cm^{-1} 3350, 3050, 1750, 1694, 1659, 1525; δ_H($CDCl_3$) 1.00 (d, *J* 6.1, 3H, CH_3), 1.32 (s, 9H, But), 2.95 (dd, *J* 6.7, 13.9, 1H, CH_2Ph), 3.11 (dd, *J* 6.2, 13.9, 1H, CH_2Ph), 3.67 (s, 3H, CO_2CH_3), 4.20–4.32 (m, 1H, C*H*OH), 4.40–4.60 (m, 2H, C*H*CHOH + C*H*CH_2Ph), 5.40–5.58 (br s, 1H, *H*NBoc), 7.10–7.33 (m, 6H, ArH + *H*NCHCH); δ_C($CDCl_3$) 19.5, 28.0, 33.6, 38.3, 52.2, 57.5, 67.2, 79.8, 126.5, 128.2, 129.1, 136.5 155.2, 171.2, 172.2; [α]D −7.7 (*c* 5, $CHCl_3$).

Communication 8/07063F

ChemComm

Model systems for flavoenzyme activity: aromatic stacking in sol-gel matrices

Michael D. Greaves, Trent H. Galow and Vincent M. Rotello*

Department of Chemistry, Lederle Graduate Research Center, University of Massachusetts at Amherst, Amherst, MA 01003, USA. E-mail: rotello@chem.umass.edu

Received (in Columbia, MO, USA) 18th September 1998, Accepted 7th December 1998

Silicate matrices effectively replicate both the isolation and preorganization found in the active sites of flavoenzymes.

The peptide scaffolding found in proteins performs two crucial roles in defining the active site environment. First, it provides isolation of this active site from unwanted interactions with water and other entities. Second, it presents reactive functionality in the geometry required for efficient recognition and catalysis. While researchers have been able to use solution-based model systems to explore key aspects of both isolation[1] and recognition,[2] the creation of models that simultaneously replicate both functions remains an intimidating prospect.[3]

One means of obtaining isolation is through the use of nanoporous[4] and mesoporous[5] media. In recent research we have demonstrated efficient hydrogen bond recognition of flavin mononucleotide (FMN)[6] in sol-gel silicates.[7] In these systems, incorporation of the flavin into the cybotactic region of the silicate effectively modeled the isolation provided by the active site. Hydrogen bond recognition of the flavin was then provided by doping with a diaminopyridine-based receptor, replicating the enzyme-cofactor hydrogen bonding found in the flavoenzymes.[8]

Aromatic–aromatic interactions are an important motif in flavoenzyme architecture (Fig. 1). As with hydrogen bonding, aromatic stacking plays a dual role in flavoenzyme function, providing efficient recognition of the flavin cofactor, and serving to modulate its reactivity.[9] In recent investigations, we created effective solution-phase models for enzyme–cofactor aromatic stacking.[10] We report here the use of silicate sol-gels to provide both isolation and preorganization for flavin–aromatic complexes, effectively replicating the role of the protein scaffolding.

Flavin-containing sols were prepared *via* the addition of dilute acid and tetraethyl orthosilicate (TEOS) to an aqueous solution of flavin mononucleotide (FMN) **1**, followed by

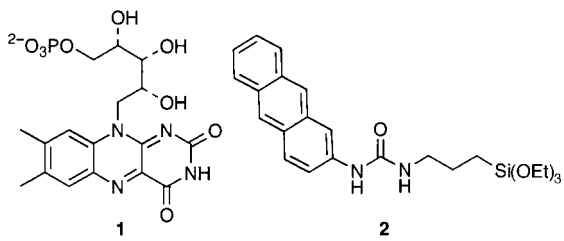

1 **2**

sonication to homogeneity. Aromatic stacking interactions were probed by addition of varying quantities of anthracene derivative *2* to the sol.[12] Sols were then poured into cuvettes and sealed: wet gels formed within 100 h.

The optical transparency of the silicate matrix allowed direct spectroscopic observation of aromatic stacking. As shown in Fig. 2, increasing quantities of receptor **2** resulted in decreased flavin fluorescence emission. This is consistent with solution-based studies, where we have established that aromatic stacking between the electron-rich anthracene and the electron-poor flavin effectively quenches flavin fluorescence.[13]

During the course of hydrolysis and gelation, there is negligible change (< 2%) in the volume of our sol-gels. We can therefore calculate an approximate pore volume by calculating

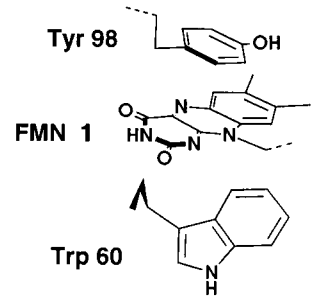

Fig. 1 Flavin binding site of the flavodoxin isolated from *Desulfovibrio vulgaris* (ref. 11).

the quantity of EtOH released during the hydrolysis of the orthosilicate. Assuming complete hydrolysis of TEOS, the final gel will be 17% silicate and 83% EtOH. Given this volume, the association constant for the FMN **1**–receptor **2** complex can be fitted to a 1 : 1 binding isotherm,[14] providing an estimated binding constant of 200 ± 50 M^{-1} (Fig. 3).[15] This is considerably higher than that observed for N^{10}-isobutylflavin **3**[16] with acylated aminoanthracene **4** (< 3 M^{-1}), demonstrating

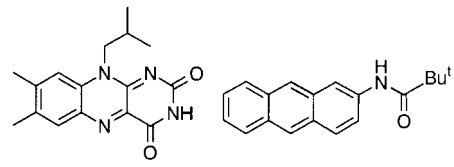

3 **4**

an active role of the silicate matrix in preorganizing the flavin **1**–receptor **3** complex in the sol-gel. This result is consistent with our previous studies,[17] further demonstrating this unusual matrix-assisted recognition enhancement.

In summary, we have demonstrated that aromatic stacking to a sol-gel-bound flavin can be established through addition of an

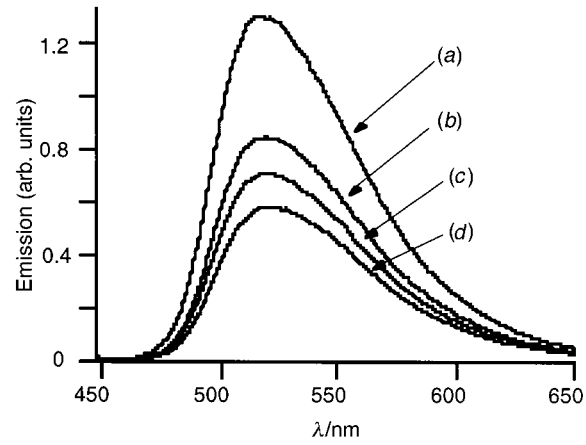

Fig. 2 Flavin fluorescence emission profiles of sol-gels containing FMN **1** and receptor **2**: (*a*) 0, (*b*) 10, (*c*) 20 and (*d*) 30 equiv. **2**. [FMN] = 0.0196 mmol dm^{-3}. Excitation wavelength = 445 nm; uncertainty of fluorescence values = ±5%.

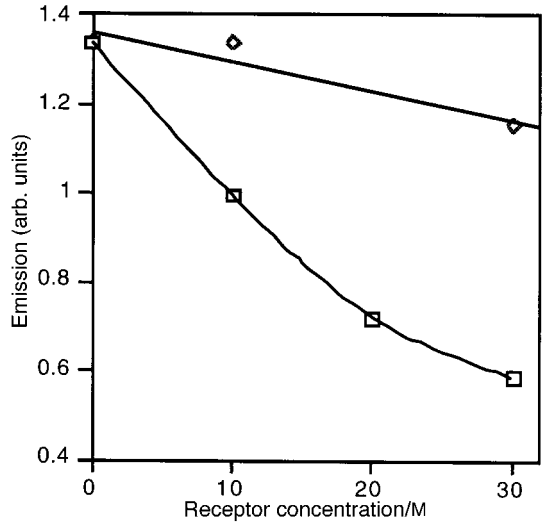

Fig. 3 Plot of flavin (**1**/**3**) fluorescence emission *vs.* receptor (**2**/**4**) concentration (□) **1** + **2** in sol-gel and (◇) **3** + **4** in EtOH. [FMN] = 0.0196 mmol dm^{-3}, [**3**] = 0.236 mmol dm^{-3} (calculated concentration of FMN inside the porous sol-gel matrix).

anthracene-based receptor. This interaction is greatly enhanced in the sol-gel relative to solution-phase studies. This indicates that the silicate matrix replicates the two-fold role of the protein scaffolding of flavoenzymes: isolation of the active site,[18] and preorganization of the active site functionality. Application of silicate sol-gels to the creation of functional flavoenzyme models is currently underway, and will be reported in due course.

Notes and references

1 D. J. Cram, *Nature*, 1992, **356**, 29; D. J. Cram, R. Jaeger and K. Deshayes, *J. Am. Chem. Soc.*, 1993, **115**, 10 111; R. Breslow, *Acc. Chem. Res*., 1995, **28**, 146; N. Branda, R. Wyeler and J. Rebek, *Science*, 1994, **263**, 1222; R. G. Chapman, G. Olovsson, J. Trotter and J. C. Sherman, *J. Am. Chem. Soc.*, 1998, **120**, 6252. For examples of molecular imprinting, see: B. Santora, A. Larsen and M. Gagne, *Organometallics*, 1998; **17**, 3138; S. Lee, I. Ichinose and T. Kunitake, *Langmuir*, 1998, **14**, 2857.

2 E. Gallo and S. Gellman, *J. Am. Chem. Soc.*, 1993, **115**, 9774; S. Zimmerman and T. Murray, *Tetrahedron Lett.*, 1994, 4077; J. Nowick, J. Chen and G. Noronha, *J. Am. Chem. Soc.*, 1993, **115**, 7636; G. Das and A. Hamilton, *J. Am. Chem. Soc.*, 1994, **116**, 11 139.

3 For dendritic systems that combine isolation and recognition. see C. Gorman, B. Parkhurst, W. Y. Su and K.-Y. Chen, *J. Am. Chem. Soc.*, 1997, **119**, 1141; S. Zimmerman, Y. Wang, P. Bharathi and J. Moore, *J. Am. Chem. Soc.*, 1998, **120**, 2172.

4 K. Balkus, L. Ball, B. Gnade and J. Anthony, *Chem. Mater.*, 1997, **9**, 380; Y. Xu and C. Langford, *J. Phys. Chem. B*, 1997, **101**, 3115; K. Yoon, Y. Park and J. Kochi, *J. Am. Chem. Soc.*, 1996, **118**, 12 710; S. Vasenkov and H. Frei, *J. Am. Chem. Soc.*, 1998, **120**, 4031. For a recent review see: R. J. Gorte, *Recent Advances and New Horizons in Zeolite Science and Technology. Studies in Surface Science and Catalysis, No. 102*, ed. H. Chon, S. Woo and S.-E. Park, Elsevier, Amsterdam, 1996.

5 D. Avnir, D. Levy and R. Reisfeld, *J. Phys. Chem.*, 1984, **88**, 5956; U. Narang, J. D. Jordan, F. V. Bright and P. N. Prasad, *J. Phys. Chem.*, 1994, **98**, 8101; F. Nishida, J. M. McKiernan, B. Dunn, J. I. Zink, C. J. Brinker and A. J. Hurd, *J. Am. Ceram. Soc.*, 1995, **78**, 1640; L. M. Ilharco, A. M. Santos, M. J. Silva and J. M. G. Martinho, *Langmuir*, 1995, **11**, 2419; K. Y. Parish, D. Habibi and V. Mohammadi, *J. Organomet. Chem.*, 1989, **369**, 17; A. Slama-Schwok, D. Avnir and M. Ottolenghi, *J. Am. Chem. Soc.*, 1991, **113**, 3984; A. Rosenfeld, D. Avnir and J. Blum, *J. Chem. Soc., Chem. Commun.*, 1993, 583. For recent reviews, see D. Avnir, *Acc. Chem. Res.*, 1995, **28**, 328; B. Dunn and J. I. Zink, *Chem. Mater.*, 1997, **9**, 2280.

6 For other studies of encapsulated biomolecules, see: L. Ellerby, C. Nishida, F. Nishida, S. Yamanaka, B. Dunn, J. Valentine and J. I. Zink, *Science*, 1992, **255**, 1113; S. Braun, S. Shtelzer, S. Rappoport, D. Avnir and M. Ottolenghi, *J. Non-Cryst. Solids*, 1992, **147** and **148**, 739; I. Pankratov and O. Lev, *J. Electroanal. Chem.*, 1995, **393**, 35.

7 For a detailed review of the fundamentals of sol-gel technology, see: C. J. Brinker and G. W. Scherer, *Sol-Gel Science*, Academic Press, San Diego, 1990; L. Hench and J. West, *Chem. Rev.*, 1990, **90**, 33; A. M. Buckley and M. Greenblatt, *J. Chem. Educ.*, 1994, **71**, 599.

8 E. Breinlinger, A. Niemz and V. Rotello, *J. Am. Chem. Soc.*, 1995, **117**, 5379.

9 B. Stockman, T. Richardson and R. Swenson, *Biochemistry*, 1994, **33**, 15 298.

10 E. Breinlinger and V. Rotello, *J. Am. Chem. Soc.*, 1997, **119**, 1165.

11 W. Watt, A. Tulinsky, R. P. Swenson and K. D. Watenpaugh, *J. Mol. Biol.*, 1991, **218**, 195.

12 Synthesized in 75% yield from 2-aminoanthracene and 3-(triethoxysilyl)propyl isocyanate.

13 *N*-Alkylurea analogs of **2** shows essentially identical quenching behavior as for **2**, demonstrating that hydrogen bonding to the urea is not involved in flavin recognition.

14 Solution studies have shown that additional anthracene–flavin interactions have little effect on flavin fluorescence, allowing selective monitoring of the 1 : 1 complex. The large excesses of receptor **2** used should minimize the effect of 2 : 1 receptor flavin binding on the receptor available for the first binding event.

15 The uncertainty presented is the asymptotic standard error. As this system is not in the standard state, the calculated K_a value is for comparison purpose only.

16 N^{10}-Isobutylflavin **3** was used for these studies due to the low solubility of **1** in EtOH.

17 M. Greaves and V. Rotello, *J. Am. Chem. Soc.*, 1997, **119**, 10 569.

18 At the concentrations of flavin **1** used in these sol-gel experiments, there is no deviation from ideal fluorescence dependence on concentration. This indicates that there are no flavin–flavin interactions occurring, demonstrating site isolation of the flavin species.

Communication 8/07317A

1,8-Diazabicyclo[6.6.6]eicosa-4,11,17-triyne: a flexible cage for protons, copper(I) and silver(I)

Andreas Kunze, Rolf Gleiter* and Frank Rominger

Organisch-Chemisches Institut der Universität Heidelberg, Im Neuenheimer Feld 270, D-69120 Heidelberg, Germany. E-mail: rolf.gleiter@urz.uni-heidelberg.de

Received (in Liverpool, UK) 16th October 1998, Accepted 30th November 1998

X-Ray structure analysis of the diprotonated cage of 3 and its silver(I) and copper(I) complexes reveals in all three cases the *in,in* conformation and a significant shortening of the intrabridgehead distance from 5.05 Å in 3 to 4.85 Å for 3·2H$^+$, 4.23 Å for 3·Cu$^+$ and 4.61 Å for 3·Ag$^+$.

Investigations of bicyclic compounds with nitrogen atoms at the bridgehead positions prove that mono- and di-protonation depends on the intrabridgehead distance and on the conformation(s) at the nitrogen atoms.[1] In the case of 1,6-diazabicyclo-[4.4.4]tetradecane **1**, where the nitrogen atoms adopt the *in,in*

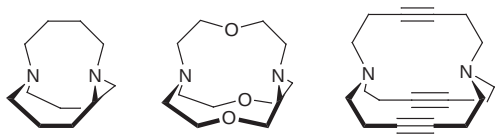

1 **2** **3**

conformation,[2] monoprotonation yields a very stable species due to a very strong intramolecular hydrogen bond between the two bridgehead positions,[2] rendering diprotonation rather difficult.[3] For the [1.1.1]cryptand **2**,[4–6] which also shows the *in,in* conformation, inside protonation of both nitrogens has been reported. This finding can be traced back to the larger N···N distance in **2** [3.88(2) Å][5] as against in **1** [2.806(3) Å].[2] In **2**·2H$^+$ the N···N distance was found to be enlarged to 3.91(1) Å.[5] Reports on the accommodation of ions other than H$^+$ in bicyclic bridgehead diamines are sparse. For the encapsulation of Li$^+$ in **2**[6] the other functions were held at least partly responsible.

Our recently prepared 1,8-diazabicyclo[6.6.6]eicosa-4,11,17-triyne **3**[7] resembles a stretched **1** and shows an even larger N···N distance [5.049(2) Å] than **2**. However, the steric effects of the bridges, as encountered in **1** and related species, should be reduced due to the linear and rigid triple bonds. Therefore we studied the reactions of **3** with protons and metal ions.

The protonation of **3** with TFA was investigated in $CDCl_3$, CD_3OD and D_2O as solvents.† In $CDCl_3$ 1.5 equiv. of TFA are necessary to generate **3**·H$^+$, while in CD_3OD only 0.5 equiv. are required. Monoprotonation reduces the symmetry of **3** (D_3) to C_3, which yields six signals in the ^{13}C NMR spectrum of **3**·H$^+$. In the ^{1}H NMR spectrum (CD_3OD, 200 MHz) only four lines are found at δ 2.43, 2.79, 3.43 (in a ratio of 2 : 1 : 1) and 7.89 (the proton at the nitrogen atom). Five equivalents of TFA in $CDCl_3$ have to be added to obtain a two-fold protonation of **3**.† The shape of the ^{1}H NMR spectra of **3**·H$^+$ and **3**·2H$^+$ prove that the rapid equilibration between the two enantiomorphic helical conformations found in **3** is still present.

In all cases the protonation equilibrium is achieved instantly after addition of the acid. Even deprotonation succeeds easily with molar amounts of KOH. In **3**·H$^+$ and **3**·2H$^+$ we find a fast intermolecular proton exchange with solvents such as CD_3OD and D_2O. This behaviour is in contrast to the experiences gained from **1** and **2** and can be classified as the reaction of a normal tertiary amine. X-Ray investigations of **3**·2H$^+$ show‡ that both bridgehead hydrogens are inside the cage [Fig. 1(*a*)].

Interestingly, the encapsulation of two protons in the cavity of **3** causes a contraction of the N···N distance by 0.2 Å to 4.845(3) Å (see Table 1) and an increase of the inward pyramidization of the nitrogens by about 3° to *ca.* 112°, which is close to the ideal tetrahedral angle. The torsional angle between the triple bonds is reduced to 42.7(5)°. The distance between the two bridgehead protons in **3**·2H$^+$ amounts to 3.066(3) Å. An intramolecular proton exchange of **3**·H$^+$ in 1,1,2,2-tetrachloro[$^2H_2$]ethane could not be detected up to 130 °C.

Stirring a solution of **3** under argon in CH_2Cl_2 with a small excess of MOTf (M = Cu, Ag) at room temperature for three days leads to 1 : 1 complexes for both metals in almost quantitative yields. The spectroscopic properties of **3**·Cu$^+$ and **3**·Ag$^+$ suggest that the metal is situated in the center of the cage.† NMR and IR studies give no hints of a binding interaction between the metal ion and the surrounding triple bonds, so it can be said that the ligand coordinates mainly with the bridgehead nitrogens, effecting a linear N–M$^+$–N geometry. The structural assignment is supported by X-ray investigations of single crystals of both complexes.‡ It is seen [Fig. 1(*b*), (*c*)] that the metal ion is located in the center of the cage, forcing the bridgehead positions even closer together. **3**·Ag$^+$ displays, like **3**, D_3 symmetry, while **3**·Cu$^+$ reveals C_{3h} symmetry. The N–

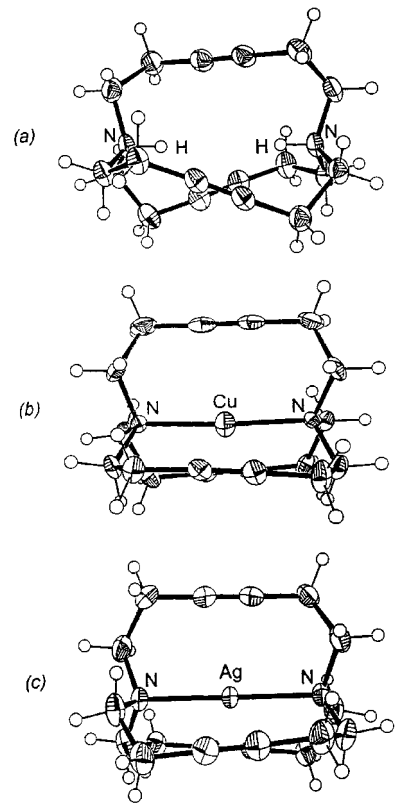

Fig. 1 ORTEP plots (50% ellipsoid probability) of the molecular structures of (*a*) **3**·2H$^+$, (*b*) **3**·Cu$^+$ and (*c*) **3**·Ag$^+$.

Table 1 Most relevant distances and angles for **3**, **3**·2H$^+$, **3**·Cu$^+$ and **3**·Ag$^+$ (standard deviations given in parentheses)

	3[a]	**3**·2H$^+$	**3**·Cu$^+$	**3**·Ag$^+$[b]
N···N/Å	5.049(2)	4.845(3)	4.227(5)	4.614(5) *4.630(5)*
N–M/Å	—	—	2.110(2), 2.118(2)	2.306(3), 2.308(3) *2.313(3), 2.317(3)*
M–X[c]/Å	—	—	2.460(4)–2.576(4)	2.493(4)–2.527(4) *2.498(4)–2.539(4)*
Θ[d] (°)	55.5(3)	42.5(3)–42.9(3)	6.3(3)–7.9(3)	8.2(3) *16.2(3)*
d(C≡C)/Å	1.188(2)	1.192(4)	1.189(6)–1.195(6)	1.194(6)–1.199(6) *1.195(6)–1.204(6)*

[a] Ref. 7. [b] Data in italics refer to the second independent complex cation in the asymmetric unit. [c] M–X is the distance between the metal and the center of the triple bonds. [d] Torsional angle between the triple bonds.

M$^+$–N bond angles for **3**·Cu$^+$ and **3**·Ag$^+$ amount to 176.6(3) and 178.9(3)°, respectively. Relevant data for **3**·Cu$^+$ and **3**·Ag$^+$ are collected in Table 1 and compared with **3** and **3**·2H$^+$.

As a consequence of the shortening of the N···N distance in **3**, the torsion angle between the triple bonds is reduced considerably in **3**·Cu$^+$ and **3**·Ag$^+$. The distances between the centers of the alkyne groups and the metal ions [**3**·Cu$^+$: 2.460(4)–2.576(4), **3**·Ag$^+$: 2.493(4)–2.539(4) Å] are larger than for other alkyne silver or copper complexes [Cu$^+$–center of alkyne : 2.02(1) Å, Ag$^+$–center of alkyne : 2.33(1) Å].[8] In both metal complexes the bridgehead atoms show an ideal tetrahedral conformation. The mean N–Ag$^+$ and N–Cu$^+$ distances [2.311(3) and 2.114(2) Å, respectively] are rather expanded with regard to the values reported for homoleptic two-coordinated silver(I) amine complexes, *e.g.* $Ag(NH_3)_2NO_3$ [2.121(1) Å][9] and comparable complexes of copper(I) (average value: 1.88 Å).[10] Many of the known mononuclear two-coordinated copper(I) complex cations deviate considerably from the ideal linear structure to coordinate further ligands and come up to the preferred four-coordinate tetrahedral geometry. Although in **3**·Cu$^+$ potential ligands (the triple bonds) are within reach, this tendency seems to be effectively blocked due to the extended N–Cu$^+$–N arrangement.

The triflate salts of **3**·Cu$^+$ and **3**·Ag$^+$ are stable to air and not light sensitive. None of the silver(I) halides is obtained by treatment of solutions of **3**·Ag$^+$ TfO$^-$ in CH_2Cl_2 or MeOH with Me_2NH_2Cl, Et_3NHBr and Bu_4NI at room temperature, indicating remarkable stability. The aptitude of **3** as a flexible ligand for further metal ions is currently under investigation.

We thank the Deutsche Forschungsgemeinschaft (SFB 247), the Fonds der Chemischen Industrie, DEGUSSA AG and the BASF Aktiengesellschaft, Ludwigshafen, for financial support.

Notes and references

† *Selected data* for **3**·2H$^+$($CF_3CO_2^-$)$_2$: δ_H(CD_3OD, 200 MHz) 3.01 (t, *J* 5.6, 12H), 3.60 (t, *J* 5.4, 12H), 7.87 (s, 2H); δ_C(CD_3OD, 50.3 MHz) 16.6, 55.5, 81.1, 113.2, 114.1, 118.9, 119.8, 158.6, 159.4, 160.3, 161.0. For **3**·Cu$^+$ TfO$^-$: δ_H(CD_2Cl_2, 300 MHz) 2.63 (s, 24H); δ_C(CH_2Cl_2, 50.3 MHz) 18.9, 53.0, 80.3; Calc. for $C_{18}H_{24}N_2{}^{65}Cu$: 331.1235, found: 331.1241. For **3**·Ag$^+$ TfO$^-$: δ_H(CD_3OD, 500 MHz) 2.64 (s, 12H), 2.69 (s, 12H); δ_C(CD_3OD, 125 MHz) 18.9, 54.1, 79.0; Calc. for $C_{18}H_{24}N_2{}^{107}Ag$: 375.0990, found: 375.0986.

‡ *Crystal data* for **3**·2H$^+$ ($CF_3CO_2^-$·CF_3CO_2H)$_2$: $C_{26}H_{28}F_{12}N_2O_8$, *M* = 724.50, colourless crystals from $CDCl_3$, monoclinic, *a* = 16.0744(1), *b* = 10.2190(2), *c* = 18.9058(3) Å, *β* = 91.5930(1)°, *V* = 3104.35(8) Å^3, ρ_c = 1.55 Mg m^{-3}, *T* = 200(2) K, space group *C*2/*c*, *Z* = 4, *μ*(Mo-K*α*) = 0.16 mm^{-1}, 11183 reflections collected, 2687 independent reflections (R_{int} = 0.0239), R_1 (*F*) = 0.046, wR_2 (F^2) = 0.112. The structure contains two hydrogen-bonded trifluoroacetate dimers as anions for each dication.

For **3**·Cu$^+$ TfO$^-$: $C_{19}H_{24}CuF_3N_2O_3S$, *M* = 481.00, colourless crystals from MeOH, monoclinic, *a* = 11.7163(4), *b* = 7.4458(3), *c* = 23.4107(8) Å, *β* = 99.8520(1)°, *V* = 2012.17(13) Å^3, ρ_c = 1.59 Mg m^{-3}, *T* = 200(2) K, space group $P2_1/n$, *Z* = 4, *μ*(Mo-K*α*) = 1.24 mm^{-1}, 14503 reflections collected, 3478 independent reflections (R_{int} = 0.0291), R_1 (*F*) = 0.029, wR_2 (F^2) = 0.069. The copper atom is refined with a free site occupancy factor (it refines to a partial site occupancy of 0.8), because the copper position is partially occupied by a proton (20% occupancy). 10% of the complex cations are disordered, showing a D_3 symmetry like **3**·Ag$^+$.

For **3**·Ag$^+$ (TfO$^-$·0.25 CH_2Cl_2): $C_{19.25}H_{24.50}AgCl_{0.50}F_3N_2O_3S$, *M* = 546.56, colourless crystals from CH_2Cl_2, triclinic, *a* = 13.4273(2), *b* = 13.9115(3), *c* = 14.0299(3) Å, *α* = 65.5820(1), *β* = 73.2750(1), *γ* = 64.6590(1)°, *V* = 2137.02(7) Å^3, ρ_c = 1.70 Mg m^{-3}, *T* = 200(2) K, space group $P\bar{1}$, *Z* = 4, *μ*(Mo-K*α*) = 1.15 mm^{-1}, 15934 reflections collected, 7079 independent reflections (R_{int} = 0.0200), R_1 (*F*) = 0.032, wR_2 (F^2) = 0.075. Two independent complex cations in the asymmetric unit. The unit cell contains four complex cations, four triflate anions and one disordered CH_2Cl_2 molecule. CCDC 182/1102. Crystallographic data is available as .cif files from the RSC web site, see: http://www.rsc.org/suppdata/cc/1999/171

1 Reviews: R. W. Alder, *Acc. Chem. Res.*, 1983, **16**, 321; *Chem. Rev.*, 1989, **89**, 1215; *Tetrahedron*, 1990, **46**, 683; R. W. Alder and S. P. East, *Chem. Rev.*, 1996, **96**, 2097.
2 R. W. Alder, A. G. Orpen and R. B. Sessions, *J. Chem. Soc., Chem. Commun.*, 1983, 999.
3 R. W. Alder, A. Casson and R. B. Sessions, *J. Am. Chem. Soc.*, 1979, **101**, 3652.
4 J. Cheney, J. P. Kintzinger and J.-M. Lehn, *Nouv. J. Chem.*, 1978, **2**, 411.
5 H. J. Brügge, D. Carboo, K. van Deuten, A. Knöchel, J. Kopf and W. Dreissig, *J. Am. Chem. Soc.*, 1986, **108**, 107.
6 J. Cheney and J. M. Lehn, *J. Chem. Soc., Chem. Commun.*, 1972, 487.
7 V. Wolfart, R. Gleiter, C. Krieger and H. Pritzkow, *Tetrahedron Lett.*, 1998, **39**, 513.
8 R. Gleiter, M. Karcher, D. Kratz, M. C. Ziegler and B. Nuber, *Chem. Ber.*, 1990, 1461.
9 D. M. P. Mingos, J. Yan, S. Menzer and D. J. Williams, *J. Chem. Soc., Dalton Trans.*, 1995, 319.
10 B. J. Hathaway, *Comprehensive Coordination Chemistry*, ed. G. Wilkinson, R. D. Gillard and J. A. McCleverty, Pergamon Press, 1987, vol. 5, p. 551.

Communication 8/08068B

ChemComm

Weak hydrogen bonding between acetylenic groups: the formation of diamondoid nets in the crystal structure of tetrakis(4-ethynylphenyl)methane†

Elena Galoppini*[a] and Richard Gilardi[b]

[a] *Department of Chemistry, Rutgers University, Newark NJ 07102, USA. E-mail: galoppin@andromeda.rutgers.edu*
[b] *Laboratory for the Structure of Matter, The Naval Research Laboratory, Washington, D.C. 20375, USA*

Received (in Columbia, MO, USA) 5th October 1998, Accepted 7th December 1998

The crystal structure of tetrakis(4-ethynylphenyl)methane 1 shows interwoven diamondoid lattices formed by weak hydrogen bonds between the acetylenic groups, while 1,3,5,7-tetrakis(4-ethynylphenyl)adamantane 2 crystallizes in a non-symmetrical network.

Organic crystals or polymers having large and dimensionally-fixed cavities are expected to exhibit unprecedented structural and physical properties.[1] A particularly attractive kind of network with a regular array of cavities can be obtained, in theory, by connecting the four vertices of tetrahedral organic molecules.[1e,2] This mode of assembly has been termed diamondoid due to its resemblance to the lattice structure of diamond.

Tetraphenylmethane and adamantane are useful building blocks for diamondoid networks. We are studying a series of derivatives bearing acetylenic groups on all four vertices. Ethynes are versatile functional groups for connecting building blocks because they possess rigid-rod geometry, complex with metals and undergo coupling and polymerization reactions.[3]

Fortuitously, the crystal structure‡ of the first model compound, tetrakis(4-ethynylphenyl)methane **1**, contained highly symmetric diamondoid networks formed by van der Waals association, or weak hydrogen bonding, between acetylenic groups. Crystal structures reported by others for a series of terminal alkynes show that the acidic C≡CH groups act as hydrogen donors and form close contacts with hydrogen bonding groups and also with π-systems, including ethynyl and phenyl groups.[4] These kinds of interactions possess the properties of weak (1–2.2 Kcal mol^{-1}) hydrogen bonds and are called C(alkyne)H···π hydrogen bonds.[4a]

While numerous examples exist of diamondoid networks formed by strong hydrogen bonding groups, such as carboxylic acids[1e] and pyridones,[1c] or by metal complexes,[1d] only a few involve van der Waals interactions, such as Br···N and Br···Ph.[4a] To the best of our knowledge, the crystal structure of **1** is the first diamondoid network sustained by C≡CH···C≡C close contacts. Interestingly, C≡CH···Ph interactions, often observed in the crystal structures of phenylsubstituted alkynes,[4a] were not observed in **1**.

Compound **1**§ was prepared in two steps and 67% yield from the known tetrabromide **3**[5] (Scheme 1). Compound **1** crystallizes in a body-centered space group, $I\bar{4}$, and molecules sit on unit cell center and corner sites that require S_4 symmetry (Fig. 1). A three-dimensional network is formed by weak hydrogen bonds between the alkynyl groups from four separate molecules that meet (*i.e.* come close) at nodes in the network that are also S_4 in their local symmetry. The molecule at the center of the cell forms linkages only to molecules that are 1.5 unit cells up and down in the *c* axis direction; they, in turn, link to other molecules that are 3.0 *c* axis translations above and below the origin molecule, and in so doing form cages that resemble super-adamantane models, which are outlined in Fig. 2. The super-adamantane cages are distorted, with a cross-cage distance of 21.7 Å (3 unit cell lengths) in the *c* direction, and two equal cross-cage distances of only 18.3 Å perpendicular to the *c* axis. The structural topology mimics closely that of tetrakis(4-bromophenyl)methane,[1a] which crystallizes in the same space group, and has nodes where four bromine atoms approach one another.

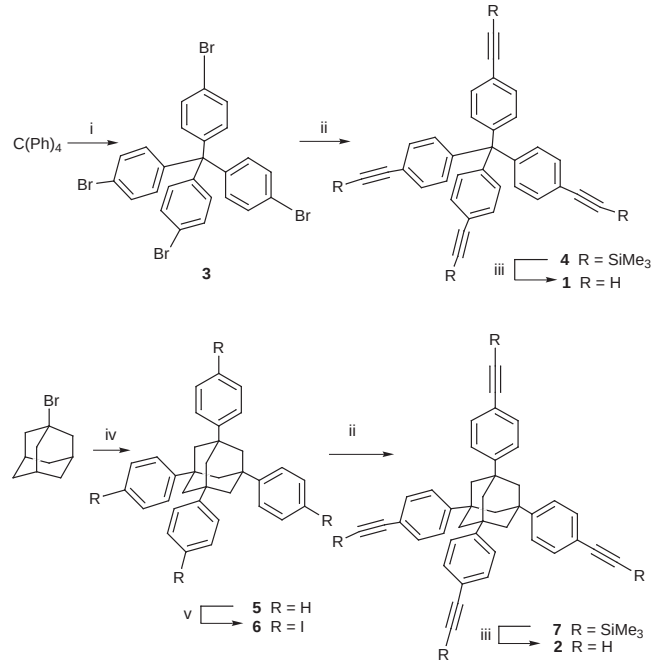

Scheme 1 *Reagents and conditions*: i, Br_2, Fe (ref. 5); ii, Et_3N, CuI, $[Ph_3P]_2PdCl_2$, $Me_3SiC{\equiv}CH$, reflux, 81%; iii, TBAF, MeCN, 85%; iv, $AlCl_3$, C_6H_6, reflux, 50% (ref. 7); v, $(CF_3CO_2)_2IPh$, I_2, $CHCl_3$, 70% (ref. 7).

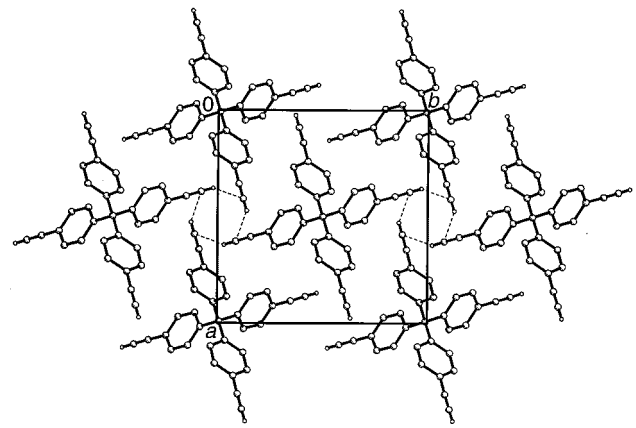

Fig. 1 Crystal structure of **1**. Molecules sit on four-fold S_4 sites at (0, 0, 0) and (0.5, 0.5, 0.5). The quartet-clusters of H-bonds shown about the S_4 sites (0.5, 0, −0.25) and (0.5, 1.0, −0.25) are 5.43 Å (*viz*. 3/4*c*) below the plane passing through the central atom. The C≡CH···C≡C distance is 2.76 Å, and the H-bond makes an angle of 152° with CH and 86° with C≡C.

† Experimental details and extra crystallographic views are available from the RSC web site, see: http://www.rsc.org/suppdata/cc/1999/173/

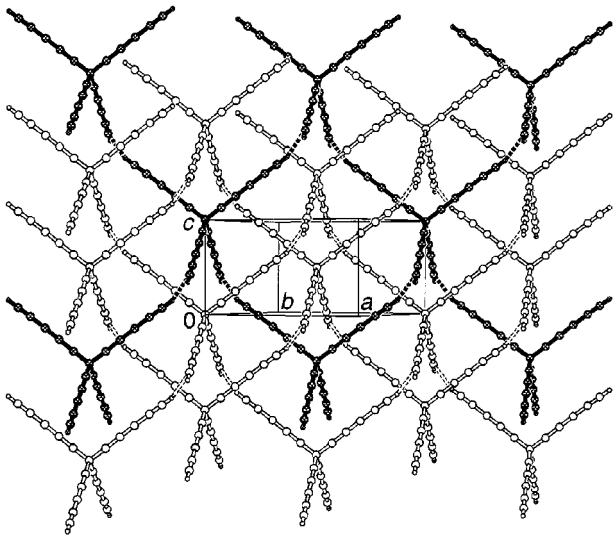

Fig. 2 A schematic view of the three interwoven diamondoid nets, one of which is accented in bold. For clarity, the phenyl groups have been replaced by three 'atoms' in a straight line.

The repetition of a single linked cage by crystal lattice translations produces a three-dimensional network, but origin molecules located at +*c* and +2*c* serve as generators of two more networks which penetrate the holes of the first network, and coexist without (close) interaction. The assembly is thus comprised of three identical interwoven diamondoid networks (Fig. 2). The hydrogen bonded alkyne moieties are neither perpendicular (inter-line angle of 90°) nor antiparallel (180°), but approach at an intermediate inclination, with an inter-linear angle of 110.6° between lines passing through the ethynes of H-bonded neighbors in the cluster. The inter-alkyne hydrogen bond H4B···C4B (2.76 Å), is the only intermolecular distance less than the expected van der Waals' contact (2.90 Å).[6] Hydrogen atom positions were normalized to give linear 1.08 Å C–H bonds before calculating all H-bond parameters. The closest C–H approach is to the terminal C atom; distances to the other alkyne C atom and to the midpoint of the alkyne bond are greater.

To assess whether a diamondoid motif would occur upon changing the tetrahedral core, we prepared 1,3,5,7-tetrakis(4-ethynylphenyl)adamantane **2**§ (Scheme 1.)[7] In the crystal structure‡ of **2**, both C≡CH···C≡C and C≡CH···Ph interactions are present, but the lattice is not diamondoid. Compound **2** crystallizes from benzene–hexane in a monoclinic packing arrangement (*C*2/*c*), with two molecules of **2** and a half-molecule of benzene in the asymmetric unit of the crystal (Fig. 3). Crystals of **2** grown from a few solvents other than benzene also showed asymmetric lattices.

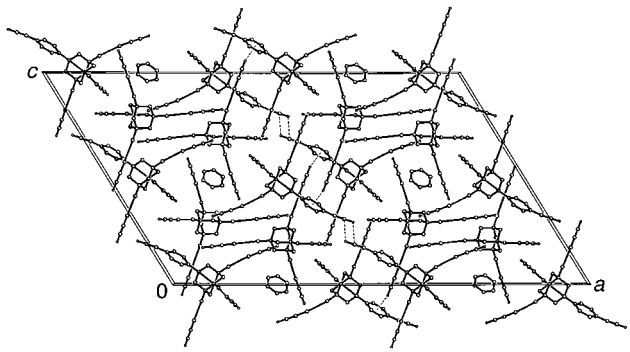

Fig. 3 Crystal structure of **2**. Sixteen molecules of **2** and four benzene molecules occupy each cell; those on the bottom and top faces are shown twice. For clarity, the phenyl groups have been replaced by three 'atoms' in a straight line.

In contrast to **1**, where all alkynes are involved in extended CH··π networks, only two of eight independent alkyne termini of **2** participate in close contacts. One alkyne hydrogen atom points directly at the face of a neighboring near-perpendicular phenyl ring, with CH···C(Ph) approaches of 2.55, 2.60 and 2.75 Å, a typical CH··π interaction mode. The other close contact is an almost antiparallel (side-by-side) approach between two C≡CH termini related by a 2-fold rotation, with a C···H distance of 2.60Å and a C···C distance of 3.17Å (expected[6] van der Waals contacts are 2.9 and 3.4 Å). Similar alkynyl contacts of both types have been reported before.[2a,8]

In summary, the crystal structure of **1** is the first example of a diamondoid packing motif formed by weak hydrogen bonding between acetylenic groups. We are currently investigating hydrogen bonding of **1** and **2** with other compounds and expanding the family of ethynyl-substituted tetrahedral building blocks.

This work was supported by the U.S. National Science Foundation (CHE-9709330) and the Office of Naval Research. We thank Ms Jagruti Patel for synthesizing **3**.

Notes and references

‡ Intensity data for **1** and **2** were measured on a Bruker diffractometer with Cu-Kα radiation (λ = 1.54178 Å) at T = 293 K. Structures were solved by direct methods, aided by program XS, and refined with full-matrix least-squares program XL, from SHELXTL (ref. 9). *Crystal data* for **1**: $C_{33}H_{20}$, M = 416.49, tetragonal space group $I\bar{4}$; a = b = 12.9197(4), c = 7.2357(5) Å, V = 1207.8(1) Å^3, Z = 2, and D(X-ray) = 1.145 mg mm^{-3}. Clear colorless 0.54 × 0.26 × 0.17 mm crystal; 1204 data measured to a 2θ max of 116°. Absorption correction by integration over crystal volume (μ = 0.493 mm^{-1}). Least-squares refinement on F^2 differences; R-factors: R = 0.0367, $wR2$ = 0.0993 for all 848 unique refl. For **2**: $C_{42}H_{32}$·1/4(C_6H_6), M = 556.20, monoclinic space group $C2/c$, a = 48.460(4), b = 10.5467(13), c = 28.759(3) Å, β = 121.896(4)°, V = 12479(2) Å^3, Z = 16, and D(X-ray) = 1.184 mg mm^{-3}. Clear colorless 0.48 × 0.11 × 0.05 mm crystal; 8609 data measured to 2θ = 90°[$<I>$ was measured to be < 2σ(I) at higher angles]. Absorption correction by integration over crystal volume (μ = 0.504 mm^{-1}). Least-squares refinement on F^2 differences varied a total of 785 parameters. R factors were R = 0.0574 for 2985 unique reflections with [I > 2σ(I)], and R = 0.1141, $wR2$ = 0.1376 for all 5051 unique reflections. CCDC 182/1111. The crystallographic data is available in CIF format from the RSC web site, see: http://www.rsc.org/suppdata/cc/1999/173/

§ *Selected data* for **1**: δ_H NMR (500 MHz, $CDCl_3$) 7.36 (d, J 4.5, 8H), 7.32 (d, J 4.5, 8H), 3.04 (s, 4 H, C≡C*H*); δ_C (125 MHz, $CDCl_3$) 146.17, 131.64, 130.72, 120.25, 83.13 (*C*≡CH), 77.60 (C≡C*H*), 64.77 (*C*Ph$_4$). HRMS (FAB): calc. for $C_{33}H_{20}$: 416.1565, found 416.1565. For **2**: δ_H (500 MHz, $CDCl_3$) 7.46 (d, J 8.5, 8H), 7.39 (d, J 8.5, 8H), 3.03 (s, 4 H, C≡C*H*), 2.10 (br s, 12H, CH_2); ^{13}C δ_C (125 MHz, $CDCl_3$) 149.65, 132.23, 124.99, 120.06, 83.43 (*C*≡CH), 76.90 (C≡*C*H), 46.70 [*C*(ad)-Ph], 39.27 (*C*H$_2$) HRMS (FAB): calc. for $C_{42}H_{32}$: 536.2504, found 536.2504.

1 (*a*) D. S. Reddy, D. C. Craig and G. R. Desiraju, *J. Am. Chem. Soc.*, 1996, **118**, 4090 and references cited therein; (*b*) J. S. Moore, *Nature*, 1995, **374**, 495; (*c*) X. Wang, M. Simard and J. D. West, *J. Am. Chem. Soc.*, 1994, **116**, 12119; (*d*) M. Zaworotko, *Chem. Soc. Rev.*, 1994, 283; (*e*) O. Ermer, *J. Am. Chem. Soc.*, 1988, **110**, 3747.
2 (*a*) P. E. Eaton, E. Galoppini and R. Gilardi, *J. Am. Chem. Soc.*, 1994, **116**, 7588; (*b*) K. S. Feldman, C. M. Kraebel, M. Parvez, *J. Am. Chem. Soc.*, 1993, **115**, 3846.
3 P. J. Stang and F. Diederich, *Modern Acetylene Chemistry*, Wiley-VCH, 1995.
4 (*a*) T. Steiner, E. B. Starikov, A. Amado and J. J. C. Teixeira-Dias, *J. Chem. Soc., Perkin Trans. 2*, 1995, 1321; (*b*) M. A. Viswamitra, R. Radhakrishnan, J. Bandekar and G. R. Desiraju, *J. Am. Chem. Soc.*, 1993, **115**, 4868.
5 L. M. Wilson and A. C. Griffin, *J. Mater. Chem.*, 1993, **3**, 991.
6 R. S. Rowland and R. Taylor. *J. Phys. Chem.*, 1996, **100**, 7384.
7 Synthesis of **5** and **6**: V. R. Eichert and L. J. Mathias, *Macromolecules*, 1994, **27**, 7015.
8 H. E. Zimmerman and Z. Zhu, *J. Am. Chem. Soc.*, 1995, **117**, 5245.
9 G. Sheldrick, SHELXTL96, *Acta Crystallogr., Sect. A*, 1990, **46**, 467.

Communication 8/07993E

ChemComm

A novel entry to 5a-carba-hexopyranoses from carbohydrates based on a 6-*exo-dig* radical cyclization: synthesis of 5a-carba-β-D-mannopyranose pentaacetate

Ana M. Gómez,* Gerardo O. Danelón, Eduardo Moreno, Serafín Valverde and J. Cristóbal López*

Instituto de Química Orgánica General (CSIC), Juan de la Cierva 3, 28006 Madrid, Spain.
E-mail: clopez@cc.csic.es

Received (in Cambridge, UK) 12th November 1998, Accepted 24th November 1998

Carbohydrate-derived 2,3:4,6-diacetonides which are homologated at C-1 by reaction with phenyl acetylide undergo a 6-*exo-dig* radical cyclization, from a radical located at C-5, to yield highly functionalized cyclohexanes that are correlated with carba-sugars.

The term 'carba-sugar' is currently used to describe monosaccharide analogs having a methylene group instead of the ring oxygen atom.[1] Carba-sugars derived from hexopyranoses, 'carba-pyranoses' (*e.g.* **1**), were first prepared more than three decades ago by McCasland and co-workers[2] prior to their isolation from natural sources as components of important antibiotics.[3] Many of these substances, owing to their close structural resemblance to carbohydrates, are endowed with an interesting range of biological activities[4] which has triggered the development of different synthetic approaches for their preparation.[1,5,6] However, to the best of our knowledge only one synthetic approach involving radical ring closure[7] leading to 6-deoxy-5a-carba-pyranosides has been reported.[8] A very recent report by Maudru, Singh and Wightman[9] on the synthesis of carba-pyranoses by 6-*exo-dig* radical cyclization of carbohydrate derived alkynes prompts us to disclose our own results in this area.

As a continuation of our interest in the synthesis of highly functionalized carbocycles[10] from carbohydrates,[11] we turned our attention to the preparation of 5a-carba-hexopyranosides by radical ring closure of carbohydrate derived alkynes. Here we report some preliminary results which have resulted on the synthesis of 5a-carba-β-D-mannose pentaacetate **13**. Our general approach, outlined in Scheme 1 for D-mannose, correlates retrosynthetically the methylene group of the carba-pyranoside (*e.g.* **1**) with an exocyclic double bond in a highly functionalized cyclohexane (*e.g.* **2**). The latter could thus be obtained by a 6-*exo-dig* radical cyclization of a carbohydrate derived alkyne (*e.g.* **3**) easily derived from a pyranose 2,3:4,6-diacetonide derivative (*e.g.* **4**).

Accordingly mannose diacetonide **4** (Scheme 2), prepared in one single step from D-mannose by kinetic acetonation,[12] was treated with lithium phenylacetylide to yield, as a very major isomer, diol **5** in 65% isolated yield.† Chemoselective protection of the prop-2-ynylic hydroxy group could be accomplished by the use of either ethyl chloroformate (**6a**, 60%)[13] or TBDMSCl (**6b**, 65%).‡ The hydroxy group at C-5 in **6a**, or **6b**, was next treated with phenyl chlorothioformate[14] to furnish derivatives **7a** (85%) and **7b** (80%), respectively, which upon reaction with Bu_3SnH and AIBN[15] (toluene, 90 °C, 0.02 M) afforded tricyclic derivatives **8**§ and **9**§ in 95% combined yield. The synthetic scheme was next continued with compound **8b**§ [two isomers: δ 2.89 (ddt, $J_{4,5}$ = $J_{5,6ax}$ = 10.8 Hz, $J_{5,6eq}$ = 4.5 Hz, $J_{5,Holef}$ = 2.8 Hz, H-5 one isomer), 2.48 (ddt, $J_{4,5}$ = $J_{5,6ax}$ = 11.1 Hz, $J_{5,6eq}$ = 5.1 Hz, $J_{5,Holef}$ = 2.3 Hz, H-5 other isomer)]. Accordingly, after a change in the protecting group at

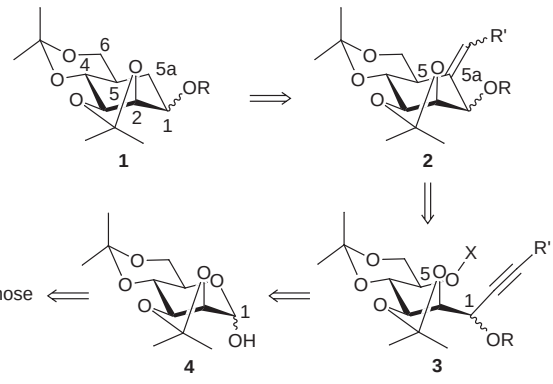

Scheme 1

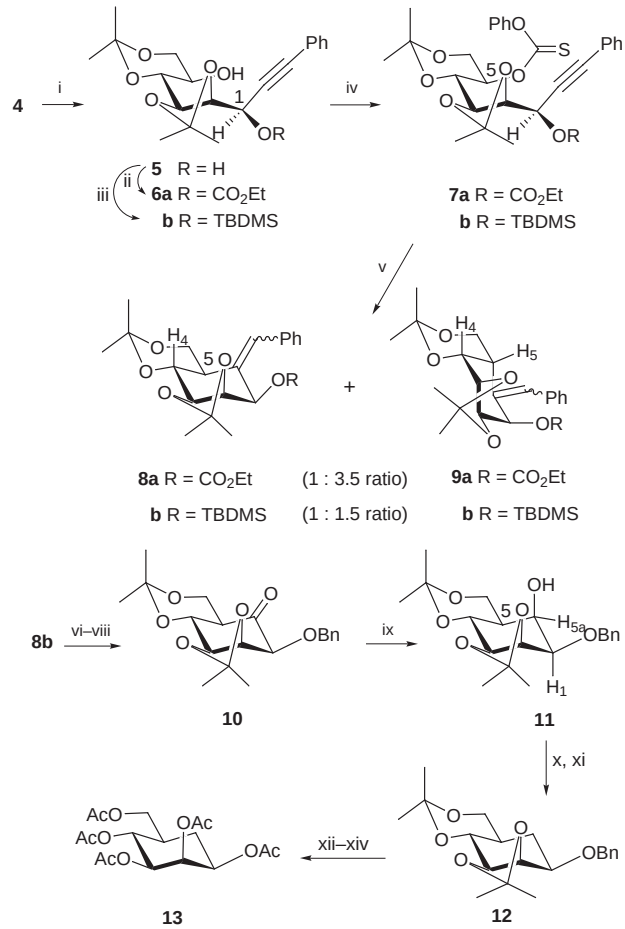

Scheme 2 *Reagents and conditions*: i, PhC≡CLi, THF, −78 °C; ii, $ClCO_2Et$, Py, CH_2Cl_2, 0 °C; iii, TBDMSCl, Et_3N, DMAP, CH_2Cl_2; iv, ClC(S)OPh, Py, MeCN, 85 °C, 1 h; v, Bu_3SnH, AIBN, toluene (0.02 M), 90 °C; vi, TBAF, THF; vii, HNa, Bu_4NI, BnBr; viii, O_3, MeOH–CH_2Cl_2 (1:1), −78 °C, then Me_2S; ix, BH_3·SMe_2, THF; x, HNa, CS_2, MeI; xi, Bu_3SnH, AIBN, toluene, 90 °C; xii, H_2, Pd/C, MeOH; xiii, AcOH–THF–H_2O (4:2:1), 60 °C; xiv, Ac_2O, Py.

C-1 in **8b** (OTBDMS→OBn), ozonolysis was carried out to yield ketone **10**, which upon reduction ($BH_3 \cdot SMe_2$) gave, in a stereoselective manner, the highly functionalized cyclohexane **11** ($J_{5a,1}$ = 3.8 Hz) (75%, three steps). The hydroxy function at C-5a was deoxygenated under radical conditions, *via* its xanthate,[14,15] to afford 5a-carba-D-mannopyranoside derivative **12** (85%, two steps). Hydrolysis of the acetals followed by hydrogenation and acetylation gave 5a-carba-β-D-mannose pentaacetate **13**[16]¶ (87%, three steps).

In our opinion, several aspects of the synthetic scheme deserve further comment: (i) the choice of a 2,3:4,6-diacetonide derivative has reduced the protecting group manipulations in the synthetic scheme to a minimum; (ii) the selection of a phenylacetylide as the radical acceptor was made on the basis of the beneficial effects of the phenyl group in alkyne cyclizations;[17,18] (iii) unlike other approaches to carba-sugars from carbohydrates,[8,9] in this synthetic scheme an hexose is correlated with its corresponding carba-pyranoside; (iv) the present method permits access to fully functionalized cyclohexanes (*e.g.* **11**) of potential interest in the synthesis of biologically active compounds;[4] (v) by changing the protecting group of the hydroxy function α to the radical acceptor some stereocontrol has been attained in the cyclization reaction in favor of the isomer with *trans* 6,6-ring fusion[19] (**8**, Scheme 2); (vi) similar chemistry carried out on **9a** or **9b** would allow access to 5a-carba-α-L-gulopyranose.

In conclusion we have disclosed a novel entry into functionalized cyclohexane derivatives and carba-sugars from monosaccharides by 6-*exo-dig* cyclization of alk-6-ynyl radicals. Our approach complements the one recently described by Maudru *et al*.[9] in the sense that it allows for functionalization at all positions of the cyclohexane ring. The application of this synthetic scheme to other pyranose derived diacetonides is currently under study.

This research was supported with funds from the Dirección General de Enseñanza Superior (grants: PB96-0822 and PB97-1244). A. M. G. thanks the Consejo Superior de Investigaciones Científicas for financial support. G. O. D. thanks the Agencía Española de Cooperacion Internacional for a MUTIS scholarship.

Notes and references

† Compound **5** was the major isomer observed in the crude reaction mixture and could be easily separated by chromatography. The stereochemistry at C-1 was probed at a later stage on the synthesis. The corresponding epimer at C-1 was also observed (> 4:1 ratio) together with some isomeric 2,3:5,6-diacetonides (^{13}C NMR).

‡ Compounds resulting from the reaction of both hydroxy groups were always present, in yields ranging from 10–15%, and could be easily separated by chromatography.

§ Compounds **8a** and **8b** existed as two isomers (*ca.* 1:1 ratio), corresponding to the orientation of the phenyl group in the exocyclic double bond. Conversely, only one isomer at the phenyl group was observed for the *cis*-fused products **9a** and **9b**.

¶ The spectral properties (^1H NMR, C_6D_6, 400 MHz) were in accord with those reported in the literature (ref. 16): $[\alpha]_D$ +2.0 (*c* 0.6, $CHCl_3$), lit.,[16a] +2.9 (*c* 1.1, $CHCl_3$); lit.,[16b] +2.53 (*c* 1.67, $CHCl_3$); lit.,[16c] +2.9 (*c* 1.28, $CHCl_3$).

1 T. Suami and S. Ogawa, *Adv. Carbohydr. Chem. Biochem.*, 1990, **48**, 21.
2 G. E. McCasland, S. Furuta and L. J. Durham, *J. Org. Chem.*, 1966, **31**, 1516; 1968, **33**, 2835; 1968, **33**, 2841.
3 T. Iwasa, H. Yamamoto and M. Shibata, *J. Antibiot.*, 1970, **32**, 595; T. W. Miller, B. H. Arison and G. Albers-Schonberg, *Biotechnol. Bioeng.*, 1973, **15**, 1075.
4 S. Ogawa, in *Carbohydrate Mimics*: *Concepts and Methods*, ed. Y. Chapleur, Wiley-VCH, Weinheim, 1998, p. 87; S. Ogawa, in *Carbohydrates in Drug Design*, ed. Z. J. Witczak and K. A. Nieforth, Marcel Dekker, New York, 1997, p. 433; T. Suami *Top. Curr. Chem.*, 1990, **154**, 257 and references cited therein.
5 S. Ogawa, in *Studies in Natural Products Chemistry*, ed. A-U Rahman, Elsevier Science, 1993, vol. 13, p. 187; T. Suami, *Pure Appl. Chem.*, 1987, **59**, 1509.
6 A. V. R. L. Sudha and M. Nagarajan, *Chem. Commun.*, 1998, 925; R. Angelaud and Y. Landais, *Tetrahedron Lett.*, 1997, **38**, 8841; R. Verduyn, S. H. van Leeuwen, G. A. van der Marel and J. H. van Boom, *Recl. Trav. Chim. Pays-Bas*, 1996, **115**, 67; H. A. J. Carless and S. S. Malik, *J. Chem. Soc., Chem. Commun.*, 1995, 2447; D. A. Entwistle and T. Hudlicky, *Tetrahedron Lett.*, 1995, **36**, 2591; L. Pingli and M. Vandewalle, *Synlett*, 1994, 228; M. Yoshikawa, N. Murakami, Y. Yokokawa, Y. Inoue, Y. Kuroda and I. Kitagawa, *Tetrahedron*, 1994, **50**, 9619; D. S. Larsen, N. S. Trotter and R. J. Stoodley, *Tetrahedron Lett.*, 1993, **34**, 8151; T. K. M. Shing, Y-X Cui and Y. Tang, *Tetrahedron*, 1992, **48**, 2349; J. L. Aceña, O. Arjona, R. Fernández de la Pradilla, J. Plumet and A. Viso, *J. Org. Chem.*, 1992, **57**, 1945; S. V. Ley and L. L. Yeung, *Synlett*, 1992, 291; S. Cai, M. R. Stroud, S. Hakomori and T. Toyokuni, *J. Org. Chem.*, 1992, **57**, 6693; R. Blattner and R. J. Ferrier, *J. Chem. Soc., Chem. Commun.*, 1987, 1008.
7 W. B. Motherwell and D. Crich, *Free Radical Chain Reactions in Organic Synthesis*, Academic Press, London, 1992; D. P. Curran, *Synthesis* 1989, 417; D. P. Curran, *Synthesis* 1989, 489.
8 H. Redlich, W. Sudau, A. K. Szardenings and R. Vollerthun, *Carbohyr. Res.*, 1992, **226**, 57.
9 E. Maudru, G. Singh and R. H. Wightman, *Chem. Commun.*, 1998, 1505.
10 R. J. Ferrier and S. Middleton, *Chem. Rev.*, 1993, **93**, 2779; B. Fraser-Reid and R Tsang, *Strategies and Tactics in Organic Synthesis*, Academic Press, New York, 1989, vol. 2, p. 123.
11 A. M. Gómez, S. Mantecón, S. Valverde and J. C. López, *J. Org. Chem.*, 1997, **62**, 6612; J. C. López, A. M. Gómez and S. Valverde, *J. Chem. Soc., Chem. Commun.*, 1992, 613.
12 J. Gelas and D. Horton, *Carbohydr. Res.*, 1978, **67**, 371.
13 J. J. Gaudino and C. S. Wilcox, *J. Am. Chem. Soc.*, 1990, **112**, 4374.
14 M. J. Robins, J. S. Wilson and F. Hansske, *J. Am. Chem. Soc.*, 1983, **105**, 4059.
15 D. H. R. Barton and S. W. McCombie, *J. Chem. Soc., Perkin Trans. 1*, 1975, 1574.
16 (*a*) L. Pingli and M. Vandewalle, *Tetrahedron*, 1994, **50**, 7061; (*b*) T. Takahashi, H. Kotsubo, T. Namiki and T. Koizumi, *J. Chem. Soc., Perkin Trans. 1*, 1990, 3065; (*c*) H. Paulsen, W. von Deyn and W. Röben, *Liebigs Ann. Chem.*, 1984, 433.
17 D. L. J. Clive, P. L. Beaulieu and L. Set, *J. Org. Chem.*, 1984, **49**, 1314.
18 R. E. McDevitt and B. Fraser-Reid, *J. Org. Chem.*, 1994, **59**, 3250.
19 D. P. Curran, N. A. Porter and B. Giese, *Stereochemistry of Radical Reactions*, VCH, Weinheim, 1996, p. 53.

Communication 8/08848I

ChemComm

Structural isomers of $M(dca)_2$ molecule-based magnets. Crystal structure of tetrahedrally coordinated sheet-like β-$Zn(dca)_2$ and β-$Co/Zn(dca)_2$, and the octahedrally coordinated rutile-like α-$Co(dca)_2$, where dca^- = dicyanamide, $N(CN)_2^-$, and magnetism of β-$Co(dca)_2$

Paul Jensen, Stuart R. Batten, Gary D. Fallon, Boujemaa Moubaraki, Keith S. Murray* and David J. Price

Department of Chemistry, Monash University, Clayton, Victoria 3168, Australia.
E-mail: keith.s.murray@sci.monash.edu.au

Received (in Cambridge, UK) 10th November 1998, Accepted 15th December 1998

β-$Zn(dca)_2$ and 0.12% Co(II) doped β-$Zn(dca)_2$ contain tetrahedrally coordinated metal ions within a corrugated sheet network structure [dca = dicyanamide, $N(CN)_2^-$], β-$Co(dca)_2$ is a spin-canted antiferromagnet (T_N = 9 K), while the rutile-like octahedral α-form is a ferromagnet.

We have recently described an important new class of molecule-based magnets of type $M(dca)_2$ which possess a rutile-like single net structure.[1] In this α-structural type, the metal ions are octahedrally coordinated to six dicyanamide (dca) ligands *via* the nitrile and amide N-donor atoms, each dca therefore being a 3-connector. The Co(II) and Ni(II) compounds are ferromagnets, with T_c = 9 and 20 K respectively, while the Cu(II) compound is a near-paramagnet, with Jahn–Teller distorted Cu–N(amide) bond lengths. α-$Mn(dca)_2$ and α-$Fe(dca)_2$ are spin-canted antiferromagnets with T_N values of 16 and 19 K, respectively.[2] Kepert and Kurmoo[3] and Miller and Epstein and coworkers[4] have subsequently reported some of the same α-type compounds. Here, we describe a structural isomer of the β-type in which the metal ions are each tetrahedrally coordinated to four dca ligands *via* nitrile N-donor atoms to form an infinite sheet structure. This structure has been refined for colourless crystals of β-$Zn(dca)_2$ and for deep blue crystals of Co(II) doped β-$Zn(dca)_2$. As indicated earlier by Köhler,[5] the blue β-$Co(dca)_2$ phase can be prepared by removal of pyridine from $Co(dca)_2(pyridine)_2$. We report here antiferromagnetic coupling and magnetic order in β-$Co(dca)_2$ prepared in this way and compare these to the magnetic behaviour observed in the ferromagnetic α-isomer.

β-$Zn(dca)_2$ was prepared by reaction of $Zn(NO_3)_2{\cdot}6H_2O$ with sodium dicyanamide in water in a 1:2 mole ratio. Colourless crystals were obtained by slowly diffusing the reagents together. The 0.12% Co(II) doped crystals were prepared by mixing hot aqueous solutions of $Zn(NO_3)_2{\cdot}6H_2O$ and $Co(NO_3)_2{\cdot}6H_2O$ with one of Na(dca). Deep blue crystals formed from the pink solution. Doubling of some of the C–N bands from coordinated dca occurs in the IR spectrum probably because of the presence of two structurally distinct dca ligands in $Zn(dca)_2$ and in $Co/Zn(dca)_2$.†

The structures of α-$Co(dca)_2$, β-$Zn(dca)_2$ and 0.12% β-$Co/Zn(dca)_2$ were solved by single-crystal X-ray crystallography. The structure of α-$Co(dca)_2$ is isomorphous with the other members of the α-$M(dca)_2$ compounds discussed above.[1–4] It possesses a rutile-like structure with octahedral cobalt ions and three-connecting dca ligands [Co-N(nitrile) 2.092(2) Å, Co–N(amide) 2.150(3) Å].‡ These values are obviously much closer together than in the Jahn–Teller distorted Cu [1.975(1) and 2.478(2) Å, respectively],[1] and are shorter than those found in Mn [2.189(1) and 2.290(2) Å].[2] In all three structures the metal–amide bonds are longer than the metal–nitrile bonds.

As both β-isomer structures are isomorphous, we will discuss only the $Zn(dca)_2$ structure in detail.‡ The structure consists of tetrahedral Zn atoms [N–Zn–N 108.05(9)–111.9(2)°]bridged by two-connecting dicyanamide ligands [Zn–N 1.958(4), 1.936(4) and 1.960(3) Å]. The kinked nature of the dca bridge, aided by some bending at the coordinating nitrogen donors [C–N–Zn 155.3(3), 165.4(4) and 171.9(4)°], allows the tetrahedral ions to be bridged into a corrugated square-grid sheet structure (Fig. 1). The sheets stack in the direction of the *c* axis and are interdigitated. As a result, the shortest Zn···Zn distances (4.447 Å) are between sheets, with the intrasheet Zn···Zn distances (*via* the dca bridges) being 7.584 and 7.606 Å. The structure of the 3D rutile-like α isomer is obviously markedly different to the 2D sheet structure for the β isomer described here. The former contains octahedral metal ions and three-connecting dca ligands, while the latter contains tetrahedral metal ions and two-connecting dca ligands (*i.e.* the amide nitrogens do not coordinate).

The structures described above of β-$Zn(dca)_2$ were determined at 123 K. The room temperature structure was also determined,‡ and found to possess a different space group (*Cmcm*, *vs Pnma* at 123 K). Further investigation showed a reversible phase change occurring between 210 and 220 K. A second phase change occurred at 120 K which resulted in fragmentation of the crystal. The topology and connectivity of the structure in the room temperature phase is the same as in the 123 K phase. The phase change arises due to ordering of one of the two crystallographically unique dca ligands (dca1). At room temperature dca1 is disordered over two positions, which are related by a mirror plane. The ligand 'leans over', with its mean plane making an angle of 16.6° to this mirror plane (on which lie the metal atoms and nitrile nitrogen atoms of dca1). The mirror plane arises because the lean of dca1 is disordered equally between the two alternative directions. In the 123 K structure, however, this ligand becomes ordered, with all the dca1 ligands in a sheet tilting in the one direction only, and the mirror plane symmetry is lost.

The deep blue β-$Co(dca)_2$ was produced by depyridination under vacuum of $Co(dca)_2(pyridine)_2$.[5] Although the powder was largely amorphous and diffracted extremely weakly, the pattern was suggestive of being isomorphous with β-$Zn(dca)_2$. The visible spectra (diffuse reflectance) of neat β-$Co(dca)_2$ and of Co doped $Zn(dca)_2$ are identical thus indicating that the tetrahedral coordination geometry around Co(II) is the same; λ_{max}/nm 602, 565(sh), 483w (sh). Upon exposure to the

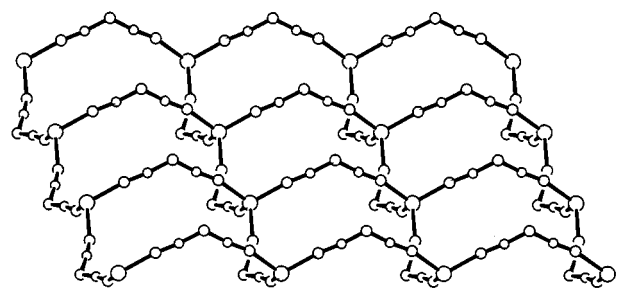

Fig. 1 The puckered, square-grid sheets of β-$Zn(dca)_2$.

atmosphere, the powder turns from blue to pink. Again, although the diffraction was very weak, the X-ray powder diffraction pattern was suggestive of the presence of the rutile-like α-Co(dca)$_2$. The diffuse reflectance visible spectra was also now reminiscent of the α phase; λ_{max}/nm = 1131(br), 510, 481.

The magnetic moment, per mol of Co, of the 0.12% Co(II) doped Zn(dca)$_2$ sample remains constant at 4.6 μ_B over the range 300–15 K. This was anticipated for a magnetically dilute tetrahedral d^7 ion having a $^4A_2$ ground state influenced by spin–orbit coupling. Together with the lack of any observed long-range order under small applied-fields, the data are consistent with random doping of the diamagnetic Zn(II) sites by Co(II), much like traditional doping into zinc oxide hosts. In contrast, the magnetic properties of neat β-Co(dca)$_2$ are indicative of antiferromagnetic coupling and a magnetic phase change occurring at *ca*. 9 K, due to spin canted antiferromagnetism (weak ferromagnetism). This contrasts markedly with α-Co(dca)$_2$ which displays a ferromagnetic transition, also at 9 K.[1] In a magnetic field of 1 T, the effective magnetic moment, per Co, of the β-isomer decreases a little from 4.55 μ_B at 300 K to 4.3 μ_B at 22 K before increasing sharply to reach a maximum of 4.45 μ_B, then decreasing rapidly towards 2.39 μ_B at 2 K (Fig. 2). The corresponding χ values show small deviation from Curie-Weiss behaviour above 25 K with $\theta = -4.5$ K [*cf.* α-Co(dca)$_2$, $\theta = +6.1$ K]. Long range magnetic order is clearly evident in the magnetisation data measured in small applied fields. It can be seen in Fig. 2 that the field-cooled (FCM) and zero-field cooled (ZFCM) magnetisation values increase rapidly below 9.5 K under fields of 10, 50 and 100 Oe. The temperature at which the FCM and ZFCM data diverge changes a little with field *viz.* 9.0 K (10 Oe), 8.83 K (50 Oe), 8.65 K (100 Oe). The ZFCM data likewise pass through a field-dependant maximum.

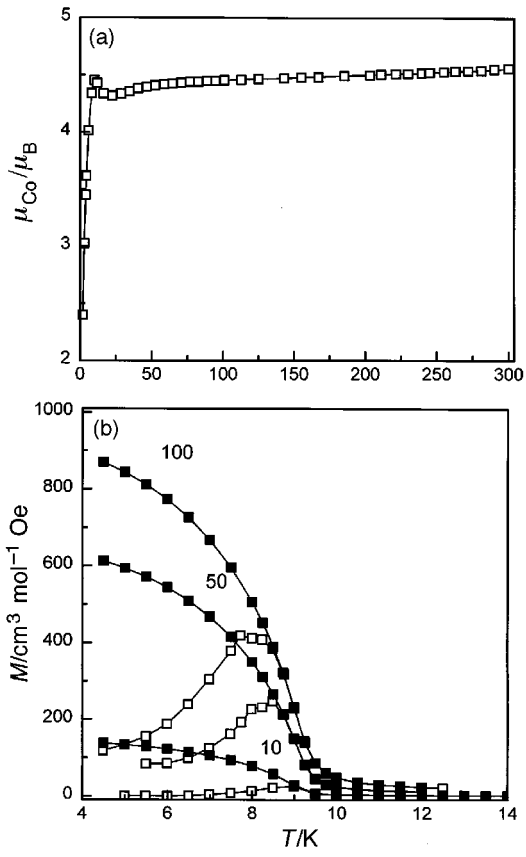

Fig. 2 (a) Plot of μ(per Co) *vs* temperature for β-Co(dca)$_2$ in a field of 1 T. (b) Plots of field-cooled (FCM) (■) and zero-field cooled (ZFCM) (□) magnetisation *vs* temperature for β-Co(dca)$_2$ in fields of 10, 50 and 100 Oe.

A powder sample of β-Co(dca)$_2$ displays hysteresis in magnetisation with a coercive field of 538 Oe and remanent magnetisation of 0.22 $N\mu_B$ at 2 K. High field magnetisation data in fields of up to 5 T show small diversions from linearity without reaching saturation and with a small value of only 2.37 $N\mu_B$ at 5 T. This contrasts markedly with the rapid saturation behaviour noted in the ferromagnetic α-isomer and is indicative of antiferromagnetic coupling. The nature of the ordered state is therefore one of a spin-canted antiferromagnet as was also found in α-Mn(dca)$_2$ and α-Fe(dca)$_2$. Such ordering is becoming increasingly common in homometallic molecular magnets.[2–4,6]

This work was supported by a grant (to K. S. M.) and a fellowship (to S. R. B.) from the Australian Research Council. The help of Mr R. Mackie, Physics Department, Monash University with the powder XRD measurements is gratefully acknowledged.

Notes and references

† IR (cm^{-1}, Nujol) Zn(dca)$_2$: ν_{as}(C≡N) 2298m, 2280m; ν_s(C≡N) 2209s; ν_{as}(C–N) 1417(sh), 1408s, ν_s(C–N) 964 vw.

‡ *Crystal data* for α-Co(dca)$_2$: C_4N_6Co, M = 191.02, orthorhombic, *Pnnm* (no. 58), a = 7.0433(2), b = 5.9748(3), c = 7.4039(4) Å, U = 311.57(2) Å^3, T = 123 K, Z = 2, F(000) = 186, D_c = 2.036 g cm^{-3}, μ(Mo-Kα) = 26.81 cm^{-1}, pink acicular crystal (0.10 × 0.03 × 0.03 mm), 4200 total reflections ($2\theta_{max}$ = 56.5°), 473 independent reflections (R_{int} = 0.047), 336 observed [$I > 3\sigma(I)$], refined against F, 29 parameters, R_1 [$I > 3\sigma(I)$] = 0.0281, R_w = 0.0285, goodness of fit = 2.57.

For β-Zn(dca)$_2$ at 123 K: C_4N_6Zn, M = 197.46, orthorhombic, *Pnma* (no. 62), a = 7.6060(3), b = 7.5844(3), c = 11.8422(4) Å, U = 683.14(8) Å^3, Z = 4, F(000) = 384, D_c = 1.920 g cm^{-3}, μ(Mo-Kα) = 35.28 cm^{-1}, colourless tablet (0.20 × 0.16 × 0.08 mm), 9157 total reflections ($2\theta_{max}$ = 56.4°), 1019 independent reflections (R_{int} = 0.048), 700 observed [$I > 3\sigma(I)$], refined against F, 61 parameters, R_1 [$I > 3\sigma(I)$] = 0.0225, R_w = 0.0226, goodness of fit = 2.24.

For 0.12% Co doped β-Zn(dca)$_2$: structure refined assuming 100% Zn, C_4N_6Zn, M = 197.46, orthorhombic, *Pnma* (no. 62), a = 7.6070(3), b = 7.5828(4), c = 11.8468(6) Å, U = 683.35(10) Å^3, T = 123 K, Z = 4, F(000) = 384, D_c = 1.919 g cm^{-3}, μ(Mo-Kα) = 35.27 cm^{-1}, blue tablet (0.20 × 0.20 × 0.07 mm), 8876 total reflections ($2\theta_{max}$ = 56.5°), 1020 independent reflections (R_{int} = 0.059), 667 observed [$I > 3\sigma(I)$], refined against F, 61 parameters, R_1 [$I > 3\sigma(I)$] = 0.0273, R_w = 0.0244, goodness of fit = 2.25.

For β-Zn(dca)$_2$ at 293 K: orthorhombic, *Cmcm* (no. 63), a = 7.5526(3), b = 12.2167(8), c = 7.5882(4) Å, U = 700.15(7) Å^3, Z = 4, F(000) = 384, D_c = 1.873 g cm^{-3}, μ(Mo-Kα) = 34.41 cm^{-1}, colourless prism (0.3 × 0.2 × 0.1 mm), 2534 total reflections ($2\theta_{max}$ = 60°), 567 independent reflections (R_{int} = 0.036), 512 observed [$I > 2\sigma(I)$], refined against F^2, 39 parameters, R_1 [$I > 2\sigma(I)$] = 0.0390, wR_2 (all data) = 0.1246, goodness of fit = 1.217.

CCDC 182/1120. See http://www.rsc.org/supp.data/cc/1999/177/for crystallographic files in .cif format.

1 S. R. Batten, P. Jensen, B. Moubaraki, K. S. Murray and R. Robson, *Chem. Commun.*, 1998, 439.
2 K. S. Murray, S. R. Batten, B. Moubaraki, D. J. Price and R. Robson, *Mol. Cryst. Liq. Cryst.*, in press.
3 C. Kepert and M. Kurmoo, *Mol. Cryst. Liq. Cryst.*, in press.
4 C. R. Kmety, J. L. Manson, Q. Huang, J. W. Lynn, R. W. Erwin, J. S. Miller and A. J. Epstein, *Mol. Cryst. Liq. Cryst.*, in press.
5 H. Köhler, *Z. Anorg. Allg. Chem.*, 1964, **331**, 237.
6 A. Escuer, R. Vicente, M. A. S. Goher and F. A. Mautner, *Inorg. Chem.*, 1997, **36**, 3440.

Communication 8/08777F

ChemComm

The carbonylation of methyl iodide and methanol to methyl acetate catalysed by palladium and platinum iodides

Jun Yang, Anthony Haynes and Peter M. Maitlis

The Department of Chemistry, The University of Sheffield, Sheffield, UK S3 7HF. E-mail: P.Maitlis@Sheffield.ac.uk

Received (in Cambridge, UK) 25th November 1998, Accepted 8th December 1998

Palladium(II) salts catalyse the carbonylation of methyl iodide in methanol to methyl acetate (5 atm CO, 140 °C) in the presence of a large excess of iodide, even without amine or phosphine co-ligands; platinum(II) salts show similar reactions but are a little less effective.

The substantial current interest in reactions catalysed by palladium–phosphine or palladium–amine[1,2] complexes prompts us to disclose new data on methanol carbonylation catalysts. We find that palladium(II), in the presence of an excess of iodide, catalyses the carbonylation of methyl iodide in methanol to methyl acetate at 5 atm CO, 140 °C. Under these conditions phosphine or amine co-ligands are not required.

The BP–Monsanto process for making acetic acid, methyl acetate, and/or acetic anhydride from methanol relies in its key (organometallic) steps on the carbonylation of methyl iodide catalysed by a rhodium and iodide system.[3] The *Cativa* process recently developed by BP Chemicals uses a closely related but more effective system based on a promoted iridium/iodide catalyst.[4,5] A number of other catalyst systems have been examined,[6] but because of the economic importance of the process, the search for new catalysts continues.

Although various carbonylation reactions involving palladium complexes have been described, they generally require co-ligands such as amines or phosphines.[7] If they are not present, the process is quickly deactivated with the formation of (inactive) palladium metal.

A palladium catalysed carbonylation of methyl iodide would be expected to comprise a cycle with individual steps similar to those found for rhodium and iridium, and since palladium complexes generally undergo carbonylation, migratory insertion and reductive elimination very easily, the slow rate determining step in the methyl iodide carbonylation cycle is probably the oxidative addition. In rhodium and iridium chemistry this step is enhanced by a more nucleophilic metal centre,[8] which can be achieved for example, by increasing the electron density at the metal with basic ligands. This could account for the reported use of ligands such as bipy in the palladium catalysed carbonylations.

We first investigated methyl iodide carbonylation using chelate N-ligands ('N–N'), including bipyridyl and the very convenient Ar-BIAN ligands [bis(arylimino)acenaphthenes, derived from acenaphthenequinone and an aromatic primary amine, $ArNH_2$, Ar = phenyl, 4-tolyl, *etc.*] which can easily be 'tuned' by changes in the aryl substituents.[2] Reactions related to methanol carbonylation have also been modelled on palladium complexes, for example,[2]

$$[Pd(tmeda)(Me)(OR)] + CO\ (1\ atm,\ 25°C) \xrightarrow{Me_2CO} MeCO_2R + Pd^0\ [tmeda = Me_2NCH_2CH_2NMe_2;\ R = Ph,\ CH(CF_3)_2]$$

but we found no catalytic turnover (< 1 in 16 h) on carbonylating the chelate-iodomethyl complexes, [Pd('N–N')-(Me)(I)] in neat methanol.

However, catalytic reactions occurred in the presence of methyl iodide (Table 1). The complexes [Pd(4-Tol-BIAN)-(Me)(I)], and [Pd(bipy)(Me)(I)], $[Pd(PPh_3)_2Cl_2]$ all gave turnovers in the range 10–20/16 h; the Ar-BIAN ligands were slightly better than bipy, and both were comparable to triphenylphosphine.

Substantial further improvements were achieved on addition of 40–100 equiv. per palladium of either a base or an ionic iodide.† Under our operating conditions the highest turnovers (*ca.* 110/16 h) were found using $[Pd(PPh_3)_2Cl_2]$ and Bu_4NI as additive. Slightly lower turnovers were obtained for other additives such as triethylamine, LiI, and other quaternary ammonium iodides. Higher amounts of a given iodide led to higher turnovers. Addition of small amounts of water (100–500 equiv./Pd) led to decreased turnovers but did not quench the reaction. Separate investigations showed that the role of amines was to generate the quaternary ammonium iodides by reaction with MeI.

When the solution containing $[Pd(PPh_3)_2Cl_2]$ and Bu_4NI was examined by ^{31}P NMR spectroscopy at the end of a catalytic reaction, there was no sign of PPh_3 coordinated to palladium. The only signal (δ 22.2) that could be detected was due to $[PPh_3Me]I$.

Thus the PPh_3 has become detached during the catalysis. To examine whether the ligand plays an important role, we investigated the catalytic behaviour of simple salts of palladium without any amine or phosphine co-ligands. Palladium iodide proved to be an effective catalyst by itself in the presence of excess iodide (but with no other stabilising ligand), giving a typical turnover of *ca.* 75/16 h.

A rather parallel reactivity sequence was provided by platinum. Again here $[PtI_4]^{2-}$ (formed *in situ*) was effective (turnover *ca.* 70/16 h), as were phosphine and amine complexes $[PtL_2Cl_2]$ [L_2 = $(PPh_3)_2$ > 4-Tol-BIAN ≈ bipy, ≈ $\{P(C_6H_{11})_3\}_2$].‡ Again, ^{31}P NMR examination of the catalyst solution using $[Pt(PPh_3)_2Cl_2]$ at the end of the reaction showed

Table 1 Carbonylation of methyl iodide and methanol to methyl acetate promoted by palladium or platinum complexes and anionic iodide[a]

Catalyst	Iodide additive/mmol	Turnover
[Pd(4-Tol-BIAN)(Me)(I)][b]	—	< 1
[Pd(4-Tol-BIAN)(Me)(I)][c]	—	10 ± 2
[Pd(4-Tol-BIAN)(Me)(I)]	—	20 ± 5
$[PdCl_2(PPh_3)_2]$	—	9 ± 2
$[PdCl_2(PPh_3)_2]$	Bu_4NI (0.4) or $(C_5H_{11})_4NI$ (0.4)	110 ± 5
$[PdCl_2(PPh_3)_2]$	LiI (1) or Et_3N (1)	95 ± 10
$[PdCl_2(PPh_3)_2]$	Bu_4NI (0.4) + water (100–500)	60 ± 5
$[PdCl_4]^{2-}$	Bu_4NI (0.5) or LiI (1)	80 ± 5
$[PdI_2]$	LiI (1)	70 ± 5
$[PtCl_2(PPh_3)_2]$	—	9 ± 2
$[PtCl_2(PPh_3)_2]$	Bu_4NI (0.4)	30 ± 5
$[PtI_4]^{2-}$	Bu_4NI (0.5) or LiI (1)	65 ± 5
$[Ni(NO_3)_2]$	Bu_4NI (0.5) or LiI (1)	15 ± 5
$[NiCl_2(PPh_3)_2]$	Bu_4NI (0.4)	15 ± 5

[a] *Conditions*: catalyst (0.01 mmol), methyl iodide (6 mmol, except where indicated) and iodide (as specified), and methanol (50 mmol) in Fisher–Porter tubes operating at a pressure of 5 atm CO, 140 °C, for 16 h. Analysis of the product (methyl acetate) was by GC (PE 8700; 10 m supel-Q-plot column, FID). Total turnover = number of equivalents of methyl acetate produced per equivalent of catalyst. [b] As *a* above but without any methyl iodide. [c] As for *a* above but with 0.6 mmol methyl iodide.

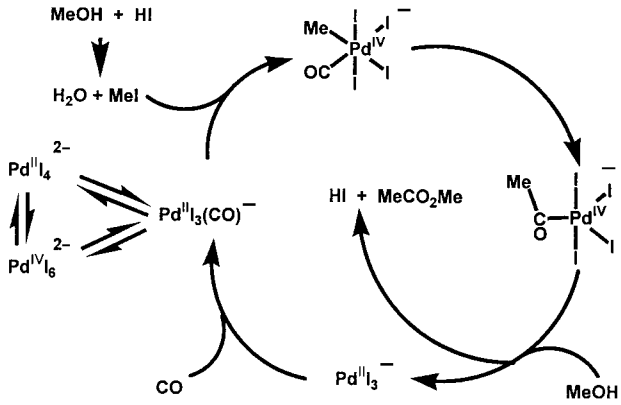

Scheme 1 A possible catalytic cycle for methanol carbonylation based on Pd^{II}/Pd^{IV}.

the presence of only $[PPh_3Me]I$ (δ 22.2). When K_2PtCl_4 + MeOH + MeI + Bu_4NI + CO (5 atm/16 h/140 °C) was used as the catalyst system, a ν(CO) 2063 cm^{-1} was observed in the IR spectrum of the residue once the volatiles had been removed. This is precisely the wavenumber quoted by Calderazzo and coworkers for $[Pt(CO)I_3]^-$,[9] and suggests that this species is involved in our catalytic cycle. No metal carbonyl was detected at the end of our palladium catalysed reactions, but Calderazzo and coworkers noted that $[Pd(CO)I_3]^-$ readily lost all its CO when the pressure was removed, and thus it is not surprising that we did not observe it.

Palladium catalysed methanol carbonylation, in the presence of very large amounts of specific promoters, such as sulfolane, and preferably an amine (*e.g.* 2,2′-bipyridyl) has been described in patents by van Leeuwen (Shell).[10] Those methanol carbonylation reactions required both quite severe conditions (for example, 182 °C/110 bar CO) and the addition of promoters such as bipyridyl; methanol carbonylation in the absence of such promoters was not claimed and platinum salts were specifically excluded from the Shell patents.

There do not appear to have been any reports of platinum catalysed carbonylations to methyl acetate, though the carbonylation of methanol to methyl formate has been noted,[6] and Kozitsyna and Moiseev reported that an unusual diphenylphosphido–platinum species in the presence of BF_3 did catalyse the carbonylation of methyl acetate to acetic anhydride.[11]

Nickel in the presence of iodide has long been known to catalyse methanol carbonylation, but only under drastic conditions (200–300 atm/230–350 °C).[12] We have tried nickel catalysts under our conditions and find activity but at quite a low level in the presence of 50–100 equiv. of iodide.

In summary, we have shown that, in the presence of excess iodide, palladium and platinum salts catalyse the carbonylation of methyl iodide in methanol to methyl acetate at 5 atm CO, 14 °C. The reactions taking place are best described by,

$$MeI + MeOH + CO \rightarrow MeCO_2Me + HI$$

followed by,

$$HI + MeOH \rightarrow MeI + H_2O$$

Catalytic cycles involving either M^{II}/M^{IV} or M^0/M^{II} (M = Pd, Pt) seem possible and an example of the former is illustrated in Scheme 1. It may be noted that iodide can stabilise Pd^{IV} as in Cs_2PdI_6.[13]

We thank BP Chemicals for support and Dr G. Sunley for carrying out some extra experiments.

Notes and references

† Bromide and chloride were also effective as promoters but less so than iodide.

‡ The ligands do seem to have a (second order) effect on the reaction; for example the tricyclohexylphosphine complexes $[M\{P(C_6H_{11})_3\}_2Cl_2]$ (M = Pd, Pt) are significantly less effective than the corresponding triphenylphosphine complexes. An effect of the counter-cation is also evident. Both these points are currently under investigation.

1 B. L. Shaw, *New J. Chem.*, 1998, 77; B. L. Shaw, S. D. Perera and E. A. Staley, *Chem. Commun.*, 1998, 1361.
2 I. Toth and C. Elsevier, *J. Am. Chem. Soc.*, 1993, **115**, 10 388; G. M. Kapteijn, A. Dervisi, M. J. Verhoef, M. A. F. H. van den Broek, D. M. Grove and G. van Koten, *J. Organomet. Chem.*, 1996, **517**, 123.
3 P. M. Maitlis, A. Haynes, G. J. Sunley and M. J. Howard, *J. Chem. Soc., Dalton Trans.*, 1996, 2187.
4 K. E. Clode, D. J. Watson and C. J. E. Vercauteren (BP Chemicals) EP 616997, priority date, 26/3/93; K. E. Clode, (BP Chemicals) EP 786447, priority date, 26/3/93; C. S. Garland, M. F. Giles and G. J. Sunley (BP Chemicals) EP 643034, priority date, 10/9/93; C. S. Garland, M. F. Giles, A. D. Poole and G. J. Sunley (BP Chemicals) EP 728726, priority date, 21/2/95; M. J. Baker, M. F. Giles, C. S. Garland and G. Rafaletos (BP Chemicals) EP 749948, priority date, 21/6/95; see also, *Chem. Br.*, 1996, 483; M. Howard, *Abstracts, XI International Symposium on Homogeneous Catalysis*, St. Andrews, 1998, p. M2.
5 T. Ghaffar, H. Adams, P. M. Maitlis, G. J. Sunley, M. J. Baker and A. Haynes, *Chem. Commun.*, 1998, 1023.
6 T. W. Dekleva and D. Forster, *Adv. Catal.*, 1986, **34**, 81.
7 See, for example, P. M. Maitlis, *Organic Chemistry of Palladium, Vol. II, Catalytic Reactions*, Academic Press, New York, 1971, p. 18; R. F. Heck, *Palladium Reagents in Organic Synthesis*, Academic Press, New York, 1985, p. 341; J. Tsuji, *Palladium Reagents and Catalysts*, Wiley, Chichester, 1995.
8 D. Forster, *J. Am. Chem. Soc.*, 1975, **97**, 951; C. E. Hickey and P. M. Maitlis, *J. Chem. Soc., Chem. Commun.*, 1984, 1609; A. Fulford, C. E. Hickey and P. M. Maitlis, *J. Organomet. Chem.*, 1990, **398**, 311; J. Rankin, A. D. Poole, A. C. Benyei and D. J. Cole-Hamilton, *Chem. Commun.*, 1997, 1835.
9 B. P. Andreini, D. Belli Dell'Amico, F. Calderazzo and G. Pelizzi, *J. Organomet. Chem.*, 1988, **354**, 369; B. P. Andreini, D. Belli Dell'Amico, F. Calderazzo, M. G. Venturi, G. Pelizzi and A. Segre, *J. Organomet. Chem.*, 1988, **354**, 357.
10 P. W. N. van Leeuwen (Shell Internationale Research Maatschappij BV) EP 0090443; priority date 30/3/82; P. W. N. van Leeuwen and C. F. Roobeek (Shell Internationale Research Maatschappij BV) EP 0133331; priority date 25/7/83.
11 N. Yu Kozitsyna and I. I. Moiseev, *Kinet. Katal.*, 1990, **31**, 251; 1992, **32**, 975.
12 W. Reppe, H. Kroeper, N. von Kutepow and H. J. Pistor, *Annalen*, 1953, **582**, 72; see also A. A. Kelkar, R. S. Ubale, R. M. Deshpande and R. V. Chaudhari, *J. Catal.*, 1995, **156**, 290.
13 D. Sinram, C. Brendel and B. Krebs, *Inorg. Chim. Acta*, 1982, **64**, L131; see also G. Thiele, K. Brodersen, E. Kruse and B. Holle, *Chem. Ber.*, 1968, **101**, 2771.

Communication 8/09197H

Unique guest inclusion within multi-component, extended-cavity resorcin[4]arenes

Leonard R. MacGillivray*[a] and Jerry L. Atwood*[b]

[a] *Steacie Institute for Molecular Sciences, National Research Council of Canada, Ottawa, Ontario, Canada K1A 0R6. E-mail: lmacgil@ned1.sims.nrc.ca*

[b] *Department of Chemistry, University of Columbia-Missouri, Columbia, Missouri, 65211 USA. E-mail: chemja@showme.missouri.edu*

Received (in Cambridge, UK) 12th November 1998 Accepted 9th December 1998

Co-crystals involving *C*-methylcalix[4]resorcinarene 1 and substituted pyridines obtained from $MeNO_2$–benzene and MeCN–benzene yields multi-component complexes 1·4(4-picoline)·$MeNO_2$ 2 and 1·4(1,10-phenanthroline)·MeCN·benzene 3 in which the cavity of 1 is extended by four pyridines supramolecularly and the included solvent serves as a guest.

There is currently a great deal of interest in utilizing noncovalent forces for the construction of multi-component host frameworks (*e.g.* molecular capsules) that display recognition properties analogous to their monomolecular predecessors (*e.g.* carcerands).[1–3] These frameworks typically involve replacing covalent bonds with supramolecular synthons that retain the structural integrity of the parent host molecule. Notably, in addition to providing access to systems which are difficult to obtain using conventional molecular synthesis,[3] such frameworks can display properties not found in the molecular analog (*e.g.* reversible formation)[4] which, in some instances, can bear relevance in understanding related biological phenomena (*e.g.* virus formation).[5]

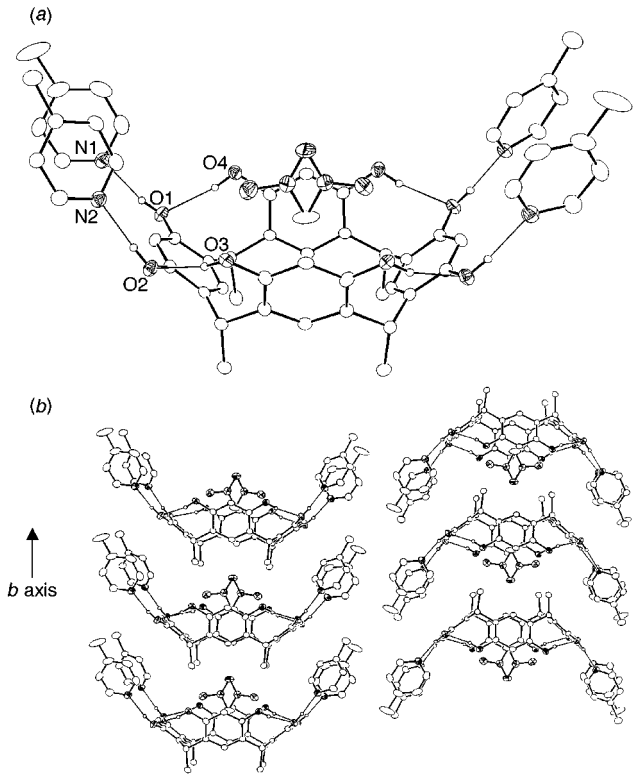

Fig. 1 ORTEP perspective of (*a*) the six-component assembly **2**, and (*b*) self-inclusion displayed by **2**. Selected interatomic distances (Å): O(1)···O(4) 2.840(3), O(1)···N(1) 2.740(3), O(2)···O(3) 2.806(3), O(2)···N(2) 2.704(3).

Along these lines, we have recently shown that it is possible to extend the cavities of resorcin[4]arenes (*e.g. C*-methylcalix[4]resorcinarene **1**) supramolecularly using aromatic-based hydrogen bond acceptors.[2] Our initial attempt at a discrete system, **1**·4(py)·py (py = pyridine), consisted of six molecules comprised of two different components in which four molecules of py participate in four O–H···N hydrogen bonds, as two stacked dimers, along the upper rim of **1**, to form a cavity large enough to host a fifth py. Here, we now demonstrate that it is possible to isolate a guest within a discrete supramolecular cavity based upon **1**, in **1**·4(4-pic)·$MeNO_2$ **2** (4-pic = 4-picoline), which is different than that of the 'substituents' hydrogen bonded to the upper rim of the macrocycle. By employing similar conditions used to form **2**, we also demonstrate that is possible to expand the chemistry of these systems to a chelating agent, 1,10-phenanthroline (1,10-phen), in **1**·4(1,10-phen)·MeCN·benzene **3**, which assembles to form both conventional and bifurcated O–H···N hydrogen bonds along the upper rim of **1**. Such observations are important since, in addition to showing that it is possible to fully mimic host–guest properties of monomolecular calix[4]arenes supramolecularly, they confirm generality in this approach with respect to both upper rim substitution and guest inclusion.

Addition of **1** (0.020 g) to a boiling aliquot of 4-pic (2 ml) yielded a yellow precipitate. Attempts to grow crystals of this material suitable for single crystal X-ray analysis failed. The precipitate was then heated and $MeNO_2$ (3 ml) followed by benzene (2 ml) were added dropwise, with continuous heating, according to eqn. (1), until the solid dissolved. Yellow crystals of **2** suitable for X-ray analysis formed, upon cooling, within a day. The formulation of **2** was confirmed by single crystal X-ray analysis† and ^{1}H NMR spectroscopy.

1 + 4-pic (excess) + $MeNO_2$ (excess) + benzene (excess) → **1**·4(4-pic)·$MeNO_2$ **2** (1)

A view of the six-component complex **2** is shown in Fig. 1(*a*). In a similar way to **1**·4(py)·py,[2] four molecules of 4-pic have assembled along the upper rim of **1** such that they form stacked dimers and participate in four O–H···N hydrogen bonds with two opposite resorcinol units of **1** [O···N separations (Å): O(1)···N(1) 2.740(4), O(2)···N(2) 2.704(4)]. Unlike **1**·4(py)·py, however, the cavity created by the five molecules is occupied by a guest which is different than the walls of the host. Specifically, a molecule of $MeNO_2$, which lies disordered across a crystallographic two-fold rotation axis, has assembled within **1** and interacts with **1** *via* C–H···π-arene interactions. Thus, by selecting a guest with an appropriate size, shape, and chemical exterior to assemble within **1**·4(4-pic), full structural mimicry, in a single step and virtually quantitative yield, of those host–guest properties displayed by upper rim substituted monomolecular calix[4]arenes has been achieved.[9] In other words, this approach to discrete, extended cavity frameworks based upon **1** is not limited to two component **1**·4(pyr)·pyr (where pyr = pyridine, substituted monopyridines) systems.[2]

A view of the crystal structure of **2** is shown in Fig. 1(*b*). Unlike **1**·4(py)·py, **2** self-assembles in the solid state such that

the complexes self-include and lie in an antiparallel fashion along the crystallographic *b* axis. Indeed, the ability of **2** to exhibit self-inclusion may be attributed to the small size the $MeNO_2$ guest which, unlike **1**·4(py)·py, allows neighbouring molecules of **1** to assemble within the cavities created by the 4-pic moieties.‡

That this approach to discrete extended cavity frameworks based upon **1** may be expanded to a system involving a bifurcated hydrogen bond and a different guest is demonstrated by **3**. When **1** (0.020 g) was added to a boiling aliquot of MeCN (4 ml) in the presence of 1,10-phen (0.027 g) a white microcrystalline solid formed. Attempts to grow single crystals of this material suitable for single crystal X-ray analysis failed. Colorless crystals of **3** suitable for X-ray analysis were obtained by redissolving the solid, by heating, in the presence of benzene (2 ml), according to eqn. (2), and allowing the solution to slowly cool. The formulation of **3** was confirmed by single crystal X-ray analysis§ and ^{1}H NMR spectroscopy.

1 + 4(1,10-phen) + MeCN (excess) + benzene (excess) → **1**·4(1,10-phen)·MeCN·benzene**3** (2)

A view of the seven-component complex **3** is shown in Fig. 2. In a similar way to **2**, four molecules of 1,10-phen have assembled along the upper rim of **1** and lie approximately orthogonal to two opposite resorcinol units of the macrocycle. Unlike **2**, however, in addition to conventional O–H···N forces, the phenanthroline moiety interacts with **1** *via* a bifurcated hydrogen bond. In particular, three phenanthroline units participate in conventional O–H···N hydrogen bonds [O···N separations (Å): O(1)···N(1,2) 2.77(1), 3.20(1); O(2)···N(3,4) 2.67(1), 3.38(1); O(5)···N(5,6) 2.73(1), 3.40(1)] while a fourth participates in a bifurcated interaction [O···N separations (Å): O(6)···N(7,8) 2.77(1), 3.00(1)]. Interestingly, in the case of the former, the longest O···N separations are associated with the 'outer' region of the upper rim of **1** while, in the case of the latter, the longest distance is associated with the 'inner' region. As a consequence of these forces, a cavity has formed, inside which a molecule of MeCN is located, interacting with **1**, in a similar way to the $MeNO_2$ guest of **2**, *via* C–H···π-arene interactions.¶ The molecule of benzene, which completes **3**, is then observed to lie sandwiched between two opposite phenanthroline moieties, in a region above a resorcinol unit of **1**, such that the aromatic participates in two edge-to-face π–π interactions with the bipyridines.[10] To the best of our knowledge, in addition to **3**, an assembly involving 'resorcinol' and a chelating agent such as 1,10-phen has not been observed.

In a similar way to **1**·4(py)·py,[2] **3** self-assembles in the solid state such that the cavities of **1** lie at approximately right angles to each other. Thus, in a similar way to the guest of **1**·4(py)·py, the 1,10-phen moieties, owing to their size and location above **1**, preclude self-inclusion of **1** as observed in **2**.

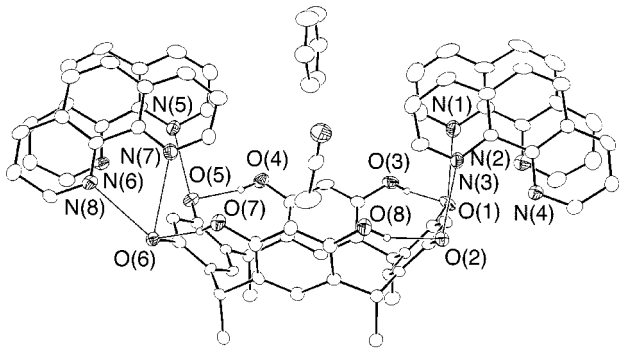

Fig. 2 ORTEP perspective of the seven-component assembly **3**. Selected interatomic distances (Å): O(1)···O(3) 2.73(1), O(1)···N(1) 2.77(1), O(1)···N(2) 3.20(1), O(2)···O(8) 2.76(1), O(2)···N(3) 2.67(1), O(2)···N(4) 3.38(1), O(4)···O(5) 2.75(1), O(5)···N(5) 2.73(1), O(5)···N(6) 3.40(1), O(6)···O(7) 2.78(1), O(6)···N(8) 2.77(1), O(6)···N(7) 3.00(1).

The results reported herein demonstrate that by using appropriately functionalized molecular components, it is possible to mimic host–guest properties of calix[4]arenes supramolecularly with respect to both upper rim substitution and guest inclusion. With these observations realized, focus can be placed upon determining if mimicry of those methods that involve sterochemical control to extending the cavity of **1** (*e.g.* C_4 *vs.* C_{2v}) can be achieved.[11] If one also considers that this approach stemmed from a crystal engineering design strategy,[12] such observations attest to the utility in using a supramolecular synthon, such as the resorcinol-based system[13] employed here, for rational solid state design.

We are grateful for funding from the National Science Foundation and the Natural Sciences and Engineering Research Council of Canada (doctoral scholarship, L. R. M.).

Notes and references

† *Crystal data* for **2**: monoclinic, space group $P2/c$, a = 11.481(1), b = 7.566(1), c = 29.501(2) Å, β = 96.434(1)°, U = 2546.5(3) Å^3, D_c = 1.28 g cm^{-3}, Mo-Kα radiation (λ = 0.71070 Å) for Z = 2. Least-squares refinement based on 2523 reflections with $I_{net} > 2.0\sigma(I_{net})$ (out of 3304 unique reflections) led to a final value of R = 0.048. Aromatic and hydroxy hydrogen atoms were placed by modelling the moieties as rigid groups with idealised geometry, maximising the sum of the electron density at the calculated hydrogen positions. Structure solution was accomplished using SHELXS-86 (ref. 6) and refinement was conducted using SHELXL93 (ref. 7) locally implemented on a pentium-based IBM compatible computer. Structure refinements and production of the figures were accomplished with the aide of RES2INS (ref. 8).

‡ We also note an O4···O4′ (O-4′ $-x$ + 1, $+y$, $-z$ + 1.5) separation of 3.025(3) Å between self-included strands of adjacent layers which suggests a weak hydrogen bond involving a disordered hydroxy hydrogen atom.

§ *Crystal data* for **3**: orthorhombic, space group $P2_12_12_1$, a = 14.504(1), b = 15.752(1), c = 31.097(2) Å, U = 7104.3(6) Å^3, D_c = 1.29 g cm^{-3}, Mo-Kα radiation (λ = 0.71070 Å) for Z = 4. Least-squares refinement based on 6469 reflections with $I_{net} > 2.0\sigma(I_{net})$ (out of 9237 unique reflections) led to a final value of R = 0.068. Aromatic hydrogen atoms were placed by modelling the moieties as rigid groups with idealised geometry, maximising the sum of the electron density at the calculated hydrogen positions. Structure solution and refinement was conducted as described for **2**. CCDC 182/1117.

¶ We note that the included MeCN lies slightly tilted towards one of the resorcinol units of **1** such that the positioning of the molecule conforms to the cavity defined by the 1,10-phen moieties.

1 T. H. Heinz, D. M. Rudkevich and J. Rebek, Jr., *Nature*, 1998, **394**, 764.
2 L. R. MacGillivray and J. L. Atwood, *J. Am. Chem. Soc.*, 1997, **119**, 6931.
3 R. K. R. Jetti, S. S. Kuduva, D. S. Reddy, F. Xue, T. C. W. Mak, A. Nangia and G. R. Desiraju, *Tetrahedron Lett.*, 1998, **39**, 913.
4 J. de Mendoza, *Chem. Eur. J.*, 1998, **4**, 1373.
5 L. R. MacGillivray and J. L. Atwood, *Nature*, 1997, **389**, 469.
6 G. M. Sheldrick, *Acta. Crystallogr., Sect. A*, 1990, **46**, 467.
7 G. M. Sheldrick, SHELXL93, University of Göttingen, Germany, 1993.
8 L. J. Barbour, RES2INS, University of Missouri-Columbia, Missouri, USA, 1997.
9 R. K. Juneja, K. D. Robinson, C. P. Johnson and J. L. Atwood, *J. Am. Chem. Soc.*, 1993, **115**, 3818.
10 W. L. Jorgensen and D. L. Severance, *J. Am. Chem. Soc.*, 1990, **112**, 5525.
11 A. Shivanyuk, E. F. Paulus, V. Böhmer and W. Vogt, *J. Org. Chem.*, 1998, **63**, 6448.
12 G. R. Desiraju, *Angew. Chem., Int. Ed. Engl.*, 1995, **34**, 2311.
13 T. Dewa, K. Endo and Y. Aoyama, *J. Am. Chem. Soc.*, 1998, **120**, 8933.

Communication 8/08835G

Observations on the versatility of methylenecyclopropanes as olefinic components in the intramolecular Pauson–Khand reaction

Hervé Corlay,[a] Eric Fouquet,[b]† Emmanuel Magnier[b] and William B. Motherwell*[b]

[a] *Department of Chemistry, Imperial College of Science, Technology and Medicine, South Kensington, London, UK SW7 2AY*

[b] *Department of Chemistry, Christopher Ingold Laboratories, University College London, 20 Gordon Street, London, UK WC1H 0AJ. E-mail: w.b.motherwell@ucl.ac.uk*

Received (in Cambridge, UK) 21st September 1998, Accepted 9th December 1998

Cyclopropyl tethered methylenecyclopropanes can function in the intramolecular Pauson–Khand reaction either as simple alkene components, or give rearranged hydroindenones in which neither of the two carbon atoms of the alkyne component form part of the cyclopentenone unit in the product.

Extensive and elegant studies by Binger[1] have established that transition metal mediated reactions of alkylidenecyclopropanes with olefinic and acetylenic acceptors provide a valuable method for cyclopentanoid construction. The essentially contemporaneous introduction of the intramolecular variant by ourselves[2a] and by the Nakamura group[2b] has led, *via* a series of systematic studies using both nickel(0) and palladium(0) catalysts,[2] to greatly improved levels of regiocontrol, and recent detailed stereochemical studies by Lautens[2h] have further enhanced the synthetic potential of this methodology.

Within this framework, it was therefore of interest to extend our studies to encompass the intramolecular variant of the highly useful Pauson–Khand reaction[3] using such substrates. Our primary objective, as encapsulated in Fig. 1(*a*), was to attach the tethering chain to the cyclopropyl unit, and hence to examine the possibility of generating highly strained tricyclic systems. During the course of our own work, a systematic study describing the contrasting tethering connectivity implied in Fig. 1(*b*) has been published.[4] In this latter case, however, as in the similarly precedented concept of using the enhanced reactivity of an allylidene cyclopropane as the diene component in Diels–Alder reactions,[5] a spiro fused cyclopropyl adduct is necessarily formed.

In the first instance, we elected to study the behaviour of the readily prepared[2f,g] methylenecyclopropanes **1a** and **1b** using octacarbonyldicobalt and the mild amine *N*-oxide protocol developed by Schreiber[6] (Scheme 1). The obtention of the

Fig. 1

1a R = H
b R = C_9H_{19}

2a 41%
b 38%

Scheme 1 *Reagents and conditions*: i, $Co_2(CO)_8$ (1.0 equiv.), benzene, room temp., 1 h; ii, NMO (6 equiv.), benzene, reflux, 2 h.

† Present address: Laboratoire de Chimie Organique et Organométallique, URA CNRS no. 35, Université Bordeaux 1, 351 Cours de la Libération, 33405 Talence Cedex, France.

tricyclic adducts **2a** and **2b** confirmed the validity of this approach and the isolation of **2b** as a single diastereoisomer also established, as expected, that the *trans* stereochemistry of the substituents around the methylenecyclopropane was preserved in the cycloaddition product.

We were therefore encouraged to extend the scope of this approach to the methylenecyclopropane **1c**, in which the additional methyl group was expected to lead to the formation of the adducts **2**, containing two contiguous quaternary carbon centres (Table 1). In the event, under the previously described reaction conditions, the anticipated tricyclic product **2c** was not formed, and initial spectral data clearly indicated that cyclopropyl ring opening had occurred to give a bicyclic hydroindenone derivative containing an exocyclic carbon–carbon double bond. The full complexity of this bizarre rearrangement and the precise structures **3** of the rearranged cycloadducts were only revealed however through a careful systematic study of further substrates **1d–f** in which the progressive incorporation of additional substituents on the cyclopropyl ring and on the alkyne provided regio- and stereo-chemical markers to trace the outcome of the reaction in terms of carbon atom connectivity (Table 1, entries 1–4). The relative location and stereochemistry of the substituents in cycloadducts **3c–f** was rigorously established using a combination of 2D NMR, NOESY and

Table 1 Reaction of compounds **1c–f**

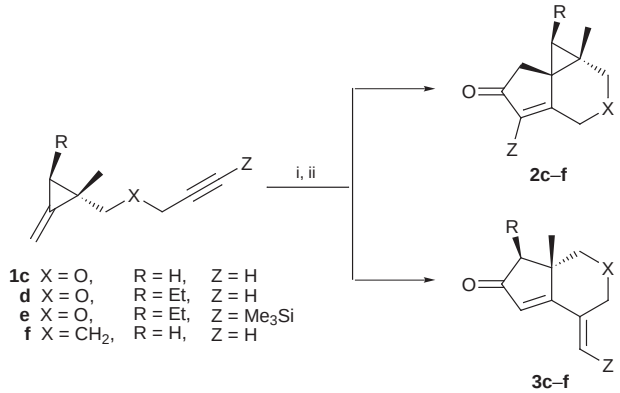

1c X = O, R = H, Z = H
d X = O, R = Et, Z = H
e X = O, R = Et, Z = Me_3Si
f X = CH_2, R = H, Z = H

Entry	Substrate	Reaction conditions[a] Solvent	*t*/h	*T*/°C	Products (% yield)
1	**1c**	benzene	1	reflux	**3c** (51)
2	**1d**	benzene	2	reflux	**3d** (47)
3	**1e**	benzene	1.5	reflux	**2e** (10), **3e** (40)
4	**1f**	benzene	1	reflux	**3f** (51)
5	**1c**	THF	10	room temp.	**2c** (44), **3c** (12)
6	**1d**	benzene	24	room temp.	**2d** (20), **3d** (26)
7	**1e**	THF	2	reflux	**2e** (28), **3e** (28)

[a] *Reagents and conditions*: i, $Co_2(CO)_8$ (1.0 equiv.), benzene, room temp., 1 h; ii, NMO (6 equiv.) and reaction conditions above.

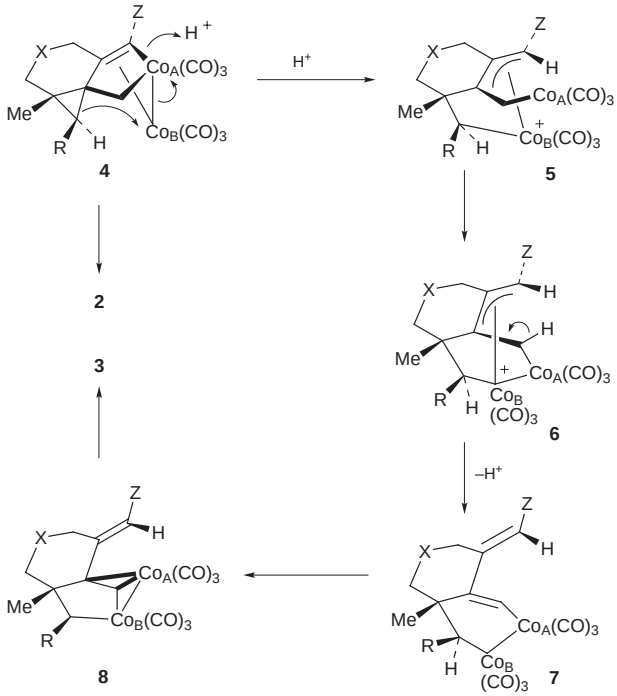

Scheme 2

HMBC experiments. Thus, careful scrutiny of structures **3** uncovers the remarkable fact that *neither* of the two carbon atoms of the tethered alkyne have been incorporated into the cyclopentenone unit of the final product in this intramolecular variant of the Pauson–Khand reaction. It was also of interest to note that cyclisation proceeded smoothly using the all-carbon tethering chain in the terminal alkyne **1f**, thereby providing a concise route to the usefully functionalised bicyclo[4.3.0]non-1-en-3-one **3f** (entry 4). From both a mechanistic and preparative standpoint the preservation of the original cisoid geometry of the substituents (R and CH_3) around the cyclopropyl ring in the rearranged adducts is also significant, as is the fact that **3e** was isolated as a single geometrical isomer, most probably of *E* configuration.

Finally, from a preparative standpoint, we have also been able, through a judicious choice of experimental conditions, to suppress the rearrangement pathway, and hence to redirect the course of the reaction towards the formation of our originally desired tricyclic systems, as shown for the prototypical substrates **1c**, **1d** and **1e** (Table 1, entries 5, 6 and 7).

From the foregoing examples, it is clear that the presence of the additional methyl group is necessary in order to isolate the skeletally rearranged products **3**. While detailed mechanistic speculation is premature at this stage, it seems reasonable to postulate that the formation of the standard metallacycle **4** (Scheme 2) occurs in all cases as an early common intermediate. At lower temperatures and preferably in the presence of a more coordinating cosolvent such as THF, the major reaction pathway then follows the normal sequence of events to give products of type **2**. At higher temperatures in refluxing benzene, however, the relief of strain in those substrates possessing the additional methyl group engenders rearrangement. A formal mechanistic rationale involves 'edge' attack[7] on the proximal bond of the cyclopropyl ring by the suitably aligned neighbouring cobalt atom (Co_B) to give a π-allyl complex whose protonolysis on the sp^2 carbon would lead to the cation **5**. Such an opening would proceed with retention of configuration at the migrating terminus. Formation of the metallacycle **6** followed by proton loss to liberate the diene system then leads to **7** which can either rearrange or formally be considered as an equivalent of the necessary metallacyclic framework **8** for insertion of carbon monoxide and reductive elimination to afford products of type **3**.

The inherent reactivity of the methylenecyclopropane unit in the present intramolecular variant of the Pauson–Khand reaction can therefore be harnessed, by virtue of controlling a bifurcated reaction pathway, either for the construction of tricyclic systems with preservation of the cyclopropyl ring, or for the preparation of heavily functionalised and stereochemically complex bicyclo[4.3.0]non-1-en-3-one derivatives.

We acknowledge the Centre National de la Recherche Scientifique (CNRS) and the Royal Society for the award of a Fellowship (to E. F.), Atochem for the provision of a studentship (to H. C.) and the Ministère des Affaires Etrangères for a Bourse Lavoisier (E. M.). We also thank Drs W. J. Kerr, D. A. Widdowson and especially Dr P. Kočovský for very helpful mechanistic discussions. We are also grateful to the University of London Intercollegiate Research School (ULIRS) for mass spectral measurements.

Notes and references

1 For reviews see P. Binger and H. M. Büch, *Top. Curr. Chem.*, 1987, **135**, 77; T. Ohta and H. Takaya, in *Comprehensive Organic Synthesis*, ed. B. M. Trost and I. Fleming, Pergamon, Oxford, 1991, vol. 5, p. 1185.

2 (*a*) R.T. Lewis, W.B. Motherwell and M. Shipman, *J. Chem. Soc., Chem. Commun.*, 1988, 948; (*b*) S. Yamago and E. Nakamura, *J. Chem. Soc., Chem. Commun.*, 1988, 1112; S. Yomago and E. Nakamura, *Tetrahedron*, 1989, **45**, 2887; (*c*) S. A. Bapuji, W. B. Motherwell and M. Shipman, *Tetrahedron Lett.*, 1989, **30**, 7107; (*d*) W. B. Motherwell and M. Shipman, *Tetrahedron Lett.*, 1991, **32**, 1103; (*e*) R. T. Lewis, W. B. Motherwell, M. Shipman, A. M. Z. Slawin and D. J. Williams, *Tetrahedron*, 1995, **51**, 3289; (*f*) H. Corlay, R. T. Lewis, W. B. Motherwell and M. Shipman, *Tetrahedron*, 1995, **51**, 3303; (*g*) H. Corlay, W. B. Motherwell, A. M. K. Pennell, M. Shipman, A. M. Z. Slawin, D. J. Williams, P. Binger and M. Stepp, *Tetrahedron*, 1996, **52**, 4883; (*h*) M. Lautens, Y. Ren and P. H. M. Delanghe, *J. Am. Chem. Soc.*, 1994, **116**, 8821, M. Lautens and Y. Ren, *J. Am. Chem. Soc.*, 1996, **118**, 9597 and 10668.

3 For recent reviews, see N.E. Schore, *Org. React.*, 1991, **40**, 1; N. E. Schore, in *Comprehensive Organic Synthesis*, ed. B. M. Trost and I. Fleming, Pergamon, Oxford, 1991, vol. 5, p. 1037.

4 A. Stolle, H. Becker, J. Salaün and A. de Meijere, *Tetrahedron Lett.*, 1994, **35**, 3517 and 3521; S. Bräse, S. Schömenauer, G. McGaffin, A. Stolle and A. de Meijere, *Chem. Eur. J.*, 1996, **2**, 545. For reports on intermolecular Pauson-Khand reactions of methylenecyclopropanes, see W. A. Smit, S. L. Kireev, O. M. Nefedov and V. A. Tarasov, *Tetrahedron Lett.*, 1989, **30**, 4021; H. Corlay, I. W. James, E. Fouquet, W. B. Motherwell and J. Schmidt, *Synlett*, 1996, 990.

5 S. Halazy, W. Dumont and A. Krief, *Tetrahedron Lett.*, 1981, 4737; A. Krief and F. Zutterman, *J. Org. Chem.*, 1983, **48**, 1135; L. Paquette, G. Wells and G. Wickham, *J. Org. Chem.*, 1984, **49**, 3618.

6 S. Shambayati, W. E. Crowe and S. L. Schreiber, *Tetrahedron Lett.*, 1990, **31**, 5289.

7 For an excellent overview of metal-mediated cyclopropane ring opening and leading references, see P. Kočovský, J. Šrogl, M. Pour and A. Gogoll, *J. Am. Chem. Soc.*, 1994, **116**, 186.

Communication 8/07333C

A remarkably stable indium trihydride complex: synthesis and characterisation of $[InH_3\{P(C_6H_{11})_3\}]$

David E. Hibbs, Cameron Jones* and Neil A. Smithies

Department of Chemistry, University of Wales, Cardiff, PO Box 912, Park Place, Cardiff, UK CF1 3TB. E-mail: jonesca6@cardiff.ac.uk

Received (in Cambridge, UK) 27th November 1998, Accepted 15th December 1998

The reaction of $[InH_3(NMe_3)]$ with $P(C_6H_{11})_3$ affords the first example of a phosphine–indium trihydride complex, $[InH_3\{P(C_6H_{11})_3\}]$, which exhibits remarkable thermal stability; the X-ray crystal structure of the complex is described.

The utility of Lewis base adducts of AlH_3 and GaH_3 as chemical vapour deposition precursors to thin films of the group 13 metal[1] or semiconducting materials[2] has led to their chemistry being extensively studied over the last decade.[3] Until very recently no corresponding InH_3 complexes were known, presumably because of thermal instability that arises from the weakness of the In–H bond. We have reversed this situation with the syntheses of $[InH_3\{CNPR^iC_2Me_2NPr^i\}]$ **1** and $[InH_3(NMe_3)]$ **2**,[4,5] the former being stabilised by coordination to a highly nucleophilic 'Arduengo' carbene. Despite this, **1** is not stable in the solid state above −5 °C (decomp. > −20 °C in solution) and **2** is only stable in dilute solutions below −30 °C. It seems likely that if InH_3 complexes are to find similar applications to their aluminium and gallium counterparts, then examples will need to be found that are stable at room temperature. Herein we report the synthesis and structural characterisation of such a compound, $[InH_3(PCy_3)]$ **3** (Cy = cyclohexyl), which represents the first example of a phosphine adduct of InH_3, and the first InH_3 complex to have had its hydride ligands located by X-ray crystallography.

Treatment of an ethereal solution of $[InH_3(NMe_3)]$[5] with 1 equiv. of PCy_3 at −40 °C led to the high yield formation (71%) of **3** after recrystallisation from toluene (Scheme 1). Interestingly, **3** could not be formed from the direct reaction of PCy_3 with $LiInH_4$ (LiH elimination) which is in contrast to the high yield preparation of $[GaH_3(PCy_3)]$ **4** from the reaction of $LiGaH_4$ and PCy_3 in diethyl ether.[6] In addition, there was no evidence for the formation of **3** from the reaction of a 1 : 1 mixture of PCy_3 and anhydrous HCl with $LiInH_4$ in diethyl ether at −40 °C {*cf.* the formation of $[AlH_3(PCy_3)]$ **5** by a similar route[7]}.

Compound **3** is remarkably thermally stable and decomposes in the solid state only at temperatures in excess of 50 °C to indium metal, hydrogen gas and PCy_3 (*cf.* **4**, decomp. > 130 °C;[6] **5**, decomp. > 160 °C[7]). At room temperature (25 °C) crystalline samples of **3** showed only minimal decomposition over a period of 7 days under an argon atmosphere, as determined from the ^{1}H NMR of the sample after that period. Surprisingly, **3** also displays considerable stability to oxygen and moisture in the solid state as it shows no decomposition in air over 24 h at room temperature. In benzene solutions samples of **3** are less stable but still take *ca.* 1 h to decompose at 25 °C. As has been suggested for **4** and **5**, the unusual stability of **3** can probably be attributed to the steric properties of the phosphine ligand.

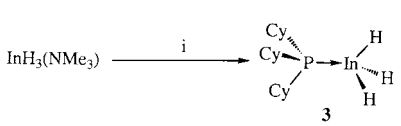

3

Scheme 1 *Reagents and conditions*: i, PCy_3, $-NMe_3$, Et_2O, −40 °C, 2 h.

The solution NMR data† for **3** support its proposed structure. Its ^{1}H NMR spectrum exhibits the expected resonances for the phosphine ligand in addition to a broad hydride resonance that integrates for three hydrogens at δ 5.61 (*cf.* δ 5.58 in **1**[4,5]) which is significantly downfield with respect to the related resonances in **4** (δ 4.32[6]) and **5** (δ 4.25[7]). The ^{31}P NMR spectrum of **3** displays a singlet at δ 7.43 which can be compared to δ 11.1 for the free ligand.[7] A strong, broad In–H stretching absorbance was observed at 1661 cm^{-1} (*cf.* 1640 cm^{-1} for **1**[5]) in its IR spectrum (Nujol mull). This is at a lower frequency than the corresponding M–H stretches in **4** (1800 cm^{-1})[6] and **5** (1750 cm^{-1})[7] and reflects the relative weakness of the M–H bonds in **3**. No molecular ion was seen in the mass spectrum of **3** but a fragment corresponding to the free phosphine ligand was observed.

An X-ray crystal structure analysis‡ of **3** (Fig. 1) was carried out and it was found to be isomorphous to its aluminium and gallium counterparts, **5** and **4**, respectively. The quality of the X-ray data allowed the three hydride ligands to be located from difference maps and their positional and isotropic thermal parameters to be refined. The complex is monomeric and shows no evidence of intermolecular interactions through bridging hydrides. As in **4**, the metal centre has a slightly flattened tetrahedral geometry [P–In–H 101.4° (av.), H–In–H 116.2° (av.)] with an average In–H distance of 1.68 Å. This distance compares well with the only other structurally characterised terminal In–H bond in a neutral complex, *viz.* 1.69(3) Å in $[InH\{2\text{-}Me_2NCH_2(C_6H_4)\}]_2$.[8] Not surprisingly both these distances are shorter than bridging In–H distances, *e.g.* 1.87 Å (av.)

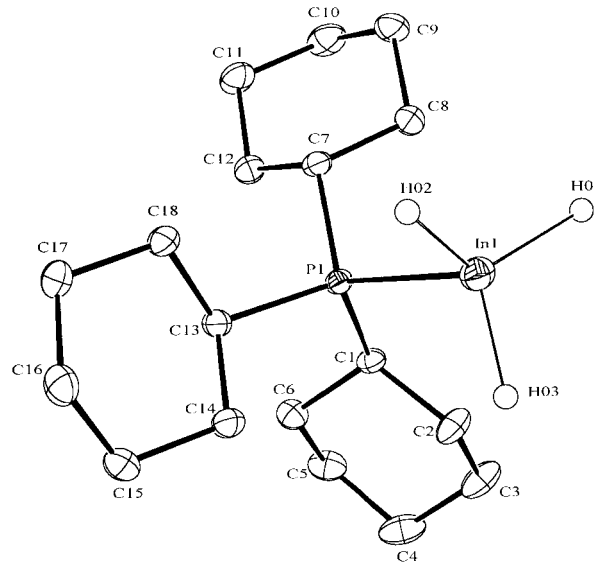

Fig. 1 Molecular structure of $[InH_3\{P(C_6H_{11})_3\}]$ **3**. Selected bond lengths (Å) and angles (°): In(1)–P(1) 2.6474(6), In(1)–H(01) 1.81(2), In(1)–H(02) 1.62(3), In(1)–H(03) 1.62(3), P(1)–C(13) 1.8433(17), P(1)–C(7) 1.8448(17), P(1)–C(1) 1.8632(17); P(1)–In(1)–H(01) 103.4(7), P(1)–In(1)–H(02) 97.3(11), P(1)–In(1)–H(03) 103.6(11), H(01)–In(1)–H(02) 121.3(13), H(01)–In(1)–H(03) 111.0(13), H(02)–In(1)–H(03) 116.4(16).

in $[Li(tmeda)_2][Me_3In–H–InMe_3]$.[9] The In–P distance in **3** [2.6474(6) Å] is in the normal region for such interactions though is slightly longer than In–P distances in four co-ordinate tertiary phosphine adducts of indium halides, *e.g.* 2.569 Å in $[InI_3(PPr^i_3)]$[10] and 2.603 Å in $[InI_3(PPh_3)]$.[11]

The remarkable thermal stablity of **3** has prompted us to begin an investigation of its chemistry and the preparation of a range of related phosphine– and arsine–indium hydride complexes. The results of these investigations will form the basis of a later publication.

We gratefully acknowledge financial support from the EPSRC (studentship for N. A. S.).

Notes and references

† *Spectroscopic data* for **3**: ^{1}H NMR (400 MHz, C_6D_6, $SiMe_4$, 298 K) δ 0.92–1.75 (m, 33H, C_6H_{11}), 5.61 (br s, 3H, In–H); ^{13}C NMR (100.6 MHz, C_6D_6, 298 K) δ 26.6 (s, CH_2), 27.7 (d, CH_2, $^2J_{PC}$ 10.2 Hz), 30.5 (s, CH_2), 31.8 (d, CH, $^1J_{PC}$ 13.0 Hz); ^{31}P NMR (36.3 MHz, C_6D_6, 85% H_3PO_4, 298 K) δ 7.43, IR ν 1661 cm^{-1} (s, br, In–H str.); MS EI *m/z* (%): 280 (PCy_3^+, 63), 197 (PCy_2^+, 100), 114 (PCy^+, 78).

‡ *Crystal data* for **3**: $C_{18}H_{36}InP$ M = 398.26 triclinic, space group $P\bar{1}$, a = 8.1147(10), b = 10.897(2), c = 11.4273(10) Å, α = 74.940(9), β = 88.665(10), γ = 81.840(10)°, V = 965.8(2) Å^3, Z = 2, D_c = 1.369 g cm^{-3}, $F(000)$ = 416, μ = 12.98 cm^{-1}, crystal 0.20 × 0.20 × 0.20 mm, radiation Mo-Kα (λ = 0.71073 Å), 150(2) K.

All crystallographic measurements were made using an Enraf-Nonius CAD4 diffractometer. The structure was solved by heavy atom methods (SHELXS86)[12] and refined on F^2 by full matrix least squares (SHELX93)[13] using all unique data. All non-hydrogen atoms are anisotropic with H-atoms [except those attached to In(1)] included in calculated positions (riding model). Neutral-atom complex scattering factors were employed.[13] Empirical absorption corrections were carried out by the DIFABS method.[14] Final R (on F) and wR (on F^2) were 0.0199 and 0.0513 for $I > 2\sigma(I)$, and 0.229 and 0.559 for all data. CCDC 182/121. See http://www.rsc.org/suppdata/cc/1999/185 for crystallographic files in .cif format.

1 M. G. Simmonds and W. L. Gladfelter, in *The Chemistry of Metal CVD*, ed. T. Kodas and M. Hampden-Smith, VCH, Weinheim, 1994 and references therein.
2 J. N. Kidder, H. K. Yun, J. W. Rogers and T. P. Pearsall, *Chem. Mater.*, 1998, **10**, 777.
3 C. Jones, G. A. Koutsantonis and C. L. Raston, *Polyhedron*, 1993, **12**, 1829; M. G. Gardiner and C. L. Raston, *Coord. Chem. Rev.*, 1997, **166**, 1; *Chemistry of Aluminium, Gallium, Indium and Thallium*, ed. A. J. Downs, Blackie, Glasgow, 1993 and references therein.
4 D. E. Hibbs, M. B. Hursthouse, C. Jones and N. A. Smithies, *Chem. Commun.*, 1998, 869.
5 M. D. Francis, D. E. Hibbs, M. B. Hursthouse, C. Jones and N. A. Smithies, *J. Chem. Soc., Dalton Trans.*, 1998, 3249.
6 J. L. Atwood, K. D. Robinson, F. R. Bennett, F. M. Elms, G. A. Koutsantonis, C. L. Raston and D. J. Young, *Inorg. Chem.*, 1992, **31**, 2673.
7 F. R. Bennett, F. M. Elms, M. G. Gardiner, G. A. Koutsantonis, C. L. Raston and N. K. Roberts, *Organometallics*, 1992, **11**, 1457.
8 C. Kümmel, A. Meller and M. Noltemeyer, *Z. Naturforsch., Teil B*, 1996, **51**, 209.
9 D. E. Hibbs, M. B. Hursthouse, C. Jones and N. A. Smithies, *Organometallics*, 1998, **17**, 3108.
10 S. M. Godfrey, K. J. Kelly, P. Kramkowski, C. A. McAuliffe and R. G. Pritchard, *Chem. Commun.*, 1997, 1001.
11 M. A. Brown, D. G. Tuck and E. J. Wells, *Can. J. Chem.*, 1996, **74**, 1535.
12 G. M. Sheldrick, *Acta Crystallogr., Sect. A*, 1990, **46**, 467.
13 G. M. Sheldrick, SHELXL-93 Program for Crystal Structure Refinement, University of Göttingen, Germany, 1993.
14 N. P. C. Walker and D. Stuart, *Acta Crystallogr., Sect. A*, 1983, **39**, 158.

Communication 8/09279F

Unexpected formation of 3,3a,4,7a-tetrahydrobenzofuran-2,5-diones as well as arene carboxylic acids upon formal double *exo* nucleophilic addition of $R^1R^2C^-COO^-$ to anisolechromium tricarbonyl complexes

Moncef Bellassoued,*[a] Evelyne Chelain,[a] Jérôme Collot,[a] Henri Rudler*[b] and Jacqueline Vaissermann[b]

[a] *Laboratoire de Synthèse Organométallique associé au CNRS, Université de Gergy-Pontoise, 5 Mail Gay Lussac, Neuville-sur-Oise, 95031 Cergy-Pontoise Cedex, France*

[b] *Laboratoire de Synthèse Organique et Organométallique, UMR 7611 and Laboratoire de Chimie des Métaux de Transition, URA 419, Université Pierre et Marie Curie T 44-45, 4 place Jussieu, 75252 Paris Cedex 5, France. E-mail: rudler@ccr.jussieu.fr*

Received (in Liverpool, UK) 16th November 1998, Accepted 30th November 1998

Bis(trimethylsily)ketene acetals of the general structure 2 (R^1 = H, Me, R^2 = Me, Et, Pr^i, CMe = CH_2) react at −78 °C in the presence of Bu^{t}OK with a series of arenechromium tricarbonyl complexes 3 to give as expected, after oxidation with I_2 followed by silica gel chromatography, arylcarboxylic acids 7. In the case of anisolechromium tricarbonyl 8, besides the *m*-methoxyarylcarboxylic acids, tetrahydrobenzofuran-2,5-diones 11, are formed as the result of a double nucleophilic addition.

Complexation of an arene group to $Cr(CO)_3$ allows, *via* an addition–oxidation sequence, the introduction of various substituents on the arene nucleus and, as a result, the construction of complex molecules.[1] Although a large array of substituted aryls bearing various functional groups (CN, CO_2R, *etc*.) have been prepared since the pioneering work of Semmelhack and Card,[2,3] a method to directly introduce a carboxylic acid has still been lacking.

During our investigations directed towards the synthesis of pyrrole-containing aryl acids from arenechromium tricarbonyl complexes,[4] we were faced with this problem. Here we describe a successful approach based on the interaction of arenechromium tricarbonyl complexes with potassium enolates originating from bis(trimethylsilyl)ketene acetals[5,6] which leads to not only arylcarboxylic acids, but also to the unexpected formation of γ-functionalized cyclohexenones from anisole.

The following set of transformations allowed the reactivity of such potassium enolates towards arenechromium tricarbonyl to be assessed.

Thus, a solution of complex **3** (R = OPh, 1.53 g, 5 mmol) and of the ketene acetal **1** (1.36 g, 7.5 mmol) in THF (10 ml) was treated at −78 °C with a slight excess of Bu^{t}OK (1 M) in THF (8 ml) in the presence of HMPA (6 ml). After 1.5 h at this temperature, a solution of I_2 (6.20 g, 5 equiv.) in THF (15 ml) cooled to −78 °C was slowly added. The solution was then progressively warmed to room temperature overnight. Treatment with Et_2O and aqueous sodium bisulfite, followed by extraction with Et_2O and evaporation of the solvents *in vacuo*, left an oil which was chromatographed on silica gel. Elution with mixtures of light petroleum–Et_2O gave the aryl ester **4** (0.72 g, 52%) (Scheme 1).[7] Under the same conditions, the silyl enol ether of butyrolactone **5** led to α-phenylbutyrolactone **6** (30%).[7]

The bis(trimethylsilyl) acetals **2** behaved similarly. For example, a solution of complex **3** (R = OPh, 0.6 g, 2 mmol) and acetal **2** (R^1 = H, R^2 = Me, 0.9 g, 4 mmol) in THF (10 ml) was treated at −78 °C with a THF solution of Bu^{t}OK (5 ml) in the presence of HMPA (3 ml), then with I_2 (2.1 g) in THF (10 ml) to give, after workup and silica gel chromatography as above, fenoprofen **7** (0.38 g, 79%).[7] This transformation is of a general scope giving the known acids in fairly good yields (Table 1).

Surprisingly, in the case of complex **8**, derived from anisole, the course of the reaction was different. Under exactly the same

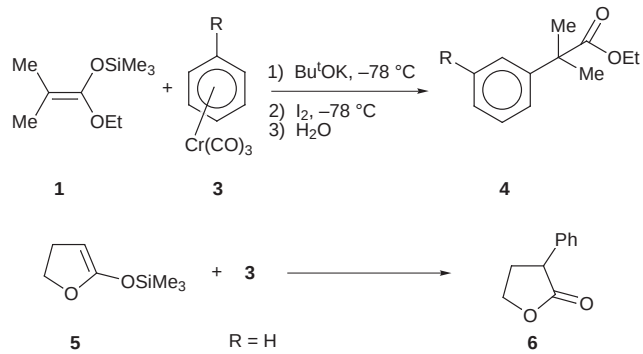

Scheme 1

reaction conditions, this complex gave with **2** (R^1 = H, R^2 = Pr^i) a mixture of two compounds which could be separated by silica gel chromatography. The physical data of the less polar product corresponded to those of the expected arylcarboxylic acid **9c** (41%).[7] The ^{13}C NMR spectrum of the more polar compound (23%), obtained as white crystals, mp 72 °C, showed signals at δ 195.50, 142.73 and 131.49, typical for a cyclohexenone, and also signals at δ 175.92 and 72.27, which agree with the presence of a γ-lactone. The ^1H NMR spectrum is also in accord with the presence of these two functional groups, with signals at δ 6.76 (dd) and 6.19 (d) for the protons of the double bond, and at δ 5.15 (dm) for a proton geminated to oxygen. Taken together, these data are fully consistent with **11c**, 3-isopropyl-3,3a,4,7a-tetrahydrobenzofuran-2,5-dione (Scheme 2).[7] **11a** and **11b** (together with the known acids) were

Table 1

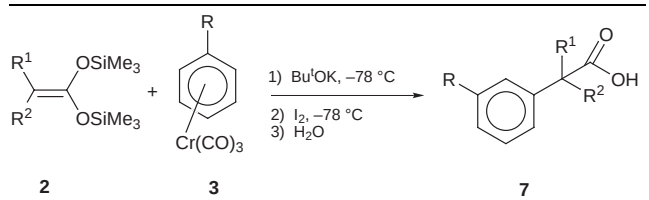

Entry	**2**/equiv.	R^1	R^2	R	Yield of **7** (%)
1	2	H	Me	H	68
2	2	H	Me	OPh	79
3	2	H	Et	H	66
4	1.5	H	Et	OPh	61
5	2	H	Pr^i	H	94
6	1.5	H	Pr^i	OPh	85
7	2	Me	Me	H	63
8	2	Me	Me	OPh	77
9	1	H	CMe=CH_2	H	23

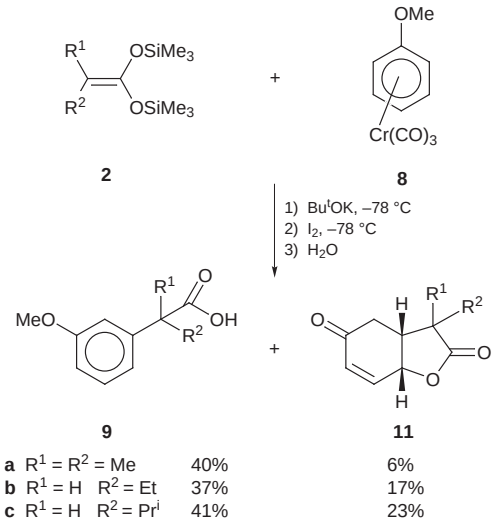

Scheme 2

obtained under the same conditions. A final confirmation of the structure came from a radiocrystallographic study on **11a**, shown in the CAMERON projection in Fig. 1.[8]

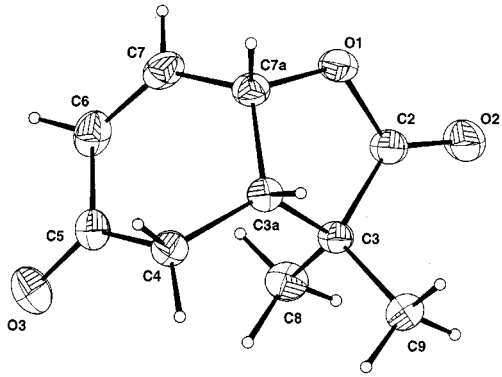

Fig. 1 X-Ray structure of **11a**. Important bond distances (Å): C(5)–O(3), 1.209(2); C(6)–C(7), 1.313(3); C(7a)–O(1), 1.457(2); O(1)–C(2), 1.351(2): C(2)–O(2), 1.193(2).

As expected for anisole,[9,10] addition of the enolate to the arenechromium system took place at the *meta* position to give **10**, but it was followed by the concomitant formation of a cyclohexenone (originating from the dienol ether) and of a lactone (originating from the trimethylsilyl carboxylate group). Although the formation of 3-substituted cyclohexenones *via* nucleophilic addition to anisolechromium tricarbonyl complexes is a known and important process,[11–13] the formation of fused systems containing a 4-substituted cyclohexenone such as **11** has to the best of our knowledge not been observed up to now.

The mechanism of this transformation, which corresponds to a formal (3 + 2) cycloaddition, is still a matter of speculation. Nevertheless, the presence of the methoxy group is fundamental since no lactones were detected in its absence (*vide supra*): its role is probably to activate the γ-position or to stabilize a crucial intermediate for the ring-closing step. Moreover, two observations could militate in favour of two successive *exo* addition reactions, the second one taking place after the oxidation step, probably on an iodinated ring. First, **11** could not be detected before the iodine treatment of the intermediate **10**,[14,15] second, the *cis* junction of the two rings could indicate that the carboxylato group enters also in an *exo* way although isomerization of a *trans*-fused system to a *cis*-fused one could occur during the purification step (Scheme 3).

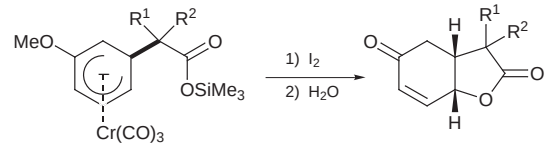

Scheme 3

To summarise, arylcarboxylic acids can be obtained in one step from readily available bis(trimethylsilyl)ketene acetals and arenechromium tricarbonyl complexes together with products resulting from an intramolecular trapping reaction. Work is in progress to establish the mechanism of the latter transformation, to find the conditions that would make the bicyclic lactones the exclusive products of the reaction, and to attempt their enantioselective synthesis since in the case of **11b**,**c** three contiguous chiral centers are formed with high diastereoselectivity.

Notes and References

1 M. F. Semmelhack, *Comprehensive Organic Synthesis*, ed. B. M. Trost and I. Fleming, Pergamon, Oxford, 1991, vol. 4, p. 517; E. P. Kündig, *Pure Appl. Chem.*, 1985, **57**, 1855.
2 M. F. Semmelhack and H. T. Hall, *J. Am. Chem. Soc.*, 1974, **96**, 7091.
3 R. J. Card and W. S. Trayhanovsky, *Tetrahedron Lett.*, 1973, 3823.
4 A. Parlier, M. Rudler, H. Rudler, R. Goumont, J. C. Daran and J. Vaissermann, *Organometallics*, 1994, **13**, 4708.
5 C. Ainsworth and Y. N. Kuo, *J. Organomet. Chem.*, 1973, **46**, 73.
6 M. Bellassoued and M. Gaudemar, *Tetrahedron Lett.*, 1990, **31**, 209.
7 *Selected data* for **4**: δ_H(200 MHz, $CDCl_3$) 7.32–7.27 (m, 3H), 7.05–7.01 (m, 5H), 6.85–6.95 (m, 1H), 4.13 (q, *J* 8, 2H), 1.55 (s, 6H), 1.17 (t, *J* 8, 3H). δ_C(50 MHz, $CDCl_3$) 176.42, 157.12, 147.08, 129.7, 129.55, 123.21, 120.64, 118.7, 111.7, 60.90, 46.50, 26.51, 14.08. MS (EI) *m/z* 284 (M^+). For **6**: δ_H (200 MHz, CDCl) 7.40–7.25 (m, 5H), 4.50–4.25 (m, 2H), 3.60 (dd, *J* 9.5, 1H), 2.77–2.61 (m, 1H), 2.51–2.35 (m, 1H). δ_C(50 MHz, $CDCl_3$) 177.6, 136.76, 128.62, 128.0, 127.7, 66.64, 45.57, 31.64. MS (EI) *m/z* 212 (M^+). For **7** (R = OPh): δ_H (200 MHz, $CDCl_3$) 11.0 (br s, 1H), 7.38–6.87 (m, 9H), 3.49 (t, *J* 6, 1H), 2.10 (m, 1H), 1.77 (m, 1H), 0.92 (t, *J* 7.2, 3H). δ_C(50 MHz, $CDCl_3$) 180.43, 157.50, 157.07, 149.43, 129.87, 123.44, 123.87.44, 123.0, 119.01, 118.82, 117.70, 53.30, 26.40, 12.20. MS (EI) *m/z* 256 (M^+). For **11a**: mp 69 °C; δ_H(200 MHz, $CDCl_3$) 6.84 (dd, *J* 10.2, 3.4, 1H), 6.14 (d, *J* 10.2, 1H), 5.10 (dd, *J* 3.4, 0.8, 1H), 2.81 (dd, *J* 13.8 and 6.4, 1H), 2.51 (ddd, *J* 13.8, 10.6 and 6.4), 1.25 (s, 3H), 1.09 (s, 3H). δ_C(50 MHz, $CDCl_3$) 196.17, 180.24, 141.61, 132.12, 70.97, 43.32, 35.25, 24.71, 20.05.
8 *Crystal data* for **11a**: colorless plates monoclinic space group $P2_1/n$, a = 11.369(3), b = 6.145(3), c = 13.537(4) Å, β = 105.53(2)°, Z = 4, R = 0.0476, R_w* = 0.0564, GOF = 1.11. Collected reflections 2505, independent reflections, 2186 (θ = 1–28°, Mo-Kα radiation, R_{int} = 0.0079). The obtained structure model was first refined anisotropically for all non-hydrogen atoms and isotropically for the hydrogen atoms using 1549 reflections. CCDC 182/1116.
9 M. F. Semmelhack, J. J. Harrison and Y. Thebtaranonth, *J. Org. Chem.*, 1979, **44**, 3275.
10 J. C. Boutonnet, F. Rose-Munch and E. Rose, *Tetrahedron Lett.*, 1985, **26**, 3989.
11 M. F. Semmelhack and A. Yamashita, *J. Am. Chem. Soc.*, 1980, **102**, 5924.
12 H. G. Schmalz and K. Schellhaas, *Angew. Chem., Int. Ed. Engl.*, 1997, **35**, 2146.
13 A. J. Pearson and A. V. Gontcharov, *J. Org. Chem.*, 1998, **63**, 152.
14 M. F. Semmelhack, H. T. Hall, M. Yoshifuji, G. Clark, T. Bargar and K. Hirotsu, *J. Am. Chem. Soc.*, 1979, **101**, 3535.
15 E. P. Kündig and D. P. Simmons, *J. Chem. Soc., Chem. Commun.*, 1983, 1320.

Communication 8/08072K

Preparation, characterisation and slow quantitative dissociation of a novel asymmetric *N*-unsubstituted dialkylsulfimide

Anthony D. M. Curtis,[a] Ray McCague,[b] Christopher A. Ramsden*[a] and Muhammad R. Raza[a]

[a] *Department of Chemistry, Keele University, Keele, Staffordshire, UK ST5 5BG. E-mail: cha33@cc.keele.ac.uk*
[b] *Chirotech Technology Ltd.,Cambridge Science Park, Milton Road, Cambridge, UK CB4 4WE*

Received (in Liverpool, UK) 26th October, 1998, Accepted 8th December 1998

(±)-*S*-Imino-4,5-dihydro-3*H*-dinaphtho[2,1-*c*:1′,2′-*e*]thiepine, a novel asymmetric *N*-unsubstituted sulfimide, undergoes slow, quantitative N–S bond cleavage in $CDCl_3$ solution at 20 °C with a half-life of 20 h.

Sulfimides, sulfoxides and sulfur ylides **1** (X = NR, O or CR_2) belong to a general family of 'non-classical' molecules that are associated with three-centre, four-electron [3*c*-4*e*] bonds.[1]† This large family includes 1,3-dipoles, *e.g.* **2**,[2] and hypervalent compounds, *e.g.* **3**.[3,4] Whether represented by 1,3-dipolar,

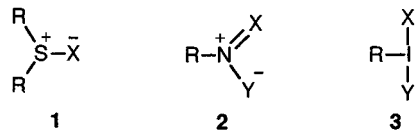

1 **2** **3**

hypervalent or hetero-ylide structures, the fundamentally similar bonding in these non-classical molecules leads to common modes of reaction.[1] These include '*syn*-addition' and 'ligand coupling': in the latter mode of reaction the [3*c*-4*e*] bond is transformed into a lone pair and either a σ-bond between ligands X and Y (*e.g.* 1,3-dipoles **2** and hypervalent molecules **3**) or a second lone pair on a single ligand X (*e.g.* ylides and hetero-ylides **1**).[1] Transfer of nitrene or an alkylnitrene from a chiral sulfimide **1** (X = NH or N–alkyl) to prochiral substrates is a potentially useful application of ligand coupling and this has prompted us to seek a suitably reactive chiral *N*-unsubstituted sulfimide for evaluation.

N-Unsubstituted diarylsulfimides **1** (R = Ar, X = NH) are stable compounds and relatively unreactive, decomposing to the diarylsulfide only at 100 °C or above.[5–7] In contrast, the dialkyl derivatives **1** (R = alkyl, X = NH) are reported to be very unstable with respect to decomposition to the dialkylsulfide.[7–9] To be synthetically useful a suitable sulfimide should be sufficiently stable for convenient preparation but ideally should be reactive at ambient temperature. The sulfide precursor must also be accessible and robust enough to facilitate recovery and regeneration of the sulfimide. We have now identified a novel chiral *N*-unsubstituted sulfimide that fulfils these requirements. In particular, we report the preparation of the asymmetric (C_1) unsubstituted sulfimide **4** from the dissymmetric (C_2) sulfide **5** and its slow and quantitative first-order thermal dissociation back to the sulfide precursor **5** (Scheme 1). The process **4** → **5** can be formally classified as a ligand coupling in which the ligand is nitrene (:NH), and in principle this reaction provides a source of singlet nitrene in a chiral environment. This behaviour

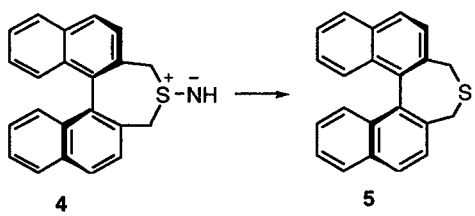

4 **5**

Scheme 1

is consistent with the general classification described above but the ease of dissociation is surprising since thioethers are not particularly good leaving groups in related reactions.[10] Since the enantiomers of sulfide **5** can be separated using column chromatography (triacetylcellulose),[11] sulfimide enantiomers **4** can be separately prepared by amination of homochiral sulfide **5** and, furthermore, homochiral sulfide regenerated during reactions of sulfimide enantiomers **4** can be recycled without the need for resolution.

Initially we attempted to prepare the novel sulfimide **4** *via* the *N*-tosyl derivative **6**. Treatment of the racemic sulfide **5**[11] in CH_2Cl_2 with chloramine-T (1.12 equiv.) and hexadecyltributylphosphonium bromide (0.06 equiv.) gave the (±)-*N*-tosylsulfimide **6**, mp 225 °C (decomp.) (86%).‡ All attempts to

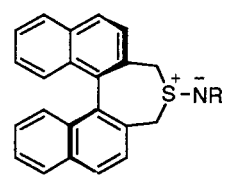

6 R = Ts
7 R = CONHPh

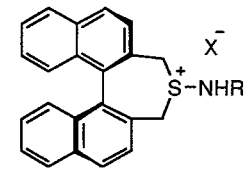

8 R = H, X = OMes
9 R = Ts, X = Cl

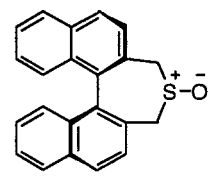

10

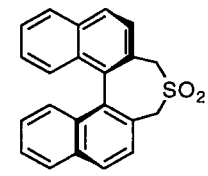

11

obtain the free sulfimide **4** by acid catalysed removal of the tosyl group[5,6] were unsuccessful. In an alternative approach, reaction of the sulfide **5** with *O*-mesitylenesulfonylhydroxylamine[12] (1.5 equiv.) gave the (±)-*S*-aminosulfonium salt **8**, mp 199 °C (decomp.) (87%). All spectroscopic properties of compounds **6** and **8** supported the assigned structures. In particular, the ^{1}H NMR spectrum ($CDCl_3$) of the salt **8** showed two pairs of doublets (*J* 12 and 14.5 Hz) at δ 3.71, 3.94, 4.42 and 4.78 due to the four non-equivalent methylene protons.

For direct comparison of spectroscopic properties we have also made the asymmetric (C_1) sulfoxide **10** and the dissymmetric (C_2) sulfone **11**. Oxidation of the sulfide **5** with sodium perborate tetrahydrate (1.0 equiv.) in glacial AcOH gave the novel sulfoxide **10**, mp 239–241 °C (92%) and use of 2 equiv. gave the novel sulfone **11**, mp > 260 °C (75%). As expected the ^{1}H NMR spectrum ($CDCl_3$) of the sulfoxide showed four discrete doublets (δ 3.26, 3.51, 3.92 and 4.36), (*J* 12 or 14 Hz) for the non-equivalent methylene protons. In $CDCl_3$ the spectrum of the sulfone showed only a singlet (δ 4.11) for the four methylene protons but in C_6D_6 solution two doublets (δ 3.49, *J* 14 Hz and δ 3.62, *J* 14 Hz) consistent with the dissymmetric structure **11** were observed.

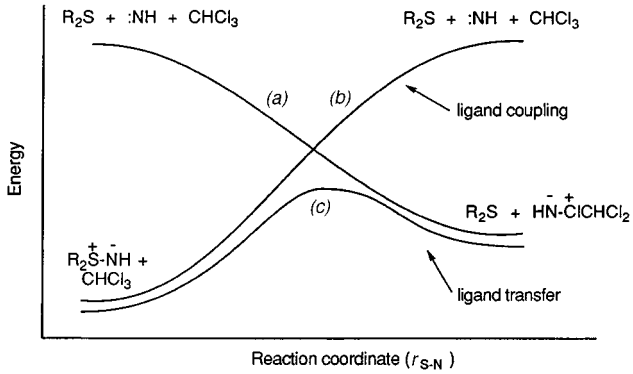

Fig. 1 A bond forming–bond breaking analysis and the possible role of solvent in the S–N bond dissociation of *N*-unsubstituted sulfimides.

The salt **8** can be converted into the free sulfimide **4** in solution by treatment with a number of bases including LDA, DBU and DABCO. The *N*-unsubstituted sulfimide **4** is too unstable to be isolated but is sufficiently stable in solution at room temperature to allow investigation of its properties, and it appears to be indefinitely stable in solution at 0 °C and below. Treatment of a toluene solution of compound **8** at −80 °C with LDA (1.0 equiv.) followed by addition of phenyl isocyanate (3.0 equiv.) gave the adduct **7**, mp 142 °C (decomp.) (67%). In a similar manner the *N*-tosylsulfimide **6** (88%), identical to an authentic sample, was obtained *via* the salt **9** by *in situ* treatment of the sulfimine **4** with TsCl. The ^{1}H NMR spectrum of the free sulfimide **4** in $CDCl_3$ solution was obtained by treatment of the salt **8** with 1 equiv. of base. Using DBU, a spectrum with two pairs of doublets (δ 3.03, 3.56, 3.72 and 4.16), (*J* 12 or 14 Hz) assignable to the four non-equivalent methylene protons was obtained. As expected, this spectrum closely resembles that of the stable and closely related sulfoxide **10** and the signals are up-field relative to those for the corresponding protons in the cation **8**. In agreement with their C_1 symmetry, non-equivalence of the CH_2 groups was also observed in the ^{13}C NMR spectra of sulfimide **4** (δ 54.25 and 56.59) and sulfoxide **10** (δ 54.62 and 57.08). In contrast, the C_2 symmetric sulfide **5** and sulfone **11** each show a single CH_2 signal, which appear at δ 32.35 and δ 58.24, respectively.

When an NMR sample of the sulfimide **4** was re-examined after 24 h the spectrum showed that a significant amount of the sulfide **5** was present. The rate of transformation of the sulfimide, generated in $CDCl_3$ solution using LDA (1.0 equiv.), was followed by monitoring the decay of the proton doublet at δ 4.16 using $CHCl_2CHCl_2$ in a sealed capillary (δ 5.96) as internal reference. Slow but quantitative transformation to the sulfide **5** took place over a period of 4 days, during which the sulfide proton signals appeared and simultaneously the sulfimide signals decayed. The dissociation **4** → **5** has a half-life (*ca.* 20 h) which is independent of concentration, suggesting reaction kinetics that are first-order or pseudo-first-order. We have not yet been able to determine the fate of the NH fragment, the products of which may include N_2 and NH_3.[5–9]

Thermal dissociation of a simple *N*-unsubstituted sulfimide to a sulfide and singlet nitrene at room temperature is an unexpected process in which an electron-rich nitrogen atom is transformed in one step into an electron-deficient nitrogen. In the gas phase this process is also extremely endothermic. Using the AM1 semi-empirical MO method,[13] we have calculated the energy of dissociation for the process Me_2S^+–N^-–H → Me_2S + NH to be 106.8 kcal mol^{-1} and to have an energy profile of the type described by the curve (*b*) in Fig. 1. Solvation of the sulfimide and sulfide are unlikely to change this profile but solvation of the nitrene may be significant. Singlet nitrene has a low energy, unoccupied p-orbital that can interact with a lone pair on solvent molecules such as $CHCl_3$ to form a hetero-ylide (*i.e.* HN^-–Cl^+–R). Participation of the solvent may therefore facilitate the reaction by providing an alternative mechanism ('ligand transfer') as shown by curve (*c*) in the Bell–Evans–Polanyi analysis[14] in Fig. 1. This mechanism is consistent with pseudo-first-order kinetics and the proposed iminochlorinane intermediate is analogous to the isolable iminoiodinanes, *e.g.* TsN^--I^+Ph.[15] This mode of stabilisation of singlet nitrenes is consistent with experimental observations that CH_2Cl_2 stabilises the singlet-state character of nitrenes.[16] A similar model for lone pair stabilisation of nitrenes has been proposed by Gleiter and Hoffmann.[17] NMR studies in inert solvents to eliminate solvent participation, *e.g.* saturated hydrocarbons, were precluded by solubility and availability. When the sulfimide **4** was generated in C_6D_6 solution sulfide formation still occurred but the reaction was not as clean as in $CHCl_3$: a very complex mixture of additional products was observed and none were formed in any significant amount.

In conclusion, we have obtained a chiral *N*-unsubstituted sulfimide having sufficient levels of stability and reactivity to enable studies of its nitrene transfer onto prochiral substrates. Cleavage of the S–N bond probably occurs by interaction with solvent (ligand transfer) to give a reactive intermediate rather than by formation of the free nitrene (ligand coupling). These preliminary results may be relevant to the role of solvent in nitrene mediated reactions. We plan further investigations of the chemistry and modes of reaction of this interesting system and related species.

Notes and references

† These bonds are sometimes described as two-centre, four-electron [2*c*-4*e*] bonds but in this context 'centre' strictly refers to the centres of the three atomic orbitals that interact to form molecular orbitals. In these bonds two of the atomic orbitals happen to be on the same atom but it is important to retain the description [3*c*-4*e*] to emphasise the similarity of bonding and properties to closely related systems, *e.g.* **2** and **3**.

‡ All new compounds were characterised by spectroscopy and elemental analysis.

1 J. I. Musher, *Angew. Chem., Int. Ed., Engl.*, 1969, **8**, 54; C. A. Ramsden, *Chem. Soc. Rev.*, 1994, **23**, 111.
2 *1,3-Dipolar Cycloaddition Chemistry*, ed. A. Padwa, Wiley-Interscience, New York, 1984.
3 A. Varvoglis, *Hypervalent Iodine Chemistry in Organic Synthesis*, Academic Press, London, 1997.
4 R. M. Moriarty, R. K. Vaid and G. F. Koser, *Synlett*, 1990, 365.
5 N. Furukawa, T. Omata, T. Yoshimura, T. Aida and S. Oae, *Tetrahedron Lett.*, 1972, 1619.
6 T. Yoshimura, T. Omata, N. Furukawa and S. Oae, *J. Org. Chem.*, 1976, **41**, 1728.
7 S. Oae and N. Furukawa, *Sulfilimines and Related Derivatives*, ACS Monograph 179, American Chemical Society, Washington, DC, 1983.
8 R. Appel and W. Büchner, *Chem. Ber.*, 1962, **95**, 2220; R. Appel and W. Büchner, *Angew. Chem., Int. Ed. Engl.*, 1959, **71**, 701; R. Appel, W. Büchner and E. Guth, *Liebigs Ann. Chem.*, 1958, **618**, 53.
9 J. B. Lambert, C. E. Mixan and D. S. Bailey, *J. Am. Chem. Soc.*, 1972, **94**, 208.
10 C. A. Ramsden and H. L. Rose, *J. Chem. Soc., Perkin Trans. 1*, 1997, 2319.
11 I. G. Stará, I. Stary, M. Tichy, J. Závada and P. Fiedler, *J. Org. Chem.*, 1994, **59**, 1326.
12 Y. Tamura, J. Minamikawa and M. Ikeda, *Synthesis*, 1977, 1.
13 M. J. S. Dewar, E. G. Zoebisch, E. F. Healy and J. J. P. Stewart, *J. Am. Chem. Soc.*, 1985, **107**, 3902.
14 M. J. S. Dewar, *The Molecular Orbital Theory of Organic Chemistry*, McGraw-Hill, New York, 1969, p. 284.
15 G. Besenyei, S. Németh and L. I. Simándi, *Tetrahedron Lett.*, 1993, 6105.
16 R. C. Belloli and V. A. LaBahn, *J. Org. Chem.*, 1975, **40**, 1972; R. C. Belloli, M. A. Whitehead, R. H. Wollenberg and V. A. LaBahn, *J. Org. Chem.*, 1974, **39**, 2128; G. R. Felt, S. Linke and W. Lwowski, *Tetrahedron Lett.*, 1972, 2037; D. S. Breslow and E. I. Edwards, *Tetrahedron Lett.*, 1972, 2041.
17 R. Gleiter and R. Hoffmann, *Tetrahedron*, 1968, **24**, 5899.

Communication 8/08356H

ChemComm

Crystallographic evaluation of the mobility of 2-naphthoic acid included in heptakis(2,6-di-*O*-methyl)-β-cyclodextrin

Kazuaki Harata

Biomolecules Department, National Institute of Bioscience and Human-Technology, 1-1 Higashi, Tsukuba, Ibaraki 305-8566, Japan. E-mail: harata@nibh.go.jp

Received (in Columbia, MO, USA) 15th September 1998, Accepted 4th December 1998

Analysis of anisotropic temperature factors of the title compound revealed the rigid-body thermal motion of 2-naphthoic acid, which has root mean squared amplitudes of 0.3 Å for translational motion and 6° for libration.

Cyclodextrins are cyclic oligosaccharides consisting of glucose units and form inclusion complexes with a variety of guest molecules. X-Ray structures of numerous crystalline complexes of cyclodextrins and their derivatives have revealed guest molecules included in the macrocyclic cavity.[1] The guest molecules have relatively high mobility in the host cavity because they are weakly bound by van der Waals forces, electrostatic forces, hydrogen bonds, *etc*. instead of chemical bonds. However, no attention has been paid to the mobility of included guest molecules. Analysis of not only the mean structure of inclusion but also the mobility of the guest molecule is essential to elucidate the characteristics of included guests. The crystallographic temperature factor is a measure of the mobility of the atoms, groups or molecules.[2] Analysis of temperature factors is expected to provide information on the dynamic state of guest molecules in crystalline complexes. Here we deal with the thermal motion of 2-naphthoic acid included in heptakis(2,6-di-*O*-methyl)-β-cyclodextrin. The crystal structure of the 1 : 1 complex has been reported.[3]† The naphthalene ring of the guest molecule is inserted into the host macrocycle from the O6 side while the carboxy group protrudes outside the host cavity.

The molecular fluctuation of 2-naphthoic acid was evaluated by the TLS method[4] which has been applied for the analysis of thermal motion of molecular crystals.[4,5] The anisotropic temperature factor is expressed by a linear combination of translation (T), libration (L) and screw motion (S), as described in eqn. (1), where G_{ijkl} and H_{ijkl} are functions of the atomic coordinates.

$$u_{ij} = \Sigma G_{ijkl}\boldsymbol{L}_{kl} + \Sigma H_{ijkl}\boldsymbol{S}_{kl} + \boldsymbol{T}_{ij} \quad (1)$$

Tensor elements for these motions were determined by the least-squares fit to observed anisotropic temperature factors. The quantity minimized was $\Sigma w_{ij}(\Sigma G_{ijkl}\boldsymbol{L}_{kl} + \Sigma H_{ijkl}\boldsymbol{S}_{kl} + \boldsymbol{T}_{ij} - u_{ij})$.[2] The inverse value of the estimated standard deviation of u_{ij} was used as weight w_{ij}. The center of libration was so determined that the $\boldsymbol{S}$ tensor was symmetrical. The tensors of $\boldsymbol{T}$, $\boldsymbol{L}$, and $\boldsymbol{S}$ are given in Table 1. From the eigenvalues of $\boldsymbol{T}$ and $\boldsymbol{L}$ tensors, the root mean squared amplitudes of translational and rotational vibration were estimated as 0.35, 0.27 and 0.27 Å and 4.6, 5.1 and 7.7°, respectively, for the three principal axes. Therefore, 2-naphthoic acid has a rotational vibration of about 6° and a translational vibration of about 0.3 Å. The discrepancy factor for observed and calculated values of u_{eqv} (Table 2), $\Sigma|u_{eqv}^{obs} - u_{eqv}^{cal}|\Sigma u_{eqv}^{obs} = 0.048$, indicates that the magnitude of atomic thermal motion is mostly derived from the rigid-body motion. In contrast, the discrepancy factor of 0.24 for u_{ij} is large. The reason is obvious from the comparison between observed and reproduced temperature factors as shown in Fig. 1. Differences in the orientation of thermal ellipsoids are observed for C5, C6, C7, C8, O1 and O2 and significant disagreements are found in off-diagonal u_{ij} elements for these atoms. A possible explanation for the disagreement is the effect of torsional vibration of the carboxy group around the C2–C11 bond. The local motion of the carboxy group affects the libration parameters and as a result disagreement also occurs for C5, C6, C7 and C8, which are located on the other end of the guest molecule. Such internal motion is coupled with the rigid-body motion and not distinguishable. The TLS model was also applied for the host molecule, but the discrepancy factors of 0.31 and 0.50 for u_{eqv} and u_{ij}, respectively, indicate that the thermal motion of the host molecule is not a simple rigid-body motion because of the high conformational flexibility of the macrocyclic ring.

As shown in Fig. 1, the largest translational motion is in the direction of the short axis of the naphthalene ring. Intermolecular contacts with host molecules impose restrictions on the movement of the guest molecule. Motion in the direction perpendicular to the molecular plane is prohibited by a methyl group and CH_2 groups,[2] which are marked with asterisks in Fig. 1. The carboxy group, which is coplanar with the naphthalene ring within an atomic deviation of 0.05 Å, forms a water-mediated hydrogen-bond bridge with an adjacent host molecule. The C1, C4, C5 and C8 atoms of the naphthalene ring have contacts with the O6 oxygen atoms of the host of 3.5–3.8 Å. Two methyl groups of an adjacent host molecule related *via* a two-fold screw axis are inserted from the secondary hydroxy side and have contacts with the C6 and C7 atoms of the naphthalene ring with a shortest distance of 3.5 Å. The center of libration (O1) is shifted by 0.83 Å towards the C2 atom from the

Table 1 TLS tensors

$\boldsymbol{T}/10^{-3}$ Å^2	$\boldsymbol{L}/10^{-3}$ rad^2	$\boldsymbol{S}/10^{-3}$ rad Å
$\begin{pmatrix} 86 & -7 & -22 \\ -7 & 76 & 8 \\ -22 & 8 & 105 \end{pmatrix}$	$\begin{pmatrix} 13 & 3 & -4 \\ 3 & 10 & -3 \\ -4 & -3 & 10 \end{pmatrix}$	$\begin{pmatrix} -2 & -3 & -2 \\ -3 & 2 & 0 \\ -2 & 0 & 0 \end{pmatrix}$

Table 2 Observed and calculated u_{eqv} (Å^2)

Atom	u_{eqv}^{obs}	u_{eqv}^{cal}	Atom	u_{eqv}^{obs}	u_{eqv}^{cal}	Atom	u_{eqv}^{obs}	u_{eqv}^{cal}
C1	0.097	0.103	C6	0.141	0.142	C11	0.109	0.113
C2	0.095	0.093	C7	0.139	0.137	O1	0.124	0.115
C3	0.107	0.099	C8	0.117	0.127	O2	0.168	0.154
C4	0.117	0.113	C9	0.088	0.100			
C5	0.133	0.136	C10	0.103	0.105			

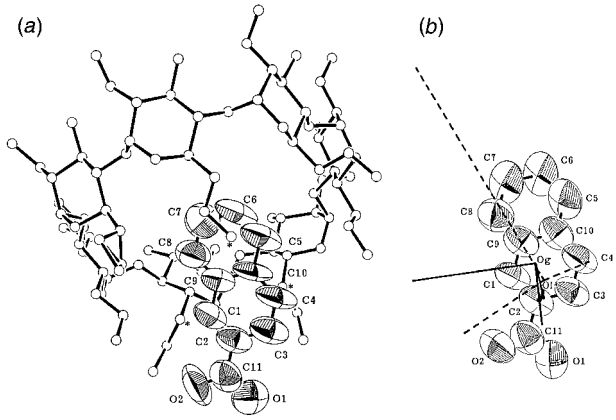

Fig. 1 ORTEP drawings of (*a*) observed and (*b*) reproduced thermal motion of 2-naphthoic acid. Principal axes of translation (solid lines) are drawn from the center of gravity (Og). The length of the axes corresponds to eigenvalues of the ***T*** tensor. Dashed lines denote principal axes of libration drawn from the center of libration (Ol).

center of gravity (Og). The largest libration is around the principal axis located on the guest plane,which makes an angle of about 30° with the long axis of the naphthalene ring. In cyclodextrin complexes, guest molecules generally have greater thermal motion than the host molecules. The present result demonstrates that rigid-body motion is predominant in the thermal motion of the guest molecule and is interpreted in terms of the TLS model.

Notes and references

† *Crystal data*: $C_{56}H_{98}O_{35}\cdot C_{11}H_8O_2\cdot 3H_2O$, M = 1557.6, space group $P2_12_12_1$, a = 15.436(2), b = 18.922(1), c = 27.852(2) Å, Z = 4, D_x = 1.270 g cm^{-3}. X-Ray diffraction data were collected on a Nonius CAD4 diffractometer at 293 K. The structure was refined for 4458 reflections with $F_o > 3\sigma(F)$ to the R value of 0.073.

1 K. Harata, *Chem. Rev.*, 1998, **98**, 1803.
2 B. T. M. Willis and A. W. Pryor, *Thermal Vibrations in Crystallography*, Cambridge University Press, London, 1975.
3 K. Harata, *J. Chem. Soc., Chem. Commun.*, 1993, 2347.
4 V. Schomaker and K. N. Trueblood, *Acta Crystallogr., Sect. B*, 1968, **24**, 63.
5 M. Kaftory and D. Dunitz, *Acta Crystallogr., Sect. B*, 1976, **32**, 617.

Communication 8/07168C

ChemComm

Confinement of C_{70} in an extended saddle shaped nickel(II) macrocycle

Peter D. Croucher, Jodie M. E. Marshall, Peter J. Nichols and Colin L. Raston*

Department of Chemistry, Monash University, Clayton, Melbourne, Victoria 3168 Australia.
E-mail: c.raston@sci.monash.edu.au

Received (in Columbia, MO, USA) 5th October 1998, Accepted 8th December 1998

Saddle shaped {2,3,6,8,11,12,15,17-octamethyldibenzo-[*b*,*i*]1,4,8,11-tetraaza(1,4)annulene}nickel(II), Ni(OMTAA), acts as a heterotropic divergent receptor molecule with C_{70} forming a 1 : 1 complex in the solid state, where the extended supramolecular array consists of zigzag alternating C_{70}–Ni(OMTAA) chains and corrugated sheets of close contact C_{70} molecules.

Host–guest chemistry of globular molecules including fullerenes,[1–18] carboranes,[19] and P_4E_3 (E = S, Se),[1,20] has recently gained prominence in forming inclusion nanostructures, crystal engineering, and in their purification. A major challenge in forming supermolecules involving such molecules is gaining control over the inherently weak host–guest interactions. Complementarity of curvature and maximising the number of points/area of van der Waals contact are important factors in the formation of stable host–guest complexes, at least in the absence of hydrogen bonding, and electrostatic and coordination interactions. Competition between the host–host, host–guest and guest–guest interactions is important in determining the structure of the resulting supramolecular array. This is particularly evident in fullerene chemistry where interfullerene interactions play a major role in the structures of inclusion complexes.[5–15] The interactions of solvent with all species and crystal packing forces provide additional variables.

Recently we reported that Ni(TMTAA), Fig. 1 (R = H), acts as a divergent heterotopic receptor with C_{60}, 1,2-dicarbododecaborane and the chalcogenides P_4S_3 and P_4Se_3;[1,20] the saddle shape of the host arises from otherwise unfavourable interactions between the –{NC(Me)}$_2$CH– methyl groups and the hydrogen atoms on the aromatic rings. Here we report the structure of a 1 : 1 inclusion complex of C_{70} in an extended nickel(II) macrocycle, Ni(OMTAA) (Fig. 1, R = Me). It is noteworthy that there is only one structurally authenticated inclusion complex of C_{70}, a 2 : 1 complex with calix[6]arene.[5]

[Ni(OMTAA)C_{70}] crystallised from a 2 : 1 toluene solution of the two constituents with the host in excess.† The X-ray structure determination‡ revealed that a 1 : 1 complex formed, a molecule of each component comprising the asymmetric unit. Surprisingly it is isostructural to that complex formed between Ni(TMTAA) and C_{60}. It appears that the larger macrocycle and fullerene allows for a similar packing to that of the smaller macrocycle and fullerene. However, the interplay between the fullerene and the host is, in the present structure, complicated somewhat by the long axis present in C_{70}. There are close contacts between the two supramolecular synthons involving the nickel centre, Ni···C 3.20(1) and 3.22(1) Å for the phenylene and {NC(Me)}$_2$CH– lined faces respectively. The extended structure has each fullerene in each saddle in a zigzag motif, Fig. 2. A third macrocycle–fullerene interaction is observed between a pseudo-cavity, defined by the backside face of a phenyl ring and one methyl group from each of the {NC(Me)}$_2$CH– moieties, and a third fullerene residing with its long axis running within the long pseudo-mirror-plane of the Ni(OMTTA) molecule, Fig. 2(a). The interaction is comprised of a π···π stacking of a five membered ring of the fullerene and the phenyl of the host, ring centroid–ring centroid distance 3.30(1) Å; methyl groups in close contact with the fullerene have C···C distances at 3.44(1) and 3.20(1) Å respectively for

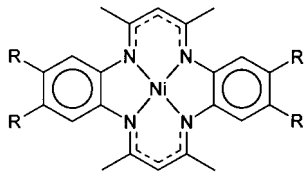

Fig. 1 Ni(TMTAA), R = H, and Ni(OMTAA), R = CH_3.

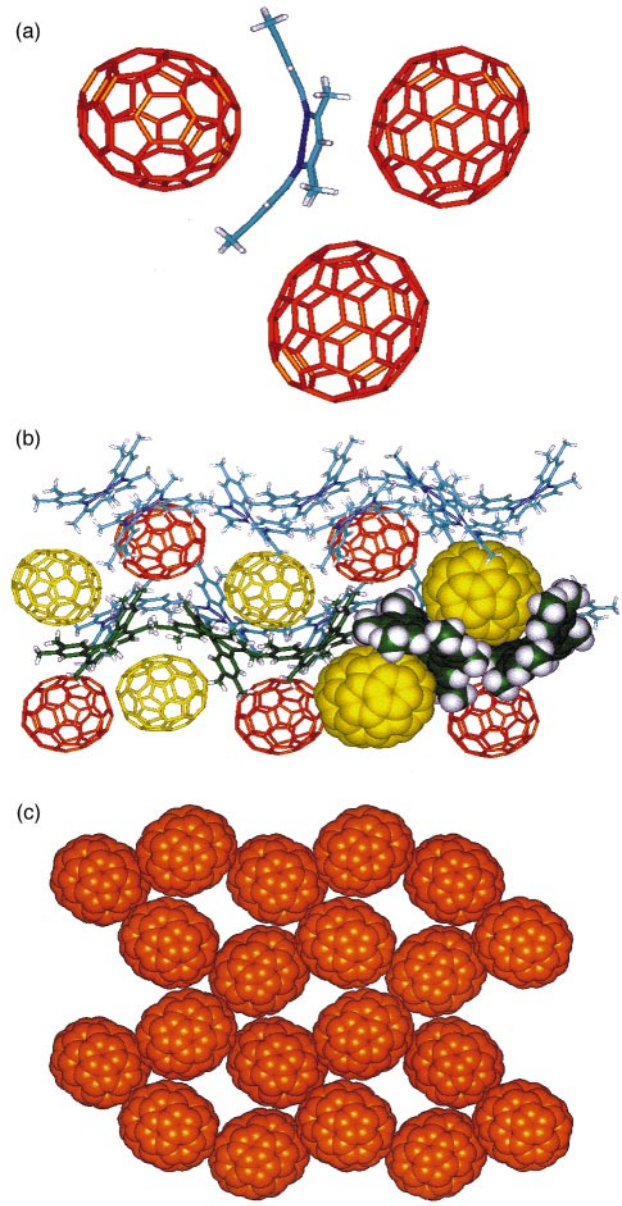

Fig. 2 Structure of [Ni(OMTAA)C_{70}] showing (a) three guest interactions for each macrocycle. (b) The alternating sheets of close-contact fullerenes and Ni(OMTAA) molecules respectively. (c) The corrugated sheet of close contact fullerenes in [Ni(OMTAA)C_{70}].

{NC(Me)}$_2$CH– and 3.17(1) and 2.93(1) Å for the phenyl methyls.

Rather than lie flat across the phenylene face of Ni(OMTAA), the C_5 axis of C_{70} intersects with NiN_4 plane at 33.(1)° along the valley formed by the phenyl rings, and at 15.1(1)° across the valley, and lies almost flat against the {NC(Me)}$_2$CH– face, corresponding angle 15.4(1)°. The elliptical fullerene makes close contact with five other fullerenes forming a two-dimensional corrugated sheet consisting of slightly offset fullerene chains, Fig. 2(b). Within each ridge or trough, the C_5 axes of each C_{70} are arranged in a zigzag fashion with a five-membered ring of one fullerene and a six-membered ring of another fullerene in the chain π-stacking, albeit with a slight deviation from coplanarity, making a point of closest contact at 3.14(1) Å. One of the poles of the fullerene, *i.e.* the five-membered ring through which the C_5 axis passes, forms a classical π···π stacking interaction with that of an adjacent fullerene such that one of the participating fullerenes is on a ridge, the other in a trough. The fourth and fifth close contact points to each fullerene run at right angles to the grain of the sheet, as defined by the ridges and troughs, and continue on to form a chain which has the C_5 axes aligned in a zigzag fashion and contiguous fullerenes alternating between ridge and trough positions. These points are those of closest contact to each fullerene, C···C 3.05(1) Å. Interestingly, the C_5 axes of the C_{70} in this structure and one of the C_5 axes of C_{60} in the [Ni(OMTAA)C_{60}] structural analogue are aligned similarly within their respective supramolecular arrays despite the spherical nature of the C_{60}.

The pole of the fullerene not involved in the π···π interfullerene interaction, aligns itself with one of the {NC(Me)}$_2$CH– methyl groups making a C···C point of close contact at 3.05(1) Å. Four other fullerene molecules make van der Waals contact with the phenylmethyl and {NC(Me)}$_2$CH– methyl groups of Ni(OMTAA). The phenylmethyl groups at one end of the Ni(OMTAA) molecule make two van der Waals contact points with those of an adjacent molecule of opposite curvature to form an S-shaped fragment –CH_3···CH_3 2.88(1) Å. A second host–host interaction involves offset side-by-side molecules, again with opposing curvature, such that the central {NC(Me)}$_2$CH– proton aligns itself with the aromatic proton of its neighbour H···H 2.91(1) Å {NC(Me)}$_2$CH– methyl groups make close contact at 2.89(1) Å and crystallographic symmetry makes the third contact point identical to the first. Ni(OMTAA) makes van der Waals contact with two further host molecules through the methyl groups on both the phenyl and {NC(Me)}$_2$CH– moieties. Consequently, the supramolecular array consists of sheets of fullerene layered between intercalating sheets of Ni(OMTAA) [Fig. 2(c)].

The 1 : 1 complex [Ni(OMTAA)C_{70}] is isostructural with [Ni(OMAA)C_{60}] despite the difference in host shape and increased host–host interaction. This finding gives insight into now studying the supramolecular chemistry of higher fullerenes *via* extending the arms of the nickel macrocycle to accommodate the large fullerenes in an isostructural system.

We thank the Australian Research Council for support of this work.

Notes and references

† [Ni(OMTAA)C_{70}] was obtained by mixing hot toluene solutions of the nickel(II) macrocycle (20 mg, 0.04 mmol) and C_{70} (16 mg, 0.02 mmol) and cooling the resultant solution slowly whereupon black plate-like crystals of the complex were deposited. Cold toluene was added quickly to the cooled mixture and the crystals were removed by filtration and washed with dichloromethane until the filtrate became colorless giving [Ni(OMTAA)C_{70}] (20 mg, 80% yield).

‡ *X-Ray crystallography*: [Ni(OMTAA)C_{70}]: data were collected on an Enraf Nonius CCD and were corrected for Lorenzian and polarisation but not absorption. The structure was solved using TEXSAN. All non-hydrogen atoms were refined anisotropically using a full-matrix least-squares refinement against *F*. Hydrogen atoms were included at calculated positions with a riding model. *Crystal data*. $C_{96}H_{30}N_4Ni$, M = 1298.02, monoclinic, space group $P2_1/n$, a = 14.9165(5), b = 18.8797(7), c = 19.5635(4) Å, β = 105.490(1)°, U = 5309.3(3) Å^3, Z = 4, D_c = 1.624 g cm^{-3}, Mo-Kα radiation, λ = 0.71073 Å, T = 123 K, μ = 4.35, 4235 reflections observed, 910 parameters, R = 0.0649, wR_2 = 0.0474. CCDC 182/1105. See http://www.rsc.org/suppdata/cc/1999/193/ for crystallographic files in .cif format.

1 P. C. Andrews, J. L. Atwood, L. J. Barbour, P. J. Nichols and C. L. Raston, *Chem. Eur. J.*, 1998, **4**, 8, 1382.
2 J. L. Atwood, G. A. Koustantonis and C. L. Raston, *Nature*, 1994, **368**, 229.
3 K. Tsubaki, K. Tanaka, T. Kinoshita and K. Fuji, *Chem. Commun.*, 1998, 895; T. Haino, M. Yanase and Y. Fukazawa, *Tetrahedron Lett.*, 1997, **38**, 3739; A. Ikeda and S. Shinkai, *Chem. Rev.*, 1997, **97**, 1713; A. Ikeda, M. Yoshimura and S. Shinkai, *Tetrahedron Lett.*, 1997, **38**, 2107; K. Araki, K. Akao, T. Suzuki and S. Shinkai, *ibid*, 1996, **37**, 73; T. Suzuki, K. Nakashima and S. Shinkai, *Tetrahedron Lett.*, 1995, **36**, 249; T. Suzuki, K. Nakashima and S. Shinkai, *Chem. Lett.*, 1994, 699; R. M. Williams, J. M. Zwier and J. W. Verhoeven, *J. Am. Chem. Soc.*, 1994, **116**, 6965; R. M. Williams and J. W. Verhoeven, *Recl. Trav. Chim. Pays-Bas*, 1992, **111**, 531.
4 A. Drljaca, C. Keppert, L. Spiccia, C. L. Raston, C. A. Sandoval and T. D. Smith, *Chem. Commun.*, 1997, 195.
5 J. L. Atwood, L. J. Barbour, C. L. Raston and I. B. N. Sudria, *Angew. Chem., Int. Ed. Engl.*, 1998, **37**, 981.
6 Z. Yoshida, H. Takekuma, S. Takekuma and Y. Matsubara, *Angew. Chem., Int. Ed. Engl.*, 1994, **33**, 1597.
7 T. Haino, M. Yanase and Y. Fukuzawa, *Angew. Chem., Int. Ed. Engl.*, 1997, **36**, 259.
8 T. Haino, M. Yanase and Y. Fukuzawa, *Angew. Chem., Int. Ed. Engl.*, 1997, **37**, 997.
9 C. L. Raston, J. L. Atwood, P. J. Nichols, I. B. N. Sudria, *Chem. Commun.*, 1996, 2615.
10 J. W. Steed, P. C. Junk, J. L. Atwood, M. J. Barnes, C. L. Raston and R. S. Burkhalter, *J. Am. Chem. Soc.*, 1994, **116**, 10 346; J. L. Atwood, M. J. Barnes, M. G. Gardiner and C. L. Raston, *Chem. Commun.*, 1996, 1449.
11 N. S. Isaacs, P. J. Nichols, C. L. Raston, C. A. Sandoval and D. Young, *Chem. Commun.*, 1997, 1839.
12 L. Y. Chiang, J. W. Swirczewski, K. Liang and J. Millar, *Chem. Lett.*, 1994, 981.
13 Q. Zhu, D. E. Cox, J. E. Fischer, K. Kniaz, A. R. McGhie and O. Zhou, *Nature*, 1992, **355**, 712.
14 J. D. Crane, P. B. Hitchcock, H. W. Kroto, R. Taylor and D. R. M. Walton, *J. Chem. Soc., Chem. Commun.*, 1992, 1764.
15 P. W. Stephens, D. Cox, J. W. Lauher, L. Milhaly, J. B. Wiley, P. Allemand, A. Hirsch, K. Holczer, Q. Li, J. D. Thompson and F. Wudl, *Nature*, 1992, **355**, 331.
16 A. Izuoka, T. Tachikawa, T. Sugawara, Y. Saito and H. Shinohara, *Chem. Lett.*, 1992, 1049.
17 A. Izuoka, T. Tachikawa, T. Sugawara, Y. Suzuki, M. Konno, Y. Saito and H. Shinohara, *J. Chem. Soc., Chem. Commun.*, 1992, 1472.
18 J. D. Crane and P. B. Hitchcock, *J. Chem. Soc., Dalton Trans.*, 1993, 2537.
19 A. Harada and S. Takahashi, *J. Chem. Soc., Chem. Commun.*, 1988, 1352; P. D. Godfrey, W. J. Grigsby, P. J. Nichols and C. L. Raston, *J. Am. Chem. Soc.*, 1997, **119**, 9283; R. J. Blanch, M. Williams, G. D. Fallon, M. G. Gardiner, R. Kaddour and C. L. Raston, *Angew. Chem., Int. Ed. Engl.*, 1997, **36**, 504.
20 P. C. Andrews, J. L. Atwood, L. J. Barbour, P. D. Croucher, P. J. Nichols and C. L. Raston, in preparation.

Communication 8/07990K

Chiral 1,2-ethanediyl-spaced quaterpyridines give a library of cyclic and double helicates with copper(I)

Gerhard Baum,[b] Edwin C. Constable,*[a] Dieter Fenske,[b] Catherine E. Housecroft[a] and Torsten Kulke[a]

[a] *Institut für Anorganische Chemie, Spitalstrasse 51, CH-4056 Basel, Switzerland. E-mail: constable@ubaclu.unibas.ch*

[b] *Institut für Anorganische Chemie, Universität Karlsruhe (TH), Engesserstraße, 76128 Karlsruhe, Germany*

Received (in Cambridge, UK) 25th November, 1998 Accepted 10th December 1998

A new enantiomeric pair of ligands in which a 2,2′:6′,2″:6″,2‴-quaterpyridine has been split into two 2,2′-bipyridine binding domains by a CH_2CH_2 spacer has been prepared: reaction with Ag(I) gives dinuclear double helicates whereas Cu(I) gives a library of $\{CuL\}_n^{n+}$ complexes (n = 2,3,4,5) of which the compounds with n = 2,3 have been structurally characterised as double helicates and cyclohelicates respectively.

It is established that oligopyridines can give helicates upon coordination to metal centres[1,2] and that structural development of the ligand allows subtle control to be exerted over the consequences of helication; for example, chiral ligands may be used to give a diastereomeric excess of left- or right-handed helicates[3,4] or spacers may be introduced which might lead to the formation of closed circular structures.[4–8] To date, only two examples of cyclohelicates with chiral ligands have been reported, and in each case the reactions were diastereoselective, giving trinuclear[8] or hexanuclear[4] solid state complexes. Here we report the formation of a library of $\{CuL\}_n^{n+}$ species from reactions of a new chiral helicand based upon a spaced 2,2′:6′,2″:6″,2‴-quaterpyridine (qtpy).

The new chiral ligands all-(*S*)-**1** and all-(*R*)-**2** were obtained in 80–85% yield using standard methods and were fully characterised. The ligands exhibited equal and opposite optical rotations in chloroform (**1**: $[\alpha]_D^{23°}$ +82.2°; **2**: $[\alpha]_D^{23°}$ −82.3°) and circular dichroism (CD) spectra. The spectra exhibited two principal absorptions (**1**: $\Delta\varepsilon_{255}$ +5.8, $\Delta\varepsilon_{307}$ −1.7; **2**: $\Delta\varepsilon_{255}$ −6.2, $\Delta\varepsilon_{301}$ +2.4) which correspond to π–π* transitions in the electronic spectra at 256 and 299 nm. The ligands are chiral analogues of **3** which has been shown to form dicopper(I) double helicates[9–12] and we were interested in comparing the diastereoselectivities obtained upon the formation of double helicates with **1** and **2** with the corresponding qtpy ligands **4** and **5**.[13]

Ultrasonication of a 1:1 stoichiometric mixture of AgO_2CCH_3 or $[Cu(MeCN)_4][PF_6]$ and **1** or **2** in MeOH (Ag or Cu) or MeCN (Cu) gave solutions from which colourless or orange hexafluorophosphate salts of stoichiometry $[\{AgL\}_n][PF_6]_n$ or $[\{CuL\}_n][PF_6]_n$ were isolated in near quantitative (≥97%) yield after recrystallisation of the initial precipitates by the diffusion of diethyl ether vapour into MeOH or MeCN solutions. In each case, the compounds only exhibited a single spot on tlc analysis (SiO_2, MeCN, H_2O, aqueous KNO_3).

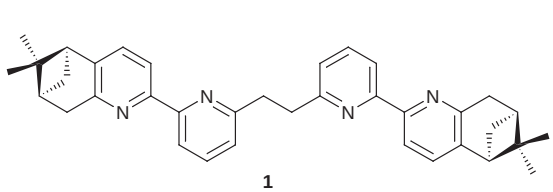

1

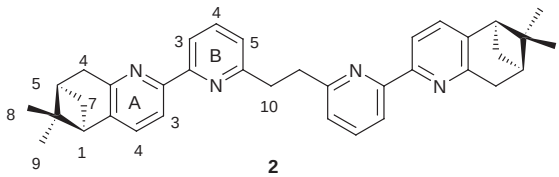

2

To simplify the discussion, only complexes with **1** will be explicitly discussed. Those with **2** parallel the behaviour exactly. In the case of the silver complex, both ES (MeCN or MeOH) and MALDI TOF (2,6-dihydroxybenzoic acid matrix) mass spectrometry showed an intense peak at *m/z* 1414 corresponding to $\{[Ag_2(\mathbf{1})_2][PF_6]\}^+$ but no peaks corresponding to higher nuclearity species and suggesting a double-helical formulation. This is further supported by the observation of a single solution species in the ^{1}H NMR spectrum (CD_3CN). The signals corresponding to H^{5B}, $H^{4A,4B}$ and the ethylene bridge protons are broadened at ambient temperature but show no change over a temperature range −40 to +75 °C suggesting that a low energy intramolecular process is responsible for the broadening rather than a chemical exchange process. The complex is optically active and solutions in MeCN exhibit $[a]_D^{23}$: +73.1° and CD spectra with $\Delta\varepsilon_{220}$ +26, $\Delta\varepsilon_{298}$ −31 and De_{322} +64. The band at 322 nm with a large $\Delta\varepsilon$ is characteristic of a double helicate and the sign of $\Delta\varepsilon$ allows the unambiguous assignment of *P* helical chirality to the double helix obtained with **1** and *M* helical chirality to the complex with **2**.[3,13,14] To conclude, the reaction of **1** or **2** with AgO_2Ac leads only to dinuclear double helicates.

The case of the copper(I) complexes was far more complicated. Solutions in CD_3OD exhibited two subspectra in a ratio of 10:7 and comparison of chemical shifts with the double-helical copper(I) complexes of **3** strongly suggested the formation of a mixture of *P* and *M* dinuclear double helicates. Recrystallisation from MeOH yielded orange needles together with smaller amounts of fluffy solid consisting of small orange crystals. The ^{1}H NMR spectrum of the fluffy crystalline solid (in CD_3OD) corresponded to the dominant species, but within 10 min the solution had equilibrated to give the 10:7 ratio of complexes, the most characteristic signals of which are doublets assigned to H^{5B} at δ 7.16 and 7.03 for the major and minor species respectively. The ES MS of either type of crystal in MeOH revealed only peaks assigned to $\{[Cu_2(\mathbf{1})_2][PF_6]\}^+$ and $[Cu_2(\mathbf{1})_2)]^{2+}$. The needles consisted of a 1:1 mixture of the two species and a solid state structural determination confirmed the formulation as a dinuclear double helicate.†

The structural determination of the complex $\{[Cu_2(\mathbf{2})_2][PF_6]_2\}_2 \cdot 3Et_2O$ showed that the needles were a *quasi*-racemate containing equal amounts of the diastereomeric *P* and *M* double helicates in the crystal (Fig. 1). Each copper is in a distorted four coordinate environment and the bond angles and distances are typical with Cu–N distances of 1.995(4)–2.072(4) Å and bite angles of 81.2–82.2°. The Cu···Cu distances in the individual cations are 5.885 and 5.958 Å comparable to the complexes of **3**[10] but much longer than those with **4** and **5**.[13]

Dissolution of any of the crude solids, or the crystalline materials obtained from MeOH in CD_3CN resulted in orange solutions whose ^{1}H NMR spectra contained between three and

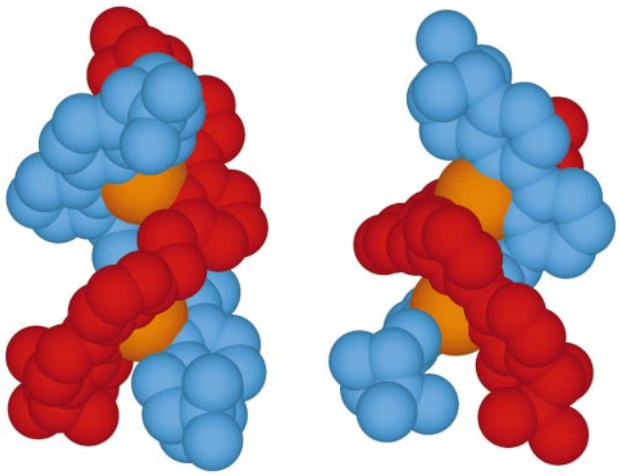

Fig. 1 The solid state structures of the *M* and *P* cations in $[Cu_2(\mathbf{2})_2][PF_6]_2 \cdot 3Et_2O$; hydrogen atoms have been omitted for clarity.

five species (as monitored by the upfield H^{5B} resonances) depending upon the concentration of the sample. Systematic and reversible changes in the spectra and speciation occurred upon varying the concentration, or upon titrating CD_3OD into CD_3CN solutions (or *vice versa*). ES MS studies of the MeCN or MeOH solutions revealed the presence of ions assigned to $[Cu_2(\mathbf{1})_2)]^{2+}$, $\{[Cu_2(\mathbf{1})_2][PF_6]\}^{+}$, $[Cu_3(\mathbf{1})_3]^{3+}$, $\{[Cu_4(\mathbf{1})_4][PF_6]\}^{3+}$ $\{[Cu_5(\mathbf{1})_5][PF_6]_2\}^{2+}$ and $\{[Cu_5(\mathbf{1})_5][PF_6]_3\}^{3+}$ (all charges confirmed by partial mass isotopomer distribution) and allowed the assignment of the subspectrum containing a δ 5.94 resonance for H^{5B} to the trinuclear species. Higher concentrations favoured the formation of higher nuclearity species and at concentrations below 10^{-4} M only the dinuclear species were present in MeCN according to both ^{1}H NMR and ESMS measurements.

Diffusion of Et_2O vapour into MeCN solutions of the complexes at an initial concentration that the NMR studies indicated significant amounts of the trinuclear species should be present resulted in the formation of triangular orange crystals, fresh solutions of which only exhibited (in CD_3OD) the subspectrum containing the δ 5.94 ^{1}H NMR resonance; upon standing the mixture of complexes was regenerated. A solid state structure determination† revealed a pair of diastereomeric *P* and *M* cyclic $[Cu_3(\mathbf{1})_3]^{3+}$ cations (Fig. 2). The bond angles and distances are similar to those in $[Cu_2(\mathbf{2})_2][PF_6]_2$ and the three Cu centres are in a distorted tetrahedral geometry (bite angles 80.0–82.4°, Cu–N 1.981–2.048 Å) and describe a triangle with Cu···Cu distances of 6.905–6.983 Å. The pinene groups point outwards giving the cation an outer diameter of *ca*. 20.5 Å and a height of 8 Å. The shortest distance between the ligands is around 3.7 Å (C···C) or 2.2 Å (shortest H···H), making the cavity at the centre of the triangle too small to include any guests. By

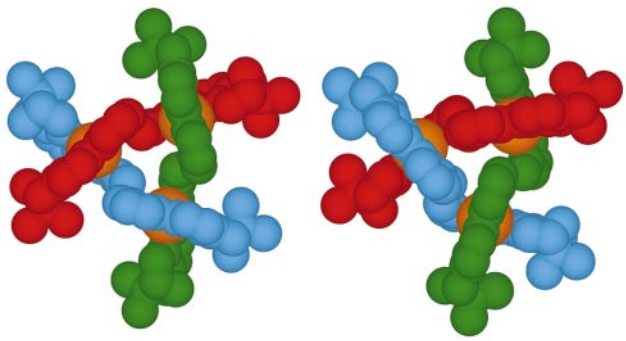

Fig. 2 The solid state structures of the *M* and *P* cyclohelicate cations in $[Cu_3(\mathbf{1})_3][PF_6]_2 \cdot 0.75MeCN$, hydrogen atoms have been omitted for clarity.

analogy, we assume that the higher nuclearity species are also cyclohelicates.

In both of the complexes structurally characterised, the spacer reduces interactions between the chiral substituents and the other ligand strand such that the diastereoselectivity is reduced[13] and in the solid state, *quasi*-racemates are obtained. In contrast to previously reported cyclohelicates, which in the solid state exhibited diastereoselective formation of *P* or *M* helicates, our system shows no solid state diastereoselectivity. In contrast, modest diastereoselectivity is shown in solution; equilibrated MeOH solutions containing only the 10:7 mixture of diastereomers of the dinuclear double helicate have CD responses indicating an excess of the *P* helicate with **1** and the *M* helicate with **2**.

Detailed studies of the speciation and chiroptical properties of these systems are underway; however, we have established that in MeCN solution a library[5] of copper(I) helicates is formed. We should like to thank the Schweizerischer Nationalfonds zur Förderung der wissenschaftlichen Forschung and the University of Basel for support.

Notes and references

† *Crystal data* for $C_{144}H_{152}Cu_4F_{24}N_{16}P_4 \cdot 3(C_2H_5)_2O$: M = 3163.22, triclinic, a = 12.576(3), b = 16.179(3), c = 21.058(4) Å, α = 96.86(3), β = 95.34(3), γ = 111.00(3)°, U = 3928.5(14) Å^3, θ 2.44–28.16°, Z = 1, D_c = 1.337 Mg m^{-3}, space group $P\bar{1}$ (no. 1), Mo-Kα radiation (λ = 0.71073 Å), μ(Mo-Kα) = 6.6 cm^{-1}, F(000) = 1646, T = 200 K, 27400 independent reflections [23672, $I > 2.0\sigma(I)$]. Refinement converged at a final R = 0.0565, wR = 0.1520. Minimum and maximum final residual electron density 0.66 and 0.91 e Å^{-3}.

For $4(C_{108}H_{114}Cu_3N_{12}P_3F_{18}) \cdot 3CH_3CN$: M = 8 945.86, cubic, a = 36.533(5) Å, U = 48759(12) Å^3, θ 1.6–23.3°, Z = 4, D_c = 1.219 Mg m^{-3}, space group $I2_13$ (no. 199), Mo-Kα radiation (λ = 0.71073 Å), μ(Mo-Kα) = 6.33 cm^{-1}, F(000) = 18 504, T = 200 K, 11702 independent reflections [4801, $I > 2.0s(I)$]. Refinement converged at a final R = 0.1098, wR = 0.2730. Minimum and maximum final residual electron density 0.57 and 1.41 e Å^{-3}. In both structures the hexafluorophosphate anions were disordered and crystallographically imperfect models were adopted to allow subsequent refinement of the cations of interest.

Data collected were measured on a STOE IPDS Image Plate diffractometer; structure solution SHELXL-97, SHELXS-97. CCDC 182–1115. See http://www.rsc.org/sappdata/cc/1999/195/ for crystallographic files in .cif format.

1 E. C. Constable, in *Comprehensive Supramolecular Chemistry*, ed. J.-M. Lehn. Pergamon, Oxford, 1996, vol. 9, p. 213.
2 C. Piguet, G. Bernardinelli and G. Hopfgartner, *Chem. Rev.*, 1997, **97**, 2005.
3 G. Baum, E. C. Constable, D. Fenske, C. E. Housecroft and T. Kulke, *Chem. Commun.*, 1998, 2659 and references therein.
4 O. Mamula, A. von Zelewsky and G. Bernardinelli, *Angew. Chem., Int. Ed. Engl.*, 1998, **37**, 290 and references therein.
5 B. Hasenknopf, J.-M. Lehn, B. O. Kniesel, G. Baum, and D. Fenske, *Angew. Chem., Int. Ed. Engl.*, 1996, **35**, 1838; B. Hasenknopf, J. M. Lehn, N. Boumedine, A. Dupont-Gervais, A. Van Dorsellaer, B. O. Kneisel and D. Fenske, *J. Am. Chem. Soc.*, **1997**, **45**, 10956.
6 P. L. Jones, K. J. Byrom, J. C. Jeffery, J. A. McCleverty, and M. D. Ward, *Chem. Commun.*, 1997, 1361.
7 P. W. N. Baxter, J.-M. Lehn and K. Rissanen, *Chem. Commun.*, 1997, 1323.
8 C. Provent, S. Hewage, G. Brand, G. Bernardinelli, L. J. Charbonnière, and A. F. Williams, *Angew. Chem., Int. Ed. Engl.*, 1997, **36**, 1287.
9 Y. He and J.-M. Lehn, *Chem. J. Chin. Univ.*, 1990, **6**, 183.
10 M.-T. Youinou, R. Ziessel and J.-M. Lehn, *Inorg. Chem.*, 1991, **30**, 2144.
11 J.-M- Lehn and R. Ziessel, *Helv. Chim. Acta*, 1988, **71**, 1511.
12 A. Juris and R. Ziessel, *Inorg. Chim. Acta*, 1994, **225**, 251.
13 G. Baum, E. C. Constable, D. Fenske, T Kulke, *Inorg. Chem. Commun.*, 1998, **1**, 80; *Chem. Commun.*, 1997, 2043; G. Baum, E. C. Constable, D. Fenske, C. E. Housecroft and T Kulke, *Chem. Eur. J.*, submitted.
14 M. Ziegler and A. von Zelewsky, *Coord. Chem. Rev.*, in press.

Communication 8/09230C

Novel amine-modified TiO_2–SiO_2 aerogel for the demanding epoxidation of substituted cyclohexenols

Marco Dusi, Christian A. Müller, Tamas Mallat and Alfons Baiker*

Laboratory of Technical Chemistry, Swiss Federal Institute of Technology, ETH-Zentrum, CH-8092 Zürich, Switzerland. E-mail: baiker@tech.chem.ethz.ch

Received (in Cambridge, UK) 29th October 1998, Accepted 3rd December 1998

Amine additives provided high selectivity (up to 98%) in the epoxidation of sensitive alkyl-substituted cyclohexenols with a TiO_2–SiO_2 aerogel and Bu^{t}OOH; heterogenization of the catalyst system resulted in a new bifunctional catalyst.

Recently, active and selective titania–silica epoxidation catalysts have been prepared by the solution sol-gel technique.[1–4] The advantages of this preparation method are the intimate molecular-scale mixing of Ti in the silica matrix and high surface area of the materials. The drying conditions have also been recognized to play an important role: removal of the solvent entrapped in the tenuous gel network by semicontinuous extraction with supercritical CO_2 at near ambient temperature results in mesoporous textural properties, providing access of bulky reactants to the active sites.[2] An aerogel with a TiO_2 content of 20 wt% (20LT), prepared by this method, showed outstanding performance in the epoxidation of cyclic olefins with alkyl hydroperoxides.[5,6]

In the epoxidation of primary and secondary allylic alcohols, high selectivities were achieved in the presence of (basic) zeolite 4 Å or $NaHCO_3$ used as additives.[7] There are also some other examples in the literature on the enhancement of epoxide selectivity when the acidity of a Ti- and Si-containing catalyst is tuned by alkali metal exchange or addition of an inorganic base to the reaction mixture.[8–11] In the epoxidation of alkyl-substituted cyclohexenols, such as 3-methylcyclohex-2-en-1-ol **1** and 3,5,5-trimethylcyclohex-2-en-1-ol (isophorol), 20LT provided the epoxides only as minor products (< 10% selectivity). Unfortunately, the acid-catalyzed side reactions could not be suppressed by any of the known methods. For comparison, good to high yields of the epoxides of alkyl-substituted cyclohexenols were obtained by stoichiometric oxidations,[12–15] but no efficient catalytic method is available yet for this type of epoxidation reaction.[16]

Here we report a new strategy for the selective epoxidation of alkyl-substituted cyclohexenols by adjusting the surface properties of titania–silica with small amounts of amines. The epoxidation of 3-methylcyclohex-2-en-1-ol **1** with TBHP (*tert*-butyl hydroperoxide) was chosen as a model reaction (Scheme 1).

A 20LT aerogel was prepared by the solution sol-gel method as described previously.[2] The solvent was extracted semi-continuously with supercritical CO_2 at 40 °C and 240 bar. The raw aerogel was calcined in air at 400 °C for 5 h. X-Ray analysis showed that the amorphous material possessed a good Ti dispersion, high surface area (S_{BET} = 680 m^2 g^{-1}) and mesoporous structure (mean pore diameter: 9 nm, pore size maximum: 40 nm, pore volume: 1.5 cm^3 g^{-1}).

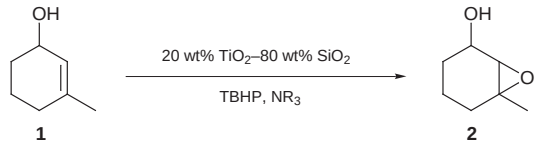

1 **2**

Scheme 1

Prior to epoxidation, 0.1 g 20LT was dried *in situ* in Ar at 200 °C for 16 h. Under standard conditions, epoxidation was carried out at 60 °C in Ar using 10 mmol substrate, 2.5 mmol TBHP, 0.1 g activated molecular sieves 4 Å, the amine modifier, 0.5 ml dodecane (internal standard) and toluene (total volume: 10 ml). Conversion and selectivities were determined by GC analysis and iodometric titration. The conversion of **1** is related to the stoichiometric initial amount of TBHP (4:1) and given in mol% of the maximal attainable value, and the epoxide selectivity is quoted with reference to the substrate consumed.

In the absence of amine the allylic alcohol **1** was readily converted non-oxidatively, and the epoxide **2** was only a minor product (Table 1). Major reactions were the acid-catalyzed isomerization and dehydration of **1**, and oligomerization of **1** and **2**. Note that the epoxidation activity of titania–silica is attributed to the Lewis acidity of the $(Si–O)_4Ti$ sites, whereas the surface silanol groups represent Brønsted acidic sites active in the aforementioned side reactions.[17,18] Addition of 1 or 10 mol% amine (related to **1**) suppressed the acid-catalyzed side reactions and good to high epoxide selectivity was achieved. Interestingly, no correlation between the basicity of the amine additive and the epoxide selectivity could be established.

The amount of amine additive played an important role in the selectivity enhancement, as illustrated in Fig. 1. Only 1 mol% of triazine was sufficient to suppress the acid-catalyzed reactions and reduce the conversion of **1** to 100% or below. Note that the substrate:TBHP molar ratio was 4:1, and that the conversion is related to the initial amount of TBHP. Addition of 5 mol% of triazine afforded the highest epoxide yield of 56%, correspond-

Table 1 Epoxidation of 3-methylcyclohex-2-en-1-ol **1** using amines as additives (under standard conditions)

				Epoxide selectivity (%) related to[b]	
Entry	Additive	pK_a	$t_{30\%}$[a]/min	**1**	Peroxide
1	—	—	1.3	3	34
2[c]	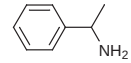	9.4	120	82	49
3[c]		0.65	36	90	80
4[c,d]		–1.7	9.2	92	86
5[e]		10.9	43	73	83
6[e]	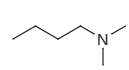	10.0	9	98	*ca.* 100

[a] Time needed for 30% conversion of **1**. [b] Determined at $t_{30\%}$. [c] 10 mol% amine (based on **1**) was used. [d] Ethylbenzene was used as internal standard. [e] 1 mol% amine (based on **1**) was used.

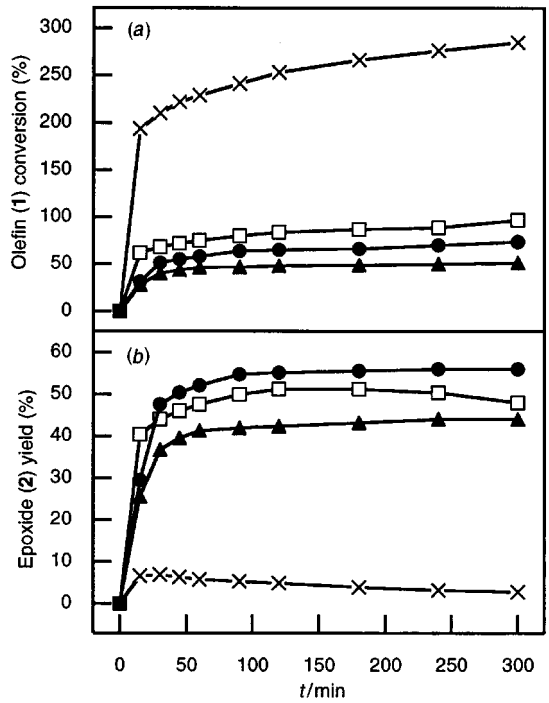

Fig. 1 Influence of the amount of triazine on (*a*) the conversion of **1** (related to the initial amount of TBHP) and (*b*) the yield of **2**: (×) 0, (□) 1, (●) 5 and (▲) 10 mol% based on **1**.

ing to over 90% epoxide selectivity at medium conversion. The results show that the amounts of amine additives quoted in Table 1 may be far from the optimum values.

On the basis of preliminary kinetic studies we propose that the amines have a rather complex effect. At low concentrations they interact mainly with the surface silanol groups, and deactivate (block) these Brønsted sites. This positive effect on selectivity depends only marginally on the pK_a value of the amine, as all amines tested are more basic than the oxygen atom of **1**. At higher concentrations, interaction of the amines with the Ti site seems to be dominant, leading to lower epoxidation activity. This effect is similar to the detrimental influence of alcoholic solvents, which was suggested to be due to their competition with TBHP for the active sites.[17] Also, at high amine concentrations (usually ⩾5mol%) the base-catalyzed ring opening of **2** became important.

Intrigued by the good results of the epoxidation of **1** with Me_2NBu as additive, we prepared a new catalyst with immobilized aminoalkyl groups. An aerogel containing 10 wt% TiO_2 was designed with surface $Me_2N(CH_2)_3$ groups (designated $10LT_A$). To a solution of $(MeO)_4Si$ (135 mmol) and $Ti(acac)_2(OPr^i)_2$ (12.5 mmol) (75% in Pr^iOH) in Pr^iOH (10 ml), the hydrolysant consisting of water (750 mmol) and HNO_3 (15 mmol) in Pr^iOH (40 ml) was added at room temperature. After 6 h stirring, a solution of $Me_2N(CH_2)_3Si(OMe)_3$ (15 mmol) in Pr^iOH (82 ml) was added. The solution gelated within 12 h. After ageing for 7 days at room temperature, the solvent was removed by extraction with supercritical CO_2 at 40 °C and 230 bar. On the basis of a thermoanalytical investigation, the amine-modified aerogel was calcined only at 100 °C for 1 h, in order to avoid decomposition of the $Me_2N(CH_2)_3$ groups. The BET surface area of the mesoporous calcined sample amounted to 312 $m^2\ g^{-1}$. The pore volume was 1.0 $cm^3\ g^{-1}$ and the average cylindrical pore diameter was calculated to be 11.6 nm. The good titania dispersion (relative contribution of Si–O–Ti entities) was confirmed by FT-IR from the ratio of Si–O–Ti (950 cm^{-1}) and Si–O–Si (1210 cm^{-1}) peak areas.

This catalyst also converted the allylic alcohol **1** selectively to the epoxide **2**. At 30% conversion of **1**, which was attained in 18 min, the epoxide selectivity was 78%. As compared to the reaction with 20LT and Me_2NBu (Table 1), the lower epoxide selectivity of $10LT_A$ is likely due to the too high amine content. The catalyst was also tested in the epoxidation of *trans*-hex-2-en-1-ol. Under conditions similar to the oxidation of **1** but at 90 °C, the epoxide yield was 48% after 1 h reaction time. Recycling $10LT_A$ twice (after washing and drying) afforded 33 and 31% yields. The lower yields were partly due to catalyst loss during recycling (17%), and the difference between the performance of fresh and used catalysts decreased at higher reaction times. Epoxide selectivity was barely influenced by recycling (70 and 72% for the first and third runs, respectively). Besides, $10LT_A$ did not catalyze the epoxide ring opening reaction, indicating the suppressed acidity of this amine-modified catalyst.

We have attempted to apply amine modifiers in the epoxidation of other cyclic allylic alcohols. The epoxidation of isophorol over 20LT without amine additive at 363 K resulted in byproducts mainly by non-oxidative reactions, and only 10% epoxide selectivity at 221% conversion (related to initial TBHP concentration) was obtained in 1h. Using $PhMeCHNH_2$ (1 mol%) the side reactions were diminished and 58% epoxide selectivity at 72% substrate conversion was achieved. The influence of alkyl substituents on the epoxidation of cyclohexenols is presently under investigation.

In conclusion, in the epoxidation of alkyl-substituted cyclic allylic alcohols with a titania–silica aerogel and TBHP, small amounts of amines suppress the acid-catalyzed, non-oxidative side reactions. In the best case, 1 mol% of Me_2NBu (related to 3-methylcyclohex-2-en-1-ol reactant) afforded 98% epoxide selectivity at 30% conversion, and over 70% epoxide yield at high conversion. On the basis of this observation, a novel bifunctional, recyclable catalyst has been developed. This modified aerogel contains both Lewis acidic $[(SiO)_4Ti]$ and Lewis basic $[C_3H_6N(CH_3)_2]$ sites. It is hoped that tuning the acid–base and redox properties will further improve the performance of this catalyst.

Financial support by Hoffmann-La Roche AG, Switzerland and the 'Kommission für Technologie und Innovation' is gratefully acknowledged.

Notes and references

1 S. Thorimbert, S. Klein and W. F. Maier, *Tetrahedron*, 1995, **51**, 3787.
2 D. C. M. Dutoit, M. Schneider and A. Baiker, *J. Catal.*, 1995, **153**, 165.
3 S. Klein, J. A. Martens, R. Parton, K. Vercruysse, P. A. Jacobs and W. F. Maier, *Catal. Lett.*, 1996, **38**, 209.
4 H. Kochkar and F. Figueras, *J. Catal.*, 1997, **171**, 420.
5 R. Hutter, T. Mallat, D. Dutoit and A. Baiker, *Top. Catal.*, 1996, **3**, 421.
6 R. Hutter, T. Mallat and A. Baiker, *J. Chem. Soc., Chem. Commun.*, 1995, 2487.
7 M. Dusi, T. Mallat and A. Baiker, *J. Mol. Catal. A: Chem.*, 1999, **138**, 15.
8 G. J. Hutchings, D. F. Lee and A. R. Minihan, *Catal. Lett.*, 1996, **39**, 83.
9 A. Sato, J. Dakka and R. A. Sheldon, *Stud. Surf. Sci. Catal.*, 1994, **84**, 1853.
10 R. Hutter, T. Mallat, A. Peterhans and A. Baiker, *J. Catal.*, 1997, **172**, 427.
11 B. Notari, *Adv. Catal.*, 1996, **41**, 253.
12 W. Adam and A. K. Smerz, *Tetrahedron*, 1995, **51**, 13039.
13 D. Ye, F. Fringuelli, O. Piermatti and F. Pizzo, *J. Org. Chem.*, 1997, **62**, 3748.
14 K. Mori, B. G. Hazra, R. J. Pfeiffer, A. K. Gupta and B. S. Lindgren, *Tetrahedron*, 1987, **43**, 2249.
15 X. Lusinchi and G. Hanquet, *Tetrahedron*, 1997, **53**, 13727.
16 S. M. Brown, S. G. Davies and J. A. A. de Sousa, *Tetrahedron: Asymmetry*, 1991, **2**, 511.
17 R. A. Sheldon, in *Aspects of homogeneous catalysis*, ed. R. Ugo, Reidel, Dordrecht, 1981, vol. 4, p. 3.
18 E. Jorda, A. Tuel, R. Teissier and J. Kervennal, *J. Catal.*, 1998, **175**, 93.

Communication 8/08374F

Generation of a glutathione peroxidase-like mimic using bioimprinting and chemical mutation

Junqiu Liu,[a] Guimin Luo,*[a] Shujuan Gao,[a] Kun Zhang,[a] Xinfan Chen[b] and Jiacong Shen[c]

[a] *The National Laboratory of Enzyme Engineering, Jilin University, Changchun 130023, PR China. E-mail: gmluo@mail.jlu.edu.cn*
[b] *Department of Materials Science, Jilin University, Changchun 130023, P.R. China*
[c] *Key Laboratory for Supramolecular Structure and Spectroscopy of Jilin University, Changchun 130023, PR China*

Received (in Cambridge, UK) 28th October 1998, Accepted 15th December 1998

Molecular imprinting of albumin with *N*,*S*-bis(2,4-dinitrophenyl)glutathione (GSH-2DNP), a glutathione (GSH) derivative, leads to an imprinted protein with GSH binding sites; chemical mutation of the protein results in formation of an artificial enzyme with high glutathione peroxidase (GPX) activity.

The catalytic efficiency of an enzyme is dependent on its ability to recognise substrates, and the generation of recognition sites for substrates plays an important role in enzyme imitation.[1] In general, two strategies have been used to generate this recognition, the monoclonal antibody technique and molecular imprinting.[2,3] Glutathione peroxidase (GPX, EC 1.11.1.9) is an important antioxidative enzyme that catalyzes the reduction of a wide variety of hydroperoxides by glutathione (GSH).[4] The enzyme is composed of four identical subunits; the active site in each subunit contains a selenocysteine residue (catalytic group) and a GSH binding site.[5] Based on the structure of this enzyme, we have previously developed a strategy for generating catalytic antibodies with GSH binding sites and GPX activity using monoclonal antibody preparation technology and chemical mutation.[6] This study shows that the binding site for substrate GSH and the catalytic moiety selenocysteine are critical factors for catalysis.

Here we describe a new strategy for generating a GPX mimic with a GSH binding site using bioimprinting and chemical mutation. The method consists of five basic steps: (i) unfolding the conformation of the starting protein under acid conditions; (ii) addition of the imprinting molecule (or template), to allow it to interact with the denatured protein to form a new conformation with substrate binding sites; (iii) crosslinking the protein with a bifunctional reagent to fix the new conformation of the protein; (iv) dialysis of the protein to remove the imprinting molecules; and (v) conversion of the active serine residues in the binding site of the crosslinked protein into selenocysteines to incorporate catalytic groups. Thus, there are both substrate binding sites and catalytic groups in the printed protein and thus it should display an enzyme activity.

We chose a GSH derivative, *N*,*S*-bis(2,4-dinitrophenyl)glutathione (GSH-2DNP), as the imprinting molecule. The unstable thiol group and amino group of GSH were protected by reaction with 2,4-dinitrofluorobenzene to give GSH-2DNP. The derivative is structurally similar to the substrate molecule GSH. After the conformation of the starting protein (egg albumin) had been unfolded by denaturation, the imprinting molecule (GSH-2DNP) was allowed to interact with the unfolded protein to form a new conformation *via* hydrogen bonds, ion pairing and hydrophobic interactions. The new conformation was then fixed using glutaraldehyde. The cavities, which were left in the printed protein after removing GSH-2DNP by dialysis, were able to recognize the substrate GSH. The serine residues located in the binding sites of the imprinted protein were active and could be converted into the catalytic groups of GPX (selenocysteines) by chemical mutation.[6,7]

The preparation of the imprinted enzyme is as follows: egg albumin (1 ml of a 1 mg ml^{-1} solution) was adjusted to pH 3.0 with 0.1 M HCl and stirred at room temperature for 1 h. The imprinting molecule, GSH-2DNP (5 mg), was added to the protein solution and stirred for 1 h. The pH was then adjusted to 8.0 with 0.1 M NaOH and glutaraldehyde solution (1%; 100 μl) was added. The reaction mixture was stirred at 5 °C for 12 h and dialyzed for 48 h against 50 mM phosphate buffer, pH 7.0. The dialyzed solution was activated by adding 10 μL of phenylmethanesulfonyl flouride (20 mg ml^{-1} solution in MeCN) and incubated at 25 °C for 3 h. A portion of 1 M NaHSe (100 μl; 100 μmol) prepared according to the method of Klayman and Griffin[8] was added to the activated solution, and incubated at 40 °C for 30 h under nitrogen atmosphere. The solution was oxidized by air at 4 °C for 5 h and was centrifuged to remove the solid selenium. The crude imprinted protein was purified by gel filtration on a superose B-12 column, and the first peak was collected; the crosslinked protein in this peak proved to be the dimer by HPLC. The non-printed protein was also prepared from egg albumin using the same conditions in the absence of GSH-2DNP, and used as a control.

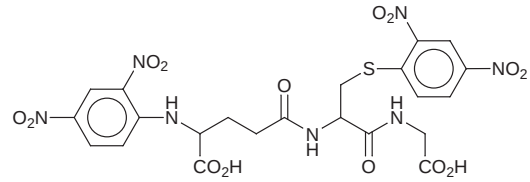

GSH-2DNP

The selenium content was determined by 5,5′-dithiobis(2-nitrobenzoic acid) titration,[7] and 1.89 ± 0.15 equiv. of selenium

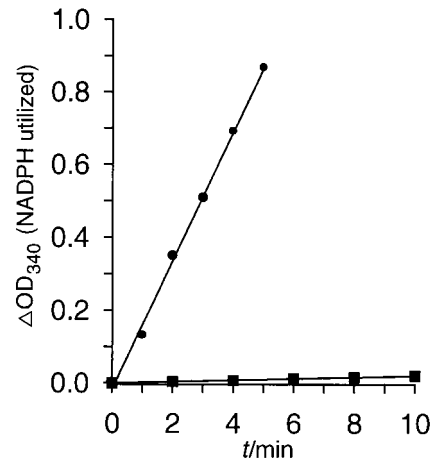

Fig. 1 Printed and non-printed protein-catalyzed reduction of H_2O_2 by GSH: (●) printed protein and (■) non-printed protein. The catalytic reaction containing GSH (1 mM), H_2O_2 (0.5 mM), glutathione reductase (1 unit), NADPH (0.25 mM) and 0.2 μM enzyme mimic (pH 7.0 at 25 °C) was monitored *via* NADPH decrease in absorbance at 340 nm. The absorbance change was corrected for the background reaction between H_2O_2 and GSH.

per printed protein molecule was detected. The GPX activity of the printed protein was measured by a coupled enzyme system containing glutathione reductase, GSH, NADPH and H_2O_2.[6] The printed protein-catalyzed reduction of H_2O_2 by GSH was initiated by adding the substrate H_2O_2. The initial rate of the printed protein (0.2 μM)-catalyzed removal of H_2O_2 (with NADPH) by GSH was found to be 8.2×10^{-3} M min^{-1} during the initial 5 min of reaction (Fig. 1). However, the initial rate of the non-printed protein (0.2 μM)-catalyzed reaction was only 9.5×10^{-5} M min^{-1}. The GPX activities of the printed and non-printed proteins were calculated to be 817 ± 28 and 10 ± 3 U μmol^{-1}, respectively. The printed protein displays a high GPX-like activity and is only seven times less than that of the native GPX from rabbit liver (5780 U μmol^{-1}).[6] Compared with ebselen (PZ51, 0.99 U μmol^{-1}), the best GPX mimic known,[6] the GPX activity of the printed protein is 820 times that for PZ51. The apparent catalytic rate constant for H_2O_2 (k_{cat}) was measured to be 785 min^{-1} ([GSH] = 1 mM).

It was found that GSH-2DNP inhibited the GPX activity of the printed protein, while the GPX activity of the non-printed protein was unaffected by GSH-2DNP, indicating that specific binding sites for the imprinting molecule have been obtained.

Thus, bioimprinting of albumin with a GSH derivative led to the generation of cavities for binding GSH. The high catalytic activity of the printed protein and the inhibition by the imprinting molecule provide strong evidence that the catalysis achieved is a function of specific binding sites generated by protein imprinting. Although the formation of active sites requires further investigation, the initial results suggest that this approach is a new method for generating imprinted enzymes with high GPX activity.

Notes and references

1 G. Wulff, *Angew. Chem., Int. Ed. Engl.*, 1995, **34**, 1812.
2 R. A. Lerner, S. J. Benkovic and P. G. Schultz, *Science*, 1991, **252**, 659.
3 S. Saraswathi and M. H. Keyes, *Enzyme Microb. Technol.*, 1984, **6**, 98.
4 S. C. Gamble, *J. Chem. Technol. Biotechnol.*, 1997, **68**, 123.
5 O. Epp, R. Ladenstein and A. Wendel, *Eur. J. Biochem.*, 1983, **133**, 51.
6 G. M. Luo, Z. Q. Zhu, L. Ding, Q. A. Sun, Z. Liu and J. C. Shen, *Biochem. Biophys. Res. Commun.*, 1994, **198**, 1240.
7 I. M. Bell, M. L. Fisher, Z. P. Wu and D. Hilvert, *Biochemistry*, 1993, **32**, 3754.
8 D. L. Klayman and T. S. Griffin, *J. Am. Chem. Soc.*, 1973, **95**, 197.

Communication 8/08347I

ChemComm

Template-directed synthesis of bi-functionalized organo-MCM-41 and phenyl-MCM-48 silica mesophases

Simon R. Hall,[a] Christabel E. Fowler,[a] Benedicte Lebeau[b] and Stephen Mann*[a]†

[a] *Department of Chemistry, University of Bath, Bath, UK BA2 7AY*
[b] *Laboratoire des Matériaux Minéraux, CNRS UPRES-A 7016-NSCMu, 3 rue Alfred Werner, 68093 Mulhouse Cedex, France*

Received (in Cambridge, UK) 18th November 1998, Accepted 4th December 1998

Template-directed co-condensation was used to synthesize organo-functionalized MCM-41 silica hexagonal mesophases containing binary combinations of covalently linked phenyl and amino, thiol or allyl moieties; similar methods were used to prepare a phenyl-functionalized organo-MCM-48 silica with cubic structure.

The direct synthesis of ordered MCM-41 silica mesophases containing covalently coupled organic moieties has been recently reported.[1–5] These materials could have important uses in optical applications,[5] catalysis,[6,7] metal-ion extraction[8] and adsorption processes.[9] Here we extend the method of template-directed co-condensation to the synthesis of MCM-41 structures containing two distinct types of covalently linked organic functionalities. We show that allyl, thiol or amine moieties can be incorporated along with phenyl residues into the hexagonally ordered mesophase. In addition, we report the direct synthesis of an organo-MCM-48 cubic mesophase with covalently linked phenyl functionalities by adaptation of a previously reported method involving hydrothermal phase transformation.[10]

Bifunctionalized organosilica–surfactant mesophases with hexagonal MCM-41-type structure were synthesized at room temperature and pressure from alkaline solutions of hexadecyltrimethylammonium bromide (CTAB) containing varying molar ratios of tetraethoxysilane (TEOS), phenyltriethoxysilane (PTES), and another organotrialkoxysilane [$(RO)_3Si–R'$, R′ = CH_2CHCH_2 (allyltrimethoxysilane, ATMS), $(CH_2)_3NH_2$ (3-aminopropyltriethoxysilane, APTES) or $(CH_2)_3SH$ (3-mercaptopropyltriethoxysilane, MPTES). The molar composition of a typical synthesis was: 0.12 CTAB : 0.50 NaOH : 1.0 total siloxane : 130 H_2O.‡ Acidic extraction of the surfactant from the as-synthesized products was used to prepare the corresponding organo-functionalized mesoporous silica materials.

Transmission electron microscopy (TEM) [Fig. 1(a)] and small-angle X-ray powder diffraction (SAXRD) indicated that well ordered hybrid mesophases were formed when the total amount of organotrialkoxysilanes in the synthesis mixture was *ca.* 20 mol% or less. Under these conditions, it was possible to covalently link two organic functionalities into the ordered silica framework without disruption of the long range mesoscopic order established by self-assembly of the surfactant template. For example, materials perpared from 10 mol% of PTES and 10 mol% of ATMS, MPTES or APTES, showed four reflections that were assigned to the (100), (110), (200) and (210) reflections of hexagonally ordered MCM-type structures with unit cell parameters between 4.4 and 4.6 nm.§ The *d* spacings were similar to those reported for non-functionalized MCM-41, as well as ordered organosilica mesophases prepared from co-condensation of TEOS and a single organotrialkoxysilane.[1,3] Bifunctionalized mesoporous derivatives, prepared by surfactant extraction, were generally less ordered than the as-synthesized products, except for materials prepared from PTES and APTES which showed four diffraction peaks.§ In each case, significant contractions in the unit cell length to values below 4 nm were observed.BET data gave a surface area of 1220 $m^2\ g^{-1}$ and pore diameter of *ca.* 3.5 nm for a surfactant-extracted material prepared from 5 mol% of phenyl- and 5 mol% amino-trialkoxysilanes.

MCM-41 type materials prepared from 20 mol% PTES and 20 mol% ATMS showed evidence for extensive structural disorder (broad reflections at d = 3.61 and 1.87 nm) and lattice contraction (a = 4.17 nm) in the as-synthesized materials, presumably due to the decreasing number of fully condensed Si (Q^4) centres associated with the higher levels of organosiloxane linkages. Surfactant extraction gave only a single, broad ill defined peak, indicative of collapse of the partially ordered channel structure in these hybrid materials.

Incorporation of the covalently linked organic groups was confirmed by ^{29}Si solid-state CP NMR spectroscopy which showed distinct resonances for siloxane [Q^n = $Si(OSi)_n(OH)_{4-n}$, n = 2–4] and organosiloxane [T^m = $RSi(OSi)_m(OH)_{3-m}$, m = 1–3] environments (graphical abstract). The integrated signal due to the latter approximately doubled when

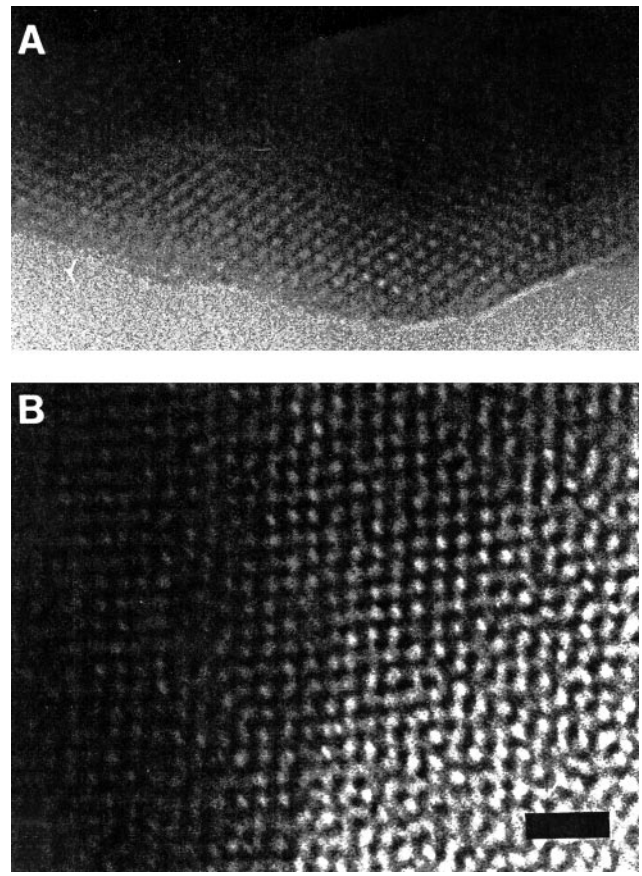

Fig. 1 TEM micrographs of (A) as-synthesized bi-functionalized phenyl-amino-MCM-41 mesophase (10 mol% PTES/10 mol% APTES) showing hexagonally ordered channel structure, (B) phenyl-functionalized MCM-48 mesophase (10 mol% PTES) showing cubic structure viewed down the < 110 > zone. Scale bar (both micrographs) = 10 nm.

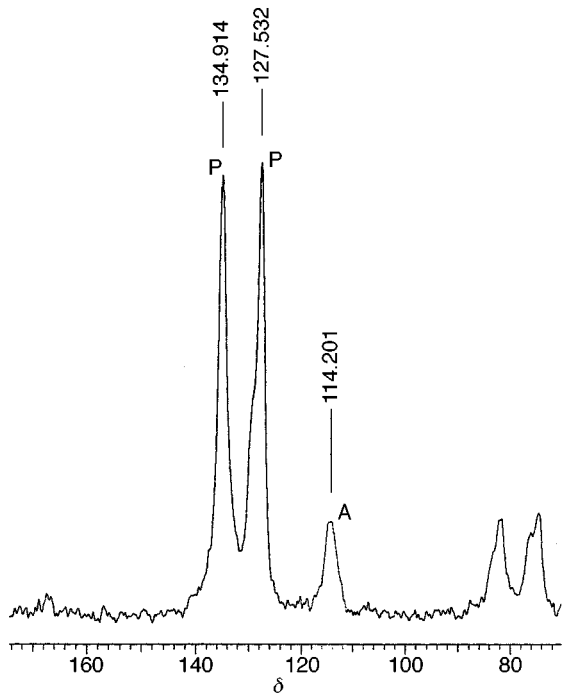

Fig. 2 ^{13}C CP MAS NMR spectrum for a bifunctionalized organo-MCM-41 mesophase showing resonances for intact phenyl (P) and allyl (A) moieties.

the total amount of organoalkoxysilanes in the synthesis mixture was increased from 20 to 40%. In most cases, the Q^3 and T^2 linkages were predominant, indicating that the organosilica mesophases contained significant amounts of uncondensed Si–OH centres. The bifunctional nature of the materials was confirmed by ^{13}C CP MAS NMR studies which showed intact phenyl moieties along with unmodified allyl, amine or thiol groups (Fig. 2).¶ This was consistent with FTIR spectra of the surfactant-extracted materials which showed characteristic absorption bands for the covalently-linked organic residues.‖

Organosilica–surfactant mesophases were also synthesized at 100 °C from alkaline solutions of hexadecyltrimethylammonium chloride (CTACl) containing varying molar ratios of TEOS and PTES, APTES, MPTES or ATMS; typically the molar composition was: 0.64 CTACl : 0.25 NaOH : 1.0 total siloxane : 62 H_2O.** Under these conditions, which utilise lower surfactant concentrations than are normally required for MCM-48 synthesis, the cubic mesophase is formed by an ethanol-induced phase transformation of a MCM-41 precursor.[10] SAXRD data for a functionalized silica mesophase prepared from 10 mol% PTES gave four reflection peaks at d = 3.93, 3.52, 2.15 (broad) and 1.79 nm that were indexed to the (211), (220), (400)/(420) and (431) reflections, respectively, of a cubic *Ia*3*d* mesophase with unit cell length of 9.62 nm. TEM images confirmed the formation of an ordered MCM-48-type material [Fig. 1(b)] and ^{13}C CP NMR showed resonances (δ 127.5, 135.0) corresponding to the covalently linked phenyl moieties. FTIR peaks at 702 and 3000–3100 cm^{-1} also confirmed the presence of the phenyl functionality. SAXRD profiles of the surfactant extracted, phenyl-functionalized MCM-48 silica showed three main reflections (d = 3.93, 2.10, 1.49 nm) which were indexed to the (100), (110) and (210) peaks of a hexagonally ordered organo-mesoporous material. The apparent structural collapse of the cubic material in the absence of the surfactant was consistent with TEM images which showed a marked decrease in the amount of cubic pore order in the sample. BET analysis gave a surface area of 1040 $m^2\ g^{-1}$ for the surfactant extracted product.

Analogous samples functionalized with amino, thiol or allyl groups gave only broad XRD peaks, with no evidence of an ordered organo-MCM-48 (or MCM-41) mesophase. ^{13}C CP NMR and FTIR data on these samples indicated that the organic groups were not incorporated to any significant extent into the silica materials. This suggests that APTES, MPTES and ATMS did not undergo significant condensation, or that the functional groups are labile under the reaction conditions, or both. In particular, the elevated temperature of the synthesis method is likely to increase the rate of formation of the Q^n centres at the expense of the T^m linkages.

Our results suggest that bifunctionalization of the MCM-41 mesostructure could provide a general route to multi-component inorganic–organic hybrids and their (partially) ordered mesoporous derivatives. Such materials extend the complexity of self-organized inorganic matter and should be useful in processes requiring controlled confinement, for example where the channel reactivity needs to be coupled with the hydrophobic/hydrophilic balance of the localized environment. Because the 3-D channel network of MCM-48 is less susceptible to pore blockage compared with the linear channel structure of MCM-41, organoMCM-48 materials could have specific technological advantages. However, significant advances are required to improve the structural stability of these organized materials.

We thank Dr David C. Apperley (University of Durham) for solid-state NMR data, Dr S. J. Roser (University of Bath) for help with SAXRD data, and the EPSRC for financial support to S. R. H.

Notes and references

† Current address: School of Chemistry, University of Bristol, Bristol, UK BS8 1TS. E-mail: s.mann@bris.ac.uk

‡ In a typical preparation (mol% PTES : ATMS : TEOS = 10 : 10 : 80), 1.6 g CTAB was dissolved in a solution of 70.2 g of distilled deionized H_2O containing 20 g of 1.0 M NaOH, 0.59 g ATMS and 0.87 g PTES added, and the mixture stirred vigorously for 5 min; 5.99 g TEOS was then added and the mixture stirred for 24 h at room temp. The white precipitate was filtered, washed with distilled deionized H_2O, and dried for 10 h at 100 °C *in vacuo*. Acid extraction was performed by stirring a suspension of the solid product (0.99 g dm^{-3}) in 1.0 mol dm^{-3} HCl in EtOH under reflux at 75 °C for 24 h. The extracted material was then filtered, washed with ethanol and dried in a vacuum oven at 100 °C for 10 h.

§ SAXRD d spacings/nm [*hkl* = (100), (110), (200) and (210), unless specified]: MCM-41 materials (10 mol% per functionality); PTES-ATMS, as-synthesized, 3.83, 2.20, 1.92, 1.52, a = 4.42; surfactant-extracted, 3.26 (100), a = 3.64. PTES-MPTES, as-synthesized, 3.86, 2.20, 1.91, 1.44, a = 4.45; surfactant-extracted, 3.07 (100), a = 3.54. PTES-APTES, as-synthesized, 4.03, 2.29, 1.99, 1.49, a = 4.65; surfactant-extracted, 3.17 (100), 2.11 (200), a = 3.66.

¶ ^{13}C CP MAS NMR data (δ): phenyl, 127, 129, 130, 134; allyl, 114, 135; thiol, 23.0, 41.4; amino, 16.8, 44.8.

‖ FTIR data (cm^{-1}): phenyl, 668, 702, 1430, 3000–3100; allyl, 800, 1420; thiol, 2550–2590 (weak); amino, 3400, 1620–1650.

** For MCM-48 functionalized with 10 mol% PTES, 0.67 g of solid NaOH was dissolved in 17 g of distilled deionized H_2O and 6.50 g of TEOS and 0.63 g PTES added under vigorous stirring, and the solution left for 5 min 27.8 g of CTACl solution was added and the mixture left to stir for 15 min, then poured into a stoppered PTFE bottle, and heated without stirring at 100 °C for 72 h. After cooling to room temperature, the solid product was recovered by filtration, washed with distilled, deionized H_2O, and dried for 10 h at 100 °C *in vacuo*. Surfactant extracted materials were prepared as for the MCM-41 samples.

1 S. L. Burkett, S. D. Sims and S. Mann, *Chem. Commun.*, 1996, 1367.
2 D. J. MacQuarrie, *Chem. Commun.*, 1996, 1961.
3 C. E. Fowler, S. L. Burkett and S. Mann, *Chem. Commun.*, 1997, 1679.
4 M. H. Lim, C. F. Blanford and A. Stein, *J. Am. Chem. Soc.*, 1997, **119**, 4090.
5 C. F. Fowler, B. Lebeau and S. Mann, *Chem. Commun.*, 1998, 1825.
6 M. H. Lim, C. F. Blanford and A. Stein, *Chem. Mater.*, 1998, **10**, 467.
7 J. H. Clark and D.J. MacQuarrie, *Chem. Commun.*, 1997, 853.
8 X. Feng, G. E. Fryxell, L. Q. Wang, A. Y. Kim, J. Liu and K. M. Kemner, *Science*, 1997, **276**, 923.
9 C. M. Bambrough, R. C. T. Slade, R. T. Williams, S. L. Burkett, S. D. Sims and S. Mann, *J. Colloid. Interface Sci.*, 1998, **201**, 220.
10 R. Schmidt, M. Stocker, D. Akporiaya, E. H. Torstad and A. Olsen, *Microporous Mater.*, 1995, **5**, 1.

Communication 8/09008D

Reaction of (dimethylvinylidene)carbene with indole-3-carbaldehyde and its application in the synthesis of β-(dehydroprenyl)indole-based natural products

Jyh-Horng Sheu,* Chun-An Chen and Buo-Horng Chen

Department of Marine Resources, National Sun Yat-Sen University, Kaohsing, 804, Taiwan.
E-mail: sheu@mail.nsysu.edu.tw

Received (in Cambridge, UK) 9th November 1998, Accepted 7th December 1998

Reaction of (dimethylvinylidene)carbene with indole-3-carbaldehyde gives various dehydroprenyl-based indoles. Efficient synthesis of the indole natural products yuehchukene and murrapanine, using this reaction as a key step, is also described.

The cyclopropanation of nucleophilic olefins with (dimethylvinylidene)carbene **1**, generated by the elimination of hydrogen halide from propargyl halides or halloallenes (Scheme 1),

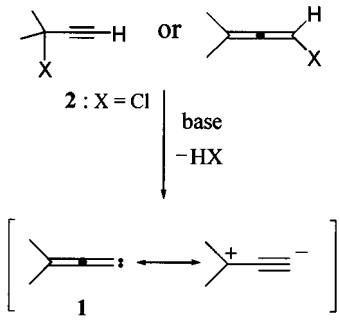

Scheme 1

represents an important carbon–carbon bond-forming process, involving introduction of a dehydroprenyl group into organic substrates,[1–6] and has found use in natural product synthesis.[7,8] Interaction of **1** with indole itself[9] and α- and/or β-methyl indoles has been studied,[10] however, reaction between **1** and indoles containing an electron-withdrawing group at C-2 or C-3 has not been investigated. In connection with our previous studies on the regioselectivity of **1** towards different olefins[11] and synthesis of β-(dehydroprenyl)indoles,[12] we have investigated the reaction of **1** with indole-3-carbaldehyde. We report herein the preliminary results of this work directed to the introduction of a dehydroprenyl unit onto the β-carbon of indole. Application of this reaction in the synthesis of indole natural products containing a β-dehydroprenyl group is also described.

Treatment of 3-chloro-3-methylbut-1-yne **2** with aq. KOH, a catalytic amount of dibenzo-18-crown-6 and THF in the presence of indole-3-carbaldehyde **3** under reflux gave a mixture which was separated to afford two bis-indoles, 3-[3-methyl-1-(3-formylindol-1-yl)but-2-enyl]indole **4**† (44%) and 3-[(*E*)-3-methyl-3-(3-formylindol-1-yl)but-1-enyl]indole **5**‡ (6%), and 3-(1,1-dimethylprop-2-ynyl)indole **6**[9] (8%). Alkyne **6** was considered to be derived from the electrophilic addition of the carbene **1** at C-3 to the β-carbon of anion **7** and subsequent decarbonylation. Electrophilic addition of the carbene at C-1 to the β-carbon of the indolide anion **7** and subsequent decarbonylation, on the other hand, would lead to the formation of indole **8**, a tautomer of β-(dehydroprenyl)-indole **9**, as the reactive intermediate. Further condensation of anion **7** at the C-2 and C-4 positions of the side-chain of **8** could give β-prenylindoles **4** and **5**, respectively. The mechanism of this reaction was proposed as portrayed in Scheme 2. The formation of **4** and **5** revealed that β-dehydroprenylation of indole had taken place, but that the product was unstable in the form of **8** or its tautomer **9** under the above reaction conditions, and had undergone *in situ* Michael condensation with anion **7**.

Interaction of carbene **1** with α- and/or β-methylindoles, and indole itself, has been shown to give mostly ring expansion of the cyclopropane intermediates, which were assumed to be formed by addition of carbene to the nucleophilic 2,3-double bond of indoles, to give 3-vinylquinolines.[9,10] However, the

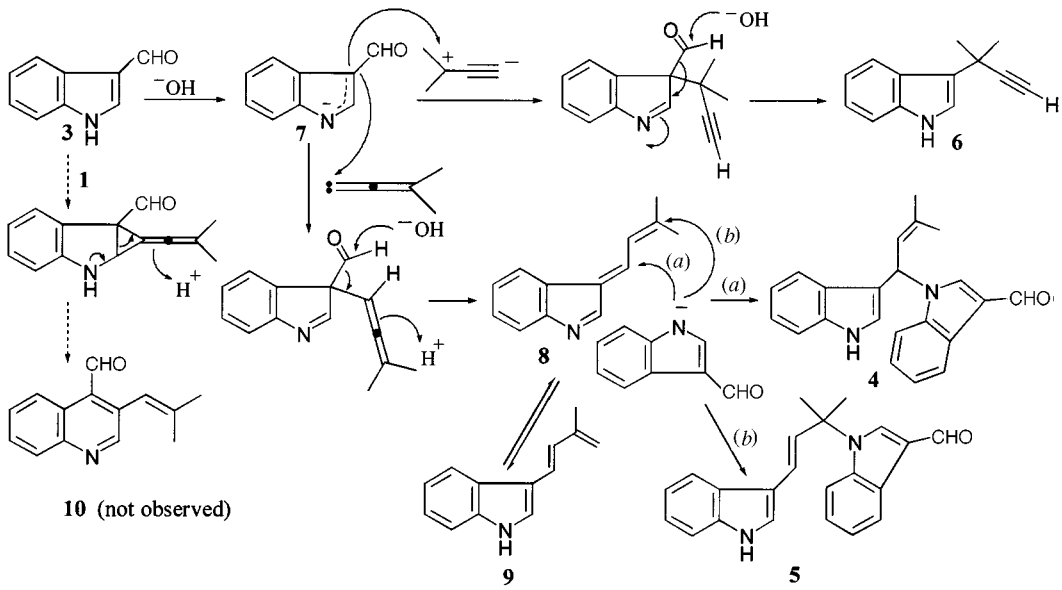

Scheme 2

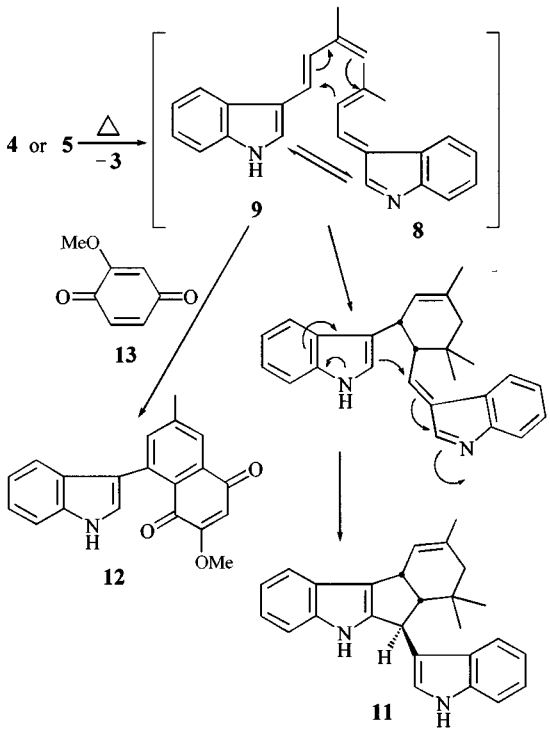

Scheme 3

reaction of **1** with **3** did not give the expected quinoline **10**, probably due to the stronger acidity of indole-3-carbaldehyde **3** in comparison with α- and/or β-methylindoles and indole itself. Thus, interaction of indole **3** with base gave indolide anion **7**, which reacted predominantly *via* nucleophilic attack by C-3 upon carbene **1**, and led to the formation of dehydroprenylindoles and/or the following prenylindoles. This study shows that the presence of an electron-withdrawing group, in this case the formyl group at the β-position of indole, could prevent the formation of quinoline and steer the reaction towards β-alkylation products.

The above reaction provides a new method for the β-prenylation of indole in a simple and efficient manner. Furthermore, elimination of **3** from both **4** and **5** to give β-(dehydroprenyl)indole **9** should be achieved easily as the anion **7** is stable due to delocalisation of the negative charge, and is considered to be a good leaving group. Thus, the above reaction may be useful for the synthesis of β-(dehydroprenyl)indole-base compounds. In order to demonstrate the potential of this carbon–carbon bond-forming reaction we applied the above reaction as a key step in the synthesis of two bioactive indole natural products, yuehchukene **11**[13,14] and murrapanine **12**,[15] which were isolated from *Murraya* species. The structures of these two compounds reveal that they are derived from β-(dehydroprenyl)indole **9**. We found that heating both **4** and **5** in a neutral solution of ethylene glycol at 165–170 °C yielded yuehchukene in 42% yield. Thermal reaction of **4** and **5** with methoxyquinone **13** (3 equiv.) under the above reaction conditions afforded murrapanine in 65% yield. The above one-step reactions are considered to give β-(dehydroprenyl)indole **9** first *via* elimination of **3** (recovered quantitatively), followed by subsequent Diels–Alder reaction (Scheme 3) as described previously.[12] The dehydroprenyl unit of the carbon skeleton of natural products **11** and **12** were constructed completely from carbene **1** in this synthesis. It is worth mentioning here that this is the first synthesis of a dehydroprenylated indole natural products using (dimethylvinylidene)carbene **1** as the isoprenoid unit of the carbon skeleton.

In conclusion this is the first reaction of vinylidenecarbene with indoles having an electron-withdrawing substituent on the 2,3-double bond. The above reaction provides an efficient method for introducing an appropriate 'isoprene' group into the β-position of indole, making use of inexpensive and readily available propargyl chloride **2** and indole-3-carbaldehyde **3** as starting materials. The above result suggests that reaction of vinylidenecarbene with indoles containing different functional groups at C-2 and C-3 should be further investigated. The scope of this chemistry is now being explored in our laboratory.

This work was supported by a grant from the National Science Council of Republic of China (NSC-87-2113-M-110-015) awarded to J.-H. S.

Notes and references

† *Selected data* for **4** : ν_{max}(KBr)/cm^{-1} 3256, 1636, 1614, 1386; δ_H(300 MHz, $CDCl_3$) 1.84 (s, 3 H), 1.86 (s, 3 H), 5.68 (d, 1 H, *J* 8.4), 6.56 (d, 1 H, *J* 8.4), 7.04–8.35 (m, 10 H), 8.38 (br s, 1 H, NH), 9.86 (s, 1 H); *m*/*z* 328 (M^+).

‡ *Selected data* for **5** : ν_{max}(KBr)/cm^{-1} 3260, 1640, 1612, 1396, 956; δ_H(300 MHz, $CDCl_3$) 1.94 (s, 6 H), 6.48 (d, 1 H, *J* 16.2), 6.70 (d, 1 H, *J* 16.2), 7.12–8.35 (m, 10 H), 8.41 (br s, 1 H, NH), 10.03 (s, 1 H); *m*/*z* 328 (M^+).

1 H. D. Hartzler, *J. Am. Chem. Soc*., 1961, **83**, 4990.
2 T. B. Patrick, *Tetrahedron Lett*., 1974, 1407.
3 T. Sasaki, S. Eguchi, M. Ohno and F. Nakata, *J. Org. Chem*., 1976, **41**, 2408.
4 T. Harada, Y. Nozaki and A. Oku, *Tetrahedron Lett*., 1983, **24**, 5665.
5 H. D. Hartzler, *J. Am. Chem. Soc*., 1961, **83**, 4997.
6 H. D. Hartzler, *J. Org. Chem*., 1964, **29**, 1311.
7 R. W. Mills, R. D. H. Murray and R. A. Raphael, *J. Chem. Soc*., *Chem. Commun*., 1971, 555.
8 D. Michelot, G. Linstrumelle and S. Julia, *J. Chem. Soc*., *Chem. Commun*., 1974, 10.
9 E. Wenkert, E. C. Angell, V. F. Ferreira, E. L. Michelotti, S. R. Pittre, J.-H. Sheu and C. S. Swindell, *J. Org. Chem*., 1986, **51**, 2343.
10 S. R. Landor, V. Rogers and H. R. Sood, *J. Chem. Soc*., *Perkin Trans. 1*, 1976, 2103.
11 J.-H. Sheu, C.-F. Yen, Y.-L. Chan and J.-F. Chung, *J. Org. Chem*., 1990, **55**, 5232; J.-H. Sheu, C.-F. Yen, C.-W. Huang and Y.-L. Chan, *Tetrahedron Lett*., 1991, **32**, 5547; J.-H. Sheu, C.-F. Yen and C.-W. Huang, *J. Chin. Chem. Soc*., 1993, **40**, 59.
12 J.-H. Sheu, Y.-K. Chen and Y.-L. V. Hong, *Tetrahedron Lett*., 1991, **32**, 1045; J.-H. Sheu, Y.-K. Chen and T.-L. V. Hong, *J. Org. Chem*., 1993, **58**, 5784; J.-H. Sheu, Y.-K. Chen, H.-F. Chung, P.-J. Sung and S.-F. Lin, *Heterocycles*, 1996, **43**, 1751; J.-H. Sheu, Y.-K. Chen, H.-F. Chung, S.-F. Lin and P.-J. Sung, *J.Chem. Soc*., *Perkin Trans. 1*, 1998, 1959.
13 Y.-C. Kong, K.-F. Cheng, R. C. Cambie and P. G. Waterman, *Chem. Commun*., 1985, 47.
14 Y.-C. Kong, K.-H. Ng, K.-H. Wat, A. Wang, I. F. Saxena, H.-F. Cheng, P. P. H. But and H.-T. Chang, *Planta Med*., 1985, **44**, 304.
15 T.-S. Wu, M.-J. Liou, C.-J. Lee, T.-T. Jong, A. T. McPhail, D. R. McPhail and K.-H. Lee, *Tetrahedron Lett*., 1989, **30**, 6649.

Communication 8/08733D

ChemComm

Intramolecular non-bonded interaction between selenium and oxygen as revealed by ^{17}O and ^{77}Se NMR spectroscopy and natural bond orbital analysis

Hiroto Komatsu, Michio Iwaoka and Shuji Tomoda*

Departement of Life Sciences, Graduate School of Arts and Sciences, The University of Tokyo, Komaba, Meguro-ku, Tokyo 153-8902, Japan. E-mail: tomoda@selen.c.u-tokyo.ac.jp

Received (in Cambridge, UK) 20th October 1998, Accepted 30th November 1998

^{17}O and ^{77}Se NMR spectroscopic measurement and natural bond orbital (NBO) analysis of 2-formyl- and 2-hydroxymethyl-benzeneselenenyl derivatives (ArSeX; X = Cl, Br, CN, SPh, SeAr, Me: Ar = C_6H_4CHO, $C_6H_4CH_2OH$) provided strong evidence for the intramolecular non-bonded interaction between selenium and oxygen due to orbital interaction between the oxygen lone pair and the low-lying σ^*_{SeX} antibonding orbital ($n_O \rightarrow \sigma^*_{SeX}$).

Non-bonded interactions involving selenium are an important factor that often dictates the structure and reactivity of organoselenium compounds, some of which are known to be useful for asymmetric synthesis[1] as well as for enzyme-mimetic catalytic reactions.[2] We have recently studied the non-bonded interaction between selenium and nitrogen (Se···N)[3] and selenium and fluorine (Se···F)[4] to characterize the mechanism of the interactions. While the former interaction is stabilized chiefly *via* orbital interaction (donor–acceptor interaction),[3] the stabilization mechanism of the latter may be slightly more electrostatic in nature.[4] From the viewpoint of electronegativity scale,[5] it is expected that the interaction between selenium and oxygen (Se···O) may be intermediate. However the results of the recent publications on the mechanism of Se···O interactions are variable to leave the interaction mechanism of Se···O uncertain.[6]

Herein we report the first systematic NMR study of Se···O interactions. The conclusions drawn from the present NMR study have been corroborated by *ab initio* molecular orbital calculations combined with natural bond orbital (NBO) analysis proposed by Weinhold.[7]

Model compounds, ^{17}O-enriched 2-formylbenzeneselenenyl derivatives (**1a–f**) and 2-(hydroxymethyl)benzeneselenenyl derivatives (**2a–f**), were synthesized from the corresponding

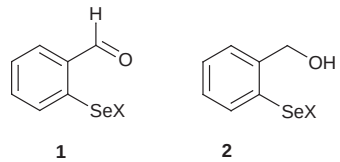

1 **2**

a: X = Cl
b: X = Br
c: X = CN
d: X = SPh (**d'**: X = SMe)
e: X = SeAr (**e'**: X = SeMe)
f : X = Me

^{17}O-enriched diselenide (**1e**) according to literature methods.[8] These compounds were obtained in spectrally pure form except for **1d** and **2d**, which slowly disproportionated into the corresponding diselenides (**1e** and **2e**) at room temperature.

Since ^{17}O nuclear spin is a quadrupole, attempts at observing the one-bond spin–spin coupling constant between the non-bonded ^{17}O and ^{77}Se ($^1J_{Se\cdots O}$), which was thought to provide direct information as to the intramolecular non-bonded interaction between these nuclei, was unsuccessful. The ^{17}O NMR chemical shift data (δ_O) for compounds **1** and **2**, obtained at 67.70 MHz, are collected in Table 1 along with those of ^{77}Se NMR chemical shift (δ_{Se}), measured at 95.35 MHz. Three notable features are seen from Table 1.

First, within the series of compounds **1**, a monotonous downfield shift of δ_O is observed on going from **1a** to **1f** (δ_O = 493.0 → 561.6), while exactly the opposite trend is apparent for δ_O for **2** (δ_O = 24.9 → 10.6). Secondly, δ_O values for **1** (δ_O = 493.0–561.6), each of which possesses an sp^2-hybridized oxygen, are shifted toward upfield ($\Delta\delta_O$ = −76 to −7) compared with that of a reference benzaldehyde, which lacks the selenium moiety (δ_O = 569),[9] whereas δ_O values for **2** (δ_O = 24.9–10.6), each of which bears an sp^3-hybridized oxygen, are shifted downfield ($\Delta\delta_O$ = 24.2–9.9) compared to that of reference compound benzyl alcohol (δ_O = 0.7).[10] The mutually inverse effect on the relative chemical shift ($\Delta\delta_O$) precludes the possibility of major inductive through-bond electronic effects of the selenium moiety (SeX). These experimental data strongly suggest that a Se···O interaction (attractive or repulsive) may exist at least in one of these compound series. It should be noted that the absolute magnitude of these shifts ($\Delta\delta_O$) steadily decrease on going from **a** through **f** for both series. Thirdly, comparison of ^{77}Se chemical shifts (δ_{Se}) between compounds **1** and **2** possessing the same substituent X reveals that the former (1114.1–259.5) is considerably lower than the latter (987.1–157.2), clearly suggesting that there should be a stronger Se···O interaction in series**1** than in **2** ($\Delta\delta_{Se}$ = 25.3–190.0): the significant downfield shift may be caused on the selenium nucleus by the anisotropic deshielding effect of the formyl C=O bond of **1** if the selenium lies coplanar with the C=O bond.

It is well known[11] that a linear dependence of ^{17}O NMR chemical shift on the amount of electronic charge on the oxygen atom generally exists within a series of structurally similar compounds: for an sp^2-hybridized oxygen atom, the higher the charge, the larger the magnitude of upfield shift of ^{17}O NMR chemical shift, while exactly the opposite trend is observed for sp^3-hybridized oxygen. According to this rule, the dependence of the chemical shift (δ_O) on substituent X seen from Table 1 suggests that for both series of compounds (**1** and **2**) the electronic charge on the oxygen atom in the conformation with

Table 1 ^{17}O and ^{77}Se NMR chemical shifts (δ_O and δ_{Se}) of **1** and **2**[a]

		1			**2**			
	X	δ_O[b]	$\Delta\delta_O$[c]	δ_{Se}[d]	δ_O[b]	$\Delta\delta_O$[e]	δ_{Se}[d]	$\Delta\delta_{Se}$[f]
a	Cl	493.0	−76	1114.1	24.9	+24.2	987.1	127.0
b	Br	515.9	−53	1029.5	23.2	+22.5	839.5	190.0
c	CN	548.0	−21	426.7	22.0	+21.3	314.5	111.8
d	SPh	556.6	−12	621.7	16.0	+15.3	501.8	119.9
e	SeAr	559.3	−10	458.5	13.3	+12.6	433.2	25.3
f	Me	561.6	−7	259.5	10.6	+9.9	157.2	102.3

[a] Measured in $CDCl_3$ at 298 K. [b] Measured at 67.70 MHz with D_2O as an external standard. [c] Relative ^{17}O NMR chemical shift with respect to PhCHO (δ_O = 569).[9] [d] Measured at 95.35 MHz with Me_2Se as an external standard. [e] Relative ^{17}O NMR chemical shift with respect to $PhCH_2OH$ in acetone (δ_O = 0.7).[10] [f] $\Delta\delta_{Se} = \delta_{Se}(\mathbf{1}) - \delta_{Se}(\mathbf{2})$.

Se···O interaction should decrease monotonously on going from **a** to **f**.

Strong theoretical evidence for the existence of attractive Se···O interaction as well as for the definitive trend of the electronic charge at oxygen atom for both series of compounds has been obtained with *ab initio* molecular orbital calculations[12] and natural bond orbital (NBO) analysis.[7] See http://www.rsc.org/suppdata/cc/1999/205 for summary of results as electronic supplementary information. Initial conformational search of **1** and **2** at the RHF/3-21G* level indicated two stable conformational isomers for both series of model compounds (Scheme 1). Conformer **A**, in which the O–Se–X angle is nearly 180°, has a close Se···O contact, whereas conformer **B**, in which the Se–X bond is almost perpendicular to the plane of the phenyl ring, does not. For all model compounds calculated with 6-31G(d,p) basis for C, H, N, O, S, and Cl and Huzinaga's 43321/4321/311(d) basis set for Se and for Br,[13] conformer **A** was found to be more stable by ΔE_{tot} = 0.44–9.99 kcal mol^{-1}, strongly suggesting that the Se···O interaction may be attractive in all cases in consonant with the trends manifested by the ^{17}O and ^{77}Se NMR chemical shift data.

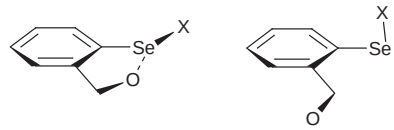

A **B**

Scheme 1

Natural population analysis (NPA) of these conformers indicates the following three intriguing points with regard to the electron population at oxygen atom in conformers **A** and **B** (q_A and q_B). First, the populations at the oxygen atom of **2** (*ca.* −0.8 e) are uniformly greater than those of **1** (*ca.* −0.6 e) irrespective of substituent X. Secondly, relative oxygen populations with respect to the reference compounds (PhCHO for **1** and $PhCH_2OH$ for **2**) for conformer **A** (Δq_A) are negative, indicating that Se···O interaction might induce a small increment of electron density at the oxygen and that this is larger in **1** (Δq_A = 0.000 to −0.025) than in **2** (Δq_A = −0.001 to −0.008). Thirdly, such a tendency is attenuated on going from **a** to **f** for both series, which may imply that the magnitude of the Se···O interaction is diminished in this order. In full agreement with the previous observation[11] on the linear relationship between the charge at oxygen and ^{17}O NMR chemical shift, Δq_A indeed exhibits a linear correlation with $\Delta\delta_O$ (r^2 = 0.89 and 0.90 for series **1** and **2**, respectively), indicating that conformer **A** is more stable for both series **1** and **2**.

NBO deletion analysis, which is known to be an effective method of quantitative evaluation of attractive orbital interaction alone,[7] has been applied to conformer **A** for both compound series to estimate the strength of the Se···O interaction due to orbital interaction mechanism (E_{del}). Series **1** has E_{del} = 16.6–6.1 kcal mol^{-1} and **2** has E_{del} = 6.8–1.9 kcal mol^{-1}. A remarkable linear correlation was observed between the Se···O distance ($d_{Se\cdots O}$) and the NBO deletion energy (E_{del}) for each series (r^2 = 0.98 for **1** and 0.96 for **2**), which may suggest that the attractive Se···O interaction should arise chiefly from orbital interaction. NBO second-order perturbation analysis indicated that the major orbital interaction is that between the oxygen lone pair (n_O) and the low-lying σ^*_{SeX} antibonding orbital ($n_O \rightarrow \sigma^*_{SeX}$). It is apparent that this interaction energy explains most of E_{del} in all cases. Interestingly an excellent linear correlation was observed between the relative chemical shift ($\Delta\delta_O$) and E_{del} for each series of model compounds. For series **1**, the slope of the correlation is negative (r^2 = 0.96), whereas for **2** it is positive (r^2 = 0.90), indicating that both upfield shift for series **1** and downfield shift for series **2** should be roughly proportional to the magnitude of the Se···O interaction due to orbital interaction mechanism (E_{del}). It is particularly noteworthy that highly electronegative substituent (X), such as CN, shows almost no deviation from linearity, which may preclude the possibility of electrostatic mechanism of Se···O interaction in these compounds.

In summary, the linear correlations among the three parameters for conformer **A** of both series **1** and **2** namely, $\Delta\delta_O$, E_{del} and Δq_A, are in full accord with the existence of attractive nonbonded Se···O interactions, the major mechanism of which is most likely to be the orbital interaction between the oxygen lone pair (n_O) and the low-lying σ^*_{SeX} antibonding orbital. Possible enhanced strength of the attractive Se···O interaction in **1** *cf.* **2** may be most simply explained in terms of π-conjugation between the formyl group and the phenyl ring in **1**, which may encumber free rotation around the C(Ph)–CH bond to generate a stable conformation of **1** with a Se···O distance that is shorter ($d_{Se\cdots O}$ = 2.58–2.86 Å) than those of **2** ($d_{Se\cdots O}$ = 2.82–3.17 Å).

This work is supported by the Grant-in Aid for Scientific Research (Nos. 09239207, 07854034 and 06854029) from the Ministry of Education, Science, Sports and Culture of Japan.

Notes and references

1 K. Fujita, M. Iwaoka and S. Tomoda, *Chem. Lett.*, 1994, 923; K. Fujita, K. Murata, M. Iwaoka and S. Tomoda, *Tetrahedron*, 1997, **53**, 2029; T. Wirth, *Liebigs Ann./Recueil*, 1997, 2189.

2 M. Iwaoka and S. Tomoda, *J. Chem. Soc., Chem. Commun.*, 1992, 1165; M. Iwaoka and S. Tomoda, *J. Am. Chem. Soc.*, 1994, **116**, 2557; R. Kaur, H. B. Singh and R. P. Patel, *J. Chem. Soc., Dalton Trans.*, 1996, 2719; T. Wirth, S. Häuptli and M. Leuenberger, *Tetrahedron: Asymmetry*, 1998, **9**, 547.

3 M. Iwaoka and S. Tomoda, *J. Am. Chem. Soc.*, 1996, **118**, 8077.

4 M. Iwaoka, H. Komatsu and S. Tomoda, *Chem. Lett.*, 1998, 969.

5 L. C. Allen, *J. Am. Chem. Soc.*, 1989, **111**, 9003.

6 B. M. Goldstein, S. D. Kennedy and W. J. Hennen, *J. Am. Chem. Soc.*, 1990, **112**, 8265; F. T. Burling and B. M. Goldstein, *J. Am. Chem. Soc.*, 1992, **114**, 2313; D. H. R. Barton, M. B. Hall, Z. Lin, S. I. Parekh and J. Reibenspies, *J. Am. Chem. Soc.*, 1993, **115**, 5056.

7 A. E. Reed and F. Weinhold, *J. Chem. Phys.*, 1983, **78**, 4066; A. E. Reed, R. B. Weinstock and F. Weinhold, *J. Chem. Phys.*, 1985, **83**, 735; A. E. Reed and F. Weinhold, *J. Chem. Phys.*, 1985, **83**, 1736; A. E. Reed, L. A. Curtiss and F. Weinhold, *Chem. Rev.*, 1988, **88**, 899.

8 **1e** was synthesized by the reaction of **2e**[14] with chlorotrimethylsilane in dimethyl sulfoxide. **1e** was then exposed to oxygen-exchange in HCl–dioxane by using 22% ^{17}O-enriched H_2O. ^{17}O-enriched **2e** was synthesized by reduction of **1e** with $NaBH_4$ in MeOH. Other model compounds were derived from ^{17}O-enriched **1e** and **2e** by applying previous methods.[3] All compounds were characterized by ^{1}H, ^{13}C, ^{17}O and ^{77}Se NMR spectra. **1a–c**, **1f**[15] and **2e**[14] are known compounds.

9 D. W. Boykin and A. L. Baumstark, in *^{17}O NMR Spectroscopy in Organic Chemistry*, ed. D. W. Boykin, CRC Press, Florida, 1991, p. 205.

10 P. Balakrishnan, A. L. Baumstark and D. W. Boykin, *Tetrahedron Lett.*, 1984, 169.

11 M.-T. Béraldin, E. Vauthier and S. Fliszár, *Can. J. Chem.*, 1982, **60**, 106; G. Jaccard, P.-A. Carrupt and J. Lauterwein, *Magn. Reson. Chem.*, 1988, **26**, 239.

12 Gaussian 94 was used for all calculations performed in this paper: M. J. Frisch, G. W. Trucks, H. B. Schlegel, P. M. W. Gill, B. G. Johnson, M. A. Robb, J. R. Cheeseman, T. A. Keith, G. A. Petersson, J. A. Montgomery, K. Raghavachari, M. A. Al-Laham, V. G. Zakrzewski, J. V. Ortiz, J. B. Foresman, J. Cioslowski, B. B. Stefanov, A. Nanayakkara, M. Challacombe, C. Y. Peng, P. Y. Ayala, W. Chen, M. W. Wong, J. L. Andres, E. S. Replogle, R. Gomperts, R. L. Martin, D. J. Fox, J. S. Binkley, D. J. Defrees, J. Baker, J. P. Stewart, M. Head-Gordon, C. Gonzalez and J. A. Pople, Gaussian, Inc., Pittsburgh, PA, 1995.

13 *Gaussian Basis Sets for Molecular Calculations*, ed. S. Huzinaga, Elsevier, Amsterdam, 1984.

14 M. Iwaoka and S. Tomoda, *Phosphorus Sulfur Silicon Relat. Elem.*, 1992, **67**, 125.

15 G. Llabrès, M. Baiwir, J.-L. Piette and L. Christiaens, *Org. Magn. Reson.*, 1981, **15**, 152.

Communication 8/08126C

Synthesis of a chiral dendrimer based on polyfunctional amino acids

Andreas Ritzén and Torbjörn Frejd*

Organic Chemistry 1, Department of Chemistry, Lund University, PO Box 124, SE-221 00, Lund, Sweden. E-mail: torbjorn.frejd@orgk1.lu.se

Received (in Liverpool UK) 24th November 1998, Accepted 10th December 1998

A chiral, nonracemic dendrimer of generation two based on aromatic bis- and tris-amino acids has been synthesised.

The design and synthesis of functional dendrimers has been the focus of much research during the last ten years.[1,2] Chiral, nonracemic dendrimers with well-defined stereochemistry are a particularly interesting subclass, with potential applications in asymmetric catalysis and chiral molecular recognition.[3] For biological applications, polyionic, water-soluble dendrimers will be of interest.[4] Here we report the synthesis of a chiral, nonracemic dendrimer **14** (see Scheme 2) based on synthetic, di- and tri-functional amino acids.

The dendrimer **14** is assembled from nine units of the bis-amino acid **7** and one unit of protected phenyltrisalanine **12**.[5] The synthesis of **7** is described in Scheme 1, and is based on a Heck coupling–hydrogenation protocol which has been used in our laboratory before.[5–7] Starting from 4-aminophenylacetic acid **1**, iodination with ICl gave **2**.[8] Removal of the amino group *via* stepwise diazotization and reduction proved difficult, and *in situ* generation of the diazonium salt in refluxing EtOH was the only satisfactory method found. Under these conditions, the diazonium salt was immediately reduced by EtOH giving **3** as

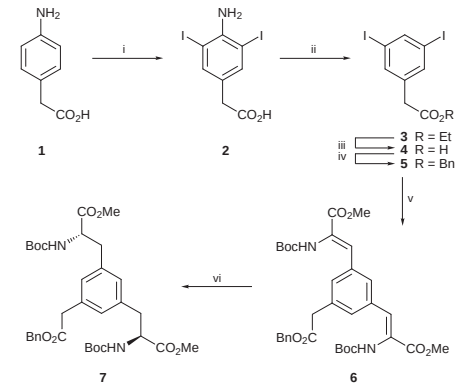

Scheme 1 *Reagents and conditions*: i, ICl (2.0 equiv.), HCl (1 M), room temp. 18 h, 65%; ii, H_2SO_4, $NaNO_2$ (3.0 equiv.), EtOH (99.5%), reflux, 1 h, 55%; iii, NaOH (2 M), reflux, 3 h, then HCl, 92%; iv, $KHCO_3$ (1.1 equiv.), BnBr (1.1 equiv.), DMF, 60 °C, 2 h, 58%; v, H_2C=C(NHBoc)CO_2Me (2.0 equiv.), $Pd(OAc)_2$ (0.10 equiv.), $NaHCO_3$ (5.0 equiv.), $Bu_4N^+Cl^-$ (2.0 equiv.), DMF, 60 °C, 8 h, 43%; vi, {Rh(COD)[(S,S)-Et-DuPHOS]}$^+OTf^-$ (0.009 equiv.), H_2 (40 psi), MeOH, room temp., 6 h, > 99%, > 98%, ee dr > 99 : 1.

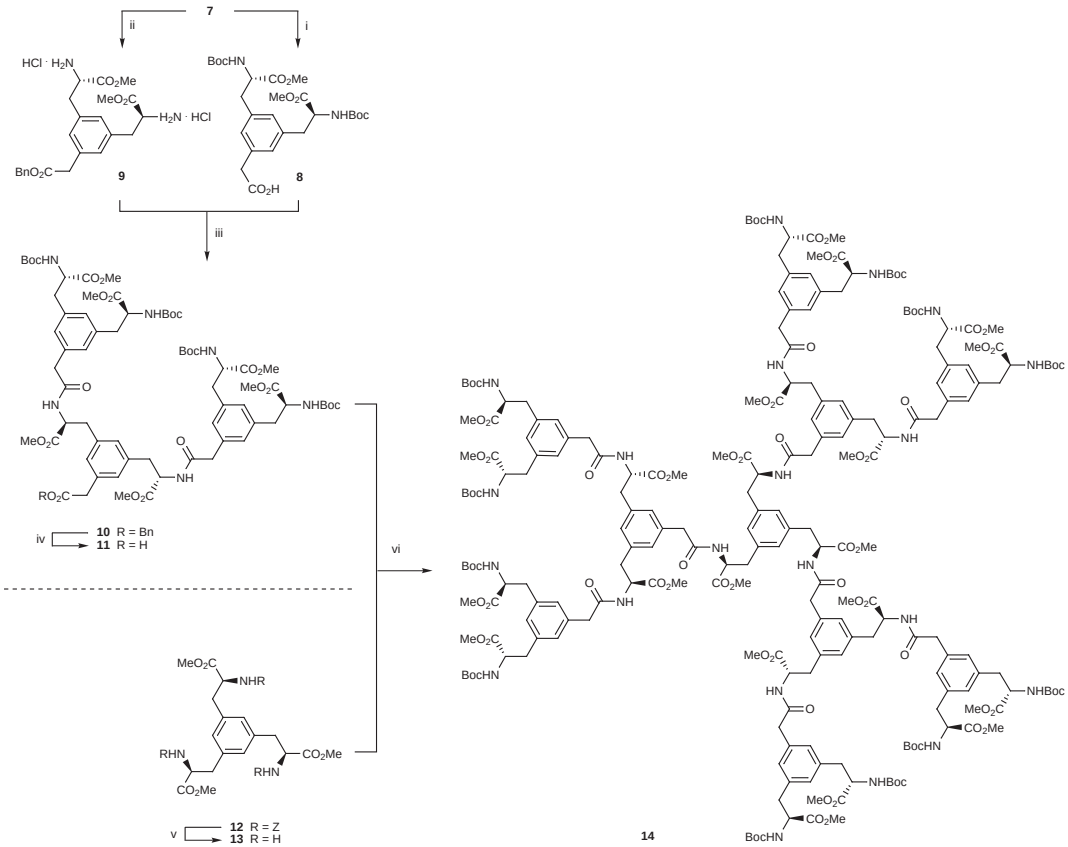

Scheme 2 *Reagents and conditions*: i, Pd/C (5%), EtOH (99.5%), H_2 (1 atm), room temp., 3 h; ii, 3 M HCl in EtOAc, 30 min, room temp.; iii, **8** (2.0 equiv.), TFFH (2.4 equiv.), DIEA (4.8 equiv.), DMF, room temp., 5 min, then **9** (1.0 equiv.), room temp., 1 h, then repeat acylation with **8** (1.0 equiv.), TFFH (1.2 equiv.), Pr^i_2NEt (2.4 equiv.), 57% overall from **7**; iv, Pd/C (5%), EtOH (99.5%), H_2 (1 atm), room temp., 3 h; v, Pd/C (5%), EtOH (99.5%), H_2 (1 atm), room temp., 6 h; vi, **11** (4.0 equiv.), TFFH (4.4 equiv.), Pr^i_2NEt (8.8 equiv.), DMF, room temp., 5 min, then **13** (1.0 equiv.), room temp., 1 h, 87% overall from **12**.

the ethyl ester, which had to be replaced by a benzyl ester to give **5**. Unfortunately, reduction of the diazonium salt of **2** with benzyl alcohol failed. Heck coupling with methyl 2-[(*tert*-butoxycarbonyl)amino]acrylate[7] gave the unsaturated derivative **6**, which was hydrogenated with a chiral Rh^{I}-Et-DuPHOS† catalyst[9] to give **7**.

The convergent synthesis of dendrimer **14** from **7** and **12** is shown in Scheme 2. Since **14** is a polyamide related to a peptide, but possibly more sterically congested, an efficient peptide coupling reagent with minimum steric bulk and high reactivity was desired for the formation of the amide bonds. Based on these considerations, we chose to use TFFH[10]† for the amide bond formations. To this end, hydrogenolysis of **7** yielded **8**, while acidolysis of **7** with HCl in EtOAc (generated from AcCl and EtOH) gave **9**. Acylation of **9** with 2 equiv. of **8** using TFFH proved difficult, and a substantial amount of monoacylated material was recovered. To achieve satisfactory results, **9** had to be acylated twice, first with 2 equiv. of **8** and then with 1 equiv., in two consecutive operations. With this procedure, the dendritic wedge **10** was formed in 57% yield from **7**.

Hydrogenolysis of **10** yielded the free acid **11**, and similar treatment of **12** yielded triamine **13**. Acylation of **13** with 4 equiv. of **11** using TFFH finally yielded dendrimer **14** in 87% yield after a single acylation. This coupling thus proceeded with higher efficiency than that leading to the dendritic wedge **10** above. The reason for this counterintuitive outcome is unclear at present. The identity of **14** was confirmed by NMR and MALDI MS analyses (calc. 4488.9 [M + Na], found 4488.7).

While **14** was synthesised in fully protected form, deprotection of the methyl esters, the Boc groups, or both, will yield a polyionic compound with potentially interesting properties. Studies in this direction are in progress in our laboratory.

We thank the Swedish Natural Science Research Council, the Crafoord Foundation, the Knut and Alice Wallenberg Foundation, and the Royal Physiographic Society in Lund for financial support, and Mr Hasse Karlsson, Department of Medical Biochemistry, Göteborg University, for recording the MALDI mass spectrum.

Notes and references

† List of abbreviations: (*S*,*S*)-Et-DuPHOS = 1,2-bis[(2*S*,5*S*)-2,5-diethylphospholano]benzene, TFFH = *N*,*N*,*N*′,*N*′-tetramethyl-2-fluoroformamidinium hexafluorophosphate.

1 H.-F. Chow, T. K.-K. Mong, M. F. Nongrum and C.-W. Wan, *Tetrahedron*, 1998, **54**, 8543.
2 G. R. Newkome, C. N. Moorefield and F. Vögtle, *Dendritic Molecules, Concepts, Syntheses, Perspectives*, VCH, Weinheim, 1996.
3 H. W. I. Peerlings and E. W. Meijer, *Chem. Eur. J.*, 1997, **3**, 1563.
4 D. K. Smith and F. Diederich, *Chem. Eur. J.*, 1998, **4**, 1353.
5 A. Ritzén and T. Frejd, *Tetrahedron: Asymmetry*, 1998, **9**, 3491.
6 A. Ritzén, B. Basu, S. K. Chattopadhyay, F. Dossa and T. Frejd, *Tetrahedron: Asymmetry*, 1998, **9**, 503.
7 A.-S. Carlström and T. Frejd, *Synthesis*, 1989, 414.
8 J. W. Barnett, F. A. Robinson and B. M. Wilson, *J. Chem. Soc.*, 1947, 202.
9 M. J. Burk, J. E. Feaster, W. A. Nugent and R. L. Harlow, *J. Am. Chem. Soc.*, 1993, **115**, 10125.
10 L. A. Carpino and A. El-Faham, *J. Am. Chem. Soc.*, 1995, **117**, 5401.

Communication 8/09195A

Strong intramolecular π–π interactions favor the formation of 2 : 1 (L : M) lanthanide complexes of tris(2-benzimidazolylmethyl)amine

Raphaël Wietzke,[a] Marinella Mazzanti,*[a] Jean-Marc Latour[b] and Jacques Pécaut[b]

[a] *Laboratoire de Reconnaissance Ionique and* [b] *Laboratoire de Chimie de Coordination Service de Chimie Inorganique et Biologique, Département de Recherche Fondamentale sur la Matière Condensée, CEA-Grenoble, 38054 Grenoble, Cedex 09, France. E-mail: mazzanti@drfmc.ceng.cea.fr*

Received (in Basel, Switzerland) 8th October 1998, Accepted 13th December 1998

Reaction of the tripodal ligand tris(2-benzimidazolylmethyl)amine with lanthanides(III) in the presence of counterions ClO_4^-, OTf^- or Cl^- results, even for ligand to metal ratios lower than 2, in the formation of bisligand complexes showing strong p–p interactions between the benzimidazole rings both in solution and in the solid state.

The search for strongly luminescent lanthanide complexes has motivated the synthesis of lanthanide(III) complexes containing only neutral aromatic N-donor ligands.[1] So far, such complexes have been reported only for the tridentate ligand terpyridine (terpy) and for terpy analogues containing benzimidazole side arms.[2,3] These tris(ligand) complexes are formed in a non-aqueous solvent, in absence of coordinating anions and at ligand to metal ratios L/M ⩾ 3. The high stability against ligand dissociation shown by the benzimidazole derivative has been attributed to the presence of intramolecular π stacking interactions.[4] We have recently synthesized, and characterized by crystallographic and NMR studies, some 1 : 1 lanthanide(III) complexes of the tripodal neutral N-donor ligands tris[(2-pyridyl)methyl]amine (tpa) and tris[(2-pyrazinyl)methyl]-amine.[5] Attempts to add a second ligand to these complexes in the presence of coordinating counterions failed. On the other hand, in the presence of non-coordinating anions, addition of an excess of tripodal ligand to the mono(ligand) complexes resulted in the formation of hydroxo-derivatives.[6] In order to investigate whether π–π interactions could stabilize the 2 : 1 complexes, we studied lanthanide(III) complexation by the tripodal N-donor ligand tris(2-benzimidazolylmethyl)amine (ntb), and analogue of tpa in which the pyridine arms are replaced by a benzimidazole. Indeed, ntb demonstrates a strong stabilization of the 2 : 1 complexes in solution as well as in the solid state.

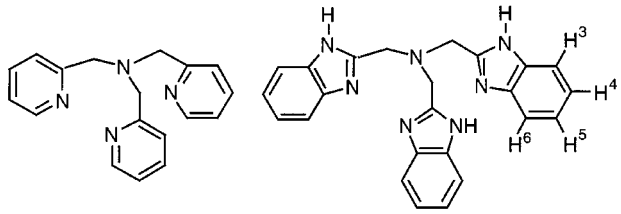

Reaction of $Ln(ClO_4)_3 \cdot 6H_2O$ (Ln = La, Nd, Eu) with 2 equiv. of ntb in acetonitrile yields complexes $[Ln(ntb)_2][ClO_4]_3 \cdot 2MeCN \cdot 3Et_2O$ (**1**, Ln = La; **2**, Ln = Nd; **3**, Ln = Eu) in which the two tripodal ligands encapsulate the lanthanide ion and shield it entirely from solvent molecules (see below).† Reaction of $LuCl_3 \cdot 6H_2O$ with ntb in a 2 : 1 (ntb/Lu) ratio in methanol yields also the bis(ligand) complex $[Lu(ntb)_2]Cl_3 \cdot 7H_2O \cdot 0.5MeOH$ **4**. This is the first example, to our knowledge, in which a neutral N-donor ligand displaces all the strongly coordinating chloride ions. An X-ray diffraction study‡ allowed the determination of the crystal structures of the complexes **1**–**4**, which all present the same structural arrangement for the cation $[Ln(ntb)_2]^{3+}$. The crystal structure of the cation $[Eu(ntb)_2]^{3+}$ is shown in Fig. 1. The coordination geometry is best described as a distorted bicapped trigonal antiprism, in which the lanthanide ion is eight-coordinated by two tetradentate ligands with a pseudo-C_3 symmetric arrangement. The most important feature of these structures is the presence of strong π–π interactions[7] between the benzimidazole rings as shown by the interplanar distances and angles reported in Table 1. Very recently preliminary results on the crystal structures of supramolecular networks using $[Ln(ntb)_2][ClO_4]_3$ as building blocks have been reported.[8] In these structures the stacking interactions between the benzimidazole units are completely lost probably due to the hydrogen-bonding interaction with the 4,4′-bipyridyl space present in the assembly.

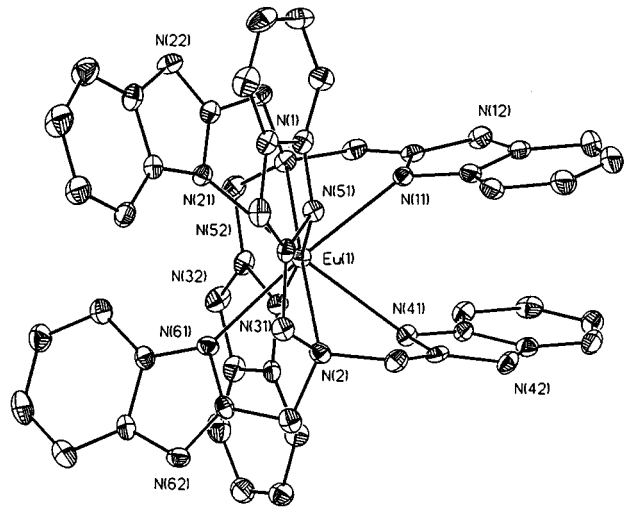

Fig. 1 Crystal structure of the cation of $[Eu(ntb)_2]^{3+}$ **3** with thermal ellipsoids at 30% probability. Selected bond lengths (Å): Eu–N(1) 2.713(4), Eu–N(2) 2.725(4), Eu–N(31) 2.507(4), Eu–N(11) 2.504(4), Eu–N(51) 2.503(4), Eu–N(641) 2.500(4), Eu/N(21) 2.496(4), Eu–N(61) 2.479(4).

The titration of $Ln(OTf)_3$ (Ln = La, Eu, Lu) with ntb in anhydrous acetonitrile was followed by ^1H NMR spectroscopy under a dry argon atmosphere. For a metal to ligand ratio of 1 : 1 two sets of signals were observed (Fig. 2) which were assigned to the 1 : 1 and 2 : 1 ntb complexes. The presence of the two complexes in solution was confirmed by electrospray mass spectrometry. Comparison of the chemical shift of the benzimidazole ring protons in the 1 : 1 and 2 : 1 complexes of lanthanum

Table 1 Interplane distances and angles between the planes of the benzimidazole rings

	α_1/°	d_1/Å	α_2/°	d_2/Å	α_3/°	d_3/Å
$[La(ntb)_2][ClO_4]_3$	13.3	3.55	12.2	3.50	34.0	3.48
$[Nd(ntb)_2][ClO_4]_3$	13.9	3.38	14.5	3.53	34.3	3.40
$[Eu(ntb)_2][ClO_4]_3$	15.3	3.30	15.4	3.38	34.6	3.47
$[Lu(ntb)_2]Cl_3$	16.7	3.15	19.9	3.18	2.31	3.20

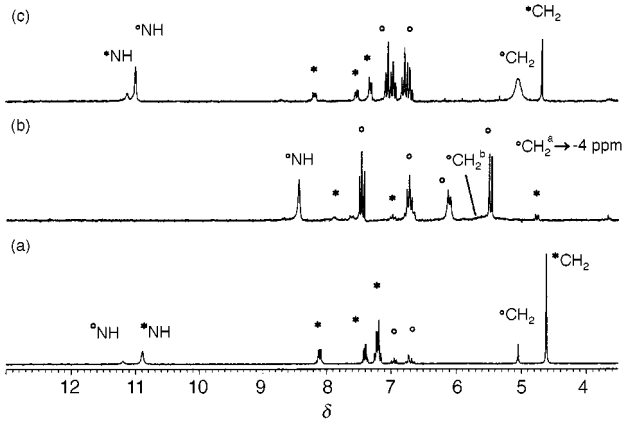

Fig. 2 ^{1}H NMR spectra at 298 K of: (a) a 1 : 1 mixture of $La(OTf)_3$ and ntb in anhydrous acetonitrile; (b) a 1 : 1 mixture of $Eu(OTf)_3$ and ntb in acetonitrile; (c) a 1 : 1 mixture of $Lu(OTf)_3$ and ntb in acetonitrile [(*) indicates the 1 : 1 complex and (○) indicates the 2 : 1 complex].

reveals an upfield shift of 0.4–1.00 ppm for the bis(ntb) complex in agreement with the presence of intramolecular π-stacking interactions in solution.[9] Integration of the NMR signals of the two species gave an approximate value of the ratio (K_2/K_1) of the stepwise formation constants of the 2 : 1 and 1 : 1 complexes. This ratio varies along the series: 0.03 for La, 14 for Eu, 3 for Lu. While for La, $K_1 > K_2$, the value of the ratio K_2/K_1 indicates, in the case of Eu and Lu, a strong preference of the ntb ligand for the formation of the 2 : 1 complexes. This is a rare behavior in coordination chemistry which has only previously been observed twice for lanthanides in presence of tripodal amines with phenolato or phosphinato donors.[10,11] As expected, this ratio is dependent on the counter anion, with the coordinating anions opposing the formation of the 2 : 1 complex. In this respect, it is striking that the bis(ntb) complex already exists in methanol solution of $LuCl_3·6H_2O$ and ntb in a 1 : 1 ratio, as shown by ^{1}H NMR and ESMS.

The high formation constant in water solution of the 2 : 1 complex of the tripodal aminophenol ligand reported by Orvig and coworkers[10,11] was attributed to an entropic effect associated with the release of water molecules. On the other hand, the entropy changes associated with the complexation of strongly basic polydentate amines with lanthanide perchlorate in anhydrous acetonitrile are large and negative and the complexes are enthalpy stabilized.[10] In the Ln–ntb system it is unlikely that an entropy effect related to a change in coordination number is responsible for the observed anomaly ($K_2 > K_1$). The preference for the bis(ntb) complexes might be rather of enthalpic origin and related to the strong π–π interactions found in solution as well as in the solid state.

As a consequence of this π–π stacking of the ligands the metal is completely shielded from the solvent since no water molecule is coordinated to the lanthanide ions in the solid state. This is also true in solution, since comparison of the luminescence lifetimes of $[Tb(ntb)_2](OTf)_3$ in MeOH and MeOD gave a value for the number of coordinated methanol molecules close to zero ($q = 0.35 \pm 0.5$).[12]

This work was supported by the Commissariat à l'Energie Atomique. We thank Colette Lebrun for recording the mass spectra.

Notes and references

† Elemental analyses for complexes **1**–**4**: Calc. for $[La(ntb)_2][ClO_4]_3·3H_2O$, $C_{48}H_{48}Cl_3N_{14}O_{15}La$: C, 44.15; H, 3.70; N, 15.01. Found: C, 43.86; H, 3.80; N, 14.99. Calc. for $[Nd(ntb)_2][ClO_4]_3$, $C_{48}H_{42}Cl_3N_{14}O_{12}Nd$: C, 45.71; H, 3.69; N, 15.88. Found: C, 45.84; H, 3.37; N, 15.59. Calc. for $[Eu(ntb)_2][ClO_4]_3·2H_2O$, $C_{48}H_{46}Cl_3N_{14}O_{14}Eu$: C, 44.41; H, 3.74; N, 14.90. Found: C, 44.31; H, 3.56; N, 15.07. Calc. for $[Lu(ntb)_2]Cl_3·6H_2O$, $C_{48}H_{54}Cl_3N_{14}O_6Lu$: C, 47.87; H, 4.52; N, 16.28. Found: C, 47.66; H, 4.46; N, 15.91%.

‡ *Crystal data*: **1**: $[La(ntb)_2][ClO_4]_3·2MeCN·3Et_2O$, $C_{64}H_{78}N_{16}O_{15}Cl_3La$, M = 1556.68, monoclinic, $P2_1/c$, a = 18.4451(4), b = 25.0336(6), c = 16.9564(4) Å, β = 111.7940(10)°, V = 3903.0(13) Å^3, Z = 4, D_c = 1.422 g cm^{-3}, μ = 0.771 mm^{-1}, 9937 independent reflections ($2\theta_{max}$ = 26) were collected at 173 K. Refinement using the SHELXTL 5.05 package on all data converged at $R_1[F > 4\sigma(F)]$ = 0.0767, wR_2 = 0.1827.

2: $[Nd(ntb)_2][ClO_4]_3·2MeCN·3Et_2O$, $C_{64}H_{78}N_{16}O_{15}Cl_3Nd$, M = 1562.01, monoclinic, $P2_1/c$, a = 18.2235(7), b = 24.8434(10), c = 16.8575(7) Å, β = 111.79(1), V = 7086.5(5) Å^3, Z = 4, D_c = 1.464 g cm^{-3}, μ = 0.921 mm^{-1}. 12398 independent refelections ($2\theta_{max}$ = 26) were collected at 293 K. Refinement using the SHELXTL 5.05 package on all data converged at $R_1[F > 4\sigma(F)]$ = 0.0618, wR_2 = 0.1250.

3 $[Eu(ntb)_2][ClO_4]_3·2MeCN·3Et_2O$, $C_{64}H_{78}N_{16}O_{15}Cl_3Eu$, M = 1569.73, monoclinic, $P2_1/c$, a = 18.1861(4), b = 24.8563(6), c = 16.9481(4) Å, β = 111.93(1), V = 7106.9(3) Å^3, Z = 4, D_c = 1.467 g cm^{-3}, μ = 1.070 mm^{-1}. 12490 independent reflections ($2\theta_{max}$ = 26) were collected at 173 K. Refinement using the SHELXTL 5.05 package on all data converged at $R_1[F > 4\sigma(F)]$ = 0.0481, wR_2 = 0.0865.

4 $[Lu(ntb)_2]Cl_3·7H_2O·0.5MeOH$, $C_{48.5}H_{58}N_{14}Cl_3O_{7.5}Lu$, M = 1238.41, orthorhombic, $Pbcn$, a = 28.03400(10), b = 14.87580(10), c = 27.7355(3) Å, V = 11566.5(2) Å^3, Z = 8, D_c = 1.422 g cm^{-3}, μ = 1.905 mm^{-1}. 10926 independent reflections ($2\theta_{max}$ = 26) were collected at 293 K. Refinement using the SHELXTL 5.05 package on all data converged at $R_1[F > 4\sigma(F)]$ = 0.0867, wR_2 = 0.2266.

To prevent loss of solvent, all the crystals were coated with a light hydrocarbon oil and quickly transferred to a stream of cold nitrogen on the diffractometer.

All data sets were collected using a Siemens SMART CCD area detector three-circle diffractometer (Mo-Kα radiation, graphite monochromator, λ = 0.71073 Å). Non-hydrogen atoms were refined anisotropically and hydrogen atoms were included in calculated positions. For complex **4**, one water molecule was refined isotropically due to a disorder problem. CCDC 182/1127. See http://www.rsc.org/suppdata/cc/1999/209/ for crystallographic files in .cif format.

1 N. Sabbatini, M. Guardigli and J.-M. Lehn, *Coord. Chem. Rev.*, 1993, **123**, 201.
2 G. H. Frost, F. A. Hart, C. Heath and M. B. Hursthouse, *Chem. Commun.*, 1969, 1421.
3 C. Piguet, A. F. Williams, G. Bernardinelli and J.-C. G. Bünzli, *Inorg. Chem.*, 1993, **32**, 4139.
4 S. Petoud, J.-C. G. Bünzli, F. Renaud, C. Piguet, K. J. Schenk and G. Hopfgartner, *Inorg. Chem.*, 1997, **36**, 5750.
5 R. Wietzke, M. Mazzanti, J.-M. Latour, J. Pecaut, P.-Y. Cordier and C. Madic, *Inorg. Chem.*, 1998, **37**, 6690.
6 R. Wietzke, M. Mazzanti, J.-M. Latour and J. Pecaut, unpublished results.
7 W. D. Horrocks, Jr. and D. R. Sudnick, *Acc. Chem. Res.*, 1981, **14**, 384.
8 E. C. Constable and M. D. Ward, *J. Am. Chem. Soc.*, 1990, **112**, 1256.
9 C.-Y. Su, B.-S. Kang, H.-Q. Liu, Q.-G. Wang and T. C. W. Mak, *Chem. Commun.*, 1998, 1551.
10 P. Caravan, T. Hedlund, S. Liu, S. Sjöberg and C. Orvig, *J. Am. Chem. Soc.*, 1995, **117**, 11 230.
11 M. P. Lowe, P. Caravan, S. J. Rettig and C. Orvig, *Inorg. Chem.*, 1998, **37**, 1637.
12 J. H. Forsberg, *Coord. Chem. Rev.*, 1973, **10**, 195.

Communication 8/07831I

A new pillared structure with double-layers of alumina

Fathi Kooli,* Takayoshi Sasaki and Mamoru Watanabe

National Institute for Research in Inorganic Materials, 1-1 Namiki. Tsukuba, Ibaraki 305-0044 Japan.
E-mail: kooli@nirim.go.jp

Received (in Cambridge, UK) 2nd November 1998, Accepted 4th December 1998

Addition of a suspension of exfoliated titanate nanosheets into an Al_{13} pillaring solution produced a novel pillared structure associated with double layers of Al_{13} cations, which can be converted to a mesoporous alumina-pillared titanate with a 2.4 nm spacing by subsequent heat-treatment.

Pronounced interest has been focused on preparation of layered metal oxides pillared with inorganic compounds. The pillaring process is effective for the formation of porous materials such as molecular sieves, catalyst supports, *etc*.[1] In general, most layered oxides are not easily pillared with bulky inorganic cations owing to their inaccessibility to their interlayer space. It is required to develop new intercalation techniques to form large pillars in layered oxides. One of these technique is the pre-pillaring method, in which the interlayer spacing of the oxides is expanded with long-alkylamine chains[2] followed by intercalation of large inorganic polyoxocations such as $[AlO_4Al_{12}(OH)_{24}(H_2O)_{12}]^{7+}$ ('Al_{13}').

For swollen smectite clays, many routes have been examined to prepare new materials which are thermally more stable and more porous than those pillared by conventional techniques. For example, a pillared montmorillonite with a basal spacing of 2.6 nm was prepared by refluxing or hydrothermally treating a mixed solution of Al_{13} polyoxocations and a salt of a rare earth element (*e.g*. Ce or La nitrate) at 130–200 °C.[3,4] This spacing is much larger than those normally reported for pillared clays,[1] and is believed to result from the formation of large polymeric Ce/La-bearing Al_{13} polyoxocations upon hydrothermal treatment of the solution.[3]

Recently, delamination of various layered host materials has been studied extensively,[5] and restacking of the exfoliated single layers in the presence of the bulky cations gives an alternative route to pillared materials.[6] Sasaki *et al.*[7,8] reported that a layered protonic titanate with lepidocrocite-type structure was exfoliated into its single layers in a tetrabutylammonium hydroxide solution. Here, applying this exfoliation route, we found a novel pillared structure with a double-layer arrangement of Al_{13} polyoxocations. By heat-treatment, this phase was converted into a mesoporous alumina-pillared titanate characterized by a larger interlayer spacing and higher specific surface area in comparison with comparable materials produced *via* a pre-pillaring method.

The layered protonic titanate ($H_{0.7}Ti_{1.83}\square_{0.17}O_4\cdot H_2O$, 1 g) was exfoliated into single sheets upon treatment with 200 cm^3 of a tetrabutylammonium hydroxide (TBAOH) solution (0.016 mol dm^{-3}) for 7 days at room temperature. The ratio of TBA cations to protons in the titanate was adjusted to unity, which is a favorable condition for delamination.[8] The Al_{13} solution was prepared by moderately hydrolyzing an aluminium nitrate solution (0.2 mol dm^{-3}) with tetramethylammonium hydroxide (TMAOH) at room temperature. The OH/Al molar ratio was adjusted to 2.5, where Al_{13} polyoxocations are predominant. The colloidal suspension of the titanate was poured into the Al_{13} solution and aged overnight under stirring at 80 °C. The ratio of Al (mmol)/titanate (g) was 16. The product was collected by centrifugation, washed with distilled water, and dried in air.

Fig. 1(a) shows a powder X-ray diffraction pattern of the protonated titanate with a basal distance of 0.94 nm.[9] The colloidal suspension did not display basal reflections, indicating that the titanate single-sheets were dispersed in the aqueous medium.[8] Addition of the titanate suspension to the Al_{13} solution gave a product with a basal diffraction series of 2.6 nm [Fig. 1(b)]. This new phase with larger spacing has not been reported previously for Al_{13}-pillared materials prepared under such mild conditions. Two possibilities may explain this high expansion: (i) the co-presence of TBA and Al_{13} cations in the interlayer space or (ii) the incorporation of a large amount of aluminium polyoxocations. Thermogravimetry showed only a small broad exothermic peak around 370 °C following a weight loss of 4%, suggesting only a small amount of residual organic cations in the pillared material. After this weight loss, the material had a gallery height of 2.5 nm, and thus indicates that possibility (i) is not valid. Therefore, it can be concluded that the large expansion is mainly due to the presence of a large amount of aluminium polyoxocations in the interlayer space.

The new phase shows two noticeable features in terms of structural and compositional data as compared with the Al_{13}-monolayer pillared titanate: (i) a large interlayer distance of 2.6 *vs*. 1.6 nm (corresponding to intercalation of a monolayer of

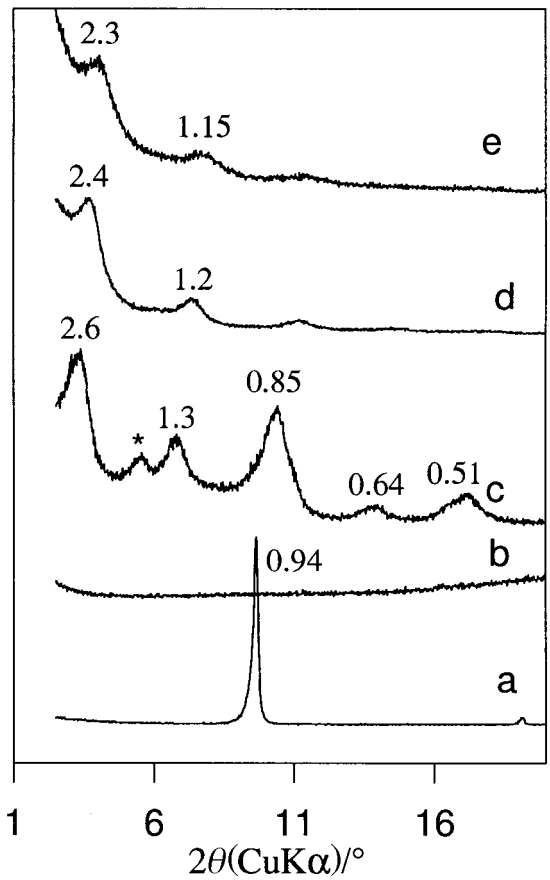

Fig. 1 PXRD patterns of (a) protonated titanate, (b) colloidal suspension of exfoliated titanate and (c) the resulting product prepared after exfoliation and reaction with Al_{13} solution. (d) and (e) correspond to the product (c) heat-treated at 500 and 600 °C, respectively. (*) phase at 1.6 nm (see text).

Al_{13} cations).[10,11] By taking into account the basal spacing of the protonated titanate which accommodates a monolayer of H_2O and H_3O^+, the net interlayer expansion may be estimated as 1.94 nm [= 2.6 − (0.94 − 0.28)]. This is approximately double that of 0.94 nm [= 1.6 − (0.94 − 0.28)] for the monolayered phase.[11] (ii) A double amount of Al_{13} cations. On the basis of chemical analysis, the new product has a composition of $(Al_{13})_{0.22}Ti_{1.83}\square_{0.17}O_4 \cdot 2.88\ H_2O$ whereas the amount of Al_{13} cations in the 1.6 nm phase has been reported to be close to 0.11 mol per chemical formula.[11]

These two features strongly suggest that the titanate obtained in this study accommodates Al_{13} cations in a double-layer arrangement. Nazar *et al*.[12] identified a new aluminium polyoxycation cluster formed by the dimerization of two Al_{12} polyoxocations (tentatively formulated as $Al_{24}O_{72}$) which was facilitated by refluxing an Al_{13} solution at high temperatures. This new polyoxycation is about 1.4 nm in size and considerably larger than Al_{13} cations (*ca*. 1 nm).[13] The expected spacing for the intercalation of such a dimeric polyoxocation, however, does not approximate to the large interlayer expansion observed in this study. Furthermore, the formation of the 2.6 nm phase under mild conditions at room temperature should be noted, which excludes formation of the $Al_{24}O_{72}$ polyoxocation.

The Al_{13} polyoxocations are generally believed to hold a theoretical charge of 7+ while the above empirical formula suggests a 3.2+ charge for Al_{13}. A similar situation has also been reported for Al_{13}-intercalated montmorillonite clay.[14] Thus the actual aluminium polyoxocation will probably be modified from $(Al_{13})^{7+}$. Neighboring Al_{13} polyoxocations in a bilayer are expected to mutually condense *via* apical water molecules. Such condensation should be effective in relaxing the electrostatic repulsion between the polyoxocations and lead to charge balance with the host layers interleaving the bilayer. A simple model for the condensation would give the following composition for the modified Al_{13} as $[AlO_4Al_{12}(OH)_{24}O_2(H_2O)_8]^{3+}$.

The intercalation of Al_{13} would probably be irreversible, since the interlayer gallery was little changed before and after treatment of the Al_{13}-product in a solution of sodium chloride (1 mol cm^{-3}) overnight at 80 °C. The pillared structure of the present material was preserved up to 600 °C, while the basal spacing shrunk from 2.6 to 2.4 nm [Fig. 1(c) and 1(d)]. The shrinkage could be attributed to dehydroxylation of the aluminium species upon heating. The pillared material collapsed at 600 °C and TiO_2 and α-Al_2O_3 started to crystallize. The trace '1.6 nm', phase also collapsed.

The sample calcined at 500 °C had a type IV nitrogen adsorption isotherm (in the IUPAC classification) with a large hysteresis loop of type H4.[15] The specific surface area was *ca*. 300 $m^2\ g^{-1}$ with a pore volume of 0.25 mL liquid nitrogen per gram of material. The surface area of the pillared titanate was greatly enhanced in comparison with protonic titanate (1–2 $m^2\ g^{-1}$), and also much higher than those of pillared titanates, (100–200 $m^2\ g^{-1}$).[10,11] The average pore diameter is 3.5 nm and the pore size distribution shows a maximum at *ca*. 4.0 nm. Further study is now being conducted to clarify the effect of different experimental parameters on the physico-chemical properties of these materials.

Notes and references

1 K. Ohtsuka, *Chem. Mater*., 1997, **9**, 2039.
2 A. Clearfield and B. D. Robert, *Inorg. Chem*., 1988, **27**, 3237.
3 J. Sterte. *Clays Clay Miner*., 1991, **39**, 167
4 E. Booij, J. T. Kloprogge and A. Rob Van Veen. *Clays Clay Miner*., 1996, **44**, 774.
5 A. Jacobson, *Mater. Sci. Forum*, 1994, **152**–**153**, 1.
6 L. F. Nazar, S. W. Liblong and X. T. Yin, *J. Am. Chem. Soc*., 1991, **113**, 5889.
7 T. Sasaki, M. Watanabe, H. Hashizume, H. Yamada and H. Nakazawa, *J. Am. Chem. Soc.*, 1996, **118**, 8329.
8 T. Sasaki and M. Watanabe. *J. Am. Chem. Soc.*, 1998, **120**, 4682.
9 T. Sasaki, M. Watanabe, Y. Michiue, Y. Komatsu, F. Izumi and S. Takenouchi, *Chem. Mater*., 1995, **7**, 1001.
10 S. Cheng and T.-C. Wang, *Inorg. Chem*., 1989, **28**, 1283.
11 F. Kooli, T. Sasaki and M. Watanabe, *Microporous Mesoporous Mater*., in press.
12 L. F. Nazar, G. Fu and D. Bain, *J. Chem. Soc., Chem. Commun*., 1992, 251.
13 G. Johanson, *Ark. Kemi*., 1962, **20**, 305.
14 J. Bovey and W. Jones, *J. Mater. Chem*, 1995, **5**, 2027.
15 K. S. W. Sing, D. H. Everett, R. A. W. Haul, L. Moscou, R. Pierotti, J. Rouquerol and T. Sieminiewska, *Pure Appl. Chem*., 1985, **57**, 603.

Communication 8/08453J

Photoinduced electron transfer from pyrene to methylviologen in polystyrene latex dispersions as studied by diffuse reflectance laser flash photolysis

K. Nakashima,*[a] T. Miyamoto[a] and S. Hashimoto[b]

[a] *Department of Chemistry, Faculty of Science and Engineering, Saga University, 1 Honjo-machi, Saga 840-8502, Japan. E-mail: nakashik@cc.saga-u.ac.jp*

[b] *Department of Chemistry, Gunma College of Technology, 580 Toriba-machi, Maebashi, Gunma 371-0845, Japan*

Received (in Cambridge, UK) 22nd September 1998, Accepted 15th Decemer 1998

Fluorescence and diffuse reflectance flash photolysis studies revealed that photoinduced electron transfer from pyrene to methylviologen was enhanced in polystyrene latex dispersions, and also that the back electron transfer was markedly suppressed in the dispersions, resulting in effective charge separation.

Latex particles represent a new type of organic solid material which can be employed as a micro-substrate for photoreactions. The surface consists of organic polymers embedded sparsely with functional groups such as sulfate, carboxyl or amino groups. This structure leads latex particles to have two types of adsorption sites on the surface: (1) the polymer matrix which affords continuous adsorption domains to non-polar and low polarity adsorbates, and (2) the functional group which gives discrete adsorption sites to ionic and highly polar species. Such a feature is not found in any other solid materials which are employed as adsorbents. Furthermore, latex particles have many other advantageous features as described in previous papers.[1,2]

We have investigated several photoreactions, such as electronic energy transfer[3,4] and electron transfer,[2,5] on the surface of polystyrene (PS) and poly(butyl methacrylate) latexes in aqueous dispersions, and demonstrated the usefulness of the latexes as micro-substrates for the photoreactions. Here, we report photoinduced electron transfer (PET) from pyrene (Py) to methylviologen (MV^{2+}) in PS latex dispersions.

The PS latex was synthesized by standard emulsion polymerization in the presence of sodium dodecyl sulfate. The latex was purified by repeated dialysis. The diameter of the latex particles was determined to be 85 nm with an Otsuka ELS-800 dynamic light scattering spectrophotometer. Fluorescence spectra were recorded on a Hitachi F-4000 spectrofluorometer. Transient absorption spectra were observed with a nanosecond diffuse reflectance laser photolysis system, the set-up of which was similar to that described previously.[6]

We measured fluorescence spectra of Py in the absence and presence of MV^{2+} [Fig. 1(a)]. It is well known that the fluorescence of Py is quenched by MV^{2+} through PET as follows:[7,8]

$$\mathrm{Py} + h\nu_a \rightarrow \mathrm{Py}^* \quad (1)$$

$$\mathrm{Py}^* + \mathrm{MV}^{2+} \xrightarrow{\mathrm{PET}} \mathrm{Py}^{\cdot+} + \mathrm{MV}^{\cdot+} \quad (2)$$

$$\downarrow \text{Fluorescence}$$

$$\mathrm{Py} + h\nu_f$$

Thus, we can observe the PET reaction by monitoring the fluorescence quenching of Py. As seen from Fig. 1(a), the fluorescence of Py is effectively quenched by MV^{2+} in the latex dispersion even when the MV^{2+} concentration is at a level of μM, which is several tens of times smaller than that needed for quenching in aqueous solutions. This means that PET in the latex dispersions takes place several tens of times more efficiently than in aqueous solutions. The marked enhancement of PET can be ascribed to the increase in local concentrations of the donor and acceptor on the latex surface, as confirmed by the adsorption isotherms (data not shown). The effective adsorption of the donor (Py) onto the latex surface is also evidenced by the vibronic fine structure of the fluorescence. The intensity ratio between the band I and III [the so-called I_1/I_3 value; Fig. 1(a)] is well known to be a measure of polarity around the probe.[9,10] The I_1/I_3 value obtained is 1.13 for the latex dispersion, which is much closer to the values for benzene (1.05)[10] and propan-1-ol (1.09)[10] than that for water (1.81). This means that most of the Py molecules are located on the latex particles.

There are generally two purposes for employing solid surfaces as substrates for PET: (A) to enhance PET by condensing and orienting the reactants, and (B) to suppress the back electron transfer to achieve effective charge separation.[11] We have shown in Fig. 1 the usefulness of the PS latex particles for realizing purpose (A). To examine (B), we intended to observe transient absorption spectra. As the latex dispersion is very turbid, a conventional (*i.e.* transmittance mode) flash photolysis technique is of no use for the system. Therefore, we employed the diffuse reflectance mode. The transient absorption spectra for the PS latex dispersion containing Py and MV^{2+} are shown in Fig. 2. The band at 408 nm is assigned to the $MV^{\cdot+}$ cation radical, and the band at 461 nm to the $Py^{\cdot+}$ cation radical [Fig. 2(a)]. We note from Fig. 2 that these radical bands remain for > 1 ms. If we consider that charge recombination between the products usually takes place on the time scale of picoseconds or nanoseconds in homogeneous solutions, we can see

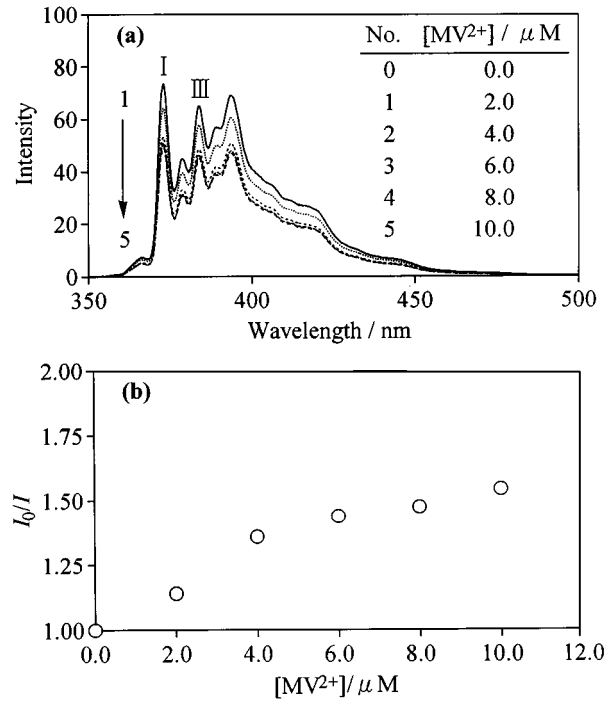

Fig. 1 Fluorescence spectra (a) and Stern–Volmer plot (b) for a Py/MV^{2+} pair in a PS latex dispersion. Concentrations: [Py] = 0.514 μM, [PS] = 1.00 g L^{-1}. The samples are excited at 334 nm. The spectra are corrected by subtracting background scattering of excitation light.

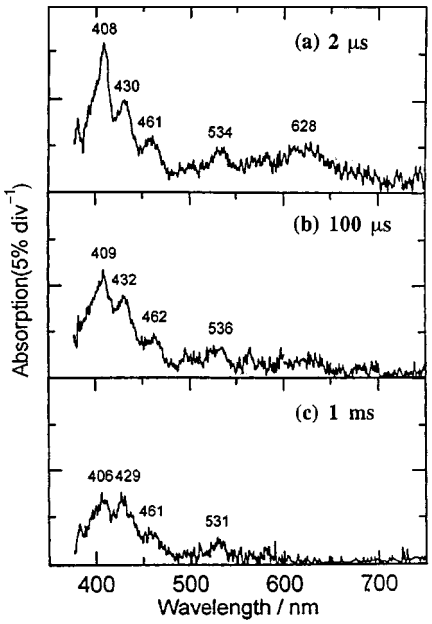

Fig. 2 Transient absorption spectra of a Py/MV^{2+} pair in a PS latex dispersion. Concentrations: [Py] = 250 μM, [MV^{2+}] = 300 μM, [PS] = 54.2 g L^{-1}.

that the back electron transfer is markedly suppressed in the latex dispersion. Thus, the present result demonstrates the usefulness of the latex system for performing effective charge separation.

In order to understand the remarkable effect of the latex system on suppression of charge recombination, we show in Fig. 3 a schematic diagram for behavior of the reactants and products of the PET reaction on the latex surface. Before the PET reaction, Py molecules are mostly adsorbed onto the continuous PS area by hydrophobic interaction, while MV^{2+} molecules are adsobed onto the sulfate groups by electrostatic attraction. After the PET reaction, both of the products will be

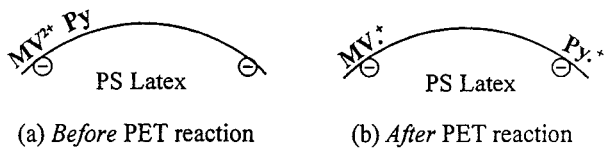

Fig. 3 Schematic representation for the behavior of Py, MV^{2+} and their PET reaction products on a PS latex surface.

fixed at the sulfate groups owing to electrostatic interaction. The fixation of the products seems to result in suppression of the back electron transfer.

Recently, Hsiao and Webber investigated PET reactions from pyrene and anthracene derivatives to a viologen analogue using a PS latex dispersion.[12] They also observed a remarkable increase in the efficiency of charge separation for some donor–acceptor pairs, although the forward PET reactions were not improved by the use of the latex dispersion. They ascribed the remarkable increase in the yield of the charge separation to a 'compartmentalization effect' of the latex particles. It is likely that there are compartments (holes) on the latex surface which accommodate limited types of the products and/or reactants. The existence of such compartments is also suggested in our experiments for the present system and also for another system.[2] The Stern–Volmer plot [Fig. 1(b)] shows a downward curve, indicating that the fluorescence of Py is partly protected from quenching by MV^{2+} on the PS latex particles. We can attribute this protected quenching to the likelihood that some portion of Py molecules on the latex surface is incorporated into the holes in the latex particles (see ref. 2 for detailed discussion). In conclusion, it seems that both a 'fixation effect' and 'compartmentalization effect' play an important role in PET processes in latex systems.

Note and references

1 K. Nakashima, N. Kido, A. Yekta and M. A. Winnik, *J. Photochem. Photobiol. A: Chem*., 1997, **110**, 207.
2 K. Nakashima, S. Tanida, T. Miyamoto and S. Hashimoto, *J. Photochem. Photobiol. A: Chem*., 1998, **117**, 111.
3 K. Nakashima, J. Duhamel and M. A. Winnik, *J. Phys. Chem*., 1993, **97**, 10702.
4 K. Nakashima, Y. S. Liu, P. Zhang, J. Duhamel, J. Feng and M. A. Winnik, *Langmuir*, 1993, **9**, 2825.
5 K. Nakashima and N. Kido, *Photochem. Photobiol*., 1996, **64**, 296.
6 S. Hashimoto, N. Fukazawa, H. Fukumura and H. Masuhara, *Chem. Phys. Lett*., 1994, **223**, 493.
7 R. D. Stramel, C. Nguyen, S. E. Webber and M. A. J. Rodgers, *J. Phys. Chem*., 1988, **92**, 2934.
8 D. Fornasiero and F. Grieser, *J. Chem. Soc., Faraday Trans*., 1990, **86**, 2955.
9 K. Kalyanasundaram and J. K. Thomas, *J. Am. Chem. Soc*., 1977, **99**, 2039.
10 D. C. Dong and M. A. Winnik, *Photochem. Photobiol*., 1982, **35**, 17.
11 K. Kalyanasundaram, *Photochemistry in Microheterogeneous Systems*, Academic Press, New York, 1987.
12 J.-S. Hsiao and S. E. Webber, *J. Phys. Chem*., 1993, **97**, 8289; J.-S. Hsiao and S. E. Webber, *J. Phys. Chem*., 1993, **97**, 8296.

Communication 8/07368F

Bis(2-methoxyethyl)aminosulfur trifluoride: a new broad-spectrum deoxofluorinating agent with enhanced thermal stability

Gauri S. Lal,* Guido P. Pez, Reno J. Pesaresi and Frank M. Prozonic

Air Products and Chemicals Inc, 7201, Hamilton Boulevard, Allentown, PA 18195-1501, USA.
E-mail: lalgs@apci.com

Received (in Corvallis, OR, USA) 2nd November 1998, Accepted 7th December 1998

Bis(2-methoxyethyl)aminosulfur trifluoride (Deoxo-Fluor™) is effective for the conversion of alcohols to alkyl fluorides, aldehydes/ketones to the corresponding *gem*-difluorides and also for the transformation of carboxylic acids to their trifluoromethyl derivatives; it is a less thermally sensitive, broader-spectrum alternative to the traditional dialkylaminosulfur trifluoride (DAST) deoxofluorination reagents.

In view of the importance of organofluorine compounds in the pharmaceutical and agrochemical industries, efforts aimed at the development of simple, safe and efficient methods for their synthesis have escalated in recent years.[1–5] The conversion of carbon–oxygen to carbon–fluorine bonds by nucleophilic fluorinating sources (deoxofluorination) represents one such technique which has been widely used for the selective introduction of fluorine into organic molecules.[6] This transformation has been accomplished routinely with the dialkylaminosulfur trifluorides, such as DAST (NEt_2SF_3), for laboratory scale reactions.[7] However, utilization of DAST for larger scale applications has been limited by its well known thermal instability.[8,9] DAST and related dialkylaminosulfur trifluorides are said to undergo catastrophic decomposition (explosion or detonation) with gas evolution on heating to > 90 °C.[10]

We now report on bis(2-methoxyethyl)aminosulfur trifluoride (Deoxo-Fluor) **1**, a new deoxofluorinating agent which is a less thermally sensitive and very effective alternative to DAST. It permits the facile conversion of alcohols to alkyl fluorides, aldehydes/ketones to the corresponding *gem*-difluorides, and also the transformation of carboxylic acids to the corresponding trifluoromethyl derivatives with, in some cases, superior performance to DAST.

Deoxo-Fluor reagent is obtained in a manner analogous to that of DAST[9] by reacting the *N*-trimethylsilyl derivative of bis(2-methoxyethyl)amine with SF_4 in Et_2O at −30 °C. The crude product is distilled (60 °C, 0.1 mmHg) to afford a light yellow oil in 70% yield [$\delta_H(CDCl_3)$ 3.5 (t, 4H), 3.15 (t, 4H), 3.05 (s, 6H); $\delta_F(CDCl_3)$ 55 (s, br, 2F), 28 (s, br, 1F]. A comparison of the thermal stability of Deoxo-Fluor and DAST, as determined by differential scanning calorimetry (DSC), is illustrated in Fig. 1. While the onset of decomposition is almost the same for both compounds (~140 °C), DAST degrades much more rapidly and with somewhat larger heat evolution (1700 *vs.* 1100 J g^{-1} for **1**). Deoxo-Fluor showed a much more gradual exotherm over a wider temperature range. These preliminary results indicate that the latter should be safer to use than DAST on a larger, practical scale.

The broad applicability of **1** for the deoxofluorination of organic substrates is illustrated by its reaction chemistry, as shown in Table 1. Primary, secondary and tertiary alcohols react at relatively low temperatures (−78 °C to ambient), giving moderate to excellent yields of the corresponding alkyl fluorides. Fluorination of the anomeric hydroxy group of the sugar was particularly effective, giving the desired compound in 95% yield. The fluorination of aldehydes and ketones con-

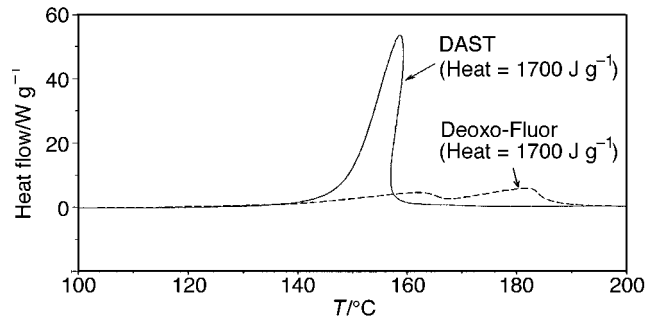

Fig. 1 DSC plots for the thermal decomposition of DAST and Deoxo-Fluor **1** (ref. 13). Samples were in hermetically sealed gold pans; scan rate 10 °C min^{-1}.

Table 1 Fluorination of model compounds with the Deoxo-Fluor reagent **1**

Substrate	**1**/equiv.	Solvent	*T*/°C	*t*/h	Product	Yield (%)
$PhCH_2CH_2OH$	1.1	CH_2Cl_2	room temp.	16	$PhCH_2CH_2F$	85
$MeCH(OH)CO_2Et$	1.1	CH_2Cl_2	room temp.	3	$MeCHFCO_2Et$	73
$Me_2C(OH)CO_2Et$	1.1	CH_2Cl_2	room temp.	8	Me_2CFCO_2Et	89
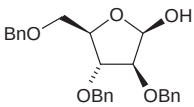	1.1	CH_2Cl_2	0	0.5	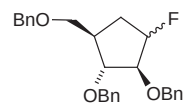	95[a]
PhCHO	1.7	CH_2Cl_2	reflux	16	$PhCHF_2$	95
4-*tert*-butylcyclohexanone	1.7	CH_2Cl_2	room temp.	16	1-*tert*-butyl-4,4-difluorocyclohexane	85
$PhOCH_2COMe$	1.7	CH_2Cl_2	room temp.	16	$PhOCH_2CF_2Me$	98
PhCOMe	1.5	neat	85	16	$PhCF_2Me$	92
$PhCO_2H$	1.1	CH_2Cl_2	0	0.5	PhCOF	96
$Me(CH_2)_8CO_2H$	1.1	CH_2Cl_2	0	0.5	$Me(CH_2)_8COF$	96
PhCOF	2.0	neat	85	48	$PhCF_3$	58
$Me(CH_2)_8COF$	2.0	neat	85	48	$Me(CH_2)_8CF_3$	63

[a] Ratio α:β = 9:91.

ducted in CH_2Cl_2 at room temperature in the presence of 0.1 equiv. of HF, generated *in situ* with added EtOH, afforded excellent yields of the corresponding *gem*-difluoro products from both aliphatic and aromatic carbonyl compounds. The relatively greater thermal stability of **1** was exploited for the fluorination of electron-deficient ketones and carboxylic acids, which are traditionally less reactive substrates. As illustrated in Table 1, **1** reacted readily with carboxylic acids, giving acyl fluorides. These were subsequently converted to the trifluoromethyl derivatives on heating for an extended period in the neat reagent at 90 °C. DAST has not been generally employed for the fluorination of carboxylic acids and we are only aware of one report of such an application.[11]

The broad-spectrum reactivity of the Deoxo-Fluor reagent coupled with its potentially greater margin of safety in use and commercial availability[12]should lead to its widespread application for the synthesis of specialty organofluorine compounds. Detailed studies of its thermal behavior and reactivity with a wider range of functional groups are in progress.

Notes and references

1 J. T. Welch and S. Eshwarakrishan, *Fluorine in Bioorganic Chemistry*, Wiley, New York, 1991.

2 R. Filler and K. Kirk, *Biological Properties of Fluorinated Compounds*, A. J. Elliott, *Fluorinated Pharmaceuticals* and R. W. Lang, *Fluorinated Agrochemicals* in *Chemistry of Organic Fluorine Compounds II*, ed. M. Hudlicky and A. E. Pavlath, ACS Monograph 187, American Chemical Society, Washington, DC, 1995.

3 D. Cartwright, *Recent Developments in Fluorine-Containing Agrochemicals*, in *Organofluorine Chemistry, Principles and Commercial Applications*, ed. R. E. Banks, B. E, Smart and J. C. Tatlow, Plenum, New York, 1994.

4 R. Filler, in *Organofluorine Compounds in Medicinal and Biomedicinal Applications*, ed. R. Filler, Y. Kobayashi and L. M. Yagupolskii, Elsevier, Amsterdam, The Nederlands, 1993.

5 *New Fluorinating Agents in Organic Synthesis*, ed. L. German and S. Zemskov, Springer-Verlag, Heidelberg, New York, 1989.

6 M. Hudlicky, *Fluorination with Diethylaminosulfur Trifluoride and related Aminosulfuranes*, in *Org. React.*,, 1988, **25**, 513.

7 W. J. Middleton, *J. Org. Chem*., 1975, **40**, 574.

8 J. Cochran, *Chem. Eng. News*, 1979, **57**, 4.

9 W. J. Middleton, *Chem. Eng. News*, 1979, **57**, 43.

10 P. A. Messina, K. C. Mange and W. J. Middleton, *J. Fluorine Chem*., 1989, **42**, 137.

11 $PhCF_3$ was reportedly produced in 50% yield by heating *in situ* prepared PhCOF with excess DAST in diglyme for 20 h at 80 °C: W. J. Middleton, *US Pat.* 3,914,265 (1975).

12 From Aldrich Chemical Co, Milwaukee, WI 53201 and Air Products and Chemicals, Inc. 7201 Hamilton Boulevard, Allentown, PA, USA 18195-1501.

13 The exotherm peak for DAST appears skewed, as the sample heats faster than the furnace, then cools to readjust to the temperature program.

Communication 8/08517J

Typeset and printed by Black Bear Press Limited, Cambridge, England

ChemComm
FEATURE ARTICLE

Recent developments in Ramberg–Bäcklund and episulfone chemistry

Richard J. K. Taylor†

Department of Chemistry, University of York, York, UK Y010 5DD. E-mail: rjkt1@york.ac.uk

Received (in Cambridge, UK) 24th August 1998, Accepted 11th September 1998

A brief historical review of the Ramberg–Bäcklund rearrangement is presented along with a summary of its applications to the synthesis of bioactive target molecules. Recent developments in this area originating from the author's laboratories, mostly from the past five years, are reviewed. These include: (i) the isolation of episulfones from the Ramberg–Bäcklund rearrangement, (ii) the preparation of episulfones by the oxidation of episulfides, (iii) the generation and synthetic applications of episulfone α-anions, (iv) the epoxy-Ramberg–Bäcklund rearrangement, (v) the tandem conjugate addition-Ramberg–Bäcklund rearrangement, and (vi) utilisation of the Ramberg–Bäcklund rearrangement in natural product synthesis and related areas, including recent applications for the synthesis of *C*-glycosides.

(*a*) Introduction

Since its discovery in 1940,[1] the Ramberg–Bäcklund rearrangement, the base-mediated conversion of α-halogenated sulfones into regio-defined alkenes (Scheme 1), has attracted a considerable amount of interest from both synthetic and mechanistic viewpoints.[2] The development of the Meyers' modification (Scheme 2),[3] in which the sulfone undergoes *in situ* halogenation-Ramberg–Bäcklund rearrangement, has further extended the synthetic utility of this process.

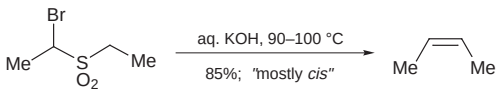

Scheme 1

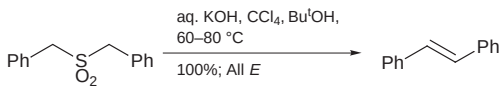

Scheme 2

The strengths of the procedure from a synthetic perspective are: (i) the ease with which the requisite sulfones can be constructed and the conjunctive nature of the sequences, (ii) the unambiguous location of the resulting alkene moiety and the applicability of the procedure to all alkene substitution patterns including tetrasubstituted variants, (iii) the efficiency with which strained alkenes (*e.g.* cyclobutenes, unsaturated cyclophanes)[2,3] can be prepared, (iv) the applicability of the procedure to conjugated polyene synthesis, either by using allylic sulfones[2] or *via* the vinylogous[4] and Michael-induced[5] variants of the Ramberg–Bäcklund rearrangement. Predictably high stereocontrol is not a feature of the Ramberg–Bäcklund rearrangement, but in general *Z*-alkenes predominate when mild bases are employed, whereas stronger bases favour *E*-alkenes.[2]

The utility of the Ramberg–Bäcklund rearrangement can be seen from applications to the synthesis of natural products and related analogues. Recent examples from other groups, shown in Fig. 1, include a formal total synthesis of brassinolide,[6] the total syntheses of (+)-solamin,[7] (+)-eremantholide A[8] and (−)-conduritol E derivatives,[9] the preparation of enediyne[10] and ciguatoxin[11] analogues, and the synthesis of an advanced intermediate to the *C*-aryl glycoside chrysomycin A.[12]

In terms of the mechanism of the Ramberg–Bäcklund reaction, considerable progress was made in the 1950s and 1960s.[2] Elegant studies by Bordwell, Neureiter, Paquette and others have resulted in the general acceptance of the mechanistic sequence illustrated in Scheme 3. Indirect support was obtained for the intermediacy of episulfones (thiirane 1,1-dioxides): they were prepared by other procedures (*e.g. via* addition of diazoalkanes to sulfenes[13]) and then it was established that they gave alkenes under the conditions normally employed for the Ramberg–Bäcklund rearrangement.[14]

My interest in synthetic and mechanistic aspects of the Ramberg–Bäcklund rearrangement was stimulated by Dr D. Neville Jones, my Ph.D. supervisor. Although a considerable amount of research had already been carried out by that time, I became convinced that the full potential of the process had yet to be realised. However, it was a number of years before the opportunity arose to make any personal contributions to this area of chemistry. This article summarises these recent contributions and includes some, as yet, unpublished results.

(*b*) The isolation of episulfones from α-halo sulfones

As part of a programme to synthesise novel sulfur-containing analogues of thromboxane A_2,[15] Richard Batten, Guy Casy, Vinod Kansal, Simon Lane, Stephen Quick, Alan Sutherland and Stamatis Vassiliou developed a number of procedures to prepare substituted thianes.[15,16] This presented an opportunity to explore some novel Ramberg–Bäcklund chemistry, investigating the utility of the rearrangement for the conversion of

Richard Taylor graduated from the University of Sheffield and then carried out his PhD under the supervision of Dr D. Neville Jones working in the area of thiasteroid synthesis. After postdoctoral periods with Dr Ian T. Harrison (Syntex Research, Palo Alto; prostaglandin synthesis) and Professor Franz Sondheimer, University College London; annulene synthesis), he was appointed to a lectureship at the Open University in Milton Keynes (1975–1979). A move to the University of East Anglia, Norwich, followed and in 1993 he was appointed to a Chair of Organic Chemistry at the University of York. His research interests centre on the synthesis of bioactive natural products and related compounds, and the development of new synthetic methodology utilising organometallic and organosulfur chemistry. His awards include the Royal Society of Chemistry's Hickinbottom Fellowship for independent creativity in experimental organic chemistry (1985–1987) and the Royal Society of Chemistry's Tilden Medal and Lectureship (1999/2000). He is currently UK Regional Editor of the international journal Tetrahedron and a member of the Executive Board of Tetrahedron Publications.

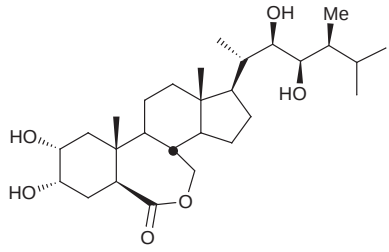

Brassinolide

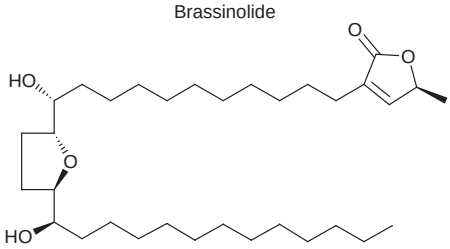

Solamin

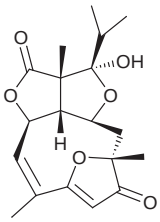

Eremantholide A

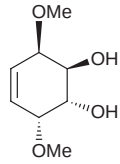

1,4-Dimethyl conduritol E

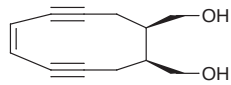

Bioactive enediyne analogue

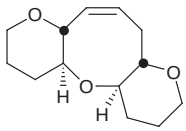

Ciguatoxin analogue

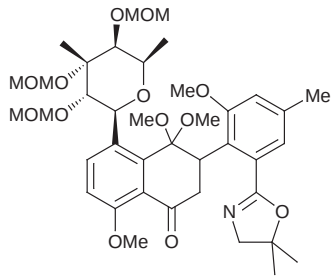

Chrysomycin A precursor

Fig. 1 Bioactive target molecules prepared using the Ramberg–Bäcklund rearrangement.

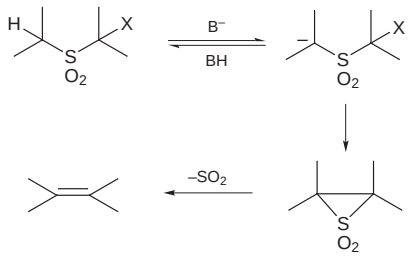

Scheme 3

thiane dioxides into cyclopentenoid natural products [see section (*f*)].[17] As part of this study, Alan Sutherland carried out the Ramberg–Bäcklund rearrangement of α-iodo sulfone **1** at low temperature. Surprisingly, because these reactions were generally very clean, two products were obtained (Scheme 4). The expected cyclopentene **3** was accompanied by a major crystalline by-product (69% yield) which no longer contained an iodide group, but neither did it possess alkenyl protons or carbons in its NMR spectra. We eventually concluded that the mystery by-product had to be the episulfone **2** (this finally being confirmed by X-ray crystallography). Episulfone **2** was stable

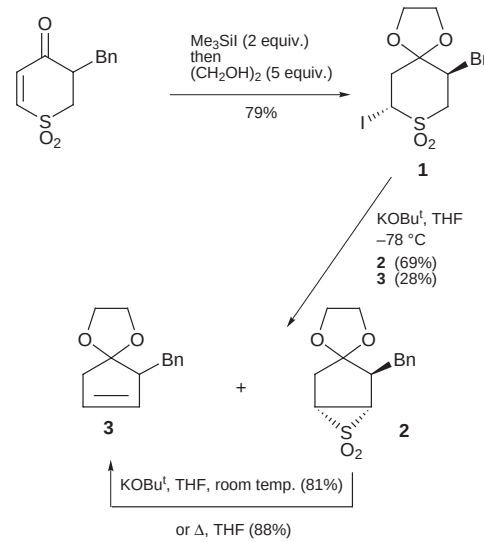

Scheme 4

for months on storage at −18 °C but, as expected, gave cyclopentene **3** on thermolysis or treatment with base. This was the first time that an episulfone had been isolated from an α-halo sulfone under the conditions of the Ramberg–Bäcklund reaction and it provided unambiguous proof of its intermediacy in the rearrangement process.[18]

After the initial discovery, the reaction conditions conditions were optimised and Alan Sutherland, Stephen Jeffery, Simon Pyke, Wendy Loughlin, Richard Ewin and Carlos Morales prepared the 'parent' episulfone **4** and a range of stable, functionalized analogues from α-halo sulfones in high yields (Fig. 2).[19,20] All of the compounds have been fully characterised and X-ray crystal structures were obtained on compounds **2** and **5**. It is not essential to use α-iodo sulfones in this process: episulfone **5** was also prepared from the corresponding α-bromo (74%) and α-chloro (85%) sulfones.

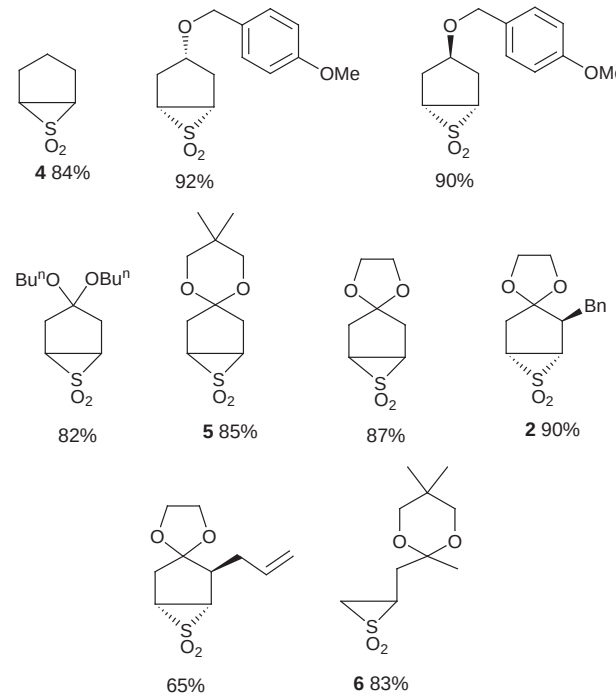

Fig. 2 Episulfones prepared from α-iodo sulfones (isolated yields shown).

Although most of the episulfone isolation programme was carried out using thiane dioxides, we believe that this procedure

for episulfone preparation is likely to be widely applicable: this is illustrated by the efficient conversion of an acyclic α-iodo sulfone into episulfone **6**.[20] In addition, Simpkins recently reported the preparation of 1-ethyl-2-methylepisulfone from the corresponding acyclic α-iodo sulfone using a similar procedure.[21]

(*c*) Preparation of episulfones by the oxidation of episulfides

Having disproved one widely accepted belief concerning episulfones—that they cannot be prepared from α-halo sulfones—we turned our attention to another. A wide range of organic sulfides, both acyclic and cyclic, are readily oxidised to give the corresponding sulfoxides and sulfones. Episulfides (thiiranes), however, have proved anomalous: under controlled conditions they can be oxidised to episulfoxides but, despite many attempts,[22] there were no authenticated[23] reports of episulfones being prepared from either episulfides or episulfoxides by an oxidative pathway. Given the accessibility of episulfides, we decided to reinvestigate their oxidation. The choice of oxidant was prompted by the recent report[24] that methyl(trifluoromethyl)dioxirane (TFDO) converts sulfides directly into sulfones *via* sulfurane intermediates, and does not proceed by way of sulfoxides. Such a procedure seemed to be ideally suited to the preparation of episulfones from episulfides, particularly as a convenient *in situ* method for preparing TFDO from Oxone® ($KHSO_5$ triple salt) and 1,1,1-trifluoroacetone has been described by Yang *et al.*[25] Paul Johnson therefore investigated the oxidation of propene episulfide **7** under these conditions (Scheme 5). This particular episulfide was chosen because it is commercially available and gives a reasonably stable and well characterised episulfoxide **8**.[26]

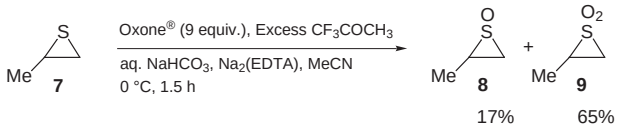

Scheme 5

To our delight, and somewhat surprisingly in view of previous studies, treatment of propene episulfide **7** with Oxone®/trifluoroacetone under Yang's conditions gave the corresponding episulfone **9** in 65% isolated yield, together with 17% of episulfoxide **8**, after chromatography. Having made this discovery, we went on to demonstrate that a range of episulfones can be prepared by the Oxone®/trifluoroacetone oxidative procedure (Fig. 3).[27]

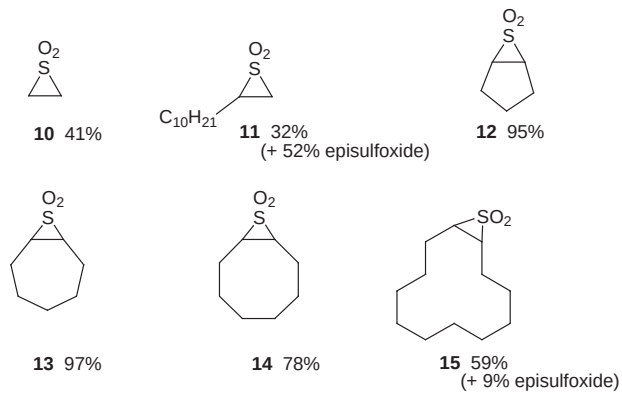

Fig. 3 Oxone®/trifluoroacetone preparation of episulfones **10–15**.

The ease with which bicyclic episulfones can be obtained is particularly noteworthy as the standard diazoalkane/sulfene methodology is not readily applicable to such systems. It should be noted that a preliminary study using 'isolated' TFDO, which readily oxidises a range of sulfides to sulfones,[24] has revealed that it converts episulfides into episulfoxides in good yield but that, surprisingly, episulfones are not formed in any significant amount. More research is needed, but it seems likely that the active oxidant in the Oxone®/trifluoroacetone mixture which promotes episulfone production is not TFDO but some other peroxidic species.

(*d*) The generation and synthetic applications of episulfone α-anions

With straightforward routes now available for episulfone preparation we decided to investigate their synthetic applications. Simon Pyke therefore set out to generate α-sulfonyl anions from episulfones and examine their trapping reactions with electrophiles. We thought that this methodology could provide a useful new procedure for the stereocontrolled synthesis of alkenes with a range of substitution patterns: this is illustrated in Scheme 6 for the production of tri- and tetrasubstituted alkenes.

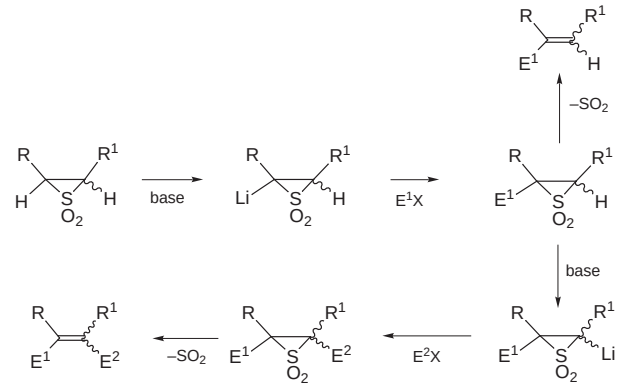

Scheme 6

In order to establish the viability of this proposal we chose to study the deprotonation-trapping of episulfone **5** due to its accessibility, stability, and the fact that stereoisomeric alkylated episulfones and alkenes are not possible, therefore simplifying product analysis. Extensive experimentation with a range of bases and electrophiles gave only trace amounts of the required adducts (as the alkenes).[28] Wendy Loughlin then achieved success using an *in situ* trapping approach in which the electrophilic trapping agent is premixed with the substrate before the addition of the base (Scheme 7). Using this

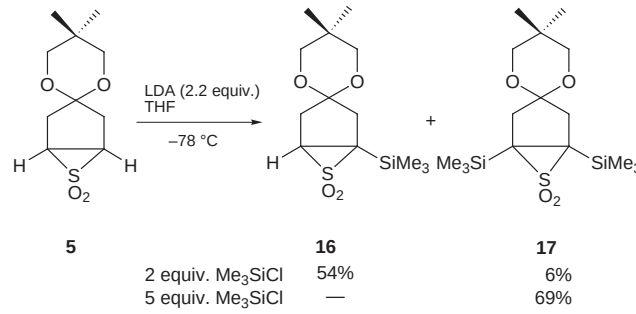

Scheme 7

procedure, with trimethylsilyl chloride as the electrophile, we could produce good yields of mono- or di-silyl adducts, **16** or **17** respectively, depending on the excess of electrophilic trapping agent. Andy Graham prepared a good quality crystal of disilylated episulfone **17** and its structure was confirmed by

Madeleine Moore and Giles Wilson using X-ray crystallography: this is the first reported X-ray structure of a tetrasubstituted episulfone and the long carbon–carbon episulfone bond length (1.686 Å) is particularly noteworthy.[29]

Using similar procedures, Wendy Loughlin and Andy Graham prepared a range of silyl and stannyl episulfone adducts (Fig. 4), most as relatively stable, fully characterised crystalline solids.[29] Carbon-based electrophiles were also employed successfully, although the yields of the adducts were rather low. Complementary research on episulfone α-anions has recently been described by Simpkins *et. al.*,[21,30] and they have shown that *C*-alkylation and hydroxyalkylation can be performed much more efficiently by use of the Bu^t-P$_4$-phosphazene base.

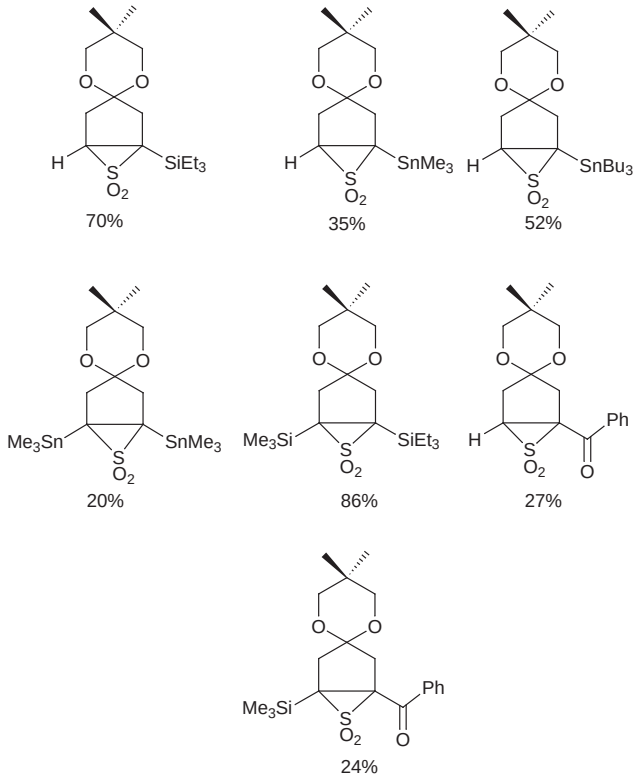

Fig. 4 Episulfones prepared from episulfone α-anions (isolated yields shown).

The functionalized episulfones were efficiently converted into novel 1,2-bis(silyl)alkenes, vinylsilanes and vinylstannanes by treatment with potassium *tert*-butoxide or thermolysis (Scheme 8).

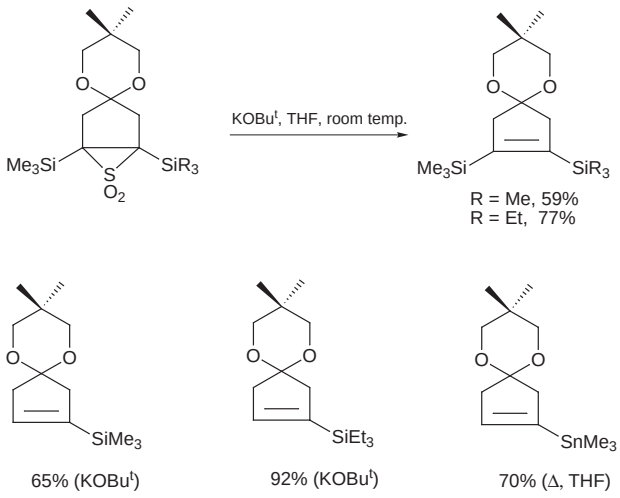

Scheme 8

(*e*) New variants of the Ramberg–Bäcklund rearrangement

More recently, we have developed two novel variants of the Ramberg–Bäcklund rearrangement.

(*i*) The epoxy-Ramberg–Bäcklund reaction

The first of these variants was suggested in discussion with Mark Gamble. We envisaged a new variant of the Ramberg–Bäcklund rearrangement in which the leaving group is incorporated into a three membered ring (Scheme 9). A major advantage of this new variant compared to the traditional Ramberg–Bäcklund rearrangement is that alkene formation is accompanied by the introduction of allylic functionality. Thus, the epoxy-Ramberg–Bäcklund reaction would provide a new method for the synthesis of allylic alcohols from readily available sulfonyl oxiranes.

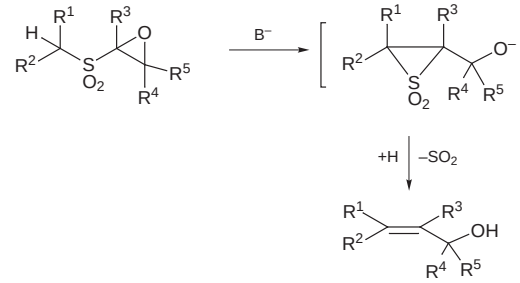

Scheme 9

Initial studies to establish the viability of this idea were carried out by Arne Grumann, who had what we believed to be the ideal starting material, **18**, to hand (Scheme 10). Thus, the required epoxide **19** was easily prepared but, despite a considerable amount of effort, we were unable to devise conditions to effect the ring contraction to give cyclopentenol.

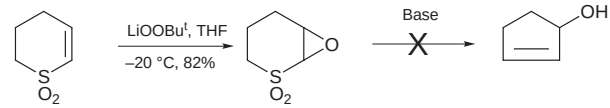

18 **19**

Scheme 10

We reasoned that the spirocyclic intermediate required for this transformation would be just too strained when starting with a bicyclic epoxide. When Paul Evans started his research in this area we therefore investigated an acyclic system (Scheme 11).

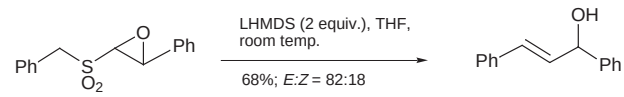

Scheme 11

We were delighted to observe the success of this new process and Paul Evans and Paul Johnson have since applied it to a range of substrates (Fig. 5).[31,32] As can be seen, the epoxy-Ramberg–Bäcklund reaction can be employed to prepare mono-, di- and tri-substituted alkenes, is often high yielding and can exhibit a high degree of stereoselectivity.

We are currently optimising this epoxy-Ramberg–Bäcklund reaction, exploring the thiirane and aziridine variants, and optimising a tandem epoxidation-epoxy-Ramberg–Bäcklund procedure (Scheme 12). We are also utilising the methodology for the synthesis of natural products such as sphingosine.

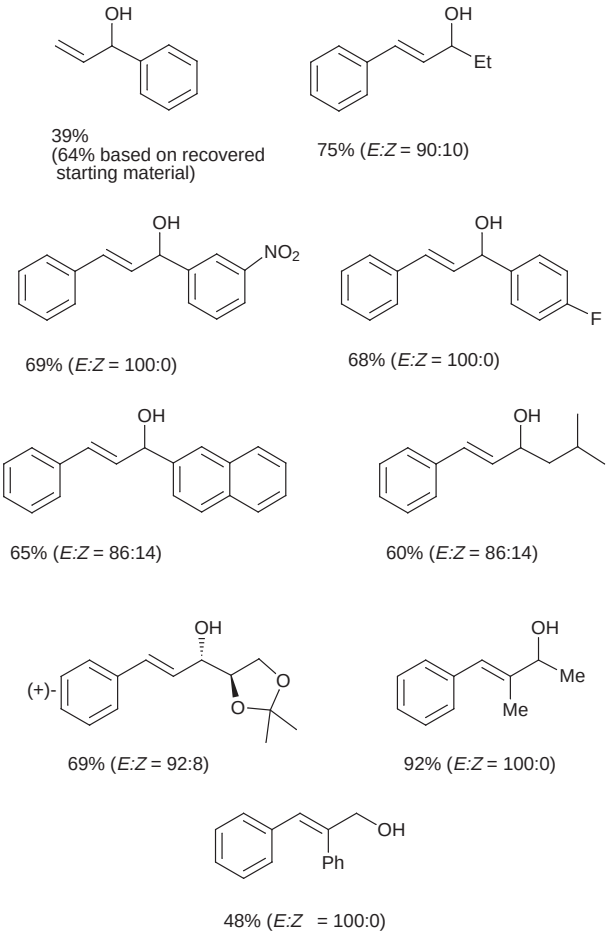

Fig. 5 Products of the epoxy-Ramberg–Bäcklund rearrangement (using LiOBu^t in THF; isolated yields shown).

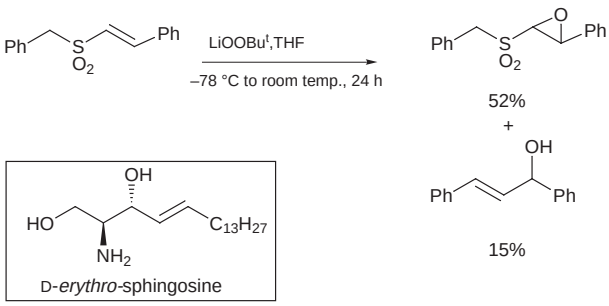

Scheme 12

(*ii*) Tandem conjugate addition-Ramberg–Bäcklund rearrangements

Serendipity played a major part in the discovery of the second variant of the Ramberg–Bäcklund rearrangement. Paul Evans was attempting to prepare sulfonyl aziridines to study the feasibility of the aziridine-Ramberg–Bäcklund rearrangement. However, treatment of bromovinyl sulfone **20** with amines did not produce the corresponding aziridines, as expected,[33] but generated allylamines **21** instead (Scheme 13).

We presume that this process proceeds by the sequence shown in Scheme 13, *i.e.* conjugate addition to bromovinyl sulfone **20** followed by α-sulfonyl anion equilibration and Ramberg–Bäcklund rearrangement. This process is related to the Michael-induced Ramberg–Bäcklund (MIRB) reaction shown in Scheme 14.[5] The MIRB process is of limited utility, however, due to the apparent requirement for a dienyl sulfone (**22**, n = 2); similar reactions involving vinyl sulfones (n = 1) are unknown.

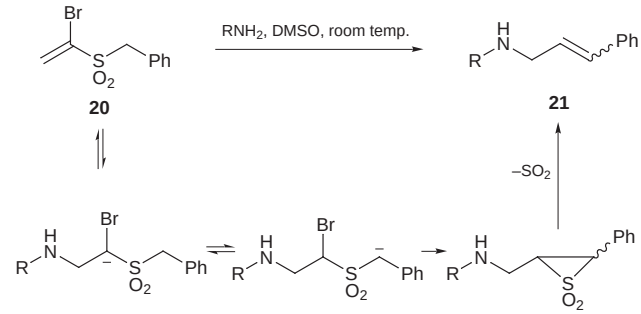

Scheme 13

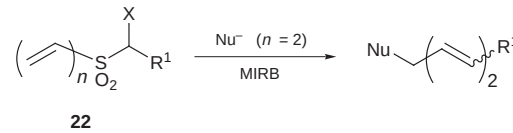

Scheme 14

The novel tandem conjugate addition Ramberg–Bäcklund sequence was investigated with several other nucleophiles (Scheme 15).[34] We believe that this is a generally useful procedure as bromovinyl sulfones are readily prepared from the corresponding vinyl sulfones by a bromination–dehydrobromination sequence and they are excellent Michael acceptors. Thus, thiolates, alkoxides, amines and malonates all gave successful addition-rearrangements. The stereochemical outcome of the these reactions reflects the basicity of the reaction medium: with amines as nucleophiles/bases, *cis*-isomers predominate, whereas the more basic conditions employed in the other processes favoured formation of the *trans*-alkenes.

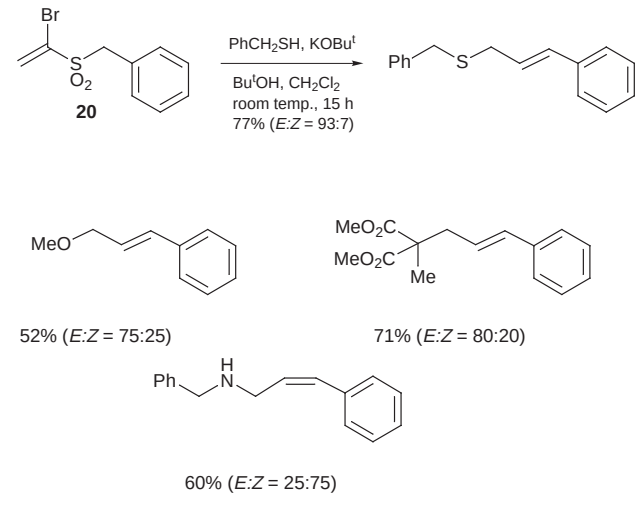

Scheme 15

(*f*) Applications of the Ramberg–Bäcklund rearrangement in natural product and bioactive target molecule synthesis

We have utilised the Ramberg–Bäcklund rearrangement for the synthesis of a number of natural products and related compounds of biological interest.

(*i*) Cyclopentene-based natural products and related compounds

As referred to earlier, Guy Casy, Simon Lane and Stephen Quick developed a general organocopper-based route to convert

3-alkoxycarbonylthiin-4-ones **23** into 2,3-disubstituted 2,3-dihydrothiin-4-ones **24** as part of a programme to prepare thiathromboxane A_2 (**25**) and novel thiathromboxane analogues (Scheme 16).[15,16] We envisaged utilising the Ramberg–Bäcklund rearrangement to convert the sulfones derived from these 2,3-disubstituted 2,3-dihydrothiin-4-ones into 2,3-disubstituted cyclopentenones as shown in Scheme 16. We wrote to Professor Leo Paquette outlining our ideas. Receiving an encouraging response, Guy Casy prepared dioxide **26** by oxidation of the corresponding sulfide and introduced the iodide substituent with concomitant ketone protection giving adduct **27**. Ramberg–Bäcklund rearrangement proceeded smoothly to produce cyclopentene **28** which was converted into either the non-conjugated cyclopentenone **29**, or its conjugated isomer **30**, by acidic hydrolysis.[17] Matsuyama's group reported the use of the Ramberg–Bäcklund rearrangement to prepare cyclopentenes at about the same time.[35]

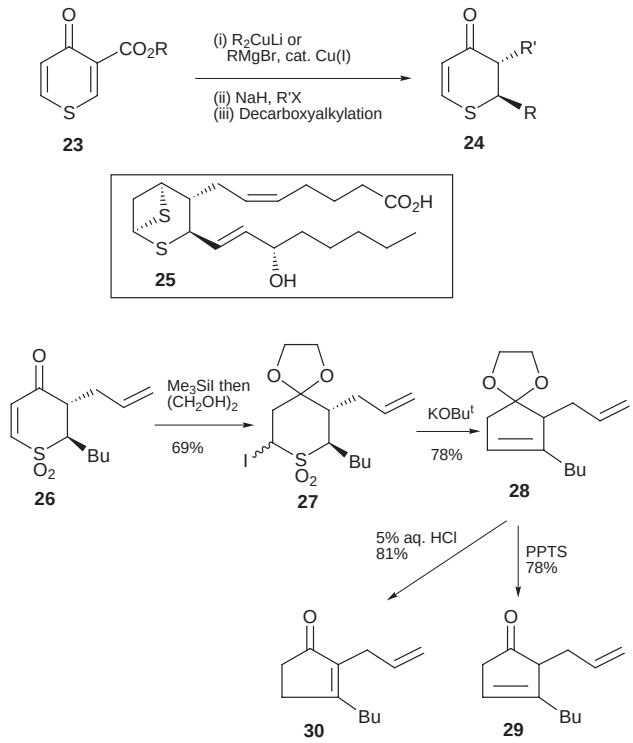

Scheme 16

Guy Casy went on to utilise this mild Ramberg–Bäcklund route to cyclopentenes as part of a formal total synthesis of the naturally occurring antibacterial agent tetrahydrodicranenone B (**33**), as shown in Scheme 17.[17] α-Iodo sulfone **31**, prepared using similar organocopper methodology to that shown in Scheme 16, underwent Ramberg–Bäcklund rearrangement to give cyclopentene **32** which can be converted into tetrahydrodicranenone B in three efficient steps using the chemistry developed by Moody, Roberts and Toczek.[36]

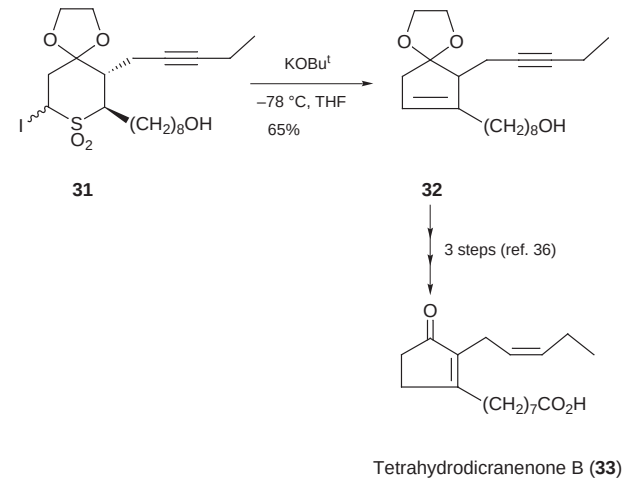

Scheme 17

Arne Grumann later employed a similar Ramberg–Bäcklund ring contraction, this time on α-bromo sulfone **36**, as the key step in the first synthesis of *trans*-carbovir **38** (Scheme 18).[37] *cis*-Carbovir is a fraudulent nucleoside which acts as a potent inhibitor of HIV reverse transcriptase. The 5-substituted unsaturated thiane **34** was prepared from thioacrolein *via* a hetero-Diels–Alder process. An important subsequent step involved conjugate addition of ammonia to unsaturated sulfone **35** to produce α-bromo sulfone **36** in an efficient and stereoselective manner. The use of α-bromo-α,β-unsaturated sulfones as precursors to Ramberg–Bäcklund substrates should be generally useful methodology (see also Scheme 15). Ramberg–Bäcklund reaction of **36** followed by deprotection gave amine hydrochloride **37** which was elaborated using the Traube method to complete the synthesis of *trans*-carbovir.[37]

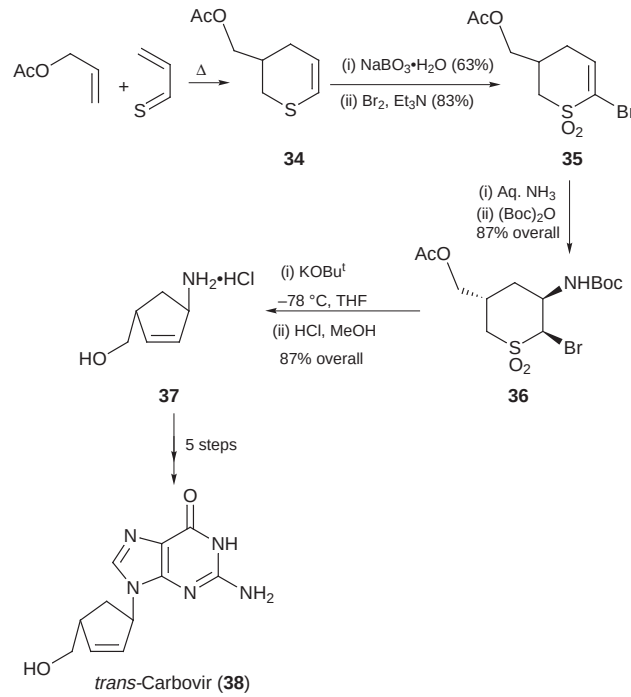

Scheme 18

About this time we became interested in synthetic applications of amino acids. Mark Gamble first prepared amino cyclopentanes using glutamic acid-derived sulfones.[38] He then studied the cyclisation reactions of methionine-derived sulfones such as **39** (Scheme 19). The cyclisation to produce the enantiomerically pure thiane dioxide **40** proceeded in high yield and the product was subsequently elaborated to give α-bromo sulfone **41**. This compound underwent Ramberg–Bäcklund rearrangement to give the protected amino cyclopentenone **42**, unfortunately in racemic form.[39] Attempts to desulfurise the cyclic sulfones in this sequence were unsuccessful but Tim Ockendon and Peter O'Brien found that the sulfoxides corresponding to **39** also underwent cyclisation, and Raney nickel desulfurisation of intermediates such as **43** provided a method for preparing protected *anti*-1,2-amino alcohols like **44**.[39]

(*ii*) Unsaturated amino acid synthesis

The interest in methionine chemistry referred to in the previous section provided the stimulus for Marcel Schaeffer to investigate the Ramberg–Bäcklund reactions of L-methionine-derived α-chloro sulfones [Scheme 20(*a*)]. He showed that

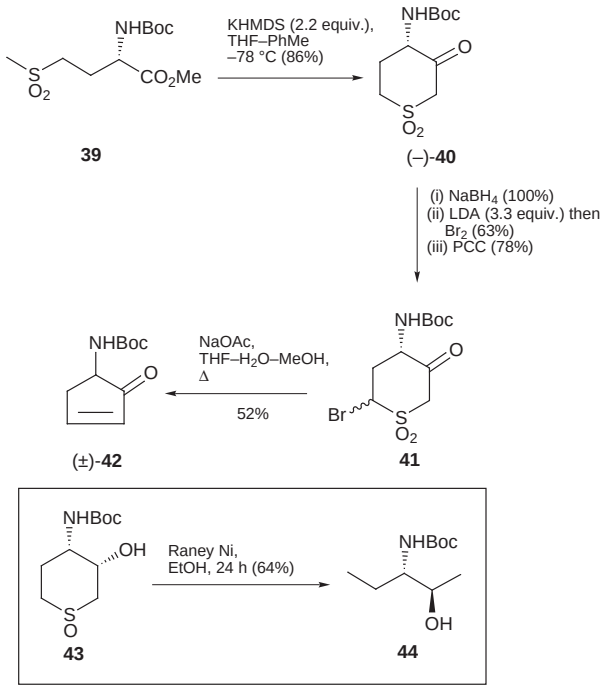

Scheme 19

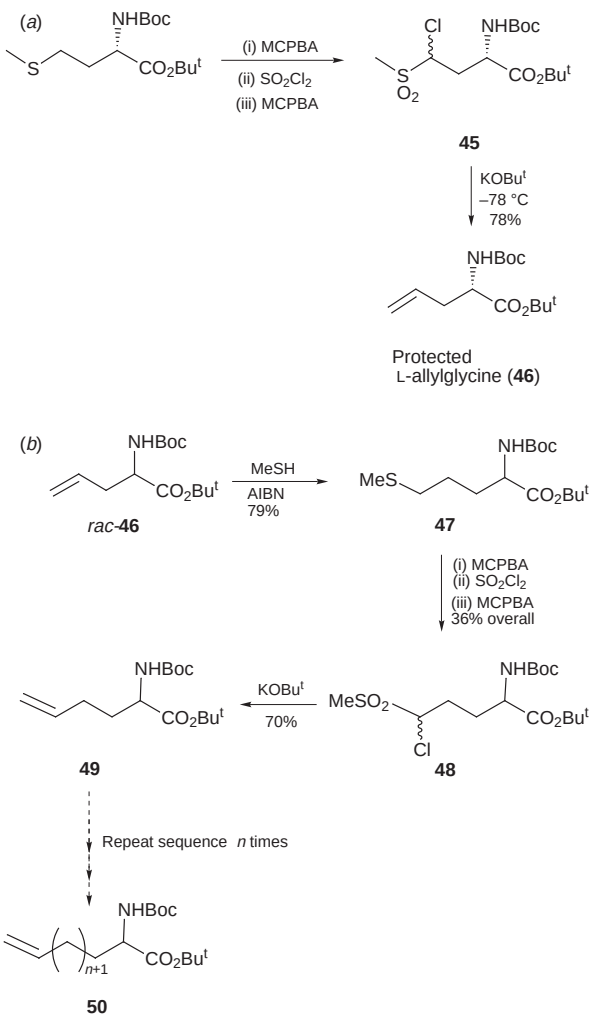

Scheme 20

chloro sulfone **45** underwent efficient conversion into allyl glycine derivative **46** and demonstrated, with Zhao-Xia Guo, that racemisation could be avoided by carrying out the reaction at −30 °C or lower.[40]

In unpublished and unoptimised work, Zhao-Xia Guo went on to demonstrate that this sequence could be employed in an iterative manner [Scheme 20(*b*)]. Thus, the radical addition of methanethiol to the protected allylglycine **46** gave sulfide **47** which was easily elaborated *via* α-chloro sulfone **48** to give butenyl glycine derivative **49**. In principle, this sequence could be employed to prepare the series of unsaturated amino acid derivatives **50** (n = 0,1,2 *etc*.).

In order to complete the sequence, Tim Ockendon attempted to prepare the corresponding vinyl glycine derivative **53** (Scheme 21). He utilised a modified version of the sulfinyl

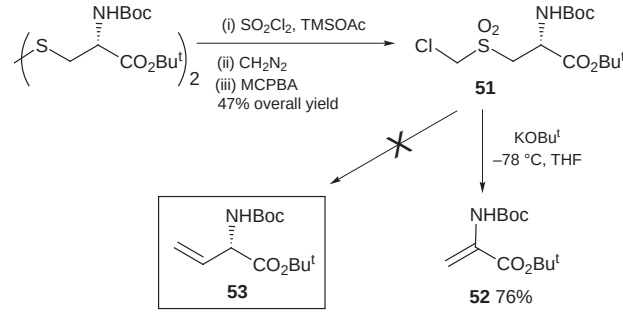

Scheme 21

chloride procedure developed by Ottenheijm *et al*.[41] to prepare α-chloro sulfone **51** in a regioselective manner. Unfortunately, treatment of **51** under standard Ramberg–Bäcklund conditions gave 1,2-elimination, producing alkene **52**, and none of the required product **53** was observed. We were, however, able to prepare the corresponding vinyl glycinol **56** using Ramberg–Bäcklund methodology (Scheme 22). α-Chloro sulfone **54** was thus converted into alkene **55** which was desilylated to give the known[42] alcohol **56** in enantiomerically pure form.

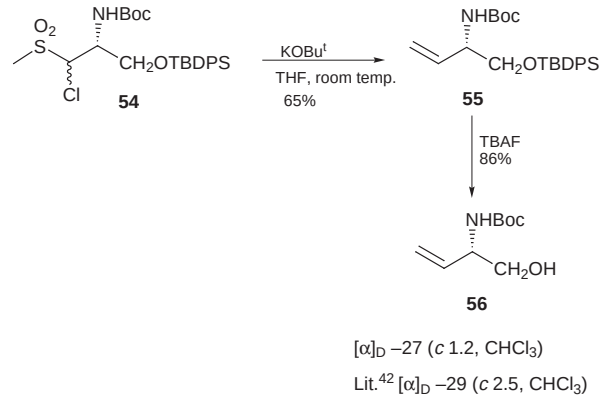

Scheme 22

(*iii*) *exo*-Glycal synthesis

As part of a project to design and synthesise novel analogues of sialyl Lewis^x,[43] Paul Murphy prepared a number of thioglycosides **57**. These compounds provided us with the opportunity to obtain the corresponding *S*-glycoside dioxides **58** and investigate their Ramberg–Bäcklund rearrangements (Scheme 23).

The sequence illustrated in Scheme 23 leads to *exo*-glycals **59**. The parent 1-*exo*-methylene compounds (**59**, R = R′ = H) have been used as glycosidase inhibitors[44] and are valuable synthetic intermediates.[45–51] Scheme 24 summarises synthetic applications of the glucose-derived *exo*-methylene compound **60**. The corresponding substituted *exo*-glycals **59** (R, R′ ≠ H) are also of considerable interest.[52]

A number of procedures have been published for the preparation of *exo*-methylene glycals[44–51] but the method of

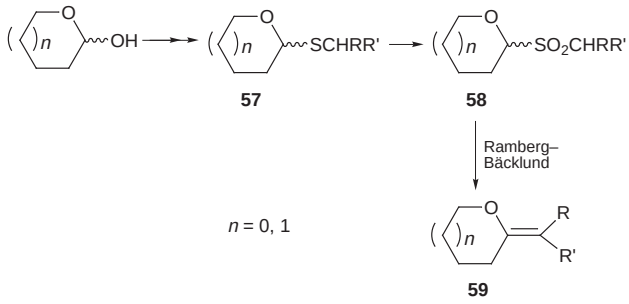

Scheme 23

choice would appear to be methylenation of the corresponding lactones using dicyclopentadienyl(dimethyl)titanium (or the Tebbe reagent).[47,51] There is no general method to prepare substituted *exo*-glycals **59** (R, R′ ≠ H), however.[53] Paul Murphy, Frank Griffin and Duncan Paterson therefore set out to explore the Ramberg–Bäcklund route to *exo*-glycals.[54,55] Scheme 25 summarises some of the procedures used to prepare the *S*-glycosides[56] and thus the sulfones needed for the Meyers' variant of the Ramberg–Bäcklund rearrangement.[3] Similar procedures were used to prepare related glucose-derived sulfones and *S*-glycoside dioxides derived from other sugars.

We were delighted to observe that the required transformations to produce *exo*-glycals proceeded efficiently using

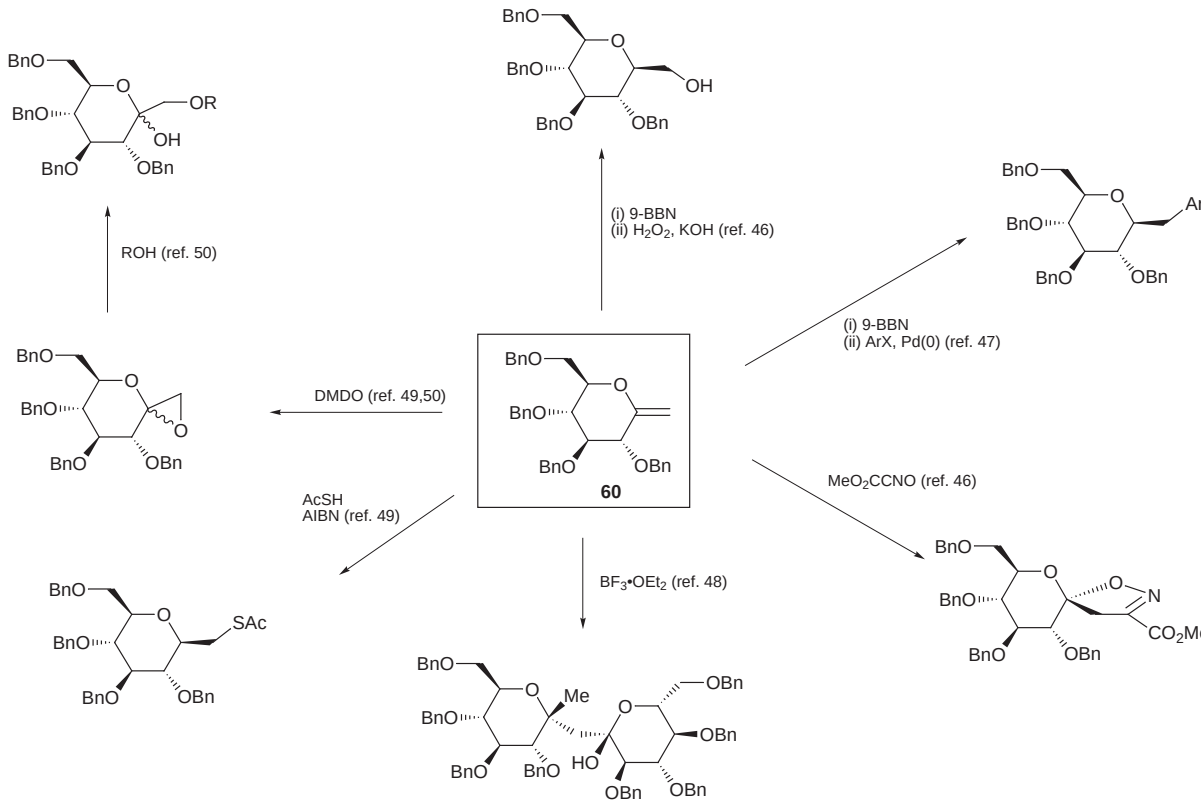

Scheme 24

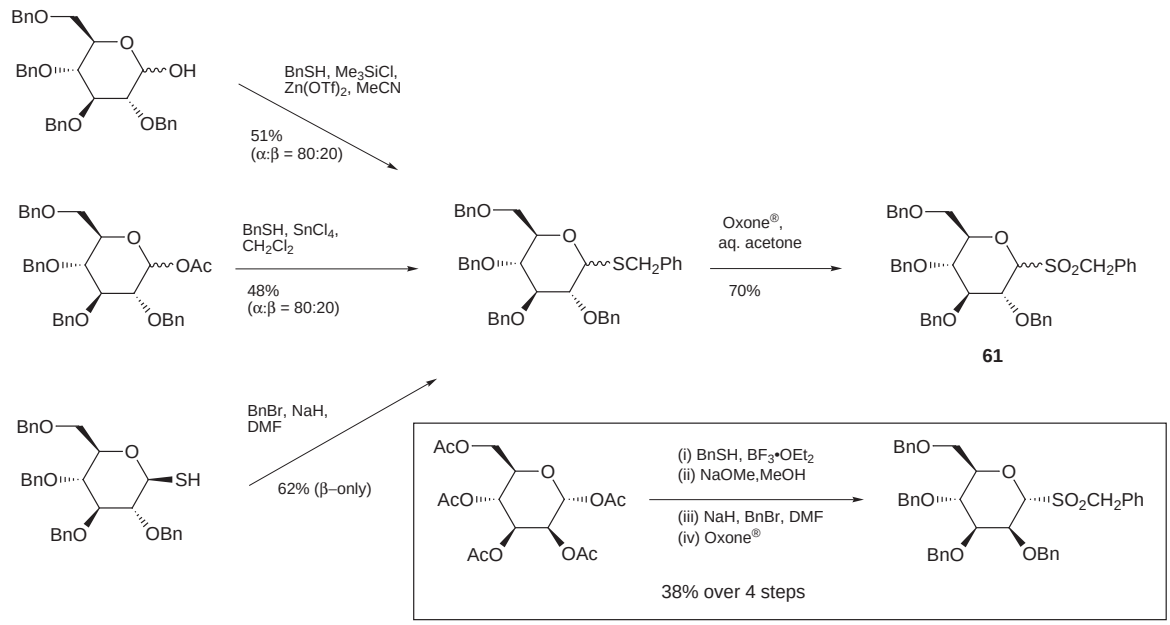

Scheme 25

Meyers' original conditions[3a] (CCl_4, KOH) and the modified conditions (CBr_2F_2, KOH, Al_2O_3) recently reported by Chan *et al*.[3b] This is shown in Scheme 26 for the glucose derived benzyl sulfone **61**: phenyl glycal **62** was produced in reasonable yield using the Meyers' conditions and excellent yield by the Chan procedure, the *Z*-product predominating in both cases.

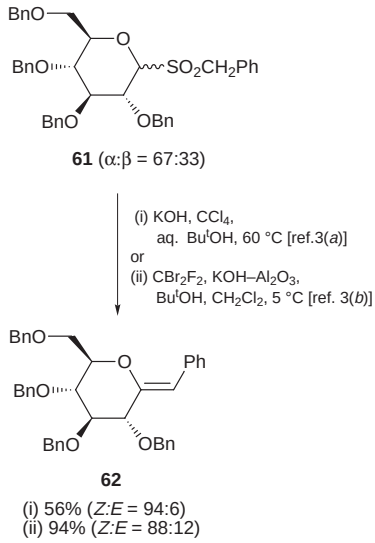

Scheme 26

We then proceeded to prepare a range of *exo*-glycals using this Ramberg–Bäcklund methodology (Fig. 6). As can be seen, the glucose-derived methylene compound **63a** was prepared, as were the phenyl, methyl and ethyl substituted alkenes **63b–d** (all with the *Z*-alkene predominating). Although unoptimised, galactose, mannose, xylose, fucose and ribose derived alkenes **63e–i** were equally accessible. Tetrasubstituted alkenes **63j–l** were also prepared by this methodology, although in these cases the required transformation was only observed using the Meyers' conditions. Further work is needed to optimise these yields, but the availability of highly hindered glycals, particularly adamantene derivative **63l**, is noteworthy.

The ease with which anomeric carbanions eliminate C-2 alkoxides to give *endo*-glycals has been a longstanding problem in *C*-glycoside synthesis until recently.[57] It should be noted that the Ramberg–Bäcklund methodology is compatible with 2-alkoxy substituents. Investigations are therefore underway to probe the mechanisms of these reactions.[54]

As mentioned, *exo*-glycals have proved to be valuable glycosidase inhibitors[44,52] but for our methodology to be of use in this area it is important to be able to remove the hydroxy group protection without reducing or hydrolysing the enol ether moiety. Benzyl protection is not suitable for this purpose and Duncan Paterson has explored the compatibility of other protecting groups with the Ramberg–Bäcklund conditions (Scheme 27). Sulfone **64**, protected by *tert*-butyldimethylsilyl (TBDMS) groups, was therefore prepared. Ramberg–Bäcklund rearrangement of **64** proceeded smoothly and desilylation was accomplished using tetrabutylammonium fluoride (TBAF). This two step sequence produced the unprotected enol ether **65** (which was acetylated for characterisation purposes).

We have also investigated synthetic applications of these novel *exo*-glycals. As shown in Scheme 28, Marie-Lyne Alcaraz utilised the *Z*-phenyl derivative **62** in a formal synthesis of the *C*-glycoside **68**, recently reported as a new β-glycosidase inhibitor by Schmidt and Dietrich.[58] Thus, hydroboration using borane–THF followed by oxidation gave a separable 25 : 75 mixture of α- and β-alcohols **66** and **67** in 65% overall yield. Schmidt and Dietrich converted alcohol **67** into enzyme inhibitor **68** in five high yielding steps.[58] The advantage of our new procedure is the brevity of the synthetic route: Schmidt and

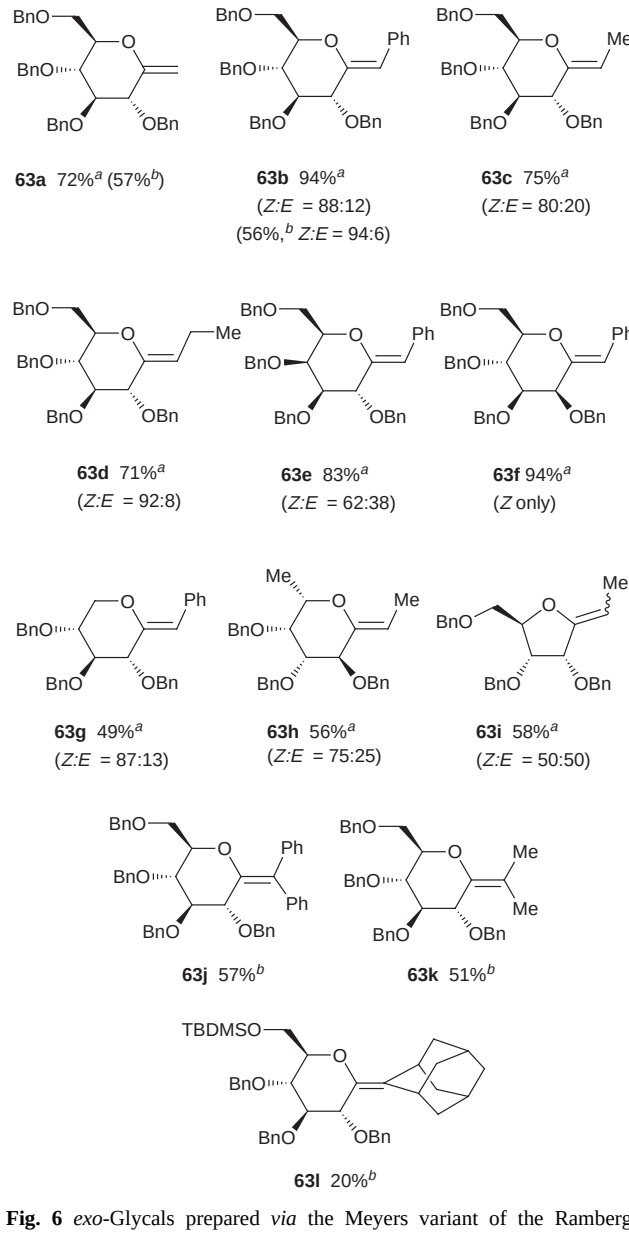

Fig. 6 *exo*-Glycals prepared *via* the Meyers variant of the Ramberg–Bäcklund rearangement. [a] Using CF_2Br_2 [ref. 3(*b*)]. [b] Using CCl_4 [ref. 3(*a*)].

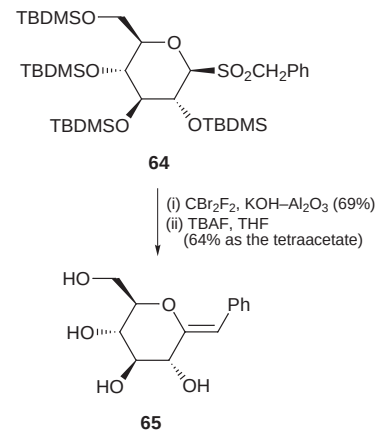

Scheme 27

Dietrich required eight steps to prepare alcohol **67** from D-glucal.[58]

Frank Griffin employed this new methodology to prepare the spirocyclic sugars **73** and **74** (Scheme 29). These compounds,

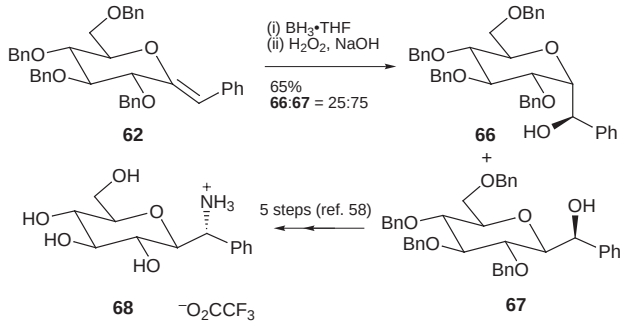

Scheme 28

which are simplified analogues of natural products such as papulacandin D,[59] have recently been prepared by a photolytic route.[60] In our new synthesis (Scheme 29), the benzylated thioglucose derivative **69**[56b] was alkylated giving sulfide **70** which was oxidised to sulfone **71**, both steps proceeding in good yield. The Ramberg–Bäcklund rearrangement proceeded smoothly on the unprotected alcohol **71** using Chan's CBr_2F_2 conditions[3b] giving *exo*-glycal **72** in 73% yield. Cyclisation was effected by treatment of enol ether **72** with camphorsulfonic acid (CSA) in methanol to produce a separable mixture of spiroacetals **73** and **74** (30 : 70) in 75% yield.

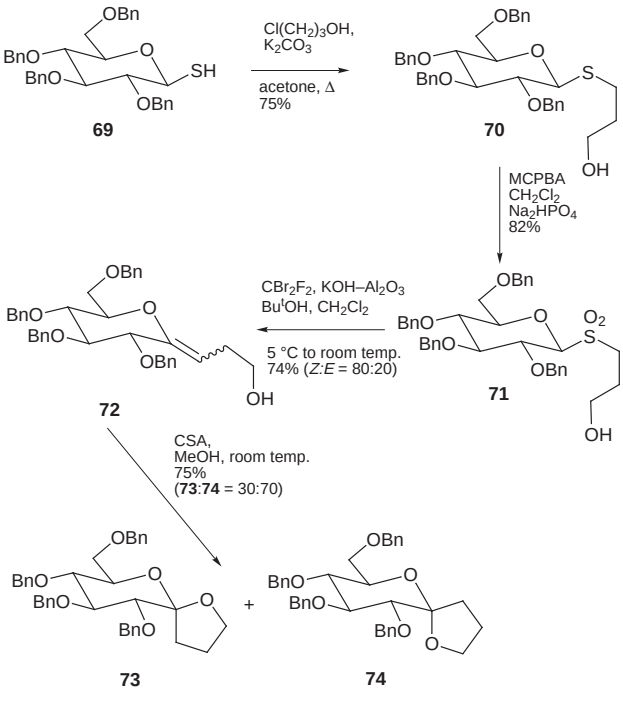

Scheme 29

We are currently optimising this Ramberg–Bäcklund methodology for *exo*-glycal synthesis, and exploring its applications for the synthesis of more complex *C*-glycosides and *C*-disaccharides. For example, routes to carba-glycopeptides[61] **75** and carba-disaccharides[62] such as methyl carba-isomaltoside **76** using the Ramberg–Bäcklund chemistry are currently being investigated.[63]

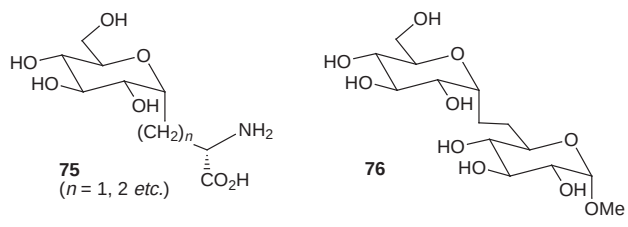

Summary

Major advances have been made in Ramberg–Bäcklund and episulfone chemistry over the past few years. Procedures have been developed which enable episulfones to be produced from α-halo sulfones or from episulfides by oxidation. Episulfone deprotonation-trapping reactions have been developed to provide a new method of preparing novel vinylsilanes and vinylstannanes, and new variants of the Ramberg–Bäcklund rearrangement have been discovered which produce functionalised products such as allylic alcohols and amines. Mild conditions have been developed for the classical Ramberg–Bäcklund rearrangement and applied to the synthesis of cyclopentene-based natural products and unsaturated amino acids. In addition, the Meyers' variant of the Ramberg–Bäcklund rearrangement has been utilised in a new route to *exo*-glycals commencing from *S*-glycoside dioxides. Ongoing work to further apply this new methodology, for example to the synthesis of sphingosines and novel *C*-disaccharides, promises further interesting and useful discoveries ahead.

Acknowledgements

This article is dedicated to Dr D. Neville Jones, who taught me all about the Ramberg–Bäcklund rearrangement (and many other things) and stimulated a life-long interest in organosulfur chemistry, and to Dr Ian Harrison, who extended this interest in organosulfur compounds and also introduced me to prostaglandins, thromboxanes and other arachidonic acid metabolites. Without the influence of these two outstanding teachers and scientists none of the research described in this article would have been possible.

I would like to pay tribute to the co-workers mentioned in the text for their practical skills, intellectual contributions and, in particular, for their enthusiasm when ploughing what has usually been a lone furrow alongside the organometallic and natural product teams. I would also like to thank the industrial collaborators and other group members for their contributions over the years and the EPSRC for financial support.

This article was written during a period as short term visitor at the University of Auckland in May–June, 1998: I would like to thank Professor Paul Woodgate and all of his colleagues for their stimulating company and for making the visit so memorable.

Notes and references

1 L. Ramberg and B. Bäcklund, *Ark. Kemi. Mineral. Geol*., 1940, **27**, **Band 13A**, 1 (*Chem. Abstr*., 1940, **34**, 4725).
2 For reviews see: L. A. Paquette, *Org. React*., 1977, **25**, 1; S. Oae and Y. Uchida (ch. 12) and S. Braverman (ch. 13), in *The Chemistry of Sulfones and Sulfoxides*, Ed. S. Patai, Z. Rappoport and C. J. M. Stirling, Wiley, Chichester, 1988; J. M. Clough, in *Comprehensive Organic Synthesis*, ed. B. M. Trost and I. Fleming, Pergamon, Oxford, 1991, vol. 3, ch. 3.8.
3 (*a*) C. Y. Meyers, A. M. Malte and W. S. Matthews, *J. Am. Chem. Soc*., 1969, **91**, 7510; (*b*) see also T.-L. Chan, S. Fong, Y. Li, T.-O. Man and C. D. Poon, *J. Chem. Soc*., *Chem. Commun*., 1994, 1771 and references cited therein.
4 R. B. Mitra, M. V. Natekar and S. D. Virkar, *Indian J. Chem*., 1971, **13**, 251; see also E. Block, M. Aslam, V. Eswarakrishnan, K. Gebreyes, J. Hutchinson, R. Iyer, J.-A. Lafitte and A. Wall, *J. Am. Chem. Soc*., 1986, **108**, 4568 and references cited therein.
5 J. J. Burger, T. B. R. A. Chen, E. R. de Waard and H. O. Huisman, *Tetrahedron*, 1981, **37**, 417 and references cited therein.
6 T. Schmittberger and D. Unguen, *Tetrahedron Lett*., 1997, **38**, 2837.
7 B. M. Trost and Z. Shi, *J. Am. Chem. Soc*., 1994, **116**, 7459.
8 R. K. Boeckman, Jr., S. K. Yoon and D. K. Heckendorn, *J. Am. Chem. Soc*., 1991, **113**, 9682.
9 V. Cerè, F. Peri and S. Pollicino, *Tetrahedron Lett*., 1997, **38**, 7797.
10 K. C. Nicolaou, G. Zuccarello, C. Riemer, V. A. Estavez and W.-M. Dai, *J. Am. Chem. Soc*., 1992, **114**, 7360.
11 E. Alvarez, M. T. Díaz, L. Hanxing and J. D. Martín, *J. Am. Chem. Soc*., 1995, **117**, 1437.

12 D. J. Hart, G. H. Merriman and D. G. J. Young, *Tetrahedron*, 1996, **52**, 14 437.
13 N. H. Fischer, *Synthesis*, 1970, 393; G. Opitz, K. Reith and T. Ehlis, *Chem. Ber*., 1990, **123**, 1563, 1989 and references cited therein.
14 F. G. Bordwell, J. M. Williams, E. B. Hoyt and B. B. Jarvis, *J. Am. Chem. Soc*., 1968, **90**, 429 and references cited therein.
15 G. Casy, S. Lane and R. J. K. Taylor, *J. Chem. Soc., Perkin Trans. 1*, 1986, 1397; S. Lane, S. J. Quick and R. J. K. Taylor, *J. Chem. Soc., Perkin Trans. 1*, 1985, 893.
16 G. Casy, A. G. Sutherland, R. J. K. Taylor and P. G. Urben, *Synthesis*, 1989, 767; V. K. Kansal and R. J. K. Taylor, *J. Chem. Soc., Perkin Trans. 1*, 1984, 703; R. J. Batten, J. D. Coyle, R. J. K. Taylor and S. Vassiliou, *J. Chem. Soc., Perkin Trans. 1*, 1982, 1177; R. J. Batten, J. D. Coyle and R. J. K. Taylor, *Synthesis*, 1980, 910.
17 G. Casy and R. J. K. Taylor, *J. Chem. Soc., Chem. Commun*., 1988, 454; *Tetrahedron*, 1989, **45**, 455.
18 A. G. Sutherland and R. J. K. Taylor, *Tetrahedron Lett*., 1989, **30**, 3267;
19 S. M. Jeffery, A. G. Sutherland, S. M. Pyke, A. K. Powell and R. J. K. Taylor, *J. Chem. Soc., Perkin Trans. 1*, 1993, 2317.
20 R. A. Ewin, W. A. Loughlin, S. M. Pyke, J. C. Morales and R. J. K. Taylor, *Synlett*, 1993, 660.
21 N. S. Simpkins, *Phosphorus, Sulfur Silicon*, 1997, **120/121**, 197.
22 For a review which discusses attempts to prepare episulfones by episulfide oxidation, see U. Zoller, in *The Chemistry of Sulfones and Sulfoxides*, ed. S. Patai, Z. Rappoport and C. J. M. Stirling, Wiley, Chichester, 1988, ch. 9, pp. 413–419.
23 The only literature claim to the successful oxidation of an episulfide to an episulfone (D. C. Dittmer and G. C. Levy, *J. Org. Chem*., 1965, **30**, 636) was later disproved (U. Jacobsson, T. Kempe and T. Norin, *J. Org. Chem*., 1974, **39**, 2722).
24 G. Asensio, R. Mello and M. E. González-Núñez, *Tetrahedron Lett*., 1996, **37**, 2299.
25 D. Yang, M. K. Wongand and Y. C. Yip, *J. Org. Chem*., 1995, **60**, 3887.
26 K. Kondo and A. Negishi, *Tetrahedron*, 1971, **27**, 4821.
27 P. Johnson and R. J. K. Taylor, *Tetrahedron Lett*., 1997, **38**, 5873.
28 S. M. Jeffery, S. M. Pyke, A. G. Sutherland and R. J. K. Taylor, Poster presentation at The First Anglo-Norman Chemistry Colloquium, Rouen, 1991.
29 A. E. Graham, W. A. Loughlin and R. J. K. Taylor, *Tetrahedron Lett*., 1994, **34**, 7281; A. E. Graham, W. A. Loughlin, M. H. Moore, S. M. Pyke, G. Wilson and R. J. K. Taylor, *J. Chem. Soc., Perkin Trans. 1*, 1996, 661.
30 A. P. Dishington, R. E. Douthwaite, A. Mortlock, A. B. Muccioli and N. S. Simpkins, *J. Chem. Soc., Perkin Trans. 1*, 1997, 323.
31 P. Evans and R. J. K. Taylor, *Tetrahedron Lett*., 1997, **38**, 3055.
32 P. Evans, P. Johnson, O. Ort and R. J. K. Taylor, unpublished work.
33 J.-M. Gaillot, Y. Gelas-Mialhe and R. Vessière, *Can. J. Chem*., 1979, **57**, 1958 and references cited therein.
34 P. Evans and R. J. K. Taylor, *Synlett*, 1997, 1043.
35 H. Matsuyama, Y. Miyazawa, Y. Tokai and M. Kobayashi, *J. Org. Chem*., 1987, **52**, 1703 and references cited therein.
36 C. J. Moody, S. M. Roberts and J. Toczek, *J. Chem. Soc., Chem. Commun*., 1986, 1292.
37 A. Grumann, H. Marley and R. J. K. Taylor, *Tetrahedron Lett*., 1995, **36**, 7767.
38 M. P. Gamble, G. M. P. Giblin and R. J. K. Taylor, *Synlett*, 1995, 779.
39 M. P. Gamble, G. M. P. Giblin, J. G. Montana, P. O'Brien, T. P. Ockendon and R. J. K. Taylor, *Tetrahedron Lett*., 1996, **37**, 7457.
40 Z.-X. Guo, M. J. Schaeffer and R. J. K. Taylor, *J. Chem. Soc., Chem. Commun*., 1993, 874.
41 H. C. J. Ottenheijm, R. M. J. Liskamp, S. P. J. M. van Nispen, H. A. Boots and M. W. Tijhuis, *J. Org. Chem*., 1981, **46**, 3273; J. Drabowicz, B. Bujnicki and B. Dudzinski, *Synth. Commun*., 1994, **24**, 1207.
42 A. McKillop, N. Lewis, R. J. Watson and R. J. K. Taylor, *Synthesis*, 1994, 31.
43 P. V. Murphy, R. E. Hubbard, D. T. Manallack, J. G. Montana and R. J. K. Taylor, *Tetrahedron Lett*., 1998, **39**, 3273.
44 C. F. Brewer, E. J. Hehre, J. Lehmann and W. Weiser, *Liebigs Ann*., 1984, 1078 and references cited therein.
45 C. S. Wilcox, G. W. Long and H. Suh, *Tetrahedron Lett*., 1984, **25**, 395.
46 T. V. RajanBabu and G. S. Reddy, *J. Org. Chem*., 1986, **51**, 5458.
47 C. R. Johnson and B. A. Johns, *Synlett*, 1997, 1406.
48 L. Lay, F. Nicotra, L. Panza, G. Russo and E. Caneva, *J. Org. Chem*., 1992, **57**, 1304.
49 J. Gervay, T. M. Flaherty and D. Holmes, *Tetrahedron*, 1997, **53**, 16 355.
50 F. Nicotra, L. Panza and G. Russo, *Tetrahedron Lett*., 1991, **32**, 4035.
51 R. Csuk and B. I. Glänzer, *Tetrahedron*, 1991, **47**, 1655 and references cited therein; M. H. Ali, P. M. Collins and W. G. Overend, *Carbohydr. Res*., 1990, **205**, 428.
52 A. Vasella, C. Witzig, C. Waldraff, P. Uhlmann, K. Briner, B. Bernet, L. Panza, and R. Husi, *Helv. Chim. Acta*, 1993, **76**, 2847 and references cited therein.
53 M. Lakhrissi and Y. Chapleur, *Angew. Chem., Int. Ed. Engl*., 1996, **35**, 750 and references cited therein.
54 F. K. Griffin, P. V. Murphy, D. E. Paterson and R. J. K. Taylor, *Tetrahedron Lett*., 1998, **39**, 8179.
55 M.-L. Alcaraz, F. K. Griffin, D. E. Paterson and R. J. K. Taylor, *Tetrahedron Lett*., 1998, **39**, 8183.
56 (*a*) P. Li, L. Sun, D. W. Landry and K. Zhao, *Carbohydrate Res*., 1995, **275**, 179 and references cited therein; (*b*) S. A. Holick, S. H. L. Chiu and L. Anderson, *Carbohydr. Res*., 1976, **50**, 215 and references cited therein.
57 D. Mazéas, T. Skrydstrup and J.-M. Beau, *Angew. Chem., Int. Ed. Engl*., 1995, **34**, 909 and references cited therein. For a recent reference in this area see C. Jaramillo, G. Corrales and A. Fernández-Mayoralas, *Tetrahedron Lett.*, 1998, **39**, 7783.
58 R. R. Schmidt and H. Dietrich, *Angew. Chem., Int. Ed. Engl*., 1991, **30**, 1328.
59 A. G. M. Barrett, M. Peña and J. A. Willardsen, *J. Chem. Soc., Chem. Commun*., 1995, 1145 and 1147 and references cited therein.
60 A. Martín, J. A. Salazar and E. Suárez, *J. Org. Chem*., 1996, **61**, 3999.
61 J. R. Axon and A. J. Beckwith, *J. Chem. Soc., Chem. Commun*., 1995, 549; T. Fuchs and R. R. Schmidt, *Synthesis*, 1998, 753 and references cited therein.
62 P. K. Goekjian, T.-C. Wu, H.-Y. Kang and Y. Kishi, *J. Org. Chem*., 1991, **56**, 6422; M. H. D. Postema, *C-Glycoside Synthesis*, CRC Press, Boca Raton, 1995; D. E. Levy and C. Tang, *The Chemistry of C-Glycosides*, Pergamon, Oxford, 1995; Y. Du and J. Linhardt, *Tetrahedron*, 1998, **54**, 9913 and references cited therein.
63 F. K. Griffin, D. E. Paterson and R. J. K. Taylor, unpublished results.

Paper 8/06615I

Aufbau synthesis of a mixed-metal anion receptor cage

Ramón Vilar, D. Michael P. Mingos,* Andrew J. P. White and David J. Williams

Department of Chemistry, Imperial College of Science Technology and Medicine, London, UK SW7 2AY. E-mail: d.mingos@ic.ac.uk

Received (in Basel, Switzerland) 26th October 1998, Accepted 8th December 1998

The isolation and structural characterisation of square planar [Ni(atu)$_2$] (Hatu = amidinothiourea) has provided a rational basis to synthesise the novel mixed-metal cage compounds [Ni$_4$Pd$_2$(atu)$_8$X]X$_3$ (X = Cl, Br); one of these cages (when X = Cl) has been crystallographically characterised showing that the chloride anion is encapsulated in the centre of the cage forming eight hydrogen-bonds with N–H groups from the ligands and two Lewis acid–base interactions with two palladium(II) ions.

The inclusion of guest molecules into host structures has attracted great interest over the past two decades.[1] This interest has been stimulated by the potential properties of these supermolecules as chemical sensors,[2] nanoscale devices[3] and systems with biological markers.[4] Whilst the supramolecular chemistry of cationic or neutral guests has been widely studied,[5] that of anions has received much less attention.[6] Examples of molecular containers (such as squares and cages) have been reported to selectively encapsulate anionic guests.[7] The incorporation of transition metal centres into such molecular containers may either enhance their Lewis acidity or introduce magnetic, electrochemical and luminescent properties into the host molecules.[8]

Recently we have reported the selective encapsulation of anions (Cl **1**, Br **2**) inside the hexanuclear nickel cages [Ni$_6$(atu)$_8$]$^{4+}$ (Hatu = amidinothiourea and atu is its deprotonated form).[9] These cages self-assemble according to eqn. (1) only in the presence of the templating anions F$^-$, Cl$^-$ and Br$^-$.

$$4\,Ni(ClO_4)_2 + 8\,Hatu \longrightarrow 4\,[Ni(atu)_2] \xrightarrow{2\,NiX_2} [Ni_6(atu)_8X]X_3 \quad (1)$$

X = Cl **1**, Br **2**

Hatu =

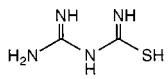

Here, we report the synthesis and structural characterisation of the square planar precursor [Ni(atu)$_2$] **3**. The isolation of this complex has made it possible to rationally synthesise the new mixed-metal cage compounds [Ni$_4$Pd$_2$(atu)$_8$X]X$_3$ (X = Cl **4**, X = Br **5**) which retain the basic octahedral metal framework observed in **1** and **2** but selectively include the palladium ions in *trans*-positions. Although there are a number of examples of anion encapsulation by homonuclear cages, few examples of mixed metal cages have previously been reported.

When a solution of Ni(ClO$_4$)$_2$ in methanol was mixed with 2 equivalents of amidinothiourea [Hatu = H$_2$NC(=NH)-NHC(=NH)SH] a dark orange solution was obtained from which a crystalline material was separated after addition of diethyl ether. A single crystal analysis of the compound confirmed its formulation as *trans*-[Ni(atu)$_2$] (Fig. 1).

Amidinothiourea can coordinate to metal centres using either two nitrogens (N,N) or one nitrogen and one sulfur (N,S). The molecular structure of **3** reveals the coordination mode to be N,N′. This is in striking contrast to what is observed in the only other structurally characterised complex of this ligand, with palladium, where N,S coordination occurs.[10] This suggested that the non-coordinated sulfur atoms in **3** are available for coordination to additional metal centres. This was partially

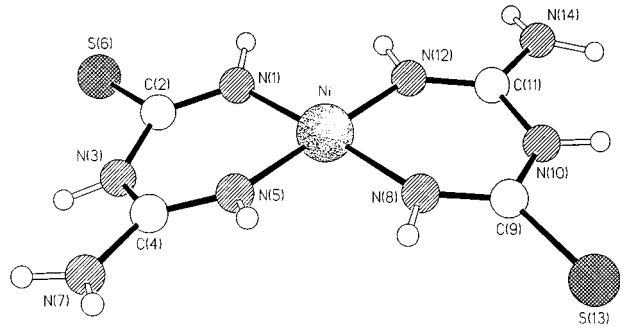

Fig. 1 The molecular structure of one of the independent molecules present in the crystals of **3**. Ni–N distances are in the range 1.843(5)–1.872(4) Å.

corroborated when addition of NiX$_2$ salts (X = Cl, Br) to this solution yielded the recently reported hexanickel cages **1** and **2**, albeit with an isomerisation of the square-planar complex from *trans*- to *cis*-.

When a solution of [Pd(PhCN)$_2$Cl$_2$] in CH$_2$Cl$_2$ was added to a solution of **3** in methanol (in a 1 : 2 ratio) a change in colour to a brighter orange was immediately observed. After 2 h the volume of methanol was reduced and diethyl ether added. A crystalline material precipitated and was formulated as [Ni$_4$-Pd$_2$(atu)$_8$Cl]Cl$_3$ **4** on the basis of spectroscopic and elemental analyses.† Crystals suitable for crystallographic analysis were obtained by slow evaporation of diethyl ether into a methanol solution of **4**. The molecular structure of **4** is shown in Fig. 2.

The X-ray analysis‡ revealed the presence of an octahedral Ni$_4$Pd$_2$ mixed-metal cage complex with one of the chloride anions encapsulated at its centre. The overall geometry is very similar to that of the all-nickel counterpart **1**,[9] but with the nickel atoms in the *trans*-positions replaced by palladium atoms (*vide infra*). The geometry at each nickel centre is square-planar with Ni–N distances ranging between 1.847(5) and 1.887(9) Å,

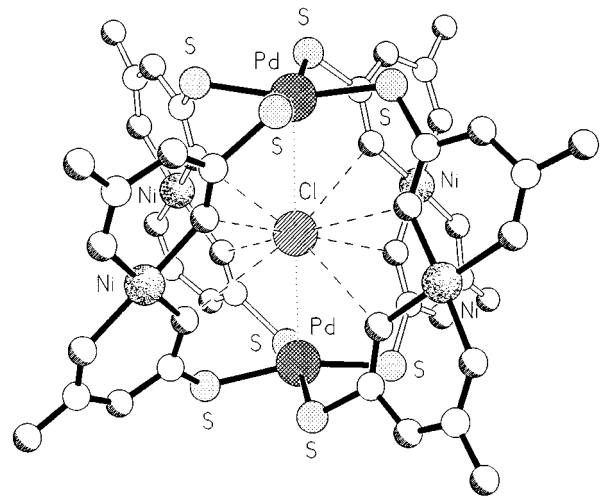

Fig. 2 The molecular structure of the mixed-metal cage cation **4** showing the encapsulation of a chloride anion. The Ni–N distances are in the range 1.847(5)–1.887(9) Å, Pd–S between 2.315(2) and 2.323(2) Å and N···Cl 3.29–3.39 Å; the Pd···Cl distances are 3.169(2) and 3.190(2) Å.

whereas that at the palladium centres is distinctly pyramidal, the palladium atoms lying *ca.* 0.31 Å out of the planes of their substituents towards the encapsulated chloride anion [the Pd–S distances range between 2.315(2) and 2.323(2) Å]. As in **1** the anion is displaced slightly towards one of the MS_4 metal atoms, the Pd···Cl distances being 3.169(2) and 3.190(2) Å. The 'retaining' N–H···Cl hydrogen-bonds have N···Cl distances ranging between 3.29 and 3.39 Å. The cage as a whole exhibits a small helical twist with the north and south PdS_4 units being rotated by *ca.* 17° with respect to each other about the Pd···Pd vector. Although the cage has helicity, the crystals are racemic, there being equal numbers of Δ and Λ forms present. The 'non-encapsulated' chloride anions link adjacent cages *via* additional N–H···Cl hydrogen-bonds, with the voids formed between the cages being filled by the methanol and diethyl ether solvent molecules.

An intriguing difference between the hexanickel cages **1** and **2**,[9] and the mixed-metal Ni–Pd cages reported in this paper (**4** and **5**) is their colour: the former are dark green while the later are dark orange. Ni(II) square planar complexes are generally red or orange. However, the coordination of ligands above or below the square-plane commonly results in a change in their colour to dark green or blue.[11] This has been attributed to interactions between these ligands and the metal d_{z^2} orbital in the axial positions of the square planar unit. The change in colour for **1** and **2** underlines the importance of the acceptor–donor interaction between the NiS_4 units and the encapsulated halide.

The generality of the *aufbau* process for the synthesis of **4** is supported by the ability to synthesise the analogous bromide species. When a mixture of $Ni(ClO_4)_2$/2 Hatu was reacted with $[Pd(PhCN)_2Br_2]$ an orange product was obtained. This product was recrystallised from methanol–diethyl ether and was formulated on the basis of IR, ^{1}H NMR and elemental analyses as the cage compound $[Ni_4Pd_2(atu)_8Br]Br_3$ **5**.

The formation of the above complexes can be rationalised on the basis of the sequence of reactions shown in eqn. (2).

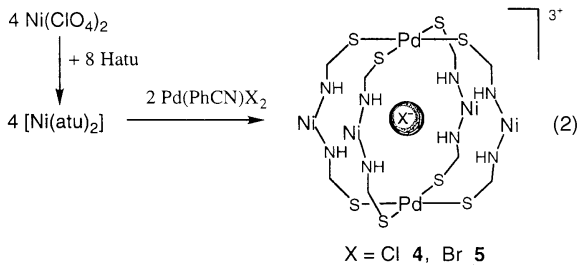

(2)

These results have demonstrated that the formation of octahedral cage complexes of amidinothiourea, which are capable of encapsulating halide anions, are not limited to the self-assembly processes but can be built up using well defined coordination chemistry principles. The isolation of mixed-metal cages such as those described above, open up the possibility of fine tuning the chemical and spectroscopic properties of this interesting class of anion receptor molecules.

We thank EPSRC for financial support and BP plc for endowing D. M. P. M's chair.

Notes and references

† **4**: yield (crystalline material): 37% [based on the initial $Ni(ClO_4)_2$]; ^{1}H NMR (CD_3OD) δ 7.9 (br, NH). IR(KBr): ν/cm^{-1} 3434m, 3332m (N–H), 1658vs (C–N), 1598s (C–S), 1174s. Electronic spectrum (MeOH): λ_{max} = 441 nm; Anal. Calc. for $C_{16}H_{40}N_{32}S_8Ni_6Cl_4{\cdot}5H_2O{\cdot}0.5CH_2Cl_2$: C, 12.3; H, 3.1; N, 26.9; Cl, 10.6. Found: C, 12.0; H, 3.1; N, 26.4; Cl, 9.5%.

5: yield (crystalline material): 46% [based on the initial $Ni(ClO_4)_2$]; ^{1}H NMR (CD_3OD) δ 8.0 (br, NH). IR(KBr): ν/cm^{-1} 3434m, 3332m (N–H), 1658vs (C–N), 1598s (C–S), 1174s. Electronic spectrum (MeOH): λ_{max} = 445 nm; Anal. Calc. for $C_{16}H_{40}N_{32}S_8Ni_6Br_4{\cdot}CH_3OH$: C, 11.7; H, 2.5; N, 25.8; Br, 18.5. Found: C, 11.2; H, 2.8; N, 23.8; Br, 18.7%.

‡ *Crystal data*: for **3**: $C_4H_{10}N_8S_2Ni{\cdot}0.67Me_2SO$, M = 345.1, monoclinic, space group $P2_1/c$ (no. 14), a = 8.776(1), b = 12.142(1), c = 18.806(1) Å, β = 99.77(1)°, V = 1974.9(3) Å^3, Z = 6 (one of the two independent molecules has C_i symmetry), D_c = 1.741 g cm^{-3}, μ(Cu-Kα) = 61.0 cm^{-1}, F(000) = 1068, T = 173 K; yellow plates, 0.20 × 0.12 × 0.03 mm, Siemens P4/RA diffractometer, ω-scans, 2678 independent reflections. The structure was solved by direct methods and the major occupancy non-hydrogen atoms were refined anisotropically using full matrix least-squares based on F^2 to give R_1 = 0.047, wR_2 = 0.103 for 2136 independent observed absorption corrected reflections [$|F_o| > 4\sigma(|F_o|)$, $2\theta \leqslant 120°$] and 306 parameters.

For **4**: $C_{16}H_{40}Cl_4N_{32}S_8Ni_4Pd_2{\cdot}6.5CH_3OH{\cdot}Et_2O$, M = 1809.1, monoclinic, $P2_1/c$ (no. 14), a = 19.271(2), b = 15.586(2), c = 25.250(4) Å, β = 104.10(1)°, V = 7356(2) Å^3, Z = 4, D_c = 1.634 g cm^{-3}, μ(Cu-Kα) = 89.4 cm^{-1}, F(000) = 3676, T = 183 K; orange prisms, 0.42 × 0.33 × 0.23 mm, Siemens P4/RA diffractometer, ω-scans, 10 934 independent reflections. The structure was solved by direct methods and the major occupancy non-hydrogen atoms were refined anisotropically using full matrix least-squares based on F^2 to give R_1 = 0.053, wR_2 = 0.135 for 8789 independent observed absorption corrected reflections [$|F_o| > 4\sigma(|F_o|)$, $2\theta \leqslant 120°$] and 831 parameters. CCDC 182/1122.

1 J.-M. Lehn, *Supramolecular Chemistry-Concepts and Perspectives*, VCH, Weinheim, 1995.
2 M. A. Mortellaro and D. G. Nocera, *J. Am. Chem. Soc.*, 1996, **118**, 7414; T. W. Swager, *Acc. Chem. Res.*, 1998, **31**, 201.
3 P. N. W. Baxter, in *Comprehensive Supramolecular Chemistry*, J. P. Sauvage and M. Wais Hosseini (volume editors), Elsevier, Exeter, 1996, vol. 5, p. 165.
4 R. J. Pieters and F. Diederich, *Chem. Commun.*, 1996, 2255; K. Konishi, S. Kimata, K. Yoshida, M. Tanaka and T. Aida, *Angew. Chem., Int. Ed. Engl.*, 1996, **35**, 2823.
5 B. Dietrich, in *Comprehensive Supramolecular Chemistry*, G. W. Gokel, Elsevier, Exeter, 1996, vol. 1, p. 153.
6 P. D. Beer, *Chem. Commun.*, 1996, 689; D. M. Rudkevich, W. Verboom, Z. Brzozka, M. J. Palys, W. P. R. V. Stauthamer, G. J. van Hummel, S. M. Franken, S. Harkema, J. F. J. Engbersen and D. N. Reinhoudt, *J. Am. Chem. Soc.*, 1994, **116**, 4341; W. Xu, J. J. Vittal, R. J. Puddephatt, *ibid.*, 1995, **117**, 8362; *Supramolecular Chemistry of Anions*, ed. A. Bianchi, E. García-España, K. Bowman-James, Wiley–VCH, Weinheim, 1997; M. C. T. Fye, P. T. Glink, S. Menzer, J. F. Stoddart, A. J. P. White and D. J. Williams, *Angew. Chem., Int. Ed. Engl.*, 1997, **36**, 2068; N. S. Fender, I. A. Kahwa, A. J. P. White and D. J. Williams, *J. Chem. Soc., Dalton Trans.*, 1998, 1729.
7 M. M. G. Antonisse and D. N. Reinhoudt, *Chem. Commun.*, 1998, 443.
8 M. Fujita, in *Comprehensive Supramolecular Chemistry*, J. P. Sauvage and M. Wais Hosseini (volume editors), Elsevier, Exeter, 1996, vol. 9, p. 253; C. J. Jones, *Chem. Soc. Rev.*, 1998, **27**, 289; M. Fujita and K. Ogura, *Bull. Chem. Soc. Jpn.*, 1996, **69**, 1471; B. Olenyuk, A. Fechtenkötter and P. J. Stang, *J. Chem. Soc., Dalton Trans.*, 1998, 1707.
9 R. Vilar, D. M. P. Mingos, A. J. P. White and D. J. Williams, *Angew. Chem., Int. Ed. Engl.*, 1998, **37**, 1258.
10 L. Coghi, M. Lanfranchi, G. Pelizzi and P. Tarasconi, *Tranistion Met. Chem.*, 1978, **3**, 69; T. Tada, Y. Kushi and Y. Yoneda, *Bull. Chem. Soc. Jpn.*, 1982, **55**, 1063; P. Lemoine, M. Chiadmi, V. Bissery, A. Tomas and B. Viossat, *Acta Crystallogr., Sect. C*, 1996, **52**, 1430; R. O. C. Hart, S. G. Bott, J. L. Atwood and S. R. Cooper, *J. Chem. Soc., Chem. Commun.*, 1992, 894.
11 F. A. Cotton and G. Wilkinson, *Advanced Inorganic Chemistry*, John Wiley and Sons, New York, 5th edn., 1988, pp. 748–752.

Communication 8/08303G

Dearomatising cyclisations of lithiated *N*-benzylbenzamides

Anjum Ahmed, Jonathan Clayden* and Samreen A. Yasin

Department of Chemistry, University of Manchester, Oxford Road, Manchester, UK M13 9PL. E-mail: j.p.clayden@man.ac.uk

Received (in Liverpool, UK) 22nd October 1998, Accepted 3rd December 1998

On treatment with Bu^{t}Li in the presence of HMPA, *N*-benzylbenzamides undergo anionic cyclisation with dearomatisation to give an extended amide enolate which reacts with electrophiles to yield bicyclic cyclohexadiene derivatives.

Dearomatisation is an attractive strategy for the synthesis of functionalised six-membered ring compounds,[1] and the Birch reduction has long been the most important dearomatising reaction of substituted benzene rings.[2] More recent methods include addition to chromium–arene complexes, oxidations wtih *Pseudomonas putida*,[3] MAD-promoted nucleophilic attack on aromatic aldehydes and ketones,[4] or radical cyclisation.[5] We have recently described a dearomatising anionic cyclisation of naphthalenes, in which a lithiated tertiary 1-naphthamide undergoes intramolecular attack on the naphthalene ring to generate a benzo[*e*]isoindolinone.[6] We now report that similar conditions promote the dearomatising cyclisation of simple benzamides to give tetrahydroisoindolones.

N-Benzylbenzamides **1** and **2** undergo benzylic deprotonation (α to nitrogen) on treatment with Bu^{t}Li, and the α-lithiated species can be alkylated with MeI or BnBr to yield **4**–**6** (Scheme 1).[7] When we carried out this deprotonation in the presence of HMPA, the organolithium **3** was no longer stable over a period of hours at −78 °C, and slowly underwent a new kind of dearomatising anionic cyclisation.[8] Adding MeI after 16 h gave no **4** or **6**, but instead a regio- and stereo-isomeric mixture of cyclised isoindolinones **8** or **9** in 71–73% yield (Scheme 2). In a similar manner, an aqueous quench provided tetrahydroisoindolones **10** and **11**, which are surprisingly resistant to air oxidation, in yields of 80–89%.

At least 6 equiv. of HMPA are essential for high-yielding cyclisations at −78 °C: in pure THF the organolithium **3** (R = Bn) survived for 16 h and returned **2** in quantitative yield upon aqueous quench. DMPU (*N*,*N*'-dimethylpropyleneurea) can be used in place of HMPA, but acceptable yields are then obtained only if the temperature is raised to −40 °C for the 16 h period. TMEDA fails to promote the cyclisation. Organolithium cyclisations are often faster in the presence of lithium-coordinating additives such as HMPA, DMPU or TMEDA:[9] these are assumed to work by promoting dissociation of the organolithium to an ion pair.[10] It would then be the ion pair which cyclises, by a mechanism which is as yet unclear, but may be electrocyclic. Besides our naphthamide cyclisation,[6] there

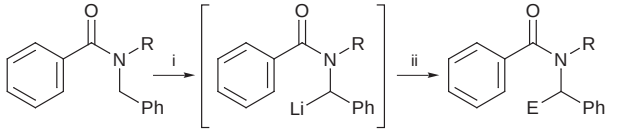

1 R = Bu^t
2 R = Bn
3
4 R = Bu^t, E = Me; 96%
5 R = Bu^t, E = Bn; 80%[a]
6 R = Bn, E = Me; 45%[b]

Scheme 1 *Reagents and conditions*: i, Bu^{t}Li (3 equiv.), THF −78 °C, 6 h; ii, MeI or BnBr. [a] HMPA added 5 min before BnBr. In the absence of HMPA, only starting material was recovered. [b] Deprotonated in presence of HMPA (−78 °C, 20 min). Remainder consists largely of cyclised material as described below.

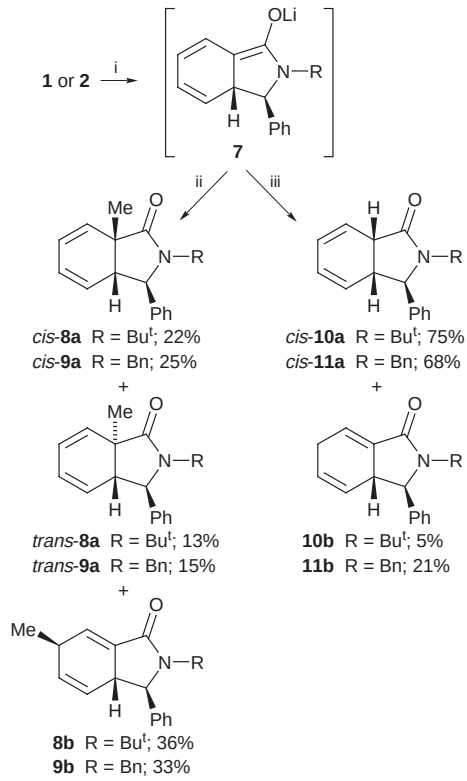

Scheme 2 *Reagents and conditions*: i, Bu^{t}Li (1.3 equiv.), HMPA (6 equiv.), THF, −78 °C, 16 h; ii, MeI; iii, H_2O.

are few precedents for cyclisation of an organolithium onto an aromatic ring,[11] and only one which results in loss of aromaticity.[12] Curran has described a closely related radical cyclisation of an *N*-benzyl-*N*-*tert*-butylbenzamide[13] which yields a rearomatised isoindolone.

Whatever the detailed mechanism of the cyclisation, it must produce the extended enolate **7**, with the phenyl group lying *exo* to the 6,5-fused ring system. Enolate **7** evidently reacts both α and γ to the amide carbonyl group,[14] leading to the observed mixture of regioisomers.† We observed only one stereoisomer of the γ-alkylated compounds **8b**–**11b**; we assigned their stereochemistry by means of an X-ray crystal structure of **8b**

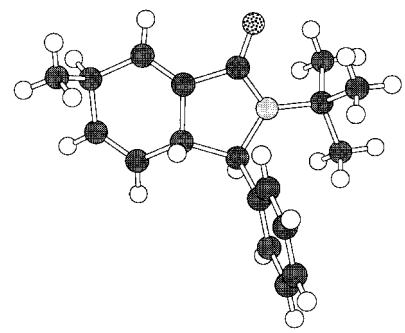

Fig. 1 X-Ray crystal structure of **8b** (R = Bu^t).

Table 1 Cyclisation results with various electrophiles

Entry	E^+	E	Yield (%)[a] **12** (total)	*cis*-**12a**	*trans*-**12a**	**12b**	α : γ ratio **12a** : **12b**[b]	*cis*-**12a**: *trans*-**12a**[b]
1	NH_4Cl	H	80[c]	75	0	5	3.5 : 1	> 20 : 1
2	MeI	Me	71[d]	22	13	36	1 : 1	1.3 : 1
3	MeOTs	Me	56[d]	43	5	8	7 : 1	6 : 1
4	MeOTf	Me	47[d]	34	13	0	20 : 1	2 : 1
5	allyl-Br	allyl	73	46	0	27	3 : 1	> 4 : 1
6	BnBr	Bn	65	61	0	4	1.6 : 1	> 20 : 1
7	EtI	Et	11	—	—	—	*ca.* 1 : 1	—
8	EtOTs	Et	30	30	0	0	*ca.* 6 : 1	> 20 : 1

[a] Isolated yield. [b] Ratio by ^{1}H NMR analysis. [c] **12** (E = H) is identical with **10**. [d] **12** (E = Me) is identical with **8**.

(Fig. 1), which shows the cyclohexadiene ring as a boat bearing the methyl group pseudoaxially.‡ The α-alkylated compounds **8a** and **9a** were formed as stereoisomeric mixtures, with the *cis* ring junction favoured (as in the related naphthamide series[6]). Their relative stereochemistry was elucidated by NOE studies. The major stereoisomers are formed by attack of the electrophile on the *exo* face of the bicyclic enolate **7**.

The same three classes of products, in varying ratios, were obtained when other electrophiles were used to quench the cyclisation, as shown in Scheme 3 and Table 1. Harder alkylating agents apear to favour α-attack on **6** (MeOTf > MeOTs > MeI); more sterically demanding alkylating agents appear to be more stereoselective.

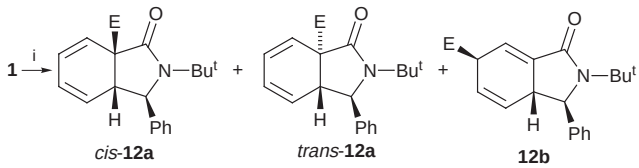

Scheme 3 *Reagents and conditions*: i, Bu^{t}Li (1.3 equiv.), HMPA (6 equiv.), THF, −78 °C, 16 h; ii, E^+.

It was also possible to improve the regioselectivity of the alkylation step by varying the enolate counterion or solvent. Table 2 shows the result of reforming the enolate **7** with Bu^{s}Li, LiHMDS, NaHMDS or KHMDS, and alkylating it with BnBr (Scheme 4). The lithium enolate generated by deprotonation with Bu^{s}Li reacts more regioselectively than the same enolate formed by the reaction in the presence of HMPA, and the presence of hexamethyldisilazane leads almost solely to the α-alkylated product. The sodium and potassium enolates reacted less regioselectively, but the potassium enolate gave an almost quantitative yield of isolated regioisomers.

Table 2 Alkylations using various bases

Entry	Base	Yield (%)[a] *cis*-**12a** (E = Bn)	**12b** (E = Bn)	α : γ ratio **12a** : **12b** (E = Bn)[b]
1	Bu^{s}Li	57[c]		3 : 1
2	LiHMDS	70	7	10 : 1
3	NaHMDS	39	21	3.5 : 1
4	KHMDS	75	17	4 : 1

[a] Isolated yield. [b] By ^{1}H NMR analysis. [c] Isolated yield of mixture.

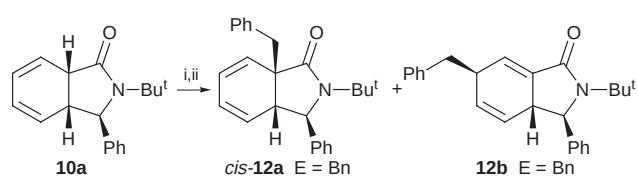

Scheme 4 *Reagents and conditions*: i, base (2 equiv.); ii, BnBr.

We are grateful to the EPSRC, Merck, Sharp and Dohme, and Zeneca Agrochemicals for CASE awards (to A. A. and S. A. Y.), to Dr M. Rowley (Merck, Sharp and Dohme) and Dr M. Turnbull (Zeneca Agrochemicals) for helpful discussions, to Dr M. Helliwell for determining the X-ray crystal structure of **8b**, and to the Royal Society for an Equipment Grant. The optimisation of the conditions for the cyclisation was assisted by an observation made by Sharon Jaeger.[15]

Notes and references

† The ratio of **10a** : **10b** is kinetically controlled: **10a** and **10b** do not interconvert under the conditions of the aqueous work-up, nor even in Bu^{t}OK–Bu^{t}OH at 80 °C.

‡ *Crystal data* for **8b**: colourless plates, $C_{19}H_{23}NO$, triclinic, space group *P*1, *a* = 8.316(1), *b* = 15.316(2), *c* = 6.424(2) Å, α = 93.10(2), β = 92.74(2), γ = 79.96(1)°, 3491 reflections measured, 3273 unique, *R* = 0.068, R_w = 0.055. CCDC 182/1112.

1 T. Bach, *Angew. Chem., Int. Ed. Engl.*, 1996, **35**, 729; L. N. Mander, *Synlett*, 1991, 134.
2 P. W. Rabideau and Z. Marcinow, *Org. React.*, 1992, **42**, 1.
3 H. A. J. Carless, *Tetrahedron: Asymmetry*, 1992, **3**, 795.
4 K. Maruoka, M. Ito and H. Yamamoto, *J. Am. Chem. Soc.*, 1995, **117**, 9091; S. Saito, K. Shimada, H. Yamamoto, E. Martínez de Marigorta and I. Fleming, *Chem. Commun.*, 1997, 1299.
5 J. Boivin, M. Yousfi and S. Z. Zard, *Tetrahedron Lett.*, 1997, **38**, 5985.
6 A. Ahmed, J. Clayden and M. Rowley, *Chem. Commun.*, 1998, 297; A. Ahmed, J. Clayden and M. Rowley, *Tetrahedron Lett.*, 1998, **39**, 6103.
7 P. Beak and D. B. Reitz, *Chem. Rev.*, 1978, **78**, 275; P. Beak, W. Zajdel and D. B. Reitz, *Chem. Rev.*, 1984, **84**, 471.
8 For cyclisations of α-nitrogen-substituted organolithiums onto other acceptors see, for example, C. A. Broka and T. Shen, *J. Am. Chem. Soc.*, 1989, **111**, 2981; I. Coldham and R. Hufton, *Tetrahedron*, 1996, **52**, 12541; I. Coldham, R. Hufton and D. J. Snowden, *J. Am. Chem. Soc.*, 1996, **118**, 5322; I. Coldham, M. M. S. Lang-Anderson, R. E. Rathmell and D. J. Snowden, *Tetrahedron Lett.*, 1997, **38**, 7621.
9 W. F. Bailey, X.-L. Jiang and C. E. McLeod, *J. Org. Chem.*, 1995, **60**, 7791; W. F. Bailey and X.-L. Jiang, *J. Org. Chem.*, 1996, **61**, 2596.
10 R. W. Hoffmann, R. Koberstein, B. Remacle and A. Krief, *Chem. Commun.*, 1997, 2189.
11 G. W. Klumpp and R. F. Schmitz, *Tetrahedron Lett.*, 1974, **15**, 2911; A. Krief, B. Kenda, P. Barbeaux and E. Guittet, *Tetrahedron*, 1994, **50**, 7177.
12 J. K. Crandall and T. A. Ayers, *J. Org. Chem.*, 1992, **57**, 2993.
13 D. P. Curran and H. Liu, *J. Chem. Soc., Perkin Trans. 1*, 1994, 1377.
14 The surprising (see I. Fleming, *Frontier Orbitals and Organic Chemical Reactions*, Wiley, New York, 1976, pp. 45–46) lack of regioselectivity in the reactions of these extended enolates is possibly due to their bicyclic nature. For comparable examples of extended amide enolates, see R. K. Haynes, S. M. Starling and S. C. Vonwiller, *J. Org. Chem.*, 1995, **60**, 4690; M. Yamaguchi, M. Hamada, H. Nakashima and T. Minami, *Tetrahedron Lett.*, 1987, **28**, 1785.
15 S. E. Jaeger, Ph.D. thesis, University of Manchester, 1996.

Communication 8/08218I

Ionic cleavage of Ti–Co and Zr–Co bonds: the role of the nucleophilicity of the late transition metal in the reactive behaviour of early–late heterobimetallics

Martin Schubart,[a] Gemma Mitchell,[a] Lutz H. Gade,*[b] Thomas Kottke,[a] Ian J. Scowen[c] and Mary McPartlin[c]

[a] *Institut für Anorganische Chemie der Universität Würzburg, Am Hubland, 97074 Würzburg, Germany*
[b] *Laboratoire de Chimie Organométallique et de Catalyse, Institut LeBel, Université Louis Pasteur, 4, rue Blaise Pascal, 67070 Strasbourg, France. E-mail: gade@chimie.u-strasb.fr*
[c] *School of Applied Chemistry, University of North London, Holloway Road, London, UK N7 8DB*

Received (in Basel, Switzerland) 2nd November 1998, Accepted 8th December 1998

The ionic cleavage of Ti–Co and Zr–Co bonds occurs upon reaction with Bu^{t}NC and the products [MeSi{SiMe$_2$N(*p*-Tol)}$_3$Ti(CNBu^t)$_2$][Co(CO)$_4$] 3 and[MeSi{SiMe$_2$N(*p*-Tol)}$_3$Zr(CNBu^t)$_3$][Co(CO)$_4$] 4 were characterized by single crystal X-ray diffraction; the importance of the nucleophilicity of the late transition metal fragment in reactions of the unsupported early–late heterobimetallics is demonstrated.

In many cases, early–late heterobimetallic complexes display the reactive behaviour of pairs of metal nucleophiles and electrophiles which are 'masked' by the existence of a metal–metal bond and which is cleaved during the course of the reaction.[1–5]

In order to assess the validity of the concept of combining metal nucleophilicity and electrophilicity we decided to reduce the basicity of the late transition metal fragment to the degree at which polar additions to suitable unsaturated substrates no longer take place.[6] Instead, the heterolytic cleavage of the metal–metal bond and 'solvation' of the Ti-group fragment by the substrate was thought to be a possible reaction pathway yielding the *extremely rare* case of an ionic dissociation of the metal–metal bond between transition elements *without* concomitant redox reaction.[7] Redox disproportionation is observed in the well known reaction of $Co_2(CO)_8$ with donor ligands.[8] Here, we wish to give a first account of these investigations which led to the conversion of metal–metal bonded dinuclear complexes to fairly stable organometallic salts. More importantly, we could demonstrate that subsequent addition of a stronger metal nucleophile led to the re-formation of the polar metal–metal bond.

The objects of study were the heterobimetallic complexes [MeSi{SiMe$_2$N(*p*-Tol)}$_3$M-Co(CO)$_4$] (M = Ti **1**, Zr **2**)[9] in which the late transition metal fragment is characterized by low nucleophilicity.[6] Reaction of **1** and **2** with Bu^{t}NC in toluene led to the clean conversion to products which contain two and three molecules of isocyanide associated with every Ti and Zr centre, respectively, as established by elemental analysis. The formation of both compounds **3** and **4** occurred cooperatively, *i.e.* without detection of intermediates, and the products crystallized directly from the reaction mixture in yields of 75 and 77%, respectively. A single ν(CO) band at 1875 cm^{-1} in the IR spectra of both compounds indicated the presence of the tetracarbonyl cobaltate anion[10] and their low solubility in the aromatic reaction medium indicated an ionic species. In both cases it proved to be possible to obtain single crystals of the apparently salt-like compounds directly from the reaction mixture. It was therefore possible to establish their structure by X-ray crystallography and to confirm their formulation as [MeSi{SiMe$_2$N(*p*-Tol)}$_3$Ti(CNBu^t)$_2$][Co(CO)$_4$] **3** and [MeSi{SiMe$_2$N(*p*-Tol)}$_3$Zr(CNBu^t)$_3$][Co(CO)$_4$] **4** (Scheme 1).†

The [Co(CO)$_4$]$^-$ anion in the crystal structure of **3** was found to be highly disordered which precluded the complete refinement of the structural data. However, the presence of the pentacoordinate titanium complex cation [MeSi{SiMe$_2$N(*p*-Tol)}$_3$Ti(CNBu^t)$_2$]$^+$ could be established unambiguously. In contrast, the X-ray diffraction experiment performed on a single crystal of compound **4** yielded a data set of good quality and permitted full refinement of the structure which is depicted in Fig. 1.‡

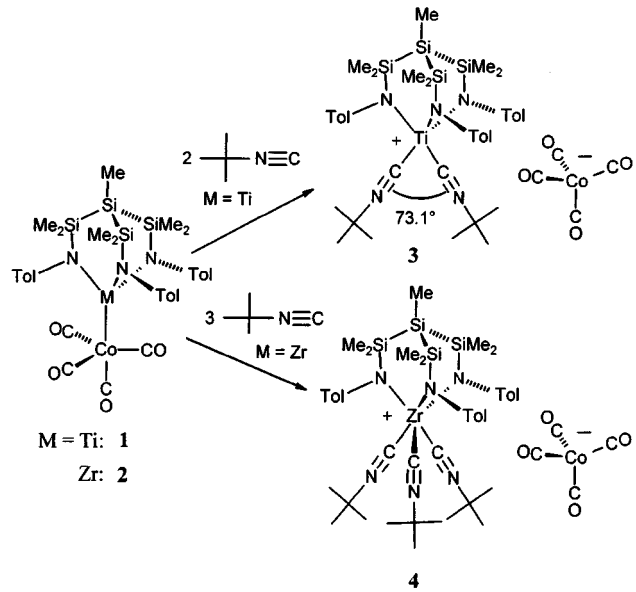

Scheme 1 Ionic cleavage of the Ti–Co and Zr–Co bonds.

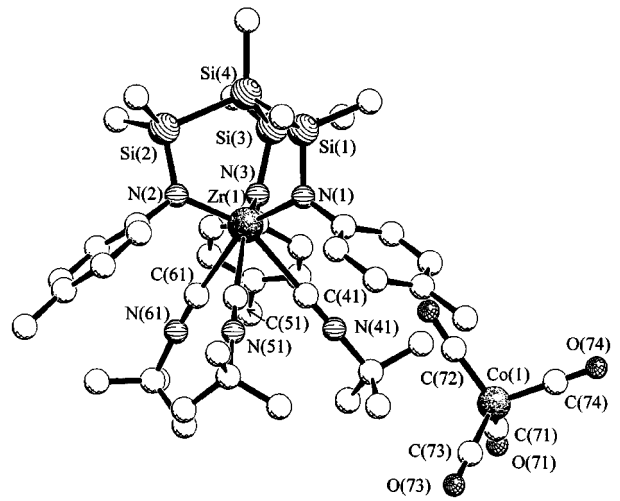

Fig. 1 Molecular structure of **4** in the crystal. Principal bond lengths (Å) and interbond angles (°): Zr(1)–N(1) 2.074(4), Zr(1)–N(2) 2.076(5), Zr(1)–N(3) 2.082(5), Zr(1)–C(41) 2.431(7), Zr(1)–C(51) 2.448(7), Zr(1)–C(61) 2.440(7), Co(1)–C(71) 1.7332(9), Co(1)–C(72) 1.722(8), Co(1)–C(73) 1.769(8), Co(1)–C(74) 1.741(8); N(1)–Zr(1)–N(2) 105.8(2), N(1)–Zr(1)–N(3) 108.0(2), N(2)–Zr(1)–N(3) 108.9(2), C(41)–Zr(1)–C(51) 70.6(2), C(41)–Zr(1)–C(61) 72.1(2), C(51)–Zr(1)–C(61) 71.4(2).

The crystal structure of **4** clearly establishes the ionic cleavage of the metal–metal bond by which the slightly distorted tetrahedral $[Co(CO)_4]^-$ anion [OC–Co–CO′ 107.2–110.5°] and the trigonally distorted octahedral cation $[MeSi\{SiMe_2N(p\text{-}Tol)\}_3Zr(CNBu^t)_3]^+$ were generated. Owing to the sixfold coordination at the Zr-centre the Zr–N distances [2.073(4), 2.077(5), 2.082(5) Å] are somewhat greater than those found in previously reported four-coordinate tripodal amidozirconium complexes, in particular, the Zr–Co dinuclear complex **2** [2.037(5), 2.044(5), 2.032(5) Å].[9] Remarkably, the Zr–C bond lengths of the coordinated isocyanide ligands [2.439(7), 2.448(7), 2.430(7) Å] are significantly greater than those found in all known structurally characterized isocyanide–zirconium species [Zr–C 2.31–2.37 Å].[11]

In view of the previously observed insertions of isocyanides into the highly polar metal–metal bonds of unsupported early–late heterobimetallics[3] it was of particular interest to explore how the complex salts **3** and **4** would react with the strong metal nucleophile $[RuCp(CO)_2]^-$. In principle, two reaction pathways were conceivable, the direct nucleophilic attack at the C-atom of a coordinated, and thus activated, isocyanide ligand generating the metallaiminoacyl complexes. Alternatively, rapid nucleophilic substitution of the isocyanide ligands could intially lead to the M–Ru heterodinuclear complexes **5** and **6** which would over a period of several hours insert the displaced isocyanide. The latter was established by NMR and IR spectroscopy in the reaction of **3** with $K[RuCp(CO)_2]$ in C_6D_6. Almost instantaneous formation of the M–Ru complex **5** was observed[3] which, subsequently, was partially converted to the insertion product **7** (Scheme 2).‡ This result is pertinent to the previously proposed mechanism of the insertion of unsaturted polar substrates into the metal–metal bonds, which we derived from a kinetic study, and supports the notion that predissociation of the heterodinuclear complex and addition of the ionic fragments to the substrate does not appear to be the decisive step.[4] Rather, as proposed by us, the substrate coordinates to the early transition metal centre in the dinuclear complex, thus lablizing and polarizing the metal–metal bond which is cleaved in the subsequent rearrangement of the nucleophilic metal fragment to give the insertion product.

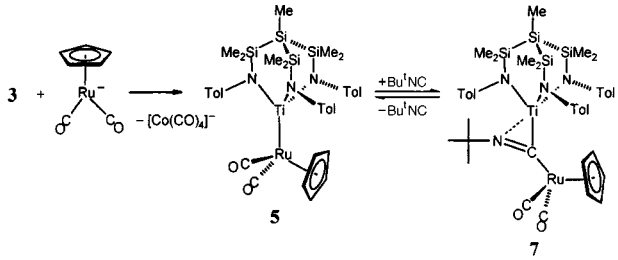

Scheme 2 Reaction of **3** with $K[RuCp(CO)_2]$, initially yielding the Ti–Ru complex **5** which subsequently reversibly inserts Bu^tNC.

In view of the incomplete insertion of Bu^tNC into the metal–metal bonds we studied the reaction leading to **7** in more detail by reacting **5** with varying amounts of isocyanide and determining the conversion of **5** to **7** by ^1H NMR spectrocopy as well as the reverse reaction taking place upon dissolution of isolated solid **7**. The insertion/de-insertion equilibrium depicted in Scheme 2 could thus be established for **5** and **7** with an equilibrium constant $K = [\mathbf{7}]/[\mathbf{5}][Bu^tNC] = 0.91\ dm^3\ mol^{-1}$ in toluene at 298 K.

We thank the Deutsche Forschungsgemeinschaft, the Fonds der Chemischen Industrie, the European Commission (TMR network and Erasmus Program), the EPSRC and the DAAD and British Council for funding. We dedicate this paper to Professor Bernt Krebs, Universität Münster, on the occasion of his 60th birthday.

Notes and references

† *Selected spectroscopic and analytical data*: **3**: ^1H NMR (C_6D_6) δ 0.22 (s, CH_3Si), 0.42 [s, $Si(CH_3)_2$], 1.21 [s, $CNC(CH_3)_3$], 2.24 [s, $CH_3C_6H_4$], 6.88–7.09 (m, Tol). ^{13}C {^1H} NMR (C_6D_6) δ −14.1 (CH_3Si), 2.4 [$Si(CH_3C_6H_4)$], 30.2 [$CNC(CH_3)_3$], 57.7 [$CNC(CH_3)_3$], 125.5 (Tol, C^2), 129.3 (Tol, C^3), 129.8 (Tol, C^4), 149.3 (C NR), 150.0 (Tol, C^1), IR (benzene): 2140, 2107 [m, ν(NC)], 1875 [ν(CO)] cm^{-1}. **4**: ^1H NMR (C_6D_6) δ 0.25 (s, CH_3Si), 0.38 [s, $Si(CH_3)_2$], 1.07 [s, $CNC(CH_3)_3$], 2.29 [s, $CH_3C_6H_4$], 6.79 [d, ^3J(HH) 8.0 Hz, Tol], 7.03 (d, Tol). ^{13}C {^1H} NMR (C_6D_6) δ −16.8 (CH_3Si), 1.8 [$Si(CH_3)_2$], 20.8 ($CH_3C_6H_4$), 29.0 [$CNC(CH_3)_3$], 57.7 [$CNC(CH_3)_3$], 125.9 (Tol, C^2), 129.3 (Tol, C^3), 132.3 (Tol, C^4), 147.6 (C NR), 149.4 (Tol, C^1). IR (benzene): 2145s, 2120m [ν(NC)], 1875 (ν(CO)] cm^{-1}. **7**: ^1H NMR (C_6D_6) δ 0.34 (s, CH_3Si), 0.58 [s, $Si(CH_3)_2$], 1.00 [s, $CNC(CH_3)_3$], 2.18 [s, $CH_3C_6H_4$], 4.55 (s, C_5H_5), 6.90 [d, ^3J(HH) 8.4 Hz, tol], 7.01 (d, Tol). ^{13}C {^1H} NMR (C_6D_6) δ −14.3 (CH_3Si), 2.9 [$Si(CH_3)_2$], 20.8 ($CH_3C_6H_4$), 28.3 [$CNC(CH_3)_3$], 62.4 [$CNC(CH_3)_3$], 89.9 (C_5H_5), 125.6 (Tol, C^2), 129.3 (Tol, C^3), 130.0 (Tol, C^4), 14.1 (Tol, C^1), 200.5 (CO), 266.1 (TiC=N). IR (benzene): 2043s, 1985s [s, ν(CO)] cm^{-1}.

‡ *Crystal data*: for **3**: $C_{42}H_{60}CoN_5O_4Si_4Ti$, monoclinic, space group *Cc*, *a* = 20.8267(15), *b* = 14.1970(13), *c* = 17.590(3) Å β = 90.481(10)° *V* 5167.8(10) A^3, *Z* = 4, D_c = 1.180 g cm^{-3} *T* = 291(2) K, μ = 0.608 cm^{-1}; Siemens P4 diffractometer, 3396 measured data (1.74 < θ < 21.00°), semi-empirical absorption corrections (ψ-scans, relative T_{max} = 0.89039, T_{min} = 0.83523), 3075 independent reflections, R_{int} = 0.0373, R_1 0.0748, wR_2 = 0.1748 [$I > 2\sigma(I)$], *S* = 0.959 for 422 parameters.

For **4**: $C_{61}H_{85}CoN_6O_4Si_4Zr$, monoclinic, space group $P2_1/c$, *a* = 24.622(5), *b* = 14.092(3), *c* = 21.316(4) Å, β = 109.97(3)° *V* = 6952(2) A^3, *Z* = 4, D_c = 1.174 g cm^{-3}, *T* = 183(2)K, μ = 0.502 mm^{-1}; Siemens P4 diffractometer, 12997 measured data (3.01 < θ < 23.63°), semi-empirical absorption corrections (ψ-scans, relative T_{max} = 0.36434, T_{min} = 0.33836), 9816 independent reflections, R_{int} = 0.0650, R_1 0.0676, wR_2 = 0.0799 [$I > 2\sigma(I)$], *S* = 1.010 for 697 parameters. Programs: SHELXTL 5.03, Siemens Analytical X-Ray Instruments Inc., 1994, Madison WI, CCDC 182/1124.

1 M. Herberhold and G.-X. Jin, *Angew. Chem., Int. Ed. Engl.*, 1994, **33**, 964; C. P. Casey, *J. Organomet. Chem.*, 1990, **400**, 205; G. S. Ferguson, P. T. Wolczanski, L. Parkanyi and M. Zonnevylle, *Organometallics*, 1988, **7**, 1967; T. A. Hanna, A. M. Baranger and R. G. Bergman, *J. Am. Chem. Soc.*, 1995, **117**, 665.

2 S. Friedrich, H. Memmler, L. H. Gade, W.-S. Li and M. McPartlin, *Angew. Chem., Int. Ed. Engl.*, 1994, **33**, 676; S. Friedrich, H. Memmler, L. H. Gade, W.-S. Li, I. J. Scowen, M. McPartlin and C. E. Housecroft, *Inorg. Chem.*, 1996, **35**, 2433; S. Friedrich, L. H. Gade, I. J. Scowen and M. McPartlin, *Angew. Chem., Int. Ed. Engl.*, 1996, **35**, 1338; S. Friedrich, L. H. Gade, I. J. Scowen and M. McPartlin, *Organometallics*, 1995, **14**, 5344.

3 B. Findeis, M. Schubart, C. Platzek, L. H. Gade, I. J. Scowen and M. McPartlin, *Chem. Commun.*, 1996, 219.

4 H. Memmler, U. Kauper, L. H. Gade, I. J. Scowen and M. McPartlin, *Chem. Commun.*, 1996, 1751.

5 A. Schneider, L. H. Gade, M. Breuning, G. Bringmann, I. J. Scowen and M. McPartlin, *Organometallics*, 1998, **17**, 1643.

6 R. G. Pearson, H. Sobel and J. Songstad, *J. Am. Chem. Soc.*, 1968, **90**, 316.

7 Examples of ionic dissociation of polar metal–metal bonds which have been studied carefully in solution. D. A. Roberts, W. C. Mercer, S. M. Zahurak, G. L. Geoffroy, C. W. DeBrosse, M. E. Cass and C. G. Pierpont, *J. Am. Chem. Soc.*, 1982, **104**, 910; P. S. Bearman, A. K. Smith, N. C. Tong and R. Whyman, *Chem. Commun.*, 1996, 2061.

8 G. Fachinetti, G. Fochi, T. Funaioli and P. F. Zanazzi, *Angew. Chem., Int. Ed. Engl.*, 1987, **26**, 680 and references therein.

9 G. Jansen, M. Schubart, B. Findeis, L. H. Gade, I. J. Scowen and M. McPartlin, *J. Am. Chem. Soc.*, 1998, **120**, 7239.

10 A. R. Manning, *J. Chem. Soc. A*, 1968, 1135.

11 P. Berno, C. Floriani, A. Chiesi-Villa and C. Rizzoli, *J. Chem. Soc., Dalton Trans.*, 1991, 3085; B. Temme, G. Erker, R. Fröhlich and M. Grehl, *Angew. Chem., Int. Ed. Engl.*, 1994, **33**, 1480; T. Brackemeyer, G. Erker and R. Fröhlich, *Organometallics*, 1997, **16**, 531; W. Ahlers, B. Temme, G. Erker, R. Fröhlich and T. Fox, *J. Organomet. Chem.*, 1997, **527**, 191.

Communication 8/08498J

The synthesis and ring-opening metathesis polymerization of peptide functionalized norbornenes

Stefano C. G. Biagini,[a] R. Gareth Davies,[a] Vernon C. Gibson,*[b] Matthew R. Giles,[b] Edward L. Marshall,[b] Michael North*[a] and David A. Robson[b]

[a] *Department of Chemistry, University of Wales, Bangor, Gwynedd, UK LL57 2UW. E-mail: m.north@bangor.ac.uk*
[b] *Department of Chemistry, Imperial College of Science, Technology and Medicine, Exhibition Road, South Kensington, London, UK SW7 2AY. E-mail: v.gibson@ic.ac.uk*

Received (in Liverpool, UK) 20th October 1998, Accepted 15th December 1998

Norbornene monomers bearing two and three amino acid residues have been synthesized and the ring-opening metathesis polymerization of the monomers investigated using Mo(=CHCMe$_2$Ph)(=N-2,6-Pr$^i_2$C$_6$H$_3$)(OR)$_2$, [R = CMe$_3$ 1a, CMe$_2$CF$_3$ 1b, CMe(CF$_3$)$_2$ 1c].

The preparation of macromolecular biomimetic compounds requires careful control of the primary, secondary, and tertiary structures of the polymeric material. Typically, polymerization processes have failed to address these requirements due to lack of control over the polydispersity of the polymer which needs to be as near to monodisperse as possible, or due to the limited diversity of functional groups present in the final polymer.[1] Ring-opening metathesis polymerization (ROMP) using well-defined transition metal initiators, gives products with a narrow molecular weight distribution, and offers a high degree of control over the final molecular weight of the products. The latest generation initiators have also allowed the introduction of a wide range of functionalities within ROMP products. Furthermore, the living nature of the polymerization allows the preparation of block copolymers.[2]

We have previously described the use of ROMP methodology in the synthesis of biomimetic polymers based upon amino acids,[3] antibiotics[4] and nucleic acids.[5] Other workers have also reported the preparation of carbohydrate derived polymers.[6] Here we describe our initial results towards the preparation of polymers incorporating peptide units. Our strategy was based upon the preparation of the monomers by coupling norbornene derivatives **2a**,**b**[7] to different amino acid and peptide moieties. This would allow the introduction of peptides chosen for their specific folding pattern (*e.g.* α-helical) and thus provide further control of the macrostructure of the polymer product. The well-defined initiators Mo(=CHCMe$_2$Ph)(=N-2,6-Pr$^i_2$C$_6$H$_3$)(OR)$_2$ [R = CMe$_3$ **1a**, CMe$_2$CF$_3$ **1b**, CMe(CF$_3$)$_2$ **1c**] developed by Schrock and co-workers[8] were employed for the ROMP reactions.

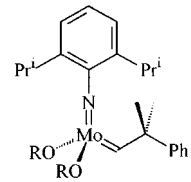

1a; R = Me$_3$C
1b; R = (CF$_3$)Me$_2$C
1c; R = (CF$_3$)$_2$MeC

Acids **2a**,**b** could be converted into the corresponding acid chlorides† **3a**,**b** by reaction with oxalyl chloride and DMF (Scheme 1). Compounds **3a**,**b** are crystalline solids and are convenient starting materials for the synthesis of the desired peptides **4**–**8a**,**b**. Thus, reaction of compounds **3a**,**b** with the methyl esters of alanine,‡ phenylalanine, phenylglycine, or proline gave monomers **4**–**7a**,**b** respectively, whilst reaction of **3a**,**b** with the dipeptide derivative phenylalanyl–phenylalanine methyl ester gave tripeptide derivatives **8a**,**b**.

Preliminary studies indicated that both the *exo*- and *endo*-isomers of monomers **4**–**8** could be polymerized by initiators **1a**–**c**. However, the polymerization of the *exo*-monomers was more facile (in line with previous reports of the ROMP of *endo*- and *exo*-norbornene derivatives[8]) and the isolated polymers were easily characterized, so monomers **4**–**8a** were selected for a more detailed study. The polymerization of each of monomers **4**–**8a** was then investigated as shown in Scheme 2, utilizing each of initiators **1a**–**c**, the results being given in Table 1. In each case, the polymerization was first carried out using 10 equiv. of monomer **4**–**8a** to allow the propagating alkylidene resonance to be detected by ^{1}H NMR spectroscopy, and the polymerization was then repeated using approximately 100 equiv. of the monomer to prepare a larger sample of the polymer. The initiators **1a**–**c** were tolerant of the amide bond(s)

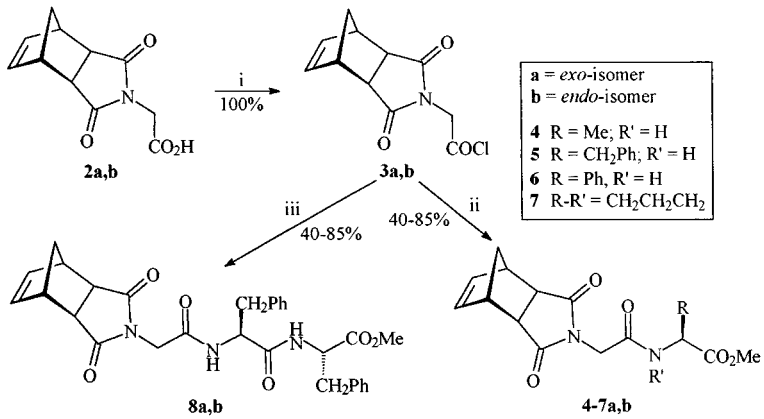

Scheme 1 *Reagents*: (i) (COCl)$_2$, DMF; (ii) Cl$^-$ H$_3^+$NCH(R)CO$_2$Me, Et$_3$N; (iii) Cl$^-$ H$_3^+$NCH(CH$_2$Ph)CONHCH(CH$_2$Ph)CO$_2$Me, Et$_3$N.

Table 1 Physical and selected spectroscopic data for the polymers derived from monomers **4a**–**8a**

Monomer	Catalyst	δ_H Mo=C*H*R	%*cis*[a]	T_g[b]/°C	M_n(calc)[c]	M_n[d]	M_w[d]	PDI[e]	$[\alpha]_D$[f]
4a	**1c**	12.48	60	133	15 300	12 000	14 700	1.22	−54
5a	**1a**	11.58	8	123	19 000	15 000	20 100	1.34	+79
	1b	11.99	44	161	19 000	18 600	29 000	1.56	+59
	1c	12.40	69	110	13 350	12 900	16 300	1.26	+63
6a	**1a**	11.56	13	165	9 950	6 900*	7 120*	1.03	+61**
	1b	11.97	57	150	18 400	17 800	24 700	1.39	+57**
	1c	12.44	74	149	16 200	7 100	7 400	1.03	+56**
7a	**1a**	11.60	9	179	13 360	21 600	25 200	1.17	−64
	1b	12.00	45	161	17 000	17 200	19 400	1.13	−56
	1c	12.60	71	154	18 700	29 500	32 700	1.13	−58
8a	**1a**	11.57	[g]	134	14 000	9 200*	9 500*	1.04	+24
	1b	12.20	[g]	120	17 400	7 000*	7 200*	1.03	+27
	1c	12.45	[g]	106	13 400	7 800*	8 100*	1.03	+19

[a] Determined by ^{1}H NMR spectroscopy. [b] Determined by TMA analysis. [c] Calculated from the monomer to initiator ratio. [d] M_n and M_w values were obtained by GPC using $CHCl_3$ as eluent, a differential refractometry detector, and two PLgel 10 μl mixed columns calibrated using polystyrene standards ranging in molecular weight from 1560 to 10^6 except where indicated by *. In these cases, the polymers were not soluble in $CHCl_3$, so molecular weight data were obtained by MALDI-TOF mass spectrometry. The experimentally determined M_ns are lower than M_n(calc) reflecting the tendency of MALDI-TOF to detect components of lower mass preferentially.[9] [e] Calculated as M_w/M_n. [f] Measured in $CHCl_3$ except where indicated by ** when DMSO was used as solvent. [g] Determination of the %cis alkenes in the polymer was not possible due to signal overlap.

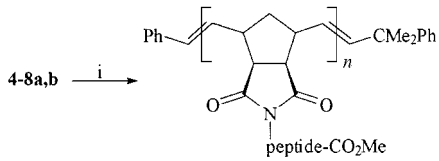

Scheme 2 *Reagents*: (i) a, **1a**–**c**, CH_2Cl_2, b, PhCHO.

in monomers **4**–**8a**, even when the polymerizations were left for three days. However, the polymers derived from monomer **4a** using initiators **1a**,**b** were found to be insoluble in organic solvents and so could not be fully characterized. These polymers are therefore not included in Table 1. Monomer **4a** contains the two amino acids (glycine and alanine) with the least hydrophobic sidechains and this probably accounts for the poor solubility of polymers derived from this monomer, as all of the other monomers gave polymers which were soluble in at least some organic solvents.

The ^{1}H NMR results show the expected trend of increasing *cis*–*trans* ratio associated with using initiators possessing increased fluorination of the ancillary ligands.[2] This trend is also apparent in the glass transition temperatures (T_g), which decrease with increasing *cis* content. All of the polymers were optically active which suggests that the chirality of the amino acids has been preserved during the polymerizations as has previously been observed for amino acid derived monomers.[3] The fact that all of the polymers derived from the same monomer have similar specific rotations suggests that the chemical environment around the peptide chains is not significantly affected by changes in the stereochemistry of the polymer backbone. All of the polymers exhibited low PDIs, and in each case, a propagating alkylidene signal could be observed in the ^{1}H NMR spectrum, indicating that the polymers were formed by a living polymerization process.

In conclusion, we have shown that peptide derived norbornenes **4**–**8** are suitable substrates for ROMP using well-defined molybdenum-based initiators. It is possible to control the stereochemistry of the polymers by varying the structure of the initiator. Our work in this area is continuing and further results using peptides that are known to adopt preferred conformations will be reported in due course.

The authors thank the EPSRC for financial support and studentships to R. G. D. and D. A. R., and Ciba-Geigy and the EPSRC for a studentship to M. R. G. Mass spectra were acquired by the EPSRC national service centre, and T_g data were obtained by the ULIRS service for thermomechanical analysis (TMA) at Birkbeck College, University of London. The staff of these services are thanked for their efforts.

Notes and references

† All new compounds exhibited satisfactory spectroscopic and analytical properties.

‡ All chiral amino acids discussed in this manuscript have the (*S*)-configuration.

1 D. Philp and J. F. Stoddart, *Angew. Chem., Int. Ed. Engl.*, 1996, **35**, 1154.
2 K. J. Ivin and J. C. Mol, *Olefin Metathesis and Metathesis Polymerization*, Academic Press, London, 1997; R. H. Grubbs and W. Tumas, *Science*, 1989, **243**, 907; R. R. Schrock, *Acc. Chem. Res.*, 1990, **23**, 158; W. J. Feast and V. C. Gibson, in *Chemistry of the Metal-Carbon Bond*, ed. F. R. Hartley, Wiley, New York, 1989, vol. 5.
3 M. P. Coles, V. C. Gibson, L. Mazzariol, M. North, W. G. Teasdale, C. M. Williams and D. Zamuner, *J. Chem. Soc., Chem. Commun.*, 1994, 2505; S. C. G. Biagini, M. P. Coles, V. C. Gibson, M. R. Giles, E. L. Marshall and M. North, *Polymer*, 1998, **39**, 1007.
4 S. C. G. Biagini, V. C. Gibson, M. R. Giles, E. L. Marshall and M. North, *Chem. Commun.*, 1997, 1097.
5 V. C. Gibson, E. L. Marshall, M. North, D. A. Robson and P. J. Williams, *Chem. Commun.*, 1997, 1095.
6 K. H. Mortell, M. Gingras and L. L. Kiessling, *J. Am. Chem. Soc.*, 1994, **116**, 12 053; C. Fraser and R. H. Grubbs, *Macromolecules*, 1995, **28**, 7248; K. H. Mortell, R. V. Weatherman and L. L. Kiessling, *J. Am. Chem. Soc.*, 1996, **118**, 2297; K. Nomura and R. R. Schrock, *Macromolecules*, 1996, **29**, 540.
7 S. C. G. Biagini, S. M. Bush, V. C. Gibson, L. Mazzariol, M. North, W. G. Teasdale, C. M. Williams, G. Zagotto and D. Zamuner, *Tetrahedron*, 1995, **51**, 7247.
8 R. R. Schrock, J. S. Murdzek, G. C. Bazan, J. Robbins, M. DiMare and M. O'Reagan, *J. Am. Chem. Soc.*, 1990, **112**, 3875; G. C. Bazan, E. Khosravi, R. R. Schrock, W. J. Feast, V. C. Gibson, M. B. O'Reagan, J. K. Thomas and W. M. Davis, *J. Am. Chem. Soc.*, 1990, **112**, 8378; G. C. Bazan, R. R. Schrock, H.-N. Cho and V. C. Gibson, *Macromolecules*, 1991, **24**, 4495.
9 P. M. Lloyd, K. G. Suddaby, J. E. Varney, E. Scrivener, P. J. Derrick and D. M. Haddleton, *Eur. Mass. Spectrom.*, 1995, **1**, 293.

Communication 8/08189A

A novel ruthenium-catalysed tandem diyne cycloisomerisation—cross metathesis process

Roland Stragies, Matthias Schuster and Siegfried Blechert*

Institut für Organische Chemie, Sekr. C3, Technische Universität Berlin, Straße des 17. Juni 135, 10623 Berlin, Germany. E-mail: sibl@wap0105.chem.tu-berlin.de

Received (in Cambridge, UK) 7th October 1998, Accepted 21st December 1998

Ruthenium-catalysed cycloisomerisation of hepta-1,6-diynes in the presence of functionalised terminal olefins yields five-membered cyclic products with variable unsaturated side chains and is applicable to the synthesis of highly functionalised hetero- and carbocycles.

The development of well-defined catalysts tolerating a variety of functional groups has significantly widened the scope of olefin metathesis as a synthetic method.[1] Whereas there are numerous examples for the ring closing metathesis (RCM) of dienes and its application in the field of natural product synthesis,[2] little is known about comparable reactions involving alkynes.[3] Only the RCM of enynes has found synthetic application.[4] Very recently, Fürstner and Seidel[5] reported the RCM of diynes to macrocyclic cycloalkynes and acyclic alkynes as stoichiometric by-products. Herein, we describe a tandem process that consists of a diyne cyclisation to a small ring and a cross metathesis with a terminal alkene and its application to the synthesis of functionalised unsaturated carbo- and heterocycles.

Recently, we presented a selective yne–ene cross metathesis.[6] This reaction was found to be initiated by attack of the catalytic ruthenium–alkylidene complex at the triple bond (Scheme 1), thus, resulting in the formation of a conjugated alkylidene complex. Reaction of this reactive intermediate with the alkene component gives the cross coupling product in a selective manner. In the course of systematic investigations into the metathesis of alkynes[7] it has now been found that the introduction of a second triple bond into the alkyne component at a certain distance leads to an initial diyne cycloisomerisation event without affecting the subsequent cross coupling step.

In the initial experiments hepta-1,6-diyne **4a** was employed. We decided to use allyltrimethylsilane as the alkene component, since it has previously been proven to be a highly efficient cross metathesis coupling agent.[8] When **4a** and 3 equiv. of allyltrimethylsilane were reacted with 10 mol% of the ruthenium catalyst $Cl_2(PCy_3)_2Ru{=}CHPh$ (Cy = cyclohexyl) [Ru] introduced by Grubbs and coworkers,[9] a carbocyclic product (**5a**) was isolated in 65% yield (Scheme 2).† In contrast, all attempts to perform the same reaction under catalysis of Schrock's molybdenum catalyst[10] $PhMe_2CCH{=}Mo{=}N[2,6\text{-}(^iPr_2C_6H_3)][OCMe(CF_3)_2]_2$ ([Mo]) failed. This result is not surprising considering reports describing a [Mo]-catalysed cyclopolymerisation[11] of **4a**.

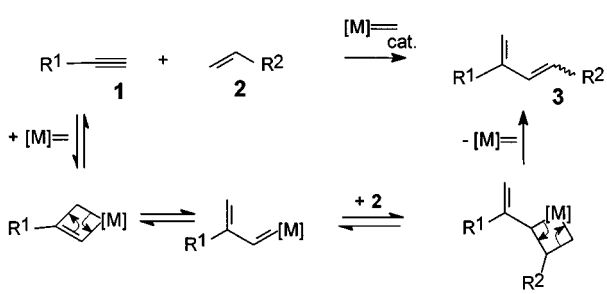

Scheme 1 Reaction path of yne–ene cross metathesis.

Accordingly, all further experiments were conducted under catalysis of [Ru] using the standard conditions mentioned above.‡ Like **4a**, simple N- and O-containing symmetrical diynes are also transformed into heterocyclic products as demonstrated by the synthesis of dihydropyrroles **5b** and **5c** and dihydrofuran **5d**. We also attempted to prepare S-containing heterocycles from diynic sulfides, sulfoxides, and sulfones. Although these heptadiynes have been described as suitable substrates for the [Mo]-catalysed cyclopolymerisation process,[12] rapid isomerisation into the corresponding allenes and no metathesis was observed under our reaction conditions. To further investigate the scope of the reaction we employed various functionalised terminal olefins as alkene components. The use of protected alcohols resulted in formation of the heterocyclic products **6a–c** in acceptable yields. In addition, a terpene derivative and an N- and O-protected amino alcohol were successfully transformed into **6e** and **6f**, respectively. These examples demonstrate that structurally diverse olefins undergo the tandem reaction. With the exception of compounds containing sterically demanding substituents (**6c**, *E*/*Z* = 5 : 1; **6f**, *E*/*Z* = 2.5 : 1) all products were isolated as *E*/*Z* isomer mixtures (1 : 1–1 : 1.5). This lack of selectivity is a common problem of cross metathesis.[1,8] With respect to a second problem often encountered in methathetical cross couplings, the tendency of the coupling partners to self-react, the tandem process proved to be remarkably selective. In all reactions only traces of alkene homodimer were identified. To study the accessibility of six- and seven-membered heterocycles we prepared the appropriate diynic precursors **7** and **8**, respectively. However, no cyclisation took place in the presence of allyltrimethylsilane under standard reaction conditions. Instead, products resulting from yne–ene cross metathesis of the silane with one or both triple bond(s) were identified. This finding indicates the importance of the distance between the two triple

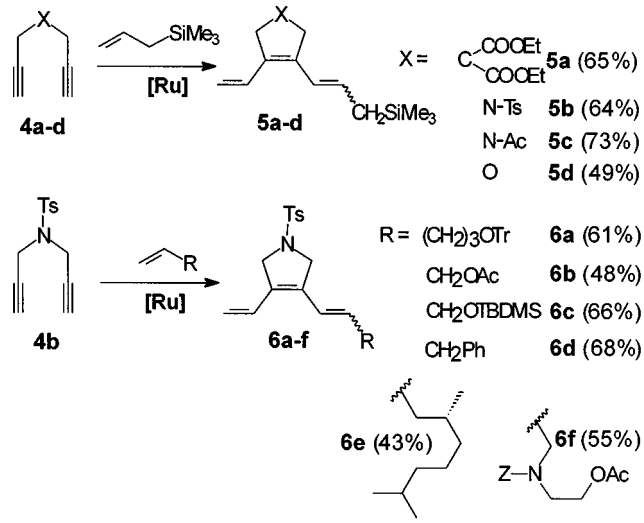

Scheme 2 Products of diyne cycloisomerisation–cross metathesis tandem reactions.

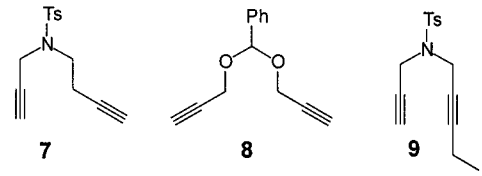

bonds for the cycloisomerisation step. The failure of **9** containing a disubstituted triple bond to undergo the cyclisation might be attributed to a kinetic barrier caused by the additional ethyl substituent.

The [Ru]-catalysed reaction of unsymmetrical diyne **10** with allyltrimethylsilane (Scheme 3) demonstrates that the cyclisation–cross metathesis tandem process shows regioselectivity. Considering that **11a** and **11b** were formed in a 4 : 1 ratio under standard conditions, higher selectivities could be observed using different substituents or reaction partners under optimised conditions.

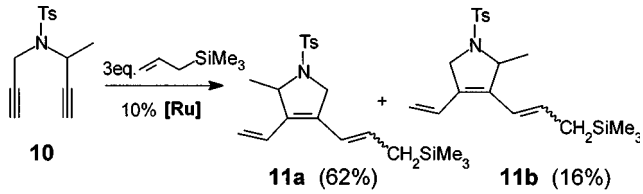

Scheme 3 [Ru]-catalysed reaction of asymmetric diyne **10** with allyltrimethylsilane giving regioisomeric **11a** and **11b**.

For the novel tandem process described above the reaction path depicted in Scheme 4 is proposed. The reaction is assumed to start with the reversible addition of the catalytic carbene complex at one of the triple bonds. Intramolecular addition of the resulting conjugated ruthenium–alkylidene complex to the second triple bond gives rise to a cyclic carbene complex, which directly cross-reacts with the alkene component.

In summary, a new tandem metathesis reaction suitable for the synthesis of functionalised carbo- and heterocycles has been developed. The reaction shows atom economy[13] and combines the cyclisation of a hepta-1,6-diyne with a cross metathesis. A variety of differently substituted five-membered carbo- and heterocycles has been prepared. We are currently exploring the possibility of enhancing the regio- and stereoselectivity of the reaction.

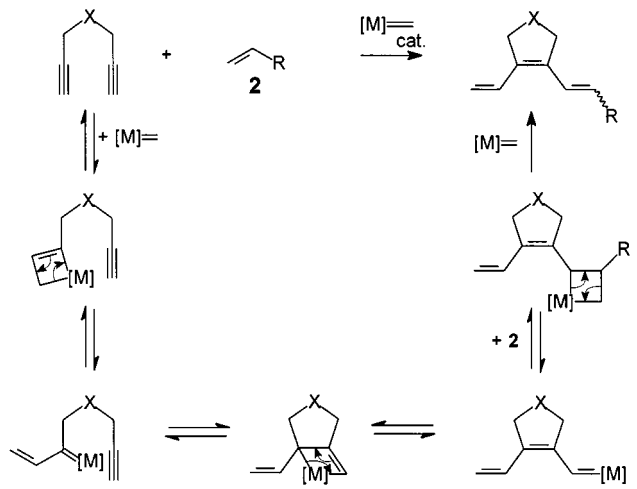

Scheme 4 Proposed pathway of the diyne cycloisomerisation–cross metathesis tandem reaction.

Notes and references

† Synthesis of **5a** employing standard reaction conditions: **4a** (100 mg, 0.424 mmol) and allyltrimethylsilane (140 mg, 1.27 mmol) was dissolved in dry CH_2Cl_2 (3 mL). [Ru] (35 mg, 0.04 mmol) was added and the mixture was stirred for 12 h. The solvent was removed under vacuum and the residue was chromatographed on silica gel using Bu^{t}OMe–hexane (v/v = 1/9) to give **5a** {101 mg, 68%, *E*/*Z*-ratio: 1.1/1); R_f = 0.6, Bu^{t}OMe–hexane (v/v = 1/4)}; (*E*)-**5a**: δ_H (400 MHz, $CDCl_3$) 6.75 (dd, 1H, *J* 19, 11), 6.29 (d, 1 H, *J* 15), 5.71 (dt, 1H, *J* 15, 8), 5.10 (m, 2H), 4.20 (q, 4H, *J* 7), 3.21 (s, 2H), 3.05 (s, 2H), 1.73 (t, 6H, *J* 7), 1.25 (d, 2H, *J* 8), 0.00 (s, 9H). (*Z*)-**5a**: δ_H (400 MHz, $CDCl_3$) 6.67 (dd, 1H, *J* 19, 11), 6.08 (d, 1H, *J* 12), 5.53 (dt, 1H, *J* 12, 8), 5.10 (m, 2H), 4.20 (q, 4H, *J* 7), 3.37 (s, 2H), 3.21 (s, 2H), 1.73 (t, 6H, *J* 7), 1.61 (d, 2H, *J* 8), 0.02 (s, 9H). δ_C (67.9 MHz, $CDCl_3$) 172.00 (Cq), 171.95 (Cq), 135.06 (Cq), 133.97 (Cq), 130.60 (CH), 130.18 (CH), 129.94 (CH), 129.54 (CH), 121.61 (CH), 119.46 (CH), 114.35 (CH_2), 113.42 (CH_2), 61.52 (CH_2), 57.54 (Cq), 56.78 (Cq), 44.30 (CH_2), 41.41 (CH_2), 40.53 (CH_2), 39.49 (CH_2), 24.42 (CH_2), 21.48 (CH_2), 13.94 (CH_3), −1.89 (CH_3), −1.98 (CH_3). IR (film) 3470(w), 2981(m), 2955(m), 2906(m), 1732(s), 1670(w), 1456(w), 1446(m), 1367(m), 1250(s), 1187(s), 1071(s), 837(s), 760, 695 cm^{-1}. HRMS: Calcd. for [M$^+$] $C_{19}H_{30}O_4Si$: 350.1913. Found 350.1924.

‡ In all reactions the starting material was completely consumed. In some cases traces of symmetrically disubstituted cyclic products resulting from cycloisomerisation followed by double-cross metathesis were the only identifiable by-products.

1 General reviews on olefin metathesis: R. H. Grubbs and S. Chang, *Tetrahedron*, 1998, **54**, 4413; M. Schuster and S. Blechert, *Angew. Chem.*, 1997, **109**, 2124; *Angew. Chem., Int. Ed. Engl.*, 1997, **36**, 2036; K. J. Ivin and J. C. Mol, *Olefin Metathesis and Metathesis Polymerisation*, Academic Press, New York, 1997.

2 Reviews emphasizing RCM and its application in organic synthesis: R. H. Grubbs, S. J. Miller and G. C. Fu, *Acc. Chem. Res.*, 1995, **28**, 446; S. K. Armstrong, *J. Chem. Soc., Perkin Trans. 1*, 1998, 371.

3 Cross metatheses of alkynes has been reported before ref. 5: D. Villemin and P. Cadiot, *Tetrahedron Lett.*, 1982, **23**, 5139; N. Kaneta, K. Hikichi, S. Asaka, M. Uemura and M. Mori, *Chem. Lett.*, 1995, 1055; J. Sancho and R. R. Schrock, *J. Mol. Catal.*, 1982, **15**, 75; R. R. Schrock, *Polyhedron*, 1995, **22**, 3177.

4 A. Kinoshita and M. Mori, *Synlett*, 1994, 1020; A. Kinoshita and M. Mori, *J. Org. Chem.*, 1996, **61**, 8356; S.-H. Kim, W. J. Zuercher, N. B. Bowden and R. H. Grubbs, *J. Org. Chem.*, 1996, **61**, 1073; W. J. Zuercher, M. Scholl and R. H. Grubbs, *J. Org. Chem.*, 1998, **63**, 4291.

5 A. Fürstner and G. Seidel, *Angew. Chem.*, 1998, **110**, 1758; *Angew. Chem., Int. Ed.*, 1998, **37**, 1734.

6 R. Stragies, M. Schuster and S. Blechert, *Angew. Chem.*, 1997, **109**, 2628; *Angew. Chem., Int. Ed. Engl.*, 1997, **36**, 2518.

7 For example, see: J.-U. Peters and S. Blechert, *Chem. Commun.*, 1997, 1983.

8 O. Brümmer, A. Rückert and S. Blechert, *Chem. Eur. J.*, 1997, **3**, 441; W. E. Crowe, D. R. Goldberg and Z. J. Zhang, *Tetrahedron Lett.*, 1996, **37**, 2117.

9 P. Schwab, M. B. France, J. W. Ziller and J. W. Grubbs, *Angew. Chem.*, 1995, **107**, 2179; *Angew. Chem., Int. Ed. Engl.*, 1995, **34**, 2039.

10 R. R. Schrock, J. S. Murdzek, G. C. Bazan, J. Robbins, M. DiMare and M. O'Regan, *J. Am. Chem. Soc.*, 1990, **112**, 3875.

11 R. R. Schrock, *Acc. Chem. Res.*, 1990, **23**, 158.

12 Y.-S. Gal and S.-K. Choi, *J. Polym. Sci., Sect. A*, 1993, **31**, 345.

13 B. M. Trost, *Angew. Chem.*, 1995, **107**, 285; *Angew. Chem., Int. Ed. Engl.*, 1995, **34**, 259.

Communication 8/07843B

X-Ray structure and solvolytic activity towards phosphate diesters of a zirconium(IV) complex

Eugen Stulz and Christian Leumann*

Department of Chemistry and Biochemistry, University of Bern, Freiestrasse 3, CH-3012 Bern, Switzerland. E-mail: leumann@ioc.unibe.ch

Received (in Basel, Switzerland) 20th November 1998, Accepted 8th December 1998

The X-ray structure of the complex $Zr^{IV}(acac)_2$(salicylideneaminoethanol) [$Zr(acac)_2$(sae)] could be solved, and the reactivity of the complex towards phosphate diester solvolysis was investigated showing substantial rate acceleration over background in benzene–methanol solution (*ca.* 10^8) and in aqueous medium (*ca.* 10^5).

The development of artificial nucleases is an attractive feature in the design of new compounds for application in antisense therapy, or as new tools in gene technology.[1] Predominantly metal complexes as activators for phosphate ester hydrolysis are under intense investigation, since metal ions are known to promote phosphoester transesterification reactions with high rate accelerations.[2] Especially with dinuclear Co(II) complexes[3] and with lanthanide ions,[4] including high-valent Ce(IV)[5] and Th(IV),[6] remarkable activities were observed.

We have investigated complexes of Zr(IV)[7] as activators for phosphate ester solvolysis, because of (i): its high stable oxidation state +IV (ideally suited for electrostatic activation); (ii): its hard Lewis acid character (promising strong interactions with phosphates);† and (iii): its maximum coordination number of eight. In general, tetravalent metal ions are known to hydrolyse phosphate esters more efficiently than tervalent ions.[8] The hydrolytic activity of Zr^{4+} towards phosphate diesters has first been described 60 years ago.[9] Only recently, while our investigations were underway, two reports addressing the hydrolytic activity of $ZrCl_4$ with bis(*p*-nitrophenyl) phosphate (BNPP) **1**[10] appeared. However, neither catalytic behaviour nor a detailed structure of the complexes used were disclosed. Here we report, for the first time, the catalytic activity of the Zr(IV) complex $Zr(acac)_2$(sae) **2** (sae = salicylideneaminoethanol) in phosphate diester solvolysis.

The Zr(IV) complex **2** was prepared from $Zr(acac)_4$ and the ligand H_2sae according to a known procedure.[11] Recrystallisation of **2** from hot toluene produced crystals suitable for X-ray analysis. Complex **2** crystallises in a centrosymmetric dimeric form, **2**–**2**, with the inversion centre in between the two zirconium atoms held together *via* two oxygens of the aminoethanolato-sidechains.‡ The geometry of the zirconium ligand sphere is dodecahedral. Extension to the maximum coordination number eight around zirconium can be considered to be the driving force for dimerisation. Fig. 1 shows the refined structure of **2**–**2**.§ Considerable changes in the UV–VIS spectrum of **2** were observed upon changing from aprotic to protic solvents. This indicates a weak acid–base interaction between zirconium and the protic solvents, and is in accordance with **2** existing predominantly in the monomeric, solvated form under these conditions.

The reactivity of **2** towards phosphate diester cleavage was investigated in C_6D_6–methanol (1 : 1) as solvent owing to the low solubility of **2** in pure protic solvents. The progress of the solvolysis reaction was monitored by ^{31}P NMR spectroscopy.

Upon mixing of **2** (4 mM) with dimethylphosphate (DMP) **3** (16 mM) in C_6D_6–MeOH (1 : 1) the ^{31}P NMR spectra showed a small, broad signal (δ −6; 4.2%) and a large, sharp signal (δ 2.8; 95.8%). The former signal was assigned to zirconium-complexed DMP, the latter refers to free DMP **3**. From this a dissociation constant of 76.2 mM was calculated. This value is significantly higher than the previously reported dissociation constant of $ZrCl_4$ with **1** in water (K_M = 1.3 mmol dm^{-3}).[10b]

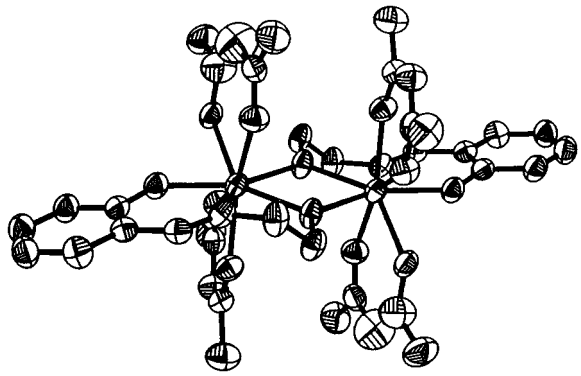

Fig. 1: ORTEP plot of **2**–**2**. Thermal ellipsoids are drawn at the 50% probability level; hydrogens are omitted for clarity.

Analysis by ^{31}P NMR spectroscopy [C_6D_6–MeOH (1 : 1)] revealed that the 'RNA-model' 2-hydroxypropyl phenyl phosphate (HPP) **4** (δ −5.2) reacts in the presence of catalytic amounts of **2** to initially give the cyclic phosphate (cHP) **5** (δ 15.5), which further reacts with methanol to give a mixture of the two isomeric methyl hydroxypropyl phosphates (MHP) **6a** (δ 2.3) and **6b** (δ 1.1) in comparable ratios (Scheme 1). The reactions were performed in unbuffered¶ solutions at 28 °C with either variable concentrations in complex **2** ([**2**] = 1, 2, 3, 4 mM) at constant phosphate concentration ([**4**] = 24 mM) or *vice versa* ([**4**] = 8, 12, 24, 28 mM; [**2**] = 2 mM). The variations of phosphate concentrations *vs.* reaction time were fitted to the model for a consecutive irreversible first-order reaction[12] and gave the pseudo first-order rate constants k_1 and k_1' (Fig. 2).

At constant zirconium concentration (2 mM) the rate constants k_1 (2.77×10^{-4} s^{-1}) and k_1' (1.18×10^{-4} s^{-1}) were independent of phosphate concentration thus proving the catalytic reactivity of **2**. At constant phosphate concentrations (24 mM) a linear dependence on the concentration of complex

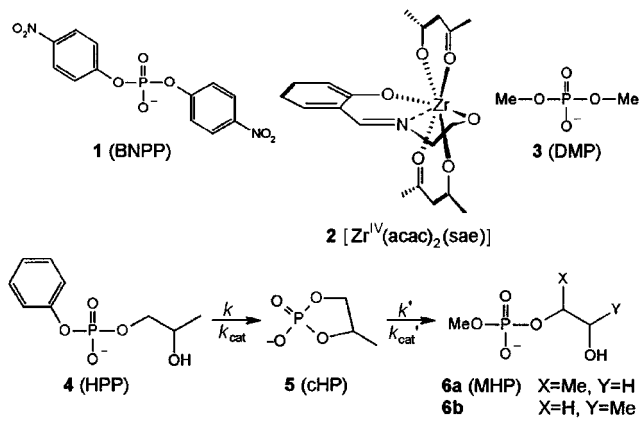

Scheme 1

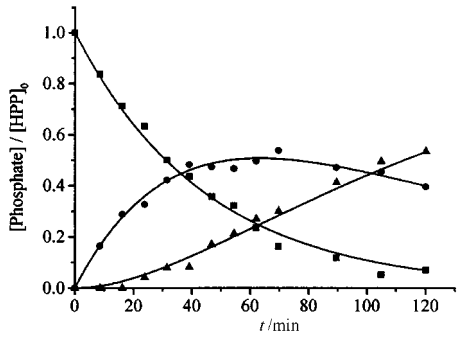

Fig. 2 Time dependent variation of the concentrations of HPP **4** (■), cHP **5** (●), MHP **6** (▲) with curve fitting according to the equations for a consecutive irreversible first-order reaction.[12] [**2**] = 2 mM, [**4**] = 8 mM.

2 is observed. From this linear correlation, the second-order rate constants were determined to be k_2 = 0.14 dm^3 mol^{-1} s^{-1} and k_2' = 0.058 dm^3 mol^{-1} s^{-1}. These values are slightly lower than the reported values for the hydrolysis of 2-hydroxypropyl *p*-nitrophenyl phosphate with Zr^{4+} (2.2 dm^3 mol^{-1} s^{-1}),[10a] but indicate a reactivity that is comparable to that of lanthanide complexes.[13]

From the kinetic measurements the initial rates v_0 for the cyclisation reaction **4**→**5** were also evaluated. The plots of log (v_0) *vs.* log ([**2**]) (with [**4**] = const. = 24 mM) or *vs.* log ([**4**]) (with [**2**] = const. = 2 mM) revealed that the reaction is first order in both reactants giving a clean overall second-order reaction. This indicates that the active species is a distinct 1 : 1 complex between **2** and phosphate diester. The initial rates (for [**2**] = const.) allowed an analysis according to Michaelis–Menten kinetics. From the Eadie–Hofstee plot, the values K_M = 68.6 mmol dm^{-3} and k_{cat} = 0.013 s^{-1} could be obtained. The K_M value is almost identical to the dissociation constant of **3** with **2** (76.2 mmol dm^{-3}), obtained by direct ^{31}P NMR measurement, and therefore represents a true dissociation constant for a 1 : 1 Zr(IV)–phosphate complex. The discrepancy between this K_M value and that for the system $ZrCl_4$ and **1** (1.3 mmol dm^{-3})[10b] indicates activity of higher order Zr(IV) complexes in the latter case formed upon mixing of $ZrCl_4$ with water.

Compared to the uncatalysed reaction ($k_{1,0}$ = 1.9 × 10^{-11} s^{-1}; $k_{1,0}'$ = 1.24 × 10^{-11} s^{-1})¶ the reaction rates k_{cat} and k_{cat}' (determined from the pseudo first-order reaction rates $k_1' K_M$/[**2**]; k_{cat}' = 0.0043 s^{-1}) represent a rate acceleration of 6.8 × 10^8 for the cyclisation of **4**→**5** and 3.5 × 10^8 for the re-esterification **5**→**6**. These rate accelerations agree well with the reported reactivity of Zr^{4+}.[10] In contrast to earlier reports, however, the transesterification reactions described here were catalytic in zirconium and proceed *via* a well defined 1 : 1 Zr(IV) : phosphate stoichiometry.

We investigated also the reactivity of **2** towards **4** in the presence of water (C_6D_6–MeOH–H_2O 5 : 5 : 1; T = 40 °C). The best conditions for solubility of **2** were found to be in buffered solution (100 mM Tris-HCl) at pH 9.0 (**2** dissociates under acidic conditions and is barely soluble at higher pH values; no pH rate profile could therefore be measured). In this system the activity of **2** ([**2**] = 1.5 mM, [**4**] = 12 mM) dropped significantly to a rate acceleration of only 75 over background (k_1 = 9.7 × 10^{-7} s^{-1}; $k_{1,0}$ = 1.3 × 10^{-8} s^{-1}), but catalytic turnover was still observed. This loss of reactivity may be due to the deactivation of the zirconium in the presence of water or hydroxide.

In aqueous medium without organic cosolvents (H_2O; pH 7.0; 10 mM Tris-HCl; 10 mM KCl and $MgCl_2$; 5 mM $CaCl_2$. T = 37 °C), catalyst **2** ([**2**] = 4.5 × 10^{-5} M, nearly sat. soln.) hydrolysed **1** ([**1**] = 1.6 × 10^{-5} M) with an observed pseudo first-order rate constant $k_{1,obs}$ = 1.5 × 10^{-5} s^{-1}. This leads to a rate acceleration of 2.9 × 10^5, compared to the uncatalysed reaction (5.1 × 10^{-11} s^{-1}).[14] No significant background reaction was observed under these conditions, therefore hydrolysis of **1** is not due to the salts added to mimic physiological conditions. Although this reaction was performed with excess **2** over **1**, it shows that **2** is still highly active towards **1** even in water.

In conclusion, we have shown that the Zr(IV) complex **2** exhibits substantial activity towards phosphate diesters in transesterification or hydrolysis, despite the fact that **2** is charge-neutral and cannot compensate for the negative charge of the substrates.

We thank Professor Helen Stoeckli-Evans (Université de Neuchâtel, Switzerland) for collecting the X-ray diffraction data of **2** and the 'Stipendienfonds der Basler Chemischen Industrie' for financial support.

Notes and references

† A preliminary ^{1}H NMR experiment in D_2O using $Zr(OAc)_4$ (68 mM), which should give polymeric structures to a lesser extent than $ZrCl_4$ (S. Hannane, F. Bertin and J. Bouix, *Bull. Soc. Chim. Fr.*, 1994, **131**, 262) and dimethyl phosphate (DMP **3**, 270 mM) showed rapid formation (< 2 min) of a Zr(IV)–DMP complex (δ 3.55, broad signal; free DMP: δ 3.43). The signals were not enough resolved to allow determination of an association constant, but approximately 2 equiv. DMP were complexed. This agrees with other observations.[10b]

‡ *Crystallographic data*: $C_{38}H_{46}N_2O_{12}Zr_2$; M = 905.21; triclinic, $P\bar{1}$, a = 11.6425(2), b = 12.0019(2), c = 15.7179(3) Å, α = 89.321(3), β = 70.008(3), γ = 86.675(3)°, V = 2060.4(7) Å^3, T = 223 K, Z = 2 (dimers), μ = 0.566 mm^{-1}; 16331 total reflections; 7494 independent reflections; R_{int} = 0.0711, R_1 = 0.0889; $R(\sigma)$ = 0.1133, wR_2 = 0.1252. CCDC 182/1123. See http://www.rsc.org/suppdata/cc/1999/239/ for crystallographic files in .cif format.

§ In the unit cell, **2**–**2** appears as two symmetrically independent molecules. The structural differences however are rather small and mainly occur in the conformation of the acac-ligands along the O···O-edges. This is a known structural feature of Zr(IV)–acac complexes (R. B. VonDreele, J. J. Stezowski and R. C. Fay, *J. Am. Chem. Soc.*, 1971, **93**, 2887; J. V. Silverton and J. L. Hoard, *Inorg. Chem.*, 1963, **2**, 243). For simplicity reasons, Fig. 1 only shows one of the two conformers.

¶ The background rate constants were measured at [NaOMe] = 1 mM to be $k_{2,0}$ = 2.93 × 10^{-3} dm^3 mol^{-1} s^{-1} and $k_{2,0}'$ = 1.97 × 10^{-3} dm^3 mol^{-1} s^{-1}. The pH of C_6D_6–MeOH (1 : 1) was 8.2 corresponding to [MeO$^-$] = 6.3 × 10^{-9} M and did not change during the catalytic and background reactions. With $k_{1,0}$ = $k_{2,0}$ [MeO$^-$] the first order background rate constants were extrapolated to the conditions used in the catalysed reactions.

1 E. Kövári and R. Krämer, *J. Am. Chem. Soc.*, 1996, **118**, 12 704; J. Chin, *Acc. Chem. Res.*, 1991, **24**, 145; D. Magda, R. A. Miller and J. L. Sessler, *J. Am. Chem. Soc.*, 1994, **116**, 7439; R. Häner, J. Hall and G. Ryhs, *Helv. Chim. Acta*, 1997, **80**, 487.
2 M. Yashiro, A. Ishikubo and M. Komiyama, *Chem. Commun.*, 1997, 83; J. H. Kim and J. Chin, *J. Am. Chem. Soc.*, 1992, **114**, 9792; Y. Matsumoto and M. Komiyama, *J. Chem. Soc., Chem. Commun.*, 1990, 1050; E. L. Hegg, K. A. Deal, L. L. Kiessling and J. N. Burstyn, *Inorg. Chem.*, 1997, **36**, 1715.
3 N. H. Williams and J. Chin, *Chem. Commun.*, 1996, 131.
4 J. R. Morrow and W. C. Trogler, *Inorg. Chem.*, 1988, **27**, 3387.
5 J. Sumaoka, Y. Azuma and M. Komiyama, *Chem. Eur. J.*, 1998, **4**, 205.
6 R. A. Moss, J. Zhang and K. Bracken, *Chem. Commun.*, 1997, 1639.
7 Taken in part from the Ph.D. thesis of E. S. (E. Stulz, *Zr(IV)–Komplexe als Nuclease-Mimetika*, Dissertation Universität Bern, 1998). Preliminary results were presented as a poster at the 36th IUPAC Congress in Geneva, Switzerland, August 1997 (*Chimia*, 1997, **7**, 462).
8 B. K. Takasaki and J. Chin, *J. Am. Chem. Soc.*, 1994, **116**, 1121.
9 E. Bamann, *Angew. Chem.*, 1939, **52**, 186.
10 (*a*) R. A. Moss, J. Zhang and K. G. Ragunathan, *Tetrahedron Lett.*, 1998, **39**, 1529; (*b*) R. Ott and R. Krämer, *Angew. Chem.*, 1998, **110**, 2064.
11 P. K. Mishra, V. Chakravortty and K. C. Dash, *Transition Met. Chem.*, 1991, **16**, 73.
12 A. Fersht, *Enzyme Structure and Mechanism*, Freeman, New York, 2nd edn. 1985, p. 133. This method is applicable because the reactions were catalytic in **2** and went to complete formation of **6a** and **6b**.
13 J. R. Morrow, L. A. Buttrey and K. A. Berback, *Inorg. Chem.*, 1992, **31**, 16; J. R. Morrow, L. A. Buttrey, V. M. Shelton and K. A. Berback, *J. Am. Chem. Soc.*, 1992, **114**, 1903 and references therein.
14 J. Chin, M. Banaszczyk, V. Jubian and X. Zou, *J. Am. Chem. Soc.*, 1989, **111**, 186.

Communication 8/09101C

Complexation of stable carbenes with alkali metals

Roger W. Alder,* Michael E. Blake, Christel Bortolotti, Simone Bufali, Craig P. Butts, Emma Linehan, Josep M. Oliva, A. Guy Orpen and Michael J. Quayle

School of Chemistry, University of Bristol, Cantock's Close, Bristol, UK BS8 1TS. E-mail: rog.alder@bristol.ac.uk

Received (in Liverpool, UK) 13th November 1998, Accepted 10th December 1998

Stable diaminocarbenes, including imidazol-2-ylidenes, undergo complexation with lithium, sodium and potassium species; the crystal structure of a complex of 1,3-diisopropyl-3,4,5,6-tetrahydropyrimid-2-ylidene 1 with $KN(SiMe_3)_2$ is reported.

There is a vast literature concerning carbene complexes of metals. N-Heterocyclic carbenes are reported to complex with 48 elements, but Group 1 metals are notable by their absence.[1] We report ^{13}C NMR shift evidence concerning interaction between stable ylidic diaminocarbenes **1**–**3** and imidazol-2-ylidene **4** with lithium, sodium and potassium species in toluene and THF solutions, and the X-ray structure of $[\mathbf{1}\cdot KN(SiMe_3)_2]_2$. Since carbenes like **1**–**4** are often generated by C-deprotonation of formamidinium and related cations by bases with alkali metal counterions (*e.g.* $KOBu^t$, NaH, and LDA),[2–6] the observation of complexation with these ions is important in understanding of the properties of these carbenes in solution.

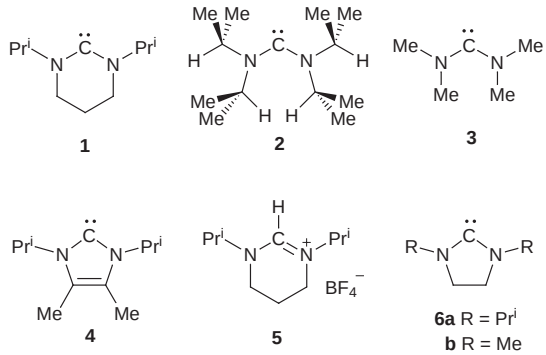

Carbene **1** can be prepared in 40% yield by deprotonation of **5** with $NaN(SiMe_3)_2$ in THF at −78 °C, exchange of solvent to toluene to permit azeotropic removal of $HN(SiMe_3)_2$, followed by distillation of **1**, which melts close to ambient temperature (all operations involving diaminocarbenes were performed under dry N_2). Precursor **5** is conveniently made by refluxing an equimolar mixture of $Pr^iNH(CH_2)_3NHPr^i$ and NH_4BF_4 in $HC(OEt)_3$ as solvent, with azeotropic removal of EtOH. Diaminocarbene **1** is the first example where the N–C–N group is part of a six-membered ring, and appears to be thermodynamically stable to dimerisation, unlike the five-membered ring analogue **6a**.[7] Thus **1** is stable when generated from **5** using a deficiency of base, but generation of **6a** under these conditions leads to rapid dimerisation, due to catalysis by the dihydroimidazolium precursor.[8]

A solution of free **1** in toluene-d_8 shows resonances at δ_C 236, 58, 36, 22 and 21. The ^{13}C shift of the carbene centre in stable carbenes typically occurs between δ_C 200 and 300,[2–6] but is substantially shielded in known metal complexes, and so provides a sensitive probe for complexation. The chemical shift of the carbene centre in **1** depends on the amount and nature of the alkali metal species present in toluene-d_8 solution (limiting shifts are given in Table 1), but is only affected by the presence of massive amounts (*ca.* 6 equiv.) of $LiN(SiMe_3)_2$ in THF-d_8, presumably because of competition from the solvent for Li. The chemical shifts of **1** and **3**, and of their complexes with Li^+, Na^+ and K^+ ions, have been calculated (Table 1), using the B3LYP/6-31G*/GIAO method.[9] The changes observed on complexation in solution are, not surprisingly, smaller than those calculated for complexation to the bare cations.

Addition of 12-crown-4 in portions to solutions of **1** in toluene-d_8 generated from **5** using lithium 2,2,6,6-tetramethylpiperidide (LiTMP) leads to quantitative precipitation of $LiBF_4\cdot$12-crown-4 (no NMR signals for free 12-crown-4 are observed until > 1 equiv. has been added), with the ^{13}C NMR shift of the carbene centre moving smoothly from δ_C 218 to 236, indicating that the equilibrium between free **1** and the lithium complex is fast on the NMR timescale. It appears that the $LiBF_4$ formed in the reaction is soluble until the 12-crown-4 is added. On the other hand, portionwise addition of 2 equiv. of $LiN(SiMe_3)_2$ in toluene-d_8 to a solution of free **1** in toluene-d_8, generated using $NaN(SiMe_3)_2$ as described above, leads to the ^{13}C signal moving to δ_C 218, but subsequent addition of 12-crown-4 leads to a limiting shift of δ_C 224, suggesting the formation of a soluble tertiary complex containing 12-crown-4, $LiN(SiMe_3)_2$ and carbene **1**.

Portionwise addition of 2 equiv. of $NaN(SiMe_3)_2$ to free **1** in toluene-d_8 leads to the chemical shift moving smoothly to δ_C 224. When 15-crown-5 is then added in portions, the chemical

Table 1 Limiting observed and calculated ^{13}C NMR chemical shifts for the carbene centre of carbenes **1**, **3** and **4**

		Free	Li complex		Na complex		K complex	
Carbene	Conditions	δ_C	δ_C	[Li]/[carbene]	δ_C	[Na]/[carbene]	δ_C	[K]/[carbene]
1	THF-d_8, $MN(SiMe_3)_2$	237.4	221.2	8.3	—	—	—	—
	Toluene-d_8, $MN(SiMe_3)_2$	236.1	216.8	15.2	221.3	11.1	226.7	17.2
	GIAO calc.[a]	232.7	190.2	—	198.5	—	200.3	—
3	Toluene-d_8, $MN(SiMe_3)_2$	—	238.4	—	—	—	—	—
	THF-d_8, LiTMP	—	244.0	2.6	—	—	—	—
	THF-d_8, LiTMP + LiOTf	—	240.2	5.0	—	—	—	—
	GIAO calc.	246.9	202.9	—	—	—	—	—
4	Toluene-d_8, $MN(SiMe_3)_2$	206.8	195.7	7.0	196.4	7.1	201.1	4.2

[a] For the $[carbene–K]^+$ species, σ is estimated from B3LYP/LANL2DZ calculations, since there is no 6-31G* basis set for K.

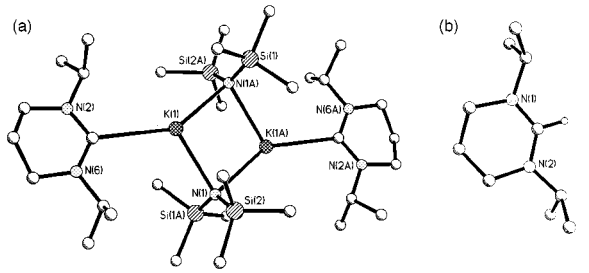

Fig. 1 (a) Molecular structure of $[\mathbf{1}\cdot KN(SiMe_3)_2]_2$. (b) Molecular structure of the cation of **5**.

Table 2 Structural parameters for **1** and related species

	$C_{carbene}$–N distance/Å	N–$C_{carbene}$–N angle (°)
$[\mathbf{1}\cdot KN(SiMe_3)_2]_2$	1.345(2)	116.3(2)
DFT structure for **1**	1.353	116.2
5	1.310(2)	125.1(2)
2	1.372(6) (av.)	121.0(5)

shift moves back to δ_C 236 as the free carbene is released. In a similar way, the addition of 2 equiv. of $KN(SiMe_3)_2$ in toluene leads to a chemical shift of δ_C 228. On standing, crystals were obtained from this solution and subjected to X-ray structure determination.† The structure [Fig. 1(a)] shows that dimeric molecules are present with the $N(SiMe_3)_2$ groups acting as bridging ligands. The K···C distance of 3.00 Å is much greater than the M···C distances for non−alkali metal complexes of imidazol-2-ylidenes,[1] which are typically < 2.3 Å. The Cambridge Structural Database[10] yielded no data on potassium complexes with σ-bound sp^2 carbon ligands. However, in the infinite chain structure of $(Me_3Si)_3CK$, the K···C distance is 3.10 Å,[11] while $Me_3Sn(Cl)N{\equiv}CK$ possesses a significantly shorter K···C distance of 2.75 Å,[12] and in KCN itself, the K···C distance is 2.8 Å.[13] Thus the K···C distance in $[\mathbf{1}\cdot KN(SiMe_3)_2]_2$ appears to be normal, but suggests that the interaction is largely of an electrostatic ion–dipole nature. Mixed complexes of $KN(SiMe_3)_2$ with $LiN(SiMe_3)_2$ and with $NaN(SiMe_3)_2$, displaying a similar dimeric core structure but with two THF ligands co-ordinated to the potassium, show K···O(THF) distances of 2.69 and 2.71 Å respectively.[14] In the light of this structural evidence, it is not surprising that complexation of **1** is more difficult to observe in THF solution.

The structural parameters of the carbene ligand itself are similar to those obtained from B3LYP/6-31G* DFT calculations for free **1**, and to those observed for **2** (Table 2). In the complex, the isopropyl groups are oriented away from the bulky $N(SiMe_3)_2$ groups, as might be expected. However, the same conformation is observed‡ for **5** [Fig. 1(b)], and is also calculated to be preferred by free **1**. The decrease in the N–$C_{carbene}$–N angle on deprotonation of **5** is striking, but some decrease has been observed in every other comparable case.[2,3,5] The increase in the $C_{carbene}$–N distance on deprotonation of **5** is also in line with previous examples, and suggests some decrease in π-bonding in **1** compared with **5**.

Complexation with alkali metal species also occurs with imidazol-2-ylidene **4**, although the upfield shifts are somewhat less than for **1** (Table 1). Bis(diisopropylamino)carbene **2** is much more hindered that **1** due to the buttressing effect of the isopropyl groups,[4] and we see little evidence for complexation in this case. Conversely, the least hindered carbenes[15] like **3** should be better ligands and their behaviour may be affected by the presence of metal species even in THF. This carbene has been generated using LDA or LiTMP bases and all attempts so far to remove the lithium species have resulted in precipitates which could not be separated without destroying the carbene. The question of alkali metal co-ordination to **3** and bis(*N*-piperidyl) carbene is particularly important with regard to the rates and mechanism of dimerisation of these carbenes. Metal ions might act as Lewis acid catalysts for dimerisation, as is observed for protons,[8,15] but strong complexation should eventually suppress dimerisation. Preliminary results suggest the latter effect is dominant, thus reaction of $HC(NMe_2)_2\cdot Cl$ with LiTMP in toluene-d_8 leads to a solution of **3** in which its half-life is extended to many days as compared to a few hours in THF. Addition of 2.4 equiv. of LiOTf to THF solutions of **3** generated using 2.6 equiv. of LiTMP leads to an upfield shift (Table 1) and halves the rate of dimerisation. The half-life of **3** in the absence of lithium may therefore be quite short, although Denk *et al*.[7] have reported that **6b**, which is surely less hindered than **3**, can be observed at ambient temperatures when prepared by reaction of the corresponding thione with potassium metal. The dimerisation of **3**, and the influence of metal species on this process, are the subject of continuing studies.

We thank EPSRC for support (grant GR/K76160) and for studentships to M. E. B. and M. J. Q; J. M. O. thanks the EEC for support (TMR contract ERBFMBICT97).

Notes and references

† *Crystal data* for $[\mathbf{1}\cdot KN(SiMe_3)_2]_2$: $C_{32}H_{76}K_2N_6Si_4$, M = 735.55, colourless block, 0.52 × 0.46 × 0.42 mm, triclinic, $P\bar{1}$ (no. 2), a = 9.413(1), b = 10.937(3), c = 12.306(2) Å, α = 73.97(2), β = 73.132(12), γ = 69.426(10)°, V = 1113.5(3) Å^3, T = 173 K, Z = 1, μ = 0.348 mm^{-1}, 11499 reflections measured, 5034 independent, 4058 observed, 202 parameters. The structure was solved by direct methods and refined on F^2. R_1 = 0.0266 for observed data and 0.0343 for all data.

‡ *Crystal data* for **5**: $C_{10}H_{21}BF_4N_2$, M = 256.10, colourless block, 0.4 × 0.4 × 0.2 mm, orthorhombic, $P2_12_12_1$ (no. 19), a = 8.434(1), b = 10.467(3), c = 15.389(4) Å, V = 1358.57(5) Å, T = 173 K, Z = 4, μ = 0.112 mm^{-1}, 8599 reflections measured, 3095 independent, 2184 observed, 199 parameters, 94 restraints. The structure was solved by direct methods and refined on F^2. R_1 = 0.0394 for observed data and 0.0664 for all data. The BF_4 counterion was disordered over two sites and restrained in geometry. CCDC 182/1119. The crystallographic data is available in CIF format from the RSC web site, see: http://www.rsc.org/suppdata/cc/1999/241/

1 W. A. Herrmann and C. Köcher, *Angew. Chem., Int. Ed. Engl.*, 1997, **36**, 2162.
2 A. J. Arduengo III, R. L. Harlow and M. Kline, *J. Am. Chem. Soc.*, 1991, **113**, 361; A. J. Arduengo III, H. V. R. Dias, R. L. Harlow and M. Kline, *J. Am. Chem. Soc.* 1992, **114**, 5530.
3 A. J. Arduengo III, J. R. Goerlich and W. J. Marshall, *J. Am. Chem. Soc.*, 1995, **117**, 11027.
4 R. W. Alder, P. R. Allen, M. Murray and A. G. Orpen, *Angew. Chem., Int. Ed. Engl.*, 1996, **35**, 1121.
5 A. J. Arduengo, III, J. R. Goerlich and W. J. Marshall, *Leibigs Ann/Recl.*, 1997, 365.
6 R. W. Alder, C. P. Butts and A. G. Orpen, *J. Am. Chem. Soc.*, 1998, **120**, 11 526.
7 M. K. Denk, A. Thadani, K. Hatano and A. J. Lough, *Angew. Chem., Int. Ed. Engl.*, 1997, **36**, 2607.
8 D. M. Lemal, R. A. Lovald and K. I. Kawano, *J. Am. Chem. Soc.*, 1964, **86**, 2518.
9 GIAO shielding constants σ were converted to chemical shifts using $\delta = \sigma_{TMS} - \sigma$.
10 Cambridge Structural Database, Version 5.15, April 1998 release, 181,309 structures searched; F. H. Allen and O. Kennard, *Chem. Des. Automation News*, 1993, **8**, 1 and 31.
11 C. Eaborn, P. B. Hitchcock, K. Izod, A. J. Jaggar and J. D. Smith, *Organometallics*, 1994, **13**, 753.
12 S. E. Johnson and C. B. Knobler, *Organometallics*, 1992, **11**, 3684.
13 R. M. Bozorth, *J. Am. Chem. Soc.*, 1922, **44**, 317.
14 P. G. Williard and M. A. Nicholls, *J. Am. Chem. Soc.*, 1991, **113**, 9671.
15 R. W. Alder and M. E. Blake, *Chem. Commun*., 1997, 1513.

Communication 8/08951E

ChemComm

Biosynthesis of dictyopterene A: stereoselectivity of a lipoxygenase/hydroperoxide lyase from *Gomphonema parvulum* (Bacillariophyceae)

Marc Hombeck, Georg Pohnert and Wilhelm Boland*

Max-Planck-Institute for Chemical Ecology, Tatzendpromenade 1a, D-07745 Jena, Germany. E-mail: Boland@ice.mpg.de

Received (in Liverpool, UK) 29th October 1998, Accepted 21st December 1998

(9*S*)-Hydroperoxyicosatetraenoic (9*S*-HPETE) acid is shown to be an intermediate in the biosynthesis of dictyopterene A in the freshwater diatom *Gomphonema parvulum*; the stereochemistry of (9*S*)-HPETE and the position of the hydrogen atom at C(16) lost during fatty acid cyclisation and oxidative cleavage of the hydroperoxide were investigated using trapping experiments and chirally deuterium labelled fatty acids.

Fatty acid derived C_8 and C_{11} hydrocarbons like finavarrene **7**, hormosirene **5** or dictyopterene A **6** act as pheromones in marine brown algae (Scheme 1).[1] The same compounds occur in heterocontophytic diatoms[2,3] and in higher plants,[4] however here, their biological function is unknown. Brown algal derived cyclopropanes and cycloheptadienes are secreted as mixtures of enantiomers with often well defined compositions that depend on species and habitat. Hormosirene **5** is a particularly interesting example. Both enantiomers are known and, in general, the ee of the secreted mixtures (52–92% ee) is characteristic for the species, sometimes even for the habitat.[1] This raises questions about how the stereochemistry of the cyclopropane is established and how the ratio of enantiomers is controlled in the biosynthetic pathway.

In earlier work we demonstrated that both brown algae[5] and diatoms[2] exploit the pool of unsaturated C_{20} fatty acids for the biosynthesis of C_8 and C_{11} hydrocarbons. Cell free extracts of the diatom *G. parvulum* were shown to oxidatively cleave deuterium labelled arachidonic acid into two isotopically labelled fragments, namely **6** and 9-oxononadienoic acid **9**. Performing the transformation in the presence of $^{18}O_2$ resulted in incorporation of one ^{18}O in the C(9)-aldehyde group. This suggests an initial functionalisation of the fatty acid to

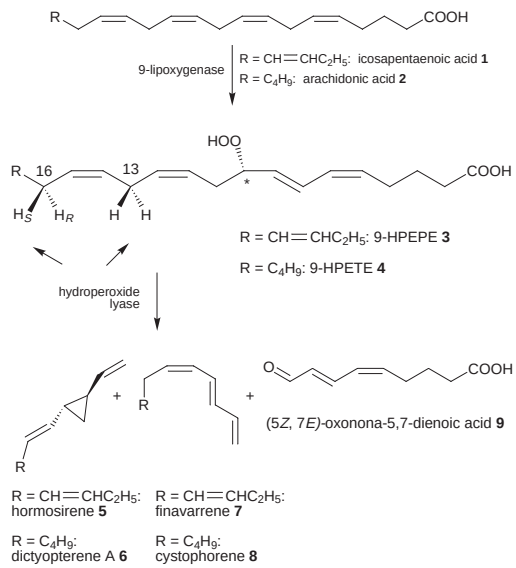

Scheme 1 Biosynthesis of C_9 and C_{11} hydrocarbons in the diatom *G. parvulum*.

9-hydroperoxyicosatetraenoic acid (9-HPETE) **4** followed by oxidative cleavage of the reactive intermediate into the bifunctional **9** and the olefin **6**. By analogy, the more highly unsaturated icosapentaenoic acid **1** could serve as the precursor for **5** (Scheme 1)

In principle, the configuration and ee of cyclopropanes **5** and **6** could be controlled either by the ee of the 9-OOH group directing all subsequent steps, by selective abstraction of one enantiotopic hydrogen atom at the methylene group of C(16), or by the folding of the fatty acids within the enzyme active site. To evaluate the influence of the two different stereogenic centres on the reaction course, we approached the absolute configuration and ee of the postulated **4** intermediate by a trapping experiment yielding 9-hydroxyicosatetraenoic acid (9-HETE). The hydrogen atom eliminated from C(16) was identified by using chiral, deuterium labelled arachidonic acid precursors and MS analysis of the metabolites after GLC separation on chiral stationary phases.

G. parvulum produces icosapentaenoic acid **1** derived **5** as the major volatile product (56% ee)[2] and small amounts of the arachidonic acid metabolites, **6** (24% ee) and cystophorene **8**. Addition of (labelled) arachidonic acid to a cell free extract of *G. parvulum* resulted in an 800-fold increase in the amount of **6** and **8** and the extracted metabolites could be analysed by MS without significant interference from a background of unlabelled, natural products. When the experiment was carried out in the presence of excess glutathione and glutathione peroxidase,† a system known to reduce hydroperoxy fatty acids rapidly and universally,[6] 9-HETE could be isolated together with small amounts of various autooxidation products. In the absence of glutathione and glutathione peroxidase no free **4** or 9-HETE could be detected. Independent experiments with synthetic 9-HETE excuded this compound as biosynthetic intermediate of **6** and confirmed the involvement of **4** *en route* to **6, 8** and **9** (Scheme 1). Following RP-HPLC purification and esterification of 9-HETE with *N*-(dimethylaminopropyl)-*N*′-ethylcarbodiimide–hydrochloride in aqueous MeOH,[7] the ee of the resulting ester was determined by HPLC on cyclodextrin as the chiral stationary phase.‡ On comparison with authentic compounds (SIGMA, Deisenhofen, Germany), the configuration of the hydroxy acid was established as (9*S*)-HETE (71% ee), reflecting the configuration and the ee of the unstable precursor **4**. The ee of (9*S*)-HPETE formed by the intact system should be even higher, since significant autooxidation of **2** occurred during the experiment with the crude enzyme preparation. Comparison of this value with the very low ee of the product (1*S*,2*R*)-**6** (24% ee, GLC on γ-cyclodextrin), clearly demonstrated that the HOO group of **4** at C(9) is not controlling the product stereochemistry.

To identify which hydrogen atom at C(16) is lost during olefin formation, the enzyme preparation was incubated with deuterium labelled (16*S*)-[15,16-$^2H_2$]-**2a** or (16*R*)-[15,16-$^2H_2$]-**2b**. The chiral precursors were synthesised from chiral epoxyheptanol-derived Wittig reagents of type **10** and 14-oxotetradecatrienoic acid methyl ester[8,9] **11** in 96 and 95% ee respectively[10] (Scheme 2).

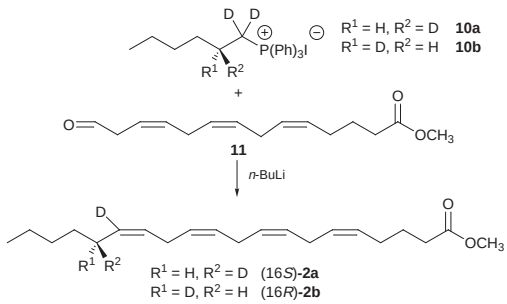

Scheme 2 Synthesis of deuterated (16*S*)-[15,16-$^2H_2$]-**2a** and (16*R*)-[15,16-$^2H_2$]-**2b**.

The olefinic metabolites of **2a**,**b** were extracted by solid-phase microextraction (SPME)[2] and analysed by GC-MS, using a chiral stationary phase for separation of the enantiomers (*vide supra*). Administration of (16*S*)-[15,16-$^2H_2$]-arachidonic acid **2a** yielded [1′,2′-$^2H_2$]dictyopterene A **6** with a molecular ion at 152 Da, confirming the presence of two deuterium atoms in each of the two enantiomers (Fig. 1A). Incubation of (16*R*)-[15,16-$^2H_2$]-arachidonic acid **2b** afforded labelled **6** showing, for both enantiomers, the same pattern of molecular ions at *m/z* 152 (45%) and 151 (55%). Thus, due to a kinetic isotope effect (KIE), the expected C(16)-H_R was not exclusively attacked, but also the C(16)-H_S generating a mixture of [1′,2′-$^2H_2$]-**6** and [1′-^{2}H]-**6** from (16*R*)-**2b**. In addition, larger amounts of [7,7-$^2H_2$]-**8**, the product of a hydrogen atom loss from C(13), were produced (Fig. 1B). Both dideuterated compounds apparently resulted from reaction paths which avoided the abstraction of the kinetically unfavoured C(16)-^2H_R of **2b**.

The isotope effect was quantified by incubating the crude enzyme preparation with excess of an equimolar mixture of **2** and [16,16-$^2H_2$]-**2**. Product analysis by GC-MS revealed that the unlabeled precursor was the preferred substrate for the formation of **6** (**6**:[2′^{2}H]-**6** = 4.5:1) and confirmed loss of the hydrogen atom as rate limiting. Moreover, in the same experiment labelled **8** was produced in excess ([7,7-$^2H_2$]-**8**:**8** = 6.5:1) indicating that a single enzyme is responsible for the production of **8** and **6**. If a second lyase, removing hydrogen atoms from C(13) of the precursor had been present in the crude enzyme preparation, a ratio of [$^2H_2$]-**8**:**8** = 1:1 should have resulted due to the absence of a KIE for this position. Thus, the dynamic product channelling, following the administration of

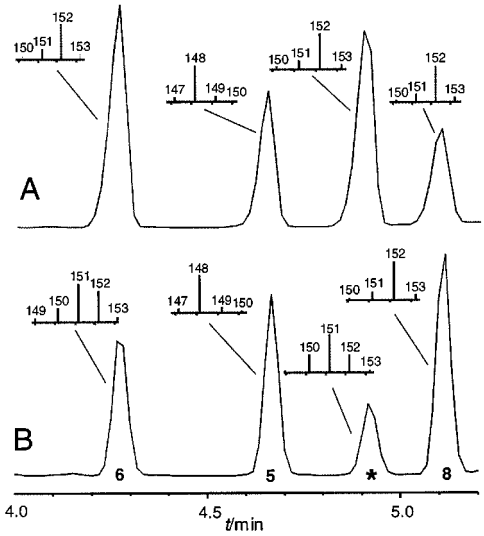

Fig. 1 GC-profile of labelled and unlabelled C_{11} hydrocarbons in *G. parvulum* with inserts of their mass spectra showing the region of the molecular ion. (A) after treatment with (16*S*)-[15,16-$^2H_2$]-**2a**. (B) after treatment with (16*R*)-[15,16-$^2H_2$]-**2b**. The large amount of 6-butylcyclohepta-1,4-diene (*) (dictyotene) results from a thermal [3.3]-sigmatropic rearrangement of **6** in the injection port of the GC and does not reflect the actual concentration of dictyotene in the hydrocarbon mixture.

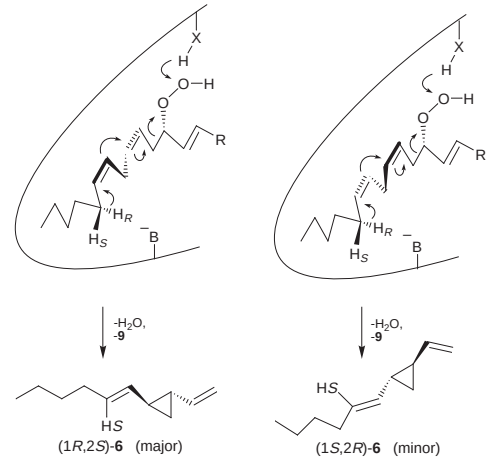

Scheme 3 Proposed folding alternatives of intermediate **4** at the active centre of the *G. parvulum* hydroperoxide lyase leading to enantiomers of **6**. Whether or not the transformation proceeds *via* ionic or radical intermedates remains to be established.

labelled and unlabelled precursors, is highly indicative of a single hydroperoxide lyase exerting only a limited control on the orientation of the substrate at the active site, generating either predominately **6** or **8**, depending on the ease of hydrogen abstraction. Accordingly, the rather low ee of **6** could be also attributed to the limited control over the folding of **4** in the enzyme active site, as illustrated in Scheme 3.

Although the model of limited control over the substrate orientation at the active centre and during the catalytic process, is in accord with the experimental findings, the involvement of two enzymes, each responsible for the (predominant) production of a distinct enantiomer, cannot be ignored. Further work with isolated enzymes is required to provide a conclusive answer to the question on the origin of enantiomeric mixtures of C_{11} hydrocarbons in diatoms and marine brown algae.

Financial support by the Deutsche Forschungsgemeinschaft, Bonn, and the Fonds der Chemischen Industrie, Frankfurt, is gratefully acknowledged. We thank the BASF AG, Ludwigshafen, and the Bayer AG, Leverkusen, for generous supply of chemicals and solvents. We also thank Professor D. Czarnecki, Loras College, Dubuque, Iowa, USA, for stock cultures of the diatoms, and Professor H. G. Floss, Seattle, USA, for laboratory facilities.

Notes and References

† *Ca.* 10^7 cells of *G. parvulum* in phosphate buffer (5 ml, 0.01 M, pH 7) were sonicated and the cell debris was removed by centrifugation. The supernatant was treated with glutathione (0.1 g, reduced form) and glutathione peroxidase (10 units) prior to addition of **2** (30 μl, 10% in EtOH). After 3 h 9-HETE was detected by RP-HPLC (Econosphere, C18, MeOH–H_2O–HAc 75:25:0.25, UV 235 nm for monitoring).

‡ The enantiomers were separated on a Chiralcel OB column[11] (Daicel Chem. Ind., hexane–propan-2-ol 99:1, 1 ml min^{-1}, baseline separation, UV 235 for monitoring).

1 W. Boland, *Proc. Natl Acad. Sci. U.S.A.*, 1995, **92**, 37.
2 G. Pohnert and W. Boland, *Tetrahedron*, 1996, **52**, 10 073.
3 T. Wendel and F. Jüttner, *Phytochemistry*, 1996, **41**, 1445.
4 W. Boland and K. Mertes, *Eur. J. Biochem.*, 1985, **147**, 83.
5 K. Stratmann, W. Boland and D. G. Müller, *Angew. Chem., Int. Ed. Engl.*, 1992, **31**, 1246.
6 A. Hamberg and W. H. Gerwick, *Arch. Biochim. Biophys.*, 1993, **305**, 115.
7 M. K. Dhaon, R. K. Olsen and K. Ramasamy, *J. Org. Chem.*, 1982, **47**, 1962.
8 M. Hombeck and W. Boland, *Tetrahedron*, 1998, **54**, 11 033.
9 K. B. Sharpless and T. Katsuki, *J. Am. Chem. Soc.*, 1980, **102**, 5974.
10 M. Hombeck and W. Boland, *J. Org. Chem.*, in preparation.
11 V. Di Marzo, L. De Petrocellis, C. Gianfrani and G. Cimino, *Biochem. J.*, 1993, **295**, 23.

Communication 8/08409B

The total synthesis of (−)-α-kainic acid using titanium-mediated diene metallabicyclisation methodology

Andrew D. Campbell,[a] Tony M. Raynham[b] and Richard J. K. Taylor*[a]

[a] *Department of Chemistry, University of York, York, UK YO10 5DD. E-mail: rjkt1@york.ac.uk*
[b] *Roche Discovery Welwyn, Welwyn Garden City, Hertfordshire, UK AL7 3AY*

Received (in Cambridge, UK) 2nd November 1998, Accepted 11th December 1998

Titanium-mediated diene metallabicyclisation–elimination–functionalisation has been utilised for the preparation of *syn*-3,4-disubstituted and *syn,syn*-2,3,4-trisubstituted pyrrolidines in high yield and excellent stereoselectivity; this methodology has been employed in a total synthesis of (−)-α-kainic acid starting from L-serine.

(−)-α-Kainic acid **1**, isolated from the marine algae *Digenea simplex*[1] and *Centrocerus clavulatum*[2] and from the Corsican

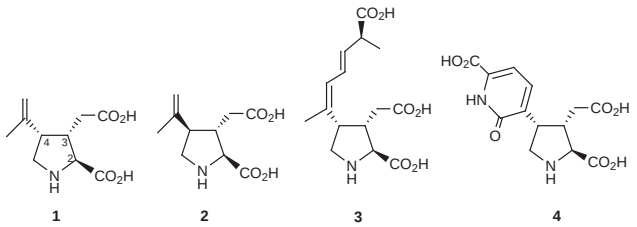

1 **2** **3** **4**

moss *Alsidum helminthocorton*,[3] has generated a great deal of interest because of its potent neuroexcitatory activity. With the discoveries of α-allokainic acid **2**, the domoic acid family (*e.g.* domoic acid **3**) and the acromelic acid family (*e.g.* acromelic acid A **4**), the synthetic community has been stimulated to design efficient, stereocontrolled routes to 2,3,4-trisubstituted pyrrolidines.[4]

Given our interest in the kainoid area,[5] and our ongoing research into synthetic applications of diene metallabicyclisation reactions,[6] we envisaged a new approach to kainic acid as shown in Scheme 1. Thus, zirconium- or titanium-mediated metallabicyclisation of diene **5** should produce the metallabicycle **6** which would be expected to undergo rapid β-elimination to generate the archetypal kainoid 4-isopropenyl substituent. This sequence would produce organometallic reagent **7** which could then be functionalised to introduce the requisite 3-carboxymethyl substituent of the kainoids.

Other cyclisation–elimination approaches to the kainoids have been investigated but stereochemical control has been poor.[7] Similar problems were encountered when we explored the zirconium-mediated sequence outlined in Scheme 1, although a successful synthesis of (−)-α-kainic acid was accomplished.[8] Here we describe the use of Sato's (η_2-propene)Ti(OPr^i)$_2$ reagent[9] in the metallabicyclisation–elimination sequence, and demonstrate that the procedure produces 3,4-disubstituted and 2,3,4-trisubstituted pyrrolidines with extremely high stereoselectivity. We then describe the application of this methodology to the synthesis of (−)-α-kainic acid **1**: to the best of our knowledge, this is the first application of diene metallabicyclisation–elimination methodology in natural product synthesis.

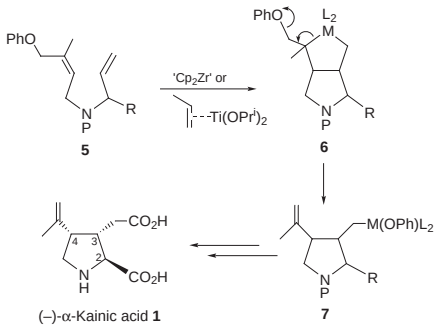

Scheme 1

Model studies were first carried out to assess the viability of the (η_2-propene)Ti(OPr^i)$_2$ procedure for the stereoselective preparation of pyrrolidines (Table 1).† As can be seen (entry 1), treatment of diene **8** with Ti(OPr^i)$_4$/2 Pr^{i}MgCl produced, after protonation, the 3,4–disubstituted pyrrolidine **9a** in an excellent yield with a 6:1 ratio of *syn:anti* diastereomers. The alkyl–titanium intermediate could also be halogenated giving alkyl halides **9b** and **9c** in good yield.

Cyclisation of the trisubstituted alkenes **10** and **12** also proceeds efficiently and with excellent *syn*-selectivity giving **11** as the only product (entries 2 and 3). Further studies are in progress to rationalise this much improved stereoselectivity. We next looked at the titanium-mediated cyclisation–elimination reaction of the 2-methyl substituted system **13**. We were delighted to observe that in this case the high C-3/C-4 *syn*-selectivity was retained, as only the two separable diastereoisomers **14** and **15** were isolated.‡ Remarkably,[9c] the major product was the *syn, syn*-diastereomer **14** in which all three substituents were on the same face of the pyrrolidine. This stereochemical assignment was confirmed by comparison of the ^{1}H NMR spectra of **14** and **15** with **9a** and related systems,[8] and

Table 1 Titanium-mediated diene metallabicyclisation–elimination–trapping reactions (*cis*:*trans* ratios determined by ^{1}H NMR spectroscopy)

	Starting diene	Electrophile	Major product	Yield (%) (*syn:anti*)
1	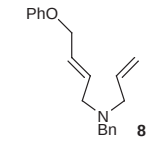 **8**	H^+ (**9a**) I_2 (**9b**) Br_2 (**9c**)	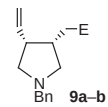 **9a–b**	**9a** E = H, 85% (6:1) **9b** E = I, 72% (6:1) **9c** E = Br, 67% (6:1)
2	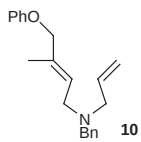 **10**	H^+	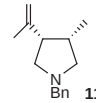 **11**	84% (*syn* only)
3	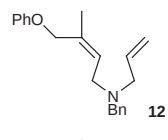 **12**	H^+	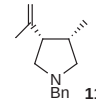 **11**	86% (*syn* only)
4	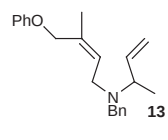 **13**	H^+	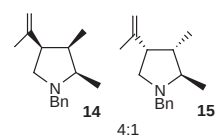 **14** **15** 4:1	74%

by NOE studies (*e.g.* H-2 and H-4 enhanced by irradiation at H-3). It has been demonstrated that all *syn*-analogues of kainic acid can be epimerised at C-2 to give the kainoid structure.[10] Thus, a titanium-mediated metallabicyclisation approach for the synthesis of kainic acid could commence with L-serine and include an epimerisation step after cyclisation. The strategy has now been implemented successfully (Scheme 2).

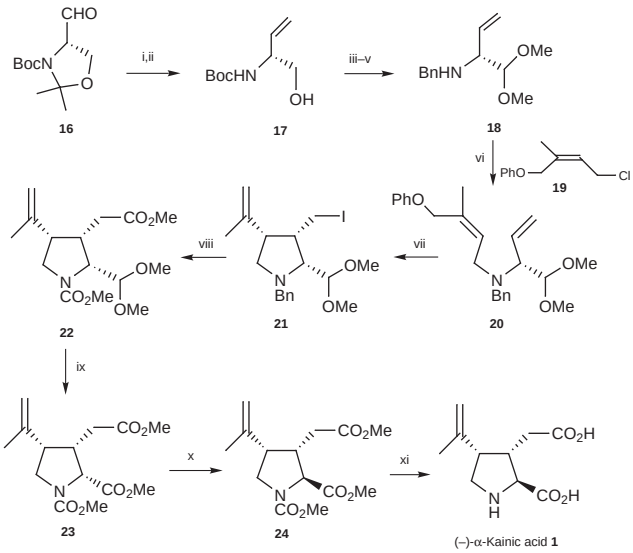

Scheme 2 *Reagents and conditions*: i, $Ph_3P^+CH_3Br^-$ KHMDS, THF, −78 °C (80%); ii, Dowex (H^+) resin, aq. MeOH (93%); iii, Dess–Martin oxidation; iv, HCl/MeOH; v, PhCHO, $NaBH(OAc)_3$, $ClCH_2CH_2Cl$ (31% for 3 steps); vi, K_2CO_3, cat. NaI, MeCN, reflux (88%); vii, $Ti(OPr^i)_4$, Pr^iMgCl (2 equiv.), Et_2O, −50 °C to room temp., then I_2, 0 °C [56% (78% based on recovered **20**)]; viii, Bu^tLi (2.2 equiv.), Et_2O, −80 °C, then excess $ClCO_2Me$, −80 °C, then excess $ClCO_2Me$, $ClCH_2CH_2CI$, reflux, 2 h (61%); ix, Jones' oxidation then CH_2N_2 (65%); x, LiHMDS (2.5 equiv.), THF, 0 °C, then MeOH (80%); xi, NaOH/MeOH, reflux (70%).

Thus, L-serine was converted into the (*S*)-Garner aldehyde **16** using our improved procedure.[11] Wittig methylenation and acid hydrolysis gave the Boc protected vinylglycinol **17**[11,12] which underwent Dess–Martin oxidation to a very unstable aldehyde which was immediately subjected to *N*-Boc deprotection–acetal formation to give an amino acetal which was then reductively aminated with benzaldehyde to give **18** in 31% yield over three steps. The ee of this amine was shown to be 93% by comparison with racemic material using HPLC on a chiral column [Chiralpak AS, 1:99 Pr^iOH–hexane, R_t 324 s (*vs*. 287 s)]. This is the first preparation of an acetal-protected vinylglycinal, a compound that could be useful in other synthetic applications. Alkylation with allyl chloride **19** then gave the cyclisation precursor **20** in 88% yield.§ Allyl chloride **19** was prepared by Horner–Wadsworth–Emmons elaboration of 2-phenoxyacetone with methyl diethyl phosphonoacetate (94%, *E*:*Z* = 2:1) followed by chromatographic separation, reduction of the resulting α,β-unsaturated ester (DIBAL-H) and chlorination (TsCl, DMAP).

Ti^{II}-mediated cyclisation–iodination of **20** gave the *syn*,*syn*-pyrrolidine **21** as the only cyclised product in 56% yield (78% based on recovered diene **20**). Lithium–halogen exchange and quenching with excess methyl chloroformate gave **22** in 61% overall yield. Jones' oxidation cleaved the acetal and oxidised the aldehyde produced to the corresponding acid which was treated with CH_2N_2 to give ester **23**. Compound **23** is a protected derivative of the so-called β-kainic acid: the titanium methodology provides a very convenient stereoselective route to these compounds which are reported to have interesting anti-convulsant properties.[13]

Epimerisation at C-2 was successfully achieved using LiHMDS (2.5 equiv.) and quenching with MeOH.[10*b*] Using this procedure, complete conversion into the epimeric ester **24** was observed [TLC (SiO_2: EtOAc–light petroleum, 1:2) **23**, R_f 0.30; **24**,[14] R_f 0.31]. Saponification of **24** was accompanied by *N*-deprotection giving (−)-α-kainic acid **1**, which was spectroscopically consistent with authentic material and corresponded well in terms of polarimetry {$[\alpha]_D$ −15.2 (*c* 0.95, H_2O); lit.,[15] −15.0 (*c* 0.5, H_2O)} and mp [mp 244–247 °C (decomp.); lit.,[15] mp 237–243 °C (decomp.)].

In conclusion, we have developed a new enantioselective synthesis of (−)-α-kainic acid **1** which has as its cornerstone a totally stereoselective titanium-mediated diene metallabicyclisation process. The total synthesis is high yielding (3.5% in twelve steps from commercially available material). This new route contrasts to other cyclisation–elimination approaches to the kainoids where stereochemical control has been poor,[7] and although our procedure does require epimerisation at C-2 to obtain the kainoid structure, it also provides a route to β-kainoids. In addition, kainoid analogues with a range of different substituents at C-3 and C-4 are available *via* this route. From a general methodological viewpoint, the new procedure for the stereoselective preparation of *syn*,*syn*-2,3,4-trisubstituted pyrrolidines is noteworthy.

We are grateful to the BBSRC and Roche Discovery Welwyn for a CASE award (A. D. C.).

Notes and references

† All new compounds were fully characterised spectroscopically and by HRMS/elemental analysis.

‡ During the course of our studies Sato *et al.* also reported the stereoselective synthesis of a 2,3,4-trisubstituted pyrrolidine *via* titanium-mediated diene metallabicyclisation [ref. 9(*c*)], although their system was not suitable for elaboration to produce kainoids.

§ Initial studies were carried out with a protected alcohol as the C-2 substituent. Metallabicyclization was successful and completely stereoselective, but problems were encountered when trying to adjust the oxidation state of the C-2 substituent.

1 S. Murakami, T. Takemoto and Z. Shimizu, *J. Pharm. Soc. Jpn.*, 1953, **73**, 1026.
2 G. Impellizzeri, S. Mangiafico, G. Oriente, M. Piatelli, S. Sciuto, E. Fattorusso, S. Magno, S. Santacroce and D. Sica, *Phytochemistry*, 1975, **14**, 1549.
3 G. Balansard, M. Pellegrini, C. Cavalli and P. Timon-David, *Ann. Pharm. Fr.*, 1983, **41**, 77.
4 A. F. Parsons, *Tetrahedron*, 1996, **52**, 4149.
5 A. F. Parsons and R. J. K. Taylor, *J .Chem. Soc., Perkin Trans. 1*, 1994, 1945.
6 A. J. Bird, R. J. K. Taylor and X. Wei, *Synlett*, 1995, 1237.
7 S.-E. Yoo, S.-H. Lee, K.-Y. Yi and N. Jeong, *Tetrahedron Lett.*, 1990, **31**, 6877; M.-P. Bertrand, S. Gastaldi and R. Nourguier, *Tetrahedron Lett.*, 1996, **37**, 1229; O. Miyata, Y. Ozawa, I. Ninomiya and T. Naito, *Synlett*, 1997, 275; see also M. D. Bachi and A. Melman, *J. Org. Chem.*, 1997, **62**, 1896.
8 A. D. Campbell, T. M. Raynham and R. J. K. Taylor, unpublished results.
9 (*a*) K. Harado, H. Urabe and F. Sato, *Tetrahedron Lett.*, 1995, **36**, 3203; (*b*) Y. Takayama, Y. Gao and F. Sato, *Angew. Chem., Int. Ed. Engl.*, 1997, **36**, 851; (*c*) Y. Takayama, S. Okamoto and F. Sato, *Tetrahedron Lett.*, 1997, **38**, 8351.
10 (*a*) S. Takano, Y. Iwabuchi and K. Ogasawara, *J. Chem. Soc., Chem. Commun.*, 1988, 1204; (*b*) A. Rubio, J. Esquerra, A. Escribano, M. J. Remuiñán and J. J. Vaquero, *Tetrahedron Lett.*, 1998, **39**, 2171.
11 A. D. Campbell, T. M. Raynham and R. J. K. Taylor, *Synthesis*, 1998, 1707; see also A. McKillop, R. J. K. Taylor, R. J. Watson and N. J. Lewis, *Synthesis*, 1994, 31 and references cited therein.
12 Z.-Y. Wei and E. Knaus, *Synthesis*, 1994, 1463.
13 J. F. Collins, A. J. Dixon, G. Badman, G. De Sarro, A. G. Chapman, G. P. Hart and B. S. Meldrum, *Neurosci. Lett.*, 1984, **51**, 371.
14 S. Takano, K. Inomata and K. Ogasawara, *J. Chem. Soc., Chem. Commun.*, 1992, 169.
15 W. Oppolzer and K. Thirring, *J. Am. Chem. Soc.*, 1982, **104**, 4978.

Communication 8/09598A

ChemComm

Sulfur oxidation in supercritical carbon dioxide: dramatic pressure dependant enhancement of diastereoselectivity for sulfoxidation of cysteine derivatives

R. Scott Oakes, Anthony A. Clifford, Keith D. Bartle, Mark Thornton Pett† and Christopher M. Rayner*

School of Chemistry, University of Leeds, Leeds, UK LS2 9JT. E-mail: chrisr@chem.leeds.ac.uk

Received (in Liverpool, UK) 3rd December 1998, Accepted 8th December 1998

The diastereoselective sulfoxidation of chiral sulfides derived from methionine and cysteine has been investigated in conventional solvents and in supercritical carbon dioxide ($scCO_2$); use of *tert*-butyl hydroperoxide and Amberlyst™ 15 ion exchange resin is particularly effective for sulfoxide formation, and with cysteine derivatives shows a dramatic pressure-dependant increase in diastereoselectivity (up to > 95% de) in $scCO_2$ compared with conventional solvents, where no diastereoselectivity is observed; the stereochemical configuration of the major product of the oxidation of Cbz-CysSMe-OMe has been confirmed as *anti* using X-ray crystallography.

The development of new methods for addressing environmental problems associated with organic synthetic procedures continues to be one of the major challenges facing synthetic organic chemists, and will remain so for the foreseeable future. Supercritical carbon dioxide ($scCO_2$) is currently being investigated as an environmentally friendly solvent by a number of research groups, and has been demonstrated as being an effective medium for a limited number of organic transformations (*vide infra*). Supercritical fluids are substances above their critical temperatures and pressures, whose properties are intermediate between those of gases and liquids, and which can be controlled by both temperature and pressure.[1] Pure carbon dioxide has a critical temperature of 31 °C and critical pressure of 74 atmospheres, both of which are readily achievable using commercially available equipment. Advantages include: low toxicity, ready availability, ease of removal and disposal and/or recycling. Other advantages which are particularly relevant for carrying out reactions in $scCO_2$ are: fine control of solvent properties by changes in temperature and pressure; the ability to homogenise reaction substrates, electrically neutral metal complexes and gases like oxygen and hydrogen; enhanced diffusion rates; and potential for product processing.[2]

Supercritical fluids have also been shown to be excellent media for a number of reactions.[3] In our laboratories, we have recently shown that it is possible to fine tune the *endo*/*exo* selectivity of the Diels–Alder reaction between cyclopentadiene and methyl acrylate by controlling the density of the reaction medium by varying the temperature and pressure of the $scCO_2$.[4] However, in this case, the changes observed were modest, and gave no real preparative advantage. We now report some results which clearly show definite advantages of carrying out reactions in $scCO_2$ in addition to the environmental and processing reasons stated above.

We have recently developed a new method for the oxidation of simple sulfides to sulfoxides in conventional solvents and $scCO_2$[5] using *tert*-butyl hydroperoxide (TBHP) as oxidant with Amberlyst 15 ion exchange resin catalyst (Scheme 1).[6] High yields and excellent selectivity for sulfoxide formation are obtained, even with an excess of oxidant, and this method provides an attractive alternative to procedures currently available for use under conventional conditions as well as in $scCO_2$.[7]

We now report the results of studies on the oxidation of more complex substrates, which have potential for diastereoselective oxidation, to see whether using $scCO_2$ as solvent has any particular advantages in addition to the environmental and product processing benefits mentioned above.

Recent studies on the sulfoxidation of cysteine derivatives have shown that, although in general they may be expected to give diastereoselective oxidation, this can in practice be difficult to achieve without significant substituent modification, requiring preparation of the MEM esters of *S*-benzyl (or larger) derivatives for good results, with no significant selectivity being observed with the methyl esters[8] or reported for *S*-methyl derivatives.[8,9] With this in mind, we chose to investigate the oxidation of a range of conventionally protected cysteine and methionine derivatives, firstly as more complex examples of substrates for oxidation, but also to determine if carrying out the reaction in $scCO_2$ had any significant effect on the diastereoselectivity of the reaction.

Initial studies using our TBHP/Amberlyst reagent system showed that oxidation of Cbz-methionine methyl ester proceeded efficiently in either toluene or $scCO_2$, but with no diastereoselectivity as determined by ^1H NMR analysis, presumably due to the remote nature of the existing chiral centre and the sulfur atom in the substrate.‡ A potentially more promising substrate, CBz methyl cysteine methyl ester, was oxidised in high yield, but also gave no appreciable diastereoselectivity in toluene or CH_2Cl_2 in accord with previous literature results.[8] On attempting the reaction in $scCO_2$ (200 bar, 40 °C), high yields were obtained (Scheme 1), but also significant diastereoselectivity (Fig. 1). As from our previous work on the Diels–Alder reaction,[4] we were aware that the density of the medium, controlled by varying either temperature or pressure, can have an effect on reaction selectivity, and it may be possible to fine tune the reaction conditions to optimise such selectivity. In this case, by varying the pressure at a constant temperature of 40 °C, we were able to optimise the diastereoselectivity of the reaction to > 95% de (Fig. 1). This is a particularly dramatic enhancement considering that no selectivity was observed under conventional reaction conditions.

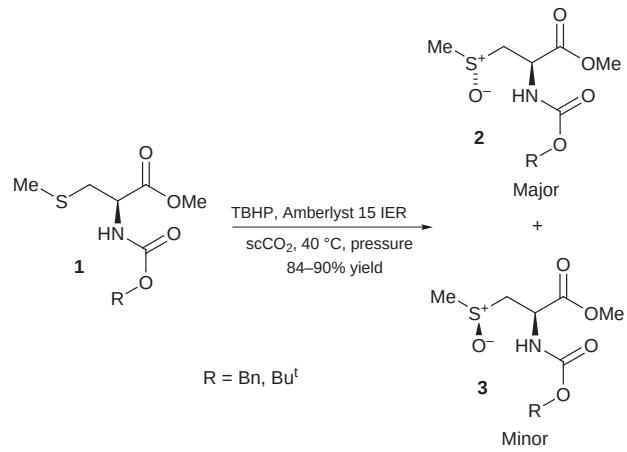

Scheme 1

† Author to whom communications regarding X-ray crystal structure determination should be addressed.

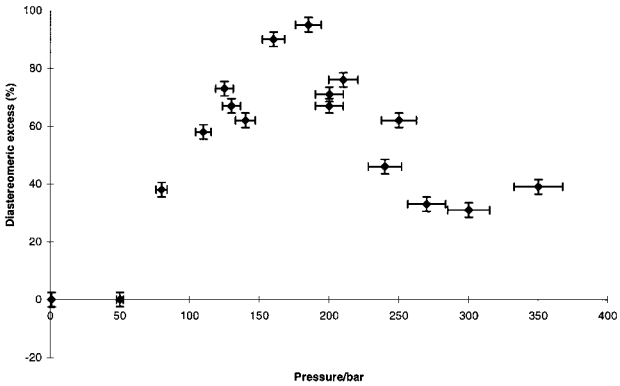

Fig. 1 Variation of diastereoselectivity for oxidation of Cbz-CysSMe-OMe.

Similar effects were also observed in the case of Boc methyl cysteine methyl ester, although with less impressive selectivities (up to 31% de). Note that in both cases, at a constant temperature, the selectivity rises to a maximum at around 180 bar then falls off as pressure is increased further. The relative stereochemistry of the major isomer for the oxidation of Cbz-CysSMe-OMe has been confirmed as the *anti* isomer **2** (R = Bn) by X-ray crystallography§ (Fig. 2).

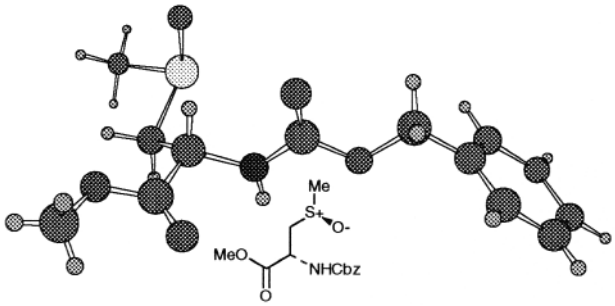

Fig. 2 X-Ray crystal structure of major diastereomer from oxidation of Cbz-CysSMe-OMe in $scCO_2$.

We had previously rationalised this kind of fine-tuning of reaction conditions by the adjustment of the nearest neighbour solvent molecules with respect to the transition states.[4] This would be particularly important for processes with highly ordered transition states such as Diels–Alder reactions. In the case of this work, the situation is less clear and factors such as hydrogen bonding and/or conformation[10] may also play an important role. The fact that essentially no diastereoselectivity is observed in conventional solvents, however, strongly suggests that the nature of the reaction medium is playing a crucial role in inducing the stereoselective reaction.

Whilst the actual reasons for this effect may be the subject of some debate, there is no doubt that it is potentially very important in the area of stereoselective synthesis, particularly if it can be shown to be applicable to other types of reaction, with similar levels of amplification of stereoselectivity. We are currently investigating both the causes and generality of this effect, and the results of these studies will be reported in due course.

We are very grateful to the following members of the Leeds Cleaner Synthesis Group and their respective companies for funding and useful discussions: Dr Andrew Bridge, Rhône-Poulenc Rorer; Dr Mike Loft, GlaxoWellcome; Dr Jo Negri, Pfizer Central Research; Dr Nick Troughton, Solvay Interox; and Dr Ken Veal, SmithKline Beecham Pharmaceuticals.

Notes and references

‡ Experimental procedure: As with all reactions under high pressure, adequate safety precautions must be taken. For carrying out reactions in $scCO_2$, a stainless steel cyclindrical vessel was used with a volume of 20 ml. The seal between vessel and lid is maintained by a Viton high pressure 'O'-ring. Stirring is accomplished using a remote magnetic stirrer. A Swagelok pressure relief valve with a release pressure of 6000 psi is employed as a safety precaution. The pressure is measured utilising a Farnells Electronics™ pressure transducer (0–5000 psi). Reagents can be injected into the system *via* a Rheodyne injector valve. The system is pressurised using a Varian™ 8500 syringe pump, which draws from a BOC 100.00 CP grade CO_2 cylinder (*ca*. 50 bar head pressure), and has a cooled pump head. Temperature control is achieved by locating the vessel in a modified GC oven. Diastereomeric ratios were determined by ^{1}H NMR analysis to ±2.5% de. Errors along the pressure axis were set at 5% to allow for inaccuracies in other variables such as temperature, reagent quantities and volumes, and pressure.

Amberlyst™ 15 resin (0.5 g), the sulfide (up to 4.0 mmol) and a magnetic stirrer were placed in the reaction vessel described above, at room temperature. The vessel was sealed and pressurised to *ca*. 50 bar with CO_2 and the oven temperature maintained at 40 °C. Agitation was started at a rate of 600 rpm. The pressure was increased to *ca*. 100–120 bar, at which point the TBHP (1.1 equiv. of *ca*. 4.0 M solution in toluene) was injected and the pressure further increased to the desired reading. Agitation was maintained at this temperature and pressure for 24 h. On completion, the pressure was released slowly *via* a vent into a CH_2Cl_2 trap (20 ml). When atmospheric pressure was reached, the reaction vessel was washed through with CH_2Cl_2 (2 × 1 ml, at 50 bar). The vessel was opened and the Amberlyst™ 15 washed with MeOH (2 × 5 ml) and removed by filtration. The solutions were combined and the solvent was removed *in vacuo*. Column chromatography of the residue gave the desired sulfoxides in 82–97% yield.

§ *Crystal data* for **2** (R = Bn) (ref. 11): $C_{13}H_{17}NO_5S$, M = 299.34, orthorhombic, space group $P2_12_12_1$, a = 7.87930(10), b = 8.19550(10), c = 22.0906(4) Å, V = 1426.50(4) Å^3, T = 100(2) K, Z = 4, D_c = 1.394 Mg m^{-3}, μ(MoKα) = 0.245 mm^{-1}, 27208 reflections collected, 2747 independent reflections, R(int) = 0.0282, all non-H atoms anisotropic, all H-atoms constrained to idealised positions. Final R indices [based on 2724 reflections with $I > 2\sigma(I)$], R_1 = 0.0256, wR_2 = 0.0706. The absolute structure of the molecule was confirmed by the refinement of an enantiopole parameter to −0.02(6). CCDC 182/1113. Crystallographic data is available in CIF format from the RSC web site, see: http://www.rsc.org/suppdata/cc/1999/247/

1 A. A. Clifford, *Fundamentals of Supercritical Fluids*, Oxford University Press, 1998; A. A. Clifford, in *Supercritical Fluids*, ed. E. Kiran and J. M. H. Levelt Sengers, Kluwer, Dordrecht, 1994, p. 449.
2 See for example: L. E. McMahon, P. Timmins, A. C. Williams and P. York, *J. Pharm. Sci*., 1996, **85**, 1064; J. W. Tom, G. B. Lim, P. G. Debendetti and R. K. Prud'homme, in *Supercritical Fluid Engineering Science—Fundamentals and Applications*, ed. E. Kiran and J. F. Brennecke, ACS Symp. Ser. 514, 1993, ch. 11; P. G. Debendetti, *Supercritical Fluids*, ed. E. Kiran and J. M. H. Levelt Sengers, Kluwer, Dordrecht, 1994, p. 719.
3 For recent examples see: M. A. Carroll and A. B. Holmes, *Chem. Commun*., 1998, 1395; D. K. Morita, D. R. Pesiri, S. A. David, W. H. Glaze and W. Tumas, *Chem. Commun*., 1998, 1397; M. G. Hitzler, F. R. Smail, S. K. Ross and M. Poliakoff, *Chem. Commun*., 1998, 359; D. R. Pesiri, D. K. Morita, W. Glaze and W. Tumas, *Chem. Commun*., 1998, 1015; G. R. Haas and J. W. Kollis, *Tetrahedron Lett*., 1998, **39**, 5923.
4 A. A. Clifford, K. Pople, W. J. Gaskill, K. D. Bartle and C. M. Rayner, *J. Chem. Soc., Faraday Trans*., 1998, **94**, 1451.
5 R. S. Oakes, A. A. Clifford, K. D. Bartle, and C. M. Rayner, unpublished results.
6 Other sulfonic acid-based catalysts have been reported: F. Bonadies, F. De Angelis, L. Locati and S. Scettri, *Tetrahedron Lett*., 1996, **37**, 7129; G. W. Breton, J. D. Fields and P. J. Kropp, *Tetrahedron Lett*., 1995, **36**, 3825.
7 C. M. Rayner and C. P. Baird, *J. Chem. Soc., Perkin Trans. 1*, 1998, 1973.
8 S. Nakamura, K. Goto, M. Kondo, S. Naito, Y. Tsuda and K. Shishido, *Bioorg. Med. Chem. Lett*., 1997, **7**, 2033; C. H. Levenson and R. B. Meyer Jr., *J. Med. Chem*., 1984, **27**, 228.
9 Variable selectivities (up to 88% de) have been reported for the oxidation of N-protected β-amino phenyl sulfides using TEMPO and sodium hypochlorite, see: R. Siedlecka and J. Skarzewski, *Synlett*, 1996, 757; A. Lewanowicz, J. Lipinski, R. Siedlecka, J. Skarzewski and F. Baert, *Tetrahedron*, 1998, **54**, 6571.
10 H. Yamada, T. Kazuoka and A. Sera, *J. Am. Chem. Soc*., 1988, **110**, 7552 and references cited therein.
11 G. M. Sheldrick, *Acta Crystallogr., Sect A*, 1990, **46**, 467; G. M. Sheldrick, G. M. Sheldrick, SHELXL-97 (Release 2), Program for refinement of crystal structures, University of Göttingen, 1998.

Communication 8/09434I

Aldehydes and ketones as dipolarophiles: application to the synthesis of oxapenams

Mark D. Andrews,[a] Giles A. Brown,[a] Jonathan P. H. Charmant,[a] Torren M. Peakman,[a] Arlene Rebello,[a] Kenneth E. Walsh,[a] Timothy Gallagher*[a] and Neil J. Hales*[b]

[a] *School of Chemistry, University of Bristol, Bristol, UK BS8 1TS. E-mail: t.gallagher@bristol.ac.uk*
[b] *Zeneca Pharmaceuticals, Mereside, Alderley Park, Macclesfield, UK SK10 4TG*

Received (in Liverpool, UK) 6th November 1998, Accepted 4th December 1998

2-Substituted (6a–e) and 2, 2-disubstituted oxapenams (6f–g) are obtained in one step by thermolysis of the β-lactam-based oxazolidinone 4 in the presence of aldehydes and reactive ketones respectively; the *C(6)*-substituted oxazolidinone variant 7 reacts with hexafluoroacetone to give the enantiomerically pure oxapenam 8.

β-Lactams continue to represent a versatile and commercially significant class of antibiotics and the promise of an enhanced or novel biological profile has done much to stimulate the design and synthesis of new structural variants.[1] The oxygen-based clavams, of which the potent β-lactamase inhibitor clavulanic acid[2] is the best known example, also includes oxapenams **1**[3] and oxapenems **2**,[4] together with the isomeric isoclavams **3**.[5] These oxygen-containing bicyclic β-lactams,

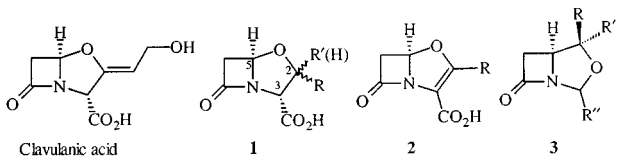

which constitute an interesting and comparatively new class of β-lactams, incorporate significant strain as compared to their more stable sulfur-based analogues (penams). As a consequence, oxapenams are thermally and hydrolytically sensitive molecules, which places a significant demand on the range and efficiency of approaches that may be employed for the synthesis of these compounds.[6]

Here we describe a flexible but also very direct route for the synthesis of both 2-substituted and 2,2-disubstituted oxapenams represented by general structure **1**. The process that has been developed is summarised in Scheme 1 and involves a formal 1,3-dipolar cycloaddition reaction (to establish the bicyclic skeleton of the oxapenams) by exploiting aldehydes and reactive ketones as 1,3-dipolarophiles.[7] The successful application of this chemistry to oxapenams not only represents a novel entry to this class of molecule but also represents a significant

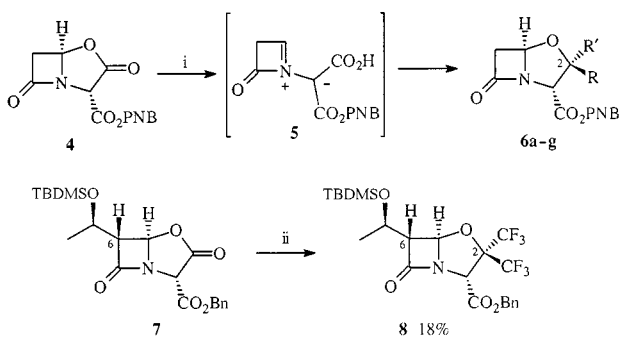

Scheme 1 *Reagents and conditions:* i, aldehyde/ketone (1.1–1.5 equiv.), MeCN, 81 °C, 24–48 h, then chromatography (for R and R′, see Table 1); ii, CF_3COCF_3, MeCN, 81 °C, 24 h.

extension to the recently reported azomethine ylide approach to bicyclic β-lactams.[8]

Thermolysis of the readily available β-lactam-based oxazolidinone **4** (PNB = $CH_2C_6H_4$-4-NO_2)[8] (which was carried out using deoxygenated MeCN, either at reflux or in a sealed tube at 81 °C) in the presence of either an aldehyde or a ketone (1.1–1.5 equiv.) provides racemic oxapenams **6a–g** in a single step albeit in moderate (19–56%) yield. The scope of this chemistry is illustrated by the examples shown in Table 1 and a

Table 1 Synthesis of oxapenams **6a–g**

Aldehyde/ketone	Oxapenam	Yield (%) (*exo* : *endo*)
PhCHO	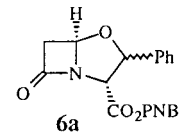 **6a**	19 (1 : 1)
4-$O_2NC_6H_4CHO$	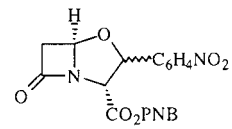 **6b**	21 (1 : 1)
4-ClC_6H_4CHO	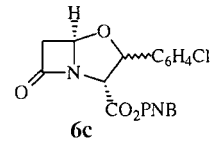 **6c**	26 (1 : 1)
4-$F_3CC_6H_4CHO$	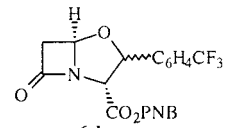 **6d**	21 (1 : 1)
C_6F_5CHO	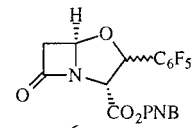 **6e**	40 (1 : 1.5)
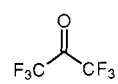	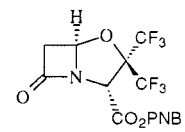 **6f**	56
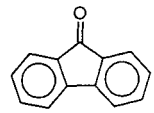	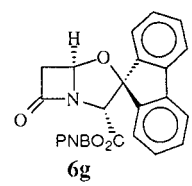 **6g**	25

range of 2-substituted oxapenams (derived from aldehydes) and 2,2-disubstituted oxapenams (derived from ketones) have been obtained. The same cycloaddition sequence has also been applied to the C(6)-substituted oxazolidinone variant **7**, which underwent reaction with hexafluoroacetone to provide the enantiomerically pure 2,2-bis(trifluoromethyl)oxapenam **8** {$[\alpha]_D^{24}$ +34.1 (*c* 0.09, CH_2Cl_2)} in 18% isolated yield.

The most important feature of the process shown in Scheme 1 is the very direct nature of this entry to oxapenams, which compensates for the modest yields observed. While aldehydes and reactive ketones appear to be reactive towards the azomethine ylide **5** (produced by fragmentation of **4**),[8c] a number of ketones (cyclohexanone, cyclopentanone, diethyl 2-oxomalonate, pyridine-4-carbaldehyde), either failed to trap or to give characterisable products. This may indicate the relative instability of the product oxapenams to either the thermal reaction conditions and/or chromatographic isolation, and such factors are likely contributors to the modest yields of oxapenams **6** that have been obtained.†

The cycloaddition pathway shown in Scheme 1 is, however, efficient in terms of the level of both regio- and stereo-control observed, but we were also concerned to establish this stereochemical outcome rigorously. Assignments in this area have often been based on the presumption that the thermodynamically more stable *trans* relationship between *C(3)* and *C(5)* predominates and by application of an empirical observation, the Bentley–Hunt rule.[6c] The reliability of this rule, and consequently its value as a diagnostic tool, has recently been questioned.[9] We, like others,[3c] have relied on NOE difference spectroscopy to assign the stereochemistry of oxapenams. With aldehydes, approximately equal amounts of the *exo* and *endo* adduct C(2) diastereomers were isolated and in the case of both **6d** and **6e**, the *exo* and *endo* isomers were separated and relative stereochemistry—C(2) *vs.* C(3) *vs.* C(5)—was assigned on the basis of NOE difference spectroscopy.‡ Only the oxapenam (clavam) regioisomer has been detected in the cases that we have examined and the thermodynamically more stable *trans* relationship between C(3) and C(5) (as defined by NOE and X-ray crystallography) is favoured; this latter stereochemical outcome is consistent with that observed previously in the synthesis of carbapenams, Δ^1-carbapenems and penams.[8]

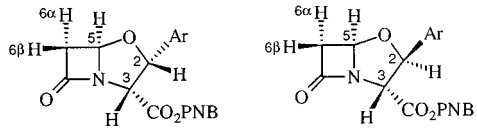

exo-**6d**, Ar = $C_6H_5CF_3$ *endo*-**6d**, Ar = $C_6H_5CF_3$
exo-**6e**, Ar = C_6F_5 *endo*-**6e**, Ar = C_6F_5

The structure of the hexafluoroacetone adduct **6f** has been established by X-ray crystallographic analysis§ which confirmed both the regiochemistry of the cycloaddition reaction (clavam *vs*. isoclavam) and the relative stereochemistry between C(3) and C(5).

In summary, utilisation of aldehydes and reactive ketones as dipolarphiles for the azomethine ylide strategy provides a very direct entry to both 2-substituted and 2,2-disubstituted oxapenams. This not only represents a novel route to an unusual class of bicyclic β-lactams but also enhances the scope and value of the underlying cycloaddition based methodology.

We thank Zeneca Pharmaceuticals for a Studentship (to G. A. B.), the EPSRC (Grant GR/K88569) and the University of Bristol for a University Research Fellowship (to T. G.), and we acknowledge use of the EPSRC's Chemical Database Service at Daresbury.[10]

Notes and references

† Thermolysis of **4** in the presence of dibenzosuberone gave the corresponding cycloadduct in only 6% yield after 24 h, but on continued heating (to 48 h), complete decomposition of this product was observed. In a qualitative sense, we have observed a correlation between enhanced thermal and chromatographic stability of oxapenams and an increase in the electron withdrawing nature of the C(2) substituent(s).

‡ NOE difference analysis involved irradiation of all ring protons (H2, H3, H4, H6α and H6β). The proton irradiated is indicated in bold and the proton(s) enhanced are shown in brackets. *Exo*-**6d**: **H2** δ 5.61 (H3, H6β, *ortho* protons of $C_6H_4CF_3$); **H3** δ 5.08 (H2); **H5** δ 5.85 [H6α, H6β (weak)]; **H6α** (H5, H6β); **H6β** [H6α, H2, H5 (weak)]; *endo*-**6d**: **H2** δ 5.53 (H5, *ortho* protons of $C_6H_4CF_3$); **H3** δ 4.43 (*ortho* protons of $C_6H_4CF_3$); **H5** δ 5.53 [H2, H6α, H6β (weak)]; **H6α** (H5, H6β); **H6β** [H6α, H5 (weak)]. Similar observations (with the exception of the aromatic proton enhancements) were recorded for *exo*- and *endo*-**6e**. *Exo* and *endo* adducts for the other entries shown in Table 1 were readily correlated using ^{1}H NMR data. As illustrated for *exo*- and *endo*-**6d**, chemical shifts (300 MHz, CD_3CN) followed a clear pattern with signals for H2, H3 and H5 corresponding to the *exo* isomer consistently appearing at lower field than those associated with the isomeric *endo* adduct. The structure of cycloadduct **8** was also established by NOE spectroscopy. All new compounds have been characterised by spectroscopic methods and either microanalysis or high resolution mass measurement.

§ *Crystal data* for **6f**: $C_{15}H_{10}F_6N_2O_6$, M = 428.3, orthorhombic, space group *Pbca*, a = 11.658(1), b = 8.055(1), c = 36.764(5) Å, U = 3264.6(8) Å^3, Z = 8, μ = 0.177 mm^{-1}, 2344 unique data, θ < 23.3 °, R_1 = 0.032. CCDC 182/1118. The crystallographic data is available in CIF format, see: http://www.rsc.org/suppdata/cc/1999/249/

1 R. D. G. Cooper, in *Topics in Antibiotic Chemistry*, ed. P. G. Sammes, Ellis Horwood Ltd., Chichester, 1980, vol. 3, p. 39; W. Dürckheimer, J. Blumbach, R. Lattrell and K. H. Scheunemann, *Angew. Chem., Int. Ed. Engl.*, 1985, **24**, 180; *Recent Advances in the Chemistry and Biology of β-Lactams and β-Lactam Antibiotics*, ed. G. I. Georg, *Bioorg. Med. Chem. Lett.* (Symposia-in-print No 8), 1993, **3**, 2159.

2 T. T. Howarth, A. G. Brown and T. J. King, *J. Chem. Soc., Chem. Commun.*, 1976, 266; D. Brown, J. R. Evans and R. A. Fletton, *J. Chem. Soc., Chem. Commun.*, 1979, 282. The latter authors coined the term 'clavam'.

3 (*a*) M. Wanning, H. Zähner, B. Krone and A. Zeeck, *Tetrahedron Lett.*, 1981, **22**, 2539; (*b*) D. L. Pruess and M. Kellett, *J. Antibiot.*, 1983, **36**, 208; (*c*) J. E. Baldwin, R. M. Adlington, J. S. Bryans, A. O. Bringhen, J. B. Coates, N. P. Crouch, M. D. Lloyd, C. J. Schofield, S. W. Elson, K. H. Baggaley, R. Cassels and N. Nicholson, *Tetrahedron*, 1991, **47**, 4089.

4 W. Nagata, *Pure Appl. Chem.*, 1989, **61**, 325; M. Murakami, T. Aoki, M. Matsuura and W. Nagata, *J. Antibiot.*, 1990, **43**, 1441; H. R. Pfaendler, W. Hendel and U. Nagel, *Z. Naturforsch. Teil B.*, 1992, **47**, 1037; H. Wild and W. Hartwig, *Synthesis*, 1992, 1099; H. Wild, *Tetrahedron Lett.*, 1993, **34**, 285; H. R. Pfaendler, F. Weisner and K. Metzger, *Bioorg. Med. Chem. Lett.*, 1993, **3**, 2211; M. Botta, M. Crucianelli, R. Saladino, C. Mozzetti and R. Nicoletti, *Tetrahedron*, 1996, **52**, 10205; H. R. Pfaendler and C. Medicus, *Bioorg. Med. Chem. Lett.*, 1997, **7**, 623; P. Couture and J. Warkentin, *Can. J. Chem.*, 1998, **76**, 241.

5 J. Brennan, G. Richardson and R. J. Stoodley, *J. Chem. Soc., Chem. Commun.*, 1980, 49; G. H. Hakimelahi and G. Just, *Can. J. Chem.*, 1981, **59**, 941; J. Brennan, G. Richardson and R. J. Stoodley, *J. Chem. Soc., Perkin Trans. 1*, 1983, 649; D. Häbich, P. Naab and K. Metzger, *Tetrahedron Lett.*, 1983, **24**, 2559; B. H. Lee, A. Biswas and M. J. Miller, *J. Org. Chem.*, 1986, **51**, 106.

6 Synthetic routes to oxapenams: (*a*) S. Oida, A. Yoshida and E. Ohki, *Chem. Pharm. Bull.*, 1978, **26**, 448; (*b*) T. Kobayashi, Y. Iwano and K. Hirai, *Chem. Pharm. Bull.*, 1978, **26**, 1761; (*c*) P. H. Bentley and E. Hunt, *J. Chem. Soc., Perkin Trans. 1*, 1980, 2222; (*d*) J. C. Müller, V. Toome, D. L. Pruess, J. F. Blount and M. Weigele, *J. Antibiot.*, 1983, **36**, 217; (*e*) A. G. Brown, D. F. Corbett, J. Goodacre, J. B. Harbridge, T. T. Howarth, R. J. Ponsford, I. Stirling and T. J. King, *J. Chem. Soc., Perkin Trans. 1*, 1984, 635; (*f*) S. De Bernardo, J. P. Tengi, G. J. Sasso and M. Weigele, *J. Org. Chem.*, 1985, **50**, 3457; (*g*) D. Hoppe and T. Hilpert, *Tetrahedron*, 1987, **43**, 2467; (*h*) B. Furman, Z. Kaluza and M. Chmielewski, *J. Org. Chem.*, 1997, **62**, 3135; (*i*) O. Neuss, B. Furman, Z. Kaluza and M. Chmielewski, *Heterocycles*, 1997, **45**, 265.

7 O. Tsuge and S. Kanemasa, *Advanced Heterocyclic Chemistry*, ed. A. R. Katritzky, Academic Press, San Diego, 1989, vol. 45, p. 231.

8 (*a*) S. R. Martel, R. Wisedale, T. Gallagher, L. D. Hall, M. F. Mahon, R. H. Bradbury and N. J. Hales, *J. Am. Chem. Soc.*, 1997, **119**, 2309; (*b*) D. Planchenault, R. Wisedale, T. Gallagher and N. J. Hales, *J. Org. Chem.*, 1997, **62**, 3438; (*c*) S. R. Martel, D. Planchenault, R. Wisedale, T. Gallagher and N. J. Hales, *Chem. Commun.*, 1997, 1987.

9 B. Furman, P. Krajewski, Z. Urbanczyk-Lipkowska, J. Frelek, Z. Kaluza, L. Kozerski and M. Chmielewski, *J. Chem. Soc., Perkin Trans. 2*, 1998, 1737.

10 D. A. Fletcher, R. F. McMeeking and D. J. Parkin, *J. Chem. Inf. Comput. Sci.*, 1996, **36**, 746.

Communication 8/08688E

ChemComm

Diastereoselective iodoamidation of 3-acetyloxybut-1-enylamines: simple synthesis of a precursor of aza sugars involving a pyrrolidine ring

Woo Song Lee, Ki Chang Jang, Jin Hyo Kim and Ki Hun Park*

Department of Agricultural Chemistry, Gyeongsang National University, Chinju 660-701, Korea.
E-mail: khpark@gshp.gsnu.ac.kr

Received (in Cambridge, UK) 20th November 1998, Accepted 23rd December 1998

3-Acetyloxybut-1-enylamines 3–9 were easily transformed using iodine to pyrrolidine derivatives 3a–9a, precursors for aza sugars, *via* a diastereoselective iodoamidation.

Since the discovery that polyhydroxylated pyrrolidines are potent glycosidase inhibitors with potential therapeutic utility in the treatment of various diseases such as diabetes,[1] cancer[2] and viral infections,[3] much attention has been concentrated on the development of convenient and efficient routes to these compounds. In general, synthetic routes to aza sugars require azide displacement/reduction and intramolecular N-alkylative cyclisation with protecting group manipulation,[4] starting from carbohydrates or non-carbohydrates. Here we report the highly diastereoselective iodoamidation of 3-acetlyoxybut-1-enylamines **1** for the preparation of pyrrolidine derivatives **2** (*e.g.* anisomycine,[5] 3,4-dihydroxyprolinol,[6] swainsonine[7] and lentiginosine[8]) (Scheme 1).

The requisite substrates **3**–**9** were prepared easily by the usual method from commercially available L-tyrosin, L-phenylalanine and L-serine.[9]† Fortunately, each diastereomeric allylic alcohol given by the Grignard reaction could be isolated in pure form by column chromatography. We chose the 9-phenylfluoren-9-yl (Pf) group for protection of the amine since this protecting group has been shown to inhibit deprotonation at the α-position of α-amino aldehydes.[10] α-Amino aldehydes having the Pf group are very stable to Grignard reaction conditions.[11]

Compound **3** was treated with I_2 under biphasic conditions (aq. $NaHCO_3$–THF–Et_2O = 2 : 1 : 1) at room temperature for 3 h to give the all *trans* pyrrolidine **3a** (*vide infra*) as the sole product in high yield *via* a diastereoselective iodoamidation. Although THF, MeOH, CH_2Cl_2 and MeCN have been found to be acceptable solvents for iodoamidation, these solvents required much longer reaction times and resuted in 35–50% recovery of the starting material. As shown in Table 1, the optimum reaction conditions involved biphasic conditions to improve reactivity and affording pyrrolidine **3a**.

Treatment of **4** under the same conditions afforded a 25 : 1 ratio of the *cis* and *trans* isomers of pyrrolidine **4a**. Compounds **5** and **6** were cyclized according to these standard conditions to give the expected the corresponding pyrrolidines *trans*-**5a** and *cis*-**6a** in high yield, respectively. Compound **7** was also exposed to the same reaction conditions to give *cis*-**7a** in a ratio of 20 : 1 in 66% yield. In the case of starting materials *trans*-**8** and *cis*-**9**,‡ this solvent mixture was not suitable. Thus, compounds **8** and **9** were treated with I_2 in THF to give the corresponding *trans*-**8a** and *cis*-**9a** in 92% (based on 65% conversion) and 88% (based on 80% conversion) yields, respectively (Table 2). The structures of all pyrrolidines **3a**–**9a** were confirmed by their characteristic spectroscopic data.§

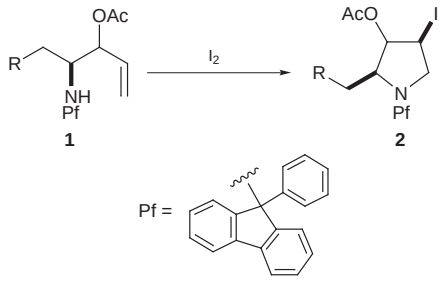

Scheme 1

The relative stereochemistries of the products **3a** and **4a** were determined from their ^{1}H NMR spectra based on the coupling constant values and 2D NOE experiments. For *trans*-**3a**, proton H_3 (t like, $J_{2,3}$, $J_{3,4}$ = 5.1 Hz) adjacent to the acetyloxy group gave weak correlation with protons (H_2 and H_4) adjacent to the *p*-tolylmethyl and iodine groups, but strong NOE cross peaks were observed between H_2–H_4 and H_2–H_{5b}, thereby allowing one to assign its relative stereochemistry. In pyrrolidine *cis*-**4a**, proton H_3 (t like, $J_{2,3}$, $J_{3,4}$ = 6.9 Hz) adjacent to the acetyloxy group displayed strong mutual correlation with the protons (H_2 and H_4) adjacent to the *p*-tolylmethyl and iodine groups, thereby verifying the structure of *cis*-**4a** as shown in Fig. 1.

Based on the coupling constant values in the high-field ^{1}H NMR spectra of *trans*-**3a** and *cis*-**4a**, the stereochemistries of *trans*-**5a** (H_3, t like, $J_{2,3}$, $J_{3,4}$ = 5.1 Hz) and *cis* **6a** (H3, t like, $J_{2,3}$, $J_{3,4}$ = 6.9 Hz) could be determined from each coupling constant value. The stereochemistries of *trans*-**8a** (H3, dd, $J_{2,3}$ = 4.8, $J_{3,4}$ = 3.4 Hz) and *cis* **9a** (H3, dd, $J_{2,3}$ = 2.4, $J_{3,4}$ = 4.2 Hz) were also confirmed using coupling constant values.

Although numerous construction methods for the electrophilic cyclisation have been developed,[12] the closest literature precedent to this haloamidation has been independently studied by the groups of Takahata[13] and Yoshida.[14] Takahata has shown that iodine-induced lactamization of γ,δ-unsaturated thioimidates proceeds regioselectively to provide γ-lactams. Yoshida has reported that *N*-(*p*-tolylsulfonyl)pent-4-enylamines were subjected to stereoselective haloamidation to afford mainly *cis* substituted pyrrolidines. Although these methodologies have been proven to be useful protocols, they are of limited use for the direct synthesis of polyhydroxylated aza sugars because these reactions proceed *via* 5-*exo*-*trig* cyclisation. Thus, we are the first to observe chiral induction on the pyrrolidine ring through an diastereoselective iodoamidation and to succeed in

Table 1 Solvent effects in stereoselective iodoamidation[a]

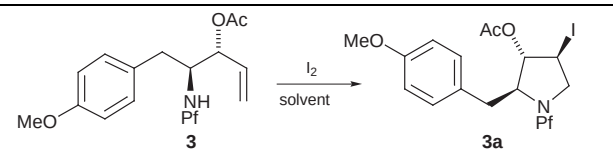

Solvent	I_2/equiv.	*t*/h	Yield (%)[b]
THF	3.0	15	48[c]
MeOH	3.0	18	45[d]
CH_2Cl_2	3.0	6	50[e]
MeCN	3.0	6	60[f]
Biphase[g]	3.0	3	92

[a] All reactions were carried out under room temperature. [b] Isolated yield. [c] 48% Recovery of starting material. [d] 40% Recovery of starting material. [e] *50% Recovery of starting material.* [f] 35% Recovery of starting material. [g] $NaHCO_3$–THF–Et_2O = 2 : 1 : 1.

Table 2 Diastereoselective iodoamidation of 3-acetoxybut-1-enylamines with iodine

Substrates[a]	Conditions	Products[b]	Yield[c]
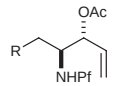 **3** R = *p*-tolyl	I_2,biphase,[d] room temp. 3 h	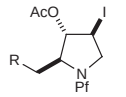 **3a**	92% (sole)
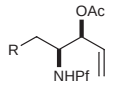 **4** R = *p*-tolyl	I_2,biphase, room temp. 3.5 h	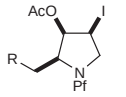 **4a**	90% (25 : 1)
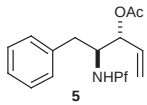 **5**	I_2,biphase, room temp. 3 h	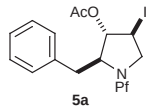 **5a**	90% (62 : 1)
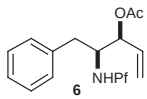 **6**	I_2,biphase, room temp. 3 h	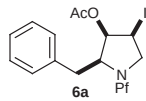 **6a**	90% (5 : 1)
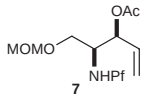 **7**	I_2,biphase, room temp. 10 h	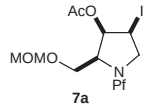 **7a**	66% (21 : 1)
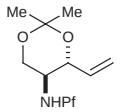 **8**	I_2,THF, room temp. 10 h	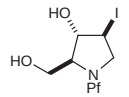 **8a**	92%[e] (20 : 1)
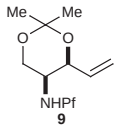 **9**	I_2,THF, room temp. 10 h	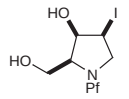 **9a**	88%[f] (sole)

[a] All allylic alcohols are enantiomeric pure. [b] The stereochemistry was signed by ^{1}H NMR and 2D NOE experiments. [c] Isolated yields. [d] 3 equiv. of I_2, aq. $NaHCO_3$–THF–Et_2O = 2 : 1 : 1. [e] Based on 65% conversion of starting material and 35% cleavage of the isopropylidene group of **8**. [f] Based on 80% conversion of starting material and 20% cleavage of the isopropylidene group of **9**.

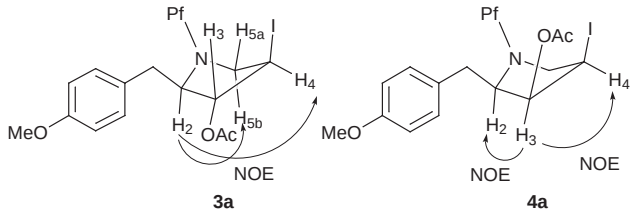

Fig. 1 NOE interactions derived from NOESY experiments.

using a strong electron-donating group, 9-phenylfluoren-9-yl (Pf), on an amine moiety.

In conclusion, we found that optically active starting materials **1** as chiral building blocks are converted easily to pyrrolidine derivatives **2** *via* a diastereoselective iodoamidation. These species should be valuable for the total synthesis of polyhydroxylated aza sugars having a pyrrolidine ring and may be suitable for substitution with various nucleophiles (NaN_3, amines, alcohols, thiols and Grignard compounds), giving novel aza sugar derivatives. Thus, we are currently investigating the preparation of all six diasteromers of anisomycin and other 3,4-dihydroxyprolinols.

This work was supported by a grant from the High-technology Development Project for Agriculture, Forestry and Fisheries. We thank the Korea Science and Engineering Foundation for a fellowship supporting the Postdoctoral research of Dr Woo Song Lee.

Notes and references

† Starting materials **3**–**9** were prepared by a sequential reaction, namely, free animo acids were treated with TMSCl in MeOH to give methyl esters, the amino groups of which were protected with PfBr in CH_2Cl_2. The methyl esters were then subjected to reduction and Swern oxidation to afford aldehydes, which were reacted with vinylmagnesium bromide to give separable allylic alcohols.

‡ The relative stereochemistries of the corresponding acetonides *trans*-**8** (J = 8.1 Hz for the proton on oxygen) and *cis*-**9** (J = 1.0 Hz for the a proton on oxygen) were confirmed by coupling constant analysis.

§ *Selected data* for **3a**: colorless prisms, mp 67–68 °C; $[\alpha]_D^{22}$ +33.0 (*c* 1.3, $CHCl_3$); δ_H (500 MHz, $CDCl_3$) 1.61 (3H,s), 2.37 (1H, dd, *J* 4.0, 13.6), 2.44 (1H, dd, *J* 6.7, 10.1), 2.67 (1H, dd, *J* 9.7, 13.6), 2.73 (1H, m), 3.00 (1H, dd, *J* 2.7, 10.2), 3.28 (1H, dt, *J* 4.3, 5.1), 3.71 (3H, s), 4.56 (1H, t-like, $J_{2,3}$, $J_{3,4}$ 5.1), 6.72 (2H, d, *J* 8.7), 6.89 (2H, d, *J* 8.7), 7.23–7.34 (13H, m). For **4a**: colorless prisms, mp 70–71 °C; $[\alpha]_D^{20}$ −22.9 (*c* 1.2, $CHCl_3$); δ_H (500 MHz, $CDCl_3$): 2.08 (3H, s), 2.19 (1H, dd, *J* 3.4, 14.1), 2.65 (1H, dd, *J* 3.7, 9.2), 2.86 (1H, dd, *J* 10.9, 14.1), 3.17 (1H, dd, *J* 9.2, 11.2), 3.43 (1H, ddd, *J* 3.5, 7.2, 10.8), 3.55 (1H, ddd, *J* 3.7, 7.2, 8.1), 5.17 (1H, t like, $J_{2,3}$, $J_{3,4}$ 6.9), 6.65 (2H, d, *J* 8.7), 6.87 (2H, d, *J* 8.7), 7.24–7.75 (13H, m).

1 S. Horri, H. Fukase, T. Matsuo, Y. Kameda, N. Asano and K. Matsui, *J. Med. Chem*., 1986, **29**, 1038.
2 M. A. Spearman, J. C. Jamieson and J. A. Wright, *Exp. Cell Res*., 1987, **168**, 116; K. Tsukamoto, A. Uno, S. Shimada and G. Imokaw, *Clin. Res*., 1989, **37A**, 722.
3 A. Karpas, G. W. J. Fleet, R. A. Dwek, S. Petursson, S. K. Mamgoong, N. G. Ramsden, G. S. Jacob and T. W. Rademacher, *Proc. Natl. Acad. Sci. U.S.A.*, 1988, **85**, 9229; G. W. J. Fleet, *FEBS Lett*., 1988, **237**, 128.
4 G. Kinast and M. Schedel, *Angew. Chem. Int. Ed. Engl*., 1981, **20**, 805; A. Vasella and R. Voeffray, *Helv. Chim. Acta*, 1982, **65**, 1134; H. Iida, N. Yamazaki and C. Kibayashi, *J. Org. Chem*., 1987, **52**, 3337; D. Beaupere, B. Stasik, R. Uzan and G. Demailly, *Carbohydr. Res*., 1989, **191**, 163; C. H. von der Osten, A. J. Sinskey, C. F. Barbas, R. L. Pederson, Y.-F. Wang and C.-H. Wong, *J. Am. Chem. Soc*., 1989, **111**, 3924; G. W. J. Fleet, N. M. Carpenter, S. Petursson and N. J. Ramsden, *Tetrahedron Lett*., 1990, **31**, 409; A. Straub, F. Effenberger and P. Fischer, *J. Org. Chem*., 1990, **55**, 3926.
5 D. P. Schumacher and S. S. Hall, *J. Am. Chem. Soc*., 1982, **104**, 6076; H. H. Baer and M. Zamkanei, *J. Org. Chem*., 1988, **53**, 4786; R. Ballini, E. Marcantoni and M. Petrini, *J. Org. Chem*., 1992, **57**, 1316.
6 G. W. J. Fleet, S. J. Nicolas, P. W. Smith, S. V. Evans, L. E. Fellows and R. J. Nash, *Tetrahedron Lett*., 1985, **26**, 3127; N. Asano, K. Oseki and K. Matsui, *J. Med. Chem*., 1994, **37**, 3710.
7 H. Setoi, H. Takeno and M. Hashimoto, *J. Org. Chem*., 1985, **50**, 3948; R. B. B. III, J.-R. Choi, W. D. Montgomery and J. K. Cha, *J. Am. Chem. Soc*., 1989, **111**, 2580.
8 S. Nukui, M. Sodeoka, H. Sasaki and Shibasaki, *J. Org. Chem*., 1995, **60**, 398.
9 F. J. Sardina and H. Rapoport, *Chem. Rev*., 1996, **96**, 1825.
10 W. D. Lubell and H. Rapoport, *J. Am. Chem. Soc*., 1987, **109**, 236.
11 M. Gerspacher and H. Rapoport, *J. Org. Chem*., 1991. **56**, 3700.
12 S. Robin and G. Rousseau, *Tetrahedron*, 1998, **54**, 13681.
13 H. Takahata, T. Tamotsu and Y. Takao, *J. Org. Chem*., 1989, **54**, 4812; H. Takahata, K. Yamazaki, T. Takamatsu, T. Yamazaki and T. Momose, *J. Org. Chem*., 1990, **55**, 3947.
14 Y. Tamaru, S. Kawamura, K. Tanaka and Z. Yoshida, *Tetrahedron Lett*., 1984, **25**, 1063; Y. Tamaru, S.-i. Kawamura, T. Bando, K. Tanaka, M. Hojo and Z.-i. Yoshida, *J. Org. Chem*., 1988, **53**, 5491.

Communication 8/09083A

Antipodal forms of cephem derivatives *via* stereochemical manipulations of the cephalosporin nucleus

Francesco De Angelis,*[a] Cristina Mozzetti,[b] Alessandra Di Tullio[a] and Rosario Nicoletti[b]

[a] *Dipartimento di Chimica, Ingegneria Chimica e Materiali, Università dell'Aquila, Coppito, L'Aquila, I-67010 Italy. E-mail: deangelis@axscaq.aquila.infn.it*

[b] *Dipartimento di Chimica,Università di Roma 'La Sapienza', Roma, Italy*

Received (in Cambridge, UK) 16th November 1998, Accepted 16th December 1998

Two complementary strategies have been developed in order to convert a cephalosporin derivative, characterized by the 'natural' absolute configuration of the two stereogenic centers, into its enantiomer, as an optically pure compound.

In the field of bioactive molecules asymmetry plays a fundamental role;[1] chiral drugs, in particular, are developed as single enantiomers,[2] since the optical antipode of the active compound must be regarded as a different substance with possible different biological targets. In the course of our studies aimed at developing cephem derivatives with altered biological activity, we sought a means of synthesizing, in homochiral form, bis-epimeric (relative to the stereochemistry of the natural compound) cephalosporins, starting from a commonly available β-lactam precursor (Scheme 1). Totally stereoselective syntheses of β-lactams with altered chirality have already been described by other research groups, but they have principally focused their attention on penam derivatives, usually in mono-epimeric forms, or on monobactam compounds.[3] A route to a cephalosporin enantiomer has been recently disclosed, where 6-aminopenicillanic acid (6-APA) has been used as the starting material.[4] Here we report on two alternative strategies which lead to the cephalosporin enantiomers of natural occurring (6*R*,7*R*)-cephalosporins, starting from 7-aminodesacetoxy-cephalosporanic acid (7-ADCA) **1**. In view of this target we have explored pathways to both epimeric forms, at C-6 and C-7, of the protected cephem derivative **2** obtained from **1**, followed by epimerization of the other stereogenic center to finally produce the cephalosporin antipodal form **3**.

The first strategy we describe here (Scheme 2) for the epimerization at the C-6 position exploits the well-known chlorinolysis of the thiazolidine ring of penicillins first developed by Kukolja,[5] followed by reconstruction of the isomerically modified skeleton.[6] Although this procedure is also cited by other authors,[4,7] and also worked well in our hands on penam derivatives, it failed when, in our case, it was applied on the cephem derivative, leaving the substrate **2** unreacted in the presence of added chloride ion, or it led to decomposition products under forced conditions. After many exploratory reactions, **2** was converted in high yields into a 2 : 3 mixture of the azetidinone sulfenyl chloride **4** and the chloro derivative **5** by reaction with an equimolar amount of chlorine and a slight excess amount of $TiCl_4$, at −15 °C. The two compounds were then isolated by chromatography over deactivated silica gel. In marked contrast to the penam congeners,[5] in our case only the *trans* isomers were produced. It is also worth noting that the allylic sulfenyl chloride **4**, in the presence of chlorine or of a Lewis acid, is highly susceptible to nucleophilic displacement of SCl_2 with formation of the unwanted derivative **5**. This compound in fact can also be readily prepared from **4** by treatment with 1 equiv. of chlorine. On the other hand, **4** formed as the only isolable product when **2**, as a solid powder, was rapidly treated with an excess of freshly distilled sulfuryl chloride, at 0 °C, and practically at the same time the reaction quenched with a large amount of toluene. The ring closure step was performed by treatment of **4** with 1 equiv. of $SnCl_2$ dihydrate, in dioxane, at the reflux temperature for 15 min to give a 1 : 2 mixture of the *cis*/*trans* isomers **2** and **6**, which were separated by chromatography on silica gel.

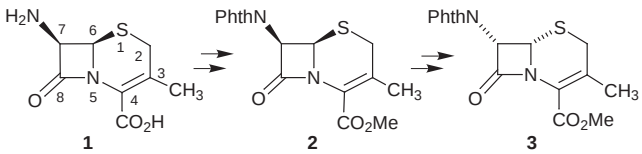

Scheme 1

Oxidation of **6** with MCPBA gave a 1 : 1 mixture of the two sulfoxide epimers **7** and **8**,[8] which were separated by taking advantage of their marked difference in solubility. The (1*R*)-sulfoxide **8**, in contrast to its epimer **7**, is practically insoluble at room temperature in many solvents such as methanol, acetone and THF; **7** in fact was completely recovered as a pure compound by treating the reaction mixture with EtOAc. Compound **7** was then equilibrated by base to partially give the stereoisomer **9** (a 2 : 1 mixture in favour of **7**), with a *cis* arrangement of the β-lactam hydrogens. The equilibrium position between the two epimers, verified also by starting from the *cis* isomer, was slowly reached with Et_3N in CH_2Cl_2, but very rapidly with a stronger base like DBU; in both cases there

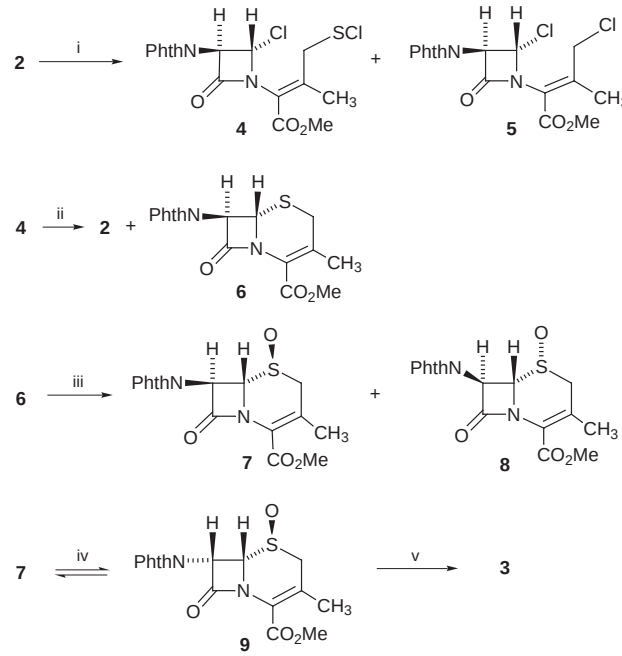

Scheme 2 *Reagents and conditions*: i, $Cl_2/TiCl_4$, CH_2Cl_2, −15 °C, 87% (**4** : **5** *ca.* 2 : 3) [or SO_2Cl_2 (instant treatment), 0 °C, to give only **4**, 66%]; ii, $SnCl_2 \cdot 2H_2O$, 1,4-dioxane, reflux, 15 min, 45% (**6** : **2** *ca.* 2 : 1); iii, MCPBA, $CHCl_3$, 25 °C, 3 h, 95% (**7** : **8** *ca.* 1 : 1); iv, DBU, CH_2Cl_2, 25 °C, immediate reaction (**9** : **7** *ca.* 1 : 2); v, PBr_3, CH_2Cl_2, 0 °C, immediate reaction, 52%.

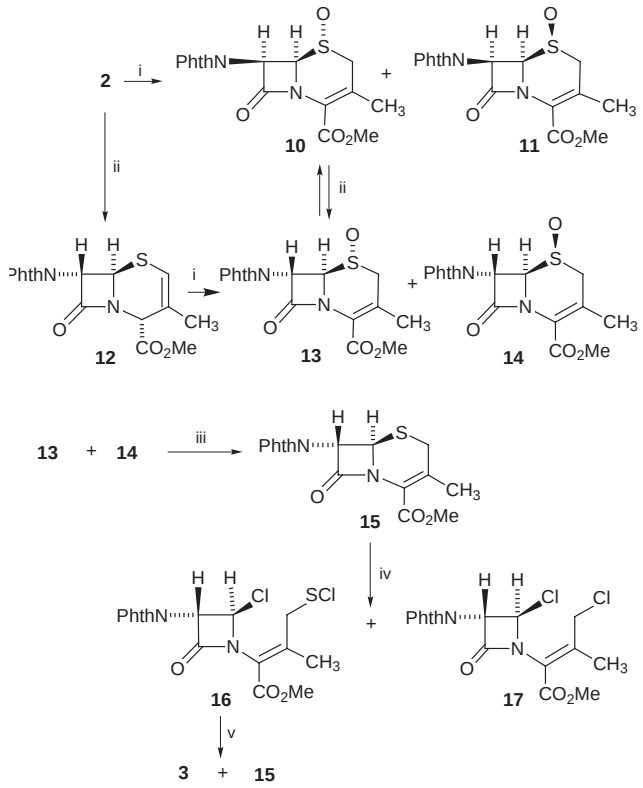

Scheme 3 *Reagents and conditions*: i, MCPBA, $CHCl_3$, 25 °C, 3 h (**10** : **11** *ca*. 9 : 1, 78%; **13** : **14** *ca*. 1 : 1, 84%); ii, DBU, CH_2Cl_2, 25 °C (**2** to **12**, 2 h; **13** : **10**, *ca*. 2:1, immediate reaction); iii, PBr_3, CH_2Cl_2, 0 °C, 10 min, 90%; iv, Cl_2, CH_2Cl_2, −15 °C, 10 min, 70% (**16** : **17** *ca*. 5 : 2)[or SO_2Cl_2 (instant treatment), 0 °C, 60% (**16** : **17** *ca*. 5 : 1)]; v, $SnCl_2{\cdot}2H_2O$, 1,4-dioxane, reflux, 15 min, 47% (**3** : **15** *ca*. 1 : 2).

is no loss of material and the remaining *trans* isomer was quantitatively recovered by chromatography. (1*R*)-Sulfoxide **8**, probably because of its very low solubility even in DMSO, does not seem to undergo equilibration at any observable rate. Finally, reduction of **9** with PBr_3[9] gave the enantiomer **3** of derivative **2** of 7-ADCA as an optically pure compound. As expected, the enantiomers gave equal and opposite CD spectra, thus showing also the stereochemical correctness of the individual reaction steps.[10] It is worth pointing out that the 7-phthalimido group, besides being relatively chemically stable, could play an important role in determining the isomer ratio in the epimerization steps. It is also easily removable,[11] thus giving potential access to pharmacologically useful 7-amidic substitution.

In order to complete the general strategy to the stereochemical manipulation of the cephem nucleus, we have also developed a complementary, which, *mutatis mutandis*, ideally represents the 'mirror image' of the one we have just described (see Scheme 3). Partial epimerization at C-7 was realized by base treatment of the cephalosporin (1*R*)-sulfoxide derivative **10**:[9] **13**, which is the enantiomer of **7**, formed in 65% yield, the remaining 35% being the starting *cis* isomer **10**. More conveniently, complete epimerization at C-7 in **2** occurred by treatment with DBU to give the Δ^2-derivative **12**. Oxidation of **12** to the sulfoxides **13** and **14** was the necessary step in order to obtain retro-isomerization of the double bond to Δ^3. Compound **15**, which is the optical antipode of **6**, was obtained by PBr_3 reduction at the sulfoxide moieties of the two S-1 epimers. According to this procedure, the overall yield from **2** to **15** was practically quantitative.

The enantiomer **16** of the sulfenyl chloride **4** was then obtained (together with **17**) by chlorinolysis (Cl_2 or SO_2Cl_2) of the C-6–S-1 bond. In this case, the presence of $TiCl_4$ was not only unnecessary, but even lowered the reaction rate and yields. Pure **16** then followed the same destiny as its enantiomer **4**: ring closure gave a 2 : 1 mixture of **15** together with, once more, the required enantiomer **3** of the natural cephem derivative **2**. Chromatographic separation afforded **3** as a chemically and optically pure material (overall yield 6.0%, starting from **2**; recovered isomers, to be re-used in the reaction sequel, were not taken into account), which showed identical chemical–physical properties to the sample obtained by the other reaction pathway.[10]

In conclusion, the present work describes a versatile 'circular' strategy, exemplified by two complementary reaction sequences, to convert a natural cephalosporin derivative into its optical antipode. The chemical transformations involved, even if the overall efficiency of the routes is low due to the yields of some stages being poor, appear significative in the cephalosporin chemistry context. Along the reaction paths, in fact, all the possible stereoisomers of cephalosporin sulfides and sulfoxides, susceptible of further chemical elaborations, have been encountered.[12]

Funds are from Italian CNR (Consiglio Nazionale delle Ricerche) and the Ministry of University and Scientific and Technological Research. Thanks are due to Dr M. C. Gaudiano for CD spectra.

Notes and references

1 E. J. Ariens, *Med. Res. Rev.*, 1986, **6**, 451.
2 S. C. Stinson, *Chem. Eng. News*, 1992, **70**, 46; 1993, **71**, 38.
3 A. Vlietinck, E. Roets, P. Claes, G. Janssen and H. Vanderhaeghe *J. Chem. Soc., Perkin Trans. 1*, 1973, 937; J. E. Baldwin, R. Y. Chan and J. D. Sutherland, *Tetrahedron Lett.*, 1994, **35**, 5519; D. R. Wagle, C. Garai, M. G. Monteleone and A. K. Bose, *Tetrahedron Lett.*, 1988, **29**, 1649; C. Somoza and O. A. Mascaretti, *Tetrahedron*, 1988, **44**, 7007.
4 T. Fekner, J. E. Baldwin, R. M. Adlington and C. J. Schofield, *Chem. Commun.*, 1996, 1989.
5 S. Kukolja, *J. Am. Chem. Soc.*, 1971, **93**, 6267.
6 S. Kukolja, *J. Am. Chem. Soc.*, 1971, **93**, 6269.
7 J. E. Baldwin and D. P. Hesson, *J. Chem. Soc., Chem. Commun.*, 1976, 667; R. G. Micetich, R. Singh, W. O. Merlo, D. M. Tetteh, C. C. Shaw and R. B. Morin, *Heterocycles*, 1984, **22**, 2757.
8 At difference with our case, it is well-known [R. D. G. Cooper and D. O. Spry, in *Cephalosporins and Penicillins, Chemistry and Biology*, ed. E. H. Flynn, Academic Press, New York and London, 1972, p. 209] that oxidation with MCPBA of *N*-phthalimido-*cis*-penam and cephem derivatives affords almost exclusively the (1*R*)-sulfoxide.
9 C. F. Murphy and J. A. Webber, in *Cephalosporins and Penicillins, Chemistry and Biology*, ed. E. H. Flynn, Academic Press, New York and London, 1972, p. 137.
10 Spectral data in agreement with the reported structures were obtained for all compounds. In particular, the *cis* and *trans* arrangements of the β-lactam protons, as well as the chirality at S-1 of the sulfoxide derivatives, were precisely indicated by ^{1}H NMR spectroscopy: P. V. De Marco and R. Nagarajan, in *Cephalosporins and Penicillins, Chemistry and Biology*, ed. E. H. Flynn, Academic Press, New York and London, 1972, p. 330 and pp. 349–353: *Selected data* for **8**: mp = 176–179 °C; $[\alpha]_{365}$ + 238, $[\alpha]_D$ + 1 (*c* 0.2, EtOH); δ_H(200 MHz, $CDCl_3$) 2.38 (s, 3H), 3.28 (AB system, *J* 14, 2H), 3.86 (s, 3H), 5.15 (d, *J* 4, 1H), 5.75 (d, *J* 4, 1H), 7.88 (m, 4H); ν_{max}(Nujol)/cm^{-1} 1787 (br, C=O β-lactam), 1729 (br, C=O ester and imide); *m*/*z* (EI) 358 [M$^+$].
11 S. Kukolja and S. R. Lammert, *J. Am. Chem. Soc*., 1975, **97**, 5582; T. Kamiya, M. Hashimoto, O. Nakaguchi and T. Oku, *Tetrahedron*, 1979, **35**, 323.
12 The only epimer absent in the routes described is the enantiomer of sulfoxide **11**, which can be obtained, together with **9**, by direct oxidation of **3**.

Communication 8/08911F

ChemComm

Novel spiro-polymers with enhanced solubility

Saad Makhseed and Neil B. McKeown*

Department of Chemistry, University of Manchester, UK M13 9PL. E-mail: neil.mckeown@man.ac.uk

Received (in Cambridge, UK) 2nd November 1998, Accepted 11th December 1998

Well-defined spiro-polymers which are freely soluble in organic solvents can be prepared from the ketal-forming reaction between pentaerythritol and either a diketone bearing alkyl solubilising groups or a diketone which generates a contorted polymeric structure.

Ladder polymers are of interest as high performance materials due to their great rigidity, lack of rotational freedom and high thermal stability which arises because mass deterioration requires the scission of two covalent bonds within the same cyclic subunit.[1] However, they are difficult materials to make due to the need for an efficient polymerisation reaction that forms cyclic inter-monomer linkages. Spiro-polymers are a subclass of ladder polymers in which adjacent rings share a common atom.[1,2] Spiro-polyketals such as **1a**, readily prepared from pentaerythritol **2** and cyclohexane-1,4-dione **3a** (Scheme 1), are particularly attractive synthetic targets because the two bonds of the cyclic ketal-linking group form almost simultaneously during polymerisation. In addition, ketal formation is an efficient equilibrium process which can be driven to completion by the removal of water. Unfortunately, the regular structure of **1a** results in a highly crystalline material which has poor solubility in all solvents, including refluxing toluene. This leads to the formation of low molar mass products due to precipitation at an early stage of the polymerisation and prohibits molecular mass determination of the resulting material.[3,4] In addition, the possibility that **1a** is cross-linked by non-cyclic acetal linkages cannot be disproved by solution-based structural characterisation.

Our interests lie in the utilisation of spiro-polyketals as molecular-scale scaffolding for the assembly of rigid polymeric networks. However, soluble materials are required in order to assess the efficiency of ketal formation for macromolecule construction and to facilitate solution-based molecular mass determination. There are two common strategies for the improvement of the solubility of rigid polymers; decorating the polymer with solubilising groups (*e.g.* alkyl groups)[5] or introduction of structural irregularities which reduce the linearity of the polymer.[6] Here we describe the use of both of these approaches for obtaining soluble spiro-polyketals.

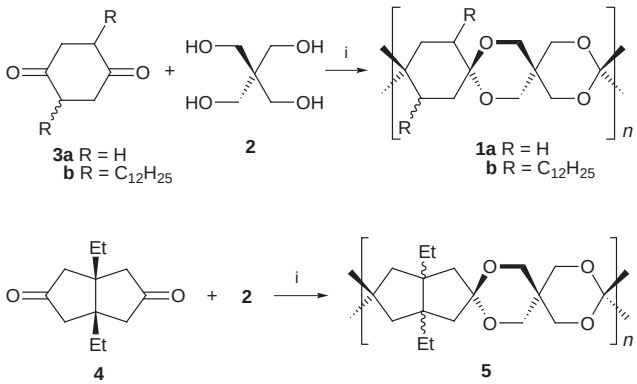

Scheme 1 *Reagents and conditions*: i, TsOH, toluene, reflux, 48 h.

The replacement of **3a** with 2,5-didodecylcyclohexane-1,4-dione **3b**, prepared by the base catalysed dialkylation of dimethyl 2,5-dioxocyclohexane-1,4-dicarboxylate followed by ester hydrolysis and decarboxylation,[7] in the spiro-polymerisation with **2** gives **1b** in good yield. This material is soluble in aprotic solvents (*e.g.* THF, CH_2Cl_2) and has ^{1}H and ^{13}C NMR spectra which are consistent with the proposed structure. Analysis using gel permeation chromatography (GPC) of a THF solution of **1b** (Table 1), using a calibration based on polystyrene standards, and NMR end-group analysis indicates only a modest degree of polymerisation ($<DP> \approx 8$–10), however, even this figure represents at least 24 spirocycles per molecule, on average.

It is known that alkyl chains adjacent to the ketone group have an adverse steric effect on ketal formation.[8] Therefore, we sought a diketone which could accommodate alkyl solubilising groups at sites where they would not interfere with ketal formation. The readily prepared 1,5-dialkylbicyclo[3.3.0]-octane-3,7-diones satisfy this criteria. It was found that 1,5-diethylbicyclo[3.3.0]octane-3,7-dione **4**, prepared from dimethyl 3-oxopentane-1,5-dioate and hexane-3,4-dione using the Weiss–Cook reaction,[9,10] undergoes ketalisation with **2** to give polymer **5** in good yield (Scheme 1). Despite the absence of long alkyl solubilising groups, polymer **5** is freely soluble in aprotic organic solvents (*e.g.* toluene, THF, CH_2Cl_2, DMSO). This solubility must arise from the non-linearity of the dione precursor **4** which results in a randomly contorted structure similar to the dynamic random coil configuration adopted by flexible polymers in solution (Fig. 1).

Both GPC and ^{13}C NMR end-group analysis (Table 1) indicates that **5** has a reasonable average molecular mass for a polymer derived from small-scale step-growth polymerisation ($<DP> \approx 28$–30). End groups give rise to clear signals corresponding to the carbonyl group (δ 215), the methylene groups adjacent to the carbonyl (δ 47.2; Fig. 2) and the methylene groups on the terminal pentaerythritol (δ 70.1). Calculation of average molecular mass was based on comparing the sum of the intensities of the two types of end-group methylene carbon signals with the combined intensity of the two types of methylene units within the main body of the polymer at δ 43.0–45.5 (Fig. 2) and 63.5–65.0. The apparent

Table 1 Yield, molecular mass data and glass transition temperatures for polymers **1b** and **5**. Molecular mass data is a range obtained for several samples

Polymer	Yield (%)	$<M_n>$ (gpc)	$<M_w>/<M_n>$	$<M_n>$ (NMR)	T_g/°C
1b	85	(5–6) × 10^3	1.6–1.8	(4–5) × 10^3	45[a]
5	88	(12–14) × 10^3	1.8–2.5	(8–9) × 10^3	180

[a] Sample appears to be partially crystalline (m.p. = 120 °C).

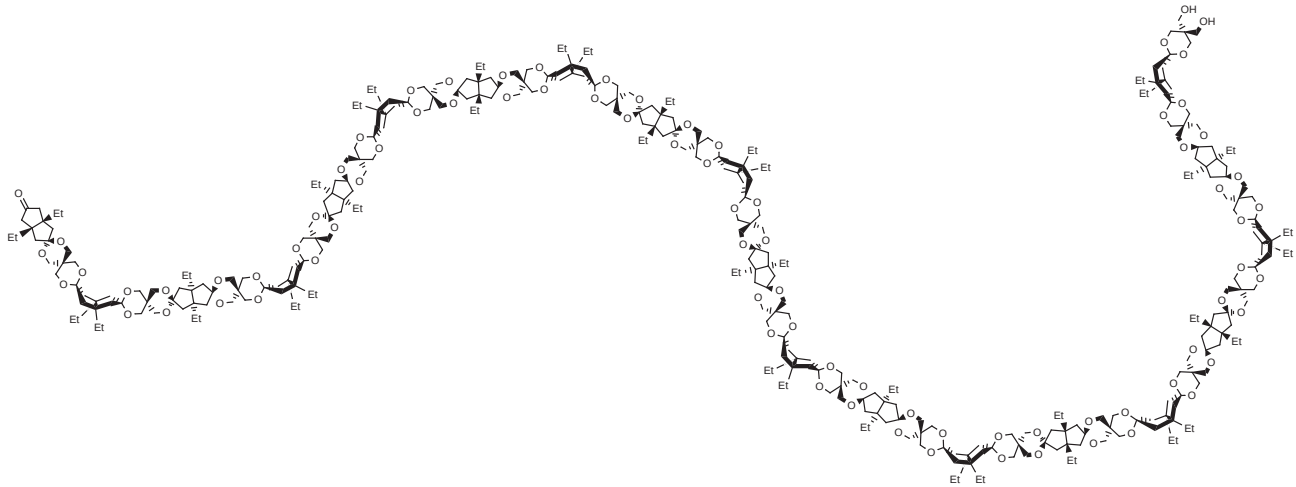

Fig. 1 A two-dimensional representation of the contorted configuration of polyketal **5** resulting from the bent shape of diketone **4**.

overestimation of the molecular mass by GPC, with respect to the absolute value estimated from end-group analysis, is attributable to the greater hydrodynamic volume per unit mass of rigid polymer **5** as compared to the polystyrene standards used for calibration. The observation of both ketone and alcohol end-groups in the ^{13}C NMR spectrum suggests that reaction conditions (*e.g.* higher concentration, longer reaction time) could be found for obtaining polymer **5** with greater molecular mass.

The irregular structure and low flexibility of polymer **5** results in it being a glassy solid with a high glass transition temperature (Table 1). Thermogravimetric analysis indicates that this material is stable up to 280 °C and it appears indefinitely stable in the solid phase but, unless suitable precautions are taken, it possesses only limited stability in solution towards hydrolysis. This study confirms that spiropolymers of reasonable molecular mass can be achieved by ketal formation. In particular, the use of unhindered but non-linear diketones such as **4** gives well-defined (*i.e.* not cross-linked) soluble polyketals which possess an unusual combination of rigidity and structural irregularity.

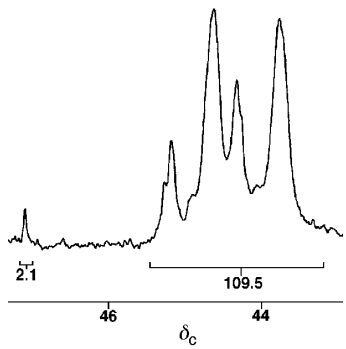

Fig. 2 Detail from the ^{13}C NMR spectrum of polyketal **5** showing the signal due to the methylene group adjacent to the terminal carbonyl (δ 47.2) and the methylene units derived from diketone **4** in the main body of the polymer (δ 43.0–45.5). Average molecular mass calculations used the stated intensities of these peaks together with those derived from the terminal pentaerythritol methylene signal (δ 70.1) and another well-defined group of signals at δ 63.5–65.0 from the pentaerythritol methylene signals in the main body of the polymer.

We thank Kuwait University for the provision of a studentship (S. M.).

Notes and references

1 W. J. Bailey, in *The Encyclopaedia of Polymer Science and Engineering*, Wiley, New York, 1993, Index vol., p. 158.
2 S. Nakamura, in *Polymeric Materials Encyclopaedia*, ed. J. C. Salamone, Academic Press, NewYork, 1996, vol. 10, p. 7854.
3 W. J. Bailey and A. A. Volpe, *J. Polym. Sci. (A-1)*, 1970, **8**, 2109.
4 R. W. Alder and B. S. R. Reddy, *Polymer*, 1994, **35**, 5765.
5 For example, M. Rehahn, A.-D. Schlüter, G. Wegner and W. J. Feast, *Polymer*, 1989, **30**, 1060.
6 J. M. G. Cowie, *Polymers: Chemistry and Physics of Modern Materials*, Blackie, Glasgow, 1991.
7 J. R. Anderson and O. Jørgensen, *J. Chem. Soc., Perkin Trans. 1*, 1979, 3095.
8 P. J. Kocienski, *Protecting Groups*, Thieme, Stuttgart, 1994.
9 U. Weiss and J. M. Edwards, *Tetrahedron Lett.*, 1968, 4885.
10 S. H. Bertz, J. M. Cook, A. Gawrish and U. Weiss, *Org. Synth.*, 1990, **Coll. Vol. 7**, 50.

Communication 8/08457B

Addition of nucleophiles to electron-deficient alkenes: structural studies on the incipient reaction and the zwitterionic intermediate

Paul C. Bell and John D. Wallis*

Chemical Laboratory, School of Physical Sciences, University of Kent, Canterbury, UK CT2 7NH. E-mail: jdw@ukc.ac.uk

Received (in Liverpool, UK) 2nd November 1998, Accepted 1st December 1998

Three distinct interactions between a Me_2N group and an electron-deficient alkene located in the *peri* positions of a naphthalene ring comprise an almost complete cyclisation, an incipient reaction, and a less favourable orientation of the nitrogen lone pair with respect to the alkene, which can be related to the electronic characteristics of the alkene substituents; the cyclised material is zwitterionic and is composed of the enolate of a β-dicarboxylic diester and a trialkylarylammonium cation.

Insight into bond forming and bond breaking processes in chemical reactions have been gained by analysing the geometries of interaction between pairs of functional groups which have been measured by X-ray diffraction.[1] Most notably, a reaction coordinate for the addition of a nucleophile to a carbonyl group was constructed from the structures of a range of molecules in which a tertiary amino group and a carbonyl group were held in close proximity.[2–4] Kirby and Jones studied the spontaneous cleavage of tetrahydropyranyl acetals and glucosides, and were able to show correlations between the length of the exocyclic C–O bond and reactivity.[5–7] Similar studies have been made on the addition of nucleophiles to triple bonds, notably nitriles[8–10] and alkynes.[11–13] The addition of a nucleophile to an electron-deficient carbon–carbon double bond is a very important reaction in organic synthesis. To begin a study of the correlation between the bond formation and bond breaking processes in this type of reaction, we have measured the interactions between a Me_2N group and different electron-deficient alkenes located in the *peri* positions of naphthalenes **1**–**3** by X-ray crystallography.† The quite distinct molecular

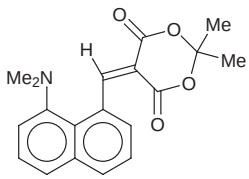

1

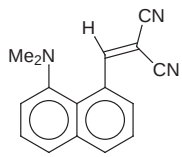

2

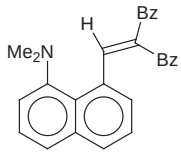

3

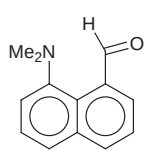

4

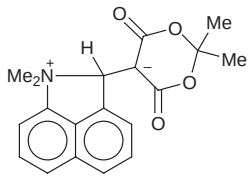

5

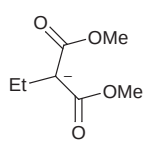

6

structures of these three compounds are presented in Fig. 1, and selected details of their molecular geometries are given in Table 1.

Results for compound **1** show that the nucleophilic addition of the Me_2N group to the alkene is almost complete, and that the structure lies much nearer to the zwitterionic formulation **5** in which a trialkylarylammonium cation and the enolate of a β-dicarboxylic diester coexist. The hexamethylguanidinium salt of the enolate of dimethyl ethylmalonate, **6**, has been reported previously.[14] In the zwitterion **5** the carbon–nitrogen bond [1.651(3) Å] is nearly fully formed, and the π bond of the alkene is almost completely broken [1.471(3) Å, *cf.* 1.510(6) Å in **6**]. The newly formed five-membered ring adopts a half chair conformation with the largest torsion angle [17.1(2)°] about the new N(1)–C(11) bond so that the *N*-methyl groups are displaced by different amounts from the naphthalene plane [C(18), −1.512(3); C(19), 0.860(3) Å].

In contrast, structures **2** and **3** are closer to their uncyclised formulations. However, there is a stronger interaction between the functional groups in **2** than in **3** as indicated by the shorter N(1)···C(11) distance, the lengthening of the alkene bond, and the orientation and in-plane displacement of the Me_2N group into a more favourable position for bond formation with the alkene. Thus, the N(1)···C(11) separations in **2** and **3** [2.413(2) and 2.679(2) Å respectively] are *ca*. 0.8 and 0.5 Å within the sum of the van der Waals radii for these atoms, and the alkene bond is lengthened to 1.354(2) Å in **2** whereas it is only 1.341(2) Å in **3**. Both substituents in **3** are displaced in the plane of the aromatic system in the same sense by *ca*. 2° away from their idealised positions; the Me_2N group is moved towards the other *peri* substituent, which has moved away. In comparison to this, the structure of **2** shows an increase of a further 2° in the displacement of the Me_2N group towards the alkene, but the alkene is displaced by 2° towards the Me_2N group, indicative of a larger attraction between these groups. The larger N(1)···C(11) separation in **3** is partly attained by an increase in the exocyclic

Table 1 Selected molecular geometry for **2**, **3** and **5** presented in order of decreasing attractive interaction between the *peri* groups

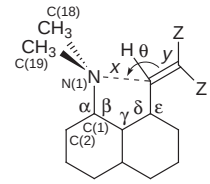

	x/Å	*y*/Å	α (°)	β (°)	γ (°)	δ (°)
5	1.651(3)	1.471(3)	128.6(2)	108.8(2)	113.3(2)	109.9(2)
2	2.413(2)	1.354(2)	124.3(2)	115.9(1)	120.4(1)	120.2(1)
3	2.679(2)	1.341(2)	122.3(2)	118.3(2)	123.5(2)	122.5(2)

	ε (°)	θ (°)	C(18)–N(1)–C(1)–C(2)	C(19)–N(1)–C(1)–C(2)	Naphthalene–alkene angle[a]
5	131.4(2)	114.9(2)	−71.9(2)	49.5(3)	65.5(1)
3	120.3(1)	112.5(1)	−81.5(2)	49.2(2)	64.0(2)
2	117.6(2)	118.0(1)	−105.0(2)	25.9(3)	54.4(1)

[a] Angle between naphthalene system and the plane of the alkene.

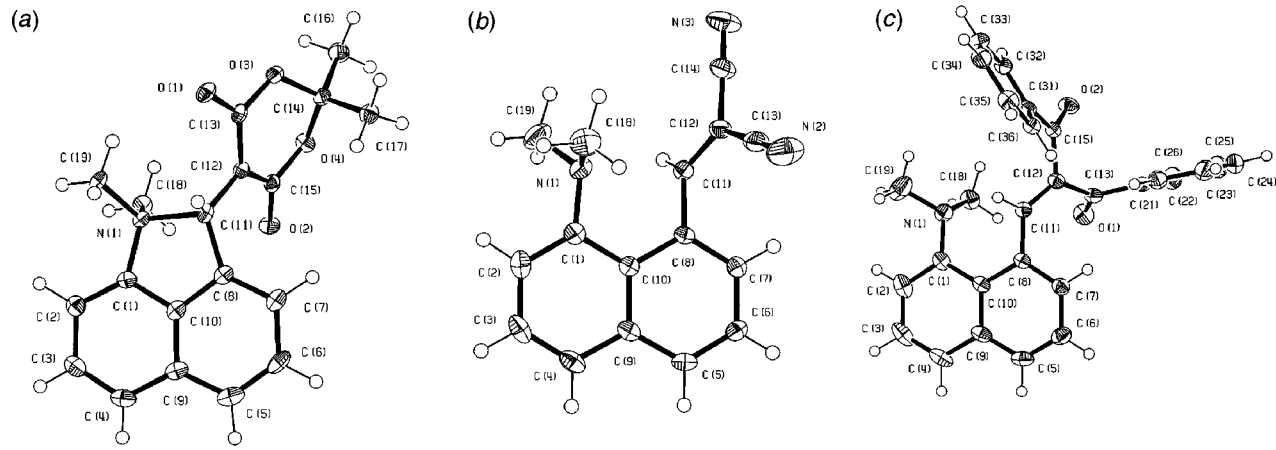

Fig. 1 The structures of molecules (*a*) **5**, (*b*) **2** and (*c*) **3** with atomic displacement parameters drawn at the 50% level.

bond angle at C(10) by *ca*. 3° in the naphthalene system. Furthermore, while the Me_2N group in **3** is oriented such that the axis of its lone pair would lie at 30° to the N(1)···C(11) vector, and thus poorly aligned with the α-C atom of the alkene, in **2** the alignment is considerably better, with the axis of the lone pair lying only 13° away from the N(1)···C(11) vector. Indeed, the orientation of the Me_2N group in **2** is very similar to that in the cyclised material **5**. There is evidence in **2** for a slight pyramidalisation at the alkene's α-C atom, C(11), where this atom deviates from the plane of its three neighbours by 0.087(7) Å towards the amino nitrogen atom. The failure of the nitrogen lone pair to be attracted to the alkene in **3** is due to the reduced conjugation of the carbonyl groups with the double bond. The torsion angles between the carbonyl groups and the alkene bond are 52.2(3) and –146.6(2)°. In **2** the cylindrical π-system of the nitrile groups ensure conjugation with the alkene, and compound **5** has cyclised since the carbonyl groups are held in conjugation with the developing carbanionic centre by the dioxane ring. The degrees of interaction between the *peri* groups in the three compounds studied mirror the pK_as of the methylene derivatives used to prepare them from **4**.[15] In contrast, the intrinsic rate constant for the reaction of secondary amines with benzylidene derivatives containing the same electron-attracting β-substituents as structures **1**–**3** is highest for the dinitrile $PhHC{=}C(CN)_2$.[16]

The structure of zwitterion **5** is particularly interesting. The enolate grouping shows an asymmetric geometry with the $^{-}$C(12)–C(13)=O(1) fragment showing a greater degree of enolate character than the $^{-}$C(12)–C(15)=O(2) moiety as indicated by a longer C=O bond [1.236(2) *cf*. 1.224(2) Å] and shorter C–C bond [1.409(3) *cf*. 1.428(2) Å]. This higher enolate character may be induced by the formation of a particularly short intermolecular hydrogen bond by O(1) with the naphthalene ring hydrogen atom *ortho* to the positively charged ammonium substituent [O(1)···H(2), 2.20(2) Å, O(1)···H(2)–C(2), 164(2)°]. In addition, each carbonyl oxygen atom makes an intramolecular contact with a methyl hydrogen atom and is involved in further intermolecular contacts with hydrogen atoms (O···C range: 2.38–2.53 Å). Similar contacts were observed between enolate **6** and hexamethylguadinium ions (2.31–2.59 Å) although in this case the enolate geometry was symmetrical [$^{-}$C–C: 1.412 and 1.413, C=O, 1.229 and 1.233 Å).

NMR studies on **2, 3** and **5** dissolved in $CDCl_3$ are consistent with **5** retaining its cyclic zwitterionic structure. The chemical shift for the *N*-methyl groups in **5** (δ 3.37) is *ca*. 0.7 ppm downfield of the corresponding resonances in **2** and **3**, and the shift of the methine hydrogen (δ 7.06) is *ca*. 1.6 ppm upfield of those for the alkenyl hydrogens in **2** and **3**. In the ^{13}C NMR spectrum of **5** the ring sp^3 carbon atom resonates at δ 99.1 and the signal from the carbanionic carbon occurs at δ 69.8. Further work to build up a more detailed picture of the reaction coordinate for nucleophilic addition to an alkene is in progress.

We thank the EPSRC for a studentship, SmithKline Beecham for financial support, the EPSRC mass spectrometry service for data, the EPSRC X-ray crystallography service for three data sets, and the Cambridge Structural Database.[17] We thank Professor R. F. Hudson and Professor A. Williams for helpful discussions.

Notes and references

† *Crystal data* for **2**: $C_{16}H_{13}N_3$, M_r = 247.29, monoclinic, a = 13.606(10), b = 9.042(5), c = 11.073(10) Å, β = 103.38(2)°, V = 1325.3 Å^3, Z = 4, $P2_1/a$, D_c = 1.24 g cm^{-3}, μ = 0.08 mm^{-1}, 2677 unique reflections, 2082 with $F > 4\sigma(F)$, R = 0.050, wR = 0.128. For **3**: $C_{28}H_{23}NO_2$, M_r = 405.47, monoclinic, a = 11.2537(4), b = 11.4933(5), c = 16.7819(6) Å, β = 93.884(2)°, V = 2165.6 Å^3, Z = 4, $P2_1/n$, D_c = 1.24 g cm^{-3}, μ = 0.08 mm^{-1}, 5350 unique reflections, 3759 with $F > 4\sigma(F)$, R = 0.057, wR = 0.164. For **5**: $C_{19}H_{19}NO_4$, M_r = 325.35, monoclinic, a = 9.918(3), b = 12.7145(9), c = 12.2801(8) Å, β = 90.99(1)°, V = 1548.3 Å^3, Z = 4, $P2_1/c$, $D_{c.}$ = 1.40 g cm^{-3}, μ = 0.1 mm^{-1}, 2381 unique reflections, 1724 with $F > 4\sigma(F)$, R = 0.040, wR = 0.095.

X-Ray diffraction data were collected at 150 K using Mo-Kα radiation located and refined with isotropic displacement parameters. CCDC 182/1110. Crystallographic data is available in CIF format from the RSC web site, see: http://www.rsc.org/suppdata/cc/1999/257

1 H.-B. Bürgi and J. D. Dunitz, *Structure Correlation*, VCH, Weinheim, 1994, vol. 1.
2 H.-B. Bürgi, J. D. Dunitz and E. Schefter, *J. Am. Chem. Soc.*, 1973, **95**, 5065.
3 W. B. Schweizer, G. Procter, M. Kaftory and J. D. Dunitz, *Helv. Chim. Acta*, 1978, **61**, 2783.
4 A. S. Cieplak, in ref. 1, ch. 6.
5 A. J. Briggs, R. Glenn, P. G. Jones, A. J. Kirby and P. Ramaswamy, *J. Am. Chem. Soc.*, 1984, **106**, 6200.
6 P. G. Jones and A. J. Kirby, *J. Am. Chem. Soc*., 1984, **106**, 6207.
7 P. G. Jones and A. J. Kirby, *J. Chem. Soc., Chem. Commun*., 1986, 444.
8 G. Procter, D. Britton and J. D. Dunitz, *Helv. Chim. Acta*, 1981, **64**, 471.
9 D. Britton and C. J. Cramer, *Acta Crystallogr*., 1996, **B52**, 344.
10 P. N. W. Baxter, J. A. Connor, D. C. Povey and J. D. Wallis, *J. Chem. Soc., Chem. Commun*., 1991, 1135.
11 C. R. Rice and J. D. Wallis, *J. Chem. Soc., Chem. Commun*., 1973, 572.
12 M. Pilkington, J. D. Wallis, G. T. Smith and J. A. K. Howard, *J. Chem. Soc., Perkin Trans. 2*, 1996, 1849.
13 H. S. Bengaard, S. Larsen, H. O. Sorensen, K. J. Robinson and J. D. Wallis, *Acta Crystallogr., Sect. C*, 1998, **54**, in the press.
14 M. T. Reetz, C. Bingel and K. Harms, *J. Chem. Soc., Chem. Commun*., 1993, 1558.
15 C. F. Bernasconi, *Tetrahedron*, 1989, **45**, 4017.
16 C. F. Bernasconi and M. Panda, *J. Org. Chem*., 1987, **52**, 3042.
17 F. H. Allen and O. Kennard, *Chem. Des. Automatic News*, 1993, **8**, 1 and 31.

Communication 8/08488B

New insights into the origin of NO_2 in the mechanism of the selective catalytic reduction of NO by propene over alumina

Frederic C. Meunier,* John P. Breen and Julian R. H. Ross

Centre for Environmental Research, University of Limerick, Limerick, Ireland. E-mail: frederic.meunier@ul.ie

Received (in Cambridge, UK) 2nd November 1998, Accepted 24th December 1998

The formation of NO_2 as a reaction intermediate in the selective catalytic reduction of NO by C_3H_6 in the presence of a large excess of O_2 over alumina is shown not to occur through the direct oxidation of NO by O_2.

Selective catalytic reduction (SCR) of NO_x by hydrocarbons has received much attention as a possible means to control the emissions from diesel and lean-burn engines. The work by Burch *et al.* has unveiled many of the features of the NO reduction over Pt-based materials.[1,2] Yet, the mechanisms of SCR reactions over alumina, one of the most active metal oxides for the SCR of NO by hydrocarbons,[3] and alumina promoted by metal oxides such as CoO_x remain unclear.[4] It has been suggested that when using propene as a reductant, the initial step of the SCR reaction is the oxidation of NO by O_2 to form NO_2 which in turn reacts with the reducing agent to form N_2.[5–7] The results of the experiments reported in this paper bring a new insight into the formation of NO_2 over alumina during the propene-SCR of NO, resulting in a necessary re-evaluation of the current theories on the reaction mechanism.

The γ-alumina used in these experiments was supplied by Alcan (AA400, 150 $m^2\ g^{-1}$) and was calcined in air at 923 K for 6 h prior to use. The reactants (NO and C_3H_6) and products of reaction (CO_2, CO, NO_2, N_2O, NH_3) were analysed by FT-IR spectroscopy (7 m path length Foxboro® gas-cell fitted in a Nicolet® 550 FT-IR). No hydrogen cyanide nor any other products were detected in the experiments reported here. The N_2 concentration was calculated during steady state conditions on the basis of a 100% nitrogen balance on the other N-containing products detected. A quartz microreactor (4 mm internal diameter) was used for the catalytic tests, the catalytic bed being held in place by quartz wool plugs. No reaction was observed when the reactants were passed through the reactor in the absence of a catalyst bed. The results reported here were obtained at steady state conditions and were found to be reproducible.

Fig. 1(*a*) shows the NO_2 yield obtained during the oxidation of NO (500 ppm) by O_2 (2.5%) over alumina and Fig. 1(*b*) shows the calculated NO_2 yield obtained at the thermodynamic equilibrium of the reactions described by eqn. (1) as a function of temperature:

$$NO + \tfrac{1}{2}\,O_2 \leftrightarrow NO_2 \qquad (1)$$

As it has often been reported in the literature, the alumina catalyst exhibited very poor activity for the NO oxidation reaction with yields of NO_2 attaining equilibrium conversions only at temperatures above 900 K. Fig 1(*c*) shows the NO yield obtained during the decomposition of NO_2 to $NO + \frac{1}{2}\,O_2$ (the reverse reaction of that discussed above) and Fig. 1(*d*) shows the calculated NO yield obtained at the thermodynamic equilibrium of the same reaction as a function of temperature. The activity of the alumina for the backward reaction of eqn. (1) was somewhat greater than that of the forward reaction but yet again the equilibrium limit was only reached at a temperature of about 900 K.

Fig. 2 shows the propene conversion [Fig. 2(*a*)] and yields of the different N-containing products of the reaction between NO (500 ppm), propene (500 ppm), and O_2 (2.5%) over alumina at 813 K and at varying *W*/*F*s (ratio of catalyst weight to feed flow rate). Fig. 3(*a*) shows the varying molar ratios of NO_2/NO obtained from the results of the experiments shown in Fig. 2. The NO_2/NO ratio at the thermodynamic equilibrium of reaction (1) at 813 K calculated using the initial concentration values of NO and O_2 is shown in Fig. 3(*b*). The conversion of propene [Fig. 2(*a*)] increased with increasing *W*/*F* values, reaching 100% conversion at $W/F = 180$ mg s cm^{-3}. The yield of N_2 [Fig. 2(*b*)] followed a similar trend to that of propene conversion, increasing steadily with increasing *W*/*F* values and then levelling off when all the propene was converted, *i.e.* at

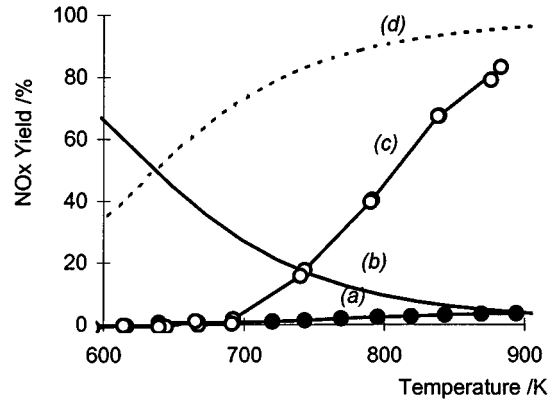

Fig. 1 *(a)* Experimental NO_2 yield (●) obtained during the oxidation of NO over γ-Al_2O_3 and (*b*) NO_2 yield limit (—) associated with the thermodynamic equilibrium of the reaction $NO + \frac{1}{2}\,O_2 \leftrightarrow NO_2$ as function of temperature. *(c)* Experimental NO yield (○) obtained during the decomposition of NO_2 to $NO + \frac{1}{2}\,O_2$ over γ-Al_2O_3 and (*d*) NO yield limit (---) associated with the thermodynamic equilibrium of the reaction $NO + \frac{1}{2}\,O_2 \leftrightarrow NO_2$ as function of temperature. Feed: 500 ppm NO or NO_2 + 2.5% O_2 in Ar, $W/F = 60$ mg s cm^{-3}.

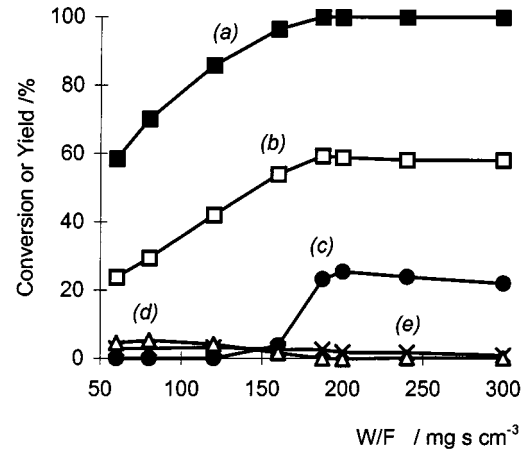

Fig. 2 Selective catalytic reduction of NO using propene over γ-Al_2O_3 at 813 K: (*a*) propene conversion (■), (*b*) N_2 yield (□), (*c*) NO_2 yield (●), (*d*) NH_3 yield (Δ) and (*e*) N_2O yield (×) as a function of the *W*/*F*. Feed: 500 ppm NO + 500 ppm C_3H_6 + 2.5% O_2 in Ar, 200 mg of alumina.

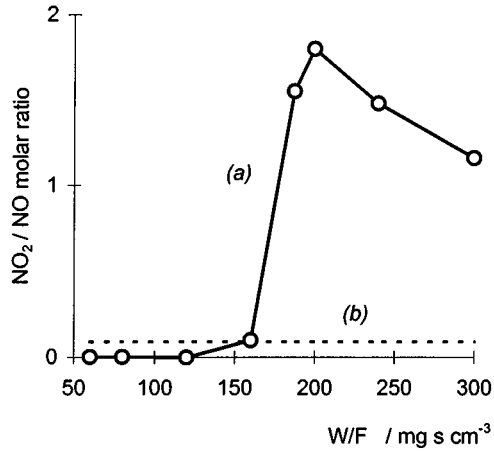

Fig. 3 Selective catalytic reduction of NO using propene over γ-Al_2O_3 at 813 K as a function of the *W*/*F*: NO_2 to NO ratio (*a*) experimental (○) and (*b*) at the thermodynamic equilibrium of the reaction NO + $\frac{1}{2}$ O_2 ↔ NO_2 (---). Feed: 500 ppm NO + 500 ppm C_3H_6 + 2.5% O_2 in Ar, 200 mg of alumina.

W/*F*s greater than 180 mg s cm^{-3}. The striking feature of Fig. 2 is the sharp rise in the production of NO_2 [Fig. 2(*c*)] as soon as the conversion of propene reaches 100%. At propene conversions lower than 95%, the presence of NO_2 was not detected (*i.e.* < 2.5 ppm). Upon completion of the conversion of propene, the NO_2 yield reached a value of approximately 25% (corresponding to 127 ppm of NO_2). With further increase in the values of *W*/*F*, the NO_2 yield gradually decreased. The gradual decrease in the concentration of NO_2 was accompanied by a similar increase in the concentration of NO (not shown in Fig. 2) while the concentrations of all the other products of reaction were either steady (N_2) or decreased (N_2O and NH_3). Interestingly, Fig. 3 shows that in the region of 100% propene conversion (*W*/*F* ≥ 180 mg s cm^{-3}), the experimental values of the molar ratios of NO_2/NO were greater than 1. Hence, these values were more than 10 times greater than the value of the thermodynamic equilibrium ratio of NO_2/NO (*i.e.* 0.09) calculated at the same temperature. The same results were obtained whether the *W*/*F* was varied with increasing or decreasing values.

Further experiments carried out using the same reactant concentrations, at constant *W*/*F* (60 mg s cm^{-3}) and varying temperature also showed that, at the temperature of 100% conversion of propene, there was a sharp increase in the yield of NO_2. At 843 K, propene conversion was not complete and NO_2 was not detected; however, at 873 K propene was fully converted and NO_2 yields of 30% were obtained (this value again being well in excess of levels obtained from equilibrium calculations). The sharp increase in the NO_2/NO ratio at the temperature of 100% conversion of propene was the same regardless of whether the reaction temperatures were increased or decreased.

It is evident from the results of experiments described in this paper that NO_2 could not be observed when propene was present in the product streams. This can be explained by the work of a number of different authors,[4,6,7] who have shown that alumina is very active for the reduction of NO_2 by propene to form N_2. However, upon complete combustion of the propene, the NO_2 could not be reduced and was therefore detected in the reactor effluent. Fig. 2 and 3 show that the maximum NO_2/NO ratio occurred at a *W*/*F* value of 200 mg s cm^{-3}, and at higher *W*/*F*s the ratio decreased towards the equilibrium ratio. This was probably due to the slow decomposition of the NO_2 to NO and O_2 (in the absence of propene) which Fig. 1(*c*) shows can occur over the alumina catalyst. Surprisingly, the catalytic data reported on alumina in this paper and the corresponding thermodynamic calculations show that most of the NO_2 observed upon completion of propene conversion during the SCR of NO did not arise from the direct oxidation of NO by O_2 [eqn. (1)]. A mechanism involving the direct reaction of NO, O_2 and NO_2 could not exceed thermodynamic limits. Therefore, the current model of the alkene-SCR reaction over alumina-based catalysts needs to be re-evaluated.[5–7]

At least two alternative solutions could be proposed to explain the formation of the high concentrations of NO_2 observed. First, a mechanism involving consecutive steps could occur in which a nitro or a nitrite compound, *e.g.* nitromethane CH_3NO_2, is formed along with CO (or CO_2) from the reaction of propene, O_2 and NO [eqn. (2-1)]. Organic nitro or nitrite species have often been quoted as possible intermediates of SCR reactions.[8] The subsequent oxidation of this organo-NO_x species would yield NO_2 [eqn. (2-2)]

$$C_3H_6 + \tfrac{3}{2}\,O_2 + 2\,NO \rightarrow 2\,CH_3NO_2 + CO \qquad (2\text{-}1)$$

$$CH_3NO_2 + \tfrac{7}{4}\,O_2 \rightarrow NO_2 + CO_2 + \tfrac{3}{2}\,H_2O \qquad (2\text{-}2)$$

Overall, eqn. (2-1) and (2-2) combine to give:

$$C_3H_6 + 5\,O_2 + 2\,NO \rightarrow 2\,NO_2 + 2\,CO_2 + CO + 3\,H_2O \qquad (2\text{-}3)$$

This mechanism is supported by the fact that thermodynamic calculations show that the reactions given by eqn. (2-1) and (2-2) are strongly exergonic over the temperature range investigated here (*e.g.* $\Delta G°_{813K}$ = −298 kJ mol^{-1} and −734 kJ mol^{-1}, respectively). Regarding a second possible mechanism, the oxygen needed to form the NO_2 could be supplied by another molecule of NO, *i.e.* in a disproportionation reaction, and not by the O_2. An example of mechanism of SCR of NO involving a disproportionation of NO to N_2 and NO_2 was proposed by Smits and Iwasawa .[9] These authors suggested that one of the roles of the hydrocarbon, NO and O_2 was to form a radical molecule R* (*e.g.* 1-nitro-*sec*-propyl) which in turn could propagate the disproportionation reaction:

$$4\,NO\ (+R^*) \leftrightarrow N_2 + 2\,NO_2\ (+R^*) \qquad (3)$$

The thermodynamics of the disproportionation reaction described by eqn. (3) essentially favour the right hand-side of the equation at temperatures below 600 °C (and are independent of the concentration of O_2) and therefore this mechanism could be responsible for the high yields of NO_2 observed. Hence, one of the possible role of the alumina (a known mild oxidiser) during alkene-SCR reactions would be to allow the formation of organic-nitro or nitrite species [eqn. (2)] and/or the formation of a hydrocarbon-based propagator [eqn. (3)]. Experiments using $N^{18}O$ and $^{16}O_2$ are planned and should give some evidence of the origin of the oxygen in NO_2 (*i.e.* by observing either $N^{18}O^{18}O$ or $N^{18}O^{16}O$) to determine which of the two models proposed is the most likely.

The conclusion of this work is that the formation of NO_2 during the propene-SCR of NO over alumina is not obtained by direct oxidation of NO by O_2 but that a more complex mechanism has to be considered.

Part of this work was funded by the European Community, through the Environment and Climate Programme, Contracts E5V5-CT94 and ENV4-CT97-0658.

Notes and references

1 R. Burch and T. C. Watling, *Catal. Lett.*, 1997, **43**,19.
2 R. Burch, P. Fornasiero and T. C. Watling, *J. Catal*., 1998, **176**, 204.
3 H. Hamada, *Catal. Today*, 1994, **22**, 21.
4 J. Yan, M. C. Kung, W. M. H. Sachtler and H. H. Kung, *J. Catal*., 1997, **172**, 178.
5 H. Hamada, Y Kintaichi, M. Sasaki and T. Ito, *Appl. Catal*., 1991, **70**, L15.
6 H. Hamada, Y. Kintaichi, M. Inaba, M. Tabata, T. Yoshinari and H. Tsuchida, *Catal. Today*, 1996, **29**, 53.
7 N. Okazaki, S. Osada and A. Tada, *Appl. Surf. Sci.*, 1997, **121/122**, 396.
8 C. Yokoyama and M. Misono, *J. Catal*., 1994, **150**, 9.
9 R. H. H. Smits and Y. Iwasawa, *Appl. Catal. B*, 1995, **6**, L201.

Communication 8/08465C

Hybrid P-chiral diphosphines for asymmetric hydrogenation

Duncan Carmichael, Henri Doucet and John M. Brown*

Dyson Perrins Laboratory, South Parks Road, Oxford, UK OX1 3QY. E-mail: bjm@ermine.ox.ac.uk

Received (in Liverpool, UK) 6th November 1998, Accepted 8th December 1998

A family of diphosphine ligands has been prepared by Michael addition of *o*-anisylphenyl phosphide to diethyl vinylphosphonate and elaboration to phospholanes based on hexane-2,5-diol or mannitol; some preliminary results of Rh-complex catalysed hydrogenations are reported.

The scope of asymmetric hydrogenation of alkenes has been gradually extended both in reactant structure and catalyst efficiency over many years.[1] For rhodium catalysis, the early work of the Monsanto group using the P-chiral diphosphine DIPAMP has provided an enduring standard.[2] Only phospholane ligands in the DUPHOS and BPE series have exhibited superior enantioselectivity over a broad front.[3]

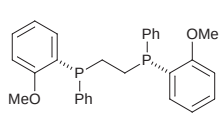

1 (*R*,*R*)-DIPAMP

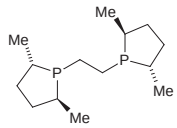

2 (*S*,*S*)-MeBPE

It is a commonly held belief that C_2 symmetric diphosphine (or diol or diamine) ligands are endowed with superior properties in catalysis, their attractiveness augmented by ease of synthesis.[4] An alternative view, stated most clearly by Achiwa and co-workers,[5] is that intermediates in a catalytic cycle lack the intrinsic symmetry of the ligand and consequently the two chelating atoms must fulfil different roles. The implication is that lack of symmetry may be a positive advantage in an appropriate case. In previous work we have endeavoured to separate the functions of the two chelating phosphorus atoms in asymmetric hydrogenation.[6] The synthesis of a new class of unsymmetrical ligands permits that approach to be extended further.

Our basic idea was to combine the phosphorus moieties of DIPAMP **1** and BPE **2** in a single ligand. The synthesis is based on conjugate addition of racemic phosphineborane **3**[7] to diethyl vinylphosphonate (Scheme 1).[8] Alane reduction of the product **4** gave the primary phosphineborane **5**. Following deboronation, stepwise double nucleophilic displacement on the cyclic sulfate **6**[9] *via* BuLi deprotonation permitted synthesis of the target compounds **7a** and **8a** as a diastereomeric mixture in good yield. These were separated by MPLC, with some difficulty (EtOAc–pentane). The analogous compounds **10a-OH** and **11a-OH**, prepared from the mannitol derivative **9**,[10] proved much more amenable to chromatographic separation, and subsequently afforded the pure methyl ethers **10a-OMe** and **11a-OMe**.[11] The absolute configuration of product boranes was established by CD in comparison with that of the diborane from *(S,S)*-DIPAMP, the phospholane part being essentially CD transparent in the 240-400 nm region. This set of procedures gives access to a family of unsymmetrical 1,2-phosphinoethane ligands as their stable diborane complexes.[12]

In most cases hydrogenation experiments were carried out by *in situ* deboronation[13] and reaction with $(COD)_2RhBF_4$ to generate the catalyst. In initial studies of the hydrogenation of simple dehydroamino acids and esters, two questions were posed: Is the enantioselectivity governed predominantly by one of the two phosphorus nuclei in the ligand? Does the alternative

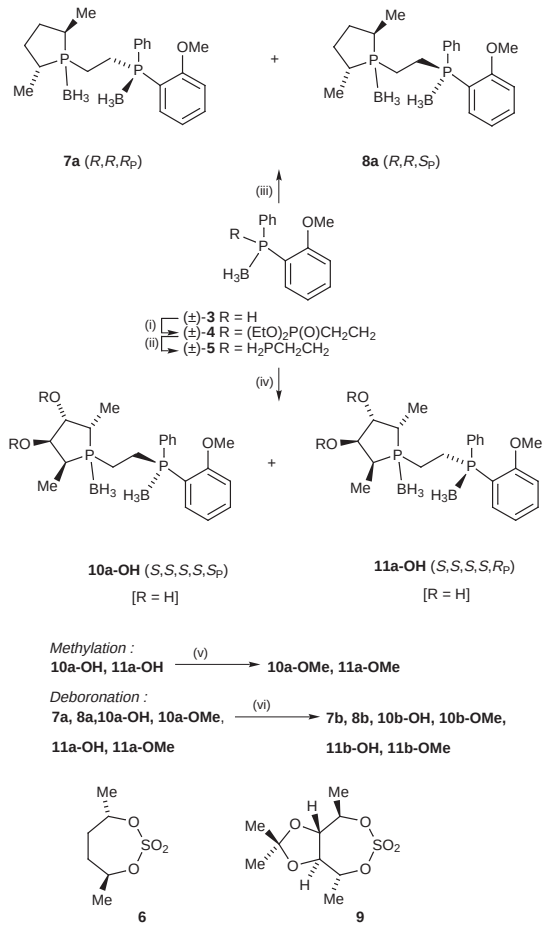

Scheme 1 *Reagents*: (i) CH_2=CHP(O)$(OEt)_2$, KOBu^t, THF, 95%; (ii) DABCO, C_7H_8; AlH_3, Et_2O; H_2O then CaH_2; (iii) BuLi, THF, −78 °C then **6** then further BuLi; Me_2S•BH_3, 45% overall; (iv) BuLi, −78 °C then **9**; then repeat; Me_2S•BH_3, 30% isolated overall for (ii), (iv); (v) NaH, MeI, THF, ⩾80%; (vi) HBF_4•OMe_2 then $NaHCO_3$.

match or mismatch of arylphosphine and phospholane chirality have a significant effect on enantioselectivity? The results recorded in Table 1 provide answers to these points but also some surprises. A broad conclusion from these and parallel results is that the 'matched' ligand[14] gives significantly higher ees than the 'mismatched' ligand, and also that the phospholane configuration is dominant in defining the stereochemical course of hydrogenation, but to an extent that depends on the substrate. In the case of the bulkier pivalamide **13** and benzamide **14**, the configuration of the arylphosphine part plays a very minor role. In comparison to the mannitol derived ligands **11**, the simple phospholanes **7b** and **8b** gave significantly inferior results in these and related cases and were thus investigated in less detail.

Further results of interest came from a study of the itaconate esters and half-esters recorded in Table 2. Here the mismatched diastereomers of ligand **10b** gave poor ees and are not included. For the 1-substituted monoester **15**, the hydroxy ligand **11b-OH** gives a superior ee to its methyl ether. The reverse is true for the 3-substituted monoester **16**, where the methyl ether **11b-OMe**

Table 1

Substrate	Catalyst precursor	Ee (%)
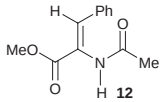 **12**	**10b-OMe**	19 *S*
	11b-OMe	85 *S*
	10b-OH	43 *S*
	11b-OH	**92** *S*
	7b	38 *S*
	8b	60 *R*
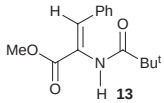 **13**	**10b-OMe**	58 *S*
	11b-OMe	67 *S*
	10b-OH	82 *S*
	11b-OH	**88** *S*
	7b	5 *R*
	8b	36 *R*
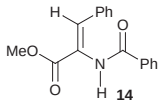 **14**	**11b-OMe**	77 *S*
	10b-OH	72 *S*
	11b-OH	**90** *S*[a]

Conditions: substrate : catalyst 100 : 1, $(COD)_2RhBF_4$ as precursor ($HBF_4{\cdot}OMe_2$ deboronation *in situ*), 1.3 bar, MeOH, 1–3 h. [a] TfO^- instead of BF_4^-.

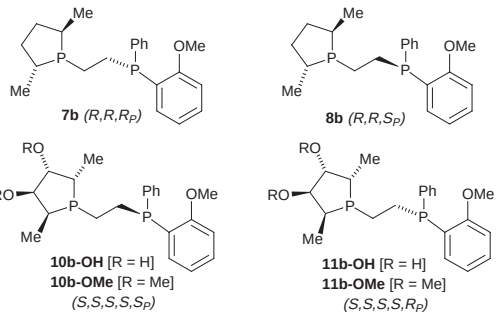

provides the product of higher enantioselectivity. Changing the solvent from MeOH to CH_2Cl_2 led to inferior rates and selectivities in both these cases.

These preliminary results indicate that, contrary to expectation, the enantioselectivity is sensitive to remote oxygen substituents in the phospholane ring. Inspection of molecular models indicates that the MeO- or HO- groups are axial in the 5-membered ring of the phospholane, and in the vicinity of substituents on the coordinated alkene. Hence the opportunity exists for cooperative association through H-bonding between ligand and coordinated reactant.[15] The combination of good enantioselectivities in simple unoptimised reactions make this an attractive series of ligands for further investigation with the potential for rational structural alteration, and the impetus of additional synthetic power and mechanistic information arising from the distinct role of the two ligating atoms. The results nicely complement those of Börner and co-workers on asymmetric hydrogenation with mannitol-derived diphospholanes.[16]

Table 2

Substrate	Catalyst precursor	Ee (%)
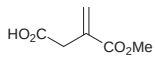 **15**	**11b-OMe**	85 *R*
	11b-OH	**95** *R*
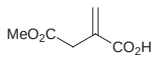 **16**	**11b-OMe**	**93** *R*[a]
	11b-OH	87 *R*
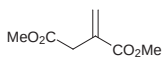 **17**	**11b-OMe**	**85** *R*
	11b-OH	80 *R*[a]

Conditions: substrate : catalyst 100 : 1, $(COD)_2RhBF_4$ as precursor, ($HBF_4{\cdot}OMe_2$ deboronation *in situ*), 1.3 bar, MeOH, 1–3 h. [a] 94% ee for **16** with TfO^- instead of BF_4^-.

We thank EPSRC, DTI and Chiroscience (Dr Ulrich Berens), Glaxo-Wellcome (Dr Andrew Payne), Robinson Bros. (Dr Kelvyn Soars), SB (Dr Peter Sheldrake) and Zeneca FCMO (Dr A. John Blacker) for support under the LINK Asymmetric Synthesis Programme. We thank CNRS for support for leave of absence (to D. C.). Johnson-Matthey kindly provided a loan of $RhCl_3{\cdot}3H_2O$ and we thank Dr Ulrich Berens (Chirotech) for a generous sample of the enantiomerically pure diol. We thank Dr A. Boerner (Rostock) for a useful exchange of information (ref. 16).

Notes and references

1 H. Takaya, T. Ohta and R. Noyori, *Catalytic Asymmetric Synthesis*, VCH, Weinheim, 1993, ch. 1; R. Noyori, *Asymmetric Catalysis in Organic Synthesis*, Wiley, NY, 1994, ch. 2; A. Pfaltz, *Houben-Weyl Methods of Organic Chemistry, Vol. E21d 2.5.1.2*, ed. G. Helmchen, R. W. Hoffmann, J. Mulzer and E. Schaumann, Thieme, Stuttgart, 1995.

2 B. D. Vineyard, W. S. Knowles, M. J. Sabacky, G. L. Bachman and D. J. Weinkauff, *J. Am. Chem. Soc.*, 1977, **99**, 5946.

3 M. J. Burk, F. Bienewald, M. Harris and A. Zanotti-Gerosa, *Angew. Chem., Int. Ed.*, 1998, **37**, 1931; M. J. Burk, C. S. Kalberg and A. Pizzano, *J. Am. Chem. Soc.*, 1998, **120**, 4345, and earlier references.

4 J. K. Whitesell, *Chem. Rev.*, 1989, **89**, 1581; B. M. Trost and D. L. Van Vranken, *Angew. Chem., Int. Ed. Engl.*, 1992, **31**, 228.

5 K. Inoguchi, S. Sakuraba and K. Achiwa, *Synlett*, 1992, 169; T. Morimoto, M. Chiba and K. Achiwa, *Chem. Pharm. Bull.*, 1993, **41**, 1149; T. V. RajanBabu and A. L. Casalnuovo, *J. Am. Chem. Soc.*, 1996, **118**, 6325.

6 J. A. Ramsden, J. M. Brown, M. B. Hursthouse and A. I. Karalulov *Tetrahedron: Asymmetry*, 1994, **5**, 2033; J. A. Ramsden, T. Claridge and J. M. Brown, *J. Chem. Soc., Chem. Commun.*, 1995, 2469.

7 T. Imamoto, T. Oshiki, T. Onozawa, T. Kusumoto and K. Sato, *J. Am. Chem. Soc.*, 1990, **112**, 5244; T. Imamoto, T. Yoshizawa, K. Hirose, Y. Wada, H. Masuda, K. Yamaguchi and H. Seki, *Heteroatom Chem.*, 1995, **6**, 99; M. Ohff, J. Holz, M. Quirmbach and A. Börner, *Synthesis*, 1998, 1391.

8 *C.f.* K. Bourumeau, A.-C. Gaumont and J.-M. Denis, *Tetrahedron Lett.*, 1997, **38**, 1923.

9 M. J. Burk, J. E. Feaster, W. A. Nugent and R. L. Harlow *J. Am. Chem. Soc.*, 1993, **115**, 10 125.

10 In 90% yield from the corresponding diol, L. F. Wiggins and D. J. C. Wood, *J. Chem. Soc*., 1950, 1566; Y. Le Merrer, A Dureeault, C. Greck, D. Micas-Languin, G. Gravier and J. C. Depezay, *Heterocycles*, 1983, **25**, 541.

11 The absolute configuration of all product boranes was established by CD in comparison with that of the diborane from (*S,S*)-DIPAMP, the phospholane part being essentially CD transparent in the 240–400 nm region. We warmly thank Dr Guiliano Siligardi, KCL, for this data.

12 Full details of the synthesis will be published separately; D. Carmichael and J. M. Brown *Tetrahedron: Asymmetry*, in preparation.

13 L. McKinstry and T. Livinghouse, *Tetrahedron Lett.*, 1994, **35**, 9319.

14 (*R,R*)-DIPAMP (ref. 2) and the (*S,S*)-phospholane MeBPE (ref. 8) both give *S*-amino acids on Rh asymmetric hydrogenation, hence **8b** and **11b** constitute the configurationally matched ligands and **7b**, **10b** the mismatched ligands.

15 M. Sawamura and Y. Ito, *Chem. Rev*., 1992, 92, 857; J. Holz, M. Quirmbach and A. Borner, *Synthesis*, 1997, 983, and references cited therein.

16 J. Holz, M. Quirmbach, U. Schmidt, D. Heller, R. Stürmer and A. Börner, *J. Org. Chem*., 1998, **63,** 8031.

Communication 8/08711C

Perfluoroheptadecan-9-one: a selective and reusable catalyst for epoxidations with hydrogen peroxide

Michiel C. A. van Vliet, Isabel W. C. E. Arends and Roger A. Sheldon*

Laboratory of Organic Chemistry and Catalysis, Delft University of Technology, Julianalaan 136, 2628 BL Delft, The Netherlands.E-Mail: secretariat-ock@stm.tudelft.nl

Received (in Cambridge, UK) 25th November 1998, Accepted 16th December 1998

Perfluoroheptadecan-9-one is a selective and mild catalyst for the epoxidation of a wide variety of alkenes with hydrogen peroxide; after the reaction the catalyst can be easily recovered and reused without noticable decomposition.

Following the seminal publication of Horváth and Rábai[1] in 1994 there has been increasing interest in the concept of fluorous biphasic catalysis.[2] The use of catalysts soluble in the fluorous phase facilitates catalyst separation from substrate and products which are soluble in a second (*e.g.* hydrocarbon) phase. Attachment of long perfluoroalkyl groups ('fluorous ponytails') to *e.g.* phosphine ligands, renders metal complexes soluble in fluorocarbons and insoluble in most organic solvents. In most cases catalytic activity is preserved only when the perfluoroalkyl group is not directly attached to the ligand but is separated by a spacer, mostly a $–CH_2CH_2–$ group.[2] In this way the electronic properties of the ligand are not significantly affected by the strongly electron-withdrawing perfluoroalkyl moiety.

A few examples of the application of fluorous biphasic chemistry to catalytic oxidations have been reported.[3] In all the reported cases the unique electron-withdrawing properties of the perfluoroalkyl group were not exploited. On the other hand, the use of hexafluoroacetone as a mild and selective catalyst for the epoxidation of alkenes with highly concentrated hydrogen peroxide (Scheme 1) has been known for more than 25 years.[4]

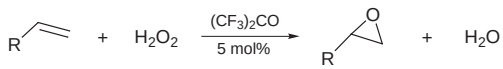

Scheme 1

Although rates are rather low, the reaction proceeds under very mild conditions and affords very acid-sensitive epoxides in high yields. A major disadvantage, however, is the high volatility of hexafluoroacetone and its application at reflux temperature (80 °C) requires a cryogenic condensor to avoid loss of the catalyst. Our approach to improve this catalyst was to replace the trifluoromethyl groups by larger perfluoroalkyl groups. The advantages are clear: the catalyst is less volatile† and the use of long perfluoroalkyl groups render it highly soluble in a fluorous phase and sparingly soluble in common organic solvents.

As is shown in Table 1 perfluoroheptadecan-9-one[5] was *ca.* four times as active as hexafluoroacetone in the epoxidation of cyclooctene with anhydrous H_2O_2[6] in refluxing EtOAc. Screening of several solvents revealed that polar, non-basic solvents, such as halogenated hydrocarbons and trifluoroethanol, were superior. Perfluoroheptadecan-9-one was only sparingly soluble in halogenated hydrocarbons. When 5 mol% was used it did not dissolve completely even in boiling 1,2-dichloroethane. Addition of 10 vol% of a cosolvent, *e.g.* EtOH or EtOAc, increased the solubility of the catalyst, resulting in a higher reaction rate. In this case the two requirements, anhydrous hydrogen peroxide and the need for a cosolvent, could be met by using hydrogen peroxide in EtOAc, easily prepared by azeotropic drying.[6]

Table 2 shows the results for epoxidation of several alkenes catalyzed by perfluoroheptadecan-9-one in refluxing 1,2-dichloroethane. Most epoxides are obtained in excellent yields, except for extremely acid-sensitive epoxides like camphene

Table 1 Epoxidation of cyclooctene with anhydrous H_2O_2 in EtOAc catalysed by perfluoroketones[a]

Catalyst	Initial rate mol mol^{-1} h^{-1}	Yield (%)[b]
$CF_3C(O)CF_3$	2.4	82
$C_6F_5C(O)CF_3$	1.3	74
$C_8F_{17}C(O)C_8F_{17}$	10	98

[a] Conditions: 5 mmol cyclooctene, 1 mmol n-decane (internal standard), 0.25 mmol perfluoroketone (5 mol%), 10 mmol H_2O_2 in 10 ml EtOAc. Reflux under N_2. Analysis by GC. [b] After 24 h.

Table 2 Epoxidation with anhydrous H_2O_2 in dichloroethane–EtOAc catalysed by perfluoroheptadecan-9-one[a]

Alkene	Initial rate/ mol mol^{-1} h^{-1}	*t*/h	Yield (%)
Cyclooctene	42	2	100
Cyclooctene[b]	41	2	96
Cyclooctene[c]	—	2	12
Cyclohexene	48	2	92
1-Methylcyclohexene	70	0.5	97
Methylenecyclohexane	15	2	64
Limonene	77	0.5	72
α-Pinene[d]	38	0.5	55
Camphene[d]	23	1.5	49
2-Methylundec-1-ene	28	1.5	96
Dec-1-ene	4.4	18	72

[a] Conditions: 5 mmol alkene, 1 mmol n-decane (internal standard), 0.25 mmol perfluoroheptadecan-9-one (5 mol%), 10 mmol H_2O_2 in 1 ml EtOAc and 10 ml 1,2-dichloroethane. Reflux under N_2. Analysis by GC. [b] 5 mol% of recovered catalyst was used. [c] No catalyst was added. [d] 5 mol% of Na_2HPO_4 was added.

Table 3 Epoxidation with 60% H_2O_2 in trifluoroethanol catalysed by perfluoroheptadecan-9-one[a]

Alkene	Initial rate/ mol mol^{-1} h^{-1}	*t*/h	Yield (%)
Cyclooctene	80	2	100
Cyclooctene[b]	82	2	100
Cyclooctene[c]	—	2	50
Cyclohexene[d]	34	1	64
1-Methylcyclohexene[d]	175	0.5	89
Methylenecyclohexane[d]	47	0.5	62
2-Methylundec-1-ene[d]	13	2	63
Dec-1-ene[d]	1.9	18	57

[a] Conditions: 5 mmol alkene, 1 mmol diglyme (internal standard), 0.25 mmol perfluoroheptadecan-9-one (5 mol%), 10 mmol H_2O_2 in 5 ml trifluoroethanol. Reflux under N_2. Analysis by GC. [b] 5 mol% of recovered catalyst was used. [c] No catalyst was added. [d] 5 mol% of Na_2HPO_4 was added.

oxide and α-pinene oxide. These epoxides can be obtained in moderate yields by buffering the reaction mixture with a small amount of base (Na_2HPO_4).

Simple cooling of the reaction mixture in an ice-bath (0 °C) gave crystallisation of the catalyst. Filtration and washing with a small amount of cold solvent gave the pure catalyst in about 80% yield. Quantitative GC measurements showed that the catalyst was not decomposed under the reaction conditions and was completely removed from the reaction mixture after filtration.‡ An interrupted catalytic experiment§ showed that no catalytically active material was present in the filtrate. A catalytic experiment on a larger scale (1 g of catalyst) gave a recovery of the catalyst of 92% after cooling to 0 °C and filtration. The recovered catalyst was still active in epoxidation with the same rates and yield.

The reaction could also be performed with 60% aqueous hydrogen peroxide in boiling trifluoroethanol. This solvent is known to be an excellent solvent in combination with aqueous hydrogen peroxide.[7] Table 3 shows the results for the epoxidation of several alkenes catalysed by perfluoroheptadecan-9-one in boiling trifluoroethanol. The yields are moderate to high, but the formation of acid-sensitive epoxides is only possible when the reaction medium is buffered by a phosphate buffer (*e.g.* 5 mol% of Na_2HPO_4). In this solvent simple cooling of the reaction mixture also resulted in crystallisation of the catalyst, but the recovery was generally lower than in dichloroethane. GC measurements indicated that a part of the catalyst remained dissolved in the reaction mixture after filtration.

We are currently investigating the scope of perfluoro ketones as catalysts for oxidations with hydrogen peroxide.

Notes and references

† Hexafluoroacetone is a gas. Perfluoroheptadecan-9-one is a solid with a melting point of 110 °C and an atmospheric boiling point of about 170 °C.

‡ The *ca.* 20% loss of the catalyst is attributed to losses incurred during sampling and mechanical losses associated with the small scale of the reactions (200 mg of catalyst).

§ A standard catalytic experiment was interrupted by cooling to 0 °C at 70% conversion. The catalyst was removed by filtration. The filtrate was again heated under reflux. The reaction proceeded but with a rate about 30 times lower; comparable to the blank reaction.

1 I. T. Horváth and J. Rábai, *Science*, 1994, **266**, 72; I. T. Horváth, *Acc. Chem. Res.*, 1998, **31**, 641; see also D. W. Zhu, *Synthesis*, 1993, 953.

2 I. T. Horváth and J. Rábai, *US Pat.* 5463082 (1995), to Exxon Research and Engineering Company; I. T. Horváth, G. Kiss, R. A. Cook, J. E. Bond, P. A. Stevens, J. Rábai and E. J. Mozeleski, *J. Am. Chem. Soc.*, 1998, **120**, 3133.

3 G. Pozzi, S. Banfi, A. Manfredi, F. Montanari and S. Quici, *Tetrahedron*, 1996, **52**, 11879; G. Pozzi, I. Colombani, M. Miglioli, F. Montanari and S. Quici, *Tetrahedron*, 1997, **53**, 6145; G. Pozzi, M. Cavazzini, S. Quici and S. Fontana, *Tetrahedron Lett.*, 1997, **38**, 7605–8; J.-M. Vincent, A. Rabion, V. K. Yachandra and R. H. Fish, *Angew. Chem., Int. Ed. Engl.*, 1997, **36**, 2346; G. Pozzi, F. Montanari and S. Quici, *Chem. Commun.*, 1997, 69; G. Pozzi, F. Cinato, F. Montanari and S. Quici, *Chem. Commun.*, 1998, 877.

4 L. Kim, *Br. Pat.*, 1399639 (1972) to Shell Internationale Research Maatschappij N.V.; R. P. Heggs and B. Ganem, *J. Am. Chem. Soc.*, 1979, **101**, 2484; A. J. Biloski, R. P. Heggs and B. Ganem, *Synthesis*, 1980, 810; P. A. Ganeshpure and W. Adam, *Synthesis*, 1996, 179.

5 L. S. Chen, G. J. Chen and C. Tamborski, *J. Fluorine Chem.*, 1984, **26**, 341.

6 G. Legemaat, W. Drenth, M. Schmidt, G. Prescher and G. Goor, *J. Mol. Catal.*, 1990, **62**, 119.

7 T. M. Shryne and L. Kim, *US Pat.* 4024165 (1977) to Shell Oil Company.

Communication 8/09204D

ChemComm

Highly efficient oxidation of alcohols and aromatic compounds catalysed by the Ru-Co-Al hydrotalcite in the presence of molecular oxygen

Tsuyoshi Matsushita, Kohki Ebitani and Kiyotomi Kaneda*

Department of Chemical Science and Engineering, Graduate School of Engineering Science, Osaka University, 1-3 Machikaneyama, Toyonaka, Osaka 560-8531, Japan. E-mail: kaneda@cheng.es.osaka-u.ac.jp

Received (in Cambridge, UK) 20th November 1998, Accepted 15th December 1998

The ruthenium hydrotalcite having cobalt cations, Ru-Co-Al-CO_3 HT, is an effective heterogeneous catalyst for the oxidation of various kinds of alcohols in the presence of molecular oxygen.

From the standpoints of atom economy and environmental friendliness,[1,2] much attention has been paid to the development of selective oxidations catalysed by metal compounds using molecular oxygen as oxidant.[3–6] Hydrotalcites of layered mineral materials consist of cationic Brucite layers separated by layers of anionic species.[7] Changing the element ratios in the Brucite layer and selection of different anionic species enables tuning of the surface basicity.[8] Additionally, various metal elements can be introduced into the Brucite layer *via* the isomorphic substitution of Mg^{II} or Al^{III} cations at the octahedral sites, which are expected to be the active sites of the catalysts.[3] Thus, the interaction of introduced metal cations (M^1) with other cations (M^2) through M^1–O–M^2 bonds would lead to unique catalytic reactions using the functionalised hydrotalcites. Here, we have designed a highly active catalyst of the hydrotalcite containing Ru and Co cations for the oxidation of various alcohols and hydrocarbons in the presence of molecular oxygen. This heterogeneous catalyst has the advantages of using molecular oxygen and a simple work-up procedure over other homogeneous oxidizing reagents.[1] Furthermore, this hydrotalcite is reusable without appreciable loss of activity and selectivity for the above oxidation.

Various Ru hydrotalcites having divalent metal cations M^{II} in place of Mg^{II} ($Ru:M^{II}:Al = 0.3:3.0:1.0$) were prepared according to a modified version of a procedure in the literature.[7] A representative example is for the hydrotalcite having cobalt, aluminum, and ruthenium in the Brucite layer and CO_3 anions in the interlayer (Ru-Co-Al-CO_3 HT). A mixture of $RuCl_3{\cdot}3H_2O$ (1.53 mmol), $CoCl_2{\cdot}6H_2O$ (15.3 mmol) and $AlCl_3{\cdot}6H_2O$ (5.10 mmol) were dissolved in distilled water (10 ml). To an aqueous solution of Na_2CO_3 (13.3 mmol) and NaOH (46.4 mmol) was slowly added the above solution, and then the resulting mixture was heated at 65 °C for 18 h with stirring. The obtained slurry was cooled to room temperature and filtered, washed with distilled water and dried at 110 °C for 12 h, yielding 2.05 g of powder. The structure of the powder was confirmed by its X-ray diffraction pattern, and the basal spacing was estimated to be 7.9 Å, which is similar to that of the Ru–Mg–Al–CO_3 HT (7.92 Å); calc. for Ru-Co-Al-CO_3 HT ($Ru:Co:Al = 0.3:3.0:1.0$): Co, 20.1; Al, 7.4; Ru, 7.0%. Found: Co, 19.5; Al, 7.4; Ru, 7.3%. X-Ray photon spectroscopy (XPS) for the Ru-Co-Al-CO_3 HT: Co $2p_{3/2}$ = 780.6 eV, FWHM = 3.1 eV; Ru $3d_{5/2}$ = 282.7 eV, FWHM = 2.0 eV. XPS for the Ru-Mg-Al-CO_3 HT: Ru $3d_{5/2}$ = 281.7 eV, FWHM = 2.5 eV. The XPS peak positions are refered to Al_{1s} at 73.7 eV].

A typical example for the oxidation of alcohols is as follows (Scheme 1). Into a reaction vessel with a reflux condensor were placed cinnamyl alcohol (0.80 g, 6.0 mmol), the Ru-Co-Al-CO_3 HT (0.90 g) and toluene (15 ml). The resulting mixture was stirred at 60 °C under an O_2 atmosphere. After 40 min, the hydrotalcite was separated by filtration. GC analysis of the filtrate showed a quantitative yield of cinnamaldehyde. Removal of the solvent under reduced pressure was followed by column chromatography on silica to yield cinnamaldehyde (0.707 g, 89%). Isolated hydrotalcites were washed with aqueous 10% Na_2CO_3 (30 ml) and water, and could be reused without appreciable loss of activity for the above oxidation; the first, second and third runs of the experiment using the spent hydrotalcites gave cinnamaldehyde with > 92% GC yield.

Ru hydrotalcites having divalent metal cations in place of Mg^{II} were examined as catalysts for the oxidation of cinnamyl alcohol in the presence of molecular oxygen, as shown in Table 1. Generally, cinnamaldehyde is the main product under the

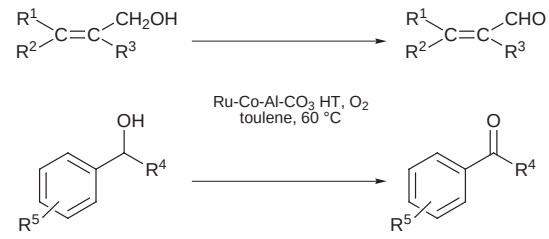

Scheme 1

Table 1 The oxidation of cinnamyl alcohol with various Ru hydrotalcites[a]

Entry	Catalyst	Time	Conversion (%)	Yield[b] (%)	Heat of adsorption[c]/ J g^{-1}
1	Ru-Co-Al-CO_3 HT	40 min	100	94	13.4
2	Ru-Mn-Al-CO_3 HT	40 min	99	92	13.3
3	Ru-Fe-Al-CO_3 HT	40 min	64	50	12.9
4	Ru-Zn-Al-CO_3 HT	40 min	23	23	6.6
5	Ru-Mg-Al-CO_3 HT	40 min	31	20	32.1
		8 h	100	95[d]	
6[e]	Co-Al-CO_3 HT + Ru-Mg-Al-CO_3 HT	40 min	33	22	

[a] Reaction conditions: cinnamyl alcohol (2.0 mmol), catalyst (0.30 g), toluene (5 ml), 60 °C, O_2 atmosphere. [b] Yields of cinnamaldehyde were determined by GC analysis using internal standards, based on cinnamyl alcohol. [c] The basicity of the hydrotalcites was estimated by calorimetric heats of benzoic acid adsorption (ref. 8). [d] Cited from ref. 3. [e] The physical mixture of the two catalysts which contained the same amounts of Ru and Co as entry 1 was used.

Table 2 The oxidation of various alcohols with Ru-Co-Al-CO_3 HT[a]

Entry	Substrate	Product	Time	Conversion (%)	Yield[b] (%)
1	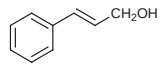	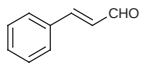	40 min	100	94 (89)[c]
2	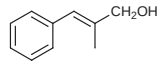	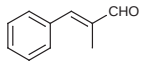	1.5 h	100	100
3	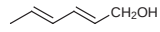	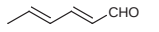	2 h	99	90
4	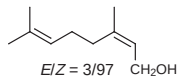 *E*/*Z* = 3/97	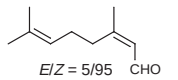 *E*/*Z* = 5/95	12 h	86	80
5	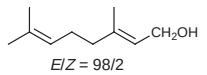 *E*/*Z* = 98/2	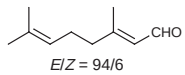 *E*/*Z* = 94/6	12 h	89	71
6	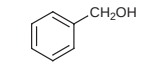	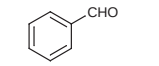	1 h	100	96
7	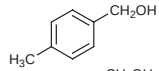	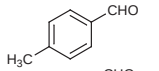	50 min	100	100
8	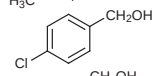	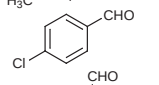	1.5 h	100	95
9	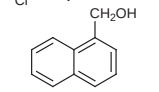	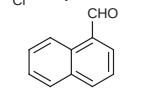	1 h	100	92
10	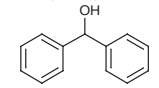	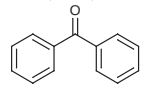	1 h	100	96 (98)
11	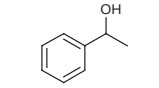	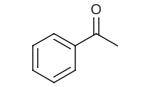	1.5 h	100	100
12	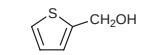	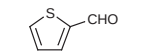	40 min	100	91
13	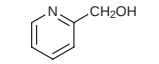	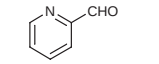	7 h	99	91
14	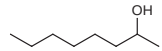	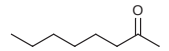	2 h	100	97 (82)

[a] Reaction conditions: substrate (2 mmol), Ru-Co-Al-CO_3HT (0.3 g), toluene (5 ml), 60 °C, O_2 atmosphere. [b] Yields of aldehydes and ketones were determined by GC analysis using internal standards, based on alcohols. [c] Values in parentheses are isolated yields. In the case of the product isolation experiments, the reaction scale was three times as much as that given in footnote (*a*).

above conditions. The hydrotalcite with Ru cations in the Brucite layer, Ru-Mg-Al-CO_3 HT, has been previously found to be a good catalyst (entry 5).[3] Substitution of Mg ions with Co ions in the Brucite layer of the above Ru-Mg-Al-CO_3 HT drastically enhanced the catalytic activity (entries 1 and 5). The Ru-Mn-Al-CO_3 HT was also an effective catalyst, while the introduction of Fe and Zn cations resulted in low yields of cinnamaldehyde.

Oxidation of various kinds of alcohols using the Ru-Co-Al-CO_3 HT in toluene was carried out at 60 °C. Typical results for the oxidation of aromatic and aliphatic alcohols were summarized in Table 2. Cinnamyl alcohol and its derivative gave α,β-unsaturated aldehydes in almost quantitative yield (entries 1 and 2). In the cases of benzylic alcohols, the corresponding aldehydes were obtained in high yield (entries 6–11). It is notable that benzoic acids (over-oxidation products) were barely detected under the above conditions. Further, the hydrotalcite catalyst is applicable for the oxidation of aliphatic allylic alcohols (entries 3–5) and heterocyclic alcohols including sulfur and nitrogen species in spite of slow reaction rates (entries 12 and 13).† A secondary saturated alcohol, octan-2-ol, was smoothly converted into the corresponding ketone (entry 14), while primary saturated alcohols such as octan-1-ol showed extremely low reactivity for this oxidation. Interestingly, the hydrotalcite could also efficiently oxygenate the benzylic

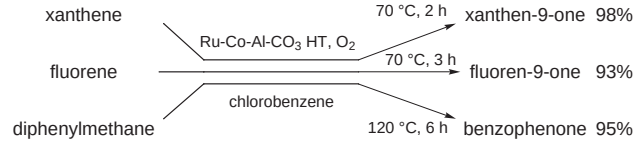

Scheme 2

positions of aromatic compounds, *i.e.* xanthene, fluorene and diphenylmethane, to give the corresponding ketones (Scheme 2).

The hydrotalcite catalyst was easily separated from the reaction mixture and was reusable without an appreciable loss of activity and selectivity for the above oxidations.

In the oxidation of cinnamyl alcohol, the Co-Al-CO_3 HT (Co : Al = 3 : 1) barely catalysed the oxidation, and the activity of Ru-Co-Al-CO_3 HT was much higher than that of a physical mixture of Co-Al-CO_3 HT and Ru-Mg-Al-CO_3 HT (Table 1, entry 6). These results indicate that it is the synergism derived from interaction of Co and Ru cations in the Ru-Co-Al-CO_3 HT that enhances the catalytic activity. The XPS results show that the oxidation state of the Ru cations of Ru-Co-Al-CO_3 HT was higher than that of Ru-Mg-Al-CO_3 HT; the Ru $3d_{5/2}$ electron binding energy of Ru-Co-Al-CO_3 HT was similar to that of RuO_3.[9] Presumably, the Ru cation species with higher oxidation states, *i.e.* Ru^{IV} to Ru^{VI}, induced by the introduction of Co cations are responsible for high catalytic activity in the above oxidation.[5] From Table 1, the basicity of hydrotalcites is not correlated with the catalytic activity for the oxidation.[3] At present, we think that substitution of Mg cations with divalent Co cations in the Brucite layer might lead to generation of an active species having a high oxidation state for the Ru ions, *e.g.* Ru=O species.[10]

In conclusion, the ruthenium hydrotalcite having Co cations was found to be an effective heterogeneous catalyst for the oxidation of various kinds of alcohols in the presence of molecular oxygen. This heterogeneous oxidation can be regarded as an environmentally benign chemical process because of the use of molecular oxygen, the simple work-up procedure and the reusability of the hydrotalcite catalyst.

Notes and references

† The oxidations of aliphatic allylic alcohols and 2-pyridylmethanol hardly proceeded in the presence of the Ru-Mg-Al-CO_3 HT under these reaction conditions.

1 G. W. Parshall and S. D. Ittel, *Homogeneous Catalysis*, 2nd edn., Wiley, New York, 1992; C. L. Hill, *Advances in Oxygenated Processes*, ed. A. L. Baumstark, JAI, London, 1998, vol. 1, p. 1; M. Hudlucky, *Oxidations in Organic Chemistry*, ACS Monograph, Washington, DC, 1990; R. A. Sheldon and J. K. Kochi, *Metal-Catalyzed Oxidations of Organic Compounds*, Academic Press, London, 1981.

2 B. M. Trost, *Science*, 1991, **254**, 1471; *Angew. Chem., Int. Ed. Engl.*, 1995, **34**, 259.

3 Hydrotalcite: K. Kaneda, T. Yamashita, T. Matsushita and K. Ebitani, *J. Org. Chem.*, 1998, **63**, 1750.

4 Co: Y. Ishii, T. Iwahama, S. Sakaguchi, K. Nakayama and Y. Nishiyama, *J. Org. Chem.*, 1996, **61**, 4520.

5 Ru: M. Matsumoto and N. Watanabe, *J. Org. Chem.*, 1984, **49**, 3435; S.-I. Murahashi, T. Naota and N. Hirai, *J. Org. Chem.*, 1993, **58**, 7318; I. E. Markó, P. R. Giles, M. Tsukazaki, I. Chellé-Regnaut, C. J. Urch and S. M. Brown, *J. Am. Chem. Soc.*, 1997, **119**, 12 661.

6 Pd: K. Kaneda, M. Fujii and K. Morioka, *J. Org. Chem.*, 1996, **61**, 4503; K. Kaneda, Y. Fujie and K. Ebitani, *Tetrahedron Lett.*, 1997, **38**, 9023; T. Nishimura, T. Onoue, K. Ohe and S. Uemura, *Tetrahedron Lett.*, 1998, **39**, 6011; K. P. Peterson and R. C. Larock, *J. Org. Chem.*, 1998, **63**, 3185.

7 F. Cavani, F. Trifirò and A. Vaccari, *Catal. Today*, 1991, **11**, 173.

8 K. Kaneda, S. Ueno and T. Imanaka, *J. Chem. Soc., Chem. Commun.*, 1994, 797; K. Kaneda, S. Ueno and T. Imanaka, *J. Mol. Catal. A: Chem.*, 1995, **102**, 135.

9 H. Y. H. Chan, C. G. Takoudis and M. J. Weaver, *J. Catal.*, 1997, **172**, 336.

10 W.-H. Fung, W.-Y. Yu and C.-M. Che, *J. Org. Chem.*, 1998, **63**, 2873.

Communication 8/09082C

Buta-2,3-dienylstannanes, effective reagents for regioselective buta-1,3-dienylation of aldehydes and acetals

Meiming Luo, Yoshiharu Iwabuchi and Susumi Hatakeyama*

Faculty of Pharmaceutical Sciences, Nagasaki University, Nagasaki 852-8521, Japan.
E-mail: susumi@net.nagasaki-u.ac.jp

Received (in Cambridge, UK) 20th November 1998, Accepted 11th December 1998

Two buta-2,3-dienylstannanes, 1-tri-*n*-butylstannylbuta-2,3-diene and 1-triphenylstannylbuta-2,3-diene, have been prepared and shown to react with aldehydes and acetals under Lewis acid catalyzed conditions producing (buta-1,3-dien-2-yl)methanol derivatives in high yields.

Recently, buta-2,3-dienylsilanes **1** (M = SiR_3)[1,2] and buta-2,3-dienylboronates **1** [M = $B(OR)_2$],[3] have appeared as useful reagents for the synthesis of (buta-1,3-dien-2-yl)methanol derivatives **2** from aldehydes and acetals. In addition, we have demonstrated that these dienols **2** are valuable precursors for the syntheses of a variety of natural products.[1,4] As part of our interest in developing a catalytic asymmetric reaction of a buta-2,3-dienylmetal **1** with an aldehyde using a chiral Lewis acid,† we directed our attention to buta-2,3-dienylstannanes **1** (M = SnR_3) which are unprecedented as synthetic reagents. Here, we report the first practical syntheses of 1-tri-*n*-butylstannylbuta-2,3-diene **3** and 1-triphenylstannylbuta-2,3-diene **4** and their Lewis acid catalyzed reactions with aldehydes and acetals.

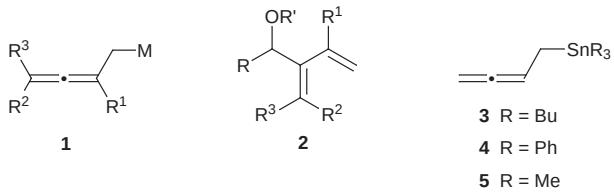

Reich and co-workers reported[5] that treatment of 1,4-bis(trimethylstannyl)but-2-yne with HCl in $CDCl_3$ caused protomonodestannylation to give 1-trimethylstannylbuta-2,3-diene **5**. However, to the best of our knowledge, the results of this NMR experiment have not been further examined in detail. This situation allowed us to examine in detail protomonodestannylations of 1,4-bis(trialkylstannyl)but-2-ynes as one possible route to buta-2,3-dienylstannanes (Scheme 1). After many discouraging results, we eventually found good reaction conditions wherein large quantities of 1-tri-*n*-butylstannylbuta-2,3-diene **3** are obtained with > 95% purity from 1,4-bis(tri-*n*-butylstannyl)but-2-yne **7**. Thus, treatment of **7**, prepared by the reaction of 1,4-dichlorobut-2-yne **6** with tri-*n*-butylstannyllithium,‡ with concentrated HCl in a 16:1 mixture of Et_2O and THF at 0 °C gave **3** cleanly in 90% yield.§ This HCl-promoted protomonodestannylation also turned out to proceed in a reasonable yield (77%) in Et_2O although the reaction was rather sluggish even at room temperature. When THF was used as solvent for this reaction, the yield of **3** decreased to 42%, possibly because of its further protodestannylation giving buta-1,3-diene. It is important to note that purification of **3** by silica gel column chromatography caused isomerization to 2-tri-*n*-butylstannylbuta-1,3-diene **8**. The ratio of **3** and **8** was at best 1 : 1 under these unsatisfactory conditions and varied depending upon the amount of silica gel used. This isomerization, however, could be completely suppressed by use of silica gel pretreated with Et_3N. Compound **3** thus purified was thermally stable and no isomerization occurred during distillation.

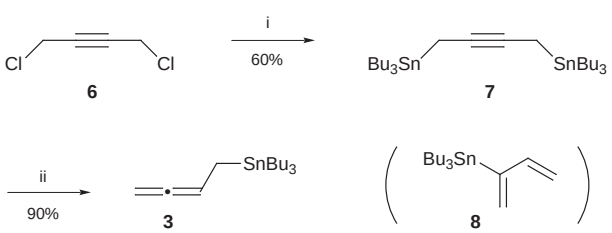

Scheme 1 *Reagents and conditions*: i, Bu_3SnLi, THF, −78 °C; ii, conc. HCl, Et_2O–THF, 0 °C.

We also investigated the reaction of Ph_3SnCl or Bu_3SnCl with the Grignard reagent **9**[6] prepared from chloroprene (2-chlorobuta-1,3-diene) (Scheme 2). We found that, in the case of Ph_3SnCl, the reaction occurred preferentially at the C4 position to give a 88 : 12 mixture of 1-triphenylstannylbuta-2,3-diene **4** and 2-triphenylstannylbuta-1,3-diene **10** in quantitative yield. Recrystallization of this mixture from *n*-hexane afforded pure **4** in 73% yield.¶ Interestingly, as previously reported,[7] Bu_3SnCl reacted with the Grignard reagent **9** with complete C2 selectivity to give 2-tri-*n*-butylstannylbuta-1,3-diene **8** quantitatively.

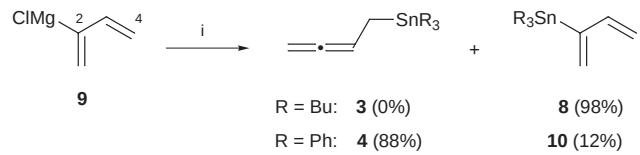

Scheme 2 *Reagents and conditions*: i, Bu_3SnCl or Ph_3SnCl, THF, −78 °C.

Having developed practical methods for the preparation of buta-2,3-dienylstannanes **3** and **4**, we then investigated their Lewis acid catalyzed reactions with various aldehydes and acetals (Scheme 3). Table 1 summarizes Lewis acid catalyzed additions of **3** and **4** to aldehydes. It is evident that this reaction has broad applicability for the preparation of **12** (R^2 = H) and $BF_3{\cdot}Et_2O$ is the catalyst of choice, except for the two examples listed in entries 8 and 10. It is also apparent that **3** is much more reactive than **4** in this reaction. Compound **3** was found to gradually isomerize to **8** under these conditions, whereas compound **4** did not undergo such Lewis acid catalyzed isomerization.

As can be seen from Table 2, both **3** and **4** again reacted with acetals in good yields. The mixed titanium reagent [$3TiCl_4{\cdot}Ti(OPr^i)_4$] was found to give better results than $BF_3{\cdot}Et_2O$, especially in the cases of aliphatic acetals (entries 1, 2, 10 and 11). Conversely, the reaction of cinnamaldehyde dimethyl acetal with **3** took place almost quantitatively under $BF_3{\cdot}Et_2O$

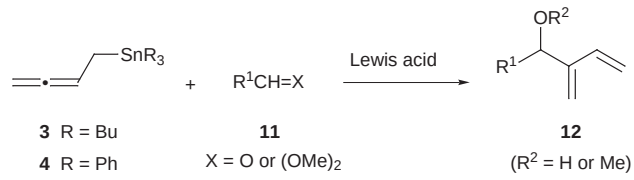

Scheme 3

Table 1 Lewis acid catalyzed addition of **3** and **4** to aldehyde **11** (X = O) giving **12** (R^2 = H)[a]

Entry	**3** or **4**	R^1	Lewis acid	Solvent	*t*/h	Yield (%)[b]
1	**3**	$Ph(CH_2)_2$	$BF_3{\cdot}Et_2O$	CH_2Cl_2	2	57
2	**3**	$Ph(CH_2)_2$	$BF_3{\cdot}Et_2O$	toluene	9	92
3	**3**	$Ph(CH_2)_2$	$TiCl_4$	CH_2Cl_2	10	17[c]
4	**3**	$Ph(CH_2)_2$	$3TiCl_4{\cdot}Ti(OPr^i)_4$	toluene	8	44[c]
5	**3**	$Ph(CH_2)_2$	MgI_2	CH_2Cl_2	4	51[d]
6	**3**	$PhCH_2$	$BF_3{\cdot}Et_2O$	toluene	12	83
7	**3**	$PhCH_2$	$TiCl_4$	CH_2Cl_2	0.3	64
8	**3**	(*E*)-PhCH=CH	$BF_3{\cdot}Et_2O$	toluene	10	0[e]
9	**3**	Ph	$BF_3{\cdot}Et_2O$	toluene	9	96
10	**4**	Ph	$BF_3{\cdot}Et_2O$	CH_2Cl_2	10	0[e]
11	**4**	Ph	$3TiCl_4{\cdot}Ti(OPr^i)_4$	CH_2Cl_2	10	40 (65)[f]
12	**3**	*n*-C_7H_{15}	$BF_3{\cdot}Et_2O$	toluene	12	87
13	**4**	*n*-C_7H_{15}	$BF_3{\cdot}Et_2O$	CH_2Cl_2	23	85
14	**3**	*c*-C_6H_{11}	$BF_3{\cdot}Et_2O$	toluene	12	90
15	**4**	*c*-C_6H_{11}	$BF_3{\cdot}Et_2O$	CH_2Cl_2	16	86

[a] All reactions were carried out at −78 °C in the indicated solvent (0.13 mol dm^{-3}) using buta-2,3-dienylstannane (2 equiv.), aldehyde (1 equiv.), and Lewis acid (1 equiv.) unless stated otherwise. [b] Isolated yield. [c] The aldehyde was partly cyclyzed to indan-1-ol which underwent further reaction to produce several by-products. [d] The reaction was carried out at room temperature. [e] Most of the aldehyde was recovered. [f] Yield in parenthesis based on the consumed aldehyde.

Table 2 Lewis acid catalyzed addition of **3** and **4** to acetal **11** (X = $(OMe)_2$) giving **12** (R^2 = Me)[a]

Entry	**3** or **4**	R^1	Lewis acid	Solvent	*t*/h	Yield (%)[b]
1	**3**	$Ph(CH_2)_2$	$BF_3{\cdot}Et_2O$	toluene	12	0[c]
2	**3**	$Ph(CH_2)_2$	$3TiCl_4{\cdot}Ti(OPr^i)_4$	toluene	5	95
3	**3**	$PhCH_2$	$3TiCl_4{\cdot}Ti(OPr^i)_4$	toluene	5	81
4	**3**	(*E*)-PhCH=CH	$BF_3{\cdot}Et_2O$	toluene	10	99
5	**3**	(*E*)-PhCH=CH	$3TiCl_4{\cdot}Ti(OPr^i)_4$	toluene	10	48
6	**3**	Ph	$BF_3{\cdot}Et_2O$	toluene	10	89
7	**3**	Ph	$3TiCl_4{\cdot}Ti(OPr^i)_4$	toluene	4	89
8	**4**	Ph	$BF_3{\cdot}Et_2O$	toluene	10	86
9	**4**	Ph	$3TiCl_4{\cdot}Ti(OPr^i)_4$	CH_2Cl_2	6	70
10	**3**	*n*-C_7H_{15}	$BF_3{\cdot}Et_2O$	toluene	9	0[c]
11	**3**	*n*-C_7H_{15}	$3TiCl_4{\cdot}Ti(OPr^i)_4$	CH_2Cl_2	4	86
12	**4**	*n*-C_7H_{15}	$3TiCl_4{\cdot}Ti(OPr^i)_4$	CH_2Cl_2	7	91
13	**3**	*c*-C_6H_{11}	$3TiCl_4{\cdot}Ti(OPr^i)_4$	CH_2Cl_2	4	96
14	**4**	*c*-C_6H_{11}	$3TiCl_4{\cdot}Ti(OPr^i)_4$	CH_2Cl_2	8	89

[a] Reactions were carried out at −78 °C in the indicated solvent (0.13 mol dm^{-3}) using buta-2,3-dienylstannane (**3**: 2 equiv. **4**: 1.2 equiv.), acetal (1 equiv.) and Lewis acid (1 equiv.). [b] Isolated yield. [c] Most of the aldehyde was recovered.

catalyzed conditions and $3TiCl_4{\cdot}Ti(OPr^i)_4$ produced poor result in this particular case (entries 4 and 5).

In conclusion, we have successfully synthesized two buta-2,3-dientylstannanes, 1-tri-*n*-butylstannylbuta-2,3-diene **3** and 1-triphenylstannylbuta-2,3-diene **4**, in >95% isomeric purity for the first time. These buta-2,3-dienylstannanes react with various aldehydes and acetals regioselectively in a 1,3-rearrangement fashion to give (buta-1,3-dien-2-yl)methanol derivatives in excellent yields. In comparison with the related silicon[1] and boron reagents,[3] buta-2,3-dienylstannanes have the advantage of broad applicability in buta-1,3-dienylations of both aldehydes and acetals. The development of a catalytic asymmetric reaction of buta-2,3-dienylstannanes with aldehydes is the focus of current investigations.

This work was supported by the Japan Society for the Promotion of Science (postdoctoral fellowship for M. L.). We gratefully acknowledge the Tosoh Corporation (Nanyo Research Laboratory, Japan) for providing chloroprene.

Notes and references

† A catalytic asymmetric version of this process using either buta-2,3-dienylsilanes or buta-2,3-dienylboronates has not been successfully achieved yet.

‡ Prepared according to Reich's method for 1,4-bis(trimethylstannyl)but-2-yne (ref. 5).

§ Experimental procedure for **3**: To a stirred solution of **7** (7.93 g, 12.5 mmol) in Et_2O (80 ml) with cooling in an ice bath was added a mixture of concentrated HCl (1.3 ml) and THF (5 ml). After stirring at 0 °C for 8 h, the reaction mixture was basified with 5% NaOH (10 ml) and extracted with Et_2O. The extract was washed with water, dried over $MgSO_4$, and concentrated *in vacuo*. Purification by column chromatography [SiO_2 (30 g) pretreated with Et_3N (30 g); *n*-hexane] afforded **3** (3.86 g, 90%), bp 150 °C (0.2 mmHg) (Kugelröhr).

¶ Experimental procedure for **4**: A flame-dried flask was charged with THF (30 ml) and Grignard reagent **9** (1.6 mol dm^{-3} in THF, 12.5 ml, 20 mmol) under argon and then a solution of Ph_3SnCl (7.71 g, 20 mmol) in THF (15 ml) was added dropwise at −78 °C. After being stirred at −78 °C for 30 min, the reaction mixture was quenched with 5% NaOH (10 ml) and extracted with Et_2O. The extract was dried over $MgSO_4$, concentrated *in vacuo*, and chromatographed [SiO_2 (30 g) pretreated with Et_3N (30 g); *n*-hexane] to give an 88 : 12 mixture of **4** and **10** as a colorless viscous oil (8.05 g) which solidified during overnight storage in a refrigerator. Recrystallization of this crystalline solid from *n*-hexane afforded **4** (5.86 g, 73%) as colorless crystals (mp 54–55 °C).

1 For a review on buta-2,3-dienylsilanes, see: S. Hatakeyama, *J. Synth. Org. Chem. Jpn.*, 1997, **55**, 793.
2 T. Nishiyama, T. Esumi, Y. Iwabuchi, H. Irie and S. Hatakeyama, *Tetrahedron Lett.*, 1998, **39**, 43.
3 B. Zheng and M. Srebnik, *J. Org. Chem.*, 1995, **60**, 486; R. Soundararajan, G. Li and H. C. Brown, *J. Org. Chem.*, 1996, **61**, 100; B. Zheng and M. Srebnik, *Synth. Commun.*, 1996, **26**, 393.
4 S. Hatakeyama, M. Yoshida, T. Esumi, Y. Iwabuchi, H. Irie, T. Kawamoto, H. Yamada and M. Nishizawa, *Tetrahedron Lett.*, 1997, **38**, 7887.
5 H. J. Reich, I. L. Reich, K. E. Yelm, J. E. Holladay and D. Gschneidner, *J. Am. Chem. Soc.*, 1993, **115**, 6625.
6 S. Nunomoto and Y. Yamashita, *J. Org. Chem.*, 1979, **44**, 4788.
7 E. Wada, S. Kanemasa, I. Fujiwara and O. Tsuge, *Bull. Chem. Soc. Jpn.*, 1985, **58**, 1942; G. S. Bates, M. D. Fryzuk and C. Stone, *Can. J. Chem.*, 1987, **65**, 2612.

Communication 8/09081E

Epitaxial growth of WO_{3-x} needles on (10 $\bar{1}$0) and (01 $\bar{1}$0) WC surfaces produced by controlled oxidation with CO_2

Andrew P. E. York,[a] Jeremy Sloan[a,b] and Malcolm L. H. Green*[a]

[a] *Inorganic Chemistry Laboratory, University of Oxford, South Parks Road, Oxford, UK OX1 3QR. E-mail: malcolm.green@chem.ox.ac.uk*

[b] *Department of Materials, University of Oxford, Parks Road, Oxford, UK OX1 3PH*

Received (in Bath, UK) 23rd September 1998, Accepted 4th January 1999

The controlled oxidation with CO_2 of both high surface area (high S_g) and low surface area WC to form WO_{3-x} needles, has been observed *in situ*, inside a controlled environment transmission electron microscope (CETEM), and also *ex situ*, in a standard flow reactor; the tungsten oxide needles, which consist mainly of distorted γ-$WO_{2.72}$, propagate in an epitaxial fashion from the (10 $\bar{1}$0) and (01 $\bar{1}$0) surfaces of the parent WC crystals; possible mechanisms for the formation of the needles are proposed.

Recently, WC was shown to be an active catalyst for the conversion of methane and carbon dioxide to synthesis gas (CO + H_2).[1,2] During the course of these studies, it was found that catalyst deactivation due to oxidation of WC by CO_2 leads to the formation of tungsten oxides, which are inactive for methane reforming. Such materials are, however, useful in a wide variety of applications including some catalytic processes (*e.g.* metathesis),[3] in optoelectronic devices,[4] as gas sensor materials,[5] and have recently been developed as precursor materials for the synthesis of inorganic fullerene-like (IF) materials based on 2H-WS_2 layered chalcogenide structures.[6–8] While using CETEM to probe the deactivation mechanism of the carbide, we observed the propagation of oxygen deficient tungsten oxide needles from specific crystal faces of the parent carbide. We describe here their *in situ* and *ex situ* formation from both high and low surface area WC particles by controlled oxidation with CO_2.

High surface area (high S_g) WC (40 m^2 g^{-1}) was synthesised by reacting WO_3 with a mixture of 20% CH_4–H_2 (100 ml min^{-1}), ramping the temperature from room temperature to 750 °C at a rate of 1 °C min^{-1}.[2] This material was then characterised by XRD and found to be hexagonal WC with an average particle size radius of 7.62 nm (Scherrer method). The low surface area (low S_g) WC (Alfa Chemicals, 99.5%) exhibited average particle sizes of *ca.* 2.5 μm, estimated by high resolution transmission electron microscopy (HRTEM).

The oxidation of WC in the presence of CO_2 was initially investigated *in situ* in a 400 kV CETEM, described previously.[9,10] Cooling effects due to the thermal conductivity of CO_2 have been taken into account in the reaction temperatures quoted. Both WC samples were heated, under differential pumping conditions, in the temperature range 550–650 °C with an introduced partial pressure of 5 mbar CO_2. The onset of oxidation for high S_g WC was observed at 550–560 °C by formation of WO_{3-x} needles from the surfaces of the WC crystals. For low S_g WC, needle growth started at 580–590 °C, suggesting a slightly higher activation energy for this oxidation. In both cases, needle growth could be observed *in situ* in real time and Fig. 1(a) shows a typical example of growth observed from a cluster of high S_g WC crystallites after *ca.* 20 min at 580 °C. In the case of low S_g (*i.e.* large particle size) WC, parallel multiple needle growth was also observed from the facets of individual WC crystallites. Fig. 1(b) shows six WO_{3-x} needles growing from the (01 $\bar{1}$0) facet of a WC with its [10 $\bar{1}$0] zone axis orientated parallel to the electron beam (SAED not shown). This reaction was subsequently repeated *ex situ* for

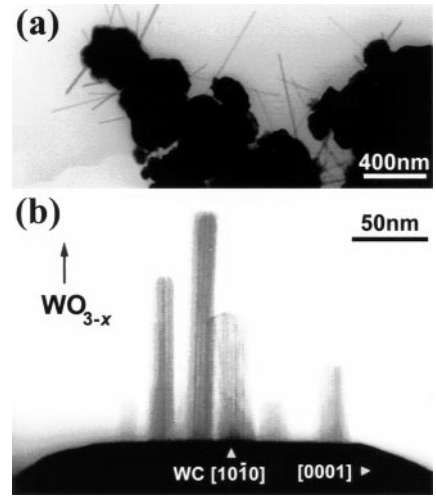

Fig. 1 (a) Micrograph showing WO_{3-x} needle formation from clusters of high S_g WC observed by CETEM. (b) Micrograph showing multiple parallel WO_{3-x} needle growth occurring from the (10 $\bar{1}$0) (alternatively (01 $\bar{1}$0)) face of a single WC crystal in the same [01 $\bar{1}$0] orientation as the example in Fig. 2 (SAED pattern not shown).

both the low and high S_g carbides in a standard flow reactor at ambient pressure and in the temperature range 600–800 °C using a CO_2 flow rate of 100 ml min^{-1} for 24 h. At 750–800 °C, the yield of WO_{3-x} needles from WC from both specimens was quantitative. Partially oxidised WC showing epitaxial needle growth was observed in samples oxidised at 600–750 °C.

For the low S_g WC, it was possible to correlate the WO_{3-x} needle growth with respect to either the (10 $\bar{1}$0) or the (01 $\bar{1}$0) face of the parent carbide; growth from the hexagonal (0001) face was not observed. The middle section of Fig. 2 shows a HRTEM micrograph of the interface between a WO_{3-x} needle grown on the surface of a WC crystallite. The inset indexed SAED pattern **I** (obtained from **I′**) corresponds to a [01 $\bar{1}$0] projection of the parent carbide. The dense microstructure of this crystal is visible below the carbide/oxide interface in the micrograph. Inset **II** is a fast Fourier transform (FFT) computed from region **II′** in the micrograph and shows the calculated diffraction behaviour of the oxide needle. The indicated strong reflections in the centre of **II** correspond to the 0.375 nm layers in the oxide needle. Diffuse streaking in the horizontal rows of diffraction maxima (small arrowheads) correspond to planar disorder occurring parallel to the needle axis (indicated by arrow **A**, micrograph). Substructure reflections, two of which are denoted **A** and **B**, are also visible along these rows. Inset **III**, obtained from the oxide/carbide interface (region **III′**), is an FFT showing the composite diffraction behaviour at the interface. In this pattern, the strong reflections corresponding to the oxide layers are now aligned along [10 $\bar{1}$0] of the WC pattern (large arrow). It is significant that reflection **A** (and its equivalents) from the oxide is now coincident with the WC 0001 reflection (and its equivalents) in **III**, suggesting that the

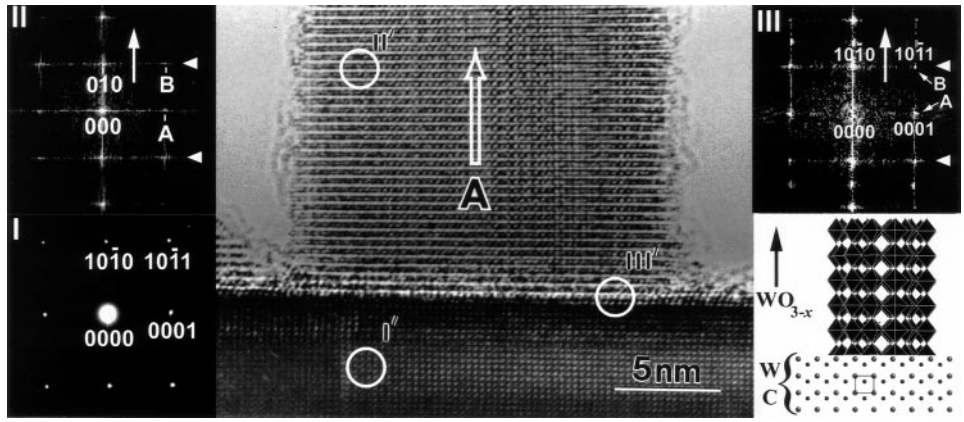

Fig. 2 Micrograph showing the interface between WO_{3-x} needle and WC parent crystal. The inset patterns correspond to: **I**, [01 $\bar{1}$0] SAED pattern obtained from region **I′** corresponding to the parent WC crystal; **II** FFT obtained from region **II′** corresponding to the WO_{3-x} needle; and **III**, FFT obtained from region **III′** corresponding to the WO_{3-x}/WC interface. At the lower right is a schematic representation of the composite microstructure at the interface. The unit cell of the parent carbide (a = 0.2907 nm; c = 0.2837 nm) is indicated.

substructure of the oxide is constrained by that of the carbide, as in a template relationship. This could also be a source of the strain and disorder indicated by the streaking in **II** and **III**. A schematic representation of the overall microstructure is given at the lower right of Fig. 2.

The projection of the oxide in **II** and **III** closely resembles a [001] projection of the phase γ-$WO_{2.72}$ and reflections **A** and **B** (corresponding to 0.284 and 0.220 nm, respectively), are close to (006) and (016) (corresponding to 0.276 and 0.223 nm, respectively) of this oxide.[11,12] Also, the microstructures of the epitaxially grown oxide and γ-$WO_{2.72}$ are very similar as revealed by a comparison of an enlarged region of Fig. 2 [Fig. 3(a)] and an image simulation[13] calculated for a [001] projection of the latter [Fig. 3(b)].

The possible mechanisms for needle formation from the carbides should be addressed. It is proposed that the first step in the formation of the oxide needles is the dissociation of carbon dioxide on the WC surface, according to reaction (1), in agreement with the proposed mechanism for the reforming of methane published by Green and coworkers.[1,2,14] According to this mechanism, oxidation of WC by CO_2 is solely a surface phenomenon and gas-phase dioxygen is not involved.

$$WC + CO_2 = WO_x + CO \quad (1)$$

After the formation of surface oxide, two possible needle propagation mechanisms may be envisaged: (i) an insertion/diffusion mechanism whereby the oxide forms layer-by-layer resulting in platelets that are pushed from below as oxidation diffuses into the carbide crystal; and (ii) a gas-phase reaction involving the transport of oxide from the carbide surface to the oxide needle tips. If mechanism (i) were responsible, progressive consumption of the carbide crystals from the inside should have been observed, but this was not the case.

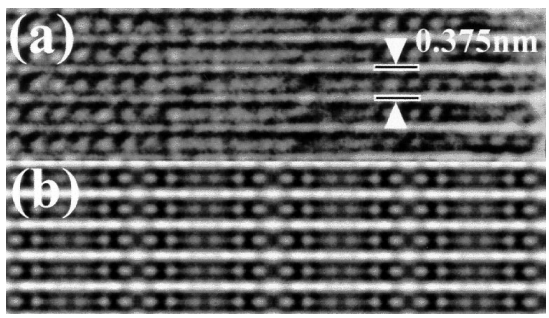

Fig. 3 (a) Enlargement of a segment of the WO_{3-x} needle in Fig. 2. (b) Image simulation calculated for a [001] projection of γ-$WO_{2.72}$ computed using a 1.4 nm thick foil at −70 nm defocus. There is a close (though not perfect) correspondence between the two microstructures.

Mechanism (ii) allows for the epitaxial growth of the needles from the WC crystal surfaces which is apparently observed. Possible support for this is given by the observation of amorphous material on the surface of the needle and the carbide (see Fig. 2) which may correspond to the sublimate feedstock. In addition, the vapour pressure of WO_3 at 550 and 650 °C, and 1 atm (*i.e.* similar conditions to those employed for *ex situ* needle growth) is 5×10^{-4} and 0.0193 mmHg respectively,[15] indicating that tungsten oxide will have a significant presence in the gas-phase. Therefore, we propose that needle growth proceeds *via* mechanism (ii).

The epitaxial growth of orientated WO_{3-x} needles on (10 $\bar{1}$0) and (01 $\bar{1}$0) WC facets by controlled oxidation has been demonstrated. Such a process may, with further development, allow greater control over the stoichiometry and morphology of the produced tungsten oxide needles. We will discuss the issues raised by this work more fully in a future publication.

A. P. E. Y. is grateful to CANMET for financial support; we would also like to thank Ron Doole of the Department of Materials for his assistance with the CETEM.

Notes and references

1 A. P. E. York, J. B. Claridge, A. J. Brungs, S. C. Tsang and M. L. H. Green, *Chem. Commun.*, 1997, 39.
2 A. P. E. York, J. B. Claridge, A. J. Brungs, S. C. Tsang and M. L. H. Green, *Stud. Surf. Sci. Catal.*, 1997, **110**, 711.
3 A. G. Basrur, S. R. Patwardhan and S. N. Vyas, *J. Catal.*, 1991, **127**, 86.
4 S. Passerini, B. Scrosati, V. Hermann, C. Holmblad and T. Bartlett, *J. Electrochem. Soc.*, 1994, **141**, 1025.
5 H. T. Sun, C. Cantalini, L. Lozzi, M. Passacantando, S. Santucci and M. Pelino, *Thin Solid Films*, 1996, **287**, 258.
6 R. Tenne, L. Margulis, M. Genut and G. Hodes, *Nature*, 1993, **360**, 444.
7 L. Margulis, G. Salitra, R. Tenne and M. Talianker, *Nature*, 1993, **365**, 113.
8 M. Homyonfer, B. Alperson, Y. Rosenberg, L. Sapir, S. R. Cohen, G. Hodes and R. Tenne, *J. Am. Chem. Soc.*, 1997, **119**, 2693.
9 R. C. Doole, G. M. Parkinson and J. M. Stead, *Inst. Phys. Conf. Series*, 1991, **119**, 157.
10 R. C. Doole, G. M. Parkinson, J. L. Hutchison, M. J. Goringe and P. J. F. Harris, *JEOL News*, 1992, **30E**, 14.
11 A. Magnéli, *Ark. Kemi*, 1949, **1**, 223.
12 A. Magnéli, Powder Diffraction File card 5-392 (ASTM, Philadelphia Pennsylvania).
13 P. A. Stadelmann, *Ultramicroscopy*, 1987, **21**, 131.
14 J. B. Claridge, A. P. E. York, A. J. Brungs, C. Márquez-Alvarez, J. Sloan, S. C. Tsang and M. L. H. Green, *J. Catal.*, 1998, **180**, 85.
15 *Gmelins Handbuch der Anorganischen Chemie*, ed. R. J. Meyer, Verlag Chemie, Berlin, 1933, vol. 54, p. 122.

Communication 8/07403H

Modification of [M]-MSU-X mesoporous silicate pore morphology by post-synthesis treatment

Stephen A. Bagshaw*

Advanced Materials Group, Industrial Research Limited, PO Box 31-310, Lower Hutt, New Zealand.
E-mail: s.bagshaw@irl.cri.nz

Received (in Cambridge, UK) 26th November 1998, Accepted 24th December 1998

[M]-MSU-X mesoporous silicates prepared from selected low concentration non-ionic polyethylene oxide surfactants have been subjected to post synthesis hydrothermal treatment which significantly modifies the pore morphologies forming stable hexagonal or lamellar structures through an internal dissolution-redirection mechanism.

The development of synthetic methods to improved templated mesostructured materials[1–3] for catalytic and molecular sieving applications is attracting considerable attention. The search for inexpensive and environmentally benign routes to specialised materials and fine chemicals is also an area of considerable scientific and technological interest. Recent work has shown that mesostructured silica,[4] metallo-silicates[5] and alumina[6] may be templated by inexpensive and non-toxic non-ionic polyethylene oxide (PEO) and tri-block co-polymer surfactants under near ambient reaction conditions.[4]

The pore architectures of these so-called MSU-X molecular sieve materials were described as three-dimensional interconnecting networks of 'worm-like' channels.[7,8] Hexagonal mesoporous silicas have previously been reported[9,10] from very high alkyl-PEO surfactant concentrations (50 wt%) and strongly acidic reaction media. Here we describe an improved yet very simple, inexpensive and environmentally benign synthesis route to [M]-MSU-X mesoporous silicates that exhibit worm-like, hexagonal and lamellar pore architectures. A possible mechanism for the pore rearrangement is briefly discussed.

[M]-MSU-X mesostructures have been prepared from selected members of the Brij® series of commercially available alkyl-PEO surfactants. These materials have been found to consistently exhibit greater lattice regularity than any of the Tergitol 15-S®, Triton® or Pluronic® series of surfactants that have been previously employed at low surfactant concentration (Fig. 1).[4–6,7] If any [M]-MSU-1 material with worm-like pore morphology was dried and treated in water at 373 K under autogenous pressure for approximately 72 h its pore symmetry became significantly reordered and thermally induced lattice contraction upon calcination became almost negligible. Only when high regularity [M]-MSU-1 materials prepared from the Brij® series of surfactants were treated however, were lamellar and hexagonally symmetric structures observed.

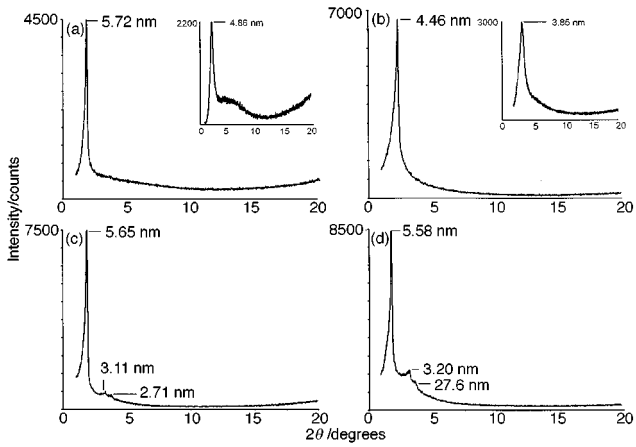

Fig. 1 XRD patterns of 7SAB Brij 76 templated [Ti]-MSU-1 (a) as-prepared, (b) calcined, (c) hydrotreated 72 h and (d) hydrotreated 72 h and calcined. Inset (a): as-prepared 5SAB Tergitol 15-S-12 templated [Ti]-MSU-1, (b) calcined 5SAB-C. (λ = 0.179026 nm.)

[Si]-, [Al]-, [Zr]- and [Ti]-MSU-1 silicates were prepared according to a method previously reported utilising the $N^0(N^+)X^-I^+$ assembly route.[5] Reordered [M]-MSU-1 materials were then prepared by treating the dried samples in distilled water (1 g sample per 30 mL water) at 100 °C in a sealed container for predetermined times.[11] The samples were recovered, dried in air and, in this instance, calcined at 600 °C for 4 h to remove the template. A Tergitol 15-S-12 templated [Ti]-MSU-1 sample is labeled 5SAB and a Brij 76 templated [Ti]-MSU-1 sample is labeled 7SAB, with suffixes HT-3 for 72 h hydrothermal treatment and C for calcination.

Low-angle powder X-ray diffraction (XRD) analyses (Fig. 1) show the single and multiple reflection patterns of [Ti]-MSU-1 samples in the as-prepared, hydrothermally treated and calcined forms. The as-prepared samples [Fig. 1(a)] exhibit intense first-order d_{100} reflections indicative of mesostructures possessing non-ordered worm-like pore structures with no long-range symmetry. It is however, immediately apparent from comparison of the peak widths and intensities, that the relations between structural repeat units are considerably more regular in the Brij 76 templated sample (Fig. 1) than in the Tergitol 15-S-12 templated sample (Fig. 1 inset). Calcination produced lattice contractions in the order of 20% and intensity increases of the d_{100} reflections that have been previously well documented.[1–10] Hydrothermal treatment of the as-prepared 7SAB sample for 72 h however, results in the appearance of two additional reflections [Fig. 1(c)]. The *d* spacings are not simple multiples, which would be expected for a lamellar system so are therefore probably best described by a hexagonal symmetry or at the very least, to pore symmetry similar to that observed for hexagonal MCM-41 type materials.[1,2] The appearance of additional XRD reflections were not observed for materials prepared from other non-ionic surfactant templates, such as Tergitol 15-S-12, although there is evidence for improvement in the pore ordering of all [M]-MSU-X materials.[12]

An important consequence of the hydro-treatment is that calcination of the treated samples results in negligible lattice contractions. This result indicates that the hydro-treatment causes hydrolysis and condensation of the silicate structure beyond that caused during the initial formation reaction.

Nitrogen adsorption isotherms of the various samples reflect important differences between [M]-MSU-X mesostructures prepared with Brij® surfactants, over other surfactants, and hydrothermally treated samples. The isotherm of 7SAB-C is characteristic of a material with pore diameter in the small mesoporous region exhibiting a shallow step with a definite point of inflexion at P/P_0 = 0.25 and no hysteresis of the desorption branch. Samples prepared with other PEO surfactants (*e.g.* 5SAB-C) generally exhibit no point of inflexion in the same region, indicating slightly smaller pore diameters

Table 1 Textural properties of worm-like and hexagonally symmetric[Ti]-MSU-1 mesoporous metallo-silicates

[Ti]-MSU-1 sample	d_{100} lattice spacing[a]/ nm	Lattice contraction[b] (%)	BET surface area[c]/ $m^2\ g^{-1}$	Pore diameter[d]/nm	Pore volume[e]/ $cm^3\ g^{-1}$	Wall thickness[f,g]/nm
5SAB	4.85					
5SAB-C	3.85	21	800	1.8[h]	0.35	2.0
5SAB-HT-3	4.55					
5SAB-HT-3C	4.50	0.7	970	2.4[i]	0.70	2.1
7SAB	5.70					
7SAB-C	4.45	22	920	2.2[a]	0.50	2.3
7SAB-HT-3	5.65					
7SAB-HT-3C	5.60	1.2	970	3.6[b]	1.10	2.0

[a] ±0.05 nm. [b] ±0.1%. [c] 10 $m^2\ g^{-1}$. [d] ±0.5 nm. [e] ±0.05 $cm^3\ g^{-1}$. [f] ±0.5 nm. [g] Wall thicknesses calculated by subtracting pore diameter from d_{100} lattice spacing value assuming that the d_{100} value is equivalent to the distance between adjacent pore centres. [h] Average pore diameter calculated from adsorption isotherm using HK model for cylindrical pores. This model tends to over-estimate pore diameters if pores are above 2.0 nm diameter. [i] Average pore diameter calculated from adsorption isotherm using BJH model for cylindrical pores. This model tends to under-estimate pore diameters.

(Table 1).[7] After hydrothermal treatment the shallow step is replaced by a well defined, high volume step in the upper capillary condensation region of the isotherm (P/P_0 = 0.55) indicative of well defined mesopores. Some hysteresis of the desorption branch becomes evident which may be a result of necking of the pores but is also possibly a consequence of the high adsorption partial pressure given that hysteresis is generally observed in mesostructured materials where the adsorption step is above P/P_0 = 0.45.

Selected area transmission electron micrograph (TEM) of the as-prepared materials (not presented) display the worm-like pore architecture previously reported for MSU-X materials.[4] Fig. 2 suggests that as a result of the hydrothermal treatment, the worm-like pore morphology has largely been replaced by a structure exhibiting ordering in two dimensions. In the present image the most obvious new feature appears as a lamellar phase coincident with the preexisting worm-like structure. When this evidence is combined with XRD data and the fact that the samples are calcined it seems reasonable to conclude that regular pores exist both parallel and perpendicular to the electron beam and that areas of hexagonal symmetry are being observed.

We suggest that hydrothermal treatment of templated silicate mesostructures causes structural modification through a dissolution/reprecipitation mechanism. Initially a diffuse inner layer of silica at the pore/template interphase, as invoked by Edler and White,[13] dissolves at the elevated temperature of the treatment. This dissolved silica reaches supersaturation within the interphase and then reprecipitates into a more dense phase on the pore wall. Only when the template is retained within the pore void can this dissolved silica be redirected to form on the pore walls. Such behaviour is observed for S^+I^- MCM-41 materials[11,13] but not for $S^+X^-I^+$ nor $S^\circ I^\circ$ templating.[12] It is by no means obvious that it would be observed in $N^+X^-I^0$ or $N^0\ I^0$ templated systems.

The data presented here however show definite beneficial effects of hydrothermal treatment on the non-ionically templated silicate systems. The exact mechanism whereby the worm-like pore morphology transforms into the more regular arrangement is currently under investigation. We are also currently investigating possible improvements in the molecular sieving and catalytic properties of the modified samples over regular MSU-X materials in the isomerisation of terpene substrates.

The author gratefully acknowledges the assistance of the New Zealand Lotteries grant board and Karen Reader for TEM analyses. This work was funded as part of a contract with the New Zealand Foundation for Research Science and Technology.

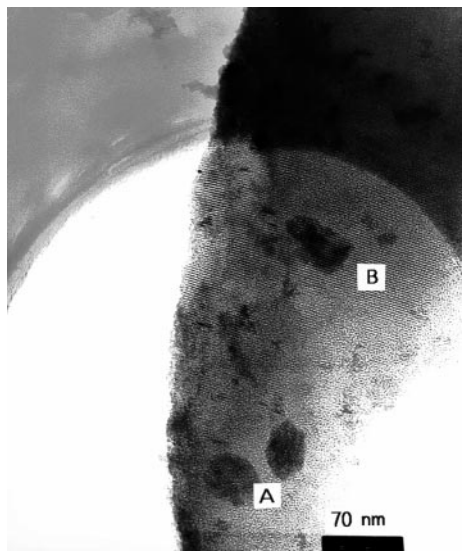

Fig. 2 Representative transmission electron micrograph of sample 7SAB-HT-3C displaying areas of (A) worm-like and (B) and hexagonal/lamellar symmetries.

Notes and references

1 C. T. Kresge, M. E. Leonowicz, W. J. Roth, J. C. Vartuli and J. S. Beck, *Nature*, 1992, **359**, 710.
2 G. Huo, D. I. Margolese, U. Ciesla, P. Feng, T. E. Gier, P. Sieger, R. Leon, P. M. Petroff, F. Schuth and G. D. Stucky, *Nature*, 1994, **368**, 317.
3 P. T. Tanev and T. J. Pinnavaia, *Science*, 1995, **267**, 865.
4 S. A. Bagshaw, E. Prouzet and T. J. Pinnavaia, *Science*, 1995, **269**, 1242.
5 S. A. Bagshaw, T. Kemmitt and N. B. Milestone, *Microporous Mesoporous Mater.*, 1998, **22**, 419.
6 S. A. Bagshaw and T. J. Pinnavaia, *Angew. Chem., Int. Ed. Engl.*, 1996, **35**, 1102.
7 E. Prouzet and T. J. Pinnavaia, *Angew. Chem., Int. Ed. Engl.*, 1997, **36**, 516.
8 R. Richer and L. Mercier, *Chem. Commun.*, 1998, 1775.
9 G. S. Attard, J. C. Glyde and C. S. Gottner, *Nature*, 1995, **378**, 366.
10 D. Zhao, J. Feng, Q. Huo, N. Melosh, G. H. Freidrikson, B. F. Chmelka and G. D. Stucky, *Science*, 1998, **279**, 548.
11 Q. Huo, D. I. Margolese and G. D. Stucky, *Chem. Mater.*, 1996, **8**, 1147.
12 S. A. Bagshaw, *Stud. Surf. Sci. Catal.*, 1998, **117**, 381.
13 K. J. Edler, P. A. Reynolds, J. W. White and D. Cookson, *J. Chem. Soc., Faraday Trans.*, 1997, **93**, 199.

Communication 8/09254K

$[\{Cu(bipy)(H_2O)Pt(CN)_4\}_2]\cdot 2H_2O$: the first synthesis and crystal structure of a discrete heterometallic square cyano-bridged compound with terminal cyano ligands

Larry R. Falvello* and Milagros Tomás*

Department of Inorganic Chemistry and Aragón Materials Science Institute, University of Zaragoza-C.S.I.C., Plaza San Francisco s/n E-50009 Zaragoza, Spain. E-mail: falvello@LRF1.unizar.es

Received (in Basel, Switzerland) 21st September 1998, Accepted 13th December 1998

The synthesis and crystal structure of a square cyano-bridged compound with terminal cyano ligands are presented together with a discussion of the influence of H_2O molecules on the stability of the terminal cyanides and therefore on the discrete nature of the compound.

The particular characteristics of the cyanide group have accorded it wide-ranging interest in various research areas.[1,2] One of the more interesting characteristics of $C\equiv N^-$ is its ability to act either as a terminal or as a bridging ligand. When it acts as a bridging ligand between metal atoms it usually gives rise to polymeric compounds[2] with 1-D, 2-D or 3-D networks. Except for some clusters such as those with the 'Mo_6Cl_8' core,[3] few discrete cyanide-containing molecules with more than three metal atoms have been synthesized and structurally characterized; and particularly rare are those with cyano–metal rings.[1]

Although square or distorted square cyano-bridged fragments, both homo- and hetero-nuclear, have been found embedded in polymeric compounds,[4–6] only very few discrete molecules with square cyano-bridged structures have been reported,[1] characterized mostly on the basis of molecular weight determinations.[7] Only two, the homonuclear compounds $[Cp_2Ti(CN)]_4$ and $[(\eta^2\text{-tmtch})Cu(CN)]_4$ (tmtch = 3,3,6,6,-tetramethyl-1-thia-4-cycloheptyne) have been fully characterized by single-crystal X-ray diffraction studies.[8] No structures of heteronuclear, square, cyano-bridged compounds have been reported.

It may be that the scant information available to date on discrete cyano-bridged ring compounds is the result of a scarcity of appropriate cyano-containing starting materials and the difficulty of obtaining crystalline compounds suitable for X-ray diffraction studies. We report here the synthesis of a discrete cyano-bridged ring using a 'stoichiometrically inappropriate' starting material and the preparation of single crystals by an unconventional method.

Polymerization can easily occur when the starting cyano compound contains more cyano groups than those required for the formation of the discrete ring. So it would seem that appropriate starting materials for obtaining discrete square homometallic $\{M(CN)\}_4$ or heterometallic $\{M(CN)M'(CN)\}_2$ rings should contain an average of one cyano group per metal. In fact, $[(\eta^2\text{-tmtch})Cu(CN)]_4$ was obtained beginning with CuCN, with only one CN group per metal center; and $[Cp_2Ti(CN)]_4$ was prepared using a starting material, $\{Cp_2TiCl\}_2$, which only incorporates one CN group per Ti upon reacting with NaCN.

Structures of discrete square cyano-bridged compounds with terminal CN groups are not known, but there are some examples of other kinds of compounds with terminal CN groups that do not form polymers.[6,9] For instance, in the compound $[\{Cu(dien)M(CN)_6\}_n][Cu(dien)(H_2O)(\mu\text{-}CN)M(CN)_5]_n$,[6] in addition to an unbounded chain of fused heterometallic rings, the discrete dianionic unit with five terminal cyanides, is also present.

$[Pt(CN)_4]^{2-}$ compounds can react using the basic character of the Pt atom and have been extensively studied for their formation of conducting metal stacks.[10] $[Pt(CN)_4]^{2-}$ can also form complexes using its terminal CN ligands, giving rise to polynuclear compounds with 3-D networks such as in $[NMe_4][CuPt(CN)_4]$[11] or 2-D networks as in the Hofmann-type clathrates $[M(NH_3)_2Pt(CN)_4]$.[5] 1-D networks have been proposed for Zr or Hf in $[M(\eta^5\text{-}C_5H_5)_2Pt(CN)_4]_n$, although no X-ray diffraction data are available owing to the amorphous character of the solids.[12] $[Pt(CN)_4]^{2-}$ also reacts with rare earth metals, forming interesting 1-D networks that contain both terminal and bridging cyano groups.[13] However, to our knowledge no discrete heteronuclear compounds derived from $[Pt(CN)_4]^{2-}$ and containing bridging CN ligands, have been structurally characterized.

The reaction of $[NBu_4]_2[Pt(CN)_4]$ with $Cu(NO_3)_2\cdot 2.5H_2O$ and 2,2′-bipyridyl produces the immediate precipitation of the deep blue solid $[\{Cu(bipy)(H_2O)Pt(CN)_4\}_2]\cdot 2H_2O$ **1**.† The IR spectrum of compound **1** shows four absorptions in the CN region: 2208, 2195, 2156 and 2149 cm^{-1}. Those at 2208 and 2195 cm^{-1} correspond in all likelihood to the two *cis*-bridging CN groups, since bridging CN usually appears at higher energy than does terminal CN.[2] Thus, the bands at 2156 and 2149 cm^{-1} correspond to the two *cis*-terminal CN ligands. Crystals suitable for X-ray diffraction can be obtained—together with a variety of other compounds—by an unusual procedure, dissolution of compound **1** in a concentrated solution of NH_4OH and then slow evaporation of the NH_3. Compound **1** is very insoluble, and its solubility in NH_4OH is probably due to the coordination of NH_3 to the copper, which breaks the bridging cyanide system. The evaporation of the NH_3 regenerates the tetranuclear compound. This method, breaking the bridging cyanide system and slow regeneration of the insoluble compound, can probably be applied to the crystallization and even formation of other compounds, especially cyanide complexes. The magnetic properties and the nature of the other compounds are presently under study. Fig. 1 shows a view of one molecule of $[\{Cu(bipy)(H_2O)Pt(CN)_4\}_2]$.‡ The molecule consists of two $Pt(CN)_4$ fragments and two $Cu(bipy)(H_2O)$ moieties held together by CN bridges. The bridging cyanide ligands bind to platinum through their carbon atoms and to the copper centers through nitrogen, and the *cis*-disposition of the bridging CN moieties at each of the metal centers yields the square shape of the core of the complex. The molecule sits on a crystallographic inversion center. The square planar coordination about each platinum center is completed by two terminal CN groups. Each Cu center has a terminal chelating bipy ligand, which is nearly coplanar with the square core of the complex. The coordination about copper is completed by an apical aqua ligand [Cu–O 2.227(6) Å], giving a distorted square pyramidal coordination environment. As the molecule is centric, the two square pyramids at opposite corners of the Pt_2Cu_2 square have opposite polarities. There is also one unligated molecule of water in the crystallographic asymmetric unit, or two per molecule of complex **1**. Both the ligated [O(1)] and unligated [O(2)] water

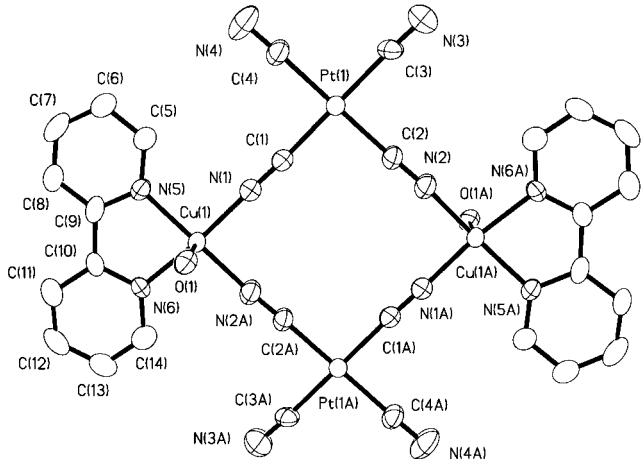

Fig. 1 Crystal structure of **1** with atom labelling scheme (50% probability ellipsoids). Hydrogen atoms and solvent molecules are omitted for clarity. Selected bond lengths (Å) and angles (°): Pt(1)–C(1) 1.973(8), Pt(1)–C(2) 1.973(7), Pt(1)–C(3) 1.985(8), Pt(1)–C(4) 1.987(8); Cu(1)–N(1) 1.958(7), Cu(1)–N(2A) 1.961(6), Cu(1)–N(5) 2.010(6), Cu(1)–N(6) 1.994(6), Cu(1)–O(1) 2.228(6), C(1)–N(1) 1.145(10), C(2)–N(2) 1.144(10), C(3)–N(3) 1.114(11), C(4)–N(4) 1.136(10); N(5)–Cu(1)–N(6) 81.5(3).

molecules are involved in significant hydrogen bonds. The bound water molecule acts as an H-bond donor to the terminal nitrogen atom N(4) of another molecule, with O(1)···N(4′) 2.82(1) Å. The free water molecule acts as a hydrogen bond donor to terminal nitrogen atom N(3) of two different molecules, with O(2)···N(3′) 2.85(1) Å and O(2)···N(3″) 2.94(1) Å. So the terminal nitrogen atoms of both pendant cyanide ligands serve as hydrogen bond acceptors in the extended structure. There is also a hydrogen bond between the bound and free water moieties, with O(1)···O(2) 2.76(1) Å.

The fact that the apical water molecule in the coordination environment of copper is not substituted by cyanide nitrogen to give rise to an extended structure can be explained as the result of several factors. First of all, the fifth and sixth coordination constants of copper are relatively small, especially when the first four ligands are nitrogen donors.[14] So a factor internal to the molecule, the propensity of copper not to accept a fifth nitrogen donor, may be responsible for the incorporation of water and the concomitant impediment to polymer formation. It remains true, however, that cases exist in which cyanide participates in a copper coordination environment consisting of five nitrogen atoms; the $[(Cu(dien)M(CN)_6\}_n]^{n-}$ chain is just such an example.

The hydrogen bonding that is found in the solid is also a key factor, and may be crucial, in determining the structure that we observe, since the formation of significant hydrogen bonds satisfies the nucleophilicity of the terminal nitrogen atoms and serves as a blocking factor, both spatially and electronically, against coordination of these nitrogen atoms to other metal centers.

In conclusion, the use of a starting material with excess cyanide in an environment favorable to the formation of hydrogen bonds with the cyanide nitrogen as acceptor, can give rise to discrete molecules with terminal cyanide ligands such as the tetranuclear square heterometallic complex **1**.

Funding by the Dirección General de Enseñanza Superior (Spain) under grant PB95-0792 is gratefully acknowledged. The authors thank Dr J. M. Williams for helpful suggestions.

Notes and references

† *Experimental procedure and selected data*: an acetone solution of 0.200 g (0.254 mmol) of $[NBu_4]_2[Pt(CN)_4]$ was added to an aqueous solution of 0.058 g (0.25 mmol) of $Cu(NO_3)_2{\cdot}2.5H_2O$ and bipy (0.040 g, 0.25 mmol). The precipitate of complex **1** was filtered off after being stirred for 15 min. The solid was washed with acetone and dried (77% yield). Crystals suitable for X-ray analysis were obtained by dissolving compound **1** in a concentrated solution of NH_4OH and then letting the NH_3 evaporate slowly. Satisfactory elemental analysis was obtained. IR: ν(OH): 3504–3261 cm^{-1}; bipy: 1612, 1605 and 773 cm^{-1}.

‡ (a) *Crystal structure data*: crystal dimensions, 0.32 × 0.26 × 0.12 mm; monoclinic, space group $P2_1/c$; a = 8.5573(8), b = 26.064(3), c = 7.5950(7) Å, β = 91.976(9)°, V = 1693.0(3) Å^3; D_c = 2.177 Mg m^{-3}; $2\theta_{max}$ = 55.0°; Mo-Kα radiation, $\lambda(\bar{\alpha})$ = 0.71073 Å; ω–θ scans; T = 298–299 ± 1 K; L_p corrections applied; μ = 9.53 mm^{-1}; max., min. relative transmission = 1.000, 0.370; absorption corrections based on 26 ψ-scans of reflections with bisecting-mode Eulerian equivalent χ ranging from −27 to +50°; 4251 data measured, 3863 unique, R_{int} = 0.0274; structure solution by direct methods; 3863 data used in refinement to F^2, no σ limit; 222 parameters. All hydrogen atoms were observed in a difference Fourier map, but those of the bipy ligand were placed at idealized positions and refined as riding atoms with isotropic displacement parameters set to 1.2 times the equivalent isotropic displacement parameters of their respective parent carbon atoms. The hydrogen atoms of the H_2O moieties were initially placed at the positions at which they were located in the difference Fourier map and were refined as riding atoms with independent isotropic displacement parameters. $R1$ = 0.0383 [calculated for 3125 $|F| > 4\sigma(|F|)$]; $wR2$ = 0.1050 for all F^2; quality of fit = 1.046. Max., min. residual difference density: +1.31, −1.20 e Å^{-3}. (b) *Crystallographic software*: data reduction and L_p corrections, XCAD4B (K. Harms, 1995); absorption corrections and molecular graphics, SHELXTL Rel. 5.05/VMS, ©1996, Siemens Analytical X-Ray Systems, Inc., Madison, WI; direct methods, SHELXS-97, ©1997, George M. Sheldrick; structure refinement, SHELXL-97, ©1997, George M. Sheldrick. CCDC 182/1126. See http://www.rsc.org/suppdata/cc/1999/273/ for crystallographic files in .cif format.

1 H. Vahrenkamp, A. Geib and G. N. Richardson, *J. Chem. Soc., Dalton Trans.*, 1997, 3643.
2 K. R. Dunbar and R. A. Heintz, *Prog. Inorg. Chem.*, 1997, **45**, 283.
3 D. H. Johnston, C. L. Stern and D. F. Shriver, *Inorg. Chem.*, 1993, **32**, 5170.
4 G. W. Beall, W. O. Milligan, J. Korp and I. Bernal, *Inorg. Chem.*, 1977, **16**, 2715; H. J. Buser, D. Schwarzenbach, W. Petter and A. Ludi, *Inorg. Chem.*, 1977, **16**, 2704.
5 T. Iwamoto, T. Nakano, M. Morita, T. Miyoshi, T. Miyamoto and Y. Sasaki, *Inorg. Chim. Acta*, 1968, **2**, 313.
6 G. O. Morpurgo, V. Mosini, P. Porta, G. Dessy and V. Fares, *J. Chem. Soc., Dalton Trans.*, 1981, 111; D. G. Fu, J. Chen, X. S. Tan, L. J. Jiang, S. W. Zhang, P. J. Zheng and W. X. Tang, *Inorg. Chem.*, 1997, **36**, 220.
7 F. Stocco, G. Stocco, W. M. Scovell and R. S. Tobias, *Inorg. Chem.*, 1971, **10**, 2639; B. L. Shaw and G. Shaw, *J. Chem. Soc.*, 1971, 3533.
8 P. Schinnerling and U. Thewalt, *J. Organomet. Chem.*, 1992, **431**, 41; F. Olbrich, J. Kopf and E. Weiss, *J. Organomet. Chem.*, 1993, **456**, 293.
9 S. Takano, T. Naito and T. Inabe, *J. Mater. Chem.*, 1998, **8**, 511; M. Zhou, B. W. Pfennig, J. Steiger, D. Van Engen and A. B. Bocarsly, *Inorg. Chem.*, 1990, **29**, 2456.
10 J. R. Ferraro and J. M. Williams, *Introduction to Synthetic Electrical Conductors*, Academic Press, New York, 1987, pp. 139–204.
11 R. W. Gable, B. F. Hoskins and Richard Robson, *J. Chem. Soc., Chem. Commun.*, 1990, 762.
12 J. A. Abys, G. Ogar and W. M. Risen, *Inorg. Chem.*, 1981, **20**, 4446.
13 D. W. Knoeppel and S. G. Shore, *Inorg. Chem.*, 1996, **35**, 1747; D. W. Knoeppel and S. G. Shore, *Inorg. Chem.*, 1996, **35**, 5328.
14 B. J. Bathaway, in *Comprehensive Coordination Chemistry*, ed. G. Wilkinson, R. D. Gillard and J. A. McCleverty, Pergamon Press, Oxford, 1987, vol. 5, pp. 533–774.

Communication 8/07324D

Oxidized caesium/nanoporous carbon materials: solid-base catalysts with highly-dispersed active sites

Mark G. Stevens, Denise Chen and Henry C. Foley*

Center for Catalytic Science and Technology, Department of Chemical Engineering, University of Delaware, Colburn Laboratory, Academy Street, Newark, Delaware, 19716, USA. E-mail: foley@che.udel.edu

Received (in Bloomington, IN, USA) 23rd October 1998, Accepted 6th January 1999

By vapor depositing Cs metal on nanoporous carbon materials and then oxidizing, a solid-base catalyst is produced that is quite active for the aldol condensation of acetone to isophorone.

In previous work we have shown that Cs/NPC materials are very powerful base catalysts.[1] The materials prepared from vapor deposition of elemental Cs provide a greater than 9 : 1 ratio of the less stable *cis*-but-2-ene over the *trans* isomer in the isomerization of but-1-ene at 273 K. They have a strong affinity for hydrogen,[2] since they can cleave the energetic C–H bond in benzene to promote condensation to biphenyl. Therefore, we sought to explore the activity of the oxidized state of Cs/NPC as a catalyst.

By preparing nanoporous carbon (NPC) with methods discussed previously,[1–4] we obtain high carbon solids that contain nanopores[3,4] with dimensions narrowly distributed around a mode of 0.5 nm and transport pores[5] with dimensions near 10 nm. These transport pores are *critical* for access to the catalytic sites contained in the nanopores.[6] Into these nanopores, the vapor of elemental caesium is rapidly and strongly adsorbed in a highly dispersed state.[1] The resultant materials are paramagnetic,[1] and EPR measurements[2] indicate that electrons of Cs are donated to the carbon. Since the Cs is atomically dispersed within the nanopores, oxidation should yield basic sites that are highly dispersed throughout the carbon. In contrast, aqueous impregnation of Cs salts will lead to large crystallites formed within the macro- and meso-pores.

Utilizing X-ray diffraction as a structural probe, upon exposure of the Cs/NPC to air we find a set of sharp lines superimposed upon the broad background of NPC (Fig. 1). These lines are consistently produced by air exposure of samples prepared in the range of 10–15 wt.% Cs. The lines do not correspond to those exhibited by the various Cs oxides, hydroxides or carbonates whose powder X-ray patterns are well known. It is interesting that when the Cs level is raised to 65 wt.% and the sample is air exposed, the X-ray pattern consists of just four sharp lines at 2θ = 13.05, 26.19, 39.72, and 53.88° (Cu-Kα radiation, λ = 0.15406 nm), corresponding to *d*-spacings of 6.781, 3.400, 2.267, and 1.700 Å, respectively, indicating that a crystalline form of Cs hydrous oxide has formed.[7] It is plausible that the X-ray pattern for air exposed Cs/NPC prepared at the lower loading of Cs corresponds to an intermediate hydrous oxide structure.

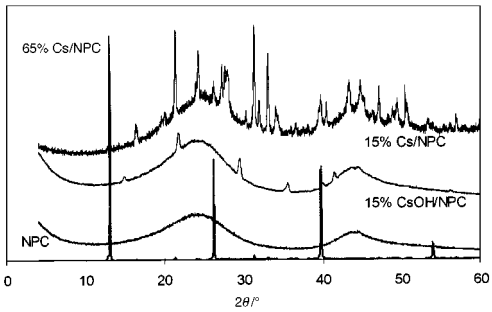

Fig. 1 Scaled XRD plots of NPC, 15% Cs on NPC, 65% Cs on NPC and 15% CsOH on NPC. Radiation used was Cu-Kα (λ = 0.15406 nm).

To determine if this oxide of vapor-deposited Cs on NPC led to a different level of activity than that obtained by impregnation with an aqueous salt, we chose to study the base-catalyzed aldol-condensation of acetone. Starting with Cs/NPC, this reaction would be expected to rapidly oxidize the Cs/NPC *in situ*, since water is a by-product of the coupling steps. Secondly, since the condensation products may react further to produce higher molecular weight species, inclusion of transport porosity within the carbon support should be critical to avoid rapid catalyst deactivation.

The liquid phase isophorone process[8] operates at 6–10% acetone conversion with a sodium hydroxide catalyst, an isophorone yield around 70% and losses due to heavies production. A more energy-intensive, vapor-phase process is also employed in which the acetone is passed over solid oxide type bases. Both processes incur a great deal of separations costs, requiring as many as four distillation columns operating under vacuum to reduce further by-product formation. In 1995, isophorone sold for \$4+/lb and the sole United States supplier was Union Carbide. The total world capacity was ≈156 MM lb./yr. Isophorone's uses range from a high-boiling, low-evaporative solvent for synthetic polymers to an insecticide (when converted to 3,5-xylenol). The fastest growing market for isophorone is as a building block for light-stable polyurethane.[9]

The base-catalyzed condensation of acetone (Scheme 1) begins with the extraction of the acidic α-proton to form the enolate anion, which attacks a second acetone to form the tetrahedral alkoxide ion intermediate, which is protonated to form the aldol. At elevated temperatures the aldol releases water to form mesityl oxide, which can undergo subsequent condensation steps. Upon the condensation of the aldol to form the

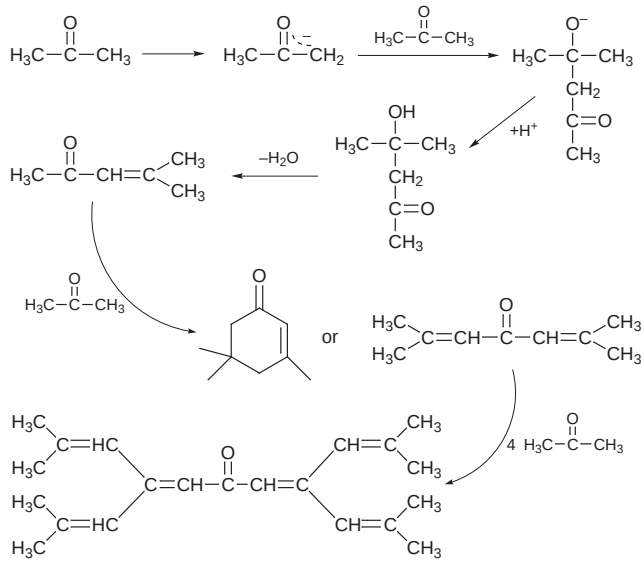

Scheme 1 The base-catalyzed, aldol-condensation reaction of acetone.

disubstituted enone, the material may simply form the conjugated diene-one product or the industrially significant, cyclic isophorone. The conjugated nature of the enone product allows for continued additions, forming higher molecular weight species that can accumulate rapidly in an all-nanoporous catalyst, thus restricting access to the active sites within the nanopores and shutting down reaction.

Experiments were carried out in a gas-phase flow reactor.† A steady argon flow (150 cm^3 min^{-1}) carried acetone vapor from a room-temperature gas sparger through the heated catalyst bed. Unreacted acetone and the heavier products were condensed and analyzed quantitatively by gas chromatography and mass spectrometry. The major product was isophorone along with mesityl oxides and higher-molecular-weight species that were lumped into a fraction called 'heavies'. Acetone conversion and selectivity to isophorone obtained over the vapor-deposited Cs/NPC catalyst for various temperatures are displayed in Table 1. Acetone conversion and selectivity to isophorone both maximize at 225–250 °C. At 20 °C isophorone selectivity drops due to increased mesityl oxide formation. At temperatures above 250 °C the activity of the catalyst dropped even though the selectivity to isophorone remained high. This was most likely due to the accumulation of heavy products in the pores. Each catalyst dropped to $< 20\%$ of its initial activity within 5 h and gained approximately 10% of its initial weight. At 225 and 250 °C the turnovers (mol of acetone converted/mol Cs) before catalyst deactivation were at a maximum of ≈ 10 (Table 1).

Significantly, the effect of air exposure on the catalyst before reaction was to *increase* its initial activity. Catalyst samples that were not air-exposed before reaction did not produce isophorone in the first hour on stream. After this induction period, however, they behaved as the air exposed samples did.

When compared to catalysts prepared by vapor deposition of elemental Cs, those samples that were prepared with CsOH solution‡ were less active and less selective. The selectivity to isophorone over the catalyst prepared by vapor deposition was *ca.* 60% throughout the experiment, whereas the selectivity for the solution-impregnated sample began at 45% and declined to 30%. Both materials gained approximately 10% of their initial weight in non-volatile compounds.

The vapor deposition of Cs led to catalysts that maintained their high selectivity to isophorone even as their activities dropped. The selectivity to isophorone remained 60% over a conversion range from 0–20%. As the acetone conversion approached 20% the loss in selectivity due to heavies formation became more significant. Attempts made to achieve higher conversions were not successful since the catalyst deactivated more rapidly due to non-volatile product accumulation.

Finally, as control experiments, we tested the NPC support alone without Cs and a sample of Cs-loaded NPC containing only nanopores.§ Neither material led to any significant acetone conversion. The Cs on all-nanoporous carbon catalyst, however, did increase in mass by an amount equal to 10% of its initial mass.

The GCMS data obtained indicate that the higher-energy, non-cyclic trimer was the species that led to heavies formation; none of the heavy materials identified contained cyclic fragments. This makes sense since the protons that are active for base extraction are α to the carbonyl or conjugated. The non-cyclic trimer has 12 of these active protons and the isophorone has only 3 that are not sterically hindered. Hence the key to reducing heavies formation and deactivation is to promote ring formation over oligomerization. Since the heat of formation and the activation energy to form the non-cyclic products are higher, a reduction in temperature should favor the isophorone product. Also, ring formation should have a lower (more negative) $\Delta S^{\ddagger}$, therefore, a decrease in temperature should again favor its formation. Secondly, any variable that reduces the overall conversion or catalyst basicity should reduce heavies formation. Thus, less basic metals such as potassium or sodium, lower acetone concentrations in the feed, and shorter contact times in the reactor should favor isophorone production.

Caesium, vapor-deposited into the carbon and then oxidized, is more active than Cs deposited from a salt in aqueous solution. The Cs hydrous oxide that results from oxidation of the vapor-deposited element is certainly a different phase; by examining the X-ray diffraction patterns of the two materials we were able to confirm this. The samples prepared with the CsOH solution showed patterns indicative of large hydroxide crystals. In contrast, the used vapor-deposited Cs/NPC material displayed an X-ray diffraction pattern with sharp lines, but the lines did not match any of the known caesium hydroxides or oxides. This set of results points to a new approach in the synthesis and use of solid Brønsted bases for continuous-flow organic synthesis. By preparing a carbon with both nanopores and mesopores, we can vacuum deposit cesium in a highly dispersed state, convert it to an active form *via* oxidation, and provide the necessary avenues for rapid molecular ingress and egress.

Table 1 Conversion, carbon selectivity towards isophorone and Cs^0 turnovers at various temperatures. Argon flow rate: 150 cm^3 mol^{-1} saturated with acetone at 25 °C

T/°C	Conversion (%) (per g Cs)	Isophorone selectivity (%)	Cs Turnovers
200	6.1	54	5.34
225	11.9	61	10.43
250	11.4	60	10.04
275	5.2	57	4.56
300	3.8	57	3.38

This work was supported by the Department of Energy, Office of Basic Energy Sciences; the Delaware Research Partnership; and the E. I. duPont deNemours and Co., Inc.

Notes and references

† A Tylan mass flow controller regulated an argon (Matheson Grade) carrier-gas flow. The argon flow served two purposes: to purge the reactor system of air and to carry acetone at its room-temperature vapor pressure from a bubbler to the reactor. The reactor consisted of a ½″ o.d. quartz tube heated by heat tape, the temperature of which was regulated by an Omega PID temperature controller. The catalyst was placed in the heated zone of the reactor between two plugs of glass wool. After leaving the reactor, the acetone–argon stream was cooled and condensed into a catch pot by a shell and tube condenser, through which flowed −10 °C chilled glycol. Samples were taken by removing all the liquid from the catch pot with a syringe inserted through a serum cap, weighed, spiked with a biphenyl standard, and analyzed on a Varian GC with an FID detector.

‡ A sample of CsOH/NPC was prepared by stirring the NPC with 50% CsOH solution for 1 h, filtering, and vacuum drying at 350 °C for 24 h.

§ NPC prepared by the pyrolysis of poly(furfuryl alcohol) alone at 850 °C for 8 h under helium produces a purely nanoporous material with no pores larger than 2 nm.

1 M. G. Stevens and H. C. Foley, *Chem. Commun.*, 1997, 519.
2 M. G. Stevens, K. M. Sellers, S. Subramoney and H. C. Foley, *Chem. Commun.*, 1998, in press.
3 H. C. Foley, M. S. Kane and J. F. Goellner, in *Access in Nanoporous Materials*, ed. J. J. Pinnavaia and M. F. Thorpe, Plenum, New York, 1995.
4 D. S. Lafyatis, J. Tung and H. C. Foley, *Ind. Eng. Chem. Res.*, 1994, **30**, 865.
5 M. S. Kane, L. C. Kao, R. Mariwala, D. F. Hilscher and H. C. Foley, *Ind. Eng. Chem. Res.*, 1996, **35**, 3319.
6 G. Malinoski, W. H. Bruning, *J. Am. Chem. Soc.*, 1967, **89**, 5063.
7 M. G. Stevens, S. Subramoney and H. C. Foley, *Chem. Phys. Lett.*, 1998, **292**, 352.
8 K. Schmitt, *Chem. Ind.*, 1966, **18**, 204.
9 K. Othmer, *Encyclopedia of Chemical Technology*, Wiley, New York, 4th edn., 1995, vol. 14 p. 1000.

Communication 8/08249I

ChemComm

Low symmetry metal complexes: chloro cysteine ethyl ester-*N,S* triphenylphosphine palladium(II), a new regioselective hydrocarboxylation catalyst for 2-phenylpropanoic acid, and its crystal structure

Julio Real,*[a] Montserrat Pagès,[a] Alfons Polo,[b] J. Francesc Piniella[c] and Ángel Álvarez-Larena[c]

[a] *Departament de Química, Universitat Autònoma de Barcelona, E-08193, Bellaterra, Barcelona, Spain. E-mail: real@cc.uab.es*

[b] *Departament de Química, Facultat de Ciències, Universitat de Girona, E-17071 Girona, Spain. E-mail: dqapo@xamba.udg.es*

[c] *Servei de Difracció de Raigs-X and Unitat de Cristallografia i Mineralogia, Universitat Autònoma de Barcelona, E-08193, Bellaterra, Barcelona, Spain*

Received (in Basel, Switzerland) 23rd November 1998, Accepted 28th December 1998

The hydrochlorides of cysteamine, cysteine ethyl ester and penicillamine methyl ester, react with $Pd(PPh_3)_4$ to yield low symmetry complexes of palladium(II) that incorporate the *N,S*-aminothiolato ligand and triphenylphosphine; the complex with cysteine ethyl ester, structurally characterized by X-ray diffraction, proved to be an effective catalyst for the hydrocarboxylation of styrene with high selectivity (98%) towards 2-phenylpropanoic acid.

Low symmetry complexes of the transition metals in general, and the platinum group metals in particular, are of interest because of their potential as selective catalysts in homogeneous reactions. Geometric and electronic asymmetry is associated with increased stability of one of the possible key intermediates, which should give rise to improved selectivity. The preferred ligands in many selective catalytic reactions are sophisticated diphosphines. However, these are often even more expensive than the precious metal itself. This report is part of our efforts to evaluate the use of inexpensive, low symmetry ligands from the chiral pool, in structurally well characterised complexes, to promote selective homogeneous catalytic reactions.[1]

Cysteine ligand type containing complexes are not very common,[2] but we have shown that chelate assisted oxidative addition to Pt(0) is a reaction that can introduce acidic hydrogen containing cysteamine and cysteine ethyl ester ligands in the coordination sphere of the metal.[3] However, in the case of palladium the expected metal complexes would contain the often-unstable Pd–H bond. In a new approach, we have added an acid to quench the possible palladium hydride in order to obtain stable palladium(II) complexes in one step. The stoichiometric addition of acid has been achieved by the use of the hydrochlorides of the ligands.

The hydrochlorides of cysteamine ($HSCH_2CH_2NH_2{\cdot}HCl$), cysteine ethyl ester [$HSCH_2C^*H(CO_2Et)NH_2{\cdot}HCl$] and also penicillamine methyl ester [$HSCMe_2C^*H(CO_2Me)NH_2{\cdot}HCl$] reacted with $Pd(PPh_3)_4$ to yield the corresponding *N,S*-aminothiolato chloro triphenylphosphine complexes in good yield, with displacement of three PPh_3 ligands, oxidation of the metal and evolution of hydrogen (Scheme 1). In this way, complexes **1**–**3** were obtained as stable crystalline solids.† The *cis*-P,S coordination was established by single crystal X-ray analysis. Complex **2** exhibits a very short Pd–S distance of 2.253(2) Å that is effectively equal to the Pd–P distance of 2.254(2) Å, owing to the non-bridging coordination of the sulfur and the low *trans* influence of the chloro ligand.‡[4] Complexes **1**–**3** are stable in solution and do not form sulfur-bridged dimers or polymers, even when exposed to air. In these complexes four very different atoms coordinate the metal, but only when the asymmetric carbon containing cysteine and penicillamine are used, is the symmetry plane of the square planar complex broken and the compounds become optically active. Fig. 1 shows that in the solid state,[5] the ethyl carboxylate substituent in the chelate ring of **2** adopts an axial orientation and the oxygen of the carbonyl group approaches the coordinated nitrogen.§

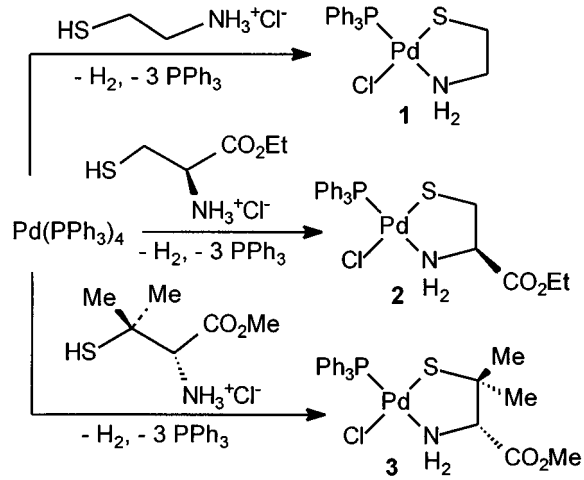

Scheme 1

Catalytic hydrocarboxylation of olefins is an interesting reaction for the synthesis of the pharmacologically useful 2-arylpropionic acids, provided that a selective catalyst towards the branched acid is used.[6] Complex **2** has been subjected to a preliminary evaluation in the hydrocarboxylation of styrene as a model aryl olefin, with oxalic acid under CO pressure and no added co-catalysts. Complex **2** has been found to be active, and its selectivity in 2-phenylpropanoic acid (2-PP) was very high (Table 1). Hydrogenation was the main side reaction, and it was always under 0.2%. In low conversion conditions (*i.e.*, when the reaction was stopped after 2 h), yields increased steadily with temperature. After 24 h, 75% conversions were reached and selectivities as high as 98% in branched acid (2-PP) were maintained. However, at 100 and 120 °C, lower than expected conversions were observed. This result, together with the fact that after depressurisation of the reactor, palladium black is observed,¶ lead us to believe that the catalytic species suffers degradation under such reaction conditions. The catalytic reaction is faster at higher temperatures, but so is the decomposition of the catalyst.

The 2-phenylpropanoic acid product is racemic in all cases. Considering the fact that the reaction medium is strongly acidic, and that as proposed[7] it is reasonable to think that two free coordination sites are needed for this reaction, we are suggesting at this stage structure **A** for the active species. The relatively low bulk of **A** is consistent with branched selectivity. Also, the lack

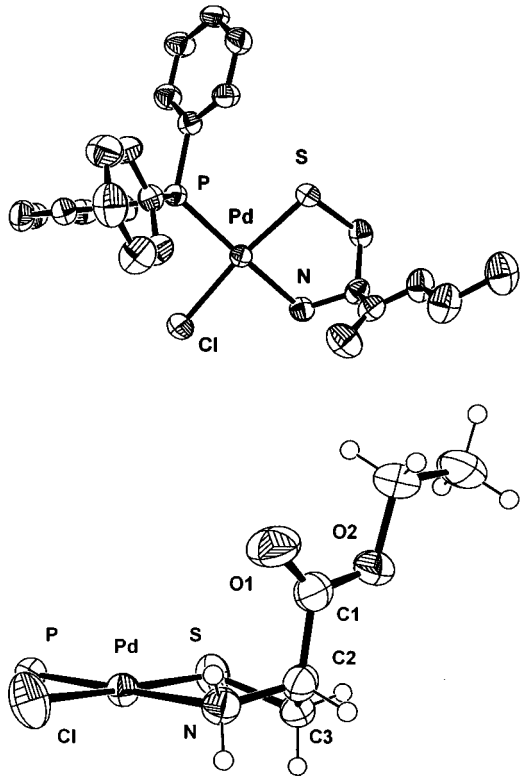

Fig. 1 The above projection of complex **2** includes all non-hydrogen atoms (ORTEP-III, 50% probability). In the nearly eclipsed projection below, the aryl rings have been omitted and the hydrogen atoms have been included, to fully appreciate the axial position of the ethoxycarbonyl group. The C1–C2 bond forms an angle of 84.5(3)° with the coordination plane of the metal and the O1–C1–C2–N torsion angle is 12.1(8)°. Selected distances (Å) and angles (°): Pd–S 2.253(2), Pd–P 2.254(2), Pd–N 2.097(5), Pd–Cl 2.349(2), S–C3 1.826(6), N–C2 1.483(7), C1–C2 1.509(8), C2–C3 1.482(8), C1–O1 1.192(7), C1–O2 1.323(8); S–Pd–P 92.92(6), S–Pd–N 85.7(1), Cl–Pd–P 93.63(6), Cl–Pd–N 87.7(1).

Table 1 Complex **2** as a catalyst in the hydrocarboxylation of styrene. Conversion and selectivity towards 2-phenylpropanoic acid (2-PP) in the reaction of styrene with oxalic acid under CO, at different temperatures over 2 and 24 h[a]

	2 h		24 h	
T/°C	Conversion (%)	Selectivity (%)	Conversion (%)	Selectivity (%)
60	0.6	—	30	98
80	7	98	75	98
100	12	97	68	97
120	16	97	67	96

[a] Conditions: 2 mmol styrene + 2.5 mmol $H_2ox{\cdot}2H_2O$ in 10 mL of DME solvent; [styrene]/[**2**] = 50; CO pressure: 30 bar. No oxygen or co-catalysts present.

of chiral induction would be consistent with structure **A**, in which the asymmetric centre is displaced away from the metal. At this point, we rule out complete detachment of the sulfur ligand in the active species, because the activities and selectivities observed with **2** were not those of a simple Pd(II) + PPh_3 system with a phosphine/palladium ratio of unity, which is the ratio in complex **2**.‖ Furthermore, relevant results by Claver, van Koten and coworkers[8] with aryl aminothiolato complexes

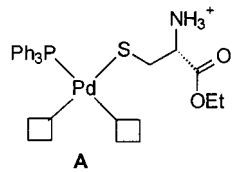

A

of palladium, seem to indicate that sulfur ligands promote high branched selectivity.

From a purely practical, synthetic point of view complex **2**, which is readily prepared from affordable, easily accessible reagents, catalyses the conversion of styrene to 2-phenylpropanoic acid (98%) by reaction with oxalic acid under CO (30 bar), with a 75% yield at 80 °C in 24 h. Further work on the synthesis, structure and evaluation of this novel class of compounds in catalysis is under way and will be reported in due course.

This work was financially supported by the DGICYT, project PB91-0663-CO3; and the CICYT and DGR, project QFN95-4725-CO3. We thank C. Claver for supplying a pre-print of ref. 8. M. P. thanks the UAB for a temporary teaching appointment as her only support towards her doctorate.

Notes and references

† Synthesis of **1**: A solution of $HSCH_2CH_2NH_2{\cdot}HCl$ (0.52 mmol) in methanol (5 ml) was slowly added to $Pd(PPh_3)_4$ (0.52 mmol) in toluene (20 ml) and stirred under nitrogen at 60 °C for 3 h to afford an orange solution. Concentration of the solution caused precipitation of the product as an orange solid, which was purified by recrystallization in acetone–diethyl ether to yield $[PdCl(SCH_2CH_2NH_2)(PPh_3)]$ **1** as dark orange crystals (65% yield). The same procedure can be used for compounds **2** and **3**. Compounds **1**–**3** gave satisfactory spectral (^1H, ^{31}P and ^{13}C NMR and IR) and analytical data.

‡ *Crystal data* for **2**: $C_{23}H_{25}ClNO_2PPdS$; M = 552.32; orthorhombic, a = 7.929(5), b = 10.330(2), c = 28.769(6) Å, V = 2356(2) Å^3; T = 293 K; space group $P2_12_12_1$, Z = 4; μ = 10.8 cm^{-1}; 2069 independent reflections for 277 parameters; $R(F)$ = 0.023 for 1910 reflections with $I > 2\sigma(I)$ and $R_w(F^2)$ = 0.063 for all 2069 reflections; S = 1.129; Flack parameter 0.01(4). CCDC 182/1134. See http://www.rsc.org/suppdata/cc/1999/277/ for crystallographic files in .cif format.

§ The IR stretching frequencies for the CO and NH_2 groups, and the distance between the oxygen and hydrogen atoms O1···H–N of 2.18(4) Å, do not support the existence of hydrogen bonding. The eclipsed conformation could be favoured by an electrostatic interaction between the negatively charged oxygen and a positively charged *quaternary* nitrogen.

¶ Powder X-ray diffraction showed it to be finely divided metal, and not palladium sulfide of any crystallinity. This palladium black does not catalyse the reaction, even when triphenylphosphine is added.

‖ Working in the same conditions as used for **2**, we have found the selectivity of $PdCl_2$ or $PdCl_2(MeCN)_2$ plus 1 equiv. of PPh_3 to be 85–88% in 2-PP, although the second precursor is faster.

1 H.-U. Blaser, *Chem.Rev.*, 1992, *92*, 935; W. A. Herrmann and B. Cornils, *Angew. Chem. Int. Ed. Engl*., 1997, **36**, 1048.
2 H. S. Laurie in *Comprehensive Coordination Chemistry*, ed. G. Wilkinson, R. D. Gillard and J. A. McCleverty, Pergamon, Oxford, 1987, vol. 2, pp. 739–776; K. A. Mitchell and C. M. Jensen, *Inorg. Chem.*, 1995, **34**, 4441; K. A. Mitchell, K. C. Streveler and C. M. Jensen, *Inorg. Chem.*, 1993, **32**, 2608; K. S. Wyatt, K. N. Harrison and C. M. Jensen, *Inorg. Chem.*, 1992, **31**, 3867; L. Kumar, N. R. Kandasamy and T. S. Srivastava, *Inorg. Chim. Acta*, 1982, **67**, 139; G. Pneumatikakis and N. Hadjiliadis, *J. Inorg. Nucl. Chem.*, 1979, **41**, 429; P. de Meester, D. J. Hodgson, H. C. Freeman and C. J. Moore, *Inorg. Chem.*, 1977, **16**, 1494; M. G. B. Drew and A. Kay, *J. Chem., Soc. A*, 1971, 1846; M. G. B. Drew and A. Key, *Inorg. Phys. Theor.*, 1971, 1851.
3 J. Real, A. Polo and J. Duran, *Inorg. Chem. Commun.*, 1998, **1**, 457.
4 SHELX-97: G. M. Sheldrck, University of Göttingen, Germany, 1997.
5 M. N. Burnett and C. J. Johnson, ORTEP-III: Oak Ridge Thermal Ellipsoid Plot Program for Crystal Structure Illustrations, Oak Ridge National Laboratory Report ORNL-6895, 1996. PC version used: L. J. Farrugia, *J. Appl. Crystallogr.*, 1997, 565.
6 I. Tkachenko, in *Comprehensive Organometallic Chemistry*, ed. G. Wilkinson, F. G. A. Stone and E. W. Abel, Pergamon, Oxford, 1987, vol. 8, pp. 101–223; H. Alper, J. B. Woell, B. Despeyroux and D. J. H. Smith, *J. Chem. Soc., Chem. Commun.*, 1983, 1270; H. Alper and N. Hamel, *J. Am. Chem. Soc.*, 1990, **112**, 2803; B. El Ali and H. Alper, *J. Org. Chem.*, 1993, **58**, 3595; *J. Mol. Catal.*, 1992, **77**, 7; J.-Y. Yoon, E. J. Jang, K. H. Lee and J. S. Lee, *J. Mol. Catal. A*, 1997, **118**, 181.
7 B. El Ali and H. Alper, *J. Mol. Catal.*, 1993, **80**, 377; 1992, **77**, 7.
8 D. Kruis, N. Ruiz, M. D. Janssen, J. Boersma, C. Claver and G. van Koten, *Inorg. Chem. Commun.*, 1998, **1**, 295.

Communication 8/09130G

ChemComm

Reduction of sulfur monoxide on a hexanuclear ruthenium complex

Teiji Chihara,*[a] Takahiro Tase,[b] Haruo Ogawa[b] and Yasuo Wakatsuki*[a]

[a] *The Institute of Physical and Chemical Research (RIKEN), Wako, Saitama 351-0198, Japan. E-mail: waky@postman.riken.go.jp*

[b] *Department of Chemistry, Tokyo Gakugei University, Koganei, Tokyo 184-8501, Japan*

Received (in Cambridge, UK) 23rd December 1998, Accepted 12th January 1999

The sulfur monoxide unit, which originates from a gaseous SO_2 molecule trapped on a Ru_6-cluster, is easily reduced either by CO or H_2 to the sulfide ligand with concomitant skeletal cluster rearrangement, where the resulting cluster shape depends largely on the amount of the reducing agent taken up by the cluster.

Removal of SO_2 from combustion gases by reduction to sulfur is of great research interest because harmless S_8 is often a more desirable product than oxidized forms such as SO_4^{2-}.[1,2] The heterogeneous system, 0.5% Ru/γ-Al_2O_3, is one of the most active agents for the catalytic reduction of SO_2 with H_2 in the gas phase.† The presence of Al_2O_3 is crucial, since Ru metal alone has no catalytic activity.[3] It is likely that, aside from the role of Al_2O_3 as the carrier of fine metal particles, the Lewis acid character of Al_2O_3 assists in the reduction.[4,5] On the basis of the often-referred cluster–surface analogies,[6] reduction of SO_2 on high nuclearity metal clusters would be a good model for SO_2 reactions on metal particles.[1,7] Shriver and coworkers found that the cluster-bound SO_2 in the trinuclear cluster $[Fe_3H(CO)_9(SO_2)]^-$ is transformed to a μ_3-SO ligand on reduction with Na·Ph_2CO, but prior acetylation of the ligating SO_2 to give an AcOSO ligand was necessary for its complete reduction to the sulfide complex $[Fe_3(CO)_9S]^{2-}$.

Although $[Fe_3(CO)_9(SO)]^{2-}$ represents the first example of a cluster-bound SO made by reductive cleavage of SO_2, addition of excess reducing agent to the isolated SO complex resulted in degradation of the cluster, and hence reactivity of this highly important intermediate could not be studied.[8] In the high nuclearity cluster complex, $[Ru_6C(CO)_{15}(\mu\text{-}SO_2)]^{2-}$, which we recently prepared, the bound SO_2 can easily be converted to an SO ligand, $Ru_6C(CO)_{15}(\mu_3\text{-}SO)$ **1**, by addition of a Lewis acid such as BF_3.[9] Herein we describe the first reduction-reactivity of the SO ligand on polynuclear cluster complexes, which may have relevance to a stepwise reduction of SO_2 on heterogeneous metal surfaces.

A dichloroethane solution of **1** was heated at 70 °C for 6 h under one atmosphere of CO. A dark-purple crystalline complex was isolated in 74% yield after chromatography on silica gel, and was structurally characterized as $Ru_6C(CO)_{16}S$ **2**.‡ As shown in Scheme 1, the reaction is accompanied by incorporation of an additional CO into the cluster, cleavage of two of the metal–metal bonds and swinging of the S-capped metal triangle to open the upper part of the original octahedral metal skeleton of **1** (Scheme 1). An 88-electron Os cluster having a related structure, $Os_6(CO)_{16}(\mu_4\text{-}S)(\mu_3\text{-}S)$, has been isolated by Adams and Yang as one of the products of the thermolysis of $HOs_3(CO)_{10}(\mu\text{-}SPh)$.[10]

The reduction of SO to S on the cluster was also achieved by reaction with H_2. A dichloroethane solution of complex **1** was allowed to react with H_2 (10 atm) and 1.5 equiv. CO in an autoclave. After 6 h at 70 °C, four complexes were isolated after silica-gel column chromatography: the known trinuclear complex, $Ru_3(CO)_9(\mu_2\text{-}H)_2(\mu_3\text{-}S)$ (12%),[11] red–purple crystalline $Ru_6C(CO)_{16}(H)_2S$ (**3**, 30%), dark-orange crystals of $Ru_6C(CO)_{16}(H)_4S$ (**4**, 9%), and a brown powder (*ca.* 15%) which appears to be a heptanuclear ruthenium complex containing sulfur and CO as determined by elemental analysis, IR, and

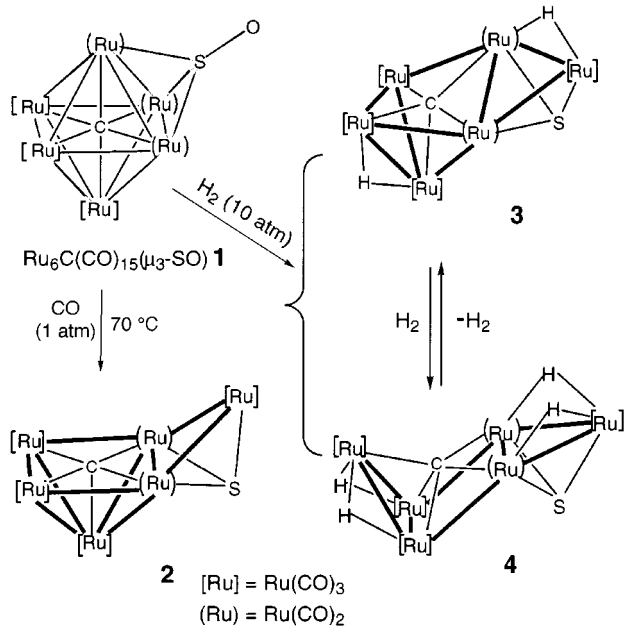

Scheme 1

ESMS. The new compounds **3** (Fig. 1) and **4** (Fig. 2) were characterized by single-crystal X-ray diffraction analyses.‡ Complex **3** has a shape analogous to that of **2** but, as a result of cleavage of an additional metal–metal bond [Ru3···Ru6 3.920(1) Å], the pentagonal unit is now very much distorted. Two new hydride ligands, which are bridging the Ru1–Ru3 and Ru5–Ru6 bonds, supply the electrons needed to break the

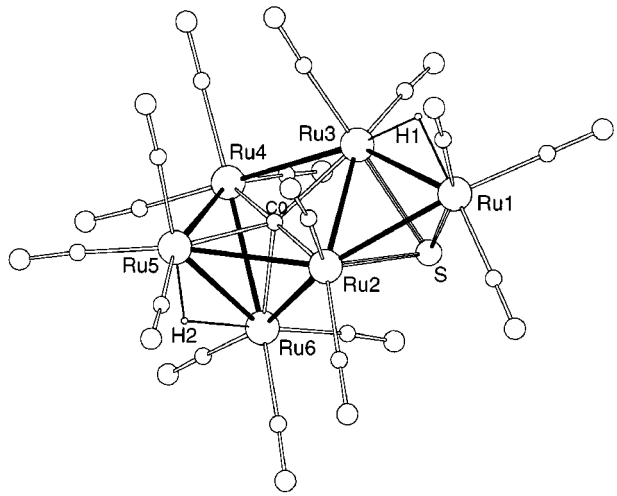

Fig. 1 X-Ray crystal structure of $Ru_6C(CO)_{16}(H)_2S$ **3**. Selected bond distances (Å): Ru1–Ru2 2.8071(5), Ru1–Ru3 2.8603(5), Ru2–Ru3 2.7308(5), Ru2–Ru5 2.8656(5), Ru2–Ru6 2.8765(5), Ru3–Ru4 2.9794(5), Ru3···Ru6 3.920(1), Ru4–Ru5 2.9261(5), Ru4–Ru6 2.8358(5), Ru5–Ru6 2.8249(5), Ru1–S 2.318(1), Ru2–S 2.383(1), Ru3–S 2.389(1).

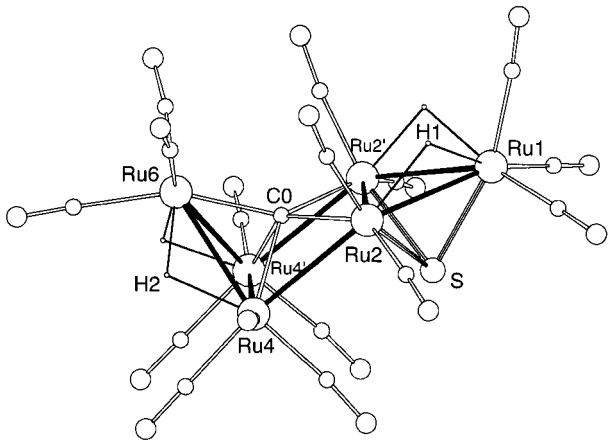

Fig. 2 X-Ray crystal structure of $Ru_6C(CO)_{16}(H)_4S$ **4**. Selected bond distances (Å): Ru1–Ru2 2.854(1), Ru2–Ru3 2.721(1), Ru2–Ru4 2.869(1), Ru4–Ru5 2.808(1), Ru4–Ru6 2.860(1), Ru2···Ru6 3.8939(1), Ru1–S 2.359(4), Ru2–S 2.375(3).

metal–metal bond. In complex **4**, two more hydrogen atoms are present and one more metal–metal bond (either Ru2–Ru5 or Ru2–Ru6 in **3**) has been broken. The solid-state molecular structure of **4** has a mirror plane that passes through Ru1, Ru6, and the carbide carbon atom (C0) of the chair-like cluster skeleton. The carbide ligand is well exposed, its distances from the metal square Ru2–Ru2′–Ru4–Ru4′ and the metal triangle Ru4–Ru4′–Ru6 are 0.39 and 0.80 Å, respectively. A carbon atom of this type has attracted much interest as being relevant to metal-surface bound carbon atoms in heterogeneous catalysis.[12]

Despite the large change in skeletal shape, complexes **3** and **4** are interconvertible cleanly, although slowly, at room temperature. The transformation was monitored by observing the characteristic IR bands of these complexes in the ν(CO) region. Keeping a dichloromethane solution of **3** under 15 atm H_2 at room temperature gave **4** in 80% conversion after 2 weeks, while formation of any other by-products was not detected. The reverse reaction was more facile. When a dichloromethane solution of **4** was allowed to stand under argon for 4 days, dihydrogen was released to generate **3** almost quantitatively. In contrast, **2** did not react with H_2 under similar conditions. The reactions are summarized in Scheme 1. Further, it may be mentioned that the trinuclear complex $Ru_3(CO)_9(\mu\text{-}H)_2(\mu_3\text{-}S)$ obtained as a minor product in the present reaction of **1** with H_2 (*vide supra*) has a structure[11] similar to that of the S-capped metal triangle moiety in **4**. It is interesting that recent reports have described facile metal–metal bond cleavage on solid metal surfaces induced by adsorption of small molecules such as H_2.[13]

In conclusion, reduction of sulfur oxide to S on high nuclearity clusters should take place smoothly either by CO or H_2 once the cluster bound SO_2 is transformed to SO. The first step, reduction of SO_2 to SO, appears more difficult since $[Ru_6C(CO)_{15}(\mu\text{-}SO_2)]^{2-}$ or $Ru_6C(CO)_{16}(\mu\text{-}SO_2)$ do not react under similar conditions. Either much more severe conditions or assistance by a Lewis acid will be required for the initial reduction process.

Notes and references

† In homogeneous dinuclear metal systems, pioneering works for catalytic and stoichiometric reduction of SO_2 by H_2 have been reported by Kubas *et al.*[14,15] and Neher and Lorenz.[16]

‡ *Crystal data*: for **2**: $C_{17}O_{16}Ru_6S$, M = 1098.66, triclinic, space group $P\bar{1}$, a = 8.8781(4), b = 10.6179(5), c = 15.1237(11) Å, α = 83.354(5), β = 82.280(4), γ = 74.894(3)°, U = 1352.8(1) Å^3, Z = 2, T = 21 °C, μ = 34.15 cm^{-1}, for 6279 unique reflections R = 0.022 and GOF = 1.26.

For **3**: $C_{17}H_2O_{16}Ru_6S$, M = 1100.67, monoclinic, space group $P2_1/n$, a = 16.2771(14), b = 9.7107(7), c = 17.6042(9) Å, β = 96.174(5)°, U = 2766.4(3) Å^3, Z = 4, T = 21 °C, μ = 33.40 cm^{-1}, for 4739 unique reflections R = 0.023 and GOF = 1.17.

For **4**: $C_{17}H_4O_{16}Ru_6S{\cdot}CH_2Cl_2$, M = 1187.62, orthorhombic, space group *Pnnm*, a = 23.7389(26), b = 12.0440(7), c = 17.5965(12) Å, U = 3315.6(5) Å^3, Z = 4, T = 21 °C, μ = 29.51 cm^{-1}, for 2869 unique reflections R = 0.044 and GOF = 3.55. CCDC 182/1141. See http://www.rsc.org/suppdata/cc/1999/279/ for crystallographic files in .cif format.

1 G. J. Kubas, *Acc. Chem. Res.*, 1994, **27**, 183.
2 D. J. Mulligan and D. Berk, *Ind. Eng. Chem. Res.*, 1989, **28**, 926.
3 D. C. Moody, R. R. Ryan and K. V. Salazar, *J. Catal.*, 1981, **70**, 221.
4 J. A. Ripmeester, *J. Am. Chem. Soc.*, 1982, **105**, 2925.
5 E. P. Parry, *J. Catal.*, 1963, **2**, 371.
6 E. L. Muetterties, T. N. Rhodin, E. Bard, C. F. Brucker and W. R. Dretzer, *Chem. Rev.*, 1979, **79**, 91.
7 J. L. Vidal, R. A. Fiato, L. A. Cosby and R. L. Pruett, *Inorg. Chem.*, 1978, **17**, 2574.
8 G. B. Karet, C. L. Stern, D. M. Norton and D. F. Shriver, *J. Am. Chem. Soc.*, 1993, **115**, 9979.
9 T. Chihara, H. Kubota, M. Fukumoto, H. Ogawa, Y. Yamamoto and Y. Wakatsuki, *Inorg. Chem.*, 1997, **36**, 5488.
10 R. D. Adams and L.-W. Yang, *J. Am. Chem. Soc.*, 1982, **104**, 4115.
11 R. D. Adams and D. A. Katahira, *Organometallics*, 1982, **1**, 53.
12 J. B. Bradley, *Adv. Organomet. Chem.*, 1983, **22**, 1.
13 H. Tanaka, J. Yoshinobu and M. Kawai, *Surf. Sci.*, 1995, **327**, L505.
14 A. Toupadakis, J. G. Kubas and C. J. Burns, *Inorg. Chem.*, 1992, **31**, 3810.
15 G. J. Kubas and R. R. Ryan, *J. Am. Chem. Soc.*, 1985, **107**, 6138.
16 A. Neher and I.-P. Lorenz, *Angew. Chem., Int. Ed. Engl.*, 1989, **28**, 1342.

Communication 8/09980D

ChemComm

Fast carbonyl exchange in the solid state for β-cyclodextrin/(arene)Cr(CO)$_3$ inclusion complexes

Silvio Aime,* Holly C. Canuto, Roberto Gobetto and Fabio Napolitano

Dipartimento di Chimica I.F.M., Università di Torino, Via P. Giuria 7, 10125 Torino, Italy. E-mail: aime@ch.unito.it

Received (in Basel, Switzerland) 20th November 1998, Accepted 28th December 1998

The exchange of carbonyls is a common feature for metal carbonyl compounds in solution whereas in the solid state high interatomic potential energy barriers cause this occurrence to be highly unlikely; it is shown that the compartmentalization of (arene)Cr(CO)$_3$ in the β-cyclodextrin cavity removes any constraint and thereby facilitates the rotation of the Cr(CO)$_3$ group in the solid state.

Cyclodextrins (CDs) that are naturally occurring oligomers of amylose which consist of six to eight glucose units are known to form inclusion compounds with various moieties including neutral molecules and organometallic complexes.[1] The ability of the cyclodextrin molecule to include guest compounds into its internal hydrophobic cavity has been extensively studied and found to be dependent on the size of the internal cavity which can vary from 5 to 7 to 8 Å for α-, β- and γ-cyclodextrins respectively.

Although properties of cyclodextrin inclusion compounds have been studied extensively there have been relatively few reports on their molecular dynamics in the solid state. With regards to organometallic complexes, reports on the inclusion compound formed between ferrocene and β-cyclodextrin (β-CD) indicated that inclusion into the cavity altered the dynamics in the solid state of the guest molecule compared to that observed for the pure compound.[2–5]

We were interested in investigating motion in the solid state of other previously reported inclusion compounds formed between β-cyclodextrin and organometallic complexes whose solid state dynamics of the pure compound had been well documented. This was found to be the case for (arene)Cr(CO)$_3$

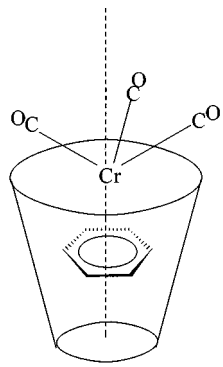

(arene = C_6H_6, C_6H_5Me, $C_6H_4Me_2$) complexes where the motion in the solid state had been previously investigated by several authors.[6–8]

It was found that in a polycrystalline sample of $(C_6H_6)Cr(CO)_3$, the arene rotates freely along its principal coordination axis whereas the carbonyl moiety is rigid on the NMR timescale at ambient temperature. Calculations based upon the X-ray crystal structure showed that there is a large potential energy barrier for the rotation of the $Cr(CO)_3$ unit as a consequence of the strong interatomic interactions with the neighbouring molecules.[9,10] This situation is clearly depicted in the ^{13}C CP MAS NMR spectrum [Fig. 1(*a*)] which shows single resonances for the C_6H_6 ligand at δ 95 and the carbonyl group (isotropic peak at δ 234) each showing the typical spinning side band (SSB) manifold which for the carbonyl resonance is indicative of a chemical shift anisotropy of *ca*. 390 ppm. Such a value has been commonly observed for solid state specimens of metal carbonyls containing terminal bound CO.[11]

In the β-CD/$(C_6H_6)Cr(CO)_3$ adduct the arene is reorienting freely as observed in the polycrystalline specimen.[6] This is proven firstly by the observation of a single ^{13}C resonance for the benzene ring in the ^{13}C CP MAS NMR spectrum [Fig. 1(b)] at the same chemical shift as the pure compound. Further support for the occurrence of free arene rotation is gained by looking at the ^{2}H NMR solid state spectrum of the inclusion compound containing as a guest molecule the perdeuterated $(C_6D_6)Cr(CO)_3$ isotopomer.† A typical powder pattern[12] with an inner separation between the main components of 71.0 kHz is observed at 300 K. This behaviour is consistent with the occurrence of a fast-exchange regime (> 10^8 s^{-1}) for the arene ring executing six-site nearest-neighbour jumps within the β-cyclodextrin cavity.

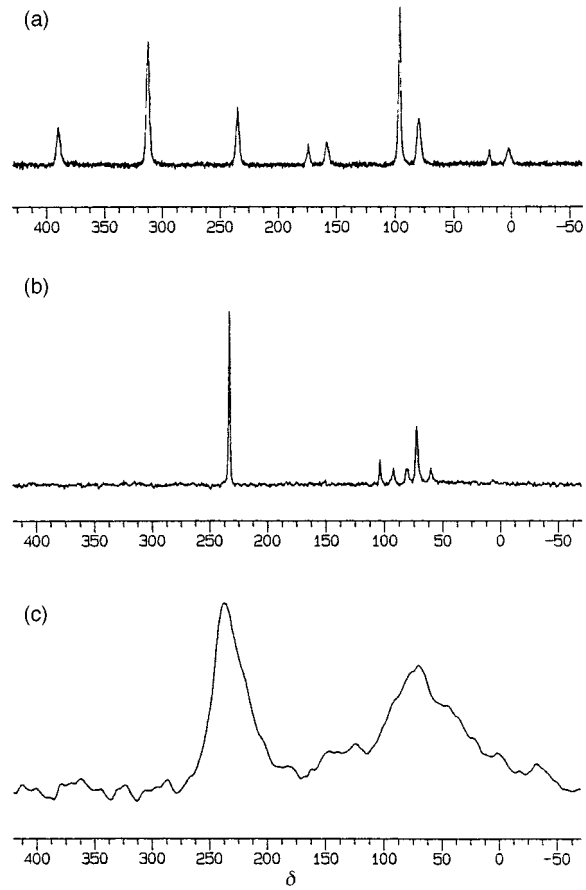

Fig. 1 Solid state ^{13}C NMR spectra recorded at 67.8 MHz for (a) CP MAS of $(C_6H_6)Cr(CO)_3$, (b) CP MAS of β-CD/$(C_6H_6)Cr(CO)_3$ adduct and (c) CP-static β-CD/$(C_6H_6)Cr(CO)_3$ adduct. All spectra was recorded for ^{13}CO enriched‡ samples, with cross polarization (contact time 5 ms) and a recycle delay of 20 s. For (a) and (b) the sample spinning speed was 5000 Hz.

Contrary to what is observed for the polycrystalline sample, in the inclusion compound, the carbonyl moiety acquires a substantial mobility which averages out the CSA responsible for the appearance of the SSB manifold in the high field ^{13}C NMR spectra of metal carbonyls under magic angle spinning [Fig. 1(b)]. Thus the ^{13}C CP MAS NMR spectrum of $(C_6H_6)Cr(CO)_3$ compartmentalized in the β-CD cavity is strictly analogous to the solution spectrum.

At ambient temperature the T_1 of the ^{13}CO resonance in the crystalline $(C_6H_6)Cr(CO)_3$ specimen is *ca.* 30 s, a value significantly shorter than those reported[13] for binary metal carbonyl resonances. This behaviour is likely to be the result of the dipolar interaction to the arene protons modulated by the intramolecular motion of the π-bonded C_6H_6 ring. At the same temperature and magnetic field strength, the T_1 of the CO resonance in the inclusion compound is only 1 s. This observation clearly indicates a high mobility of the carbonyl moiety. It is also worth noting that, in chloroform solution at 6.7 T and 298 K, the T_1 of the carbonyl resonance of $(C_6H_6)Cr(CO)_3$ is 23 s. Indeed the concurrence of a short T_1 and of the lack of the SSB manifold allows the attainment of higher sensitivity of the ^{13}C NMR spectrum of the included species than that of the crystalline sample and even of the solution spectrum.

Further evidence of the dynamic state of the carbonyl moiety has been obtained by recording the static spectrum of the inclusion compound [Fig. 1(c)]. The ^{13}CO resonance displays a bandwidth at half height of *ca.* 20 ppm, *i.e.* remarkably smaller than that commonly found in the static spectra of metal carbonyls.[11]

The motion of the carbonyl ligands is still in fast exchange also at temperatures as low as −100 °C where the ^{13}C CP MAS NMR spectrum is identical to that recorded at ambient temperature. This observation unambiguously shows that the high rotational barrier of the carbonyls[14] is overcome when the metal complex is included in the CD.

The observation of a narrow ^{13}C NMR carbonyl resonance in the static spectrum and the almost negligible asymmetry of its shape appear to be in agreement with the fast rotation of the $M(CO)_3$ unit around its principal coordination axis. A consequence of this type of motion is that the anisotropy of the axially symmetric ^{13}CO tensor is reduced by a factor of $(3\cos^2\beta - 1)/2$ where β is the angle between the principal chemical shift tensor axis and the rotational axis.[15] In the case of the β-CD/$(C_6H_6)Cr(CO)_3$ adduct the structure of the guest molecule[16] is such that the angle β is close to the value of the magic angle. Thereby rotation about the principal rotation axis would be expected to decrease the chemical shift anisotropy to a value close to zero also in the static spectrum.[14] An isotropic (or almost isotropic) reorientation of the whole molecule, which in principle would justify the absence of chemical shift anisotropy, has to be ruled out on the basis of the features of the deuterium NMR spectrum which is typical of a C_6 rotation.

The scrambling of carbonyls is a very common feature in metal carbonyl compounds in solution but it is highly unlikely in the solid state. Our findings show that the stereochemical non-rigidity of the carbonyl moieties may be re-established in a solid sample provided that the intermolecular interactions responsible for the high potential energy barriers in the crystalline framework of the pure compound are removed.

The observed behaviour would seem to suggest that the β-CD cavity provides a lower energy pathway for the rotation of the $M(CO)_3$ group.

Analogous results have been obtained by recording the ^{13}C CP MAS spectra of the inclusion complexes of β-CD with (toluene)$Cr(CO)_3$ and (*o*-xylene)$Cr(CO)_3$.

This work has been carried out with the support of the EU-TMR Program (Contract No. FMRX CT 96 0091). H. C. C. gratefully acknowledges the EU-SOCRATES Program for supporting her leave from QMW College (University of London).

Notes and references

† ^{13}C enriched $(C_6H_6)Cr(CO)_3$ was prepared by irradiating the compound in a benzene solution under 1 atm of ^{13}CO (99% enriched) using a 125 W high pressure mercury lamp for 2 h.[17]

‡ $(C_6D_6)Cr(CO)_3$ was obtained by reacting $(C_6H_6)Cr(CO)_3$ in a 1 : 1 mixture of C_6D_6 and $(CD_3)_2CO$ in a sealed vessel at 142 °C for 18 h, in a manner similar to that previously reported for other arene substitutions in ref. 18.

1 J. Szejtli, *Chem. Rev.*, 1998, **98**, 1743.
2 Z. Narankiewicz, A. L. Alexander, L. Bondareva, I. A. Mamedyarova, M. N. Nefedova and V. I. Sokolov, *J. Inclusion Phenom.*, 1991, **11**, 233.
3 F. Imashiro, D. Kuwahara, N. Kitazaki and T. Terao, *Magn. Reson. Chem.*, 1992, **30**, 796.
4 D. Kuwahara, F. Imashiro and T. Terao, *Chem. Phys. Lett.*, 1993, **204**, 5.
5 H.-J. Schneider, F. Hacket and V. Rudiger, *Chem. Rev.*, 1998, **98**, 1755.
6 P. Delise, G. Allegra, E. R. Mognaschi and A. Chierico, *J. Chem. Soc., Faraday Trans. 2*, 1975, **71**, 207.
7 G. W. Wagner and B. Hanson, *Inorg. Chem.*, 1987, **26**, 2019.
8 S. Aime, D. Braga, R. Gobetto, F. Grepioni and A. Orlandi, *Inorg. Chem.*, 1991, **30**, 951.
9 D. Braga and F. Grepioni, *Organometallics*, 1992, **11**, 717.
10 D. Braga, *Chem. Rev.*, 1992, **92**, 633.
11 J. W. Gleeson and R. W. Vaughan, *J. Chem. Phys.*, 1983, **78**, 5384.
12 M. I. Altbach, Y. Hiyama, R. J. Wittebort and L. G. Butler, *Inorg. Chem.*, 1990, **29**, 741.
13 T. H. Walter, L. Reven and E. Oldfield, *J. Phys. Chem.*, 1989, **93**, 1320.
14 P. J. Barrie, C. A. Mitsopoulou, M. Motevalli and E. W. Randall, *J. Chem. Soc., Dalton Trans.*, 1997, 353.
15 R. Tycko, G. Dabbagh, G. B. M. Vaughan, P. A. Heiney, R. M. Strongin, M. A. Cichy and A. B. Smith III, *J. Chem. Phys.*, 1993, **99**, 7554.
16 G. Allegra and P. Corradini, *J. Am. Chem. Soc.*, 1959, **81**, 2271.
17 T. C. Flood, E. Rosenberg and A. Sarhangi, *J. Am. Chem. Soc.*, 1977, **99**, 4334.
18 C. A. L. Mahaffy and P. L. Pauson, *J. Chem. Res.* (*S*), 1979, 126.

Communication 8/09100E

A catalytic symmetrical etherification

Laurence Bagnell, Teresa Cablewski and Christopher R. Strauss*

CSIRO Molecular Science, Bag 10, Clayton South,Victoria 3169, Australia. E-mail: chris.strauss@molsci.csiro.au

Received (in Cambridge, UK) 17th November 1998, Accepted 5th January 1999

A novel, catalytic, thermal etherification produces minimal waste and can be carried out under almost neutral conditions.

Most methods for etherification use either strongly acidic or basic conditions.[1–3] Their disadvantages have been summarised by Lemaire and co-workers, who explored hydrogenolysis of hemiacetals as an alternative.[4] The long-established Williamson synthesis[5] is still the most common procedure. It involves substitution of an alkyl halide (RX) by a strongly basic alkoxide or phenoxide (*e.g.* KOR or NaOR) and so is unsuitable if base catalysed elimination of HX from RX can compete.[6,7] A stoichiometric amount of waste salt (KX or NaX) is also produced. Importantly, inorganic salts account for the bulk of industrial chemical wastes.[7] Besides polluting soil and ground water, salts can lower the pH of atmospheric moisture and have been implicated in the formation of acid-dew.[8] Hence, their minimisation is essential.

Our research is directed toward technologies and methodologies for environmentally benign organic chemistry.[6,9] We now report a catalytic etherification that produces minimal organic waste and that can be carried out without the addition of acid or base.[10]

For a symmetrical ether, an excess of alcohol (ROH) and a catalytic amount of RX are heated. A solvolytic displacement reaction[11*a*] between RX and ROH affords R_2O along with HX or its elements [hereafter referred to as HX; eqn. (1)]. The liberated HX reacts with another molecule of ROH to form water and to regenerate RX [eqn. (2)]. If the rates of these forward reactions are comparable, the concentration of HX will be low throughout and that of RX will remain relatively constant. Although HX and RX are stoichiometric reactants or products in eqn. (1) and (2), they do not appear in the sum [eqn. (3)]. The net process involves condensation of two molecules of ROH to give R_2O plus water.

$$RX + ROH \rightleftharpoons R_2O + HX \quad (1)$$

$$HX + ROH \rightleftharpoons RX + H_2O \quad (2)$$

$$2\,ROH \rightleftharpoons R_2O + H_2O \quad (3)$$

A widely accepted mechanism of etherification catalysed by strong acids (commonly, sulfuric acid is used) involves protonation of the hydroxy function of an alcohol to give the corresponding oxonium ion as a better leaving group.[1,2] The reaction then can proceed through substitution by another molecule of the alcohol or by elimination of water, followed by acid-catalysed addition of the alcohol to the resulting olefin. Although the overall reaction is also satisfied by eqn. (3), the solution would remain acidic throughout.

By contrast, the present process requires participation by the counterion X^- and utilises ostensibly neutral conditions. For it to operate efficiently, X^- should be a good leaving group [to satisfy eqn. (1)], an effective nucleophile [to accommodate eqn. (2)] and a weak base to minimise competing elimination reactions.[12] Bromide and iodide possess these properties.[13] To the best of our knowledge, a critical participatory role for the counterion of the acid has not previously been envisaged or recognised.

The examples presented in Table 1 were obtained by heating the reactants in glass-lined pressure vessels without water removal. Conversions rather than yields have been quoted, owing to the catalytic nature of the systems, and by-product formation was negligible in all cases. Neat Bu^nOH was unreactive at 200 °C (entry 1), but in the presence of a catalytic amount of Bu^nBr it afforded $Bu^n{}_2O$ without significant consumption of the haloalkane (entry 2). A comparable result was obtained with $PhCH_2CH_2OH$ at 220 °C (entries 4 and 5). Styrene or 1-phenylethyl derivatives, that might have been anticipated through mechanisms involving elimination, were not detected. Cyclopropylmethanol, although highly acid-labile,[14] was stable at reflux (entry 6), but in the presence of a catalytic amount of cyclopropylmethyl bromide, it condensed to form bis(cyclopropylmethyl) ether, without significant depletion of the bromide or rearrangement (entry 7), until the conversion was approximately 50%. This result indicated that the concentration of acid was not sufficiently high to affect the cyclopropylmethyl group.

As the reaction further progressed though, phase separation occurred and HBr accumulated in the aqueous medium. Consequently, the rate of etherification slowed and the unreacted alcohol and the product ether were decomposed by the acid to give cyclobutyl and homoallyl alcohols along with mixtures of ethers containing cyclopropyl, cyclobutyl and homoallyl functionalities.[14]

Nonetheless, the examples in Table 1 demonstrated the process, its applicability for base- or acid-labile compounds (entries 5 and 7, respectively) and the catalytic role of RX.

Table 1 Example reactions and conditions

Entry	Starting material(s)	*T* /°C	*t*/h	Major product(s)	Conversion(%)
1	Bu^nOH	200	2	no reaction	—
2	Bu^nOH (10 ml) + Bu^nBr (1 mol)	200	1	$Bu^n{}_2O$	26
3[*a*]	Bu^nOH (10 mol) + Bu^nBr (1 mol) + LiBr (1 mol	200	1	$Bu^n{}_2O$	54
4	$PhCH_2CH_2OH$	220	22	$(PhCH_2CH_2)_2O$	< 1
5[*a*]	$PhCH_2CH_2OH$ (10 mol) + $PhCH_2CH_2Br$ (1 mol)	220	21	$(PhCH_2CH_2)_2O$	76
6	Cyclopropylmethanol	120	24	no reaction	
7[*a,b*]	Cyclopropylmethanol (10 mol) + cyclopropylmethyl bromide (0.9 mol)	115	24	bis(cyclopropylmethyl) ether	51
8[*a,c,d,e*]	Bu^sOH (10 mol) +Bu^sBr (1 mol)	150	5	$Bu^s{}_2O$(1 : 1 mixture of diastereoisomers)	8
9[*a,c,d,e*]	Bu^sOH (10 mol) +Bu^sBr (1 mol) +LiBr (1 mol)	150	5	$Bu^s{}_2O$(1 : 1 mixture of diastereoisomers)	18

[*a*] Concentration of bromo derivative essentially unchanged after the reaction. [*b*] Extended heating led to acid catalysed decomposition. See text. [*c*] Optically pure Bu^sOH also afforded a 1 : 1 mixture of diastereoisomers, suggestive of an S_N1 mechanism. [*d*] Prolonged heating led to some evolution of gas. [*e*] Neat Bu^sOH did not react at 150 °C for 5 h.

The pathway was investigated by heating $PhCH_2CH_2OH$ with Bu_4NBr (not entered in Table 1). After 20 h at 200 °C, $(PhCH_2CH_2)_2O$ was not detected (but $PhCH_2CH_2OBu^n$ was produced by Hoffmann degradation, in low conversion). $PhCH_2CH_2Br$ and $(PhCH_2CH_2)_2O$ formed only after a few drops of acid (HOAc) were added to the reaction mixture, followed by further heating. This experiment indicated that the presence of X^- was insufficient to drive the reaction and that HX was required. We have also found that the process can be started from eqn. (2). In an example, HBr (9 mol%) was heated with $PhCH_2CH_2OH$ at 200 °C. After 3 h, the product mixture was no longer acidic and contained $PhCH_2CH_2Br$ (9%) and $(PhCH_2CH_2)_2O$ (6%) along with unreacted $PhCH_2CH_2OH$. These results were all consistent with the pathway in eqn. (1)–(3) and indicated that mechanisms proposed for acid-catalysed etherification[1,2] may in some cases need to accommodate possible participatory roles of the counterion.

As mentioned above, although hydroxy and alkoxy functions are not readily displaced from carbon atoms, protonation in strong acid greatly facilitates their leaving.[1,2] Indeed, HBr and HI have been employed as cleavage agents for ethers for well over a century.[15] Conversely, the rate of solvolytic displacement of alkyl halides by alcohols [the forward reaction in eqn. (1)] can be accelerated by a small amount of water.[11b] However, excess water would shift unfavourably the position of equilibrium in eqn. (2) and promote the reverse reaction in eqn. (3). These opposing factors indicate that, for etherification, depletion of water should be beneficial but complete removal may be detrimental. Also, when the concentration of alcohol is 10–50 times larger than that of RX, the first order rate constant of eqn. (1) can rise considerably.[16] Thus the rate and extent of reaction in eqn. (1) will depend on the relative concentrations of RX and ROH as well as on the concentration of water present. Entries 3 and 9 were consistent with reports that the addition of alkaline metal salts also can accelerate solvolytic processes,[17] including the rate of ionisation of RX.[18] Our results and published data[11,16–18] indicate that the catalytic process would operate most effectively at low to moderate conversions and should be amenable to continuous processing. This aspect and the preparation of unsymmetrical and polyethers will be discussed elsewhere.

Notes and references

1 H. Feuer and J. Hooz, *The Chemistry of the Ether Linkage*, ed. S. Patai, Interscience, London, 1967, ch. 10, pp. 445–498.
2 N. Baggett, *Comprehensive Organic Chemistry*, series ed. D. Barton and W. D. Ollis, vol. ed., J. F. Stoddart, Pergamon, Oxford, 1979, vol. 1, pp. 799–852.
3 O. Mitsunobu, *Comprehensive Organic Synthesis*, series ed. B. M. Trost and I. Fleming, vol. ed., E. Winterfeldt, Pergamon, New York, 1991, vol. 6, pp. 1–31.
4 V. Bethmont, F. Fache and M. Lemaire, *Tetrahedron Lett*., 1995, **36**, 4235.
5 A. W. Williamson, *J. Chem. Soc*., 1852, **4**, 229.
6 T. Cablewski, A. F. Faux and C. R. Strauss, *J. Org. Chem*., 1994, **59**, 3408; K. D. Raner, C. R. Strauss, R. W. Trainor and J. S. Thorn, *J. Org. Chem.*, 1995, **60**, 2456.
7 R. A. Sheldon, *Chem. Ind. (London)*, 1997, 12.
8 H. Okochi, T. Kajimoto, Y. Arai and M. Igawa, *Bull. Chem. Soc. Jpn*., 1996, **69**, 3355.
9 C. R. Strauss and R. W. Trainor, *Aust. J. Chem*., 1995, **48**, 1665; J. Li, A. W.-H. Mau and C. R. Strauss, *Chem. Commun*., 1997, 1275; L. Bagnell, M. Bliese, T. Cablewski, C. R. Strauss and J. Tsanaktsidis, *Aust. J. Chem*., 1997, **50**, 921; J. An, L. Bagnell, T. Cablewski, C. R. Strauss and R. W. Trainor, *J. Org. Chem*., 1997, **62**, 2505.
10 A patent application has been filed.
11 (*a*) A. Streitwieser Jr., *Solvolytic Displacement Reactions*, McGraw-Hill, New York, 1962, p. 2; (*b*) pp. 34–38.
12 C. K. Ingold, *Structure and Mechanism in Organic Chemistry*, 2nd edn., Cornell University Press, 1969, ch. 7, pp. 418–561.
13 E. S. Gould, *Mechanism and Structure in Organic Chemistry*, Holt, Rinehart and Winston, New York, 1959, ch. 8, pp. 250–313.
14 C. C. Lee and A. J. Cessna, *Can. J. Chem*., 1980, **58**, 1075 and references cited therein.
15 E. Staude and F. Patat, *The Chemistry of the Ether Linkage*, ed. S. Patai, Interscience, London, 1967, ch. 2, pp. 21–80.
16 E. Gelles, E. D. Hughes and C. K. Ingold, *J. Chem. Soc*., 1954, 2918.
17 S. Winstein, E. Clippinger, A. H. Fainberg and G. C. Robinson, *J. Am. Chem. Soc*., 1954, **76**, 2597.
18 J. F. Bunnett and D. L. Eck, *J. Org. Chem*., 1971, **36**, 897; L. C. Manege, T. Ueda and M. Hojo, *Bull. Chem. Soc. Jpn*., 1998, **71**, 589.

Communication 8/08980I

ChemComm

Turning up the heat: synthesis of octanuclear chromium(III) carboxylates

Ian M. Atkinson,[b] Cristiano Benelli,[c] Mark Murrie,[a] Simon Parsons[a] and Richard E. P. Winpenny*[a]

[a] *Department of Chemistry, The University of Edinburgh, West Mains Road, Edinburgh, UK EH9 3JJ*
[b] *School of Molecular Science, James Cook University, Queensland 4811, Australia*
[c] *Department of Chemistry, University of Florence, Via Maragliano 77, 50144 Florence, Italy*

Received (in Basel, Switzerland) 26th October 1998, Accepted 13th December 1998

Two new octanuclear Cr(III) carboxylate complexes are reported illustrating a temperature dependent route to high nuclearity species.

A vast amount of research is currently focused on the investigation of magnetic exchange interactions in polynuclear assemblies and more specifically upon molecules which possess high spin ground states. Although the use of carboxylate ligands has proved a rich source of high nuclearity complexes for both manganese[1] and iron[2] similar studies with chromium(III) carboxylates have thus far been much more restricted. This is probably due to the relative kinetic inertness of Cr(III) and the inherent stability of the low nuclearity complexes—in particular oxo-centred Cr(III) triangles—once formed. Further reaction of $\{Cr_3O\}$ units has so far only produced $\{Cr_4O_2\}$ cores[3] despite the fact that these units can be thought of as building blocks in the formation of larger structures for Mn[1] and Fe.[2] The most significant exception is a report of a dodecanuclear Cr cage with pivalate ligands, formed by heating an ill-defined material of stoichiometry '$[Cr(OH)(O_2CCMe_3)_2]$' under an inert atmosphere.[4] We now report that this reaction is applicable to other carboxylates and other metals, and that the topology of the resulting cages can be controlled by temperature. We also show that electrospray mass spectrometry (ESMS) is an excellent tool for demonstrating nuclearity of such cages in solution.

Reaction of $Cr(NO_3)_3{\cdot}9H_2O$ (0.050 mol) with KO_2CPh (0.178 mol) in H_2O (500 cm^3) at *ca.* 80 °C gives a blue precipitate in >90% yield which has solubility in several organic solvents. ESMS† of this material dissolved in CH_2Cl_2–MeOH indicates a structure based on a typical oxo-centred $\{Cr_3O\}$ unit $[Cr_3O(O_2CPh)_6(H_2O)_2(OH)]$ **1**: *m/z* (% intensity) found (calc.) = 950.7 (67%) (951.7, M^+). Higher *m/z* peaks assigned as MeOH adducts with consistent isotopic splitting patterns are also seen. Unfortunately whether **1** is trimeric or contains oligomers of trimers is not certain.

Complex **1** undergoes complicated thermal rearrangements upon heating. Heating **1** at 210 °C *in vacuo* for 2 h caused elimination of H_2O yielding a pale green–blue powder. Extraction with CH_2Cl_2 followed by slow evaporation of the solution over a period of seven months at ambient temperature gave crystals of $[Cr_8(OH)_8(O_2CPh)_{16}]$ **2** (yield *ca.* 15%).‡ The structure of **2** (Fig 1)§ reveals eight octahedrally coordinated Cr atoms linked by eight bridging hydroxides and sixteen 1,3-bridging O_2CPh ligands forming a sixteen membered ring. The hydroxide ligands line the cavity in the centre of the 'wheel' pointing alternately slightly above and below the Cr_8 ring. Eight of the O_2CPh ligands bridge Cr atoms around the outside of the 'wheel' almost in-plane with the wheel, while the remaining eight ligands bridge alternately above and below the ring at an angle of *ca.* 90° forming two hydrophobic pockets.

The wheel may be formed in small amounts from the thermolysis and crystallise slowly, however the ESMS of the crude green–blue powder formed after thermolysis shows the predominant species present to be of similar mass to oxo-centred triangles, but with the MeOH adducts having greater relative intensity compared with **1** than in the spectra prior to heating. The balance of evidence is that heating to 210 °C disrupts the triangular units of **1**, probably by driving off terminally coordinated water, with **2** forming during crystallisation. ESMS of redissolved crystals of **2** did not show any significant peaks due to polynuclear species.

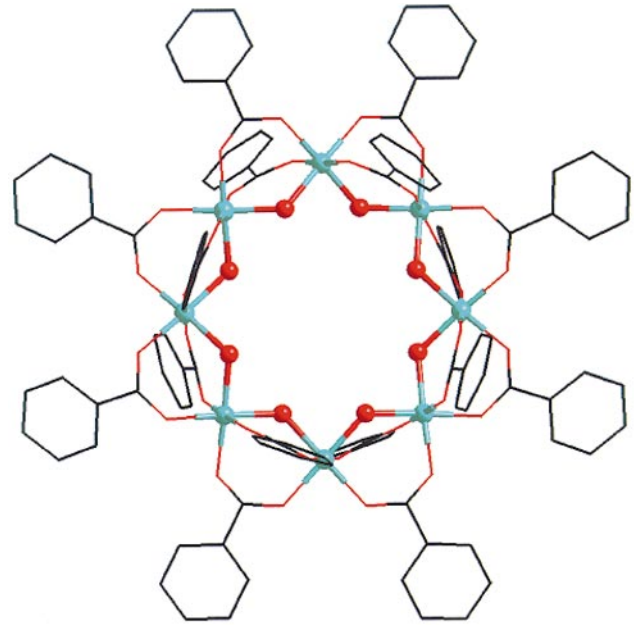

Fig. 1 The structure of **2**. Bond length ranges: Cr–O(benzoate) 1.925–2.002, Cr–O(hydroxide) 1.930–1.969 Å (av. esd 0.013 Å). Bond angle ranges: *cis* at Cr 84.5–95.6, *trans* at Cr 175.2–179.5° (av. esd 0.6°) (Cr, blue; O, red, μ-OH ball, other O atoms line; C, black lines).

Heating **1** at 400 °C under a stream of N_2 for 1 h eliminates more H_2O, yielding a dark green solid. Extraction with CH_2Cl_2 followed by addition of Pr^nOH (1:3, v/v) gave crystals of $[Cr_8O_4(O_2CPh)_{16}]$ **3** after 7 d in 70% yield.‡ The structure of **3** (Fig. 2)§ shows a distorted $\{Cr_4O_4\}^{4+}$ cubane core where each μ_4-oxide bridges to a further Cr atom creating a larger Cr_4 tetrahedron. The structure can also be considered to be formed from two orthogonal distorted $\{Cr_4O_2\}$ butterfly units and has non-crystallographic T_d symmetry. Twelve of the sixteen O_2CPh ligands link the cubane Cr atoms to the outer Cr atoms while four of the O_2CPh ligands are found in the unusual bidentate bridging mode capping the final two coordination sites on the outer Cr atoms. This coordination leads to the outer Cr sites being considerably more distorted from octahedral geometry than the Cr atoms of the central cubane. The Cr–O bond lengths to these chelating benzoates are also longer, which suggests these groups may be substituted which might allow new chemistry to be performed at these sites. Peaks in the ESMS are seen, both prior to crystallisation and for pure **3**, at *m/z* (% intensity) found (calc.) = 1232.3 (27%) [1231.9, (**3** + $2Na)^{2+}$]; 1220.1 (31%) [1220.4, (**3** + $Na)^{2+}$]; 1088.1 (100%) [1087.8, (**3** − 2 $O_2CPh)^{2+}$]. In contrast to **2** therefore, we can conclude that **3** is present in solution, and is the major product of the thermolysis.

The Cr(III) starting materials are perfectly set up to promote oligomerisation *via* conversion of coordinated H_2O to hydrox-

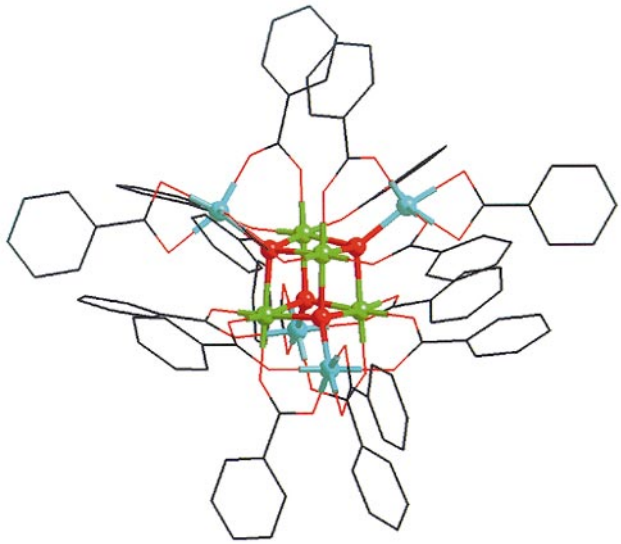

Fig. 2 The structure of **3**. Bond length ranges: Cr–O(1,3-bridging benzoate) 1.927–1.985, Cr–O(chelating benzoate) 2.009–2.056, Cr–O(oxide) 1.966–2.039 Å (av. esd 0.008 Å). Bond angle ranges: *cis* at Cr (metal atoms of central cubane) 81.7–99.1, *trans* at Cr(cubane) 172.8–179.7, *cis* at Cr (outer metal atoms) 64.7–109.4, *trans* at Cr (outer metal atoms) 154.9–74.2° (av. esd, 0.3°) (Cr atoms of central heterocubane, green; outer Cr, blue; O, red, μ_4-O ball, other O atoms line; C, black lines).

ide or oxide bridges rather than relying upon the serendipitous formation of such bridges in solution reactions. Furthermore, controlling the temperature of these rearrangement reactions permits isolation of different nuclearity products and we believe this route is applicable to other metals. IR and elemental analysis strongly suggests that the iron analogue of **3** can be made by the same route. The structure of **3** is also very similar to a mixed-valent Co cage, made by an entirely different route, with benzoate ligands which has been reported by Christou *et al*.[9] No other cages containing this metal-array have been described.

Preliminary magnetic measurements on both **2** and **3** indicate antiferromagnetic exchange between the Cr centres. The susceptibility data¶ for **2** could be modelled with one exchange parameter, $J = 12.0\ cm^{-1}$; while for **3** two exchange terms were required: $J_1 = 2.1\ cm^{-1}$, and represents the exchange between Cr atoms within the central heterocubane (green in Fig. 2), while $J_2 = 3.4\ cm^{-1}$, models the exchange between the central Cr atoms and the outer tetrahedron. The latter model is not ideal at present, but the fit is sufficiently good to be satisfied that these exchange parameters are broadly correct.

We thank the EPSRC(UK) for funding for a diffractometer, an electrospray mass spectrometer and for a Fellowship (to M. M.), and NATO and COST Action 518 for supporting the collaboration between Edinburgh and Florence.

Notes and references

† Electrospray mass spectra were obtained on a Finnegan LCQ spectrometer with the sample dissolved in CH_2Cl_2 which was added to MeOH prior to injection into the spectrometer.

‡ Satisfactory elemental analyses were obtained for **2** and **3**.

§ *Crystal data*: for $C_{106}H_{84}Cr_8O_{40}\cdot 1.5CH_2Cl_2$ **2**: monoclinic, space group *C*2/*c*, $a = 24.219(7)$, $b = 23.534(7)$, $c = 23.318(10)$ Å, $\beta = 95.37(5)°$, $V = 13232(8)$ Å^3, $M = 2541.1$, $Z = 4$ (the molecule lies on a twofold axis), $\mu = 0.764\ mm^{-1}$, $T = 150.0(2)$ K, $R1 = 0.1344$.

For $C_{112}H_{80}Cr_8O_{36}\cdot 5\ CH_2Cl_2$ **3**: monoclinic, space group $P2_1/c$, $a = 16.165(8)$, $b = 45.24(3)$, $c = 17.638(10)$ Å, $\beta = 110.52(5)°$, $V = 12079(12)$ Å^3, $M = 2842.4$, $Z = 4$, $\mu = 0.993\ mm^{-1}$, $T = 150.0(2)$ K, $R1 = 0.1025$.

Data collection, structure solution and refinement were performed using programs SIR92,[5] DIRDIF[6] and SHELXL-97.[7] All crystals of **2** were badly twinned leading to the poor refinement which is sufficient to unambiguously derive connectivity. Diffuse lattice solvent (1.5 CH_2Cl_2 per formula unit) was treated by the van der Sluis-Spek method.[8] Only Cr and O atoms were refined anisotropically. Full details have been deposited and will be published later. CCDC 182/1128. See http://www.rsc.org/suppdata/cc/1999/285/ for crystallographic files in .cif format.

¶ Variable-temperature magnetic measurements on **2** and **3** in the region 1.8–325 K were made using a SQUID magnetometer (Quantum Design) with samples sealed in gelatine capsules. Diamagnetic corrections for sample holders and samples were applied to the data. The data were fitted with Hamiltonians: for **2,** $H = JS_xS_{x+1} + JS_8S_1$ ($1 \leqslant x \leqslant 7$); and for **3**, $H = J_1(S_1S_2 + S_1S_3 + S_1S_4 + S_2S_3 + S_2S_4 + S_3S_4) + J_2\{S_5(S_1 + S_2 + S_4) + S_6(S_2 + S_3 + S_4) + S_7(S_1 + S_2 + S_3) + S_8(S_1 + S_3 + S_4)\}$.

1 For example: R. Sessoli, H.-L. Tsai, A. R. Schake, S. Wang, J. B. Vincent, K. Folting, D. Gatteschi, G. Christou and D. N. Hendrickson, *J. Am. Chem. Soc*., 1993, **115**, 1804; R. C. Squire, S. M. J. Aubin, K. Folting, W. E. Streib, G. Christou and D. N. Hendrickson, *Inorg. Chem*., 1995, **34**, 6463; E. K. Brechin, W. Clegg, M. Murrie, S. Parsons, S. J. Teat and R. E. P. Winpenny, *J. Am. Chem. Soc*., 1998, **120**, 7365.

2 For example: W. Micklitz, V. McKee, R. L. Rardin, L. E. Pence, G. C. Papaefthymiou, S. G. Bott and S. J. Lippard, *J. Am. Chem. Soc*., 1994, **116**, 8061; A. K. Powell, S. L. Heath, D. Gatteschi, L. Pardi, R. Sessoli, G. Spina, F. Del Giallo and F. Pieralli, *J. Am. Chem. Soc.*, 1995, **117,** 2491; S. P. Watton, P. Fuhrmann, L. E. Pence, A. Caneschi, A. Cornia, G. L. Abbati and S. J. Lippard, *Angew. Chem., Int. Ed. Engl.*, 1997, **36**, 2774.

3 A. Bino, R. Chayat, E. Pedersen and A. Schneider, *Inorg. Chem*., 1991, **30**, 856; T. Ellis, M. Glass, A. Harton, K. Folting, J. C. Huffman and J. B. Vincent, *Inorg. Chem*., 1994, **33**, 5522.

4 A. S. Batsanov, G. A. Timko, Y. T. Struchkov, N. V. Gérbéléu and K. M. Indrichan, *Koord. Khim*., 1991, **17**, 662.

5 A. Altomare, G. Cascarano, C. Giacovazzo and A. Guagliardi, SIR92, *J. Appl. Crystallogr*., 1993, **26**, 343.

6 P. T. Beurskens, G. Beurskens, W. P. Bosman, R. de Gelder, S. Garcia-Granda, R. O. Gould, R. Israel and J. M. M. Smits, DIRDIF-96 program system, University Crystallography Laboratory, University of Nijmegen, 1996.

7 G. M. Sheldrick, University of Göttingen, 1997.

8 P. van der Sluis and A. L. Spek, *Acta Crystallogr., Sect. A*, 1990, **46**, 194.

9 K. Dimitrou, J.-S. Sun, K. Folting and G. Christou, *Inorg. Chem.*, 1995, **34**, 4160.

Communication 8/08304E

Uncatalysed hydrogen-transfer reductions of aldehydes and ketones

Laurence Bagnell and Christopher R. Strauss*

CSIRO Molecular Science, Bag 10, Clayton South, Victoria 3169, Australia. E-mail: chris.strauss@molsci.csiro.au

Received (in Cambridge, UK) 17th September 1998, Accepted 5th January 1999

Aldehydes and ketones are reduced to the corresponding alcohols by transfer hydrogenation at high temperature with EtOH, Pr^{n}OH or Pr^{i}OH as hydrogen donors in the absence of catalysts and base.

Hydrogen-transfer occurs when covalently bonded hydrogen changes its site of attachment, either inter- or intra-molecularly.[1] The reduction of aldehydes and ketones usually involves unlike donors and acceptors.[2–4] It has been long considered that catalysts are required,[3] that alcohols are preferred hydrogen donors[5] and that base promotion is beneficial.[4,6] For example, Meerwein–Ponndorf–Verley (MPV) reductions are typically conducted using a stoichiometric amount of $Al(OPr^i)_3$ and excess Pr^{i}OH.[4,7] However, such conditions can give substantial amounts of side-products[4] and generate environmentally undesirable salts during work-up.[8]

Our work toward the development of cleaner processes for preparative organic chemistry has produced new thermolytic methods.[9] Now we report hydrogen-transfer reactions that employ elevated temperatures without added metallic catalysts, acids or bases.

The starting aldehydes and ketones were heated with low-boiling alcohols in stainless steel autoclaves, with or without glass liners, at 220–230 °C. After cooling, the products were isolated by rotary evaporation and/or distillation. Solvent extraction was avoided and recycling of the unreacted volatile alcohols was facilitated.

Initially, EtOH, Pr^{n}OH or Pr^{i}OH were evaluated as the sources of hydrogen, with PhCHO as the reductant. BzOH was formed at comparable rates in these alcohols, including in all-glass systems. After treating PhCHO for 24 h in Pr^{i}OH at 225 °C (entry 1 in Table 1), the product mixture comprised BzOH (92% isolated yield), starting material (4%) and (*E*)-4-phenylbut-3-en-2-one (the aldol by-product from the reaction of the starting PhCHO with Me_2CO formed by oxidation of the Pr^{i}OH; 2%). $PhCO_2H$ and $PhCO_2Bz$ (possible by-products from Cannizzarro and Tishchenko reactions, respectively) were either present in trace amounts or not detected. Thus, the reaction proceeded slowly but selectively and competing processes were retarded in the absence of added base.

A similar result was obtained for the reduction of cinnamaldehyde (entry 2).[10] The major product was (*E*)-cinnamyl alcohol. 3-Phenylpropanol (up to 7%) was formed by reduction of the double bond followed by that of the aldehydic function. The stability of cinnamyl alcohol under similar conditions (entry 7) confirmed this reduction sequence.

High-boiling hydrocarbons have been used by others as hydrogen donors for the reduction of carbonyl compounds, at temperatures around 400 °C.[11,12] However, in contrast with the present work (which employed considerably lower temperatures), α,β-unsaturated carbonyl compounds were selectively hydrogenated at the carbon–carbon double bond, while the carbonyl group remained intact.[11]

Herein, cyclohexanone and acetophenone afforded cyclohexanol and 1-phenylethanol, respectively (entries 5 and 6). The rate of reduction of ketones was slower than that for aldehydes. Dehydration of the products was not observed.

To the best of our knowledge, this is the first report of synthetic hydrogen-transfer reductions by low-boiling alcohols such as Pr^{i}OH, Pr^{n}OH or EtOH, alone. Significantly, in all cases so far examined, the products were the same as those reported for corresponding MPV reactions.[13] A co-ordinating metal was not added to our experiments, so despite the similarities of the products, an alternative mechanism is obligatory to that proposed for MPV reactions by Jackman and Mills[14] and widely accepted.[4,6,15]

In summary, this environmentally benign method of selective transfer-hydrogenation employs inexpensive, renewable reagents and affords minimal waste, with no inorganic salts introduced or formed. It offers considerable promise for cleaner processing and for biomimetic applications. Investigation of the converse approach, *i.e.* the use of low-boiling aldeydes and ketones for Oppenauer-type oxidations[16] of alcohols, is underway.

Notes and references

1 For classification, see E. A. Braude and R. P. Linstead, *J. Chem. Soc.*, 1954, 3544.
2 Cannizzarro and Tishchenko reactions are exceptions.
3 See the reviews on catalytic transfer hydrogenation: G. Brieger and T. J. Nestrick, *Chem. Rev*., 1974, **74**, 567.; R. A. W. Johnstone, A. H. Wilby and I. D. Entwistle, *Chem. Rev*., 1985, **85**, 129.
4 C. F. de Grauw, J. A. Peters, H. van Bekkum and J. Huskens, *Synthesis*, 1994, 1007.
5 See for example, E. C. Kleiderer and E. C. Kornfeld, *J. Org. Chem*., 1948, **13**, 455.

Table 1 Example reactions and conditions[a]

Entry	Starting material	*T*/°C	*t*/h	Major product	Yield[b] (%)
1	PhCHO	225[c]	24	BzOH	92[d]
2	(*E*)-PhCH=CHCHO	227[c]	27	(*E*)-PhCH=CHCH$_2$OH	83
3	*p*-Anisaldehyde	225[c]	29	*p*-methoxybenzyl alcohol	81
4	*n*-Dodecanal	225[c]	29	*n*-dodecanol	68
5	Cyclohexanone	226[c]	22	cyclohexanol	50
6	Acetophenone	225[c]	24	1-phenylethanol	24
7	(*E*)-PhCH=CHCH$_2$OH	225[c]	29	no reaction	0
8	4-Chlorobenzaldehyde	225[c]	29	4-chlorobenzyl alcohol	91
9	3-Bromo-4-methoxybenzaldehyde	226[c]	29	3-bromo-4-methoxybenzyl alcohol	74

[a] All reactions were performed in Pr^{i}OH. [b] When yields were low to moderate, the residue was mainly starting material. [c] At 220 and 232 °C, the vapour pressure of Pr^{i}OH is 4 and 5 MPa, respectively. [d] In a typical experiment, a solution of PhCHO (2.2 g) and Pr^{i}OH (150 ml) was heated in a sealed autoclave at 225 °C for 29 h. The product was concentrated by fractional distillation and then purified by distillation under reduced pressure.

6 R. M. Kellogg, in *Comprehensive Organic Synthesis*, series ed. B. M. Trost and I. Fleming, vol. ed. I. Fleming, Pergamon, Oxford, 1993, vol. 8, p. 79.
7 Recently, a bidentate aluminium complex, prepared *in situ* from Me_3Al and 2,7-dimethyl-1,8-biphenylenediol in the presence of Pr^iOH or 1-phenylethanol, was reported for catalytic reductions of aldehydes and ketones. See T. Ooi, T. Miura, and K. Maruoka, *Angew. Chem. Int. Ed.*, 1998, **37**, 2347.
8 R. A. Sheldon, *CHEMTECH*, 1994, **24**(3), 38.; R. A. Sheldon, *Chem. Ind.* (*London*), 1997, 12.
9 T. Cablewski, A. F. Faux and C. R. Strauss, *J. Org. Chem*., 1994, **59**, 3408.; K. D. Raner, C. R. Strauss, R. W. Trainor and J. S. Thorn, *J. Org. Chem.*, 1995, **60**, 2456.; C. R. Strauss and R. W. Trainor, *Aust. J. Chem*., 1995, **48**, 1665.; J. Li, A. W.-H. Mau and C. R. Strauss, *Chem. Commun*., 1997, 1275.; L. Bagnell, M. Bliese, T. Cablewski, C. R. Strauss and J. Tsanaktsidis, *Aust. J. Chem*., 1997, **50**, 921.; J. An, L. Bagnell, T. Cablewski, C. R. Strauss and R. W. Trainor, *J. Org. Chem*., 1997, **62**, 2505.
10 When this reaction was attempted in MeOH, the dimethyl acetal of cinnamaldehyde resulted.
11 C. Ruchardt, M. Gerst and J. Ebenhoch, *Angew. Chem., Int. Ed. Engl*., 1997, **36**, 1406.
12 C. Choi and L. M. Stock, *J. Org. Chem*., 1984, **49**, 2871.
13 A. L. Wilds, *Org. React.*, 1944, **2**, 178.
14 L. M. Jackman and J. A. Mills, *Nature*, 1949, **164**, 789.
15 E. C. Ashby, *Acc. Chem. Res*., 1988, **21**, 414.
16 C. Djerassi, *Org. React.*, 1951, **6**, 207.

Communication 8/08977I

An unusual ring expansion from the Zav'yalov pyrrole synthesis: formation of oxacino[2,3-*c*]pyrroles

Christopher D. Gabbutt,[a] John D. Hepworth,[a] B. Mark Heron,*[a] Mark R. J. Elsegood[b] and William Clegg[b]

[a] *Department of Chemistry, University of Hull, Hull, UK HU6 7RX. E-mail: b.m.heron@chem.hull.ac.uk*
[b] *Department of Chemistry, University of Newcastle, Newcastle upon Tyne, UK NE1 7RU. E-mail: w.clegg@ncl.ac.uk*

Received (in Liverpool, UK) 18th November 1998, Accepted 22nd December 1998

Enamino acids 2 and 5 undergo a facile cyclisation to afford the pyrrole 3 and isoindole 6 ring systems; a novel two atom ring expansion ensues when derivatives 5b,d are subjected to the cyclisation conditions, resulting in the formation of the new oxacino[2,3-*c*]pyrrole system, the structure of which is confirmed by X-ray crystallography.

The pyrrole unit[1] occurs in a diversity of natural products, pharmaceutical agents and polymers.[2] The synthesis of this ring system has been the subject of intense activity and has featured in a number of review articles.[3,4] Despite such activity, routes to 2,5-unsubstituted pyrroles and routes which involve the formation of the C-2–C-3 bond are particularly rare.[4] There are several routes to pyrroles that utilise 1,3-dicarbonyl compounds and α-amino acids as the starting components, but in all of these examples the resulting pyrrole retains a carboxylate function at C-2.[5] In 1973, Zav'yalov reported an efficient route to the pyrrole system (Scheme 1),[6] which has been scarcely utilised in the last 25 years.[7] We now report the application of this methodology to the synthesis of some novel substituted pyrroles and fused analogues and describe a unique ring expansion reaction to afford the new oxacino[2,3-*c*]pyrrole system.

Dimethylaminomethylene ketones **1** and **4** were obtained by standard protocols.[8] Their addition–elimination reaction with a range of α-amino acids in aq. EtOH containing NaOAc gave the crystalline enamino acids **2** and **5** in high yields (Scheme 2).†

Heating a solution of enamino acids **2a**,**b** and **5a**,**c** in Ac_2O containing Et_3N proceeded with the instantaneous formation of a deep red colour which was accompanied by the vigorous evolution of CO_2 (lime water bubbler) as the internal reaction temperature reached reflux. In the case of **5b**,**d**, however, evolution of CO_2 was only slight. After *ca*. 30 min the reaction mixture was allowed to cool and was subjected to an aqueous work-up. TLC examination of the crude reaction mixtures typically revealed the presence of a fast running major component contaminated with dark base line material rendering initial purification by flash chromatography easy.

The cyclisation of enamino acid **2a** proceeded with the expected regioselectivity of cyclisation on to the more electrophilic ketonic carbonyl group rather than the ester function to afford a single pyrrole, **3a**, confirmed by the presence of signals in its ^{1}H NMR spectrum associated with the ethyl ester moiety. Of particular note is the efficient preparation of **3b**. Existing routes to compounds of this type are often laborious and low yielding.[3c,f,h,4] Formation of the pyrroles **3** and isoindoles **6** and **9** is chemoselective, and in no instances did we observe the presence of any α-amino ketones resulting from a Dakin–West reaction.[9]

The ^{13}C NMR spectra of **7** (from **5b**) and **8** (from **5d**) contained an additional low field signal at δ 168.9 (OAc) and 192.8 (C=O), respectively, when compared to the isoindoles **6a** and **b**. Elemental analysis and HRMS for **7** and **8** confirmed that both contained an additional CO_2 unit. The structure of **8**‡ was established as the oxacino[2,3-*c*]pyrrole by X-ray crystallography (Fig. 1). The ^{1}H NMR spectrum of **8**§ displayed marked broadening of the signals associated with the aliphatic functions indicating that the molecule is undergoing conformational interconversion. The resolution of the spectrum was improved when it was recorded at low temperature (253 K).

It is evident from the ^{1}H NMR data that the eight-membered ring of **8** is in equilibrium between a number of conformers.[10] However, **7** does not display this behaviour, probably as a

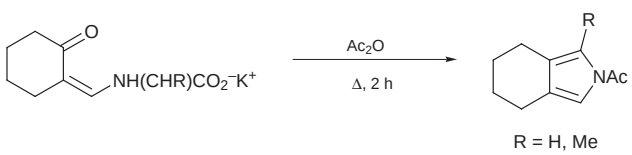

Scheme 1

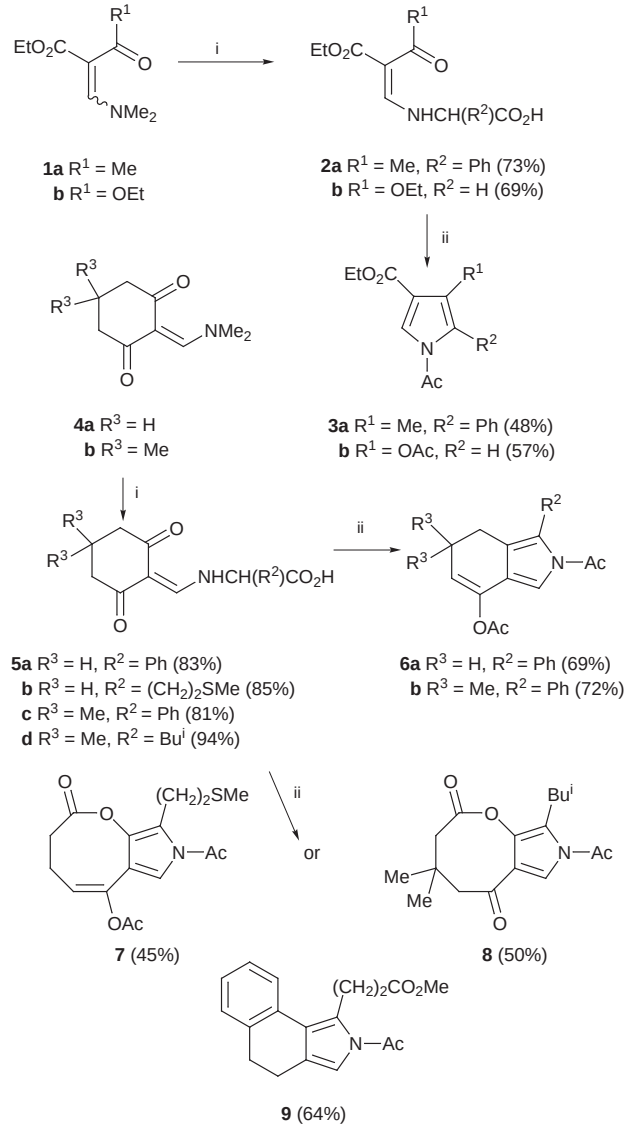

Scheme 2 *Reagents and conditions*: i, α-amino acid (1.05 equiv.) NaOAc.3H_2O (1.05 equiv.) eq. EtOH, Δ; ii, Ac_2O, Et_3N (1.1 equiv.), Δ.

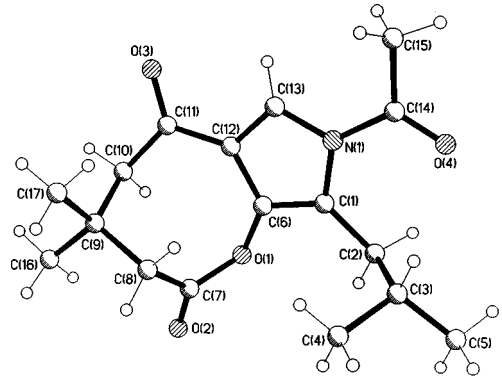

Fig. 1 X-Ray crystallographic structure of the oxacino[2,3-*c*]pyrrole **8**.

consequence of the rigidity imparted to the ring by the enol acetate function.

Scheme 3 depicts a possible mechanism for the formation of the isoindoles **6** and oxacinopyrrole **8**. It is well established that the acylation of *N*-substituted amino acids proceeds with the formation of mesoionic 1,3-oxazolium-5-olates (munchnones) and evidence has accrued that these are tautomeric with *N*-acyl ketenes.[11] The mesoionic heterocycle **10** may react by two distinct pathways. We propose that, when R = phenyl, the extended conjugation imparts stability to the munchnone tautomer which then attacks the proximal C=O group. The alkoxide species thus generated forms the lactone **11** with concomitant oxazole ring cleavage. Cycloreversion of CO_2 and subsequent *O*-acylation completes the route to the dihydroisoindoles **6a**,**b**. Conversely, **10** is destabilised when R = alkyl and the munchnone undergoes ring–chain tautomerism to the *N*-acyl ketene **12**. Intramolecular acylation of the enamine function affords the spirocycle **13**. Oxetane ring formation and subsequent ring cleavage of **14** effects the ring expansion to the oxacinopyrrole system. It is noteworthy that the formation of the oxacinopyrroles only occurs with the combination of an α-alkyl amino acid and a cyclohexane-1,3-dione; replacement of either one of these components results in the formation of the pyrrole or isoindole as, for example, **9** which is derived from 2-hydroxymethylene-1-tetralone and glutamic acid 5-methyl ester.

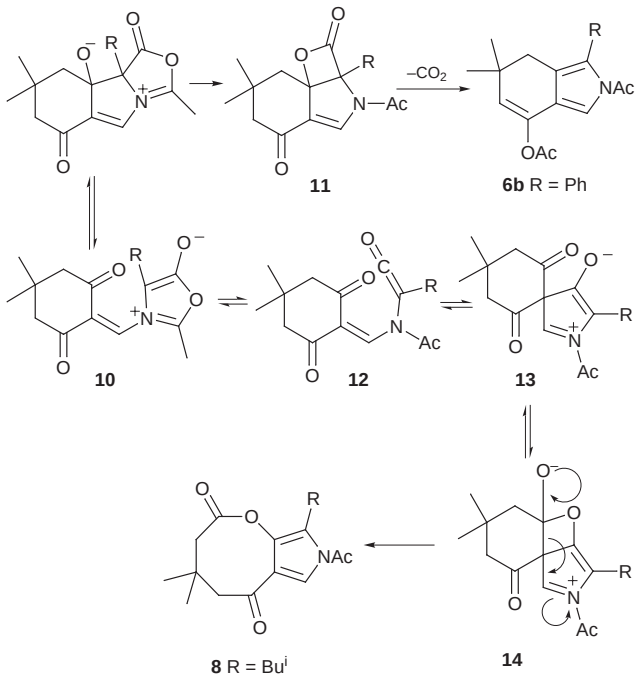

Scheme 3

In conclusion, this pyrrole synthesis is highly versatile and permits access to 2,5-unsubstituted pyrroles, 3-hydroxypyrrole derivatives, isoindoles and the novel oxacino[2,3-*c*]pyrroles.

We thank the EPSRC for the provision of a mass spectrometry service at the University of Wales, Swansea.

Notes and references

† All new compounds were fully characterised by ^{1}H and ^{13}C NMR, HRMS and elemental analyses.

‡ *Crystal data* for **8**: $C_{17}H_{23}NO_4$, M = 305.36, triclinic, space group $P\bar{1}$, a = 7.7540(11), b = 8.8328(12), c = 12.476(2) Å, α = 78.530(14), β = 89.250(12), γ = 81.025(9)°, U = 827.0(2) Å^3, D_c = 1.226 g cm^{-3}, Z = 2, Cu-Kα radiation (λ = 1.54184 Å), μ = 0.71 mm^{-1}, T = 160 K, $R1$ = 0.0471 ($F^2 > 2\sigma$), $wR2$ = 0.1095 (all data) for 2778 unique data and 205 parameters. CCDC 182/1130. Crystallographic data is available in CIF format from the RSC web site, see: http://www.rsc.org/suppdata/cc/1999/289/

§ *Selected data* for **8**: from **5d** (49.5%) after elution from silica with 40% EtOAc in hexane, as colourless cubes from EtOAc–hexane, mp = 152.5–153.5 °C, ν_{max}(KBr)/cm^{-1} 2962, 1766, 1742, 1670, 1594, 1524, 1274, 1189 cm^{-1}; δ_H($CDCl_3$, 253 K) 0.82 (3H, d, J 6.6, CHCH_3), 0.94 (3H, d, J 6.6, CHCH_3), 1.07 (3H, s, 7-CH_3), 1.27 (3H, s, 7-CH_3), 1.87 [1H, m, J 6.6, CH(CH_3)$_2$], 2.25 (1H, d, J 12.3, CH_2), 2.37 (1H, d, J 12.3, CH_2), 2.64–2.70 [1H, m, CH_2CH(CH_3)$_2$], 2.65 (3H, s, NAc), 2.79–2.83 [1H, m, CH_2CH(CH_3)$_2$], 2.92 (1H, d, J 12.3, CH_2), 2.99 (1H, d, J 12.3, CH_2), 7.70 (1H, s, 1-H); δ_C($CDCl_3$, 299 K) 22.1, 23.5, 28.2, 29.4, 33.2, 34.6, 42.5, 53.4, 120.0, 122.3, 126.5, 137.4, 169.0, 169.4, 192.8. Found C, 66.85; H, 7.60; N, 4.55; M$^+$ 305.1627. $C_{17}H_{23}NO_4$ requires C, 66.85; H, 7.60; N, 4.60%; M$^+$ 305.1627.

1 G. B. Jones and B. J. Chapman, in *Comprehensive Heterocyclic Chemistry II*, ed. A. R. Katritzky, C. W. Rees and E. F. V. Scriven, Pergamon, Oxford, 1996, vol. 2, p. 1.

2 G. W. Gribble, in *Comprehensive Heterocyclic Chemistry II*, ed. A. R. Katritzky, C. W. Rees and E. F. V. Scriven, Pergamon, Oxford, 1996, vol. 2, p. 207.

3 (*a*) J. M. Patterson, *Synthesis*, 1976, 281; (*b*) R. Bonnett and S. A. North, *Adv. Heterocycl. Chem.*, 1981, **29**, 341; (*c*) R. J. Sundberg, in *Comprehensive Heterocyclic Chemistry*, ed. A. R. Katritzky and C. W. Rees, Pergamon, Oxford, 1984, vol. 3, p. 313; (*d*) L. N. Sobenina, A. I. Mikhaleva and B. A. Trofimov, *Russ. Chem. Rev.*, 1989, **58**, 163; (*e*) R. A. Jones (ed.) *Chem. Heterocycl. Compds.*, 1990, **48-1**, 1; (*f*) H. McNab and L. C. Monahan in, R. A. Jones (ed.) *Chem. Heterocycl. Compds.*, 1992, **48-2**, 525; (*g*) P. Lue and J. V. Greenhill, *Adv. Heterocycl. Chem.*, 1996, **67**, 207; (*h*) R. A. Mattocks, *J. Chem. Soc., Perkin Trans. 1*, 1978, 896.

4 R. J. Sundberg, in *Comprehensive Heterocyclic Chemistry II*, ed. A. R. Katritzky, C. W. Rees and E. F. V. Scriven, Pergamon, Oxford, 1996, vol.2, p. 119.

5 H. Pleninger and H. Husseine, *Synthesis*, 1970, 587; E. Campaigne, G. M. Shutske and J. C. Payne, *J. Heterocycl. Chem.*, 1977, **14**, 329; S. Mataka, K. Takahashi, Y. Tsuda and M. Tashiro, *Synthesis*, 1982, 157; G. H. Walizei and E. Breitmaier, *Synthesis*, 1989, 337; J. B. Paine III, J. R. Brough, K. R. Buller and E. E. Erikson, *J. Org. Chem.*, 1987, **52**, 3986; A. Alberola, J. M. Andrés, A. González, R. Pedrosa and M. Vicente, *J. Chem. Soc., Perkin Trans. 1*, 1990, 2681; H. K. Hombrecher and G. Horter, *Synthesis*, 1990, 389.

6 S. I. Zav'yalov, I. F. Mustafaeva, N. I. Aronova and N. N. Makhova, *Izv. Akad. Nauk SSSR, Ser. Khim. (Engl. Transl.)*, 1973, 2505.

7 N. J. Bach, E. C. Kornfeld, N. D. Jones, M. O. Chaney, D. E. Dorman, J. W. Paschal, J. A. Clemens and E. B. Smalstig, *J. Med. Chem.*, 1980, **23**, 481; D. Berney, *Helv. Chim. Acta*, 1982, **65**, 1694; V. Cecchetti, A. Fravolini and F. Schiaffella, *J. Heterocycl. Chem.*, 1982, **19**, 1045; M. A. Ansari and J. C. Craig, *Synth. Commun.*, 1991, **21**, 1971.

8 C. D. Gabbutt, J. D. Hepworth and B. M. Heron, *J. Chem. Soc., Perkin Trans. 1*, 1992, 2603.

9 N. L. Allinger, G. L. Wang and B. B. Dewhurst, *J. Org. Chem.*, 1974, **39**, 1730; G. L. Buchanan, *Chem. Soc. Rev.*, 1988, **17**, 91.

10 T. P. Smith, in *Comprehensive Heterocyclic Chemistry II*, ed. A. R. Katritzky, C. W. Rees and E. F. V. Scriven, Pergamon, Oxford, 1996, vol. 9, p. 429.

11 R. Knorr and R. Huisgen, *Chem. Ber.*, 1970, **103**, 2598.

Communication 8/09033E

Scandium triflate catalyzed *in situ* Prins-type cyclization: formations of 4-tetrahydropyranols and ethers

Wen-Chun Zhang, Ganapathy S. Viswanathan and Chao-Jun Li*

Department of Chemistry, Tulane University, New Orleans, Louisiana 70118, USA.
E-mail: cjli@mailhost.tcs.tulane.edu

Received (in Corvallis, OR, USA) 11th November, 1998, Accepted 16th December 1998

The reaction of aldehydes with homoallyl alcohols catalyzed by scandium triflate generates tetrahydropyran-4-ol and ethers in good yields.

The acid-catalyzed olefin–aldehyde condensation, known as the Prins reaction, is one of the fundamental reactions for carbon–carbon bond formation.[1] However, the synthetic application of this important reaction has been under-explored due to the classical conditions of strong acids (*e.g.* sulfuric acid) and high reaction temperatures, which often generate a mixture of a range of products. The importance of the tetrahydropyran ring is exemplified by the ring's function as the backbone of various carbohydrates and natural products.[2] Its importance calls for the continuing search for methods of synthesizing tetrahydropyran derivatives.[3] Recently, during our investigation of indium-mediated reactions under solventless conditions,[4] we observed the formation of tetrahydropyran-4-ols and 4-bromotetrahydropyran derivatives. In order to explain the formation of the tetrahydropyran derivatives, we postulated that the product was generated through a tandem carbonyl allylation–hemiacetal formation–Prins reaction. We speculated that the reaction of a homoallyl alcohol with an aldehyde should generate the

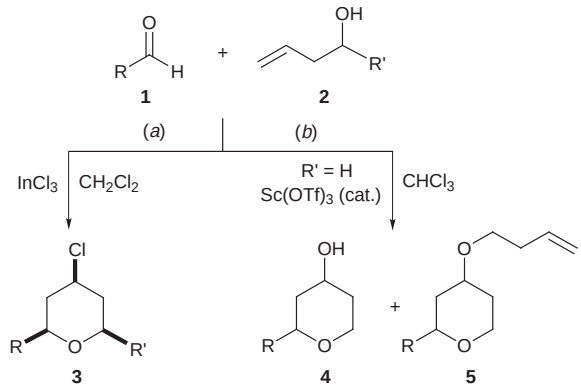

Scheme 1

Table 1 Tetrahydropyran derivatives *via* $Sc(OTf)_3$ catalyzed Prins-type cyclization

Entry	RCHO	Product (% yield) 4	Product (% yield) 5	Overall yield (%)
1	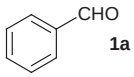 **1a**	**4a** (14)	**5a** (63)	77
2	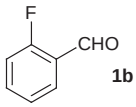 **1b**	**4b** (19)	**5b** (50)	69
3	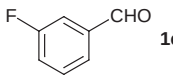 **1c**	**4c** (12)	**5c** (57)	69
4	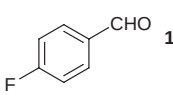 **1d**	**4d** (16)	**5d** (69)	85
5	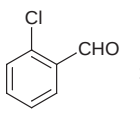 **1e**	**4e** (13)	**5e** (71)	84
6	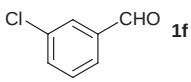 **1f**	**4f** (11)	**5f** (65)	76
7	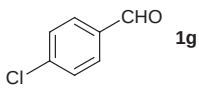 **1g**	**4g** (15)	**5g** (68)	83
8	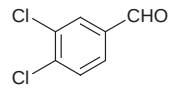 **1h**	**4h** (17)	**5h** (49)	66
9	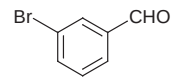 **1i**	**4i** (14)	**5i** (72)	86
10	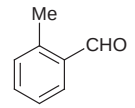 **1j**	**4j** (20)	**5j** (58)	78
11	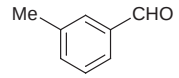 **1k**	**4k** (13)	**5k** (62)	75
12	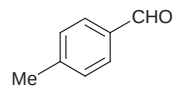 **1l**	**4l** (18)	**5l** (64)	82
13	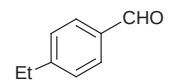 **1m**	**4m** (10)	**5m** (56)	66
14	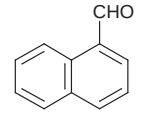 **1n**	**4n** (9)	**5n** (70)	79

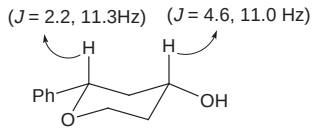

Fig. 1 Coupling constants in **4a**.

corresponding tetrahydropyran derivatives. Subsequently, by controlling the reaction conditions, we have developed an efficient synthesis of 4-chlorotetrahydropyrans **3** mediated by indium trichloride [Scheme 1, route (*a*)].[5] We also conceived that if we replaced the chloride ion with a non-nucleophilic anion, then the tetrahydropyranol **4** or its ether **5** would become the major products [route (*b*)]. However, to do so we would need a Lewis acid to facilitate the Prins reaction. It appears that the scandium triflate chemistry developed by Kobayashi and others would be the best choice for this reaction.[6] Here, we report that the reaction of aldehydes with homoallyl alcohols catalyzed by scandium triflate generates the corresponding desired products readily (Scheme 1).[7]

When a mixture of benzaldehyde and but-3-en-1-ol was stirred with $Sc(OTf)_3$ in $CHCl_3$ under a refluxing temperature overnight, 63% of a tetrahydropyran ether **5a** was isolated together with 14% of the corresponding tetrahydropyranol **4a**.† Measurement of the coupling constants of the benzylic hydrogen (J = 2.2 and 11.3 Hz) as well as the hydrogen on the carbon bearing the hydroxy group (J = 4.6 and 11.0 Hz) of the tetrahydropyranol **4a** indicated a structure where the hydroxy and the phenyl groups are in a *cis* relationship and are equatorial (Fig. 1). The formation of other stereoisomers is negligible as shown by the ^{1}H NMR measurement of the crude reaction mixture. A variety of other aromatic aldehydes reacted similarly generating the corresponding products (Table 1) in good isolated (overall) yields. Aliphatic aldehydes were less effective for the reactions. Other solvents that we have tested (such as CH_2Cl_2, hexane, toluene,THF and Et_2O) were not as effective as $CHCl_3$ for the reaction. The catalytic cycle of this Prins-type reaction is postulated in Scheme 2. A similar mechanism has been used to explain a cross-allylation of aldehydes by Nokami and co-workers very recently.[8] In conclusion, we have developed an effective $Sc(OTf)_3$-catalyzed Prins-type reaction to form tetrahydropyranols and related ether derivatives. The conditions for the catalyzed reaction are much milder than the classical Prins reaction using strong acids. Presently, we are evaluating a range of synthetic potentials of this catalyzed reaction.

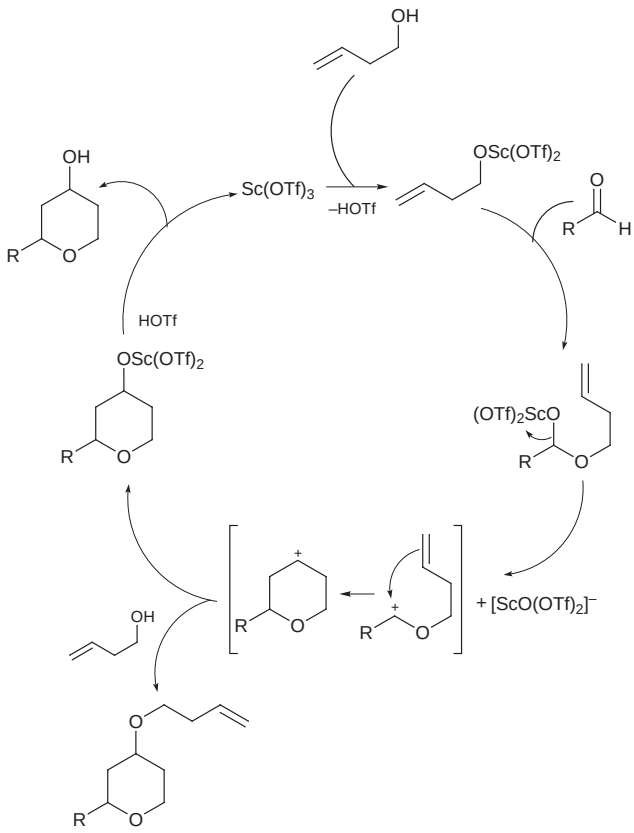

Scheme 2 Proposed mechanism for the $Sc(OTf)_3$ catalyzed tetrahydropyran formations.

We are grateful to US NSF-EPA, LEQSF and the NSF Early CAREER Award program for partial support of this research.

Notes and references

† Typical experimental procedure: A mixture of **1** (2 mmol), but-3-en-1-ol **2** (4 mmol) and scandium triflate (5 mol%) was mixed in $CHCl_3$ (5 ml). The reaction mixture was refluxed under nitrogen overnight. After concentrated *in vacuo*, the crude reaction mixture was subjected to column chromatography on silica gel eluting with hexane–EtOAc (gradient eluent: 27 : 1 to 3 : 1) to yield products **4** and **5**.

1 For reviews, see: E. Arundale and L. A. Mikeska, *Chem. Rev.*, 1952, **51**, 505; D. R. Adams and S. P. Bhatnagar, *Synthesis*, 1977, 661.
2 K. C. Nicolaou and E. J. Sorensen, *Classics in Total Synthesis*, VCH, Weinheim, 1996.
3 The best known method in this regard is probably the hetero-Diels–Alder reaction with Danishefsky's diene; for examples, see: S. J. Danishefsky, W. H. Pearson and D. F. Harvey, *J. Am. Chem. Soc.*, 1984, **106**, 2456; S. J. Danishefsky and C. J. Maring, *J. Am. Chem. Soc.*, 1989, **111**, 2193.
4 X. H. Yi, J. X. Haberman and C. J. Li, *Synth. Commun.*, 1998, **28**, 2999.
5 J.Yang, G. S. Viswanathan and C. J. Li, *Tetrahedron Lett.*, in the press. Such compounds were also accessible through $TiCl_4$ and $AlCl_3$ catalyzed allylsilane reactions of aldehydes and cross−coupling between homoallyl alcohols and aldehydes, however, when both substituents are aromatic, the reaction provided no or a low yield of the product, see: Z. Y. Wei, J. S. Li, D.Wang and T. H. Chan, *Tetrahedron Lett.*, 1987, **28**, 3441; F. Perron and K. F. Albizati, *J. Org. Chem.*, 1987, **52**, 4130; Z. Y. Wei, D. Wang, J. S. Li and T. H. Chan, *J. Org. Chem.*, 1989, **54**, 5768; L. Coppi, A. Ricci and M. Taddei, *J. Org. Chem.*, 1988, **53**, 913. Very recently, Rychnovsky and co-workers reported an interesting $SnBr_4$-mediated segment-coupling Prins cyclization, see: S. D. Rychnovsky, Y. Hu and B. Ellsworth, *Tetrahedron Lett.*, 1998, **39**, 7271.
6 For a leading reference, see: S. Kobayashi and I. Hachiya, *J. Org. Chem.*, 1994, **59**, 3590; For a related review, see: S. Kobayashi, *Synlett*, 1994, 689.
7 All products have been fully characterized and produced satisfactory ^{1}H and ^{13}C NMR, IR and elemental analysis results. For a $Yb(OTf)_3$ catalyzed allylation of aldehydes with allylsilane to generate homoallyl alcohols, see: Y. Yang, M. Wang and D. Wang, *Chem. Commun.*, 1997, 1651.
8 J. Nokami, K. Yoshizane, H. Matsuura and S. Sumida, *J. Am. Chem. Soc.*, 1998, **120**, 6609.

Communication 8/08960D

ChemComm

A robust structural motif in inclusion crystals of norbile acids

Michihiro Sugahara, Kazuki Sada and Mikiji Miyata*

Material and Life Science, Graduate School of Engineering, Osaka University, 2-1 Yamadaoka, Suita, Osaka 565-0871, Japan. E-mail: miyata@ap.chem.eng.osaka-u.ac.jp

Received (in Cambridge, UK) 16th November 1998, Accepted 8th January 1999

Four norbile acids (norcholic, nordeoxycholic, norchenodeoxycholic and norlithocholic acids) include various organic compounds and have a common robust motif in their crystal structures based on a cyclic hydrogen bond network and steric complementarity in the lipophilic parts.

The development of robust structural motifs in the crystalline state has attracted much attention as 'supramolecular synthons'[1] for the design of molecular cavities in nanoporous organic materials. However, most focus on directional strong intermolecular interactions such as multiple hydrogen bonding groups.[2] The design of robust motifs using steric complementarity or other weak interactions is still in its infancy: layer structures of long alkyl compounds,[3] herring-bone motifs or π–π stacking of polyaromatic compounds[4] or tetraarylporphyrins[5] are known. We describe here a novel robust motif based on the steric complementarity of the liophilic parts in inclusion crystals of norbile acids.

Norbile acids (**1a**–**4a)** were prepared from commercially available bile acids (**1b**–**4b**) by degradation of the side chain.[6]

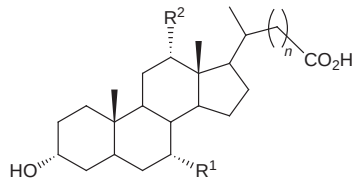

n = 1	**1a** R^1 = OH, R^2 = OH	**2a** R^1 = H, R^2 = OH
	3a R^1 = OH, R^2 = H	**4a** R^1 = H, R^2 = H
n = 2	**1b** R^1 = OH, R^2 = OH	**2b** R^1 = H, R^2 = OH
	3b R^1 = OH, R^2 = H	**4b** R^1 = H, R^2 = H

Trace formation of inclusion crystals was investigated by recrystallization from more than eighty organic compounds. The guest incorporation and stoichiometries were determined by thermogravimetric analysis, IR spectroscopy and using a Karl Fischer moisture content meter. Table 1 shows the guest compounds, the host–guest ratios and the structural type of the host assemblies. Inclusion compounds of **2a** have already been reported by us,[7] and the other three norbile acids also form inclusion crystals with many organic compounds as **2a** does. In some cases, **1a** includes guest compounds as well as one molecule of water. Compared to the lack of inclusion ability of **4b**,[8] various organic compounds are included in **4a**.

The X-ray diffraction patterns of the inclusion crystals indicate that they exhibit several types of host framework, depending on the guest molecules. It is noteworthy that the B type structure in Table 1 is observed in the crystal structures of all four norbile acids. The crystal structures of the inclusion crystals of acetone were further characterized by X-ray crystallography (Fig. 1).† They are all isostructural, despite the different number and locations of the hydroxy groups in the steroidal skeleton. This remarkable structural feature is a bilayer structure that is formed by hydrogen bonding between the hydrophilic faces (α-faces) of the steroidal plane and van der Waals association between the lipophilic faces (β-faces). In the hydrophilic layer, a cyclic hydrogen-bond network involves two hydroxy groups in the 3-positions and two carboxylic acids in the side chains from four different host molecules (Fig. 2). This cyclic hydrogen bond network forms a wavy sheet structure, which stacks in an antiparallel manner without any void space in the liopophilic layers. A caged inclusion cavity forms between the side chains due to the unbalanced molecular structure with the wide steroidal plane and the rod-like side chain. The guest compounds are included in 2:1 host–guest stoichiometry in the cavity.

In contrast, bile acids have diverse crystal structures. That is, **1b** and **2b** form bilayer structures,[9] while **3b** and **4b** form helical[10] and non-layer[8] structures, respectively. In these cases all hydrogen bond groups contribute to the formation of such

Table 1 Guest molecules of **1a**, **2a**, **3a** and **4a**, and their host–guest ratios and molecular assembly modes[a]

	1a		**2a**		**3a**		**4a**	
Guest (G1)	H : G1 : G2	Mode	H : G1 : G2	Mode	H : G1 : G2	Mode	H : G1 : G2	Mode
MeOH	1 : 1	A	1 : 0 : 1		1 : 1	B	1 : 1	A
EtOH	1 : 1	A	1 : 1	C	1 : 1	A	1 : 1	A
PrOH	2 : 1	B	1 : 1	C	1 : 1	A	2 : 1	B
Pr^{i}OH	2 : 1 : 1	B	1 : 1	C	2 : 1	B	2 : 1	B
BuOH	2 : 1	B	2 : 1 : 1	B	2 : 1	B	1 : 0 : 1	
Bu^{s}OH	nc		1 : 1	C	2 : 1	B	2 : 1	B
Ethylene glycol	1 : 1	A	1 : 0 : 1		1 : 1	A	2 : 1	B
Acetone	2 : 1 : 1	B	2 : 1	B	2 : 1	B	2 : 1	B
MeCOEt	2 : 1 : 1	B	2 : 1	B	2 : 1	B	2 : 1	B
MeCOPr	2 : 1	B	2 : 1	B	2 : 1	B	2 : 1	B
Pentane-2,4-dione	2 : 1	B	2 : 1	B	2 : 1	B	2 : 1	B
γ-Valerolactone	2 : 1 : 1	B	2 : 1	B	2 : 1 : 1	B	2 : 1	B
MeCN	2 : 1 : 1	B	1 : 1	B	1 : 1	B	1 : 1	B
EtCN	2 : 1 : 2	B	2 : 1	B	2 : 1	B	2 : 1	B
Acrylonitrile	2 : 1	B	2 : 1	B	2 : 1	B	2 : 1	B

[a] G2 = water; mode A = bilayered cage (I); mode B = bilayered cage (II); mode C = monolayered; H : G = host–guest molar ratio; nc = not crystalized; GF = homocrystals of host without incorporation of the guest.

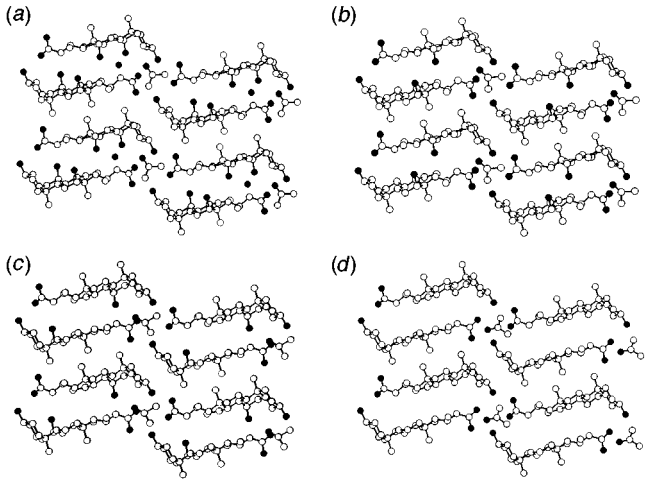

Fig. 1 Crystal structures of (a) **1a**·with acetone·water (2:1:1), (*b*) **2a**·acetone (2:1), (*c*) **3a**·acetone (2:1) and (*d*) **4a**·acetone (2:1), respectively. Hydrogen atoms are omitted for clarity and the empty and closed cycles represent carbon and oxygen atoms, respectively.

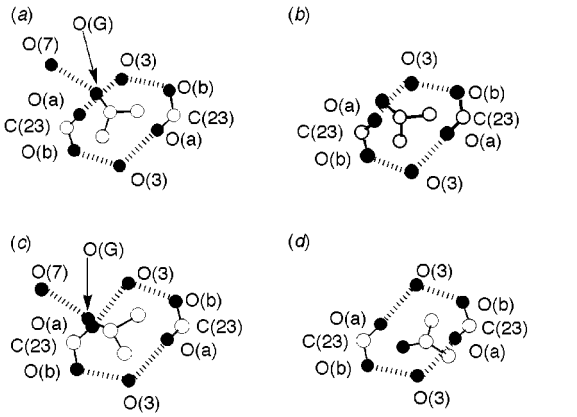

Fig. 2 Hydrogen bond networks of (*a*) **1a**, (*b*) **2a**, (*c*) **3a** and (*d*) **4a** with acetone, respectively. The empty and closed cycles represent carbon and oxygen atoms, respectively. The distances of the cyclic host–host hydrogen bond sequence, O(3)H•••O(23a)=C–O(23b)H•••O(3)•••O(23a)=C–O(23b)H•••O(3) are 2.63, 2.73, 2.61 and 2.79 Å for **1a**, 2.64, 2.75, 2.61 and 2.79 Å for **2a**, 2.71, 2.64, 2.76 and 2.65 Å for **3a**, 2.72, 2.60, 2.79 and 2.62 Å for **4a**.

host-inherent assemblies involving different hydrogen bond networks. In the case of norbile acids, however, the groups at the 7 and 12 positions do not join the networks, yielding the common assembly mentioned above. This is attributed to the side chains being shortened by one methylene group. The restrained chains have carboxy groups orientated in different directions, explaining the different hydrogen bond networks. Moreover, the wavy structure of the host molecules causes steric complementarity of the lipophilic β-faces. Accordingly, the molecules form the wavy layers which stack with good complementarity, leading to the robust structural motif.

This paper describes the new robust motif in the crystal structures of the norbile acids. The robustness is mainly caused by steric complementarity between the lipophilic layers. Molecular recognition and guest-dependent polymorphism of the host assemblies is currently under investigation.

Footnotes and references

† *Crystal data* for (*a*) **1a**·acetone·water (2:1:1), (*b*) **2a**·acetone (2:1), (*c*) **3a**·acetone (2:1) and (*d*) **4a**·acetone (2:1): (a) $C_{46}H_{76}O_{10}$•C_3H_6O•H_2O (−63.9 °C), M = 865.20, triclinic, space group $P1$, a = 10.657(1), b = 15.309(6), c = 7.556(2) Å, α = 93.75(1), β = 106.19(2), γ = 79.15(2)°, V = 1162.6(5) Å^3, Z = 1, D_c = 1.236 g cm^{-3}; (b) $C_{46}H_{76}O_8$•C_3H_6O (-63.8 °C), M = 815.18, triclinic, space group $P1$, a = 10.5710(9), b = 15.269(2), c = 7.583(3) Å, α = 92.47(2), β = 104.61(2), γ = 80.221(9)°, V = 1167.1(4) Å^3, Z = 1, D_c = 1.160 g cm^{-3}; (c) $C_{46}H_{76}O_8$•C_3H_6O (-62.8 °C), M = 815.18, triclinic, space group $P1$, a = 10.490(1), b = 15.257(1), c = 7.567(3) Å, α = 92.758(3), β = 104.24(2), γ = 79.999(8)°, V = 1155.9(4) Å^3, Z = 1, D_c = 1.171 g cm^{-3}; (d) $C_{46}H_{76}O_6$•C_3H_6O (−63 °C), M = 783.18, triclinic, space group $P1$, a = 10.466(4), b = 15.243(2), c = 7.555(3) Å, α = 92.36(2), β = 103.08(3), γ = 80.78(2)°, V = 1158.8(6) Å^3, Z = 1, D_c = 1.122 g cm^{-3}. (a) 3609, (b) 3696, (c) 3603 and (d) 3462 reflections were unique, and (a) 3534, (b) 3619, (c) 3531 and (d) 3351 observed reflections with $I > 1.5\sigma(I)$ were used for further calculations after Lorentz and polarization corrections. In the case of **4d**, the guest molecule is disordered so that the position and thermal parameters of the guest molecule were refined isotropically as a ridged model. A total of (a) 550, (b) 523, (c) 523 and (d) 476 parameters were refined to final residuals (a) R = 0.152 and R_w = 0.256, (b) R = 0.134 and R_w = 0.220, (c) R = 0.130 and R_w = 0.221 and (d) R = 0.149 and R_w = 0.267 (refinement on F^2). CCDC 182/1137. Crystal data are available in CIF format from the RSC web site, see: http://www.rsc.org/suppdata/cc/1999/293.

1 G. R. Desiraju, *Crystal Engineering: The Design of Organic Solids*, Elsevier, New York, 1989; G. R. Desiraju, *Angew. Chem., Int. Ed. Engl*., 1995, **34**, 2311; J. L. Atwood, J. E. D. Davies, D. D. MacNicol and F. Vogtle, *Comprehensive Supramolecular Chemistry*, Pergamon, New York, 1996, vol. 6; M. C. T. Fyfe and J. F. Stoddart, *Acc. Chem. Res*., 1997, **30**, 393 .

2 V. Ramamurthy and D. F. Eaton, *Chem. Mater.*, 1994, **6**, 1128; J. Wang, M. Simard and J. D. Wuest, *J. Am. Chem. Soc*., 1994, **116**, 12 119; V. A. Russell, C. C. Evans, W. Li and M. D. Ward, *Science*, 1997, **276,** 575.

3 J. H. Fendlar, *Membrane Mimetic Chemistry*, Wiley, New York, 1982; T. Kunitake, in *Comprehensive Supramolecular Chemistry*, ed. J. L. Atwood, J. E. D. Davies, D. D. MacNicol and F. Vogtle, Pergmon, New York, 1996, vol. 9, p. 351.

4 A. Gavezzotti, *J. Am. Chem. Soc.*, 1989, **111**, 1835; G. R. Desiraju and A. Gavezzotti, *J. Chem. Soc., Chem. Commun*., 1989, 621.

5 M. P. Byrn., C. J. Curtis, I. Goldberg, Y. Hsiou, S. I. Khan, P. A. Sawin, S. K. Tendick and C. E. Strouse, *J. Am. Chem. Soc*., 1991, **113**, 6549; M. P. Byrn, C. J. Curtice, Y. Hsiou, S. I. Khan, P. A. Sawin, S. K. Tendick, A. Terzis and C. E. Strouse, *J. Am. Chem. Soc*., 1993, **115**, 9480; I. Goldberg, H. Kruptishky, Z. Stein, Y. Hsiou and C. E. Strouse, *Supramol. Chem.*, 1995, **4**, 203; I. Goldberg, H. Krupitsky, Z. Stein, and C. E. Strouse, *J. Inclusion Phenom.*, 1994, **18**, 177.

6 C. D. Schteingart and A. F. Hofman, *J. Lipid Res*., 1988, **29**, 1387.

7 K. Sada, M. Sugahara, Y. Nakahata, Y. Yasuda, A. Nishio and M. Miyata, *Chem. Lett*., 1998, 31.

8 K. Arora, G. Germain and J. P. Declercq, *Acta Crystallogr., Sect. B*, 1976, **32**, 415.

9 M. Miyata and K. Sada, in *Comprehensive Supramolecular Chemistry*, ed. D. D. MacNicol, F. Toda and R. Bishop, Pergmon, New York, 1996, vol. 6, p. 147.

10 P. J. Rizkallah, M. M. Harding, P. F. Lindley, A. Aigner and A. Bauer, *Acta Crystallogr., Sect. B*, 1990, **46**, 262.

Communication 8/08900K

Hydrogen bonded driven anion binding by dicationic [1$_4$]imidazoliophanes

Ermitas Alcalde,*[a] Carmen Alvarez-Rúa,[b] Santiago García-Granda,[b] Esther García-Rodriguez,[b] Neus Mesquida[a] and Lluïsa Pérez-García[a]

[a] *Laboratori de Química Orgànica, Facultat de Farmàcia,Universitat de Barcelona, E-08028Barcelona, Spain. E-mail: betaines@farmacia.far.ub.es*

[b] *Departamento de Química Física y Analítica, Facultat de Química, Universidad de Oviedo,E-33006Oviedo, Spain*

Received (in Liverpool, UK) 2nd November 1998, Accepted 21st December 1998

Imidazolium units represent the main structural motifs for the formation of unconventional C–H···Cl$^-$ hydrogen bonds which become the noncovalent forces driving the anion interactions exibited by dicationic [1$_4$]imidazoliophanes in the solid state, while C–H···O hydrogen bonds with water play a crucial role in governing the conformation of the solid–state aggregates, as well as in solution, wherein NMR studies also reveal the importance of hydrogen bonds in controlling the tendency to anion binding.

The molecular diversity within molecular *hosts* permits the design of new architectures with capacity for specific biological or physical properties.[1] The increasing interest in anion recognition phenomena is mainly directed towards synthetic receptors based on positively charged moieties.[2] Consequently, the primary noncovalent driving forces are controlled by electrostatic interactions,[2] whereas hydrogen bonding forces[3] are known to play a significant role in a few host systems.[4] Developing the chemistry of heterocyclic betaines, we have reported the first examples of quadrupolar architectures within [1$_4$]heterophanes built up from imidazolium methylene triazo-

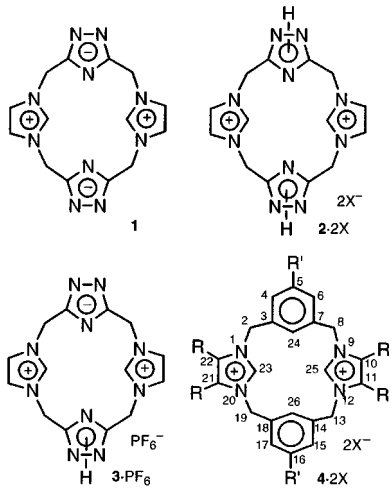

late subunits, *e.g.* the bis-betaine **1**, as well as its precursors the dicationic macrocycle **2** and betaine **3**.[5] We now report the synthesis and structural properties of simple dicationic [1$_4$]heterophanes **4·2X** containing two imidazolium nuclei in a 1,3-alternating manner as models for anion recognition.

The dicationic phanes **4·2X** were prepared following a '3+1' convergent approach (Scheme 1), efficiently applied for synthesizing the dicationic azolophane **2**. Thus, macrocyclization of the trinuclear compounds **5a**–**c**† with 1,3-bis(halomethyl)benzenes **6** or **7** produced the title phanes **4a**–**c·2X**.‡

The targeted macrocycles were characterized on the basis of their spectroscopic data.§ Furthermore, the structure of macrocycles **4a·2Cl·2H$_2$O** and **4b·2Cl·3.5H$_2$O** were confirmed by X-ray crystallography.¶‖

Concerning **4a·2Cl·2H$_2$O**, the dication **4a** adopts a chair-like conformation (Fig.1 and 2). Regarding hydrogen bonds,** in

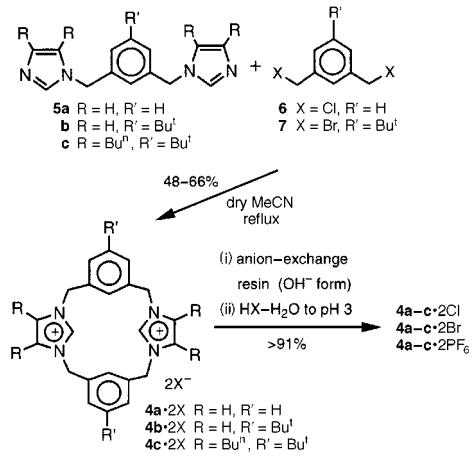

Scheme 1 '3+1' Convergent synthesis of dicationic imidazoliophanes **4·2X**.

the highly directional C–H···Cl$^-$ interactions (θ *ca.* 160°), each chlorine counterion is three-centered between a *m*-xylyl hydrogen atom, *e.g.* H6, and the acidic hydrogen atom on the imidazolium ring, *e.g.* H10, the latter being the shortest hydrogen bond interaction (2.54 Å, θ = 157°).†† Moreover, there are *weak* interactions with water.**

The molecular shape of dication **4b** assumes a cone-like conformation in contrast with the partial cone-like arrangement observed for **4a**. However, both dications **4a** and **4b** have similar molecular cavity dimensions: a square of 5 Å side.[5] The assemblages depicted in Fig. 3 show that the asymmetric unit of **4b·2Cl·3.5H$_2$O** contains two different dication—**A** and **B**. Dication **A** has the propensity to form hydrogen bonds with one of the chlorine counterions (Cl2), meanwhile dication **B** interacts with one water molecule (O7).‖**

For the title dications **4a–c·2X** (X = Cl$^-$, Br$^-$, PF_6^-) reported, the ^{1}H NMR spectra showed a sharp singlet for the methylene

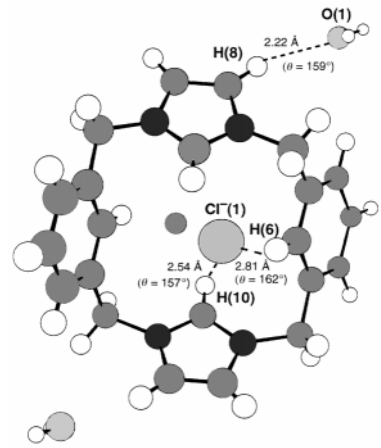

Fig. 1 Molecular structure of **4a·2Cl·2H$_2$O**, showing the non-covalent interactions.

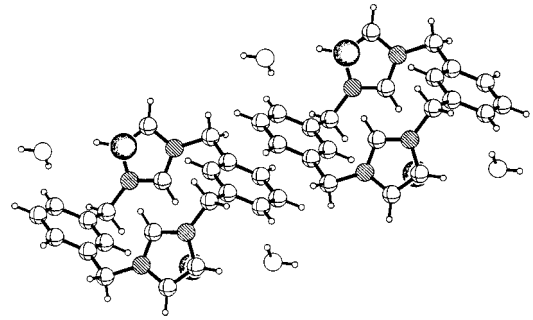

Fig. 2 Unit cell diagram for **4a·2Cl·2H$_2$O**.

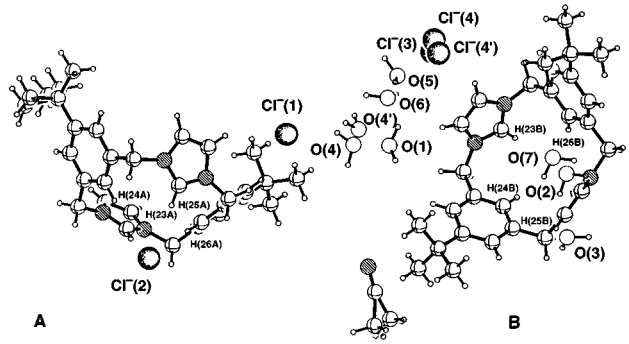

Fig. 3 Unit cell diagram for **4b·2Cl·3.5H$_2$O·0.5CH$_3$N**.

proton atoms, indicating the rapid interconversion of the different possible conformations, comparable to those of [1$_4$]azolophane **2·2X**.[5]‡‡ Moreover, the δ_H values of H-23 and H-25 (Im$^+$) together with H-24 and H-26 (aromatic fragments) are sensitive to the nature of the anion and to the solvent polarity, moving to lower fields.

As a consequence of the hydrogen bonding with the counteranion present in the macrocycle, the acidic H-23 and H-25 hydrogen atoms are shifted downfield in comparison with standard values for these protons within azolophanes (*e.g.* **2·2X**) and a variety of *N*-azolylimidazolium salts with different spacers.[5,8] Furthermore, significant changes in δ_H were induced by addition of various tetrabutylammonium salts [*ca*. 6 mM] to a DMSO-d_6 solution of the model dication **4c·2PF$_6$** [*ca*. 3 mM]. The major deshielding effect observed was up to 302 Hz for the imidazolium ring protons H-23 and H-25, and followed the order $H_2PO_4^- > F^- > CH_3CO_2^- > CN^- > Cl^-$.

In summary, a convergent '3 + 1' synthesis led to model dicationic heterophanes based on imidazolium units as molecular recognition motifs for anions. Structural studies both in solution and in the solid-state reveal that dications **4·2X** are unusual hydrogen bond donor-rich organic macrocycles, and their anion interactions are controlled by hydrogen bonding networks. These simple dicationic systems may be exploited for template phenomena and transport processes.

This work was supported by DGICYT (MEC, Spain) through grants PB95-0268, PB96-0556, and the Comissionat per a Universitats i Recerca de la Generalitat de Catalunya through grant 97SGR75. C. A.-R. thanks MEC for a F.P.I. fellowship. N. M. thanks the Universitat de Barcelona for a fellowship.

Notes and references

† Protophanes **5a–c** (ref. 6) were obtained by reaction of conveniently substituted imidazoles with a 1,3-bis(halomethyl)benzene **6** or **7** (ref. 7).

‡ Counterion exchange was performed by treatment of the [1$_4$]heterophanes **4a–c·2X** with a strongly basic anion exchange resin (ref. 8) followed by immediate collection of the eluates in acid solutions (either aq. HCl, aq. HBr or aq. HPF_6) to pH 3–4, following a standard protocol (ref. 5, 8).

§ As for ES mass spectra, the heterophanes **4a·2X** revealed characteristic peaks for the successive loss one and two counterions.

¶ *Crystal data* for **4a·2Cl·2H$_2$O:** $C_{22}H_{26}Cl_2N_4O_2$, M = 449.37, colorless crystal, 0.53 × 0.53 × 0.43 mm^3 size, monoclinic, a = 8.627(2), b = 15.788(1), c = 8.735(2) Å, β = 113.38(1)°, V = 1092.0(3) Å^3, space group $P2_{1/c}$, Z = 2, ρ = 367 g cm^{-3}, Mo-Kα radiation (graphite crystal monochromator, λ = 0.71073 Å), μ = 0.324 mm^{-1}, T = 200(2) K. Of 2828 reflections measured, 1910 were unique with R_{int} = 0.019, of which only 1674 reflections were observed with $I > 2\sigma(I)$, final GoF = 1.076, refined to R_1 = 0.027, wR_2 = 0.067. For **4b·2Cl·3.5H$_2$O·0.5CH$_3$CN**: $(C_{30}H_{38}N_4Cl_2)\cdot 3.5H_2O\cdot 0.5CH_3CN$, M = 609.13, colorless crystal, 0.26 × 0.23 × 0.26 mm^3 size, triclinic, a = 12.240(4), b = 12.837(5), c = 21.579(8) Å, α = 90.50(3), β = 96.55(4), γ = 98.03(3)°, V = 3334(2) Å^3, space group $P\bar{1}$, Z = 4, ρ = 1.213 g cm^{-3}, Mo-Kα radiation (graphite crystal monochromator, λ = 0.71073 Å), μ = 0.233 mm^{-1}, T = 200(2) K. Of 12321 reflections measured, 11718 were unique with R_{int} = 0.0509 and 5375 observed with $I > 2\sigma(I)$, final GoF = 1.029, refined to R_1 = 0.1032, wR_2 = 0.2512. Data collected on a Nonius CAD-4 single-crystal diffractometer, ω–2Θ scans. Lorent and polarization corrections were applied and the data were reduced to F_o^2 values. The structures were solved by direct methods using the program SHELXS (ref. 9), were further refined using SHELXL (ref. 10), and the major occupancy non-hydrogen atoms refined anisotropically. The hydrogen atoms, located by Fourier difference synthesis, were isotropically refined with a common thermal parameter. Crystals of compound **4b·2Cl** were very unstable, and were mounted on a X-TEMP2 device (ref. 11). CCDC 182/1132.

‖ The atom numbering system is not the same as that obtained from the X-ray analysis.

** For **4a·2Cl**, the most relevant geometrical data for hydrogen bonds, distances (Å) and angles (°) (with esds) are: C(10)–H(10), 0.976 (19), C(10)···Cl$^-$(1), 3.456 (2), H(10)···Cl$^-$(1), 2.538 (19), C(10)–H(10)···Cl$^-$(1),156.7 (1.5); C(6)–H(6), 1.005 (18), C(6)···Cl$^-$(1), 3.781 (2), H(6)···Cl$^-$(1), 2.811 (19), C(6)–H(6)···Cl$^-$(1), 162.3 (1.3). Concerning interactions with water, the C–H···O hydrogen bond connects the trifurcated acceptor (O1) with the cationic ring, *e.g*. H8, the *m*-xylene ring, *e.g*. H2, and the spacer, *e.g.* H27.

†† Steiner (ref. 12) pointed out that hydrogen bonds from C–H groups to halide ions are only rarely discussed in the literature, even though stronger C–H donors exhibit CH···Hal$^-$ distributions of similar shape as for O/N–H donors and can be analyzed in the same way. As for the (NN)C(sp^2)–H fragment, the mean C–H···Cl$^-$ distance of 2.54 Å was found (ref. 12). Within NH···Hal$^-$ bonds, we should mention the calix[4]pyrroles described by Sessler (ref. 13) as anion binding agents in CH_2Cl_2 solution and in the solid state. Both in the chloride and fluoride complexes, the anions occupy a perching position above the main plain of the nitrogen atoms.

‡‡ ^{1}H NMR spectra were recorded at room temperature (22 °C) on a Varian Gemini 300 spectrometer operating at 300 MHz, in polar aprotic solvents (DMSO-d_6, CD_3CN).

1 M. C. T. Fyfe and J. F. Stoddart, *Acc. Chem. Res*., 1997, **30**, 393.
2 *Supramolecular Chemistry of Anions*, ed. A. Bianchi, K. Bowman-James and E. García-España, Wiley-VCH, New York, 1997; F. P. Schmidtchen and M. Berger, *Chem. Rev*., 1997, **97**, 1609.
3 G. A. Jeffrey, *An Introduction to Hydrogen Bonding*, Oxford University Press, Oxford, 1997; *The Crystal as a Supramolecular Entity*, ed. G. R. Desiraju, Wiley, Chichester, 1996.
4 For some examples on C–H···anion hydrogen bonds, see: S. Shinoda, M. Tadokoro, H. Tsukube and R. Arakawa, *Chem. Commun*., 1998, 181; B. Koning, R. Hulst, A. Bouter, J. Buter, A. Meetsma and R. M. Kellogg, *Chem. Commun*., 1997, 1065; M. C. T. Fyfe, P. T. Glink, S. Menzer, J. F. Stoddart, A. J. P. White and D. J. Williams, *Angew. Chem., Int. Ed. Engl.*, 1997, **36**, 2068; R.E. Cramer, V. Fermin, E. Kuwabara, R. Kirkup, M. Selma, K. Aoki, A. Adeyemo and H. Yamakazi, *J. Am. Chem. Soc*., 1991, **113**, 7033.
5 E. Alcalde, M. Alemany, L. Pérez-García and M. L. Rodríguez, *J. Chem. Soc., Chem. Commun.*, 1995, 1239 and references cited therein; E.Alcalde, M. Alemany and M. Gisbert, *Tetrahedron*, 1996, **52**, 15171.
6 P. K. Dahl and F. H. Arnold, *J. Am. Chem. Soc*., 1991, **113**, 7417.
7 S. S. Moore, T. L. Tarnowski, M. Newcomb and D. J. Cram, *J. Am. Chem. Soc*., 1977, **99**, 6398.
8 E. Alcalde, I. Dinarés, J. Frigola, C. Jaime, J.-P. Fayet, M.-C. Vertut, C. Miravitlles and J. Rius, *J. Org. Chem*., 1991, **56**, 4223.
9 M. G. Shieldrick, *Acta. Crystallogr*., 1990, **A46**, 467.
10 G. M. Sheldrick, *Crystallographic Computing*, ed. G. H. D. Flack, P. Parkanyi and K. Simon, Oxford University Press, Oxford, 1993, p. 111.
11 T. Kottke and D. Stalke, *J. Appl. Crystallogr*., 1993, **26**, 615.
12 T. Steiner, *Acta. Crystallogr*., 1998, **B54**, 456 and references cited therein.
13 P. A. Gale, J. L. Sessler and V. Král, *Chem. Commun*., 1998, 1.

Communication 8/08503J

Heterolytic dihydrogen activation in an iridium complex with a pendant basic group

Dong-Heon Lee,[a] Ben P. Patel,[a] Eric Clot,[b] Odile Eisenstein*[b] and Robert H. Crabtree*[a]

[a] *Department of Chemistry, Yale University, New Haven, CT, 06520-8107 USA. E-mail: robert.crabtree@yale.edu*
[b] *LSDSMS (UMR 5636), Case courrier 14, Université de Montpellier 2, 34095 Montpellier cedex 5, France. E-mail: eisenst@gauss.lsd.univ-montp2.fr*

Received (in Bloomington, IN, USA) 4th November 1998, Accepted 22nd December 1998

Experimental and theoretical studies show that H_2 reacts with an Ir phosphine complex having a basic pendant amino group to give either an H_2 or an Ir–H···H–N hydrogen-bonded hydride complex, depending on the basicity of the phosphine ligands.

Heterolytic hydrogen activation by a transition metal complex can occur by deprotonation of an intermediate dihydrogen complex by an external base, as shown in several studies.[1–6] We have shown that appending an NH_2 group at the 2-position of a cyclometalated 7,8-benzoquinolinate ligand (bq-NH_2) can lead to ligand binding *via* both M–L bonds and –N–H···L hydrogen bonds.[7] Since the pendant NH_2 group is basic, we have now examined the possibility that the pendant group can act as an internal base to deprotonate an adjacent H_2 ligand.

We have compared the reactivity of a series of bq-NH_2 complexes with that of the corresponding unsubstituted benzoquinolinate analogue (bq-H) that lacks the pendant group. In the comparison bq-H system, the known cationic aqua complex, $[IrH(bq\text{-}H)(OH_2)(PPh_3)_2]BF_4$ **1**, reacts with H_2 to give a cationic H_2 complex, **2**, previously characterized in detail.[8] Addition of Bu^{t}Li as base leads to deprotonation of the H_2 ligand to form the known neutral dihydride, $[IrH_2(bq\text{-}H)(PPh_3)_2]$ **3** (Scheme 1).

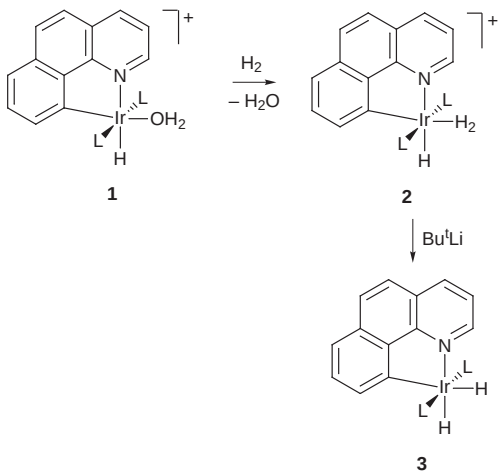

1 **2** **3**

Scheme 1

The aqua complex, $[IrH(bq\text{-}NH_2)(OH_2)(PPh_3)_2]BF_4$ **4a**, in the new pendant amine system also reacts with H_2 to give, not the corresponding H_2 complex, **5a**, but *via* heterolytic activation to give the dihydride, **6a**, instead (Scheme 2). Complex **6a** was fully characterized as $[IrH_2(bq\text{-}NH_3)(PPh_3)_2]BF_4$ and its identity is shown, for example, by the spectral data. The reaction is accompanied by the loss of both the ^{1}H NMR triplet hydride resonance at δ −16.4 and the amino resonance at δ 6.1 characteristic of **4a**, and the appearance of two sharp, mutually coupled (dt, $^2J_{HH'}$ 8.5; $^2J_{PH}$ 14.6 Hz) hydride resonances at δ −23.2 and −25.7, and a broad resonance at δ 3.8, which are respectively assigned to the *cis*-hydrides and the NH_3^+ protons.

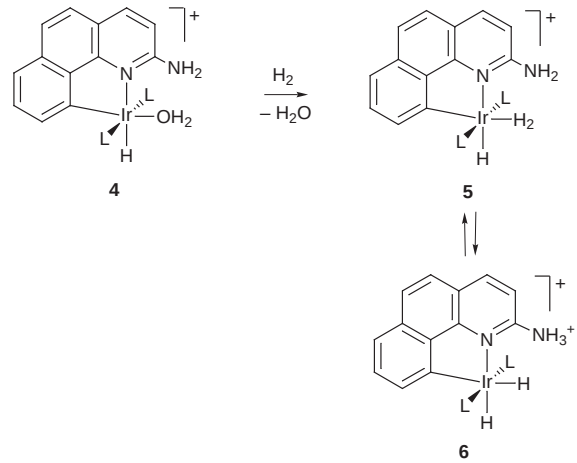

4 **5** **6**

Scheme 2 L = PPh_3, **a**; $PMePh_2$, **b**; PEt_2Ph, **c** or PBu^n_3, **d**.

This conversion is completely reversible: removing the dihydrogen gas from the solution with a stream of dinitrogen causes the resonances at δ −23.2 and −25.7 to disappear, and the signal at δ −16.1 to reappear in the ^{1}H NMR spectrum. Complex **6a** readily loses H_2 in the solid state, and as a result we were unable to isolate it for elemental analysis or IR studies.

Theoretical work (DFT-B3PW91)† on the model systems $[IrH(bq\text{-}NH_2)(H_2)(PH_3)_2]^+$ **7a** and $[IrH_2(bq\text{-}NH_3)(PH_3)_2]^+$ **8a** gave the unexpected result that the H_2 complex is the more stable form by 12 kcal mol^{-1}, contrary to the result in the experimental system. In considering why there might be a difference between the experimental pair **5**/**6** and the theoretical model pair **7**/**8** (Scheme 3), we considered the possibility that the change from PPh_3 to PH_3 was responsible. If so, we felt that the more basic alkyl phosphines would be a better experimental comparison.

Accordingly, we studied the species, $[IrH(bq\text{-}NH_2)(OH_2)(P\text{-}Bu^n_3)_2]BF_4$ **4d**, made *via* the standard route,[7,8] where the aryl groups have been replaced by alkyls. Hydrogen was passed for 1 min at −80 °C in the presence of anhydrous $MgSO_4$ to facilitate removal of water. Even with such a small change, we find that the H_2 complex, **5d**, is now formed on reaction with H_2, not the dihydride **6d**. The identity of the H_2 complex followed from the ^{1}H NMR data, which show two separate resonances below 230 K, a broad one at δ −4.7 for the coordinated H_2 molecule and a sharp one at δ −17.2 for the

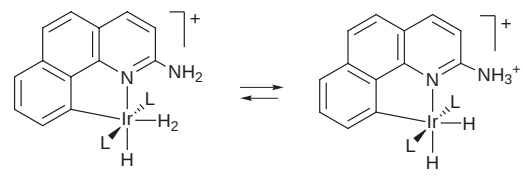

7 **8**

Scheme 3 L = PH_3, **a**; PH_2F, **b**; PHF_2, **c**; PF_3, **d**.

Table 1 IR data for [IrH(bq-NH_2)(CO)$(L)_2$](BF_4) which shows the order of donor power of the phosphines studied

Ligand (L)	ν_{CO}/cm^{-1}
PPh_3 (**9a**)	2026.5
$PMePh_2$ (**9b**)	2021.8
PEt_2Ph (**9c**)	2015.3
PBu^n_3 (**9d**)	2004.6

classical hydride. These chemical shifts are close to those for the unsubstituted analogue [IrH(bq-H)$(H_2)(PPh_3)_2$]BF_4 **2**.[8] The HD complex (d^1-**5b**)shows a $^1J_{HD}$ coupling of 29.3 Hz.

Similar results were obtained with other basic phosphines, PEt_2Ph and $PMePh_2$, so the result is general. In no case was an equilibrium seen between dihydrogen complex **5** and hydride **6**. This implies that moving to a more basic phosphine decreases the acidity of the coordinated H_2 ligand in **5** and correspondingly increases the basicity of the terminal hydride in **6**. This results in the proton moving completely from the NH_3^+ group of **6** to the terminal hydride to give **5** on changing from PPh_3 to any of the more basic phosphines.

This large change of structure is rather surprising for such a relatively small change in ligand, and we wanted to verify that the basicity of the phosphines was indeed varying in the expected manner. Reaction of the aqua complex, **4** with CO (1 atm) in CH_2Cl_2 gave the carbonyl species [IrH(bq-NH_2)(CO)$(L)_2$]BF_4 (**9**, L = PPh_3, **a**; $PMePh_2$, **b**; PEt_2Ph, **c**; PBu^n_3, **d**). The IR data obtained for these complexes (Table 1) verifies that the basicity is indeed higher for the more highly alkylated phosphines. Having only one CO but two L groups makes this system much more sensitive to change of phosphine than Tolman's LNi$(CO)_3$ system,[9] but the trends are essentially the same.

Returning to the theoretical work, we have a rare case where the quantum model PH_3 is inadequate to reproduce the experimental observations on a PPh_3 complex. In order to model the more electron-accepting PR_3 groups, we have now moved to PFH_2 (**7b**/**8b**), PF_2H (**7c**/**8c**), and PF_3 (**7d**/**8d**); of course these are far more electron-withdrawing than the experimental PPh_3 group, but we were only interested in seeing if the correct trends could be reproduced. Indeed, as shown in Table 2, the calculated energies for **7** and **8** do alter in the expected fashion, confirming that the acid/base character of the Ir–H/Ir–(H_2) system shows an unexpectedly strong dependence on the nature of the phosphine.

Table 2 The theoretical structural (Å) and energetic parameters (kcal mol^{-1}) of dihydrogen complex **7** and dihydride **8** with change of phosphine

	7		**8**		
Ligand	d_{HH}	$d_{H\cdots H}$	d_{NH}	$d_{H\cdots H}$	ΔE^a
PH_3	0.861	1.854	1.135	1.412	−12
PFH_2	0.851	1.829	1.090	1.548	−2.5
PF_2H	0.856	1.873	1.093	1.502	+0.5
PF_3	0.847	1.849	1.073	1.618	+3.0

[a] E(**8**) − E(**7**) is reported, so negative values imply the dihydrogen complex is more stable.

The structural parameters of **7** and **8** from the theoretical work (Table 2) are in good agreement with the solid state structure of [IrH(bq-NH_2)(CO)$(L)_2$]PF_6 for which experimental structural data is available.[10] For all phosphine ligands, **7** and **8** both correspond to energy minima. In **7**, the dihydrogen ligand is always coplanar with the *cis*-Ir–H bond and the pendant NH_2 group is coplanar and conjugated with the bq ligand. As expected, the H–H distance in **7** decreases (from 0.861 to 0.847 Å) with increasing F substitution on the phosphine (Table 2) showing the effects of the diminished back-donation along the series. In **8**, the N–H bond interacting with the hydride *via* a dihydrogen bond[11] is elongated, especially for PH_3 (d_{NH} = 1.135 Å) where the hydride is the most basic and the dihydrogen bond distance is the shortest ($d_{H\cdots H}$ = 1.412 Å). The compounds cannot be isolated because they lose hydrogen too readily, consistent with the presence of a strong N–H···H–Ir interaction. This 1.4 Å H···H distance is significant because it is considerably shorter than any so far suggested for a dihydrogen bond, consistent with a particularly strong interaction, and is even in the range proposed for stretched dihydrogen complexes, so the species could even be considered as representing an arrested intermediate stage of heterolytic H_2 activation. Going from PH_3 to PF_3 leads to an elongation of $d_{H\cdots H}$ to 1.618 Å, however, beyond the upper limit of 1.6 Å proposed for stretched H_2 complexes, showing the strong sensitivity of the structure to the nature of the phosphine.

This work shows that the very strong dependence[1,2,20] of the pK_a of the H_2 ligand has interesting effects on the reactivity of these complexes toward H_2 and on the structure of the resulting hydrides even with relatively small changes in the ligand sphere. The pK_a of the H_2 ligand seems to be unusually sensitive to back bonding effects, even though the changes in d_{HH} are relatively modest (Table 2). From a theoretical standpoint, great care should be taken in modelling such systems.

We thank the NSF (R. H. C.), the University of Montpellier and CNRS (O. E.) for funding and Bruno Chaudret (Toulouse) for discussions.

Notes and references

† *Computational details*: All the calculations were performed with the Gaussian 94 set of programs[12] at the B3PW91 level[13,14] level. Iridium was represented with the Hay–Wadt relativistic core potential (ECP) for the 60 innermost electrons and its associated double-ζ basis set.[15] Phosphorus atoms were also represented with Los Alamos ECPs and their associated double-ζ basis set[16] augmented by a polarisation d function.[17] A 6-31G(d,p) basis set[18,19] was used for the atoms bound directly to Ir (H, C, and N) and for the atoms of the amido group (N and H), all the other atoms have been described with a 6-31G basis set.[18] Full geometry optimisations within C_s symmetry (the bq-NH_2 ligand is planar) have been carried out within the framework of DFT (B3PW91).

1 D. M. Heinekey and W. J. Oldham Jr., *Chem. Rev.*, 1993, **93**, 913.
2 R. H. Crabtree, *Angew. Chem., Int. Ed. Engl.*, 1992, **32**, 789.
3 P. J. Brothers, *Prog. Inorg. Chem.*, 1981, **28**, 1.
4 J. Huhmann-Vincent, B. L. Scott and G. J. Kubas, *J. Am. Chem. Soc.*, 1998, **120**, 6808.
5 K. T. Smith, M. Tilset, R. Kuhlman and K. G. Caulton, *J. Am. Chem. Soc.*, 1995, 117, 9473.
6 M. Schlaf, A. J. Lough, P. A. Maltby and R. H. Morris, *Organometallics*, 1996, 15, 2270.
7 B. P. Patel and R. H. Crabtree, *J. Am. Chem. Soc.*, 1996, **118**, 13105.
8 R. H. Crabtree, M. Lavin and L. Bonneviot, *J. Am. Chem. Soc.*, 1986, **108**, 4032.
9 A. Tolman, *Chem Rev.*, 1977, **77**, 313.
10 K. Gruet, D.-H. Lee and R. H. Crabtree, unpublished work.
11 R. H. Crabtree, P. E. M. Siegbahn, O. Eisenstein, A. L. Rheingold and T. F. Koetzle, *Acc. Chem. Res.*, 1996, **29**, 348; A. J. Lough and R. H. Morris, *Inorg. Chem.*, 1995, **34**, 1549.
12 Gaussian 94, Revision B.3, M. J. Frisch, G. W. Trucks, H. B. Schlegel, P. M. W. Gill, B. G. Johnson, M. A. Robb, J. R. Cheeseman, T. Kerth, G. A. Petersson, J. A. Montgomery, K. Raghavachari, M. A. Al-Laham, V. G. Zakrzewski, J. V. Ortiz, J. B. Foresman, C. Y. Peng, P. Y. Ayala, W. Chen, M. W. Wong, J. L. Andres, E. S. Replogle, R. Gomperts, R. L. Martin, D. J. Fox, J. S. Binkley, D. J. Defrees, J. Baker, J. P. Stewart, M. Head-Gordon, C. Gonzalez and J. A. Pople, Gaussian Inc, Pittsburgh PA, 1995.
13 A. D. Becke, *J. Chem. Phys.*, 1993, **98**, 5648
14 J. P. Perdew and Y. Wang, *Phys. Rev. B*, 1992, **45,** 13244
15 P. J. Hay and W. R. Wadt, *J. Chem. Phys.*, 1985, **82**, 299
16 W. R. Wadt and P. J. Hay, *J. Chem. Phys.*, 1985, **82**, 284
17 A. Hölwarth, M. Böhme, S. Dapprich, A. W. Ehlers, A. Gobbi, V. Jonas, K. Köhler, R. Stegmann, A. Veldkamp and G. Feenking, *Chem. Phys. Lett.*, 1993, **208**, 237.
18 W. J. Hehre, R. Ditchfield and J. A. Pople, *J. Chem. Phys.*, 1972, **56**, 2257
19 P. C. Harihan and J. A. Pople, *Theor. Chim. Acta*, 1973, **28**, 213.
20 G. Jia and R. H. Morris, *J. Am. Chem. Soc.*, 1991, **113**, 875.

Communication 8/08601J

ChemComm
FEATURE ARTICLE

New approaches to rate enhancement in heterogeneous catalysis

Graham J. Hutchings

Department of Chemistry, Cardiff University, PO Box 912, Cardiff, UK CF1 3TB

Received (in Cambridge, UK) 12th August 1998, Accepted 29th October 1998

Rate enhancement, or promotion, of heterogeneous catalysts has long been viewed as an empirical subject, and many catalysts have been designed on the basis of large catalyst screening programmes. This paper addresses recent advances in this topic and indicates that much progress is being made on the basis of a molecular approach, in contrast to the previous empirical methodology, and in particular highly effective enantioselective heterogeneous catalysts can be designed. Two catalyst systems are selected for detailed discussion, namely enantioselective hydrogenation using cinchona-modified platinum catalysts and the modification of zeolites with chiral molecules.

Introduction

The design of high activity heterogeneous catalysis is considered crucial for the successful operation of the chemical industry. Most bulk chemical and petrochemical processes could not be operated commercially without a heterogeneous catalyst. Recently, there has been an increased awareness that heterogeneous catalysts could significantly improve a large number of fine chemical processes. Historically, most people would consider that current commercial heterogeneous catalysts are designed mainly by empirical large scale testing programmes. While this is not strictly true, there remains one area that has received very limited attention and this concerns the effect of rate enhancement, or promotion, of heterogeneous catalysts caused by additional catalyst components that are often inactive for the reaction if used alone. This is a subject that has been almost exclusively studied in industrial laboratories and the results are typically only disclosed in the patent literature. Most commercially operated catalysts involve promoters; for example, the effect of the addition of K^+ to the Fe Fischer Tropsch synthesis or ammonia synthesis catalysts is well known.[1] The dichotomy between academic and industrial research is well exemplified in the research concerning oxides and phosphates as catalysts for heterogeneous hydrocarbon oxidation. Most academic studies are concerned with the reaction mechanism on non-promoted systems whereas most industrial studies are concerned with promoted catalysts.[2,3] The origin of the rate enhancement effects observed in these complex systems remains obscure[2] mainly because the precise structure of the active site is unknown. This problem is best exemplified by vanadium phosphate catalysts for the oxidation of butane to maleic anhydride, since even though they have been the subject of over a thousand research papers and patents[2,4] the structure of the active site remains a matter of debate. However, recent detailed electron microscopy[5] and *in situ* laser Raman spectroscopy studies[6] are starting to make progress in this area. This lack of detailed knowledge concerning the structure of the active site in heterogeneous catalysts makes it almost impossible to adopt a molecular approach to this subject which is essential if progress is to be made. This is not a disadvantage that is shared by related subject areas of surface science, homogeneous catalysis and theoretical studies, since all of these use a molecular approach. If significant progress is to be made in heterogeneous catalysis then a similar molecular approach has to be adopted. In this paper it is shown that the latest research approaches in the design of heterogeneous catalysts are using a molecular approach and that progress is being made in the understanding of rate enhancement in heterogeneous catalysts. Two systems have been selected as examples of recent work, namely enantioselective hydrogenation using cinchona-modified platinum catalysts and the modification of zeolites with chiral molecules. Both of these examples have been selected since they demonstrate the advantages of rate enhancement in enantioselective catalysis since, in the absence of rate enhancement, the unmodified active sites are not less active than modified sites, and in some cases are more active, and hence the attainment of high enantioselectivities requires the absence of unmodified sites. However, when rate enhancement is observed, then unmodified sites are not a significant source of reaction and do not interfere with enantioselective reactions.

The author has 23 years experience in the study and design of heterogeneous catalysts, particularly oxides and zeolites. His early career involved nine years in ICI in both research and production. In 1984 he left industry for an academic position at the University of Witwatersrand in Johannesburg prior to returning to the UK in 1987 to help establish the Leverhulme Centre for Innovative Catalysis at the University of Liverpool. In 1997 he was appointed as Head of Department and Professor of Physical Chemistry at Cardiff University.

Enantioselective hydrogenation using cinchona-modified platinum

The hydrogenation of α-ketoesters using modified heterogeneous catalysts has been extensively studied, particularly for the reaction of ethyl pyruvate using modified Pt catalysts,[7–9] although recent studies have begun to generalise this system to a broader range of substrates and metals.[10] The reaction was originally described by Orito *et al.*,[11–14] and has been become the most intensively studied heterogeneous enantioselective catalytic reaction. The reason for this interest is that it is viewed by many workers as a model reaction on which to base other enantioselective studies. The approach adopted, *i.e.* the creation of a chiral active site by the adsorption of pure enantiomers onto a metal surface, has also proved successful in the related studies by Izumi[15] for the hydrogenation of β-ketoesters with tartrate-modified nickel catalysts. The early work on this reaction has been extensively reviewed,[7–9,16,17] and consequently only the important features of the reaction will be described here.

Extensive studies have revealed that hydrogenation of α-ketoesters in the presence of cinchona alkaloids as modifiers is best carried out using Pt catalysts (Fig. 1).[9,11–14,18] The Pt can be supported on a diverse range of materials, Al_2O_3, SiO_2, TiO_2, C, and the best results have been obtained using 5%Pt/Al_2O_3.[19]

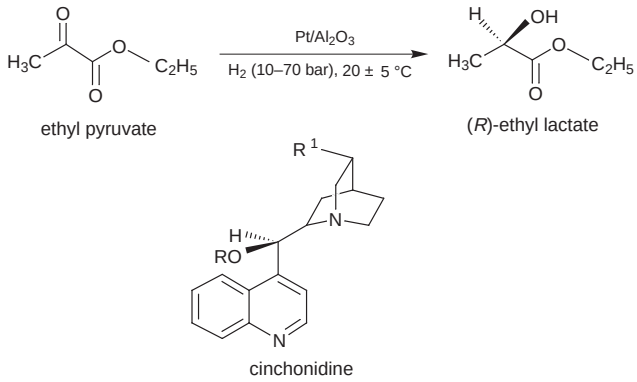

Fig. 1 Hydrogenation of ethyl pyruvate using Pt/Al_2O_3 catalysts modified with cinchonidine.

Interestingly, zeolites have also been successfully used as supports,[20–22] but no advantages for the specific use of microporous materials are apparent when compared with Al_2O_3 or other non-microporous supports. The optimum Pt particle size is considered to be > 2 nm, and catalysts with smaller Pt particle sizes have been shown to be less selective. It is generally agreed that the reason for the structure sensitivity remains a matter for debate. Some researchers[9] consider that the relatively flat low index planes are more suitable for adsorption of the cinchona modifier; however, Augustine *et al.*[23] dispute this and argue that the corner and ad-atoms are the active centres. Evidence in favour of the former viewpoint comes from heat pretreatment of the catalyst, which can be expected to stabilise low index planes, which shows an increase in enantioselectivity.

Most research effort for this reaction has concentrated on the optimisation of the enantioselection, and, specifically, on the design of the chiral modifier for the supported Pt catalyst with ethyl pyruvate as the substrate, and a selection of the results is summarised in Table 1. Early work focused on the method of

Table 1 Hydrogenation of ethyl pyruvate with Pt/Al_2O_3 using chinchona related modifiers[a]

Modifier[b]			
R	R^1	Solvent	ee (%)[c]
H	Et	Acetic acid	90
Me	Et	Acetic acid	95
H	CH_2OH	Acetic acid	91
(*R*)-Lactate	Et	Acetic acid	44
(*S*)-Lactate	Et	Acetic acid	46
(*R*)-Benzyllactate	Et	Ethanol	20
(*S*)-Benzyllactate	Et	Ethanol	25

[a] Source ref. 16, *reaction conditions*: 50–100 mg Pt/Al_2O_3, 10 ml ethyl pyruvate, 20 ml solvent, ambient temperature, 100 bar. [b] R and R^1 as in Fig. 1. [c] Best ee reported for (*R*)-enantiomer.

modification by cinchona alkaloids and it was recognised that the choice of solvent was important for the attainment of high ee. The highest ee is obtained when acetic acid is used as solvent and the ee was found to increase in the order: ethanol < toluene < acetic acid when either 10,11-dihydrocinchonidine or 10,11-dihydro-*O*-methylcinchonidine were used as modifiers, and ethyl pyruvate or ethyl 4-phenyl-2-oxobutyrate were used as substrates. From this early work it was concluded[16] that the minimal requirements for an efficient modifier for the hydrogenation of α-ketoesters is the presence of a basic nitrogen centre in close proximity to one or more chiral centres and an aromatic ring system, with best results being obtained with planar ring systems, *e.g.* quinolyl or naphthyl. To date it is generally agreed that 10,11-dihydrocinchonidine is the most effective modifier for high pressure hydrogenation of ethyl pyruvate. However, recent extensive studies by Baiker[24] have indicated the efficacy of mechanistic studies for the design of new chiral modifiers in enantioselective hydrogenation that can be used to replace the cinchona alkaloids.

The mechanism by which enantioselection occurs has been a matter of some speculation in recent years, and most recently has become a matter of intense debate.[25,26] Most researchers agree that the cinchona modifier interacts with the metal catalyst surface to form a new enantioselective catalytic site. Augustine *et al.*[23] proposed that the cinchona molecule is adsorbed through the quinoline N atom adjacent to a Pt ad-atom, where the substrate and H coadsorb with the N interacting with a CO group of the substrate. Baiker and coworkers[27–30] have utilised molecular simulations of the interaction between the substrate and the modifier and have suggested that protonated cinchonidine interacts with the oxygen atom of the CO bond that is subsequently hydrogenated, and that this interaction activates the substrate and thereby leads to the observed rate enhancement. An alternative proposal concerning the origin of the enantioselection, the shielding effect model, has been proposed by Margitfalvi and coworkers.[31,32] This model also uses molecular simulations as an integral part of the study. It is proposed that the modifier and the substrate preferentially form a 1:1 complex in solution, and this activated complex is subsequently hydrogenated by adsorbed hydrogen on the metal surface. Recently, we have considered these approaches using molecular simulations,[33] and it is clear that molecular simulation studies are playing a valuable role in aiding the design of new chiral modifiers, but there remains a central problem with this approach, namely that the platinum metal surface is not included in these simulations. Since the interaction between the cinchona and the platinum surface is considered to be crucial, this represents a major flaw. The alternative approach involving a more rigorous quantum mechanics calculation would prove to be too costly in computing time at present, and only relatively simple systems have been studied to date.

One of the most important observations for the Pt/cinchona catalyst system is the observation that the rate of hydrogenation of the α-diketone is significantly enhanced on the addition of the cinchona modifier (Table 2). A rate enhancement is

Table 2 Effect of cinchona modifier on the rate of hydrogenation of ethyl pyruvate with Pt/Al_2O_3 catalysts[a]

Modifier[b]	Modification time/h	Solvent	Rate/mmol^{-1} g^{-1}
None	—	None	50
None	—	Ethanol	35
C	1	Ethanol	1100–1300
DHC	1	Ethanol	1100–1300
DHC	18	Ethanol	1490

[a] Data taken from ref. 10, H_2 pressure 10 bar, 20 °C. [b] C = cinchonidine, DHC = 10,11-dihydrocinhonidine.

observed with cinchonidine and 10,11-dihydrocinchonidine. The same effect is observed when Pt colloids are used as catalysts (Table 3), and this indicates that the nature of the

Table 3 Enantioselective hydrogenation of ethyl pyruvate with Pt colloids using 10,11-dihydrocinchonidine as modifier[a]

Solvent	ee (%)	Relative rate[b]
Ethanol[c]	0	1
Ethanol	45	6
Toluene	15	2
Isopropanol	50	4

[a] Data taken from ref. 16. [b] Rates relative to hydrogenation rate in absence of modifier. [c] No modifier present.

support may not be of great significance for this effect. To date, the origin of the rate enhancement has not been determined, partly due to the fact that most studies have concentrated on the

optimisation of enantioselection. It is tempting to link the observation of the rate enhancement effect with the enantioselection that is achieved with this catalyst system. However, the rate enhancement is observed for racemic hydrogenation. For example Blaser *et al.*[19] have shown that aniline, triethylamine and quinuclidine all enhanced the rate of racemic hydrogenation of ethyl pyruvate when added to the Pt/Al_2O_3 catalyst and that there was a relationship between the pK_a of the nitrogen base and the degree of rate enhancement. The rate enhancement observed with cinchonidine is much higher than that predicted by pK_a considerations alone, indicating that other factors are important. Interestingly, Rylander[34] had previously noted that racemic amines could enhance the rate of hydrogenation of ketones. It is possible that the rate enhancement observed in the Pt/cinchona system is similar in origin to that observed in a number of homogeneously catalysed reactions (*e.g.* the enantioselective oxidation catalysts based on Mn–salen complexes[35]). It can be considered that the Pt/cinchona system will be a catalyst where the nature of the active site will be identified at the molecular level in the near future using a combination of experimental and theoretical studies.

Work we have carried out[36] on a related reaction, the hydrogenation of α,β-unsaturated aldehydes, has also shown a rate enhancement effect. We modified the surface of a Cu/Al_2O_3 catalyst with thiophene and this enhanced the rate of formation of the unsaturated alcohol, this being the first example of the catalytic activity of copper being promoted by sulfur. In this case, the thiophene modifier dissociates and the active site is considered to involve the interaction between a sulfur atom and the copper surface, based on detailed spectroscopic study.

Zeozymes: catalysts of the future

In recent years, the use of zeolites as high activity/high selectivity catalysts has received significant interest. The one clear driving force for these studies is that the three dimensional structure of the zeolite and, in particular, the structure of the active site are well known from detailed spectroscopic and diffraction studies. In zeolites all the atoms are on the surface and hence this class of materials enable a link to be formed with the elegant and detailed surface spectroscopic studies on single crystal surfaces, since both approaches allow heterogeneous catalysis to be studied at the molecular level with well-defined systems that can be probed with surface sensitive techniques. For zeolites, since all atoms are on the surface, normal bulk techniques (NMR, FTIR and X-ray diffraction) become surface sensitive techniques. Three distinct approaches are apparent in the recent literature, and these involve (a) using zeolites as supports for homogeneous catalysts or grafting active complexes onto mesoporous materials, (b) encapsulating large homogeneous complexes using a *ship-in-a-bottle* technique, and (c) chiral modification of zeolite surfaces.

(a) The first approach was exemplified by Corma *et al.*[37] for the hydrogenation of prochiral alkenes using Rh and Ni complexes supported on zeolite Y. Enantioselective hydrogenation using homogeneous Rh complexes is well documented,[38] and the rationale for this work was the requirement to find a less expensive heterogeneous route to pharmaceutical chemicals. Corma *et al.*[37] utilised Rh and Ni complexes with a range of ligands derived from proline. The complexes were anchored through silanol groups onto either silica or zeolite Y. The zeolite was prepared by steam calcination at 1027 °C of an 80% exchanged NH_4^+ zeolite Y, followed by treatment with citric acid. The zeolite is described as having a 'supermicropore' system (pore size 1.2–3.0 nm). These catalysts were found to be highly active for the hydrogenation of *N*-acyldehydrophenylalanine derivatives. They observed that the rate of hydrogenation was enhanced when the catalyst was supported on the zeolite compared to the rate observed for the non-supported complex or for the silica supported material, and they suggest that the confinement within the pores of the zeolite may play a role in the observed rate enhancement. However, in other cases, the same group have shown that reactions promoted by zeolite-supported catalysts are slower than those promoted by silica-supported complexes.[39] Hence, this approach cannot be considered to be a general method of securing rate enhancement.

A similar approach has been exemplified in the study of Ti-containing silicates, although in this case the Ti atoms are components of the active site and do not act as a promoter. On the basis of the developments in wider pore zeolites and related materials[40,41] Thomas *et al.*[42–44] have shown that titanium metallocenes grafted onto MCM-41 can act as effective oxidation catalysts with higher activity than Ti-MCM-41 catalysts when the Ti is incorporated into the silicate framework. Thomas *et al.*[42] have based their catalyst design on the concepts of interfacial coordination chemistry, surface organometallic chemistry and shape selective catalysis. However, other researchers[45] have shown that Ti-MCM-41 catalysts can be synthesised with very high activities.

(b) Encapsulation of large complexes within the micropores of zeolites has been pioneered by the studies of Jacobs *et al.*[46,47] The initial examples of this approach[46] involved the encapsulation in zeolites Y and X of iron phthalocyanine complexes, and these were shown to be active for the oxidation of alkanes with H_2O_2 as a mimic for cytochrome 450, the biological oxidation catalyst. Subsequently, complexes of manganese(II) with bipyridene (bpy) have been examined in detail.[47] In solution, the catalytic efficacy of these materials is limited by their catalase activity, *i.e.* their tendency to decompose hydrogen peroxide catalytically. When *cis*-$[Mn(bpy)_2]^{2+}$ complexes are encapsulated within the micopores of zeolite Y and X, however, they can act as effective alkene epoxidation catalysts without complications of competing processes such as self-oxidation or catalase activity. The catalysts are able to epoxidise a broad range of alkenes, and high epoxide selectivities (> 60%) are observed with hex-1-ene, cyclohexene, dodec-1-ene and cyclododecene. Owing to the acidic nature of the zeolites used, the products of the acid catalysed ring opening reactions were observed at extended reaction times. These catalysts are, therefore, further examples of a bifunctional catalyst combining oxidation and acid catalytic functions. The encapsulated *cis*-$[Mn(bpy)_2]^{2+}$ catalysts are remarkably stable, and are found to remain active for up to 1000 cycles for the oxidation of cyclohexene with H_2O_2. The catalyst can also be reused following drying at 47 °C and it is reported that repeated catalyst regeneration is possible, indicating that encapsulation of the *cis*-$[Mn(bpy)_2]^{2+}$ complex reduces the rate of oxidative destruction. The authors report that after repeated regeneration no changes in catalytic activity or spectroscopic properties of the complex could be observed. Electronic, rather than steric, factors were considered to control the reaction of the encapsulated catalysts and the hydrogen peroxide is considered to be activated by the formation of a high-valent manganese species [for example Mn(IV)=O], and it is the oxygen associated with this species that is inserted into the alkene C=C double bond.

Ogunmumi and Bein[48] and Sabater *et al.*[49] have extended the use of encapsulation to prepare heterogeneous catalysts for enantioselective epoxidation. The catalysts are based on the recently developed Jacobson homogeneous oxidation catalyst. Ogunmumi and Bein[48] and Sabater *et al.*[49] have also reported the successful encapsulation of Mn(III) salen complexes into zeolite Y using a *ship-in-a-bottle* approach previously used in the work of Jacobs and coworkers. Assembly of the reagents within the zeolite supercages leads to entrapped complexes that are too large to diffuse out of the zeolite host. The encapsulated complexes were characterised using vibrational and electronic spectroscopies together with ESR spectroscopy to confirm that the Mn(III) salen complex had been formed. The epoxidation of

prochiral alkenes was studied using sodium hypochlorite as oxidant. Bein has reported high ee for the epoxidation of *cis*-β-methylstyrene and there are indications that the encapsulated complex does not leach from the host zeolite. Turnover numbers based on Mn are not high, and the regeneration and reuse of catalysts is an issue that has yet to be confirmed. This approach essentially uses the advances made in homogeneous catalyst systems and it is not anticipated that the encapsulation process can be expected to lead to further enhancement in catalytic performance.

(c) Modification of zeolites by pure enantiomers is the most recent of the approaches to be developed, although clearly it has its basis in the well-studied catalysts for enantioselective hydrogenation based on Pt/cinchona and Ni/tartrate. An initial report on the use of a zeolite as host for chiral induction was by Sundarabubu *et al.*[50] In this study two zeolites NaY and NaX were modified by (−)-ephedrine and modest ee (< 10%) in the photolysis of ketones capable of undergoing the Norrish–Yang reaction. The most important observation related to the nature of the enantiomer that is enhanced in reactions using the two selected zeolites. In NaY, (−)-ephedrine showed enantioselectivity in favour of the (+) isomer of the product; however, the same chiral modifier favoured the (−)-isomer in NaX, although to a lesser extent. This remarkable effect was attributed to differences in the supercage free volume, as this was found to be different for the two modified zeolites.

The concept of modification of zeolite supercages to create the chiral environment required to favour the formation of one of a pair of diastereoisomeric transition states, a necessary condition for enantioselection, has been pioneered in our recent research. We selected chiral dithiane oxides since these were readily available to us with high optical purity, and as they provide a number of heteroatoms to ensure that the modifier is firmly anchored within the zeolite. A surprising early result we obtained is that the dithiane oxides are remarkably stable within the zeolite: they were only decomposed thermally at temperatures > 400 °C, and they were not racemised by adsorption in the zeolite. We selected the dehydration of butan-2-ol as an example of a simple acid catalysed reaction that can in principle demonstrate both enantioselectivity [differentiation between (*R*)- and (*S*)-butan-2-ol] and product selectivity (formation of but-1-ene, *cis*- and *trans*-but-2-ene).

Our initial experiments were carried out using zeolite Y modified with racemic 1,3-dithiane 1-oxide. We found that the dithiane oxide-modified zeolite Y is considerably more active than unmodified zeolite Y by several orders of magnitude, and that this activity was maintained without significant loss over several days. Under our reaction conditions, unmodified zeolite Y only became active at temperatures above 150 °C and required a reaction temperature of 225 °C to achieve 90% conversion, whereas the modified zeolite gave 90% conversion at 115 °C. We have now observed this effect with a number of other dithiane oxides (Fig. 2).[50,51] These early results show that modification of zeolite Y with the dithiane oxide creates a new high activity acid site. As noted previously, it is this observation of rate enhancement that we consider of crucial importance in the design of novel enantioselective catalysts. Since the active sites in the modified zeolite are considerably more active than those of the unmodified zeolite, we believed that the modified zeolite could form the basis of a new enantioselective catalyst. Our initial experiments confirm that this can indeed be observed, and the results are given in Table 4.[50] In these experiments, we reacted racemic butan-2-ol over zeolite Y which had been modified with an enantiomerically enriched dithiane 1-oxide. The chiral acid catalyst is selective for the reaction of one of the enantiomers preferentially, even though both enantiomers are present in equal concentration at the inlet to the reactor.

Modification of zeolite H-Y with dithiane oxide (**I**) leads to the creation of a catalyst that has enhanced activity for the acid

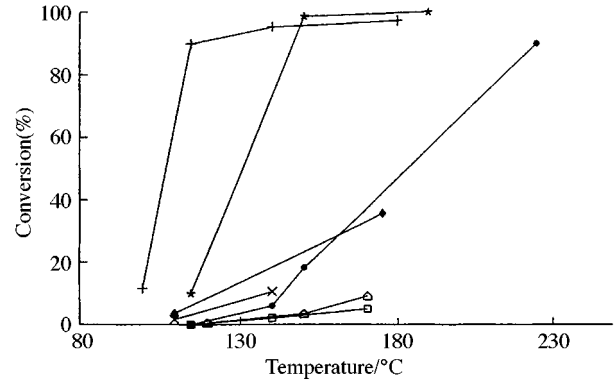

Fig. 2 Effect of temperature on the conversion of butan-2-ol over zeolite Y, key: (●) Zeolite H-Y (LZY 82, Union Carbide), (+) Zeolite H-Y (LZY 82) after modification with 1,3-dithiane 1-oxide, (★) Zeolite H-Y (LZY 82) after modification with 2-methyl-1,3-dithiane 1-oxide, (□) Zeolite H-Y (Crossfield), (X) Zeolite H-Y (Crossfield) with 1,3-dithiane 1-oxide, (⌂) Zeolite H-Y (Crossfield) after modification with 2-phenyl-1,3-dithiane 1-oxide and (◆) H-Y (LZY 82) after modification with 1,3-dithiane, reaction conditions: catalyst (0.3 g) reacted with butan-2-ol (3.2×10^{-3} mol h^{-1}) prevaporised in nitrogen (4.3×10^{-2} mol h^{-1}).

catalysed dehydration of butan-2-ol when compared with the unmodified zeolite or when modified with the corresponding dithiane (**II**). This effect is observed both for samples prepared by addition of the modifier to the synthesis gel and for the post

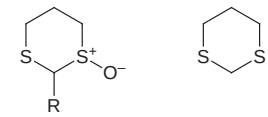

I **II**

synthesis modification of two different commercial samples of zeolite Y (Crossfield and Union Carbide). When the modifier is added to the synthesis gel, the resulting zeolite contains only a small quantity of the modifier, but the effect is still apparent.[52]

The interaction of alcohols with the acid forms of zeolites has been well studied in recent years, and for butanols it is generally considered that the adsorbed species that is formed initially is a butoxide species adsorbed at the active site that is formed from the dehydration of butan-2-ol. *In situ* FTIR spectroscopy confirmed that, in the present study, a butoxide species is formed on reaction of the butan-2-ol with both the unmodified zeolite and the dithiane oxide modified zeolite.[48] Consistent with the enhanced reactivity observed with the flow reactor studies, the *in situ* FTIR spectroscopy experiments reveal that the alkoxide species is formed at a significantly lower temperature for the dithiane oxide modified zeolite than for the unmodified zeolite.

All these data indicate that when the dithiane oxide is added to the zeolite, a new high activity site is formed, and it was concluded that the degree of rate enhancement observed can be related to the presence of extra-framework aluminium. This must, however, act in combination with the Brønsted acid site of the bridging hydroxy group associated with the zeolite framework aluminium, since the dehydration reaction investigated is catalysed by Brønsted acidity. A number of studies have indicated that a combination of extra-framework (Lewis acid sites) and framework (Brønsted acid sites) aluminium can give enhanced acidity in zeolite catalysts. Haag and Lago[53] showed that steaming zeolites at 500 °C with low levels of water vapour can lead to an increase in the activity of the zeolite for acid catalysed reactions. Mirodatos and Bartemeuf[54] showed that superacid sites could be created in mordenite by a steaming procedure. These effects were subsequently explained by Fritz and Lunsford[55] in terms of the initial dealumination of the zeolite to form non-framework aluminium that imparts, presumably through an electrostatic effect, strong acidity of the

Table 4 Reaction of racemic butan-2-ol over zeolite Y modified by enantiomerically enriched dithiane oxides

Catalyst[a]				Product composition[c]/× 10^{-3} mol h^{-1}				Butan-2-ol conversion (%)		
Zeolite	Modifier	*T*/°C	Conversion (%)[b]	But-1-ene	But-2-ene	(*R*)-Butan-2-ol	(*S*)-Butan-2-ol	*R*	*S*	Relative rate
Y[d]	(*R*)-**I**, R = H	110	0.5	—	0.037	3.673	3.640	0.002	0.035	1 : 17.5
Y[d]	(*R*)-**I**, R = H	120	1.3	0.015	0.085	3.669	3.581	0.006	0.094	1 : 15.7
Y[d]	(*R*)-**I**, R = H	150	9.9	0.105	0.620	3.657	2.968	0.018	0.707	1 : 39.3
Y[e]	(*S*)-**I**, R = Ph	110	4.2	0.020	0.271	3.399	3.660	0.276	0.015	18.4 : 1
Y[e]	(*S*)-**I**, R = Ph	120	7.5	0.044	0.507	3.260	3.594	0.415	0.081	5.1 : 1

[a] **I** = Dithiane 1-oxide (see text). [b] Total conversion of (*R*) and (*S*)-butan-2-ol. [c] Flow rate: 10^{-3} mol h^{-1}. [d] Zeolite Y (Crossfield NaY, ion exchanged with NH_4NO_3 and calcined at 550 °C), modified with (*R*)-1,3-dithiane 1-oxide, 1 molecule per supercage (0.1 g), tested in a convential glass microreactor with racemic butan-2-ol (7.35×10^{-3} mol h^{-1}), prevaporized in a nitrogen diluent (6.7×10^{-3} mol h^{-1}). [e] Zeolite Y (ultrastabilized LZY 82, Union Carbide) modified with (*S*)-2-phenyl-1,3-dithiane,1 molecule per supercage (0.1 g), tested in a convential glass microreactor with racemic butan-2-ol (7.35×10^{-3} mol h^{-1}), prevaporized in a nitrogen diluent (6.2×10^{-3} mol h^{-1}).

remaining framework Brønsted acid sites. This leads to an increase in acidity of the zeolite, and, for simple acid catalysed reactions such as cracking, an enhanced activity is observed. In the present work, the high activity site is considered to be formed by the specific interaction of the dithiane oxide with both the extra-framework aluminium and the Brønsted acid site associated with the framework aluminium (Fig. 3). Supporting

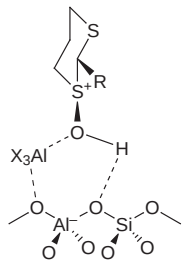

Fig. 3 Schematic representation of the structure of the high activity site formed on addition of 1,3-dithiane 1-oxide to zeolite H-Y (AlX_3 denotes extra-framework aluminium species).

evidence for this proposed model comes from detailed ^{27}Al MAS NMR spectroscopy studies and molecular simulations[56,57] that have shown that the dithiane oxide interacts strongly with the extra-framework aluminium atoms.

The formation of high activity acid sites enables these modified zeolites to be used as enantioselective catalysts, since, although only one active site per supercage is modified, it is many orders of magnitude more active than the remaining unmodified sites. When the dithiane oxide is used in the enantiomerically enriched form, the active sites are able to discriminate between the enantiomers of butan-2-ol. This important effect is achieved by enantioselective rate enhancement, *i.e.* both enantiomers react faster in the chiral environment than in the absence of the chiral modifier, but one reacts faster than the other.

The activation energies for the dehydration of the separate enantiomers over the zeolites doped with the enantiomerically enriched dithiane oxides were found to be identical within experimental error (105 ± 5 kJ mol^{-1}). In addition, it was noted that the enantiomeric discrimination obtained from the reaction of racemic butan-2-ol is higher than that based on the conversions of the separate enantiomers. The apparent inconsistency can be resolved by regarding the modified zeolite as if it were an enzyme (a zeozyme) operating with its active sites saturated with substrate and, due to this saturation, the alcohol–catalyst complexation constant does not appear in the experimental kinetics. The conversions of the separate enantiomers then yield the relative reactivities in the catalytic step, whereas the results using the racemate reflect the enantioselection, not only of the catalytic step, but also of the competitive binding of the substrates. Present indications, supported by molecular modelling studies, are that the latter effect is the larger.[52,56,57]

It is important to note that the reactants and products in this reaction are gas phase. However, the reactant butan-2-ol is present at high partial pressures, and, at the lower temperature used in this study, which is only 12 °C above the boiling point of butan-2-ol, it is possible that condensation may occur in the micropores of the zeolite. This effect would not, however, be expected to contribute significantly to the results obtained at the higher temperatures, where enantioselection is still observed, albeit briefly. We consider that these results provide the first example of a gas-phase enantioselective reaction heterogeneously catalysed by a zeolite. Although the initial approach described here has concerned the design of a catalyst that consumes chiral molecules, the study should be viewed, in effect, as a proof of the concept that a zeolite can be modified so that it preferentially catalyses the reaction of one enantiomer of a chiral substrate in the presence of both. In view of the immense range of microporous zeolites available together with the large number of enantiomerically pure modifiers, we consider that this approach will provide the basis for the generic design of a new type of enantioselective catalysts. As further evidence for this viewpoint, we have recently shown[58] that Cu^{2+}-exchanged zeolites HY modified by chiral oxazolines are highly effective catalysts for the enantioselective aziridination of alkenes employing [*N*-(*p*-tolylsulfonyl)imino)]phenyliodinane (PhI=NTs) as the nitrogen source. (Fig. 4, Table 5) and that

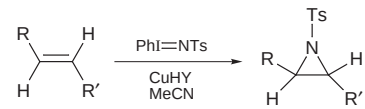

Fig. 4 Aziridination of alkenes using CuHY as catalyst.

the Mn^{3+}-exchanged Al-MCM-41 modified by a chiral salen ligand is an enantioselective epoxidation catalyst using iodosyl benzene as oxidant.[59]

These examples, it is hoped, demonstrate that a molecular approach can be taken to the design of novel high activity/selectivity heterogeneous catalysts. The approach proposed for the design of heterogeneous catalysts is similar in concept to that of the 'ligand accelerated reaction' described by Berrisford *et al.*[60] and exemplified in extensive homogeneous catalytic systems. In addition, it should be noted that the approach detailed in the present paper can also be useful in the design of chiral catalysts supported on different materials, *e.g.* amorphous oxides, organic polymers and dendrimers. In the future it is expected that the approaches outlined herein will become standard and that, in particular, the design of heterogeneous catalysts will involve an interplay between experimental and theoretical studies using catalysts with known structures. The recent work also demonstrates that rate enhancement in heterogeneous catalysis is now being studied at the molecular level, in contrast to the earlier approaches well exemplified in many patents published on this topic.

Acknowledgements

The work described in this paper has involved extensive collaboration with many colleagues and students in recent

Table 5 Representative bis(oxazolines) for the enantioselective aziridination of alkenes

Oxazoline	Alkene[a]	*T*/°C	Yield(%)	e.e.(%)[c]
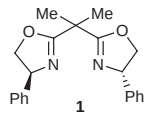 **1**	*trans*-β-Methyl cinnamate	–10	8 (21)	61 (70)
	trans-β-Methylstyrene	–10	74	36
	Styrene	–10	82	44
	Styrene	25	87	29
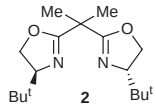 **2**	Styrene	–20	64	0
	Styrene[b]	–20	15 (89)	18 (63)
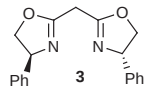 **3**	Styrene	25	78 (75)	10 (10)
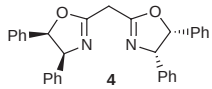 **4**	Styrene	25	73 (74)	0 (15)
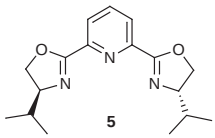 **5**	Styrene	–10	4	61

[a] Unless otherwise specified reaction conditions were: solvent MeCN, alkene: PhI = NTs = 5:1 molar ratio. [b] Styrene was used as solvent. [c] Enantioselectivity determined by chiral HPLC. Absolute configurations of major products, determined by optical rotation, are (*S*) for *trans*-β-methylstyrene and *trans*-β-methylcinnamate, (*R*) for styrene values in parentheses indicate yields obtained from homogeneous reactions.

years, including: Phil Page, Don Bethell, Dave Willock, Colin Rochester, Frank King, Fred Hancock, Richard Wells, Paul Collier, Saskia Feast, Chris Langham and Ifedi Okoye.

Notes and references

1 M. V. Twigg, *Catalyst Handbook*, Wolfe, London, 2nd edn., 1989.
2 G. J. Hutchings, *Appl. Catal.*, 1991,**72**, 1.
3 G. J. Hutchings, *Catal. Today*, 1993, **16**, 139.
4 G. J. Hutchings, C. J. Kiely, M. T. Sananes and J. C. Volta, *Catal. Today*, 1998, **40**, 273.
5 C. J. Kiely, A. Burrows, S. Sajip, G. J. Hutchings, M. T. Sananes, A. Tuel and J. C. Volta, *J. Catal.*, 1996, **162**, 31.
6 G. J. Hutchings, A. Desmartin-Chomel, R. Olier and J. C. Volta, *Nature*, 1994, **368**, 41.
7 H. U. Blaser, H. P. Jalett, D. M. Monti, A. Baiker and J. T. Wherli, *Stud. Surf. Sci. Catal.*, 1991, **67**, 147.
8 A. Biaker, *Stud. Surf. Sci. Catal.*, 1996, **101**, 51.
9 G. Webb and P. B. Wells, *Catal. Today*, 1992, **12**, 319.
10 T. J. Hall, P. Johnston, W. A. H. Vermeer, S. R. Watson and P. B. Wells, *Stud. Surf. Sci. Catal.*, 1996, **101**, 221; I. M. Sutherland, A. Ibbotson, R. B. Moyes and P. B. Wells, *J. Catal.*, 1990, **125**, 77; P. A. Meheux, A. Ibbotson and P. B. Wells, *J. Catal.*, 1991, **128**, 387; K. E. Simons, A. Ibbotson, P. Johnston, H. Plum and P. B. Wells, *J. Catal.*, 1994, **150**, 321; G. Bond and P. B. Wells, *J. Catal.*, 1994, **150**, 329.
11 Y. Orito, S. Imai, S. Niwa and G.-H. Nguyen, *J. Synth. Org. Chem. Jpn.*, 1979, **37**,173.
12 Y. Orito, S. Imai and S. Niwa, *Nippon Kagaku Kaishi*, 1979, 1118.
13 Y. Orito, S. Imai and S. Niwa, *Nippon Kagaku Kaishi*, 1980, 670.
14 Y. Orito, S. Imai and S. Niwa, *Nippon Kagaku Kaishi*, 1982, 137.
15 Y. Izumi, *Adv Catal.*, 1983, **32**, 215.
16 H. U. Blaser, H. P Jalett, M. Müller and M. Studer, *Catal. Today*, 1997, **37**, 441.
17 H. U. Blaser, *Tetrahedron: Asymmetry*, 1991, **2**, 843.
18 H. U. Blaser and M. Müller, *Stud. Surf. Sci. Catal.*, 1991, **59**, 73.
19 H. U. Blaser, H. P. Jalett, D. M. Monti, J. F. Reber and J. T. Wherli, *Stud. Surf. Sci. Catal.*, 1988, **41**, 153.
20 U. Böhmer, K. Morgenschweiss and W. Reschetilowski, *Catal. Today*, 1995, **24**,195.
21 W. Reschetilowski, U. Böhmer and K. Morgenschweiss, *Chem.-Ing.-Tech.*, 1995, **67**, 205.
22 W. Reschetilowski, U. Böhmer and J. Wiehl, in *Chiral Reactions in Heterogeneous Catalysis*, ed. G. Jannes and V. Dubois, Plenum Press, New York, 1995, p. 111.
23 R. L. Augustine, S. K. Tanielyan and L. K. Doyle, *Tetrahedron: Asymmetry*, 1993, **4**, 1803.
24 A. Baiker, *J. Mol. Catal. A*, 1997, **115**, 473.
25 D. G. Blackmond, *J. Catal.*, 1998, **176**, 267.
26 T. Mallat and A. Baiker, *J. Catal.*, 1998, **176**, 271.
27 K. E. Simons, G. Wang, T. Heinz, T. Giger, T. Mallat, A. Pfaltz and A. Baiker, *Tetrahedron: Asymmetry*, 1995, **6**, 505.
28 A. Baiker, T. Mallat, B. Minder, O. Schwalm, K. E. Simons and J. Weber, in *Chiral Reactions in Heterogeneous Catalysis*, ed. G. Jannes and V. Dubois, Plenum Press, New York, 1995, p. 95.
29 O. Schwalm, B. Minder, J. Weber and A. Baiker, *Catal. Lett.*, 1994, **23**, 271.
30 O. Schwalm, J. Weber, B. Minder and A. Baiker, *J. Mol. Struct.* (*THEOCHEM*), 1995, **330**, 353.
31 J. L. Margitfalvi, M. Hegedüs and E. Tfirst, *Tetrahedron: Asymmetry*, 1996, **7**, 571.
32 J. L. Margitfalvi, M. Hegedüs and E. Tfirst, *Stud. Surf. Sci. Catal.*, 1996, **101**, 241.
33 G. J. Hutchings and D. J. Willock, *Top. Catal.*, 1998, **5**, 177.
34 P. N. Rylander, *Catalytic Hydrogenation in Organic Synthesis*, Academic Press, London, 1979.
35 S. B. Chang, J. M. Galvin and E. N. Jacobsen, *J. Am. Chem. Soc.*, 1994, **116**, 6937.
36 G. J. Hutchings, F. King, I. P. Okoye, M. B. Padley and C. H. Rochester, *J. Catal.*, 1994, **148**, 453; F. King, I. P. Okoye, M. B. Padley and C. H. Rochester, *J.Catal.*, 1994, **148**, 463; M. B. Padley, C. H. Rochester, G. J. Hutchings and F. King, *J. Catal.*, 1994, **148**, 438.
37 A. Corma, M. Iglesias, C. del Pino and F. Sànchez, *Proc. 10th Int. Cong. Catal.*, Elsevier, Amsterdam, 1993, p. 2293.
38 R. Noyari, *Chem. Soc. Rev.*, 1989, 187.
39 A. Corma, M. Iglesias, F. Mohino and F. Sönchez, *J. Organometal. Chem.*, 1977, **544**, 147.
40 J. M. Thomas, *Nature*, 1994, **368**, 289.
41 J. M. Thomas and G. N. Greaves, *Science*, 1994, **265**, 1675.
42 T. Maschmeyer, F. Rey, G. Sankar and J. M. Thomas, *Nature*, 1995, **378**, 159.
43 R. Oldroyd, J. M. Thomas, T. Maschmeyer, P. A. MacFaul, D. W. Snelgrove, K. I. Ingold and D. M. Wayner, *Angew. Chem. Int. Ed. Engl.*, 1996, **35**, 2787.
44 T. Maschmeyer, R. D. Oldroyd, G. Sankar, J. M. Thomas, I. J. Shannon, J. A. Klepetko, A. F. Masters, J. K. Beattie and C. R. A. Catlow, *Angew. Chem., Int. Ed. Engl.*, 1997, **36**, 1639.
45 A. Corma, J. L. Jorda, M. T. Navarro and R. Rey, *Chem. Commun.*, 1998, 1899.
46 R. F. Parton, L. Uytterhoeven and P. A. Jacobs, in *Heterogeneous Catalysis and Fine Chemicals* ed. M. Guisnet), Elsevier, Amsterdam, 1995, p. 395.
47 P. P. Knops-Gerrits, D. De Vos, F. Thibault-Starzyk and P. A. Jacobs, *Nature*, 1994, **369**, 543.
48 S. B. Ogunmumi and T. Bein, *Chem. Commun.*, 1997, 901.
49 M. J. Sabater, A. Corma, A. Domenech, V. Fornés and H. Garcia, *Chem. Commun.*, 1997, 1285.
50 G. Sundarababu, M. Leibovitch, D. R. Corbin, J. R. Scheffer and V. Ramamurphy, *Chem. Commun.*, 1996, 2159.
51 S. Feast, D. Bethell, P. C. B. Page, F. King, C. H. Rochester, M. R. H. Siddiqui, D. J. Willock and G. J. Hutchings, *J. Chem. Soc., Chem. Commun.*, 1995, 2409.
52 S. Feast, M. R. H. Siddiqui, R. Wells, D. J. Willock, F. King, C. H. Rochester, D. Bethell, P. C. B. Page and G. J. Hutchings, *J. Catal.*, 1997, **167**, 533.
53 W. O. Haag and R. M. Lago, *US Pat.*, 1982, 4326994.
54 C. Mirodatos and D. Bartemeuf, *J. Chem. Soc., Chem. Commun.*, 1981, 39.
55 P. O. Fritz and J. H. Lunsford, *J. Catal.*, 1989, **118**, 85.
56 S. Feast, D. Bethell, P. C. B. Page, M. R. H. Siddiqui, D. J. Willock, G. J. Hutchings, F. King and C. H. Rochester, *Stud. Surf. Sci. Catal.*, 1996, **101**, 211.
57 D. J. Willock and G. J. Hutchings, *Top. Catal.*, 1998, **5**, 177.
58 C. Langham, P. Piaggio, D. Bethell, D. F. Lee, P. McMorn, P. C. B. Page, D. J. Willock, C. Sly, F. E. Hancock, F. King and G. J. Hutchings, *Chem. Commun.*, 1998, 1601
59 P. Piaggio, P. McMorn, C. Langham, D. Bethell, P. C. B. Page, F. E. Hancock and G. J. Hutchings, *J. Nouv. Chem.*, in press
60 D. J. Berrisford, C. Bolm and B. Sharpless, *Angew. Chem., Int. Ed. Engl.*, 1995, **34**, 1059.

Paper 8/06376A

15-Deoxy-16-(*m*-tolyl)-17,18,19,20-tetranorisocarbacyclin: a simple TIC derivative with potent anti-apoptotic activity for neuronal cells

Masaaki Suzuki,*[a] Koichi Kato,[b] Yumiko Watanabe,[c] Takumi Satoh,[c] Kiyoshi Matsumura,[c] Yasuyoshi Watanabe[c] and Ryoji Noyori*[b]

[a] *Department of Biomolecular Science, Faculty of Engineering, Gifu University, Yanagido 1-1, Gifu 501-1193, Japan. E-mail: suzukims@apchem.gifu-u.ac.jp*

[b] *Department of Chemistry and Research Center for Materials Science, Nagoya University, Chikusa, Nagoya 464-8602, Japan. E-mail: noyori@chem3.chem.nagoya-u.ac.jp*

[c] *Department of Neuroscience Osaka Bioscience Institute, Furuedai 6-2-4, Suita, Osaka 565-0874, Japan*

Received (in Cambridge, UK) 30th September 1998, Accepted 7th January 1999

Biologically remarkable 15-deoxy-TIC has been realised by the removal of the C(15) chiral centre in 15*R*-TIC, a stable ligand for a CNS-type prostacyclin receptor (IP_2); this deoxy derivative exhibits ten-fold higher affinity and selectivity than 15*R*-TIC for the IP_2 receptor in correlation with the anti-apoptotic activity for neuronal cells.

In response to the increasing requirement for the development of specific molecular probes for the elucidation of the role of prostaglandin (PG) in brain functions,[1] we have designed (15*R*)-16-(*m*-tolyl)-17,18,19,20-tetranorisocarbacyclin **1** (15*R*-TIC) which has high binding affinity and selectivity for a novel prostacyclin (PGI_2) receptor subtype (IP_2) in the central nervous system (CNS).[2] This was utilised to visualise the specific location of the IP_2 receptor for both *in vitro* and *in vivo* systems by autoradiography of rat brain slices[3] and the positron emission tomography (PET) of a living rhesus monkey[4] using tritium-labelled ligand **2** and ^{11}C-labelled ligand **4**,[5] respectively.

The *R* configuration of C(15) in **1** was surprising, because the configuration of this hydroxy-bearing chiral centre in hormonal PGs is generally *S*.[6] In addition, 15*S*-TIC **3**, a C(15) stereoisomer of **1**, exhibited high binding affinity for both PGI_2 receptors, IP_1 and IP_2, as peripheral and CNS types, respectively.[2,3] These findings led us to speculate that the configuration of hydroxy-bearing C(15) in **1** may not be crucial for the binding with the IP_2 receptor and, therefore, that a common structure capable of more specifically recognising the IP_2 receptor could be hidden between these tolylisocarbacyclin structures, **1** and **3**. Accordingly, our interest has been directed to elucidating the essential structural elements necessary to discriminate between the two receptors, particularly focusing on the elimination of the C(15) chirality. Described herein is the synthesis of a 15-deoxy-TIC derivative with superb biological properties.

The title compound **5**, among other synthesised derivatives, exhibited the highest binding affinity and selectivity for the IP_2 receptor. As outlined in Scheme 1, the synthetic strategy consists of the stepwise construction of the *E*-olefin in the ω side-chain instead of the one-step Julia coupling,[7] because the starting aldehyde **6** is unstable under strongly basic conditions.[8] Thus aldehyde **6**[9] was condensed with (formylmethylene)-triphenylphosphorane in benzene at 80 °C to give (*E*)-α,β-unsaturated aldehyde **7** in 64% yield. Carbonyl reduction of **7** using $NaBH_4$ in MeOH, followed by methoxycarbonylation of the resulting allylic alcohol with $ClCO_2Me$ in the presence of

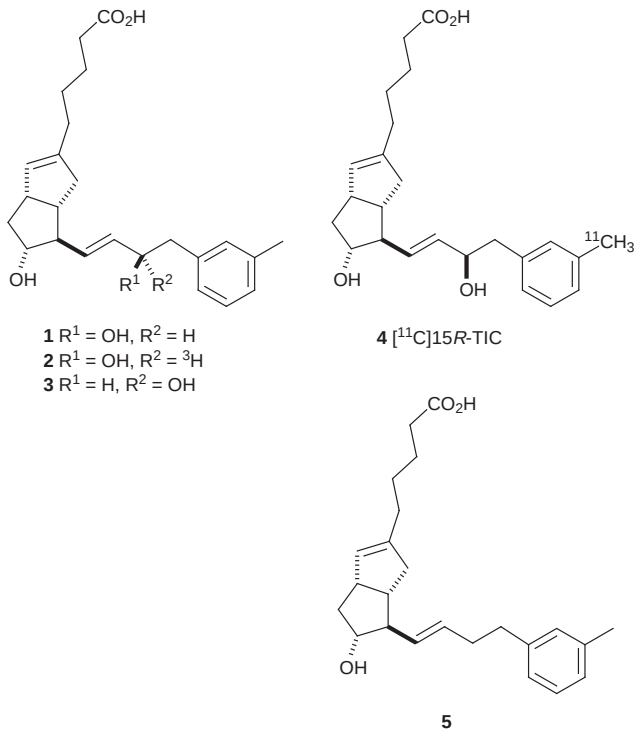

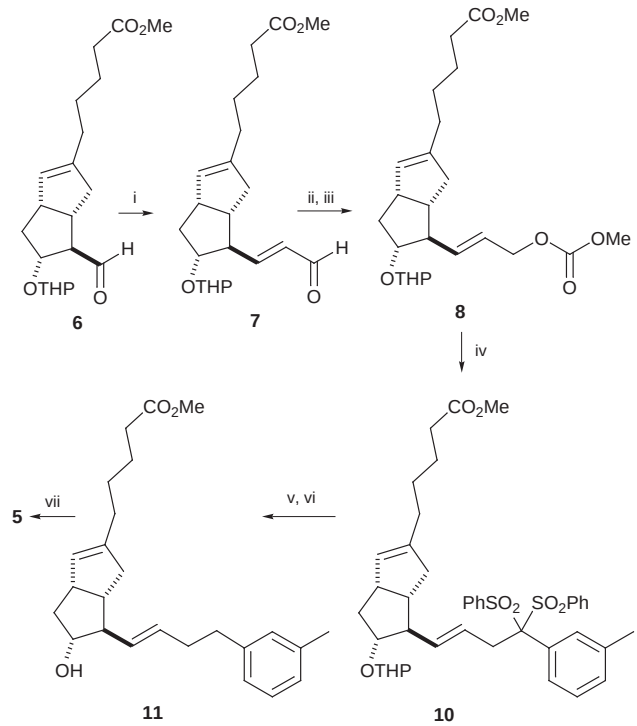

Scheme 1 *Reagents and conditions*: i, $Ph_3PCHCHO$, benzene, reflux; ii, $NaBH_4$, MeOH; iii, $ClCO_2Me$, DMAP, CH_2Cl_2; iv, $Pd_2(dba)_3$, $CHCl_3$, dppe, *m*-$CH_3C_6H_4CH(SO_2Ph)_2$ **9**, THF, 50 °C; v, Mg, MeOH; vi, TsOH, MeOH; vii, aq. NaOH, MeOH.

DMAP in CH_2Cl_2 gave the allyl carbonate **8** in 91% overall yield. The cross-coupling between the allyl carbonate **8** and the sulfone **9** was conducted at 50 °C in THF in the presence of a catalytic amount of $Pd_2(dba)_3$/dppe (1:2 ratio),[10] giving the sulfone **10** in 97% yield.† Reductive removal of the $PhSO_2$ group in **10** with Mg metal in MeOH and subsequent deprotection of the tetrahydropyranyl group with TsOH in MeOH gave the 15-deoxy derivative **11** in 84% overall yield. Finally, alkaline hydrolysis of **11** afforded the desired 15-deoxy-16-(*m*-tolyl)-17,18,19,20-tetranorisocarbacyclin, referred to as 15-deoxy-TIC **5**, in 94% yield.‡

The binding assay was conducted for the neuronal PGI_2 receptor proteins in frozen tissue sections containing the thalamus and the nucleus tractus solitarius (NTS) as representative of the IP_2 and IP_1 receptors, respectively, using C(15) tritium-labelled 15*S*-TIC ([^{3}H]15*S*-TIC)[2] as a standard radioligand. The 50% inhibitory concentrations of the binding (IC_{50} values) were determined by the degree of displacement of 10 nM [^{3}H]15*S*-TIC bound to each receptor by nonradioactive TIC derivatives. Accordingly, 15-deoxy-TIC **5** binds with the CNS-type IP_2 receptor (IC_{50} value = 3 nM) ten times more strongly than 15*R*-TIC **1** while maintaining the weak binding for IP_1 receptor (IC_{50} value = 1 μM).§ As a result, the binding selectivity for the IP_2 receptor [$IC_{50(IP1)}/IC_{50(IP2)}$] increased by a factor of 10. The importance of the length of the ω side-chain, the tolyl group and 13,14 double bond was clarified by a study of the structure binding affinity relationships. Thus the elimination of the hydroxy group at C(15) markedly enhanced the binding affinity and selectivity.

Since the discovery of 15*R*-TIC **1**,[2] we have pursued the biofunction of various TICs in the brain and developed CNS-specific PGI_2 ligands that exhibit neuronal survival-promoting activity both *in vitro* and *in vivo*.[11] The difference of the potency of the binding affinity between **1** and **5** is actually correlated well with the biological activity. Thus 15-deoxy-TIC **5** showed an inhibitory effect on apoptosis of neuronal cells induced by high oxygen (50%) atmosphere at ten-fold lower concentration than 15*R*-TIC **1** (IC_{50} = 30 and 300 nM, respectively). It should be noted that **5** did not exhibit any significant inhibitory effect on platelet aggregation, up to 400 nM, while PGI_2 derivatives which bind to the IP_1 receptor showed a very potent inhibitory effect at several nM.¶

Overall, we have found the essential structure that has conspicuous biological properties by rational molecular modification. The structural simplification by removal of the C(15) chirality will increase chemical or biological tolerance[12] to give a promising anti-apoptotic agent, particularly for chemotherapy of CNS neurons damaged with oxidative stress and ischemia.[11] Future progress will be reported in due course.

This work was supported in part by Grant−in−aids for Scientific Research on Priority Area No. 09273102 and the COE program No. 07CE2004 from the Ministry of Education, Science, Sports and Culture, Japan.

Notes and references

† The sulfone **9** was prepared in 60% overall yield by mixing of *m*-methylbenzaldehyde and PhSH in the presence of TMSCl in CH_2Cl_2 (25 °C, overnight) followed by treatment with Oxone in aq. MeOH (25 °C, 5 h). *Selected data* for **9**: δ_H (270 MHz, $CDCl_3$) 2.22 (s, 3, CH_3), 5.40 (s, 1, CH), 7.1–7.2 (m, 4, arom.), 7.45 (t, 4, *J* = 7.4, arom.), 7.62 (t, 2, *J* 7.4, arom.), 7.79 (d, 4, *J* 7.4 Hz, arom.); δ_C (67.5 MHz, $CDCl_3$) 21.3, 88.7, 125.5, 128.6, 128.8, 129.8, 131.3, 134.5, 138.0, 138.6.

‡ *Selected data* for **5**: δ_H (270 MHz, $CDCl_3$) 1.4–2.1 (m, 10, 4 CH_2, CH, OH), 2.2–2.5 (m, 10, 2 CH_2, CH_3, CH_2CO, CH), 2.6–2.8 (m, 2, benzylic CH_2), 2.90–3.05 (br, 1, allylic CH), 3.63 (dt, 1, *J* 6.9, 9.4, CHO), 5.23 (dd, 1, *J* 8.9, 15.3, vinylic in chain), 5.28 (s, 1, vinylic in ring), 5.53 (dd, 1, J 6.9, 15.3, vinylic in chain), 6.97 (d, 1, *J* 7.9, arom.), 6.98 (s, 1, arom.), 7.00 (d, 1, *J* 7.4, arom.), 7.17 (t, 1, *J* 7.7, arom.); δ_C (67.5 MHz, $CDCl_3$) 21.4, 24.4, 27.1, 30.5, 33.6, 34.5, 35.8, 39.3, 39.6, 44.3, 45.6, 58.6, 77.9, 125.6, 126.5, 128.1, 128.4, 129.4, 132.1, 132.2, 137.8, 141.3, 141.8, 178.3.

§ The displacement of [^{3}H]15*R*-TIC **2** binding with the IP_2 receptor by **5** gave a similar result.

¶ The biological activity was examined at Teijin Co.

1 O. Hayaishi, *FASEB J.*, 1991, **5**, 2575; K. Matsumura, Y. Watanabe, H. Onoe and Y. Watanabe, *Neuroscience*, 1995, **65**, 493; H. Wise, in *Progress in Drug Research*, ed. E. Jucker, Birkhäuser Verlag, Basel, Switzerland, 1997, vol. 49, p. 123.

2 M. Suzuki, K. Kato, R. Noyori, Y. Watanabe, H. Takechi, K. Matsumura, B. Långström and Y. Watanabe, *Angew. Chem., Int. Ed. Engl.*, 1996, **35**, 334; H. Takechi, K. Matsumura, Yu. Watanabe, K. Kato, R. Noyori, M. Suzuki and Y. Watanabe, *J. Biol. Chem.*, 1996, **271**, 5901.

3 Y. Watanabe, K. Matsumura, H. Takechi, K. Kato, H. Morii, M. Björkman, B. Långström, R. Noyori, M. Suzuki and Y. Watanabe, unpublished work.

4 Y. Watanabe, M. Suzuki, M. Björkman, K. Matsumura, Y. Watanabe, K. Kato, H. Doi, H. Onoe, S. Sihver, Y. Andersson, K. Kobayashi, O. Inoue, A. Hazato, L. Lu, M. Bergström, R. Noyori and B. Långström, *Abstr. Pap. Neuroimage*, Aarhus, May 16–18, 1997, vol. **5**, p. A1.

5 M. Suzuki, H. Doi, M. Björkman, Y. Andersson, B. Långström, Y. Watanabe, R. Noyori, *Chem. Eur. J.*, 1997, **3**, 2039; Björkman, Y. Andersson, H. Doi, K. Kato, R. Noyori, M. Suzuki, Y. Watanabe and B. Långström, *Acta Chem. Scand.*, 1998, **52**, 635.

6 N. H. Andersen and P. W. Ramwell, *Arch. Intern. Med.*, 1974, **133**, 30; P. W. Collins and S. W. Djuric, *Chem. Rev.*, 1993, **93**, 1533. For some exceptions in marine products, see: A. J. Weinheimer and R. L. Spraggins *Tetrahedron Lett.*, 1969, 5185; R. J. Light and B. Samuelsson *Eur. J. Biochem.*, 1972, **28**, 232.

7 M. Julia and J.-M. Paris, *Tetrahedron Lett.*, 1973, 4833; P. J. Kocienski, B. Lythgoe and S. Ruston, *J. Chem. Soc., Perkin Trans. 1*, 1978, 829.

8 B. Achmatowicz, E. Baranowska, A. R. Daniewski, J. Pankowski and J. Wicha, *Tetrahedron*, 1988, **44**, 4989.

9 H. Hemmerle and H.-J. Gais, *Angew. Chem., Int. Ed. Engl.*, 1989, **28**, 349; M. Suzuki, H. Koyano, R. Noyori, H. Hashimoto, M. Negishi, A. Ichikawa and S. Ito, *Tetrahedron*, 1992, **48**, 2635.

10 J. Tsuji, I. Shimizu, I. Minami and Y. Ohashi, *Tetrahedron Lett.*, 1982, 4809.

11 T. Satoh, Y. Ishikawa, Y. Kataoka, Y. Cui, H. Yanase, K. Kato, Yu. Watanabe, K. Nakadate, K. Matsumura, H. Hatanaka, R. Noyori, M. Suzuki and Y. Watanabe, unpublished work.

12 K. E. Atkins, W. E. Walker and R. M. Manyik, *Tetrahedron Lett.*, 1970, 3821; D. E. Bergbreiter and D. A. Weatherford, *J. Chem. Soc., Chem. Commun.*, 1989, 883; E. Änggård and B. Samuelsson, *J. Biol. Chem.*, 1964, **239**, 4097.

Communication 8/07613H

ChemComm

A new and enantioselective indolizidine synthesis by *meso*-epoxide α-deprotonation–transannular N–C insertion

David M. Hodgson* and Lesley A. Robinson

Dyson Perrins Laboratory, Department of Chemistry, University of Oxford, South Parks Road, Oxford, UK OX1 3QY. E-mail: david.hodgson@chem.ox.ac.uk

Received (in Liverpool, UK) 19th November 1998, Accepted 5th January 1999

Enantioselective α-deprotonation–rearrangement of *N*-Boc hexahydroazonine oxide 10 using organolithiums in the presence of (-)-sparteine 3 gives the ester 12 in up to 89% ee.

We recently reported the enantioselective α-deprotonation–rearrangement of medium-sized (8-, 9- and 10-membered) cycloalkene-derived achiral epoxides using a secondary organolithium in combination with a chiral ligand such as (−)-sparteine **3**, which gives bicyclic alcohols in good yields and ees (77–84% ee, *e.g.* Scheme 1, X = CH_2).[1] However, only a single functional group is generated in the desymmetrised bicycles. One strategy to enhance the utility of this transformation would be to examine heterocycloalkene-derived achiral epoxides. Here we communicate our preliminary results concerning the synthesis and novel rearrangement chemistry of an azacyclic epoxide of this type (**1**, X = NR).

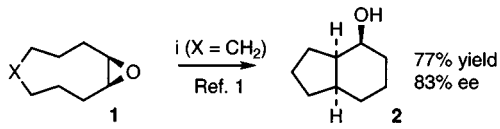

Scheme 1 *Reagents and conditions*: i, Pr^iLi (2.4 equiv.), (−)-sparteine **3** (2.5 equiv.), Et_2O, −98 °C (5 h) to 25 °C (15 h).

An important aspect of the study of transannular reactions of a medium-sized heterocycle concerns the potential problem of preparing the substrate.[2] However, application of methodology[3] used in the synthesis of the azacycloundecene system found in manzamine C led to a highly satisfactory route to the azacyclic epoxide **9** (Scheme 2). Thus, cyclisation under dilute conditions of the ditosylate **6** of the known diol **5** (readily available from cycloocta-1,5-diene)[4] gave the reduced azonine **7** in 62% yield; to the best of our knowledge this is the most efficient cyclisation reported which gives a simple reduced azonine.[2]

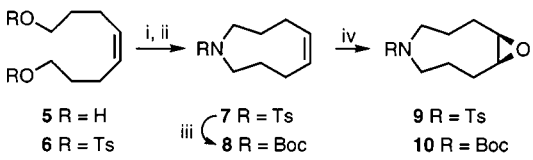

Scheme 2 *Reagents and conditions*: i, TsCl (4.9 equiv.), Py, 0 °C (5 h) to 25 °C (15 h), 74%; ii, $TsNH_2$ (1.7 equiv), NaOH (200 equiv.), Bu_4NI (1.4 equiv.), toluene–H_2O, reflux, 5 h, 62%; iii, Na naphthalenide (2.5 equiv.), THF, −78 °C, then HCl(g), then Et_3N (1.5 equiv.), Boc_2O (1.5 equiv.), DMAP (0.1 equiv.), CH_2Cl_2, 25 °C, 64% from **7**; iv, $MeCO_3H$ (1.2 equiv.), Na_2CO_3 (3 equiv.), NaOAc (0.02 equiv.), CH_2Cl_2, 0 °C (10 min) to 25 °C (15 h), 82% (R = Ts), 87% (R = Boc).

Subjection of the epoxide **9**, derived from reduced azonine **7**, to typical asymmetric rearrangement conditions[1] [Bu^sLi (2.4 equiv.) and (−)-sparteine **3** (2.5 equiv.) in Et_2O at −78 °C for 5 h, followed by warming to 25 °C over 15 h, *cf.* Scheme 1] led only to the recovery of starting epoxide **9**, whereas quenching the reaction with D_2O led to essentially complete *o*-deuterium incorporation into the tosyl group of the recovered starting material (64%). An attempt to induce reaction at the epoxide group subsequent to *ortho*-deprotonation using double the quantities of reagents indicated above led to no identifiable products; an alternative protecting group was therefore required. Removal of the tosyl group from **7** using sodium naphthalenide and immediate Boc reprotection of the amine hydrochloride salt gave the reduced azonine **8** (64%). Epoxidation provided **10**, which could potentially undergo deprotonation with an organolithium either α to the epoxide oxygen, or α to nitrogen. Beak has reported a 6-*exo-tet* cyclisation onto an epoxide *via* deprotonation α to NBoc; the deprotonation site was however also benzylic in this case.[5] Beak has also reported that the rate of deprotonation of Boc-protected azacycles decreases on moving from pyrrolidine to piperidine to perhydroazepine.[6] In the event, reaction of the epoxide **10** with Bu^sLi (2.4 equiv. in Et_2O at −78 °C for 5 h, followed by warming to 25 °C over 15 h) led to an inseparable 1 : 1 mixture of epimers (due to the stereogenic centre in the Bu^s group, *vide infra*) of ketone **11a** (48%, 70% based on recovered epoxide **10**, Scheme 3).

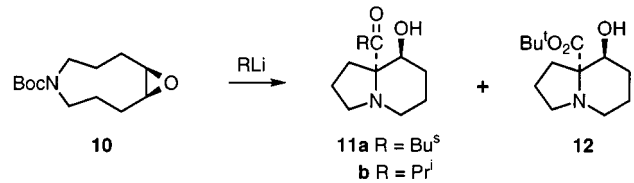

Scheme 3

In contrast, reaction of the epoxide **10** with Bu^sLi, under the same conditions but in the presence of TMEDA (2.5 equiv.), led to the formation of ester **12** as the major product (**12** : **11a**, 8 : 1 by ^1H NMR analysis; 74% isolated yield of **12**). Using (−)-sparteine **3** as the ligand in an otherwise identical experiment gave an equal mixture of **11a** and **12** (66% ee for **12**).† Experiments were then carried out to examine the possibility of increasing both the proportion and ee of ester **12** formed from epoxide **10** (Table 1).

Maintaining the reaction at −78 °C for 18 h and then quenching at this temperature gave ester **12** in improved ee (74%, Table 1, entry 1), but the ketone **11a** predominated. However, repeating the same procedure at −98 °C significantly improved the proportion of ester **12** (**12** : **11a**, 5 : 1) and increased the ee of **12** to 79% (entry 2). Using Pr^iLi at −98 °C gave mainly the ester **12** (**12** : **11a**, 10 : 1) and with the highest level of asymmetric induction (89% ee, entry 3),‡ as also observed with our earlier work on cycloalkene-derived epoxides.[1] Using (−)-α-isosparteine **4** as ligand with either Bu^sLi or Pr^iLi slowed the reaction considerably (entries 4 and 5), particularly in conjunction with Bu^sLi; the ees were also reduced compared with the corresponding (−)-sparteine **3** reactions. In an attempt to allow Pr^iLi/(−)-α-isosparteine **4** to completely consume the epoxide **10**, the reaction was left for 40 h at −98 °C (entry 6), but it still remained only 50% complete after this time and no change in the ee of ester **12** was observed. The use of catalytic amounts of ligand was also investigated

Table 1 Effect of experimental conditions on the yields and enantioselectivities of formation of indolizidine **12** from epoxide **10** using ligand/RLi in Et_2O

Entry[a]	Ligand	RLi	**10** : **11** : **12**[b]	Yield of **12**[c] (%)	Ee of **12** (%)
1[d]	**3**	Bu^{s}Li	0 : 1.6 : 1.0	32 (20)	74
2	**3**	Bu^{s}Li	0.1 : 0.2 : 1.0	58 (50)	79
3	**3**	Pr^{i}Li	0.3 : 0.1 : 1.0	57 (49)	89
4	**4**	Bu^{s}Li	5.0 : 0 : 1.0	14	64
5	**4**	Pr^{i}Li	2.0 : 0.1 : 1.0	29	79
6[e]	**4**	Pr^{i}Li	1.3 : 0.1 : 1.0	40	78
7[f]	**3**	Pr^{i}Li	0.7 : 0.6 : 1.0	36	82
8[f]	**4**	Pr^{i}Li	1.2 : 0.1 : 1.0	33	77
9[e,f]	**4**	Pr^{i}Li	0.4 : 0.2 : 1.0	54	89

[a] Ratio of ligand : RLi : epoxide **10**, 2.45 : 2.4 : 1 and carried out at −98 °C with a reaction time of 18 h unless otherwise indicated. [b] Ratios determined by ^{1}H NMR analysis of the crude reaction mixture. [c] Yield of **12** as measured by ^{1}H NMR analysis using methyl diphenylacetate as an internal standard. Isolated yields given in parentheses. [d] Carried out at −78 °C. [e] Reaction time 40 h. [f] Ratio of ligand : RLi : epoxide **10**, 0.24 : 2.4 : 1.

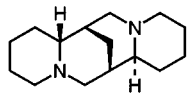

(−)-**3**

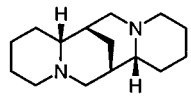

(−)-**4**

(entries 7–9) with interesting results. Using 24 mol% (−)-sparteine **3** (10 mol% with respect to Pr^{i}Li), high levels of ee (82%) were still achieved, but the reaction was found to be much slower. In contrast, (−)-α-isosparteine **4** was more effective when used in a catalytic fashion (entry 8), with no apparent change in the ee (compare entry 5). Repeating this last reaction but leaving it for 40 h at −98 °C allowed the reaction to proceed further to completion and also gave a much higher level of ee (entry 9).

The structures of indolizidinols **11** and **12** were assigned by extensive spectroscopic investigations and were later further supported by X-ray crystallographic analysis of ketone **11b**.§ A mechanistic explanation for the formation of the indolizidinols is that they arise *via* lithiation α to the epoxide oxygen to give **13**, followed by transannular reaction using the N lone pair to give an ammonium ylide **14** which undergoes [1,2] migration of the exocyclic N substituent (Scheme 4); direct insertion of the lithiated epoxide into the exocyclic C–N bond is also possible. Incorporation of the organolithium to give the ketones **11** could occur before or after the transannular reaction. The latter

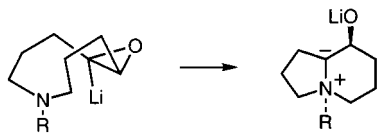

13 **14**

Scheme 4

process seems most likely, since reducing the equivalents of organolithium from 2.5 improves (at the expense of conversion of starting epoxide **10**) the ratio of ester **12** : ketone **11**, and in a separate experiment ester **12** could be quantitatively converted to ketone **11b** using Pr^{i}Li (1.1 equiv., −78 °C for 1 h, followed by warming to 0 °C over 2 h).

Insertion of a lithiated epoxide into a C–N bond has not previously been reported and the present study illustrates an example of this process leading to a new and enantioselective entry to the important indolizidine framework. Further studies on the scope of this process are in progress and will be reported in due course.

We thank the EPSRC for a Research Grant (GR/L39940: postdoctoral support to L. A. R.), the EPSRC National Mass Spectrometry Service Centre for mass spectra and Dr D. J. Watkin and Professor K. Prout (Chemical Crystallography Laboratory, University of Oxford) for assistance with the X-ray structure analysis.

Notes and references

† Ees were determined by GC (Chrompack chirasil-dex 25 m × 0.32 mm ID column; 6 psi, 120 °C). The absolute configurations of the predominant indolizidinol enantiomers are not known but can be tentatively assigned as shown in Scheme 3 by analogy with the selectivity for deprotonation at the *R* configured epoxide stereocentre with (−)-sparteine **3** observed in our earlier medium-ring studies (ref. 1).

‡ Freshly distilled (−)-sparteine (70 mm^3, 0.30 mmol) in Et_2O (1 cm^3) was added dropwise over 0.5 h to a stirred solution of Pr^{i}Li [1.09 mol dm^{-3} in light petroleum (boiling range 40–60 °C); 270 mm^3, 0.29 mmol] in Et_2O (1 cm^3) at −98 °C. The reaction mixture was allowed to stir for 1 h at −98 °C before the epoxide **10** (30 mg, 0.12 mmol) in Et_2O (1 cm^3) was added dropwise over 0.5 h. The reaction mixture was stirred for 18 h at this temperature and then H_3PO_4 (0.5 mol dm^{-3} in water; 1 cm^3) added slowly dropwise. After warming to room temperature the organic layer was removed and the aqueous layer extracted with Et_2O (3 × 5 cm^3). The combined organic extracts were dried ($MgSO_4$) and then evaporated under reduced pressure. Purification of the residue by column chromatography [(SiO_2, 50% Et_2O–light petroleum (boiling range 40–60 °C) → 100% Et_2O] gave the ester **12** (14.8 mg, 49%); $[\alpha]_D^{21}$+48.6 (*c* 0.3 in $CHCl_3$).

§ *Crystal data* for **11b**: $C_{12}H_{20}NO_2$, *M* = 210.29, orthorhombic, space group $P2_12_12_1$ (No. 19), *a* = 5.807(7), *b* = 13.393(2), *c* = 15.477(3) Å, *V* = 1203.7(3) Å^3, *Z* = 4. 1038 independent reflections measured at 173 K on an Enraf-Nonius DIP2000 diffractometer. Mo-Kα radiation. 718 reflections with $I > 8\sigma(I)$ and 137 variables yield R = 0.064, R_w = 0.063. CCDC 182/1138. Crystal data are available in CIF format from the RSC web site, see: http://www.rsc.org/suppdata/cc/1999/309/

1 D. M. Hodgson, G. P. Lee, R. E. Marriott, A. J. Thompson, R. Wisedale and J. Witherington, *J. Chem. Soc., Perkin Trans. 1*, 1998, 2151.
2 P. A. Evans and A. B. Holmes, *Tetrahedron*, 1991, **47**, 9131.
3 Y. Torisawa, A. Hashimoto, M. Nakagawa, H. Seki, R. Hara and T. Hino, *Tetrahedron*, 1991, **47**, 8067.
4 D. Raederstorff, A. Y. L. Shu, J. E. Thompson and C. Djerassi, *J. Org. Chem.*, 1987, **52**, 2337.
5 P. Beak, S. Wu, E. K. Yum and Y. M. Jun, *J. Org. Chem.*, 1994, **59**, 276.
6 P. Beak and W. K. Lee, *J. Org. Chem.*, 1993, **58**, 1109.

Communication 8/09105F

Synthesis and structure of arene soluble *N,N′*-bis(di-*tert*-butylsalicylidene)ethylenediamine yttrium complexes

William J. Evans,* Cy H. Fujimoto and Joseph W. Ziller

Department of Chemistry, University of California, Irvine, Irvine, California 92697-2025 USA.
E-mail: wevans@uci.edu

Received (in Columbia, MO, USA) 23rd September 1998, Accepted 9th December 1998

YCl_3 reacts with 1 and 2 equiv. of the dipotassium salt of *N,N′*-bis(3,5-di-*tert*-butylsalicylidene)ethylenediamine (K_2salen′) and thf to form the arene soluble complexes, [(salen′)Y(μ-Cl)(thf)]$_2$ and (thf)$_2$K[Y(salen′)$_2$], respectively, which provide comparative structural information on the use of this ligand *vis-à-vis* bis(cyclopentadienyl) ligand sets.

Efforts to extend the range of ancillary solubilizing and stabilizing environments for yttrium and the lanthanide metals beyond the common cyclopentadienyl ligand and its analogs have led to the exploration of alternative, polydentate anionic ligands containing various combinations of oxygen and nitrogen donor atoms.[1] Among the ligands examined have been substituted Schiff base derivatives of *N,N′*-bis(salicylidene)-ethylenediamine (H_2salen), a ligand which has been successfully used with both main group and transition metals.[2–8] Salen derivatives are attractive since they can be prepared and derivatized easily and inexpensively[2] and even bi- and tridentate Schiff bases have been shown to be effective ligands for lanthanides.[3] Initial studies[6] of the di-*tert*-butyl substituted analog *N,N′*-bis(3,5-di-*tert*-butylsalicylidene)ethylenediamine, H_2salen′,[7] suggested that this ligand would be of limited use with the f-elements compared to cyclopentadienyl ligands since synthetic routes using common precursors such as YCl_3 and Y[N(SiMe$_3$)$_2$]$_3$, led to insoluble, presumably oligomeric complexes.[6] Only by use of the specialized silylamide, [N(SiHMe$_2$)$_2$]$^-$,[9] was a fully characterizable complex, (salen′)Y[N(SiHMe$_2$)$_2$](thf) **1** obtained.[6] We report here that by using the potassium salt, K_2salen′, obtained from H_2salen′ and KH, soluble complexes can be obtained directly from YCl_3.

YCl_3 reacts with 1 equiv. of K_2salen′ in thf over a 6 h period to form the arene soluble complex [(salen′)Y(μ-Cl)(thf)]$_2$ **2** which was identified by NMR and IR spectroscopy, elemental analysis,† and X-ray diffraction,‡ Fig. 1. Complex **2** crystallizes from benzene as a thf-solvated asymmetric dimer in which one salen′ ligand adopts a nearly planar orientation [Y(2)] and the other is non-planar.

Both yttrium ions in **2** have seven-coordinate distorted capped trigonal prismatic geometries, but Cl(1) occupies the capping position for the Y(1) trigonal prism and N(3) is the cap for Y(2). The distortions of the trigonal prisms also differ: the dihedral angles of the planes of the trigonal faces are 16.6° for Y(1) and 5.4° for Y(2). The salen′ ligand attached to Y(1) has a 119.8° dihedral angle between the planes of the phenyl rings, whereas the salen′ around Y(2) has a more planar orientation, with an 8.4° dihedral angle. The analogous angle in **1** is 108°.[6] In contrast, (salen′)InCl[8] is a monomer in which the salen′ donor atoms are planar. The monomeric structure may be more favorable for indium since it is less electropositive and *ca.* 0.1 Å smaller than yttrium.

Since **2** is similar to the important general class of bis(cyclopentadienyl) halide precursors [(C$_5$H$_4$R)$_2$Y(μ-Cl)]$_2$, comparison of the structural parameters of the [Y(μ-Cl)]$_2$ unit in **2** with those of the structurally characterized cyclopentadienyl examples in which R = H,[10] SiMe$_3$[11] and PPh$_2$,[12] allows evaluation of the salen′$^{2-}$ ligand set *vs.* two C$_5$H$_4$R$^-$ ligands. As shown in Table 1, the Y–Cl distances in **2** are larger than those

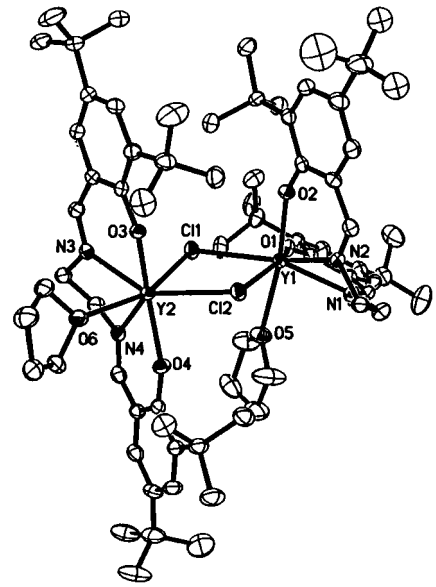

Fig. 1 Structure of [(salen′)Y(μ-Cl)(thf)]$_2$ **2** with thermal ellipsoids drawn at the 50% probability level.

Table 1 Structural data on complexes containing the [Y(μ-Cl)]$_2$ unit

Formula	Coordination number	Y–Cl/Å	Y–Cl–Y/°	Cl–Y–Cl/°	Ref
[(salen′)Y(μ-Cl)(thf)]$_2$	7	2.734(1)–2.759(1)	102.60(3)–103.13(3)	76.34(3)–76.52(3)	This work
[Cp$_2$Y(μ-Cl)]$_2$	8	2.677(3) 2.691(3)	98.58(4)	81.44(4)	10
[(Me$_3$SiC$_5$H$_4$)$_2$Y(μ-Cl)]$_2$	8	2.684(1) 2.704(1)	98.4(1)	81.6(1)	11
syn-[(Ph$_2$PC$_5$H$_4$)$_2$Y(μ-Cl)]$_2$	8	2.655(2) 2.680(2)	97.19(7) 97.43(7)	82.34(7) 82.99(7)	12
anti-[(Ph$_2$PC$_5$H$_4$)$_2$Y(μ-Cl)]$_2$	8	2.657(2) 2.657(2)	99.30(7)	80.69(7)	12

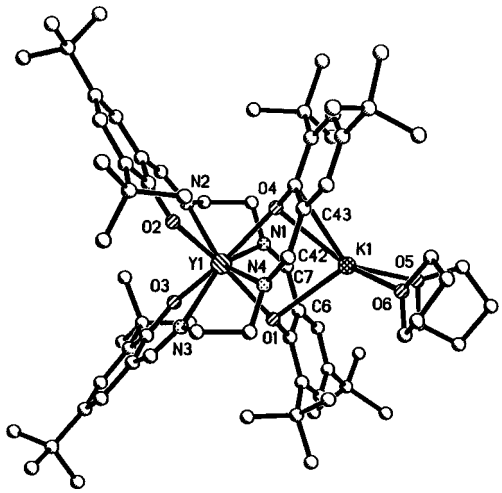

Fig. 2 Ball-and-stick model (for clarity) of $(thf)_2K[(salen')_2Y]$ **3**.

in the $[(C_5H_4R)_2Y(\mu\text{-}Cl)]_2$ complexes, even though **2** is formally seven coordinate and the other complexes are eight coordinate. This difference is accompanied by slightly smaller Cl–Y–Cl angles and slightly larger Y–Cl–Y angles.

Reaction of 2 equiv. of K_2salen′ with YCl_3 also provides an arene soluble product, $(thf)_2K[(salen')_2Y]$ **3**. The coordination environment in **3** (Fig. 2) differs from the 'sandwich' type of coordination which has been postulated for lanthanide complexes containing two disalicylidene-1,2-phenylenediamine ligands.[4] The yttrium in **3** is surrounded by a distorted eight-coordinate square antiprismatic coordination geometry with the N(2) and O(2) of one salen′ ligand and the N(3) and O(3) of the other ligand in one square face and the other donor atoms of the two ligands, N(1), N(4), O(1) and O(4), in the other square face. The dihedral angles between the arene rings in the salen′ ligands are similar: 20.9 and 22.5°. The Y–O distances [2.245(4)–2.356(3) Å] in this eight-coordinate complex are larger than those [2.143(2) and 2.16 Å] in seven-coordinate **2** and six-coordinate **1**, respectively. The Y–N distances [2.556(4)–2.618(4) Å] are also larger than the largest Y–N distances in **2** and **1** [2.492(3) and 2.44 Å, respectively].

The potassium in **3** is coordinated to two thf oxygen atoms at distances of 2.608(6) and 2.683(3) Å and an oxygen atom from each salen′ at 2.720(4) and 2.724(4) Å. The next closest distances involve C(48) [3.141(5) Å] and C(1) [3.180(5) Å], both of which are comparable to the potassium–phenyl carbon distance of 3.191(5) Å in $KBPh_4$.[13] The potassium distances to N(4) [3.245(5) Å], N(1) [3.362(4) Å], C(43) [3.431(5) Å], C(42) [3.434(5) Å], C(6) [3.454(5) Å] and C(7) [3.464(5) Å] are longer, but are within the 3.288(9)–3.534(13) Å range of K-donor atom long distance interactions cited in potassium aryloxide literature.[14] The structure of **3** demonstrates the flexibility of the salen′ ligand: two of these large ligands can be accommodated at one yttrium center and can incorporate a counter-cation to make an arene soluble product. The cyclopentadienyl analog, which would be a $[(C_5H_4R)_4Y]^-$ complex, is not known for yttrium.[15]

These results show that the salen′ ligand is viable both synthetically and structurally for metals the size of yttrium. This ligand can take the place of two cyclopentadienyl ligands in a chloride complex to provide a bridged species with slightly modified structural parameters as well as a bis(salen′) complex which has no cyclopentadienyl analog. Electronically, this salen′ should be quite different from cyclopentadienyl ligand sets and the ramifications of this difference are under investigation.

For support of this research, we thank the Division of Chemical Sciences of the Office of Basic Energy Sciences of the Department of Energy.

Notes and references

† Addition of YCl_3 (975 mg, 5 mmol) to a stirred solution of K_2salen′ (2.69 g, 4.74 mmol, from KH and H_2salen′ in thf) in 70 mL of thf caused the white suspension of K_2salen′ to disappear immediately. A clear yellow solution with white insoluble material began to form. After 6 h, the reaction mixture was filtered and the solvent was removed by rotary evaporation to give an oil. Trituration with hexanes generated a yellow powder and removal of the volatiles by rotary evaporation left **2** as a yellow powder (3.10 g, 90%). $\delta_H(C_4D_8O$, 400 MHz) 8.25 (s, 2H), 7.36 (d, *J* 2.8, 2H), 7.03 (d, *J* 2.4, 2H), 3.89 (br, 4H), 1.45 (s, 18H), 1.25 (s, 18H); $\delta_c(C_4D_8O$, 100 MHz) 169.5, 129.4, 130.5, 63.3, 30.3, 31.9. Isopiestic molecular weight in thf: calc. 1357; found, 1190. IR(KBr): 2953s, 2861m, 1738m, 1716m, 1620s, 1533m, 1461m, 1435m, 1410m, 1353w, 1256w, 1200w, 1159w, 1102w, 1159w, 1102w, 1056w, 1025w cm^{-1}. Anal. Calc. for $C_{36}H_{54}N_2O_3YCl$: C, 62.92; H, 7.85; N, 4.07. Found: C, 62.80; H, 7.62; N, 3.97%.

Following the procedure above, addition of YCl_3 (150 mg, 0.77 mmol) to K_2salen′ (929 mg, 1.6 mmol) gave **3** as a dark orange powder (820.9 mg, 95%). $\delta_H(C_4D_8O$, 500 MHz) 8.14 (s, 2H), 7.07 (d, *J* 2.75, 2H), 6.80 (s, *J* 2.75, 2H), 4.29 (br, 4H), 1.26 (s, 18H), 1.14 (s, 18H); $\delta_c(C_4D_8O$, 125 MHz) 169.3, 128.2, 130.7, 64.3, 30.3, 32.0. IR(KBr): 2955s, 2860m, 1625m, 1530s, 1437m, 1408m, 1349w, 1308w, 1261m, 1197w, 1161w, 1056m br, 797m cm^{-1}. Anal. Calc. for $C_{80}H_{124}KN_4O_8Y$: C, 68.73; H, 8.94; N, 4.01. Found: C, 68.24; H, 8.94; N, 3.84%.

‡ *Crystallographic data*: **2**·2.5C_7H_8: $C_{72}H_{108}N_4O_6Y_2Cl_2$·2.5$C_7H_8$, *M* = 1604.68, monoclinic, space group $P2_1/n$, *a* = 14.4421(7), *b* = 21.3531(10), *c* = 29.7693(14) Å, β = 103.333(1)°, *V* = 8932.9(7) $Å^3$, *Z* = 4, *T* = 158 K, μ = 1.403 mm^{-1}, Mo-Kα radiation, graphite monochromator. The raw frame data were processed using SAINT and SADABS and subsequent calculations were carried out with SHELXTL. The structure was solved by direct methods and refined on F^2 by full-matrix least-squares techniques. Hydrogen atoms were included using a riding model. At convergence, *wR*2 = 0.1492 and GOF = 1.028 for 900 variables refined against 21112 unique data [as comparison, for refinement on *F*, *R*1 = 0.0618 for those 13184 data with $I > 2.0\sigma(I)$].

3: $C_{80}H_{124}KN_4O_8Y$, *M* = 1397.84, space group $P2_1/n$, *a* = 16.3521(9), *b* = 25.6261(14), *c* = 19.1803(10) Å, β = 97.7470(10), *V* = 7964.0(7), *Z* = 4, *T* = 158 K, μ = 0.838 mm^{-1}, Mo-Kα radiation, graphite monochromator. Data analysis was as above. At convergence, *wR*2 = 0.2546 and GOF = 1.031 for 747 variables refined against all 18592 unique data [as comparison, for refinement on *F*, *R*1 = 0.1038 for those 10540 data with $I > 2.0\sigma(I)$]. CCDC 182/1125.

1 F. A. Hart, *Comprehensive Coordination Chemistry*, ed. G. Wilkinson, R. D. Gillard and J. A. McCleverty, Pergamon, Oxford, 1987, vol. 3, ch. 39 and references therein; W. J. Evans, *New J. Chem.*, 1995, **19**, 525; I. Santos and N. Marques, *New J. Chem.*, 1995, **19**, 551.
2 D. E. Fenton and P. A. Vigato, *Chem. Soc. Rev.*, 1988, **17**, 69; D. A. Atwood, *Coord. Chem. Rev.*, 1997, **165**, 267.
3 P. Blech, C. Floriani, A. Chiesi-Villa and C. Guastini, *J. Chem. Soc., Dalton Trans.*, 1990, 3557.
4 H. Chen and R. D. Archer, *Inorg. Chem.*, 1994, **33**, 5195 and references therein.
5 G. B. Deacon, T. Feng, D. C. R. Hockless, P. C. Junk, B. W. Skelton and A. H. White, *Chem. Commun.*, 1997, 341.
6 R. Anwander, T. Priermeier and O. Runte, *Chem. Commun.*, 1996, 1385.
7 D. A. Atwood, M. S. Hill, J. A. Jegier and D. Rutherford, *Organometallics*, 1997, **16**, 2659; M. S. Hill, P. R. Wei and D. A. Atwood, *Polyhedron*, 1998, **17**, 811.
8 M. S. Hill and D. A. Atwood, *Main Group Chem.*, 1998, **2**, 191.
9 W. A. Herrmann, R. Anwander, F. C. Munck, W. Scherer, V. Dufand, N. W. Huber and G. R. J. Artus, *Z. Naturforsch., Teil B*, 1994, **49**, 1789.
10 E. B. Lobkovskii, G. L. Soloveichik, B. M. Bulychev and A. B. Erofeev, *Zh. Strukt. Khim.*, 1984, **25**, 170.
11 W. J. Evans, M. S. Sollberger, J. L. Shreeve, J. M. Olofson, J. H. Hain and J. W. Ziller, *Inorg. Chem.*, 1992, **31**, 2492.
12 R. Broussier, G. Delmas, P. Perron, B. Gautheron and J. L. Petersen, *J. Organomet. Chem.*, 1995, **511**, 185.
13 E. Weiss, *Angew. Chem., Int. Ed. Engl.*, 1993, **32**, 1501.
14 W. J. Evans, M. A. Ansari, J. W. Ziller and S. I. Khan, *J. Organomet. Chem.*, 1998, **553**, 141.
15 H. Schumann, J. A. Meese-Marktscheffel and L. Esser, *Chem. Rev.*, 1995, **95**, 865.

Communication 8/07470D

Not all short C–H···O contacts are hydrogen bonds: the prototypical example of contacts to C=O⁺–H

Thomas Steiner†

Department of Structural Biology, Weizmann Institute of Science, Rehovot 76100, Israel

Received (in Cambridge, UK) 17th November 1998, Accepted 23rd December 1998

Intermolecular contacts between C–H groups and the charged moiety X=O⁺–H show a pronounced negative directionality, *i.e.* short contacts are associated with strongly bent angles; this indicates that these interactions do not represent hydrogen bonds, although they are occasionally short with H···O distances down to 2.5 Å.

After a long period of dispute, it has in recent years become accepted that directional and cohesive C–H···O interactions represent hydrogen bonds.[1,2] Because carbon acidities span a very wide range,[3] the strengths of C–H···O hydrogen bonds cover also a wide range that overlaps at one end with strengths of O–H···O hydrogen bonds,[4] and on the other end it merges with van der Waals interactions.[5] In this context, it is of importance to ask whether *all* short C–H···O contacts are hydrogen bonds, or if there are exceptions. This matter has been addressed by several authors. In particular, short intramolecular C–H···O contacts,[6] short contacts with second-nearest neighbours,[7] compressed C–H···O interactions[8] and inter-anion C–H···O contacts[9] have been mentioned as possibly destabilizing. All these studies, however, remained limited in scope. In the present work, a whole class of short C–H···O contacts that do not represent hydrogen bonds will be presented, and structural consequences of this lack of hydrogen bond nature will be shown. The analytical tool used is the crystal correlation method, which has not been applied for this purpose before.

In hydrogen bonding X–H···A, it is a prerequisite that the acceptor A is a basic entity, and the donor X–H must be at least slightly acidic. Alternatively, in an electrostatic approach, one can give as a basic requirement that the acceptor A must carry a negative partial charge, or at least must have a sterically accessible region of negative charge concentration. This would mean that intermolecular contacts X–H···$A^{\delta+}$ do not fulfill the primary conditions for hydrogen bonding, and even if they occur experimentally, they should not be classified as hydrogen bonds. To look into the matter of intermolecular C-H···O contacts that are not hydrogen bonds, contacts to O atoms of the kind $O^{\delta+}$ are, therefore, a relevant system. Candidates are the O atoms in species like H_3O^+ and $X{=}OH^+$. In the latter, the positive charge need not be localized on the O-atom, but charge delocalization with substantial contribution of the resonance form $X{=}OH^+$ should be sufficient. Examples are systems like $P{=}OH^+ \leftrightarrow P^+{-}OH$, $>N{-}C{=}OH^+ \leftrightarrow >N^+{=}C{-}OH$, and so on.

In crystals, there is not even one example of a short contact X–H···$O^{\delta+}$ formed by an O–H or N–H group.‡ However, relatively short contacts of C–H groups to $O^{\delta+}$ do occur occasionally within frameworks of strong hydrogen bonds and ionic interactions. As an example, the crystal structure of acetamidium nitrate[10] is shown in Fig. 1. A methyl C–H group forms a short contact to a nitrate O atom (H···O = 2.28 Å), which is clearly suggestive of a C–H···$O^{\delta-}$ hydrogen bond. This C–H group also forms an inter-cation C–H···$O^{\delta+}$ contact with H···O = 2.60 Å. When considering only interatomic distances, this contact too might be interpreted as a weak hydrogen bond, and such a view could even be supported by the suitable orientation of the electron lone pair of the protonated amide O atom. On the other hand, when looking at the overall electrostatic situation, and when considering the complete absence of related O/N–H···$O^{\delta+}$ 'hydrogen bonds' in crystals, this C–H···$O^{\delta+}$ interaction would rather be taken as forced by optimization of the strong interionic interctions. In view of such conflicting arguments, further evidence in favour of or against the interpretation as a hydrogen bond is clearly needed.

One of the characterstics of hydrogen bonding is the *directionality*. In optimal geometry, the donor is oriented linearly at the acceptor, and any deviation from linearity incurs an energetic disadvantage. The weaker hydrogen bond types can be easily distorted from optimal geometry so that large deviations from linearity occur frequently, but a statistical preference for linearity is discernible even for the very weak C–H···O hydrogen bonds formed by methyl groups.[11] This property can be used as a test criterion in assessing whether a particular type of intermolecular C–H···O contact is a hydrogen bond or not. In a CSD analysis‡ of intermolecular C–H···$O^{\delta+}$

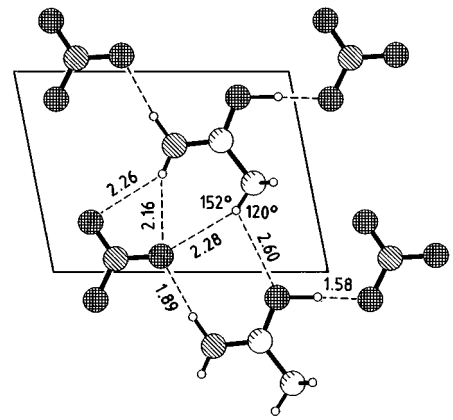

Fig. 1 Crystal structure of acetamidium nitrate (ref. 10); geometries are given for normalized H atom positions.

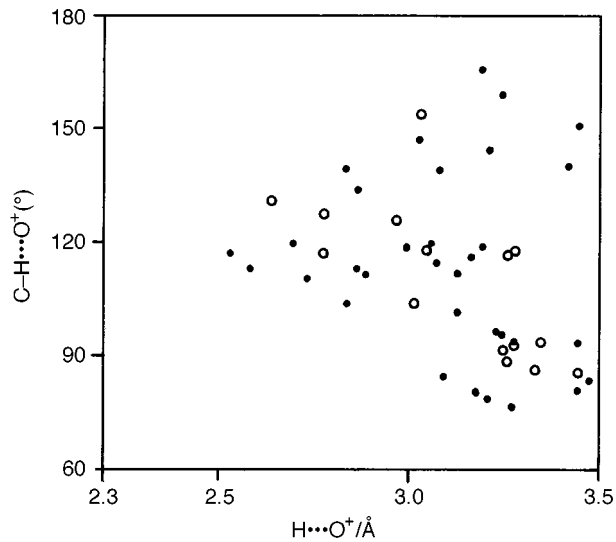

Fig. 2 Scatterplot of C–H···O angles against H···O distances in C–H···O contacts involving fragments (●) **1** and (○) **2**.

† On leave from: Institut für Kristallographie, Freie Universität Berlin, Takustraße 6, D-14195, Berlin, Germany. E-mail: steiner@chemie.fu-berlin.de

Table 1 The structural data set under study

CSD reference code‡	Ref.	C=O⁺H type	C–H type	Charge on CH donor molecular	Counterion to C = O⁺H	Shortest H···O$^{\delta+}$/Å
BIFKEG	12(*a*)	**2**	$>CH_2$	0	NO_3^-	2.64
BIFKIK	12(*a*)	**2**	$>CH_2$	0	ClO_4^-	2.78
CAPRLC	12(*b*)	**1**	$>CH_2$	+1	Cl^-	2.59
DAHRAF	12(*c*)	**2**	$-CH_3$	+1	$F_3C\text{-}SO_3^-$	2.97
ENANLC	12(*d*)	**1**	$>CH_2$	+1	Cl^-	2.86
FUVMUE	12(*e*)	**1**	$-CH_3$	+1	$F_3C\text{-}SO_3^-$	2.73
MACMHC	12(*f*)	**1**	$-CH_3$	+1	Cl^-	3.08
MACMNO	10	**1**	$-CH_3$	+1	NO_3^-	2.60
VAYLAI	12(*g*)	**1**	$-CH_3$	+1	NO_3^-	2.53

Table 2 Mean geometries of different kinds of C–H···O interactions with H···O < 3.0 Å as compared with C–H···H–C van der Waals contacts

Interaction type	[*n*]	H···O (Å)	C···O (Å)	C–H···O/H (°)
C≡C–H···O=C[a]	44[a]	2.36(4)	3.31(2)	152(2)
C=CH_2···O=C[a]	124[a]	2.67(1)	3.56(2)	143(1)
CH_2–CH_3···O=C[a]	767[a]	2.761(6)	3.590(7)	137.1(7)
CH_2–CH_3···H–C[a]	3975[a]			128.6(3)
C–H···O$^{\delta+}$	15	2.78(4)	3.45(5)	121(3)

[a] From ref. 11.

contacts, data quantities sufficient for statistical analysis were found only for the O atoms in OH groups of the cationic fragments **1** and **2**, which represent protonated acetamide and

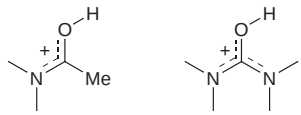

1 **2**

urea skeletons. In both fragments, the positive charge is delocalized, but this involves only small groups of atoms. Fragments which allow charge dilution over larger atom groups than in urea were generally not considered.

For C–H···O contacts formed by fragments **1** and **2**, the scatterplot of C–H···O angles against the H···O distance is shown in Fig. 2, and some additional information is given in Table 1. The overall appearence of the scatterplot is very different from those obtained for hydrogen bonds. For these, short contacts are associated with relatively linear angles.[1] The shortest contacts in Fig. 2 have H···O distances slightly longer than 2.5 Å, but are all associated with strongly bent angles around 120°. No C–H···O$^{\delta+}$ contact is found which is at the same time short and linear, and relatively linear angles occur only at long distances > 3.0 Å. This could be termed a 'negative directionality', which is clearly incompatible with a hydrogen bond nature of the interaction. In order to compare the typical contact geometry with those of clear C–H···O hydrogen bonds and of C–H···H-C van der Waals contacts, mean distances and angles are listed for H···O < 3.0 Å in Table 2. The van der Waals contacts have isotropic directionality characteristics, associated with a mean C–H···H angle of 128.6°.[11] C–H···O hydrogen bonds are on average more linear than van der Waals contacts, whereas C–H···O contacts of fragments **1** and **2** are more bent, with a mean angle of 121(3)°. This indicates that these C–H···O contacts are neither hydrogen bonds, nor are they of the van der Waals type, but the H atom is rather repelled by the O atom, in a sense pushed out of the way.

A look at Table 1 shows that the data sample is chemically diverse. Most of the C–H···O contacts represent inter-cation interactions, but there are also examples of C–H groups in uncharged molecules. This means that the interaction is not specific to a particular narrow family of molecules, or to cation–cation contacts, but is of more general relevance. Actually, short but bent C-H···O$^{\delta+}$ contacts are found in the CSD also for O-atoms in P = OH$^+$, S = OH$^+$ and H_3O^+ but for these, the data quantities are too small to allow reasonable statistical analysis. It is of importance that the C–H groups involved are all of the very weakly polar types $>CH_2$ and $-CH_3$ (Table 1), for which the unfavourable electrostatic interaction H$^{\delta+}$···O$^{\delta+}$ is expected to be only relatively weak. The more polar kinds of C–H[3,5] apparently avoid short contacts to O$^{\delta+}$ as efficiently as do the strongly polar groups O–H and N–H.

The data in Fig. 2 and Table 2 clearly show that contacts of the kind C–H···O$^{\delta+}$ should not be considered as hydrogen bonds, even though they are occasionally relatively short. It is not the contact distances that lead to this conclusion, but the contact *directionalities*. A look at the data quantities in Table 2 also shows that short C–H···O$^{\delta+}$ contacts are a rare phenomenon when compared to C–H···O hydrogen bonding. There are two important conclusions: (i) not every single short C–H···O contact occurring in crystals is a hydrogen bond, and (ii) considering only contact distances is an unsuitable approach in the analysis of hydrogen bonds, and of intermolecular interactions in general.

The author thanks the Minerva Foundation (Munich) for granting a fellowship to stay at the Weizmann Institute of Science in the research group of Professor Joel L. Sussman.

Notes and references

‡ Cambridge Structural Database (CSD),[13] spring 1998 update with 181 309 entries, ordered and error-free organic crystal structures with $R < 0.08$, H-atom positions normalized.

1 T. Steiner, *Chem. Commun.*, 1997, 727; *Cryst. Rev.*, 1996, **6**, 1.
2 G. R. Desiraju, *Acc. Chem. Res.*, 1991, **24**, 290; 1996, **29**, 441.
3 V. R. Pedireddi and G. R. Desiraju, *J. Chem. Soc., Chem. Commun.*, 1992, 988.
4 H. Bock, R. Dienelt, H. Schödel and Z. Havlas, *J. Chem. Soc., Chem. Commun.*, 1993, 1792; T. Steiner, J. van der Maas and B. Lutz, *J. Chem. Soc., Perkin Trans. 2*, 1997, 1287; B. M. Kariuki, K. D. M. Harris, D. Philp and J. M. A. Robinson, *J. Am. Chem. Soc.*, 1997, **119**, 12679.
5 T. Steiner, *New J. Chem.*, 1998, 1099.
6 P. Coppens, *Acta Crystallogr.*, 1964, **17**, 573.
7 T. Steiner and W. Saenger, *J. Am. Chem. Soc.*, 1993, **115**, 4540.
8 P. Seiler, L. Isaacs and F. Diederich, *Helv. Chim. Acta*, 1996, **79**, 1047
9 D. Braga, F. Grepioni, E. Tagliavini, J. J. Novoa and F. Mota, *New J. Chem.*, 1998, 755.
10 A. I. Gubin, A. I. Yanovskii, Y. T. Struchkov, B. A. Berimzhanov, N. N. Nurakhmetov and M. Z. Buranbaev, *Cryst. Struct. Commun.*, 1980, **9**, 745.
11 T. Steiner and G. R. Desiraju, *Chem. Commun.*, 1998, 891.
12 (*a*) J. W. H. M. Uiterwijk, S. Harkema, D. N. Reinhoudt, K. Daasvatn, H. J. J. den Hertog and J. Geevers, *Angew. Chem., Int. Ed. Engl.*, 1982, **21**, 450; (*b*) F. K. Winkler, and J. D. Dunitz, *Acta Crystallogr., Sect. B*, 1975, **31**, 278; (*c*) G. Maas, *Acta Crystallogr., Sect. C.*, 1985, **41**, 1133; (*d*) F. K. Winkler and J. D. Dunitz, *Acta Crystallogr., Sect. B.*, 1975, **31**, 273; (*e*) T. Gramstad, S. Husebye, K. Maartmann-Moe and J. Saebo, *Acta Chem. Scand., Ser. B*, 1987, **41**, 1; (*f*) E. Benedetti, B. di Blasio and P. Baine, *J. Chem. Soc., Perkin Trans. 2*, 1980, 500; (*g*) A. I. Gubin, M. Z. Buranbaev and N. N. Nurakhmetov, *Kristallografiya*, 1988, **33**, 506.
13 F. H. Allen and O. Kennard, *Chem. Des. Autom. News*, 1993, **8**, 1.

Communication 8/08974D

ChemComm

Functional silica aerogel from metastable lamellar composite

Yizhu Guo and Ana R. Guadalupe*

Department of Chemistry, PO Box 23346, University of Puerto Rico, San Juan, Puerto Rico 00931. E-mail: aguadalu@upracd.upr.clu.ed

Received (in Cambridge, UK) 6th October 1998, Accepted 7th January 1999

A functional aerogel composed of interconnected silica nanoparticles has been synthesized from a metastable lamellar composite based on a novel type of cooperative interaction between silica and surfactant species.

Silica aerogels possess an attractive and unique set of properties, [1,2] including extremely low densities, high surface area, low thermal conductivity and low dielectric permittivity. The pore structure of aerogels is formed by the controlled condensation of small (polymeric or colloidal) primary particles which are usually generated and aggregated by a sol–gel process. [1,3] Typically, an alkoxysilane precursor is used to produce an alcogel in acidic or basic alcoholic solution by a one- or two-step sol–gel process, then the alcogel is subject to air-exchange without destroying the gel structure generally by supercritical drying. A highly pursued goal in aerogel technology is the elimination of the supercritical drying step, because it is the most expensive and risky step in the production of aerogels. While the structure–property relationship of aerogels is readily manipulated through the choice of precursors and polymerization conditions, research in new aerogel chemistry and compositions is necessary for performance improvement and novel applications.[4]

Here we report the synthesis of a functional aerogel from a metastable lamellar surfactant–silica composite, eliminating the intermediate alcogel formation. We demonstrate that the surfactant mesostructure facilitates and stabilizes the formation of monodispersed silica nanoparticles, that aggregate into a highly porous solid. The porous, skeletal structure is maintained after removal of surfactant. This procedure provides a novel non-supercritical drying technique for the production of aerogels and reveals a new aerogel chemistry for functional, highly porous materials.

Bis[(3-triethoxysilyl)propyl]tetrasulfide (SIS, purchased from Petrarch systems) was chosen as the silane precursor. The sulfur chain (–S_4–) in the SIS molecule has been demonstrated to have a high affinity for heavy metals (*e.g.* mercury and silver).[5] Thus, functionalized aerogels would be a potential sorbent for the recovery of heavy metals, as shown for thiol-monolayer modified molecular sieves M41S.[6] The precursor was added dropwise into 5% aqueous sodium dodecyl sulfate (SDS, purchased from Aldrich) solution under vigorous stirring. Then 0.1 M HCl was added dropwise as the catalyst. The composition (molar ratio) of the final solution was SIS : SDS : HCl : H_2O = 1 : 1.5 : 0.05 : 600. A bean curd-like, milky-white gel formed and floated in a clear solution after 2–3 days under ambient conditions. In contrast, no gel formed in the solution without SIS, or a light yellow precipitate formed in the solution without SDS.

Fig. 1 shows the small angle X-ray diffraction patterns of the gel samples dried at room temperature [curve (a)] and at 100 °C for 4 h at atmospheric pressure [curve (b)]. The room temperature-dried gel exhibited well defined (001), (002), and (003) peaks characteristic of lamellar structure, with the largest *d* value of 35.13 Å. By contrast only poorly-defined (001) and (002) peaks were observed for the heated gel, and the *d* value decreased to 28.79 Å, indicating that the lamellar structure of the gel (SDS/SIS sol–gel composite) is thermally unstable.

Fig. 2 shows typical TEM micrographs of the ethanol-washed room temperature-dried SDS/SIS sol–gel composite. It is clear that a three-dimensional highly porous skeleton structure characteristic of aerogel[7] is formed from the SDS/SIS sol–gel composite after removing the surfactant. Closer examination reveals that the network is constructed by interconnected nanoparticles. These nanoparticles are narrowly distributed with a diameter around 38 nm. The aerogel thus prepared exhibited low bulk density (*ca.* 0.2 g cm^{-3}).

A possible mechanism for the SIS aerogel formation from a metastable lamellar SDS/SIS sol–gel composite is proposed in Scheme 1. A high SDS concentration in water leads to a lyotropic lamellar liquid-crystalline phase consisting of bilayer sheets[8] (A). Addition of the hydrophobic silica precursor, SIS, into the aqueous media under vigorous agitation resulted in the formation of SIS droplets promoted and stabilized by the presence of SDS (B). Meanwhile, mediated by Na^+ counter ions, SDS bilayers bend around the SIS droplets.[9,10] Upon closing, these sheets form lamellar vesicles,[11–13] encapsulating the SIS droplets (C). The hydrolysis and condensation (*i.e.* polymerization) of SIS then occurs in these lamellar vesicles. Aggregation of these lamellar droplets is facilitated[9,14–16] by dehydration of the surfactant head groups and an increase in counter ion binding caused by the release of ethanol in the SIS hydrolysis process. Upon aggregation, a bean curd-like gel

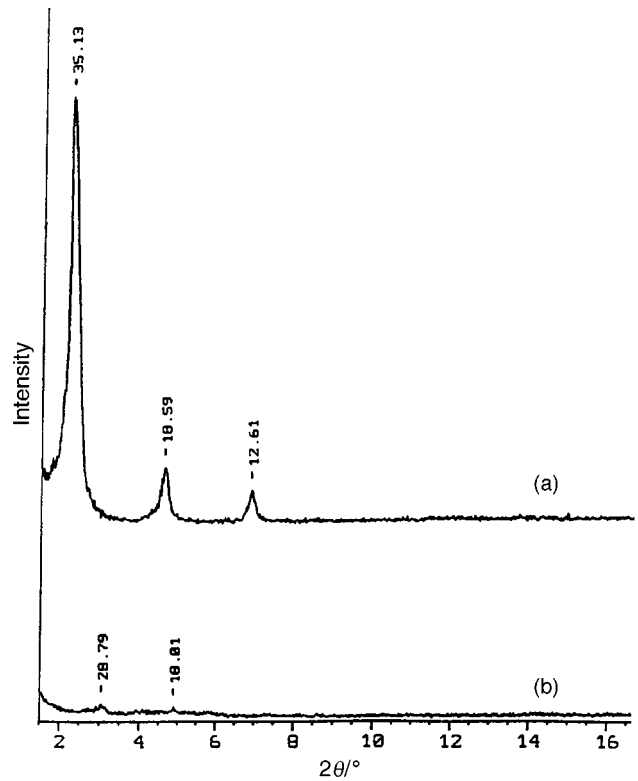

Fig. 1 Small angle X-ray diffraction patterns of the SDS/SIS sol–gel composites dried at room temperature (a) and dried at 100 °C under ambient pressure (b).

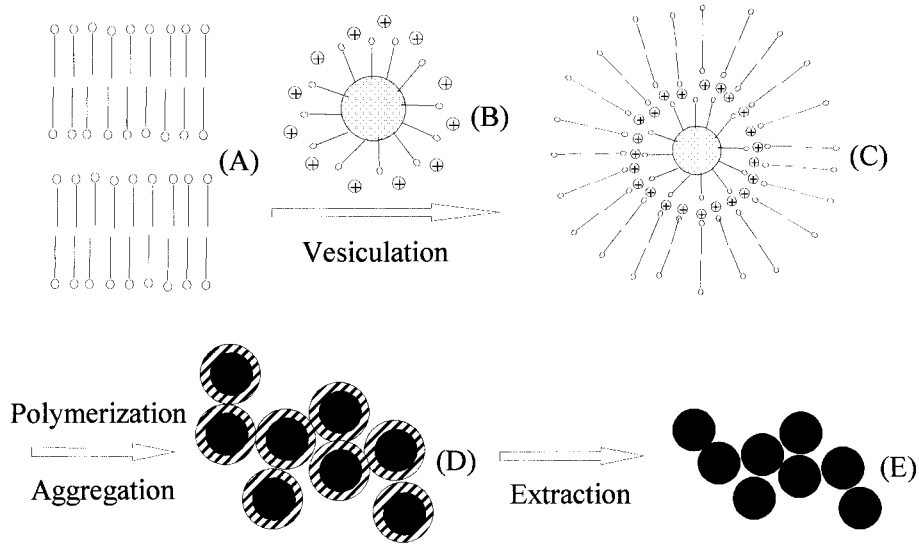

Scheme 1

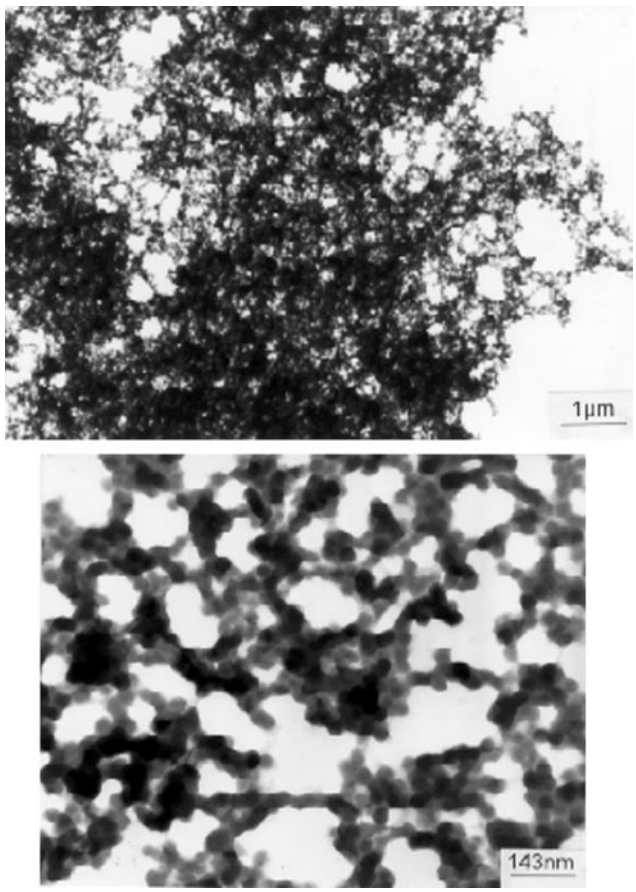

Fig. 2 Transmission electron microscopy micrographs of the ethanol-washed room temperature-dried SDS/SIS sol–gel composite at low (top) and high (bottom) magnifications.

formed (D). At SDS concentrations of ⩾5%, bean curd-like gels are readily formed. A higher concentration (> 10%) results in SDS crystallization. Removal of SDS by alcohol extraction resulted in the SIS aerogel (E), most probably because of the highly hydrophobic interactions among the SIS sol–gel nanoparticles.

In conclusion, we have developed a novel approach for the production of a functionalized aerogel from a surfactant/SIS sol–gel composite. This technique allows atmospheric pressure drying so eliminating expensive and risky supercritical drying. The highly porous characteristics combined with the high affinity of the sulfur chain for heavy metals hold promising and immediate environmental application in the recovery of heavy metals.

This project was supported by DoE-EPSCoR (046138). Special thanks are given to Victor Pantojas from the UPR Materials Characterization Center for his help with the XRD experiment and to Camillo Cangany from the Research Center for Minority Institutions (RCMI, RP-03051), Medical Science Campus, University of Puerto Rico.

Notes and references

1 N. Husing and U. Schubert, *Angew. Chem. Int. Ed.*, 1998, **37**, 22.
2 M. Wu, T. Fujiu and G. L. Messing, *J. Non-Cryst. Solids*, 1990, **121**, 407.
3 *Sol-Gel Science: the Physics and Chemistry of Sol-Gel Processing*, ed. C. J. Brinker and G. W. Scherer, Academic Press, Inc., New York, 1990.
4 R. W. Pekala and L. W. Hrubesh, *J. Non-Cryst. Solids*, 1995**, 186**, Vii.
5 Y. Z. Guo and A. R. Guadalupe, *J. Pharm. Biomed. Anal*., in press.
6 X. Feng, G. E. Fryxell, L. Q. Wang, A. T. Kim, J. Liu and K. M. Kemner, *Science*, 1997, **276**, 923.
7 D. W. Hua, J. Anderson, J. Di Gregorio, D. M. Smith and G. J. Beaucage, *J. Non-Cryst. Solids*, 1995, **186,** 142.
8 P. Ekwall, in *Advances in Liquid Crystals*, ed. G. H. Brown, Academic Press, New York, 1975, vol. 1, p. 1.
9 A. Sein and J. B. F. N. Engberts, *Langmuir*, 1995, **11**, 455.
10 Q. Huo, D. I. Margolese, U. Ciesla, P. Feng, T. E. Gier, P. Sieger, R. Leon, P. M. Petroff, F. Schuth and G. D. Stucky, *Nature*, 1994, **368**, 317.
11 D. Allan, P. Thomas and R. H. Michell, *Nature*, 1978**, 276**, 289.
12 B. W. Ninham and D. F. Evans, *Faraday Discuss. Chem. Soc.*, 1986, **81**, 1.
13 H. Hauser, *Biochim. Biophys. Acta*, 1984, **772**, 37.
14 P. J. Missel, N. A. Mazer, M. C. Carey and G. B. Benedek, in *Solution Behaviour of Surfactants*, ed. K. L. Mittal and E. J. Fendler, Plenum Press, New York, 1982, vol. 2, p. 373.
15 J. Marra, *J. Phys. Chem.*, 1986, **90**, 2145.
16 D. D. Miller, L. J. Magid and D. F. Evans, *J. Phys. Chem.*, 1990, **94**, 5921.

Communication 8/07762B

A novel protocol for *N*-methyl-γ-amino-β-hydroxy acids from oxazolidinones

G. Vidyasagar Reddy,* G. Venkat Rao and D. S. Iyengar*

Discovery Laboratory, Organic Division – II, Indian Institute of Chemical Technology, Hyderabad-500 007, India. E-mail: iyengar@iict.ap.nic.in

Received (in Cambridge, UK) 29th October 1998, Accepted 18th December 1998

A new two step methodology for *N*-methyl-γ-amino-β-hydroxy acids from oxazolidinones is described

Optically active *N*-methyl-γ-amino-β-hydroxy acids are a class of nonproteinogenic amino acids present in a variety of biologically active compounds, *e.g.* Hapalosin,[1] a multidrug resistance active compound containing 3-hydroxy-4-*N*-methylamino-5-phenylpentanoic acid, and Dolastatine 10,[2] an anticancer compound containing 3-hydroxy-4-*N*-methylamino-5-methylheptanoic acid. Due to their promising biological activity, they have become an interesting class of compounds in the pharmaceutical industry. Although there are methods[3] available for preparation of *syn* and *anti* isomers of γ-amino-β-hydroxy acids, there is no effective method available to make their *N*-methylated analogues. The literature methods[4] of their preparation involves the treatment of *N*-protected-γ-amino-β-hydroxy acid with NaH followed by MeI. However, this method suffers due to competitive reactions such as the β-elimination resulting in the formation of α,β-unsaturated acid derivatives, and pyrrolidinone ring formation. The other problems associated with this method are *O*-methylation and *N*-deprotection, resulting in a complex mixture of products. In view of this, alternative methods have been developed.[5] Herein, we report an elegant, entirely novel, short and efficient protocol for the title compounds involving two new reactions, *viz*. (a) Wittig reaction of oxazolidinones (**1**→**2**) and (b) a reductive process of their corresponding α,β-unsaturated esters (**2**→**3**) (Scheme 1).

N-Cbz-oxazolidinones[6] (**1**) obtained from *N*-Cbz-α-amino acids by the reaction of paraformaldehyde in the presence of catalytic TsOH, were subjected to the Wittig reaction with Ph_3PCHCO_2Et to give α,β-unsaturated esters (**2**) in excellent yields. Since there was no enhancement of the signal in the NOE experiment between the olefinic proton and the methine proton in the ring, the olefin geometry was assumed to be '*E*'.

The reaction of α,β-unsaturated ester **2a** with $NaCNBH_3$–TMSCl under N_2 atmosphere afforded an easily separable mixture of *syn* and *anti* *N*-Cbz-*N*-methyl-γ-amino-β-hydroxy acids **3a** (syrup; $[\alpha]_D^{24}$ −29.4 (*c* 1, MeOH)) and **4a** (syrup; $[\alpha]_D^{25}$ −26.6, (*c* 1, MeOH)) in a ratio of 4:1 in 94% combined yield (Scheme 1).

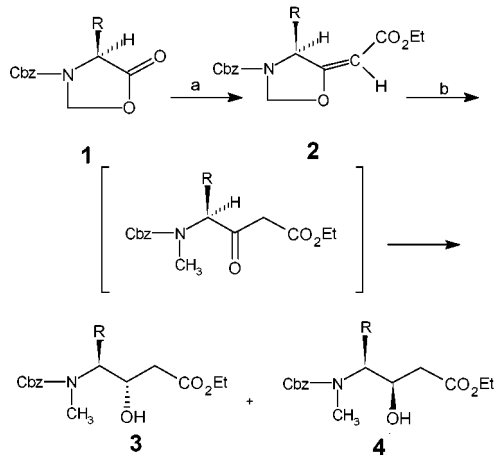

Scheme 1 *Reagents and conditions:* a, Ph_3P=CHCOOEt, toluene, reflux, 3 h; b, $NaCNBH_3$, TMSCl, CH_3CN, N_2, rt, 30 min.

As expected the major isomer **3a** was found to be *syn* from the ^{1}H-NMR of the corresponding oxazolidinone[7] **8** obtained by the treatment of **3a** with NaH in DMF (J = 4.5 Hz for ring protons 4-H and 5-H, Scheme 2), which may be explained by the Felkin–Anh model[8] (Fig. 1). This was further confirmed by converting the minor *anti* isomer **4a** into the known compound **7** (oil; $[\alpha]_D^{25}$ −43.7 (*c* 1, MeOH); lit.[4c] $[\alpha]_D^{25}$ −41.2, (*c* 1, MeOH)) and by comparing specific rotations and spectral data with those of reported values which are found to be in good agreement (Scheme 3).

In order to probe the generality of the reaction, the process was further applied to **2b**–**2c.** *N*-Cbz-*N*-methyl-γ-amino-β-hydroxy acids (**3b**,**c**, **4b**,**c**) obtained using this methodology are shown in Scheme 1 (Table 1). All the compounds obtained were fully characterized by spectral data.[9] Important characteristic NMR signals of **3a** [δ_H 2.80 (s, 3H, N-CH_3), 1.30 (t, 3H, J 6.4, CH_3), 4.20 (q, 2H, J 6.4, CH_2)] clearly indicate the *N*-methyl group and ethyl esters. The spectroscopic data and optical rotations are in accordance to those of reported values.

In summary, we report an entirely novel, straightforward and practical methodology for *N*-methyl-γ-amino-β-hydroxy acids,

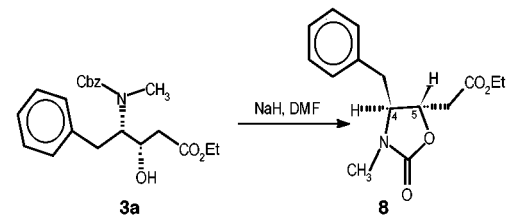

Scheme 2

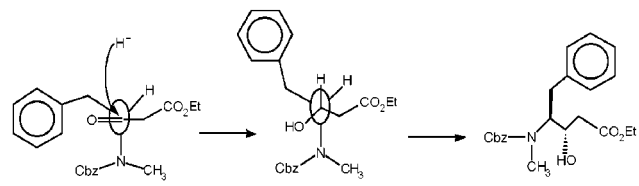

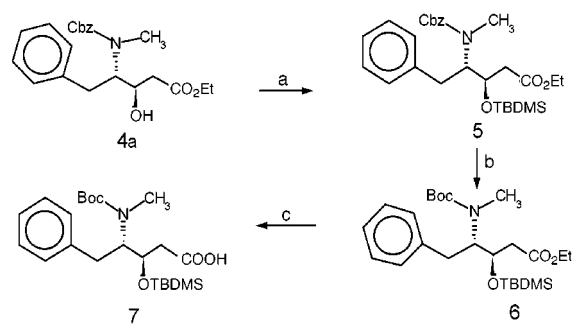

Scheme 3 *Reagents and conditions :* a, TBDMSCl, imidazole, DMF, rt, 10 h, 95%; b, 10% Pd–C/H_2, Boc_2O, MeOH, rt, 12 h, 98%; c, 2M NaOH, THF, rt, 4 h, 92%.

Table 1 Preparation of *N*-Cbz-*N*-methyl-γ-amino-β-hydroxy acids from oxazolidinones

		2		**3** and **4**
S. No	R	Yield (%)	$[\alpha]_D^{25}$ [a]	Yield (ratio)[b]
A	$PhCH_2$	96	−13.8	94 (4 : 1)[c]
B	Me_2CHCH_2	94	45.2	92 (3:1)[d]
C	$MeCH_2CHMe$	96	25.6	96 (3:1)[d]

[a] Specific rotations were measured with c = 1 in MeOH. [b] Yield (%) are combined yields. Ratio is [c] based on isolated yield, [d] based on crude ^{1}H-NMR.

key precursors of the potential bioactive molecules and enzyme inhibitors, for the first time. The present methodology enables the synthesis of a variety of *N*-methyl-γ-amino-β-hydroxy acids with ease, and hence offers a practical alternative to the earlier methodologies. Further work is in progress and will be reported in due course.

G. V. S. R. and G. V. R. thank the CSIR (India) for their fellowships.

Notes and references

1 K. Strattmann, D. L. Burgoyne, R. E. Moore, G. M. L. Patterson and C. D. Smith, *J. Org. Chem.*, 1994, **59**, 7219.

2 G. R. Pettit, S. B. Singh, D. L. Herald, P. Llyoyd, D. Kantosci, D. Burkett, J. Barkoczy, F. Hogan and T. R. Wardlaw, *J. Org. Chem*., 1994, **59**, 6287.

3 P. Castejon, A. Moyano, M. A. Pericas and A. Riera, *Tetrahedron*, 1996, **52**, 7063.

4 (*a*) T. Shioiri, K. Hayashi and Y. Hamada, *Tetrahedron*, 1993, **49**, 1913; (*b*) I. Maugras, J. Poncet and P. Jouin, *Tetrahedron*, 1990, **46**, 2807; (*c*) T. Okuno, K. Ohmori, S. Nishiyama, S. Yamamura, K. Nakamura, K. N. Houk and K. Okamoto, *Tetrahedron*, 1996, **52**,14 723.

5 F. Roux, V. Maugras, J. Poncet, G. Niel and P. Jouin, *Tetrahedron*, 1994, **50**, 5345; S. Kano, Y. Yuasa and S. Shibuya, *Hetereocycles*, 1990, **31**, 1597; S. Kano, T. Yokomatsu and S. Shibuya, *J. Org. Chem*., 1989, **54**, 513.

6 D. B. Ishai, *J. Am. Chem. Soc*., 1957, **79**, 5736.

7 C. Beier, E. Schaumann and G. Adiwidjala, *Synlett*, 1998, 41.

8 J. Mulzer, in *Houben-Weyl Methods of Organic Chemistry*, 4th edn., vol. E21a, ed. G. Helmchen, R. W. Hoffmann, J. Mulzer and E. Schaumann, Thieme, Stuttgart, 1995, p. 75.

9 *Selected data* for **2a**: Colorless syrup; δ_H 1.30 (3H, t, J 6.4, CH_2CH_3), 3.00–3.40 (2H, m, $PhCH_2$), 4.20 (2H, q, J 6.4, CH_2CH_3), 4.80–4.90 (1H, m, *CH*Bn), 5.05 (2H, s, $PhCH_2O$), 5.20–5.32 (1H, br s, N-CH_2), 5.35 (1H, s, olefin), 5.60 (1H, br s, N-CH_2), 7.00–7.40 (10H, m, Ar) ; δ_C 14.3 (C-9), 38.7 (CH_2Ph), 59.5 (C-8), 59.8 (C-4), 67.7 (C-11), 91.0 (C-2), 126.7 (Ar), 128.0 (Ar), 128.2 (Ar), 128.3 (Ar), 128.6 (Ar), 129.7 (Ar), 130.5 (Ar), 132.5 (Ar), 136.3 (C-6), 154.2 (C-10), 167.1 (C-5), 171.5 (C-7); *m*/*z* 382 (M^+ + H). For **2b**: Colorless syrup; δ_H 0.82 (3H, d, J 6.7, CH_3), 1.00 (3H, d, J 6.7, CH_3), 1.22 (3H, t, J 6.2, CH_2CH_3), 1.30–1.80 (3H, m), 4.10 (2H, q, J 6.2, CH_2CH_3), 4.90 (1H, d, J 4.5), 5.12 (2H, ABq, J_{gem} 13.5, CH_2Ph), 5.22 (1-H, s, olefin), 5.50 (1H, br s, N-CH_2), 5.65 (1H, br s, N-CH_2), 7.30 (5H, m, Ar); δ_C 14.2 (C-9), 20.8 (CH_3), 23.5 (CH_3), 24.9 (CH_2), 39.9 (*C*H), 57.6 (C-8), 59.4 (C-4), 67.9 (C-11), 89.9 (C-2), 128.2 (Ar), 128.4 (Ar), 135.4 (C-6), 154.0 (C-10), 166.6 (C-5), 172.1 (C-7); *m*/*z* 348(M^+ + H). For **2c**: Colorless syrup; δ_H 0.88 (3H, t, J 6.2, CH_3CH_2), 1.20 (3H, d, J 6.8, CH_3), 1.28 (3H, t, J 6.2, CH_2CH_3), 1.30–1.50 (2H, m, CH_2CH_3), 2.00–2.20 (1H, m, $CH(CH_3)CH_2CH_3$), 4.10 (2H, q, J 6.2, CH_2CH_3), 4.92 (1H, d, J 4.6, N-CH), 5.15 (2H, ABq, J_{gem} 14.0, OCH_2Ph), 5.30 (1H, s, olefin), 5.40 (1H, br s, N-CH_2), 5.62 (1H, br s, N-CH_2), 7.30 (5H, m, Ar); δ_C 11.7 (CH_3), 14.0 (C-9), 16.2 (CH_3), 23.6 (CH_2), 39.1 (*C*H), 59.3 (C-8), 63.9 (C-4), 67.7 (C-11), 90.6 (C-2), 128.0 (Ar), 128.1 (Ar), 128.2 (Ar), 135.4 (C-6), 154.2 (C-10), 166.6 (C-5), 171.4 (C-7); *m*/*z* 348 (M^+ + H). For **3a**: Colorless syrup; $[\alpha]_D^{25}$ −29.4, (*c* 1, MeOH); δ_H 1.25 (t, 3H, CH_3), 2.40–2.55 (m, 2H, CH_2Ph), 2.80 (s, 3H, N-CH_3), 2.95–3.10 (m, 2H, CH_2CO_2), 4.00–4.18 (quartet overlapped with multiplet, 4H, CH_2CH_3 and *CH*NH and *CH*OH), 4.90–5.20 (m, 2H, $PhCH_2O$), 7.05–7.35 (m, 10H, Ar); δ_C 14.1, 30.6, 39.4, 58.6, 59.2, 59.9, 69.8, 79.2, 126.2, 128.2, 128.5, 128.7, 129.5, 130.2, 132.3, 154.4, 171.4; *m*/*z* 386 (M^+ + H). For **4a**: Colorless syrup; $[\alpha]_D^{25}$ −26.6 (*c* 1, MeOH); δ_H 1.20 (t, 3H, CH_3), 2.30–2.45 (m, 2H, CH_2Ph), 2.75 (s, 3H, N-CH_3), 3.00–3.20 (m, 2H, CH_2CO_2), 4.00–4.20 (quartet overlapped with multiplet, 4H, CH_2CH_3 and *CH*NH and *CH*OH), 5.00–5.15 (m, 2H, $PhCH_2O$), 7.10–7.35 (m, 10H, Ar); *m*/*z* 386 (M^+ + H). For **7**: Colorless oil; $[\alpha]_D^{25}$ −43.7 (*c* 1, $CHCl_3$); lit.[4c] $[\alpha]_D^{25}$ −41.2 (*c* 1, $CHCl_3$); δ_H 0.09 (s, 3H, Si-CH_3), 0.20 (s, 3H, CH_3-Si), 0.95 (s, 9H, $(CH_3)_3C$-Si), 1.35 (s, 9H, $(CH_3)_3C$), 2.35–2.50 (m, 2H, CH_2Ph), 2.75 (s, 3H, N-CH_3), 2.90–3.05 (m, 2H, CH_2CO_2), 4.25–4.40 (m, 2H, *CH*-NH and *CH*-OH), 7.10–7.35 (m, 5H, Ph); δ_C −4.7, −4.6, 14.2, 18.3, 25.6, 30.5, 35.7, 39.9, 56.2, 60.9, 71.1, 76.9, 79.2, 126.3, 128.0, 129.2, 138.7, 155.0, 171.5; *m*/*z* 324 (M^+ + H).

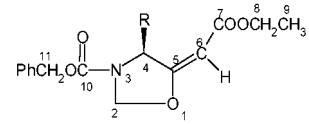

2a R = $PhCH_2$
2b R = Me_2CHCH_2
2c R = $MeCH_2CHMe$

Communication 8/08379G

The crystal and molecular structure of 2,7-di-*tert*-butyl-4,5,9,10-tetraphenylbenzo[1,2,:4,5]dicyclobutadiene: an exceptionally long C–C aromatic bond

Roland Boese,[a] Jordi Benet-Buchholz,[a] Amnon Stanger[b], Koichi Tanaka[c] and Fumio Toda[c]

[a] *Institut für Anorganische Chemie der Universität-GH, Universitätsstrasse 5-7, D-45117, Essen, Germany. E-mail: boese@structchem.uni-essen.de*

[b] *Department of Chemistry and The Lise Meitner-Minerva Center for Computational Quantum Chemistry, Technion - Israel Institute of Technology, Haifa 32000, Israel*

[c] *Department of Applied Chemistry, Faculty of Engineering, Ehime University, Matsuyama, Ehime 790-8577, Japan*

Received (in Cambridge, UK) 23rd December 1998, Accepted 4th January 1999

The X-ray determined structure of the title compound is reported; it was found that the annelated bonds are the longest observed in a benzene derivative [1.540(5) Å]; *ab initio* calculations (at the B3LYP/6-31G* and MP2/6-31G* levels of theory) were used in order to understand the electronic and structural properties of the compound.

Strain imposed on aromatic compounds alters the properties of the aromatic systems. Of particular interest is strain that is imposed in the σ-plane, namely, perpendicular to the π-system. When the strain is imposed in an angular manner (schematically shown in **1**) it causes the localization of the aromatic bonds.[1] When imposed in a linear manner (as in the title compound) the aromatic moiety changes dramatically.[2] However, in the particular case of benzo[1,2:4,5]dicyclobutadiene **2** it was predicted that this system should show two types of isomerism:[3] bond-stretch isomerism (**2a** with D_{2h} symmetry *vs.* **2b** and **2c** with C_{2v} symmetry) and Kekulé isomerism (*i.e.* **2b** *vs.* **2c**). As the title derivative of **2** was prepared some years ago,[4] and the study of its chemical and physical properties has not yielded conclusive answers,[5] and in light of the controversial issue of bond-stretch isomerism,[6] it was decided to characterize the structure crystallographically.

The title compound **3** was made as previously published.[4] Crystals suitable for X-ray analysis of this highly sensitive compound[4] were obtained by careful recrystallization from *p*-xylene. Five data sets of different crystals of different quality and at various temperatures were collected. All of them showed the same features that are presented in Fig. 1 (the essential bonding parameters can be found in the figure caption). In the monoclinic system (space group *C*2/*c*, a = 21.3735(5), b = 6.11890(10), c = 23.4144(6) Å, β = 99.8480(10)°, Z = 4),[7] the molecular structure was found to possess C_2 symmetry with some unexpected bond distances, especially in the central ring. To the best of our knowledge, the C(1)C(2) distance is the longest distance ever found in a benzene ring. The geometry is not expected to be essentially influenced by intermolecular contacts, which are mostly beyond van der Waals contacts; the closest are at H(9B) and H(12A) with 2.22 Å (C–H distances expanded to 1.08 Å).

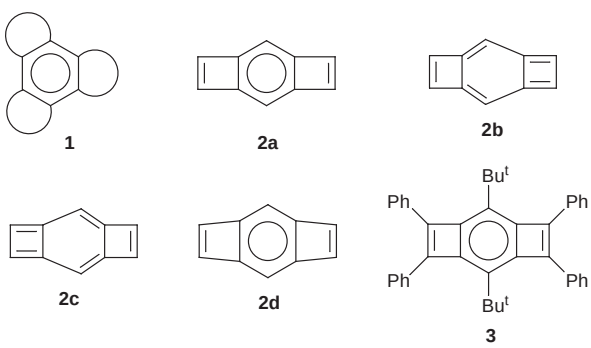

Although Schulman and Disch[3] predicted unusual structures for **2**, all the structural features of **3** are different than those predicted theoretically. The symmetry of the benzobicyclobutadiene skeleton in **3** is D_{2h}, as in **2a**, but the bond lengths are closer to a hybrid of the two theoretical C_{2v} *isomers* **2b** and **2c**.[8a] However, the annelated bonds in **3** are shorter than the average of the respective bonds in **2b** and **2c**. Also, it looked like the more stable isomer was not the one that was experimentally found.[8b] In order to resolve this dichotomy, we decided to study the issue using *ab initio* calculations on **2** at higher theoretical levels.

GAUSSIAN 94[9] was used. The systems under study were optimized at the B3LYP/6-31G* and MP2/6-31G* theoretical levels, which have been shown to produce reliable structures for small-ring annelated benzene systems.[1c,10] Table 1 summarizes the geometry of the systems obtained at these levels of theory. It was found that there are only two bond-stretch isomers, both possessing D_{2h} symmetry. One is similar to **2a**, and the second one, **2d**, does not correspond to **2b** (or **2c**) but is similar that one found in the crystal structure of **3**. Furthermore, **2d** is theoretically predicted to be 2.4 and 3.7 kcal mol^{-1} (at B3LYP/6-31G* and MP2/6-31G*, respectively) more stable than **2a**.

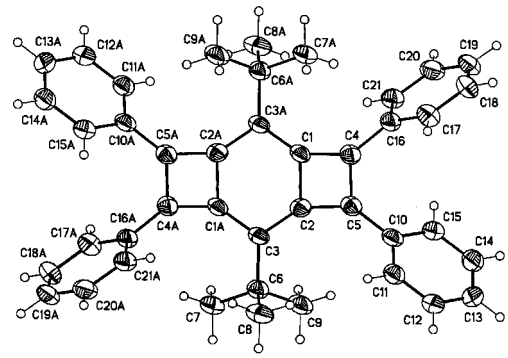

Fig. 1 Ellipsoid representation (50%) of **3**. Important distances (Å) and angles (°): C(1)–C(2) 1.540(5), C(2)–C(3) 1.416(5), C(1A)–C(3) 1.407(5), C(1)–C(4) 1.402(5), C(2)–C(5) 1.412(5), C(4)–C(5) 1.471(5), C(3)–C(6) 1.524(5), C(4)–C(16) 1.479(5), C(5)–C(10) 1.455(5), C(10)–C(11) 1.397(6), C(11)–C(12) 1.378(5), C(12)–C(13) 1.382(6), C(13)–C(14) 1.364(6), C(14)–C(15) 1.387(6), C(10)–C(15) 1.405(6), C(16)–C(17) 1.388(6), C(17)–C(18) 1.385(6), C(18)–C(19) 1.362(6), C(19)–C(20) 1.374(6), C(20)–C(21) 1.397(6), C(16)–C(21) 1.394(6), H(15)···H(17) 3.34; C(2)–C(3)–C(1A) 109.7(3), C(1)–C(2)–C(3) 123.7(3), C(2)–C(1)–C(3A) 126.0(3), C(1)–C(2)–C(5) 88.5(3), C(2)–C(1)–C(4) 88.6(3), C(1)–C(4)–C(5) 91.7(3), C(2)–C(5)–C(4) 91.0(3), C(10)–C(5)–C(4)–C(16) 11.3(6), C(5)–C(2)–C(3)–C(6) −3.1(8), C(5)–C(4)–C(16)–C(17) −64.5(5), C(4)–C(5)–C(10)–C(11) 136.1(4).

Table 1 Calculated (B3LYP/6-31G* and MP2/6-31G*) geometries and relative energies of the two isomers of **2**

	Isomer	Level	R_1	R_2	R_3	R_4	ΔE/kcal mol^{-1}
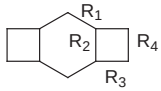	**2d**	B3LYP/6-31G*	1.3888	1.5641	1.3916	1.4583	−2.4
	2a	B3LYP/6-31G*	1.3944	1.4026	1.5430	1.3456	0
	2d	MP2/6-31G*	1.3898	1.5545	1.3921	1.4587	−3.7
	2a	MP2/6-31G*	1.3943	1.4082	1.5361	1.3456	00

Table 2 Bond-length differences between the calculated geometries of **2d** (at B3LYP/6-31G* and MP2/6-31G*) and **4** and **3**

	X	Level	ΔR_1	ΔR_2	ΔR_3	ΔR_4	Average error
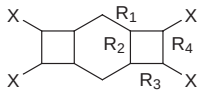	H (**2d**)	B3LYP/6-316*	−0.023	+0.024	−0.016	−0.013	0.019
	H (**2d**)	MP2/6-31G*	−0.023	+0.015	−0.016	−0.015	0.018
	Vinyl (**4**)	B3LYP/6-31G*	−0.021	−0.011	−0.001	+0.014	0.012

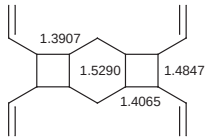

Fig. 2 B3LYP/6-31G* structure of **4** at D_{2d} symmetry (the experimentally found isomer).

Both isomers have been shown to be minima on the potential surface by frequencies calculations.

Although the agreement between the calculated and observed structures is reasonable, we have calculated the structure of the 4,5,9,10-tetraethenyl derivative of **2** (**4**), to see if the alkenyl substitution (that mimics the phenyl substitution in **3**) is responsible for (at least some) of the geometrical differences between the calculated and measured structures. Fig. 2 shows the geometry of **4** (at D_{2h} symmetry)[11] and Table 2 presents an error survey of the studied systems. The numbers in Table 2 suggest that (i) B3LYP/6-31G* and MP2/6-31G* describe the system with about the same accuracy,[12] and (ii) that at least a part of the discrepancy between the measured and calculated structures is due to the substitution. This can be concluded from the fact that the average error values for **4** are 37% smaller than for **2**, and that the sign of the error for different bonds is different.

We are currently studying the issue of interconversion between the two isomers theoretically, and are trying to prepare other derivatives of the title compound that may yield the other bond-shift isomer.

We thank The American – Israeli Binational Science Foundation, the Lise-Meitner-Minerva Center for Computational Quantum Chemistry, the VPR fund at the Technion and the Fonds der Chemischen Industrie for financial support.

Notes and references

1 (*a*) R. Boese, D. Bläser, W. E. Billups, M. M. Haley, A. H. Maulitz, D. L. Mohler and K. P. C. Vollhardt, *Angew. Chem., Int. Ed. Engl.*, 1994, **33**, 313; (*b*) N. L. Frank and J. S. Siegel, in *Advances in Theoretical Interesting Molecules*, JAI Press, London 1995, vol. 3, p. 209; (*c*) A. Stanger, *J. Am. Chem. Soc.*, 1991, **113**, 8277; (*d*) A. Stanger, *J. Am. Chem. Soc.*, 1998, **120**, 12 034.

2 J. M. Schulman, R. L. Disch, H. Jiuo and P. v. R. Schleyer, *J. Phys. Chem.*, in the press and references therein; K. P. C. Vollhardt and D. B. Mohler, in *Advances in Strain in Organic Chemistry*, ed. B. Halton, JAI Press, London, 1996, vol. 5, p. 121.

3 J. M. Schulman and R. L. Disch, *J. Am. Chem. Soc.*, 1993, **115**, 11 153.

4 F. Toda and M. Ohi, *J. Chem. Soc., Chem. Commun.*, 1975, 506.

5 F. Toda, N. Dann, K. Tanaka and Y. Tekehira, *J. Am. Chem. Soc.*, 1977, **99**, 4529; F. Toda and P. Garratt, *Chem. Rev.*, 1992, **92**, 1685.

6 See, for example, A. Bashall, V. C, Gibson, T. P. Kee, M. McPartlin, O. B. Robinson and A. Shaw, *Angew. Chem.*, 1991, **103**, 1021; *Angew. Chem., Int. Ed. Engl.*, 1991, **30**, 980; G. Parkin, *Acc. Chem. Res.*, 1992, **25**, 455; G. Parkin, *Chem. Rev.*, 1993, **93**, 887; K. Yoon, G. Parkin and A. L. Rheingold, *J. Am. Chem. Soc.*, 1993, **114**, 2210.

7 *Crystal data* for **2**: $C_{42}H_{38}$, crystal dimensions $0.13 \times 0.11 \times 0.07$ mm^3, green, mounted with polyfluorinated oil and measured on a Siemens SMART-CCD diffractometer (three-axis platform) with Mo-Kα-radiation at 130 K; a = 21.3735(5), b = 6.11890(10), c = 23.4144(6) Å, β = 99.8480(10)°, V = 3017.07(7) Å^3; monoclinic crystal system, Z = 4, D_c = 1.195 g cm^{-3}, μ = 0.067 mm^{-1}, space group $C2/c$, data collection of 8535 intensities ($2\Theta_{max}$ = 45°, one run 0.3° ω-scans, 120 frames at ϕ = 0°, four runs 0.3° ϕ-scans with 600 frames at angles 135, 143, 156 and 169° in ω, more than 97% of the data covered), absorption correction with Siemens SADABS (R_{merg} before/after = 0.115/0.063, max/min equivalent transmission = 1.00/0.60), 1910 independent intensities (R_{merg} = 0.103), 1479 'observed' data [$F_o \geqslant 4\sigma(F)$], structure solution with direct methods (Siemens SHELXS) and refined on F^2 (Siemens SHELXTL-Plus, ver. 5.01) (190 parameters), the hydrogen atom positions were calculated and refined as riding groups with 1.2-fold (1.5 for methyl groups) isotropic U values. $R1$ = 0.0827, $wR2$ = 0.2251, $w^{-1} = \sigma^2(F_o^2) + (0.103P)^2 + 6.50P$, where $P = [(\max F_o^2) + (2F_c^2)]/3$, max/min residual electron density = 0.264/−0.246 eÅ^{-3}. CCDC 182/1129.

8 According to Schulman and Disch (ref. 4): (*a*) the experimentally obtained structure is a transition state between the two Kekulé isomers **2b** and **2c**, and (*b*) **2a** was predicted to be more stable than **2b** by 17.9–20 kcal mol^{-1}.

9 GAUSSIAN 94, Revision E.1, M. J. Frisch, G. W. Trucks, H. B. Schlegel, P. M. W. Gill, B. G. Johnson, M. A. Robb, J. R. Cheeseman, T. Keith, G. A. Petersson, J. A. Montgomery, K. Raghavachari, M. A. Al-Laham, V. G. Zakrzewski, J. V. Ortiz, J. B. Foresman, J. Cioslowski, B. B. Stefanov, A. Nanayakkara, M. Challacombe, C. Y. Peng, P. Y. Ayala, W. Chen, M. W. Wong, J. L. Andres, E. S. Replogle, R. Gomperts, R. L. Martin, D. J. Fox, J. S. Binkley, D. J. Defrees, J. Baker, J. P. Stewart, M. Head-Gordon, C. Gonzalez and J. A. Pople, Gaussian, Inc., Pittsburgh PA, 1995.

10 N. L. Frank, K. K. Baldridge and J. A. Siegel, *J. Am. Chem. Soc.*, 1995, **117**, 2102.

11 The discussion presented here for **4** regards the tetraethenyl derivative of isomer **2d**. However, **2a** also has a stable tetravinyl derivative. The two bond-shift isomers (*i.e.* **2a** and **2d**) also have other stable derivatives that show this isomerism, such as the tetrahydroxy and tetracyano derivatives (A. Stanger, unpublished results). These are, however, beyond the scope of this paper.

12 The agreement between the experimental and calculated structures is even better if the experimental σ value (0.005 Å for all the discussed bonds) is considered.

Communication 8/09116A

Photoinduced switching of metal complexation by quinolinospiropyranindolines in polar solvents

Greg E. Collins,*[a] Ling-Siu Choi,[a] Kenneth J. Ewing,[a] Veronique Michelet,[b] Corinne M. Bowen[b] and Jeffrey D. Winkler*[b]

[a] *Naval Research Laboratory, Chemistry Division, Code 6116, Washington DC 20375-5342, USA. E-mail: gcollins@ccf.nrl.navy.mil*

[b] *Department of Chemistry, The University of Pennsylvania, Philadelphia, Pennsylvania 19104, USA*

Received (in Columbia, MO, USA) 5th October 1998, Accepted 11th January 1999

The first demonstration of rapid and reversible, photoinduced switching of metal complexation from a quinolinospiropyranindoline–metal complex in aqueous solution is presented.

The design and synthesis of functional molecules with molecular switching characteristics is currently an area of intense activity and tremendous potential significance to the fields of molecular electronics and sensor device fabrication.[1] The development of new materials for application in sensing transducers has traditionally been plagued by non-reversible interactions between the analyte and sensing receptor, a factor resulting in one-time use sensors. Innovative efforts to overcome this problem have typically relied upon the incorporation of both the complexation or recognition site and a light- or potential induced rejection mechanism into a single sensing molecule.[2,3] Spiropyrans[4,5] and spirooxazines[6,7] have shown particular promise in this regard due to the photochemically-mediated interconversion of 'open' and 'closed' forms (*e.g.* **1**⇆**2**) upon exposure to UV or visible light, respectively. The introduction of metal ion complexation sites to take advantage of the spiropyranindoline ⇆ merocyanine interconversion leads to the photoreversible ejection of complexed metal ions.[4] To our knowledge, there are no published accounts of photoreversible metal ion complexation by these compounds in aqueous media. The reason for this is simple: stabilization of the merocyanine isomer in water prevents the photoinduced ejection of trapped metal ions. Photoreversible metal complexation in water is critical to the eventual application of these materials to sensor transducers operated in aqueous systems for environmental monitoring. Here we describe the molecular design issues critical to promoting photoreversible metal complexation for spirobenzopyrans in polar solvents, and present the first demonstration of rapid and reversible, photoinduced switching of metal complexation from a quinolinospiropyranindoline–metal complex in aqueous solution.

Two 8-hydroxylquinoline-derived spiropyranindolines **1a** (R = H)[4,8] and **1b** (R = NO_2),[4] which differ only by the addition of a nitro group *para* to the pyran oxygen, are shown in Scheme 1.

While the denticity of 8-hydroxyquinoline for metal ions is well precedented, our initial expectation was that the stability of the metal/merocyanine complex **3a** would prevent photoisomerization to **1a** with concomitant release of metal ion. Spirobenzopyran **1b** was, therefore, prepared to promote photoreversibility of metal complexation by withdrawing electron density away from the phenolate oxygen and decreasing the denticity of **2b**. Spirobenzopyran **1b** does indeed exhibit significant, photoreversible metal complexation in organic solvents with low polarity, such as tetrahydrofuran. Unfortunately, there is little to no observable reversibility in solvents of higher polarity, such as acetonitrile. The inability to achieve the conversion of **3b** to **1b** *via* irradiation can be explained by the enhanced stabilization of the zwitterionic merocyanine form, **2b**, by the nitro group which serves to delocalize the phenoxide anion in **2b**.[9] This stabilizing effect of the nitro group in **2b** is underscored by the rapid conversion of **1b** in the dark to the colored, merocyanine form **2b** in solvents with dielectric constants higher than that of tetrahydrofuran. Note from Scheme 1 that in addition to the solvent dependent generation of **2** under dark conditions, the concentration of **2** is further enhanced under UV light illumination. Ultimately, the lifetime of any free zinc ions ejected into solution is significantly attenuated due to the rapid recomplexation event, **2b**→**3b**.

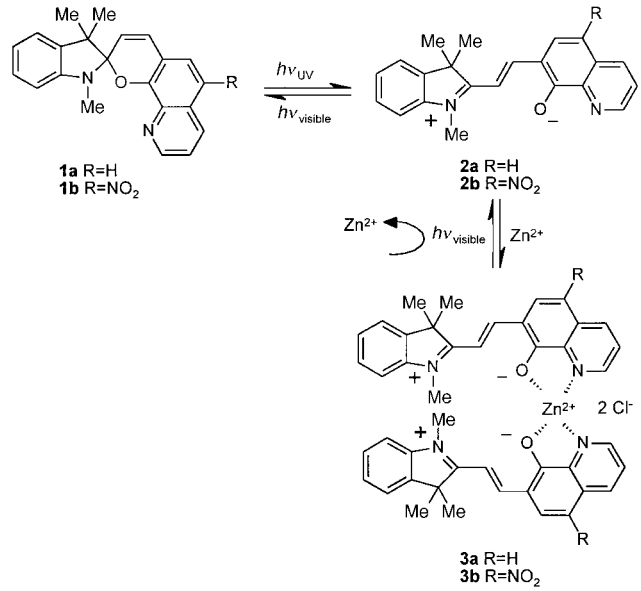

Scheme 1 Photoreversible equilibria of quinolinospiropyranindoline (**1a**, R = H) and nitroquinolinospiropyranindoline (**1b**, R = NO_2).

The thermodynamic stability of the closed quinolinospiropyranindoline, **1**, must be enhanced to promote photoreversibility of metal complexation of **3** in polar solvents. The simplest way of doing this is to remove the nitro group *para* to the phenoxide anion, as in **1a**. Evidence for the improved stability of **1a** relative to **1b** is apparent from the colorless solution, indicative of the closed spiropyran, obtained for **1a** in acetonitrile (2.4×10^{-5} M; Fig. 1A, spectrum a). The dark addition of 0.5 equivalents of Zn^{2+} to this solution of **1a** in acetonitrile (Fig. 1A, spectrum b) results in the formation of a bright red complex **3a**, with Zn^{2+} in a 2 : 1 ligand : metal ratio, based upon stoichiometric determinations using the molar ratio absorbance method.

Exposure of a solution of **3a** in acetonitrile to visible light (150 W tungsten flood lamp) causes the temporary ejection of the complexed metal ion, and a transition to the colorless, closed form of the quinolinospiropyranindoline (**3a**→**1a**). Evidence for this shift is shown in Fig. 1A, which shows the effect of exposure of a solution of **3a** to visible light as a function of time.

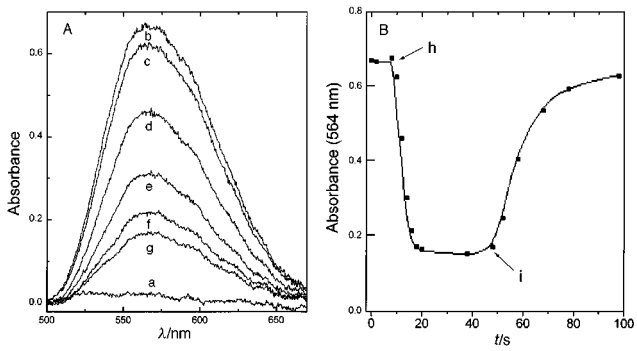

Fig. 1 (A) UV–VIS spectra of 2.4×10^{-5} M **1a** in acetonitrile with (a) no Zn^{2+} added; (b) 1.2×10^{-5} M Zn^{2+} added; and solution (b) after exposure to visible light for (c) 2, (d) 12, (e) 14, (f) 16, (g) 20 s. (B) Switching behavior observed in the absorbance intensity at 564 nm with visible light on at 8 s (h) and off at 48 s (i).

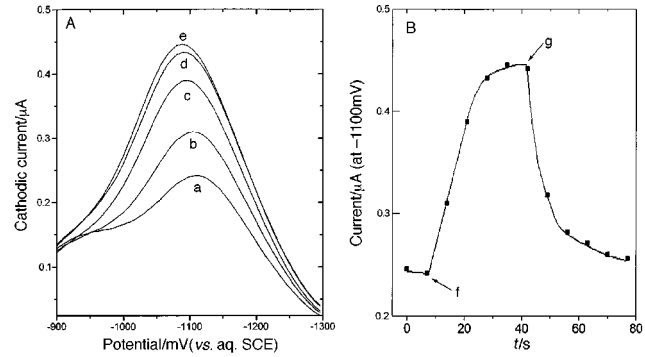

Fig. 2 (A) Cathodic reduction of free Zn^{2+} ions in a 4 : 1 water–acetonitrile solution containing 2.4×10^{-5} M **1a** and 1.2×10^{-5} M Zn^{2+} after exposure to visible light for (a) 0, (b) 7, (c) 14, (d) 21, (e) 28 s. (B) Switching behavior observed in the cathodic reduction of free Zn^{2+} ions in solution with visible light on at 7 s (f) and off at 42 s (g).

This amazing effect can be monitored visually without the aid of a spectrometer, the transition from a strongly colored, red complex to a nearly colorless solution (78% reduction in absorbance at 564 nm, Fig. 1A) indicating that the complex **3a** is undergoing photoisomerization to the closed spirobenzopyran form **1a** and ejecting the complexed Zn^{2+} ion in the process. The photochemically mediated ejection of the metal ion from **3a** is fast, with an 8 s response time following the onset of visible light irradiation (Fig. 1B). Immediately following the cessation of light, the free metal ion is quickly recomplexed (50 s time response) as the equilibrium shifts back to its original state (**1a**→**3a**). In contrast, ejection of Zn^{2+} ion from a solution of **3b** in acetonitrile upon irradiation with visible light is minimal (14%), a result which can be ascribed to the enhanced stability of **2b** in polar solvents, as described above. This rapid switching behavior in the metal complexation properties of spiropyranindoline **1a** is an important step toward the development of molecular devices and sensors.[10]

While UV–VIS spectroscopy monitors equilibria pertaining to the ligand, electrochemistry can be used to monitor equilibria associated with the metal ion. Square wave voltammetry was utilized (1) as a complementary technique to confirm the ejection of metal ions from the merocyanine complex, and (2) to assess the extent of reversible rejection of complexed zinc from both **3a** and **3b** in aqueous solution (a 4 : 1 water–acetonitrile solution was utilized due to solubility constraints). Initially, a control experiment was run on a solution of 1.2×10^{-5} M Zn^{2+} in order to identify the peak position and intensity of the Zn^{2+} cathodic wave (−1100 mV *vs.* aq. SCE). Exposure of the control solution to visible light had no effect on the voltammogram prior to the addition of the spiropyranindolines. Both **1a** and **1b** (2.4×10^{-5} M) led to rapid complexation of Zn^{2+}, resulting in the near elimination of the free Zn^{2+} potential peak. Because of the rapid increase in current associated with the reduction of water, we were unable to identify any cathodic waves corresponding to the reduction of **3a** or **3b**. Unlike the irradiation of **3b** with visible light, which resulted in no change in the free Zn^{2+} cathodic wave at −1100 mV, complex **3a** exhibited an ejection of 8% of the complexed Zn^{2+} ions into the aqueous solution (Fig. 2A). The rate of recomplexation of ejected Zn^{2+} ions in water (Fig. 2B) was nearly twice as fast as that observed in acetonitrile (light on, 14 s response time; light off, 28 s response time, both in an unstirred solution). The attenuation in the extent of photoreversible metal ejection and the more rapid metal ion recomplexation are both indicators of the enhanced stabilization effect water has on the merocyanine form, **2a**, when compared to the solvent, acetonitrile.

In conclusion, we have demonstrated a rapid, switching type mechanism for photoreversible metal complexation by quinolinospiropyranindoline **1a** in aqueous solution. Modifications of these systems designed to enhance the photoreversibility in aqueous media are currently under investigation in our laboratories.

The authors gratefully acknowledge the Office of Naval Research for financial support (N-00014-93-1-0836 to J. D. W.).

Notes and references

1 *Nanotechnology*, ed. B. C. Crandall and J. Lewis, MIT Press, Cambridge, MA, 1992.
2 K. Kimura, R. Mizutani, M. Yokoyama, R. Arakawa, G. Matsubayashi, M. Okamoto and H. Doe, *J. Am. Chem. Soc.*, 1997, **119**, 2062.
3 T. Saji and I. Kinoshita, *J. Chem. Soc., Chem. Commun.*, 1986, 716.
4 J. D. Winkler, C. M. Bowen and V. Michelet, *J. Am. Chem. Soc.*, 1998, **120**, 3237.
5 M. Inouye, K. Akamatsu and H. Nakazumi, *J. Am. Chem. Soc.*, 1997, **119**, 9160.
6 K. Kimura, M. Kaneshige, T. Yamashita and M. Yokoyama, *J. Org. Chem.*, 1994, **59**, 1251.
7 T. Tamaki and K. Ichimura, *J. Chem. Soc., Chem. Commun.*, 1989, 1477.
8 F. Przystal and J. P. Phillips, *J. Heterocycl. Chem.*, 1967, **4**, 131.
9 T. Bercovici, R. Heiligman-Rim and E. Fischer, *Mol. Photochem.*, 1969, **1**, 23.
10 In addition to Zn^{2+}, the photoreversibility of complexation by NQSP and QSP was examined using UV–VIS spectroscopy for the following metals: Zn^{2+}, Hg^{2+}, Cd^{2+}, Pb^{2+}, Cu^{2+}, Ni^{2+}, Co^{2+}, Mg^{2+}, Ca^{2+} and Al^{3+}. NQSP in THF exhibited photoreversibility for Hg^{2+}, Cd^{2+}, Pb^{2+}, Mg^{2+}, Ca^{2+} and Al^{3+}, while QSP in THF and MeCN exhibited photoreversibility for only Zn^{2+} and Al^{3+}.

Communication 8/07994C

Stereochemical control of *cis*- and *trans*-$TiCl_2$ groups in six-coordinate complexes [(L)$TiCl_2$] (L^{2-} = N_2O_2-donor Schiff base) and reactions with trimethylaluminium to form cationic aluminium species

Jonathan P. Corden, William Errington, Peter Moore* and Malcolm G. H. Wallbridge

Department of Chemistry, University of Warwick, Coventry, UK CV4 7AL. E-mail: p.moore@warwick.ac.uk

Received (in Cambridge, UK) 29th October 1998, Accepted 7th January 1999

The first example of a *cis*-configuration of the $TiCl_2$ group in a six-coordinate titanium complex [(L)$TiCl_2$], involving a tetradentate N_2O_2-donor Schiff base ligand (L^{2-}), is reported, and reactions of such complexes with trimethyl aluminium have been shown to generate cationic aluminium species.

There is an increasing interest in the use of group 4 metallocenes, and related compounds, such as the chiral bis(indenyl) complexes involving zirconium and hafnium, in combination with aluminium trialkyls or methylaluminoxane (MAO), as alkene polymerisation catalysts.[1–4] The use of other group 4 coordination compounds in such processes may also be possible, and the d^0 metal complexes [(L)MCl_2] (M = Ti, Zr), derived from the disodium salts of the tetradentate Schiff bases H_2L (Scheme 1), is one system being explored,[5] since the zirconium derivative, containing a *cis*-$ZrCl_2$ group, has already been shown to be catalytically active in the presence of an aluminium trialkyl.[6]

The stereochemistry of the MCl_2 group is an important feature of the overall structure with respect to catalytic activity, and therefore it is of significance that to date all reported titanium derivatives [(L)$TiCl_2$] exhibit a *trans*-geometry for the $TiCl_2$ fragment,[7,8] instead of the *cis*-arrangements (Scheme 1) that are analogous to that in the *ansa*-metallocenes. The *cis*-structure is, however, more common with the [(L)MCl_2] complexes of the heavier and larger group 4 elements (M = Zr, Hf),[9,10] and has also been observed with an oxovanadium(IV) species [(L)V(O)OMe].[11] It is significant that even in complexes with the same Schiff base ligand, for example the *N*,*N*'-ethylenebis(acetylacetoiminate) dianion ($acen^{2-}$), the zirconium complex [(acen)$ZrCl_2$] adopts the *cis*-structure, whereas the corresponding titanium compound reverts to the *trans*-geometry.[8,9] Since titanium is the group 4 element that is often used in catalytic reactions, it is desirable to be able to control the stereochemistry at the metal centre. We now report the synthesis of the first *cis*-titanium Schiff base complexes, using easily accessible Schiff bases, together with some reactions of these species with aluminium trialkyls.

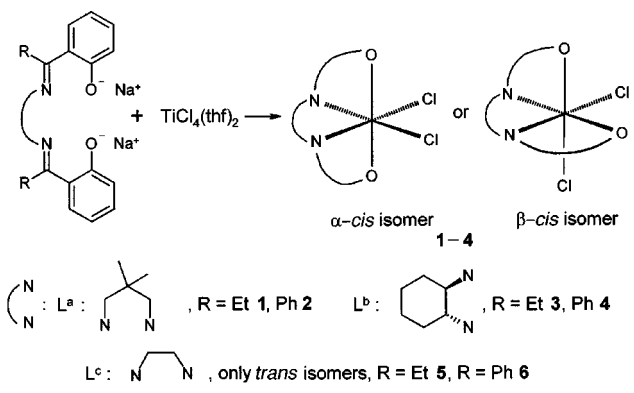

Scheme 1

Our present studies on titanium–Schiff base complexes, where we have isolated a series of *trans*-[(L)$TiCl_2$] complexes,[12] have indicated that substantial steric effects within the ligand are required to achieve a folding of the ligand such that it takes up a *cis*-geometry as shown in Scheme 1. Following molecular mechanics and dynamics calculations on [(L)$TiCl_2$] derivatives, it appeared that complexes **1**–**4** should adopt a folded configuration, leading to a *cis*-geometry at the metal centre. The four neutral ligands were prepared in high yield (> 90%) by condensation of the appropriate diamine (using *trans*-cyclohexane-1,2-diamine for L^b) and keto derivatives, and converted to the new metal complexes [(L)$TiCl_2$] (50–60% yield) by the reaction shown in Scheme 1.†

The X-ray structure of [(L)$TiCl_2$] complex **3**‡ (Fig. 1) shows a distorted octahedral arrangement around the titanium centre, with a folded ligand and a β-*cis*-geometry for the complex. The Cl–Ti–Cl angle is 86.9(1)°. The variation in the ligand geometry has little effect on the bond distances involving the metal. The Ti–O and Ti–N distances are *ca.* 1.82 and 2.19 Å respectively, similar to those reported for the numerous *trans*-[(L)$TiCl_2$] complexes,[7,8] while the Ti–Cl distances are all *ca.* 2.35 Å in both the *trans*- and *cis*-derivatives [2.323(2) and 2.391(3) Å in **3**]. Similarities in the spectroscopic data (IR, NMR) between **3** and the other three [(L)$TiCl_2$] complexes **1**, **2** and **4** indicate that these also probably form *cis*-structures, but we are still attempting to obtain suitable crystals to allow definitive X-ray studies to be undertaken.

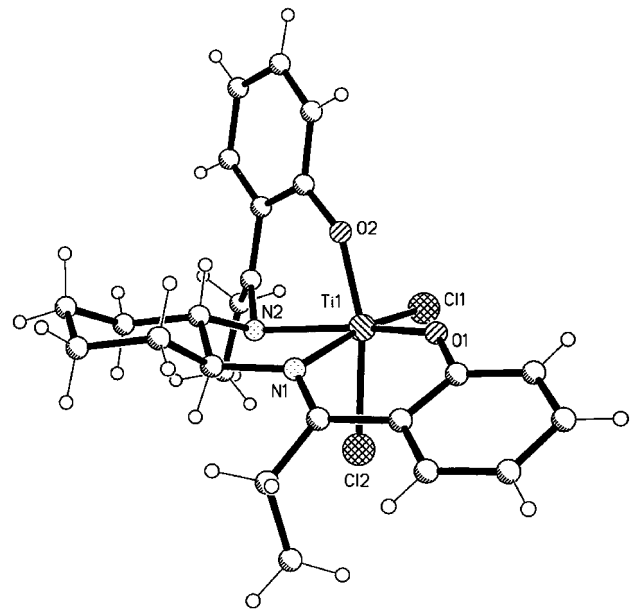

Fig. 1 Molecular structure of **3**. Selected bond lengths (Å) and angles (°): Ti(1)–O(1) 1.796(5), Ti(1)–O(2) 1.827(5), Ti(1)–N(1) 2.186(5), Ti(1)–N(2) 2.205(6), Ti(1)–Cl(1) 2.323(2), Ti(1)–Cl(2) 2.391(3); O(1)–Ti(1)–O(2) 99.5(2), N(1)–Ti(1)–N(2) 76.6(2), N(2)–Ti(1)–Cl(1) 99.67(16); Cl(1)–Ti(1)–Cl(2) 86.89(9).

We have confirmed that the titanium complexes **1**–**4** act as catalysts for the polymerisation of ethene in the presence of MAO, although they are not as active as the *ansa*-titanocenes.§ Since MAO often contains an appreciable quantity of trimethyl aluminium (TMA, ≈15% by weight in the present case) we have investigated the action of TMA on some $[(L)TiCl_2]$ complexes. In a series of ^{1}H NMR experiments we have used titrations with TMA to show that complete reaction is achieved when a molar ratio $[(L)TiCl_2]$: TMA of 1 : 2 is attained. In more detailed experiments on the related *trans*-$[(L^c)TiCl_2]$ complexes, red–brown solids of composition $[\{(L^c)TiCl_2\}\cdot 2AlMe_3]$ were obtained in *ca.* 40% yield by the addition of a hexane solution of TMA to the Schiff base complex (2 : 1 mole ratio) in toluene, and subsequent removal of the solvent. The ^{1}H NMR spectrum of each adduct shows two singlet resonances, with appropriate relative intensities, for the two coordinated $AlMe_3$ molecules (the derivatives with **5** and **6** gave resonances at δ −0.21, −0.41 and −0.34, −0.53 respectively, arising from the methyl groups of the two different $AlMe_3$ molecules) in addition to the resonances from L^c. Thus two different sites for coordination of the TMA are indicated, but we have no definitive evidence to indicate the structures of these species at present. If the initially formed red solution from **5** is allowed to stand, colourless, air-reactive crystals are quickly deposited (yield *ca.* 5%), and these were identified from X-ray data‡ as the unexpected ionic species $[(L^c)(AlMe)(AlMe_2)]^+[AlCl_3Me]^-$ (**7;** Fig. 2). Part of the structure of the cation in **7** resembles the previously reported *neutral* species $[(L^c)AlR']$ [L^c, R = H; R' = Me, Et] which have the metal atom bonded centrally above the N_2O_2 plane.[13,14] In the present case, where the cation is present, the compound contains additionally an $AlMe_2$ fragment bonded symmetrically to two oxygen atoms of the Schiff base. The $[AlCl_3Me]^-$ anion is discrete, with no significant interactions with the cation, and adopts the expected slightly distorted tetrahedral structure. Cationic aluminium alkyl complexes have recently been shown to act as transition metal-free alkene polymerisation catalysts,[15] in addition to the already established cationic group 4 species.[3] The role of the aluminium alkyl as a cocatalyst with group 4 compounds is still the subject of debate, but as a consequence of the present results it is now clear that for some titanium complexes the addition of TMA is capable of generating cationic species of aluminium in solution. It is significant that no titanium atom is present in the cation, but the titanium species is clearly involved in the overall reaction since the $[AlCl_3Me]^-$ anion arises by halide abstraction from the titanium centre. Although we have not yet been able to identify the nature of the titanium species remaining in solution, it is of interest that under our conditions we have not yet observed the formation of any Ti(III) or Ti–Me species, as have been found in other studies involving TMA and the different but closely related complex *trans*-$[(L^c)TiCl_2]$ [(L^c; R = H)].[16]

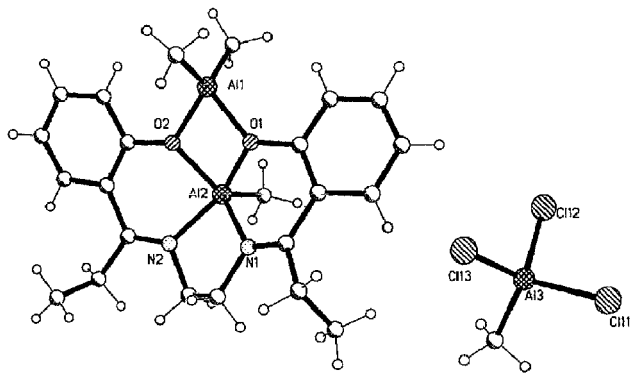

Fig. 2 Molecular structure of **7**. Selected bond lengths (Å) and angles (°): Al(1)–O(1) 1.845(6), Al(1)–O(2) 1.868(6), Al(2)–O(1) 1.873(6), Al(2)–O(2) 1.877(6), Al(2)–N(2) 1.945(7), Al(2)–N(1) 1.960(8); O(1)–Al(1)–O(2) 77.4(2), O(1)–Al(2)–O(2) 76.5(2), O(1)–Al(2)–N(2) 149.6(3), O(2)–Al(2)–N(2) 88.2(3), O(1)–Al(2)–N(1) 88.2(3), O(2)–Al(2)–N(1) 136.2(3), N(2)–Al(2)–N(1) 85.0(3).

We are continuing our studies to determine both the nature of the titanium species remaining in solution, and the effect that variations in the Schiff bases has on the overall reaction involved.

We thank EPSRC for grants in support of this work, the X-ray crystallographic service (University of Wales, Cardiff) for collecting the data on compound **3**, and B.P. Chemicals (Sunbury) for advice (Dr I. R. Little) and collaboration involving a CASE award to J. P. C.

Notes and references

† *Typical procedure*: sodium hydride (2 mol) was added slowly to a solution of the ligand (1 mol) in THF, the suspension was stirred until the evolution of H_2 was complete, and the mixture then refluxed for 2 h. The solution–suspension was cooled to −78 °C and a solution of $[TiCl_4(thf)_2]$ (1 mol) in thf was then added slowly. The resultant suspension was stirred at 50 °C for 5 h, and then filtered through a fine filter stick. The filtrate was evaporated to dryness, and the solid obtained was washed with hot toluene to remove any thf (yield *ca.* 40%). A higher yield (50–60%) can be obtained by extracting the original solid filtered off (mainly NaCl) with toluene. All the new compounds were fully characterised by IR, mass and NMR spectroscopy and elemental analysis.

‡ *Crystal data* for **3**: $C_{24}H_{28}Cl_2N_2O_2Ti\cdot CHCl_3$, M = 614.65, T = 150(2) K, monoclinic, space group $P2_1/c$, a = 16.446(3), b = 9.796(2), c = 18.160(4) Å, β = 111.32(3)°, U = 2725.3(9) Å3, Z = 4, μ = 0.831 mm^{-1}. 12060 reflections (4283 independent) were collected in the range θ 2.29–25.12° using a Delft Instruments FAST TV area detector diffractometer. Final $R1$ = 0.053 and $wR2$ = 0.129.

For **7**: $C_{24}H_{34}Al_3Cl_3N_2O_2$, M = 569.82, T = 230(2) K, orthorhombic, $Pna2_1$, a = 15.7057(15), b = 9.7173(9), c = 19.5089(15) Å, U = 2977.4(5) Å^3, Z = 4, μ = 0.419 mm^{-1}. 5592 reflections (3804 independent) were collected in the range θ 2.09–23.00° using a Siemens SMART CCD area-detector diffractometer. Final $R1$ = 0.074 and w$R2$ = 0.161. Refinement was by full-matrix least squares on F^2 for all data using SHELXL-97.[17] Hydrogen atoms were added at calculated positions and refined using a riding model. CCDC 182/1135. See http://www.rsc.org/suppdata/cc/1999/323/ for crystallographic files in .cif.format.

§ Preliminary polymerisation tests using a 1000-fold excess of MAO with the neutral compounds **1**–**4**, in toluene solution at 23 °C and ethene at 30 psi, show they possess low activities of *ca.* 20–100 (g polymer) (mmol catalyst)$^{-1}$ h^{-1}, while similar runs with several analogous *trans*-$[TiCl_2]$ complexes show a much lower activity (< 1) for these systems.

1 F. R. W. P. Wild, L. Zsolnai, G. Huttner and H.-H. Brintzinger, *J. Organomet. Chem.*, 1982, **232**, 233.
2 H.-H. Brintzinger, D. Fischer, R. Mulhaupt, B. Rieger and R. M. Waymouth, *Angew. Chem., Int. Ed. Engl.*, 1995, **34**, 1143.
3 M. Bochmann, *J. Chem. Soc., Dalton Trans.*, 1996, 255 and references therein.
4 H. Sinn and W. Kaminsky, *Adv. Organomet. Chem.*, 1980, **18**, 99.
5 A. S. Guram and R. F. Jordan, *Comprehensive Organometallic Chemistry*, ed. M. F. Lappert, 2nd edn., Pergamon, Oxford, 1995, vol. 4, p. 589.
6 E. B. Tjaden, D. C. Swenson, R. F. Jordan and J. L. Peterson, *Organometallics*, 1995, **14**, 371.
7 C. Floriani, E. Solari, F. Corazza, A. Chiesi-Villa and C. Gaustini, *Angew. Chem., Int. Ed. Engl.*, 1989, **28**, 64 and references therein.
8 M. Mazzanti, J.-M. Rosset, C. Floriani, A. Chiesi-Villa and C. Gaustini, *J. Chem. Soc., Dalton Trans.*, 1989, 953.
9 F. Corazza, E. Solari, C. Floriani, A. Chiesi-Villa and C. Gaustini, *J. Chem. Soc., Dalton Trans.*, 1990, 1335.
10 P. Woodman, P. B. Hitchcock and P. Scott, *Chem. Commun.*, 1996, 2735.
11 S. A. Fairhurst, D. L. Hughes, U. Kleinkes, G. J. Leigh, J. R. Sanders and J. Weisner, *J. Chem. Soc., Dalton Trans.*, 1995, 321 and references therein.
12 J. P. Corden, W. Errington, P. Moore and M. G. H. Wallbridge, unpublished work.
13 J. T. Leman, J. Braddock-Wilking, A. J. Coolong and A. R. Barron, *Inorg. Chem.*, 1993, **32**, 4324.
14 S. J. Dzugan and V. L. Goedken, *Inorg. Chem.*, 1986, **25**, 2858.
15 M. P. Coles and R. F. Jordan, *J. Am. Chem. Soc.*, 1997, **119**, 8125.
16 D. G. Kelly, A. J. Toner, N. M. Walker, S. J. Coles and M. B. Hursthouse, *Polyhedron*, 1996, **15**, 4307.
17 G. M. Sheldrick, Program for the Refinement of Crystal Structures, University of Göttingen, Germany, 1997.

Communication 8/08372J

A formal synthesis of (+)-pyripyropene A using a biomimetic epoxy-olefin cyclisation

Varinder K. Aggarwal,*[a] Paul A. Bethel[a] and Robert Giles[b]

[a] *Department of Chemistry, University of Sheffield, Sheffield, UK S3 7HF*
[b] *SmithKline Beecham, Old Powder Mills, Tonbridge, Kent, UK TN11 9AN*

Received (in Liverpool, UK) 4th November 1998, Accepted 7th January 1999

Bicyclic ester 2, a key intermediate in the first total synthesis of (+)-pyripyropene A 1, was synthesised from geraniol in 11 steps, utilising an epoxy-olefin biomimetic cyclisation as the key step.

Pyripyropenes A–L, isolated by Õmura and co-workers[1] from a fermentation broth of *Aspergillus fumigatus*, are the most effective naturally occurring inhibitors of acyl-CoA: cholesterol acyltransferase (ACAT), the enzyme responsible for intracellular esterification of cholesterol. Inhibition of the ACAT enzyme represents a new approach to the prevention and treatment of atherosclerosis and hypercholesterolemia[2] since evidence suggests that ACAT inhibitors may lower plasma cholesterol levels and prevent the accumulation of cholesteryl esters in arterial lesions.

The most active member of the family, (+)-pyripyropene A **1**, was synthesised by Õmura and Smith from (+)-Wieland–Miescher ketone **3** in 19 steps[3] (Scheme 1).

We envisioned a short biomimetic route to the decalin subunit **2**, a key intermediate in the Õmura–Smith synthesis (prepared in 10 steps from **3**), utilising an epoxy-olefin cyclisation[4] of allyl silane **10**. Although a biomimetic polyene cyclisation has been used to prepare the simplest member of the family, pyripyropene E **4**,[5] it was surprising that this strategy had not been adopted for pyripyropene A **1** as the required epoxide contains a neighbouring alcohol group and as such could be easily obtained in enantiomerically pure form by Sharpless epoxidation.[6] Such epoxy alcohols (protected as ethers) have been successfully employed in epoxy-olefin cyclisations.[7]

The known allylic alcohol **5**, derived from geraniol in 5 steps,[7] was converted to bromide **6** upon treatment with MsCl/Et_3N followed by LiBr at −78 °C. (Scheme 2).[8] Low temperature and a controlled amount of LiBr were required to minimise opening of the epoxide. The relatively unstable bromide **6** was then employed in the alkylation step with the dianion of methyl acetoacetate[9] to afford β-keto ester **7** in 78% yield. Upon treatment of β-keto ester **7** with $BF_3{\cdot}OEt_2$ in CH_2Cl_2, epoxy-olefin cyclisation ensued but the oxabicycle **8** was formed exclusively.[10] To promote carbon over oxygen cyclisation, the carbonyl group had to be masked or removed and several possibilities were apparent from the literature. (i) Conversion of β-keto ester **7** into the silyl enol ether **12**.[11]

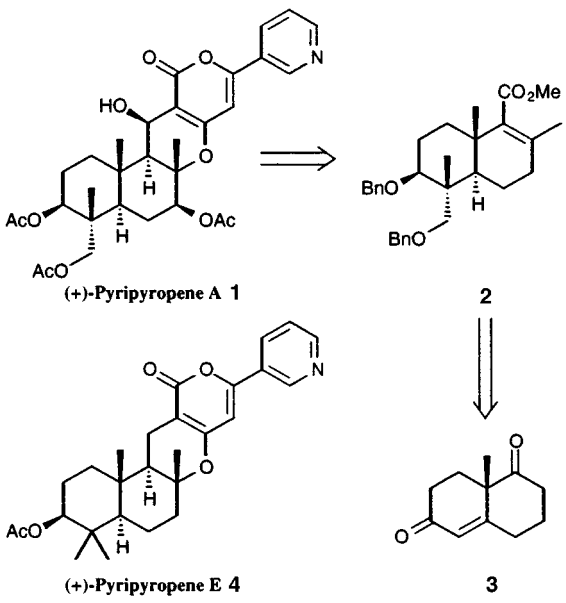

Scheme 1

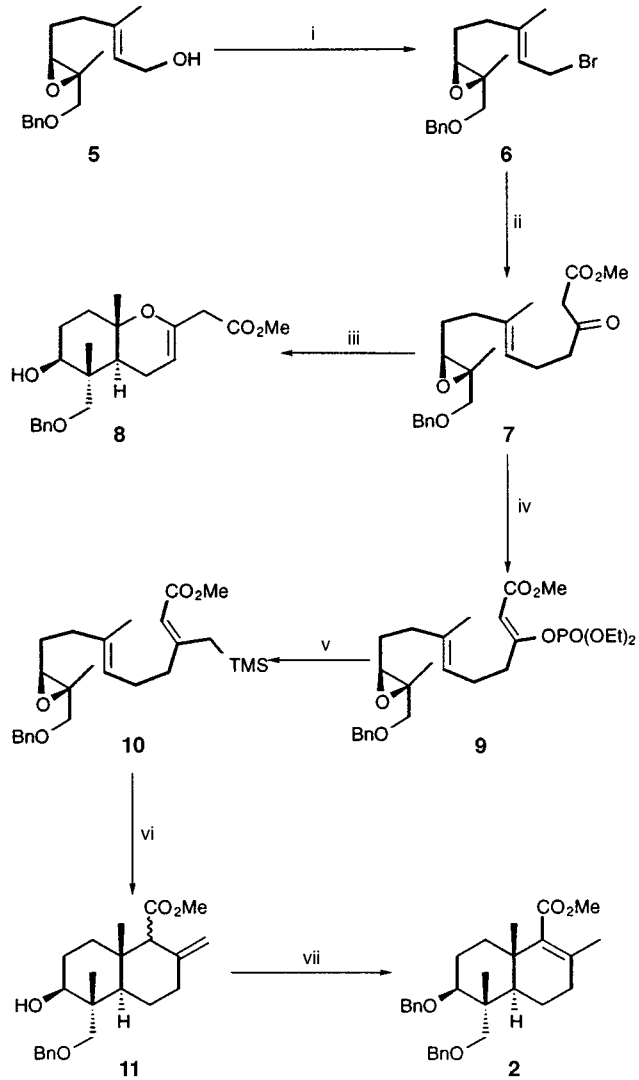

Scheme 2 *Reagents and conditions*: i, MsCl, Et_3N, THF, −78 °C, then LiBr (3 equiv.), acetone, −78 °C, 50 min, 87%; ii, methyl acetoacetate, NaH, Bu^nLi, THF, 0 °C, then **6**, 78%; iii, $BF_3{\cdot}OEt_2$, CH_2Cl_2, 60%; iv, NaH, $(EtO)_2POCl$, Et_2O, 93%; v, $TMSCH_2MgCl$, $Ni(acac)_2$ (cat.), Et_2O, 0 °C, 54%; vi, $BF_3{\cdot}OEt_2$, CH_2Cl_2, 54%; vii, NaH, BnBr, THF, reflux, 51%.

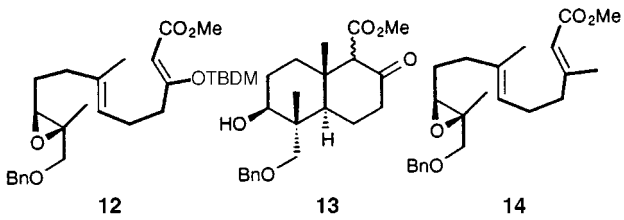

However, cyclisation of this substrate only provided a low yield (26% from **7**) of **13**. (ii) Conversion of β-keto ester **7** into the unsaturated ester **14**.[12] However, it is known that unsaturated esters are poor terminating groups for polyolefin cyclisation.[13] (iii) Conversion of β-keto ester **7** into allylsilane **10**.[14] Weiler had shown that allylsilanes bearing ester groups were sufficiently nucleophilic to undergo epoxy-olefin cyclisation.[14] This route was eventually successful. Thus, conversion of β-keto ester **7** to *Z*-enol phosphate **9** [NaH, $(EtO)_2POCl$, Et_2O] followed by coupling with $TMSCH_2MgCl$ in the presence of nickel(II) bisacetylacetonate furnished the cyclisation substrate, *Z*-allylsilane **10**.

Both the nature of the protecting group on oxygen[15] and cyclisation conditions were critical to the success of the key step. Treatment of the allylsilane **10** with $BF_3{\cdot}OEt_2$ at room temperature gave the required decalin in 54% yield as a 3:2 mixture of epimeric hydroxy esters **11**. In contrast, the use of $SnCl_4$ or $MeAlCl_2$ (Corey's preferred cyclisation catalyst)[4b–d] resulted in chlorohydrins **16** and **18** (Scheme 3). Attempts to cyclise the unprotected epoxy alcohol **15** failed;[16] only mixtures of unidentifiable acyclic and monocyclic products were observed with $BF_3{\cdot}OEt_2$ and the use of $MeAlCl_2$ resulted in the formation of chlorohydrins **17** and **19** as shown in Scheme 3. The use of $SnCl_4$ yielded bicyclic ethers **20** and **21** along with chlorohydrin **17**.

All that remained to complete the formal synthesis was isomerisation of the exocyclic double bond and benzylation of the free alcohol. However, attempts to isomerise the alkene **11** into conjugation with the ester using $RhCl_3$[17] resulted in the formation of the trisubstituted alkene **22** instead.[18] Fortuitously,

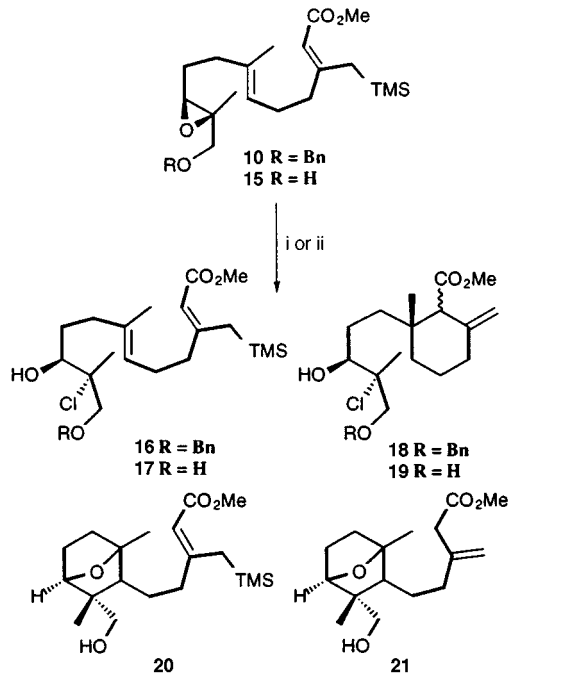

Scheme 3 *Reagents and conditions*: i, $MeAlCl_2$, CH_2Cl_2, room temp.; ii, $SnCl_4$, CH_2Cl_2, room temp.

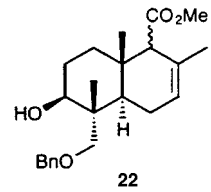

benzylation of alcohol **11** using an excess of NaH in THF and BnBr[19] resulted in concomitant isomerisation of the alkene and provided **2** directly in 51% yield. Decalin **2** was spectroscopically identical[20] to that reported by Ōmura and Smith.[3]

We thank the EPSRC and SmithKline Beecham for a CASE award and Meng Fang Wang for initial studies.

Notes and references

1 Y.-K. Kim, H. Tomoda, H. Nishida, T. Sunazuka, R. Obata and S. Omura, *J. Antibiot.*, 1994, **47**, 154; S. Omura, H. Tomoda, Y.-K. Kim and H. Nishida, *J. Antibiot.*, 1993, **46**, 1168; H. Tomoda, Y.-K. Kim, H. Nishida, R. Masuma and S. Omura, *J. Antibiot.*, 1994, **47**, 148; H. Tomoda, N. Tabata, D.-J. Yang, H. Takayanagi, H. Nishida and S. Omura, *J. Antibiot.*, 1995, **48**, 495; T. Sunazuka and T. Nagamitsu, *J. Synth. Org. Chem. Jpn.*, 1988, **56**, 478.

2 D. R. Sliskovic and A. D. White, *Trends Pharmacol. Sci.*, 1991, **12**, 194.

3 A. B. Smith III, T. Nagamitsu, T. Sunazuka, R. Obata, H. Tomoda, H. Tanaka, Y. Harigaya and S. Omura, *J. Org. Chem.*, 1995, **60**, 8126.

4 For a review, see: (*a*) S. K. Taylor, *Org. Prep. Proced. Int.*, 1992, **24**, 247. For recent examples, see: (*b*) E. J. Corey and M. Sodeoka, *Tetrahedron Lett.*, 1991, **32**, 7005; (*c*) E. J. Corey, G. Luo and L. S. Lin, *J. Am. Chem. Soc.*, 1997, **119**, 9927; (*d*) E. J. Corey, G. Luo and L. S. Lin, *Angew. Chem., Int. Ed.*, 1998, **37**, 1126. For mechanistic studies, see: (*e*) E. J. Corey and D. D. Staas, *J. Am. Chem. Soc.*, 1998, **120**, 3526.

5 K. A. Parker and L. Resnick, *J. Org. Chem.*, 1995, **60**, 5726; A. B. Smith III, T. Kinsho, T. Sunazuka and S. Omura, *Tetrahedron Lett.*, 1996, **37**, 6461.

6 B. K. Sharpless, Y. Gao, R. M. Hanson, J. M. Klunder, S. Y. Ko and H. Masamune, *J. Am. Chem. Soc.*, 1987, **109**, 5765.

7 S. P. Tanis, Y.-H. Chuang and D. B. Head, *J. Org. Chem.*, 1988, **53**, 4929.

8 F. E. Ziegler, S. I. Klein, U. K. Pati and T.-F. Wang, *J. Am. Chem. Soc.*, 1985, **107**, 2730.

9 L. Weiler and S. N. Huckin, *J. Am. Chem. Soc.*, 1974, **96**, 1082.

10 β-Keto esters are known to cyclise through oxygen rather than carbon, see: T. R. Hoye, A. J. Caruso and M. J. Kurth, *J. Org. Chem.*, 1981, **46**, 3550; J. D. White, R. W. Skeean and G. L. Trammell, *J. Org. Chem.*, 1985, **50**, 1939.

11 S. R. Harring, E. D. Edstrom and T. Livinghouse, *Adv. Heterocycl. Nat. Prod. Synth.*, 1992, **2**, 299.

12 L. Weiler and F.-W. Sum, *Can. J. Chem.*, 1979, **57**, 1431.

13 E. E. van Tamelan, *Acc. Chem. Res.*, 1968, **1**, 111.

14 L. Weiler and R. J. Armstrong, *Can. J. Chem.*, 1986, **64**, 584.

15 Tanis showed that the benzyl ether of the epoxy alcohol was superior to silyl protected analogues: See ref. 7.

16 For successful examples of (epoxy alcohol)-olefin cyclisations, see: T. Frejd, L. Pettersson and G. Magnusson, *Tetrahedron Lett.*, 1987, **28**, 2753; M. E. Jung, Y. M. Cho and Y. H. Jung, *Tetrahedron Lett.*, 1996, **37**, 3; G. Stork, T. Doi and L. Liu, *Tetrahedron Lett.*, 1997, **38**, 7471. In each case, the system was set up to prepare monocycles only.

17 J. Andrieux, D. H. R. Barton and H. Patin, *J. Chem. Soc., Perkin Trans. 1*, 1977, 359.

18 From molecular modelling it was found that **22** was lower in energy than the conjugated tetrasubstituted double bond isomer.

19 The optimised procedure required refluxing **11** with NaH (5 equiv.) in THF for 4 h followed by addition of BnBr and refluxing for a further 2 h. Less isomerisation was observed if **11** was refluxed with NaH for a shorter time.

20 By ^1H NMR, ^{13}C NMR, mass and IR analyses.

Communication 8/08644C

ChemComm

Synthesis and spectroscopy of Ru(II)-bridged DNA hairpins

Frederick D. Lewis,* Sara A. Helvoigt† and Robert L. Letsinger*

Department of Chemistry, Northwestern University, 2145 Sheridan Road, Evanston, IL 60208, USA. E-mail: lewis@chem.nwu.edu

Received (in Columbia, Mo, USA) 28th October 1998, Accepted 11th January 1999

A difunctional Ru(II) complex has been prepared which can be incorporated into synthetic oligonucleotides by means of standard solid-phase methodology and the properties of several oligonucleotide conjugates capable of forming Ru(II)-bridged hairpins have been investigated.

There is continuing interest in the development of oligonucleotide conjugates containing luminescent or redox-active transition metal complexes.[1] These conjugates have been investigated as alternatives to the use of radioactive isotopes for gene sensing, as site specific photonucleases, and as luminescent probes for the study of energy transfer and electron transfer in duplex DNA. In most of the conjugates investigated to date the metal complex is attached post-synthetically to the 5′-end of an oligonucleotide by means of a flexible tether.[2] Flexible tethers[3] and rigid linkers[4] with metal-binding ligands have also been used to modify nucleosides which can be incorporated using standard solid-phase methodology at a specific position in a synthetic oligonucleotide. Hybridization of conjugates with flexible tethers results in the formation of duplexes in which the metal complex may be intercalated, groove bound, or only weakly associated with the duplex. Uncertainty about the location of the metal complex can complicate the interpretation of electron and energy transfer measurements. Our interest in photoinduced electron transfer in duplex DNA[5] led us to undertake the synthesis of oligonucleotide conjugates in which a difunctional metal complex forms a linker connecting two oligonucleotides. We report here the synthesis and spectral properties of the first Ru(II)-linked oligonucleotides which possess complementary sequences capable of forming hairpin structures.

Preparation of synthetic oligonucleotides with a linking metal complex by standard solid state synthesis required the development of a difunctional ligand in which one functional group can be protected and the other activated. Our solution to this problem is outlined in Scheme 1. The difunctional diamidobipyridine ligand dabp (**1a**‡) was prepared from 2,2′-bipyridine-4,4′-dicarboxylic acid following the method developed for the synthesis of analogous arenedicarboxamides.[6] Reaction of this ligand with $[Ru(bpy)_2Cl_2]\cdot 2H_2O$[7] afforded the complex $[Ru(bpy)_2(dabp)]^{2+}$ **2a**, isolated as the PF_6^- salt.[8] Synthesis of the mono-protected complex $[Ru(bpy)_2(DMT\text{-}dabp)][PF_6]_2$ **2b** was best accomplished *via* reaction of the monoprotected dabp ligand **1b** with $[Ru(bpy)_2Cl_2]\cdot 2H_2O$. Repeated efforts to convert **2b** to **2c** using standard conditions led to recovery of **2b**. We found that **2c** is moderately stable when prepared in a glove box, but is rapidly hydrolyzed to **2b** upon exposure to moisture.

The instability of **2c** necessitated a modified protocol for oligonucleotide synthesis. The 3′-segment of the oligonucleotide was prepared according to standard solid phase procedures.[9] After removal of its 5′-DMT protecting group, the column was brought into a dry box and the oligonucleotide coupled with **2c**, using tetrazole as the activator. The column was returned to the automatic synthesizer to complete the synthesis of the oligonucleotide. The coupling efficiency for Ru incorporation, as determined by monitoring release of the dimethoxytrityl cation, was > 95%. Obtained by this procedure were the Ru-linked oligonucleotides dT_4–$Ru(bpy)_2(dabp)^{2+}$–dA_4, dG_3–$Ru(bpy)_2(dabp)^{2+}$–dC_3, and dGCAATTGC–$Ru(bpy)_2(dabp)^{2+}$–dGCAATTGC, **3**–**5**.[10] After removal from the solid support and deprotection the oligonucleotides were purified by HPLC and appear as a single peak on both ion exchange and reverse phase HPLC.[6]

The absorption spectrum of $[Ru(bpy)_2(dabp)]^{2+}$ **2a** displays maxima at 468 nm (ε = 8538 $dm^3\ mol^{-1}\ cm^{-1}$) and 288

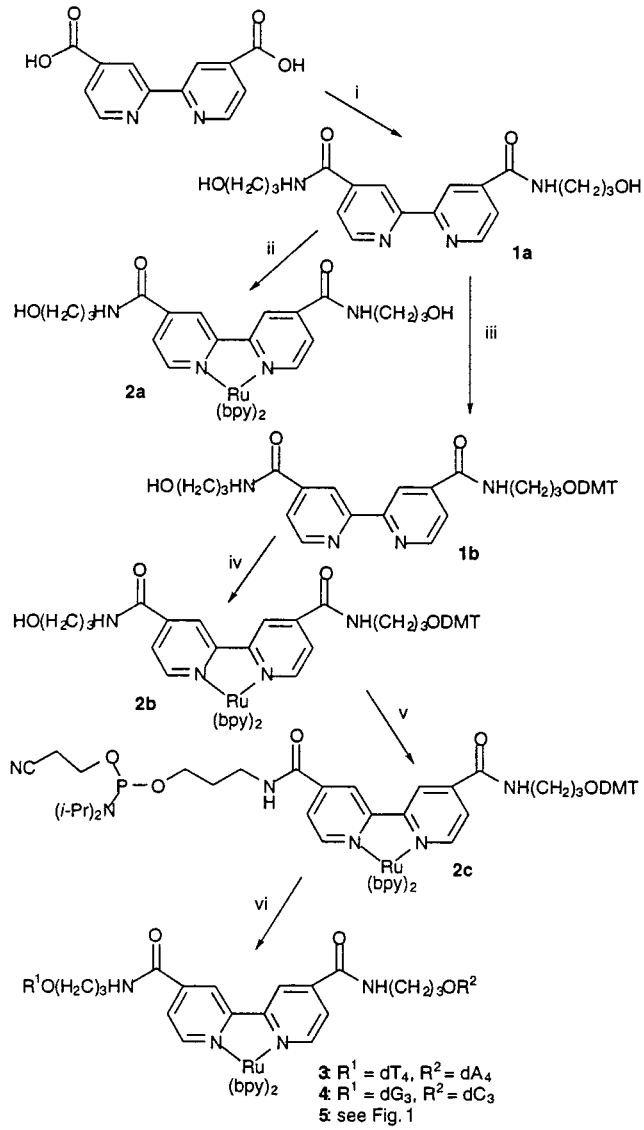

Scheme 1 *Reagents and conditions*: i, a, $SOCl_2$, $PhCH_2NEt_3Cl$, $C_2H_4Cl_2$, reflux; b, $HOCH_2CH_2CH_2NH_2$, Et_3N, THF, MeOH, 50%; ii, $[Ru(bpy)_2Cl_2]\cdot 2H_2O$, 95% ethanol, 90%; iii, a, dimethylaminopyridine, pyridine; b, dimethoxytrityl (DMT) chloride, pyridine, 38%; iv, same as ii, 88%; v, (2-cyanoethyl)diisopropylchloride phosphoramidite, Et_3N, dry acetonitrile, glove box, not isolated; vi, see text, Expidite™ nucleic acid synthesis system.

† Present address: Nanophase Technologies Corp., 453 Commerce St., Burr Ridge, IL 60521, USA.

(43 550) which are red-shifted with respect to those of $[Ru(bpy)_3]^{2+}$, as previously observed for Ru(II) complexes with a single bipyridine-4,4′-dicarboxamide ligand.[11] The spectra of **3**–**5** have maxima below 300 nm for the nucleobases which overlap the shorter wavelength Ru^{2+} band. The 260 nm bands of **3**–**5**, but not the 468 nm bands exhibit hypochromism. The complex **2a** and conjugates **3**–**5** display a single broad emission band with a maximum at 665 nm, similar to that reported for other Ru(II) complexes possessing a single bipyridine-4,4′-dicarboxamide ligand.[11] The luminescence quantum yields and decay times are summarized in Table 1. The neighboring nucleobases have little effect on the photophysical behavior of the Ru(II) complex, in accord with previous observations for $[Ru(bpy)_3]^{2+}$ covalently attached to oligonucleotides.[3]

Table 1 Emission lifetimes and quantum yields for complexes **2a**, **3**, **4** and **5**

Complex	τ/ns	Φ_e[a]
2a	850	0.013
3	815	0.018
4	790	0.016
5	608	0.019

[a] Values are reported relative to $[Ru(bpy)_3][PF_6]_2$ in water (Φ_e = 0.042) and calculated according to published procedures (J. N. Demas and G. A. Crosby, *J. Phys. Chem.*, 1971, **75**, 991).

Molecular modeling indicates that the conjugates **3**–**5** can adopt low energy hairpin conformations as shown schematically in Fig. 1; however, these conjugates also might form duplexes in which the Ru(II) complexes occupy bulges on opposite strands. In the case of **5** a value of T_M = 50 °C is obtained from the thermal dissociation profile in 0.1 M NaCl. This value is independent of concentration (1.0–5.0 μM). In the case of **4** the observed value of T_M = 50 °C in 1.0 M NaCl is higher than that calculated for either a GGG/CCC duplex [T_M(calc.) = −42 °C] or for two such duplex segments [T_M(calc.) = 20 °C] with no contribution from the Ru(II) linkers and no cooperativity in melting of the two segments.[12] This evidence supports the tentative assignment of a hairpin *vs.* duplex structures for **4** and **5**. The conjugates **3** and **4** have broad thermal dissociation profiles (not shown) and values of T_M (< 20 and 50 °C, respectively, in 1.0 M NaCl) lower than those of the analogous stilbene dicarboxamide-bridged hairpins (T_M = 49 and > 80 °C, respectively, in 1.0 M NaCl).[7] This may reflect a better fit for the stilbene *vs.* Ru(II) linker across the double helix. The broad thermal dissociation profiles for **3**–**5** may reflect multiple conformations for the hairpin loop region as well as the presence of two diastereomeric octahedral complexes.

The preliminary results reported here provide a potentially versatile method for the introduction of a bipyridyl-complexed metal ion at a specific location in a synthetic conjugate. The three conjugates prepared in this study have complementary arms and thus are capable of forming hairpin structures with a bridging metal complex. Whereas the precise structures of these conjugates remain to be established, the metal complex is likely located at the end of a duplex region of a hairpin structure. The excited Ru(II) complex selected for this study is not quenched by nucleobases, however excited state redox potentials can be tuned over a wide range by variation of the nonbridging ligands or metal.[13] Similarly, the use of nucleobase analogs such as 6-oxoguanine or 7-deazaguanine which have low oxidation potentials should increase the driving force for photoinduced electron transfer.[14] In addition, hybridization of metal linked conjugates possessing noncomplementary arms with unlabelled oligonucleotides should position the metal center near a specific location in the unlabelled strand. Thus the availability of difunctional metal complexes which can be introduced into oligonucleotides *via* automated phosphoramidite chemistry serves to extend structural diversity currently available with monofunctional metal complexes.[2–4] The long lifetimes and moderately large fluorescence quantum yields make these Ru(II) complexes particularly well-suited for studies of long range energy and electron transfer.

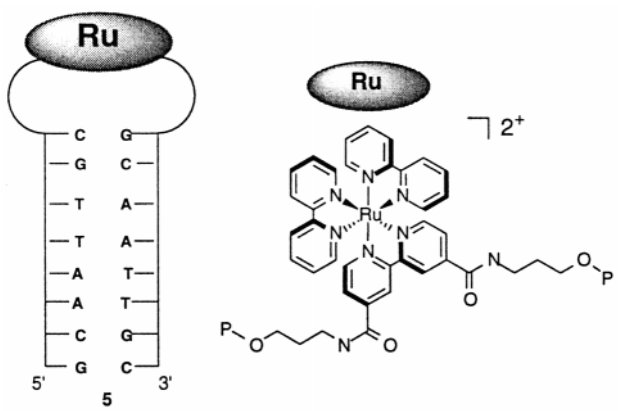

Fig. 1 Schematic structure for the hairpin conformation of **5**.

This work has been supported by the Division of Chemical Sciences, Offices of Basic Energy Sciences, US Department of Energy.

Notes and references

‡ *Selected data* for **1a**: ES/MS (DMSO–H_2O): *m/z* 359 NMR (DMSO-d_6, ^{1}H): δ 8.95 (t, 2H), 8.85 (d, 2H), 8.75 (s, 2H), 7.8 (d, 2H), 4.5 (t, 2H), 3.5 (t, 4H), 3.3 (t, 4H), 1.7 (q, 4H). For **1b**: NMR (DMSO-d_6, ^{1}H): δ 9.9 (t, 2H), 9.85 (d, 2H), 9.75 (d, 2H); 7.8 (dd, 2H), 7.35 (d, 2H), 7.2 (m, 5H), 6.8 (d, 4H), 3.65 (s, 6H), 3.4 (m, 8H), 1.85 (q, 2H), 1.7 (q, 2H). For **2a**: ES/MS (MeCN): *m/z* 917 ($[Ru(bpy)_2dabp][PF_6]^+$), 386 ($[Ru(bpy)_2dabp]^{2+}$). UV–VIS (MeCN): 468 nm (ε = 8538 dm^3 mol^{-1} cm^{-1}); 350 (6847), 288 (43550), 236 (37107). For **2b**: ES/MS (MeCN): *m/z* 1219 ($[Ru(bpy)_2$(DMT-dabp)$][PF_6]^+$); 537 ($[Ru(bpy)_2$(DMT-dabp)$]^{2+}$). UV–VIS (MeCN): 468, 350, 288, 236 nm. For **2c**: NMR (MeCN, ^{31}P): δ +140 (two singlets).

1 A. Sigel and H. Sigel, *Interactions of Metal Ions with Nucleotides, Nucleic Acids, and Their Constituents*, Marcel Dekker Inc., New York, 1996, vol. 32, p. 814; A. Sigel and H. Sigel, *Probing of Nucleic Acids by Metal Ion Complexes of Small Molecules*, Marcel Dekker Inc., New York, 1996, vol. 33, p. 678.

2 For selected examples, see: W. Bannwarth, D. Schmidt, R. L. Stallard, C. Hornung, R. Knorr and F. Müller, *Helv. Chim. Acta*, 1988, **71**, 2085; C. J. Murphy, M. R. Arkin, Y. Jenkins, N. D. Ghatlia, S. H. Bossman, N. J. Turro and J. K. Barton, *Science*, 1993, **262**, 1025; T. J. Meade and J. F. Kayyem, *Angew. Chem., Int. Ed. Engl.*, 1995, **34**, 352; E. Meggers, D. Kusch and B. Giese, *Helv. Chim. Acta*, 1997, **80**, 640.

3 J. Tesler, K. A. Cruickshank, K. S. Schanze and T. L. Netzel, *J. Am. Chem. Soc.*, 1989, **111**, 7221; C. Moucheron, A. Kirsch-De Mesmaeker and J. M. Kelly, *J. Photochem. Photobiol. B. Biol.*, 1997, **40**, 91.

4 D. J. Hurley and Y. Tor, *J. Am. Chem. Soc.*, 1998, **120**, 2194.

5 F. D. Lewis, T. Wu, Y. Zhang, R. L. Letsinger, S. R. Greenfield and M. R. Wasielewski, *Science*, 1997, **277**, 673; F. D. Lewis and R. L. Letsinger, *J. Biol. Inorg. Chem.*, 1998, **3**, 215.

6 R. L. Letsinger and T. Wu, *J. Am. Chem. Soc.*, 1995, **117**, 7323.

7 B. P. Sullivan, D. J. Salmon and T. J. Meyer, *Inorg. Chem.*, 1978, **17**, 3334.

8 K. A. Opperman, S. L. Mecklenburg and T. J. Meyer, *Inorg. Chem.*, 1994, **33**, 5295.

9 T. Brown and D. J. S. Brown, in *Oligonucleotides and Analogues; A Practical Approach*, ed. E. Eckstein, IRL Press, New York, 1991, pp. 1–24.

10 *tert*-Butyl hydroperoxide (1.0 M dichloromethane) was used as the oxidizer instead of I_2 for the completion of the synthesis. Overall yields ranged from 3–5% after purification.

11 A. Juris, V. Balzani, F. Barigelletti, S. Campanga, P. Belser and A. Von Zelewsky, *Coord. Chem. Rev.*, 1988, **84**, 85.

12 J. SantaLucia, Jr., *Proc. Natl. Acad. Sci. USA*, 1998, **95**, 1460.

13 I. Ortmans, C. Moucheron and A. Kirsch-De Mesmaeker, *Coord. Chem. Rev.*, 1998, **168**, 233.

14 C. Sheu and C. S. Foote, *J. Am. Chem. Soc.*, 1995, **117**, 6439; S. O. Kelly and J. K. Barton, *Chem. Biol.*, 1998, **5**, 413.

Communication 8/08491B

ChemComm

Predictable solid state structures incorporating the C≡C–H···O$_2$N supramolecular synthon

James M. A. Robinson, Douglas Philp,* Benson M. Kariuki and Kenneth D. M. Harris*

School of Chemistry, University of Birmingham, Edgbaston, Birmingham, UK B15 2TT. E-mail: d.philp@bham.ac.uk

Received (in Cambridge, UK) 23rd November 1998, Accepted 4th December 1998

Terminal alkynes interact with nitro groups in a symmetrically bifurcated manner to form ribbon-like structures in the solid state.

It is widely accepted that although C–H groups are relatively poor hydrogen bond donors, many C–H···O interactions share some of the characteristics of stronger hydrogen bonds that are formed with more conventional hydrogen bond donors such as N–H and O–H.[1] Attempts to quantify donor and acceptor strengths in C–H···O interactions have shown[2,3] that, as expected, the strongest interactions are formed by pairing the most acidic C–H hydrogens, such as Cl_3C–H and C≡C–H, with the best oxygen acceptors, which include P=O and H_2O. Although the oxygens of the nitro group appear to be poor hydrogen bond acceptors when compared to oxygen atoms in other bonding environments, they do participate in other noteworthy interactions such as the polarisation-induced halogeno···nitro motif. In particular, the iodo···nitro supramolecular synthon[4] **1** has been utilised in several recent examples[5] of crystal engineering. Recently, our analysis[6] of the structures of substituted benzene derivatives containing alkynes and/or halogens has suggested that there may be recognition characteristics which are shared between terminal alkynes and halogen atoms. For this reason, we felt that a logical development of the iodo···nitro synthon **1** (Fig. 1) would be the substitution of the iodine by a terminal alkyne to give the synthon **2**, with the expectation that it would retain the novel bifurcated interaction. Furthermore, such studies should provide additional insight into the characteristics of C–H···O hydrogen bonds to nitro groups. Here we describe the crystal structures of 1-ethynyl-4-nitrobenzene **3** and the 1:1 co-crystal [**4**·**5**] of 1,4-dinitrobenzene **4** and 1,4-diethynylbenzene **5**; both structures contain the supramolecular synthon **2**.

Small needle-like crystals of **3** were grown by the slow evaporation of solvent from a solution of **3** in a MeOH–H_2O mixture. However, poor crystal quality, coupled with a tendency for crystal twinning, made structure solution impossible from single crystal X-ray diffraction data. Therefore, the structure was solved from powder X-ray diffraction data using the Monte Carlo method.[7] The crystal structure of **3**† contains (Fig. 2*a*) linear ribbons of **3** which are connected by the alkynyl···nitro motif **2** to create infinite chains of molecules linked by C≡C–H···O hydrogen bonds as the major intermolecular interaction. The two C–H···O distances ($d_{H\cdots O}$ = 2.47 and 2.36 Å) are significantly less than the sum of the van der Waals radii,[8] (Σ_{vdw} = 2.65 Å). The adjacent ribbons of molecules are not coplanar, but are stepped to form corrugated layers. Thus, the aromatic protons of each molecule in a ribbon form a number of minor C–H···O interactions with the nitro groups of the molecules in adjacent ribbons ($d_{H\cdots O}$ range 2.4–2.9 Å).

In order to assess whether the alkynyl···nitro interaction in motif **2** could be used as a robust supramolecular synthon in crystal engineering applications, we attempted a co-crystallisation between two molecular components with the potential to form motif **2**. Whereas the structure of **3** contains *da*··*da* ··*da* interaction arrays based on one molecular component (where *da* is a component containing self-complementary donor and acceptor sites), we aimed to design and construct a structure based on *dd*··*aa*··*dd* arrays using two molecular components (Fig. 1).

Single crystals of [**4**·**5**] suitable for single crystal X-ray diffraction studies were grown by slow evaporation of solvent from a solution of a 1:1 mixture of **4** and **5** in benzene. The crystal structure of [**4**·**5**]‡ (Fig. 2*b*) bears a strong resemblance to that of **3** in that linear molecular ribbons arise from infinite chains of molecules linked by motif **2**. Again, the alkynyl···nitro interaction is not symmetrically bifurcated, with a small difference between the two C–H···O distances ($d_{H\cdots O}$ = 2.54 and 2.61 Å); additional C–H···O contacts ($d_{H\cdots O}$ 2.6–2.7 Å) are also formed between ribbons, as seen for **3**.

The C–H···O distances observed in the alkynyl···nitro motifs in both **3** and [**4**·**5**] are relatively long compared to other C–H···O interactions involving terminal alkynes.[3] This observation can be attributed to the acknowledged poor hydrogen bond accepting properties of the oxygens of the nitro group, although distance alone cannot be a taken as a quantitative indication of the interaction strength. Therefore, we have attempted to further characterise the alkynyl···nitro interaction using infra-red spectroscopy and *ab initio* quantum mechanical calculations.

The difference (denoted $\Delta\nu_{\equiv C-H}$) between the C–H stretching frequency for the 'free' alkyne (as determined for a dilute solution of the alkyne in CCl_4) and for the hydrogen bonded alkyne in the solid gives a qualitative indication of the strength of the C–H···O interaction. Typically, the range in magnitude of $\Delta\nu_{\equiv C-H}$ for alkynyl C–H···O interactions vary from long, and

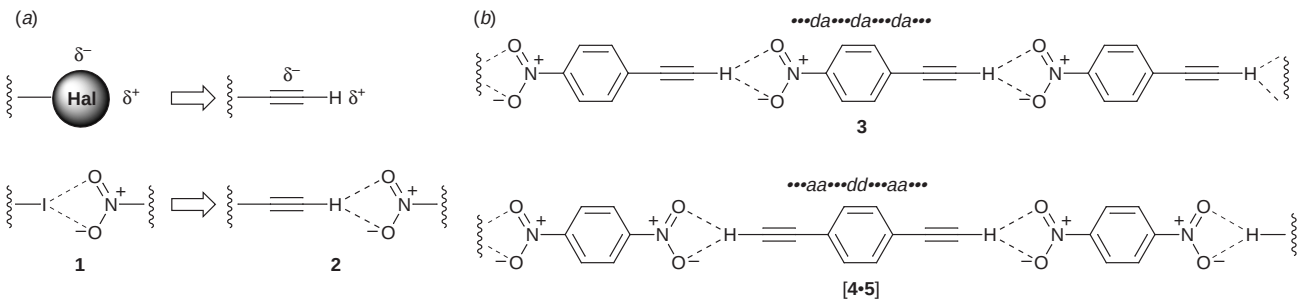

Fig. 1 (*a*) The polarisation pattern found in terminal alkynes is similar to that for halogens. Thus, the established iodo···nitro synthon **1** can be evolved into the alkynyl···nitro synthon **2**. (*b*) The synthon **2** can be used to form linear molecular ribbons, either using one molecular component as in **3** or two components as in [**4**·**5**].

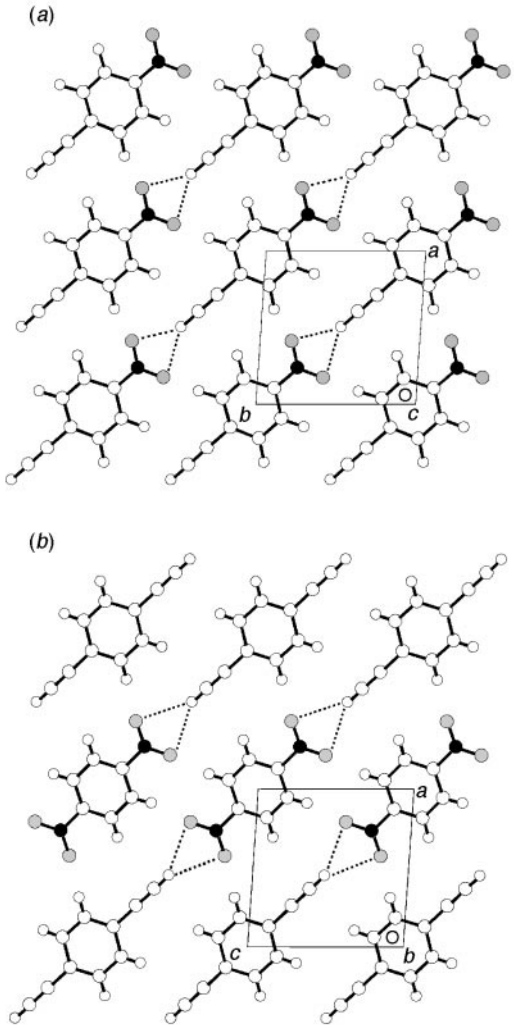

Fig. 2 The crystal structures of (*a*) **3** and (*b*) [**4·5**] both show linear molecular ribbons which are held together by the alkynyl···nitro synthon**2**. The black and shaded spheres represent nitrogen and oxygen atoms respectively; the dotted lines represent C≡C–H···O_2N interactions.

thus presumably very weak, interactions (*ca*. 15 cm^{-1}, $d_{H\cdots O}$ = 2.92 Å)[9] to much shorter, stronger interactions (*ca*. 145-200 cm^{-1}, $d_{H\cdots O}$ < 2.0 Å)[10] with most red-shifts falling[9] in the range 40–100 cm^{-1}. The infra-red spectra for polycrystalline samples of **3** and [**4·5**] obtained from the same batches used for the X-ray diffraction data collections were measured§ in KBr disks. The $\Delta\nu_{\equiv C-H}$ for **3** (57 cm^{-1}) and [**4·5**] (50 cm^{-1}) represents an appreciable red shift of indicative of a moderately strong interaction, which is comparable to alkyne C–H···O interactions which involve supposedly much better oxygen acceptors (such as OH groups).

Ab initio quantum mechanical calculations were performed¶ at the MP2/6-31G(d,p) level using an ethyne–nitrobenzene aggregate as a model system for the alkynyl···nitro interactions. The energy of interaction (ΔE_{int}), corrected for basis set superposition error (BSSE), for the alkynyl···nitro C–H···O_2N interaction was calculated to be −8.0 kJ mol^{-1}. Although this interaction energy is less than that calculated[11] for the alkynyl···water C–H···O interaction (−12.2 kJ mol^{-1}), surprisingly, it is comparable to the estimated[12] interaction energy for the bifurcated iodo···nitro motif (−10 kJ mol^{-1}).

In conclusion, we have demonstrated that, by virtue of common recognition features, halogens and terminal alkynes can be exchanged to create a new supramolecular synthon incorporating a C≡C–H···O_2N interaction which, by FTIR spectroscopy and quantum mechanical calculations, has been shown to possess a significant binding energy.

This research was supported by the University of Birmingham and the EPSRC (Quota award to J. M. A. R. and Postdoctoral Fellowship to B. M. K.). We are grateful to the EPSRC and CCLRC for the award of synchrotron beam-time at the Daresbury Laboratory.

Notes and references

† *Crystal data* for **3**: [$C_8H_5NO_2$], M = 147.13 g mol^{-1}, triclinic, space group $P\bar{1}$, a = 6.8261(8), b = 7.9213(9), c = 7.4743(7) Å, α = 116.581(4), β = 91.556(4), γ = 92.749(9)°, V = 360.5(1) $Å^3$, Z = 2, λ = 1.3 Å, T = 295(2) K. The sample was loaded into a capillary (1.0 mm diameter). Data were measured on the high-resolution powder diffraction station 2.3 at the Synchrotron Radiation Source, Daresbury Laboratory, for a total of 100 min. Data were recorded in the 2θ range 5 to 67° in 0.01° steps. The powder diffraction pattern was indexed using ITO (ref. 13) and the structure was solved by the Monte Carlo method (ref. 7). The geometry of the molecule was restrained during the Rietveld refinement which was carried out using GSAS (ref. 14). Non-hydrogen atom positions were refined with fixed isotropic displacement parameters (0.025 $Å^2$) and hydrogen atoms were placed in calculated positions. Final refinement gave R_p = 0.067, R_{wp} = 0.097.

‡ *Crystal data* for [**4·5**]: [$C_6H_4N_2O_4{\cdot}C_{10}H_6$], M = 294.26 g mol^{-1}, triclinic, space group $P\bar{1}$, a = 7.059(3), b = 7.555(2), c = 6.939(3) Å, α = 91.86(4), β = 93.849(9), γ = 89.669(9)°, V = 369.0(3) $Å^3$, Z = 1, λ = 0.71069 Å, T = 296(2) K, μ = 0.097 mm^{-1}, 1142 independent reflections (R_{int} = 0.065), R = 0.061, wR_2 = 0.155. CCDC 182/1108.

§ Infra-red spectra were recorded on a Perkin–Elmer Paragon 1000 FTIR spectrometer at 293 K. Solid state spectra were recorded as KBr disks. Solution spectra (concentration *ca.* 2 mM) were recorded in CCl_4 in an Aldrich Demountable liquid-cell kit with a pathlength of 0.5 mm. All spectra were recorded at a resolution of 2 cm^{-1}.

¶ *Ab initio* quantum mechanical calculations, including geometry optimisations, were performed using GAMESS (ref. 15) (the version dated 18 May 1997 was used for all calculations). Corrections for BSSE for the optimised coordinates were obtained by the full counterpoise procedure using CADPAC (ref. 16).

1 For recent discussions of the properties of C–H···O interactions, see T. Steiner, *Chem. Commun*., 1997, 727; T. Steiner and G. R. Desiraju, *Chem. Commun*., 1998, 891.
2 T. Steiner, *J. Chem. Soc*., *Chem. Commun*., 1994, 2341.
3 T. Steiner, *New J. Chem*., 1998, 1099.
4 For a recent discussion of the term 'supramolecular synthon' see A. Nangia and G. R. Desiraju, *Top. Curr. Chem*., 1998, **198**, 57.
5 F. H. Allen, B. S. Goud, V. J. Hoy, J. A. K. Howard and G. R. Desiraju, *J. Chem. Soc*., *Chem. Commun*., 1994, 2729; V. R. Thalladi, B. S. Goud, V. J. Hoy, F. H. Allen, J. A. K. Howard and G. R. Desiraju, *Chem. Commun*., 1996, 401; J. A. R. P. Sarma, F. H. Allen, V. J. Hoy, J. A. K. Howard, R. Thaimattam, K. Biradha and G. R. Desiraju, *Chem. Commun*., 1997, 101.
6 J. M. A. Robinson, B. M. Kariuki, K. D. M. Harris and D. Philp, *J. Chem. Soc*., *Perkin Trans. 2*, 1998, 2459.
7 K. D. M. Harris, M. Tremayne, P. Lightfoot and P. G. Bruce, *J. Am. Chem. Soc*., 1994, **116**, 3543; M. Tremayne, B. M. Kariuki and K. D. M. Harris, *Angew. Chem*., *Int. Ed. Engl*., 1997, **36**, 770; M. Tremayne, B. M. Kariuki and K. D. M. Harris, OCTOPUS (Monte Carlo Technique For Powder Structure Solution).
8 R. S. Rowland and R. Taylor, *J. Phys. Chem*., 1996, **100**, 7384.
9 T. Steiner, J. van der Mass, A. M. M. Schreurs, J. Kroon and M. Tamm, *Chem. Commun*., 1998, 171.
10 T. Steiner, J. van der Maas and B. Lutz, *J. Chem. Soc*., *Perkin Trans. 2*, 1997, 1287; B. M. Kariuki, K. D. M. Harris, D. Philp and J. M. A. Robinson, *J. Am. Chem. Soc*., 1997, **119**, 12 679.
11 D. Philp and J. M. A. Robinson, *J. Chem. Soc*., *Perkin Trans. 2*, 1998, 1643.
12 F. H. Allen, J. P. M. Lommerse, V. J. Hoy, J. A. K. Howard and G. R. Desiraju, *Acta Crystallogr*., *Sect. B*, 1997, **53**, 1006.
13 J. W. Visser, *J. Appl. Crystallogr*., 1969, **2**, 89.
14 A. C. Larson and R. B. Von Dreele, Los Alamos Laboratory Report No. LA-UR-86-748, 1987.
15 M. W. Schmidt, K. K. Baldridge, J. A. Boatz, S. T. Elbert, M. S. Gordon, J. H. Jensen, S. Koseki, N. Matsunaga, K. A. Nguyen, S. J. Su, T. L. Windus, M. Dupuis and J. A. Montgomery, *J. Comput. Chem*., 1993, **14**, 1347.
16 CADPAC, The Cambridge Analytical Derivatives Package, Issue 6.1, Cambridge 1996.

Communication 8/09115C

ChemComm

Electrodeposition of mesoporous tin films

Adam H. Whitehead, Joanne M. Elliott, John R. Owen* and George S. Attard

Dept. of Chemistry, University of Southampton, Southampton, UK SO17 1BJ. E-mail: jro@soton.ac.uk

Received (in Bath, UK) 10th November 1998, Accepted 12th January 1999

Mesoporous metallic tin has been electrodeposited, from the homogeneous hexagonal mesophase of a series of amphiphilic non-ionic surfactants, with a controllable repeat structure in the range of 5–10 nm.

It has been reported that mesoporous silica may be prepared by a sol–gel route from silicon alkoxides in the presence of a low concentration of a cationic surfactant.[1] Similarly the formation of several mesoporous metal oxides has been reported.[2] It has also been shown that nanostructured silica may be formed in the presence of surfactant concentrations high enough to form homogeneous liquid crystalline mesophases.[3,4] Under these conditions the nanostructure of the silica was a cast of the architecture of the liquid crystalline phase in which it was formed. In other words the liquid crystal phase acted as a direct template for the silica.

There have been very few reports of the formation of nanostructured metals although Attard *et al.* have used a direct templating method to prepare mesoporous platinum as both a powder[5] and coherent film.[6] The platinum film was electrodeposited from a homogeneous hexagonal (H_I) mesophase of a range of octaethylene glycol monoalkyl ethers with aqueous hexachloroplatinic acid. The following work reports on the electrochemical synthesis of mesoporous tin films (H_I-eSn) using a route similar to that employed for platinum. Mesoporous tin could be expected to offer advantageous properties over existing negative electrodes in lithium ion batteries.

Tin was electrodeposited from five electrolytes containing oligoethylene glycol monoalkyl ether surfactants (E1–E5, Table 1) and one electrolyte without surfactant (N1).† After deposition the cells were disassembled and the electrodes bearing the electrodeposited tin (H_I-eSn) were repeatedly washed with *ca.* 200 ml of absolute ethanol to remove the electrolyte. Gravimetric measurements of the deposits revealed that the current efficiency was > 94%, based on the two electron reduction of Sn^{II} to Sn.

Small angle X-ray diffractograms of the tin deposits were recorded over the range 2θ 0.7–3.0° (Cu-Kα radiation), which revealed a single peak for each film prepared from the templating electrolytes E1–E5, but not for the reference electrolyte N1, Table 2. Hence the X-ray peak may be taken to indicate that the templated electrodes possessed a spatially periodic structure with a characteristic repeat distance in the range 5–10 nm which was not an artefact of the X-ray technique. The repeat distance was noted to depend on the type of surfactant used and to be increased by the presence of *n*-heptane. As may be expected, if a direct templating mechanism were operating, the repeat distances of the tin films were similar to those obtained for the respective electrolytes from which they were deposited, Table 2. In addition, the repeat distance for tin deposited from E1 was of the same order of magnitude as that observed for H_I-ePt using $C_{16}EO_8$.[6]

Table 1 Electrolyte compositions

		Electrolyte composition (w/o)		
Electrolyte	Surfactant	0.2 M $SnSO_4$, 0.3 M H_2SO_4	*n*-Heptane	Surfactant
E1	$C_{16}EO_8$	50	0	50
E2	$C_{18}EO_{10}$[a]	50	0	50
E3	$C_{18}EO_{20}$[a]	40	0	60
E4	$C_{16}EO_8$	47	5	48
E5	$C_{18}EO_{10}$[a]	50	3.5	46.5

[a] Nominal surfactant formula.

Table 2 Repeat distances of electrolytes and corresponding tin films based on XRD measurements. Also shown are the second cycle lithium extraction capacities of the films from electrochemical measurements

Electrolyte	Repeat distance of electrolyte/Å	Repeat distance tin film/Å	Lithium extraction capacity/C g^{-1}
E1	58 ± 3	60 ± 6	2510
E2	61 ± 3	66 ± 6	2080
E3	82 ± 4	81 ± 8	2060
E4	63 ± 3	63 ± 5	2570
E5	84 ± 4	85 ± 9	2120
N1	—	—	1260

Transmission electron microscopy (TEM) revealed mesoporosity in the samples, although a regular structure could not be assigned unambiguously, Fig. 1.

Further analysis of tin samples with a loading of 1.2 mg cm^{-2} was undertaken after drying under vacuum at 100 °C for 24 h. The dried samples were used as the working electrodes of non-aqueous electrochemical cells with lithium foil counter and reference electrodes and a 1 M $LiCF_3SO_3$–ethylene carbonate–diethyl carbonate electrolyte.

Using these cells ac impedance measurements were carried out over the frequency range 5 kHz to 5 Hz with a dc bias potential of 2 V *vs.* $Li–Li^+$ and oscillator level of 15 mV p–p.

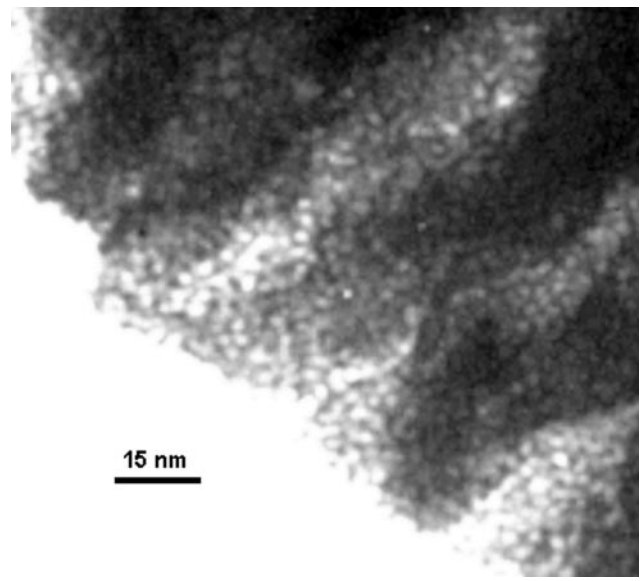

Fig. 1 Typical TEM image of a tin sample deposited from a templating electrolyte (E4).

These measurements showed the tin to act as a blocking electrode at low frequencies, as would be expected in the absence of faradaic reactions. From the values of the electrode capacitance it appeared that the samples prepared from the $C_{16}EO_8$-based electrolytes (E1 and E4), had a surface area 35 ± 10 times greater than that of rolled tin foil (9.0 μF cm^{-2}, Advent metals) of the same geometric surface area. However, an E1 sample dried at 180 °C under vacuum had a surface area enhancement of only 2 ± 1. Such a decrease in surface area may be understood in terms of a reduction in the number of accessible mesopores, which might occur by a surface melting phenomenon at below the bulk melting point of tin (232 °C).[9,10] For comparison tin deposited from the Brij-based electrolytes (E2, E3 and E5) had surface areas only slightly larger than the reference sample (N1), with surface enhancements of 8 ± 3 and 6 ± 2 respectively.

It has been noted previously that the electrochemical alloying of lithium may cause tin to undergo a volume expansion of up to 259%.[11] This expansion and any subsequent contraction, on removal of lithium, tends to create stresses within the tin alloy, leading to disintegration of the structure.[12] As loose tin–lithium particles would not be expected to be in good electrical contact with the bulk of the sample the amount of lithium that may be extracted should give an indication of the extent of pulverisation. It would be expected that extensive mesoporosity would significantly reduce internal stresses during expansion and thus decrease the mechanical degradation of the electrodes.

In order to examine the electrodeposited tin, lithium was inserted and extracted using a pulsed coulometric titration regime,[13] between the potential limits of 0.05 and 0.95 V *vs.* Li–Li^+. The magnitude of the insertion and extraction current densities was 350 μA cm^{-2} (equivalent to 290 mA g^{-1} of tin). The second cycle extraction capacities are shown in Table 2, from which it may be noted that the H_I-eSn samples all showed higher extraction capacities than the non-templated tin (from N1). The samples prepared from the mixed chain length surfactants (E2, E3 and E5) had similar extraction capacities to one another, *ca.* 2100 C g^{-1}. However, the single chain length surfactants (E1 and E4) provided tin samples with the highest extraction capacities, although still below the theoretical maximum of 3570 C g^{-1}.[14] Nevertheless, it may be noted that the H_I-eSn extraction capacities were much higher than those of commercial lithium battery negative electrode materials (coke and graphite) which are typically < 1350 C g^{-1}.[15]

In conclusion mesoporous H_I-eSn films were prepared from a series of templating electrolytes. In addition tin deposited from the $C_{16}EO_8$-based electrolytes (E1 and E4) holds promise for use as a negative electrode material for rechargeable lithium ion batteries.

We thank Mr N. R. B. Coleman and Prof. P. N. Bartlett for their support and advice, and Dr C.G. Göltner for the TEM studies. This work was supported by Southampton Innovations Ltd and the EPSRC.

Notes and references

† Electrodeposition procedure: of the surfactants, octaethylene glycol monohexadecyl ether ($C_{16}EO_8$, > 98% Fluka), had a narrow distribution of both alkyl and oxyethylene chain lengths, whereas the others contained a broader mixture of chain lengths: Brij 76 (average composition of $C_{18}EO_{10}$, Aldrich) and Brij 78 (average composition of $C_{18}EO_{20}$, Aldrich). Templating electrolytes were prepared by mixing the surfactants with an aqueous solution of ≈0.2 M $SnSO_4$ and ≈0.3 M H_2SO_4. E4 and E5 also contained *n*-heptane which was expected to act as a swelling agent, increasing the radii of the cylindrical aggregates of the H_I phase and hence the pore size in the templated electrodeposit. The concentrations of surfactant, aqueous solution and *n*-heptane (Table 1) were chosen such that a H_1 phase of each lyotropic liquid crystal was formed, as verified from the characteristic optical textures when viewed through a polarising microscope.[7]

Although the $C_{16}EO_8$-based electrolytes (E1 and E4) were used at room temperature (22 ± 2 °C) the $C_{18}EO_{10}$-based electrolytes (E2 and E5) required heating to 45 °C, and the $C_{18}EO_{20}$-based electrolyte (E3) to 50 °C, in order to improve ionic conductivity and ensure that a homogeneous H_I phase was formed. All solutions and electrolytes were freshly prepared immediately prior to commencing electrodeposition of tin.

Reference samples were prepared from a non-templating plating electrolyte, N1, with the composition, 0.15 M $SnSO_4$, 0.6 M H_2SO_4, 0.28 M 4-hydroxybenzene sulfonic acid and 0.055 M *p*-cresol.[8] Tin was deposited galvanostatically from N1 with a current density of 5 mA cm^{-2}. Tin was deposited potentiostatically from E1–E5 by applying −100 mV across a two-electrode cell, with a tin counter electrode and copper or gold working electrode of area *ca.* 0.5 cm^2.

1 J. S. Beck, J. C. Vartuli, W. J. Roth, M. E. Leonowicz, C. T. Kresge, K. D. Schmitt, C. T-W. Chu, D. H. Olson, E. W. Sheppard, S. B. McCullen, J. B. Higgins and J. L. Schenkler, *J. Am. Chem. Soc.*, 1992, **114**, 10 834.
2 N. Ulagappan and C. N. R. Rao, *Chem. Commun.*, 1996, **14,** 1685.
3 G. S. Attard, M. Edgar, J. W. Emsley and C. G. Göltner, *MRS Symp. Proc.*, 1996, **425**, 149.
4 G. S. Attard, J. C. Glyde and C. G. Göltner, *Nature*, 1995, **378**, 366.
5 G. S. Attard, C. G. Göltner, J. M. Corker, S. Henke and R. H. Templer, *Angew. Chem., Int. Ed. Engl.*, 1997, **36**, 1315.
6 G. S. Attard, P. N. Bartlett, N. R. B. Coleman, J. M. Elliott and J. R. Owen and J.-H. Wang, *Science*, 1997, **278**, 838
7 D. J. Mitchell, G. J. T. Tiddy, L. Waring, T. Bostock and M. P. McDonald, *J. Chem. Soc., Faraday Trans. 1*, 1983, **79**, 975.
8 D. Pletcher, *Industrial Electrochemistry*, Chapman and Hall, 1982 p. 407.
9 E. Søndergård, R. Kofman, P. Cheyssac, F. Celestini, T. Ben David and Y. Lereah, *Surf. Sci.*, 1997, **388**, L1115.
10 Y. Oshima and K. Takayanagi, *Surf. Rev. Lett.*, 1996, **3**, 1199.
11 I. A. Courtney and J. R. Dahn, *J. Electrochem. Soc.*, 1997, **144**, 2045.
12 J. Yang, M. Winter and J. O. Besenhard, *Solid State Ionics*, 1996, **90**, 281.
13 A. H. Whitehead, M. Perkins and J. R. Owen, *J. Electrochem. Soc.*, 1997, **144**, L92.
14 J. Wang, I. D. Raistrick and R. A. Huggins, *J. Electrochem. Soc.*,1986, **133**, 457.
15 M. Winter, J. O. Besenhard, M. E. Spahr and P. Novak, *Adv. Mater.*, 1998, **10**, 725.

Communication 8/08775J

Tuning the pore size from micro- to meso-porous in thermally stable aluminophosphates

Saúl Cabrera,[a] Jamal El Haskouri,[a] Carmen Guillem,[a] Aurelio Beltrán-Porter,[a] Daniel Beltrán-Porter,[a] Sagrario Mendioroz,[b] M. Dolores Marcos*[a] and Pedro Amorós*[a]

[a] *Institut de Ciència dels Materials de La Universitat de València (ICMUV), Dr. Moliner 50, 46100-Burjassot (València), Spain. E-mail: loles.marcos@uv.es; pedro.amoros@uv.es*

[b] *Instituto de Catálisis y Petroleoquímica, Campus Universidad Autónoma, Cantoblanco, 28049-Madrid, Spain*

Received (in Bristol, UK) 16th December 1998, Accepted 12th January 1999

Thermally stable porous aluminophosphates (ICMUV-3) with P/Al molar ratios in the range 0.15 ⩽ P/Al ⩽ 0.75 and showing continuously adjustable pore sizes from 13 to 37 Å have been prepared through a surfactant-assisted procedure without changing the surfactant length and/or addition of organic expansors.

Since the discovery in 1982 of three-dimensional aluminium phosphates (ALPOs),[1] their chemistry has aroused great interest mainly due to the attainment of microporous structures showing a broad range of physicochemical properties of potential application in fields such as catalysis or molecular sieving.[2,3] Control of pore geometry and diameter are key to many of these applications, especially in the case of those that rely on size or shape selectivity and ready access to pore system. The synthesis of ALPO molecular sieves, as for zeolites, involves the use of organic agents as 'templates'.[4] In this sense, the synthetic strategy developed by Mobil scientists to obtain mesoporous silicas by use of micellar aggregates of surfactants as 'templates',[5] was also seen as very promising for the preparation of aluminophosphates. Thus, Stucky and coworkers[6] were the first to extend the surfactant templating strategy to the synthesis of non-silica-based mesostructures, mainly metal oxides. However, in the case of the ALPO system this method has not been as fruitful as for silica-based materials. Although lamellar[7] and hexagonal MCM-41-type mesostructured ALPOs[8,9] have been prepared through surfactant-assisted synthetic strategies, the preparation of the corresponding mesoporous materials was not possible because their mesostructure collapsed upon calcination during surfactant removal. More recently, the preparation of two thermally stable mesoporous ALPOs using cationic surfactants has been described: Kevan and coworkers[10,11] have reported the synthesis of non-ideal mesoporous aluminophosphates (0.16 ⩽ P/Al ⩽ 0.60) with a constant pore size around 35 Å, and Kuroda and coworkers[12,13] have described the isolation of mesoporous ALPO's showing pore diameters modulated in the range 18–39 Å by changing the chain lengths of the surfactants and using organic cosurfactants as pore expansors.

We report here, a novel method to prepare thermally stable mesoporous aluminophosphates, denoted ICMUV-3, allowing a continuous adjustment of the pore sizes simply by regulation of both the P/Al molar ratio and the water content in the mother-solution.

Mesoporous ICMUV-3 materials have been prepared using cetyltrimethylammonium bromide (CTABr) as surfactant structural directing agent in an aqueous TEA (triethanolamine) medium with a molar ratio in the starting solution Al : *x*P : 0.3CTABr : 3.8TEA : *y*H_2O, (*x* = 0.12–1.5, *y* = 131–185). In a typical sample preparation, Al(OBu^s)$_3$ (5.1 ml, 0.02 mol) was slowly added to liquid TEA (10 ml; 0.075 mol) and heated at 160 °C. After 30 min, the solution was cooled at 120 °C and 2.1 g of CTABr (0.006 mol) added. Then, it was cooled at room temperature and mixed with 43 ml (2.4 mol) of distilled water. The resulting solution (pH$_i$ = 10–11) was then combined with a given amount of diluted phosphoric acid (0.55 mol in 10 ml of water) under vigorous stirring (pH$_f$ = 8–9), and the formation of a white solid was observed. This mesostructured solid was washed with warm water and air dried. In order to obtain the corresponding mesoporous material, the surfactant was thermally removed by stepped treatments under flowing air atmosphere (2 h at 300 °C, 2 h at 400 °C and finally at 500 °C during 2 h). All the samples were analyzed and characterized by X-ray powder diffraction techniques (Seifert 3000TT diffractometer using Cu-Kα radiation), TEM (Philips CM10 instrument operated at 120 kV), electron probe microanalysis EPMA (Philips SEM-515 instrument), N_2 adsorption–desorption isotherms (Micromeritics ASAP2010 analyzer) and ^{27}Al MAS NMR (Varian Unity-300 spectrometer operating at 300 MHz.

EPMA analysis shows that each ICMUV-3 mesoporous sample has a constant and well defined composition, showing in each case a homogeneous distribution of phosphorus atoms in the framework. Hence, monophasic character of the solids can be assumed. In all cases, ICMUV-3 solids have a non-ideal ALPO stoichiometry (P/Al < 1). ^{27}Al MAS NMR spectroscopy for as-synthesized and calcined ICMUV-3 materials show two resonance signals at δ *ca.* 0 and 50. These signals are indicative of six- and four-coordinate metal centers, respectively. A relative intensity increase of the signal assigned to the four-coordinate Al centers is observed as the P/Al ratio increases both in mesostructured and mesoporous solids. Also, an increase of that signal is observed after calcination.

Selected XRD patterns of as-synthesized and mesoporous ICMUV-3 samples are shown in Fig. 1. All solids present at least one very intense peak at low 2θ values (d_{100} = 28–57 Å). It should be remarked that the position of this peak closely follows the variation of the P/Al molar ratio in the solids: the

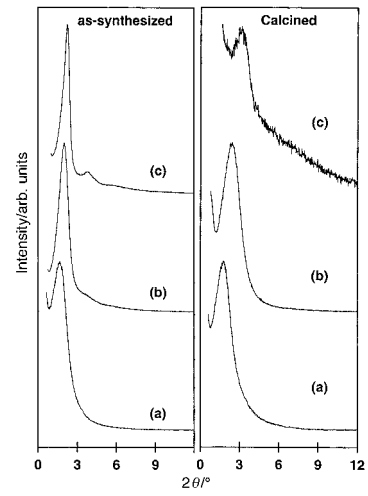

Fig. 1 Representative X-ray powder diffraction patterns of both as-synthesized and porous ICMUV-3 solids; (a) P/Al = 0.17, (b) P/Al = 0.55, (c) P/Al = 0.74.

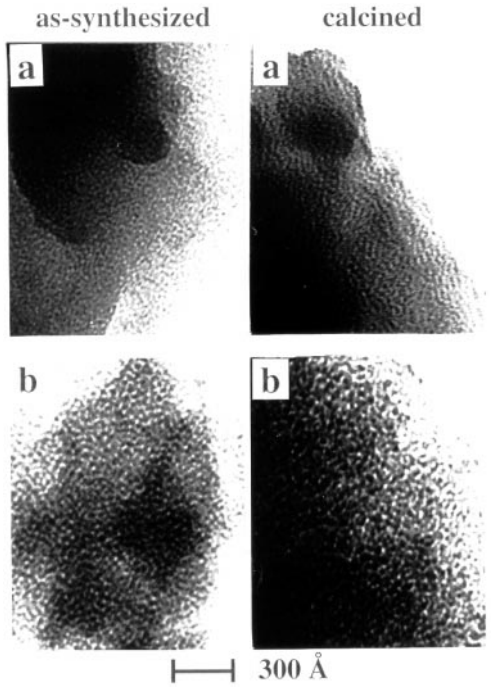

Fig. 2 Typical TEM images of as-synthesized and mesoporous ICMUV-3 solids having a P/Al molar ratio of (a) 0.17 and (b) 0.74.

peak appears at lower *d*-spacing as the P/Al ratio increases. Additionally, as-synthesized ICMUV-3 materials with high phosphorus content (P/Al > 0.4) show XRD peaks that can be assigned to the (110) and (200) reflections assuming an hexagonal MCM-41-type cell.[5] When comparing as-synthesized solids (mesostructured) with the corresponding mesoporous materials, we can see that calcination results in an intensity decrease and a broadening of the XRD peak together with a significant shift towards higher 2θ values. In general, these effects increase as the phosphorus content in the solids does.

Representative TEM images of both as-synthesized and mesoporous ICMUV-3 materials are shown in Fig. 2. On the lines of the XRD observations, it can be noted that while the as-synthesized solids show hexagonal (though disordered) pore distributions, the pore packing motif in the mesoporous materials can be better described as wormhole-like.

All ICMUV-3 aluminophosphates show one well defined step in their N_2 adsorption isotherm. Two different behaviours are, however, observed: while solids with low P/Al ratio present type IV isotherms, materials with high P/Al ratio show type I behaviour. The presence of hysteresis loops in the type IV desorption isotherms, as well as their sharp curvature, suggests the existence of a certain blocking in the pore system of the solids with lower P/Al molar ratio. Similar isotherm curves have been previously observed in aluminas prepared through a related surfactant-assisted procedure.[14,15] As can be seen in Fig. 3, average pore diameters (BJH model) for ICMUV-3 solids seem to agree with XRD data, and a continuous pore size modulation in the 13–37 Å range has been observed. From these data, an almost constant pore wall dimension of 16 Å for all ICMUV-3 solids is obtained.

Besides the pore size adjustment, it is possible to achieve a second and additional tuning by the sole adjustment of the H_2O/TEA molar ratio in the mother-solution, in a similar way we have previously described for pure aluminas.[14] Indeed, for a fixed P/Al molar ratio, such pore size modulation allows us to modify the pore dimensions in a range of *ca.* ± 3 Å by adjusting the H_2O/TEA molar ratio from 34 to 49.

Hence, the synthetic procedure here described has allowed us to obtain porous aluminophosphates with continuously adjustable pore sizes ranging from micro- (13 Å, 480 $m^2\ g^{-1}$) to mesoporous (37 Å, 650 $m^2\ g^{-1}$) by simple adjustment of the P/Al molar ratio in the initial mixture. Though the modulation in pore size is continuous, two groups of materials can be differentiated: those with low phosphorus content, whose behaviour is close to that of pure aluminas, and those with high phosphorus content, which likely approach the conventional behaviour of ALPOs. Mesoporous materials with P/Al ratios corresponding to the second group present a more ordered pore distribution.

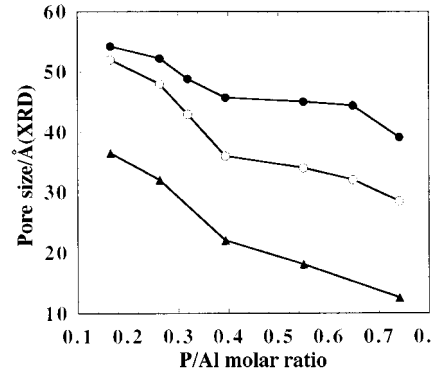

Fig. 3 Evolution of the d_{100} low reflection of both the as-synthesized (●) and porous (○) ICMUV-3 and the average pore size (▲) with the P/Al molar ratio.

We conclude that thermally stable micro/mesoporous aluminophosphates with continuously adjustable pore sizes can be prepared in aqueous/TEA through the surfactant assisted procedure using CTABr. Taking into account the ready formation of stable TEA–Al^{3+} complexes,[14,16] the principal role played by TEA can be postulated as a 'hydrolysis retarding agent'. In this way, its presence in the reaction medium is essential for the isolation of mesostructured ICMUV-3 solids by allowing a satisfactory balance between the two principal processes which take place in solution: the hydrolysis and condensation reactions of aluminium cations in water–phosphoric media and the self-assembling between organic and inorganic moieties.

This research was supported by D. G. E. S. under grant PB95-1094. J. E. H. and S. C. thank the A. E. C. I. for doctoral grants.

Notes and references

1 S. T. Wilson, B. M. Lok, C. A. Messina, T. R. Cannon and E. M. Flanigan, *J. Am. Chem. Soc.*, 1982, **104**, 1176.
2 M. E. Davis, C. Saldariaga, C. Montes, J. Garces and C. Crowder, *Nature*, 1988, **331**, 698.
3 R. J. Francis and D. O'Hare, *J. Chem. Soc., Dalton Trans.*, 1998, 3133.
4 M. E. Davis and R. F. Lobo, *Chem. Mater.*, 1992, **4**, 756.
5 C. T. Kresge, M. E. Leonowicz, W. J. Roth, J. C. Vartuli and J. S.Beck, *Nature*, 1992, **359**, 710.
6 Q. Huo, D. I. Margolese, U. Ciesla, P. Feng, T. E. Gier, P. Sieger, R. Leon, P. M. Petroff and G. D. Stucky, *Nature*, 1994, **368**, 317.
7 A. Sayari, V. R. Karra, J. S. Reddy and I. L. Moudrakovski, *Chem. Commun.*, 1996, 411.
8 P. Feng, Y. Xia, J. Feng, X. Bu and G. D. Stucky, *Chem. Commun.*, 1997, 949.
9 B. T. Holland, P. K. Isbester, C. F. Blanford, E. J. Munson and A. Stein, *J. Am. Chem. Soc.*, 1997, **119**, 6796.
10 D. Zhao, Z. Luan and L. Kevan, *Chem. Commun.*, 1997, 1009.
11 Z. Luan, D. Zhao, H. He, J. Klinowski and L. Kevan, *J. Phys. Chem. B*, 1998, **102**, 1250.
12 T. Kimura, Y. Sugahara and K. Kuroda, *Chem. Commun.*, 1998, 559.
13 T. Kimura, Y. Sugahara and K. Kuroda, *Microporous Mesoporous Mater.*, 1998, **22**, 115.
14 S. Cabrera, J. El Haskouri, J. Alamo, A. Beltrán, D. Beltrán, S. Mendioroz, M. D. Marcos and P. Amorós, *Adv. Mater.*, in press.
15 S. A. Bagshaw and T. J. Pinnavaia, *Angew. Chem., Int. Ed. Engl.*, 1996, **35**, 1102.
16 K. F. Waldner, R. M. Laine, S. Dhumrongvaraporn, S. Tayaniphan and R. Narayanan, *Chem. Mater.*, 1996, **36**, 516.

Communication 8/09833F

Unique catalytic properties of Pt and tungstophosphoric acid supported on MCM-41 for the reduction of NO_x in the presence of water vapour

Andreas Jentys,* Walter Schießer and Hannelore Vinek

Vienna University of Technology, Institute for Physical Chemistry, Getreidemarkt 9/156, A-1060 Wien, Austria. E-mail: jentys@tuwien.ac.at; http://www.physchem.tuwien.ac.at/catalysis/

Received (in Cambridge, UK) 6th October 1998, Accepted 21st December 1998

Pt and tungstophosphoric acid supported on MCM-41 type materials show a pronounced increase in the activity during the catalytic reduction of NO_x with propene in the presence water vapour.

To combine the advantages of zeolites[1–4] and oxide based systems,[5,6] we studied the potential of transition metal containing mesoporous molecular sieves with the MCM-41 type structure for the catalytic reduction of NO_x.[7,8] As the acid sites of these materials are only weakly acidic,[9] we also impregnated the catalysts with tungstophosphoric acid ($H_3PW_{12}O_{40}\cdot 6H_2O$) in order to generate strongly acidic sites.[10]

Siliceous mesoporous molecular sieves with the MCM-41[8] type structure, synthesised with $C_{16}TMABr$,[11] were impregnated with aqueous solutions of $PtCl_4$ (Pt/MCM-41),[12] of $H_3PW_{12}O_{40}$ (HPW/MCM-41) and of $PtCl_4$ and $H_3PW_{12}O_{40}$ (Pt + HPW/MCM-41). For comparison Pt/SiO_2 (Degussa Aerosil 200) and Pt/γ-Al_2O_3 (170 $m^2\ g^{-1}$), also prepared by impregnation, were used. The metal and tungstophosphoric acid loading of all catalysts investigated are summarised in Table 1.

The characterisation of the support (MCM-41) was carried out by XRD, N_2 BET and IR spectroscopy.[9] The siliceous MCM-41 type material showed four Bragg reflections (*d*-spacing: 39 Å) and a sharp step in the N_2 isotherm at $p/p_0 \approx 0.4$. The dispersion of the metal, determined by volumetric H_2 chemisorption after reduction for 2 h at 773 K in H_2 (heating rate 15 K min^{-1}), was 64% for the Pt/MCM-41 catalyst. The BET surface areas of Pt/MCM-41 and Pt + HPW/MCM-41 were 1000 and 470 $m^2\ g^{-1}$, respectively.[10]

Catalytic properties were studied in a reaction system using a chemiluminescence NO_x analyser and a gas chromatograph (TCD and FID) to determine the concentrations of the reactants and products. The concentrations of the reactants were 1010 ppm NO, 1010 ppm C_3H_6, 4.9 vol% O_2, 0–8 vol% H_2O (balance He). The reactions reported were carried out at 573 K and at a space velocity of 11 000 h^{-1} ($w/F = 6 \times 10^{-2}$ g s cm^{-3}), the activity reported was measured after 2 h on stream. Before the reaction all catalysts were activated in He at 773 K for 1 h. TPD indicated that at this temperature H_2O was completely removed from the Pt + HPW/MCM-41 catalyst.

A comparison of the activity and selectivity (determined at the temperature of maximum NO_x conversion) is given in Table 1. The use of siliceous mesoporous molecular sieves as the Pt support improved the activity and the selectivity towards N_2 formation compared to Pt supported on dense SiO_2.[6] After the co-impregnation of MCM-41 with Pt and tungstophosphoric acid the activity decreased to a level comparable to Pt/SiO_2 and Pt/Al_2O_3, while MCM-41 based catalysts containing tungstophosphoric acid only showed a significantly lower activity. The main product of these reactions, however, was N_2O, which is characteristic for Pt group metals supported on oxides.[13] Transition metals supported on zeolites, such as Fe/ZSM5, show generally a higher N_2 yield, but are only active above 650 K.[14]

The conversions of NO_x over Pt/MCM-41 and Pt + HPW/MCM-41 at 573 K as a function of the water vapour concentration are compared in Fig. 1. At this temperature, the activity and selectivity of the catalysts in the absence of water vapour were almost identical. With increasing H_2O vapour concentration the activity of Pt + HPW/MCM-41 increased, until a maximum was reached at 2.0 vol% H_2O, where the NO_x conversion was 25% (relative %) higher compared to the water-free reaction conditions. A further increase led to a decrease in the activity; however, even at 8.5 vol% water vapour the activity was 10% higher compared to the water-free reaction conditions. In contrast, for Pt/MCM-41 a continuous decrease in the activity with increasing H_2O concentration was observed.

The activity changed almost instantaneously with the addition of 2.5 vol% water vapour into the gas stream (see Fig. 2). After switching back to water-free reaction conditions the activity immediately returned to the initial value on Pt/MCM-41. On Pt + HPW/MCM-41 it decreased to a constant level, which was 12% above the initial activity, and only after an additional heating for 1 h at 773 K in He could the initial activity be restored.

In contrast to the published results,[3,14,15] this is the first time that a pronounced increase in catalytic activity during the reduction of NO_x with hydrocarbons in the presence of H_2O vapour has been observed. The activity of the Pt + HPW/MCM-41 catalyst is significantly improved in the presence of up to 8.5 vol% water vapour compared to water free reaction conditions, while the activity of Pt/MCM-41 was slightly suppressed in the presence of water vapour.

To elucidate the reason behind these unique catalytic properties, the formation of acidic surface sites resulting from the deposition of tungstophosphoric acid on MCM-41 was

Table 1 Composition and catalytic properties of the catalysts

Sample	Pt (wt%)	Tungstophosphoric acid (wt%)	Max. NO_x conversion (%)	Temp. for max. NO_x conversion/K	Selectivity to N_2[a] (%)
Pt/MCM-41	1.61	0	62	493	35
Pt + HPW/MCM-41 (0 vol% H_2O)	1.61	30	47	543	36
Pt + HPW/MCM-41 (2 vol% H_2O)	1.61	30	51	553	37
HPW/MCM-41 (0 vol% H_2O)	0	30	22	593	32
HPW/MCM-41 (2 vol% H_2O)	0	30	19	593	35
Pt/SiO_2	1.61	0	51	513	29
Pt/Al_2O_3	1.62	0	46	543	34

[a] *vs.* formation of N_2O (reported at the temperature at the highest NO_x conversion).

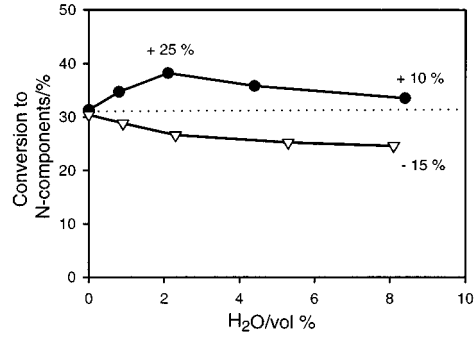

Fig. 1 Activity of (▽) Pt/MCM-41 and (●) Pt + HPW/MCM-41 as a function of water vapour concentration (573 K).

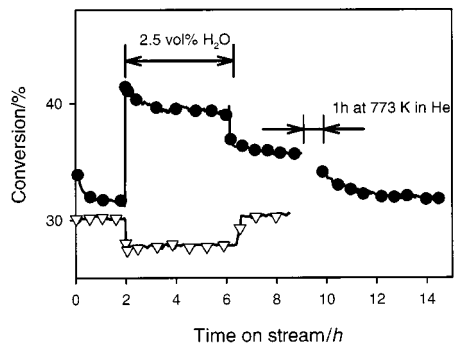

Fig. 2 Changes in activity of (▽) Pt/MCM-41 and (●) Pt + HPW/MCM-41 during a stepwise change of the water vapour concentration between 0 and 2.5 vol% at 573 K.

investigated by following the adsorption of pyridine using IR spectroscopy. The spectra shown in Fig. 3 were normalised to the structural vibrations of MCM-41 between 2100 and 1770 cm^{-1}, the other experimental details are described in ref. 9. After activation in vacuum ($\approx 10^{-6}$ mbar) at 773 K, pyridine was adsorbed with a partial pressure of 10^{-1} mbar at 423 K on Pt + HPW/MCM-41 and on siliceous MCM-41. Subsequently, the tungstophosphoric acid containing sample was hydrated by the co-adsorption of 9×10^{-1} mbar H_2O. The bands at 1449 and 1600 cm^{-1}, present after adsorption of pyridine on MCM-41 and on Pt + HPW/MCM-41, are assigned to hydrogen-bonded pyridine formed on Lewis acid sites. Brønsted acid sites, indicated by the bands at 1540 and 1614 cm^{-1}, were only present on Pt + HPW/MCM-41. After the co-adsorption of H_2O the concentration of Brønsted acid sites on Pt + HPW/MCM-41 increased by about 75%, while the concentration of Lewis acid sites was not affected by the presence of water vapour.

In recent work[16–18] it was shown that hydrated tungstophosphoric acid supported on SiO_2 forms protonated NO species (*i.e.* NOH^+) upon adsorption of NO and that the adsorbed NO is almost completely decomposed (70–100% NO conversion) into N_2 and N_2O ($\approx$ 50% selectivity to N_2) in the presence of O_2 and

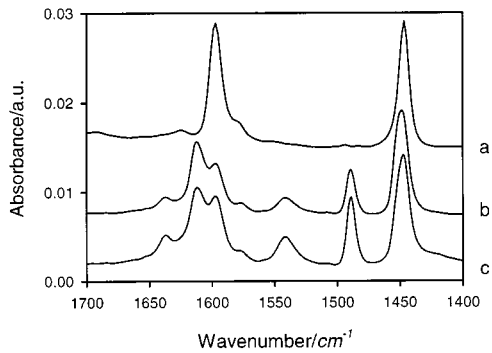

Fig. 3 Difference IR spectra after adsorption of pyridine at 423 K: (a) 10^{-1} mbar pyridine on siliceous MCM-41, (b) 10^{-1} mbar pyridine on Pt + HPW/MCM-41 and (c) 10^{-1} mbar pyridine and 9×10^{-1} mbar H_2O on Pt + HPW/MCM-41.

H_2O around 700 K. This reaction was only observed on hydrated tungstophosphoric acid and, therefore, could be the additional reaction pathway accounting for the improved activity of the Pt + HPW/MCM-41 catalyst in the presence of water vapour.

The reactions reported here however, were carried out at a much lower temperature (573 K), where the NO_x conversion over the Pt-free HPW/MCM-41 catalyst was only 8%. Also, the activity of the HPW/MCM-41 catalyst was not influenced by the presence of water vapour. Therefore, we assume that the direct reaction on tungstophosphoric acid is not the main route contributing to the overall activity in these experiments and that Pt and tungstophosphoric acid are essential to achieve the additional activity observed in the presence of water vapour.

We propose two reaction pathways in order to explain the additional activity observed on the Pt + HPW/MCM-41 catalyst in the presence of water vapour: (i) NOH^+, formed on the hydrated tungstophosphoric acid, disproportionates and the carbonaceous species formed on the Pt clusters react with the O atoms to form CO_2, while N recombines and desorbs as N_2. This reaction mechanism is similar to that described for $C_3H_6/NO/O_2$ reactions, with an additionally proposed reaction pathway for the formation of N^{-}* and O^{-}* on the surface of the hydrated tungstophosphoric acid; (ii) in the other reaction pathway we suppose that C_3H_6 adsorbs on the hydrated tungstophosphoric acid. The C_xH_y species, formed upon adsorption on the Brønsted acid sites, react with NO^{-}* adsorbed on the metal. The presence of highly acidic Brønsted sites on the hydrated tungstophosphoric acid (see Fig. 3) generates additional adsorption sites, which increases the local concentration of hydrocarbons on the perimeter of the metal clusters and thus give rise to the higher activity in the presence of water vapour.

In both mechanisms proposed an additional pathway is described, which is not present on Pt/MCM-41 or on dehydrated Pt + HPW/MCM-41 catalysts. However, at the moment we can not unequivocally decide which of the two routes described is responsible for the catalytic effects observed.

The work was supported by the Fonds zur Förderung der Wissenschaftlichen Forschung under project P10874 CHE and by the Österreichische Nationalbank under project 7119.

Notes and references

1 M. Iwamoto, H. Furukawa, Y. Mine, F. Uemura, S. Mikuriya and S. Kagawa, *J. Chem. Soc., Chem. Commun.*, 1986, 1271.
2 Y. Li and J. Armor, *Appl. Catal. B*, 1992, **1**, L31.
3 X. Feng and W. K. Hall, *J. Catal.*, 1997, **166**, 368.
4 M. Iwamoto, H. Yahiro, H. K. Shin, M. Watanabe, J. Guo, M. Konno, T. Chikahisa and T. Murayama, *Appl. Catal. B*, 1994, **5**, L1.
5 H. Hamada, Y. Kintaichi, M. Sasaki and Y. Ito, *Appl. Catal.*, 1991, **75**, L1.
6 R. Burch and P. J. Millington, *Catal. Today*, 1995, **26**, 185.
7 J. N. Armor, *Catal. Today*, 1977, **38**, 163.
8 C. T. Kresge, M. E. Leonowicz, W. J. Roth, J. C. Vartuli and J. S. Beck, *Nature*, 1992, **359**, 710.
9 A. Jentys, N. H. Pham and H. Vinek, *J. Chem. Soc., Faraday Trans.*, 1996, **92**, 3287.
10 I. V. Kozhevnikov, A. Sinnema, R. J. J. Jansen, K. Pamin and H. van Bekkum, *Catal. Lett.*, 1995, **30**, 241.
11 C. F. Cheng, D. H. Park and J. Klinowski, *J. Chem. Soc., Faraday Trans.*, 1997, **93**, 193.
12 A. Jentys, W. Schießer and H. Vinek, *Catal. Lett.*, 1997, **47**, 193.
13 M. D. Amiridis, T. Zhang and R. J. Farrauto, *Appl. Catal. B*, 1996, **10**, 203.
14 H. Y. Chen and W. M. H. Sachtler, *Catal. Lett.*, 1998, **50**, 125.
15 S. Sumiya, M. Saito, H. He, Q. C. Feng, N. Takezawa and K. Yoshida, *Catal. Lett.*, 1998, **50**, 87.
16 R. L. McCormick, S. K. Boonrueng, A. M. Herring and M. S. Graboski, *Proc. ACS Annual Meeting, Las Vegas, 1997*, p. 791.
17 A. M. Herring and R. L. McCormic, *J. Phys. Chem. B*, 1998, **102**, 3175.
18 R. L. McCormick, S. K. Boonrueng and A. M. Herring, *Catal. Today*, 1998, **42**, 145.

Communication 8/07758D

Linear dimerisation of but-1-ene in biphasic mode using buffered chloroaluminate ionic liquid solvents

B. Ellis,[a] W. Keim[b] and P. Wasserscheid*[b]

[a] *BP Chemicals Sunbury-on-Thames, Middlesex, UK TW16 7LN*
[b] *Institut für Technische Chemie und Petrolchemie der RWTH Aachen, Worringer Weg 1, 52074 Aachen, Germany. E-mail: wasserscheidp@itc.rwth-aachen.de*

Received (in Cambridge, UK) 28th October 1998, Accepted 15th January 1999

The use of a buffered ionic liquid as a solvent for catalysts known to produce linear dimers from but-1-ene has been explored; this resulted in a significant enhancement of the activity of known catalysts, combined with the retention of both dimer selectivity and product linearity; in addition, the biphasic mode of operation allows easy catalyst recovery and recycle.

The dimerisation and oligomerisation of olefins in the presence of homogeneous Group VIII transition metal catalysts has been studied extensively. With higher olefins, the products typically consist of mixtures of branched isomers. Few catalysts are known which catalyse the linear dimerisation and oligomerisation of C_4-olefins. Linear C_8-olefin dimers are highly-desirable intermediates for the production of C_9-plasticizers, exhibiting better thermal properties than those produced from highly-branched C_8-olefin dimer feedstock (IFP Dimersol, Hüls).

To our knowledge, the best system for producing linear dimers from higher olefins originated from our group in 1979,[1] namely a catalyst based on square planar Ni-*O,O′* chelating systems, with an easily replacable group such as cod, methallyl, allyl, *etc.*, *e.g.* (cod)Ni(hfacac) **1**.

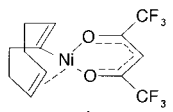

1

The above catalyst is active in organic solvents at > 50 °C, but reaches its maximum activity at 90 °C, with a turnover frequency of 500 h^{-1} with but-1-ene as feedstock. With an overall dimer selectivity of 85%, the selectivity to the linear dimer product is typically as high as 75%. Although the product quality produced by catalyst **1** is of industrial interest, the combination of high ligand costs, low catalyst activity and difficult catalyst recovery from the homogenous reaction mixture, has so far prevented industrial development.

Recently, a new approach has been adopted for catalyst separation and recycling in oligomerisation reactions, involving the use of a solvent known as an ionic liquid, which is simply a salt mixture of melting point below ambient. A well studied example involves salt mixtures of aluminium halides in combination with suitable substituted organic cations such as 1-butyl-3-methylimidazolium or 1-butylpyridinium cations.[2–4]

The oligomerisation of propene and butenes using ionic liquids as catalyst/solvent has been described by Chauvin *et al.*[5–8] These authors used a slightly acidic ionic liquid of the type [cation]X/AlX_3/$AlEtCl_2$ as a solvent for a Ni(II)-catalyst precursor known to produce highly-branched dimer products. Use of the ionic liquid solvent imparted significantly higher activity to highly branched dimer products with high activity. Moreover, the high solubility of the Ni-complex but poor solubility of the olefins produced in the ionic liquid facilitated a simple decantation step allowing complete catalyst separation.

In the case of butene oligomerisation[7] using [Ni-$(MeCN)_6$][BF_4]$_2$ as catalyst, the distribution of butene dimers, typically 39 ± 1% dimethylhexenes, 56 ± 2% monomethylheptenes and 6 ± 1% *n*-octenes, was reported to be independent of the addition of phosphine ligands. Moreover, the product mix was independent of feedstock, with both but-1-ene and but-2-ene yielding the same dimer distribution, with only 6% of the high-value linear dimer.

In the present article, we report the use of slightly acidic 1-butyl-4-methylpyridinium chloroaluminates, buffered with weak organic bases, as solvents for the linear dimerisation of but-1-ene in biphasic mode catalysed by the Ni-complex **1**.

The ionic liquids were initially prepared by mixing 1-butyl-4-methylpyridiniumchloride (4-MBP Cl) with $AlCl_3$. The Ni-catalyst **1** was dissolved in this binary mixture. Additional alkali metal chloride or organic bases were added afterwards to adjust the desired melt composition. The oligomerisation reactions were carried out in a glass autoclave. After the reaction the remaining organic layer was hydrogenated for determination of the linearity of the dimer products (determination of products by GC–MS and comparison with authentic samples).

It was found that **1** is deactivated by basic chloroaluminate ionic liquids ($X_{AlCl_3} < 0.5$) owing to excess free Cl^- anions, which probably block the free coordination sites of the catalyst (Table 1, entry 1). In acidic chloroaluminate ionic liquids ($X_{AlCl_3} > 0.5$) a large number of branched higher oligomers was formed, with only 8% dimer products formed. Clearly, the dimerisation activity of **1** is swamped by the fast cationic oligomerisation reaction initiated by the intrinsic acidicity of the ionic liquid solvent (Table 1, entry 2). Both results fit well to previous observations with other Ni-catalyst in the oligomerisation of monoolefins and are already described elsewhere in some detail.[5]

It is known that cationic side reactions catalysed by the ionic liquid itself can be avoided if a chloroethylaluminate melt is used as catalyst solvent.[5] However, with **1** the use of this melt as solvent leads to an immediate catalyst decomposition (Table 1, entry 3). At −10 °C, rapid decomposition could be avoided but the linearity of the dimer products was still low (Table 1, entry 4). Probably, even at this low temperature, $AlEtCl_2$ transfers ethyl-groups to the Ni and destroys the Ni-*X,Y* chelating system, which is known to be responsible for the desired high linearity.[1] Moreover, $AlEtCl_2$ is known to exhibit isomerisation activity[9] for converting but-1-ene rapidly into the thermodynamic distribution of butenes (*ca.* 4% but-1-ene at room temperature). While dimer selectivity was enhanced using a mixed system of the form 4-MBP/$AlCl_3$/$AlEtCl_2$ as used by Chauvin *et al.* in previous oligomerisation, dimer linearity was still unsatisfying low at 37% (Table 1, entry 5).

As an alternative way to avoid cationic side reactions, we tested **1** in buffered ionic liquids. The Lewis acidity of ionic liquids is routinely buffered by the addition of alkali metal chloride.[10] Since excess alkali metal chloride does not dissolve in the neutralised resulting ionic liquid, buffering in this manner is very efficient. Our dimerisation experiments were carried out in buffered ionic liquids with and without excess of solid alkali metal chloride. In the first case (Table 1, entry 6), almost no Ni-catalysed dimerisation was observed. Obviously, the slightly Lewis-acidic Ni-catalyst center is 'buffered' by the excess of

Table 1 Catalytic results with Ni-complex **1** in different ionic liquid systems.

Entry	Ionic liquid system (mol% composition)	T/°C	TOF[a]/h^{-1}	$S(C_8)$[b] (%)	$L(C_8)$[c]
1	4-MBPCl/$AlCl_3$ (0.65/0.35)	25	0	—	—
2	4-MBPCl/$AlCl_3$ (0.45/0.55)	25	[d]	8	41
3	4-MBPCl/$AlEtCl_2$ (0.36/0.64)	25	0[e]		
4	4-MBPCl/$AlEtCl_2$ (0.36/0.64)	−10	61	96[f]	12
5	4-MBPCl/$AlCl_3$/$AlEtCl_2$ (0.43/0.53/0.04)	25	415	73	37
6	4-MBPCl/$AlCl_3$ (0.45/0.55) buffered with excess LiCl[g]	25	[h]	—	—
7	4-MBPCl/$AlCl_3$ (0.33/0.66) buffered with excess LiCl[i]	25	[d]	16	28
8	4-MBPCl/$AlCl_3$ (0.45/0.55) buffered with excess LiCl[i]	25	7500	75	30
9	4-MBPCl/$AlCl_3$/pyrrole (0.43/0.53/0.04)	25	1350	86	56
10	4-MBPCl/$AlCl_3$/*N*-methylpyrrole (0.43/0.53/0.04)	25	2100	98[f]	51
11	4-MBPCl/$AlCl_3$/chinoline (0.43/0.53/0.04)	25	1240	98[f]	64
12	4-MBPCl/$AlCl_3$/pyridine (0.43/0.53/0.04)	25	550	78	33
13	4-MBPCl/$AlCl_3$/2,6-dimethylpyridine (0.43/ 0.53/0.04)	25	2480	55	68
14	4-MBPCl/$AlCl_3$/2,6 di-*tert*-butylpyridine (0.43/0.53/0.04)	25	2100	49	32

General conditions: 4 g ionic liquid, 0.04 g **1**, 12 g but-1-ene, reaction time was varied to reach comparable conversions of 15–20%. [a] Turnover frequency (TOF) in mol of butene converted per mol of Ni per h. [b] Selectivity to dimer product in %. [c] Selectivity to linear dimer in the dimer fraction of the product in %. [d] The product is mainly formed by a cationic oligomerisation mechanism of the acidic ionic liquid. The calculation of a turnover frequency related to the amount of nickel catalyst would be meaningless in this case. [e] Catalyst decomposes and forms a black solid of elemental Ni. [f] No products resulting from a parallel cationic side reaction are detected. [g] Ionic liquid was buffered with excess of dry LiCl (dried for 14 days over P_2O_5 at 150 °C). The ionic liquid used for reaction contained solid excess LiCl. [h] Traces of cationic oligomers. [i] Ionic liquid was buffered with excess of dry LiCl (dried 14 days over P_2O_5 at 150 °C). Solid excess LiCl was filtered off. The ionic liquid used for reaction was a clear liquid and contained no solid excess LiCl.

solid alkali metal chloride to a non-reactive Ni-species. Without excess of solid alkali metal chloride, the extent of cationic side reaction is dominated by the chemical behaviour termed 'latent acidity'.[11,12] Even very weak bases (B:) form an $AlCl_3$ adduct in neutral buffered melts. The additional driving force for this reaction apparently results from the precipitation of the solid alkali metal chloride: $AlCl_4^- + Li^+ + B: \rightleftharpoons B:AlCl_3 + LiCl$ (s). In our experiments, the but-1-ene feedstock seems to react as such a weak base. We found that the extent of cationic side reaction correlates well with the $Al_2Cl_7^-$ content of the melt from which the buffered ionic liquid was prepared (Table 1, entries 7, 8). However, a comparison of entries 2 and 8 clearly demonstrates the efficiency of an alkali metal chloride buffer in suppressing the formation of cationic oligomers.

Alternatively, we looked for new methods to buffer acidic ionic liquids so as to avoid the precipitation of an alkali metal chloride. We found that a slightly acidic melt buffered with small amounts of weak organic bases provides a solvent which allows a selective, ligand-controlled, biphasic reaction with the Ni-catalyst **1**. The function of the base is to trap any free acidic species in the melt which may initiate cationic side reaction (Table 2).

The base has to be system-adapted to provide high solubilty in the ionic liquid in question, while at the same time being non-coordinating with respect to the catalytic active Ni-center. Possible bases are any cyclic, heterocyclic or aliphatic, aromatic or non-aromatic bases which have these properties. Specially favorable are pyrrole, *N*-methylpyrrole and chinoline (Table 1, entries 9–11).

Experiments with different pyridine derivatives as buffer are interesting in two different respects (Table 1, entries 12–14): While the pyridine-buffered but-1-ene oligomerisation shows a significantly lower activity, this is not the case for the 2-substituted pyridines. This is probably due to a stronger coordination of the unsubstituted pyridine to the active center during reaction, in contrast to the sterically more demanding pyridine derivatives. Moreover, the $S(C_8)$ selectivity clearly decreases with the steric demand of the *o*-substitutent on the pyridine. Assuming that the $S(C_8)$ can be regarded as an indicator of the efficiency of the buffering process, this is a clear sign for a considerable contribution of a sterically demanding step in the buffering process. If only superacidic protons were responsible for the observed cationic side reaction in acidic ionic liquids, these should be perfectly buffered by a strong base like 2,6-di-*tert*-butylpyridine, which is not the case. It is assumed therefore that the reaction $Al_2Cl_7^- + \text{base} \rightleftharpoons AlCl_3\text{–base} + AlCl_4^-$ plays a major role in the buffering process.

Table 2 Function of the added organic base B

$$Al_2Cl_7^- + B \rightleftharpoons B\text{-}AlCl_3 + AlCl_4^-$$

$$B\text{-}AlCl_3 + HCl \rightleftharpoons HB^+ + AlCl_4^-$$

$$Al_2Cl_7^- + HCl + B \rightleftharpoons HB^+ + 2\,AlCl_4^-$$

Overall, the buffering procedures reported here facilitate use of an ionic liquid solvent for catalyst **1**, permitting reaction to take place in biphasic reaction mode with facile catalyst separation and catalyst recycling. The high intrinsic dimer linearity of catalyst **1** is maintained, but with significant enhancement of catalyst activity over that observed in toluene solvent.

In addition, our new concept of producing a latent-acidic chloroaluminate ionic liquid, by buffering a slightly acidic melt with weak organic bases, could prove to be useful in other transition metal catalysed reactions. In contrast to the known systems,[4–7] it avoids any addition of alkylaluminium and thereby allows the use of reduction-sensitive metal complexes at higher temperatures.

We wish to thank Drs M. Jones and M. Atkins of BP Chemicals for their helpful discussions and financial support for this programme and Prof. Ken Seddon for his fruitful advice.

Notes and references

1 W. Keim, B. Hoffmann, R. Lodewick, M. Peukert, G. Schmitt, J. Fleischhauer and U. Meier, *J. Mol. Catal.*, 1979, **6**, 79.
2 H. L. Chum, V. R. Koch, L. L. Miller and R. A. Osteryoung, *J. Am. Chem. Soc.*, 1975, **97**, 3264.
3 J. S. Wilkes, J. A. Levisky, R. A. Wilson and C. L. Hussey, *Inorg. Chem.*, 1982, **21**, 1263.
4 K. R. Seddon, *J. Chem. Technol. Biotechnol.*, 1997, **68**, 351.
5 Y. Chauvin, B. Gilbert and I. Guibard, *J. Chem. Soc., Chem. Commun.*, 1990, 1715.
6 Y. Chauvin, S. Einloft and H. Olivier, *Ind. Eng. Chem. Res.*, 1995, **34**, 1149.
7 Y. Chauvin, H. Olivier, C. Wyrvalski, L. Simon and E. de Souza, *J. Catal.*, 1997, **165**, 275.
8 Y. Chauvin, S. Einloft and H. Olivier, *US Pat.* 5 550 304, 1996.
9 Y. Chauvin, L. Mußmann and H. Olivier, *Angew. Chem.*, 1995, **107**, 2941.
10 T. J. Melton, J. Joyce, J. T. Maloy, J. A. Boon and J. S. Wilkes, *J. Electrochem. Soc.*,1990, **137**, 3865.
11 I. C. Quarmby and R. A. Osteryoung, *J. Am. Chem. Soc.*, 1994, **116**, 2649.
12 R. A. Osteryoung, I. C. Quarmby, R. A. Mantz and L. M. Goldenberg, *Anal. Chem.*, **66**, 1994, 3558.

Communication 8/08346K

ChemComm

The elimination–addition mechanism of nucleophilic substitution at an alkylphosphonyl centre: stereospecificity, non-stereospecificity and the alkylidineoxophosphorane (phosphene) intermediate

Martin J. P. Harger* and Deborah K. Jones

Department of Chemistry, The University, Leicester, UK LE1 7RH

Received (in Liverpool, UK) 1st December 1998, Accepted 13th January 1999

The substitution reactions of $R'_2CHP(O)(NMeR^*)Cl$ (R'_2CH = fluoren-9-yl; R* = CHMePh) with secondary amines (Me_2NH, Et_2NH, Pr^iNHEt) are largely stereospecific or non-stereospecific depending on the bulk of the amine and its concentration; two elimination–additon pathways, differing in whether or not the phosphene intermediate $R'_2C{=}P(O)NMeR^*$ becomes liberated, may be responsible.

Methyleneoxophosphoranes, or phosphenes, are the phosphorus analogs of sulfenes.[1] Like other three-coordinate P^V species they generally have only a fleeting existence in solution.[2] They have been generated in some oxidation,[3] fragmentation[4] and rearrangement[5] reactions, but unlike sulfenes they have not been implicated as intermediates in nucleophilic substitution.[6] A possible exception is the conversion of the fluorenylphosphonamidic chloride **1** into the phosphonic

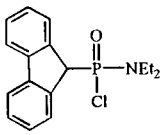

1

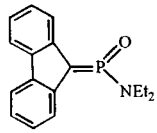

2

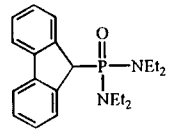

3

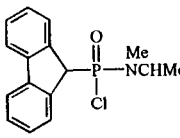

4

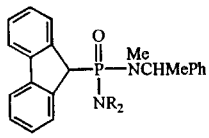

5

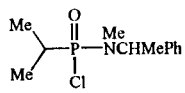

6

diamide **3** with Et_2NH.[7] On steric grounds (substrate and nucleophile) this should proceed very slowly, at least by the normal associative $S_N2(P)$ mechanism,[8] but in fact it proceeds quite readily.[7] It may be that in this case the acidity of the C_α–H bond in the substrate makes a dissociative elimination–addition mechanism, with a phosphene intermediate **2**, more accessible than is usual. We hoped that a stereochemical study, using a substrate related to **1**, would help to clarify the role of phosphene intermediates in nucleophilic substitution.

The phosphonamidic chloride **4** was prepared by treating fluoren-9-ylphosphonic dichloride[7] with (S)-(−)-PhMeCHNHMe (2.5 equiv.) in CH_2Cl_2 (1 : 1 v/v amine–CH_2Cl_2). Chromatography (silica gel; 1 : 6 EtOAc–light petroleum) and crystallisation afforded pure (≥99%) samples of the individual diastereoisomers of **4**: sample **A**, mp 145–147 °C; $\delta_P(CDCl_3)$ 43·0; $\delta_H(CDCl_3)$ 4.99 (d, J_{PH} 29, >CH), 1.61 (d, J_{PH} 12.5, NMe) and 0.68 (d, J_{HH} 7, CH*Me*); sample **B**, mp 103.5–104.5 °C; $\delta_P(CDCl_3)$ 43.15; $\delta_H(CDCl_3)$ 4.98 (d, J_{PH} 30, >CH), 1.62 (d, J_{PH} 13, NMe) and 1.33 (d, J_{HH} 7, CHMe).†

The two samples (**A** and **B**) of the substrate **4** were allowed to react with Et_2NH (large excess) as a 1.2 mol dm^{-3} solution in $CHCl_3$ at 31 °C. In both cases the phosphonic diamide **5** (R = Et), *m/z* 418 (M^+, 10%) and 253 ($M^+ - C_{13}H_9$, 100), was obtained as an unequal mixture of diastereoisomers: $\delta_P(CDCl_3)$ 34.25; $\delta_H(CDCl_3)$ 4.93 (d, J_{PH} 27, >CH), 2.18 (d, J_{PH} 9.5, NMe), 1.48 (d, J_{HH} 7, CH*Me*) and 0.80 (t, J_{HH} 7, NCH_2*Me*) (major from **A**); $\delta_P(CDCl_3)$ 34.65; $\delta_H(CDCl_3)$ 4.96 (d, J_{PH} 26, >CH), 1.82 (d, J_{PH} 9.5, NMe), 0.96 (t, J_{HH} 7, NCH_2*Me*) and 0.81 (d, J_{HH} 7, CH*Me*) (major from **B**). Monitoring the reactions by ^{31}P NMR spectroscopy showed that stereoisomerisation of the substrate was slight (≤3%) up to 50% completion (*t* = 9.5 h for **A**, 6 h for **B**) and the diastereoisomer ratio of the product did not change significantly as the reaction progressed. The observed product diastereoisomer ratios, 33 : 67 from **A** and 77 : 28 from **B**, can therefore be taken as a true indication of how the diastereoisomers of the substrate **4** react with Et_2NH.

The reactions clearly fall between the extremes of complete stereospecificity (product diastereoisomer ratios 0 : 100 and 100 : 0) and complete non-stereospecificity (ratios same; not necessarily 50 : 50). A likely explanation is that two mechanisms are operating in parallel, one stereospecific and the other non-stereospecific. The obvious candidates for these are $S_N2(P)$ and elimination–addition (EA). In the former the five-coordinate intermediate or transition state would be formed by attack of the nucleophile opposite the leaving group, resulting in inversion of configuration at phosphorus, while in the latter the trigonal three-coordinate phosphene intermediate would be susceptible to attack at either of its diastereotopic faces.

Consistent with that picture is the behaviour of **4** with other amines. Me_2NH differs little from Et_2NH in basicity but, for steric reasons, it is much more nucleophilic towards a tetrahedral P=O centre [≥100 times with $Pr^iP(O)(NEt_2)Cl$ as substrate[7]]. The $S_N2(P)$ pathway should therefore be more important with Me_2NH and increased stereospecificity was indeed observed; using 1.2 mol dm^{-3} Me_2NH in $CHCl_3$ the product **5** (R = Me) [$\delta_P(CDCl_3)$ 35.15 and 34.3] was formed with diastereoisomer ratios of 6 : 94 from **A** and 97 : 3 from **B**. Conversely, Pr^iNHEt is much less nucleophilic than Et_2NH and reduced stereospecificity was observed; with 1.2 mol dm^{-3} Pr^iNHEt the product diastereoisomer ratios were 42 : 58 and 52 : 48 [$\delta_P(CDCl_3)$ 34.3 and 34.2]. Nonetheless, there are two reasons why the competing $S_N2(P)$–EA picture seems unsustainable.

First, the reaction of the fluorenyl substrate **4** with Me_2NH is some 50 times *faster* than the corresponding reaction of the analogous isopropyl compound **6** [$\delta_P(CDCl_3)$ 58.75 and 58.45 (diastereoisomers); product $\delta_P(CDCl_3)$ 42.6 and 41.9].† We would not expect $S_N2(P)$ to be less sterically hindered when the alkyl group on phosphorus is fluorenyl rather than isopropyl, and some evidence supports that view: methanolysis of the phosphonamidic chlorides **4** and **6** under non-basic conditions (MeOH containing 0.2 mol dm^{-3} AgOTf) is 10–20 times *slower* for the fluorenyl compound ($t_{½}$ *ca.* 10 min for **6** but 3 h for **4** at 31 °C). The high reactivity of **4** with Me_2NH thus seems irreconcilable with a mechanism that is predominantly $S_N2(P)$, notwithstanding the high stereospecificity of the reaction.‡

Second, inclusion of a small amount of the strong base 1,8-diazabicyclo[5.4.0]undec-7-ene (DBU) (2 equiv.; 0.07 mol dm^{-3}) increases the rate of the reaction of the fluorenyl substrate **4** with Me_2NH (1.2 mol dm^{-3}) *ca.* 100-fold but does not accelerate the reaction [$S_N2(P)$] of the isopropyl analogue **6**. Crucially, the stereochemistry of the reaction of **4** is unaffected

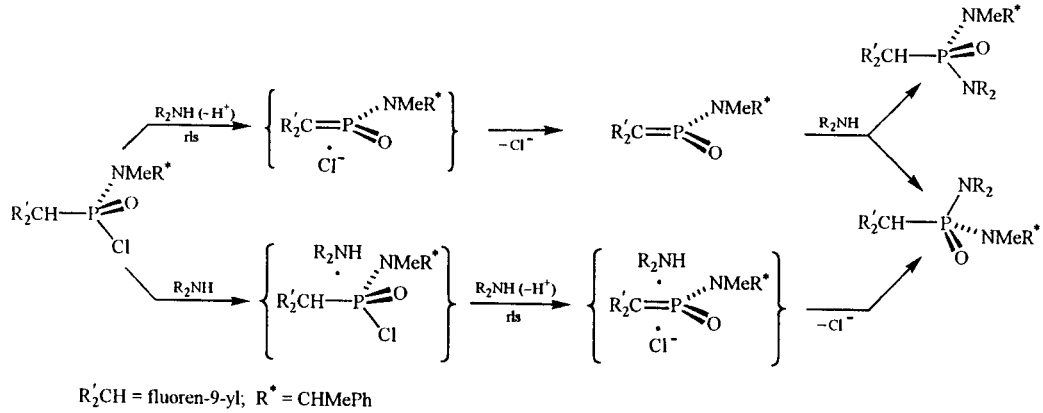

Scheme 1

by the presence of DBU, *i.e.* the reaction is still largely stereospecific [product **5** (R = Me) diastereoisomer ratio 97 : 3 from **B**]. The implication is clear: the stereospecific pathway, like its nonstereospecific counterpart, is base-induced and is not $S_N2(P)$.

One further observation is pertinent. When the Et_2NH concentration was reduced to 0.2 mol dm^{-3} substrate **4** gave the product **5** (R = Et) with a diastereoisomer ratio of 42 : 58 from **A** and 55 : 45 from **B**. This reduced stereospecificity implies that the stereospecific pathway is kinetically of a higher order in amine.

As a whole the results point to two EA pathways, one first order in amine and nonstereospecific, the other second order in amine and stereospecific (or practically so). In the former (Scheme 1, top pathway) the amine acts only as a base in the rate-limiting elimination step, and the resulting phosphene intermediate recombines with the chloride ion, or diffuses away and becomes free before reacting with the nucleophile. In the latter (Scheme 1, bottom pathway) there is preassociation:[9] the nucleophile is already in place when elimination occurs, the phosphene is trapped before it can diffuse away, and the nucleophile becomes attached to that face of the phosphene which is not shielded by the chloride ion.§ Of the two pathways the one involving preassociation will be more sensitive to the bulk of the amine and its concentration. As the amine changes from Me_2NH to Et_2NH to Pr^iNHEt, or the concentration of amine decreases, the contribution of the stereospecific pathway declines; the free phosphene intermediate plays an increasingly important part and the overall reaction becomes increasingly nonstereospecific.

Notes and references

† The new compounds **4** and **6** and the products derived from them were fully characterised by NMR spectroscopy (^{31}P and ^{1}H), mass spectrometry, and elemental analysis and/or accurate mass measurement.

‡ The reaction of **4** with Me_2NH is of an order > 1 in amine; this may also point to a mechanism that is not $S_N2(P)$.

§ The elimination step of the EA mechanism probably involves rapid reversible removal of the C_α proton followed by rate-limiting elimination of chloride from the conjugate base (reversible ElcB) [in the reaction of the 9-deuterio analogue of substrate **1** with Et_2NH, D/H exchange is much faster than substitution (ref. 7)]; for simplicity this detail is omitted from Scheme 1.

1 J. F. King, *Acc. Chem. Res.*, 1975, **8**, 10; J. F. King, J. Y. L. Lam and S. Skonieczny, *J. Am. Chem. Soc.*, 1992, **114**, 1743; J. F. King and R. Rathore, in *The Chemistry of Sulfonic Acids, Esters and their Derivatives*, ed. S. Patai and Z. Rappoport, Wiley, Chichester, 1991, ch. 17.

2 M. Regitz and G. Maas, *Top. Curr. Chem.*, 1981, **97**, 71; F. H. Westheimer, *Chem. Rev.*, 1981, **81**, 813.

3 Th. A. van der Knaap, Th. C. Klebach, R. Lourens, M. Vos and F. Bickelhaupt, *J. Am. Chem. Soc.*, 1983, **105**, 4026.

4 L. D. Quin, J.-S. Tang, G. S. Quin and G. Keglevich, *Heteroatom Chem.*, 1993, **4**, 189; G. Keglevich, K. Újszászy, L. D. Quin and G. S. Quin, *Heteroatom Chem.*, 1993, **4**, 559; G. Keglevich, K. Újszászy, G. S. Quin and L. D. Quin, *Phosphorus, Sulfur, Silicon*, 1995, **106**, 155.

5 M. Regitz and H. Eckes, *Tetrahedron*, 1981, **37**, 1039; D. I. Loewus, *J. Am. Chem. Soc.*, 1981, **103**, 2292; T. Kawashima, Y. Miki, T. Tomita and N. Inamoto, *Chem. Lett.*, 1986, 501.

6 G. Cevasco and S. Thea, *J. Chem. Soc., Perkin Trans. 2*, 1993, 1103; 1994, 1103.

7 M. J. P. Harger and B. T. Hurman, *J. Chem. Soc., Perkin Trans. 1*, 1998, 1383.

8 G. R. J. Thatcher and R. Kluger, *Adv. Phys. Org. Chem.*, 1989, **25**, 99; A. Yliniemala, T. Uchimara, K. Tanabe and K. Taira, *J. Am. Chem. Soc.*, 1993, **115**, 3022; G. R. J. Thatcher and A. S. Campbell, *J. Org. Chem.*, 1993, **58**, 2272 and references cited in these.

9 W. P. Jencks, *Acc. Chem. Res.*, 1980, **13**, 161; *Chem. Soc. Rev.*, 1981, **10**, 345.

Communication 8/09407A

Role of oxygen transients in the facile scission of C–O bonds of alcohols on Zn surfaces

K. R. Harikumar and C. N. R. Rao*

Solid State and Structural Chemistry Unit and CSIR Centre of Excellence in Chemistry, Indian Institute of Science, Bangalore 560012, India. E-mail: cnrrao@sscu.iisc.ernet.in

Received (in Cambridge, UK) 19th October 1998, Accepted 23rd December 1998

The alkoxy species produced by the interaction of alcohols with Zn surfaces undergoes C–O bond scission at 150 K giving hydrocarbon species, but this transformation occurs even at 80 K when alcohol–oxygen mixtures are coadsorbed, due to the oxygen transients.

Studies of the decomposition of methanol on transition metal surfaces have shown that the methoxy species formed around 150 K, undergoes C–O bond scission on some of the surfaces at relatively high temperatures giving hydrocarbon species.[1–4] Ethanol transforms to the alkoxy species on transition metal surfaces and undergoes C–O or C–C bond scission depending on the surface.[5,6] Interaction of propan-2-ol with transition metal surfaces also produces the alkoxy species and the C–O bond scission occurs at high temperatures on some of the surfaces yielding hydrocarbon species.[5,7] We have investigated the interaction of methanol on polycrystalline as well as (0001) Zn surfaces by electron spectroscopic techniques and found that the methoxy species produced around 120 K undergoes C–O bond scission at 150 K and above, giving rise to hydrocarbon species. We show the C(1s) and O(1s) spectra of methanol on a Zn(0001) surface in Fig. 1(a) and (b) respectively to illustrate the transformations. The C(1s) features due to the methoxy and hydrocarbon species are seen at 286 and 285 eV respectively at 150 K. The O(1s) spectrum shows a feature due to the methoxy species at 532 eV which disappears above 150 K. The alkoxy species formed initially undergoes C–O bond scission on the Zn(0001) surface in the cases of both ethanol and propan-2-ol. The stability of the alkoxy species increases from methanol to propan-2-ol, the alkoxy species being formed in the latter even at 80 K. Thus, in all the three alcohols, hydrogen abstraction occurs to give the alkoxy species, followed by the scission of the C–O bond forming the hydrocarbon species at 150 K. These changes are corroborated by vibrational energy loss spectroscopy. The above transformations of alcohols (ROH, R = alkyl group) on the Zn(0001) surface can be represented as follows:

$$\mathrm{ROH(a)} \rightarrow \mathrm{RO(a)} + \mathrm{H(a)} \quad (1)$$

$$\mathrm{RO(a)} \rightarrow \mathrm{R(a)} + \mathrm{O(a)} \quad (2)$$

We were interested in examining the effect of $O^{\delta-}$ type reactive oxygen transients on the interaction of alcohols with the Zn(0001) surface, since such species are known to readily abstract hydrogen from NH_3 and other molecules.[8,9] For this purpose, we have investigated the coadsorption of a 3 : 1 mixture of methanol and oxygen on the Zn(0001) surface. Typical C(1s) and O(1s) spectra are shown in Fig. 1(c) and (d) respectively. In the C(1s) spectrum, the feature due the methoxy species at 286 eV appears at 80 K, along with a weak feature at 287 eV due to chemisorbed methanol. More importantly, a relatively intense feature due to the hydrocarbon species with a C(1s) binding energy around 285 eV also occurs at 80 K. The O(1s) spectrum shows the presence of chemisorbed methanol and the methoxy species at 80 K with O(1s) binding energies at 533.6 eV and 532 eV respectively. A feature around 530 eV due to the oxidic species emerges progressively with increasing temperature. Coadsorption of oxygen with methanol appears to give rise to the short-lived reactive $O^{\delta-}$ type of transient species which readily abstracts hydrogen from methanol even at 80 K, the OCH_3 species subsequently giving the $(CH)_x$ species through C–O bond scission. It should be noted that the coadsorption of methanol and oxygen on a Cu(110) surface only yields OCH_3 and formate[10]

Coadsorption of a 3 : 1 mixture of ethanol and oxygen on the Zn(0001) surface also results in the formation of the alkoxy and the hydrocarbon species at 80 K, with a progressive increase in the hydrocarbon species with increase in temperature. In Fig. 2(a) we show typical C(1s) spectra to illustrate the transformations. Coadsorption of a 3 : 1 mixture of propan-2-ol and oxygen on the Zn(0001) surface gives a high proportion of the hydrocarbon species at 80 K as can be seen from Fig. 2(b). It should be recalled that amongst the three alcohols studied, the proportion of the alkoxy species formed on Zn surfaces is highest in the case of propan-2-ol. Since the formation of the alkoxy species precedes the C–O bond scission, the ease of

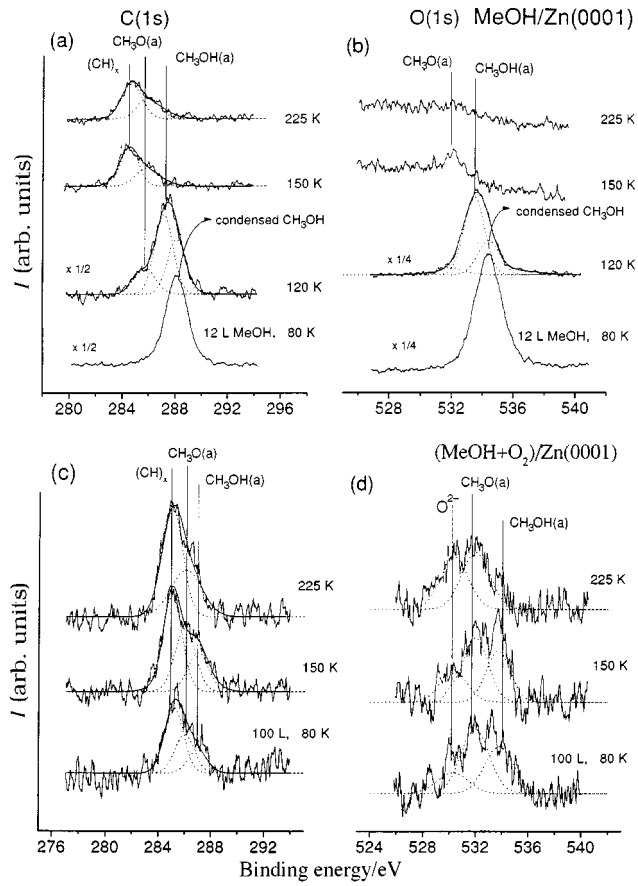

Fig. 1 (a) C(1s) and (b) O(1s) spectra of CH_3OH adsorbed on a Zn(0001) surface. CH_3OH was first adsorbed at 80 K and the surface progressively warmed to 225 K. (c) C(1s) and (d) O(1s) spectra of a 3 : 1 mixture of CH_3OH and O_2 adsorbed on Zn(0001). The mixture was adsorbed at 80 K and the surface progressively warmed to 225 K.

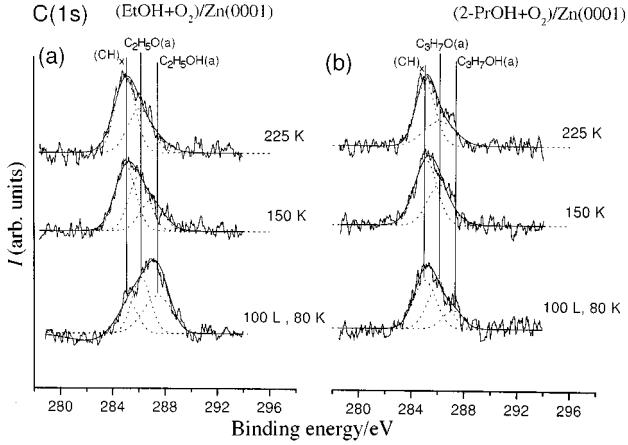

Fig. 2 C(1s) spectra of (a) of a 3 : 1 mixture of C_2H_5OH and O_2 and (b) of a 3 : 1 mixture of propan-2-ol and O_2 adsorbed on a Zn(0001) surface. The alcohol–oxygen mixture was adsorbed at 80 K and the surface progressively warmed to 225 K.

formation of the hydrocarbons will be related to the abundance of the alkoxy species. It is known that adsorption of alcohols on ZnO surfaces gives rise to alkenes, aldehydes and ketones.[11] However, in the present study on Zn surfaces, we only observe the formation of hydrocarbons.

The formation of the $(CH)_x$ type species at 80 K by the interaction of alcohol–oxygen mixtures with Zn surfaces suggests that the C–O bond scission is favoured by the oxygen transient. We represent these transformations as follows:

$$Zn + 1/2O_2 \rightarrow Zn + O^{\delta-}(a) \quad (3)$$

$$ROH + O^{\delta-}(a) \rightarrow RO(a) + OH(a) \quad (4)$$

$$RO(a) \rightarrow R(a) + O(a) \quad (5)$$

$$2OH(a) \rightarrow H_2O + O^{2-}(a) \quad (6)$$

We consider the occurrence of C–O bond scission in alcohols at as low a temperature as 80 K to be significant, considering that such scission occurs at 150 K in the absence of oxygen on the Zn(0001) surface and at much higher temperatures on other transition metal surfaces.

Notes and references

1 R. J. Levis, J. Zhicheng and N. Winograd, *J. Am. Chem. Soc.*, 1989, **111**, 4605.
2 M. Rebholz, V. Matolin, R. Prins and N. Kruse, *Surf. Sci.*, 1991, **251/252**, 1117.
3 J. Wang and R. I. Masel, *J. Am. Chem. Soc.*, 1991, **113**, 5850.
4 S. Chaturvedi and D. R. Strongin, *J. Phys. Chem. B*, 1998, **102**, 2970; B.-R. Sheu and D. R. Strongin, *J. Catal.*, 1995, **154**, 379.
5 M. Bowker and R. J. Madix, *Surf. Sci.*, 1982, **116**, 549; J. B. Benziger and R. J. Madix, *J. Catal.*, 1980, **65**, 36.
6 C. J. Houtman and M. A. Barteau, *J. Catal.*, 1991, **130**, 528.
7 B. C. Wiegand, P. Uvdal, J. G. Serafin and C. M. Friend, *J. Phys. Chem.*, 1992, **96**, 5063; B. C. Wiegand, P. Uvdal, J. G. Serafin and C. M. Friend, *J. Am. Chem. Soc.*, 1991, **113**, 6686.
8 M. W. Roberts, *Chem. Soc. Rev.*, 1996, 437.
9 A. F. Carley, P. R. Davies and M. W. Roberts, *Chem. Commun.*, 1998, 1793; G. U. Kulkarni, C. N. R. Rao and M. W. Roberts, *J. Phys. Chem.*, 1996, **99**, 3310; G. U. Kulkarni, C. N. R. Rao and M. W. Roberts, *Langmuir*, 1995, **11**, 2572.
10 P. R. Davies and G. G. Mariotti, *Chem. Commun.*, 1996, 2319; P. R. Davies and G. G. Mariotti, *Catal. Lett.*, 1997, **43**, 261.
11 M. Bowker, R. W. Petts and K. C. Waugh, *J. Catal.*, 1986, **99**, 53 and references therein.

Communication 8/08076C

Is samarium diiodide an inner- or outer-sphere electron donating agent?

Rasmus J. Enemærke, Kim Daasbjerg* and Troels Skrydstrup*

Department of Chemistry, Aarhus University, Langelandsgade 140, 8000 Aarhus C, Denmark. Fax: +45 8619 6199. E-mail: kdaa@kemi.aau.dk

Received (in Liverpool, UK) 26th November 1998, Accepted 14th January 1999

From the measured value of $E°$ (SmI_2^+–SmI_2) in THF and using free energy plots, the electron transfer between samarium diiodide and acetophenone was shown to be clearly of inner-sphere nature; on the other hand, with benzyl bromide it is closer to an outer-sphere process.

Twenty years have almost passed since the first introduction of samarium diiodide (SmI_2) as a reagent for organic synthesis by Kagan and coworkers.[1] The rich chemistry of this polyvalent one-electron reductant has not been surpassed by any other reagent and it still continues to astound with its ability to promote an array of sequential reactions comprising of carbon radicals and anions.[2] It is surprising though that very little is known concerning the mechanistic details of the electron transfer processes (inner- or outer-sphere) taking place between Sm(II) and organic substrates.[3] In this paper, we describe the nature of the electron transfer between SmI_2 and two substrates, namely benzyl bromide and acetophenone.

Paramount for the comprehension of electron transfer processes involving SmI_2, is that the standard potential of the SmI_2^+–SmI_2 couple in THF be well defined. It is noteworthy that these fundamental measurements have not been performed even after 20 years of existence of SmI_2 in the organic chemistry community. The potential cited today by organic chemists for the Sm(III)–Sm(II) couple of −1.80 V *vs.* SCE was determined in 1948 by polarographic measurements in water,[4] which is simply not compatible with current studies.†

Hence, we set out to investigate the redox properties of SmI_2 and SmI_3 by means of cyclic voltammetry in a supporting electrolyte solution of NBu_4I (0.02 M) and NBu_4PF_6 (0.2 M) in THF.‡ Fig. 1 shows three of the voltammograms recorded for SmI_2 at different sweep rates v in the range 0.02–0.5 V s^{-1}. The peak separation increases from *ca.* 150 to 300 mV as a function of v. As the peak potentials and currents acquired in the voltammograms of SmI_2 are in good agreement with the corresponding values obtained for SmI_3, it appears that the same reaction mechanism is in play no matter which of the two compounds is the starting point for the electrochemical investigation. A working model was therefore set up, as illustrated in Scheme 1, involving a heterogeneous electron transfer step and a fast established chemical equilibrium, where SmI_2^+ coordinates strongly with I^- present in the electrolyte solution.

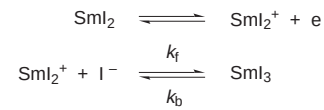

Scheme 1

In order to determine the standard potential (or more correctly the formal potential) $E°$ of SmI_2^+–SmI_2 from the cyclic voltammograms, the association constant ($K = k_f/k_b$) for SmI_3 is required. A rough estimate of $K \approx 10^7$ dm^3 mol^{-1} could be obtained simply by comparing conductivity measurements performed on SmI_3 and NBu_4I in THF since the association constant for NBu_4I in THF has been estimated previously.[7] However, the electrochemical measurements were carried out with substantial amounts of supporting electrolyte present in THF and K may be somewhat different in this more polar medium. Being cautious and selecting 1 and 10^4 as the limiting values of $K[I^-]$, digital simulations of the voltammograms (see Fig. 1) were carried out on the basis of the above reaction scheme.§ Simulations revealed that $K[I^-]$ is $< 10^4$ if the chemical equilibrium should be established quickly with a large k_b and without k_f exceeding the diffusion-controlled limit. The shape of the experimental cyclic voltammograms was presumably somewhat influenced by adsorption phenomena and therefore the main emphasis in the simulation procedure was to describe the reproducible development in the experimentally obtained peak potentials and currents as a function of v. This led to a value for $E°$ of −1.41 ± 0.08 V *vs.* Fc^+–Fc and for the logarithm of the standard heterogeneous rate constant $k°$ (in cm s^{-1}) of −2.20 ± 0.70. Comparing these values of $E°$ and log $k°$ with those obtained if the chemical equilibrium reaction is neglected (−1.51 V and −2.92, respectively) illustrates the importance of including follow-up or preceding reactions in electrochemical measurements.

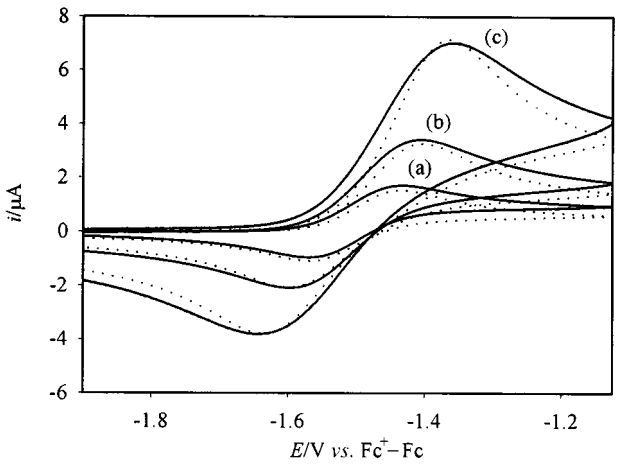

Fig. 1 Cyclic voltammograms of 2.5 mM SmI_2 recorded in THF–0.2 M NBu_4PF_6 + 0.02 M NBu_4I at a glassy carbon electrode (diameter = 1 mm) at sweep rates of (a) 0.02, (b) 0.1 and (c) 0.5 V s^{-1}. The dotted curves represent simulated curves based on the following parameters: $E°$ = −1.41 V, $k_f[I^-]$ = 1.5 × 10^5 s^{-1}, k_b = 3.8 × 10^3 s^{-1}, $k°$ = 0.0065 cm s^{-1}, D = 5.4 × 10^{-6} cm^2 s^{-1}, transfer coefficient α = 0.5 and capacitance C_d = 10^{-7} F.

The outer- or inner-sphere electron donor abilities of SmI_2 towards a given substrate can now be assessed by comparing the reactivity of SmI_2 and a corresponding outer-sphere electron donor.[8] In this way the degree of electronic interaction between SmI_2 and the substrate in the transition state can be estimated. The first reaction studied was the reduction of benzyl bromide, in which the rate-controlling step is the initial electron transfer forming the benzyl radical. As representatives of outer-sphere electron donors, four radical anions of aromatic compounds were selected having potentials $E°_A$ close to that of SmI_2^+.[8] The rate constants k_{ET} for the electron transfer reactions between the radical anions and benzyl bromide were measured¶ and depicted in free energy plots of log k_{ET} *vs.* $E°_A$ (Fig. 2). The value of k_{ET} (= 0.34 dm^3 mol^{-1} s^{-1}) corresponding to the $E°$ of SmI_2^+ = −1.41 V can be interpolated from the straight line

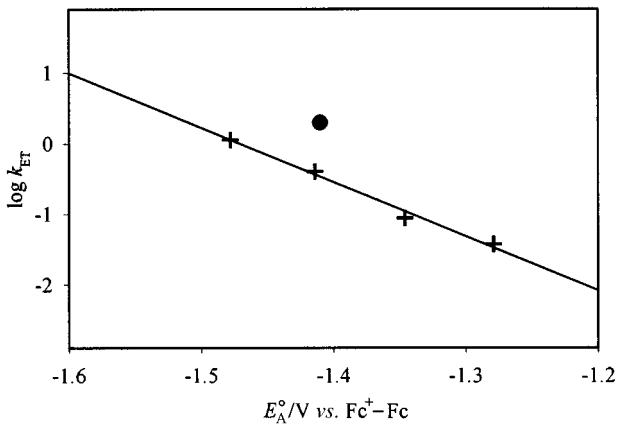

Fig. 2 Electron transfer rate constants (+) for the reaction between radical anions of aromatic compounds (2,3-dimethylanthraquinone, anthraquinone, 2,3-dimethylnaphthoquinone and 1,2-benzanthraquinone) and benzyl bromide as well as the rate constant (●) of the reaction between SmI_2 and benzyl bromide in THF–0.2 M NBu_4PF_6–0.02 M NBu_4I.

through the four points determined by linear least square analysis. Included in Fig. 2 is the rate constant k_{obs} of the reaction between SmI_2 and benzyl bromide (= 2.0 dm^3 mol^{-1} s^{-1}) with a position slightly above the line. The value of k_{obs}/k_{ET} thus obtained is 5.9 which indicates that the electron transfer process does have inner-sphere character. Nevertheless, the ratio is relatively small and it suggests that the electronic interaction between SmI_2 and benzyl bromide in the transition state amounts to only a few kcal mol^{-1}.‖

As a representative for the class of carbonyl compounds, which are involved in many SmI_2-induced electron transfer reactions, we studied the reduction of acetophenone. For SmI_2 the reaction leads to the formation of a metal-complexed ketyl radical in the rate-controlling step. However, the procedure used for measuring k_{ET} for benzyl bromide can not be employed in this case since the electron transfer from aromatic radical anions to acetophenone, forming its radical anion, involves an energetically unfavourable equilibrium reaction. Still, the rate constant for the electron transfer process between an outer-sphere donor of E° = −1.41 V and acetophenone can be estimated on the basis of the equations of Marcus and Eyring (using a collision frequency of 3×10^{11} dm^3 mol^{-1} s^{-1}).[11] The E° of acetophenone is −2.52 V as measured by cyclic voltammetry, and if the reorganization energy of the reaction is assumed to be in the range 20–30 kcal mol^{-1}, k_{ET} can be calculated as *ca.* 10^{-8} dm^3 mol^{-1} s^{-1}. The rate constant k_{obs} for the reaction between SmI_2 and acetophenone was measured¶ to be 7 dm^3 mol^{-1} s^{-1} so in this case k_{obs}/k_{ET} approaches 10^9. This is a substantial value compared with the result for benzyl bromide and the mechanism in this case clearly can be classified as an inner-sphere electron transfer process with a strong electronic interaction in the transition state.

In conclusion, we provide the E° value for the SmI_2^+–SmI_2 couple in THF, and apply it to describe the mechanism of electron transfer from SmI_2 to two organic substrates. We are currently using the above methodology to investigate the mechanism of SmI_2-based reductions of other functionalities.

Notes and references

† Shabangi and Flowers recently measured the oxidation potential of SmI_2 in THF–0.1 M NBu_4PF_6 but did not investigate the mechanism of the electrode reaction nor its thermodynamic significance (ref. 5). The peak potential was −1.33 V *vs.* Ag–$AgNO_3$ (−1.21 V *vs.* Fc^+–Fc) at a sweep rate of 0.1 V s^{-1}.

‡ The experimental set-up for the electrochemical experiments was as described in ref. 6. The working electrode was a glassy carbon disk of diameter 1 mm. All potentials were reported *vs.* the ferrocenium–ferrocene (Fc^+–Fc) redox couple, the potential of which was measured to 0.52 V *vs.* SCE in THF–0.2 M NBu_4PF_6. Experiments were carried out at 20 °C. NBu_4I was added to the cell in order to suppress any ligand-exchange of I^- by PF_6^- in either SmI_2 or SmI_3. UV-spectral investigations revealed that at least 10 mM of NBu_4I must be present in the electrolyte solution (THF–0.2 M NBu_4PF_6) for the UV-spectrum to resemble that of SmI_2 or SmI_3 in THF alone. The upper concentration limit of NBu_4I was 30 mM, set by its solubility.

§ Digisim 2.1 software (Bioanalytical Systems Inc) was used for digital simulation. The diffusion coefficients of SmI_2 and SmI_2^+, *D*, were assumed to be equal. In the experiments, variation of the NBu_4I concentration in the range 10–30 mM had no detectable effect on the position of the peak potentials. This was attributed to the small dissociation constant of NBu_4I in THF ($\approx 10^{-6}$ mol dm^{-3})[7] and the resulting low concentration of free iodide. The concentration of iodide was assumed to be reasonably constant throughout the whole scan range due to the equilibrium reaction with NBu_4I and thus included in the forward rate constant k_f in the simulations. At lower concentrations of NBu_4I the cyclic voltammetric waves were shifted in a positive direction though being complicated by ligand exchange reactions involving PF_6^- from NBu_4PF_6.

¶ The reaction kinetics was followed by UV–VIS spectroscopy using a dip-probe technique (ref. 9). The decay of SmI_2 in the presence of a substrate was detected at 560 and 620 nm. No build-up of intermediates during the reaction could be detected in the wavelength range 300–800 nm. The presence of supporting electrolyte had no influence on the reaction rate. The kinetics for benzyl bromide and acetophenone followed the same rate law described by: $d[SmI_2]/dt = -nk_{obs}[SmI_2][substrate]$, where n = 2 for benzyl bromide and n = 1 for acetophenone. k_{obs} was determined under pseudo-first-order conditions using an excess of substrate.

‖ This is true even if one takes into account that the k_{obs}/k_{ET} ratio obtained should be considered as a minimum value;[10] the self-exchange reorganisation energy of the SmI_2^+–SmI_2 couple is somewhat higher than for the aromatic radical anions as indicated by the relatively low value of k° measured by cyclic voltammetry.

1 P. Girard, J. L. Namy and H. B. Kagan, *J. Am. Chem. Soc.*, 1980, **102**, 2693.
2 For recent reviews on the application of SmI_2: G. A. Molander and C. R. Harris, *Chem. Rev.*, 1996, **96**, 307; G. A. Molander and C. R. Harris, *Tetrahedron*, 1998, **54**, 3321; T. Skrydstrup, *Angew. Chem., Int. Ed. Engl.*, 1997, **36**, 345.
3 R. G. Finke, S. R. Keenan and P. L. Watson, *Organometallics*, 1989, **8**, 263.
4 A. Timnick and G. Glockler, *J. Am. Chem. Soc.*, 1948, **70**, 1347.
5 M. Shabangi and R. A. Flowers II, *Tetrahedron Lett.*, 1997, **38**, 1137.
6 B. Svensmark and S. U. Pedersen, *Acta Chem. Scand. Ser. A*, 1986, **40**, 607.
7 I. Svorstøl, H. Høiland and J. Songstad, *Acta Chem. Scand. Ser. B*, 1984, **38**, 885; C. Treiner and J. C. Justice, *Comptes Rendus*, 1969, **269**, 1364.
8 H. Lund, K. Daasbjerg, T. Lund and S. U. Pedersen, *Acc. Chem. Res.*, 1995, **28**, 313; J.-M. Savéant, *Adv. Phys. Org. Chem.*, 1990, **26**, 1 and references therein.
9 S. U. Pedersen, T. Lund, K. Daasbjerg, M. Pop, I. Fussing and H. Lund, *Acta Chem. Scand.*, 1998, **52**, 657; S. U. Pedersen, T. B. Christensen, T. Thomasen and K. Daasbjerg, *J. Electroanal. Chem.*, 1998, **454**, 123.
10 K. Daasbjerg and H. Lund, *Acta Chem. Scand.*, 1993, **47**, 597; H. Balslev, K. Daasbjerg and H. Lund, *Acta Chem. Scand.*, 1993, **47**, 1221.
11 R. A. Marcus, *Annu. Rev. Phys. Chem.*, 1964, **15**, 155.

Communication 8/09277J

2,5-Di(2-pyridyl)phospholes: model compounds for the engineering of π-conjugated donor–acceptor co-oligomers with a chemically tunable HOMO–LUMO gap

Caroline Hay,[a] Delphine Le Vilain,[a] Valérie Deborde,[a] Loïc Toupet[b] and Régis Réau*[a]

[a] *UMR 6509 CNRS-Université de Rennes, Campus de Beaulieu, 35042 Rennes Cedex, France. E-mail: regis.reau@univ-rennes1.fr*

[b] *UMR 6626 CNRS-Université de Rennes, GMCM, Campus de Beaulieu, 35042 Rennes Cedex, France*

Received (in Liverpool, UK) 28th October 1998, Accepted 23rd December 1998

2,5-Di(2-pyridyl)phospholes possess an extended π-conjugated system with a charge transfer structure; high yielding chemical modifications involving the phosphorus atom allow fine tuning of the HOMO–LUMO gap.

The control of both the structure and HOMO–LUMO gap of linear π-conjugated oligomers is the focus of considerable interest. These compounds have been investigated in order to simulate the electronic and electrochemical properties of the corresponding polymers and they are now emerging as efficient molecular wires in electronics applications.[1] Group 15 and 16 heterocyclopentadienes have been widely used as building blocks for the design of well-defined linear π-conjugated oligomers.[1] However, there are only a few instances of phospholes having been used for such a purpose,[2] although they display particular properties which make them attractive synthons. Firstly, the aromaticity of phospholes is generally much lower than that of furan, pyrrole or thiophene.[3] This is a consequence of the inherent pyramidal geometry of the tricoordinate phosphorus atom which disrupts efficient orbital interaction within the five-membered ring. This property should have an impact on the molecular engineering of the HOMO–LUMO separation of linear π-conjugated systems since π-electron delocalization along the chain is favoured when the backbone features heterocycles of low resonance energy.[1a,3c] Secondly, and in contrast to thiophene or pyrrole, phospholes possess a heteroatom which retains a versatile reactivity.[3a,b] This may offer the possibility of tuning the HOMO–LUMO gap *via* chemical modifications. Recently, Mathey *et al.* prepared various α-oligophospholes (n = 2–4) and oligomers containing α-thienyl- or α-furyl-α-phospholyl links.[2a–e] X-Ray diffraction studies performed on these derivatives showed that they deviate notably from planarity. This rotational disorder prevents extended π-conjugation because the orbital overlap varies approximately with the cosine of the twist angle. A recent strategy to effect a coplanar arrangement in linear π-conjugated polymers involved constructing alternating [A-B] derivatives where the A and B units are electron-deficient and electron-rich, respectively.[4] These derivatives are considered to have a charge-transfer structure with double bond character between the A-B units. As the parent phosphole can be considered as a very electron-rich heterocyclopentadiene,[3c] we decided to investigate the preparation of derivatives based on alternating pyridine and phosphole rings with a well defined 2,5-linkage. Herein, we describe an efficient synthesis of the simplest model, namely a 2,5-di(2-pyridyl)phosphole, and we show the possibility of tuning its HOMO–LUMO gap through chemical modifications.

The target phospholes were prepared according to Fagan's method[5] which involves the reaction of zirconacyclopentadienes with dihalogenophosphines. In order to obtain the desired 2,5-substitution pattern, diynes **1a**,**b** possessing a flexible spacer were employed (Scheme 1).[6] A Sonogashira coupling of hexa-1,7-diyne with 2-bromopyridine allowed an efficient and large-scale preparation of derivatives **1a** (92%) and **1b** (94%). These compounds reacted at −78 °C with 'zirconocene'[6] *via* a regioselective ring-closing diyne coupling to give the corresponding zirconacyclopentadienes which were characterised by NMR spectroscopy. Isolation of the zirconium-containing metallacycles was not necessary; addition of 1.1 equiv. of $PhPCl_2$ to the reaction mixture at −78 °C afforded the desired phospholes **2a**,**b** in a 'one-pot' procedure. They were isolated as air-stable yellow powders after purification by chromatography (alumina) in 70 and 73% yield, respectively. Phospholes **2a**,**b** have been characterised by high resolution mass spectrometry and elemental analyses and they exhibit the expected NMR spectroscopic data. In the ^{13}C NMR spectrum, the endocyclic P–C_α carbon atoms of **2a** give a singlet, which is not unusual for phospholes,[2e,3a,b] while the other endocyclic carbon and the C_{ipso} atoms of the aromatic rings of compounds **2a**,**b** all appear as doublets with classical J_{PC} coupling constants.

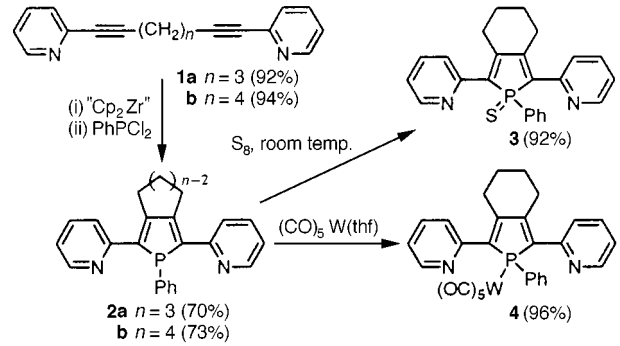

Scheme 1

The crystal structure of derivative **2b** (Fig. 1) reveals that, as expected, the phosphorus atom is strongly pyramidalized [Σ(CPC angles) = 299.3°] and that the endocyclic P–C bond lengths [1.801(4) and 1.804(4) Å] approach that of a P–C single bond (1.84 Å). These data compare well with those observed for a 2,5-dialkynylphosphole[2c] [Σ(CPC angles) = 292.4°; P–C,

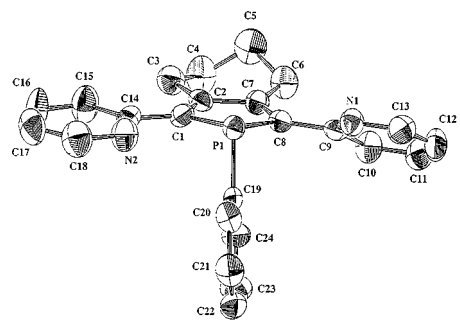

Fig. 1 ORTEP view of **2b**. Selected bond lengths (Å): P–C(1) 1.806(6), C(1)–C(2) 1.354(8), C(2)–C(7) 1.478(9), C(7)–C(8) 1.356(9), C(8)–P 1.806(6).

1.815–1.821 Å] and 1,2,5-triphenylphosphole[7] [P–C, 1.822 Å], two compounds for which it is proposed that ring delocalization is almost switched off, with the endocyclic subunit being conjugated with the C_2 and C_5 substituents.[3a,b] Of particular importance, the two bond lengths between the pyridyl rings and the slightly puckered phosphole ring [1.464(5) and 1.467(5) Å] have values that lie between those associated with single and double bonds, and the dihedral angles (25.6 and 7.0°) are relatively small, allowing an extended π-conjugation. These structural data clearly show that in 1-phenyl-2,5-di(2-pyridyl)phospholes the dienic moiety of the phosphole ring is conjugated with the two pyridine rings and not with the phosphorus atom.

The UV–VIS data for compounds **2a**,**b** and of the related 2,5-diphenylphosphole **2c** are given in Table 1. Derivative **2c** was isolated in only 10% yield according to the strategy presented in Scheme 1 starting from 1,8-diphenylocta-1,7-diyne.[6b] Interestingly, the λ_{max} observed for 2,5-pyridylphospholes **2a**,**b** are comparable, and notably longer to that of the 2,5-diphenylphosphole **2c** ($\Delta\lambda_{max}$ > 36 nm). This observation, which is in line with the conclusion drawn from the solid state structure, highlights the importance of the alternating electron-deficient/electron-rich ring structure of derivatives **2a**,**b** which favours the delocalization of the π-system.

The next question was whether chemical transformation involving the phosphorus atom, which is not involved in the π-delocalized system, would significantly modify the HOMO–LUMO gap? Treatment of phosphole **2b** with elemental sulfur and $W(CO)_5$(thf) afforded derivatives **3** and **4**, respectively, in near quantitative yields. The molecular formulae of **3** and **4** were established by multinuclear NMR spectroscopy, high resolution mass spectrometry and elemental analyses. These chemical transformations resulted in a blue shift of λ_{max} relative to phosphole **2b** (Table 1), the effect being more pronounced for the sulfide **3** ($\Delta\lambda_{max}$ = 26 nm) than for the complex **4** ($\Delta\lambda_{max}$ = 17 nm). In order to evaluate the relative contribution of geometric effects (degree of planarity) on values of λ_{max} in this series, derivative **4** was subjected to an X-ray diffraction study (Fig. 2). The structural data for complex **4**† are very similar to those observed for the free phosphole **2b**, suggesting that the coordination of the metal did not result in a dramatic steric perturbation. As observed for the free ligand, the three heteroatoms are pointing in the same direction. Note that the sum of the CPC angles is 298.7° (**2b**, 299.3°) and that the two endocyclic P–C bonds [1.818(4) and 1.824(4) Å] are slightly longer than those of **2b** [1.801(4) and 1.804(4) Å]. The twist angles between the pyridyl and the phosphole rings (11.3 and 0.0°) are smaller than those observed for the non-coordinated phosphole **2b** (25.6 and 7.0°). Since the pyridine–phosphole–pyridine moiety of **2b** is more planar when coordinated, the origin of the blue shift observed on going from **2b** to **4** is likely to be due to electronic factors. It seems reasonable to propose that both oxidation with sulfur and the coordination of the phosphorus atom decreases the electron-density of the phosphole ring, leading to a decrease in the degree of charge transfer in the π-linear conjugated pyridine–phosphole–pyridine system. As expected, this effect is more pronounced for sulfide **3** than for complex **4**.

Derivatives **2a**,**b** and **4** are air-stable in the solid state and also in THF solution for days. Preliminary stability tests by thermogravimetric analysis and differential scanning calorimetry under nitrogen show that derivative **2a** (mp 186 °C) and **2b** (mp 192 °C) are stable up to 201 and 211 °C, respectively, whereas complex **4** (mp > 204 °C) decomposes at 204 °C.

The synthesis of alternating pyridine–phosphole co-oligomers with a well-defined 2,5-linkage is under active investigation.

We thank the Conseil Régional Bretagne for financial support of this work.

Table 1 UV–VIS data in THF for compounds **2a–c**, **3** and **4**

Compound	λ_{max}/nm	log ε
2a	390	3.96
2b	395	4.02
2c	354	4.20
3	364	3.28
4	373	4.01

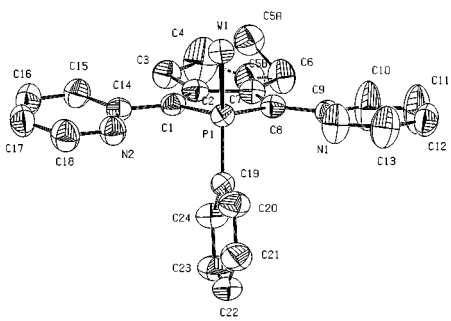

Fig. 2 ORTEP view of **4**. CO ligands have been omitted for clarity. Selected bond lengths (Å): P–C(1) 1.820(5), C(1)–C(2) 1.356(5), C(2)–C(7) 1.466(8), C(7)–C(8) 1.352(5), C(8)–P 1.819(4).

Notes and references

† *Crystal data* for **2b**: Samples were studied on a CAD4 NONIUS diffractometer with graphite monochromatized Mo-Kα (λ = 0.71073 Å) at 293(1) K. The whole structures were refined with SHELXL97. ORTEP views with 50% probability were realized with PLATON98.

Crystal data for **2b**: $C_{24}H_{21}N_2P$, M = 368.42; crystal size 0.32 × 0.22 × 0.18 mm, monoclinic, space group $P2_1/n$, a = 8.619(2), b = 14.127(2), c = 16.116(4) Å, β = 104.53(6)°, U = 1899.5(7) Å^{-3}, Z = 4, D_c = 1.288 g cm^{-3}, μ = 1.55 cm^{-1}, $F(000)$ = 776, 4398 reflections measured, 4128 were independent [1643 with $I > 2\sigma(I)$], 245 variables refined, R_1 = 0.0654 (wR_2 = 0.1221).

Crystal data for **4**: $C_{29}H_{21}N_2O_5PW$, M = 692.33; crystal size 0.40 × 0.22 × 0.12 mm, triclinic, space group $P\bar{1}$; a = 9.943(2), b = 11.122(9), c = 13.590(5) Å, α = 78.34(3), β = 72.90(2), γ = 66.90(3)°, U = 1315(1) Å^{-3}, Z = 2, D_c = 1.749 g cm^{-3}, μ = 44.96 cm^{-1}, $F(000)$ = 676, 5715 reflections measured, 5377 were independent [4764 with $I > 2\sigma(I)$], 343 variables refined, R_1 = 0.0278 (wR_2 = 0.0686).

CCDC 182/1131. Crystallographic data is available in CIF format from the RSC Web site, see: http://www.rsc.org/suppdata/cc/1999/345/

1 (*a*) J. Roncali, *Chem. Rev.*, 1997, **97**, 173; (*b*) J. M. Tour, *Chem. Rev.*, 1996, **96**, 537; (*c*) A. Kraft, A. Gimsdale and A. Holmes, *Angew. Chem., Int. Ed.*, 1998, **37**, 402; (*d*) I. Jestin, P. Frère, P. Blanchard and J. Roncali, *Angew. Chem., Int. Ed.*, 1998, **37**, 942.

2 (*a*) E. Deschamps, L. Ricard and F. Mathey, *Angew. Chem., Int. Ed. Engl.*, 1994, **33**, 1158; (*b*) M.-O. Bevierre, F. Mercier, L. Ricard and F. Mathey, *Angew. Chem., Int. Ed. Engl.*, 1990, **29**, 655; (*c*) S. Holand, F. Gandolfo, L. Ricard and F. Mathey, *Bull. Soc. Chim. Fr.*, 1996, **133**, 33; (*d*) E. Deschamps and F. Mathey, *J. Org. Chem.*, 1990, **55**, 2494; (*e*) E. Deschamps, L. Ricard and F. Mathey, *Heteroatom Chem.*, 1991, **3**, 377; (*f*) S. H. Mao and T. Don Tilley, *Macromolecules*, 1997, **30**, 5566.

3 (*a*) F. Mathey, *Chem. Rev.*, 1988, **88**, 437; (*b*) L. D. Quin, in *Comprehensive Heterocyclic Chemistry*, ed. A. R. Katritzky, Pergamon, Oxford, 1996, p. 757; (*c*) I. Albert, T. Marks and M. Ratner, *J. Am. Chem. Soc.*, 1997, **119**, 6575; (*d*) A. Dransfeld, L. Nyulaszi and P. v. R. Schleyer, *Inorg. Chem.*, 1998, **37**, 4413.

4 (*a*) For recent contributions see: Q. T. Zhang and J. M. Tour, *J. Am. Chem. Soc.*, 1998, **120**, 5355; F. Demanze, A. Yasser and F. Garnier, *Macromolecules*, 1996, **29**, 4267; (*b*) S. Yamaguchi, Y. Itami and K. Tamao, *Organometallics*, 1998, **17**, 4910.

5 P. J. Fagan, W. A. Nugent and J. C. Calabresse, *J. Am. Chem. Soc.*, 1994, **116**, 1880.

6 (*a*) E. Negishi and T. Takahashi, *Acc. Chem. Res.*, 1994, **27**, 124; (*b*) B. Lucht, S. Mao and T. Don Tilley, *J. Am. Chem. Soc.*, 1998, **120**, 4354; (*c*) B. Lucht and T. Don Tilley, *Chem. Commun.*, 1998, 1645.

7 W. P. Ozbirn, R. A. Jacobson and J. C. Clardy, *J. Chem. Soc., Chem. Commun.*, 1971, 1062.

Communications 8/08408D

A novel pentamanganese(II) cluster produced by a controlled self assembly process; an exact match between the coordination algorithm of the metals and the ligand binding site arrangement

Craig J. Matthews,[a] Zhiqiang Xu,[a] Sanat K. Mandal,[a] Laurence K. Thompson,*[a] Kumar Biradha,[b] Karen Poirier[b] and Michael J. Zaworotko†[b]

[a] *Department of Chemistry, Memorial University of Newfoundland, St. John's, NFLD, Canada A1B 3X7. E-mail: lthomp@morgan.ucs.mun.ca*

[b] *Department of Chemistry, St. Mary's University, Halifax, NS, Canada B3H 3C3*

Received (in Cambridge, UK) 17th November 1998, Accepted 13th January 1999

The tetradentate ligand phaap combines a bridging alkoxide oxygen and diazine and pyridine nitrogen donors, with five critically positioned binding sites, and on reaction with $Mn(ClO_4)_2{\cdot}6H_2O$ undergoes a controlled self assembly to produce a unique trigonal bipyramidal oxygen bridged metal cluster with an exact match between the coordination requirements of the five six-coordinate metals and the donor arrangements of the six coordinated ligands.

The continued investigation of low molecular weight models for the oxygen evolving manganese complex of photosystem (II) has produced a range of homotetranuclear complexes, which have been bridged by oxygen centres and involved a variety of geometric arrangements, *e.g.* dimer of dimers, butterfly, cubane and adamantane type structures and mixed valence aggregates.[1–4] These have primarily been synthesized using strategies that utilize pre-organized macrocyclic hosts[1] or by employing self assembly reactions involving 'simple' carboxylates,[5] and substituted pyridonates.[6] The former method is a more rational approach because of the reduced tendency to form large aggregates, whereas the latter approaches often generate high nuclearity clusters that are difficult to predict in advance. There has also been a parallel increase in the number of higher nuclearity polymanganese aggregates, some of which possess manganese ions of variable oxidation state, and display single molecule magnetic behaviour.[7] However homopentanuclear Mn^{II} clusters[8] are poorly represented and their chemistry virtually unknown, while mixed oxidation state Mn_5 systems are rare ($Mn^{III}_4Mn^{II}$,[9] $Mn^{II}_4Mn^{III}$[10]). This situation can perhaps be attributed to the apparent lack of a general strategy for the synthesis of high nuclearity clusters, although several groups are attempting to overcome the problem by using *e.g.* small nuclearity clusters as 'building blocks'.[11]

We have discovered that it is possible to combine the attributes of a bridging donor (alkoxide), and terminal donors in

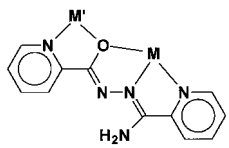

phaap

one 'planar' tetradentate ligand phaap which is capable of acting in a polynucleating, bridging capacity to aggregate several transition metal centres into an alkoxo-bridged cluster in an apparently controlled way. A number of square tetranuclear, homometallic (Ni^{II}, Co^{II}, Cu^{II}), and heterometallic ($Co^{II}_2Fe^{III}_2$, $Fe^{III}Cu^{II}_3$) complexes of phaap have been produced,[12] but with Mn^{II} the preferred arrangement is a pentanuclear cluster.

Reaction of phaap with $Mn(ClO_4)_2{\cdot}6H_2O$ in aqueous methanol produced an orange product (90% yield),‡ which gave orange crystals of $[Mn_5(phaap - H)_6](ClO_4)_4 \cdot 3.5MeOH{\cdot}H_2O$ **1** from ethanol suitable for structural analysis.§ A similar pentanuclear nitrate cluster complex $\{[Mn_5(phaap - H)_6](NO_3)_4{\cdot}5H_2O\}$¶ is produced by reaction of phaap with manganese(II) acetate in methanol followed by addition of $NaNO_3$.[12] The structure of the cation in **1** is unique (Fig. 1), with three pairs of almost parallel tetradentate ligands arranged around a pentanuclear, trigonal bipyramidal manganese(II) core, with each ligand filling five metal coordination sites and providing an alkoxide type bridge between adjacent pairs of pseudo-octahedral manganese atoms. The NH_2 ends of the ligands terminate at the equatorial manganese centers, and the O ends terminate at the apical centers, with each tetradentate (N_3O) ligand bridging each adjacent pair of metal centers along the six non-equatorial edges of the trigonal bipyramid. This arrangement provides an exact match between the coordination environment provided by the ligands and the coordination requirements of the five pseudo-octahedral metal centers. Within the Mn_5 core (Fig. 2) each apical metal atom is linked to an equatorial metal atom by an oxygen bridge, and each equatorial metal atom is linked to the apical pair of manganese atoms by two oxygen bridges. The equatorial manganese atoms are quite distorted, with *cis* and *trans* ligand angles as low as 70 and 140° respectively. The apical manganese centres have more normal pseudo-octahedral angles. Mn–N and Mn–O distances fall in the ranges 2.14–2.41 and 2.14–2.22 Å, respectively.

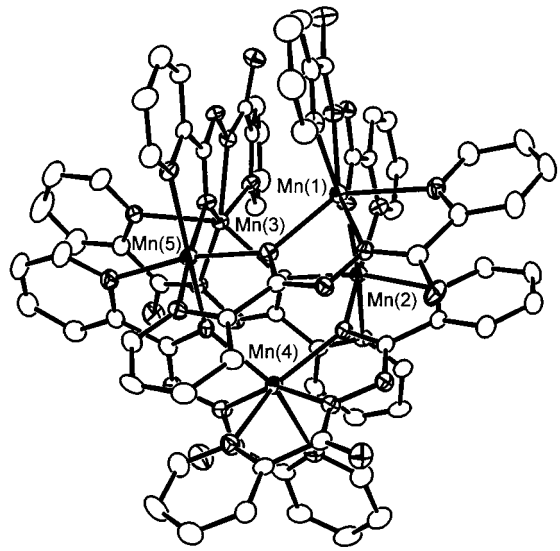

Fig. 1 Structural representation of the cation $[Mn_5(phaap - H)_6]^{4+}$ (40% probability thermal ellipsoids). Mn(1)–Mn(2) 3.9474(14), Mn(1)–Mn(5) 3.9630(12), Mn(3)–Mn(5) 3.9208(14), Mn(4)–Mn(5) 3.9059(13), Mn(2)–Mn(3) 3.9116(12), Mn(2)–Mn(4) 3.9190(13), Mn–N 2.144–2.403, Mn–O 2.140–2.218 Å.

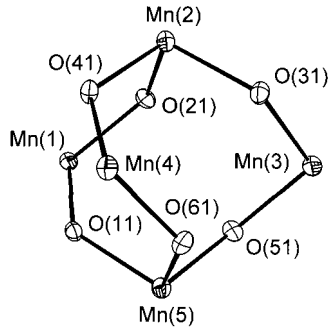

Fig. 2 Structure of the trigonal-bipyramidal core in $[Mn_5(phaap - H)_6]^{4+}$.

Adjacent Mn···Mn separations fall in the range 3.90–3.97 Å, with Mn–O–Mn angles in the range 128–131°. Within each ligand N–N distances average 1.399 Å, indicating single bond character, while average C–O and C–$N_{diazine}$ distances of 1.311 and 1.297 Å, respectively, indicate some charge delocalization within each N–C–O framework.

Variable temperature magnetic susceptibility measurements were carried out on a powdered sample of **1** in the temperature range 5–300 K.‖ Magnetic moments (per mole) drop smoothly from 13.4 μ_B at 296 K to 5.8 μ_B at 5 K, indicating the presence of antiferromagnetic coupling within the pentanuclear manganese(II) core, and the likelihood of an $S = 5/2$ ground state. This is consistent with the presence of oxygen bridges between the manganese(II) centres. An evaluation of the exchange coupling will be described elsewhere.

Electrochemical studies carried out in acetonitrile (1.0 mM, 0.1 M NEt_4ClO_4; Pt working electrode, Pt counter electrode, SSCE reference electrode) revealed three sequential, reversible, one electron waves (cyclic voltammetry; $\Delta E_p = \approx 90$ mV for each wave, and remains essentially constant from 100–1000 mV s^{-1}) in the range 0.6–1.0 V (Fig. 3), with equal current heights (coulometry at 1.1 V required 3.0 equivalents of charge for full oxidation to a brown colored solution, and with the potential set at 0.5 V after oxidation 3.0 equivalents of charge were required for full reduction to the original yellow orange colored solution) corresponding to the formation of a Mn^{II}_2-Mn^{III}_3 species. The Mn^{III} sites are assumed to be those in the equatorial plane. An irreversible wave at $E_{1/2} = 1.5$ V, similar to an irreversible wave observed in an acetonitrile solution of the zinc perchlorate complex, is associated with ligand oxidation. No EPR signal (X band) was observed for the $Mn^{II}_2Mn^{III}_3$ solution at ambient temperature, but in the UV–VIS spectrum an intense band appears at 937 nm ($\varepsilon = 720$ dm^3 mol^{-1} cm^{-1}), which is absent in the spectrum of **1**. On prolonged standing the spectrum reverts to that of the Mn^{II}_5 species.

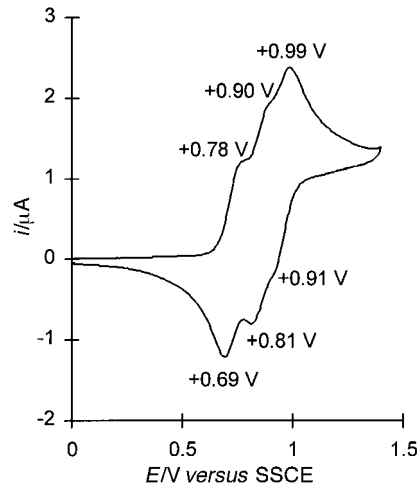

Fig. 3 Cyclic voltammetry for $[Mn_5(phaap - H)_6](ClO_4)_4$ in acetonitrile (1.0 mM, 0.1 M NEt_4ClO_4; Pt working electrode, Pt counter electrode, SSCE reference electrode; BAS CV27 Voltammograph; 100 mV s^{-1}).

The aggregation of five six-coordinate manganese(II) centres (thirty coordination positions) into an alkoxo-bridged, trigonal bipyramidal cluster by the six phaap ligands (thirty donor atoms) can be regarded as directed synthesis followed by self assembly, where the coordination site arrangement presented by the ligands matches exactly the coordination algorithm of the five metals. The fact that this geometrical arrangement seems to be unique for Mn^{II} may arise from the coordination flexibility of this metal ion due to its high spin d^5 electron configuration and zero crystal field stabilization energy.

This research work was supported by NSERC (Natural Sciences and Engineering Research Council of Canada).

Notes and references

† Present address; University of Winnipeg, Winnipeg, MB, Canada R3B 2E9.

‡ Ligand phaap (0.241 g, 1.00 mmol) was added to a hot solution of $Mn(ClO_4)_2·6H_2O$ (0.362 g, 1.00 mmol) in methanol–water (4 : 1) and the mixture stirred for 30 min, resulting in the formation of an orange precipitate. Found (vacuum dried recrystallized sample): C, 40.81; H, 2.93; N, 19.83. Calc. for $Mn_5(C_{12}H_{10}N_5O)_6(ClO_4)_4$ **1**: C, 40.91; H, 2.86; N, 19.88. IR (Nujol mull, cm^{-1}): ν(NH) 3441, 3336 ; ν(CN) 1649; $\nu(ClO)_4$ 1087, 620. UV–VIS. (Nujol mull): 541 nm (sh), 426 (sh): (MeCN) 579 nm ($\varepsilon = 63$ dm^3 mol^{-1} cm^{-1}). $\mu_{RT} = 5.8$ μ_B.

§ *Crystal data* for $C_{75.5}H_{76}Cl_4N_{30}Mn_5O_{26.5}$ **1**; $M = 2248.17$, triclinic, space group $P\bar{1}$, $a = 13.3249(7)$, $b = 18.8617(9)$, $c = 20.9513(10)$ Å, $\alpha = 85.3696(9)$, $\beta = 74.1679(10)$, $\gamma = 74.3330(9)°$, $V = 4877.6(4)$ Å^3, $\lambda = 0.71073$ Å, $Z = 2$, $D_c = 1.531$ g cm^{-3}, $T = 193(2)$ K, orange plate (0.10 × 0.20 × 0.40 mm), $\mu = 0.828$ mm^{-1}. Data were collected using a Siemens Smart three-circle diffractometer, equipped with a CCD area detector using graphite-monochromatized Mo-Kα X-radiation, and with an LT-II low temperature device. Diffracted data were corrected for absorption using the SADABS program. (G. M. Sheldrick, SADABS. Empirical Absorption Correction Program. University of Göttingen: Göttingen, Germany, 1996). SHELXTL (G. M. Sheldrick, SHELXTL 5.04/VMS, An integrated system for solving, refining and displaying crystal structures from diffraction data. Siemens Analytical X-ray Instruments Inc., Madison, WI) was used for the structure solution and the refinement based on F^2. All the non-hydrogen atoms were refined anisotropically. Hydrogen atoms were fixed at idealized positions with isotropic U values set 1.2 × U (atom connected), and not refined. H atoms on one badly disordered methanol were not included. For 1260 parameters $R1 = 0.0637$, $wR2 = 0.1473$, for 11531 unique reflections with $I > 2.0\sigma(I)$ (12481 independent reflections), for 2θ in the range 2.02–46.0° (GOF = 1.085). CCDC 182/1142. See http://www.rsc.org/suppdata/cc/1999/347/ for crystallographic files in .cif format.

¶ The analogous nitrate complex has comparable pentanuclear core dimensions [$a = 17.968(7)$, $b = 20.444(8)$, $c = 13.429(8)$ Å, $\alpha = 108.67(4)$, $\beta = 102.71(4)$, $\gamma = 84.60(3)°$, $V = 4557(4)$ Å^3, $Z = 2$, space group $P\bar{1}$, $R = 0.076$, $R_w = 0.091$ (Rigaku AFC6S); Mn···Mn 3.91–4.01 Å, Mn–O–Mn 128–131°].

‖ SQUID magnetometer (Quantum Design MPMS5S) with a field of 2000 Oe. Diamagnetic corrections for the sample holder and with sample were applied.

1 V. McKee, *Adv. Inorg. Chem.*, 1993, **40**, 323 and references therein.
2 R. Hage, *Recl. Trav. Chim. Pays-Bas*, 1996, **115**, 385.
3 G. Christou, *Acc. Chem. Res.*, 1989, **22**, 328.
4 V. L. Pecoraro, *Photochem. Photobiol.*, 1988, **48**, 249.
5 G. Christou, *Magnetism: A Supramolecular Function*,. ed. O. Kahn, Kluwer, Dordrecht, 1996, p. 383.
6 S. Parsons and R. E. P. Winpenny, *Acc. Chem. Res.*, 1997, **30**, 89.
7 A. Caneschi, D. Gatteschi and R. Sessoli, *J. Chem. Soc., Dalton Trans.*, 1997, 3963.
8 S. Brooker, V. McKee and T. Metcalfe, *Inorg. Chim. Acta*, 1996, **246**, 171.
9 M. S. Lah and V. L. Pecoraro, *J. Am. Chem. Soc.* ,1989, **111**, 7258.
10 R. A. Reynolds III and D. Coucouvanis, *Inorg. Chem.*, 1998, **37**, 170.
11 E. Libby, K. Folting, C. J. Huffman, J. C. Huffman and G. Christou, *Inorg. Chem.*, 1993, **32**, 2549.
12 C. J. Matthews, Z. Xu, L. Zhao, D. O. Miller and L. K. Thompson, unpublished results.

Communication 8/08970A

Rationalisation of the IR stretching frequencies of Brønsted acid centres in microporous solids

Dewi W. Lewis*[a] and German Sastre[b]

[a] *Department of Chemistry, University College London, 20 Gordon St., London, UK WC1H 0AJ. E-mail: d.w.lewis@ucl.ac.uk*

[b] *Instituto de Tecnologia Quimica UPV-CSIC, Universidad Politecnica de Valencia, Av. Los Naranjos s/n, 46022 Valencia, Spain*

Received (in Cambridge, UK) 7th December 1998, Accepted 15th January 1999

The relative position of the O–H stretching frequency of Brønsted acid sites in microporous solids is found to be correlated with the gradient norm of the electrostatic potential and, unlike previous attempts to provide a unified picture of the vibrational properties in such solids, the correlation is found for all structural and compositional variants studied to date.

Both aluminosilicate and aluminophosphate-based crystalline microporous solids can be prepared so that they possess acidic properties, rendering them suitable as solid acid catalysts. The predominant acid function in such materials is a Brønsted acid centre characterised by a protonated oxygen bridging two tetrahedrally coordinated atoms, T–O(H)–T′, where T is typically Si, Al, P. The relative acidity of different centres is typically estimated from the IR vibrational frequency of the hydroxyl bond, ν(O–H) and, more realistically, through the shift in this frequency on the sorption of small probe molecules.[1] Over the years, a number of attempts have been made to provide a rationalisation of the relative position of the stretching frequency of the Brønsted hydroxyl, ν(O–H), with the use of Sanderson electronegativity[2] being the most successful. However, this approach is found only to be valid for low concentrations of acid sites when the acid centres can be considered homogeneous and cannot, therefore, be applicable in the case of either low Si/Al zeolites,[3] or for SAPO materials, where Si-islands can form. Furthermore, the electronegativity is dependant only on composition[2] and hence differences in acidity between different structures with the same composition cannot be accounted for. Deviations are also found once acid sites are considered to be 'perturbed' as a consequence of being present in small cavities. In such cases, a $1/r^2$ relationship between the bathochromic shift observed and near neighbour oxygen distances in the same ring as the acid site has been proposed.[2] The latter observation has been taken by many authors as suggesting that the shift is proportional to the size of the cavity in which the proton vibrates and have assigned IR bands based on this assumption alone, without any consideration of the local environment not part of the immediate cavity. However, no general descriptor or rationalisation has been suggested which is consistent regardless of material structure and composition. Furthermore, there exists little theoretical evaluation of the correlations described above.

We have applied standard lattice energy minimisation and Mott–Littleton methodologies[4] to determine the equilibrium geometries of acid sites in a variety of structures and compositions of both aluminosilicates and silicoaluminophosphates and subsequently used a lattice dynamics approach to calculate the vibrational properties; the GULP code[5] was used throughout. The model consists of formally charged ions which also interact through short-range interatomic potentials (two- and three-body terms) coupled with a shell model description of polarisation; the parameters used are those of Sanders *et al.*[6] and Gale and Henson,[7] with the hydroxyl model being a modification of that derived for NaOH.[8,9] The model has been extensively demonstrated to reproduce experimental structures and also gives good agreement with experimental vibrational properties; although a -150 cm^{-1} correction for anharmonicity is required for O–H stretching frequencies.[9] The results presented here have been corrected thus unless otherwise stated.

The ability of the model to reproduce the experimentally observed vibrational properties is illustrated in Fig. 1. Not only are the relative shifts in ν(O–H) between the different structures reproduced but also the range of vibrations noted within a structure are in good agreement. Our calculations also reproduce the observed bands; for example, in SSZ-13 we calculate two bands at 3593 and 3575 cm^{-1} and in mordenite we observe two bands at 3600 and 3572 cm^{-1}, compared to 3603, 3579 and 3612, 3585 cm^{-1} respectively from experiment. Similarly, we calculate shifts to lower wavenumber with decreasing Si/Al in FAU.

Thus, together with previous studies, the data strongly suggests that this particular potential model is suitable for determining the relative positions of vibration frequencies across a broad range of microporous systems. But what properties of the structure correlate with the resulting vibrations? Do the calculated sites and geometries correlate with features such as cavity size discussed above?

We previously demonstrated that short-range interactions which manifest themselves as local geometry changes, particularly in the T–O–T′ bond angle are not adequate to identify variations in vibrational properties.[10] For example, identical T–O–T′ angles at different sites within the same structure can

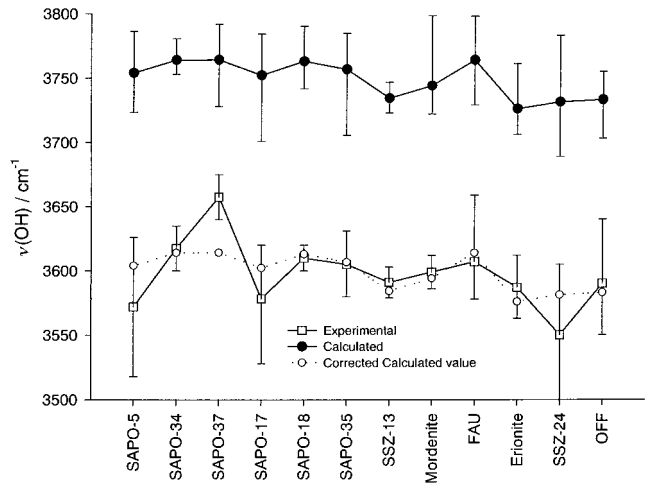

Fig. 1. Comparison of calculated (●) and experimental (□) ν(O–H) values. Shown as data points are the mean values of all noted signals; from experiment each peak position noted in published spectra has been included, whilst our calculations include all sites considered regardless of relative energy. The bars signify the minimum and maximum values found with no consideration of relative peak strength (in the case of experiment) or likely population (in the case of the calculated values). Once the anharmonicity correction term[9] of -150 cm^{-1} is applied to the calculated values (○), close agreement is found with the experimental value of ν(O–H).

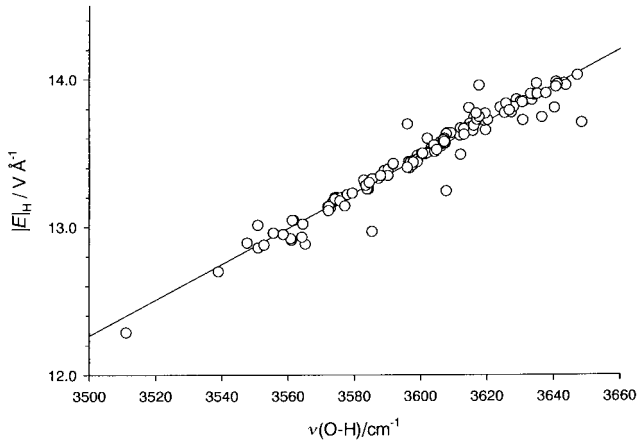

Fig. 2 Correlation of the gradient norm of the electrostatic potential at the proton ($|E|_H$) with the calculated stretching frequency (corrected for anharmonicity), ν(O–H). Acid centres considered include; isolated sites in high Si/Al aluminosilicates, sites in low Si/Al and in Si/Al = 1 aluminosilicates and isolated and island sites of SAPOs, in the structure types indicated in Fig. 1.

possess radically different values of ν(O–H). Instead, we consider (as have others) that the long-range Coulombic interactions are dominant and have previously observed a remarkable correlation between ν(O–H) and the gradient norm of the electrostatic potential at the proton, $|E|_H$, when considering the acidity of SAPOs.[10,11] Extending this idea to the range of structures now considered, it is clear from Fig. 2 that such a correlation appears quite general. We do not, however, observe a consistent correlation between ν(O–H) and the size of the cavity in which the proton is vibrating (Fig. 3) as is often claimed. Furthermore, we do not find that consideration of near neighbour O–H distances[2] can be used to identify likely shifts in

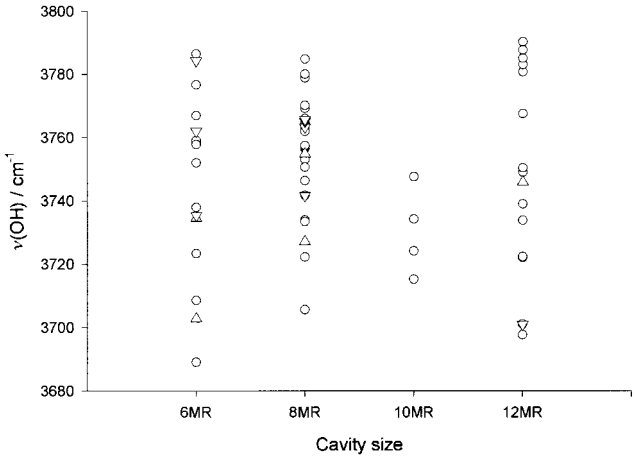

Fig. 3 Calculated vibrational frequencies and cavity size for isolated Brønsted acid sites. All data are presented as open circles whilst highlighted are the values for SAPO-17 (▽) and Offretite (△) which clearly show that cavity size alone cannot account for the relative position of ν(O–H); similar-sized cavities exhibit a wide range of values, whilst in some materials protons in large cavities have higher ν(O–H) than smaller cavities.

ν(O–H). For example, we observe a number of cases where we obtain almost identical ν(O–H) for protons vibrating within different sized cavities of the same material; in SAPO-17 we calculate that protons in both 8MR and 6MR sites vibrate at 3613–3616 cm^{-1}, whilst we also determined other sites in 6MR vibrating at a lower value of 3592 cm^{-1}.[11] In SAPO-35 we determined that three of the lowest frequency vibrations, at 3607 cm^{-1}, are present in 8MR whilst a proton in a 6MR gave a signal at 3616 cm^{-1},[11] which may have been expected to shift to lower values if the cavity size and reduction in nearest oxygen distances arguments held.[2] This apparent lack of correlation can be readily rationalised; consideration of the cavity size does not take into account the interactions between the proton and oxygens which are 'behind' the proton; and near-neighbour oxygens not directly in the same ring may be closer, and thus more influential, than those in the ring, particularly for larger cavities.

In summary therefore, we have identified that interatomic potential calculations are able to reproduce the vibrational properties of Brønsted acid sites in a wide structural and compositional range of microporous solids. We find that the relative position of ν(O–H) can be correlated with the gradient norm of the electrostatic potential at the proton, providing a direct correlation between the structure and the resulting vibration. Note, however, that simple consideration of the electrostatic potential of the framework 'hosting' the acid sites does not provide such insights; lattice relaxation is significant. Thus, we believe, these calculations can be used to verify and assign observed IR bands to specific acid sites in such structures. Furthermore, they may indeed provide a unifying rationalisation of stretching frequencies in such materials. Current work is focused on understanding further the correlation with electrostatic potential and the contribution of the electrostatic field to proton transfer.

We thank the Instituto de Tecnologia Quimica for a postdoctoral research grant (G. S.) and the Royal Society for further funding (D. W. L.). We also thank Dr J. D. Gale for many useful discussions.

Notes and references

1 A. Zecchina and C. O. Areán, *Chem. Soc. Rev.*, 1996, **25**, 187.
2 P. A. Jacobs and W. J. Mortier, *Zeolites*, 1982, **2**, 226.
3 J. Dwyer, F. R. Fitch and E. E. Nkang, *J. Phys. Chem.*, 1983, **87**, 5402.
4 *Computer Simulation of Solids*, ed. C. R. A. Catlow and W. C. Mackrodt, Spinger-Verlag, Berlin 1982.
5 J. D. Gale, *J. Chem. Soc., Faraday Trans.*, 1997, **93**, 629.
6 M. J. Sanders, M. Leslie and C. R. A. Catlow, *J. Chem. Soc., Chem. Commun.*, 1984, 1271.
7 J. D. Gale and N. J. Henson, *J. Chem. Soc., Faraday Trans.*, 1994, **90**, 3175.
8 P. Saul, C. R. A. Catlow and J. Kendrick, *Philos. Mag. B*, 1985, **51**, 107.
9 K.-P. Schröder, J. Sauer, M. Leslie, C. R. A. Catlow and J. M. Thomas, *Chem. Phys. Lett.*, 1992, **188**, 320.
10 G. Sastre and D. W. Lewis, *J. Chem. Soc., Faraday Trans.*, 1998, **94**, 3049.
11 G. Sastre and D. W. Lewis, *Proc. 12th International Zeolites Conference*, Baltimore MRS, in press.

Communication 8/09509D

Evidence for a ruthenium dihydride species as the active catalyst in the $RuCl_2(PPh_3)$-catalyzed hydrogen transfer reaction in the presence of base

Attila Aranyos,[a] Gábor Csjernyik,[a] Kálmán J. Szabó*[b] and Jan-E. Bäckvall*[b]

[a] *Department of Organic Chemistry, University of Uppsala, Box 531, SE-751 21 Uppsala, Sweden*
[b] *Department of Organic Chemistry, Arrhenius Laboratory, Stockholm University, SE-106 91 Stockholm, Sweden. E-mail: kalman@organ.su.se; jeb@organ.su.se*

Received (in Cambridge, UK) 26th November 1998, Accepted 8th January 1999

The role of the base in $RuCl_2(PPh_3)_3$-catalyzed hydrogen transfer reactions is to generate a highly active $RuH_2(PPh_3)_3$ catalyst from the dichloride *via* two consecutive alkoxide displacement–β-elimination sequences.

In 1991 we reported on a dramatic rate acceleration in the $RuCl_2(PPh_3)_3$-catalyzed transfer-hydrogenation of ketones upon addition of a catalytic amount of base.[1] The accelerating effect of the base was in the order of 10^3–10^4, and this provided a viable procedure for transfer hydrogenation. This remarkable effect was subsequently extended to other hydrogen transfer reactions,[1b] and by using it in the reversed direction, procedures for ruthenium-catalyzed Oppenauer oxidation were developed.[2] Further developments of the ruthenium-catalyzed transfer hydrogenations[3,4] into enantioselective versions have been recently realized by several groups.[5–10]

The effect of base in the iridium-catalyzed[10b–11] transfer hydrogenation has also been observed, but the role of base has remained unclear.[12] In our previous work on the use of $RuCl_2(PPh_3)_3$ **1** as a catalyst we proposed that a ruthenium alkoxide is formed with a subsequent β-elimination[13] to give a ketone and $Ru(H)Cl(PPh_3)_3$ **2**. The latter was proposed to act as the active catalyst. We have now studied the mechanism of this reaction and found that formation of a ruthenium dihydride species is responsible for the dramatic rate acceleration.

The reaction of $RuCl_2(PPh_3)_3$ **1** with isopropanol in the presence of base was studied by ^1H NMR spectroscopy with the aim of detecting complexes, which are possible active catalytic intermediates in transfer hydrogenation reactions. Treatment of $RuCl_2(PPh_3)_3$ with isopropanol and KOH at room temperature under argon gave a doublet of a triplet at δ −10.15 (J_{PH} 35.2, 42.2 Hz) and a broad singlet at δ −7.07 in an integral ratio of 3 : 1.[14] According to literature data the multiplet at δ −10.15 was assigned as $RuH_2(PPh_3)_3$ **3′**[15] and the singlet at δ −7.07 as $Ru(H_2)H_2(PPh_3)_3$.[16] Thus, the mole ratio between the complexes is 6 : 1. To further establish the assignments, reference samples of $RuH_2(PPh_3)_4$ **3**[17] and $Ru(H_2)H_2(PPh_3)_3$[16] were prepared according to literature procedures. Addition of **3** to the reaction sample increased the multiplet at δ −10.15. The doublet of triplet coupling pattern and the presence of free PPh_3 according to ^{31}P NMR clearly indicate that in solution $RuH_2(PPh_3)_4$ **3** dissociates a phosphine to give $RuH_2(PPh_3)_3$ **3′**. Also, addition of $Ru(H_2)H_2(PPh_3)_3$ to the reaction sample increased the broad singlet at δ −7.07. Furthermore, the ^{31}P NMR of the reaction sample and the reference samples established the assignments made. It is not yet clear which role $Ru(H_2)H_2(PPh_3)_3$ plays in the catalytic reaction but it is known[15a,18] that in the presence of ketones $Ru(H_2)H_2(PPh_3)_3$ easily dissociates its H_2 ligand. This will generate the active catalyst $RuH_2(PPh_3)_3$ **3′** and also lead to some 'hydrogen-leakage' in the hydrogen transfer reaction.[19]

The observation that a ruthenium dihydride complex is formed when $RuCl_2(PPh_3)_3$ reacts with isopropanol in the presence of base has interesting mechanistic implications for $RuCl_2(PPh_3)_3$-catalyzed hydrogen transfer reactions. To obtain further evidence for a dihydride species as the active catalyst, we studied the catalytic hydrogen transfer between cyclopentanol and acetone employing three different catalyst sources: $RuCl_2(PPh_3)_3$ **1**, $Ru(H)Cl(PPh_3)_3$ **2**,[20] and $RuH_2(PPh_3)_4$ **3**[17] [Fig. 1, eqn. (1)].

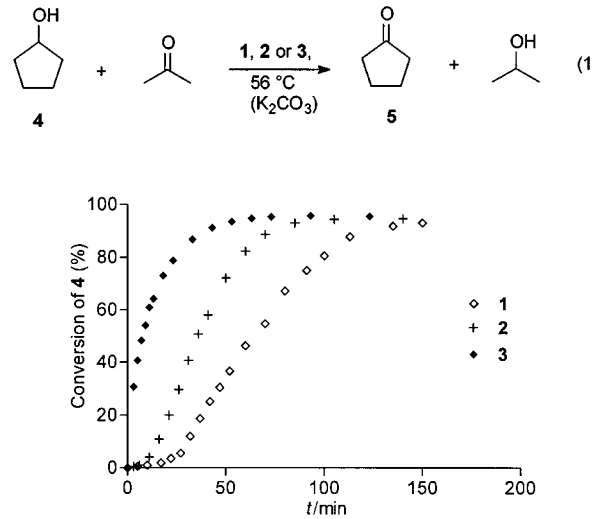

Fig. 1 Ruthenium-catalyzed hydrogen transfer from cyclopentanol to acetone with $RuCl_2(PPh_3)_3$ **1**, $Ru(H)Cl(PPh_3)_3$ **2**, or $RuH_2(PPh_3)_4$ **3** at 56 °C in the presence of K_2CO_3. In each experiment 0.2 mol% of ruthenium catalyst was employed.

The conversion of **4** to **5** was monitored by GC. Significant differences were observed in the reaction rates for the three catalyst precursors. Thus, there were observable induction periods for the complexes **1** and **2**, with the longest induction period for **1**. For the dihydride complex **3** there was a fast initial rate, without any sign of an induction period. Catalyst **3** showed identical reactivity also in the absence of base, whereas **1** and **2** were inactive under these conditions. The longer induction period for **1** compared to **2** is explained by eqns. (2) and (3). The two chlorides in **1** are removed in two consecutive alkoxide displacement–β-elimination sequences whereas for **2** only one such sequence is requried [eqn. (3)].[21,22]

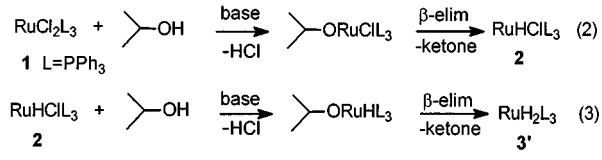

The mechanism for the ruthenium-catalyzed hydrogen transfer is depicted in Scheme 1. It is interesting that once the ruthenium dihydride has been generated the base is no longer required, which was confirmed by experiments (*vide supra*).

Additional support for a dihydride as the active catalyst was obtained from stoichiometric reactions of **2** and **3′** with acetone in toluene-d_8 [eqns. (4) and (5)] monitored by ^1H NMR. Thus, it was found that monohydride **2** did not react with acetone at

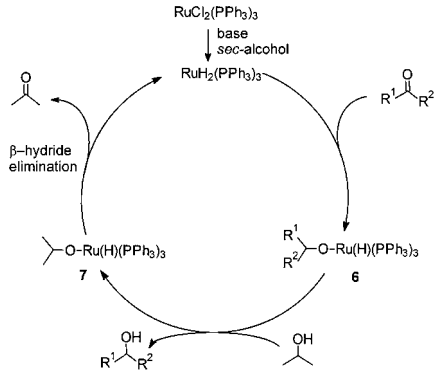

Scheme 1 Mechanism of $RuCl_2(PPh_3)_3$-catalyzed hydrogen transfer.

56 °C, whereas the dihydride **3′** (generated from **3** *in situ*) rapidly ($t_{\frac{1}{2}} \approx 5$ min) reduced acetone to isopropanol. This rules out **2** as the active catalyst. In the catalytic system (Scheme 1), where there is a large excess of alcohol, it is likely that proton transfer from isopropanol to the alkoxy group in **6** takes place. This leads to an exchange of alkoxy groups on ruthenium to give **7**. In eqn. (5) there is no excess of alcohol and a formal reductive elimination to give a Ru(0) species would predominate.

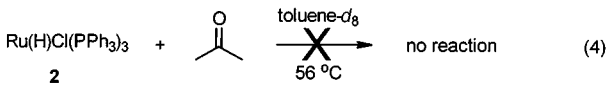

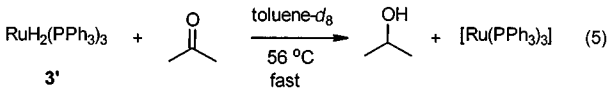

Apparently, exchange of the chloride ligand of **2** to a hydride **3′** leads to dramatic changes in the electronic structure of the ruthenium catalyst, which facilitates the hydride addition to a ketone. Preliminary theoretical calculations on the formaldehyde complex **8** and the corresponding alkoxy adduct **9** for ruthenium monohydride (X = Cl) and ruthenium dihydride (X = H) were performed at the DFT/DZ + P level of theory.[23] The calculations show that for the monohydride **8** (X = Cl) the reaction is thermodynamically unfavored by 5.3 kcal mol^{-1} (Fig. 2). This implies that the alkoxy chloride **9** (X = Cl) is unstable and will undergo facile β-elimination to give the keto compound and the hydride.[24] In the case of the dihydride complex the equilibrium is slightly shifted toward adduct **9**, the free energy difference being about 1 kcal mol^{-1}.

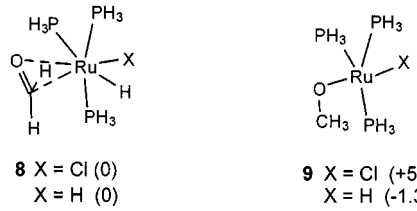

8 X = Cl (0)
X = H (0)

9 X = Cl (+5.3)
X = H (-1.3)

Fig. 2 Energies (kcal mol^{-1}) of structures **8** and **9** for dihydride (X = H) and monohydride (X = Cl).

In conclusion, the experimental results indicate that ruthenium dihydride $RuH_2(PPh_3)_3$ is the active catalyst in base-accelerated $RuCl_2(PPh_3)_3$-catalyzed hydrogen transfer reactions.[25] Furthermore, it is shown that the monohydride **2** is not the active catalyst. Theoretical calculations support the observation that a chlororuthenium monohydride is unreactive towards hydride addition to a keto group.

This work was supported by the Swedish Natural Science Research Council and the Parallelldatorcentrum, Stockholm.

Notes and references

1 (*a*) J. E. Bäckvall, R. L. Chowdhury and U. Karlsson, *J. Chem. Soc., Chem. Commun.*, 1991, 473; (*b*) G.-Z. Wang and J. E. Bäckvall, *J. Chem. Soc., Chem. Commun.*, 1992, 980.

2 G.-Z. Wang and J. E. Bäckvall, *J. Chem. Soc., Chem. Commun.*, 1992, 337; M. L. S. Almeida, M. Beller, G.-Z. Wang and J. E. Bäckvall, *Chem. Eur. J.*, 1996, **2**, 1533.

3 For other recent advancements on ruthenium-catalyzed transfer hydrogenations see: (*a*) H. Yang, M. Alvarez, N. Lugan and R. Mathieu, *J. Chem. Soc., Chem. Commun.*, 1995, 1721; (*b*) E. Mizushima, M. Yamaguchi and T. Yamagishi, *Chem. Lett.*, 1997, 237.

4 For reviews on hydrogen transfer reactions see: R. A. W. Johnstone, A. H. Wilby and I. D. Entwistle, *Chem. Rev.*, 1985, **85**, 129; P. A. Chaloner, M. A. Esterulas, F. Joo and L. A. Oro, *Homogeneous Hydrogenation*, Kluwer Academic Publishers, Dordrecht, The Netherlands, 1994, pp. 87–118; G. Zassinovich, G. Mestroni and S. Gladiali, *Chem. Rev.*, 1992, **92**, 1051; J. E. Bäckvall, R. L. Chowdhury, U. Karlsson and G.-Z. Wang, in *Perspective in Coordination Chemistry*, ed. A. F. Williams, C. Floriani and A. E. Merbach, *Verlag Helvetica Chimica Acta*, Basel, 1992, pp. 463–486.

5 J. P. Genêt, V. Ratovelomanana-Vidal and C. Pinel, *Synlett*, 1993, 478; P. Krasik and H. Alper, *Tetrahedron*, 1994, **50**, 4347.

6 S. Hashiguchi, A. Fujii, J. Takehera, T. Ikariya and R. Noyori, *J. Am. Chem. Soc.*, 1995, **117**, 7562; R. Noyori and S. Hashiguchi, *Acc. Chem. Res.*, 1997, **30**, 97.

7 T. Langer and G. Helmchen, *Tetrahedron Lett.*, 1996, **37**, 1381.

8 T. Sammakia and E. L. Stangeland, *J. Org. Chem.*, 1997, **62**, 6104.

9 (*a*) M. Palmer, T. Walsgrove and M. Wills, *J. Org. Chem.*, 1997, **62**, 5226; (*b*) K. J. Haack, S. Hashiguchi, A. Fujii, J. Takehera, T. Ikariya and R. Noyori, *Angew. Chem., Int. Ed. Engl.*, 1997, **36**, 285; (*c*) F. Touchard, P. Gamez, F. Fache and M. Lemaire, *Tetrahedron Lett.*, 1997, **38**, 2275; (*d*) D. A. Alonso, D. Guijarro, P. Pinho, O. Temme and P. G. Andersson, *J. Org. Chem.*, 1998, **63**, 2749 and references therein.

10 For other metal systems see: (*a*) D. Müller, G. Umbricht, B. Weber and A. Pfaltz, *Helv. Chim. Acta.*, 1991, **74**, 232; (*b*) S. Gladiali, G. Chelucci, G. Chessa, G. Delogu and F. Soccolini, *J. Organomet. Chem.*, 1987, **327**, C15; (*c*) P. Kvintovics, B. R. James and B. Heil, *J. Chem. Soc., Chem. Commun.*, 1986, 1810.

11 R. Uson, L. A. Oro, R. Sariego and M. A. Esteruelas, *J. Organomet. Chem.*, 1981, **214**, 399.

12 In a recent publication Noyori[9b] discussed the role of base in ruthenium-catalyzed hydrogen transfer and proposed a monohydride amide complex as the reactive intermediate (catalyst) in his system.

13 For related β-hydride elimination from iridium alkoxide complexes see: O. Blum and D. Milstein, *J. Am. Chem. Soc.*, 1995, **117**, 4582.

14 The ^1H NMR spectrum was recorded in benzene-d_6 after removal of isopropanol.

15 (*a*) D. E. Linn and J. Halpern, *J. Am. Chem. Soc.*, 1987, **109**, 2969; (*b*) R. U. Kirss, T. C. Eisenschmid and R. Eisenberg, *J. Am. Chem. Soc.*, 1988, **110**, 8564.

16 L. S. Van Der Sluys, G. J. Kubas and K. G. Caulton, *Organometallics*, 1991, **10**, 1033.

17 R. O. Harris, N. K. Hota, L. Sadavoy and J. M. C. Yuen, *J. Organomet. Chem.*, 1968, **54**, 259; J. J. Levison and S. D. Robinson, *J. Chem. Soc. A*, 1970, 2947.

18 Y. Lin and Y. Zhou, *J. Organomet. Chem.*, 1990, **381**, 135.

19 D. J. Cole-Hamilton and D. Morton, *J. Chem. Soc., Chem. Commun.*, 1988, 1154; D. Morton, D. J. Cole-Hamilton, I. D. Utuk, M. Paneque-Sosa and M. Lopez-Poveda, *J. Chem. Soc., Dalton Trans.*, 1989, 489.

20 (*a*) P. S. Hallman, B. R. McGarvey and G. Wilkinson, *J. Chem. Soc. A*, 1968, 3143; (*b*) B. N. Chaudret, D. J. Cole-Hamilton, R. S. Nohr and G. Wilkinson, *J. Chem. Soc., Dalton Trans.*, 1977, 1546.

21 The conversion of Ru–Cl into Ru–H on reaction of $[RuCl_2(COD)]_x$ with base and a secondary alcohol to give dihydride complexes was recently reported: S. P. Nolan, T. R. Belderrain and R. H. Grubbs, *Organometallics*, 1997, **16**, 5569; see also ref. 20*b*.

22 It has been proposed that a dihydride is formed from $RuHCl(CO)(P^iPr_3)_2$ (analogous to **2**) and isopropanol in the presence of KOH: M. A. Esteruelas, E. Sola, L. A. Oro, H. Werner and U. Meyer, *J. Mol. Catal.*, 1988, **45**, 1.

23 (*a*) The theoretical calculations were carried out by using a Becke-type[23b] three parameter hybrid-functional (B3PW91) in connection with the LANL2DZ basis set augmented with d-polarization functions on the C, O and P atoms and p-polarization functions on Ru-*H* and CH_2O atoms; (*b*) A. D. Becke, *J. Chem. Phys.*, 1993, **98**, 5648.

24 For related calculations (Hartree–Fock) on **8** (X = Cl) and **9** (X = Cl) see: H. Itagaki, N. Koga, K. Morokuma and Y. Saito, *Organometallics*, 1993, **12**, 1648.

25 Recently, Mizushima *et al.*[3b] reported results, which suggest that ruthenium dihydride complex **3**, is the active catalyst in hydrogen transfer reactions; see also ref. 18.

Communication 8/09236B

'Inverse crown ether' complexes: extension to potassium through the synthesis of $[\{[(Me_3Si)_2N]_4K_2Mg_2(O_2)\}_\infty]$, a peroxo-centred macrocycle linked into infinite chains by intermolecular $K\cdots CH_3(SiMe_2)$ interactions

Alan R. Kennedy,[a] Robert E. Mulvey,*[a] Colin L. Raston,[b] Brett A. Roberts[a] and René B. Rowlings[a]

[a] *Department of Pure and Applied Chemistry, University of Strathclyde, Glasgow, UK G1 1XL. E-mail: r.e.mulvey@strath.ac.uk*

[b] *Department of Chemistry, Monash University, Clayton, Victoria, 3168, Australia*

Received (in Cambridge, UK) 11th December 1998, Accepted 18th January 1999

The title compound represents the first potassium example of a novel class of amide-supported heterobimetallic macrocycle having a dicationic $(N_4K_2Mg_2)^{2+}$ octagonal ring framework surrounding a dianionic $(O_2)^{2-}$ core.

In the conventional host–guest chemistry of crown ether complexes,[1] the series of oxygen centres within the macrocyclic ligand host provide an electron-rich cavity tailor-made for the entertainment of electron-poor metal cation guests. Recently, however, we have described a remarkable new type of macrocyclic complex which conversely has a series of metal cations within its cyclic ring framework and an oxygen anion within the cavity of the ring.[2] Their generalised structural formula is depicted in **1**. Best regarded as 'inverse crown ether'

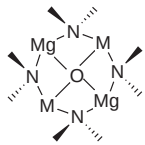

1

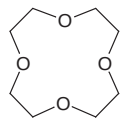

[12]crown-4

complexes, their ring motifs in containing four Lewis acidic metal sites can be thought of in effect as the inverse of [12]crown-4 with its four Lewis basic ligand sites. Preceding this work, the collection of [12]mercuracarborand-4 complexes developed by Hawthorne and coworkers[3] have been similarly interpreted as 'anti-crown', charge-reversed analogues of [12]crown-4, but, in this case, no oxygen anions are involved; instead the softer acid Hg centres bind anions such as Cl^-, Br^-, I^- or *closo*-$B_{10}H_{10}^{2-}$. Returning to the inverse crown ether complexes, three have been reported previously. Two are dilithium-dimagnesium amides, $[\{(Me_3Si)_2N\}_4Li_2Mg_2(O_2)_x(O)_y]$[4] **2** and $[(Me_2CCH_2CH_2CH_2Me_2CN)_4Li_2Mg_2(O)]$[2] **3**; while the third is a disodium analogue $[\{(Me_3Si)_2N\}_4Na_2Mg_2(O_2)_x(O)_y]$[2] **4**. Here, in this paper, we extend this novel class of heterobimetallic macrocyclic complex to the next member of the alkali metal family, potassium, through the synthesis and structural characterisation of the dipotassium-dimagnesium amide $[\{[(Me_3Si)_2N]_4K_2Mg_2(O_2)\}_\infty]$ **5**. Though also based on an eight-membered $(N_4M_2Mg_2)$ ring system, the crystal structure of **5** differs in two major respects from those of its lithium and sodium congeners: first, the $(N_4K_2Mg_2)$ ring is not molecular, but polymerises through intermolecular $K\bullet\bullet\bullet CH_3(SiMe_2)$ interactions; second, throughout the bulk polymer the cavities of the 2+ charged rings are filled exclusively by peroxo (O_2^{2-}) dianions, *i.e.* no oxide (O^{2-}) ions are present.

In the fortuitous preparation of the first inverse crown ether complex, we concluded that mixtures of butyllithium, dibutylmagnesium and the sterically demanding amine hexamethyldisilazane were highly efficient oxygen scavengers.[4] Thus, any oxygen contaminant available in solution would be readily sequestered by the reaction system and then precipitated in the form of the stable peroxo–oxo centred mixed-metal macrocycle **2**. With this insight we subsequently deliberately added molecular oxygen to other reaction solutions of this type. This strategy was used in the preparations of **3** and **4**. The preparation of **5** essentially mimicked that of its lighter alkali metal counterparts. Like **2**, it was initially obtained unexpectedly (in a low yield of 2%) by the reaction shown in eqn. (1): here, oxygen

$$\text{'BuK'} + Bu_2Mg + 3(Me_3Si)_2NH \xrightarrow{\text{trace of } O_2} {}^1/_x[\{(Me_3Si)_2N\}_4K_2Mg_2(O_2)] + \text{other products} \quad (1)$$

was not deliberately added to the solution; though, significantly, neither the amine reactant nor the solvents (hexane, heptane, *p*-xylene) were deoxygenated beforehand. Note also that the potassium reagent used was not pure butylpotassium, but rather the unrefined solid isolated from the metal–metal exchange reaction between butyllithium and potassium *tert*-butoxide.[5] Repeating the preparation in a Schlenk tube adapted with a calcium chloride drying tube at its inlet, gave substantially larger amounts of colourless, crystalline **5** (best yield to date, 23%).† While we attribute this improvement to the intentional introduction of atmospheric oxygen, the possibility that minute traces of moisture are involved cannot be completely dismissed. However, in a control experiment, following the same procedure carried out in eqn. (1), a stoichiometric amount of deoxygenated H_2O was additionally introduced to the reaction solution. A white solid precipitated out within a few minutes and would not redissolve on warming. The isolated solid exhibited distinct melting point characteristics from those of **5**;† even more significantly, its IR spectrum revealed the presence of a strong O–H band at 3695 cm^{-1} [characteristic of $Mg(OH)_2$] before the mull was exposed to air. Clearly this solid is not **5**.

The octagonal ring structure of **5** (Fig. 1)‡ consists of alternating nitrogen and metal atoms. Like metal atoms occupy transannular positions, and each one coordinates (side-on) to the O_2^{2-} ion in the core of the ring. These ring molecules are not discrete, but link through intermolecular $K\cdots CH_3(SiMe_2)$ interactions (one per K centre) to form one-dimensional infinite chains (Fig. 2) which propagate along the *a* direction. Selected bond lengths and bond angles are given in the legend to Fig. 1. The O–O bond length [1.583(1) Å] is close to that [1.541(9) Å] in the heptalithium-tetrarubidium mixed alkoxide peroxide $[\{(Bu^tOLi)_5(Bu^tORb)_4(Li_2O_2)\cdot 2TMEDA\}_\infty]$.[6] While the Mg centre engages this dianion in a symmetrical manner (Mg–O: mean, 2.012 Å; difference, 0.005 Å), the interaction with the K centre is lopsided (K–O: mean, 2.843 Å; difference, 0.121 Å). The extra atoms (from Me_3Si groups, see below) in the coordination sphere of the K centre may be a factor in this asymmetry. One might be inclined to explain the 100% peroxide incorporation within the ring cavity in terms of the 'soft' nature of potassium; but, the true explanation must be more profound as there is no regular pattern to the peroxide:

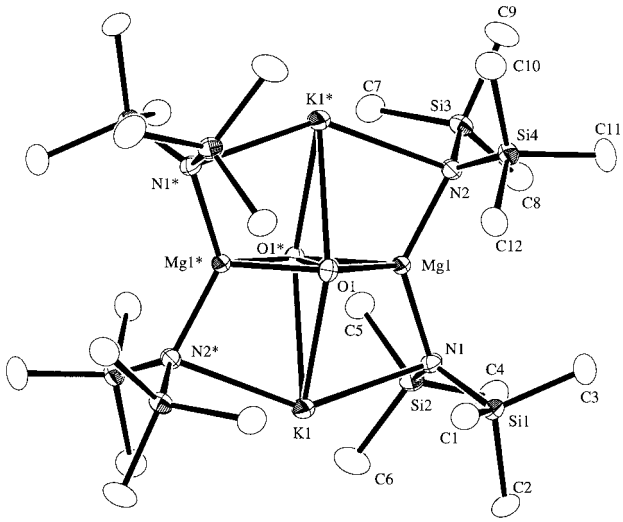

Fig. 1 Double asymmetric unit of **5**. Hydrogen atoms have been omitted for clarity. Selected bond lengths (Å) and bond angles (°): K1–O1 2.782(1), K1–O1* 2.903(1), K1–N1 2.855(1), K1–N2* 2.804(1), Mg1–O1 2.015(1), Mg1–O1* 2.010(1), Mg1–N1 2.044(1), Mg1–N2 2.043(1), K1–N1–Mg1 83.95(3), K1*–N2–Mg1 83.11(4). * $1 - x, y, z$.

oxide ratios found in **2**, **3** and **4** (*i.e.* 72 : 28, 0 : 100, 32 : 68 respectively). Clearly, the hard/moderately hard/soft demarcation normally associated with the Li/Na/K series is not the sole factor here. Kinetic influences must also be at work. The ($N_4K_2Mg_2$) ring in **5** is essentially planar [sum of endocyclic bond angles, 1074.6 *cf.* 1073.7° for the ($N_4Na_2Mg_2$) ring in **4**]. A salient feature running through the series of inverse crown ether complexes is that the Mg atoms are always displaced towards the centre of the ring as a result of strong Mg–O bonding. The magnitude of this displacement increases with increasing size of the alkali metal partner in the ring, as evidenced by the *endo*cyclic N–Mg–N bond angles in **2** [193.3° (approximate value owing to Li/Mg substitutional disorder in crystal)], **4** (218.4°) and **5** (227.8°). Likewise, the small Li cation in **2** and **3** is pulled towards the centre of the ring through strong Li–O bonding, resulting in endocyclic N–Li–N bond angles > 180°. Conversely, the heavier alkali metal cations in **4** and **5** occupy peripheral ring sites with endocyclic N–M–N

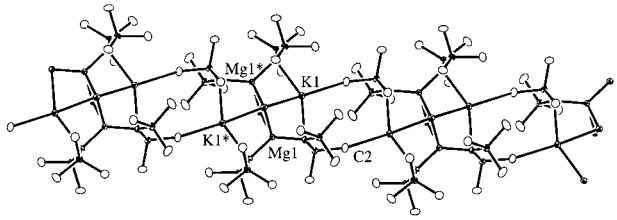

Fig. 2 View showing extended chain arrangement of **5**. Intermolecular K···$CH_3(SiMe_2)$ interactions are shown; intramolecular ones are omitted for clarity.

bond angles significantly < 180° [159.84(2)° in **4**, 142.44(3)° in **5**], reflecting longer, weaker Na–O/K–O bonding. In contrast, there is considerably less variation in the endocyclic M–N–Mg bond angles throughout the series [range: 76.58(7)–83.95(3)°]. The final feature of note in **5** is the short K···$CH_3(SiMe_2)$ contacts. Measuring 3.246(2) Å, the shortest of these are intermolecular ones (K1···C2*) which link the ($N_4K_2Mg_2$) rings together through near-linear K···C–Si units [angle, 157.29(7)°]. Interestingly, intermolecular Na···C–Si contacts of a similar length [3.275(2) Å] appear in **4**,[2] but these are normally accorded less significance when the smaller size of Na is taken into account (ionic radii: Na^+, 1.02 Å; K^+, 1.38 Å). However, the similar intermolecular contacts seen in **4** and **5** raises the question as to whether the former truly consists of discrete molecules. Intramolecular K···C–Si contacts [lengths: 3.317(2), 3.359(1) and 3.397(2) to C7, C1 and C6, respectively] also contribute to the bonding in **5**. These agostic-type interactions[7] are comparable to those in other recently reported potassium structures,[8] most pertinently in [{$(Me_3Si)_2NK$}$_2$] (shortest, 3.34 Å).[9]

We thank the EPSRC (for studentship to R. B. R.) and Monash University (for providing B. A. R. with a travel grant to allow him to work at Strathclyde).

Notes and references

† Satisfactory microanalyses have been obtained. **5** proved to be too insoluble in arene solvents for a useful, diagnostic ^{1}H NMR spectrum to be obtained. It starts to decompose at 80 °C and gradually darkens to a black solid at 140 °C. On the other hand, the white solid from the control reaction fails to melt below 300 °C and does not change colour.

‡ *Crystal data* for **5**: $C_{24}H_{72}K_2Mg_2N_4O_2Si_8$, M = 800.34, triclinic, space group $P\bar{1}$, a = 11.102(4), b = 12.907(6), c = 8.906(3) Å, α = 107.63(3), β = 100.47(3), γ = 96.34(4)°, U = 1177.3(9) Å^3, Z = 1, λ = 0.71069 Å, μ = 0.457 mm^{-1}, T = 123 K, R = 0.0229, R_w = 0.0404 for 5156 reflections with $I > 2\sigma(I)$. 5673 reflections measured with $2\theta < 55°$. Refinement on F, to convergence, with isotropic H atoms gave a maximum residual electron density of 0.323 e Å^{-3} . Program used Texsan. CCDC 182/1145. See http://www.rsc.org/suppdata/cc/1999/353/ for crystallographic files in .cif format.

1 G. Gokel, in *Crown Ethers and Cryptands*, The Royal Society of Chemistry, Cambridge, 1991.
2 A. R. Kennedy, R. E. Mulvey and R. B. Rowlings, *Angew. Chem.*, 1998, **110**, 3321; *Angew. Chem., Int. Ed. Engl.*, 1998, **37**, 3180.
3 X. Yang, C. B. Knobler, Z. Zheng and M. F. Hawthorne, *J. Am. Chem. Soc.*, 1994, **116**, 7142.
4 A. R. Kennedy, R. E. Mulvey and R. B. Rowlings, *J. Am. Chem. Soc.*, 1998, **120**, 7816.
5 L. Lochmann, J. Pospisil and D. Lim, *Tetrahedron Lett.*, 1966, 256.
6 W. Clegg, A. M. Drummond, R. E. Mulvey and S. T. Liddle, *Chem. Commun.*, 1998, 2391.
7 K. W. Klinkhammer, *Chem. Eur. J.*, 1997, **3**, 1418.
8 W. Clegg, S. Kleditzsch, R. E. Mulvey and P. O'Shaughnessy, *J. Organomet. Chem.*, 1998, **558**, 193.
9 K. F. Tesh, T. P. Hanusa and J. C. Huffman, *Inorg. Chem.*, 1990, **29**, 1584.

Communication 8/09681C

ChemComm

3-Methyl-α-himachalene is confirmed, and the relative stereochemistry defined, by synthesis as the sex pheromone of the sandfly *Lutzomyia longipalpis* from Jacobina, Brazil

J. Gordon C. Hamilton,[a] Antony M. Hooper,[b] Kenji Mori,[c] John A. Pickett*[b] and Satoshi Sano[c]

[a] *School of Life Sciences, University of Keele, Keele, Staffordshire, UK ST5 5BG*
[b] *IACR-Rothamsted, Harpenden, Hertfordshire, UK AL5 2JQ. E-mail: john.pickett@bbsrc.ac.uk*
[c] *Department of Chemistry, Science University of Tokyo, Kagurazaka 1-3, Shinjuku-ku, Tokyo 162-8601, Japan*

Received (in Cambridge, UK) 7th January 1999, Accepted 11th January 1999

The structure of the sex pheromone produced by the male sandfly *Lutzomyia longipalpis*, from the Jacobina region of Brazil, previously proposed tentatively as the novel homosesquiterpene 3-methyl-α-himachalene is confirmed by synthesis and biological activity; the relative stereochemistry is defined as 1*RS*,3*RS*,7*RS* by comparing the natural product with the four synthetic diastereoisomers.

The sandfly *Lutzomyia longipalpis* (Lutz and Neiva) (Diptera: Psychodidae) is the vector of the protozoan parasite *Leishmania chagasi* (Cunha and Chagas) (Kinetoplastida: Trypanosomatidae), the causative agent of visceral leishmaniasis in the New World. Male *L. longipalpis* release a sex pheromone from glands on the tergites of the abdomen[1] which is highly attractive to females.[2] The sex pheromone gland of *L. longipalpis* from Jacobina (Bahia State) in northeastern Brazil produces several compounds but only the principal volatile component is responsible for the attraction of females.[3] It was proposed, mostly on the basis of mass spectrometry of the natural product and of products of microchemical reactions, that the pheromone comprised the novel homosesquiterpene 3-methyl-α-himachelene.[4] The sex pheromones of other sympatric and allopatric populations of *L. longipalpis* are different;[5] for example, that from the Lapinha region of Brazil (Minas Gerais State) has been tentatively proposed as another novel sesquiterpene, 9-methylgermacrene-B.[6] The purpose of this work was to test the proposed structure for the Jacobina *L. longipalpis* sex pheromone by synthesis of 3-methyl-α-himachalene **1**.

The synthetic route adopted followed the intramolecular Diels–Alder methodology employed by Wenkert and Naemura[7] for α-himachalene and is described in Scheme 1. Diene **7** comprised a mixture of *E*/*Z* isomers (77 : 23–90 : 10) by ^{1}H NMR spectroscopy. The subsequent cyclisation of the keto enediene **8** in xylene under reflux gave a mixture of cyclic products, which could be separated by medium pressure liquid chromatography into enantiomeric pairs of diastereoisomers **9a**–**d**.† Final conversion to the diastereoisomeric 3-methyl-α-himachalenes **1a**–**d**‡ was achieved quantitatively using the Tebbe reagent. Assignment of structures **9a**–**d** was by correlation and two dimensional NOE spectroscopy (Fig. 1). Compounds **9a** and **9c** were designated as *cis*-fused by the ring junction protons showing a NOE to each other. The relative stereochemistry of the methyl group could be determined for **9c** by a NOE to the ring junction proton of C-1, a signal not seen for **9a**. The relative stereochemistries of the C-3 methyl group of *trans*-fused **9b** and **9d** were also elucidated by NOE experiments. A NOE was observed between the C-1 proton of **9b** and one of the C-6 methyl groups, while the *other* C-6 methyl group showed a NOE to the C-3 methyl, which therefore lies on the *opposite* face to the C-1 proton (Fig. 1). The structures of **1a**–**d** were inferred from **9a**–**d** and in comparison with NMR data for natural α-himachalene.[4] Mass spectra were obtained by GC-MS.§

Co-injection of natural product with the diastereoisomers, using high-resolution capillary GC on columns of different polarity (Table 1) gave peak enhancement only with diastereoisomer **1c**. In the case of chiral GC, only one enantiomer of **1c** enhanced the natural product peak. The ^{1}H NMR results reported,[6] although incomplete, showed good agreement with only those for structure **1c**. The mass spectrum for the natural product[6] was almost identical with that for **1c**, with greater differences from those for **1a**, **1b** and **1d**. All had a base peak at *m*/*z* 94, different from that for α-himachalene (*m*/*z* 93), which was suggested as likely when the earlier tentative structural prediction was made.[6] Bioassays¶ involving attraction of female *L. longipalpis* and conducted in a Y-tube olfactometer showed that only diastereoisomer **1c** and the natural pheromone extract were active and both showed high statistical significance. This was in agreement with the chromatographic and spectral data, giving the sex pheromone structure as (1*RS*,3*RS*,7*RS*)-3-methyl-α-himachalene, *i.e.* (1*RS*,3*RS*,7*RS*)-2-methylene-3,6,6,9-tetramethylbicyclo[5.4.0]undec-8-ene (**1c**). The *cis* stereochemistry of the natural product is analogous

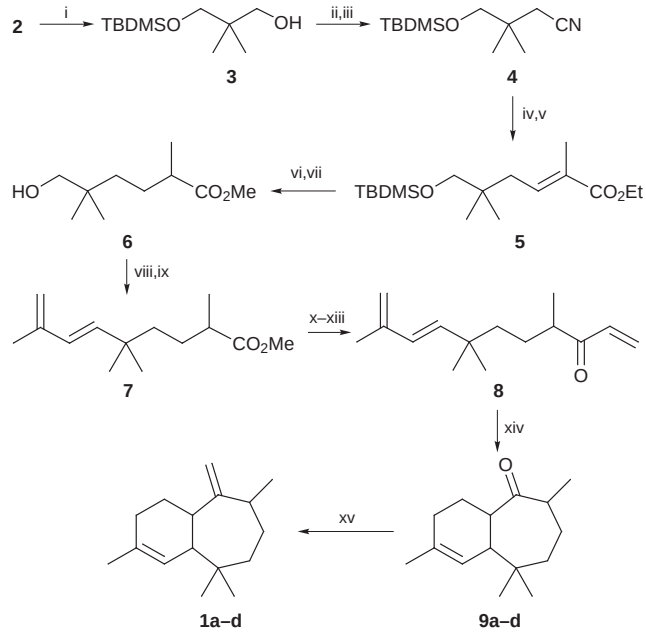

Scheme 1 *Reagents and conditions:* i, NaH (1.0 equiv.), TBDMSCl (1.1 equiv.), THF, 94%; ii, TsCl, Py, $CHCl_3$; iii, NaCN, DMSO, heat, 94% (2 steps); iv, DIBALH, CH_2Cl_2, H_3O^+, 67%; v, $CH_3C{=}(PPh_3)CO_2Et$, benzene, reflux, quant.; vi, Mg, MeOH, 88%; vii, aq. HF, Me_3CN, 97%; viii, Swern oxidation; ix, $Ph_3P{=}CHCMe{=}CH_2$, THF, reflux, 56% (2 steps); x, $LiAlH_4$, Et_2O, 92%; xi, PCC, MS 4A, CH_2Cl_2; xii, $CH_2{=}CHMgBr$, THF, 70% (2 steps); xiii, Dess–Martin oxidation, 86%; xiv, xylene, reflux, 62%; xv, Tebbe reagent, quant.

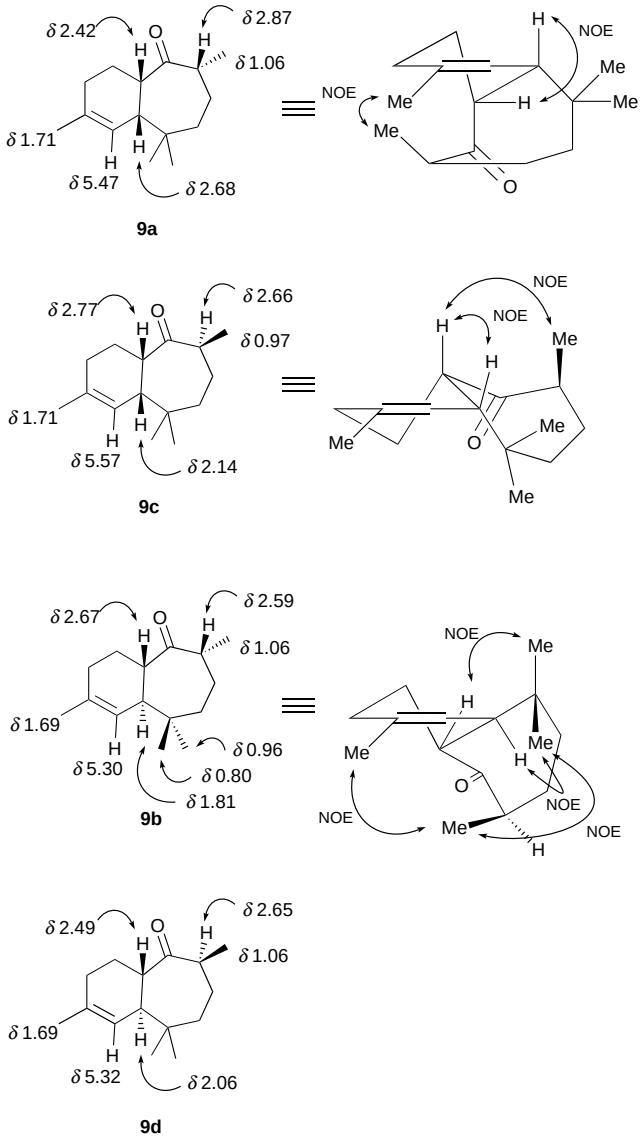

Fig. 1 Assignment of the relative stereochemistry of **9a**–**d**.

Table 1 Retention times of all isomers of 3-methyl-α-himachalene **1a**–**d** by GC and peaks enhanced on coinjection with natural material of *L. longipalpis* from Jacobina

	Retention time/min	
Compound	HP-5 (a siloxane)[a]	Chiral GC (β-cyclodextrin)[b]
1a	16.67	37.01
		No chiral separation
1b	16.03	35.15
		36.35
1c	14.73[c]	32.50
		33.01[c]
1d	14.71	32.58
		33.36

[a] 0.32 mm id × 30 m × 25 μm film thickness, 40 to 150 °C at 5 °C min^{-1}. [b] 0.25 mm id × 30 m × 25 μm film thickness, 40 to 180 °C at 3 °C min^{-1}. [c] Peaks enhanced on coinjection with natural material.

to that of natural α-himachalene, with absolute stereochemistry 1*R*,7*R*.[8] The absolute stereochemistry of the pheromone is now under further investigation, although the bioassay results suggest no interference with biological activity by the sample containing both enantiomers. Attempts are being made to scale-up the synthesis for field and pest control studies.

Notes and references

† *Selected data* for **9a**: R_f 0.64; δ_H 0.70 (s, 3H, 6-CH_3), 1.01 (s, 3H, 6-CH_3), 1.06 (d, *J* 6.5, 3-CH_3), 1.71 (br s, 3H, 9-CH_3), 2.42 (m, 1H, 1-H), 2.68 (br s, 1H, 7-H), 2.87 (m, 1H, 3-H), 5.47 (br s, 1H, 8-H). For **9b**: R_f 0.64; δ_H 0.80 (s, 3H, 6-CH_3), 0.96 (s, 3H, 6-CH_3), 1.06 (d, *J* 6.5, 3-CH_3), 1.69 (br s, 9-CH_3), 1.81 (m, 1H, 7-H), 2.67 (m, 1H, 1-H), 2.59 (m, 1H, 3-H), 5.30 (br s, 1H, 8-H). For **9c**: R_f 0.61; δ_H 0.85 (s, 3H, 6-CH_3), 0.97 (d, *J* 6.5, 3-CH_3), 1.07 (s, 3H, 6-CH_3), 1.71 (br s, 9-CH_3), 2.14 (br s, 1H, 7-H), 2.66 (m, 1H, 3-H), 2.77 (m, 1H, 1-H), 5.57 (br s, 1H, 8-H). For **9d**: R_f 0.61; δ_H 0.77 (s, 3H, 6-CH_3), 1.01 (s, 3H, 6-CH_3), 1.06 (d, *J* 6.5, 3-CH_3), 1.69 (br s, 9-CH_3), 2.06 (m, 1H, 7-H), 2.49 (m, 1H, 1-H), 2.65 (m, 1H, 3-H), 5.32 (br s, 1H, 8-H). R_f values in hexane–EtOAc 10:1.

‡ *Selected data* for **1a**: δ_H 0.81 (s, 3H, 6-CH_3), 0.94 (s, 3H, 6-CH_3), 1.10 (d, *J* 7, 3-CH_3), 1.70 (br s, 3H, 9-CH_3), 4.82 (s, 1H, 2-C$H_a$$CH_b$), 4.86 (s, 1H, 2-$CH_aCH_b$), 5.49 (br s, 1H, 8-H). For **1b**: δ_H 0.71 (s, 3H, 6-CH_3), 0.94 (s, 3H, 6-CH_3), 1.06 (d, *J* = 7, 3-CH_3), 1.69 (br s, 9-CH_3), 4.76 (s, 1H, 2-C$H_a$$CH_b$), 4.86 (s, 1H, 2-$CH_aCH_b$), 5.30 (br s, 1H, 8-H). For **1c**: δ_H 0.96 (s, 3H, 6-CH_3), 1.00 (s, 3H, 6-CH_3), 1.01 (d, *J* 7, 3-CH_3), 1.68 (br s, 9-CH_3), 4.76 (s, 1H, 2-C$H_a$$CH_b$), 4.81 (s, 1H, 2-$CH_aCH_b$), 5.51 (br s, 1H, 8-H). For **1d**: δ_H 0.70 (s, 3H, 6-CH_3), 0.94 (s, 3H, 6-CH_3), 0.97 (d, *J* 7, 3-CH_3), 1.67 (br s, 9-CH_3), 4.75 (s, 1H, 2-C$H_a$$CH_b$), 4.79 (s, 1H, 2-$CH_aCH_b$), 5.31 (br s, 1H, 8-H).

§ GC–MS: 0.32 mm id × 50 m HP-1(a siloxane × 0.52 μm film thickness, 30 to 250 °C at 5 °C min^{-1}; EI at 70 EV, 250 °C (VG-Autospec, Fisons Instruments), elution order **1d**, **1c**, **1b**, **1a**. *Selected data* for **1a**: *m*/*z* 94 (100%), 79 (55), 121 (54), 41 (52), 93 (51), 91 (41), 107 (40), 105 (35), 69 (35), 55 (34), 119 (32), 81 (29), 95 (24), 77 (24), 148 (23), 149 (19), 133 (18), 65 (18), 203 (16), 161 (16), 175 (15), 53 (15), 39 (15), 218 (11, M^+). For **1b**: *m*/*z* 94 (100%), 121 (87), 105 (61), 91 (58), 79 (57), 55 (56), 41 (53), 148 (51), 107 (50), 136 (47), 93 (46), 69 (43), 175 (35), 119 (33), 39 (31), 42 (28), 77 (28), 133 (27), 95 (23), 161 (22), 218 (21), 81 (21), 92 (20), 27 (20), 67 (19), 123 (18), 162 (18), 131 (17), 148 (17), 147 (16), 120 (15), 43 (15). For **1c**: *m*/*z* 94 (100%), 41 (69), 93 (63), 107 (61), 79 (59), 121 (58), 175 (53), 91 (46), 105 (45), 69 (44), 55 (43), 119 (40), 203 (38), 81 (36), 77 (32), 133 (26), 67 (26), 95 (25), 149 (24), 148 (23), 147 (21), 39 (21), 43 (20), 29 (20), 109 (20), 43 (20), 162 (19), 27 (19), 218 (18, M^+), 123 (17), 161 (16), 136 (15), 67 (15). For **1d**: *m*/*z* 94 (100%), 121 (65), 79 (50), 93 (49), 107 (45), 41 (44), 91 (40), 136 (39), 105 (38), 119 (38), 148 (36), 69 (32), 55 (31), 175 (30), 81 (27), 77 (26), 133 (25), 149 (24), 218 (23 M^+), 95 (22), 161 (18), 147 (17), 67 (16), 109 (15), 53 (15).

¶ Virgin female sandflies were removed from larval rearing pots within 10 h after eclosion to ensure that they were unmated. They were provided with a saturated sugar solution on cotton wool and subsequently maintained for 5–6 days in Barraud cages (18 × 18 × 18 cm). Bioassays were conducted in a glass (9 mm internal diameter) Y-tube olfactometer. Zero grade air was passed (2 ml min^{-1}) through two charcoal filters into the test and control arms (10 cm long). The olfactometer was connected to the air supply by Teflon tubing. A filter paper disk (1.5 cm diameter) was inserted into the Teflon tubing at the connection with the olfactometer test and control arms. During bioassays pheromone extracts or synthetic chemicals in hexane were placed on one of the filter paper disks. Hexane in the same quantity as for the test arm was placed on the other filter paper disk. The female sandfly was introduced into the third arm (10 cm long) of the olfactometer and its response observed for 5 min. Female attraction to **1c** and extract prepared from 5–7 day old male *L. longipalpis* was highly significant (χ^2 = 6.2 × 10^{-7} and P = 1.4 × 10^{-26}, respectively). Females were not significantly attracted to **1a**, **1b** or **1d**, nor to a natural α-himachalene sample at the same levels.

1 R. P. Lane, A. Phillips, D. H. Molyneux, G. Procter and R. D. Ward, *Ann. Trop. Med. Parasitol.*, 1985, **79**, 225
2 I. E. Morton and R. D. Ward, *Med. Vet. Entomol.*, 1989, **3**, 219
3 J. G. C. Hamilton, M. J. Dougherty and R. D. Ward, *J. Chem. Ecol.*, 1994, **20**, 141; M. J. Dougherty, P. Guerin and R. D. Ward, *Physiol. Entomol.*, 1995, **20**, 23
4 J. G. C. Hamilton, G. W. Dawson and J. A. Pickett, *J. Chem. Ecol.*, 1996, **22**, 2331
5 J. G. C. Hamilton and R. D. Ward, *Parassitologia*, 1991, **33** (Suppl 1), 283; J. G. C. Hamilton, R. D. Ward, M. J. Dougherty, C. Ponce, E. Ponce, H. Noyes and R. Zeledon, *Ann. Trop. Med. Parasitol.*, 1996, **90**, 533
6 J. G. C. Hamilton, G. W. Dawson and J. A. Pickett, *J. Chem. Ecol.*, 1996, **22**, 1477
7 E. Wenkert and K. Naemura, *Synth. Commun.*, 1973, **3**, 45
8 T. C. Joseph and S. Dev, *Tetrahedron*, 1968, **24**, 3841

Communication 9/00242A

ChemComm

Highly active Pd^{II} cyclometallated imine catalysts for the Heck reaction

Manuela Ohff, Andreas Ohff and David Milstein*

Department of Organic Chemistry, The Weizmann Institute of Science, 76100 Rehovot, Israel.
E-mail: comilst@wiccmail.weizmann.ac.il

Received (in Cambridge, UK) 18th December 1998, Accepted 14th January 1999

The new cyclopalladated, phosphine-free imine complexes 1–3 are exceptional catalysts for the Heck arylation, leading to more than a million turnovers in some cases; the catalysts are very thermally and air stable and are recovered unchanged after the catalysis.

The Heck arylation of alkenes [eqn. (1)] is a useful synthetic method that is attracting much current interest.[1] Normally, palladium phosphine complexes are utilized, and the reactions

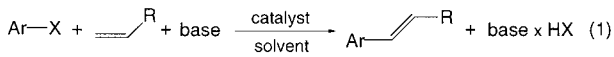

are conducted under an inert atmosphere. Recently, very efficient catalysis using palladium complexes incorporating cyclometallated phosphines,[2,3] chelating diphosphines,[4] carbene ligands[5] and dimethylglycine[6]† have been reported. We have reported that palladium complexes of tridentate PCP-type ligands are excellent catalysts, and have provided evidence which renders the traditional Pd^0/Pd^{II} cycle unlikely in that case.[6] The issue of a possible Pd^{II}/Pd^{IV} cycle in Heck catalysis is currently under debate.[4,7,8] and a new mechanism involving Pd^{IV} intermediacy in Heck catalysis has been suggested.[9]

We report here[10] that the palladium imine complexes **1**–**3** are outstanding catalysts for this reaction with turnover numbers

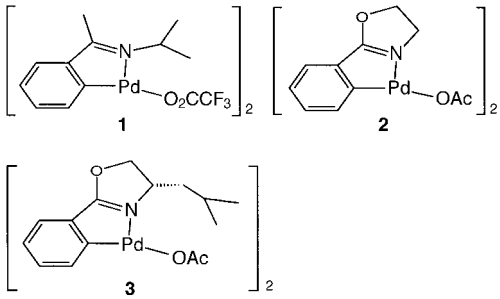

(TON) of more than 10^6 in some cases. These readily prepared Pd^{II} catalysts are exceedingly thermally stable and are not sensitive to oxygen. The use of phosphine free, nitrogen-based ligands in the Heck reaction is very rare and was reported for bidentate nitrogen ligands. However, low catalytic activity was observed.[11]‡

The new dimeric imine complexes **1**–**3** in which the metal center is stabilized by a five-membered ring, were readily prepared by treatment of $Pd(O_2CCF_3)_2$ or $Pd(OAc)_2$ with the corresponding imines in THF.§ Complex **1** was characterized by X-ray analysis (Fig. 1).¶ X-Ray structures of other palladated imine complexes were reported.[12]

Complexes **1**–**3** show extremely high activity in the catalytic arylation of olefins with aryl iodides and bromides (Table 1). Because of the stabilizing metallated ligand system, the complexes are very thermally stable and no degradation is observed under the reaction temperatures. These complexes are also not sensitive to oxygen and moisture and the reactions can be carried out in air, with no change in efficiencies or yield. The catalyst remains highly active after the reaction is complete, and upon addition of more substrates catalysis is resumed. At the end of the catalysis, the acetate or trifluoroacetate moieties are substituted to give the corresponding palladiumhalide complex. Conveniently, catalyst **1** can be formed *in situ* under the reaction conditions from $Pd(OAc)_2$ and the readily available imine ligand, leading to similar results.

While very high TONs and yields are observed for catalysts **1**–**3**, complex **1** exhibits higher turnover rates. Of the solvents tested, *N*-methylpyrrolidone (NMP) was found to be the best. The reaction can be carried out also in solvents of lower polarity (dioxane) or non-polar ones (mesitylene), although at lower rates. Pure solvent and starting materials should be used in the highly catalytic reactions. Both Na_2CO_3 and NEt_3 were used as bases, although the reaction was faster with the soluble amine, leading to a turnover rate of *ca.* 8×10^4 h^{-1} and 100% yield with iodobenzene and methyl acrylate.

In a typical experiment, a slight excess of the olefin is added to a solution of the aryl halide in freshly distilled NMP, followed by addition of an equimolar amount of $NaHCO_3$ or NEt_3. The catalyst is added and the mixture is stirred at 140 °C for the specified time. The reaction mixture is analyzed by gas chromatography and is worked up by addition of water and extraction of the organic phase with CH_2Cl_2. After evaporation of the volatiles, the essentially pure product is characterized by NMR and IR spectroscopy. Selected results are listed in Table 1.

As expected, the reaction outcome depends on the halide and on the olefin. With iodobenzene and methyl acrylate, essentially complete conversions are obtained with very high turnover numbers of up to 1.4×10^6, which are among the highest observed so far.‖ Methyl crotonate and styrene also react normally, while significantly lower rates are obtained with non-activated alkenes. Chlorobenzene was only marginally reactive.[13]** The observed TON of 137 100 in the case of bromobenzene is similar to the one that we reported for PCP-type ligands[6] but the reaction was slower in the latter case. As

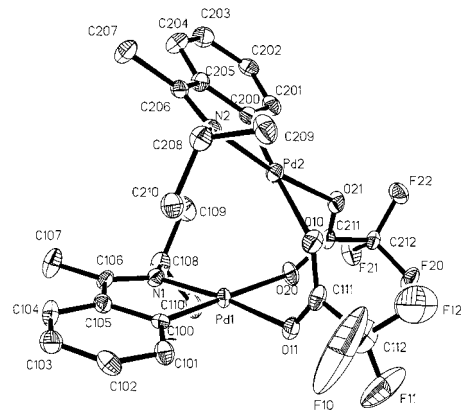

Fig. 1 Perspective view (ORTEP) of complex **1**. Bond distances (Å) and angles (°) (errors in last digits in parentheses) are: Pd(1)–C(100) 1.942(6); Pd(1)–N(1) 2.035; Pd(1)–O(11) 2.065(5); Pd(1)–O(20) 2.174(4); N(1)–C(106) 1.295(8); C(100)–C(105) 1.422(9); C(105)–C(106) 1.450(9); C(100)–Pd(1)–N(1) 81.0(2); C(100)–Pd(1)–O(11) 92.7(2); C(100)–Pd(1)–O(20) 178.3(2).

Table 1 Results of the Heck reaction with the imine catalyst **1**–**3**

ArX[a]	Alkene[a]	Solvent[b]	Base	Catalysts (mmol/10^{-5})	*t*/h	*T*/°C	TON	Yield (%)[c]
PhI	methyl acrylate	NMP	Na_2CO_3	**1** (3.5)	9	140	142900	100[d]
PhI	methyl acrylate	Dioxane	Na_2CO_3	**1** (3.5)	40	140	36900	25[d]
PhI	methyl acrylate	NMP	NEt_3	**1** (3.5)	1	140	142900	100[d]
PhI	methyl acrylate	DMA	NEt_3	**1** (3.5)	16	140	93700	66[d]
PhI	methyl acrylate	Dioxane	NEt_3	**1** (3.5)	16	140	107200	75[d]
PhI	methyl acrylate	Mesitylene	NEt_3	**1** (3.5)	16	140	130300	93[d]
PhI	methyl acrylate	NMP	Na_2CO_3	**1** (0.46)	32	140	1087000	100[d]
PhI	methyl acrylate	NMP	NEt_3	**1** (0.35)	18	140	1429000	100[d]
PhI	styrene	NMP	Na_2CO_3	**1** (3.5)	80	140	105700	74[e]
PhI	methyl crotonate	NMP	Na_2CO_3	**1** (3.5)	39	140	140000	98[f]
4-MeO-C_6H_4I	methyl acrylate	NMP	Na_2CO_3	**1** (3.5)	12	140	138600	97[g]
PhBr	methyl acrylate	NMP	Na_2CO_3	**1** (3.5)	43	140	137100	96[d]
4-CHO-C_6H_4I	methyl acrylate	NMP	Na_2CO_3	**1** (3.5)	25	140	140000	98[h]
PhI	methyl acrylate	NMP	Na_2CO_3	**2** (3.5)	22	140	142900	100[d]
PhI	methyl acrylate	NMP	Na_2CO_3	**3** (3.5)	22	140	142900	100[d]
PhI	dihydropyran	NMP	Na_2CO_3	**3** (70)	68	120	4300	60[i]
PhI	indene	NMP	Na_2CO_3	**3** (70)	115	120	5100	72[j]
PhI	cyclohexene	NMP	Na_2CO_3	**3** (70)	68	120	3000	42[i]
PhI	dihydrofuran	NMP	Na_2CO_3	**3** (70)	22	140	7100	100[i]
PhI	dihydrofuran	NMP	NEt_3	**3** (10.5)	24	120	38100	80[i]
PhBr	methyl acrylate	NMP	Na_2CO_3	**2** (7.0)	130	140	132900	93[d]

[a] Amounts: ArX, 5 mmol; alkene, 6 mmol; Na_2CO_3, 3.5 mmol; NEt_3 7 mmol. [b] NMP = *N*-methylpyrrolidone; DMA = *N*,*N*-dimethylacetamide. [c] Determined by GC, based on the aryl halide. [d] Methyl *trans*-cinnamate. [e] Stilbene, *cis*:*trans* = 1:7. [f] Methyl *trans*-3-methylcinnamate:methyl *cis*-3-methylcinnamate:3-methylenebenzenepropanoic acid methyl ester:methyl 4-phenylbut-2-enoate (10:1:1:1). [g] Methyl *trans*-*p*-methoxycinnamate. [h] Methyl *trans*-*p*-formylcinnamate. [i] Mixture of isomers of the phenyl derivatives of the olefins. [j] Mixture of isomers, main product: 2-phenylindene.

far as we are aware, our results with the relatively inactive bromobenzene and the commonly used acrylate esters are unsurpassed.

In summary, the metallated imine palladium(II) complexes show exceedingly high catalytic activity and yields in the Heck reaction, including reactions of the non-activated bromobenzene. The activities observed are among the highest reported for the Heck reaction. The new catalyst system is very thermally and air stable. Further investigations aimed at clarification of the scope and mechanism of these reactions are in progress.

We thank Dr L. J. W. Shimon for the X-ray analysis of complex **1**. This work was supported by The Israel Science Foundation, Jerusalem, Israel, and by the MINERVA Foundation, Munich, Germany. M. O. thanks the Deutsche Forschungsgemeinschaft for a fellowship. A. O. thanks the Minerva Foundation for a fellowship. D. M. is the holder of the Israel Matz Professorial Chair of Organic Chemistry.

Notes and references

† The role of the dimethylglycine additive is unclear and stabilized palladium colloids may be involved in this case. See ref. 6.

‡ With phenanthroline ligands, only 40 TON or less were obtained. Bipyridine and bis-oxazoline ligands were inactive with methyl acrylate and resulted in very low yields and turnovers with other alkenes. See ref. 11.

§ **1**: $\delta_H(C_6D_6)$ 0.85, 1.15 (d, $^3J_{HH}$ 6.6, 3H, CH_3), 1.06 (s, 3H, CH_3), 3.20 (sept, $^3J_{HH}$ 6.6, 1H, CH), 6.46, 7.29 (m, 1H, H_{aryl}), 6.77 (m, 2H, H_{aryl}); $\delta_C(C_6D_6)$ 14.0, 20.8, 21.9, 54.4 (s, CH/CH_3), 116.8 (q, J_{CF} 288, CF_3), 124.3, 126.7, 129.6, 132.5 (s, C_{aryl}), 166.0 (q, $^2J_{CF}$ 38, OC=O), 179.2 (s, C=N). For **2**: $\delta_H(C_6D_6)$ 2.22 (s, 3H, CH_3), 2.62, 2.82, 3.00, 3.24 (m, 1H, CH_2), 6.71, 6.84 (m, $^3J_{HH}$ 7.6/7.4, 1H, H_{aryl}), 7.01 (d, $^3J_{HH}$ 7.4, 1H, H_{aryl}), 7.48 (d, $^3J_{HH}$ 7.6, 1H, H_{aryl}); $\delta_C(C_6D_6)$ 24.5 (s, CH_3), 49.6, 69.7 (s, CH_2), 123.4, 125.1, 130.1, 132.1, 131.8, 149.2 (s, C_{aryl}), 174.4 (s, C=N), 181.1 (s, OC=O). For **3**: $\delta_H(C_6D_6)$ 0.70 (d, $^3J_{HH}$ 6.6, 6H, CH_3), 0.84 (m, 1H, left part of CH_2), 1.14 (m, 1H, CH), 1.82 (ddd, 1H, right part of CH_2), 2.16 (s, 3H, CH_3), 3.09 (m, 1H, CH), 3.37 (m, 2H, CH_2), 6.75 (t, $^3J_{HH}$ 7.6, 1H, H_{aryl}), 6.87, 7.13 (m, $^3J_{HH}$ 7.6, 1H, H_{aryl}), 7.50 (d, $^3J_{HH}$ 7.6, 1H, H_{aryl}); $\delta_C(C_6D_6)$ 21.8, 23.5, 24.6, 25.2 (s, CH/CH_3), 43.5, 75.5 (s, CH_2), 60.4 (s, CH), 123.5, 125.2, 130.2, 132.0, 132.4, 149.3 (s, C_{aryl}), 173.2 (s, C=N), 181.1 (s, OC=O).

¶ *Crystal data* for **1**: $C_{26}H_{28}N_2O_4F_6Pd_2$, M = 759.30, yellow, plates, 0.2 × 0.2 × 0.05 mm^3, monoclinic, $P2(1)/c$ (No. 14), a = 17.044(3), b = 16.976(3), c = 19.725(4) Å, β = 97.75° (3), from 25 reflections, T = 110 K, V = 5655(2) Å^3, Z = 8, D_c = 1.784 Mg m^{-3}, μ = 1.346 mm^{-1}, Mo-Kα, 12993 independent reflections, R_{int} = 0.0481, final R_1 = 0.0618. CCDC 182/1144. Crystallographic data are available in .cif format from the RSC web site, see: http://www.rsc.org/suppdata/cc/1999/357

‖ As far as we are aware, this is the highest TON reported for a quantitative Heck reaction. A TON of 1120000 was reported for the reaction of iodobenzene with methyl acrylate after 13 days at 95 °C, but the yield was 56%. See ref. 3.

** Catalysis with chlorobenzene was accomplished by addition of NaI and $NiBr_2$. However, the reaction was very slow, resulting in 10% yield and 190 TON after 21 h at 140 °C.

1 Reviews: R. F. Heck, *Palladium Reagents in Organic Synthesis*, Academic Press, London, 1985; R. F. Heck, *Comprehensive Organic Synthesis*, ed. B. M. Trost and I. Flemming, Pergamon, Oxford, New York, 1991, vol. 4, p. 833; V. V. Grushin and H. Alper, *Chem. Rev.*, 1994, **94**, 1047; A. de Meijere and F. E. Meyer, *Angew. Chem., Int. Ed. Engl.*, 1994, **33**, 2379; W. Carbri and I. Candiani, *Acc. Chem. Res.*, 1995, **28**, 2.

2 W. A. Herrmann, C. Brossmer, K. Öfele, C.-P. Reisinger, T. Riermeier, M. Beller and H. Fisher, *Angew. Chem., Int. Ed. Engl.*, 1995, **34**, 1844; M. Beller, T. H. Riermeier, S. Haber, H.-J. Kleiner and W. A. Herrmann, *Chem. Ber.*, 1996, **129**, 1259; W. A. Herrmann, C. Brossmer, C.-P. Reisinger, T. H. Riermeier, K. Öfele and M. Beller, *Chem. Eur. J.*, 1997, **3**, 1357.

3 B. L. Shaw, S. D. Perera and E. A. Staley, *Chem. Commun.*, 1998, 1361.

4 B. L. Shaw and S. D. Perera, *Chem. Commun.*, 1998, 1863.

5 W. A. Herrmann, M. Elison, J. Fischer, C. Köcher and G. R. J. Artus, *Angew. Chem., Int. Ed. Engl.*, 1995, **34**, 2371.

6 M. T. Reetz, E. Westermann, R. Lohmer and G. Lohmer, *Tetrahedron Lett.*, 1998, **39**, 8449.

7 M. Ohff, A. Ohff, M. E. van der Boom and D. Milstein, *J. Am. Chem. Soc.*, 1997, **119**, 11687.

8 M. Beller and T. H. Riermeier, *Eur. J. Inorg. Chem.*, 1998, **1**, 29.

9 B. L. Shaw, *New. J. Chem.*, 1998, **22**, 77.

10 M. Ohff, A. Ohff and D.Milstein, *Israel Patent Appl.*, 121346 (filed on 20.07.1997).

11 W. Cabri, I. Candiani, A. Bedeschi and R. Santi, *Synlett*, 1992, 871.

12 For example, G. Zhao, Q. G. Wang and T. C. Mak, *J. Chem. Soc., Dalton Trans.*, 1998, 1241.

13 For high yield Heck reactions with chlorobenzene and other unactivated aryl chlorides, see Y. Ben-David, M. Portnoy, M. Gozin and D. Milstein, *Organometallics*, 1992, **11**, 1995; M. Portnoy, Y. Ben-David and D. Milstein, *Organometallics*, 1993, **12**, 4734; M. T. Reetz, G. Lohmer and R. Schwickardi, *Angew. Chem., Int. Ed.*, 1998, **37**, 481.

Communication 8/09883B

Synthesis, characterization and thin film formation of end-functionalized organometallic polymers

Maria Peter,[a] Rob G. H. Lammertink,[a] Mark A. Hempenius,[a] Menno van Os,[b] Marcel W. J. Beulen,[c] David N. Reinhoudt,[c] Wolfgang Knoll[b] and G. Julius Vancso*[a]

[a] *Faculty of Chemical Technology, Department of Polymer Materials Science and Technology, University of Twente, PO Box 217, NL-7500 AE Enschede, The Netherlands. E-mail: G.J.Vancso@ct.utwente.nl*
[b] *Max-Planck-Institut für Polymerforschung, Ackermannweg 10, D-55128 Mainz, Germany*
[c] *Department of Supramolecular Chemistry and Technology/MESA Research Institute, University of Twente, PO Box 217, NL-7500 AE Enschede, The Netherlands*

Received (in Bristol, UK) 9th November 1998, Accepted 12th January 1999

Poly(ferrocenyldimethylsilanes) (PFS) end-functionalized by ethylene sulfide form stable, electroactive layers on Au.

Interfacial electron transfer plays a fundamental role in a large number of biological and technical processes. Progress in the area of self-assembled monolayers resulted in a number of synthetic and physical developments which now allow one to perform systematic studies of surface electrochemistry of well defined molecular thin films of thiols terminated by (electroactive) ferrocene moieties, immobilized on Au.[1] Surface immobilization of redox active compounds, such as ferrocene derivatives, with a well defined structure and with a variable surface concentration of the electroactive centers offers the possibility of the control of charge transfer. We have undertaken a systematic study of thiol end-functionalized ferrocenylsilane polymers obtained by anionic polymerization.

In this contribution we describe the synthesis, molecular characterization and thin film properties of poly(ferrocenyldimethylsilane) (PFS), end-functionalized by ethylene sulfide (ES), denoted ES–PFS. This organometallic polymer has been chosen as it exhibits interesting electrochemical and other potentially useful properties owing to its unique structure which incorporates ferrocene units and Si atoms in the main chain.[2]

Poly(ferrocenyldimethylsilane) homopolymer and its thiol end-functionalized derivative were synthesized by anionic ring-opening polymerizations. The synthesis of the homopolymer has been described elsewhere.[3] ES–PFS was synthesized by treating an end-reactive living homopolymer with ethylene sulfide as shown in Scheme 1.

Molecular characterization of ES–PFS was carried out by ^{1}H NMR, GPC, FTIR and elemental analysis. GPC measurements were carried out in THF in order to determine the molar mass and its distribution. The molar mass of ES–PFS was referenced to a polystyrene calibration curve. The number average molar mass, M_n, was found to be 12.4×10^3. This value was expected from the molar ratio of monomer to initiator. The polydispersity ratio (M_w/M_n) was found to be equal to 1.11. The molar mass of the polymer was also estimated by end-group analysis using ^{1}H NMR[4] and a value of 12.3×10^3 was obtained. Thus, an excellent agreement between the molar masses according to the two techniques was found. The peak found in the ^{1}H NMR spectrum at δ 2.57 (spectrum not shown) was assigned to the methylene group next to sulfur in the end-group. The assignments of the ^{1}H NMR resonances at δ 4.00 3.80 correspond to the protons (4H) from the cyclopentadienyl rings, while the resonance at δ 0.28 corresponds to the 6H from the methyl groups attached to Si. Spectroscopic characterization of ES–PFS was undertaken by FTIR of ES–PFS in KBr pellets. The absorbances assigned to the C–H vibrations in the ferrocene rings and in the methyl, and methylene groups can be observed in the FTIR spectra. Results from elemental analysis are in a good agreement with the theoretically expected values [theoretical values (mass%): C, 59.14; H, 5.8; S, 0.97 and experimentally found values: C, 58.33; H, 5.92; S, 0.62].

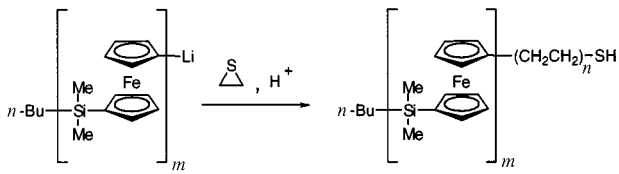

Scheme 1

Thin films of ES–PFS were prepared by immersing gold substrates[5] into 0.1 and 1.0 mg ml^{-1} solutions of the polymers in toluene for 48 h to ensure maximum coverage. The samples were subsequently rinsed with toluene and dried in a nitrogen stream. The films were characterized by contact angle measurements, XPS and FTIR. Contact angles with water were measured to evaluate the wetting properties and the uniformity of the ES–PFS layers on gold. Advancing contact angles were found to be *ca.* 95° and receding contact angles *ca.* 76°, respectively, indicating a hydrophobic surface. Peaks associated with C 1s, Fe 2p (from the ferrocene ring), Si 2s (from the polymer backbone) and S 2p (from the end-function) can be distinguished in the XPS spectra of ES–PFS layers. This indicates that the polymer is immobilized on the gold surface. FTIR spectra of the monolayers taken in grazing incidence with perpendicularly polarized light confirm the presence of the end-functionalized polymer on the Au substrate. The observed vibration frequencies are in good agreement with literature data.[6]

Surface plasmon resonance spectroscopy (SPRS) experiments were carried out in order to study the adsorption kinetics of end-functionalized ES–PFS on gold in comparison with PFS, and to determine the optical thickness of the layers.[7] The formation of a thin film of ES–PFS on the gold surface results in an angular shift of the resonance angle [Fig. 1(a)] which is a function of the thickness and the refractive index. Curve 2 in Fig. 1(a) was recorded following 50 h of total sorption time. An average value of 39.8 Å was found for the limiting optical thickness of the polymer (refractive index n = 1.687) described in this study. The refractive index was determined previously by profilometry followed by ellipsometry. Measurements of the time dependence of optical reflectivity showed that a monolayer is formed with fast kinetics [Fig. 1(b)]. At between 800 and 3000 min the reflectivity remained constant. The adsorption of non-functionalized PFS on the gold surface did produce a small angular shift [Fig. 1(c)] from which an average thickness of 11.0 Å was determined. Curve 2 in Fig. 1(c) was measured following 800 min of total sorption time. The time dependence of the reflectivity showed [Fig. 1(d)] that in the case of non-functionalized polymer the adsorption rates are slower. In order to check whether the predominant process is physi- or chemisorption, the polymer films were washed after deposition using toluene. The layer formed of non-functionalized polymers

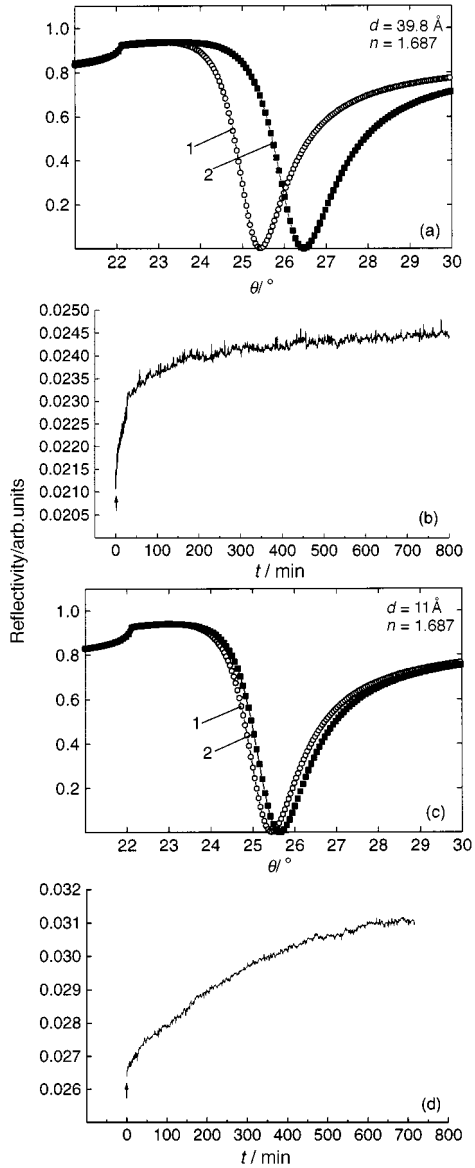

Fig. 1 (a) Angular reflectivity scans recorded in air (1) at bare Au/LaSFN9 (Berliner Glass) and (2) after immobilization of ES–PFS (c = 1.0 mg ml^{-1}) on Au/LaSFN9. (b) Time dependence of reflectivity for ES–PFS in toluene (c = 1.0 mg ml^{-1}) at an angle of incidence θ = 78° (the arrow indicates the injection of the polymer solution). (c) Angular reflectivity scans recorded in air (1) at bare Au/LaSFN9 (Berliner Glass) and (2) after adsorption of PFS (c = 1.0 mg ml^{-1}) on Au/LaSFN9. (d) Time dependence of reflectivity for PFS in toluene (c = 1.0 mg ml^{-1}) at an angle of incidence θ = 77° (the arrow indicates the injection of the polymer solution).

could be easily removed which indicated that only physisorption occurred for this polymer. The films of the end-functionalized ES–PFS were stable against washing with toluene indicating predominant chemisorption.

Atomic force microscopy (AFM) was used to image the film topography. Well defined, triangular, monoatomic terraces of Au(111) were prepared by annealing sputtered Au substrates, on glass, in a H_2 flame. Tapping mode atomic force microscopy[8] (AFM) height and phase imaging were used to characterize the morphology of ES–PFS layers on Au(111). Owing to the adsorption of the end-functionalized polymer, corresponding AFM images exhibit a globular surface structure (Fig. 2), instead of the atomically smooth terraces of bare Au(111). The contours of the underlying triangular terraces of Au(111) can still be observed on the AFM images even for the specimen showing the chemisorbed polymer film.

The electrochemical behavior of ES–PFS layers in comparison with the physisorbed PFS layers was investigated by cyclic voltammetry. The experiments were performed on layers of physisorbed, non-functionalized PFS and end-functionalized,

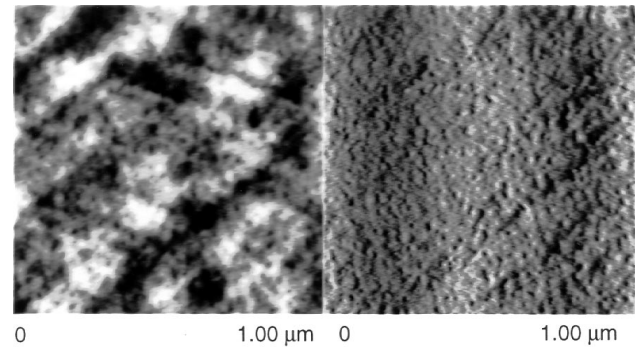

Fig. 2 Tapping mode height (left, z = 10 nm) and phase (right, z = 9°) images recorded for ES–PFS layers on Au(111).

chemisorbed films of ES–PFS before and after immersion in pure toluene for 24 h. The current observed for the end-functionalized ES–PFS showed only a small change prior to, and following immersion into toluene. This can be considered as an indication for the fact that the end-functionalized PFS forms a stable layer on gold. For the non-functionalized physisorbed PFS the change in the intensity of the current in the cyclic voltammograms prior to, and following immersion into the solvent was significant (Fig. 3).

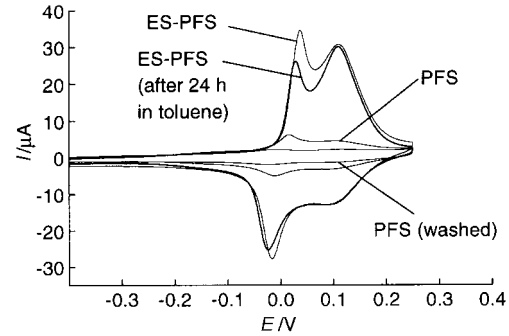

Fig. 3 Cyclic voltammograms of PFS, PFS (after 24 h in toluene), ES–PFS and ES–PFS (after 24 h in toluene) layers on gold at v = 50 mV s^{-1} scan rate (reference electrode Hg–$HgSO_4$, auxiliary electrode Pt, 0.1 M $NaClO_4$ electrolyte solution).

Further work is aimed at *in situ* studies of the electrochemical behavior of end-functionalized poly(ferrocenylsilane) layers on Au substrates by electrochemical AFM at different degrees of oxidation.

The authors would like to thank Mr H. Schönherr for his help with AFM experiments and for many helpful discussions. The contributions of Mr P. G. H. Kosters in the FTIR experiments, Mr A. H. J. van den Berg in the XPS measurements, and Mr C. J. Padberg with the GPC are acknowledged.

Notes and references

1 L. H. Dubois and R. G. Nuzzo, *Annu. Rev. Phys. Chem.*, 1992, **43**, 437; K. Chen, F. Xu, C. A. Mirkin, R.-K. Lo, K. S. Nanjundaswami, J.-P. Zhou and J. T. McDevitt, *Langmuir*, 1996, **12**, 2622.
2 I. Manners, *Can. J. Chem.*, 1998, **76**, 371; D. A. Foucher, R. Ziembinsky, B.-Z. Tang, P. M. Macdonald, J. Massey, C. R. Jaeger, G. J. Vancso and I. Manners, *Macromolecules*, 1993, **26**, 2878.
3 R. Rulkens, Y. Ni and I. Manners, *J. Am. Chem. Soc.*, 1994, **116**, 12 121; R. Rulkens, A. J. Lough and I. Manners, *J. Am. Chem. Soc.*, 1994, **116**, 797.
4 See, *e.g.*: D. Campbell and J. R. White, *Polymer Characterization*, Chapmann and Hall, London, 1989, p 12.
5 U. B. Steiner, W. R. Caseri and U. W. Suter, *Langmuir*, 1998, **14**, 347.
6 D. D. Popenoe, R. S. Deinhammer and M. D. Porter, *Langmuir*, 1992, **8**, 2521.
7 E. F. Aust, S. Ito, M. Sawodny and W. Knoll, *Trends Polym. Sci.*, 1994, **2**, 313.
8 S. N. Magonov and M. H. Whangbo, *Surface Analysis with STM and AFM*, VCH, Weinheim, 1996.

Communication 8/09259A

Determination of absolute configuration using circular dichroism: Tröger's Base revisited using vibrational circular dichroism

A. Aamouche, F. J. Devlin and P. J. Stephens*

Department of Chemistry, University of Southern California, Los Angeles, CA 90089-0482, USA.
E-mail: stephens@chem1.usc.edu

Received (in Corvallis, OR, USA) 5th November 1998, Accepted 21st December 1998

A new methodology for predicting the Vibrational Circular Dichroism (VCD) spectra of chiral molecules using Density Functional Theory (DFT) and Gauge-Invariant Atomic Orbitals (GIAOs) permits the direct determination of the absolute configuration of organic molecules in solution; application to Tröger's Base leads to the opposite absolute configuration from that deduced from electronic CD, confirming the conclusion arrived at from X-ray analysis of a diastereoisomeric salt.

Chiral molecules exhibit circular dichroism (CD).[1] The CD of enantiomers is of identical magnitude and opposite sign at all frequencies. The CD of a molecule can therefore be used to obtain its absolute configuration (AC). Application of CD to the determination of AC requires a methodology predicting the sign (or signs) of the CD for one (or more) transition of the molecule.

In practice there are two main choices to be made in utilizing CD for AC determination. First, the specific spectral region to be used must be selected. Currently, CD can be routinely measured from the mid-infrared[2] to the vacuum ultraviolet[3] encompassing both vibrational and electronic transitions. Second, the methodology to be used in predicting the CD of the transitions to be studied must be chosen. This can range from empirical correlation to *a priori ab initio* quantum mechanical calculation.

Historically, Electronic CD, measured in the near-infrared–visible–ultraviolet spectral region, has been the predominant choice of chemists.[4] Vibrational CD (VCD),[5] measured in the infrared spectral region, has been little utilized since the first measurements in the early 1970s.[6] This can be attributed primarily to the absence of a practical methodology for reliably predicting VCD intensities.

The purpose of this report is to demonstrate that recent developments in *ab initio* Density Functional Theory[7] now make practicable the prediction of VCD intensities in large organic molecules with an accuracy sufficient to permit ACs to be reliably deduced using VCD spectroscopy. The key to this advance has been the development and implementation[8] of analytical derivative techniques for calculating Atomic Axial Tensors (AATs)[9] using Gauge-Invariant Atomic Orbitals (GIAOs).[10] We report a study of the VCD spectrum of Tröger's Base **1**.

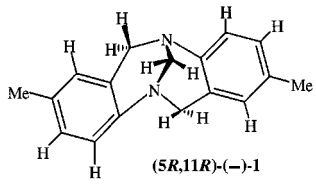

(5*R*,11*R*)-(−)-**1**

Tröger's Base was first resolved in 1944.[11] Its AC was first assigned in 1967[12] by means of the CD of electronic transitions associated with the aromatic rings. The Coupled Oscillator method[13] (also often referred to as the Exciton Coupling method[14]) was used to elucidate the AC from the CD spectrum. In 1991, on the basis of the X-ray structure of a salt of **1** with a chiral anion of known AC, it was reported that the original AC assignment was incorrect.[15]

The unpolarized absorption and CD spectra of **1** over the range 800–1700 cm^{-1} are shown in Fig. 1 and 2, together with the corresponding predicted DFT spectra. DFT calculations were carried out *via* the GAUSSIAN program[16] using the hybrid functional[17] B3PW91[18] and the 6-31G* basis set[19] (321 basis functions) as described previously.[20] All calculations use direct, analytical derivative methods. The calculations are carried out within the harmonic approximation [9] and therefore predict only fundamental transitions. The fundamentals are numbered (1 being lowest) in Fig.1(*b*) and 2(*b*). Comparison of the predicted and experimental absorption spectra (Fig. 1) leads to the assignment detailed in Fig. 1(*a*). In assigning the spectrum we allow for the overall shift of the predicted spectrum to higher frequency, due predominantly to the neglect of anharmonicity in the calculation,[21] and make use not only of frequencies but also of intensities (without the latter, assignment would be much more difficult). We note that almost all observed bands are assignable to fundamentals: only two bands are clearly observed which cannot be so assigned. This confirms the excellence of the harmonic approximation for the mid-IR spectral region. The fundamentals most easily and unambiguously assigned are those corresponding to bands which are resolved from neighboring bands and of significant intensity. The 25 fundamentals 34, 35, 38, 42–44, 50–64, 69, 70, 82 and 83 are in this category. The remaining 29 fundamentals are either unresolved and/or weak; their assignment is less definitive.

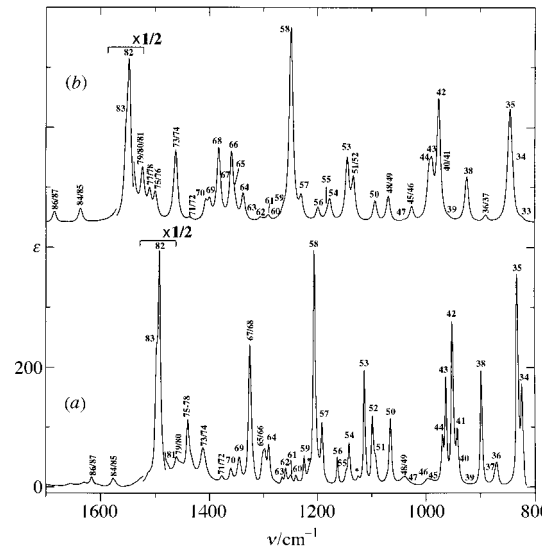

Fig. 1 Mid-IR absorption spectra of **1**: (*a*) Experimental spectrum in CCl_4 solution; 0.20 M (−)-**1**, 156 μ pathlength (800–1480 and 1525–1700 cm^{-1}); 0.10 M (−)-**1**,104 μ pathlength (1480–1525 cm^{-1}); resolution 1 cm^{-1}; (*b*) DFT/B3PW91/6-31G* spectrum; band shapes are Lorentzian (γ = 4.0 cm^{-1}). Fundamentals are numbered. Asterisks indicate bands assigned as non-fundamentals.

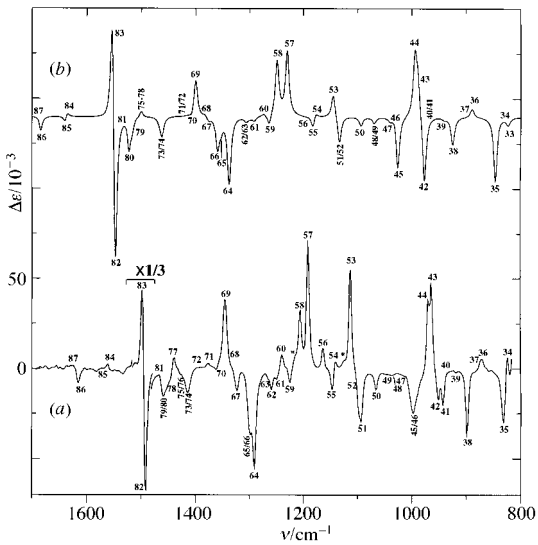

Fig. 2 Mid-IR VCD spectra of **1**: (*a*) Experimental spectrum of (−)-**1** in CCl_4 solution; concentrations and pathlengths are as in Fig. 1. Resolution 4 cm^{-1}. The spectrum is one-half of the difference in spectra of (−)-**1** and (+)-**1**. Scan time of each spectrum was 1 h. VCD was measured using a Bomem/BioTools Chiral*IR* spectrometer; (*b*) DFT/B3PW91/6-31G* spectrum of (5*R*,11*R*)-**1**; band shapes are Lorentzian (γ = 4.0 cm^{-1}). Fundamentals are numbered. Asterisks indicate bands assigned as non-fundamentals.

In Fig. 2 the experimental VCD spectrum is for the (−)-isomer of **1** and the calculated VCD spectrum is for the (5*R*,11*R*)-enantiomer. The assignment of the experimental VCD spectrum follows from the assignment of the absorption spectrum and is shown in Fig. 2(*a*). Comparison of the calculated and experimental spectra shows that predicted VCD signs and intensities are in excellent overall agreement with experimental signs and intensities. The comparison of calculated and experimental VCD signs and intensities is most straightforward for the 25 fundamentals resolved in the absorption spectrum. Of these, VCD is clearly observed for 19: fundamentals 35, 38, 42–44, 50, 53–60, 62, 64, 69, 82 and 83. In every case except for one (56) the predicted sign agrees with the experimental sign. We conclude directly that (−)-**1** has the (5*R*,11*R*) AC. This result is opposite to that arrived at from the electronic CD of **1** and consistent with the conclusion deduced by X-ray crystallography.[15]

Complete quantitative analysis of the spectra, based on the assignments shown in Fig. 1 and 2, is accomplished using Lorentzian fitting.[20] The absorption spectrum yields the frequencies and dipole strengths; the VCD spectrum yields the rotational strengths. In Fig. 3 we plot the experimental rotational strengths obtained for the 19 fundamentals resolved in the VCD spectrum against the corresponding calculated rotational strengths. In Fig. 3(*a*) and 3(*b*) the calculated rotational strengths are for the (5*R*,11*R*) and (5*S*,11*S*) enantiomers respectively. Perfect agreement of calculated and experimental rotational strengths for the correct enantiomer leads to a straight line of slope +1; comparison to the opposite enantiomer leads to a slope of −1. The plots in Fig. 3 simultaneously confirm the correctness of the identification of the (−)-isomer with the (5*R*,11*R*) AC and define the quantitative reliability of the DFT methodology.

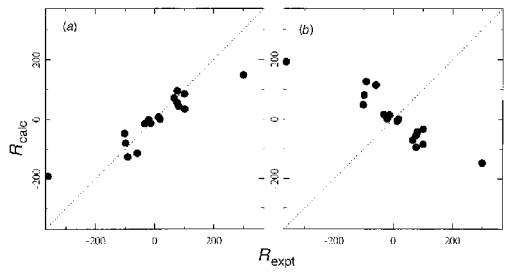

Fig. 3 Comparison of calculated and experimental rotational strengths for (*a*) (5*R*,11*R*)-**1** and (−)-**1**; (*b*) (5*S*,11*S*)-**1** and (−)-**1**. Experimental rotational strengths were obtained by Lorentzian fitting (ref. 20). The dashed line is of slope +1.

The advantages of Vibrational CD over Electronic CD are clearly exposed by this study. VCD can be measured for many transitions, in contrast to the small number of transitions generally accessible to Electronic CD measurement. The widths of vibrational transitions are much narrower than of electronic transitions, leading to more highly resolved spectra. VCD intensities depend only on ground electronic state properties and are more easily and reliably predicted than Electronic CD intensities which depend on excited electronic states in addition. The DFT/GIAO methodology for predicting VCD intensities is general and of high accuracy; it is not necessary to resort to simplified models to interpret VCD spectra. Recent developments incorporated in GAUSSIAN 98[16] have greatly enhanced the efficiency of DFT/GIAO calculations; 6-31G* calculations are now practicable for molecules possessing more than 100 atoms.

We are grateful to NIH for support (GM051972); and to Elf Aquitaine, Inc. for a post-doctoral fellowship (to A. A.).

Notes and references

1 E. Charney, *The Molecular Basis of Optical Activity: Optical Rotatory Dispersion and Circular Dichroism*, Wiley, New York, 1979.
2 L. A. Nafie, in *Advances in Applied Fourier Transform Infrared Spectroscopy*, ed. M. W. Mackenzie, Wiley, New York, 1988, ch. 3, p. 67; T. A. Keiderling, in *Practical Fourier Transform Infrared Spectroscopy*, Academic Press, New York, 1990, ch. 5, p. 203.
3 W. C. Johnson, Jr., *Rev. Sci. Instrum.*, 1971, **42**, 1283; A. Gedanken and M. Levi, *Rev. Sci. Instrum.*, 1977, **48**, 1661; P. Snyder, *Photochem. Photobiol*., 1986, **44**, 237.
4 P. Crabbe, *Optical Rotatory Dispersion and Circular Dichroism in Organic Chemistry*, Holden-Day, 1965.
5 P. J. Stephens and M. A. Lowe, *Annu. Rev. Phys. Chem.*, 1985, **36**, 213; L. A. Nafie, *Annu. Rev. Phys. Chem.*, 1997, **48**, 357.
6 G. Holzwarth, E. C. Hsu, H. S. Mosher, T. R. Faulkner and A. Moscowitz, *J. Am. Chem. Soc.*, 1974**, 96**, 251; L. A. Nafie, J. C. Cheng and P. J. Stephens, *J. Am. Chem. Soc.* **1975**, *97*, 3842; c) L. A. Nafie, T. A. Keiderling and P. J. Stephens, *J. Am. Chem. Soc.*,1976, **98**, 2715.
7 *Chemical Applications of Density Functional Theory*, ACS Sympp. Ser. 629, ed. B. B. Laird, R. B. Ross and T. Ziegler, ACS, Washington, D.C., 1996.
8 J. R. Cheeseman, M. J. Frisch, F. J. Devlin and P. J. Stephens, *Chem. Phys. Lett.*, 1996, **252**, 211.
9 P. J. Stephens, *J. Phys. Chem.*, 1985, **89**, 748; P. J. Stephens, *J. Phys. Chem.* ,1987, **91**, 1712.
10 Also referred to as London orbitals.
11 V. Prelog and P. Wieland, *Helv. Chim. Acta*, 1944, **27**, 1127.
12 S. F. Mason, G. W. Vane, K. Schofield, R. J. Wells and J. S. Whitehurst, *J. Chem. Soc. B*, 1967, 553.
13 Ref. 1, ch. 4.
14 N. Harada and K. Nakanishi, *Circular Dichroic Spectroscopy: Exciton Coupling in Organic Stereochemistry*, University Science Books, 1983.
15 S. H. Wilen, J. Z. Qi and P. G. Williard, *J. Org. Chem.*, 1991, **56**, 485.
16 GAUSSIAN 95 (Development Code) and GAUSSIAN 98, Gaussian, Inc., Pittsburgh, PA, 1998.
17 A. D. Becke, *J. Chem. Phys.*, 1993, **98**, 1372; A. D. Becke, *J. Chem. Phys.*, 1993, **98**, 5648.
18 P. J. Stephens, F. J. Devlin, C. F. Chabalowski and M. J. Frisch, *J. Phys. Chem.*, 1994, **98**, 11623.
19 W. J. Hehre, P. R. Schleyer, L. Radom and J. A. Pople, *Ab Initio Molecular Orbital Theory*, Wiley, New York, 1986.
20 P. J. Stephens, J. R. Cheeseman, M. J. Frisch, C. S. Ashvar and F. J. Devlin, *Mol. Phys.*, 1996, **89**, 579; F. J. Devlin, P. J. Stephens, J. R. Cheeseman and M. J. Frisch, *J. Phys. Chem.*,1997, **101**, 6322; F. J. Devlin, P. J. Stephens, J. R. Cheeseman and M. J. Frisch, *J. Phys. Chem.*, 1997, **101**, 9912.
21 J. W. Finley and P. J. Stephens, *J. Mol. Struct. (THEOCHEM)*, 1995, **357**, 225.

Communication 8/08677J

Encapsulation of WC within 2H-WS_2 inorganic fullerene-like cages

Aude Rothschild,[a] Jeremy Sloan,*[b,c] Andrew P. E. York,[b] Malcolm L. H. Green,[b] John L. Hutchison[c] and Reshef Tenne[a]

[a] *Department of Materials and Interfaces, Weizmann Institute, Rehovot, 76100, Israel*
[b] *Inorganic Chemistry Laboratory, University of Oxford, South Parks Road, Oxford, UK OX1 3QR. E-mail: Jeremy.Sloan@chem.oxford.ac.uk*
[c] *Department of Materials, University of Oxford, Parks Road, Oxford, UK OX1 3PH*

Received (in Bristol, UK) 11th November 1998, Accepted 12th January 1999

The preparation of WC encapsulated within 2H-WS_2 inorganic fullerene-like (IF) cages by sulfidisation is described; the encapsulates were prepared from both high surface area (high S_g) and low surface area (low S_g) WC precursors; for low S_g WC, partial conversion of the carbide to the sulfide only was achieved with 2–20 IF layers obtained around carbide particles, resulting in WC/2H-WS_2 composites; the amount of conversion obtained in the case of the high S_g WC depended on the method of preparation of the precursor; total conversion to 2H-WS_2 was obtained from a precursor obtained by carburisation of small WO_3 particles, while only partial conversion was obtained in the instance of high S_g WC prepared from ball-milled low S_g WC.

Inorganic fullerene-related structures (IFs) of the form 2H-MX_2 with M = W, Mo and X = S, Se can be prepared by a variety of routes including gas–solid[1–4] and vapour phase[5] reaction between a sulfidising agent and a metal oxide, by STM induction from amorphous MoS_3 films[6] and also by chemical-transport reactions.[7] Such materials owe their fullerene-like properties to the fact that they can incorporate non-six membered moieties that result in the formation of both curved and closed multiple layered structures similar to those formed by graphitic carbon.[8] These materials have found uses in tribological applications[9] and also in nanoscale electronic devices.[10] We describe here the encapsulation of 2H-WS_2 IF material around particles of the corresponding monocarbide. This result is novel as WC is a much denser and more metallic material than the oxide or sulfide precursors previously used to synthesize IFs.

The low S_g WC used in these experiments exhibited average particle sizes of 0.3–2.5 μm and was obtained from Alfa Chemicals (99.5%). The high S_g WC was prepared by two methods. First, WC (α-form) with a surface area of 40 $m^2\ g^{-1}$ and particle diameters in the range 200–2000 Å was prepared by reacting WO_3 with a mixture of 20% CH_4–H_2 (100 ml min^{-1}), ramping the temperature from 20 to 750 °C at the rate of 1 °C min^{-1}.[11] The carburisation of this precursor was verified in the bulk by X-ray powder diffraction (XRD) using a Philips 1729 diffractometer equipped with Cu-Kα_1 radiation operated at 40 kV and 30 mA. The second high S_g sample was prepared by grinding the commercially available low S_g WC in a ball milling apparatus for 48 h. This technique also produced a precursor with particle sizes in the range 200–2000 Å. All of the sulfidisations were carried out in a standard flow reactor at a temperature of 820 °C using a mixture of forming gas (5% H_2–95% N_2) at 110 ml min^{-1} and H_2S at a flow rate of 4 ml min^{-1}. All precursors and their resulting encapsulates were characterised by electron diffraction (ED) and high resolution transmission electron microscopy (HRTEM).

In general, IFs prepared from the low S_g (*i.e.* large particle size) WC precursor materials were completely covered by the encapsulating 2H-WS_2 network which varied from between 2 and 20 2H-WS_2 layers per encapsulate. The size of the resulting encapsulates were found to be in the same range as the precursor particles (see above), although some slight expansion in size had probably occurred as a result of the conversion from the relatively dense carbide to the much bulkier sulfide [Fig. 1(a)]. For these relatively large encapsulates, there was no obvious crystallographic relationship between the hexagonal $P\bar{6}m2$ WC structure [Fig. 1(a)] and the encapsulating $P6_3/mmc$ 2H-WS_2 network [Fig. 1(a)]. In Fig. 1(b), for example, is shown a large carbide encapsulate (denoted **WC**) coated with a non-uniform 2H-WS_2 'skin', the external form of which was determined by the adventitious morphology of the precursor rather than by the encapsulate microstructure. On the surface of the encapsulate in Fig. 1(b), a small 2H-WS_2 nanotube (denoted **N**) has formed on the surface of the encapsulate that presumably originated from an asperity occurring on the surface of the unreacted WC precursor. A further point is that, regardless of the length of the sulfidisation step, the 2H-WS_2 material did not penetrate beyond a depth of *ca.* 100 Å into the WC encapsulates, except where assisted by surface irregularities of the type giving rise to the prominent feature in Fig. 1(b).

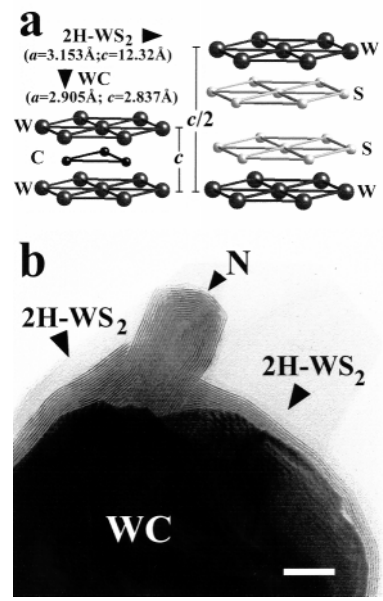

Fig. 1 (a) Schematic depictions of the hexagonal $P\bar{6}m2$ WC and $P6_3/mmc$ 2H-WS_2 structures showing the differences in *c vs.* stacking. (b) HRTEM micrograph showing 2H-WS_2 encapsulated low S_g WC particle. A small asperity in the original precursor particle has led to the formation of a small nanotube (**N**) on the surface of the encapsulate (scale bar ≈ 140 Å).

In the instance of encapsulates formed from the high S_g WC originating from carburised WO_3, near complete conversion to 2H-WS_2 IF structures was achieved. In the example shown in Fig. 2(a), a completely reacted and ellipsoidal 2H-WS_2 structure (overlapping with other IF material) is visible. A '$\bar{C}$'-shaped shard of IF material (denoted **S**) is also visible in the lower left region of the micrograph. Even in structures originating from relatively larger precursor particles than those giving rise to the structures in Fig. 2(a), fully reacted IFs were generally obtained.

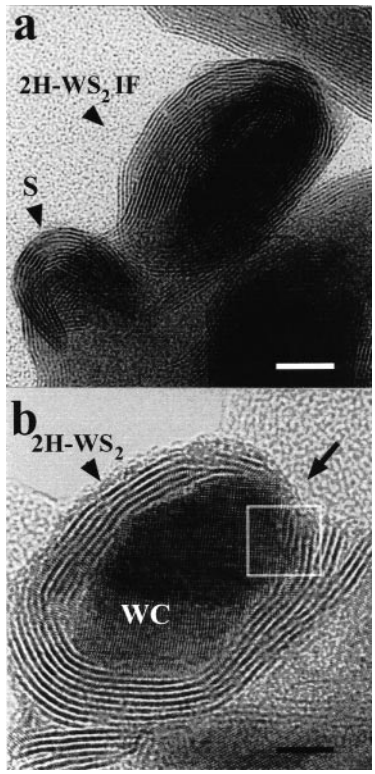

Fig. 2 (a) HRTEM micrograph showing a 2H-WS_2 IF nanoparticle originating from a high S_g precursor formed by carburisation of small WO_3 particles. A small C-shaped shard (**S**) of IF material is visible in the lower left of the micrograph (scale bar ≈ 75 Å). (b) 2H-WS_2 IF encapsulated high S_g particle formed from a ball milled WC precursor (scale bar ≈ 50 Å).

This total conversion can be explained in terms of fairly high residual oxygen content present in the carburised precursor, which may be either present in the main bulk of the WC particles as oxycarbide or on the surfaces of the carbide particles as an oxidised passivated layer.

The main difference between IF materials grown from the precursor originating from the carburised WO_3 particles and the ball-milled WC precursor is that the latter product still contained unreacted carbide. Furthermore, as with encapsulates formed from the low S_g (*i.e.* large particle size) WC precursor, the number of encapsulating shells formed around the encapsulate was limited to 2–20 regardless of the length of the sulfidisation step. In Fig. 2(b), we see a small carbide encapsulate formed from a ball milled WC particle encased in a 2H-WS_2 IF 'shell' of variable thickness up to 10 layers. Note that in the upper right region of the micrograph, a small break in the coverage is visible (arrowed) but the 2H-WS_2 coverage of most of the observed encapsulates was generally found to be complete. These smaller encapsulates yielded information with respect to the growth mechanism of the encapsulating sulfide material from the carbide. In Fig. 3(a) we see a fast Fourier transform (FFT) calculated from the WC/2H-WS_2 interface obtained from the region indicated by the superimposed square in Fig. 2(b). The main calculated reflections in the FFT can be indexed according to an [01$\bar{1}$0] projection of WC. Superimposed upon the pattern, a blurred reflection corresponding to the (0002) planes of encapsulating 2H-WS_2 is visible. Note that this reflection is aligned along the [0001] direction with respect to the carbide. In Fig. 3(b) the microstructure of the carbide (denoted **WC**) in relation to the encapsulating sulfide (denoted **2H-WS_2**) is shown. A small disordered region of carbide (denoted **DS**) is visible at the lower middle of the micrograph caused either by mechanical deformation of the carbide during the ball-milling process or by stacking faults present in the

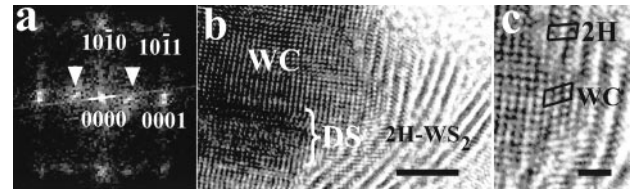

Fig. 3 (a) Calculated ED pattern, obtained from a FFT of the indicated region in Fig. 2(b) corresponding to the WC/2H-WS_2 interface. The 0002 reflections of the sulfide are arranged along [0001] with respect to the carbide. (b) HRTEM micrograph showing the WC/2H-WS_2 interface. A distorted region (**DS**) is visible in the carbide microstructure (scale bar ≈ 35 Å). (c) Enlargement of the WC/2H-WS_2 interface showing intergrowth between two layers of the distorted carbide structure (**WC**) and one layer of the sulfide (**2H**; scale bar ≈ 10 Å).

original material. In a further enlargement [Fig. 3(c)], we see that two distorted layers of the carbide (denoted **WC**) intergrow with one layer (denoted **2H**) of the sulfide. This type of growth may be important in terms of initiating the propagation of the 2H-WS_2 encapsulating material. However, we see from the lower magnification micrographs of both the low S_g and high S_g WC encapsulates [*i.e.* Fig. 1(b) and 2(b)] that the adventitious morphology of the precursor plays a more important rôle in terms of determining the overall shape of the obtained encapsulates. This is in accordance with the previous observations for WO_{3-x} oxides encapsulated within 2H-WS_2 IF materials.[12]

The consequence of encapsulation of WC inside 2H-WS_2 IF shells with respect to the composite physical properties will be to enhance considerably the structural rigidity of the resulting 2H-WS_2/WC encapsulates, which may enhance their performance in tribological applications. This would be an interesting result as WC is one of the hardest known materials. Furthermore, the inclusion of the more metallic metal carbide within the sulfide should also enhance the conductive properties of the resulting composite material.

The authors are indebted to the UK–Israel Science and Technology program which is governed jointly by the British Council and the Israel Ministry of Science. A. R. is indebted to the French Ministry of Foreign Affairs (Lavoisier program) for additional financial support.

Notes and references

1 R. Tenne, L. Margulis, M. Genut and G. Hodes, *Nature*, 1993, **360**, 444.
2 L. Margulis, G. Salitra, R. Tenne and M. Talianker, *Nature*, 1993, **365**, 113.
3 Y. Feldman, G.L. Frey, M. Homyonfer, V. Lyakhovitskaya, L. Margulis, H. Cohen, G. Hodes, J. L. Hutchison and R. Tenne, *J. Am. Chem. Soc.*, 1996, **118**, 5362.
4 T. Tsirlina, Y. Feldman, M. Homyonfer, J. Sloan, J. L. Hutchison and R. Tenne, *Fullerene Sci. Technol.*, 1998, **6**, 157.
5 Y. Feldman, E. Wasserman, D. J. Srolovitz and R. Tenne, *Science*, 1995, **267**, 222.
6 M. Homyonfer, Y. Mastai, M. Hershfinkel, V. Volterra, J. L. Hutchison and R. Tenne, *J. Am. Chem. Soc.*, 1996, **188**, 7804.
7 M. Remškar, Z. Škraba, M. Regula, C. Ballif, R. Sanjinés and F. Lévy, *Adv. Mater.*, 1998, **10**, 246.
8 S. Iijima, *Nature*, 1991, **354**, 56.
9 L. Rapoport, Y. Bilik, Y. Feldman, M. Homyonfer, S. R. Cohen and R. Tenne, *Nature*, 1997, **387**, 791.
10 M. Homyonfer, B. Alperson, Y. Rosenberg, L. Sapir, S. R. Cohen, G. Hodes and R. Tenne, *J. Am. Chem. Soc.*, 1997, **119**, 2693.
11 A. P. E. York, J. B. Claridge, A. J. Brungs, S. C. Tsang and M. L. H. Green, *Stud. Surf. Sci. Catal.*, 1997, **110**, 711.
12 J. Sloan, J. L. Hutchison, R. Tenne, Y. Feldman, T. Tsirlina and M. Homyonfer, *J. Solid State Chem.*, in press.

Communication 8/09273G

ChemComm

A simple photo-affinity labeling protocol

Hong-yu Li, Ying Liu, Kan Fang, and Koji Nakanishi*

Department of Chemistry, Columbia University, New York, NY 10027, USA. E-mail: kn5@columbia.edu

Received (in Corvallis, OR, USA) 3rd December 1998, Accepted 28th December 1998

After photo-crosslinking and proteolysis of a photoaffinity labeled ligand to its receptor, the ester group incorporated in the ligand is cleaved by an amine with specific functionality, which displaces the bulk of the ligand from the peptide fragments, and facilitates subsequent tandem mass spectrometric sequencing.

With the very rapid advancement in analytical methods, the technique of photoaffinity labeling has become an increasingly central tool for investigating 3D interactions between ligands and receptors on a molecular basis.[1] Although photoaffinity labeling was introduced over thirty years ago by Westheimer,[2] the protocol remains basically unchanged. It involves synthesis of radioactive and photo-labeled ligands, incubation, photolysis, proteolysis and sequencing of radiolabeled peptide fragments by amino acid sequencer. However, in the case of membrane-bound receptors, the isolation of cross-linked peptide fragments from a sticky peptide mixture has been a particularly challenging and occasionally impossible task; nevertheless, photoaffinity labeling is the only general method to investigate such ligand–receptor interactions at a molecular level.[1]

Recently we introduced the protocol of using the bifunctional photoaffinity probe (BPP)[3] **1** coupled with tandem mass spectrometry (MS) to facilitate the often tedious photoaffinity studies dealing with membrane-bound receptors (Fig.1).

The ligand-BPP moiety which is bound to biotin through a linker is incubated with the receptor and irradiated with 350 nm light leading to site **A** photolysis and photocrosslinking. This is followed by receptor proteolysis and a second irradiation with 350 nm light, but under mildly basic conditions, upon which site

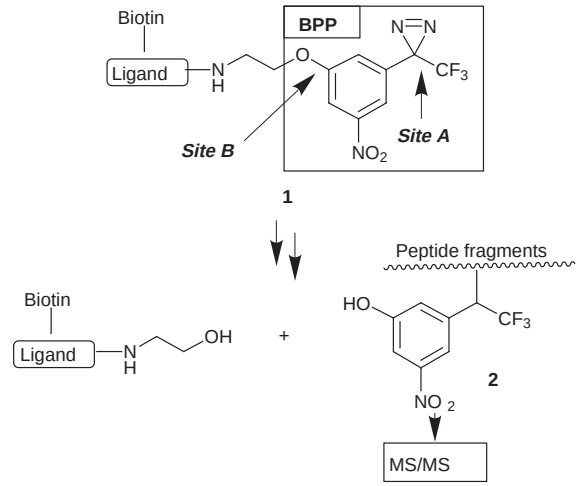

Fig. 1 Bifunctional photoaffinity probe (BPP).

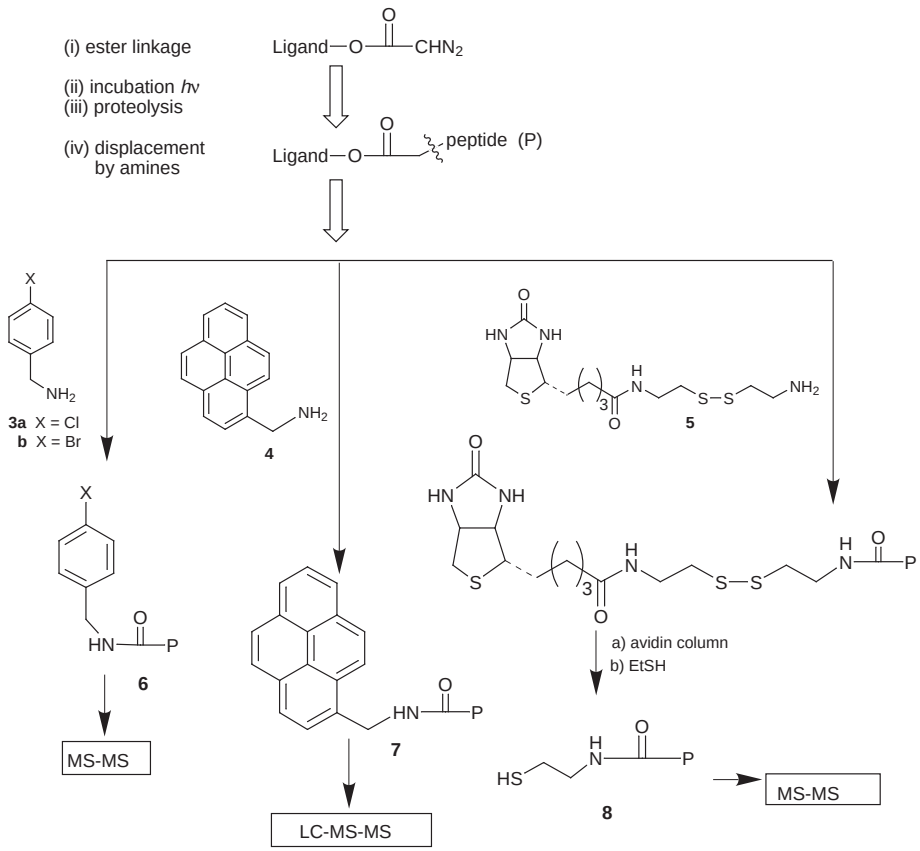

Fig. 2 General scheme of the protocol.

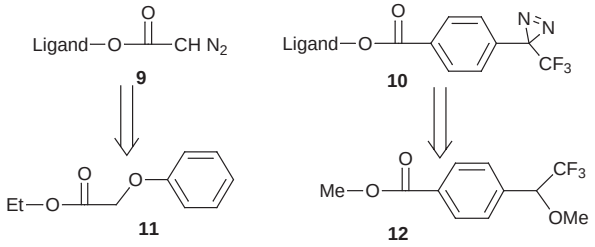

Fig. 3 Model compounds for the aminolysis reaction.

B cleavage occurs to detach the bulk of the ligand from the crosslinked peptide fragment; the ligand moiety and non-crosslinked fragments are separated from crosslinked fragment **2**, which is sequenced by tandem MS. This protocol is currently being applied to a particular ligand–receptor pair.

In the following, we introduce an alternative to further facilitate the photoaffinity crosslinking and sequencing processes. In the case of BPP, the ligand moiety was removed by a second photolysis performed under mild base conditions. In this revised protocol which does not use BPP, the ligand moiety is removed by aminolysis of a labile ester bond, as summarized in Fig. 2: (i) esterification of the hydroxy group with the appropriate photolabel, *e.g.* diazoacetate; (ii) incubation of ligand with its receptor followed by photolysis; (iii) enzymatic and/or chemical cleavage of the receptor; (iv) ester aminolysis and removal of the ligand moiety using amines **3**–**5**†‡ with functionalities for identification and/or purification purposes, *e.g.* bromine or chlorine atoms as tags for MS identification (**3**), fluorescence tag for HPLC detection (**4**), biotin tag for purification with immobilized avidin (**5**); (v) sequencing of tagged peptide fragments by tandem MS (MS/MS).[4–6]

Here, aminolysis performs the dual function of removing the undesired ligand moiety[7–9] and introducing the tag for MS sequencing, as well as purification. Namely, benzylamines **3** carry the isotopic halogen atoms[10] for facile MS identification, pyren-1-ylmethylamine **4** introduces a fluorescent tag[11] for chromatographic detection, if necessary, prior to MS, while biotinylated amine **5** with a cleavable disulfide bond is useful for separation of cross-linked peptide fragment(s) by avidin chromatography.[12,13]

A wide variety of photolabeling probes can be adapted to the protocol either directly or *via* short linkers, *e.g.* ethanolamine and glycolic acid, to modify either the ligand or the photolabile probes before linking. The aminolysis was checked with model compounds **11** and **12**, the products that might be produced from photolabeled ligands **9** and **10** (Fig. 3), respectively.

Ester **11** was converted into the amide upon treatment with 150 equiv.‡ of amines **3a**, **3b**, **4**, and **5**,§ 50° C, 1 day, in yields of 75, 61, 64 and 52%, respectively. Aminolysis of ester **11** with base **3a**, performed in the presence of four peptides Gly-Gly-Phe, Lys-Phe, Gly-Leu-Tyr and Phe-Tyr, resulted in a 62% transformation, demonstrating that peptide bonds are not affected; the sluggish aminolysis of aromatic esters was accelerated upon addition of NaCN,¶ in which case 70% of ester **12**‖ was aminolized overnight by 100 equiv. of amine **3a** in pyridine.** The disulfide bond in the biotinylated amide derived from **5** and **11** was readily cleaved by EtSH to give product **8** (P = phenoxymethyl) without biotin, suited for tandem MS analysis, in quantitative yield.††

The present simple protocol, which provides an alternative to the BPP approach, is currently being applied to an actual ligand–receptor system.

This work was supported by NIH Grant AI 100187. We are grateful to Drs Yasuhiro Itagaki and Masaru Hashimoto, and Mr Jinsong Guo, for discussions.

Notes and references

† Pyren-1-ylmethylamine hydrochloride and 4-bromobenzylamine hydrochloride are commercially available (Aldrich). The free pyren-1-ylmethylamine and 4-bromobenzylamine were obtained by passing their hydrochlorides through an ion exchange column (OH^- type). If pyren-1-ylmethylamine were brominated, the fluorophore will serve as a MS tag as well.

‡ Although the amino group in Lys in the peptide would be deactivated by protonation or hydrogen bonding, in principle, it can aminolyze the ester. Therefore, excess amine is required, which also accelerates the reaction.

§ Amine **5** was made by the coupling of cystamine and (+)-biotin 4-nitrophenyl ester.

¶ NaCN is a very mild catalyst. It is likely that the attack of cyanide anion occurs only on the ester bond without damage of the peptide fragment (ref. 14).

‖ Ester **12** was readily prepared from the photoaffinity labeling probe 4-(1-azi-2,2,2-trifluoroethyl)benzoic acid (ref. 15) by photolysis and then methylation.

** The aminolysis works in a wide spectrum of polar solvents, such as water, EtOH, MeOH, pyridine, *etc.*

†† *Selected data* for amides: Amide from **3a** and **11**: *m/z* (EI) found: 275.0721 [$(M)^+$ $C_{15}H_{14}O_2N_3{}^{35}Cl$], calc.: 275.0713. Amide from **3a** and **12**: *m/z* (EI) found: 357.0739 [$(M)^+$ $C_{17}H_{15}O_2N^{35}ClF_3$], calc.: 357.0743. Amide from **3b** and **11**: *m/z* (FAB) found: 319.0210 [$(M + 1)^+$ $C_{15}H_{14}O_2NBr^{79}$], calc.: 319.0208. Amide from **4** and **11**: *m/z* (EI) found: 365.1422 [$(M)^+$ $C_{25}H_{19}O_2N$], calc.: 365.1416. Amide from **5** and **11**: *m/z* (FAB) found: 513.1688 [$(M + 1)^+$ $C_{22}H_{33}O_4N_4S_3$], calc.: 513.1664.

1 F. Kotzyba-Hibert, I. Kapfer and M. Goeldner, *Angew. Chem., Int. Ed. Engl.*, 1995, **34**, 1296 (Review).
2 A. Singh, E. R. Thorton and F. H. Westheimer, *J. Biol. Chem.*, 1962, **237**, 3006.
3 K. Fang, M. Hashimoto, S. Jockusch, J. N. Turro and K. Nakanishi, *J. Am. Chem. Soc.*, 1998, **120**, 8543.
4 R. Orlando, P. T. M. Kenny, C. Moquin-Pattey, K. Lerro and K. Nakanishi, *Org. Mass Spectrom.*, 1993, **28**, 1395.
5 X. Yu, Z. Wu and C. Fenselau, *Biochemistry*, 1995, **34**, 3377.
6 L. E. Ball, J. E. Oatis Jr., K. Dharmasiri, M. Busman, J. Wang, L. B. Cowden, A. Galijatovic, N. Chen, R. K. Crouch and D. R. Knapp, *Protein Sci.*, 1998, **7**, 758.
7 H. K. Bell, *Tetrahedron Lett.*, 1986, **27**, 2263.
8 T. Hogberg, P. Strom, M. Ebner and S. Ramsby, *J. Org. Chem.*, 1987, **52**, 2033.
9 E. M. Suh and Y. Kishi, *J. Am. Chem. Soc.*, 1994, **116**, 11205.
10 H. Y. Li, S. Matsunaga and N. Fusetani, *J. Med. Chem.*, 1995, **38**, 338.
11 C. V. Kumar, A. Buranaprapuk, G. J. Opiteck, M. B. Moyer, S. Jockusch and N. J. Turro, *Proc. Natl. Acad. Sci. U.S.A.*, 1998, **95**, 10361.
12 Y. Hatanaka, M. Hashimoto and Y. Kanaoka, *J. Am. Chem. Soc.*, 1998, **120**, 453.
13 M. A. Shogren-Knaak and B. Imperiali, *Tetrahedron Lett.*, 1998, **39**, 8241.
14 S. Hunig and R. Schaller, *Angew. Chem., Int. Ed. Engl.*, 1982, **21**, 36.
15 M. Nassal, *Liebigs Ann. Chem.*, 1983, 1510.

Communication 8/09507H

ChemComm

Transformation of fusicocca-2,10(14)-dien-8β-ol into fusicoccin J by the fusicoccin-producing fungus, *Phomopsis (Fusicoccum) amygdali*. Support for the intermediacy of fusicocca-2,10(14)-diene in the fusicoccin biosynthesis

Nobuo Kato,*[a] Chang-Shan Zhang,[a] Naoto Tajima,[b] Akira Mori,[a] Antonio Granit[c] and Takeshi Sassa*[b]

[a] *Institute of Advanced Material Study, Kyushu University, Kasuga, Fukuoka 816-8580, Japan. E-mail: kato-n@cm.kyushu-u.ac.jp*

[b] *Department of Bioresources, Faculty of Agriculture, Yamagata University, Tsuruoka, Yamagata 997-8555, Japan. E-mail: tsassa@tds1.tr.yamagata-u.ac.jp*

[c] *Department of Plant Pathology, University of Bari, I-70126 Bari, Italy*

Received (in Cambridge, UK) 4th December 1998, Accepted 6th January 1999

(+)-Fusicocca-2,10(14)-diene, isolated recently by the authors, is most likely a genuine hydrocarbon intermediate in the biosynthesis of fusicoccin, as its 8β-hydroxy derivative is smoothly and efficiently converted into fusicoccin J by the fusicoccin-producing fungus, *Phomopsis (Fusicoccum) amygdali* F6.

Fusicoccin A (**1**)[1] and J (**2**)[2] and their congeners, produced by the phytopathogenic fungus *Phomopsis (Fusicoccum) amygdali*, possess potent H^+–ATPase activating activity.[3] Their

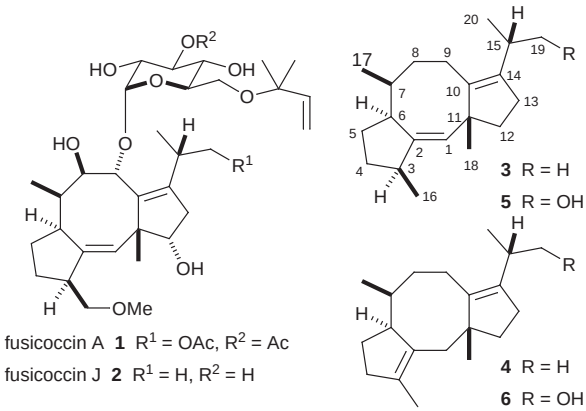

action is at the center of interest, since the fusicoccin-binding 14-3-3 proteins are regarded as key proteins in intracellular signal transductions in both plant and animal cells.[4]

Earlier studies on the fusicoccin biosynthesis have postulated fusicocca-1,10(14)-diene **3** as the hydrocarbon intermediate.[5] However, we have recently isolated fusicocca-2,10(14)-diene **4**, a double bond isomer of **3**, from *P. amygdali* F6† as a main hydrocarbon constituent.[6] This fact called our attention to the initially-forming fusicoccane hydrocarbon in the fusicoccin biosynthesis. To clarify the true hydrocarbon intermediate, feeding experiments of synthetic derivatives of both **3** and **4** have been carried out. The results reported here strongly suggest that **4**, not **3**, is the genuine hydrocarbon.

For feeding experiments of synthetic intermediary substrates, we chose hydrophilic monohydroxylated derivatives of **3** and **4**, which should have suitable solubility in the culture medium. As a preliminary study, feeding experiments (*vide infra*) using fusicocca-1,10(14)-dien-19-ol **5** and its isomer **6**[6] were carried out. Feeding of **5** showed no significant formation of the corresponding metabolites and the production of fusicoccins fell off clearly as monitored on TLC with a control mixture of metabolites, indicating that **5** seemed to perturb the biological processes. On the other hand, **6** gave a new metabolite {$[\alpha]_D^{22}$ + 35.8 (*c* 0.30, $CHCl_3$)}, whose structure was elucidated as fusicocca-2,10(14)-diene-8β,16,19-triol **7** from its spectral data (Scheme 1).‡

These results led the authors to suspect that 8β-hydroxylation at the non-allylic position occurs at an early stage of the biosynthesis. Therefore, we turned our attention to the transformations of the 8β-hydroxylated derivatives of **3** and **4**. The 8α-hydroxy-substituents of **8** and **9**[6] were epimerized by an oxidation–reduction process. Then, the 19-hydroxy group was removed by $LiEt_3BD$ reduction of the corresponding mesylate providing the deuterated compounds **10** and **11**.

A solution of 60 mg of **10** or **11** in a small amount of EtOH was added equally (10 mg each) to six cultures of the fungus strain F6 which had been growing for 2 or 3 days at 25 °C.§ After additional cultivation for 3 days, the combined culture filtrate was extracted with EtOAc at pH 9.0.

From the feeding experiment of **10**, which has the 1,10(14)-diene system typical for fusicoccin, 50 mg of **2** and 13 mg of a new non-natural metabolite {mp 126–127 °C, $[\alpha]_D^{22}$ + 16.6 (*c* 0.41, $CHCl_3$)} were obtained. The structure of the latter was elucidated to be 16-demethoxy-6′-*O*-de-*tert*-pentenyl [19-$^2H_1$]fusicoccin J (**12**) from its spectral data (Scheme 2).

The molecular formula is $C_{26}H_{41}DO_8$; FAB MS: *m/z* 506.2844 [(M + Na)$^+$, $C_{26}H_{41}DO_8Na$ requires, 506.2840]. ^1H and ^{13}C NMR ($CDCl_3$–CD_3OD 5 : 1, +40 °C, 600 and 150 MHz, respectively) signals are fully assignable by 2D measurements. Diagnostic signals are as follows; δ_H 1.02 (2H, br d, *J* 6.8; H19, deuterated methyl), 1.09 (3H, d, *J* 7.0; H16), 1.18 (3H, s; H18), 3.18 (sextet, *J* 6.8; H15), 3.46 (dd, *J* 9.5, 9.3; H4′), 3.50 (dd, *J* 9.5, 3.8; H2′), 3.63 (ddd, *J* 9.5, 3.5, 3.3; H5′), 3.67 (dd, *J* 11.7, 3.5; H6′), 3.72 (t, *J* 6.2; H12), 3.75 (dd, *J* 9.5, 9.3; H3′), 3.77 (dd,

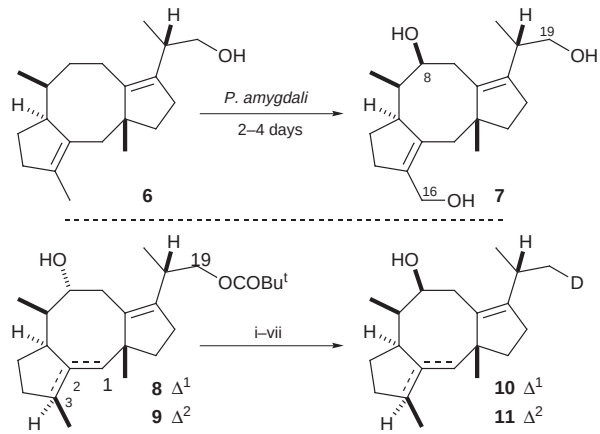

Scheme 1 *Reagents and conditions*: i, $(ClCO)_2$, DMSO then Et_3N, CH_2Cl_2 (Δ^1, 86%; Δ^2, 97%); ii, DIBAL-H, THF [Δ^1, 24% (**8**, 42%); Δ^2, 52% (**9**, 15%)]; iii, TBDMSCl, imidazole, CH_2Cl_2; iv, LAH, THF; v, MsCl, Py (3 steps, Δ^1, 83%; Δ^2, 73%); vi, $LiEt_3BD$, THF; vii, Bu_4NF, THF (2 steps, Δ^1, 87%; Δ^2, 86%).

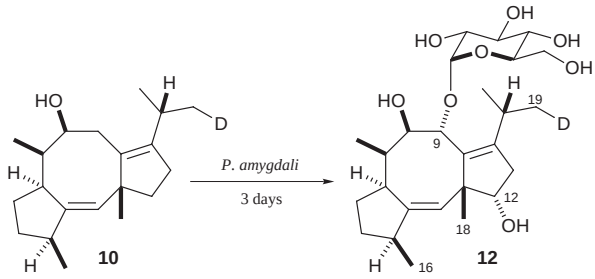

Scheme 2

J 11.7, 3.3; H6′), 3.80 (d, *J* 9.9; H9), 3.92 (dd, *J* 9.9, 4.6; H8), 4.95 (d, *J* 3.8; H1′) and 5.20 (t, *J* 1.8; H1); δ_C 19.73 (C16), 21.01 (t, C19, deuterated carbon), 61.83 (C6′), 70.59 (C4′), 71.82 (C5′), 72.37 (C2′), 73.90 (C3′), 77.55 (C9), 78.62 (C8), 80.22 (C12) and 101.87 (C1′). These data clearly reveal that **12** was generated only from feeded **10**; the C9 and C12 positions were hydroxylated; α-glucosidation occurred at C9. The C16 methyl was preserved intact. The stereochemistry of the hydroxylated positions was confirmed with NOE enhancements of H9 and H12 upon irradiation of H18. The glucosidic linkage between C1′ and C9 was deduced from HMBC correlations of C9/H1′ and C1′/H9. Thus, although **12** is a fusicoccin type-glucoside, it lacks the hydroxylation of its C16-methyl group. The fusicoccin J (**2**) obtained in this feeding experiment was natural; no deuterated substance was detected by NMR spectroscopy. Identification of **12** suggests that 12α-hydroxylation of fusicoccin precedes the prenylation of its glucosyl moiety.

The result obtained from the feeding experiment using **11** was more striking and conclusive for the elucidation of the biosynthetic pathway of **2**. Fusicoccin J (**2**, 51 mg) isolated from the culture broth of this experiment was found to have a remarkable amount of the deuterated substance (**2**-*d*). Incorporation of **11** into **2**-*d* was easily recognized by ^{1}H, ^{13}C NMR ($CDCl_3$, 600 and 150 MHz, respectively) and mass spectra. The distinguishable signals between **2** and **2**-*d* are δ_H 1.04 (2H, br d, *J* 6.8; **2**-*d* H19, deuterated methyl)/1.06 (3H, d, *J* 6.8; **2**-H19) and 3.169 (sextet, *J* 6.8; **2**-*d* H15)/3.174 (septet, *J* 6.8; **2** H15); δ_C 20.44 (**2**-*d* C20)/20.47 (**2** C20), 20.98 (t, **2**-*d* C19, deuterated carbon)/21.27 (**2** C19) and 27.78 (**2**-*d* C15)/27.86 (**2** C15). In the FAB mass spectrum, the ratios of **2** $(M + H)^+$/**2**-*d* $(M + H)^+$ and **2** $(M + Na)^+$/**2**-*d* $(M + Na)^+$ are close to 1 : 1; *m/z* 581 (7.9%)/582 (7.9%) and 603 (6.3%)/604 (6.7%); FAB-MS: *m/z* 603.3513 ($C_{32}H_{52}O_9Na$ requires, 603.3509) and 604.3577 ($C_{32}H_{51}DO_9Na$ requires, 604.3572). At least 40% of fusicoccin J was derived from the feeded substrate **11**, the double bond of which had originally been located at the C2–C3 position.

Thus, these results clearly demonstrate that the C16 methyl has to be allylic for its conversion into the methoxymethyl group. Therefore **4**, actually isolated from mycelia of the fungus, is most likely the genuine hydrocarbon intermediate in the biosynthetic pathway of fusicoccin.

Our interests are currently focused on the identification of non-deuterated **11** from the fungus and on the chemical mechanism of the double bond isomerization occurring during the conversion of **11** to **2**. The transformation from **10** to **12** by the fungus can be regarded as the creation of an 'artificial fusicoccin' from a '*pseudo*-biosynthetic intermediate'. Efforts on this line are also in progress.

Notes and references

† The fungus strain F6 produces fusicoccin J as a main metabolite (*ca*. 120 μg ml^{-1}) in the culture medium indicated below.
‡ Details will be reported in a full paper.
§ The composition of the culture medium was as follows; 8.0% commercial sugar, 1.0% corn steep liquor, 0.5% peptone and 0.5% NaCl in 100 ml of deionized water .

1 A. Ballio, M. Brufani, C. G. Casinovi, S. Cerrini, W. Fedeli, R. Pellicciari, B. Santurbano and A. Vaciago, *Experientia*, 1968, **24**, 631; K. D. Barrow, D. H. R. Barton, E. B. Chain, U. F. W. Ohnsorge and R. Thomas, *Chem. Commun.*, 1968, 1198.
2 A. Ballio, C. G. Casinovi, V. D'Alessio, G. Grandolini, G. Randazzo and C. Rossi, *Experientia*, 1974, **30**, 844; K. D. Barrow, D. H. R. Barton, E. Chain, D. Bageenda-Kasujja and G. Mellows, *J. Chem. Soc., Perkin Trans. 1*, 1975, 877.
3 E. Marré, *Ann. Rev. Plant Physiol.*, 1979, **30**, 273.
4 B. De Boer, *Trends Plant Sci.*, 1997, **2**, 60.
5 A. Banerji, R. B. Jones, G. Mellows, L. Phillips and K.-Y. Sim, *J. Chem. Soc., Chem. Commun.*, 1976, 2221; G. Randazzo, A. Evidente, R. Capasso, F. Colantuoni, L. Tuttobello and A. Ballio, *Gazz. Chim. Ital.*, 1979, **109**, 101.
6 N. Kato, C.-S. Zhang, T. Matsui, H. Iwabuchi, A. Mori, A. Ballio and T. Sassa, *J. Chem. Soc., Perkin Trans. 1*, 1998, 2473.

Communication 8/09496I

Novel alkaline earth supported catalysts for thiophene synthesis

Barry W. L. Southward,*[a] Lance S. Fuller,[b] Graham J. Hutchings,[c] Richard W. Joyner[d] and Russell A. Stewart[b]

[a] *Catalysis Research Centre, Department of Chemistry, University of Reading, Whiteknights, Reading, UK RG6 6AD. E-mail: b.w.l.southward@reading.ac.uk*
[b] *Inspec Fine Chemicals Ltd., Four Ashes, Wolverhampton, UK WV10 7BP*
[c] *Department of Chemistry, University of Wales at Cardiff, PO Box 912, Cardiff, UK CF1 3TB*
[d] *Nottingham Trent University, Burton Street, Nottingham, UK NG1 4BU*

Received (in Liverpool, UK) 10th December 1998, Accepted 15th January 1999

3-Methylthiophene can be synthesised in yields > 95 mol% from the reaction of 2-methylbutanol and CS_2 over MgO-supported potassium-promoted '$Fe_{0.95}Cr_{0.05}OOK$'; catalysts using γ-Al_2O_3 or other alkaline earth oxides as supports are less effective.

The derivatives of the sulfur-containing heterocycle thiophene have been widely used for many years as raw materials in the production of agrochemicals, dyes and pharmaceuticals.[1] As a consequence the synthesis of such compounds on an industrial scale (1000 tonnes per annum) is of significant economic importance and provides considerable incentive for research. Currently market demand is met by two heterogeneous catalytic processes involving the reaction of organic oxygenates (alcohols, carbonyls, α,β-unsaturated aldehydes) with a suitable sulfur source (CS_2 or H_2S) over γ-Al_2O_3-based catalysts at high temperatures (> 450 °C).[2,3] However, the synthesis of substituted thiophenes by standard high temperature vapour phase methods has been found to be far less efficient than the synthesis of the unsubstituted parent molecule, with yields decreasing from > 90% for thiophene to *ca.* 40–50% for 3-methylthiophene.[2,3] Here we address this problem and present initial results for catalysts based upon alkaline earth oxide-supported $Fe_{0.95}Cr_{0.05}OOK$ catalysts which give yields of 3-methylthiophene (3MT) > 95 mol% from the reaction of 2-methylbutanol and CS_2.

Catalysts were prepared by dissolution of 95 : 5 wt% Fe_2SO_4 : Cr_2SO_4 in distilled water (80 °C), with constant stirring. K_2CO_3 solution (2 : 1 K : Me^{3+}) was added, followed by the weight balance of support (85%). The mixture was evaporated to a paste, dried (120 °C, 24 h) and calcined (air, 24 h, 700 °C). Samples were then pelleted and sieved (0.6–1.0 mm), prior to testing for 3-methylthiophene synthesis in a fixed bed microreactor.[4] All reactions involved passing a reagent stream of 2-methylbutanol (2MB), CS_2 and N_2 (1 : 1.5 : 80 molar ratio) at a GHSV of 12 000 h^{-1} over 1.0 g of catalyst. Product analysis was performed by on-line GC FID analysis with a carbon balance of 98–100% for all data quoted, based upon conversion of 2MB.

Previously we have demonstrated that a mixed α-$Fe_{0.95}Cr_{0.05}OOH$ material is a highly efficient low temperature 3MT synthesis catalyst.[5,6] Further data have shown that the activity, selectivity and thermal stability of this material may be enhanced by addition of 7.5% K_2CO_3. This is postulated as being linked to the formation of mixed MOOK species (M = Fe or Cr).[6a] In addition, Stobbe *et al.*[4] have shown MgO-supported FeoOK to be an active and selective dehydrogenation catalyst. Hence we have examined the activity of MgO-supported $Fe_{0.95}Cr_{0.05}OOK$ for 3MT synthesis.

The effect of temperature on the performance of $Fe_{0.95}Cr_{0.05}OOK$/MgO for 3MT synthesis is illustrated in Fig. 1 and Table 1. Initially there is negligible 2MB conversion, however, for T > 325 °C there are dramatic increases in conversion and 3MT yield. This is initially coupled with a significant production of thiophene arising from β-methyl scission, as reflected in the concomitant increases in light fractions. However, at temperatures > 425 °C there is a plateau of activity with 3MT yields > 95 mol%, at 100 mol% conversion of 2MB. This contrasts with the data obtained for the current commercially utilised catalyst (7.5% K_2CO_3-promoted Cr_2O_3/γ-Al_2O_3), which gave a peak yield of *ca.* 78 mol% 3MT at 475 °C. In this case the selectivity of the catalyst is limited by extensive side reactions such as cracking and β-methyl fission which not only limit 3MT selectivity but are also known to have a deleterious effect on catalyst lifetime due to coke build-up.[6a]

In a further set of experiments the effect of support on the activity of the FeCrOOK phase was examined (Table 1). It is apparent that the choice of support has a marked effect on catalyst performance, with optimum activity being obtained for the MgO case. The use of alternative alkaline earth oxide supports resulted in significant decreases in overall activity and 3MT selectivity down the group. Moreover, the selectivity towards 2-methylbutene also increased with the increasing basicity of the support. Conversely, while there is minimal production of the alkene on the acidic FeCrOOK/γ-Al_2O_3, more cracking of the alcohol is observed and the peak of 3MT synthesis activity (*ca.* 95 mol%) is observed at 500 °C. Furthermore, the 3MT production increases linearly with temperature for the γ-Al_2O_3 variant with no observed plateau temperature, further hindering its industrial application.

The high activity of these materials is consistent with previous findings[5–7] and is ascribed to the presence of $Fe_{0.95}Cr_{0.05}OOK$. Attempts to characterise this phase *via* X-ray

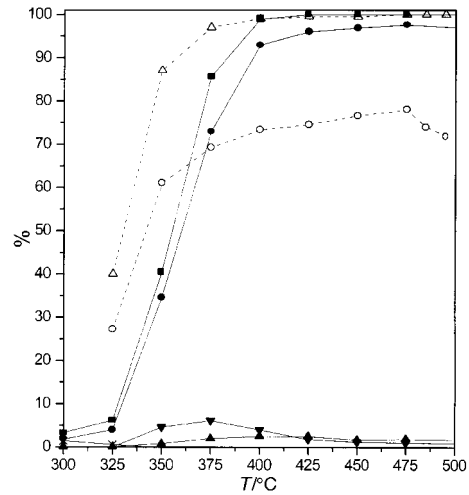

Fig. 1 3MT synthesis performance comparison of $Fe_{0.95}Cr_{0.05}OOK$/MgO and the current industrial catalyst (7.5 K_2CO_3/11% Cr_2O_3/γ-Al_2O_3). Gas hourly space velocity (GHSV) = 12 000 h^{-1}, all samples taken after 15 min equilibration at temperature. (△) indcat conversion of 2MB, (○) indcat 3MT mol% yield, (■) 2MB conversion FeCrOOK, (●) 3MT yield FeCrOOK, (▼) thiophene yield FeCrOOK, (▲) cracked fractions FeCrOOK, (x) 2-methylbutene FeCrOOK.

Table 1 The activity of supported 'FeCrOOK' for 3MT synthesis

Catalyst	Activity/ mol%	*T*/°C 300	325	350	375	400	425	450	475	500
	3MT yield	1.8	4.0	34.5	72.9	92.9	96.0	96.9	97.6	97.0
	2MB conv	3.3	6.2	40.3	85.6	98.9	100	100	100	100
FeCrOOK/MgO	Thiophene	0.0	0.1	4.6	9.0	5.2	0.8	0.4	0.6	0.7
	Cracked	1.4	0.1	0.8	3.6	0.8	3.2	2.6	1.8	2.3
	2MeButene	0.1	2.1	0.4	0.0	0.0	0.0	0.0	0.0	0.0
	3MT	1.5	1.2	1.5	3.3	13.3	35.3	49.6	67.0	52.5
FeCrOOK/CaO	2MB conv	3.1	3.3	4.8	11.3	30.2	51.3	63.5	79.4	68.4
	2MeButene	1.4	2.0	3.3	7.8	16.1	14.5	12.1	10.9	14.8
	3MT	0.7	0.4	1.1	1.1	2.3	4.4	8.6	12.3	11.2
FeCrOOK/SrO	2MB conv	1.6	1.4	2.7	3.6	7.5	12.0	19.9	24.3	24.8
	2MeButene	0.6	0.6	1.3	2.2	4.8	7.1	10.6	11.4	13.1
	3MT	0.4	0.9	1.2	1.4	3.1	3.9	4.9	6.7	7.4
FeCrOOK/BaO	2MB conv	1.6	2.2	3.2	4.1	6.9	9.4	12.8	17.5	17.0
	2MeButene	0.9	1.1	1.8	2.5	3.6	5.3	7.7	10.5	9.3
Ind. Cat+	3MT	—	27.2	60.9	69.8	73.3	74.6	78.0	74.1	72.1
	2MB conv	—	40.1	87.0	97.2	99.0	99.5	100	100	100
7.5% K/11% Cr_2O_3/MgO	3MT	0.0	5.4	14.6	19.2	29.1	40.1	82.9	90.9	94.1
	2MB Conv	4.2	12.4	26.9	33.4	45.7	61.3	95.9	97.2	99.0

Table 2 Normalised activities of catalysts for 3MT synthesis

Catalyst	Surface area/ $m^2\ g^{-1}$	NA[a]	CrUV[b]
FeCrOOK/MgO	30	15.12	919200
Industrial catalyst[c]	125	2.90	4000
FeCrOOK/γ-Al_2O_3	220	1.60[d]	97300
Cr_2O_3/MgO	30	9.87	1200
7.5% K Cr_2O_3/MgO	30	14.58[d]	20100

[a] Normalised activity (moles of 3MT per hour per square metre surface area of catalyst). [b] Cr_2O_3. Utilisation value (normalised activity per mole of Cr_2O_3) (nominal values reflecting the effective use of Cr). [c] 7.5 K_2CO_3/11% Cr_2O_3/γ-Al_2O_3. [d] Based upon yield at 500 °C, *cf.* 475 °C for all other samples.

diffraction were unsuccessful, with only support oxide and K_2SO_4 being detected. Similarly, whilst X-ray photon spectroscopy analysis indicated the presence of Fe^{3+} as oxide/oxide hydroxide,[8] no Cr^{3+} (present at 0.3 wt%) was detected. Thus we ascribe the high selectivity to a synergistic phase formation. This premise is suggested by the lower activity of K-promoted Cr_2O_3/MgO (Tables 1, 2) and further supported by the lower intrinsic activity of Fe, *cf.* Cr for heterocycle synthesis.[6a] A comparison of normalised activities and Cr utilisation values (Table 2) supports the claim that activity is not merely due to mixed supported oxides. These findings are also consistent with the work of Stobbe *et al.*[6] who have shown FeOOK to be a specific phase of high dehydrogenation function, a feature which has been found to be of specific importance in the thiophene synthesis mechanism.[5–7]

These data briefly summarise initially findings regarding the activity of this highly promising new class of catalysts.[7] Ongoing trials are assessing their lifetime performance, regeneration characteristics and suitability for industrial application.

We are grateful for the financial support of this work by Synthetic Chemicals Ltd, now Inspec Fine Chemicals Ltd. The contribution of Mr F. P. Getton is also acknowledged.

Notes and references

1 L. S. Fuller, *Thiophene and Thiophene Derivatives, Kirk-Othmer Encyclopaedia of Chemical Technology*, 4th edn., Wiley, New York, 1997, p. 34.
2 J. Barrault, M. Guisnet, R. Lucien and R. Maurel, *J. Chem. Res.*, 1978, (*S*) 207; (*M*) 2634 (US Pat. 4,143,052).
3 N. R. Clark and W. E. Webster, *Br. Pat.* (1,345,203 (assigned to Synthetic Chemicals Ltd).
4 D. E. Stobbe, F. R. van Buren, A. J. van Dillen and J. W. Geus, *J. Catal.*, 1992, **135**, 533.
5 B. W. L. Southward, Lance S. Fuller, G. J. Hutchings, R. W. Joyner and R. A. Stewart, *Chem. Commun.*, 1998, 2541.
6 (*a*) B. W. L. Southward, PhD Thesis, University of Liverpool, 1993; (*b*) B. W. L. Southward, L. S. Fuller, G. J. Hutchings, R. W. Joyner and R. A. Stewart, *Eur. Pat.* 751,138.
7 B. W. L. Southward, L. S. Fuller, G. J. Hutchings, R. W. Joyner and R. A. Stewart, *Eur. Pat.* 751,139.
8 NIST XPS database.

Communication 8/09675I

ChemComm

A novel layered templated lithium zinc phosphate prepared by an unusual solution mediated technique

Torben R. Jensen*[a]† and Rita G. Hazell[b]

[a] *Chemistry Department, University of Southern Denmark, Odense University, DK-5230 Odense M, Denmark*
[b] *Chemistry Department, University of Aarhus, DK-8000 Aarhus C, Denmark*

Received (in Bristol, UK) 11th November 1998, Accepted 12th January 1999

A novel layered lithium zinc phosphate $LiZn(HPO_4)(PO_4)\cdot H_3NCH_2CH_2NH_3\cdot H_2O$ containing ethylenediamine(en), having a long nucleation time, is prepared by moderate temperature solution mediated conversion of a microporous zinc phosphate; its crystal structure is also reported.

Synthetic microporous and layered materials are of considerable interest for a wide variety of industrial and chemical applications, *e.g*. catalysis, ion exchange or intercalation.[1] These materials have expanded their range of compositions tremendously from the original zeolite type aluminium silicate minerals and now include phosphates, arsenates, vanadates, and chalcogenides.[2] Orthophosphates are possibly the fastest expanding group of inorganic materials and recently templated iron phosphates were discovered, arising from the development of new solvothermal synthesis techniques.[3]

Solvothermal synthesis using organic amine ions as templates is a common route to novel open framework materials and detailed knowledge of the synthesis mechanism, including nucleation and crystal growth, is of importance for the design of new materials.[4] The formation of a Mn substituted aluminium phosphate (Mn-AlPO-5, AFI structure) was investigated using *in situ* synchrotron radiation powder diffraction. The crystal growth followed a first order kinetic model after a nucleation period; clearly, lowering the synthesis temperature increases the nucleation time.[5] Similar main features were found for the crystallisation of a microporous oxyfluorinated gallophosphate, ULM-5.[6] Changing the composition of reactants for the ULM-5 synthesis revealed the presence of an intermediate phase; decreasing the synthesis temperature increases the time of stability of the intermediate.[6] In general microporous and layered materials are topologically metastable and convert to more dense phases upon heating dry or in water, *i.e*. approaching higher density and higher thermodynamic stability. In some cases microporous materials can transform to other microporous or layered materials upon prolonged solvothermal treatment at a constant moderate temperature. The materials prepared by such solution mediated conversion might not be attainable increasing the synthesis temperature as the system enters the stability field of other more dense phases. β-$LiZnPO_4\cdot H_2O$, a new variant of the zeolite ABW structure, was initially prepared at room temperature by solution mediated conversion of α-$LiZnPO_4\cdot H_2O$ having a nucleation period of *ca*. 3 months.[7] Variation of the composition of the reaction mixture revealed that β-$LiZnPO_4\cdot H_2O$ could be prepared with a nucleation period of several days.[7] Ambient temperature solution mediated conversion of one metastable phase to another is probably useful in a wide range of chemical compositions for discovering new materials and the method might be characterised as a *chemie douche* technique.[8] Another approach utilises slow diffusion of the reactants in a silica gel. After a nucleation period of *ca*. 3 weeks at ambient conditions crystals of new layered templated aluminium and gallium phosphates appeared.[9]

The method of solution mediated conversion is utilised in the present study preparing zinc hydrogenphosphates containing rubidium or caesium and a new layered templated lithium zinc phosphate $LiZn(HPO_4)(PO_4)\cdot H_2en\cdot H_2O$ **1**; all the materials have long nucleation time.

We have discovered a new rubidium zinc hydrogenphosphate, $Rb_2Zn_2(HPO_4)_3$ prepared at 51 °C with nucleation time of *ca*. 4.5 months [monoclinic, space group $P2_1/c$, a = 12.5880(4), b = 12.7170(8), c = 7.5827(8) Å, β = 96.100(1)°]. This material has a complex crystal structure with spiralling chains of ZnO_4 and HPO_4 tetrahedra.[10] At ambient conditions we also prepared a new layered caesium zinc hydrogenphosphate, $CsZn_{2.5}(HPO_4)_3\cdot 2H_2O$, by a solution mediated conversion after a nucleation period of *ca*. 2 months [triclinic, space group $P\bar{1}$, a = 8.3918(6), b = 9.8254(8), c = 9.9090(7) Å, α = 111.17(1), β = 111.75(1), γ = 97.56(1)°].[11]

The synthesis of **1** was performed in the system $Li/Zn/PO_4$–en–H_2O; a gel was left to stand at 21 °C in a sealed flask preventing evaporation.‡ After 1 day a microporous zinc phosphate, $Zn_2(PO_4)_2\cdot H_2en$, DAF-3,[12] formed and after *ca*. 3 months crystallisation of **1** was observed thus, DAF-3 is a metastable, intermediate phase. The material DAF-3 has only been obtained as microcrystalline powder, whereas **1** can be obtained as larger crystals. This is probably due to very different time-scales of nucleation and crystal growth for the two materials. A faster and more direct preparative route for **1** might exist but not at much higher temperatures owing to formation of more dense phases, *e.g*. δ_l-$LiZnPO_4$.[13]

The crystal structure of **1** was investigated by single crystal X-ray diffraction providing a detailed structural model including all hydrogen positions in space group $C2/c$.§ **1** is built from regular tetrahedra of PO_4, ZnO_4 and LiO_4 forming two types of chains running in the (010) direction; zigzag four ring chains of alternating PO_4 and ZnO_4 and chains of corner sharing LiO_4, each LiO_4 tetrahedron having one oxygen from crystal water. These chains are alternately connected by HPO_4 tetrahedra forming layers held together by hydrogen bonding through ethylenediamine and water. Fig. 1 shows the *ac* projection of the crystal structure of **1**. Half the H_2en ions were found across a symmetry centre and are connecting the zigzag chains. The other H_2en ions connecting LiO_4 chains in different sheets are placed across the twofold axes of the space group $C2/c$ in such a way that the individual H_2en ions do not obey this symmetry, necessitating a disordered structural model in $C2/c$ or lowering the symmetry to Cc. The refinement in Cc was unstable unless all except this dication was constrained to keep the centrosymmetric relation. In fact the least squares program, KRYSTAL,[14] has been modified to allow symmetry operations which apply to a specified number of atoms only. The two models have the same number of parameters and gave similar R-values. We therefore chose the $C2/c$ solution.

1 is the first layered material in the system M_2O–ZnO–P_2O_5–H_2O–amine, M = alkali metal, with only one other member, reported as $Na_{67}(NMe_4)_{12}Zn_8(ZnPO_4)_{96}\cdot 192H_2O$, an analogue to zeolite X.[15] The latter is partly templated by hydrated sodium ions and partly by the amine ions. A large number of alkali metal containing microporous and some layered materials have been described, *e.g*. two ABW type polymorphs of $LiZnPO_4\cdot H_2O$ denoted α and β,[7,13a] but **1** is the first compound with alkali metal–oxygen–alkali metal contact, although Zn–O–Zn linkages are known, but rare.[16] Fig. 2 shows the connectivity of

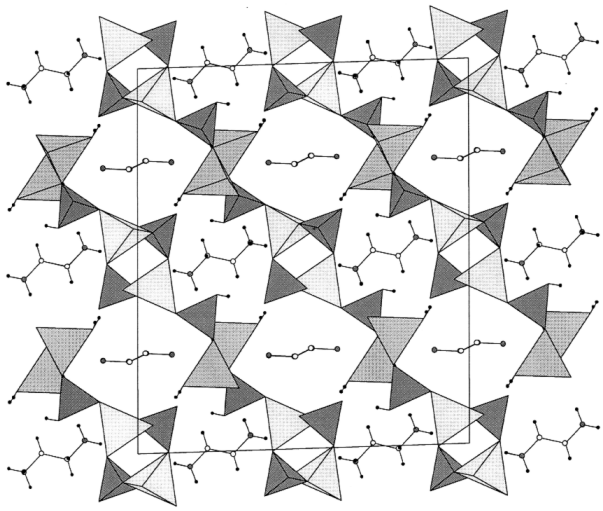

Fig. 1 The crystal structure of **1**; the *ac* projection. PO_4 (dark) and ZnO_4 (light) tetrahedra forming four-ring chains along with LiO_4 (medium dark) chains are running in the (010) direction, connected by HPO_4 tetrahedra to form layers, which are assembled by linking ethylenediamine ions. H atoms small size dark circles, C and N atoms larger medium dark circles.

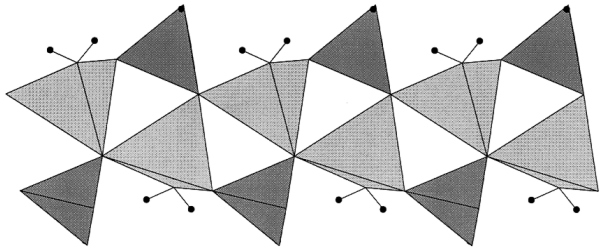

Fig. 2 The Li–O–Li chains running along the *b* axis in the crystal structure of **1**. Hydroxyl hydrogen and H atoms in the water molecules coordinated to Li shown as small size dark circles, PO_4 dark and LiO_4 medium dark tetrahedra.

the Li–O–Li chains in the crystal structure of **1**. These chains are similar to the Zn–O–Zn chains in a newly reported H_2en containing zinc phosphate, $Zn_6(HPO_4)(PO_4)_4{\cdot}H_2en{\cdot}H_2O$.[16b] The material **1** has a rare layered crystal structure assembled by linking amine ions.

A Danish Technical Research Council PhD grant is gratefully acknowledged. The Siemens SMART diffractometer at Chemistry Department, Aarhus University was partly financed by Carlsbergfondet.

Notes and references

† Present address: Condensed Matter Physics and Chemistry Department, Risø National Laboratory, DK-4000 Roskilde, Denmark. E-mail: trj@gamma.dou.dk

‡ *Synthesis*: $LiZn(HPO_4)(PO_4){\cdot}H_2en{\cdot}H_2O$ **1** was prepared by dissolving $LiOH{\cdot}H_2O$ (1.833 g), LiCl (1.867 g) and $Zn(MeCO_2)_2{\cdot}2H_2O$ (9.639 g) in water. H_3PO_4 85% (10.022 g) and then ethylenediamine (en) (4.6 mL) were added under stirring forming a white gel with composition, 0.99 Li_2O : 1 ZnO : 0.98 P_2O_5 : 1.92 en : 43 H_2O, *c*(PO_4) *ca*. 1.7 M, pH = 4.95. A portion of this gel was left to stand at ambient conditions, *ca*. 21 °C, in a sealed bottle preventing evaporation. After *ca*. 24 h DAF-3 was formed as a microcrystalline powder [$a = b = 14.7073(8)$, $c = 8.946(1)$ Å, refined from 103 powder diffraction reflections, in accordance with ref. 12] and after *ca*. 3 months DAF-3 partly transformed to **1**.

§ *Single crystal diffraction*: A transparent, plate-like crystal of **1** was selected for data collection on a Siemens SMART diffractometer equipped with a CCD detector and graphite monochromatised Mo-Kα radiation, λ = 0.71073 Å. Approximately one hemisphere of data was collected in narrow frames covering 0.3° in ω in three sets at different φ angles using a detector to crystal distance of 40.0 mm. Data were corrected for Lorentz-polarisation effects and for absorption using an empirical method (SADABS) giving 1616 unique reflections.

Details of data collection: θ_{max} = 24.5°, T = 120(2) K, measured reflections 4108, R_{int} = 0.027, Transmission (max. min.): 0.93, 0.80. A structural model was found using direct methods and the program SIR97.[17] The program KRYSTAL was used for the structure refinement.[14] The H atom positions were found in the difference Fourier maps and thermal parameters were kept isotropic; all other atoms were refined with anisotropic temperature factors. Scattering factors of neutral atoms were applied throughout this work. The refinement converged at R = 0.027 and R_w = 0.035, with 183 parameters refined using full matrix least squares based on F^2 and a weighting scheme, $w = \{[\sigma_{cs}(F^2) + 0.03F^2]^{-2}$. Figures were prepared using the program Atoms Ver. 4.0.[18]

Crystal data for **1**: M = 343.41, monoclinic, space group *C*2/*c*, (no. 15), a = 18.068(2), b = 5.3034(6), c = 21.065(3) Å, β = 91.992(2)°, U = 2017.3(4) Å^3, Z = 8, μ = 2.794 mm^{-1}, D_c = 2.261 g cm^{-3}. CCDC 182/1146. See http://www.rsc.org/suppdata/cc/1999/371/ for crystallographic files in .cif format.

1 S. T. Sie, *Advanced Zeolite Science and Applications*, ed. J. C. Jansen, M. Stöcker, H. G. Karge and J. Weitkamp, *Stud. Surf. Sci. Catal*., 1994, **85**, 587; G. Alberti, M. Casciola, U. Costantino and R. Vivani, *Adv. Mater*., 1996, **8**, 291.
2 (*a*) M. Estermann, L. B. McCusker, C. Baerlocher, A. Merrouche and H. Kessler, *Nature*, 1991, **352**, 320; (*b*) S.-L Wang, K.-F. Hsu and Y.-P. Nieh, *J. Chem. Soc., Dalton Trans*., 1994, 1681; (*c*) T. R. Jensen, P. Norby, J. C. Hanson, E. M. Skou and P. C. Stein, *J. Chem. Soc., Dalton Trans*., 1998, 527; (*d*) V. Soghomonian, Q. Chen, R. C. Haushalter, J. Zubieta and C. J. O'Connor, *Science*, 1993, **259**, 1596; (*e*) J. A. Hanko and M. G. Kanatzidis, *Angew. Chem., Int. Ed. Engl.*, 1998, **37**, 342 and references therein.
3 (*a*) T. E. Gier and G. D. Stucky, *Nature*, 1991, **349**, 508; (*b*) K.-H. Lii and Y.-F. Huang, *Chem. Commun*., 1997, 1311; (*c*) K.-H. Lii, Y.-F. Huang, V. Zima, C.-Y. Huang, H.-M. Lin, Y.-C. Jiang, F.-L. Liao and S.-L. Wang, *Chem. Mater*., 1998, **10**, 2599.
4 R. J. Francis and D. O'Hare, *J. Chem. Soc., Dalton Trans.*, 1998, 3133.
5 A. Nørlund Christensen, T. R. Jensen, P. Norby and J. C. Hanson, *Chem. Mater*., 1998, **10**, 1688.
6 R. J. Francis, S. J. Price, S. O'Brien, A. M. Fogg, D. O'Hare, T. Loiseau and G. Férey, *Chem. Commun.*, 1997, 521.
7 T. R. Jensen, *J. Chem. Soc., Dalton Trans*., 1998, 2261.
8 J. Gopalakrishnan, *Chem. Mater*., 1995, **7**, 1265.
9 M. A. Leech, A. R. Cowley, K. Prout and A. M. Chippindale, *Chem. Mater*., 1998, **10**, 451.
10 T. R. Jensen, R. G. Hazell, T. Vosegaard and H. J. Jakobsen, *Inorg. Chem.*, to be submitted.
11 T. R. Jensen and R. G. Hazell, *J. Chem. Soc., Dalton Trans.*, to be submitted.
12 R. H. Jones, J. Chen, G. Sankar and J. M. Thomas, *Zeolites and Related Microporous Materials: State of the Art 1994*, ed. J. Weitkamp, H. G. Karge, H. Pfeifer and W. Hölderich, *Stud. Surf. Sci. Catal*., 1994, **84**, 2229.
13 (*a*) W. T. A. Harrison, T. E. Gier, J. M. Nicol and G. D. Stucky, *J. Solid State Chem*., 1995, **114**, 249; (*b*) T. R. Jensen, P. Norby, P. C. Stein and A. M. T. Bell, *J. Solid State Chem*., 1995, **117**, 39.
14 A. Hazell, KRYSTAL, An integrated system of crystallographic programs, Aarhus University, Denmark, 1995.
15 W. T. A. Harrison, T. E. Gier, K. L. Moran, J. M. Nicol, H. Eckert and G. D. Stucky, *Chem. Mater*., 1991, **3**, 27.
16 (*a*) Tianyou Song, M. B. Hursthouse, Jiesheng Chen, Jianing Xu, K. M. Abdul Malik, R. H. Jones, Ruren Xu and J. M. Thomas, *Adv. Mater*., 1994, **6**, 679; (*b*) S. B. Harmon and S. C. Sevov, *Chem. Mater*., 1998, **10**, 3020; (*c*) See also refs. 2*b* and 2*c*.
17 A. Altomare, G. Cascarano, C. Giacovazzo, A. Guagliardi, M. C. Burla, G. Polidori and M. Camalli, *J. Appl. Crystallogr*., 1994, **27**, 435.
18 E. Dowty, Program ATOMS version 4.0, Shape Software, 521 Hidden Valley Road, Kingsport, TN 37663, 1997.

Communication 8/09272I

Thiacalixarenes as cluster keepers: synthesis and structural analysis of a magnetically coupled tetracopper(II) square

Gilles Mislin,[a] Ernest Graf,[a] Mir Wais Hosseini,*[a] Alexander Bilyk,*[b] Annegret K. Hall,*[b] Jack M. Harrowfield,*[b] Brian W. Skelton*[c] and Allan H. White*[c]

[a] *Laboratoire de Chimie de Coordination Organique (URA 422 CNRS), Université Louis Pasteur, F-67000 Strasbourg, France. E-mail: hosseini@chimie.u-strasbg.fr*
[b] *Special Research Centre for Advanced Minerals and Materials Processing, University of Western Australia, Nedlands, WA 6907, Australia*
[c] *Crystallography Centre and Department of Chemistry, University of Western Australia, Nedlands, WA 6907, Australia*

Received (in Basel, Switzerland) 25th November 1998, Accepted 17th December 1998

An X-ray structure determination of an antiferromagnetic copper complex of *p-tert*-butyltetrathiacalix[4]arene has shown it to contain a square, phenoxo- and sulfur-bridged cluster of four Cu(II) ions sandwiched between two fully deprotonated calixarenes, thus forming a ditopic, divergent receptor; as prepared, the complex has each cavity occupied by a molecule of dichloromethane.

Inclusion based molecular network koilates may be obtained using cavity-containing molecules, koilands 'hollow molecular units', and connector molecules.[1] So far, study of such materials has been mainly oriented towards the understanding of structural characteristics. A development which remains to be achieved is the design and preparation of functional inclusion molecular networks. Calix[4]arene[2] derivatives, *e.g.* **1**, offer particular promise in this regard, as the fusion of calixarene units by bridging through entities such as Si(IV)[3] readily enables the divergent orientation of cavities of a size and nature sufficient to accommodate a variety of guests. The fact that a number of different metals (including Ti, Nb, Al, Zn, Mg and Eu)[4] may be used similarly as bridges adds a further dimension to the possible utility of these materials.

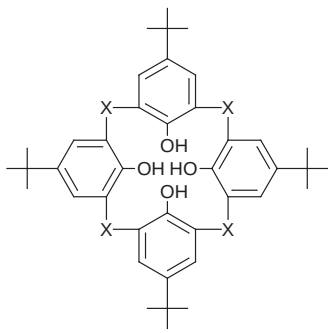

1 X = CH_2
2 X = S

As a means of enhancing selectivity in metal ion binding, the functionalisation of calixarenes with sulfur-containing groups has been quite widely investigated.[2,5,6] In general, this has involved quite difficult synthetic chemistry but the recent discovery[7] of a facile, high-yielding pathway to the tetrathiacalix[4]arene **2**, in which thiaether sulfur has replaced the methylene groups of calix[4]arene itself, has offered considerable prospects for expansion of the applications of such molecules.[8] Oxidation of the thiaether bridges to sulfoxide[9] and sulfone[10,11] groups offers a unique way of converting **2** to a number of interesting derivatives. Here, as part of a programme to systematically evaluate the metal ion coordinating ability of these new calixarenes (Fig. 1), we report the structure of a copper derivative, $Cu_4(\mathbf{2})_2$, of **2** in which a hollow molecular

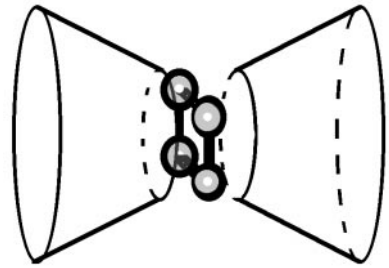

Fig. 1 Schematic representation of a hollow molecular unit obtained by fusion of two tetrathiacalix[4]arenes by four metal centres.

unit is apparent. In the case of this transition metal, coordination to the calixarene appears to involve only oxygen and sulfur donor sites, though it is anticipated that, as with the simple calixarenes, other metals may be bound through interactions with, for example, the phenyl-ring π-electrons.[12]

Upon heating a dimethylformamide (DMF) solution of compound **2**, hydrated copper acetate and Et_3N, a dark blue–black, crystalline complex was obtained.† The ^1H NMR spectrum of a solution of the complex in $CDCl_3$ at 298 K showed only a single, broad resonance, indicating that the complex was paramagnetic. Under the same conditions, an electron spin resonance could not be detected [a phenomenon known for many multinuclear Cu(II) systems,][13] but SQUID measurements of magnetic susceptibility (4–298 K; Fig. 2) could be interpreted, in the light of the structural information described below, in terms of antiferromagnetic coupling (J = 103 ± 1 cm^{-1}) of four equivalent Cu(II) ions arranged in a

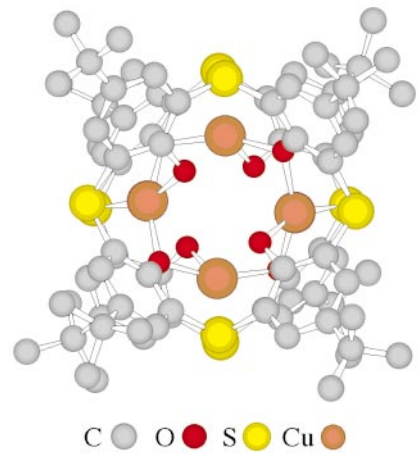

Fig. 2 A lateral view of the solid state structure of the tetranuclear copper complex possessing two cavities occupied each by one CH_2Cl_2 molecule. For clarity, H atoms are omitted.

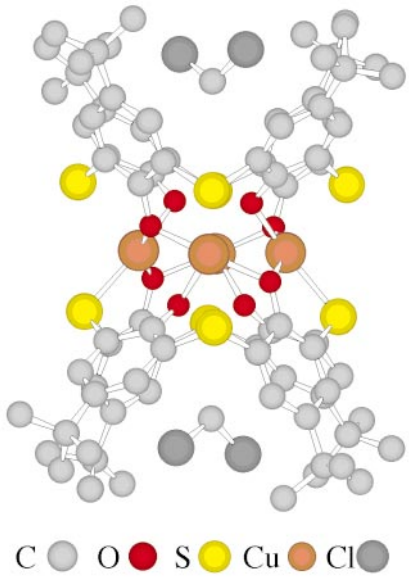

Fig. 3 Top view of the crystal structure of the tetranuclear copper complex showing the square arrangement of the metal centres and their bridging by phenoxide groups.

square. The coupling is appreciably stronger than in a previously characterised Cu_4 square array,[14] presumably as a consequence of a smaller separation between the metal atoms.

Single crystals (black tablets) of $Cu_4(\mathbf{2})_2$ suitable for X-ray crystallography were readily obtained on addition of ethanol to a solution of the complex in dichloromethane.‡ Two inequivalent $Cu_4(\mathbf{2})_2$ units are found within the unit cell but the differences between them are subtle and will be described elsewhere. In both, the Cu_4 array, sandwiched between two thiacalix entities in a 'cone' conformation similar to that of the free ligand,[8] is close to exactly square, with each copper in a six-coordinate O_4S_2 donor-atom environment. The coordination sphere is far from regular, with one Cu–O bond *ca.* 0.5 Å longer than the other three and one Cu–S bond *ca.* 0.3 Å longer than the other. Fourfold symmetry for the $Cu_4(\mathbf{2})_2$ unit is broken by the inclusion of one molecule of CH_2Cl_2 within each of the divergent cavities of this hollow molecular building block (Fig. 2 and 3). Comparison with an analogous copper complex of *p*-*tert*-butylcalix[4]arene is not possible since no such structure has been determined but it has been suggested[7] that the far better extractant activity of **2** relative to **1** may be associated with the presence of the additional sulfur-donor centres and thus it is significant that the present structure demonstrates their involvement in the coordination of Cu(II). Other structures we are in the process of refining show that this mode of binding is certainly not restricted to Cu(II).

In summary, we note that this structure is both the first known of a Cu(II) complex of any calixarene and the first known of any complex of the tetrathiacalix[4]arene **2**. It is also that of the first intentionally synthesised paramagnetic koiland (hollow molecular building block), though others have been identified.[4] The use of this hollow molecular unit in the formation of magnetic inclusion networks in the crystalline phase is under current investigation.

Notes and references

† The *p*-*tert*-butylthiacalix[4]arene **2** (270 mg, 0.37 mmol) was dissolved in DMF (8 mL) containing Et_3N (10 drops) and the resulting solution was added to a solution of $Cu(OAc)_2{\cdot}H_2O$ (150 mg, 0.75 mmol) in DMF (5 mL). EtOH (20 mL) was added to the dark brown solution and this was heated at reflux for 4 h. The reaction mixture was cooled to room temperature and filtered. The crude black solid was recrystallised twice from CH_2Cl_2–EtOH to give the product as black prisms (190 mg, 57%). MS (FAB) *m/z* 1685 (M^+ 1685, calc. 1689). Anal. Calc. for $C_{80}H_{88}O_8S_8Cu_4{\cdot}CH_2Cl_2$: C, 54.87; H, 5.12; S, 14.47. Found: C, 54.80; H, 5.06, S, 14.27%. UV–VIS: λ_{max}/nm (ε_{max}/dm^3 mol^{-1} cm^{-1}): 310 (4.29 × 10^5), 356 (6.41 × 10^3), 418 (4.57 × 10^3), 572 (2.77 × 10^3).

‡ *Crystal/refinement data*: $[Cu_4(C_{40}H_{44}O_4S_4)_2{\cdot}2CH_2Cl_2]{\cdot}CH_2Cl_2$, M = 1943.1, monoclinic, space group $P2_1/c$, a = 16.877(1), b = 28.872(2), c = 39.128(3) Å, β = 95.770(1)°, V = 18969 Å^3. D_c (Z = 8 dimers) = 1.361 g cm^{-3}, 160847 (*i.e.* $2\theta_{max}$ = 58° sphere) 'SAINT'/'SADABS' processed CCD reflections ('$T_{min,max}$' = 0.33, 0.89) merged to 33502 unique (R_{int} = 0.048), 13828 with $|F| > 4\sigma|F|$, refining to conventional R, R_w on $|F|$ 0.059, 0.058 {anisotropic thermal parameters (non-hydrogen atoms), (x, y, z, U_{iso}) H included constrained at estimates}. Solvent occupancies were set at unity after trial refinement. CCDC 182/1133. See http://www.rsc.org/suppdata/cc/1999/373/ for crystallographic files in .cif format.

1 M. W. Hosseini and A. De Cian, *Chem. Commun.*, 1998, 727.
2 C. D. Gutsche, *Calixarenes Revisited, Monographs in Supramolecular Chemistry, No. 1*, ed. J. F. Stoddart, RSC, Cambridge, 1998.
3 X. Delaigue, M. W. Hosseini, A. De Cian, J. Fischer, E. Leize, S. Kieffer and A. Van Dorsselaer, *Tetrahedron Lett.*, 1993, **34**, 3285.
4 M. M. Olmstead, G. Sigel, H. Hope, X. Xu and P. Power, *J. Am. Chem. Soc.*, 1985, **107**, 8087; F. Corazza, C. Floriani, A. Chiesi-Villa and C. Guastini, *J. Chem. Soc., Chem. Commun.*, 1990, 1083; J. L. Atwood, S. G. Bott, C. Jones and C. L. Raston, *J. Chem. Soc., Chem. Commun.*, 1992, 1349; J. L. Atwood, P. C. Junk, S. M. Lawrence and C. L. Raston, *Supramol. Chem.*, 1996, **7**, 15; A. Bilyk, J. M. Harrowfield, B. W. Skelton and A. H. White, *J. Chem. Soc., Dalton Trans*, 1997, 4251 and references therein.
5 X. Delaigue, J. M. Harrowfield, M. W. Hosseini, A. De Cian, J. Fischer and N. Kyritsakas, *J. Chem. Soc., Chem. Commun.*, 1994, 1579; X. Delaigue, M. W. Hosseini, N. Kyritsakas, A. De Cian and J. Fischer, *J. Chem. Soc., Chem. Commun.*, 1995, 609; X. Delaigue, J. M. Harrowfield, M. W. Hosseini, M. Mocerino, B. W. Skelton and A. H. White, *Aust. J. Chem.*, 1998, **51**, 111.
6 D. M. Roundhill, *Prog. Inorg. Chem.*, 1995, **43**, 533.
7 H. Kumagai, M. Hasegawa, S. Miyanari, Y. Sugawa, Y. Sato, T. Hori, S. Ueda, H. Kamiyama and S. Miyano, *Tetrahedron Lett.*, 1997, **38**, 3971; T. Sone, Y. Ohba, K. Moriya, H. Kumada and K. Ito, *Tetrahedron Lett.*, 1997, **38**, 10689.
8 H. Akdas, L. Bringel, E. Graf, M. W. Hosseini, G. Mislin, J. Pansanel, A. De Cian and J. Fischer, *Tetrahedron Lett.*, 1998, **39**, 2311.
9 G. Mislin, E. Graf, M. W. Hosseini, A. De Cian and J. Fischer, *Chem. Commun.*, 1998, 1345.
10 N. Iki, H. Kumagai, N. Morohashi, K. Ajima, M. Hasegawa and S. Miyano, *Tetrahedron Lett.*, 1998, **39**, 7559.
11 G. Mislin, E. Graf, M. W. Hosseini, A. De Cian and J. Fischer, *Tetrahedron Lett.*, 1998, **39**, submitted.
12 J. M. Harrowfield, M. I. Ogden, W. R. Richmond and A. H. White, *J. Chem. Soc., Chem. Commun.*, 1991, 1159; R. Asmuss, V. Böhmer, J. M. Harrowfield, M. I. Ogden, W. R. Richmond, B. W. Skelton and A. H. White, *J. Chem. Soc., Dalton Trans.*, 1993, 2427.
13 E. I. Solomon, U. M. Sundaram and T. E. Machonkin, *Chem. Rev.*, 1996, **96**, 2563.
14 P. Chaudhuri, I. Karpenstein, M. Winter, M. Lengen, C. Butzlaff, E. Bill, A. X. Trautwein, U. Flöcke and H.-J. Haupt, *Inorg. Chem.*, 1993, **32**, 888.

Communication 8/09184F

ChemComm

Zeolite-like crystal structure of an empty microporous molecular framework

Cameron J. Kepert† and Matthew J. Rosseinsky*

Inorganic Chemistry Laboratory, Department of Chemistry, University of Oxford, South Parks Road, Oxford, UK OX1 3QR. E-mail: matthew.rosseinsky@chem.ox.ac.uk

Received (in Cambridge, UK) 15th December 1998, Accepted 7th January 1999

The rigidity of the coordination polymer framework of $Ni_2(4,4'\text{-bipy})_3(NO_3)_4$ is demonstrated quantitatively by determination of the structures of both ethanol-loaded and desolvated forms, showing only a small relaxation of the structure on guest loss.

The synthesis of extended molecular frameworks[1] robust to guest exchange[2] and linked by coordinate or hydrogen bonds has led to suggestions that such frameworks would be suitable for applications in separations and heterogeneous catalysis.[3] To date, however, there has been no direct proof by structure refinement that a completely desolvated coordination polymer can retain the same open-framework geometry (as defined by quantitative analysis of diffracted intensities) once the solvent template/guest occupying the putative void space has been removed, preventing a detailed assessment of claims for zeolite-like behaviour. Previous single crystal studies are restricted to cell dimension measurement on partly desolvated systems without structure analysis.[4] Here, we report the guest exchange chemistry and the first full crystallographic characterisation of a microporous molecular framework coordination polymer in both the solvated and completely desolvated state. Guest loss is fully reversible on a single crystal and causes no observable increase in crystal mosaicity. The refinement of data collected *in situ* on the desolvated crystal proves that the open-channel geometry is retained in the total absence of the guest, demonstrating a direct structural and chemical link with the large family of zeolite frameworks and obviating the possible problem of guest resorption on cooling present in *ex situ* studies.

Crystals of **A**, $Ni(bpy)_{3/2}(NO_3)_2{\cdot}EtOH$ (bpy = 4,4′-bipyridine), were grown and sealed in capillaries containing mother-liquor to prevent desolvation. Isomorphous salts containing water and CS_2 have recently been reported by other workers.[5,6] Our structural refinement‡ reveals the interposition of chiral bilayers of opposite handedness to form a tongue-and-groove type structure (as represented schematically in the inset of Fig. 1). The bilayers, which take the form of the 8^210 network,[7] result from the T-shaped coordination about nickel of three bpy units (Fig. 1). The pseudo-square-pyramidal nickel coordination is completed by two nitrate groups. Of the two crystallographically distinct bpy units, one links the nickel centres to form parallel chains in the *ab* plane and the other links neighbouring layers of chains along *z*. Although the layered array of coordinate bonds between Ni and bpy suggests two-dimensional interactions, closer inspection of the structure reveals C–H···O hydrogen bonds between the nitrate anions bound directly to the metal and the bpy groups of every second bilayer (Fig. 1). This interlayer interaction acts together with the Ni–bpy coordinate bonds within the bilayer to impart a three-dimensional character to the structure, which may be considered as the interpenetration of two semi-regular $6^4(6,10)^1$-type 3-D networks.[7]

The interlocking of the bilayers produces channels of dimensions 6 by 3 Å parallel to *a* which are occupied in the as-grown material by ethanol. The ethanol molecule forms a single hydrogen bond to one of four neighbouring nitrate groups coordinated to nickel. These guests are liberated slowly at room temperature (50% of the ethanol is lost within 1 h at 25 °C under dry N_2). Complete and rapid guest desorption occurs with heating to 100 °C, beyond which the empty framework material $Ni(bpy)_{3/2}(NO_3)_2$ **B** is stable to 230 °C. The desolvated phase has been shown to have microporosity by N_2 sorption measurements[5] and will take up H_2O at room temperature, with other guests including MeOH, EtOH and Pr^iOH.

The structural consequences of desorption were studied by single crystal X-ray diffraction. The evolution of the unit cell on desorption is shown in Fig. 2, as measured *in situ* by heating a crystal at 20 K h^{-1} under dry dinitrogen. With complete desolvation of the lattice at 375 K there is a 2.4% decrease in cell volume. The robust nature of the framework is reflected in the retention of similar mosaicity of the crystal upon desolvation, allowing structural refinement of the empty co-ordination polymer framework. The refined structure and flat nature of the final difference Fourier maps demonstrate that empty channels, of dimensions 6 × 3 Å, are retained on desolvation (Fig. 3). Guest loss does not involve symmetry change or channel volume collapse, unlike the extended hydrogen bonded network of $[Co(H_2O)_6]H_2(TC\text{-}TTF){\cdot}2H_2O$.[8] Quantitative assessment of

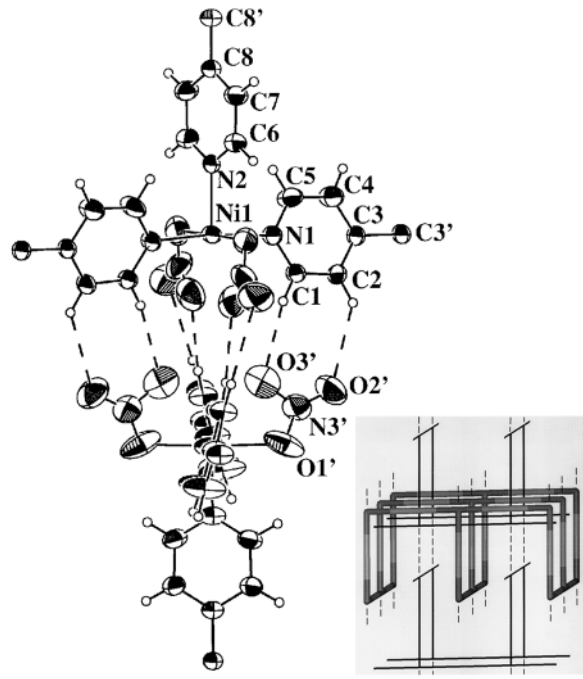

Fig. 1 The structural motif of **A** and **B**, showing labelling of all atoms in the asymmetric unit of the empty molecular framework **B** at 375 K (30% probability thermal ellipsoids). The T-shaped coordination of 4,4′-bpy about Ni gives rise to the formation of interlocking two-dimensional bilayers, as represented diagramatically in the inset. For clarity one of the interlocking bilayers is highlighted. The chains represent linear Ni(bpy) strands in the *ab* plane connected into bilayers of chains at different heights along *c* by bpy groups. The torsion angle between the two sets of chains in a bilayer relaxes upon guest loss as described in the text. Multiple hydrogen bonding interactions impart a 3D nature to the framework structure (C1···O3′ 3.536(7), H1···O3′ 2.35, C2···O2′ 3.412(7), H2···O2′ 2.76 Å). Each dashed line in the inset represents eight of the C–H···O interactions in the main figure.

the channel volume[9] reveals that it is almost unchanged: the calculated ethanol-filled volume of **A** is 808.0 Å^3 per unit cell (20.6% of crystal volume) compared to a void volume of 793.8 Å^3 (20.1%) in **B**. Removal of the ethanol atoms from the refined structure followed by treatment of the data with the SQUEEZE routine[9] suggested a cavity electron population of 24.6 e$^-$ per formula unit in **A**, agreeing well with 26 e$^-$ for one ethanol molecule. Similar analysis of the data from **B** yields a cavity population of only 0.8 e$^-$ per formula unit, demonstrating there is no significant ordered or disordered electron density in the channels. The average shift in framework atomic positions with desorption is 0.06 Å, and the observed Ni–bpy distances remain unchanged within error, as found for the T–O distances in hydrated and dehydrated Cu zeolite Y.[10] The main structural relaxation of the framework is a subtle scissor-like action of the bilayers, leading to a decrease in the bilayer torsion angle (defined in Fig. 1) from 65.5 to 63.9°. This small distortion accompanies a 2.3% decrease in *a* and a 0.9% increase in *b*. The multitude of hydrogen bonding interactions between bilayers imparts stability to the structure in the *z* direction, as evidenced by the small decrease in *c* of 1.0%.

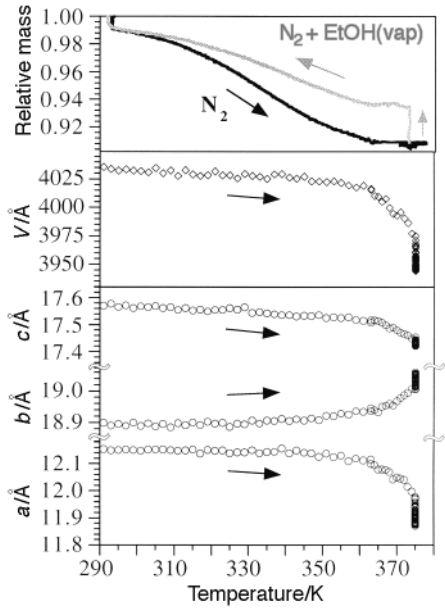

Fig. 2 Evolution of the mass, orthorhombic unit cell volume (Å^3) and axial parameters (Å) during the desorption transition **A** → **B**, as measured by thermogravimetry and single crystal X-ray diffraction. The grey curve of the TGA plot is of the sorption transition **B** → **A**, performed by cooling **B** under 5 Pa partial pressure of EtOH vapour in a stream of dry N_2.

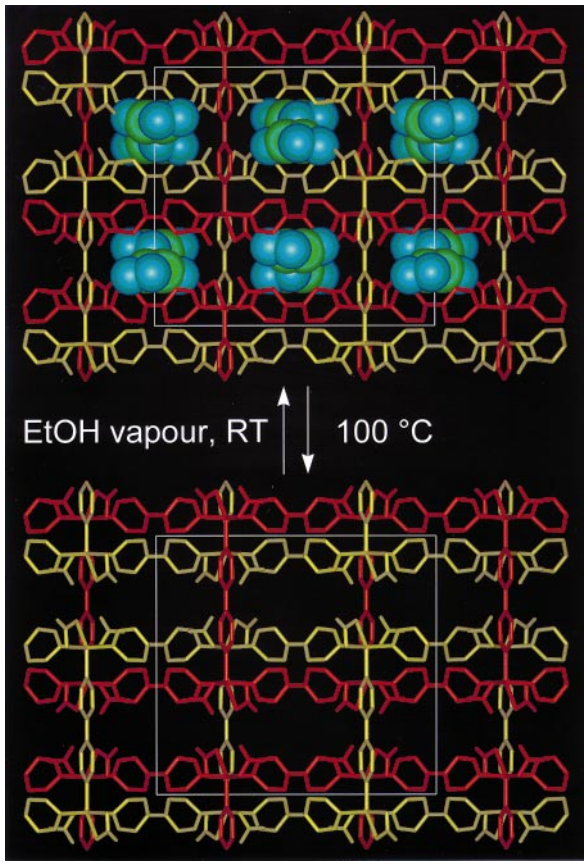

Fig. 3 Structural projections down the *a*-axis, drawn to scale, showing the complete removal of disordered ethanol molecules from **A** to form **B**. The desolvated structure, **B**, contains empty one-dimensional channels running along the *x* direction which occupy 20% of the crystal volume and have dimensions 6 × 3 Å. Adjacent bilayers are shown in yellow and red, with the C and disordered O atoms of the guest as green and blue spheres.

The present structure refinements represent the first definitive demonstration of the retention of structural integrity of a coordination polymer framework upon complete desolvation, confirming the analogy with zeolites suggested by sorption and powder diffraction measurements.

C. J. K. thanks Christ Church, Oxford for a Junior Research Fellowship.

Notes and references

† Present address: School of Chemistry, University of Sydney, NSW 2006, Australia. E-mail: cameron.kepert@chem.ox.ac.uk.

‡ *Single crystal X-ray data*: for **A**: $C_{17}H_{18}N_5Ni_1O_7$, M = 463.07, T = 293(2) K, orthorhombic, space group *Ccca*, blue platelet, a = 12.156(2), b = 18.891(3), c = 17.584(3) Å, V = 4038.0(12) Å^3, Z = 8, D_c = 1.523 Mg m^{-3}, μ = 1.841 mm^{-1}. Data were collected on an Enraf-Nonius CAD4 diffractometer with Cu-Kα (λ = 1.54180 Å) radiation. The structure was solved with SHELXS-86 and refined within SHELXL-93.[11] Refinement with full matrix least-squares on F_o^2 (data/restraints/parameters = 866/17/130) converged to $R1$ = 0.0848, $wR2$ = 0.2028 [for 413 data with $I > 2\sigma(I)$]; $R1$ = 0.1728, $wR2$ = 0.2435 (all data). Disorder in the nitrate and bpy ligands was modelled as described in the .cif file.

For **B**: $C_{15}H_{12}N_5Ni_1O_6$, M = 417.01, T = 375(2) K, orthorhombic, space group *Ccca*, blue platelet, a = 11.883(1), b = 19.049(1), c = 17.415(1) Å, V = 3942.0(5) Å^3, Z = 8, D_c = 1.405 Mg m^{-3}. Data were collected on an Enraf-Nonius DIP2000 diffractometer equipped with Mo-Kα (λ = 0.71073 Å) radiation, Eu/Ba image plate detectors and an Oxford Instruments nitrogen gas cryostream. The structure was refined with SHELXL-93[11] from data reduced with the HKL suite of programs.[12] Full matrix least-squares refinement on F_o^2 (data/restraints/parameters = 1957/0/124) converged to $R1$ = 0.0676, $wR2$ = 0.2085 [for 1480 data with $I > 2\sigma(I)$]; $R1$ = 0.0819, $wR2$ = 0.2210 (all data). μ = 1.023 mm^{-1}. CCDC 182/1136. See http://www.rsc.org/suppdata/cc/1999/375/ for crystallographic files in .cif format.

1 B. F. Hoskins and R. Robson, *J. Am. Chem. Soc.*, 1990, **112**, 1546.
2 O. M. Yaghi, G. M. Li and H. L. Li, *Nature*, 1995, **378**, 703.
3 H. Li, M. Eddaoudi, T. L. Groy and O. M. Yaghi, *J. Am. Chem. Soc.*, 1998, **120**, 8571; K. Endo, T. Koike, T. Sawaki, O. Hayashida, H. Masuda and Y. Aoyama, *J. Am. Chem. Soc.*, 1997, **119**, 4117; M. Fujita, Y. J. Kwon, S. Washizu and K. Ogura, *J. Am. Chem. Soc.*, 1994, **116**, 1151.
4 P. Brunet, M. Simard and J. D. Wuest, *J. Am. Chem. Soc.*, 1997, **119**, 2737; D. Venkataraman, G. B. Gardner, S. Lee and J. S. Moore, *J. Am. Chem. Soc.*, 1995, **117**, 11600.
5 M. Kondo, T. Yoshitomi, K. Seki, H. Matsuzaka and S. Kitagawa, *Angew. Chem., Int. Ed. Engl.*, 1997, **36**, 1725.
6 K. N. Power, T. L. Hennigar and M. J. Zaworotko, *New J. Chem.*, 1998, **22**, 177.
7 A. F. Wells, *Three-Dimensional Nets and Polyhedra*, Wiley-Interscience, 1977.
8 C. J. Kepert, D. Hesek, P. D. Beer and M. J. Rosseinsky, *Angew. Chem., Int. Ed. Engl.*, 1998, **37**, 3158.
9 A. L. Spek, *Acta Crystallogr., Sect. A*, 1990, **46**, C.
10 I. E. Maxwell and J. J. de Boer, *J. Phys. Chem.*, 1975, **79**, 1875.
11 G. M. Sheldrick, SHELXS-86 and SHELXL-93 Programs for the solution and refinement of crystal structures, Universitat Göttingen 1986 and 1993.
12 Z. Otwinowski and W. Minor, in *Methods in Enzymology*, ed. C. W. Carter and R. M. Sweet, Academic Press, New York, 1996, p. 276.

Communication 8/09746A

$[NHMe_3][Cu(CS_4)]$: a two-dimensional network involving an unprecedented μ_3-η^1:η^1:η^2 coordination mode of perthiocarbonate to copper(I)

Guo-Cong Guo and Thomas C. W. Mak*

Department of Chemistry, The Chinese University of Hong Kong, Shatin, New Territories, Hong Kong, China. E-mail: tcwmak@cuhk.edu.hk

Received (in Cambridge, UK) 11th December 1998, Accepted 21st December 1998

The new complex $[NHMe_3][Cu(CS_4)]$, which was obtained by solvothermal synthesis, contains a two-dimensional $^2{}_\infty[Cu(CS_4)^-]$ network consolidated by an unprecedented μ_3-η^1:η^1:η^2 coordination mode of the perthiocarbonate dianion.

The reaction of transition metal chelate polysulfides with carbon disulfide to form metal perthiocarbonates was first reported by Coucouvanis and Draganjac in 1982,[1] and up to now the few known examples in the literature include $[Ni(CS_4)_2]^{2-}$,[2] $[MoS(CS_4)_2]^{2-}$,[1,3] $[(CS_4)Mo_2S_4(CS_4)]^{2-}$,[1,3] $[(CS_4)Mo_2O_2S_2(CS_4)]^{2-}$,[3] $[Mn(CO)_3(CS_4)]_2^{2-}$,[4] $[Mn(CS_4)_2Cl]^{3-}$ [5] and $[Zn(CS_4)\{Me_2NCH_2CH_2N(Me)CH_2CH_2NMe_2\}]$.[6] These compounds are now generally synthesized by (i) the reaction of metal polysulfides with CS_2,[1,2b,3–6] (ii) the reaction of metal salts with K_2CS_4, [2a] or (iii) the oxidation of metal thiocarbonates with iodine or sulfur.[2a] Recently we employed the hydro(solvo)thermal technique to synthesize transition metal polychalcogenides using K_2E_n (E = S, Se and Te; n = 2–6) as mineralizers,[7] and herein we report the crystal structure of $[NHMe_3][Cu(CS_4)]$,† which was obtained in an analogous way.

The common coordination mode of the perthiocarbonate anion to a metal ion is bidentate, forming a nearly planar five-membered chelate ring [Fig. 1(a)], except for $[Mn(CO)_3(CS_4)]_2^{2-}$ in which each CS_4^{2-} ligand chelates to one Mn atom to form a planar five-membered ring with its perthio sulfur atom further coordinated to the other Mn atom to generate a discrete dimeric anion [Fig. 1(b)]. Single-crystal X-ray analysis has shown that the perthiocarbonate ligand in the present $[NHMe_3][Cu(CS_4)]$ complex exhibits an unprecedented μ_3-η^1:η^1:η^2 coordination mode, which bridges adjacent copper ions along the [−1 1 1] and [−1 1 −1] directions to form a two-dimensional network (Fig. 2).‡ To our knowledge, hitherto in all known metal perthiocarbonates only two terminal sulfur atoms of the CS_4^{2-} ligand bond to metal atom(s), but in $[NHMe_3][Cu(CS_4)]$ the third terminal sulfur atom has been found to be involved in metal coordination for the first time.

The anionic network $^2{}_\infty[Cu(CS_4)^-]$ can be regarded as constructed from a basic building unit, namely the centrosymmetric $Cu_2(CS_4)_2$ dimer as illustrated in Fig. 1(b). The unit cell contains two crystallographically independent dimers, which cross-link each other through interaction between the non-chelating, third terminal sulfur atom of each CS_4^{2-} ligand and an adjacent copper atom to form a puckered network as shown in Fig. 2. The network has two non-equivalent, though similar, irregular polygonal openings with wall-to-wall interatomic distances ranging from 5.4 to 10.3 Å. The crystal structure of $[NHMe_3][Cu(CS_4)]$ consists of a parallel stacking of these two-dimensional networks, with an interlayer separation of 7.83 Å, to form channels running along the [1 0 0] direction, in each of which the ordered $NHMe_3^+$ cations are arranged in a zigzag column (see corresponding figure in the Table of Contents).

Each copper atom exhibits distorted tetrahedral coordination geometry, with Cu–S bond distances in the range 2.265(1)–2.4517(9) Å that vary according to the coordination mode of the sulfur atom: S (chelate) < S (bridging) < perthio S (chelate) < perthio S (bridging). There are two kinds of nearly planar rings in the $Cu_2(CS_4)_2$ dimer, namely five-membered $CuSCS_2$ and four-membered Cu_2S_2, which make a dihedral angle of 71.2°. In β-$[Cu(S_4)]_n^{n-}$ the basic construction unit that generates a chain-like structure, namely a $Cu_2(S_4)_2$ dimer,[8] is structurally analogous to the present $Cu_2(CS_4)_2$ dimer but, unlike the CS_4^{2-} ligand, the S_4^{2-} ligand symmetrically chelates the copper atom

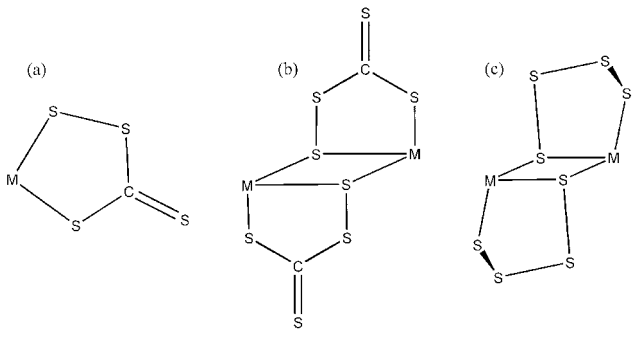

Fig. 1 Coordination modes of the perthiocarbonate dianion.

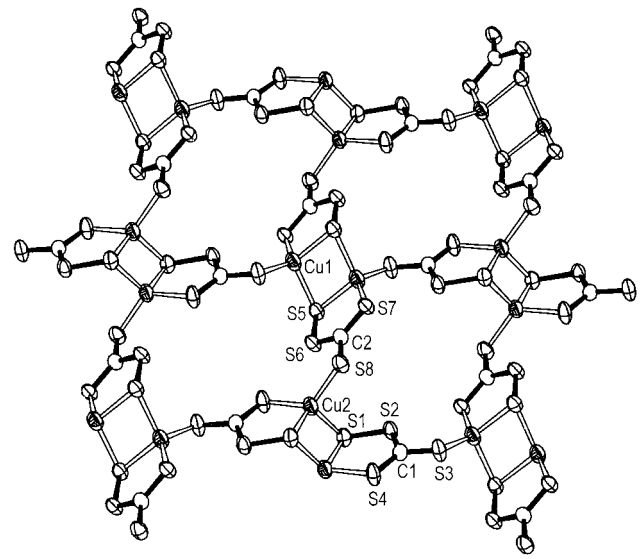

Fig. 2 Two-dimensional $^2{}_\infty[Cu(CS_4)^-]$ network viewed along the [1 0 0] direction. The thermal ellipsoids are drawn at the 70% probability level. Selected interatomic distances (Å), bond lengths (Å), and bond angles (°): Cu(1)···Cu(1)^i 2.8438(9), Cu(1)–S(3)^{ii} 2.2797(8), Cu(1)–S(5)^i 2.3530(9), Cu(1)–S(5) 2.4517(9), Cu(1)–S(7)^i 2.2681(9), Cu(2)···Cu(2)^{iii} 2.7361(8), Cu(2)–S(1) 2.4386(9), Cu(2)–S(1)^{iii} 2.3785(8), Cu(2)–S(4)^{iii} 2.265(1), Cu(2)–S(8) 2.3016(9), S(1)–S(2) 2.057(1), S(3)–C(1) 1.693(3), S(4)–C(1) 1.684(3), S(5)–S(6) 2.045(1), S(7)–C(2) 1.694(3), S(8)–C(2) 1.711(3); S(7)^i–Cu(1)–S(3)^{ii} 128.32(4), S(7)^i–Cu(1)–S(5)^i 95.79(3), S(3)^{ii}–Cu(1)–S(5)^i 111.75(3), S(7)^i–Cu(1)–S(5) 107.67(3), S(3)^{ii}–Cu(1)-S(5) 104.48(3), S(5)^i–Cu(1)–S(5) 107.45(3), S(4)^{iii}–Cu(2)–S(8) 123.32(4), S(4)^{iii}–Cu(2)–S(1)^{iii} 94.36(3), S(8)–Cu(2)–S(1)^{iii} 113.95(3), S(4)^{iii}–Cu(2)–S(1) 107.89(4), S(8)–Cu(2)–S(1) 106.03(3), S(1)^{iii}–Cu(2)–S(1) 110.79(3). Symmetry codes: ^{i} $-x+1, -y, -z+2$; ^{ii} $x, y, z-1$; ^{iii} $-x, -y+1, -z+3$.

to form a puckered five-membered ring [Fig. 1(c)]. Obviously, the principal difference between the CS_4^{2-} and S_4^{2-} ligands is that the *exo* sulfur atom of a chelating CS_4^{2-} ligand is capable of binding to another metal atom, as found in the present $[Cu(CS_4)]^-$ anion. The average non-bonded Cu···Cu distance in $[NHMe_3][Cu(CS_4)]$ is 0.16 Å longer than that found in β-$[Cu(S_4)]_n^{n-}$.[8]

The CS_4^{2-} ligand in the title compound exhibits electron delocalization similar to that found in $[Mn(CS_4)_2Cl]^{3-}$,[5] $[Ni(CS_4)_2]^{2-}$ [2b] and one of the two non-equivalent anions in $K_2CS_4{\cdot}MeOH$.[9] The S–S bond distances in both delocalized and localized CS_4^{2-} ligands in transition metal complexes, with the possible exception of $[Mo_2(S)_2(\mu\text{-}S)_2(CS_4)_2]^{2-}$,[1,3] are all longer than those found in $K_2CS_4{\cdot}MeOH$; this is attributable to M–S π bonding within the MCS_3 ring that results in weakening of the S–S bond, as is the case commonly found in metal complexes containing a chelating S_4^{2-} ligand.[10] Generally, polychalcogeno complexes of d^2 and d^8 metals show a pronounced E–E bond alternation pattern within the ME_4 (E = S, Se and Te) ring whereas d^{10} metal complexes do not. Thus lengthening of the S–S bond distance in $[NHMe_3][Cu(CS_4)]$, as compared to those in $K_2CS_4{\cdot}MeOH$,[9] is consistent with additional binding of the perthio sulfur atom to the copper center. A similar case was found in $[Mn(CO)_3(CS_4)]_2^{2-}$ [4] in which the S–S bond distance is longer than that in $[Mn(CS_4)_2Cl]^{3-}$.[5]

Recently it has been pointed out that the formation of carbon–heteroatom bonds in amines, ethers and sulfides by reductive elimination can be incorporated into a number of catalytic processes,[11] and interesting speculations as to the possible significance of C–S forming processes in the biosynthesis of metalloenzymes have been proposed.[12] The identity of the perthiocarbonate dianion in the title compound is firmly established, as the measured C–S distances are in good agreement with those of known perthiocarbonate complexes. However, the formation of C–S bonds to yield CS_4^{2-} in the synthesis of $[NHMe_3][Cu(CS_4)]$ is presumably much more complex under hydrothermal conditions, causing partial degradation of the tetramethylammonium ion to yield the trimethylammonium ion while providing the source of carbon. In this context it is noted that in $[Mn(CO)_3(CS_4)]_2^{2-}$, the carbon atom of the CS_4^{2-} ligand arises from a carbonyl group in the reaction between $[(CO)_5MnMn(CO)_4Br]^-$ and S_8 in 4-methylpentan-2-one and not from the solvent.[4]

This work is supported by Hong Kong Research Grants Council Earmarked Grant CUHK 4179/97P and Direct Grant A/C 2060129 of The Chinese University of Hong Kong.

Notes and references

† *Synthesis*: $[NHMe_3][Cu(CS_4)]$ was prepared by reacting CuCl (37.1 mg, 0.375 mmol), K_2S_4 [7a] (232.0 mg, 1.125 mmol), NMe_4Br (115.4 mg, 0.75 mmol), and 0.4 mL EtOH in a Pyrex ampoule of *ca.* 7 mL capacity. The ampoule was flame-sealed under vacuum, heated in a furnace to 100 °C for 144 h, and then cooled to 60 °C at 6 °C h^{-1}. Dark red prismatic crystals were isolated and washed with ethanol (estimated yield *ca.*10 %). The crystals are air-stable and insoluble in water and most organic solvents.

‡ *Crystal data*: $[NHMe_3][Cu(CS_4)]$, $C_4H_{10}CuNS_4$, M = 263.91, triclinic, space group $P\bar{1}$ (no. 2), a = 9.254(1), b = 10.737(1), c = 10.887(1) Å, α = 78.62(1), β = 74.18(1), γ = 68.22(1)°, U = 960.9(2) Å^3, T = 293 K, Z = 4, D_c = 1.824 g cm^{-3}, $F(000)$ = 536, μ(Mo-Kα) = 30.72 cm^{-1}, absorption corrections applied using ABSCOR,[13] relative transmission factors in the range 0.936–1.0. A total of 3210 reflections were collected in the 2θ range 4.0–53.5° ($-11 \leqslant h \leqslant 10$, $-13 \leqslant k \leqslant 0$, $-13 \leqslant l \leqslant 13$), 3095 of which with $I > 2\sigma(I)$ were considered as observed. The structure was solved by direct methods and the $NHMe_3^+$ and CS_4^{2-} ions, which exhibit normal molecular dimensions, were readily identified. Anisotropic refinement of all non-hydrogen atoms was carried out by full-matrix least squares on F^2 using the Siemens SHELXTL (PC Version)[14] package of crystallographic software, 181 variables, $R1 = \Sigma\,||Fo| - |F_c||/\Sigma\,|F_o| = 0.0436$, $wR2 = \{\Sigma\,[w(F_o^2 - F_c^2)^2]/\Sigma\,[w(F_o^2)^2]\}^{1/2} = 0.1146$, GOF = 1.119, min., max. residual electron density +0.522, −0.754 e Å^{-3}. CCDC reference 182/1149.

1 D. Coucouvanis and M. Draganjac, *J. Am. Chem. Soc*., 1982, **104**, 6820.
2 (*a*) D. Coucouvanis and J. P. Fackler, Jr., *J. Am. Chem. Soc*., 1967, **89**, 1346; (*b*) D. Coucouvanis, P. R. Patil, M. G. Kanatzidis, B. Detering and N. C. Baenziger, *Inorg. Chem*., 1985, **24**, 24.
3 D. Coucouvanis, M. E. Draganjac, S. M. Koo, A. Toupadakis and A. I. Hadjikyriacou, *Inorg. Chem*., 1992, **31**, 1186.
4 H. Alper, F. Sibtain, F. W. B. Einstein and A. C. Willis, *Organometallics*, 1985, **4**, 604.
5 S.-B. Yu and R. H. Holm, *Polyhedron*, 1993, **12**, 263.
6 R. J. Pafford and T. B. Rauchfuss, *Inorg. Chem*., 1998, **37**, 1974.
7 (*a*) G.-C. Guo, R. W. M. Kwok and T. C. W. Mak, *Inorg. Chem*., 1997, **36**, 2475; (*b*) G.-C. Guo and T. C. W. Mak, *J. Chem. Soc., Dalton Trans.*, 1997, 709; (*c*) G.-C. Guo and T. C. W. Mak, *Inorg. Chem*., 1998, **37**, 6538.
8 M. D. Kanatzidis and Y. Park, *J. Am. Chem. Soc*., 1989, **111**, 3767.
9 W. A. Bueno, A. Lautie, C. Sourisseau, D. Zins and M. Robineau, *J. Chem. Soc., Perkin Trans. 2*, 1978, 1011.
10 M. G. Kanatzidis and S.-P. Huang, *Coord. Chem. Rev*., 1994, **130**, 509; M. Draganjac, E. Simhon, L. T. Chan, M. G. Kanatzidis, N. C. Baenziger and D. Coucouvanis, *Inorg. Chem*., 1982, **21**, 3321; H. D. Block and R. Allmann, *Cryst. Struct. Commun*., 1975, **4**, 53; C. E. Briant, M. T. Calhorda, T. S. A. Hor, N. D. Howells and D. M. P. Mingos, *J. Chem. Soc., Dalton Trans*., 1983, 1325.
11 D. Baranano and J. F. Hartwig, *J. Am. Chem. Soc*., 1995, **117**, 2937; K. Osakada, M. Maeda, Y. Nakamura and T. Yamamota, *J. Chem. Soc., Chem. Commun*., 1986, 442; J. P. Wolfe and S. L. Buchwald, *J. Am. Chem. Soc*., 1997, **119**, 6054; S. Wagaw, B. H. Yang and S. L. Buchwald, *J. Am. Chem. Soc*., 1998, **120**, 6621; G. W. Parshall, *Homogeneous Catalysis*, Wiley-Interscience: New York, 1980; G. Mann, D. Baranano, J. F. Hartwig, A. L. Rheingold and I. A. Guzei, *J. Am. Chem. Soc*., 1998, **120**, 9205; P. M. Boorman, M. Wang and M. Parvez, *J. Chem. Soc., Chem. Commun.*, 1995, 999.
12 P. M. Boorman, X. Gao, H.-B. Kraatz, V. Mozol and M. Wang, in *Transition Metal Sulfur Chemistry*, ed. E. I. Stiefel and K. Matsumoto, ACS Symp. 653, 1996, p. 197.
13 ABSCOR—An Empirical Absorption Correction Based on Fourier Coefficient Fitting, T. Higashi, Rigaku Corporation, Tokyo, 1995.
14 SHELXTL/PC Version 5 Reference Manual, Siemens Energy & Automation, Inc., Madison, WI, 1996.

Communication 8/09683J

ChemComm

An insight into ion-transport by calixarenes; the structure of the dipotassium complex of *p-tert*-butylcalix[8]arene crystallised from a protogenic, coordinating solvent [ethanol/diethylcarbonate (10 : 1)]

Nicholas P. Clague,[a] William Clegg,[b,c] Simon J. Coles,[c] Jonathan D. Crane,[a]* David J. Moreton,[d] Ekkehard Sinn,[a] Simon J. Teat[c] and Nigel A. Young[a]

[a] *Department of Chemistry, The University of Hull, Cottingham Road, Kingston-upon-Hull, UK HU6 7RX. E-mail: j.d.crane@chem.hull.ac.uk*
[b] *Department of Chemistry, University of Newcastle upon Tyne, Newcastle, UK NE1 7RU*
[c] *CCLRC, Daresbury Laboratory, Daresbury, Warrington, Cheshire, UK WA4 4AD*
[d] *BP Chemicals (Additives) Ltd., Hull Research Centre, Saltend, Hull, UK HU12 8DS*

Received (in Basel, Switzerland) 2nd December 1998, Accepted 20th January 1999

The structure of the dipotassium complex of the dianion of *p-tert*-butylcalix[8]arene crystallised from a protogenic, coordinating solvent (ethanol–diethylcarbonate, 10 : 1) shows that the metal ions are bound above and below the cavity of the calix[8]arene, which adopts a 'pinched' conformation.

The binding of metal ions to the calixarenes and their O-pendant derivatives is an area of intense research interest, in particular with regard to selective metal ion coordination and transport.[1] The discovery that the parent calixarenes effect the transport of Group 1 metal ions in [water | organic solvent | water] liquid membrane systems stimulated great interest in this family of compounds.[2] Recent research has concentrated on metal ion binding to O-pendant derivatives of the calixarenes (mostly calix[4]arenes in which the pendant groups are generally predominant in the metal ion binding and the calixarene is used in a preorganising role), and a great deal of X-ray crystallographic structural information has been accumulated for these systems.[1] In contrast, there is a paucity of structural data for Group 1 metal ion complexes of the parent calixarenes; the only reported structures are the Cs^+ complex of the mono-anion of *p-tert*-calix[4]arene (H_4L), $Cs(H_3L)(MeCN)$, which beautifully illustrates the importance of $\pi\cdots M^+$ interactions in these systems,[3] and two Li^+ complexes of fully deprotonated *p-tert*-butylcalix[4]arene: $Li_5L(OH)(hmpa)_4$ and $Li_8L_2(hmpa)_4$ (hmpa = hexamethylphosphoramide).[4] It has been proposed that the larger calix[*n*]arenes ($n \geqslant 6$) are able to bind and transport more than one metal ion at a time, and that this may be a result of their ability to adopt 'pinched' conformations.[5] However, as yet there are no crystal structures that detail the conformation of a larger calixarene upon binding to the Group 1 metal ions, the number of metal ions that may bind, the site(s) of metal ion binding, the effects of metal ion binding upon the pattern of hydrogen-bonding within the calixarene cavity or the number and disposition of other ligands bound to the metal ions (presumably water in the ion transport systems).

In this context, we herein report the preparation and crystal structure of the dipotassium complex of the dianion of *p-tert*-butylcalix[8]arene (H_8L'). The reaction of H_8L' (0.5 mmol) with 8 equiv. of KOH or $KOBu^t$ in ethanol–diethylcarbonate (10 : 1, 100 cm^3) under a dry atmosphere yielded colourless crystals of the dipotassium salt $K_2(H_6L')(EtOH)_{4.67}\{(EtO)_2CO\}_{1.33}$ **1** upon standing for 72 h. The same product was also isolated when ethanol–dimethylcarbonate (10 : 1) was used as solvent, indicating alcohol exchange of the dialkylcarbonate under these conditions.

The molecular structure of **1** is shown in Fig. 1. The molecule of **1** lies on a crystallographic inversion centre with the K^+ ions lying above and below the cavity of the calix[8]arene and a K(1)···K(1a) distance of 4.424(2) Å. The K^+ ion is six coordinate with a distorted octahedral geometry comprising three calix[8]arene ArOH ligands in a *fac* arrangement and two ethanol ligands, and is completed by a diethylcarbonate or ethanol ligand with occupancies of 0.66 and 0.34, respectively. The calix[8]arene is doubly deprotonated and adopts a 'pinched' conformation with two ArOH groups bridging the K^+ ions at the 'pinch' (Fig. 2). There are structurally characterised precedents for the doubly bridged $K_2(\mu\text{-OAr})_2$ moiety with the deprotonated acidic phenols 2,4,6-$(CF_3)_3C_6H_2OH$ and 2,4,6-$(NO_2)_3C_6H_2OH$.[6,7] However, in **1** the bridging phenol ligands remain protonated; the free refinement of the three unique calix[8]arene ArOH protons indicates that the formally deprotonated phenol, O(3), is furthest from the K^+ ions and all three calix[8]arene ArOH protons are involved in strong intra-calix[8]arene hydrogen-bonding. There is an additional hydrogen-bond between O(3) and one of the ethanol ligands (Fig. 2), and presumably the overall hydrogen-bonding arrangement favours the observed deprotonation of O(3). The presence of protons on the bridging phenol ligands is also consistent with their greater K–O bond distances (av. 2.92 Å) compared with the terminal ligands (av. 2.73 Å) and the reported examples of the $K_2(\mu\text{-OAr})_2$ moiety (av. 2.76 Å).

The isolation of a neutral, molecular, dipotassium complex from this protogenic, coordinating solvent medium is consistent with the ion transport properties of *p-tert*-butylcalix[8]arene. It is probable that the calix[8]arene complex responsible for K^+

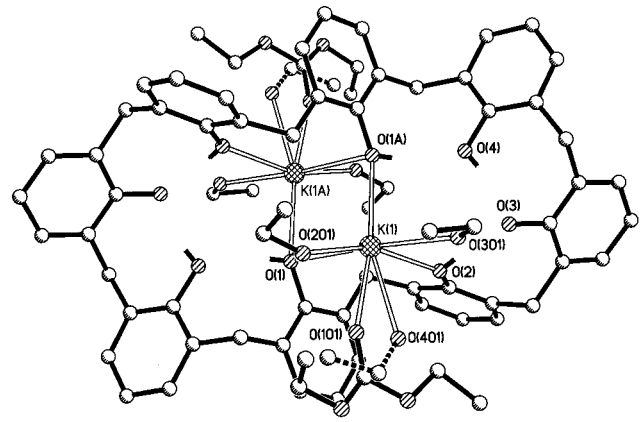

Fig. 1 Molecular structure of **1**. For clarity *tert*-butyl groups and C–H hydrogens have been omitted. Selected bond lengths (Å) and angles (°): K(1)–O(1) 2.949(2), K(1)–O(1a) 2.8963(19), K(1)–O(2) 2.7205(19), K(1)–O(101) 2.825(4), K(1)–O(201) 2.616(4), K(1)–O(301) 2.726(3); K(1)–O(401) 2.780(12); K(1)–O(1)–K(1a) 98.37(5), O(1)–K(1)–O(1a) 81.63(6), O(1)–K(1)–O(2) 97.28(6), O(1)–K(1)–O(301) 172.32(7), O(1a)–K(1)–O(101) 169.01(11), O(1a)–K(1)–O(401) 163.4(1), O(2)–K(1)–O(201) 160.68(11): symmetry operation; *a*, $-x$, $2-y$, $2-z$.

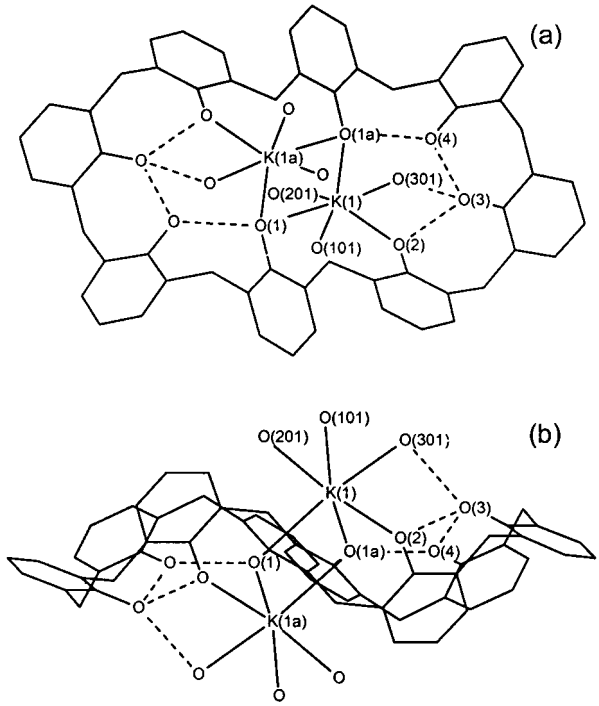

Fig. 2 Schematic representations of **1** showing the arrangement of hydrogen-bonds (O···O): (*a*) from above, (*b*) edge on. The *p*-*tert*-butyl groups are omitted for clarity and only the coordinated oxygen atom, O(101), of the partial occupancy diethylcarbonate ligand is shown. Hydrogen-bonds: O(1a)···O(4) 2.627(3), O(2)···O(3) 2.508(3), O(3)···O(4) 2.486(2), O(3)···O(301) 2.673(3), O(101)···O(201) 2.523(7) Å. (There are no other O···O interactions < 3.1 Å.)

ion transport in [water | organic solvent | water] liquid membrane systems is similar to **1** but with the ethanol and diethylcarbonate ligands replaced by water molecules. In this regard it is noteworthy that by comparison with the disposition of the ethanol molecules in **1**, these water molecules would be involved in intramolecular hydrogen-bonding to at least one of the ArOH groups of the calixarene cavity and probably also to each other, thus minimising unfavourable interactions with the organic solvent during ion transport.

This work was supported by the EPSRC, BP Chemicals (Additives) Ltd., (Industrial CASE studentship to NPC) and the University of Hull.

Notes and references

† *Crystal data*: $C_{104}H_{148.66}K_2O_{16.66}$, M_r = 1743.7, monoclinic, space group $P2_1/n$, a = 16.1867(3), b = 12.1515(2), c = 26.4092(4) Å, β = 105.827(2)°, U = 4997.57(15) Å^3, Z = 2, D_c = 1.159 g cm^{-3}, μ = 0.157 mm^{-1}, $F(000)$ = 1888. Crystal dimensions 0.10 × 0.05 × 0.03 mm. Data were collected at 160 K employing a wavelength of 0.6879 Å, on a Bruker AXS SMART CCD area detector diffractometer with a silicon (111) crystal monochromator and a palladium coated focusing mirror on the single crystal diffraction station (no. 9.8) at Daresbury Laboratory Synchrotron Radiation Source.[8] Coverage of a hemisphere of reciprocal space was achieved by 0.2° increments in ω, with θ_{min} = 1.80° and θ_{max} = 26.99° (index ranges $-20 \leqslant h \leqslant 17$, $-12 \leqslant k \leqslant 15$, $-34 \leqslant l \leqslant 34$). Corrections were applied to account for incident beam decay. A solution was provided *via* direct methods and refined by full-matrix least squares on F^2. 25725 reflections were measured, producing 10828 unique data with R_{int} = 0.0372. 649 parameters with 110 restraints refined to R_1 = 0.0802 and wR_2 = 0.2475 [$I > 2\sigma(I)$] with S = 1.060 and residual electron density extremes of 1.229 and −0.779 e Å^{-3}. Notes on the refinement: twofold orientational disorder was resolved for two independent *tert*-butyl groups and for one the minor components were refined isotropically with no hydrogen atoms; substitutional disorder of diethylcarbonate and ethanol was also modelled [refined occupancies 0.656:0.344(5)] as alternative ligands to K(1) with the aid of geometrical and displacement parameter constraints. CCDC 182/1151. See http://www.rsc.org/suppdata/cc/1999/379/ for crystallographic files in .cif format.

‡ A satisfactory elemental analysis for **1** could not be obtained due to the crystals rapidly desolvating upon removal from the solvent. The analysis of samples dried to constant weight in air over several days were consistent with decomposition to a formulation of $K_2(H_8L)(HCO_3)_2(H_2O)_5$. (Found C, 68.09; H, 7.67%. Calc. for $C_{90}H_{124}K_2O_{19}$: C, 68.07; H, 7.87%.)

1 M. A. McKervey, M. J. Schwing-Weill and F. Arnaud-Neu, in *Comprehensive Supramolecular Chemistry*, ed. G. W. Gokel, 1996, Pergamon, Elsevier Science Ltd., Oxford, UK, vol. 1, p. 537; D. M. Roundhill, *Prog. Inorg. Chem*., 1995, **43**, 533.
2 S. R. Izatt, R. T. Hawkins, J. J. Christensen and R. M. Izatt, *J. Am. Chem. Soc*., 1985, **107**, 63.
3 J. M. Harrowfield, M. I. Ogden, W. R. Richmond and A. H. White, *J. Chem. Soc., Chem. Commun*., 1991, 1159.
4 M. G. Davidson, J. A. K. Howard, S. Lamb and C. W. Lehmann, *Chem. Commun*., 1997, 1607.
5 C. D. Gutsche, *Acc. Chem. Res*., 1983, **16**, 161.
6 *The United Kingdom Chemical Database Service*, D. A. Fletcher, R. F. McMeeking and D. Parkin, *J. Chem. Inf. Comput. Sci*., 1996, **36**, 746.
7 S. Brooker, F. T. Edelmann, T. Kottke, H. W. Roesky, G. M. Sheldrick, D. Stalke and K. H. Whitmire, *J. Chem. Soc., Chem. Commun*., 1991, 144; Y. Kobuke, K. Kokubo and M. Munakata, *J. Am. Chem. Soc*., 1995, **117**, 12 751.
8 R. J. Cernik, W. Clegg, C. R. A. Catlow, G. Bushnell-Wye, J. V. Flaherty, G. N. Greaves, I. D. Burrows, D. J. Taylor, S. J. Teat and M. Hamichi, *J. Synchrotron Rad*., 1997, **4**, 279; W. Clegg, M. R. J. Elsegood, S. J. Teat, C. Redshaw and V. C. Gibson, *J. Chem. Soc., Dalton Trans*., 1998, 3037.

Communication 8/09401B

Control of proton transfer by hydrogen bonding in the protonated forms of the binucleophilic complex [{η⁵-$C_5H_4CH(CH_2)_4NMe$}Ir(PPh_3)H_2]

M. Mar Abad, Isabelle Atheaux, André Maisonnat* and Bruno Chaudret

Laboratoire de Chimie de Coordination du CNRS, UPR 8241, lié par conventions à l'Université Paul Sabatier et à l'Institut National Polytechnique, 205 route de Narbonne, 31077 Toulouse Cedex 4, France.
E-mail: maisonat@lcc-toulouse.fr

Received (in Basel, Switzerland) 23rd November 1998, Accepted 16th January 1999

Proton transfer reactions between both nucleophilic sites of a dihydrido iridium complex containing the 4-*N*-methylpiperidylcyclopentadienyl ligand and their dependance with the hydrogen bonding ability of the solvent medium are studied by NMR.

Proton transfer reactions in organometallic and bioinorganic chemistry are of fundamental interest and recent reviews deal with their thermodynamic, kinetic or mechanistic aspects.[1,2] In this context, considerable attention has been focussed on the protonation or deprotonation of transition metal hydrides and on the role of dihydrogen and hydrogen-bonded complexes as possible intermediates. It is widely recognized that hydrogen bonding, in its conventional aspect,[3,4] plays a fundamental role on proton transfer reactions.[5] It may also be supposed to play a decisive role in its non-conventional aspect, *i.e.* as a weak intramolecular hydrogen–hydrogen attractive interaction between a conventional hydrogen-bond donor and a transition metal hydride.[6]

The nucleophilic character of the iridium dihydride complex [(η⁵-C_5H_5)Ir(PR_3)H_2] has been used during the past few years to prepare new cationic polyhydrides displaying in ^{1}H NMR quantum mechanical exchange couplings.[7] The recent synthesis of a piperidino-substituted cyclopentadienyl ligand[8,9] gives the opportunity to prepare an iridium dihydride containing a second nucleophilic site and convenient to study both the possibility of hydrogen bonding and the dynamics of proton transfer.

The new dihydrido iridium complex [(η⁵-C_5H_4pip)Ir(PPh_3)H_2] **3**, [pip = *N*-methylpiperidyl, $CH(CH_2)_4NMe$] has been prepared by usual methods starting from the salt Na(C_5H_4pip) recently described, and involving the intermediate preparation of the bis(ethylene) and diiodide iridium complexes [(η⁵-C_5H_4pip)Ir(C_2H_4)$_2$] **1** and [(η⁵-C_5H_4pip)Ir(PPh_3)I_2] **2**.

For the three complexes, **1**–**3**, the ^{1}H NMR spectra show respectively AA′BB′ (**1**) or AA′BB′X (**2** and **3**) patterns in the range δ 4.50–5.50 for the Cp protons, a sharp resonance at δ *ca.* 2.2 for the methyl group linked to nitrogen and second order signals in the range δ 1.2–3.0 for piperidyl ring protons. Electron saturation in **1**–**3** rules out the coordination of the piperidyl nitrogen to the metal as in the parent rhodium complex [(η⁵-C_5H_4pip)Rh(C_8H_{14})$_2$].[8]

The equivalent hydrides of **3** resonate at δ −17.52 (CD_2Cl_2, 293 K, J_{PH} 30.2 Hz) in the ^{1}H NMR and the ν_{Ir-H} vibrations appear at 2128 cm^{-1} in the IR spectrum (KBr pellet), in the terminal Ir–H region. Protonation of **3** was first carried out in the presence of 2 equiv. of $HBF_4{\cdot}Et_2O$. The reaction leads to the expected dicationic species **4** resulting from the protonation of both amino and metal dihydrido nucleophilic sites as shown in Scheme 1.

The formation of an ammonium group is revealed (^{1}H NMR) by the appearance of a new broad signal in the low-field region at δ 8.75 (CD_2Cl_2, 293 K), and by a down-field shift of the methyl resonance of the methylpiperidyl group which appears in **4** as a doublet centered at δ 2.92 ($^3J_{HH}$ 4.2 Hz). The IR spectrum exhibits new absorption bands at 2950 cm^{-1} attributed to the ν_{N-H} vibration of the ammonium group and in the ν_{Ir-H} region at 2029 cm^{-1} (KBr pellet). In the ^{31}P{^{1}H} NMR spectrum, the diprotonation of **3** is accompanied by an up-field shift of the phosphorus nucleus of the PPh_3 ligand, from δ 13.25 for the starting material to δ 7.20 for the diprotonated product **4**. The high-field ^{1}H NMR spectrum exhibits, at room temperature, a new doublet centered at δ −12.26 (CD_2Cl_2, J_{P-H} 6.6 Hz). As in the case of the cyclopentadienyl parent iridium cations [(η⁵-C_5H_5)Ir(PR_3)H_3^+],[7] this signal is highly temperature dependent and decoalesces (≈ 11.7 kcal mol^{-1}) at lower temperature into an AB_2X spin system (δ_A −12.73, δ_B −11.55) displaying large temperature dependent $J_{H_A-H_B}$ coupling constants *i.e.* 278 Hz at 183 K and 446 Hz at 203 K, attributed to quantum mechanical exchange couplings.

Acidification at room temperature of **3** in CH_2Cl_2 with slightly less than 1 equiv. of $HBF_4{\cdot}Et_2O$ gave the trihydride monocation **6** (Scheme 1) in which only the iridium hydride was protonated. This complex differs from the diprotonated product **4** mainly in that it exhibits neither the typical ammonium resonance in the low-field region of the ^{1}H NMR nor the ν_{N-H} vibration in the IR. The other spectroscopic data are somewhat similar to those observed for **4**. Typically, the ^{31}P{^{1}H} NMR spectrum exhibits a singlet at δ 7.80 (CD_2Cl_2). The ^{1}H NMR spectrum in the high-field region exhibits a broad resonance centered at δ −12,36 which decoalesces by decreasing the temperature into typical resonances for a AB_2 spin system (^{1}H{^{31}P}) characterized, as previously observed for the diprotonated derivative, by large and highly temperature dependant $J_{H_a-H_b}$ coupling constants, *i.e.* 295 Hz at 183 K, 368 Hz at 193 K, 464 Hz at 203 K and 634 Hz at 213 K. These coupling constants are slightly larger than those measured for the dication **4** at similar temperatures. According to recent observations,[10] this could suggest some degree of hydrogen-bonding interaction between the hydride ligands and the piperidyl nitrogen lone pair. This Ir(H)$_3$···N≡hydrogen-bonding interaction could also rationalize, (i) the observation in complex **6** of a slightly higher

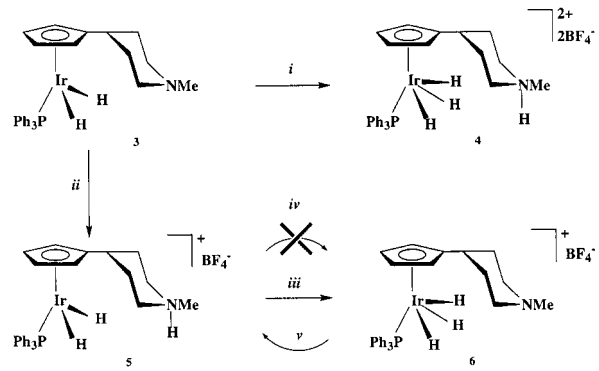

Scheme 1 Summary of the reactions run in the NMR tube; i, $HBF_4{\cdot}Et_2O$ (2 equiv.), CD_2Cl_2, 293 K; ii, $HBF_4{\cdot}Et_2O$ (1 equiv.), CD_2Cl_2, 193 K; iii, 293 K; iv, in presence of THF or PPh_3O (10%), 293 K; v, addition of THF, 293 K.

energy barrier for the classical site to site proton exchange in the $[Ir(H)_3^+]$ group than in complex **4** and (ii) the low-field shift of the methyl resonance of the methylpiperidyl group which appears at δ 2.80 in **6** (instead of δ 2.20 and 2.92, respectively, observed for the starting material and complex **4**), although the added proton is clearly coordinated to the iridium atom.

^{1}H NMR monitoring demonstrates that the initial step of the protonation of **3** at 183 K with 1 equiv. of $HBF_4{\cdot}Et_2O$ consists in the quantitative formation of a piperidinium group observed at δ 12.3 (br) the dihydrido iridium part of the molecule being unchanged. The methyl resonance, which appears at δ 2.91 is downfield shifted, whereas the characteristic signals of the cyclopentadienyl protons and of the hydrido ligands are very similar to those observed for **3** *i.e.* two multiplets at δ 5.02 and 4.85 for the cyclopentadienyl protons and a broad doublet at δ −17.56 (J_{HP} 29.6 Hz) for the hydrides. When the reaction mixture is quickly warmed up to room temperature over a few minutes and then cooled again at 183 K, it is possible to follow by ^{1}H NMR the disappearance of the broad piperidinium resonance at δ 12.3 and of the hydride resonance at δ −17.56 and the growth of the characteristic signals of the trihydrido monocation **6**. The migration of the added proton from the piperidyl to the iridium dihydrido groups is not reversible.

When the protonation of **3** by 1 equiv. of $HBF_4{\cdot}Et_2O$ is carried out in presence of THF in the ratio THF/CD_2Cl_2 = 10/90, the initial step remains the protonation of the piperidyl group to give **5** but the migration of the added proton to give **6** is not observed. However, instead of proton transfer, ^{1}H NMR studies at various temperatures and various concentrations reveal an interesting intramolecular proton exchange process between the piperidyl amino group and iridium (Fig. 1). The coalescence was reached at 293 K (200 MHz) and ΔG^* at coalescence temperature of this purely kinetic phenomenon can be estimated[11] at 12 kcal mol^{-1}.

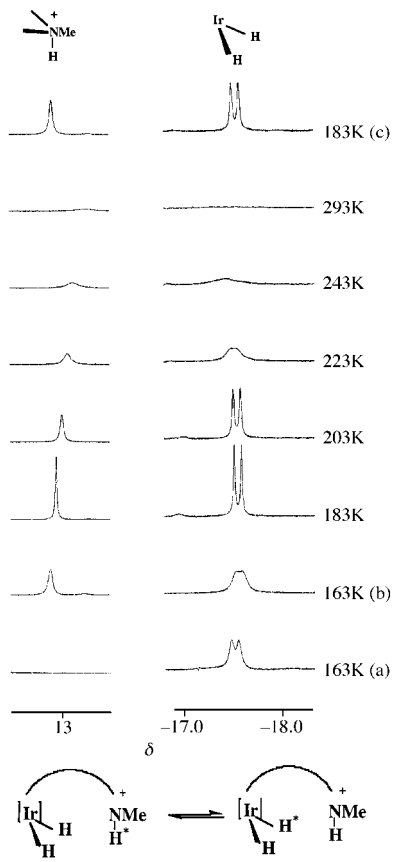

Fig. 1 Temperature dependance of the ^{1}H NMR spectra (CD_2Cl_2, 400 MHz), in the high- and low-field regions, in the presence of THF, (a) of the starting material **3** at 163 K, (b) after addition of 1 equiv. of $HBF_4{\cdot}Et_2O$ at 163 K, (c) after increasing progressively the temperature from 163 to 293 K and then cooling to 183 K.

This indicates a thermodynamic stabilization of the dihydrido piperidinium form **6** for the monoprotonated product which probably involves a weak hydrogen-bonding interaction between oxygen lone-pair of THF and the piperidinium proton. Furthermore, the observation of proton exchange with a low activation energy, involves a spatial proximity of both nucleophilic sites. This proximity could be explained by the existence of non-conventional intramolecular Ir–H···H–N hydrogen bonds such as those recently described by the groups of Crabtree[12,13] and Morris.[14]

As complementary experimental facts, it is of interest (i) that the addition of few drops of THF to a CD_2Cl_2 solution of the trihydrido cation **6** causes the immediate and total reverse transfer of the proton from the iridium hydride to the piperidyl sites to give **5** which experiences the low barrier exchange process described above and (ii) that the addition of $OPPh_3$, a weak base having a great capacity for formation of hydrogen bond,[15] to **6** causes again the total reverse transfer of the proton but the piperidinium species so obtained was stabilized to such an extent that the exchange of proton was not observed in the experimental conditions used.

In conclusion, we describe the synthesis of a new series of piperidylcyclopentadienyl iridium hydride complexes. We demonstrate that the kinetic site of protonation is the amino group of the piperidyl moiety whereas the thermodynamic one is dependent on the intermolecular hydrogen bonds present in the medium. In the absence of hydrogen bonding to solvent, the product of protonation at Ir is the thermodynamically stable one. The products of protonation at Ir and at N have similar stability in THF which allows the observation of an intramolecular proton transfer process and the product of protonation at N is the most stable in the presence of $OPPh_3$ owing to the formation of strong hydrogen bonds. This therefore further demonstrates the importance of hydrogen bonding for controlling the reactivity of hydrido organometallic complexes.

We are grateful to the CNRS for financial support of this work and to Johnson Matthey for a loan of ammonium chloroiridate. We thank Francis Lacassin for the NMR experiments.

Notes and references

1 S. S. Kristjansdottir and J. R. Norton, in *Transition Metal Hydrides*, ed. A. Dedieu, VCH, 1992, pp. 309–359.
2 K. W. Kramarz and J. R. Norton, *Prog. Inorg. Chem.*, 1994, **42**.
3 *The Hydrogen Bond*, ed. P. Schusfer, G. Zundel and C. Sandorfy, North-Holland, Amsterdam, New York, and Oxford, 1976.
4 G. A. Jeffrey and W. Saenger, in *Hydrogen Bonding in Biological Structures*, Springer, Berlin, 1991.
5 E. S. Shubina, N. V. Belkova and L. M. Epstein, *J. Organomet. Chem.*, 1997, **536**–**537**, 17.
6 B. P. Patel, J. Wessel, W. Yao, J. C. Lee Jr., E. Peris, T. F. Koetzle, G. P. A. Yap, J. B. Fortin, J. S. Ricci, G. Sini, A. Albinati, O. Eisenstein, A. L. Rheingold and R. H. Crabtree, *New J. Chem.*, 1997, **21**, 413; A. Caballero, F. A. Jalon and B. R. Manzano, *Chem. Commun.*, 1998, 1879; H. S. Chu, C. P. Lau, K. Y. Wong and W. T. Wong, *Organometallics*, 1998, **17**, 2768.
7 D. M. Heinekey, J. M. Millar, T. F. Koetzle, N. G. Payne and K. W. Zilm, *J. Am. Chem. Soc.*, 1990, **112**, 909.
8 P. C. McGowan, C. E. Hart, B. Donnadieu and R. Poilblanc, *J. Organomet. Chem.*, 1997, **528**, 191.
9 A. I. Philippopoulos, N. Hadjiliadis, C. E. Hart, B. Donnadieu, P. C. McGowan and R. Poilblanc, *Inorg. Chem.*, 1997, **36**, 1842.
10 J. A. Ayllon, S. Sabo-Etienne, B. Chaudret, S. Ulrich and H.-H. Limbach, *Inorg. Chim. Acta*, 1997, **259**, 1.
11 *NMR Spectroscopy*, H. Günther, John Wiley, Chichester, 1980, pp. 234–280.
12 J. C. Lee, E. Peris, A. L. Rheingold and R. H. Crabtree, *J. Am. Chem. Soc.*, 1994, **116**, 11 014.
13 E. Peris, J. C. Lee, J. R. Rambo, O. Eisenstein and R. H. Crabtree, *J. Am. Chem. Soc.*, 1995, **117**, 3485.
14 S. Park, R. Ramachandran, A. J. Lough and R. H. Morris, *J. Chem. Soc., Chem. Commun.*, 1994, 2201.
15 H. R. Hays and D. J. Peterson, in *Organic Phosphorus Compounds*, ed. G. M. Kosolapoff and L. Maier, Wiley-Interscience, New York, 1972, vol. 3, pp. 388–391.

Communication 8/09126I

Halide enhancement of the luminescence of $Cd_{10}S_4$ thiolate clusters

Richard D. Adams,* Bin Zhang, Catherine J. Murphy* and Lee K. Yeung

Department of Chemistry and Biochemistry, University of South Carolina, Columbia, SC 29208, USA.
E-mail: Adams@psc.sc.edu; Murphy@psc.sc.edu

Received (in Bloomington, IN, USA) 3rd December 1998, Accepted 13th January 1999

New halide-substituted cluster anions $[Cd_{10}S_4X_4(SR)_{12}]^{4-}$ (R = Ph, X = I, 2a; R = *p*-MeC_6H_4, X = I, 3a or Br, 3b) of the $[Cd_{10}S_4(SR)_{16}]^{4-}$ family have been prepared and characterized; investigations of their luminescence show that the introduction of the halide groups produces red shifts and significant enhancements in their emission intensities.

Semiconductor quantum dots are colloidal semiconductor particles, *ca.* 10–200 Å in diameter, that exhibit interesting optoelectronic properties due to quantum confinement of photogenerated electron–hole pairs.[1] Synthetic challenges in the field include narrowing the size distribution of the particles, and effective capping of surface atoms. A 'bottom-up' approach to the synthesis of well defined quantum dots begins with molecular clusters based on a semiconductor core.[1a] For CdS, one of the most studied quantum dot materials, molecular clusters having 10, 17 and 32 cadmium atoms in the core have been synthesized.[2] Here, we report the synthesis, crystallographic and spectroscopic characterization of new halide substituted molecular clusters derived from the $Cd_{10}S_4(SR)_{12}$ core. The halide ligands profoundly affect the spectral distribution and intensity of the observed photoluminescence relative to that of the parent cluster anion $[Cd_{10}S_4(SPh)_{16}]^{4-}$ **1**.

The new cluster anions $[Cd_{10}S_4X_4(SR)_{12}]^{4-}$ (R = Ph, X = I, **2a**; R = *p*-MeC_6H_4, X = I, **3a** or Br, **3b**) were synthesized by a modification of the procedure used for the synthesis of the parent $[Cd_{10}S_4(SPh)_{16}]^{4-}$.[2b]† The structures of **3a** and **3b** were determined crystallographically as their NEt_4 salts,‡ and an ORTEP diagram of **3b** is shown in Fig. 1. The cluster has S_4 symmetry and the $[Cd_{10}S_4(SR)_{12}]$ core of **3a** and **3b** is similar to those of the parent **1**.[2b]

The principal difference between **3a**,**b** and **1** is the presence of a terminally coordinated halide ligand on each of the four external cadmium atoms of the cluster.

The compounds are colorless to pale yellow, and the principal features in the UV–VIS spectra are intraligand bands at 250–300 nm.[3] The tetramethylammonium salt of the parent cluster **1** has been reported to show weak broad luminescence at *ca.* 530–550 nm in acetonitrile.[4] Under our conditions the parent cluster **1** emits broadly at *ca.* 430 nm. Interestingly, the halide clusters **2a, 3a** and **3b** show considerably more intense emission, readily visible to the naked eye under ultraviolet illumination, with apparent maxima at *ca.* 490 and 540 nm

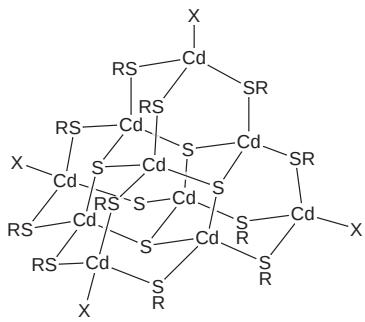

R = Ph; X = SPh, **1** or I, **2a**
R = C_6H_4Me-*p*; X = I, **3a** or Br, **3b**

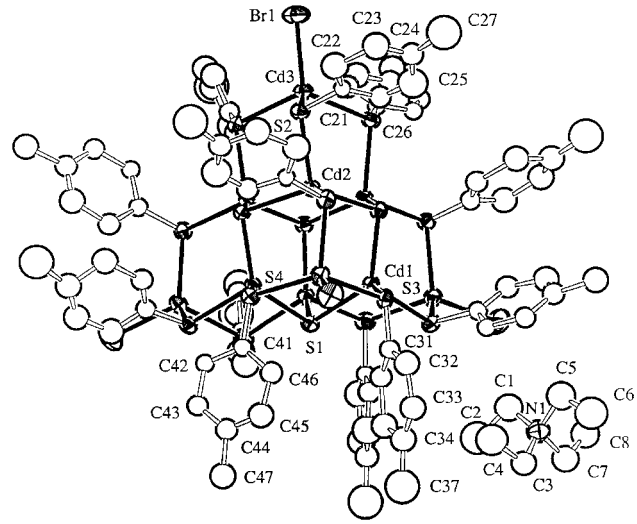

Fig. 1 An ORTEP diagram of the molecular structure of $[NEt_4]_4[Cd_{10}S_4(SC_6H_4Me\text{-}p)_{12}Br_4]$, **3b**.

(Fig. 2). For **3b**, emission spectra were also acquired on a single crystal taken from the diffractometer and was found to be identical to that taken in DMSO solution. For all compounds, the excitation spectra had maxima in the range 350–390 nm, lying in the absorption tail of the much more prominent intraligand bands.

The existence of multiple excited states, the domination of observed broad emission by a low-lying state with low oscillator strength, and the large Stokes shift have been documented in the case of a Cd_{32} cluster, and it was speculated that its *ca.* 500 nm emitting state was an intrinsic charge transfer state within the cluster.[2e] Calculations of the ground and excited states of the related Cd_4 cluster $[Cd_4(SPh)_{10}]^{2-}$ suggest that the lowest energy transition in this molecule is more localized, a

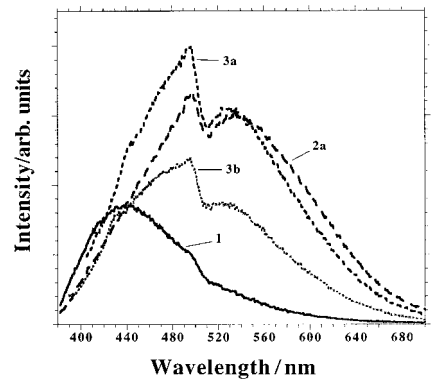

Fig. 2 Uncorrected emission spectra of 1.7×10^{-3} M **1**, 1.7×10^{-3} M **2a**, 1.6×10^{-3} M **3a** and 1.8×10^{-3} M **3b** in DMSO solution at room temperature. To ensure sample purity, single crystals of each compound, characterized by X-ray diffraction, were dissolved in DMSO and data was acquired within hours of dissolution. The excitation wavelengths employed were the maxima for each compound: 350 nm for **1**, 360 nm for **2a,** 380 nm for **3a** and 390 nm for **3b**. All other parameters were identical.

mixture of thiolate to Cd 5s ligand-to-metal charge transfer (LMCT) and intraligand charge transfer bands.[5] The sizes of Cd_{10} clusters reported here are in between these; time-resolved spectroscopy experiments are in progress to elucidate the details of the electronic structure of the halide–Cd_{10} clusters.§

Copper(I) halide clusters of the type $Cu_4X_4L_4$ also show complex emission spectra, and *ab initio* calculations have demonstrated that the two observed emissive states are likely halide-to-ligand charge transfer and 'cluster-centered' states; the cluster-centered states are a complex mixture of halide-to-metal charge transfer and metal-centered states.[6] For some of the compounds in this series, the emission spectra are insensitive to the nature of the halide, which was rationalized on the basis of competing trends in halogen electronegativities and ionization energies.[6] In these Cu_4 clusters, the electronic states of the halide are crucial to the photoluminescence of the cluster. Our results clearly demonstrate that halide ligands produce a strong enhancement in the intensity of photoluminescence from the excited states of our Cd_{10} clusters.

This work was funded by the Office of Naval Research grant no. N00014-97-1-0806.

Notes and references

† *Synthesis* of $[NEt_4]_4[Cd_{10}S_4I_4(SC_6H_4Me\text{-}p)_{12}]\cdot 2H_2O$ **3a**: $Cd(NO_3)_2\cdot 4H_2O$ (0.767 g) in MeOH (15 mL) was added to a solution of *p*-thiocresol (0.943 g) and triethylamine (1.146 mL) in methanol (15 mL) at 25° C. Then NEt_4I (0.474 g) in MeOH (15 mL) was added. After all the precipitate had dissolved, the solvent was removed *in vacuo*. The residue was dissolved in acetonitrile (35 mL) and powdered sulfur (0.048 g) was added to the clear solution at 25 °C. This reaction was complete in < 2 min. Isolated yield (24% based on Cd). ^{113}Cd NMR (CD_3CN) δ 559.54 (6 Cd), 434.28 (4 Cd). Anal. Calc: C, 36.71; H, 4.46; N, 1.48. Found: C, 37.12; H, 3.90; N 1.70%. Compound **2a** was prepared similarly using benzenethiol in place of *p*-thiocresol. Compound **3b** was prepared similarly to **3a** by substituting NEt_4Br for NEt_4I. For **3b**: ^{113}Cd NMR (CD_3CN) δ 560.86 (6 Cd), 411.57 (4 Cd).

‡ The compounds $[NEt_4]_4[Cd_{10}S_4I_4(SC_6H_4Me\text{-}p)_{12}]\cdot 2H_2O$ **3a** and $[NEt_4]_4[Cd_{10}S_4Br_4(SC_6H_4CH_3)_{12}]$ **3b** both crystallize in the tetragonal crystal system: space group $P\bar{4}2_1c$. For **3a**: M = 3795.31, $a = b$ = 20.1542(8) Å, c = 18.7192(5) Å, Z = 2, 1545 reflections, R = 0.048, λ = 0.71069 Å, D_c = 1.61 g cm^{-3}, μ(Mo-Kα) = 23.71 cm^{-1}, T = 293 K. For **3b**: M = 3571.27, $a = b$ = 20.3321(6) Å, c = 18.9573(7) Å, Z = 2, 1524 reflections, R = 0.051, λ = 0.71069 Å, D_c = 1.56 g cm^{-3}, μ (Mo-Kα) = 26.84 cm^{-1}, T = 293 K. Anion **1** was also characterized crystallographically in the form of its NEt_3H salt: space group $P\bar{4}2_1c$. For $[NEt_3H][Cd_{10}S_4(SC_6H_5)_{16}]$, **1**: M = 3489.89, $a = b$ = 20.3001(3) Å, c = 18.0263(5) Å, Z = 2, 2084 reflections, R = 0.040, λ = 0.71069 Å, D_c = 1.56 g cm^{-3}, μ(Mo-Kα) = 17.27 cm^{-1}, T = 293 K. CCDC 182/1147.

§ The smallest CdS molecular cluster that has been reported to be emissive is $[Cd_4(SC_6H_4NO_2)_{10}]^{2-}$, which emits at 500 nm, albeit with a lifetime of *ca.* 200 ps or shorter; the transition has been assigned as a cluster-to-nitrobenzene charge transfer. D. I. Yoon, D. C. Selmarten, H. Lu, H.-J. Liu, C. Mottley, M. A. Ratner and J. T. Hupp, *Chem. Phys. Lett.*, 1996, **251**, 84. For the NMe_4 salt of **1** the emissive state has been assigned as metal-to-ligand charge transfer; see ref. 4*a*. Ref. 4*a* also reports very weak emission from $[Cd_4(SC_6H_5)_{10}]^{2-}$, with a wavelength maximum at *ca.* 500 nm and a lifetime of *ca.* 400 ps.

1 (*a*) H. Weller, *Curr. Opin. Colloid Interfac. Sci.*, 1998, **3**, 194; (*b*) A. P. Alivisatos, *J. Phys. Chem.*, 1996, **100**, 13 226; (*c*) A. P. Alivisatos, *Science*, 1996, **271**, 933; (*d*) H. Weller, *Adv. Mater.*, 1993, **5**, 88; (*e*) H. Weller, *Angew. Chem., Int. Ed. Engl.*, 1993, **32**, 41; (*f*) Y. Wang, *Adv. Photochem.*, 1995, **19**, 179; (*g*) Y. Wang and N. Herron, *J. Phys. Chem.*, 1991, **95**, 525; (*h*) M. L. Steigerwald and L. E. Brus, *Acc. Chem. Res.*, 1990, **23**, 183; (*i*) A. Henglein, *Chem. Rev.*, 1989, **89**, 1861; (*j*) M. G. Bawendi, M. L. Steigerwald and L. E. Brus, *Annu. Rev. Phys. Chem.*, 1990, **41**, 477. (*k*) R. R. Chandler and J. L. Coffer, *J. Phys. Chem.*, 1993, **97**, 9767; (*l*) J. K. Lorenz and A. B. Ellis, *J. Am. Chem. Soc.*, 1998, **120**, 10 970.

2 (*a*) C. J. Murphy, *J. Cluster Sci.*, 1996, **7**, 341; (*b*) $[Cd_{10}S_4(SPh)_{16}]^{4-}$: I. G. Dance, A. Choy and M. L. Scudder, *J. Am. Chem. Soc.*, 1984, **106**, 6285; (*c*) $[Cd_{17}S_4(SPh)_{28}]^{2-}$: G. S. H. Lee, D. C. Craig, I. Ma, M. L. Scudder, T. D. Bailey and I. G. Dance, *J. Am. Chem. Soc.*, 1988, **110**, 4863; (*d*) $Cd_{17}S_4(SCH_2CH_2OH)_{26}$: T. Vossmeyer, G. Reck, L. Katsikas, E. T. K. Haupt, B. Schulz and H. Weller, *Science*, 1995, **267**, 1476; (*e*) $Cd_{32}S_{14}(SPh)_{36}$: N. Herron, J. C. Calabrese, W. E. Farneth and Y. Wang *Science*, 1993, **259**, 1426; (*f*) $Cd_{32}S_{14}[SCH_2CH(OH)Me_3]_{36}$: T. Vossmeyer, G. Reck, B. Schulz, L. Katsikas and H. Weller, *J. Am. Chem. Soc.*, 1995, **117**, 12 881; (*g*) S. Behrens, M. Bettenhausen, A. C. Deveson, A. Eichhofer, D. Fenske, A. Lohde and U. Woggon, *Angew. Chem., Int. Ed. Engl.*, 1996, **35**, 2215; (*h*) S. Behrens, M. Bettenhausen, A. Eichhofer and D. Fenske, *Angew. Chem., Int. Ed. Engl.*, 1997, **36**, 2797.

3 R. Bertonocello, M. Bettinelli, M. Casarin, C. Maccato, L. Pandolfo and A. Vittadini, *Inorg. Chem.*, 1997, **21**, 4707.

4 (*a*) T. Turk, U. Resch, M. A. Fox and A. Vogler, *J. Phys. Chem.*, 1992, **96**, 3818; (*b*) N. Herron, Y. Wang and H. Eckert, *J. Am. Chem. Soc.*, 1990, **112**, 1322.

5 H.-J. Liu, J. T. Hupp and M. A. Ratner, *J. Phys. Chem.*, 1996, **100**, 12204.

6 M. Vitale, C. K. Ryu, W. E. Palke and P. C. Ford, *Inorg. Chem.*, 1994, **33**, 561.

Communication 8/09443H

meso-Substituted expanded porphyrins: new and stable hexaphyrins

Maria G. P. M. S. Neves,[a] Rosália M. Martins,[a] Augusto C. Tomé,[a] Armando J. D. Silvestre,[a] Artur M. S. Silva,[a] Vitor Félix,[a] Michael G. B. Drew[b] and José A. S. Cavaleiro*[a]

[a] *Department of Chemistry, University of Aveiro, 3810 Aveiro, Portugal. E-mail: jcavaleiro@dq.ua.pt*
[b] *Department of Chemistry, University of Reading, Whiteknights, Reading, UK RG6 6AD*

Received (in Liverpool, UK) 16th November 1998, Accepted 8th January 1999

New hexapyrrolic macrocycles have been synthesized and characterized by UV–VIS, mass and NMR spectroscopy and X-ray crystallography.

In recent years there has been considerable research directed towards the synthesis and study of systems involving expanded porphyrin macrocycles. Such systems are finding applications in the fields of medicine, neutral substrate binding and anion recognition.[1]

Recent studies have shown that inverted[2] and expanded[3] porphyrins can be formed during the Rothemund synthesis of porphyrins. Very recently the synthesis of an interesting expanded porphyrin, the hexaphenylhexaphyrin **1**, has been reported.[4] The poor stability of that compound hampered its spectroscopic characterisation.

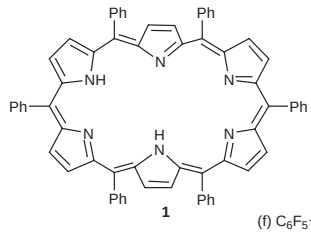

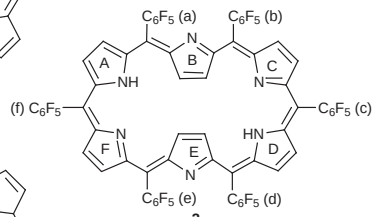

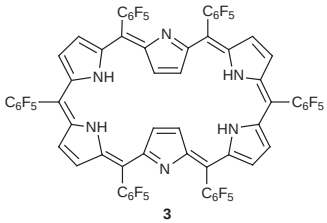

Here we report the synthesis and characterisation by spectroscopic techniques of stable *meso*-hexa(pentafluorophenyl)hexaphyrins **2** and **3**; the structure considered for **2** was also confirmed by X-ray crystallography. These new compounds were obtained during the Rothemund synthesis of *meso*-tetra(pentafluorophenyl)porphyrin under modified experimental conditions:[5] addition of pentafluorobenzaldehyde to a refluxing mixture of glacial AcOH and $PhNO_2$, followed by the dropwise addition of pyrrole. The final mixture was refluxed for 45 min, the solvents were removed by distillation, and the residue was then purified by silica gel column chromatography. The first fraction to be collected contained the expected porphyrin (15%), and a more polar bluish fraction was then eluted (*ca.* 1%). Thin layer chromatographic (TLC) analysis of this fraction revealed the presence of two main compounds with blue and violet colours: $\lambda_{max}(CH_2Cl_2)$/nm (log ε) 591 (4.95), 762 (3.82) and 568 (5.64), 712 (4.67), respectively (Fig. 1).

Both compounds show, in their mass spectra (LSIMS), the same molecular ions at *m/z* 1462, which correspond to molecules formed from six pyrroles and six pentafluorobenzaldehyde units. The fact that both compounds show the same molecular ions was an unexpected observation, since they can be interconverted by hydrogenation–dehydrogenation processes: by reacting the blue compound with DDQ in $CHCl_3$ the violet one is obtained and reduction of the violet compound with $TsNHNH_2$ gives the blue one.

Surprisingly, the ^{1}H NMR spectra of these compounds show that they have aromatic features: for the major (violet) compound, signals at δ −2.43, −1.98, 9.11 and 9.49 are observed. The analysis of this spectrum, together with the HETCOR (^{1}H/^{13}C) spectrum, revealed that the singlet (4H) at δ −2.43 correlates with the carbon resonance at δ 122.9. The very broad singlet at δ −1.98 shows no correlation with carbons and was, thus, attributed to N*H* protons. This signal became more narrow when the proton spectrum was registered at 273.1 K. Based on these spectra, and on the ^{19}F NMR spectrum (*vide infra*), the structure **2** is proposed for this macrocycle. For the blue compound the hydrogenated structure **3** is considered, based mainly on its mass and NMR spectra and its dehydrogenation to **2**. The ^{1}H NMR spectrum of the blue compound is significatively different from that of compound **2**: signals at δ 2.55 (4H, s), 4.40 (br s), 7.63 (4H, d, *J* 4.7) and 7.73 (4H, d, *J* 4.7) are observed; there are no signals at negative δ values. The signal at δ 4.40 is due to the N*H* protons since it disappears after shaking with D_2O. From the HETCOR (^{1}H/^{13}C) experiment we can observe a correlation between the singlet at δ 2.55 and the resonance at δ 119.4 while the doublets at δ 7.63 and 7.73 correlate, respectively, with the carbon resonances at δ 130.2 and 129.2. From the NMR spectra of the blue product it is obvious that there are no sp^3 carbons in this reduced compound.

The fact that both compounds show the same ion at *m/z* 1462 can be explained by a fast hydrogenation of **2** to **3** during the acquisition of the mass spectra.† This was confirmed by the use of deuterated nitrobenzyl alcohol as matrix: **2** gives a signal at *m/z* 1466, corresponding to the addition of '2D' plus the exchange of the two N*H* by N*D*; **3** gives a set of signals at *m/z* 1463–1466 corresponding to the successive exchange of the four N*H* by N*D*.

For compound **2**, the resonance at δ −2.43 corresponds to the 'inner', strongly shielded, four β-protons of the two inverted pyrrole rings (B and E). Since the N*H* protons resonate at δ −1.98 we can say that they are 'inside' the macrocycle and not in the inverted pyrrole rings. The 'outer' β-pyrrolic protons appear as two doublets (4H each) at δ 9.11 and 9.44; they correlate, in the HETCOR (^{1}H/^{13}C) spectrum, with the carbon resonances at δ 132.5 and 135.0, respectively. This last observation confirms that each pyrrole ring (A, C, D and F) has

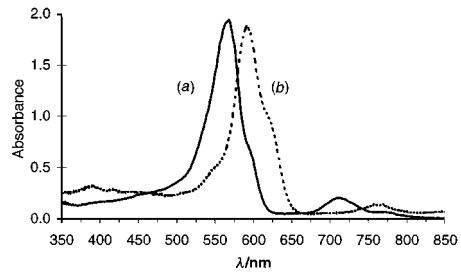

Fig. 1 Electronic spectra of compounds (*a*) **2** and (*b*) **3**.

non-equivalent β-pyrrolic carbons and protons. The resonances of all α-pyrrolic carbons (δ 156.3 for rings B, E and 149.5, 149.7 for the other rings) were determined by the connectivities found in the HMBC spectrum. The resonances of the *meso* carbons appear at δ 106.2 and 117.4, whereas those of the pentafluorophenyl rings appear as multiplets with low intensity (due to both relaxation processes and coupling with the fluorine atoms).

From the ^{19}F NMR spectrum of **2** (Table 1), by comparing the relative signal integrals, we can conclude that there are two types of pentafluorophenyl rings in a 2 : 1 ratio. This result is also compatible with the proposed structure: the two *meso*-pentafluorophenyl rings (c) and (f) are in a different environment than the other four phenyl rings.

The acidic character of the N*H* protons and the stability of *meso*-hexa(pentafluorophenyl)hexaphyrin **2** was demonstrated by the following experiments: (i) addition of several drops of a solution of NaOD (in D_2O) to a $CDCl_3$ solution of this compound, followed by a gentle shaking, led to the appearance of two signals (δ −2.43 and −5.91) in the negative region of the ^{1}H NMR spectrum; (ii) after a more vigorous shaking, only the resonance at δ −5.91 was observed for the β-H of rings B and E. This strong shielding of the 'inner' protons suggests the conversion of the macrocycle into the corresponding dianion; (iii) the neutralization of this solution allowed us to recover the *meso*-hexa(pentafluorophenyl)hexaphyrin **2**.

All the NMR results discussed here support the proposed structure **2** for this new 26π electron macrocycle. The final proof for the structure of this compound was obtained by X-ray single crystal diffraction.

The X-ray structure of **2**‡ is presented in Fig. 2. The macrocycle displays a nonplanar conformation [see Fig. 2(*b*)] with four *exo* pyrrolic rings (A, C, D and F) and two *endo* rings (B and E). π-Electron delocalization in the macrocyclic core is apparent from the observed range of bond lengths: 1.33(1)–1.39(1) Å for the N–Cα bonds and 1.39(1)–1.42(1) Å for the Cα-C*meso* bonds. On the other hand, the range found for the C–C bond lengths in the pyrrole rings suggest that these bonds have some double or single bond character: 1.36(1)–1.32(1) Å for the Cβ–Cβ bonds and 1.42(1)–1.46(1) Å for the Cα–Cβ bonds. The six pentafluorophenyl rings are tilted by 47.3(1), 43.3(1), 51.0(1), 68.4(1), 78.8(1) and 81.4(1)° relative to the least-square plane defined by the atoms of the macrocyclic core. Consequently, the average bond length between the *meso* carbons and pentafluorophenyl rings of 1.50(1) Å indicates an absence of a π interaction between those rings and the macrocyclic core.

This set of structural features is consistent with a 26π electron aromatic current ring extended over the nitrogens, the α-pyrrolic carbons and the *meso* carbons of the macrocyclic ring.

The nonplanarity of the macrocycle is due to its large dimensions [N(39)···N(45) 2.93(1), N(18)···N(24) 2.82(1), N(24)···N(39) 7.58(1) and N(18)···N(45) 7.60(1) Å] and the bulk of the *meso*-pentafluorophenyl rings. In order to minimise the steric interactions, the macrocycle looses the planarity of its core, leading an average deviation of 0.536(8) Å of the atoms belonging to the macrocyclic core from the least-squares plane defined by their atomic positions.

We thank FCT, Lisbon, for funding the Research Unit No. 62/94 and Mr Pedro Domingues (University of Aveiro) for the mass spectra.

Table 1 ^{19}F NMR chemical shifts (ppm, from TFA) observed in the spectrum of the *meso*-hexa(pentafluorophenyl)hexaphyrin **2**

	(a), (b), (d) and (e) phenyl rings	(c) and (f) phenyl rings
o-F	−136.19 (4F)	−135.63 (2F)
m-F	−162.22 (4F)	−159.61 (2F)
p-F	−151.94 (2F)	−149.08 (1F)

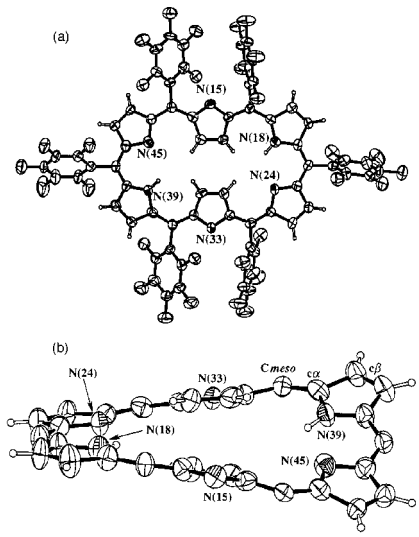

Fig. 2 (*a*) Top and (*b*) side views of **2** (thermal ellipsoids at the 40% probability level). The side view shows the nonplanarity of the macrocyclic core. In both views only the labelling scheme for nitrogen atoms is presented, and in (*b*) the phenyl rings are omitted for clarity.

Notes and references

† A similar hydrogenation process was observed during the acquisition of the mass spectrum of the *meso*-tetra(pentafluorophenyl)porphyrin.

‡ *Crystal data* for **2**: $C_{66}H_{14}F_{30}N_6$, M = 1460.83; monoclinic, space group $P2_1/c$, a = 10.911(10), b = 27.242(23), c = 19.466(21) Å, β = 90.31(1)°, V = 5786(10) Å^3, Z = 4, D_c = 1.677 g cm^{-3}, μ = 0.168 mm^{-1}. A violet needle-like crystal was mounted in a Lindmann capillary under saturated atmosphere of the mother-liquor. The X-ray data were collected with graphite monochromated Mo-Kα radiation (λ = 0.71073 Å) on a Mar-research image plate system at Reading University. The crystal was positioned at 75 mm from the plate. An exposure time of 5 min was used per 2º frame collected. Data analysis was performed with the XDS program (ref. 6). Intensities were not corrected for absorption effects. 12030 reflections collected in the range 2.0 < θ < 26.1 (*hkl* range indices: 0 ⩽ h ⩽ 11, −33 ⩽ k ⩽ 33, −19 ⩽ l ⩽ 19) were merged in the Laue symmetry group 2/*m* to 7246 unique reflections with a R_{int} = 0.0454. The structure was solved by direct methods and refined by full-matrix least-squares methods on F^2 using the SHELX-97 package (ref. 7) Anisotropic parameters were used for all non-hydrogen atoms. The hydrogen atoms were included in the refinement in geometric positions with a U_{iso} = 1.2U_{eq} of the parent nitrogen atom. In agreement with ^{1}H NMR results, two geometric arrangements for two N–H protons were considered: one proton at N(39) and one at N(18) or alternatively one proton at N(24) and the other at N(45). The first arrangement was considered as correct since it gave a slightly lower R value (0.0789) than the second (0.0795). The final refinement of 920 parameters converged to R and wR values of 0.0785 and 0.2094 and GOF = 0.862 for the data with I > 2σ(I). The final R and wR values for all *hkl* data were 0.2304 and 0.2750, respectively. In the last difference Fourier map the residual electronic density was in the range of −0.341 to 0.281 e Å^{-3}. Molecular diagrams were made with ZORTEP (ref. 8). CCDC 182/1139. Crystal data are available in CIF format from the RSC web site, see: http://www.rsc.org/suppdata/cc/1999/385/

1 A. Jasat and D. Dolphin, *Chem. Rev*., 1997, **97**, 2267; B. Franck and A. Nonn, *Angew. Chem., Int. Ed. Engl*., 1995, **34**, 1795.
2 P. J. Chmielewski, L. Latos-Grazynski, K. Rachlewicz and T. Glowiak, *Angew. Chem., Int. Ed. Engl*., 1994, **33**, 779; H. Furuta, T. Asano and T. Ogawa, *J. Am. Chem. Soc*., 1994, **116**, 767.
3 P. J. Chmielewski, L. Latos-Grazynski and K. Rachlewicz, *Chem. Eur. J*., 1995, **1**, 68.
4 C. Bruckner, E. D. Sternberg, R. W. Boyle and D. Dolphin, *Chem. Commun.*, 1997, 1689.
5 A. M. d'A. Rocha Gonsalves, J. M. T. Varejão and M. M. Pereira, *J. Heterocycl. Chem.*, 1985, 1228.
6 W. Kabsch, *J. Appl. Crystallogr*., 1988, **21**, 916.
7 G. M Sheldrick, SHELX-97, University of Göttingen, 1997.
8 L. Zsolnai, ZORTEP, University of Heidelberg, 1994.

Communication 8/08952C

Use of 2-methyl-1-phenylpropan-2-yl hydroperoxide (MPPH) as a mechanistic probe for the heterolytic *versus* homolytic O–O bond cleavage of *tert*-alkyl hydroperoxide by iron(III) porphyrin complex

Wonwoo Nam,* Hye J. Choi, Hui J. Han, So H. Cho, Ha J. Lee and So-Yeop Han

Department of Chemistry and Center for Cell Signaling Research, Ewha Womans University, Seoul 120-750, Korea. E-mail: wwnam@mm.ewha.ac.kr

Received (in Cambridge, UK) 18th December 1998, Accepted 14th January 1999

The mechanism of the O–O bond cleavage of *tert*-alkyl hydroperoxide by iron(III) porphyrin complexes has been studied using 2-methyl-1-phenylpropan-2-yl hydroperoxide (MPPH) as a mechanistic probe; the hydroperoxide O–O bond is cleaved both heterolytically and homolytically and partitioning between the two pathways significantly depends on the reaction conditions such as the pH of the reaction solutions and the nature of porphyrin and axial ligands.

The reactions of iron(III) porphyrin complexes with alkyl hydroperoxides have been intensively studied as biomimetic models for heme-containing enzymes such as cytochromes P-450, peroxidases and catalases, with the intention of elucidating the mechanism of O–O bond activation and the structure of reactive intermediates.[1] Traylor *et al.* proposed that the O–O bond of hydroperoxides is heterolytically cleaved by the iron porphyrins, giving the formation of a high-valent iron oxo porphyrin cation radical intermediate **1** (Scheme 1, pathway A).[2] In contrast, Bruice *et al.*[3] and others[4] provided evidence that the initial step of the hydroperoxide O–O bond cleavage is homolysis, resulting in the formation of a ferryl–oxo complex, **2**, and an alkoxyl radical (Scheme 1, pathway B). Despite the intensive study for the last two decades, the nature of the O–O bond cleavage of ROOH by the iron(III) porphyrin complexes has been controversial and still remains unclear.

In recent years, 2-methyl-1-phenylpropan-2-yl hydroperoxide (MPPH) has been shown to be an excellent mechanistic probe capable of distinguishing between free alkoxyl radical chemistry and radical-free (enzyme mimetic) chemistry in non-porphyrin iron(III) complex-catalyzed oxidations of hydrocarbons by *tert*-alkyl hydroperoxides.[5] When the O–O bond of MPPH is cleaved homolytically by the iron complexes, an alkoxyl radical (MPPO·) is generated [eqn. (1)]. Then, the

$$Fe^{III} + PhCH_2CMe_2OOH \xrightarrow{\text{homolysis}} Fe^{IV}{=}O + PhCH_2CMe_2O^{\bullet} + H^+ \quad (1)$$
(MPPH) (MPPO•)

alkoxyl radical undergoes an extremely rapid β-scission, giving PhCHO and $PhCH_2OH$ [eqn. (2)].[5] In contrast, heterolytic

$$PhCH_2CMe_2O^{\bullet} \xrightarrow{-Me_2CO} PhCH_2^{\bullet} \xrightarrow{+O_2} \longrightarrow PhCHO + PhCH_2OH \quad (2)$$
(MPPO•)

reduction of MPPH by the iron complexes yields an alcohol (MPPOH) [eqn. (3)]. Therefore, the mechanism of the O–O

$$Fe^{III} + PhCH_2CMe_2OOH \xrightarrow{\text{heterolysis}} Fe^{V}{=}O + PhCH_2CMe_2OH \quad (3)$$
(MPPOH)

bond cleavage of *tert*-alkyl hydroperoxides can be determined by analyzing the products derived from the decomposition of MPPH by iron complexes. Another mechanistic probe often used to interpret the mechanism of the O–O bond cleavage of ROOH by iron(III) porphyrin complexes is to analyze the products yielded in the epoxidation of olefins such as (*Z*)-stilbene.[6] When **2** is formed *via* homolysis (Scheme 1, pathway B), **2** affords a low yield of epoxide products with a loss of stereospecificity.[7] In contrast, **1**, which is generated *via* heterolysis (Scheme 1, pathway A), is capable of epoxidizing olefins stereospecifically. We therefore studied iron(III) porphyrin complex-catalyzed olefin epoxidation reactions using the aforementioned two mechanistic probes (*i.e.* MPPH as an oxidant and (*Z*)-stilbene as a substrate), in order to clarify the mechanism of the O–O bond cleavage of *tert*-alkyl hydroperoxides by iron(III) porphyrin complexes.

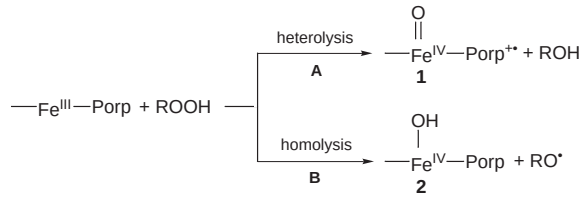

Scheme 1

The catalytic epoxidation of (*Z*)-stilbene by MPPH was carried out in the presence of water-soluble iron(III) porphyrin complexes in buffered H_2O–MeOH–MeCN solutions.† Among the tested iron porphyrins (see Fig. 1), $Fe(TDFPPS)^{3-}$ showed the greatest reactivity for giving a high yield of *cis*-stilbene oxide with a trace amount of *trans*-stilbene oxide, whereas other iron porphyrins gave a small amount of *cis*-stilbene oxide (*vide infra*). Fig. 2 shows the result of product studies obtained in the (*Z*)-stilbene epoxidation by $Fe(TDFPPS)^{3-}$ and MPPH at pH 3–8. The epoxidation reaction was found to depend on the pH of the reaction solutions[8] and the yield of *cis*-stilbene oxide formed was higher at low pH values, as we have observed previously.[9] Interestingly, the amounts of *cis*-stilbene oxide and MPPOH yielded in the reactions were similar, demonstrating that the reaction of $Fe(TDFPPS)^{3-}$ and MPPH involves heterolysis of the hydroperoxide to generate $(TDFPPS)^{+\cdot}Fe^{IV}{=}O$ as a reactive intermediate responsible for the (*Z*)-stilbene epoxidation. In addition to the heterolysis of MPPH by $Fe(TDFPPS)^{3-}$,

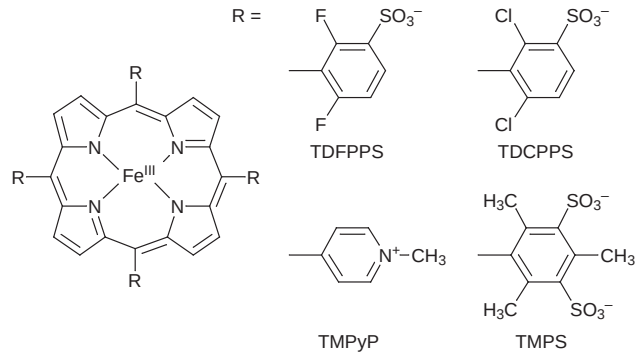

Fig. 1 Structures and abbreviated names of iron(III) porphyrin complexes used in this study.‡

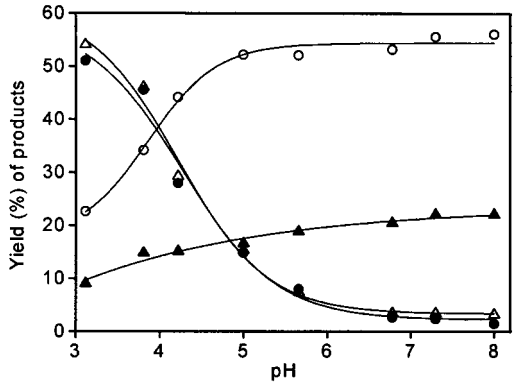

Fig. 2 Plot of the percent yield of products (●, *cis*-stilbene oxide; △, MPPOH; ▲, $PhCH_2OH$; ○, PhCHO) *vs.* pH of reaction solutions for the catalytic epoxidation of (*Z*)-stilbene by $Fe(TDFPPS)^{3-}$ and MPPH. The percent yields are calculated on the basis of MPPH used. See footnote † for detailed experimental procedures.

homolysis of MPPH took place concurrently even at low pH values, as demonstrated by the observation of the formation of PhCHO and $PhCH_2OH$ [eqn. (2)]. As the pH of the reaction solution increased, the yields of *cis*-stilbene oxide and MPPOH products decreased and the amounts of the PhCHO and $PhCH_2OH$ increased. These results indicate that the O–O bond cleavage of MPPH was shifted from heterolysis to homolysis as the pH of the reaction solutions increased.

In addition to the pH effect on hydroperoxide O–O bond cleavage, we found that there are other important factors that control the type of O–O bond cleavage of *tert*-alkyl hydroperoxides. As shown in Table 1, the O–O bond cleavage was significantly affected by the porphyrin ligands bound to iron and the general trend appeared to be that more electronegatively-substituted iron porphyrins gave a high percentage of heterolysis, whereas homolysis prevailed in the reactions with less electronegatively-substituted iron porphyrins. This result is consistent with the observation that electron-deficient iron porphyrins are effective catalysts in the epoxidation of olefins by H_2O_2 and ROOH.[10] We also found, by studying the epoxidation of (*Z*)-stilbene with $Fe(TDFPPS)^{3-}$ and MPPH in the presence of imidazoles, that there is a significant axial ligand effect on the ratio of the heterolytic and homolytic O–O bond cleavage of *tert*-alkyl hydroperoxides.[4b,11,12] Interestingly, the presence of imidazoles such as 5-chloro-1-methylimidazole and 1-phenylimidazole increased the yields of *cis*-stilbene oxide and MPPOH products, whereas 1-methylimidazole and 1,2-dimethylimidazole did not alter the ratio of heterolysis to homolysis significantly (data not shown), indicating that the nature of the axial ligand bound to iron is another important factor determining the type of the hydroperoxide O–O bond cleavage.[11–13]

In summary, we demonstrated unambiguously that the O–O bond of *tert*-alkyl hydroperoxides is cleaved both heterolytically and homolytically,[11] depending on the reaction conditions such as pH and the electronic nature of the porphyrin and axial ligands. These results rationalize the long-standing dichotomy of the interpretations for the O–O bond cleavage mechanism of ROOH by iron(III) porphyrin complexes, mainly suggested by Traylor[2] and Bruice[3] and co-workers.

Table 1 Product yields formed in the epoxidation of (*Z*)-stilbene by MPPH catalyzed by iron porphyrin complexes at pH 3.2[a]

	Yields (%)[b]			
Iron porphyrins	*cis*-Stilbene oxide	MPPOH	$PhCH_2OH$	PhCHO
$Fe(TDFPPS)^{3-}$	51	54	8	21
$Fe(TDCPPS)^{3-}$[c]	33	38	12	41
$Fe(TMPyP)^{5+}$	2	7	14	59
$Fe(TMPS)^{7-}$[c]	12	19	18	44

[a] See footnote † for detailed reaction procedures. [b] Based on MPPH used. [c] Reactions were run for 8 h.

This research was supported by the Korea Science and Engineering Foundation (96-0501-01-01-3), the MOST through the Women's University Research Fund, and Ewha Womans University (1998).

Notes and references

† MPPH was prepared according to literature procedures[5] and the purity of MPPH was determined to be 100% by NMR. In a typical reaction, MPPH (4 mM, introduced as a 0.2 M solution in MeOH) was added to a reaction solution containing $Fe(TDFPPS)^{3-}$ (0.04 mM, introduced as 0.01 M solution in H_2O) and (*Z*)-stilbene (6 mM, introduced as 0.3 M solution in MeOH) in a solvent mixture (5 mL) of buffered H_2O (2.5 mL)–MeOH (1.0 mL)–MeCN (1.5 mL) in order to make the reaction mixture homogeneous. Reactions at pH 3 were performed in formate buffer (0.1 M), at pH 4–5 in acetate buffer (0.1 M), and at pH 6–8 in phosphate buffer (0.1 M), and the pH was adjusted by adding either HCl (3 M) or NaOH (3 M) solutions as necessary. The reaction mixture was stirred in air for 4 h at 25 °C, and then analyzed by *Orom Vintage 2000* HPLC equipped with a variable wavelength UV-200 detector. Detection was made at 215 and 254 nm.

‡ All iron(III) porphyrin complexes used in this study were obtained from Mid-Century Chemical. Abbreviations used: TDFPPS, [*meso*-tetrakis(2,6-difluoro-3-sulfonatophenyl)porphyrin; TDCPPS, *meso*-tetrakis(2,6-dichloro-3-sulfonatophenyl)porphyrin; TMPyP, *meso*-tetrakis(*N*-methylpyridin-4-ylium)porphyrin; TMPS, *meso*-tetrakis(2,5-disulfonatomesityl)-porphyrin.

1 M. Sono, M. P. Roach, E. D. Coulter and J. H. Dawson, *Chem. Rev.*, 1996, **96**, 2841; T. G. Traylor and P. S. Traylor, in *Active Oxygen in Biochemistry*, ed. J. S. Valentine, C. S. Foote, A. Greenberg and J. F. Liebman, Blackie Academic and Professional, Chapman and Hall, London, 1995, pp. 84–187; B. Meunier, *Chem. Rev.*, 1992, **92**, 1411.
2 T. G. Traylor, C. Kim, W.-P. Fann and C. L. Perrin, *Tetrahedron*, 1998, **54**, 7977 and refs. therein.
3 O. Almarsson and T. C. Bruice, *J. Am. Chem. Soc.*, 1995, **117**, 4533 and refs. therein.
4 (*a*) F. Minisci, F. Fontana, S. Araneo, F. Recupero, S. Banfi and S. Quici, *J. Am. Chem. Soc.*, 1995, **117**, 226; (*b*) S. E. J. Bell, P. R. Cooke, P. Inchley, D. R. Leanord, J. R. Lindsay Smith and A. Robbins, *J. Chem. Soc., Perkin Trans. 2*, 1991, 549; (*c*) R. Labeque and L. J. Marnett, *J. Am. Chem. Soc.*, 1989, **111**, 6621.
5 P. A. MacFaul, D. D. M. Wayner and K. U. Ingold, *Acc. Chem. Res.*, 1998, **31**, 159; P. A. MacFaul, K. U. Ingold, D. D. M. Wayner and L. Que, Jr., *J. Am. Chem. Soc.*, 1997, **119**, 10594; P. A. MacFaul, I. W. C. E. Arends, K. U. Ingold and D. D. M. Wayner, *J. Chem. Soc., Perkin Trans. 2*, 1997, 135; I. W. C. E. Arends, K. U. Ingold and D. D. M. Wayner, *J. Am. Chem. Soc.*, 1995, **117**, 4710.
6 G.-X. He and T. C. Bruice, *J. Am. Chem. Soc.*, 1991, **113**, 2747; A. J. Castellino and T. C. Bruice, *J. Am. Chem. Soc.*, 1988, **110**, 158.
7 J. T. Groves, Z. Gross and M. K. Stern, *Inorg. Chem.*, 1994, **33**, 5065.
8 A. Hadasch, A. Sorokin, A. Rabion and B. Meunier, *New J. Chem.*, 1998, 45; R. Song, A. Sorokin, J. Bernadou and B. Meunier, *J. Org. Chem.*, 1997, **62**, 673; S. M. S. Chauhan, P. P. Mohapatra, B. Kalra, T. S. Kohli and S. Satapathy, *J. Mol. Catal. A: Chem.*, 1996, **113**, 239.
9 S. J. Yang and W. Nam, *Inorg. Chem.*, 1998, **37**, 606 and refs. therein.
10 Y. J. Lee, Y. M. Goh, S.-Y. Han, C. Kim and W. Nam, *Chem. Lett.*, 1998, 837; T. G. Traylor, C. Kim, J. L. Richards, F. Xu and C. L. Perrin, *J. Am. Chem. Soc.*, 1995, **117**, 3468; J. F. Bartoli, P. Battioni, W. R. De Foor and D. Mansuy, *J. Chem. Soc., Chem. Commun.*, 1994, 23.
11 A. J. Allentoff, J. L. Bolton, A. Wilks, J. A. Thompson and P. R. Ortiz de Montellano, *J. Am. Chem. Soc.*, 1992, **114**, 9744.
12 D. Mansuy, P. Battioni and J.-P. Renaud, *J. Chem. Soc., Chem. Commun.*, 1984, 1255.
13 K. Yamaguchi, Y. Watanabe and I. Morishima, *J. Am. Chem. Soc.*, 1993, **115**, 4058.

Communication 8/09876J

Synthesis and X-ray structure of a cluster complex with facial coordination of cyclooctatetraene to a Co_2Ni triangle

Hubert Wadepohl,* Stefan Gebert, Rüdiger Merkel and Hans Pritzkow

Anorganisch-chemisches Institut der Ruprecht-Karls-Universität, Im Neuenheimer Feld 270, D-69120 Heidelberg, Germany. E-mail: bu9@ix.urz.uni-heidelberg.de

Received (in Basel, Switzerland) 4th January 1999, Accepted 16th January 1999

The reaction between $[(\eta\text{-}C_5H_5)NiCo_3(CO)_9]$ and cyclooctatetraene yields $[Co_2Ni(CO)_6(\mu_3\text{-}\eta^2:\eta^3\text{-}C_8H_8)]$ with a cyclooctatetraene ligand in the facial coordination mode to a heterometallic Co_2Ni triangle.

The facial coordination of the cyclic π-perimeters C_nH_n (n = 5–8) to a molecular metal cluster is well documented.[1–4] Examples include the complexes $[\{(\eta\text{-}C_5H_5)Rh\}_3(\mu_3\text{-}H)(\mu_3\text{-}C_5H_5)]$,[5] $[\{(CO)_3M\}_3(\mu_3\text{-}C_6H_6)]$ (M = Ru, Os),[6] $[\{(CO)_2Ru\}_3(\mu_3\text{-}SBu^t)(\mu_3\text{-}C_7H_7)]$[7] and $[\{(CO)Ni\}_3\{\mu_3\text{-}(CF_3)_2C_2\}(\mu_3\text{-}C_8H_8)]$.[8] In such complexes, the C_nH_n ligand bonds to a triangular array of three metal atoms, which may even be part of a larger cluster moiety. This coordination geometry is frequently related to the adsorption states of the corresponding hydrocarbons on atomically flat (single crystal) metal surfaces.[9] Similar adsorbates are key intermediates in the industrially enormously important catalytic hydrocarbon reforming processes.[10] Curiously, although heteronuclear cluster complexes are quite commonplace, to our knowledge only one compound has been reported with a facial coordination of a cyclic conjugated unsaturated hydrocarbon to a cluster face comprised of two different types of metal atoms, *viz.* an Ru_2Pt face in $[Ru_6Pt_3(CO)_{18}\{\mu_3\text{-}\eta^2:\eta^2\text{-}C_6H_5(CH_2)_2Ph\}(\mu_3\text{-}H)_4]$ **1**.[11] Our prime interest in such species comes from the well known fact that metal alloys and supported bimetallic clusters can have catalytic properties which may be vastly different from those of the pure metals.[12] Complexes such as **1** may be important stepping stones on the way towards an understanding of some of the factors which control how these catalysts work on the molecular level. Recently we reported on the simple one-pot synthesis of the complexes $[Co_4(CO)_6(\mu_3\text{-}C_7H_7)(\eta^5\text{-}C_7H_9)]$ **2** and $[Co_4(CO)_6(\mu_3\text{-}C_8H_8)(\eta^4\text{-}C_8H_8)]$ **3**, starting from the binary carbonyl $[Co_4(CO)_{12}]$ and cycloheptatriene or cyclooctatetraene, respectively.[13] The products **2** and **3** provide a convenient entrance to large families of tri- and tetra-nuclear cluster complexes with facial C_7H_7 and C_8H_8 ligands.[3,13] Here, we report the synthesis and characterisation of a cluster complex containing a C_8H_8 ligand in the facial coordination mode to a Co_2Ni metal triangle. This is the first example of facial C_8H_8 coordination to a heterometallic face of a cluster, and only the second throughout the whole series $M_m(\mu_3\text{-}C_nH_n)$ (n = 5–8).

Reaction of the tetranuclear complex $[(\eta\text{-}C_5H_5)NiCo_3(CO)_9]$ **4** with an excess of cyclooctatetraene in refluxing *n*-heptane gave a dark red microcrystalline precipitate in 25% yield. The presence of a face-capping C_8H_8 ligand in this product was indicated by the NMR spectra.† However, no resonances were observed for a cyclopentadienyl ligand. The IR spectrum‡ indicated terminal and bridging carbonyl ligands; the large number of bands in the ν_{CO} region pointed to a rather low molecular symmetry. The structure of the product was eventually determined by a single crystal X-ray structure analysis.§ The molecular structure, $[M_3(CO)_6(\mu_3\text{-}C_8H_8)]$, is shown in Fig. 1, together with selected bond parameters. Unfortunately, the identity of the metal atoms M (cobalt or nickel) could not be determined unambiguously from the diffraction data.

The observed diamagnetism of the complex requires the composition of either $[Co_2Ni(CO)_6(C_8H_8)]$ or $[Ni_3(CO)_6(C_8H_8)]$. XPS analysis of a sample film deposited from solution on a gold foil gave the atomic ratio Co : Ni = 2 : 1. The isotope pattern starting with *m/z* 448 of the peak due to the molecular ion in the field desorption mass spectrum is also only consistent with the formulation $[Co_2Ni(CO)_6(\mu_3\text{-}C_8H_8)]$ **5**. The novel complex **5** is isoelectronic with its anionic tricobalt analog, $[Co_3(CO)_6(\mu_3\text{-}C_8H_8)]^-$ **6**, which was obtained in high yield by reductive degradation of **3**.[3]

The mean metal metal separation in **5** is 2.514 Å, shorter than in the tricobalt complex **6** (2.528 Å[14]). An even shorter mean metal metal distance (2.438 Å) was found in $[NiCo_2(\mu_2\text{-}CO)_3(PMe_3)_6]$, where D_{3h} symmetry is imposed on the molecule by the lattice symmetry (Co and Ni atoms are necessarily disordered).[15] This contraction of the metal triangles can be attributed to the effect of exchanging a cobalt for the smaller nickel atom. In both **5** and **6**, the lengths of the three individual metal metal bonds differ only by a maximum of 0.02 Å. In the only two structurally characterised cluster complexes with triangular Co_2Ni faces comprised of equally substituted apices disorder of the metals was found, indicating a close similarity of Co–Co and Co–Ni bonds.[15,16] For **5**, we cannot completely rule out some static disorder of the metal triangle, but there are no unusual shapes or orientations of the anisotropic displacement ellipsoids, and all the peaks in the Fourier synthesis are well defined.

The bridging C_8H_8 ligand attains an $\eta^2:\eta^3:\eta^3$ coordination mode with respect to the metal triangle. The carbocyclic ring is non-planar and approaches a chair conformation (Fig. 2). Carbon–carbon bond lengths within the $\mu_3\text{-}C_8H_8$ vary barely significantly within the range 1.396(8)–1.434(8) Å. The ligand

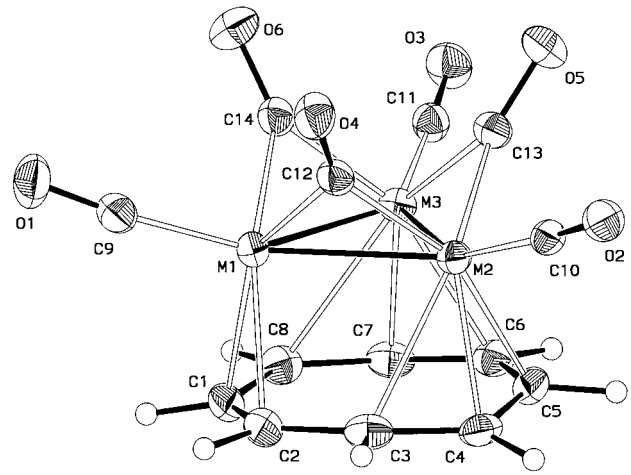

Fig. 1 Molecular structure of $[Co_2Ni(CO)_6(\mu_3\text{-}C_8H_8)]$ **5**. Selected bond lengths (Å) and angles (°): M1–M2 2.512(1), M1–M3 2.503(1), M2–M3 2.526(1), M1–C1 2.118(5), M1–C2 2.140(5), M2–C3 2.333(5), M2–C4 2.087(5), M2–C5 2.236(5), M3–C6 2.190(5), M3–C7 2.088(5), M3–C8 2.427(5), C1–C2 1.396(8), C1–C8 1.434(8), C2–C3 1.417(8), C3–C4 1.418(7), C4–C5 1.411(7), C5–C6 1.432(8), C6–C7 1.412(7), C7–C8 1.404(7), C2–C1–C8 133.2(5), C1–C2–C3 134.4(5), C2–C3–C4 136.5(5), C3–C4–C5 131.6(5), C5–C6–C7 134.8(5), C6–C7–C8 132.8(5), C7–C8–C1 136.5(5) (M = Co, Ni).

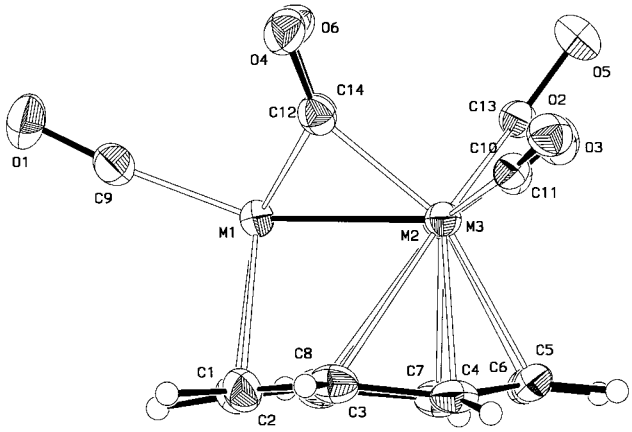

Fig. 2 Side view of **5** showing the conformation of the μ_3-C_8H_8 ring.

shell of the cluster is completed by three terminal and three edge-bridging carbonyl ligands. In solution, both the carbonyl and C_8H_8 ligands in **5** display fluxional behaviour. Only one ^{13}C NMR resonance is observed for the six carbonyl ligands, indicating a 'merry-go-round' type exchange process which involves both the terminal and bridging CO ligands. The observation of only one ^{13}C and ^1H NMR resonance for the μ_3-C_8H_8 ring is consistent with a rapid rotation of this ligand on top of the metal triangle. A high degree of fluxionality is generally characteristic for C_8H_8 ligands capping a Co_3 cluster face.[3] Evidently, the activation barrier for this process is not appreciably increased on coordination to the Co_2Ni triangle.

During the formation of **5**, the presence of [(η-C_5H_5)$Co(CO)_2$] **7** in the reaction mixture was observed by IR spectroscopy. It is therefore likely, that the reaction involves an intra- or inter-molecular transfer of the cyclopentadienyl ligand from the nickel to a cobalt atom, which then leaves the cluster in the form of **7**. Vahrenkamp and coworkers have previously noted a similar role of an intermolecular nickel-to-cobalt transfer of a cyclopentadienyl ligand during metal exchange reactions in tri- and tetra-nuclear cluster complexes.[17]

We thank the Sonderforschungsbereich 247 der Universität Heidelberg and the Fonds der chemischen Industrie for support. H. W. acknowledges the award of a Heisenberg Fellowship by the Deutsche Forschungsgemeinschaft. Special thanks are due to Professor Ch. Wöll (Ruhr-Universität Bochum) for the XPS analysis.

Notes and references

† ^1H NMR (C_6D_6, 200 MHz) δ 3.42 (s); ^{13}C NMR (C_6D_6) δ 71.8 (C_8H_8), 185.1 (CO).

‡ IR (CH_2Cl_2) ν_{CO}/cm^{-1} 2059s, 2020vs, 2003vs, 1883vs, 1853m, 1834m.

§ *Crystal data* for $[Co_2Ni(CO)_6(\mu_3\text{-}\eta^2:\eta^3\text{-}C_8H_8)]\cdot C_6H_6$: $C_{20}H_{14}Co_2NiO_6$, M = 526.91, monoclinic, space group $P2_1/n$, a = 10.203(5), b = 16.674(8), c = 11.902(6), β = 101.19(2), V = 1986.3(17) Å^3, Z = 4, μ(Mo-Kα) = 2.51 mm^{-1}, T = 203 K. Crystals obtained from a benzene solution at 10 °C were found to be twinned and consisted of two interpenetrating individuals with different orientation. 4951 intensity data were collected based on the orientation matrix of the individual which gave stronger reflections. Deletion of overlapping reflections resulted in 3454 unique data ($-13 \leqslant h \leqslant 13$, $0 \leqslant k \leqslant 22$,$0 \leqslant l \leqslant 15$; $2\theta_{max}$ = 56°). The structure was solved by direct methods and refined by full-matrix least squares based on F^2. All metal atoms were refined as cobalt. All non-hydrogen atoms were treated anisotropic, hydrogen atoms were located from difference Fourier syntheses and refined with isotropic displacement parameters, wR_2 = 0.094 (all data), R_1 = 0.040 [2261 reflections with $F_o > 4\sigma(F_o)$], GOF = 1.035. CCDC 182/1148. See http://www.rsc.org/suppdata/cc/1999/389/ for crystallographic files in .cif format.

1 H. Wadepohl, *Angew. Chem.*, 1992, **104**, 253.
2 D. Braga, P. J. Dyson, F. Grepioni and B. F. G. Johnson, *Chem. Rev.*, 1994, **94**, 1585.
3 H. Wadepohl, *Coord. Chem. Rev.*, 1999, in the press.
4 H. Wadepohl and A. Metz, in *Metal Clusters in Chemistry*, ed. P. Braunstein, L. Oro and P. R. Raithby, Wiley-VCH 1998, in the press.
5 E. O. Fischer, O. S. Mills, E. F. Paulus and H. Wawersik, *Chem. Commun.*, 1967, 643; O. S. Mills and E. F. Paulus, *J. Organomet. Chem.*, 1968, **11**, 587.
6 M. P. Gomez-Sal, B. F. G. Johnson, J. Lewis, P. R. Raithby and A. H. Wright, *J. Chem. Soc. Chem. Commun.*, 1985, 1682; B. F. G. Johnson, J. Lewis, M. Martinelli, A. H. Wright, D. Braga and F. Grepioni, *J. Chem. Soc., Chem. Commun.*, 1990, 364.
7 T. A. Cresswell, J. A. K. Howard, F. G. Kennedy, S. A. R. Knox and H. Wadepohl, *J. Chem. Soc., Dalton Trans.*, 1981, 2220.
8 J. L. Davidson, M. Green, F. G. A. Stone and A. J. Welch, *J. Chem. Soc., Dalton Trans.*, 1979, 506.
9 G. A. Somorjai, *Pure Appl. Chem.*, 1998, **60**, 1499; *J. Phys. Chem.*, 1990, **94**, 1013.
10 G. A. Somorjai, *Chemistry in Two Dimensions: Surfaces*, Cornell University Press, Ithaca, 1981, ch. 9.
11 R. D. Adams, T. S. Barnard, Zhaoyang Li, Wengan Wu and J. H. Yamamoto, *J. Am. Chem. Soc.*, 1994, **116**, 9103.
12 J. H. Sintfelt, *Sci. Am.*, 1985, **253**(**9**), 96.
13 H. Wadepohl, S. Gebert, H. Pritzkow, D. Braga and F. Grepioni, *Chem. Eur. J.*, 1998, **4**, 279.
14 H. Pritzkow, unpublished work.
15 H.-F. Klein, M. Mager, U. Flörke, H.-J. Haupt, M. Breza and R. Boca, *Organometallics* 1992, **11**, 2912.
16 V. G. Albano, G. Ciani and P. Chini, *J. Chem. Soc., Dalton Trans.*, 1974, 432.
17 H. Beurich, R. Blumhofer and H. Vahrenkamp, *Chem. Ber.*, 1982, **115**, 2409.

Communication 9/00002J

Porous platinum fibers synthesized using supercritical fluid

H. Wakayama* and Y. Fukushima

Toyota Central R&D Labs., Inc., Nagakute, Aichi, 480-1192, Japan. E-mail: e0980@mosk.tytlabs.co.jp

Received (in Cambridge, UK) 26th October 1998, Accepted 19th January 1999

Porous platinum fibers replicating both the shape and nanopore structure of activated carbon fibers have been prepared in supercritical fluid media.

Several techniques have been developed recently for fabricating nanostructured materials using templates, such as molecular[1] and surfactant arrays,[2,3] latex spheres,[4] block copolymers[5] and carbon nanotubes.[6–8] One of us has reported the synthesis of highly ordered mesoporous silica or silica–alumina using hexagonally packed aggregates of surfactants as templates.[3] In the case of porous metal, platinum black is synthesized electrochemically. Recently, Attard *et al.* have reported the production of mesoporous platinum materials.[9–11] The shape of the porous platinum materials are restricted to powders[9] or films.[10] The fabrication of such structures that can be used directly without any binders or substrates has remained an experimental challenge. The control of macroscopic shape is quite important in applying such porous materials as catalysts, electrodes, sensors and capacitors. We show here the synthesis of porous platinum fibers replicating morphologies, with both the porous structure and fibrous shape of base activated carbon fibers, using supercritical fluid as a medium. Supercritical fluids have large diffusion coefficients,[12] low viscosity and controllable solubility[13] and are expected to carry effective amounts of precursor into small spaces and to be effective media in replicating a template with porous structure such as activated carbon.

Acetone (5 ml) along with $Pt(acac)_2$ (0.5 g) (acac = acetylacetonate) was placed in a stainless steel vessel (50 ml). A stainless steel basket containing 1 g of activated carbon fibers (Touyoubou co. BW103) was then placed in the vessel. The activated carbon fibers in the cage were not in contact with the liquid acetone or the Pt precursor. The closed vessel was filled with CO_2 and kept at 423 K and 32 MPa for 2 h in an oil bath. Then, the base activated carbon was removed by oxidation using YAMATO Scientific O_2 plasma equipment (PC-103, RFG-500) at 500 W in O_2 (160 ml min^{-1}) for 8 h. The fibrous shape of the cloth was retained even after removal of the activated carbon fiber cloth.

As shown in Fig. 1(a), the sample treated with oxygen plasma shows three characteristic X-ray diffraction peaks which correspond to (111), (200) and (220) peaks for metallic platinum. No peaks due to platinum oxide were detected in the XRD pattern in the sample treated with oxygen plasma while XRD peaks from activated carbon disappear for the sample treated with oxygen plasma. The crystalline sizes of platinum metal calculated from the half widths of the (111), (200) and (220) reflections in the XRD pattern were estimated to be *ca*. 10 nm.

Thermogravimetry(TG) showed that the weight loss up to 1273 K in air flow was only 3% for the Pt-coated sample after removal of activated carbon. This confirmed that no activated carbon was present in the treated sample in O_2 plasma.

Scanning electron micrographs (SEM) (Fig. 2) showed the morphology of base activated carbon fibers (A) and Pt-coated samples after the removal of activated carbon in O_2 plasma (B–D), revealing fibrous shapes with almost the same diameter as that of activated carbon fibers. The product, the structure of which is a cast-off skin of the base activated carbon fibers, consisted of fused particles of 20–80 nm in diameter.

In the Pt coating process, the temperature and the pressure in the vessel was 423 K and 32 MPa, beyond the critical temperature (304 K) and pressure (7.38 MPa) of CO_2. The Pt precursor [$Pt(acac)_2$] at the bottom of the vessel dissolves in supercritical CO_2 and acetone and is carried into the pores of the activated carbon fiber. $Pt(acac)_2$ adsorbed on the surface of the activated carbon will react with hydroxyl units and adsorbed water molecules. During the treatment in O_2 plasma, the sample was heated to 453 K and adsorbed $Pt(acac)_2$ on the activated carbon is reduced to Pt metal. Because of the low surface concentration of Pt precursor on activated carbon, the Pt metal sintered into particles.

The BET surface area of the Pt porous fiber calculated measuring N_2 adsorption isotherms was 47 m^2 g^{-1}, larger than that found for platinum black (20–30 m^2 g^{-1}).

Recently Attard *et al.* produced mesoporous platinum powder denoted Hi-ePt of surface area 22 ± 2 m^2 g^{-1} [9] and platinum film denoted Hi-Pt of surface area 60 ± 6 m^2 g^{-1}.[10] The shapes of these Pt porous materials, however, were limited

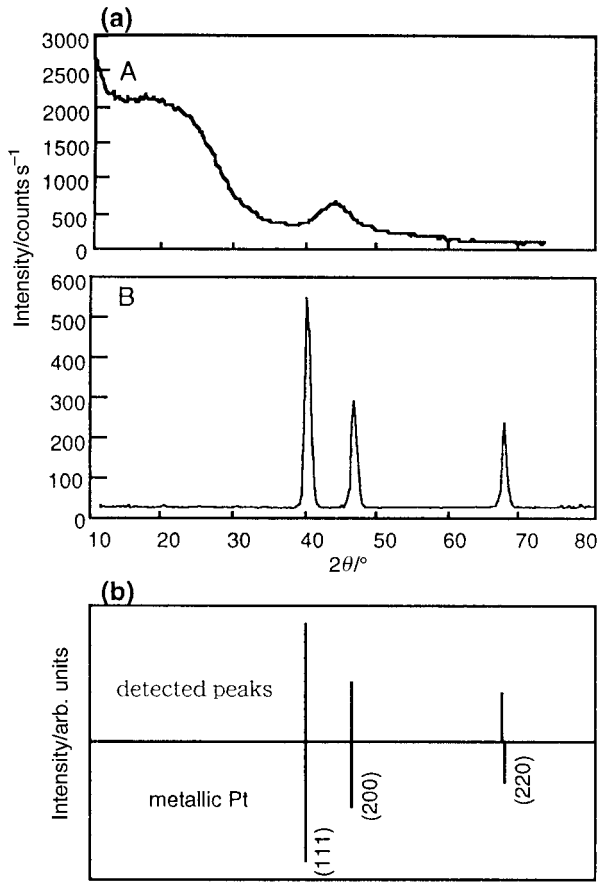

Fig. 1 (a) X-Ray diffraction patterns of (A) activated carbon fiber and (B) Pt-coated sample after the removal of activated carbon in O_2 plasma. These spectra were recorded on a RIGAKU RINT-2000 with Cu-Kα radiation. (b) Comparison between detected XRD peaks from the sample treated with oxygen plasma and ASTM-JPCDS data for platinum metal (PDF No.4-802).

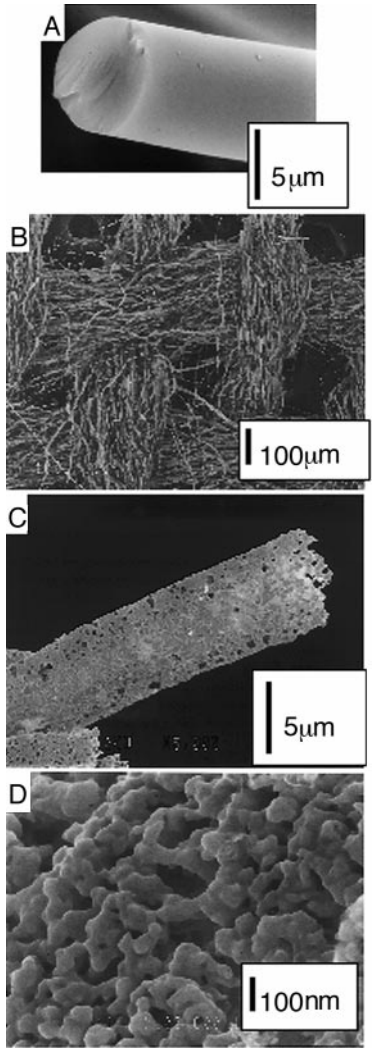

Fig. 2 Scanning electron micrographs of (A) base activated carbon fiber and (B)–(D) Pt-coated sample after the removal of activated carbon in O_2 plasma. These micrographs were obtained on a JEOL JSM-890.

to granules or films. Removing the base material after coating the metal precursor using supercritical fluid makes it possible to produce metallic materials with a similar shape to that of the base. The morphology of porous metal can thus be controlled through the choice of the shape of base activated carbon. Supercritical fluids can even carry precursor molecules into micropores (*ca*. 1 nm diameter) without condensation into the liquid phase. Thus, the coating process with supercritical fluids provides a new effective method for obtaining castoff skins using fine structures of base porous materials. Porous platinum structures with high surface area will show great advantages for catalytic applications and encouraging results were obtained for the synthesized porous Pt fibers as a catalyst for CO oxidation.[14]

The authors thank Ms Sasaki and Dr Inagaki for useful discussions and Mr Kadoura for taking the SEM micrographs.

Notes and references

1 W. N. Meier and D. H. Olson, *Atlas of Zeolite Structure Types*, Butterworths, London, 2nd edn., 1988.
2 C. T. Kresge, M. E. Leonowicz, W. J. Roth, J. C. Vartuli and S. Beck, *Nature*, 1992, **359**, 710.
3 S. Inagaki, Y. Fukusima and K. Kuroda, *J. Chem. Soc., Chem. Commun.*, 1993, **8**, 680.
4 O. D. Velev, T. A. Jede, R. F. Loba and A. M. Lenhoff, *Nature*, 1997, **389**, 447.
5 M. Templin, A. Franck, A. D. Chsne, H. Leist, Y. Zhang, R. Ulrich, V. Schandler and U. Wiesner, *Science*, 1997, **278**, 1795.
6 P. M. Ajayan, D. Stephan, Ph. Redlich and C. Colliex, *Nature*, 1995, **357**, 564.
7 C. N. R. Rao, B. C. Satishkumar and A. Govindaraj, *Chem. Commun.*, 1997, **16**, 1581.
8 B. C. Satishkumar, A. Govindaraj, Erasmus M. Vogl, Lipika Basumallick and C. N. R. Rao, *J. Mater. Res.*, 1997, **12**, 604.
9 G. S. Attard, C. G. Goltner, J. M. Corker, S. Henke and R. H. Templer, *Angew. Chem., Int. Ed. Engl.*, 1997, **36**, 1315.
10 G. S. Attard, P. N. Bartlett, N. R. B. Coleman, J. M. Elliott, J. R. Owen and J. H. Wang, *Science*, 1997, **278**, 838.
11 G. S. Attard, N. R. B. Coleman and J. M. Elliott, *Stud. Surf. Sci. Catal.*, 1998, **117**, 89.
12 J. M. Dobbs, J. M. Wong, R. J. Lahiere and K. P. Johnston, *Ind. Eng. Chem. Res.*, 1987, **26**, 56.
13 P. Etesse, J. A. Zega and R. Kobayashi, *J. Chem. Phys.*, 1992, **97**, 2022.
14 13.3 mg of a platinum cloth sample was placed in a quartz tube (20 mm in diameter). 1% CO, 1% H_2 and 7.5% of O_2 in a nitrogen carrier stream were introduced into the tube at 3300 ml min^{-1}. The sample was heated up to 773 K at a rate of 12 K min^{-1}. 50% of CO was converted into CO_2 at 475 K and almost all of the CO was converted into CO_2 above 484 K.

Communication 8/08255C

ChemComm

The first transition metal cholesteryl-phosphine complexes

Daravong Soulivong,[a] Dominique Matt*[a] and Raymond Ziessel*[b]

[a] *Groupe de Chimie Inorganique Moléculaire, Université Louis Pasteur (ULP), CNRS-UMR 7513, 1 rue Blaise Pascal, F-67008 Strasbourg, France. E-mail: dmatt@chimie.u-strasbg.fr*

[b] *Laboratoire de Chimie, d'Electronique et de Photonique Moléculaire, Ecole de Chimie, Polymères et Matériaux (ECPM-ULP), CNRS-UPRES A 7008, 25 rue Becquerel, 67087 Strasbourg Cedex 2, France. E-mail: ziessel@chimie.u-strasbg.fr*

Received (in Cambridge, UK) 19th November 1998, Accepted 14th January 1999

Novel optically pure cholesteryl-phosphine ligands (3α-PPh_2chol and 3β-PMe_2chol) have been synthesized and were shown to form stable and highly soluble Pd(II) and Pt(II) complexes; as revealed by an X-ray analysis the (chol)-P···P(chol) fragment of the square planar *trans*-[PtI_2(3β-PMe_2chol)$_2$] complex adopts a staggered arrangement (V-shape).

As part of our ongoing research for new catalytic and mesomorphic molecular materials it was of interest to design multifunctional ligands based on steroidal phosphines. Surprisingly, very little work has been devoted to cholesteryl-derived phosphines[1] and it appears that no complexes have been reported until now with such hybrid ligands. The cholesteryl fragment offers many advantages in terms of chirality,[2] liquid-crystalline behaviour,[3] lipophilicity,[4] optical and molecular recognition.[5] We now report a convenient synthesis of 5-cholestene derivatives substituted at the C_3-carbon atom with phosphino groups (PPh_2 and PMe_2) and present their coordinative properties towards precious metals.†

Phosphine L^1 was prepared in 73% isolated yield‡ by reacting 5-cholestene-3β-methanesulfonate (3β-MsO-chol)[6] with Ph_2PLi as shown in Scheme 1. The ligand is characterized by a ^{31}P NMR signal at δ −18.6 and by an $[\alpha]_D^{589}$ of +15.8° (*c* = 1, CH_2Cl_2). The phosphino subunit occupies the α position of the C_3-carbon atom as unambiguously proven by a positive NOE effect of 8% found between the olefinic H-6 proton and the *ortho* P-phenyl atoms. It is noteworthy that there is no indication for the formation of the 3β substituted isomer, an observation that is in keeping with an S_N2 substitution reaction. A complete assignment of proton and carbon signals was made using NOESY, ^1H–^{13}C COSY, ^{13}C-DEPT and HMBC pulse sequences (for selected data and atom labelling see Table 1). The corresponding phosphine oxide which was readily obtained by oxidation is characterised by a ^{31}P NMR signal at δ +35.6, and a strong IR absorption band at 1187 cm^{-1} ($\nu_{P=O}$). Reaction of 2 equiv. of L^1 with [MCl_2(PhCN)$_2$] afforded quantitatively‡ the corresponding *trans*-[$MCl_2(L^1)_2$] complexes (**1** M = Pd, **2** M = Pt; Scheme 1). Both complexes are *highly* soluble in *hydrocarbons* and insoluble in protic solvents.

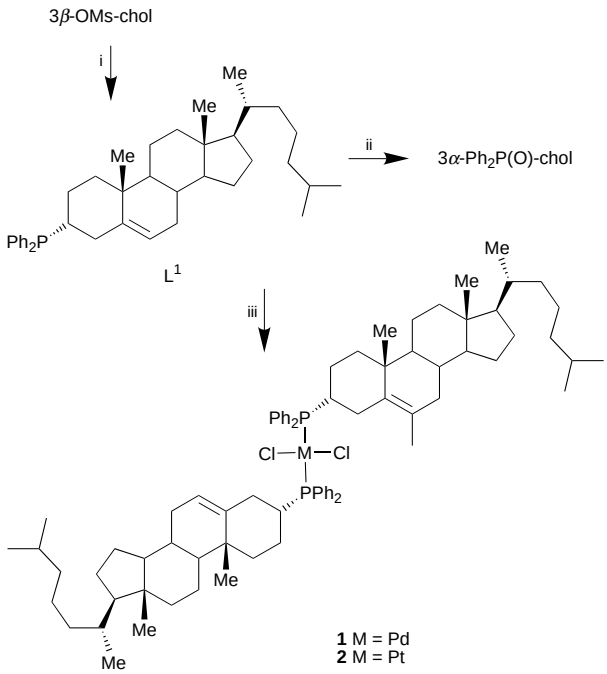

Scheme 1 *Reagents and conditions*: i, Ph_2PLi, THF, 25 °C, 3 d; ii, air, CH_2Cl_2; iii, [$MeCl_2$(PhCN)$_2$], CH_2Cl_2 (M = Pd, Pt).

In contrast to the reaction described above yielding exclusively a C_3-α-substituted product, we discovered that treatment in THF at −78 °C at 3β-Cl-chol with 2 equiv. of PMe_2K (prepared[7] by quantitative reduction of Me_2P–PMe_2 in decaline) gave a mixture of compounds from which 3β-PMe_2-chol (L^2) could be isolated in 47% yield (as the major compound, Scheme 2). Selected spectroscopic data for L^2 are: δ_P −41 and $[\alpha_D]^{589}$ of −33.7° (*c* = 1, CH_2Cl_2). The α-stereochemistry of L^2 could unequivocally be established using 2D proton NMR spectroscopy ($^3J_{H\text{-}3\alpha/H\text{-}4\beta}$ 11 Hz and $^3J_{H\text{-}3\alpha/H\text{-}4\alpha}$ 15 Hz) and was further confirmed by an X-ray diffraction study (*vide infra*). The 3α-PMe_2-chol isomer was also formed in this reaction (β/α ratio 7/3) but could not be obtained in a pure form. Note, the ^{31}P NMR signal of the latter isomer (δ_P −54) is considerably shifted with respect to the β form; such shielding effects have previously been observed on going from 4-methyl-$P_{axial}Me_2$-cyclohexane to its $P_{equatorial}$-isomer.[8] We also note that Me_2P–PMe_2 (δ_P −58) was detected in the reaction mixture.

The sparingly soluble complexes **3** (M = Pd) and **4** (M = Pt) were obtained in high yield by reaction of L^2 with [$MCl_2(SEt)_2]_2$. Metathesis of **4** with NaI in acetone–THF resulted in the formation of the soluble *trans*-[$PtI_2(L^2)_2$] complex **5** (Scheme 2), the molecular structure of which was determined by a single-crystal X-ray analysis¶ (Fig. 1). This study confirmed the α-stereochemistry of the cholesteryl-phosphine ligand L^2. The platinum atom is in a square-planar environment with the two P-atoms occupying *trans* positions. Interestingly, the molecule possesses a C_2-axis perpendicular to the metal plane, with the two steroidal backbones located on the same side of the coordination plane. Observing the molecule perpendicularly to the P···P axis, the two chol subunits adopt a V-shaped arrangement, as shown in Fig. 1; the relative organization of the steroidal fragments is probably controlled by van der Waals forces between cholesteryl units of neighboring molecules. In the crystallographic cell (Fig. 1) the molecules are arranged in a head-to-tail fashion, a situation which is reminiscent of that found in some chol-derivatives displaying liquid-crystalline behaviour.[3] The shortest chol–chol intermolecular distances are in the order of 2.5 Å (1 − *x*, 1 − *y*, *z*). Note, the situation found here contrasts with the solid state

Table 1 Selected NMR data [^{1}H(500 MHz), ^{13}C{^{1}H} (125 MHz), $CDCl_3$] for L^1 and L^2

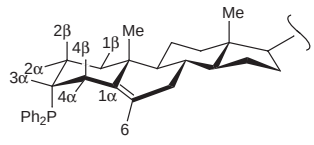

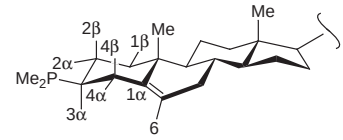

C atom		δ_C (J/Hz)	δ_H (J/Hz)	δ_C (J/Hz)	δ_H (J/Hz)
1	CH_2	34.99 (d, $^3J_{CP}$ 10)	1.59 (β), 1.82 (α)	40.28 (d, $^3J_{CP}$ 13)	1.08 (β), 1.92 (α)
2	CH_2	24.15 (d, $^2J_{CP}$ 12)	1.58 or 1.94 (α),[a] 1.97 (β)	24.95 (d, $^2J_{CP}$ 13)	1.39 (β), 1.64 (α)
3	CH	35.05 (d, J_{CP} 9)	2.72 (β)	40.88 (d, J_{CP} 8)	1.18 (α)
4	CH_2	33.94 (d, $^2J_{CP}$ 15)	1.91 (α), 2.66 (β)	35.03 (d, $^2J_{CP}$ 13)	2.03 (α), 2.13 (β)
5	C	140.03 ($^3J_{CP}$ 0)		142.85 (d, $^3J_{CP}$ 11)	
6	CH	121.96	5.17 (br d, $^3J_{HH}$ 5.0)	119.63	5.30 (d, $^3J_{HH}$ 5.0)
	PCH_3			11.46 (d, J_{CP} 14)	1.00 (d, $^2J_{HP}$ 1.9)
	PCH_3			11.38 (d, J_{CP} 14)	0.99 (d, $^2J_{HP}$ 2.0)

[a] Tentative assignment.

structure of a related bis(cholesteryldiethylphosphinite)Pd(II) complex where no significant intermolecular interactions were observed.[2c]

In summary, chol-derived phosphines with a wide range of physical properties should now be accessible with this synthetic protocol. Further studies are in progress to elucidate the mechanism and driving force leading to the formation of the new 3β-PMe_2chol ligand. We are also continuing to explore the potential of these new ligands in three major directions: (i) formation of three-dimensional scaffoldings to generate metallomesogens, (ii) the use of these functional phosphines for Wittig olefinations and finally (iii) the study of their transition metal complexes as precursors in asymmetric catalysis.

We warmly thank Drs A. Burger (ULP) and J.-F. Biellmann (ULP-CNRS) and Prof. M. Rohmer (ULP) for fruitful discussion. The CNRS is acknowledged for partial financial support.

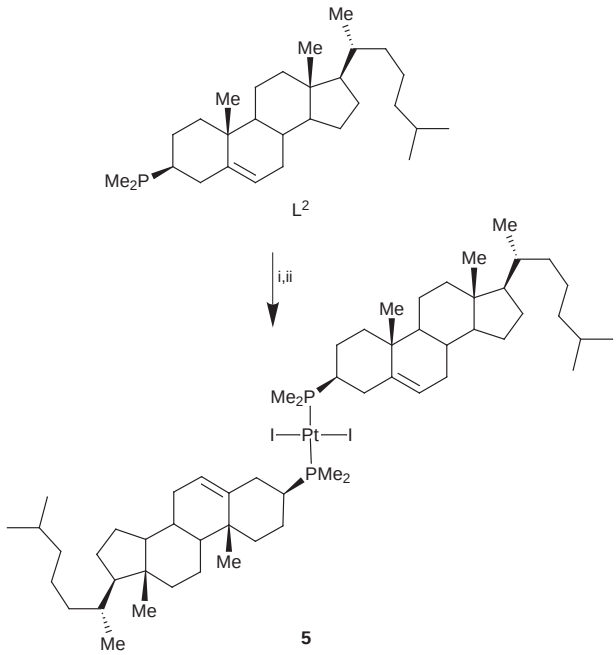

Scheme 2 *Reagents and conditions*: i, $[PtCl_2(SEt_2)_2]$, THF; ii, NaI, acetone–THF.

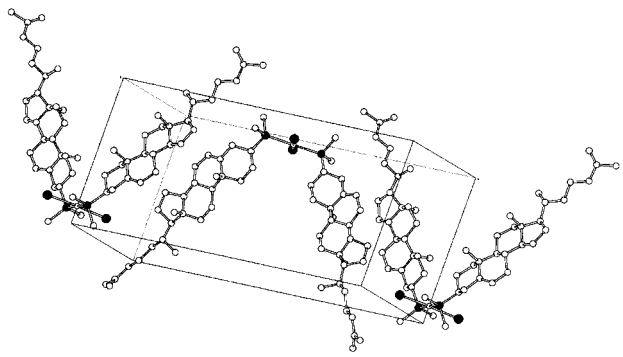

Fig. 1 Solid state structure of complex **5** showing the organization of the cholesteryl fragments. Selected bond lengths (Å): Pt–I 2.584(1), Pt–P 2.332(3), P–C(1) 1.81(2), P–C(2) 1.82(2), P–C(3) 1.85(1).

Notes and references

† On the basis of spectroscopic evidence, including EI and FABMS and elemental analysis the structures of the new ligands and complexes were unequivocally authenticated. See http://www.rsc.org/suppdata/cc/1999/393/ for selected data for L^1, 3α-$Ph_2P(O)$chol, L^2 and **1**–**5**.

‡ Obtained by precipitation with MeOH: L^1 was recrystallized from Et_2O–MeOH and complexes **1** and **2** were obtained analytically pure after precipitation.

¶ *Crystal data* for **5**•2$CHCl_3$•H_2O: $C_{58}H_{102}P_2I_2Pt$•2$CHCl_3$•H_2O, M = 1567.08, orthorhombic, space group $P2_12_12$, yellow crystals, a = 29.557(1), b = 9.069(3), c = 12.422(4), V = 3329.7 Å^3, Z = 2, D_c = 1.563, μ = 14.161 mm^{-1}, $F(000)$ = 1580. Data were collected on a Philips PW1100/16 diffractometer (graphite Cu-Kα radiation, 1.5418 Å) at −100 °C. 2353 reflections collected ($3 \leqslant 2\theta \leqslant 54°$), 2143 data with $I > 3\sigma(I)$. The structure was solved using the Nonius OpenMoleN[10] package and refined by full matrix least-squares with anisotropic thermal parameters for all non hydrogen atoms except for the solvent molecules (the latter are disordered in the crystallographic structure). The absolute configuration was determined by refining Flack's x parameter equal to 0.02(2). Final results: $R(F)$ = 0.046, $wR(F)$ = 0.066, GOF = 1.029, 310 parameters, largest difference peak = 1.037 e Å^{-3}. CCDC 182/1143. See http://www.rsc.org/suppdata/cc/1999/393/ for crystallographic files in .cif format.

1 Y. Nagao and L. Horner, *Phosphorus*, 1976, **6**, 139.
2 See, for example: (*a*) S. Hanessian, Y. Leblanc and P. Lavallee, *Tetrahedron Lett.*, 1982, **23**, 4411; (*b*) Don E. Gibbs and C. Larsen, *Synthesis*, 1984, 410; (*c*) P. Berdagué, J. Courtieu, H. Adams, N. A. Bailey and P. Maitlis, *J. Chem. Soc., Chem. Commun.*, 1994, 1589; (*d*) L. Knerr, X. Pannecoucke, G. Schmitt and B. Luu, *Tetrahedron Lett.*, 1996, **37**, 5123.
3 R. Deschenaux, J.-L. Marendaz, J. Santiago and J. W. Goodby, *Helv. Chim. Acta*, 1995, **78**, 1215; R. Deschenaux, M. Even and D. Guillon, *Chem. Commun.*, 1998, 537.
4 A. Kreimeyer, F. André, C. Gouyette and T. Huynh-Dinh, *Angew. Chem., Int. Ed.*, 1998, **37**, 2853.
5 T. Nishi, A. Ikeda, T. Matsuda and S. Shinkai, *J. Chem. Soc., Chem. Commun.*, 1991, 339.
6 M. Aburatani, T. Takeuchi and K. Mori, *Synthesis*, 1987, 181.
7 H. Niebergall and B. Langenfeld, *Chem. Ber.*, 1962, **95**, 64.
8 M. D. Gordon and L. D. Quin, *J. Am. Chem. Soc.*, 1976, **98**, 15.
9 J. P. Starck, A. Milton, Y. Nakatani and G. Ourisson, *Bull. Chem. Soc. Fr.*, 1994, **131**, 210.
10 OpenMoleN, Interactive Structure Solution, Nonius B.V., Delft, The Netherlands, 1997.

Communication 8/09041F

Typeset and printed by Black Bear Press Limited, Cambridge, England

Transition metal-catalysed addition reactions of H–heteroatom and inter-heteroatom bonds to carbon–carbon unsaturated linkages *via* oxidative additions

Li-Biao Han and Masato Tanaka*

National Institute of Materials and Chemical Research, Tsukuba, Ibaraki 305-8565, Japan.
E-mail: mtanaka@ccmail.nimc.go.jp

Oxidative addition of inter-heteroatom bonds comprising B, Si, Ge, Sn, P, S, Se and Te with late transition metal complexes readily takes place at room temperature and triggers a variety of catalytic additions of the bonds to carbon–carbon unsaturated linkages. The new catalytic reactions are regio- and stereoselective and provide high yield syntheses of synthetically versatile heteroatom compounds.

Introduction

Transition metal complex catalysis in heteroatom chemistry is experiencing vigorous growth these days. This is partly because heteroatom-to-carbon bonds can be very reactive and versatile intermediates in synthetic organic chemistry. In addition, heteroatom compounds can exhibit biological activity. Furthermore heteroatom compounds, inclusive of polymeric ones, are useful as such or as precursors in various applications such as ceramics, heat-resistant materials, semiconductors and electroluminescent materials. Although metal complex-catalysed substitution reaction with heteroatom nucleophiles such as palladium-catalysed amination of organic halides[1] has been fairly well studied, metal complex-catalysed addition reactions of H–heteroatom and inter-heteroatom bonds (H–E, E–E′; E, E′ = heteroatom) to carbon–carbon unsaturated bonds have not been extensively explored until recently. The newly developed addition reactions generally give the products selectively in high yields under mild reaction conditions and hence are particularly attractive from the synthetic point of view. Although mechanistic details may vary depending on the heteroatom compounds used, most of the additions are overall envisioned to proceed *via* a simple sequence of events comprising (i) oxidative addition of an inter-heteroatom bond (E–E′) to a transition metal complex, (ii) insertion of an alkene or alkyne, and reductive elimination (Scheme 1). Exceptional

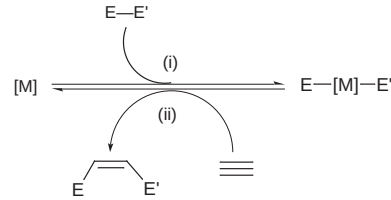

Scheme 1

reactions in this category that have been rather well studied include those of group 14 element compounds such as Si–H, Sn–H, Si–Si, Si–Sn, Si–CN and some of them are exploited in industry.[2] Transition metal-catalysed additions of B–H bonds, which provide a possibility to control regio-, stereo- and chemoselectivity in the hydroboration processes, have also been well studied.[3] This article focuses on the recent progress in the transition metal-catalysed additions of groups 13, 15 and 16 (B, N, P, S and Se) heteroatom compounds that are considered to proceed *via* a mechanism similar to Scheme 1. Since additions of group 14 element compounds and the catalysed hydroborations have been subjects of numerous review articles, they will not be discussed here.

Metal-catalysed additions of B–E bonds (E = B, Si, Sn, S)

In 1993, Miyaura and Suzuki reported addition reactions of diborons with alkynes (Scheme 2).[4] The addition of bis(pinacolato)diboron **1** to alkynes proceeds efficiently in the presence of a catalytic amount of $Pt(PPh_3)_4$ to afford the *cis*-bis(boryl)alk-

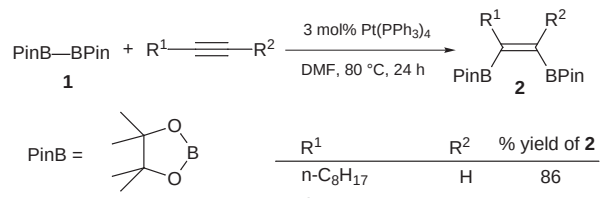

R^1	R^2	% yield of **2**
n-C_8H_{17}	H	86
Cy	H	78
Pr	Pr	86
Ph	Ph	79
Ph	H	79
CH_2=$CH(CH_2)_4$	H	85
$Cl(CH_2)_3$	H	83
$NC(CH_2)_3$	H	79
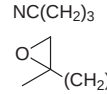	H	87
$MeOC(O)(CH_2)_4$	H	89

Scheme 2

Li-Biao Han was born in Shandong, China in 1965. He finished his university education at Osaka University in 1988 and received his PhD in 1993 under the supervision of Professor N. Sonoda. After several years postdoctoral research experience, he joined the National Institute of Materials and Chemical Research in 1997.

Masato Tanaka is the Director of the Department of Organic Chemistry of the National Institute of Materials and Chemical Research. He is also an Adjunct Professor of the Department of Industrial Chemistry, Science University of Tokyo. He received his PhD from Kyoto University in 1974 for his work on carbonylation and was a research associate with Professor Howard Alper at the University of Ottawa in 1977–1978. He won several awards, including the Progress Award in Synthetic Organic Chemistry (1986), a Commendation by the Minister of State for Science and Technology (1987), the Divisional Award of the Chemical Society of Japan (1994), and the Wilhelm Manchot Research Professorship (Pinguin Foundation, Germany, 1998).

enes **2** in high yields. In this diboration both terminal and internal alkynes are reactive as substrates. The reaction is accelerated in polar solvents such as DMF and MeCN, but also proceeds in non-polar solvents like hexane to give the products in good yields. $Pt(CO)_2(PPh_3)_2$ also exhibits high activity, but others such as $Pd(PPh_3)_4$ and $RhCl(PPh_3)_3$ that are efficient catalysts for hydroboration[3] are ineffective. Mechanistic studies by these authors and others have disclosed that oxidative addition of the B–B bond to the Pt complex is a key reaction that triggers the catalysis.[4–6] Indeed, $Pt(PPh_3)_4$ reacts with **1** to give a *cis* complex **3**, which reacts with an alkyne (but not with alkene) to afford the adduct (Scheme 3). Since a detailed study

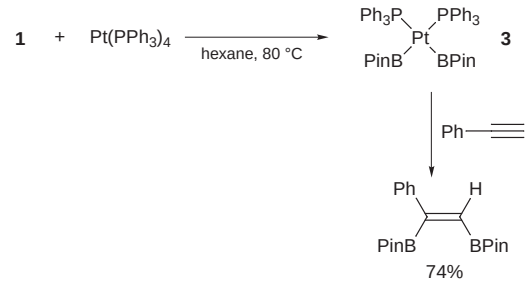

Scheme 3

on the reaction of *cis*-$Pt(BCat)_2(PPh_3)_2$ (Cat = $C_6H_4O_2$) with alkynes revealed that the addition reaction was strongly retarded by an addition of a free phosphine to the reaction mixture, dissociation of a phosphine ligand from **3′** generating three coordinate species is believed to precede the insertion of an alkyne (Scheme 4).

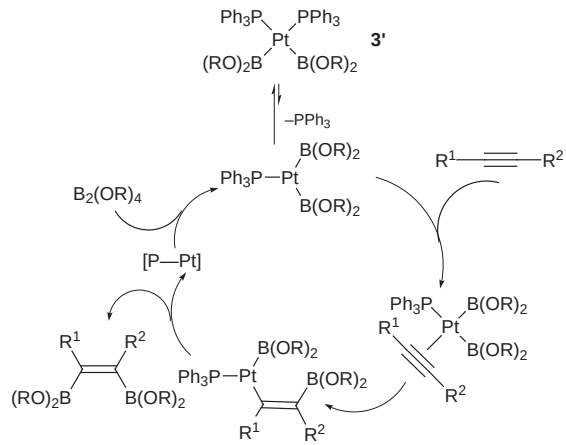

Scheme 4

1,3-Dienes also react bis(pinacolato)diboron **1** in the presence of $Pt(PPh_3)_4$ to form *Z*-1,4-adducts in high yields with excellent selectivities (Scheme 5).[7] Interestingly, when a

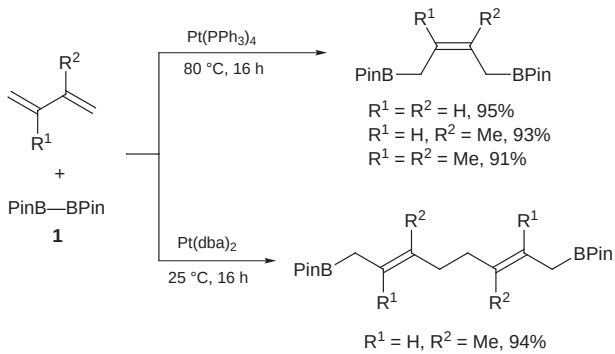

Scheme 5

phosphine-free platinum complex, $Pt(dba)_2$, is employed as catalyst, a 1:2 adduct of the diboron to the diene is obtained. Regioselectivity in the reaction of penta-1,3-diene varies depending on the platinum complex catalyst being phosphine-ligated or phosphine-free. Thus, 1,4-addition to penta-1,3-diene takes place with $Pt(PPh_3)_4$ to form **4**, whereas the same reaction with $Pt(dba)_2$ selectively affords the 1,2-addition product **5** (Scheme 6).

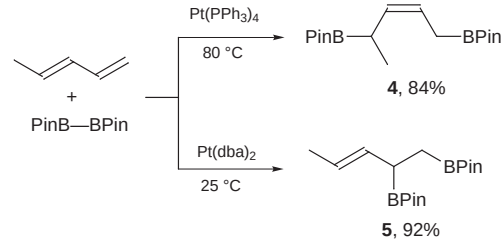

Scheme 6

In contrast to the facile additions to alkynes, $Pt(PPh_3)_4$ does not catalyse the additions of diborons to alkenes. In 1995, Baker and co-workers briefly described that a phosphine–gold(I) complex was able to catalyse the addition of a diboron to styrenes to give desired 1,2-diboronate esters.[8] Very recently, phosphine-free platinum complexes such as $Pt(cod)_2$ and $Pt(dba)_2$ have been found to efficiently catalyse the diborations of terminal alkenes and strained cyclic alkenes to afford the addition products in high yields (Scheme 7).[9]

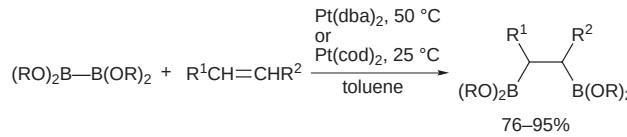

$(RO)_2B$ = PinB or CatB
Alkenes: ethylene, hex-1-ene, styrene, 4-methoxystyrene, 6-chlorohex-1-ene, cyclopentene, norbornene *etc.*

Scheme 7

Palladium- or platinum-catalysed additions of other B–heteroatom bonds are also rapidly emerging. We have found a highly stereo- and regio-selective Pd-catalysed addition of a B–Sn reagent to alkynes, which represents the first addition reaction of a bond comprising groups 13 and 14 elements to unsaturated carbon linkages (Scheme 8).[10] The addition of **6** to

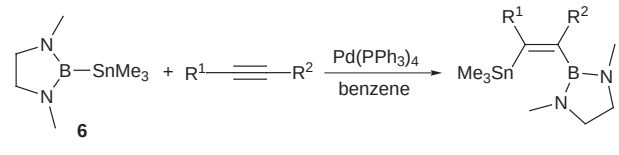

R^1 = n-C_6H_{13}, R^2 = H, 83%
R^1 = Ph, R^2 = H, 73%
R^1 = R^2 = Ph, 78%

Scheme 8

terminal alkynes takes place rapidly even at room temperature to afford *cis*-adducts in high yields, although the presence of an N–B bond in the starting diboron reagent retarded the diborations of alkynes.[4] Both terminal and internal alkynes are reactive substrates. The reactions of terminal alkynes end up with the boryl group selectively attached to the terminal carbons. Mechanistic studies have substantiated that oxidative addition of the B–Sn bond of **6** to the palladium centre is involved in the catalytic cycle. In one case such an adduct was isolated and was fully characterized (Scheme 9) and the adduct proved to exhibit a high activity when employed as catalyst. Diynes also readily react with **6**; highly regio- and stereo-selective borylstannylative carbocyclization takes place to

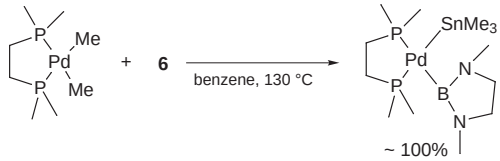

Scheme 9

afford good yields of 1-(borylmethylidene)-2-(stannylmethylidene)cycloalkanes (Scheme 10).[11] Simple addition products to

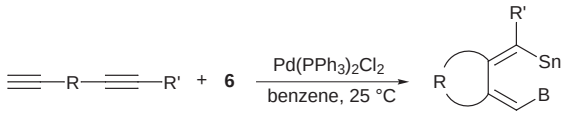

R = $(CH_2)_3$, R' = H, 92%
R = $(CH_2)_4$, R' = H, 84%
R = $(CH_2)_2$, R' = H, 97%
R = $CH_2N(Ts)CH_2$, R' = H, 82%
R = CH_2OCH_2, R' = H, 93%
R = $CH_2C(CO_2Et)_2CH_2$, R' = Et, 86%

Scheme 10

the triple bonds are not found in the reaction mixture. It is surprising that even a very strained four-membered ring can be selectively formed nearly quantitatively starting with a hexa-1,5-diyne as substrate. An enyne compound also undergoes the borylstannylative carbocyclization (Scheme 11). These carbo-

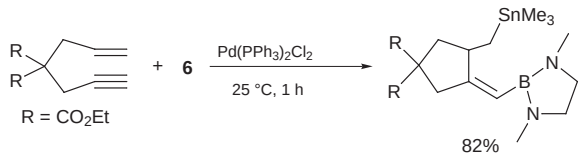

R = CO_2Et

Scheme 11

cyclization reactions are very regioselective; the boryl group is selectively introduced to the more reactive unsaturated linkage, *i.e.* the terminal C≡C rather than internal one in the unsymmetrical diyne system and the C≡C rather than the C=C in the enyne system. On the basis of these experiments, the triple bond insertion to the Pd–B bond (in preference to the Pd–Sn bond) is believed to follow the oxidative addition of **6** in the catalytic cycle. The reaction of 1,3-dienes requires narrower tuning of the nature of the ligand. Triphenylphosphine–palladium complexes that were active in the reactions of alkynes, diynes, and enyne compounds are not so efficient with dienes. 4-Ethyl-2,6,7-trioxa-1-phosphabicyclo[2.2.2]octane [$P(OCH_2)_3CEt$ = etpo] proved to be the ligand of choice, the use of which results in more than 80% yields of 1,4-adducts (Scheme 12).[12]

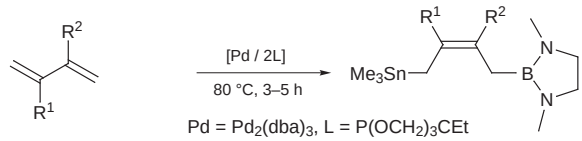

Pd = $Pd_2(dba)_3$, L = $P(OCH_2)_3CEt$

R^1 = CH_3, R^2 = H, 83%
R^1 = R^2 = H, 95%
R^1 = R^2 = CH_3, 87%

Scheme 12

In contrast to the B–Sn additions to alkynes, analogous B–Si additions are not straightforward and do not proceed efficiently under similar conditions. The $Pd_2(dba)_3$/etpo catalyst system is again the catalyst of choice but heating (typically 110 °C) is required for the reaction to take place (Scheme 13). The

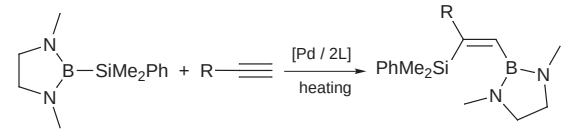

Pd = $Pd_2(dba)_3$, L = $P(OCH_2)_3CEt$
R = n-C_6H_{13}, 92%
R = Ph, 97%

Scheme 13

$Pd_2(dba)_3/PMe_3$ system, which was among the better catalysts for the additions of disilanes or digermanes,[13] also exhibits respectable performance.[14] Both the regio- and stereo-selectivities of the B–Si addition to terminal alkynes are similar to those found in the B–Sn addition to give the *cis* adduct with the boryl group bound to the terminal carbon predominantly. Unlike the borylstannylative carbocyclization in which the cyclization products were exclusively produced, the reaction of octa-1,7-diyne with the silylborane is not selective but gives a mixture of a cyclization product and a simple addition product (Scheme 14) when catalysed by the $Pd_2(dba)_3$/etpo catalyst

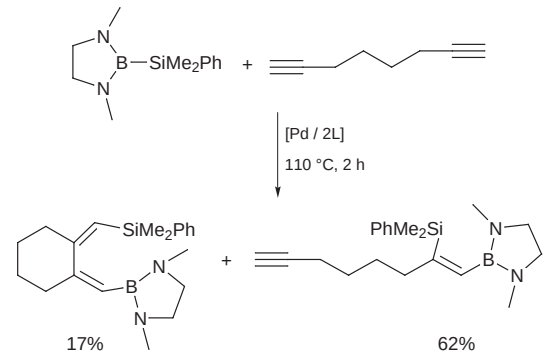

Scheme 14

system. The palladium(0)–*tert*-alkyl isocyanide catalyst systems, which were efficient for the addition of Si–Si bonds,[15] are also active catalysts for the addition of another B–Si reagent to alkynes to produce similar *cis*-addition products (Scheme 15).[16]

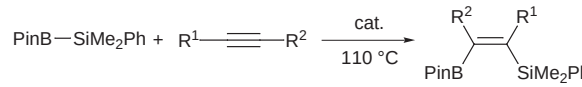

cat. = $Pd(OAc)_2/Bu^tCH_2CMe_2NC$
R^1 = Ph, R^2 = H, 82%
R^1 = THPO$(CH_2)_2$, R^2 = H, 88%
R^1 = MEMO$(CH_2)_3$, R^2 = H, 85%
R^1 = c-Hex-1-enyl, R^2 = H, 82%
R^1 = Me_3Si, R^2 = H, 73%
R^1 = R^2 = Ph, 74%
R^1 = R^2 = Bu, 24%

Scheme 15

Successful addition of the Si–B reagent to alkenes has been achieved by using platinum complex catalysts (Scheme 16).[17] Thus, refluxing a mixture of the silylborane and 1-alkenes in dioxane in the presence of $Pt(CH_2{=}CH_2)(PPh_3)_2$ affords the adducts **7** with the boryl group bonded to the internal carbon of the double bond; note that the regioselectivity is the reverse of that found in addition reactions of terminal alkynes. Besides **7**, significant amounts of 1-boryl-1-silylalkanes **8** are also formed in the reactions of 1-alkenes.[18] Interestingly, the palladium(0)–*tert*-alkyl isocyanide complexes and $Pd(PPh_3)_4$, both of which are efficient in the Si–B and Sn–B additions to alkynes, respectively, do not show catalytic activity towards the addition to alkenes.

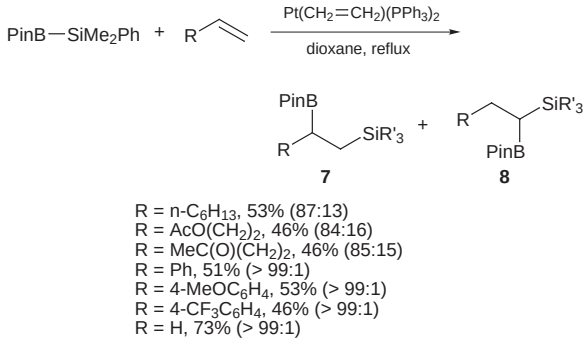

R = n-C_6H_{13}, 53% (87:13)
R = $AcO(CH_2)_2$, 46% (84:16)
R = $MeC(O)(CH_2)_2$, 46% (85:15)
R = Ph, 51% (> 99:1)
R = 4-$MeOC_6H_4$, 53% (> 99:1)
R = 4-$CF_3C_6H_4$, 46% (> 99:1)
R = H, 73% (> 99:1)

Scheme 16

The palladium-catalysed addition of B–S bonds to terminal alkynes is another example of metal catalysed B–heteroatom bond additions.[19] The reaction takes place in THF to afford the adduct in high yields and selectively with the boryl group bound to the terminal carbons, as for the B–Si and B–Sn additions. Isolation of the adducts is hampered by the very high susceptibility of the C–B bond to cleavage, but the product generated *in situ* can be used for further manipulations, *e.g*. the Suzuki–Miyaura coupling reaction, without isolation (Scheme 17). A catalytic cycle starting with the oxidative addition of the

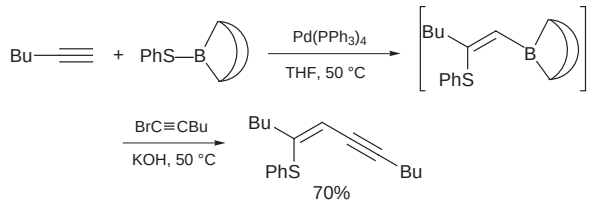

Scheme 17

B–S bond to Pd has been proposed for this reaction, but the mechanistic detail remains to be clarified.

Metal-catalysed additions of N–H, P–H and P–Se bonds

Compared to other heteroatom compounds, only a few metal-catalysed additions of group 15 element compounds are known. Although catalytic additions of N–H bonds to unsaturated bonds are highly attractive from the practical viewpoint,[20] only limited success has been achieved.[21] Milstein and co-workers have demonstrated that aniline oxidatively adds cleanly to an electron-rich Ir^{I} complex, $[Ir(PEt_3)_2(C_2H_4)Cl]$, to produce an Ir^{III} anilido hydrido complex. Despite its low catalytic efficiency, the Ir^{III} anilido hydrido complex undergoes insertion of norbornene leading to a new complex containing a chelating aminoalkyl ligand, from which the addition product is formed through reductive elimination (Scheme 18).[22] A catalytic system generated from $[RhCl(PEt_3)_2]_2$ and LiNHPh in aniline has also been used for hydroamination of norbornene, in which a rhodium anilido complex is probably involved as key catalytic species. Another adduct arising from addition of an *ortho* C–H bond of aniline to norbornene is also formed in addition to the desired hydroamination product (Scheme 19).[23] Recently, asymmetric hydroamination of norbornene with aniline was reported by use of an Ir^{I}–binap catalyst system, albeit in low chemical yields.[24] An addition of fluoride ion to the reaction mixture enhances the catalytic activity to give 22% chemical yield and 95% ee of the *exo*-2-(phenylamino)norbornane (Scheme 20). Palladium-catalysed hydroamination of allenes has also appeared recently (Scheme 21).[25] Addition of acetic acid facilitates the reaction, but the detailed reaction mechanism remains to be clarified.

Transition metal-catalysed additions of phosphorus compounds *via* oxidative addition are still very rare. Pringle and

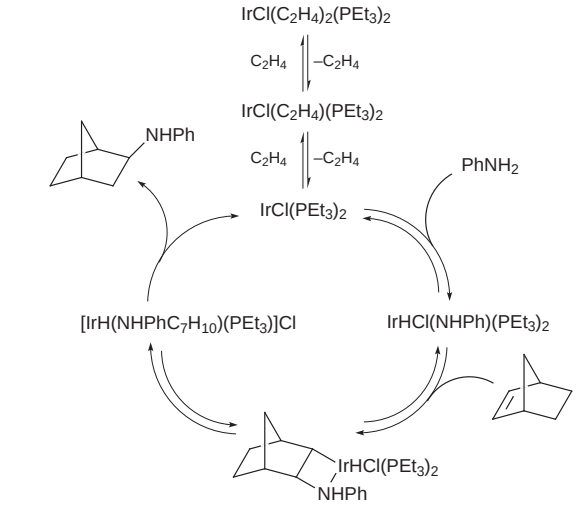

Scheme 18

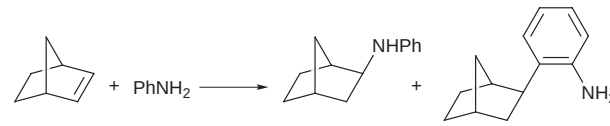

Scheme 19

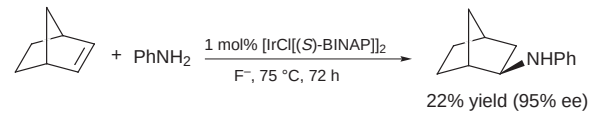

Scheme 20

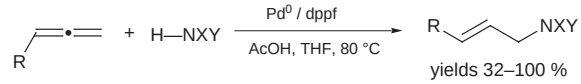

X = Y = CH_2CO_2Et, CH_2Ph, Ph
X = β-Naphthyl, Y = Ph
R = Ph, *p*-MeC_6H_4, *p*-$CF_3C_6H_4$, $Ph(CH_2)_2$, n-Octyl, *p*-$F_3COC_6H_4$

Scheme 21

coworkers have reported that PH_3 reacts with acrylonitrile in the presence of $Pt[P(CH_2CH_2CN)]_3$ to give $P(CH_2CH_2CN)_3$ (Scheme 22).[26] The reaction has been proposed to proceed *via*

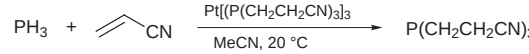

Scheme 22

oxidative addition of the P–H bond to platinum. A recent mechanistic study has confirmed this idea, showing furthermore that the reaction is likely proceed through insertion of acrylonitrile into the Pt–P (but not Pt–H) bond, followed by a C–H reductive elimination (Scheme 23).[27]

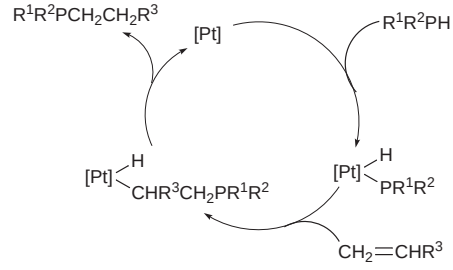

Scheme 23

We also have found that oxidative addition of the H–P bonds of hydrogen phosphonates $[(RO)_2P(O)H]$ with Pt^0 complexes

readily takes place to afford the corresponding hydrido(phosphoryl) complex quantitatively. Heating the complex with phenylacetylene formed a vinylphosphonate (Scheme 24).[28]

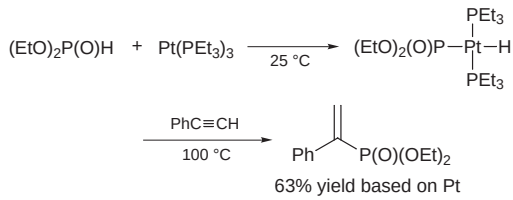

Scheme 24

Accordingly, catalytic addition of hydrogen phosphonates to alkynes readily proceeds when palladium complexes are used as catalysts (hydrophosphorylation). Markovnikov adducts are normally formed in high yields and with high selectivities (Scheme 25). When oct-4-yne was employed as substrate, only

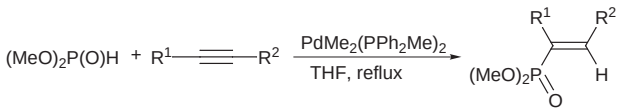

R^1 = n-C_6H_{13}, R^2 = H, 95%
R^1 = Ph, R^2 = H, 93%
R^1 = 4-MeC_6H_4, R^2 = H, 90%
R^1 = NC$(CH_2)_3$, R^2 = H, 94%
R^1 = cyclohex-1-en-1-yl, R^2 = H, 89%
R^1 = Me_3Si, R^2 = 41%
R^1 = R^2 = Pr, 82%

Scheme 25

the *cis*-adduct was selectively obtained. Among the complexes screened, $Pd(CH_2{=}CH_2)(PPh_3)_2$ and $PdMe_2(PPh_2Me)_2$ show highest activity. The frequently employed $Pd(PPh_3)_4$ also catalyses the addition, albeit slowly. Pd^{II} complexes such as $PdCl_2$, $Pd(OAc)_2$, $PdCl_2(PPh_3)_2$ and $PdCl_2(PhCN)_2$ are totally ineffective, presumably because of the difficulty of these precursor complexes being reduced to Pd^0 active species. When $PdMe_2(PPh_2Me)_2$ is used as precursor, Pd^0 species **10** is readily formed through the sequence shown in Scheme 26,[29] and the

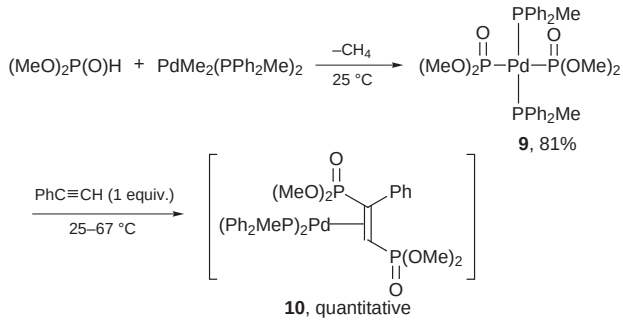

Scheme 26

species **10** does catalyse the addition of $(MeO)_2P(O)H$ to phenylacetylene efficiently.

Unlike the reaction of alkynes with hydrogen phosphonates, the reactions with $Ph_2P(O)H$ in the presence of $Pd(PPh_3)_4$ catalyst proceeds under very mild conditions (hydrophosphinylation) and selectively forms *anti*-Markovnikov products through *cis*-addition (Scheme 27).[30] The P–H bond of $Ph_2P(O)H$ also undergoes oxidative addition with Pd^0 and Pt^0 complexes to afford *cis*-MH[P(O)Ph_2][PPh_2(OH)](PEt_3) (M = Pd, Pt) (Scheme 28).[30,31] Although platinum complex **11a** does not react with oct-1-yne upon heating, **11b** does react in benzene at room temperature to afford two regioisomeric alkenylpalladium species. Heating the reaction mixture at 70 °C affords the

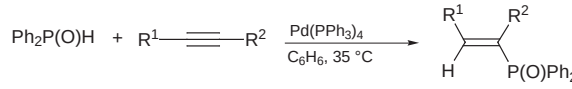

R^1 = n-C_6H_{13}, R^2 = H, 81%
R^1 = $HO(CH_2)_2$, R^2 = H, 86%
R^1 = Ph, R^2 = H, 79%
R^1 = R^2 = H, 51%
R^1 = 4-MeC_6H_4, R^2 = H, 83%
R^1 = R^2 = Pr, 61%
R^1 = NC$(CH_2)_3$, R^2 = H, 73%
R^1 = R^2 = Ph, 85%

Scheme 27

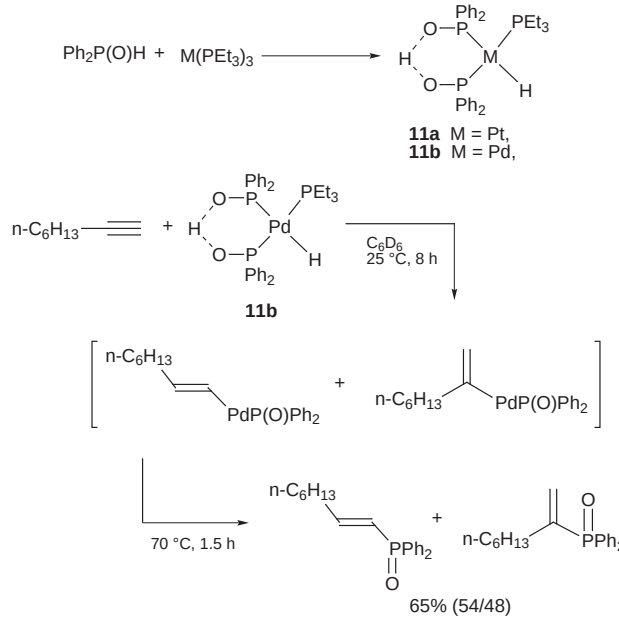

Scheme 28

corresponding alkenylphosphine oxides. This result indicates that the catalysis proceeds through insertion of an alkyne into the Pd–H bond (hydropalladation) followed by reductive elimination of the alkenyl and phosphinyl ligands forming the product, which differs from the platinum-catalysed addition of PH_3 to acrylonitrile (*vide supra*).[27]

Very interestingly, the regioselectivity of the hydrophosphinylation of alkynes can be easily switched by addition of only one drop of $Ph_2P(O)OH$ to the reaction mixture (Scheme 29).[32]

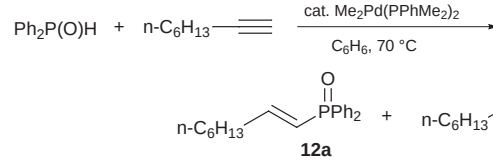

mol% $Ph_2P(O)OH$ added	% yield of **12** (**a**/**b**)
0	75 (88/12)
1	92 (21/79)
5	99 (5/95)
10	96 (4/96)

Scheme 29

Thus, when an equimolar mixture of $Ph_2P(O)H$ and oct-1-yne in C_6D_6 was heated at 70 °C for 2 h in the presence of a catalytic quantity (5% relative to the substrate) of *cis*-$Me_2Pd(PPhMe_2)_2$, isomeric **12b** and **12a** were formed in 75% total yield with a ratio of 12:88. However, another reaction run in the presence of only 1 mol% (relative to the substrate) of $Ph_2P(O)OH$ under otherwise identical conditions resulted in 92% total yield and a **12b**/**12a** ratio of 79:21. The regioselectivity for **12b** was further improved with an increase in the quantity of $Ph_2P(O)OH$ to

achieve nearly quantitative formation of the adducts in a ratio of 95:5 in the presence of 5 mol% $Ph_2P(O)OH$. Besides the phosphinic acid, dibutyl phosphate and phosphoric acid work as well to give **12b** as the major product. However, the reversal is not observed with HMPA, acetic acid or benzoic acid. To explain the reversal we propose another reaction mechanism, in which a new palladium species **13** plays a key catalytic role (Scheme 30). Complex **13′** was indeed generated and isolated

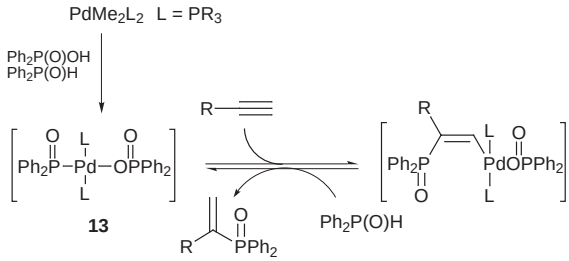

Scheme 30

when $PdMe_2(PR_3)_2$ was treated with $Ph_2P(O)H$ and $Ph_2P(O)OH$ (Scheme 31). In addition, species **13′**, when used as

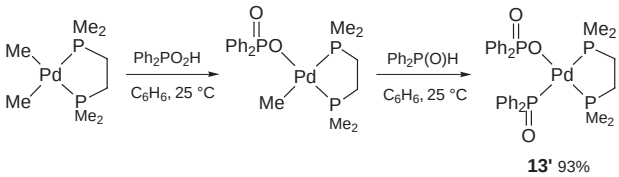

Scheme 31

catalyst in the addition reaction of $Ph_2P(O)H$ to oct-1-yne, exhibited essentially the same activity and regioselectivity as the combination of $PdMe_2(dmpe)_2$ [dmpe = 1,2-bis(dimethylphosphino)ethane] and $Ph_2P(O)OH$.

Besides P–H bonds, oxidative additions of other P–heteroatom bonds also proceed and catalytic addition reactions can be designed. For instance, a selenophosphate readily reacts with Pd^0 and Pt^0 complexes to generate seleno(phosphoryl)metal(II) species (Scheme 32). *cis*-Additions of the selenophosphate to

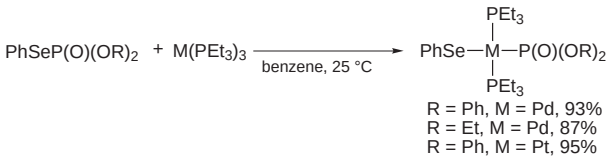

Scheme 32

terminal alkynes also readily proceed to afford the adducts regio- and stereo-selectively with the phosphoryl group bound to the terminal carbons (Scheme 33).[33]

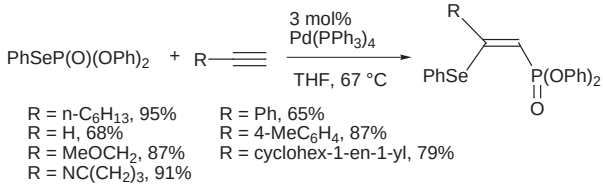

Scheme 33

Metal-catalysed additions of chalcogen compounds

Metal-catalysed addition reactions of chalcogen reagents to carbon–carbon unsaturated bonds did not attract much attention until the pioneering work reported by Ogawa, Sonoda and their co-workers.[34] In the presence of $Pd(OAc)_2$, thiophenol and selenophenol react with terminal alkyne to produce Markovnikov *cis*-addition products in good yields with high regioselectivity (Scheme 34).[35] Allenes[36] and conjugated en-

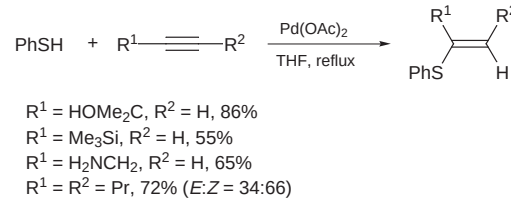

Scheme 34

ynes[37] similarly react with PhSH (Schemes 35 and 36). A very interesting thioformylation reaction also proceeds when the

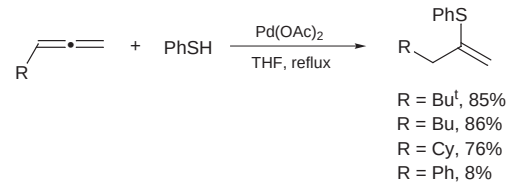

Scheme 35

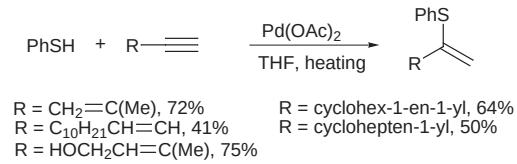

Scheme 36

addition of PhSH to alkynes was carried out under a CO atmosphere in the presence of a catalytic amount of Rh^I complex (Scheme 37).[38] $Pd(OAc)_2$, which is a good catalyst for the addition of PhSH, does not exert activity towards the

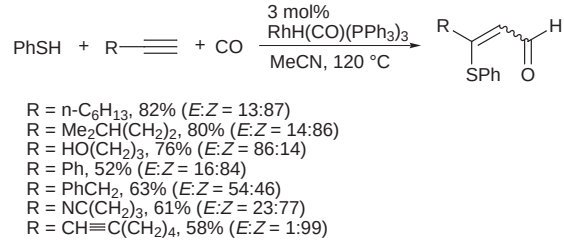

Scheme 37

thioformylation reaction. The use of $Pd(PPh_3)_4$ and $PdCl_2(PPh_3)_2$ resulted in a rather complicated mixture. On the other hand, addition of chalcogen–chalcogen bonds (S–S and Se–Se) to alkynes is efficiently catalysed by $Pd(PPh_3)_4$ to give predominantly the *cis*-addition products in good yields (Scheme 38).[39] When the reaction is run under a CO atmosphere, the simple addition of the dichalcogenides is suppressed, resulting in a selective carbonylative addition to produce the *Z* products in high yields (Scheme 39). A very interesting variation is the reaction of alkynes bearing an OH group at a proper position (propargylic alcohols, for example); a novel thiolative lactonization takes place to afford the corresponding lactons in good yields (Scheme 40).[40] The metal-catalysed additions of S–S bonds are applicable to other substrates. For example, $(ArS)_2$ undergoes telomerization with isocyanides (C=NAr′) in the

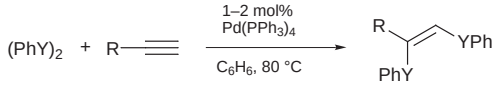

Y = S: R = $Me_2CH(CH_2)_2$, 98%
R = $Me_2(HO)C$, 89%
R = Me(HO)CH, 87%
R = $HOCH_2$, 79%
R = $HO(CH_2)_2$, 80%
R = Me_3Si, 54%
R = H_2NCH_2, 66%
R = Ph, 85%
R = $CH_2{=}CHCH_2(CO_2Et)_2CCH_2$, 55%

Y = Se: R = $Me_2CH(CH_2)_2$, 79%
R = $Me_2(HO)C$, 96%
R = $HO(CH_2)_2$, 84%
R = Me_3Si, 66%
R = H_2NCH_2, 90%
R = $CH_2{=}CHCH_2OCH_2$, 58%

Scheme 38

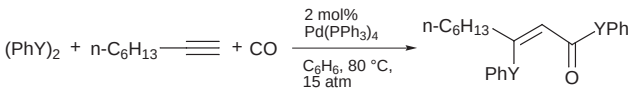

Y = S, 56%; Y = Se, 87%

Scheme 39

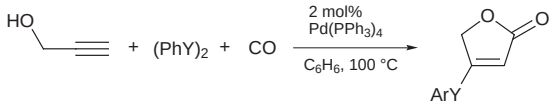

Y = S, 43%; Y = Se, 53%

Scheme 40

presence of $Pd(PPh_3)_4$ to furnish novel telomeric products, $(ArS(C{=}NAr')_nSAr)$ (Scheme 41).[41]

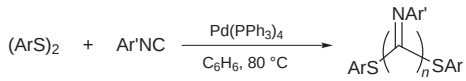

Scheme 41

Oxidative additions of S–H and S–S bonds to transition metal complexes have long been known[42] and are probably involved in the foregoing catalytic reactions. Related C–S bond scissions by metal complexes have also been extensively studied for modeling the hydrodesulfurization (HDS) process. However, similar studies on other chalcogen compounds are rare.[43] A recent systemic study on the reaction of Ph_2Y (Y = S, Se, Te) with group 10 transition metal complexes $M(PEt_3)_n$ (M = Ni, Pd, Pt; n = 3, 4) has revealed the formation of corresponding *trans*-$MPh(YPh)(PEt_3)_2$ complexes in high yields (Scheme 42).[44] However, the reaction of $PhTePr^i$ with $Pt(PEt_3)_3$ clearly

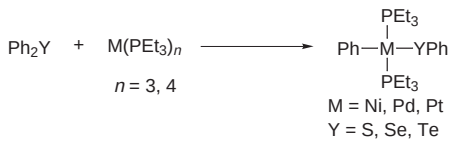

Scheme 42

suggests that *cis*-$PtPh(TePr^i)(PEt_3)_2$ is the initial product, which isomerizes rapidly to the thermodynamically more stable *trans*-form on standing (Scheme 43). The ease of the oxidative

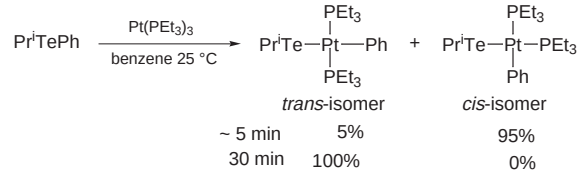

Scheme 43

addition decreases in the order of C–Te > C–Se > C–S, which is the reverse of the order of their bond strengths and has similarity to the trend found with organic halides. The C–Te bond is extremely reactive; its oxidative addition to Pd^0 is even faster than the corresponding iodide (Scheme 44)! Oxidative

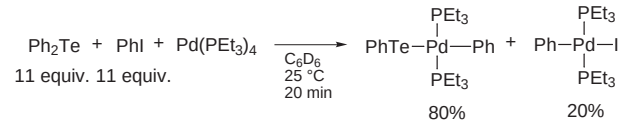

Scheme 44

addition of chalcogenides to the palladium and platinum complexes seems quite general. In practice, chalcogenides of Si, Ge and Sn were more reactive in the oxidative addition reaction than their corresponding C–chalcogen bonds.[45] The reactivity trends were S–Si < Se–Si < Te–Si, and Si–Se < (Ge–Se) < Sn–Se, *i.e.* a heavier element bond reacted more readily. Obviously, these results have suggested new clues for the manipulations of chalcogen compounds using transition metal catalysts.[46] For example, we have found the addition of $PhSSiCl_3$ to terminal alkynes is efficiently catalysed by Pt^0 complexes to produce the *Z* adducts in high yields regioselectively with the Si moiety bound to the terminal carbons (Scheme 45).[47] Similar to the additions of $PhSeSiMe_3$ and

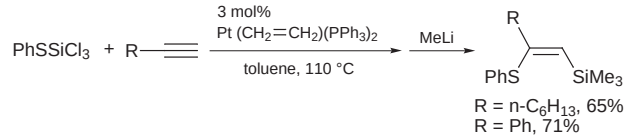

R = n-C_6H_{13}, 65%
R = Ph, 71%

Scheme 45

$PhSeGeMe_3$ to phenylacetylene catalysed by $Pd(PPh_3)_4$ (Scheme 46),[34] this reaction is envisioned to proceed *via*

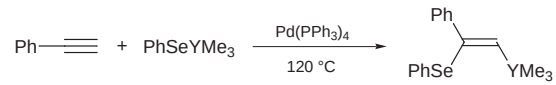

Y = Si, 21%; Ge, 36%

Scheme 46

oxidative addition of the S–Si bond. However, there is no need to prepare starting $PhSSiCl_3$ in advance, since $PhSSiCl_3$ is generated *in situ* from $(PhS)_2$ and $(SiCl_3)_2$. In a new protocol, the same adduct can be obtained regio- and stereo-selectively in good yields, by simply heating a mixture of a disulfide, $(SiCl_3)_2$ and an alkyne in the presence of the platinum catalyst (Scheme 47). Possible byproducts coming from additions of the disulfide and/or disilane are not formed at all.

Conclusion

As described in this article, the simple combination of the classical elemental processes, oxidative addition, insertion of unsaturated compounds and reductive elimination, proves powerful for the design of new catalytic reactions in heteroatom chemistry. We believe homogeneous catalysis will find more opportunities not only in organic synthesis but in organometallic synthesis. Accumulation of knowledge concerning the chemistry of transition metal–heteroatom bonds is a pre-

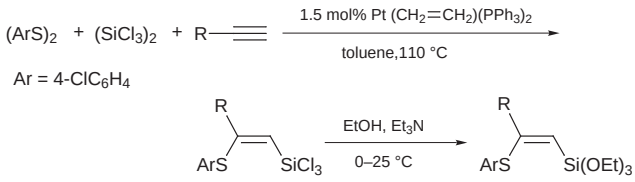

R = n-C_6H_{13}, 83% R = $Cl(CH_2)_3$, 79%
R = $PhCH_2$, 76% R = $NC(CH_2)_3$, 81%
R = Ph, 62% R = $Bu^tMe_2SiO(CH_2)_4$, 72%
R = 4-ClC_6H_4, 65% R = $Bu^tCO_2(CH_2)_2$, 87%
R = 4-MeC_6H_4, 60% R = cyclohex-1-en-1-yl, 51%

Scheme 47

requisite for this goal. Research along the line covering a wider range of elements is being actively pursued in our group.

Acknowledgments

We are indebted to our co-workers whose names appear in the references. Financial support from the Japan Science and Technology Corporation (JST) through the CREST program is gratefully acknowledged.

Notes and references

1 For example: M. Beller, *Angew. Chem., Int. Ed. Engl.*, 1995, **34**, 1316; A. S. Guram, R. A. Rennels and S. L. Buchwald, *Angew. Chem., Int. Ed. Engl.*, 1995, **34**, 1348; J. P. Wolfe, S. Wagaw and S. L. Buchwald, *J. Am. Chem. Soc.*, 1996, **118**, 7215; R. A. Widenhoefer and S. L. Buchwald, *Organometallics*, 1996, **15**, 2755; R. A. Singer, J. P. Sadighi and S. L. Buchwald, *J. Am. Chem. Soc.*, 1998, **120**, 213; G. Mann, J. F. Hartwig, M. S. Driver and C. Fernandez-Rivas, *J. Am. Chem. Soc.*, 1998, **120**, 827; J. Louie, F. Paul and J. F. Hartwig, *Organometallics*, 1996, **15**, 2794; M. S. Driver and J. F. Hartwig, *J. Am. Chem. Soc.*, 1996, **118**, 7217; J. F. Hartwig, *Synlett.*, 1997, 329.

2 *Comprehensive Handbook on Hydrosilylation*; ed. B. Marciniec, Pergamon, Oxford, UK, 1992; K. A. Horn, *Chem. Rev.*, 1995, **95**, 1350; H. K. Sharma and K. H. Pannell, *Chem. Rev.*, 1995, **95**, 1351; S. Murai and N. Chatani, *J. Synth. Org. Chem., Jpn.*, 1993, **51**, 421; C. A. Recatto, *Aldrichim. Acta*, 1995, **28**, 85; R. J. P. Corriu and J. J. E. Moreau, *J. Organomet. Chem.*, 1972, **40**, 73; Y. Ichinose, H. Oda, K. Oshima and K. Utimoto, *Bull. Chem. Soc. Jpn.*, 1987, **60**, 3468; K. Kikukawa, H. Umekawa, F. Wada and T. Matsuda, *Chem. Lett.*, 1988, 881; H. X. Zhang, F. Guibe and G. Balavoine, *J. Org. Chem.*, 1990, **55**, 1857; T. N. Mitchell, A. Amamria, H. Killing and D. Rutschow, *J. Organomet. Chem.*, 1983, **241**, C45; H. Killing and T. N. Mitchel, *Organometallics*, 1984, **3**, 1318; E. Piers and R. T. Skerlj, *J. Chem. Soc., Chem. Commun.*, 1986, 626; T. N. Mitchell and U. Schneider, *J. Organomet. Chem.*, 1991, **407**, 319 and references cited therein.

3 K. Burgess and M. J. Ohlmeyer, *Chem. Rev.*, 1991, **91**, 1179; I. Beletskaya and A. Pelter, *Tetrahedron*, 1997, **53**, 4957.

4 T. Ishiyama, N. Matsuda, N. Miyaura and A. Suzuki, *J. Am. Chem. Soc.*, 1993, **115**, 11018; T. Ishiyama, N. Matsuda, M. Murata, F. Ozawa, A. Suzuki and N. Miyaura, *Organometallics*, 1996, **15**, 713.

5 C. N. Iverson and M. R. I. Smith, *J. Am. Chem. Soc.*, 1995, **117**, 4403; C. N. Iverson and M. R. I. Smith, *Organometallics*, 1996, **15**, 5155.

6 G. Lesley, P. Nguyen, N. J. Taylor, T. B. Marder, A. J. Scott, W. Clegg and N. C. Norman, *Organometallics*, 1996, **15**, 5137.

7 T. Ishiyama, M. Yamamoto and N. Miyaura, *Chem. Commun.*, 1996, 2073.

8 R. T. Baker, P. Nguyen, T. B. Marder and S. A. Westcott, *Angew. Chem., Int. Ed. Engl.*, 1995, **34**, 1336.

9 T. Ishiyama, M. Yamamoto and N. Miyaura, *Chem. Commun.*, 1997, 689; C. N. Iverson and M. R. Smith III, *Organometallics*, 1997, **16**, 2757.

10 S.-y. Onozawa, Y. Hatanaka, T. Sakakura, S. Shimada and M. Tanaka, *Organometallics*, 1996, **15**, 5450.

11 S.-y. Onozawa, Y. Hatanaka, N. Choi and M. Tanaka, *Organometallics*, 1997, **16**, 5389.

12 S-y. Onozawa, Y. Hatanaka and M. Tanaka, *Tetrahedron Lett*, in the press.

13 T. Hayashi, A. M. Kawamoto, T.-a. Kobayashi and M. Tanaka, *J. Chem. Soc., Chem. Commun.*, 1990, 563; H. Yamashita, M. Catellani and M. Tanaka, *Chem. Lett.*, 1991, 241; H. Yamashita and M. Tanaka, *Chem. Lett.*, 1992, 1547; T. Hayashi, H. Yamashita, T. Sakakura, Y. Uchimaru and M. Tanaka, *Chem. Lett.*, 1991, 245; H. Yamashita, N. P. Reddy and M. Tanaka, *Macromolecules*, 1993, **26**, 2143.

14 S.-y. Onozawa, Y. Hatanaka and M. Tanaka, *Chem. Commun.*, 1997, 1229.

15 Y. Ito, M. Suginome and M. Murakami, *J. Org. Chem.*, 1991, **56**, 1948; M. Suginome, H. Oike, S.-S. Park and Y. Ito, *Bull. Chem. Soc. Jpn.*, 1996, **69**, 289.

16 M. Suginome, H. Nakamura and Y. Ito, *Chem. Commun.*, 1996, 2777.

17 M. Suginome, H. Nakamura and Y. Ito, *Angew. Chem., Int. Ed. Engl.*, 1997, **36**, 2516.

18 Similar 1,1-adducts were formed in dehydrogenative double silylation of 1-alkenes with 1,2-bis(dimethylsilyl)benzene. See M. Tanaka, Y. Uchimaru and H.-J. Lautenschlager, *J. Organomet. Chem.*, 1992, **428**, 1.

19 T. Ishiyama, K.-i. Nishijima, N. Miyaura and A. Suzuki, *J. Am. Chem. Soc.*, 1993, **115**, 7219.

20 M. B. Gasc, A. Lattes and J. J. Perie, *Tetrahedron*, 1983, **39**, 703; L. S. Hegedus, *Angew. Chem., Int. Ed. Engl.*, 1988, **27**, 1113; J.-J. Brunet, D. Neibecker and F. Niedercorn, *J. Mol. Catal.*, 1989, **49**, 235.

21 Hydroaminations catalysed by organolanthanides have been developed. However, they will not be discussed here since they proceed *via* a different mechanism from that shown in Scheme 1. See P. J. Walsh, A. M. Baranger and R. G. Bergman, *J. Am. Chem. Soc.*, 1992, **114**, 1708; M. A. Giardello, V. P. Conticello, L. Brard, M. R. Gagne and T. J. Marks, *J. Am. Chem. Soc.*, 1994, **116**, 10241; Y. Li and T. J. Marks, *Organometallics*, 1996, **15**, 3770; Y. Li and T. J. Marks, *J. Am. Chem. Soc.*, 1996, **118**, 9295; A. Haskel, T. Straub and M. S. Eisen, *Organometallics*, 1996, **15**, 3773.

22 A. L. Casalnuovo, J. C. Calabrese and D. Milstein, *J. Am. Chem. Soc.*, 1988, **110**, 6738.

23 J.-J. Brunet, G. Commenges, D. Neibecker and K. Philippot, *J. Organomet. Chem.*, 1994, **469**, 221.

24 R. Dorta, P. Egli, F. Zürcher and A. Togni, *J. Am. Chem. Soc.*, 1997, **119**, 10857.

25 M. Al-Masum, M. Meguro and Y. Yamamoto, *Tetrahedron Lett.*, 1997, **38**, 6071.

26 P. G. Pringle and M. B. Smith, *J. Chem. Soc., Chem. Commun.*, 1990, 1701.

27 D. K. Wicht, I. V. Kourkine, B. M. Lew, J. M. Nthenge and D. S. Glueck, *J. Am. Chem. Soc.*, 1997, **119**, 5039.

28 L.-B. Han and M. Tanaka, *J. Am. Chem. Soc.*, 1996, **118**, 1571.

29 L.-B. Han and M. Tanaka, unpublished results.

30 L.-B. Han, N. Choi and M. Tanaka, *Organometallics*, 1996, **15**, 3259.

31 W. B. Beaulieu, T. B. Rauchfuss and D. M. Roundhill, *Inorg. Chem.*, 1975, **14**, 1732; P. W. N. M. van Leeuwen, C. F. Roobeek, R. L. Wife and J. H. G. Frijns, *J. Chem. Soc., Chem. Commun.* 1986, 31.

32 L.-B. Han, R. Hua and M. Tanaka, *Angew. Chem., Int. Ed.*, 1998, **37**, 94.

33 L.-B. Han, N. Choi and M. Tanaka, *J. Am. Chem. Soc.*, 1996, **118**, 7000.

34 A. Ogawa and N. Sonoda, *J. Synth. Org. Chem., Jpn.*, 1996, **54**, 894; A. Ogawa and N. Sonoda, *J. Synth. Org. Chem., Jpn.*, 1993, **51**, 815

35 H. Kuniyasu, A. Ogawa, K.-I. Sato, I. Ryu, N. Kambe and N. Sonoda, *J. Am. Chem. Soc.*, 1992, **114**, 5902; H. Kuniyasu, A. Ogawa, K.-I. Sato, I. Ryu and N. Sonoda, *Tetrahedron Lett.*, 1993, **34**, 2491.

36 A. Ogawa, J.-i. Kawakami, N. Sonoda and T. Hirao, *J. Org. Chem.*, 1996, **61**, 4161.

37 J.-E. Bäckvall and A. Ericsson, *J. Org. Chem.*, 1994, **59**, 5850.

38 A. Ogawa, M. Takeba, J.-i. Kawakami, I. Ryu, N. Kambe and N. Sonoda, *J. Am. Chem. Soc.*, 1995, **117**, 7564.

39 H. Kuniyasu, A. Ogawa, S.-I. Miyazaki, I. Ryu, N. Kambe and N. Sonoda, *J. Am. Chem. Soc.*, 1991, **113**, 9796; Y. Gareau and A. Orellana, *Synlett.*, 1997, 803.

40 A. Ogawa, H. Kuniyasu, N. Sonoda and T. Hirao, *J. Org. Chem.*, 1997, **62**, 8361.

41 H. Kuniyasu, K. Sugoh, M. S. Su and H. Kurosawa, *J. Am. Chem. Soc.*, 1997, **119**, 4669

42 For references, see ref. 34, 39 and 41 and literature cited therein.

43 Reviews: R. J. Angelici, *Acc. Chem. Res.*, 1988, **21**, 387; R. J. Angelici, *Coord. Chem. Rev.*, 1990, **105**, 61; R. A. Sánchez-Delgado, *J. Mol. Catal.*, 1994, **86**, 287. For other examples, see K. Matsubara, R. Okamura, M. Tanaka and H. Suzuki, *J. Am. Chem. Soc.*, 1998, **120**, 1108 and references cited therein.

44 L.-B. Han, N. Choi and M. Tanaka, *J. Am. Chem. Soc.*, 1997, **119**, 1795.

45 L.-B. Han, S. Shimada and M. Tanaka, *J. Am. Chem. Soc.*, 1997, **119**, 8133.

46 L.-B. Han and M. Tanaka, *Chem. Commun.*, 1998, 47; T. Stüdemann, V. Gupta, L. Engman and P. Knochel, *Tetrahedron Lett.*, 1997, **38**, 1005.

47 L.-B. Han and M. Tanaka, *J. Am. Chem. Soc.*, 1998, **120**, 8249.

Paper 8/06537C

Conversion of a new chiral reagent Δ-[Ru(bpy)$_2$(dmso)Cl]PF$_6$ to Δ-[Ru(bpy)$_2$(dmbpy)]PF$_6$Cl with 96.8% retention of chirality (dmbpy = 4,4′-dimethyl-2,2′-bipyridine)

Dusan Hesek,[a] Yoshihisa Inoue,*[a] Simon R. L. Everitt,[a] Hitoshi Ishida,[a] Mieko Kunieda[a] and Michael G. B. Drew[b]

[a] *Inoue Photochirogenesis Project, ERATO, JST, 4-6-3 Kamishinden, Toyonaka 565-0085, Japan. E-mail: inoue@chem.eng.osaka-u.ac.jp*

[b] *Department of Chemistry, The University of Reading, Whiteknights, Reading, UK RG6 6AD*

Received (in Cambridge, UK) 14th September 1998, Accepted 25th January 1999

The new chiral ruthenium bis(bpy) sulfoxide reagent, Δ-*cis*-[Ru(bpy)$_2$(dmso)Cl]PF$_6$ (100% ee following HPLC resolution) is used to prepare Δ-[Ru(bpy)$_2$(dmbpy)][PF$_6$]Cl in excellent yield (97%) with almost complete retention of absolute configuration (96.8%), as confirmed by X-ray crystallographic studies on a single enantiomer of [Ru(bpy)$_2$(dmbpy)][PF$_6$]Cl (obtained without resolution or chromatographic methods) and by analysis of the optical properties of both the precursor and product.

Optically pure octahedral ruthenium complexes have been known for many years, and are important synthetic targets.[1] Many synthetic procedures are known for their preparation but almost all of these processes rely on a resolution technique at the final stage in the preparation.[2,3] Although a diastereoselective synthesis using the so-called chiragen ligands has been reported,[4–6] the absence of a *general* asymmetric synthesis of ruthenium tris(bpy) complexes necessitates a compromise position. The preparation, and resolution of an enantiomerically pure precursor, which is stable enough to be handled, yet sufficiently reactive to allow a quantitative conversion to the desired complex, ideally with no loss of optical activity during this transformation represents such a compromise. The envisioned precursor should also comprise simple materials, that can be easily combined, then readily separated. Such methodology has been reported previously by Hua and von Zelewsky[7,8] who have developed [Ru(bpy)$_2$(py)$_2$]$^{2+}$, and by Keene and coworkers,[1,3,9] who have developed [Ru(bpy)$_2$(CO)$_2$]$^{2+}$. Both of these complexes have been resolved and subsequently applied in the synthesis of enantiomerically pure ruthenium tris(bpy) complexes in a stereoselective fashion. We have sought to add to this highly interesting work by searching for a new ruthenium complex which bears the aforementioned properties, since the availability of the widest possible range of chiral reagents permits the synthetic inorganic chemist to carefully tune the reaction conditions according to the type of product that is required. Herein we wish to report that such a precursor has been realized during the course of our research into the photochemical properties of octahedral ruthenium complexes.[10] Racemic *cis*-[Ru(bpy)$_2$Cl$_2$] **1** is converted to *cis*-[Ru(bpy)$_2$(Me$_2$SO)Cl]Cl **2** when it is heated at 85 °C in dry, deaerated Me$_2$SO for 5 h. After evaporation of the solvent, the racemic product is treated with ether and hot acetone to remove excess Me$_2$SO. The Δ- and Λ-enantiomers of **2** can be readily and completely separated by HPLC,† using a chiral stationary phase during which a counter ion exchange of Cl$^-$ to PF$_6^-$ occurs, and the enantiomers are found not to interconvert, even upon heating in Me$_2$SO for 2 h. NMR techniques allow us to confirm the sulfoxide product,‡ and IR shows that the sulfoxide is S-, not O-bonded, as demonstrated by the S-ligated sulfoxide stretching frequency at 1120 cm^{-1}.[11] It is important to note that **2**·Cl$^-$ is soluble in polar/protic solvents [much more so than Ru(bpy)$_2$Cl$_2$], but is slightly unstable upon prolonged exposure to light, slowly decomposing over several hours if left uncovered. However, the light sensitivity is not so high that completely dark conditions are required, and short exposure times do not result in any noticeable photodegradation.

Stereochemistry at the metal center is almost completely retained when resolved Δ-**2**·PF$_6$ (ee = 100%) is heated to 75 °C for 2 h with 4,4′-dimethyl-2,2′-bipyridine **3** (dmbpy) in a mixture of ethanol and acetic acid (8 : 1), affording Δ-[Ru(bpy)$_2$(dmbpy)][PF$_6$]Cl **4** in 97% yield, with an ee of 96.8% (Scheme 1). Thus, the dmso precursor reacts with near quantitative conversion, and shows almost complete stereoretention, rendering it suitable as a chiral reagent in the stereocontrolled synthesis of ruthenium tris(bpy) complexes.

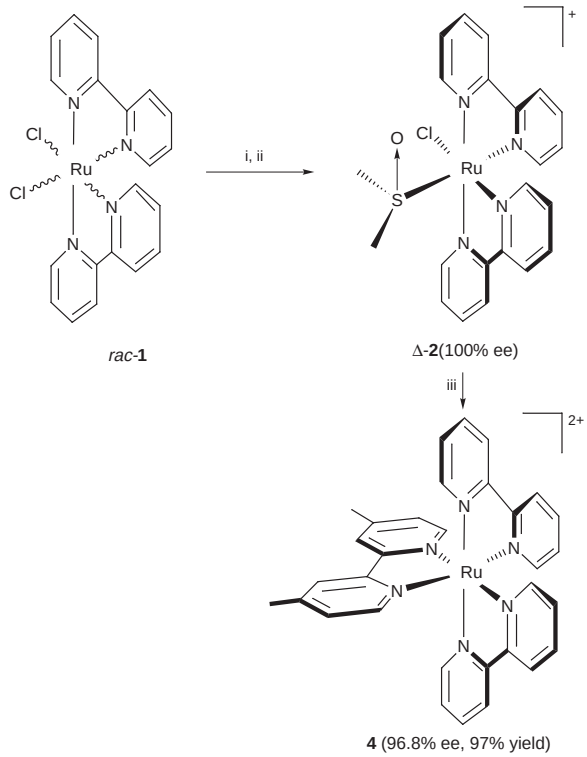

Scheme 1 *Reagents and conditions*: i, DMSO, 85 °C, 5 h; ii, HPLC resolution; iii, dmbpy, EtOH–AcOH, 75 °C, 2 h.

The circular dichroism (CD) and UV–VIS spectra of both Δ-**2** and **4** are shown in Fig. 1. The main features of the CD spectra are the ligand centered bands at *ca*. 275 nm, and the MLCT bands at *ca*. 450 nm. Assignments are based on previously reported data for **1** and related ruthenium complexes.[12–14] The spectra of Δ-**2** and **4** are supported by strong, independent structural data. It should be noted that because the synthesis was stereoretentive, *no resolution procedure* was applied either in the synthesis or in the purification. The material obtained was

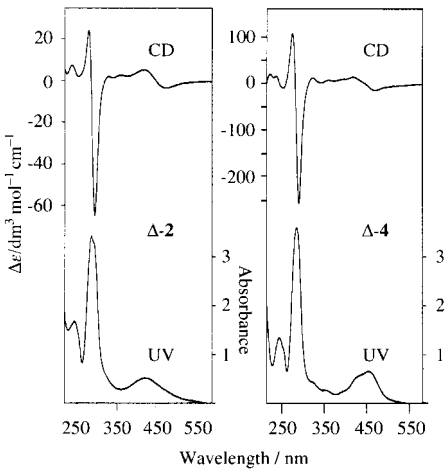

Fig. 1 CD and UV–VIS spectra of Δ-**2** and Δ-**4**.

subsequently shown to be enantiomerically pure by CD spectroscopy and HPLC. A crystal of **4** was grown from this sample using an EtOH–MeCN mixed solvent and subjected to X-ray analysis. The chirality was established as Δ using the method of Bijvoet[15] as indicated by the Flack parameter and *R* factor tests. The structure obtained is shown in Fig. 2.§ This study is therefore of high interest, as there are very few examples of the X-ray structures of enantiomerically pure ruthenium polypyridyl complexes in the literature which are accompanied by CD spectra.[3] The absolute configuration at the metal centre was also confirmed by comparison of the CD spectra and X-ray crystal structure of **4** with the previously recorded X-ray crystal structure of Λ-[Ru(dmbpy)$_2${4,4′-bis[(*R*)-(+)-α-phenylethylamido]-2,2′-bipyridine}][PF_6]$_2$ which has known stereocentres, and was therefore solved with complete certainty.[16] In **4**, the metal is in an octahedral environment with Ru–N distances ranging from 2.055(5) to 2.077(5) Å.

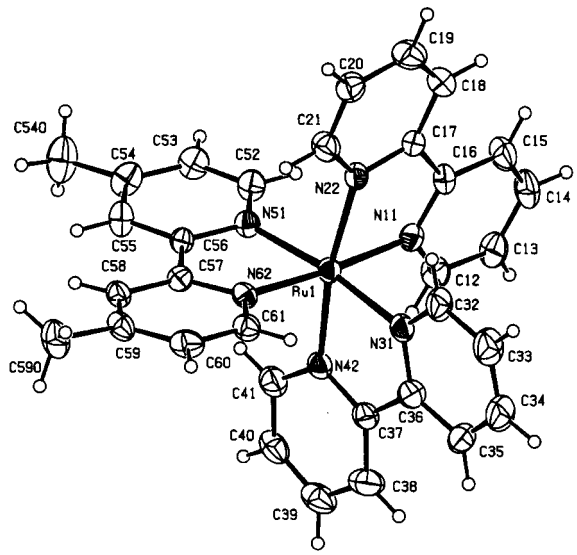

Fig. 2 ORTEP view of molecule $\mathbf{4}^{2+}$ from $\mathbf{4}\cdot 2PF_6^-$ with thermal ellipsoids at 30% probability.

In summary, *cis*-[Ru(bpy)$_2$(Me_2SO)Cl]PF_6 **2** can be prepared using very simple experimental techniques. This ruthenium bis(bpy) sulfoxide is stable (in the absence of strong light), and can be readily resolved to give the new, enantiomerically pure chiral reagent. This can be used for the synthesis of ruthenium tris(bpy) complexes with almost complete stereoretention at the metal centre, as exemplified by the preparation of **4**, which has been confirmed by CD and X-ray methods. To date, only two other complexes have been reported that can be used in this manner, and these have received a good deal of attention, demonstrating the importance of this type of reagent.[1,3,7–9] The synthesis outlined above is both simple and reliable, affording a product with a high enantiomeric excess, in near quantitative yield. This easy to handle chiral sulfoxide reagent is already beginning to prove invaluable in the synthesis of complicated, enantiomerically enriched/pure ruthenium tris(bpy) complexes (for example, the synthesis of a novel tetrakis[ruthenium tris(bipyridine)]calix[6]arene derivative with good diastereomeric purity[17]), and its use in this role will be the subject of future reports from our laboratories.

Notes and references

† HPLC was carried out using a CHIRACEL OD-R column (Diacel Chemical Industries Ltd.) (20 mm diameter × 250 mm length) with aqueous $NaPF_6$ (1 mol dm^{-3}) as the mobile phase. For a flow rate of 3 ml min^{-1}, retention times of 16.90 min for Δ-**2**, 34.6 min for Δ-**4** and 29.6 min for Λ-**4** were observed.

‡ *Selected data* for Δ-**2**: ^{1}H NMR (CD_3CN) δ 10.12 (d, *J* 5.6, 1H, Ha-6), 9.63 (dd, *J* 5.6 Hz, 1.3 Hz, 1H, Hd-6), 8.68 (d, *J* 8.4 Hz, 1H, Hd-3), 8.53 (m, 2H, Ha,b-3), 8.44 (d, *J* 8.4 Hz, 1H, Hc-3), 8.27 (t, *J* 7.6 Hz, 1H, Hd-4), 8.12 (t, *J* 7.6 Hz, 1H, Ha-4), 7.93 (m, 2H, Hb,c-4), 7.86 (d, *J* 5.2 Hz, 1H, Hc-6), 7.84 (t, *J* 8.0 Hz, 1H, Hd-5), 7.73 (t, *J* 8.0 Hz, 1H, Ha-5), 7.24 (m, 2H, Hb,c-5), 7.20 (d, *J* 4.8 Hz, 1H, Hb-6), 3.13 (s, 3H, CH_3), 2.06 (s, 3H, CH_3). Anal. Calc. for $C_{22}H_{22}Cl_2N_4ORuS\cdot H_2O$ (*M* = 580.0) C, 45.51; H, 4.17; N, 9.65. Found: C, 44.98; H, 3.96; N, 9.41%.

§ $C_{34}H_{31}F_{12}N_7P_2Ru$, *M* = 928.67, orthorhombic, space group $P2_12_12_1$, *a* = 13.731(11), *b* = 20.496(9), *c* = 13.521(8) Å, *V* = 3805 Å^3, *Z* = 4, μ = 0.591 mm^{-1}, D_c = 1.621 Mg m^{-3}; 8740 independent reflections were measured on a Rigaku 4-circle diffractometer. Refinement on F^2 *via* SHELXL (G. M. Sheldrick, 1997, program for crystal structure refinement) gave an *R* of 0.0519 for 6197 reflections with $I > 2\sigma(I)$. Flack parameter −0.07(5). Reverse coordinates gave *R* = 0.0542. CCDC 182/1152. See http://www.rsc.org/suppdata/cc/1999/403/ for crystallographic files in .cif format.

1 F. R. Keene, *Coord. Chem. Rev.*, 1997, **166**, 121.
2 N. C. Fletcher, P. C. Junk, D. A. Reitsma and R. F. Keene, *J. Chem. Soc., Dalton Trans.*, 1998, 133.
3 T. J. Rutherford, P. A. Pellegrini, J. Aldrich-Wright, P. C. Junk and F. R. Keene, *Eur. J. Inorg. Chem.*, 1998, 1677.
4 H. Mürner, P. Belser and A. von Zelewsky, *J. Am. Chem. Soc.*, 1996, **118**, 7989.
5 H. Mürner, H. Stoeckli-Evans and A. von Zelewsky, *Inorg. Chem.*, 1996, **35**, 3931.
6 P. Hayoz, A. von Zelewsky and H. Stoeckli-Evans, *J. Am. Chem. Soc.*, 1993, **115**, 5111.
7 X. Hua and A. von Zelewsky, *Inorg. Chem.*, 1995, **34**, 5791.
8 X. Hua and A. von Zelewsky, *Inorg. Chem.*, 1991, **30**, 3796.
9 T. J. Rutherford, M. G. Quagliotto and F. R. Keene, *Inorg. Chem.*, 1995, **34**, 3857.
10 D. Hesek, Y. Inoue and S. R. L. Everitt, *Chem. Lett.*, 1999, 109.
11 I. P. Evans, A. Spencer and G. Wilkinson, *J. Chem. Soc., Dalton Trans.*, 1973, 204.
12 B. Bosnich, *Inorg. Chem.*, 1968, **7**, 2379.
13 P. S. Braterman, B. C. Noble and R. D. Peacock, *J. Phys. Chem.*, 1986, **90**, 4913.
14 K. Kalyanasundaram, *Coord. Chem. Rev.*, 1982, **46**, 159.
15 J. M. Bijvoet, A. F. Peerdeman and A. J. van Bommel, *Nature*, 1951, **168**, 271.
16 D. Hesek, Y. Inoue, S. R. L. Everitt, H. Ishida, M. Kunieda and M. G. B. Drew, unpublished results.
17 D. Hesek, Y. Inoue, S. R. L. Everitt, H. Ishida, M. Kunieda and M. G. B. Drew, *Tetrahedron: Asymmetry*, 1998, **9**, 4089.

Communication 8/09698H

ChemComm

Rate constants for the reaction of cumylperoxyl radicals with Bu_3SnH and $(TMS)_3SiH$

Chryssostomos Chatgilialoglu,*[a] Vitaliy I. Timokhin,*[b] Andriy B. Zaborovskiy,[b] Daria S. Lutsyk[b] and Ruslan E. Prystansky[b]

[a] *I.Co.C.E.A., Consiglio Nazionale delle Ricerche, Via Gobetti 101, I-40129 Bologna, Italy. E-mail: chrys@area.bo.cnr.it*

[b] *Department of Physico-Chemistry, Institute of Physical Chemistry, National Academy of Sciences of Ukraine, 3A Naukova Street, 290053, Lviv, Ukraine*

Received (in Liverpool, UK) 13th December 1998, Accepted 18th January 1999

The rate constants for the reaction of a cumylperoxyl radical with Bu_3SnH and $(TMS)_3SiH$ were determined at 72.5 °C to be 1600 and 66 M^{-1} s^{-1}, respectively, by using inhibited hydrocarbon oxidation methodologies.

In the last two decades, radical chain reactions have proven to be valuable in synthetic organic chemistry.[1a] The majority of such chain processes have been carried out by using Bu_3SnH or $(TMS)_3SiH$, which are the most widely used reagents under reduction conditions.[1] For a synthetically useful radical chain reaction the intermediates must be *disciplined*. The concept of discipline[2] in free radical reactions is strictly connected with the kinetic information of each individual step, although upon first consideration, the importance of the kinetic knowledge might be less apparent in planning a synthetic strategy.

The reaction of peroxyl radicals with organic substrates is one of the most important classes of reactions in chemistry,[3] being the key step of several processes, *e.g.* autoxidation of synthetic polymers, lipid peroxidation and DNA damage. The use of alkylperoxyl radicals in synthesis is limited to a few procedures.[4,5] In one of them, the conversion of halides to alcohols has recently been approached by tin hydride reduction under aerobic conditions.[5] The reaction sequence that has been suggested is shown in Scheme 1. Examples in which the alkyl radical rearranges itself prior to the reaction with molecular oxygen are reported,[5] although in some cases the reaction is sluggish and gives undesired products.[6] Nakamura and co-workers were able to run these experiments under conditions where hydroperoxides were isolated in good yields.[7] In one case, the $(TMS)_3SiH$ mediated halide to alcohol transformation was reported to give a moderate yield.[7] In all these transformations, the reaction of a peroxyl radical with a tin or silicon hydride is crucial. Kinetic information regarding this step is not available. In their recent mechanistic studies on model DNA damage, Greenberg and co-workers[8] arbitrarily assumed the rate constants for the ROO• radical with Bu_3SnH to be 5×10^3 M^{-1} s^{-1} at 55 °C in THF. Following these considerations, the knowledge of the rate constants for the reaction of peroxyl radicals with Bu_3SnH and $(TMS)_3SiH$ turns out to be necessary for better synthetic planning as well as a reference reaction for mechanistic studies.

Herein we report the rate constants of a cumylperoxyl radical with $(TMS)_3SiH$ and Bu_3SnH which have been determined by using inhibited hydrocarbon oxidation methodologies.[9,10] In particular, two different kinetic approaches were used for the two reducing agents, depending on the presence or absence of an induction period when they are used as antioxidants. Scheme 2 shows that the initiation and propagation steps are identical for the two methods, whereas the termination steps are different.

Providing that conditions can be found in which *termination 1* is applied, the rate constant for H-atom abstraction from the silane by cumylperoxyl radicals can be obtained from eqn. (1),[9]

$$\frac{(-\mathrm{d}[O_2]/\mathrm{d}t)_0}{(-\mathrm{d}[O_2]/\mathrm{d}t)} - \frac{(-\mathrm{d}[O_2]/\mathrm{d}t)}{(-\mathrm{d}[O_2]/\mathrm{d}t)_0} = \frac{fk_{SiH}[(TMS)_3SiH]_0}{(2k_tR_i)^{1/2}} \quad (1)$$

where $(-\mathrm{d}[O_2]/\mathrm{d}t)$ and $(-\mathrm{d}[O_2]/\mathrm{d}t)_0$ represent the initial rate of oxidation of cumene with or without $(TMS)_3SiH$.‡ The stoichiometric factor f, which is the number of cumylperoxyl radicals trapped by each molecule of silane, is assumed to be equal to 2.§ The inhibition of thermally initiated (0.021 M of AIBN at 345.5 K) oxidation of pure cumene by $(TMS)_3SiH$ (concentration range of 1.84×10^{-4} to 6.13×10^{-4} M) is found to be the case. Fig. 1 shows that the oxidation rate of cumene decreases upon increasing the concentration of silane without an induction period. On the other hand, Fig. 1 also shows the linear regression analysis of eqn. (1), whose slope provides $2k_{SiH}/(2k_t R_i)^{1/2}$ to be 7.1×10^2 M^{-1}. Since the rate of radical production[11]

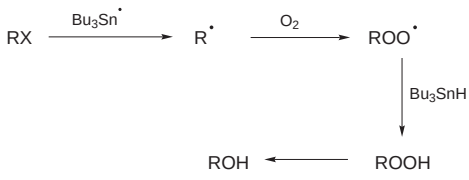

Scheme 1

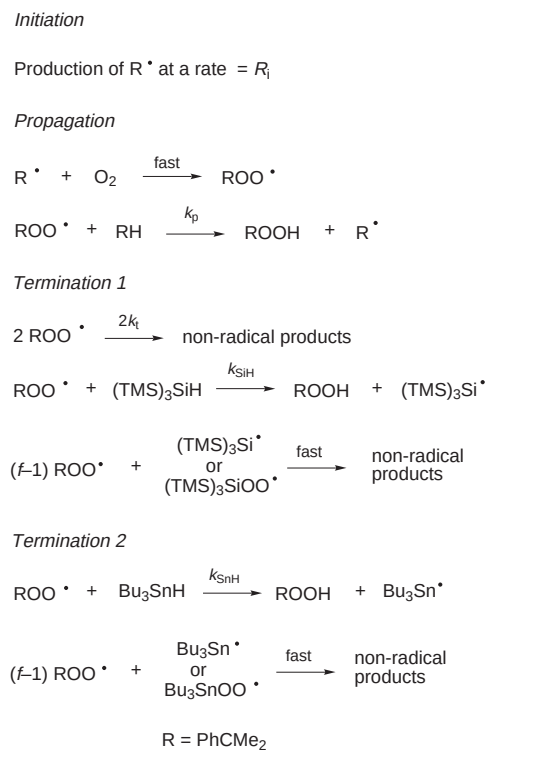

Scheme 2

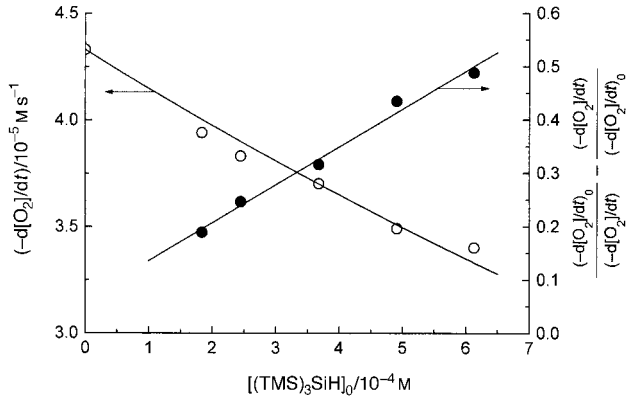

Fig. 1 Plots of (○) $-d[O_2]/dt$ and (●) $(-d[O_2]/dt)_0/(-d[O_2]/dt) - (-d[O_2]/dt)/(-d[O_2]/dt)_0$ *vs.* $[(TMS)_3SiH]$; [AIBN] = 0.021 M at 345.5 K.

and the termination for cumylperoxyl radicals[12] are $R_i = 1.09 \times 10^{-6}$ M s^{-1} and $2k_t = 3.2 \times 10^4$ M^{-1} s^{-1}, respectively, we calculated $k_{SiH} = 66.3$ M^{-1} s^{-1} at 345.5 K.

The inhibition of thermally initiated (0.0172 M of AIBN at 345.5 K) oxidations of pure cumene by Bu_3SnH (concentration range of 1.07×10^{-3} to 3.20×10^{-3} M) shows an induction period (τ). *Termination 2* in Scheme 2 describes the inhibition mechanism and the initial rate of oxidation (before exiting from the induction period), given by eqn. (2), of peroxyl radicals

$$(-d[O_2]/dt) = \frac{k_p[RH]_0 R_i}{f k_{SnH}[Bu_3SnH]_0} \quad (2)$$

trapped by each molecule of Bu_3SnH. The use of Boozer *et al.*'s induction period method,[13] of which an example is illustrated in Fig. 2 (*i.e.* suppression of the oxygen uptake by the presence of Bu_3SnH) allows the determination of the τ values. Then the stoichiometric factor f can be obtained from $f = R_i\tau/[Bu_3SnH]_0$.[9,10] All the data are summarized in Table 1. From the slope of the linear plot between $-d[O_2]/dt$ and $1/[Bu_3SnH]_0$, the

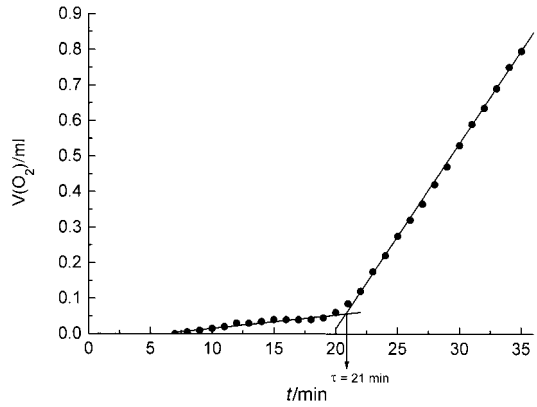

Fig. 2 Oxygen consumption during the AIBN-initiated (0.0172 M) oxidation of cumene in the presence of 2.64×10^{-3} M of Bu_3SnH at 345.5 K.

Table 1 Kinetic data for the oxidation of cumene in the presence of Bu_3SnH[a]

$(d[O_2]/dt)$[b]/M s^{-1}	$[Bu_3SnH]_0$/M	v	τ/min	f
10.94×10^{-6}	1.07×10^{-3}	11.8	10	0.52
7.01×10^{-6}	1.64×10^{-3}	7.5	15	0.51
3.15×10^{-6}	2.64×10^{-3}	3.4	21	0.44
4.67×10^{-6}	3.20×10^{-3}	5.0	20	0.35

[a] [AIBN] = 0.0172 M, $R_i = 0.89 \times 10^{-6}$ M s^{-1} at 345.5 K. [b] $d[O_2]/dt = (d[O_2]/dt)_{exp} - R_i$.

$k_p[RH]_0R_i/fk_{SnH}$ was found to be 11.6×10^{-9} s^{-1}.§ Taking $k_p = 1.3$ M^{-1} s^{-1},[12] $[RH]_0 = 7.188$ M, $R_i = 0.89 \times 10^{-6}$ M s^{-1},[11] and an average of $f = 0.46$, we calculated $k_{SnH} = 1559$ M^{-1} s^{-1} at 345.5 K.

In summary, the rate constants of 66 and 1600 M^{-1} s^{-1} at 345.5 K were obtained for the reaction of cumylperoxyl radicals with $(TMS)_3SiH$ and Bu_3SnH, respectively. Therefore, the alkylperoxyl radicals abstract a hydrogen atom from the tin hydride 24 times faster than from the silane. $(TMS)_3SiH$ is a notably less reactive hydrogen donor than Bu_3SnH, mainly due to the *ca.* 5 kcal mol^{-1} difference in bond dissociation energies.[14] For comparison, primary alkyl radicals and acyl radicals abstract hydrogen from the silane five and 16 times slower, respectively, than from the tin hydride at the same temperature and in much faster processes.[14]

Notes and references

† This relation can be used when the initial oxidation rate and the initiation rate remain essentially constant under the experimental conditions.
‡ This is possible if the reactions in *termination 1* dominate the systems and if the products of these reactions are not active towards initiation.
§ Since the chain length of oxidation [*i.e.* $\nu = (-d[O_2]/dt)_{exp}/R_i$] is less than 12, the initial rate of oxidation is corrected for oxygen absorption by the initiator, and nitrogen evolution from the initiator, *i.e.* $-d[O_2]/dt = (-d[O_2]/dt)_{exp} - R_i$, where the $(-d[O_2]/dt)_{exp}$ is the experimental initial rate of cumene oxidation.

1 (*a*) For example, see: D. P. Curran, N. Porter and B. Giese, *Stereochemistry of Radical Reactions*, VCH, Weinheim, 1995; W. B. Motherwell and D. Crich, *Free Radical Chain Reactions in Organic Synthesis*, Academic Press, London, 1992; (*b*) For reviews on $(TMS)_3SiH$, see: C. Chatgilialoglu, *Acc. Chem. Res.*, 1992, **25**, 188; C. Chatgilialoglu, C. Ferreri and T. Gimisis, in *The Chemistry of Organic Silicon Compounds*, ed. S. Rappoport and Y. Apeloig, Wiley, London, 1998, vol. 2, pp. 1539–1579.

2 A terminology introduced by Barton. For example, see: D. H. R. Barton, *Aldrichim. Acta*, 1990, **23**, 3; D. H. R. Barton and S. I. Parekh, *Half a Century of Free Radical Chemistry*, CUP, Cambridge, UK, 1993.

3 For some representative reviews, see: K. U. Ingold, *Acc. Chem. Res.*, 1969, **2**, 1; N. A. Porter, in *Organic Peroxides*, ed. W. Ando, Wiley, Chichester, 1992; C. von Sonntag and H.-P. Schuchmann, *Angew. Chem., Int. Ed. Engl.*, 1991, **30**, 1229; C. Walling, in *Active Oxygen in Chemistry*, ed. C. S. Foote, J. C. Valentine, A. Greenberg and J. F. Liebman, Blackie, London, 1995, pp. 24–65.

4 For example, see: G. L. Hill and G. M. Whitesides, *J. Am. Chem. Soc.*, 1974, **96**, 870; D. H. R. Barton, D. Crich and W. B. Motherwell, *J. Chem. Soc., Chem. Commun.*, 1985, 1066; H. C. Brown, M. M. Midland and G. W. Kabalka, *Tetrahedron*, 1986, **42**, 5523.

5 E. Nakamura, T. Inubushi, S. Aoki and D. Machii, *J. Am. Chem. Soc.*, 1991, **113**, 8980; S. Moutel and J. Prandi, *Tetrahedron Lett.*, 1994, **35**, 8163; S. Mayer and J. Prandi, *Tetrahedron Lett.*, 1996, **37**, 3117; M. Sawamura, Y. Kawaguchi, K. Sato and E. Nakamura, *Chem. Lett.*, 1997, 705; M. Sawamura, Y. Kawaguchi and E. Nakamura, *Synlett*, 1997, 801.

6 For example, see: D. L. Boger and J. A. McKie, *J. Org. Chem.*, 1995, **60**, 1271.

7 E. Nakamura, K. Sato and Y. Imanishi, *Synlett*, 1995, 525.

8 K. A. Tallman, C. Tronche, D. J. Yoo and M. M. Greenberg, *J. Am. Chem. Soc.*, 1998, **120**, 4903.

9 E. T. Denisov and I. V. Khudyakov, *Chem. Rev.*, 1987, **87**, 1313; E. T. Denisov, *Liquid-Phase Reaction Rate Constants*, Plenum, New York, 1974; N. M. Emanuel, E. T. Denisov and Z. K. Maizus, *Liquid Phase Oxidation of Hydrocarbons*, Plenum, New York, 1967.

10 J. A. Howard, Y. Ohkatsu, J. H. B. Chenier and K. U. Ingold, *Can. J. Chem.*, 1973, **51**, 1543; J. H. B. Chenier, S. B. Tong and J. A. Howard, *Can. J. Chem.*, 1978, **56**, 3047; S. Korcek, J. H. B. Chenier, J. A. Howard and K. U. Ingold, *Can. J. Chem.*, 1972, **50**, 2285.

11 J. P. Van Hook and A. V. Tobolsky, *J. Am. Chem. Soc.*, 1958, **80**, 779; E. Niki, Y. Kamija and N. Ohta, *Bull. Chem. Soc. Jpn.*, 1969, **42**, 3220.

12 D. G. Hendry, *J. Am. Chem. Soc.*, 1967, **89**, 5433.

13 C. E. Boozer, G. S. Hammond, C. E. Hamilton and J. N. Sen, *J. Am. Chem. Soc.*, 1955, **77**, 3233.

14 C. Chatgilialoglu, *Chem. Rev.*, 1995, **95**, 1229.

Communication 8/08894B

The thiyl radical-mediated isomerization of *cis*-monounsaturated fatty acid residues in phospholipids: a novel path of membrane damage?

Carla Ferreri,[ab] Cristina Costantino,[a] Laura Landi,[c] Quinto G. Mulazzani[d] and Chryssostomos Chatgilialoglu*[a]

[a] *I.Co.C.E.A., Consiglio Nazionale delle Ricerche, Via P. Gobetti 101, 40129 Bologna, Italy. E-mail: chrys@area.bo.cnr.it*
[b] *Dipartimento di Chimica Organica e Biologica, Università di Napoli 'Federico II', Via Mezzocannone 16, 80134 Napoli, Italy*
[c] *Dipartimento di Biochimica 'G. Moruzzi', Università di Bologna, Via Irnerio 48, 40126 Bologna, Italy*
[d] *F.R.A.E., Consiglio Nazionale delle Ricerche, Via P. Gobetti 101, 40129 Bologna, Italy*

Received (in Liverpool, UK) 10th December 1998, Accepted 19th January 1999

Thiyl radicals, generated from biologically relevant thiols under biomimetic conditions, reversibly attack the double bonds of unsaturated phospholipids containing *cis*-fatty acid residues either in lipid solutions or lipid vesicles, thus producing phospholipids containing *trans*-fatty acid residues in high yield.

Radical-based damage of biologically relevant molecules has increasingly attracted the interest of researchers from different scientific fields, from chemistry to medicine. To the best of our knowledge, reported radical processes involving membrane phospholipids are limited to lipid peroxidation,[1] and to a recently reported homolytical cleavage of lysophospholipids.[2]

In cell membranes, the *cis* configuration of unsaturated fatty acid residues regulates the self-organization of phospholipids. The enzymatic *cis–trans* isomerization[3] has recently been found to affect the lipid assembly since the *trans* arrangement resembles the structure of saturated fatty acids.[4] From a chemical perspective, the *cis* to *trans* conversion of double bonds is a thermodynamically favoured process,[5,6] which can also occur by the reversible addition of a free radical.[7] In this context, thiyl radicals are very efficient isomerizing agents.[7,8] We report herein that thiyl radicals are also able to induce the isomerization of *cis*-monounsaturated phospholipids. This process was observed using lipid solutions and, more interestingly, liposome vesicles which model the cell membrane.[9] We have shown that phospholipids containing *trans*-fatty acid residues are produced in high yield.

Dioleoyl phosphatidyl choline (DOPC) was the substrate of choice since it represents the main natural component of cell membranes.[10] It is also known that the oxidizability of this substrate is very low.[11] A first set of experiments was carried out with a *tert*-butyl alcohol solution of DOPC, since it is known that phospholipids do not aggregate in this solvent.[12] A $CHCl_3$ solution of DOPC (3 ml; 0.15 mmol of oleate contents) was evaporated in a test tube under an argon stream. Bu^{t}OH (1 ml), $HOCH_2CH_2SH$ (0.075 mmol) and AMVN (0.030 mmol) were added and the solution degassed with argon.† The reaction mixture was warmed to 54 °C and aliquots (100 μl) were processed at different times. Alternatively, Bu^{t}OH (1 ml) and $HOCH_2CH_2SH$ (0.007 mmol) were added and the solution was divided into aliquots of 100 μl in different tubes followed by saturation with N_2O prior to γ-irradiation.[13] After transesterification[14] of the phospholipids at different reaction times, the methyl oleate/methyl elaidate ratios were obtained by GC analysis. Fig. 1(*a*) and (*b*) show the time profiles of methyl elaidate (*i.e.* the *trans* isomer) formation. In all cases the conversion of the starting material to the equilibrium mixture was quantitative and in the absence of thiol the isomerization did not occur [Fig. 1(*a*) and (*b*)].

The mechanism that we conceived for this transformation includes hydrogen abstraction from the thiol, the addition of thiyl radicals to the *cis* double bond of oleic acid residues, half-rotation about the carbon–carbon bond of the radical intermediate, and ejection of the thiyl radical by β-scission (Scheme 1).[7] It is worth pointing out that the final isomeric composition is in agreement with the difference in the thermodynamic stability between methyl elaidate and methyl oleate.[7]

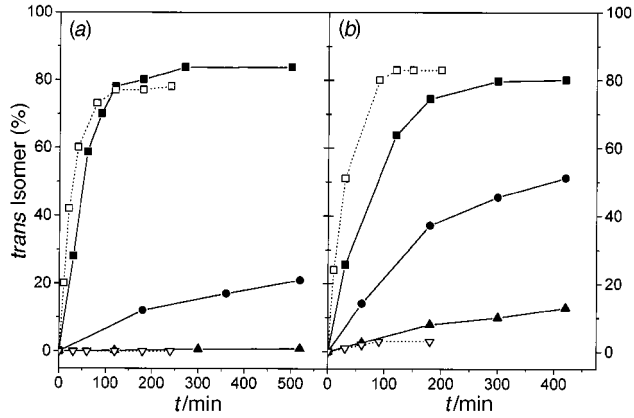

Fig. 1 Time profiles of *trans* isomer formation (*i.e.* methyl elaidate): (*a*) AMVN at 54 °C or AAPH at 37 °C: (□) DOPC with 75 mM $HOCH_2CH_2SH$ in Bu^{t}OH; (▽) DOPC without thiol in Bu^{t}OH; (■) LUVET with 75 mM $HOCH_2CH_2SH$; (●) LUVET with 75 mM of GSH; (▲) LUVET with 75 mM CySH. (*b*) γ-Radiolysis (32 Gy min^{-1}) at 22 °C: (□) DOPC with 7 mM $HOCH_2CH_2SH$ in Bu^{t}OH; (▽) DOPC without thiol in Bu^{t}OH; (■) LUVET with 7 mM $HOCH_2CH_2SH$; (●) LUVET with 7 mM GSH; (▲) LUVET with 7 mM CySH.

As far as the model membranes are concerned, large unilamellar vesicles (LUVET) made by the extrusion technique[15] were tested both by azo compounds and γ-irradiation using $HOCH_2CH_2SH$ or, alternatively, two other biologically-related thiols such as glutathione (GSH) and cysteine (CySH).‡

For the thermal initiation, we used the hydrophilic azo compound AAPH, by dissolving it with the thiol in the external

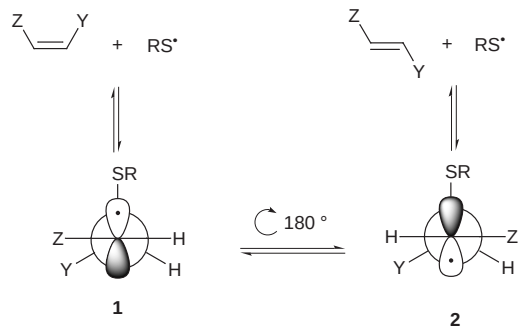

Scheme 1

aqueous phase of the LUVET. A comparison of the time profiles given by the three different thiols is shown in Fig. 1(*a*). The isomerization is probably due to the thiyl radicals, provided that they are able to migrate into the lipophilic compartment, and attack the double bond of the phospholipids as described in Scheme 1. As a matter of fact, the isomerization rate follows the lipophilicity order of the three compounds[16] (*i.e.* $HOCH_2CH_2SH$ > GSH > CySH) and indicates that the CyS• radical is unable to induce isomerization.

For the γ-irradiation experiments the time profiles are shown in Fig. 1(*b*). The isomerization with CySH is not straightforward. In order to explain these results, we suggest that under γ-radiolysis the initial radicals,§ which are more reactive than those derived from the thermal decomposition of AAPH, can abstract either the thiol hydrogen or the β-hydrogen with respect to the SH moiety which is activated by the neighbouring groups [eqn. (1)].[17] We also suggest that the HS• radical obtained by β-

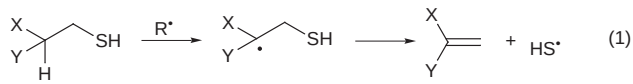

(1)

fragmentation is able to migrate into the lipophilic compartment and isomerize the double bond. The viability of eqn. (1) was confirmed by a series of control experiments. In particular, Fig. 2(*a*) shows the isomerization trends of LUVET with compounds **3** and **4** which are expected to generate MeS• radicals *via* a

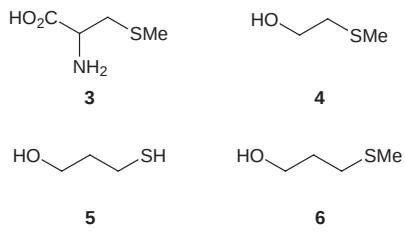

reaction analogous to eqn. (1). On the other hand, using compounds **5** and **6**, isomerization occurs only with the former, the latter being inactive [Fig. 2(*a*)]. Fig. 2(*b*) shows a comparison of experiments with LUVET and $HOCH_2CH_2SH$ under two different dose rates. The higher efficiency of the *cis–trans* isomerization at a low dose rate is probably due to a decrease in competing reactions involving thiyl radicals.

In conclusion we have shown that phospholipids containing *trans*-unsaturated fatty acids are the major products of the thiyl radical attack on natural phospholipids. We have also modelled the occurrence of such a reaction in cell membranes using naturally occurring thiols. Furthermore, the role played by thiols in this process is in antithesis to their action as radioprotectors.[18] The *cis–trans* interconversion of unsaturated lipids has to be considered, together with autooxidation, when examining cellular damage caused by radical attack, since it can determine changes in barrier properties and functions of biological membranes. Therefore, accurate analyses of the cellular lipid content are required. Further work on the *cis–trans* isomerization of mono- and poly-unsaturated phospholipids and its biological implications is in progress.[19]

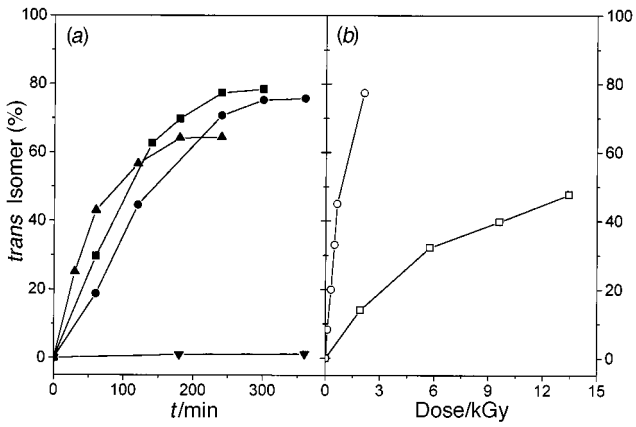

Fig. 2 (*a*) Time profiles of *trans* isomer formation (*i.e.* methyl elaidate) from the γ-radiolysis (32 Gy min^{-1}) of LUVET with (■ **3**, (●) **4**, (▲) **5** or (▼) **6** (all 7 mM). (*b*) *trans*-Isomer formation (*i.e.* methyl elaidate) *vs.* dose from the γ-radiolysis of LUVET with 7 mM $HOCH_2CH_2SH$.

Notes and references

† Dioleoyl phosphatidyl choline (DOPC) as a solution in $CHCl_3$ (20 mg ml^{-1}) and the radical initiators azobis(2,4-dimethylvaleronitrile) (AMVN) and azobis(2-amidinopropane) hydrochloride (AAPH) were commercially available and used without further purification.

‡ A $CHCl_3$ solution of DOPC (3 ml; 0.15 mmol of oleate contents) was evaporated to a thin film in a test tube under an argon stream. Degassed phosphate buffer (1 ml; Na_2HPO_4 10 mM, NaCl 0.14 M, pH 7.2) was added and MLV were formed by vortex stirring for 7 min under argon atmosphere. LUVET were prepared by membrane extrusion through 100 nm polycarbonate filters with LiposoFast™ (ref. 15). To these suspensions the required amounts of thiol (0.075 mmol) and AAPH (0.030 mmol) were consecutively added. The samples were then warmed to 37 °C under argon and aliquots (100 μl) were processed at different times. For γ-irradiation experiments, LUVET were prepared as described above in which Pr^iOH (0.12-0.35 mM depending from the nature of thiol) replaced the initiator in the aqueous phase. The suspension was divided into different Pyrex test tubes, flushed for 15 min with N_2O and irradiated at different times.

§ Radiolysis of water leads to species e_{aq}^- , HO• and H•. The presence of N_2O transforms the e_{aq}^- to HO• radicals. The presence of Pr^iOH transforms the majority of the above mentioned species into Me_2C•OH radicals which are believed to further react with thiols to generate thiyl radicals (ref. 13).

1 For reviews, see E. Niki, in *Organic Peroxides*, ed. W. Ando, Wiley, New York, 1992, pp. 764–787; L. C. R. Barclay, *Can. J. Chem.*, 1993, **33**, 1.
2 S. N. Muller, R. Batra, M. Senn, B. Giese, M. Kisel and O. Shadyro, *J. Am. Chem. Soc.*, 1997, **119**, 2795.
3 R. Holtwick, F. Meinhardt and H. Keweloh, *Appl. Environ. Microbiol.*, 1997, **63**, 4292; B. Loffeld and H. Keweloh, *Lipids*, 1996, **31**, 811; H. Keweloh and H. J. Heipieper, *Lipids* , 1996, **31**, 129.
4 R. L. Wolff and B. Entressangles, *Biochim. Biophys. Acta***,** 1994, **1211**, 198.
5 For a review, see P. E. Sonnet, *Tetrahedron*, 1980, **36**, 557.
6 For catalytic hydrogenation of oils, see L. Ovesen, T. Leth and K. Hausen, *Lipids*, 1996, **31**, 971 and references cited therein.
7 C. Chatgilialoglu, M. Ballestri, C. Ferreri and D. Vecchi, *J. Org. Chem.*, 1995, **60**, 3826.
8 For a review, see C. Chatgilialoglu and M. Guerra, in *Supplement S: The Chemistry of Sulfur-containing Functional Groups*, ed. S. Patai and Z. Rappoport, Wiley, London, 1993, pp. 363–394.
9 *Liposomes a practical approach*, ed. R. R. C. New, IRL Press, Oxford, 1990.
10 L. L. M. Van Deenen, in *Progress in the Chemistry of Fats and Other Lipids. Vol. VIII*, ed. R. T. T. Helman, Pergamon, Oxford, 1965, pp. 1–127.
11 C. Schöneich, U. Dillinger, F. von Bruchhausen and K.-D. Asmus, *Arch. Biochem. Biophys*., 1992, **292**, 456.
12 L. R. C. Barclay, J. M. McNeil, J. J. VanKessel, B. Forrest, N. A. Porter, L. S. Lehman, K. J. Smith and J. C. Ellington Jr., *J. Am. Chem. Soc.*, 1984, **106**, 6740.
13 C. Schöneich, M. Bonifacic and K.-D. Asmus, *Free Radical Res. Commun*., 1989, **6**, 393.
14 Transesterification in alkaline medium is preferable, as reported by: J. F. K. Kramer, V. Fellner, M. E. R. Dugan, F. D. Sauer, M. M. Mossoba and M. P. Yurawecz, *Lipids*, 1997, **32**, 1219.
15 R. C. MacDonald, R. I. MacDonald, B. Ph. M. Menco, K. Takeshita, N. K. Subbarao and L. Hu, *Biochim. Biophys. Acta*, 1991, **1061**, 297.
16 G. L. Newton, J. A. Aguilera, T. Kim, J. F. Ward and R. C. Fahey, *Radiat. Res.*, 1996, **134**, 215 and references cited therein.
17 For example, see R. Zhao, J. Lind, G. Merenyi and T. E. Eriksen, *J. Am. Chem. Soc.*, 1994, **116**, 12 010; M. S. Akhlaq and C. von Sonntag, *J. Am. Chem. Soc.*, 1986, **108**, 3542.
18 G. Stark, *Biochim. Biophys. Acta* , 1991, **1071**, 103 and references cited therein.
19 After completion of this manuscript, the following paper on thiyl-induced *cis–trans* isomerization of linoleate derivatives has appeared: J. Schwinn, H. Sprinz, K. Drößler, S. Leistner and O. Brede, *Int. J. Radiat. Biol*., 1998, **74**, 359.

Communication 8/09674K

Enantioselective epoxidation of *trans*-disubstituted alkenes by D_2-symmetric chiral dioxoruthenium(VI) porphyrins

Rui Zhang, Wing-Yiu Yu, Tat-Shing Lai and Chi-Ming Che*

Department of Chemistry, The University of Hong Kong, Pokfulam Road, Hong Kong. E-mail: cmche@hkucc.hku.hk

Received (in Cambridge, UK) 10th November 1998, Accepted 4th December 1998

A series of D_2-symmetric chiral *trans*-dioxoruthenium(VI) porphyrins can effect enantioselective epoxidation of *trans*-β-methylstyrene in up to 70% ee, and 76% ee is attained for the oxidation of cinnamyl chloride; the facial selection for the *trans*-alkenes epoxidation is explained by a 'head-on approach' model.

The design of new metal catalysts for highly enantioselective epoxidation of unfunctionalized *trans*-disubstituted alkenes remains a challenge in the field of asymmetric oxidation.[1] A clue to this problem would be to prepare reactive, and yet isolable, chiral metal–oxo complexes which can act upon *trans*-alkenes to give epoxides in better enantioselectivities than the *cis*-counterparts.[2] If such complexes can be obtained, the structure–enantioselectivity relationship established by studying their stoichiometric alkene epoxidations could assist future design for better metal catalysts. Here, we show that a series of *trans*-dioxoruthenium(VI) complexes with D_2 symmetric porphyrins bifacially encumbered by four chiral threitol units (Fig. 1) can react favorably with *trans*-alkenes in exceptional %ee. Also, our findings do not reconcile with the 'side-on approach' model proposed for the oxo-metalloporphyrin-mediated alkene oxidations.

The D_2-symmetric porphyrins $H_2L^{1–3}$* and the [Ru^{II}-$L^{1–3}$*(CO)(EtOH)] precursors were prepared by the literature methods.[3] Treating the ruthenium(II) carbonyl complexes with *m*-chloroperoxybenzoic acid in dichloromethane for 5 min gave [$Ru^{VI}(L^{1–3}*)O_2$] **1a–c**, which were isolated as dark red–purple crystalline solids (80% yield). Complexes **1a–c** are diamagnetic and stable in solid and in solution for hours at room temperature. The oxidation state marker band at 1018 (**1a**), 1019 (**b**,**c**) together with an intense asymmetric O=Ru=O stretch at 818 (**1a**), 821 (**1b**), 819 cm^{-1} (**1c**) observed in their IR spectra are consistent with a Ru(VI) formulation.

At room temperature, complex **1a** in the presence of pyrazole (Hpz) oxidized styrene in a degassed benzene solution to give styrene oxide in 64% yield and 62% ee (Table 1, entry 1). The enantioselectivity was slightly improved (65% ee) when the reaction was carried out at 0 °C, and the %ee is comparable to the best reported value of 69% ee by employing the chiral Mn–porphyrin catalysts.[3] However, the other dioxoruthenium(VI) derivatives bearing *gem*-diethyl (**1b**) and *gem*-cyclopentyl groups (**1c**) at the threitol units afforded slightly lower ee of 60 and 55% respectively. A paramagnetic bis(pyrazolato)ruthenium(IV), [$Ru^{IV}(L^{1–3}*)(pz)_2$] **2** (μ_{eff} = 2.9 μ_B), was isolated by column chromatography at the end of the epoxidation reactions.[4] It is noteworthy that when styrene reacted with **1a** without Hpz; styrene oxide with only 40% ee was obtained and [$Ru^{II}(L^{1}*)(CO)$] was isolated. To account for the ee discrepancy, we propose that a ruthenium(II) species produced by further reduction of the putative Ru(IV) intermediate would racemize the chiral styrene oxide by an epoxide ring opening pathway previously suggested by Groves *et al.* (Scheme 1).[5]

More importantly, **1a** reacted with *trans*-β-methylstyrene in degassed benzene to give the *trans*-epoxide in 67% ee at room temperature, and up to 70% ee was attained when performing the reaction at 0 °C (entry 3). Notably, the oxidation of cinnamyl chloride furnished the corresponding epoxide in 76% ee and 70% yield (entry 4). Indeed, few reported metalloporphyrin-catalyzed asymmetric epoxidation systems are

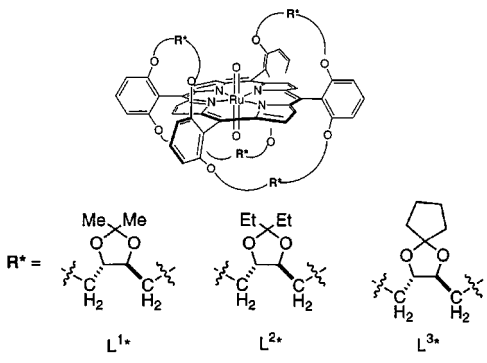

Fig. 1

Table 1 Stoichiometric epoxidation of some aromatic alkenes by [$Ru^{VI}(L^{1}*)O_2$] (1a)

Entry	Alkene	Solvent	Epoxide yield[a] (%)	%ee (abs. config.)[b]
1	Ph	C_6H_6	64[c]	62 (*R*)
		C_6H_6	62	40 (*R*)[d]
		CH_2Cl_2	39	41 (*R*)
		MeCN	13	33 (*R*)
2	Cl	C_6H_6	75	60 (*R*)
3	Ph, Me	C_6H_6	90 (>99 % *trans*)	67 (1*S*,2*R*)
		C_6H_6 (0 °C)	90 (>99 % *trans*)	70 (1*S*,2*R*)
		CH_2Cl_2	58 (>99 % *trans*)	32 (1*S*,2*R*)
		EtOAc	82 (>99 % *trans*)	38 (1*S*,2*R*)
4	Ph, Cl	C_6H_6	70	76 (1*S*,2*R*)
5	Ph, Me	C_6H_6	75 (> 99% *cis*)	40 (1*S*,2*R*)
		CH_2Cl_2	68 (95% *cis*, 5% *trans*)	18 (1*S*,2*R*)
6		C_6H_6	88	20 (1*S*,2*R*)

Reaction conditions: to a degassed benzene solution (1 cm^3) containing alkene (1 mmol) and pyrazole (0.3 mmol) was added the dioxoruthenium(VI) complex (0.015–0.03 mmol) under an argon atmosphere. The reaction mixture was stirred at room temperature (or otherwise noted) for 12 h, and the aliquot was analyzed by gas chromatography for product identification and quantification. [a] Yields are based on the amount of the oxidant used. [b] Enantiopurities (%ee) of the epoxides were determined by GC equipped with a chiral capillary column (J & W Scientific cyclodex-B or G-TA). Absolute configuration was determined by comparing with authentic chiral samples. [c] Benzaldehyde (27%) and phenylacetaldehyde (12%) were also detected. [d] Reaction was carried out without pyrazole.

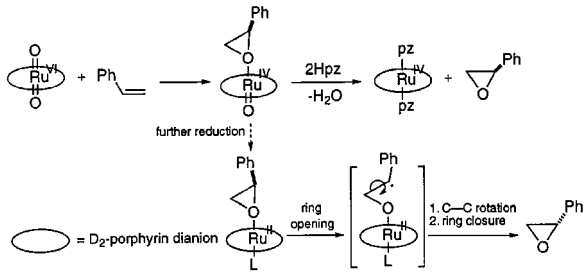

Scheme 1

known to attain >20% ee for the *trans*-β-methylstyrene oxidation.[3,6] We had previously reported that a chiral D_4-symmetric dioxoruthenium(VI) complex can effect epoxidation of *cis*-β-methylstyrene in much higher enantioselectivity of 76% ee *vs*. 20% ee for the *trans*-isomer.[7] In this work, when *cis*-β-methylstyrene (entry 5) and 1,2-dihydronaphthalene (entry 6) reacted with **1a**, the *cis*-epoxides (>99% stereoretention) were produced in only 40 and 20% ee, respectively. Oxidation of *trans*- and *cis*-β-methylstyrene by complexes **1b** and **1c** also resulted similar *trans* preference albeit in lower enantioselectivities, for instance when **1b** was the oxidant, the *trans*- and *cis*-epoxides with 50 and 28% ee resulted respectively.

The asymmetric alkene epoxidations by **1a** also exhibit remarkable solvent dependence.[8] The *trans*-β-methylstyrene oxidation by **1a** displays clean pseudo-first-order kinetics: $-d[Ru(VI)]/dt = k_{obs}[Ru(VI)]$, where $k_{obs} = k_2[alkene]$ and k_2 is the second-order rate constant of the reaction. Upon changing solvent from benzene to dichloromethane, the k_2 value halves: 9.04×10^{-4} (C_6H_6), 4.15×10^{-4} dm^3 mol^{-1} s^{-1} (CH_2Cl_2) at 298 K. It is noted that the %ee of the *trans*-epoxide also decreases in a similar fashion: 67% ee (C_6H_6) *vs.* 32% ee (CH_2Cl_2). By contrast, no solvent effect has been observed for the analogous reactions of the D_4-chiral dioxoruthenium(VI) porphyrin. Since the alkene oxidation is highly stereospecific (Table 1, entries 3 and 5), therefore, the %ee of the epoxide should be determined only by facial selectivity at the rate-limiting association of the C=C bond with the Ru=O group (Scheme 2).[9] We suspect that polar solvent may aggregate around the threitol units through dipole–dipole interaction thereby affecting the facial approach of the alkene.

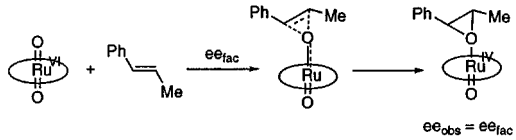

Scheme 2

In literature, *cis–trans* stereoselectivity in the metalloporphyrin-catalyzed alkene epoxidations is generally explained by the 'side-on approach'.[10] Yet, in this case, this model cannot account for the observed *trans* preference. Here, we propose a 'head-on approach' model in which the molecular plane of the C=C bond lies perpendicular to the Ru=O axis (Scheme 3). Since the *cis vs. trans* stereoselectivity should arise from the steric interaction between the incoming alkene and the porphyrin ligand, the 'head-on approach' of a *trans*-alkene molecule to oxo–metalloporphyrins can also be feasible according to previous studies.[11]

The asymmetric epoxidation of *trans*-β-methylstyrene can become catalytic using 2,6-dichloropyridine *N*-oxide (Cl_2pyNO) or O_2 as terminal oxidant. Similarly the catalytic *trans*-alkene oxidation is more enantioselective than that of the analogous *cis*-β-methylstyrene oxidation. For example, with Cl_2pyNO (0.146 mmol) as terminal oxidant and benzene as solvent, the *trans*-β-methylstyrene (1 mmol) oxidation furnished the *trans*-epoxide in 50% ee (70% yield, turnover = 70); whereas the oxidation of the *cis* analogue afforded the *cis*-epoxide in only 7% ee (70% yield, turnover = 66) under the same conditions. On the other hand, **1a** can also effect aerobic asymmetric *trans*-β-methylstyrene epoxidation in benzene (9 atm O_2, 40 h) to give the *trans*-epoxide in 59% ee (turnover = 7).

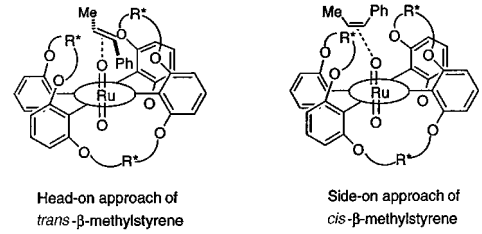

Scheme 3

We acknowledge support from The University of Hong Kong and The Hong Kong Research Grants Council, ERB003 and HKU7092/98P.

Notes and references

† Characterization data for the dioxoruthenium(VI) and bis(pyrazolato)-ruthenium(IV) porphyrin complexes: [$Ru^{VI}(L^{1*})O_2$ **1a**: ^{1}H NMR (300 MHz, $CDCl_3$): δ 8.65 (d, *J* 4.7 Hz, 4H), 8.55 (d, *J* 4.7 Hz, 4H), 7.77 (t, *J* 6.5 Hz, 4H), 7.22–7.38 (m, *m*-H overlapped with a solvent peak, 8H), 4.91 (d, *J* 10.4 Hz, 4H), 4.62 (d, *J* 9.0 Hz, 4H), 4.43 (t, *J* 9.0 Hz, 4H), 4.22 (d, *J* 10.1 Hz, 4H), 3.76 (d, *J* 9.0 Hz, 4H), 2.60 (t, *J* 8.5 Hz, 4H), 0.77 (s, 12H), −0.78 (s, 12H). UV–VIS (CH_2Cl_2) λ_{max}/nm (log ε/dm^3 mol^{-1} cm^{-1}): 442 (5.12), 536 (4.07). FABMS *m/z*: 1379 (M^+, 18%), 1363 (M^+, 18%), 1363 ($M^+ - O$, 30%), 1347 ($M^+ - 20$, 100%).

[$Ru^{VI}(L^{2*})O_2$] **1b**: ^{1}H NMR (300 MHz, $CDCl_3$): δ 8.64 (d, *J* 4.7 Hz, 4H), 8.53 (d, *J* 4.7 Hz, 4H), 7.74 (m, 4H), 7.37–7.30 (m, *m*-H overlapped with a solvent peak, 8H), 4.98 (d, *J* 10.4 Hz, 4H), 4.60 (d, *J* 8.8 Hz, 4H), 4.44 (t, *J* 8.9 Hz, 4H), 4.23 (d, *J* 10.4 Hz, 4H), 3.74 (d, *J* 8.8 Hz, 4H), 2.63 (t, *J* 8.7 Hz, 4H), 1.02 (m, 8H), 0.53 (t, *J* 7.2 Hz, 12H), −0.25 (m, 8H), −1.37 (t, *J* 7.3 Hz, 12H). UV–VIS (CH_2Cl_2): λ_{max}/nm (log ε/dm^3 mol^{-1} cm^{-1}) 443 (5.15), 534 (4.02). FABMS: *m/z* 1491 (M^+, 9%), 1475 ($M^+ - O$, 20%), 1459 ($M^+ - 2O$, 100%).

[$Ru^{VI}(L^{3*})O_2$] **1c**: ^{1}H NMR (300 MHz, $CDCl_3$): δ 8.67 (d, *J* 4.6 Hz, 4H), 8.56 (d, *J* 4.6 Hz, 4H), 7.76 (m, 4H), 7.20–7.37 (m, *m*-H overlapped with a solvent peak, 8H), 4.88 (d, *J* 9.3 Hz, 4H), 4.60 (d, *J* 9.4 Hz, 4H), 4.64 (t, *J* 9.0 Hz, 4H), 4.24 (d, *J* 10.1 Hz, 4H), 3.77 (d, *J* 8.6 Hz, 4H), 2.57 (t, *J* 8.6 Hz, 4H), 0.83 (m, 12H), 0.60 (m, 12H), 0.32 (m, 4H), −1.16 (m, 4H). UV–VIS (CH_2Cl_2) λ_{max}/nm (log ε/dm^3 mol cm^{-1}): 441 (5.03), 535(4.02). FABMS *m/z*: 1483 (M^+, 8%), 1467 ($M^+ - O$, 22%), 1451 ($M^+ - 2O$, 100%).

[$Ru^{IV}(L^{1*})(pz)_2$] **2a**: IR(KBr): 1006 cm^{-1} (oxidation state marker band). FABMS *m/z*: 1483 (M^+, 100%), 1415 ($M^+ -$ pz, 10%), 1347 ($M^+ - 2$ pz, 20%). Anal. Calc. for $C_{78}H_{76}N_8O_{19}Ru \cdot 3H_2O$: C, 60.89; H, 5.33; N, 7.28. Found: C, 60.77; H, 5.31; N, 7.25%. UV–VIS ($CHCl_3$) λ_{max}/nm (logε/dm^3 mol^{-1} cm^{-1}): 425 (5.09), 517 (4.04), 550 (sh).

1 E. N. Jacobsen, in *Comprehensive Organometallic Chemistry II*, ed. G. Wilkinson, F. G. A. Stone, E. W. Abel and L. S. Hegedus, Pergamon, New York, 1995, vol. 12, ch. 11.1; For chiral ruthenium complexes catalyzed asymmetric epoxidation of *trans*-alkenes, see: N. End and A. Pfaltz, *Chem. Commun.*, 1998, 589.
2 Z. Gross, S. Ini, M. Kapon and S. Cohen, *Tetrahedron Lett.*, 1996, **37**, 7325.
3 J. P. Collman, V. J. Lee, C. J. Kellen-Yuen, X. Zhang, J. A. Ibers and J. I. Brauman, *J. Am. Chem. Soc.*, 1995, **117**, 692.
4 C.-J. Liu, W.-Y. Yu, S.-M. Peng, T. C.-W. Mak and C.-M. Che, *J. Chem. Soc., Dalton Trans.*, 1998, 1805.
5 J. T. Groves, K. T. Ahn and R. Quinn, *J. Am. Chem. Soc.*, 1988, **110**, 4217.
6 The best reported ee is 83% for the oxidation of *trans*-β-methylstyrene using chiral Cr–salen catalysts, see: C. Bousquet and D. C. Gilheany, *Tetrahedron Lett.*, 1995, **36**, 7739.
7 T.-S. Lai, R. Zhang, K.-K. Cheung, H.-L. Kwong and C.-M. Che, *Chem. Commun.*, 1998, 1583; T.-S. Lai, H.-L. Kwong, R. Zhang and C.-M. Che, *J. Chem. Soc., Dalton Trans.*, 1998, 3559.
8 Z. Gross and S. Ini, *J. Org. Chem.*, 1997, **62**, 5514.
9 W. Zhang, N. H. Lee and E. N. Jacobson, *J. Am. Chem. Soc.*, 1994, **116**, 425; W.-H. Fung, W.-Y. Yu and C.-M. Che, *J. Org. Chem.*, 1998, **63**, 7715.
10 J. T. Groves and R. S. Myers, *J. Am. Chem. Soc.*, 1983, **105**, 5791.
11 D. Ostovic and T. C. Bruice, *Acc. Chem. Res.*, 1992, **25**, 314.

Communication 8/08776H

Synthesis of microporous zirconosilicates containing ZrO_6 octahedra and SiO_4 tetrahedra

Sudhakar R. Jale,* Adeola Ojo and Frank R. Fitch

BOC Gases, Technology, 100 Mountain Avenue, Murray Hill, NJ 07974, USA. E-mail: sudhakar.jale@us.gtc.boc.com

Received (in Bloomington, IN, USA) 6th November 1998, Accepted 22nd January 1999

Three novel crystalline zirconosilicate molecular sieves, analogous to elpidite, umbite and gaidonnayite minerals, containing zirconium in octahedral coordination and silicon in tetrahedral coordination are synthesized.

The isomorphous substitution of various metal ions into crystalline inorganic frameworks has been a very active area of research over the last two decades. By substituting metal ions with different oxidation states and electronegativities, it is possible to modify the acid strength and the ion-exchange capacities of zeolites.[1] Most of the isomorphous substitutions in zeolite frameworks involve the incorporation of the metal ions into tetrahedral positions. It has been shown that Ti,[2] Zr[3] and Sn[4] can form crystalline silicate materials,[5] where Si is in tetrahedral coordination and Ti, Zr or Sn is in octahedral coordination. Since these metal ions are in 4+ oxidation state and in octahedral coordination, this results in two negative charges on the framework for each of the metal ions incorporated.

In 1990, Chapman[6] reported two titanosilicate minerals (vinogradovite and zorite) containing Ti in octahedral coordination. Subsequently, Engelhard Corporation developed microporous titanium silicate molecular sieves, described as ETS-4[7] and ETS-10,[8] which contain silicon in tetrahedral coordination and titanium in octahedral coordination. Until now, only titanosilicates have been synthesized with large pore openings. Similarly to titanium, zirconium also forms a variety of silicate minerals having zirconium in octahedral coordination. Until now, zirconosilicate minerals have been synthesized at temperatures between 300 and 700 °C and pressures of up to 700 bar.[9]

Here, for the first time, we report the synthesis of gaidonnayite and umbite zirconosilicate minerals. We have also been able to synthesize elpidite at 200 °C under autogeneous pressure. The synthesis of zirconosilicates has been carried out using sodium silicate, zirconyl chloride, potassium fluoride, sodium hydroxide, potassium hydroxide, hydrochloric acid and tetramethylammonium bromide using the gel compositions reported in Table 1. All these chemicals were obtained from Aldrich. The syntheses were carried out hydrothermally at 200 °C under static conditions. After the specified crystallization time, the product was filtered off, washed with deionized water and dried at room temperature.

The XRD patterns of all three zirconosilicates shown in Fig. 1 match well with mineral counterparts. Umbite and gaidonnayite belong to $P2_12_12_1$ and $P2_1nb$ space groups, respectively[11,12] and all three minerals have an orthorhombic unit cell. The samples calcined at 400 °C have XRD patterns identical to those of as-synthesized materials, indicating a good thermal stability. Thermogravimetric analysis of calcined and rehydrated elpidite and umbite samples showed 7 and 11 wt% loss, respectively between 35 and 300 °C. The BET surface area of zirconosilicates measured at liquid nitrogen temperature was negligible, showing that the pore size is less than the kinetic diameter of the nitrogen molecule. However, based on the structural data and the water adsorption measurements (type I isotherm), they can be classified as microporous materials. Recently, the titanium analogue of umbite also has been shown to adsorb water but not nitrogen.[10]

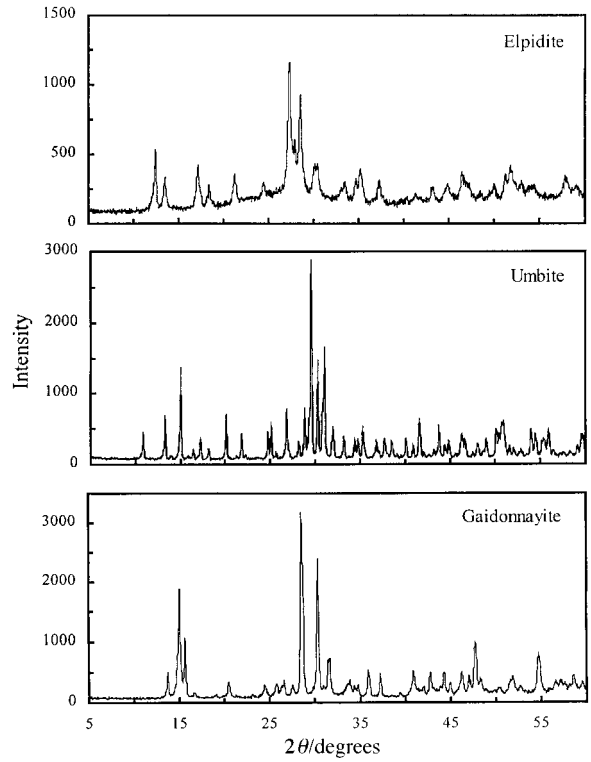

Fig. 1 The XRD patterns of zirconosilicates analogous to elpidite, gaidonnayite and umbite minerals.

Chemical analysis data of well crystalline, pure forms of zirconosilicates are summarized in Table 2. The Si/Zr ratios of elpidite, umbite and gaidonnayite are 5.1, 4.3 and 3.0, respectively. The chemical formulas of umbite[11]

Table 1 Gel composition and crystallization times in the synthesis of zirconosilicates

Compound	SiO_2	ZrO_2	K_2O	Na_2O	R_2O^a	HCl	KF	H_2O	*t*/d
Elpidite	1.0	0.17	0.10	—	—	1.59	0.33	29.8	35
Gaidonnayite	1.0	0.20	0.25	1.17	0.20	0.40	0.50	35.0	19
Umbite	1.0	0.10	0.27	0.52	—	0.20	0.53	30.8	32
Umbite	1.0	0.10	1.19	0.23	0.3	0.20	0.50	36.8	2

[a] R = Tetramethylammonium bromide.

Table 2 Chemical analysis of zirconosilicates

Compound	LOI[a] (wt%)	Si/Zr	Si/Al	Si/ (Al + Zr)	Na + K)/ (2Zr + Al)
Elpidite	10.7	5.07	59.78	4.67	0.78
Umbite	10.2	4.25	90.34	4.06	1.20
Gaidonnayite	10.3	3.06	60.52	3.06	1.02

[a] LOI = loss of ignition.

($K_2ZrSi_3O_9·H_2O$), elpidite[9] ($Na_2ZrSi_6O_{15}·3H_2O$) and gaidonnayite[12] ($K_2ZrSi_3O_9·2H_2O$) are reported in the literature. The calculated chemical formulas of umbite ($M_{2.4}ZrSi_4O_{11}$), elpidite ($M_{1.6}ZrSi_5O_{13}$) and gaidonnayite ($M_2ZrSi_3O_9$) materials synthesized in this study are slightly different from those reported in the literature.

Owing to an aluminium impurity in the source materials, there is always some aluminium in these materials. If both Al and Zr are in the framework, this ratio should be 1.0. A deviation from this value indicates that either there is an excess of alkali metal ion (possibly due to the presence of defects) or a part of these metals are not substituted into the framework. The lower ratio for elpidite is most probably due to the presence of some amorphous material.

The ion-exchange capacity of umbite was tested by refluxing in 0.5 M NaCl solution. The original sample contains 29% Na and 71% K, while the Na-exchanged sample had 81% Na and 21% K cations adding up to a (Na + K)/(2Zr + Al) ratio of 1.02. Since zirconium has two negative charges, two cations are required to balance the charge. The Si/Zr and Si/Al ratios of this sample were 3.6 and 76.6, respectively. These results confirm that at least 80% of the cations are exchangeable and most of the Zr and Al are present in the framework. Upon ignition, umbite lost about 13% of its weight as water, which is close to the value obtained by TGA.

The hydroxide concentration in the gel influences the rate of hydrolysis of the metal ions and also the rate at which the condensation of these species into the framework structures takes place. In general, an increase in the hydroxide concentration decreases the nucleation time and accelerates the crystal growth. As can be seen in Table 1, by increasing the hydroxide concentration and also by partially replacing sodium by potassium, the crystallization time of umbite was reduced from 38 to 2 days. We have been able to synthesize at least three more zirconosilicates by changing the OH^- ion concentration. However, the structures of these materials are not yet identified.

In conclusion, we have demonstrated the synthesis of microporous zirconosilicates analogous to minerals under hydrothermal conditions at temperatures significantly lower than those used previously in the literature. These zirconosilicates might be useful adsorbents for kinetic separation of smaller gaseous molecules such as water from a mixture with other components.

Notes and references

1 R. Szostak in *Molecular Sieves*, Blackie Academic and Professional, New York, 1998, p. 208.
2 P. A. Sandomirskii and N. V. Belov, *Sov. Phys. Crystallogr.*, 1979, **24**, 686.
3 S. Ghose, C. Wan and C. Y. Chao, *Can. Mineral.*, 1980, **18**, 503.
4 F. Liebau, in *Structural Chemistry of Silicates*, Springer-Verlag, Berlin, 1985.
5 J. L. Guth, in *Zeolite Microporous Solids: Synthesis, Structure and Reactivity*, ed. E. G. Derouane, F. Lemos, C. Naccache and F. R. Ribeiro, Kluwer Academic Publishers, Dordrecht, 1992, p. 49.
6 D. M. Chapman, *Zeolites*, 1990, **10**, 730.
7 S. M. Kuznicki, *US Pat.*, 4 853 202, 1989.
8 S. M. Kuznicki, *US Pat.*, 4 938 939, 1990.
9 G. Baussy, R. Caruba, A. Baumer and G. Turco, *Bull. Soc. Fr. Minéral. Cristallogr.*, 1974, **97**, 433.
10 Z. Lin, J. Rocha, P. Brandão, A. Ferreira, A. Esculcas, J. D. Pedrosa de Jesus, A. Philippou and M. Anderson, *J. Phys. Chem. B*, 1997, **101**, 7114.
11 G. D. Ilyushin, *Inorg. Mater.*, 1993, **29**, 971.
12 A. Roberts and M. Bonardi, *Geol. Surv. Can.*, 1983, **83**–**1**, 480.

Communication 8/08709A

Side-chain alkylation of toluene with propene on caesium/nanoporous carbon catalysts

Mark G. Stevens, Melony R. Anderson and Henry C. Foley*

Center for Catalytic Sciences and Technology, Department of Chemical Engineering, University of Delaware, Colburn Laboratory, Academy Street, Newark, Delaware 19716, USA. E-mail: foley@che.udel.edu

Received (in Bloomington, IN, USA) 13th November 1998, Accepted 11th January 1999

Caesium/nanoporous carbon materials are powerful solid-base catalysts, promoting the side-chain alkylation of toluene with propene in a continuous flow reactor at conditions as mild as 150 °C and 50 psig.

When a strong base, such as Na metal, is employed as a catalyst, alkylation occurs at the benzylic hydrogen of the side chain. During the later 1950s, many researchers[1–5] explored this chemistry, most notably, Pines *et al.*[1,2,4] Recently, there has been much interest in examining novel solid-base catalysts for larger scale reactions such as side-chain alkylation of toluene with methanol[6–9] and olefins.[10,11] To date, however, there are no industrial processes that take advantage of this chemistry to produce alkylbenzenes from lower-cost toluene.[12] As early as 1964 Foster[10] had shown that graphite intercalation compounds of alkali metals readily promoted the side-chain alkylation of toluene with ethylene, but reaction was slow, required high pressure and it was not clear if the alkali metal had remained intercalated in the graphite.

In contrast to the graphite intercalation compounds of alkali metals, which exfoliate readily,[13] we have shown that Cs entrapped in nanoporous carbon is well dispersed and very strongly bound.[14] Preparing nanoporous carbon (NPC) with macropores provides for facile molecular ingress and egress to the catalytic sites.[15]

We have shown that Cs/NPC is active enough to break the C–H bond in benzene (110 kcal mol^{-1}) and to promote its condensation to biphenyl.[16] Given this result, we expected the catalyst to remove the more facile benzylic hydrogen from toluene readily, and if an olefin such as propene were present, to produce *n*-butylbenzene and isobutylbenzene. At the same time in the case of propene, cyclization and release of dihydrogen could lead to the dicyclic products 1-methylindan, 1,2,3,4-tetrahydronaphthalene and 2-methylindan.

Batch, liquid phase reactions† of toluene and propene over this nanoporous carbon catalyst containing *ca.* 10 wt% Cs produced *n*-butylbenzene, isobutylbenzene and 2-methylindan. Table 1 displays the results of several experiments carried out at 150 °C and at various conversions. The major product was isobutylbenzene. Propene was the limiting reactant in all these experiments. Once the propene was consumed, secondary reactions began to become important. As was the case in the reaction of benzene over Cs/NPC,[16] aromatic-ring coupling produced species such as bibenzyl, dimethylbiphenyls, and methyldiphenylmethanes. Additionally, cyclization of isobutylbenzene produced 2-methylindan. If 1-methylindan and 1,2,3,4-tetrahydronaphthalene were produced, they remained below our detection limits. Both side reactions should produce H_2 and GC measurements of the vapor phase over the products confirmed that H_2 indeed had been produced. Control experiments using carbon without C_2 produced no detectable reaction. At higher conversions, the catalyst achieved over nine turnovers based on the total moles of Cs, a lower limit value that confirms the catalytic nature of the reaction.

In a second set of experiments, to avoid the possible complication of Cs leaching into the liquid phase, toluene was converted to butylbenzenes in the vapor phase using a tubular flow reactor. A mixture of toluene in propene (5 mol %) was circulated over the catalyst at temperatures from 150–400 °C and 4 bar,‡ (Fig. 1, Table 2). The increase in the availability of propene reduced the toluene coupling to an undetectable level. Propene coupling, however, did occur with the excess propene in the system to form C_6 compounds such as 4-methylpentene, cyclohexane, hex-1-ene and dimethylbutenes. Above 150 °C, *ca.* 10% of the propene that reacted went to the C_6 products, indicating the potential utility of Cs/NPC as a catalyst for producing higher-molecular-weight olefin monomers. This propene coupling may also account for the decrease in activity at > 250 °C. At 350 and 400 °C the catalysts gained mass (3.6 and 6.0% of their initial mass, respectively). This suggests that deactivation arose due to the formation of propene oligomers in the pores, resulting in a loss of diffusive transport to the catalytically active sites. The sample of catalyst used at 400 °C not only gained mass, but also was coated with a hexane-soluble, waxy film.

We find that Cs/NPC yields high iso/normal butylbenzene ratios (≥10). This indicates that the predominant mechanism proceeds *via* surface anions and through the formation of the benzyl anion from the toluene substrate. Pines and Stalick[17]

Table 1 Results of batch study[a]

Conversion (%)		Toluene selectivity (%)				
Toluene	Propylene	Coupled	Isobutyl	*n*-Butyl	Indan	Turn-over
0.03	0.40	0.00	100.00	0.00	0.00	0.039
0.12	1.41	0.00	82.99	0.00	17.01	0.137
1.03	18.84	0.44	70.44	9.17	19.94	2.367
1.06	18.35	0.55	72.47	9.83	17.14	2.452
3.49	38.19	1.29	70.23	13.76	14.72	3.934
6.82	≈100.00	2.49	71.66	13.16	12.69	10.657
7.12	≈100.00	3.19	73.11	11.95	11.75	9.274

[a] Conversion of toluene and propylene and selectivity were calculated from GC of the liquid phase. Turnovers were calculated by titrating the used catalyst for Cs content with H_2SO_4. All products were identified by GCMS.

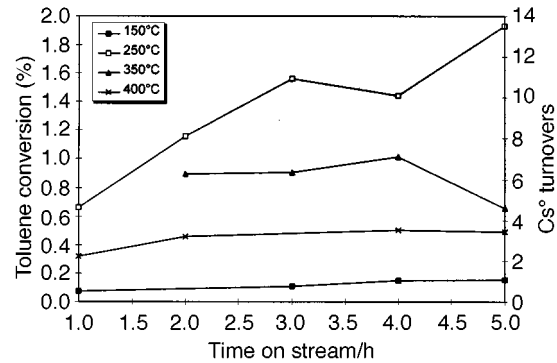

Fig. 1 Vapor-phase conversion and catalyst turnovers *versus* time on stream at 4 bar gas pressure (5% toluene in propylene) and temperature. Conversion of toluene, was calculated from GC of the liquid phase. Turnovers were calculated by titrating the used catalyst for Cs content with H_2SO_4.

Table 2 Results of gas-phase, continuous experiments[a]

		Toluene selectivity (%)				
T/°C	Propene selectivity	Isobutyl-benzene	*n*-Butyl-benzene	Methyl-indan	Tetra-hydro-naph-thalene	Catalyst weight gain (%)
150	100.0	94.7	2.6	2.7	0.0	< 0.1
250	89.4	72.3	8.2	15.8	3.6	< 0.1
350	93.0	79.8	7.6	10.7	1.9	3.6
400	93.5	85.5	9.6	5.0	0.0	6.0

[a] Propylene selectivity to alkylation products was calculated by comparing the amount of propylene converted to C_6 byproducts to the toluene conversion. Conversion and selectivity of toluene, were calculated from GC measurements of the liquid phase. Products identified by GCMS.

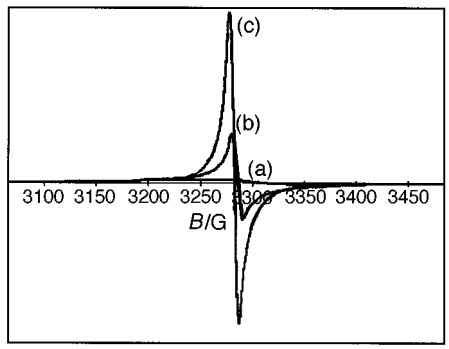

Fig. 2 EPR differential plot of: (a), carbon precursor; (b), carbon loaded with 30% Cs; (c), carbon loaded with 3% Cs.

have shown that a large normal to iso ratio is the best indicator of an anionic rather than free-radical mechanism.

That the chemistry over Cs/NPC should proceed through anions rather than radicals makes good sense based on characterization of the Cs/NPC by EPR spectroscopy. Our EPR measurements (Fig. 2) show the existence of such radical anions, and the measured g-value of 2.0026[16] indicates that the unpaired electrons are transferred from the Cs to the carbon. The EPR spectra also show that more unpaired electrons are present at low Cs levels (3 wt%) than at high loadings (30 wt%). Previously, we found that the electronic character of the material goes from strongly paramagnetic to weakly paramagnetic and diamagnetic with increased Cs content.[14] This transformation arises from spin pairing within the polyaromatic nanodomains as additional electrons are added. Based on these results, at the intermediate Cs loadings (10 wt%) used for the catalysts examined here, the material should behave as much, or more, like a Lewis base than as a radical. We conclude that radical anions, represented as $Cs_n/NPC^{n-y\cdot S}$ where $y = [1 + (-1)^{n+1}]/2$, and the corresponding spin-paired multiply charged anions (formed by addition or removal of one electron) catalyze this reaction and drive the chemistry toward isobutylbenzene formation. The same intermediate anions which produce isobutylbenzene also can react intramolecularly to form the corresponding bicyclic compounds and also through an anion mechanism.

In conclusion, we have shown the Cs/NPC materials to be powerful Lewis bases which promote the side-chain alkylation of toluene at unprecedentedly mild conditions.

This work was supported by the Department of Energy, Office of Basic Energy Sciences; the Delaware Research Partnership; and the E. I. duPont deNemours and Co., Inc.

Notes and references

† Batch reactions were performed in a stainless-steel, 'tubing-bomb' reactor (2.54 cm. o.d., 1.77 cm i.d. 15 cm long, capped with a valve assembly, total internal volume: 15 cm). Catalyst and toluene were loaded in an argon-atmosphere glove box. The reactor was sealed with a titanium gasket, removed from the glove box, charged with propene and placed in a fluidized sand bath maintained at the reaction temperature.

‡ A recirculating vaporizer/condenser reactor was constructed for the experiments. Propene (maintained at 4 bar with live feed) cycled through the system at 1500 sccm in the following order: bubbled through a temperature controlled (298 K) vessel containing 100 ml of toluene; the toluene rich (5 mol%) propene passed through a flow controller, a diaphragm pump and to the catalyst bed; the stream was heated to reaction temperature and flowed through the catalyst bed (1.5 g of catalyst containing 10 wt%/Cs 0.025 s/pass contact time); the reacted stream then returned to the bottom of the toluene vessel to repeat the cycle.

1 H. Pines and V. Mark, *J. Am. Chem. Soc.*, 1956, **78**, 4316.
2 L. Schaap and H. Pines, *J. Am. Chem. Soc.*, 1957, **79**, 4967.
3 S. E. Voltz, *J. Org. Chem.*, 1957, **22**, 48.
4 H. Pines and D. Wunderlich, *J. Am. Chem. Soc.*, 1958, **80**, 6001.
5 R. M. Schramm and G. E. Langlois, *J. Am. Chem. Soc.*, 1960, **82**, 4912.
6 P. Tundo, *Continuous Flow Methods in Organic Synthesis*, Ellis Horwood Ltd, Chichester, UK, 1991.
7 M. L. Unland and G. E. Baker *US Pat.* 4 140,726, 1979.
8 L. Huei-Cheng, *US Pat.* 4 463 204 1984.
9 L. H. Slaugh and T. F. Brownscombe, *US Pat.* 5 015 796 1991.
10 W. E. Foster, *US Pat.* 3 160 670, 1964.
11 *US Pat.* 3 316 315.
12 K. Othmer, *Encyclopedia of Chemical Technology*, Wiley, New York, 4th edn., 1995, vol. 2, p. 94.
13 F. J. Salzano and S. Aronson, *J. Chem. Phys.*, 1966, **45**, 6.
14 M. G. Stevens and H. C. Foley, *Chem. Commun.*, 1997, 519.
15 H. C. Foley, *Microporous Mater.*, 1995, **4**, 407.
16 M. G. Stevens, K. M. Sellers, S. Subramoney and H. C. Foley, *Chem. Commun.*, 1998, 2679.
17 H. C. Pines and W. M. Stalick, *Base-catalyzed Reactions of Hydrocarbons and Related Compounds*, Academic Press, New York, 1997.

Communication 8/08948E

ChemComm

Palladium-catalysed asymmetric allylic alkylation using new chiral phosphinite–nitrogen ligands derived from D-glucosamine

Koji Yonehara, Tomohiro Hashizume, Kenji Mori, Kouichi Ohe* and Sakae Uemura*

Department of Energy and Hydrocarbon Chemistry, Graduate School of Engineering, Kyoto University, Sakyo-ku, Kyoto 606-8501, Japan. E-mail: uemura@scl.kyoto-u.ac.jp

Received (in Cambridge, UK) 24th December 1998, Accepted 25th January 1999

Novel phosphinite–nitrogen chiral ligands synthesized from D-glucosamine furnish a high level of enantiomeric excess (up to 96% ee) in palladium-catalysed allylic alkylation.

Palladium-catalysed allylic alkylation is known as a powerful synthetic tool for the construction of carbon–carbon bonds.[1] Enantioselective versions of the reaction have been explored and large enantiomeric excesses have been achieved using various C_2- and C_1-symmetric bidentate chiral ligands.[2] While they are excellent ligands, expensive chiral sources and tedious synthetic steps are sometimes needed for their synthesis. Recently carbohydrates have attracted a great deal of interest as a source of chiral ligands, because they exist widely in nature and have many chiral centres in their skeletons.[3,4] Now, we report the synthesis of novel phosphinite–nitrogen chiral ligands from commercial D-glucosamine hydrochloride (2-amino-2-deoxy-D-glucopyranoside hydrochloride), which have been less frequently used as chiral ligands,[4,5] and their application to the Pd-catalysed allylic alkylation.

First, we prepared compound **1** according to the procedures illustrated in Scheme 1. *N*-Acylation of D-glucosamine hydrochloride with $(Pr^iCO)_2O$ and NaOMe, and the protection of both 4,6- and 1,3-positions by benzylidene and acetyl groups gave D-glucopyranoside **2** in good yield. This compound could be readily converted into oxazoline derivative **3** using $SnCl_4$ without removing the benzylidene protecting group.[6] Deacetylation of the 3-position followed by treatment with Ph_2PCl and Et_3N gave phosphinite–nitrogen chiral ligand **1**. This ligand was easily oxidized by air in solution, but was relatively stable in the solid state.

Asymmetric allylic substitution of 1,3-diphenyl-3-acetoxyprop-1-ene with dimethyl malonate in the presence of *N*,*O*-bis(trimethylsilyl)acetamide (BSA) and KOAc was carried out with the palladium complex generated *in situ* by mixing chiral ligand **1** and $[Pd(\eta^3\text{-}C_3H_5)Cl]_2$. The results are summarized in Table 1. In the presence of only 0.25 mol% Pd complex, the reaction proceeded very smoothly with high enantioselectivity. The best result was obtained when the reaction was carried out in toluene at 0 °C (entries 1–5).

Next, we synthesized phosphinite–nitrogen ligands **5**–**9**† by the procedure described in Scheme 1 using anhydrides or acid chlorides such as BnCOCl, $(Bu^tCO)_2O$, PhCOCl, $(Bu^iCO)_2O$ and Ac_2O, and applied them to the palladium-catalysed asymmetric allylic alkylation under the previously determined optimum conditions (entries 6–10).‡ As can be seen in Table 1, a dramatic substituent effect on the enantiomeric excess was observed. The use of the ligand **5** (R = Bn) or **6** (R = Bu^t) (entries 6 and 7) gave lower enantioselectivities compared with the case of ligand **1**. On the contrary, the use of the ligand **7** (R = Ph) or **8** (R = Bu^i) increased the selectivity (entries 8 and 9). Furthermore, it was noted that the highest enantiomeric excess (96% ee) was achieved using ligand **9** (R = Me) (entry 10).

We suppose that nucleophilic attack occurs predominantly at the allyl terminus *trans* to the Pd–P bond in the π-allylpalladium complex.[8] Since the (*S*)-product was obtained as the major enantiomer, the reaction probably proceeds through *endo* intermediate **A** rather than *exo* intermediate **B**, as shown in

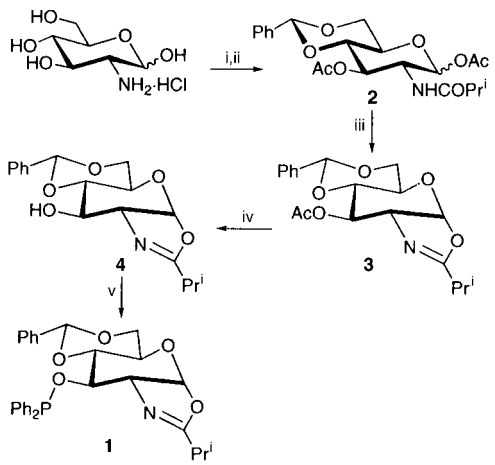

Scheme 1 *Reagents and conditions*: i, $(Pr^iCO)_2O$, MeONa, MeOH, room temp., 24 h, 82%; ii, PhCHO, $ZnCl_2$, room temp., 5 h, then Ac_2O, pyridine, room temp., 24 h, 43% (2 steps); iii, $SnCl_4$, CH_2Cl_2, room temp., 1 h, 52%; iv, K_2CO_3, MeOH, room temp., 1 h, 73%; v, Ph_2PCl, Et_3N–THF (1 : 1), cat. DMAP, room temp., 15 min, 46%.

Table 1 Palladium-catalysed asymmetric allylic alkylation with chiral ligands **1** and **5**–**9**[a]

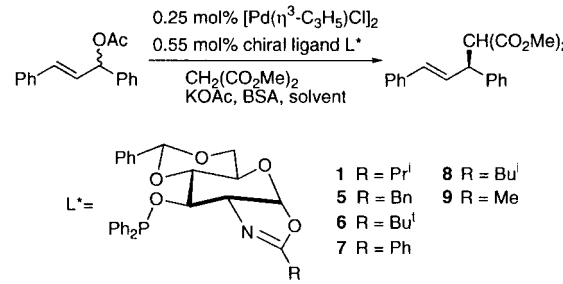

Entry	L*	Solvent	*T*/°C	*t*/h	Ee (%)[b]
1	**1**	CH_2Cl_2	room temp.	1	85 (*S*)
2	**1**	THF	room temp.	0.5	86 (*S*)
3	**1**	toluene	room temp.	1	88 (*S*)
4	**1**	toluene	60	0.5	84 (*S*)
5	**1**	toluene	0	6	90 (*S*)
6	**5**	toluene	0	18	78 (*S*)
7	**6**	toluene	0	6	83 (*S*)
8	**7**	toluene	0	6	94 (*S*)
9	**8**	toluene	0	6	95 (*S*)
10	**9**	toluene	0	6	96 (*S*)

[a] The reaction was carried out under Ar using 1,3-diphenyl-3-acetoxyprop-1-ene (1.0 mmol), dimethyl malonate (3.0 mmol), BSA (3.0 mmol), KOAc (0.05 mmol), solvent (2.0 ml), $[Pd(\eta^3\text{-}C_3H_5)Cl]_2$ (0.25 mol%) and L* (0.55 mol%). Product was isolated in quantitative yield. [b] Measured by HPLC; the absolute configuration was determined by optical rotation (ref. 7).

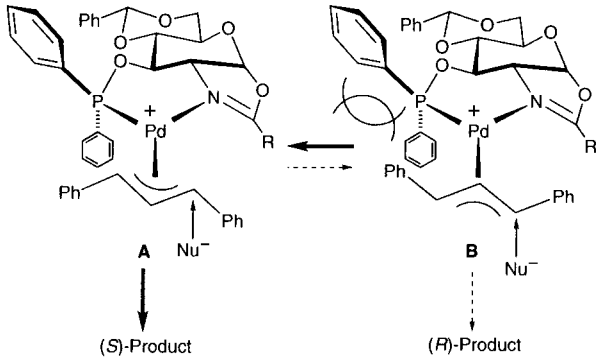

Scheme 2

Scheme 2. In the transition state, the steric repulsion in **A** between the phenyl group on phosphorous and the substrate appears smaller than that in **B**.

In summary, we have demonstrated that the novel chiral ligands **1** and **5**–**9** are very efficient ligands for asymmetric allylic alkylation, using only 0.25 mol% Pd complex to provide a high enantioselectivity (up to 96% ee). These ligands can be prepared in six steps using commercial D-glucosamine hydrochloride as an inexpensive natural chiral source. They are a new type of P–N ligands using only the chirality of D-glucosamine, which is communicated to the coordination sphere built with both phosphorous and nitrogen. To the best of our knowledge, this is the first example of the application of phosphinite–nitrogen chiral ligands[9] to asymmetric allylic alkylation. Application of these ligands to other asymmetric reactions is now in progress.

Notes and references

† *Selected data* for **9**; δ_H 2.05 (d, *J* 1.1, 3H), 3.61–3.69 (m, 2H), 3.76 (t, *J* 8.5, 1H), 4.23–4.32 (m, 2H), 4.36 (dd, *J* 3.3, 8.5, 1H), 5.35 (s, 1H), 5.98 (d, *J* 7.4, 1H), 7.23–7.53 (m, 15H); δ_C 14.3, 62.9, 68.6, 69.4 (d, *J* 5.2), 79.6 (d, *J* 3.6), 82.3 (d, *J* 20.2), 101.2, 102.2, 126.0–136.9 (16 C), 141.9 (d, *J* 21.3), 142.2 (d, *J* 16.4), 165.0; δ_P 114.5; $[\alpha]_D^{20}$ −75.7 (*c* 0.25, $CHCl_3$).

‡ Procedure for the Pd-catalysed enantioselective allylic alkylation: To a stirring solution of $[Pd(\eta^3\text{-}C_3H_5)Cl]_2$ (0.91 mg, 2.5×10^{-3} mmol) in toluene was added ligand **9** (2.62 mg, 5.5×10^{-3} mmol) under Ar atmosphere. After 30 min, racemic 1,3-diphenyl-3-acetoxyprop-1-ene (0.25 g, 1.0 mmol) was added and the solution was stirred for 30 min. *N*,*O*-Bis(trimethylsilyl)acetamide (0.74 ml, 3.0 mmol), dimethyl malonate (0.35 ml, 3.0 mmol) and KOAc (4.8 mg, 0.05 mmol) were then added at 0 °C and the solution was stirred at this temperature. After the reaction was completed (6 h), the solvent was evaporated *in vacuo* and column chromatography on silica gel (hexane–EtOAc 5 : 1) of the residue yielded the pure product. The enantiomeric excess was determined to be 96% ee by HPLC (Daicel Chiralcel AD column, 1.0 ml min^{-1}, hexane–Pr^iOH 95 : 5).

1 J. Tsuji, *Palladium Reagents and Catalysis, Innovations in Organic Synthesis*, Wiley, New York, 1995.
2 For an overview see: B. M. Trost and D. L. Van Vranken, *Chem. Rev.*, 1996, **96**, 395.
3 N. Nomura, Y. C. Mermet-Bouvier and T. V. RajanBabu, *Synlett*, 1996, 745; P. Barbano, A. Currao, J. Herrmann, R. Nesper, P. S. Pregosin and R. Salzmann, *Organometallics*, 1996, **15**, 1879; A. Albinati, P. S. Pregosin and K. Wick, *Organometallics*, 1996, **15**, 2419; K. Boog-Wick, P. S. Pregosin and G. Trabesinger, *Organometallics*, 1998, **17**, 3254; K. Boog-Wick, P. S. Pregosin, M. Wörle and A. Albinati, *Helv. Chim. Acta*, 1998, **81**, 1622.
4 B. Gläser and H. Kunz, *Synlett*, 1998, 53.
5 T. V. RajanBabu, T. A. Ayers, G. A. Halliday, K. K. You and J. C. Calabrese, *J. Org. Chem.*, 1997, **62**, 6012.
6 V. K. Srivastava, *Carbohydr. Res.*, 1982, **103**, 286.
7 J. Sprinz and G. Helmchen, *Tetrahedron Lett.*, 1993, **34**, 1769.
8 The phosphorous atom is a better π-acceptor than the nitrogen atom in π-allyl–palladium complexes bearing a P–N bidentate ligand. For examples, see: B. Åkermark, B. Krakenberger, S. Hansson and A. Vitagliano, *Organometallics*, 1987, **6**, 620; P. E. Blöchl and A. Togni, *Organometallics*, 1996, **15**, 4125; E. Peña-Cabrera, P.-O. Norrby, M. Sjögren, A. Vitagliano, V. De Felice, J. Oslob, S. Ishii, D. O'Neill, B. Åkermark and P. Helquist, *J. Am. Chem. Soc.*, 1996, **118**, 4299; H. Steinhagen, M. Reggelin and G. Helmchen, *Angew. Chem., Int. Ed. Engl.*, 1997, **36**, 2108.
9 Some imino-phosphinite ligands and their application to other asymmetric reactions have been reported: C. G. Arena, F. Nicolo, D. Drommi, G. Brunò and F. Faraone, *J. Chem. Soc., Chem. Commun.*, 1994, 2251; R. Sablong, C. Newton, P. Dierkes and J. A. Osborn, *Tetrahedron Lett.*, 1996, **37**, 4933; R. Sablong and J. A. Osborn, *Tetrahedron Lett.*, 1996, **37**, 4937.

Communication 8/10041A

Thermally stable coordinatively unsaturated alkyl complexes resistant to β-hydride elimination: $Tp^{iPr}M–CH_2CH_3$ (M = Co, Fe)

Nobuhiko Shirasawa, Munetaka Akita,* Shiro Hikichi and Yoshihiko Moro-oka*

Research Laboratory of Resources Utilization, Tokyo Institute of Technology, 4259 Nagatsuta, Midori-ku, Yokohama 226-8503, Japan. E-mail: makita@res.titech.ac.jp

Received (in Cambridge, UK) 3rd December 1998, Accepted 27th January 1999

Coordinatively unsaturated hydrocarbyl complexes bearing β-hydrogen atoms, $Tp^{iPr}M–CH_2CH_3$ [M = Fe, Co; Tp^{iPr} = hydrotris(3,5-diisopropylpyrazolyl)borate], 14e and 15e species, respectively, are prepared; they are resistant to β-hydride elimination.

'18-Electron (EAN) rule' and 'β-hydride elimination' are usually key principles in predicting stability of organometallic compounds.[1] In a previous paper, we reported a complex which does not obey the 18e rule: the coordinatively unsaturated 14e η^1-allyliron complex supported by the Tp^{iPr} ligand [Tp^{iPr} = hydrotris(3,5-diisopropylpyrazolyl)borate], $Tp^{iPr}Fe–CH_2$-$CH{=}CH_2$.[2] Although η^3 (π)-coordination of the allyl ligand would give a 16e species, closer to the coordinatively saturated 18e configuration, X-ray crystallography of the allyliron complex revealed that the η^1 (σ)-coordination of the allyl ligand to the iron center led to the highly coordinatively unsaturated 14e species. Our communication was followed by a recent report by Parkin *et al.*, who disclosed the synthesis and unusual reactivity of the related methyliron complex, [$PhTp^{Bu^t}$]Fe–Me [$PhTp^{Bu^t}$ = PhB (3-Bu^t-pz)$_3$, pz = pyrazolyl],[3] and thus the study on the coordinatively unsaturated hydrocarbyl complexes of late transition metals has attracted increasing attention.[4] During the course of our study, we have succeeded in the synthesis and characterization of coordinatively unsaturated alkyl complexes resistant to β-hydride elimination.

Reaction of the Fe and Co chloride complexes **1** with ethylmagnesium bromide in THF afforded pale yellow (**2a**) and blue products (**2b**), respectively, after removal of the inorganic salts by filtration through a Celite pad followed by crystallization from pentane [eqn. (1)]. X-Ray crystallography of the Co

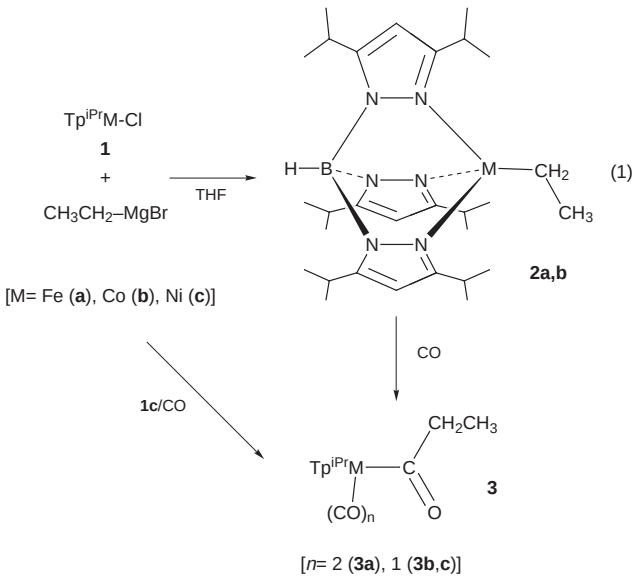

complex **2b** [Fig. 1(a)]† revealed the formation of the ethyl complex with tetrahedral coordination geometry as judged by the similar N–Co distances and N–Co–CH_2 angles [Co1–N11 2.049(6), Co1–N21 2.017(7), Co1–N31 2.025(7) Å; N11–Co1–C1 123.1(3), N21–Co1–C1 125.2(3), N31–Co1–C1 124.5(3)°]. The Co–CH_2 distance [Co1–C1 2.01(1) Å] falls in the accepted range of the Co–C σ-bond lengths. The structural parameters are comparable to those of the allyliron complex mentioned above.[2] The iron complex **2a** was also assigned to $Tp^{iPr}Fe–CH_2CH_3$ with tetrahedral structure, on the basis of its cell parameters† similar to those of **2b**, but could not be refined satisfactorily due to the low quality of the crystals. In contrast to the Co and Fe complexes, the reaction of the Ni complex **1c** afforded an intractable mixture of products from which no characterizable product could be isolated.

In order to further confirm the presence of a M–C bond in **2**, the ethyl complexes **2a**,**b** were subjected to carbonylation. Stirring a toluene solution of **2a**,**b** for 1 h under CO atmosphere (1 atm) produced **3a**,**b**, respectively. Their IR spectra containing

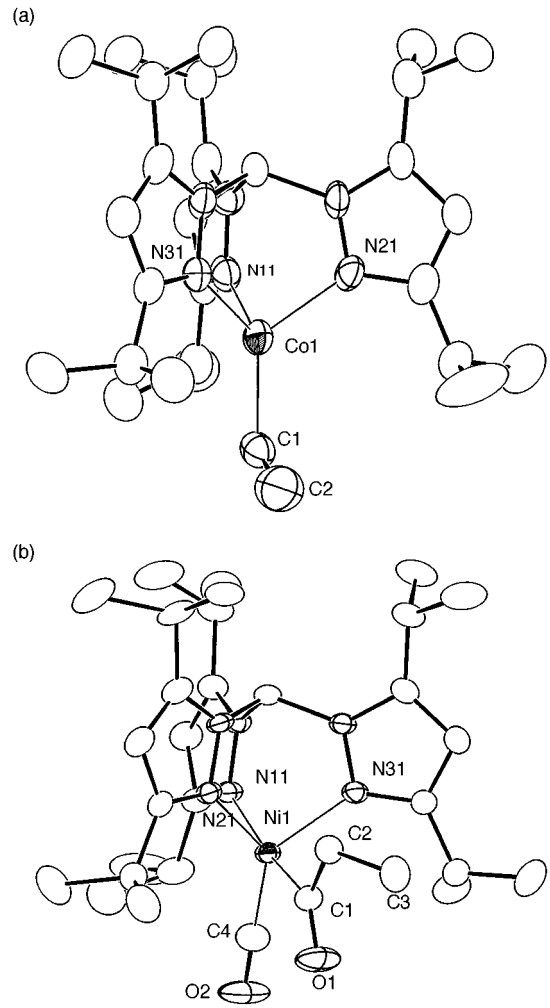

Fig. 1 Molecular structures of **2b** (a) and **3c** (b) drawn at the 30% probability level.

ν(CO) and ν(C=O) vibrations suggest formation of acyl complexes.‡ The diamagnetic iron complex **3a** was characterized on the basis of its ^{1}H and ^{13}C NMR spectra indicating the $(CO)_2Fe–C(=O)CH_2CH_3$ functional group in addition to the κ^3-Tp^{iPr} ligand, and its IR spectrum suggests the presence of two rotamers as observed for $TpFe(CO)_2–C(=O)CH_3$.[5] The assignment of the monocarbonyl structure of the cobalt complex **3b** is based on the single ν(CO) absorption. Interestingly, although the ethylnickel complex **2c** could not be isolated from the Grignard reaction mentioned above, the reaction under CO atmosphere produced the acyl complex **3c**, which was characterized spectroscopically and structurally [Fig. 1(b)].† The Ni center adopts a trigonal bipyramidal structure with the N11–Ni1–C1 axis, where the κ^3-Tp^{iPr} ligand occupies the two basal and one apical coordination sites and the acyl and CO ligands occupy the remaining apical and coordination sites, respectively, as judged by the interligand angles [N11–Ni1–C1 171.7(1) ($\approx$180°); N21–Ni1–C1 89.8(2), N31–Ni1–C1 87.7(1), C1–Ni1–C4 87.2(2), N11–Ni1–N21 85.1(1), N11–Ni1–N31 86.6(1), N11–Ni1–C4 101.1(2)° ($\approx$90°); N21–Ni1–N31 98.9(1), N21–Ni1–C4 131.0(2), N31–Ni1–C4 129.8(2)° ($\approx$120°)]. In accord with this view, the axial N–Ni distance is slightly longer than the equatorial ones [Ni1–N11 2.058(3) Å > Ni1–N21 2.018(3), Ni1–N31 2.034(3) Å]. As for the Ni(CO)–C(=O)Et part, the structure of the acyl part is normal [Ni1–C1 1.947(4), O1–C1 1.192(5) Å; Ni1–C1–O1 124.2(3), Ni1–C1–C2 115.7(3), C1–C2–C3 112.2(4)°], and the CO ligand is coordinated to the Ni center in a typical η^1-fashion [Ni1–C4 1.767(5), O2–C4 1.126(6) Å; Ni1–C4–O2 177.0(4)°]. Thus the successful characterization of the acyl complexes **3** supports the presence of the M–CH_2CH_3 functional group in the starting complexes **2**. The formation of the acyl complexes **3** *via* addition and insertion of CO molecules is in contrast to the result of carbonylation of the related iron–alkyl complex, [$PhTp^{Bu^t}$]Fe–Me, giving the Fe(I) carbonyl complex, [$PhTp^{Bu^t}$]Fe–CO.[3] The difference may arise from the highly sterically demanding $PhTp^{Bu^t}$ ligand, which would hinder formation of penta- or hexa-coordinated species leading to the acyl structure.

When the ethyl complexes **2a**,**b** were heated in heptane for 5 h at 110 °C, only small amounts of ethane [10 (**2a**) and 8% (**2b**) yields] were detected together with trace amounts of ethene by GLC analysis of the gas phase. In contrast, hydrogenolysis (2 atm; 16 h at room temperature) produced ethane in 60 (**2a**) and 91% (**2b**) yields and protonolysis with aqueous HCl afforded ethane in 66 (**2a**) and 96% (**2b**) yields. Thus complexes **2** bearing β-hydrogen atoms were found to be resistant to 'β-hydride elimination'.

The ethyl-iron and -cobalt complexes prepared in the present study are highly coordinatively unsaturated 14e (Fe: **2a**) and 15e species (Co: **2b**), respectively, which are quite sensitive to air and moisture. It is remarkable that, despite their coordinatively unsaturated electronic structures, they are resistant to β-hydride elimination and are stable at room temperature. The magnetic moments [μ = 5.0 μ_B (**2a**), 4.2 μ_B (**2b**)] close to the calculated spin only magnetic moments [4.90 (S = 2), 3.87 (S = 3/2)] and EHMO calculations indicate that the ethyl complexes **2** are high spin species and all their non-bonding d-orbitals are fully or half occupied. The stability of the ethyl complexes **2** may be interpreted in terms of the lack of a vacant coordination site (a vacant non-bonding d-orbital)[1] and the high spin electronic configurations should be a result of the tetrahedral coordination geometry regulated by the tripodal Tp^{iPr} ligand. Their electronic structure, however, should be flexible. Upon interaction with an appropriate substrate the electronic configuration may be changed so as to form a vacant coordination site and accommodate a substrate into the coordination sphere as typically exemplified by carbonylation giving the acyl complexes **3**.

We are grateful to the Ministry of Education, Science, Sports, and Culture of the Japanese Government (Grants-in-Aid for Scientific Research: No. 08102006 and 09238105) for financial support of this research.

Notes and references

† X-Ray diffraction measurements were made on a Rigaku RAXIS IV imaging plate area detector with graphite-monochromated Mo-Kα radiation. The structures were solved by using the teXsan crystal structure analysis package. *Crystal data*: **2b**: $C_{26}H_{51}N_6BCo$, M = 553.5, T = −60 °C, monoclinic, space group $P2_1/c$, a = 10.309(3), b = 16.21(2), c = 19.207(5) Å, β = 100.02(2)°, V = 3160(4) Å^3, Z = 4, D_c = 1.16 g cm^{-3}, μ = 5.7 cm^{-1}, R_1 = 0.083 for the 3267 unique data with $F_o > 4\sigma(F_o)$ and 347 parameters, wR_2 = 0.224 for all 4201 unique data.

3c: $C_{31}H_{51}BN_6NiO_2$, M = 609.3, T = −60 °C, monoclinic, space group $P2_1/n$, a = 9.968(5), b = 15.820(2), c = 21.570(2) Å, β = 97.02(2)°, V = 3376(1) Å^3, Z = 4, D_c = 1.20 g cm^{-3}, μ = 6.1 cm^{-1}, R_1 = 0.084 for the 5974 unique data with $F_o > 4\sigma(F_o)$ and 431 parameters, wR_2 = 0.238 for all 6368 unique data. The disordered C25, C26, C28, C29, C38 and C39 parts were refined taking into account the minor components. CCDC 182/1153. See http://www.rsc.org/suppdata/cc/1999/417/ for crystallographic files in .cif format.

Cell parameters for **2a**: T = −60 °C, monoclinic, space group $P2_1/c$, a = 10.465(4), b = 16.18(1), c = 19.200(8) Å, β = 100.87(1)°, V = 3193(3) Å^3.

‡ *Selected spectral data*: **2a**: 2543 cm^{-1} (ν_{BH}). **2b**: 2541 cm^{-1} (ν_{BH}). **3a**: 2553 (ν_{BH}), 2024, 2000, 1957, 1930 (ν_{CO}), 1668, 1620 cm^{-1} ($\nu_{C=O}$). $\delta_H(CD_2Cl_2)$ 6.39 (2H, 2, pz), 6.36 (1H, s, pz), 3.67 (q, J 7.0 Hz, CH_2). $\delta_C(CD_2Cl_2)$ 259.5 [s, Fe–C(=O)], 215.0 (s, Fe–CO), 56.8 (t, J 130 Hz, CH_2), 10.3 (q, J 128 Hz, CH_2CH_3). **3b**: 2540 (ν_{BH}), 1999 (ν_{CO}), 1636 cm^{-1} ($\nu_{C=O}$). **3c**: 2547 (ν_{BH}), 2009 (ν_{CO}), 1682 cm^{-1} ($\nu_{C=O}$). $\delta_H(CD_2Cl_2)$ 5.84 (3H, s, pz), 1.88 (q, J 7.4 Hz, CH_2), 0.45 (t, J 7.4 Hz, CH_2CH_3). $\delta_C(CD_2Cl_2)$ 225.9 (s, Ni–C(=O)), 187.4 (s, Ni–CO), 40.7 (t, J 132 Hz, CH_2), 11.1 (q, J 127 Hz, CH_2CH_3).

1 A. Yamamoto, *Organotransition Metal Chemistry*, Wiley-Interscience, New York, 1986; J. P. Collman, L. S. Hegedus, J. R. Norton and R. G. Finke, *Principles and Applications of Organotransition Metal Chemistry*, University Science Books, Mill Valley, CA, 1987; R. H. Crabtree, *The Organometallic Chemistry of the Transition Metals*, Wiley-Interscience, New York, 2nd edn., 1994.

2 M. Akita, N. Shirasawa, S. Hikichi and Y. Moro-oka, *Chem. Commun.*, 1998, 973.

3 J. L. Kisko, T. Hascall and G. Parkin, *J. Am. Chem. Soc.*, 1998, **120**, 10 561.

4 Several examples of coordinatively unsaturated hydrocarbyl complexes kinetically stabilized by bulky ligands are known. See, for example: B. K. Bower and H. G. Tennent, *J. Am. Chem. Soc.*, 1972, **94**, 2512; A. Kose, E. Solari, C. Floriani, A. Chiesi-Villa, C. Rizzoli and N. Re, *J. Am. Chem. Soc.*, 1994, **116**, 9123; R. C. Kerber, *Comprehensive Organometallic Chemistry II*, ed. E. W. Abel, F. G. A. Stone and G. Wilkinson, Pergamon, Oxford, 1995, vol. 7, ch. 2.3.1.

5 F. A. Cotton, B. A. Frenz and A. Shaver, *Inorg. Chim. Acta*, 1973, **7**, 161.

Communication 8/09441A

ChemComm

Phthalocyanine-containing polystyrenes

Saad Makhseed, Anthony Cook and Neil B. McKeown*†

Department of Chemistry, University of Manchester, Manchester, M13 9PL UK. E-mail: neil.mckeown@man.ac.uk

Received (in Cambridge, UK) 4th January 1999

An unsymmetrical phthalocyanine derivative containing a single styrene unit, prepared using a mixed phthalonitrile cyclotetramerisation, can undergo free radical polymerisation to give well-defined polystyrenes in which the macrocyclic components aggregate even in dilute solution.

Phthalocyanine (Pc) and its derivatives possess interesting electronic, optical and catalytic behaviour.[1] There has been much interest in the synthesis of phthalocyanine-containing polymers suitable for the exploitation of Pc functionality.[2] Previously, Pc has been incorporated into intractable network polymers,[3] rigid polysiloxanes in which the silicon(IV) ion is held within the central cavity of the macrocycle,[4] main-chain liquid crystalline polymers,[5] polymers formed by the coordination of bidentate ligands with metal ion containing Pcs,[6] dendrimers which comprise a Pc ring at their core,[7] and polymers in which the Pc is a component of a side-chain attached to the polymer backbone.[8] Here we describe the synthesis of polystyrenes with Pc-containing side-chains. The widespread use of polystyrene as the substrate for polymer-supported catalysts, its excellent processability and its optical clarity make these materials attractive synthetic targets with numerous potential applications.

The synthetic route to the Pc-containing styrene monomers is given in Scheme 1. The strategy is to prepare an unsymmetrical phthalocyanine, which possesses six solubilising alkyl side-chains and a single reactive hydroxy functionality for the attachment of the styrene group, *via* a mixed cyclotetramerisation of suitable phthalonitrile precursors. In order to protect the hydroxy group during the base catalysed Pc forming reaction, 4-hydroxyphthalonitrile[9] was first reacted with methoxyethoxymethyl chloride (MEM chloride) to give **1**. The MEM moiety not only acts as a protecting group during the mixed cyclotetramerisation reaction between **1** and an excess of 4,5-bis(dodecyloxy)phthalonitrile[8] but its relative polarity, as compared to that of the dodecyloxy side-chains, also facilitates chromatographic separation of the required unsymmetrical Pc **2** from the Pc by-products.[10] Removal of the MEM group followed by the reaction of the resulting Pc **3** with 1-bromo-11-(4-vinylphenoxy)undecane[11] gives the desired Pc-containing styrene monomer **4**. Spectroscopic and elemental analysis of **4** was consistent with its proposed structure.†

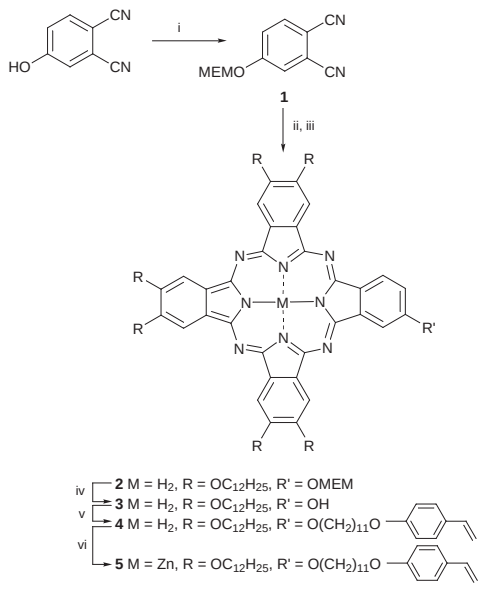

Scheme 1 *Reagents and conditions*: i, MEMCl, pyridine; ii, 4,5-bis(dodecyloxy)phthalonitrile, $C_5H_{11}OLi$, $C_5H_{11}OH$, 135 °C; iii, AcOH; iv, PPTS, $C_5H_{11}OH$, 135 °C; v, 1-bromo-11-(4′-vinylphenoxy)undecane, K_2CO_3, DMF, 50 °C; vi, $Zn(OAc)_2$, $C_5H_{11}OH$, 135 °C.

The long alkyl spacing group between the styrene unit and the Pc ring is designed to minimise any detrimental steric effect on the polymerisation reaction due to the large macrocycle. Indeed, free radical polymerisation of **4** can be achieved with high conversion (> 85%) to give soluble polymers of reasonable molar mass ($M_n > 40 \times 10^3$ amu) and with relatively narrow polydispersity ($M_w/M_n \sim 1.5$) as measured by gel permeation chromatography (GPC) against commercial polystyrene standards (Table 1). The optimum conditions for polymerisation proved to be a 0.05 mmol ml^{-1} concentration of monomer **4** in benzene solution using a 5 mol% concentration of AIBN relative to **4**. Prior complexation of **4** to zinc(II), to give monomer **5**,† resulted in polymers of higher mass.

It is possible to vary the concentration of Pc functionality within the resulting materials by preparing random copolymers from styrene and Pc **4** or **5**. Interestingly, the molecular masses obtained for these copolymers were consistently higher than those of unsubstituted polystyrene obtained under the same conditions. This prompted us to perform control experiments in which styrene was polymerised with or without added unreactive metal-free octakis(dodecyloxy)-Pc (ODPc) or its zinc(II) derivative (ZnODPc). The polystyrene prepared in the presence of ODPc or ZnODPc proved to have significantly higher mass and lower polydispersity than that prepared in its absence (Table 1). This unexpected result was attributed to the Pc removing the residual oxygen which remained after conventional deoxygenation using a repeated freeze–thaw degassing process. It is well-established from various spectroscopic and electronic conductivity studies that Pcs interact strongly with molecular oxygen. Zinc(II)-containing Pcs are particularly efficient at interacting with oxygen and this may explain why monomer **5** is particularly well-suited to free radical polymerisation.

UV–VIS absorption spectra of the polymers dissolved in toluene reveal that there are strong cofacial interactions between the Pc side-chains. This is apparent from the large bathochromic shift of the primary Q-band of the Pc from 690 to 620 nm. We believe that these interactions are primarily intramolecular because even very dilute solutions show this effect, whereas solutions of monomer **4** or **5** of similar concentration display an unperturbed Q-band (Fig. 1). UV–VIS spectra of the copolymers also display the broad absorption band resulting from self-association. High resolution ^1H NMR spectroscopy clearly shows the presence of the dodecyloxy groups attached to the Pc side-chains, however the aromatic protons are indicated only by a single very broad signal centred at δ 6.9, presumably due to intramolecular association of the Pc units. NMR spectra of the copolymers show clear signals originating from the polystyrene backbone, however, only broadened resonances from the alkyl component of the Pc-containing side-chain are apparent. This

Table 1 Polymerisation data for Pc-containing styrenes prepared using the conditions described in the text. Each figure for conversion and M_n is an average of several runs.

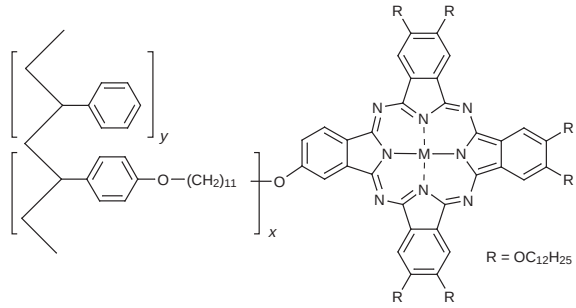

Monomer(s)	*x* (%)	*y* (%)	Conversion (%)	$< M_n >$ (amu)	$< M_w > / < M_n >$
4	100	0	87	44×10^3	1.6
5	100	0	90	53×10^3	1.3
4 + styrene	0.5	99.5	95	72×10^3	1.7
5 + styrene	20	80	95	46×10^3	1.5
5 + styrene	0.5	99.5	94	80×10^3	1.7
Styrene + ODPc	0	100	89	8×10^3	1.7
Styrene + ZnODPc	0	100	90	10×10^3	1.7
Styrene	0	100	88	7×10^3	2.0

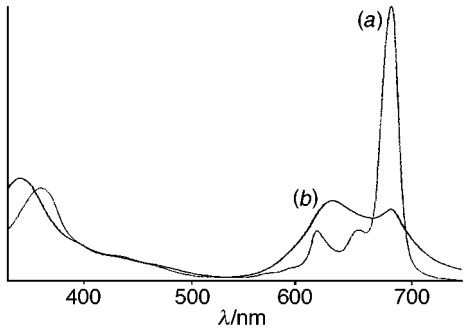

Fig. 1 UV–VIS absorption spectrum for (*a*) the monomer **5** and (*b*) the polystyrene derived from **5** (x = 100%).

observation reinforces the evidence from UV–VIS spectroscopy that Pc self-association is a feature of the dilute solution behaviour of the copolymers even for those which possess only a small degree of Pc side-chain substitution (~0.5 mol% concentration).

Unlike the precursors and monomers **2**–**5** which form a columnar mesophase at elevated temperatures, thin films of the Pc-containing homopolymers are birefringent solids up to their decomposition temperatures (~300 °C). The copolymers are isotropic glassy solids with well-defined glass transition temperatures. Thin films of the copolymers, fabricated by spin-coating or by melt processing, are optically clear and highly coloured. The non-scattering nature of these films make them suitable for optical studies.

This work illustrates the compatibility of Pc-containing styrene monomers with free radical polymerisation to produce well-defined macromolecules. It allows the design of novel, readily processed functional materials including polymeric dyes, polymer supported Pc-catalysts, photobactericidal polymers[12] and polymers for various optical applications.

We thank Kuwait University (S. M.) and the EPSRC (A. C.) for the provision of studentships.

Notes and references

† *Selected data* for **4**: λ(toluene)/nm 700, 664, 646, 398, 342; ν (thin film)/cm^{-1} 3422 (NH); δ_H(benzene-d_6, 500 MHz, 60 °C) −3.40 (2H, br s), 0.99 (18H, t), 1.30–1.85 (108H, br m), 2.08–2.24 (12H, br m), 3.78 (2H, t), 4.24 (12H, br s), 4.40 (2H, br s), 5.06 (1H, d), 5.56 (2H, d), 6.64 (1H, dd), 6.85 (2H, d), 7.27 (2H, d), 7.68 (1H, br s), 8.30–8.70 (7H, br m), 9.12 (1H, br s); *m/z* (MALDI) 1906 (M^+). For **5:** λ(toluene)/nm 679, 612, 360; δ_H(benzene-d_6, 500 MHz, 60 °C) 1.01 (18H, t), 1.40–1.70 (96H, br m), 1.72–1.88 (12H, br m), 2.08–2.24 (12H, br m), 3.80 (2H, t), 4.12–4.26 (12H, br m), 4.36 (2H, br s), 5.06 (1H, d), 5.56 (2H, d), 6.64 (1H, dd), 6.85 (2H, d), 7.27 (2H, d), 7.65 (1H, br s), 8.15–8.65 (7H, br m), 9.12 (1H, br s); *m/z* (MALDI) 1971 (M^+).

1 N. B. McKeown, *Phthalocyanine Materials: Synthesis, Structure and Function*, Cambridge University Press, Cambridge, 1998.
2 D. Wöhrle, in *Phthalocyanines: Properties and Applications*, ed. C. C. Leznoff and A. P. B. Lever, VCH, NY, 1989, vol. 1, p. 58.
3 D. Wöhrle, U. Marose and R. Knoop, *Makromol. Chem.*, 1985, **186**, 2209.
4 R. D. Joyner and M. E. Kenney, *Inorg. Chem.*, 1962, **1**, 717.
5 5. G. C. Bryant, M. J. Cook, T. G. Ryan and A. J. Thorne, *Tetrahedron*, 1996, **52**, 809.
6 M. Hanack and M. Lang, *Adv. Mater.*, 1994, **6**, 819.
7 M. Brewis, G. J. Clarkson, A. M. Holder and Neil B. McKeown, *Chem. Commun.*, 1998, 969.
8 J. F. Van der Pol, E. Neeleman, R. J. M. Nolte, J. W. Zwikker and W. T. Drenth, *Makromol. Chem.*, 1989, **190**, 2727.
9 D. Wöhrle and G. Knothe, *Synth. Commun.*, 1989, **19**, 3231.
10 P. Humberstone, G. J. Clarkson, N. B. McKeown and K. E. Treacher, *J. Mater. Chem.*, 1996, **6**, 315.
11 A. Cook, S. Greenfield and N. B. McKeown, manuscript in preparation.
12 R. Bonnett, D. G. Buckley, T. Burrow, A. B. B. Galia, B. Saville and S. P. Songca, *J. Mater. Chem.*, 1993, **3**, 323.

Communication 9/00069K

The first total synthesis of a type II manumycin antibiotic, (+)-TMC-1 A: the total syntheses of (−)-LL-C10037β and (+)-manumycin B

J. J. Cronjé Grové, Xudong Wei and Richard J. K. Taylor*

Department of Chemistry, University of York, Heslington, York, UK YO10 5DD. E-mail: rjkt1@york.ac.uk

Received (in Cambridge, UK) 8th January 1999, Accepted 22nd January 1999

A procedure using Na[PhSeB(OEt)$_3$] is reported for conversion of the type I epoxy ketone manumycins into the type II β-hydroxyketone variants; using this procedure, (−)-LL-C10037β and (+)-TMC-1A have been prepared for the first time; the first synthesis of (+)-manumycin B, which provides full stereochemical clarification of the natural product, is also described.

The most recent additions to the manumycin family of antibiotics are the TMC-1 natural products **1**–**5** which were isolated from *streptomyces* sp. A-230 in 1996 by Kohno and co-workers and shown to be cytotoxic to a range of tumour cell lines *in vitro*.[1] This new group of compounds differ from most of the manumycin family,[2–6] *e.g.* manumycin A **6** and manumycin B **7**,† in that they possess a β-hydroxy ketone in place of the more common epoxy ketone unit. Sattler, Thiericke and Zeeck have termed[3] the β-hydroxy ketone subset, which also includes manumycin D **5**,[1,4] type II manumycins and the epoxy ketone subset type I manumycins. The same structural relationship is seen in the less complex anti-tumour natural products LL-C10037β **8** and LL-C10037α **9**.[7]

Despite their promising biological properties and interesting structures, synthetic approaches to the TMC-1 antibiotics have not been reported to date. We have recently developed a synthetic route to the type I manumycins and utilised it to prepare (+)-manumycin A[5] and other members of the family.[2,6] Regioselective reduction of the α,β-epoxy ketone group of the type I manumycins should produce the type II variants. Thus, TMC-1A **1** should be available by the reduction of manumycin B **7**.†

In order to establish the validity of this strategy, we first investigated the conversion of LL-C10037α **9** into LL-C10037β **8** as shown in Scheme 1.

The (+)-enantiomer of LL-C10037α (also known as MT 35214) was prepared using our published procedure.[6] The reagent of choice for the epoxy ketone reduction proved to be Na[PhSeB(OEt)$_3$],[8] generated *in situ* by $NaBH_4$ reduction of PhSeSePh. Model studies showed that this reagent displays exceptional tolerance towards the sensitive functional groups present within the target molecules. Treatment of (+)-**9** with a freshly prepared solution of Na[PhSeB(OEt)$_3$] in EtOH at 0 °C resulted in the formation of (−)-LL-C10037β **8**, after oxidative work-up, in an unoptimised but respectable yield of 63%.‡ Compound **8** is extremely sensitive to acid and readily undergoes dehydration–aromatisation. All spectroscopic data (IR, UV, NMR) for **8** were entirely consistent with those published[7] for the natural product. In addition, the optical rotation of (−)-**8** corresponded well to the literature data for the enantiomeric natural product {$[\alpha]_D$ −34.8 (*c* 0.9, MeOH); lit.,[7] +26.3 (*c* 0.26, MeOH)} and satisfactory HRMS data were obtained [Found: MH^+, 186.07681. $C_8H_{12}NO_4$ requires 186.07663 (1 ppm error)]. This study therefore produced the first synthesis of LL-C10037β and established the methodology for an assault on TMC-1 A. Due to the ready availability of the enantiomerically pure amine (−)-**10**, prepared utilising the Wynberg chiral phase transfer technology developed for our synthesis of (+)-manumycin A,[5,6] the (+)-enantiomer of TMC-1 A was targeted (Scheme 2).

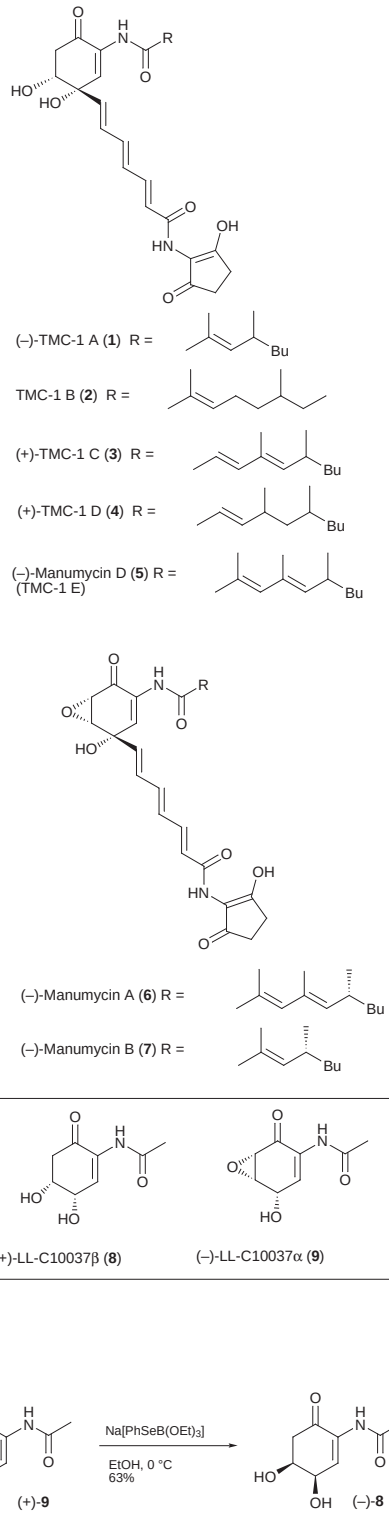

Scheme 1

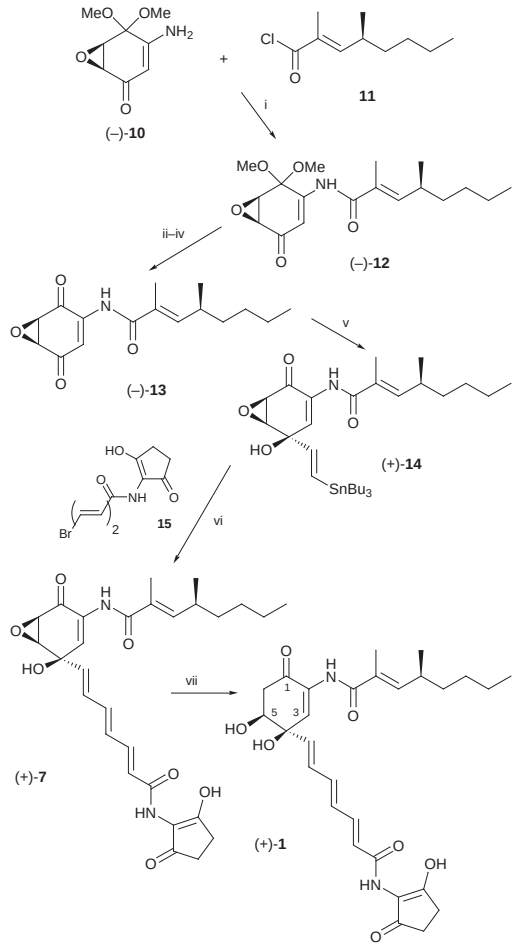

Scheme 2 *Reagents and conditions*: i, Bu^{t}OLi, THF (89%); ii, $LiEt_3BH$, THF, −78 °C (95%); iii, montmorillonite K10, CH_2Cl_2, room temp. (90%); iv, PDC, CH_2Cl_2, room temp (76%); v, (*E*)-$Bu_3SnCH{=}CHLi$, THF, −78 °C (28%); vi, [5% $PdCl_2(Ph_3P)_2$, DIBAL-H], THF–DMF, room temp. (71%); vii, Ph_2Se_2, $NaBH_4$, EtOH, 0 °C (66%).

Evans' oxazolidinone methodology was employed to prepare (*S*)-(+)-2-methylpropanal which was converted into acid chloride **11** using standard methodology.[5] Acylation of (−)-**10** in the presence of lithium *tert*-butoxide[2] afforded amide (−)-**12** in an excellent yield of 89%. Direct deprotection of the acetal was attempted but was unsuccessful due to aromatisation; amide (−)-**12** was therefore converted into the corresponding epoxy quinone (−)-**13** *via* a three step reduction–deprotection–oxidation sequence in good overall yield. The enantiomeric quinone, (+)-**13**, was obtained by Hara *et al.* by chromic acid degradation of manumycin B.[9] The NMR data and optical rotation of quinone (−)-**13** corresponded well to those of its enantiomer {*e.g.* $[\alpha]_D$ −16.5 (*c* 1.1, $CHCl_3$); lit.,[9b] +16.0 (*c* 0.2, $CHCl_3$)}.

Quinone (−)-**13** was elaborated *via* the addition of (*E*)-$Bu_3SnCH{=}CHLi$:[10] a mixture of mono- and di-adducts was obtained from which vinylstannane (+)-**14** was isolated in 28% yield after chromatography. The expected[2,5] *syn*-hydroxy epoxide structure was confirmed by the diagnostic coupling constant between H-3 and H-5 (*J* 2.7 Hz). Stille coupling between vinylstannane (+)-**14** and dienyl bromide **15**[11] proceeded efficiently (71%) to give (+)-manumycin B **7** as a bright yellow solid (mp 96–97 °C; lit.,[4] 94 °C) which displayed spectroscopic, chromatographic and polarimetric data entirely consistent with it being the enantiomer of the natural product. This is the first synthesis of manumycin B and it confirms that, as proposed,[5] it does indeed have the *syn*-hydroxy epoxide configuration illustrated (rather than the corresponding *anti*-arrangement described in the original structure elucidation[4]).

Treatment of (+)-manumycin B **7** with $Na[PhSeB(OEt)_3]$ using the reaction conditions developed in the model studies resulted in the formation of a polar, light sensitive, dark yellow solid in an isolated yield of 66%. All spectroscopic and chromatographic data proved to be consistent with the literature[1] values for the natural antibiotic, TMC-1 A [*e.g.* $\delta_C(CDCl_3$, 500 MHz) 191.8 (C-1), 132.0 (C-2), 126.2 (C-3), 73.5 (C-4), 71.8 (C-5), 40.5 (C-6); lit.,[1] ($CDCl_3$, 400 MHz) 191.8 (C-1), 132.2 (C-2), 126.0 (C-3), 73.6 (C-4), 71.9 (C-5), 40.6 (C-6)]. The optical rotation of the product {$[\alpha]_D$ +58.6 (*c* 0.5, $CHCl_3$) was consistent with it being the enantiomer of (−)-TMC-1 A **1** {lit.[1] −55.0 (*c* 0.1, $CHCl_3$)}. This study therefore confirms structure **1** for (−)-TMC-1 A and establishes the 4′*R* configuration for the side chain methyl group.

In summary, we have devised a procedure for converting the type I epoxy ketone manumycins into the type II β-hydroxy ketone variants. Using this procedure, (−)-LL-C10037β and (+)-TMC-1A have been prepared for the first time and the structures of the natural products confirmed. The first synthesis of (+)-manumycin B is also reported, thereby correcting the published stereochemical assignment and confirming the *syn*-hydroxy epoxide structure. It seems likely that manumycin B is the biosynthetic proecursor of TMC-1 A, and therefore that the chemical synthesis described above is biomimetic.

We thank the Foundation for Research Development (South Africa) and the EPSRC for research fellowships (J. J. C. G. and X. W., respectively). We are also grateful to Dr T. A. Dransfield and Miss H. Fish (University of York) for their expert assistance with mass spectrometry and NMR spectroscopy, and to Dr S.-i. Ikeda[9b] for spectra and physical data for epoxyquinone (+)-**13**.

Notes and references

† Manumycin B (ref. 4) is shown with the revised *syn*-hydroxy epoxide stereochemistry suggested in ref. 5 and the 4′*R* configuration of the side chain methyl substituent established in ref. 5(*b*).

‡ All new compounds were fully characterised spectroscopically and by HRMS/elemental analysis.

1 J. Kohno, M. Nishio, K. Kawano, N. Nakanishi, S.-i. Suzuki, T. Uchida and S. Komatsubara, *J. Antibiot.*, 1996, **49**, 1212.
2 For a recent article listing all of the manumycin family, see R. J. K. Taylor, L. Alcaraz, I. Kapfer-Eyer, G. Macdonald, X. Wei and N. J. Lewis, *Synthesis*, **1998**, 775.
3 I. Sattler, R. Thiericke and A. Zeeck, *Nat. Prod. Rep.*, 1998, **15,** 221.
4 I. Sattler, C. Gröne and A. Zeeck, *J. Org. Chem.*, 1993, **58**, 6583.
5 (*a*) L. Alcaraz, G. J. Macdonald, J. P. Ragot, N. Lewis and R. J. K. Taylor, *J. Org. Chem*., 1998, **63**, 3526; (*b*) L. Alcaraz, G. J. Macdonald, J. P. Ragot, N. Lewis and R. J. K. Taylor, *Tetrahedron*, in the press.
6 G. J. Macdonald, L. Alcaraz, N. J. Lewis and R. J. K. Taylor, *Tetrahedron Lett.*, 1998, **39**, 5433.
7 B. Shen, Y. G. Whittle, S. J. Gould and D. A. Keszler, *J. Org. Chem*., 1990, **55**, 4422; M. D. Lee, A. A. Fantini, G. O. Morton, J. C. James, D. B. Borders and R. T. Testa, *J. Antibiot*., 1984, **37**, 1149.
8 M. Miyashita, T. Suzuki, M. Hoshino and A.Yoshikoshi, *Tetrahedron*, 1997, **37**, 12 469 (see ref. 12 therein for other methods of achieving this transformation).
9 (*a*) M. Hara, K. Akasaka, S. Akinaga, M. Okabe, H. Nakano, R. Gomez, D. Wood, M. Uh and F. Tamanoi, *Proc. Natl. Acad. Sci*., *U.S.A.*, 1993, **90**, 2281. (*b*) S.-i. Ikeda, Tokyo Research Laboratories, Kyowa Hakko Kogyo Co. Ltd., personal communication.
10 E. J. Corey and R. H. Wollenberg, *J. Org. Chem.*, 1975, **40,** 3788.
11 G. Macdonald, L. Alcaraz, X. Wei, N. J. Lewis and R. J. K. Taylor, *Tetrahedron*, 1998, **54**, 9823.

Communication 9/00261H

Natural bond orbital analysis of hyperconjugative stabilization effects in the transition states of cyclohexanone reduction with $LiAlH_4$

Shuji Tomoda* and Takatoshi Senju

Department of Life Sciences, Graduate School of Arts and Sciences, The University of Tokyo, Komaba, Meguro, Tokyo 153-8902, Japan. E-Mail: tomoda@selen.c.u-tokyo.ac.jp

Received (in Cambridge, UK) 23rd November 1998, Accepted 22nd January 1999

Natural bond orbital (NBO) analysis of the transition states of cyclohexanone reduction with $LiAlH_4$ located at the B3LYP/6-31+G(d) level along the intrinsic reaction coordinate (IRC) strongly indicate that the antiperiplanar effect involving the incipient bond may not be important as a controlling factor of π-facial selection in carbonyl reduction.

Since Cieplak[1] proposed the theory of π-facial stereoselectivity in 1981, the direction of the antiperiplanar hyperconjugative stabilization effects (hereafter abbreviated as 'the AP effect') in the transition states of nucleophilic carbonyl addition have been the subject of intense investigation in both theoretical and experimental organic chemistry.[2] While the Felkin–Anh model[3] postulated the AP effect between the filled electron-rich incipient bond and the vacant vicinal antiperiplanar bonds, Cieplak predicted the opposite electronic property in common organic reactions, proposing exactly the reverse AP effect.[1] Herein we report the first transition state of the reduction of cyclohexanone with $LiAlH_4$ together with the natural bond orbital (NBO)[4] analysis of the AP effects along the intrinsic reaction coordinate towards the transition state.

The structures of the axial (*ax*-TS) and equatorial (*eq*-TS) transition states of cyclohexanone reduction with $LiAlH_4$ optimized at the B3LYP/6-31+G(d) level are shown in Fig. 1. The zero point vibrational energy corrected relative electronic energy was 1.36 kcal mol^{-1}, slightly favoring the *ax*-TS in agreement with experiment. Each transition state had a single imaginary vibrational frequency corresponding to the stretching vibration of the incipient bond (ν_i = 377.7 and −392.6 cm^{-1} for *ax*-TS and *eq*-TS, respectively). The incipient bond distances for $LiAlH_4$ transition states were 1.531 and 1.556 Å for *ax*- and *eq*-TS, respectively, which are far shorter than the unrealistically long incipient bonds of LiH transition states [2.739 (*ax*-TS) and 2.510 (*eq*-TS) Å; B3LYP/6-31+G(d)]. In contrast to the LiH cases, the relative earliness of *ax*- and *eq*-TS with $LiAlH_4$ in terms of the incipient bond length suggests that the latter is moderately earlier than the former. Such a trend is also seen in the bond lengths of other parts of the structures, such as the C=O, Al–H and O–Li bond distances. Thus the incipient bond for *ax*-TS may be stronger than that for *eq*-TS. The hydride approaching angles in the $LiAlH_4$ transition structures [109.8 (*ax*-TS) and 109.5° (*eq*-TS)] are greater by ~ 20° than those for the LiH cases [85.6 (*ax*-TS) and 90.3° (*eq*-TS)] The former values are similar to the average angle of nucleophile approach (107°) observed by crystallographic investigation of some crystalline ketones.[5] The torsion angles of the cyclohexanone moiety along C2–C1–C6–C5 are 44.2 and 63.8° for *ax*- and *eq*-TS, respectively. The latter is much more distorted than the LiH transition states [42.5 (*ax*-TS) and 56.5° (*eq*-TS)]. The magnitude of the torsional strain of the cyclohexanone moieties of $LiAlH_4$ transition states relative to ground-state cyclohexanone optimized at the B3LYP/6-31+G(d) level was 11.9 and 10.9 kcal mol^{-1} for *ax*-TS and *eq*-TS, respectively [single point calculation at the MP2/6-31+G(d) level]. As such, *ax*-TS is slightly (1.0 kcal mol^{-1}) more distorted than *eq*-TS, in sharp contrast to the LiH case previously reported.[6] It is therefore concluded that the torsional strain is not responsible for π-facial stereoselectivity in cyclohexanone reduction as pointed out previously by Frenking using the LiH transition states.[7]

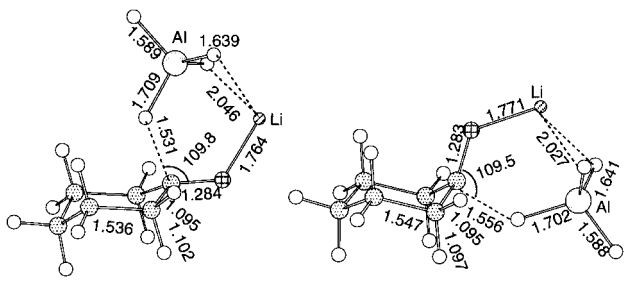

Fig. 1 Selected structural parameters for the transition states of cyclohexanone reduction with $LiAlH_4$ obtained at the B3LYP/6-31+G(d) level. Bond lengths are in Å and angles are in degrees. *E* indicates the total electronic energy.

It is expected that the magnitude of the AP effects may be initially significant, but should gradually be diminished along the IRC toward the transition state for the following two reasons. First, as the reaction proceeds, the strength of the incipient bond increases, causing some energy increase in the antibonding (σ‡*) level of the incipient bond accompanied by energy reduction of its bonding (σ‡) level. This may cause reduction of both (Cieplak and Felkin–Anh) antiperiplanar stabilization mechanisms involving the incipient bond. Secondly, as the reaction proceeds, hybridization of the carbonyl carbon (C1) changes from sp^2 to sp^3, and therefore the length of the intervening σ_{C1-C2} bond increases to cause inevitable reduction in the magnitude of the antiperiplanar hyperconjugation toward transition state. Consequently it is expected that antiperiplanar hyperconjugation mechanisms may operate effectively in the early stages and that the difference in the magnitude between the two π-faces of the carbonyl plane may be reduced steadily along the reaction coordinate toward the transition state, where it may vanish completely.

To evaluate the relative magnitude of the AP effects in the $LiAlH_4$ transition states, a natural bond orbital (NBO) program[4] combined with intrinsic reaction coordinate (IRC) calculations with GAUSSIAN 94[8] were applied at the B3LYP/6-31+G(d) level. IRC calculation clearly showed that the above structures with negative frequencies (Fig. 1) were indeed the transition states. As shown in Fig. 2, structural analysis of the reaction along the IRC indicated a steady decrease in the AP effects towards the transition states. The percentage elongation of the vicinal antiperiplanar bonds (relative to the corresponding bonds of ground-state cyclohexanone optimized at the same level) in *eq*-TS (0.33–0.14%) is always greater than that in *ax*-TS (0.13–0.05%) along the reaction coordinate. It should be noted here that elongation of the antiperiplanar bonds is reduced to almost zero (0.05%) in *ax*-TS (IRC = 0) in agreement with the above prediction. The relative magnitude of the transition state AP effects (*ax*-TS vs. *eq*-TS) as well as the marginal AP effect in *ax*-TS clearly indicate that if the AP effects were the

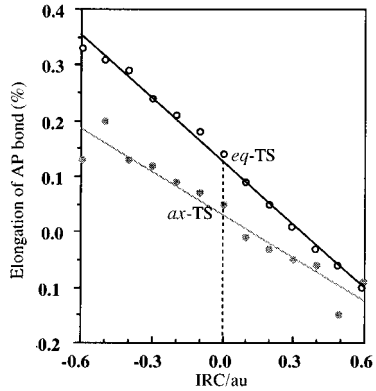

Fig. 2 Elongation of vicinal antiperiplanar bonds along the IRC for cyclohexanone reduction with $LiAlH_4$ [B3LYP/6-31+G(d)].

major mechanism of facial stereoselection in cyclohexanone reduction, stereoselectivity opposite to the experimental result must be observed, contrary to the predictions of both conventional models.[1,3]

In agreement with the above theoretical outcomes, NBO analysis along the IRC toward the transition states suggested that a small amount of electronic charge was removed from the vicinal antiperiplanar bonds all the way along the transition states [0.015–0.008 electrons for the *eq*-attack and 0.011–0.005 electrons for the *ax*-attack based on the bond population for the corresponding antiperiplanar bonds of cyclohexanone optimized at the B3LYP/6-31+G(d) level] and that they monotonously decreased along IRC as shown in Fig. 3. The small reduction in the amount of electrons in the antiperiplanar bonds clearly indicated that the Cieplak hyperconjugation effect should be greater than the Felkin–Anh hyperconjugation effect. The electron population of the incipient bond ($\sigma^{\ddagger}$) determined with natural resonance theoretical (NRT) analysis[4] was 0.696 and 0.663 for *ax*- and *eq*-TS, respectively. These values strongly suggest significantly electron-deficient incipient bonds in the transition states for cyclohexanone reduction in agreement with Cieplak's proposal.[1] Thus the greater AP effect at *eq*-TS compared with *ax*-TS as indicated by the percentage elongation of the antiperiplanar bonds (*ax*-TS = 0.05% and *eq*-TS = 0.14%) as well as by the magnitude of electron transfer (*ax*-TS = 0.005 *e* and *eq*-TS = 0.008 *e*) strongly suggests that the AP effect may not be an essential mechanism of π-facial stereoselection.

It was found that within the framework of modern molecular orbital methods operational direction of the AP effect involving an incipient bond is not necessarily consistent with a preferred direction of hydride attack, as seen in the following transition state examples of $LiAlH_4$ reduction obtained at the B3LYP/6-31+G(d) level. The 3,5-dithiacyclohexanone reduction with $LiAlH_4$, the *eq*-attack of which is preferred to the *ax*-attack,[9] shows unusual behavior of the AP effect: the C2–S3 bond in *eq*-TS is shortened (−0.11%), while the C2–H*ax* bond in *ax*-TS is elongated (+0.25%) relative to the starting ketone. The

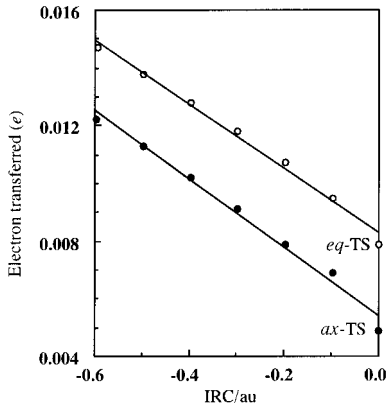

Fig. 3 Plot of the electron population moved from an antiperiplanar bond against the IRC for cyclohexanone reduction with $LiAlH_4$ [B3LYP/6-31+G(d)].

reduction in the NBO[5] electron population in the antiperiplanar bonds at C2 and C6 (−0.012 and 0.000 for *ax*- and *eq*-TS, respectively) was also consistent with this interesting trend. It is clear that the experimental stereochemistry cannot be explained in terms of the AP effect. Apparently the AP effect is more significant in *ax*-TS, although *ax*-TS is less stable by 1.39 kcal mol^{-1} than *eq*-TS.

Another intriguing case is the adamantanone system. It has long been known that adamantanone is less reactive in hydride reduction than cyclohexanone,[10] despite the theoretical observation that the AP effects are much greater in adamantanone than in cyclohexanone. The $LiAlH_4$ transition state of the parent adamantan-2-one shows more than twice (+0.34% elongation of the C–C bond) as large AP effects as those of cyclohexanone (+0.05 and +0.14% for *ax*- and *eq*-TS, respectively). While 5-methyladamantan-2-one shows only a marginal difference in percentage elongation of the vicinal antiperiplanar C–C bond between the *syn*- (+0.40%) and *anti*-TS (+0.38%) (relative to the ground-state 5-methyladamantan-2-one), 5-fluoroadamantan-2-one, which gives preferential *syn*-attack in $NaBH_4$ reduction (63 : 37),[11] shows a larger AP effect in *anti*-TS (+0.48%) than in *syn*-TS (+0.39%) relative to the ground-state 5-fluoroadamantan-2-one. In both of these cases, the *syn*-TS is more stable than the *anti*-TS by 0.12 (5-methyladamantan-2-one) and 0.23 (5-fluoroadamantan-2-one) kcal mol^{-1}. Another case which shows similar behavior is 5-azaadamantan-2-one *N*-oxide, which prefers 96% *syn*-attack upon reduction with $NaBH_4$.[12] The $LiAlH_4$ reduction transition states of this compound show elongation of the vicinal antiperiplanar bonds of +1.00% (*anti*-TS) and +0.95% (*syn*-TS) relative to the parent ketone. Virtually no difference in the magnitude of the AP effects over two carbonyl faces is evident.

The present analysis strongly suggests that the transition state effects are most likely to have minor effects on facial selection. This 'unusual' behavior may be readily understood if one considers the mechanism (the direction of the force vector on hydride nucleus) of the AP effect which operates against the incipient bond formation: the effect causes elongation of the incipient bond against the force vector on hydride directed toward bond formation with the carbonyl. We emphasize again that the difference in the magnitude of the driving force of the reaction generated over the two π-faces of the carbonyl plane through orbital interactions[13] between ketone and hydride should be the origin of π-facial stereoselectivity in cyclohexanone reduction.[14]

Notes and references

1 A. S. Cieplak, *J. Am. Chem. Soc*., 1981, **103,** 4540.
2 B. W. Gung, *Tetrahedron*, 1996, **52**, 5263.
3 M. Chérest and H. Felkin, *Tetrahedron Lett*., 1968, 2205; N. T. Anh and O. Eisenstein, *Nouv. J. Chim.*, 1976, **1**, 61.
4 A. E. Reed, L. A. Curtiss and F. Weinhold, *Chem. Rev*., 1988, **88**, 899; E. D. Glendening and F. Weinhold, *Natural Resonance Theory I. General Formalism*, in Technical Report of Theoretical Chemistry Institute, No. 803 (1994).
5 H. B. Bürgi, J. D. Dunits and E. Shefter, *J. Am. Chem. Soc*., 1973, **95**, 5065.
6 Y.-D. Wu, J. A. Tucker and K. N. Houk, *J. Am. Chem. Soc*., 1991, **113**, 5018.
7 G. Frenking, K. F. Köhler and M. T. Reez, *Angew. Chem., Int. Ed. Engl*., 1991, **30**, 1146.
8 GAUSSIAN 94 (Revision D.1 and E.2), Gaussian, Inc., Pittsburgh, PA, 1997.
9 Y. M. Kobayashi, J. Lambrecht, J. C. Jochims and U. Burkert, *Chem. Ber*., 1978, **111**, 3442; J. C. Jochims, Y. M. Kobayashi and E. Skrzelewski, *Tetrahedron Lett*., 1974, 571 and 575.
10 P. Geneste, G. Lamaty, C. Moreau and J-P. Roque, *Tetrahedon Lett*., 1970, 5011.
11 C. K. Cheung, L. T. Tseng, M.-H. Lin, S. Srivastava and W. J. le Noble, *J. Am. Chem. Soc*., 1986, **108**, 1598.
12 J. M. Hahn and W. J. le Noble, *J. Am. Chem. Soc*. 1992, **114**, 1916.
13 G. Klopman, *J. Am. Chem. Soc*., 1968, **90**, 223; L. Salem, *J. Am. Chem. Soc*., 1968, **90**, 543; I. Fleming, *Frontier Orbitals and Organic Chemical Reactions*, Wiley, London, 1977.
14 S. Tomoda and T. Senju, *Tetrahedron*, 1997, **53**, 9057.

Communication 8/09117J

A new synthetic path to *peri*-naphthisoxazoles by oxidative intramolecular cyclization of some β,γ-unsaturated oximes

John C. Barnes, William M. Horspool* and George Hynd

Department of Chemistry, The University of Dundee, Dundee, Scotland, UK DD1 4HN.
E-mail: w.m.horspool@dundee.ac.uk

Received (in Liverpool, UK) 7th December 1998, Accepted 27th January 1999

Some β,γ-unsaturated oximes undergo an unprecedented intramolecular cycloaddition to an aryl group to afford *peri*-naphthisoxazoles when they are irradiated in the presence of $PhI(OAc)_2$ and I_2 or HgO and I_2 in benzene or by thermal reaction with NaOCl and Et_3N in CH_2Cl_2.

As part of a general study of the reactivity of β,γ-unsaturated oximes[1] we have examined their reactions in the presence of reagents known to yield free radicals. A survey of the literature on iminoxyl radicals suggests that such radicals have not been generated photochemically in solution previously. Therefore, the methodology for the generation of alkoxyl radicals was used as a model. Two methods, $PhI(OAc)_2$–I_2 in 1,2-dichloroethane[2] and HgO–I_2 in benzene[3] have been used extensively by several groups and these methods were utilised in this study. Thus we report the photochemical reactions of the β,γ-unsaturated oximes **1** with both these reagent systems.

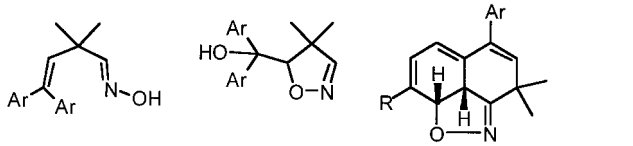

1a Ar = Ph
b Ar = *p*-BrC_6H_4
c Ar = *p*-ClC_6H_4
d Ar = *p*-$CH_3C_6H_4$

2a Ar = Ph
b Ar = *p*-$CH_3C_6H_4$

3a Ar = Ph, R = H
b Ar = *p*-BrC_6H_4, R = Br
c Ar = *p*-ClC_6H_4, R = Cl
d Ar = *p*-$CH_3C_6H_4$, R = CH_3

The oximes **1** are readily prepared from the corresponding aldehydes. These are synthesised following the method originally reported by Zimmerman and co-workers[4] and more recently extended by Armesto *et al.*[1] Typically irradiation (λ > 280 nm) of the oxime **1a** in benzene in the presence of HgO–I_2 (3 equiv. of each) resulted in the formation of two products. The ^{13}C and ^1H NMR spectra of the more polar component showed it to be the known hydroxydihydroisoxazole **2a** (13%) previously reported by Armesto *et al.*[5]

The ^1H NMR spectrum of the less polar but major component of the mixture showed this to be considerably different from the hydroxydihydroisoxazole **2a**. The identification of this product was not easy by conventional means although the integral and the number of vinylic signals in the ^1H NMR spectrum suggested that addition to one of the aromatic rings had taken place. X-Ray diffraction† showed this product to be a *peri*-naphthisoxazole, 6-phenyl-8,8-dimethyl-10-aza-11-oxatricyclo[7.2.1^{1,9}.0^{5,12}]dodeca-2,4,6,9-tetraene **3a** (55%) (Fig. 1).

The irradiation of the oxime **1a** in 1,2-dichloroethane in the presence of $PhI(OAc)_2$–I_2 (1.2 equiv.), best carried out with a low wattage tungsten lamp, was more efficient and cleaner than in the presence of HgO–I_2, yielding only the *peri*-naphthisoxazole **3a** in 77% yield and recovered starting material. Other derivatives of the oxime behaved similarly and **1b** and **1c** were converted into the corresponding *peri*-naphthisoxazoles **3b** and **3c** in yields of 67 and 68%, respectively.

The formation of the *peri*-naphthisoxazole products from these irradiations suggests that they might arise from a conventional intramolecular 1,3-dipolar addition of a nitrile oxide to an arene. However, there appears to be no literature precedent for the addition of such a 1,3-dipole to a benzene moiety, although there are reports of additions to heteroarenes.[6] Neither are we aware of a precedent for the formation of a nitrile oxide *via* an iminoxyl radical. Thus it was important to verify whether or not the conventional route to nitrile oxides would also yield *peri*-naphthisoxazoles.

The method selected was reaction of the oxime **1b** (250 mg, 0.94 mmol) with NaOCl (0.21 ml of an 8% solution, 1.68 mmol) and Et_3N (10 mg, 0.1 mmol) in CH_2Cl_2 (10 ml).[7] The mixture was stirred at room temperature for 4 days. This indeed yields the same *peri*-naphthisoxazole **3b** obtained by the photochemical route. However, in this instance the yield is only 44% and the reaction time is much longer (4 days). Similar thermal reactivity was observed with the oxime **1d**, which gave the *peri*-naphthisoxazole **3d** in 47%. Interestingly the irradiation of oxime **1d** using either HgO–I_2 or $PhI(OAc)_2$–I_2 failed to yield a *peri*-naphthisoxazole and gave only the corresponding hydroxydihydroisoxazole **2b** in yields varying from 24–45%. Thus there appears to be a difference between the photochemical and the thermal cyclization.

It is most likely that both of the photochemical reactions involve the homolytic fission of OI bonds. There are many literature examples of hypoiodites formed from alcohols using both of the methods utilised here.[2,3] It is reasonable to assume that oximes will also yield hypoiodites and, therefore, these should also undergo OI bond fission with the formation of, in this instance, iminoxyl radicals such as **4**. The cycloaddition could involve this species with the formation of an intermediate such as **5**.

Final cycloaddition and loss of a hydrogen would yield the product. Alternatively the iminoxyl radical could lose a hydrogen to afford the nitrile oxide **6** that would then undergo cycloaddition. We have not resolved this dilemma since it is clear that the conventional path to nitrile oxides also affords the cycloadducts. The one thing that is obvious is that the paths appear to be subtly different. This is seen by the failure of **1d** to undergo the photochemical cyclization while the thermal reaction of **1d** affords **3d**. Currently experiments are in hand to try to resolve this difference.

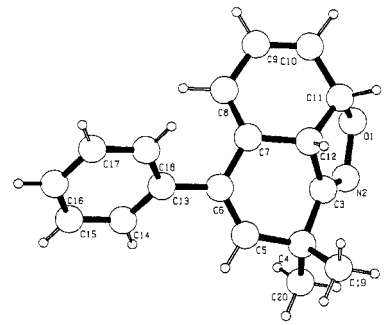

Fig. 1 X-Ray structure of **3a**.

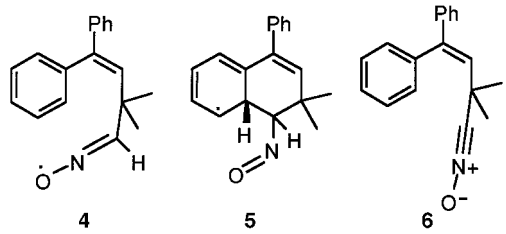

4 5 6

We thank the University of Dundee and the EC (ERBCHRXCT930151) for financial support and the EPSRC National Crystallographic Service (University of Wales, Cardiff) for data collection.

Notes and references

† *Crystal data* for **3a**: $C_{18}H_{17}NO$, M = 263.33, orthorhombic, $P2_12_12_1$, a = 8.6306(7), b = 10.610(2), c = 15.119(4) Å, V = 384.4(5) Å^3, Z = 4, D_c = dimensions 0.18 × 0.14 × 0.14 mm was used. Reflections collected / unique 5768 / 2125 [R(int) = 0.0686] collected on the EPSRC FAST system at University of Wales, Cardiff. Structure solved by direct methods (SHELXS-97) (ref. 8) and refined anisotropically using full-matrix least-squares based on F^2 (SHELXL-97/2). Hydrogen atoms of the tricyclic portion located and refined, other hydrogen atoms placed on calculated positions, all isotropic. Largest difference peak and hole 0.225 and −0.159 e Å^{-3}, R_1 = 0.030, wR_2 = 0.068 for 1792 independent observed reflections [$|F_o| > 4\sigma_F$, $2\theta \leq 50°$. The absolute chirality of **3a** could not be unambiguously determined. CCDC 182/1156. Crystal data are available in CIF format from the RSC web site, see: http://www.rsc.org/suppdata/cc/1999/425

1 See for example: D. Armesto, M. J. Ortiz, A. Ramos, E. P. Mayoral and W. M. Horspool, *J. Org. Chem.*, 1994, **59**, 8115; D. Armesto, A. Ramos and E. P. Mayoral, *Tetrahedron Lett.*, 1994, **35**, 3785; D. Armesto, A. Ramos, M. J. Ortiz, M. J. Mancheno and E. P. Mayoral, *Recl. Trav. Chim. Pays-Bas*, 1995, **114**, 514; D. Armesto, M. G. Gallego, W. M. Horspool and A. Ramos, *J. Chem. Soc., Perkin Trans. 1*, 1996, 107; D. Armesto, A. Ramos, M. J. Ortiz, W. M. Horspool, M. J. Mancheno, O. Caballero and E. P. Mayoral, *J. Chem. Soc., Perkin Trans. 1*, 1997, 1535.

2 J. I. Concepcion, C. G. Francisco, R. Hernandez, J. A. Salazar and E. Suarez, *Tetrahedron Lett*., 1984, **25**, 1553; J. I. Concepcion, C. G. Francisco, R. Freire, R. Hernandez, J. A. Salazar and E. Suarez, *J. Org. Chem*., 1986, **51**, 402; M. Angeles, J. A. Salazar and E. Suarez, *J. Org. Chem*., 1996, **61**, 3999.

3 H. Suginome and S. Yamada, *J. Org. Chem*., 1984, **49**, 3753; H. Suginome and Y. Nakayama, *J. Chem. Soc., Perkin. Trans. 1*, 1992, 1843; K. Orito, K. Yorita and H. Suginome, *Tetrahedron Lett*., 1991, **32**, 5999; K. Kobayashi, Y. Kanno, S. Seko and H. Suginome, *J. Chem. Soc., Perkin. Trans. 1*, 1992, 3111; H. Suginome, Y. Nakayama, H. Harada, H. Hachiro and K. Orito, *J. Chem. Soc., Chem. Commun*., 1994, 451; H. Suginome, T. Kondoh, C. Gogonea, V. Singh, H. Goto and E. Osawa, *J. Chem. Soc., Perkin. Trans. 1*, 1995, 69; H. Suginome, K. Orito, K. Yorita, M. Ishikawa, N. Shimoyama and T. Sasaki, *J. Org. Chem*., 1995, **60**, 3052.

4 H. E. Zimmerman and A. C. Pratt, *J. Am. Chem. Soc.*, 1970, **92**, 6259.

5 D. Armesto, F. Langa, R. P. Ossorio and W. M. Horspool, *J. Chem. Soc., Chem. Commun*., 1990, 123.

6 P. Caramella, G. Cellerino, C. A. Corsico, G. Invernizzi, P. Grunanger, K. N. Houk and F. M. Albini, *J. Org. Chem*., 1976, **41**, 3349; P. Caramella, G. Cellerino, P. Grunanger, F. M. Albini and M. R. R. Cellerino, *Tetrahedron*, 1978, **34**, 3545; P. Caramella, G. Cellerino, K. N. Houk, F. M. Albini and C. Santiago, *J. Org. Chem*., 1978, **43**, 3006; P. Caramella, G. Cellerino, P. Grunanger, F. M. Albini and M. R. R. Cellerino, *Tetrahedron*, 1978, **34**, 3545; V. Librando, U. Chiacchio, A. Corsaro and G. Gumina, *Polycyclic Aromat. Comp.*, 1996, **11**, 313.

7 G. A. Lee, *Synthesis*, 1982, 508.

8 G. M. Sheldrick, in preparation for *J. Appl. Crystallogr.*

Communication 8/09610D

Stereoselective construction of the tetracyclic scalarane skeleton from carvone

Antonio Abad,* Consuelo Agulló, Ana C. Cuñat and M. Carmen Llosá

Departamento de Química Orgánica, Universidad de Valencia, Dr. Moliner 50, 46100 Burjassot, Valencia, Spain. E-mail: antonio.abad@uv.es

Received (in Liverpool, UK) 4th January 1999, Accepted 25th January 1999

The tetracyclic scalarane skeleton 22 has been constructed from (*S*)-(+)-carvone using two intramolecular Diels–Alder reactions as key synthetic steps.

An increasing number of compounds of the relatively new family of the scalarane sesterterpenoids, which show structures based on the hypothetical scalarane skeleton **1**, have been isolated from different marine organisms.[1] These compounds

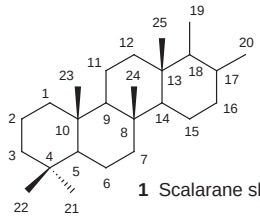

1 Scalarane skeleton

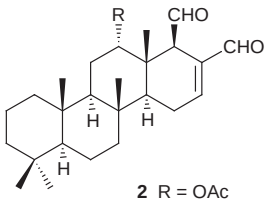

2 R = OAc

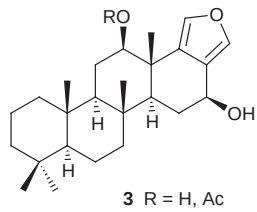

3 R = H, Ac

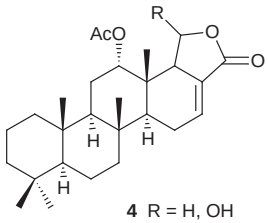

4 R = H, OH

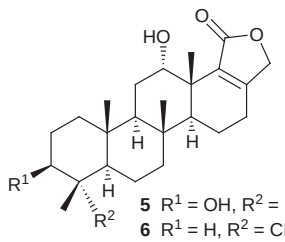

5 R^1 = OH, R^2 = Me
6 R^1 = H, R^2 = CH_2OH

seem to play an important ecological function[2] and some of them exhibit potentially useful biological activities, including antiinflammatory,[3] cytotoxic[4] and antifeedant[5] properties. Most of the members of this group of sesterterpenes possess a 1,4-dialdehyde moiety at C19–C20, either as actual aldehyde groups or latent as γ-butenolide or furan rings, as well as a C12 oxygenated function as common structural features. Recently some compounds with an additional oxygenated function at the C3 position have also been isolated.[6] Some representative compounds are scalaradial **2**, scalarafurans **3**, scalarolides **4**[4] and sesterstatins **5** and **6**.[7]

In spite of their interesting biological activities and challenging structures, this family of sesterterpenes has received little synthetic attention. To the best of our knowledge, only the synthesis of several compounds with the basic scalarane skeleton starting from manool,[8] methyl isocopalate[9] and methyl copalate,[10] as well as the total enantioselective biomimetic synthesis of scalarenedial[11] **2** (R = H) have been published. However, none of these syntheses solves the incorporation of the oxygenated function at the C12 position.

As part of our continuing interest in the synthesis of polycyclic natural products from readily available chiral building blocks,[12] we sought an efficient route to the scalarane sesterterpenes from carvone and we report herein a stereoselective general approach to the tetracyclic ABCD carbon framework. Explicitly, we describe the efficient preparation of the compound **22**, which has the scalarane skeleton and functionalisation suitable for further elaboration into some of the more representative natural scalaranes. The synthesis of **22** is effected using (*S*)-carvone as a C-ring synthon which is incorporated into the tetracyclic framework following a C→CD→ABCD ring annulation strategy, using two intramolecular Diels–Alder (IMDA) reactions as key synthetic steps.[13]

The synthesis commences with the preparation of the propargyl (prop-2-ynyl) compound **15**, precursor of the IMDA reaction that allows the construction of the CD ring subunit (Scheme 1). The known dialkylated carvone **9**, obtained in 70% overall yield from (*S*)-carvone by two consecutive alkylations with MeI and 3-iodopropanaldehyde diethyl acetal,[12a] was stereoselectively converted into the α-epoxy ketone **10** in 92% yield by treatment with alkaline H_2O_2. Treatment of **10** with the lithium derivative of methoxymethyl(diphenyl)phosphine oxide

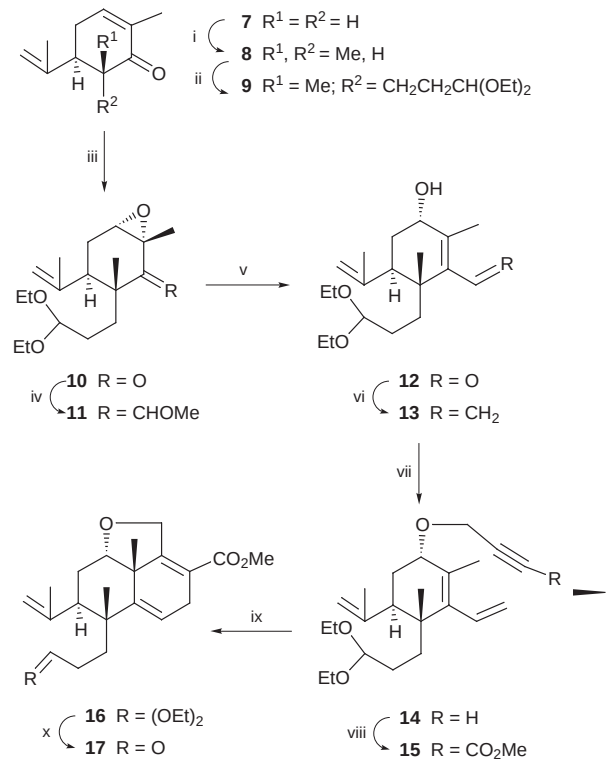

Scheme 1 *Reagents and conditions*: i, LDA, THF, −10 °C then CH_3I; ii, LDA, HMPA–THF, −78 °C then $(EtO)_2CHCH_2CH_2I$, 70% from **7**; iii, H_2O_2, NaOH, MeOH, room temp., 92%; iv, $Ph_2P(O)CH(Li)OMe$, THF, −78 °C then NaH, DMF, from 0 °C to room temp.; v, chromatography on silica gel, 77% from **10**; vi, $Ph_3P{=}CH_2$, THF, −20 °C, 85%; vii, Bu^n_4NI, $BrCH_2CCH$, 60% NaOH, room temp., 97%; viii, BuLi, THF, −78 °C then HMPA, $CNCO_2Me$, 87%; ix, toluene, 105 ºC, 99%; x, PPTS, acetone–H_2O, reflux, 87%.

in THF at low temperature afforded a mixture of crystalline β-hydroxyphosphine oxides, which were subjected to *syn* elimination by treatment with NaH in DMF at 0 °C to give a mixture of isomeric vinyl ethers **11**. Direct chromatographic purification of this mixture on silica gel resulted in chemoselective hydrolysis of the vinyl ether moiety and consecutive opening of the epoxide, providing the desired unsaturated hydroxy aldehyde **12** cleanly and efficiently (77% overall yield from epoxy ketone **10**).† Methylenation of **12** under Wittig conditions then gave dienol **13** in 85% yield, which was transformed into the propargyl ether **14** in very high yield by reaction with propargyl bromide under phase-transfer conditions. Sequential treatment of compound **14** with BuLi and methyl cyanoformate in the presence of added HMPA provided **15** in 87% yield, which underwent a smooth IMDA cycloaddition upon heating in a sealed tube at 105 °C overnight in anhydrous toluene. The reaction takes place very cleanly to give the tricyclic system **16** in nearly quantitative yield.[14]

After successfully accomplishing the synthesis of the CD ring fragment, attention was turned towards the construction of the AB rings, for which we followed a parallel route to that previously used by us for the preparation of a related system (Scheme 2).[12c] Removal of the aldehyde acetal function of **16** with PPTS in aqueous acetone afforded the aldehyde **17** in 87% yield. Wittig reaction of **17** with (α-formylethylidene)triphenylphosphorane provided the chain-extended aldehyde **18**, which by subsequent standard Wittig methylenation afforded the compound **19** in 78% overall yield. Heating a solution of this compound in toluene and a small amount of propylene oxide in a sealed tube at 185 ºC for 6 days afforded the pentacyclic compound **20**, with the expected *trans–anti–trans* fused ABC ring system of the scalarane framework, in 85% yield after column chromatography.

Completion of the synthesis of compound **22** was effected as follows. First **20** was submitted to Simmons-Smith cyclopropanation conditions to chemo- and stereoselectively cyclopropanate the ring A double bond, an indirect way of introducing the geminal dimethyl group at C-4 of the natural scalaranes. Finally, cleavage of the dihydrofuran ring of **21** occurred smoothly and cleanly by treatment with Ac_2O and zinc iodide, being accompanied by simultaneous lactonisation to give the scalarane-type compound **22**‡ in 86% overall yield for the last two steps.

The synthesis of **22** from (*S*)-(+)-carvone is thus completed in 15 synthetic operations in 17% overall yield. We believe that this compound constitutes an attractive intermediate for the synthesis of the more representative scalaranes. Work is currently in hand to further elaborate this intermediate towards scalaradial.§

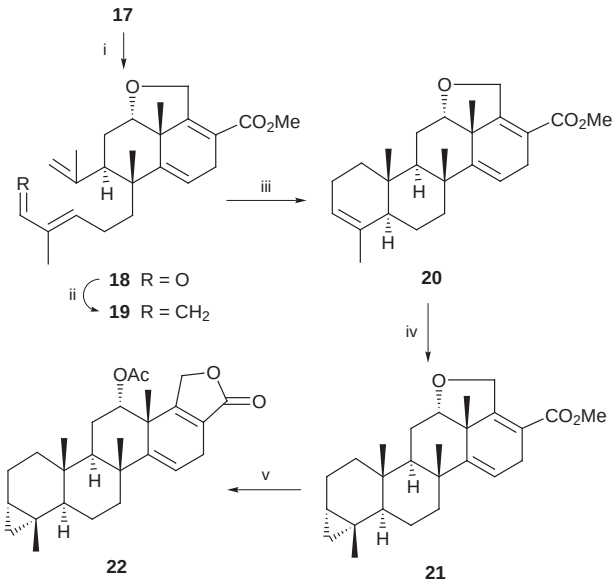

Scheme 2 *Reagents and conditions*: i, Ph_3P=CMeCHO, benzene, reflux, 87%; ii, Ph_3P=CH_2, THF, −20 °C, 90%; iii, toluene, 185 °C, 85%; iv, Et_2Zn, CH_2I_2, toluene, room temp., 89%; v, ZnI_2, $(MeCO)_2O$, room temp., 96%.

Financial support from DGICYT (Grant PB95-1088) is gratefully acknowledged. Special thanks are due to Dr Roberto M. Sotelo (Programa Intercampus América Latina/España 1997 from Universidad Tecnológica Nacional de Avelladena, Argentina) for the repetition of some reactions.

Notes and references

† Alternative procedures to effect the same transformation using different mild acidic conditions also promoted hydrolysis of the acetal moiety.

‡ All new compounds give satisfactory analytical and spectral data. *Selected data* for **16**: $[\alpha]_D^{21}$ −21.3 (*c* 2.8, $CHCl_3$); δ_H(300 MHz, $CDCl_3$) δ 5.75 (1H, dd, *J* 6.9, 1.8), 4.82 and 4.72 (1H each, each br s), 4.78 (1H, dd, *J* 15.5, 2.7), 4.58 (1H, dd, *J* 15.5, 3.8), 4.4 (1H, dd, *J* 5.3, 5.2), 4.17 (1H, dd, *J* 8.6, 4.5), 3.71 (3H, s), 3.61 and 3.44 (2H each, each m), 3.28 (1H, dd, *J* 20.7, 6.9), 2.73 (1H, m), (3H, s), 1.16 (6H, t, *J* 6.5), 1.11 (3H, s), 1.06 (3H, s). For **20**: $[\alpha]_D^{21}$ −44.7 (*c* 3.3, $CHCl_3$); mp 159–160 °C (from EtOH); δ_H(400 MHz, $CDCl_3$), 5.65 (1H, dd, *J* 6.5, 1.5), 5.27 (1H, br s), 4.96 (1H, dd, *J* 14, 2.4), 4.31 (1H, dd, *J* 14, 3.5), 3.92 (1H, dd, *J* 4.5, 1.7), 3.74 (3H, s), 3.34 (1H, dd, *J* 20.7, 6.5), 2.65 (1H, dddd, *J* 20.7, 3.5, 2.4, 1.5), 1.61 (3H, br s), 1.19 (3H, s), 1.107 (3H, s), 0.786 (3H, s). For **22**: $[\alpha]_D^{21}$ +82 (*c* 2.8, $CHCl_3$); mp 217–220 °C (from EtOH–acetone); δ_H(400 MHz, $CDCl_3$) 5.73 (1H, dd, *J* 4.6, 2.9), 4.93 (1H, dd, *J* 3.0, 2.2), 4.82 (1H, ddd, *J* 16.5, 3.3, 1.5), 4.48 (1H, ddd, *J* 16.5, 2.4, 2.3), 2.96 (1H, m), 2.82 (2H, m), 1.95 (3H, s), 1.42 (3H, s), 1.25 (3H, s), 0.98 (3H, s), 0.8 (1H, m), 0.82 (3H, s), 0.55 (1H, m), 0.44 (1H, dd, *J* 9.5, 4), 0.35 (1H, ddd, *J* 18.8, 12.7, 6.9), −0.03 (1H, dd, *J* 5.3, 4.0).

§ This transformation requires the establishment of a *trans* CD ring fusion. An initial experiment showed that the hydrogenation of the C14–C15 double bond of the alcohol resulting from hydrolysis of the acetate group of **22**, with $[Ir(cod)(py)(PCy_3)]PF_6$ takes place chemo- and stereo-selectively to give the required *trans* CD ring fusion.

1 J. D. Connolly and R. A. Hill, in *Dictionary of Terpenoids*, 1st edn., Chapman and Hall, London, 1991, vol. 3, p. 1110; D. J. Faulkner, *Nat. Prod. Rep.*, 1997, **14**, 259 and previous reviews of this series.
2 R. P. Walker, J. E. Thompson and D. J. Faulkner, *J. Org. Chem.*, 1980, **45**, 4876.
3 K. B. Glaser, M. L. Sung, Y. W. Lock, J. Bauer, D. Kubrak and A. Kreft, *Bioorg. Med. Chem. Lett.*, 1994, **4**, 1873, and references cited therein.
4 A. Rueda, E. Zubía, M. J. Ortega, J. L. Carballo and J. Salvá, *J. Org. Chem.*, 1997, **62**, 1481 and references cited therein.
5 B. Terem and P. J. Scheuer, *Tetrahedron*, 1986, **42**, 4409; M. A. Becerro, V. J. Paul and J. Starmer, *Marine Ecology Progress Series*, 1998, **168**, 187.
6 N. Tsuchiya, A. Sato, T. Hata, N. Sato, K. Sasagawa and T. Kobayashi, *J. Nat. Prod.*, 1998, **61**, 468.
7 G. R. Pettit, Z. A. Cichacz, R. Tan, M. S. Hoard, N. Melody and R. K. Petitt, *J. Nat. Prod.*, 1998, **61**, 13.
8 W. Herz and J. S. Prasad, *J. Org. Chem.*, 1982, **47**, 4171; V. Ragoussis and M. Liapis, *J. Chem. Soc., Perkin Trans. 1*, 1990, 2545; N. Ungur, M. Gavagnin and G. Cimino, *Nat. Prod. Lett.*, 1996, **8**, 275.
9 M. González-Sierra, R. M. Cravero, M. A. Laborde and E. A. Rúveda, *J. Chem. Soc., Perkin Trans. 1*, 1985, 1227.
10 T. Nakano, M. I. Hernández, A. Martín and J. D. Medina, *J. Chem. Soc., Perkin Trans. 1*, 1988, 1349.
11 E. J. Corey, G. Luo and S. Lin, *J. Am. Chem. Soc.*, 1997, **119**, 9927.
12 (*a*) A. Abad, C. Agulló, M. Arnó, A. C. Cuñat, B. Meseguer and R. J. Zaragozá, *J. Org. Chem.*, 1998, **63**, 5100; (*b*) A. Abad, C. Agulló, M. Arnó, M. L. Marín and R. J. Zaragozá, *Synlett*, 1997, 573; (*c*) A. Abad, C. Agulló, M. Arnó, A. Cantín, A. C. Cuñat, B. Meseguer and R. J. Zaragozá, *J. Chem. Soc., Perkin Trans. 1*, 1997, 1837.
13 For previous works which use carvone and an IMDA reaction for the construction of other polycyclic natural products, see: V. H. Rawal and S. Iwasa, Abstracts of Papers, 204th National Meeting of the American Chemistry Society, Washington, DC, American Chemical Society, Washington, 1992, ORGN 35; T. K. M. Shing, Q. Jiang and T. C. W. Mak, *J. Org. Chem.*, 1998, **63**, 2056. For reviews of the intramolecular Diels–Alder reaction, see: W. R. Roush, in *Comprehensive Organic Synthesis*, ed. B. M. Trost and I. Fleming, Pergamon, Oxford, 1991, vol. 5 (ed. L. A. Paquette), ch. 4.4, p. 513 and references cited therein.
14 A related strategy has been previously used for the synthesis of the AB rings of the labdane diterpene forskolin, see: M. I. Colombo, J. Zinczuk and E. A. Rúveda, *Tetrahedron*, 1992, **48**, 963.

Communication 9/00081J

Photoinduced electron transfer in sexithiophene/fullerene derivative blends: evidence of long-lived spin correlated radical pairs

Luigi Pasimeni,*[a] Anna Lisa Maniero,[a] Marco Ruzzi,[a] Maurizio Prato,[b] Tatiana Da Ros,[b] Giovanna Barbarella[c] and Massimo Zambianchi[c]

[a] *Department of Physical Chemistry, University of Padova, Via Loredan 2, I-35131 Padova, Italy*
[b] *Department of Pharmaceutical Sciences, University of Trieste, Piazzale Europa 1, I-34127 Trieste, Italy. E-mail: prato@univ.trieste.it*
[c] *I.Co.CEA, Area Ricerca C.N.R., Via Gobetti 101, I-40129 Bologna, Italy*

Received (in Cambridge, UK) 19th November 1998, Accepted 15th January 1999

Photoinduced electron transfer between sexithiophene and fullerene derivatives in the solid phase has been studied by transient EPR spectroscopy: spin correlated radical pairs were observed having a lifetime of 10 μs and mean distance of 20 Å.

Several classes of electron donor–acceptor (D–A) systems have been investigated displaying through-bond and through-space mechanisms of photoinduced electron transfer (PET), the latter mechanism being responsible for the charge-separated state in D–A blends. Among other systems,[1] the PET process has been fully investigated in blends of thiophene polymers and oligomers and C_{60} as building blocks.[2,3]

The thiophene–C_{60} combination is particularly attractive because of the tunable donor properties of the thiophenes[4–6] (depending on their chain length and substituents) and the acceptor properties of C_{60}. PET from π-conjugated polymers and oligomers of thiophene derivatives to C_{60} have been studied mainly by photoinduced absorption (PIA) spectroscopy and light-induced electron paramagnetic resonance (LEPR).[1] Using PIA spectroscopy, it was found that the forward electron transfer is extremely fast (ps time scale), while the rate for back electron transfer can be many orders of magnitude lower.

Compounds **1**[7] and **2**[8] (Scheme 1) were prepared as described previously. Mixed films of sexithiophene/fullerene composites were prepared by dissolving the donor and acceptor mixture (1 : 1 molar ratio) in toluene in quartz tubes. After evaporating the solvent at a pressure of 10^{-1} Torr, the tubes were sealed under vacuum. The EPR experiments consisted of laser excitation followed by time-resolved direction of the signal.†

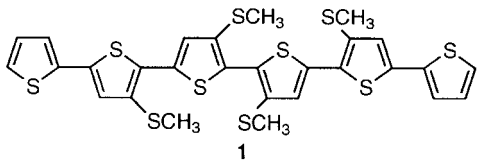

1

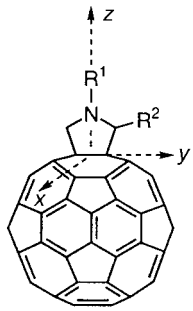

2 $R^1 = CH_2CH_2OCH_2CH_2OCH_2CH_2OCH_3$; $R^2 = H$

Scheme 1 Schematic view of possible structure of the **1**/**2** radical pair.

Field-swept spectra of **1**/**2** blends obtained at variable delay time from the laser pulse, are shown in Fig. 1(a) and (b). Within 0.5 μs from the laser pulse the signal reaches its maximum, then the spectrum intensity decays to zero within several microseconds.

The spectrum at its maximum intensity, shown in Fig. 1(c), is typical of spin correlated radical pairs.[9,10] Upon excitation and photoinduced electron transfer, the D^+A^- radical pair produced is characterized by two radicals having different g factors, g_D and g_A that interact by spin exchange and dipolar interactions, with J and D the constants that express their strength, respectively. Thorough analysis of the spectrum allows one to obtain information about the structure of the charge separated radical pair.

The basic EPR spectrum of a spin-correlated radical pair, created in a singlet or a triplet configuration, consists of four peaks arranged as two doublets with equal splittings determined by the spin–spin interaction between the radicals. Both doublets have one component emissive (e) and the other absorptive (a), reflecting the non-equilibrium populations of the four-electron

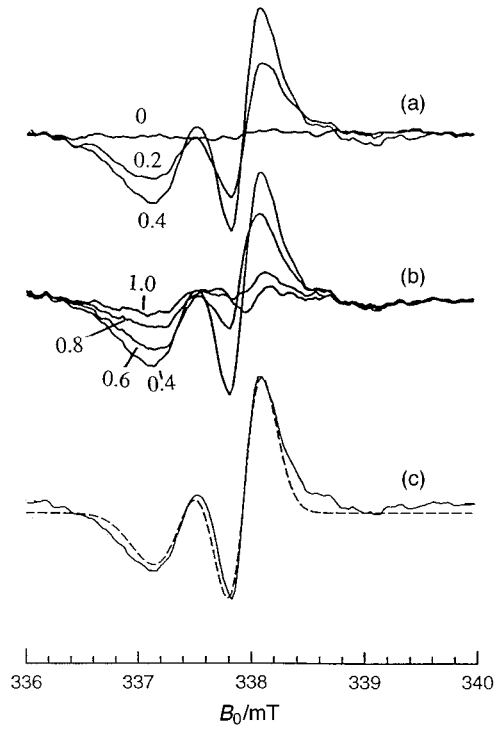

Fig. 1 Growth (a) and decay (b) of the field-swept transient EPR spectra recorded at different delay times from the laser pulse and at 120 K in **1**/**2** blends are shown. (c) Spectrum at the maximum intensity (delay time 0.4 μs, solid line) and its computer simulation (dashed line). The values of g_D = 2.0030 and g_A = 1.9998 factors were used assumed as isotropic. The value of g_A is typical of the monoanion of a C_{60} adduct.

spin states. In case of hyperfine interactions with magnetic nuclei of one or both radicals of the pair, each doublet may become a more complicated multiplet. For non-oriented samples, the EPR signal has to be averaged over all the orientations of the radical pair with respect to the direction of the external field.

As shown in Fig. 1(a)–(c), the characteristic e/a/e/a pattern for a singlet born radical pair was observed in the whole time range of the experiment, extending from 0.1 to 20 μs. Simulation of the spectrum requires the knowledge of several structural parameters like the components of g_D and g_A tensors and the D and J values, although it is known that the lineshape depends most critically on the relative orientation of the principal axes of the g_D and g_A tensors and the spin–spin dipolar tensor.[10] Because of the lack of structural information on the radical pair, we have calculated the spectrum lineshape for different structural arrangements and different D and J values, and the fitting reported in Fig. 1(c) gave $D = -0.15$ mT and $J = 0.01$ mT, while principal axes of g_D and g_A, and of spin–spin dipolar tensors are assumed parallel. We have found that the spectrum lineshape is rather sensitive to the relative orientation of g and dipolar tensors, but the spread of resonant fields is scarcely affected by the above assumption. An isotropic hyperfine constant of 0.06 mT due to two equivalent hydrogen nuclei on the donor was also included.[11] In the averaging procedure over all orientations of the radical pair the stick diagram at a fixed orientation was convoluted with an envelope function in order to mimic the line broadening due to relaxation and residual unresolved hyperfine splittings. The simulated spectrum is shown in Fig. 1(c).

In order to model the structure of the pair having the charge-separated state we calculated the electron dipolar tensor for which the spin densities on the sexithiophene and on the fullerene moieties are needed. We considered for **1** the spin distribution calculated for sexithiophene,[11] while that for **2** was obtained from a HF calculation on the neutral *N*-methyl analog of **2** by taking the squares of the LUMO coefficients. The dipole–dipole interaction was calculated with the point dipole approximation, justified by the large distance between the two electrons. When the sexithiophene molecule is arranged as shown in Scheme 1, coplanar with the pyrrolidine ring, and its short in-plane axis is parallel to the z axis, the experimental value of $D = -0.15$ mT is reproduced when the centers of mass of the two molecules are 20 Å apart, a distance consistent also with the $J = 0.01$ mT value. This electron–hole (e–h) separation distance seems rather large as compared to the 10.25 Å value calculated for fullerene-doped *N*-poly(vinylcarbazole).[12] This finding supports that, in our case, a secondary radical pair is formed after e–h hopping from a more tightly bound primary pair (primary pair). It is suggested that a multistep process may occur as illustrated in Scheme 2. After the absorption of light from the donor and the exciplex formation ^{1}(AD)* the primary pair (A^-D^+) is generated by PET with the forward rate constant

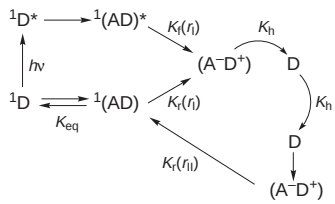

Scheme 2 Schematic representation of the multistep process experienced by the electron–hole pair generated by PET. Primary pair (A^-D^+) may either recombine by rate constant $K_r(r_I)$ or may give rise by hopping of charges (K_h hopping rate constant) to a secondary pair (A^-SD^+). The latter in turn recombines with rate constant $K_r(r_{II}) < K_r(r_I)$ or transforms into subsequent pairs until it leads to radicals trapped at impurity sites.

$K_f(r_I)$, where r_I is the distance of closest approach between donor and acceptor molecules. Then, the primary (e–h) state evolves in time either by recombining to the neutral ^{1}(AD) state with backward rate constant $K_r(r_I)$ or it transforms into a secondary (A^-SD^+) pair where the active role of spacer neutral molecules (S) is to increase the e–h distance. In our case the primary pair eludes observation, since its lifetime must be < 100 ns, as shown by the signal growth in Fig. 1. In the secondary pair the dipolar and exchange interactions as well as the recombination rate constant $K_r(r_{II})$ are reduced and its lifetime falls into the ms domain. Further hopping of charges within the material eventually leads to radicals trapped at impurity sites, providing probably the light-induced EPR signals observed under continuous illumination.[13]

The phenomenon described in this work seems to be peculiar to the specific sexithiophene **1**. In fact, attempts to reproduce the same results with other methylsulfanyl-sexithiophenes[14] were unsuccessful.

In conclusion, we have shown that in blends of sexithiophene **1** with fullerene derivatives **2**, radical pairs are generated by PET that evolve in the ms domain as detected by transient EPR spectra. The resulting charge separated states are much longer than for covalently linked dyads[14] and this suggests that, analogously to other systems,[1] the blends presented here might be well suited for use in photovoltaic and optoelectronic systems.

Notes and references

† The sample was irradiated by a Lambda Physik LPX 100 XeCl excimer laser ($\lambda = 308$ nm, ≈ 10 mJ pulse^{-1}) which fed a Coumarin 47 dye laser with emitting light at 450 nm (pulse duration ≈ 20 ns). A modified Bruker ER 200D X-band (9.5 GHz) EPR spectrometer was used equipped with a fast microwave preamplifier and a broad band (10 kHz–6.5 MHz) video amplifier, whose upper frequency value limits the time resolution of the experimental to *ca.* 150 ns. The time-dependent EPR signal was digitized in a transient recorder (LeCroy 9450 digital oscilloscope) at a maximum acquisition rate of 400 megasamples s^{-1}. Typical two-dimensional (2D) EPR spectra have been recorded by collecting the time profile of the signal at different settings of the resonant magnetic field through the spectrum.

1 N. S. Sariciftci, L. Smilowitz, A. J. Heeger and F. Wudl, *Science*, 1992, **258**, 1474.
2 K. Yoshino, X. Hong Yin, S. Morita and A. A. Zakhidov, *Jpn. J. Appl. Phys.*, 1993, **32**, L140.
3 R. A. J. Janssen, M. P. T. Christiaans, K. Pakbaz, D. Moses, J. C. Hummelen and N. S. Sariciftci, *J. Chem. Phys.*, 1995, **102**, 2628 and references therein.
4 G. Horowitz, F. Garnier, A. Yassar and R. Hajlaoui, *Adv. Mater.*, 1996, **52**, 52.
5 D. Fichou, J.-M. Nunzi, F. Charra and N. Pfeffer, *Adv. Mater.*, 1994, **6**, 64.
6 S. C. Veenstra, G. G. Malliaras, H. J. Brouwer, F. J. Esselink, V. V. Krasnikov, P. F. van Hutten, J. Wildeman, H. T. Jonkman, G. A. Sawatzky and G. Hadziioannou, *Synth. Met.*, 1997, **84**, 971.
7 G. Barbarella, M. Zambianchi, R. Di Toro, M. Colonna, L. Antolini and A. Bongini, *Adv. Mater.*, 1996, **8**, 325.
8 P. Wang, B. Chen, R. M. Metzger, T. Da Ros and M. Prato, *J. Mater. Chem.*, 1997, **7**, 2397.
9 J. R. Norris, A. L. Morris, M. C. Thurnauer and J. Tang, *J. Chem. Phys.*, 1990, **92**, 4239.
10 G. Kothe, S. Weber, E. Ohmes, M. C. Thurnauer and J. R. Norris, *J. Am. Chem. Soc.*, 1994, **116**, 7729.
11 M. Bennati, K. Nemeth, P. R. Surjan and M. Mehring, *J. Chem. Phys.*, 1996, **105**, 4441.
12 Y. Wang and A. Suna, *J. Phys. Chem. B*, 1997, **101**, 5627.
13 A. L. Maniero, L. Pasimeni, G. Barbarella, M. Zambianchi and M. Prato, in *Fullerenes and Photonics IV*, ed. Z. H. Kafafi, SPIE Proceedings, San Diego, 1997, vol. 3142, p. 112.
14 H. Imahori and Y. Sakata, *Adv. Mater.*, 1997, **9**, 537.

Communication 8/09036J

Methyl exchange on silicon during the addition of methylmagnesium iodide to a cyanohydrin *O*-silyl ether

Cécile Arbez-Gindre, Valérie Berl and Jean-Pierre Lepoittevin*

Laboratoire de Dermatochimie, Université Louis Pasteur, Clinique Dermatologique, CHU, F-67091 Strasbourg, France. E-mail: jplepoit@chimie.u-strasbg.fr

Received (in Cambridge, UK) 16th December 1998, Accepted 20th January 1999

Reaction of [^{13}C]methylmagnesium iodide (99 atom% ^{13}C) with cyanohydrin *O*-trimethylsilyl ether 1, followed by acidic hydrolysis, led to the formation of a methyl ketone derivative 2a that was only partially labelled (60 ± 5 atom% ^{13}C); this loss of labelling occurred through a methyl exchange reaction on silicon as shown by the presence on intermediate 2b of [^{13}C]methyl groups on silicon (30 atom% ^{13}C).

The addition of Grignard reagents to cyanohydrin *O*-silyl ethers is a highly efficient method for synthesising α-hydroxy ketones[1,2] or β-amino alcohols[1,3] (Scheme 1). This reaction which has found numerous applications in the synthesis of natural products,[4–6] provides easy access to type **2** α-hydroxy ketones from cyanohydrin *O*-trimethylsilyl ether **1**.

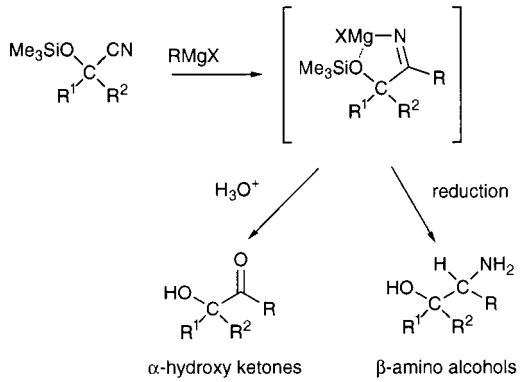

Scheme 1

During studies of the allergenic potential of corticosteroids[7,8] and their interactions with skin proteins by ^{13}C NMR spectroscopy, we were interested in the synthesis of the [21-^{13}C] intermediate **2**. Addition of 2.2 equiv. of [^{13}C]methylmagnesium iodide (99 atom% ^{13}C) to **1** in toluene–Et_2O (4 : 1) at 60 °C for 26 h, followed by acidic hydrolysis, gave a mixture of **2a** and **2b** (Scheme 2) with a combined yield of 79%. However, ^{1}H NMR analysis of these products gave surprising results. In addition to the expected doublet at δ 2.25 (J_{C-H} = 128 Hz) which confirmed the formation of a [^{13}C]methyl ketone, a singlet at δ 2.25 was seen accounting for 40 ± 5% of the ^{1}H integration and due to the presence of [^{12}C]methyl ketone. Moreover, in addition to the expected singlet at δ 0.1, and characteristic of methyl groups on silicon (compound **2b**), we observed a doublet (J_{C-H} = 118 Hz) which is consistent with the presence of [^{13}C]methyl groups on silicon.

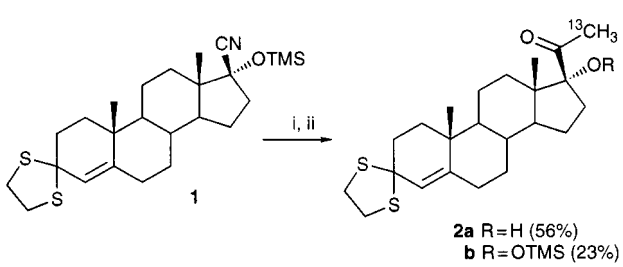

Scheme 2 *Reagents and conditions*: i, $^{13}CH_3MgI$, Et_2O, toluene, 26 h, 55–60 °C; ii, HCl 10%, acetone, THF, 14 h, room temp.

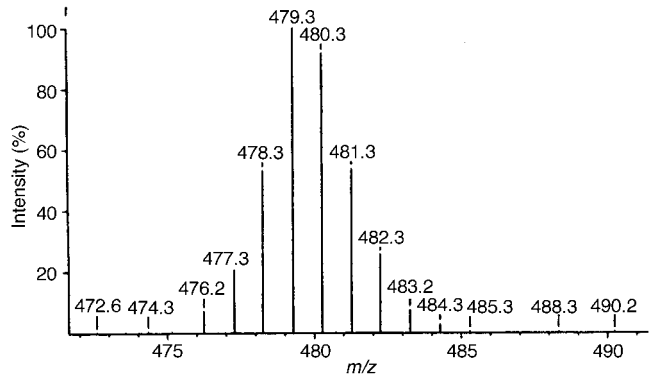

Fig. 1 Mass spectrum of compound **2b** (molecular peak).

This clearly indicates that the 21-methyl position was only partially labelled (60 ± 5 atom% ^{13}C) and that some methyl groups on silicon were also partially labelled (30 atom% ^{13}C). A mass spectrum of compound **2b** (electronic impact, Fig. 1) confirmed this finding and showed an almost statistical distribution of [^{13}C]methyl groups on the molecule.[9]

Addition of Grignard reagents to nitriles proceeds *via* rapid nitrogen complexation, followed by a slow addition of the alkyl group, to form an intermediate imine.[10–12] The presence of 30 atom% ^{13}C on the silyl group indicated that 0.9 equiv. of methyl had been exchanged. If this process occurred before the addition reaction on the nitrile, this would lead to a 1.3 : 0.9 mixture of ^{13}C/^{12}C on the Grignard and therefore to 60 atom% ^{13}C labelling of the methyl ketone.

Thus, our finding could support the idea of a methyl exchange reaction occurring before the Grignard reagent addition on the nitrile, even if we do not know the effect of a potential complexation of methyl magnesium iodide with trimethylsilyl ether on this exchange process.

Notes and references

1 W. R. Jackson, H. A. Jacobs, G. S. Jayatilake, B. R. Matthews and K. G. Watson, *Aust. J. Chem.*, 1990, **43**, 2045.
2 J. R. Luly, C. N. Hsiao, N. BaMaung and J. J. Plattner, *J. Org. Chem.*, 1988, **53**, 6109.
3 W. R. Jackson, H. A. Jacobs, B. R. Matthews, G. S. Jayatilake and K. G. Watson, *Tetrahedron Lett.*, 1990, **31**, 1447.
4 M. Gill, M. J. Kiefer, D. A. Lally and A. Ten, *Aust. J. Chem.*, 1990, **43**, 1497.
5 G. Pattenden, N. A. Pegg and R. W. Kenyon, *J. Chem. Soc., Perkin Trans. 1*, 1991, 2363.
6 I. Oprean, H. Ciupe, L. Gansca and F. Hodosan, *J. Prakt. Chem.*, 1987, **329**, 283.
7 J. P. Lepoittevin, J. Drieghes and A. Goossens, *Arch. Dermatol.*, 1995, **131**, 31.
8 M. Matura, J. P. Lepoittevin, C. Arbez-Gindre and A. Goossens, *Contact Dermatitis*, 1998, **38**, 106.

9 *M* calculated for $C_{26}H_{42}O_2S_2Si$: 478.24.
10 P. Canonne, G. B. Foscolos and G. Lemay, *Tetrahedron Lett.*, 1980, **21**, 155.
11 E. C. Ashby, L. C. Chao and H. M. Neumann, *J. Am. Chem. Soc.*, 1973, **95**, 4896.
12 F. Effenberger, B. Gutterer and J. Syed, *Tetrahedron: Asymmetry*, 1995, **6**, 2933.

Communication 8/09782H

Radical cation Diels–Alder reaction between indoles and exocyclic 1,3-dienes with incorporated intentional cleaving points

Thomas Peglow,[a] Siegfried Blechert*[a] and Eberhard Steckhan[b]

[a] *Institut für Organische Chemie der Technischen Universität Berlin, Strasse des 17. Juni 124, 10623 Berlin, Germany. E-mail: sibl@wap0105.chem.tu-berlin.de*

[b] *Kekulé-Institut für Organische Chemie und Biochemie der Universität, Gerhard-Domagk-Strasse 1, 53121 Bonn, Germany*

Received (in Liverpool, UK) 4th January 1999, Accepted 27th January 1999

A photoinduced electron transfer catalyzed radical cation Diels–Alder reaction between exocyclic dienes, containing an N–O or N–N bond as an intentional cleaving point in the ring moiety, and indoles yields, after cleavage of the N–O or N–N bond, highly functionalized tetrahydrocarbazole derivatives, products of a formal Diels–Alder reaction between indole and open chain 1,3-dienes.

The indole skeleton is a fundamental structural unit of numerous alkaloids and biologically active compounds.[1] Since indole could prove to be an appropriate starting material for further alkaloid synthesis if suitable chemistry can be developed from this parent skeleton, attempts have been made to use the 2,3-double bond of indole in Diels–Alder cycloaddition reactions. However, the electron-rich indole shows only a low tendency to act as a dienophile. Its use mainly has been limited to Diels–Alder reactions with inverse electron demand under application of electron-poor heterodienes such as tetrazine derivatives or tetrachlorothiophene 1,1-dioxide.[2] In bimolecular Diels–Alder reactions with normal electron demand, indole can act as a dienophile if electron-withdrawing groups are present in the 1- and 3-position, but long reaction times and high temperatures are necessary.[3]

In contrast, we demonstrated the very efficient application of electron-rich indole in radical cation Diels–Alder reactions with electron-rich dienes under mild reaction conditions using photoinduced electron transfer (PET).[4,5] However, so far only a few, mainly unfunctionalized simple *endo*- and *exo*-cyclic dienes, *e.g.* cyclohexa-1,3-diene[4] and 1,2-dimethylidenecyclohexane derivatives[5] have been employed, leading to carbocyclic ring-anellated and bridged tetrahydrocarbazole derivatives, respectively. Open-chain 1,3-dienes without a rigid s-*cis*-conformation of the double bonds failed to undergo this PET-catalyzed cycloaddition reaction.

In order to broaden the synthetic scope of this reaction, we focused our investigations on the application of readily accessible functionalized exocyclic dienes, especially those which contain an intentional cleavage point in the ring moiety, thus representing the equivalents of open-chain 1,3-dienes. The rapid construction of multi-functionalized carbazoles according to this approach should be of interest with respect to indole alkaloid synthesis. In the following, our preliminary results are reported.

We started our studies with the five-membered exocyclic diene **2**[6] as a representative functionalized diene (Scheme 1).

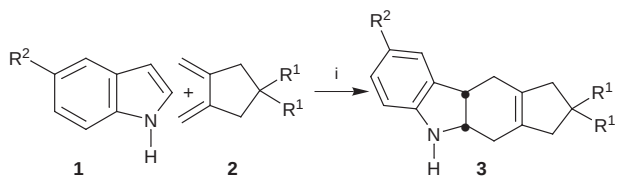

Scheme 1 *Reagents and conditions:* i, 5 mol% photosensitizer, CH_2Cl_2, $\lambda \geqslant 345$ nm, 1000 W, 20 ° C, 1.5 h.

Due to the ease of preparation of a wide variety of these exocyclic dienes *via* an enyne cyclisation reaction,[7] these compounds are promising starting materials for the anticipated carbazole synthesis. Indeed, irradiation of diene **2**, indoles **1** and catalytic amounts of the photosensitizer triphenylpyrylium tetrafluoroborate (TPP) or tris(4-methoxyphenyl)pyrylium tetrafluoroborate (TAP) at $\lambda \geqslant 345$ nm gave good yields of Diels–Alder products **3**. Only the *cis*-fused tetrahydrocarbazoles were obtained (Scheme 1, Table 1, entries 1 and 2).

Encouraged by these results, we turned our interest to exocyclic dienes with an intentional cleavage point in the ring moiety. As potentially ring-cleavable groups we selected the N–O and N–N bonds in compounds **5** and **10** (Schemes 2 and 3). For the rapid synthesis of the hydroxylamine-derived exocyclic dienes **5** we developed a tandem-reaction initiated by a palladium-mediated allylic amination of **4** and followed by a Heck reaction (Scheme 2). The phenyl group attached to the diene moiety was chosen to stabilize the intermediate **7** and should control the regiochemistry of the anticipated cycloaddition reaction with these asymmetrical dienes (Scheme 3).[5]

Irradiation at $\lambda \geqslant 345$nm of dienes **5**, indoles **1** and catalytic amounts of either TPP or TAP gave good to moderate yields of Diels–Alder products **8** and **9** under complete regiocontrol (Scheme 3, Table 1, entries 3–9). The somewhat lower yields obtained with dienes **5** as compared to the five-membered diene **2** might be rationalized by an increased steric demand of these phenyl substituted dienes **5**. As above, in all cases the bridge is *cis*-configured, but, due to the stereogenic carbon bearing the phenyl group, 1:1 mixtures of diastereomers were obtained. An

Table 1 Reaction of dienes **2**, **5** and **10** with indoles **1**

Entry	Diene	R^1	Indole	R^2	Cycloadduct (% yield)	Photo-sensitizer
1	**2**	CO_2Et	**1b**	CO_2Me	**3a** (61)	TPP
2	**2**	CO_2Et	**1d**	NO_2	**3b** (80)	TAP
3	**5a**	Ts	**1a**	H	**8a** (15), **9** (13)	TPP
4	**5a**	Ts	**1a**	H	**9** (39)	TAP
5	**5a**	Ts	**1b**	CO_2Me	**8b** (50)	TPP
6	**5a**	Ts	**1c**	CN	**8c** (61)	TPP
7	**5a**	Ts	**1d**	NO_2	**8d** (61)	TAP
8	**5b**	Ac	**1d**	NO_2	**8e** (63)	TAP
9	**5c**	CO_2Et	**1d**	NO_2	**8f** (60)	TAP
10	**10a**	Ac	**1d**	NO_2	**11a** (58)	TAP
11	**10b**	COPh	**1d**	NO_2	**11b** (60)	TAP

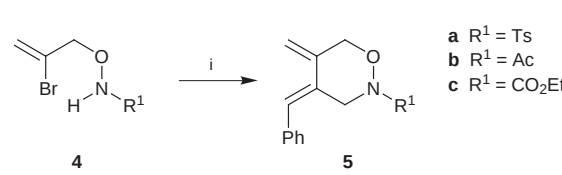

Scheme 2 *Reagents and conditions:* i, $PhCH{=}CHCH_2OCO_2Me$ (1 equiv.), K_2CO_3 (2 equiv.), 5 mol% $Pd(OAc)_2$, 30 mol% PPh_3, MeCN, 20 °C, 2 h, then heated to 80 °C, 16 h, 60–70%.

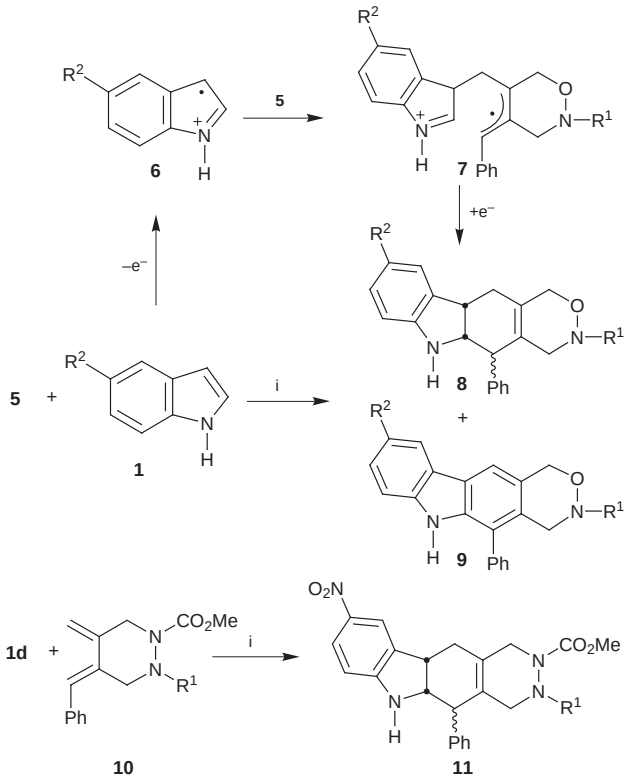

Scheme 3 *Reagents and conditions:* i, 5 mol% photosensitizer, CH_2Cl_2, $\lambda \geqslant 345$ nm, 1000 W, 20 ° C, 1.5 h.

exception is the diastereoselective (> 20 : 1) formation of **8a**, where the hydrogens at the bridge are *cis* relative to the phenyl group, probably owing to a selective aromatization of the other diastereomer giving **9**. Except for reactions with indole **1d**, this aromatization is a major follow-up reaction when TAP is used as sensitizer, but it can be completely suppressed when switching to TPP (except for indole **1a**, see Table 1, entry 3). A further feature of this reaction is the strong dependence of the yields upon the difference between the electronic character of the starting materials: the smaller the difference of the HOMO energies of the starting materials (decreasing from **1a** to **1c**/**d** in reaction with dienes **2** and **5**) the higher the obtained yield of the cycloadduct (see Table 1, entries 1–7).[8]

Variation of the electron-withdrawing group attached to the hydroxylamine component showed no effect on the cycloaddition reaction (Table 1, entries 7–9) and the yields obtained with the hydrazide-derived dienes **10**[9] are comparable to those received with the hydroxylamine derivatives **5** (Scheme 3, Table 1, entries 10 and 11). This was quite surprising because hitherto the incorporation of carbamate and amide groups in the diene was crucial to PET catalyzed reactions with indoles.[10]

As expected, the weak N–O bond of the cycloadducts is easily reductively cleaved with sodium amalgam[11] giving tetrahydrocarbazole **12** in almost quantitative yield (Scheme 4). The nitro group on the indole skeleton remained unchanged under these reaction conditions.Thus, in only four steps a highly functionalized tetrahydrocarbazole derivative is obtained in

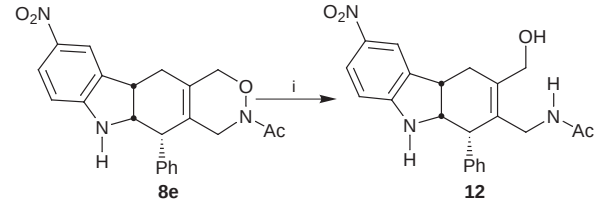

Scheme 4 *Reagents and conditions:* i, Na_2HPO_4 (4.7 equiv.), 15× by weight Na(Hg), EtOH, 0 → 20 °C, 20 h, 94%.

reasonable yield for further synthesis. Further experiments to explore the synthetic potential of this PET-catalyzed cycloaddition reaction are being continued in our laboratories.

This work was supported by the Volkswagen Stiftung (I/71748) and the Fonds der Chemischen Industrie.

Notes and references

1 M. Hesse, *Indolalkaloide*, Verlag Chemie, Weinheim, 1974; R. J. Sundberg, *The Chemistry of Indoles*, Academic Press, New York, 1970; W. A. Remers, in *The Chemistry of Heterocyclic Compounds*, ed. W. J. Houlihan, Wiley-Interscience, New York, 1973, vol. 25, part I, ch. 1; R. A. Jones, in *Comprehensive Heterocyclic Chemistry*, ed. R. A. Katritzky and C. W. Reese, Pergamon, New York, 1984, vol. 4, p. 201.

2 M. S. Raasch, *J. Org. Chem.*, 1980, **45**, 856; A. Padwa, Y. Gareau, B. Harrison and A. Rodriguez, *J. Org. Chem.*, 1992, **57**, 3540; G. Seitz and T. Kaempchen, *Arch. Pharm.*, 1976, **309**, 679; M. Takahashi, H. Ishida and M. Kohmoto, *Bull. Chem. Soc. Jpn.*, 1976, **49**, 1725; G. Seitz and R. Mohr, *Chem. Ztg.*, 1987, **111**, 81; S. C. Benson, C. A. Palabrica and J. K. Snyder, *J. Org. Chem.*, 1987, **52**, 4610; D. L. Boger and S. M. Sakya, *J. Org. Chem.*, 1988, **53**, 1415; S. C. Benson, J. L. Gross and J. K. Snyder, *J. Org. Chem.*, 1990, **55**, 3257; S. C. Benson, J.-H. Li and J. K. Snyder, *J. Org. Chem.*, 1992, **57**, 5285.

3 F. Wenkert, P. D. R. Moeller and S. R. Piettre, *J. Am. Chem. Soc.*, 1988, **110**, 7188; G. A. Kraus, J. Raggon, P. J. Thomas and D. Bougie, *Tetrahedron Lett.*, 1988, **44**, 5605; G. A. Kraus, D. Bougie, R. A. Jacobsen and Y. Su, *J. Org. Chem.*, 1989, **54**, 2425.

4 A. Gieseler, E. Steckhan, O. Wiest and F. Knoch, *J. Org. Chem.*, 1991, **56**, 1405; O. Wiest, E. Steckhan and F. Grein, *J. Org. Chem.*, 1992, **57**, 4034.

5 O. Wiest and E. Steckhan, *Tetrahedron Lett.*, 1993, **34**, 6391; U. Haberl and E. Steckhan, *Diplomarbeit*, Universität Bonn, 1995; U. Haberl, E. Steckhan and S. Blechert, *Int. Symposium of the VW-Stiftung on Intra- and Intermolecular Electron Transfer*, October 1996, Abstract Poster 16.

6 R. Grigg, P. Stevenson and T. Worakun, *Tetrahedron*, 1988, **44**, 4967.

7 For a review, see: B. M. Trost, *Acc. Chem. Res.*, 1990, **23**, 34.

8 It has been previously shown that for an efficient radical cation Diels–Alder reaction, the oxidation potentials, which correspond to the HOMO energies, of diene and dienophile should not differ by much more than 500 mV; a smaller difference normally results in higher yields; J. Mlcoch and E. Steckhan, *Angew. Chem.*, 1985, **97**, 429; J. Mlcoch and E. Steckhan, *Tetrahedron Lett.*, 1987, **28**, 1081; M. Martiny, E. Steckhan and T. Esch, *Chem Ber.*, 1993, **126**, 1671.

9 Prepared *via* a Heck reaction analogous to dienes **5**.

10 S. Blechert and E. Steckhan, unpublished results.

11 G. E. Keck, S. Fleming, D. Nickell and P. Weider, *Synth. Commun.*, 1979, **9**, 281.

Communication 9/00078J

TEMPO-modified graphite felt electrodes: attempted enantioselective oxidation of *rac*-1-phenylethanol in the presence of (−)-sparteine

E. M. Belgsir[a] and H. J. Schäfer*[b]

[a] *Laboratoire de Catalyse en Chimie Organique, UMR CNRS-Université de Poitiers n°6503, 40, avenue du Recteur Pineau, 86022 Poitiers cedex, France*

[b] *Organisch-Chemisches Institut der Universität Münster, Corrensstraße 40, 48149 Münster, Germany. E-mail: schafeh@uni-muenster.de*

Received (in Liverpool, UK) 15th December 1998, Accepted 22nd January 1999

At a TEMPO-modified graphite felt electrode (TMGFE) *rac*-1-phenylethanol 2 is not enantioselectively oxidised in the presence of (−)-sparteine 1, but instead 1 is dehydrogenated to its iminium salt; 2 is oxidised in solution by the oxoammonium salt 6 in the absence of 1, but not on the TMGFE in the range 0–1.0 V *vs.* Ag/AgNO$_3$.

Oxoammonium[1] salts, generated by oxidation of aminoxyl radicals by chemical oxidants or at the anode, have been successfully used for the selective oxidation of alcohols. Of particular interest in this connection was the invention of TEMPO-modified graphite felt electrodes (TMGFE).[2–7] In the presence of (−)-sparteine **1**, it was reported that a TMGFE can oxidise enantioselectively (*S*)-1-phenylethanol (*S*-**2**) in *rac*-**2** leaving 46.2% of **2** as the (*R*)-isomer with 99.6% ee.[7] We failed to reproduce these very interesting results and therefore studied this conversion by cyclic voltammetry and controlled potential electrolysis.[8]

Fig. 1 shows voltammograms recorded at the TMGFE in 0.2 M $NaClO_4$ MeCN solution.[9] The charge, Q_P, involved during oxidation of TEMPO and reduction of $TEMPO^+$ is equal and stable within 30 cycles. Deconvolution and integration of these peaks permits evaluation of the concentration, $C_{NO\cdot}$, of the active aminoxyl radicals at the electrode.[10] It was found that $C_{NO\cdot}$ never exceeds 1 μmol cm^{-3} ($0.4 < C_{NO\cdot} < 0.6$ μmol cm^{-3}).[11] By potential controlled coulometry a density of 0.43 μmol cm^{-3} of active radicals was found, which is consistent with the results obtained *via* cyclic voltammetry.

Electrolysis in a divided cell (Nafion® 117 membrane) under previously reported conditions[7] (10 mmol of **1**, 10 mmol of *rac*-**2** and 5 mmol of tetraline **3** used as standard in 25 ml of 0.2 M $NaClO_4$ MeCN solution) afforded after consumption of 752.6 C, which is sufficient to oxidise about 80% of (*S*)-**2**, no acetophenone **4**, but **2** was almost quantitatively recovered (96%). However, 78% of **1** was oxidized, presumably into the corresponding iminium salt. It has been reported[12–14] that tertiary amines can be dehydrogenated to iminium salts by oxoammonium salts.

With a five-fold lower concentration of *rac*-**2**, **1** and **3** under otherwise the same conditions, the current decreased to 5% after consumption of 64 C. GC of the crude product gave 0.03 mmol of α-tetralol and 0.01 mmol of α-tetralone from **3** and 0.11 mmol of aphylline[15] **5** from **1**, which corresponds to more

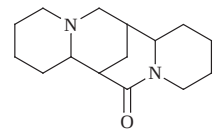

Aphylline **5**

than 80% of the experimental quantity of electricity. The amount of iminium salt of **1** is difficult to evaluate, but it corresponds approximately to the missing quantity of electricity. Compound **4** could not be detected. In an undivided cell no conversion of **2** was found in the presence of **1** at oxidation potentials ranging from 0.53 to 1.10 V *vs.* Ag/AgNO$_3$.

These results led us to investigate the electrochemical behaviour of **1** by cyclic voltammetry (Fig. 2). As expected, **1** is oxidized both on graphite felt and on TMGFE. Under potentiodynamic conditions the TMGFE are inactive towards the *rac*-**2** oxidation between 0 and 0.8 V *vs.* Ag/AgNO$_3$ (Fig. 3), but at 1.0 V *vs.* Ag/AgNO$_3$ an oxidation wave starts even in the absence of the chiral base. It is well known that secondary alcohols are readily oxidised by oxoammonium salts in solution.

This is also found with 4-acetylamino-2,2,6,6-tetramethyl-1-oxopiperidinium **6** as a tetrafluoroborate salt. Species **6** was selected for the homogeneous oxidation because of its similar structure to the immobilized aminoxyl radical, which is also substituted with an amide group at C-4. In the absence of **1** with 1 mmol of *rac*-**2** and 1 mmol of **6** (tetrafluoroborate salt) in 5 ml of MeCN, 50% acetophenone **4** was obtained after 10 min. When **6** (2 mmol) was added to a mixture of *rac*-**2** (2 mmol) and **1** (2 mmol) in 5 ml of MeCN the solution turned immediately to an orange colour, however no *rac*-**2** was converted. The orange

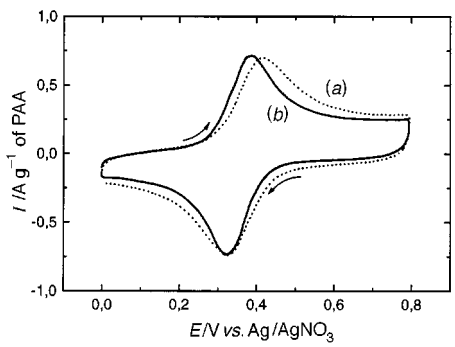

Fig. 1 Voltammograms recorded at 10 mV s^{-1} in 0.2 M $NaClO_4$–MeCN unstirred solution: (*a*) non-crosslinked and non-methylated TMGFE and (*b*) crosslinked and methylated TMGFE ($0.5 \times 1 \times 1$ cm^3).

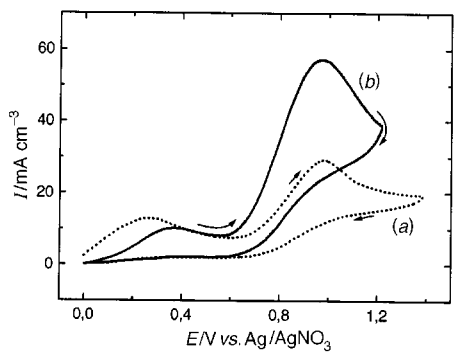

Fig. 2 Voltammograms recorded in 0.2 M $NaClO_4$–MeCN unstirred solution at 10 mV s^{-1} in the presence of 2 mmol (−)-sparteine: (*a*) on a graphite felt electrode and (*b*) on TMGFE ($0.5 \times 1 \times 1$ cm^3).

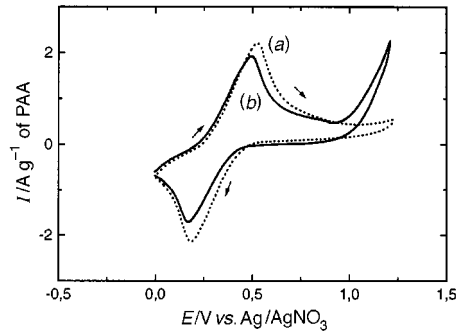

Fig. 3 Voltammograms of a TMGFE ($0.5 \times 1 \times 1$ cm^3) recorded in 0.2 M $NaClO_4$–MeCN stirred solution at 10 mV s^{-1} (*a*) in the absence and (*b*) in the presence of 1 mmol of phenylethanol.

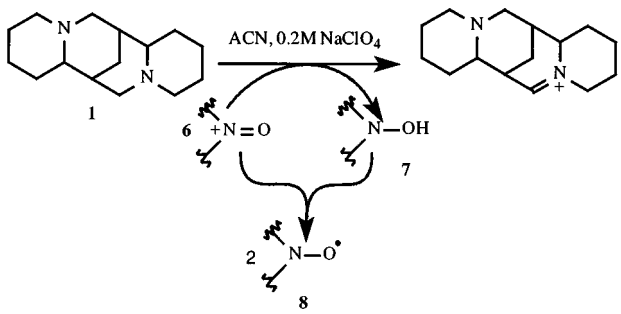

Scheme 1

colour is due to the formation of the radical *via* a fast symproportionation[1] (Scheme 1).

The results above demonstrate that the TMGFEs are not active below 0.8 V *vs.* $Ag/AgNO_3$ towards *rac*-**2** oxidation, which is easily oxidised in solution by **6**, whereby 4-acetamido-2,2,6,6-tetramethyl-1-hydroxypiperidine **7** is formed as a reduction product of **6**. The difference in these two processes is that in homogeneous oxidation **8** is regenerated *via* a base catalysed symproportionation of **6** and **7**, whilst at the TMGFE the immobilised **7** has to be oxidized.

In the absence of a base, the inactivity of the TMGFE towards the oxidation of *rac*-**2** could be due to a slow oxidation of immobilised **7**. Therefore we investigated the electrochemical behaviour of **7** by cyclic voltammetry (Fig. 4). In an unstirred solution, the CV exhibits during the first cycle a very weak oxidation of **7** into **6**, which is reduced during the negative sweep at 0.32 V *vs.* $Ag/AgNO_3$ into **8**. The current of **7** amounts to only 0.5% of that of **8** at the same concentration. In the presence of lutidine **9**, the current increases about twenty-fold, however it is still only 10% of that of **8** at the same concentration. The role of the added base appears to be connected with the regeneration of the active oxidant immobilised onto the electrode,[16] because we demonstrated that in solution **6** can oxidise *rac*-1-phenylethanol without any organic or mineral base.

The TMGFE is thus active for alcohol oxidation, but only in the presence of an electrochemically inert base which can be used in acetonitrile. (−)-Sparteine as base appears to be unsatisfactory, because it is oxidized by **6** prior to the alcohol.

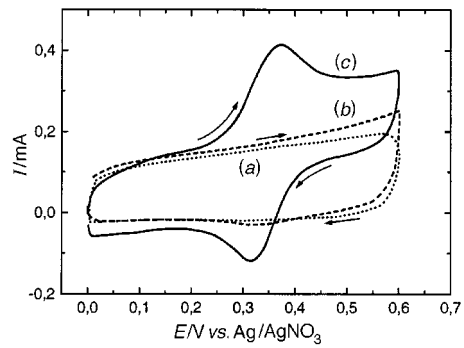

Fig. 4 Voltammograms of a graphite rod electrode recorded in 0.2 M $NaClO_4$–MeCN solution at 10 mV s^{-1} (*a*) in supporting electrolyte only, (*b*) in the presence of 0.2 mmol of **7** and (*c*) in the presence of both 0.2 mmol of **7** and 0.2 mmol of lutidine **9**.

This work was supported by a NATO Fellowship to Dr E. M. Belgsir and by the Arbeitsgemeinschaft Industrieller Forschungsvereinigungen (AIF Nr. 11621 N/1).

Notes and references

1 A. E. J. de Nooy, A. C. Besemer and H. van Bekkum, *Synthesis*, 1996, 1153; and references cited therein.
2 T. Osa, Y. Kashiwagi, K. Mukai, A. Oshawa and J. Bobbitt, *Chem. Lett.*, 1990, 75.
3 Y. Kashiwagi, A. Ohsawa, T. Osa, Z. Ma and J. M. Bobbitt, *Chem. Lett.*, 1991, 581.
4 Y. Kashiwagi, H. Ono and T. Osa, *Chem. Lett.*, 1993, 257.
5 T. Osa, Y. Kashiwagi, Y. Yanagisawa and J. Bobbitt, *J. Chem. Soc., Chem. Commun.*, 1994, 2535.
6 Y. Yanagisawa, Y. Kashiwagi, F. Kurashima, J.-I. Anzai, T. Osa and J. Bobbitt, *Chem. Lett.*, 1996, 1043.
7 Y. Kashiwagi, Y. Yanagisawa, F. Kurashima, J.-I. Anzai, T. Osa and J. M. Bobbitt, *Chem. Commun.*, 1996, 2745.
8 The preparation of TEMPO-modified graphite felt electrodes (TMGFE) was carried out following a previously described procedure (ref. 2–7). The graphite felt electrodes (Le Carbone Lorraine, VG 4000) were refluxed in MeOH for 4 h, dried and dipped in a 0.25% polyacrylic acid (PAA, Aldrich)–methanol (Merck) solution and then carefully dried. Subsequently, the coated electrodes were treated with 4 equiv. of 4-amino-2,2,6,6-tetramethylpiperidin-1-oxyl [with respect to the amount of carboxylic acid (evaluated by weight) at the electrode] in the presence of 4.8 equiv. of DCC (ACROS) in DMF (ACROS) at room temperature for 80–90 h. Thereafter the electrodes were crosslinked with 3.3 equiv. of 1,6-diaminohexane (Fluka) in the presence of DCC for 80 h and were subsequently alkylated (CH_2N_2 or Me_2SO_4 or Et_2SO_4). Following this procedure, no difference was found between the electrodes alkylated in ethereal Et_2O or Me_2SO_4 or Et_2SO_4. If alkylation is carried out before the amide linkage formation, the concentration, $C_{NO\cdot}$, of the active aminoxyl radical decreases but the electrochemical behaviour is similar to that observed with the other electrodes. Increasing PAA thickness did not increase significantly $C_{NO\cdot}$ and did not improve the activity of the electrode even if the reaction time of each preparative step was increased proportionally. Amide linkage formation was also carried out before the coating procedure but the resulting film was very unstable.
Electrochemical measurements and electrolyses were performed in a 0.2 M $NaClO_4$ (ACROS)–MeCN (Merck) solution (dried on molecular sieves 3Å) using a HEKA PG28 generator-potentiostat. Chromatographic analyses were carried out using a Shimadzu chromatograph equipped with a capillary column [HP5 (Hewlett Packard) or FS Hydrodex β-PM (Macherey Nagel)]. *rac*-1-Phenylethanol, acetophenone, tetraline and (−)-sparteine were purchased from Aldrich. The work-up of the electrolyses solution consisted of evaporating the MeCN, then the residue was dissolved in EtOAc, filtered and subjected to chromatography.
9 Conversely to the results reported by Osa *et al.* (ref. 2), no large difference was observed between the peak potentials when the PAA on the electrode was crosslinked and methylated or untreated.
10 $C_{NO\cdot} = Q_P/nFV$, where n is the number of electrons, F is the Faraday equivalent and V the volume of the graphite felt electrode.
11 According to Osa and co-workers, the density evaluated by titration was 50 times higher (24 μmol cm^{-3}) and seems to be very stable from one article to the other (ref. 3–7). However, the quantity of electricity estimated from their voltammogram (ref. 5) is equal to 33.6 mC and corresponds to 0.7 μmol cm^{-3}.
12 D. H. Hunter, D. H. R. Barton and W. J. Motherwell, *Tetrahedron Lett.*, 1984, **25**, 603.
13 D. H. Hunter, J. S. Racok, A. W. Rey and Y. Z. Ponce, *J. Org. Chem.*, 1988, **53**, 1278.
14 J. M. Bobbitt and Zhenkun Ma, *Heterocycles*, 1992, **33**, 641.
15 Structure assignment was performed by comparison of the mass spectra obtained by GC–MS with spectra from the NIST library.
16 A. Deronzier, D. Limosin and J. C. Moutet, *Electrochim. Acta*, 1987, **32**, 1643.

Communication 8/09789E

Novel zwitterionic complexes of Ti(IV) *via* reaction of Lewis acids $M(C_6F_5)_3$ (M = B, Al) with a titanium diene complex (η^5-$C_5Me_4SiMe_2N^tBu$)Ti(1,3-pentadiene)

Alan H. Cowley,* Gregory S. Hair, Brian G. McBurnett and Richard A. Jones*

Department of Chemistry and Biochemistry, The University of Texas at Austin, Austin, Texas 78712, USA. E-mail: cowley@mail.utexas.edu

Received (in Columbia, MO, USA) 2nd December 1998, Accepted 21st January 1999

The reaction of (η^5-$C_5Me_4SiMe_2N^tBu$)Ti(1,3-pentadiene) with $B(C_6F_5)_3$ or $Al(C_6F_5)_3$ in 1:1 mole ratio in hexane solution at room temperature results in the formation of titanium borate or aluminate zwitterions which both feature stabilisation of the Ti(IV) centre by two agostic Ti···H–C interactions.

It has been demonstrated recently that Cp_2Zr(butadiene) reacts readily with $B(C_6F_5)_3$ to afford a zirconium borate zwitterion (**1**) that is an active catalyst for α-olefin polymerization.[1] An important structural facet of this zwitterion is the presence of a weak dative interaction between an *ortho*-fluorine of one of the BC_6F_5 groups and an otherwise vacant coordination site on zirconium.[2] We report here (i) the first structurally characterised example of a new type of titanium borate zwitterion that does not involve intramolecular F→metal stabilisation,† and (ii) the first example of an analogous titanium aluminate zwitterion. In addition, both complexes feature stabilisation of the Ti(IV) metal centre by two agostic C–H···Ti interactions.

It has been reported[3] that, when treated with $B(C_6F_5)_3$, the bridged monocyclopentadienyl titanium diene complex (η^5-$C_5Me_4SiMe_2N^tBu$)Ti(1,3-pentadiene) **2** forms an active olefin polymerization catalyst. We have found that the reaction of **2** with an equimolar quantity of $B(C_6F_5)_3$ in hexane at 25 °C affords a virtually quantitative yield of a dark green crystalline solid (mp 156–157 °C) with an empirical composition (η^5-$C_5Me_4SiMe_2N^tBu$)Ti(1,3-pentadiene)·$B(C_6F_5)_3$ **3**.‡ An X-ray diffraction study of **3** (Fig. 1)§ revealed a zwitterionic structure in which the $B(C_6F_5)_3$ group is bound to the terminal $–CH_2$ carbon atom (C(1)) of the original pentadiene ligand. The C(2)–C(3) and C(3)–C(4) bond distances and the C(2)–C(3)–C(4) bond angle of the coordinated diene are similar to those reported by Erker *et al.*[1] for **1** hence the C(2)–C(3)–C(4) moiety can be regarded as being η^3-attached to the metal. However, the metal–C(2)–C(1) bond angle in **3** is considerably more acute (74.08(10)°) than the corresponding bond angle in **1** such that the Ti–C(1)–B fragment is almost linear (Ti–C(1)–B = 174.1(1)°), the Ti–C(1) distance is short (2.360(2) Å), and the C(1)–B distance is longer in **3** (1.705(3) Å) than in **1** (1.633(9) Å). Collectively, the foregoing structural features strongly suggested the presence of agostic C–H···Ti interactions for the CH_2 hydrogens of C(1). This surmise was confirmed in the later stages of refinement of the X-ray structure. Both hydrogen atoms attached to C(1) were located and refined with isotropic thermal parameters and show relatively short Ti···H distances (Ti–H(1A) = 2.20(2); Ti–H(1B) = 2.27(2) Å). Further support for the existence of the proposed agostic interactions stemmed from the observation of a C–H stretching frequency at 2669 cm^{-1} in the IR spectrum (Nujol mull). ^1H, ^{13}C, and ^{11}B NMR spectroscopic data¶ are also consistent with the X-ray analysis, thus implying that the solid state structure persists in solution. The ^{11}B chemical shift for **2** (δ −8.4) falls in the region observed for four-coordinate boron.[4] Three additional points are worth noting regarding the NMR data. Firstly, a two-dimensional ^1H–^{13}C study (at 500 and 125 MHz) revealed that the N–^{t}Bu and *Me*CHCHCHCH$_2$ signals overlap at δ −1.05. Secondly, the carbon attached to boron, C(1), is not observed in the ^{13}C NMR spectrum, and finally there is a ≈1.0 ppm difference in the ^1H chemical shifts for the C(1) methylene protons. The primary cause of this difference in chemical shifts is probably the existence of the chiral centre at titanium. However, other possible contributors include (i) the influence of the ring current from the tetramethylcyclopentadienyl group and (ii) only one H atom may be agostic in solution.

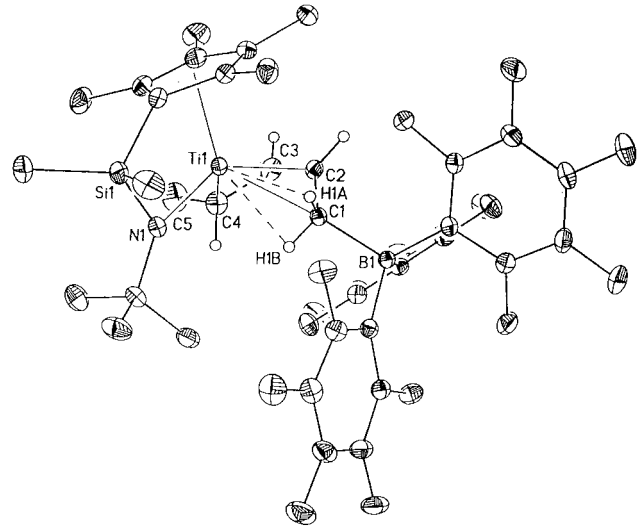

Fig. 1 X-Ray crystal structure of **3**. Selected bond distances (Å) and angles (°) for **3** (the corresponding values for **4** are shown in parentheses with Al(1) replacing B(1)): Ti(1)–C(1) 2.360(2) (2.355(2)), Ti(1)–C(2) 2.282(2) (2.261(3)), Ti(1)–C(3) 2.327(2) (2.344(3)), Ti(1)–C(4) 2.233(2) (2.271(3)), Ti(1)–H(1A) 2.20(2) (2.27(3)), Ti(1)–H(1B) 2.27(2) (2.45(3)), C(1)–B(1) 1.706(3) (2.052(3)), C(1)–C(2) 1.494(3) (1.479(5)), C(2)–C(3) 1.382(3) (1.386(5)), C(3)–C(4) 1.413(3) (1.416(5)), C(4)–C(5) 1.505(3) (1.512(5)), B(1)–C(1)–C(2) 116.8(2) (108.3(2)), C(1)–C(2)–C(3) 125.8(2) (126.6(3)), C(2)–C(3)–C(4) 125.8(2) (125.4(3)), C(3)–C(4)–C(5) 121.9(2) (120.3(3)). Thermal ellipsoids are drawn at the 30% level.

The reaction of **2** with $Al(C_6F_5)_3$ in hexane solution at 25 °C afforded high yields of **4**, the aluminium analogue of **3**.‡ To our knowledge, this represents the first example of a titanium aluminate zwitterion of this type. Structural authentication was provided by an X-ray crystallographic study§ which demonstrated that the geometry of **4** is very similar to that of **3** (Fig. 2). Two agostic Ti–H–C interactions are present with Ti–H(1A) and Ti–H(1B) distances of 2.27(3) and 2.45(3) Å, respectively. As in the case of **3**, NMR spectroscopic data indicate that the solution and solid state structures are very similar. The only significant difference in the ^1H and ^{13}C NMR spectra for **3** and **4** is that in the latter there is no overlap of the N–^{t}Bu and diene methyl ^1H resonances.

We are grateful to the National Science Foundation and the Robert A. Welch Foundation for financial support.

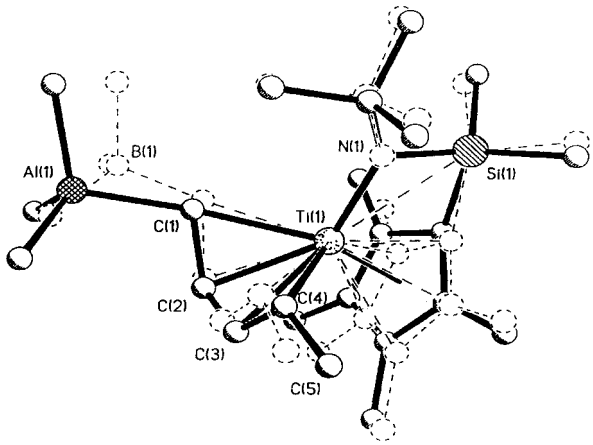

Fig. 2 Comparison of the ball-and-stick structures of **3** and **4**.

Notes and references

† A referee has suggested that the structural differences between the title compounds and the zirconium borate zwitterion (**1**) may be due to the greater electron deficiency at titanium.

‡ *Experimental procedures*: **3**: all manipulations were performed under an atmosphere of dry nitrogen or under vacuum using a Vacuum Atmospheres drybox or standard Schlenk techniques. All solvents were dried prior to use. A solution of $B(C_6F_5)_3$ (1.06 g, 2.07 mmol) in hexane (75 ml) was added to a solution of **2** (0.754 g, 2.06 mmol) in hexane at 25 °C with stirring. A dark green precipitate of **3** formed immediately and was collected and dried under vacuum. X-Ray quality crystals of **3** were grown by slow cooling of concentrated hexane solutions from 50 °C to room temperature. Isolated yield: 1.43 g, 80%; ^{1}H NMR assay indicated that the reaction is essentially quantitative. (Found: C, 52.02; H, 4.19; Ti, 5.45. Calc. for $C_{38}H_{35}BF_{15}NSiTi$: C, 52.02; H, 4.02; Ti 5.46%). Compound **4** was prepared in a similar fashion to that described for **3**.

§ *Crystal data*: **3**, $C_{38}H_{35}BF_{15}NSiTi$, M = 877.47, triclinic, space group $P\bar{1}$, a = 10.243(1), b = 11.376(1), c = 16.419(2) Å, α = 78.67(1), β = 79.45(1), γ = 84.85(1)°, U = 1841.3(3) Å^3, Z = 2, μ = 3.72 cm^{-1}, D_c = 1.583 Mg m^{-3}, F(000) = 892, λ = 0.71073 Å, T = 183 K. Data for **3** and **4** were collected on a Siemens P4 diffractometer. Of a total of 9281 collected reflections, 8284 were unique. The structure was solved by direct methods. The hydrogens on the coordinated diene were located; the remaining hydrogens were placed in calculated positions (C–H, 0.96 Å). Refinement was by full matrix least squares on F^2 with anisotropic displacement parameters for the non-located H atoms. Final R indices [$I > 2\sigma(I)$], $R1$ = 0.0410, $wR2$ = 0.1092.

4, $C_{45}H_{43}AlF_{15}NSiTi$, M = 985.77, monoclinic, space group $P2_1/n$, a = 10.879(3), b = 38.665(6), c = 11.069(2) Å, β = 107.19(2)°, U = 4448(1) Å^3, Z = 4, μ = 3.36 cm^{-1}, D_c = 1.472 Mg m^{-3}, F(000) = 2016, λ = 0.71073 Å, T = 183 K. Of a total of 12 132 collected reflections, 10 205 were unique. The structure was solved by direct methods. The hydrogens on the coordinated diene were located; the remaining hydrogens were placed in calculated positions (C–H, 0.96 Å). Refinement was by full matrix least squares on F^2 with anisotropic displacement parameters for the non-located H atoms. Final R indices [$I > 2\sigma(I)$], $R1$ = 0.0536, $wR2$ = 0.1116. CCDC 182/1160. See http://www.rsc.org/suppdata/cc/1999/437/ for crystallographic files in .cif format.

¶ NMR data for **3**: ^{1}H NMR (500 MHz, C_6D_6) δ −0.37 (s, CH_2-diene, 1H), 0.35 (br s, $SiCH_3$, 3H), 0.58 (s, SiMe, 3H), 0.88 (br s, CH_2-diene, 1H), 1.05 (s, N^{t}Bu + CH_3-diene, 12H), 1.22 (s, CpMe, 3H), 1.28 (s, CpMe, 3H), 1.29 (s, CpMe, 3H), 1.85 (s, CpMe, 3H), 3.26 (m, CH-diene, 1H), 3.90 (m, CH-diene, 1H), 4.91 (m, CH-diene, 1H). ^{13}C{^{1}H} NMR (125 MHz, C_6D_6) δ 6.42 (s, $SiCH_3$), 6.81 (s, $SiCH_3$), 10.83 (s, $CpCH_3$), 12.19 (s, $CpCH_3$), 14.37 (s, $CpCH_3$), 14.46 (s, $CpCH_3$), 18.74 (s, CH_3(diene)), 33.79 (s, CH_3-^{t}Bu), 61.42 (s, C-^{t}Bu), 90.32 (s, CH-diene), 110.52 (s, C(Cp)), 112.04 (s, CH-diene), 127.45 (s, CpMe(Cp)), 130.56 (s, CH-diene), 132.75 (s, CMe(Cp)), 134.85 (s, CMe(Cp)), 137.88 (s, CMe(Cp)), 136.50 (m, $C(C_6F_5)$), 138.50 (m, CF), 147.69 (m, CF), 149.55 (m, CF). ^{19}F NMR (282 MHz, C_6D_6) δ −129.0 (m, *o*-F, 6F), −157.9 (m, *p*-F, 3F), −163.1 (m, *m*-F, 6F). ^{11}B NMR (96 MHz, C_6D_6) δ −8.4.

NMR data for **4**: ^{1}H NMR (500 MHz, C_6D_6) δ −0.09 (d, CH_2-diene, 1H, ^3J = 3.8), 0.33 (s, $SiCH_3$, 3H), 0.54 (s, $SiCH_3$, 3H), 0.72 (d, CH_2-diene, 1H, ^3J = 15.5), 1.05 (s, N^{t}Bu, 9H), 1.12 (d, CH_3-diene, 3H, ^3J = 5.8), 1.15 (s, $CpCH_3$, 3H), 1.18 (s, $CpCH_3$, 3H), 1.31 (s, $CpCH_3$, 3H), 1.73 (s, $CpCH_3$, 3H), 3.02 (qd, CH-diene, 1H), 4.14 (m, CH-diene, 1H), 4.69 (dd, CH-diene, 1H, ^3J = 9.93, 13.75). ^{13}C{^{1}H} NMR (125 MHz, C_6D_6) δ 6.26 (s, $SiCH_3$), 7.36 (s, $SiCH_3$), 10.71 (s, $CpCH_3$), 11.84 (s, $CpCH_3$), 14.02 (s, $CpCH_3$), 14.98 (s, $CpCH_3$), 18.87 (s, CH_3-diene), 33.93 (s, CH_3^{t}Bu), 60.91 (s, C-^{t}Bu), 89.83 (s, CH-diene), 109.36 (s, C(Cp)), 112.44 (s, CH-diene), 127.45 (s, CH-diene), 130.75 (s, CMe(Cp)), 133.12 (s, CMe(Cp)), 135.49 (s, CMe(CP)), 136.20 (m, CF), 138.25 (s, CMe(Cp)), 149.47 (m, CF). ^{19}F NMR (282 MHz, C_6D_6) δ −121.9 (m, *o*-F, 6F), −153.9 (m, *p*-F, 3F), −161.9 (m, *m*-F, 6F).

1 (*a*) B. Temme, G. Erker, J. Karl, H. Luftmann, R. Fröhlich and S. Kotila, *Angew. Chem., Int. Ed. Engl.*, 1995, **34**, 1755; (*b*) B. Temme, J. Karl and G. Erker, *Chem. Eur. J.*, 1996, **2**, 919; (*c*) J. Karl, G. Erker and R. Fröhlich, *J. Am. Chem. Soc.*, 1997, **119**, 11 165.

2 For other examples of a zirconium borate zwitterion featuring Zr···F stabilisation, see J. Ruwwe, G. Erker and R. Fröhlich, *Angew. Chem., Int. Ed. Engl.*, 1996, **35**, 80; Y. Sun, R. E. v. H. Spence, W. E. Piers, M. Parvez and G. P. A. Yap, *J. Am. Chem. Soc.*, 1997, **119**, 5132.

3 D. D. Devore, F. J. Timmers, D. L. Hasha, R. K. Rosen, T. J. Marks, P. A. Deck and C. L. Stern, *Organometallics*, 1995, **14**, 3132.

4 R. G. Kidd, in *NMR of Newly Accessible Nuclei*, vol. 2, ed. P. Laszlo, Academic Press, New York, 1983.

Communication 8/09438A

3-Ethynylcyclopropene: a highly suspicious crystal structure

Steven S. Wesolowski, Jason M. Gonzales, Paul v. R. Schleyer and Henry F. Schaefer III*

Center for Computational Quantum Chemistry, University of Georgia, Athens, Georgia 30602-2525, USA. E-mail: hfsiii@arches.uga.edu

Received (in Corvallis, OR, USA) 7th December 1998, Accepted 25th January 1999

High level *ab initio* structures for 3-ethynylcyclopropene contain a typical cyclopropene C=C double bond of 1.296 Å, in sharp contrast to a recent X-ray structure in which the C=C double bond (1.255(2) Å) is purported to be the shortest yet observed among all hydrocarbons.

Baldridge *et al.* recently reported an X-ray crystal structure for 3-ethynylcyclopropene **1** in which the 'curiously short' 1.255 Å double bond is 'the shortest crystallographically observed C=C double bond known in any hydrocarbon.'[1] Their computed geometry at the spin restricted Hartree–Fock (RHF) level gave a double bond length of 1.27 Å, and inclusion of correlation effects *via* density functional theory† increased their best theoretical estimate to 1.28 Å, 0.03 Å longer than the experimentally inferred value. This discrepancy was not resolved. The authors suggested that the 'deviation could come from difficulties in approximating the orbital arrangement in **1**',[1] *i.e.* that their theoretical levels might not be definitive. Given this disturbing structural difference coupled with reassurances that crystal packing effects and high angle refinement procedures should have only a 'very small effect' in the X-ray structure,[1b] we investigated the structure of **1** using high level coupled cluster techniques.

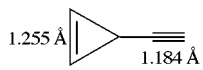

1

We optimized‡ the C_s structure of **1** using the coupled cluster singles and doubles method[8] with a perturbative triples correction [CCSD(T)][9,10] within a TZ2P + f basis set.§ For wavefunction expansions dominated by a single reference determinant, the CCSD(T) approach within a suitable basis set is well known to accurately reproduce structural parameters. At the level chosen, bond lengths between heavy (non-hydrogen) atoms within closed shell molecules are typically in error relative to gas phase experimental values by less than 0.008 Å.[16,17]

Comparison of the TZ2P + f/CCSD(T) and X-ray structures (Fig. 1) reveals a substantial difference in the double bond length and a smaller difference in the triple bond length of the ethynyl group. The *ab initio* double and triple bonds are respectively 0.041 and 0.027 Å longer than those of their X-ray counterparts. Indeed, the only structural parameters in good agreement are the single bond linkage of the ethynyl group and the majority of bond angles. The exceptional similarity of our TZ2P + f/CCSD(T) double and triple bonds to microwave values for the related fragment molecules in Fig. 2 (cyclopropene,[18] propyne,[19] and acetylene[18]) supports the study of substituent effects by Baldridge *et al.* in suggesting that there are no strong adjacent orbital interactions affecting either of these bonds in **1**. Indeed, the X-ray C=C cyclopropene distance in 3-vinylcyclopropene is 1.279 Å (0.024 Å longer than the X-ray distance in **1**).[20]

At every correlated level employed (Table 1) the double bond is more than 0.035 Å longer than experiment. Although the X-ray structure r_α is inherently different from the theoretical equilibrium geometry r_e, differences of this magnitude seem unlikely. Appreciable bond contraction is observed upon increasing the DZP basis to TZ2P with both the MP2 and CCSD(T) methods, and the convergence of these bonds with respect to the basis set was examined further at the MP2 level. However, additional polarization functions [TZ2P + f and TZ2P(f,d)] or even upgrading the basis set on carbon to quadruple-ζ quality (cc-pVQZ/TZ) has only a small effect

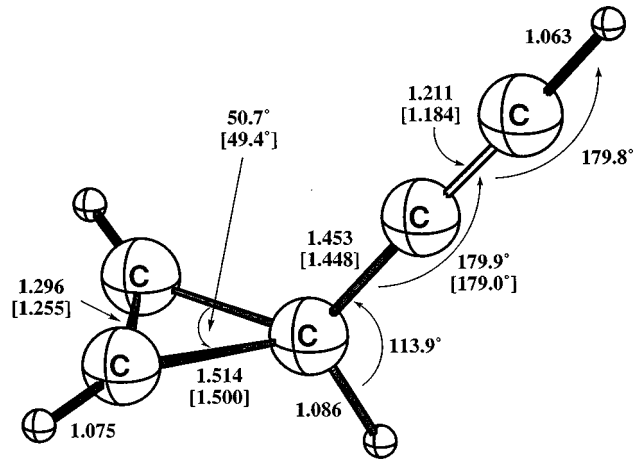

Fig. 1 The structure of 3-ethynylcyclopropene **1** optimized at the TZ2P + f/CCSD(T) level of theory. Bond lengths are in Å and bond angles are in degrees. Experimental bond lengths and angles are given in brackets.

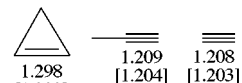

2 **3** **4**

Fig. 2 Theoretical TZ2P + f/CCSD(T) and gas phase experimental [in brackets] bond lengths (Å) in cyclopropene (**2**), propyne (**3**), and acetylene (**4**).

Table 1 The double and triple bond lengths in **1** as a function of level of theory

Method	$d_{C=C}$/Å	$d_{C\equiv C}$/Å
DZP/RHF	1.2841	1.1973
TZ2P + f/RHF	1.2691	1.1840
DZP/BHLYP	1.2904	1.2066
DZP/B3PW91	1.3047	1.2200
DZP/B3LYP	1.3058	1.2207
DZP/MP2	1.3216	1.2387
DZP/CCSD	1.3168	1.2288
DZP/CCSD(T)	1.3233	1.2353
TZ2P/MP2	1.2957	1.2151
TZ2P/CCSD(T)	1.2981	1.2122
TZ2P + f/MP2	1.2939	1.2146
TZ2P(f,d)/MP2	1.2942	1.2145
(cc-pVQZ/TZ)/MP2	1.2899	1.2112
TZ2P + f/CCSD(T)	**1.2957**	**1.2112**
Experiment	**1.255(2)**	**1.184(2)**

(< 0.006 Å) on these bonds, and a similar conclusion for CCSD(T) structures is expected.

Clearly, a high level theoretical equilibrium structure has been obtained which has no extraordinary features and differs dramatically from the X-ray geometry. What is the reason for this disagreement? Our computational reexamination at higher levels than employed earlier[1] increase, rather than decrease, the discrepancies with experiment. Hence, it seems unlikely that the theoretical predictions are incorrect. Solid state effects were considered by the experimentalists, but discounted.[1] Are inaccuracies in the X-ray structure possible? A referee (an expert crystallographer) reexamined the X-ray data in detail, but could find 'neither reasonable nor unreasonable problems with the original work.' Hence, no plausible explanation for the differences exist at present. Further insights will largely hinge on the availability of experimental gas phase data and future solutions of X-ray and neutron diffraction structures for related 3-substituted cyclopropenes.

This research was supported by the US National Science Foundation, grant number CHE-9527468. S. S. W. was supported by a Department of Defense Graduate Fellowship and a Robert S. Mulliken Graduate Fellowship. The authors thank Dr Holger Bettinger, Dr T. Daniel Crawford and Professor John F. Stanton for insightful discussions concerning this research.

Notes and references

† Estimate based on results using the B3PW91 hybrid functional within DZ(2df,2p) and 8s6p3d basis sets. See ref.1.

‡ Methods used in this work include spin restricted Hartree–Fock (RHF), second order Møller–Plesset perturbation theory (MP2), density funnctional theory (DFT), CCSD and CCSD(T). No orbitals are frozen or deleted in the coupled cluster and MP2 procedures. The DFT functionals used are B3LYP, BHLYP and B3PW91 composed of permutations of the correlation functionals of Lee *et al.* (LYP)[2] and Perdew and Wang (PW91)[3] with the exchange functionals of Becke: (B3)[4] and (BH).[5] Stationary point structures are completely optimized within the C_s symmetry constraints using analytic gradient techniques until residual Cartesian coordinate gradients are less than 10^{-6} au. SCF quadratic force constants were determined *via* analytic second derivatives to establish stationary structures as minima. All computations were carried out using the ACESII[6] and Gaussian94[7] program packages.

§ Five basis sets are employed throughout this study. The smallest is a double-ς plus polarization (DZP) basis consisting of the standard Huzinaga–Dunning[11,12] set of contracted Gaussian functions with sets of five d-type and three p-type polarization functions from Dunning's correlation-consistent double-ς (cc-pVDZ) basis sets[13] added to the carbon and hydrogen atoms, respectively. A TZ2P basis set was formed from the Huzinaga–Dunning[11,14] sp sets augmented with two sets of polarization functions from Dunning's cc-pVTZ sets[13,15] (two sets of five d-type functions on C and two sets of p functions on H), and the TZ2P + f and TZ2P (f,d) basis sets include further sets of seven f-type functions (α = 0.761) on C plus a set of five d-type functions (α = 1.057) on H. The cc-pVQZ/TZ set contains Dunning's[13] cc-pVQZ and cc-pVTZ functions centered on the carbon and hydrogen atoms, respectively. The DZP, TZ2P, TZ2P + f, TZ2P (f,d), and cc-pVQZ/TZ basis sets contain 95, 156, 191, 211 and 331 contracted Gaussian functions, respectively.

1 (*a*) K. K. Baldridge, B. Biggs, D. Bläser, R. Boese, R. D. Gilbertson, M. M. Haley, A. H. Maulitz and J. S. Siegel, *Chem. Commun.*, 1998, 1137; (*b*) note 7 in this paper.
2 C. Lee, W. Yang and R. G. Parr, *Phys. Rev. B*, 1988, **37**, 785.
3 J. P. Perdew and Y. Wang, *Phys. Rev. B*, 1992, **45**, 13 244.
4 A. D. Becke, *J. Chem. Phys.*, 1993, **98**, 5648.
5 A. D. Becke, *J. Chem. Phys.*, 1993, **98**, 1372.
6 J. F. Stanton, J. Gauss, J. D. Watts, W. J. Lauderdale and R. J. Bartlett, ACES II. The package also contains modified versions of the MOLECULE Gaussian integral program of J. Almlöf and P. R. Taylor, the ABACUS integral derivative program written by T. U. Helgaker, H. J. Aa. Jensen, P. Jørgensen and P. R. Taylor, and the PROPS property evaluation integral code of P. R. Taylor.
7 M. J. Frisch, G. W. Trucks, H. B. Schlegel, P. M. W. Gill, B. G. Johnson, M. A. Robb, J. R. Cheeseman, T. Keith, G. A. Petersson, J. A. Montgomery, K. Raghavachari, M. A. Al-Laham, V. G. Zakrzewski, J. V. Ortiz, J. B. Foresman, J. Cioslowski, B. B. Stefanov, A. Nanayakkara, M. Challacombe, C. Y. Peng, P. Y. Ayala, W. Chen, M. W. Wong, J. L. Andres, E. S. Replogle, R. Gomperts, R. L. Martin, D. J. Fox, J. S. Binkley, D. J. Defrees, J. Baker, J. P. Stewart, M. Head-Gordon, C. Gonzalez and J. A. Pople, Gaussian 94, Revision C.3, Gaussian, Inc., Pittsburg, PA, USA, 1995.
8 G. D. Purvis and R. J. Bartlett, *J. Chem. Phys.*, 1982, **76**, 1910.
9 K. Raghavachari, G. W. Trucks, J. A. Pople and M. Head-Gordon, *Chem. Phys. Lett.*, 1989, **157**, 479.
10 R. J. Bartlett, J. D. Watts, S. A. Kucharski and J. Noga, *Chem. Phys. Lett.*, 1990, **165**, 513; erratum: 1990, **167**, 609.
11 S. Huzinaga, *J. Chem. Phys.*, 1965, **42**, 1293.
12 T. H. Dunning, *J. Chem. Phys.*, 1970, **53**, 2823.
13 T. H. Dunning, *J. Chem. Phys.*, 1989, **90**, 1007.
14 T. H. Dunning, *J. Chem. Phys.*, 1971, **55**, 716.
15 D. E. Woon and T. H. Dunning, *J. Chem. Phys.*, 1993, **98**, 1358.
16 T. J. Lee and G. E. Scuseria, in *Quantum Mechanical Electronic Structure Calculations with Chemical Accuracy*, ed. S. R. Langhoff, Kluwer Academic Publishers, Dordrecht, 1995, pp. 47–108.
17 This agrees with the very recent comparison of Botschwina *et al.* of the cc-pVQZ/CCSD(T) bond lengths of NCCCNC with r_e data deduced from microwave analysis. C. Bartel, P. Botschwina, H. Bürger, A. Guarnieri, Ä. Heyl, A. Huckauf, D. Lentz, T. Merzliak and E. Mkadmi, *Angew. Chem.*, 1998, **110**, 3036.
18 R. J. Berry and M. D. Harmony, *Struct. Chem.*, 1990, **1**, 49.
19 M. LeGuennec, J. Demaison, G. Wlodarczak and C. J. Marsden, *J. Mol. Spectrosc.*, 1993, **160**, 471.
20 R. Boese, D. Bläser, W. E. Billups, M. M. Haley, W. Luo and B. E. Arney, *J. Org. Chem.*, 1994, **59**, 8125.

Communication 8/09612K

Metallomesogens presenting blue phases in a glassy state and in metallomesogen/nematic mixtures

Julio Buey,[a] Pablo Espinet,*[a] Heinz-S. Kitzerow*[b] and Jochen Strauss[b]

[a] *Departamento de Química Inorgánica, Facultad de Ciencias, Universidad de Valladolid, E-47005 Valladolid, Spain. E-mail: espinet@qi.uva.es*

[b] *Department of Chemistry, University of Paderborn, Warburger Str. 100, 33098 Paderborn, Germany*

Received (in Cambridge, UK) 13th January 1999, Accepted 3rd February 1999

Two palladium complexes are described with very high helical twisting power and producing blue phases, in one case preserved in a glassy state for several days.

Blue phases (BPs)[1] have been the subject of intensive studies during the last decade in the field of chiral liquid crystals because of their anomalous physical and structural features such as Bragg reflections in the visible wavelength, and the occurrence of liquid single crystals (liquid crystal droplets with the shape of solid crystals).[2] These phases are sometimes observed in a narrow range of temperature, typically 2–3 °C, between the cholesteric (N*) and the isotropic (I) phases, in compounds with very small pitch (*p*). Up to three different phases can be observed at zero field,[3] labelled as BPI (body centered cubic structure), BPII (simple cubic structure) and BPIII (structure still under discussion).[4] Although many organic mesogens displaying BPs are known, the first example of a metallomesogen[5] displaying a blue phase has been reported only recently.[6,7] Here we describe two structural types of metallomesogen leading to blue phases. For one of them the BP is preserved in a glassy state for several days. These compounds have been found in the same family of orthometallated compounds that yielded the first ferroelectric[8] and the first cholesteric metallomesogen.[9]

The new chiral complexes **1** and **2** were prepared as described

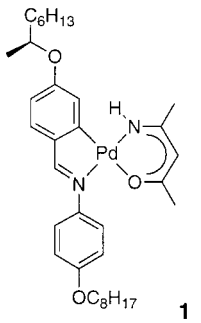

1

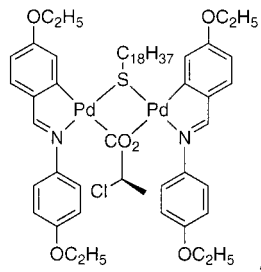

2

elsewhere for similar compounds.[9,10] Their mesogenic properties were studied by optical microscopy and differential scanning calorimetry (DSC) at 5 °C min^{-1}, and the pitch (*p*) and handedness of the cholesteric helix were determined using the modified Grandjean–Cano method.[11] All these data are summarized in Table 1. It should be noted that the complexes display both cholesteric and blue phases in their pure state, but their high viscosity prevents a good alignment of the samples as well as the growing of well shaped BP single crystals to be studied by the Kossel method.[12] For these reasons Cano and Kossel experiments were performed on mixtures of the compounds with the nematic host ZLI-1275 (Merck). The ability of the chiral compounds to induce helical phases on mixing with the nematic host is represented either by the helical twisting power $htp = 1/pc$ (c = concentration of the dopant), or by the molecular twisting power, $mtp = M/px_mr$,[13] where M is the molecular weight, p the pitch, x_m the weight fraction of the chiral dopant and ρ the mass density of the cholesteric solution. The latter quantity is particularly suitable to characterize the twisting power of a molecule.

The mononuclear complex **1** exhibits monotropic BPII and BPI phases at reasonably low temperatures, as well as a very strong selective reflection. The appearance of these phases is in agreement with the estimated pitch of pure **1** ($\approx$ 350 nm). Due to the high viscosity and the low transition temperatures of the material, both phases are retained in a glassy state at room temperature. Thus in contrast to the usual problems, for studying BPs, which require sophisticated temperature control, glassy samples of **1** can be observed, handled, and even stored for days very easily. Kossel experiments could only be carried out on mixtures of **1** and ZLI-1275. For one of the mixtures (62.6 wt% of **1**, deep blue selective reflection at r.t.), three different Kossel diagrams were observed at 47 °C. The first one (Fig. 1a) shows the main ring corresponding to a BPII crystal viewed in its [100] orientation; the second (Fig. 1b) a BPI crystal in the [110] orientation; and the third (Fig. 1c) is the sum of both diagrams, suggesting the coexistence of BPI and BPII crystals in the sample. In order to increase the selective reflection wavelength for the BPII modification, a more dilute mixture was prepared (52.6 wt% of **1**, green selective reflection at r.t.), but in this case only the BPI modification was observed (Fig. 1d).

Moreover, **1** has good solubility in the nematic host, very high *htp* (*i.e.* very low pitch), and a *p* value almost invariant with temperature (17.43 wt% of **1**, Fig. 2). The value of its molecular twisting power is as high as for most chiral dopants used in commercial applications, but still one order of magnitude below the highest value reported for calamitic chiral dopants (DL21 : 28300 m^2 mol^{-1}).[14]

The dinuclear compound **2** also displays a monotropic BPI phase, in the range 98–94 °C, appearing under the microscope

Table 1 Phase transition data and characterisation of the helix for complexes **1** and **2**

Complex	Transition[a]	T/°C	ΔH/kJ mol^{-1}	p^d/μm	htp^d/(mm wt%)$^{-1}$	mtp^d/m^2 mol^{-1}	Handedness
(*S*)-**1**	C–I	85.4	36.5	1.9–2.9	20–30	1500–2400	Right
	I–BPII–BPI–N*[b]	46.1	−0.3[c]				
(*R*)-**2**	C–I	134.1	36.8	−7 to −14[e]	−14 to −26.5[e]	−1600 to −3000	Left
	I–BPI[b]	98.0	−0.3[c]				
	BPI–N*	94.0					

[a] See ref. 1. [b] Monotropic transitions not resolved by DSC. [c] Combined enthalpies. [d] In mixtures with ZLI-1275. [e] See text.

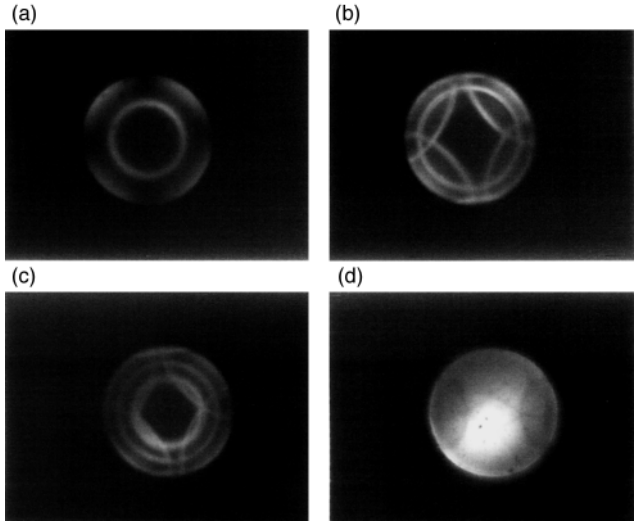

Fig. 1 Kossel diagrams of mixtures of 62.6 wt% of **1** in ZLI-1275 at 47 °C (a–c), and 52.06 wt% at 47 °C (d).

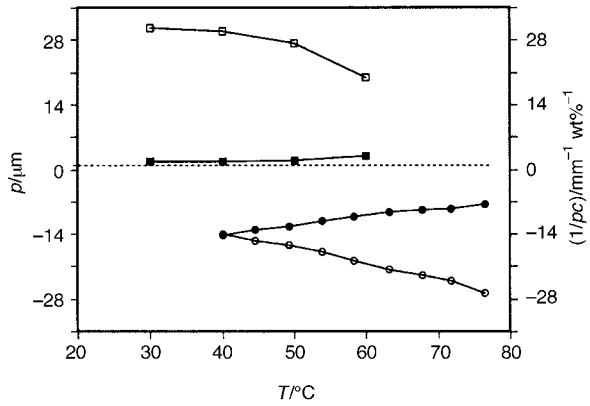

Fig. 2 Temperature dependence of the cholesteric pitch p (■, **1**; ●, **2**) and the helical twisting power $1/pc$ (□. **1**; ○, **2**) in mixtures of 17.43 wt% of **1** in ZLI-1275, or 5.01 wt% of **2** in ZLI-1275.

in its platelet texture. At the lower temperature, some crystallization occurs. Complex **2** gave rather high and temperature-dependent p values (measured on a 5.01 wt% mixture with ZLI-1275, the amount of **2** being limited by its low solubility), leading to estimated p values for pure **2** ranging from ≈350 nm at 76 °C to ≈700 nm at 40 °C. As previously reported for related systems,[9] this strong temperature dependence of p is possibly associated with the occurrence of two conformers in a temperature-dependent thermodynamic equilibrium.[15]

In summary, the mononuclear complex **1** shows a very low p value which is almost temperature independent, and a good solubility in a nematic matrix. Its enantiomer is easily available using the enantiomeric alcohol. These properties are very good for its application as chiral dopant.[16] Furthermore, the glassy state of **1** allows the stabilization of a blue phase for several days. Further studies on these fascinating materials are in progress.

This work was sponsored by the Spanish Comisión Interministerial de Ciencia y Tecnología (Project MAT96-0708), the Junta de Castilla y León (Project VA23/97), and the Deutsche Forschungsgemeinschaft (Sfb 335).

Notes and references

1 For reviews on BPs see: H. Stegemeyer, Th. Blümel, H. Hiltrop, H. Onusseit and F. Porsch, *Liq. Cryst.*, 1986, **1**, 3; P. P. Crooker, *Liq. Cryst.*, 1989, **5**, 751; T. Seidemann, *Rep. Prog. Phys.*, 1990, **53**, 659; H. S. Kitzerow, *Mol. Cryst. Liq. Cryst.*, 1991, **202**, 51.
2 D. L. Johnson, J. H. Flack and P. P. Crooker, *Phys. Rev. Lett.*, 1980, **45**, 641; *Phys. Lett. A*, 1981, **82**, 247.
3 P. P. Crooker and H.-S. Kitzerow, *Condens. Mater. News*, 1992, **1**, 6.
4 J. B. Becker and P. J. Collings, *Mol. Cryst. Liq. Cryst. A*, 1996, **265**, 163; T. C. Lubensky and H. Stark, *Phys. Rev. E*, 1996, **53**, 714; J. Englert, L. Longa and H. R. Trebin, *Liq. Cryst.*, 1996, **21**, 243.
5 For reviews see: A. M. Girour-Godquin and P. M. Maitlis, *Angew. Chem., Int. Ed. Engl.*, 1991, **30**, 375; P. Espinet, M. A. Esteruelas, L. A. Oro, J. L. Serrano and E. Sola, *Coord. Chem. Rev.*, 1992, **117**, 215; *Inorganic Materials*, ed. D. Bruce and D. O'Hare, John Wiley and Sons, Chichester, 1992; S. A.Hudson and P. M. Maitlis, *Chem. Rev.*, 1993, **93**, 861; *Metallomesogens*, ed. J. L. Serrano, VCH, Weinheim, 1995.
6 T. Seshadri and H.-J. Haupt, *Chem. Commun.*, 1998, 735.
7 There is a previous report on metal complexes exhibiting some phases intermediate between the N* and the isotropic liquid, hence suspected to be BPs. However, they could not be unequivocally characterized as such, apparently because of the strong optical absorption of the samples: W. Pyzuk and Y. Galyametdinov, *Liq. Cryst.*, 1993, **15**, 265.
8 P. Espinet, J. Etxebarría, M. Marcos, J. Pérez, A. Remón and J. L. Serrano, *Angew. Chem., Int. Ed. Engl.*, 1989, **28**, 1065; M. J. Baena, J. Barberá, P. Espinet, A. Ezcurra, M. B. Ros and J. L. Serrano, *J. Am. Chem. Soc.*, 1994, **116**, 1899.
9 M. J. Baena, J. Buey, P. Espinet, H.-S. Kitzerow and G. Heppke, *Angew. Chem., Int. Ed. Engl.*, 1993, **32**, 1201.
10 J. Buey and P. Espinet, *J. Organomet. Chem.*, 1996, **507**, 137.
11 G. Heppke and F. Oestreicher, *Z. Naturforsch., Teil A*, 1977, **32**, 899.
12 P. E. Cladis, T. Garel and P. Pieranski, *Phys. Rev. Lett.*, 1986, **57**, 2841; H.-S. Kitzerow, PhD Thesis, Technische Universität Berlin, 1989.
13 C. S. Bak and M. M. Labes, *J. Chem. Phys.*, 1975, **62**, 3066.
14 G. Heppke, D. Lötzsch and F. Oestreicher, *Z. Naturforsch, Teil A*, 1986, **41**, 1214.
15 G. Heppke, D. Lötzsch and F. Oestreicher, *Z. Naturforsch., Teil A*, 1987, **42**, 279; L. Komitov, S. T. Lagerwall, B. Stebler, G. Anderson and K. Flatiscler, *Ferroelectrics*, 1991, **114**, 167; A. J. Slaney, I. Nishiyama, P. Styring and J. W. Goodby, *J. Mater. Chem.*, 1992, **2**, 805; P. Styring, J. D. Vuijk, I. Nishiyama, A. J. Slaney, J. W. Goodby, *ibid.*, 1993, **3**, 399; J. W. Goodby, A. Slaney, I. Nishiyama, J. Vuijk, P. Styring and K. Toyne, *Mol. Cryst. Liq. Cryst.*, 1994, **243**, 231.
16 These and related materials have been tested as chiral dopants in commercial cells: J. Buey and P. Espinet, *Spanish Pat. Appl.*, P9602436, 1996; J. Buey, P. Espinet, R. García and B. Rodríguez, *Spanish Pat. Appl.* P9701817, 1997.

Communication 9/00374F

Selective C_α–C_β bond cleavage by water in allenylidene and alkenylvinylidene ruthenium complexes

Claudio Bianchini,* Maurizio Peruzzini,* Fabrizio Zanobini, Carlos Lopez, Isaac de los Rios and Antonio Romerosa

Istituto per lo Studio della Stereochimica ed Energetica dei Composti di Coordinazione, ISSECC, CNR, Via J. Nardi, 39 - 50132 Firenze, Italy. E-mail: bianchin@fi.cnr.it; peruz@fi.cnr.it

Received (in Basel, Switzerland) 4th January 1999, Accepted 27th January 1999

The Ru(II) complex *mer,trans*-[(PNP)RuCl$_2$(PPh$_3$)] [PNP = MeCH$_2$CH$_2$N(CH$_2$CH$_2$PPh$_2$)$_2$] reacts in refluxing THF with propargyl alcohols HC≡CCRR′OH (R = R′ = Me, Ph; R = Me, R′ = Ph) yielding either the allenylidene complex *fac,cis*-[(PNP)RuCl$_2${C=C=CPh$_2$}] or the alkenylvinylidene derivatives *fac,cis*-[(PNP)RuCl$_2${C=C(H)C(R)=CH$_2$}] (R = Me, Ph); treatment of all these complexes in CH$_2$Cl$_2$ or THF with water results in the formation of the ruthenium carbonyl *fac,cis*-[(PNP)RuCl$_2$(CO)] and free alkenes H$_2$C=CRR′ (R = R′ = Me, Ph; R = Me, R′ = Ph) *via* regioselective C_α–C_β bond cleavage.

Understanding and rationalizing the reactivity of transition metal complexes containing allenylidene ligands, M=C=C=CR$_2$, is a topic of much current interest in organometallic chemistry.[1–3] Sound motivations arise from the increasing applications of allenylidene complexes, especially of ruthenium derivatives, to various catalytic reactions involving C–C bond formation.[4]

As a general trend, nucleophiles may attack either the C_α or C_γ carbon atom in allenylidene ligands affording Fischer-type carbenes or alkynyl compounds, respectively.[5] The addition of water has been found to take place selectively at C_α to give unsaturated hydroxycarbenes.[6] At least in one case, however, there was the suspicion that water might be able to cleave a C–C bond in an allenylidene ligand but no experimental evidence was reported supporting this hypothesis.[7] The question regarding the hydrolytic C–C bond cleavage in allenylidenes and homologous ligands is not of trivial importance given the wide use of their metal complexes as catalyst precursors in a variety of homogeneous processes, especially in reactions where new C–C bonds are formed.[4,8] For this reason, we decided to investigate the reactions of both allenylidene and alkenylvinylidene complexes with water. Ruthenium was the metal of choice as it is known to effectively stabilize cumulene complexes and it also constitutes the essential ingredient in many C–C bond forming reactions.[4,8]

Following the well known Selegue's synthetic protocol,[9] the neutral allenylidene complex *fac,cis*-[(PNP)RuCl$_2$-{C=C=CPh$_2$}] **2** was obtained in 78% yield by refluxing *mer,trans*-[(PNP)Ru(Cl)$_2$(PPh$_3$)] **1**[10] and 1,1-diphenylprop-2-yn-1-ol in THF (Scheme 1).†

Complex **2**[11] was authenticated by means of standard spectroscopic techniques as well as a single-crystal X-ray analysis (Fig. 1).‡ The crystallographic study confirmed the *fac* stereochemistry of the PNP ligand and the *trans* disposition of the diphenylallenylidene ligand and the nitrogen donor atom.[12]

While π-alkyne coordination (**A**) and alkyne to vinylidene tautomerization (**B**) are common steps to any propargyl alcohol activation, the eventual dehydration process of the hydroxyvinylidene intermediate may occur with different regioselectivity (Scheme 2). Either allenylidene (**C**) or alkenylvinylidene derivatives may indeed form depending on the presence of hydrogens on the carbon atom proximal to the OH group. If there are no hydrogens, the allenylidene products are stable,

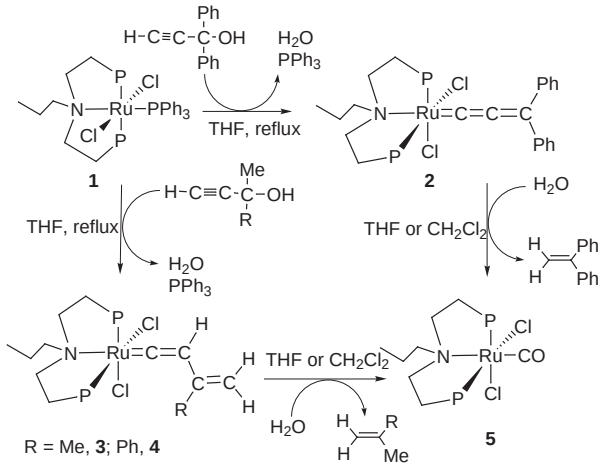

Scheme 1

otherwise they may tautomerize to alkenylvinylidenes (**E**). Alternatively, the alkenylvinylidene ligand may form *via* direct elimination of water from the hydroxyvinylidene intermediate (**D**).[13]

Within this mechanistic picture, it was not surprising to find that **1** reacts with either 1,1-dimethyl- or 1-methyl,1-phenylpropyn-1-ol yielding the alkenylvinylidenes *fac,cis*-[(PNP)RuCl$_2${C=C(H)C(R)=CH$_2$}] (R = Me, **3**; Ph, **4**).[11]‡ It was surprising instead to discover that both the allenylidene

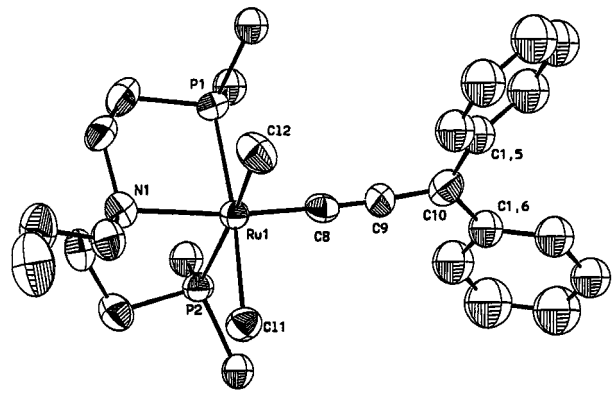

Fig. 1 ORTEP drawing of complex **2**.[18] For sake of clarity only the *ipso* carbon atoms of the phenyl substituents in the PNP ligand are reported. Selected distances (Å) and angles (°): P(1)–Ru(1) 2.314(2), P(2)–Ru(1) 2.289(2), N(1)–Ru(1) 2.335(5), Ru(1)–Cl(1) 2.449(2), Ru(1)–Cl(2) 2.461(2), Ru(1)–C(8) 1.858(7), C(8)–C(9) 1.221(9), C(9)–C(10) 1.376(10), N(1)–Ru(1)–P(1) 82.69(14), N(1)–Ru(1)–P(2) 83.11(15), N(1)–Ru(1)–Cl(1) 90.15(14), N(1)–Ru(1)–Cl(2) 87.96(15), N(1)–Ru(1)–C(8) 173.4(2), P(1)–Ru(1)–P(2) 100.17(8), P(1)–Ru(1)–Cl(1) 171.95(6), P(1)–Ru(1)–Cl(2) 88.49(8), P(1)–Ru(1)–C(8) 90.66(19), P(2)–Ru(1)–Cl(1) 82.52(7), P(2)–Ru(1)–Cl(2) 166.62(6), P(2)–Ru(1)–C(8) 98.35(19), Cl(1)–Ru(1)–Cl(2) 87.59(8), Cl(1)–Ru(1)–C(8) 96.5(2), Cl(2)–Ru(1)–C(8) 91.67(19), Ru(1)–C(8)–C(9) 175.8(6), C(8)–C(9)–C(10) 171.1(7).

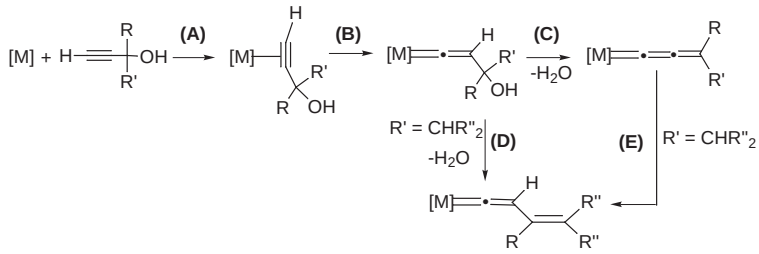

Scheme 2

complex **2** and the alkenylvinylidenes **3** and **4** are transformed by water (5 equiv.) into the known carbonyl derivative *fac*,*cis*-[(PNP)$RuCl_2$(CO)] (**5**)[14] and the corresponding free alkene $H_2C{=}CRR'$ (R = R′ = Ph; R = Me or Ph, R′ = Me). The quantitative formation of 1 equiv. of alkene was shown by GC–MS analysis and NMR spectroscopy (^{1}H, ^{13}C) on both reaction mixtures and samples isolated by TLC. The hydrolysis reactions are quite fast at reflux temperature in either THF or CH_2Cl_2 but take place also at room temperature. When D_2O was employed in the place of H_2O, the alkene was found to regioselectively incorporate two *gem* deuterium atoms ($D_2C{=}CRR'$) indicating that both terminal hydrogens come from water. Finally, the selective incorporation of ^{18}O in the carbonyl complex **5**-^{18}O, $\nu(C^{18}O)$ 1899 cm^{-1}, was observed when the hydrolysis reactions were carried out with $H_2{}^{18}O$ confirming that the C_α–C_β bond scission in either allenylidene or alkenylvinylidene ligand was brought about by water and not by adventitious oxygen.[15]

In conclusion, for the first time it has been shown that both allenylidene and alkenylvinylidene ruthenium complexes, dissolved in organic solvents, may react with water producing CO ligands and free alkene *via* regioselective cleavage of the C_α–C_β bond. The hydrolysis of metal vinylidenes has recently been reported to give carbonyl species and the saturated hydrocarbon derived from the homologation of the vinylidene substituent.[15] From allenylidene and alkenylvinylidene complexes, unsaturated hydrocarbons are selectively formed, which may open the door to the alternative synthesis of high-added value alkenes or alkenes selectively deuterated at the unsubstituted end.

This work was supported by the bilateral program «Azione Integrata» between the University of Florence (Italy) and Almeria (Spain) and by the EC contracts INTAS 96-1176 and INCO ERBIC15CT960746.

Notes and references

† Satisfactory elemental analyses were obtained for **2** (red purple crystals), **3** (pink crystals), and **4** (pink red crystals). Selected spectroscopic data for **2**: IR ($\nu_{C=C=C}$) 1916m cm^{-1}. ^{31}P{^{1}H} NMR (CD_2Cl_2, 85% H_3PO_4, 294 K), δ 49.12 (s). ^{13}C{^{1}H} NMR (CD_2Cl_2, TMS, 294 K), δ 304.3 (t, $^2J_{CP}$ 19.2 Hz, C_α), 233.8 (s, C_β), 150.8 (s, C_γ). For **3**: IR ($\nu_{C=C}$) 1610s cm^{-1}. ^{1}H NMR ($CDCl_3$, TMS, 294 K), δ 5.16 (t, $^4J_{HP}$ 3.3 Hz, 1H, CH), 4.63 and 4.15 (d, $^2J_{HH}$ 1.8 Hz, 1H each, CH_2), 2.28 [s, 3H, CH_3(alkenylvinylidene)]. ^{31}P{^{1}H} NMR ($CDCl_3$, 85% H_3PO_4, 294 K), 47.81 (s). ^{13}C{^{1}H} NMR ($CDCl_3$, TMS, 294 K), δ 313.5 (t, $^2J_{CP}$ 18.0 Hz, C_α), 126.6 (s, C_δ), 114.2 (s, C_β), 18.5 [s, CH_3(alkenylvinylidene)], confirmed by a DEPT-135 experiment, C_γ, not assigned. For **4**: IR ($\nu_{C=C}$) 1617s cm^{-1}. ^{1}H NMR (CD_2Cl_2, TMS, 294 K), 5.73 and 5.25 (d, $^2J_{HH}$ 1.6 Hz, 1H each CH_2), 5.10 (t, $^4J_{HP}$ 8.2 Hz, 1H, CH). ^{31}P{^{1}H} NMR (CD_2Cl_2, 85% H_3PO_4, 294 K), δ 49.20 (s). ^{13}C{^{1}H} NMR (CD_2Cl_2, TMS reference, 294 K), 350.3 (t, $^2J_{CP}$ 17.5 Hz, C_α), 150.2 (s, C_γ), 122.6 (s, C_δ), 113.5 (s, C_β), confirmed by a DEPT-135 experiment.

‡ *Crystal data*: $C_{46}H_{45}Cl_2NP_2Ru$, M_w = 845.79, monoclinic, space group $P2_1/c$, a = 11.881(9), b = 13.446(2), c = 25.264(5) Å, β = 98.00(5)°, V = 3997(3) Å^3, Z = 4, D_c = 1.406 g cm^{-3}, T = 293(2) K, μ(Mo-Kα) = 0.640 mm^{-1}; red crystal, crystal size 0.23 × 0.35 × 0.29 mm, Enraf Nonius CAD4 diffractometer, 5545 independent reflections. The structure was solved by direct methods (SIR92)[16] and refined ($F_0{}^2$) using the program SHELX-93.[17] An empiric absorption correction was applied *via* ψ scan (0.97–1.00). The final R, R_w indices [$I > 2\sigma(I)$] were 0.0644, 0.1544 for 220 parameters (non-hydrogen atoms anisotropic, hydrogen atoms in idealised positions, C–H = 0.96 Å). CCDC 182/1164.

1 E. O. Fischer, H.-J. Halder, A. Franck, F. H. Köhler and G. Huttner, *Angew. Chem., Int. Ed. Engl.*, 1976, **15**, 623; H. Berke, *Angew. Chem., Int. Ed. Engl.*, 1976, **15**, 624.

2 For the general reactivity of allenylidenes, see: (*a*) M. A. Esteruelas, A. V. Gómez, A. M. López, E. Oñate and N. Ruiz, *Organometallics*, 1998, **17**, 4959 and references therein; (*b*) R. Wiedemann, P. Steinert, O. Gevert and H. Werner, *J. Am. Chem. Soc.*, 1996, **118**, 2495; (*c*) H. Fischer, G. Roth, D. Reindl and C. Troll, *J. Organomet. Chem*., 1993, **454**, 133; (*d*) V. N. Kalinin, V. V. Deunov, M. A. Lusenkova, P. V. Petrovsky and N. E. Kolobova, *J. Organomet. Chem.*, 1989, **379**, 303; (*e*) D. Touchard and P. H. Dixneuf, *Coord. Chem. Rev.*, 1998, **178**–**180**, 409; (*f*) M. I. Bruce, *Chem. Rev.*, 1998, **98**, 2797.

3 For theoretical studies, see: (*a*) M. A. Esteruelas, V. Gómez, A. M. López, J. Modrego and E. Oñate, *Organometallics*, 1997, **16**, 5826; (*b*) B. E. R. Schilling, R. Hoffmann and D. L. Lichtenberger, *J. Am. Chem. Soc.*, 1979, **101**, 585.

4 A. Fürstner, M. Picquet, C. Bruneau and P. H. Dixneuf, *Chem. Commun*., 1998, 1315; B. M. Trost and J. A. Flygare, *J. Am. Chem. Soc.*, 1992, **114**, 5476.

5 (*a*) V. Cadierno, M. P. Gamasa, J. Gimeno, M. C. López-Gonzalez, J. Borge and S. Garcia-Granda, *Organometallics*, 1997, **16**, 4453; (*b*) C. Bohanna, B. Callejas, A. J. Edwards, M. A. Esteruelas, F. J. Lahoz, L. A. Oro, N. Ruiz and C. Valero, *Organometallics*, 1998, **17**, 373; (*c*) D. Touchard, P. Haquette, A. Daridor, A. Romero and P. H. Dixneuf, *Organometallics*, 1998, **17**, 3844; (*d*) D. Pilette, K. Ouzzine, H. Le Bozec, P. H. Dixneuf, C. E. F. Rickard, and W. R. Roper, *Organometallics*, 1992, **11**, 809.

6 M. A. Esteruelas, A. V. Gómez, F. J. Lahoz, A. M. López, E. Oñate and L. A. Oro, *Organometallics*, 1996, **15**, 3423.

7 The iridium ethenyl complex Ir(CR=CRCR=CR)$(PPh_3)_2$(CO)(η^1-CH=CH_2) (R = CO_2Me) was indeed obtained by reacting Ir(CR=CRCR=CR)$(PPh_3)_2$(CO)Cl (R = CO_2Me) with HC≡CCH_2OH. The hydrolysis of an undetected allenylidene intermediate was hypothesized: J. M. O'Connor and K. Hilbner, *Chem. Commun*., 1995, 1209.

8 C. Bruneau and P. H. Dixneuf, *Acc. Chem. Res*., 1999, in press.

9 J. P. Selegue, *Organometallics*, 1982, **1**, 217.

10 C. Bianchini, P. Innocenti, D. Masi, M. Peruzzini and F. Zanobini, *Gazz. Chim. Ital.*, 1992, **122**, 461.

11 Complexes **2**–**4** exhibit a rich chemistry which will be detailed in due course; C. Bianchini and M. Peruzzini, manuscript in preparation.

12 X-Ray authenticated Ru(II)-diphenylallenylidenes include: [CpRu(P-$Me_3)_2${C=C=CPh_2}], ref. 9; [(η^5-C_9H_7)Ru$(PPh_3)_2${C=C=CPh_2}], ref. 5(*b*); [RuCl($Pr^i{}_2CH_2CH_2OMe)_2${C=C=CPh_2}](OTf), M. Martin, O. Gevert and H. Werner, *J. Chem. Soc., Dalton Trans*., 1996, 2275; [$RuCl_2$(η^2-$Pr^i{}_2CH_2CH_2OMe$)(η^1-*P*-$Pr^i{}_2CH_2CH_2OMe$){C=C=CPh_2}], H. Werner, A. Stark, P. Steinert, C. Grünwald and J. Wolf.

13 (*a*) J. P. Selegue, B. A. Young and S. L. Logan, *Oragnometallics*, 1991, **10**, 1972; (*b*) V. Cadierno, M. P. Gamasa, J. Gimeno, J. Borge and S. Garcia-Granda, *Organometallics*, 1997, **16**, 3187.

14 C. Bianchini, P. Innocenti, M. Peruzzini, A. Romerosa and F. Zanobini, *Organometallics*, 1996, **15**, 272.

15 The hydrolysis of related vinylidene species has been studied in detail, see: C. Bianchini, J. A. Casares. M. Peruzzini, A. Romerosa and F. Zanobini, *J. Am. Chem. Soc.*, 1996, **118**, 4585.

16 A. Altomare, G. Cascarano, C. Giacovazzo, A. Guagliardi, C. Burla, G. Polidori and M. Camalli, *J. Appl. Crystallogr.*, 1994, **27**, 435.

17 G. M. Sheldrick, SHELX-93, University of Göttingen, 1993.

18 C. K. Johnson, ORTEP, Oak Ridge, TN, 1976.

Communication 9/00011I

Ethylene polymerization over chromium complexes grafted onto MCM-41 materials

R. Ramachandra Rao, Bert M. Weckhuysen* and Robert A. Schoonheydt

Centrum voor Oppervlaktechemie en Katalyse, Departement Interfasechemie, K.U. Leuven, Kardinaal Mercierlaan 92, 3001 Heverlee, Belgium. E-mail: Bert.Weckhuysen@agr.kuleuven.ac.be

Received (in Bristol, UK) 9th November 1998, Accepted 1st February 1999

Chromium acetylacetonate [$Cr(acac)_3$] complexes have been grafted onto the surface of Al-MCM-41 materials and were characterised by combined DRS–EPR spectroscopies and TGA; these materials were found to be active for the polymerisation of ethylene.

The recent discovery of the M41S family of mesoporous crystalline solids with sharply distributed pore diameters in the range 2–10 nm has greatly increased the range of supports for preparing heterogeneous catalysts.[1] Among them, MCM-41 is the most studied. It possesses a hexagonally arranged array of uniform pores. Brönsted acidity may be generated in MCM-41 by isomorphous substitution of Al^{3+} for Si^{4+}.[2–4] Recently, transition metal complexes encapsulated in mesoporous molecular sieves have been shown to exhibit high catalytic activity in oxidation reactions. Examples are $[Mn(bipy)_2]^{2+}$ complexes in the oxidation of styrene[5*a*] and Schiff base complexes in the aerial oxidation of alkylaromatics.[5*b*] Supported chromium oxides, in particular Cr/SiO_2 and $Cr/Ti/SiO_2$, are industrially very important catalysts for the production of high-density polyethylene (HDPE) and linear low-density polyethylene (LLDPE).[6] Based on the pore size of the mesoporous solids, it was our view that the MCM-41 material should be an excellent support for grafting chromium complexes. Here, we report on the characterisation and catalytic activity of well defined $Cr(acac)_3$ complexes grafted onto MCM-41 materials. The goal of this study is two-fold: (1) to characterise chromium complexes grafted onto MCM-41 by spectroscopic methods and (2) to obtain novel and catalytically active materials for ethylene polymerisation.

Al-MCM-41 was prepared at 100 °C in a Teflon autoclave for 24 h.[7] The gel composition of the starting material was $1Al_2O_3 : 31SiO_2 : 2.2(HDTMABr)_2O : 3.16(TEA)_2O : 1.89 Na_2O : 795H_2O$ (HDTMABr = hexadecyltrimethylammonium bromide, TEA = tetraethylammonium). This material after drying at 60 °C and calcination at 500 °C, was used for impregnation with a solution of $Cr(acac)_3$ in methanol under an N_2 atmosphere. The final product after calcination contained 1.5 wt% Cr and had a Si/Al ratio of 27.

The XRD patterns of calcined Al-MCM-41 and calcined Cr(acac)–Al-MCM-41 are identical to those previously reported for MCM-41 materials,[1–5] and confirm the hexagonal mesoporous structure. The *d*-spacings of Al-MCM-41 and Cr(acac)–Al-MCM-41 were 3.71 and 3.84 nm, respectively, while the surface area and pore volume of the Al-MCM-41 catalyst were 860 $m^2\ g^{-1}$ and 1.8 ml g^{-1}, respectively. TG analysis of the Cr(acac)–Al-MCM-41 catalyst showed two weight losses at 230 and 330 °C; *i.e.* acac ligands were removed in two stages. Thus, the supported Cr-complex is stable up to 200 °C in oxygen. In the first stage one ligand is removed as acetylacetone with the aid of the surface protons of MCM-41. In the second stage, the ligands which are not interacting with framework oxygens are removed by oxidation or pyrolysis. The amount of acac molecules per chromium atom was found to be 2.65, which suggests that there are two types of complexes present on the surface: one which has only two acac ligands, and a second with three acac ligands which has partial H-bonding with framework oxygen atoms (Scheme 1).

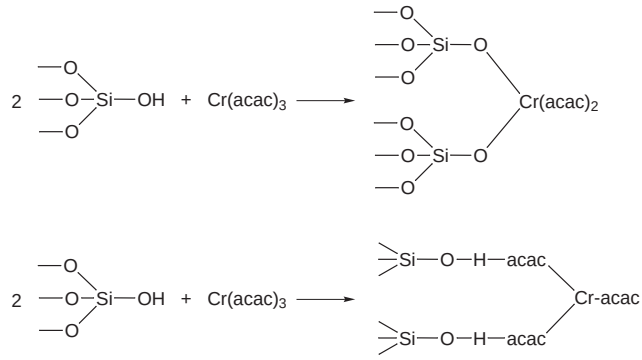

Scheme 1

The as-synthesized $Cr(acac)_n$–Al-MCM-41 (with $n = 2$ or 3) material has been characterised by combined DRS–EPR spectroscopies to study the coordination environment of Cr. Diffuse reflectance spectra are shown in Fig. 1. At room temperature, three absorption bands at 327, 389 and 562 nm are observed, which are typical for Cr^{3+}.[8] EPR reveals an intense signal with $g_{eff} \approx 4$, and zero field parameters D and $E \neq 0$ (Fig. 2). This is indicative for a strongly distorted Cr^{3+} complex.[9] During calcination in O_2, the intensity of the DRS band at 562 nm decreases with increasing calcination temperature. At 500 °C, two new DRS bands at 280 and 370 nm became apparent. These bands are charge transfer transitions of Cr^{6+}.[8] A fraction of Cr^{3+} could not be oxidised to $Cr^{6+/5+}$, which suggests that small clusters of Cr_2O_3 were formed on the catalyst surface. This has been confirmed by EPR spectroscopy. Indeed, the EPR spectra have a characteristic broad signal around $g = 2$ of clustered Cr^{3+} in pseudo-octahedral coordination.[9] In addition, small amounts of Cr^{5+} with $g_{\|} = 1.910$ and $g_{\perp} = 1.978$ have been detected.

Ethylene polymerization was carried out over calcined $Cr(acac)_n$–Al-MCM-41 in a quartz flow cell at 100 °C with 2 bar of pure ethylene. DRS and EPR spectra were recorded at regular time intervals in order to monitor the chromium

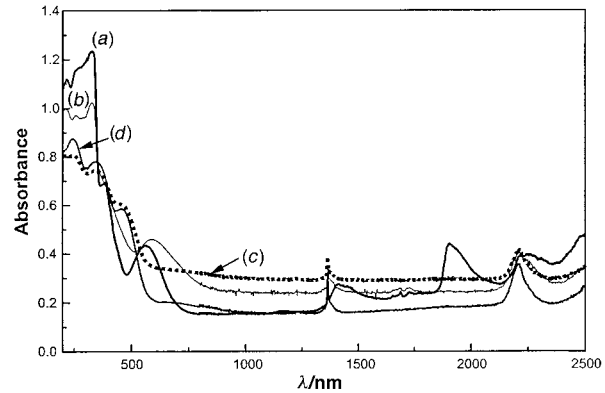

Fig. 1 Diffuse reflectance spectra of the $Cr(acac)_n$–Al-MCM-41 material after heating in O_2 at (*a*) 20, (*b*) 200, (*c*) 400 and (*d*) 500 °C.

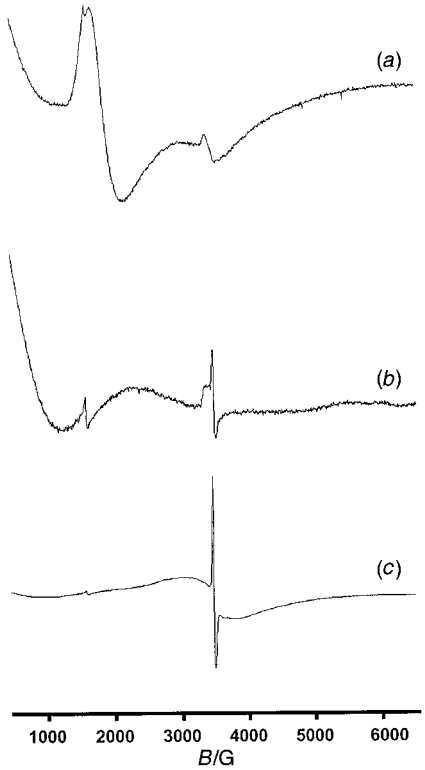

Fig. 2 Electron paramagnetic resonance spectra of Cr(acac)$_n$–Al-MCM-41 material after heating in O_2 at (*a*) 20, (*b*) 500 °C and (*c*) after 120 min reaction of ethylene at 100 °C.

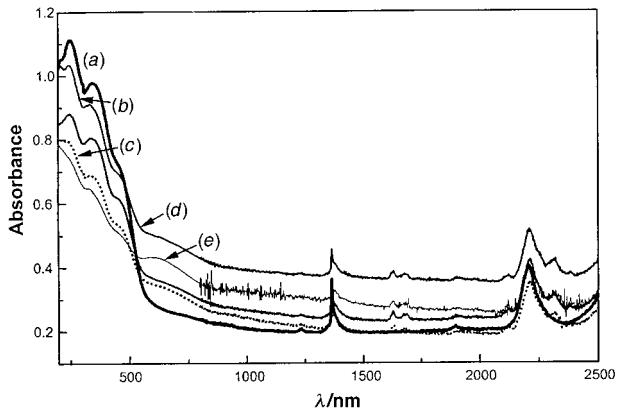

Fig. 3 Diffuse reflectance spectra of the Cr(acac)$_n$–Al-MCM-41 exposed to ethylene at 100 °C as a function of the reaction time: (*a*) 10, (*b*) 15, (*c*) 30, (*d*) 45 and (*e*) 120 min.

oxidation state during the reaction. $Cr^{6+/5+}$ is readily reducible upon interaction with ethylene, and the corresponding DRS spectra are shown in Fig. 3. After 2 h of reaction, a broad and ill defined absorption band is observed with maximum around 600 nm. This maximum is indicative for the formation of Cr^{3+}.[8] This observation has been confirmed by EPR spectroscopy. Indeed, the corresponding EPR spectrum [Fig. 2(*c*)] is dominated by a broad $g = 2$ signal, due to Cr^{3+}, and a sharp axial signal typical for Cr^{5+}.[9] In addition, new features in the NIR region of the DRS spectra were observed (Fig. 3). To further investigate this behaviour, a detailed FTIR study was performed for the catalytic materials exposed to ethylene. A band at *ca.* 1476 cm^{-1} was observed, due to the CH_2 bending mode of polyethylene.[10]

Ethylene polymerisation over Cr(acac)$_n$–Al-MCM-41 materials was then further studied at 100 °C for 2 h in a catalytic reactor, in which the ethylene consumption is reflected by a pressure decrease in the reactor system. Typical results are shown in Fig. 4. It is clear that, depending on the initial ethylene

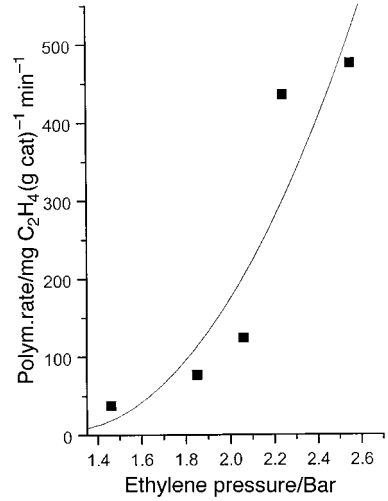

Fig. 4 Polymerization rate over Cr(acac)$_n$–Al-MCM-41 catalyst as a function of the initial ethylene pressure at 100 °C.

pressure, high polymerization rates between 50 and 500 mg ethylene (g catalyst)$^{-1}$ min^{-1} were obtained. After reaction the catalyst was dispersed in the polyethylene formed during reaction, and the formation of polyethylene was confirmed *via* FTIR spectroscopy.

Summarising, the present study demonstrates that Cr(acac)$_3$ complexes can be grafted onto Al-MCM-41 materials. It results in a novel catalytic system, which is able to polymerise ethylene at relatively low pressures. Further research has to be directed towards the influence of the pore diameter of MCM-41 on the polymer characteristics.

R. R. R. is thankful for a junior postdoctoral fellowship of the K. U. Leuven, while B. M. W. is a postdoctoral fellow of the Fonds voor Wetenschappelijk Onderzoek-Vlaanderen (F. W. O.). This work was financially supported by the Geconcerteerde Onderzoeksactie (G. O. A.) of the Flemish Government and by the F. W. O.

Notes and references

1 C. T. Kresge, M. E. Leonowicz, W. J. Roth, J. C. Vartuli and J. S. Beck, *Nature*, 1992, **359**, 710.
2 R. Mokaya, W. Jones, Z. Luan, M. D. Alba and J. Klinowski, *Catal. Lett.*, 1996, **37**, 113.
3 A. Corma, V. Fornes, M. T. Navarro and J. Perez-Pariente, *J. Catal.*, 1994, **148**, 569.
4 R. Mokaya and W. Jones, *Chem. Commun.*, 1998, 1839.
5 (*a*) S. S. Kim, W. Zhang and T. J. Pinnavaia, *Catal. Lett.*, 1997, **43**, 149; (*b*) I. C. Chisem, J. Rafelt, M. T. Shieh, J. Chisem, J. H. Clark, R. Jachuck, D. Macquarrie, C. Ramshaw and K. Scott, *Chem. Commun.*, 1998, 1949.
6 S. L. Fu, M. P. Rosynek and J. H. Lunsford, *Langmuir*, 1991, **7**, 1179; B. M. Weckhuysen and R. A. Schoonheydt, *Catal. Today*, 1999, in press.
7 J. Rathousky, A. Zukal, O. Franke and G. Schulz-Ekloff, *J. Chem. Soc., Faraday Trans.*, 1994, **90**, 2821.
8 B. M. Weckhuysen, I. E. Wachs and R. A. Schoonheydt, *Chem. Rev.*, 1996, **96**, 3327.
9 B. M. Weckhuysen, R. A. Schoonheydt, F. A. Mabbs and D. Collison, *J. Chem. Soc., Faraday Trans.*, 1996, **92**, 2431.
10 C. N. R. Rao, *Chemical Applications of Infrared Spectroscopy*, Academic Press, 1963.

Communication 8/09260E

The facile synthesis of 1,2,3-trisubstituted pyrroles from the reaction of chlorocarbenes with 1-azabuta-1,3-dienes

Yuri N. Romashin,[a] Michael T. H. Liu*[a] and Roland Bonneau[b]

[a] *Department of Chemistry, University of Prince Edward Island, P.E.I.,Canada C1A 4P3. E-mail: liu@upei.ca*
[b] *LPCM, Laboratoire de Chimie Physique A, Université de Bordeaux 1, 33405 Talence Cedex, France*

Received (in Corvallis, OR, USA) 4th December 1998, Accepted 4th January 1999

1,2,3-Trisubstituted pyrroles have been synthesized in good yield from the reaction of chlorocarbenes with 1-azabuta-1,3-dienes.

Carbenes and metal carbenoids are useful intermediates in the synthesis of nitrogen-containing heterocyclic compounds of biological importance. Most of the work has been devoted to the reactions of carbenes and metal carbenoids with azomethines that result in aziridines, pyrrolidines, oxazolidines and β-lactams.[1,2] The literature has only two examples where pyrroles appeared as the end product.[3,4] Introducing dimethyl acetylenedicarboxylate to a reaction mixture of *N*-benzylideneaniline and dichlorocarbene, generated by alkaline hydrolysis of $CHCl_3$, results in the formation of a pyrrole derivative in low yield.[3] Thermolysis of chromium carbene complexes with 1-azabuta-1,3-dienes leads to the formation of 1,2,3-trisubstituted pyrroles in good yield.[4] However, no pyrroles could be detected in the reaction of dichlorocarbene with 1-azabuta-1,3-dienes, where dichloroaziridines were isolated in high yield.[3,5] Pyrroles represent an important major class of heterocycles. Their prominence encourages the continuing evolution of new synthetic methods.[6] Our experiments produced a facile one-step synthesis of 1,2,3-trisubstituted pyrroles based on the reaction of arylchlorocarbenes with a variety of 1-azabuta-1,3-dienes under photolytic or thermal conditions.

We propose that the reaction of singlet carbene such as arylchlorocarbene with 1-azabuta-1,3-dienes goes through an azomethine ylide[3] **4** *via* a reaction between the vacant 2p-orbital of the carbene and the nitrogen non-bonding electron pair (Scheme 1). The formed ylide then undergoes intramolecular ring-closure to form a dihydropyrrole **5**, followed by HCl elimination to produce pyrroles.

The arylchlorocarbenes **2** were generated from arylchlorodiazirines **1**[7] by photolysis or thermolysis. We prepared the 1-azabuta-1,3-dienes **3** (R^1 = Me, Bn; R^2 = Me, Ph) from cinnamaldehyde or crotonaldehyde and methyl or benzyl amines. We purified them by distillation under reduced pressure. The chlorocarbenes **2** react rapidly with 1-azabuta-1,3-dienes **3** to presumably yield dihydropyrroles **5**. In all cases, the elimination of HCl from **5** to give pyrroles **6** is instantaneous since no trace of **5** could be found. Yields and melting points of pyrroles **6** are presented in Table 1 and their spectral data[8] compare well with those previously reported for **6a**,**d**.[2,6,9] The yields of pyrroles **6** obtained from photolysis (30–55%) and thermolysis (40–65%) are comparable.†

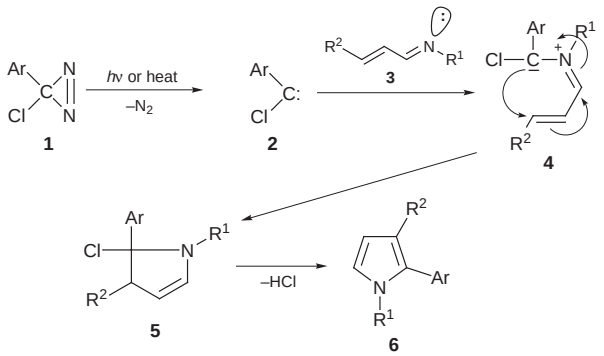

a Ar = Ph, R^1 = Me, R^2 = Ph
b Ar = *p*-MeC_6H_4, R^1 = Me, R^2 = Ph
c Ar = *p*-ClC_6H_4, R^1 = Me, R^2 = Ph
d Ar = Ph, R^1 = Bn, R^2 = Ph
e Ar = *p*-MeC_6H_4, R^1 = Bn, R^2 = Ph
f Ar = *p*-ClC_6H_4, R^1 = Bn, R^2 = Ph
g Ar = *p*-MeC_6H_4, R^1 = Bn, R^2 = Me

Scheme 1

Table 1 Isolated yields for 1,2,3-trisubstituted pyrroles **6**

					Yield (%)	
Product **6**	Ar	R^1	R^2	Mp/°C	*hν*	Heat
a	Ph	Me	Ph	96–96.5	50	54
b	*p*-MeC_6H_4	Me	Ph	95–96	51	65
c	*p*-ClC_6H_4	Me	Ph	112–113	48	52
d	Ph	Bn	Ph	116–117[a]	40	50
e	*p*-MeC_6H_4	Bn	Ph	132–133	55	58
f	*p*-ClC_6H_4	Bn	Ph	147–148	50	56
g	*p*-MeC_6H_4	Bn	Me	viscous oil	30	40

[a] Only the mp for **6d** has been reported: lit., 117–118 °C (ref. 6).

Photolyses were carried out by irradiation (350 nm) of solutions of the chlorodiazirines **1** (1 mmol) and 1-azabuta-1,3-dienes **3** (2.5 mmol) in hexane (50 ml) at 25 °C for 24 h. For the thermolysis reactions solutions of chlorodiazirines **1** (1 mmol) and the 1-azabuta-1,3-dienes **3** (2.5 mmol) were refluxed in absolute benzene (10 ml) for 3 h. After workup, the pyrroles **6** were purified by column chromatography on silica gel with hexane–Et_2O (10 : 1) as eluent, followed by crystallization from Pr^iOH–hexane (1 : 3).

M. T. H. Liu wishes to thank the NSERC of Canada for generous financial support.

Notes and references

† All compounds reported herein gave satisfactory microanalysis data.

1 A. Padwa and M. D. Weingarten, *Chem. Rev.*, 1996, **96**, 223; A. Padwa and S. F. Hornbruckle, *Chem. Rev.*, 1991, **91**, 263; A. F. Khlebnikov and R. R. Kostikov, *Russ. Chem. Bull.*, 1993, **42**, 653; M. P. Doyle and D. C. Forbes, *Chem. Rev.*, 1998, **98**, 911; L. S. Hegedus, J. Montgomery, Y. Narukawa and D. S. Snustad, *J. Am. Chem. Soc.*, 1991, **113**, 5784.
2 E. Vedejs and J. W. Grissom, *J. Am. Chem. Soc.*, 1988, **110**, 3238.
3 R. R. Kostikov, A. F. Khlebnikov and V. Y. Bespalov, *J. Phys. Org. Chem.*, 1993, **6**, 83.
4 T. N. Danks and D. Velo-Rego, *Tetrahedron Lett.*, 1994, **35**, 9443.
5 R. R. Kostikov, A. F. Khlebnikov and K. A. Ogloblin, *Zh. Org. Khim.*, 1977, **13**, 1857.
6 B. M. Trost and E. Keinan, *J. Org. Chem.*, 1980, **45**, 2741.
7 W. H. Graham, *J. Am. Chem. Soc.*, 1965, **87**, 4396.
8 *Selected data* for **6a**: δ_H(60 MHz, $CDCl_3$) 3.53 (3H, s), 6.46 (1H, d, *J* 3), 6.76 (1H, d, *J* 3), 7.1–7.5 (10H, m). For **6b**: δ_H (60 MHz, $CDCl_3$) 2.33 (3H, s), 3.47 (3H, s), 6.38 (1H, d, *J* 3), 6.72 (1H, d, *J* 3), 7.1–7.4 (9H, m). For **6c**: δ_H(60 MHz, $CDCl_3$) 3.48 (3H, s), 6.43 (1H, d, *J* 3), 6.76 (1H, d,

J 3), 7.1–7.5 (9H, m); *m/z* 267 [M^+]. For **6d**: δ_H(300 MHz, $CDCl_3$) 5.00 (2H, s), 6.50 (1H, d, *J* 3), 6.80 (1H, d, *J* 3), 7.1–7.4 (15H, m). For **6e**: δ_H(300 MHz, $CDCl_3$) 2.34 (3H, s), 5.00 (2H, s), 6.52 (1H, d, *J* 3), 6.78 (1H, d, *J* 3), 7.1–7.4 (14H, m). For **6f**: δ_H(300 MHz, $CDCl_3$) 5.00 (2H, s), 6.52 (1H, d, *J* 3), 6.82 (1H, d, *J* 3), 7.1–7.4 (14H, m). For **6g**: δ_H(300 MHz, $CDCl_3$) 2.07 (3H, s), 2.37 (3H, s), 5.00 (2H, s), 6.17 (1H, d, *J* 3), 6.67 (1H, d, *J* 3), 7.1–7.4 (9H, m).

9 I. Saito, A. Yazaki and T. Matsuura, *Tetrahedron Lett.*, 1976, 2459.

Communication 8/09508F

ChemComm

A new type of supramolecular entanglement in the silver(I) coordination polymer $[Ag_2(bpethy)_5](BF_4)_2$ [bpethy = 1,2-bis(4-pyridyl)ethyne]

Lucia Carlucci, Gianfranco Ciani* and Davide M. Proserpio

Dipartimento di Chimica Strutturale e Stereochimica Inorganica and Centro CNR, Via G. Venezian 21, 20133 Milano, Italy. E-mail: davide@csmtbo.mi.cnr.it

Received (in Basel, Switzerland) 21st December 1998, Accepted 27th January 1999

The polymeric compound $[Ag_2(bpethy)_5](BF_4)_2$, obtained from $AgBF_4$ and 1,2-bis(4-pyridyl)ethyne (bpethy) in molar ratio 1:3, contains infinite molecular ladder motifs with monodentate ligands as sidearms on both sides, that are threaded through the squares of adjacent polymeric units in a mutual relationship, to give infinite 'polythreaded' bidimensional layers.

Two topical areas in metal-directed supramolecular chemistry,[1] that have attracted much interest in recent times, deal, respectively, with (*i*) the construction of fascinating interwoven/intertwined molecular arrays, such as catenanes, rotaxanes, knots and helicates,[2] and (*ii*) the crystal engineering of polymeric networks,[3] which are often interpenetrated.[4] Though these two fields are characterized by different objectives, the self-assembly of extended coordination frames has recently produced noteworthy examples of structural motifs typical of the former area involved in polymeric systems, such as polyrotaxanes,[5] polypseudo-rotaxanes,[6] and polycatenated molecular ladders[7] and multiple layers.[8] The stimulating current developments in the supramolecular chemistry of intertwined organic systems have revealed a variety of novel structural motifs that might have a parallel relevance also in coordination chemistry. New possible molecular modules are, for example, self-complementary units, represented by rings (or polygons) bearing one sidearm (see **1** in Scheme 1), which can self-assemble *via* non-covalent bonds to give supramolecular oligomeric or polymeric species, with the sidearm of each unit threaded through the ring of the lateral unit (see **1A**, **1B** and **1C**). Systems like these, called 'supramolecular daisy chains', have been recently discussed in the presentation of a plerotopic organic monomer that gives an array of the **1A** type.[9] A variation of the previous motif **1** can be the addition of a second sidearm, as in **2**, that can oligomerize or polymerize *via* a mutual threading involving adjacent units, as in **2A** and **2B**. On passing from finite to infinite molecular modules one can imagine the extension of rings **1** and **2** into polymeric ladder species (such as **3** and **4**, respectively). Indeed, different examples of molecular ladders have been described within coordination polymers,[7,10] including a species like **4** (called a molecular 'railroad').[11] Supramolecular assembling of **3** and **4** with identical adjacent motifs can produce, *inter alia*, two-dimensional entanglements characterized by 'polythreading' (as in **3A**) or 'mutual polythreading' (as in **4A**). We report here the characterization of an example of a type **4A** supramolecular entanglement in a coordination polymer obtained from the self-assembly of $AgBF_4$ and 1,2-bis(4-pyridyl)ethyne (bpethy). Many reactions with different silver salts in varied conditions have been carried out, but only linear $[Ag(bpethy)]^+$ polymers were isolated using metal-to-ligand molar ratios up to 1:2. We have therefore attempted reactions with a higher excess of the ligand, and from $AgBF_4$ and bpethy in molar ratio 1:3 in $MeCN–Et_2O$ we have obtained a derivative characterized by single crystal X-ray analysis as the novel species $[Ag_2(bpethy)_5](BF_4)_2$.†

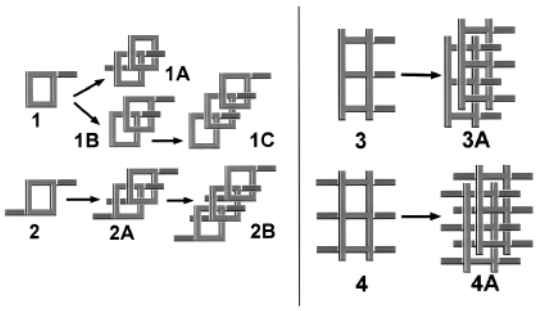

Scheme 1

The structure is comprised of ladder-like polymeric units, shown in Fig. 1, bearing, as extensions of each rung (C), two additional monodentate dangling bpethy molecules (A), that are folded in opposite directions on the two sides of the ladder. The Ag···Ag distances are 13.93 Å along the siderails and 14.48 Å within the rungs.

The coordination geometry at the silver centres (see Fig. 1, top) is flattened tetrahedral. The two rows of lateral arms form dihedral angles with the ladder plane of *ca.* 137°, resulting in a stretched zigzag shaped section (see Fig. 1, bottom). In contrast, the related 'railroad' polymer of $[Ni_2(4,4'\text{-bpy})_5(H_2O)_4](ClO_4)_4\cdot 3(4,4'\text{-bpy})\cdot 4H_2O$ is flat,[11] because the Ni^{2+} centres are octahedral and all the 4,4′-bipyridyl groups lie almost coplanar. The square grids, in this species, are smaller (11.39 × 11.34 Å).

All the ladders of $[Ag_2(bpethy)_5](BF_4)_2$ run in the same direction, [−1 0 1], and are closely disposed on layers. The ladder planes are stacked parallel at a distance of 3.51 Å and display an inclination of *ca.* 22° with respect to the average plane of the layer (see Fig. 2, top). The most interesting

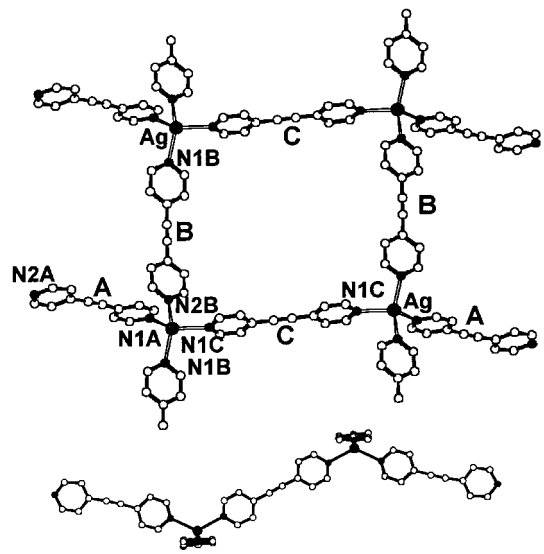

Fig. 1 Two views of a single molecular ladder motif. The top view shows the three types of bpethy ligands (A, B and C, the latter lying on inversion centres). The Ag–N bond lengths are in the range 2.300(2)–2.424(2) Å; two of the N–Ag–N angles are significantly larger [N1B–Ag–N2B 139.92(8), N1A–Ag–N1C 125.00(9)°] than the other four [in the range 95.52(8)–103.01(8)°].

structural feature, however, consists of the fact that the terminal bpethy ligands of each ladder are threaded into the squares of the adjacent ladders, in a mutual relationship. The length of the ligands is such that the threading involves not only the first but also the second nearest neighbouring ladders. Each square is therefore penetrated by four bpethy molecules, two entering by one side and two by the opposite one, as shown in Fig. 2 and 3, thus resulting in a supramolecular entanglement originated by five polymeric units. The aromatic rings of all the threaded molecules are parallel to those of the ligands of the ladder rungs. An extended system of stacked rings is thus formed, with π–π interactions [plane separation 3.5–3.6(1) Å, lateral offset 1.9–3.0(1) Å] that stabilize the whole entanglement.[12] An additional stabilization can be attributed to weak attractive CH–π interactions,[13] involving H atoms of the terminal (A) and of the rung ligands (C), that point toward the centres of the rings and of the C≡C moieties of the siderail ligands (B) (H···bar distances and C–H···bar angles: 2.66–2.79 Å, 144–168°, with bar = the baricentre of the π system). The schematic representation of the 'mutual polythreading' in this species given in Fig. 2 (bottom) shows that two adjacent ladders are displaced by *ca.* 1/4 of the polymer period along the direction of extension. The sequence of the ladders in a layer is therefore of the *ABCDABCD* type. The entangled layers stack along the crystallographic ***b*** axis, leaving interlayer voids that are occupied by the BF_4^- anions.

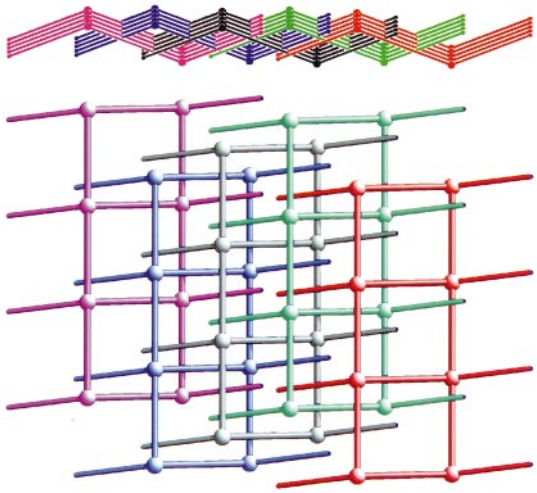

Fig. 2 Two schematic views of the entangled ladders: approximately down the direction of propagation (top), and down the perpendicular to the polythreaded layer, showing the relative displacement of the adjacent ladders (bottom).

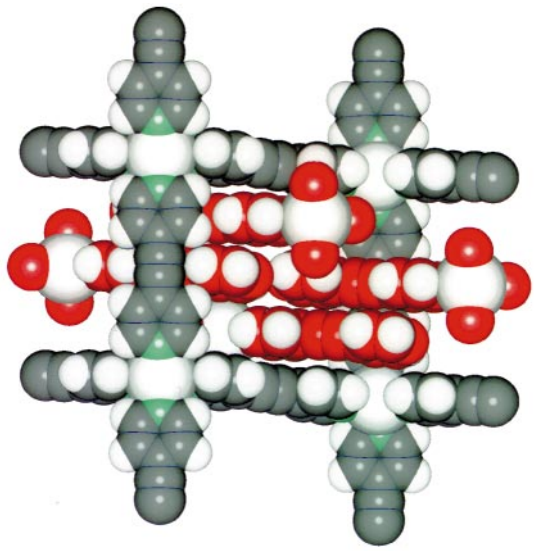

Fig. 3 Sphere packing representation of a square unit of the ladders, showing the four threading bpethy molecules (with the non-hydrogen atoms in red).

A variety of appealing interpenetrated frameworks has been recently described in coordination polymer chemistry.[4] While interpenetration requires breaking of links to separate the individual nets, other types of polymeric supramolecular architectures can be, in principle, disentangled by simply unthreading the components. These species are much less known, at present, and include examples such as infinite double-helices,[6] a clothlike warp-and-weft sheet structure,[14] and bilayer species interdigitated in a gear-like (or tongue and groove) fashion.[15] The fascinating 'polythreaded' structure here described belongs to this class of polymers and can be considered a model of a new type of infinite entanglement, that can be extended to other systems.

Notes and references

† *Crystal data*: $C_{60}H_{40}Ag_2B_2F_8N_{10}$, M = 1290.38, triclinic, space group $P\bar{1}$ (no. 2), a = 10.397(1), b = 11.109(1), c = 13.696(2) Å, α = 80.65(1)°, β = 69.11(1)°, γ = 69.66(1)°, U = 1384.4(3) Å^3, Z = 1, μ(Mo-Kα) = 0.784 mm^{-1}, 21682 reflections measured, 8249 unique (R_{int} = 0.0251), final $R1$ and $wR2$ values 0.0373 and 0.0978 for 5299 independent reflections [$I > 2\sigma(I)$]. The data collection was performed at 293 K on a Siemens SMART CCD area-detector by the ω-scan method, within the limits $2 < \theta < 31°$. The structure was solved by direct methods (SIR97) and refined by full-matrix least-squares (SHELX97). Anisotropic thermal parameters were assigned to all the non-hydrogen atoms but to the minor component (28%) of the disordered anion. CCDC 182/1163. See http://www.rsc.org/suppdata/cc/1999/449/ for crystallographic files in .cif format.

1 *Comprehensive Supramolecular Chemistry*, ed. J.-M. Lehn, Pergamon Press, Oxford, 1995.
2 See, *e.g.*: J.-C. Chambron and J.-P. Sauvage, *Chem. Eur. J.*, 1998, **4**, 1362; P. R. Ashton, V. Balzani, A. Credi, O. Kocian, D. Pasini, L. Prodi, N. Spencer, J. F. Stoddart, M. S. Tolley, M. Venturi, A. J. P. White and D. J. Williams, *Chem. Eur. J.*, 1998, **4**, 590; P. J. Stang, *Chem. Eur. J.*, 1998, **4**, 19; G. Baum, E. C. Constable, D. Fenske and T. Kulke, *Chem. Commun.*, 1997, 2043; H. Sleiman, P. N. W. Baxter, J.-M. Lehn, K. Airola and K. Rissanen, *Inorg. Chem.*, 1997, **36**, 4734; C. Piguet, G. Bernardinelli and G. Hopfgartner, *Chem. Rev.*, 1997, **97**, 2005; M. Fujita and K. Ogura, *Coord. Chem. Rev.*, 1996, **148**, 249;
3 B. F. Hoskins and R. Robson, *J. Am. Chem. Soc.*, 1990, **112**, 1546; R. Robson, B. F. Abrahams, S. R. Batten, R. W. Gable, B. F. Hoskins and J. Liu, *Supramolecular Architecture*, ACS, Washington DC, ch. 19, 1992.
4 S. R. Batten and R. Robson, *Angew. Chem., Int. Ed.*, 1998, **37**, 1461.
5 D. M. L. Goodgame, S. Menzer, A. M. Smith and D. J. Williams, *Angew. Chem., Int. Ed Engl.*, 1995, **34**, 574; D. Whang and K. Kim, *J. Am. Chem. Soc.*, 1997, **119**, 451; B. F. Hoskins, R. Robson and D. A. Slizys, *J. Am. Chem. Soc.*, 1997, **119**, 2952.
6 L. Carlucci, G. Ciani, D. W. v. Gudenberg and D. M. Proserpio, *Inorg. Chem.*, 1997, **36**, 3812.
7 M. Fujita, Y. J. Kwon, O. Sasaki, K. Yamaguchi and K. Ogura, *J. Am. Chem. Soc.*, 1995, **117**, 7287; A. J. Blake, N. R. Champness, A. Khlobystov, D. A. Lemenovkii, W.-S. Li and M. Schröder, *Chem. Commun.*, 1997, 2027.
8 F.-Q. Liu and T. D. Tilley, *Inorg. Chem.*, 1997, **36**, 5090.
9 P. R. Ashton, I. Baxter, S. J. Cantrill, M. C. T. Fyfe, P. T. Glink, J. F. Stoddart, A. J. P. White and D. J. Williams, *Angew. Chem., Int. Ed.* 1998, **37**, 1294.
10 P. Losier and M. J. Zaworotko, *Angew. Chem., Int. Ed. Engl.*, 1996, **35**, 2779; D. Venkataraman, S. Lee, J. S. Moore, P. Zhang, K. A. Hisch, G. B. Gardner, A. C. Covey and C. L. Prentice, *Chem. Mater.*, 1996, **8**, 2030.
11 O. M. Yaghi, H. Li and T. L. Groy, *Inorg. Chem.*, 1997, **36**, 4292.
12 See, *e.g.*: C. H. Hunter, *Chem. Soc. Rev.*, 1994, 101; C. Chipot, R. Jaffe, B. Maigret, D. A. Pearlman and P. A. Kollman, *J. Am. Chem. Soc.*, 1996, **118**, 11217.
13 See, *e.g.*: H.-C. Weiss, D. Bläser, R. Boese, B. M. Doughan and M. H. Haley, *Chem. Commun.*, 1997, 1703; Y. Umezawa, S. Tsuboyama, K. Honda, J. Uzawa and M. Nishio, *Bull. Chem. Soc. Jpn.*, 1998, **71**, 1207.
14 P. M. Van Calcar, M. M. Olmstead and A. L. Balch, *J. Chem. Soc., Chem. Commun.*, 1995, 1773.
15 M. Kondo, T. Joshitomi, K. Seki, H. Matsuzaka and S. Kitagawa, *Angew. Chem., Int. Ed. Engl.*, 1997, **36**, 1725; K. N. Power, T. L. Hennigar and M. J. Zaworotko, *New J. Chem.*, 1998, 177.

Communication 8/09361J

Phospha-alkyne hydro-osmiation: synthesis of $[Os\{\kappa^1P,\kappa^1P'\text{-}P{=}CRP(=CHR)\}Cl(CO)(PPh_3)_2]$ (R = CMe_3)

Anthony F. Hill,*[a] Cameron Jones*[b] and James D. E. T. Wilton-Ely[a]

[a] *Centre for Chemical Synthesis, Department of Chemistry, Imperial College of Science Technology and Medicine, South Kensington, London, UK SW7 2AY. E-mail: a.hill@ic.ac.uk*

[b] *Department of Chemistry, Cardiff University, Cardiff, UK CF1 3TB. E-mail: jonesca6@cardiff.ac.uk*

Received (in Cambridge, UK) 8th January 1999, Accepted 20th January 1999

The reaction of $[OsHCl(CO)(PPh_3)_2(BTD)]$ (BTD = 2,1,3-benzothiadiazole) with P≡$CCMe_3$ provides the novel complex $[Os\{\kappa^1P,\kappa^1P'\text{-}P{=}CRP(=CHR)Cl(CO)(PPh_3)_2]$ (R = CMe_3) which features both phospha-alkenyl and phospha-alkene donors within the same metallacycle.

We have recently described the facile hydroruthenation of phospha-alkynes by the ruthenium complexes $[RuHCl(CA)(PPh_3)_3]$ (A = O **1a**, S **1b**).[1] The phospha-alkenyl complexes $[Ru(P{=}CHCMe_3)Cl(CA)(PPh_3)_2]$ (A = O **2a**, S **2b**) which results are remarkable for a number of reasons. Firstly, the metal centre is coordinatively unsaturated, as a result of a non-linear Ru–P–C phospha-alkenyl spine. Secondly, the phospha-alkenyl ligand is unusually simple, in that it lacks the previously requisite kinetic or thermodynamic stabilisation conferred by bulky or π-dative substituents.[2] Finally but perhaps most significantly, the phospha-alkenyl ligand serves as a versatile precursor for the preparation of a range of novel complexes of otherwise inaccessible organophosphorus ligands including the unusual phospha-alkenes $XP{=}CHCMe_3$ (X = H, Me, ClHg, $AuPPh_3$, HgPh).[3] The successful synthesis and synthetic utility of the complexes **2a** and **2b** immediately raises the question of the generality of the phospha-alkyne hydrometallation strategy. Encouragingly, Nixon and coworkers have recently reported the hydrozirconation of a *coordinated* phospha-alkyne by the Schwarz' reagent to provide a synthetically useful P-zirconated phospha-alkene complex $[ZrPt(\mu\text{-}PCHCMe_3)Cl(dppe)(\eta\text{-}C_5H_5)_2]$.[4] Furthermore the hydrostannylation of phospha-alkynes has now been reported, although in this case the process lacks the regioselectivity offered by the two transition metal systems.[5] Herein we report the hydro-osmiation of a phospha-alkyne, leading to a novel osmacycle which includes both phospha-alkene and phospha-alkenyl donor components.

In contrast to the ruthenium complexes **2a** and **2b**, treating $[OsHCl(CO)(PPh_3)_3]$ **1c** with an excess of P≡$CCMe_3$ fails to result in any appreciable reaction. We have encountered a similar lack of reactivity of **1c** towards alkynes and attributed this to the lack of phosphine lability under mild conditions. However, prior conversion of **1c** to the more labile complex $[OsHCl(CO)(PPh_3)_2(BTD)]$ **3a** (BTD = 2,1,3-benzothiadiazole) provides a reagent capable of alkyne hydro-osmiation under ambient conditions providing convenient access to the complexes $[Os(CH{=}CHR)Cl(CO)(PPh_3)_2(BTD)]$.[6] It is noteworthy that whilst the analogous ruthenium complex $[RuHCl(CO)(PPh_3)_2(BTD)]$ **3b**[7] also hydrometallates alkynes to provide coordinatively saturated σ-alkenyl complexes $[Ru(CH{=}CHR)Cl(CO)(PPh_3)_2(BTD)]$,[8] we find that treating **3b** with an excess of P≡$CCMe_3$ results in the exclusive formation of *coordinatively unsaturated* **2a** with no indication of BTD coordination. In a similar manner the acetonitrile complex $[RuHI(CO)(NCMe)(PPh_3)_2]$ reacts with P≡$CCMe_3$ to provide the new phospha-alkenyl complex $[Ru(P{=}CHCMe_3)I(CO)(PPh_3)_2]$ **2c** which despite being coordinatively unsaturated, fails to recoordinate the liberated acetonitrile ligand (Scheme 1). The formulation of **2c** follows unambiguously from spectroscopic and microanalytical data,† amongst which the ^{31}P NMR data are particularly informative. The phospha-alkenyl ligand gives rise to a triplet resonance at δ 462.7 [$J(P_2P)$ 13.1 Hz] due to coupling to the two chemically equivalent phosphine phosphorus nuclei. This resonance is shifted slightly to higher field of that for **2a** [δ 450.4, $J(P_2P)$ 10.0 Hz]. Whilst **2a** is air stable both as a solid and in solution, solutions of the more electron rich complex **2c** are rapidly decomposed by air.

The reaction of **3a** with P≡$CCMe_3$ was then investigated and surprisingly *ultimately* found not to provide the analogous phospha-alkenyl complex $[Os(P{=}CHCMe_3)Cl(CO)(PPh_3)_2]$. Rather, the product **4** obtained after 18 h at room temperature was found to incorporate two equivalents of phospha-alkyne. Even when the reaction was performed with a deficiency of phospha-alkyne, no species other than **3a** and **4** could be spectroscopically observed to accumulate during the course of the reaction. In the absence of crystals suitable for an X-ray diffraction study, the complex **4** is formulated as the metallacyclic phospha-alkenyl–phospha-alkene complex

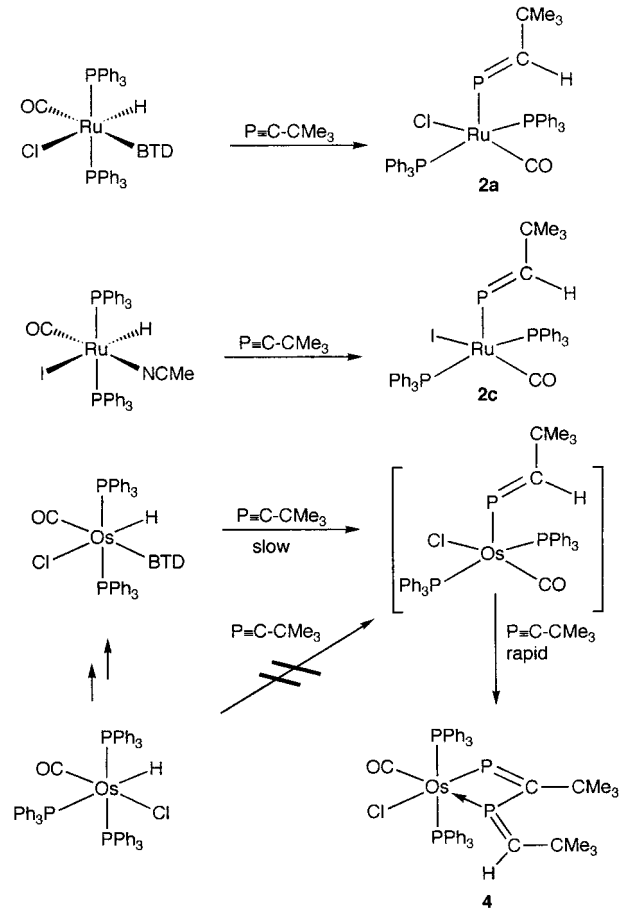

Scheme 1

$[Os\{\kappa^1P,\kappa^1P'\text{-}P{=}C(CMe_3)P(=CHCMe_3)\}Cl(CO)(PPh_3)_2]$ on the basis of spectroscopic, micro-analytical and FABMS data.† Characteristic data pertaining to the '$OsCl(CO)(PPh_3)_2$' unit are unremarkable, with interest focusing on those associated with the novel metallacycle: Two Bu^t chemical environments follow from the appearance of two singlet resonances in the ^{1}H NMR spectrum (δ 0.90, 0.70) in addition to a doublet resonance at δ 6.83 [^2J(PH) 12.6 Hz] corresponding to the vinylic (neopentylidene) proton. The ^{31}P NMR spectrum consists of three resonances: the two phosphine ligands give rise to a double-doublet resonance [δ −1.35, J(PP) 12, 18 Hz] confirming their mutually *trans* disposition, straddling the molecular symmetry plane; the phospha-alkenyl resonance appears as a slightly broadened singlet at δ 578.9 whilst the phospha-alkene phosphorus nucleus is manifest as an apparent triplet at δ 111.9 [J(PP) 19 Hz], indicating that the net coupling between the two phosphorus nuclei of the metallacycle is negligible. Only one isomer is formed with respect to the osmium stereochemistry, and since our recent structural studies of various σ-P phospha-alkene complexes suggest a moderate π-acidity,[3] it seems reasonable that it is the isomer shown (phospha-alkene *trans* to π-basic chloride) which is formed.

The metallacycle in **4** is unique in possessing both phospha-alkenyl and phospha-alkene ligating groups, although other metallacyclic phospha-alkenyl complexes have been reported, *viz*. $[Os\{P{=}C(CF_3)O\}(CO)_2(PPh_3)_2]$,[9] $[Rh\{P{=}C(CMe_3)\text{-}C{=}CH_2\}Cl(PPr^i_3)_2]$,[10] and the λ^5-phospha-alkenyl complex $[Ru\{P(=O){=}C(CMe_3)C(=O)\}(CNCMe_3)_2(PPh_3)_2]$,[11] (spectroscopic data of which support our formulation). The route by which **4** is formed presumably involves a slow insertion of one equivalent of $P{\equiv}CCMe_3$ into the osmium hydride bond to provide transiently the phospha-alkenyl complex $[Os(P{=}CHCMe_3)Cl(CO)(PPh_3)_2]$, followed by a rapid insertion of a second equivalent of phospha-alkyne into the Os–P bond and subsequent metallacyclisation. It is therefore noteworthy that treating the ruthenium complexes **2a** or **2c** with an excess of phospha-alkyne fails to result in any discernible reaction. Thus our very modest attempt to generalise what appears a simple reaction, phospha-alkyne hydrometallation, has highlighted the diversity of reactivity available to phospha-alkynes through coordinative activation by transition metals.

A. F. H. gratefully acknowledges the Leverhulme Trust and the Royal Society for the award of a Senior Research Fellowship. Osmium and ruthenium salts were generously provided by Johnson Matthey Chemicals Ltd.

Notes and references

† *Selected data* for new complexes. Satisfactory elemental microanalytical data obtained. **2c**: IR(CH_2Cl_2): 1936 [ν(CO)] cm^{-1}. (Nujol): 1925 [ν(CO)], 1660, 1247, 1157, 1119, 968, 862, 849 cm^{-1}. NMR ($CDCl_3$, 25 °C): ^{1}H, δ 0.90 [d, 9H, CH_3, J(HP) 1.32 Hz], 6.41 [dt, 1H, PCH, J(HP) 4.48 J(HP_2) 0.75 Hz], 7.32–7.68 (m, 30H, PPh). ^{31}P{^{1}H}, δ 462.7 [t, P=C, 1 P, J(P_2P) 13 Hz], 33.1 [d, 2 P, PPh_3, J(PP_2) 14 Hz]. FABMS: *m/z* (%) = 883 (2) $[M]^+$, 853 (3) $[M - CO]^+$, 781 (19) $[M - PCHCMe_3]^+$, 755 (6) $[M - I]^+$, 654 (15) $[M - I - PCHCMe_3]^+$, 625 (14) $[M - CO - I - PCHCMe_3]^+$. **4**: IR ($CH_2Cl_2$): 1940 [$\nu$(CO)] cm^{-1}. (Nujol): 1934 [ν(CO)], 1718, 1311, 1263, 1089vs, 971, 931, 852 cm^{-1}. NMR ($CDCl_3$, 25 °C): ^{1}H, δ 0.70, 0.90 (s × 2, 9H × 2, CH_3), 6.83 [br d, 1H, PCH, J(PH) 12.6 Hz], 7.33, 7.66 (m × 2, 30H, Ph). ^{31}P{^{1}H}, δ 578.9 (br s, 1 P), 111.9 [t, 1 P, J(PP) 19], −1.35 [dd, 2 P, J(PP) 12, 18 Hz] ^{13}C{^{1}H}: 226.1 [br d, P=CHR, J(PC) 68.0], 185.7 (m, OsCO), 134.6 [t, $C^{3,5}$ of Ph, J(P_2C) 4.4], 133.3 [t, C^1 of Ph, J(P_2C) 25.9], 129.9 (s, C^4 of Ph) 127.8 [t, $C^{2,6}$ of Ph, J(P_2C) 4.9], 48.0 (br s, P_2CCMe_3), 36.0 [d, $CHCMe_3$, J(PC) 4.3], 30.5 [d, CH_3, J(PC) 11.9 Hz], 29.8 (br s CH_3). NB: the neopentylidyne carbon resonance was not unambiguously identified and possibly lies beneath the phosphine resonances. FABMS: *m/z* (%) = 999 (7) $[M + H_2O]^+$, 979 (1) $[M]^+$, 779 (3) $[M - PCHCMe_3]^+$, 737 (6) $[M + H_2O - PPh_3]^+$, 707 (2) $[M + H_2O - CO - PPh_3]^+$.

1 R. B. Bedford, A. F. Hill and C. Jones, *Angew. Chem., Int. Ed. Engl.*, 1996, **35**, 547; R. B. Bedford, A. F. Hill, C. Jones, A. J. P. White, D. J. Williams and J. D. E. T. Wilton-Ely, *Organometallics*, 1998, **17**, 4744.

2 For a recent review on the chemistry of phospha-alkenyl complexes, see: L. Weber, *Angew. Chem., Int. Ed. Engl.*, 1996, **35**, 271.

3 R. B. Bedford, D. E. Hibbs, A. F. Hill, M. B. Hursthouse, K. M. A. Malik and C. Jones, *Chem. Commun.*, 1996, 1895; R. B. Bedford, A. F. Hill, C. Jones, A. J. P. White, D. J. Williams and J. D. E. T. Wilton-Ely, *J. Chem. Soc., Dalton Trans.*, 1997, 139, 1113; R. B. Bedford, A. F. Hill, C. Jones, A. J. P. White, D. J. Williams and J. D. E. T. Wilton-Ely, *Chem. Commun.*, 1997, 179; A. F. Hill, C. Jones, A. J. P. White, D. J. Williams and J. D. E. T. Wilton-Ely, *J. Chem. Soc., Dalton Trans.*, 1998, 1419.

4 M. H. A. Benvenutti, N. Cebac and J. Nixon, *Chem. Commun.*, 1997, 1327.

5 M. Schmidz, R. Göller, U. Bergsträßer, S. Leininger and M. Regitz, *Eur. J. Inorg. Chem.*, 1998, 227.

6 A. F. Hill and J. D. E. T. Wilton-Ely, *J. Chem. Soc., Dalton Trans.*, 1998, 3501.

7 N. W. Alcock, A. F. Hill and M. S. Roe, *J. Chem. Soc., Dalton Trans.*, 1990, 1737.

8 M. C. J. Harris and A. F. Hill, *J. Organomet. Chem.*, 1992, **438**, 209; M. C. J. Harris and A. F. Hill, *Organometallics*, 1991, **10**, 3903.

9 D. S. Bohle, G. R. Clark, C. E. F. Rickard and W. R. Roper, *J. Organomet. Chem.*, 1988, **353**, 355; D. S. Bohle, C. E. F. Rickard and W. R. Roper, *J. Chem. Soc., Chem. Commun.*, 1985, 1594.

10 P. Binger, J. Haas, A. T. Herrmann, F. Langhauser and C. Krüger, *Angew. Chem., Int. Ed. Engl.*, 1991, **30**, 310.

11 A. F. Hill, C. Jones, A. J. P. White, D. J. Williams and J. D. E. T. Wilton-Ely, *Chem. Commun.*, 1998, 367.

Communication 9/00257J

Selective synthesis of 1-stanna-2-boraferrocenes: novel bidentate Lewis acids *via* an unexpected rearrangement reaction

Frieder Jäkle, Alan J. Lough and Ian Manners*

Department of Chemistry, University of Toronto, 80 St. George Street, Toronto, Ontario, Canada M5S 3H6. E-mail: imanners@alchemy.chem.utoronto.ca

Received (in Bloomington, IN, USA) 25th November 1998, Accepted 22nd January 1999

Ferrocene based bidentate Lewis acids of the general formula 1,2-fc(BR_2)(SnR_3) are obtained in one step from 1,1′-distannaferrocenes and chloroboranes *via* an unexpected rearrangement reaction.

Bidentate Lewis acids have attracted increasing attention owing to their potential in selective anion recognition,[1] self-assembly with Lewis bases,[2] as catalysts in acid catalyzed organic transformations[3] and as cocatalysts in Ziegler–Natta olefin polymerization.[4] Systems with two different acidic centers are still very rare although they might give rise to very specific binding properties.[5–7] In particular, the combination of Lewis acidic tin(IV) and boron centers permits fine-tuning of the Lewis acidity by well known selective substituent exchange reactions at either of the metal centers. As part of our general interest in the area of tin- and boron-substituted ferrocene derivatives, here, we report on a selective, one step synthesis of ferrocene based bidentate Lewis acids from readily available 1,1′-disubstituted stannaferrocenes.[8,9]

When 1,1′-bis[trimethylstannyl]ferrocene **1**[10] was treated with 1 equiv. of BCl_3 or $PhBCl_2$ in hexanes at −78 °C and the reaction mixture was allowed to slowly warm to 0 °C, the 1-stanna-2-boraferrocenes **2a** and **2b** were obtained as red oils after removal of all volatile material in high vacuum (Scheme 1). During the course of this reaction, one of the stannyl groups is replaced by a boryl substituent, which is accompanied by an unexpected rearrangement reaction. The boryl group in **2a** and **2b** is found exclusively *ortho* to the remaining stannyl substituent whereas the proton has transferred to the other Cp ring leaving an unsubstituted Cp ligand in **2a** and **2b**.† The reactions were conveniently followed by ^{1}H, ^{11}B and ^{119}Sn NMR spectroscopy.‡ The ^{11}B NMR spectra of **2a** and **2b** display a broad signal (**2a**: δ 51.1, **2b**: δ 57.2) in the expected range for aryldichloroboranes and diarylchloroboranes, respectively. In the ^{119}Sn NMR spectra of **2a** and **2b** a singlet (**2a**: δ −5.1, **2b** δ −9.9) is found at a similar chemical shift as observed for the starting material **1** (δ −6.3) indicating that a trimethylstannyl moiety is still attached to the ferrocene core. The most striking feature in the ^{1}H NMR spectra is a singlet with the intensity of five protons in the region typical of unsubstituted ferrocene Cp rings (**2a**: δ 3.92, **2b**: δ 3.93). The NMR signals for the methyl protons are particularly useful to monitor the substitution pattern on tin and boron, because of coupling between the ^{117}Sn and ^{119}Sn nuclei and adjacent methyl groups. For **2a** and **2b** one singlet with tin satellites is found [**2a**: δ 0.28, (9H), **2b**: δ 0.18, (9H)].

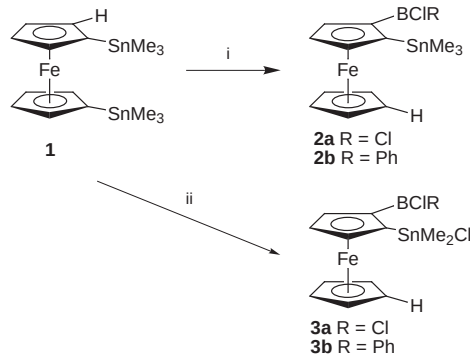

Scheme 1 *Reagents and conditions*: i, $RBCl_2$, hexanes, −78 °C to room temp.; ii, 2 $RBCl_2$, hexanes, −78 °C to room temp.

In order to investigate whether a second tin-boron exchange can take place, **1** was reacted with 2 equiv. of the haloboranes. If a similar reaction path as described for the formation of **2** is followed, either the formation of a 1,2-diboraferrocene or a rearranged 1,1′-diboraferrocene would be expected (Scheme 1). However, a ligand exchange on the remaining tin center to form **3a** and **3b** (73 and 53% isolated yield after recrystallization from hexanes at −55 °C, respectively) took place and no spectroscopic evidence for the formation of bisborylated ferrocenes was found.‡§ The ^{11}B NMR spectra of **3a** and **3b** show broad singlets (**3a**: δ 49.8, **3b**: δ 56.6) in the same range as observed for **2a** and **2b**. However, the exchange of a methyl for a chloro substituent on tin is evidenced by a pronounced high field shift in the ^{119}Sn NMR spectra (**3a**: δ 102.1, **3b**: δ 85.9). The planar chirality of **3a** and **3b** leads to two different signals in the ^{1}H NMR spectra for the methyl groups on tin [**3a**: δ 0.69, (3H), δ 0.52, (3H), **3b**: δ 0.82, (3H), δ 0.66 (3H)]. It is significant to note that **3b** was also detected as a byproduct in the 1 : 1 reaction between **1** and $PhBCl_2$ accompanied by a small amount of unreacted **1** accounting for a relatively low yield of **2b** in comparsion to **2a** (estimated yields based on ^{1}H NMR spectroscopy for **2a**: 95%, **2b**: 50%). By contrast, **3a** is only formed if **1** is reacted with an excess of BCl_3.

To remove any traces of Me_3SnCl or Me_2SnCl_2 from crude **2a** and **2b**, both compounds were kept at 50 °C for 3 h in high vacuum. Surprisingly, this led to another very selective rearrangement reaction giving almost exclusively **4a** and **4b**, which are obtained in good isolated yields by recrystallization from hexanes (Scheme 2). In both compounds a chloro substituent on boron has exchanged with a methyl group on the tin center.

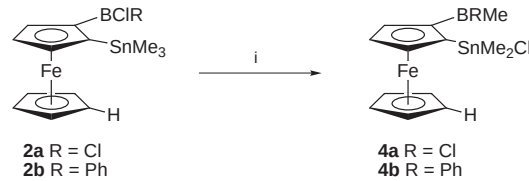

Scheme 2 *Conditions*: i, 50 °C in high vacuum, 3 h.

The ^{11}B NMR spectra of **4a** and **4b** display a broad singlet (**4a**: δ 61.5, **4b** δ 67.5) which is shifted by about 10 ppm to lower field in comparison to **2a**,**b** and **3a**,**b**. On the other hand, the ^{119}Sn NMR spectrum of **4a** and **4b** (**4a** δ 89.8, **4b** δ 95.3) shows a singlet at a similar chemical shift as for **3a** and **3b**. Three singlets are observed for the methyl groups in the ^{1}H NMR spectra of **4a** and **4b**, but only two of them display tin satellites.§ The NMR spectroscopic data therefore clearly confirm a rearranged structure in comparison to **1** and the proposed substituent exchange reactions between **2**, **3** and **4**.

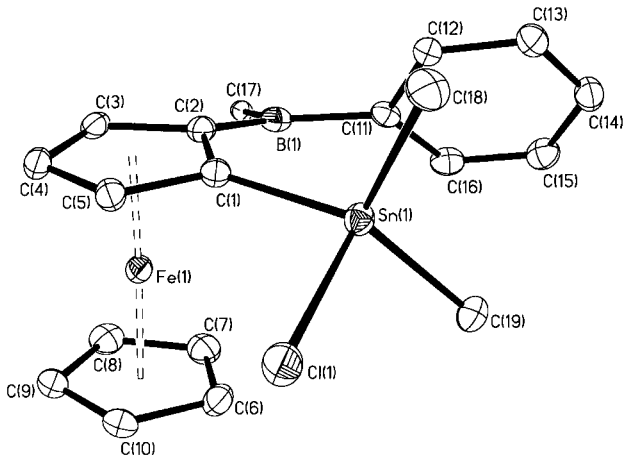

Fig. 1 Molecular structure (ORTEP drawing) of **4b**. Selected bond lengths (Å): Sn(1)–C(1) 2.121(4), Sn(1)–C(18) 2.130(4), Sn(1)–C(19) 2.121(4), Sn(1)–Cl(1) 2.404(1), B(1)–C(2) 1.536(6), B(1)–C(11) 1.571(5), B(1)–C(17) 1.623(5).

In order to further confirm the assigned rearranged structures and to distinguish unambiguously between a 1,2-substituted and a 1,3-substituted ferrocene moiety, a single crystal X-ray diffraction study of compound **4b** was undertaken.¶ Dark red crystals of **4b** were obtained from hexanes at −30 °C. A racemic mixture of both of the two possible enantiomers due to the planar chirality in **4b** is found in the single crystal used for X-ray crystallography. The structure (Fig. 1) confirmed that the proposed rearrangement reactions (see Schemes 1 and 2) had taken place. No interaction between the tin bound chlorine atom and the Lewis acidic boron center is evident. However, the boron atom is bent towards the iron atom as observed previously in the crystal structure of dibromoborylferrocene [**4b**: α^* = 12.2(3)°, $FcBBr_2$: α^* = 17.7, 18.9°; α^* = 180° − centroid (C1–C5)–C(2)–B angle] suggesting some iron–boron interaction.[11] A smaller degree of iron–boron interaction in **4b** in comparison to $FcBBr_2$ is reflected in a significantly longer B–C(Cp) bond length [**4b**: 1.536(6) Å, $FcBBr_2$: 1.474(9), 1.482(8) Å] and a longer Fe–B distance [**4b**: 3.087(5) Å, $FcBBr_2$: 2.840 Å]. The tin atom is only slightly bent away from the Cp plane [**4b**: α^* = 2.7(2)°, α^* = 180° − centroid(C1–C5)–C(1)–Sn angle].

In summary, reaction of **1** with haloboranes provides a mild, simple one step synthesis of novel bidentate ferrocene based Lewis acids. In contrast, the direct borylation of ferrocene with BCl_3 requires extended reaction times at elevated temperature.[12] The reaction sequence involves an interesting substituent rearrangement from one Cp ring to the other. Currently, we are investigating mechanistic details of the observed rearrangement reactions, the use of 1-stanna-2-boraferrocenes as bidentate Lewis acids in selective anion recognition including the effect of their planar chirality[13] and their potential as precursors for other 1,2-substituted ferrocenes.

We wish to acknowledge a DFG postdoctoral fellowship for F. J. and I. M. is grateful to the Alfred P. Sloan Foundation for a Research Fellowship (1994–1998), NSERC for an E. W. R. Steacie Fellowship (1997–1999), and the University of Toronto for a McLean Fellowship (1997–2003).

Notes and references

† The similarity of the Cp proton NMR resonances of **2a**,**b**, **3a**,**b** and **4a**,**b** suggests a 1,2-substitution pattern analogous to that found by X-ray diffraction for **4b**.

‡ *Selected spectroscopic data*: For **2a**: ^{1}H NMR (400 MHz, C_6D_6, 20 °C): δ 4.71 [dd, *J* (HH) = 1.2, 2.4 Hz, 1H, Cp-H3], 4.53 [ps.t, *J* (HH) 2.4 Hz, 1 H, Cp-H4), 4.46 [dd, *J* (HH) 1.2, 2.4 Hz, 1 H, Cp-H5], 3.92 (s, 5H, Cp), 0.28 [s/d, *J* (^{117}SnH) 52, *J* (^{119}SnH) 55 Hz, 9 H, SnMe]; ^{13}C NMR (100.5 MHz, C_6D_6, 20 °C): δ 85.2 (Cp-C3), 80.8, 79.4 (Cp-C4,5), 70.7 (Cp), −1.7 (SnMe), not observed (*ipso*-Cp); ^{11}B NMR (160.4 MHz, C_6D_6, 20 °C): δ 51.1 ($h_{1/2}$ 320 Hz); ^{119}Sn NMR (111.8 MHz, C_6D_6, 20 °C): δ −5.1. **3a**: ^{1}H NMR (300 MHz, C_6D_6, 20 °C): δ 5.24 [dd, *J* (HH) 1.2, 2.4 Hz, 1 H, Cp-H3], 4.51–4.55 (m, 2H, Cp-H4,5), 3.87 (s, 5 H, Cp), 0.69 [s/d, *J* (^{117}SnH) 61, *J* (^{119}SnH) 64 Hz, 3H, SnMe), 0.52 [s/d, *J* (^{117}SnH) 60, *J* (^{119}SnH) 62 Hz, 3H, SnMe]; ^{13}C NMR (75.5 MHz, C_6D_6, 20 °C): δ 86.2 (Cp-C3), 81.1, 80.7 (Cp-C4,5), 71.7 (Cp), 2.5, 1.1 (SnMe), not observed (*ipso*-Cp); ^{11}B NMR (160.4 MHz, C_6D_6, 20 °C): δ 49.8 ($h_{1/2}$ 350 Hz); ^{119}Sn NMR (111.8 MHz, C_6D_6, 20 °C): δ 102.1; MS (70 eV, EI): *m/z* (%): 450 (100) [M^+], 435 (28) [$M^+ - CH_3$], 420 (73) [$M^+ - 2\ CH_3$]. **4a**: ^{1}H NMR (400 MHz, C_6D_6, 20 °C): δ 5.33 [dd, *J* (HH) 1.2, 2.4 Hz, 1 H, Cp-H3], 4.54 [ps.t, *J* (HH) 2.4 Hz, 1H, Cp-H4,] 4.22 [dd, *J* (HH) 1.2, 2.4 Hz, 1H, Cp-H5], 3.85 (s, 5H, Cp), 0.86 (s, 3H, BMe), 0.82 [s/d, *J* (^{117}Sn, H) 63, *J* (^{119}SnH) 65 Hz, 3H, SnMe], 0.65 [s/d, *J* (^{117}SnH) 60, *J* (^{119}SnH) 62 Hz, 3H, SnMe]; ^{13}C NMR (75.5 MHz, C_6D_6, 20 °C): δ 84.8 (Cp-C3), 80.0 (Cp-C4,5), 70.3 (Cp), 2.7, 1.3 (SnMe), not observed (*ipso*-Cp, BMe); ^{11}B NMR (160.4 MHz, C_6D_6, 20 °C): δ 61.5 ($h_{1/2}$ 400 Hz); ^{119}Sn NMR (111.8 MHz, C_6D_6, 20 °C): δ 89.8; MS (70 eV, EI): *m/z* (%): 430 (100) [M^+], 415 (27) [$M^+ - CH_3$], 400 (78) [$M^+ - 2\ CH_3$].

§ Satisfactory elemental analyses for compounds **3a**,**b** and **4a**,**b** have been obtained.

¶ *Crystallographic data*: $C_{19}H_{22}BClFeSn$, *M* = 471.2, monoclinic, space group $P2_1/n$, *a* = 11.051(1), *b* = 14.166(1), *c* = 11.791(1) Å, β = 95.83(1)°, *U* = 1836.3(6) Å^3, *Z* = 4, D_c = 1.704 g cm^{-3}, μ = 2.291 mm^{-1}, 3145 observed reflections [$I > 2\sigma(I)$], R = 0.0307; R_w = 0.0786, GOF = 1.068. Data were collected on a Nonius Kappa CCD diffractometer at 150.0(1) K. The structure was solved by direct methods (SHELXS97) and refined by full-matrix least squares (SHELXL97) based on F^2 with all reflections. Non-hydrogen atoms were refined anisotropically, and hydrogen atoms were included in calculated positions. CCDC 182/1154. See http://www.rsc.org/suppdata/cc/1999/453/ for crystallographic files in .cif format.

1 M. M. G. Antonisse and D. N. Reinhoudt, *Chem. Commun.*, 1998, 443.
2 F. P. Gabbaï, A. Schier and J. Riede, *Angew. Chem., Int. Ed.*, 1998, **37**, 622.
3 T. Ooi, T. Miura and K. Maruoka, *Angew. Chem., Int. Ed.*, 1998, **37**, 2347.
4 K. Köhler, W. E. Piers, A. P. Jarvis, S. Xin, Y. Feng, A. M. Bravakis, S. Collins, W. Clegg, G. P. A. Yap and T. B. Marder, *Organometallics*, 1998, **17**, 3557.
5 H. E. Katz, *J. Am. Chem. Soc.*, 1986, **108**, 7640.
6 B. Wrackmeyer, U. Dörfler, W. Milius and M. Herberhold, *Z. Naturforsch., Teil B*, 1996, **51**, 851.
7 J. J. Eisch and B. W. Kotowicz, *Eur. J. Inorg. Chem.*, 1998, 761.
8 H. Braunschweig, R. Dirk, M. Müller, P. Nguyen, R. Resendes, D. P. Gates and I. Manners, *Angew. Chem., Int. Ed. Engl.*, 1997, **36**, 2338.
9 F. Jäkle, R. Rulkens, G. Zech, D. A. Foucher, A. J. Lough and I. Manners, *Chem. Eur. J.*, 1998, **4**, 2117.
10 Z. Dawoodi, C. Eaborn and A. Pidcock, *J. Organomet. Chem.*, 1979, **170**, 95; purity of 1,1′-$(fcSnMe_3)_2$ >95% by ^{1}H NMR spectroscopy.
11 A. Appel, F. Jäkle, T. Priermeier, R. Schmid and M. Wagner, *Organometallics*, 1996, **15**, 1188.
12 T. Renk, W. Ruf and W. Siebert, *J. Organomet. Chem.*, 1976, **120**, 1.
13 G. Wagner and R. Herrmann, in *Ferrocenes*, ed. A. Togni and T. Hayashi, VCH, Weinheim, New York, Basel, Cambridge, Tokyo, 1995, p. 173.

Communication 8/09276A

A novel eight-membered Cu_4I_4 ring supported by sulfur atoms of an $M(mnt)_2$ moiety: syntheses and crystal structures of $(NBu^n_4)_2[M(mnt)_2Cu_4I_4]$ (M = Ni, Pd, Pt; mnt = 1,2-dicyano-1,2-ethylenedithiolato) with doubly-bridged one-dimensional chain structures

Kunihisa Sugimoto,[a] Takayoshi Kuroda-Sowa,*[a] Masahiko Maekawa[b] and Megumu Munakata[a]

[a] *Department of Chemistry, Kinki University, Higashi-Osaka, Osaka 577-8502, Japan. E-mail: kuroda@chem.kindai.ac.jp*

[b] *Research Institute for Science and Technology, Kinki University, Higashi-Osaka, Osaka 577-8502, Japan*

Received (in Cambridge, UK) 14th December 1998, Accepted 29th January 1999

Crystal structure analyses of the title compounds revealed that they have almost the same structure with a novel eight-membered Cu_4I_4 ring supported by an $M(mnt)_2$ moiety, two cyano groups out of the four of which coordinate to two copper(I) ions in neighboring molecules, resulting in the formation of a unique doubly-bridged one-dimensional chain structure.

There is considerable growing interest in copper(I) coordination polymer chemistry due to a variety of fascinating multi-dimensional structures and the possibility for developing new functional materials.[1] Molecules having cyano groups sometimes can be good bridging ligands since their moderate coordination abilities to copper(I) ions make it possible to obtain single crystals suitable for X-ray analyses.[2] In order to add functionality to copper(I) polymers, we chose $[M(mnt)_2]^{n-}$ (M = Ni, Pd, Pt; mnt = 1,2-dicyano-1,2-ethylenedithiolato; n = 1, 2) as bridging ligands for copper(I) ions. Conducting and magnetic properties of compounds containing $[M(mnt)_2]^{n-}$ moieties have been extensively studied.[3] However, mixed metal coordination compounds containing a $M(mnt)_2$ moiety are rare. A series of compounds with μ-bridging silver(I) ions, $[Ag(PR_3)_2]_2M(mnt)_2$,[4] is the only known example so far to our knowledge.[5] Here, we report the syntheses and structures of new mixed metal coordination polymer compounds, $(NBu^n_4)_2[M(mnt)_2Cu_4I_4]$ (M = Ni **1**, Pd **2**, Pt **3**), which represent the first examples of $M(mnt)_2$ functioning as a bridging ligand. They have novel eight-membered Cu_4I_4 rings supported by sulfur atoms of $M(mnt)_2$.

Reddish black crystals of **1**–**3** were prepared by reaction of CuI and $(NBu^n_4)_2[M(mnt)_2]$[6] in THF at room temperature followed by diffusion with diethyl ether.† Single crystal X-ray structure analyses of **1**–**3**‡ showed that all three compounds have essentially the same structure. Fig. 1 displays an ORTEP drawing of the molecular structure of **1** with the atom numbering scheme. The $Ni(mnt)_2$ moiety retains its original planar structure and there is no significant change in Ni–S bond lengths compared to those of the parent compound. One side of the $Ni(mnt)_2$ moiety is covered by an eight-membered ring of Cu_4I_4 with copper atoms being close to the mnt sulfur atoms (Cu–S 2.35 Å av.). Each copper atom is located almost directly above the corresponding sulfur atom, and not between two sulfur atoms like for the bridging mode observed in $[Ag(PR_3)_2]_2M(mnt)_2$ compounds.[4] Within the eight-membered ring, copper and iodine atoms are connected alternately with Cu–I distances ranging from 2.517(3) to 2.643(1) Å. This eight-membered ring is considered to be a new isomeric form of the Cu_4X_4 arrangement with cubane- and step-like conformations having been reported previously for $[Cu_4X_4L_n]$ complexes.[7] The molecule has a C_2 symmetry axis lying normal to the $Ni(mnt)_2$ plane through the Ni atom. There are two independent copper atoms, Cu(1) and Cu(2): the former has a distorted tetrahedral coordination with two I, one S and one N atom while

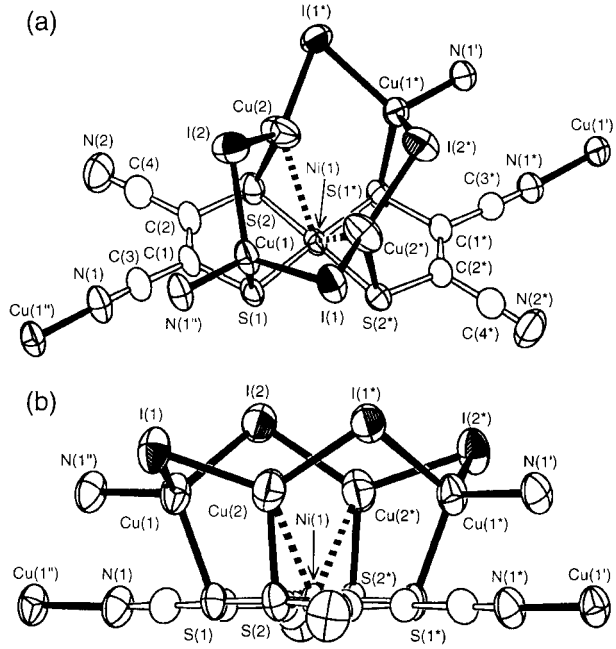

Fig. 1 (a) Top and (b) side views of ORTEP drawings of the $[Ni(mnt)_2Cu_4I_4]^{2-}$ dianion in **1**.

the latter§ shows a distorted trigonal planar coordination with two I and one S atom. It should be noted that the Ni(1)···Cu(2) distance of 2.887(4) Å is shorter than the sum of the van der Waals radii, indicating a weak interaction.

The nitrogen atom coordinating to the Cu(1) atom is from the cyano group in the neighboring molecule. This means that two cyano groups out of four in a molecular unit of **1** coordinate to two Cu(1) atoms in neighboring molecules, resulting in the formation of a doubly-bridged one-dimensional chain structure as shown in Fig. 2. This is the first example in which a $Ni(mnt)_2$ moiety acts as a bridging ligand in a coordination polymer. The chains run parallel along the *c*-axis direction, being separated from each other by bulky $NBu^n_4{}^+$ cations as shown in Fig. 3. A pressed pellet of **1** after exposure to iodine vapor for seven days gave an electrical conductivity of 1.6×10^{-3} S cm^{-1} at room

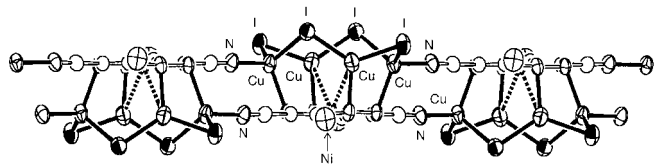

Fig. 2 View of the doubly-bridged anionic polymer $\{[Ni(mnt)_2Cu_4I_4]^{2-}\}_\infty$ in **1**.

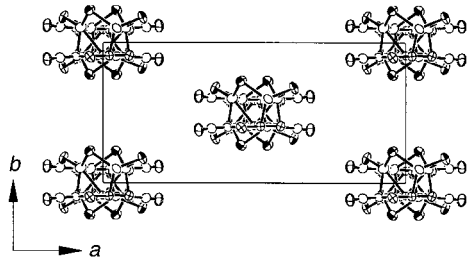

Fig. 3 Molecular packing of **1** viewed from the *c*-axis direction. The $NBu^n{}_4^+$ cations are omitted for clarity.

temperature, while the undoped material is an insulator. In spite of the polymeric structure in the solid state, **1** is soluble in THF. A ^{13}C NMR spectrum measured in d_8-THF shows two peaks at δ 115.4 and 126.0 which are shifted from those observed for $Ni(mnt)_2^{2-}$ (δ 118.1 and 125.4). These shifts indicate the presence of a slightly modified $Ni(mnt)_2^{2-}$ framework, probably $[Ni(mnt)_2Cu_4I_4]^{2-}$, in solution. The Cu–S bonds in **1** are expected to be strong enough to be maintained in THF solution whereas Cu–N(cyano) bonds are expected to dissociate. The weakness of the Cu–N(cyano) bond is exemplified by the observation of uncoordinated cyano groups in the crystal structure.

The structures of **2** and **3** are almost the same as that of **1**. The main differences are the M···Cu(2) distances which are 2.947(2) and 2.856(4) Å for Pd(1)···Cu(2) and Pt(1)···Cu(2), respectively. These distances are also shorter than the sum of the van der Waals radii, indicating weak interactions between these metal atoms. The consistency of the framework in changing the center metal atom indicates that the Cu–S interaction is dominant in determining the framework of their molecular units. Effects of changing cations as well as changing halogens on the molecular framework and the conductivity are under investigation.

In summary, we have characterized novel mixed metal compounds **1**–**3**, which have an eight-membered Cu_4I_4 ring supported by an $M(mnt)_2$ moiety. Two cyano groups out of four in the $M(mnt)_2$ moiety coordinate to two Cu(I) ions in neighboring molecules, resulting in the formation of a unique doubly-bridged one-dimensional chain structure. This is the first example showing that the $M(mnt)_2$ moiety acts as a bridging ligand for metal ions.

This work was supported in part by a Grant-in-Aid for Science Research from the Ministry of Education, Science and Culture, Japan. The authors are grateful to Kinki University for the financial support and to Messrs. N. Takamoto and M. Kawaguchi for their assistance.

Notes and references

† *Procedure* for **1**: a suspension of $(NBu^n{}_4)_2[Ni(mnt)_2]$ (41.2 mg, 0.05 mmol) and CuI (38 mg, 0.2 mmol) in THF (15 ml) was stirred for 24 h at room temp. The resultant solution was filtered and the filtrate was poured into a glass tube. The same amount of ether was added slowly and the tube was sealed. After standing for one week at room temp. reddish black crystals of $(NBu^n{}_4)_2[Ni(mnt)_2Cu_4I_4]$ **1** were obtained (14.7 mg, 18.5%). Similar methods were used for the preparation of **2** and **3**. Reddish black crystals of $(NBu^n{}_4)_2[Pd(mnt)_2Cu_4I_4]$ **2**, (20.1 mg, 24.6%) and $(NBu^n{}_4)_2[Pt(mnt)_2Cu_4I_4]$ **3**, (21.7 mg, 25.2%) were obtained.

‡ *Crystal data*: for **1**: $I_4NiCu_4S_4N_6C_{40}H_{72}$; M = 1585.79, monoclinic, space group $C2/c$ (no. 15), a = 29.22(2), b = 11.457(3), c = 20.430(5) Å, β = 121.87(2)°, U = 5808(4) Å^3, Z = 4, μ(Mo-Kα) = 4.062 mm^{-1}, 6665 unique reflections (R_{int} = 0.033), of which 4529 were observed [$I > 2\sigma(I)$]. At final convergence $R1$ [$I > 2\sigma(I)$] = 0.0402, $wR2$ (all data) = 0.1339 for 273 variables, S = 1.262; For **2**: $I_4PdCu_4S_4N_6C_{40}H_{72}$; M = 1633.49, monoclinic, space group $C2/c$ (no. 15), a = 29.260(5), b = 11.458(7), c = 20.714(4) Å, β = 122.57(1)°, U = 5852(3) Å^3, Z = 4, μ(Mo-Kα) = 4.017 mm^{-1}, 6727 unique reflections (R_{int} = 0.035), of which 3933 were observed [$I > 2\sigma(I)$]. At final convergence $R1$ [$I > 2\sigma(I)$] = 0.0447, $wR2$ (all data) = 0.1391 for 273 variables, S = 1.074. For **3**: $PtI_4Cu_4S_4N_6C_{40}H_{72}$; M = 1633.49, monoclinic, space group $C2/c$ (no. 15), a = 29.179(3), b = 11.462(4), c = 20.735(2) Å, β = 122.602(6)°, U = 5841(1) Å^3, Z = 4, μ(Mo-Kα) = 6.028 mm^{-1}, 6706 unique reflections (R_{int} = 0.058), of which 4201 were observed [$I > 2\sigma(I)$]. At final convergence $R1$ [$I > 2\sigma(I)$] = 0.0435, $wR2$ (all data) = 0.1040 for 273 variables, S = 0.982. All data collections were performed on a Rigaku AFC5R or AFC7R diffractometer using the ω–2θ scan technique ($2\theta_{max}$ = 55.0°). The structures were solved by direct methods. The non-hydrogen atoms were refined anisotropically. The final cycle of a least-squares refinement converged including the atomic coordinates and anisotropic thermal parameters for all non-hydrogen atoms. CCDC 182/1155. See http://www.rsc.org/suppdata/cc/1999/455/ for crystallographic files in .cif format.

§ The second copper atom was found to be disordered. 92% at Cu(2) and 8% at Cu(3) which is dislocated 0.91 Å from Cu(2) atom towards [I(2*)].

1 J. Lehn, *Angew. Chem., Int. Ed. Engl.*, 1990, **29**, 1304; B. F. Hoskins and R. Robson, *J. Am. Chem. Soc.*, 1990, **112**, 1546; M. Munakata, L. P. Wu and T. Kuroda-Sowa, *Bull. Chem. Soc. Jpn.*, 1997, **70**, 1727.

2 M. Munakata, L. P. Wu, T. Kuroda-Sowa, M. Maekawa, Y. Suenaga and K. Furuichi, *J. Am. Chem. Soc.*, 1996, **118**, 3305; M. Munakata, L. P. Wu, M. Yamamoto, T. Kuroda-Sowa and M. Maekawa, *J. Am. Chem. Soc.*, 1996, **118**, 3117; M. Munakata, G. L. Ning, T. Kuroda-Sowa, M. Maekawa, Y. Suenaga and T. Horino, *Inorg. Chem.*, 1998, **37**, 5651; T. Kuroda-Sowa, T. Horino, M. Yamamoto, Y. Ohno, M. Maekawa and M. Munakata, *Inorg. Chem.*, 1997, **36**, 6382.

3 J. S. Miller and A. J. Epstein, *Prog. Inorg. Chem.*, 1976, **20**, 1; J. S. Miller and A. J. Epstein, *J. Coord. Chem.*, 1979, **8**, 191; M. M. Ahmad and A. E. Underhill, *J. Chem. Soc., Dalton Trans.*, 1982, 1065; A. T. Coomber, D. Beljonne, R. H. Friend, J. L. Brédas, A. Charlton, N. Robertson, A. E. Underhill, M. Kurmoo and P. Day, *Nature*, 1996, **380**, 144.

4 D. Coucouvanis, N. C. Baenziger and S. M. Johnson, *Inorg. Chem.*, 1974, **13**, 1191; F. J. Hollander, Y. L. Ip and D. Coucouvanis, *Inorg. Chem.*, 1976, **15**, 2230; M. Ebihara, M. Tsuchiya, M. Yamada, K. Tokoro and T. Kawamura, *Inorg. Chim. Acta*, 1995, **231**, 35.

5 F. H. Allen, O. Kennard and R. Taylor, *Acc. Chem. Res.*, 1983, **16**, 146.

6 E. Billing, R. Williams, I. Bernal, J. H. Waters and H. B. Gray, *Inorg. Chem.*, 1964, **3**, 663.

7 M. R. Churchill and K. L. Kalra, *Inorg. Chem.*, 1974, **13**, 1065; M. R. Churchill and K. L. Kalra, *Inorg. Chem.*, 1974, **13**, 1427; L. M. Engelhardt, P. C. Healy, J. D. Kildea and A. H. White, *Aust. J. Chem.*, 1989, **42**, 107; M. Hakansson, S. Jagner, E. Clot and O. Eisenstein, *Inorg. Chem.*, 1992, **31**, 5389; G. Hu, G. J. Mains and E. M. Holt, *Inorg. Chim. Acta*, 1995, **240**, 559.

Communication 8/09708I

C_3-Symmetrical lanthanide podates organized by intramolecular trifurcated hydrogen bonds

Fabien Renaud,[a] Claude Piguet,*[a] Gérald Bernardinelli,[b] Gérard Hopfgartner[c] and Jean-Claude G. Bünzli[d]

[a] *Department of Inorganic, Analytical and Applied Chemistry, University of Geneva, 30 quai E. Ansermet, CH-1211 Geneva 4, Switzerland. E-mail: Claude.Piguet@chiam.unige.ch*
[b] *Laboratory of X-ray Crystallography, 24 quai E. Ansermet, CH-1211 Geneva 4, Switzerland*
[c] *F. Hoffmann-La Roche Ltd, Pharmaceuticals Division, PRNK 68/152, CH-4070 Basle, Switzerland*
[d] *Institute of Inorganic and Analytical Chemistry, BCH, University of Lausanne, CH-1015 Lausanne, Switzerland*

Received (in Basel, Switzerland) 15th December 1998, Accepted 20th January 1999

The protonated tripodal podand $[L^6 + H]^+$ forms stable and organized monometallic podates $[Ln(L^6 + H)]^{4+}$ where Ln^{III} is facially nine-coordinated by three wrapped unsymmetrical tridentate binding units. An unusual trifurcated hydrogen bond assists the organisation of the covalent tripod.

Symmetrical tridentate binding units containing a central pyridine ring L[1–4] are promising receptors for the design of triple helical nine-coordinate lanthanide(III) building blocks $[Ln(L^1 - 2H)_3]^{3-}$ and $[Ln(L^i)_3]^{3+}$ (i = 2–4) with pre-

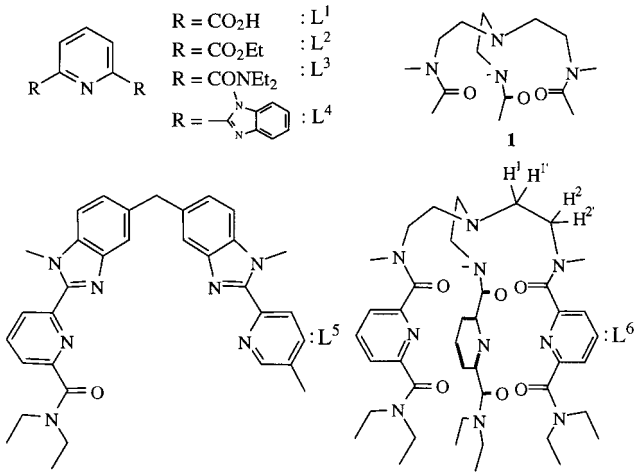

determined physico-chemical properties.[1] Good structural and electronic control has also been demonstrated for unsymmetrical tridentate ligands whose facial orientation in the final C_3-symmetrical complexes is provided by a non-covalent tripod in the heterobimetallic d–f triple-stranded helicates (HHH)-$[LnM(L^5)_3]^{5+}$ (M = Fe^{II}, Co^{II}, Zn^{II}).[1,2] Surprisingly, covalent tripods which are systematically used for organizing unsymmetrical bidentate binding units around octahedral d-block metal ions in monometallic[3] and polymetallic[4] podates have rarely been involved in the related arrangement of tridentate binding units around tricapped trigonal prismatic f-block ions.[5–7] Here, we report the preparation and complexation properties of the new podand L^6 which is designed to encapsulate nine-coordinate lanthanide ions into a tricapped trigonal prismatic geometry.

The podand L^6 is obtained in one step (yield 84%) from the condensation of tris[2-(*N*-methylaminoethyl)]amine (Me-tren)[8] with an excess of 6-(*N*,*N*-diethylcarbamoyl)pyridine-2-carboxylic acylchloride.[2] Potentiometric titration of L^6 with trifluoromethanesulfonic acid in water–acetonitrile (95 : 5) in the pH range 7.0–2.0 (0.1 M $NaClO_4$) reveals a single pK_a = 4.66(1) which is attributed to the protonation of the apical nitrogen atom of the Me-tren tripod by comparison with pK_a = 5.19(2) found for the model compound **1** in the same conditions. When this titration is monitored by ^{1}H NMR in $(CD_3)_2SO$, the methylene protons $H^{1,1'}$ and $H^{2,2'}$ undergo the expected downfield shifts [$\Delta\delta(H^{1,1'})$ = 0.9 ppm, $\Delta\delta(H^{2,2'})$ = 0.3 ppm] resulting from the protonation of the apical nitrogen atom.[9] However, pK_a($[L^6 + H]^+$) and pK_a($[\mathbf{1} + H]^+$) are six orders of magnitude lower than that of the triethylammonium cation (pK_a = 11.01) which strongly suggests that the protonated apical nitrogen adopts an *endo* conformation stabilized by an intramolecular trifurcated hydrogen bond with the surrounding oxygen atoms of the side arms as previously described for protonated cryptands[10] and tris(2-hydroxyethyl)amine podands.[11] The severely reduced hydrophilicity of the resulting clipped conformation accounts for the drastic destabilization of the protonated form in polar media.[10,11]

ESMS titrations of L^6 in acetonitrile with $Ln(ClO_4)_3{\cdot}xH_2O$ (Ln = Sm–Lu; x = 6–9) show the exclusive formation of the 1 : 1 complexes $[LnL^6]^{3+}$ while signals corresponding to $[LnL^6]^{3+}$ and $[Ln(L^6)_2]^{3+}$ are detected for large Ln^{III} ions (Ln = La–Pr). This qualitative speciation is confirmed by spectrophotometric data obtained in the same conditions and fitted to eqn. (1) for Ln = Sm–Lu and eqns. (1) and (2) for Ln = La–Nd (Table 1). The formation of 1 : 2 complexes $[Ln(L^6)_2]^{3+}$ in acetonitrile is limited to light Ln^{III} (Ln = La–Pr) as a result of their larger ionic radii which make them more accessible in $[LnL^6]^{3+}$ for further complexation, as previously reported for hexadentate podands with twelve-coordinated Ln^{III}.[12]

$$Ln^{3+} + L^6 \leftrightarrow [LnL^6]^{3+} \quad \log(\beta_{11}) \quad (1)$$

$$Ln^{3+} + 2L^6 \leftrightarrow [Ln(L^6)_2]^{3+} \quad \log(\beta_{12}) \quad (2)$$

$$Ln^{3+} + [L^6 + H]^+ \leftrightarrow [Ln(L^6 + H)]^{4+} \quad \log(\beta_{11}^H) \quad (3)$$

No clear size-discriminating effect is observed for $\log(\beta_{11})$, but the stability constants are large enough to ensure the quantitative formation of $[LnL^6]^{3+}$ in solution for ligand concentrations > 1 mM and a stoichiometric ratio $Ln : L^6$ = 1. This is confirmed by ^{1}H and ^{13}C NMR spectra (0.05 M in CD_3CN at 298 K) which indicate that $[LnL^6]^{3+}$ (Ln = Ce–Lu) exist as inert and compact C_3-symmetrical complexes. Spectrophotometric titrations of $[L^6 + H]^+$ by $Ln(ClO_4)_3$ in acetonitrile can be fitted to eqn. (3) and give $\log(\beta_{11}^H)$ = 6.7(2), 6.4(2) and 6.4(5) for Ln = Sm, Y and Lu, respectively. The only marginal decrease of $\log(\beta_{11}^H)$ compared to $\log(\beta_{11})$ points to a remarkable preorganization of the protonated podand in $[L^6 + H]^+$ which essentially overcomes the increased electrostatic

Table 1 Selected thermodynamic formation constants of $[Ln(L^6)_i]^{3+}$ (i = 1,2) in acetonitrile at 298 K

Ln	$\log(\beta_{11})$	$\log(\beta_{12})$	Ln	$\log(\beta_{11})$
La	8.3(2)	13.6(2)	Sm	7.0(4)
Ce	8.5(7)	13.3(9)	Dy	7.4(3)
Pr	8.0(7)	12.9(9)	Lu	8.0(6)

repulsion occurring upon complexation to Ln^{3+}. X-Ray quality prisms of $[Eu(L^6 + H)](CF_3SO_3)_3(PF_6)\cdot 0.5MeCN$ **2** can be grown from a solution containing a mixture of triflate and hexafluorophosphate anions. The crystal structure of **2** confirms the presence of a protonated cationic podate $[Eu(L^6 + H)]^{4+}$ located on a crystallographic threefold axis passing through N1, H01 and Eu.†

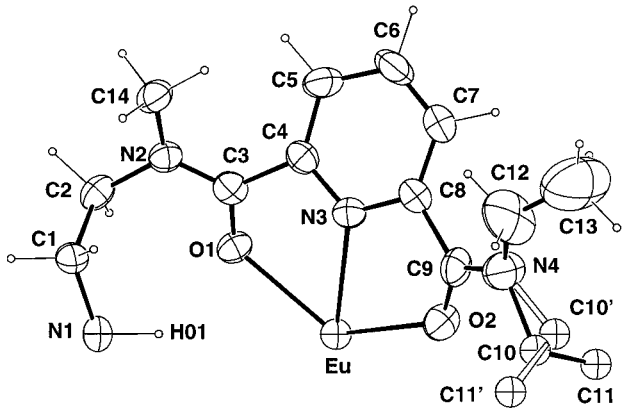

Fig. 1 Atomic numbering scheme of the cation $[Eu(L^6 + H)]^{4+}$ in **2**. Ellipsoids are represented at 40% probability level. The disordered ethyl group [C(10), C(11)] is represented with arbitrary fixed U_{iso} (0.04 Å^2) for clarity. Selected bond and contact distances (Å) and angles (°) in **2**: Eu–O(1) 2.404(8), Eu–N(3) 2.568(7), Eu–O(2) 2.395(7), N(1)···H(01) 1.10(1), N(1)···O(1) 3.02(1), O(1)···H(01) 2.167(8), O(1)–Eu–N(3) 63.5(3), O(1)–Eu–O(2) 125.5(2), N(3)–Eu–O(2) 62.4(4), N(1)–H(01)···O(1) 131.8(4).

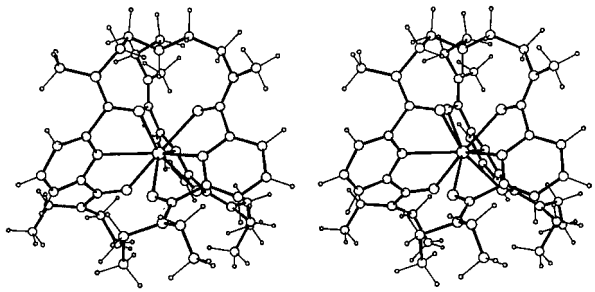

Fig. 2 ORTEP stereoview of the cation $[Eu(L^6 + H)]^{4+}$ perpendicular to the threefold axis.

The three tridentate binding units of the podand are tricoordinated to Eu^{III} whose coordination sphere is best described as a slightly distorted tricapped trigonal prismatic site in which the six oxygen atoms of the carboxamide units occupy the vertices of the prism and the three pyridine nitrogen atoms cap the rectangular faces. The Eu atom lies almost in the equatorial plane defined by the threefold symmetry related nitrogen atoms N(1), N(1′), N(1″) [deviation 0.0281(1) Å], but is significantly closer to the lower oxygen tripod [1.649(1) Å from {O(2), O(2′), O(2″)} and 1.780(1) Å from {O(1), O(1′), O(1″)}]. The Eu–N and Eu–O distances are standard[7] and the triple-helical podate adopts a conical shape which is exemplified by the larger non-bonded O···O distances observed between the oxygen atoms of the lower tripod {O(2), O(2′), O(2″)} [O(2)···O(2′) 3.01 Å, O(1)···O(1′) 2.80 Å] and which strongly contrasts with the cylindrical arrangement of the helical strands found in $[Eu(L^3)_3]^{3+}$.[7] The remarkable trifurcated hydrogen bond observed between atom N(1) (*endo* conformation) and atoms O(1), O(1′) and O(1″)[13] provides three fused and helically twisted seven-membered rings [N(1)–C(1)–C(2)–N(2)–C(3)–O(1)–H(01)] which contribute to the rigidity and the compact arrangement of the tripod. The podate $[Eu(L^6 + H)]^{4+}$ can be thus described as two helical fractions (*i.e.* the covalent tripod and the coordinated strands) which are put on top of each other. The two helical domains display opposite helicity leading to an irregular conical amphiverse *PM* (or *MP*) helix.[14]

Protonation of the apical *endo* nitrogen atoms associated with intramolecular hydrogen bonds is thought to play a crucial role in the stability, rigidity and organization of the final podate as similarly suggested by Shanzer and coworkers for lateral interstrand hydrogen bonding in related podates with d-block metal ions.[4] Preliminary photophysical studies in the solid state and in solution confirm that the C_3-symmetrical structure of the cation $[Eu(L^6 + H)]^{4+}$ is maintained in acetonitrile in agreement with paramagnetic NMR data. The high-resolution emission spectra of $[Eu(L^6 + H)]^{4+}$ display only two components for the $^5D_0 \rightarrow {}^7F_1$ transition[2,7] and three components for the transition $^5D_0 \rightarrow {}^7F_2$ which are diagnostic for a C_3-symmetrical arrangement of the donor atoms around Eu^{III}. The luminescence quantum yield of $[Eu(L^6 + H)]^{4+}$ in acetonitrile is small ($\Phi_{abs} = 1.5 \times 10^{-4}$) as a result of inefficient ligand-centered $^1\pi\pi^* \rightarrow {}^3\pi\pi^*$ intersystem crossing, but the edifice displays a good resistance toward hydrolysis: addition of 10 M water in acetonitrile has only a minor effect on the emission spectrum of $[Eu(L^6 + H)]^{4+}$ and its associated $Eu(^5D_0)$ lifetime [1.96(3) ms in absence of water and 1.29(5) ms with 10 M water], while a drastic quenching of the luminescence was observed for $[Eu(L^3)_3]^{3+}$ after the addition of 1 M water.[7] A comparison between the quenching efficiencies of H_2O *vs.* D_2O using the empirical Horrocks' equation[15] allows one to estimate $q = 0.2 \pm 0.5$ water molecule coordinated to Eu^{III} in acetonitrile containing 10 M of water. Such a small number can be accounted for by second sphere interactions. We conclude that a combination of the podand effect with secondary weak intramolecular interactions allows a precise control of facial nine-coordinate trigonal prismatic site around Ln^{III}, thus offering promising possibilities for the development of pre-organized anchors in heteropolymetallic lanthanide-containing supramolecular complexes.

Notes and references

† *Crystal data*: $C_{45}H_{61}N_{10}O_{15}F_{15}PS_3Eu\cdot 0.5CH_3CN$, $M = 1566.6$; trigonal, space group $R\bar{3}$, $Z = 6$, $a = 13.2949(5)$, $c = 61.020(3)$ Å, $V = 9340.6(8)$ Å^3, $\mu = 9.43$ mm^{-1}, $F(000) = 4758$, $D_c = 1.67$ g cm^{-3}, 5097 measured reflections, 2552 unique reflections of which 2179 were observables [$|F_o| > 4\sigma(F_o)$]; R_{int} for equivalent reflections 0.049. Full-matrix least-squares refinement based on F using weight of $1/[\sigma^2(F_o) + 0.0001(F_o^2)]$ gave final values $R = 0.065$, $wR = 0.062$, and $S = 2.33(4)$ for 285 variables and 2179 contributing reflections. CCDC 182/1150.

1 For reviews, see: C. Piguet and J.-C. G. Bünzli, *Chimia*, 1998, **52**, 579; C. Piguet, *Chimia*, 1996, **50**, 144.
2 S. Rigault, C. Piguet, G. Bernardinelli and G. Hopfgartner, *Angew. Chem., Int. Ed.*, 1998, **37**, 169.
3 G. Serratrice, H. Boukhalfa, C. Beguin, P. Baret, C. Caris and J.-L. Pierre, *Inorg. Chem.*, 1997, **36**, 3898.
4 S. Blanc, P. Yakirevich, E. Leize, M. Meyer, J. Libman, A. vanDorsselaer, A.-M. Albrecht-Gary and A. Shanzer, *J. Am. Chem. Soc.*, 1997, **119**, 4934 and references therein.
5 S. J. Archibald, A. J. Blacke, S. Parsons, M. Schröder and R. E. P. Winpenny, *J. Chem. Soc., Dalton Trans.*, 1997, 173; N. Brianese, U. Casellato, S. Tamburini, P. Tomasin and P. A. Vigato, *Inorg. Chim. Acta*, 1998, **272**, 235.
6 J. Xu, S. J. Franklin, D. W. Whisenhunt and K. N. Raymond, *J. Am. Chem. Soc.*, 1995, **17**, 7245.
7 F. Renaud, C. Piguet, G. Bernardinelli, J.-C. G. Bünzli and G. Hopfgartner, *Chem. Eur. J.*, 1997, **3**, 1646.
8 H. Schmidt, C. Lensink, S. K. Xi and J. G. Verkade, *Z. Anorg. Allg. Chem.*, 1989, **578**, 75.
9 P. Caravan and C. Orvig, *Inorg. Chem.*, 1997, **36**, 236.
10 L. R. MacGillivray and J. L. Atwood, *J. Org. Chem.*, 1995, **60**, 4972.
11 C. Castellari and S. Ottani, *Acta Crystallogr., Sect. C*, 1996, **52**, 2619.
12 P. L. Jones, A. J. Amoroso, J. C. Jeffery, J. A. McCleverty, E. Psillakis, L. H. Rees and M. D. Ward, *Inorg. Chem.*, 1997, **36**, 10.
13 R. Taylor, O. Kennard and W. Versichel, *Acta Crystallogr., Sect. B*, 1984, **40**, 280.
14 J. H. Brewster, *Top. Curr. Chem.*, 1974, **47**, 29; C. Piguet, G. Bernardinelli and G. Hopfgartner, *Chem. Rev.*, 1997, **97**, 2005.
15 W. deW. Horrocks Jr. and D. R. Sudnick, *J. Am. Chem. Soc.*, 1979, **101**, 334.

Communication 8/09742I

ChemComm

Bidirectional asymmetric allylboration and the synthesis of C_2 symmetric 3-methylenepentane-1,5-diols

Anthony G. M. Barrett,* D. Christopher Braddock and Pieter D. de Koning

Imperial College of Science, Technology and Medicine, South Kensington, London, UK SW7 2AY. E-mail: m.stow@ic.ac.uk

Received (in Liverpool, UK) 16th October 1998, Accepted 27th January 1999

The double allylboration of aldehydes using 1,3-bis(diisopinocampheylboryl)-2-methylenepropane under Brown's salt-free conditions provides C_2 symmetric 3-methylenepentane-1,5-diols in excellent enantiomeric excess.

C_2 Symmetric 3-methylenepentane-1,5-diols **1** are versatile synthetic intermediates[1] and a number of procedures have been reported for their synthesis.[2,3] Most of these methods entail the

1 **2**

double addition of an aldehyde to the 2-methylpropene dianion, or a synthetic equivalent. However, the reported syntheses are neither diastereo- nor enantio-selective as only 1 : 1 mixtures of the C_2 **1** and *meso* **2** diastereomers were obtained. As an extension of the Brown asymmetric allylboration reaction,[4] we were interested in preparing the enantiomeric bis(diisopinocampheylborane)s (*S,S*)- and (*R,R*)-**4** and investigating their double allylboration reactions. In this regard, we were encouraged by a report detailing the use of 1,3-bis(dipropylboryl)-2-methylenepropane in double allylboration reactions, affording 1 : 1 mixtures of the desired 3-methylenepentane-1,5-diols **1** (racemic) and **2** (*meso*).[3]

Treatment of an ethereal suspension of 1,3-dilithio-2-methylenepropane, prepared from 2-methylpropene **3**, Bu^{n}Li and TMEDA in hexane,[5] with 2 equiv. of the commercially available (1*S*)-(+)-*B*-chlorodiisopinocampheylborane (DIP-Cl™) afforded the corresponding bis(diisopinocampheylborane) (*S,S*)-**4** (Scheme 1). The corresponding enantiomeric borane (*R,R*)-**4** was prepared from (1*R*)-(−)-DIP-Cl™.† *In situ* reaction with benzaldehyde followed by an alkaline H_2O_2 work-up gave an inseparable mixture of 3-methylene-1,5-diphenylpentane-1,5-diols **1** and **2** (R = Ph) (60%), which were readily separated from the accompanying product of mono-allylboration, 3-methyl-1-phenylbut-3-en-1-ol (**5**) (R = Ph) (30%) (Scheme 1). The diastereomeric ratio (dr) of the mixture of diols **1** and **2** (R = Ph) was estimated to be 8 : 2 (by ^{1}H NMR spectroscopy), in favour of the desired C_2 symmetric isomer **1**.

While this was a promising result, the moderate dr of the C_2 symmetric diol **1** as well as the significant amount of alcohol **5** formed necessitated changes to the reaction conditions. Reasoning that alcohol **5** arose from 3-lithio-2-methylpropene as a result of incomplete dianion formation,[5,6] the 1,3-dilithio-2-methylenepropane was isolated by filtration (35–50%) prior to the addition of the DIP-Cl™. The subsequent allylboration reaction was conducted under Brown's 'salt-free' conditions[7] in order to improve the selectivity. Gratifyingly, these modifications afforded the desired product **1** (R = Ph) with excellent diastereo- and enantio-selectivity (see Table 1, entry 1), and reduced the yield of the alcohol by-product **5** to less than 5%.

A range of aldehydes were allowed to react with both enantiomers of reagent **4**‡ to afford the corresponding C_2 symmetric 3-methylenepentane-1,5-diols **1** in moderate yields (Table 1)§ but with excellent diastereoselectivities (> 80% de)

Table 1 Preparation of C_2 symmetric 3-methylenepentane-1,5-diols **1**

Entry	Reagent	Aldehyde	Yield (%)	Dr[a]	Ee (%)[a]	Config.
1	(*S,S*)-**4**	PhCHO	55 R = Ph	84 : 16	> 95	(*R,R*)
2	(*S,S*)-**4**	Pr^{i}CHO	41 R = Pr^i	93 : 7	> 95	(*R,R*)
3	(*R,R*)-**4**	Pr^{i}CHO	38 R = Pr^i	91 : 9	> 95	(*S,S*)
4	(*S,S*)-**4**	EtCHO	45 R = Et	93 : 7	> 95	(*S,S*)
5	(*S,S*)-**4**	Bu^{i}CHO	53 R = Bu^i	93 : 7	> 95	(*S,S*)
6	(*S,S*)-**4**	C_5H_{11}CHO	43 R = C_5H_{11}	92 : 8	> 95	(*S,S*)
7	(*S,S*)-**4**	4-O_2N-C_6H_4CHO	51 R = 4-O_2N-C_6H_4	95 : 5	> 95	(*R,R*)
8	(*S,S*)-**4**	4-MeO-C_6H_4CHO	55 R = 4-MeO-C_6H_4	95 : 5	> 95	(*R,R*)
9	(*S,S*)-**4**	3-O_2N-C_6H_4CHO	47 R = 3-O_2N-C_6H_4	94 : 6	> 95	(*R,R*)
10	(*S,S*)-**4**		38 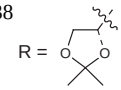	66 : 14.5 : 1	—	(*R,R*)[b]
11	(*R,R*)-**4**		50 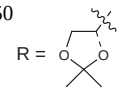	160 : 22 : 1	—	(*S,S*)[b]
12	(*R,R*)-**4**	(*S*)-citronellal	57 (*S*)-Me_2C=C$(CH_2)_2$CHMeCH$_2$ 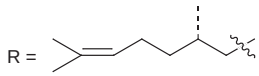	46 : 6 : 1	—	(*R,R*)[b]
13	(*S,S*)-**4**	2-O_2N-C_6H_4CHO	0 R = 2-O_2N-C_6H_4	—	—	—
14	(*S,S*)-**4**	Bu^{t}CHO	0 R = Bu^t	—	—	—

[a] The diastereomeric ratio (dr) is the ratio **1** : **2**. Both the dr and the ee are estimated from the corresponding bis-Mosher esters (ref. 8). [b] The stereochemical descriptor refers to the central 3-methylenepentanediol entity.

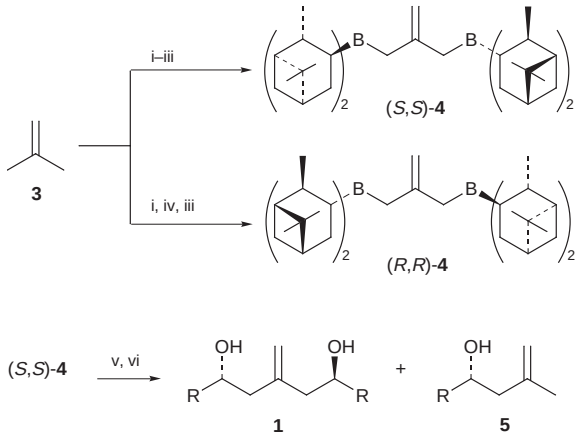

Scheme 1 *Reagents and conditions*: i, Bu^{n}Li, TMEDA, hexane; ii, (+)-DIP-Cl™, Et_2O; iii, pentane, filtration; iv, (−)-DIP-Cl™, Et_2O; v, RCHO, Et_2O or THF, −78 °C; vi, 30% H_2O_2, 4 mol dm^{-3} NaOH, 20 °C.

and enantioselectivities (> 95% ee).¶ Both pivaldehyde and 2-nitrobenzaldehyde failed to provide the corresponding adducts **1** presumably on account of steric congestion (Table 1, entries 13 and 14). In the case of the homochiral aldehydes (Table 1, entries 10, 11 and 12) substantial reagent control of the selectivity was observed, with largely a single isomer being isolated in both the mismatched (entry 10) and matched (entry 11) cases.

The absolute stereochemical course of the reaction was determined by an X-ray crystallographic analysis of the bis-(*S*)-(−)-Mosher ester **6**.‖ This study unequivocally established both the relative and absolute stereochemistry of the diol and, by implication, all of the other diols in Table 1. Additional confirmation of the absolute stereochemistry was obtained from a comparison of the optical rotation of dihydroxy ketone **7**

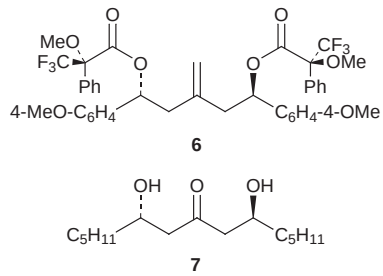

{$[\alpha]_D^{25}$ +45.8, (*c* 0.2 in $CHCl_3$)}, obtained *via* ozonolysis of diol **1** (R = C_5H_{11}) (97%), with that previously reported for the antipode {$[\alpha]_D^{25}$ −40.4, (*c* 0.2 in $CHCl_3$)}.[9]

This study further demonstrates the utility of pinene-derived compounds in asymmetric synthesis. The direct conversion of aldehydes into highly enantiomerically enriched C_2 symmetric 3-methylenepentane-1,5-diols **1** *via* an experimentally simple procedure should be of considerable application in organic synthesis.

We thank Parke Davis Warner Lambert for generous support of this programme of research, Glaxo Wellcome Research Ltd. for the generous research endowment (to A. G. M. B.), the Wolfson Foundation for establishing the Wolfson Centre for Organic Chemistry in Medical Science at Imperial College and the EPSRC.

Notes and references

† A solution of the salt-free bis(diisopinocampheylborane) **4** in Et_2O was found to be stable for up to 3 days at room temperature under an argon atmosphere. After this time the reagent deteriorated markedly as evidenced by substantially reduced yields.

‡ In a typical procedure a solution of (1*S*)-(+)-*B*-chlorodiisopinocampheylborane (5.4 g; 16.8 mmol) in dry Et_2O (20 ml) was added to a vigorously stirred suspension of 1,3-dilithio-2-methylenepropane·2(TMEDA) (2.3 g; 7.7 mmol) in dry Et_2O (20 ml) at 0 °C and the mixture was stirred at 20 °C for 3 h under argon. The Et_2O was removed *in vacuo* and the residue was dissolved in dry pentane (50 ml) and filtered under argon. The residual salts were washed with a further portion of dry pentane (50 ml). The combined pentane extracts were evaporated under reduced pressure and the resulting oil was dissolved in dry Et_2O (50 ml) under argon and cooled to −78 °C. 4-Methoxybenzaldehyde (2.5 ml; 20.5 mmol) was added and the resulting solution was stirred for 3 h at −78 °C. H_2O_2 (30%; 4 ml; 32 mmol) and aqueous NaOH (4 mol dm^{-3}; 8 ml; 32 mmol) were added simultaneously and the mixture was stirred for 18 h at 20 °C. Water (20 ml) was added and the mixture was extracted with Et_2O (3 × 20 ml). The ethereal extracts were dried and concentrated to give a clear residue, which was chromatographed (EtOAc–hexanes, 2 : 3) to give (1*R*,5*R*)-1,5-bis(4-methoxyphenyl)-3-methylenepentane-1,5-diol (1.377 g; 55%) as a white solid.

§ The reported yields are relative to the amount of 1,3-dilithio-2-methylenepropane. All new compounds were fully characterised by spectroscopic data, combustion analysis and HRMS.

¶ Diastereoselectivites and enantioselectivities were determined by preparation of the corresponding bis-Mosher esters (ref. 8) and ^{1}H NMR analysis.

‖ Full details of the X-ray crystallographic study will be reported elsewhere.

1 For example, see F. Alonso, E. Lorenzo and M. Yus, *Tetrahedron Lett.*, 1997, **38**, 2187.
2 R. B. Bates, W. A. Beavers, B. Gordon III and N. S. Mills, *J. Org. Chem.*, 1979, **44**, 3800; J. Klein, A. Medlik-Balan, A. Y. Meyer and M. Chorev, *Tetrahedron*, 1976, **32**, 1839; T. Imai and S. Nishida, *Synthesis*, 1993, 395; C. Gómez, D. J. Ramón and M. Yus, *Tetrahedron*, 1993, **49**, 4117; G. Majetich, H. Nishidie and Y. Zhang, *J. Chem. Soc., Perkin Trans. 1*, 1995, 453; S.-K. Kang, D.-C. Park, C.-H. Park and S.-B. Jang, *Synth. Commun.*, 1995, **25**, 1359; C.-J. Li, *Tetrahedron Lett.*, 1995, **36**, 517; Y. Masuyama, M. Kagawa and Y. Kurusu, *Chem. Commun.*, 1996, 1585; A. Krief and W. Dumont, *Tetrahedron Lett.*, 1997, **38**, 657 and references cited therein.
3 Y. N. Bubnov, M. E. Gurskii and D. G. Pershin, *Bull. Acad. Sci. USSR, Div. Chem. Sci.*, 1987, **36**, 1107.
4 H. C. Brown and P. K. Jadhav, *J. Am. Chem. Soc.*, 1983, **105**, 2092; W. R. Roush, *Allyl Organometallics*, in *Comprehensive Organic Synthesis*, ed. B. M. Trost, I. Fleming and C. H. Heathcock, Pergamon, Oxford, 1991, vol. 2, pp. 1–53 and references cited therein; A. G. M. Barrett and P. W. H. Wan, *J. Org. Chem.*, 1996, **61**, 8667 and references cited therein.
5 J. J. Bahl, R. B. Bates, W. A. Beavers and N. S. Mills, *J. Org. Chem.*, 1976, **41**, 1620.
6 H. C. Brown, P. K. Jadhav and P. T. Perumal, *Tetrahedron Lett.*, 1984, **25**, 5111.
7 U. S. Racherla and H. C. Brown, *J. Org. Chem.*, 1991, **56**, 401.
8 J. A. Dale, D. L. Dull and H. S. Mosher, *J. Org. Chem.*, 1969, **34**, 2543.
9 R. Annunziata, M. Cinquini, F. Cozzi and A. Restelli, *J. Chem. Soc., Perkin Trans. 1*, 1985, 2293.

Communication 8/08070D

Anion pillaring of layered silver coordination networks

George K. H. Shimizu,*† Gary D. Enright, Chris I. Ratcliffe and John A. Ripmeester

Steacie Institute for Molecular Sciences, National Research Council of Canada, Ottawa, Ontario, K1A 0R6, Canada. E-mail: gshimizu@ucalgary.ca

Received (in Columbia, MO, USA) 5th October 1998, Accepted 29th January 1999

Silver *p*-toluenesulfonate and the dithia ligand, 1 form a layered framework where the sulfonate anion serves to 'pillar' the network, as in clay-like solids, allowing for inclusion of benzene.

The generation of microporous metal-organic networks, patterned after naturally occurring solids, is a burgeoning field of research.[1,2] Relative to their wholly inorganic cousins, these 'mineralomimetic'[3] coordination networks offer the promise of greater functionality, inherent to the incorporation of organic moieties, generally at the cost of the thermal or chemical stability of the framework.

Clays are a family of layered compounds, many of which have reactive sites in the interlayer space suitable for acid catalysis and anion exchange. A common strategy to enhance the efficacy of clays is to 'pillar' the interlayer region with a large ion, thereby offering greater access to the interlayer.[4] We recently reported the self-assembly of $AgBF_4$ and the dithia ligand, **1**, to yield an infinite layered network, structurally

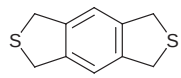

1

analogous to an anionic clay, which swells to different degrees depending on the solvent.[5] As part of our ongoing study of how closely this family resembles clay-like materials, we present a new complex, formed between **1** and silver *p*-toluenesulfonate, AgOTs. This complex maintains the previously observed lamellar motif but also incorporates a coordinating anion to 'pillar' the interlayer region and allow for selective inclusion of benzene.

AgOTs in MeCN was added to a MeCN solution of **1** in a 1 : 1 molar ratio. Diffusion of benzene into this solution gave colourless, plate-like crystals of $\{Ag(\mathbf{1})OTs\cdot 0.5C_6H_6\}_\infty$, **2**, suitable for an X-ray analysis.‡ The structure of **2** (Fig. 1), reveals the formation of an infinite two-dimensional array consisting of cationic Ag(**1**) layers reinforced by a coordinating *p*-toluenesulfonate anion. The geometry at the metal centre is a distorted trigonal monopyramid comprised of three thioether donors, where the Ag–S angles sum to 355°, and a sulfonate oxygen (Ag–S1 = 2.5347(6) Å, Ag–S2a = 2.6077(7) Å, Ag–S2b = 2.5739(6) Å, Ag–O3 = 2.574(2) Å). Each molecule of **1** is asymmetrically ligated to three different silver ions (Fig. 2). That is, the sulfur donor on one side of the ligand coordinates to two silver ions while the sulfur atom on the other side of the ligand bonds to only one, consistent with the $Ag(\mathbf{1})BF_4$ complexes.[5] However, in contrast to the BF_4^- complex, the Ag(**1**) network in **2** does not form perfectly flat layers. In complex **2**, a corrugated motif is adopted (Fig. 2), as necessitated by the distorted trigonal geometry at the Ag^I centre. The dihedral angle formed by the central benzene rings of adjacent molecules of **1** is 48.50(9)°. In **2**, ligand **1** is observed solely in the *anti* conformation, with respect to the orientation of the sulfur donors in the slightly puckered pentagonal rings.

The toluenesulfonate anion is coordinated to the silver ions and orients itself at an angle of 24.2(1)° to the mean lamellar plane. The interlayer distance in **2** is 11.230(1) Å (*cf.* 10.085(1) Å in the BF_4 salt), defined as the perpendicular distance between Ag^I ions. Thus, the anion serves as a pillar to prop the lamellae apart and allow for inclusion of 0.5 molecules of benzene per asymmetric unit. This structure is analogous to that of a pillared anionic clay. The crystals readily lose the benzene upon standing but DSC/TGA reveals the desolvated network to be thermally stable to 190 °C, similar to the BF_4^- complexes.[5]

The ligand–ligand separation, measured perpendicular to the plane of the central benzene ring in **2**, is 3.940(1) Å. The maximum breadth of the *p*-toluenesulfonate ion, taken as the spherical diameter of the SO_3 group, was calculated as 4.92 Å.[6] Although the average spherical diameter of the anion is larger than the inter-ligand distance, the anions are not aligned directly adjacent to each other. For comparison, in the complex, $\{Ag(\mathbf{1})(MeCN)_2(BF_4)\}_\infty$, the inter-ligand distance[5] is 3.826(1) Å and the ionic diameter of a BF_4 ion is 4.79 Å.[6] Thus, in **2**, the lamellae have expanded to incorporate a slightly larger anion.

Interestingly, if one compares the metal centres in this structure with the two previously observed $Ag(\mathbf{1})(solv)BF_4$ (solv = $(MeCN)_2$ or PhCN) structures, one observes a different

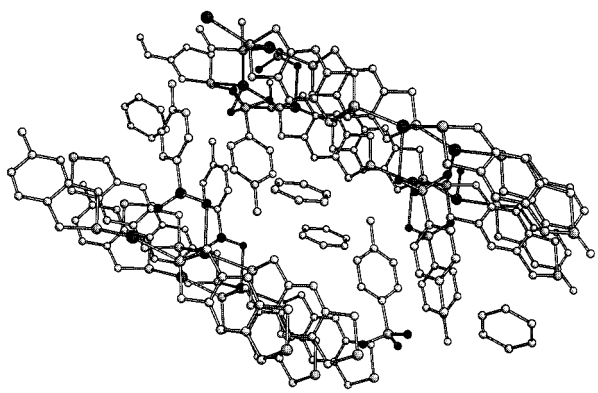

Fig. 1 View of the lamellar network formed by the complex, $\{Ag(\mathbf{1})OTs\cdot 0.5C_6H_6\}_\infty$, showing the 'pillaring' effect of the OTs anions and the inclusion of benzene in the resultant void space.

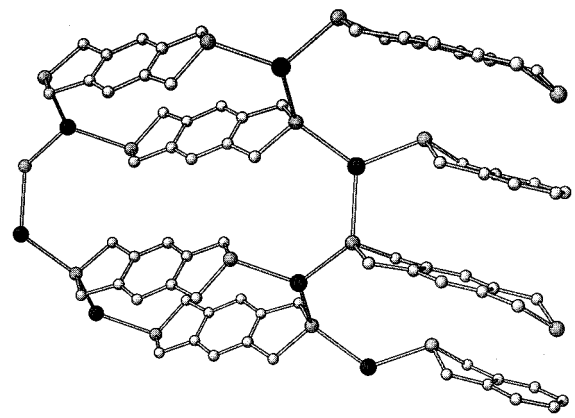

Fig. 2 View of the corrugated structure of the cationic Ag(**1**) layers and the distorted trigonal geometry at Ag^I.

coordination geometry in each case, a distorted trigonal monopyramid in the present case, and trigonal bipyramidal and near perfect trigonal monopyramidal for the MeCN and PhCN adducts of the $AgBF_4$ compounds, respectively. However, in each case, the overall motif adopted is that of a layered network. Silver(I) is well known to have a particularly pliant coordination sphere, as illustrated by these and other examples.[7] A number of studies exist where completely different structures are observed with silver(I) and a given ligand by varying the anion.[8] The tendency of the Ag(**1**)X system, where X is a monovalent anion, to adopt lamellar networks represents the manifestation of a structural constraint built into the dithia ligand, **1**, and the operation of a 'Lamellar Chelate Effect'.[5]

An attempt was made to generate compound **2** *via* anion exchange from the compound $\{Ag(\mathbf{1})(MeCN)_2BF_4\}_\infty$. The BF_4 salt was stirred, as a heterogeneous suspension, in a 0.1 M aqueous solution of sodium *p*-toluenesulfonate for 30 minutes. The solid was filtered off, washed with copious amounts of water, and analyzed by solid-state ^{13}C CP MAS NMR. The spectrum revealed a *ca.* 20% exchange of OTs for BF_4. This process was repeated twice more with the same solution resulting in a *ca.* 40% exchange. A likely scenario, consistent with clay-like behaviour, is that exchange occurs primarily around the periphery of the layered structure thus rendering the core sites inaccessible. Experiments in which exchanges with successively larger anions, also incorporating catalytic amounts of 'swelling' solvents, are in progress.

Notes and references

† Current address: Department of Chemistry, University of Calgary, 2500 University Drive N.W., Calgary, Alberta, T2N 1N4, Canada.

‡ Crystal data for **2**: $C_{20}H_{20}AgS_3O_3$, M = 512.42, monoclinic, space group $P2_1/n$, a = 11.8117(5), b = 7.8813(5), c = 22.3316(10) Å, β = 102.245(5)°, V = 2031.6(2) Å^3, Z = 4, D_c = 1.675 g cm^{-3}, μ(Mo-Kα) = 1.32 mm^{-1}, crystal size 0.04 × 0.20 × 0.20 mm. Data were collected with a Siemens SMART CCD diffractometer using graphite-monochromatized Mo-Kα radiation. A total of 22941 reflections ($3 < 2\theta/° < 57.4$) were processed of which 5244 were unique and 4171 were considered significant with $I_{net} > 2.5\sigma(I_{net})$. The structure was solved by direct methods and refined using the NRCVAX suite of programs.[9] Final residuals were R = 0.029 and R_w = 0.028 (GOF = 1.92) for 324 parameters. CCDC 182/1159.

1 L. J. Barbour, G. W. Orr and J. L. Atwood, *Nature*, 1998, **393**, 671; G. B. Gardner, D. Venkataraman, J. S. Moore and S. Lee, *ibid.*, 1995, **374**, 792; B. F. Abrahams, B. F.Hoskins, D. M. Michail and R. Robson, *ibid.*, 1994, **369**, 727; O. M. Yaghi, G. Li and H. Li, *ibid.*, 1995, **378**, 703; K. A. Hirsch, S. R. Wilson and J. S. Moore, *Chem. Eur. J.*, 1997, **3**, 765; M. Bertelli, L. Carlucci, G. Ciani, D. M. Proserpio and A. Sironi, *J. Mater. Chem.*, 1997, **7**, 1271; M. Fujita, Y. J. Kwon, O. Sasaki, K. Yamaguchi and K. Ogura, *J. Am. Chem. Soc.*, 1995, **117**, 7287; M. Yamamoto, L. P. Wu, T. Kuroda-Sowa, M. Maekawa, Y. Suenaga and M. Munakata, *Inorg. Chim. Acta*, 1997, **258**, 87; J. R. Black, N. R. Champness, W. Levason and G. Reid, *J. Chem. Soc., Chem. Commun.*, 1995, 1277; A. J. Blake, N. R. Champness, S. S. M. Chung, W.-S. Li and M. Schröder, *Chem. Commun.*, 1997, 1675; S. Subramanian and M. J. Zaworotko, *Angew. Chem.*, 1995, **107**, 2295; *Angew. Chem., Int. Ed. Engl.*, 1995, **34**, 2127; F.-Q. Liu and T. D. Tilley, *Inorg. Chem.*, 1997, **36**, 5090.

2 C. L. Bowes and G. A. Ozin, *Adv. Mater.*, 1996, **8**, 13; R. Robson, B. F. Abrahams, S. R. Batten, R. W. Gable, B. F. Hoskins and J. Lui in *Supramolecular Architecture, Synthetic Control in Thin Films and Solids*, ed. T. Bein, ACS Symp. Ser. 499, American Chemical Society, Washington, DC, 1992, pp. 256–273.

3 T. Iwamoto, S. Nishikiori, T. Kitazawa and H. Yuge, *J. Chem. Soc., Dalton Trans.*, 1997, 4127.

4 M. A. Occelli and H. Robson, in *Expanded Clays and Other Microporous Solids*, Academic Press, New York, 1992.

5 G. K. H. Shimizu, G. E. Enright, C. I. Ratcliffe, J. A. Ripmeester and D. D. M. Wayner, *Angew. Chem.*, 1998, **110**, 1510, *Angew. Chem., Int. Ed. Engl.*, 1998, **37**, 1407. As a control, the monothia derivative of **1** was synthesized and complexation with silver(I) was studied. Without the enhanced stability provided by the layer formation, neither the AgOTs nor $AgBF_4$ salts formed stable complexes; in fact, the $AgBF_4$ salt underwent immediate photolysis and decomposition.

6 A value for the ionic volumes was calculated using Moldraw software. A qualitative value of the ionic diameter was determined by assuming a spherical ion and doubling the value of the radius from $V = \frac{4}{3}\pi r^3$. To obtain the spherical radius of the SO_3 group of the *p*-toluenesulfonate, an SO_4 group was employed.

7 Moore and coworkers have recently performed a comprehensive search of the Cambridge Structural Database to quantify occurrences of metal ion geometries, see D. Venkataraman, Y. Du, S. R. Wilson, P. Zhang, K. Hirsch and J. S. Moore, *J. Chem. Educ.*, 1997, **74**, 915. Their results, available at http://sulfur.scs.uiuc.edu, indicate that silver(I) may adopt anywhere from a two- to six-coordinate geometry but that three- and four-coordinate geometries are most common.

8 K. A. Hirsch, S. R. Wilson, J. S. Moore, *Inorg. Chem.*, 1997, **36**, 2960; H. A. Jenkins, S. J. Loeb and A. Malats-i-Riera, *Inorg. Chim. Acta*, 1996, **246**, 207; D. Affandi, S. J. Berners-Price, Effendy, P. J. Harvey, P. C. Healy, B. E. Ruch and A. H. White, *J. Chem. Soc., Dalton Trans.*, 1997, 1411; D. Fortin, M. Drouin, M. Turcotte and P. D. Harvey, *J. Am. Chem. Soc.*, 1997, **119**, 531.

9 E. J. Gabe, Y. LePage, J.-P. Charland, F. L. Lee and P. S. White, *J. Appl. Crystallogr.*, 1989, **32**, 384.

Communication 8/07991I

Novel supported catalyst for hydrodesulfurization reaction

Maria Wojciechowska,* Mariusz Pietrowski and Sławomir Łomnicki

A. Mickiewicz University, Faculty of Chemistry, 60-780 Poznań, ul. Grunwaldzka 6, Poland.
E-mail: emawoj@main.amu.edu.pl

Received (in Cambridge, UK) 18th September 1998, Accepted 20th January 1999

Thanks to a combination of the high activity of ruthenium and unique properties of a new support, magnesium fluoride, a system highly active in the hydrodesulfurization reaction was obtained.

The petrochemical industry faces a difficult problem of satisfying increasingly restrictive standards for fuels. In particular this problem concerns the reduction of the content of sulfur, nitrogen and aromatic components in the fuels produced, which can be achieved by application of various hydrotreatment processes of crude fuels (HDS, HDN, HDM, HYD and HYC). The sulfided catalysts applied at present, containing molybdenum, cobalt, nickel and tungsten supported on alumina will not be able to comply with future standards of fuel quality. Thus it is necessary to prepare new catalysts for hydrotreatment, which apart from high activity, should be characterized by high HDS selectivity.

In 1981, Pecoraro and Chianelli[1] showed that among transition metal sulfide catalysts, ruthenium systems were the most active. Further studies revealed the dependence of activity of sulfided ruthenium catalysts and the support used. For example Ru supported on alumina[2,3] was found to have different HDS properties than Ru supported on carbon.[4]

The present results concern thiophene HDS activity at atmospheric pressure. Thiophene was introduced into the reactor by bubbling a stream of pure hydrogen at a rate of 15 $cm^3\ min^{-1}$ through a thiophene saturator, maintained in an ice bath at 0 °C. The concentration of thiophene in the feed steam (total flow rate 20 $cm^3\ min^{-1}$) was maintained at *ca.* 2.5×10^{-4} mol l^{-1} by adjusting the H_2 flow rate through the saturator. The gas mixtures were analyzed by on-line gas chromatography.

The Ru/MgF_2 catalysts were prepared by conventional impregnation with $Ru_3(CO)_{12}$, surface area of the support = 40 $m^2\ g^{-1}$. Magnesium fluoride was obtained from the reaction of $MgCO_3$ with a 1 : 1 aqueous solution of HF.[5] The precipitate was then dried at 110 °C for 24 h and calcined in air at 400 °C for 4 h. The specific properties of magnesium fluoride: hardness, resistance to calcination in oxygen and well developed porous structure enable its application as an active support and owing to the absence of lattice oxygen anions, opens up great possibilities for the study of the structure and texture of the catalyst[5,6] as well as reaction mechanisms.[7,8] Additionally the presence of anions of higher electronegativity than oxygen anions leads to the expectation of the appearance of strong interactions between the support and the supported active phase.

The Ru/MgF_2 system containing 1.61% weight of ruthenium was found to be more active than similar samples supported on alumina or silica (Fig. 1). All samples were pretreated in two ways: S, sulfidation in 10% H_2S–H_2 and (ii) OS, calcination in air followed by sulfidation in 10% H_2S–H_2.

As can be seen in Fig. 1, preliminary calcination in air distinctly increases the activity of the samples (apart from those supported on silica). This effect can be explained by much easier sulfidation of calcined samples, which proceeds by the exchange of surface oxygen ions of RuO_2 clusters by sulfur atoms.

Fig. 2 presents the product distribution of thiophene HDS over Ru/MgF_2 and Ru/Al_2O_3. The selectivity of hydrogenation

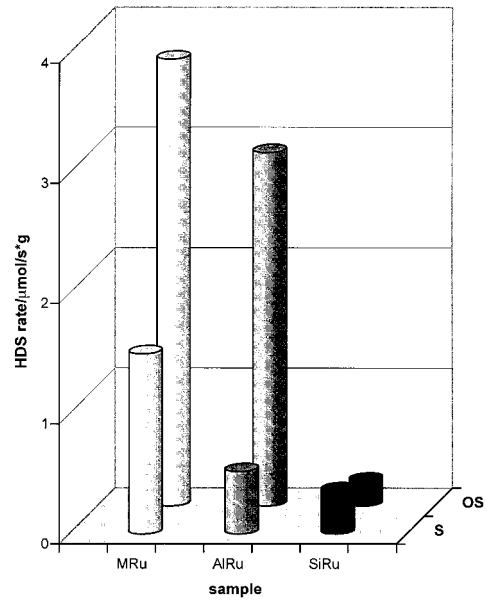

Fig. 1 Comparision of the HDS activity over Ru/MgF_2 (MRu), Ru/Al_2O_3 (AlRu) and Ru/SiO_2 (SiRu) catalysts at 400 °C. S, sulfided in 10% H_2S–H_2, 400 °C, 2 h; OS, calcined in air at 400 °C, 4 h, sulfided in 10% H_2S–H_2; 400 °C, 2 h. The rate of HDS of thiophene is given by HDS rate = *FXC/W*, where *F* is the total flow rate of feed, *X* the fractional conversion, *C* the concentration of thiophene in the feed and *W* the catalyst weight.

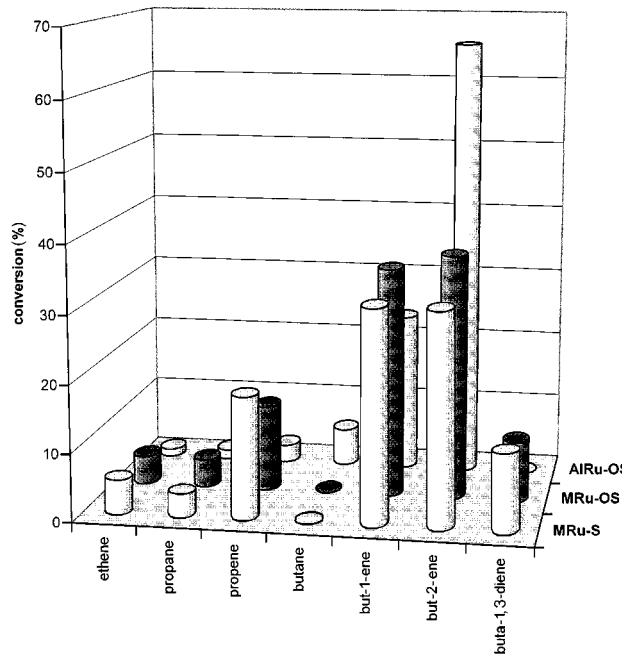

Fig. 2 Product distribution of thiophene HDS over Ru/MgF_2 (MRu) and Ru/Al_2O_3 (AlRu) catalysts. S, sulfided in 10% H_2S–H_2, 400 °C, 2 h; OS, calcined in air at 400 °C, 4 h, sulfided in 10% H_2S–H_2, 400 °C, 2 h.

Table 1 Selectivity of hydrogenation and isomerization

Sample	S_{hyd}	S_{iso}
MRu-S	0.00	1.00
MRu-OS	0.00	0.94
AlRu-OS	0.06	0.36

(S_{hyd}) is defined as the ratio of the formation rates of butane *vs.* butenes, whereas the ratio of but-1-ene *vs.* but-2-enes represents the selectivity of isomerization (S_{iso}).

From the above data the conclusion can be made that Ru/MgF_2 catalysts are very selective systems in the HDS process, much less hydrogenation occurs simultaneously with hydrodesulfurization (Table 1) in comparison with Ru/Al_2O_3. This, together with very high HDS activity is a clear advantage of Ru/MgF_2 catalysts compared with other ruthenium systems supported on different supports.

Since the work of Ledoux *at al.*[9] and Qusro and Massoth,[10] which found a distinct correlation between the HDS activity of thiophene and dibenzothiophene, the results of the HDS reaction for thiophene can be a model example for general conclusions of the hydrodesulfurization activity of the Ru/MgF_2 system.

The lack of tetrahydrothiophene in the reaction products together with the presence of buta-1,3-diene suggests the reaction pathway shown in Scheme 1.[11]

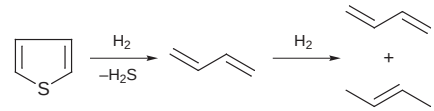

Scheme 1

The catalytic tests for model catalytic reactions of the described samples show a correlation between the thiophene HDS activity and the number of medium strength acidic sites.

Notes and references

1 T. A. Pecoraro and R. R. Chianelli, *J. Catal.*, 1981, **67**, 430.
2 M. Nagai, K. Koizumi and S. Omi, *Catal. Today*, 1997, **35**, 393.
3 Y. J. Kuo and B. J. Tatarchuk, *J. Catal.*, 1988, **112**, 229.
4 M. J. Ledoux, O. Michaux and G. Agostini, *J. Catal.*, 1986, **102**, 275.
5 J. Haber and M. Wojciechowska, *J. Catal.*, 1988, **110**, 23.
6 J. Haber and M. Wojciechowska, *Catal. Lett.*, 1991, **10**, 271.
7 M. Wojciechowska, J. Haber, S. Łomnicki and J. Stoch, *J. Mol. Catal.*, in press.
8 M. Wojciechowska, J. Haber and S. Łomnicki, *Arch. Environ. Protect.*, 1997, **23**, 7.
9 M. J. Ledoux, C. P. Huu, Y. Segura and F. Luck, *J. Catal.*, 1990, **121**, 70.
10 Q. Qusro and F. E. Massoth, *Appl. Catal.*, 1987, **29**, 375.
11 K. F. McCarthy and G. L. Schrader, *J. Catal.*, 1987, **103**, 261.

Communication 8/07002D

$C_{120}OS$: the first sulfur-containing dimeric [60]fullerene derivative

Sabine Giesa,[ab] Jürgen H. Gross,[a] William E. Hull,[c] Sergei Lebedkin,[d] Andrei Gromov,[b] Rolf Gleiter[a] and Wolfgang Krätschmer*[b]

[a] *Organisch-Chemisches Institut der Universität, Im Neuenheimer Feld 270, D-69120 Heidelberg, Germany*
[b] *Max-Planck-Institut für Kernphysik, Postfach 103980, D-69029 Heidelberg, Germany. E-mail: w.kraetschmer@mpi-hd.mpg.de*
[c] *Central Spectroscopy Department, German Cancer Research Center, Im Neuenheimer Feld 280, D-69120 Heidelberg, Germany*
[d] *Forschungszentrum Karlsruhe, Institut für Nukleare Festkörperphysik, Postfach 3640, D-76021 Karlsruhe, Germany*

Received (in Liverpool, UK) 16th December 1998, Accepted 26th January 1999

$C_{120}OS$ has been synthesised by thermal reaction of $C_{120}O$ and sulfur, isolated by HPLC, and characterised by MALDI-TOF-MS, LT-FAB-MS, XPS, Raman, UV-VIS, IR and ^{13}C-NMR spectroscopy; all data are consistent with a molecule of C_s symmetry with the fullerene cages linked by furan- and thiophene-like bridging units.

Following thermal reactions of the $C_{60}/C_{60}O/C_{60}O_2$ system in the solid state, various dimeric fullerene derivatives, *e.g.* $C_{120}O$,[1,2] $C_{120}O_2$ [3,4] and C_{119},[5] have been isolated and characterised. Since ethers and thioethers exhibit similar chemical behavior, we reasoned that it should be possible to synthesise sulfur analogues of the mono- and dimeric [60]fullerene oxides. Several efforts to prepare them in toluene or *o*-dichlorobenzene (ODCB) solutions using typical sulfur-transferring reagents such as Lawesson's reagent,[6] titanocene pentasulfide[7] or sulfur activated with $AlCl_3$, failed. Therefore, we performed the thermolysis of a 1 : 1 (wt%) mixture of solid $C_{120}O$[1,2] and elemental sulfur for 24 h at 230 °C under Ar at atmospheric pressure. The result was the well-known decay of $C_{120}O$ into C_{60} (*ca.* 5–10% with respect to the total amount of fullerene) as well as the production of $C_{120}OS$ (up to 70%). $C_{120}OS$ was also produced by direct heating of $C_{60}/C_{60}O$ mixtures with sulfur, but with lower yields. The product mixtures were dissolved in ODCB and analysed by high-performance liquid chromatography (HPLC)† and matrix-assisted laser desorption/ionisation time-of-flight mass spectrometry (MALDI-TOF-MS). $C_{120}OS$, purified by two-stage HPLC, is a stable, dark brown solid, and its solubility in ODCB is *ca.* 1 mg ml^{-1}

As in the case of the oxides of [60]fullerene dimers,[1,3,4] negative-ion matrix-assisted laser desorption/ionisation time-of-flight mass spectrometry (MALDI-TOF-MS) was used to detect the molecular anion radical, $M^{-\bullet}$, of $C_{120}OS$ (M_r 1489.38) at *m/z* 1489 (Fig. 1).‡ The fragment ions at *m/z* 720, 736 and 752, respectively, can be assigned to C_{60}, $C_{60}O$ and $C_{60}S$. Unfortunately, the observed molecular weight is also consistent with the formula $C_{120}O_3$, and the weak signal at *m/z* 752 may be interpreted as $C_{60}O_2$. The low abundance of ^{34}S (4.2%) and the experimental error in the measurement of the isotopic pattern did not allow us to distinguish between $C_{120}O_3$, $C_{120}OS$ or even C_{124}. Therefore, high-resolution negative-ion low-temperature fast-atom bombardment mass spectrometry (HR-LT-FAB-MS)[8,9] was used to obtain exact masses for $C_{120}OS$ isotopomers, confirming $C_{120}OS$ as the molecular formula.§ The results were: $^{12}C_{120}OS$, *m/z* 1487.9748 (calc. 1487.9670, error +5.2 ppm); $^{12}C_{119}{}^{13}COS$, *m/z* 1488.9764 (calc. 1488.9703, +4.1 ppm); $^{12}C_{118}{}^{13}C_2OS$, *m/z* 1489.9811 (calc. 1489.9737, +5.0 ppm).

Direct confirmation of the presence of sulfur in $C_{120}OS$ was obtained by X-ray photoelectron spectroscopy (XPS).¶ Sulfur was detected *via* the binding energies of 2p electrons which were measured as 163.2 eV ($S_{2p}{}^{3/2}$) and 164.4 eV ($S_{2p}{}^{1/2}$) and are consistent with a thioether moiety and not an S–O linkage (binding energy for sulfoxides: *ca.* 168 eV[10]).

Because of the low solubility of $C_{120}OS$ in ODCB, a sample was prepared for NMR studies with enrichment to *ca.* 7% ^{13}C.[4] The 125 MHz ^{13}C-NMR spectrum exhibited in the sp^3 region four signals with equal integrals and in the sp^2 region 54 resolved signals for 56 distinguishable sp^2 carbons, *i.e.* two pairs of carbons were coincident, giving two peaks with integral 2.‖ This spectrum is consistent with a dimer structure having two-fold symmetry and no carbon atom lying on a symmetry element. The four distinguishable sp^3 sites (eight carbon atoms) led us to a plausible structure which is homologous with the B isomer of $C_{120}O_2$.[3,4,11] The replacement of an oxygen atom in one of the furanoid bridges in C_{2v} $C_{120}O_2$(B) with sulfur results in a structure of C_s symmetry, denoted here as *syn*-**1** (stereo image in Fig. 2).** A total of six possible C_s isomers with *syn* or *anti* bridges (O, S atoms on the same or opposite sides of the cyclobutane bridging unit) were modeled with HyperChem 4.5 using the semi-empirical AM1 and PM3 methods. The *syn*-**1**

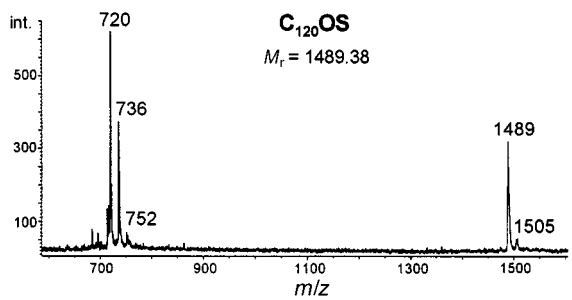

Fig. 1 The MALDI-TOF mass spectrum of $C_{120}OS$ in a 9-nitroanthracene matrix (negative-ion reflector mode) shows the molecular anion radical $M^{-\bullet}$ at *m/z* 1489 and fragment ions at *m/z* 720, 736 and 752.

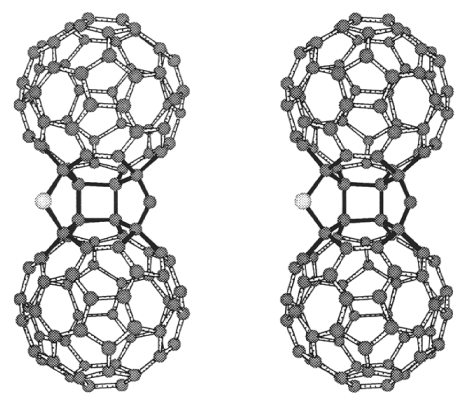

Fig. 2 Stereo pair for the lowest-energy structure of $C_{120}OS$ with C_s symmetry (denoted *syn*-**1**); furan, cyclobutane and thiophene bridges are attached to the 6,6, 5,6 and 6,6 junctions, respectively.

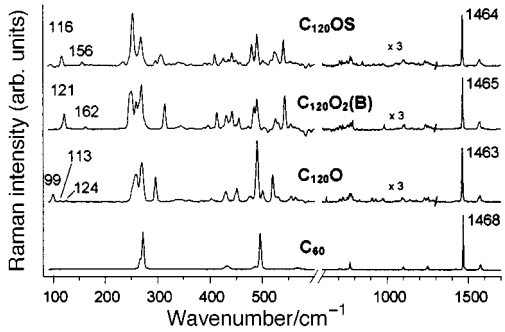

Fig. 3 FT-Raman spectra of solid C_{60}, $C_{120}O$, $C_{120}O_2$(B) and $C_{120}OS$. The region below 200 cm^{-1} is associated with 'rigid-body' cage–cage vibrations.

structure, with 6,6-5,6-6,6 junctions in each cage for the furan–cyclobutane–thiophene bridges (so-called *hph* junctions[11]), has the lowest energy and no double bonds within the pentagons. The next low-energy structure, *syn*-**2** with *php* junctions is 64 kcal mol^{-1} higher in energy. The *syn*-**1** structure can be readily formed from $C_{120}O$, which has 6,6 (*h*) furan junctions, by addition of a sulfur atom to the 6,6 junction next to the C–C bridging bond in one cage (in our nomenclature the so-called *cis*-**1** *anti* junction[4]) followed by the formation of C–S–C and C–C inter-cage bonds to the corresponding *cis*-1 6,6 junction in the opposite fullerene cage.

It has been shown that low-frequency vibrational modes in fullerene dimers are very sensitive to the details of the bridging structure.[4,12] The Raman spectra of C_{60}, $C_{120}O$, $C_{120}O_2$ and $C_{120}OS$ have been obtained under comparable conditions in the solid state (Fig. 3).†† The Raman spectra of $C_{120}OS$ and $C_{120}O_2$(B) are very similar in the range 100–600 cm^{-1}, but differ significantly from the spectrum of $C_{120}O$. In particular, two cage–cage vibrations were observed at 116 and 156 cm^{-1} for $C_{120}OS$ and at 121 and 162 cm^{-1} for $C_{120}O_2$(B), while three bands were found at 99, 113 and 124 cm^{-1} for $C_{120}O$. These results imply that $C_{120}OS$ and $C_{120}O_2$(B) have very similar bridging units and provide strong support for the NMR-consistent structure of $C_{120}OS$ with C_s symmetry (Fig. 2). The C–S–C bridge in $C_{120}OS$ has longer bonds and weaker force constants compared to the C–O–C bridge, and this is expected to result in lower cage–cage vibration frequencies in $C_{120}OS$ compared with $C_{120}O_2$(B), in agreement with the observed spectra.

The FTIR spectrum of $C_{120}OS$ (KBr micropellet) is also quite similar to that of $C_{120}O_2$(B) with bands at 1646, 1459, 1424, 1257, 1189, 1102, 1006, 965, 884, 790, 764, 549, 526 and 471 cm^{-1}. Finally, the UV-VIS spectrum of $C_{120}OS$ in n-hexane resembles that of $C_{120}O_2$(B) with peaks at 222, 274, 284 and 312 nm and weak bands at 422, 430, 464 and 486 nm.

In conclusion, $C_{120}OS$ is the first sulfur-containing dimeric [60]fullerene derivative to be synthesised and characterised by spectroscopic methods. All data are consistent with the lowest-energy modeled structure in which two fullerene cages are linked *via* furan and thiophene bridging rings with a *cis*-**1** configuration of 6,6 junctions. This structure is homologous to the lowest-energy dimeric oxide $C_{120}O_2$(B).

S. G., S. L., A. G. and W. K. thank the Deutsche Forschungsgemeinschaft for financial support (S. L.: Sonderforschungsbereich 551 'Kohlenstoff aus der Gasphase: Elementarreaktionen, Strukturen, Werkstoffe'). The authors are especially indebted to Professor M. Grunze and C. Yan for the XPS spectrum. The technical assistance of Mrs M. Schickedanz (HPLC), Mrs R. Alberts and Mrs A. Krupp (preparation of $C_{120}O$) is gratefully acknowledged.

Notes and references

† $C_{120}OS$ was separated from C_{60} and $C_{120}O$ using a 250 × 4.6 mm Cosmosil Buckyprep column (elution with 9 : 1 toluene–n-hexane, flow rate 1 ml min^{-1}, detection at 340 nm). Elution times for C_{60}, $C_{120}O$ and $C_{120}OS$ were 8.9, 16.1 and 19.2 min, respectively.

‡ MALDI-TOF mass spectra were acquired in the negative-ion reflector mode with a Bruker Biflex instrument (Bruker-Franzen Analytik, Bremen, Germany) using 10 mg ml^{-1} 9-nitroanthracene in acetone as matrix.

§ Negative-ion LT-FAB-MS was performed with a JMS-700 instrument (JEOL, Tokyo, Japan). Solid $C_{120}OS$ was dissolved in 3 μl 1-chloronaphthalene containing 10% 3-nitrobenzyl alcohol and then cooled in liquid nitrogen.[8] High-resolution measurements were made with narrow scans of the accelerating voltage. Internal mass calibration was achieved using $[(H_2SO_4)_nHSO_4]^-$ cluster ions generated from concentrated sulfuric acid. This technique was found to yield hydride adduct formation of about one third of the total molecular ion intensity superimposing the isotopic peaks and shifting the *m/z* values systematically to the high mass side (*ca.* 3 ppm).[9]

¶ XPS was obtained with an LH-12 XP spectrometer (Leybold Heraeus, Hanau, Germany). A polycrystalline gold target was placed in a concentrated solution of $C_{120}OS$ for 40 h under argon atmosphere, rinsed with ODCB and toluene and finally dried under an argon gas flow.

‖ ^{13}C-NMR measurements were performed at 125.76 MHz with a Bruker AM-500 spectrometer using standard Fourier transform techniques and a 5 mm ^{1}H/^{13}C dual probehead (Bruker Analytik GmbH, Rheinstetten, Germany). The sample contained *ca.* 0.3 mg $C_{120}OS$ (7% ^{13}C) in 0.28 ml ODCB-d_4 (saturated solution) with *ca.* 17 mM $Cr(acac)_3$ added. Parameters: temperature 20 °C, rf pulse width 5.9 μs (70° flip angle), repetition time 2.0 s, 151200 transients in 84 h). Chemical shifts for sp^2 carbons (except where noted each resonance represents two carbons): δ (ppm rel. TMS) 152.10, 149.24, 149.09, 148.65, 148.35, 148.21, 147.90, 147.63, 147.29, 146.93, 146.82, 146.54, 146.45, 146.28, 146.09, 145.81, 145.75, 145.60, 145.33, 145.27, 145.15, 145.08, 145.04, 144.97, 144.94, 144.74, 144.72, 144.61, 144.60, 144.50 (4C), 144.39, 144.37, 144.34, 144.23, 144.05, 143.89, 143.76, 143.74, 143.65, 142.93 (4C), 142.47, 142.37, 142.19, 142.18, 141.93, 141.85, 141.17, 141.15, 140.50, 139.83, 138.55, 138.06, 137.38, 134.31; sp^3: 92.40, 80.24, 72.44, 67.38.

** Theoretically, there are putative $C_{120}O_3$ structures with C_s symmetry, *e.g.* four epoxy derivatives of $C_{120}O_2$(B), but these would exhibit 5 or 6 sp^3 carbon signals and an sp^2 pattern inconsistent with the observed spectrum.

†† Bruker FRA 106 spectrometer (Bruker Optik GmbH, Karlsruhe, Germany) using Nd:YAG laser excitation at 1064 nm (resolution 2 cm^{-1}).

1 S. Lebedkin, S. Ballenweg, J. Gross, R. Taylor and W. Krätschmer, *Tetrahedron Lett.*, 1995, **36**, 4971.
2 A. B. Smith, H. Tokuyama, R. M. Strongin, G. T. Furst, W. J. Romanow, B. T. Chait, U. A. Mirza and I. Haller, *J. Am. Chem. Soc.*, 1995, **117**, 9359.
3 A. Gromov, S. Lebedkin, S. Ballenweg, A. G. Avent, R. Taylor and W. Krätschmer, *Chem. Commun.*, 1997, 209.
4 A. Gromov, S. Lebedkin, W. E. Hull and W. Krätschmer, *J. Phys. Chem. A*, 1998, **102**, 4997.
5 A. Gromov, S. Ballenweg, S. Giesa, S. Lebedkin, W. E. Hull and W. Krätschmer, *Chem. Phys. Lett.*, 1997, **267**, 460.
6 S. Scheibye, R. Shabana and S. O. Lawesson, *Tetrahedron*, 1982, **38**, 993; M. P. Cava and M. I. Levinson, *Tetrahedron*, 1985, **41**, 5061.
7 R. Steudel and R. Strauss, *J. Chem. Soc., Dalton Trans.*, 1984, 1775.
8 J. H. Gross, *Rapid. Commun. Mass Spectrom.*, 1998, **12**, 1833.
9 J. H. Gross, S. Giesa and W. Krätschmer, *Rapid Commun. Mass Spectrom.*, in the press.
10 *Handbook of X-Ray Photoelectron Spectroscopy*, ed. C. D. Wagner, W. M. Riggs, L. E. Davis, J. F. Moulder and G. E. Mullenberg, Perkin-Elmer Corp. Physical Electronics Division, 6509 Flying Cloud Drive, Eden Prairie, Minnesota 55 344, 1978.
11 J. W. Fowler, D. Mitchell, R. Taylor and G. Seifert, *J. Chem. Soc., Perkin Trans. 2*, 1997, 1901.
12 S. Lebedkin, A. Gromov, S. Giesa, R. Gleiter, B. Renker, H. Rietschel and W. Krätschmer, *Chem. Phys. Lett.*, 1998, **285**, 210.

Communication 8/09831J

ChemComm

π-Mediated rearrangements and 1,2-H shifts of indanylcarbenes

Robert A. Moss,* Wei Ma and Ronald R. Sauers*

Department of Chemistry, Rutgers University, New Brunswick, New Jersey 08903, USA.
E-mail: moss@rutchem.rutgers.edu

Received (in Corvallis, OR, USA) 15th December 1998, Accepted 29th January 1999

Absolute rate constants determined for 1,2-C and 1,2-H migrations of cyclobutyl-, cyclopentyl-, benzocyclobutenyl- and benzocyclopentenyl-(chloro)- or -(acetoxy)-carbenes reveal that 'phenyl' carbon migrations are preferred to alternative 1,2-C shifts due to π-electronic effects.

The 1,2-C migration of 'phenyl' carbon *a* is strongly preferred to that of 'benzyl' carbon *b* in benzocyclobutenylcarbenes **1-Cl**, **1-F** and **1-OAc**, whilst the 1,2-H shift is virtually non-

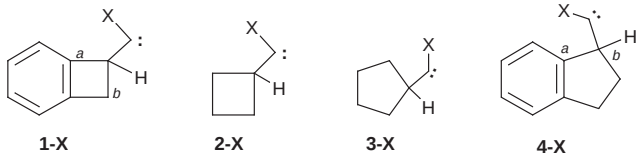

1-X **2-X** **3-X** **4-X**

X = Cl, OAc, or F (for **1**)

competitive.[1] The 1,2-C shift specificity is attributable to mediation by the phenyl π-system.[1] Given the somewhat unusual nature of cyclobutylcarbenes,[2] such as **2-Cl**[3] and **2-OAc**,[4] where relief of strain may drive the 1,2-C shift ring expansion, we now extend our studies to cyclopentylcarbenes **3-Cl** and **3-OAc**, as well as their benzo derivatives, the indanylcarbenes **4-Cl** and **4-OAc**. The results imply that, despite dominant reassertion of the 1,2-H shift with carbenes **3-X** and **4-X**, π-assisted 1,2-C_a migrations remain favored over unassisted C_b shifts.

All carbenes were generated from appropriate diazirine precursors. 3-Chloro-3-cyclopentyldiazirine (λ_{max} 348, 364 nm, pentane) was prepared in 35% yield by NaOCl oxidation[5] of cyclopentanecarboximidamide·HCl,[6] whereas 3-acetoxy-3-cyclopentyldiazirine (13%, λ_{max} 342, 354 nm, pentane) was obtained from a 'modified' Graham oxidation (LiOAc, NaOCl)[4] of the same amidine.† For the indanyl precursors, indan-1-one was converted (40%) to 1-cyanoindane[7] with tosylmethyl isocyanide and NaOEt in DME. The cyanoindane gave 58% of indane-1-carboximidamide·HCl upon reaction with $MeClAlNH_2$ (toluene, 80 °C, 30 h),[8] and the amidine was oxidized to 3-chloro-3-(indan-1-yl)diazirine (30%, λ_{max} 330, 346, 360 nm, pentane) with NaOCl,[5] or to the analogous acetoxydiazirine (9%, 338, 352 nm, pentane) with LiOAc/NaOCl.[4]† All diazirines were purified by chromatography on silica gel and characterized by NMR and UV spectroscopy.

Carbenes **3-X** and **4-X** were generated by photolysis (λ > 320 nm, 25 °C) and by thermolysis (78 °C) of pentane solutions of the diazirines (A = 0.5–0.7 at λ_{max}). Products were identified by GC-MS, and confirmed by comparisons with independently synthesized samples, or were isolated and characterized by NMR and GC-MS. All new products gave acceptable elemental analyses or high resolution MS molecular ions. All major products (> 5%) were characterized.

From **3-Cl**, we obtained only 1,2-H shift product **5**, which was synthesized from cyclopentanone and Ph_3P=CHCl. Carbene **3-OAc** gave enol acetate **6** by 1,2-H shift, and dione **7** by

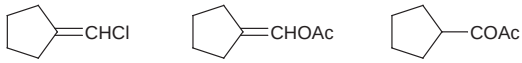

5 **6** **7**

1,2-Ac migration[4,9] in ratios of 1.17 : 1 (*hν*) or 1.23 : 1 (78 °C); no 1,2-C shift product was observed. Authentic **6** was readily obtained by reaction of cyclopentanecarbaldehyde with Ac_2O,[10] whilst **7** was prepared from the same starting material *via* conversion to *E*/*Z*-1-cyclopentylpropene with Ph_3P=CHMe, followed by oxidation with $KMnO_4$.[11]

Indan-1-yl(chloro)carbene (**4-Cl**) produced H-shift products (*E*/*Z*)-**8-Cl**, as well as the isomeric 1,2-C shift products

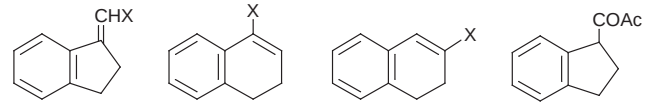

8-X **9-X** **10-X** **11**

1-chloroindene (**9-Cl**, *via* C_a migration) and 2-chloroindene (**10-Cl**, *via* C_b migration). The GC product distribution (**8-Cl** : **9-Cl** : **10-Cl**) was 8.2 : 1.0 : 0.03 (*hν*) or 10.0 : 1.0 : 0.03 (78 °C). Authentic chloroindenes were prepared by reactions of α-tetralone (for **9-Cl**) or β-tetralone (for **10-Cl**) with PCl_5 in benzene.[12] Alkenes **8-Cl** (*E*/*Z* ~ 5) were synthesized in 60% yield by NaOH-induced elimination of HCl from 1-dichloromethylindane, itself prepared by reaction of photogenerated **4-Cl** with HCl in pentane.

From acetoxyindanylcarbene, **4-OAc**, we obtained H-shift products (*Z*/*E*)-**8-OAc**, C-shift products **9-OAc** (*via* C_a migration) and **10-OAc** (*via* C_b migration), and the acetyl migration product, dione **11**. The **8-OAc** : **9-OAc** : **10-OAc**: **11** product distributions were 9.0 : 1.0 : 0.29 : 5.3 (*hν*) and 10.3 : 1.0 : 0.24 : 5.2 (78 °C). Authentic samples of **8-OAc**, **9-OAc** and **10-OAc** were synthesized by reactions of indane-1-carbaldehyde, α-tetralone or β-tetralone, respectively, with Ac_2O;[10] whilst dione **11** was identified by its GC-MS and associated cracking pattern.

Absolute rate constants (reproducibility ~ ±15%) for the carbenic rearrangements were determined at 25 °C by laser flash photolysis (LFP)[9] of pentane solutions of the appropriate diazirines (A_{max} = 0.5–0.7 at λ_{max}) at 351 nm, using the pyridine ylide method.[4,9,13] Growth of the carbene–pyridine ylide was monitored at 390 nm. Details of this methodology, as applied to the carbenic rearrangements, have been described.[4,9]

The absolute rate constants determined for the aggregate rearrangements of carbenes **3-Cl**, **3-OAc**, **4-Cl** and **4-OAc** were (where appropriate) partitioned into k_H, k_C and k_{Ac}, in accord with the product distributions given above. In the case of **4-Cl**, the product distribution is likely biased by rearrangement directly from the excited diazirine,[1,3a,14] so that we partitioned the aggregate rate constant using the 78 °C thermolysis product distribution. Excited state diazirine rearrangements are not expected in the acetoxycarbene series.[4,15] The partitioned rate constants appear in Table 1, together with related data for carbenes **1-Cl** and **1-OAc**,[1] **2-Cl**[3] and **2-OAc**,[4] Me_2CHCCl[16] and $Me_2CHCOAc$.[4] The **2-Cl** rate constants are corrected for excited diazirine contributions,[3] whereas the 78 °C thermal product distribution is given for **1-Cl**.[1]

The most immediate observation from Table 1 is the dominance of the 1,2-H shift in the chemistry of the five-membered ring carbenes. In the absence of strain relief to drive the ring expansion, as in cyclobutylcarbenes **2-OAc** and **2-Cl**,

Table 1 Absolute rate constants of carbenic rearrangements

	Rate constants/s^{-1}			
Carbene	1,2-H	1,2-C_a	1,2-C_b	1,2-Ac
Me_2CHCCl[a]	$>10^8$			
$Me_2CHCOAc$[b]	4.0×10^6			4.0×10^6
2-Cl[c]	1.2×10^7	5.6×10^7	[d]	
2-OAc[b]	1.3×10^4	3.2×10^4	[d]	4.0×10^5
3-Cl[e]	2.2×10^7			
3-OAc[e]	2.9×10^6			2.4×10^6
1-Cl[f,g]	(1.0)	(92)	(7.0)	
1-OAc[f]		8.5×10^6	$< 8.5 \times 10^4$	
4-Cl[e]	1.4×10^7	1.5×10^6	4.5×10^4	
4-OAc[e]	1.4×10^5	1.6×10^4	4.7×10^3	8.5×10^4

[a] Ref. 16. [b] Ref. 4. [c] Ref. 3*a*. [d] $C_b = C_a$. [e] This work. [f] Ref. 1. [g] Only the 78 °C product distribution is available; cf. ref. 1.

where k_C exceeds k_H by factors of 2.5–4.7,‡ the 1,2-H shift is preferred. In cyclopentylcarbenes[17] **3-Cl** and **3-OAc**, it is preferred by a factor of at least 50.§

More to the point, the π-mediation effects, detected in the benzocyclobutenylcarbenes **1-X**,[1] also appear to operate with benzocyclopentenylcarbenes **4-X**, where phenyl carbon (C_a) migrations exceed C_b shifts by factors of 33 (X = Cl) or 3.4 (X = OAc). Importantly, the C_a migrations are *accelerated* by the benzo units whatever the outcome of the k_H *vs*. k_C competition; comparisons of **1-OAc** to **2-OAc**, **4-Cl** to **3-Cl** and **4-OAc** to **3-OAc** reveal significant $k_C(a)$ enhancements.

Other themes may be discerned in Table 1. Anticipated decreases in both k_H and k_C are observed as consequences of replacing carbenic Cl by OAc 'spectator' substituents.[4] These decreases are common to isopropyl-, cycloalkyl- and benzocycloalkenyl-carbenes. Additionally, k_{Ac} is slowed ⩾28 times in the benzocycloalkenylcarbenes **1-OAc** and **4-OAc**, relative to Pr^iCOAc or **3-OAc**, which may well reflect stabilization of the former carbenes' vacant p orbitals by the same homo-π donation[1] that is central to the π-mediation of their C_a migrations. (The ten-fold decrease in k_{Ac} of **2-OAc**, relative to Pr^iCOAc, is attributable to enhanced electron donation by the cyclobutyl moiety.[3c,4])

We conclude that π-mediation of carbenic 1,2-C migrations is not an isolated occurrence, but may occur generally in appropriate systems.

This paper is dedicated to the memory of Professor Robert R. Squires. We thank Ms Dina Merrer and Mr Shunqi Yan for assistance with the LFP experiments. We are grateful to the National Science Foundation for financial support.

Notes and references

† Both chloro and acetoxy diazirines are produced, but are separable by silica chromatography with 1:2 CH_2Cl_2–pentane.

‡ Additionally, 1,2-H migration is disfavored in cyclobutylcarbenes due to the unfavorable imposition of δ+ on the cyclobutyl carbon during hydride migration (ref. 4).

§ The experimental results are mirrored by calculations at the B3LYP/6-311 + G(d,p)//MP2/6-31G(d) level with ZPE corrections (GAUSIAN 94, Revision B.1) which give E_a for the 1,2-H and 1,2-C shifts of **2-Cl** as 6.0 and 5.6 kcal mol^{-1}, modestly favoring 1,2-C migration, as compared to E_a = 1.9 and 8.1 kcal mol^{-1} for the analogous reactions of **3-Cl**, where 1,2-H migration is strongly preferred.

1 R. A. Moss, S. Xue and R. R. Sauers, *J. Am. Chem. Soc.*, 1996, **118**, 10 307.
2 D. H. Paskovich and P. W. N. Kwok, *Tetrahedron Lett.*, 1967, 1227.
3 (*a*) R. A. Moss and G.-J. Ho, *J. Phys. Org. Chem.*, 1993, **6**, 126; (*b*) R. A. Moss and G.-J. Ho, *Tetrahedron Lett.*, 1990, **31**, 1225; (*c*) R. A. Moss, M. E. Fantina and R. C. Munjal, *Tetrahedron Lett.*, 1979, 1227.
4 R. A. Moss, S. Xue, W. Ma and H. Ma, *Tetrahedron Lett.*, 1997, **38**, 4379.
5 W. H. Graham, *J. Am. Chem. Soc.*, 1965, **87**, 4396.
6 A. W. Dox and F. C. Whitmore, *Org. Synth.*, 1941, **Coll. Vol. I**, 5*f*.
7 A. Tetsuya, K. Shoji, A. Yoshiaki and N. Shunsaku, *Chem. Pharm. Bull.*, 1978, **26**, 1776.
8 R. S. Garigipati, *Tetrahedron Lett.*, 1990, **31** 1969. R. A. Moss, W. Ma, D. C. Merrer and S. Xue, *Tetrahedron Lett.*, 1995, **36**, 8761.
9 R. A. Moss, S. Xue, W. Liu and K. Krogh-Jespersen, *J. Am. Chem. Soc.*, 1996, **118**, 12 588.
10 T. J. Cousineau, S. L. Cook and J. A. Secrist III, *Synth. Commun.*, 1979, **9**, 157.
11 K. B. Sharpless, R. F. Lauer, O. Repic, A. Y. Teranishi and D. R. Williams, *J. Am. Chem. Soc.*, 1971, **93**, 3303.
12 S. Mondal and A. J. Bhattacharya, *Curr. Sci.*, 1984, **53**, 676.
13 J. E. Jackson, N. Soundararajan, M. S. Platz and M. T. H. Liu, *J. Am. Chem. Soc.*, 1988, **110**, 5595.
14 M. Nigam, M. S. Platz, B. M. Showalter, J. P. Toscano, R. Johnson, S. C. Abbot and M. M. Kirchhof, *J. Am. Chem. Soc.*, 1998, **120,** 8055; W. R. White III and M. S. Platz, *J. Org. Chem.*, 1992, **57**, 2841; J. A. LaVilla and J. Goodman, *Tetrahedron Lett.*, 1990, **31**, 5109.
15 R. A. Moss and D. C. Merrer, *Tetrahedron Lett.*, 1998, **39**, 8067.
16 R. Bonneau, M. T. H. Liu and M. T. Rayez, *J. Am. Chem. Soc.*, 1989, **111**, 5973; M. T. H. Liu and R. Bonneau, *J. Am. Chem. Soc.*, 1966, **22**, 63.
17 W. Kirmse and G. Wächterhäuser, *Tetrahedron*, 1966, **22**, 63.

Communication 8/09769K

ChemComm

An unexpected intermolecular chiral biaryl coupling reaction induced by a hypervalent iodine(III) reagent: synthesis of potential precursor for ellagitannin

Mitsuhiro Arisawa, Saori Utsumi, Makiko Nakajima, Namakkal G. Ramesh, Hirofumi Tohma and Yasuyuki Kita*

Graduate School of Pharmaceutical Sciences, Osaka University, 1-6, Yamada-oka, Suita, Osaka 565-0871, Japan. E-mail: kita@phs.osaka-u.ac.jp

Received (in Cambridge, UK) 11th December 1998, Accepted 28th January 1999

A novel phenyliodine(III) bis(trifluoroacetate) (PIFA)-induced intermolecular chiral biaryl coupling reaction has been accomplished using α-D-glucose derivatives as chiral templates.

Chiral biaryl compounds serve as important building blocks in the synthesis of natural products including ellagitannins, which have diverse pharmacological activities, such as inhibition of HIV reverse transcriptase,[1] DNA topoisomerase I mediated relaxation[2] and antioxidant activity.[3] In addition they are also used as chiral catalysts in asymmetric reactions.[4] Although several kinds of asymmetric biaryl coupling reactions leading to ellagitannin have been reported,[5] most of them involve the use of heavy metal reagents, such as $Pb(OAc)_4$, CuCN and Cu–pyridine, affording the products in moderate yields.

In recent years, use of hypervalent iodine(III) reagents has gained importance as a non- or low-toxic alternative to heavy metal reagents, to perform a variety of organic transformations. In continuation of our research on the use of hypervalent iodine(III) reagents in organic synthesis, we reported efficient nucleophilic substitution reactions on electron-rich aromatic compounds using a variety of nucleophiles such as N_3,[6] OAc, β-dicarbonyl compounds,[7] SCN and SPh.[8] Very recently, a hypervalent iodine(III)-induced intramolecular biaryl coupling reaction of phenol ether derivatives leading to dibenzo heterocyclic compounds has been reported by us.[9] The facile nature of this reaction prompted us to explore the possibility of using chiral templates in the above coupling reaction with a view to obtaining optically active biaryl compounds. Here we report the first example of an asymmetric intermolecular biaryl coupling reaction induced by phenyliodine(III) bis(trifluoroacetate) (PIFA) with α-D-glucose derivatives as the chiral auxiliary.

Our strategy to obtain the chiral biaryl compounds involves the following three step sequence: (a) synthesis of substituted aroyl derivatives of chiral diols, (b) biaryl coupling reaction using hypervalent iodine(III) reagent and (c) removal of the chiral auxiliary. Accordingly, aroyl derivatives of diols derived from glucose, menthane-3,8-diol, pinane-2,3-diol and hydrobenzoin have been synthesized and their biaryl coupling reaction examined using PIFA. Interestingly, except for the glucose-derived diol derivatives, none of the others were found to participate in the coupling reaction. Thus, the 1,2-diaroyl derivatives (**1a**, **b**)† of protected α-D-glucose underwent a smooth coupling reaction in the presence of PIFA–BF_3•Et_2O, unexpectedly in an intermolecular fashion, to afford the dimers (**2a**, **b**)† in good yields and with high diastereoselectivity

Table 1 Novel chiral biaryl coupling reaction using PIFA

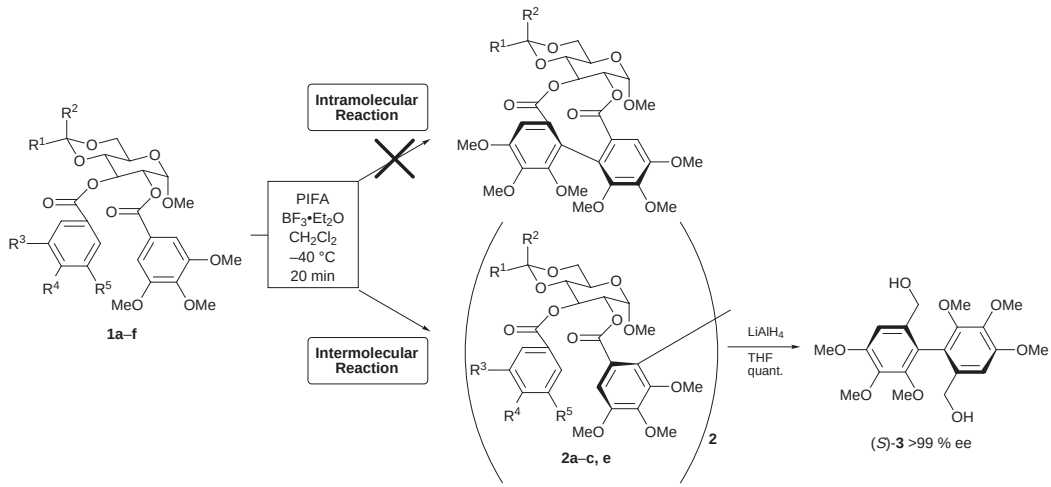

Run	Substrate	R^1	R^2	R^3	R^4	R^5	Yield (%)[a]	De (%)
1	**1a**	Me	Ph	OMe	OMe	OMe	79 (90)	> 99
2	**1b**	Ph	H	OMe	OMe	OMe	44 (68)	> 99
3	**1c**	Me	Ph	OEt	OEt	OEt	37 (59)	> 99
4	**1d**	Me	Ph	OMe	H	OMe	0[b]	—
5	**1e**	Me	Ph	H	OMe	OMe	30 (38)	> 99
6	**1f**	Me	Ph	H	H	H	0[b]	—

[a] Yields in parenthesis indicate the conversion yields based upon the consumed starting material. [b] Complex mixture.

(Table 1). It is quite surprising that the reaction proceeds in an intermolecular fashion and not in the expected intramolecular way. Even more surprising is that only the aromatic ring attached to the C-2 carbon of the sugar moiety underwent the coupling reaction, while the aromatic ring on the C-3 carbon of the sugar remained intact. However, it has been observed that the substituent on the C-3 aromatic ring exerts a great influence on this biaryl coupling reaction. High yields of the products were obtained in the case where the aromatic ring on the C-3 carbon of the sugar was substituted with three methoxy groups at the 3', 4' and 5' positions. Bulkier substituents on the C-3 aromatic ring reduce the yield of the desired product, while no reaction was observed at all with the unsubstituted one. Noteworthy is that only the α-D-glucopyranoside derivative is effective in bringing about this coupling reaction. No coupling reaction took place with the diaroyl derivatives of methyl-β-D-glucopyranoside. Substituted diaroyl derivatives derived from other carbohydrate molecules such as galactose or mannose proved unsuccessful for this reaction. Furthermore, the choice of the Lewis acid used to activate PIFA seems to be critical. Among tested Lewis acids such as BF_3•Et_2O, BF_3•Bu_2O, BCl_3, $ZnBr_2$, $TiCl_4$, $SnCl_4$, Et_2AlCl, $FeCl_3$, $MgCl_2$, $Sn(OTf)_3$ and TMSOTf, only BF_3•Et_2O was found to be an efficient activator in the present case.

In order to obtain the chiral biaryl compound, the coupled adducts (**2a**–**c**, **e**) were treated with $LiAlH_4$. In all cases, the optically active biphenyl compound (**3**) was obtained in quantitative yield, with the regeneration of the chiral sugar auxiliary, which can be used for successive reactions. The optical purity of **3** was determined by HPLC to be >99%, according to the procedure of Meyers.[5d,10]

A plausible explanation for this unexpected intermolecular coupling reaction could be that the sugar moiety and the trimethoxybenzoyl group present at the C-3 carbon of the sugar have a spacial interaction, thereby favorably positioning the aromatic ring on the C-2 carbon to couple with another like molecule.

In summary, we have encountered an unexpected intermolecular biaryl coupling reaction induced by PIFA. The reaction proceeds in high yields and with remarkable diastereoselectivity. The importance of chiral biaryl compounds in organic synthesis as well as in biological sciences, coupled with the use of a hypervalent iodine(III) reagent as a low-toxic reagent, render this method attractive for the synthesis of optically active biphenyl compounds. Detailed investigation of this interesting reaction is in progress.

Notes and references

† *Preparation of* **1a**: A solution of methyl-4,6-*O*-(1′-methylbenzylidene)-α-D-glucopyranoside (ref. 11) (2.22 g, 7.5 mmol), DMAP (183 mg, 1.5 mmol), DCC (3.25 g, 15.75 mmol) and 3,4,5-trimethoxybenzoic acid (3.18 g, 15.0 mmol) in CH_2Cl_2 (125 ml) was stirred at room temperature for 12 h. The precipitate was filtered and the mother liquor was subjected to column chromatography (*n*-hexane–AcOEt = 3 : 2), giving **1a** (4.68 g, 6.83 mmol, 91.0 %) as colorless needles. Mixed benzoates **1c**–**f** were synthesized from methyl-4,6-*O*-(1′-methylbenzylidene)-2-(3′,4′,5′-trimethoxybenzoyl)-α-D-glucopyranoside, which in turn was regioselectively prepared from methyl-4,6-*O*-(1′-methylbenzylidene)-α-D-glucopyranoside using 1-(benzoyloxy)-benzotriazole (ref. 12).

Preparation of **2a**: To a stirred solution of **1a** (34.2 mg, 0.050 mmol) in CH_2Cl_2 (0.50 ml) was added a solution of PIFA (21.5 mg, 0.050 mmol) and BF_3•Et_2O (0.013 ml, 0.100 mmol) in CH_2Cl_2 (0.50 ml) at −40 °C under nitrogen atmosphere, and the reaction was stirred at the same temperature for 20 min. The reaction was quenched by the addition of saturated $NaHCO_3$, extracted with CH_2Cl_2, washed with brine, dried over Na_2SO_4 and evaporated. After column chromatography (*n*-hexane–AcOEt = 1 : 1), **2a** (27.0 mg, 0.0197 mmol, 79%) and **1a** (4.0 mg, 12%) were obtained as colorless needles. *Selected data* for **2a**: mp 168.0–170.0 °C (from Et_2O); δ_H(500 MHz, $CDCl_3$) 1.47 (6H, s), 3.32 (6H, s), 3.45 (6H, s), 3.57–3.63 (4H, m), 3.80 (6H, s), 3.82 (6H, s), 3.91 (6H, s), 3.92 (12H, s), 3.96–4.06 (4H, m), 4.64 (2H, dd, *J* 9.77, 3.66), 4.75 (2H, d, *J* 3.66), 5.86 (2H, dd, *J* 9.77, 9.77), 7.20 (2H, s), 7.33 (4H, s), 7.33–7.37 (10H, m); δ_C(75.0 MHz, $CDCl_3$) 31.78, 55.13, 55.65, 56.25, 60.39, 60.82, 60.95, 62.99, 63.73, 70.10, 72.32, 73.01, 97.50, 102.15, 107.06, 109.31, 124.56, 124.54, 125.14, 126.59, 128.13, 128.83, 140.29, 142.65, 145.51, 150.87, 152.03, 153.09, 165.22, 165.41; IR ν_{max}(KBr)/cm^{-1} 1728, 1338, 1223 cm^{-1}; *m/z* (FAB) 1366 (M^+); HRMS (FAB): calc. for $C_{70}H_{78}O_{28}Na$ 1389.4578, found 1389.4561. Anal. calc. for $C_{70}H_{78}O_{28}$: C, 61.49; H, 5.75. Found: C, 61.09; H, 5.73.

1 G. I. Nonaka, I. Nishioka, M. Nishizawa, T. Yamagishi, Y. Kashiwada, G. E. Dutschman, A. J. Bodner, R. E. Kilkuskie, T.-C. Cheng and K.- H. Lee, *J. Nat. Prod.*, 1990, **53**, 587.

2 (*a*) K. F. Bastow, I. D. Bori, Y. Fukushima,Y. Kashiwada, T. Tanaka, G. I. Nonaka, I. Nishioka and K.-H. Lee, *Planta Med.*, 1993, **59**, 240; (*b*) D. E. Berry, L. MacKenzie, E. A. Shultis, J. A. Chan and S. M. Hecht, *J. Org. Chem.*, 1992, **57**, 420.

3 For example, H. Okamura, A. Mimura, Y. Yakou, M. Niwano and Y. Takahara, *Phytochemistry*, 1993, **33**, 557.

4 R. Noyori, *Chem. Soc. Rev.*, 1989, **18**, 187; S. Inoue, H. P. Takaya, K. Tani, S. Otsuka, T. Sato and R. Noyori, *J. Am. Chem. Soc.*, 1990, **112**, 4897.

5 (*a*) K. S. Feldman and S. M. Ensel, *J. Am. Chem. Soc.*, 1993, **115,** 1162; (*b*) K. S. Feldman, S. M. Ensel and R. D. Minard, *J. Am. Chem. Soc.*, 1994, **116**, 1742; (*c*) K. S. Feldman and S. M. Ensel, *J. Am. Chem. Soc.*, 1994, **116,** 3357; (*d*) T. D. Nelson and A. I. Meyers, *J. Org. Chem.*, 1994, **59**, 2577; (*e*) B. H. Lipshutz, Z.-P. Liu and F. Kayser, *Tetrahedron Lett.*, 1994, **35**, 5567; (*f*) K. S. Feldman and A. Sambandam, *J. Org. Chem.*, 1995, **60**, 8171; (*g*) K. F. Feldman and R. S. Smith, *J. Org. Chem.*, 1996, **61**, 2606; (*h*) A. I. Meyers, *J. Heterocyclic Chem.*, 1998, **35**, 991; (*i*) K. S. Feldman and K. L. Hunter, *Tetrahedron Lett.*, 1998, **39**, 8943; (*j*) D. Dai and O. R. Martin, *J. Org. Chem.*, 1998, **63**, 7628.

6 Y. Kita, H. Tohma, M. Inagaki, K. Hatanaka and T. Yakura, *Tetrahedron Lett.*, 1991, **32**, 4321.

7 Y. Kita, H. Tohma, K. Hatanaka, T. Takada, S. Fujita, S. Mitoh, H. Sakurai and S. Oka, *J. Am. Chem. Soc.*, 1994, **116**, 3684.

8 (*a*) Y. Kita, T. Takada, S. Mihara and H. Tohma, *Synlett*, 1995, 211; (*b*) Y. Kita, T. Takada, S. Mihara, B. A. Whelan and H. Tohma, *J. Org. Chem.*, 1995, **60**, 7144.

9 (*a*) Y. Kita, M. Gyoten, M. Otsubo, H. Tohma and T. Takada, *Chem. Commun.*, 1996, 1481; (*b*) T. Takada, M. Arisawa, M. Gyoten, R. Hamada, H. Tohma and Y. Kita, *J. Org. Chem.*, 1998, **63**, 7698.

10 We followed the protocol of Meyers *et al.*, while determining the ee of the biphenyl compound **3**. According to them [ref. 5(*d*)] in such cases, HPLC was found to be a more reliable method for the determination of ee than by optical rotation. They encountered a discrepancy in the optical rotation of a similar compound.

11 A. Lipták and P. Pügedi, *Angew. Chem., Int. Ed. Engl.*, 1983, **22**, 255.

12 S. Kim, H. Chang and W. J. Kim, *J. Org. Chem.*, 1985, **50**, 1751.

Communication 8/09680E

ChemComm

Synthesis and characterisation of microporous titanoniobosilicate ETNbS-10

João Rocha,*[a] Paula Brandão,[a] Júlio D. Pedrosa de Jesus,[a] Andreas Philippou[b] and Michael W. Anderson[b]

[a] *Department of Chemistry, University of Aveiro, 3810 Aveiro, Portugal. E-mail: rocha@dq.ua.pt*
[b] *Department of Chemistry, UMIST, PO Box 88, Manchester, UK M60 1QD*

Received (in Cambridge, UK) 24th December 1998, Accepted 2nd February 1999

The synthesis, structural characterisation and catalytic activity in *tert*-butanol dehydration of microporous titanoniobosilicate ETNbS-10 are reported.

ETS-10 is a novel microporous framework titanosilicate consisting of 'TiO_2' rods, which run in two orthogonal directions, surrounded by tetrahedral silicate units.[1–3] The pore structure consists of 12-rings, 7-rings, 5-rings and 3-rings and has a three-dimensional wide-pore channel system whose minimum diameter is defined by 12-ring apertures. In an attempt to improve the acid characteristics of ETS-10, silicon has been isomorphously substituted by boron, aluminium and gallium.[4–6] A vanadosilicate with the structure of ETS-10 has also been reported.[7] We now wish to report the synthesis, structural characterisation and catalytic activity in the dehydration of *tert*-butanol, of niobium-substituted ETS-10.

ETNbS-10 materials with Nb/Ti molar ratios (ICP) of 0.12, 0.38 and 0.47 were prepared using a modification of the ETS-10 synthesis. An alkaline solution was made by mixing 10.00 g sodium silicate (Na_2O 8% m/m, SiO_2 27% m/m, Merck), 15.03 g H_2O, 0.80 g NaOH (Merck), 0.96 KF (Aldrich), 0.38 g KCl (Panreac), 1.02 g NaCl (Aldrich) 4.63 g $TiCl_3$ (15% m/m solution of $TiCl_3$ in 10% m/m HCl, Merck) and 1.50 g $Nb(HC_2O_4)_5$ (Niobium Products). 0.10 g seed of ETS-10 was added to the resulting gel. This gel, with a composition 5.6 Na_2O : 2.4 K_2O : 10.0 SiO_2 : TiO_2 : 0.30 Nb_2O_5 : 266 H_2O, was autoclaved under autogeneous pressure for 3 days at 230 °C. The crystalline product was filtered, washed with distilled water and dried at ambient temperature, the final product being an off-white microcrystalline (2–3.5 μm) powder. The samples were characterised by powder X-ray diffraction (XRD), high-resolution and scanning electron microscopies (HREM and SEM, respectively), infrared (TFIR) and Raman spectroscopies, ^{29}Si and ^{93}Nb solid state NMR.

The ETNbS-10 samples with Nb/Ti 0.12 and 0.38 are essentially pure. SEM and powder XRD reveal that the sample with Nb/Ti 0.47 also contains some quartz (< 10%) and, in addition, a small amount of an unknown niobosilicate. The HREM images of this sample (not shown) and ETS-10[2,3] are very similar. The powder XRD patterns of ETS-10 and ETNbS-10 samples (not shown) are virtually identical and show no significant shift in any reflection. This is to be expected because Ti(IV) and Nb(V) have very similar ionic radii.

The total mass losses between 30 and 700 °C of ETNbS-10 (*ca.* 11%, Nb/Ti 0.12) and ETS-10 (*ca.* 12.5%) are similar. Nitrogen adsorption isotherms of ETNbS-10 and ETS-10 materials are of type I with maximum uptakes of *ca.* 0.11 and 0,12 g/g, respectively. However, due to the presence of quartz and niobosilicate dense impurities the maximum uptake of ETNbS-10 with Ti/Nb 0.47 is much smaller (*ca.* 0.06 g/g).

Fig. 1(a) shows the ^{29}Si magic-angle spinning (MAS) NMR spectra of ETS-10 and ETNbS-10 (Ti/Nb 0.47). In ETS-10 there are two types of silicon chemical environments, Si(3Si, 1Ti) and Si(4Si, 0Ti), which give the two groups of resonances at δ −94 to −97 and δ *ca.* −103.7, respectively.[3] the spectrum reveals a further crystallograpic splitting of the Si(3Si, 1Ti) site. ETNbS-10 gives a ^{29}Si MAS NMR spectrum similar to that of ETS-10. However, all resonances broaden considerably and, in particular the ETS-10 peak at δ −103.7, shifts slightly to low frequency. Due to this broadening, the ETS-10 line splitting at δ *ca.* −96.5 is no longer resolved. This seems to indicate the framework insertion of Nb because studies on Al-substituted ETS-10 have shown that the broadening of the ^{29}Si MAS NMR resonances is due to lattice distortion upon Al incorporation.[6] However, in ETNbS-10 Nb is likely to replace Ti and not Si. We note in passing that ETS-10 and an ETS-10 sample impregnated with niobium give very similar ^{29}Si MAS NMR spectra.

The central-transition ^{93}Nb MAS NMR spectrum [Fig. 1(b)] of ETNbS-10 contains a broad (full-width-at-half-maximum, FWHM, *ca.* 240 ppm) asymmetric resonance at δ *ca.* 100 relative to solid Nb_2O_5. This is consistent with niobium being present in distorted octaedral coordination.[8]

Raman spectra (Fig. 2) provide perhaps the best evidence for the isomorphous substitution of Ti by Nb in the ETS-10 framework. ETS-10 gives a main strong and sharp band at *ca.* 735 cm^{-1}, assigned to the TiO_6 octahedra. As the samples Nb content increases this peak shifts slightly and broadens and, simultaneously, a band grows at *ca.* 664 cm^{-1}. The latter is typical of NbO_6 octahedra in microporous niobosilicates: titanoniobosilicate synthetic analogues of the mineral nenadkevichite give a similar band at 668 cm^{-1},[8] while a recently reported niobosilicate (AM-11) gives a band at 687 cm^{-1}.[9] The FTIR spectrum of ETS-10 (not shown) displays bands at 446, 550 and 746 cm^{-1}, associated with the TiO_6 octahedra. As the Nb content of the samples increases the intensity of these bands decreases, while a new band at 918 cm^{-1} is seen. This is a

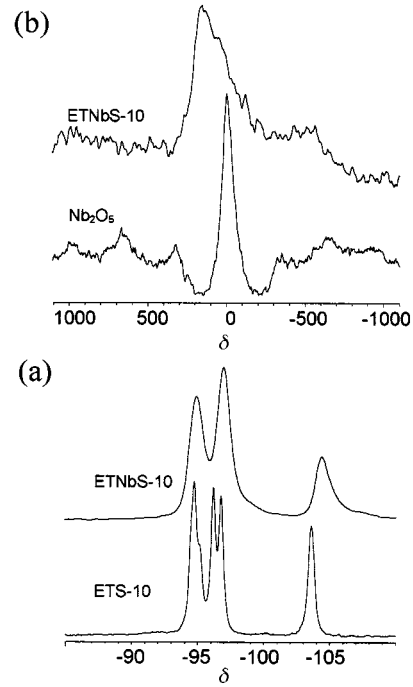

Fig. 1 (a) ^{29}Si MAS NMR spectra of ETS-10 and ETNbS-10 (Nb/Ti 0.47). (b) ^{93}Nb MAS NMR spectra of Nb_2O_5 and ETNbS-10 (Nb/Ti 0.47). The ^{29}Si and ^{93}Nb spectra were recorded at 79.5 and 97.84 MHz on a Bruker MSL 400P spectrometer using spinning rates of 5 and 32 kHz, respectively.

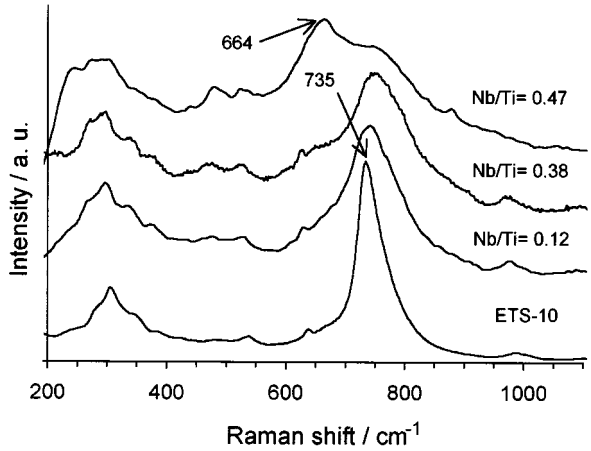

Fig. 2 Stokes-shifted Raman spectra of ETS-10 and ETNbS-10 materials (the Nb/Ti ratios are depicted). The spectra were measured using a Renishaw imaging microscope model 2000.

further indication that Nb replaces Ti in the ETS-10 framework.

A preliminary characterisation of the acid–base properties of ETNbS-10 was performed by means of *tert*-butanol dehydration. The main product of this catalytic process is isobutene an essential ingredient in methyl *tert*-butyl ether (MTBE) synthesis. The product distributions for ETNbS-10 and (for comparison) ETS-10 are given in Table 1. It is apparent that the former dehydrates *tert*-butanol to isobutene with remarkably high activity and selectivity. This finding coupled with the large pore volume of this material point to its potential in catalysis. These results are in accord with a recent study on *tert*-butanol dehydration over AM-6, ETS-10 and Al-substituted ETS-10 which has shown that the basic sites are responsible for the excellent catalytic performance of the materials.[10]

Table 1 A comparison between the catalytic performance of the ETS-10 and ETNbS-10 materials under identical reaction conditions[a]

	ETS-10	Ti/Nb = 0.12	Ti/Nb = 0.47
Conversion	44.0	71.2	99.7
Isobutene	43.56	65.0	95.0
C_5–C_9	0.44	6.2	4.7

[a] Catalyst activation at T = 400 °C and P = 1 atm for 3 h. WHSV = 2 h^{-1}, TOS = 60 min. T = 250 °C, Ar carrier gas flow 30 ml min^{-1}.

This work was supported by PRAXIS XXI and FEDER.

Notes and references

1 S. M. Kuznicki, *US Pat.*, 4,853,202, 1989.
2 M. W. Anderson, O. Terasaki, T. Ohsuna, A. Phillippou, S. P. Mackay, A. Ferreira, J. Rocha and S. Lidin, *Nature*, 1994, **367**, 347.
3 M. W. Anderson, O. Terasaki, O. Ohsuna, P. J. O'Malley, A. Philippou, S. P. MacKay, A. Ferreira, J. Rocha and S. Lidin, *Philos. Mag. B*, 1995, **71**, 813.
4 J. Rocha, P. Brandão, M. W. Anderson, T. Ohsuna and O. Terasaki, *Chem. Commun.*, 1998, 667.
5 M. W. Anderson, A. Philippou, A. Ferreira, Z. Lin and J. Rocha, *Angew. Chem., Int. Ed. Engl.*, 1995, **34**, 1003.
6 M. W. Anderson, J. Rocha, Z. Lin, A. Philippou, I. Orion and A. Ferreira, *Microporous Mater.*, 1996, **6**, 195.
7 J. Rocha, P. Brandão, Z. Lin, M. W. Anderson, V. Alfredsson and O. Terasaki, *Angew. Chem., Int. Ed. Engl.*, 1997, **36**, 100.
8 J. Rocha, P. Brandão, Z. Lin, A. P. Esculcas and M. W. Anderson, *J. Phys. Chem.*, 1996, **100**, 14978.
9 J. Rocha, P. Brandão, A. Philippou and M. W. Anderson, *Chem. Commun.*, 1999, 2687.
10 A. Philippou, M. Naderi, J. Rocha and M. W. Anderson, *Catal. Lett.*, 1998, **53**, 221.

Communication 8/10042J

Improvement of hydrothermal stability of MCM-41 mesoporous molecular sieve

Debasish Das, Chou-Mei Tsai and Soofin Cheng*

Department of Chemistry, National Taiwan University, Taipei 106, Taiwan. E-mail: chem1031@ccms.ntu.edu.tw

Received (in Cambridge, UK) 17th December 1998, Accepted 25th January 1999

Addition of cations such as tetraalkylammonium or sodium ions to the synthesis gel results in considerable improvement of the hydrothermal stability of mesoporous molecular sieve MCM-41.

The recent development of the mesoporous molecular sieve MCM-41 by the workers of Mobil[1,2] has attracted much attention because of the potential of these materials for use as catalysts or catalyst supports. The structure of MCM-41 consists of a hexagonal array of one-dimensional channels of uniform mesopores with pore diameter in the range 15–100 Å, depending on the nature of the template and synthesis conditions. The presence of these very large uniform pores opens up the possibilities for shape-selective conversions of bulky molecules such as those encountered in the manufacture of fine chemicals and pharmaceuticals.[3]

The main drawback of MCM-41 molecular sieve for practical applications is its rather low hydrothermal stability. The hexagonal arranged silica framework is stable when surfactant template molecules are present. However, the calcined samples, which have no templates in the pores, have very poor structural stability, especially in hot water. By contrast, the crystal structure of pure silica MCM-41 was found to be retained up to 850 °C[4] or in a 100% steam flow under atmospheric pressure at 500 °C.[5] Nevertheless, the structure of MCM-41 collapses if it is placed in hot water or aqueous solution for an extended period of time. Partial substitution of Si by other atoms like Ti or Al was reported to improve the thermal and hydrothermal stability to some extent.[6] It was also reported that improved hydrothermal stability could be achieved by adjusting the gel pH several times during the hydrothermal crystallization process.[7] However, this pH adjustment is a tedious process and the high pressure crystallization reaction has to be interrupted repeatedly. Here, we report that significant improvement in the hydrothermal stability of MCM-41 can be achieved by simply adding different tetraalkylammonium (TAA^+) or sodium ions to the synthesis gel and without the necessity of multiple pH adjustment steps.

The hydrothermal crystallization procedure described earlier[8] was slightly modified to obtain MCM-41 samples. The synthesis gel was prepared by adding sodium silicate solution (*ca.* 3.7% NaOH, *ca.* 7.0% SiO_2), to a clear solution containing cetyltrimethylammonium bromide (CTMABr, 99+%) and tetraalkylammonium (TAA^+) or sodium bromide salts. After stirring the mixture for *ca.* 10 min at room temp., a measured amount of 1.10 M sulfuric acid (p.a. grade) was added to the gel and the pH value was adjusted to *ca.* 9.5–10. The molar ratio of the final gel composition is $SiO_2 : 0.48CTMA^+ : (0–0.96)TAA^+ : 0.39Na_2O : 0.29H_2SO_4 : 50–110H_2O$. The gel mixture was stirred for 2 h at room temp. and then transferred into polypropylene bottles and statically heated at 100 °C for 4 days under autogenerated pressure. The final solid material obtained was filtered off, washed until free of Br^- ions, dried and calcined at 560 °C.

The hydrothermal stability of the synthesized samples was investigated by mixing *ca.* 0.2 g of the calcined sample with 20 g deionised water and heating in a closed bottle at 100 °C under static conditions for different time periods. After hydrothermal treatment, the samples were filtered, washed with deionised water and dried at 70 °C overnight. The hydrothermal stability was monitored by following the peak intensities of the X-ray diffraction patterns recorded on a Scintag X1 diffractometer using Cu-Kα radiation (λ = 0.154 nm). Nitrogen adsorption/desorption isotherms at liquid N_2 temperature were measured using a Micromeritics ASAP 2100 system. Prior to the experiments, samples were outgassed at 300 °C for *ca.* 6–8 h under vacuum (10^{-3} Torr). Mesopore size distribution was calculated from the desorption branch of the isotherm by the BJH (Barrett–Joyner–Halenda) method using the Halsey equation. ^{29}Si MAS NMR spectra were acquired at 59.62 MHz with 30° pulse duration of 2.0 ms, 60 s recycle delay using a Bruker MSL-300 spectrometer.

The effect of added TAA^+ cation concentration was studied by using tetrapropylammonium cation. It was found that with TPA^+/surfactant molar ratios up to 2.0, the MCM-41 structure could be obtained. Further increase in TPA^+ concentration results in either poorly crystalline or amorphous material. Highly ordered MCM-41 samples were obtained at TPA^+/surfactant ratios of 0.6–1.4. XRD patterns of the samples showed a very intense (100) diffraction peak and three additional higher order peaks with lower intensities. This suggests that these samples have a high degree of long range ordering of the structure and well formed hexagonal pore arrays. The specific surface area, A_{BET}, as determined from the linear part of the BET equation (p/p_o = 0.05–0.3), shows that these samples have a very high surface area of *ca.* 1000 $m^2\ g^{-1}$. All the samples show typical type IV adsorption isotherms of cylindrical mesopores with a sharp inflection at $p/p_0 \approx 0.3$. Pore size distribution curves show a remarkably narrow pore size distribution with a pore size of *ca.* 27 Å. The pore wall thickness as estimated from the difference of the X-ray unit cell parameter (a_o) and the peak pore diameter was found to be *ca.* 18–19 Å for the calcined samples.

The XRD patterns of the water-treated samples show that all the samples synthesized with the addition of TPA^+ are quite stable to hydrothermal treatment at 100 °C for 4 days. The intensity of the (100) peak remains very strong although the other higher order peaks become smaller. The slight shift of the (100) peak position towards higher 2θ values indicates the contraction of the pores due to an increase in pore wall thickness.

The effect of addition of cations other than TPA^+ is shown in Fig. 1 and the physical properties of the MCM-41 samples prepared with different cations are also listed in Table 1. A cation/surfactant molar ratio of 1.4 was used in the synthesis. It can be seen that highly ordered MCM-41 materials were also obtained with TMA^+, TEA^+ and even Na^+ ions. The BET surface areas, A_{BET}, of these samples are in the range 1010–1070 $m^2\ g^{-1}$. Mesopore size distribution analysis showed a very narrow distribution with a peak pore diameter of *ca.* 27 Å. By contrast, earlier workers reported that without any pH adjustment steps, addition of salts like sodium chloride resulted in poorly ordered MCM-41 samples.[7]

The MCM-41 crystalline structures were well retained after hydrothermal treatment of the calcined samples at 100 °C for 4 days (Fig. 1). Only slight decreases of the (100) peak intensity and the long-range structural ordering were observed. The surface area and pore volume of the water-treated samples were

Table 1 Physical properties of MCM-41 samples prepared with different additional cations

Cation	Treatment	A_{BET}/ $m^2\ g^{-1}$	Mesopores			Peak pore diameter/Å	Wall thickness/Å
			$A_{BJH}/m^2\ g^{-1}$	$V_{BJH}/cm^3\ g^{-1}$	D_{BJH}/Å		
TPA^+	Calcined	1030	1126	0.76	27.0	27.0	17.2
	Water-treated	1030	1053	0.70	26.6	24.0	20.6
TEA^+	Calcined	1010	1155	0.80	27.7	27.0	18.5
	Water-treated	940	1130	0.76	26.9	24.2	21.2
TMA^+	Calcined	1045	1234	0.87	28.2	27.0	19.4
	Water-treated	960	1175	0.79	26.9	24.2	20.6
Na^+	Calcined	1020	1159	0.80	27.6	27.1	17.9
	Water-treated	920	1079	0.72	26.7	24.1	19.2
—	Calcined	1070	1216	0.83	27.3	26.8	19.3
	Water-treated	705	369	0.23	24.9	—[a]	—[a]

[a] The pore size distribution was too broad and irregular to determine the peak diameter.

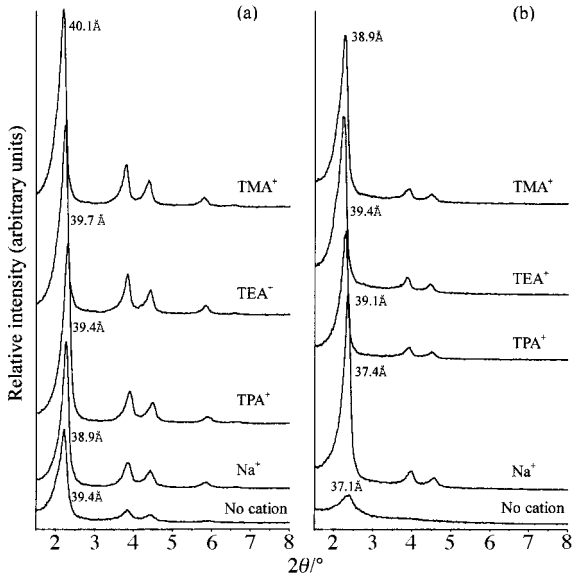

Fig. 1 XRD patterns of the MCM-41 samples prepared with the addition of different cations; (a) calcined samples and (b) after hydrothermal treatment at 100 °C for 4 days.

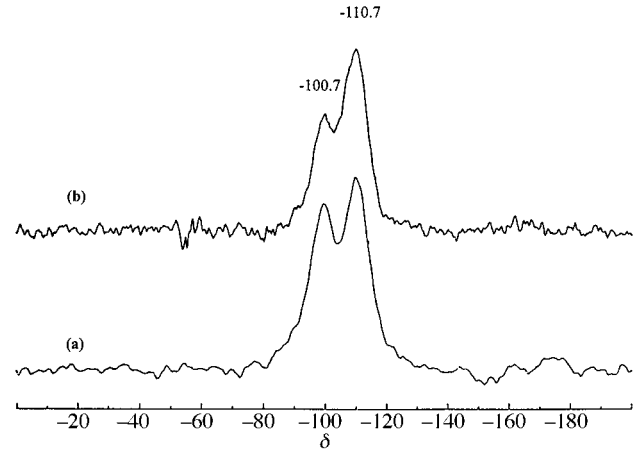

Fig. 2 ^{29}Si MAS NMR spectra of MCM-41 samples prepared (a) without additional cations and (b) with TPA^+ ions.

slightly lower than those of the calcined samples. From the nature of the adsorption isotherms and the pore size distribution curves, the pore size distribution was slightly broadened for TAA^+ and Na^+ modified samples after water treatment, but the mesoporous structure was unaltered. Also, the peak pore diameter shifts slightly towards lower values due to increased pore wall thickness. By contrast, for a sample prepared without addition of TAA^+ or extra Na^+ ions, the hexagonal pattern almost disappeared after hydrothermal treatment. The mesopore area of the unmodified sample decreases drastically after hydrothermal treatment, indicating severe disintegration of the mesostructure. It is also noted here that samples prepared without additional cations have similar pore wall thickness to those prepared by adding different cations. Hence, the increased hydrothermal stability is not related to the pore wall thickness as reported earlier.[9]

It appears that during the formation of the surfactant–silicate mesostructure, the electrostatic interaction between the cationic surfactant micelles and the surrounding silicate anions is altered by the presence of the additional cations. ^{29}Si MAS NMR spectra of the samples prepared with and without TPA^+ are shown in Fig. 2. It can be seen that the Q_4/Q_3 ratio in the as-synthesized samples was much higher for that prepared in the presence of TPA^+. The higher Q_4/Q_3 ratio indicates that there is increased condensation between the silanol groups during the formation of the mesostructure.

These results suggest that MCM-41 type mesoporous materials with a high degree of hydrothermal stability can be directly obtained without tedious pH adjustment steps by adding additional cations in the synthesis gel. Although the exact roles of these additional cations are still not clear, their presence seems to facilitate increased condensation of the silanol groups during the formation of the mesostructure. The highly condensed silica wall is considered to have better structural stability under hydrothermal treatment conditions.

Financial support from the China Petroleum Corporation, Taiwan is gratefully acknowledged. One of the authors (D. D.) thanks the National Science Council, Taiwan for a post-doctoral fellowship.

Notes and references

1 C. T. Kresge, M. E. Leonowicz, W. J. Roth, J. C. Vartuli and J. S. Beck, *Nature*, 1992, **359**, 710.
2 J. S. Beck, J. C. Vartuli, W. J. Roth, M. E. Leonowicz, C. T. Kresge, K. D. Schmitt, C. T. W. Chu, D. H. Olson, E. W. Sheppard, S. B. McCullen, J. B. Higgins and J. L. Schlenker, *J. Am. Chem. Soc*., 1992, **114**, 10834.
3 A. Corma, V. Fornés, M. T. Navarro and J. Pérez-Pariente, *J. Catal*., 1994, **148**, 569.
4 C. Y. Chen, H. X. Li and M. E. Davis, *Microporous Mater*., 1993, **2**, 17.
5 J. M. Kim, J. H. Kwak, S. Jun and R. Ryoo, *J. Phys. Chem*., 1995, **99**, 16742.
6 L. Y. Chen, S. Janicke and G. K. Chuah, *Microporous Mater*., 1997, **12**, 323.
7 R. Ryoo and S. Jun, *J. Phys. Chem*., 1997, **101**, 317.
8 H. P. Lin, C. Y. Mou and S. Cheng, *Microporous. Mater*., 1997, **10**, 111.
9 N. Coustel, F. Di Renzo and F. Fajula, *J. Chem. Soc*., *Chem. Commun*., 1994, 967.

Communication 8/09815H

ChemComm

Diels–Alder reactions of dienylboron compounds with unactivated dienophiles: an application of boron tethering for substituted cyclohexenol synthesis

Robert A. Batey,* Avinash N. Thadani and Alan J. Lough†

Department of Chemistry, University of Toronto, Toronto, Ontario, Canada M5S 3H6.
E-mail: rbatey@alchemy.chem.utoronto.ca

Received (in Corvallis, OR, USA) 7th December 1998, Accepted 27th January 1999

An efficient tethered intramolecular Diels–Alder reaction of 1,3-dienylboronates with various allyl and homoallyl alcohols under thermal conditions is described.

The use of Diels–Alder reactions is one of the most commonly encountered strategies for the formation of six-membered rings, particularly in natural product synthesis.[1,2] The reaction has been further augmented by using synthetic equivalents of either the diene or dienophile.[1] For instance, alkenylboron dienophiles have been used as synthetic equivalents to enols.[3–5] 1,3-Dienylboronates are versatile synthetic equivalents for hetero-subsituted dienes, since the allylboronate cycloadducts can be transformed to desirable substituted cyclohexene derivatives.[6] However, a major impediment to the use of 1,3-dienylboronate dienes in Diels–Alder reactions is the need for activated dienophile partners (*e.g*. *N*-phenylmaleimide or methylacrylate). Narasaka has demonstrated that phenylboronic acid can be used to create a temporary O–B–O tether between a diene and dienophile containing free hydroxy groups.[7] Inspired by Narasaka's work, we reasoned that tethering[8–10] *via* a C–B–O connection would enable the reaction of 1,3-dienylboron compounds with dienophiles containing hydroxy groups, such as allylic and homoallylic alcohols (*vide infra*). Here we report the first examples of Diels–Alder reactions of 1,3-dienylboron compounds with unactivated dienophiles.

Tethering of dienylboronate precursors **1** to a dienophilic component **2** allows *in situ* formation of mixed boronic esters, followed by intramolecular Diels–Alder reaction to the allylboracycles **3** (Scheme 1). Oxidation of the C–B bond in the adducts **3**, with retention of stereochemistry, leads to the formation of cyclohexenols, which are valuable precursors in natural porduct synthesis. Overall, **1** acts as a masked 1-hydroxydiene equivalent in the Diels–Alder reaction. In comparison to existing silicon-tethered Diels–Alder methodology, this approach uses the more readily synthesized dienylboronates as precursors. The use of a C–B–O rather than an O–B–O tether[7] is important, since in most cases O–B–O tethers are not applicable.

The dienylboronates **1** are formed *via* standard hydroboration methodology from the corresponding enynes. Thus, hydroboration of **4** and **7** with dicyclohexylborane afforded the corresponding dicyclohexyl(dienyl)boranes. The boron–cyclohexyl bonds were then preferentially oxidized with $Me_3N(O)$ to afford the desired dienylboronate (Table 1 and 2) without concomitant oxidation of the boron–diene bond.[6a,11] Since dienylboronates are subject to disproportionation, they were generally used *in situ* without purification. Thermal Diels–Alder reaction was conducted in the presence of an appropriate dienophile, in a degassed toluene solution, with 5 mol% of 2,6-di-*tert*-butyl-4-methylphenol (BHT) as a free radical inhibitor, using a sealed tube and a heating bath of the appropriate temperature. Oxidation with $Me_3N(O)$ or basic H_2O_2 then afforded racemic cyclohexene diols **5** and **6** in good yields (Tables 1 and 2).

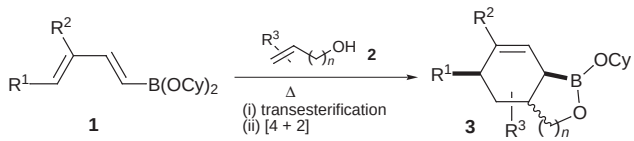

Scheme 1

The constraining effects of the tether both accelerate the rate of cycloaddition, and control the regio- and stereoselectivity of the reaction. We have not been able to isolate cycloadducts in those cases where the initial tethering step cannot occur. For instance, no cycloaddition reaction was observed between ethane-1,2-diyl dienyl boronates and cinnamyl alcohol, allyl alcohol or methyl cinnamyl ether, even after prolonged heating at 220 °C.

Table 1 Tethered Diels–Alder reactions of **4**

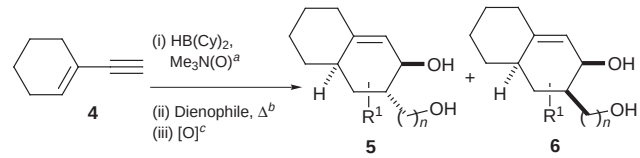

Entry	Dienophile	*T*/°C	*t*/h	Yield (%)[d]	Dr (**5** : **6**)[e]
1	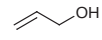	190	48	60[f]	40 : 60
2	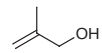	190	48	40	50 : 50
3	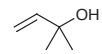	190	5	82	55 : 45
4	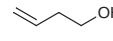	190	120	71	89 : 11
5	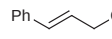	190	6	75	95 : 5
6	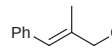	190	12	68	27 : 73
7	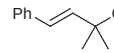	150	0.5	62	85 : 15
8	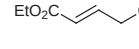	80	16	77	84 : 16
9	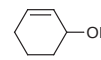	190	24	70	25 : 75
10	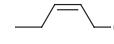	190	36	50	[g]

[a] 1 equiv. $HB(Cy)_2$, THF, 0 °C to room temp., 1 h; 2 equiv. $Me_3N(O)$, THF, 0 °C to room temp., 2 h. [b] [Boronate] = *ca*. 0.3 M, $PhCH_3$, 5 mol% BHT. [c] 5 equiv. $Me_3N(O)$, C_6H_6, 80 °C, 24 h or 3 equiv. NaOH/3 equiv. H_2O_2, THF–H_2O, 2 h. [d] Yields are for chromatographically purified material and are calculated from **4**. [e] The diastereomeric ratios (**5** : **6**) are based upon NMR analysis of the crude products. [f] 6% of the corresponding enone was isolated. [g] Only **5** was isolated along with 6% of a byproduct presumably derived from **6**.

† To whom correspondence concerning the crystallographic data should be addressed.

Table 2 Tethered Diels–Alder reactions of **7**

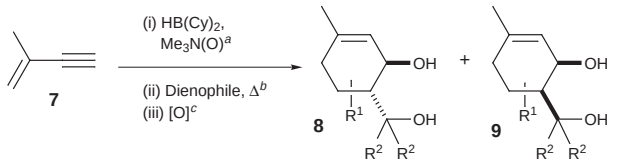

Entry	Dienophile	*T*/°C	*t*/h	Yield (%)[d]	Dr (**5** : **6**)[e]
1	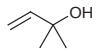	190	1	81	55 : 45
2	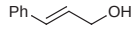	190	6	65	75 : 25
3	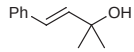	150	0.5	62	75 : 25

[a] 1 equiv. $HB(Cy)_2$, THF, 0 °C to room temp., 1 h; 2 equiv. $Me_3N(O)$, THF, 0 °C to room temp., 2 h. [b] [Boronate] = *ca.* 0.3 M, $PhCH_3$, 5 mol% BHT. [c] 5 equiv. $Me_3N(O)$, C_6H_6, 80 °C, 24 h or 3 equiv. NaOH/3 equiv. H_2O_2, THF–H_2O, 2 h. [d] Yields are for chromatographically purified material and are calculated from **7**. [e] The diastereomeric ratios (**8** : **9**) are based upon NMR analysis of the crude products.

Although the tethered reactions are completely regioselective, they occur with varying diastereoselectivity depending on the substituents present on the dienophile. The presence of an activating electron-withdrawing group on the dienophile results in faster reactions (Table 1, entries 5 and 7). In comparison to the reaction using allyl alcohol (Table 1, entry 1), reaction with activated *E*-allylic alcohols favours the formation of the *trans*-substituted compounds **5** (Table 1, entries 5 and 8). This is expected, since the activating phenyl or ester groups are *endo* with respect to the diene in the transition state. The use of a longer tethering chain as exemplified by homoallyl alcohol (Table 1, entry 4) results in longer reaction times compared to allyl alcohol (Table 1, entry 1), but again favours the *trans*-substituted adduct **5**. Conversely, the presence of a *gem*-dimethyl group in the tethering chain results in shorter reaction times, because of the Thorpe–Ingold effect (Table 1, entries 3 and 6). The stereochemistry of compound **5** (Table 1, entry 5)[12] and compound **6** (Table 1, entry 9)[13] were confirmed by single crystal X-ray analysis. In the latter case the dienylboronate is delivered to the same face of the cyclohexenol ring as the hydroxy group.

Dienylboronates derived from **7** were also used as Diels–Alder precursors (Table 2). The yields are slightly lower in these cases due to the greater propensity of the dienylboronate towards polymerization. One of the enantiomers of compound **8** (Table 2, entry 1) has been used as an intermediate in the synthesis of *ent*-Δ^1-tetrahydrocannabinol.[14]

In summary, we have demonstrated a new dienylboronate tethered Diels–Alder reaction, one of the few methods allowing the use of unactivated dienophiles. The effect of the substituents on the dienophile and the length of tether on the efficacy and diastereoselectivity of the reaction was investigated. The ready availability of various enynes as precursors and the synthetic flexibility of the C–B bond in the cycloadducts is anticipated to provide access to a variety of functionalized cyclohexene derivatives.

We thank the Natural Sciences and Engineering Research Council of Canada (NSERC) for financial support of this work. A. N. T. thanks the NSERC for a Postgraduate Scholarship. R. A. B. thanks the University of Toronto, Astra Pharma Inc. and Astra Research Centre of Montreal, for additional support. We thank Dr A. B. Young for mass spectroscopic assistance.

Notes and references

1 For a review on intermolecular Diels–Alder reactions, see: W. Oppolzer, in *Comprehensive Organic Synthesis*, ed. B. M. Trost, I. Fleming and L. A. Paquette, Pergamon, Oxford, 1991, vol. 5, pp. 315–399.

2 For reviews on intramolecular Diels–Alder reactions, see: W. R. Roush, in *Comprehensive Organic Synthesis*, ed. B. M. Trost, I. Fleming and L. A. Paquette, Pergamon, Oxford, 1991, vol. 5, pp. 513–550; D. Craig, *Chem. Soc. Rev.*, 1987, **16**, 187; A. G. Fallis, *Can. J. Chem.*, 1984, **62**, 183.

3 For the first example of the use of an organoboron compound in an intermolecular Diels–Alder reaction, see: D. S. Matteson and J. O. Waldbillig, *J. Org. Chem.*, 1963, **28**, 366.

4 For examples of the use of alkenylboron compounds as dienophiles in intermolecular Diels–Alder reactions, see: D. A. Singleton, in *Advances in Cycloaddition*, ed. M. Lautens, JAI Press, Greenwich, CT, 1997, vol. 4, pp. 121–148.

5 For examples of the use of alkenylboron compounds as dienophiles in intramolecular Diels–Alder reactions, see: D. A. Singleton and Y.-K. Lee, *Tetrahedron Lett.*, 1995, **36**, 3473; R. A. Batey, D. Lin, A. Wong and C. L. S. Hayhoe, *Tetrahedron Lett.*, 1997, **38**, 3699.

6 (*a*) M. Vaultier, F. Truchet, B. Carboni, R. W. Hoffmann and I. Denne, *Tetrahedron Lett.*, 1987, **28**, 4169; (*b*) X. Wang, *J. Chem. Soc., Chem. Comm.*, 1991, 1515; (*c*) P.-Y. Renard and J.-Y. Lallemand, *Bull. Soc. Chim. Fr.*, 1996, **133**, 143; (*d*) G. Ohanessian, Y. Six and J.-Y. Lallemand, *Bull. Soc. Chim. Fr.*, 1996, **133**, 1143; (*e*) L. Garnier, B. Plunian, J. Mortier and M. Vaultier, *Tetrahedron Lett.*, 1996, **37**, 6699; (*f*) P.-Y. Renard and J.-Y. Lallemand, *Tetrahedron: Asymmetry*, 1996, **7**, 2523; (*g*) P.-Y. Renard, Y. Six and J.-Y. Lallemand, *Tetrahedron Lett.*, 1997, **37**, 6589.

7 K. Narasaka, S. Shimada, K. Osoda and N. Iwasawa, *Synthesis*, 1991, 1171; S. Shimada, K. Osoda and K. Narasaka, *Bull. Chem. Soc. Jpn.*, 1993, **66**, 1254.

8 The most common tethering approach for Diels–Alder reactions uses carbon–metalloid or carbon–metal precursors. The constraining effects of the tether both accelerate the rate of cycloaddition, and control the regio- and stereo-selectivity of the reaction. The majority of examples employ a C–Si–O tether, such as in the reactions of dienylsilanes: K. Tamao, K. Kobayashi and Y. Ito, *J. Am. Chem. Soc.*, 1989, **111**, 6478; K. J. Shea, A. J. Staab and K. S. Zandi, *Tetrahedron Lett.*, 1991, **32**, 2715; K. J. Shea, K. S. Zandi, A. J. Staab and R. Carr, *Tetrahedron Lett.*, 1990, **31**, 5885; R.-M. Chen, W.-W. Weng and T.-Y. Luh, *J. Org. Chem.*, 1995, **60**, 3272.

9 For reviews on silicon-tethered reactions, see: L. Fensterbank, M. Malacria and S. McN. Sieburth, *Synthesis*, 1997, 813; M. Bols and T. Skrydstrup, *Chem. Rev.*, 1995, **95**, 1253.

10 For the use of alkenylboronic acids as dienophiles in tethered Diels–Alder reactions, see: R. A. Batey, A. N. Thadani and A. J. Lough, *J. Am. Chem. Soc.*, 1999, **121**, 450.

11 R. W. Hoffmann and S. Dresely, *Synthesis*, 1988, 103.

12 *Crystal data* for **5**·0.5(H_2O): $C_{17}H_{22}O_2$·0.5(H_2O), M = 267.35, orthorhombic, a = 20.2986(7), b = 5.8725(3), c = 25.2100(14) Å, U = 3005.1(2) Å^3, T = 293 K, space group $Pca2_1$ (no. 29), Z = 8, μ(Mo-Kα) = 0.077 mm^{-1}, 29314 reflections measured, 3874 unique (R_{int} = 0.064) which were used in all calculations. The final *wR(F*^{2}*)* was 0.1610 (all data). Single crystals of **5**·0.5(H_2O) were obtained *via* slow evaporation of a solution of **5** in EtOAc–hexanes, mounted in inert oil and transfered to the diffractometer. The structure was solved using direct methods and refined by full-matrix least-squares on *F*^{2}.

13 *Crystal data* for **6**: $C_{14}H_{22}O_2$, M = 222.32, monoclinic, a = 6.0121(2), b = 12.1615(4), c = 16.7127(5) Å, U = 1221.96 (7) Å^3, T = 293 K, space group $P2_1/c$ (no. 14), Z = 4, μ(Mo-Kα) = 0.078 mm^{-1}, 10537 reflections measured, 2468 unique (R_{int} = 0.038) which were used in all calculations. The final *wR(F*^{2}*)* was 0.1553 (all data). Single crystals of **6** were obtained *via* slow evaporation of a solution of **6** in EtOAc–hexanes, mounted in inert oil and transfered to the diffractometer. The structure was solved using direct methods and refined by full-matrix least-squares on *F*^{2}. CCDC 182/1161.

14 D. A. Evans, E. A. Shaughnessy and D. M. Barnes, *Tetrahedron Lett.*, 1997, **38**, 3193; P. Stoss and P. Merrath, *Synlett*, 1991, 553; L. Crombie, W. M. L. Crombie, S. V. Jamieson and C. J. Palmer, *J. Chem. Soc., Perkin Trans. 1*, 1988, 1243; R. Mechoulam, N. K. McCallum and S. Burstein, *Chem. Rev.*, 1976, **76**, 75.

Communication 8/09615E

ChemComm
FEATURE ARTICLE

Atom-transfer reactions catalyzed by methyltrioxorhenium(VII)—mechanisms and applications

James H. Espenson

Ames Laboratory and Department of Chemistry, Iowa State University, Ames, IA 50011, USA. E-mail: espenson@ameslab.gov

Received (in Cambridge, UK) 25th November 1998, Accepted 23rd December 1998

Methyltrioxorhenium activates hydrogen peroxide by an electrophilic mechanism, transferring a single oxygen atom to many substrates without the intervention of free-radical intermediates. The reactions proceed without by-products, unlike those of most chemical (stoichiometric) oxidizing agents. In separate chemistry, the rhenium catalyst brings about the transfer of oxygen atoms between a pair of closed-shell molecules.

Introduction

This review focuses on the catalytic chemistry of the compound methyltrioxorhenium, CH_3ReO_3, abbreviated as MTO. With but eight atoms, the small MTO molecule functions as a versatile catalyst for a considerable breadth of reactions. The essence of its chemistry is the transfer of an oxygen atom from one species to another. The oxygen source is often hydrogen peroxide; molecular oxygen is not activated. Oxygen transfer between two other substrates, as in $X + YO \rightarrow XO + Y$, is a separate process catalyzed by MTO.

Our research has been directed toward two aspects of the catalytic chemistry: gaining an understanding of the mechanisms by which different MTO reactions occur and using that understanding to predict and carry out other useful transformations. These two outlooks reinforce one another. The solubility of MTO in aqueous and most organic media adds to its versatility; the solvent can be chosen to meet requirements of the substrates, to facilitate product isolation, to enable kinetics studies, or as a matter of convenience. MTO is air-stable also, which enhances its general usefulness in catalytic systems; on the other hand, with but rare exception it does not catalyze autoxidation reactions.

The MTO molecule is isoelectronic and isostructural with the dangerously explosive permanganic acid, $HMnO_4$. MTO is rather more like perrhenic acid, $HReO_4$ or $HO–ReO_3$, in that both are quite mild oxidants. Indeed, with one known exception, the catalytic chemistry of MTO does not involve its redox reactivity; the rhenium atom remains in oxidation state VII. An exception, to be dealt with in due course, involves the intermediacy of the rhenium(v) compound $CH_3ReO_2{\cdot}L_2$, with L = solvent or incidental ligand. Let us note at the outset that the methyl group of MTO, or an aspect it confers on the system, is somehow essential. The isoelectronic perrhenic acid does not catalyze the reactions presented here, likely because ReO_4^- is anionic.

This review divides the reactions of MTO and its derivatives into these groups: (1) interactions with hydrogen peroxide, (2) O-atom transfer from hydrogen peroxide, leading to simple and complex transformations, (3) reactions proceeding by C–H activation, (4) non-oxidative rearrangement and coupling reactions, (5) the use of bromide ions as a co-catalyst, and (6) extensions to some nitrene and carbene chemistry.

The MTO catalyst

MTO remains the premier member of a now-sizable family of compounds $R–ReO_3$ in which the organic group R may be alkyl, vinyl, aralkyl, allyl, alkynyl, or cyclopentadienyl. MTO shows the greatest thermal stability (T_{dec} > 300 °C) of any member of the series, aside perhaps from $(\eta^5\text{-}C_5Me_5)ReO_3$, a catalytically-inactive compound with an 18e electronic configuration. The preparative aspects and the structural chemistry of MTO and numerous derivatives have been thoroughly reviewed recently,[1] and thus need be dealt with only cursorily here. MTO has the expected $\psi\text{-}T_d$ structure of a four-coordinate compound of a d^0 metal center.[2] Coordination compounds, such as MTO·L and $MTO{\cdot}L_2$, where L is an anionic or uncharged Lewis base, have been characterized.[3–5] They have five- and six-coordinate structures. MTO–ligand systems are highly labile, and the ^1H NMR signals for the methyl protons of MTO and MTO·L coalesce to a singlet owing to the lability of the system on the NMR timescale. At 298 K in acetonitrile, the first binding constant of pyridine to MTO is 200 L mol^{-1} whereas that of the better donor 4-picoline is 730 L mol^{-1} and that of the sterically encumbered 2,6-di-*tert*-butyl-4-methylpyridine is < 1 L mol^{-1}.[6] Under the conditions studied, binding of a second pyridine in solution was not detected.

MTO is not prone to decomposition in solvents containing water by pathways involving acid. If this appears remarkable, then it is useful to recall that this feature is common to many

James Espenson was born in Los Angeles, California and attended school there and in its environs. He entered the California Institute of Technology, obtaining his B.S. degree in 1958. He enrolled for graduate study in the University of Wisconsin and wrote his PhD thesis under the supervision of Edward L. King in 1962. Following that he was a postdoctoral associate at Stanford University with Henry Taube during 1962–63. He was appointed Instructor of Chemistry at Iowa State University in 1963 and jointly Assistant Chemist at the Ames Laboratory of the (then) US Atomic Energy Commission. Promotions followed in due course: to Assistant Professor (1965), Associate Professor (1967), Professor (1971). He was named Distinguished Professor in 1988, and continues to hold a joint appointment at the Ames Laboratory, where he is Program Director.

Espenson has been named the John A. Wilkinson teaching award winner, Fellow of the Alfred P. Sloan foundation, Fellow of the Japan Society for the Promotion of Science, and Fellow of the American Association of the Advancement of Science. He is the author of more than 300 research publications and of the book Chemical Kinetics and Reaction Mechanisms *(2nd edn., 1995).*

other methyl–metal compounds and ions. Solutions of $HgCH_3^+$, $TlCH_3^{2+}$, $CH_3AuOH_2^{2+}$, to cite a few heavy metal derivatives, are stable toward strong acid.[7] Certain methylated first-row metals are also stable in strongly acidic solutions, such as $CH_3Co(dmgH)_2{\cdot}L$ and its relatives, including methylcobalamin. This aspect suggests, correctly, that MTO might be stabilized during catalytic turnovers by the addition of acid in semi-aqueous and aqueous media, and by the use of aprotic solvents in other instances. It is rarely useful to insist upon dry solvents for MTO-catalyzed reactions, especially since the family of reactions for which MTO is most often used, activation of hydrogen peroxide, forms water as a stoichiometric product.

Peroxorhenium compounds—structure, equilibrium, kinetics

Key to the activation of hydrogen peroxide is its interaction with MTO, yielding an equilibrium mixture of two peroxorhenium compounds, denoted **A** and **B**, both η^2-peroxo complexes of rhenium(VII). The existence of the η^2–peroxo groups comes as no surprise. This is the prevalent mode of coordination between peroxide and many d^0-metal centers.[8] The structural formulas of **A** and **B** are shown in Scheme 1.

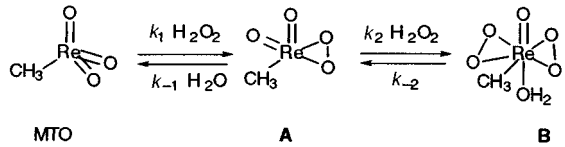

Scheme 1

The structure of the diperoxo complex **B** has been determined crystallographically. Rhenium adopts the structure of a pentagonal bipyramid, with axial oxo (167 pm) and aqua (225 pm) groups. In the equatorial positions are the methyl group (213 pm) and the four peroxo oxygens (191 pm).[9] The water molecule is also coordinated to **B** in solution; its ^1H signal can be seen below −55 °C in d_8-THF.[9,10] No such signal was found for **A**, however, implying the absence of a coordinated water molecule or its exceptional lability.[10]

Both **A** and **B** have been detected by their methyl resonances in the ^1H and ^{13}C NMR spectra, and by their optical signals. Of these, the easier to locate is **B**, since it more readily builds to appreciable concentrations. The binding of peroxide to rhenium is cooperative, as will be explained two paragraphs hence. As a consequence, except for particular concentrations of hydrogen peroxide, **A** does not rise to levels comparable to those of MTO and **B** at equilibrium, although the NMR and optical signals of **A** can easily be seen if the peroxide concentration is not so high as to favor **B** exclusively. Because the reactions between MTO and hydrogen peroxide are equilibrium processes, it is not permitted to evaluate properties of **B**, such as its absorption spectrum, by dissolving the isolated solid. Certain erroneous values, such as absorption coefficients, have been reported as a result. Partial dissociation of **B** will occur, depending on the concentration of total rhenium and peroxide. Instead, one must obtain the spectrum of **B** by determinations in solutions containing some excess of peroxide, or by extrapolation from the least-squares fitting of the mathematical expression relating absorbance and the individual molar absorptivities:

$$\bar{\varepsilon} = \frac{\text{Absorbance}}{b[\text{Re}]_T} = \frac{\varepsilon_{\text{MTO}} + \varepsilon_{\mathbf{A}}K_1[H_2O_2] + \varepsilon_{\mathbf{B}}K_1K_2[H_2O_2]^2}{1 + K_1[H_2O_2] + K_1K_2[H_2O_2]^2}$$

That is not to say that the equilibria in Scheme 1 are instantaneously established. In fact, the four rate constants defined therein have been evaluated under different conditions of solvent and temperature. One such experiment showing time-resolved spectral changes accompanying this reaction is shown on the cover.[11]

These steps play an important role in governing the rate of catalytic turnovers. Table 1 summarizes the values of the equilibrium and rate constants for the two reaction steps in aqueous solution[12] and in acetonitrile, and Table 2 presents the molar absorptivities and chemical shifts of compounds **A** and **B**.[13]

Table 1 Equilibrium and rate constants at 298 K for the formation of the peroxorhenium compounds **A** and **B** in aqueous solution and in acetonitrile containing 2.6% water

	K	k_f/L mol^{-1} s^{-1}	k_r/s^{-1}
Step 1:	16.1 (aq.)	80 (aq.)	10 (aq.)
	209 (AN)	0.81 (AN)	3.9×10^{-3} (AN)
	261 (MeOH)		
Step 2:	132 (aq.)	5.2 (aq.)	4×10^{-2} (aq.)
	660 (AN)	4.5×10^{-2} (AN)	6.8×10^{-5} (AN)
	814 (MeOH)		

Table 2 Values of molar absorptivities and chemical shifts for MTO, **A**, and **B**

			NMR: δ	
	Compound	λ_{max} (log ε)	^1H	^{13}C
	MTO	206 (3.78)	2.1[d]	19.09[e]
		228 (3.56)[a,b]		
	A	320 (2.85)[c]	2.4[d]	
	B	360 (3.08)[c]	2.7[d]	31[f]

[a] In aqueous solution. [b] Ref 55. [c] In CH_3CN. [d] In THF; Ref 13. [e] In $CDCl_3$ at 28 °C; Ref 56. [f] In D_2O at 20 °C; Ref 9.

The unusual features of the data in Table 1 are these: (1) the second peroxide has a larger binding constant than the first, that is to say, they show cooperativity; (2) the step with the greater driving force is the slower. Both of these trends also hold in other solvents. Cooperativity is perhaps the consequence of an increasing Re–O bond order as the number of oxo groups decreases; **B** is favored as a consequence. The slowness of the second binding step compared to the first may reflect both the increased crowding of the coordination positions and the decreased electrophilic character of rhenium once the first peroxide has been added. In organic solvents the binding constants are generally larger than in water, and the rate constants smaller; indeed, the step represented by k_2 often poses a significant kinetic barrier to product formation by the path in which **B** is the intermediate.

Activation parameters have been reported for the first step. The values in aqueous solution for k_1 are: $\Delta H_1^{\ddagger}$ = 24.5 kJ mol^{-1}, $\Delta S_1^{\ddagger}$ = −212 J K^{-1} mol^{-1}, $\Delta V_1^{\ddagger}$ = −10.6 cm^3 mol^{-1}.[14] These values have been interpreted according to Scheme 2.

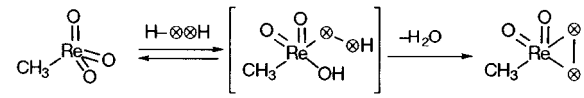

Scheme 2

Exchange of oxygen atoms between water and hydrogen peroxide is forbiddingly slow.[15] The same is true for peroxo-rhenium complexes: the oxo and peroxo oxygens remain distinct. Oxygen atoms are, however, rapidly exchanged between MTO and water. At first this seems anomalous, in that the Re=O bonds are short and robust. However a process analogous to that just shown for peroxide easily provides a pathway for facile exchange (Scheme 3).

These reactions are the prelude to the activation of H_2O_2 by MTO. In all of this, there is no indication that organic hydroperoxides associate with MTO or are activated by it.

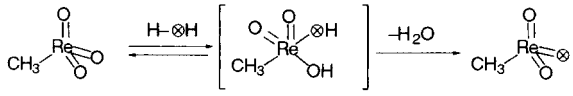

Scheme 3

Evidently the formation of the η^1-O_2^{2-} structure is crucial. Over very long times, MTO does decompose in the presence of alkyl hydroperoxides, such as Bu^{t}OOH and Am^{t}OOH. These reactions occur by radical pathways involving RO$^\bullet$ and ROO$^\bullet$ intermediates, among others.[16] They stand alone as examples of single-electron reactivity of MTO.

Catalyst deactivation

The decomposition of MTO is strongly accelerated by increases in the concentration of hydroxide ions. Even in strongly acidic media, pH < 3, the rate law shows a pH-dependence that implicates a first-order kinetic dependence on [OH$^-$].[17] The full

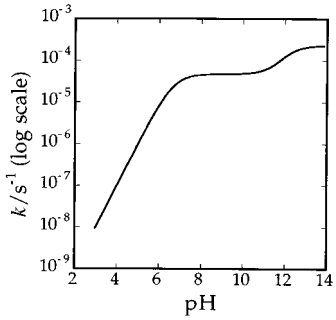

Fig. 1 The pH–rate profile for the decomposition of MTO with numerical values referring to 298 K. The reaction is strongly base-catalyzed, with two plateaus corresponding to the stepwise acid ionization of MTO_{aq}.

rate–pH profile, shown in Fig. 1, is consistent with this net reaction showing the evolution of methane:

$$CH_3ReO_3 + H_2O = CH_4 + ReO_4^- + H^+$$

The two plateaus seen in the pH profile correspond to the successive acid ionization reactions of MTO_{aq}, corresponding to $CH_3ReO_3(OH)^-$ and $CH_3ReO_3(OH)_2^{2-}$. The respective equilibrium constants, expressed as pK_a values, lie in the ranges 6.7–7.5 and 11.7–11.9 at 298 K.[10,17,18] The rate equation for the reaction at pH $< \approx 6$ is $v = k$[MTO][OH$^-$], with $k = 8.6 \times 10^2$ L mol^{-1} s^{-1} at 298 K ($\Delta H^\ddagger = 15.9$ kJ mol^{-1}).[17]

These reactions are slow enough that they tend not to cause difficulty in catalysis, although their instability toward base generally precludes the use of an alkaline medium. As will be shown, the decomposition of MTO in the presence of hydrogen peroxide occurs more rapidly and usually comprises the greater problem. Irreversible decomposition of MTO in peroxide-containing solutions forms methanol primarily, according to these net reactions:[10]

$$CH_3ReO_3 + H_2O_2 = CH_3OH + ReO_4^- + H^+$$

The rate law can be written

$$\frac{d[ReO_4^-]}{dt} = k\frac{[CH_3ReO_3][H_2O_2]}{[H^+]}$$

from which one infers that the reaction can be represented by any of these bimolecular partners: **A** + OH$^-$ ($k_{298} = 3.1 \times 10^9$ L mol^{-1} s^{-1}), $CH_3ReO_3 + HO_2^-$ ($k_{298} = 2.0 \times 10^8$ L mol^{-1} s^{-1}), or, improbably, $CH_3ReO_3(OH)^- + H_2O_2$. The first two are in principle resolvable by isotopic labeling, but oxygen exchange between H_2O and ReO_4^- occurs too rapidly to permit a definitive experiment. [19] Because HO_2^- is a more potent nucleophile than OH$^-$, it seems likely that their reactions with MTO are analogous. We therefore describe the reaction as shown below.

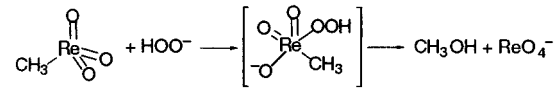

Concurrently, oxygen is evolved as a consequence of the MTO-catalyzed decomposition of hydrogen peroxide ($2H_2O_2 \rightarrow 2H_2O + O_2$), which we infer takes place from **B**:[10,13]

$$CH_3Re(O)(\eta^2\text{-}O_2)_2 \rightarrow CH_3ReO_3 + O_2$$

Photochemical deactivation

Irradiation of **B** by light filtered so as to allow only $\lambda > 400$ nm, to prevent direct photolysis of hydrogen peroxide itself, leads to the slow fading of its yellow color. In acetonitrile this process gives a quantitative yield of perrhenic acid and principally methyl hydroperoxide.[13] The main photoreaction is:

$$CH_3Re(O)(\eta^2 - O_2)_2 + H_2O \xrightarrow{h\nu} ReO_4^- + CH_3OOH + H^+$$

A small concentration of methanol was formed as well; the higher the concentration of hydrogen peroxide, the lower the yield of methanol. In methylene chloride and THF at higher energies, with monochromatic light between 365 and 248 nm, $^3O_2$ was formed.[20] The conclusion was reached that the coupling of initially formed oxygen atoms, ^3O, was responsible.

Peroxide activation by MTO: reaction kinetics

Hydrogen peroxide will oxidize certain electron-rich substrates, but the reactions are generally rather slow without the MTO catalyst. In a few cases both the uncatalyzed and the MTO-catalyzed rate constants have been determined. The catalytic enhancements for MTO often amount to a factor of 10^5–10^6. Many other substrates, ones that seem not to react with hydrogen peroxide, do so quite successfully once MTO has been added. In this section certain aspects of the chemical kinetics will be presented, and the subject of the chemical mechanisms will be taken up in the next section.

The reaction scheme is simply described: **A** and **B** separately react with substrate **X**, converting it to the product **XO**. In so doing, **A** is converted to MTO and **B** to **A**. The respective rate constants are designated k_3 for **A** and k_4 for **B**. These steps couple with those in Scheme 1, which enter as kinetic or sometimes equilibrium reactions depending on the various values pertaining to a given substrate and solvent, and to the concentrations employed. The analysis of the kinetic data has many features in common with that for enzyme-catalyzed reactions and the Michaelis–Menten formalism. This approximation has been termed the 'improved steady-state' method.[21] To illustrate the difference between it and the ordinary steady-state treatment, we show a simple case, the conversion of starting material S to product P *via* intermediate I. The expressions for the reaction rates are:

Reaction Scheme

$$S \underset{k_{-1}}{\overset{k_1}{\rightleftharpoons}} I \xrightarrow{k_2} P$$

Steady-state

$$v = \frac{d[P]}{dt} = \frac{k_1k_2[S]}{k_{-1} + k_2}$$

Improved steady-state

$$v = \frac{d[P]}{dt} = \frac{k_1k_2[S]}{k_{-1} + k_2 + k_1[S]}$$

The improved steady-state mathematics affords the advantage that the intermediate need not be maintained at a small fraction of the concentration of S, as it must in the ss formalism. That E·S may attain a concentration comparable to E is a vital

feature of the Michaelis–Menten equation in that it provides a model to account for the experimentally observed phenomenon that the reaction rates rise initially with [S] and then tend toward a plateau. This effect, known as saturation kinetics, is not found in the ss analysis.[22]

For MTO it is also not valid to adopt the ss model in that it would require that [**A**] and [**B**] always << [MTO]. The improved ss treatment gives this result:

$$-\frac{d[X]}{dt} = \frac{k_1k_3[Re]_T[H_2O_2][X] + \frac{k_1k_2k_4[Re]_T[X][H_2O_2]^2}{k_4[X]+k_{-2}}}{k_{-1}+k_3[X]+k_1[H_2O_2]+\frac{k_1k_2[H_2O_2]^2}{k_4[X]+k_{-2}}}$$

This equation appears to be more formidable than it really is. With the rate constants k_1, k_{-1}, k_2, and k_{-2} known from studies of the MTO–H_2O_2 reactions in the absence of substrate, only k_3 and k_4 remain as unknowns.

Under certain conditions this form simplifies. The parameters involved may be ones the experimenter can control to some extent, such as concentrations, but the parameter list also includes rate constants that will, of course, differ relatively among substrates, often by a large amount. Thus the conditions needed for simplification need to be scrutinized individually for different substrates and concentration ranges. Two of the useful simplifications are these:

(a) at the relatively low concentrations of hydrogen peroxide, such that **B** is not significant,

$$-\frac{d[X]}{dt} = \frac{k_1k_3[Re]_T[H_2O_2][X]}{k_{-1}+k_3[X]+k_1[H_2O_2]}$$

This form has been useful at times mostly because **A** and **B** usually (but not always) are quite comparable in their reactivity (*i.e.*, k_3 and k_4 are of the same magnitude, as illustrated later).

(b) at quite high peroxide concentrations, where **B** is the only significant form,

$$-\frac{d[X]}{dt} = k_4[X][Re]_T$$

This approach has proved useful when the parameters permit its application. One test, but not the only one, is that the reaction rates are peroxide-independent when this form applies.

This is an outline of the kinetics analysis. The reader is referred to the referenced publications for further detail.[23] In the balance of this review, rate constants will be given without further explanation as to their origin.

Peroxide activation by MTO: isotopic tracer

Isotopic labeling was carried out to define the source of the oxygen atom transferred to the substrate. It consisted of the use of MTO and water labeled with oxygen-18 (recall that this pair rapidly exchanges) and hydrogen peroxide labeled with oxygen-16. GC–MS determinations showed that only PhS(^{16}O)Me was formed, implying that the catalytic reaction transfers a peroxo oxygen to the substrate. As **A** (shown here) or **B** reacts, we have Scheme 4.

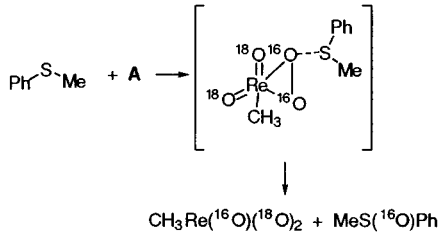

Scheme 4

As the cycle repeats, $CH_3Re(^{16}O)(^{18}O)_2$ continues to revert to $CH_3Re(^{18}O)_3$ by exchange with water. The repeated recycling with $H_2{}^{16,16}O_2$ generates **A** and **B** with $^{16,16}O_2{}^{2-}$ groups that then transfer oxygen-16. The necessary control experiments were carried out to verify that this was a valid experiment.[23]

Peroxide activation by MTO: reactivity of different substrates

In order to present and discuss the structure–reactivity relationships, it is desirable first to examine the relative magnitudes of k_3 and k_4. Values of these rate constants for selected substrates are presented in Table 3. These are by no means all of the data,

Table 3 Comparisons of the rate constants k_3 for **A** and k_4 for **B** in their reactions with different substrates

Substrate	k_3/L mol^{-1} s^{-1} [a]	k_4/k_3 [a]	Ref.
PhSMe	2.65×10^3	0.36	23
Ph_2S	1.18×10^2	0.27	23
PPh_3	7.3×10^5	3.0	57
$P(C_6F_5)_3$	1.30×10^3	2.7	57
trans-PhCH=CHOMe	14.2	0.90	24
trans-PhCH=CHMe	0.51	0.43	24
Cl^-	5.6×10^{-2}	2.3	12
Br^-	3.5×10^2	0.49	42
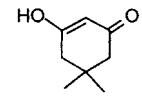	0.19	0.58	58
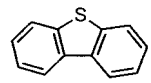	10.2	2.1	59
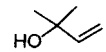	$k_3 \approx 0$ $k_4 = 7.6 \times 10^{-3}$	>>1	28

[a] The solvent is 1:1 acetonitrile–water at pH 1 except for the halide ions in aqueous solution at pH 0 and the allylic alcohol where 4:1 acetonitrile–water was used.

but they are representative of the substrates. Save for the special case of the allylic alcohol to which we return in a later section, the numerical values presented make the case quite emphatically: k_3 and k_4 are of the same magnitude. Sometimes the one is a little larger, sometimes the other. A factor of three in either direction encompasses all of the variations. The similarity of the values for a given substrate is particularly striking in that the rate constants themselves span a factor of 10^8. The proof we have advanced for the comparable reactivity has been verified repeatedly; it rests on the quantitative interpretation of the kinetic effects of the concentrations of hydrogen peroxide and substrate. This demonstration has included epoxidation reactions.[24] This method has been commented on and accepted by others.[25] Despite this, certain statements and diagrams persist in identifying **A** as inactive and **B** as the only active form of the catalyst; see, for example, Fig. 1 in a 1996 reference.[20]

The inductive effect of substituents within a family of related substrates allows one to probe the electron demand in the transition state. Several such results are summarized in Table 4. In every case, the rate increases with electron-donating substituents on an aryl group and *vice versa*. These effects are regular, but mild. The four reactions in the series have Hammett reaction constants in the range −0.63 to −1.19. Each of them displays the trend that electron-donating substituents increase the rate of reaction with **A**, and *vice versa*. In keeping with that, it is instructive to examine the kinetic effects of substituting methyl groups on the double bond of aliphatic alkenes. Table 5 presents a subset of the data, which clearly show that the more alkyl groups on the double bond, the greater the reaction rate. Because of the substituent effects, and supported by the isotopic labeling, we propose a transition state for this reaction in which the nucleophilic reagent **X** (including electron-rich alkenes) attacks a peroxo-oxygen of the rhenium catalyst.

Table 4 Effect of substituents on the aryl group of different substrates on the relative rate constants (k_3/k_{3H}) for the reactions with **A**

Substituent:	4-MeO	4-Me	3-Me	H	4-F	4-Cl	4-Br	4-CF_3	4-NH_3^+	4-NO_2
σ:	−0.27	−0.17	−0.069	0	0.06	0.23	0.23	0.54	0.73	0.78
Substrate										
$ArNMe_2$		1.33		1.00 [a]	0.69		0.47			0.10
ArSMe		1.6		1.00 [b]		0.61			0.22	
Ar_3P		1.29		1.00 [c]		0.66		0.47		
$ArCH{=}CH_2$	5.45	1.59	1.09	1.00 [d]						

[a] Relative to k_{3H} = 18.4 L mol^{-1} s^{-1} at 25.0 °C in methanol; ρ = −1.19.[60] [b] Relative to k_{3H} = 2.65 × 10^3 L mol^{-1} s^{-1} in 1 : 1 acetonitrile–water at pH 1 and 25.0 °C; ρ = −0.98.[23] [c] Relative to k_{3H} = 7.3 × 10^5 L mol^{-1} s^{-1} in 1 : 1 acetonitrile–water at pH 1 and 25.0 °C; ρ = −0.63.[57] [d] Relative to k_{3H} = 1.1 × 10^{-1} L mol^{-1} s^{-1} in 1 : 1 acetonitrile–water at pH 1 and 25.0 °C; ρ = −0.93.[24]

Table 5 Kinetic effects on k_4/L mol^{-1} s^{-1} at 298 K in two solvents for epoxidation reactions arising from the substitution of alkyl groups on the double bond.[61]

Structural formula	No. Alkyl groups	MeOD	CH_3CN-H_2O
	1	0.013	0.098
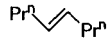	2	0.048	0.25
	3	0.26	3.92
	4	1.33	8.93

In keeping with those results, it is instructive to examine the k_3 values themselves for different types of nucleophilic reagents **X**. The most reactive group are the phosphines, the least the alkenes. A display of these values is presented in Fig. 2. The rate constants span eight orders of magnitude, roughly 10^6–10^{-2} L mol^{-1} s^{-1}. An inspection of the entries in this figure confirm that this is a general trend.

A further manifestation of these effects is seen in a different variation of the substituent effects. Substitution of electronegative substituents into the molecule greatly reduces its reactivity. For example, compare these rate constants:[23]

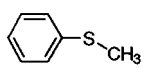

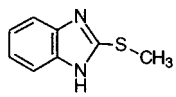

When successive oxidation steps are found, as with this conversion: $R_2S \rightarrow R_2SO \rightarrow R_2SO_2$ for which the successive rate constants are in an approximate 35 : 1 ratio.[26] Likewise, once a 1,3-diene has been converted to the epoxide (preferentially, at the more alkylated double bond) there is little tendency to form the di-epoxide.

From these various approaches, it is possible to argue that the role of MTO is to polarize the normally nucleophilic peroxide anion to the extent that it can itself be attacked by nucleophiles. Other high-valent metal complexes from such elements as Mo(VI), W(VI), Os(VIII), Cr(VI), and V(V), often oxo species themselves and possessed of a d^0 electron configuration, can activate peroxide by a similar mechanism.[27]

This brings us to the rather special case of allylic alcohols, represented by the last entry to Table 3. A comparison of these rate constants at first suggests the same effect, save that the electronegative hydroxy group gives rise to a remarkably small kinetic deceleration by comparison with other examples. But the allylic alcohols constitute the seemingly unique instance

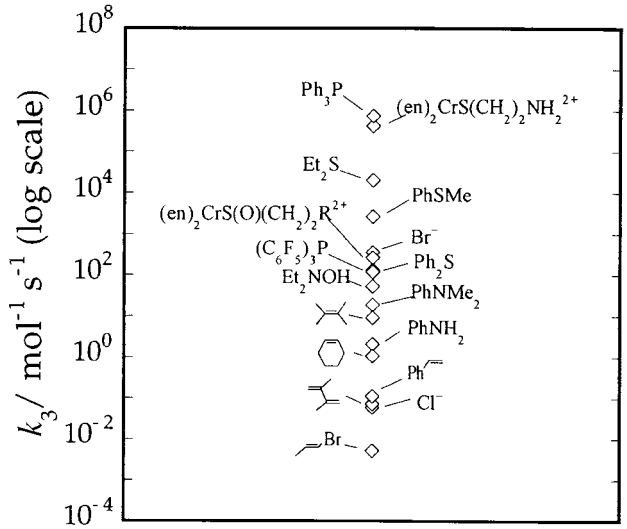

Fig. 2 A display of selected compounds showing the value of each rate constant k_3 at 298 K. Note that the reactivity spans a factor of ≈10^8; note that the axis has a logarithmic scale.

(see Table 3) in which k_3 is negligible compared with k_4, implying a special mechanism open only to catalyst **B**.[28]

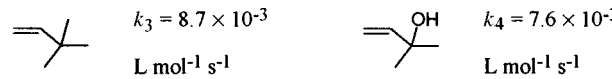

We suggest that these findings manifest the overriding importance of hydrogen bonding in this transition state, a point of view reinforced by data on stereoselectivity in the same system.[28b] We have concluded that the transition state features hydrogen bonding to a *different* peroxo group than that transferring the oxygen atom. This transition state is depicted below, along with one reaction showing that diasteroselectivity can consequently be realized with allyl alcohols.

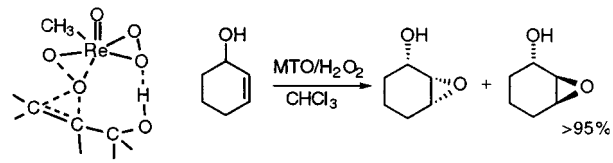

Peroxide activation by MTO: comparisons to dimethyldioxirane 

Aside from the obvious structural analogy between **A**, **B**, and DMDO, the similarities in reactivity are notable. To cite just a

few points, DMDO reacts *stoichiometrically* with many of the same substrates that **A** and **B** do, such as *N,N*-dimethylanilines,[29] alkenes,[30,31] and thioethers.[32] Beyond that, the correlation between the rate constant k_4 for **B** and that for DMDO is striking. Fig. 3 presents on a log–log scale the one set of values against another. The slopes of these lines are 0.84 for aliphatic alkenes and 1.18 for styrenes. Were it not for this, no reason would arise to question the previously given explanation that catalysis by MTO arises from the ability of Re(VII) to polarize the coordinated peroxide anion. But surely the saturated carbon center of DMDO is incapable of activating its peroxide group in the same fashion. The remarkable correlations between the MTO and DMDO reactions require that attributes common to both reagents be sought. Features such as bond and angle strain are, qualitatively, common to both groups of peroxides. The final accounting for the electronic structures remains to be made, and speculation at this point is unnecessary.

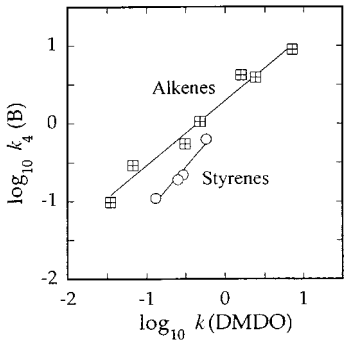

Fig. 3 The rate constants for the epoxidation of styrenes and of aliphatic alkenes by two reagents, dimethyldioxirane and the diperoxorhenium complex **B**, are shown as a linear free-energy correlation. The slopes of the lines are 1.18 (R = 0.982) and 0.84 (R = 0.987).

Peroxide activation by MTO: stabilization of epoxides

Some of the reactions that can follow epoxide formation are deleterious, the most notorious of which is loss of epoxides to acid-catalyzed ring-opening. Generally, but not universally, this is considered an undesirable event. The addition of acid to the solutions, in an effort to stabilize the catalyst, is not allowed. The acidity of the water molecule coordinated to **B**, which has been given as pK_A = 3.8,[9] provides a built-in method for loss of the epoxide. If one attempts to circumvent this effect by the use of a Brønsted base or a buffer, then the inherent base-sensitivity of **B** (especially) immediately prevails, and the catalytic reaction ceases.[10,17,18] A Lewis base such as pyridine serves to stabilize the catalyst against decomposition at the same time eliminating the acidity of the medium and thus preserving the epoxide.[33,34] Representative values of the equilibrium constants (L mol^{-1}) at 298 K for binding Lewis bases to MTO are as shown here for nitrogen bases in acetonitrile[6] and for the phosphorus derivatives in benzene.[35]

(*p*-Tol)$_3$P	2.0
3-NCC$_5$H$_4$N	7.2
(*p*-Tol)$_3$PO	5.3×10^1
C$_5$H$_5$N	2.0×10^2
C$_5$H$_5$NO	2.1×10^2
4-MeC$_5$H$_4$N	7.3×10^2

Coordination of a Lewis base to MTO evidently prevents its being attacked by HOO$^-$, which is the most serious pathway for its loss. [10] The coordination is not so tight, however, as to preclude the necessary formation of the peroxorhenium compounds. A further helpful effect of the Lewis base, if it is also a Brønsted base, is to accelerate the conversion of MTO to **A** and to **B**, which greatly reduces the time the system needs to maintain its integrity. If the epoxide-stabilizing reagent is, for example, a pyridine, then it will be oxidized concomitantly. For example, for α-methyl styrene in acetonitrile at 296 K, the competing reaction rates are: [6]

$v_i^{Py-NO} = k[MTO]_0[Py]_0 \quad k = 0.42 \pm 0.01$ L mol^{-1} s^{-1}
$v_i^{Epox} = k[MTO]_0[\alpha\text{-MeSty}]_0 \quad k = 0.22 \pm 0.04$ L mol^{-1} s^{-1}

The development of methods to prevent catalyst deactivation continues to be an active area, owing to the importance of transforming alkenes to epoxides, and the last work still remains incomplete.

Peroxide activation by MTO: reactions with steps subsequent to O-atom addition

Certain other reactions that follow oxygen-atom transfer from **A** or **B** to the substrate are an inherent part of the process. Here are some examples:

Secondary hydroxylamines yield an intermediate that is converted to the final nitrone product in a rapid elimination reaction following the first step:

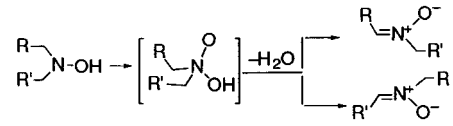

4-Hydroxyalkenes, following epoxide formation undergo cyclization to form substituted tetrahydrofurans;[36] with related molecules the cyclization rates are seen to fall in the expected order favoring these ring sizes 5 > > 6 > 3 > 7 > 8:[37]

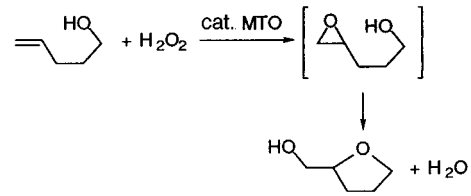

δ,γ-Unsaturated hydroxycarboxlyic acids, again following epoxidation, yield hydroxy lactones:[38]

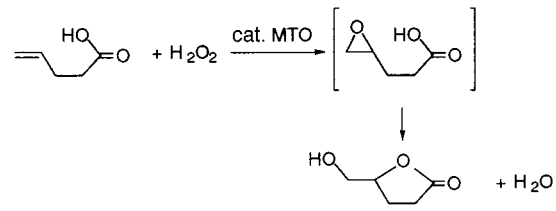

Silyl enol ethers provide a convenient an efficient route to α-hydroxy ketones by way of an epoxide; the product yields are generally ≥95%:[39]

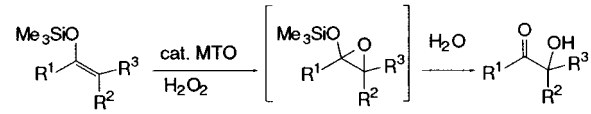

Particularly useful is the MTO-catalyzed oxidation of *N,N*-dimethylhydrazones derived from aldehydes which produces nitriles in > 90% yield.[40] This reaction begins in the usual manner, with the transfer of an oxygen atom from **A** or **B** to the more basic (amine) nitrogen. Following that, a Cope-type elimination reaction[41] yields the nitrile and dimethylhydrox-

ylamine. The latter is independently oxidized to the nitrone, $CH_3N(=CH_2)O$, as described previously.

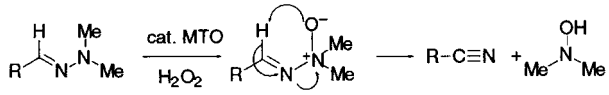

During the course of these studies we have developed a particular solvent formulation that preserves the catalyst quite well. It consists of a mixture of acetonitrile, acetic acid, and pyridine (94.5 : 5 : 0.5). The role of pyridine is to accelerate the cycling of MTO and its peroxides, as in Scheme 1, with acetic acid preventing the mixture from becoming so basic that the catalyst is irreversibly deactivated.

Peroxide activation by MTO: reactions involving the breaking of C–H bonds

In every one of the reactions presented to this point, an oxygen atom was transferred from a peroxorhenium complex to an electron-rich atom or center. In contrast, arenes and secondary alcohols are oxidized by a different mechanism.

MTO–hydrogen peroxide converts methyl arenes to quinones, yielding preferentially the *para* isomer:

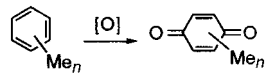

These tend to be sluggish reactions. A higher level of MTO is employed, typically 10% of the arene, and a temperature of 57 °C in glacial acetic. The yields are high, but the conversions not, since the catalyst is gradually deactivated. *o*-, *m*-, and *p*-Dimethylbenenes gave the quinones in 12–15% conversion after 3.5 h; 1,2,4-trimethylbenzene gave 75% conversion in 4 h, along with 33% of the hydroquinone. The data are scant, but a plausible mechanism for the first and most difficult step, phenol formation, is as given in Scheme 5.

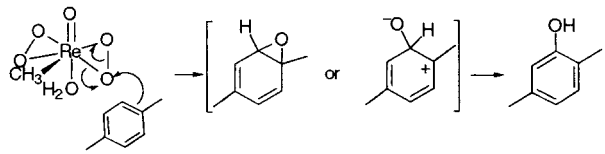

Scheme 5

The oxidation of secondary alcohols by hydrogen peroxide is also catalyzed by MTO; again the reaction faces a substantial kinetic barrier. Representative rate constants at 298 K for the reaction between **B** and the alcohols are 1.02×10^{-4} L mol^{-1} s^{-1} for 4-methyl-α-methylbenzyl alcohol and 4.9×10^{-5} L mol^{-1} s^{-1} for 4-chloro-α-methylbenzyl alcohol. There was a kinetic isotope effect of 3.2 for the α C–H bond of 1-phenylethanol (1,2,2,2-D_4). When the same alcohol was labeled with ^{18}O, 80% of the oxygen was retained in the ketone. Tests for the possible intervention of a free radical intermediate were carried out; the evidence was entirely negative. A mechanism featuring hydride abstraction is proposed, the first time for the H_2O_2/MTO system (Scheme 6)

Peroxide activation by MTO: bromide ions as co-catalyst

The ability of the MTO/H_2O_2 system to oxidize Br^- to BrO^- (ref. 42) (see Table 3) affords a means of developing a different oxidizing species in solution, one capable of adopting a different mechanism. Actually, the useful species is Br_2, not BrO^-/HOBr, since the reaction between HOBr and Br^- is

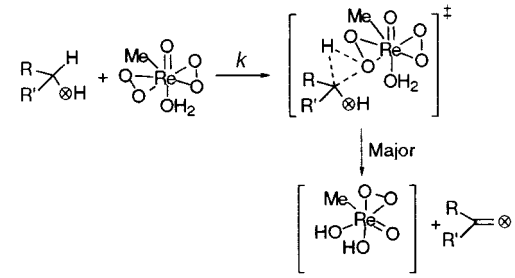

Scheme 6

exceptionally rapid.[43] This approach offers two advantages: it opens a new mechanism in place of oxygen-atom transfer and accomplishes what amounts to a bromine reaction without using any substantial concentration of that element, obviating waste disposal costs for bromide solutions.

Sec-phenylethanol, for example, is oxidized by MTO/H_2O_2 42-times more rapidly when a catalytic concentration of bromide is present (1.1 mM HBr and 200 mM alcohol) as compared to the same reaction in its absence. The reason is that Br_2 carries out hydride abstraction, which **A** and **B** do not.[44] The sequence is the following:

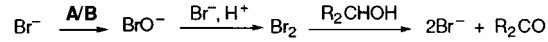

MTO-catalyzed reactions not involving hydrogen peroxide

Rearrangement reactions of a single substrate

Alcohols to ethers. MTO is the first transition metal complex in trace quantity to catalyze the direct formation of ethers from alcohols. These reactions occur in various aprotic solvents (benzene, toluene, dichloromethane, acetone, *etc.*) and in the alcohols themselves. Aromatic alcohols react best; for example benzyl alcohol is converted in 30% yield to the ether; the conversion is 36%, the balance being comprised of 3% PhCHO and 3% $PhCH_3$. This required 2 d at room temperature; after that time none of the catalyst remained. The intermediates characterized and inferred for the reaction of MTO with hydrogen peroxide and for its exchange with water indicate the following mechanism (Scheme 7) from which the ether can be formed by reductive elimination.[45]

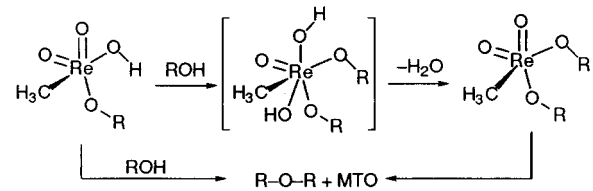

Scheme 7

We noted that (a) no reaction occurred with alcohols containing an electron-withdrawing group at the *para* position such as NO_2, Br, and Cl, (b) an olefin was formed from 2,2-dimethyl-1-phenylpropan-1-ol, and (c) alcohols underwent disproportionation catalyzed by MTO. It seems that these reactions occur through a carbocation intermediate (Scheme 8).

This scheme further reports that MTO catalyzes the reactions between amines, aryl and alkyl, and alcohols, leading to amine products.[45]

1,3-Transposition of allylic alcohols.[46] MTO catalyzes the approach to equilibrium in reactions such as those shown in Table 6. Yields of the isomerized alcohol are often less than

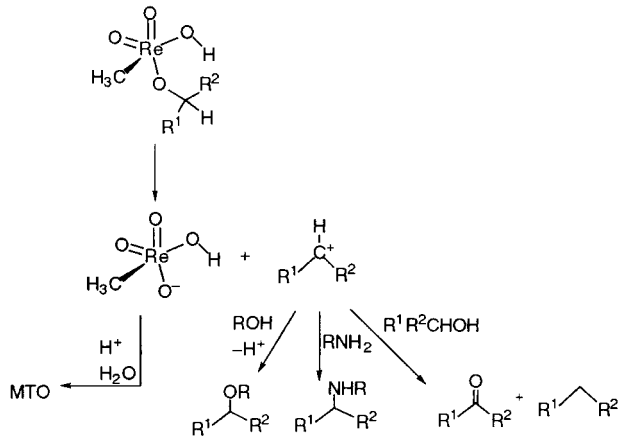

Scheme 8

100%, due to the reverse reaction. This equilibrium was confirmed by the use of deuterium labeling; the isotopomers of 2-cyclohexen-1-ol are interconverted by this degenerate reaction:

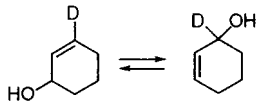

The equilibrium constant was found to be 1.20 ± 0.02 in benzene at ~23 °C, demonstrating an appreciable equilibrium isotope effect. The reaction is sharply inhibited by traces of water. The use of $CH_3Re(^{18}O)_3$ resulted in no incorporation of oxygen-18 into the alcohol product. Because of that we must discard a mechanism related to that presented for ether formation. A mechanism to account for the various lines of evidence, including the inhibition of water that competes with the allyl alcohol and leads to the dead-end species $CH_3Re(O)_2(OH)_2$, is depicted in Scheme 9.

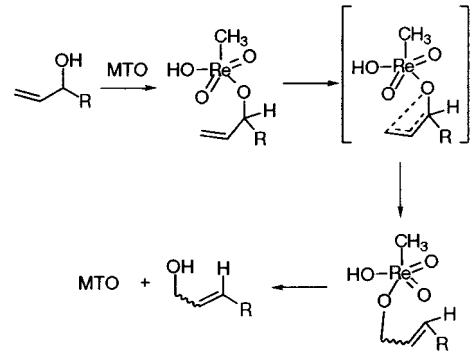

Scheme 9

MTO-catalyzed cyclotrimerization of aldehydes. This reaction yields 1,3,5-trioxanes:

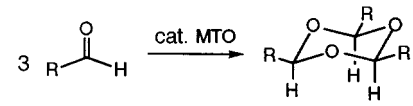

This reaction was carried out successfully for nineteen anhydrous aldehydes.[47] The stereochemistry was established by NMR and by X-ray crystallography in one instance; oxygen-18 labeling of MTO showed that just one of the three oxygen atoms in the product derived from MTO. Yields are generally high, >90%. Although many trioxanes can be isolated at room temperature, several of the reactions need to be carried out at −30 °C, lest the products revert to the parent aldehyde. Indeed, all of the trimeric products revert to the aldehyde thermally. The mechanism has not been established, but the structures shown for several of the reactions are suggestive of a sequence in which an adduct with four-membered ring, derived from the interaction of MTO and one aldehyde, is further homologated (Scheme 10).

Table 6 Equilibrium reactions for the 1,3-transposition of allylic alcohols.[62]

Substrate	Product	Time	% Product at equilibrium
	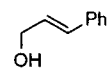	5 d	63
	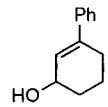	10 h	98
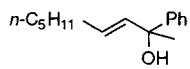	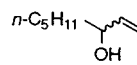	3 d	52
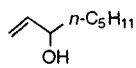	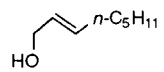	1 d	33
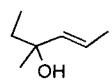	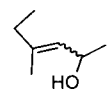	2 d	30
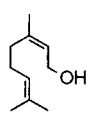	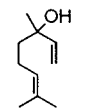	2.5 d	86

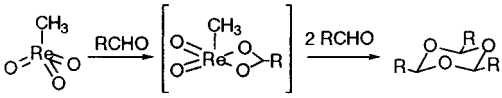

Scheme 10

Atom transfer reactions not involving hydrogen peroxide

The reactions referred to in this section are of the general form YO + X → Y + XO. One example is the reaction between epoxides and triphenylphosphine. Without MTO no reaction occurs despite its spontaneity ($\Delta G° \approx -230$ kJ mol^{-1}). The catalyst causes this general transformation:[48]

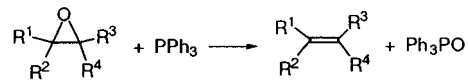

The reaction gives high yields (≥79%) in benzene at room temperature, seems to be quite general, and proceeds with preservation of the relative stereochemistry about the C–C bond of the epoxide. Two distinctly different, plausible mechanisms can be suggested from other results. In the first, the epoxide and MTO form a dialkoxyl (glycolato) rhenium complex. This reaction has been well established independently.[49] Following that the phosphine abstracts an oxygen, leading to the products and the regeneration of the catalyst (Scheme 11).

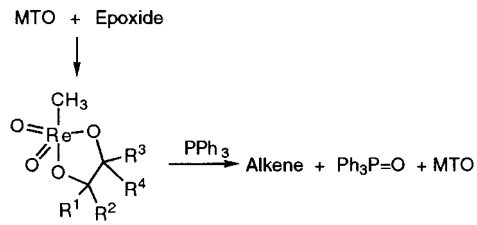

Scheme 11

A certain level of support for this scheme is afforded by the determination that the independently-prepared dialkoxylrhenium complex reacts with triphenylphosphine in the required manner.

The second plausible explanation starts with the reaction between triphenylphosphine and MTO. Methyldioxorhenium(V) is formed; the Re(V) is coordinated by phosphine (L) to an extent dependent on their concentrations; a compound in which Re(VII) is present in the molecular unit has been characterized: $CH_3Re(O)_2L_2 \cdot MTO$.[50] This species is known to abstract an oxygen atom from substrates that have a bond to oxygen weaker than that present in MTO, 465 kJ for MTO(aq) = CH_3ReO_2(aq) + O(aq).[51] Based on these ideas, this alternative reaction scheme can be proposed, in which L represents phosphines or other ligands coordinated to Re(V) (Scheme 12).

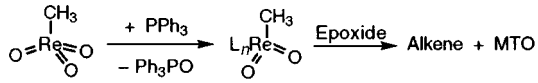

Scheme 12

It would be premature at this stage to decide between the two. Several related transformations have also been found. Thus MTO is an effective catalyst, when accompanied by triphenylphosphine, for converting tertiary amine oxides [*e.g.*, Ar-N(O)Me_2 and C_5H_5NO] to amines, triphenylphosphine oxide being formed concomitantly. These reactions were studied in benzene, but there is no reason to believe other solvents would not serve as well.[48]

Sulfoxides are converted into sulfides in high yield (65–77%) by the same procedure. Reactions have been carried out in benzene at room temperature for aryl and alkyl sulfoxides.[48] On the other hand, attempts to excise an oxygen atom from a sulfone have failed. Among other factors, one notes that sulfoxides have an S–O bond enthalpy of ≈330 kJ mol^{-1}, whereas for sulfones this is ≈440 kJ mol^{-1}.

The bond enthalpies along the series Ar_3EO (E = P, As, Sb) are such that oxygen is preferentially bound to phosphorus. Uncatalyzed oxygen exchange is not significant. With MTO catalytic reactions occur, converting ArAs(Sb)O and Ar_3P to ArAs(Sb) and Ar_3PO. The involvement of the Re(V) complex, CH_3ReO_2 or its ligated derivatives, seems likely.

Coupling reactions using the MTO catalytic template

Ketones and aldehydes do not react with epoxides in the absence of MTO. With the MTO catalyst, 1,3-dioxolanes are formed, often but not invariably in high yields from reactions carried out for two days in chloroform.[52] The net equation is shown below.

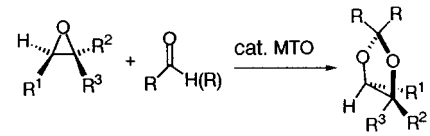

The reaction proceeds in two steps: in the first, as described in the preceding section, a dialkoxylrhenium complex is formed, and then attacked by the carbonyl compound. Each step proceeds with inversion of configuration, the resultant being that the dioxolane retains the structure of the parent epoxide.

Carbene and nitrene transfer reactions

As one examines the structures of **A** and **B**, it is natural to inquire whether one (both?) of the oxygen atoms of the coordinated peroxide might be replaced with isoelectronic nitrene (NR) or carbene (CR_2) equivalents. Taking **A** for

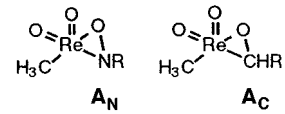

example, might the intermediates $\mathbf{A_N}$ or $\mathbf{A_C}$ be made? And, if successful, would these species transfer a group (presumably the less electronegative nitrene or carbene fragment) to a suitable substrate? Attempts to prepare $\mathbf{A_N}$ by the reactions of MTO with hydroxylamines, this being the example from isoelectronic substitutions in Scheme 1, have met with no success. Not only that, but such mixtures showed no evidence of catalytic activity toward substrates that react with MTO/H_2O_2.

We consequently turned to organic azides and diazoalkanes as sources of the putative NR and CR_2 groups for incorporation into an active form of MTO. A certain level of success has been realized, as represented by the subsequent MTO-catalyzed conversions, when ethyl diazoacetate was used. Aryl imines were transformed to aziridines, carbonyl compounds to epoxides, and alkenes to epoxides (Scheme 13)[53,54]

The model in terms of an $\mathbf{A_C}$-like carbene donor holds some appeal, but attempts to identify such species have not been successful. It may be that MTO releases a free carbene to carry out this chemistry, an idea that finds credence in the sensitivity of these reactions to moisture, a feature not found in most MTO-catalyzed reactions.

In summary

The catalyst methyltrioxorhenium has proved its abilities and its versatility. It seems assured of a useful place in the repertoire of

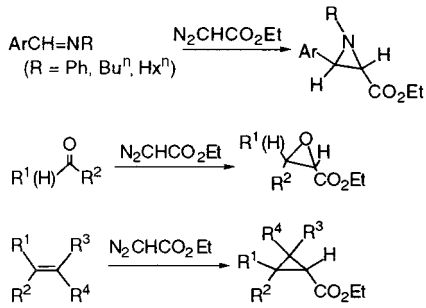

Scheme 13

catalysts that activate hydrogen peroxide and also provide other pathways for oxygen atom transfer. The fact that MTO is soluble in different media, and retains its catalytic activity therein, enhances its usefulness. Other substances act as catalysts for peroxide reactions, among them molybdates, tungstates, and other Mo(VI) and W(VI) complexes.[27] But MTO, advantageously, does not engage in any oligomerization or pH-dependent equilibria, unlike molybdate and tungstate, greatly simplifying the characterization of its reaction mechanisms.

Acknowledgements

I am grateful to my coworkers in this area, whose names are given in the referenced publications. Support is acknowledged from the US Department of Energy, Office of Basic Energy Sciences, Division of Chemical Sciences under contract W-7405-Eng-82 for research concerning the MTO catalyst, particularly selective oxidation reactions, and the development and study of catalytic organic reactions; to the National Science Foundation (CHE–9007283) for support of research in the area of O-atom transfer, and to the donors of The Petroleum Research Fund, administered by the American Chemical Society, for partial support of research concerning organic transformations.

References

1 C. C. Romão, F. E. Kühn and W. A. Herrmann, *Chem. Rev.*, 1997, **97**, 3197.
2 W. A. Herrmann, P. Kiprof, K. Rydpal, J. Tremmel, R. Blom, R. Alberto, J. Behm, R. W. Albach, H. Bock, B. Solouki, J. Mink, D. Lichtenberger and N. E. Gruhn, *J. Am. Chem. Soc.*, 1991, **113**, 6527.
3 W. A. Herrmann, J. G. Kuchler, G. Weichselbaumer, E. Herdtweck and P. Kiprof, *J. Organomet. Chem.*, 1989, **372**, 351.
4 J. Takacs, M. R. Cook, P. Kiprof, J. G. Kuchler and W. A. Herrmann, *Organometallics*, 1991, **10**, 316.
5 W. A. Herrmann, J. G. Kuchler, P. Kiprof and J. Riede, *J. Organomet. Chem.*, 1990, **395**, 55.
6 W.-D. Wang and J. H. Espenson, *J. Am. Chem. Soc.*, 1998, **120**, 11335.
7 R. S. Tobias, *Organomet. Chem. Rev.*, 1966, **1**, 93–129.
8 G. Strukul, R. Ros and R. A. Michelin, *Inorg. Chem.*, 1982, **21**, 495.
9 W. A. Herrmann, R. W. Fischer, W. Scherer and M. U. Rauch, *Angew. Chem., Int. Ed. Engl.*, 1993, **32**, 1157.
10 M. Abu-Omar, P. J. Hansen and J. H. Espenson, *J. Am. Chem. Soc.*, 1996, **118**, 4966.
11 Dr P. D. Metelski is acknowledged for preparing this experiment and display.
12 P. J. Hansen and J. H. Espenson, *Inorg. Chem.*, 1995, **34**, 5839.
13 W.-D. Wang and J. H. Espenson, *Inorg. Chem.*, 1997, **36**, 5069.
14 O. Pestovsky, R. van Eldik, P. Huston and J. H. Espenson, *J. Chem. Soc., Dalton Trans.*, 1995, 133.
15 H. Taube, *Rec. Chem. Prog.*, 1956, **17**, 277.
16 K. A. Brittingham and J. H. Espenson, *Inorg. Chem.*, in press.
17 G. Laurenczy, F. Lukács, R. Roulet, W. A. Herrmann and R. W. Fischer, *Organometallics*, 1996, **15**, 848.
18 J. H. Espenson, H. Tan, S. Mollah, R. S. Houk and R. D. Eager, *Inorg. Chem.*, 1998, **37**, 4621.
19 R. K. Murmann, *J. Phys. Chem.*, 1967, **71**, 974.
20 I. Hatzopulos, H.-D. Brauer, M. R. Geisberger and W. A. Herrmann, *J. Organomet. Chem.*, 1996, **520**, 201.
21 J. H. Espenson, *Chemical Kinetics and Reaction Mechanisms*, McGraw-Hill Inc., New York, 2nd edn. 1995.
22 It is this author's opinion that certain disagreements about steady-state kinetics trace to the failure to make a clear distinction between ss and improved-ss treatments: see R. Breslow, *J. Chem. Educ.*, 1990, **67**, 228; D. B. Northrop, *J. Chem. Educ.*, 1993, **70**, 999; R. Breslow, *J. Chem. Educ.*, 1993, **70**, 999.
23 K. A. Vassell and J. H. Espenson, *Inorg. Chem.*, 1994, **33**, 5491.
24 A. Al-Ajlouni and J. H. Espenson, *J. Am. Chem. Soc.*, 1995, **117**, 9243.
25 K. P. Gable, *Adv. Organomet. Chem.*, 1997, **41**, 127.
26 D. W. Lahti and J. H. Espenson, unpublished results.
27 G. Strukul, *Catalytic Oxidations with Hydrogen Peroxide as Oxidant*, Kluwer Academic Publishers, Dordrecht, 1992.
28 (*a*) H. A. Riley and J. H. Espenson, *Inorg. Chem.*, in press; (*b*) W. Adam, A. Corna, A. Martinez, C. M. Mitchell, T. I. Ready, M. Renz and A. K. Smerz, *J. Mol. Catal. A*, 1997, **117**, 357.
29 P. C. Buxton, J. N. Ennis, B. A. Marples, V. Waddington and T. R. Boehlow, *J. Chem. Soc., Perkin Trans. 2*, 1998, 265.
30 A. L. Baumstark, E. Michelena-Baez, A. M. Navarro and H. D. Banks, *Heterocycl. Commun.*, 1997, **3**, 393.
31 A. L. Baumstark and L. Vasquez, *J. Org. Chem.*, 1988, **53**, 3437.
32 W. A. Schenk, J. Frixch, W. Adam and F. Prechtl, *Angew. Chem., Int. Ed. Engl.*, 1994, **106**, 1699.
33 J. Rudolph, K. L. Reddy, J. P. Chiang and K. B. Sharpless, *J. Am. Chem. Soc.*, 1997, **119**, 6189.
34 C. Coperet, H. Adolfsson and K. B. Sharpless, *Chem. Commun.*, 1997, 1565.
35 M. D. Eager and J. H. Espenson, unpublished information.
36 H. Tan and J. H. Espenson, submitted for publication.
37 F. A. Carey and R. J. Sundberg, *Advanced Organic Chemistry*, Plenum Press, Part A, 3rd edn., New York, 1990, p. 163.
38 H. Tan and J. H. Espenson, in press.
39 S. Stanković and J. H. Espenson, *J. Org. Chem.*, 1998, **63**, 4129.
40 S. Stanković and J. H. Espenson, *Chem. Commun.*, 1998, 1579.
41 R. Fernandez, C. Gasch, J. Lassaletta, J. Llera and J. Vazquez, *Tetrahedron Lett.*, 1993, **34**, 141.
42 J. H. Espenson, O. Pestovsky, P. Huston and S. Staudt, *J. Am. Chem. Soc.*, 1994, **116**, 2869.
43 A. Mohammed and H. A. Liebhafsky, *J. Am. Chem. Soc.*, 1934, **56**, 1680.
44 R. Stewart, in *Oxidation Mechanisms: Applications to Organic Chemistry*, W. A. Benjamin Inc., New York, 1964.
45 Z. Zhu and J. H. Espenson, *J. Org. Chem.*, 1996, **61**, 324.
46 J. Jacob, J. H. Espenson, J. H. Jensen and M. S. Gordon, *Organometallics*, 1998, **17**, 1835.
47 Z. Zhu and J. H. Espenson, *Synthesis* 1998, 417.
48 Z. Zhu and J. H. Espenson, *J. Mol. Catal.*, 1995, **103**, 87.
49 Z. Zhu, A. Al-Ajlouni and J. H. Espenson, *Inorg. Chem.*, 1996, **35**, 1408.
50 W. A. Herrmann, P. W. Roesky, M. Wang and W. Scherer, *Organometallics*, 1994, **13**, 4531.
51 M. M. Abu-Omar, E. H. Appleman and J. H. Espenson, *Inorg. Chem.*, 1996, **35**, 7751.
52 Z. Zhu, J. H. Espenson, *Organometallics*, 1997, **16**, 3658.
53 Z. Zhu and J. H. Espenson, *J. Org. Chem.*, 1995, **60**, 7090.
54 Z. Zhu and J. H. Espenson, *J. Am. Chem. Soc.*, 1996, **118**, 9901.
55 I. A. Begnan, J. Behm, M. R. Cook and W. A. Herrmann, *Inorg. Chem.*, 1991, **30**, 2165.
56 W. A. Herrmann, J. G. Kuchler, J. K. Felixberger, E. Herdtweck and W. Wagner, *Angew. Chem., Int. Ed. Engl.*, 1988, **27**, 394.
57 M. M. Abu-Omar and J. H. Espenson, *J. Am. Chem. Soc.*, 1995, **117**, 272.
58 M. M. Abu-Omar and J. H. Espenson, *Organometallics*, 1996, **15**, 3543.
59 K. N. Brown and J. H. Espenson, *Inorg. Chem.*, 1996, **35**, 7211.
60 Z. Zhu and J. H. Espenson, *J. Org. Chem.*, 1995, **60**, 1326.
61 A. Al-Ajlouni and J. H. Espenson, *J. Org. Chem.*, 1996, **61**, 3969.
62 J. Jacob, J. H. Espenson, J. H. Jensen and M. S. Gordon, *Organometallics*, 1998, **37**, 1835.

Paper 8/09222B

ChemComm

Water-soluble iridium and rhodium complexes with tris(hydroxymethyl)phosphine and their catalysis in biphasic hydrogenation and hydroformylation

Atsushi Fukuoka,*[a]† Wataru Kosugi,[a] Fumiaki Morishita,[a] Masafumi Hirano,[a] Louise McCaffrey,[b] William Henderson[b] and Sanshiro Komiya*[a]

[a] *Department of Applied Chemistry, Tokyo University of Agriculture and Technology, Koganei, Tokyo, 184-8588, Japan*

[b] *Department of Chemistry, University of Waikato, Private Bag 3105, Hamilton, New Zealand*

Received (in Cambridge, UK) 28th October 1998, Accepted 5th February 1999

Novel water-soluble Ir and Rh complexes with tris(hydroxymethyl)phosphine catalyse the selective hydrogenation of the C=O bond of cinnamaldehyde and the hydroformylation of pent-1-ene both under biphasic conditions.

The use of aqueous/organic biphasic systems is attracting growing interest in catalytic reactions by transition metal complexes.[1] The biphasic systems have benefits in catalyst separation and recycling, and the reduction or elimination of organic solvents is also advantageous for the development of economical and environmentally friendly processes. The key for such biphasic catalysis is to use water-soluble phosphines as ligands. Since the launch of the commercial propylene hydroformylation process by Ruhrchemie/Rhône-Poulenc,[2] sulfonated derivatives of PPh_3 such as $PPh_2(C_6H_4$-*m*-$SO_3Na)$ (TPPMS) and $P(C_6H_4$-*m*-$SO_3Na)_3$ (TPPTS) have been widely used as ligands in hydroformylation, hydrogenation, and related reactions catalysed by transition metals.[1,3]

Tris(hydroxymethyl)phosphine, $P(CH_2OH)_3$ (THMP) is a highly water-soluble phosphine and has unique reactivity towards a number of reagents to give functionalised hydroxymethylphosphines.[4] Although many transition metal complexes of THMP are known,[5] there are limited examples of catalytic reactions using the THMP complexes. Chatt *et al.* reported the first examples of THMP complexes of Rh, Pd and Pt; however, these complexes showed low catalytic activities in hydrogenation and hydroformylation of olefins.[5a] Recently, Pringle and coworkers showed high efficiency of THMP complexes of Pt, Pd and Ni in catalytic hydrophosphination of formaldehyde,[6] and biphasic hydrogenation of sorbic acid was reported using THMP complexes of Ru.[7] In this study, we have prepared novel THMP complexes of Ir and Rh, and their catalytic performances have been tested for hydrogenation of cinnamaldehyde and hydroformylation of pent-1-ene.

Reaction of $[IrCl(cod)]_2$ (cod = cycloocta-1,5-diene) with THMP[5c] (P/Ir ratio = 3) in THF at room temperature under N_2 readily precipitated a white powder, which was purified by recrystallisation from EtOH–Et_2O to give $[Ir(cod)\{P(CH_2OH)_3\}_3]Cl$ **1** in 91% yield [eqn. (1)]. Complex **1** was characterised by analytical and spectroscopic methods.‡ Electrospray mass spectroscopy (ESMS) of **1** in MeOH at a cone voltage of 20 V gave a single peak at *m*/*z* 673 due to $[Ir(cod)(THMP)_3]^+$ with the same isotope pattern as calculated. In the $^{31}P\{^1H\}$ NMR of **1** in $(CD_3)_2SO$, only a singlet peak was observed at δ −17.5, which was shifted lower than free THMP at δ −25.7. A variable-temperature NMR study was performed

$$[IrCl(cod)]_2 + 6\ P(CH_2OH)_3 \xrightarrow[\text{room temp.}]{\text{THF}} \underset{\mathbf{1}}{2\ [Ir(cod)\{P(CH_2OH)_3\}_3]Cl} \quad (1)$$

using CD_3OD as a solvent. Similarly, only a singlet peak was observed at δ −17.6 with a half width of 5 Hz at 20 °C. On cooling to −80 °C, the singlet peak was gradually shifted lower to δ −15.7 and slightly broadened (half width 12 Hz), and the NMR spectral change was reversible on warming again to 20 °C. The broadening of the peak suggests that **1** is fluxional in this temperature range. When THMP was added to **1**, the peaks of **1** and THMP were independently seen at 20 °C in the $^{31}P\{^1H\}$ NMR, thus excluding the intermolecular exchange of the ligands. In accordance with the $^{31}P\{^1H\}$ NMR, the ^1H NMR of **1** gave a doublet (J_{HP} 4.5 Hz) due to CH_2 of THMP at δ 4.12 and a broad peak due to OH at δ 5.53, and these peaks were shifted to lower field than those of free THMP [CH_2 at δ 3.85 (t, *J* 5.1 Hz) and OH at δ 4.68 (q, *J* 5.1 Hz)]. The ^1H NMR data including integrals and elemental analysis also support the formation of five-coordinate complex **1**.

One might expect that $[IrCl(THMP)_2]_2$ or $[Ir(cod)(THMP)_2]Cl$ would also be formed in the reaction of $[IrCl(cod)]_2$ and THMP; however, in the presence of 3 equiv. of THMP complex **1** is exclusively formed. This type of $[Ir(cod)L_3]^+$ complex is known for compact phosphines,[8a] and $[Ir(cod)(PMe_3)_3]Cl$ was prepared from the reaction of $[IrCl(cod)]_2$ with 3 equiv. of PMe_3.[8b]

Similar reaction of $[RhCl(cod)]_2$ with THMP (P/Rh ratio = 3) in THF at room temperature under N_2 gave a complicated mixture, and isolation of products was unsuccessful. On the other hand, the reaction with 4 equiv. of THMP precipitated a yellow powder, and recrystallisation from EtOH–CH_2Cl_2 gave *cis*-$[RhH_2\{P(CH_2OH)_3\}_4]Cl$ **2** in 74% yield based on Rh.‡ The formation of the hydride complex was unexpected; however, the presence of Rh–H was confirmed by ^1H NMR and IR. In the ^1H NMR of **2** in $(CD_3)_2SO$, RhH was observed at δ −11.26 with couplings to Rh and P (J_{RhH} 120.8 Hz, J_{PH} 12.9 Hz), which is characteristic for *cis*-$[RhH_2(PR_3)_4]^+$.[9] In the IR spectrum, ν_{RhH} appeared at 2007 cm^{-1}. The $^{31}P\{^1H\}$ NMR gave two doublets of triplets with equal intensity at δ 21.2 (J_{RhP} 86, J_{PP} 22 Hz) and 34.9 (J_{RhP} 97, J_{PP} 22 Hz), showing the *cis* geometry of **2**. ESMS and elemental analysis also support the structure of **2**.

The hydride origin is not clear at this moment. THMP itself is a reactive agent, and the reactions of THMP such as deprotonation and elimination of formaldehyde were reported in the preparation of THMP complexes of Pt[6] and Ru.[5f] Other possible hydride sources are the cod ligand, the solvents (THF, EtOH, Et_2O and CH_2Cl_2), or a trace of water included in the reaction mixture.§ The possibility of cod is excluded, since a quantitative amount of free cod was observed in the reaction of $[RhCl(cod)]_2$ with THMP (P/Rh = 4) in $(CD_3)_2SO$. In the $^{31}P\{^1H\}$ NMR of this reaction, the resonances of **2** and THMP oxide (δ 44) were detected, thus suggesting that a trace of water can react with Ru intermediates to give **2** and THMP oxide. When D_2O was added to **2** in $(CD_3)_2SO$, the Rh–H and OH peaks in ^1H NMR were significantly decreased, and the peaks completely disappeared in pure D_2O. This result shows a facile

† Present address: Catalysis Research Center, Hokkaido University, Sapporo 060-0811, Japan. E-mail: fukuoka@cat.hokudai.ac.jp

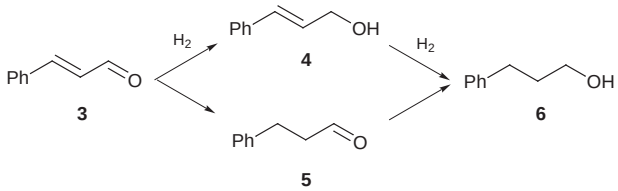

Scheme 1

Table 1 Biphasic hydrogenation of cinnamaldehyde catalysed by [Ir(cod){$P(CH_2OH)_3$}$_3$]Cl **1**[a]

Run	THMP/**1**[b]	H_2[c]/atm	*T*/°C	Conv. of **3** (%)	Selectivity (%)[d]		
					4	**5**	**6**
1	0	30	100	90	76	2	22
2	0	100	100	99	88	2	9
3	5	90	100	20	97	3	0
4	5	90	125	97	97	2	0.3

[a] *Conditions*: **1** 0.015 mmol, cinnamaldehyde 7.5 mmol, water/benzene = 5 ml/5 ml, reaction time 24 h. [b] Molar ratio of added THMP to **1**. [c] Initial pressure at room temperature. [d] (Mol of product)/(mol of converted **3**) × 100.

H–D exchange of Rh–H with D_2O, indicating that Rh–H has protic character.

Hydrogenation of cinnamaldehyde **3** in the biphasic water/benzene media was performed as a test reaction of the catalysis using complex **1** (Scheme 1). Selective hydrogenation of the C=O bond would give cinnamyl alcohol **4**, which is more valuable than hydrocinnamaldehyde **5** from the C=C bond hydrogenation and hydrocinnamyl alcohol **6** from the complete hydrogenation of both the C=O and C=C bonds.[3c] Under the conditions of 100 °C and 30 atm, with complex **1**, the conversion of **3** was 90% and the proportion of **4**:**5**:**6** was 76:2:22 (Table 1, run 1). At the H_2 pressure of 100 atm, the proportion was 88:2:9, with 99% conversion (run 2). The addition of 5 equiv. of THMP to **1** at 90 atm decreased the conversion to 20%; however, the selectivity of **4** was increased to 97% (run 3). Interestingly, under the conditions of 125 °C and 90 atm in the presence of 5 equiv. of THMP, the conversion was 97% and the proportion of **4**:**5**:**6** was 97:2:0.3 (run 4). The role of added THMP in the catalytic mechanism is being studied.

Rh complex **2** catalysed the biphasic hydroformylation of pent-1-ene to give oxo aldehydes. Under the conditions of 100 °C, CO/H_2 20 atm/20 atm, water/benzene 4 ml/4 ml, and substrate/catalyst ratio 90, pent-1-ene was quantitatively converted to hexanal (43% yield) and 2-methylpentanal (57%) in 20 h.

In all the catalytic hydrogenation and hydroformylation reactions, the substrates and products were recovered from the benzene layer, and the catalysts were present in the water layer. In order to test the catalyst stability three catalytic runs were repeated, recycling the same water layer containing **1** or **2**. No decrease was observed in the reaction rates and product selectivities, showing the reliable stability of THMP complexes **1** and **2**.

We are grateful to the Asia 2000 Foundation of New Zealand for financial support.

Notes and references

‡ *Selected data*: **1**: ^{1}H NMR [300 MHz, $(CD_3)_2SO$]: δ 2.12 and 2.41 (br, total 8H, cod CH_2), 3.90 (br, 4H, cod CH=), 4.12 [d, J_{PH} 4.5 Hz, 18H, $P(CH_2OH)_3$], 5.53 [br, 9H, $P(CH_2OH)_3$]. $^{31}P\{^1H\}$ NMR [122 MHz, $(CD_3)_2SO$]: δ −17.5 (s). ESMS (20 V, MeOH) *m*/*z* 673 ([Ir(cod){$P(CH_2OH)_3$}$_3$]$^+$). Mp 115–117 °C (decomp.). Anal. Found: C, 29.05; H, 5.41. Calc. for $C_{17}H_{39}O_9P_3ClIr$: C, 28.84; H, 5.55%. Molar electrical conductivity Λ (MeOH, 24 °C) 9.05 S cm^2 mol^{-1}. Halogen check (the Beilstein test): positive. Air-stable. Soluble in water, MeOH, EtOH, 2-PrOH, and Me_2SO, but insoluble in benzene, hexane, acetone, or CH_2Cl_2. **2**: IR (KBr, cm^{-1}) 2007 (ν_{RhH}). ^{1}H NMR [300 MHz, $(CD_3)_2SO$]: δ −11.26 (m, J_{RhH} 120.8, J_{PH} 12.9 Hz, 2H, RhH), 3.91 and 3.99 [d, J_{PH} 4.5 Hz, total 24H, $P(CH_2OH)_3$], 5.45 and 5.51 [br, 12H, $P(CH_2OH)_3$]. $^{31}P\{^1H\}$ NMR [122 MHz, $(CD_3)_2SO$]: δ 21.2 (dt, J_{RhP} 86, J_{PP} 22 Hz, 2P, *trans* to H), 34.9 (dt, J_{RhP} 97, J_{PP} 22 Hz, 2P, *trans* to P). ESMS (20 V, MeOH) *m*/*z* 601 ([RhH_2{$P(CH_2OH)_3$}$_4$]$^+$). Mp 145–150 °C (decomp.). Anal. Found: C, 22.48; H, 5.82. Calc. for $C_{12}H_{38}O_4P_4ClRh$: C, 22.64; H, 6.02%. Λ (MeOH, 24 °C) 8.04 S cm^2 mol^{-1}. Halogen check (the Beilstein test): positive. Stability and solubility are similar to those of **1**.

§ The THF solvent had no contamination of alcohols, which was confirmed by NMR. In the preparation of **2**, $RhCl(THMP)_4$ was not observed in the crude product but **2** was already formed in 70–80% yield with other uncharacterised species.

1 B. Cornils and W. A. Herrmann, in *Applied Homogeneous Catalysis with Organometallic Compounds*, ed. B. Cornils and W. A. Herrmann, VCH, Weinheim, 1996, p. 575; W. A. Herrmann and C. W. Kohlpaintner, *Angew. Chem., Int. Ed. Engl.*, 1993, **32**, 1524; P. Kalck and F. Monteil, *Adv. Organomet. Chem.*, 1992, **34**, 219; I. T. Horvath, *J. Mol. Catal. A*, 1997, 117; K. Nomura, *J. Mol. Catal. A*, 1998, **130**, 1.

2 E. G. Kuntz, *CHEMTECH*, 1987, 570; B. Cornils and E. Wiebus, *CHEMTECH*, 1995, 33.

3 (*a*) M. E. Davis, *CHEMTECH*, 1992, 498; (*b*) R. V. Chaudhari, B. M. Bhanage, R. M. Deshpande and H. Delmas, *Nature*, 1995, **373**, 502; (*c*) J. M. Grosselin, C. Mercier, G. Allmang and F. Grass, *Organometallics*, 1991, **10**, 2126; (*d*) E. Fache, C. Santini, F. Senocq and J. M. Basset, *J. Mol. Catal.*, 1992, **72**, 337; (*e*) G. Papadogianakis, L. Maat and R. A. Sheldon, *J. Chem. Soc., Chem. Commun.*, 1994, 2659.

4 N. J. Goodwin, W. Henderson and J. K. Sarfo, *Chem. Commun.*, 1996, 1551; N. J. Goodwin, W. Henderson, B. K. Nicholson, J. K. Sarfo, J. Fawcett and D. R. Russell, *J. Chem. Soc., Dalton Trans.*, 1997, 4377.

5 (*a*) J. Chatt, G. J. Leigh and R. M. Slade, *J. Chem. Soc., Dalton Trans.*, 1973, 2021; (*b*) D. L. Dubois and A. Miedanar, *J. Am. Chem. Soc.*, 1987, **109**, 113; (*c*) J. W. Ellis, K. N. Harrison, P. A. T. Hoye, A. G. Orpen, P. G. Pringle and M. B. Smith, *Inorg. Chem.*, 1992, **31**, 3026; (*d*) S. Komiya, H. Awata, S. Ishimatsu and A. Fukuoka, *Inorg. Chim. Acta*, 1994, **217**, 201; (*e*) V. S. Reddy, D. E. Berning, K. V. Katti, C. L. Barnes, W. A. Volkert and A. R. Ketring, *Inorg. Chem.*, 1996, **35**, 1753; (*f*) L. Higham, A. K. Powell, M. K. Whittlesey, S. Wocadlo and P. T. Wood, *Chem. Commun.*, 1998, 1107.

6 P. A. T. Hoye, P. G. Pringle, M. B. Smith and K. Worboys, *J. Chem. Soc., Dalton Trans.*, 1993, 269.

7 B. Drießen-Hölscher and J. Heinen, *J. Organomet. Chem.*, 1998, **570**, 141.

8 (*a*) G. J. Leigh and R. L. Richards, in *Comprehensive Organometallic Chemistry*, ed. G. Wilkinson, F. G. A. Stone and E. W. Abel, 1982, vol. 5, p. 600; (*b*) J. S. Merola and R. T. Kacmarcik, *Organometallics*, 1989, **8**, 778.

9 R. A. Jones, F. M. Real, G. Wilkinson, A. M. R. Galas, M. B. Hursthouse and K. M. A. Malik, *J. Chem. Soc., Dalton Trans.*, 1980, 511.

Communication 8/08350I

ChemComm

Cyclopropanation in the reaction of $[M(CO)_3Tp]^-$ [M = Mo, W; Tp = hydridotris(pyrazolyl)borate] with $I(CH_2)_3I$ and the insertion of isocyanide into metal–acyl bonds

Harry Adams, Rachel J. Cubbon, Mark J. Sarsfield and Mark J. Winter*

Department of Chemistry, The University, Sheffield, UK S3 7HF. E-mail: mark.winter@sheffield.ac.uk

Received (in Basel, Switzerland) 21st December 1998, Accepted 27th January 1999

Treatment of $I(CH_2)_3I$ with anions $[M(CO)_3Tp]^-$ (M = Mo, W) leads to an η^2-acyl cyclopropanation product $M(CO)_2\{\eta^2\text{-}C(O)(c\text{-}C_3H_5)\}Tp$ which decarbonylates to give π-allyl complexes and reacts with CNBu^t by formal insertion of isonitrile into the metal–acyl bond.

We have described earlier reactions between dihaloalkanes such as $I(CH_2)_3I$ and $[M(CO)_n(\eta^5\text{-}C_5H_5)]^-$ (n = 3, M = Mo, W; n = 2, M = Fe) which lead to the formation of the cyclic carbene complexes $MI(CO)_{n-1}\{=\overline{C(CH_2)_3O}\}(\eta^5\text{-}C_5H_5)$.[1,2] We are interested in these compounds in connection with their ability to act as precursors for compounds which undergo migrations to carbene. While examining related compounds but containing the hydridotris(pyrazolyl)borato (Tp) ligand, we discovered a remarkable cyclopropanation process and highly unusual insertions of isonitrile into metal acyl bonds.

The reaction between $[W(CO)_3Tp]^-$ **1** with $I(CH_2)_3I$ affords small quantities of the η^2-acyl cyclopropyl complexes $W\{\eta^2\text{-}C(O)(c\text{-}C_3H_5)\}(CO)_2Tp$ **2**. The η^2-ligand is suggested by the solution IR spectrum (ν_{CO}1958 and 1824 cm^{-1}) which is typical of previously reported η^2-acyl complexes.[3] Other spectroscopic and spectrometric methods suggest the presence of the cyclopropyl group in complex **2**, but given that the few known cyclopropyl acyl complexes are formed from preconstructed cyclopropyl rings,[4] it was felt necessary to confirm this unusual result by X-ray crystallography (Fig. 1). The cyclopropyl ring is orientated approximately perpendicular to the plane of the η^2-acyl group while the η^2-acyl group itself is best regarded as occupying a single coordination site of a slightly distorted octahedral tungsten. In the solid state, the acyl group does not lie on a mirror plane, and there is likely to be a low energy solution fluxional process as has been demonstrated *via* EHMO calculations on the complex $Mo\{\eta^2\text{-}C(O)Me\}(CO)_2Tp$ **3**. This process is described as a rapid net rocking motion of the acyl group about the plane of symmetry which bisects the angle between the carbonyls and the two pyraozole groups *cis* to the acyl group.[3]

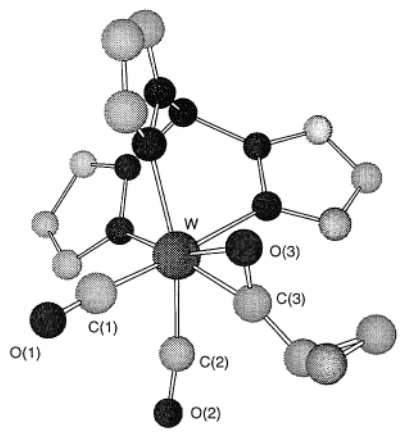

Fig. 1 Molecular structure of $W\{\eta^2\text{-}C(O)(c\text{-}C_3H_5)\}(CO)_2Tp$ **2**. Selected bond lengths (Å) and angles (°), W–C(3) 2.02(2), C(3)–O(3) 1.25(2), O(3)–W 2.217(10), C(1)–W–C(2) 80.6(6), C(3)–W–O(3) 34.0(4).

During the formation of **2**, monitoring by IR spectroscopy shows additional bands associated with the hydride $WH(CO)_3Tp$ (by comparison with an authentic sample made by the analogous route known to give $MoH(CO)_3Tp$).[5] Further, IR and NMR evidence indicates the presence of the η^2-acyl **4** in the reaction mixture. The inference that the anion $[W(CO)_3Tp]^-$ acts as a base and removes a proton from the η^2-acyl **4** (to give **5**) so inducing cyclization to give **2** is supported by the observation that addition of proton sponge [1,8-bis(dimethylamino)naphthalene] to the reaction mixture prevents the formation of $WH(CO)_3Tp$ and increases the isolated yield of **2** to 74%. Therefore, the mechanism for cyclopropyl formation is believed to proceed (Scheme 1) *via* a deprotonation α to the acyl carbon and ring closure process. That the position α to the η^2-acyl ligand in general is acidic is reinforced by earlier observations which show an α proton in complexes such as $Mo(\eta^2\text{-}COMe)(CO)_2Tp$ **3** is removed by base such as Bu^{n}Li or KH[6] and our finding that deprotonation of **2** with LDA followed by acidification or alkylation of the resulting anion affords the functionalized derivatives $W(CO)_2\{\eta^2\text{-}C(O)(c\text{-}C_3H_4R)\}Tp$ (**6**, R = Me; **7** M = D; **8**, R = allyl). The corresponding reaction of the molybdenum anion $[Mo(CO)_3Tp]^-$ **9** with $I(CH_2)_3I$ in the presence of proton sponge affords complex **10** (68%).

Complex **2** displays further interesting reactivity. Thermolysis or photolysis of **2** results in decarbonylation and ring opening of the cyclopropyl function to give the η^3-allyl complex **11**.[7] By way of partial comparison, an earlier report describes the ring opening of the cyclopropyl methyl complex $Mo(CO)_3(CH_2\text{-}c\text{-}C_3H_5)(\eta\text{-}C_5H_5)$ in refluxing hexane to give the η^3-allyl $Mo(CO)_2(\eta^3\text{-}C_3H_4Me)(\eta\text{-}C_5H_5)$.[8] Mechanistic insight into the formation of **11** in this way is given by the photolysis or thermolysis of the deuterated material $W(CO)_2\{\eta^2\text{-}C(O)(c\text{-}C_3H_4D)\}Tp$ **7** which affords $W(CO)_2(\eta^3\text{-}C_3H_4D)Tp$ **12** with > 95% deuterium labelling at the central carbon of the allyl group. Since no D-scrambling occurs, it is clear that the ring-opening process involves C–C bond cleavage between the two CH_2 groups and rearrangement to give **12**. The corresponding photolysis (but not thermolysis) of **6** affords the allyl derivative **13**.

Addition of CNBu^t to a solution of **2** in THF results in a remarkable reaction (48 h at ambient temperature for completion) leading to the α-keto-η^2-iminoacyl **14** together with the seven-coordinate Tp tungsten η^1-acyl complex **15**. There are examples of η^1-α-ketoacyl complexes in the literature (however their formation is concurrent with oxidation at the metal centre[9]) and at least one example of a α-keto-η^1-iminoacyl[10] (but made from a pre-assembled ketoimidoyl group). Because of this unusual reaction, the structure of **14** was confirmed by X-ray crystallography (Fig. 2).† The iminoacyl bond length [C(12)–N(7) 1.257(14)Å] of **14** is in the range of those reported for other η^2-iminoacyl complexes.[11] Stirring a solution of **15** in THF over three days results in only partial conversion of **14** with formation of unidentified decomposition products. Consequently, it may well be that in the reaction of **2** with CNBu^t to

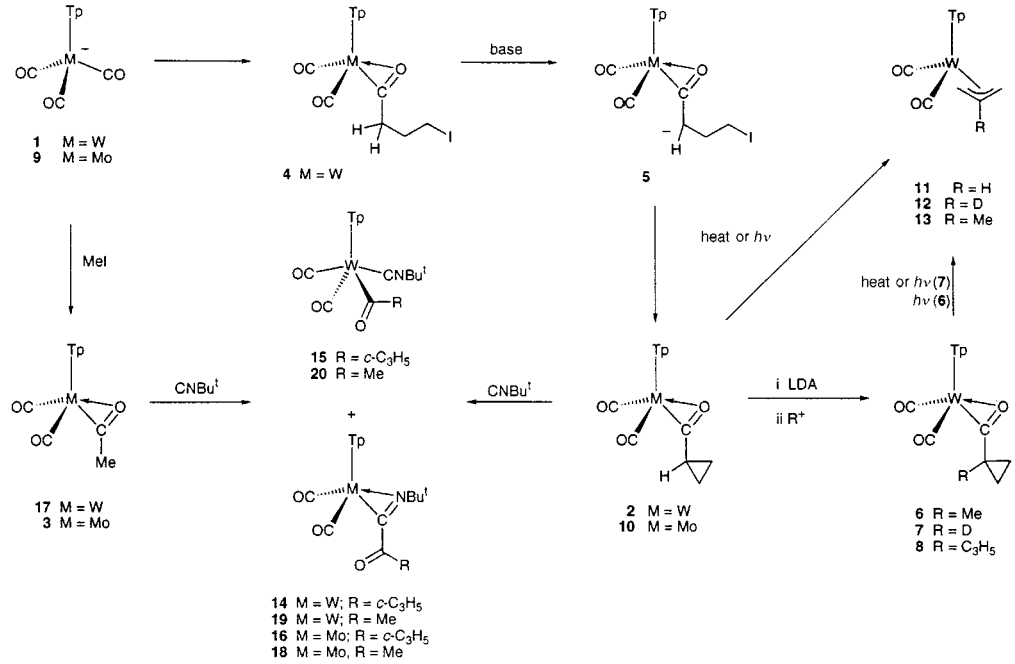

Scheme 1

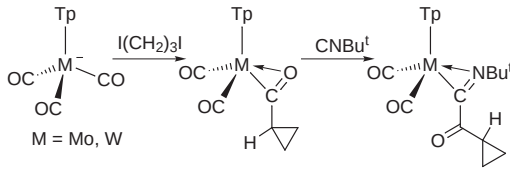

Scheme 2

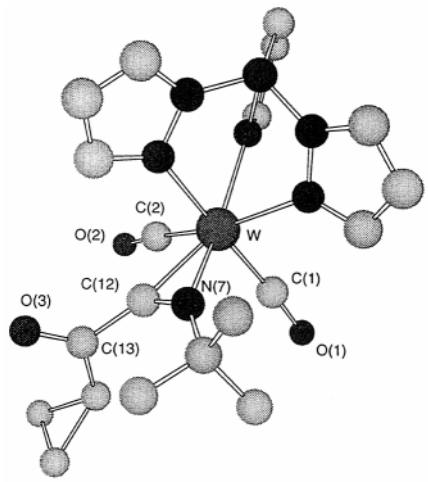

Fig. 2 Molecular structure of W{η^2-C(NBu^t)CO(*c*-C_3H_5)}$(CO)_2$Tp **14**. Selected bond lengths (Å) and angles (°), W–C(12) 2.101(11), C(12)–N(7) 1.257(14), N(7)–W 2.190(8), C(1)–W–C(2) 80.0(5), C(12)–W–N(7) 34.0(4).

form **14**, a route *via* **15** is not the major path leading to **14**. The insertion of isonitrile into metal acyl bonds of this type is reasonably general. Thus, CNBu^t reacts with the molybdenum species **10** to form **16** and we also find that the complexes M{η^2-C(O)Me}$(CO)_2$Tp (**3**, M = Mo;[3] **17** M = W) react with CNBu^t to give the insertion products $M(CO)_2$\{η^2-C(NBu^t)(COR)}Tp (**18** M = Mo; **19**, M = W). In the tungsten case, the η^1-acyl **20** is also isolable.

We are pleased to acknowledge assistance from the EPSRC for a postgraduate studentship award to M. J. S.

Notes and references

† *Crystal data*: **2**: triclinic, space group $P\bar{1}(C_1^1$ no. 2) a = 8.328(2), b = 9.478(2), c = 12.201(3) Å, α = 75.27(2), β = 77.89(2), γ = 74.17(2)°, U = 885.8(4) Å^3; D_c = 1.957 g cm^{-3}, Z = 2. Mo-Kα radiation ($\bar{\lambda}$ = 0.71073 Å), μ(Mo-Kα) = 6.548 mm^{-1}, F(000) = 500. Data were collected in the range 3.5 < 2θ < 45°(ω-scan), 2024 independent reflections [$|F|/\sigma(|F|)$ > 4.0], final R = 0.0546, with allowance for the thermal anisotropy of all non-hydrogen atoms.

14, monoclinic, space group $P2_1/n$ [a non standard setting of $P2_1/c$ (C_{2h}^5, no. 14], a = 8.016(2), b = 36.229(7), c = 9.501(2) Å, β = 112.84(3)°, U = 2542.9(10) Å^3; D_c = 1.628 g cm^{-3}, Z = 4. Mo-Kα radiation ($\bar{\lambda}$ = 0.71073 Å), μ(Mo-Kα) = 4.581 mm^{-1}, F(000) = 1224. Data were collected in the range 4.5 < 2θ < 45°(ω-scan), 2761 independent reflections [$|F|/\sigma(|F|)$ > 4.0], final R = 0.0449 with allowance for the thermal anisotropy of all non-hydrogen atoms. CCDC 182/1162.

1 M. J. Winter, N. A. Bailey, D. A. Dunn, C. N. Foxcroft, G. R. Harrison and S. Woodward, *J. Chem. Soc., Dalton Trans.*, 1988, 1449.
2 H. Adams, N. A. Bailey, M. Grayson, C. Ridgway, A. J. Smith, P. Taylor and M. J. Winter, *Organometallics*, 1990, **9**, 2621.
3 M. D. Curtis, K.-B. Shiu and W. M. Butler, *J. Am. Chem. Soc.*, 1986, **108**, 1550.
4 F. J. Manganiello, L. W. Christensen and W. H. Jones, *J. Organomet. Chem.*, 1982, **235**, 327.
5 M. D. Curtis and K.-B. Shiu, *Inorg. Chem.*, 1985, **24**, 1213.
6 J. L. Templeton, C. A. Ruskins, M. A. Collins, A. S. Gamble and T. L. Tonker, *J. Am. Chem. Soc.*, 1989, **111**, 2550.
7 S. Trofimenko, *J. Am. Chem. Soc.*, 1969, **91**, 588.
8 K. H. Pannell, R. N. Kapoor, M. Wells and T. Giasolli, *Organometallics*, 1987, **6**, 663.
9 G. L. Geoffroy, J. B. Sheridan, S. L. Bassner and C. Kelley, *Pure Appl. Chem.*, 1989, **61**, 1723.
10 A. Mantovani, G. Facchin, T. Boschi and B. Crociani, *J. Organomet. Chem.*, 1981, **206**, C11.
11 L. D. Durfee and I. P. Rothwell, *Chem. Rev.*, 1988, **88**, 1059.

Communication 8/09887E

Geometric and electronic structure of metal-cage fullerenes, $C_{59}M$ (M = Pt, Ir) obtained by laser ablation of electrochemically deposited films

Josep M. Poblet,*[a] Jordi Muñoz,[a] Krzysztof Winkler,[b,c] Mark Cancilla,[b] Akari Hayashi,[b] Carlito B. Lebrilla*[b] and Alan L. Balch*[b]

[a] *Departament de Quimica Fisica i Inorganica, Universitat Rovira i Virgili, Imperial Tarraco 1, 43005 Tarragona, Spain*

[b] *Department of Chemistry, University of California, Davis, California 95616, USA. E-mail: albalch@udavis.edu*

[c] *Department of Chemistry, Institute of Chemistry, University of Bialystok, Bialystok, Poland*

Received (in Bloomington, IN, USA) 4th December 1998, Accepted 9th February 1999

Laser ablation of electrochemically deposited $C_{60}M_n$ [M = Pt, $Ir(CO)_2$] films produces $[C_{59}M]^+$ whose electronic and geometric structures have been investigated by density functional theory.

A number of clusters based on a fullerene-like cage with heteroatoms incorporated into the cage framework have been observed in mass spectrometric studies. These clusters include examples where boron,[1] nitrogen,[2] silicon,[3] and niobium[4] are incorporated into the cages. The dimer, $\{C_{59}N\}_2$, has been prepared *via* a chemical route and isolated.[5] Recently, Branz *et al.* reported gas phase studies that generated $C_{60}M_x$ and $C_{70}M_x$ by evaporation of the metal into the fullerene vapor.[6] Subsequent photofragmentation of $C_{60}M_x$ and $C_{70}M_x$ produced clusters with the compositions, $C_{59-2n}M$ and $C_{69-2n}M$ with M = Fe, Co, Ni, Rh, Ir and n = 0, 1, 2. Here we report complementary studies that show that $C_{59-2n}M$ and $C_{69-n}M$ can be formed by laser ablation of electrochemically deposited films that are believed to contain polymeric, covalently bound chains: $\cdots C_{60}ML_nC_{60}ML_nC_{60}ML_n\cdots$, where ML_n = $Ir(CO)_2$ or Pt.[7]

Fig. 1 shows the results of laser ablation studies of the electrochemically deposited $C_{60}\{Ir(CO)_2\}_n$ film, which was obtained by electrochemical reduction of a toluene–acetonitrile (4 : 1 v/v) solution of C_{60} and $Ir(CO)_2Cl(NH_2C_6H_4Me\text{-}p)$ as described previously.[7] The lower trace shows the entire spectrum in the positive ion mode from laser desorption with a 340 nm N_2 laser from a film of $C_{60}\{Ir(CO)_2\}_n$. The spectrum reveals a strong $[C_{60}]^+$ peak at *m/z* 720 with the usual set of lower mass peaks due to loss of C_2 units from the fullerene. At higher mass the second most intense feature in the spectrum is a multiplet that is indicative of the presence of $[C_{59}Ir]^+$. Additionally a feature is seen at *m/z* 877 that corresponds to the presence of $[C_{57}Ir]^+$. Inset 1 shows an expansion of the spectroscopic multiplets for the $[C_{59}Ir]^+$ and $[C_{57}Ir]^+$ features and comparison with the calculated spectra based on the natural abundances of isotopes of C and Ir. No other iridium containing peaks are seen in the spectrum, the other peaks in the spectrum between those of $[C_{57}Ir]^+$ and $[C_{60}]^+$ correspond to the fullerene ions, $[C_{70-2n}]^+$. There is also no evidence in this spectrum for the presence of the $[C_{60}Ir_n]^+$ ions which were a prominent feature of the mass spectra that were obtained by Branz *et al.*[6] in their studies of the reactions of C_{60} and iridium vapors that led to the prior detection of $[C_{59}Ir]^+$.

Fig. 2(a) shows the corresponding spectral features for formation of $[C_{69}Ir]^+$ that was obtained by desorption from a film prepared by electrochemical reduction of a solution of C_{70} and $Ir(CO)_2Cl(NH_2C_6H_4Me\text{-}p)$. Fig. 2(b) shows the spectral features for the formation of $[C_{59}Pt]^+$ which was obtained by desorption from a film of $C_{60}Pt_n$ prepared by electrochemical reduction of a solution of C_{60} and $PtCl_2(pyridine)_2$. In the negative ion mode, the spectra from all three films show only the features due to $[C_{60}]^-$ and its fragmentation products; no evidence for the existence of $[C_{59}Ir]^-$, $[C_{69}Ir]^-$ or $[C_{59}Pt]^-$ was seen. We believe that the ions, $[C_{59}Ir]^+$, $[C_{69}Ir]^+$ and $[C_{59}Pt]^+$, are formed during the laser ablation process from $(\eta^2\text{-}C_{60})M$ units that are present in the electrochemically deposited films.

In order to understand the electronic and geometrical structures of these heterofullerenes, the optimal geometries have been computed by means of DFT calculations† under the

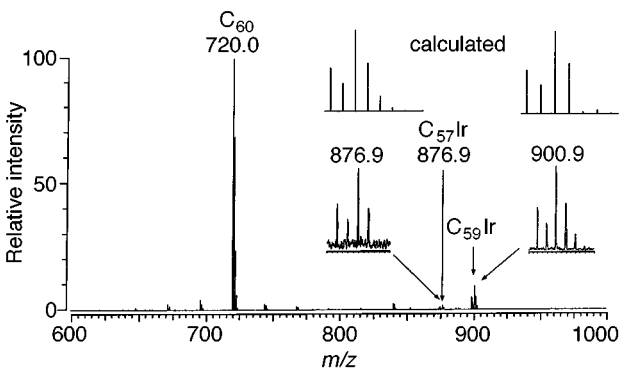

Fig. 1 Mass spectra (positive ion mode) obtained by laser ablation of electrochemically deposited films from C_{60} and $Ir(CO)_2Cl(NH_2C_6H_4Me\text{-}p)$. Inserts show expansions of the multiplets observed for $[C_{59}Ir]^+$ and $[C_{57}Ir]^+$ and comparisons with the calculated spectra.

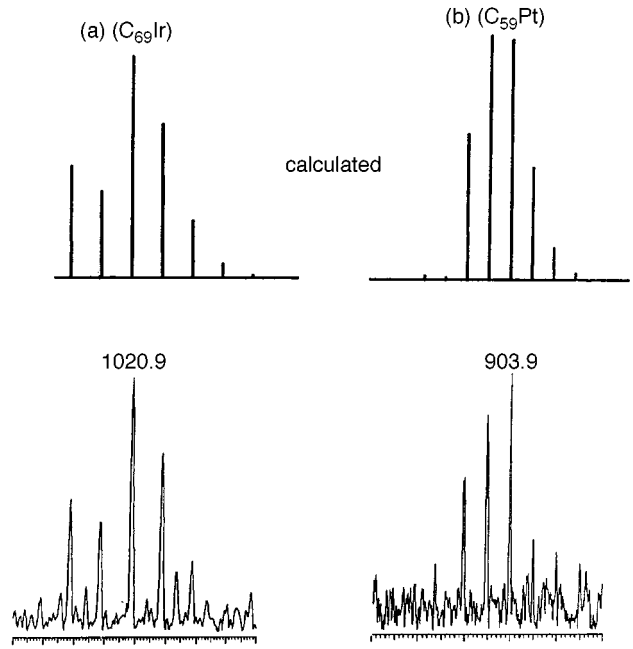

Fig. 2 Mass spectra (positive ion mode) obtained by laser ablation of electrochemically deposited films from (a) C_{70} and $Ir(CO)_2Cl(NH_2C_6H_4Me\text{-}p)$; and (b) C_{60} and $PtCl_2(py)_2$.

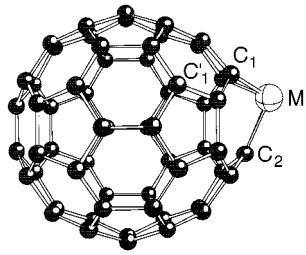

$C_{59}Ir$, $C_{59}Pt$

Fig. 3 A drawing of the geometric structure of $C_{59}Ir$ (and $C_{59}Pt$) obtained from density functional calculations. Selected bond lengths (Å) and angles (°): C_1–Pt 1.992, C_2–Pt 1.934, C_1–Pt–C_1' 78.5, C_1–Pt–C_2 96.7, C_1–Ir 1.954, C_2–Ir 1.905, C_1–Ir–C_1' 81.7, C_1–Ir–C_2 92.3.

Table 1 Computed energies (in eV) of C_{60} and metal–fullerene compounds

	C_{60}	$C_{59}Pt$	$C_{59}Ir$	$(\eta^2\text{-}C_{60})\text{-}Pt(PH_3)_2$	$(\eta^2\text{-}C_{60})\text{-}\{Pt(PH_3)_2\}_2$
IP	8.28	7.39	7.10	7.35	6.82
EA	3.49	3.56	3.71	3.08	2.73
E(LUMO)	−5.37	−5.34	−5.08	−4.86	−4.45
E(HOMO)	−7.03	−6.05	−5.64	−6.22	−5.97

restrictions of C_s symmetry. The computed geometries, which correspond to the substitution of one carbon atom by a metal atom, are similar for M = Pt and Ir. The optimization yields a geometry with a local distortion in the vicinity of the metal atom (Fig. 3). The computed M–C bond lengths are 1.954 and 1.905 Å for $C_{59}Ir$ and 1.992 and 1.934 Å for $C_{59}Pt$.

The electronic configuration of $C_{59}Pt$ is a closed-shell singlet in which the HOMO–LUMO gap was computed to be 0.7 eV. The triplet structure with one electron in the HOMO and another in the LUMO was also optimized but its relative energy with respect to the singlet structure was quite high (10.1 kcal mol^{-1}). Mulliken population analysis indicates that there is significant charge transfer from metal to the carbon fragment, since the net charge on platinum is +1.3 e. The electronic populations of the s, p and d platinum orbitals are 2.38, 6.03 and 8.24 e, respectively. Other models of space partitioning predict less charge transfer. Hirshfeld and Voronoi procedures assign a net charge of +0.5 e to the platinum atom.[8,9] The metal orbitals in $C_{59}Pt$ are spread through a range of molecular orbitals and each of the molecular orbitals in the metallofullerene has a low metal contribution. Specifically, the participation of the metal orbitals is 19% in the HOMO and 17% in the LUMO. The ground state for the analog iridium cluster is a doublet of symmetry A′ in which the spin density is quite delocalized with 0.22 e on the metal center, 0.27 e on C(2) and the rest of the spin density delocalized through the carbon cage in smaller increments. Hirshfeld and Voronoi population analyses suggest that the charge on the iridium atoms is *ca.* 0.35 e, and that the charge transfer from the metal to fullerene is somewhat lower than in the platinum analog.

In order to get more information about the physical properties of these clusters we have also computed the vertical ionization potentials (IP) and electron affinities (EA). These data and the energies of the HOMOs and LUMOs are presented in Table 1 for C_{60}, $C_{59}Pt$, $C_{59}Ir$, $(\eta^2\text{-}C_{60})Pt(PH_3)_2$ and $(\eta^2\text{-}C_{60})\{Pt(PH_3)_2\}_2$. Substitution of a carbon by a metal increases the energy of the HOMO in both $C_{59}Pt$ and $C_{59}Ir$ relative to C_{60}. As a consequence of this increase, the IP's of the substituted fullerenes are lower than those of C_{60} itself.

Smalley and coworkers[10] estimated from photoelectron spectra an EA of *ca.* 2.60–2.80 eV for C_{60}. Although present DFT calculations probably predict an excessively high value for C_{60}, the computed relative EAs for $(\eta^2\text{-}C_{60})\{Pt(PH_3)_2\}_n$ (n = 1 and 2) are in very good concordance with the electrochemical studies of Fagan and coworkers who proposed that coordination of one $Pt(PR_3)_2$ group to C_{60} lowers the EA of the carbon cluster by 0.34 eV while coordination of two groups to C_{60} decreases the EA by 0.70 eV.[11]

The energies of the LUMOs in $C_{59}Pt$ and C_{60} are very similar, −5.34 and −5.37 eV, respectively. Consequently, the difference between the EAs of C_{60} and $C_{59}Pt$ was computed to be very small (0.05 eV). The added electron in $C_{59}Ir$ goes to a half-filled orbital at an energy of −5.64 eV, which is 0.27 eV lower than the energy of the LUMO of C_{60}. Thus, the EA of $C_{59}Ir$ is 0.22 eV higher than the EA of C_{60}.

The ability of $C_{59}Pt$ to coordinate PH_3 or CO was also analyzed. For both molecules, the DFT calculations yielded an optimal geometry in which the metal has a tetrahedral coordination with three quasi identical Pt–C bond lengths. The new computed Pt–ligand bond distances are 2.409 Å for PH_3 and 1.983 Å for CO. The corresponding bonding energies were calculated to be 14.2 and 6.2 kcal mol^{-1}, respectively. In the case of $C_{59}PtCO$, the ground state is a triplet since the HOMO and LUMO are quasi degenerate orbitals.

We thank the National Science Foundation (Grant CHE 9610507) for financial support, Johnson Matthey for a loan of platinum and iridium salts, and L. Voss, Dr A. de Bettencourt-Dias and Dr C. Bo for assistance. DFT calculations have been carried out on workstations purchased with funds provided by the DGICYT of the Government of Spain and by the CIRIT of Generalitat of Catalunya (Grants no. PB95-0639-C02-02 and SGR97-17).

Notes and references

† *Computation*: gradient corrected DFT calculations were carried out with the ADF program.[12] We used the local density approximation with Vosko–Wilk–Nusair parametrization for correlation.[13] Becke's non-local corrections to the exchange energy and Perdew's non-local corrections to the correlation energy were added.[14] Slater basis sets of double-ζ + polarization quality were used to describe the valence electrons of C, O, P and H. For iridium and platinum, the 5sp electrons were described by double-ζ Slater functions, 5d and 6s by triple-ζ functions, and 6p by a single orbital.

1 T. Guo, C. Jin and R. E. Smalley, *J. Phys. Chem.*, 1991, **95**, 4948.
2 W. Andreoni, F. Gygi and M. Parinello, *Chem. Phys. Lett.*, 1992, **190**, 159.
3 T. Kimura, T. Sugai and H. Shinohara, *Chem. Phys. Lett.*, 1996, **256**, 269.
4 D. E. Clemmer, J. M. Hunter, K. B. Shelimov and M. F. Jarrold, *Nature*, 1994, **372**, 248.
5 J. C. Hummelen, B. Knight, J. Pavlovich, R. Gonzalez and F. Wudl, *Science*, 1995, **269**, 1554.
6 W. Branz, I. M. L. Billas, N. Malinowski, F. Tast, M. Heinebrodt and T. P. Martin, *J. Chem. Phys.*,1998, **109**, 3425.
7 A. L. Balch, D. A. Costa and K. Winkler, *J. Am. Chem. Soc.*, 1998, **120**, 9614.
8 F. L. Hirshfeld, *Theor. Chim. Acta*, 1977, **44**, 129.
9 G. Voronoi, *J. Reine Angew. Mathematik*, 1908, **134**, 198.
10 S. H. Yang, C. L. Pettiette, J. Concienciao, O. Cheshnowsky and R. E. Smalley, *Chem. Phys. Lett.*, 1991, **139**, 233.
11 S. A. Lerke, B. A. Parkinson, D. H. Evans and P. J. Fagan, *J. Am. Chem. Soc.*, 1992, **114**, 7807.
12 (*a*) ADF2.3 User's Guide, Chemistry Department, Vrije Universiteit, Amsterdam, The Netherlands, 1997; (*b*) E. J. Baerends D. E. Ellis and P. Ros, *Chem. Phys.*, 1973, **2**, 41; (*c*) G. te Velde and E. J. Baerends, *J. Comput. Phys.*, 1992, **99**, 84.
13 S. H. Vosko, L. Wilk and M. Nusair, *Can. J. Phys.*, 1980, **58**, 1200.
14 A. D. Becke, *J. Chem. Phys.*, 1986, **84**, 4524; *Phys. Rev. A*, 1988, **38**, 3098; J. P. Perdew, *Phys. Rev. B*, 1986, **33**, 8882; 1986, **34**, 7606.

Communication 8/09550G

Predictions for possible new, doubly and triply bridged oxides and peroxides of C, N, P, and S

Pekka Pyykkö

Department of Chemistry, University of Helsinki, P.O.B. 55 (A. I. Virtasen aukio 1), FIN--00014 Helsinki, Finland. E-mail: Pekka.Pyykko@helsinki.fi

Received (in Cambridge, UK) 2nd December 1998, Accepted 16th February 1999

By regarding the $X^{2-,3-}$ oxoanions of main group elements as pseudochalcogenides or pseudopnicogenides, and possibly cutting the peroxide bridges to oxide bridges, one arrives at a series of so far experimentally unknown oxides and peroxides, X_2, having high, but not exceedingly high energies.

Pseudohalides, such as CN^-, are known to form corresponding pseudohalogens, like NC–CN. Similarly, certain divalent and trivalent polyatomic anions, $X^{2-,3-}$, can be regarded as pseudochalcogenides and pseudopnicogenides. They can in principle form the corresponding neutral molecules X_2.[1] Now, consider an oxoanion, such as $X^{2-} = CO_3^{2-}$ from this point of view. The corresponding neutral X_2 dimer is $(CO_3)_2$, for which we consider the structure {O=C(–O–O–)$_2$C=O} **1**. If the peroxide bridges are shortened to oxide ones, the structure O=C(μ-O)$_2$C=O **2** is obtained. We here point out the possible existence of an entire class of such compounds. Further variations on the theme are obtained by replacing some or all of the oxygens by sulfurs, by adding or omitting terminal oxygens, by replacing them with halogen atoms, or by varying the total charge.

Related singly bridged peroxide systems are known. Peroxodisulfate, $S_2O_8^{2-}$, is one of the most powerful oxidizing agents.[2] Note that below we discuss the neutral S_2O_8. The peroxydicarbonate, $C_2O_6^{2-}$ is known. We here discuss the neutral C_2O_6. The diphosphate **9** is six electrons short of $2PO_4^{3-}$. These proposed oxidized oxoanion dimer molecules, if they can be made, are likely to be even stronger oxidants than the known peroxo compounds.

Triply bridged, 'confacial tetrahedral geometries' are rare.[3,4] We are not aware of experimentally known molecules with (–O–)$_3$ bridges.

The second-order Møller-Plesset or B3LYP density functional calculations were performed using GAUSSIAN 94. The obtained structures are reported in Table 1 and shown in Fig. 1. It was checked that all geometries correspond to local minima. The vibrational frequencies for species **1**–**5** are shown in Fig. 2. The pseudochalcogen corresponding to carbonate **1** is found to have a relatively low energy, Table 2. In the calculated structure the two coaxial carbonate planes are rotated through 37.8°. Double peroxide bridges are previously known in the cyclic peroxides of type R$_2$C(–OO–)$_2$CR$_2$.[5] We now replace the –CR$_2$ groups by –C=O groups.

Perhaps the most interesting result is that carbon dioxide would be able to form the metastable planar dimer **2** only about 200 kJ mol^{-1} above two monomers. Both this dimer and a $(CO_2)_3$ trimer have been recently discussed by Lewars.[6] He finds for the dimer **2** at the MP2/6-31G* level a barrier of 41 kJ mol^{-1}, which would make it a possible low-temperature species, that merits further studies. The structure of **2** does not offend chemical intuition, although the four-ring is strained. Furthermore the structures, vibrational frequencies and heats of formation are very similar at the four levels [(a)–(d)] of approximation. Four-rings with two opposite > C=O groups and two opposite > N–Ph groups are known.[7] If the ring oxygens are replaced with sulfur atoms, the resulting dimers **3** and **5** are only *ca.* 100 kJ mol^{-1} above two carbonyl sulfide or carbon disulfide monomers, respectively. The alternative $C_2O_2S_2$ structure **4** lies higher.

Of the present ten species, one is experimentally known. High-pressure experiments on CS_2 are thought to yield **5**, identified on the basis of an IR band at 1150 cm^{-1}.[8] The present calculations find a b_{1u} vibration with large intensity (814 km mol^{-1}) at 1125 cm^{-1} at the B3LYP/6-31G* level (c). The corresponding frequency for **2** and **3** is predicted to occur at

Table 1 Calculated geometries for the peroxide-bridged dimers X_2 corresponding to anions $X = EO_n^{q-}$. The geometries of the corresponding oxygen-bridged species are also given. E–O$_t$ is the terminal and E–O$_b$ the bridging distance, respectively. α is the dihedral E–O–O–E angle. Some sulfur analogues are included

				Distance/pm			Angle/°	
X	Species	No.	Symmetry	E–O$_t$	E–O$_b$	O–O	O$_t$–E–O$_b$	α
CO_3^{2-}	O=C(–O–O–)$_2$C=O	**1**[a]	D_2	119.9	137.4	147.8	123.3	65.7
	O=C(–O–)$_2$C=O	**2**[a]	D_{2h}	118.4	140.2	—	133.0	
	O=C(–O–)$_2$C=O	**2**[b]	D_{2h}	117.3	139.5	—	132.9	
	O=C(–O–)$_2$C=O	**2**[c]	D_{2h}	117.6	139.6	—	133.2	
	O=C(–O–)$_2$C=O	**2**[d]	D_{2h}	116.7	139.3	—	133.2	
	O=C(–S–)$_2$C=O	**3**[c]	D_{2h}	118.7	182.6	—	130.1	
	S=C(–O–)$_2$C=S	**4**[c]	D_{2h}	159.3	138.9	—	133.5	
	S=C(–S–)$_2$C=S	**5**[c]	D_{2h}	161.3	179.2	—	131.2	
	F–C(–O–)$_3$C–F	**6**[a]	D_{3h}	129.2	145.0	—	123.5	
NO_3^-	N(–O–)$_3$N	**7**[a]	D_{3h}	—	150.1	—	127.2	
NO_4^{3-}	O=N(–O–)$_3$N=O	**8**[a]	D_{3h}	116.4	161.7	—	126.1	
PO_4^{3-}	O=P(–O–O–)$_3$P=O	**9**[c]	D_3	146.0	165.0	148.7	115.9	36.4
SO_4^{2-}	O$_2$S(–O–O–)$_2$SO$_2$	**10**[c]	C_{2h}	143.8[e]	169.2	146.2	103.8, 110.7	76.3

[a] MP2/6-31G*. [b] MP2/cc-pVTZ. [c] DFT B3LYP/6-31G*. [d] DFT B3LYP/cc-pVTZ. [e] Both equal.

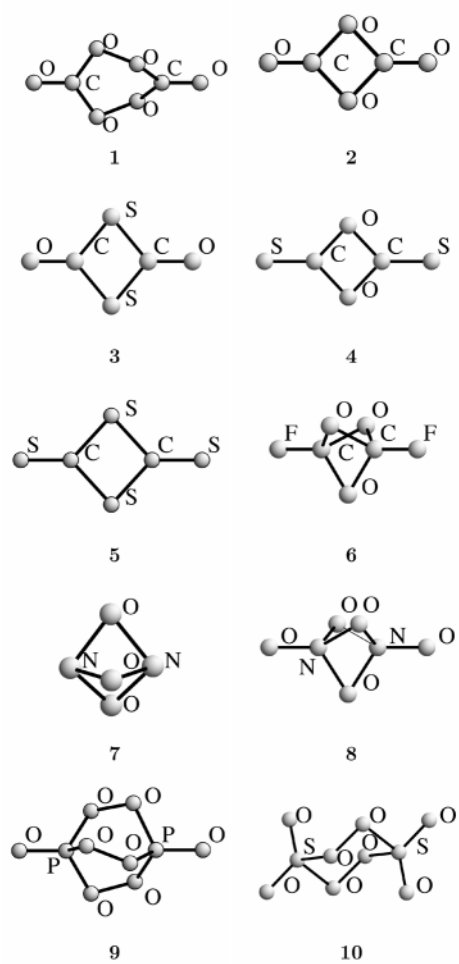

Fig. 1 The calculated structures of species **1**–**10**

Table 2 Calculated heats of formation, ΔH (kJ mol^{-1}), with respect to the reference compounds given, without zero-point energy corrections. For footnotes, see Table 1

Molecule	Reference	ΔH
1[a]	$2CO + H_2O_2 - 2H_2$	−9
2[a]	$2CO_2$	206
2[b]	$2CO_2$	196
2[c]	$2CO_2$	174
2[d]	$2CO_2$	202
3[c]	2OCS	111
4[c]	2OCS	225
5[c]	$2CS_2$	115
6[a]	$CO + CO_2 + F_2$	−19
7[a]	$N_2 + \frac{3}{2}O_2$	653
	$ON–NO_2$	552

1951 (a) or 1950 (d) and 1863 (c) cm^{-1}, respectively, Fig. 2. As the dimerisation energies for **3** and **5** are comparable, compression of OCS should result in **3**.

Compound **6** has a favourable heat of formation, as seen from Table 2. Its e′ and a_2'' frequencies at 1187 and 1419 cm^{-1} have intensities of 320 and 820 km mol^{-1}, respectively, at MP2/6-311G* level.

The trigonal bipyramidal, D_{3h}, structure **7** of N_2O_3 is calculated to lie at very high energy, 552 kJ mol^{-1} above the experimentally known $ON–NO_2$ structure. The vibrational frequencies of the high-energy form are, however, all positive and quite large (e″ 525, e′ 648 (42), 732(3), a_2'' 722(41), a_1' 848, 1120 cm^{-1}). It is a possible high-energy species. The IR

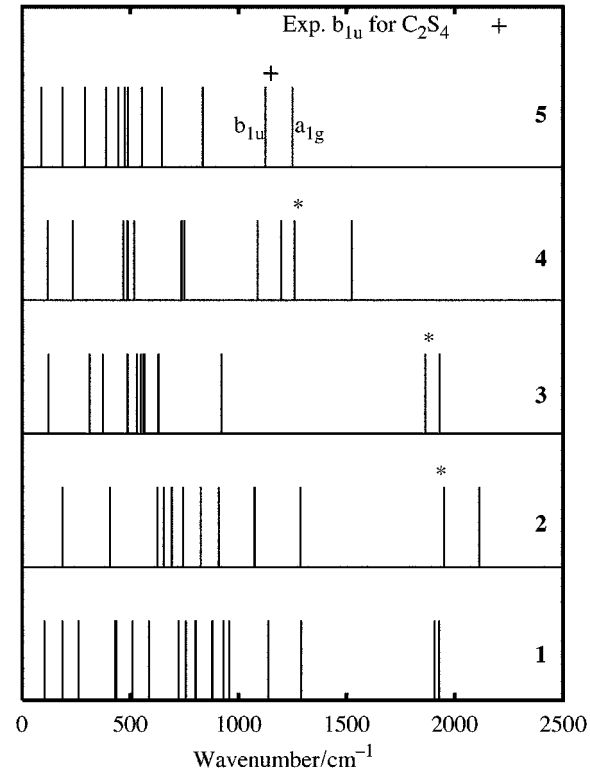

Fig. 2 The calculated vibrational frequencies of species **1**–**5**. The predicted, intensive b_{1u} vibration frequencies of **2**–**4** are marked with a star.

intensities (in parentheses) are quite low and the static dipole moment is zero. For the valence isoelectronic P_2S_3, the D_{3h} structure is calculated to lie only slightly above the lowest 'W' one.[9]

The structure of **8** is of the same type as that calculated for $[O=Si(–O–)_3Si=O]^{2-}$ by Cederbaum and coworkers.[10] The corresponding $C_2O_5^{2-}$ was here found to be unstable, having two negative frequencies.

Concluding, we suggest that the carbonyl sulfide dimer **3** is likely and the carbon dioxide dimer **2** conceivable as a synthetic goal. The latter has already been proposed by Lewars[6] as a possible low-temperature species.

The proposed molecules might have applications as strong oxidants or as high-energy species.

This study is supported by The Academy of Finland.

Notes and references

1 A. M. Golub, H. Köhler and V.V. Skopenko, *Chemistry of Pseudohalides*, Elsevier, Amsterdam, 1986, p. 469.
2 F. A. Cotton and G. Wilkinson, *Advanced Inorganic Chemistry*, Wiley, New York, 1988, p. 524.
3 C. Zheng, R. Hoffmann and D. R. Nelson, *J. Am. Chem. Soc.*, 1990, **112**, 3784.
4 C. Horn, I. Dance, D. Craig, M. Scudder and G. Bowmaker, *J. Am. Chem. Soc.*, 1998, **120**, 10 549.
5 *Houben-Weyl, Methoden der organischen Chemie, 4:e Auflage, Band VIII, Sauerstoffbindungen III*, ed. E. Müller, Georg Thieme Verlag, Stuttgart, 1952, p. 31.
6 E. Lewars, *J. Mol. Struct. (THEOCHEM)*, 1996, **363**, 1.
7 Ref. 5, p. 221.
8 S. F. Agnew, R. E. Mischke and B. I. Swanson, *J. Phys. Chem.* 1988, **92**, 4201.
9 L. L. Lohr and D. Sundholm, *J. Mol. Struct.*, 1997, **413**–**414**, 495.
10 T. Sommerfeld, M. K. Scheller and L. Cederbaum, *J. Chem. Phys.*, 1996, **104**, 1464.

Communication 8/09416K

Aerobic oxidation of a disulfide to its sulfonate leading to supramolecular pyridine-2-sulfonato Cu(II) and Zn(II) complexes

Kentaro Kimura, Takahiro Kimura, Isamu Kinoshita,* Nobuaki Nakashima, Ken'ichi Kitano, Takanori Nishioka and Kiyoshi Isobe

Department of Molecular Materials Science, Graduate School of Science, Osaka City University, Sugimoto, Sumiyoshi-ku, Osaka 558-8585, Japan. E-mail: isamu@sci.osaka-cu.ac.jp

Received (in Cambridge, UK) 7th December 1998, Accepted 1st February 1999

A one-dimensional copper(II) complex with pyridine-2-sulfonate donors, [{Cu(3-mpSO$_3$)$_2$}$_n$] (3-mpSO$_3$ = 3-methylpyridine-2-sulfonate), is formed *via* the air oxidation of 3-mpds (2,2′-bis(3-methylpyridyl)disulfide) in the presence of CuBr$_2$, and a mononuclear zinc complex, [Zn(3-mpSO$_3$)$_2$(H$_2$O)$_2$], which has two-dimensional H-bonded networks and luminescent properties in solid state, is prepared by the reaction of ZnBr$_2$ with 3-mpSO$_3$H.

A variety of complexes with pyridine derivatives have been extensively investigated as a motif in supramolecular architecture.[1] On the other hand, one of the pyridine derivatives, pyridine-2-sulfonate, has been used for studies on ligand effects on GoAgg^{II} oxidation and chromic acid oxidation,[2] which can be expected to serve as a simple chelating ligand. Luminescent complexes of pyridine-2-sulfonate with several lanthanoids have also been prepared.[3] However, except for a silver(I) complex preliminarily reported by Charbonnier *et al*.[4] and a cobalt(III) complex recently reported by Murata *et al*.,[5] there is no report on the crystal structures of pyridine-2-sulfonato complexes.

In the present work, a supramolecular entity with a pyridine-2-sulfonate donor has been unexpectedly found in the reaction of 2,2′-bis(3-methylpyridyl)disulfide (3-mpds) with CuBr$_2$ under aerobic conditions, where the air oxidation of 3-mpds to 3-methylpyridine-2-sulfonate (3-mpSO$_3$) took place to afford a one-dimensional copper(II) complex, [{Cu(3-mpSO$_3$)$_2$}$_n$] **1**. By using the sulfonato ligand we have also synthesized a photoluminescent complex, [Zn(3-mpSO$_3$)$_2$(H$_2$O)$_2$] **2**, which is assembled by intermolecular hydrogen bonds in the solid state.†

Addition of a methanolic suspension of 3-mpds[6,7] in air to a methanol solution of CuBr$_2$ immediately afforded brown and red crystals, which were removed by filtration after 2 days.‡ The filtrate was allowed to stand for a month, yielding green crystals of sulfonato complex [{Cu(3-mpSO$_3$)$_2$}$_n$] **1**.§

As shown in Fig. 1, the molecular structure of **1** consists of an infinite one-dimensional chain of octahedrally co-ordinated centrosymmetric copper atoms, bridged by 3-mpSO$_3$ ligands. Two 3-mpySO$_3$ ligands are co-ordinated to the Cu ion to form a basal plane with two five-membered chelate rings in a *trans* fashion. The apical sites are occupied by two oxygen atoms of the 3-mpSO$_3$ ligands bridging to the adjacent Cu centres; the axial Cu–O bond lengths are longer than the corresponding equatorial ones by 0.44 Å.

Oxidation of 2,2′-dipyridyl disulfide to pyridine-2-sulfinate in the presence of the Cu(II) ion and water under both aerobic and anaerobic conditions has already been reported by Seff *et al*.[8] In general, further oxidation of disulfides or sufinate compounds to the corresponding sulfonates requires a strong oxidizing agent such as hydrogen peroxide or halogen.[5,9] Surprisingly, in the present experiment, 3-mpds was oxidized to 3-mpSO$_3$ even under relatively mild oxidative conditions. Such an oxidation phenomenon is considered to be a preceding process of oxidative desulfurization and to be a mimic of the metabolism of sulfur *in vivo*.[10]

The sulfonato zinc complex, [Zn(3-mpSO$_3$)$_2$(H$_2$O)$_2$] **2**, was obtained from the reaction of ZnBr$_2$ with 3-mpSO$_3$H[6,11] in water, and the molecular structure is shown in Fig. 2.¶ The zinc ion is co-ordinated by two 3-mpSO$_3$ ligands through the aromatic nitrogens in *trans* positions and sulfonate oxygens in *cis* positions and by two water molecules *cis* to each other. This N$_2$O$_4$ donor set forms the octahedral co-ordination geometry around the Zn atom. As depicted in Fig. 3, all of the co-ordinated water molecules and the unco-ordinated sulfonate oxygens are used for intermolecular hydrogen bonds (O(2)···O(4) 2.818(2) Å, O(3)···O(4) 2.723(2) Å), forming two-dimensional H-bonded networks parallel to the *bc* plane. Interestingly, the zinc complex **2** in the solid state displays luminescence with maximum peaks at 345 and 490 nm at room temperature when excited at 311 nm (Fig. 4). The higher energy emission is presumably a fluorescence. On the other hand, the

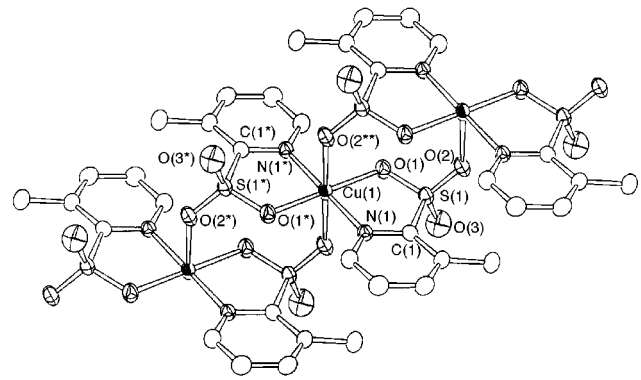

Fig. 1 One-dimensional infinite structure of [{Cu(3-mpSO$_3$)$_2$}$_n$] **1** along the *c* axis, showing three of the copper centres. Selected bond lengths (Å) and angles (°): Cu(1)–O(1) 1.977(2), Cu(1)–N(1) 1.985(2), Cu(1)–O(2**) 2.419(2), O(1)–Cu(1)–N(1) 94.74(7), O(1)–Cu(1)–O(1*) 180.0, N(1)–Cu(1)–N(1*) 180.0, Cu(1)–O(1)–S(1) 119.1(1), O(1)–S(1)–C(1) 102.0(1), S(1)–C(1)–N(1) 114.0(2), Cu(1)–N(1)–C(1) 117.8(2).

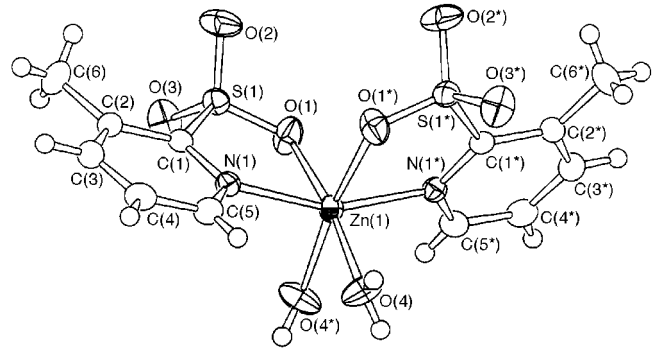

Fig. 2 The molecular structure of [Zn(3-mpSO$_3$)$_2$(H$_2$O)$_2$] **2**. Selected bond lengths (Å) and angles (°): Zn(1)–O(1) 2.155(1), Zn(1)–O(4) 2.095(1), Zn(1)–N(1) 2.109(1), O(1)–Zn(1)–N(1) 79.90(5), O(4)–Zn(1)–O(4*) 83.51(9), Zn(1)–O(1)–S(1) 120.37(7), O(1)–S(1)–C(1) 104.82(8), S(1)–C(1)–N(1) 114.6(1), Zn(1)–N(1)–C(1) 120.0(1).

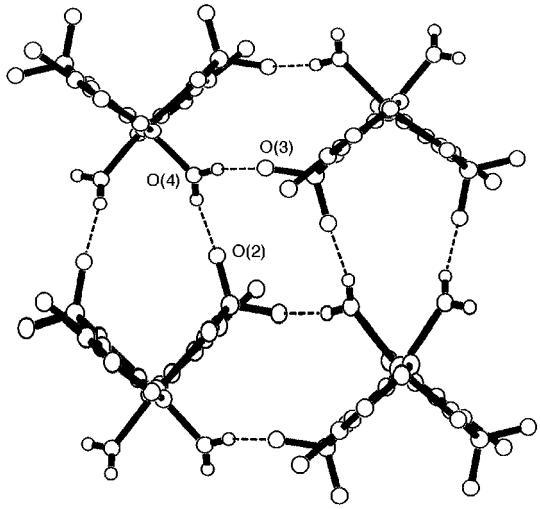

Fig. 3 H-Bonded network of complex **2** parallel to the *bc* plane. The intermolecular H-bonds are drawn as dashed lines. All hydrogen atoms except for the co-ordinated H_2O are omitted for clarity. H-bond lengths (Å): O(2)···O(4) 2.818(2), O(3)···O(4) 2.723(2).

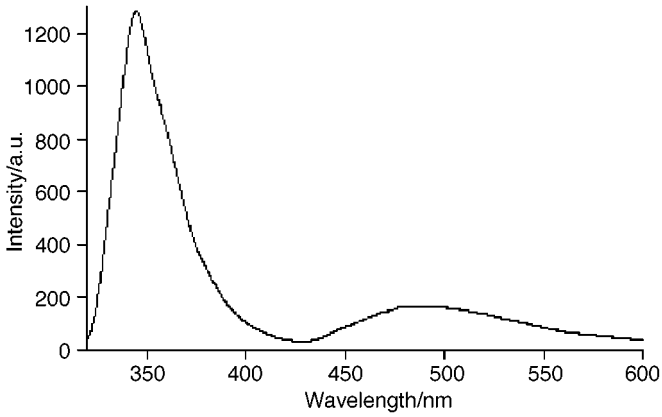

Fig. 4 Emission spectrum of complex **2** in the solid state at room temperature when excited at 311 nm.

lower energy emission can be assigned to a phosphorescence (τ = 0.15 s).

In preliminary experiments, crystals of Mn(II) and Co(II) complexes with 3-mpSO$_3$ ligands prepared in the same manner have proved to be isomorphous with those of complex **2**. Comparative studies of their chemical and physical properies are in progress.

The authors gratefully acknowledge Ms. Tamaki Nagasawa (Osaka City University) for elemental analyses. This work was financially supported by Grants-in-Aid from the Ministry of Education, Japan (No. 06640731 and 09874135).

Notes and references

† *Crystal data*: intensity data were collected on a Rigaku AFC-7S diffractometer with graphite-monochromated Mo-Kα radiation (λ = 0.71069 Å) at 296 K, using the ω–2θ scan technique to a maximum 2θ value of 60.0°.

[{Cu(3-mpSO$_3$)$_2$}$_n$] **1**: $C_{12}H_{12}CuN_2O_6S_2$, M = 407.90, green prismatic crystal (0.36 × 0.20 × 0.10 mm), triclinic, space group $P\bar{1}$, a = 7.7242(8), b = 9.7417(8), c = 4.9584(7) Å, α = 103.837(9), β = 98.12(1), γ = 93.227(8)°, V = 357.07(7) Å^3, Z = 1, D_c = 1.897 Mg m^{-3}, F(000) = 207, μ(Mo-Kα) = 1.855 mm^{-1}, 2293 reflections, of which 2069 were independent (R_{int} = 0.025). R = 0.033, R_w = 0.051, $\Delta\rho_{max}$ = +0.28 and $\Delta\rho_{min}$ = −0.76 e Å^{-3} (teXsan software).

[Zn(3-mpSO$_3$)$_2$(H$_2$O)$_2$] **2**: $C_{12}H_{16}N_2O_8S_2Zn$, M = 445.77, colorless prismatic crystal (0.62 × 0.34 × 0.28 mm), monoclinic, space group $C2/c$, a = 19.058(1), b = 7.381(1), c = 14.321(1) Å, β = 126.176(4)°, V = 1626.2(3) Å^3, Z = 4, D_c = 1.821 Mg m^{-3}, F(000) = 912, μ(Mo-Kα) = 1.813 mm^{-1}, 2630 reflections, of which 2556 were independent (R_{int} = 0.021). R = 0.027, R_w = 0.038, $\Delta\rho_{max}$ = +0.30 and $\Delta\rho_{min}$ = −0.47 e Å^{-3} (teXsan software). CCDC 182/1157. See http://www.rsc.org/suppdata/cc/1999/497/ for crystallographic files in .cif format.

‡ X-Ray diffraction analysis revealed that the brown and red products were [CuBr$_2$(3-mpds)] and [CuBr(3-mpts)] (3-mpts = 2,2′-bis(3-methylpyridyl)trisulfide), respectively.

§ Complex **1**: (Calc. for $C_{12}H_{12}CuN_2O_6S_2$: C, 35.33; H, 2.97; N, 6.87. Found: C, 35.15; H, 2.89; N, 6.82%). Although the yield of complex **1** is low (*ca*. 5%), the formation of this complex *via* the air oxidation of 3-mpds is reproducible. When Cu(ClO$_4$)$_2$·6H$_2$O was applied to the reaction, the oxidation of 3-mpds was terminated at the formation of 3-methylpyridine-2-sulfinate as reported by Seff *et al*. for the oxidation of 2,2′-dipyridyl disulfide. The direct reaction of 3-mpSO$_3$H with CuBr$_2$ in aqueous methanol afforded another polymorph with complex **1** in a better yield.

¶ *Selected data* for complex **2**: (Calc. for $C_{12}H_{16}N_2O_8S_2Zn$: C, 32.33; H, 3.62; N, 6.29. Found: C, 32.30; H, 3.58; N, 6.26%). ^{1}H NMR (300 MHz, CD$_3$OD, TMS): δ 2.61 (s, 6H, CH$_3$), 7.49 (dd, 2H, ^3J = 7.7 Hz, ^3J = 4.8 Hz, β-H), 7.89 (d, 2H, ^3J = 7.7 Hz, γ-H), 8.51 (d, 2H, ^3J = 4.8 Hz, α-H).

1 J.-M. Lehn, *Supramolecular Chemistry*, VCH, Weinheim, 1995, pp. 89 and 139.
2 E. About-Jaudet, D. H. R. Barton, E. Csuhai and N. Ozbalik, *Tetrahedron Lett*., 1990, **31**, 1657; J. Rocek and T-Y. Peng, *J. Am. Chem. Soc.*, 1977, **99**, 7622.
3 G. Kallistratos, U. Kallistratos and H. Mündner, *Chim. Chron. New Ser*., 1982, **11**, 249.
4 F. Charbonnier, R. Faure and H. Loiseleur, *Cryst. Struct. Commun*., 1981, **10**, 1129.
5 M. Murata, M. Kojima, A. Hioki, M. Miyagawa, M. Hirotsu, K. Nakajima, M. Kita, S. Kashino and Y. Yoshikawa, *Coord. Chem. Rev*., 1998, **174**, 109.
6 E. C. Horning, *Organic Synthesis*, John Wiley & Sons, Inc., New York, 1955, vol. 3, pp. 136–139; J. R. Thirtle, *J. Am. Chem. Soc.*, 1946, **68**, 342.
7 D. N. Harpp and J. G. Gleason, *J. Org. Chem.*, 1970, **35**, 3259.
8 L. S. Higashi, M. Lundeen, E. Hilti and K. Seff, *Inorg. Chem.*, 1977, **16**, 310.
9 R. K. Henderson, E. Bouwman, A. L. Spek and J. Reedijk, *Inorg. Chem*., 1997, **36**, 4616; W. G. Jackson and A. M. Sargeson, *Inorg. Chem*., 1988, **27**, 1068.
10 E. S. Raper, *Coord. Chem. Rev*., 1994, **129**, 91; S. Oae and T. Okuyama, *Organic Sulfur Chemistry: Biochemical Aspects*, CRC Press, Ann Arbor, 1992, pp. 1–43.
11 A. M. Comrie and J. B. Stenlake, *J. Chem. Soc*., 1958, 1853.

Communication 8/09513B

Dual reaction behaviour of an *in situ* generated nitrilium phosphane ylide complex towards carbon–sulfur π-systems

Rainer Streubel* and Christoph Neumann

Institut für Anorganische und Analytische Chemie der Technischen Universität Braunschweig, Postfach 3329, D-38106 Braunschweig, Germany. E-mail: r.streubel@tu-bs.de

Received (in Basel, Switzerland) 15th December 1998, Accepted 8th February 1999

[3 + 2] Cycloaddition of *in situ* generated nitrilium phosphane ylide complex 4b with phenylisothiocyanate yielded *N*-piperidino-substituted Δ³-1,3,2-thiazaphospholene complex 5 regioselectively, whereas with benzyl *N*,*N*-dimethyl dithiocarbamate ester the thiaphosphirane 9 is obtained; these reactions, a 1,3-dipolar cycloaddition and a transylidation, shed first light on the reactivity of a nitrilium phosphane ylide complex towards different C,S π-systems.

Betaines **I**,[1] **II**,[1b,2] **III**, **IV**[3] and **V**[4] with a phosphorus atom in the central 1,3-dipole skeleton are of increasing interest in phosphorus and heterocyclic chemistry (Scheme 1).[5] Recently, we gained strong evidence for the transient formation of nitrilium phosphane ylide complexes (**V**) by employing dialkyl cyanamides and different trapping reagents such as dimethyl acetylene dicarboxylate[6] or nitriles.[7] Although we gained some evidence that transiently formed 2*H*-azaphosphirene complexes[7] and, under some circumstances, transition states of the 2 : 1 donor–acceptor adduct-type, with nitriles as donors and a terminal phosphanediyl complex as acceptor,[8] may be involved in transylidation processes, those reactions are not completely understood. To shed more light on this process and to exploit synthetically the transylidation methodology, we have now started to investigate the reaction behaviour of transiently formed nitrilium phosphane ylide complexes towards different C,S π-systems such as isothiocyanates and dithiocarbamates.

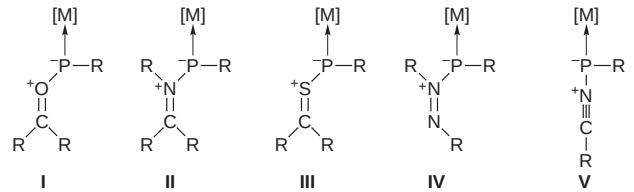

Scheme 1 1,3-Dipole complexes ([M] = metal complex fragment, R denotes ubiquitous organic substituents).

Thermal ring-opening of the 2*H*-azaphosphirene complex **1**[9] in toluene in the presence of 2 equiv. of 1-piperidinonitrile **2** and 2 equiv. of phenylisothiocyanate **3** furnished the Δ³-1,3,2-thiazaphospholene complex **5**, regioselectively; neither regioisomers nor isomers resulting from a cycloaddition reaction of intermediately formed **4b** with the C,N π-system of **3** have been observed. Employment of benzyl *N*,*N*-dimethyl dithiocarbamate ester **6** under the same reaction conditions gave the thiaphosphirane **9** exclusively; neither five-membered heterocycles, formed by reaction of **4b** with **6**, nor the corresponding thiaphosphirane complex **8** could be detected spectroscopically (Scheme 2). It is remarkable that this reaction did not change, even when benzonitrile was employed as solvent. Therefore, the formation of both heterocycles is explained by reactions of the *in situ* generated nitrilium phosphane ylide complex **4b**, which leads either to **5** *via* [3 + 2] cycloaddition or to **9** *via* an intersystem-transylidation-type reaction giving 1,3-dipole complex **7**, which undergoes ring-closure to **8** and subsequent decomplexation to give **9** as the final product. Because a transient formation of terminal phosphanediyl complex $[(OC)_5WPCH(SiMe_3)_2]$ can be achieved *via* thermally induced

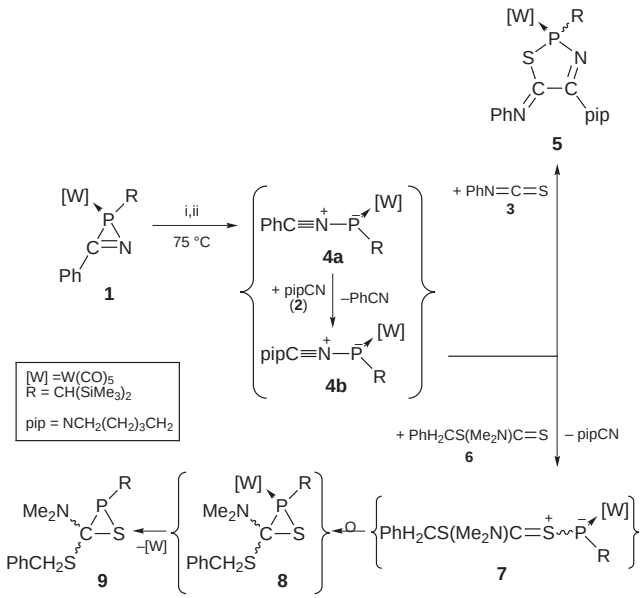

Scheme 2 *Reagents and conditions*: i, 1 mmol of **1** was treated with 6 mmol of phenylisothiocyanate and 2 mmol 1-piperidinonitrile in 2 ml of toluene at 75 °C for 1.5 h. Work-up by column chromatography at low temperature and crystallization from pentane afforded **5** as a yellow solid (28%, mp. 98 °C); ii, 1 mmol of **1** was treated with 5 mmol of benzyl *N*,*N*-dimethyldithiocarbamate ester in 3 ml of toluene at 75 °C for 2 h.Work-up by column chromatography at low temperature afforded **9** as a pale yellow oil (13%).

ring-cleavage of **4a** in toluene,[4] we repeated the reaction of **1** and **6** in toluene in the absence of **2** and obtained, once more, thiaphosphirane **9** as the only phosphorus-containing product. This result also supports the assumption of complex **7** as a highly reactive intermediate in this reaction course.

The compositions of the Δ³-1,3,2-thiazaphospholene complex **5** and the thiaphosphirane **9** are confirmed by elemental analyses and mass spectrometry;† the structural formulation is based on their characteristic NMR spectral data† in solution. The connectivity of the heterocyclic ring atoms of complex **5** was also confirmed by X-ray structure analysis, although the refinement was unsatisfactory because of heavily disordered substituents at the five-membered ring system; therefore, the structure will not be further discussed here.

The phosphorus nucleus of **5** displays a resonance at δ 105.8, which is significantly high-field shifted compared to Δ³-1,3,2-oxazaphospholene complexes (δ 190–205[6]), with a markedly decreased phosphorus–tungsten coupling constant of 287.1 Hz (*cf.* 300–306 Hz[6]). The carbon atom resonances of the heterocycle appear at δ 157.7 and 160.9 with phosphorus–carbon coupling constants of 9.2 and 12.8 Hz, respectively. Similarly to Δ³-1,3,2-oxazaphospholene complexes, these carbon resonances display small carbon–phosphorus coupling constants; this seems to be a characteristic phenomenon for such heterocyclic ring systems. The phosphorus and the ring carbon atom of the thiaphosphirane **9** display resonances at low field

[δ(^{31}P) 36.4; δ(^{13}C) 106.5; *cf.* ref. 10], which indicates a deshielding influence of the two directly bonded electronegative N- and S-atoms of the *exo*-substituents on the atoms of the thiaphosphirane ring.

We are currently investigating the reactivity of *in situ* generated nitrilium phosphane ylide complexes towards other heterocumulene systems.

This work was supported by the Fonds der Chemischen Industrie and by the Deutsche Forschungsgemeinschaft.

Notes and references

† Satisfactory elemental analyses were obtained for complexes **5** and **9**. NMR data were recorded in $CDCl_3$ solution at 50.3 (^{13}C) and 81.0 MHz (^{31}P), using TMS and 85% H_3PO_4 as standard references; *J*/Hz. *Selected spectroscopic data* for **5**: ^{13}C NMR: δ 157.7 (d, $^{(2+3)}J_{PC}$ 9.2, PSC), 160.9 (d, $^{(2+3)}J_{PC}$ 12.8, PN=C), 197.5 (d, $^{2}J_{PC}$ 7.9, *cis*-CO), 200.9 (d, $^{2}J_{PC}$ 30.0, *trans*-CO); ^{31}P NMR: δ 105.8 (d, $^{1}J_{PW}$ 287.1); *m/z* (EI) 759 (M^+). **9**: ^{13}C NMR: δ 106.5 (s, PSC); ^{31}P NMR: δ 36.4; *m/z* (EI) 401 (M^+).

1 (*a*) Y. Inubushi, N. H. Tran Huy, L. Ricard and F. Mathey, *J. Organomet. Chem.*, 1997, **533**, 83; (*b*) R. Streubel, A. Ostrowski, H. Wilkens, F. Ruthe, J. Jeske and P. G. Jones, *Angew. Chem., Int. Ed. Engl.*, 1997, **36**, 378.
2 N. H. Tran Huy, L. Ricard and F. Mathey, *Heteroatom. Chem.*, 1998, **9**, 597.
3 N. H. Tran Huy, L. Ricard and F. Mathey, *New J. Chem.*, 1998, **22**, 75.
4 R. Streubel, H. Wilkens, A. Ostrowski, C. Neumann, F. Ruthe and P. G. Jones, *Angew. Chem., Int. Ed. Engl.*, 1997, **36**, 1492.
5 K. B. Dillon, F. Mathey and J. F. Nixon, *Phosphorus: The Carboncopy*, Wiley, Chichester, 1998, p. 19.
6 H. Wilkens, J. Jeske, P. G. Jones and R. Streubel, *Chem. Commun.*, 1998, 1529.
7 H. Wilkens, F. Ruthe, P. G. Jones and R. Streubel, *Chem. Eur. J.*, 1998, **4**, 1542.
8 H. Wilkens and R. Streubel, *Phosphorus Sulfur Silicon Relat. Elem.*, 1998, **124**/**125**, 83.
9 R. Streubel, A. Ostrowski, S. Priemer, U. Rohde, J. Jeske and P. G. Jones, *Eur. J. Inorg. Chem.*, 1998, 257.
10 K. Toyota, H. Takahashi, K. Shimura and M. Yoshifuji, *Bull. Soc. Chem. Jpn.*, 1996, **69**, 141.

Communication 8/09741K

Incompletely condensed silasesquioxanes as models for zeolite defect sites: an FTIR and density functional study

Simon Krijnen,* Roelant J. Harmsen, Hendrikus C. L. Abbenhuis, Jan H. C. Van Hooff and Rutger A. Van Santen

Schuit Institute of Catalysis, Eindhoven University of Technology, PO Box 513, 5600 MB Eindhoven, The Netherlands. E-mail: simon@sg3.chem.tue.nl

Received (in Cambridge, UK) 10th December 1998, Accepted 16th February 1999

FTIR hydroxyl vibration bands in highly dealuminated zeolites could be unambiguously assigned to well defined hydroxyl clusters present at defect sites by the use of density functional calculations on incompletely condensed silasesquioxane complexes which, in addition, provided useful spectroscopic references.

Because of their defined cage like structures, it is expected that silasesquioxane complexes are not only suitable for mimicking silica surfaces[1] but can be considered as parts of zeolites as well, resembling for instance the zeolite double-four-ring (D4R). In this respect, the studies on defect sites as a part of zeolite research, in which still much is unknown about the precise zeolitic structure,[2] could profit from useful reference data obtained from silsesquioxane chemistry. Especially the assignment of zeolite defect sites by means of FTIR analysis, despite the numerous reports on these defects,[3–7] is surrounded by controversy.

In this report, we elucidated the FTIR assignment of the different possible defect sites in zeolite structures with incompletely condensed silasesquioxane complexes as references and by using computational chemistry. This powerful combination is a new approach in this field and results in a molecular level understanding of the actual hydroxyl clusters, which form the different zeolite defect sites (Fig. 1). Furthermore, a reaction of these hydroxyl clusters with different probe molecules will enable us to distinguish between defect sites located inside or outside the zeolite microporous system.

In general, the major part of the various hydroxyl bands found upon aluminium extraction out of a zeolite framework can be categorised roughly into two regions. The first is a relatively broad band between 3500 and 3560 cm^{-1} and the second, which is in most cases somewhat sharper, is present between 3680 and 3730 cm^{-1}. These bands are referred to as the 3500 and 3700 cm^{-1} bands, respectively. It is important to note that both bands can be found in various dealuminated zeolites such as ZSM-5,[3] beta,[4] faujasite[5] and mordenite,[6,7] which indicates that the different defect sites are not unique for one particular zeolite but have a more general character. The assignment of the two different hydroxyl bands which arise upon dealumination is not straightforward. A dealumination study of Wu *et al.*[6] showed a similar behaviour of both bands upon Si/Al ratio. A study by Moreno and Poncelet, however, showed a significantly different response of the 3500 and 3700 cm^{-1} bands as a function of temperature, indicating a different origin of these bands.[7]

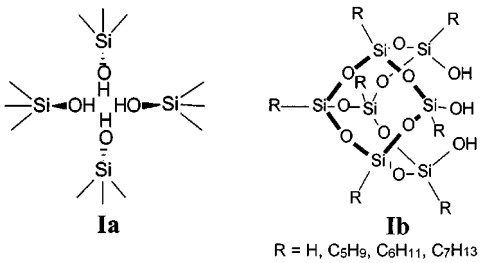

Fig. 1 A two-dimensional representation of a hydroxyl nest in a zeolite (**Ia**), in comparison with the incompletely condensed silasesquioxane complex (**Ib**).

The FTIR spectrum of dealuminated mordenite clearly shows the broad band at 3500 cm^{-1} and the band around 3700 cm^{-1}, as can be seen from Fig. 2A [dealumination with nitric acid resulted in a Si/Al ratio increase from 6.7 (spectrum a) to 39 (b), 47 (c) 79 (d) and 150 (e)]. Furthermore, the Brønsted acid band around 3610 cm^{-1} is only just apparent. This band decreases with decreasing aluminium content (increasing Si/Al) and is practically gone at Si/Al = 150, as can be seen from Fig. 2A (spectrum e). Since the 3500 cm^{-1} band is shifted about 240 cm^{-1} to lower frequency compared to the isolated silanols (present at 3745 cm^{-1}) we assume that these OH bonds are highly weakened due to their mutual hydrogen bonding. Moreover, the broad appearance of this band is indicative of a strong disturbance caused by the hydrogen bridges. The shift of the 3700 cm^{-1} band is only *ca.* 40 cm^{-1} (compared to the isolated silanol band) and is considerably less broad in comparison with the 3500 cm^{-1} band. This different appearance of the 3700 cm^{-1} band implies again that this band arises from a different, but still moderately disturbed, OH species.

Incompletely condensed silasesquioxanes contain OH groups and, as such, can be used for modelling OH clusters in zeolites. Some of these complexes, which can be considered as possible models for defect sites in zeolites, are shown in Table 1. Clearly, a zeolite-like T-atom vacancy can be recognised in complex **Ib** (see also Fig. 1), whereas complex **III** represents an isolated, non-hydrogen bridged OH group at the outer surface of the zeolite, and complex **II** can be considered as a hydrated Si–O–Si bridge. The geometry of these complexes was fully optimised.† Complex **III** as a model for isolated OH groups has the highest calculated frequency for its OH stretching vibration. This frequency of 3697 cm^{-1} is in good agreement with the measured FTIR frequency for the isolated OH stretching vibration of this complex at 3705 cm^{-1} (measured in pressed KBr pellets). A shift of *ca.* 300 cm^{-1} is obtained for the

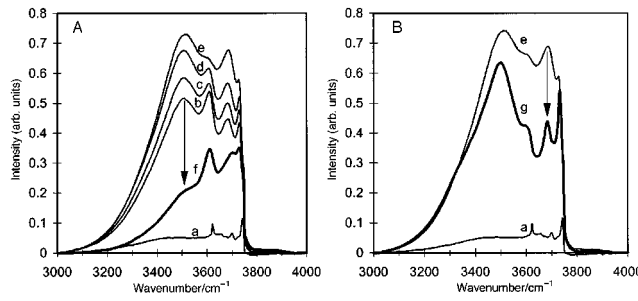

Fig. 2(A) FTIR spectra of parent Na-mordenite (a), which was dealuminated using 7 M (b), 9 M (c), 10 M (d) or 14 M (e) aqueous HNO_3 at reflux for 4 h (10 ml g^{-1}); sample 'b' subjected to a titanation using gaseous $TiCl_4$ at 400 °C (f). (B) FTIR spectra of parent Na-mordenite (a), which was dealuminated using 14 M (e) aqueous HNO_3 at reflux conditions for 4 h (10 ml g^{-1}); sample 'e' subjected to an aqueous phase titanation using a buffered 0.05 M $(NH_4)_2TiF_6$ solution (g).

calculated main bands of complex **I**, the silasesquioxane model for a zeolite T-atom vacancy, *i.e.* the actual hydroxyl nest (as plotted in Fig. 1). This shift is in good agreement with the 250 cm^{-1} shift found experimentally for the 3500 cm^{-1} band in the FTIR spectra of dealuminated zeolites (Fig. 2A). The comparable shift is a strong indication for the fact that the three membered hydroxyl nest is a reliable model for a four membered hydroxyl nest. It is important to mention the significant increase of the average OH bond distance upon hydrogen bridging, while the hydrogen bridge distance reduces to only 1.89 Å (see Table 1, complex **Ib** and **III**). Considering complex **II**, only a small shift is obtained for the OH stretching vibrations, indicative of weakly hydrogen bonded OH groups. This is confirmed by the scarcely changed OH distance and the large OH bridging distance for this complex. The small shift of the OH stretching band (22 cm^{-1} for the symmetric vibration) is in good correspondence with the measured shift of *ca.* 40 cm^{-1} for the 3700 cm^{-1} band in dealuminated zeolites. Moreover, the weaker hydrogen bridges for this type of defect site should result in a less broad signal, which is indeed obtained for the dealuminated mordenite (Fig. 2A).

Since it is concluded that the two FTIR hydroxyl bands at 3500 and 3700 cm^{-1} cannot be ascribed to the same defect site, it is interesting to know where these different defect sites are located in the zeolite microporous structure. To investigate this, the two different hydroxyl clusters are reacted with different probe molecules. Well known titanium precursors are used as probes, $TiCl_4$ and $(NH_4)_2TiF_6$, usually applied in post-synthesis procedures in the preparation of titanium zeolites.[8] The latter however, used in aqueous applications, is considered to be more bulky, especially in its hydrated form. Moreover, its siliceous analogue, $(NH_4)_2SiF_6$, is reported to be almost unable to enter the mordenite 12-ring.[9] It is assumed, therefore, that also the large $TiF_6(H_2O)_n^{2-}$ ion hardly enters the mordenite microporous structure.

Applying the different titanium precursors to the same kind of dealuminated mordenite, results in a totally different behaviour of the two above mentioned hydroxyl defect site bands. $TiCl_4$ reacts primarily with the hydroxyl nests shown by the significant decrease of the 3500 cm^{-1} band upon titanation [Fig. 2A(*f*)]. The 3700 cm^{-1} band seems hardly affected by this titanation treatment. This result is in agreement with the spectra reported earlier of dealuminated mordenite reacted with $TiCl_4$.[8c] Correspondingly, in a report concerning the titanation of dealuminated beta, the broad FTIR band present around 3500 cm^{-1} is significantly reduced upon reaction with $TiCl_4$.[10] Using aqueous $(NH_4)_2TiF_6$ as the titanium source, however, results in the opposite behaviour. The FTIR spectrum of a dealuminated mordenite titanated with this titanium source shows mainly a decrease of the 3700 cm^{-1} band [Fig. 2B(g)]. Since the 3500 cm^{-1} band was assigned to hydroxyl nests resulting from the extraction of framework aluminium, these nests are located in the zeolite micropores. The 3700 cm^{-1} band, on the other hand, was attributed to hydroxyl pairs. Since this band is affected predominantly by the titanation with the bulky $(NH_4)_2TiF_6$, we believe that these pairs are located mainly on the outer (or mesoporous) surface of the zeolite.

In conclusion, our new approach to the controversy of the assignment of the different hydroxyl bands in FTIR analysis, using silasesquioxane as models for defect sites in zeolites, is a powerful tool to clarify the different defect site structures. Based on its FTIR shift and the OH distances of the model compound **Ib**, the band at 3500 cm^{-1} must indisputably be assigned to hydroxyl nests (*i.e.* T-atom vacancies, as depicted in Fig. 1). Simultaneously, the band at 3700 cm^{-1} cannot be assigned to the same kind of hydroxyl cluster and evidence is found for the assignment of this band to a hydroxyl pair, featuring less hydrogen bonding. Regarding their location in the zeolite microporous structure, the use of titanium probe molecules shows that, in contrast to the hydroxyl nests present in the mordenite micropores, the hydroxyl pairs seem to be located primarily on the outer surface of the zeolite crystals.

Table 1 Incompletely condensed silasesquioxane complexes[a] and their calculated O–H stretching vibrations and O–H distances†

	Ib	**II**	**III**
	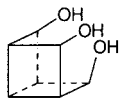	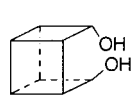	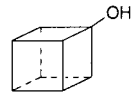
OH stretching vibrations (shift in **bold**)[b] /cm^{-1}	3403(asym)(**294**) 3396(asym)(**301**) 3331(sym) (**366**)	3698(asym)(**-1**) 3675(sym) (**22**)	3697 (**0**)
Average O—H bond distance/Å	0.996	0.980	0.978
Average O•••H bridge distance/Å	1.89	2.62	–

[a] Lines in figures represent Si–O–Si units which are terminated by hydrogen atoms at each corner. [b] The shift is defined as the difference of the calculated vibration with the 3697 cm^{-1} vibration for complex **III**.

S. K. thanks the Netherlands Institute for Catalysis Research (NIOK) for financial support. R. J. H. thanks the German Science Foundation (DFG) and the National Computing Facilities Foundation (NCF) for financial support. H. C. L. A. received a fellowship from the Royal Netherlands Academy of Arts and Sciences (KNAW).

Notes and references

† *Computational details*: calculations are based on the density functional theory (DFT)[11] as implemented in the Dgauss program (version 4.0) produced by Oxford Molecular Ltd.[12] A generalised gradient approximation to the exchange (Becke)[13] and correlation (Lee, Yang and Parr)[14] was used, and applied self-consistently. The Gaussian basis sets used are of double-zeta quality and include polarisation functions for all atoms (DZVP2).[15] A second set of basis functions, the fitting basis set, is used to expand the electron density in a set of single-particle Gaussian-type functions. All geometry optimisations were carried out fully relaxed, so as to avoid introducing unnatural strain in the molecules. The second derivatives are calculated analytically in the harmonic approximation, giving a good approximation to compute vibrational spectra.

1 F. J. Feher, D. A. Newman and J. F. Walzer, *J. Am. Chem. Soc.*, 1989, **111**, 1741.
2 R. Szostak, *Molecular Sieves, Principles of Synthesis and Identification*, Thomson Science, London, 2nd edn., 1998, p. 74.
3 G. L. Woolery, L. B. Alemany, R. M. Dessau and A. W. Chester, *Zeolites*, 1986, **6**, 14.
4 M. R. Apelian, A. S. Fung, G. J. Kennedy and T. F. Degnan, *J. Phys. Chem.*, 1996, **100**, 16 577.
5 A. Corma, V. Fornés and F. Rey, *Appl. Catal.*, 1990, **59**, 267.
6 P. Wu, T. Komatsu and T. Yashima, *J. Phys. Chem.*, 1995, **99**, 10 923.
7 S. Moreno and G. Poncelet, *Microporous Mater.*, 1997, **12**, 197.
8 (*a*) B. Kraushaar and J. H. C. Van Hooff, *Catal. Lett.*, 1988, **1**, 81; (*b*) P. Wu, T. Komatsu and T. Yashima, *J. Phys. Chem.*, 1996, **100**, 10 316; (*c*) G. P. Schindler, P. Bartl and W. F. Hölderich, *Appl. Catal. A*, 1998, **166**, 267.
9 (*a*) E. Benazzi, J. Silva, M. Ribeiro, F. Ribeiro and M. Guisnet, *Zeolites*, 1995, **16**, 393; (*b*) J. Silva, M. Ribeiro, F. Ribeiro, E. Benazzi, N. Gnep and M. Guisnet, *Zeolites*, 1995, **16**, 275.
10 S. Krijnen, P. Sánchez, B. T. F. Jakobs and J. H. C. Van Hooff, *Microporous Mesoporous Mater.*, in press.
11 P. Hohenberg and W. Kohn, *Phys. Rev. B*, 1964, **136**, 864; W. Kohn and L. J. Sham, *Phys. Rev. B*, 1965, **140**, 1133.
12 J. Andzelm and E. Wimmer, *J. Chem. Phys.*, 1992, **96**, 1280.
13 A. D. Becke, *J. Chem. Phys.*, 1986, **84**, 4524.
14 C. Lee, R. G. Parr and W. Yang, *Phys. Rev. B*, 1988, **37**, 785.
15 N. Godbout, D. R. Salahub, J. Andzelm and E. Wimmer, *Can. J. Chem.*, 1992, **70**, 560.

Communication 8/09654F

Coupling of acid–base and redox functions in mixed sulfide monolayers on gold

Marcel W. J. Beulen, Frank C. J. M. van Veggel* and David N. Reinhoudt*

Laboratory of Supramolecular Chemistry and Technology, and MESA Research Institute, University of Twente, PO Box 217, 7500 AE Enschede, The Netherlands. E-mail: d.n.reinhoudt@ct.utwente.nl

Received (in Liverpool, UK) 15th December 1998, Accepted 2nd February 1999

A mixed acid-ferrocene self-assembled sulfide monolayer on gold shows a pH-dependent electrochemical response by through-space communication between the receptor and ferrocene readout unit.

Self-assembled monolayers on gold show great promise for a variety of applications.[1] Recently, we reported the electrochemical detection by electrochemical impedance spectroscopy of the selective complexation of alkali and alkaline-earth cations (Na^+_{aq}/K^+_{aq} > 100) by self-assembled monolayers of crown ethers.[2] The advantage of electrochemically-active (*e.g.* ferrocene) monolayers is that the redox signal can be used as an internal readout.[1b] Mixed ferrocene-thiol/alkanethiol monolayers form complexes with calix[6]arene, and β- and γ-cyclodextrin from aqueous solution.[3] Rojas and Kaifer reported that the interaction of catechol or indole with a mixed monolayer of thiolated paraquat and decanethiol gives a cathodic shift of the redox potential.[4] A more general electrochemical detection of electrochemically-*inactive* compounds would be possible by decoupling the redox center and the receptor.[5] Complexation by the receptor in close proximity of the redox center should change the redox properties. Here we describe such a system in which protonation and deprotonation of a carboxylate group is detected *via* a ferrocene readout unit.

This concept was first studied in a mixed monolayer of ferrocene-thiol **1** and acid-thiol **2**[6,7] because it is known that

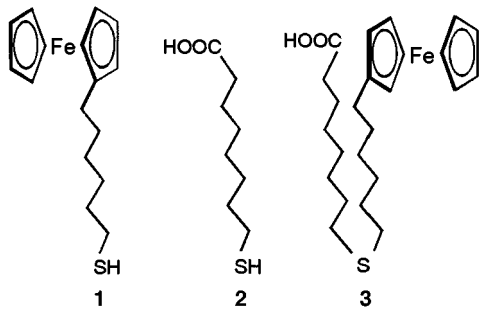

ferrocene monolayers are pH-independent.[8] Mixed monolayers were prepared from a solution containing a 1 : 3 ratio of ferrocene-thiol **1** and acid-thiol **2**.[9] The adsorbed monolayer has about half of the surface covered by ferrocene-thiol and the other half by acid-thiol (pure Fc-**1** monolayer: Q = 19.5 μC;[10] mixed Fc-**1**/acid-**2** SAM: Q = 8.6 μC). Fig. 1 shows the redox signal for the system at pH 1 and 11.[11] At high pH deprotonation of the acid group introduces a negative charge in the monolayer which stabilizes the ferrocenium ion and this results in a cathodic shift of the redox signal. The pH can be switched backward and forward leading to a small (around 10%) loss in ferrocene signal over a large number of measurements at different pHs, indicating a fairly stable system. Reductive desorption of the monolayer occurs at more cathodic potentials.[12] The cyclic voltammogram at high pH shows two very broad peaks: part of the ferrocene centers is responsive to the pH, the other part is not. Apparently, not all ferrocenes experience the same influence of deprotonation of the acid function. This is an indication of an inhomogeneous monolayer.[13]

This problem of inhomogeneity was circumvented by covalently linking the two components, which is very simply achieved in a mixed *sulfide* like **3**.[14] With this molecule, domain formation is impossible and the covalent attachment forces a 1 : 1 ratio of the binding site and the redox center. This is one of the very few examples of a monolayer adsorbate with multiple functional units.[15] We prepared monolayers of sulfide **3** that were characterized by wettability studies, X-ray photoelectron spectroscopy (XPS), time-of-flight secondary ion mass spectrometry (TOF-SIMS) and electrochemistry. Contact angles with water indicated a surface with moderate polarity and the hysteresis between the advancing and receding angle shows a disordered monolayer ($\theta_{adv/rec}$ [H_2O]: 64–20). XPS measurements of the monolayer show all the elements of the adsorbate (Fe, C, O, and S) in fair correspondence with the expected relative ratios (C : S ratio/calc. : found = 32 : 1/31 : 1). In the positive scan of the TOF-SIMS measurements the peaks for M^+ (444) and $[M + Au + H]^+$ (642) give further evidence that sulfides adsorb without C–S bond breaking on gold.[16] Electrochemical characterization showed all the characteristics of electrochemically-active monolayers, *e.g.* a linear dependence of the redox current on the scan rate. Calculation of the ferrocene charge (4.5 μC) indicates a loosely-packed monolayer, by comparison with the charge related to the pure ferrocene-thiol **1**, and mixed ferrocene-thiol **1**/acid-thiol **2** monolayers described above. The relatively high hysteresis found in the wettability studies and the moderate ferrocene coverage obtained from cyclic voltammetry confirm our previous finding[11a] that sulfides that are connected by one attachment point to gold, forming loosely-packed monolayers.[17]

The electrochemical response of the sulfide **3** monolayer is strongly influenced by the pH of the electrolyte solution (Fig. 2). The redox signal shifts cathodically but hardly broadens. This latter phenomenon is consistent with a homogeneous monolayer. These cyclic voltammograms reveal the communication between the components of the mixed sulfide monolayer, *i.e.* the redox unit senses the protonation and

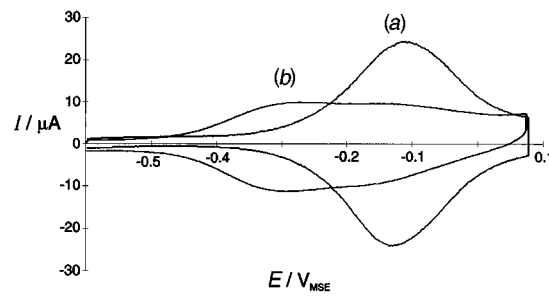

Fig. 1 Electrochemical response of a mixed ferrocene-thiol **1**/acid-thiol **2** monolayer. (*a*) pH 1, 0.1 M $HClO_4$; (*b*) pH 11, 0.1 M $NaClO_4$ + 1 mM NaOH [0 V_{MSE} = +0.61 V_{NHE}].

deprotonation of the carboxylate group. Titration with mixtures of different pH ($HClO_4$, $NaClO_4$, and NaOH) shows a strong dependence of the redox potential on the pH (Fig. 3).[18] With increasing pH values the carboxylates stabilize the ferrocenium state of the redox couple, and as a consequence the redox potential shifts cathodically. The ferrocene response curve shifts over a large pH window. It is known that the pK_a value for organic acids which in solution is about 3-4, increases for well-packed monolayers to 6–7.[19] The loose packing of monolayers of sulfides using one attachment point can result in a more exposed acid function, which will have a lower pK_a, more comparable to the solution value of 3–4. Furthermore, it is important to note that Fig. 3 is not the titration curve of the acid function in the monolayer, but the response of a complex multicomponent system to changes in the pH of the electrolyte solution. The electrochemical oxidation of ferrocene to ferrocenium might change the *apparent* pK_a of the acid function, rendering the communication mutual. A similar effect was recently described by Corn *et al.*, who showed by SPR measurements that the adsorption of the positively charged avidin on an acid-terminated monolayer shifted the apparent pK_a to lower values.[20]

A self-assembled monolayer consisting of receptor and readout units can be used to detect electrochemically-inactive compounds electrochemically. Here we have shown the pH-dependent response of mixed acid–ferrocene monolayers. At the moment we are investigating the effect on the redox signal of the ferrocene unit of the binding to the carboxylate groups of different cations. Preliminary results indicate that the binding properties of $Et_4N^+_{aq}$, and Na^+_{aq} or K^+_{aq} to the carboxylate groups (low and high binding, respectively) are reflected in the cyclic voltammograms.

Akzo Nobel Central Research is gratefully acknowledged for the XPS and SIMS measurements and CW-NWO and STW (project number 349-3332) for financial support.

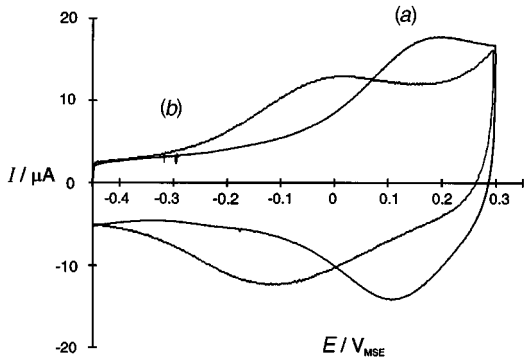

Fig. 2 Electrochemical response of a ferrocene–acid–sulfide **3** monolayer: (*a*) pH 1, 0.1 M $HClO_4$, (*b*) pH 6.5, 0.1 M $NaClO_4$ [0 V_{MSE} = +0.61 V_{NHE}].

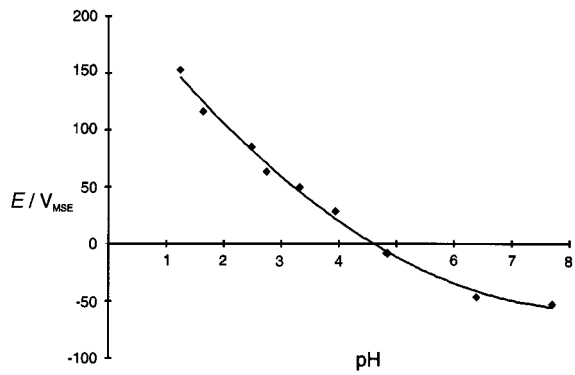

Fig. 3 Dependence of the formal potential of the ferrocene unit in a monolayer of sulfide **3** on the pH of the electrolyte solution [0 V_{MSE} = +0.61 V_{NHE}].

Notes and references

1 (*a*) A. Ulman, *An Introduction to Ultrathin Organic Films*, Academic Press, San Diego, CA, 1991; (*b*) H. O. Finklea, *Electroanalytical Chemistry*, ed. A. J. Bard and I. Rubinstein, Marcel Dekker, New York, 1996, vol. 19, pp. 109–335.

2 S. Flink, B. A. Boukamp, A. van den Berg, F. C. J. M. van Veggel and D. N. Reinhoudt, *J. Am. Chem. Soc.*, 1998, **120**, 4652.

3 L. Zhang, A. Godinez, T. Lu, G. W. Gokel and A. E. Kaifer, *Angew. Chem., Int. Ed. Engl.*, 1995, **34**, 235; H. Ju and D. Leech, *Langmuir*, 1998, **14**, 300; R. C. Sabapathy, S. Bhattacharyya, W. E. Cleland Jr. and C. L. Hussey, *Langmuir*, 1998, **14**, 3797.

4 M. T. Rojas and A. E. Kaifer, *J. Am. Chem. Soc.*, 1995, **117**, 5883.

5 An example of an *electronically*-coupled crown-annulated tetrathiafulvalene was recently shown in the literature: A. J. Moore, L. M. Goldenberg, M. R. Bryce, M. C. Petty, A. P. Monkman, C. Marenco, J. Yarwood, M. J. Joyce and S. N. Port, *Adv. Mater.*, 1998, **10**, 395.

6 Syntheses of the adsorbates ferrocene **1** and acid **2** have been described elsewhere. (*a*) Ferrocene **1**: S. E. Creager and G. K. Rowe, *J. Electroanal. Chem.*, 1994, **370**, 203; (*b*) Acid **2**: E. B. Troughton, C. D. Bain, G. M. Whitesides, R. G. Nuzzo, D. L. Allara and M. D. Porter, *Langmuir*, 1988, **4**, 365.

7 Monolayer preparation, experimental procedures, and instrumentation were previously described: E. U. Thoden van Velzen, J. F. J. Engbersen, P. J. de Lange, J. W. Mahy and D. N. Reinhoudt, *J. Am. Chem. Soc.*, 1995, **117**, 6853. Details of the electrochemical measurements: area gold working electrode: 0.44 cm^2, reference electrode: mercury sulfate electrode: 0 V_{MSE} = +0.61 V_{NHE}. The adsorption solution had a concentration of 1 mM in $CHCl_3$–EtOH (2 : 1, v/v).

8 J. J. Hickman, D. Ofer, P. E. Laibinis, G. M. Whitesides and M. S. Whrighton, *Science*, 1991, **252**, 688; J. Redepenning and J. M. Flood, *Langmuir*, 1996, **12**, 508.

9 Mixed monolayers of ferrocene-thiol and another component, such as simple alkanethiols, have previously been prepared for other purposes [see ref. 1(*b*)].

10 The experimentally found value of 19.5 μC equals 4.6×10^{-10} (mol Fc) cm^{-2} and corresponds well with values reported in literature (around 5×10^{-10} (mol Fc) cm^{-2}), see ref. 1(*b*), and: C. E. D. Chidsey, C. R. Bertozzi, T. M. Putvinski and A. M. Mujsce, *J. Am. Chem. Soc.*, 1990, **112**, 4301.

11 (*a*) Monolayers in general are electrochemically stable in a potential window of −0.8 V_{MSE}: to +0.4 V_{MSE}: M. W. J. Beulen, M. I. Kastenberg, F. C. J. M. van Veggel and D. N. Reinhoudt, *Langmuir*, 1998**,** **14**, 7463; (*b*) the acid functionality is cathodically stable to −0.8 V_{MSE}: J. A. M. Sondag-Huethorst, *Electrochemical and structural characterization of self-assembled thiol monolayers on gold*, PhD Thesis, University of Wageningen, the Netherlands, 1994.

12 C. A. Widrig, C. Chung and M. D. Porter, *J. Electroanal. Chem*, 1991, **310**, 335.

13 Mixed monolayers of two different thiols can exhibit distinctive domains, see for example: D. Hobara, M. Ota, S. Imabayashi, K. Niki and T. Kakiuchi, *J. Electroanal. Chem.*, 1998, **444**, 113.

14 Ferrocene–acid–sulfide **3** was synthesized by alkylation of 8-mercapto-octanoic acid [ref. 6(*b*)] with 6-ferrocenylhexyl bromide [ref. 6(*a*)]. *Selected data* for **3**: $\delta_H(CDCl_3)$ 4.08 (s, 7H, Fc), 4.04 (s, 2H, Fc), 2.50 (t, 4H, *J* 7.2, CH_2S), 2.40–2.25 (m, 4H, $FcCH_2$+CH_2COOH), 1.70–1.25 (m, 18H, CH_2); *m/z* (FAB-MS) 444.4 (M^+; calc. for $C_{24}H_{36}O_2SFe$: 444.2). Sulfide monolayers were prepared at an elevated temperature of 60 °C, because this increases the quality of the monolayers (see ref. 7).

15 A linear porphyrin–ferrocene–alkanethiol was recently shown to be both light-sensitive and electrochemically-active: K. Uosaki, T. Kondo, X.-Q. Zhang and M. Yanagida, *J. Am. Chem. Soc.*, 1997, **119**, 8367.

16 M. W. J. Beulen, B.-H. Huisman, P. A. van der Heijden, F. C. J. M. van Veggel, M. G. Simons, E. M. E. F. Biemond, P. J. de Lange and D. N. Reinhoudt, *Langmuir*, 1996, **12**, 6170; M. W. J. Beulen, J. Bügler, B. Lammerink, F. A. J. Geurts, E. M. E. F. Biemond, K. G. C. van Leerdam, F. C. J. M. van Veggel, J. F. J. Engbersen and D. N. Reinhoudt, *Langmuir*, 1998, **14**, 6424.

17 The loose packing of the sulfide **3** monolayer might be beneficial for our purpose because of the accessibility of the binding sites, and because the complexation and decomplexation of guests will be rapid.

18 The total electrolyte concentration was kept constant at 0.1 M.

19 C. D. Bain and G. M. Whitesides, *Langmuir*, 1989, **5**, 1370; J. Wang, L. M. Frostman and M. D. Ward, *J. Phys. Chem.*, 1992, **96**, 5224; S. E. Creager and J. Clarke, *Langmuir*, 1994, **10**, 3675; T. Randell Lee, R. I. Carey, H. A. Biebuyck and G. M. Whitesides, *Langmuir*, 1994, **10**, 741.

20 C. E. Jordan and R. M. Corn, *Anal. Chem.*, 1997, **69**, 1449.

Communication 8/09790I

Reactions of homoallylstannanes with carbon electrophiles: stereoselective cyclopropylmethylation based on the γ-effect of tin

Masanobu Sugawara and Jun-ichi Yoshida*

Department of Synthetic Chemistry and Biological Chemistry, Graduate School of Engineering, Kyoto University, Kyoto 606-8501, Japan. E-mail: yoshida@sbchem.kyoto-u.ac.jp

Received (in Cambridge, UK) 7th January 1999, Accepted 29th January 1999

Homoallylstannanes reacted with carbon electrophiles such as acetals, acid chlorides and aldehydes in the presence of Lewis acids to give the cyclopropylmethylated products with high stereoselectivities.

Enormous advances have been made in the study of the β-effect of silicon, and a number of reactions have been developed based on this effect and utilized for a variety of synthetic applications.[1] The γ-effect of silicon, however, seems to be less effective and has not been embraced as a viable principle in organic synthesis.[2] On the other hand, studies on the γ-effect of tin revealed the effectiveness of this effect[3] and have uncovered a rich variety of synthetic applications in recent years.[4] Previously, we have reported that the γ-effect of tin is stronger than the β-effect of silicon in intramolecular competition and that cationic cyclopropanation of 'tin carbenoids' with alkenes can be achieved based on the γ-effect of tin.[5] We have also been interested in the intermolecular competition between the γ-effect of tin and the β-effect of silicon. During the course of this study we found a cyclopropylmethylation reaction using homoallylstanannes that would be useful in organic synthesis.[6] We report here the preliminary results of these studies.

The intermolecular competition between the γ-effect of tin and the β-effect of silicon was examined using an electrophilic reaction of a homoallylstannane and an allylsilane. Thus, a 1 : 1 mixture of homoallyltributylstannane **2a** and allyltrimethylsilane **3** in CH_2Cl_2 was treated with 1 equiv. of benzaldehyde dimethyl acetal **1a** in the presence of TMSOTf (Scheme 1). Most of **2a** was recovered unchanged and only allylated product **5** was obtained in 87% yield. The cyclopropylmethylated product **4a** was not detected.

This result indicates that **3** is much more reactive than **2a** toward the oxonium ion ($PhCH{=}OMe^+$) generated from **1a** and suggests that the β-effect of silicon is stronger than the γ-effect of tin in intermolecular competition. In other words, the β-silyl group activates the carbon–carbon double bond more effectively toward the electrophilic reaction than the γ-stannyl group. This difference can be explained in terms of molecular orbital considerations. In the case of allylsilane **3**, the energy level of the π orbital of the carbon–carbon double bond is increased by interaction with the neighboring carbon–silicon σ orbital (σ–π interaction).[7] Therefore, the reactivity toward electrophiles is increased. In the case of homoallylstannane **2a**, however, the energy level of the π orbital should to be similar to that for normal carbon–carbon double bonds, because the interaction between the π orbital of the carbon-carbon double bond and the carbon–tin σ orbital seems to be very weak, due to the flexibility of the conformation.[8]

The next question which naturally emerged in our mind is whether the reactivity of the carbon–carbon double bond of the homoallylstannane is the same as those of simple terminal alkenes. Thus, we examined the intermolecular competition between the homoallylstannane and normal terminal alkenes. A 1 : 1 mixture of homoallylstannane **2a** and dodec-1-ene **6** was allowed to react with **1a** in the presence of TMSOTf. Although it required a slightly higher temperature, the reaction of **1a** and **2a** took place to give the cyclopropylmethylated product **4a** in 60% yield. Most of **6** was recovered unchanged (Scheme 2).

This result indicates that the homoallylstannane is definitely more reactive toward electrophiles than terminal alkenes. Therefore, there seems to exist some interaction between the carbon–tin σ orbital and the π orbital of the carbon–carbon double (**B** in Fig. 1) even if it is not particularly strong. This led us to a new aspect of the γ-effect of tin.

The following mechanism seems to be plausible. The oxonium ion is generated by the reaction of acetal **1a** with TMSOTf and then adds to the carbon–carbon double bond of homoallylstannane **2a** to give the γ-carbocation to tin. The facile γ-elimination of tin to form a cyclopropane ring takes place to give the final product **4a**.

The successful reaction of homoallylstannane **2a** and acetal **1a** prompted us to develop new reactions of homoallylstanannes with carbon electrophiles. As shown in Table 1, acetals, acid

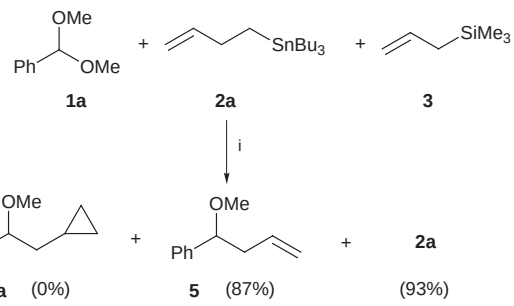

Scheme 1 *Reagents and conditions*: i, TMSOTf (1.05 equiv.), CH_2Cl_2, −78 °C, 3 h.

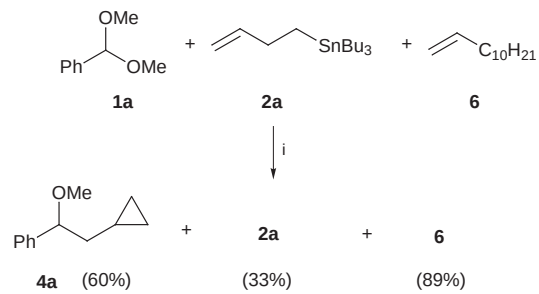

Scheme 2 *Reagents and conditions*: i, TMSOTf (1.05 equiv.), CH_2Cl_2, −50 °C, 3 h.

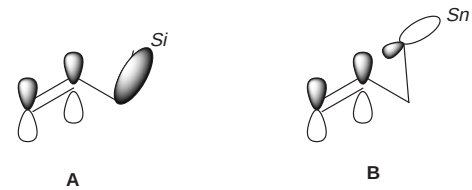

Fig. 1 σ–π Interactions in the allylsilane (**A**) and the homoallylstannane (**B**).

Table 1 Reactions of homoallylstannanes with carbon electrophiles in the presence of Lewis acids[a]

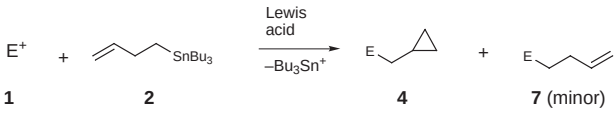

1 **2** **4** **7** (minor)

Electrophile	Homoallylstannane	4	Yield (%) 4 (*erythro* : *threo*)[c]	7
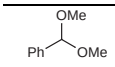 **1a**[b]	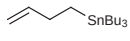 **2a** (1.3 equiv.)	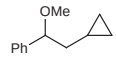 **4a**	87	<1[d]
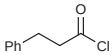 **1b**	**2a** (1.0 equiv.)	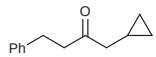 **4b**	87	12
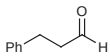 **1c**	**2a** (1.2 equiv.)	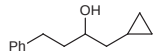 **4c**	76	7
1c	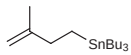 **2b** (1.3 equiv.)	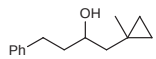 **4d**	86	10
1c	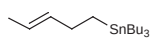 **2c** (*E*:*Z* = 88:12) (1.1 equiv.)	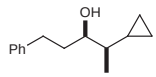 **4e**	87 (97:3)	7
 **1d**	**2c** (1.1 equiv)	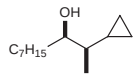 **4f**	83 (>99:1)	3[d]
 **1e**	**2c** (1.1 equiv.)	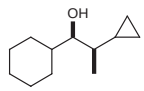 **4g**	87 (97:3)	5[d]
1e	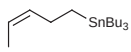 **2d** (*E*:*Z* = 1:>99) (1.2 equiv.)	**4g**	78 (68:32)	<1[d]

[a] Reaction conditions; 0.50 mmol of **1**, 1.0–1.3 equiv. of **2** and 1.1 equiv. of $TiCl_4$ in CH_2Cl_2 (1.8 ml) at −78 °C for 3 h. [b] TMSOTf (1.05 equiv.) was used instead of $TiCl_4$, at −40 °C, 3 h. [c] Determined by GLC. [d] The homoallylated product **7** was not fully characterized.

halides and aldehydes were found to be effective as carbon electrophiles. In the case of acid halides and aldehydes, $TiCl_4$ was more effective than TMSOTf. The corresponding cyclopropylmethylated products **4** were obtained in good yields together with small amounts of homoallylated by-products **7**.[2]

The diastereoselectivity of the present reaction is remarkable. For example, the *erythro* product was obtained selectively (97 : 3) starting from **1e** and (*E*)-pent-3-enyltributylstannane (*E* : *Z* = 88 : 12).[9] Presumably, the addition to the carbonyl group took place in an antiperiplanar fashion.[10] The reaction of **1e** and (*Z*)-pent-3-enyltributylstannane (*E* : *Z* = 1 : 99), however, resulted in a decrease of the selectivity (68 : 32). The low selectivity of the *cis* isomer might be explained in terms of the competition between the antiperiplanar transition state and the synclinal transition state.[11]

In summary, intermolecular competition revealed that a β-silyl group activates carbon–carbon double bonds toward electrophilic reactions more effectively than a γ-stannyl group. It was also found that the γ-stannyl group activates the carbon–carbon double bond slightly more effectively than alkyl groups. We also found that the reactions of homoallylstannanes with carbon electrophiles such as acetals, acid halides and aldehydes took place smoothly in the presence of Lewis acids. These reactions serve as a stereoselective method for cyclopropylmethylation of carbonyl compounds. Further mechanistic studies on the evaluation of the γ-effect of tin and its synthetic applications are under investigation.

Notes and references

1 For example, W. P. Weber, *Silicon Reagents for Organic Synthesis*, Springer-Verlag, Berlin, Heidelberg, 1983, p. 173; J. B. Lambert, *Tetrahedron*, 1990, **46**, 2677 and references cited therein.

2 H. Sakurai, T. Imai and A. Hosomi, *Tetrahedron Lett.*, 1977, 4045; Y. Hatanaka and I. Kuwajima, *Tetrahedron Lett.*, 1986, **27**, 719.

3 I. Fleming and C. Urch, *J. Organomet. Chem.*, 1985, **285**, 173; J. B. Lambert, L. A. Salvador and J.-H. So, *Organometallics*, 1993, **12**, 697. See also ref. 4 and 5.

4 M. Pereyre, J.-B. Quintard and A. Rahm, *Tin in Organic Synthesis*, Butterworth, London, 1987, p. 235; A. G. Davies, *Organotin Chemistry*, VCH, Weinheim, 1997 and references cited therein. See also ref. 5.

5 M. Sugawara and J. Yoshida, *J. Am. Chem. Soc.*, 1997, **119**, 11 986; M. Sugawara and J. Yoshida, *Synlett.*, 1998, 1057.

6 Cyclopropylmethylations with hetero-electrophiles by homoallylstannanes have been reported: D. J. Peterson and M. D. Robbins, *Tetrahedron Lett.*, 1972, 2135; D. J. Paterson, M. D. Robbins and J. R. Hansen, *J. Organomet. Chem.*, 1974, **73**, 237; K. C. Nicolaou, D. A. Claremon, W. E. Barnette and S. P. Seitz, *J. Am. Chem. Soc.*, 1979, **101**, 3704; Y. Ueno, M. Ohta and M. Okawara, *Tetrahedron Lett.*, 1982, **23**, 2577; J. W. Herndon and J. J. Harp, *Tetrahedron Lett.*, 1992, **33**, 6243.

7 J. C. Giordan, *J. Am. Chem. Soc.*, 1983, **105**, 6544.

8 H. C. Clark and R. C. Poller, *Can. J. Chem.*, 1970, **48**, 2670; R. S. Brown, D. F. Eaton, A. Hosomi, T. G. Traylor and J. M. Wright, *J. Organomet. Chem.*, 1974, **66**, 249.

9 The *erythro* stereochemistry was determined by comparison with an authentic sample, which was prepared by the cyclopropanation of the corresponding homoallylalcohol.

10 M. Santelli and J.-M. Pons, *Lewis Acids and Selectivity in Organic Synthesis*, CRC Press, Boca Raton, 1996, p. 91.

11 T. Hayashi, K. Kabeta, I. Hamachi and M. Kumada, *Tetrahedron Lett.*, 1983, **24**, 2865.

Communication 9/00228F

ChemComm

Efficient synthesis of non-natural ganglioside (pseudo-GM3) and fluorescent labelled lysoGM3 on the basis of polymer-assisted enzymatic strategy

Kuriko Yamada, Susumu Matsumoto and Shin-Ichiro Nishimura*

Laboratory for Bio-Macromolecular Chemistry, Division of Biological Sciences, Graduate School of Science, Hokkaido University, Sapporo 060-0810, Japan. E-mail: nishimura@polymer.sci.hokudai.ac.jp

Received (in Cambridge, UK) 14th December 1998, Accepted 12th January 1999

The versatility of polymer-assisted enzymatic synthesis of non-natural and biologically significant glycolipid derivatives was demonstrated by constructing pseudo-ganglioside GM3 1 having the trisaccharide sequence Neu5Acα-(2→6)Galβ(1→4)Glc and a fluorescent labelled lysoGM3 2.

Cell surface glycoconjugates such as glycoproteins and glycolipids are an important class of biomolecules providing a great deal of significant information on cell–cell interactions.[1] The advent of efficient and practical methods for glycoconjugate synthesis is urgently required. Enzymatic synthesis of carbohydrates with glycosyltransferases[2] and glycosidases[3] has been recognised as a promising practical alternative to chemical synthesis. Recently, we found an efficient synthetic strategy for glycoconjugates based on novel water-soluble polymer supports with specific linkers.[4–7] It was suggested that polymer **8** bearing ceramide-mimetic linkers might yield a practical procedure for the construction of natural sphingoglycolipid GM3.[6] In addition to the synthesis of naturally occurring gangliosides, our attention is now directed toward the applicability of this strategy to the synthesis of non-natural and biologically significant glycolipid derivatives. Here we report efficient syntheses of pseudo-ganglioside GM3 **1** having the

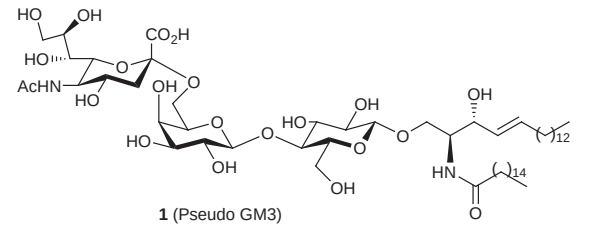

1 (Pseudo GM3)

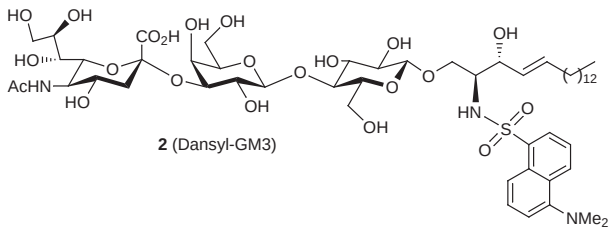

2 (Dansyl-GM3)

trisaccharide sequence Neu5Acα(2→6)Galβ(1→4)Glc and a fluorescent-labeled lysoGM3 **2** *via* enzymatic manipulations on the polymer support **8**.

Scheme 1 indicates an improved synthetic route to key glycomonomer **7**.[6] The nucleophilicity of the hydroxy group of glycosyl acceptor **4**,† *N′*-octyl-*N*²-diphenylmethylene-L-serinoamide, to the anomeric carbon of a glycosyl donor **5** was drastically enhanced by employing a Schiff base-type protective group[8] at the amino group, and the yield of the glycoside **6**†‡ was improved from 48 to 82%. Removal of the diphenylmethylene group by hydrogenation, subsequent coupling with 6-(*N*-acrylamido)hexanoic acid and *O*-deacetylation proceeded smoothly and afforded compound **7** in 78% yield from **6**. Water-soluble polymer **8** prepared from **7** by the usual radical copolymerisation with acrylamide was employed for further sugar elongation and subsequent transglycosylation reactions, as shown in Scheme 2.

In the previous report,[6] it was demonstrated that rat recombinant α(2→3)-(N)-sialyltransferase (Calbiochem®), known as an enzyme catalysing sialylation reactions of glycoprotein biosynthesis in nature, successfully transferred sialic acid residues to the glycolipid-mimetic polymer **8**. In order to evaluate the versatility of this procedure in other glycosyltransferases, we decided to synthesise non-natural ganglioside isomer **1** (pseudo GM3) utilising rat liver α(2→6)-(N)-sialyltransferase (Boehringer Mannheim). As anticipated, this enzyme also recognised polymer **8** as a 'glycoprotein-mimetic polymer' rather than as 'glycolipid-type clusters'. Novel glycopolymer **9** carrying trisaccharide Neu5Acα-(2→6)Galβ(1→4)Glc was obtained in quantitative yield and this non-natural trisaccharide moiety was subsequently transferred from polymer **9** to C16 ceramide using ceramide glycanase (CGase, Boehringer Mannheim) to afford the target glycolipid **1**† in 60% yield (11 mg) from **9** (Scheme 3). This result shows clearly that CGase exhibits broad substrate

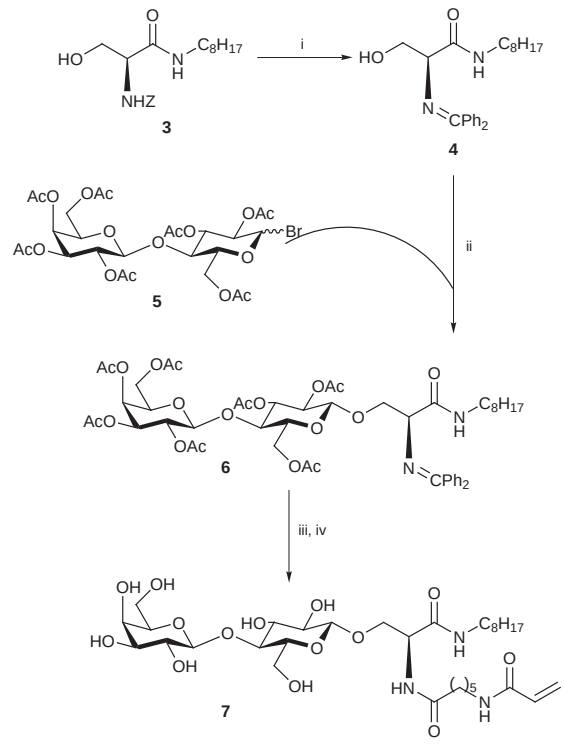

Scheme 1 *Reagents and conditions* : i, Pd-C, H_2 gas, MeOH, 25 °C, 6 h, then $Ph_2C{=}NH$ (1.0 equiv.), CSA (0.1 equiv.), CH_2Cl_2, 25 °C, 24 h, 82.3% from **3**; ii, lactosyl bromide **5** (1.2 equiv.), 4 Å molecular sieves, AgOTf (1.2 equiv.), CH_2Cl_2, 0 °C, 15 h, 82.0% from **4**; iii, Pd-C, H_2 gas, MeOH, 25 °C, 2 h, then 6-(*N*-acrylamido)hexanoic acid (1.1 equiv.), 2-ethoxy-1-ethoxycarbonyl-1,2-dihydroquinoline (1.1 equiv.), benzene, EtOH, 25 °C, 24 h, 78.0% ; iv, NaOMe (0.4 equiv.), THF, MeOH, 25 °C, 1 h, 100 % from **6**.

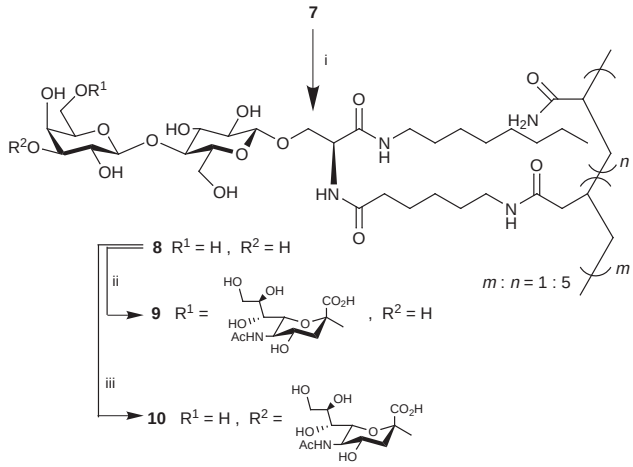

Scheme 2 *Reagents and conditions*: i, acrylamide monomer (5.0 equiv.), TMEDA (2.4 equiv.), ammonium persulfate (APS) (0.96 equiv.), DMSO, H_2O, 50 °C, 24 h, 92.0% from **7**; ii, CMP-Neu5Ac (1.2 equiv. for lactose), bovine serum albumin (BSA), calf intestinal alkaline phosphatase (CIAP) (20 units), 50 mM sodium cacodylate buffer (pH 7.40), $MnCl_2$, NaN_3, α-2,6 sialyltransferase (0.1 units, 2.7 munits per 1.0 μmol acceptor), 37 °C, 48 h, 100%; iii, CMP-Neu5Ac (1.2 equiv. for lactose), BSA, CIAP (20 units), 50 mM sodium cacodylate buffer (pH 7.40), $MnCl_2$, Triton CF-54, α-2,3 sialyltransferase (0.3 units, 8.0 munits per 1.0 μmol acceptor), 37 °C, 72 h, 100%.

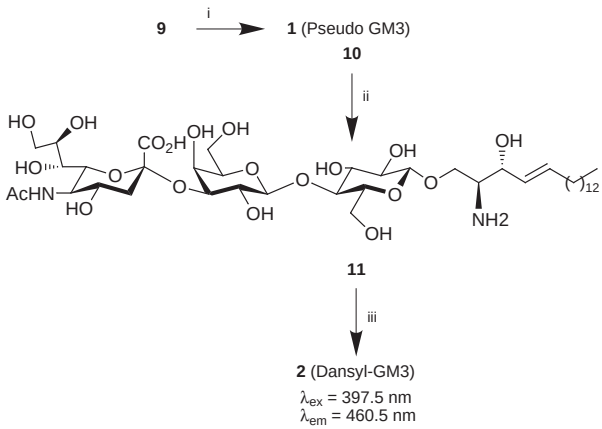

Scheme 3 *Reagents and conditions* : i, C16 ceramide (5.0 equiv.), 50 mM sodium citrate buffer (pH 6.0), Triton CF-54, ceramide glycanase from leech (0.005 units), 37 °C, 17 h, 60% from **9**; ii, D-sphingosine (5.0 equiv.), 50 mM sodium citrate buffer (pH 6.0), Triton CF-54, ceramide glycanase from leech (0.005 units), 37 °C, 17 h; iii, dansyl chloride (5.0 equiv.), Et_3N (5.0 equiv.), $CHCl_3$, 25 °C, 2 h, 50% from **10**.

specificity of transglycosylation with regard to the carbohydrate structure of glycolipids.

Next, our interest focused on the substrate specificity of the transglycosylation reaction carried out by CGase against glycosyl acceptor substrates,[9] as it will significantly influence the versatility of the present technology in the combinatorial synthesis of 'libraries of glycolipids and their mimetics'. We selected D-sphingosine (*trans*-D-erythro-2-amino-4-octadecene-1,3-diol) as a potential candidate for the synthesis of functional sphingoglycolipid derivatives, since the amino group of D-sphingosine is convenient for further modification. We were pleased to find that CGase transferred the GM3 oligosaccharide [Neu5Acα(2→3)Galβ(1→4)Glc], to the primary hydroxy group of D-sphingosine from the polymer **10** and intermediate **11** was directly dansylated to afford a fluorescent-labelled lysoGM3 **2**† in 50% yield (12 mg) from compound **10**.

In conclusion, we have demonstrated the versatility of water-soluble polymer supports in the enzymatic synthesis of non-natural and biologically important glycolipid derivatives. It should be noted that this synthetic strategy should greatly accelerate efficient combinatorial synthesis of libraries of glycolipids varying both in the carbohydrate and in the lipid portions.

This work was partly supported by a Grant-in-Aid for Scientific Research from the Ministry of Education, Science and Culture, Japan (09240101) and by a grant from the Original Industrial Technology R&D Promotion Program of the New Energy and Industrial Technology Development Organisation (NEDO).

Notes and references

† *Selected data* for **4**: δ_H(400 MHz, $CDCl_3$) 7.80–7.09 (m, 10 H, 2 × Ph), 6.92 (br s, 1 H, NH), 4.31–3.81 (m, 2 H, β-H), 4.01 (br s, 1 H, α-H), 1.32–1.24 (m, 12 H, 6 × CH_2) and 0.89 (t, 3 H, *J* 6.7, CH_3). For **6**: δ_H(400 MHz, $CDCl_3$) 7.60–7.03 (m, 10 H, 2 × Ph), 5.25 (d, 1 H, *J* 3.4, H-4′), 5.05 (dd, 1 H, *J* 8.4 and 9.0, H-3), 4.84 (dd, 1 H, *J* 3.5 and 9.2, H-2′), 4.81 (dd, 1 H, *J* 3.4 and 9.0, H-3′), 4.79 (dd, 1 H, *J* 7.6 and 9.0, H-2), 4.38 (d, 1 H, *J* 7.6, H-1), 4.32 (d, 1 H, *J* 7.8, H-1′), 4.29 (dd, 1 H, *J* 1.7 and 12.1, H-6a), 4.18 (br d, 1 H, *J* 6.5, α-H), 3.43 (dt, 1 H, *J* 1.7 and 5.2, H-5), 2.27 (s, 2 H, $NHCH_2$), 2.06–1.85 (each s, 21 H, OAc), 1.46–1.18 (m, 12 H, 6 × CH_2) and 0.79 (t, 3 H, *J* 6.7, CH_3). For **1**: δ_H(400 MHz, $CDCl_3$) 5.71 (dt, 1 H, *J* 6.7 and 14.7, Cer-5), 5.46 (dd, 1 H, *J* 7.6 and 14.7, Cer-4), 4.24 (d, 1 H, *J* 7.0, H-1′), 4.23 (d, 1 H, *J* 7.8, H-1), 2.78 (dd, 1 H, *J* 4.2 and 12.0, H-3″$_{eq}$), 2.01 (s, 3 H, NAc) and 0.81 (t, 6 H, *J* 6.7, 2 × CH_3). For **2**: δ_H(400 MHz, $CDCl_3$) 8.58–7.04 (m, 6 H, dansyl), 4.35 (d, 1 H, *J* 7.0, H-1′), 4.20 (d, 1 H, *J* 7.4, H-1), 2.73 (br d, 1 H, *J* 4.3, H-3″$_{eq}$), 1.90 (s, 3 H, NAc) and 0.88 (t, 3 H, CH_3); λ_{ex}/nm 397.5; λ_{em}/nm 460.5.

‡ In the previous report (ref. 6), the coupling reaction of **3** with **5** gave a glycoside intermediate in 48% yield.

1 Y. C. Lee and R. T. Lee, *Acc. Chem. Res*., 1995, **28**, 321.
2 O. Seiz and C.-H. Wong, *J. Am. Chem. Soc*., 1997, **119**, 8766.
3 C. H. Tran, P. Critchley, D. H. G. Crout, C. J. Britten, S. J. Witham and M. I. Bird, *J. Chem. Soc., Perkin Trans. 1*, 1998, 2295.
4 S.-I. Nishimura, K. Matsuoka and Y. C. Lee, *Tetrahedron Lett*., 1994, **35**, 5657.
5 K. Yamada and S.-I. Nishimura, *Tetrahedron Lett*., 1995, **52**, 9493.
6 S.-I. Nishimura and K. Yamada, *J. Am. Chem. Soc*., 1997, **119**, 10555.
7 K. Yamada, E. Fujita and S.-I. Nishimura, *Carbohydr. Res*., 1997, **305**, 443.
8 R. Polt, L. Szabo, J. Treiberg, Y. Li and V. Hruby, *J. Am. Chem. Soc*., 1992, **114**, 10249.
9 Y.-T. Li, B. Z. Carter, B. N. N. Rao, H. Schweingruber and S.-C. Li., *J. Biol. Chem*., 1991, **266**, 10723.

Communication 8/09729A

4 + 3 and fluorinative 4 + 3 cycloadditions of alkyne 1,4-diether dicobalt complexes

Manoj M. Patel and James R. Green*

Chemistry and Biochemistry, School of Physical Sciences, University of Windsor, Windsor, Ontario, Canada N9B 3P4. E-mail: jgreen@uwindsor.ca

Received (in Corvallis, OR, USA) 8th December 1998, Accepted 3rd February 1999

The $BF_3{\cdot}OEt_2$ mediated reactions between alkynyl diether hexacarbonyldicobalt complexes 1 and stannylsilanes 3 or 7 afford cycloheptenyne cobalt complexes 4 or fluorocycloheptyne complexes 8 depending upon the conditions of reaction.

The synthesis of seven-membered carbocyclic compounds is of much interest, due to their presence in a wide variety of natural products and due to the relative paucity of good ways to make the system.[1] The most conceptually attractive routes to the preparation of cycloheptanes are the 4 + 3 cycloaddition approaches, by virtue of the rapid assembly of the ring system and their superficial analogy to [4 + 2] cycloaddition reactions. A number of these cycloadditions have been reported,[2] most extensively those employing oxyallyl cations with dienes[3] and those condensing bis(trimethylsilyl) enol ethers with 1,4-diones.[4]

A potentially valuable variant of the 4 + 3 cycloaddition would be the reaction of sequentially formed cations from alkynyl diether complexes **1** with allyldimetal equivalents **2** or

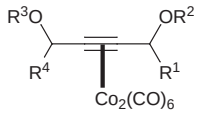

1

	R^1	R^2	R^3	R^4
a	H	Bn	Bn	H
b	H	Me	Me	H
c	H	Et	Et	H
d	Me	Me	Me	H
e	Ph	Me	Me	H
f	Me	Et	Et	Me
g	Me	TBDMS	Me	H
h	Ph	TBDMS	Me	H
i	Me	Pr^i	Me	H
j	Ph	Pr^i	Me	H

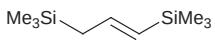

2

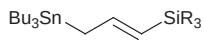

3a R = Me
b R = Et

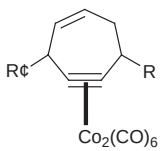

4

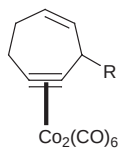

4'

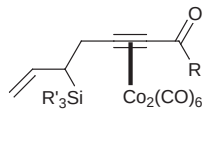

5

a R, R' = H
b R = Me, R' = H
c R = Ph, R' = H
d R, R' = Me

3. The resultant cycloheptyne complexes **4** are known to have good thermal stability,[5,6] and possess an (alkyne)hexacarbonyldicobalt function capable of synthetically important substitution[7] and cycloaddition reactions.[8] This possibility was realized by Takano's group, but they were unable to induce a Lewis acid mediated condensation between disilane **2** and **1a** to form either a cycloheptyne complex, or even useful yields of acyclic products.[9] Recent work in our laboratory has demonstrated the unexpected reactivity pathway of **2** with propargylcobalt cations bearing remote carbonyl functions, and the superiority of stannylsilanes **3** in the formation of acyclic allylation products **5**.[5]† In view of this, we have decided to investigate the viability of 4 + 3 cycloadditions between **1** and **3**.

Addition of 5 equiv. of $BF_3{\cdot}OEt_2$ to a 0 °C CH_2Cl_2 solution of **3a** and **1a** (10^{-1} M) over a period of 0.5 h gave a small amount of cycloadduct **4a** (*ca.* 10%), along with several acyclic allylation and diallylation products. Significantly improved yields of the cyclization product could be realized with methyl ether **1b** and ethyl ether **1c**, and with the triethylsilyl-substituted allyltin **3b**. Under the strictly analogous conditions, these reagent combinations afforded cycloheptenyne complex **4a** in 62 and 72% yields, respectively.

Use of reagent **3b** was investigated under these conditions with substituted alkynyl diether complexes. Methyl substituted **1d** and phenyl substituted **1e** gave cycloheptenyne complexes **4b** and **4c** as regioisomeric double bond mixtures with **4b′** (**4b** : **4b′** = 2.2 : 1) and **4c′** (**4c** : **4c′** = 1.7 : 1), respectively. In both cases, the predominant regioisomer obtained implies the preferential initial formation of the *less* substituted cation **6a**

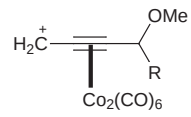

6a

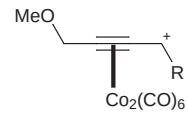

6b

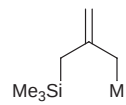

7a M = $SnBu_3$
b M = $SiMe_3$

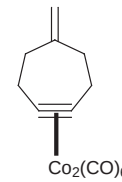

4e

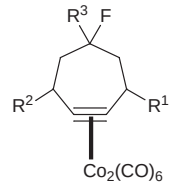

8

	R^1	R^2	R^3
a	H	H	H
b	Me	H	H
c	Ph	H	H
d	Me	Me	H
e	H	H	Me

over **6b**. Although a kinetic effect cannot be ruled out at this time, these results are consistent with the reported greater stability of less substituted propargylcobalt cations, as demonstrated by the pK_{R^+} measurements of Nicholas.[10] Dimethyl-substituted substrate **1f** gave the corresponding cycloheptenyne complexes **4d** in a more modest yield, in a 4.0 : 1 mixture of *trans* : *cis* diastereomers.‡ Finally, the isobutene dianion equivalent **7a**[11] reacted with **1c** to give methylenecycloheptyne complex **4e** in 53% yield.

Attempts were made to improve on the regiochemical selectivity for **4b** and **4c** by incorporating a bulkier ether

Table 1 4 + 3 Cycloadditions between alkynyl diether complexes **1** and allyldimetals **3** or **7**

Diether	Allyldimetal	Product	Yield[a] (%)
1b	**3b**	**4a**	62
1c	**3b**	**4a**	72
1d	**3b**	**4b + 4b′**	54 (2.2 : 1)
1e	**3b**	**4c + 4c′**	53 (1.7 : 1)
1f	**3b**	**4d**	42 (4.0 : 1)[b]
1g	**3b**	**4b**	62 (> 30 : 1)
1i	**3b**	**4b**	68 (> 30 : 1)
1h	**3b**	**4c**	37 (> 30 : 1)
1j	**3b**	**4c**	52 (> 30 : 1)
1c	**7a**	**4e**	53

[a] Ratio of regioisomers in parentheses. [b] Ratio of diastereomers *trans*-**4d** : *cis*-**4d**.

Table 2 Fluorinative 4 + 3 cycloadditions between **1** and **3** or **7**

Diether	Allyldimetal	Product	Yield[a] (%)
1c	**3b**	**8a**	**70**
1d	**3b**	**8b**	**57 (2.6 : 1)**
1e	**3b**	**8c**	**55 (2.4 : 1)**
1f	**3b**	**8d**	80 (1.9 : 1 : 0.14)[b]
1c	**7b**	**8e**	48

[a] Ratio of *trans*-**8** : *cis*-**8** in parentheses. [b] Ratio of *trans,trans*-**8d** : *cis,cis*-**8d** : *trans,cis*-**8d**.

function at the more substituted propargylic site. To this end, TBDMS ethers **1g** and **1h** and isopropyl ethers **1i** and **1j** were tested in their reactions with **3b**. Substantial improvements in regioselectivity were observed. Each of these cases resulted in the formation of the 6-substituted isomers (**4b** and **4c**) to the exclusion of the 3-substituted isomers (**4b′** and **4c′**); chemical yields were higher in both systems with the isopropyl ethers.

These cycloadditions were found to take a slightly different pathway under altered reaction conditions. Very slow addition of 5 equiv. of $BF_3{\cdot}OEt_2$ (over 12 h) to a highly dilute CH_2Cl_2 solution of **1c** and **3b** (10^{-3} M) at 0 °C resulted in the formation of fluorinated cycloheptyne complex **8a** (70% yield) to the exclusion of cycloheptenyne complex **4a**. Compound **8a** could also be obtained by rapid $BF_3{\cdot}OEt_2$ addition at 10^{-1} M concentrations, but the yield of this compound (57%) was inferior.

This fluorinative 4 + 3 cycloaddition was also found under the slow addition, high dilution conditions with the substituted diethers **1d**–**f**, giving **8b**–**d** as separable diastereomeric mixtures.[12] In monomethyl substituted **8b** and phenyl substituted **8c**, the *trans* isomers were found to predominate in a *ca.* 2.5 : 1 ratio. Stereoisomer assignments were based on the relatively upfield ^{1}H NMR chemical shift (in *cis*-**8b**) of the axial H atom geminal to fluorine (δ 4.55 in *cis*-**8b** *vs.* δ 5.11 in *trans*-**8b**), the larger vicinal coupling constants for that axial H atom ($J_{ax\text{-}ax}$ (average) = 10.9 Hz in *cis*-**8b** *vs.* $J_{eq\text{-}eq}$ (average) = 7.2 Hz in *trans*-**8b**), and a preferred chair conformation for the complexed cycloheptyne ring.[13]§¶ Dimethyl substituted **8d** was also formed as a mixture of three diastereomers, in a *trans, trans* : *cis, cis* : *trans, cis* ratio of (1.9 : 1 : 0.14). Notably, the ratio of the two diastereomers with *cis* methyl groups to the one with the *trans* orientation of methyl groups corresponds to 21 : 1. The reasons for the preferential formation of *cis*-dimethyl isomers of **8d** in the fluorocycloheptyne series, as opposed to the preferential formation of *trans*-dimethyl **4d** in the cycloheptenyne series, are not understood at this time. Finally, **1c** reacted with isobutene dianion equivalent **7b** under these conditions to afford tertiary fluoride **8e** in fair yield (48%).

In summary, rapid access into cycloheptynecobalt ring systems has been found to occur *via* both fluorinative- and non-fluorinative versions of a 4 + 3 cycloaddition reaction. Work on the preparation of more diversely substituted versions of these compound classes, and studies on the use of these compounds in the preparation of 5,7- and 6,7-ring systems, are in progress and will be reported in due course.

We are grateful to NSERC (Canada) for support of this research.

Notes and references

† These allylation products **5** may also be converted into cycloheptenyne complexes **4** (ref. 5).

‡ Diagnostic for the ^{1}H NMR based assignment of *trans*-**4d** as the major diastereomer is the existence of a 1.7% integrated NOE of the absorption for the pseudoaxial methylene proton (δ 2.00) upon irradiation of the allylic methine resonance (δ 3.75), and a 2.7% integrated NOE of the absorption for the allylic methine proton upon irradiation of the pseudoaxial methylene resonance.

§ MM2 Calculations (PC Model®) predict $J_{ax\text{-}ax}$ values of 11.8 and 11.8 Hz for the proton geminal to fluorine in *cis*-**8b**, and $J_{eq\text{-}eq}$ values of 7.0 and 7.1 Hz for the analogous proton in *trans*-**8b**.

¶ A 4.3% NOE integrated enhancement of the absorption for the propargylic methine H atom (δ 2.89) upon irradiation of the δ 4.55 resonance in *cis*-**8b** also supports the assignment of an axial orientation for these two protons.

1 D. F. Ewing, in *Rodd's Chemistry of Carbon Compounds*, 2nd edn., ed. M. Sainsbury, Elsevier, Amsterdam, 1994, vol. 2, 2nd Suppl., Pt. B, C, D, E, ch 8a. For recent work in this area, see: A. M. Montana, S. Ribes and F. Garcia, *Acta Chem. Scand.*, 1998, **52**, 453; E. J. Kantorowski, B. Borhan, S. Nazarian and M. J. Kurth, *Tetrahedron Lett.*, 1998, **39**, 2483; J. Tang, H. Shinokubo and K. Oshima, *Organometallics*, 1998, **17**, 290; J.-M. Duffault, *Synlett*, 1998, 33; B. B. Snider, N. H. Vo and S. V. O'Neil, *J. Org. Chem.*, 1998, **63**, 4732; T. Lavoisier-Gallo, E. Charonnet and J. Rodriguez, *J. Org. Chem.*, 1998, **63**, 900; H. M. L. Davies, D. G. Stafford, B. D. Doan and J. H. Hauser, *J. Am. Chem. Soc.*, 1998, **120**, 3326.

2 A. Hosomi and Y. Tominaga, in *Comprehensive Organic Synthesis*, ed. B. M. Trost, vol. ed. L. A. Paquette, Pergamon, Oxford, 1991, vol. 5, ch. 5.1; J. H. Rigby and F. C. Pigge, *Org. React.*, 1997, **51**, 351; M. Harmata, *Tetrahedron*, 1997, **53**, 6235; M. Harmata, *Adv. Cycloaddit.*, 1997, **4**, 41; P. Eilbracht and A. Hirshfelder, *Adv. Met.-Org. Chem.*, 1996, **5**, 55; H. M. R. Hoffmann, *Angew. Chem., Int. Ed. Engl.*, 1984, **23**, 1; *Angew. Chem.*, 1984, **96**, 29.

3 A. J. Demuner, L. C. A. Barbosa and D. Pilo-Veloso, *Quim. Nova*, 1997, **20**, 18; J. Mann, *Tetrahedron*, 1986, **42**, 4611; R. Noyori, *Org. React.*,1983, **29**, 163.

4 G. A. Molander and P. R. Eastwood, *J. Org. Chem.*, 1995, **60**, 8382 and references cited therein.

5 J. R. Green, *Chem. Commun.*, 1998, 1751.

6 For other known cycloheptyne- and oxacycloheptyne-cobalt complexes, see: S. L. Schreiber, M. T. Klimas and T. Sammakia, *J. Am. Chem. Soc.*, 1986, **108**, 3128; T. Nakamura, T. Matsui, K. Tanino and I. Kuwajima, *J. Org. Chem.*, 1997, **62**, 3032; N. E. Schore and S. D. Najdi, *J. Org. Chem.*, 1987, **52**, 5296; C. Yenjai and M. Isobe, *Tetrahedron*, 1998, **54**, 2509 and references cited therein.

7 A. J. M. Caffyn and K. M. Nicholas, in *Comprehensive Organometallic Chemistry II*, ed. E. W. Abel, F. G. A. Stone and G. Wilkinson, vol. ed. L. S. Hegedus, Pergamon, Oxford, 1995, vol. 12, ch. 7.1; K. M. Nicholas, *Acc. Chem. Res.*, 1987, **20**, 207.

8 N. E. Schore, in *Comprehensive Organometallic Chemistry II*, ed. E. W. Abel, F. G. A. Stone and G. Wilkinson, vol. ed. L. S. Hegedus, Pergamon, Oxford, 1995, vol. 12, ch.7.2; N. E. Schore, *Org. React.*, 1991, **40**, 1; N. E. Schore, in *Comprehensive Organic Synthesis*, ed. B. M. Trost, vol. ed. L. A. Paquette, Pergamon, Oxford, 1991, vol. 5, ch. 9.1; N. E. Schore, *Chem. Rev.*, 1988, **88**, 1081.

9 S. Takano, T. Sugihara and K. Ogasawara, *Synlett*, 1992, 70.

10 R. E. Connor and K. M. Nicholas, *J. Organomet. Chem.*, 1977, **125**, C45.

11 Closely analogous types of allyldimetal units also have been employed in the 4 + 3 cycloaddition strategies involving 1,4-dicarbonyl compounds: G. A. Molander and D. C. Schubert, *J. Am. Chem. Soc.*, 1987, **109**, 6877; A. Degl'Innocenti, P. Dembech, A. Mordini, A. Ricci and G. Seconi, *Synthesis*, 1991, 267.

12 Fluorination has also been observed in HBF_4 mediated Nicholas cyclisation reactions with allylic ethers: A. Mann, C. Muller and E. Tyrell, *J. Chem. Soc., Perkin Trans. 1* 1998, 1427.

13 The most closely analogous all-organic structures, the cycloheptenes, exist in the chair conformation: D. Ménard and M. St.-Jacques, *Tetrahedron*, 1983, **39**, 1041; L. I. Ermolaeva, V. S. Mastryukov, N. L. Allinger and A. Almenninger, *J. Mol. Struct.*, 1989, **196**, 151.

Communication 8/09641D

Dis-assembling lithium amide ladder structures: new insight through the structure of [{[$PhCH_2N(H)Li]_2$·thf}$_\infty$], a polymer of $(NLi)_2$ planar rings connected by thf-bridged $(NLi)_2$ butterfly junctions

William Clegg,[a] Stephen T. Liddle,[a] Robert E. Mulvey*[b] and Alan Robertson[b]

[a] *Department of Chemistry, University of Newcastle, Newcastle upon Tyne, UK NE1 7RU*
[b] *Department of Pure and Applied Chemistry, University of Strathclyde, Glasgow, UK G1 1XL. E-mail: r.e.mulvey@strath.ac.uk*

Received (in Cambridge, UK) 14th January 1999, Accepted 10th February 1999

One can visualise how the novel hemi-solvated polymeric ladder structure of the title compound would dis-assemble at its long, weak cisoid-$(NLi)_2$ butterfly junctions on further solvation, to release transoid-$(NLi)_2$ planar dimeric rings, the expected product of full solvation.

While our understanding of the complicated bond-making and bond-breaking processes involved in lithium amide aggregational chemistry[1,2] has deepened considerably in recent years primarily through the 'ring-laddering' principle,[3] it remains far from comprehensive. Most conspicuously, at the time of writing, there is still no example of a crystallographically characterised polymeric ladder structure of a pure (*i.e.*, donor-free) lithium amide. Mono-lithiated ethylenediamine [{$H_2NCH_2CH_2N(H)Li$}$_\infty$][4] does exist as an infinite sinusoidal wave-shaped ladder, but its NH_2 amine arms function as internal donor ligands. There is also little tangible information hitherto on the coordination chemistry taking place when coordinating solvent molecules approach a long (high oligomeric/polymeric) ladder framework. However, light has been shed on subsequent processes, specifically on the possible sequence of steps involved when lower oligomeric ladders break down to tetrasolvated $(NLi)_2$ ring dimers on gradually increasing the number of solvent ligands in the system.[5] In contrast, here, we report an unique example of a ladder structure which stays polymeric in the presence of coordinating thf molecules, in the hemi-thf complex of lithium benzylamide [{[$PhCH_2N(H)Li]_2$·thf}$_\infty$] **1**. Attention is drawn to the pattern of solvent ligation in **1**, which is without precedent in any previously reported lithium structure, amide or otherwise; and to how this extends our knowledge of the dis-assembling process in lithium amide ladder chemistry. The new structure also provides a contrast with that of the polymeric phosphide [{CyP(H)Li·thf}$_\infty$][6] which has conventional, terminal thf solvation.

Regarding the synthesis of **1**, it is a trivial matter to abstract one NH proton from benzylamine by the action of *n*-butyllithium provided a routine inert-atmosphere protocol is followed. However, obtaining a pure crystalline thf complex of the lithium benzylamide so produced is more challenging. Only pink slurries could be prepared on subjecting a 1 : 1, Bu^n-Li : $PhCH_2NH_2$ mixture with various amounts of thf (1, 2 or 6 molar equivalents). Alternatively, when excess amine was employed (*e.g.* in a 1 : 2 : 1 mixture), the known amide–amine complex [{[$PhCH_2N(H)Li]_2$·H_2NCH_2Ph}$_\infty$][7] **2** preferentially crystallised from solution. Success eventually came from a 1 : 2 : 2 mixture in hexane–toluene solution, with **1** forming as colourless crystals,† though the product was still contaminated with crystals of **2**. This product is only partially soluble in arene solvents. ^{1}H NMR spectra in d_6-benzene solution always show both benzylamine and thf molecules (in variable and inconsistent amounts) as well as *smaller* amounts of amide anions. Thus it can be reasoned that the polymeric ladder framework easily loses donor ligands, which escape into solution leaving behind a solid residue of unsolvated lithium benzylamide. In turn, the excess donor molecules in solution can dissolve a portion of this solid to generate a soluble, but weak oligomeric solvate (possibly a tetrasolvated dimer, see later). This notion of a weak solution complex is consistent with the fact that while lithium benzylamide is completely soluble in concentrated benzylamine or thf solutions, only polymeric solids are deposited from such solutions.

Pure unsolvated lithium benzylamide almost certainly has an infinite ladder structure with an alternating cisoid–transoid pattern of laterally fused $(NLi)_2$ rings. This deduction is based on the evidence that the same basic ladder framework is found in both **1** and **2**. But, of particular interest here, is the unique manner in which the solvent ligands in **1** attach themselves to this ladder framework. Spanning a four-rung section of the ladder, the central Li–N–Li(a)–N(a) ring is solvent free, while those adjacent to it, Li–N–Li(b)–N(b) and Li(a)–N(a)–Li(c)–N(c) are capped on one side by μ-bonding thf ligands, which alternate above and below the ladder plane (Fig. 1).‡ The first mentioned ring is transoid and strictly planar by virtue of its centrosymmetry. In contrast, the other two are cisoid and butterfly shaped (deviations from planarity ± 0.326 Å), with N···N hinges (folding angle 119.4°) and Li wingtips, due to the pull exerted by thf ligands, which lie on twofold rotation axes passing through oxygen atoms. As a result of symmetry, there are only three unique N–Li bond lengths in **1**: ladder edges are short [2.046(3) Å] and long [2.098(3) Å] within the non-solvent-bridged and solvent-bridged $(NLi)_2$ rings respectively; the ladder rungs are all equivalent and have an intermediate length [2.087(3) Å]. The O–Li bond lengths are also equivalent [2.146(4) Å] reflecting the symmetrical fit of the thf ligand over the puckered $(NLi)_2$ ring face.

Consideration of the architecture and dimensions of **1** leads to a more complete picture of the multistepped, ladder dis-

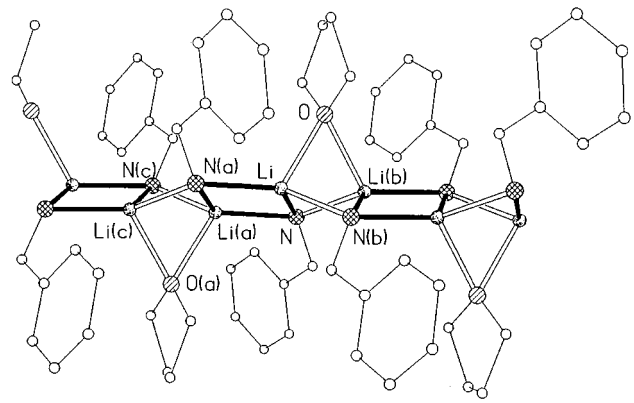

Fig. 1 Polymeric structure of **1** with atom-labelling. Hydrogen atoms are omitted for clarity. Key dimensions (Å and °): Li–N 2.087(3), Li–N(a) 2.046(3), Li–N(b) 2.098(3), Li–O 2.146(4), Li···Li(a) 2.440(6), Li···Li(b) 2.230(6), N–Li–N(a) 107.64(13), N–Li–N(b) 103.83(14), Li–N–Li(a) 72.36(13), Li–N–Li(b) 64.38(14), Li–O–Li(b) 62.60(17).

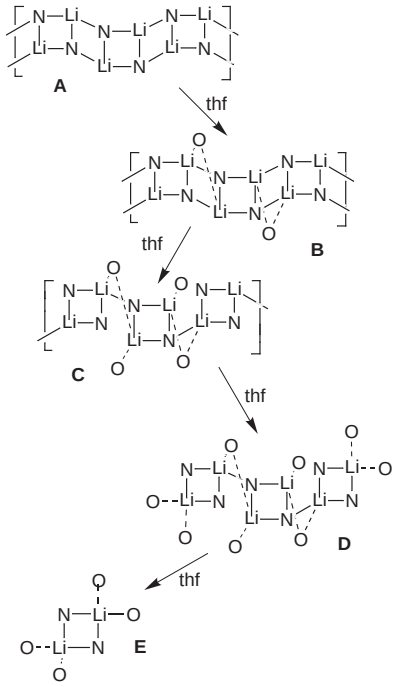

Scheme 1

assembling process than that previously outlined.[8] In particular, they provide valuable new insight into the possible early steps involved. These are included in the full sequence of steps, as we now perceive them, in Scheme 1. **A** represents the infinite ladder structure, the framework of which provides the foundation of both **1** and **2**. **B** represents the new structure **1**. This is a key structural finding as previously it was assumed that the attachment of donor ligands would automatically encourage ladder fragmentation (oligomerisation); but in **B** the polymeric arrangement is retained. Noting that lithium amide polymers are generally insoluble in arene solvents, the **A→B** transformation also has implications for the coordination chemistry developing at the solid–solution interface which eventually leads to the dissolution of the amide in an arene–thf mixture. The next transformation, **B→C**, takes place on the addition (or involvement) of more thf molecules. From the crystal structure of **1** the weakest points of the $(NLi)_\infty$ ladder framework are those bridged by the thf ligands. Logically, therefore, as the incoming thf molecules approach the metal centres in **C** (note that they all occupy identical steric environments), one of the longer, weaker N–Li edge bonds of the $(NLi)_2$ butterfly-shaped rings will cleave. This leaves the shorter, stronger bonds of the adjacent $(NLi)_2$ rings (*i.e.* those in **1** unbridged by the thf ligands) intact. The transformation **C→D** should not be regarded as a single step, polymer→oligomer one. It is more likely to be a fragmented process. To elaborate, as the solvation pattern in **C** develops along the polymer backbone, it will undoubtedly lead to increased steric repulsions caused by the presence of both bridging and terminal thf ligands. Hence, not the whole of **C**, but sections of it (possibly covering six N–Li rungs) will periodically break away from the remainder of the infinite ladder to form the oligomer **D**. Completing the sequence is the **D→E** transformation, the evidence for which is based on the structural characterisations of $[\{PhN(H)Li\}_6\cdot 8thf]$[8] and $[\{PhN(H)Li\cdot 2thf\}_2]$[9] respectively, as discussed previously. Note that the discrete $(NLi)_2$ rings in the final product **E** can be traced back to the 'unsolvated' $(NLi)_2$ rings in **1**, as both are planar and transoid.

In the specific case of lithium benzylamide, the tetra-thf solvated ring dimer possibly exists in solution. However, steric crowding probably destabilises it (note that the dibenzylamido analogue is only bis-solvated[10]) with respect to **1** which preferentially crystallises from solution. This crystallisation process is in effect the retro-counterpart of Scheme 1, and would be induced by collisions between dimers and concomitant cleavage of some thf ligands.

Finally, note that this ladder dis-assembling pathway should not be considered as all-embracing, as it is likely to be dependent on the particular donor solvent employed.

We thank the EPSRC for supporting this research.

Notes and references

† Yield of crystalline material, 28%. Our attempts to separate **1** and **2** have so far been unsuccessful. ^{1}H NMR (25 °C, 400 MHz, C_6D_6) δ −1.05 (t, NH), 0.57 (s, NH_2), 1.40 (s, CH_2, thf), 3.55 (s, OCH_2, thf, CH_2-amine), 4.27 (d, CH_2-amide), 7.07 (br m, Ph).

‡ *Crystal data*: $C_8H_{24}Li_2N_2O$, M = 298.3, orthorhombic, space group *Pbcn*, a = 22.617(5), b = 10.047(2), c = 7.594(2) Å, U = 1725.6(7) Å^3, Z = 4, D_c = 1.148 g cm^{-3}, μ = 0.53 mm^{-1} (Cu-Kα, λ = 1.54184 Å), T = 160 K; R_w = 0.1469 on F^2 values of all 1528 unique data, conventional R = 0.0509 on F values of 1151 reflections with $F_o^2 > 2\sigma(F_o^2)$, 109 parameters; final difference map within ±0.25 e Å^{-3}. CCDC 182/1165. See http://www.rsc.org/suppdata/cc/1999/511/ for crystallographic files in .cif format.

1 K. Gregory, P. v. R. Schleyer and R. Snaith, *Adv. Inorg. Chem.*, 1991, **37**, 47.
2 R. E. Mulvey, *Chem. Soc. Rev.*, 1991, **20**, 167.
3 D. R. Armstrong, D. Barr, W. Clegg, R. E. Mulvey, D. Reed, R. Snaith and K. Wade, *J. Chem. Soc., Chem. Commun.*, 1986, 869.
4 G. R. Kowach, C. J. Warren, R. C. Haushalter and F. J. DiSalvo, *Inorg. Chem.*, 1998, **37**, 156.
5 R. E. Mulvey, *Chem. Soc. Rev.*, 1998, **27**, 339.
6 E. Hey-Hawkins and S. Kurz, *Phosphorus, Sulfur, Silicon*, 1994, **90**, 281.
7 A. R. Kennedy, R. E. Mulvey and A. Robertson, *Chem. Commun.*, 1998, 89.
8 W. Clegg, L. Horsburgh, F. M. Mackenzie and R. E. Mulvey, *J. Chem. Soc., Chem. Commun.*, 1995, 2011.
9 R. v. Bülow, H. Gornitzka, T. Kottke and D. Stalke, *Chem. Commun.*, 1996, 1639.
10 P. C. Andrews, D. R. Armstrong, D. R. Baker, R. E. Mulvey, W. Clegg, L. Horsburgh, P. A. O'Neil and D. Reed, *Organometallics*, 1995, **14**, 427.

Communication 9/00392D

ChemComm

Polymorphism based on molecular stereoisomerism in tris(oxalato) Cr(III) salts of bedt-ttf [bis(ethylenedithio)tetrathiafulvalene]

Lee Martin,[a] Scott S. Turner,*[a] Peter Day,*[a] K. M. Abdul Malik,[b] Simon J. Coles[b] and Michael B. Hursthouse[b]

[a] *Davy-Faraday Research Laboratory, The Royal Institution of Great Britain, 21 Albemarle Street, London, UK W1X 4BS. E-mail: sst@ri.ac.uk; pday@ri.ac.uk*

[b] *Department of Chemistry, Cardiff University, PO Box 912, Cardiff, UK CF1 3TB*

Received (in Basel, Switzerland) 18th January 1999, Accepted 8th February 1999

Polymorphs of the charge transfer salt (bedt-ttf)$_4$[(H_3O)-$Cr^{III}(C_2O_4)_3$]·PhCN [bedt-ttf = bis(ethylenedithio)tetrathiafulvalene] which are either superconducting or semiconducting differ in the spatial distribution of Δ and Λ enantiomers of $[Cr(C_2O_4)_3]^{3-}$ within the unit cell.

Solids built from molecules give chemists the ability to create materials with structural complexities not found in traditional continuous lattice materials. Subtle changes in structure may lead to large differences in collective physical properties such as electrical transport or magnetism. For example, molecular charge transfer salts of the donor bedt-ttf, bis(ethylenedithio)-tetrathiafulvalene, exhibit room temperature electronic ground states as diverse as metallic, wide band gap semiconducting and insulating. Some even display superconductivity.[1] Their transport properties vary with the acceptor anion and different structural modifications of bedt-ttf are possible with the same anion.[2–4] The collective electronic properties of such materials depend crucially on the charge distribution, distances and relative orientations of neighbouring donor molecules in the crystal, *i.e.* on the packing motif. Motifs can be controlled by organisation of the anions, *via* 'docking' of the terminal methylene H atoms of the bedt-ttf into cavities provided by the anions organisation.[5] Anion–cation atomic contacts provide further means of self assembly within the unit cell.

The series of compounds with general formula (bedt-ttf)$_4$[$AM^{III}(C_2O_4)_3$]·PhCN (M = Fe, Cr; A = H_3O^+, K^+, NH_4^+) has been structurally characterised by room temperature and low temperature X-ray crystallography.[6–8] Their conducting and magnetic properties have been determined by single crystal resistivity measurements, SQUID magnetometry and variable temperature electron paramagnetic resonance. One polymorph of the compound with M = Cr and A = H_3O^+ (**I**)[8] has a metal to superconducting transition at T_c = 6.0(5) K. At high temperatures the bulk magnetic susceptibility is dominated by unpaired d electrons associated with the Cr(III) ion (S = 3/2). The Curie–Weiss law is obeyed from room temperature to just above T_c together with a small Pauli contribution as is usual for metallic salts. Below T_c the Meissner effect is observed and this is suppessed by an external field of 40 mT. The point symmetry about Cr is D_3 and so $[Cr(C_2O_4)_3]^{3-}$ exhibits optical isomerism although **I** is prepared from a racemic mixture of the tris(oxalato) starting material and crystallises in an achiral space group, *C*2/*c*. In contrast using enantiomerically pure $[Cr(C_2O_4)_3]^{3-}$ as a starting material we obtain another achiral phase (**II**) with identical stoichiometry to phase **I**† but with strikingly different physical properties. Transport measurements on **II** indicate semiconducting behaviour while no Meissner effect is seen and the magnetic susceptibility can be fitted to a Curie–Weiss law from ambient to low temperatures. The difference in physical properties between **I** and **II** arises from an unprecedented difference between their crystal structures namely a different spatial arrangement of the chiral enantiomers in the unit cell.

In both polymorphs‡ layers of cationic bedt-ttf molecules are interleaved by layers containing $[Cr(C_2O_4)_3]^{3-}$, H_3O^+ and PhCN. Each anionic layer forms a so-called 'honeycomb' lattice with alternate intralayer O (of H_3O^+) and Cr forming an approximately hexagonal network with benzonitrile molecules occupying the hexagonal cavities. The Cr atoms are octahedrally coordinated to three bidentate oxalate dianions, which confers the D_3 site symmetry about each transition metal. The uncoordinated O (oxalate) atoms surround a cavity occupied by H_3O^+. The area of the hexagonal cavities are almost identical and they are filled by a benzontrile molecule with little void space into which the terminal CH_2 groups of the bedt-ttf can 'dock'[5].

Despite identical stoichiometry, the organisation of the bedt-ttf layers is quite different in the two polymorphs: **I** has the so-called β″ packing motif (*C*2/*c* space group) whereas **II** presents a motif which we refer to as pseudo-κ (*Pbcn* space group). Analysis of the pseudo-κ C=C and C–S bond lengths[9] within the central ttf (tetrathiafulvalene) unit indicates that there are two different bedt-ttf molecules with charges close to 0 and +1. The +1 cations occur as face to face dimers and are surrounded by six neutral molecules. Neighbouring dimers are approximately orthogonal as in normal κ phases.[1] In the β″ phase the molecules are arranged into stacks with short S···S distances between them and bond length analysis reveals that all bedt-ttf molecules have similar but not identical positive charges close to +0.5. (Note that the sum of the bedt-ttf charges implies that in both polymorphs the water is present as H_3O^+). In **II** the centroids (centre of the ttf C=C bond) of the neutral molecules describe approximately hexagonal networks where the positively charged dimers lie close to oxalate anions, leading to H-bonding (2.51–3.05 Å) between the terminal ethylene hydrogens and oxygens (oxalate). The neutral bedt-ttf molecules are either positioned over H_3O^+ or close to the solvent.

The difference between the packing motifs of the donor cations in **I** and **II** must arise from the pattern of short atomic contacts, specifically H-bonds, between the organic and anionic layers. Evidence for such interactions between terminal CH_2 groups of bedt-ttf and the anion layer comes from translation of the $[Cr(C_2O_4)_3]^{3-}$ units within the plane of an anion layer on passing from one layer to the next. The displacement of the $[Cr(C_2O_4)_3]^{3-}$ matches the tilt of the long axis of the intervening bedt-ttf molecules, so that the contacts between H (CH_2) atoms and O (oxalate) are identical at both ends of the bedt-ttf.

The basic topography of the inorganic layers is very similar in both phases, so why should the packing of the organic donor molecules be so different? The answer lies in the distributions of enantiomeric $[Cr(C_2O_4)_3]^{3-}$. In **I** each anionic layer contains exclusively one enantiomer and the next layer contains the other giving a Δ-Λ-Δ-Λ-Δ-Λ . . . pattern. However, each anionic layer in **II** contains both Δ and Λ enantiomers arranged in rows. In adjacent layers the chiral centres are organised in an identical fashion, barring layer translation, which gives a ΔΛ-ΔΛ-ΔΛ-ΔΛ . . . pattern. In neither polymorph does relative translation of the inorganic layer affect the bedt-ttf packing motif, but only the tilt angle of the long axis of these molecules. The arrangement of the enantiomers in a single anionic layer for **I**

and **II** are shown in Fig. 1(*a*) and (*b*), respectively indicating two ways in which equal proportions of each enantiomer are accommodated in the lattice to give an achiral crystal structure. The different spatial distributions of enantiomers form the basis of the observed polymorphism and are responsible for self assembly into either pseudo κ or β″ bedt-ttf packing motifs, which determine the strikingly different electrical properties of the two phases.

The spatial relationship between the bedt-ttf packing motifs and a nearest neighbour anionic layer is given in Fig. 2(*a*) and (*b*). The bedt-ttf layer is in the foreground and superimposed, as the background, are the positions of the metal atoms and the H_3O^+ molecules (O atom is marked A) of the anion layer. The chiral environment about the metal atoms is shown as Δ or Λ, and the hexagonal honeycomb lattice marked with full lines. H-bonding interactions occur between the neighbouring O (oxalate) atoms and the H (CH_2) atoms on the extremity of each bedt-ttf. Fig. 2 shows that the two packing arrangements of the bedt-ttf are very closely related, the β″ phase being a more regular form of the pseudo-κ phase. If all enantiomers in alternate rows of **I** are changed to the other isomer then the inorganic layer topography is transformed to that of **II**. A corresponding rotation of the donor cations, maintaining the same number and disposition of H-bonds, transforms the pseudo κ phase into a phase almost identical to β″. In effect this gives a β″ phase, generated from the pseudo κ phase, which therefore contains dimers and the original pseudo-κ charge distribution.

In conclusion we have shown that there are two polymorphs of the molecular charge transfer salt (bedt-ttf)$_4$[$(H_3O)Cr(C_2O_4)_3$]·PhCN, with distinctly different, though related, packing arrangements of the bedt-ttf donor cations. The salts have either β″ or a pseudo-κ motif and they have contrasting physical properties, being superconducting or semiconducting respectively. The two modes of bedt-ttf packing are promoted by two different spatial distributions of the chiral enantiomers Δ- or Λ-$[Cr(C_2O_4)_3]^{3-}$ to give overall racemic lattices. It has been previously found that exposure to either racemic or enantiomer excess of components or additives in a crystallisation process can lead to different polymorphs of a solid.[12,13] However, to the best of our knowledge this is the first time that this specific source of polymorphism has been identified in any crystalline material. We are continuing our efforts to make related chiral compounds and to explore the supramolecular organisation in this family of organic conductors.

We acknowledge financial support from the UK Engineering and Physical Sciences Research Council.

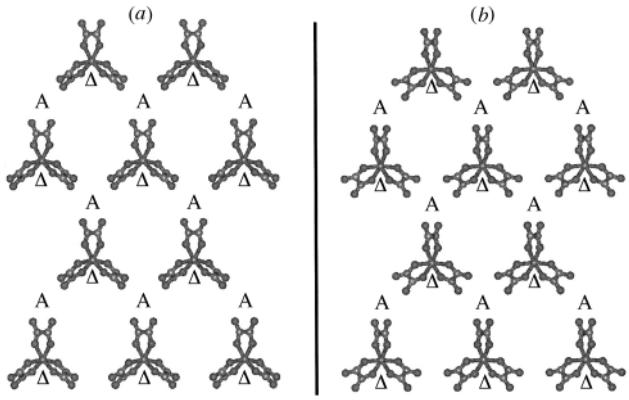

Fig. 1 Two different ways in which chiral $[Cr(C_2O_4)_3]^{3-}$ is accommodated in a single layer within (*a*) **I** and (*b*) **II**; A = H_3O^+.

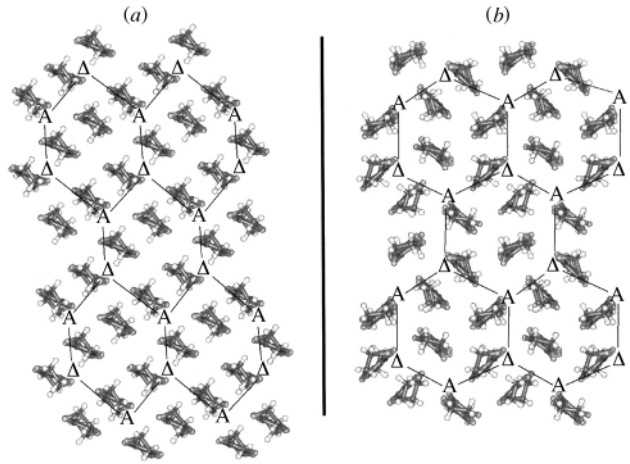

Fig. 2 The relationship between layers of bedt-ttf and $[Cr(C_2O_4)_3]^{3-}/H_3O^+$/PhCN in (*a*) **I** and (*b*) **II**.

Notes and references

† The salts were prepared by *in situ* electro-oxidation of neutral bedt-ttf at constant currents of between 0.05 and 0.2 μA, in the presence of the anion and relevant solvent. For **I** the anion source was racemic $(NH_4)_3[Cr(C_2O_4)_3]\cdot 3H_2O$.[10] The starting material used for **II** was either the pure Δ- or Λ-ammonium salt of $[Cr(C_2O_4)_3]^{3-}$, prepared by literature methods,[11] both of which gave identical products. In both syntheses the solvent was distilled and degassed just prior to use and then several drops of water were added to the electrochemical cell. All starting materials were purified by repeated crystallisation. It was noted that the crystals began to grow within two days when using racemic starting materials but only after two weeks when using a single enantiomer. The time delay confirms that at least partial racemisation must occur in the latter case prior to crystal formation.

‡ *Crystal data*: **I**: $C_{53}H_{39}CrNO_{13}S_{32}$, M = 1975.99, monoclinic, space group *C*2/*c*, a = 10.278(3), b = 20.130(4), c = 35.078(15) Å, β = 93.040(9)°, U = 7247.3(40) Å^3, T = 150(2) K, Z = 4, μ = 1.141 mm^{-1}, reflections collected = 8640, independent reflections = 4281, $R1$ = 0.0622, $wR2$ = 0.0945.

II: $C_{53}H_{39}CrNO_{13}S_{32}$, M = 1975.99, orthorhombic, space group *Pbcn*, a = 10.371(2), b = 19.518(3), c = 35.646(2) Å, U = 7216(2) Å^3, T = 150(2) K, Z = 4, μ = 1.146 mm^{-1}, reflections collected = 24400, independent reflections = 5599, $R1$ = 0.0655, $wR2$ = 0.1033.

CCDC 182/1170. See http://www.rsc.org/suppdata/cc/1999/513/ for crystallographic files in .cif format.

1 J. M. Williams, J. R. Ferraro, R. J. Thorn, K. D. Carlson, U. Geiser, H. H. Wang, A. M. Kini and M.-H. Whangbo, *Organic Superconductors* (*Including Fullerenes*): *Synthesis Structure, Properties and Theory*, Prentice Hall, Englewood Cliffs, NJ, 1992.
2 K. Bender, I. Hennig, D. Schweitzer, K. Dietz, H. Endres and H. J. Keller, *Mol. Cryst. Liq. Cryst.*, 1984, **108**, 359.
3 T. Mori, A. Kobayashi, Y. Sasaki, H. Kobayashi, G. Saito and H. Inokuchi, *Chem. Lett.*, 1984, **6**, 957.
4 H. Kobayashi, R. Kato, A.Kobayashi, Y. Nishio, K. Kajita and W. Sasaki, *Chem. Lett.*, 1986, **5**, 833.
5 H. Yamochi, T. Kamatsu, N. Matsukawa, G. Saito, T. Mori, M. Kusunoki and K. Sakaguchi, *J. Am. Chem. Soc.*, 1993, **115**, 11 319.
6 A. W. Graham, M. Kurmoo and P. Day, *J. Chem. Soc., Chem. Commun.*, 1995, 2061.
7 M. Kurmoo, A. W. Graham, P. Day, S. J. Coles, M. B. Hursthouse, J. L. Caulfield, J. Singleton, F. L. Pratt, W. Hayes, L. Ducasse and P. Guionneau, *J. Am. Chem. Soc.*, 1995, **117**, 12209.
8 L. Martin, S. S. Turner, P. Day, F. E. Mabbs and E. J. L. McInnes, *Chem. Commun.*, 1997, 1367.
9 P. Guionneau, C. J. Kepert, G. Bravic, D. Chasseau, M. R. Truter, M. Kurmoo and P. Day, *Synth. Met.*, 1997, **86**, 1973.
10 J. C. Bailar and E. M. Jones, *Inorg. Synth.*, 1959, **1**, 35.
11 G. B. Kauffman, N. Sugisaka and I. K. Reid, *Inorg. Synth.*, 1989, **25**, 139.
12 I. Weissbuch, D. Zbaida, L. Addadi, L. Leiserowitz and M. Lahav, *J. Am. Chem. Soc.*, 1987, **109**, 1869.
13 I. Kuzmenko, I. Weissbuch, E. Gurovich, L. Leiserowitz and M. Lahav, *Chirality*, 1998, **10**, 415.

Communication 9/00482C

Preparation of a new poly(arylacetylene) with a tetrathiafulvalene (TTF) unit in the side chain

Takahisa Shimizu and Takakazu Yamamoto*

Research Laboratory of Resources Utilization, Tokyo Institute of Technology, 4259 Nagatsuta, Midori-ku, Yokohama 226-8503, Japan. E-mail: tyamamoto@res.titech.ac.jp

Received (in Cambridge, UK) 11th January 1999, Accepted 16th February 1999

A new poly(arylacetylene) having a strongly electron donating unit, a tetrathiafulvalene (TTF) unit, in the side chain has been prepared by Rh-catalyzed polymerization, and optical, electrochemical and electric properties of the polymer have been revealed.

Tetrathiafulvalene (TTF) and its analogues have long attracted the attention of chemists because of their ability to form highly electrically conducting charge transfer (CT) complexes with electron acceptors.[1] Many efforts have been made to prepare polymeric materials of TTF in order to obtain mechanically tough CT adducts with a larger π-conjugation system, and preparation of π-conjugated polymers containing the TTF unit has been reported.[2] However, preparation of a poly(arylacetylene) containing the TTF unit in its side chain has not been reported. Recent synthesis of an acetylenic derivative of TTF, 2-ethynyl-TTF, by Otsubo *et al.*[3] has prompted us to carry out the polymerization of 2-ethynyl-TTF, and here we report the results of the polymerization and redox properties of the obtained polymer.

Polymerization of 2-ethynyl-TTF was carried out by using $[Rh(\mu\text{-}Cl)(\eta^4\text{-nbd})]_2$ (nbd = norbornadiene), which is known as an active catalyst for polymerization of arylacetylenes, and NEt_3 as the cocatalyst [eqn. (1)].[4] Addition of PPh_3, for modification of the catalyst, was also carried out.

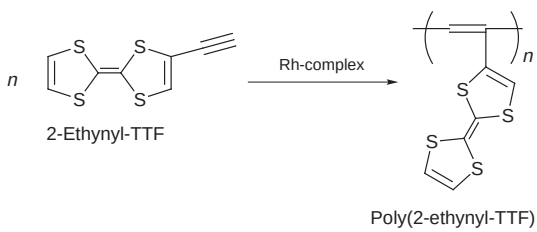

(1)

The polymerization of 2-ethynyl-TTF proceeds smoothly at room temperature and a dark-brown powder of poly(2-ethynyl-TTF) was obtained.† When the polymerization was carried out in neat NEt_3 without THF, insoluble polymer was obtained (Table 1, entry 1), although the IR spectrum of the polymer was essentially identical to those of polymers obtained in other runs. The insolubility of the polymer obtained in neat NEt_3 seems to arise from its very high molecular weight. It is reported that use of neat NEt_3, instead of other solvents, in the polymerization of phenylacetylene with the Rh catalyst leads to the formation of a polymer with a much higher molecular weight.[4c] On the other hand, carrying out the polymerization in THF (Table 1, entry 2) gave a soluble polymer having a number average molecular weight (M_n) of 11 700 in 47% yield at a high catalyst concentration of 41 mM. Lower concentration of the catalyst and shorter reaction time (entry 3) as well as addition of PPh_3 (entry 4) gave polymers with lower molecular weight. Since the Rh complex catalyst was inert over several days towards usual low molecular weight TTFs, occurrence of side reactions such as cleavage of the C–S bond of the monomer or the polymer by the catalyst was unlikely.

Table 1 Results of the polymerization of 2-ethynyl-TTF[a]

Entry	Solvent	Ligand added	Catalyst/ mM	*t*/h	Yield (%)	M_n[b]	M_w/M_n[b]
1	None	—	5	18	26	[c]	[c]
2	THF	—	41	2	47	11 700	1.23
3	THF	—	5	3	52	10 000	1.49
4	THF	PPh_3 (0.1 mM)	5	48	52	6 000	1.85

[a] Carried out in THF in the presence of NEt_3 (2.4 M) at room temperature except for entry 1 (in NEt_3). Concentration of 2-ethynyl-TTF = 0.21 M. Catalyst = $[Rh(\mu\text{-}Cl)(\eta^4\text{-nbd})]_2$. [b] Determined by GPC (polystyrene standards; eluent = DMF containing 0.006 M LiBr). [c] Insoluble.

The obtained polymers in entries 2–4 of Table 1 were soluble in some polar solvents including Me_2SO and DMF. Fig. 1 compares IR spectra of 2-ethynyl-TTF and poly(2-ethynyl-TTF). The IR spectrum of the polymer exhibits absorption bands characteristic of the TTF unit (*e.g.* 775, 793 and 1432 cm^{-1}). However, the ν(C≡C) peak (at *ca.* 2100 cm^{-1}) and the ν(C–H) peak of terminal acetylene (at *ca.* 3250 cm^{-1}) observed with 2-ethynyl-TTF completely disappear after polymerization. Poly(2-ethynyl-TTF) is stable under N_2, however, it is gradually degraded under air. Fig. 1(c) shows the IR spectrum of the polymer after exposure to air for one month. The IR spectrum exhibits new absorption peaks, which are considered to originate from OH, OOH, epoxide, and/or ether groups formed by air-oxidation. Similar air-sensitive properties and IR changes have been reported for polyacetylene[5a,b] and an analogous polymer.[5c] No apparent change in colour of the polymer, however, was observed after one month.

The ^1H NMR spectrum of poly(2-ethynyl-TTF) in $(CD_3)_2SO$ showed only broad peaks in the range δ 6.2–6.9, similar to those of reported poly(arylacetylene)s such as poly(phenylacetylene).[6] The TTF and vinyl protons are considered to overlap

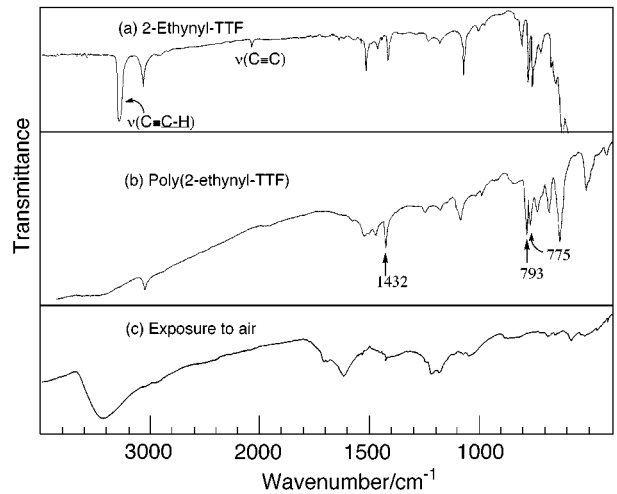

Fig. 1 IR spectra of (a) 2-ethynyl-TTF, (b) poly(2-ethynyl-TTF) (Table 1, entry 2) and (c) poly(2-ethynyl-TTF) after exposure to air for a month; (a) between NaCl crystal plates, (b) and (c) as KBr disks.

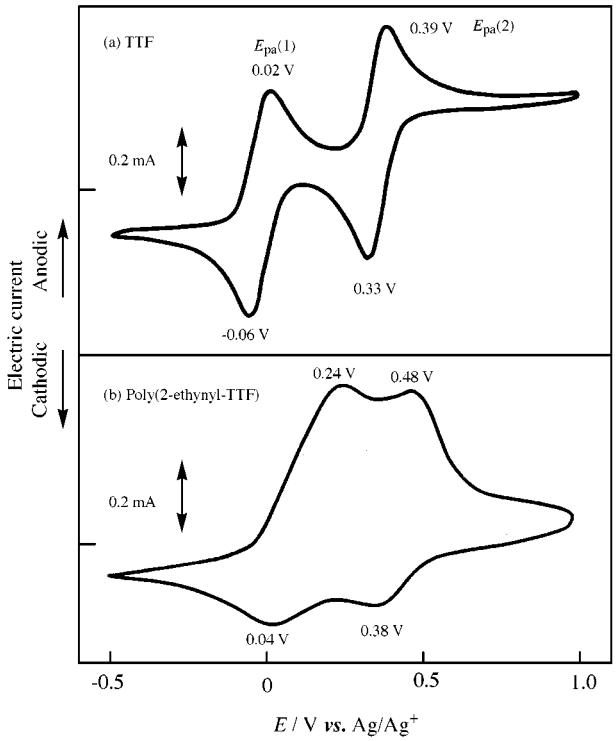

Fig. 2 Cyclic voltammograms of (a) TTF (0.10 M) and (b) poly(2-ethynyl-TTF) cast on a Pt plate (1× 1 cm) in an acetonitrile solution of $[NEt_4]BF_4$ (0.10 M). Scanning rate = 50 mV s^{-1}.

with each other to give the broad signal. The π–π* absorption band of the monomer at 395 nm disappeared after the polymerization, and poly(2-ethynyl-TTF) gives rise to a new broad absorption band at *ca*. 490 nm due to the expansion of the π-system.

Poly(2-ethynyl-TTF) is electrochemically active, and its redox behaviour has been followed by cyclic voltammetry with a film cast from a Me_2SO solution. As shown in Fig. 2(b), the cyclic voltammogram of the insoluble poly(2-ethynyl-TTF) film shows first and second E_{pa} values at 0.24 and 0.48 V *vs.* Ag/Ag$^+$ in MeCN solution containing 0.1 M $[NEt_4]BF_4$.

For TTF in solution, the two oxidation peaks, $E_{pa}(1)$ and $E_{pa}(2)$, are clearly separated with a potential difference, $E_{pa}(2) - E_{pa}(1)$, of 0.37 V [*cf*. Fig. 2(a)]. However, for the film of poly(2-ethynyl-TTF), the separation is not clear and the two peaks overlap with a smaller $E_{pa}(2) - E_{pa}(1)$ of 0.24 V. Similar differences between monomeric and π-conjugated polymeric compounds in their electrochemical redox processes have been reported for a two-step reduction of anthraquinone in a solution and π-conjugated poly(anthraquinone) in a film.[7] In Me_2SO containing 0.1 M $[NEt_4]BF_4$, both solutions of TTF and poly(2-ethynyl-TTF) give rise to $E_{pa}(1)$ and $E_{pa}(2)$ peaks at almost the same positions (0.11, 0.32 V and 0.14, 0.35 V, respectively, *vs.* Ag/Ag$^+$) although the anodic peaks of the polymer are also considerably broadened.

Poly(2-ethynyl-TTF) shows a low electrical conductivity of $< 1 \times 10^{-9}$ S cm^{-1}. The polymer reacts to give CT adducts with electron acceptors such as 7,7,8,8-tetracyanoquinodimethane (TCNQ), tetrafluorotetracyanoquinodimethane ($TCNQF_4$), dichlorodicyanoquinone (DDQ), and iodine. The ν(C≡N) band of the electron acceptors is shifted to a lower frequency by 10–50 cm^{-1} upon adduct formation, similar shifts having been reported for the CT complexes of TTF with electron acceptors.[8] Among these adducts, the CT complex with TCNQ [poly(2-ethynyl-TTF) : TCNQ = 5 : 1 molar ratio] shows the highest electrical conductivity of 2.1×10^{-3} S cm^{-1} as measured on a compressed pellet of the adduct.

Notes and references

† Analytical data of poly(2-ethynyl-TTF). Calc. for $(C_8H_4S_4)_n$: C, 42.07; H, 1.77. Found: C, 42.28; H, 1.78%.

1 See for example: G. Schukat, A. M. Richter and E. Fanghanel, *Sulfur Rep*., 1987, **7**, 155; T. Otsubo, Y. Aso and K. Takimiya, *Adv. Mater*., 1996, **8**, 203; N. L. Navor, N. Robertson: T. Weyland, J. D. Kilburn, A. E. Underhill, M. Webster, N. Svenstrup and J. Becher, *Chem. Commun*., 1996, 1363; D. Solooli, T. C. Parker, S. I. Khan and Y. Rubin, *Tetrahedron Lett*., 1998, **39**, 1327.

2 M. R. Bryce, W. Devonport, L. M. Goldenberg and C. Wang, *Chem. Commun*., 1998, 945; T. Yamamoto and T. Shimizu, *J. Mater. Chem.*, 1997, **7**, 1967; L. van Hink, G. Schukat and E. Franghanel, *J. Prakt. Chem*., 1979, **321**, 299; M. R. Bryce, A. C. Chissel, J. Gopal, P. Kathirgamanathan and D. Parker, *Synth. Met.*, 1991, **39**, 397; C. Thobie-Gautier, A. Gorgues, M. Jubault and J. Roncali, *Macromolecules*, 1993, **26**, 4094; M. Fourmigue, I. Johannsen, K. Boubekeur, C. Nalson and P. Batail, *J. Am. Chem. Soc*., 1993, **115**, 3752; S. Frenzel, S. Arndt, R. M. Gregorious and K. Müllen, *J. Mater. Chem*., 1995, **5**, 1529; A. Charlton, A. E. Underhill, G. Williams, M. Kalaji, P. J. Marphy, D. E. Hibbs, M. B. Hursthouse and K. M. A. Malik, *Chem. Commun*., 1996, 2423; L. Huchet, S. Akoudad, E, Levillain, J. Roncali and P. Bäuerle, *J. Phys. Chem.*, 1998, **102**, 7776; S. Shimada, A. Masaki, K. Hayamizu, H. Matsuda, S. Okada and H. Nakanishi, *Chem. Commun*., 1997, 1421.

3 T. Otsubo, Y. Kochi, A. Bitoh and F. Ogura, *Chem. Lett*., 1994, 2407.

4 (*a*) A. Furlani, C. Napoletano, M. Russo, A. Camus and N. Marisich, *J. Polym. Sci., Polym. Chem. Ed.*, 1989, **27**, 75; (*b*) M. Tabata, W. Yang and K. Yokota, *Polym. J*., 1990, 12, 1105; (*c*) M. Tabata, W. Yang and K. Yokota, *J. Polym. Sci., Part A, Polym. Chem*., 1994, **32,** 1113.

5 (*a*) M. Hatano, S. Kanbara and S. Okamoto, *J. Polym. Sci.*, 1961, **51**, S26; (*b*) H. W. Gibson and J. M. Pochan, *Macromolecules*, 1982, **15**, 242; (*c*) T. Yamamoto, H. Saito, K. Osakada, I. Ando and M. Kikuchi, *Polym. Bull*., 1992, **29**, 597.

6 C. I. Simionescu and V. Percec, *J. Polym. Sci., Polym. Symp*., 1980, **67**, 43; T. Masuda, H. Izumikawa, Y. Misumi and T. Higashimura, *Macromolecules*, 1996, **29**, 1167.

7 T. Yamamoto and H. Etori, *Macromolecules*, 1995, **28**, 3371; H. Etori, T. Kanbara and T. Yamamoto, *Chem. Lett*., 1994, 461.

8 T. Yamamoto, K. Sanechika and A. Yamamoto, *Inorg. Chim. Acta*, 1983, **73**, 75.

Communication 9/00300B

Hydrothermal synthesis of Mo–V–M–O complex metal oxide catalysts active for partial oxidation of ethane

Wataru Ueda,*[b] Ning Fang Chen[a] and Kenzo Oshihara[b]

[a] *Department of Environmental Chemistry and Engineering, Tokyo Institute of Technology, Nagatsuta-cho, Midori-ku, Yokohama, 226-0087 Japan*

[b] *Department of Materials Science and Engineering, Science University of Tokyo in Yamaguchi, 1-1-1 Daigaku-dori, Onoda, Yamaguchi, 765-0884 Japan. E-mail: ueda@ed.yama.sut.ac.jp*

Received (in Cambridge, UK) 27th November 1998, Accepted 19th February 1999

Mo–V–M–O (M = Al, Fe, Cr and Ti) complex metal oxide catalysts have been prepared by hydrothermal synthesis for the first time and showed activity for the partial oxidation of ethane to ethene and acetic acid.

In the last decade much progress has been made in the selective partial oxidation of light alkanes with molecular oxygen in gas phase.[1] Many types of metal oxides have been used to create catalytically active solid phases for various oxidation processes for promoting both the conversion of alkanes and the selectivity to partial oxidation products.[2] The most well known catalyst is crystalline V–P–O complex oxide for the selective oxidation of *n*-butane to maleic anhydride.[3] Crystalline forms or fine composites of complex metal oxides seem to be necessary for achieving high conversion and selectivity in alkane oxidation. It has already been shown that the Mo–V–O catalyst system, characterized by an X-ray diffraction peak near 4.0 Å (2θ = 22°, CuKα), is active for the oxidative dehydrogenation of ethane.[4,5] We have thus started studies to prepare monophasic materials or uniform fine composites of Mo–V–M–O catalysts by a hydrothermal synthetic method and recently succeeded in synthesizing solid materials which gave the same X-ray diffraction peaks and were catalytically active for the partial oxidation of ethane to ethene and acetic acid. We report here the synthetic method and the catalytic performance.

Since hydrothermal treatments at 175 °C did not give solid materials either from a mixed aqueous solution of $(NH_4)_6Mo_7O_{24}$ and NH_4VO_3 or from a solution of $(NH_4)_6Mo_7O_{24}$ and $VOSO_4$, we tried to add other metal cations for organization of Mo and V. For this purpose, Anderson-type heteropolymolybdates were chosen and metal cations such as Al, Fe, Cr, Bi, Co as heteroatoms in the Anderson structure were found to be effective organization elements. The Anderson-type heteropolymolybdates were prepared according to the reported procedure using $(NH_4)_6Mo_7O_{24}$ and metal sulfate (or alum).[6,7] The phase purity of the crystallized heteropolymolybdate samples was ascertained by XRD analysis. Hydrothermal reaction of the various Anderson-type heteropolymolybdates and $VOSO_4$ in water was carried out at 175 °C for 48 h in a PTFE lined autoclave (50 ml) without mixing. Typically, a sample, such as MoVAlO(621), where the numbers in parentheses show the atomic ratios of each element in the preparation, respectively, was synthesized in the following manner. To an aqueous solution (25 ml) of the prepared crystalline Anderson-type heteropolymolybdates, $(NH_4)_3H_6AlMo_6O_{24}\cdot 7H_2O$ (2.4 mmol) and an aqueous solution (15 ml) of $VOSO_4$ (4.8 mmol) was added dropwise with stirring at 50 °C, giving a brown–black liquid which was then allowed to undergo hydrothermal reaction in the autoclave. All reagents used were of commercially available research grade. After *ca.* 4 h reaction a small amount of black solid became observable on the wall of the autoclave and the mixed solution was black–blue. After 48 h the reaction was almost complete, yielding a substantial amount of solid in the bottom of the autoclave as well as on the wall. The obtained dark purple solid material was separated from the solution which was light green–yellow probably due to remaining V^{5+} in solution. The separated mass was washed with distilled water and dried at 40 °C overnight in air. The yield was 60 wt%. It was ascertained by XPS that the oxidation states of molybdenum and vanadium in the hydrothermally synthesized sample were 6+ and 4+, respectively, and an ICP analysis revealed that the sample contained each metal cation with a composition of $Mo_6V_{2.1}Al_{0.9}O_x$. Samples containing other metal cations (Fe, Cr, Bi or Co) were also synthesized by the same manner.

XRD patterns of the samples are shown in Fig. 1. The patterns are quite characteristic; only two sharp diffraction peaks were observed at 2θ *ca.* 22 and 45° ascribed to (00*l*) reflections and other very broad diffraction peaks appeared at 8, 11 and 27°. Mo–V–O based complex oxides giving these characteristic diffractions at 22 and 45° has already been reported in papers and patents as a key catalyst phase for acrolein oxidation to acrylic acid, ethane oxidation to ethene, and propane ammoxidation to acrylonitrile.[4–10] In these cases, however, the materials were synthesized through complicated reduction–oxidation processes in the preparation liquid and also by high-temperature heating processes, so that the materials thus prepared are multiphasic and of poor crystallinity. In the hydrothermal synthesis presented here for the first time, the preparation is very simple and highly reproducible, and sharp XRD diffraction peaks were observed, implying that the hydrothermally synthesized materials have higher crystallinity. In fact we observed rod-shape uniform crystals (0.1 μm × 0.3 μm × 10 μm on average) by SEM.

As can be seen in Fig. 1, the XRD characteristics are almost independent of the added metal cations but the relative intensities between the sharp and broad peaks are obviously different. It is, therefore, obvious that all the samples are at least

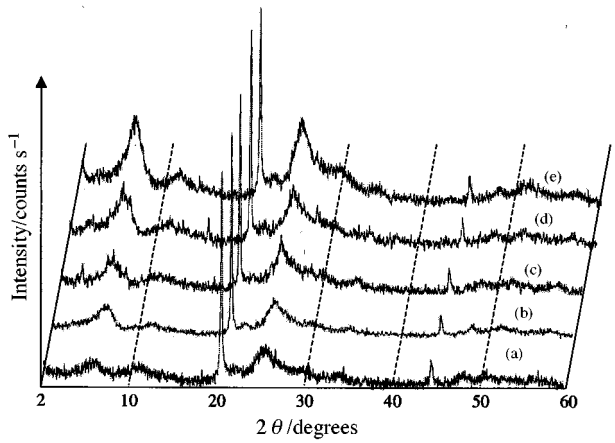

Fig. 1 XRD patterns of the hydrothermally synthesized Mo–V–M–O catalysts. XRD data were collected using a X-ray diffractometer with Cu-Kα radiation: (a) MoVCrO(621), (b) MoVFeO(661), (c) MoVBiO(621), (d) MoVAlO(621), (e) MoVCoO(621).

biphasic; one gives a set of the narrow diffraction lines and the other a set of the broad lines. For the phase giving the set of the narrow diffraction lines, we speculate, on the basis of layer-type structures proposed for Mo–V–O based oxides giving a diffraction peak at $2\theta = 22°$,[9,11] that self-organization takes place between Anderson-type heteropolyanion units and vanadyl cations under the hydrothermal reaction conditions, forming slabs with these being stacked to form a solid with a layer structure in which one crystal direction is ordered giving clear XRD peaks. Obviously we need more experimental results to clarify the structure and such work is being undertaken now.

The hydrothermally synthesized solid materials showed high catalytic activities for C_1–C_4 alkane oxidation, particularly for the production of ethene and acetic acid from direct ethane oxidation as shown in Table 1. Prior to the catalytic ethane oxidation, the catalysts were heat-treated at 410 °C for 2 h in a nitrogen stream. By this treatment the catalysts became active for the reaction but the XRD patterns did not change. When the reaction was conducted using the catalyst containing Al, Fe or Cr at 340 °C under the conditions indicated, ethane was oxidized into ethene and acetic acid quite selectively and the other products were carbon oxides. The Cr-containing catalyst tends to promote more complete oxidation. All the catalysts were highly stable under the reaction conditions, giving constant activity and selectivity. We also tried to incorporate titanium into the Mo–V–Al–O catalyst in order to improve the catalytic performance since the benificial effect of titanium has already been reported in the V–Ti–O system.[12] The catalysts MoVAlTiO were prepared by adding known amounts of $(NH_4)_2Ti(C_2O_4)_2$ into the preparative solution for hydrothermal reaction. As shown in Table 1 we observed a significant increase of the oxidation activity without significant alteration in the product selectivities. Since no additional XRD peaks were observed in the MoVAlTiO catalysts but the peaks of (00l) reflections widened, the activity increase seems to result from the increase of active area of the catalysts. As a consequence, the present result provides a new preparation route to Mo–V–O based complex oxide catalysts.

Table 1 Partial oxidation of ethane over Mo–V–M–O catalysts[a]

	Conversion (%)		Selectivity (%)			
Catalyst	C_2H_6	O_2	C_2H_4	$MeCO_2H$	CO_2	CO
MoVAlO(621)	3.9	13.2	70.4	8.1	7.6	13.9
MoVCrO(621)	4.2	18.4	55.8	10.7	12.4	21.0
MoVFeO(621)	2.6	8.4	71.0	11.2	6.8	11.0
MoVAlTiO(621-0.5)	9.1	36.3	61.5	11.9	9.1	17.5
MoVAlTiO(621-0.7)	14.7	61.3	59.6	11.5	9.9	19.0

[a] *Reaction conditions*: reaction temperature, 340 °C; catalyst weight, 1.0 g; reactant gas feed, atmospheric pressure, total flow rate, 50 ml min^{-1}; feed composition, C_2H_6:O_2:H_2O:N_2 = 30:10:20:40 (mol%).

Notes and references

1 Y. Moro-oka and W. Ueda, *Catalysis*, 1994, **11**, 223.
2 S. Albonetti, F. Cavani and F. Trifiro, *Catal. Rev.-Sci. Eng*., 1996, **38**, 413.
3 G. J. Hutchings, *Catal. Today*, 1993, **16**, 139.
4 E. M. Thorsteinson, T. P. Wilson, F. G. Young and P. H. Kasai, *J. Catal*., 1978, **52**, 116.
5 K. Ruth, R. Kieffer and R. Burch, *J. Catal*., 1998, **175**, 16; K. Ruth, R. Burch and R. Kieffer, *J. Catal*., 1998, **175**, 27.
6 L. C. W. Baker, G. Foster, W. Tan, F. Scholnick and T. P. McCutcheon, *J. Am. Chem. Soc*., 1955, **77**, 2136.
7 K. Nomiya, T. Takahashi, T. Sshirai and M. Miwa, *Polyhedron*, 1987, **6**, 213.
8 Mitsubisi Chemical, USP 5,472,925, 1995; T. Ushikubo, K. Oshima, A. Kayou, M. Vaarkamp and M. Hatano, *J. Catal*., 1997, **169**, 394; T. Ushikubo, K. Oshima, A. Kayou and M. Hatano, *Stud. Surf. Sci. Catal*., 1997, **112**, 473.
9 T. V. Andrushkevich, *Catal. Rev.-Sci. Eng*., 1993, **35**, 213.
10 Nippon Kayaku, JP 8-299797, 1996.
11 P. Courtine and E. Bordes, *Appl. Catal*., 1997, **157**, 45.
12 L. Tessier, E. Bordes and M. Gubelmann-Bonneau, *Catal. Today*, 1995, **24**, 335.

Communication 8/09278H

Synthesis of 16-desmethylepothilone B: improved methodology for the rapid, highly selective and convergent construction of epothilone B and analogues

K. C. Nicolaou,* David Hepworth, M. Ray V. Finlay, N. Paul King, Barbara Werschkun and Antony Bigot

Department of Chemistry and The Skaggs Institute for Chemical Biology, The Scripps Research Institute, 10550 North Torrey Pines Road, La Jolla, California 92037, USA and Department of Chemistry and Biochemistry, University of California San Diego, 9500 Gilman Drive, La Jolla, California 92093, USA. E-mail: kcn@scripps.edu

Received (in Corvallis, OR, USA) 21st December 1998, Accepted 4th February 1999

During a synthesis of 16-desmethylepothilone B new methods for the convergent and highly stereoselective synthesis of epothilone B and analogues were developed.

Due to their great potential as anticancer drugs with a paclitaxel-like mechanism of action, the epothilones have recently been at the focus of widespread scientific investigations.[1] In particular, significant attention has concerned chemical synthesis of the epothilone natural products, which we and others have successfully achieved.[1–3] In connection with on-going studies in the epothilone area we were interested in preparing analogues of epothilone B containing less conformationally restrained heteroaromatic side-chains, in particular the 16-desmethyl analogue **1** (Fig 1). Since this endeavour required a complete resynthesis of the epothilone macrocycle we took this opportunity to develop new methods for the swift assembly of epothilone B analogues with improved selectivities and yields.

Our aims were to combine the benefits of our highly modular and convergent approach to epothilone A and analogues *via* olefin metathesis,[1] which allowed for extremely rapid macrocycle construction, with the improved stereoselectivities inherent in our macrolactonisation strategy to epothilone B.[1] We envisioned that our approach to epothilone B analogues could be made more convergent by employing a fully functionalised C7–C12 fragment in a highly selective olefination reaction to construct the C12–C13 bond. This approach would also allow access to C26 modified analogues as previously described.[1,3*a*] Furthermore, we wished to retain a hydroxy group at the C26 position until a late stage in the synthesis and thus profit from a chemo-, regio- and stereo-selective Sharpless epoxidation.[1,3*a*] In adopting this route we were aware that a method for subsequent deoxygenation at the C26 position (adjacent to the epoxide) would have to be developed. Finally, we hoped to improve the pivotal aldol coupling step which provides the stereocentres at C6 and C7 of the macrocycle. Previously we have found this reaction to be somewhat capricious.

The thiazole aldehyde fragment **6a**† was prepared in an analogous fashion to the related epothilone B fragment with minor changes in experimental conditions (Scheme 1). An asymmetric allylboration was the key step used to introduce the stereogenic centre at C15.‡ The regioselectivity of the dihydroxylation was lower than in the epothilone B series which slightly impaired the overall yield for this fragment. The fully functionalised phosphorane **14** was prepared in short order from commercially available **7** without the need for chiral auxiliaries.

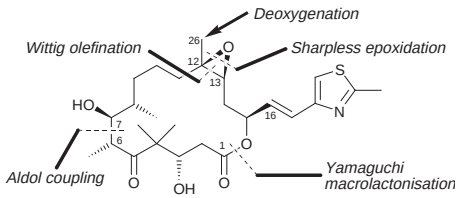

Fig. 1 Numbering and bond disconnections for **1**.

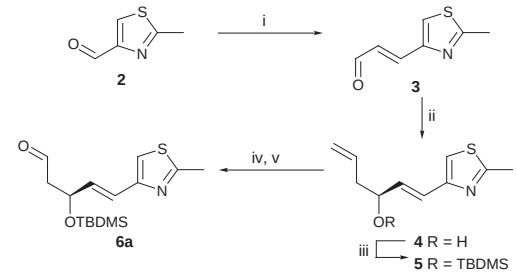

Scheme 1 *Reagents and conditions*: Ph_3P=CHCHO, CH_2Cl_2, reflux, 12 h, 82%; ii, (+)-Ipc_2B(allyl), CH_2Cl_2, Et_2O, pentane, −100 °C, 2 h, 100%; iii, TBDMSCl, imidazole, DMF, 0 → 25 °C, 2 h, 99%; iv, OsO_4 (cat.), NMO, THF, Bu^tOH, H_2O, 25 °C, 12 h, 68%; v, $NaIO_4$, MeOH, H_2O, 0 → 25 °C, 1 h, 89% (Ipc = isopinocampheyl).

The reaction sequence includes an efficient cuprate coupling,[4] and a chloroformate quench of an unstabilised ylide[5] as the key steps (Scheme 2). Control of temperature during the latter reaction is critical to obtain phosphorane of good quality.§

The all-important Wittig coupling of **14** and **6a** proceeded smoothly with excellent yield and selectivity ($E:Z > 30:1$ in all cases) to provide the coupled product **15a**, which was processed to **21a** (Scheme 3). We have since extended this approach to the natural epothilone B series **23b**, the 26-hydroxyepothilone B series **21b** and the highly flexible vinyl iodide series **21c**, which we have shown to be invaluable for producing heterocycle-modified epothilones.[1,3*b*,*c*] This route also enabled us to approach the highly epimerisation-prone aldehydes **21a**-**c** and **23b** through stereochemically 'safe' alcohol oxidation procedures.¶

We reasoned that the moderate and variable stereoselectivities obtained in the coupling of **24** with chiral aldehydes such as **21a**–**c** and **23b** may be due, at least in part, to the reversible nature of aldol reactions using ketone-derived lithium enolates.[7] In an attempt to alleviate such problems we have performed the reaction with an excess of enolate,‖ very short reaction time and a rapid low temperature quench (AcOH). Gratifyingly, the

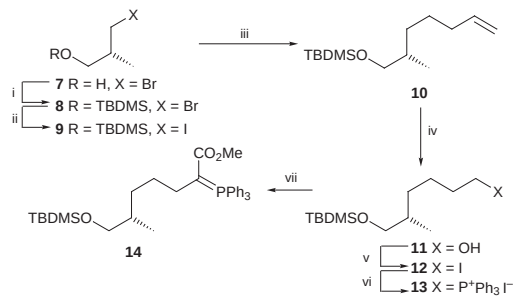

Scheme 2 *Reagents and conditions*: TBDMSCl, imidazole, DMF, 0 → 25 °C, 1 h; ii, NaI, acetone, reflux, 12 h, 99% (2 steps); iii, CH_2=$CHCH_2CH_2MgBr$, Li_2CuCl_4 (cat.), THF, 0 °C, 1 h, 96%; iv, (a) O_3, CH_2Cl_2, −78 °C, then PPh_3; (b) $NaBH_4$, EtOH, 0 °C, 30 min., 91% (2 steps); v, I_2, PPh_3, CH_3CN, Et_2O, 0 → 25 °C, 1 h, 100%; vi, PPh_3, neat, 100 °C, 2 h; vii, KHMDS, THF, 0 °C, 30 min, then MeOCOCl, −78 °C, 3 h (*ca.* 100%, 2 steps, unpurified).

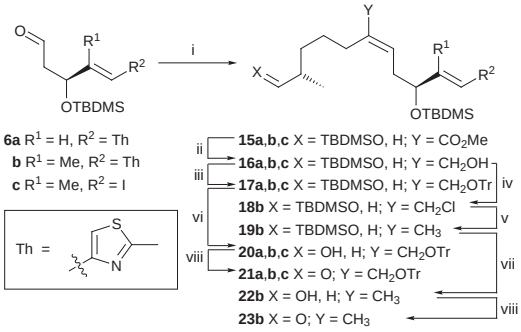

Scheme 3 *Reagents and conditions*: i, **14** (1.3 equiv. based on **12**), C_6H_6, reflux, 18 h, 84–93%; ii, DIBAL-H, THF, −78 °C, 3 h, 71–95%; iii, TrCl, DMAP, DMF, 70 °C, 18 h, 82–95%; iv, CCl_4, PPh_3, reflux, 18 h, 80%; v, $LiEt_3BH$, THF, −78 °C, 1 h, 92%; vi, HF•Py.Py, THF, 25 °C, 4 h, 66–73%; vii, CSA, MeOH, 25 °C, 1 h, 95%; viii, SO_3•Py, DMSO, Et_3N, THF, 0 °C, 1 h.

application of these conditions to aldehydes **21a–c** and **23b** lead to significant amelioration of stereoselectivity which was naturally accompanied by an improved yield of the desired aldol stereoisomer in each case (Scheme 4, Table 1). Intermediates **25a–d** were obtained in good overall yields after subsequent TBDMS-protection. Under these closely defined conditions the aldol reaction is highly reproducible and applicable to multigram quantities. These results, in terms of diastereoselectivities and yields, are at least as good as those obtained by Schinzer and co-workers in their epothilone B syntheses.[2b] Since our approach features a rather convenient protecting group strategy, we believe this development renders our modified route the most effective solution to date for epothilone B.

The TBDMS-protected aldol product **25a** was processed through to 26-hydroxy-16-desmethylepothilone B **30** in the same fashion as our published route to 26-hydroxyepothilone B (Scheme 5).[3a] As projected, the Sharpless epoxidation proceeded with complete stereo- and regio-control at the C12–C13 position. It should be noted that for this analogue series, competitive side-chain epoxidation would likely have been problematic upon use of conventional oxidants. In order to complete the synthesis, removal of the C26 hydroxy group was required. This was achieved by initial conversion to iodide **31** followed by reductive deiodination with $NaBH_3CN$[7] to provide

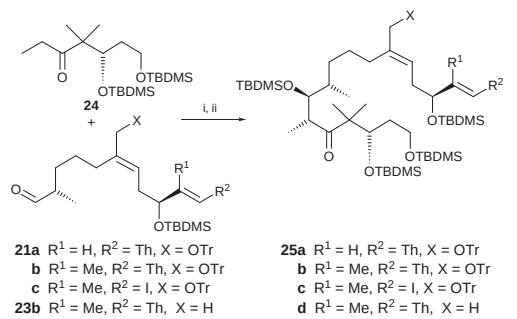

Scheme 4 *Reagents and conditions*: i, LDA (2.4 equiv.), **24** (2.3 equiv.), THF, −78 → −40 °C, 1 h, then add **21** or **23**, THF −78 °C, 2 min, then AcOH, −78 → 0 °C; ii, TBDMSOTf, 2,6-lutidine, THF, −78 → 0 °C, 1 h.

Table 1 Yields and stereoselectivities for aldol reactions

Aldehyde	Selectivity[a]	Aldol product (%)[b]	**25** (%) (2 steps)[c]
21a	⩾10 : 1	76	72
21b	⩾15 : 1	77	73
21c	⩾10 : 1	79	75
23b	⩾10 : 1	71	67

[a] Conservative estimates based upon mass recovery of the major isomer relative to all other polar impurities. [b] Often contaminated with small amounts (= 5%) of starting aldehyde. Yields are compensated. [c] Single stereoisomer free from traces of aldehyde and other impurities.

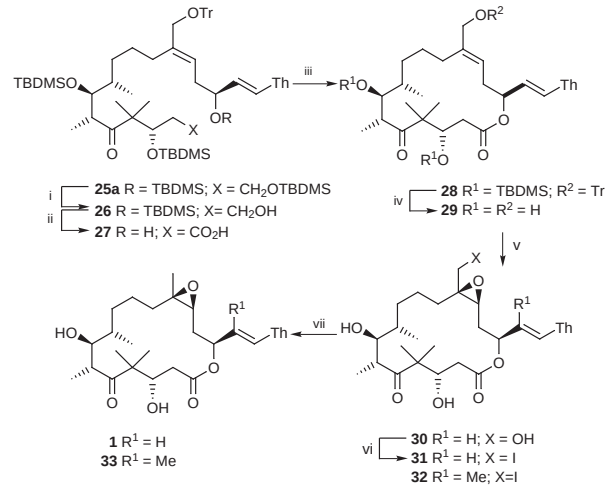

Scheme 5 *Reagents and conditions*: i, HF•Py.Py, THF, 25 °C, 3 h, 87% (after 1 recycle); ii, (a) $(COCl)_2$, DMSO, CH_2Cl_2, −78 °C, 30 min, then Et_3N, −78 → 0 °C, 30 min; (b) $NaClO_2$, Me_2C=CHMe, NaH_2PO_4, Bu^tOH–H_2O, 25 °C, 2 h; (c) TBAF, THF, 25 °C, 12 h, *ca.* 100% (3 steps); iii, 2,4,6-$Cl_3C_6H_2COCl$, Et_3N, THF, 0 °C, 1 h, then add to DMAP in toluene, 75 °C, 1 h, 73%; iv, HF•Py, THF, 0 → 25 °C, 24 h, 78%; v, (+)-diethyl L-tartrate, $Ti(Pr^iO)_4$, Bu^tOOH, CH_2Cl_2, 4 Å MS, −30 °C, 2 h, 80%; vi, (a) TsCl, Et_3N, DMAP, CH_2Cl_2, 0 → 25 °C, 1 h; (b) NaI, acetone, 25 °C, 15 h, 91% (2 steps); vii, $NaBH_3CN$, HMPA, 45 °C, 40 h, 67–70%.

our desired analogue **1** in good overall yield. Furthermore, this deoxygenation sequence has also been demonstrated for the production of epothilone B (**33**) itself from our previously reported iodide **32**. Thus, all of the synthetic methodology described herein is applicable to epothilone B, which renders our approach now *highly selective at every step*, and significantly increases the speed of access to this and related structures. Work is currently underway to assess the biological activity of **1** and related analogues of epothilone B.

We thank D.-H. Huang and Gary Siuzdak for NMR and MS studies, respectively. This research was financially supported by the National Institutes of Health USA and The Skaggs Institute for Chemical Biology, from the George Hewitt Foundation (to N. P. K.), the Deutsche Forschungsgemeinschaft (to B. W.), and grants from CaPCURE and Novartis.

Notes and references

† All new compounds exhibited satisfactory spectral and exact mass data.
‡ The ee was shown to be ⩾97% by chiral HPLC (Chiralcel OD-H column) by comparison with the racemate.
§ Due to high polarity and complex NMR spectra **14** was not purified as characterized. We observed full mass return for **12** → **14** and used the material crude using quantities assuming purity.
¶ The aldehydes were freshly prepared and not purified prior to use.
‖The unreacted ketone **24** is easily recovered by chromatography.

1 For a review of the literature to Feb. 1998, see: K. C. Nicolaou, F. Roschangar and D. Vourloumis, *Angew. Chem., Int. Ed.*, 1998, **37**, 2014.
2 For recent syntheses see: (*a*) S. A. May and P. Grieco, *Chem. Commun.*, 1998, 1597; (*b*) D. Schinzer, A. Bauer and J. Scheiber, *Synlett*, 1998, 861; (*c*) A. Balog, C. Harris, K. Savin, X.-G. Zhang, T. C. Chou and S. J. Danishefsky, *Angew. Chem., Int. Ed.*, 1998, **37**, 2675; (*d*) J. Mulzer, A. Mantoulidis and E. Öhler, *Tetrahedron Lett.*, 1998, **39**, 8633; (*e*) S. C. Sinha, C. F. Barbas III and R. A. Lerner, *Proc. Natl. Acad. Sci. U.S.A.*, 1998, **95**, 14603.
3 (*a*) K. C. Nicolaou, M. R. V. Finlay, S. Ninkovic and F. Sarabia, *Tetrahedron*, 1998, **54**, 7127; (*b*) K. C. Nicolaou, M. R. V. Finlay, S. Ninkovic, N. P. King, Y. He, T. Li, F. Sarabia and D. Vourloumis, *Chem. Biol.*, 1998, **5**, 365; (*c*) K. C. Nicolaou, N. P. King, M. R. V. Finlay, Y. He, F. Roschangar, D. Vourloumis, H. Vallberg, F. Sarabia, S. Ninkovic and D. Hepworth, *Bioorg. Med. Chem.*, 1998, in the press.
4 M. Tamura and J. Kochi, *Synthesis*, 1971, 303.
5 Y. Morimoto and H. Shirahama, *Tetrahedron*, 1996, **52**, 10631.
6 C. H. Heathcock, in *Comprehensive Organic Synthesis*, ed. B. M. Trost and I Fleming, Pergamon, Oxford, 1991, vol. 2, pp. 181–235.
7 R. O. Hutchins, D. Kandasamy, C. A. Maryanoff, D. Masilamani and B. E. Maryanoff, *J. Org. Chem.*, 1977, **42**, 82.

Communication 8/09954E

V–Zr–P oxide catalysts for highly selective oxidation of propane to acrylic acid

Yi-Fan Han, Huai-Ming Wang, Hua Cheng and Jing-Fa Deng*

Department of Chemistry, Fudan University, Shanghai 200433, People's Republic of China.
E-mail: jfdeng@srcap.stc.sh.cn

Received (in Cambridge, UK) 6th January 1999, Accepted 19th February 1999

V–Zr–P oxide catalysts have been prepared and exhibited high selectivity in the oxidation of propane to acrylic acid.

The selective oxidation of lower alkanes to other chemicals is attracting attention for economic reasons and their availability. The best-known oxidation of lower alkanes is the selective oxidation of *n*-butane to maleic anhydride over vanadium phosphorus oxide catalysts (VPO).[1] Moreover, oxidation of propane to propylene,[2–4] acrolein[5] and acrylonitrile[6] has been widely developed. It was found first by Ai[7,8] that a VPO based catalytic system could directly oxidize propane to acrylic acid effectively. The V_2O_5–P_2O_5–X_nO_m (X_nO_m = SO_3, TeO_2, Nb_2O_3, Sb_2O_3, SiO_2 and B_2O_3) type catalysts have been tested and the catalytic performance in this process is clearly improved. However, the reaction carried out on VPO catalysts at relatively high temperature (400 °C) not only results in a low selectivity to acrylic acid, but also leads to serious formation of coke on the catalyst surface and shortage of lifetime. To solve these problems, we have reported the use of a titania–silica xerogel supported VPO catalyst in this reaction[9] which showed highly selective oxidation of propane to acrylic and acetic acid at low temperature (300 °C). So far, the yield and selectivity to acrylic acid for all developed catalysts are too low to be applied at commercial level. For this reason, we sought to develop a new catalyst that possesses good performance at low temperature in order to give high yield and selectivity to acrylic acid without coking.

In our study, it was demonstrated that V–Zr–P (Zr : V = 0.5) oxide catalyst showed significant high selectivity and yield to acrylic acid at 340 °C, and had the potential for practical use.

V–Zr–P oxide catalysts were prepared by the following procedure: a mixture of V_2O_5 and $ZrOCl_2{\cdot}H_2O$ in stoichiometrical atomic ratio (Zr : V) was reduced by refluxing in a solution of isobutanol (20 ml)–benzyl alcohol (10 ml) for 12 h; a black blue or gray suspended precipitate formed. Then, an appropriate amount of 85% H_3PO_4 [atomic ratio P : (Zr + V) = 1.0] was added to the solution, which was refluxed for 6 h to give a light blue–green suspended precipitate and a black–blue solution. The precipitate was filtered off and the obtained paste was dried in an oven at 120 °C overnight. The resulting precursor was ground and sieved to obtain a 40–60 mesh size portion. VPO (V : P = 1.0) and ZrPO (Zr : P = 1.0) catalysts were also prepared by the same procedure to enable comparison. The activation of precursor and oxidation of propane were carried out in a continuous tubular flow fixed-bed microreactor. The precursor of the V–Zr–P oxide catalyst (1.0 ml) was packed into a stainless steel reactor (id: 6.0 mm, length: 20 cm) and the temperature was raised to 773 K at a rate of 20 K min^{-1} in a mixture of air–propane–water vapor (75.6 : 1.2 : 23.2) at a rate of 20 ml min^{-1} for 12 h. The sample was then cooled to the reaction temperature within 6 h.

The X-ray diffraction patterns for all the catalysts are in Fig. 1. Lines at 2θ = 23.1, 28.4 and 29.9° are attributed to $(VO)_2P_2O_7$, and those at 2θ = 22.0, 26.0 and 28.9° are attributed to $VOPO_4$, respectively.[10] It can be seen that the bare VPO catalyst is mainly constituted of $(VO)_2P_2O_7$ with some $VOPO_4$. The X-ray line due to $(VO)_2P_2O_7$ broadened and diminished with increase of the atomic ratio of Zr : V in the V–Zr–P oxides. Only small broad diffraction peaks were detected

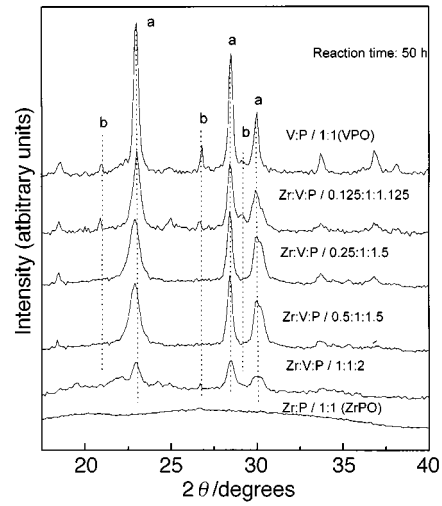

Fig. 1 XRD patterns of V–Zr–P oxide catalysts; (a) $(VO)_2P_2O_7$, (b) $VOPO_4$.

when Zr : V was raised to 1.0, indicating that $(VO)_2P_2O_7$ starts to become disordered. No distinct XRD line can be found for ZrPO, suggesting that ZrPO is an amorphous material. In addition, no zirconium phosphate was evidenced for any V–Zr–P oxides, implying that ZrPO can only disperse into the structure of VPO or form a solid solution with $(VO)_2P_2O_7$. It is also interesting to observe that the $VOPO_4$ phase disappears as Zr : V is increased to 0.25, which suggests that its formation has been suppressed.

All catalysts employed in this study were tested for the selective oxidation of propane to acrylic acid. The optimal results summarized in Table 1 show that ZrPO is inert to this reaction. For VPO catalyst, the yield and selectivity to acrylic acid are 11.2 and 48.1%, respectively. With the addition of Zr, the yield and selectivity increase sisgnificantly in comparison with the VPO catalyst. As Zr : V is changed from 0.125 to 0.5, the selectivity increases from 70.0 to 81.0% and the yield increases from 13.5 to 14.8%. With continuous increasing ratio of Zr : V to 1.0, the activity and selectivity start to decrease.

It can be seen in Fig. 2, that the temperature for achieving maximum selectivity shifts from 400 (VPO) to 340 °C (V–Zr–P

Table 1 The performance of V–Zr–P oxide catalysts[a]

V : Zr atomic ratio	*T*/°C	Conv. (mol%)	Yield (mol%)	Sel. (mol%)
1 : 1	340	16.1	12.7	70.3
1 : 0.5	340	17.5	14.8	81.0
1 : 0.25	360	18.4	14.2	71.0
1 : 0.125	380	18.5	13.5	70.0
VPO	400	23.0	11.2	48.1
ZrPO	400	—	—	—

[a] *Reaction conditions*: GHSV = 1000 h^{-1}, feed gas = air–propane–water = 73.4 : 3.2 : 23.4, time = 50 h, cat. 1.0 g; analysis: on-line gas chromatograph.

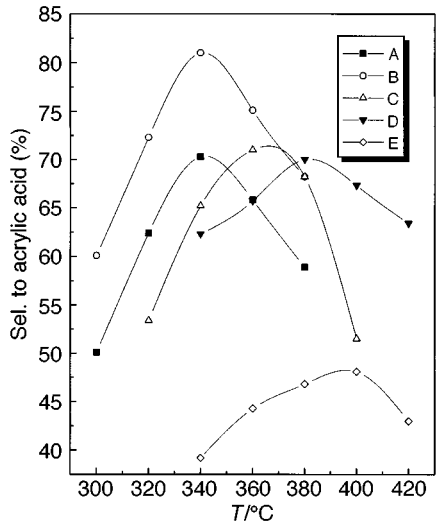

Fig. 2 Dependence of selectivity of acrylic acid on reaction temperature; (A) Zr : V : P = 1 : 1 : 2, (B) Zr : V : P = 0.5 : 1 : 2, (C) Zr : V : P = 0.25 : 1 : 2, (D) Zr : V : P = 0.125 : 1 : 2, (E) VPO. Reaction conditions: GHSV = 1000 h^{-1}, feed gas = air–propane–water vapor (73.6 : 3.2 : 23.2), time = 50 h.

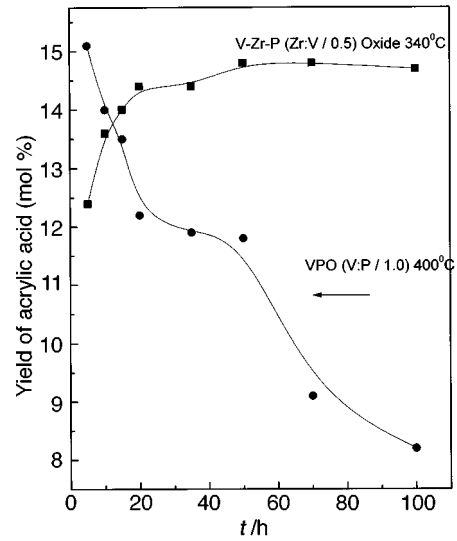

Fig. 3 Dependence of reaction time on the yield of acrylic acid. Reaction conditions: GHSV = 1000 h^{-1}, feed gas = air–propane–water vapor (73.6 : 3.2 : 23.2).

oxide, Zr : V = 0.5). It is well known that lowering temperature is favorable for reducing coke formation and beneficial in increasing the lifetime of the catalyst. Fig. 3 shows that V–Zr–P (Zr : V = 0.5) oxide catalyst shows significantly higher catalytic stability than that of VPO after 100 h of operation.

Comparison of XRD patterns with the catalytic properties of V–Zr–P oxides, as shown in Fig. 1 and Table 1, suggests a correlation of XRD line strength for $(VO)_2P_2O_7/VPOP_4$ with the catalytic performance of the catalyst. $(VO)_2P_2O_7$ most likely acts as the active phase in oxidation of propane as found in the VPO based catalytic system in oxidation of butane.[10] Further, the addition of amorphous materials in the structure of V–Zr–P oxide may effectively disperse VO_x or $(VO)_2P_2O_7$, and make an important contribution in enhancing the selectivity of catalyst.

In summary, V–Zr–P oxide catalysts exhibit satisfactory performance for selective oxidation of propane to acrylic acid. The best result, 14.8% yield and 81.0% selectivity, is shown by the catalyst with V : Zr : P = 1 : 0.5 : 1.5, at an optimum reaction temperature of 340 °C. It is clear that V–Zr–P oxide catalysts are promising for use in the selective oxidation of propane to acrylic acid.

This work was supported by the National Natural Science Foundation of China.

Notes and references

1 F. Cavani and F. Trifiro, *Catalysis*, 1994, **11**, 246.
2 G. Bellussi, G. Centi, S. Perathoner and F. Trifiro, in *Catalytic Selective Oxidation*, ed. S. T. Oyama and J. W. Hightower, American Chemical Society, Washington, DC, 1992, p. 281.
3 G. Centi, S. Perathoner, F. Trifiro, A. Aboukais, C. F. Aissi and M. Guelton, *J. Phys. Chem.*, 1992, **96**, 2617.
4 C. Mazzocchia, C. Aboumrad, C. Daigne, E. Tempesti, J. M. Herrmann and G. Thomas, *Catal. Lett.*, 1991, **10**, 181.
5 Y. C. Kim, W. Ueda and Y. Moro-oka, *Catal. Today*, 1992, **13**, 673.
6 T. Ushikubo, K. Oshima, A. Kayo, Umezawa K. Kiyono and I. Sawaki, *Eur. Pat.*, 529,853 A2, 1992, assigned to Mitsubishi Kasei Co.
7 M. Ai, *J. Catal.*, 1986, **101**, 389.
8 M. Ai, *Catal. Today*, 1992, **13**, 679.
9 Y. F. Han, H. M. Wang, H. Cheng, R. H. Jing and J. F. Deng, *New. J. Chem.*, 1998, 175.
10 *Vanadyl Pryophosphate Catalysis*, ed. G. Centi, Elsevier, Amsterdam, 1993, vol. 16, no. 1.

Communication 9/00219G

Self-assembly of a linear multicomponent porphyrin array through axial coordination

Kelly Chichak and Neil R. Branda*

Department of Chemistry, University of Alberta, Edmonton, AB, Canada T6G 2G2. E-mail: neil.branda@ualberta.ca

Received (in Columbia, MO, USA) 14th October 1998, Revised manuscript received 21st January 1999, Accepted 9th February 1999

The bis[4′-(4‴-pyridyl)-2,2′:6′,2″-terpyridine]ruthenium and osmium complexes 1a and 1b react with 2 equiv. of [Ru(TTP)(CO)(EtOH)] 4 to generate linear multicomponent arrays 3a and 3b; intramolecular phosphorescence quenching is observed for both arrays in contrast to their molecular building blocks which phosphoresce.

The rich photo- and redox chemistry of porphyrins has led to the design of sophisticated multicomponent molecular arrays held together by covalent or noncovalent interactions.[1] Efforts in this area have been spawned primarily by attempts to model solar energy capture and transfer in naturally occurring photosystems as well as to generate photoactive molecular devices.[2] One of the major concerns when designing such models is the ultimate control over the spatial organization of the chromophoric units within the arrays, where the photoinduced energy- and/or electron-transfer reactions of the resulting complexes will be governed by the supramolecular topology.

Our interests in this area are in the design and construction of molecular assemblies with well defined rigid architectures based on hybrid arrays of transition metal complexes axially coordinated to octahedral metalloporphyrins. We report here two linear multicomponent arrays **3a** and **3b** formed through the self-assembly of a central bis(terpyridine)transition metal complex linking two ruthenium(II) porphyrins *via* axial coordination.[3] The core units of triads **3a** and **3b** $[M(pytpy)_2]^{2+}$, pytpy = 4′-(4‴-pyridyl)-2,2′:6′,2″-terpyridine; M = Ru **1a**, Os **1b**] were prepared as their air-stable hexafluorophosphate salts as previously described.[4] The final triads **3a** and **3b** were prepared by adding 2 mol equiv. of [Ru(TTP)(CO)(EtOH)] **4**[5]† to 1 equiv. of $[M(pytpy)_2]^{2+}$ in acetone and gently heating (Scheme 1). Alternatively, the triads can be prepared at room temperature by adding an excess of the metalloporphyrin. In either case, the fully assembled triad complexes were isolated as red (Ru) and red–brown (Os) solids and characterized by UV–VIS spectroscopy, ^{1}H NMR spectroscopy and mass spectrometry.

The ^{1}H NMR spectra of both complexes **3a** and **3b** show significant upfield shifts for all hydrogen atoms of the $M(pytpy)_2^{2+}$ core unit as anticipated for protons lying within the shielding cone of the porphyrin (Fig. 1).[6] The anisotropic effect never completely disappears and extends over the entire distance spanned by the core unit (*ca.* 11 Å). We attribute this to an additive effect of both porphyrins forming the complex's walls. As expected, the protons immediately adjacent to the pyridine nitrogen of the core unit are the most affected and are seen to move as much as 7.5 ppm upfield upon complexation (protons H_a in Fig. 1). The smallest, but still significant, shielding effect acts upon the hydrogen atoms closest to the central metal which are shifted 0.5 ppm to higher field (protons H_c in Fig. 1).

The ^{1}H NMR studies reveal that, even in a competitive solvent such as acetone, coordination to the metalloporphyrin is strong and ligand-exchange is slow on the NMR timescale, and sharp, unchanging peaks for the statistical mixture of mono- and di-addition products were clearly visible when only 1 mol equiv. of [Ru(TTP)(CO)(EtOH)] **4** was added (Fig. 1, inset). This observation is useful when preparing complexes *in situ* and is utilitarian when constructing larger porphyrin arrays.‡

Initial photophysical studies show that the absorption spectra in the UV–VIS region of complexes **3a** and **3b** are essentially the sum of the absorption spectra of the triads' constituents. The steady-state emission properties of the triad complexes, however, differ greatly from those of their building blocks. In order

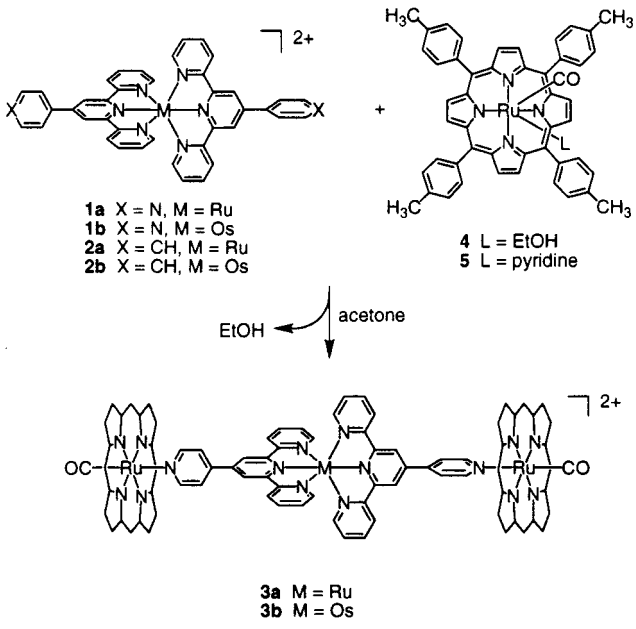

Scheme 1

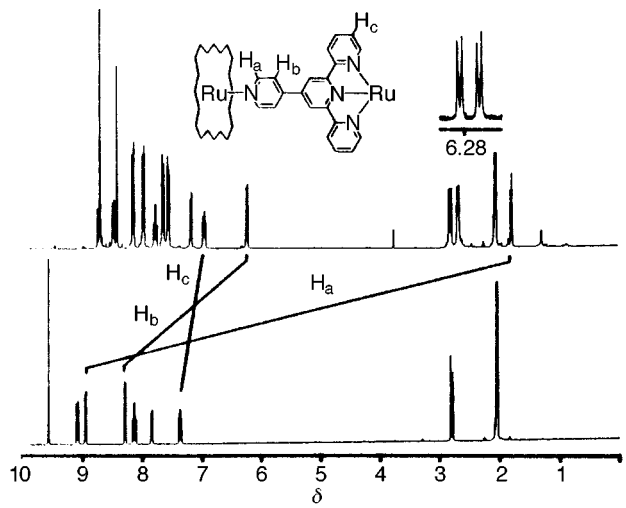

Fig. 1 ^{1}H NMR (300 MHz, acetone-d_6) spectra of $[Ru(pytpy)_2](PF_6)_2$ **1a** (bottom trace) and triad **3a** (top trace). The inset spectrum corresponds to protons H_b when only 1 mol equiv. of [Ru(TTP)(CO)(EtOH)] was added showing both mono- (peaks on the left) and bis-coordination (peaks on the right) arrays.

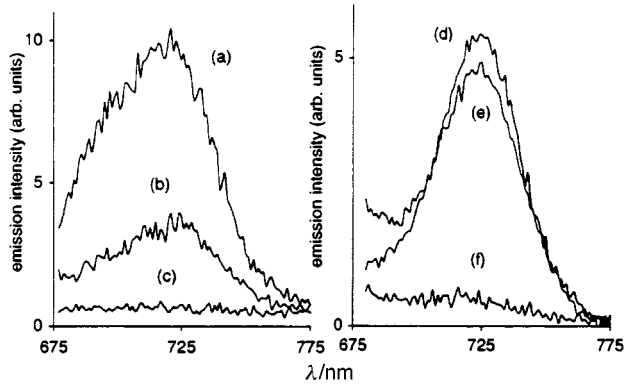

Fig. 2 Emission spectra (uncorrected) of CH_2Cl_2 solutions of (a) **2b** (λ_{ex} = 670 nm), (b) **1b** (λ_{ex} = 670 nm), (c) **3b** (λ_{ex} = 670 nm), (d) **5** (λ_{ex} = 530 nm), (e) 2 : 1 mixture of **5** and **2a** (λ_{ex} = 530 nm), (f) **3a** (λ_{ex} = 530 nm). All spectra were run in dry deoxygenated solvent.

to evaluate the photoemission properties of each of the triads' building blocks without complications from the other luminescent species, the triads composed of the two different core units **1a** and **1b** were investigated independently. The osmium core unit **1b** phosphoresces from its triplet excited state[2] at room temperature in CH_2Cl_2, but the phosphorescence of the triad **3b** is significantly quenched (Fig. 2). Here, the substantial reduction in phosphorescence intensity of the core unit on going from bis(terpyridine)osmium **1b** to triad **3b** can most likely be ascribed to ligation-induced quenching, where the porphyrin is acting as a Lewis acid for the monodentate pyridine of **1b**. This claim is supported by the complete luminescence quenching of **1b** upon *in situ* protonation with 2 equiv. of trifluoroacetic acid, although, at this stage, intramolecular triplet energy transfer from the core complex to the porphyrin cannot be completely ruled out.[9]

The lack of room temperature photoemission of the bis(terpyridine)ruthenium core unit **1a** enabled us to study the porphyrin unit, which shows substantially weaker phosphorescence intensity at room temperature in comparison with osmium core unit **1b**.[7] Again, significant phosphorescence quenching was observed for triad **3a** in comparison with the free pyridine-coordinated porphyrin species [Ru(TTP)(CO)(py)] **5** (Fig. 2). In order to rule out the existence of intermolecular phosphorescence quenching between non-coordinated chromophores, the phenyl analog of **1a**, $[Ru(phtpy)_2]^{2+}$ (phtpy = 4′-phenyl-2,2′ : 6′,2″-terpyridine) **2a**, which cannot axially coordinate to the metalloporphyrin, was prepared.[8] There was no observable intermolecular quenching of the excited state of porphyrin chromophore **5** when treated with 2 mol equiv. of **2a**, clearly indicating that the luminescence quenching occurs only when the metalloterpyridine complex is intimately coordinated to the porphyrin. We can conclude from these observations that there is effective electronic communication between chromophores within the assembled triad. A possible explanation for the luminescence quenching is that photoinduced electron-transfer occurs, followed by non-radiative decay of a charge-separated species.§ Identification of this charge-separated species and characterization of the phosphorescence quenching process within the arrays are currently under investigation.

This work was supported by a grant from the Natural Sciences and Engineering Research Council of Canada. We are grateful to the reviewers for their helpful comments and suggestions.

Notes and references

† The abbreviation TTP refers to 5,10,15,20-tetratolylporphyrinato dianion.

‡ Manuscript in preparation.

§ Excited states of metalloporphyrins are known to exhibit photoredox behaviour involving both oxidative and reductive quenching. Literature precedent suggests an electron-transfer process (see ref. 9 and references cited therein), although examples of the less frequent energy-transfer process have also been documented for covalently bound porphyrin-terpyridine hybrids (see Flamigni *et. al*. in ref. 1, for example).

1 L. Flamigni, F. Barigelletti, N. Armaroli, J.-P. Collin, J.-P. Sauvage and J. A. Gareth Williams, *Chem. Eur. J.*, 1998, **4**, 1744 and references therein; R. W. Wagner, J. Seth, S. I. Yang, D. Kim, D. F. Bocian, D. Holten and J. S. Lindsey, *J. Org. Chem.*, 1998, **63**, 5042 and references therein; T. Arimura, C. T. Brown, S. L. Springs and J. L. Sessler, *Chem. Commun.*, 1996, 2293; C. M. Drain, K. C. Russell and J.-M. Lehn, *Chem. Commun.*, 1996, 337; C. A. Hunter and R. J. Shannon, *Chem. Commun.*, 1996, 1361; R. K. Kumar, S. Balasubramanian and I. Goldberg, *Chem. Commun.*, 1998, 1435.

2 J. P. Sauvage, J.-P. Collin, J.-C. Chambron, S. Guillerez, C. Coudret, V. Balzani, F. Barigelletti, L. De Cola and L. Flamigni, *Chem. Rev.*, 1994, **94**, 993.

3 For representative examples of ruthenium(II) porphyrin arrays assembled through axial coordination, see: K. Funatsu, T. Imamura, A. Ichimura and Y. Sasaki, *Inorg. Chem.*, 1998, **37**, 4986; E. Alessio, M. Macchi, S. Heath and L. G. Marzilli, *Chem. Commun.*, 1996, 1411; M. Ikonen, D. Guez, V. Marvaud and D. Markovitsi, *Chem. Phys. Lett.*, 1994, **231**, 93 and references therein.

4 E. C. Constable and A. M. W. Cargill Thompson, *J. Chem. Soc., Dalton Trans.*, 1994, 1409.

5 K. Funatsu, A. Kimura, T. Imamura, A. Ichimura and Y. Sasaki, *Inorg. Chem.*, 1997, **36**, 1625; J. P. Collman, C. E. Barnes, P. J. Brothers, T. J. Collins, T. Ozawa, J. C. Gallucci and J. A. Ibers, *J. Am. Chem. Soc.*, 1984, **106**, 5151.

6 For previous reports of this anisotropy, see ref. 3.

7 For a detailed description of the triplet state phosphorescence of both components, see: L. M. A. Levine and D. Holten, *J. Phys. Chem.*, 1988, **92**, 714 and ref. 4.

8 E. C. Constable, J. Lewis, M. C. Liptrot and P. R. Raithby, *Inorg. Chim. Acta*, 1990, **178**, 47.

9 J.-P. Collin, A. Harriman, V. Heitz, F. Odobel and J.-P. Sauvage, *J. Am. Chem. Soc.*, 1994, **116**, 5679; A. Harriman, F. Odobel and J.-P. Sauvage, *J. Am. Chem. Soc.*,1995, **117**, 9461.

Communication 9/01231A

Baeyer–Villiger oxidations with a difference: molecular sieve redox catalysts for the low-temperature conversion of ketones to lactones

Robert Raja, John Meurig Thomas and Gopinathan Sankar

Davy Faraday Research Laboratory, The Royal Institution of Great Britain, 21 Albemarle Street, London, UK W1X 4BS. E-mail: dawn@ri.ac.uk

Received (in Liverpool, UK) 4th January 1999, Accepted 5th February 1999

Redox molecular sieve catalysts MAlPO-36 (M = Mn or Co) convert cyclopentanone, cyclohexanone, 2-methylcyclohexanone and adamantan-2-one to their corresponding lactones with high efficiency (selectivities in excess of 90%, conversions in the range 50 to 85%), in the presence of O_2 and PhCHO as sacrificial oxidant.

In 1991 Mukaiyama and co-workers reported[1] that various aldehydes could be smoothly oxidised to their corresponding carboxylic acids by molecular oxygen in the presence of $Ni^{II}(dmp)_2$ catalysts [Hdmp = 1,3-bis(*p*-methoxyphenyl)propane-1,3-dione]. They also reported[2] an efficient method for epoxidising olefins using the same catalyst, O_2 and sacrificial aldehydes (Scheme 1).

These conditions are of considerable interest in that they offer attractive alternatives to the use of environmentally less acceptable oxidants (many of which function stoichiometrically rather than catalytically) such as CrO_3, $KMnO_4$, $Pb(OAc)_4$, RuO_4 Ag_2O and $Co(acac)_3$.[3] H_2O_2 in the presence of an appropriate catalyst (*e.g.* by methyltrioxorhenium[4]) is also a good oxidant for the conversion of olefins to epoxides and cyclic ketones to lactones[5] (Scheme 2).

In pursuit of our goal to design and synthesise microporous solid catalysts for the selective aerobic oxidation of hydrocarbons, we have found that transition metal ion (framework) substituted aluminophosphates (MAlPO, where M = transition metal ions) can effectively convert alkanes[6–8] and aldehydes to their corresponding carboxylic acids. This prompted us to investigate the potential of these microporous solids for oxidation of ketones, in the presence of a sacrificial aldehyde, using air as an oxidant. Sacrificial aldehydes for the conversion of ketones to lactones (an example of Baeyer–Villiger oxidation) have been shown to be effective using various homogeneous catalysts.

Several heterogeneous catalytic systems based on hydrotalcites[9] or heteropolyoxometalates[10] have been used to effect Baeyer–Villiger oxidations. However, to the best of our knowledge, there are no reports of the use of microporous redox molecular sieves for the shape-selective conversion of ketones to lactones. Taking account of the redox properties[11] and pore dimensions of a range of metal ion substituted AlPOs, we have identified three different structures of potential catalysts that contain small amounts (up to 4 atom%) of either manganese or cobalt redox cations. The catalysts we have used are CoALPO-36, MnALPO-36, CoAlPO-5, MnAlPO-5, CoALPO-18 and MnALPO-18. The structure[12] of aluminium phosphate No. 36 (IZA structure code ATS) has well-defined, oval-shaped channels (6.5 × 7.5 Å) (Fig. 1), which, by appropriate preparative means,[7,12] may be lined with a substantial number of either cobalt or manganese ions framework-substituted in place of Al^{III} ions. Similarly, two other types of materials, AlPO-5 (AFI) and AlPO-18 (AEI) with pore dimensions of 7.3 and 3.8 Å, respectively, were synthesised with specific metal ions having identical concentrations.[11] By calcining the as-prepared MAlPOs (M = Co or Mn) samples in oxygen at 550 °C, the substituted ions may be converted[12] to their +3 oxidation states, to a degree that is dependent on the structure; the trend in the concentration of the +3 state in the three structures is AlPO-18 > AlPO-36 > AlPO-5.[11] The results of Bayer–Villiger oxidation of a number of ketones to lactones, performed with these catalysts, are given in Table 1, and a typical kinetics plot for the MnAlPO-36 catalyst is shown in Fig. 2.†

Although the mechanistic details of the aerobic oxidation of ketones to lactones reported here still requires elucidation, preliminary studies (*cf.* ref. 6) point to the fact that the active centres in the redox catalysts are the Co^{III} (or Mn^{III}) ions that line the micropores. We know that the higher conversions are effected by the framework-substituted higher valence ions in the molecular sieve catalysts for several reasons. Firstly, divalent ion substituted AlPO-36 analogues such as Mg^{2+} (or Zn^{2+}) that are not raised to higher oxidation states upon calcination in O_2 yield conversions not significantly different from those of the Mukaiyama sacrificial oxidations with benzaldehyde alone (see Table 1, entries 5 and 7). Secondly, in a parallel experiment (Table 1, entry 6) using the smaller pore CoALPO-18 (or MnALPO-18), where all the transition-metal ions are in the +3 oxidation state,[7,11] and the diameter of micropores is 3.8 Å, no catalytic conversion of cyclohexanone to ε-caprolactone occurs when benzaldehyde is used as a sacrificial oxidant because the

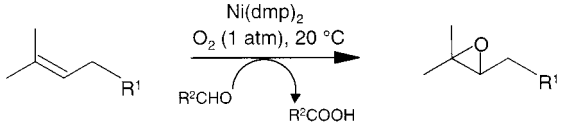

Scheme 1

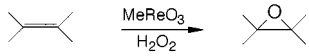

Scheme 2

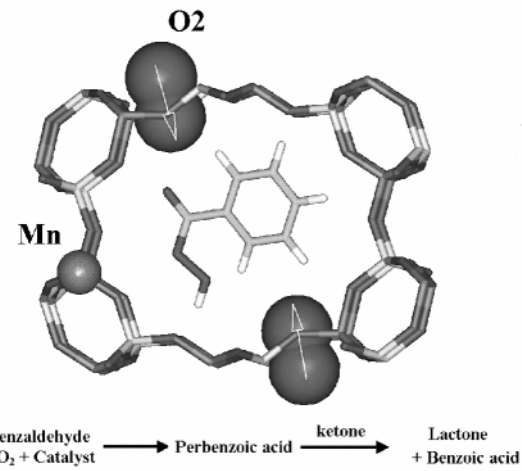

Fig. 1 Representation of the AlPO-36 catalyst, where one of the aluminium sites is occupied by manganese. The reaction scheme of the formation of the perbenzoic acid intermediate from benzaldehyde effected by Mn^{III} ions and molecular O_2 is also shown.

Table 1 Baeyer–Villiger oxidation of ketones (Mukaiyama's conditions)[a]

Entry	Substrate	Catalyst	Pore dimensions/Å	*T*/K	*t*/h	TOF[b]/h^{-1}	Conversion (%)	Lactone selectivity (%)
1	Cyclohexanone	CoALPO-36	6.5 × 7.5	323	6	250	71	98[c]
2	Cyclohexanone	CoALPO-5	7.3 × 7.3	323	6	204	60	80[c]
3	Cyclohexanone	MnALPO-36[d]	6.5 × 7.5	323	6	257	78	98[c]
4	Cyclohexanone	MnALPO-5	7.3 × 7.3	323	6	207	64	82[c]
5	Cyclohexanone	MgALPO-36	6.5 × 7.5	323	6	—[e]	20	64[c]
6	Cyclohexanone	CoALPO-18	3.8 × 3.8	323	6	—[e]	22	62[c]
7	Cyclohexanone	No Catalyst	—	323	6	—	20	65[c]
8	Cyclohexanone	CoALPO-18[f]	3.8 × 3.8	323	6	166	48	72[c]
9	Cyclopentanone	CoALPO-36	6.5 × 7.5	323	6	238	58	92[g]
10	Cyclopentanone	CoALPO-5	7.3 × 7.3	323	6	185	46	76[g]
11	Cyclopentanone	MnALPO-36	6.5 × 7.5	323	6	246	61	94[g]
12	Cyclopentanone	MnALPO-5	7.3 × 7.3	323	6	187	50	77[g]
13	Adamantan-2-one	CoALPO-36	6.5 × 7.5	353	5	220	80	99
14	Adamantan-2-one	MnALPO-36	6.5 × 7.5	353	5	224	87	99
15	2-Methylcyclohexanone	CoALPO-36	6.5 × 7.5	323	6	201	65	86
16	2-Methylcyclohexanone	MnALPO-36	6.5 × 7.5	323	6	208	72	89

[a] Reaction conditions: substrate = *ca*. 20 g; catalyst = *ca*. 0.15 g; substrate:benzaldehyde = 1:3 (mol/mol); O_2 (air) = 30 bar. [b] TOF = turnover frequency = moles of ketone converted per hour per mole of metal (Co, Mn) in the catalyst. [c] ε-Caprolactone. [d] After the reaction the catalyst was filtered off, washed thoroughly with MeOH and calcined at 550 °C for 12 h. It was then re-used twice without significant loss in catalytic activity. The reaction mixture (after 6 h) was also analysed by ICP (and atomic absorption spectroscopy) and only trace amounts (< 2 ppb) of metal were detected. In a separate experiment, the solid catalyst (entry 3) was filtered off from the reaction mixture (at 323 K) after 2 h (conversion = 29%) and the reaction was continued for a further 4 h (conversion after 6 h = 33%) with the resulting filtrate [which also had trace amounts (< 2 ppb) of metal]. No substantial increase in conversion was observed, clearly showing that the reactions are heterogeneously catalysed. [e] The TOF have not been calculated in these cases, as the conversions obtained here are non-catalytic. [f] Hexanal was used instead of benzaldehyde. [g] δ-Valerolactone.

latter is too large to gain access to the active site. (In addition, this clearly rules out the possibility of autoxidation by surface or transition metal impurities.) Further, to substantiate that the autoxidation of the aldehyde is shape-selective, we used the straight-chain hexanal, which is small enough to enter the 3.8 Å cages of the CoALPO-18 catalyst, as a sacrificial oxidant. The Baeyer–Villiger conversion of cyclohexanone to ε-caprolactone (Table 1, entry 8) freely ensues, because the hexanal gains ready access to the framework active sites and forms the peroxy acid. Thus, large-pore CoALPO-36 (or MnALPO-36) and CoAlPO-5 (or MnAlPO-5) catalysts offer easy access to bulky sacrificial oxidants (such as bezaldehyde), and oxidise a number of ketones, including adamantan-2-one, to their corresponding lactones with very high selectivity.

The implications are clear: the aldehyde is first converted by O_2 at the active sites to the corresponding peroxy acid inside the micropores, and this peroxy acid, in the manner first outlined by Criegee[5,13]—involving its initial nucleophilic attack at the carbonyl carbon—leads to the production of the lactone. In addition, as in our study of the selective oxidation of cyclohexane,[7] there appears to be a clear trend in the dependence of catalytic activity on the combination of the pore-dimension of the molecular sieve and the framework-substituted ion: the ATS structure shows higher conversion and selectivity compared to AFI, and Mn^{II} containing catalysts are slightly more active than their Co^{III} analogues. This agrees well with our estimation of the fraction of the metal ions that undergoes redox reaction.[11]

In summary, a heterogeneous redox molecular sieve catalyst first of all converts the sacrificial aldehyde involved in the Mukaiyama reaction shape-selectively (inside the micropores of the catalyst) into the active peroxy acid. This peroxy acid then converts the cyclic ketone to the lactone (outside the catalyst).

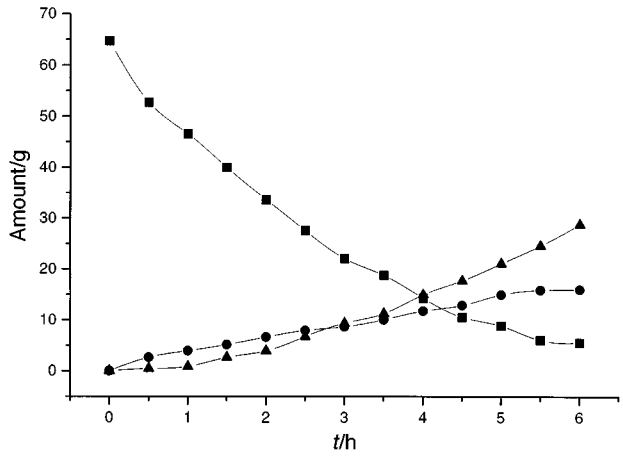

Fig. 2 Typical kinetics plot for the oxidation of cyclohexanone using MnAlPO-36, in the presence of air and benzaldehyde: (■) benzaldehyde, (●) caprolactone and (▲) benzoic acid. When the amount of aldehyde is decreased (cyclohexanone : benzaldehyde = 1 : 1), the rate of formation of the lactone decreases. We believe that the ketones compete with the aldehyde for access to the interiors of the micropores, thereby inhibiting the oxidation of the aldehyde to the peroxy acid.

Notes and references

† *Catalytic reactions.* The reactions were carried out in a high-pressure stainless steel catalytic reactor employing the conditions mentioned in Table 1. For other details see refs. 7 and 8.

1 T. Yamada, O. Rhode, T. Takai and T. Mukaiyama, *Chem. Lett.*, 1991, 5.
2 T. Yamada, T. Takai, O. Rhode and T. Mukaiyama, *Chem. Lett.*, 1991, 1.
3 M. T. Reetz and K. Töllner, *Tetrahedron Lett.*, 1995, **36**, 9461.
4 W. A. Hermann, F. E. Kühn, R. W. Fischer, W. R. Thiel and C. C. Romao, *Inorg. Chem.*, 1992, **31**, 4431.
5 G. Strukul, *Angew. Chem., Int. Ed.*, 1998, **37**, 1198.
6 R. Raja and J. M. Thomas, *Chem. Commun.*, 1998, 1841.
7 G. Sankar, R. Raja and J. M. Thomas, *Catal. Lett.*, 1998, **55**, 15.
8 J. M. Thomas, R. Raja, G. Sankar and R. G. Bell, *Nature*, 1999, in the press.
9 K. Kaneda, S. Ueno and T. Imanaka, *J. Chem. Soc., Chem. Commun.*, 1994, 797.
10 M. Hamamota, K. Nakayama, Y. Nishiyama and Y. Ishii, *J. Org. Chem.*, 1993, **58**, 6421.
11 P. A. Barret, G. Sankar, C. R. A. Catlow and J. M. Thomas, *J. Phys. Chem.*, 1996, **100**, 8977.
12 P. A. Wright, S. Natarajan, J. M. Thomas, R. G. Bell, P. L. Gai-Boyes, R. H. Jones and J. S. Chen, *Angew. Chem., Int. Ed. Engl.*, 1992, **31**, 1472.
13 R. Criegee, *Justus Liebig Ann. Chem.*, 1948, **560**, 127.

Communication 9/00080A

Unprecedented use of ^{29}Si NMR spectroscopy for a convenient determination of enantiomeric excesses of chiral α-*C*-silylated amines and alcohols†

Frederic Fortis,[a] Bernard Barbe,[b] Michel Pétraud[b] and Jean-Paul Picard*[a]

[a] *Laboratoire de Chimie Organique et Organométallique (UMR 5802), Université Bordeaux 1, F-33405 Talence, France. E-mail: j-p.picard@lcoo.u-bordeaux.fr*

[b] *Centre d'Etudes Structurales et d'Analyse des Molécules Organiques (CESAMO), Université Bordeaux 1, F-33405 Talence, France*

Received (in Liverpool, UK) 14th January 1999, Accepted 12th February 1999

The use of routine refocused-decoupled INEPT ^{29}Si NMR spectroscopy, in the presence of the chiral lanthanide shift reagent Eu(tfc)$_3$, allows convenient enantiomeric excess determination of chiral α-*C*-silylated amines and alcohols for the first time.

The constant interest in α-*C*-silylated amines, from a synthetic[1] and biological[2] point of view, has led a large number of authors to propose different syntheses for these compounds. Recently we proposed several methods giving access to 1-(trimethylsilyl)alkylamines.[3] One of these consisted of the reduction of acylsilane imines obtained *via* reductive silylation of cyanohydrins.[4]

Because of the potential biological interest of these amines and their derivatives, their synthesis in enantiomeric form is of importance. Although the literature provided us with some examples,[5] no synthesis of such chiral primary amines were described before our recent publication.[6] This led us to search for an accurate, reliable and convenient method for measuring the enantiomeric purity of the synthesized amines.

Many new NMR spectroscopic techniques for the determination of ee now exist.[7] We made our first different attempt using ^{1}H and ^{13}C NMR spectroscopy and the chiral auxiliary Eu(tfc)$_3$. We obtained poor separation and the spectra were complicated by the many protons and carbon atoms present in the compound and the lanthanide shift reagent (LSR). We turned next to ^{29}Si NMR spectroscopy, although methods exploiting the chemical shift sensitivity of this nucleus in organosilicon compounds have not so far been reported. Our experiments required the use of a routine polarization transfer technique, the ^{29}Si NMR refocused-decoupled INEPT experiment, based on the INEPT sequence,[8] which allowed us to circumvent the long relaxation time of the silicon atom. The sensitivity of this technique, which depends on the number of coupled protons, was enhanced in the case of trimethysilylated compounds. The refocusing delay time parameter (Δ = 0.02 s) was graphically chosen with the computer program SIMEPT,[9] on the basis of analytical expressions for the theoritical enhancement of decoupled INEPT spectra,[10] in order to obtain optimum enhancement, which depends on delay times. The chiral auxiliary Eu(tfc)$_3$, which converts the mixture of enantiomers into a diastereoisomeric mixture, was directly added into the NMR sample.

We studied racemic amines first. After a few minutes, the decoupled ^{29}Si NMR spectrum showed two signals of approximately the same intensity due to rapid exchange at equilibrium between the diastereoisomeric adducts and the parent racemic mixture of stereoisomers. The shift of these signals from the signal of the starting racemic mixture increased with the quantity of the europium salt added, as was the broadening of the signals. Best results were obtained with an LSR : substrate molar ratio in the 3–10% range. The results shown in the Table 1 (compounds **1**–**3**) proved the validity of the method.

In order to show that this method could be valuable for other α-*C*-silylated compounds, we also tested racemic α-*C*-silylated alcohols (Table 1, compounds **4**–**6**), synthesized by reduction of the parent acylsilanes obtained by standard methods.[11]

Table 1 Enantiomeric ratios measured for racemic α-*C*-silylated amines and alcohols

Compound		Z	R	LSR/ mol%	$\Delta\delta$ (ppm)[a]	Diastereoisomeric ratio[b]
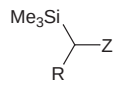	**1**	NH_2	Pr	6.2	0.021	50.7 : 49.3
	2	NH_2	C_6H_{11}	8.0	0.069	50.2 : 49.8
	3	NH_2	Bu^t	5.5	0.032	50.5 : 49.5
	4	OH	Me	6.2	0.031	50.3 : 49.7
	5	OH	Pr^i	3.2	0.138	50.1 : 49.9
	6	OH	Ph	10.0	0.031	50.3 : 49.7

[a] In $CDCl_3$ at 25 °C. ^{29}Si NMR chemical shift and separation have been shown to be solvent, substrate, LSR concentration and temperature dependent. See ref. 12. [b] Based on the integration of the ^{29}Si NMR resonances (±1%).

The ratios obtained from ^{29}Si NMR integrations confirmed that the parent mixtures were racemic and showed that this method was valuable also in these cases. However, failure was observed with α-*C*-silylated chloroalkanes, probably because the lower basicity of the chlorine atom stops the molecule complexing with Eu(tfc)$_3$.

An example of the results obtained using this technique is shown in Fig. 1.

Non-racemic mixtures of 1-(trimethylsilyl)butylamine **1** were obtained *via* asymmetric reduction of butyryltrimethylsilane imine under various conditions.[6] The NMR technique was applied to the determination of the ee of these mixtures (see example in Fig. 2) and the results were in good agreement with the mesured specific rotations (Table 2).

In summary, the $\Delta\delta_{Si}$ values of α-*C*-silylated amines and alcohols, obtained from routine refocused-decoupled INEPT experiments in the presence of Eu(tfc)$_3$, indicate that the chemical shift sensitivity of the silicon nucleus allows the determination of ee. This technique is possible because the observed silicon nucleus is close to the chiral and the complexation centers. From a practical point of view, this new and simple method (a single signal in the spectrum is converted into a double one) will be useful in the frame of the asymmetric synthesis of α-*C*-silylated amines and alcohols because it allows a rapid, convenient and accurate determination of the ee.

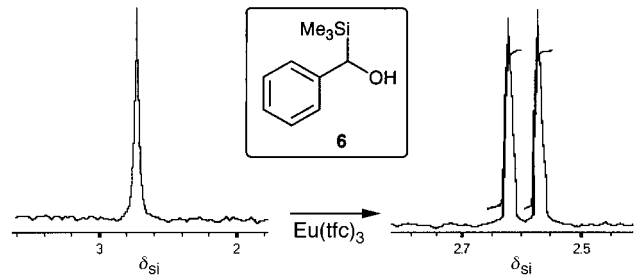

Fig. 1 ^{29}Si NMR spectra of **6** before and after the addition of Eu(tfc)$_3$.

† Part of the Thesis of F.F. (Université Bordeaux-1, 1998.

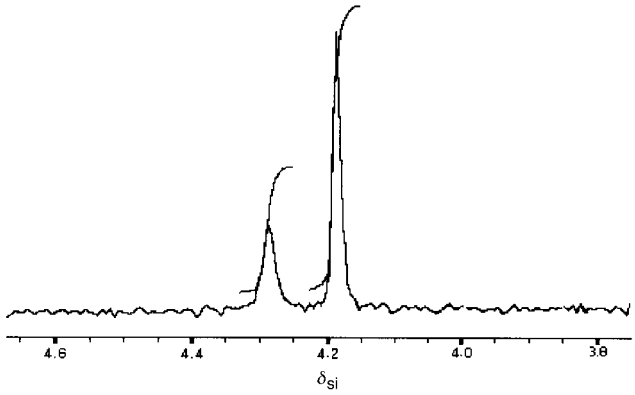

Fig. 2 ^{29}Si NMR spectra of enantioenriched 1-(trimethylsilyl)butylamine **1** after the addition of Eu(tfc)$_3$ (39% ee) (ref. 13).

Table 2 Comparison of experimental specific rotations and ees for various non-racemic mixtures of 1–(trimethylsilyl)butylamine

$[\alpha]_D^{20}$ (MeOH)	Ee (%)
+3.8	39
+2.9	31
+3.5	36
+6.1	60

Further applications of this novel technique are under investigation.

Notes and references

1 See for examples: R. Katritsky and S. Sengupta, *Tetrahedron Lett.*, 1987, **28,** 5419; V. Snieckus, *Pure Appl. Chem.*, 1990, **62,** 671 and references cited therein; J. Lasarte, C. Palomo, J.-P. Picard, J. Dunoguès and J.-M. Aizpurua, *J. Chem. Soc., Chem. Commun.*, 1989, 72; C. Palomo, J.-M. Aizpurua, J.-M. Garcia, J.-P. Picard and J. Dunoguès, *Tetrahedron Lett.*, 1990, **31**, 1921; O. Tsuge, S. Kanemasa, T. Yamada and K. Masuda, *J. Org. Chem.*, 1987, **52**, 2523; A. Padwa and W. Dent, *J. Org. Chem.*, 1987, **52**, 235.

2 See for examples: R. J. Fessenden and M. D. Coon, *J. Med. Chem.*, 1964, **7**, 561; M. Kurono, R. Unno, Y. Matsumoto, Y. Kondo, T. Mitani, T. Jomori, H. Michishita and K. Sawai, *Eur. Pat. Appl.* EP 288,002 1988 (*Chem. Abstr.*, 1989, **110**, 75808); M. Kurono, T. Suzuki, T. Suzuki, K. Hirooka, Y. Matsumoto, H. Ozawa and K. Sawai, *Eur. Pat. Appl.* EP 299,495 1989 (*Chem. Abstr.*, 1989, **111**, 7217); R. Tacke, R. Niedner, J. Frohnecke, L. Ernst and W. S. Sheldrick, *Liebigs Ann. Chem.*, 1980, 1859; R. B. Silverman and G. M. Banik, *J. Am. Chem. Soc.*, 1987, **109**, 2219. G. M. Banik, R. B. Silverman, *J. Am. Chem. Soc.*, 1990, **112**, 4499.

3 T. Constantieux, S. Grelier and J.-P. Picard, *Main Group Met. Chem.*, 1997, **20**, 503.

4 T. Constantieux and J.-P. Picard, *Organometallics*, 1996, **15**, 1604.

5 See for example: R. E. Gawley, G. Hart, M. Goicoechea-Pappas and A. Smith, *J. Org. Chem.*, 1986, **51**, 3076; R. E. Gawley, G. C. Hart and L. J. Bartolotti, *J. Org. Chem.*, 1989, **54**, 175; H. Hengelsberg, R. Tacke, K. Fritsche, C. Syldatk and F. Wagner, *J. Organomet. Chem.*, 1991, **415**, 39; S. T. Kerrick and P. Beak, *J. Am. Chem. Soc.*, 1991, **113**, 9708; D. J. Gallagher, S. T. Kerrick, and P. Beak, *J. Am. Chem. Soc.*, 1992, **114**, 5872; D. J. Gallagher, S. Wu, N. A. Nikolic and P. Beak, *J. Org. Chem.*, 1995, **60**, 8148; C. Barberis and N. Voyer, *Tetrahedron Lett.*, 1998, **39**, 6807.

6 F. Fortis and J.-P. Picard, *Tetrahedron: Asymmetry*, 1998, **9**, 3455.

7 See for example: J. A. Dale, D. L. Dull and H. S. Mosher, *J. Org. Chem.*, 1969, **34**, 2543; R. Wu, G. Hernandez, J. D. Odom, R. B. Dunlap and L. A. Silks, *Chem. Commun.*, 1996, 1125; P. Lesot, D. Merlet, A. Loewenstein and J. Courtieu, *Tetrahedron: Asymmetry*, 1998, **9**, 1871; D. Merlet, A. Loewenstein, W. Smadja, J. Courtieu and P. Lesot, *J. Am. Chem. Soc.*, 1998, **120**, 963.

8 G. A. Morris and R. Freeman, *J. Am. Chem. Soc.*, 1979, **101**, 760.

9 J.-C. Lartigue, M. Pétraud, M. Harket, B. De Jéso and M. Ratier, *Comput. Chem.*, 1996, **20**, 219.

10 K. V. Schenker and W. Von Philipsborn, *J. Magn. Reson.* 1985, **61**, 294.

11 Compound **4** from acetyltrimethylsilane (BH_3, THF, 80%): J. A. Soderquist and A. Hassner, *J. Organomet. Chem.*, 1978, **156**, C12; Compound **5** from isobutyryltrimethylsilane ($LiAlH_4$, 75%): J.-P. Picard, J.-M. Aizpurua, A. Elyusufi and P. Kowalski, *J. Organomet. Chem.*, 1990, **391**, 13; Compound **6** from benzoyltrimethylsilane ($LiAlH_4$, 82%): J.-P. Picard, R. Calas, J. Dunoguès, J. Gerval and P. Lapouyade, *J. Org. Chem.*, 1979, **44**, 420.

12 A representative procedure is as follows: 20 mg of the substrate was placed in a 5 mm NMR tube, and 4 cm^3 of dry $CDCl_3$ and Eu(tfc)$_3$ were added. The tube was sealed under nitrogen with cling-film and shaken briskly by hand to ensure complete dissolution. After 30 min, the ^{29}Si NMR spectrum (39.76 MHz) was collected (256 scans) at 300 K on a Bruker Avance DPX 200 MHz spectrometer over a spectral width of 7961 Hz with a repetition delay of 1 s between scans to allow for complete relaxation. INEPT delay time parameters choosen were τ = 0.0357 s and Δ = 0.02 s. Slight line Gaussian multiplication (−0.1 Hz) was applied to aid resolution. The FIDs were Fourier transformed and phased automatically, the same phase corrections being applied for each sample. Integration gave the relative proportions of the diastereoisomeric complexes as listed in Table 1.

13 See Table 1, Experiment 1 in ref 6.

Communication 9/00491B

New polymerization catalyzed by palladium complexes: synthesis of poly(*p*-phenylenevinylene) derivatives

Dekun Wang and Zhe Wu*

Department of Chemistry, University of Missouri-Kansas City, Kansas City, MO 64110, USA.
E-mail: zwu@cstp.umkc.edu

Received (in Corvallis, OR, USA) 4th January 1999, Accepted 9th February 1999

Palladium complexes are found to catalyze the condensation polymerization of halophenyl alkyl ketones to form polyketones, which can be readily converted to poly(phenylenevinylene) and its derivatives.

Recently, palladium-catalyzed cross-coupling reactions have received a great deal of attention. A number of important carbon–carbon bond formation processes have been realized.[1] Palladium-catalyzed coupling reactions are also of growing importance in the synthesis of macromolecules. Several important coupling reactions catalyzed by palladium complexes, such as the Stille coupling reaction,[2] the Suzuki coupling reaction,[3] and the Heck reaction,[4] as well as the reaction of a diyne or bisallene with an aryl dihalide,[5] have been successfully applied in the synthesis of macromolecules. In our ongoing program, we are interested in developing other palladium-catalyzed polymerization reactions and utilizing these reactions to synthesize important materials.

Poly(*p*-phenylenevinylene) (PPV) and its derivatives have attractive properties, such as electrical conductivity,[6] large third-order nonlinear optical response[7] and photo- and electroluminescence in the visible region.[8] However, the extended planar topology of the PPV backbone, which renders it infusible and insoluble in non-reactive media, limits its capacity for subsequent synthesis and fabrication. The problem can be overcome by synthesis of an intermediate soluble polymer, which is typically synthesized from the precursor route first developed by Wessling and Zimmerman,[9] in which the soluble precursor polymer is synthesized through a Wittig or nucleophilic displacement reaction. Thermal induced elimination to PPV can then be accomplished under mild conditions. Other routes to PPV based on this strategy were also reported.[10] We describe here our efforts in developing new polymerization methodology using aryl and ketone coupling reactions, and the application of these reactions to the synthesis of soluble poly(phenylenenevinylene) derivatives.

It was reported recently by Buchwald *et al.* that Pd^0 complexes catalyzed the coupling reaction of a ketone and an aryl halide to form an alkyl aryl ketone.[11] We envision that this reaction might be useful for polymer synthesis, providing new approaches to novel materials. We found that halophenyl alkyl ketones readily underwent condensation polymerization in the presence of a catalytic amount of Pd^0 or Pd^{II} complex, base and phosphine ligand [eqn. (1)].

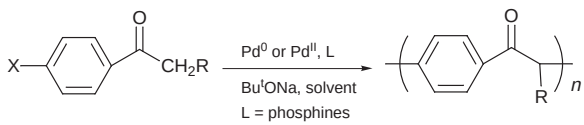

(1)

R = H, alkyl

X = Br, I

1a R = H
b R = Me
c R = Pr

We find that both mono- and bis-phosphines are effective ligands for the polymerization reactions. The influence of α-alkyl substitutent R on the polymerization (Table 1) was also examined. The α-alkyl substitutents can dramatically enhance the solubility and yield of the polymers. For example, when the α-substitutent is H (entries 1 and 2) the polymers are insoluble and are obtained in low yields. When monomers with longer alkyl substitutents were used, polymers with higher molecular weights (M_n = 11000) were obtained after fractional precipitation.

Table 1 Polymerization of 4-halophenyl alkyl ketones[a]

Entry	X	R	Yield (%)	M_n	M_w
1	Br	H	60	1800[b]	2500
2[c]	I	H	76		
3	Br	Me	70	1700	2100
4	Br	Bu	90	3200	4100
5	I	Pr	65	10100	13200

[a] $Pd(dba)_3$/BINAP was used as catalyst. [b] The polymer is slightly soluble in THF and molecular weights are determined from the soluble portion. [c] The polymer is insoluble in THF.

The polymerization was also studied in the presence of phosphines with different steric and electronic properties. As shown in Table 2, polymers were obtained in high yield and with high molecular weights in the presence of both bulky and electron-donating phosphines, such as PBu^t_3, which indicates that steric bulk and electron-donating phosphines favor the polymerizations. The results further imply that steric and electronic factors need to balance in order to achieve the optimized polymerization conditions. This observation can be understood from the fact that bulky and electron-donating ligands facilitate both oxidative addition and reductive elimination processes, which are believed to be involved in the rate-limiting steps of the catalytic cycle. We also observed that 4-iodophenyl propyl ketone, as compared to bromovalerophenone, polymerized faster and yielded higher molecular weight polymers. This observation suggests that oxidative addition of Pd^0 species to the aryl halide is also a crucial step involved in determing the rate of the polymerization.

The polymerization was also investigated in the presence of different solvents. Polar solvents seem to enhance the polymerization. For example, polymers prepared using a catalytic amount of $Pd(OAc)_2$–ligand exhibited higher molecular weights in THF than in other solvents. Better yields of polymers were also obtained in solvents such as *o*-$C_6H_4Cl_2$ and Ph_2O. No

Table 2 The effect of phosphine ligands on the polymerization[a]

Entry	Ligand	Yield (%)	Cone angle/°	*M*n	*M*w
1	PBu^t_3	63	182	11500	15200
2	PCy_3	20	170	5700	8800
3	$P(o\text{-tolyl})_3$	55	194	900	4600
4	PPh_3	30	145	700	3500
5	DPPF[b]	44		3000	6100

[a] $Pd(OAc)_2$ was used as catalyst and X = Br, R = Pr. [b] 1,1′-Bis(diphenylphosphino)ferrocene.

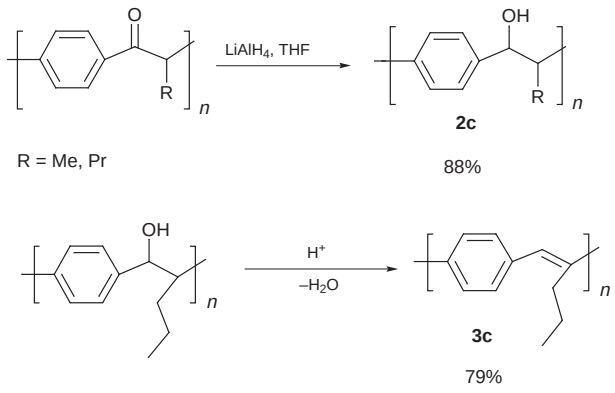

Scheme 1

polymerization was observed when DMA was used as a solvent, which may be attributed to deactivation of the catalysts.

The polymers were isolated by precipitation and the structures of the polymers were determined by spectroscopic techniques. For example, polymer **1c**† shows a peak at δ 4.67 in its ^{1}H NMR spectrum corresponding to the CH resonance. The carbonyl resonance was observed at δ 199.2 and was further confirmed by IR spectroscopy (ν = 1696 cm^{-1}). The single resonance at δ 53.2 in the ^{13}C NMR spectrum corresponds to the methine carbon in polymer **1b**, indicating that the polymerization is selective. The molecular weight was determined by gel permeation chromatography (GPC) using polystyrene as standards. The molecular weights (M_n) of the polymers obtained range from 2000 to 16 000 depending on the catalyst, ligand and solvent used.

The carbonyl groups in the polymers can be quantitatively converted to hydroxy groups using $LiAlH_4$ (Scheme 1). The ^{13}C NMR and IR spectra indicated the complete reduction of the carbonyl groups. Polymer **2c**‡ was obtained as a white solid and was insoluble in hexane. To obtain the PPV derivative, polymer **2c** was further treated with a catalytic amount of H_3PO_4 in toluene. Rapid elimination of H_2O was observed to yield polymer **3c**§ (Scheme 1). The polymer is soluble in common organic solvents, such as THF and CH_2Cl_2. The IR and ^{1}H NMR spectra indicated complete elimination. Both ^{1}H and ^{13}C NMR analysis indicated that the double bonds formed in the polymer backbone are predominantly *trans*. The polymer has a UV absorption (λ_{max} = 290 nm) and exhibits a strong blue emission at 420 nm (Fig. 1) when excitation at 290 nm is applied, which indicates that the polymer is a photoluminescence material.

We have demonstrated that palladium-catalyzed coupling of aryl halides and ketones can be used for polymer synthesis. This has led us to develop a new polymerization reaction and a novel approach to the synthesis of poly(phenylenenevinylene) derivatives. Our studies suggest that the steric and electronic properties of the ligands as well as the nature of the solvent have significant effects on the outcome of the polymerization. The polymers synthesized are soluble and exhibit photoluminescence properties. Synthesis of other electro- and/or photoluminescent polymers using this methodology are currently underway.

We thank the University of Missouri Research Board for support and Dr Zhi Xu for measurement of the fluorescence spectrum.

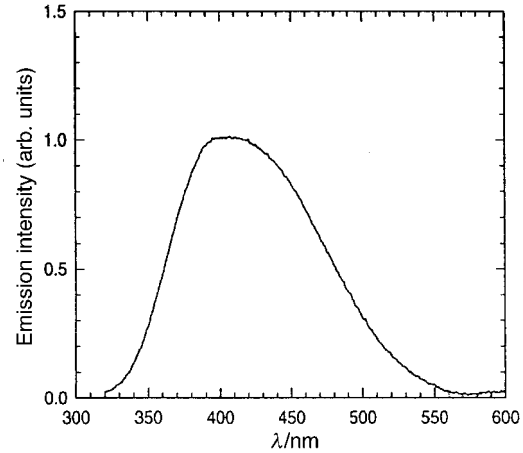

Fig. 1 Photoemission spectrum of **3c**.

Notes and references

Selected data for **1c**: $\delta_H(CDCl_3)$ 7.78 (m, 2H), 7.28 (m, 2H), 4.67 (m, 1H), 2.2–0.81 (br, 7H); $\delta_C(CDCl_3)$ 199.2 145.5, 136.2, 129.6, 128.8, 53.2, 36.7, 21.4, 14.3; ν_{max}(KBr)/cm^{-1} 3050.5, 3020.3, 2930.7, 1696.2, 1685.7, 1681.2 1270.9.

‡ *Selected data* for **2c:** $\delta_C(CD_2Cl_2)$ 7.50–6.80 (m, 4H), 4.65 (m, 1H), 3.68 (m, 1H), 2.95–0.85 (br, 8H); $\delta_C(CD_2Cl_2)$ 141.7, 128.5, 128.0, 127.6, 79.1, 34.9, 30.3, 21.1, 14.3.

§ *Selected data* for **3c**: δ_H ($CDCl_3$) 7.35–7.03 (m, 4H), 4.32–4.24 (br, 1H), 2.38–0.87 (br, 7H); $\delta_C(CDCl_3)$ 129.4, 128.6, 127.6, 126.2, 79.0, 64.5, 28.3, 21.3, 14.3.

1 L. Cassar, *J. Organomet. Chem.*, 1975, **93**, 253; N. Miyaura and A. Suzuki, *Chem. Rev.*, 1995, 2457; A. Dieck and R. F. Heck, *J. Organomet. Chem.*, 1975, **93**, 259; R. F. Heck, *Acc. Chem. Res.*, 1979, **12**, 146; M. Shibsaki, C. O. J. Boden and A. Kojima, *Tetrahedron*, 1997, **53**, 7371; J. K. Stille, *Angew. Chem., Int. Ed. Engl.*, 1986, **25**, 508; T. N. Mitchell, *Synthesis*, 1992, 803.

2 F. Babudri, S. R. Cicco, G. M. Farinola and F. Naso, *Macromol. Rapid Commun.*, 1996, **17**, 905.

3 M. Remmers, M.Schulze and G. Wegner, *Macromol. Chem. Rapid Commun*. 1996, **17**, 239.

4 D. K. Fu, B. Xu and T. M. Swager, *Tetrahedron*, 1997, **53**, 15487.

5 N. Miyaki, I. Tomita and T. Endo, *Polym. Bull.*, 1997, **39**, 677; N. Miyaki, I. Tomita and T. Endo, *Macromolecules*, 1996, **29**, 6685.

6 G. E. Wneck, J. C. W. Chien, F. E. Karasz and C. P. Lillya, *Polymer*, 1979, **20**, 1441; I. Murase, T. Ohnishi, T. Noguchi and M. Hirooka, *Synth. Met.*, 1987, **17**, 639; J. I. Jin, Y. H. Lee and H. K. Shim, *Macromolecules*, 1993, **26**, 1805.

7 D. J. William, *Angew. Chem., Int. Ed. Engl.*, 1984, **23**, 690; D. H. Hwang, J. I. Lee, H. K. Shim, W. Y. Hwang, J. J. Kim and J. I. Jin, *Macromolecules*, 1994, **27**, 6000.

8 J. H. Burroughes, D. D. C. Bradley, A. R. Brown, R. N. Marks, K. Mackay, R. H. Friends, P. L. Burns and A. B. Holmes, *Nature*, 1990, **347**, 539; G. Gustafsson, Y. Gao, G. M. Treacy, F. Klavetter, N. Colaneri and A. J. Heeger, *Nature*, 1992, **357**, 477; P. L. Burn, A. B. Holmes, A. Krat, D. D. C. Bradley, A. R. Brown, R. H. Friend and R. W. Gymer, *Nature*, 1992, **356**, 47.

9 R. A. Wessling and R. G. Zimmerman, *Chem. Abstr.*, 1969, **69**, 87735q; R. A. Wessling, *J. Polym. Sci., Polym. Symp.*, 1985, **72**, 55.

10 A. Greiner and W. Heitz, *Macromol. Chem., Rapid Commun.*, 1988, **9**, 581; V. P. Conticello, D. L. Gin and R. H. Grubbs, *J. Am. Chem. Soc.*, 1992, **114**, 9708.

11 M. Palucki and S. L Buchwald, *J. Am. Chem. Soc.*, 1997, **119**, 11108.

Communication 9/00015A

Sterically protected 1,2,3-dithiazolyl radicals: preparation and structural characterization of 4-chloro-5-pentafluorophenyl-1,2,3-dithiazolyl

Tosha M. Barclay,[a] Leanne Beer,[b] A. Wallace Cordes,[a] Richard T. Oakley,*[b] Kathryn E. Preuss,[b] Nicholas J. Taylor[b] and Robert W. Reed[b]

[a] *Department of Chemistry and Biochemistry, University of Arkansas, Fayetteville, Arkansas, 72701, USA*
[b] *Department of Chemistry, University of Waterloo, Waterloo, Ontario, Canada N2L 3G1. E-mail: oakley@sciborg.uwaterloo.ca*

Received (in Cambridge, UK) 22nd December 1998, Accepted 9th February 1999

Steric protection afforded by a pentafluorophenyl group at the 5-position facilitates the first isolation and structural characterization of a monocyclic 1,2,3-dithiazolyl as its S–S bonded dimer.

The solid state structures of many 1,3,2-dithiazolyl radicals **1** have been established by X-ray crystallography. Dimerization

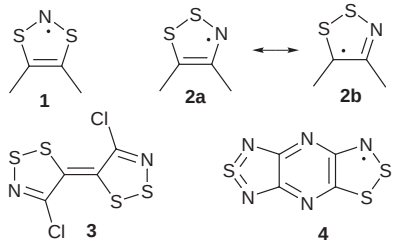

through long S–S bonds is normally observed,[1,2] but unassociated radicals are also known.[3,4] By contrast, the solid state properties of 1,2,3-dithiazolyls **2** have remained elusive, as have the structural and chemical implications of the two possible resonance formulations **2a** and **2b**. Recently, however, we demonstrated that the reduction of the 4,5-dichloro-1,2,3-dithiazolylium chloride (Appel's salt[5]) leads to C–C coupling at the 5-position, with the eventual formation of the tetrathiadiazafulvalene **3**.[6] This tendency to associate through carbon (resonance structure **2b**), and hence rearrange, illustrates one of the fundamental difficulties associated with the use of 1,2,3-dithiazolyls as building blocks for molecular conductors.[7] In our efforts to overcome this problem we have shown that delocalization of spin density away from the 5-position, as in the fused ring derivative **4**, suppresses C–C association.[8] We are now investigating the effect of sterically bulky substituents on radical association, and have found that the attachment of a pentafluorophenyl group at the 5-position provides an effective block to C–C bond formation. This has allowed us to isolate and characterize structurally, for the first time, a simple monocyclic 1,2,3-dithiazolyl radical as its S··S bonded dimer.

The synthesis of the title compound **5** involved the preparation of the corresponding dithiazolylium cation (Scheme 1) by the reaction of pentafluorophenylacetonitrile (2.6 g, 0.125 mmol) with excess (5 ml) S_2Cl_2 in 10 ml CH_2Cl_2 containing Bu^n_4NCl (0.20 g). After 10 days a canary yellow solid (2.7 g, 0.079 mmol, 63%) was filtered off and recrystallized from hot MeCN to afford orange needles of **6**, mp 211–213 °C. The reduction of **6** (0.68 g, 2.0 mmol) to **5** was very sensitive to the reaction temperature and the nature of the reducing agent. The best results were obtained using Ph_3Sb (0.38 g, 1.06 mmol) as reductant, and the reaction was performed in liquid SO_2 (5 ml) at −70 °C. After 5 min the solvent was evaporated from the still cold mixture to leave a black matrix, from which **5** (0.17 g, 0.54 mmol, 27 %) could be sublimed, at 45 °C/10^{-2} Torr, as lustrous green–black blocks, mp > 52 °C (decomp.).†

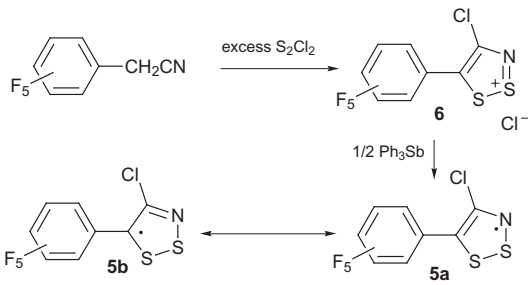

Scheme 1

Compound **5** dissolves in CH_2Cl_2 at room temperature to afford bright yellow solutions which exhibit a strong and persistent EPR signal (g = 2.0089) characteristic of a simple 1,2,3-dithiazolyl radical.[9,10] In addition to the expected triplet structure arising from hyperfine coupling to nitrogen, the spectrum (Fig. 1) also displays rich secondary structure arising from coupling to the 4-chlorine and to all five fluorines on the 5-C_6F_5 group. The a_N value (0.61 mT) is consistent with that expected for a simple 1,2,3-dithiazolyl. Cyclic voltammetry on solutions of **5** in MeCN (Pt electrodes, $Bu^n_4NPF_6$ supporting electrolyte) reveals a reversible oxidation wave with $E_{\frac{1}{2}}$(ox) = 0.38 V (*vs.* SCE) and an irreversible reduction wave with a E_{pc} (red) of −1.1 V (*vs.* SCE). The $E_{\frac{1}{2}}$(ox) potential is more anodic than that for benzodithiazolyls,[8] as expected from the more localized electron distribution in the monocyclic derivative. Indeed the potential is similar to those observed in 1,2,3,5-dithiadiazolyl radicals,[11] where spin density is formally restricted to the five-atom CN_2S_2 ring.

The crystal and molecular structures‡ of both **5** and **6** have been established by X-ray crystallography. The structure of the salt **6** (Fig. 2) consists of ion pairs in which the S–S bond of the cation is bridged by a chloride anion, with S··Cl contacts of 2.8947(16) and 2.9617(18) Å. This arrangement is reminiscent of that observed in the halide salts of 1,2,3,5-dithiadiazolylium cations.[12] The mean plane of the heterocyclic ring makes a dihedral angle of 68.6° with the plane of the C_6F_5 group. The internal structural parameters are typical of a 1,2,3-dithiazoly-

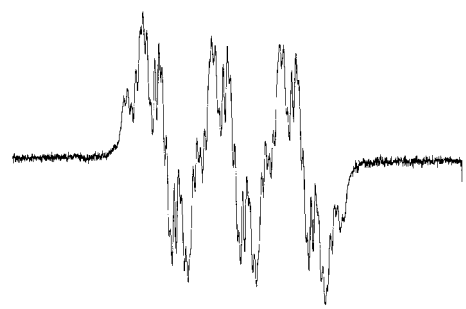

Fig. 1 EPR spectrum (293 K, CH_2Cl_2, SW = 4 mT, g = 2.0089) of radical **5**. Hyperfine coupling constants (derived by simulation with Bruker Simfonia) are a_N = 0.610, a_F = 0.175 (2 F), 0.038 (1 F), 0.031 (2 F), a_{Cl} = 0.1050 (^{37}Cl), 0.0875 (^{35}Cl) mT.

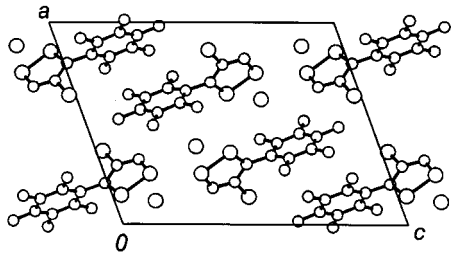

Fig. 2 PLUTO drawing of the cation/anion packing in the chloride salt of **6**. Bond distances within the heterocyclic ring are: *d*(S–S) 2.0284(4), *d*(S–N) 1.605(4), *d*(S–C) 1.673(4), *d*(N–C) 1.309(5), *d*(C–C) 1.393(2) Å.

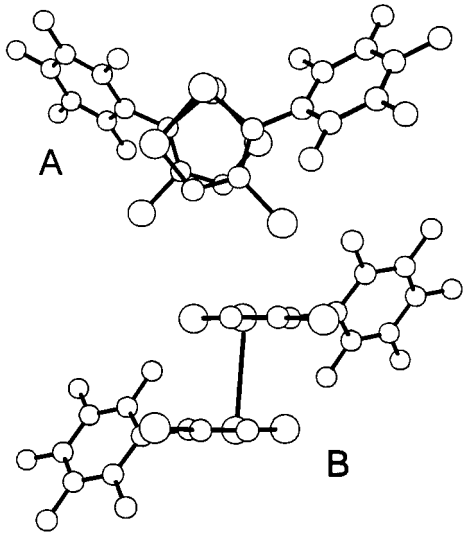

Fig. 3 PLUTO drawings of the radical dimer of **5**, showing the orientation of the overlap of the heterocyclic rings (A) and the interannular S··S contact (B). Bond distances within the heterocyclic ring are: *d*(S–S) 2.0717(8), *d*(S–N) 1.639(2), *d*(S–C) 1.724(2), *d*(N–C) 1.317(3), *d*(C–C) 1.390(3) Å.

lium salt.[13,14] In the structure of **5** the plane of the C_6F_5 group is again twisted (by 58.3°) away from the plane of the C_2S_2N ring, thereby providing the desired sterically protected 'pocket' for the 5-carbon. The radicals are nonetheless dimerized (Fig. 3). The two halves of the dimer are related by a two-fold axis, and are linked by a single interannular S··S contact of 3.2987(13) Å. This interaction is longer than the corresponding S··S interactions found in *any* known dimer of **1**, and stretches even further the conventional limit of a covalent S–S bond.[15] Taken collectively, the changes observed in the internal bond lengths (Fig. 2 and 3) upon reduction of the 6π-cation to the 7π-radical dimer are consistent with the bonding properties of the singly occupied molecular orbital of the radical.[15]

The mode of association of **5** provides an interesting lesson regarding the interplay of steric and electronic requirements. Dimerization cannot occur at the 5-carbons, for steric reasons, and so occurs through the 1-sulfurs, *i.e.* **7a**, as a result of which these atoms become hypervalent (with a S=C double bond). This arrangement is electronically *less* favored than dimerization at the 2-position, *i.e.* **7b**, which generates a hypervalent sulfur with a S=N double bond, or the more delocalized four-centre modes **7c** and **7d**, which are reminiscent of the cofacial

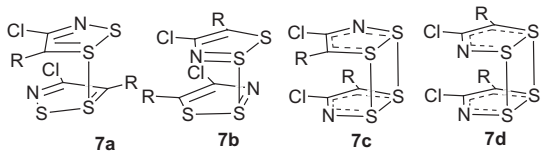

dimers commonly observed for 1,2,3,5-dithiadiazolyls.[16] Structure **7a** is, however, the *only* cofacial dimerization mode that precludes Cl/R or Cl/Cl and R/R steric interactions. The steric protection afforded by the C_6F_5 groups also affects the packing of dimers. Thus, instead of forming π-stacks, the dimers are clustered about a $\bar{4}$ site, with the dimers linked by S··S′ contacts of 3.7286(9) Å.

We thank the NSERC and the State of Arkansas for financial support. We also acknowledge the NSERC for a post-graduate scholarship to K. E. P.

Notes and references

† Satisfactory chemical analysis were obtained for compounds **5** and **6**.

‡ *Crystal data* for **5** and **6**: Data were collected at 293 K on Siemens P4 (**5**) and Enraf-Nonius (**6**) automated diffractometers with graphite-monochromated Mo-Kα radiation (λ = 0.71073 Å) using omega (**5**) and θ–2θ (**6**) scans. The structures were solved by direct methods and refined by full-matrix least-squares analysis which minimized $\Sigma w(\Delta F)^2$. Compound **5**: $ClS_2F_5NC_8$, M = 304.66, tetragonal, space group $I\bar{4}2d$, with a = 13.8634(8), c = 21.0268(4) Å, V = 4041.2(4) Å^3, Z = 16, D_c = 2.00 g cm^{-3}, μ = 0.82 mm^{-1}. 155 Parameters were refined using 1622 unique observed reflections [$I > 0.0\ \sigma(I)$] to give R = 0.029 and R_w = 0.033. Compound **6**: $Cl_2S_2F_5NC_8$, M = 340.11, monoclinic, space group $P2_1/n$, with a = 12.334(2), b = 6.0917(17), c = 15.947(3) Å, β = 110.382(16)°, V = 1123.4(4) Å^3, Z = 4, D_c = 2.01 g cm^{-3}, μ = 0.98 mm^{-1}. 163 Parameters were refined using 1502 unique observed reflections [$I > 2.0\ \sigma(I)$] to give R = 0.044 and R_w = 0.050. CCDC 182/1168.

1 G. Wolmershäuser and G. Kraft, *Chem. Ber.*, 1990, **123**, 881; G. Heckmann, R. Johann, G. Kraft and G. Wolmershäuser, *Synth. Met.*, 1991, **41**–**43**, 3287.
2 E. G. Awere, N. Burford, R. C. Haddon, S. Parsons, J. Passmore, J. V. Waszczak and P. S. White, *Inorg. Chem.*, 1990, **29**, 4821; G. Wolmershäuser, M. Schnauber and T. Wilhelm, *J. Chem. Soc., Chem. Commun.*, 1984, 573.
3 G. Wolmershäuser and R. Johann, *Angew. Chem., Int. Ed. Engl.*, 1989, **28**, 920.
4 T. M. Barclay, A. W. Cordes, N. A. George, R. C. Haddon, M. E. Itkis, M. S. Mashuta, R. T. Oakley, T. T. M. Palstra, G. W. Patenaude, R. W. Reed, J. F. Richardson and H. Zhang, *Chem. Commun.*, 1997, 873; T. M. Barclay, A. W. Cordes, N. A. George, R. C. Haddon, M. E. Itkis, M. S. Mashuta, R. T. Oakley, G. W. Patenaude, R. W. Reed, J. F. Richardson and H. Zhang, *J. Am. Chem. Soc.*, 1998, **120**, 352.
5 R. Appel, H. Janssen, M. Siray and F. Knoch, *Chem. Ber.*, 1985, **118**, 1632.
6 T. M. Barclay, A. W. Cordes, R. T. Oakley, K. E. Preuss and R. W. Reed, *Chem. Commun.*, 1998, 1039.
7 A. W. Cordes, R. C. Haddon and R. T. Oakley, *Adv. Mater.*, 1994, **6**, 798.
8 T. M. Barclay, A. W. Cordes, R. C. Haddon, M. E. Itkis, R. T. Oakley, R. W. Reed and H. Zhang, *J. Am. Chem. Soc.*, 1999, **121**, 969.
9 R. Mayer, G. Domschke and S. Bleisch, *Tetrahedron Lett.*, 1978, 4003; R. Mayer, G. Domschke, S. Bleisch, A. Bartl and A. Stăsko, *Z. Chem.*, 1981, **21**, 146, 264; R. Mayer, G. Domschke, S. Bleisch and A. Bartl, *Z. Chem.*, 1981, **21**, 326; R. Mayer, G. Domschke, S. Bleisch J. Fabian, A. Bartl and A. Stăsko, *Collect. Czech. Chem. Commun.*, 1984, **49**, 684; R. Mayer, S. Bleisch, G. Domschke, A. Tkáč and A. Stăsko, *Org. Magn. Reson.*, 1979, **12**, 532; S. R. Harrison, R. S. Pilkington and L. H. Sutcliffe, *J. Chem. Soc., Faraday Trans. 1*, 1984, **80**, 669.
10 K. F. Preston and L. H. Sutcliffe, *Magn. Reson. Chem.*, 1990, **28**, 189.
11 R. T. Boeré and K. H. Moock, *J. Am. Chem. Soc.*, 1995, **117**, 4775.
12 C. D. Bryan, A. W. Cordes, R. M. Fleming, N. A. George, S. H. Glarum, R. C. Haddon, C. D. MacKinnon, R. T. Oakley, T. T. M. Palstra, A. S. Perel, L. F. Schneemeyer and J. V. Waszczak, *J. Am. Chem. Soc.*, 1995, **117**, 6880; C. D. Bryan, A. W. Cordes, J. D. Goddard, R. C. Haddon, R. G. Hicks, C. D. MacKinnon, R. C. Mawhinney, R. T. Oakley, T. T. M. Palstra and A. S. Perel, *J. Am. Chem. Soc.*, 1996, **118**, 330.
13 J. W. Bats, H. Fuess, K. L. Weber and H. W. Roesky, *Chem. Ber.*, 1983, **116**, 1751.
14 T. M. Barclay, A. W. Cordes, J. D. Goddard, R. C. Mawhinney, R. T. Oakley, K. E. Preuss and R. W. Reed, *J. Am. Chem. Soc.*, 1997, **119**, 12136.
15 O. Knop and R. J. Boyd, *J. Am. Chem. Soc.*, 1988, **110**, 7299.
16 A. W. Cordes, R. C. Haddon and R. T. Oakley, in *The Chemistry of Inorganic Ring Systems*, ed. R. Steudel, Elsevier, Amsterdam, 1992, p. 295; A. J. Banister and J. M. Rawson, in *The Chemistry of Inorganic Ring Systems*, ed. R. Steudel, Elsevier, Amsterdam, 1992, p. 295; A. J. Banister and J. M. Rawson, *Adv. Heterocycl. Chem.*, 1995, **62**, 137.

Communication 8/09951K

ChemComm

Lifting the lid on metatungstate. ^{1}H and ^{183}W NMR study of the six electron reduced anion $[(H)_2\{W^{IV}_3(OH_2)_3\}W^{VI}_9O_{34}(OH)_3]^{3-}$

Colette Boskovic,[a] Maruse Sadek,*[b] Robert T. C. Brownlee,[b] Alan M. Bond[c] and Anthony G. Wedd*[a]

[a] *School of Chemistry, University of Melbourne, Parkville, Victoria 3052, Australia. E-mail: t.wedd@chemistry.unimelb.edu.au*
[b] *Department of Chemistry, La Trobe University, Bundoora, Victoria 3083, Australia. E-mail: m.sadek@latrobe.edu.au*
[c] *Department of Chemistry, Monash University, Clayton, Victoria 3168, Australia*

Received (in Cambridge, UK) 4th January 1999, Accepted 15th February 1999

The distribution of the eleven protons present in a six-electron reduced form of metatungstate, $[(H)_2\{W^{IV}_3(OH_2)_3\}W^{VI}_9O_{34}(OH)_3]^{3-}$, in dry CD_3CN is mapped by ^{1}H and ^{183}W NMR, allowing assessment of structural changes which accompany reduction.

The four trinuclear capping units of Keggin polyoxo anions $[X^nW^{VI}_{12}O_{40}]^{n-8}$ (T_d point symmetry; see framework in Fig. 1) are linked to define a tetrahedral cavity encapsulating atom X.[1] Six-electron reduction leads, for X^n = $2H^I$, B^{III}, Si^{IV}, to the 'poly-browns'.[1,2] X-Ray crystallographic and aqueous solution NMR data suggest effective C_{3v} point symmetry for these species, consistent with localisation of the added electrons in a single trinuclear cap whose terminal oxo ligands are protonated to aqua ligands.[3–6]

$$(W^{VI}{=}O)_3 + 6\ e^- + 6\ H^+ \rightarrow (W^{IV} \leftarrow OH_2)_3$$

The salt $(NH_4)_4[(H)_2\{W^{IV}_3(OH_2)_3\}W^{VI}_9O_{35}(OH)_2]$ **I** was synthesised by controlled potential electrolysis in aqueous HCl and converted to $(NBu_4)_3[(H)_2\{W^{IV}_3(OH_2)_3\}W^{VI}_9O_{34}(OH)_3]$ **II** by phase transfer.[7] In D_2O, **I** exhibits a single ^{1}H NMR resonance (two equivalent internal hydrogen atoms) and three ^{183}W resonances (3 : 3 : 6) consistent with effective C_{3v} point symmetry.[2–4,8] However, in dry CD_3CN, **II** exhibits five ^{1}H resonances (a–e) integrating for eleven protons and seven ^{183}W resonances (A–G) integrating for three W^{IV} and nine W^{VI} centres (Fig. 2, Table 1).

The intensities of the ^{1}H (4 : 2 : 1 : 2 : 2) and ^{183}W (1 : 2 : 2 : 2 : 2 : 2 : 1) resonances imply the presence of a mirror plane consistent with effective C_s point symmetry. It is apparent that proton exchange rates are reduced significantly in dry CD_3CN, allowing detection of surface-bound protons and differentiation of inequivalent tungsten sites. What is the driving force responsible for the effective change from T_d to C_s symmetry that accompanies the six electron reduction process?

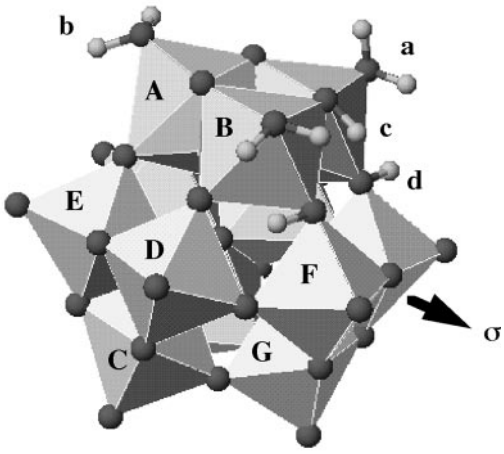

Fig. 1 Polyhedral representation of $[(H)_2\{W^{IV}_3(OH_2)_3\}W^{VI}_9O_{34}(OH)_3]^{3-}$. W atoms are centred in each 'octahedron' of O atoms.

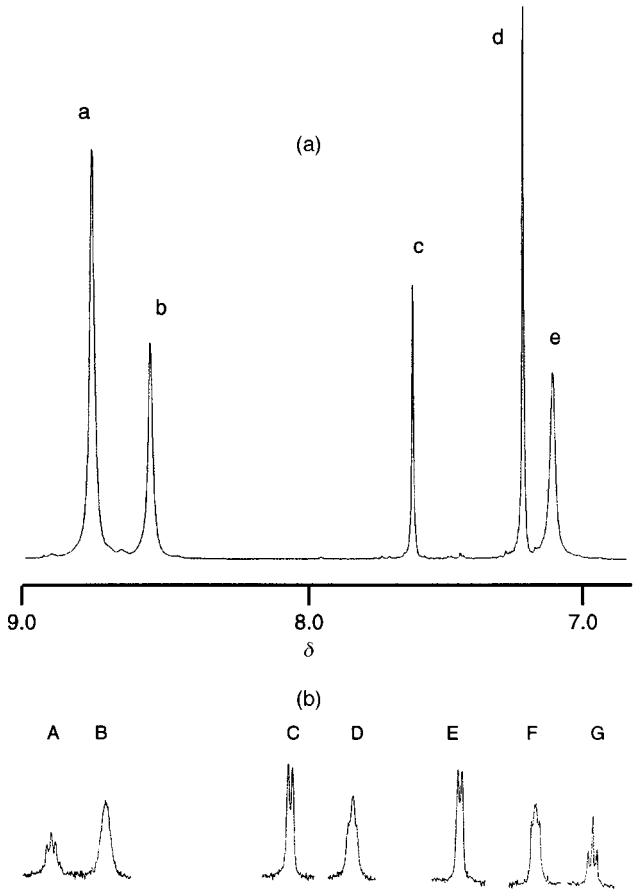

Fig. 2 NMR spectra of **II** (0.15 M) in CD_3CN (anion resonances only) (a) ^{1}H, (b) ^{183}W (99 atom% ^{183}W).

H_2O addition experiments assign resonance e to the slowly exchanging internal protons H_e and indicate that the protons H_a and H_b are in chemically similar sites.[10] Their relative intensities a : b = 4 : 2 allow assignment to the W^{IV}–aqua ligand protons. Tungsten resonances A and G of intensity 1 must be assigned to the unique W^{IV} and W^{VI} atoms lying on the mirror plane. The five resonances B–F of intensity 2 are due to five pairs of W atoms related by the mirror plane. B must be assigned to W^{IV} and so the fragments $W_AO(H_b)_2$ and $\{W_BO(H_a)_2\}_2$ are identified (Fig. 1).

A sample of II was enriched to 99 atom% ^{183}W. Its ^{183}W NMR spectrum featured resolved fine structure (13–18 Hz) assigned as $^{2}J_{WOW}$ coupling characteristic of corner-sharing WOW bridges [Fig. 2(b)].[11] Assigned resonances A and G are triplets consistent with corner-sharing to two equivalent W

Table 1 NMR data for $(NBu_4)_3[(H)_2\{W^{IV}{}_3(OH_2)_3\}W^{VI}{}_9O_{34}(OH)_3]$ **II** (0.15 M, CD_3CN)

Nucleus	Resonance	δ	$W_{1/2}$[a]/Hz	Relative intensity
^1H	H_a	8.76	7.7	3.9
	H_b	8.55	7.3	2.0
	H_c	7.61	2.5	1.0
	H_d	7.22	2.4	2.0
	H_e	7.11	8.6	2.1
^{183}W	W_A	1413.2	4.4	1
	W_B	1402.7	5.7	2
	W_C	−42.6	5.7	2
	W_D	−64.5	7.1	2
	W_E	−128.7	4.5	2
	W_F	−171.0	3.4	2
	W_G	−187.4	5.2	1

[a] For natural abundance samples.

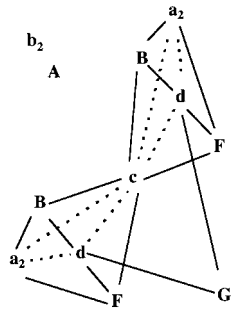

Fig. 3 Map of dipolar HH (----) and scalar WH (——) connectivities to protons H_a–H_d in **II**. Longer range interactions bd and Ad are are also observed but are omitted for clarity.

atoms (Fig. 1). On the other hand, C and E are doublets. A COSY experiment displayed a $W^{VI}W^{VI}$ cross-peak CG which allows assignment of C to the pair of tungsten atoms corner-sharing to unique atom W_G and E to the pair of tungsten atoms corner-sharing with unique atom W_A (Fig. 1). The only other $W^{VI}W^{VI}$ COSY crosspeak detected was DF and tungsten atoms W_D and W_F were assigned on the basis of multiple WOW corner-sharing interactions [Figs. 1, 2(b); *vide infra*: ref. 12].

Assignment and location of the three protons H_c and H_d were addressed initially by a HH ROESY experiment. Cross peaks ac, ad, bd and cd were detected. These dipolar interactions are mapped in Fig. 3. No interactions were observed between internal protons H_e and any of the external protons H_a–H_d.

Mapping of scalar interactions utilised WH HMQC experiments. ^{183}W–^1H coupling was not detected in the 1D spectra (*cf.* Fig. 2) implying that $^2J_{WOH} < W_{1/2} = 2$–9 Hz, allowing constraints to be set on mixing times. A spectrum is shown in Fig. 4 and the scalar connectivities are included in Fig. 3.[12]

The mapping indicates that resonances c and d may be assigned to three hydroxyl protons associated with the reduced $W^{IV}{}_3(AB_2)$ and unique $W^{VI}{}_3(GF_2)$ caps (Figs. 1, 3). Hydrogen oxide ligands $H_3O_2^-$ ligands which bridge pairs of metal atoms have been identified previously,[13] but similar stereochemistry does not appear possible here.

The C_s point symmetry of II is imposed by the positions of the three hydroxyl protons H_c and H_d (Fig. 1). The electronic feature which drives this localisation of protons is the localisation of the six added electrons in the reduced cap AB_2. In six-electron reduced $K_5[B^{III}\{W^{IV}{}_3(OH_2)_3\}W^{VI}{}_9O_{37}]\cdot 13.5H_2O$, the W^{IV}–W^{IV} bond lengths [mean 2.543(3) Å] in the reduced cap are *ca.* 0.77 Å shorter than the $W^{VI}\cdots W^{VI}$ separations in the oxidised caps.[6] The resulting mismatch in dimensions causes the boron atom to move *ca.* 0.4 Å within the internal BO_4 unit and away from the reduced cap but C_{3v} symmetry is retained. The internal cavity in **II** features two hydrogen atoms only and this anion accommodates the mismatch in a different way: three WOW links are converted to longer W(OH)W links [Fig. 1]. Ongoing work will provide more details.

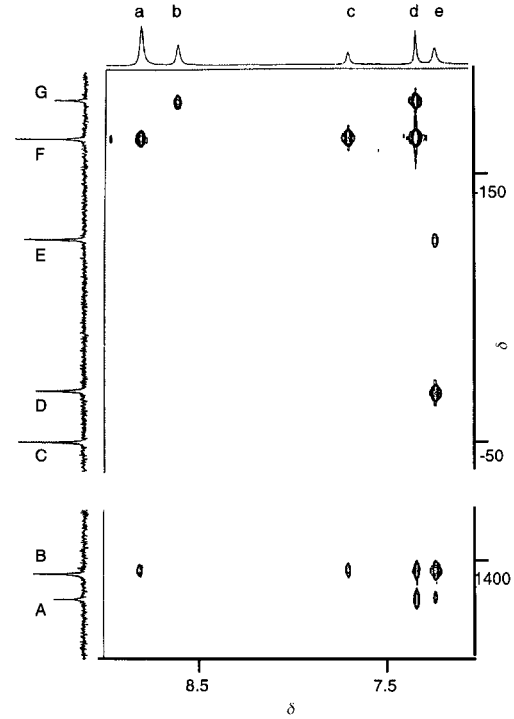

Fig. 4 ^{183}W–^1H HMQC spectrum of **II** (0.15 M, natural abundance) in CD_3CN (t_m = 60 ms; 128 × 4 K, 256 transients per increment; 25 °C).

A. M. B. and A. G. W. acknowledge support from the Australian Research Council. Associate Professor Richard Robson is thanked for stimulating discussions.

Notes and references

1 M. T. Pope, *Heteropoly and Isopoly Oxometalates*, Springer-Verlag, New York, 1983.
2 J. P. Launay, *J. Inorg. Nucl. Chem.*, 1976, **38**, 807.
3 K. Piepgrass and M. T. Pope, *J. Am. Chem. Soc.*, 1987, **109**, 1586.
4 K. Piepgrass and M. T. Pope, *J. Am. Chem. Soc.*, 1989, **111**, 753.
5 Y. Jeannin, J. P. Launay, M. A. Seid Sedjadi, *Inorg. Chem.*, 1980, **19**, 2933.
6 T. Yamase and E. Ishikawa, *J. Chem. Soc., Dalton Trans.*, 1996, 1619.
7 A solution of ammonium metatungstate in HCl was reduced to the 6e− level.[3] The ammonium salt was isolated after volume reduction and precipitation with MeOH. Phase transfer[4] mediated *via* a solution of NBu_4Br in CH_2Cl_2 led to the NBu_4Br salt.
8 J. P. Launay, M. Boyer and F. Chauveau, *J. Inorg. Nucl. Chem.*, 1976, **38**, 243.
9 ^{183}W spectra were acquired on a Bruker DRX500 spectrometer equipped with a broadband probe at 30 °C. Spectra were acquired at 20.837 MHz using a 60° pulse of 26 μs. Spectra were processed with a line broadening of 1 Hz. COSY 90 spectra were acquired using a 90° pulse of 39 μs. Experiments over the W^{VI} and W^{IV} chemical shift regions were acquired separately owing to their large separation. Gradient non-phase sensitive HMQC experiments were acquired on a Bruker DRX400 spectrometer equipped with an inverse probe at 25 °C. The probe was tuned to 400.130 MHz for ^1H and 16.671 MHz for ^{183}W. 90° pulses of 13.5, 15.3 and 25.7 μs for ^1H and 44 μs for ^{183}W were employed.
10 H_e shifts by < 0.1 ppm ($W_{1/2}$, 5–9 Hz) in the range 0–100 equiv. added H_2O. Resonances H_a, H_b and H_c, H_d broaden beyond detectability at ≈100 and 25 equiv. added H_2O, respectively.
11 J. Lefebvre, F. Chauveau, P. Doppelt and C. Brevard, *J. Am. Chem. Soc.*, 1981, **103**, 4589. Coupling characteristic of edge sharing is not resolved (ref. 4); the situation is also complicated by long range WW coupling.
12 The assignments of W_D and W_F are strengthened by the absence of Dd and the presence of Fd and Gd crosspeaks.
13 M. Ardon and A. Bino, *Struct. Bonding (Berlin)*, 1987, **65**, 1.

Communication 9/00088G

ChemComm

Unprecedented efficient hydrogenation of arenes in biphasic liquid–liquid catalysis by re-usable aqueous colloidal suspensions of rhodium

Jürgen Schulz, Alain Roucoux* and Henri Patin

Laboratoire de Chimie Organique et des Substances Naturelles, CNRS ESA 6052 Ecole Nationale Superieure de Chimie de Rennes, Avenue du Gal Leclerc, 35700 Rennes, France. E-mail: Alain.Roucoux@ensc-rennes.fr

Received (in Cambridge, UK) 19th January 1999, Accepted 18th February 1999

A reduced aqueous colloidal suspension of rhodium shows efficient activity for the catalytic hydrogenation of various benzene derivatives under biphasic conditions at room temperature and under atmospheric hydrogen pressure; the aqueous phase containing the Rh(0) particles can be re-used for further runs with a complete conservation of activity.

Among catalytic processes, hydrogenation of arenes is of great interest, in particular with the increasing industrial demand for low-aromatic diesel fuels[1] and the conversion of benzene to cyclohexane which still represents the most important industrial hydrogenation reaction.[2] Generally, the catalytic transformation is carried out with heterogeneous catalysts.[3] Recently some pure homogeneous[4] or microheterogeneous[5] systems under drastic conditions (pressure and/or high temperature) have been reported for hydrogenation of arenes.

Biphasic systems consisting of a water-phase containing catalytic species and a non-miscible organic phase continue to attract interest for economic and ecological reasons. In most cases, water-soluble homogeneous catalysts containing hydrophilic phosphines are widely used.[6] An original approach is to use colloidal metallic particles[7] finely dispersed in water. The colloidal suspension must be stabilized by highly water soluble protective agents such as polymers,[8] surfactants[9] or ionic species[10] to prevent aggregation and to facilitate recycling. Recently, our laboratory described hydrogenation of alkenes by colloidal suspension of rhodium(0) stabilized by trisulfonated molecules.[11]

Here we describe the complete hydrogenation of various benzene derivatives under biphasic liquid–liquid (water/hydrocarbon) systems by protected rhodium(0) colloids. This metal is known to reduce arenes[12] but to our knowledge, this is the first example allowing an efficient conversion with recycling at room temperature and under atmospheric hydrogen pressure.

In this system, the catalytically active aqueous suspension is made of metallic rhodium(0) particles prepared by reducing rhodium trichloride with sodium borohydride in dilute aqueous solutions of hydroxyalkylammonium salts **1a**–**d** (Scheme 1). These compounds, easily synthesized[13] by quaternization of *N*,*N*-dimethylethanolamine with the appropriate bromoalkanes, are highly water soluble. Surface tension measurements† of compounds **1a**–**1d** show that they are surfactants and self aggregate into micelles at critical micellar concentrations (cmc) of 1×10^{-2}, 2.5×10^{-3}, 1×10^{-3} and 2.5×10^{-4} mol l^{-1}. The interfacial tensions of aqueous solutions decreased from 72 to *ca*. 37 mN m^{-1}. Nevertheless, only **1c** and **1d** (alkyl chain containing 16 and 18 carbons) are efficient protective colloid agents for rhodium nanoparticles with an effective electrosteric stabilization. Transmission electron cryomicroscopic observations‡ show that the average particle size of system Rh–**1c** was 3.6 nm. The size distribution histogram was obtained on the basis of measurement of about 300 particles (Fig. 1). No evolution of distribution was observed after catalysis, consequently, these monodispersed aqueous suspensions are highly stable and can be re-used for further runs.

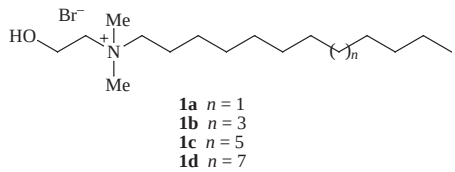

1a $n = 1$
1b $n = 3$
1c $n = 5$
1d $n = 7$

Scheme 1

The hydrogenation of benzene derivatives using the catalytic system (Rh/**1c**–**d**/water) under biphasic conditions is very selective and gives the corresponding cyclohexanes. Stable suspensions prepared in the presence of surfactant **1c** or **1d** with an optimized molar ratio **1c**,**d**/Rh = 2 give a better activity and prevent aggregation. This sytem is sufficient to maintain colloidal particles within the aqueous phase during the catalytic process and thus allows its recycling. In contrast with **1c**, CTAB (cetyltrimethylammonium bromide) gives poor results during recycling (Table 1, entry 9). This justifies the use of the hydroxyalkylammonium salt **1**. No hydrogenated intermediates are observed during the catalysis. The reaction is monitored by the volume of hydrogen consumed and gas chromatographic analysis. The conversion is usually complete after 7 h (Table 1). No induction period is observed but steric and electronic effects of substituents affect the reaction time and arenes substituted by electron-withdrawing groups react slowly (Table 1, entry 12) or not (Table 1, entry 13) whereas the reaction is favoured with electron-donating substituents. In the latter case the substrate should be preferentially adsorbed on the colloid (Table 1, entries 1–11). Analogous effects have been observed by Lemaire and coworkers.[5] The chemoselectivity of the reaction is good, with ester and ether functions remaining unaffected (Table 1, entries 6 and 12). In addition to the hydrogenation of

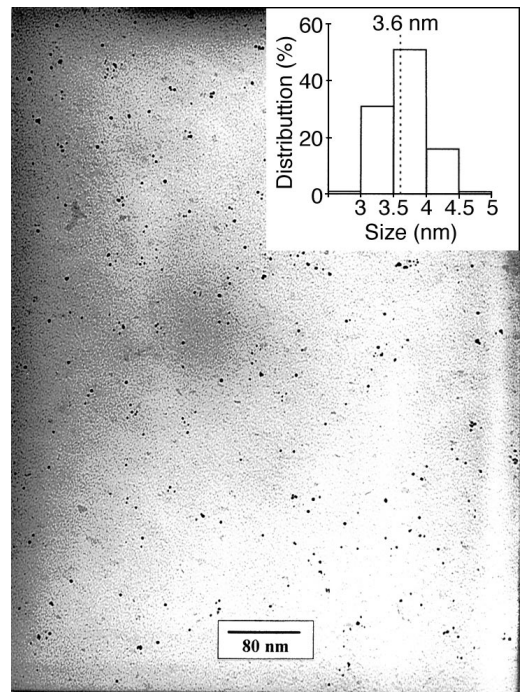

Fig. 1 TEM of Rh nanoparticles stabilized by **1c**.

Table 1 Hydrogenation of benzene derivatives under biphasic conditions[a]

Entry	Substrate	Stabilizing agent	Substrate/ Rh^0	Product yield (%)[b]	1st Run		2nd Run	
					t/h	TOF[c]/h^{-1}	*t*/h	TOF[c]/h^{-1}
1	Benzene	**1c**	100	Cyclohexane (100)	5.3	57	6.2	48
2	Benzene	**1d**	100	Cyclohexane (100)	9.1	33	13.3	23
3	Toluene	**1c**	100	Methylcyclohexane (100)	5.7	53	6.9	43
4	Ethylbenzene	**1c**	100	Ethylcyclohexane (100)	6.9	43	7.4	40
5	Cumene	**1c**	100	Isopropylcyclohexane (100)	7.8	38	8.6	35
6	Anisole	**1c**	100	Methoxycyclohexane (100)	5	60	5.3	57
7	Anisole	**1c**	500	Methoxycyclohexane (100)	23	65	24	63
8	Anisole	**1d**	100	Methoxycyclohexane (100)	8.4	36	11.5	26
9	Anisole	**CTAB**	100	Methoxycyclohexane (100)	5.1	59	24	13
10	Phenol	**1c**	100	Cyclohexanol (100)	5.2	58	5.7	53
11	Phenol	**1d**	100	Cyclohexanol (100)	5.6	54	8.4	36
12	Ethyl benzoate	**1c**	100	Ethyl cyclohexanoate (100)	9.5	32	11.9	25
13	Bromobenzene[d]	**1c**	100	—	—	—	—	—
14	Aniline	**1c**	100	Cyclohexylamine (100)	10	30	—	—
15	Styrene	**1c**	100	Ethylcyclohexane (100)	7.3	55	8.4	48
16	*o*-Xylene	**1c**	100	1,2-Dimethylcyclohexane *cis* (95), *trans* (5)	7.5	40	8.9	34
17	*m*-Xylene	**1c**	100	1,3-Dimethylcyclohexane *cis* (87), *trans* (13)	7.3	41	8.5	35
18	*p*-Xylene	**1c**	100	1,4-Dimethylcytclohexane *cis* (70), *trans* (30)	7.1	42	8.2	37

[a] *Conditions*: catalyst (3.8×10^{-5} mol), surfactant (7.6×10^{-5} mol), water (10 ml), substrate (3.8×10^{-3} mol), hydrogen pressure (1 atm), temperature (20 °C), stirred at 1500 min^{-1}. [b] Determined by GC analysis. [c] Turnover frequency defined as mol of H_2 per mol of rhodium per h. [d] Similarly PhI, PhCl and PhF are not reduced.

the aromatic ring, *exo*-C–C double bonds are hydrogenated (Table 1, entry 15). A complete hydrogenation is also observed with disubstituted benzene derivatives (Table 1, entries 16–18). The *cis*-compounds are largely the major products as usually observed in heterogeneous catalytic systems.[14] Finally, we have observed the formation of cyclohexylamine by reduction of aniline (Table 1, entry 14) but in this case, the colloidal suspension is insufficiently stable and aggregates. Accordingly the catalytic activity during the second run dramatically decreases to become negligible. We suggest a reaction between the product and the surfactant.

The durability of the catalytic system was tested by using it for four successive hydrogenations of anisole. In the first cycle, the turnover frequency (TOF) was 60 h^{-1}. Then, the aqueous phase containing the catalyst was separated from the hydrogenated product by simple decantation and re-used in a second hydrogenation cycle. In the same manner the catalyst was recycled for a third and fourth run. The aqueous suspension shows a comparable turnover activity during the four runs of catalysis. As the activity during recycling depends on the amount of colloidal particles which remain in water after decantation, an efficient biphasic catalytic system with good remaining activity at the fourth run is a demonstration of the stability of the catalytically active suspensions with compound **1c**.

In conclusion, these results show that rhodium nanoparticles, protected by hydroxyalkylammonium salts containing at least 16 carbons leading to electrosteric stabilization, can be readily used for quantitative reduction of arenes. The interfacial tension parameter can be modulated to favour the contact between the catalyst and the substrate localised in two phases. Finally, we describe an efficient recycling process for hydrogenation of benzene derivatives without loss of activity and usable under standard conditions (20 °C, 1 atm H_2).

We thank CNRS and the Region Bretagne for financial support. We would also like to thank Dr Rolland (University of Rennes 1) for helpful comments and TEM micrographs.

Notes and references

† Surface tension measurements were performed at 20 °C using the ring method with a Du Nouy tensiometer (Krüss K10T).

‡ TE Cryo-Microscopic studies were conducted using a PHILIPS CM 12 transmission electron microscope at 100 keV. Samples were prepared by a dropwise addition of the stabilized colloid in water onto a copper sample mesh covered with carbon. The colloidal dispersion was removed after 1 min using cellulose, then the samples were quickly frozen in liquid ethane before transfer to the frozen microscope.

1 A. Stanislaus and B. H. Cooper, *Catal. Rev.*, 1994, **36**, 75.
2 K. Weissermel and H. J. Arpe, in *Industrial Organic Chemistry*, VCH, New York, 2nd edn, 1993, p. 343.
3 S. Siegel, in *Comprehensive Organic Synthesis*, ed. B. M. Trost and I. Fleming, Pergamon Press, New York, 1991, vol. 9; H. Pines, *The Chemistry of Catalytic Hydrocarbon Conversions*, Academic Press, New York, 1981; M. S. Eisen and T. J. Marks, *J. Am. Chem. Soc.*, 1992, **114**, 10 358; R. D. Profilet, A. P. Rothwell and I. P. Rothwell, *J. Chem. Soc., Chem. Commun.*, 1993, 42; M. A. Keane, *J. Catal.*, 1997, **166**, 347; H. Gao and R. J. Angelici, *J. Am. Chem. Soc.*, 1997, **119**, 6937.
4 J. S. Yu, B. C. Ankianiec, M. T. Nguyen and I. P. Rothwell, *J. Am. Chem. Soc.*, 1992, **114**, 1927; I. P. Rothwell, *Chem. Commun.*, 1997, 1331; L. Plasseraud and G. Süss-Fink, *J. Organomet. Chem.*, 1997, **539**, 163.
5 K. Nasar, F. Fache, M. Lemaire, J. C. Béziat, M. Besson and P. Gallezot, *J. Mol. Catal.*, 1994, **87**, 107; F. Fache, S. Lehuede and M. Lemaire, *Tetrahedron Lett.*, 1995, **36**, 885; K. S. Weddle, J. D. Aiken III and R. G. Finke, *J. Am. Chem. Soc.*, 1998, **120**, 5653 and references therein.
6 For example, see: B. Cornils and W. A. Herrmann, in *Aqueous-Phase Organometallic Catalysis*, Wiley–VCH, Weinhem, 1998; W. A. Herrmann and C. W. Kohlpaintner, *Angew. Chem., Int. Ed. Engl.*, 1993, **32**, 1524; B. Cornils, *Angew. Chem., Int. Ed. Engl.*, 1995, **34**, 1575.
7 G. Schmid, in *Clusters and Colloids*, VCH, Weinheim, 1994, p. 459; L. N. Lewis, *Chem. Rev.*, 1993, **93**, 2693.
8 C. W. Chen and M. Akashi, *Langmuir*, 1997, **13**, 6465; A. B. R. Mayer and J. E. Mark, *J. Polym. Sci., Part A: Polym. Chem.*, 1997, **35**, 3151; L. M. Bronstein, S. N. Sidorov, A. Y. Gourkova, P. M. Valetsky, J. Hartmann, M. Breulmann, H. Cölfen and M. Antonietti, *Inorg. Chim. Acta*, 1998, **280**, 348.
9 T. Yonezawa, T. Tominaga and N. Toshima, *Langmuir*, 1995, **11**, 4601; Y. Berkovich and N. Garti, *Colloids Surf., Part A: Physicochem. Eng. Asp.*, 1997, **128**, 91.
10 C. Larpent and H. Patin, *J. Mol. Catal.*, 1988, **44**, 191.
11 C. Larpent, E. Bernard, F. Brisse-Le Menn and H. Patin, *J. Mol. Catal.*, 1997, **116**, 277.
12 O. N. Efimov, O. N. Ermenko, A. G. Ovcharenko, M. L. Khidekel and P. S. Chekrii, *Bull. Acad. Sci., USSR, Chem. Sect.*, 1969, 778; K. R. Januszkiewicz and H. Alper, *Organometallics*, 1983, **2**, 1055; J. Blum, I. Amer, K. P. C. Vollhardt, H. Schwarz and G. Höhne, *J. Org. Chem.*, 1987, **52**, 2804.
13 G. Cerichelli, L. Luchetti, G. Mancini and G. Savelli, *Tetrahedron*, 1995, **51**, 10 281.
14 H. Nagahara, M. Ono, M. Konishi and Y. Fukuoka, *Appl. Surf. Sci.*, 1997, **121**/**122**, 448.

Communication 9/00551J

Synthesis of functional 1,4-diphosphaindenes and their related anions

Patrick Rosa, Louis Ricard, François Mathey* and Pascal Le Floch*

Laboratoire 'Héteroéléments et Coordination', UMR CNRS 7653, Ecole Polytechnique, 91128 Palaiseau Cedex, France. E mail: lefloch@mars.polytechnique.fr

Received (in Liverpool, UK) 4th January 1999, Accepted 16th February 1999

Treatment of a 1-zircona-4-phosphaindene complex with PBr_3 affords a 1-bromo-1,4-diphosphaindene, which can be used as a convenient precursor for the preparation of the related 1,4-diphosphaindenyl mono- and tri-anions and (1*R*)-functional derivatives.

The search for new sophisticated ligands including sp^2-hybridised phosphorus atoms as bonding sites is a current and topical field of investigation.[1] Among these ligands, phosphinines play a significant role and continuous efforts have been made to improve the synthesis of their functional derivatives.[2] Whereas several routes towards polyfunctional mono-, bis- and tris-phosphinine based ligands[3] and macrocycles[4] have been developed, fused aromatic and non-aromatic ring systems have received much less attention. Although some polyaromatic systems are known,[5] only two examples of heterocyclic-fused ring systems incorporating the phosphinine nucleus have been described so far.[6] In view of the importance of phospholes and their related phospholide anions in coordination chemistry,[7] we decided to investigate the synthesis of 1,4-diphosphaindene species, a new type of ligand which could combine the chemistries of phosphinines and phospholes. Herein we report on these investigations.

Among the different synthetic approaches conventionally used for the synthesis of phospholes, metallacycle transfer reactions from zirconacyclopentadiene complexes appear very attractive.[8] Indeed, this simple process was used for the preparation of 1-phosphaindene ligands from η^2-benzyne zirconocene complexes, alkynes and PCl_3.[9] The recent discovery of η^2-phosphabenzyne zirconocene complexes[10] prompted us to investigate the corresponding transformation. All the experiments were conducted with the 1-zircona-4-phosphaindene complex **2** whose synthesis was previously reported from the reaction of the PMe_3 adduct of the η^2-phosphabenzyne complex with hex-3-yne. As a prelude to this work we found that the use of the Zr–Me complex **1** as precursor provided a more straighforward access to **2**. This complex turns out to be less reactive than that of its corresponding carbon counterpart. It seems likely that the decrease of electron density at the β positions of the phosphinine is responsible for this situation.[11] Preliminary experiments with PCl_3 only led to the recovery of starting material after several hours of reaction in CH_2Cl_2. Better results were obtained using $PhPCl_2$ as transfer reagent since the 1-phenyl-1,4-diphosphaindene **3** could be prepared after 5 to 10 days reaction, depending on the concentration used, in 15% yield. Finally, we found that the use of PBr_3 dramatically increased the rate of the reaction as well as the yield. After 1 h, the 1-bromo-1,4-diphosphaindene **4** was isolated in 80% yield as a slightly moisture- and oxygen-sensitive yellow oil after extraction with hexanes (Scheme 1).

The reaction of **4** with lithium is of particular interest. With a stoichiometric amount of lithium in THF at 25 °C, the monoanion **5a** is formed quantitatively according to ^{31}P NMR analysis. All available data (^{31}P, ^{1}H, ^{13}C NMR) support the structure proposed for **5a**. Whereas the ^{31}P NMR chemical shift of **5a** is comparable to those recorded for other phosphaindenyl anions, that of the phosphinine subunit experiences a dramatic upfield shift (δ 146.6 in **5a** *vs*. 176 in **4**). This observation shows

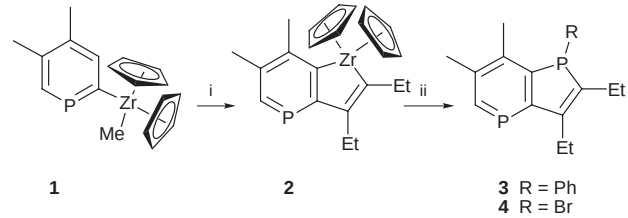

Scheme 1 *Reagents and conditions*: i, hex-3-yne, 80 °C, 3 h; ii, $PhPCl_2$, CH_2Cl_2, 5–10 d, then PBr_3, CH_2Cl_2, 1 h.

that a substantial delocalization of the negative charge occurs in **5a**. As expected, anion **5a** can be used as a convenient source of functional derivatives *via* reaction of electrophiles at the nucleophilic P atom of the phospholide unit (Scheme 2). Reactions of **5a** with $Br(CH_2)_2CN$ and MeI afford compounds **6** and **7** which were isolated in modest yields (40 and 50% respectively).† The corresponding $PSiMe_3$ derivative **8** was too sensitive towards hydrolysis to be isolated. An X-ray crystal structure analysis (Fig. 1) was carried out on the sulfide **9**‡ which was obtained by treating **7** with elemental sulfur in toluene. The structure of **9** deserves no special comment. Apparently, the phosphinine unit is not perturbed by the presence of the fused phosphole moiety as shown by the equivalency of the two C=P sp^2 bonds and by the value of the internal C–P–C angle, which is close to that recorded for other phosphinines.

Another interesting observation concerns the reduction of anion **5a**. We found that care must be taken to avoid over-reduction. Indeed, a prolonged contact with excess lithium or sodium cleanly affords a new species whose structure was ascribed to trianions **10a**,**b** on the basis of NMR data.[12] Evidence supporting the formulation proposed for **10** was given by oxidation with one equivalent of iodine, which leads back to the monoanions **5a**,**b** (Scheme 3). Further experiments aimed at developing the use in coordination chemistry of ligands such as monoanions **5**, whose synthesis was the real aim of this work, are currently under progress in our laboratories.

We are grateful to the CNRS and the Ecole Polytechnique for the financial support of this work.

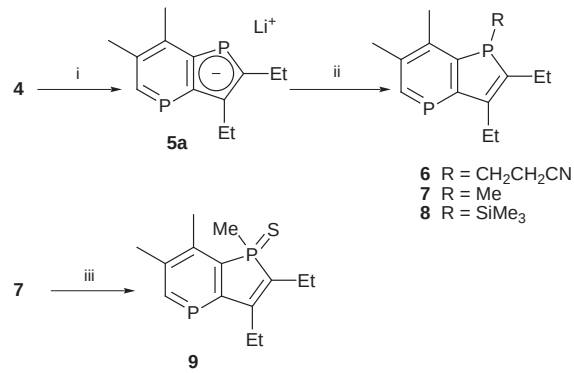

Scheme 2 *Reagents and conditions*: i, Li, THF, 30 min; ii, $BrCH_2CH_2CN$ or MeI or Me_3SiCl, THF −80 to 25 °C; iii, 1/8 S_8, toluene, 40 °C, 4 h.

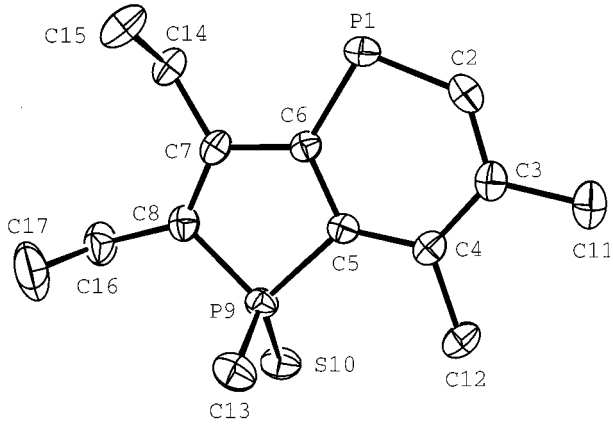

Fig. 1 Molecular structure of **9** showing the atomic number scheme. The numbering is arbitrary, not the systematic system used in the spectroscopic data. Selected interatomic distances (Å) and angles (°): P(1)–C(2) 1.734(2), C(2)–C(3) 1.377(3), C(3)–C(4) 1.419(2), C(4)–C(5) 1.388(3), C(5)–C(6) 1.417(3), C(6)–P(1) 1.730(2), C(6)–C(7) 1.480(2), C(7)–C(8) 1.349(2), C(8)–P(9) 1.797(2), P(9)–C(5) 1.813(2), C(6)–P(1)–C(2) 99.65(9), C(5)–P(9)–C(8) 93.40(8), P(9)–C(5)–C(6) 107.6(1), C(5)–C(6)–C(7) 113.9(1).

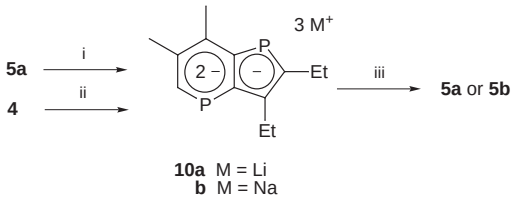

Scheme 3 *Reagents and conditions*: i, Li (excess), 1 h; ii, Na (excess), 20 min; iii, I_2 (1 equiv.), THF.

Notes and references

† All isolable compounds (**3**, **6** and **9**) gave analytical data consistent with the proposed structures. *Selected data* for **3**: δ_P(81 MHz, $CDCl_3$ unless otherwise stated) 171.5 (P_4), 6.5 (P_1). For **4**: δ_P 176.5 (P_4), 59.6 (P_1); δ_H(200 MHz, $CDCl_3$) 8.42 (d, 1H, $^2J_{H,P}$ 39.75, H_5); δ_C(50 MHz, $CDCl_3$) 172.7 (d, $^1J_{P,C}$ 50.6, C_9), 155.10 (d, $^1J_{P,C}$ 48.8, C_5). For **5a**: δ_P(C_4D_8O) 146.6 (d, $^3J_{P,P}$ 10.5, P_4), 63.7 (P_1); δ_H(C_4D_8O) 7.66 (d, 1H, $^2J_{H,P}$ 38.05, H_5); δ_C(C_4D_8O) 157.1 (dd, $^1J_{P,C}$ 36.2, $^2J_{P,C}$ 14, C_8), 156.5 (dd, $^1J_{P,C}$ 38.6, $^3J_{P,C}$ 6.8, C_2), 153.8 (dd, $^1J_{P,C}$ 42.4, $^2J_{P,C}$ 2.1, C_9); 143.9 (d, $^1J_{P,C}$ 36.9, C_5), 135.7 (dd, $J_{P,C}$ 16.5, $J_{P,C}$ 17.2, C_6 or C_7), 132.6 (dd, $^2J_{P,C}$ 23, $^2J_{P,C}$ 3.6, C_3), 122.6 (dd, $J_{P,C}$ 10.5, $J_{P,C}$ 17, C_7 or C_6). For **5b**: δ_P 153.6 (d, $^3J_{P,P}$ 10.3, P_4), 53.7 (P_1). For **6**: δ_P 174 (P_4), −1.8 (P_1). For **7**: δ_P 171.3 (P_4), −10.8 (P_1). For **8**: δ_P 170 (P_4), −43.6 (P_1). For **9**: δ_P 174 (P_4), 50.8 (P_1). For **10a**: δ_P(C_4D_8O) 34.7 (d, $^3J_{P,P}$ 13.8, P_1), 24 (P_4); δ_H(C_4D_8O) 7.20 (d, 1H, $^2J_{H,P}$ 40.1, H_5); δ_C(C_4D_8O) 150.6 (dd, $^2J_{P,C}$ 17.6, $^3J_{P,C}$ 3.9, C_6), 150 (dd, $^1J_{P,C}$ 37.1, $^2J_{P,C}$ 6.8, C_2), 146 (dd, $^1J_{P,C}$ 43.3, $^3J_{P,C}$ 4.2, C_9), 144.9 (d, $^1J_{P,C}$ 41.6, C_5), 139 (dd, $^1J_{P,C}$ 40, $^2J_{P,C}$ 10.4, C_8), 114.7 (dd, $^2J_{P,C}$ 12, $^2J_{P,C}$ 7.5, C_3), 61.1 (dd, $^3J_{P,C}$ 24.2, $^2J_{P,C}$ 8.4, C_7). For **10b**: δ_P(C_4D_8O) 39.3 (d, $^3J_{P,P}$ 12.2, P_1), 20.4 (P_4).

‡ *Crystal data* for **9**: Crystals of **9** ($C_{14}H_{20}P_2S$) were grown from MeOH. Data were collected at 123 ± 0.5 K on an Enraf-Nonius CAD4 diffractometer using Mo-Kα radiation (λ = 0.71073 Å) and a graphite monochromator. The crystal structure was solved and refined using the Enraf-Nonius MOLEN package. The compound crystallises in space group $P2_1/n$ (14), a = 9.861(1), b = 15.219(2), c = 10.715(1) Å, β = 110.95(1)°, V = 1501.89(59) Å^3, Z = 4, D_c = 1.249 g cm^{-3}, μ = 4.0 cm^{-1}, F(000) = 600. A total of 4725 unique reflexions were recorded in the range $2 \leqslant 2\theta \leqslant 60.0$ of which 1153 were considered as unobserved [$F^2 < 2.0\sigma(F^2)$], leaving 3572 for solution and refinement. Direct methods yielded a solution for all atoms. The hydrogen atoms were refined with isotropic temperature factors in the final stages of least-squares while using anisotropic temperature factors for all other atoms. A non-Poisson weighting scheme was applied with a p factor equal to 0.08. The final agreement factors were R = 0.033, R_w = 0.053, GOF = 1.10. CCDC 182/1177. Crystallographic data are available in CIF format from the RSC web site, see: http://www.rsc.org/suppdata/1999/537/

1 K. B. Dillon, F. Mathey and J. F. Nixon, in *Phosphorus: The carbon copy*, Wiley, Chichester, 1998.
2 G. Märkl, in *Multiple Bonds and Low Coordination in Phosphorus Chemistry*, ed. M. Regitz and O. J. Scherer, Thieme, Stuttgart, 1990; F. Mathey and P. Le Floch, *Chem. Ber.*, 1996, **129**, 263.
3 N. Avarvari, P. Le Floch, L. Ricard and F. Mathey, *Organometallics*, 1997, **16**, 4089.
4 N. Avarvari, N. Mézailles, L. Ricard, P. Le Floch and F. Mathey, *Science*, 1998, **280**, 1587.
5 See, for example: P. De Koe and F. Bickelhaupt, *Angew. Chem., Int. Ed. Engl.*, 1967, **6**, 567; Dimroth and H. Odenwälder, *Chem. Ber.*, 1971, **104**, 2984; G. Märkl and K. H. Heier, *Angew. Chem., Int . Ed. Engl.*, 1972, **11**, 1017; K. H. Dötz, A. Tiriliomis, K. Harms, M. Regitz and U. Annen, *Angew. Chem., Int. Ed. Engl.*, 1988, **27**, 713.
6 Two types of heterocyclic-fused phosphinines have been previously reported: an indolo derivative (see G. Märkl, G. Habel and H. Baier, *Phosphorus Sulfur*, 1979, **5**, 257) and two isostructural phoshabenzofuran and thiophene compounds (see K. H. Dötz, A. Tiriliomis and K. Harms, *Tetrahedron*, 1993, **46**, 5577).
7 F. Mathey, *Coord. Chem. Rev.*, 1994, **137**, 1.
8 P. J. Fagan and W. A. Nugent, *J. Am. Chem. Soc.*, 1988, **110**, 2310.
9 F. Nief and L. Ricard, *J. Organomet. Chem.*, 1994, **464**, 149.
10 P. Le Floch, A. Kolb and F. Mathey, *J. Chem. Soc., Chem. Commun.*, 1994, 2065; P. Rosa, P. Le Floch, L. Ricard and F. Mathey, *J. Am. Chem. Soc.*, 1997, **119**, 9417.
11 L. Nyulaszi and T. Veszpremi, *J. Phys. Chem.*, 1996, **100**, 6456.
12 Mono radical, di- and even tri-anions of phosphinines exist. Dianions have been reported as diamagnetic species although no NMR data are available, see: K. Dimroth and F. W. Steuber, *Angew. Chem., Int. Ed. Engl.*, 1967, **6**, 445; H. Weber, *Dissertation*, Universität Marburg, 1975, quoted in ref. 2.

Communication 9/00086K

Persistent vinylnitroxides

Vladimir A. Reznikov,[a] Ivan V. Ovcharenko,[b] Natalia V. Pervukhina,[a] Vladimir N. Ikorskii,[a] Andre Grand[c] and Victor I. Ovcharenko[a]*

[a] *International Tomography Center, 630090 Novosibirsk, Russia. E-mail: ovchar@tomo.nsc.ru*
[b] *Institute of Chemical Kinetics and Combustion, 630090 Novosibirsk, Russia*
[c] *CEA-CENG, Grenoble 38054, France*

Received (in Cambridge, UK) 27th January 1999, Accepted 12th February 1999

A method for the synthesis of persistent vinylnitroxides (vinylaminoxyls) has been developed and, for one of the radicals synthesized, an extremely high energy of intermolecular exchange interaction (−101 K) has been found.

Vinylnitroxides are traditionally considered transient radicals, since even EPR methods are often not powerful enough to detect them without using spin traps.[1] We succeeded in synthesizing persistent vinylnitroxides **1** and **2** and isolating them as individual solids (Scheme 1).†

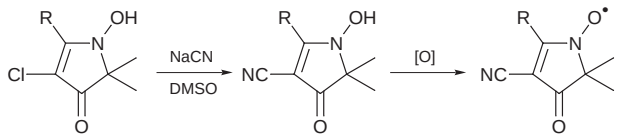

3a R = Ph
b R = *m*-pyridyl

4a R = Ph
b R = *m*-pyridyl

1 R = Ph
2 R = *m*-pyridyl

Scheme 1

The vinylnitroxides isolated are similar to nitronyl nitroxides, whose synthesis was developed by Ullman *et al.*,[2] in that they have effective delocalization of spin density. The EPR data of solutions of **1** and **2** indicate that the spin density in **1** and **2** is significantly delocalized from the N–O• group to the nitrile group [$a_{N(N–O•)}$ = 6.0 G, $a_{N(CN)}$ = 1.0 G for **1** and $a_{N(N–O•)}$ = 6.0 G, $a_{N(CN)}$ = 1.2 G for **2**).

The magnetic properties‡ of solid **1** and **2** deserve special attention. Treatment of the experimental dependence $\chi(T)$ for **1** (Fig. 1) and **2** showed that the experimental curves perfectly fit the exchange chain model[3] with parameters g = 2.04, J/k = −101 K and x = 0.02 for **1** and g = 2.01, J/k = −55 K and x = 0.03 for **2**. Due to these strong exchange interactions in solid **1** and **2**, even at room temperature the μ_{eff} values of the compounds (1.49 μ_B for **1** and 1.58 μ_B for **2**) are considerably smaller than the theoretical value of 1.73 μ_B corresponding to the presence of one unpaired electron per molecule. The effective magnetic moments of **1** and **2** continuously decrease to 0.2 and 0.4 μ_B at 2 K, respectively. In $CHCl_3$ solutions of **1** and **2**, the magnetic moments equal the theoretical value within

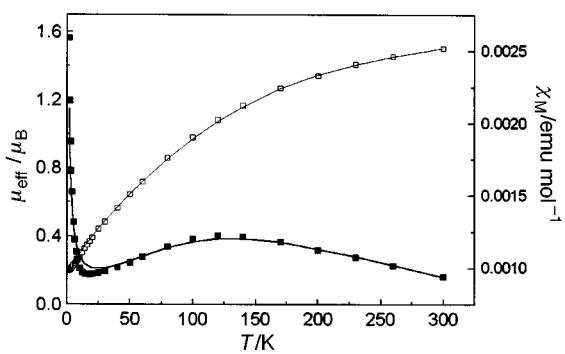

Fig. 1 Plots of effective magnetic moment (μ_{eff}) (□) and magnetic susceptibility (χ_M) (■) for **1**.

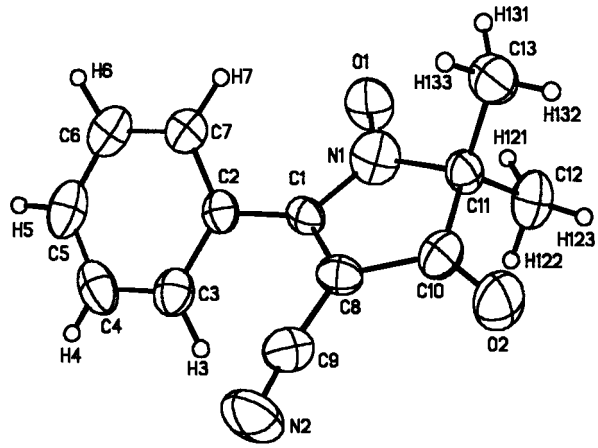

Fig. 2 ORTEP plot of the structure of **1**.

experimental error (1.70 μ_B for **1** and 1.73 μ_B for **2**) and do not change when the temperature decreases. Thus the experiment with vinylnitroxide solutions confirmed that strong spin–spin interactions are inherent in the solids. This prompted us to study the crystal structure of the vinylnitroxides. For **1** we succeeded in growing a single crystal of good quality (Fig. 2).§ In solid **1**, the shortest intermolecular contacts are at least 3 Å. Therefore, the structure of **1** should be considered molecular. However, the magnetic structure of **1**, as noted above, involves magnetic chains. The shortest intermolecular contacts in solid **1** are shown in Fig. 3. These are the nearly equal distances from the nitroxyl oxygen atom of one **1** molecule to both vinyl carbon atoms of the neighboring **1** molecule ($d_{O(N–O•)\cdots\beta\text{-}C(C=C)}$ = 3.183 Å and $d_{O(N–O•)\cdots\alpha\text{-}C(C=C)}$ = 3.296 Å). It is reasonable to assume that the 'magnetic chains' are formed by these contacts in solid **1** and are responsible for the strong exchange interactions (−101 K) in **1**.

To understand the magnetic behavior of **1** we carried out *ab initio* calculations on the electronic structure and intermolecular exchange interaction parameters in a two-radical model system [Fig. 4(*a*)]. It was found that the traditional HF (ROHF, UHF) and post-HF (direct CI, CASSCF) methods failed to give the

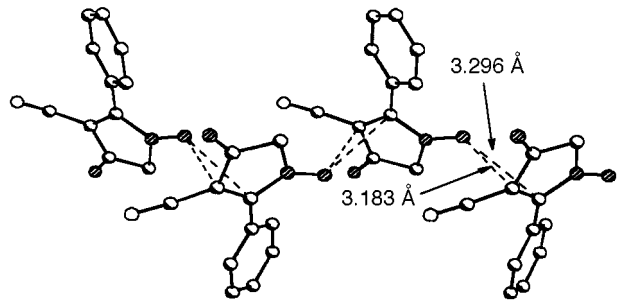

Fig. 3 Structure of the exchange chain in solid **1** (H atoms and CH_3 groups are omitted for clarity).

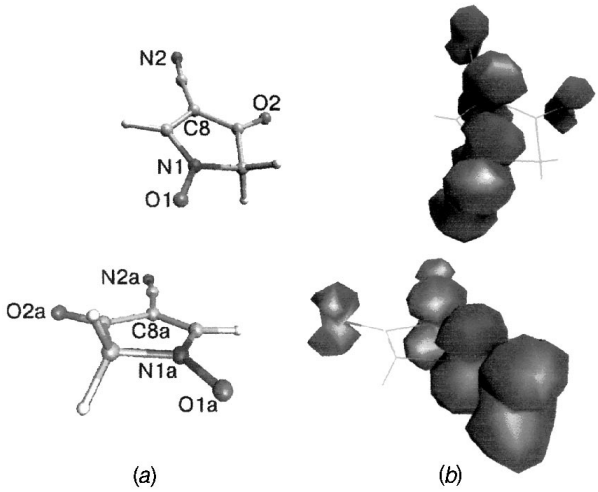

Fig. 4 Truncated (two-radical) model system (*a*) and general view of the spin density distribution for the model system (*b*).

Table 1 Exchange interaction parameters calculated in the framework of HF and DFT methods

Method	Basis set[a]	(*J*/*k*)/K
ROHF UHF	BG	$> 10^4$
CASSCF (4,6)	BG	1.5
ROHF CI(2,2)	BG	2.4
ROHF CI(2,4)	BG	2.8
ROHF CI(4,6)	BG	40.3
VWN	BG	−98.6
BP86	BG	−50.2
VWN	DZVP	−190.0
BP86	DZVP	−108.9
Experiment		−101

[a] BG: see ref. 4. DZVP: see ref. 5.

Table 2 Main calculated atomic spin densities (VWN approach)

	Basis set	
Atom	DZVP	BG
O1	0.420	0.547
N1	0.214	0.124
O2	0.101	0.107
C8	0.237	0.212
N2	0.093	0.074
O1a	0.437	0.548
N1a	0.201	0.119
O2a	0.098	0.106
C8a	0.235	0.211
N2a	0.088	0.074

sign of the exchange interaction parameter, whereas DFT/Broken Symmetry methods gave the same sign and order of the *J* parameter as in the experiment (Table 1). Analyzing the spin density distribution [Table 2 and Fig. 2(*b*)] calculated by the VWN method, one can assume that the most preferable intermolecular exchange channel passes through the vinyl β-carbon atom (C8a). The part (0.21–0.24) of the unpaired electron spin density localized on the C8a atom in one molecule contacts the spin density localized on the nitroxyl group of the neighboring molecule, causing an effective intermolecular exchange interaction between the neighboring radicals.

Thus, we succeeded in synthesizing persistent vinylnitroxides and revealed their surprising ability to form magnetic chains with strong interchain exchange interactions at long intermolecular distances (> 3 Å) in formally molecular solids. The quantum-chemical calculations adequately explain these strong exchange interactions in solid vinylnitroxides. It appeared that these strong interactions are favored by localization of the spin density of the N–O$^{\bullet}$ group of one nitroxide near the β-carbon of the vinyl group bonded to the nitroxyl group of the neighboring nitroxide.

Notes and references

† The starting 2-phenylpyrroline **3a** was obtained according to V. A. Reznikov, L. A. Vishnivetskaya and L. B. Volodarsky, *Izv. Akad. Nauk., Ser. Khim.*, **1990**, 390. The pyridine derivative was synthesized in a similar manner.

Synthesis of **4a**: 0.5 g (2 mmol) of chloropyrroline **3a** was added over 15 min to a solution of 0.2 g of NaCN (4 mmol) in 5 ml of anhydrous DMSO with stirring and cooling. The mixture was stirred further for 30 min at 20 °C and then diluted with 15 ml of water with cooling. The solution was acidified with 5% HCl to pH 3. The product precipitate was filtered off, washed with water and a 1 : 1 EtOAc–hexane mixture, and dried (80%); mp 213–216 °C (from EtOAc–MeOH); ν_{max}(KBr)/cm^{-1} 2200 (C≡N), 1675 (C=O); λ_{max}(EtOH)/nm (log ε) 245 (4.27), 346 (3.88); δ_H([$^2H_6$]DMSO) 1.35 [s, 6H, 5-(CH$_3$)$_2$], 7.64 (m, 3H), 7.84 (m, 2H, Ph); δ_C([$^2H_6$]DMSO) 20.75 [5-(CH$_3$)$_2$], 71.08 (C-5), 77.96 (C-3), 115.41 (C≡N), 125.82, 128.45, 128.84, 132.64 (Ph), 170.92 (C-2), 194.96 (C-4). The pyridine derivative **4b** was obtained in a similar manner.

Synthesis of **1**: A suspension of 0.2 g of the hydroxy compound **4b** and 2 g of MnO_2 in 10 ml of $CHCl_3$ was stirred for 30 min at 20 °C. The excess of the oxidant was filtered off, the solution was evaporated, and the residue was chromatographed on silica gel, with $CHCl_3$ as eluent (60%), mp 143–145 °C (from hexane); ν_{max}(KBr)/cm^{-1} 2200 (C≡N), 1700 (C=O), 1540, 1600 (C=C); λ_{max}(hexane)/nm (log ε) 250 (4.17), 270 (4.11), 313 (3.73), 334 (3.93), 397 (3.68), 578 (3.26) [Found (calc.): C, 68.5 (68.7); H, 4.8 (4.8); N, 12.1% (12.1%)]. An analogous procedure with the pyridine derivative **4b** afforded the corresponding radical **2** in 40% yield, mp 113–115 °C (from hexane); ν_{max}(KBr)/cm^{-1} 1705 (C=O), 1590 (C=C), 2200 (C≡N); λ_{max}(hexane)/nm (log ε) 246 (4.14), 308 (3.48), 333 (3.67), 395 (3.48), 564 (3.05) [Found (calc.): C, 55.7 (55.6); H, 4.2 (4.5); N, 15.3% (15.6%)].

‡ Magnetic susceptibility was measured with an MPMS-5S SQUID magnetometer over 2–300 K.

§ *Crystal data* for **1**: $C_{13}H_{11}N_2O_2$, M = 227.24, orthorhombic, space group *Aba*2, a = 15.334(3), b = 18.203(4), c = 8.414(2) Å, V = 2348.6(9) Å^3, Z = 8, D_c = 1.285 g cm^{-3}, λ(Mo-Kα), Enraf-Nonius CAD 4, θ region 2.60 ≤ θ ≤ 23.48°, T = 293 K, 1512 reflections collected, 847 independent (R_{int} = 0.0265), full-matrix least-squares on F^2 (SHELX 97), GOF = 0.506, final R values [847 $I_1 > 2\sigma(I)$ R_1 = 0.0204, wR_2 = 0.0251], extinction coefficient 0.0056(4). CCDC 182/1172. Crystallographic data are available in CIF format from the RSC web site, see: http://www.rsc.org/suppdata/CC/1999/539/

1 H. G. Aurich, K. Hahn and K. Stock, *Chem. Ber.*, 1979, **112**, 2776.
2 E. F. Ullman, J. H. Osiecki, D. G. B. Boocock and R. Darcy, *J. Am. Chem. Soc.*, 1972, **94**, 7049.
3 J. C. Bonner and M. E. Fisher, *Phys. Rev. A*, 1964, **135**, 640.
4 R. Poirier, R. Kari and I. G. Csizmadia, *Handbook of Gaussian Basis Sets*, Elsevier, Netherlands, 1985.
5 E. R. Davidson and D. Feller, *Chem. Rev.*, 1986, **86**, 681; N. Godbout, D. R. Salahub, J. Andzelm and E. Wimmer, *Can. J. Chem.*, 1992, **70**, 560.

Communication 9/00733D

A novel acylative ring cleavage of benzothieno[3,2-*b*]pyran-4-ols: application to the synthesis of dibenzothiophenes and fused-ring derivatives

Christopher D. Gabbutt,* John D. Hepworth, B. Mark Heron and Jean-Luc Thomas

Department of Chemistry, University of Hull, Hull, UK HU6 7RX. E-mail: c.d.gabbutt@chem.hull.ac.uk

Received (in Liverpool, UK) 26th January 1999, Accepted 11th February 1999

The benzothienopyranols 3, readily available from the ketone 1, are transformed to the carbamates 5 on treatment with *N,N*-dimethylcarbamoyl chloride, subsequent thermal electrocyclisation provides access to dibenzothiophene derivatives 6 and 11–13.

Dibenzothiophene and its congeners are not only of intrinsic interest but find applications as intermediates for the synthesis of dyes, pharmaceuticals, organic conductors and novel heterohelicenes[1,2] and hydrocarbons.[3] Dibenzothiophene and, especially, its benzologues are also of environmental concern because of their presence in fossil fuels and their combustion products.[4a,b]

The most frequently employed ring syntheses of dibenzothiophenes employ Friedel–Crafts related chemistry.[5] Routes involving the benzologation of benzo[*b*]thiophene by alternative means are less common. Thus, cycloadditions to benzo[*b*]thiophene-2,3-quinodimethanes[6] and Diels–Alder reactions of benzothienopyran-2- and 3- ones[7] have been investigated. The photodehydrocyclisation of 1-aryl-2-(thienyl)ethylenes has proved to be of value for construction of polycyclic condensed thiophenes.[4a,5,8] In contrast, benzannulation of thiophenes, in particular, benzo[*b*]thiophene, by thermal electrocyclisations has been much less studied.[5] 3-Substituted dibenzothiophene-1-carbonitriles are accessible from a tandem thermal cyclisation–elimination reaction of 2-(3-benzothienyl)-5-(dimethylamino)penta-2,4-dienonitriles.[9] More recently, 1-acetoxydibenzothiophenes have been obtained by thermolysis of 4-(2-benzothienyl)-2,3-disubstituted cyclobut-2-enones.[10]

We now report a novel thermal electrocyclisation–elimination protocol for the synthesis of dibenzothiophenes in which the key step involves formation of the carbamates **5** by an unprecedented acylative ring cleavage of benzothieno[3,2-*b*]pyran-4-ols **3** with Me_2NCOCl. The pyranols are readily prepared as shown in Scheme 1.†

2-Acetyl-3-hydroxybenzo[*b*]thiophene **1**, accessible in a single step from thiosalicylic acid,[11] was treated with 2 equiv. of LDA in THF at −40 °C to give a deep red solution of the dianion. Addition of the appropriate ketone (1 equiv.) followed by aqueous work-up provided the corresponding β-hydroxy ketone that was cyclised with methanolic-HCl to the benzothienopyranones **2a**–**g** (62–70%). Subsequent reduction gave **3a**–**g** in high yield.

Attempts to dehydrate **3a** to **4a** which, we envisaged, would function as a Diels–Alder diene, with TsOH in toluene, or with TsCl or MsCl in pyridine, failed to give a tractable product. The Chugaev-type elimination *via in situ* formation of the thiocarbonate from PhOCSCl was also unsuccessful. A mechanistically related, though little used, route to alkenes from alcohols involves the formation of carbamates, (from R_2NCOCl–pyridine), the elimination step being accomplished separately by flow pyrolysis at *ca*. 300–500 °C.[12] When **3a** was heated with Me_2NCOCl in pyridine (*ca.* 5 h) the anticipated *O*-acyl derivative was not obtained, the only isolable product was, remarkably, **5a** (mp 134–135 °C). Yields were optimised (74%) when 2 equiv. of Me_2NCOCl were used. Under the same conditions **3b**–**f** gave **5b**–**f** in excellent yields (70–90%). The ^1H NMR spectra of these compounds indicated *trans* stereochemistry of the alkene moiety.‡

We suggest that the benzothiophenes **5** are formed *via* initial *O*-acylation of **3** followed by elimination to give the pyran **4**§ which undergoes electrocyclic ring opening to the dienone **4A**. Subsequent deprotonation followed by *O*-acylation generates **5**. In accord with this proposal, it has recently been demonstrated that in solution ($CDCl_3$) 5,5-dimethyl-5*H*-thieno[3,2-*b*]pyran is in equilibrium with its dienone valence tautomer.[13]

Interestingly this elimination–acylation reaction not only affords carbamates **5** stereospecifically, but regiospecifically also. Thus **3f** gave **5f** (mp 116–118 °C, 85%) exclusively. None of the terminal alkene **7**, arising by deprotonation of the methyl

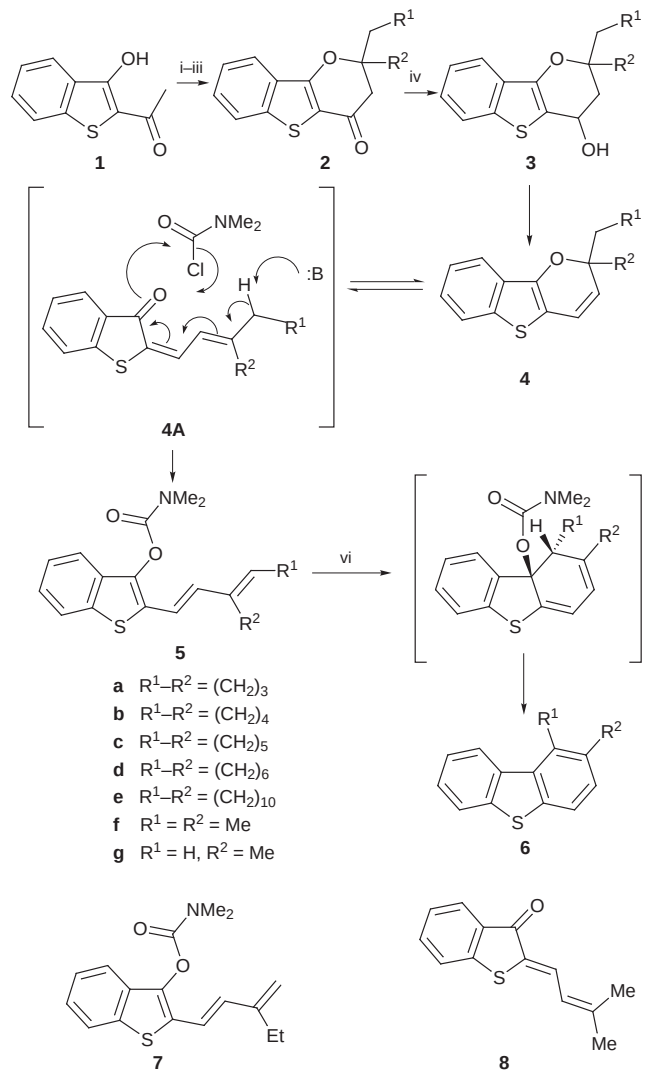

Scheme 1 *Reagents and conditions*: i, LDA, THF, −40 °C; ii, $R^1CH_2COR^2$, dil. HCl; iii, MeOH–HCl; iv, $NaBH_4$, EtOH; v, Me_2NCOCl (2 equiv.), pyridine, reflux; vi, triethylene glycol, reflux.

group in **4Af**, was observed.¶ The *E*,*E* stereochemistry of **5f** was established from its ^{1}H NMR spectrum and a NOESY experiment which confirmed the *cis* disposition of the methyl groups.

Support for the intermediacy of **4A** was provided by the behaviour of **3g**, which gave the yellow (*Z*)-dienone **8** (mp 118–120 °C, 50%),‖ *via* isomerisation of **4Ag**, as the only identifiable product. Attempts to convert **8** into **5g** by further reaction with Me_2NCOCl–pyridine were unsuccessful. Formation of the least substituted alkene is, apparently, disfavoured.

The carbamates **5** possess a contiguous triene system and have the potential to cyclise with extrusion of Me_2NCO_2H to give dibenzothiophenes. After much experimentation, it was found that when **5a**–**f** were heated in triethylene glycol (bp 285 °C) for 6 h formation of a new, non-polar compound was complete (TLC). Aqueous work-up followed by flash chromatography gave the novel fused systems **6a**–**e** (30–42%). The preparation of **6f** (28%) represents an improved route to this compound.[14] Thermal isomerisation of the *trans* alkene moiety in **5** precedes disrotatory ring closure and a concomitant E_i reaction generates **6**.

The dianion of **1** and 3-oxotetrahydrothiophene gave, ultimately, **9** and **10** (38 and 25% from the pyranol), which were

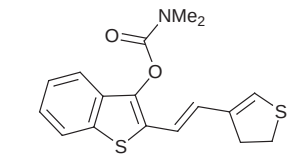

9

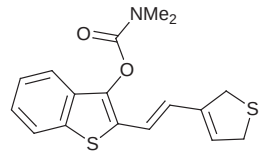

10

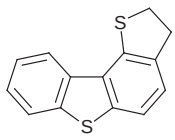

11

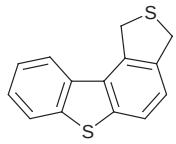

12

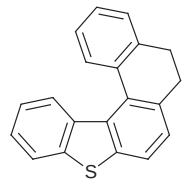

13

readily separated by flash chromatography. Thermal cyclisation provided the tetracycles **11** (mp 84–85.5 °C, 44%) and **12** (mp 79–80.5 °C, 35%) respectively. In like manner the pentacycle **13** (mp 108–109 °C, 28%) was obtained *via* 2-tetralone.

Although the yields are modest this method offers a facile entry to polycyclic thiophenes which is complementary to the current protocols. Existing procedures would not permit ready access to tetracycles **6a**–**e** nor to the isobenzothiophene **12**. Applications to the synthesis of more complex polycycles will be forthcoming.

We thank the EPSRC for provision of the mass spectrometry service at the University of Wales, Swansea, and James Robinson Ltd. for financial support to J.-L. T.

Notes and references

† All new compounds were characterised by ^{1}H and ^{13}C NMR, HRMS and elemental analysis.

‡ The *vicinal* alkene protons appeared as doublets at *ca.* δ 6.5 and 6.7, *J* 16 Hz, ($CDCl_3$) for **5a**,**b**,**e** and **f**. However, in **5c**,**d** the signals were coincidental (δ 6.59, 2H, s for both) and *trans* stereochemistry was assumed for these compounds by analogy with the other examples.

§ We are unaware of any examples in which carbamoylation with Me_2NCOCl is accompanied by *in situ* elimination. The nature of the elimination step (**3** to **4**) is a matter of conjecture but a pericyclic (*syn*) process cannot be excluded. Examples of such non-pyrolytic carbamate eliminations are rare, but the thermolysis of 1,1,3,4-tetramethyl-3-(phenylcarbamoyloxy)-2,3-dihydrosilole (CCl_4, Δ, 10 h) to 1,1,3,4-tetramethylsilole, is illustrative; A Laporterie, H. Iloughmane and J. Dubac, *Tetrahedron Lett*., 1983, 3521.

¶ Existing models that account for the stereoselectivity of ketone and enone deprotonations are not easily extrapolated to explain the outcome from **4Af**. For a review see; J.O. Williams and M. J. Kelly, in *Comprehensive Organic Functional Group Transformations*, ed. A. R. Katritzky, O. Meth-Cohn and C. W. Rees, Pergamon, Oxford, 1995, vol. 1, p. 843.

‖ Stereochemistry assigned by analogy with (*E*)- and (*Z*)-3-isobutenylidenethiophen-2(3*H*)-ones (ref. 13). Compound **8**: δ ($CDCl_3$) 7.78 (1H, d, *J* 12.2, =C*H*CHCMe_2).

1 R. K. Russell and J. B. Press, in *Comprehensive Heterocyclic Chemistry II*, ed. A. R. Katritzky, C. W. Rees and E. F. V. Scriven, Pergamon, Oxford, 1996, vol. 2, p. 679.
2 J. Larsen and K. Bechgaard, *Acta Chem. Scand*., 1996, **50**, 71, 77.
3 C. Bianchini and A. Meli, *Synlett*, 1997, 643.
4 (*a*) L. H. Klemm, *Adv. Heterocycl. Chem*., 1982, **32**, 127; (*b*) Y. Shiraishi, Y. Taki, T. Hirani and I. Komasawa, *Chem. Commun*., 1998, 2601.
5 J. Ashby and C. C. Cook, *Adv. Heterocycl. Chem*., 1974, **16**, 181; J. Nakayama, in *Comprehensive Heterocyclic Chemistry II*, ed. A. R. Katritzky, C. W. Rees and E. F. V. Scriven, Pergamon, Oxford, 1996, vol.2, p.607.
6 S. J. Collier and R. C. Storr, *Prog. Heterocycl. Chem*., 1998, **10**, 25.
7 K. Buggle, Ú. N. Ghógaín, M. Nangle and P. MacManus, *J. Chem. Soc., Perkin Trans. 1*, 1983, 1427; P. M. Jackson and C. J. Moody, *J. Chem. Soc., Perkin Trans. 1*, 1990, 681; P. M. Jackson, C. J. Moody and P. Shah, *J. Chem. Soc., Perkin Trans. 1*, 1990, 2909.
8 Y. Tominaga and R. N. Castle, *J. Heterocycl. Chem*., 1996, **33**, 523 and references cited therein.
9 J. C. Jutz, *Top. Curr. Chem*., 1979, **73**, 125; C. Jutz, R.-M. Wagner and H.-G. Löbering, *Angew. Chem., Int. Ed. Engl.*,1974, **13**, 737.
10 L. S. Liebeskind and J. Wang, *J. Org. Chem*., 1993, **58**, 3550.
11 S. Smiles and E. W. McClelland, *J. Chem. Soc*., 1921, **119**, 1810.
12 For a review see, H. McNab, in *Comprehensive Organic Functional Group Transformations*, ed. A. R. Katritzky, O. Meth-Cohn and C. W. Rees, Pergamon, Oxford, 1995, vol. 1, p. 771.
13 I. J. Turchi, J. B. Press, J. J. McNally, M. P. Bonner and K. L. Sorgi, *J. Org. Chem*., 1993, **58**, 4629.
14 M. L. Tedjamulia, Y. Tominaga R. N. Castle and M. L. Lee, *J. Heterocycl. Chem*., 1983, **20**, 1485.

Communication 9/00730J

ChemComm

A reinvestigation of the $Rh_2(OAc)_4$-catalysed decomposition of 1-diazo-4-(2-methoxyphenyl)alkan-2-ones: evidence for ionic 'ring-walk' rearrangement in norcaradiene derivatives

Paolo Manitto,* Diego Monti, Simona Zanzola and Giovanna Speranza

Dipartimento di Chimica Organica e Industriale, Università di Milano e Centro di Studio sulle Sostanze Organiche Naturali, via Venezian 21, I-20133 Milano, Italy. E-mail: manitto@icil64.cilea.it

Received (in Corvallis, OR, USA) 8th January 1999, Accepted 10th February 1999

On $Rh_2(OAc)_4$-catalysed decomposition of 1-diazo-4-(2-methoxyphenyl)butan-2-one (9) and its methyl-substituted analogue (18), norcaradienones 10 and 19, respectively, were observed as the only regioisomers resulting from intramolecular cyclopropanation, indicative of attack by the metal carbene away from the methoxy group; to explain the transformation of 10 and 19 into dihydroazulenones 15 and 23, interconversion of 10 and 19 into their isomers 14 and 22 must be invoked, and an ionic 'ring-walk' rearrangement is suggested for such an isomerization.

The intramolecular Buchner reaction, (Scheme 1)† has emerged as a prominent synthetic method[1] after the discovery by Teyssié and co-workers[2] that rhodium(II) carboxylates strongly facilitate nitrogen loss from diazo compounds **1**, probably forming carbenoid species such as **2**. Thus, either 3,4-dihydroazulen-1(*2H*)-ones **5** or 2-tetralones **6** can be obtained in good yields from the equilibrium mixtures of norcaradienones (NCD) **3** and cycloheptatrienones (CHT) **4** by addition of a base or a protic acid, respectively.

The fact that 5-methoxy-2-tetralone **7** results from 1-diazo-4-(2-methoxyphenyl)butan-2-one **9**,[3] instead of 8-methoxy-2-tetralone **8**,[1b] was explained by Cordi *et al.*[3] with the assumption that the tricyclic ketone **10** is formed through direct cyclopropanation of the benzene bond away from the methoxy group.

On the other hand, the trienone **13** could be envisaged as arising from the base-induced stabilisation of a reaction mixture consisting of the NCD/CHT couple **14**/**15**, *i.e.* of compounds formed by the attack of the carbenoid center on the 1,2-bond of the benzene ring. This direction of the intramolecular Buchner cyclisation had previously been suggested by McKervey and co-workers[1b] on the basis of the observation that the signal at *ca.* δ 5.0, which is characteristic of H-8 in 3,8a-dihydroazulen-1(*2H*)-one derivatives such as **4**,[4] was missing from the NMR spectrum of the crude product obtained by decomposition of **9**. Thus, structures **15** (instead of **11**) and **13** (instead of **12**) were assigned to the dihydroazulenone occurring in the reaction mixture and to its Et_3N-stabilised product, respectively.[1b]

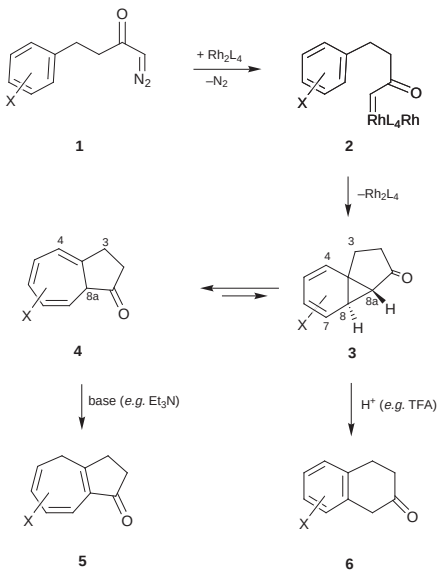

1 **2** **4** **3** **5** **6**

Scheme 1

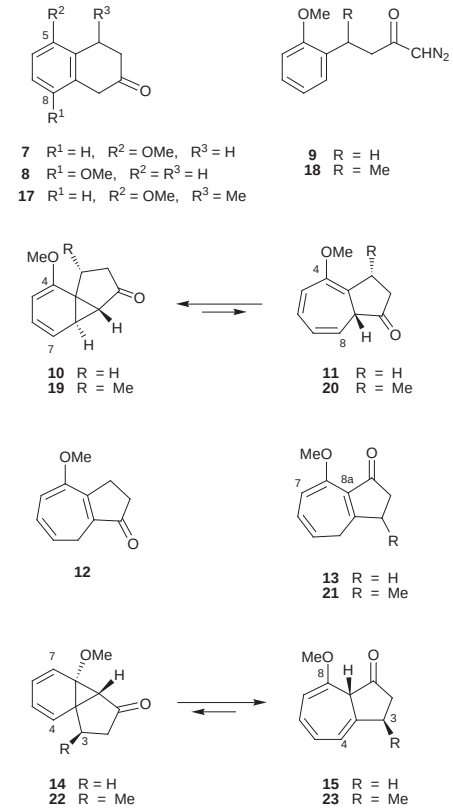

We report here spectroscopic evidence proving structure **10** for the early reaction product in the decomposition of **9** under $Rh_2(OAc)_4$ catalysis and propose a reasonable explanation for its spontaneous conversion into **15** (giving rise to **13** by Et_3N treatment) and for the formation of **7** as the final product of the TFA-ended procedure.

The decomposition of **9**[1b] was performed in CH_2Cl_2 containing catalytic amounts of $Rh_2(OAc)_4$ at 0 °C for 1 h.[1a] After the usual work-up of the reaction mixture at 0 °C, the HPLC analysis‡ of the crude product revealed the presence of two main compounds showing different electronic absorptions: λ_{max} at 280 nm for the faster moving substance and at 260, 295sh, 315sh nm for the other. Such electronic absorptions appeared to be in agreement with those expected for a norcaradiene[5,6] and for a cycloheptatriene derivative,[6] respectively. The intensity ratio of the HPLC peaks was 2 : 1 in favour of that having the shorter retention time. However, after keeping the CH_2Cl_2 solution of the crude reaction product at

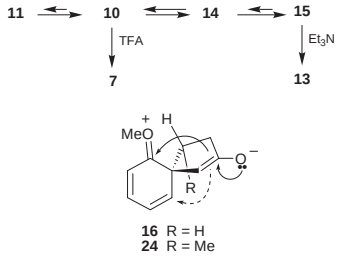

Scheme 2

room temperature overnight the peak of the faster moving substance disappeared completely. HPLC separation of the time-stabilised CH_2Cl_2 solution gave a pure compound (t_R = 11.2 min, yellowish oil, 75% yield)‡ to which the structure of 8-methoxy-3,8a-dihydroazulen-1(2*H*)-one (**15**)§ was assigned on the basis of its spectroscopic data.[1b,4] This structure was confirmed by NOE correlations (2.7 and 1.1% intensity enhancement of H-4 and H-3 by irradiation of H-3 and H-4).

Treatment of **15** with Et_3N in CH_2Cl_2 at room temperature furnished a compound (oil, 63% yield) whose spectroscopic data were consistent with the structure of a cross-conjugated dihydroazulenone,[1b,4] *i.e.* **13**.§ Thus, the occurrence of **14** as a precursor of **15** (and **13**) could be inferred. However, addition of a few drops of TFA to a CH_2Cl_2 solution of **15** or of the crude reaction product resulted in the rapid, quantitative formation of the tetralone **7**.[3]

All attempts to isolate the substance (t_R 8.7 min) accompanying **15** in the reaction mixture failed. Nevertheless, the ^{1}H NMR signals of that unstable component could be acquired by subtracting the spectra of **15** from those of the crude reaction mixture. The resulting congruent set of signals indicated a norcaradiene structure such as **10**§ having *three* olefinic hydrogens only. It must be pointed out that compound **10** does not correlate with the dihydroazulenone **15** through a direct electrocyclic reversion, but corresponds to an attack of the metal carbene on the benzene ring away from the methoxy group.

The above results can be interpreted in terms of a multiple equilibrium (Scheme 2) based on the following assumptions. The rhodium(II)-catalysed decomposition of **9** gives rise to the norcaradienone **10** (and possibly to **14,** to a lesser extent) through an intramolecular aromatic cycloaddition. Then compound **10** slowly converts into its isomer **14** (*vide infra*) which rapidly collapses to the much more stable dihydroazulenone **15**. By contrast, the NCD/CHT equilibrium[7] **10**/**11** must be assumed to be largely shifted toward the tricyclic form, *i.e* **10**. This seems plausible since it is known that hydroxy and trimethylsilyloxy groups at the 2- and/or 5-position of a cycloheptatriene ring have a strong stabilising effect on the tautomeric norcaradiene system.[8] The presence of **15** as the only final product in the reaction mixture is also consistent with the finding that among the four methoxycyclohepta-1,3,5-trienes the 1-methoxy isomer is the most stable.[9]

With regard to the possible mechanisms for the interconversion between **10** and **14** the intermediacy of a spiro derivative such as **16** (or its protonated form) seems the most likely explanation.

When 1-diazo-4-(2-methoxyphenyl)pentan-2-one **18** was decomposed by $Rh_2(OAc)_4$ in CH_2Cl_2 at 0 °C and the reaction mixture worked up in the usual manner, HPLC and ^{1}H NMR analysis revealed the presence of one reaction product. After purification by preparative HPLC this product (60% isolated yield) was shown to be the norcaradienone **19**,¶ which quickly furnished 5-methoxy-4-methyl-2-tetralone (**17**) by TFA treatment in almost quantitative yield. Compound **19** was found to be stable in CH_2Cl_2 at −20 °C for weeks; on the other hand, addition of catalytic amounts of Ph_3CBF_4 to a solution of **19** in CH_2Cl_2 caused rapid formation of the 8-methoxy-3-methyl-3,8a-dihydroazulen-1(2*H*)-one **23**,¶ which in turn gave rise to the cross-conjugated ketone **21**¶ when treated with Et_3N.

These results reinforce the above assumption concerning the occurrence of two NCD/CHT equilibria connected by ionic (cation-catalysed) interconversion of 4- and 8-methoxynorcaradienones. The fact that **19** appears to be more stable than **10** in respect to isomerization may be due to steric repulsion between the methyl group at the 3-position and the hydrogen atom at the 4-position in the spiranic intermediate **24** as well as in the tricyclic ketone **22**. In fact the methyl group in **19** was shown by NOE data¶ data to be oriented out of the plane of the six-membered ring thus minimizing its interaction with the methoxy group.

Thanks are due to MURST (Italy) for financial support.

Notes and references

† Throughout this paper azulene numbering is used for the tricyclic derivatives. A single enantiomer is depicted for all interrelated compounds.

‡ Analytical HPLC column: Merck LiChrospher 100 RP-18 (5 μm, 250 × 4 mm); eluent: MeOH–H_2O (58:42); flow rate: 1 ml min^{-1}.

§ *Selected data* for **15**: λ_{max}(MeOH)/nm (log ε) 258 (3.56), 294 (3.38), 315 (3.23); ν_{max}(film)/cm^{-1} 1752, 1707, 1610; δ_H(300 MHz, $CDCl_3$) 2.45–2.60 (2H, m, H_2-2), 2.64 (1H, br s, H-8a), 2.90 (2H, dt, *J* 2.0, 9.0, H_2-3), 3.58 (3H, s, OMe), 5.38 (1H, d, *J* 6.0, H-7), 6.18 (1H, dt, *J* 2.0, 5.5, H-4), 6.29 (1H, dd, *J* 5.5, 10.5, H-5), 6.36 (1H, dd, *J* 6.0, 10.5, H-6), assignment of the signal at δ 2.64 was confirmed by the ^{2}H NMR spectrum of a monodeuterated sample prepared from [1-^{2}H]-**9** which in turn was obtained by equilibration in CH_3OD in the presence of catalytic amount of TEA; δ_c(75 MHz, $CDCl_3$) 27.33 (t, C-3), 39.08 (t, C-2), 53.87 (d, C-8a), 56.63 (q, OCH_3), 97.06 (d, C-7), 120.58 (d, C-4), 124.42 (d, C-5), 126.66 (d, C-6), 132.81 (s, C-3a), 145.79 (s, C-8), 214.20 (s, C-1). For **13**: λ_{max}(MeOH)/nm (log ε) 232 (4.21), 266 (3.67), 323 (3.07); ν_{max}($CHCl_3$)/cm^{-1} 1698, 1612, 1554, 1439; δ_H(300 MHz, $CDCl_3$) 2.47–2.53 (2H, m, H_2-2), 2.67–2.74 (4H, m, H_2-3, H_2-4), 3.72 (3H, s, OMe), 5.50 (1H, dt, *J* 6.0, 9.5, H-5), 5.74 (1H, d, *J* 6.0, H-7), 6.09 (1H, dd, *J* 6.0, 9.5, H-6). For **10**: δ_H(300 MHz, $CDCl_3$ 1.35 (1H, br s, H-8a), 2.05–2.35 (2H, m, H_2-2), 2.80–2.90 (2H, m, H_2-3), 3.45 (1H, br d, *J* 6.5, H-8), 3.65 (3H, s, OMe), 5.51 (1H, d, *J* 8.5, H-5), 5.87 (1H, dd, *J* 6.5, 8.5, H-7), 6.14 (1H, t, *J* 8.5, H-6).

¶ *Selected data* for **19**: oil; λ_{max}(MeOH)/nm (log ε) 276 (3.70) (see ref. 6, 7); δ_H(300 MHz, $CDCl_3$), 0.95 (1H, br s, H-8a), 1.02 (3H, d, *J* 7.0, Me), 1.73 (1H, dd, *J* 9.0, 18.0, H_a-2), 2.31 (1H, dd, *J* 9.0, 18.0, H_b-2), 3.00 (1H, br d, *J* 5.0, H-8), 3.28 (1H, m, H-3), 3.67 (3H, s, OMe), 5.30 (1H, d, *J* 7.5, H-5), 5.85 (1H, dd, *J* 5.0, 9.0, H-7), 6.07 (1H, app t, *J* 8.5, H-6); selected NOE difference data: 1.02 → 3.00 (4.2%); 3.00 → 1.02 (0.5%). For **23**: yellowish oil, 51% after HPLC purification; δ_H(300 MHz, $CDCl_3$), 1.32 (3H, d, *J* 7.0, Me), 2.19 (1H, dd, *J* 7.0, 15.0, H_a-2), 2.70 (1H, br s, H-8a), 2.79 (1H, dd, *J* 7.0, 15.0, H_b-2), 3.08 (1H, m, H-3), 3.55 (3H, s, OMe), 5.40 (1H, d, *J* 5.0, H-7), 6.19 (1H, dd, *J* 2.5, 3.0, H-4), 6.32 (1H, dd, *J* 3.0, 11.0, H-5), 6.40 (1H, dd, *J* 5.0, 11.0, H-6). For **21**: oil, 35% yield after flash chromatography; δ_H(300 MHz, $CDCl_3$) 1.23 (3H, d, *J* 7.0, Me), 2.12 (1H, dd, *J* 2.0, 18.5, H_a-2), 2.76 (1H, dd, *J* 7.0, 18.5, H_b-2), 2.67 and 2.74 (2H, part AB of ABX system, J_{AB} 13.0, J_{AX} = J_{BX} 6.0, H_2-4), 2.93 (1H, m, H-3), 3.75 (3H, s, OMe), 5.29 (1H, ddd, part X of ABX system, *J* 6.0, 9.5, H-5), 5.78 (1H, d, *J* 6.5, H-7), 6.11 (1H, dd, *J* 6.5, 9.5, H-6).

1 (*a*) P. Manitto, D. Monti, S. Zanzola and G. Speranza, *J. Org. Chem.*, 1997, **62**, 6658; (*b*) M. Kennedy, M. A. McKervey, A. R. Maguire, S. M. Tuladhar and M. F. Twohig, *J. Chem. Soc., Perkin Trans. 1*, 1990, 1047.
2 A. J. Anciaux, A. Demonceau, A. F. Noels, A. J. Hubert, R. Warin and P. Teyssié, *J. Org. Chem.*, 1981, **46**, 873.
3 A. A. Cordi, J.-M. Lacoste and P. Hennig, *J. Chem. Soc., Perkin Trans. 1*, 1993, 3.
4 L. T. Scott, M. A. Minton and M. A. Kirms, *J. Am. Chem. Soc.*, 1980, **102**, 6311.
5 E. Wenkert and S. Liu, *Synthesis*, 1992, 323.
6 E. Ciganek, *J. Am. Chem. Soc.*, 1967, **89**, 1454; J. A. Berson, D. R. Hartter, H. Klinger and P. W. Grubb, *J. Org. Chem.*, 1968, **33**, 1669.
7 J. F. Liebman and A. Greenberg, *Chem. Rev.*, 1989, **89**, 1225.
8 C. S. Q. Lew, T.-H. Tang, I. G. Csizmadia and B. Capon, *J. Chem. Soc., Chem. Commun.*, 1995, 175.
9 W. H. Donovan and W. H. White, *J. Org. Chem.*, 1996, **61**, 969.

Communication 8/09991J

DMAP-promoted racemization-free deacylation of carboxthioimide† adducts: carboxthioimide as a versatile carboxy protecting group

Dah-Wei Su, Ying-Chuan Wang and Tu-Hsin Yan*

Department of Chemistry, National Chung-Hsing University, Taichung, Taiwan 400, Republic of China.
E-mail: thyan@mail.nchu.edu.tw

Received (in Cambridge, UK) 21st January 1999, Accepted 9th February 1999

The DMAP-promoted deacylation of carboxthioimide adducts can be directed to form either acid or various ester protecting groups with no detectable levels of epimerization.

The development of protecting groups of carboxy functionality which are stable under the usual reaction conditions and which can be activated by a specific reagent for nucleophilic deacylation under very mild conditions has been a challenging undertaking. Oxazolidinone-derived carboximides[1–4] as well as oxazolidinethione- and thiazolidinethione-based carboxthioimides[5,6] have proven to be valuable carboxy-protecting groups for the construction of enantiomerically pure substances. While, traditionally, the use of basic reagents ($LiOCH_2Ph$, BrMgOMe, LiOH, LiOOH, K_2CO_3/MeOH)[6,7] for the nucleophilic cleavage of imide the thioimide adducts has been the method of choice for removing the auxiliary from substances, progress in nucleophilic catalyst-promoted imide and thioimide deacylation with oxygen nucleophiles like H_2O, alcohols and phenol remains far less developed. Effecting such nucleophilic acyl substitution may have the advantage of (i) controlling the nucleophilic cleavage without causing racemization of the newly created stereocenters, (ii) promoting further useful transformations of the initial adducts without influencing the pendent functional groups, and (iii) enhancing synthetic efficiency by direct conversion of the initial adducts to various ester protecting groups. The tremendous impact of DMAP[8] in catalyzing the acylation of alcohols suggested the feasibility of DMAP as a catalyst to effect transesterification or hydrolysis of imides and thioimides. Here we report protocols whereby the thioimide transesterification promoted by DMAP can be directed to form either acid or various ester protecting groups with no detectable levels of epimerization.

The reactions of crotonyloxazolidinone-derived Diels–Alder adduct **1** with MeOH and H_2O were chosen to test the feasibility of the DMAP-promoted oxazolidinone deacylation (Scheme 1). In view of the well-documented excellent shelf lives of *N*-acyloxazolidinones,[9] we were not surprised to observe no detectable methanolysis and hydrolysis at the exocyclic carbonyl center. Believing a more polarizable auxiliary might facilitate nucleophilic attack, we turned to the deacylation of carboxthioimide derived adducts. Initial work centered on the deacylation of the Diels–Alder adduct **2** derived from the unsaturated *N*-acylthiazolidine-2-thione (*cf.* Scheme 1) which has been shown to exhibit enhanced dienophilic reactivity in a copper(II)-catalyzed asymmetric cycloaddition.[10] The requisite thioimide adduct **2** was available by treating crotonylthiazolidienethione with excess cyclopentadiene (5–10 equiv.) and 1.2 equiv. of $ZnCl_2$ in CH_2Cl_2 at 0 °C. Treatment of thioimide **2** with 1.5 equiv. of MeOH in MeCN with 20 mol% DMAP at room temperature gave the methyl ester **3a** in 96% yield along with a 93% recovery of the auxiliary (Scheme 1). The DMAP-promoted thiazolidinethione deacylation exhibited good generality. Thus, switching the nucleophile from MeOH to PhOH had little effect. The same conditions effected transesterification of **2** to afford phenyl ester **3b** in 91% yield. Similarly, DMAP (1.1 equiv.) promoted hydrolysis of **2** with H_2O as the nucleophile afforded the acid **3c**. The broad scope of the transesterification is illustrated by the tolerance of β-substituents on ethanol. Thus deacylation of **2** with 2,2,2-trichloroethanol under the same conditions gave the corresponding β-substituted ethyl ester protecting group. A labile alcohol, 2-bromoethanol, also proved to be a satisfactory nucleophile under our standard conditions in the presence of the DMAP catalyst. Trimethylsilylethanol gave similar results, albeit in a somewhat slower reaction. After 24 h, an 89% yield of 2-(trimethylsilyl)ethyl ester **3f** was obtained.‡ The utility of allyl and benzyl esters as useful carboxy-protecting groups led to our examination of allyl and benzyl alcohols, which participated equally well, giving the corresponding esters **3g** and **3h** in excellent yield (≥95%).[11] Steric hindrance plays a role; in contrast to the above, *tert*-butyl alcohol failed to react with thioimide adduct **2** under the above conditions.

The suitability of these mild conditions for oxazolidinethione deacylation is illustrated by the additional examples provided below. Camphor-based *N*-acyloxazolidinethiones such as Diels–Alder cycloadduct **4** and aldol adduct **6**[5] were utilized to test the feasibility of DMAP-promoted nucleophilic cleavage. The DMAP-promoted transesterification of cycloadduct **4**, which was prepared from the $TiCl_4$-mediated Diels–Alder reaction of camphor-based crotonyloxazolidinethione with cyclopentadiene, with benzyl alcohol proceeded more slowly

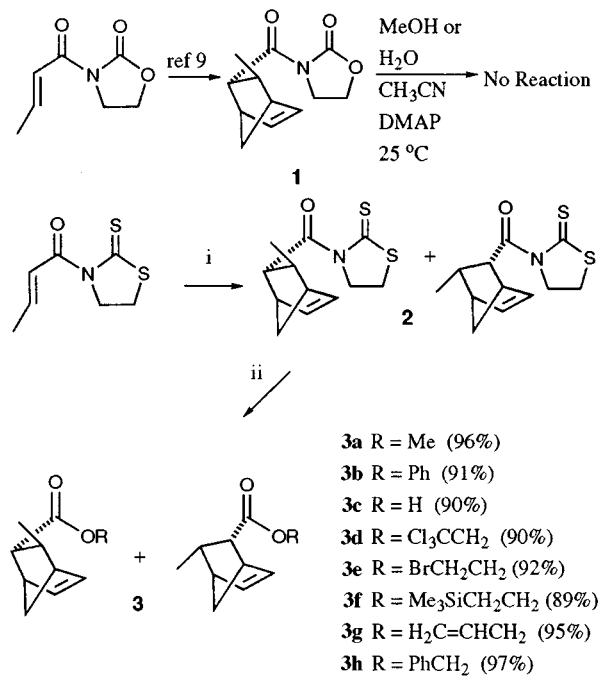

Scheme 1 *Reagents and conditions*: i, $ZnCl_2$, cyclopentadiene, CH_2Cl_2 0 °C; ii, ROH or H_2O, DMAP (0.2–1.1 equiv.), MeCN, room temp., 4–24 h.

† General IUPAC name: 3-acyl-1,3-thiazolidine-2-thione.

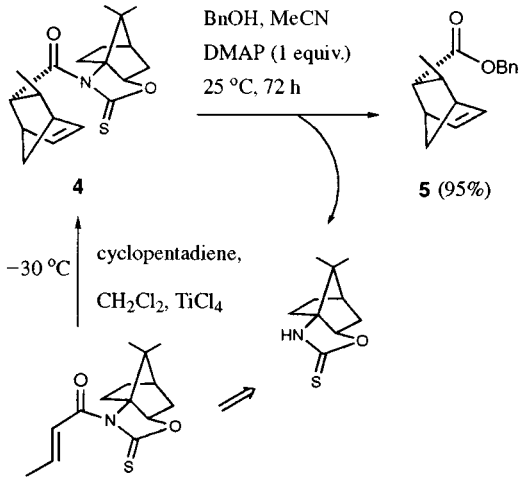

Scheme 2

but still in excellent yield (Scheme 2). After 72 h, the transesterification product **5**, $[\alpha]_D^{25}$ +129.3 (*c* 0.9, CH_2Cl_2),[9] was obtained in 95% with no detectable levels of epimerization. Using the above standard conditions, both hydrolysis and methanolysis of aldol adduct **6** were easily effected without racemization of either center (Scheme 3). The acid **6a**, $[\alpha]_D^{25}$ +13.6 (*c* 1.1, CH_2Cl_2), and ester **6b**, $[\alpha]_D^{25}$ +22.5 (*c* 1.4, CH_2Cl_2),[2] were obtained in 87 and 92% yield, respectively.

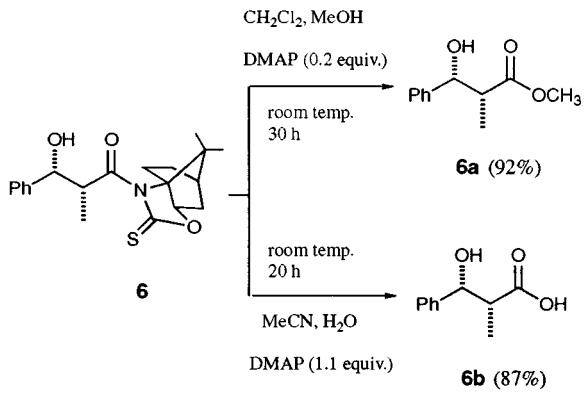

Scheme 3

In conjunction with a program directed toward the asymmetric synthesis of β-hydroxy-α-amino acids, a key intermediate toward biologically active peptides and β- and γ-lactam antibiotics,[12] we were particularly interested in bromohydrin substrates.[13] To demonstrate the utility of this protocol, we examined the transesterification of bromohydrin aldol **7**,[14] which by virtue of the ease of bromide displacement demands very mild methods. In the DMAP (0.2 equiv.) catalyzed transesterification ($PhCH_2OH$) of bromohydrin **7** at 0 °C, epoxide formation was completely suppressed and benzyl β-hydroxy-α-amino ester **8** was isolated in 96% yield with no apparent loss of stereochemistry (Scheme 4).‡ This result is in directed contrast to the BnOLi deacylation conditions for

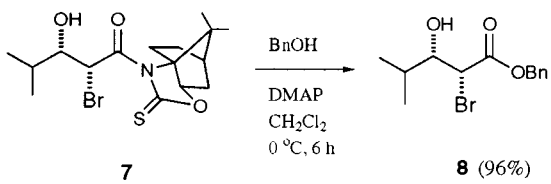

Scheme 4

oxazolidinone bromohydrins, in which benzyl α,β-epoxy esters are formed.[3]

In conclusion, we have demonstrated that carboxthioimides are very versatile and useful carboxy-protecting groups. Significantly, the thioimide transesterification *via* DMAP catalysis provides the acids or various ester protecting groups without danger of racemization. The successful control of oxazolidinethione deacylation *vs.* cyclization of nucleophiles with bromohydrin aldol adducts illustrates the power of our newly developed DMAP-promoted nucleophilic cleavage. Further details in this area will be forthcoming.

We thank the National Science Council of the Republic of China for support of this work (NSC 88-2213-M-005-006).

Notes and references

‡ *Selected data* for **3f**: δ_H(400 MHz, $CDCl_3$) 6.22 (dd, *J* 5.6, 3.2, 1H, C*H*=CH), 5.96 (dd, *J* 5.6, 2.8, 1H, C*H*=CH), 4.07 (m, 2H, OCH_2CH_2), 3.06 (m, 1H, *H*CC=C), 2.43 (m, 1H, C=CC*H*), 2.31 (dd, *J* 4.0, 4.0, 1H, *H*CC=O), 1.79 (m, 1H, *H*CCH_3), 1.37–1.52 (m, 2H, H_2CCH), 1.14 (d, *J* 7.2, 3H, $CHCH_3$), 0.92 [m, 2H, $CH_2CH_2Si(CH_3)_3$], 0.01 [s, 9H, $Si(CH_3)_3$]; δ_C(100 MHz, $CDCl_3$) 174.97, 138.59, 133.21, 62.31, 52.60, 48.79, 45.96, 45.90, 37.71, 20.96, 17.30, −1.50 (HRMS: calc. for $C_{14}H_{24}O_2Si$, 252.1546. Found 252.1545. Calc. for $C_{14}H_{24}O_2Si$: C, 66.62; H, 9.58. Found: C, 66.40; H, 9.69%). For **8**: δ_H(400 MHz, $CDCl_3$) 7.35 (br s, 5H, C_6H_5), 5.20 (2d, *J* 12.0, 2H, $C_6H_5CH_2$), 4.47 (d, *J* 3.6, 1H, CHC*H*Br), 3.53 (dd, *J* 7.2, 3.6, 1 H, CHC*H*CHBr), 1.87 (br s, 1H, O*H*), 1.78 (app. octet, *J* 7.2, 1H, $(CH_3)_2CHCH$), 1.00 (d, *J* 6.8, 3H, CH_3CHCH_3), 0.91 (d, *J* 6.8, 3H, CH_3CHCH_3); δ_C(100 MHz, $CDCl_3$) 169.18, 134.67, 128.60, 128.48, 128.25, 75.91, 67.94, 51.07, 31.61, 18.90, 17.60; $[\alpha]_D^{25}$ +15.5 (*c* 0.9, CH_2Cl_2) (HRMS: calc. for $C_{13}H_{17}O_3Br$, 300.0361. Found, 300.0355. Calc. for $C_{13}H_{17}O_3Br$: C, 51.82; H, 5.69. Found: C, 51.80; H, 5.65%).

1 Selected reviews: D. A. Evans, J. V. Nelson and T. R. Taber, *Top. Stereochem.*, 1982, **13**, 1; C. H. Heathcock, in *Asymmetric Synthesis*, ed. J. D. Morrison, Academic Press, New York, 1984, vol. 3, p. 111.
2 D. A. Evans, J. Bartrol and T. L. Shih, *J. Am. Chem. Soc.*, 1981, **103**, 2127.
3 A. Abdel-Magid, N. P. Lendon, S. E. Drake and L. Ivan, *J. Am. Chem. Soc.*, 1986, **108**, 4595.
4 H. Heathcock, *Aldrichim. Acta*, 1990, **23**, 99 and references cited therein; M. P. Bonner and E. R. Thornton, *J. Am. Chem. Soc.*, 1991, **113**, 1299; Y.-C. Wang, A.-W. Hung, C.-S. Chang and T.-H. Yan, *J. Org. Chem.*, 1996, **61**, 2038.
5 T.-H. Yan, C.-W. Tan, H.-C.Lee, H.-C. Lo and T.-Y. Huang, *J. Am. Chem. Soc.*, 1993, **115**, 2613; T.-H. Yan, A.-W. Hung, H.-C. Lee and C.-S. Chang, *J. Org. Chem.*, 1994, **59**, 8187; T.-H. Yan, A.-W.Hung, H.-C. Lee, C.-S. Chang and W.-H. Liu, *J. Org. Chem.*, 195, **60**, 3301.
6 C.-N. Hsiao, L. Liu and M. J. Miller, *J. Org. Chem.*, 1987, **52**, 2201.
7 D. A. Evans, M. D. Ennis and D. J. Mathre, *J. Am. Chem. Soc.*, 1982, **104**, 1737; D. A. Evans, M. M. Morrissey and R. L. Dorow, *J. Am. Chem. Soc.*, 1985, **107**, 4346; D. A. Evans, J. A. Ellman and R. L. Dorow, *Tetrahedron Lett.*, 1987, **28**, 1123; D. A. Evans, T. C. Britton and J. A. Ellman, *Tetrahedron Lett.*, 1987, **28**, 6141.
8 G. Hofle, W. Steglich and H. Vorbruggen, *Angew. Chem., Int. Ed. Engl.*, 1978, **17**, 569; B. Neises and W. Steglich, *Angew. Chem., Int. Ed. Engl.*, 1978, **17**, 522.
9 D. A. Evans, K. T. Chapman and J. Bisaha, *J. Am. Chem. Soc.*, 1988, **110**, 1238.
10 D. A. Evans, S. J. Miller and T. Lectka, *J. Am. Chem. Soc.*, 1993, **115**, 6460.
11 New compounds have been satisfactorily characterized spectroscopically, and elemental composition has been established by high-resolution mass spectroscopy and/or combustion analysis.
12 *Amino Acids, Peptides and Proteins*, Specialist Periodical Reports, vol. 1–16, ed. G. T. Young and R. C. Sheppard, Chemistry Society, London, 1968–1983; T. Sunazuka, T. Nagamitsu, K. Matsuzaki, H. Tanaka, S. Omura and A. B. Smith, III, *J. Am. Chem. Soc.*, 1993, **115**, 5302.
13 D. A. Evans, E. B. Sjogren, A. E. Weber and R. E. Conn, *Tetrahedron Lett.*, 1987, **28**, 39; E. J. Corey, D.-H. Lee and S. Choi, *Tetrahedron Lett.*, 1992, **33**, 6735.
14 Prepared from the $TiCl_4$-mediated aldolization of camphor-based 3-bromoacetyl-1,3-oxazolidine-2-thione with isobutyraldehyde.

Communication 9/00577C

Signal transduction mediated by artificial cell-surface receptors: activation of lactate dehydrogenase triggered by molecular recognition and phase reorganization of bile acid derivatives embedded in a synthetic bilayer membrane

Jun-ichi Kikuchi,* Katsuhiko Ariga and Kouki Ikeda

Graduate School of Materials Science, Nara Institute of Science and Technology, Ikoma, Nara 630-0101, Japan. E-mail: jkikuchi@ms.aist-nara.ac.jp

Received (in Cambridge, UK) 4th January 1999, Accepted 22nd February 1999

A bile acid derivative, *N*-(2-aminoethyl)-5β-cholan-24-amide, acts as an artificial cell-surface receptor capable of activating lactate dehydrogenase by performing double signal recognition and phase reorganization in a synthetic bilayer membrane.

Recently, bile acids have been employed as a key building block for design of artificial hosts capable of performing molecular recognition in various physical phases such as the solid state,[1] and aqueous[2] and organic media.[3] The molecular rigidity provided by the steroidal moiety is of great advantage for the functionalization of such host molecules. Meanwhile, there are few reports on bile acid derivatives, such as steroidal porphyrins[4] and cyclophanes,[5] each being a supramolecular element in bilayer membranes. We report here on the signal recognition and response of an artificial steroidal receptor, *N*-(2-aminoethyl)-5β-cholan-24-amide **2**, embedded in the bilayer membrane formed with a synthetic peptide lipid, *N*,*N*-dihexadecyl-*N*$^{\alpha}$-[6-(trimethylammonio)hexanoyl]glycinamide bromide **1**.†

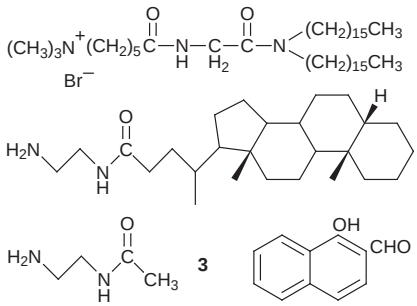

1 **2** **3** **4**

In aqueous media **1** formed a morphologically stable bilayer membrane with a gel-to-liquid crystalline phase transition at 26.0 °C (ΔH = 31.0 kJ mol^{-1}) in a manner similar to those reported for the analogous peptide lipids having a different amino acid residue.[6] Bilayer vesicles were prepared by sonication of an aqueous dispersion containing **1** and water-insoluble **2** in a 40 : 1 molar ratio with a bath-type sonicator at 80 W for 60 min in 2-[4-(2-hydroxyethyl)piperazin-1-yl]-ethanesulfonate (HEPES) buffer (100 mmol dm^{-3}, pH 7.0). The formation of single-walled bilayer vesicles was confirmed by negative-staining electron microscopy, and the vesicular size as evaluated by means of dynamic light scattering measurements was 120 nm.

Next we examined the molecular recognition behavior of the receptor **2**. 1-Hydroxy-2-naphthaldehyde **4** was effectively bound to **2** homogeneously dispersed in the bilayer vesicle by forming an imine bond between the formyl group and the amino group, as confirmed by electronic absorption spectroscopy. The binding process was reversible and in equilibrium under the present conditions. The dissociation constant for the Schiff's base was evaluated from the aldehyde-dependent absorbance changes at 440 nm to be 1.5 μmol dm^{-3} at 30.0 °C. The binding of **4** with **2** was much enhanced upon addition of copper(II) ions due to the formation of the corresponding metal chelate having an absorption maximum at 388 nm. The continuous variation method[7] applied to the present bilayer system clearly indicates that the Schiff's base and copper(II) ions form a 2 : 1 chelate accompanying the phase reorganization of the steroidal moieties in the liquid crystalline state of the membrane. Such metal-ion-induced phase reorganization behavior was reflected by an increase in the phase transition temperature and sharpening of the peak for the hybrid membrane in the dispersion states, as evaluated by differential scanning calorimetry. Thus **2** acts as an artificial host being capable of recognizing both **4** and copper(II) ions in the bilayer membrane.

We have also clarified that pig heart lactate dehydrogenase (LDH; Boehringer Manheim, Germany) was bound to the membrane surface of the cationic peptide lipid mainly through electrostatic interactions, and that the LDH activity was specifically inhibited by copper(II) ions.[8] On these grounds, we constituted an artificial signaling system with **1**, **2** and LDH as schematically shown in Fig. 1 and evaluated the signal transduction ability of the steroidal host as an artificial cell-surface receptor. We chose **4** and copper(II) ions as an external signal of the receptor **2** and the second messenger signals between **2** and LDH, respectively. Under the conditions used the metal binding affinity of the components increases in the

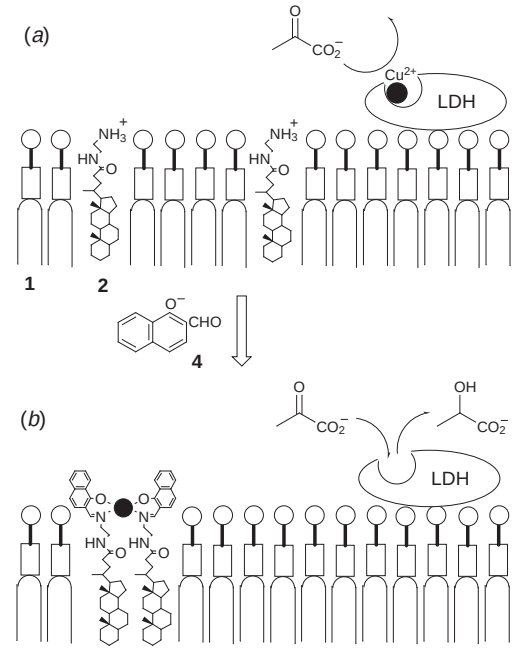

Fig. 1 Schematic illustration of switching of LDH activity mediated by an artificial cell-surface receptor **2**. (*a*) and (*b*) represent the off- and on-states of LDH in the absence and presence of an external signal **4**, respectively.

Table 1 LDH activities in an aqueous HEPES buffer (100 mmol dm^{-3}, pH 7.0) at 30.0 °C[a]

Entry	Species/μmol dm^{-3}				v_0[b]/μmol dm^{-3} s^{-1}	Activity[c] (%)
	1	**2**	**4**	Cu^{2+}		
1	0	0	0	2	0.45 (1.20)	37
2	0	0	30	2	0.37 (1.14)	32
3	1200	0	0	2	0.25 (1.17)	21
4	1200	0	30	2	0.15 (1.18)	13
5	1200	30	0	2	0.17 (1.16)	15
6	1200	30	30	2	1.00 (1.22)	82

[a] Concentrations: pyruvate, (150 μmol dm^{-3}); NADH (250 μmol dm^{-3}); LDH (170 μg dm^{-3}). [b] Initial velocity for LDH catalyzed reaction. The value in the absence of copper(II) ions is in parentheses. Values are accurate within ±3%. [c] Magnitude of v_0 in the presence of $Cu(ClO_4)_2$ relative to that of the corresponding metal-free system.

following order: **2** < LDH < the **2**–**4** complex, giving the signal transduction behaviour shown in Fig. 1. In the absence of an external signal ligand, the catalytic performance of LDH is blocked by coordination of copper(II) ions [Fig 1(*a*)], since the steroidal receptor behaves as a weak unidentate ligand for metal ions. Upon binding of the signal ligand **4** with the receptor **2**, the resulting receptor–ligand complex acts as a strong bidentate ligand to snatch the metal ion from LDH, resulting also in phase reorganization of **2** in the bilayer membrane [Fig. 1(*b*)]. Thus the LDH activity can be indirectly controlled by an external signal in the present artificial receptor system.

The catalytic activity of LDH in the reduction of pyruvate to L-lactate was evaluated spectrophotometrically by following a consumption rate (v_0) of NADH in the presence and absence of the supramolecular elements and the signaling species (Table 1). In the absence of copper(II) ions, the LDH activity was not significantly influenced by the presence of **1**, **2** and **4**. However, inactivation of LDH by copper(II) ions was highly specific, since the catalytic activity was not influenced by the presence of zinc(II) or nickel(II) ions at similar concentrations. The inhibition of LDH by copper(II) ions was reversible and competitive as analyzed by the Lineweaver–Burk plots; the inhibition constant, defined as the dissociation constant of the LDH–copper(II) complex, was 0.22 and 2.2 μmol dm^{-3} in the presence and absence of the bilayer membrane, respectively. Thus the extent of inactivation of LDH by copper(II) ions in the vesicular system was larger than that in aqueous solution (Table 1, entries 1 and 3). Inhibition of the enzymic activity by copper(II) ions was somewhat enhanced upon addition of **4** (Table 1, entry 2), and such behavior was also observed in the presence of the bilayer membrane (Table 1, entry 4). As expected, the LDH activity of the hybrid system depicted in Fig. 1(*a*) was low (Table 1, entry 5), reflecting the larger metal-binding ability of LDH than the steroidal receptor. Upon addition of the signal ligand **4** to this system, however, the LDH activity, defined as the magnitude of the initial velocity in the presence of copper(II) ions relative to that of the corresponding metal-free system, was drastically increased to 82% from 15% (Table 1, entry 6) as a consequence of the change in the metal binding mode, as shown in Fig. 1(*b*). When the receptor **2** was replaced by water-soluble **3** lacking the steroidal moiety in the supramolecular system shown in Fig. 1, the LDH activity increased only a little to 41% from 32% under similar concentration conditions. Accordingly, it is clear that the signal transduction occurrs with extremely high efficiency on the membrane surface of the hybrid molecular assembly formed from the peptide lipid **1**, the steroidal receptor **2** and LDH. The present hydrid system shows marked signal selectivity. For example, only 38% LDH activity was observed by replacement of **4** with 2-naphthaldehyde under the conditions of entry 6 in Table 1.

In conclusion, we have demonstrated here the first example of a supramolecular assembly in which an artificial cell-surface receptor is able to switch on enzymic activity *via* accompanying double signal recognition and phase reorganization. Although the reversibility in the system remains a problem, the present results may provide a useful guide for the design of supramolecular devices that mimic the signal transduction behaviour observed in biological systems such as G-protein mediated cell signaling. [9]

This work was supported by a Grant-in-Aid for Scientific Research from the Ministry of Education, Science, Sports and Culture, Japan.

Notes and references

† All new compounds gave C, H and N elemental analyses within 0.4% of theory, and ^{1}H and ^{13}C NMR spectra consistent with their structures.

1 K. Sada, N. Shiomi and M. Miyata, *J. Am. Chem. Soc.*, 1998, **120**, 10 543; D. Albert, M. Feigel, J. Benet-Buchholz and R. Boese, *Angew. Chem., Int. Ed.*, 1998, **37**, 2727.
2 V. Janout, M. Lanier and S. L. Regen, *J. Am. Chem. Soc.*, 1997, **119**, 640; J. Kikuchi, M. Inada, Y. Murakami, K. Egami and K. Suehiro, *J. Phys. Org. Chem.*, 1997, **10**, 351.
3 A. P. Davis, *Chem. Soc. Rev.*, 1993, **22**, 243; R. P. Bonar-Law and J. K. M. Sanders, *J. Am. Chem. Soc.*, 1995, **117**, 259; Y. Cheng, T. Suenaga and W. C. Still, *J. Am. Chem. Soc.*, 1996, **118**, 1813; A. P. Davis, S. Menzer, J. J. Walsh and D. J. Williams, *Chem. Commun.*, 1996, 453.
4 J. Lahiri, G. D. Fate, S. B. Ungashe and J. T. Groves, *J. Am. Chem. Soc.*, 1996, **118**, 2343.
5 Y. Murakami, J. Kikuchi and O. Hayashida, *Top. Curr. Chem.*, 1995, **175**, 133.
6 Y. Murakami and J. Kikuchi, *Bioorg. Chem. Frontiers*, 1991, **2**, 73.
7 J. Kikuchi, T. Ogata, M. Inada and Y. Murakami, *Chem. Lett.*, 1996, 771.
8 J. Kikuchi, Y. Kamijyo, H. Etoh and Y. Murakami, *Chem. Lett.*, 1996, 427.
9 A. G. Gilman, *Angew. Chem., Int. Ed. Engl.*, 1995, **34**, 1406; M. Rodbell, *Angew. Chem., Int. Ed. Engl.*, 1995, **34**, H. E. Hamm, *J. Biol. Chem.*, 1998, **273**, 669.

Communication 9/00083F

Catalytic aerogel-like materials dried at ambient pressure for liquid-phase epoxidation

J. L. Sotelo,* R. Van Grieken and C. Martos

Chemical Engineering Department, Faculty of Chemistry, Complutense University of Madrid, 28040 Madrid, Spain. E-mail: rada@eucmax.sim.ucm.es

Received (in Cambridge, UK) 18th November 1998, Accepted 19th February 1999

Titanium-containing hydrophobic silica with a pore volume and pore sizes in the range of aerogels was prepared by silylation before drying of well-dispersed mixed oxides obtained *via* a sol-gel method; it showed remarkable properties as a catalyst in the epoxidation of styrene with Bu^{t}OOH.

Environmental concern surrounding chemical processes for the production of commodity and fine chemicals has led to the development of environmentally-friendly processes based on heterogeneous catalysts. Among them, the epoxidation of olefins is a major target since the epoxide functional group is one of the most useful intermediates in organic synthesis.[1] Heterogeneous catalysts such as silica-supported titania are used on an industrial scale for propylene epoxidation using alkyl hydroperoxides as oxidant.[2]

The discovery that the Ti-substituted silicalite molecular sieve TS-1 (an isomorphous ZSM-5 zeolite) is a catalyst for selective oxidation reactions with H_2O_2[3] has promoted investigation of its use in several oxidation reactions.[4] To overcome the restriction imposed by the relatively small average diameter (*ca.* 0.55 nm) of the channel system, Ti has been incorporated into materials with larger pore sizes such as zeolite beta,[5] or hexagonal mesoporous silica (HMS).[6] Other attempts to obtain suitable epoxidation catalysts have been based on grafting of Ti compounds onto the silica surface[7] and the use of the sol-gel technique.[8] The latter has been used to obtain epoxidation catalysts ranging from amorphous microporous[9] to mesoporous titania–silica mixed oxides,[8] and even solid precursors with the appropriate properties for Ti-containing zeolite synthesis.[10]

The many potential advantages inherent to the use of sol-gel techniques in preparing epoxidation catalysts are strongly dependent on the drying method. Supercritical drying prevents the network collapse induced by capillary forces arising from the liquid–vapour interface, leading to materials with high porosity called aerogels with suitable properties to be used as catalysts,[11] although supercritical processing has numerous drawbacks due to the extreme conditions used. Recently a simpler method at ambient pressure for the preparation of aerogel-like films has been reported[12] based on the use of a silylating agent which is reacted with the hydroxy groups on the surface of an inorganic gel, preventing the irreversible shrinkage of the porous structure during drying.

We report here a simple route, based on the above mentioned silylation procedure, for the preparation of titania–silica mixed oxides with adequate textural properties and highly dispersed Ti atoms, both features leading to active catalysts in epoxidation reactions with *tert*-butyl hydroperoxide (TBHP).

The catalysts were prepared following a two-step sol-gel method. In the first step, a solution of tetraethoxysilane (TEOS) was prehydrolyzed with aqueous HCl (0.05 M) for 45 min at room temperature (samples **1**–**3**). Other catalysts were prepared by diluting TEOS in EtOH (samples **4**–**6**); the solution was prehydrolized with aqueous HCl for 90 min, since less water is added to these samples. Then, the Ti precursor [titanium(IV) butoxide, TNBT] diluted in Pr^{i}OH was added to give gel molar ratios (TEOS : H_2O : HCl : EtOH : Pr^{i}OH : TNBT) of $1:4:3.6\times10^{-3}:0:1:0.023$ for samples **1**–**3** and $1:1.25:9\times10^{-4}:2:1:0.023$ for samples **4**–**6**, with additional hydrolysis times of 20 and 75 min, respectively. The second step of the synthesis procedure increased the condensation rates by changing the pH to higher values with aqueous NH_3 (1 M) for samples **1**–**3** and dilute NH_4OH (1 M) in EtOH (1 NH_3 : 5.6 H_2O : 0.7 EtOH) for samples **4**–**6**. Once the gel point of the sol had been reached, the solid gels were aged for 48 h and samples of **1** and **4** were dried at 110 °C overnight, whereas the other catalysts were washed with *n*-hexane and treated with a TMSCl solution in *n*-hexane before drying. For comparison, a silica obtained by an analogous sol-gel procedure was impregnated with a solution of $TiCl_4$ in EtOH (Si/Ti = 54) and calcined at 550 °C for 5 h. Also, a Ti-containing HMS was provided by Dr Tuel from CNRS[13] with a Si/Ti molar ratio of 87.3. All the catalyst samples were tested in the oxidation of styrene with TBHP at 60 °C in N_2 atmosphere. Conversions and selectivities were determined by GC, ^{1}H NMR analysis and iodometric titration.

All samples were characterised by diffuse reflectance UV–VIS spectra (DR UV–VIS) in the range 190 to 500 nm. They presented a maximum absorption band centered at 220 nm, and no absorption around 330 nm was detected. Nitrogen adsorption–desorption isotherms of the samples obtained on an ASAP 2010 from Micromeritics showed a hysteresis loop corresponding to a type IV isotherm, typically assigned to mesopores present in the materials. Samples **1** and **4** present similar textural properties independent of the presence of EtOH as a diluting agent (Table 1), with BET surface areas above 600 $m^2\ g^{-1}$ pore volumes around 1 $cm^3\ g^{-1}$ and average pore sizes in the range of 50 Å as the result of the BJH analysis on the adsorption branch of the isotherm. The silylation procedure leads to a decrease in the final Ti content of the catalysts as a consequence of the reaction of TMSCl with the OH groups at the surface of

Table 1 Textural properties and chemical composition of the different tested samples

Sample	Diluted in EtOH?	Silylated?	Calcined?	Si/Ti	S_{BET}/ $m^2\ g^{-1}$	V_P (ADS)/ $cm^3\ g^{-1}$	D_P (ADS)/ Å
1	NO	NO	YES	43	682	1.0	50
2	NO	YES	NO	73	871	1.8	71
3	NO	YES	YES	69	849	1.3	68
4	YES	NO	YES	43	604	1.0	57
5	YES	YES	NO	73	723	3.0	132
6	YES	YES	YES	69	688	2.3	125

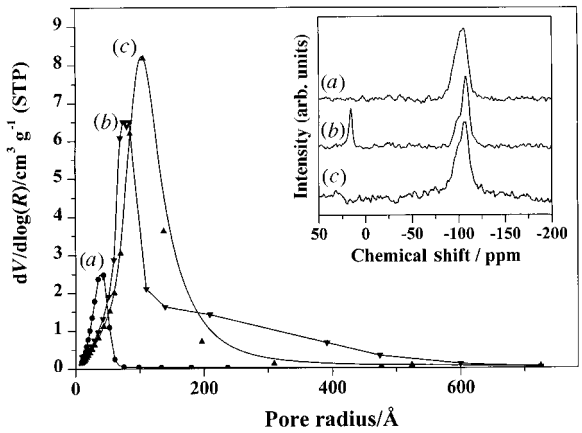

Fig. 1 Pore volume distribution (BJH analysis of the adsorption branch of the isotherm) of (*a*) **4** (xerogel), (*b*) **5** (silylated) and (*c*) **6** (silylated and calcined). Inset: ^{29}Si MAS NMR spectra of these samples are shown.

the gel, which prevents irreversible shrinkage during drying. There is a remarkable increase in the BET surface area, pore volume and mean pore size in the samples prepared with EtOH. It is interesting to note how the silylation procedure is capable of preserving at least partially the different gel structures derived from the use of increasing amounts of EtOH as solvent, something that is not shown in the textural properties of the xerogels when conventional drying is used (samples **1** and **4**). Similarly, after calcination, the differences are clearly shown not only in comparison to the xerogels but also between the materials prepared with different dilution levels, *i.e.* EtOH content. The calcination of the silylated samples leads to a decrease mainly in the pore volume of the samples compared with the uncalcined ones, showing some evidence of pore collapse. In any case, the pore volumes are clearly higher than those corresponding to xerogels and are in accordance with the textural properties of the starting non-calcined silylated samples. The used samples, after reaction, showed similar textural properties to the fresh ones.

Fig. 1 shows the pore size distribution coming from BJH analysis of the N_2 isotherms of samples **4**–**6**. There is a shift in the pore size distribution towards higher values when the silylation procedure is used, with a decrease in the size of the largest pores after calcination. The ^{29}Si MAS NMR spectra of **4**–**6** are shown in Fig. 1 (inset), recorded in a Varian 300 MHz with a spinning rate of 4 kHz. It is clearly shown how the silylation procedure decreases the large Q^3 contribution at −100 ppm in the non-silylated sample, showing up as a peak 15 ppm upfield corresponding to trimethylsilyl groups (TMS) formed in the reaction of TMSCl with the silanol groups of the gel surface.[14] The calcination procedure removes the TMS groups, with partial recovery of the surface OHs shown by the increase of the shoulder at −100 ppm. This behaviour is also seen in the IR spectra of the samples, since in the silylated catalysts there is a large decrease in the band corresponding to Si–OH vibrations (3000–3750 cm^{-1}), which is partly recovered after calcination.

Table 2 Activity of the different titanium-containing materials in the epoxidation of styrene[a]

	Conversion (%)			Selectivity (%)		
Sample	TBHP	ST	TON[b]	BADH	SO	22ET
Blank	3.9	0.6	—	13.6	86.4	0.0
Impregnated	30.2	9.8	35	1.4	81.5	17.1
Ti-HMS	45.0	16.2	77	1.0	88.3	10.7
1	39.7	15.0	35	1.4	59.9	38.7
2	35.3	12.9	50	1.9	98.1	0.0
3	35.6	13.0	48	1.1	83.9	15.0
4	41.8	15.9	37	1.4	65.7	32.9
5	45.4	16.1	63	1.4	98.6	0.0
6	41.6	17.6	66	1.2	87.8	11.0

[a] Reaction conditions: T = 60 °C, t = 3 h, autogenous pressure, no solvent, stirring speed = 300 rpm, inert atmosphere, catalyst loading = 400 mg, styrene = 100 mmol, TBHP = 40 mmol; ST = styrene; TBHP = *tert*-butyl hydroperoxide; SO = styrene oxide; BADH = benzaldehyde; 22ET = 2-phenyl-2-*tert*-butoxyethanol. [b] In moles of styrene per mole of titanium per hour.

The catalytic activities of these samples and the materials used as reference were tested in the epoxidation of styrene with TBHP. Besides the conversion of styrene and TBHP, Table 2 shows the turnover numbers (TON), relative to the total amount of Ti in the catalyst, and the selectivity of styrene towards the different products for the different catalysts, including a blank test. Different products were obtained besides the primary product, styrene oxide (SO): benzaldehyde (BADH) formed from oxidative cleavage of styrene by TBHP and 2-phenyl-2-*tert*-butoxyethanol (22ET) formed from nucleophilic attack of Bu^{t}OH on oxirane ring of the primary product.

The Ti-containing silica xerogels prepared without the use of the silylation procedure (samples **1** and **4**) show similar TON to that of the TiO_2 impregnated silica xerogel, although the selectivity towards SO is higher for the latter. Silylated samples show very high selectivity towards the epoxide with negligible formation of the product coming from the opening of the oxirane ring. The reuse of the silylated sample **5** shows a slight decrease in styrene conversion (X_{ST} = 14.2%) without any change in selectivity (S_{SO} = 98.5%). Once the silylated samples are calcined a decrease in SO selectivity is observed due to the regeneration of HO groups on the sample surface, which promotes the catalytic reaction of the epoxide with Bu^{t}OH formed from TBHP. The pore volume of the Ti-containing silica is an important factor in the preparation of these catalysts, since for comparable BET surface areas (samples **2** and **5**, for example), the higher the pore volume the thinner the pore walls; therefore there is a higher probability of the Ti atoms being located at the surface. Although at first sight the silylation procedure could lead to the complete blocking of Ti atoms at the catalyst surface, hindering their oxidation activity, not all this surface is covered by the silylating agent, as was proved by the catalytic activity of the silylated samples.

The method reported in this work is an easy and reproducible way to obtain a highly hydrophobic Ti-containing material with aerogel properties, oxidation activity comparable to Ti-HMS and higher selectivity towards epoxide formation, without the use of templates or surfactants as in the case of zeolites or micelle structured zeolitic materials.

We are grateful to Dr Tuel (CNRS) for supplying Ti-HMS, CEPSA for the X-ray fluorescence measurements. This work was supported by the EU through the Brite-Euram Project (No. Br.-1169).

Notes and references

1 K. A. Jorgensen, *Chem. Rev.*, 1989, **89**, 431.
2 R. C. Ragers, *Br. Pat.* 1 249 079, 1971.
3 M. Taramasso, G. Perego and B. Notari, *US Pat.* 4 410 501, 1983.
4 B. Notari, *Catal. Today*, 1993, **18**, 163.
5 A. Camblor, A. Corma, A. Martinez and J. Pérez-Pariente, *J. Chem. Soc., Chem. Commun.*, 1992, 583.
6 T. Tanev, M. Chibwe and T. J. Pinnavaia, *Nature*, 1994, **368**, 321.
7 M. Fraile, J. I. García, J. A. Mayoral, L. C. De Mènorval and F. Rachdi, *J. Chem. Soc., Chem. Commun.*, 1995, 539.
8 M. Schneider and A. Baiker, *Catal. Today*, 1997, **35**, 339.
9 S. Klein, J. A. Martens, R. Parton, K. Vercruysse, P. A. Jacobs and W. F. Maier, *Catal. Lett.*, 1996, **38**, 209.
10 M. A. Uguina, G. Ovejero, R. Van Grieken, D. P. Serrano and M. Camacho, *J. Chem. Soc., Chem. Commun.*, 1994, 27.
11 G. M. Pajonk, *Catal. Today*, 1997, **35**, 319.
12 S. Sai, C. Prakash, J. Brinker, A. J. Hurd Sudeep and M. Rao, *Nature*, 1995, **374**, 439.
13 S. Gonier and A. Tuel, *Zeolites*, 1995, **15**, 601.
14 H. Yokogawa and M. Yokoyama, *J. Non-Cryst. Solids*, 1995, **186**, 23.

Communication 8/09012B

ChemComm

The 20 K structure of *p*-amino-*p*′-nitrobiphenyl in the non-constraining environment of its β-cyclodextrin inclusion complex

Tom J. Brett,[a] Shuncheng Liu,[b]† Philip Coppens*[b] and John J. Stezowski*[a]

[a] *Department of Chemistry and Center for Materials Research and Analysis (CMRA), University of Nebraska-Lincoln (UNL), Lincoln, Nebraska 68588-0304, USA. E-mail: jjs@unlinfo.unl.edu*

[b] *Department of Chemistry, State University of New York at Buffalo, Buffalo, New York 14260-3000, USA. E-mail: coppens@acsu.buffalo.edu*

Received (in Columbia, MO, USA) 10th November 1998, Accepted 11th January 1999

Though *p*-amino-*p*′-nitrobiphenyl (PANB) is essentially planar in its crystalline form, it takes on a twisted conformation in its 2 : 2 crystalline inclusion complex with β-cyclodextrin (β-CD); the angles between the two phenyl rings are 40.6(2) and 42.0(1)° for the two molecules respectively, compared with 44.1(1)° for biphenyl in the gas phase, thus indicating the absence of constraints in the β-CD dimer cage.

Cyclodextrins are among the most widely used molecular hosts in the field of supramolecular chemistry.[1] They are used extensively in industry and are also chiral host molecules which can be used as models for studying weak interactions involved in molecular recognition. Room temperature diffraction studies typically show disorder, attributed to the absence of strong host–guest interactions in the inclusion complexes. Such disorder should be reduced at very low temperatures, thus allowing a more precise determination of the molecular parameters of the included species, and analysis of the influence of the geometry on the molecular conformation and electron density.

We report the synthesis and 20 K crystal structure of a *p*-amino-*p*′-nitrobiphenyl (PANB)–β-cyclodextrin (β-CD) complex. To the best of our knowledge this study represents the lowest temperature β-cyclodextrin crystallographic investigation to date. PANB has a long-lived excited triplet state, in which charge is transferred from the amine donor to the nitro acceptor group of the molecule.[2] Accordingly, a large increase in dipole moment of PANB upon excitation occurs.[3] As the diffraction analysis of molecular excited states is now becoming feasible,[4] such effects provide additional motivation for the current study.

Crystals of (β-CD–PANB)$_2$ pentaicosahydrate were prepared by adding 8 mg of PANB[5] to 20 ml of saturated aqueous β-CD. This solution was heated and stirred in a sealed flask at 85 °C for 2 h, hot filtered to remove any undissolved PANB, and allowed to cool to room temperature over 3–4 days. Small, yellow, wedge-shaped crystals of the complex were obtained.

The crystalline β-CD–PANB inclusion complex (Fig. 1) consists of face-to-face β-CD dimers including two guest PANB molecules in the extended torus.[6] The two PANB molecules pack in the β-CD dimers with overlapping phenyl rings parallel to each other. A difference map ($F_o - F_c$) calculated near the end of refinement revealed an alternate position with much lower occupancy for each of the PANB molecules. The minor component PANB molecules were included in the final cycles with a conformation restrained to be similar to that of the major PANB molecules. The refinement led to a 17% occupancy of the minor sites. Standard deviations in the molecular bond lengths and angles are satisfactory (typically 0.004 Å and 0.4° for non-hydrogen bond distances and angles, respectively). The bond lengths and angles in the two independent molecules are identical within the experimental uncertainty. They are also similar to those found in neat PANB crystals[7] (Fig. 2). In *p*-nitroaniline,[8] the nitro N–C bond is much shorter than observed in nitrobenzene,[9] the amine N–C bond is much shorter than in aniline,[10] and the aromatic ring displays alternating long and short bonds, features indicative of a quinonoid resonance form reflecting migration of charge from donor to acceptor. In β-CD–PANB, nitro N–C and amine N–C bond lengths are somewhat shorter than the corresponding bonds in nitrobenzene and aniline. But the difference is not as marked as in *p*-nitroaniline, and no significant distortions of the aromatic rings are found, thus indicating a smaller degree of charge-transfer in PANB.

Even though the bond lengths and angles are very similar in the neat crystals and in the inclusion complex, there are marked differences in overall conformation. Thus, there is a different balance between the requirements of π-conjugation of the phenyl rings and packing forces, and the steric repulsion between the *ortho* hydrogens which is reduced in the non-planar conformer. The PANB molecules in neat crystals are essentially planar [inter-ring twist angle (IRTA) of 2.3(5)° whereas in the β-CD dimer they display a twisted conformation [IRTA =

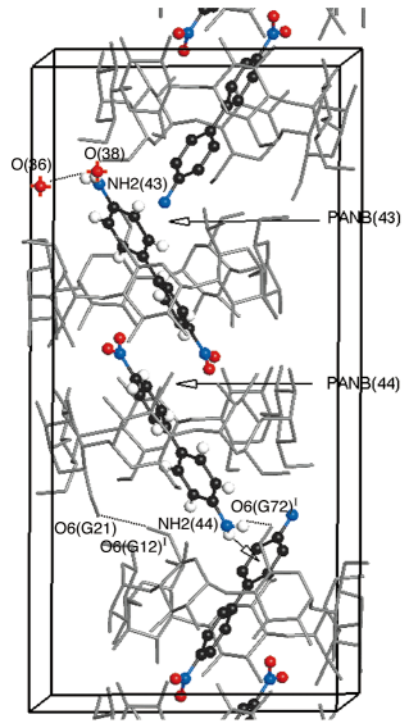

Fig. 1 Structure of the (β-CD–PANB)$_2$ complex. CDs are in grey while the atoms of the guest PANB molecules are colored as follows: carbon = black; oxygen = red; nitrogen = blue; hydrogen = white. For clarity, only the hydrogens of the PANB molecules in the assymetric unit are shown. Only water oxygen atoms involved in important guest–water interactions are shown. See text for details.

† Current address: Department of Chemistry, Capitol Normal University, Beijing 100037, China.

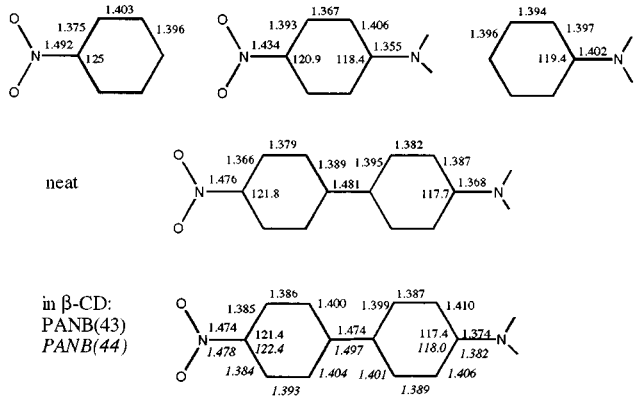

Fig. 2 Comparison of bond lengths and angles in nitrobenzene,[9] *p*-nitroaniline,[8] aniline,[10] neat PANB,[7] and the PANB molecules included in β-CD. Values reported are the average of one or two bond lengths.

40.6(2)° and 42.0(1)° for PANB(43) and PANB(44), respectively]. The difference between the two phases is similar to that observed for biphenyl, which is essentially planar in the solid state,[11] but takes on a twisted conformation in both the gas phase[12] (IRTA = 40–45°) and in its crystalline β-CD inclusion complexes [IRTA = 44.1(1)° as determined by solid state NMR[13]]. Similarly, biphenyl has been observed to take on twisted conformations in other co-crystals[14] (33,[14a] 40.5[14b] and 36.6° [14c]). *Ab initio* geometry optimization of biphenyl and PANB gives twisted conformations for the ground state of both molecules, with twist angles of 45.5 and 41.9°, respectively.[15] Evidently, the β-CD dimer interior provides a 'gas-phase-like' environment, in which the crystal packing forces that produce planar conformations in the neat crystals are no longer operative.

The host dimer entities pack in a 'screw channel' motif.[16] Host–guest interactions include both hydrogen bonding and hydrophobic interactions. The two PANB molecules reside within the β-CD dimer in the same manner, with the nitro ends of the molecules centered in the torus of the dimer. The amine ends of the PANB molecules, which may donate two hydrogen bonds and accept one, protrude from the primary ends of the dimer. One of the PANB molecules, PANB(44), serves as a hydrogen bond donor to a primary hydroxy of an adjacent β-CD dimer [NH2(44)···O6(G72)^{I} = 3.011(4) Å, ∠C6(44)–NH2(44)···O6(G72)^{I} = 111.2(3)° (I = $-x$, y − 1/2, $-z$)]. As a result, this primary hydroxy group (G72) is a +*gauche* conformer[17] with the C6–O6 bond directed towards the host cavity. The other amine hydrogen of PANB(44) is involved in a unique N–H···π face electrostatic interaction with the aniline half of a PANB molecule protruding from the primary face of the adjacent β-CD dimer. The N-to-phenyl ring plane distance is 3.277(6) Å. The two amine hydrogens of PANB(43) are involved in guest–water hydrogen bond interactions [NH2(43)···O(36) = 3.153(7) Å, ∠C6(43)–NH2(43)···O(36) = 110.8(3)°; NH2(43)···O(38)‡ = 3.275(11) Å, ∠C6(43)–NH2(43)···O(38) = 112.8(4)°]. The packing of the PANB molecules within the β-CD dimers leads to quite different intermolecular PANB interactions than exist in neat PANB crystals. The PANB molecules in the latter form an infinite chain of molecules connected by inter-molecular $NH_2\cdots NO_2$ hydrogen bonds, while such interactions are absent in the host–guest complex. Nevertheless, the donor–acceptor charge transfer, judged by the C–N bond lengths, is similar in the two crystals.

The structure determination at 20 K reveals a complex in which the guest PANB molecules are sufficiently ordered to allow an accurate and detailed structure determination. Comparison with the theoretically obtained geometry shows the guest molecules to have a conformation close to that calculated for the gas phase. The use of very low temperatures in structural analysis of host–guest complexes has significant advantages, provided, of course, that no first order phase transformations occur on cooling.

This study was supported in part by funds from CMRA UNL. Financial assistance for travel to Brookhaven National Laboratory (BNL) was provided to T. J. B. by the Warren F. and Edith R. Day Student-Aid-Fund of UNL. T. J. B. and J. J. S. (CHE-9812146), and PC (CHE-9615586) gratefully acknowledge support by the NSF. The SUNY X3 beamline at the National Synchrotron Light Source (NSLS) is supported by the Division of Basic Energy Sciences of the US Department of Energy (DE-FG02-86ER45231). Research carried out in part at the NSLS, which is supported by the US DOE, Division of Materials Sciences and Division of Chemical Sciences. Samples of β-CD were provided by Cerestar USA, Inc. (Hammond, IN).

Notes and references

‡ Calculated from average positions of disordered water O(38).

1 *Comprehensive Supramolecular Chemistry, Vol. 3, Cyclodextrins*, ed. J. L. Atwood, J. E. D. Davies, D. D. MacNicol and F. Vogtle, Pergamon, Oxford, 1996.
2 P. Piotrowiak, R. Kobetic, T. R. Schatz and G. Strati, *J. Phys. Chem.*, 1995, **99**, 2250.
3 J. Czekalla, W. Liptay and K. O. Meyer, *Ber. Bunsengesselschaft*, 1963, **67**, 465.
4 P. Coppens, D. V. Fomitchev, M. D.Carducci and K. Culp, *J. Chem. Soc., Dalton Trans.*, 1998, 865.
5 PANB was prepared by nitration of 4-nitrobiphenyl with nitric acid (H. C. Gull and E. E. Turner, *J. Chem. Soc.*, 1929, 491). The product was isolated and reduced with sodium hydrogen sulfide to give PANB (J. P. Idoux, *J. Chem. Soc., Sect. C*, 1970, 435).
6 *Crystal data*: for $(C_{42}H_{70}O_{35})_2\cdot(C_{12}H_{10}N_2O_2)_2\cdot 25.5H_2O$, M_r = 3157.81, monoclinic, $P2_1$ (no. 4), a = 15.454, b = 31.693, c = 15.255 Å, β = 102.92°, Z = 2, D_c = 1.440 g cm^{-3}, crystal size 0.094 × 0.063 × 0.063 mm. T = 20.0(1) K. Data were collected by the oscillation method at the X3A1 beamline station at the NSLS at BNL at a wavelength of 0.643 Å. A single 20 × 40 cm Fuji BAS-III imaging plate was used for data collection. The HKL suite (Z. Otwinowski, *Data Collection and Processing*, ed. L. Sawyer, N. Isaacs and S. Bailey, SERC Daresbury Laboratory, Warrington, UK, 1993, p. 56) was used for data processing (R_{merge} = 0.058). In all, 20607 unique reflections were recorded to a resolution of 0.68 Å. The structure was solved by isostructural replacement of the β-CD coordinates from an isomorphous structure. Least-squares refinement on F^2 of 1951 parameters was carried out using SHELXL97 (G. M. Sheldrick, *SHELXL97. Program for the Refinement of Crystal Structures*, University of Göttingen, Germany, 1997) and converged to a final R_1 = 0.0584, wR_2 = 0.1539, and GOF = 1.047 for 18109 reflections with $F_o > 4\sigma(F_o)$. All non-hydrogen atoms were treated anisotropically except those of the lower occupancy PANB sites which were refined as a rigid body with a single group isotropic displacement parameter. A final difference electron density map showed no distinct features with ρ_{max} = 1.352 and ρ_{min} = −0.828 e Å^{-3}. CCDC 182/1140.
7 E. M. Graham, V. M. Miskowski, J. W. Perry, D. R. Coulter, A. E. Stiegman, W. P. Schaefer and R. E. Marsh, *J. Am. Chem. Soc.*, 1989, **111**, 8771.
8 M. Colapietro, A. Domenicano, C. Marciante and G. Portalone, *Z. Naturforsch., Teil B*, 1982, **37**, 1309.
9 F. Di Rienzo, A. Domenicano and L. R. Di Sanseverino, *Acta Crystallogr., Sect. B*, 1980, **36**, 586.
10 D. G. Lister, J. K. Tyler, J. H. Høg and N. W. Larsen, *J. Mol. Struct.*, 1974, **23**, 253.
11 G. P. Charbonneau and Y. Delugeard, *Acta Crystallogr., Sect. B*, 1977, **33**, 1586.
12 O. Bastiansen, *Acta Chem. Scand.*, 1949, **3**, 408.
13 A. D. Ronemus, PhD Thesis, University of California, San Diego, 1987.
14 (*a*) T. Iwamoto, T. Miyoshi and Y. Susaki, *Acta Crystallogr., Sect. B*, 1974, **30**, 292; (*b*) A. Lipka and D. Mootz, *Z. Anorg. Allg. Chem.*, 1978, **440**, 217; (*c*) K. W. Klinkhammer, *Chemistry*, 1997, **3**, 1418.
15 *Ab initio* geometry optimizations were carried out at the HF/6-31G* level using GAUSSIAN94. Optimizations of planar, perpendicular, and twisted geometries showed the twisted conformation to be of lowest energy.
16 D. Mentzafos, I. M. Mavridis, G. LeBas and G. Tsoucaris, *Acta Crystallogr., Sect. B*, 1991, **47**, 746.
17 W. Saenger, *Inclusion Compounds*, ed. J. L. Atwood, J. E. D. Davies and D. D. MacNicol, Academic Press, London, 1984, vol. 2, 231.

Communication 8/08832B

ChemComm

A 'toothpaste tube' model for ion transport through trans-membrane channels

Peter J. Cragg,*[a] Marcus C. Allen[a] and Jonathan W. Steed[b]

[a] *School of Pharmacy and Biomolecular Sciences, University of Brighton, Cockcroft Building, Moulsecoomb, Brighton, UK BN2 4GJ. E-mail: p.j.cragg@bton.ac.uk*

[b] *Department of Chemistry, King's College London, Strand, London, UK WC2R 2LS. E-mail: jon.steed@kcl.ac.uk*

Received (in Columbia, MO, USA) 29th October 1998, Accepted 2nd February 1999

The X-ray crystal structure of the 2 : 1 Na^+ complex of the hexahomooxacalix[3]arene diethylamide derivative 1b shows capsular and nesting inclusion of the two Na^+ cations suggesting a mechanism by which Na^+ and K^+ ions are desolvated and pass through biological ion channels.

The transport of the sodium and potassium cations across biological phospholipid membranes *via* Na^+ and K^+ channel proteins is crucial to many biological processes, notably electrical signalling in the nervous system.[1–3] Key features of the transport of both Na^+ and K^+ are the high degree of selectivity of the discrimination between the two ions (factors of *ca.* 10^4) and the very rapid rate of their diffusion through the channel pore (*ca.* 10^8 ions s^{-1}).[4] Current understanding of this process has advanced markedly this year with the publication of the first X-ray crystal structure of an alkali metal channel protein.[4] This work has demonstrated that alkali metal cations diffuse in solvated form throughout most of the length of the channel before entering a cone-shaped selectivity filter. The selectivity filter discriminates on a size basis, with the cation passing through the neck of the cone with little remaining solvation shell. The high rate of throughput is explained by a 'billiard ball' effect in which incoming cations exert an electrostatic repulsion upon the metal within the selectivity filter, expelling it on to the other size of the membrane.[4] We now report the first model compound to give insight into the mechanism of this 'billiard ball' effect. This work suggests that the incoming cation is robbed of its solvation shell as it enters the cone-like selectivity filter in conjunction with a single solvent molecule in a concerted fashion, as if being squeezed through a tube of toothpaste.

Extensive work over the past fifteen years has centred around the use of the calixarenes as biological models.[5–7] However, the small size of the cone-shaped calix[4]arene does not present a significant aperture for the passage of metal cations through the annulus, although this has been suggested for K^+ recently.[8] The larger, 18-membered ring hexahomooxacalix[3]arenes of type **1**

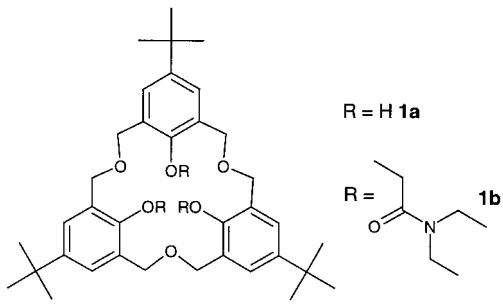

represent a more appropriate channel mimic. In biological membrane channels the inner surface of the selectivity filter is covered by successive rings of carbonyl oxygen atoms from the main chain amino acid residues.[1,4] This is simulated in the model compound **1b** discussed herein by the phenolic oxygen atoms of the oxacalix[3]arene and the carbonyl groups of the pendant amide functionalities, resulting in a three dimensional cavity comprising a double ring of six oxygen donors. The *p-tert*-butyl aryl moieties provide a hydrophobic, conical entrance to the donor site.

Reaction of pore mimic **1b** with $NaPF_6$ in water–methanol solution results in isolation of a crystalline complex of formula $[Na_2L](PF_6)_2\cdot H_2O\cdot 2MeOH$ **2** (L = **1b**). Ligand **1b** has been shown to exhibit a 1:1 binding constant for $Na^+ > 10^7$ $dm^3\ mol^{-1}$ and the transannular nucleophilic channel is an excellent size match for this cation, while being less readily able to expand sufficiently to encapsulate a K^+ ion.[9] The X-ray crystal structure of **2**† (Fig. 1) shows that the complex has a symmetrical basket, or lobster-pot shape, with one cation, Na(1) firmly encapsulated within the pocket formed by the phenolic and amide oxygen atoms, resulting in a chiral core possessing a pseudo-threefold rotation axis. In addition to the calixarene donor atoms the seven-coordinate Na(1) is also bound to a water molecule situated at the boundary between the hydrophobic cavity formed by the aryl moieties and the binding pocket. While the Na(1)–OH_2 distance is relatively long, 2.437(5) Å, the water molecule is stabilized by hydrogen bonds to the calixarene etheric bridges. Fascinatingly this water molecule also ligates a second Na^+ cation, Na(2), which is apparently in the process of entering the cavity, Na(2)–OH_2 2.277(5) Å. Cation Na(2) exhibits a highly distorted octahedral coordination geometry. In addition to a strong interaction with the intra-cavity water molecule, it is also ligated by two other solvent molecules (methanol) and forms a salt bridge to an extra-cavity PF_6^- anion. In addition to these interactions, Na(2) is strongly bound to one of the oxygen atoms of the calixarene $-CH_2OCH_2-$ bridges. The sixth and final coordination site is filled by an intriguing cation–π interaction with one of the calixarene aryl rings, Na(2)–C 3.026(6) Å. The coordination environment of Na(2) is an excellent illustration of the desolvation process which must occur in biological systems as alkali metal cations enter the conical selectivity filter as they traverse trans-membrane channel pores. The cation interacts with the macrocyclic ligand *via* a mixture of coordination and cation–π interactions, which have been strongly implicated in biochemical systems,[10,11] however, it still retains a partial solvation shell in which all three coordinated solvent molecules are involved in strong hydrogen bonding interactions either to the calixarene itself or to extra-cavity anions. In natural systems these anions are present in the form of anionic carboxylato residues of the channel protein. These second sphere coordination interactions compensate for the enthalpically unfavourable desolvation of the cation as it approaches the narrowing pore aperture. In effect the cation is squeezed into the binding pocket as a consequence of the trans-membrane concentration gradient, with solvent molecules being side-tracked by peripheral stabilising interactions. The feature of the bridging water molecule insulating one cation from another as they progress through the selectivity filter is an experimentally determined property of the K^+ channel of *Streptomyces lividans*, a protein considered to be highly representative of both K^+ and Na^+ channels.[4] Water is a small enough ligand to pass entirely through the pore in an axial coordination site and may well act as a molecular 'staple', dragging the second cation along after it as it follows the first on its passage through the channel,

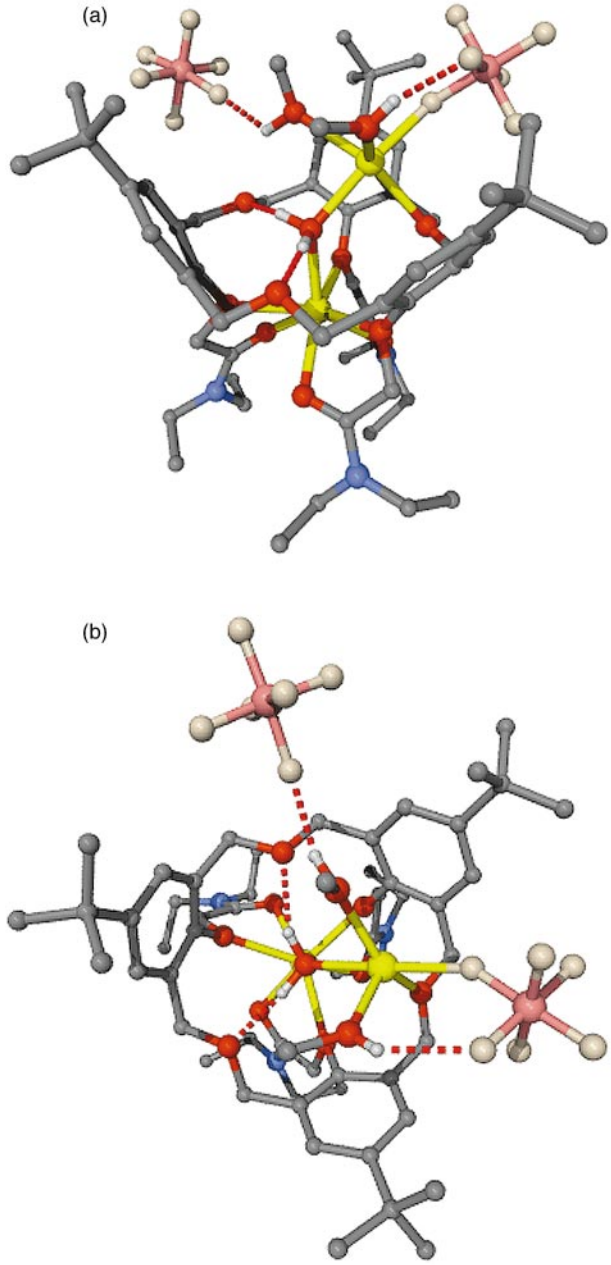

Fig. 1 (a) Side and (b) top views of the conical Na^+ channel mimic **2** showing the encapsulation of one Na^+ ion within the sodium selective cavity, while the second metal ion is beginning the process of desolvation as it enters the conical pore and forms a salt bridge to an extra-cavity hexafluorophosphate anion. The two metal ions are linked by a water molecule situated in the centre of the cavity and able to interact with the etheric oxygen atoms. Colour key: Na, yellow; O, red; N, blue; C, grey; H, small white; P, pink; F, white atoms attached to P. Hydrogen bonding interactions involving the three solvent molecules are represented by red dotted lines. Hydrogen atoms which do not take part in specific hydrogen bonding interactions are omitted for clarity. Selected distances: Na(1)–O(1A) 2.299(4), Na(1)–O(1B) 2.333(5), Na(1)–O(3B) 2.35(2), Na(1)–O(3C) 2.403(12), Na(1)–O(1C) 2.404(5), Na(1)–O(3A) 2.42(2), Na(1)–O(1) 2.437(5), Na(2)–F(1) 2.199(5), Na(2)–O(1) 2.277(5), Na(2)–O(2) 2.292(5), Na(2)–O(3) 2.348(5), Na(2)–O(2A) 2.378(5), Na(2)–C(6A) 3.027(6).

stabilized by hydrogen bonding interactions at every point. This type of mechanism is key to the understanding of the apparently contradictory features of the biological systems; their high selectivity and hence binding ability and their fast kinetics, suggesting only partial desolvation.

The model structure reported herein demonstrates conclusively, in a well-characterised system, the ability of conical channels to stack multiple cations by means of a wide variety of stabilizing interactions. Clearly identifiable features, namely inter-cation insulation by a single solvent molecule, strong cation binding and stabilising interactions conducive to desolvation, mimic closely those implicated in natural systems. Preliminary electrophysiological results‡ indicate an inward current at a potential consistent with sodium crossing the cell membrane, together with attenuation of the trans-membrane potassium current, when ligand **1b** is allowed to superfuse the cells. These initial data suggest that ligand **1b** inhibits transport of potassium and allows an influx of sodium thus performing the function of a selectivity filter on the surface of a cell. As a whole, the structure of complex **2** provides a well resolved 'snap-shot' of the cation transport process.

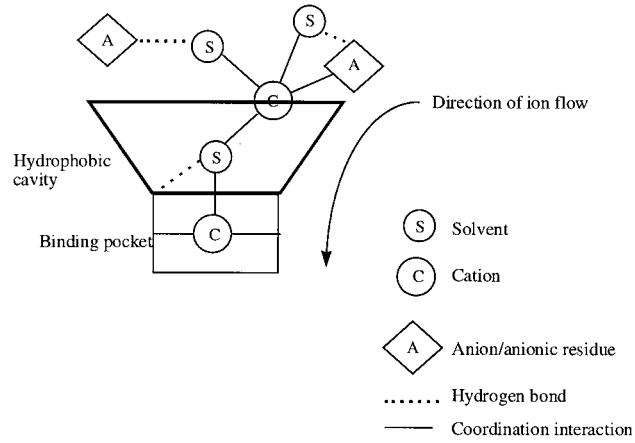

Fig. 2 Diagrammatic representation of the key structural features of **2**.

We thank the Leverhulme trust for a Fellowship (to P. J. C.) and the EPSRC and King's College London for funding the diffractometer system.

Notes and references

† *Crystal data* for **2**: $C_{56}H_{95}F_{12}N_3Na_2O_{12}P_2$, M = 1338.27, monoclinic, space group $C2/c$, a = 43.506(3), b = 13.8660(11) c = 24.2283(16) Å, β = 111.811(2)°. U = 13569.4(17) Å^3, Z = 8, μ = 1.66 cm^{-1}, T = 120 K, Reflections measured: 45 436, unique data: 11 181 (R_{int} = 0.118), parameters: 820, $R1$ [$F^2 > 2\sigma(F^2)$] 0.1095, $wR2$ (all data) 0.2683. CCDC reference number 182/1166. See http://www.rsc.org/suppdata/cc/1999/553 for crystallographic files in .cif format.

‡ Whole-cell patch clamp data from mouse neuroblastoma × rat glioma hybrid cells, NG108-15, with trans-membrane ion currents stimulated by ramping from a holding potential of −80 mV to between −180 and +60 mV.

1 B. Hille, *Ionic Channels of Excitable Membranes*, Sinauer, Sunderland, 1992.
2 Y. Kobuke, in *Advances in Supramolecular Chemistry, vol. 4*, ed. G. W. Gokel, JAI Press, Greenwich, 1997, pp. 163–210.
3 W. Kaim and B. Schwederski, *Bioinorganic Chemistry*: *Inorganic Elements in the Chemistry of Life*, Wiley, Chichester, 1994.
4 D. A. Doyle, J. M. Cabral, R. A. Pfuetzner, A. Kuo, J. M. Gulbis, S. L. Cohen, B. T. Chait and R. MacKinnon, *Science*, 1998, **280**, 69.
5 C. D. Gutsche, *Calixarenes*, ed. J. F. Stoddart, Royal Society of Chemistry, Cambridge, 1989.
6 A. Ikeda and S. Shinkai, *Chem. Rev.*, 1997, **97**, 1713.
7 L. H. Yuan, S. H. Chen, H. M. Zhao and Y. C. Ning, *Acta Chim. Sinica*, 1994, **52**, 1035.
8 P. Schmitt, P. D. Beer, M. G. B. Drew and P. D. Sheen, *Angew. Chem., Int. Ed. Engl.*, 1997, **36**, 1840.
9 H. Matsumoto, S. Nishio, M. Takeshita and S. Shinkai, *Tetrahedron*, 1995, **51**, 4647.
10 J. C. Ma and D. A. Dougherty, *Chem. Rev.*, 1997, **97**, 1303.
11 J. L. Atwood, F. Hamada, K. D. Robinson, G. W. Orr and R. L. Vincent, *Nature*, 1991, **349**, 683.

Communication 8/08492K

Unsaturated α-aminopimelic acids as potent inhibitors of *meso*-diaminopimelic acid (DAP) D-dehydrogenase

Andrew Sutherland, Jennifer F. Caplan and John C. Vederas*

Department of Chemistry, University of Alberta, Edmonton, Alberta, Canada T6G 2G2. E-mail: john.vederas@ualberta.ca

Received (in Corvallis, OR, USA) 8th January 1999, Accepted 4th February 1999

Two nonproteinogenic amino acids 5 and 6 have been efficiently prepared using an S_H2' allylstannane coupling reaction and a Wittig reaction, respectively, to effect the key steps; kinetic studies show these compounds to be reversible inhibitors of DAP dehydrogenase with K_i values of 5.3 (competitive) and 44 μM (noncompetitive), respectively.

Due to the increasing problems associated with antibiotic resistance, alternative strategies to disrupt microbial cell wall synthesis have become highly desirable.[1] The key crosslinking amino acid in the peptidoglycan cell wall layer of Gram negative bacteria is *meso*-diaminopimelic acid (DAP), the biosynthetic precursor of L-lysine, which is used as the crosslinker by many Gram positive organisms.[2] The biochemical pathway to this molecule is not present in animals, which require L-lysine in their diet, and therefore specific inhibitors of the DAP enzymes are likely to be antimicrobial agents with low mammalian toxicity. One of the enzymes used by certain bacteria[2] is *meso*-DAP D-dehydrogenase (EC 1.4.1.16), which converts L-tetrahydrodipicolinate (THDP) **1** to *meso*-DAP **3**, presumably *via* an imine **2** which is reduced stereospecifically by NADPH to generate the D-amino acid center (Scheme 1).[3] We previously demonstrated that a conformationally restricted isoxazoline analogue **4** having the DAP skeleton and a planar α-carbon attached to a basic nitrogen is a potent reversible inhibitor of DAP dehydrogenase and has antimicrobial activity.[4] However, recent X-ray crystallographic studies show that it binds in an unexpected fashion in the active site which places the L-amino acid center rather than the imine bond near the NADP moiety.[5] We now report the syntheses of two new inhibitors **5** and **6** of DAP dehydrogenase which contain a planar α-carbon but lack the characteristic basic nitrogen at the presumed reactive end of the molecule.

The synthesis of unsaturated amino acid **5** is outlined in Scheme 2. The aspartic acid derivative **7** was selectively reduced to the γ-aldehyde **8** in good yield using DIBAL-H.[6]

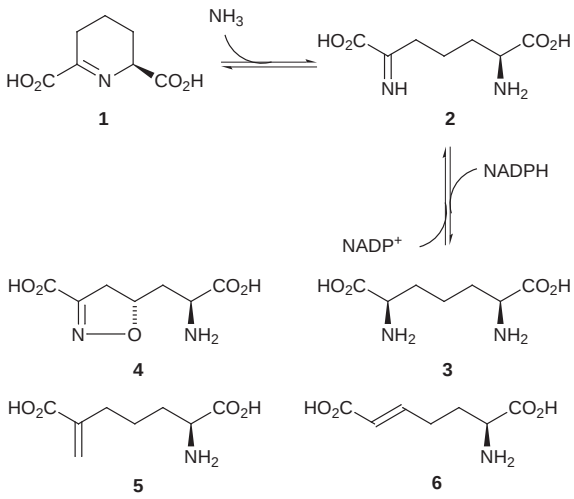

Scheme 1

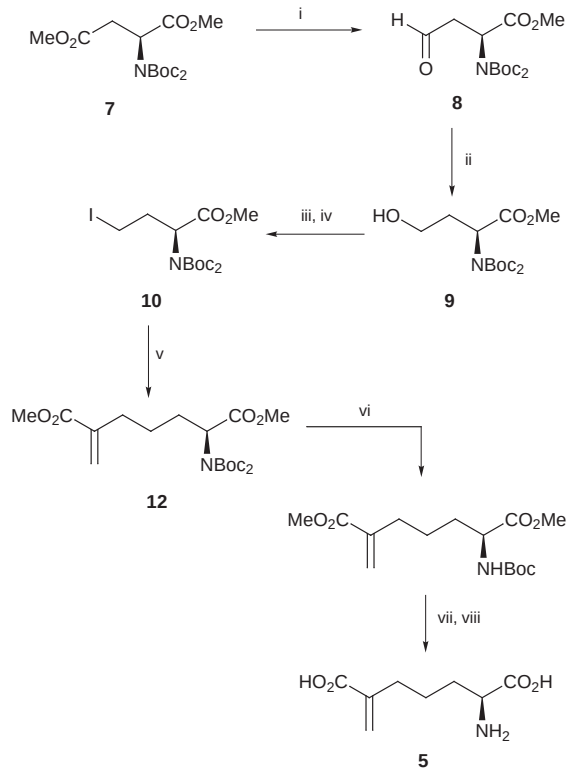

Scheme 2 *Reagents and conditions*: i, DIBAL-H (1.2 equiv.), Et_2O, −78 °C, 87%; ii, $NaBH_4$, THF, 82%; iii, MsCl, NEt_3, DMAP, CH_2Cl_2, 85%; iv, NaI, acetone, Δ 89%; v, AIBN, $MeO_2CC(=CH_2)CH_2SnPh_3$ **11**, C_6H_6, Δ, 60%; vi, TFA (1.2 equiv.), CH_2Cl_2, 76%; vii, LiOH, MeOH, H_2O, 84%; viii, TFA, CH_2Cl_2, 95%.

Further reduction gave the primary alcohol **9** which was converted to the iodide **10** using standard procedures.[7] Radical coupling of iodide **10** with stannane **11**[8] was initiated thermally using AIBN to give the protected α-aminopimelic acid analogue **12** in 60% yield. Selective removal of one of the Boc groups, followed by ester hydrolysis and finally cleavage of the second Boc group gave the parent amino acid **5** in excellent yield (20% overall for eight steps from **7**).

Reduction of the protected glutamate **13** with DIBAL-H similarly gave aldehyde **14** in good yield (Scheme 3). Wittig coupling with the stabilized ylide, methyl (triphenylphosphoranylidene)acetate, gave solely the *trans*-alkene **15**[9] which was deprotected to **6** in a similar manner as above.

With compounds **5** and **6** available, DAP D-dehydrogenase was isolated and purified from *Bacillus sphaericus* IFO 3525 as previously reported.[3a,4] Inhibition studies with this enzyme were done at pH 7.8 using the reverse reaction (oxidative deamination by $NADP^+$ of the D-amino acid center of **3** to give **1**). This produces NADPH and thereby allows continous spectrophotometric assay at 340 nm. The unsaturated amino acids **5** and **6** were first individually tested as possible substrates for DAP D-dehydrogenase in the absence of *meso*-DAP **3**, and

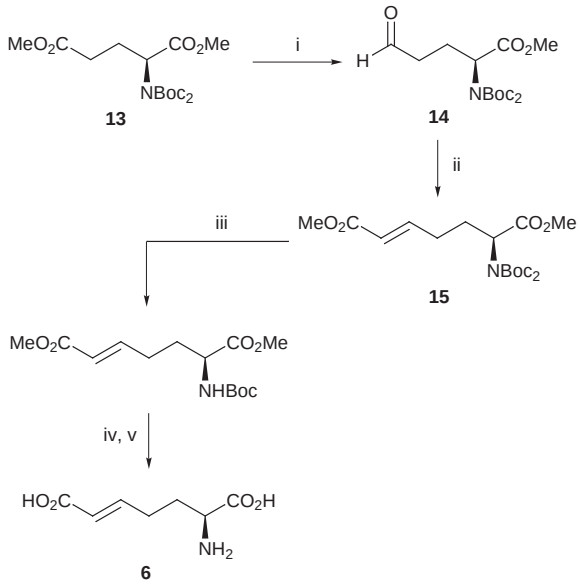

Scheme 3 *Reagents and conditions*: i, DIBAL-H, Et_2O, −78 °C, 86%; ii, $Ph_3P{=}CHCO_2Me$, THF, 85%; iii, TFA (1.2 equiv.), CH_2Cl_2, 82%; iv, LiOH, MeOH, H_2O, 98%; v, TFA, CH_2Cl_2, 87%.

as expected, showed no conversion. Subsequent inhibition studies showed both compounds to be very good but rapidly reversible inhibitors (not time-dependent) of DAP D-dehydrogenase. More detailed kinetic analyses demonstrated that **5** is a competitive inhibitor with an inhibition constant (K_i) of 5.3 μM. In contrast, a Michaelis–Menten plot for **6**, which has the double bond in the backbone, showed noncompetitive inhibition with a K_i value of 44 μM, indicating different binding modes for the two unsaturated analogues.

DAP D-dehydrogenase from *Corynebacterium glutamicum* exists as a homodimer with each monomer unit (*M ca*. 35200) possessing a similar fold but somewhat different overall conformation based on crystallographic studies.[5,10] Although there may be structural differences between the *B. sphaericus* and *C. glutamicum* enzymes,[11] their overall mechanism and inhibition by **4** are similar. Since isoxazoline **4** is a competitive inhibitor with respect to L-tetrahydrodipicolinate **1** (K_i = 4.2 μM) but a noncompetitive inhibitor with respect to *meso*-DAP (K_i = 23 μM),[4] it seems likely that the nearly equipotent noncompetitive inhibitor **6** may bind in a similar fashion. This indicates that interactions of the isoxazoline nitrogen and oxygen with active site water molecules seen in crystallographic studies may play a minor role in binding.[5] However, **5** is directly competitive with *meso*-DAP **3** and is one of the most potent substrate analogue inhibitors for this enzyme found thus far. This suggests that **5** may be a true mimic of the imine intermediate **2**, and that normal catalysis by DAP D-dehydrogenase can be blocked by conformational changes induced in the protein by binding of **4** or **6** in the adjacent subunit at a site normally occupied by THDP **1** (Fig. 1). Additional crystallographic studies with the unsaturated α-aminopimelic acid derivatives **5** and **6** may help to clarify the subunit interactions and the detailed mechanism of this enzyme. Further studies on the synthesis of DAP analogues[12] and their interactions with other DAP enzymes are in progress.

The authors thank Dr Jonathan Parrish for assistance with molecular modeling. Financial support from the Alberta Heritage Foundation for Medical Research (Fellowship to A. S.) and the Natural Sciences and Engineering Research Council of Canada (Scholarship to J. F. C. and Operating Grant) is gratefully acknowledged.

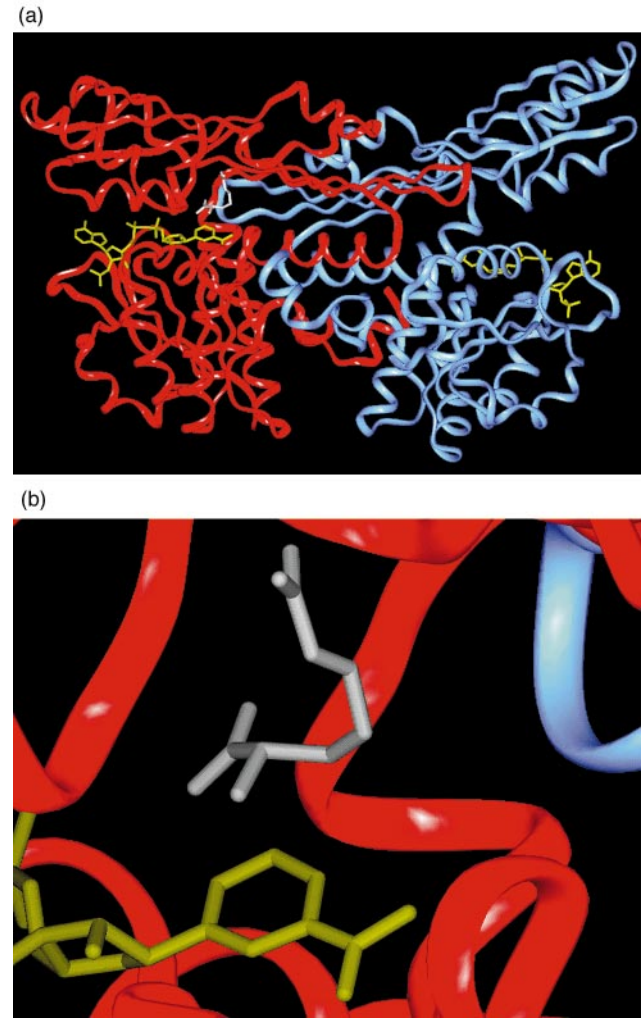

Fig. 1 (a) Model of **6** (white) docked into homodimeric DAP D-dehydrogenase (red and blue subunits) from *C. glutamicum* generated by best-fit replacement of the isoxazoline **4** in the corresponding enzyme–inhibitor crystal structure (ref. 5). These inhibitors (**4** and **6**) have their L-amino acid center proximal to the NADP moiety (yellow) and therefore cannot be oxidized by the cofactor. (b) Expansion to show the inhibitor conformation in the closed active site.

Notes and references

1 T. D. H. Bugg and C. T. Walsh, *Nat. Prod. Rep*., 1992, **9**, 199; J.-M. Ghuysen, *Int. J. Antimicrob. Agents*, 1997, **8**, 45.
2 R. J. Cox, *Nat. Prod. Rep*., 1996, **13**, 29; G. Scapin and J. S. Blanchard, *Adv. Enzymol. Relat. Areas Mol. Biol.*, 1998, **72**, 279.
3 H. Misono and K. Soda, *J. Biol. Chem*., 1980, **255**, 10599; S. J. Maniscalco, S. K. Saha and H. F. Fisher, *Biochemistry*, 1998, **37**, 14585.
4 S. D. Abbott, P. Lane-Bell, K. P. S. Sidhu and J. C. Vederas, *J. Am. Chem. Soc*., 1994, **116**, 6513.
5 G. Scapin, M. Cirilli, S. G. Reddy, Y. Gao, J. C. Vederas and J. S. Blanchard, *Biochemistry*, 1998, **37**, 3278.
6 G. Kokotos, J. M. Padron, T. Martin, W. A. Gibbons and V. S. Martin, *J. Org. Chem*., 1998, **63**, 3741.
7 M. A. Walker, K. P. Kaplita, T. Chen and H. D. King, *Synlett*, 1997, 169.
8 J. E. Baldwin, R. M. Adlington, M. B. Mitchell and J. Robertson, *Tetrahedron*, 1991, **47**, 5901.
9 The preparation of **15** by essentially the same route has been reported very recently, after our synthesis was complete: J. M. Padron, G. Kokotos, T. Martin, T. Markidis, W. A. Gibbons and V. S. Martin, *Tetrahedron: Asymmetry*, 1998, **9**, 3381.
10 G. Scapin, S. G. Reddy and J. S. Blanchard, *Biochemistry*, 1996, **35**, 13 540.
11 H. Misono, M. Ogasawara and S. Nagasaki, *Agric. Biol. Chem.*, 1986, **50**, 2729; F. Wang, G. Scapin, J. S. Blanchard and R. H. Angeletti, *Protein Sci*. 1998, **7**, 293.
12 Y. Gao, P. Lane-Bell and J. C. Vederas, *J. Org. Chem.*, 1998, **63**, 2133.

Communication 9/00297I

Photoinduced electron transfer at a gold electrode modified with a self-assembled monolayer of fullerene

Hiroshi Imahori,*[a] Takayuki Azuma,[a] Shinichiro Ozawa,[a] Hiroko Yamada,[a] Kiminori Ushida,[b] Anawat Ajavakom,[a] Hiroyuki Norieda[a] and Yoshiteru Sakata*[a]

[a] *The Institute of Scientific and Industrial Research, Osaka University, Mihoga-oka, Ibaraki, Osaka 567-0047, Japan. E-mail: imahori@sanken.osaka-u.ac.jp;sakata@sanken.osaka-u.ac.jp*
[b] *The Institute of Physical and Chemical Research (RIKEN), 2-1 Hirosawa, Wako, Saitama 351-0198, Japan*

Received (in Cambridge, UK) 21st December 1998, Accepted 22nd February 1999

A stable anodic photocurrent was observed in the presence of an electron sacrificer when a gold electrode modified with a self-assembled monolayer of C_{60} was illuminated with monochromic light, indicating the generation of a vectorial electron flow from the electron donor to the gold electrode *via* the excited states of C_{60}.

The unique three-dimensional structure of C_{60} has prompted many researchers to apply it to materials science.[1] In this context, fullerene thin films formed using a variety of methods, including Langmuir–Blodgett (LB) techniques and evaporation, have displayed interesting physical and chemical properties.[2] Self-assembled monolayers (SAMs) are useful for constructing highly ordered, two- and three-dimensional structures on substrates.[3] Several groups have already reported the preparation, electrochemistry and surface properties of C_{60} SAMs.[4–9] However, to the best of our knowledge, there have been no reports of the photoelectrochemical properties of SAMs of fullerenes. Here we report the preparation and photoelectrochemistry of a SAM of C_{60}-tethered alkanethiol **1** on a gold electrode (Fig. 1).

The synthetic route to C_{60}-linked polyalkanethiol **1** is shown in Scheme 1. It is well established that alkanethiols with a polymethylene chain form densely packed monolayers on gold surfaces. It is reported that the presence of an amido group in a chain enhances the stability of monolayers due to intermolecular hydrogen bonding.[10] Thus, it is expected that the attachment of a long alkyl chain to C_{60} with an amide linkage would allow us to produce a well-ordered C_{60} SAM on a gold electrode. Aldehyde **5** was prepared *via* six steps from 2-nitrobenzaldehyde **2**. Compound **1** was synthesized by the condensation of *N*-methylglycine, C_{60} and **5**.[11] The structures of **1** and related compounds were confirmed by spectroscopic methods including ^{1}H NMR and mass spectra.† Cyclic voltammetry of **1** in CH_2Cl_2 containing 0.1 M Bu_4NPF_6 as electrolyte exhibited reversible waves due to the first and the second reductions of C_{60} (−0.59, −1.00 V *vs.* Ag/AgCl), as shown in Fig. 2.

A monolayer of **1** was formed by the spontaneous bonding of **1** onto Au(111)/Cr/Si(100) substrates (hereafter, **1**/Au, where / represents an interface). The bonding was carried out from a 20 μM $CHCl_3$ solution for 20 h to complete the formation. After soaking, the electrode was washed well with $CHCl_3$ and dried with a stream of argon. Cyclic voltammetry of **1**/Au in CH_2Cl_2 containing 0.1 M Bu_4NPF_6 with a sweep rate of 100 mV s^{-1} showed a wave at $E_{1/2}$ = −0.63 V (*vs.* Ag/AgCl) and a second smaller wave at $E_{1/2}$ = −1.07 V, which correspond to the first and second reduction/oxidation peaks of C_{60}, respectively (Fig. 2). The values of the peak splittings (ΔE_{peak} = 210 mV) are large, compared with the ideal value in solution, indicating the slow kinetics between the C_{60} and the gold electrode due to structural constraints. Integration of the area under the curve observed for the first reduction due to the C_{60} corresponds to a surface coverage of Γ = 1.4 × 10^{-10} mol cm^{-2} (120 Å^2 molecule^{-1}),‡ which agrees well with the value (1.4 × 10^{-10} mol cm^{-2}) in similar C_{60} SAM systems.[8,9] The value is somewhat larger than the values of the hexagonal (78 Å^2

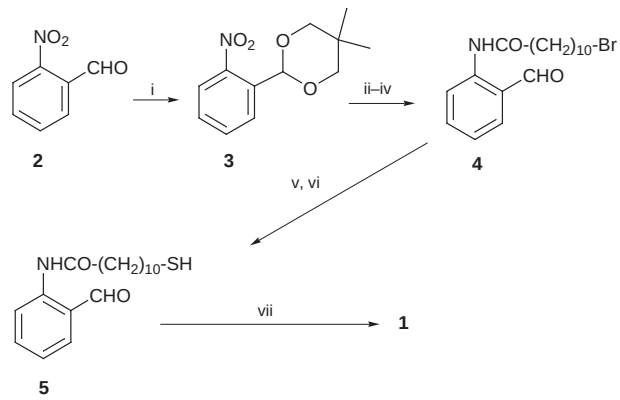

Scheme 1 *Reagents and conditions*: i, neopentyl glycol, TsOH, 91%; ii, H_2, Pd/C, 72%; iii, 11-bromoundecanoic acid, *N*-methylmorpholine, 2-chloro-4,6-dimethoxy-1,3,5-triazine, 99%; iv, H_2SO_4, TFA, 99%; v, potassium thioacetate, 80%; vi, KOH, 96%; vii, *N*-methylglycine, C_{60}, 13%.

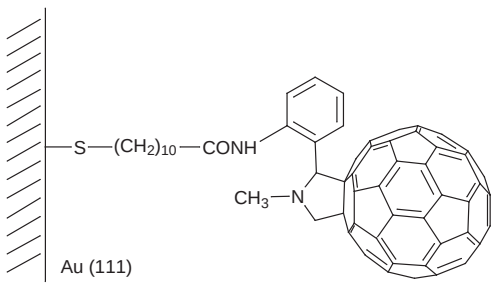

Fig. 1 A self-assembled monolayer of **1**/Au (111).

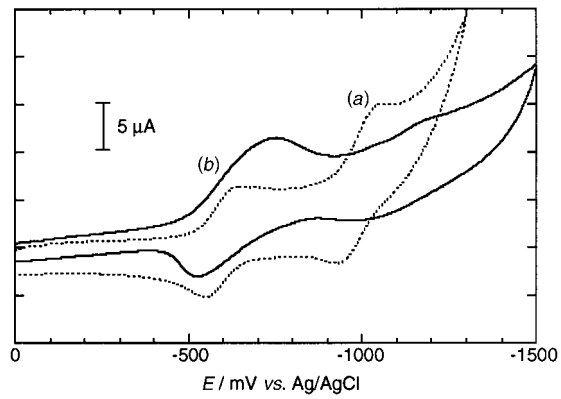

Fig. 2 Cyclic voltammograms of (*a*) **1** in CH_2Cl_2 (dotted line) and (*b*) **1**/Au in CH_2Cl_2: sweep rate 100 mV s^{-1}, electrode area 0.48 cm^2, initial potential 0 V.

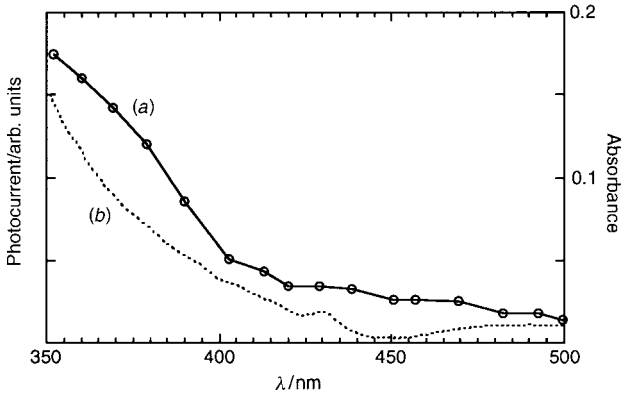

Fig. 3 Action spectrum of (*a*) C_{60} SAM cell and (*b*) absorption spectrum of **1** in $CHCl_3$ (8.88 μM).

molecule^{-1}) or the simple square (98 Å^2 molecule^{-1}) packing in similar C_{60} LB films.[12] This may be related to steric hindrance around the phenyl group on the pyrrolidine ring attached to C_{60}.

Photoelectrochemical measurements were carried out for **1**/Au in an argon-saturated 0.1 M Na_2SO_4 solution containing 50 mM ascorbic acid (AsA) as an electron sacrificer using a modified gold electrode as the working electrode, a platinum counter electrode, and a Ag/AgCl reference electrode (hereafter, Au/**1**/AsA/Pt, where / represents an interface). A stable anodic photocurrent flowed immediately after the gold electrode was irradiated and fell instantly when the illumination was terminated. The photoelectrochemical response was repeated for tens of times without any signs of attenuation when the light was switched on and off. An increment of the anodic photocurrent with an increase of positive bias to the gold electrode (−400 mV to +200 mV) in the system demonstrated that the direction of the photocurrent takes place from the cathode to the anode through the electrolyte. The intensity of the photocurrent for the Au/**1**/AsA/Pt cell is an order of magnitude larger than those of the Au/**1**/Pt cell or the bare Au/AsA/Pt cell, indicating the involvement of AsA and C_{60} for the generation of the photocurrent. The agreement of the action spectrum with the absorption of **1** in $CHCl_3$ from 350–500 nm (Fig. 3) shows that C_{60} is the photoactive species. Under excitation with $\lambda = 403 \pm 6.9$ nm light of 6.6 mW cm^{-2} and 0.1 V bias voltage, we obtained a photocurrent density of 290 nA cm^{-2}. Assuming that the absorption coefficient of **1** on the gold surface is the same as that in $CHCl_3$, absorbance of **1**/Au at 403 nm is calculated to be 7.81×10^{-4}. Given the absorbance for **1**/Au, we can estimate that the quantum yield of the Au/**1**/AsA /Pt cell is 7.5%.§ The value is at least one order of magnitude larger than those in similar photoelectrochemical cells of porphyrin SAMs[13] and comparable to those (1.2–8.2%) in similar C_{60} LB cells.[14] These results indicate that C_{60} is an excellent electron mediator as well as a good electron acceptor.[15] Based on these data together with previous results, we can propose the photocurrent generation mechanism. It is plausible that the excited singlet state (1.11 V *vs*. Ag/AgCl) and/or the triplet state (0.82 V) of the C_{60} are quenched by AsA (−0.19 V).[15] The resulting C_{60} anion radical would give an electron to the gold electrode, resulting in the recovery of the initial state. Overall, electron flow occurs from AsA to the gold electrode *via* C_{60}.

In conclusion, a photoelectrochemical cell with a gold electrode modified with a SAM of C_{60} has been constructed for the first time. The high quantum yield implies that a combination of C_{60} and SAMs is promising for applications in materials science. Our results will provide the basic information for the development of photovoltaic devices and sensors.

This work was supported by a Grant-in-Aid for COE Research and Scientific Research on the Priority Area of Electrochemistry of Ordered Interfaces and Creation of Delocalized Electronic Systems from Ministry of Education, Science, Sports and Culture, Japan. Y. S. thanks the Mitsubishi Foundation for financial support.

Notes and references

† *Selected data* for **1**: δ_H(270 MHz, $CDCl_3$) 11.84 (br s, 1H), 8.64 (d, *J* 8, 1H), 7.48 (d, *J* 8, 1H), 7.36 (t, *J* 8, 1H), 7.08 (t, *J* 8, 1H), 5.10 (s, 1H), 5.09 (d, *J* 10, 1H), 4.29 (d, *J* 10, 1H), 2.95 (s, 3H), 2.59 (q, *J* 8, 2H), 2.49 (t, *J* 8, 2H), 1.8–0.8 (m, 17H); *m*/*z* (FAB-MS) 1070 (M + H$^+$).

‡ The roughness factor (1.1) was estimated by iodine chemisorption on the Au(111) surface.

§ Absorption spectra for **1**/Au could not be obtained in reflection or transmission mode because of the low absorption coefficient of C_{60} as well as the low value of the surface coverage.

1 M. S. Dresselhaus, G. Dresselhaus and P. C. Eklund, *Science of Fullerenes and Carbon Nanotubes*, Academic Press, San Diego, 1996.
2 C. A. Mirkin and W. B. Caldwell, *Tetrahedron*, 1996, **52**, 5113.
3 A. Ulman, *Introduction to Ultrathin Organic Films*, Academic Press, San Diego, 1991.
4 J. A. Chupa, S. Xu, R. F. Fischetti, R. M. Strongin, J. P. McCauley, Jr., A. B. Smith, III, J. K. Blasie, L. J. Peticolas and J. C. Bean, *J. Am. Chem. Soc.*, 1993, **115**, 4383.
5 K. Chen, W. B. Caldwell and C. A. Mirkin, *J. Am. Chem. Soc.*, 1993, **115**, 1193.
6 W. B. Caldwell, K. Chen, C. A. Mirkin and S. J. Babinec, *Langmuir*, 1993, **9**, 1945.
7 V. V. Tsukruk, L. M. Lander and W. J. Brittain, *Langmuir*, 1994, **10**, 996.
8 X. Shi, W. B. Caldwell, K. Chen and C. A. Mirkin, *J. Am. Chem. Soc.*, 1994, **116**, 11 598.
9 F. Arias, L. A. Godínez, S. R. Wilson, A. E. Kaifer and L. Echegoyen, *J. Am. Chem. Soc.*, 1996, **118**, 6086.
10 R. C. Sabapathy, S. Bhattacharyya, M. C. Leavy, W. E. Cleland, Jr. and C. L. Hussey, *Langmuir*, 1998, **14**, 124.
11 M. Maggini, G. Scorrano and M. Prato, *J. Am. Chem. Soc.* 1993, **115**, 9798.
12 T. Nakanishi, H. Murakami and N. Nakashima, *Chem. Lett.*, 1998, 1219.
13 H. Imahori, H. Norieda, S. Ozawa, K. Ushida, H. Yamada, T. Azuma, K. Tamaki and Y. Sakata, *Langmuir*, 1998, **14**, 5335.
14 C. Luo, C. Huang, L. Gan, D. Zhou, W. Xia, Q. Zhuang, Y. Zhao and Y. Huang, *J. Phys. Chem.*, 1996, **100**, 16 685.
15 H. Imahori and Y. Sakata, *Adv. Mater.*, 1997, **9**, 537.

Communication 8/09918I

Total synthesis of deoxypyridinoline, a biochemical marker of collagen turnover

Pietro Allevi,* Alessandra Longo and Mario Anastasia

Dipartimento di Chimica e Biochimica Medica, Via Saldini 50, 20133 Milano, Italy. E-mail: allevi@unimi.it

Received (in Cambridge, UK) 11th January 1999, Accepted 9th February 1999

A convergent synthesis of deoxypyridinoline is described which involves the assembly of a suitably polysubstituted 3-hydroxypyridinium ring starting with fully protected L-lysine and L-glutamic acid.

The paper describes the synthesis[1] and complete characterization of the optically pure deoxypyridinoline **1**. This compound and pyridinoline **2** represent two crosslinks of the mature form of collagen and, at present, are the most effective biochemical markers of collagen turnover correlated with diseases such as osteoporosis, bone cancer and arthropathies.[2]

Compounds **1** and **2** were isolated from bones after several purification steps, but despite the various efforts devoted to improve their extraction, the yields are currently very poor.[3] Although in only small amounts, deoxypyridinoline **1** and pyridinoline **2** have recently been obtained in high purity from bones,[4] and their individual UV molar extinction coefficient values have been established. These values are necessary for the correct standardization of the analytical techniques normally used in clinical determinations in human urine. On the other hand it is still impossible to have a definitive validation of these parameters determined from synthetic compounds using the only multistep synthesis of the deoxypyridinoline **1** (of unspecified diastereomeric purity) and of the pyridinoline **2** (as mixture of epimers at the hydroxylated alkyl carbon) so far reported.[5] This synthesis is accomplished starting with a single fully-protected synthetic L-amino acid, prepared according to the Schoelkopf's approach. However, the enantiomeric purity of this starting building block as well as the physico-chemical parameters (UV molar extinction coefficients, optical rotations, elemental analyses) of the final compounds **1** and **2** were unreported.

In our work we decided to start from enantiomerically pure and easily available natural L-α-amino acids, in order to avoid the formation of complex diastereomeric mixtures in a possible convergent synthesis of **1**. In particular, a strategic disconnection of the pyridinium compound **1** suggested its assembly from an L-lysine residue and from two identical fragments derivable from L-glutamic acid (Scheme 1).

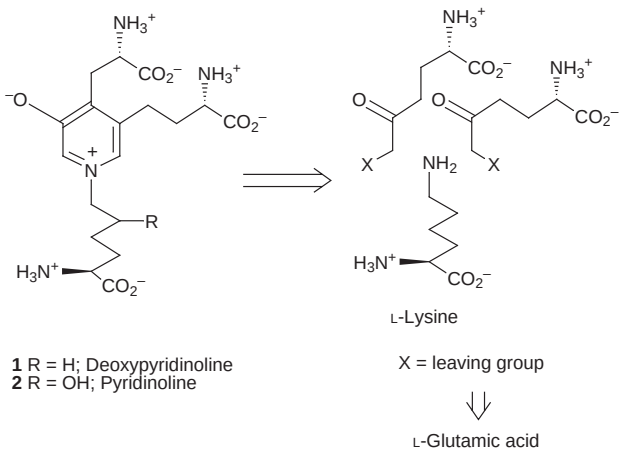

Scheme 1

With this in mind, the possibility of constructing the pyridine ring of **1** was first studied using a simpler model lacking the stereocenters and the amino acidic functionalities (Scheme 2). Easily available[6] 1-bromopentan-2-one was reacted with (*R*)-1-phenylethylamine to afford, using the best conditions (K_2CO_3, MeCN, 12 h, 25 °C), the diketoamine **3** in very high yield (80%).† Initially, various unsuccessful attempts were made to promote in the same reaction both the formation of the ketoamine **3** and its condensation to give the ketone **4**, by modulating the reaction conditions (reaction times, temperatures and/or addition of appropriate crown ethers). Subsequently, the internal condensation was attempted with the isolated and purified compound **3**. Surprisingly, treatment of amine **3** with K_2CO_3 in MeOH afforded (70% yield) a single fluorescent product, to which the structure **5**‡ could be assigned. Formation of compound **5** shows that, contrary to our expectations, the aldolic condensation occurred, followed by the oxidation of the possible intermediate cyclic ketone **4**.

The ketone **4** could be isolated and completely characterized when the reaction was performed under complete exclusion of oxygen. This compound was transformed into the pyridinium salt **5** when it was dissolved in MeOH and stirred in the presence of air and K_2CO_3. Compound **5** was also obtained, in a one-pot reaction, by mixing 1-bromopentan-2-one and (*R*)-1-phenylethylamine in an open vessel containing MeCN and K_2CO_3. When the complete formation of the ketoamine **3** was monitored, the addition of MeOH leads to the formation of the desired pyridinium salt **5**. Similar spontaneous oxidations were also recently observed[7] in other syntheses of pyridinium derivatives, but it was always impossible to map the mechanism of their formation. In our case, the isolation of compound **4** under anaerobic conditions and the observation that no tetrahydro derivative was detectable in the final reaction mixture made it possible to establish that oxygen, and not a disproportionation reaction, is responsible for the formation of pyridinium salt **5**.

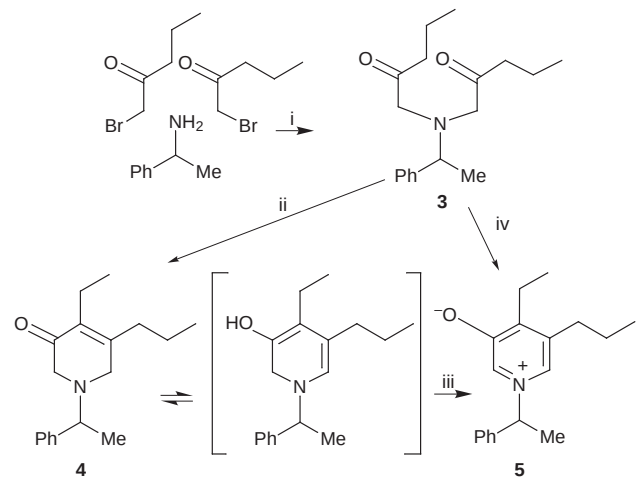

Scheme 2 *Reagents and conditions*: i, K_2CO_3, MeCN, room temp., 80%; ii, K_2CO_3, MeOH, room temp., 85%; iii, K_2CO_3, air, MeOH, room temp., 81%; iv, K_2CO_3, air, MeOH, room temp., 70%.

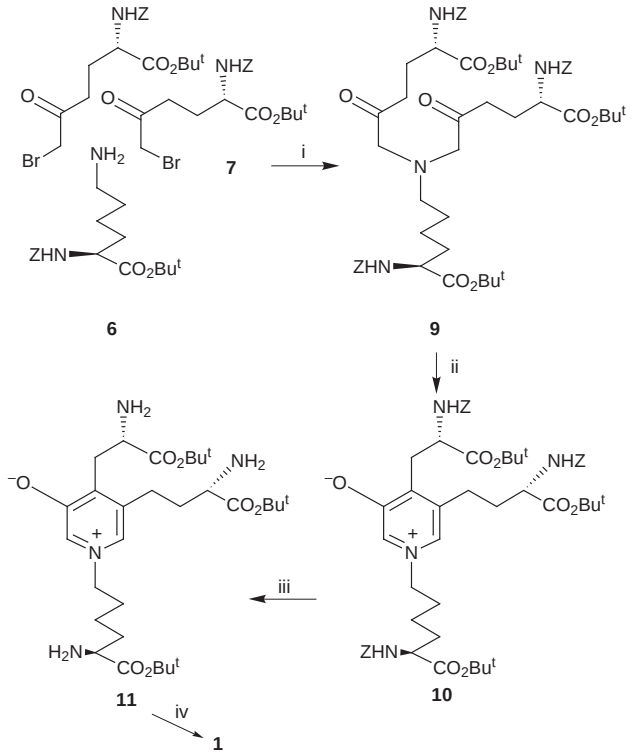

Scheme 3 *Reagents and conditions*: i, K_2CO_3, MeCN, room temp., 78%; ii, K_2CO_3, air, MeOH, room temp., 73%; iii, H_2, Pd/C, MeOH, room temp., 94%; iv, TFA, room temp., 72%.

The possibility of extending the method used for the synthesis of the simple model compound **5** to the more complex deoxypyridinoline **1** was then demonstrated by reacting under similar conditions (Scheme 3) the known[8] protected L-lysine **6** with the bromo ketone **7**§ obtained in two steps from *N*-(benzyloxycarbonyl)-L-glutamic acid 1-*tert*-butyl ester[9] **8** (Scheme 4).

Thus, the reaction in MeCN afforded the amine **9** in good yield [78% yield; an oil, $[\alpha]_D^{20}$ −0.8, $[\alpha]_{365}^{20}$ +3.1, ($CHCl_3$, 1% solution]. This amine is rather unstable in solution (decomposes in a few days) but it was transformed into the protected deoxypyridinoline **10**¶ when it was dissolved in MeOH containing K_2CO_3 and stirred in the presence of air.

Regeneration of the three protected amino groups of **10** by hydrogenolysis afforded the ester **11**‖ which, by treatment with TFA, easily gave deoxypyridinoline **1** as monotrifluoracetate salt in an epimerization-free process.[10] This salt of deoxypyridinoline **1** crystallized from aq. EtOH as a white monohydrate which was completely characterized.** Its UV molar extinction coefficients proved higher (10–20%) than those reported for the corresponding tetrachloride dihydrate salt.[4] The same difference was observed for the corresponding tetrachloride salt of **1**, which in our hands crystallized as monohydrate.

The preparation of the bromo derivative **7**, which required the activation of the ω-carboxylic group of the protected glutamic acid **8** and its substitution for an α-bromo ketone *via* an intermediate α-diazo ketone, merits comment. These transformations, well-established in the case of the shorter aspartic derivative,[11] were in our case complicated by the easy concurrent cyclisation to the known[12] (*S*)-5-(1,1-dimethylethoxy)carbonyl-1-benzyloxycarbonyl-2-pyrrolidone, cyclisation of which was not allowed in the case of the aspartic acid derivative. This cyclisation occurs during the activation of the ω-carboxylic group as an acid chloride (using $SOCl_2$ it is the only compound formed) or as mixed anhydride (using $ClCO_2Et$[13] it forms in 40% yield). Only when performing the activation with $ClCO_2Bn$ does the diazo ketone **12** [oil; $[\alpha]_D^{25}$ +16.6 ($CHCl_3$, 2% solution)] form in quantitative yield, avoiding the formation of cyclic pyroglutamate.

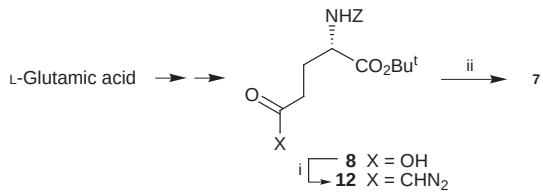

Scheme 4 Reagents and conditions: i, $ClCO_2Bn$, *N*-methylmorpholine, THF, −20 °C, then CH_2N_2, −20 °C → 0 °C, 88%; ii, HBr, AcOH, 0 °C, 64%.

Further work is currently underway to accomplish the synthesis of pyridinoline **2** by a similar convergent assembly of the pyridine nucleus starting from three L-glutamic units.

This work was supported financially by MURST COFIN progetto di ricerca 'Nuove metodologie e strategie di Sintesi di Composti di Interesse Biologico'. Dedicated to the memory of Professor Giacomino Randazzo.

Notes and references

† All new compounds gave correct elemental C, H, N and Cl analyses.

‡ *Selected data* for **5**: oil; $[\alpha]_D^{20}$ +3.3, $[\alpha]_{436}^{20}$ −13.3 ($CHCl_3$, *c* 1); δ_H(500 MHz, $CDCl_3$ 8.17 (1H, br s, pyridinium ring proton), 7.04 (1H, br s, pyridinium ring proton), 5.40 (1H, q, *J* 7.0, NC*H*CH_3), 1.96 (3H, d, *J* 7.0 Hz, NCHCH_3), 1.16 (3H, t, *J* 7.0, pyr-CH_2C*H*$_3$), 0.92 (3H, t, *J* 7.0, pyr-CH_2CH_2C*H*$_3$).

§ *Selected data* for **7**: oil; $[\alpha]_D^{20}$ −0.3, $[\alpha]_{365}^{20}$ −14.8 ($CHCl_3$, *c* 1); δ_H(500 MHz, $CDCl_3$) 4.24 [1H, ddd, *J* 8.5, 8.0, 4.5, C*H*(NHZ)CO_2Bu^t], 3.87 (2H, s, BrC*H*$_2$CO), 2.75 (1H, ddd, *J* 18.0, 8.5, 7.0, $BrCH_2COCHH$), 2.67 (1H, ddd, *J* 18.0, 8.5, 5.5, $BrCH_2COCHH$).

¶ *Selected data* for **10**: oil; $[\alpha]_D^{20}$ +5.3, $[\alpha]_{436}^{20}$ +29.2 ($CHCl_3$, *c* 1); δ_H(500 MHz, $CDCl_3$) 8.09 (1H, br s, pyridinium ring proton), 6.90 (1H, br s, pyridinium ring proton).

‖ *Selected data* for **11**: oil; $[\alpha]_D^{20}$ +32.5 ($CHCl_3$, *c* 1); δ_H(500 MHz, CD_3OD) 7.57 (1H, br s, pyridinium ring proton), 7.48 (1H, br s, pyridinium ring proton).

** *Selected data* for **1** monotrifluoroacetate monohydrate ($C_{18}H_{29}N_4O_7 \cdot CF_3CO_2^- \cdot H_2O$): $[\alpha]_D^{20}$ +33.0 ($CHCl_3$, *c* 0.98); λ_{max}(HCl 0.1 M)/nm (ε/M^{-1} cm^{-1}), 239 (3850), 293 (6480); λ_{max}(50 mM phosphate buffer, pH 7.5)/nm (ε/M^{-1} cm^{-1}) 252 (3660), 324 (6100); δ_H(500 MHz, D_2O) 8.69 (1H, br s, pyridinium ring proton), 8.62 (1H, br s, pyridinium ring proton), 4.92 (2H, t, *J* 6.5, $CH_2CH_2N^+$), 4.54 [1H, t, *J* 7.0, C*H*(NH_3^+)COO^-], 4.32 [1H, t, *J* 5.0 Hz, C*H*(NH_3^+)COO^-], 4.16 [1H, t, *J* 6.0, C*H*(NH_3^+)COO^-]; δ_C(D_2O) 175.1, 174.5, 173.6, 163.6 (q, CF_3*C*OO), 156.8, 142.1, 141.9, 136.0, 129.7, 117.5 (q, *C*F_3COO), 61.8, 55.2, 54.9, 53.6, 31.4, 30.7, 30.5, 28.6, 26.4, 21.9.

1 Presented at the 24th *Convegno Nazionale, Divisione di Chimica Organica*, Salerno (Italy) September 21–25, 1997.

2 *Inter alia*: I. T. James, A. J. Walne and D. Perrett, *Ann. Clin. Biochem*., 1996, **33**, 397; R. H. Christenson, *Clin. Biochem*., 1997, **30**, 573.

3 P. Arbault, E. Gineyts, M. Grimaux, P. Seguin and P. D. Delmas, *J. Liq. Chromatogr*., 1994, **17**, 1981; D. Fujimoto, K. Akiba and N. Nakamura, JP 54039078; (*Chem. Abstr*., 1979, **91**, 211269).

4 S. P. Robins, A. Duncan, N. Wilson and B. J. Evans, *Clin. Chem*., 1996, **42**, 1621.

5 R. Waelchli, C. H. Beerli, H. Meigel and L. Révész, *Bioorg. Med. Chem. Lett*., 1997, **7**, 2831.

6 N. D. Doktorova, L. V. Ionova, M. Y. Karpeisky, N. S. Padyukova, K. F. Turkin and V. L. Florentiev, *Tetrahedron*, 1969, **25**, 3527.

7 K. Suyama and S. Adachi, *J. Org. Chem*., 1979, **44**, 1417; Li-B. Yu, D. Chen, J. Li, J. Ramirez, P. G. Wang and S. G. Bott, *J. Org. Chem*., 1997, **62**, 208.

8 M. J. Milewska and A. Chimiak, *Tetrahedron Lett*., 1987, **28**, 1817.

9 K. Pawelczak, L. Krzyzanowski and B. Rzeszotarska, *Org. Prep. Proced. Int*., 1985, **17**, 416.

10 V. Bavetsias, A. L. Jackman, R. Kimbell, W. Gibson, F. T. Boyle and G. M. F. Bisset, *J. Med. Chem*., 1996, **39**, 73.

11 Y. Liwschitz, R. D. Irsay and A. I. Vincze, *J. Chem. Soc*., 1959, 1308.

12 D. K. Dikshit and S. K. Panday, *J. Org. Chem*., 1992, **57**, 1920.

13 P. D. Bailey and J. S. Bryans, *Tetrahedron Lett*., 1988, **29**, 2231.

Communication 9/00298G

ChemComm

Two- and three-dimensional non-interpenetrating open-networks self-assembled by μ_4-hexamethylenetetramine (hmt). Syntheses and structures of $[Ag_2(\mu_4\text{-hmt})(SO_4)(H_2O)]\cdot 4H_2O$ and $[Ag_2(\mu_4\text{-hmt})(\mu\text{-}O_2CMe)]MeCO_2\cdot 4.5H_2O$

Ming-Liang Tong, Shao-Liang Zheng and Xiao-Ming Chen*

School of Chemistry and Chemical Engineering, Zhongshan University, Guangzhou 510275, China. E-mail: cedc03@zsu.edu.cu

Received (in Cambridge, UK) 19th January 1999, Accepted 19th February 1999

Sulfate and acetate complexes comprising two-dimensional grids with square cavities and three-dimensional networks with hexagonal channels, respectively, have been prepared and characterised by X-ray single-crystal structural analysis.

Considerable research effort has recently been focused on the crystal engineering of supramolecular architectures organised by co-ordinate covalent or hydrogen bonding.[1,2] Although supramolecular co-ordination polymers have currently been constructed largely with the use of symmetrically-bridging ligands (such as 2-connectors, trigonal 3-connectors, and tetrahedral or square planar 4-connectors), the use of different synthons[1a,3,4] is one of several strategies that could be employed in the synthesis of frameworks having larger cavities or channels for possible application in separation processes and catalysis. Silver(I) is a good candidate as a simple spacer in L–M–L metallic synthons for the preparation of desired networks, and hexamethylenetetramine (hmt) as a potential tetradendate ligand seems quite suitable for self-assembly of supertetrahedral networks with metallic synthons although no supertetrahedral $[Ag_2(hmt)]$ hypothetical frame has, as yet, been isolated.[5–9] We report here the preparation and crystal structures of two novel two- and three-dimensional non-interpenetrating open-networks organised by μ_4-hmt ligand with simple spacers: $[Ag_2(\mu_4\text{-hmt})(SO_4)(H_2O)]\cdot 4H_2O$ **1** and $[Ag_2(\mu_4\text{-hmt})(\mu\text{-}O_2CMe)]MeCO_2\cdot 4.5H_2O$ **2**.

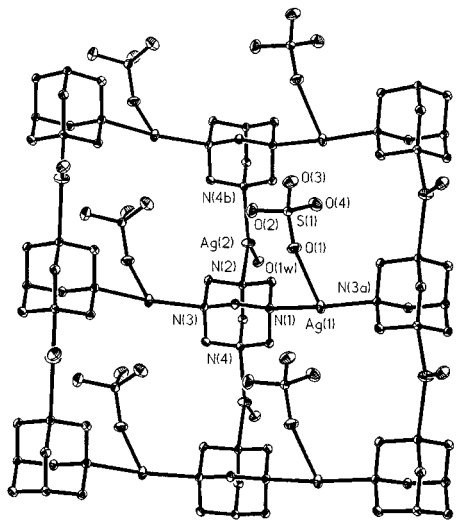

Fig. 1 ORTEP view showing the layer in **1** viewed along the *b* direction. Small open balls represent centres of mass of the hmt ligands. Relevant bonding parameters: Ag(1)–N(1) 2.292(4), Ag(1)–N(3a) 2.279(4), Ag(1)–O(1) 2.571(5), Ag(2)–N(2) 2.347(4), Ag(2)–N(4b) 2.311(4), Ag(2)–O(1w) 2.303(4) Å; N(1)–Ag(1)–N(3a) 172.81(15), N(1)–Ag(1)–O(1) 88.44(16), N(3a)–Ag(1)–O(1) 92.44(15), N(2)–Ag(2)–N(4b) 115.10(14), N(2)–Ag(2)–O(1w) 117.09(15), N(4b)–Ag(2)–O(1w) 127.80(15)°.

Both complexes were synthesised by self-assembly of the silver(I) salts with hmt, as shown in Scheme 1. An aqueous solution (5 cm^3) of hmt (0.140 g, 1.0 mmol) was added dropwise to a stirred MeCN solution (5 cm^3) of Ag_2SO_4 (0.156 g, 0.5 mmol) or $Ag(MeCO_2)$ (0.167 g, 1.0 mmol) at 50 °C for 15 min. The resulting colorless solution was allowed to stand in air at room temperature for two weeks, yielding colorless crystals [*ca.* 75% yield based on silver(I)]. Elemental analysis confirmed the formulae of **1** and **2**.† On performing the above reactions with an Ag(I) : hmt ratio of 2 : 1, crystals of **1** or **2** were correspondingly isolated in high yield, suggesting that the Ag(I) ion plays the role of a simple spacer in the self-assembly of **1** and **2**.

X-Ray crystallography‡ has established that **1** is made up of two-dimensional infinite wavy neutral layers of square units and lattice water molecules. As illustrated in Fig. 1, each square unit is organised by four Ag(I) ions in two types of geometries and four hmt molecules each at the midpoint of side and corner, respectively, in which the Ag(2) ion is in a trigonal geometry coordinated by two nitrogen atoms from different hmt ligands and one aqua ligand, while the Ag(1) atom is in a T-shaped geometry ligated by two nitrogen atoms from two hmt ligands and one monodentate SO_4^{2-} anion. Adjacent layers are connected by interlayer hydrogen bonds between the aqua

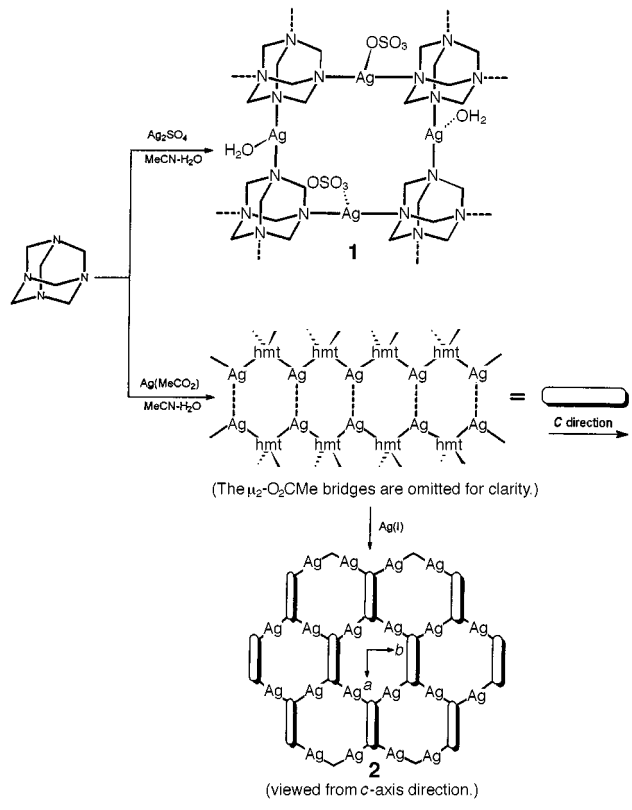

Scheme 1

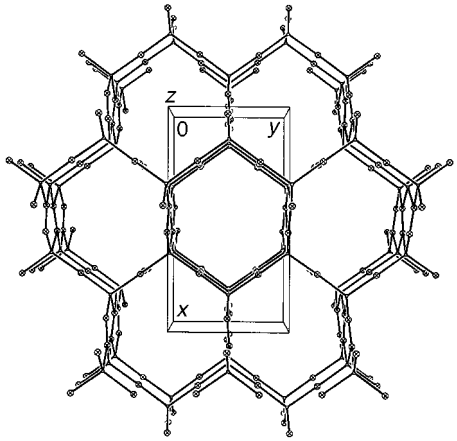

Fig. 2 View of 3-D networks in **2** along the *c*-axis direction. The μ_2-O_2CMe bridges are omitted for clarity. Small open balls represent centres of mass of the hmt ligands.

ligand and SO_4^{2-} anion with an O(1w)···O(SO_4) distance of 2.681–2.691 Å, resulting in a three-dimensional network having irregular pentagonal channels. The lattice water molecules are clathrated in these channels.

The structure of **2** consists of an open three-dimensional cationic network with hexagonal channels, acetate counterions and lattice water molecules. As shown in Scheme 1, the dimeric $Ag_2(MeCO_2)_2$ fragments are bridged by hmt ligands each using two nitrogen atoms into an infinite planar sheet with hexagonal cavities along the *c* direction. These sheets are further joined by the simple Ag(I) spacers through the two remaining nitrogen atoms of hmt ligand into a three-dimensional non-interpenetrating open-network having hexagonal channels along the *c*- and *b*-axis directions (Scheme 1 and Fig. 2). The uncoordinated acetate ions and lattice water molecules are clathrated in the channels.

In the $Ag_2(\mu$-$O_2CMe)_2$ fragments, the Ag(I) atoms are joined by two unusual non-coplanar skew–skew carboxylate bridges[10] with an Ag···Ag distance of 2.9144(8) Å, indicating a relatively strong Ag···Ag interaction;[11] each Ag(I) atom is further ligated by two nitrogen atoms from two different hmt ligands, completing a tetrahedral coordination geometry (Fig. 3).

It is noteworthy that **1** is the first two-dimensional open-network constructed by μ_4-hmt. Of the reported metal–hmt networks, hmt acts rarely in tetradendate coordination mode,[5,6,8,12–14] and only two compounds with μ_4-hmt ligand have been documented.[7,9] Moreover, the topology in **2** is, to the best of our knowledge, unprecedented. In **2**, each hexagon unit viewed from the *c*-axis direction is equivalent, and involves four Ag(I) atoms, two $Ag_2(O_2CMe)_2$ fragments and six hmt ligands, while the hexagonal units viewed from *b*-axis direction is non-equivalent and can be classified into two categories, one involves two $Ag_2(O_2CMe)_2$ fragments and two hmt ligands, another involves four Ag(I) atoms and four hmt ligands. These features are in contrast to those of the reported three-dimensional networks, a 3-D, 3-C enantiomorphic interpenetrating network in $[Ag(hmt)]PF_6 \cdot H_2O$,[6] a (3,4)-connected net in $[Ag_3(hmt)_2](ClO_4)_3 \cdot 2H_2O$,[7] and a triconnected 3D net in $[Ag_4(hmt)_3(H_2O)](PF_6)_4 \cdot 3EtOH$.[8]

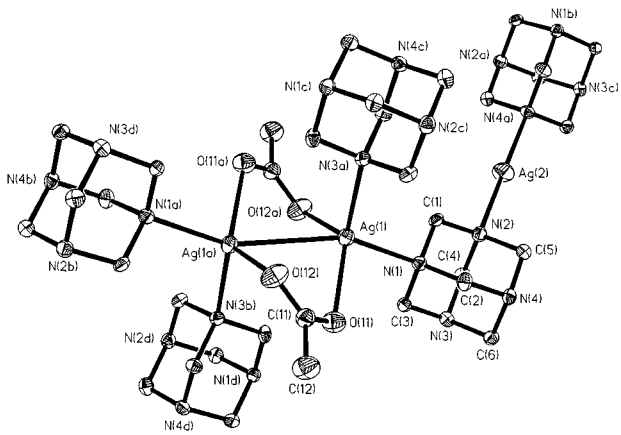

Fig. 3 Coordination environments (at 35% probability level) of the metal atoms in **2**. Relevant bonding parameters: Ag(1)–Ag(la) 2.9144(8), Ag(1)–N(1) 2.405(4), Ag(1)–N(3a) 2.403(4), Ag(2)–N(2) 2.240(4), Ag(2)–N(4a) 2.254(4), Ag(1)–O(11) 2.366(4), Ag(1)–O(12a) 2.391(4) Å; O(11)–Ag(1)–O(12a) 125.84(17), O(12a)–Ag(1)–N(3b) 108.63(14), O(12a)–Ag(1)–N(1), 91.41(15), N(1)–Ag(1)–N(3a) 115.61(14), N(1)–Ag(1)–O(11) 96.64(15), N(3a)–Ag(1)–O(12a) 108.63(14) and N(1)–Ag(2)–N(4a) 178.08(15)°.

As the self-assembly of supramolecular frameworks is highly influenced by factors such as the solvent system,[1a] template[15] and steric requirement of the counter ion,[16] our present work demonstrates that participation of counter ions plays an important role in self-assembly of these frameworks. The isolation of the title complexes and others[11,12] also suggests effective routes to constructing desired frameworks with organic molecules and metallic spacers.

This work was supported by the NSFC (No. 29625102) and Guangdong Higher Education Bureau.

Notes and references

† Anal. Calc. for $C_6H_{22}N_4O_9SAg_2$ **1**: C, 13.29; H, 4.09; N, 10.34. Found: C, 13.16; H, 4.02; N, 10.22%. Calc. for $C_{10}H_{27}N_4O_{8.5}Ag_2$ **2**: C, 21.64; H, 4.90; N, 10.09. Found: C, 21.48; H, 4.79; N, 10.04%.

‡ *Crystal data*: **1**: $C_6H_{22}N_4O_9SAg_2$, M_r = 542.08, monoclinic, space group *Cc* (no. 9), a = 6.362(6), b = 18.813(13), c = 12.552(4) Å, β = 91.64(6)°, V = 1502(2) Å^3, Z = 4, D_c = 2.398 g cm^{-3}, μ = 27.98 cm^{-1}. **2**: $C_{10}H_{27}N_4O_{8.5}Ag_2$, M_r = 555.10, orthorhombic, space group *Pbcn* (no. 60), a = 22.7015(3), b = 12.1200(2), c = 12.9889(2) Å, V = 3573.79(9) Å^3, Z = 8, D_c = 2.063 g cm^{-3}, μ = 2.240 cm^{-1}. Data collection ($2.17 \leqslant \theta \leqslant 29.06$ for **1** and $1.79 \leqslant \theta \leqslant 25.03°$ for **2**) was performed at 293 K on a Siemens R3m diffractometer (Mo-Kα, λ = 0.71073 Å). The structures were solved with direct methods (SHELXS-97)[17] and refined with full-matrix least-squares technique (SHELXL-97),[18] giving for **1** a final R_1 value of 0.0259 for 200 parameters and 2177 unique reflections with $I \geqslant 2\sigma(I)$ and wR_2 of 0.0663 for all 2177 reflections and for **2** a final R_1 value of 0.0487 for 235 parameters and 2567 unique reflections with $I \geqslant 2\sigma(I)$ and wR_2 of 0.1335 for all 3147 reflections CCDC 182/1176. See http://www.rsc.org/suppdata/cc/1999/561/ for crystallographic files in .cif format.

1 (*a*) R. Robin, B. F. Abrahams, S. R. Batten, R. W. Gable, B. F. Huskiness and J. Lieu, *Supramolecular Architecture*, ACS publications, Washington, DC, 1992, p. 256; (*b*) J. M. Lehn, *Supramolecular Chemistry*, VCH, Weinheim, 1995, ch. 9.
2 C. B. Aakeroy and K. R. Seddon, *Chem. Soc. Rev.*, 1993, 397.
3 G. R. Desiraju, *Angew. Chem., Int. Ed. Engl.*, 1995, **34**, 2311.
4 O. Ermer, *J. Am. Chem. Soc.*, 1988, **110**, 3747.
5 A. Michelet, B. Voissat, P. Khodadad and N. Rodier, *Acta Crystallogr., Sect. B*, 1981, **37**, 2171.
6 L. Carlucci, G. Ciani, D. M. Proserpio and A. Sironi, *J. Am. Chem. Soc.*, 1995, **117**, 12861.
7 L. Carlucci, G. Ciani, D. W. V. Gudenberg, D. M. Proserpio and A. Sironi, *Chem. Commun.*, 1997, 631.
8 L. Carlucci, G. Ciani, D. M. Proserpio and A. Sironi, *Inorg. Chem.*, 1997, **36**, 1736.
9 T. C. W. Mak, *Inorg. Chim. Acta*, 1984, **84**, 19.
10 Y.-X. Tong, X.-M. Chen and S. W. Ng, *Polyhedron*, 1997, **16**, 3363.
11 M. Jansen, *Angew. Chem., Int. Ed. Engl.*, 1987, **26**, 1098.
12 J. Pickardt, *Acta Crystallogr., Sect. B*, 1981, **37**, 1753.
13 H. Miyamae, H. Nishikawa, K. Hagimoto, G. Hihara and M. Nagata, *Chem. Lett.*, 1988, 1907.
14 S. R. Batten, B. F. Hoskins and R. Robson, *Inorg. Chem.*, 1998, **37**, 3432.
15 M.-L. Tong, B.-H. Ye, J.-W. Cai, X.-M. Chen and S. W. Ng, *Inorganic Chemistry*, 1998, **37**, 2645.
16 M.-L. Tong, X.-M. Chen, B.-H. Ye and S. W. Ng, *Inorg. Chem.*, 1998, **37**, 5168; L. Carlucci, G. Ciani, D. M. Proserpio and A. Sironi, *Angew. Chem., Int. Ed. Engl.*, 1995, **34**, 1895.
17 G. M. Sheldrick, SHELXS-97 User's Manual. Siemens Analytical X-ray Instrument Inc., Madison, Wisconsin, USA, 1990.
18 G. M. Sheldrick, SHELXL-97, Program for X-ray Crystal Structure Refinement, Göttingen University, Germany, 1997.

Communication 9/00508K

Sequential multistep energy transfer: enhancement of efficiency of long-range fluorescence resonance energy transfer

Shun-ichi Kawahara, Tadafumi Uchimaru* and Shigeo Murata

Department of Physical Chemistry, National Institute of Materials and Chemical Research, Agency of Industrial Science and Technology, MITI, Tsukuba Science City 305-8565, Japan. E-mail: t_uchimaru@home.nimc.go.jp

Received (in Cambridge, UK) 14th December 1999, Accepted 15th February 1999

The efficiency of long-range (*ca.* 80 Å) fluorescence energy transfer was enhanced about 1.5 times by a third chromophore located midway between two chromophores, which suggests sequential multistep energy transfer across the three chromophores.

Fluorescence resonance energy transfer (FRET)[1] is widely used to estimate chromophore separation and structure on a nanometre scale.[2] FRET in a system consisting of a fluorescent energy donor and acceptor has been extensively studied.[1b] The FRET technique has been frequently applied to probe biological and other complex systems.[3]

Recently, covalently linked porphyrin arrays have attracted much attention as biomimetic models.[4] This is because multiporphyrin assemblies are involved in the reaction centre of photosynthesis[5] and light-harvesting antenna complexes.[4] Much effort has been directed towards the development of such model systems. Covalently linked chromophore arrays will offer new opportunities for exploring long-range energy transfer and also electron transfer systems. A few reports of non-covalently linked chromophore arrays have also been described.[6]

Here we report a non-covalently linked chromophore array indicating sequential FRET across three different chromophores. We have introduced different chromophores in a duplex of oligodeoxyribonucleic acid (oligo-DNA) in a sequential manner. We have revealed that the efficiency of FRET across the two chromophores at both ends of the oligo-DNA duplex is enhanced by a third chromophore located midway between them.

6-Carboxyfluorescein (**1**), 4,7,2′,4′,5′,7′-hexachloro-6-carboxyfluorescein (**2**) and 6-carboxy-X-rhodamine (**3**) shown in Fig. 1(*a*), were used as chromophores. These chromophores were introduced at the 5′-terminal position of oligo-DNA 25-, 15-, and 10mers through an aminohexyl phosphate linker: the carboxy groups located at the 3-position of the chromophores were connected *via* amide linkages with the terminal amino group of the linker. The sequence of the oligo-DNA 15- and 10mers are complementary to that of the 25mer. Thus, these oligomers form typical B type duplexes. As shown in Fig. 2, we

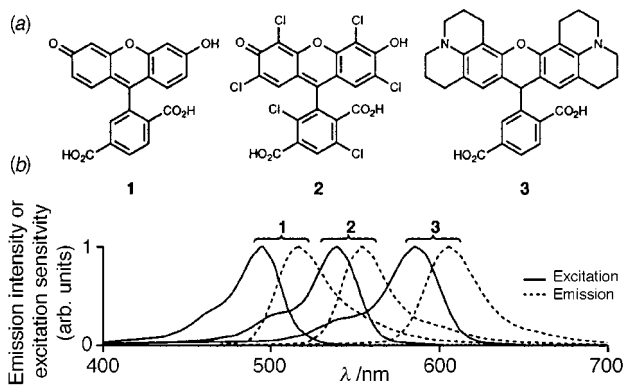

Fig. 1 (*a*) Structures of chromophores. (*b*) Excitation and emission spectra of each choromophore normalized at maximum.

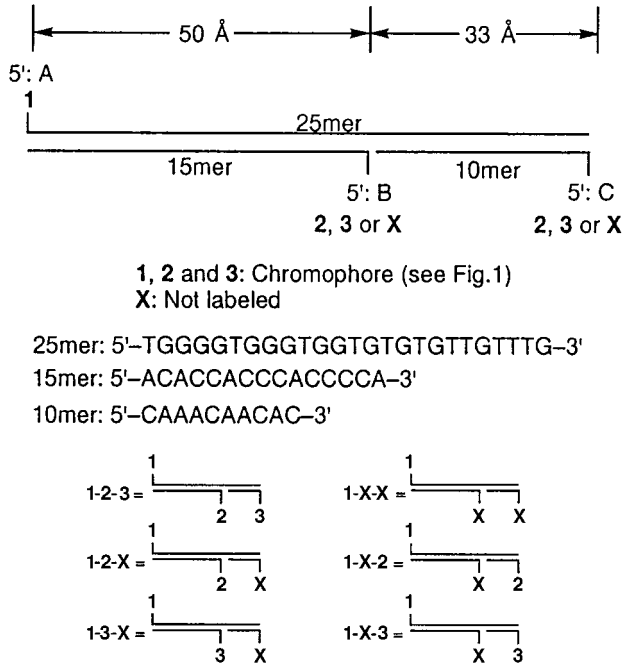

Fig. 2 DNA sequences and chromophore introduced positions.

call the 5′-terminal positions of the 25-, 15- and 10mers positions A, B, and C, respectively. Chromophore **1** was introduced at position A, while chromophores **2** and **3** were introduced at position B or C. Owing to characteristic structural features of the B type duplex, the chromophores introduced at position A, B, and C are located on the same side of the duplex chain. The distances between positions A and B and B and C are about 50 and 33 Å, respectively. Thus, position C is located *ca.* 80 Å from position A (see Fig. 2).

Fig. 1(*b*) shows the normalized emission and excitation spectra of the chromophores. The emission spectra of six duplexes (**1**-**2**-**3** through **1**-**X**-**X**,† see Fig. 2) excited at 450 nm are shown in Fig. 3(*a*) and (*b*).‡ The 450 nm light is absorbed by chromophore **1**, while the absorptions of chromophores **2** and **3** are quite weak or completely negligible at this wavelength [see Fig. 1(*b*)]. FRET from chromophore **1** to **2** or **3** was evidenced by fluorescence emission from chromophore **2** or **3**. The intensity of fluorescence from chromophore **1** was reduced as a

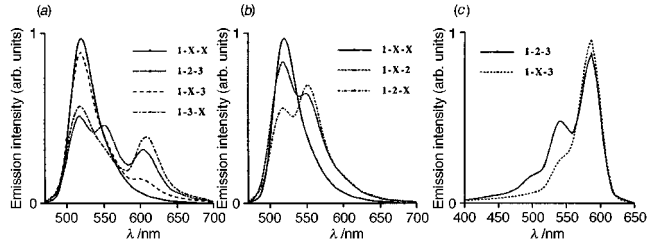

Fig. 3 (*a*) and (*b*) Emission spectra of each duplex. (*c*) Excitation spectra of **1**-**2**-**3** and **1**-**X**-**3**.

consequence of FRET across the chromophores. Correspondingly, fluorescence emission from chromophores **2** and **3** was observed. Table 1 shows the fluorescence quantum yields of each chromophore in the duplex relative to those of the same chromophore measured under the conditions without FRET.§

The results in Table 1 show that the efficiency of energy transfer from **1** to **2** or **3** decreases with the increase in the separation between the chromophores: the efficiency of energy transfer between position A and C with larger separation was lower than that between position A and B. Φ_f^{rel}(**2**) was reduced from 54% in duplex **1-2-X** to 32% in **1-X-2**. Conversely, for chromophore **1**, Φ_f^{rel}(**1**) was smaller in duplex **1-2-X** (57%) than in duplex **1-X-2** (85%). The same trend was seen for energy transfer from chromophore **1** to **3**. However, the efficiency of energy transfer from chromophore **1** to **3** was found to be lower than that from **1** to **2**. This is due to the fact that the fluorescence–absorption overlap between chromophores **1** and **3** is smaller than that between chromophores **1** and **2** [see Fig. 1(*b*)]. Φ_f^{rel}(**3**) in duplex **1-3-X** and **1-X-3** was 36 and 10%, respectively. Φ_f^{rel}(**1**) was 58 and 90%, respectively. These results indicate that our non-covalently linked chromophore arrays show normal behavior regarding energy transfer across the two chromophores.

Meanwhile, Φ_f^{rel}(**3**) was increased from 10% in **1-X-3** to 16% in **1-2-3** (see Table 1). Chromophore **2** inserted at the midway position B enhances the efficiency of the energy transfer from chromophore **1** to **3** located at positions A and C, respectively. Fluorescence excitation spectra of duplexes **1-2-3** and **1-X-3** observed at 605 nm (fluorescence maximum of chromophore **3**) are shown in Fig. 3(*c*). The excitation spectra suggested that the absolute fluorescence quantum yield of chromophore **3** was almost the same in these duplexes. Thus, we can safely conclude that the efficiency of FRET from chromophore **1** to **3** between position A and C was increased about 1.5 times due to chromophore **2** being inserted at midway position B.

Enhancement of the efficiency of energy transfer from chromophore **1** to **3** in duplex **1-2-3** can be interpreted as a consequence of sequential two-step energy transfer: energy transfer from chromophore **1** to **2** and subsequent energy transfer from chromophore **2** to **3**. Namely, chromophore **2** should work as a relay station for energy transfer, which suggests that use of an additional chromophore as a relay station should lengthen the range of energy transfer. Furthermore, sequential energy transfer *via* more than two relay stations may be possible. Such energy transfer might be called sequential multistep energy transfer. Sequential multistep energy transfer will provide us with information about the distance between chromophores with a separation larger than 100 Å, which is difficult using a simple energy transfer system consisting of just a fluorescent donor and acceptor. Thus, sequential energy transfer would be useful for research in various fields, not only in the fields of biochemistry[3] but also in the fields of supramolecular chemistry.[7]

In summary, we introduced three different chromophores in a duplex of oligo-DNA in a sequential manner. The efficiency of FRET across two chromophores was shown to be increased by a third chromophore located at the midway position between them. The third chromophore works as a relay station in energy transfer.

We thank Professor K. Tokumaru of the University of the Air for helpful discussions, and Science and Technology Agency for financial support.

Table 1 Values of Φ_f^{rel}(***n***)

Sequence	**1**	**2**	**3**
1-2-3	0.51	0.29	0.16
1-2-X	0.57	0.54	—
1-X-2	0.85	0.32	—
1-3-X	0.58	—	0.36
1-X-3	0.90	—	0.10

Notes and references

† **1-2-3** represents the oligo-DNA duplex possessing chromophores **1**, **2** and **3** at positions A, B and C, respectively. **X** means that no fluorescent chromophore is introduced at the position(s).

‡ All the fluorescence spectra were measured under the following conditions: 1 mM phosphate buffer (pH 7.0) with 0.1 M NaCl and 0.1 mM EDTA to remove the effect of contaminating metals. T = 20 °C. Concentration of oligomers = 1.0 μM. Under these conditions, three oligomers form duplexes (T_m^1 = 36–38 °C for dissociation of 10mer, T_m^2 = 60–63 °C for 15mer).

§ We derived the relative fluorescence yield, Φ_f^{apr}(***n***) in each duplex on the basis of observed fluorescence intensities of the chromophores. We employed eqn. (1), where ***n*** = **1**, **2** or **3**, Em(***n***)^{obs} = observed fluorescence

$$\Phi_f^{apr}(\boldsymbol{n}) = \left(\frac{\mathrm{Em}(\boldsymbol{n})^{obs}}{\mathrm{Em}(\boldsymbol{n})^{max}}\right)\left(\frac{\mathrm{EC}(\boldsymbol{n})}{\mathrm{EC}_{450}(\mathbf{1})}\right) \quad (1)$$

intensity of ***n*** in the FRET system excited at 450 nm, Em(***n***)^{max} = observed fluorescence intensity of ***n*** excited at the absorption maximum, EC(***n***) = extinction coefficient of **1** (48000/495 nm), **2** (79700/540 nm) and **3** (91200 /585 nm) under the present experimental conditions, and EC_{450}(**1**) = extinction coefficient of **1** at 450 nm (10800), calculated from excitation intensity and extinction coefficient at 495 nm.

However, the absorption of chromophore **2** at 450 nm cannot be completely neglected. Fluorescence emission from chromophore **2** results from not only energy transfer from **1** but also partially by direct excitation of **2** by irradiation at 450 nm. In duplex **1-2-3**, energy transfer will occur from directly excited **2** to **3**, which partially contributes to Φ_f^{apr}(**3**). We deducted these contributions of direct excitation of **2** from Φ_f^{apr}(**2**) and Φ_f^{apr}(**3**) and then derived the relative fluorescence yields of these two chromophores. Hereafter, we refer to these quantities as the relative fluorescence yields Φ_f^{rel}(***n***). The values of Φ_f^{rel}(***n***) are the fluorescence yields of emission from each chromophore solely due to the contribution of the energy transfer from chromophore **1**. For chromophore **1**, Φ_f^{apr}(**1**) = Φ_f^{rel}(**1**). In addition, for duplexes **1-3-X** and **1-X-3**, which do not possess chromophore **2**, Φ_f^{apr}(**3**) = Φ_f^{rel}(**3**). Thus, the relative fluorescence yields Φ_f^{rel}(***n***) in Table 1 do not include the contribution of fluorescence emission due to direct excitation of chromophore **2**.

1 (*a*) T. Förster, *Ann. Phys.*, 1948, **2**, 55; (*b*) B. Wieb Van Der Meer, G. Coker, III and S.-Y. S. Chen, *Resonance Energy Transfer Theory and Data*, VCH Publishers, New York, 1994.

2 A. P. de Silva, H. Q. N. Gunaratne, T. Gunnlaugsson, A. J. M. Huxley, C. P. McCoy, J. T. Rademacher and T. E. Rice, *Chem. Rev.*, 1997, **97**, 1515.

3 For example, A. I. H. Murche, R. M. Clegg, E. Kitszing, D. R. Dukett and D. M. J. Lilley, *Nature*, 1989, **341**, 763; T. Tuschl, C. Gohlke, T. M. Jovin, E. Westhof and F. Eckstein, *Science*, 1994, **266**, 785; R. C. Gupta, E. I. Golub, W. S. Marc and R. M. Charles, *Proc. Natl. Acad. Sci. USA.*, 1998, **95**, 9843.

4 D. L. Officer, A. K. Burrell and D. C. Reid, *Chem. Commun.*, 1996, 1657; A. Osuka and H. Shimizu, *Angew. Chem., Int. Ed. Engl.*, 1997, **36**, 135; J.-P. Stachan, S. Gentemann, J. Seth, W. A. Kalsbech, J. S. Lindsey, D. Holten and D. F. Bocian, *J. Am. Chem. Soc.*, 1997, **119**, 11191.

5 G. McDermott, S. M. Prince, A. A. Freer, A. M. Hawethornthwaite-Lawless, M. Z. Papiz, R. J. Cogdell and N. W. Isaacs, *Nature*, 1995, **374**, 517; S. Karrasch, P. A. Bullough and R. Ghosh, *EMBO J.*, 1995, **14**, 631.

6 P. Tecilla, R. P. Dixon, G. Slobodkin, D. S. Alavi, D. H. Waldeck and A. D. Hamilton, *J. Am. Chem. Soc.*, 1990, **112**, 9408; C. M. White, M. F. Gonzalez, D. A. Bardwell, L. H. Rees, J. C. Jeffery, M. D. Ward, N. Armaroli, G. Calogero and F. Barigelletti, *J. Chem. Soc., Dalton Trans.*, 1997, 727.

7 F. Vögtle, *Supermolecular Chemistry*, Maruzen, Tokyo, Wiley, West Sussex, 1995.

Communication 8/09728C

Synthesis of the sodium diphenylbis(cyanamido)phosphonium diylide by a new variation of the Staudinger reaction

Marc Taillefer,*[a] Nicolas Inguimbert,[a] Lothar Jäger,[b] Kurt Merzweiler[b] and Henri-Jean Cristau[a]

[a] *Ecole Nationale Supérieure de Chimie de Montpellier, ESA 5076, 8 rue de l'Ecole Normale, 34296 Montpellier cedex 05, France. E-mail: taillefe@cit.enscm.fr*

[b] *Institute of Inorganic Chemistry, University of Halle-Wittenberg D-06099 Halle/Saale, Germany*

Received (in Liverpool, UK) 3rd November 1998, Accepted 4th February 1999

The first example of a stabilized diaminophonium diazaylide, sodium diphenylbis(cyanamido)phosphonium diylide, has been synthesized by a new variation of the Staudinger reaction; the corresponding copper complex can be described as a discrete dimeric unit with $[Ph_2P(NCN)_2]^-$ in both uni- and bi-dentate modes (X-ray structure).

Lithium phosphonium diylides **1** were first discovered by Wittig in 1949.[1] As part of the study of the reactivity of these reagents,

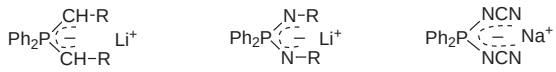

1 R = H, alkyl, C(O)R' *etc.* **2** R = alkyl **3** R = aryl **4** R = electron withdrawing group

4a

we have developed a general synthetic route to their direct precursors, the dialkyldiphenylphosphonium salts.[2] Our method thus allowed a convenient access to all types of diylides, regardless of their having non-stabilized, semi-stabilized or stabilized characters.

Thanks to their strong nucleophilic character, the phosphonium diylides **1**, until recently mainly used in coordination chemistry,[3] are excellent and versatile tools in organic synthesis.[2] Therefore, we have also developed a synthesis of their nitrogen analogs, the lithium diaminophosphonium diazaylides, in order to test their potential in synthesis.[4]

Until now our method, involving the direct dilithiation of the corresponding diaminophosphonium salts, was limited, in spite of many attempts, to the formation of non- and semi-stabilized diaminophosphonium diylides **2** and **3**.[4] We report here the synthesis of the first example of a stabilized diaminophosphonium diazaylide of type **4**, the sodium diphenylbis(cyanamido)-phosphonium diylide $Na[Ph_2P(NCN)_2]$ **4a**.

The diazaylide **4a**, which has a stronger nucleophilic character than the corresponding monoazaylide (Ph_3PNCN), has been obtained through a new variation of the Staudinger reaction, namely the reaction of Ph_2PNa with N_3CN (Scheme 1).

Under nitrogen, a solution of Ph_2PNa (30 mmol) in dry THF (80 ml) was added dropwise at 0 °C to a solution of N_3CN (65 mmol) in MeCN (80 ml). After the end of the addition, the reaction, performed under mild conditions, affords the sodium diphenylbis(cyanamido)phosphonium diylide $Na[Ph_2P(NCN)_2]$ **4a** in 80%.†

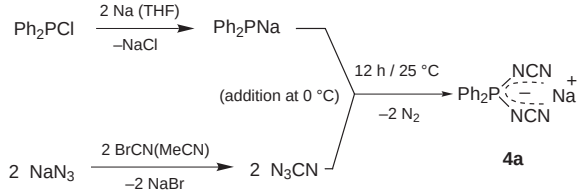

Scheme 1

The Staudinger reaction is usually described as a two-step reaction corresponding to a nucleophilic addition of a tricoordinated phosphorus center (R_3P) on an azide followed by N_2 elimination.[5] To the best of our knowledge, our reaction constitutes the first example of a Staudinger reaction involving a phosphide.

The diazaylide **4a**, whose reactivity we are currently testing in organic synthesis, may also attract interest in the field of coordination chemistry. Indeed, the corresponding non-stabilized diaminophosphonium diazaylides of type **2** are well-known bidentate ligands. The majority of the known complexes exhibit four membered MN_2P rings involving diazaylides substituted on the nitrogens by trimethylsilyl groups.[6] They are mainly represented by two categories with pentavalent phosphorus, the 1,3,2λ^5,4-diazaphosphametalletidines and the 1,3,5,7,2λ^5,6λ^5,4-tetraazadiphosphametallaspiro[3.3]bicycloheptanes.

The stabilized diazaylide $Na[Ph_2P(NCN)_2]$ **4a**, in aqueous solution with or without pyridine, forms quantitatively with metal ions (Ag^+, Ni^{2+}, Cu^{2+}) the complexes **4b**–**d** (Scheme 2).

The molecular structure of the copper complex **4d**,§ illustrated in Fig. 1, shows different structural features in comparison to corresponding complexes with non-stabilized diazaylides. Indeed, **4d** contains $[Ph_2P(NCN)_2]^-$ in two coordination modes. It can be described as a discrete dimeric unit with $[Ph_2P(NCN)_2]^-$ in both uni- and bi-dentate modes. The two copper atoms are doubly bridged by $[Ph_2P(NCN)_2]^-$ ligands, forming a 16-membered puckered cycle, which exhibits crystallographic $\bar{1}$ symmetry. The maximum deviation from the least-squares plane defined by all ring atoms amounts to −0.409(2) and +0.432(2) Å for P2 and P2′. The coordination of the copper atoms is trigonal bipyramidal. The phosphorus atoms are nearly tetrahedrally coordinated. Bonding distances and angles agree well with standard values and previous experience.[7] Lastly, it is noteworthy that, in comparison to diaminophosphonium diazaylides **2**, the $[Ph_2P(NCN)_2]^-$ anion shows different coordination properties, the preferential donor atoms being the terminal nitrogens.

The ligand properties of the $[Ph_2P(NCN)_2]^-$ anion are under investigation, as well as the synthetic potential of the corre-

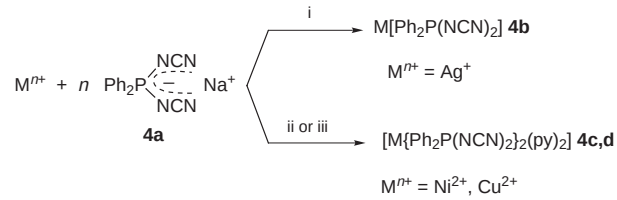

Scheme 2 Synthesis of the coordination complexes **4b** (M = Ag), **4c** (M = Ni) and **4d** (M = Cu). *Reagents and conditions*: i, **4a** (2.5 mmol), H_2O (15 ml), then $AgNO_3$ (2.7 mmol), 1 min, 25 °C,→**4b** (80%); ii, **4a** (2.5 mmol), H_2O (15 ml), then $NiCl_2·6H_2O$ (1.25 mmol), py (5 mmol), 1 min, 25 °C,→**4c** (90%); iii, **4a** (2.5 mmol), H_2O (15 ml), then $CuCl_2·2H_2O$ (1.25 mmol), py (5 mmol), 1 min, 25 °C,→**4d** (90%).‡

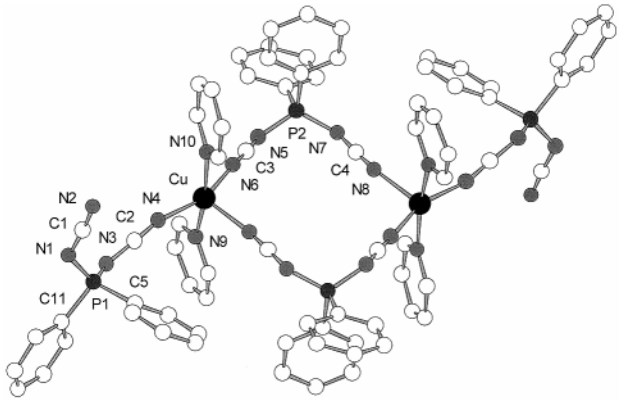

Fig. 1 Molecular structure of **4d** (dimer) in the crystal. Selected bond lengths (Å) and angles (°): Cu–N4 1.987(3), Cu–N6 1.974(3), Cu–N9 2.032(3), Cu–N10 2.042(3), Cu–N8′ 2.178(3), C1–N2 1.170(5), C1–N1 1.287(5), C2–N4 1.136(4), C2–N3 1.288(4), C3–N6 1.148(4), C3–N5 1.282(4), C4–N8 1.148(4), C4–N7 1.293(4), N1–P1 1.604(4), N3–P1 1.601(3), N5–P2 1.597(3), N7–P2 1.595(3), N2–C1–N1 174.6(5), N4–C2–N3 173.2(4), N6–C3–N5 174.9(4), N8–C4–N7 175.3(4), C1–N1–P1 124.9(3), C2–N3–P1 130.4(3), C3–N5–P2 128.4(3), C4–N7–P2 124.7(2), C2–N4–Cu 164.1(3), C3–N6–Cu 165.0(3), C4–N8–Cu′ 164.7(3). Symmetry transformations used to generate equivalent atoms A′: $-x + 1$, $-y + 1$, $-z + 2$.

sponding stabilized diazaylides **4a**–**d**. The reactivity of these reagents will be tested towards various electrophiles, particularly in aza-Wittig type reactions.

Notes and references

† Compound **4a** is a colourless solid obtained in a yield of 80%. *Selected data* for **4a**: mp 182 °C; ν_{max}(KBr)/cm^{-1} 2190vs (NCN), 2140vs (NCN) δ_P (80 MHz, [^{2}H$_6$]DMSO, 25 °C, H_3PO_4 80%) 19.23; δ_C (50.3 MHz, [^{2}H$_6$]DMSO, 25 °C, TMS) 133.1 (d, $^1J_{C,P}$ 129.3, *i*-C, C_6H_5), 131 (d, $^2J_{C,P}$ 9.6, *o*-C, C_6H_5), 128.4 (d, $^3J_{C,P}$ 12.6, *m*-C, C_6H_5), 131.5 (d, $^4J_{C,P}$ 2.3, *p*-C, C_6H_5), 119.3 (s, NCN). A correct elemental analysis for $C_{14}H_{10}N_4NaP$ was obtained.

‡ Single crystals of **4d** were obtained from a concentrated solution of the complex in 2 ml of pyridine which was overlayed with about 6 ml of n-hexane: mp 192 °C (decomp.) ν_{max}(KBr)/cm^{-1} 2230vs (NCN), 2190vs (NCN), 2180vs (NCN). A correct elemental analysis for $C_{38}H_{30}N_{10}CuP_2$ was obtained.

§ *Crystal data* for **4d**: STOE IPDS, graphite monochromated Mo-Kα radiation, λ = 0.71069 Å, T = 293 K. The structure was solved by direct methods (program system SHELXS-86) [ref. 8(*a*)]. Structure refinement on F^2 was performed using full-matrix least-squares techniques with SHELXL-93 [ref. 8(*b*)] with anisotropic displacement parameters for the non-H atoms. $C_{38}H_{30}CuN_{10}P_2$, M = 752.20, triclinic, $P\bar{1}$, a = 8.432(1), b = 13.542(1), c = 16.555(2) Å, α = 107.588(8), β = 91.82(1), γ = 98.65(1)°, V = 1775.7(4) Å^3, Z = 2, μ(Mo-Kα) = 0.749 mm^{-1}, $2\theta_{max}$ = 52.0°, reflections collected = 10554, independent reflections = 6478 [R_{int} = 0.0513], parameters = 580, $R1$ = 0.0479, $wR2$ = 0.1186 [$I > 2\sigma(I)$], $R1$ = 0.0739, $wR2$ = 0.1320 (all data), $\Delta\rho$ (max./min.) = 0.378/−0.739 e Å^{-3}. CCDC 182/1169. Crystal data are available in CIF format from the RSC web site, see: http://www.rsc.org/suppdata/cc/1999/565/

1 G. Wittig and M. Rieber, *Justus Liebigs Ann. Chem.*, 1949, **562**, 177.
2 H. J. Cristau, *Chem. Rev.*, 1994, **94**, 1299; H. J. Cristau, M. Taillefer, J. P. Urbani and A. Fruchier, *Tetrahedron*, 1996, **52**, 2005; H. J. Cristau and M. Taillefer, *Tetrahedron*, 1998, **54**, 1507; M. Taillefer and H. J. Cristau, *Tetrahedron Lett.*, 1998, **39**, 7857.
3 H. Schmidbaur, *Angew. Chem., Int. Ed. Engl.*, 1983, **22**, 907.
4 H. J. Cristau, C. Garcia, J. Kadoura and E. Torreilles, *Phosphorus Sulfur Silicon*, 1990, **49**/**50**, 151.
5 H. Staudinger and J. Meyer, *Helv. Chim. Acta*, 1919, **2**, 635; Y. Gololobov and L. F. Kasukhin, *Tetrahedron*, 1992, **48**,1353.
6 M. Witt and H. W. Roesky, *Chem. Rev.*, 1994, **94**, 1163.
7 P. Rademacher, *Strukturen Organischer Moleküle*, VCH, Weinheim, 1987, p. 56; A. G, Orpen, L. Brammer, F. H. Allen, O. Kennard, D. G. Watson and R. Taylor, *J. Chem. Soc., Dalton Trans.*, 1989, S1; L. Jäger, A. Kolbe, K. Polborn, W. Beck and M. Hvastijová, *Z. Anorg. Allg. Chem.*, 1992, **617**, 117.
8 (*a*) G. M. Sheldrick, SHELXS-86, *Acta Crystallogr., Sect. A*, 1990, **46**, 467; (*b*) G. M. Sheldrick, SHELXL-93, Program for the Crystal Structure Refinement, University of Göttingen, 1993.

Communication 8/08641I

Typeset and printed by Black Bear Press Limited, Cambridge, England

ChemComm
FEATURE ARTICLE

Temperature and solvent effects in facial diastereoselectivity of nucleophilic addition: entropic and enthalpic contribution

Gianfranco Cainelli,* Daria Giacomini and Paola Galletti

Dipartimento di Chimica 'G. Ciamician', Università degli Studi di Bologna, Italy. E-mail: cainelli@ciam.unibo.it

Received (in Cambridge, UK) 27th October 1998, Accepted 23rd December 1998

Solvent and temperature effects on facial diastereoselectivity of nucleophilic addition have been long observed but often neglected. Temperature dependent measurements according to the modified Eyring equation allow the evaluation of stereoselectivity in terms of differential enthalpy and entropy of activation, and demonstrate the paramount importance of entropic contribution in directing the facial diastereoselectivity. Even the reaction solvent proved to be important in determining the isomer ratio. In many cases Eyring plots show a non-linear behavior consisting of two linear regions intersecting at a point called the inversion temperature (T_{inv}) which, for the same reaction, depends on the nature of the solvent and correlates with their melting points. We propose that T_{inv} is the temperature value for the interconversion between two different solvation clusters which should behave like two different molecules.

Introduction

Selectivity is the keyword for organic synthesis in recent years. Among the various categories, stereoselectivity represents the main goal for researchers involved either in total synthesis or in new methodologies. Moreover, the synthetic process for a new drug or for a biologically active compound cannot avoid a correct and accurate control on the final target stereochemistry.

Nowadays, many methods are available for stereocontrolled synthesis.[1] However, in spite of excellent experimental results obtained in asymmetric induction and asymmetric catalysis, comprehension of mechanisms and identification of the molecular species involved in transferring the chiral information is still at the beginning.

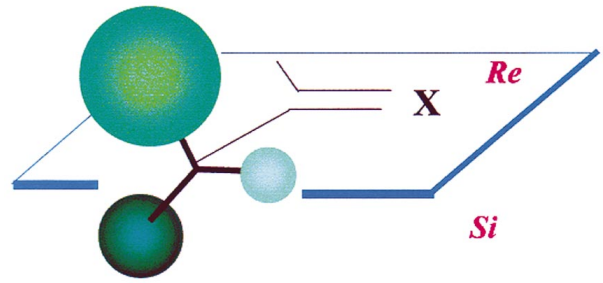

Fig. 1

The stereochemical aspect of addition reactions to carbonyls is discussed in terms of face-selectivity (Fig. 1).[2] The process will be stereotopically divergent[3] whenever, between the two competing attacks to either the *re* or *si* face, one is preferred. Such stereoselection is commonly observed in asymmetric induction on α-chiral π-compounds. In this case an addition reaction can afford two diastereoisomers (*anti* and *syn*[4]), whose kinetics are the same as those of parallel independent reactions with two different products. In a kinetically controlled process, the selectivity (*S*) is expressed as in eqn. (1), where *k* and *k*′ are

$$S = \ln (k/k') \quad (1)$$

the overall rate constants leading to the two isomers.

A lot of experimental and theoretical work deals with steric and stereoelectronic effects over face-selectivity,[4] while temperature and solvent effects have been less investigated.

Temperature-controlled diastereoselectivity

The temperature effect on diastereoselection has long been observed but often neglected. Its influence on diastereoselection is not uniform. Depending on the circumstances, upon increasing the reaction temperature the diastereoselection may decrease, but it may also be constant or even increase. In the latter case we could observe the best diastereomeric excess (de) at high temperature, a behavior that is generally not expected.

The temperature dependence in diastereofacial selectivity can be analyzed according to the Arrhenius equation for the two reaction paths [eqn. (2)], which in the framework of the Eyring

$$\ln (k/k') = -(E_a - E'_a)/RT + \ln A - \ln A' \quad (2)$$

transition state theory becomes eqn. (5) *via* eqn. (3) and (4),

$$\ln k/k' = -(\Delta G^{\ddagger} - \Delta G'^{\ddagger})/RT = -\Delta\Delta G^{\ddagger}/RT \quad (3)$$

$$\Delta G^{\ddagger} = \Delta H^{\ddagger} - T\,\Delta S^{\ddagger} \quad (4)$$

$$\ln k/k' = -(\Delta\Delta H^{\ddagger}/RT) + (\Delta\Delta S^{\ddagger}/R) \quad (5)$$

Professor Gianfranco Cainelli was born in Trento (Italy). He received the Dipl. Ing. and Doctor der Technischen Wissenschaften from the ETH Zürich. After two years as a postdoctoral fellow with Professor O. Jeger in Zürich, he moved to the Politecnico of Milan as Assistant to Professor A. Quilico and in 1968 joined the faculty of the University of Bari as full Professor. He has been Professor of Organic Chemistry at the University of Bologna since 1971.

Dr Daria Giacomini was born in San Marino (Republic of San Marino), and is a Research Associate in the Department of Chemistry 'G. Ciamician' at the University of Bologna. A graduate in Chemistry (1982), she obtained her PhD fom the University of Bologna in 1987 and held a Researcher Scientist position at the National Council of Research ICoCEA for two years before she returned to the Faculty of Science at Bologna to take up her current position (1990).

Dr Paola Galletti was born in Bologna (Italy), where she graduated in Chemistry (1994). She is now finishing her PhD in Chemistry at the University of Bologna.

where k and k' are the observed overall rate constants, and $\Delta\Delta G^{\ddagger}$ is the difference in free activation energies for *re* and *si* face attack. In diastereoselective reactions, k/k' can be expressed as the final concentration ratio of the two isomers *anti* and *syn*. Temperature dependent measurements on the basis of eqn. (5) allow the evaluation of stereoselectivity in terms of differential enthalpy and entropy of activation. It is important to underline that in diastereoselective processes, where little differential enthalpic contribution exists, temperature values in the experimentally accessible range often render the differential entropy of activation a determining contribution, especially at high temperature.[5] Under these conditions, any prediction of stereoselectivity based on classical models, such as Cram's chelated model or the Felkin-Ahn model based only on enthalpic differences, are not effective because of entropy underestimation.

Entropy and enthalpy can play in favor of opposite isomers, leading to an inversion of selectivity by temperature.[6] In this case, we get a predominance of one diastereoisomer at low temperature and the other one at high temperature. In the linear Eyring plot of ln k/k' *versus* $1/T$ (Fig. 2), reversal of de by

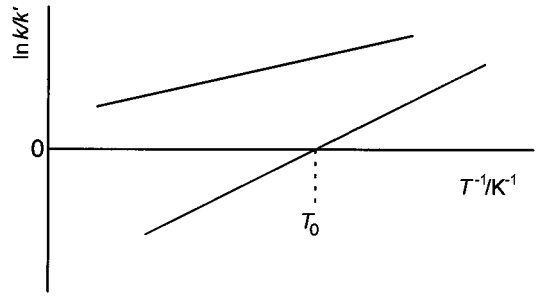

Fig. 2

reaction temperature[7] gives rise to an x-axis crossing (ln k/k' = 0, de = 0%) thus identifying an equiselective temperature T_o = $\Delta\Delta H^{\ddagger}/\Delta\Delta S^{\ddagger}$. Because of the positive value of absolute temperature, reversal of de occurs when the differential enthalpic and entropic terms have the same sign.

In this case, there exists a temperature range where $T\Delta\Delta S^{\ddagger} < \Delta\Delta H^{\ddagger}$ and another where $T\Delta\Delta S^{\ddagger} > \Delta\Delta H^{\ddagger}$. For example, in the formation of *anti* and *syn* isomers, whenever the former prevails, a negative value of the differential activation entalphy ($\Delta H^{\ddagger}_{anti} - \Delta H^{\ddagger}_{syn} = \Delta\Delta H^{\ddagger} < 0$) results. Assuming that an addition reaction is accompanied by a loss of activation entropy, $\Delta S^{\ddagger}_{anti}$ and $\Delta S^{\ddagger}_{syn}$ are both negative and the condition for the de inversion, $\Delta\Delta S^{\ddagger} < 0$, requires $|\Delta S^{\ddagger}_{anti}| > |\Delta S^{\ddagger}_{syn}|$: this means that the entropic loss in the formation of *anti* is larger than those of *syn*. As a consequence, the *anti* isomer is enthalpically driven whereas the *syn* is entropically driven: at low temperature the former prevails, while at high temperature the latter. It is important to emphasize that if both enthalpy and entropy cooperatively work in favor of the same isomer [this condition results when $\Delta\Delta S^{\ddagger}$ and $\Delta\Delta H^{\ddagger}$ have opposite signs in eqn. (5)], an inversion in the diastereomeric excess can never be obtained by solely controlling the temperature.

Eqn. (5) shows a linear correlation between $1/T$ and selectivity. However, there are experimental data that show a non-linear behavior (Fig. 3). In these cases, the corresponding Eyring plots generally consist of two linear regions intersecting at a point defining a temperature called the inversion temperature (T_{inv}).[8] This break point leads to two sets of activation parameters; one for $T < T_{inv}$ and the other for $T > T_{inv}$.

This phenomenon has been nicely reviewed by Scharf,[9] who considers the conditions for the existence of a T_{inv} in an Eyring plot showing the occurrence of two levels of selectivity in a two step reaction mechanism. He describes the T_{inv} as the temperature where a change occurs in the dominance of enthalpy and entropy in the partially selective step.

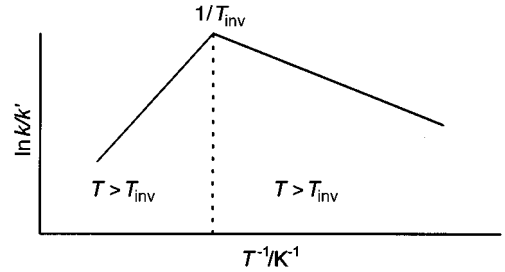

Fig. 3

More recently, Ridd[10] has interpreted non-linear Eyring plots as evidence of two potential rate determining steps in the reaction process, with only one of the two linear regions providing valid evidence on the enthalpic and entropic discrimination involved, the other coming from the transitional region in which no single stage of the reaction can be considered as rate determining.

Anyway, the debate on the very nature of inversion temperature is still open and we want to show experimental results that suggest a different interpretation.

Solvent-controlled diastereoselectivity

The solvent in which chemical processes take place is really a non-inert medium and it plays a prominent role in solution chemistry.[11] The complex interaction between solvent and solute molecules results in a gross modification of their free energies, and consequently, reactivities and stereoselectivities.

There are many examples of solvent effects on face-selectivity. In many cases a variation in the diastereomeric excess is observed[12] and other examples are known where a complete reversal of diastereoselectivity occurs because of a change in the reaction solvent. For example, some years ago, we reported a de reversal in MeMgBr addition to an *O*-triisopropylsilyloxy lactal.[13] The reaction leads to an *anti/syn* ratio of 64 : 36 in THF and 16 : 84 in Bu^{t}OMe. Very recently, Luh reported a reversal in diastereoselectivity of MeLi and Bu^{n}Li addition to hydrazones of 1,4-di-*O*-*tert*-alkoxy-L-threitols on going from THF to Et_2O.[14] These results show how the solvent plays a role in determining the prevailing isomer.

The solvent effect on face-selectivity reflects its different influence on the two diastereomeric reaction paths through a differential contribution to k and k' [eqn. (1)]. A change in the reaction medium corresponds to a change in the microscopic solute–solvent interactions. These interactions could differ in number or strength in different solvents, and they contribute to free activation energies $\Delta G^{\ddagger}$ and $\Delta G'^{\ddagger}$ in such a way that they can cause a face-selectivity reversal.

In the case of reaction in solution, it is hard to describe the system formed by reagents with their solvation shell or the solvated transition state, but some hypothesis can be considered. Two cases can be analyzed: (i) the solvent enthalpically favors and entropically disfavors an isomer whenever the solute–solvent interactions are high in strength or in number, thus stabilizing conformers with the lowest intramolecular steric interactions; (ii) the solvent entropically favors and enthalpically disfavors an isomer whenever the solute–solvent interactions are mild or low in number which results in the solvation being less ordered, thus making the system conformationally less rigid.[15]

By this brief discussion it appears to be clear that any theoretical model[4] for the analysis of stereochemical problems completely looses its predictive value by ignoring solvent effects. A detailed modelling of solvation[16] and information about its effects on the dynamics of stereoselective processes are necessary to get a deeper insight into the diastereofacial selectivity, but at the moment, research in this field is still at the beginning.

Diastereofacial selectivity in Bu^{n}Li addition to lactal imines[17]

During our studies on the stereocontrolled synthesis of 1,2-amino ethers by means of nucleophilic addition to *N*-trimethylsilyl imines of (2*S*)-lactal, we observed an impressive influence of solvent and temperature over the diastereofacial selectivity.

Bu^{n}Li cleanly reacted with *O*-protected *N*-trimethylsilyl imines of (2*S*)-lactal either in an ether (THF) or hydrocarbon (*n*-hexane) affording optically active *anti* and *syn* 1,2-amino ethers (Scheme 1). The stereochemical results are strongly dependent

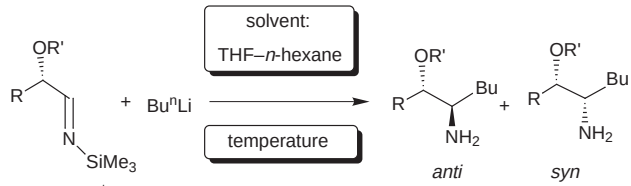

1 R' = SiBu^{t}Me$_2$, R = Me
2 R' = SiPr$^i_3$, R = Me
3 R' = Bu^t, R = Me
4 R' = SiBu^{t}Me$_2$, R = Bu^n

2a–4a **2b–4b**

Scheme 1

on solvent and temperature. We observed a complete reversal in the diastereomeric excess due to the solvent. For example, in the case of (2*S*)-*N*-trimethylsilyl-*O*-*tert*-butyldimethylsilyloxy lactal imine **1** at −90 °C in THF, we obtained an *anti/syn* ratio of 2 : 98, while in *n*-hexane the *anti/syn* ratio = 72 : 28. Moreover, a screening over a range of 150 °C showed a reversal of diastereoselection due to the reaction temperature (*e.g.* in *n*-hexane at T = −90 °C, *anti/syn* = 72 : 28, at T = 54 °C *anti/syn* = 22 : 78). In Fig. 4 the Eyring plots for all the imines **1**–**4** in THF and *n*-hexane are reported. The diastereomeric excess is defined as the difference % *anti* − % *syn*. Each imine–solvent pair showed a non-linear temperature dependence, and a characteristic inversion temperature (T_{inv}) was observed in all cases.

Diastereomeric excesses for imines **2** and **3** in THF cross the *x*-axis (de = 0%) at the equiselective temperatures T_o = −71.2 and −8.6 °C, respectively, so that a neat inversion in stereoselectivity occurred. In *n*-hexane, the imines **1**, **2** and **4** showed equiselective temperatures at T_o = −54.9, 15.4, and −36.5 °C.

In THF for $T > T_{inv}$, all the imines show a flattened trend of the de, meaning that in this range there is no temperature control of the stereoselectivity. According to eqn. (5), this result requires that the face-selection that still exists is entirely determined by $\Delta\Delta S^{\ddagger}$.

In this entropy driven region, the differentiating parameter between the four substrates is the protecting group. The *O*-TIPS and the *O*-TBDMS-*N*-TMS imines show opposite diastereofacial selectivity; for **2** the differential entropy $\Delta\Delta S^{\ddagger}$ is positive, for **1** it is negative. As a matter of fact, in one case the *anti* isomer is favored, in the other the *syn* is preferred. It is remarkable to note that for imine **1** the negative value of $\Delta\Delta S^{\ddagger}$ implies that the transition state leading to the *anti* isomer is more ordered than that which leads to the *syn* one. This result excludes the hypothesis that the prevailing *syn* isomer derives from a chelated transition state. At low temperature, all substrates give *syn* isomers. However, slopes are not markedly different and all four plots can be reproduced by translation of each other. Once again, in the face of small differential enthalpic contributions, an entropic factor determines the face-selectivity.

In *n*-hexane, imines **1**, **2** and **4** have a positive slope and exhibit a reversal of de on going from a predominance of *syn* isomers at high temperature to a predominance of *anti* isomers at lower *T*. Even the *O*-*tert*-butyl-*N*-TMS imine has a positive

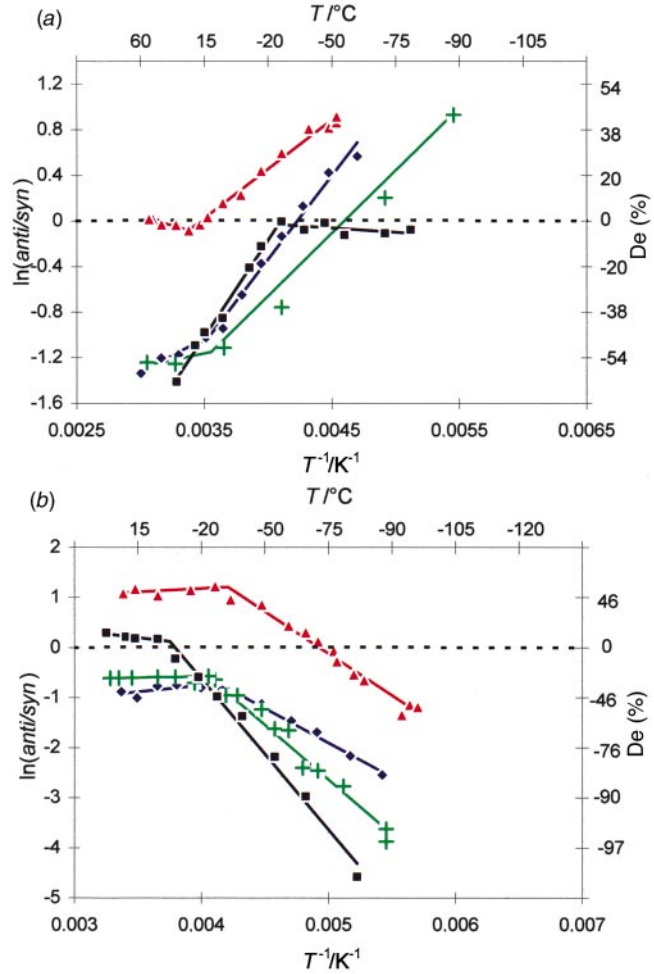

Fig. 4 Eyring plots for imines **1**–**4** in (*a*) *n*-hexane and (*b*) THF: (+) **1**, (▲) **2**, (■) **3** and (◆) **4**.

slope, and should behave in the same way as the others, but, in this case, the T_{inv} exerts a breakdown and starts up a new linear trend with a different intercept and slope, so that the de inversion is prevented.

Temperature and solvent effects on de might be attributed to different organometallic species involved. In fact, it is known that the aggregation state of Bu^{n}Li changes with these parameters.[18] However, the dynamic process that involves the aggregation state of Bu^{n}Li acts before the reacting event, so that their rate costants are identical for both diastereomers and vanish in eqn. (5). Thus a mere ground state effect would be irrelevant, but the Bu^{n}Li tendency to aggregate may to some extent influence the structure of the transition states. However, the de reversal with temperature and the existence of T_{inv} are observed in several different reactions[9,12] where no organometallic species are involved.[19]

All the activation parameters for $T > T_{inv}$ and for $T < T_{inv}$ are listed in Table 1.

It is significant to note that in all cases differential entropies and enthalpies have equal sign leading to an inversion of diastereoselectivity due to temperature, as discussed in the previous section. However, for imines **1**, **2** and **4**, but not **3**, the activation parameters for $T < T_{inv}$ showed a further switch in sign from THF to *n*-hexane, thus showing the overwhelming role of the solvent in determining the thermodynamic parameters.

Diastereofacial selectivity in Bu^{n}Li addition to 2-phenylpropanal[20]

The solvent effect obtained in the stereoselective addition of Bu^{n}Li to 2-phenylpropanal is quite peculiar (Scheme 2). We

Table 1 Differential activation parameters and inversion temperatures for Bu^{n}Li addition to imines **1**–**4**

			$T > T_{inv}$		$T < T_{inv}$		
Imine	Solvent	T_{inv}/°C	$\Delta\Delta H^{\ddagger}$/kcal mol^{-1}	$\Delta\Delta S^{\ddagger}$/cal mol^{-1}	$\Delta\Delta H^{\ddagger}$/kcal mol^{-1}	$\Delta\Delta S^{\ddagger}$/kcal mol^{-1}	$\Delta\Delta G^{\ddagger}$ (298 K)/kcal mol^{-1}
1	THF[a]	−26.8	−0.10 ± 0.01	−1.59 ± 0.02	4.3 ± 0.3	16.4 ± 1.4	0.37
1	*n*-Hexane[a]	7.9	−0.58 ± 0.22	−4.3 ± 0.7	−2.2 ± 0.4	−10.4 ± 1.7	0.71
2	THF	−35.8	−0.28 ± 0.22	1.2 ± 0.8	3.3 ± 0.2	16.4 ± 0.9	−0.63
2	*n*-Hexane	22.4	0.65 ± 0.11	2.0 ± 0.4	−1.7 ± 0.1	−5.9 ± 0.3	0.05
3	THF	−7	0.59 ± 0.18	2.4 ± 0.6	5.9 ± 0.3	22.7 ± 1.5	−0.14
3	*n*-Hexane	−28.4	−3.36 ± 0.13	−13.8 ± 0.5	0.14 ± 0.1	0.52 ± 0.5	0.75
4	THF	−31.8	−0.52 ± 0.37	−3.6 ± 1.4	2.7 ± 1.5	9.8 ± 0.7	0.05
4	*n*-Hexane	8.6	−1.17 ± 0.07	−6.2 ± 0.3	−2.9 ± 0.2	−12.3 ± 0.7	0.67

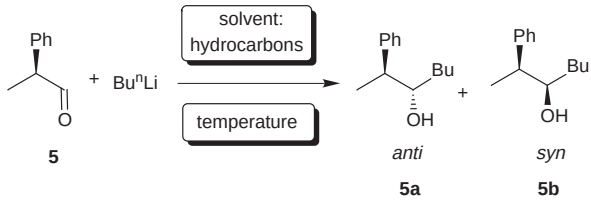

Scheme 2

established inversion temperatures in aliphatic hydrocarbons and Eyring plots for a series of linear and cyclic hydrocarbons are shown in Fig. 5.

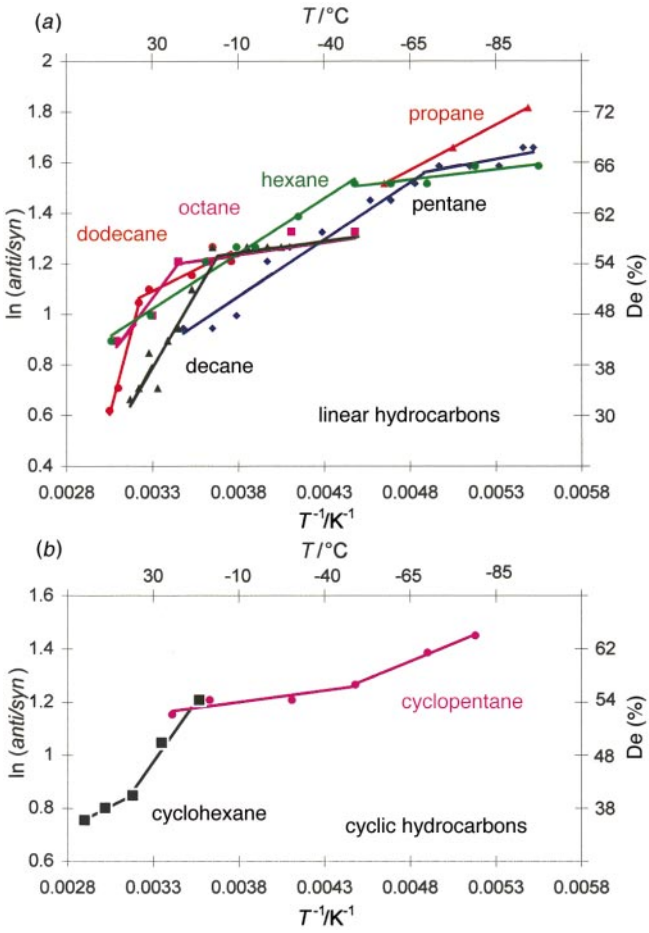

Fig. 5 Eyring plots for (*a*) linear and (*b*) cyclic hydrocarbons.

Interestingly, for cyclic and linear solvents the plot concavities are opposite. For linear hydrocarbons the pattern is consistent with the chain length of the solvent: the longer the chain, the lower the de; for example, the diastereofacial selectivity obtained with propane is doubled with respect to that of *n*-dodecane (*n*-propane de = 70%, *n*-dodecane de = 30%).

This result reveals the deep influence of solvation forces, although weak and non-specific, on the face-diastereoselectivity. The slopes of regression lines, which reflect the enthalpic contribution, flatten at low temperatures. Once more, differential entropy modulates the selectivity because only differences in the intercepts still remain when differential enthalpies vanish, and therefore the effect of solvent chain length on face-selectivity might be ascribed to entropic control. On the other hand, at high temperature, lengthening the solvent chain increases the slope, thus increasing the enthalpic contribution to de. The inversion temperatures for all linear and cyclic hydrocarbon solvents examined ranged between 205 and 317 K, increasing upon going from *n*-pentane to *n*-dodecane.

Assuming that the inversion temperature is unique to each substrate–solvent pair, all efforts to correlate inversion temperatures with classical solvent parameters, such as relative permittivity and viscosity, have failed. Interestingly, analyzing T_{inv} and the melting points of linear and cyclic hydrocarbons results in a straight line with a correlation coefficient r = 0.96 (Fig. 6).

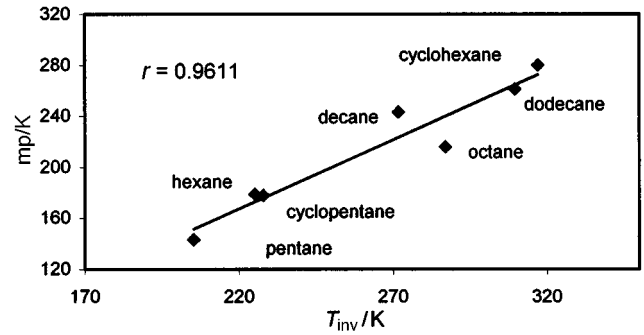

Fig. 6

Diastereofacial selectivity in the Bu^{n}Li addition to mandelic aldehyde[21]

The dependence of facial selectivity upon hydrocarbon solvents becomes more strict in the case of Bu^{n}Li addition to *O*-*tert*-butyldimethylsilyloxymandelic aldehyde **6** (Scheme 3). On this

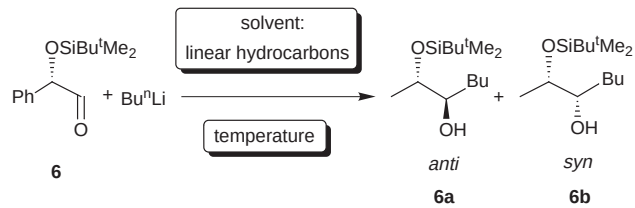

Scheme 3

substrate the reaction with Bu^{n}Li was performed in a series of linear hydrocarbons with odd and even numbers of carbon atoms.

Although this aldehyde produced diastereomeric excesses in a low range (from 20 to −10% de), in all plots an inversion

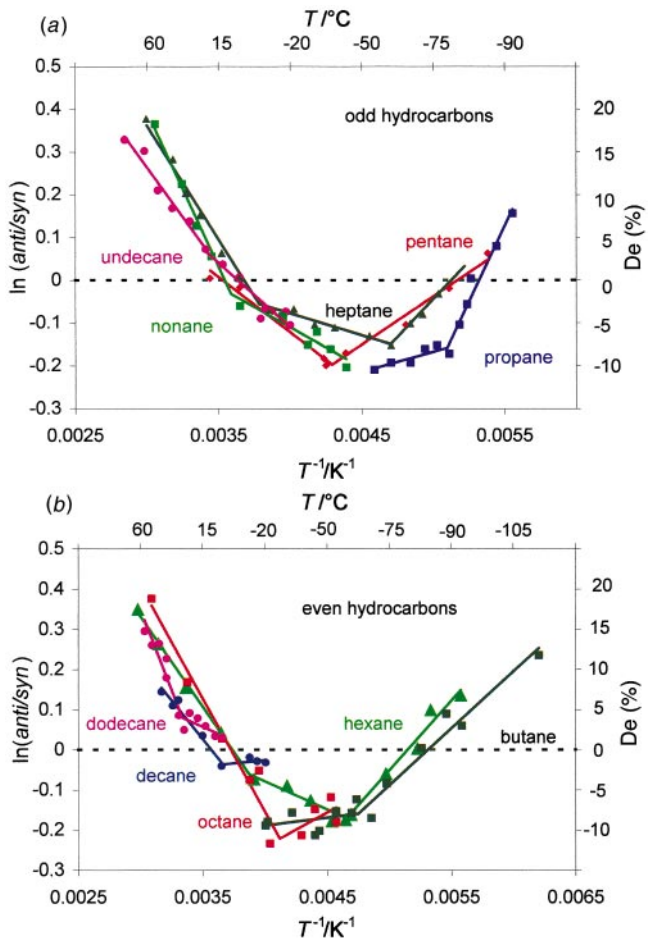

Fig. 7 Eyring plots for (*a*) odd and (*b*) even numbered hydrocarbons.

temperature was recognized (Fig. 7). Notably, this substrate exhibited the best diastereoselectivity at high temperature (T = 60.5 °C, de = 19%).

The majority of these plots cross the *x*-axis because of an opposition between the enthalpic and entropic contribution to the two isomers, as discussed above. Some plots cross the x-axis twice, once in the high and the other in the low temperature region. It is interesting to note that in the cases of *n*-hexane and *n*-heptane two inversion temperatures were obtained. It is hard to explain this experimental result as a consequence of a double change in the reaction mechanism in the light of the above mentioned interpretation of the T_{inv}.[22] As in the case of phenylpropanal **5**, the T_{inv} increases with the longer solvent alkyl chain. For mandelic aldehyde **6** each series shows a concavity opposite to that of **5**.

A plot of the inversion temperatures *versus* the number of solvent carbon atoms exhibits the same swinging feature as that for the melting points (Fig. 8). Even in this case the correlation of T_{inv} and the melting points exists, and it correlates better if we consider the odd and even series of hydrocarbons separately.

It is really surprising how the simplicity of a linear relationship between its two parameters overcomes the complexity of the physical events involved.

It is known that even and odd linear hydrocarbons differ in the crystalline form,[23] and this fact causes the melting point alternation. The same behavior has been observed for the inversion temperatures and this, along with the strict linear correlations found for both aldehydes **5** and **6**, suggests a relationship with the phase modification that occurs upon melting. An attractive possible explanation can be formulated: the inversion temperature could constitute a sort of transition between two 'phases' which, in the case of solutions, could be represented by two different solute–solvent clusters with a different order.[24] This 'phase transition' could be interpreted as the interconversion of two solute–solvent clusters having a

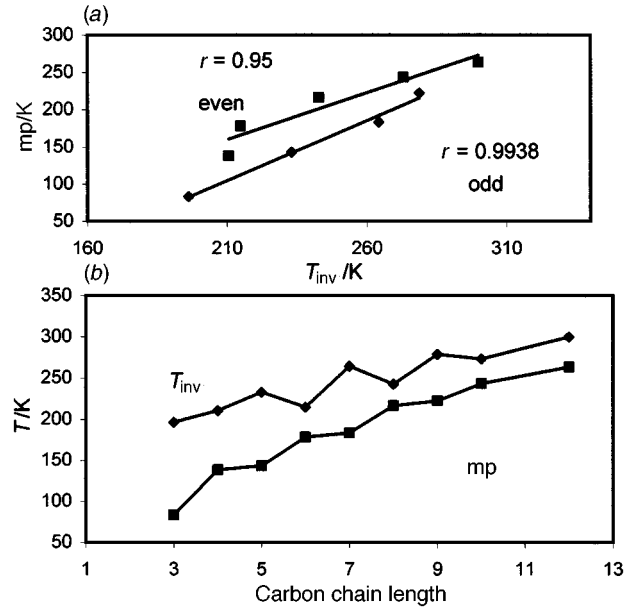

Fig. 8 (*a*) Plot of T_{inv} *vs.* mp of solvent. (*b*) Plots of T_{inv} and solvent mp *vs.* carbon chain length of solvent.

more defined tridimensional structure than generally supposed. These supramolecular structures behave like different molecules, producing a measurable change in their thermodynamic properties and therefore in the diastereoselectivity. In this hypothesis, the T_{inv} represents the interconversion temperature between two supramolecules and it does not imply any change either in the rate determining step or in the reaction mechanism.

Because of the complexity of the solvation process, it is difficult to formulate a detailed microscopic model of these supramolecules. However their interconversion could involve a solvent reorganization phenomenon due to transfer of solvent molecules between the bulk and the supramolecules or an internal rearrangement of the solvation cluster.

Conclusion

Our results confirm that not only do enthalpic contributions act in determining diastereocontrol, but even entropic factors can acquire importance with increasing reaction temperature. Indeed, whenever enthalpy and entropy favor different isomers, a de reversal can be obtained.

Solvent effects are determinant on face selectivity because solute–solvent interactions modulate the free activation energies acting on both enthalpic and entropic terms. In this way different solvents can lead to an opposite diastereoselectivity.

The correlation with melting points suggests an alternative interpretation of the very nature of inversion temperatures. We propose that T_{inv} is the temperature value for the interconversion between two different solvation clusters represented by two different supramolecules.

All these arguments support the hypothesis that the main factor in diastereofacial control is a stereospecific solvation of the π-system.[25]

Our interpretation simply constitutes an attractive proposal and an intriguing challenge for forthcoming research on stereoselectivity.

Acknowledgements

This work was supported by Ministero dell'Università e della Ricerca scientifica e Tecnologica (MURST), the University of Bologna (fund for selected topics) and CNR. We thank all students involved in this project: Argnani Miriam, Marini Andrea, Nerozzi Fabrizio, Paradisi Francesca, Scardova Lucia and Martin Walzl.

Notes and references

1 R. E. Gawley and J. Aubè, in *Principles of Asymmetric Synthesis*, Tetrahedron Organic Chemistry Series, vol.14, ed. J. E. Baldwin, F. R. S. Magnus and P. D. Magnus, Pergamon Press, Oxford, 1996; D. J. Ager and M. B. East, in *Asymmetric Synthetic Methodology*, CRC Press, 1996.

2 M. T. Reetz, *Angew. Chem., Int. Ed. Engl.*, 1984, **23**, 556.

3 N. C. DeMello and D. P. Curran, *J. Am. Chem. Soc.*, 1998, **120**, 329.

4 E. L. Eliel, S. H. Wilen and L. N. Mander, in *Stereochemistry of Organic Compounds*, Wiley, New York, 1994, p. 875.

5 B. Giese, *Acc. Chem. Res.*, 1984, **17**, 438 and references cited therein; R. E. Rosenberg and J. S. Vilardo, *Tetrahedron Lett.*, 1996, **37**, 2185.

6 See for instance: N. Hoffmann, H. Buschmann, G. Raabe and H.-D. Scharf, *Tetrahedron*, 1994, **50**, 11167; D. Awandi, F. Henin, J. Muzart and J.-P. Pete, *Tetrahedron: Asymmetry*, 1991, **2**, 1101; C. Zioudrou and P. Chrysochou, *Tetrahedron*, 1977, **33**, 2103.

7 Y. Inoue, N.Yamasaki, T. Yokoyama and A. Tai, *J. Org. Chem.*, 1992, **57**, 1332.

8 H. Buschmann, H.-D. Scharf, N. Hoffmann, M. W. Plath and J. Runsink, *J. Am. Chem. Soc.*, 1989, **11**, 5367; M. Palucki, P. J. Pospisil, W. Zhang and E. N. Jacobsen, *J. Am. Chem. Soc.*, 1994, **116**, 9333; J. Brunne, N. Hoffmann and H.-D. Scharf, *Tetrahedron*, 1994, **50**, 6819; T. Göbel and K. B. Sharpless, *Angew. Chem.*,1993, **105**, 1417, *Angew. Chem., Int. Ed. Engl.*, 1993, **32**, 1329; J. Muzart, F. Hénin, J.-P. Pète and A. M'boungou-M'Passi, *Tetrahedron: Asymmetry*, 1993, **4**, 2531; I. Tóth, I. Guo and B. E. Hanson, *Organometallics*, 1993, **12**, 477; I. E. Markò, A. Chesney and D. M. Hollinshead, *Tetrahedron: Asymmetry*, 1994, **5**, 569.

9 H. Buschmann, H.-D. Scharf, N. Hoffmann and P. Esser, *Angew. Chem.*, 1991, **103**, 480; *Angew. Chem., Int. Ed. Engl.*, 1991, **30**, 477.

10 K. J. Hale and J. H. Ridd, *J. Chem. Soc., Perkin Trans. 2*, 1995, 1601; K. J. Hale and J. H. Ridd, *J. Chem. Soc., Chem. Commun.*, 1995, 357.

11 C. Reichardt, in *Solvents and Solvent Effects in Organic Chemistry*, 2nd edn., VCH, Weinheim, 1990.

12 See for recent examples: M. T. Crimmins and A. L. Choy, *J. Am. Chem. Soc.*, 1997, **119**, 10237; R. W. Murray, M. Singh, B. L. Williams and H. M. Moncrieff, *Tetrahedron Lett.*, 1995, **36**, 2437; T. Saito, M. Kawamura and J. Nishimura, *Tetrahedron Lett.*,1997, **38**, 8231; P. Wipf and J.-K. Jung, *Angew. Chem., Int. Ed. Engl.*, 1997, **36**, 764; S. E. Denmark, N. Nakajima and O. J.-C. Nicaise, *J. Am. Chem. Soc.*, 1994, **116**, 8797; M. T. Reetz, S. Stanchev and H. Haning, *Tetrahedron*, 1992, **48**, 6813.

13 G. Cainelli, D. Giacomini and F. Perciaccante, *Tetrahedron: Asymmetry*, 1994, **5**, 1913.

14 See for instance: Y.-T. Hsieh, G.-H. Lee, Y. Wang and T.-Y. Luh, *J. Org. Chem.*, 1998, **63**, 1484.

15 B. Lecea, A. Arrieta and F. P. Cossío, *J. Org. Chem.*, 1997, **62**, 6485; C. L. Perrin, M. A. Fabian and I. A. Rivero, *J .Am. Chem. Soc.*, 1998, **120**, 1044.

16 D. J. Giesen, C. J. Cramer and D. G. Truhlar, *J. Phys. Chem.*, 1995, **99**, 7137; G. D. Hawkins, D. A. Liotard, C. J. Cramer and D. G. Truhlar, *J. Org. Chem.*, 1998, **63**, 4305; M. F. Ruiz-Lopez, X. Assfeld, J. I. Garcia, J. A Mayoral and L. Salvatella, *J. Am. Chem. Soc.*, 1993, 115, 8780; M. Sola, A. Lledos, M. Duran, J. Bertran and J.-L. M. Abboud, *J. Am. Chem. Soc.*, 1991, **113**, 2873.

17 G. Cainelli, D. Giacomini and M. Walzl, *Angew. Chem.*, 1995, **107**, 2336; *Angew. Chem., Int. Ed. Engl.*, 1995, **34**, 2150.

18 M. Schlosser, in *Organometallics in Synthesis*, Wiley, New York, 1994, p. 11.

19 Preliminary experiments using different organometallic reagents with almost certainly different aggregations, such as Bu^{t}Li and Bu^{n}MgBr, show for the same carbonyl compound the same T_{inv}.

20 G. Cainelli, D. Giacomini, P. Galletti and A. Marini, *Angew. Chem., Int. Ed. Engl.*, 1996, **35**, 2849.

21 G. Cainelli, D. Giacomini and P. Galletti, unpublished results.

22 J. Muzart, F. Hénin and S. J. Aboulhoda, *Tetrahedron: Asymmetry*, 1997, **8**, 381.

23 M. S. Searle and D. H. Williams, *J .Am. Chem. Soc.*, 1992, **114**, 10690.

24 The possibility of partial ordering of molecules in solution exists, and a temperature dependent change in this order is already manifested in a non-linear behaviour of some spectroscopic properties. See, for instance: J. B. Robert, *Mol. Phys.*, 1997, **90**, 399; M. A. Wendt, J. Meiler, F. Weinhold and T. C. Farrar, *Mol. Phys.*, 1998, **93**, 145.

25 H. Pracejus and A. Tille, *Chem. Ber.*, 1963, 854.

Paper 8/08307J

No deactivated production of hydrogen by pyrolysis of ethane over graphite-based catalysts using membrane-type reactors

Kazuhisa Murata,* Naotugu Ito, Takashi Hayakawa, Kunio Suzuki and Satoshi Hamakawa

National Institute of Materials and Chemical Research, Tsukuba, Ibaraki 305-8565, Japan.
E-mail: kmurata@nimc.go.jp

Received (in Cambridge, UK) 4th January 1999, Accepted 18th February 1999

A system consisting of a graphite catalyst and an Ag-Pd membrane reactor was found to be effective for ethane decomposition to hydrogen and carbon, where the H_2/C ratio was approximately 1.5, in accordance with the stoichiometric ratio; catalyst deactivation was not observed during reaction, since the graphite-like carbons produced by the reaction, probably also catalyze the reaction in the temperature range of 800–1000 K.

Hydrogen is expected to be used as an energy source for fuel cells such as the proton-exchange membrane (PEM) type. At present, hydrogen is typically produced *via* steam reforming and/or partial oxidation of hydrocarbon fuel.[1] Alcohols are used as precursors to hydrogen.[2] In these cases, however, carbon monoxide is a co-product. Therefore, the current PEM fuel cells require complete elimination of CO (< 1 ppm) from the hydrogen stream in order to prevent poisoning of the Pt catalyst of the cells. An alternative route is to directly decompose the hydrocarbons into hydrogen and carbon. In this case, no CO_2 is formed and the need for subsequent reactions, such as water–gas shift and CO oxidation, is eliminated. Metal oxide catalysts such as Ni/SiO_2 and Fe/Al_2O_3 are usually used for the decomposition reaction. However, over these catalysts, decomposition activity is reduced as the reaction proceeds, due to accumulation of carbon products at temperatures of 600–800 K. The undesirable formation of organic products (CH_4, C_2H_4, *etc*.) is also a significant problem.[3]

In the course of our research work on carbon-based catalysts,[4] we attempted decomposition of ethane to form hydrogen over metal-free carbon catalysts. We found that formation of hydrogen without deactivation was observed over a graphite catalyst over the temperature range 800–1000 K. The reaction was also found to be accelerated by elimination of *in situ* formed hydrogen through a Ag-Pd alloy tube. Now we report some of our results.

Commercially available carbon materials, such as activated carbon (Aldrich), C_{60} soots (MER Corp.) and graphite (Alfa) were dried at 493 K *in vacuo* for 3 h prior to use. The particle sizes of these materials were between 50–300 μ. Catalyst thus pretreated (1 g) was diluted with quartz sand (5 g)† and, for the fixed-bed reactor (FBR), placed in a quartz tube (12 mm inner diameter). An electric furnace was used for heating. The catalyst was pretreated in N_2 at 873 K for 3 h and then a premixed gas of nitrogen–ethane (2–20 vol% C_2H_6, 20 ml min^{-1}) was introduced at atmospheric pressure (W/F = 125 g h mol^{-1}).‡ For the Ag-Pd membrane reactor (PMR), a double-tubular type arrangement was used: the inner and outer tubes were Pd-Ag alloy (90Pd10Ag) (250 μ thick and 10 mm outer diameter) and quartz (1.5 mm thick and 19.5 mm inner diameter), respectively. The carbon catalysts were placed between the inner and outer tubes. The catalyst pretreatment was the same as that described above. The premixed gas was passed into the catalyst bed at atmospheric pressure (W/F = 125 g h mol^{-1}) and Ar gas (1500 ml min^{-1}) was fed through the inside of the Ag-Pd alloy tube at atmospheric pressure to remove permeated hydrogen. The organic and hydrogen products were analyzed by gas chromatography (GC) on Porapack Q and 5 Å molecular sieve columns, after 30 min on-stream at each temperature, and the yield of carbon was estimated by the mass balance of carbon [eqn. (1)].

$$C_2H_6 \rightarrow 3H_2 + 2C \quad (1)$$

As shown in Fig. 1, pyrolysis of C_2H_6 occurred at 850–1050 K in the presence of activated carbon catalyst (AC Darco G-60, **1**), and hydrogen, carbon and a small amount of organic material (methane, ethylene, benzene *etc*.) were formed. Over all these runs, the carbon yield estimated from the mass balance was in good accordance with that calculated by weighing after the reaction. The C_2H_6 conversion was as low as 47% at 948 K in the case of the fixed bed reactor (FBR) (Fig. 1). In contrast, the C_2H_6 conversion was found to be enhanced by removal of hydrogen through the Ag-Pd membrane tube and, as a result, was over 90% at 948 K. In this case, over 90% of hydrogen formed was eliminated from the reactant gas *via* permeation into the argon. For comparison, the conversion in a quartz sand/PMR system was less than that for the catalyst **1**/FBR system. Also, the conversion in a PMR system without the argon flow

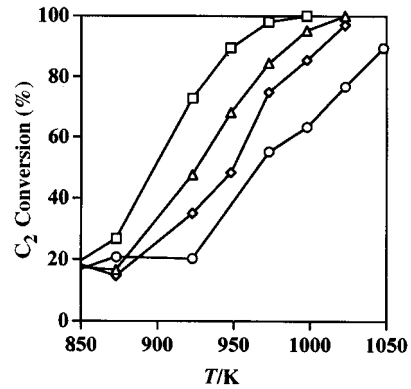

Fig. 1 Comparison of an Ag-Pd membrane reactor (PMR) with a fixed-bed reactor (FBR) for the ethane decomposition over activated carbon catalyst: catalyst = AC Darco G-60, W/F = 12 5 g h mol^{-1}, ethane: N_2 = 10 : 90. (□) PMR, (△) PMR without argon, (◇) FBR and (○) PMR without AC catalyst (quartz sand only).

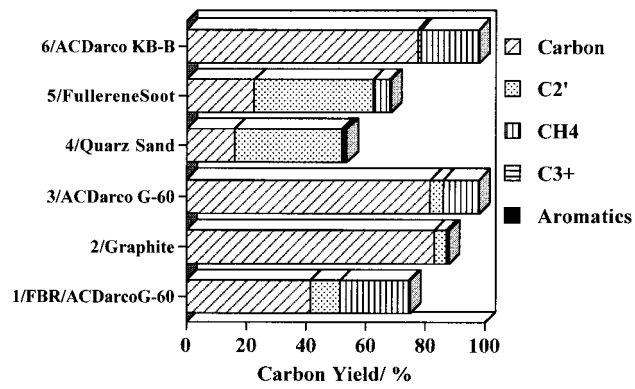

Fig. 2 Effects of carbon catalyst on the activity of ethane decomposition: T = 973 K, W/F = 125 g h mol^{-1}, ethane: N_2 = 10 : 90.

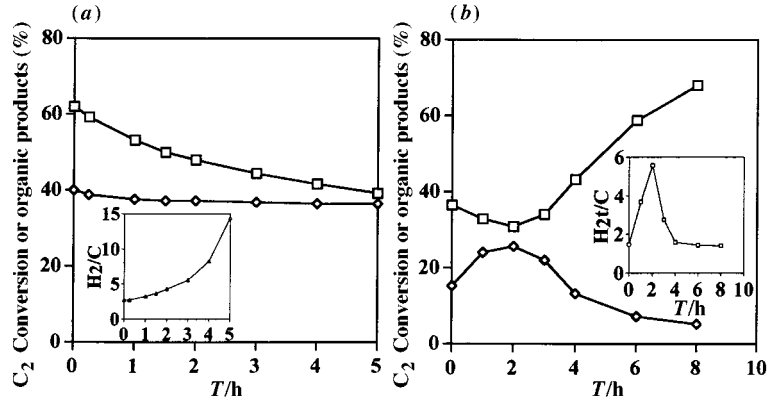

Fig. 3 Change in catalytic activity for the decomposition of ethane as a function of time. (*a*) System = AC Darco KB-B/fixed-bed reactor: (□) C_2 conversion, (◇) organic product yield. T = 923 K, W/F = 125 g h mol^{-1}, ethane: N_2 = 2 : 98. Inset: Plot of H_2/C molar ratio against time. (*b*) System = graphite/Ag-Pd membrane reactor: (□) C_2 conversion, (◇): organic products yield. T = 923 K, W/F = 125 g h mol^{-1}, ethane: N_2 = 2 : 98. Inset: Plot of H_2t/C molar ratio against time.

was between that of the PMR with argon and that of the FBR system.These findings indicate that the combined use of the carbon catalyst and the PMR system was very effective for C_2H_6 pyrolysis.

Fig. 2 shows the effects of some carbon catalyst/PMR systems on the product yields at 973 K. The efficiency of pyrolysis (carbon yield) was in the order: **2**/graphite > **6**/AC Darco G-60 > **3**/AC Darco KB-B > **1**/AC Darco G-60/FBR > **5**/C60 soots > **4**/quartz sand. In the graphite catalyst, in particular, organic by-products were formed only in *ca.* 4% yield. In the activated carbons (**3** and **6**), the yield of organic products was *ca*. 15%, although their carbon yields were close to that on graphite. The use of a fixed-bed reactor (FBR) resulted in the formation of a larger amount of organic products (> 35% yield) than that in a Pd-membrane reactor (PMR) (compare **1** and **6**). In the cases of C_{60} soots (**5**) and quartz sand (**4**), the dehydrogenation of ethane to form ethylene predominates over decomposition.

In order to shed more light on the characteristics of carbon catalyst/PMR systems, the effects of the reaction parameters on the ethane decomposition were briefly examined. The effect of the flow rate of the argon on the activity was found not to be significant under the conditions employed, provided the flow rate is above 100 ml min^{-1}. This suggested that the rate of hydrogen permeation was, in general, greater than that of ethane decomposition over the carbon catalyst under the conditions employed. The ethane conversion at 923 K increased with an increase in contact time (W/F = 25–125 g h mol^{-1}). As expected thermodynamically, lower ethane concentrations (2–20%) gave higher ethane conversions, over the temperature range from 773 to 973 K.

The mechanism of decomposition over the carbon catalysts is not clear. However, the reaction is promoted by the removal of the hydrogen formed (Fig. 1) and it seems likely that a material with a graphite-like nature is formed during decomposition, as shown by X-ray powder diffraction and H_2 temperature programmed desorption of the carbon formed, carried out by analyzing methane formed by hydrogenation of the carbon product. It is well-known that catalyst deactivation occurs as a result of the formation of graphite-like carbon[5] when metal-oxide catalysts are used in the temperature range 600–800 K. In fact, even with the activated carbon catalyst (**3**)/FBR system without metal, the ethane conversion at 923 K decreased as the reaction proceeded [Fig. 3(*a*)]; as a result, the H_2/C ratio increased due to the reduction of carbon formation and predominant formation of organic compounds [Fig 3(*a*), inset]. On the other hand, we found that the deactivation did not occur when graphite catalyst (**2**) was used, and the ethane conversion increased [Fig. 3(*b*)] as carbon was formed. In the initial stages, the H_2t/C ratio (the molar ratio of total amount of H_2 to carbon) was greater than 1.5 [the value given by stoichiometric ethane decomposition, see eqn. (1)] because of the formation of organic products (> 20%). After 5 h, however, the ratio approached 1.5, and subsequently remained constant; this indicated that the decomposition reaction occurred predominantly. This is the first example of a catalyst not being deactivated even at high ethane conversion. It is possible that the graphite-like carbon produced by the reaction also efficiently catalyzes the reaction in the membrane reactor§ over the temperature range 800–1000 K. Further investigations are currently underway to elucidate the decomposition mechanism operative in the graphite/Ag-Pd membrane reactor system.

In summary, we have found that graphite is a very good catalyst for converting ethane to hydrogen in a Ag-Pd membrane system with high activity and no deactivation. We believe this to be an excellent procedure for hydrogen production for PEM fuel cells.

Notes and references

† In order to ensure a smooth gas flow, a weight ratio of graphite : quartz of 1 : 5 was used; the results were not affected by the amount of quartz.
‡ W/F = weight of catalyst (g) over flow rate (mol h^{-1}).
§ In these cases, both graphite and PMR are important. In fact, the minimum amount of organic products was formed in the graphite catalyst/PMR system, as can be seen from Fig. 2. In the graphite/PMR system, graphite-like carbon formed over the graphite surface would not undergo successive reaction such as methane formation from hydrogen and the carbon, because almost all of the hydrogen was eliminated from the graphite surface. Thus, it seems likely that the stable graphite-like carbon product could also catalyze the reaction. On the contrary, in the AC/FBR system, the carbon product could undergo many successive reactions, since hydrogen was still present over the surface. Thus, in this case, it seems unlikely that the carbon product could catalyze the reaction.

1 N. Dave and G. A. Foulds, *Ind. Eng. Chem. Res.*, 1995, **34**, 1037.
2 M. L. Cubeiro and J. L. G. Fierro, *J. Catal.*, 1998, **179**, 150.
3 N. Z. Muradov, *Int. J. Hydrogen Energy*, 1993, **18**, 211; T. Zhang and M. D. Amiridis, *Appl. Catal. A: Gen.*, 1993, **167**, 161.
4 K. Murata and H. Ushijima, *J. Chem. Soc., Chem. Commun.*, 1994, 1157.
5 N. Z. Muradov, *Energy Fuels*, 1998, **12**, 41.

Communication 9/00009G

ChemComm

Physisorption of oxygen in narrow mesopores

Peter J. Branton,*† Katsumi Kaneko and Kenneth S. W. Sing

Department of Chemistry, Faculty of Science, Chiba University, 1-33 Yayoi, Inage, Chiba 263, Japan

Received (in Cambridge, UK) 29th January 1999, Accepted 16th February 1999

Pore filling by oxygen takes place reversibly at 77 K in pores of effective width of *ca.* 2.6 nm, whereas hysteresis is involved in the filling (by capillary condensation) of wider pores; it appears that the oxygen meniscus becomes unstable at cylindrical pore widths < *ca.* 2.9 nm.

The development of MCM-41 and other highly ordered mesoporous materials over the past decade has attracted much attention. Nitrogen adsorption measurements[1–3] at 77 K on a number of these materials have shown that the pore filling of narrow cylindrical mesopores (of effective pore width *ca.* 2–4 nm) can occur reversibly. Nitrogen isotherms given by typical 4 nm samples of MCM-41 exhibit steep and reversible pore filling risers at P/P_0 *ca.* 0.40–0.44, whereas the reversible filling of 2.5 nm pores occurs less sharply (at P/P_0 *ca.* 0.2–0.34). Samples containing wider pores always appear to give type H1 or H2 hysteresis loops.[4] These observations are consistent with the fact[5] that the lower closure points of many nitrogen hysteresis loops are located at P/P_0 *ca.* 0.42 and indicate that the mechanism of mesopore filling is dependent on the pore size.

Although nitrogen continues to be the preferred adsorptive for the characterization of porous solids, it is of interest to investigate the low-temperature adsorptive behaviour of other gases. We have studied oxygen adsorption at 77 K on a number of ordered materials comprising narrow distributions of uniform mesopores with mean pore diameters ranging from *ca.* 2 to 7 nm. Recently determined oxygen isotherms on two of these adsorbents (a narrow-pore version of MCM-41[6] and FSM-12, a modified kanemite[3]) are shown in Fig. 1 and 2, together with the corresponding α_s plots (with non-porous hydroxylated silica taken as the reference adsorbent). It can be seen that the isotherm on FSM-12 in Fig. 1 is completely reversible whereas that on the MCM-41 in Fig. 2 has a narrow type H1 hysteresis loop.

The surface areas of FSM-12 and the MCM-41 (930 and 1170 $m^2\ g^{-1}$, respectively) have been obtained by the BET-nitrogen method and analysis of the nitrogen α_s plots. By assuming these areas to be confined to the walls of non-intersecting cylindrical pores and taking the mesopore volumes as the equivalent volumes of liquid nitrogen adsorbed at $P/P_0 = 0.95$, we arrive at values of the mean pore diameter of 2.6 nm for FSM-12 and 2.9 nm for the MCM-41. If we now make the usual assumption that the same areas are available for oxygen adsorption, we obtain the apparent molecular area, $\sigma(O_2)$, values of 0.142 and 0.149 nm^2 for FSM-12 and the narrow-pore MCM-41.

With the exception of the 2.9 nm sample of MCM-41, all the ordered mesoporous adsorbents studied so far have given $\sigma(O_2) = 0.143 \pm 0.002$ nm^2 (in agreement with the value originally adopted by Brunauer and coworkers[7]). It must be kept in mind that the narrow-pore MCM-41 has a very large specific surface and an appreciable pore volume (0.87 $cm^3\ g^{-1}$) and therefore the pore walls must be extremely thin. It appears likely that this has resulted in some distortion of the surface structure, which could account for the slightly higher value of $\sigma(O_2)$.

The absence of narrow micropores is evident from the form of the α_s plots in Fig. 1 and 2. The upward deviations from linearity begin at similar relative pressures (*i.e.* P/P_0 *ca.* 0.1), but the upswing is clearly more pronounced in Fig. 2. Thus, pore filling by the 2.9 nm MCM-41 has occurred mainly over the range P/P_0 *ca.* 0.13–0.28, which would correspond to a corrected Kelvin diameter range of 2.2–3.5 nm. The apparent consistency of this range with the estimated value of 2.9 nm for the mean pore width may be misleading since the reliability of the Kelvin equation is questionable when applied to such narrow pores.[4]

The position of the lower closure point of the narrow hysteresis loop in Fig. 2 cannot be specified precisely, but it appears to be in the region of P/P_0 *ca.* 0.2. It is too early to claim that a mean pore diameter of 2.9 nm is close to the limit of stability of the oxygen meniscus at 77 K. However, it is already clear that the smaller pores in FSM-12 are not filled by the classical mechanism of capillary condensation. Furthermore, all

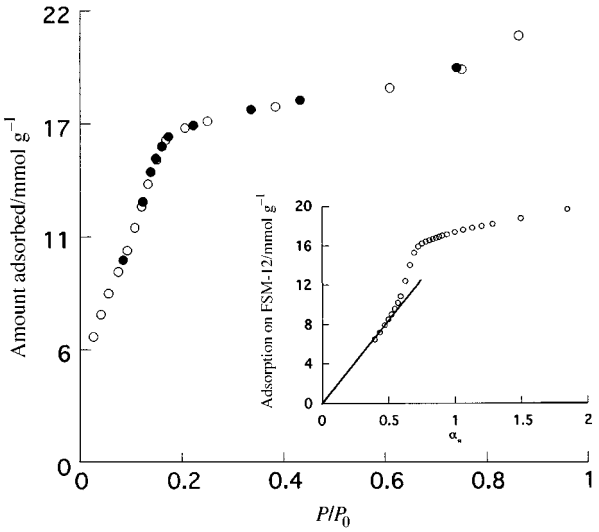

Fig. 1 Adsorption of oxygen at 77 K on FSM-12. Different symbols denote different runs. Open symbols denote adsorption, closed symbols denote desorption.

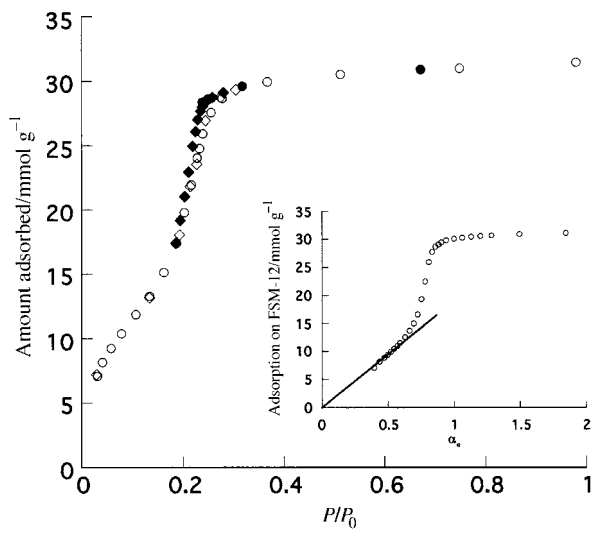

Fig. 2 Adsorption of oxygen at 77 K on MCM-41. Different symbols denote different runs. Open symbols denote adsorption, closed symbols denote desorption.

the ordered materials of wider pore-width studied so far have given hysteresis loops at relative pressures higher than 0.2. The results reported here indicate the distinctive nature of oxygen adsorption at 77 K, but more work will be required to establish its usefulness for the characterization of porous materials.

We should like to thank U. Ciesla and S. Schacht for providing the 2.9 nm sample of MCM-41.

Notes and references

† Current address: R&D Centre, British American Tobacco, Regents Park Road, Millbrook, Southampton, UK SO15 8TL.
E-mail: pjb@hantslife.co.uk

1 P. J. Branton, P. G. Hall, K. S. W. Sing, H. Reichert, F. Schuth and K. K. Unger, *J. Chem. Soc., Faraday Trans.*, 1994, **90**, 2965.
2 P. L. Llewellyn, Y. Grillet, F. Schuth, H. Reichert and K. K. Unger, *Microporous Mater.*, 1994, **3**, 345.
3 P. J. Branton, K. Kaneko, N. Setoyama, K. S. W. Sing, S. Inagaki and Y. Fukushima, *Langmuir*, 1996, **12**, 599.
4 F. Rouquerol, J. Rouquerol and K. S. W. Sing, *Adsorption by Powders and Porous Solids*, Academic Press, London, 1999, p. 417.
5 S. J. Gregg and K. S. W. Sing, *Adsorption, Surface Area and Porosity*, Academic Press, New York, 2nd edn., 1982, p. 154.
6 U. Ciesla, S. Schacht, G. D. Stucky, K. K. Unger and F. Schuth, *Angew. Chem., Int. Ed. Engl.*, 1996, **35**, 541.
7 K. M. Hanna, I. Odler, S. Brunauer, J. Hagymassy and E. E. Bodor, *J. Colloid Interface Sci.*, 1973, **45**, 27.

Communication 9/00795D

Atom-transfer within the coordination sphere of early–late heterobimetallic complexes: rapid deoxygenation of sulfoxides at low temperatures

Sylvie Fabre,[a] Bernd Findeis,[a] Dominique J. M. Trösch,[a] Lutz H. Gade,*[b] Ian J. Scowen[c] and Mary McPartlin[c]

[a] *Institut für Anorganische Chemie der Universität Würzburg, Am Hubland, 97074 Würzburg, Germany*
[b] *Laboratoire de Chimie Organométallique et de Catalyse, Institut LeBel, Université Louis Pasteur, 4, rue Blaise Pascal, 67070 Strasbourg, France. E-mail: gade@chimie.u.strasbg.fr*
[c] *School of Applied Chemistry, University of North London, Holloway Road, London, UK N7 8DB*

Received (in Basel, Switzerland) 4th January 1999, Accepted 1st February 1999

Extremely rapid oxygen transfer from sulfoxides to a carbonyl ligand to give the corresponding thioether and coordinated CO_2 is observed in the reactions of unsupported Zr–Ru heterodimetallic complexes with sulfoxides; this is interpreted to arise from the cooperative reactivity of the two complementary metal complex fragments bound to each other through a highly polar metal–metal bond.

The exploitation of the cooperative reactivity of different metal complex fragments is the underlying aim of the study of di- or tri-nuclear complexes containing highly polar metal–metal bonds between early and late transition metals.[1,2] The heteropolar addition of a metal nucleophile and electrophile to an organic substrate is the simplest manifestation of such reactivity,[3] the insertion (and subsequent cleavage) of carbonyl derivatives, which we reported recently, providing an example for this basic pattern.[4] Here we report the extremely rapid oxygen transfer from sulfoxides to coordinated CO to give CO_2 in the coordination sphere of Zr–Ru heterodi- and tri-nuclear complexes.

Metal ion mediated oxygen transfer reactions involving sulfoxides have been known for some time,[5] the most thoroughly studied systems effecting this transformation being Pt(II) complexes in acidic solution[6] and low valent Group VI complexes which are transformed to the corresponding oxo-species.[7] Deoxygenation of sulfoxides may also be achieved by some metal carbonyl derivatives under forcing conditions generating CO_2 derived from metal bound CO.[8] An important step in the labilization of the strong S–O bond is the addition of an electrophile to the oxygen atom. In reactions with early–late heterobimetallic complexes containing CO-ligands coordinated to the late transition metal *both* the electrophilic activation of the substrate and the transfer to an oxygen acceptor ligand (CO) were thought to be possible within the coordination sphere of *one* molecule.

Upon reaction of one molar equivalent of Me_2SO and Ph(Me)SO with the Zr–Ru heterodinuclear complex [MeSi(Si-Me_2NTol)$_3$ZrRuCp(CO)$_2$] (**1**)[2b] at −40 °C in toluene an immediate transformation occurred yielding products which could be isolated as yellow solids by evaporation of the solvent *in vacuo*. On the basis of their analytical and ^{1}H, ^{13}C NMR as well as IR spectroscopic properties these were formulated as [MeSi(SiMe_2NTol)$_3$Zr(μ-O_2C)RuCp(CO){S(R)R′}] (R = R′ = Me: **2a**, R = Me, R′ = Ph: **2b**) (Scheme 1). Products of higher crystallinity were obtained upon addition of a second equivalent of sulfoxide giving μ-CO_2-linked dinuclear compounds containing an O-bonded sulfoxide ligand at the zirconium centre but being otherwise of analogous composition and spectroscopic properties: [MeSi(SiMe_2NTol)$_3$Zr{OS(R)R′-κO}(μ-O_2C)RuCp(CO){S(R)R′}] (R = R′ = Me: **3a**, R = Me, R′ = Ph: **3b**).

In order to establish the structure of the reaction products unambiguously a single crystal X-ray structure analysis of **3a** was carried out.† The centre piece of the molecular structure

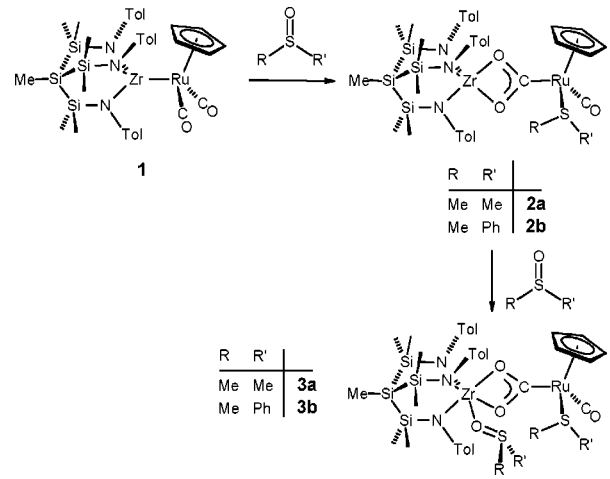

Scheme 1 Oxygen transfer upon reaction of the Zr–Ru heterodinuclear complexes with sulfoxides.

displayed in Fig. 1 is the Zr(μ-O_2C)Ru unit in which the CO_2 formed in the reaction links the two metal centres. The geometrical characteristics of the carboxylato-bridge [*d*{C(71)–O(61)} 1.276(11), *d*{C(71)–O(71)} 1.297(11) Å, *d*{Ru–C(71)} 2.082(9), *θ*{O(61)–C(71)–O(71)} 115.9(8)°] are similar to those found in a previously characterized CO_2-linked Zr–Ru

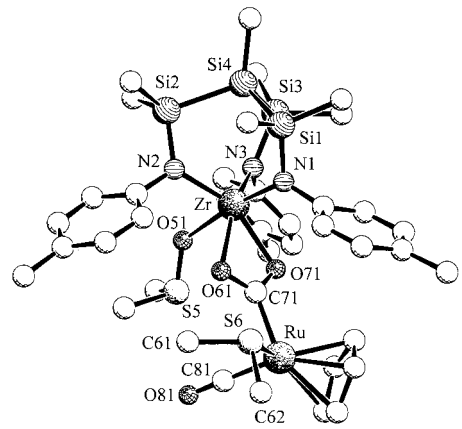

Fig. 1 Molecular structure of **3a** in the solid state. Principal bond lengths (Å) and angles (°): Ru–C(81) 1.883(14), Ru–C(71) 2.082(9), Ru–S(6) 2.364(3), Zr–N(1) 2.100(8), Zr–N(2) 2.119(8), Zr–N(3) 2.121(7), Zr–O(71) 2.221(6), Zr–O(61) 2.255(7), Zr–O(51) 2.261(7), S(5)–O(51) 1.520(7), O(61)–C(71) 1.276(11), O(71)–C(71) 1.297(11), O(81)–C(81) 1.128(13), C(81)–Ru–C(71) 87.8(4), N(1)–Zr–N(2) 99.5(3), N(1)–Zr–N(3) 101.7(3), N(2)–Zr–N(3) 104.9(3), N(1)–Zr–O(71) 90.2(3), N(2)–Zr–O(71) 152.6(3), N(3)–Zr–O(71) 97.9(3), N(1)–Zr–O(61) 92.6(3), N(2)–Zr–O(61) 95.5(3), N(3)–Zr–O(61) 152.6(3), O(71)–Zr–O(61) 58.3(2), O(61)–C(71)–O(71) 115.9(8)

heterodinuclear complex, $[Cp_2Zr(Cl)(\mu\text{-}O_2C)Ru(Cp^*)(CO)]$, reported by Gibson *et al.*[9] The metallacarboxylato unit in **3a** is almost symmetrically coordinated to the zirconium centre [*d*{Zr–O(61)} 2.255(7), *d*{Zr–O(71)} 2.221(6) Å] and together with the Me_2SO ligand [*d*{Zr–O(51)} 2.261(7)] generates the hexacoordinate zirconium complex fragment the coordination geometry of which may be viewed as being highly distorted octahedral. The dimethyl sulfide molecule formed as a consequence of the sulfoxide deoxygenation is coordinated to the Ru atom making this a chiral centre (Fig. 1).

The complexes **2a**,**b** and **3a**,**b** have several very characteristic spectroscopic properties which aid the structural assignment. As a consequence of the generation of a chiral centre at the late transition metal fragment the ^{1}H and ^{13}C NMR resonances of the $Si(CH_3)_2$ groups in the tripod ligand are diastereotopically split. The coordination of the soft donor ligand RR′S at the Ru-centres is the reason for the observation of the single ν(CO) infrared band at faily low frequency (1924–1947 cm^{-1}). The chemical shifts of the ^{13}C NMR signals assigned to the μ-CO_2 units depend quite sensitively upon the presence or absence of the additional RR′SO-donor at the Zr-centre. For **2a**,**b** they are observed at, respectively, δ 235.4 and 232.0, while the electronic readjustment within the molecule following the sulfoxide coordination at Zr leads to a significant shift of this signal to higher field [δ(^{13}C) **3a**: 225.1, **3b**: 225]. A study of this reaction employing compound **1** which was ^{13}C-labeled at the CO ligands provided support for the assumption of the role of these ligands as O-acceptors and their transformation to the bridging CO_2-unit.

The remarkable reactivity of **1** towards sulfoxides and the selectivity of the reaction raised the question of the generality of this reactive pattern of metal–metal bonded early–late heterodinuclear {$CpRu(CO)_2$} derivatives. Reaction of the heterotrinuclear complex $[CH_2(CH_2NSiMe_3)_2Zr\{RuCp(CO)_2\}_2]$ **4**[10] which contains two structurally equivalent {$CpRu(CO)_2$} units bonded to a Zr amido complex fragment with two molar equivalents of Me_2SO and Ph(Me)SO led to the immediate conversion to reaction products which were formulated on the basis of their analytical and spectroscopic properties as $[CH_2(CH_2NSiMe_3)_2Zr\{(\mu\text{-}O_2C)RuCp(CO)(SMeR)\}_2]$ (R = Me: **5a**, Ph: **5b**) in which the Zr atom is coordinated by *two* metallacarboxy units and the thioethers derived from the sulfoxides are also bonded to the Ru centres (Scheme 2).

Remarkably, all attempts to isolate, or even unambiguously detect, intermediate species in which only one metal–metal bond is cleaved failed, an observation which implies that the conversion at one centre significantly enhances the reactivity of the other. This should be compared to the results from our previous studies of simple insertion reactions of unsaturated polar substrates into these metal–metal bonds in which the reaction involving the cleavage of only one Zr–Ru bond was observed exclusively.[10] We would like to point out in this context, that in contrast to the rapid deoxygenation reactions involving the Zr–Ir complex $[Cp_2Zr(\mu\text{-}N\text{Bu}^t)IrCp^*]$ studied in Bergman's group,[1c] the presence of carbonyl ligands in **1** and **4** leads to carboxy-linked species rather than oxo complexes. The formation of a C–O and two Zr–O bonds is the thermodynamic driving force in these conversions which is sufficiently strong even to effect the displacement of an inserted isonitrile molecule from the trinuclear complex $[CH_2(CH_2NSiMe_3)_2Zr\{\eta^2\text{-}C(=NMe)M(CO)_2Cp\}\{M(CO)_2Cp\}]$ **6** (Scheme 2).

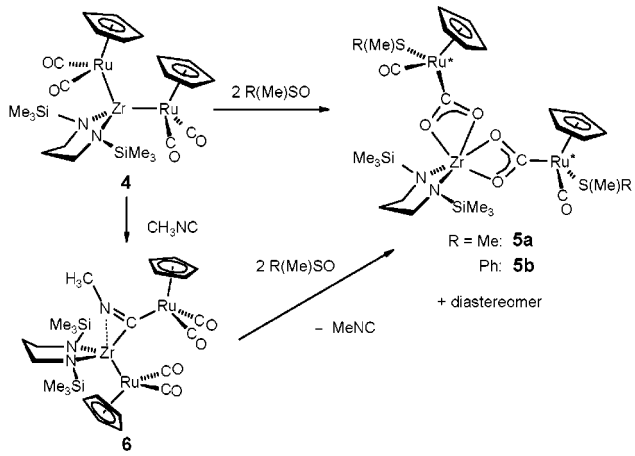

Scheme 2 Oxygen transfer upon reaction of the $ZrRu_2$ heterotrinuclear complexes with sulfoxides yielding hexacoordinate zirconium complexes containing two ruthenacarboxylato 'ligands'.

In conclusion, the reactions reported represent the first examples of transformation involving amido ligand-stabilized unsupported early–late heterobimetallics (*i.e.* containing a M–M′ bond without a bridging ligand) in which not only both metal complex fragments interact with the substrate but involvement of a coordinated ligand in an atom transfer reaction occurs. This combined and complementary reactivity of the two metal centres enables the reduction of a sulfoxide by CO under extraordinarily mild conditions.

We thank the Deutsche Forschungsgemeinschaft, the Fonds der Chemischen Industrie, the European Commission (TMR network MECATSTN), the EPSRC and the DAAD and British Council for funding. We dedicate this paper to Professor Helmut Werner, Universität Würzburg, on the occasion of his 65th birthday.

Notes and references

† *Crystal data* for **3a**: $[MeSi\{SiMe_2N(p\text{-Tol})\}_3Zr(OSMe_2\text{-}\kappa O)(\mu\text{-}O_2C)\text{-}RuCp(CO)(SMe_2)]\cdot 0.25MeC_6H_5$: $C_{40.75}H_{56}N_3O_4RuS_2Si_4Zr$, triclinic, space group $P\bar{1}$, a = 12.426(3), b = 14.510(3), c = 16.742(4) Å, α = 115.41(2), β = 96.302(13), γ = 96.682(15)°, V = 2665.0(10) Å^3, Z = 2, F(000) 1051, D_c = 1.272 g cm^{-3}, T = 296(2) K, μ = 0.683 mm^{-1}; Siemens *P*4 diffractometer, 8600 measured data (1.37 < θ < 23.00°), empirical absorption corrections (relative T_{max} 0.6108, T_{min} 0.4556), 7388 independent reflections, R_{int} = 0.0648, R_1 = 0.0709, wR_2 = 0.1523 [$I > 2\sigma(I)$], S = 0.958 for 503 parameters. Programs: SHELXTL 5.03, Siemens Analytical X-Ray Instruments Inc., 1994, Madison WI, USA and DIFABS, N. Walker and D. Stuart, *Acta Crystallogr., Sect. A*, 1983, **39**, 158. CCDC 182/1167.

1 M. Herberhold and G.-X. Jin, *Angew. Chem.*, 1994, **106**, 1016; *Angew. Chem., Int. Ed. Engl.*, 1994, **33**, 964; C. P. Casey, *J. Organomet. Chem.*, 1990, **400**, 205; T. A. Hanna, A. M. Baranger and R. G. Bergman, *J. Am. Chem. Soc.*, 1995, **117**, 665; A. M. Baranger, T. A. Hanna and R. G. Bergman, *J. Am. Chem. Soc.*, 1995, **117**, 10 041.

2 (*a*) S. Friedrich, H. Memmler, L. H. Gade, W.-S. Li and M. McPartlin, *Angew. Chem.*, 1994, **106**, 705; *Angew. Chem., Int. Ed. Engl.*, 1994, **33**, 676; (*b*) B. Findeis, M. Schubart, C. Platzek, L. H. Gade, I. J. Scowen and M. McPartlin, *Chem. Commun.*, 1996, 219; (*c*) S. Friedrich, H. Memmler, L. H. Gade, W.-S. Li, I. J. Scowen, M. McPartlin and C. E. Housecroft, *Inorg. Chem.*, 1996, **35**, 2433; (*d*) G. Jansen, M. Schubart, B. Findeis, L. H. Gade, I. J. Scowen and M. McPartlin, *J. Am. Chem. Soc.*, 1998, **120**, 7239.

3 H. Memmler, U. Kauper, L. H. Gade, I. J. Scowen and M. McPartlin, *Chem. Commun.*, 1996, 1751.

4 A. Schneider, L. H. Gade, M. Breuning, G. Bringmann, I. J. Scowen and M. McPartlin, *Organometallics*, 1998, **17**, 1643.

5 Recent review: V. Y. Kukushkin, *Coord. Chem. Rev.*, 1995, **139**, 375.

6 F. G. Bordwell and B. M. Pitt, *J. Am. Chem. Soc.*, 1955, **77**, 572; C. W. Bird, *J. Chem. Soc.*, 1968, 1230; V. Y. Kukushkin and E. Y. Pankova, *Koord. Khim.*, 1989, **15**, 531.

7 See, for example: J. P. Caradonna, P. R. Reddy and R. H. Holm, *J. Am. Chem. Soc.*, 1988, **110**, 2139 and references therein; S. Porohit, A. P. Koley, L. S. Prasad, P. T. Manoharan and S. Ghosh, *Inorg. Chem.*, 1989, **28**, 3735; S. A. Roberts, C. G. Young, W. E. Cleland, R. B. Ortega and J. H. Enemark, *Inorg. Chem.*, 1988, **27**, 3044.

8 H. Alper and E. C. H. Keung, *Tetrahedron Lett.*, 1970, 53; S. G. Davies, *J. Organomet. Chem.*, 1979, **179**, C5; H. Alper and G. Wall, *J. Chem. Soc., Chem. Commun.*, 1976, 263; V. Y. Kukushkin and A. I. Moiseev, *Zh. Obshch. Khim.*, 1990, **60**, 692.

9 D. H. Gibson, J. M. Mehta, B. A. Sleadd, M. S. Mashuta and J. F. Richardson, *Organometallics*, 1995, **14**, 4886.

10 S. Friedrich, L. H. Gade, I. J. Scowen and M. McPartlin, *Angew. Chem.*, 1996, **108**, 1440; *Angew. Chem., Int. Ed. Engl.*, 1996, **35**, 1338.

Communication 9/00010K

Ferromagnetic interactions between triphenylmethyl radicals through an organometallic coupler

O. Elsner, D. Ruiz-Molina, J. Vidal-Gancedo, C. Rovira* and J. Veciana*

Institut de Ciència dels Materials de Barcelona (CSIC), Campus Universitari de Bellaterra, 08193, Cerdanyola, Spain. E-mail: vecianaj@icmab.es; cun@icmab.es

Received (in Cambridge, UK) 13th January 1999, Accepted 22nd February 1999

A diradical consisting of two polychlorinated triphenylmethyl radical units connected by a 1,1′-metallocenylendivinylene bridge has been synthesized and characterized; EPR frozen solution experiments down to liquid helium temperature showed that the organometallic unit acts as a ferromagnetic coupler.

In the last few years, the development and study of new coupling units that promote ferromagnetic interactions between pure organic radicals has been a subject of great interest.[1] Metallocenes are excellent candidates to be used as magnetic couplers not only because of their rich chemistry but also because they are electroactive species whose oxidation state can be controlled by means of a chemical or electrochemical stimulus; moreover their oxidized states are of open-shell character. However, although such complexes have been successfully used as building blocks of molecular solids promoting intermolecular magnetic exchange interactions,[2] their use as intramolecular magnetic couplers is new. Recently, we have reported a novel family of compounds consisting of two purely organic α-nitronyl aminoxyl radicals connected by different 1,1′-metallocenylene bridges where the metallocene units were shown to act as effective magnetic couplers that transmit the magnetic interactions through their skeletons.[3] However, the small spin density located on the metallocene units of these systems and the presence of intramolecular hydrogen bonds, which determines the existence of a direct intramolecular through-space magnetic interaction, lead to the appearance of an effective antiferromagnetic interaction between the two α-nitronyl aminoxyl radical units that is very sensitive to the molecular conformation.[4] For this reason, such complexes were not suitable candidates to study and rationalize the behaviour of 1,1′-metallocenylene bridges as magnetic couplers.

In order to overcome both these factors, diradical **1,** consisting of two polychlorinated triphenylmethyl radicals connected by a 1,1′-ferrocenylendivinylene bridge, was designed. The particular structure and topology of such a diradical leads to expectation of a non-negligible spin density on the ferrocene moiety making feasible the magnetic coupling between the two organic radical units.[5] In addition, the location of both radical units far away from each other avoids any possibility of having intramolecular contacts, and consequently, a significant direct through-space magnetic interaction. Here we report the synthesis and characterization of diradical **1.** The related monoradical **2** has also been synthesized and studied for comparison purposes.

As outlined in Scheme 1, the synthetic route for preparing these radical derivatives is based on two main steps. First, a Wittig reaction between the phosphonium bromide precursor **3** and the corresponding ferrocene carbaldehyde derivative; *i.e.* ferrocene 1,1′-biscarbaldehyde and ferrocene monocarbaldehyde for radicals **1** and **2**, respectively. Second, a subsequent deprotonation and oxidation to yield the desired radicals. In the first step of the synthesis of **1**, the substituted phosphonium bromide, α,α-bis(pentachlorophenyl)-2,3,5,6-tetrachloro-α′-(triphenylphosphonium)-*p*-xylene bromide **3**, was suspended in dry THF and treated with an equimolar amount of KOBu^t. The resulting yellow ylide suspension was stirred for *ca.* 1 h and after this time ferrocene 1,1′-biscarbaldehyde was added and stirred for a further 72 h. The reaction mixture was quenched with HCl and extracted with $CHCl_3$ to give 1,1′-bis{4-[bis(pentachlorophenyl)methyl]-2,3,5,6-tetrachlorostyryl}ferrocene **4** after chromatographic purification from *n*-hexane–$CHCl_3$ (1 : 1). Finally, a THF solution of **4** was treated with an excess of tetra(*n*-butyl)ammonium hydroxide. The solution, which immediately turned purple, was stirred at room temperature for 4 h. Subsequent oxidation of the resulting dianion with *p*-chloranil yielded the 4,4′-(1,1′-ferrocenylenedivinylene)di[α,α-bis(pentachlorophenyl)-2,3,5,6-tetrachlorobenzyl] diradical **1**, which was isolated as a clathrate (**1**·2C_6H_6) after chromatographic purification (*n*-hexane–CCl_4, 1 : 1) and recrystallization from C_6H_6. This diradical is completely stable in air both in the solid state and in dilute solutions. The related monoradical derivative, the 4-(ferrocenylvinylene)-α,α-bis-(pentachlorophenyl)-2,3,5,6-tetrachlorobenzyl radical **2** was prepared following the same procedure, from the phosphonium bromide derivative **3** and ferrocene carbaldehyde. Both radicals were obtained as dark green microcrystals and were characterized by elemental analysis, cyclic voltammetry, IR, UV–VIS and EPR spectroscopies.

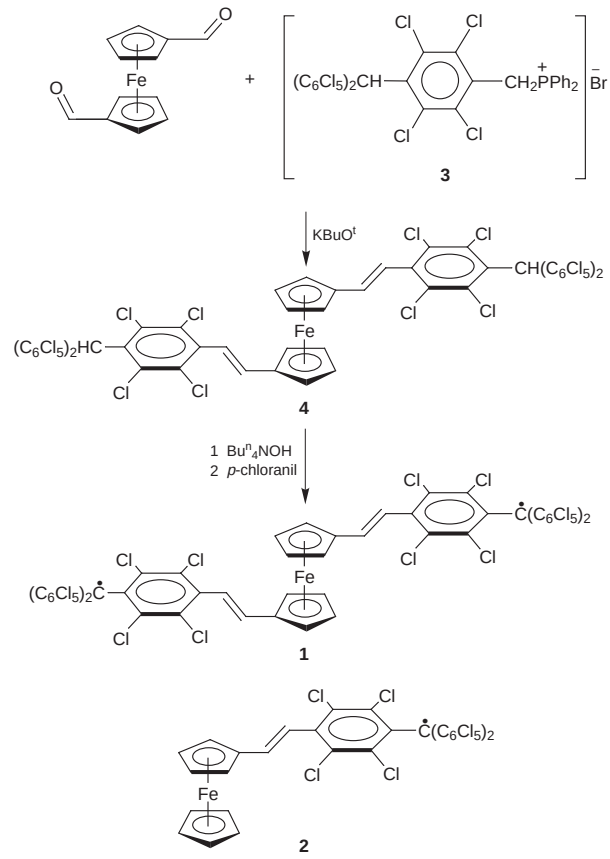

Scheme 1

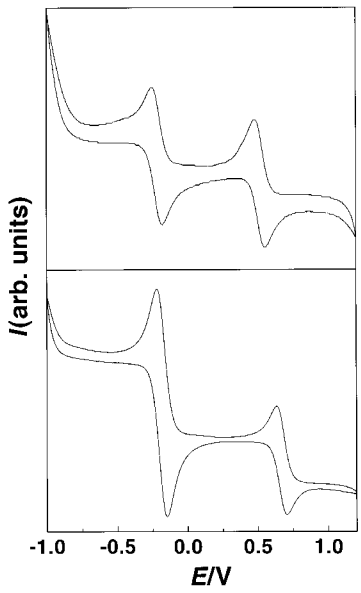

Fig. 1 Cyclic voltammograms recorded in a CH_2Cl_2 solution containing NBu_4PF_6 (0.1 M) of (a) monoradical **2** and (b) diradical **1**.

The cyclic voltammetric response of **2** shows one oxidation and one reduction process. The reversible process at +587 mV arises from the oxidation of the ferrocene unit while the reversible reduction process occurring at −177 mV is associated with the reduction of the triphenylmethyl radical unit. Cyclic voltammetry of diradical **1** (Fig. 1) shows one reversible oxidation process at +666 mV and one reversible reduction process at −181 mV that involves the simultaneous transfer of two electrons. The oxidation process was assigned, as in the monoradical species, to the oxidation of the ferrocene unit, while the reduction process was assigned to the reduction of both triphenylmethyl radical units. The fact that the oxidation process of the ferrocene unit of diradical **1** appears at a higher potential value than those observed for monoradical **2** and the unsubstituted ferrocene is the first direct evidence for the presence of an electronic interaction between the radical and the ferrocene units. Nevertheless, EPR spectroscopy provides more detailed and definitive information about the electronic structure as well as of the intramolecular electron–electron interactions in these compounds. X-Band EPR isotropic spectra of radicals **1** and **2** were obtained in toluene–CH_2Cl_2 (1 : 1). The spectra of both complexes at room temperature showed lines corresponding to the coupling of the unpaired electrons with the different nuclei with non-zero magnetic moments; *i.e.* with ^{1}H and naturally abundant ^{13}C isotope at the α and aromatic positions. Computer simulation gave the isotropic *g*-values (g_{iso}) and the isotropic hyperfine coupling constants (a_i) of the unpaired electrons with the different nuclei with non-zero magnetic moments. The g_{iso} values for diradical **1** and monoradical **2** were 2.0028 and 2.0033, respectively which are very close to that observed for other polychlorotriphenylmethyl radicals.[6] More interesting is the comparison of the isotropic hyperfine coupling constant values with the hydrogen atoms of the ethylene moieties and some of the carbon nuclei of the triphenylmethyl unit. The values of the coupling constant of diradical **1**, $a_1(^1H) \approx 0.80$ G (2H), $a_2(^1H) \leqslant 0.30$ G (2H) and $a(^{13}C) \approx 13.0$ G (1 C_α) are approximately half those found for monoradical **2**, $a_1(1^1H) \approx 1.77$ G (1H), $a_2(1^1H) \approx 0.57$ G (1H) and $a(^{13}C) \approx 29.0$ G (1 C_α) . It is then possible to conclude that the two electrons in diradical **1** are interacting with a magnetic exchange coupling constant, *J*, that fulfills $J >> a_i$. It is also worth noting that the coupling constants of diradical **1** are not exactly half of those observed for the monoradical **2** when measured under identical experimental conditions, suggesting that both molecules have small differences in the conformations of their bridges. The spectrum of diradical **1** in frozen toluene–CH_2Cl_2 (1 : 1) showed the characteristic fine structure of a triplet species and appeared to be symmetrical, indicating that this complex has a low (if any) anisotropy. The forbidden $\Delta m_s = \pm 2$ transition characteristic of a triplet species, was also observed at the half-field region of the spectrum and the intensity of the corresponding signal (I_{pp}), obtained by double integration, was measured in the range 4–100 K. The reproducibility of the results was confirmed by two independent experiments. Since the quantity $I_{pp}T$ is proportional to the population in the triplet state, the fact that $I_{pp}T$ (Fig. 2) increases with decreasing temperature indicates that the ground state of **1** is the triplet state and the singlet state should be regarded as a thermally accessible excited state.[7] A separation of +10 ±2 K (7 cm^{-1}) between both states was obtained from the fitting of the data in Fig. 2 to a Bleaney–Bowers equation.[8]

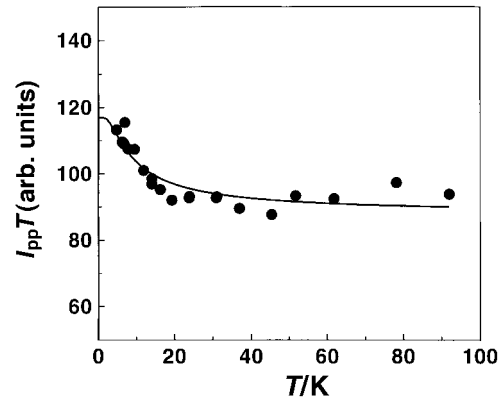

Fig. 2 Temperature dependence of $I_{pp}T$ of diradical **1**. The closed circles represent the experimental data and the continuous line the fit of experimental data to the Bleaney–Bowers equation.

In conclusion, we have shown that 1,1′-ferrocenylene bridges can act as ferromagnetic couplers when radical units with a suitable topology are connected to them. This concept can be extended to the synthesis of novel metallocene complexes bearing other organic and inorganic units providing a valuable access to this interesting class of materials.

This work was supported by grant from DGES (project PB96-0802-C02-01), CIRIT (project SGR 96-00106) and the 3MD Network of the TMR program of the E.U. (contract ERBFMRX CT980181).

Notes and references

1 D. Gatteschi, O. Kahn, J. S. Miller and F. Palacio, *Molecular Magnetic Materials*, Kluwer Academic, Dordrecht, 1991; O. Kahn, *Molecular Magnetism*, VCH Publishers, Weinheim, 1993; A. Rajca, *Chem. Rev*., 1994, **94**, 871; H. Iwamura and N. Koga, *Acc. Chem. Res*., 1993, **26**, 346.

2 J. S. Miller and A. J. Epstein, *Angew. Chem., Int. Ed. Engl*., 1994, **33**, 385 and references therein.

3 O. Jürgens, J. Vidal-Gancedo, C. Rovira, K. Wurst, C. Sporer, B. Bildstein, H. Schottenberger, P. Jaitner and J. Veciana, *Inorg. Chem*., 1998, **37**, 4547.

4 The spin density on the metallocene units linked to the α-carbon atom of α-nitronyl aminoxyl radicals is very small because the SOMO orbital has a node on this carbon atom and therefore the spin density is transmitted only by a spin polarization mechanism.

5 By contrast, for diradical **1** both unpaired electrons can be delocalized by conjugation onto the ferrocene unit according to the particular topology of the diradical promoting a larger magnetic coupling.

6 O. Armet, J. Veciana, C. Rovira, J. Riera, J. Castañer, E. Molins, J. Rius, C. Miravitlles, S. Olivella and J. Brichfeus, *J. Phys. Chem*., 1987, **91**, 5608.

7 To obtain accurate temperature measurements that ensure the validity of the experimental results, the spectrometer was equipped both with a flowing-helium Oxford ESR-900 cryostat (4.2–100 K), controlled by an Oxford ITC4 temperature control unit, and with a calibrated custom-made double temperature control system for determining accurately the sample temperature. Additional precautions to avoid undesirable saturation effects and spectral line broadening were also taken.

8 R. L. Carlin, *Magnetochemistry*, Springer-Verlag, Berlin, 1986, p. 71.

Communication 9/00371A

Size dependence of the surface plasmon enhanced second harmonic response of gold colloids: towards a new calibration method

Paolo Galletto,[a] Pierre F. Brevet,*[a] Hubert H. Girault,[a] Rodolphe Antoine[b] and Michel Broyer[b]

[a] *Laboratoire d'Electrochimie, Ecole Polytechnique Fédérale de Lausanne, CH-1015 Lausanne, Switzerland. E-mail: Pierre-francois.Brevet@epfl.ch*

[b] *Laboratoire de Spectrométrie Ionique et Moléculaire, Université Lyon 1 and UMR CNRS n° 5579, Bât 205, 43, Bd du 11 novembre 1918, 69622 Villeurbanne cedex, France*

Received (in Exeter, UK) 7th January 1999, Accepted 25th February 1999

Hyper Rayleigh scattering in solution is used for the determination of the first order hyperpolarizability $\beta_{colloid}$ of gold colloids in the size range 5–22 nm; these hyperpolarizabilities are found to range from 0.60×10^{-25} esu for 5 nm diameter colloids to up to 16.6×10^{-25} esu for 22 nm diameter colloids at the second harmonic wavelength of 532 nm; the strong size dependence of the hyperpolarisabilities reported here suggests that hyper Rayleigh scattering experiments can efficiently be used to calibrate the particle diameter of colloidal suspensions.

Gold colloids have been extensively investigated in the past owing to the potential applications of these particle suspensions. As a result, a wide range of techniques has been used for their characterisation, and in particular optical and microscopy techniques. For example, UV–VIS absorption spectroscopy and IR spectroscopy have been used to investigate the electronic properties of the particles. Also, transmission electron microscopy (TEM) measurements for deposited particles were performed to determine both the mean diameter and the size distribution of the preparations.[1,2] Recently, we have used the technique of optical surface second harmonic generation (SSHG) as a new technique for the study of noble-metal nanoparticles in diverse environmental conditions.[3,4] Indeed, it has been shown that this nonlinear optical technique is very sensitive to the surface plasmon excitation, the second harmonic signal being resonantly enhanced when the harmonic wavelength is tuned in the vicinity of the plasmon resonance. The hyper Rayleigh scattering (HRS) technique has already been used in the past for the determination of the absolute hyperpolarisability of compounds, in particular silver and gold colloids as well as SiO_2 particles.[5–7] Here, we report the use of the technique of HRS to investigate the size evolution of the first hyperpolarisability $\beta_{colloid}$ for colloids with sizes ranging from 5 to 22 nm. Within this size range, no significant surface plasmon peak shift occurs, a necessary requirement for single wavelength measurements. From the measurements and the simplicity of the experimental arrangement, we also propose this second order nonlinear technique as an efficient calibration technique for the determination of the size of nanoparticles in solution.

Colloidal gold nanoparticles with a mean particle diameter of 19 and 22 nm were prepared using the method of Turkevich *et al.*[8] Gold colloids of mean diameter 4.9 and 8.6 nm were purchased from Sigma.[9] TEM photographs of each colloidal preparation were taken and the average particle diameter along with the standard deviation were determined from at least 200 particles. The UV–VIS absorption spectrum of the gold colloid solutions presented a strong absorption band with a maximum at *ca.* 520 nm except for the 4.9 nm diameter one. Indeed, for this particle diameter, the plasmon resonance is damped owing to the size effects and therefore swamped by the sharp increase of the absorbance due to interband transitions, appearing as a mere shoulder blue shifted with respect to the true resonance location. Table 1 gives the size and the linear optical characteristics of the four gold colloidal solutions used.

The light source for the HRS experiments consisted of a Q-switched Nd : YAG laser providing pulses of 5 ns and < 4 mJ, at a repetition rate of 10 Hz at 1064 nm. The beam was focused into a 1 × 1 cm spectrophotometric cell and the experiments were performed well below the threshold for any undesirable adverse effects. A small fraction of the incident beam was directed onto a fast photodiode to monitor the intensity stability. The HRS light was collected at an angle of 90° from the incident direction by a lens and a mirror. Spectral discrimination of the second harmonic light from its linear counterpart was accomplished by two low-pass BG38 near IR filters and a 3 nm bandwidth interference filter peaked at 532 nm. The second harmonic light was then detected with a photomultiplier tube and the signal was integrated with a boxcar averager. The quadratic dependence of the HRS signal from the gold colloid solutions with the incident light intensity was always checked beforehand and the experimental conditions were first assessed on *p*-nitroaniline (pNA) in methanol. With the known value of $\beta_{MeOH} = 0.69 \times 10^{-30}$ esu, we extracted an absolute value of $\beta_{pNA} = (31 \pm 7) \times 10^{-30}$ esu in very good agreement with previous HRS measurements giving a value of $\beta_{pNA} = (34 \pm 4) \times 10^{-30}$ esu.[10]

The HRS signal $S_{2\omega}$ dependence on the incident light intensity I_0 is given according to

$$S_{2\omega} = GB^2 I_0 \, 10^{-A} \quad (1)$$

where G is a proportionality constant and A the absorbance at the harmonic wavelength. For the two component system at hand:

$$B^2 = < N_{colloid} \, \beta_{colloid}^2 + N_{H_2O} \, \beta_{H_2O}^2 > \quad (2)$$

where $N_{colloid}$ and $\beta_{colloid}$ are respectively the number density and the first hyperpolarisability of the aqueous colloids and N_{H_2O} and β_{H_2O} respectively the number density and the first hyperpolarisability of water. The factor 10^{-A} accounts for the losses due to linear absorption of the scattered light by the colloidal solution at 532 nm and was determined from the UV–VIS spectra.

HRS measurements at different number density of the 22 nm diameter colloids by dilution of the initial solution were first performed and the results are displayed in Fig. 1. A linear

Table 1 Size (mean diameter $< D >$ and dispersion), initial concentration, maximum of linear absorbance λ_{max} and first hyperpolarizability $\beta_{colloid}$ of gold colloids

Gold colloid	$< D >$/nm	Dispersion/nm	Initial concentration/ colloid dm^{-3}	λ_{max}/nm	$\beta/10^{-25}$ esu
a	4.9	0.7	4.4×10^{16}	508[a]	0.60 ± 0.09
b	8.6	1.0	6.9×10^{15}	518	2.0 ± 0.3
c	19.0	1.5	6.4×10^{14}	520	13.1 ± 2.0
d	22.0	1.7	4.6×10^{14}	520	16.6 ± 2.5

[a] Location of the shoulder of the absorbance spectrum (see text).

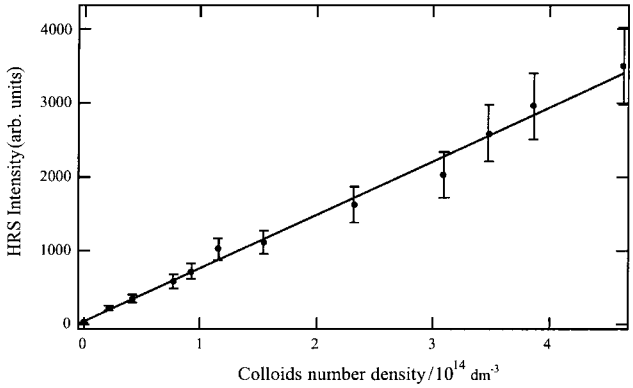

Fig. 1 HRS signal corrected for the linear absorbance at the harmonic wavelength *versus* the number density of the 22 nm gold colloids (sample d).

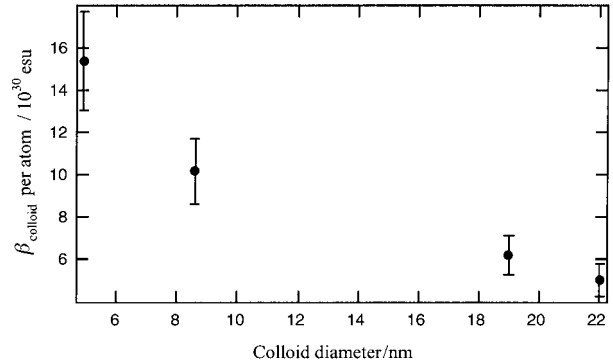

Fig. 2 Absolute value of the first hyperpolarizability $\beta_{colloid}$ calculated per gold atom in the colloid *versus* the mean diameter of the gold colloids.

behaviour is observed as expected after the correction for the absorption, and from the slope, the first hyperpolarisability of the 22 nm colloids $\beta_{colloid}$ is calculated to be $(16.6 \pm 2.5) \times 10^{-25}$ esu on the basis of $\beta_{H_2O} = 0.56 \times 10^{-30}$ esu.[7] Then, using this solution as an external reference, the first hyperpolarisability of the other colloids of size 4.9, 8.6 and 19 nm were obtained using the concentration of the initial solutions. The data are reported in the last column of Table 1. A 30-fold increase in the magnitude of the first hyperpolarisability is observed for a five-fold increase in diameter only. Such a large magnitude is however expected as it stems from the coupling between the SH field with the surface plasmon.[4] These values are rather different from the ones recently reported for 13 nm diameter gold colloids but are of the same order of magnitude as that obtained near resonance for silver colloids.[5,7] Fig. 2 shows the size dependence of the hyperpolarisability as calculated per atom, obtained dividing the value given in Table 1 by the number of gold atoms in the colloid. It is observed that the hyperpolarisabilities per atom decreases by a factor of 10 over the five-fold increase of the particle in diameter. The origin of such a behaviour may stem from the saturation of the collective effect contribution to the nonlinear optical activity when the colloid diameter gets too large.

These experiments emphasise the strong dependence of the first hyperpolarisability of the gold colloids on the particle diameter. As a result, the SH signal exhibits a 1000 fold increase in intensity for a five-fold increase in particle diameter only. For instance, for the 19 and 22 nm diameter colloids, the reported increase in the HRS signal is *ca.* 50% for a mere 16% increase in diameter. Therefore, in view of the simplicity of the experimental apparatus for these experiments, the HRS technique offers an efficient alternative to particle size determination with an external reference.

This work is supported by the European Community Training and Mobility of Researchers Programme (TMR) through the Network on Organization, Dynamics and Reactivity at Electrified Liquid–Liquid Interfaces (ODRELLI). The authors gratefully acknowledge Cyril Cayron from the Centre Interdépartemental de Microscopie Electronique (CIME) of the Ecole Polytechnique Fédérale de Lausanne for his help in the TEM measurements.

Notes and references

1 U. Kreibig and M. Vollmer, *Optical Properties of Metal Clusters* Springer, Berlin, 1995.
2 *Clusters and Colloids, from Theory to Applications*, VCH, New York, 1994.
3 R. Antoine, P. F. Brevet, H. H. Girault, D. Bethell and D. J. Schiffrin, *Chem. Commun.*, 1997, 1901.
4 R. Antoine, M. Pellarin, B. Palpant, M. Broyer, B. Prével, P. Galletto, P. F. Brevet and H. H. Girault, *J. Appl. Phys.*, 1998, **84**, 4532.
5 K. Clays, E. Hendrickx, N. Triest and A. Persoons, *J. Mol. Liq.*, 1995, **67**, 133.
6 F. W. Vance, B. I. Lemon, J. A. Ekhoff and J. T. Hupp, *J. Phys. Chem. B*, 1998, **102**, 1846.
7 F. W. Vance, B. I. Lemon and J. T. Hupp, *J. Phys. Chem. B*, 1998, **102**, 10091.
8 J. Turkevich, P. C. Stevenson and J. Hillier, *Discuss. Faraday Soc.*, 1951, **11**, 55.
9 Sigma, Product Number G1402 (4.9 nm) and G1527 (8.6 nm).
10 K. Clays and A. Persoons, *Phys. Rev. Lett.*, 1991, **66**, 2980.

Communication 9/00230H

ChemComm

Hierarchical organization of mesoporous MCM-41 ropes

Hong-Ping Lin,[a] Shang-Bing Liu,[a] Chung-Yuan Mou*[b] and Chih-Yuan Tang[c]

[a] *Institute of Atomic and Molecular Sciences Academia Sinica, PO Box 23-166, Taipei, Taiwan 106*
[b] *Department of Chemistry, National Taiwan University, Taipei, Taiwan, 106. E-mail: cymou@ms.cc.ntu.edu.tw*
[c] *Department of Zoology, National Taiwan University, Taipei, Taiwan, 106*

Received (in Cambridge, UK) 15th December 1998, Accepted 1st March 1999

Millimeter long ropes of MCM-41 materials are made from micrometer-sized fibers by self-assembly and flow-induced orientation.

Self-assembly of surfactants and aluminosilicates provides a versatile means to create various nanostructures of aluminosilicates, such as MCM-41 and MCM-48,[1,2] with potential applications in biomaterials, microelectronics and catalysis. For many applications of the mesoporous materials, these materials should be tailored not only at the nanometer scale of the pore but also at the larger scale (micro- and milli-meter) of the morphology.[3–5] Biomimetic approaches based on hierarchical organization would be a good way of building larger structures. Recent discoveries in hierarchical organization of these nanomaterials have extended the structure order to micrometer level and include tubular, spherical and fibrous morphology.[6–8] The fiber organization of mesoporous materials is particularly interesting for possible use in embedding conducting materials, from semiconductors to superconductors. We report here a simple method of making bundles of MCM-41 fibers (micrometers in diameter) into millimeter size ropes in nitric acid under a shearing flow; thus extending the previously known primary hierarchy to a higher level of secondary hierarchical structure.[8]

Since our goal is to create millimeter-scaled rope bundles of MCM-41, two sub-goals have to be met: the creation of ultralong cylindrical micelles and their parallel alignment. Previously, long fiber forms have been created by adding polymers to the surfactant,[9] and elongation is due to the polymers, not the micelles themselves. In our method we use the nitrate ion as a counter ion to create long worm-like micelles of cationic quaternary ammonium halides. Secondly, the parallel alignments of the hexagonal phase can be realized in a shearing flow. Recent studies on surfactant systems indicate that shear flow induces the formation of long cylindrical micelles and the orientation of the hexagonal phase along the flow direction.[10] Pinnavaia and coworkers found that variation in morphology of mesoporous silica could be attributed to agitation effects during synthesis.[11] Recently, it has been shown that 3-D silicate structures[12a] and 2-D films[12b] can be induced through detailed control of shear flow conditions and reaction composition.

MCM-41 materials were synthesized from quaternary ammonium halide (C_nTMAX; X = Cl or Br)–tetraethylorthosilicate (TEOS)–nitric acid (HNO_3) systems under couette flow conditions. First, into a couette flow reactor (the diameter of the stator is 8.90 cm, and the rotor is 7.92 cm), a clear aqueous solution of C_nTMAX (n = 16 or 18) was mixed thoroughly with a suitable amount of the nitric acid to form a highly viscous solution. The silica source (TEOS) was added and then stirred for 12–24 h at the designed stirring rate and temperature. The composition of gel solution is 1 C_nTMAX : (6.0–12.0) TEOS : (9.0–36.0) HNO_3 : (1000–2000) H_2O. The resultant white silica ropes were recovered by filtration and washed.

Fig. 1A shows the SEM micrograph of the calcined silica products prepared from $C_{18}TMAB$–TEOS–HNO_3–H_2O at 40 °C under a stirring rate of 500 rpm. It is found that the silica ropes are almost at the millimeter scale. The length is not uniform, but the longer ones tend also to be the thicker ones. The yield is high at *ca.* 90%. It is seen by SEM that the length and morphology of the calcined ropes are the same as the as-synthesized materials. At higher magnification, we can clearly see that the silica products consist of micrometer-sized silica fibers entwined into ropes (Fig. 1B). The corresponding higher magnification SEM image of the cross-section of the fibers shows that the micron-sized silica fibers are nearly hexagonal (Fig. 1C). From an ultrathin section TEM micrograph of the cross section of the silica fiber (Fig. 1D), one can unambiguously see that the hexagonal-shaped fibers are constituted from hexagon-arrayed MCM-41 nanochannels. Thus we have made silica ropes in second-order hierarchical structure; nanometer MCM-41 channels, micrometer fibers and millimeter sized ropes. Linear structures at each higher level are built up from the corresponding structure at lower level.

The X-ray diffraction (XRD) patterns of the as-synthesized and calcined silica ropes are shown in Fig. 2. One can clearly recognize the order of the hexagonal array of the MCM-41 structure. Both materials exhibit four sharp XRD peaks, which reflects a typically well aligned MCM-41 structure. The XRD patterns are almost flat in the range 2θ 20–30°, indicating that no amorphous silica particles are formed. The shrinkage of the d_{100} value after calcination at 560 °C for 6 h is only *ca.* 0.1–0.2 nm. This shows the nanostructure of the silica rope possesses high thermal stability.

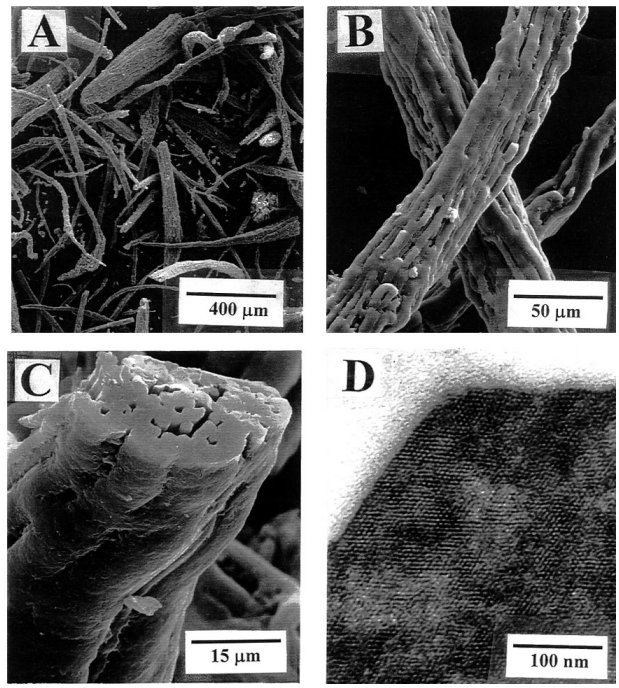

Fig. 1 SEMs of different magnifications and ultrathin TEM of millimeter-sized silica fibers obtained from the gel composition 1 $C_{18}TMACl$: 6.30 TEOS : 13.5 HNO_3 : 1002 H_2O. (A) × 50, (B) × 400, (C) × 1500, (D) ultrathin TEM of the cross section of the silica fiber.

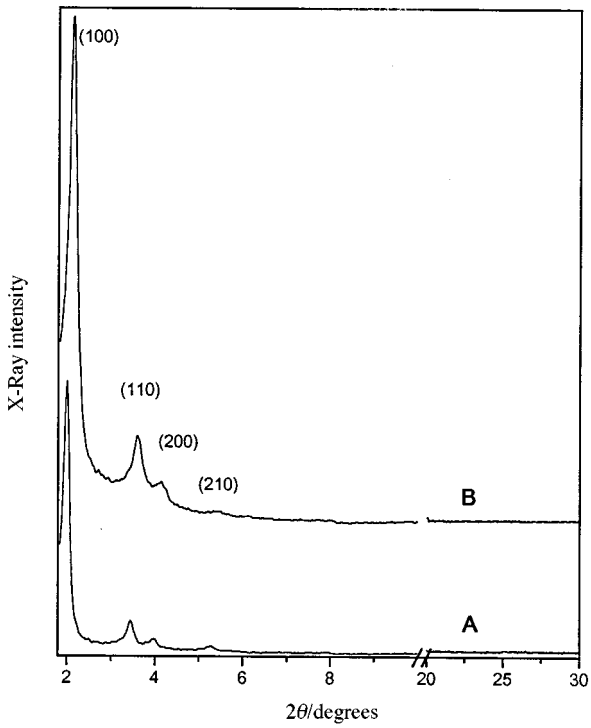

Fig. 2 XRD patterns of as-synthesized and calcined silica ropes prepared from the same gel composition of Fig. 1; (A) as-synthesized, (B) calcined.

In addition to using the surfactant C_{18}TMACl as the template, we can also fabricate millimeter-scaled silica ropes with similarly well defined XRD patterns from different C_nTMAX ($n \geqslant 16$) surfactants. The physical properties (d_{100} value, pore size, pore volume, BET surface area) of these materials after calcination are listed in Table 1. All of these mesoporous materials possess high thermal stability, large surface area and pore volume, uniformed-sized pores, the sizes of which can be varied (*i.e.* by changing the carbon chain length of surfactant) as those synthesized under basic conditions. The formation of long cylindrical micelles can be attributed to the NO_3^- anions of the nitric acid which has a stronger binding affinity to the cationic surfactant than do Br^- or Cl^- anions.[13,14] The ultra-long micelles of the $S^+NO_3^-$ acts as the template in combining with the cationic silica species (I^+), formed from the hydrolysis of TEOS, to form $S^+NO_3^-I^+$ intermediates. Then it transforms into the final mesoporous product with a constant pore size.

Table 1 Physical properties of the mesoporous silica ropes synthesized from C_nTMAX–TEOS–HNO_3–H_2O

C_nTMAX[a]	As-made d_{100} value/nm	Calcined d_{100} value/nm	BJH pore[b] size/nm	Pore volume[c]/ $cm^3\ g^{-1}$	BET surface/ $cm^2\ g^{-1}$
C_{18}TMACl	4.41	4.28	3.10	1.36	946
C_{18}TMAB	4.40	4.27	3.08	1.38	968
C_{16}TMACl	4.03	3.84	2.54	1.20	989
C_{16}TMAB	4.02	3.84	2.55	1.23	1002

[a] C_{18}TMAX systems were synthesized at 40 °C, C_{16}TMAX at 25 °C. [b] Values obtained from the adsorption portion of the N_2 adsorption–desorption isotherm. [c] Data taken at $p/p_0 = 0.9$.

The ability to control the mesoporous silica materials into a long rope form relies on the underlying physics and chemistry. From the chemical viewpoint, the NO_3^- anions of nitric acid have a strong binding strength with the cationic quaternary ammonium surfactant. Therefore the flexible and elongated rod micelles of $S^+NO_3^-$ would be formed as a supramolecalar template for the cationic silica species at a relative high concentration of nitric anions (*ca.* 0.4–0.9 M). When we use HBr or HCl as the source of acid, the morphology of the mesoporous materials is simply spherical.

From the physical viewpoint, the shearing flow also plays an important role for the formation of millimeter-scaled silica ropes. Under static condition, we obtain the mesoporous product in the facet and corrugated silica spheres as reported by Ozin's group.[6] By contrast, millimeter-sized silica ropes could only be synthesized under a steady continuous stirring.

In conclusion, mesoporous MCM-41 materials are produced in highly-ordered hierarchical form based on the combination of the elongation of the surfactant micelles using strongly binding nitrate counter ions, and the shear flow alignment which lead to formation of ropes of fibrous hexagonal nanochannels. This will provide a pathway to realize biomimetic hierarchical rope structures for other porous materials. In applications, fibrous MCM-41 materials of millimeter length could open up investigations in embedded and oriented metal and semiconductor nanorods.[15]

This research was supported by the China Petroleum Co. and the Nation Science Council of Taiwan (NSC 88-2113-M-002-027).

Notes and references

1 C. T. Kresge, M. E. Leonowicz, W. J. Roth, J. C. Vartuli and J. S. Beck, *Nature*, 1992, **359**, 710.
2 J. S. Beck, J. C. Vartuli, W. J. Roth, M. E. Leonowicz, C. T. Kresge, K. D. Schmitt, C. T.-W. Chu, D. H. Olson, E. W. Sheppard, S. B. Higgins and J. L. Schlenker, *J. Am. Chem. Soc.*, 1992, **114**, 10 834.
3 S. Mann and G. A. Ozin, *Nature*, 1996, **382**, 313; H. Yang, N. Coombs, I. Sokolov and G. A. Ozin, *Nature*, 1996, **381**, 589.
4 S. A. Davis, S. L. Burkett, N. H. Mendelson and S. Mann, *Nature*, 1997, **385**, 420.
5 Q. Hou, D. Zhao, J. Feng, K. Weston, S. K. Buratto, G. D. Stucky, S. Schacht and F. Schüth, *Adv. Mater.*, 1997, **9**, 974.
6 H. Yang, N. Coombs and G. A. Ozin, *Nature*, 1997, **386**, 692; G. A. Ozin, H. Yang, I. Sokolov and N. Coombs, *Adv. Mater.*, 1997, **9**,662.
7 S. Schacht, Q. Hou, I. G. Voigt-Martin, G. D. Stucky and F. Schüth, *Science*, 1996, **273**, 768.
8 H. P. Lin and C. Y. Mou, *Science*, 1996, **273**, 765.
9 P. J. Bruinsma, A. Y. Kim, J. Liu and S. Baskaran, *Chem. Mater.*, 1997, **9**, 2507; P. Yang, D. Zhao, B. F. Chmelka and G. D. Stucky, *Chem. Mater.*, 1998, **10**, 2033.
10 G. Schmidt, S. Muller, P. Lindner, C. Schmidt and W. Richtering, *J. Phys. Chem. B*, 1998, **102**, 507.
11 P. T. Tanev, Y. Liang and T. J. Pinnavaia, *J. Am. Chem. Soc.*, 1997, **119**, 8616.
12 (*a*) M. Lindén, S. Schacht, F. Schüth, A. Steel and K. K. Unger, *J. Porous Mater.*, 1998, **5**, 177; (*b*) H. W. Hillhouse, T. Okubo, J. W. V. Egmond and M. Tsapatsis, *Chem. Mater.*, 1997, **9**, 1505.
13 D. Nguyen and G. L. Bertrand, *J. Colloid Interface Sci.*, 1992, **150**, 143.
14 S. Berr, R. R. M. Jones and J. S. Johnson Jr., *J. Phys. Chem.*, 1992, **96**, 5611.
15 V. I. Srdanov, I. Alxneit, G. D. Stucky, C. M. Reaves and S. P. DenBaars, *J. Phys. Chem. B*, 1998, **102**, 3341.

Communication 8/09767D

The condensation of *trans*-$[PdCl_2\{(C_4H_3O)SeMe\}_2]$ with acetone: formation and crystal structure of $[Pd_2Cl_2(\mu\text{-}SeMe)_2\{MeSe(C_4H_2O)\}_2CMe_2]$

Raija Oilunkaniemi,[a] Risto S. Laitinen*[a] and Markku Ahlgrén[b]

[a] *Department of Chemistry, University of Oulu, Linnanmaa, FIN-90570 Oulu, Finland. E-mail: Risto.Laitinen@oulu.fi*

[b] *Department of Chemistry, University of Joensuu, PO Box 111, FIN-90801 Joensuu, Finland*

Received (in Basel, Switzerland) 23rd November 1998, Accepted 18th February 1999

The condensation of the furan rings in two *trans*-$[PdCl_2\{(C_4H_3O)SeMe\}_2]$ complexes with acetone and the chlorine–selenium interactions in the coordination spheres of the two palladium atoms result in the formation of a dinuclear complex $[Pd_2Cl_2(\mu\text{-}SeMe)_2\{MeSe(C_4H_2O)\}_2CMe_2]$.

Mononuclear $[ML_2X_2]$ complexes (M = Pd, Pt; L = two organic monodentate ligands containing one selenium or tellurium donor atom each, or one didentate ligand containing two chalcogen donor atoms; X = halide) form a well explored series.[1] Most of the experimental work, however, has been carried out in solution[2] and the solid state information is sparse.[3] We have recently studied the structural and bonding trends in $[MCl_2\{(C_4H_3E)E'Me\}_2]$ (M = Pd, Pt; E = S, O; E′ = Se, Te) both in solution and in the solid state.[3*i*] Surprisingly, it turned out that the crystallization of $[PdCl_2\{(C_4H_3O)SeMe\}_2]$ **1** from acetone produced a dimer $[Pd_2Cl_2(\mu\text{-}SeMe)_2\{MeSe(C_4H_2O)\}_2CMe_2]$ **2**. In this work we report the crystal structure of the dimer and discuss the route of its formation from two monomeric complexes.

The preparation of $[PdCl_2\{(C_4H_3O)SeMe\}_2]$ **1**† yields orange microcrystalline material. The product was dissolved in $CDCl_3$ and $(CD_3)_2CO$ and the ^{77}Se and $^{13}C\{^1H\}$ NMR spectra of both solutions were recorded immediately upon preparation and again after a period of four weeks.‡ The spectra of both fresh and aged samples were identical.

A chloroform solution of **1** exhibits a single ^{77}Se resonance at δ 230 consistent with the chemical shift of δ 233 reported for both $[PdCl_2\{(C_4H_3S)SeMe\}_2]$ **3** and $[PtCl_2\{(C_4H_3S)SeMe\}_2]$ **4**.[3*i*] This implies the presence of only one isomer in solution. The crystal structure determinations of **3** and **4** have shown the existence of a *trans*-isomer in the solid state.[3*i*] The ^{77}Se resonance of **1** appears as a doublet of quartets implying that selenium is bound to the methyl group and to the furyl ring with the coupling resolvable to the nearest protons [Fig. 1(a)].§

Five signals are observed in the $^{13}C\{^1H\}$ spectrum of **1**. Four resonances at δ 146, 134, 119 and 112 are due to the furyl ring carbon atoms. These values bear a logical relationship to the $^{13}C\{^1H\}$ spectra of $[MCl_2\{(C_4H_3E)E'Me\}_2]$ (M = Pd, Pt; E = S, O; E′ = Se, Te) [for detailed assignment of the resonances to individual carbon atoms, see ref. 3(*i*)]. The fifth resonance at δ 15 is assigned to the methyl carbon. NMR spectroscopy clearly shows the sole presence of monomeric *trans*-$[PdCl_2\{(C_4H_3O)SeMe\}_2]$ in chloroform solution.

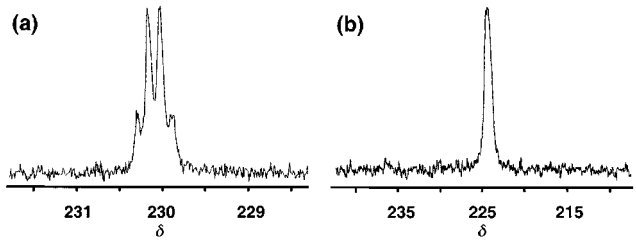

Fig. 1 The ^{77}Se NMR spectrum of $[PdCl_2\{(C_4H_3O)SeMe\}_2]$ **1** in (a) $CDCl_3$ and (b) $(CD_3)_2CO$. $^2J_{HSe}$ 11, $^3J_{HSe}$ 2 Hz.

The ^{77}Se and $^{13}C\{^1H\}$ spectra of **1** in acetone resemble those in chloroform. One ^{77}Se chemical shift is found at δ 224 and five ^{13}C resonances are observed at δ 148, 135, 118, 112 and 14. The most pronounced spectroscopic difference from the sample in chloroform is the loss of coupling information in the ^{77}Se resonance [Fig. 1(b)]. This may be due to fast exchange processes taking place in acetone solution.

Upon crystallization from acetone, a small amount of red crystals appeared together with the bulk of orange microcrystalline material of **1**.¶ The crystal structure determination of the red crystals established that **1** has condensed with acetone and dimerized, as shown in Fig. 2.‖ Both palladium atoms exhibit approximately square planar coordination sharing two bridging $MeSe^-$ ligands. The coordination planes around the two palladium atoms lie at an angle of 124.50(4)° from each other. Selected bond parameters are listed in Fig. 2. They are comparable to those observed for the related complexes and follow the trends established earlier.[3*a*,*c*,*i*]

The probable route of formation of **2** from **1** is shown in Fig. 3. The reaction can be conceived to be initiated by the

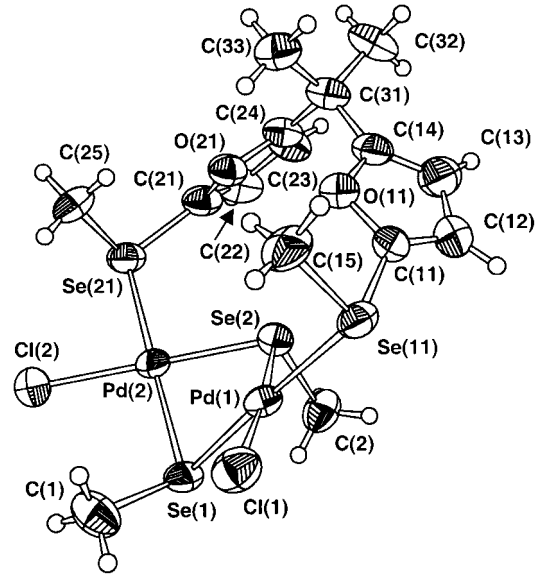

Fig. 2 The molecular structure of $[Pd_2Cl_2(\mu\text{-}SeMe)_2\{SeMe(C_4H_2O)\}_2CMe_2]$ indicating the numbering of the atoms. The thermal ellipsoids have been drawn at 50% probability level. Selected bond lengths (Å) and angles (°): Pd(1)–Se(1) 2.420(2), Pd(1)–Se(2) 2.397(1), Pd(2)–Se(1) 2.408(1), Pd(2)–Se(2) 2.396(2), Pd(1)–Se(11) 2.443(2), Pd(2)–Se(21) 2.437(1), Pd(1)–Cl(1) 2.351(2), Pd(2)–Cl(2) 2.336(3), Se(1)–C(1) 1.944(9), Se(2)–C(2) 1.962(8), Se(11)–C(11) 1.893(9), Se(11)–C(15) 1.946(8), Se(21)–C(21) 1.892(10), Se(21)–C(25) 1.960(9), C(14)–C(31) 1.49(1), C(24)–C(31) 1.52(1), C(31)–C(32) 1.52(1), C(31)–C(33) 1.56(1); Pd(1)–Se(1)–Pd(2) 85.46(4), Pd(1)–Se(2)–Pd(2) 86.23(4), Se(1)–Pd(1)–Se(2) 80.53(4), Se(1)–Pd(2)–Se(2) 80.79(4), Pd(1)–Se(11)–C(11) 109.4(3), Pd(2)–Se(21)–C(21) 110.7(3), C(14)–C(31)–C(24) 107.0(7), C(14)–C(31)–C(32) 111.0(8), C(14)–C(31)–C(33) 110.5(7), C(24)–C(31)–C(32) 108.9(7), C(24)–C(31)–C(33) 109.5(8), C(32)–C(31)–C(33) 109.8(8). The angle between the least-squares planes Pd(1)–Se(1)–Se(2)–Cl(1)–Se(11) and Pd(2)–Se(1)–Se(2)–Cl(2)–Se(21) is 124.50(4)°.

condensation of two furan rings from two separate *trans*-$[PdCl_2\{(C_4H_3O)SeMe\}_2]$ complexes by acetone. This type of condensation reaction between furan and ketones is well known.[6] Furan and acetone produce tetrametric $\{(C_4H_2O)CMe_2\}_4$ the crystal structure of which[7] shows a similar $-CMe_2-$ link between the two furan rings as **2**.

We have established[3i] that the packing in $[MCl_2\{(C_4H_3E)TeMe\}_2]$ and other related telluroether-containing palladium and platinum complexes[3d,g,h] involves close tellurium–halogen contacts. The strength of this interaction is directly proportional to the electron-withdrawing nature of the aromatic substituents bound to the tellurium atom. In the case of monomeric selenoether complexes no such halogen–chalcogen interaction is observed.[3a,c,i] The furan ring, however, may be sufficiently electrophilic to induce a chlorine–selenium interaction and form the intermediate **A**, as shown in Fig. 3. The formation of **A** is sterically very facile despite the constraint generated by the link between the two furan rings. In fact, the solid state packing of the dimer **2** involves two short intermolecular selenium–chlorine contacts of 3.505 Å and lends credibility to the intermediate **A**. Only slight rearrangement of the ligands around the two palladium atoms is needed to cleave two molecules of 2-furyl chloride and form **B**. The reaction is completed by the two $MeSe^-$ fragments that bridge the palladium atoms and thus regenerate the square-planar coordination around each.

Diorganoselenides generally act as neutral monodentate ligands without C–Se bond fission during the complexation.[1c,d] The presence of bridging $MeSe^-$ ligands in **2**, however, must be a consequence of the cleavage of the Se–C_{aryl} bond. This behaviour is consistent with the oxidative addition of organic tellurides to Pt(0) that results in the cleavage of the Te–C_{aryl} bond in preference to the Te–C_{alkyl} bond.[8]

It can be concluded that **2** is probably formed from **1** upon crystallization from acetone. Spectroscopic and compositional data indicate that the orange product obtained upon precipitation with hexane is pure monomer **1**. Upon crystallization from acetone, the solid monomer itself appears only as microcrystalline material, but small amounts of **2** build up as well formed red crystals. A systematic study on the factors affecting the formation of dimeric complex from $[MCl_2\{(C_4H_3E)SeMe\}_2]$ (M = Pd, Pt, E = O, S) and the optimization of the condensation reactions are currently in progress.

We thank Dr Maire Eloranta for inspiring discussions. Financial support from Neste Oy Foundation and Academy of Finland is gratefully acknowledged.

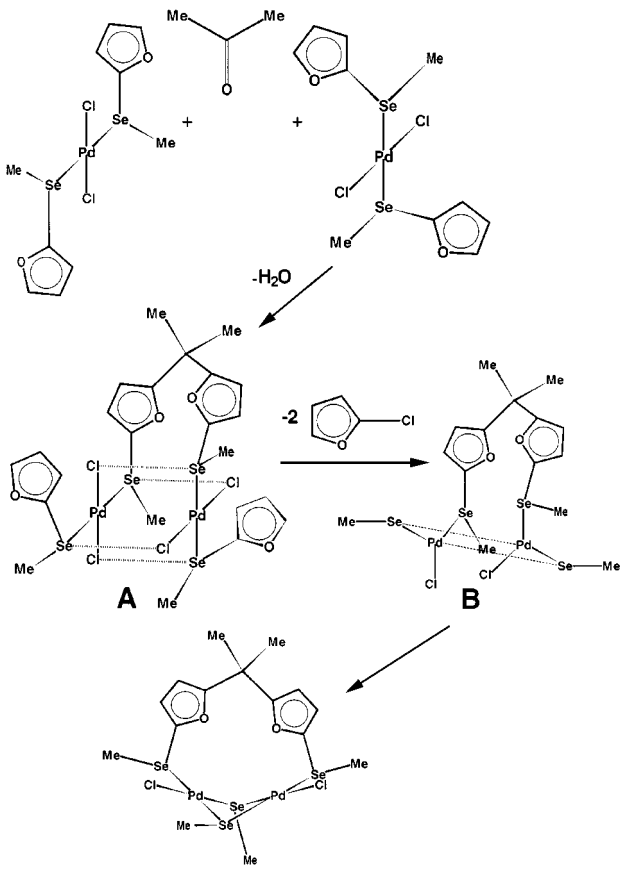

Fig. 3 Pathway of the dimerization of **1**.

Notes and references

† The general procedure for the preparation of $(C_4H_3E)E'Me$ and $[MCl_2\{(C_4H_3E)E'Me\}_2]$ (M = Pd, Pt; E = S, O; E′ = Se, Te) has been described earlier.[3i] Methyl(2-furyl)selane (0.20 g, 1.3 mmol) in 5 ml acetone was added into 20 ml of acetone solution of $[PdCl_2(PhCN)_2]$ (0.17 g, 0.44 mmol) and stirred for 3 h. The solution was concentrated and hexane added. The precipitate was filtered off, washed with hexane, and dried. Yield 0.18 g, 82%. Anal. Calc. for $C_{10}H_{12}Cl_2PdO_2Se_2$: C, 24.05: H, 2.42. Found: C, 24.10: H, 2.50%. $\delta_H(CDCl_3)$ 2.62 (6H, s), 6.46 (2H, dd, $^2J_{HH}$ 1.7, 3.4 Hz), 6.95 (2H, d, $^2J_{HH}$ 3.4 Hz), 7.66 (2H, d, $^2J_{HH}$ 1.7 Hz); $[(CD_3)_2CO]$ 2.85 (6H, s), 6.60 (2H, dd, $^2J_{HH}$ 2.1, 3.4 Hz), 7.05 (2H, br), 7.86 (2H, br).

‡ The ^{77}Se and $^{13}C\{^1H\}$ NMR spectra were recorded on a Bruker DPX 400 spectrometer operating at 76.31 and 100.61 MHz for ^{77}Se and ^{13}C, respectively. The solvent, $CDCl_3$ or $(CD_3)_2CO$, served as an internal ^2H lock. Saturated solution of SeO_2(aq) was used as an external standard for the ^{77}Se chemical shifts and $SiMe_4$ as an internal standard for the ^{13}C chemical shifts. The ^{77}Se chemical shifts are reported relative to neat Me_2Se, $[\delta(Me_2Se) = \delta(SeO_2) + 1302.6]$ and the ^{13}C shifts relative to TMS.

§ The coupling patterns of the ^{77}Se resonances in *trans*-$[PdCl_2\{(C_4H_3S)SeMe\}_2]$ **3** and *trans*-$[PtCl_2\{(C_4H_3S)SeMe\}_2]$ **4** are identical to that of **1** indicating that the structures of all three complexes **1**, **3** and **4** are similar.

¶ We were unable to obtain crystals from chloroform solution.

‖ *Crystal data* for $C_{15}H_{22}O_2Cl_2Pd_2Se_4$: M = 833.87, triclinic, $P\bar{1}$, a = 9.640(2), b = 11.557(2), c = 12.535(3) Å, α = 100.17(3), β = 105.38(3), γ = 113.52(3)°, U = 1170.0(4) Å^3, Z = 2, D_c = 2.367 g cm^{-3}, $F(000)$ = 780, μ = 7.995 mm^{-1}, T = 293 K, crystal dimensions 0.1 × 0.2 × 0.2 mm. Reflections (14164 total, 4310 unique, R_{int} = 0.0854) were collected on a Nonius Kappa CCD diffractometer using Mo-Kα radiation (λ = 0.71073 Å). Empirical absorption correction was applied to the net intensities.[4] The structure was solved by direct methods[5a] and refined on F^2.[5b] R_1 = 0.0481 and wR_2 = 0.1148 [for 2993 reflections with $F_o > 4\sigma(F_o)$] [R_1 = 0.0815 and wR_2 = 0.1302 (all data)]. CCDC 182/1175. See http://www.rsc.org/suppdata/cc/1999/585/ for crystallographic files in .cif format.

1 S. G. Murray and F. R. Hartley, *Chem. Rev.*, 1981, **81**, 365; H. J. Gysling, *Coord. Chem. Rev.*, 1982, **42**, 133; H. Gysling, in *The Chemistry of Organic Selenium and Tellurium Compounds*, ed. S. Patai and Z. Rappoport, Wiley, New York 1986, vol. 1, p. 221; E. G. Hope and W. Levason, *Coord. Chem. Rev.*, 1993, **122**, 109.

2 T. Kemmit and W. Levason, *Inorg. Chem.*, 1990, **29**, 731; P. L. Goggin, R. J. Goodfellow and S. R. Haddock, *J. Chem. Soc., Chem. Commun.*, 1975, 176; H. J. Gysling, N. Zumbulyadis and J. A. Robertson, *J. Organomet. Chem.*, 1981, **209**, C41.

3 (*a*) P. E. Skakke and S. E. Rasmussen, *Acta Chem. Scand.*, 1970, **24**, 2634; (*b*) H. J. Gysling, H. R. Luss and D. L. Smith, *Inorg. Chem.*, 1979, **18**, 2696; (*c*) R. K. Chadha, J. M. Chehayber and J. E. Drake, *Inorg. Chem.*, 1986, **25**, 611; (*d*) T. Kemmitt, W. Levason and M. Webster, *Inorg. Chem.*, 1989, **28**, 692; (*e*) T. Kemmitt, W. Levason, M. D. Spicer and M. Webster, *Organometallics*, 1990, **9**, 1181; (*f*) T. Kemmitt, W. Levason, R. D. Oldroyd and M. Webster, *Polyhedron*, 1992, **11**, 2165; (*g*) W. Levason, M. Webster and C. J. Mitchell, *Acta Crystallogr., Sect. C*, 1992, **48**, 1931; (*h*) J. E. Drake, J. Yang, A. Khalid, V. Srivastava and A. K. Singh, *Inorg. Chim. Acta*, 1997, **254**, 57; (*i*) R. Oilunkaniemi, J. Komulainen, R. S. Laitinen, M. Ahlgrén and J. Pursiainen, *J. Organomet. Chem.*, 1998, **571**, 129.

4 SHELXTL, Bruker AXP Inc., Madison, Wisconsin 53719, USA, 1997.

5 (*a*) G. Sheldrick, SHELXS-97, University of Göttingen, Germany, 1997; (*b*) G. Sheldrick, SHELXL-97, University of Göttingen, Germany, 1997.

6 R. G. Ackman, W. H. Brown and G. F. Wright, *J. Org. Chem.*, 1955, **20**, 1147; W. H. Brown and W. N. French, *Can. J. Chem.*, 1958, **36**, 371; S. Tanaka and H. Tomokuni, *J. Heterocycl. Chem.*, 1991, **28**, 991; M. De Sousa Healy and A. J. Rest, *J. Chem. Soc., Chem. Commun.*, 1981, 149; *J. Chem. Soc., Perkin Trans. 1*, 1985, 973.

7 A. Hazell, *Acta Crystallogr., Sect. C*, 1989, **45**, 137.

8 A. Khanna, B. L. Khandelwal, A. K. Saxena and T. P. Singh, *Polyhedron*, 1995, **14**, 2705.

Communication 8/09111K

Rapid and highly base selective RNA cleavage by a dinuclear Cu(II) complex

Shanghao Liu and Andrew D. Hamilton*

Department of Chemistry, Yale University, New Haven, CT, 06520, USA. E-mail: andrew.hamilton@yale.edu

Received (in Columbia, MO, USA) 21st October 1998, Accepted 9th February 1999

A bis-Cu(II) complex based on a covalently linked terpyridine and bipyridine ligand system is shown to rapidly cleave bis-ribonucleotides with remarkable selectivity for adenine bases.

Currently there is a great deal of interest in the design of catalysts for rapid and base selective RNA hydrolysis.[1,2] Such artificial ribonucleases may be useful as novel therapeutic agents for cancer and viral diseases[2f–i,3–5] or as chemical probes for RNA sequencing and structure mapping.[6] However, despite much effort none of the RNA cleaving agents developed so far has achieved the level of activity afforded by natural ribonucleases. Moreover, selective cleavage at specific base sites is a hallmark of the ribonucleases but is seen in few synthetic systems. We recently showed that dinuclear Cu(II) complex **1**

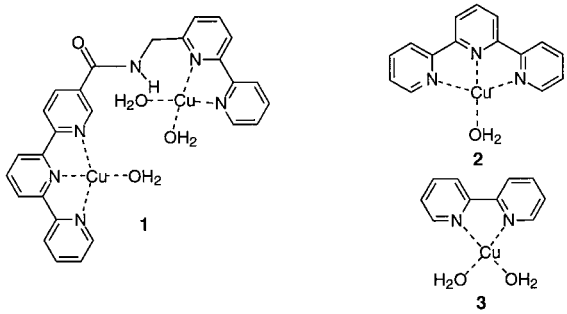

not only is more active than mononuclear complexes **2** and **3** but also exhibits remarkable base selectivity in promoting the hydrolytic cleavage of ribonucleoside 2′,3′-monophosphates, intermediates in RNA cleavage by natural ribonucleases.[7] We have now found that **1** is also highly active in promoting the hydrolysis of ribonucleotides and report here on this metal-based artificial ribonuclease that shows both potency and base selectivity.

Complex **1** was prepared as described previously.[8] The hydrolysis of RNA dimers in the presence of excess **1** was followed by HPLC.† The reaction proceeded by a transesterification–hydrolysis mechanism with ribonucleoside 2′,3′-monophosphates as intermediates (Scheme 1). All reactions followed first-order kinetics.The pH–rate profile in Fig. 1 shows

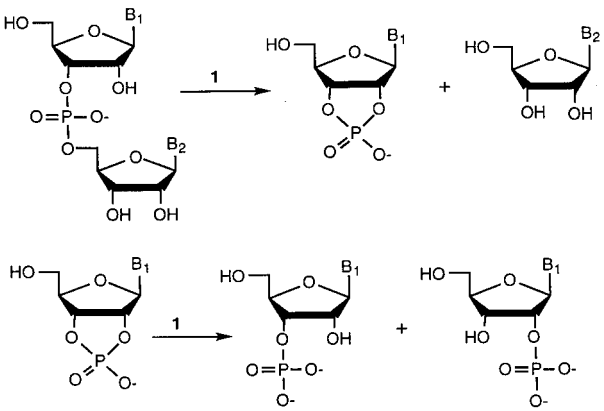

Scheme 1 Hydrolysis of RNA dimers in the presence of **1**–**3**. B_1 and B_2 are nucleobases.

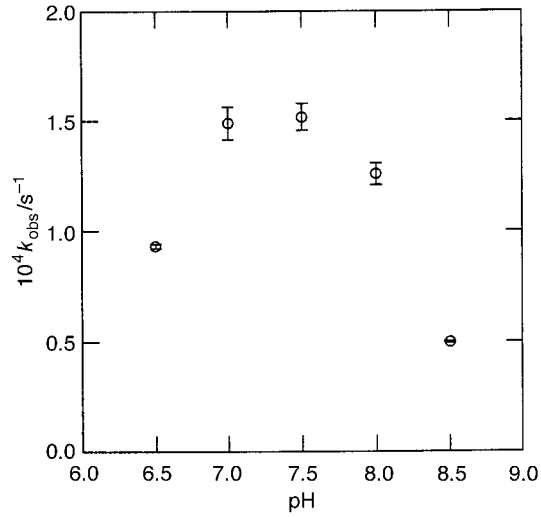

Fig. 1 pH–rate profile for the hydrolysis of ApA in the presence of **1** at 25 °C. [ApA] = 0.1 mM, [**1**] = 2.0 mM. The reaction media at pH 7.0, 7.5 and 8.0 are the HEPES buffers (0.05 M); that at pH 8.5 is the AMPSO buffer (0.05 M) and that at pH 6.5 is the MES buffer (0.05 M).

that **1** reaches its maximum activity at pH 7.5, consequently all other reactions were carried out at this pH. Table 1 summarizes the first-order rate constants and relative rates for the hydrolysis of six RNA dimers in the presence of dinuclear **1** and mononuclear **2**. All reactions with **2** as catalyst were carried out at pH 8.0 because previous work by Chin and coworkers found that related complexes reached their maximum activity near this pH in catalyzing the hydrolysis of ApA.[2c] The hydrolysis of RNA dimers in the presence of **3** was too slow to allow accurate determination of the first-order rate constants.

The remarkable base selectivity of dinuclear complex **1** is evident from the relative rates for different RNA dimers in Table 1. As in the hydrolysis of nucleoside 2′,3′-cyclic monophosphate, **1** is highly selective for adenine, hydrolyzing ApA 12, 17 and 87 times faster than CpC, UpU and GpG, respectively. The intrinsic differences in hydrolysis rate for the different dinucleotides (caused presumably by intra- or intermolecular interactions) are much smaller, with purine–purine

Table 1 First-order rate constants (k_{obs}) and relative rates (k_{rel}) for the hydrolysis of RNA in the presence of dinuclear Cu(II) complex **1** and mononuclear Cu(II) complex **2**

	Cu(II) complex **1**[a]		Cu(II) complex **2**[b]	
Substrate	$10^6 k_{obs}/s^{-1}$	k_{rel}	$10^7 k_{obs}/s^{-1}$	k_{rel}
ApA	152 ± 5	87	45 ± 2	7.8
CpC	13.2 ± 0.2	7.5	18 ± 0.1	3.1
UpU	8.7 ± 0.2	5.0	5.8 ± 0.5	1.0
GpG	1.75 ± 0.19	1.0	11.8 ± 0.2	2.0
ApC	49 ± 0.3	28	—	—
CpA	53 ± 1.0	30	—	—

[a] In pH 7.5 HEPES buffer (0.05 M) at 25 °C; [RNA] = 0.1 mM, [**1**] = 2.0 mM. [b] In pH 8.0 HEPES buffer (0.05 M) at 25 °C; [RNA] = 0.1 mM, [**2**] = 2.0 mM.

Table 2 Relative rates (k_{rel}) for the hydrolysis of RNA and nucleoside 2′,3′-monophosphates in the presence of dinuclear Cu(II) complex **1**

Substrate	k_{rel}	Substrate	k_{rel}[a]
ApA	87	2′,3′-cAMP	31
CpC	7.5	2′,3′-cCMP	5.2
UpU	5.0	2′,3′-cUMP	3.0
GpG	1.0	2′,3′-cGMP	1.0

[a] Calculated from the first-order rate constants (k_{obs}) in ref. 7.

sequences (*e.g.* ApA) being among the slowest.[9] Replacement of either adenine group in ApA by a cytidine group diminished the rate of **1**-catalysed hydrolysis threefold. This level of base selectivity is unprecedented in a simple metal-based ribonuclease mimic that lacks any appended recognition elements (such as oligonucleotide strands). Dinuclear complex **1** is also highly active: at a concentration of 2.0 mM it provides over five orders of magnitude rate acceleration for the hydrolysis of its best substrate, ApA.[10] The data in Table 1 also show that mononuclear complex **2** has moderate selectivity for adenine. Apparently, attachment of a bipyridine–Cu(II) unit to **2** not only increases its activity but also amplifies its base selectivity.

We have suggested[7] that a strong π–π stacking interaction between adenine and the bipyridine–Cu(II) unit may be the principal reason for the high selectivity of **1** for adenine in **1**-catalyzed hydrolysis of nucleoside 2′,3′-cyclic monophosphates. This same interaction also appears to be responsible for the base selectivity shown by **1** in promoting the hydrolysis of RNA. First, the base selectivities for the dinucleotide and cyclic monophosphate substrates parallel each other, as can be seen in Table 2. Second, the high selectivity of **1** for adenine in the hydrolysis of RNA dimers is insensitive to the position of the adenine group relative to the phosphate bond to be cleaved since ApC and CpA have almost identical reactivity (Table 1). These observations are more consistent with association through a less specific π–π stacking rather than more directed interactions such as hydrogen bonding and metal coordination to the nucleobases as major sources of base selectivity. Face-to-face stacking provides an interaction that is adaptable to different nucleobase positions. If hydrogen bonding or metal coordination from **1** to the nucleobases were important in stabilizing the interaction, it is probable that different base selectivities between the RNA dimers and nucleoside 2′,3′-cyclic monophosphates would result due to the different orientations and flexibilities in the two sets of substrates. Likewise, ApC and CpA should also show quite different reactivities due to the different positions of adenine in the two substrates.

In conclusion, dinuclear Cu(II) complex **1** has been shown to function as a highly active artificial ribonuclease. In addition, a remarkable selectivity among the different nucleotide bases is seen with particularly effective cleavage of adenine-containing substrates. We are currently extending these dinuclear Cu(II) complex designs to enhance the level of activity and to alter the base selectivity.

This work was supported by the National Institutes of Health (GM 53579).

Notes and references

† Hydrolysis of RNA dimers by **1** was followed by HPLC (Ranin). The following procedure is typical: 2.85 mL of **1** (2.1 mM) in a buffer solution was mixed with 0.15 mL of an RNA dimer (2.0 mM) in deionized H_2O. Aliquots (300 μL) of the reaction mixture were quenched with 50 mM EDTA (300 μL). After filtration, the quenched solution (15 μL) was injected onto a C-18 reversed-phase column and eluted for 10–15 min with 0–15% MeCN in H_2O containing 0.1% CF_3CO_2H (flow rate = 1.0 mL min^{-1}). The eluent was monitored at λ_{max} of the nucleobase (260 nm for adenine and uracil, 252 nm for guanine and 268 nm for cytidine) by a Ranin UV detector. The first-order rate constants (k_{obs}) were obtained as slopes of plots of $\ln(A_0/A_t)$ *vs.* *t*, where A_0 and A_t are the integrations of the areas of the HPLC peaks for the RNA dimer at $t = 0$ and *t*, respectively.

1 Reviews: B. N. Trawick, A. T. Daniher and J. K. Bashkin, *Chem. Rev.*, 1998, **98**, 939; M. Komiyama, *J. Biochem.*, 1995, **118**, 665; J. R. Morrow, *Adv. Inorg. Biochem.*, 1994, **9**, 41; M. W. Gobel, *Angew. Chem.*, 1994, **106**, 1201; *Angew. Chem., Int. Ed. Engl.*,1994, **33**, 1141; D. S. Sigman, A. Mazumder and D. M. Perrin, *Chem. Rev.*, 1993, **93**, 2295; J. Chin, *Acc. Chem. Res.*, 1991, **24**, 145.

2 Recent examples: (*a*) P. Hurst, B. K. Takasaki and J. Chin, *J. Am. Chem. Soc.*, 1996, **118**, 9982; (*b*) M. J. Young and J. Chin, *ibid.*, 1995, **117**, 10 577; (*c*) B. Linkletter and J. Chin, *Angew. Chem.*, 1995, **107**, 529; *Angew. Chem., Int. Ed. Engl.*, 1995, **34**, 472; (*d*) W. H. Chapman, Jr. and R. Breslow, *J. Am. Chem. Soc.*, 1995, **117**, 5462; (*e*) M. Yashiro, A. Ishikubu and M. Komoyama, *Chem. Commun.*, 1997, 83; (*f*) M. Yashiro, A. Ishikubu and M. Komiyama, *J. Chem. Soc., Chem. Commun.*, 1995, 1793; (*g*) M. Komiyama, N. Takeda, M. Irisawa and M. Yashiro, in *DNA and RNA Cleavers and Chemotherapy of Cancer and Viral Diseases*, ed. B. Meunier, Kluwer Academic Publishers, Boston, 1996, p. 321; (*h*) J. K. Bashkin, J. Xie, A. T. Daniher, L. A. Jenkins and G. C. Yeh, *ibid.*, p. 355; (*i*) R. Haner, J. Hall, D. Husken and H. E. Moser, *ibid.*, p. 307; (*j*) D. Magda, R. A. Miller, M. Wright and J. Rao, *ibid.*, p. 337; (*k*) J. R. Morrow and V. M. Shelton, *New J. Chem.*, 1994, **18**, 371; (*l*) R. Ott and R. Krämer, *Angew. Chem., Int. Ed.*, 1998, **37**, 1957.

3 C. A. Stein and J. S. Cohen, *Cancer Res.*,1988, **48**, 2659.

4 E. Uhlmann and A. Peyman, *Chem. Rev.*, 1990, **90**, 543.

5 J. F. Milligan, M. D. Matteucci and J. C. Martin, *J. Med. Chem.*, 1993, **36**, 1923.

6 For the techniques currently available for RNA sequencing and structure mapping see: T. D. Tullus, in *Bioorganic Chemistry: Nucleic Acids*, ed. S. M. Hecht, Oxford University Press, New York, 1996, p. 1244.

7 S. Liu, Z. Luo and A. D. Hamilton, *Angew. Chem., Int. Ed. Engl.*, 1997, **36**, 2678.

8 S. Liu and A. D. Hamilton, *Bioorg. Med. Chem. Lett.*, 1997, **7**, 1779.

9 T.Koike and Y. Inoue, *Chem. Lett.*, 1972, 569.

10 The background rate of hydrolysis of ApA at pH 7.5 is *ca.* 1.6×10^{-10} s^{-1}, see Y. Matsumoto and M. Komiyama, *J. Chem. Soc., Chem. Commun.*, 1990, 1050; K. Yoshinari and M. Komiyama, *Chem. Lett.*, 1990, 519.

Communication 8/08195F

Synthesis and reactions of metallo-diethynylbenzenes: building blocks for redox-active poly(phenyleneethynylene)s†

Kevin D. John and Michael D. Hopkins*

Department of Chemistry, University of Pittsburgh, Pittsburgh, Pennsylvania 15260, USA. E-mail: mdh1@vms.cis.pitt.edu

Received (in Bloomington, IN, USA) 25th November 1998, Accepted 8th February 1999

The metallo-diethynylbenzene complex W(≡CC_6H_4C≡CH-4)(dmpe)$_2$Cl, a precursor to metal-containing poly(phenyleneethynylene)s, has been prepared using alkyne-metathesis methodology and can be coupled into unsaturated organic frameworks at both the ethynyl moiety and the tungsten center and one-electron oxidized to the open-shell cation.

The unsaturation and limited conformational flexibility of phenylacetylenes (and, more generally, arylacetylenes) imparts to the polymeric materials derived from them extended π-electron systems and well defined lengths and shapes, respectively. These attributes have made poly(aryleneethynylene)s[1] the subjects of intensive research as regards their potential applications to molecular electronics,[2] photonics[3] and chemical sensing.[4] Control over the properties of poly(aryleneethynylene)s is achieved typically by changing the polymer terminating groups and the nature and connectivity of the aryl hubs. Here, we describe a different approach to functionalizing poly(aryleneethynylene)s: the replacement of triply bonded carbon atoms in the backbone with triply bonded metal centers of metal–alkylidyne complexes.[5]

Covalent alkylidyne-containing polymers analogous to poly(aryleneethynylene)s have not yet been prepared, although metal–alkylidyne coordination polymers[6] and poly(aryleneethynylene)s to which metal centers are externally coordinated[7] have been reported. Recently, Mayr *et al.* reported an important advance toward this objective with their synthesis of Fischer-type alkylidyne compounds of the form W(≡CC_6H_4I-4)$(CO)_2$(LL)X (LL = tmeda, dppe; X = Cl, Br, I),[8] which undergo cross-coupling reactions with phenylacetylenes to give compounds with phenyleneethynylene alkylidyne ligands. Simultaneously, we have been seeking to develop routes to related compounds based on Schrock's alkyne-metathesis reaction[9] because of the ease with which this methodology allows the synthesis of complexes with unsaturated alkylidyne ligands and the fact that the W(≡CR)$(OR')_3$ metathesis products allow access[10] to carbonyl-free derivatives of the type W(≡CR)L_4X. This latter point is important because W(CR)$(CO)_nL_{4-n}$X compounds typically exhibit electrochemically irreversible oxidative processes,[11] which could limit their use as building blocks for redox-active polymers. Herein we report the synthesis, *via* an alkyne-metathesis route, of W(≡CC_6H_4C≡CH-4)$(dmpe)_2$Cl **4** (dmpe = $Me_2PCH_2CH_2PMe$), some reactions that lead to its incorporation into unsaturated organic frameworks, and its redox chemistry.

Our general strategy for synthesizing compounds of the type W(≡CArC≡CH)L_4X is to begin with readily prepared unsymmetrical diynylarenes (RC≡CArC≡CR′) into which the organic functionality of importance to the properties of the final compound is preincorporated, thus minimizing the number of reaction procedures necessary once the metal center is present. The terminal C≡CH unit of the target compound is masked in the starting diynylarene by a protecting R group that is sufficiently sterically demanding to prevent alkyne metathesis at the adjacent C≡C bond. The synthetic procedure for **4** using this approach is outlined in Scheme 1. For this compound the unsymmetrical diynylarene is *p*-$Pr^nC{\equiv}CC_6H_4C{\equiv}CSiPr^i_3$, which undergoes metathesis with $W_2(OBu^t)_6$[12] exclusively at the propynyl C≡C bond to give W(≡CC_6H_4C≡C$SiPr^i_3$-4)$(OBu^t)_3$ **1**.‡ Reaction of **1** with BCl_3 and dme,[10] provides W(≡CC_6H_4C≡C$SiPr^i_3$-4)Cl_3(dme) **2**,‡ which undergoes two-electron reduction by Na/Hg amalgam in the presence of dmpe to give W(≡CC_6H_4C≡C$SiPr^i_3$-4)$(dmpe)_2$Cl **3**.‡ The target terminal ethynyl derivative **4** is then obtained by protodesilylation of **3** with $[NBu^n_4]F{\bullet}xH_2O$.‡

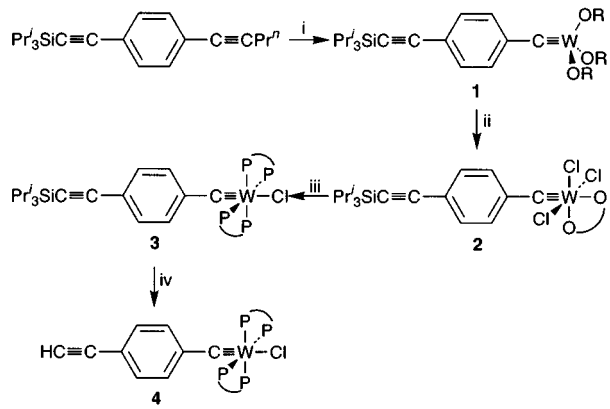

Scheme 1 *Reagents:*‡ i, 0.5 $W_2(OBu^t)_6$; ii, 3 BCl_3, dme (excess); iii, 2 dmpe, 2 Na/Hg; iv, $[NBu^n_4]F{\bullet}xH_2O$ (excess).

Compound **4** can be incorporated into extended unsaturated organic frameworks by functionalization at both the metal center and the terminal ethynyl moiety. A survey of representative reactions at these loci is presented in Scheme 2. Crucially, the fingerprint spectroscopic parameters of the ethynyl moiety (^{1}H NMR δ 2.92, $\nu_{C\equiv C}$ 2099 cm^{-1}) indicate that it is not strongly electronically perturbed relative to phenylacetylene (δ 2.93,

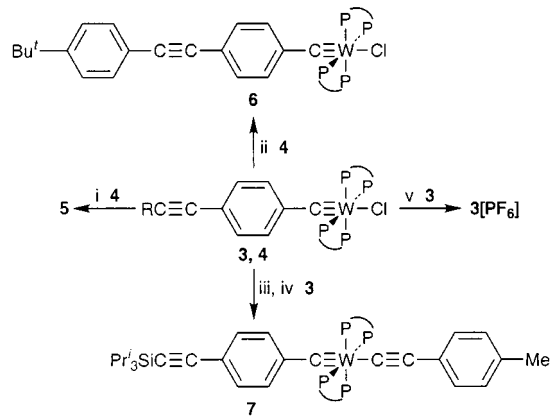

Scheme 2 *Reagents and conditions*: i, $Li[N(SiMe_3)_2]$ (1 equiv.), THF, –78 °C (10 min), MeI (excess), 0 °C (2 h); ii, *p*-$IC_6H_4Bu^t$ (1 equiv.), $PdCl_2(PPh_3)_2$/CuI (cat.), NEt_2H, 25 °C (5 h); iii, $SiMe_3(OTf)$ (1 equiv.), toluene, 25 °C (1 h); iv, LiC≡CC_6H_4Me-4 (1 equiv.), DME, 0 °C (1 h), 25 °C (1 h); v, $[C_7H_7][PF_6]$ (1 equiv.), CH_2Cl_2–MeCN (1 : 1), 0 °C (1 h).

† Dedicated to Professor Warren R. Roper on the occasion of his 60th birthday.

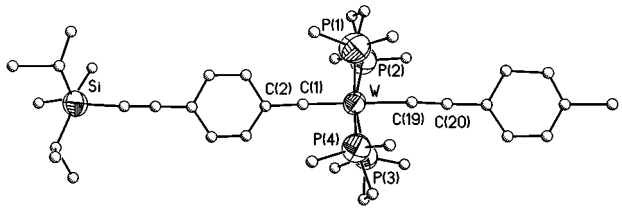

Fig. 1 Structure of W(≡CC_6H_4C≡CSiPr^i_3-4)$(dmpe)_2$(C≡CC_6H_4Me-4) **7**. Atoms are represented by spheres of arbitrary size (C) or thermal ellipsoids drawn at the 50% probability level (W, P, Si). Hydrogen atoms are omitted for clarity. Selected bond distances (Å) and angles (°): W–C(1) 1.93(3), W–C(19) 2.11(3), W–P_{av} 2.42[1]; C(1)–W–C(19) 179.3(12), C(20)–C(19)–W 174(3), C(1)–W–P_{av} 95.0(9), C(2)–C(1)–W 175(2).

2109 cm^{-1}) by the *p*-C≡W$(dmpe)_2$Cl group, and, thus, that its characteristic reactivity should be preserved. Consistent with this hypothesis, the ethynyl group of **4** can be deprotonated with Li[$N(SiMe_3)_2$] and subsequently methylated with MeI to give W(≡CC_6H_4C≡CMe-4)$(dmpe)_2$Cl **5**.‡ More importantly, the ethynyl group participates in Pd-catalyzed cross-coupling reactions with aryl halides: the reaction between **4** and *p*-$IC_6H_4Bu^t$ under standard conditions produces W[≡CC_6H_4(C≡$CC_6H_4Bu^t$-4)-4]$(dmpe)_2$Cl **6**‡ in nearly quantitative yield. At the tungsten center, substitution of the chloride ligand by unsaturated hydrocarbyl ligands can also be readily achieved. Treatment of **3** with $Me_3Si(OTf)$ to yield W(≡CC_6H_4C≡CSiPr^i_3-4)$(dmpe)_2$(OTf) followed by reaction with LiC≡CC_6H_4Me-4 provides W(≡CC_6H_4C≡CSiPr^i_3-4)$(dmpe)_2$(C≡CC_6H_4Me-4) **7**.‡ The structure of **7** (Fig. 1) is not of sufficient quality to provide quantitative insights but is interesting for the fact that it reveals that the phenyl rings are nearly coplanar, consistent with extended π conjugation in this compound.

In addition to the reaction chemistry of **3** and **4** that allows extension of their unsaturated frameworks, these compounds can be cleanly oxidized by one electron ($E_{1/2} \cong -0.8$ V *vs.* $FeCp_2^{0/+}$ in THF);[11b] accordingly, the reaction between **3** and [C_7H_7][PF_6] provides orange [W(≡CC_6H_4C≡CSiPr^i_3-4)$(dmpe)_2$Cl][PF_6] (**3**[PF_6], Scheme 2).‡ The molecular structure of **3** (unpublished results) is very similar to that of closely related [W(≡CPh)$(dmpe)_2$Br]$^+$[13] and we presume that it, too, possesses a $(d_{xy})^1$ electron configuration.

The electronic spectra of **3**–**7** indicate that their π-electron systems are extensively delocalized. These spectra exhibit characteristic bands attributable to the $(d_{xy})^2 \rightarrow (d_{xy})^1(d_{xz},d_{yz})^1$ [n→π*(W≡CR)] transition[13,14] as the lowest-energy features. This band strongly red shifts as unsaturated moieties are added to the alkylidyne ligand or to the axial site of the metal. Specifically, as the *para*-substituent on the alkylidyne ligand is changed from H [W(≡CPh)$(dmpe)_2$Cl] to C≡CSiPr^i_3 (**3**) to C≡$CC_6H_4Bu^t$-4 (**6**) the n→π* band shifts progressively to lower energy (19230, 16780 and 16500 cm^{-1}, respectively). Similarly, replacing the axial chloride ligand of **3** with C≡CC_6H_4Me-4 (**7**) results in a red shift of the n→π* band from 16780 to 15870 cm^{-1}. These red shifts must be attributed to a lowering of the energy of the π* LUMO as a result of extending the π-system, since the d_{xy} orbital is nonbonding (δ symmetry) with respect to the σ and π frameworks of the backbone.

The reactivity and physical properties of **4** suggest that this compound and its relatives should be important building blocks for new classes of poly(aryleneethynylene)s with expanded optical and redox functionality. There are no obvious reasons why the metathesis-based synthetic procedure reported here should not also yield building blocks with other aryl hubs (which are incorporated at the alkyne-metathesis step) or equatorial ligands [which are added in the course of the reduction of W(≡CArCCR)Cl_3(dme)], thus providing a high level of control over their physical properties. We are presently exploring the syntheses of such compounds.

We thank the National Science Foundation for supporting this research (Grant CHE-9700451). K. D. J. acknowledges support from Andrew W. Mellon and Lubrizol fellowships.

Notes and references

‡ Preparative details for **1**–**4** and selected NMR [CD_2Cl_2, 25 °C (^{1}H) or –10 °C (^{13}C(W≡C), ^{31}P)] and IR ($\nu_{C\equiv C}$, cm^{-1}) data are as follows. **1**: $W_2(OBu^t)_6$ (0.25 g, 0.31 mmol) and *p*-Pr^nC≡CC_6H_4C≡CSiPr^i_3 (0.20 g, 0.62 mmol) in pentane (5 mL) were stirred together for 10 min at 25 °C and allowed to stand for 12 h at –35 °C. Removal of solvent under vacuum at 25 °C gave **1** as a red–brown oil (0.31 g, 0.46 mmol, 74% yield). ^{1}H, δ 7.37 (d, 2H), 7.00 (d, 2H), 1.44 (s, 27H), 1.05 (s, 21H); ^{13}C, δ 257; IR 2159. **2**: The reaction between **1** (0.30 g, 0.45 mmol), DME (excess), and BCl_3 (1.33 mL, 1 M in heptane, 1.33 mmol),[10] gave **2** as a green powder (0.20 g, 0.31 mmol, 68% yield). ^{1}H, δ 7.66 (d, 2H), 6.76 (d, 2H), 4.42 (s, 3H), 4.26 (m, 2H), 4.07 (m, 2H), 3.90 (s, 3H), 1.12 (s, 21H); IR 2152. **3**: To a stirred, 0 °C solution of **2** (1.20 g, 1.85 mmol) in THF (150 mL) was added dmpe (0.67 g, 4.46 mmol) and Na/Hg amalgam (0.4%, 194.91 g, 3.89 mmol Na). After 12 h at 25 °C the organic phase was decanted and reduced to dryness under vacuum. The remaining solid was extracted with pentane and the extract filtered, concentrated, and layered with acetonitrile, giving **3** as a green powder (1.21 g, 1.53 mmol, 83% yield). ^{1}H, δ 7.20 (d, 2H), 6.62 (d, 2H), 1.55 (br, 8H), 1.49 (m, 12H), 1.46 (m, 12H), 1.20 (s, 21H); ^{13}C, δ 252; ^{31}P{^{1}H} 23.6; IR 2146. **4**: A stirred, –78 °C solution of **3** (0.20 g, 0.25 mmol) in THF (10 mL) was treated with [NBu^n_4]F•xH_2O (1.88 mL, 0.2 M in THF for x = 0, 0.38 mmol), warmed to 25 °C over 1 h, and then reduced to dryness under vacuum. The remaining solid was extracted with pentane and the extract filtered, concentrated, and cooled to –35 °C, giving **4** as a green powder (0.09 g, 0.14 mmol, 56% yield).^{1}H, δ 7.23 (d, 2H), 6.64 (d, 2H), 2.92 (s, 1H), 1.52 (br, 8H), 1.49 (m, 12H), 1.45 (m, 12H); ^{13}C, δ 252; ^{31}P{^{1}H}, δ 23.6; IR 2099. **5**: ^{1}H, δ 7.18 (d, 2H), 6.63 (d, 2H), 1.83 (s, 3H), 1.73 (br, 8H), 1.64 (m, 12H), 1.45 (m, 12H); ^{13}C, δ 252; ^{31}P{^{1}H} 28.5; IR 2241, 2208 (Fermi resonance). **6**: ^{1}H, δ 7.39 (d, 2H), 7.34 (d, 2H), 7.05 (d, 2H), 6.66 (d, 2H), 1.76 (br, 8H), 1.69 (m, 12H), 1.50 (m, 12H), 1.30 (s, 9H); ^{13}C, δ 253; ^{31}P{^{1}H} δ 26.8; IR 2210. **7**: ^{1}H, δ 6.98 (d, 2H), 6.89 (d, 2H), 6.86 (d, 2H), 6.73 (d, 2H), 2.22 (s, 3H), 1.77 (br, 8H), 1.68 (m, 12H), 1.62 (m, 12H), 1.08 (s, 21H); ^{13}C, δ 255; ^{31}P{^{1}H}, δ 21.3; IR 2145, 2060. **3**[PF_6]: IR 2149.

§ *Crystallographic data* for **7**: $C_{37}H_{100}ClP_4SiW$, M = 916.44, monoclinic, space group $P2_1/n$, a = 8.977(9), b = 30.30(3), c = 16.45(2) Å, β = 95.23(9)°, V = 4455(8) Å^3, Z = 4, μ = 2.847 mm^{-1}, T = 213 K, 5218 reflections measured, 4784 independent reflections, $R1$ [$I > 2\sigma(I)$] = 0.1279, $wR2$ [$I > 2\sigma(I)$] = 0.2811. Crystals of **7** diffracted weakly due to their small size; only the W, P and Si atoms could be successfully anistropically refined. CCDC 182/1174. See http://www.rsc.org/suppdata/cc/1999/589/ for crystallographic files in .cif format.

1 R. Giesa, *J. Macromol. Sci., Rev. Macromol. Chem. Phys.*, 1996, **C36**, 631.
2 P. S. Weiss, L. A. Bumm, T. D. Dunbar, T. P. Burgin, J. M. Tour and D. L. Allara, in *Molecular Electronics: Science and Technology*, ed. A. Aviram and M. Ratner, New York Academy of Sciences, New York, 1998, p. 145.
3 J. S. Moore, *Acc. Chem. Res.*, 1997, **30**, 402; W. Holzer, A. Penzkofer, S.-H. Gong, A. P. Davey and W. J. Blau, *Opt. Quantum. Electron.*, 1997, **29**, 713; W. Zhao, H. Li, R. West and J. C. Wright, *Chem. Phys. Lett.*, 1997, **281**, 105.
4 T. M. Swager, *Acc. Chem. Res.*, 1998, **31**, 201.
5 (*a*) A. Mayr and S. Ahn, *Adv. Transition Met. Coord. Chem.*, 1996, **1**, 1; (*b*) H. Fischer, P. Hofmann, F. R. Kreissl, R. R. Schrock, U. Schubert and K. Weiss, *Carbyne Complexes*, VCH, Amsterdam, 1988; (*c*) M. A. Gallop and W. R. Roper, *Adv. Organomet. Chem.*, 1986, **25**, 121.
6 T. P. Pollagi, S. J. Geib and M. D. Hopkins, *J. Am. Chem. Soc.*, 1994, **116**, 6051; H. A. Brison, T. P. Pollagi, T. C. Stoner, S. J. Geib and M. D. Hopkins, *Chem. Commun.*, 1997, 1263.
7 A. Harriman and R. Ziessel, *Coord. Chem. Rev.*, 1998, **171**, 331.
8 M. P. Y. Yu, K.-K. Cheung and A. Mayr, *J. Chem. Soc., Dalton Trans.*, 1998, 2373.
9 J. S. Murdzek and R. R. Schrock in ref. 5(*b*), p. 147.
10 M. A. Stevenson and M. D. Hopkins, *Organometallics*, 1997, **16**, 3572.
11 (*a*) E. O. Fischer, M. Schluge and J. O. Besenhard, *Angew. Chem., Int. Ed. Engl.*, 1976, **15**, 683; (*b*) D. E. Haines and M. D. Hopkins, in preparation.
12 M. H. Chisholm, B. W. Eichhorn, K. Folting, J. C. Huffman, C. D. Ontiveros, W. E. Streib and W. G. Van Der Sluys, *Inorg. Chem.*, 1987, **26**, 3183.
13 J. Manna, T. M. Gilbert, R. F. Dallinger, S. J. Geib and M. D. Hopkins, *J. Am. Chem. Soc.*, 1992, **114**, 5870.
14 A. B. Bocarsly, R. E. Cameron, H.-D. Rubin, G. A. McDermott, C. R. Wolff and A. Mayr, *Inorg. Chem.*, 1985, **24**, 3976.

Communication 8/09231A

Novel glycosylidene-spiro-heterocycles from unprecedented solvent incorporation in Koenigs–Knorr-like reactions of *C*-(1-bromo-1-deoxy-β-D-glycopyranosyl)formamides

László Somsák,* László Kovács, Viktor Gyóllai and Erzsébet Ősz

Department of Organic Chemistry, Lajos Kossuth University, Debrecen, POB 20, H-4010 Hungary. E-mail: somsak@tigris.klte.hu

Received (in Liverpool, UK) 4th January 1999, Accepted 22nd February 1999

The title compounds give glycopyranosylidene-spiro-dioxolanes 3 and 4 in acetone and *C*-(1-methylsulfanylmethoxy-α-D-glycopyranosyl)formamides 5 in DMSO in the presence of Ag_2CO_3 and AgF, respectively.

As part of an ongoing program to synthesize new anomerically bifunctional monosaccharide derivatives[1–3] as glycomimetics and their precursors we have investigated the reactions of acetylated *C*-(1-bromo-1-deoxy-β-D-glycopyranosyl)formamides (**1a**[3] and **1b**[4]) with nucleophiles under Koenigs–Knorr conditions.[5] While reaction of **1a**,**b** with 1 equiv. of water in DMSO in the presence of Ag_2O (Scheme 1) gave the expected hydroxyformamide derivatives **2a**,**b** in a crystalline state[6] [**2a**: 85%, mp 177–179 °C, $[\alpha]_D$ +36 ($CHCl_3$, *c* 1.03); **2b**: 89%, mp 143–144 °C, $[\alpha]_D$ +53 ($CHCl_3$, *c* 1.0)], a similar transformation of **1b** in acetone[7] produced the spiro compound **3b** in addition to **2b** (ratio ~1:1 by ^1H NMR spectroscopy). Using dry acetone with Ag_2CO_3 gave **3a**,**b** [**3a**: 78%, mp 165–167 °C, $[\alpha]_D$ +21 ($CHCl_3$, *c* 1.0); **3b**: 71%, mp 155–157 °C, $[\alpha]_D$ +31 ($CHCl_3$, *c* 1.0)] and small amounts of **4a**,**b** [**4a**: 6%, syrup, $[\alpha]_D$ +39, ($CHCl_3$, *c* 2.06); **4b**: 4%, syrup, $[\alpha]_D$ +57, ($CHCl_3$, *c* 1.06)] and **2a**,**b** (~5% for each) after chromatographic separation. Carrying out the reaction in dry DMSO with AgF the methylsulfanylmethoxyformamides **5a**,**b** [**5a**: 11%, syrup, $[\alpha]_D$ +21 ($CHCl_3$, *c* 1.03); **5b**: 15%, mp 155–156 °C, $[\alpha]_D$ +29 ($CHCl_3$, *c* 1.07)] could be isolated as minor products over **2a**,**b**. Experiments with **2a** showed that this compound was unchanged after one day when dissolved in acetone or DMSO either in the absence or presence of Ag_2CO_3 or AgF, respectively.

Structure elucidation† of **3**–**5** was performed by NMR (Tables 1 and 2) and MS measurements. Incorporation of acetone in **3** and **4** was indicated by a molecular ion (*m/z* 431, M^+ for each) and by two methyl singlets. The presence of one exchangable proton belonging to an sp^2-hybridized nitrogen as shown by $^{15}N/^1H$ HSQC experiments, and carbon resonances indicative of an imino ether moiety (C-10) as well as for an acetal carbon (C-8) are in accordance with the cyclic stuctures. For each derivative the vicinal proton–proton couplings showed that the sugar rings existed in the $^4C_1$ conformation. The configuration of the spiro carbons was established by the three bond heteronuclear coupling between H-5 and C-10, indicating antiperiplanar arrangement for the nuclei involved in the given conformation (see Scheme 1). This was corroborated by the characteristic downfield shifts of the sugar protons *cis* to C-10 (H-2 and H-4 in **3a**,**b**, H-5 in **4a**,**b**) following a rule established recently for glycopyranosylidene-spiro-hydantoin derivatives.[2] This effect, which is a further indirect proof of the spirocyclic structure, is attributed to the shielding anisotropy contribution of the C=NH bond which occupies a fixed position with respect to the sugar ring.

Compounds **5** had a fragment ion (*m/z* 407, $[M - CONH_2]^+$ for each) and characteristic resonances for a $CONH_2$ group and a OCH_2SCH_3 moiety. The anomeric configurations followed from the $^3J_{H\text{-}2,CONH_2}$ couplings indicating the *trans*-diaxial relationship of the two nuclei in the $^4C_1$ conformation.

Based on the experimental data available at present we think that formation of these derivatives of novel structure can most probably be explained by participation of the solvents used. The first step probably common for each transformation may be the generation of a glycosylium ion destabilized by the electron-withdrawing $CONH_2$ substituent. This intermediate can com-

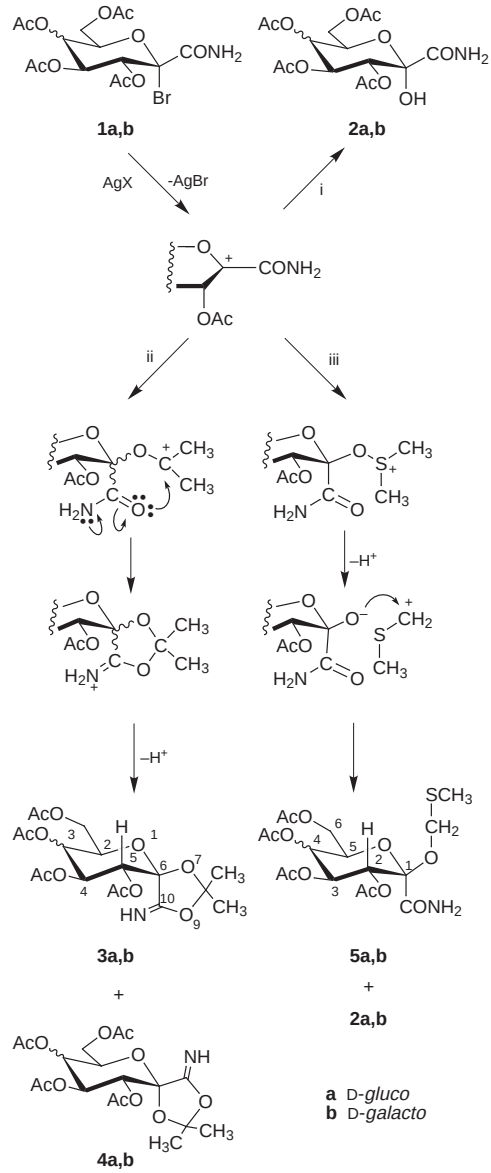

Scheme 1 *Reagents and conditions*: i, AgX = Ag_2O (1 equiv.), DMSO, H_2O (1 equiv.), 3 h, room temp.; ii, AgX = Ag_2CO_3 (1 equiv.), dry acetone, 18 h, room temp., N_2; iii, AgX = AgF (1.5 equiv.), dry DMSO, 0.5 h, room temp.

Table 1 Selected NMR data for **3** and **4** (δ/ppm, J/Hz)

	3a	**3b**	**4a**	**4b**
CH_3	1.48, 1.61	1.49, 1.69	1.61, 1.63	1.59, 1.63
CH_3	27.55, 26.91	27.63, 26.90	27.40, 26.65	27.49, 26.74
=N*H*	197.0	198.7	[a]	[a]
=N*H*	7.51	7.42	7.42	7.41
C-8	112.70	112.56	112.60	112.46
C-10	160.10	160.27	160.90	161.21
$^3J_{H\text{-}5,C\text{-}10}$	5.4	5.6	[a]	[a]
H-2 ($J_{2,3}$)	4.65 (10.2)	4.88 (1.1)	4.20 (9.5)	4.41 (1.4)
H-4 ($J_{3,4}$)	6.08 (9.8)	6.00 (3.3)	5.40 (9.0)	5.25 (3.3)
H-5 ($J_{4,5}$)	5.33 (10.2)	5.58 (10.8)	5.53 (9.8)	5.74 (11.0)

[a] Not measured because of insufficient sample quantity.

Table 2 Selected NMR data for **5**

	5a		**5b**	
	^{1}H	^{13}C	^{1}H	^{13}C
–OCH_2S–	4.78, 4.72	67.95	4.93, 4.84	67.88
–SCH_3	2.11	14.82	2.11	14.91
$CONH_2$	6.71, 5.98	168.76	6.69, 5.69	169.21
H-2 ($J_{2,3}$)	5.23 (9.0)	—	5.40 (10.6)	—
H-4 ($J_{3,4}$)	5.82 (9.0)	—	5.82 (3.2)	—
H-5 ($J_{4,5}$)	5.16 (10.0)	—	5.47 (1.4)	—
$^3J_{H\text{-}2,CONH_2}$	—	4.6	—	4.9

bine with a nucleophilic molecule present in the reaction mixture, *i.e.* water, acetone or DMSO. While deprotonation of the species obtained after combination of the glycosylium ion with a water molecule leads to the stable molecule **2**, the alkoxydimethylsulfonium intermediate (from combination with DMSO) may be deprotonated at one of the methyl groups to give **5** after a Pummerer-type rearrangement.[8] The intermediate (from combination with acetone) may be stabilized by an attack of the oxygen of the $CONH_2$ group at the positively charged carbon. The cyclic structure formed in this step can be deprotonated at the iminium moiety to result in the spirocyclic compounds **3** and **4**.

To the best of our knowledge similar solvent participation and incorporation is only known with some nitriles (mainly acetonitrile) in the sugar series.[9,10] These new, simple reactions provide ready access to novel glycopyranosylidene-spiro-heterocycles **3** and **4** that can be regarded as analogues of sugar spiro-hydantoin derivatives with important biological effects (see references in ref. 2) as well as to compounds of type **5** that can be useful orthogonally protected synthetic intermediates. The scope and limitations of the reported transformations are currently being investigated in our laboratory.

This work was supported by the Hungarian Scientific Research Fund (Grant: OTKA T 19339) and in part by OMFB (F-7/96, Hungary) and Le Ministère des Affaires Étrangères (France).

Notes and references

† Each new compound gave satisfactory elemental analysis. The NMR spectra were recorded for $CDCl_3$ solutions with reference to internal TMS in the ^{1}H, to the solvent signal in the ^{13}C, and to external NH_4Cl in the ^{15}N NMR experiments. MS: EI 70 eV.

1 L. Somsák, E. Sós, Z. Györgydeák, J.-P. Praly and G. Descotes, *Tetrahedron*, 1996, **52**, 9121.
2 E. Ősz, E. Sós, L. Somsák, L. Szilágyi and Z. Dinya, *Tetrahedron*, 1997, **53**, 5813.
3 E. Ősz, L. Somsák, L. Szilágyi, T. Docsa, B. Tóth and P. Gergely, manuscript in preparation.
4 L. Kiss and L. Somsák, *Carbohydr. Res.*, 1996, **291**, 43.
5 For a general survey on Koenigs–Knorr reactions, see: O. Lockhoff, in *Methoden der Organischen Chemie (Houben-Weyl)*, ed. H. Hagemann and D. Klamann, Thieme, Stuttgart, 1992, vol. E14a/3, p. 782.
6 These compounds have already been isolated as syrupy by-products of the reactions of **1a**,**b** with cyanate or thiocyanate ions in nitromethane (ref. 2, 3).
7 P. Z. Allen, *Methods Carbohydr. Chem.*, 1962, **1**, 372.
8 O. De Lucchi, U. Miotti and G. Modena, *Org. React.*, 1991, **40**, 157; D. Martin and G. Hauthal, *Dimethylsulfoxid*, Akademie-Verlag, Berlin, 1971, p. 302.
9 For Ritter-like reactions at the anomeric centre of monosaccharide derivatives, see as leading references: A. A. Pavia, S. N. Ung-Chhun and J.-L. Durand, *J. Org. Chem.*, 1981, **46**, 3158; D. Noort, G. A. van der Marel, G. J. Mulder and J. H. van Boom, *Synlett*, 1992, 224.
10 Our observations on the reactions of **1b** with nitriles have recently been presented: V. Gyóllai and L. Somsák, *12th International Conference on Organic Synthesis*, Venezia, Italy, June 28–July 2, 1998, OC-04, p. 25.

Communication 9/00082H

ChemComm

MCM-41–Quaternary organic tetraalkylammonium hydroxide composites as strong and stable Brønsted base catalysts

Isabel Rodriguez, Sara Iborra, Avelino Corma,* Fernando Rey and José L. Jordá

Instituto de Tecnología Química (UPV-CSIC), Avda. los Naranjos, s/n, 46022, Valencia, Spain. E-mail: itq@upvnet.upv.es

Received (in Cambridge, UK) 13th January 1999, Accepted 23rd February 1999

Quaternary organic tetraalkylammonium hydroxide grafted on MCM-41 is a strong Brønsted base catalyst, and represents a useful alternative to soluble bases in reactions such as Knoevenagel condensations, Michael additions and aldol condensations because of their high catalytic activity under mild conditions, and good stability.

The development of environmentally friendly solid catalysts for the production of fine chemicals is becoming an area of growing interest, and recyclable solid base catalysts are needed. Alkali ion-exchanged zeolites,[1,2] sepiolites,[3] alkaline oxides supported on microporous [4,5] and mesoporous aluminosilicates,[6] alkaline earth solids such as magnesium oxide,[7] aluminium–magnesium mixed oxides derived from hydrotalcites[8] and organic resins[9] can cover a wide range of basic strengths. The recently discovered family of mesoporous MCM-41 materials, with the possibility of being prepared with a wide range of pore dimensions, provides a unique inorganic support for introducing basic sites in a post-synthesis step and expanding the possibilities of the above described solid catalysts. Indeed, the reported anchored amines on MCM-41,[10] *e.g.* the immobilized 1,5,7-triazabicyclo[4.4.0]dec-5-ene on MCM-41,[11] have been shown to be efficient base catalysts. However, excluding anionic resins, the basicity of the solid inorganic catalysts developed up to now is associated with Lewis sites, and there is a need for stable catalysts containing Brønsted basic sites.

Here we report the preparation of a strong Brønsted basic catalyst obtained by preparing an inorganic–organic composite formed by an organic ammonium quaternary salt anchored on the surface of pure silica MCM-41. The truly catalytic behaviour of this material as well as the recycling characteristics is shown for Knoevenagel condensations, Michael additions and aldol condensations.

Pure silica MCM-41 with 3.7 nm pore diameter was synthesised following a well-known method from the literature.[12]

The functional tetraalkylammonium groups were anchored on the Si-MCM-41 surface by reacting 3-trimethoxysilylpropyl(trimethyl)ammonium chloride ($SiNR_4Cl$) with hydroxy groups located at the surface. This was achieved by contacting the dehydrated MCM-41 material with a solution of the appropriate amount of $SiNR_4Cl$ (provided by ABCR GMBH, 50 wt% in MeOH) in $CHCl_3$. This slurry was stirred for 1 h to allow the $SiNR_4Cl$ to diffuse inside of the pores. Then, Et_3N (molar ratio $Et_3N/SiNR_4Cl = 2$) in $CHCl_3$ was added to the above slurry. The final liquid/solid mass ratio was 20. The reaction was performed for 12 h and functionalized MCM-41 was obtained by filtration, exhaustive washing with $CHCl_3$ and CH_2Cl_2 and drying at 60 °C overnight. The MCM-41 structure was preserved.

The exchange of chloride by hydroxide anions was carried out by contacting the functionalized MCM-41 samples with a 0.21 M methanolic solution of NMe_4OH at room temperature for 10 min using a liquid/solid mass ratio of 50. The solid was recovered by filtration and extensively rinsed with MeOH, followed by vacuum drying, and the MCM-41 structure was preserved. The degree of exchange was calculated by titration of the NMe_4OH solution after exchange. The OH/N ratio found for all samples was close to 1. ^{29}Si MAS NMR spectroscopy and elemental analysis of the catalysts in the chloride and hydroxide forms show that no leaching of the anchored tetraalkylammonium occurs during the anionic exchange of chloride by hydroxide anions.

Table 1 Knoevenagel condensation between benzaldehyde **1** (10 mmol) and ethyl cyanoacetate **2a** (8 mmol) in the presence of MCM-41OH (80 mg) at 60 °C under N_2

Catalyst	Anchored NMe_4OH[a]	Intial rate[b]/ 10^{-4}	TON[c]/ 10^{-3}	Yield of **3a**
MCM-41OH1[d]	1.22	17.8	1.45	88[e]
MCM-41OH2[d]	0.88	11.0	1.25	77[e]
MCM-41OH1[f]	1.22	217	17.8	95[g]
MCM-41OH2[f]	0.88	163	18.6	90[g]
NMe_4OH[f]	0.064[h]	208[i]	32.5	100[g]

[a] In millimoles of NMe_4OH per gram MCM-41. [b] In moles of product per minute per gram of catalyst. [c] Turn over number in moles of product per minute per millimole of NMe_4OH. [d] $CHCl_3$ as solvent (5 ml). [e] 2 h reaction time. [f] Without solvent. [g] 0.5 h reaction time. [h] NMe_4OH added (in mmol). [i] In mol min^{-1}.

MCM-41OH1 was tested as a basic catalyst for the Knoevenagel condensation of benzaldehyde **1** with ethyl cyanoacetate **2a**. The reaction progress was monitored by withdrawing aliquots which were analyzed by GC, and the products were identified by GC–MS. The reaction was carried out in $CHCl_3$ at 60 °C under nitrogen atmosphere using the conditions shown in Table 1. After 2 h the conversion of ethyl cyanoacetate was 88% with 100% selectivity for the condensation product **3a** (Scheme 1).

When the condensation was carried out under the same reaction conditions described above, but in the presence of an MCM-41 sample containing a different amount of anchored tetraalkylammonium quaternary salt (MCM-41OH2), it was possible to see that the initial rate was proportional to the amount of anchored tetraalkylammonium hydroxide (Table 1), indicating that a highly homogeneous strength distribution of basic sites is obtained on these catalysts and there is total accessibility of reactants to the active centres.

The condensation was also carried out without solvent under the reaction conditions described above, and the yield, initial rate and TON obtained are given in Table 1. When the Knoevenagel condensation was carried out using other active methylene compounds, *i.e.* phenylsulfonylacetonitrile **2b**, in the presence of MCM-41OH1 at 70 °C, the reaction was completed within 1 h with 100% selectivity for phenylsulfonylcinnamonitrile **3b**.

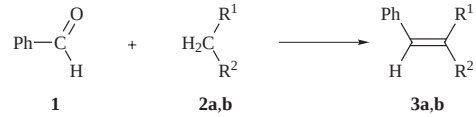

1 **2a**,**b** **3a**,**b**

a $R^1 = CN$, $R^2 = CO_2Et$
b $R^1 = CN$, $R^2 = SO_2Ph$

Scheme 1

Table 2 MCM-41OH1 as a catalyst for Michael reactions[a]

Entry	Donor	Acceptor	*T*/°C	*t*/h	Yield (%)[b]
1	Ethyl 2-oxocyclo-pentanecarboxy-late	Methyl vinyl ketone	20	1	85
2	Ethyl cyanoacetate	Methyl vinyl ketone	20	2	72 (30)
3	Ethyl cyanoacetate	Methyl vinyl ketone	60	1	58 (37)
4	Ethyl cyanoacetate	Cyclopentanone	80	2	50 (10)
5	Ethyl cyanoacetate	Cyclohexanone	80	2	35
6	Diethyl malonate	Methyl vinyl ketone	60	2	10

[a] Reaction conditions: 8 mmol of donor, 8 mmol of acceptor, 60 mg of catalyst, 2 ml MeCN under N_2. [b] Molar yield of double-addition product in parentheses.

For comparison purposes, the reaction between ethyl cyanoacetate and benzaldehyde was also carried out using NMe_4OH as a homogeneous basic catalyst (Table 1), and the initial rate per mmol of OH^- is almost twice than with the heterogeneous catalyst. Taking into account the fact that the accessibility of the reactants to the active sites on MCM-41 must be almost unrestricted, the smaller intrinsic activity shown by the heterogeneous catalyst could be explained by considering that the hydroxide group might be interacting with the remaining silanol groups located on the inner part of the MCM-41 channels.

Michael additions using different donor and acceptor substrates and requiring stronger basicities than Knoevenagel condensations were also carried out (Table 2). In all cases, products coming from side reactions such as rearrangements, dimerizations or other condensations were not observed, and extremely high selectivities for the 1,4-adduct can be achieved. This excellent selectivity must be attributed to the well-defined strong basicity of the MCM-41OH.

These results show that MCM-41OH is an efficient catalyst for Michael additions with acceptable yields and selectivities when working under mild conditions with large substrates. This is in contrast with other modified MCM-41 materials reported previously, such as Cs-MCM-41 materials, which only catalyse Michael reactions under much more drastic conditions,[6] or the MCM-TBD catalyst,[11] where the bulky immobilized 1,5,7-triazabicyclo[4.4.0]dec-5-ene reduces the pore size of the catalyst inducing a transition state shape selectivity or even limiting the accessibility of bulky reactants to the active sites.

MCM-41OH1 was also tested as a basic catalyst for the aldol condensation between benzaldehyde and 2′-hydroxyacetophenone (10 mmol and 8 mmol, respectively; 15 wt% relative to the catalyst). The solid was able to catalyse the successive aldol condensation and intramolecular Michael addition to flavanone in a solvent-free system at 130 °C. After 8 h reaction time a conversion of 65% with a selectivity of 78% for flavanone was obtained.

The MCM-41OH1 catalyst used in the Knoevenagel reaction between ethyl cyanoacetate and benzaldehyde in EtOH was reused three times, after Soxhlet extraction with CH_2Cl_2, and no leaching and/or deactivation of the catalyst was observed.

Our results prove that it is feasible to introduce strong Brønsted basic sites into the MCM-41 structure by anchoring tetraalkylammonium hydroxide salts. This new solid base catalyst is a useful alternative to soluble bases in reactions such as Knoevenagel condensations, Michael additions and aldol condensations because of its high catalytic activity under mild liquid phase conditions. The mechanical stability of the inorganic support materials ensures easy separation of the solid catalyst together with waste minimisation and the possibility of recycling.

We are grateful for financial support by the Spanish CICYT (project MAT97-1016-C02-01 and project MAT97-1016-C02-01). J. L. J thanks M. E. C. for a PhD fellowship.

Notes and references

1 A. Corma, V. Fornés, R. M. Martin-Aranda, H. García and J. Primo, *Appl. Catal*.,1990, **59**, 237.
2 D. Barthomeuf, *Stud. Surf. Sci. Catal.*, 1991, **65**, 157.
3 A. Corma and R. M. Martin-Aranda, *Appl. Catal*., 1991, **130**, 130.
4 J. C. Kim, H. X. Li, C. Y. Chen and M. E. Davis, *Microporous Mater*., 1994, **2**, 413.
5 I. Rodriguez, H. Cambon, D. Brunel and M. Laspéras, *J. Mol. Catal. A: Chem.*, 1997, **130**, 197.
6 K. R. Kloetstra and H. van Bekkum, *J. Chem. Soc., Chem. Commun*., 1995, 1005.
7 H. Moison, F. Texier-Boullet and A. Foucaud, *Tetrahedron*, 1987, **43**, 543.
8 A. Corma, V. Fornés, R. M. Martín-Aranda and F. Rey, *J. Catal*., 1992, **134**, 58
9 W. Richardhein and J. Melvin, *J. Org. Chem.*, 1991, **26**, 4874.
10 A. Cauvel, G. Renard and D. Brunel, *J. Org. Chem.*, 1997, **62**, 1325.
11 Y. V. S. Rao, D. E. De Vos and P. A. Jacobs, *Angew. Chem., Int. Ed. Engl*., 1997, **36**, 2661.
12 A. Firuzi, D. Kumar, L. M. Bull, T. Besier, P. Sieger, Q. Huo, S. A. Walker, J. A. Zasadzinski, G. Glinka, J. Nicol, D. Margolese, G. D. Stucky and B. F. Chmelka, *Science*, 1995, **267**, 1138; C. T. Kresge, M. E. Leonowicz, W. J. Roth, J. C. Vartuli and J. S. Beck, *Nature*, 1992, **395**, 710.

Communication 9/00384C

ChemComm

First donor–acceptor interaction promoted gelation of organic fluids

Uday Maitra,*[a] P. Vijay Kumar,[a] Nividh Chandra,[a] Lawrence J. D'Souza,[a] M. D. Prasanna[a] and A. R. Raju[b]

[a] *Department of Organic Chemistry, Indian Institute of Science, Bangalore 560 012, India. E-mail: maitra@orgchem.iisc.ernet.in*

[b] *Jawaharlal Nehru Center for Advanced Scientific Research, Jakkur, Bangalore 560 064, India*

Received (in Cambridge, UK) 17th December 1998, Accepted 11th February 1999

Bile acid derivatives functionalized at the 3-position with an aromatic group formed gels in organic solvents in the presence of trinitrofluorenone.

In recent years there has been considerable interest in developing new types of gelators of organic solvents.[1] Despite the recent advances, *a priori* design of a gelator for gelling a given solvent has remained a challenging task. Various non-covalent interactions like hydrogen-bonding,[2] metal coordination[3] *etc.* have been used as the driving force for the gelation process. A special class of cholesterol-based gelators were reported by Weiss,[4] and by Shinkai.[5] Gels derived from these molecules have been used for chiral recognition/sensing,[6] for studying photo- and metal-responsive functions,[7] and as templates to make hollow fiber silica.[8] Other types of organogels have been used for designing polymerized [9] and reverse aerogels,[10] and in molecular imprinting.[11] Hanabusa's group has recently reported organogels with a bile acid derivative.[12] This has prompted us to disclose our results on a novel electron donor–acceptor (EDA) interaction mediated two-component[13] gelator system based on the bile acid[14] backbone.

During the course of our investigation on bile acid-based molecular tweezers[15] it was discovered that aromatic donor-substituted bile acid derivatives such as **1**–**3**† gelatinized certain organic solvents *in the presence of* trinitrofluorenone **4** as the acceptor.‡ Interestingly, the location of the pyrene unit on the bile acid appeared to be critical, as shown by compounds **5** and **6** which did not form gels in the presence of **4**. The results from the gelation studies are summarized in Table 1. Pyrene derivative **1** in general formed highly stable gels even with less than 1% of the gelator. Compound **4** in the presence of the methyl pyrene-1-carboxylate did *not* form a gel in BuOH and $CHCl_3$.

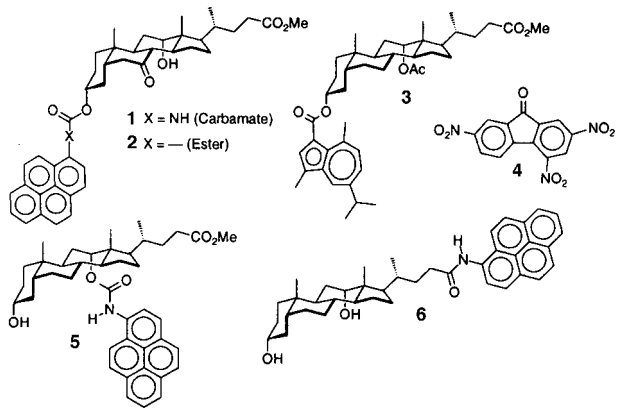

The stoichiometric requirement of the two components was easily established by measuring the T_{gel}[16] as a function of the ratio of **4**:**1** at a constant concentration of **1**. A steady increase of T_{gel} was observed with increasing amounts of **4** but after 1.25 equiv. were added there was no measurable increase, suggesting the requirement of a 1:1 stoichiometry for effective gelation. This experiment was also carried out in the reverse manner (constant concentration of **4** and variable concentration of **1**) with identical conclusion.

Table 1 Results from gelation studies[a]

Entry	Solvent	1/4	2/4	3/4
1	Bu^nOH	SG[b]	G	G
2	Bu^tOH	SG[b]	SG[b]	G
3	Bu^tOH–$CHCl_3$ (5:1 v/v)	G[c]	SG[c]	G
4	EtOH–$CHCl_3$ (3:1 v/v)	SG[b]	G[b]	G
5	Cyclohexanol	SG	SG	G
6	$CHCl_3$	G	S	S
7	*n*-Octanol	S	S	G
8	$(CH_2OH)_2$–$CHCl_3$ (3:1 v/v)	G	P	G
9	Trigol–$CHCl_3$ (3:1 v/v)	SG	P	G
10	Benzene	S	S	S
11	Cyclohexane	P	P	P
12	Cyclohexanone	S	S	S
13	$(CHCl_2)_2$	S	S	S

[a] SG = super gel (< 1 wt% gelator), G = gel (1–2 wt% of gelators), S = solution, P = precipitate. [b] These gels exhibited thixotrophy. [c] By changing the amount of $CHCl_3$ the T_{gel} could be increased or decreased.

The gels were dried in vacuum[5] and subjected to SEM analysis to examine the morphology.§ The SEM of a dried sample from **3**/**4** (Fig. 1) showed a complex three-dimensional fibrous structure with an average fiber diameter of *ca.* 2 μm. Such fibrous networks have been observed by many others, and appear to be characteristic of most gels. The SEM pictures from the xerogels derived from the other two systems did not show any obvious fibrous structure.

The gels formed from colorless **1** and **2** (and pale yellow **4**) are colored due to a charge-transfer band. The intensity of this band changes substantially during the gelation. The temperature dependence of this absorption band has been examined for **1** and **2** in $CHCl_3$ by UV-VIS spectroscopy (data for **1** are shown in Fig. 2). It is clear from this plot that the gelation process is associated with an increase in the donor–acceptor interaction because of the substantial increase in the charge transfer around

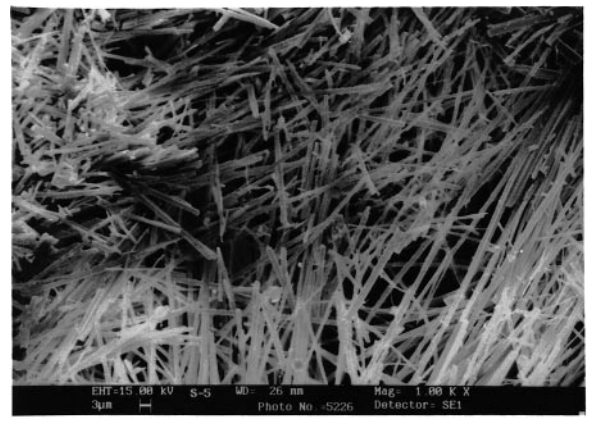

Fig. 1 Scanning electron micrograph of a dried gel derived from **3**/**4** in *n*-octanol (3% w/w) showing a fibrous network.

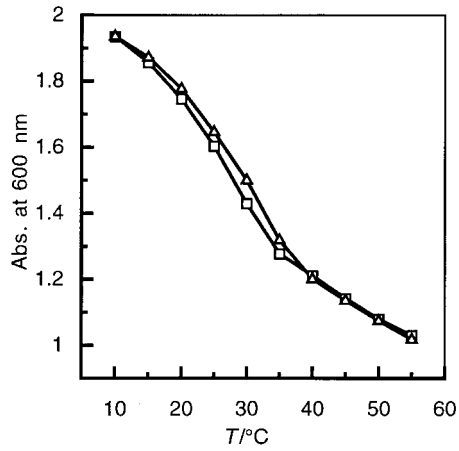

Fig. 2 Plot of A_{600} (1 mm cuvette) *vs.* temperature for gel obtained from **1** and **4** in $CHCl_3$ (62 mM each; this corresponds to 2.8% w/w of **1**): (□) cooling and (△) heating.

T_{gel}. With a true solution of **1** and **4** (in a 1 : 1 ratio) in $CHCl_3$ a monotonous increase in the absorbance was observed as the temperature was decreased in the same range. This, and the observation that no gelation occurs in the absence of **4**, suggest that the donor–acceptor interaction between the pyrene unit on the steroid and **4** is the primary driving force responsible for gelation.

Since **1** formed good gels in $CHCl_3$ (entry 6, Table 1), ^{1}H NMR spectroscopy was used to investigate the temperature dependence of the chemical shifts in $CDCl_3$. A 2.8 wt% sample was prepared in $CDCl_3$ and NMR spectra were recorded from 22 (gel) to 42 °C (fluid). Significant changes in chemical shifts were observed for the protons from **4** and the carbamate NH. A plot of the chemical shift against temperature for the C_3-H of **4** is shown in Fig. 3.[17] It is satisfying to observe that the T_{gel} determined from UV (35 °C) and NMR spectra (*ca.* 38 °C) of the same sample were comparable to that measured by the method of Takahashi *et al.*[16] (*ca.* 35 °C). The existence of hysteresis is also clear from this plot. It was also observed that the T_1 value (^{1}H) for the methoxycarbonyl group decreased from 1.48 s in the gel phase (3.8 wt %) to 1.08 s in the fluid phase (1.2 wt%) at 22 °C, suggesting reduced segmental motion of the sidechain in the gel in $CDCl_3$.

In conclusion, we have demonstrated for the first time a two-component organic gelator system which can gelatinize several organic fluids (primarily alcohols) through *donor–acceptor interaction*. The requirement of EDA for the gelation has been established from our studies, but the role of the bile acid backbone is yet to be uncovered. These systems are currently being extensively investigated to understand their structure–property relationships, three dimensional structures and material properties. We believe that these novel phases will expand our understanding of the gelation of organic fluids, and will also lead to the development of new materials for futuristic applications.[18]

We acknowledge financial support from DST, New Delhi (grant # SP/S1/G-08/96). L. J. D. and V. K. thank the U. G. C. for financial support. We also thank Professor C. N. R. Rao for help with the SEM analysis.

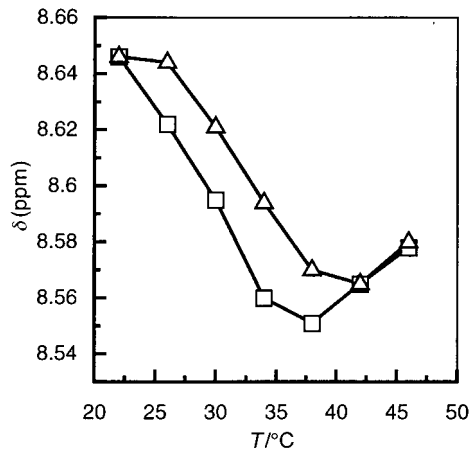

Fig. 3 Plot of chemical shift of C_3-H of **4** *vs.* temperature (the gel composition is the same as in Fig. 2): (□) cooling and (△) heating.

Notes and references

† *Selected data* of **1**: Mp 198 °C; δ_H(300 MHz, $CDCl_3$) 7.85–8.5 (m, 9H), 7.79 (br, 1H), 4.78 (m, 1H), 3.85 (m,1H), 3.67 (s, 1H), 2.73 (m, 1H), 1.1–2.4 (steroidal CH and CH_2), 1.05 (s, 3H), 0.89 (d, *J* 4.5, 3H), 0.57 (s, 3H); δ_C(75 MHz, $CDCl_3$) 211.74, 174.7, 154.4, 131.26, 130.78, 128.32, 127.57, 127.21, 126.4, 126.0, 125.17, 125.12, 125.01, 124.76, 124.64, 120.44, 74.15, 71.84, 34.76, 34.49, 33.76, 33.6, 33.43, 31.05, 30.75, 29.06, 27.42, 24.91, 24.07, 22.56, 17.31, 12.68; *m/z* 663 (M^+), 243 (100%). Compounds **2** and **3** were prepared by the direct acylation of the corresponding alcohols with the appropriate acid halides in 75 and 60% yields, respectively.

‡ *Gelation studies:* The gelator (**1**–**3**) was taken in a stoppered test tube along with an equivalent amount of **4,** the solvent (0.25 ml) was added and the mixture was heated until the solid dissolved. The solution was allowed to come to room temperature and the appearance was noted.

§ *Scanning electron micrographs:* To observe the morphology of the xerogels, 200 Å thick gold films were deposited by dc sputtering, and were examined using a Leica 440*i* SEM with a LaB_6 emitter.

1 For a comprehensive review on gelators of organic liquids see, P. Terech and R. G. Weiss, *Chem. Rev.*, 1997, **97**, 3133.
2 K. Hanabusa, K. Okui K. Karaki, T. Koyama and H. Shirai, *J. Chem. Soc., Chem. Commun.*, 1992, 1371; K. Hanabusa, M. Yamada, M. Kimura and H. Shirai, *Angew. Chem., Int. Ed. Engl.*,1996, **35**, 1949; K. Yoza, Y. Ono, K, Yoshihara, T. Akao, H. Shinmori, M. Takeuchi, S. Shinkai and D. Reinhoudt, *Chem. Commun.*, 1998, 907; V. P. Vassilev, E. E. Simanek, M. R. Wood and C.-H. Wong, *Chem. Commun.*, 1998, 1865; S. Bhattacharya, S. N. Ghanashyam Acharya and A. R. Raju, *Chem. Commun.*, 1996, 2101.
3 P. Terech, V. Schaffhauser, P. Maldivi and J. M. Guenet, *Langmuir*, 1992, **8**, 2104; C. Dammer, P. Maldivi, P. Terech and J. Guenet, *Langmuir*, 1995, **11**, 1500.
4 R. Mukkamala and R. G. Weiss, *J. Chem. Soc., Chem. Commun.*, 1995, 375; Y.-C. Lin, B, Kachar and R. G. Weiss, *J. Am. Chem. Soc.*, 1989, **111**, 5542; Y-c. Lin and R. G. Weiss, *Macromolecules*, 1987, **20**, 414.
5 K. Murata, M. Aoki, T. Susuki, T. Harada, H. Kawabata, T. Komori, F. Ohseto, K. Ueda and S. Shinkai, *J. Am. Chem. Soc.*, 1994, **116**, 6664.
6 T. D. James, H. Kawabata, R. Ludwig, K. Murata and S. Shinkai, *Tertrahedron*, 1995, **51**, 555.
7 K. Murata, M. Aoki, T. Nishi, A. Ikeda and S. Shinkai, *J. Chem. Soc., Chem. Commun.*, 1991, 1715.
8 Y. Ono, K. Nakashima, M. Sano, Y. Kanekiyo, K. Inoue, J. Hojo and S. Shinkai, *Chem. Commun.*, 1998, 1477.
9 M. de Loos, J. van Esch, I. Stokroos, R. M. Kellogs and B. L. Feringa, *J. Am. Chem. Soc.*, 1997, **119**, 12 675.
10 W. Gu, L. Lu, G. B. Chapman and R. G. Weiss, *Chem. Commun.*, 1997, 543.
11 R. J. H. Hafkamp, B. P. A. Kokke, I. M. Danke, H. P. M. Geurts, A. E. Rowan, M. C. Feiters and R. J. M. Nolte, *Chem. Commun.*, 1997, 545.
12 Y. Hishikawa, K. Sada, R. Watanabe, M. Miyata and K. Hanabusa., *Chem. Lett.* 1998, 795.
13 For other examples of two component gelator systems, see ref. 1.
14 Bile acids and their salts were shown to form gel-like aggregates in *aqueous* salt solutions: A. Rich and D. M. Blow, *Nature*, 1958, **182,** 423; N. Ramanathan, A. L. Currie and J. R. Colvin, *Nature*, 1961, **190**, 779.
15 L. J. D'souza and U. Maitra, *J. Org. Chem.*, 1996, **61**, 9494; U. Maitra, P. Rao, P. Vijay Kumar, R. Balasubramanian and L. Mathew, *Tetrahedron Lett.*, 1998, **39**, 3255.
16 T_{gel} was determined by the method of A. Takahashi, M. Sakai and T. Kato, *Polym. J.*, 1980, **12**, 335.
17 The *downfield* shift of the C–H signals upon formation of the gel is not clear to us at this time. We feel that a parallel orientation of the donor–acceptor pair (D:A) in solution may get tilted (and elongated as D:A:D:A...) upon gel formation, resulting in downfield shifts.
18 T. Kato, T. Kutsuuna, K. Hanabusa and M. Ukon, *Adv. Mater.*, 1998, **8**, 10.

Communication 8/09821B

ChemComm

A novel synthesis of chiral cyclopentyl- and cyclohexyl-amines

Pedro Pinho and Pher G. Andersson*

Department of Organic Chemistry, Uppsala University, Box 531, S-751 21 Uppsala, Sweden. E-mail: phera@kemi.uu.se

Received (in Liverpool, UK) 8th February 1999, Accepted 25th February 1999

A new route to multifunctionalised chiral cyclopentyl- and cyclohexyl-amines was developed by means of a new reaction involving the ring opening of a 2-azabicyclo-[2.2.1] or -[2.2.2] structure in high yields.

Functionalised chiral cyclopentylamines are of extreme importance in medicinal chemistry since this structural unit is present in a large number of antibiotics. The most interesting are amidomycin[1] and aristeromycin,[2] which have been shown to have antiviral properties, and carbovir[3] which is a promising antibiotic used for the treatment of AIDS[4] (Fig. 1).

We have previously reported our work on 2-azanorbornyl derivatives and their use in various reactions, *i.e.* copper-catalyzed allylic oxidation of olefins,[5a] ruthenium-catalyzed transfer hydrogenation of ketones,[5b] diethylzinc addition to both imines and aldehydes,[5c] borane reduction of ketones,[5d] rearrangement of *meso*-epoxides[5e] and preparation of cyclopentylglycine analogues.[5f] During research to modify the ligand structure, an interesting reaction was discovered that opens up a new, rapid route to substituted enantiomerically pure cyclopentylamines *via* a ring opening reaction of the bicyclic structure **A** [reaction (1)].

When attempting the preparation of the corresponding Grignard reagent of the bicyclic bromide **A**, an unexpected ring opening of the bicyclic structure occurred. Initially **C** was formed with the concurrent formation of another compound which was assigned to structure **B**. The 1 : 1 mixture of products (**B** : **C**) was inseparable by flash chromatography, but the compounds were assigned the structures displayed in reaction (1) by analysis of the spectral data of the mixture.

Despite the low selectivity, the novelty and usefulness of the ring opened product prompted us to optimize the conditions in order to favour its formation. Better results were obtained when the *N*-protecting PhEt group attached to the nitrogen in **A** was replaced by tosyl to give the corresponding tosylate **3** (Scheme 1). The electron-withdrawing properties of this group facilitate the ring opening reaction and the desired compound **4** was obtained in high yield as a single product.

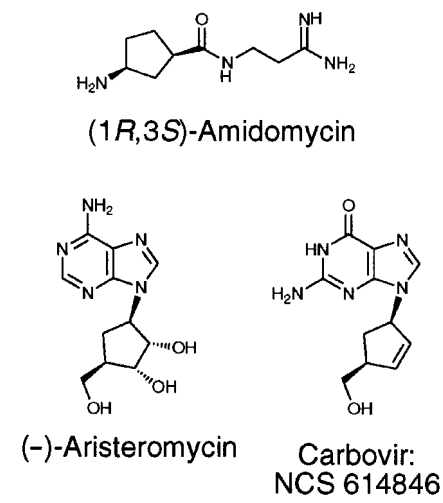

Fig. 1 Some examples of pharmaceutically active cyclopentylamines.

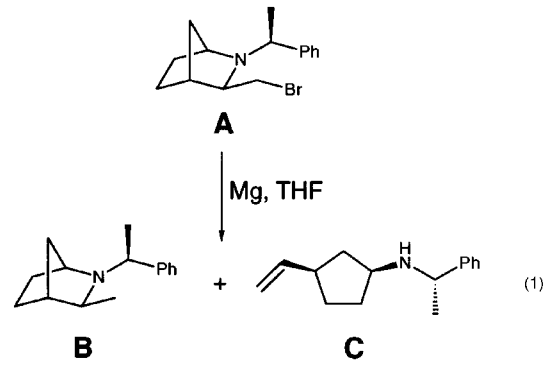

The synthetic route to the key intermediate **3** is outlined in Scheme 1. Compound **1** was obtained *via* a diasteroselective aza-Diels–Alder reaction between cyclopentadiene and the *in situ* generated imine ion of ethyl glyoxylate and (*S*)-1-phenylethylamine,[6,7] followed by simultaneous hydrogenation and hydrogenolysis to the corresponding free amino ester.[5c]

N-Tosylation and subsequent $LiAlH_4$ reduction of the ester functionality led to the alcohol **2**. The alcohol was then treated with CBr_4 and Ph_3P in CH_2Cl_2 to afford the key intermediate **3**. When treated with magnesium and tetrahydrofuran at reflux, the bicyclic bromide ring opened to give compound **4** *via* the mechanism outlined in reaction (2). Acid hydrolysis of the reaction mixture and purification of the crude residue by flash chromatography furnished the desired ring opened product in high yield.

This new methodology could also be extended to other derivatives of the 2-azanorbornyl structure. Catalytic dihydroxylation of the Diels–Alder adduct (used for the synthesis of **1**) with OsO_4 in the presence of NMO as a co-oxidant in *tert*-butyl alcohol at room temperature afforded diol **5** (Scheme 2).

Protection of diol **5** as the corresponding ketal was achieved by treatment with 2,2-dimethoxypropane and toluene-*p*-sulfonic acid in warm MeOH. Formation of product **6** required the use of slightly more than one equivalent of the acid probably due to protonation of the amine functionality, and under these conditions the reaction was completed in *ca.* 15 minutes. Solvent evaporation followed by addition of 20% aqueous NaOH and extractive work-up afforded the pure protected diol **6**. This product was treated with ammonium formate in EtOH at

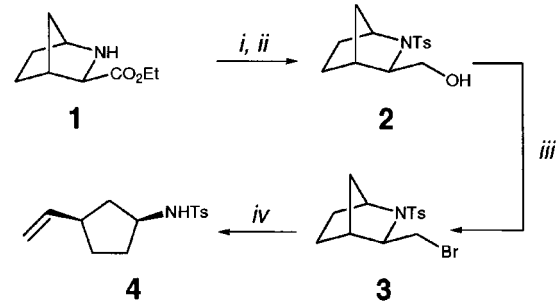

Scheme 1 *Reagents and conditions*: (i) TsCl, Et_3N, CH_2Cl_2 rt, overnight, 92%; (ii) $LiAlH_4$, THF, rt, 2 h, 95%; (iii) CBr_4, Ph_3P, CH_2Cl_2, rt, 24 h, 60%; (iv) Mg, $BrCH_2CH_2Br$, THF, reflux, 24 h, 90%.

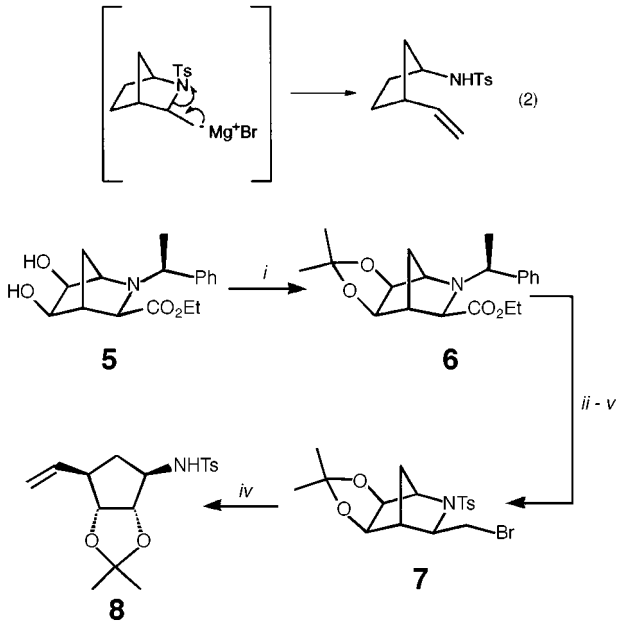

Scheme 2 *Reagents and conditions*: (i) $(MeO)_2C(CH_3)_2$, TsOH, warm MeOH, 15 min, 87%; (ii) ammonium formate, Pd/C (10%), EtOH, reflux, 1 h, 99%; (iii) TsCl, Et_3N, CH_2Cl_2, rt, overnight, 90%; (iv) $LiAlH_4$, THF, rt, 2 h, 92%; (v) CBr_4, Ph_3P, CH_2Cl_2, rt, 24 h, 59%; (vi) Mg, $BrCH_2CH_2Br$, THF, reflux, 32 h, 89%.

reflux in the presence of Pd/C (10%) to afford the corresponding free amino ester, and then submitted to the same synthetic sequence as described for **1** to yield the corresponding bromide **7**. Compound **7** ring opened to give product **8** under the conditions described for **3**, albeit in a slightly slower reaction.

By simply using cyclohexa-1,3-diene in the aza-Diels–Alder reaction, a bicyclic [2.2.2] structure was obtained.[6] Dihydroxylation of the purified adduct under the conditions described earlier yielded compound **9** (Scheme 3) which, when submitted to the same synthetic sequence as **5**, yielded the ring opened product **10**.[8] The yields for the transformation of **9** into **10** were similar to those obtained in the transformation of **5** into **8**.[9]

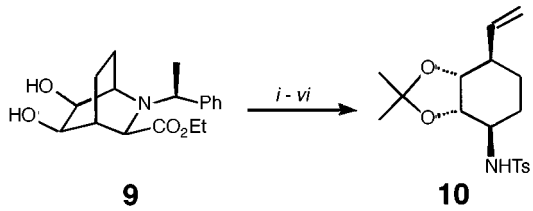

Scheme 3 *Reagents and conditions*: (i) $(MeO)_2C(CH_3)_2$, TsOH, warm MeOH, 15 min, 87%; (ii) ammonium formate, Pd/C (10%), EtOH, reflux, 1 h, 99%; (iii) TsCl, Et_3N, CH_2Cl_2, rt, overnight, 91%; (iv) $LiAlH_4$, THF, rt, 2 h, 94%; (v) CBr_4, Ph_3P, CH_2Cl_2, rt, 24 h, 62%; (vi) Mg, $BrCH_2CH_2Br$, THF, reflux, 32 h, 85%.

This work opens up a new route to cyclopentyl- and cyclohexyl-amines *via* a novel ring opening reaction of [2.2.1] and [2.2.2] azabicyclic structures. The fact that the [2.2.2] structure ring opens without increased difficulty indicates that the reaction is not only a consequence of ring strain on the [2.2.1] system.

We thank the Swedish Natural Research Council (NFR), The Swedish Foundation for Strategic Research (SSF), The Swedish Research Council for Engineering Sciences (TFR) and Astra Arcus for generous financial support.

Notes and references

1 S.-Y. Sung and A. W. Frahm, *Arch. Pharm. Pharm. Med. Chem.*, 1996, **329**, 291; S. Nakamura, K. Karasawa, N. Tanaka, H. Yonehara and H. Umezawa, *J. Antibiot., Ser. A*, 1960, 392; H. Nagata T. Taniguchi and K. Ogasawara, *Tetrahedron: Asymmetry*, 1997, **8**, 2679.

2 T. Kusaka, H. Yamamoto, M. Shibata, M. Muroi, T. Kishi and K. Mizuno, *J. Antibiot.*, 1968, 255; M. Arita, K. Adachi, H. Sawai and M. Ohno, *Nucleic Acids Res. Symp. Ser.*, 1983, **12**, 25.

3 E. L. White, W. B. Parker, L. J. Macy, S. C. Shaddix, G. McCaleb, J. A. Secrist III, R. Vince and W. M. Shannon, *Biochem. Biophys. Res. Commun.*, 1989, **161**, 393; R. Vince, M. Hua, J. Brownell, S. Daluge, F. Lee, W. M. Shannon, G. C. Lavelle, J. Qualls, O. S. Weislow, R. Kiser, P. G. Canonico, R. H. Schultz, V. L. Narayanan, J. G. Mayo, R. H. Showmaker and M. R. Boyd, *Biochem. Biophys. Res. Commun.*, 1988, **156**, 1046.

4 Other related biologically active compounds. Neplanocin A: M. Arita, K. Adachi, H. Sawai and M. Ohno, *Nucleic Acids Res. Symp. Ser.*, 1983, **12**, 25; M.-I. Lim, J. D. Moyer, R. L. Cysyk and V. E. Marquez, *J. Med. Chem.*, 1984, **27**, 1536; M.-I. Lim and V. E. Marquez, *Tetrahedron Lett.*, 1983, **24**, 5559. Guanine derivatives: A. B. Reitz, M. G. Goodman, B. L. Pope, D. C. Argentieri, S. C. Bell, L. E. Burr, E. Chourmouzis, J. Come, J. H. Goodman, D. H. Klaubert, B. E. Maryanoff, M. E. McDonnell, M. S. Rampulla, M. R. Schott and R. Chen, *J. Med. Chem.*, 1994, **37**, 3561. Adenosine analogues: Y. F. Shealy and J. D. Clayton, *J. Am. Chem. Soc.*, 1966, **88**, 3885. Tubercidin analogues: J. A. Montgomery and K. Hewson, *J. Med. Chem.*, 1967, **10**, 665. Noraristeromycin: S. M. Siddiqi, F. P. Oertel, X. Chen and S. W. Schneller, *J. Chem. Soc., Chem. Commun.*, 1993, 708. Adenosine deaminase inhibitors: H. J. Schaeffer, D. D. Godse and G. Liu, *J. Pharm. Sci.*, 1964, **53**, 1510. γ-Aminobutyric acid analogue: M. J. Milewska and T. Polonski, *Tetrahedron: Asymmetry*, 1994, **5**, 359. Carboxylic sugars and nucleosides: S. Ranganathan and K. S. George, *Tetrahedron*, 1997, **53**, 3347; M. J. Mulvihill, M. D. Surman and M. J. Miller, *J. Org. Chem.*, 1998, **63**, 4874.

5 (*a*) M. J. Södergren and P. G. Andersson, *Tetrahedron Lett.*, 1996, **37**, 7577; (*b*) D. A. Alonso, D. Guijarro, P. Pinho, O. Temme and P. G. Andersson, *J. Org. Chem.*, 1998, **63**, 2749; (*c*) D. Guijarro, P. Pinho and P. G. Andersson, *J. Org. Chem.*, 1998, **63**, 2530; (*d*) P. Pinho, D. Guijarro and P. G. Andersson, *Tetrahedron*, 1998, **54**, 7897; (*e*) M. J. Södergren and P. G. Andersson, *J. Am. Chem. Soc.*, 1998, **120**, 10760; (*f*) D. A. Alonso, S. K. Bertilsson, S. Y. Johnsson, S. J. M. Nordin, M. Södergren and P. G. Andersson, *J. Org. Chem.*, 1999, in the press.

6 L. Stella, H. Abraham, J. Feneu-Dupont, B. Tinant and J. P. Declercq, *Tetrahedron Lett.*, 1990, **31**, 2603; H. Abraham and L. Stella, *Tetrahedron*, 1992, **48**, 9707.

7 The absolute configuration of the aza-Diels–Alder adduct has been determined by means of X-ray analysis of a derivative, see: H. Nakano, N. Kumagai, C. Kabuto, H. Matsuzaki and H. Hongo, *Tetrahedron: Asymmetry*, 1995, **6**, 1233.

8 For interesting compounds containing this structure unit, see for example: G. E. Keck and S. A. Fleming, *Tetrahedron Lett.*, 1978, **48**, 4763; T. Hudlicky and H. F. Olivo, *Tetrahedron Lett.*, 1991, **32**, 6077; F. Chretien, S. I. Ahmed, A. Masion and Y. Chapleur, *Tetrahedron*, 1993, **49**, 7463; S. Grabowski, J. Armbruster and H. Prinzbach, *Tetrahedron Lett.*, 1997, **38**, 5485; H. Noguchi, T. Aoyama and T. Shioiri, *Tetrahedron Lett.*, 1997, **38**, 2883.

9 Representative spectroscopic and analytical data. (1*R*,3*S*)-1-Tosylamino-3-vinylcyclopentane (4). Magnesium metal (3.0 g, 123 mmol) was placed in a 50 mL two-neck round-bottom flask loaded with a magnetic bar. To one neck a condenser was adapted and to the other a septum. The system was evacuated and placed under argon, after which the magnesium was suspended in dry THF (3 mL). The stirring suspension was then set to reflux and a solution of compound **3** (6.0 g, 17 mmol) in dry THF (20 mL) was added in one portion *via* syringe. After stirring for 15 min a small amount of 1,2-dibromoethane was added to activate the magnesium and the mixture was heated at reflux for 24 h. The reaction was then cooled to 0 °C and quenched by addition of saturated NH_4Cl solution. After separation of the phases and extraction of the water phase with CH_2Cl_2, the combined organic layers were dried with magnesium sulfate. Solvent evaporation afforded a residue that was purified by flash chromatography to yield compound **4** (4.1 g, 15 mmol, 90%) as a white solid; mp 65–66 °C; R_f 0.11 (silica gel, pentane–ether: 80 : 20); $[\alpha]_D^{24} = -8.9$ (*c* = 1.0, CH_2Cl_2); $\nu(CH_2Cl_2)/cm^{-1}$ 3623, 3369, 2870, 1641, 1599, 1345, 1092, and 1047; $\delta_H(CDCl_3$, 400 MHz) 1.14–1.24 (1H, m), 1.38–1.45 (2H, m), 1.62–1.79 (1H, m), 1.80–1.90 (1H, m), 1.99–2.10 (1H, m), 2.34–2.42 (1H, m), 2.41 (3H, s), 3.57–3.63 (1H, m), 4.83–4.94 (2H, m), 5.65–5.75 (1H, m), 7.28 (2H, app. d, *J* 8.0), and 7.76 (2H, app. d, *J* 8.0); $\delta_C(CDCl_3$, 100 MHz) 21.5, 29.9, 32.6, 40.2, 41.8, 54.5, 113.1, 127.1, 129.6, 137.8, 141.9, and 143.2; *m/z* (EI) (rel. intensity) 264 (M^+, < 1%), 236 (25), 210 (13), 172 (14), 155 (62), 133 (44), 132 (36), 110 (41), 106 (17), 97 (12), 96 (43), 94 (13), 93 (25), 92 (35), 91 (100), 80 (21), 79 (17), and 65 (20) (Anal. Calcd. for $C_{14}H_{19}NO_2S$: C, 63.37; H, 7.22; N, 5.28. Found: C, 63.10; H, 7.07; N, 5.20%). The relative stereochemistry of this compound was determined by means of NOESY experiments.

Communication 9/01073D

First catalysis by corrole metal complexes: epoxidation, hydroxylation, and cyclopropanation

Zeev Gross,* Liliya Simkhovich and Nitsa Galili

Department of Chemistry, Technion - Israel Institute of Technology, Haifa 32000, Israel.
E-mail: chr10zg@tx.technion.ac.il

Received (in Cambridge, UK) 21st January 1999, Accepted 25th February 1999

The first ever application of corroles shows that their metal complexes are good catalysts, almost as potent as the corresponding metalloporphyrins in the oxygenation of hydrocarbons by iodosylbenzene and superior for the cyclopropanation of olefins by carbenoids.

Modified porphyrins have received increased attention in recent years, with emphasis on their syntheses, characterizations, and potential applications.[1] Some of these macrocycles form complexes with metal ions, which due to the alteration of the ligand's structure have quite different properties compared with the analogous metalloporphyrins.[2] The most interesting ligands in this respect are corroles, the one-carbon atom contracted porphyrin analogs, which may also be considered as the aromatic version of corrin—the cobalt's ligand in Vitamin B_{12}.[3] Similar to porphyrins, the corroles provide an equatorial tetradentate coordination plane, which is however trianionic and somewhat contracted (see Scheme 1). These last two properties have some remarkable effects on the coordination chemistry of corrole metal complexes (metallocorroles),[4] among which the stabilization of exceptionally high metal oxidation states is the most outstanding. The recent isolation of iron(IV) corroles[4a] and of an iron(IV) corrole radical[4b] could be relevant to catalysis by heme-enzymes and synthetic iron porphyrins, in which the analogous complexes are key intermediates.[5] But, there is still no information about corroles or their metal complexes in catalysis or in any other potential application. Presumably, it is only the lack of obvious procedures for the synthesis of corroles which prohibits such research. Thus, the first *meso*-substituted corrole—*meso*-aryl substitution is a prerequisite for a reasonable oxidation catalyst—was reported as late as 1993,[6] almost 30 years after the first reported corrole.[7] Also, in spite of the significant recent progress in corrole synthesis, even the most simple procedures reported to date require the preparation of non-commercially available starting materials.[8]

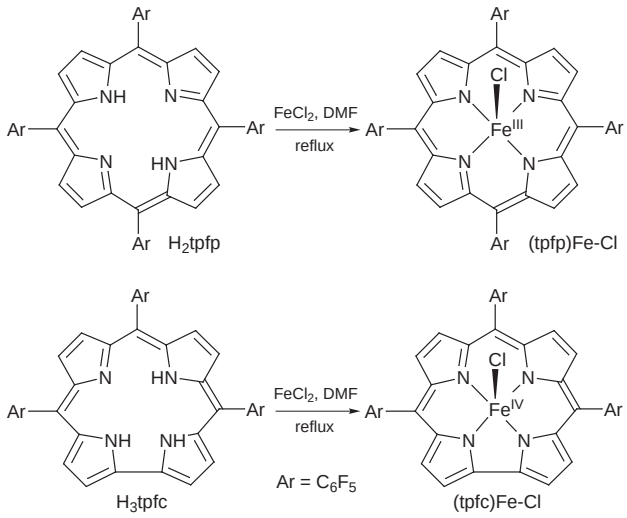

Scheme 1 Structures of *meso*-aryl substituted porphyrin and corrole, and of their iron complexes (note the different oxidation states of the metal).

We have very recently contributed to this field by disclosing the first synthesis of corroles by the direct reaction of pyrrole with aldehydes.[9] In particular, 5,10,15-tris(pentafluorophenyl)-corrole (H_3tpfc, Scheme 1) is now routinely prepared in our laboratory by this very simple and fast methodology. The structure of H_3tpfc is very similar to that of H_2tpfp, whose iron(III) complex is among the most active porphyrin-based catalysts.[10] Accordingly, we have now decided to compare the iron complexes of these two ligands as catalysts for the three main reactions catalyzed by metalloporphyrins.[11] These are the epoxidation of olefins and the hydroxylation of alkanes by iodosylbenzene, and the cyclopropanation of alkenes by carbenoids (Scheme 2).[12]

The results shown in Table 1 clearly demonstrate that (tpfc)Fe–Cl is a good catalyst in all three reactions. Still, it is not as effective as (tpfp)Fe–Cl for the epoxidation and hydroxylation of hydrocarbons. This is reflected in the higher yields of oxygenation products with (tpfp)Fe–Cl, as well as from the fact that at the end of the reactions the corrole complex, but not the analogous porphyrin complex, is completely bleached. However, for the cyclopropanation of styrene by **1a** (Scheme 2), (tpfc)Fe–Cl is superior. In addition, the catalyst is stable under the cyclopropanation conditions.

These results are reasonably accounted for by considering the proposed key intermediates in these processes, metal–oxo in oxygenation and metal–carbene in cyclopropanation.[5,12] It is well known that for iron(III) porphyrins, oxygen atom transfer from iodosyl benzene results in an oxoiron(IV) porphyrin radical intermediate, whose protection against self-destruction relies on the steric crowding of the four *meso*-aryl groups. By analogy, the oxygenation of (tpfc)Fe–Cl—an iron(IV) complex—will lead to an even more reactive intermediate. In addition, the

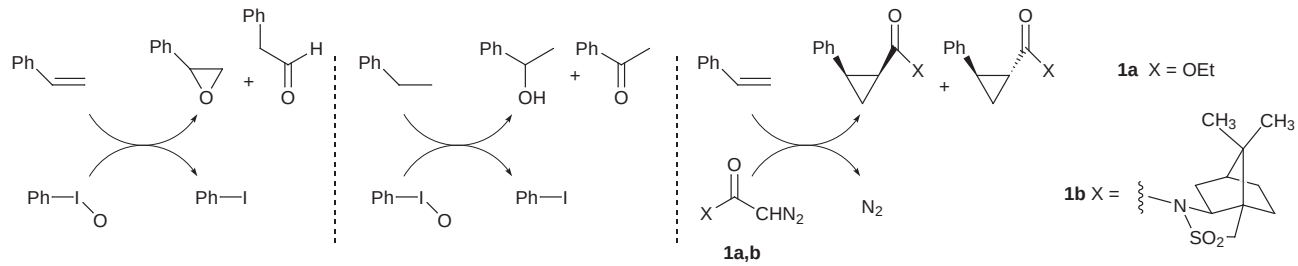

Scheme 2 Three catalytic transformations examined with (tpfc)Fe–Cl and (tpfp)Fe–Cl as catalysts.

Table 1 A comparison of (tpfc)Fe–Cl and (tpfp)Fe–Cl as catalysts for the processes shown in Scheme 1 with **1a**

	Epoxidation of styrene[a]		Hydroxylation of ethylbenzene[b]		Cyclopropanation of styrene[c]	
Products	Epoxide	Aldehyde	Alcohol	Ketone	*trans*	*cis*
With (tpfc)Fe–Cl as catalyst[d]	66%	21%	6.6%	4.2%	46%	20%
With (tpfp)Fe–Cl as catalyst[d]	90%	10%	15.7%	8.9%	40%	7%

[a] 0.36 mmol catalyst, 36 mmol iodosylbenzene, 360 mmol styrene, and 36 mmol nitrobenzene (internal standard), in 1 mL benzene, at RT for 3.5 h and 45 min, respectively. [b] 0.45 mmol catalyst, 50 mmol iodosylbenzene, 500 mmol ethylbenzene, and 50 mmol nitrobenzene (internal standard), in 1 mL benzene, overnight at RT. [c] 0.3 mM catalyst, 0.15 M **1a**, 1.5 M styrene, in 4 mL CH_2Cl_2, for 2.75 h at RT. 34 and 18% of olefins (diethyl maleate and traces of fumarate) were obtained in the reactions catalyzed by (tpfc)Fe–Cl and (tpfp)Fe–Cl, respectively. [d] Yields with regard to the limiting reagent were determined by GC relative to the internal standard.

Table 2 The results for cyclopropanation of styrene by **1a** and the unichiral carbenoid **1b**, catalyzed by the iron porphyrin complex (tpfp)Fe–Cl and the iron, cobalt, and rhodium complexes of H_3tpfc[a]

	With **1a**		With **1b**			
Catalyst	% Yield[b]	*trans*:*cis*	% Yield[c]	*trans*:*cis*	% de *trans*	% de *cis*
(tpfp)Fe–Cl	24	5.5	10	2.6	67 (*1S,2S*)	63 (*1S,2R*)
(tpfc)Fe–Cl	71	1.8	41	0.9	25 (*1S,2S*)	66 (*1S,2R*)
(tpfc)Co–PPh_3	8	2.1	[d]			
(tpfc)Rh–PPh_3	87	2.0	56	1.0	60 (*1R,2R*)	10 (*1S,2R*)

[a] 0.25–0.28 mM catalyst, catalyst : **1** : styrene = 1 : 100 : 1000, in 2 mL CH_2Cl_2, at RT under Ar. [b] Combined yields of the *trans*- and *cis*-cyclopropyl esters after 1 h, except for (tpfc)Co–PPh_3 (24 h). With (tpfc)Fe–Cl and (tpfc)Rh–$P(Ph)_3$, the reactions are complete after 1 h (the rest of **1a** is transferred into its dimerization products), while with (tpfp)Fe–Cl the reaction continues (43% yield after 3 h). [c] Combined yields of the *trans*- and *cis*-isomers after 24 h, except for (tpfp)Fe–C1 (48 h). [d] Not determined.

absence of the fourth aryl ring in (tpfc)Fe–Cl leads to reduced steric protection. Accordingly, the lower efficiency and the greater bleaching of (tpfc)Fe–Cl during catalysis may be rationalized on both electronic and steric grounds, whose relative importance still needs to be resolved. On the other hand, both factors seem to be beneficial for the cyclopropanation process. It is known that the active oxidation state in catalysis by iron(III) porphyrins is iron(II), which for (tpfp)Fe–Cl is formed *via* reduction by **1a**.[13] Thus, the results suggest that the reduction of the iron(IV) corrole is easier and that the absence of the fourth aryl group is favorable for formation of the relatively large metal–carbene intermediate. The last effect is also reflected in the relatively small *trans* : *cis* ratio of the cyclopropyl esters, 2.3 with (tpfc)Fe–Cl *vs.* 5.7 with (tpfp)Fe–Cl.

Because of the superiority of (tpfc)Fe–Cl in cyclopropanation catalysis, we turned our attention to other metal complexes of H_3tpfc, as well as to the unichiral carbenoid **1b**.[14,15] Table 2 summarizes the results of the reaction of styrene with **1a** and **1b**, catalyzed by (tpfp)Fe–Cl, (tpfc)Fe–Cl, (tpfc)Co–$P(Ph)_3$, and (tpfc)Rh–$P(Ph)_3$. Several aspects are clearly evident. First, the larger activity of the iron corrole relative to the analogous porphyrin in cyclopropanation by **1a** is further amplified in the reaction with the much bigger **1b**. Secondly, within the series of the corrole metal complexes the catalytic efficiency increases in the order of Co << Fe < Rh, similar to what is obtained with metalloporphyrins.[13] Finally, quite low *trans* : *cis* ratios are obtained for all metallocorroles, together with modest diastereomeric excesses (% de) in the reactions with **1b**. By analogy to our recent studies with the related metalloporphyrins,[14a] we anticipate that a significant increase in diastereoselectivity might be achieved by utilizing metal complexes of corroles with larger *o*-phenyl substituents. We have one such derivative,[9] but we still have to improve the synthetic methodology for its preparation.

In conclusion, this is the first report of catalysis by corrole metal complexes, and actually the first ever application of corroles. We have demonstrated that metallocorroles are good catalysts for the reactions which are traditionally investigated with metalloporphyrins. We trust that these promising preliminary results will encourage further exploration of the chemistry of corroles and their metal complexes.

This research was partially supported by 'The Technion V.P.R. Fund - R. and M. Rochlin Research Fund'.

Notes and references

1 For some excellent recent reviews, see: J. L. Sessler and S. J. Weghorn, *Expanded, Contracted, & Isomeric Porphyrins*, Pergamon, Oxford, 1997; A. Jasat and D. Dolphin, *Chem. Rev.*, 1997, **97**, 2267; E. Vogel, *J. Heterocycl. Chem.*, 1996, **33**, 1461.

2 For some recent publications, see: K. M. Kadish, P. L. Boulas, M. Kisters, E. Vogel, A. M. Aukauloo, F. D'Souza and R. Guilard, *Inorg. Chem.*, 1998, **37**, 2693; Z. Gross, I. Saltsman, R. P. Pandian and C. M. Barzilay, *Tetrahedron Lett.*, 1997, **38**, 2383; P. J. Chmielewski, L. LatosGrazynski, M. M. Olmstead and A. L. Balch, *Chem. Eur. J.*, 1997, **3**, 268.

3 S. Licoccia, and R. Paolesse, *Struct. Bond.*, 1995, **84**, 71.

4 (*a*) E. Vogel, S. Will, A. S. Tilling, L. Neumann, J. Lex, E. Bill, A. X. Trautwein, and K. Wieghardt, *Angew. Chem., Int. Ed. Engl.*, 1994, **33**, 731; (*b*) E. VanCaemelbecke, S. Will, M. Autret, V. A. Adamian, J. Lex, J. P. Gisselbrecht, M. Gross, E. Vogel and K. M. Kadish, *Inorg. Chem.*, 1996, **35**, 184; (*c*) S. Will, J. Lex, E. Vogel, V. A. Adamian, E. Van Caemelbecke and K. M. Kadish, *Inorg. Chem.*, 1996, **35**, 5577; (*d*) S. Will, J. Lex, E. Vogel, H. Schmickler, J. P. Gisselbrecht, C. Haubtmann, M. Bernard and M. Gross, *Angew. Chem., Int. Ed. Engl.*, 1997, **36**, 357.

5 J. Groves and Y. Han, *Cytochrome P450, Structure, Mechanism, and Biochemistry*, ed. P.R. Ortiz de Montellano, Plenum Press, New York, 1995, pp. 1–48.

6 R. Paolesse, S. Licoccia, M. Fanciullo, E. Morgante and T. Boschi, *Inorg. Chim. Acta*, 1993, **203**, 107.

7 A. W. Johnson and I. T. Kay, *Proc. Chem. Soc.*, 1964, 89.

8 S. Neya, K. Ohyama and N. Funasaki, *Tetrahedron Lett.*, 1997, **38**, 4113; R. Paolesse, S. Licoccia, G. Bandoli, A. Dolmella and T. Boschi, *Inorg. Chem.*, 1994, **33**, 1171.

9 Pending Israel Patent application, No.126426; Z. Gross, N. Galili and I. Saltsman, *Angew. Chem., Int. Ed.*, 1999, in the press.

10 C. K. Chang and F. Ebina, *J. Chem. Soc., Chem. Commun.*, 1981, 778.

11 (tpfp)Fe–Cl was available from our previous studies and the full characterization (including by X-ray crystallography) of (tpfc)Fe–Cl and (tpfc)Rh–$P(Ph)_3$ will be reported in the near future.

12 F. Montanari and L. Casella, *Metalloporphyrins Catalyzed Oxidations*, Kluwer, Dordrecht, 1994.

13 J. R. Wolf, C. G. Hamaker, J.-P. Djukic, T. Kodadek and L. K. Woo, *J. Am. Chem. Soc.*, 1995, **117**, 9194.

14 For the preparation of **1** and its utilization in cyclopropanation, see: (*a*) Z. Gross, N. Galili and L. Simkhovich, *Tetrahedron Lett.*, 1999, **40**, 1571; (*b*) N. Haddad and N. Galili, *Tetrahedron: Asymmetry*, 1997, **8**, 3367.

15 For the term unichiral and its advantages as compared to non-racemic, homochiral, and enantiopure, see: J. Gal, *Enantiomer*, 1998, **3**, 263.

Communication 9/00571D

Coordinatively unsaturated ruthenium allenylidene complexes: highly effective, well defined catalysts for the ring-closure metathesis of α,ω-dienes and dienynes

Alois Fürstner,*[a] Anthony F. Hill,*[b] Monika Liebl[a] and James D. E. T. Wilton-Ely[b]

[a] *Max-Planck-Institut für Kohlenforschung, Mülheim an der Ruhr, 45470 Germany. E-mail: fuerstner@mpi-muelheim.mpg.de*

[b] *Centre for Chemical Synthesis, Department of Chemistry, Imperial College of Science Technology and Medicine, South Kensington, London, UK SW7 2AY. E-mail: a.hill@ic.ac.uk.*

Received (in Cambridge, UK) 6th January 1999, Accepted 26th February 1999

The well defined, conveniently accessible and coordinatively unsaturated allenylidene complexes [$RuCl_2$(=C=C=CPh_2)(PCy_3)$_2$] and [Ru_2Cl_4(=C=C=CPh_2)(PCy_3)(η-$MeC_6H_4Pr^i$-4)] are highly effective catalysts for the ambient temperature ring-closure metathesis of α,ω-dienes and dienynes, illustrated by the facile and high yielding formation of variously functionalised 5, 6, 7, 8, 15, 16 and 18 membered mono- and bi-cyclic ring systems.

The advent of Grubbs' catalysts [$RuCl_2$(=CHR)(PR'_3)$_2$] (R = Ph, CH=CPh_2; R′ = Ph, Cy)[1] has revolutionised alkene metathesis technology by offering a combination of functional group tolerance, high activity and catalyst durability. The rapid embrace of these catalysts as tools for organic fine chemicals synthesis has been truly remarkable.[2] The possibility that complexes of unsaturated 'C_1' ligands other than alkylidenes might also serve as pre-catalysts has however received considerably less attention. Recent key observations which however presage a significant role for such ligands include (i) the demonstration that vinylidene complexes may catalyse the ring-opening metathesis polymerisation (ROMP) of strained cyclic olefins,[3] and (ii) the report by one of us of a coordinatively saturated allenylidene complex [RuCl(=C=C=CPh_2)(PCy_3)(η-$MeC_6H_4Pr^i$)]$^+$ serving as a pre-catalyst for the ring-closure of α,ω dienes.[4] The actual nature of the true catalyst(s) in this latter system is open to conjecture, given that the catalysis only proceeds at elevated temperatures. It has been shown that the pre-catalyst may be activated by prior photolysis, possibly inducing arene dissociation, although subsequent heating is still required.[5] Some insight into the possible identity of the active species has been provided by our recent demonstration that the product mixture obtained from the reaction of [Ru_2Cl_4(η-$MeC_6H_4Pr^i$)$_2$] with HC≡$CCPh_2$OH and PCy_3 under the conditions of catalysis (toluene, 80 °C) includes the coordinatively unsaturated allenylidene complexes [$RuCl_2$(=C= C=CPh_2)(PCy_3)$_2$] **1** and [Ru_2Cl_4(=C=C=CPh_2)(PCy_3)(η-$MeC_6H_4Pr^i$-4)] **2**.[6] Although prior to our report there were no known examples of coordinatively unsaturated allenylidene complexes of group 8 metals,[7] complex **2** is related to the binuclear benzylidene complex [Ru_2Cl_4(=CHPh)(PCy_3)(η-$MeC_6H_4Pr^i$-4)] reported by Grubbs,[8] whilst complex **1** represents the allenylidene analogue of Grubbs' mononuclear catalyst. Complexes **1** and **2** are conveniently prepared in high yield *via* the synthetic sequence illustrated in Scheme 1.[6] With these complexes readily in hand, we wish to report herein, results of our ongoing study of their catalytic efficacy for alkene metathesis processes.

Table 1 summarises representative ring-closure processes mediated effectively by both the mononuclear complex **1** and the binuclear derivative **2**, according to a general procedure outlined below.† To summarise the salient features which emerge: (i) In contrast to previous results with the salt [RuCl(=C=C=CPh_2)(PCy_3)(η-$MeC_6H_4Pr^i$-4)]PF_6,[4] all cyclisations proceed at room temperature and in high to excellent yield, with no need for photolytic pre-activation. (ii) Both catalysts are highly tolerant of functional groups including sulfonamide, ester, bromide, ether, siloxane, amide and fluorenylmethoxycarbonyl substituents. (iii) Both catalysts are suitable for the preparation of buta-1,3-dienes *via* the ring-closure of dienynes. (iv) Five, six, seven, eight, fifteen, sixteen and eighteen membered mono and bicyclic ring systems have been successfully prepared. These include the precursors to Exaltolid®, a musk odored perfume ingredient[9] and epilachnene, an insect repellant alkaloid isolated from the pupae of a Mexican beetle.[10] (v) In general the binuclear catalyst **2**, whilst effective, is slightly less active than the mononuclear complex **1**, requiring somewhat longer reaction times (Table 2) and providing comparable or marginally lower yields. This observation is noteworthy for two reasons: Firstly, by far the most expensive step in the preparative sequence (Scheme 1) involves the synthesis of **2** from **1**. Secondly, Grubbs has shown that for the ROMP of cycloocta-1,5-diene, the binuclear complex [Ru_2Cl_4(=CHPh)(PCy_3)(η-$MeC_6H_4Pr^i$-4)] shows a substantially greater activity (by a factor of *ca*. 20) than the mononuclear complex [$RuCl_2$(=CHPh)(PCy_3)$_2$];[8] (vi) The activities and yields observed for complex **1** suggest that it is equipotent to Grubbs' mononuclear benzylidene complex. This is mechanistically reassuring, in that following the initial cycle of catalysis, the propagating species would be expected to be identical for the two catalysts, *viz* the methylene complex [$RuCl_2$(=CH_2)(PCy_3)$_n$] (*n* = 1 or 2).

These results taken together illustrate that well defined coordinatively unsaturated allenylidene complexes provide an alternative route into the catalytic cycles which operate from the less conveniently accessible benzylidene complex [$RuCl_2$(=CHPh)(PCy_3)$_2$]. The study of synthetic approaches to allenylidene complexes, in particular those of ruthenium,[7] has matured considerably in recent times. Although **1** and **2** are, to

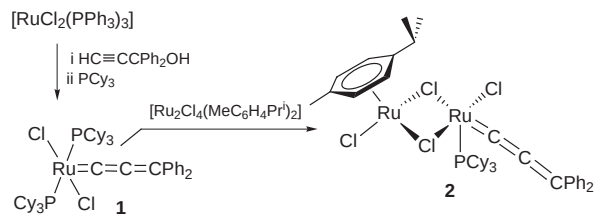

Scheme 1

Table 1. Ring-closure metathesis of α,ω-dienes and dienynes using catalysts **1** and **2**[a]

Cat.	Substrate	Product	Yield(*t*/h)
1	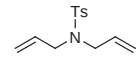		98(2)
2			88(17)
1	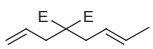		92(20)
2			89(24)
1			83(4.5)
2			75(22)
1	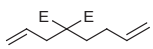	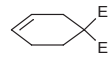	92(4)
2			94(4)
1	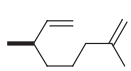	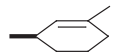	77(18)
1	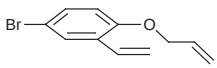	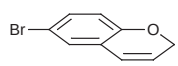	94(3)[b]
2			60(21)[b]
1		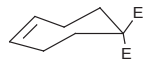	94(7)
2			94(7)
1	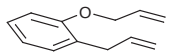	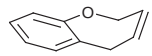	86(18)
2			77(18)
1	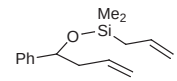	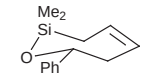	97(5)[b]
2			86(8)[b]
1	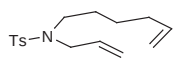	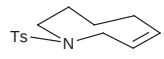	70(6)
1	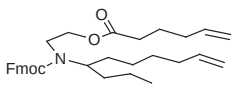	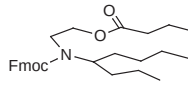	82(67)[c]
2			81(42)[c]
1	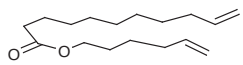	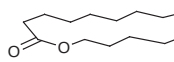	75(19)
2			69(17)
1	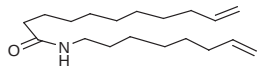	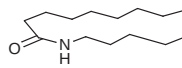	60(72)
1	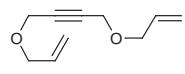	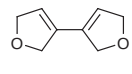	84(4)[b]
2			85(3)[b]
1	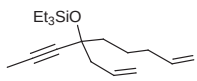	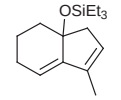	79(18)
2			81(5)[b]

[a] All reactions were carried out in CH_2Cl_2 at room temperature under Ar. E = CO_2Me, Fmoc = 9-fluorenylmethoxycarbonyl, Ts = toluenesulfonyl. [b] GC-yield. [c] Using 5 mol% of the catalyst.

Table 2

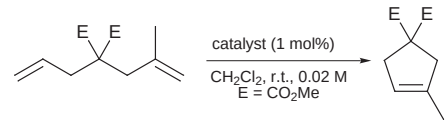

	Conversion (%, GC-yield)	
t/min	Catalyst **1**	Catalyst **2**
20	83	2.5
40	93	5
80	98	11
500	99	33

date, the only coordinatively unsaturated examples, the plethora of recently discovered ruthenium allenylidene complexes provide much scope for the further development and refinement of allenylidene-derived alkene metathesis catalysts, presaged by the high efficacy of catalysts **1** and **2**.

A. F. H. gratefully acknowledges the Leverhulme Trust and the Royal Society for the award of a Senior Research Fellowship. Ruthenium salts were generously provided by Johnson Matthey Chemicals Ltd.

Notes and references

† *N*,*N*-Bis(allyl)toluene-*p*-sulfonamide (846 mg, 3.37 mmol) and **1** (31.7 mg, 1 mol%) in CH_2Cl_2 (160 cm^3) were stirred for 2 h. The mixture was filtered through silica, freed of volatiles and the residue chromatographed (silica gel, hexane–ethyl ethanoate 4:1 eluent) to provide colorless crystals (742 mg, 98%). Mp = 123 - 124 °C. ^{1}H NMR (300 MHz, $CDCl_3$): δ 7.70 (d, 2 H, J = 8), 7.29 (d, 2 H, J = 8), 5.63 (s, 2 H), 4.10 (s, 4 H), 2.41 (s, 3 H). ^{13}C NMR (75 MHz, $CDCl_3$): δ 143.8, 134.7, 130.1, 127.8, 125.8, 55.2, 21.9. MS: *m/z* (rel. intensity): 223 (35, $[M]^+$), 155 (32), 91 (77), 68 (100), 41 (24).

1 S. T. Nguyen, R. H. Grubbs and J. W. Ziller, *J. Am. Chem. Soc.*, 1993, **115**, 9858; P. Schwab, M. B. France, J. W. Ziller and R. H. Grubbs, *Angew. Chem., Int. Ed. Engl.*, 1995, **34**, 2039; E. L. Dias, S. T. Nguyen and R. H. Grubbs, *J. Am. Chem. Soc.*, 1997, **119**, 3887.
2 A. Fürtsner, *Top. Organomet. Chem.*, 1998, **1**, 37.
3 H. Katayama and F. Ozawa, *Chem. Lett.*, 1998, 67.
4 A. Fürstner, M. Picquet, C. Bruneau and P. H. Dixneuf, *Chem. Commun.*, 1998, 1315.
5 M. Picquet, C. Bruneau and P. H. Dixneuf, *Chem. Commun.*, 1998, 2249; For a further description of photochemical effects upon ruthenium-based metathesis catalysis see A. Fürtsner and L. Ackermann, *Chem. Commun.*, 1999, 95.
6 K. J. Harlow, A. F. Hill and J. D. E. T. Wilton-Ely, *J. Chem. Soc., Dalton Trans.*, 1999, 285.
7 For a review of allenylidene complexes of ruthenium and osmium, see: A. F. Hill, in *Comprehensive Organometallic Chemistry, II*, vol **7**, pp. 348–356, ed. E. W. Abel, F. G. A. Stone and G. Wilkinson, Pergamon, Oxford, 1995.
8 E. L. Dias and R. H. Grubbs, *Organometallics*, 1998, **17**, 2758.
9 A. Fürstner and K. Langemann, *J. Org. Chem.*, 1996, **61**, 3942.
10 A. Fürstner and K. Langemann, *Synthesis*, 1997, 792.

Communication 9/00187E

Self-assembly of a bis-tridentate Py_2S_4 ligand and cadmium cation into 1- and 2-D coordination networks†

Marielle Loï,[a] Ernest Graf,[a] Mir Wais Hosseini,*[a] André De Cian[b] and Jean Fischer[b]

[a] Laboratoire de Chimie de Coordination Organique and [b] Laboratoire de Cristallochimie et Chimie Structurale, Université Louis Pasteur, F-67000 Strasbourg, UMR CNRS 7513, France. E-mail: hosseini@chimie.u-strasbg.fr

Received (in Basel, Switzerland) 18th January 1999, Accepted 16th February 1999

Using a Py_2S_4 bis-tridentate ligand and Cd(II), 1- and 2-D coordination networks were obtained and characterised in the solid state; whereas a 1-D network was obtained using the cadmium(II) dichloride salt, a 2-D network was obtained using a mixed chloride and tetrafluoroborate cadmium(II) salt; in the latter case, the inclusion of two $CHCl_3$ molecules within cavities formed by the organic and inorganic fragments was observed.

For some time now, intensive research on the design and preparation of coordination networks or polymers has been performed.[1] Although, nearly all cases reported deal with bis- or tris-monodentate systems,[2] examples of coordination polymers using bis-bidentate ligands have also been published.[3,4] On the other hand, only a few examples of characterised systems based on bis-tridentate ligands are known.[5,6]

The formation of coordination networks in the crystalline phase takes place under self-assembly conditions which require, on one hand, the reversible formation of the assembling core by complexation processes and its translation and, on the other hand, the conformity to the packing forces within the crystalline phase. Thus, for simple coordination networks, the choice of the two partners (metal, ligand) is the dominant feature. For porous coordination networks, in addition to the two partners mentioned before, one should also take into account the guest molecules initially occupying the pores. Owing to the fact that tridentate centres form rather stable and non-labile complexes with transition metals, the choice of the metal and the ligand is not obvious and therefore, not many characterised examples are available so far.

Here, we report the synthesis of a new bis-tridentate ligand and its self-assembly into 1- and 2-D coordination polymers using Cd(II) cation.

The design of the linear bis-tridentate ligand **7** (Scheme 1) is based on a combination of two pyridine moieties and four thioether groups. The two tridentate ligands are interconnected by a phenyl ring. Examples of other bis-tridentate ligands have been reported.[7]

Dealing with the metal cation, it has been shown previously that **1** forms a binuclear Cd(II) complex in which the two metal centres are bridged by two Cl^- anions.[8] This type of doubly bridged metal system has been reported for Co(II)[6b] and for Ni(II) complexes.[9]

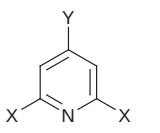

1 X = CH_2SEt, Y = H
2 X = CO_2H, Y = OH
3 X = CO_2Et, Y = Br
4 X = CH_2OH, Y = Br

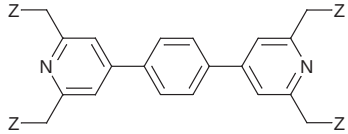

5 Z = OH
6 Z = Br
7 Z = SMe

Scheme 1

† Dedicated to Professor John A. Osborn on the occasion of his 60th birthday.

The synthesis of **7** was achieved starting from chelidamic acid **2**, which was first transformed into **3**.[10] The latter was reduced to **4**.[11] $Pd(PPh_3)_4$ catalysed coupling reaction of **4** with 1,4-phenyldiboronic acid[12] in dry THF gave **5** in 65% yield. Bromination of the latter using 33% HBr–AcOH afforded **6** in 61% yield. Finally, the treatment of **6** with NaSMe in dry THF afforded **7** in 71% yield. The latter, in addition to spectroscopic methods, was characterised by X-ray crystallography.

Upon slow diffusion at room temp. of a MeOH solution containing $CdCl_2{\cdot}xH_2O$ into a $CHCl_3$ solution of **7** (1 : 1 ratio of Cd : **7**), colourless crystals were deposited after 24 h. The X-ray study‡ showed the following features (Fig. 1): the crystal **I** (monoclinic) was composed of **7**, Cd(II), Cl^- anions, $CHCl_3$ and H_2O molecules. **7**, Cd(II) and Cl^- anions formed a neutral, infinite 1-D coordination network (Fig. 2).

Depending on the definition of the assembling core, the 1-D network $(\mathbf{7}Cd_2Cl_4)_n$ thus obtained may be described in two different ways. Considering the metallic core as a binuclear Cd_2Cl_4 unit (Fig. 2), the network may be regarded as resulting from the binding of two such units by the two PyS_2 fragments of **7** leading thus to the exo-tetranuclear Cd(II) complex and the repetition of the binding process leads to the 1-D coordination network. The same system may be also described as resulting from the bridging of consecutive exo-binuclear $\mathbf{7}{\cdot}Cd_2$ units by two Cl^- anions, and the remaining other two Cl^- anions behaving as ancillary ligands. For the ligand part, the pyridine rings were tilted by −37.6 and 38.3° with respect to the phenyl group. The CS and CN distances were roughly the same as those observed for free **7**. The coordination sphere around the Cd cations was composed of one N atom (d_{NCd} = 2.426 Å), two S atoms (d_{SCd} = 2.730, 2.747 Å) and three Cl^- anions. Among the three Cl^- present, two of them were shared between two Cd centres (d_{ClCd} = 2.591, 2.651 Å) whereas the third one was acting as an ancillary ligand (d_{ClCd} = 2.511 Å). The coordination geometry around the metal centre was distorted octahedral with S–Cd–S, Cl–Cd–Cl and N–Cd–Cl angles of 146.5, 172.0 and 175.2°, respectively. Within the $Cd_2{\cdots}Cl_4$ unit, the Cd···Cd distance was found to be 3.946 Å. The $CHCl_3$ and H_2O molecules were localised between the 1-D chains.

Interestingly, when instead of using $CdCl_2$, a mixed Cl^- and BF_4^- salt $[CdCl(BF_4)]$ was used, the same diffusion method afforded after two days another type of colourless crystal. The solid state analysis (Fig. 3)‡ showed that the crystal **II** was composed of **7**, Cd(II) cations, Cl^- and BF_4^- anions, $CHCl_3$ and MeOH molecules. **7**, Cd(II) and Cl^- anions formed a cationic infinite 2-D coordination network (Fig. 2). The latter may be described as the result of mutual interconnection of the 1-D coordination polymers described above through Cl^- anions acting now as bridging ligands. In a sense, the poor coordination ability of BF_4^- has created a Cl^- deficiency in the coordination sphere of Cd(II), made up for by an additional Cl^- bridging interaction.

Thus, the 2-D network may be regarded as the translation into two different space directions of an assembling core which may be defined $[\mathbf{7}_4Cd_4Cl_7]^+$ (Fig. 2). The charge neutrality being achieved by BF_4^- anions present in the lattice. Owing to the aromatic nature of the ligand used, the 2-D network was composed of cavities delimited in an alternating fashion by

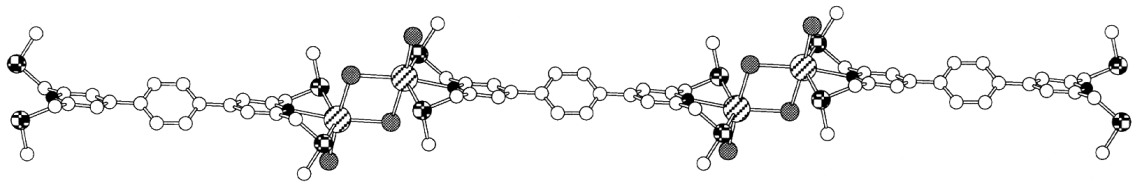

Fig. 1 A section of the X-ray structure of the 1-D coordination network **I** formed between **7** and $CdCl_2$. H atoms, anions and solvent molecules are not presented for clarity.

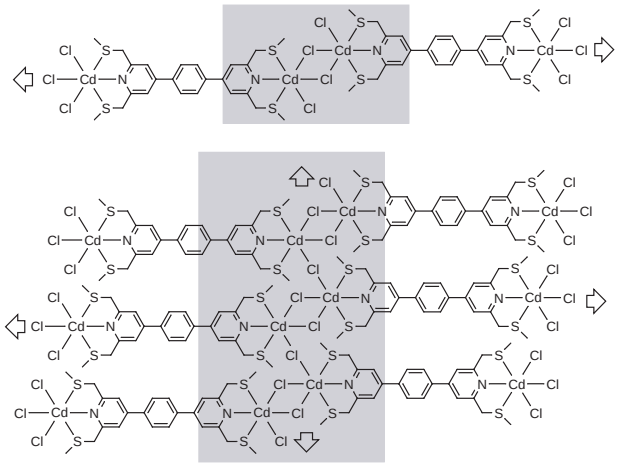

Fig. 2 Partial representation of the 1- and 2-D coordination polymers **I** and **II**.

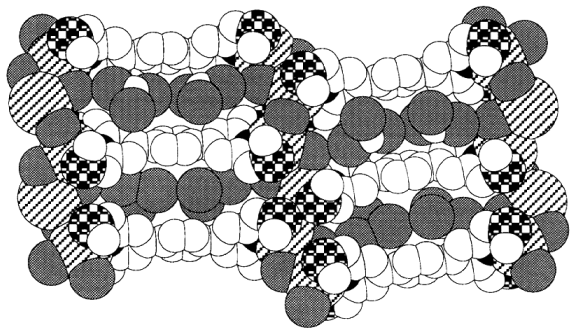

Fig. 3 A section of the X-ray structure of the 2-D coordination network **II** (see text). H atoms, anions and MeOH molecules are not presented for clarity.

organic and inorganic fragments. For **7**, the pyridine rings were tilted by −30.7 and 32.2° with respect to the phenyl group. The C–S and C–N distances were roughly the same as those observed for the free **7** and for the above-mentioned 1-D network. The coordination sphere around the Cd cations was again composed of one N atom (average d_{NCd} = 2.385 Å), two S atoms (average d_{SCd} = 2.697 Å) and three Cl^- anions. Although all three Cl^-, present in the coordination sphere of Cd cation, adopted a bridging role between the metallic centres, two of them were shared between two Cd centres (average d_{ClCd} = 2.608 Å) within the 1-D network, whereas the third one bridged two consecutive linear networks (d_{ClCd} = 2.559 Å) thus leading to a two-dimensional polymer. The coordination geometry around the metal centre was again distorted octahedral with S–Cd–S, Cl–Cd–Cl and N–Cd–Cl angles of 147.6, 169.0 and 163.6°, respectively. With the Cd_4Cl_7 unit, the Cd···Cd distances varied from 3.921 Å for the doubly bridged cations to 4.625 Å for the singly bridged centres. Interestingly, whereas MeOH and BF_4^- anions were localised between the 2-D sheets, the $CHCl_3$ molecules were included within the cyclophane type cavities composing the 2-D network.

In conclusion, using the N_2S_4 bis-tridentate ligand and Cd(II), 1- and 2-D coordination networks were obtained and characterised in the solid state. For the 2-D network the inclusion of two $CHCl_3$ molecules within cavities formed by the organic and inorganic fragments was observed. Based on the same strategy, the formation of magnetic networks using paramagnetic metal cations is currently under investigation.

Notes and references

‡ *Crystal data*: **I** (colorless, 294 K), $C_{12}H_{14}CdCl_2NS_2{\cdot}CHCl_3{\cdot}2H_2O$, M = 575.09, monoclinic, a = 29.037(1), b = 8.4340(2), c = 22.5310(8) Å, β = 126.63(1), U = 4428(2) Å^3, Z = 8, space group $C2/c$, D_c = 1.73 g cm^{-3}, Nonius Kappa CCD, Mo-Kα, μ = 1.785 mm^{-1}, 5315 data with $I > 3\sigma(I)$, R = 0.056, R_w = 0.076.

II (colorless, 173 K), $C_{24}H_{28}Cd_2Cl_3N_2S_4{\cdot}BF_4{\cdot}2CHCl_3{\cdot}CH_3OH$, M = 1161.52, orthorhombic, a = 16.3181(4), b = 14.8660(3), c = 35.9037(8) Å, U = 8709.7(6) Å^3, Z = 8, space group $Pbcn$, D_c = 1.77 g cm^{-3}, Nonius Kappa CCD, Mo-Kα, μ = 1.764 mm^{-1}, 4036 data with $I > 3\sigma(I)$, R = 0.051, R_w = 0.061. CCDC 182/1173.

1 R. Robson, in *Comprehensive Supramolecular Chemistry*, ed. J. L. Atwood, J. E. D. Davies, D. D. Macnicol and F. Vögtle, Pergamon, vol. 6, ed. D. D. Macnicol, F. Toda and R. Bishop, 1996, pp. 733; O. M. Yaghi, H. Li, C. Davis, D. Richardson and T. L. Groy, *Acc. Chem. Res*., 1998, **31**, 474.

2 T. L. Hennigar, D. C. MacQuarrie, P. Losier, R. D. Rogers and M. J. Zaworotko, *Angew. Chem., Int. Ed. Engl*., 1997, **36**, 972 and references therein; M. Loï, M. W. Hosseini, A. Jouaiti, A. De Cian and J. Fischer, *Chem. Commun.*, 1999, submitted.

3 O. J. Gelling, F. van Bolhuis and B. L. Faringa, *J. Chem. Soc., Chem. Commun.*, 1991, 917; O. Kahn, Y. Journaux and C. Mathoniere, in *Magnetism : A Supramolecular Function*, ed. O. Kahn, Kluwer, Dordrecht, Netherlands, 1996, vol. C484, pp. 531; S. Decurtins, R. Pellaux, A. Hauser and M. E. von Arx, *ibid*, p. 487; U. Velten and M. Rehahn, *Chem. Commun*., 1996, 2639.

4 C. Kaes, M. W. Hosseini, C. E. F. Rickard, B. W. Skelton and A. White, *Angew. Chem., Int. Ed.*, 1998, **37**, 920; G. Mislin, E. Graf, M. W. Hosseini, A. De Cian, N. Kyritsakas and J. Fischer, *Chem. Commun*., 1998, 2545.

5 S. J. Loeb and G. K. H. Shimizu, *J. Chem. Soc., Chem. Commun.*, 1993, 1395; A. Neels, B. Mathez Neels and H. Stoeckli-Evans, *Inorg. Chem*., 1997, **36**, 3402.

6 E. C. Constable, A. J. Edwards, D. Philips and P. R. Raithby, *Supramol. Chem*., 1995, **5**, 93.

7 H. A. Goodwin and F. Lions, *J. Am. Chem. Soc*., 1959, **81**, 6415; J.-P. Sauvage, J.-P. Collin, J.-C. Chambron, S. Guillerez, C. Coudret, V. Balzani, F. Barigelletti, L. De Cola and L. Flamigni, *Chem. Rev*., 1994, **94**, 993; P. Steenwinkel, H. Kooijman, W. J. J. Smeets, A. L. Spek, D. M. Grove and G. van Koten, *Organometallics*, 1998, **17**, 5411 and references therein.

8 F. Teixidor, L. Escriche, I. Rodrigez and J. Casabo, *J. Chem. Soc., Dalton Trans*., 1989, 1381.

9 A. J. Blake, F. Demartin, F. A. Devillanova, A. Garau, F. Isaia, V. Lippolis, M. Schröder and G. Verani, *J. Chem. Soc., Dalton Trans*., 1996, 3705.

10 H. Takalo and J. Kankare, *Acta Chem. Scand*., 1987, **41**, 219.

11 H. Takalo, *Acta Chem. Scand*., 1988, **42**, 373.

12 O. C. Musgrave, *J. Chem. Soc. C*, 1970, 488.

Communication 9/00501C

ChemComm

Pseudopolymorphism: occurrences of hydrogen bonding organic solvents in molecular crystals

Ashwini Nangia and Gautam R. Desiraju

School of Chemistry, University of Hyderabad, Hyderabad 500 046, India. E-mail: grdch@uohyd.ernet.in

Received (in Cambridge, UK) 15th December 1998, Accepted 24th February 1999

Multi-point recognition with strong and weak hydrogen bonds between solvent and solute molecules facilitates the retention of organic solvents in crystals

Pseudopolymorphism is the phenomenon wherein a compound is obtained in crystalline forms that differ in the nature or stoichiometry of included solvent molecules.[1] This subject has not been treated systematically though it is perceived to be of general importance, for example in the pharmaceutical industry.[2] In a supramolecular sense, pseudopolymorphs of a compound are different chemical systems and should be treated as such. Here, we examine the likelihood of several hydrogen bonding organic solvents in crystal structures and attempt to provide some rationalisation for these occurrences. We have not considered hydration. The presence of water in organic crystals is so widespread and the reasons for its inclusion so varied[1–3] that it would not be realistic or practicable to include it with the other solvents considered here.

The method of analysis uses the Cambridge Structural Database (CSD, version 5.15, April 1998, 181 309 entries).[4] Organic structures† containing solvent of crystallisation were retrieved and 20 common solvents found to occur at least 50 times. A few hits contain two solvents and these are included under both in Table 1. The raw frequencies of occurrence N are listed in Table 1, which also contains the numbers of fully ordered crystal structures in each case, N_{ord}.‡ Given that some solvents are used for recrystallisation more frequently than others, these N (or even N_{ord}) values cannot be taken to correspond directly to the abilities of the respective solvents to give solvated crystals. To perform an appropriate, though still approximate, correction for differences in solvent usage, all organic structures (solvated or otherwise) in the 1986 and 1996 issues of *Acta Crystallographica Section C* were examined. The number of times each solvent was used for recrystallisation alone or in combination with other solvents is given as N_{Acta} in Table 1. The quantity (N/N_{Acta}) for a particular solvent was then taken as a measure of its ability to be included in the crystal. This quantity was scaled appropriately to give the usage corrected occurrence (O_{corr}). A value of 1.00 for O_{corr} indicates a solvent that forms solvates to an extent commensurate with its usage. Values of O_{corr} much larger or much smaller than unity indicate solvents that have a greatly enhanced or a greatly reduced tendency to be included in crystals.

Table 1 Occurrences of 20 common solvents in organic crystal structures in decreasing order of O_{corr}

Solvent	N	N_{ord}	N_{Acta}	O_{corr}[a]
DMF	122	63	5	5.69
DMSO	142	70	7	4.73
Dioxane	161	83	8	4.70
p-Xylene	49	22	3	3.81
Benzene	471	271	32	3.43
THF	188	54	14	3.13
MeCN	396	181	31	2.98
AcOH	105	54	10	2.45
CCl_4	59	14	7	1.97
Toluene	266	65	36	1.72
CH_2Cl_2	455	183	77	1.38
$CHCl_3$	386	132	67	1.34
MeOH	795	433	158	1.17
Acetone	346	169	82	0.98
Pr^{i}OH	65	33	16	0.95
Cyclohexane	56	9	21	0.62
EtOAc	155	52	75	0.48
EtOH	406	168	206	0.46
Et_2O	144	54	96	0.35
Hexane	84	21	181	0.11
Total	4851	2131	1132	

[a] Calculated by the formula $(N/4851)/(N_{Acta}/1132) = 0.233\ (N/N_{Acta})$

The next step in the analysis focussed on the three solvents with the maximum values of O_{corr}. Let us consider the ordered dioxane solvates ($N_{ord} = 83$). Twenty hits contain an O–H···O hydrogen bond with specified metrics.§ In 12 of these cases, two O–H···O bonds approach a dioxane molecule as shown in the first synthon in Scheme 1. Similarly, 5 out of the 8 N–H···O hits correspond to two-point recognition with N–H groups.¶ This behaviour extends to hydrogen bonding by C–H groups. Forty six out of the 83 dioxane solvates contain a C–H···O bond to the solvent. When all the two-point cases are enumerated (13 with C–H, O–H; 8 with C–H, N–H; 40 with C–H, C–H), the total (61) is in excess of 46, indicating that in some of the cases, multiple donor groups approach the acceptor O-atom in the dioxane molecule. The overall situation is clear—when dioxane is included in an organic crystal, it is always hydrogen bonded and more importantly, to more than one donor. Generally, these donor groups (O–H, N–H, C–H) originate from different solute molecules though dioxane itself was noted to be the C–H donor in some cases (12 hits).

Multi-point recognition *via* strong and weak hydrogen bonding is also the favoured mode of association for DMSO (dimethyl sulfoxide) and DMF (dimethylformamide), both of which have a very high probability of being included in crystals. Whether the S=O group in DMSO is hydrogen bonded to an O–H, N–H or C–H group, the adjacent methyl group is invariably C–H···O bonded (25 out of 25 for O–H, 12 out of 13 for N–H, 44 out of 44 for C–H). It is interesting to note that all 44 hits that contain a C–H···O bond to DMSO as acceptor also contain a C–H···O bond from DMSO as donor. Like dioxane, DMSO shows a tendency to dimerise with itself (17 hits) or with acids (11 hits) and amides (3 hits). Many of these dimers are parts of extended hydrogen bonded networks and the various synthons shown in the scheme are not of an exclusive nature; any particular crystal structure usually contains more than one of the arrangements shown in Scheme 1. The situation with DMF is very similar. Multi-point recognition *via* C–H···O bonding from a methyl group of the solvent accounts for the majority of hits (13 out of 14 for O–H, 13 out of 16 for N–H and 29 out of 38 for C–H donors to DMF) while in 24 hits both methyl groups act as donors. As in DMSO, there is a tendency to form dimers and further these dimers extend into the general hydrogen bonding scheme. This tendency of dioxane, DMSO and DMF to self-associate as well as to form interactions with the solute improves the chances of solvent inclusion in crystals.

The final step of the analysis deals with solvates formed by EtOAc, EtOH and Et_2O. These three solvents are marked by an unusually reduced likelihood of being incorporated into solvate structures. The failure of these commonly-used solvents to be

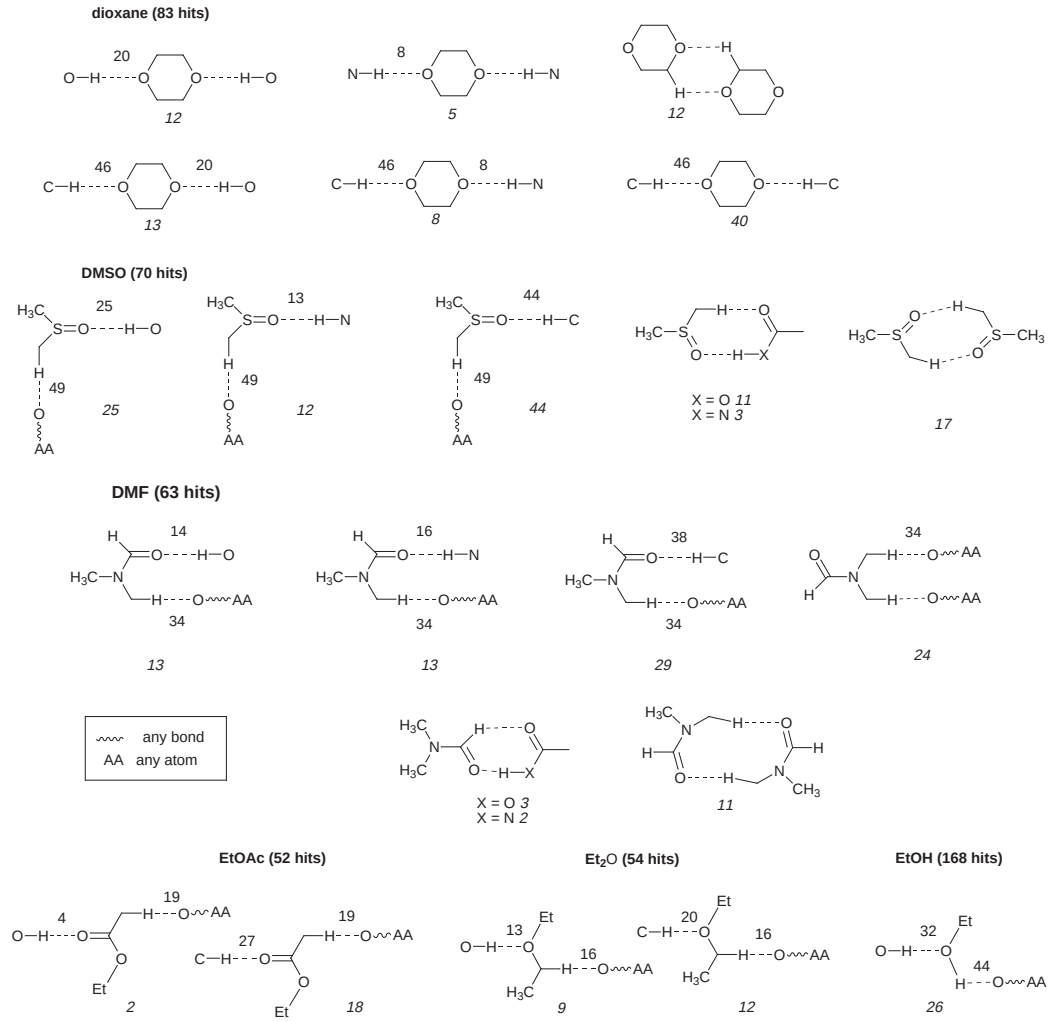

Scheme 1 Multi-point supramolecular synthons formed by the frequently included solvents dioxane, DMSO and DMF. The numbers of strong and weak hydrogen bonds among the selected hits are given near the dotted lines. The italic numbers given below each synthon represent the incidence of two-point recognition. Notice the wide prevalence of C–H···O hydrogen bonding. The reduced incorporation of the solvents EtOH, Et_2O and EtOAc is reflected in the corresponding numbers for these solvents.

thus included is accounted for in terms of their inability to effectively participate in multi-point hydrogen bonded recognition schemes. Though EtOAc has a good acceptor group, the donors are largely unactivated. Et_2O has some acceptor ability but very poor donating capability. Unlike dioxane, neither of these solvents can act as multiple acceptors. To the extent, however, that the donors in EtOAc are more activated than in Et_2O, it is incorporated in crystals better. EtOH has a very good donor and a moderate acceptor group. However, it is generally included only in alcohol and acid structures and that too as part of a cooperative network, in which capacity it is also expendable. The numerical details in Scheme 1 bear out these qualitative generalisations. Of course, there must also be other reasons for the incorporation of organic solvents in crystals. Solvents like benzene, *p*-xylene and CCl_4 are included easily but generally in rigid framework structures where they are of the correct size to act as guests in a host lattice. Nonetheless, multipoint hydrogen bonding is clearly a dominant factor that governs the inclusion of the large number of solvents that are capable of exhibiting this phenomenon.

To conclude, why is multi-point recognition of the solvent so important in the formation of pseudopolymorphic structures? Crystallisation begins with solute–solvent aggregates that contain solute–solute, solute–solvent and solvent–solvent interactions. The entropic gain in eliminating solvent molecules from these aggregates into the bulk solution, and the simultaneous enthalpic gain in forming stable solute species that contain robust supramolecular synthons, provides an adequate driving force for nucleation and crystallisation with the result that most (85%) organic crystals are unsolvated. However, when solvent molecules are attached to solute molecules in a multi-point manner *via* either strong (O/N–H···O) or weak (C–H···O) hydrogen bonds, the extrusion of solvent from the aggregates into the bulk may become sufficiently disadvantageous from an enthalpic viewpoint with the result that the solvent remains an integral part of the nucleating crystal. The formation of a solvated crystal may therefore be likened to an interruption of the sequence of events that accompany the 'normal' crystallisation of an unsolvated form.

We thank the DST (SP/S1/G19/94) for financial assistance and Dr J. A. R. P. Sarma for discussions.

Notes and references

† By the term 'organic' we mean non-metal-atom-containing (screen 57 in the CSD). This group contains 84 562 entries.

‡ CSD screens 33 (error-free), 35 (no disorder), 85 (chemical/crystallographic connectivity match), 88 (*R*-factor ≤0.10) and 153 (atom coordinates present) were applied. The H-atoms are defined in these structures. This sub-group of organic structures contains 56 492 entries.

§ Hydrogen bond metrics: O–H···O, N–H···O, $1.5< d < 2.2$ Å, $140 < \theta < 180°$; C–H···O, $2.0 < d < 3.0$ Å, $110 < \theta < 180°$. All H-atom positions were neutron-normalised.

¶ No hits were found for two-point O–H, N–H recognition.

1 T. L. Threlfall, *Analyst*, 1995, **120**, 2435.
2 S. R. Byrn, *Solid-State Chemistry of Drugs*, Academic Press, New York, 1982.
3 G. R. Desiraju, *J. Chem. Soc., Chem. Commun.*, 1991, 426.
4 F. H. Allen, J. E. Davies, J. J. Galloy, O. Johnson, O. Kennard, C. F. Macrae and D. G. Watson, *J. Chem. Inf. Comput. Sci.*,1991, **31**, 204.

Communication 8/09755K

Modification of photochemical reactivity of *trans*-2-styrylpyridine: effect of cyclodextrin complexation

H. Shayira Banu,[a] A. Lalitha,[a] K. Pitchumani*[b] and C. Srinivasan*[a]

[a] *Department of Materials Science, Madurai Kamaraj University, Madurai -625 021, India. E-mail: matsci@pronet.xlweb.com*

[b] *School of Chemistry, Madurai Kamaraj University, Madurai -625 021, India*

Received (in Cambridge, UK) 1st December 1998, Accepted 2nd March 1999

In contrast to the solution irradiation of *trans*-2-styrylpyridine, photolysis of a γ-CD complex of the base in the solid state leads to the formation of the *syn*-head-to-tail dimer in fairly good yield.

While irradiation of the free base *trans*-2-styrylpyridine (*trans*-2-SP) under nitrogen in benzene solution leads only to its isomerization to *cis*-2-SP, photolysis of *trans*-2-SP in the solid state in the presence of oxygen yields the dimer in small amounts (2.6%) along with materials formed from photooxidation.[1,2] On the other hand, irradiation of the methiodide and hydrochloride of *trans*-2-SP in the solid state causes ready dimerization; the same process in benzene solution results both in isomerization to its *cis*-form and dimerization. The structure of the dimer has been suggested as one in which the quaternized rings dimerize in alternate positions so as to reduce steric as well as charge interference.[1,2] In another study unimolecular cyclization has been reported[3] during the photolysis of 2-SP in cyclohexane in the presence of oxygen to give benzo[*f*]quinoline in 35% yield, involving the intermediacy of dihydrobenzo[*f*]quinoline along with a minor product 1-phenyl-2-(2-pyridyl)ethanol (10%).

Microheterogeneous media such as micelles, monolayer assemblies, *etc*. are employed to control and achieve some selectivity in the dimerization of 4-styrylpyridinium cations.[4] When salts of 4-styrylpyridinium ions are irradiated in hexane–aerosol OT–water reverse micelles, efficient and selective formation of the *syn*-head-to-head (72%) dimer occurs. This is in contrast to the observation of photolysis in homogeneous solution wherein 13% of the *cis*-isomer and 60% of the *syn*-head-to-tail dimer are produced.[5] When intercalated between the interlayers of clay, 4-styrylpyridinium ions selectively yield the *syn*-head-to-tail cyclodimers.[6]

Cyclodextrins (CDs) are doughnut shaped cyclic oligosaccharides consisting of six, seven or eight glucose units (α-, β- and γ-CDs, respectively) with a hydrophobic inner cavity and a hydrophilic outside. Their cavities have internal diameters varying from 4.7 to 8.3 Å, permitting them to form inclusion complexes with a variety of guest molecules.[7] The depth of the binding cavity of all three CDs is almost the same (7.8 Å). Complexation between CDs and substrates in solution has been successfully exploited to induce selectivity in some unimolecular and bimolecular photochemical reactions.[8] Tamaki and co-workers[9] were the first to explore the utility of the CD cavity in effecting regio- and stereoselective dimerization of guest molecules like anthracene-2-sulfonate and anthracene-2-carboxylate. Photodimerization of acenaphthylene[10] and coumarin[11] upon complexation into the γ-CD cavity has been reported. [2 + 2] Photocycloaddition of a symmetrical stilbene derivative to yield a mixture of dimers in the presence of γ-CD has also been reported.[12] However, inclusion of stilbenes[13,14] in β-CD results in only *cis–trans* isomerization, suggesting that the cavity free volume in cyclodextrins plays a major role in controlling the reactivity of the included olefins.

This factor, coupled with the marked observed difference in behaviour during the photolysis of 2-SP and its salt in solution and the solid state, prompted us to study the effect of CD encapsulation on the photochemical behaviour of the free base 2-SP. As the widths of the cavities of α-, β- and γ-CDs increase in a regular manner and therefore the free space available for the guest increases, it is expected that the three CDs will have a varying influence on the photolysis of 2-SP encapsulated in CD. The results of irradiation of 2-SP in the three CDs are presented here.

Irradiation of an MeCN solution of *trans*-2-SP results only in isomerization with the absence of any bimolecular dimerization or unimolecular cyclization in the photostationary state (PSS). A change in the product distribution is noticed when CD complexes of *trans*-2-SP are subjected to irradiation (Table 1).

Upon irradiation of a α-CD–*trans*-2-SP complex in the solid state, a dramatic reduction in the percentage of the *cis*-isomer was observed in the PSS compared to the solution irradiation of 2-SP. Because of the smaller width of the α-CD, a restriction is imposed by the α-CD cavity on the photoisomerization of *trans*-2-SP. A small amount of the dimer† is possibly also formed from *trans*-2-SP which has not penetrated significantly into the cavity (Table 1).

The photochemical studies of the solid β-CD complex of *trans*-2-SP reveal not only a decrease in the percentage of *cis*-2-SP, but also a notable increase in the amount of unimolecular cyclized product, benzo[*f*]quinoline (Table 1), at the expense of the *cis*-isomer. The space available in β-CD is large enough to improve *trans–cis* interconversion and facilitate the cyclization of the *cis*-isomer. A deeper penetration of the base into β-CD compared to α-CD precludes any contact between two monomers and thus rules out the formation of a dimer. Also the conformation of the *cis*-form in β-CD (Scheme 1) is such that

Table 1 Product distribution on irradiation of *trans*-2-SP in different CDs

Medium	CD : Substrate ratio	*trans*-Isomer	*cis*-Isomer	Dimer	Benzo[*f*]quinoline	X[a]
trans-2-SP in MeCN	—	7	93	—	—	—
trans-2-SP (solid)	—	80	6	5	2	7
α-CD–2-SP (solid)	1 : 1	76	16	6	1	1
β-CD–2-SP (solid)	1 : 1	74	6	1	15	4
γ-CD–2-SP (solid)	1 : 1	31	15	46	6	2
γ-CD–2-SP (solid)	1 : 2	33	7	50	10	—

[a] X = to be identified.

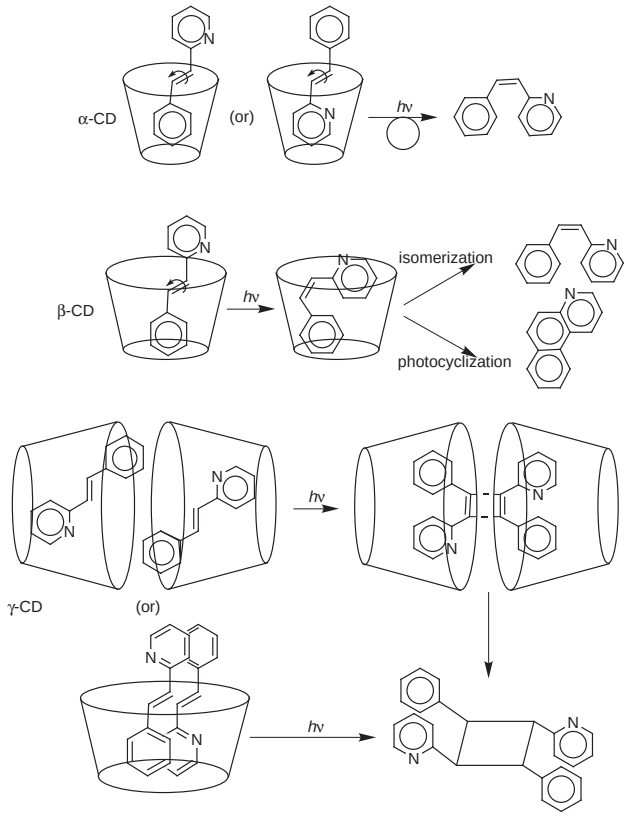

Scheme 1

the dimerization between two *cis*-molecules encapsulated in β-CD may not be easy.

In contrast to the above studies, during the photolysis of a 1 : 1 γ-CD–*trans*-2-SP solid complex a drastic decrease of *trans*-2-SP in the PSS with prominent formation of the dimer (Table 1) is observed. Since the width of the CD cavity is greatest in γ-CD among the three CDs, this free space is large enough to facilitate a marked increase in *trans–cis* photoisomerization. In the 1 : 1 complex with γ-CD the initially formed *cis*-2-SP can couple with another *cis*-2-SP molecule from the suitably oriented adjacent complex to produce the dimer (Scheme 1). The free space is so large in γ-CD that it can accommodate two molecules of the guest in the cavity of a single molecule of the host and in such a complex efficient photodimerization is expected.‡ Indeed we could prepare a 1 : 2 complex of γ-CD–*trans*-2-SP and during the photolysis of this solid complex, the yield of the dimer is slightly increased (Table 1). Since the dimer obtained in all the cases studied by us is *syn*-head-to-tail,† we presume that in the 1 : 2 complex the two *trans*-2-SP molecules are in an antiparallel alignment (Scheme 1).

Thus the observed results are significant as the dimerization is achieved with the free base while earlier reports require quaternization for effective cyclization. The present investigation suggests that it is possible to control the product of photolysis towards either unimolecular (photoisomerization and/or photocyclization) or bimolecular (photodimerization) reactions by choosing the proper CD.

2-SP was prepared and recrystallized as reported in the literature.[15] The dimer (*syn*-head-to-tail) was prepared[1] by the irradiation of 2-SP hydrochloride in benzene as a suspension for 15 h under nitrogen atmosphere using a 365 nm (8 × 8 W) annular photochemical reactor. Benzo[*f*]quinoline was prepared as reported in the literature.[3] α-CD (American Maize products, Indiana), β-CD (Aldrich) and γ-CD (American Maize Products, Indiana) were used as received. The CD complexes were prepared by a procedure reported elsewhere.[16] The CD complexes were irradiated using a 400 W (365 nm) water cooled, immersion type SAIC photoreactor. After irradiation was over, the products were extracted with $CHCl_3$ and the percentage of products were determined by PTLC. The products were characterized by ^1H NMR spectroscopy.

We wish to record our grateful thanks to the American Maize Products Company, Indiana, for the generous gift of α- and γ-CDs. Bioinformatics Centre, SBT, MKU is also acknowledged for the molecular modelling studies used in the present work. H. S. B. acknowledges financial assistance from CSIR, New Delhi.

Notes and references

† The dimer obtained in the present study is identified as the *syn*-head-to-tail dimer by its characteristic NMR pattern: $\delta_H(CDCl_3, 300\ MHz)$ 4.93 (2H, t), 5.10 (2H, t) (cyclobutyl protons), 7.11–7.59 (16H, m, ArH) and 8.66 (2H, d, Ar-H). It is also identified by its characteristic melting point, 189-190 °C (lit. 189–190 °C) (ref. 1,2).

‡ Molecular modelling studies [INSIGHT II (BIOSYM) using the DISCOVER module] were carried out to support the inclusion modes of *trans*-2-SP, *cis*-2-SP, 2 molecules of *trans*-2-SP and *cis*-2-SP inside α-, β- and γ-cyclodextrins. While 1 : 1 complexes are favoured in α-, β- and γ-CDs inclusion of two molecules of *trans*-/*cis*-2-SP is energetically allowed only in γ-CD. The results support our speculations of preferred modes of complexation. Details of the molecular modelling studies are available from the RSC website, see:http//www.rsc.org/suppdata/cc/1999/607/

1 J. L. R. Williams, *J. Org. Chem*., 1960, **25**, 1839.
2 J. L. R. Williams, S. K. Webster and J. A. Van Allan, *J. Org.Chem*., 1961, **26**, 4893.
3 P. L. Kumler and R. A. Dybas, *J. Org. Chem*., 1970, **35**, 125.
4 F. H. Quina and D. G. Whitten, *J. Am. Chem. Soc*., 1977, **99**, 877.
5 K. Takagi, B. R. Suddaby, S. L. Vadas, C. A. Backer and D. G. Whitten, *J. Am. Chem. Soc*., 1986, **108**, 7865.
6 H. Usami, K. Takagi and Y. Sawaki, *J. Chem. Soc., Faraday Trans*., 1992, **88**, 77.
7 V. Ramamurthy, *Tetrahedron*, 1986, **42**, 5753; L. Jicsinszky, E. Fenyvesi, H. Hashimoto and A. Ueno, *Cyclodextrins*, *Comprehensive Supramolecular Chemistry*, ed., J. Szejtli and T. Osa, Pergamon, Oxford, 1996, vol. 3, p. 57; A. Ueno, *Supramol. Sci*., 1996, **3**, 13; P. Bortolus and S. Monti, *Photochemistry in Cyclodextrin Cavities*, in *Advances in Photochemistry*, ed. D. C. Neckers, D. H. Volman and G. von Bünau, John Wiley, New York, 1996, vol. 21; K. Takahashi, *Chem. Rev*., 1998, **98**, 2013.
8 B. N. Rao, N. J. Turro and V. Ramamurthy, *J. Org. Chem*., 1986, **51**, 460.
9 T. Tamaki, *Chem. Lett*., 1984, 53; T. Tamaki and T. Kokubu, *J. Inclusion Phenom*., 1984, **2**, 815; T. Tamaki, T. Kokubu and K. Ichimura, *Tetrahedron*, 1987, **43**, 1484.
10 Z. Tong and Z. Zhen, *Youji Huaxue*, 1986, 44; *Chem. Abstr*., 1986, **105**, 152330g.
11 J. N. Moorthy, K. Venkatesan and R. G. Weiss, *J. Org. Chem*., 1992, **57**, 3292.
12 W. Herrmann, S. Wehrle and G. Wenz, *Chem.Commun*., 1997, 1709.
13 M. S. Syamala and V. Ramamurthy, *J. Org. Chem*., 1986, **51**, 3712.
14 M. S. Syamala, S. Devanathan and V. Ramamurthy, *J. Photochem*., 1986, **34**, 219.
15 J. L. R. Williams, R. E. Adel, J. M. Carlson, G. A. Reynolds, D. G. Borden and J. A. Ford, Jr., *J. Org.Chem*., 1963, **28**, 387.
16 G. Dasaratha Reddy, B. Jeyasree and V. Ramamurthy, *J. Org.Chem*., 1987, **52**, 3107.

Communication 8/09372E

Calix[4]arene-based Cs^+ selective optical sensor

Hai-Feng Ji, Gilbert M. Brown and Reza Dabestani*

Chemical and Analytical Sciences Division, Oak Ridge National Labotatory, PO Box 2008, MS-6100, Oak Ridge, TN 37831-6100, USA.E-mail: dabestanir@ornl.gov

Received (in Columbia, MO, USA) 4th November 1998, Accepted 15th February 1999

1,3-Calix[4]bis(9-cyano-10-anthrylmethyl)-*o*-benzocrown-6 has been synthesized as a first generation caesium selective fluorescent probe, and its emission behavior in the presence of Li^+, Na^+, K^+ and Cs^+ ions has been examined.

The chemistry of calix[4]arenes, cyclic tetramers comprising phenolic and methylene moieties, has received considerable attention in recent years.[1,2] The available sites on these macrocyclic compounds that can be easily modified to tailor them for application as ionophores in catalysis,[3] and in heavy metal absorption,[4] alkali metal complexation[2] and chemical sensors[5,6] have been examined. Calix-crown compounds show high affinity for complexation of alkali and alkaline-earth metal ions.[2,7,8] Furthermore, it has been shown that derivatives of the 1,3-alternate calix[4]crown-6 ethers exhibit high selectivity towards Cs^+ ions in both acidic and alkaline media[9–12] with distribution coefficient ratios for Cs^+/Na^+ and Cs^+/K^+ exceeding 10^4 and 10^2 respectively, based on a solvent extraction technique.[12] Self-assembled ionophores with high cation selectivity for Cs^+ ions have also been reported.[13] We have taken advantage of the high selectivity of calix[4]crown ethers to synthesize a molecular recognition agent with high specificity for Cs^+ ion complexation in the presence of other alkali metal ions using the concept of fluorescence turn-on as a platform for its detection. Crown ethers have been proposed as potential extractants for the removal of Cs from nuclear waste solutions by solvent extraction.[14] ^{137}Cs produced during the nuclear era comprises a significant fraction of the radiological materials stored in the Department of Energy's (DOE) tank waste. A recent finding[15] suggests that leakage of nuclear material (^{137}Cs in particular) into the environment from the storage tanks at Hanford sites is far greater than previously estimated. Consequently, there is considerable interest within DOE to develop a caesium selective sensor that can be utilized to perform *in situ* determination of caesium in these tanks. However, to the best of our knowledge, current technologies do not provide a chemical method for *in situ* determination of Cs^+ ion concentration in nuclear waste solutions. We have undertaken this study as part of an effort to develop a technique for such determinations.

The fluorophore reporter molecule, 9-cyanoanthracene (9CA), was covalently attached to the parent molecule 1,3-alternate conformer of calix[4]bis-*o*-benzocrown-6 to prepare a molecular recognition agent that can serve as an optical sensor. The presence of caesium ions is signaled by an increase in the emission of the 9CA group upon complexation. In the absence of caesium ions, fluorescence is partially quenched by photo-induced electron transfer (PET) from the dialkoxybenzene moiety of the crown ring to the excited singlet state of 9CA.[16,17] Upon complexation, the oxygen lone pairs will no longer participlate in PET, causing the emission of 9CA to increase.

Compound **I** 1,3-calix[4]bis(9-cyano-10-anthrylmethyl)-*o*-benzocrown-6 (Scheme 1) was synthesized[18] as the first generation of caesium selective fluorescent probes. We have examined the emission behavior of **I** in the presence of the alkali metal ions Li^+, Na^+, K^+ and Cs^+ to evaluate its selectivity. The emission of **I** in CH_2CL_2–MEOH mixture (1 : 1) is only slightly affected by the presence of either Li^+ or Na^+ ions at concentrations as high as 0.1 M (Fig. 1), ruling out the possibility of strong complexation of these ions by **I**. In the

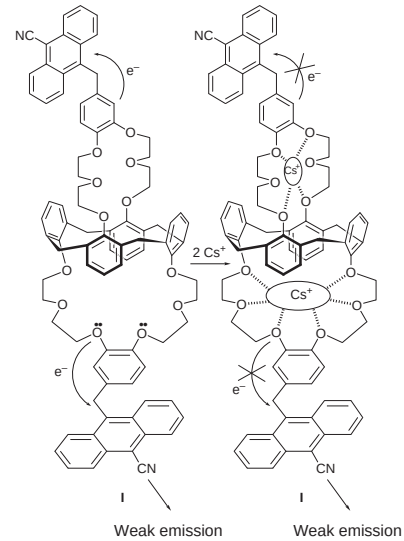

Scheme 1

presence of K^+ ions, the emission of **I** shows a slight enhancement up to a concentration of about 0.01 M, indicating some complexation of K^+ ions by **I** (Fig. 1). At higher concentrations of K^+ ions, the emission of **I** experiences a gradual decrease. The most dramatic change in the emission of **I** is observed in the presence of Cs^+ ions. As the concentration of Cs^+ ions increases, the emission of **I** increases, reaching its maximum value at a concentration of Cs^+ ions of *ca.* 10^{-3} M (Fig. 1). The observation of two plateau regions at 10^{-6} and 2×10^{-4} M Cs^+ (Fig. 1) implies that there are two sites for complexation. To the best of our knowledge, this is the first spectroscopic observation of a stepwise complexation process showing two plateau regions. The gradual quenching of the emission from **I** observed at high concentrations of K^+ and Cs^+ (Fig. 1) may be attributable to a medium effect caused by changes in the ionic strength of the solution. The magnitude of

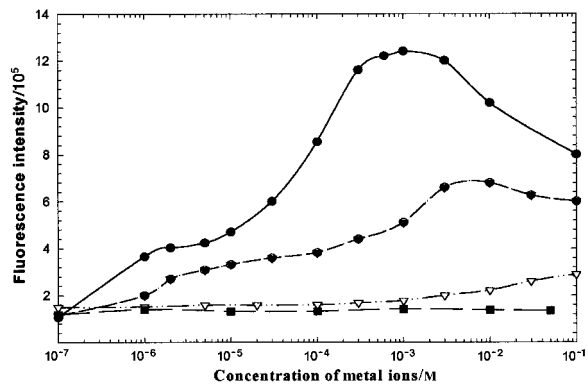

Fig. 1 Changes in the emission spectra (λ_{ex} = 320 nm) of **I** (10^{-6} M) in aerated CH_2Cl_2–MeOH (1 : 1) upon addition of alkali metal ions (acetate solution): (■) Li^+, (▽) Na^+, (▼) K^+ and (●) Cs^+.

this effect is less pronounced in the presence of Li^+ and Na^+ ions because the emission of **I** does not change significantly.

The stability constant for **I** can be estimated from the change in its fluorescence as the concentration of metal ion changes. Since **I** possesses two sites that can form a complex with Cs^+ ions (Scheme 1), eqn. (1) may be used to obtain the stability constant for complexation,[19,20] where α and χ are constants, K_{11} and K_{12} are association constants for the first and second metal ion complexation, I_o is the fluorescence intensity in the absence of metal ion, I_∞ is the intensity when no further change in fluorescence is observed upon addition of metal ion, and I is the intensity at different metal ion concentrations.

$$\frac{I - I_0}{I - I_\infty} = K_{11}[\mathrm{M}]\frac{\alpha + K_{12}\chi[\mathrm{M}]}{K_{11}[\mathrm{M}](\alpha - \chi) - \chi} \quad (1)$$

Computational fitting of the experimental fluorescence data to eqn. (1) for both K^+ and Cs^+ allows determination of parameters α, χ, K_{11} and K_{12}. Table 1 shows the values of these parameters obtained from such fits for both K^+ and Cs^+. The association constants K_{11} and K_{12} determined by us (Table 1) suggest 1 : 2 stoichiometry for calix[4]arene: K^+ (or Cs^+) and are in good agreement with the reported values for other systems that accommodate two metal ions at the complexing sites.[21] The fact that the ratio of $(K_{11}K_{12})_{Cs^+}/(K_{11}K_{12})_{K^+} = 277$ agrees reasonably well with the reported value of ~160 (for 1,2-dichloroethane) obtained *via* solvent extraction techniques[12] suggests that fluorescence spectroscopy can be used as a method to obtain the association constants for metal ion complexation. The reported quantum yields of fluorescence for **I** in the presence of different alkali metal ions shown in Table 1 are relative to 9,10-diphenylanthracene, which has $\Phi_f = 1$.[22]

Fig. 2 shows the change in fluorescence intensity profile for **I** as a function of the concentration of Cs^+ ions. The experiment was carried out *in situ* by combining equal volumes of an aqueous solution of $CsNO_3$ and a fixed concentration of **I** in CH_2Cl_2 in a quartz cell. After vigorous shaking, the two layers were allowed to separate and the fluorescence of the organic layers was obtained. The most dramatic increase in fluorescence intensity is observed over the range 10^{-3}–10^{-1} M $CsNO_3$ (Fig. 2). When the $CsNO_3$ solutions are doped with 1 M $NaNO_3$ and then added to **I** in CH_2Cl_2, the fluorescence intensity increases rapidly and then plateaus at $[Cs^+] > 1 \times 10^{-2}$ M. This rapid initial increase can be attributed to a common anion effect exerted by the presence of excess NO_3^- ions that enhances the complexation of caesium ions at low concentrations.

In conclusion, we have synthesized the first generation of caesium selective fluorescent turn-on probes based on calix[4]arene that can host two such ions upon complexation. Although the sensitivity of our probe is not as dramatic as we had hoped for practical application, we are currently exploring various ways to improve it by manipulating the parameters that have a pronounced effect on sensitivity. Along these lines, we are also examining other potential fluorophores that may induce a much stronger response upon complexation of Cs^+ ions.

This research was funded by the Environmental Management Science Program, Office of Environmental Management, U.S. Department of Energy. Oak Ridge National Laboratory is operated by Lockheed Martin Energy Research Corporation for the U.S. Department of Energy under contract number DE-AC05-96OR22464.

Table 1 Fluorescence quantum yields and association constants K_{11} and K_{12} values calculated for **I** in the presence of different alkali metal ions

Metal ion	Φ_{max}	K_{11}[a]/M^{-1}	K_{12}[a]/M^{-1}	α	χ
None	0.0082	—	—	—	—
Li^+	0.012	—	—	—	—
Na^+	0.016	—	—	—	—
K^+	0.049	6.0×10^5	5.0×10^2	1.0	2.9
Cs^+	0.096	8.3×10^6	1.0×10^4	1.0	4.5

[a] Metal ion concentration range was 10^{-7} to 2×10^{-3} M for K^+ and 10^{-7} to 1×10^{-3} M for Cs^+, respectively.

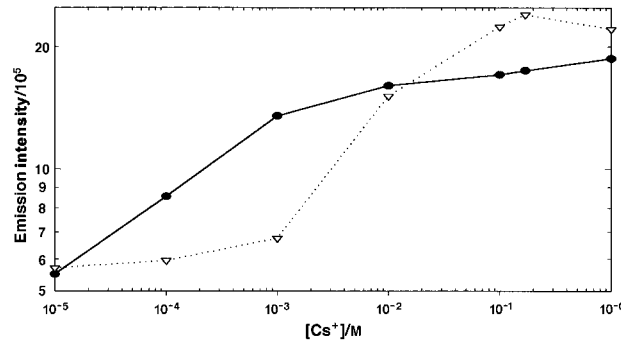

Fig. 2 Changes in the emission intensity of **I** in aerated CH_2Cl_2 as a function of Cs^+ ion concentration. Aqueous solutions of $CsNO_3$ were added to **I** in CH_2Cl_2 and after vigorous shaking the emission of the organic layer was obtained (λ_{ex} = 320 nm): (▽) without $NaNO_3$ and (●) with 1 M $NaNO_3$.

Notes and references

1 V. Bohmer, *Angew Chem., Int. Ed. Engl*., 1995, **34**, 713.
2 C. D. Gutsche, *Calixarenes*, RSC Monographs in Supramolecular Chemistry No. 1, Royal Society of Chemistry, Cambridge, UK, 1989.
3 S. Shinkai, S. Mori, H. Koreishi, T. Tsubaki and O. Manabe, *J. Am. Chem,. Soc*., 1986, **108**, 2409.
4 S. Shinkai, H. Koreishi, K. Ueda, T. Arimura and O. Manabe, *J. Am. Chem. Soc*., 1987, **109**, 6371.
5 R. J. Foster, A. Cadogan, M. T. Diaz and D. Diamond, *Sens. Actuators, B*, 1991, **4**, 325.
6 J. S. Kim, I. Y. Yu, J. H. Pang, J. K. Kim, Y-Ill. Lee, K. W. Lee and Y. Z. Oh, *Microchem. J*., 1998, **58**, 225; J. S. Kim, I. H. Suh, J. K. Kim and M. H. Cho, *J. Chem. Soc., Perkin Trans. 1*, 1998, 2307.
7 C. Asfieri, E. Dradi, A. Pochina, R. Ungaro and G. D. Andreetti, *J. Chem. Soc., Chem. Commun*., 1983, 1075.
8 D. N. Reinhoudt, J. F. Engbersen, Z. Brozozka, H. H. Van den Viekkert, G. W. Honig, A. J. Holterman and U. H. Verkerk, *Anal. Chem*., 1994, **66**, 3618.
9 Z. Asfari, C. Bressot, J. Vicens, C. Hill, J.-F. Rozol, H. Rouquette, S. Eymard, V. Lamare and B. Tourmois, *Anal. Chem*., 1995, **67**, 3133; F. Arnaud-Neu, Z. Asfari, B. Souley and J. Vicens, *New. J. Chem*., 1996, **20**, 453.
10 R. Ungaro, A. Casnati, F. Ugozzoli, A. Pochini, J.-F. Dozol, C. Hill and H. Rouquette, *Angew. Chem., Int. Ed. Engl*., 1994, **33**, 1506; A. Casnati, A. Pochini, R. Ungaro, F. Ugozzoli, F. Arnaud-neu, S. Fanni, M.-J. Schwing, R. J. M. Egberink, F. deJong and D. N. Reinhoudt, *J. Am. Chem. Soc*., 1995, **117**, 2767; I. M. Rudkevich, J. D. Mercer-Chalmers, W. Verboom, R. Ungaro, F. deJong and D. N. Reinhoudt, *J. Am. Chem. Soc*., 1995, **117**, 6124.
11 W. J. McDowell, G. N. Case, J. A. McDonough and R. A. Bartsh, *Anal. Chem*., 1992, **64**, 3013.
12 T. J. Haverlock, P. V. Bonnesen, R. A. Sachleben and B. A. Moyer, *Radiochim. Acta*, 1997, **76**, 103.
13 J. T. Davis, S. K. Tirumala and A. L. Marlow, *J. Am. Chem. Soc*., 1997, 119, 5271.
14 I. H. Gerow and M. V. Davis, *Sep. Sci. Technol*., 1979, **14**, 395; I. H., Gerow, J. E. Smith and M. V. Davis, *Sep. Sci. Technol*., 1981, **16**, 519; E. Blasius and K.-H. Nilles, *Radiochim. Acta*, 1984, **35**, 173; W. W. Schultz and L. A. Bray, *Sep. Sci. Technol*., 1987, *22*, 191; J.-F. Dozol, in *New Separation Chemistry Techniques for Radioactive Waste and Other Applications*, ed. L. Cecille, M. Casarci and L. Pietrelli, Elsevier, Amsterdam, 1991, pp. 163–172.
15 *Chem. Eng. News*, 1998, **76**, No. 37, 25.
16 R. A. Bissell, A. P. de Silva, H. Q. N. Guanratne, P. L. M. Lynch, G. E. M. Maguire, C. McCoy and K. R. A. S. Sandanayake, *Top. Curr. Chem*., Springer-Verlag, Berlin, Heidelberg, 1993, vol. 168, pp. 223–264.
17 A. P. de Silva and K. R. A. S. Sandanayake, *J. Chem. Soc., Chem. Commun*. 1989, 1183.
18 Compound **I** was prepared according to a procedure described earlier (ref. 9) with slight modifications in reagents and reaction time. A full account of this procedure will be published later.
19 D. Marquis and J.-P. Desvergne, *Chem. Phys. Lett*., 1994, **230**, 131.
20 D. Marquis, J.-P. Desvergne and H. Bouas-Laurent, *J. Org. Chem*., 1995, **60**, 7984.
21 A. D'Aprano, J. Vicens, Z. Asfari, M. Salomon and M. Iammarino, *J. Solution Chem*., 1996, **25**, 955.
22 A. Maciejewski and R. P. Steer, *J. Photochem*., 1986, **35**, 59.

Communication 8/08636B

ChemComm

Catalytic asymmetric carbon–carbon bond forming reactions: preparation of optically enriched 2-aryl propionic acids by a catalytic asymmetric hydroboration–homologation sequence†

Austin C. Chen, Li Ren and Cathleen M. Crudden*

Department of Chemistry, University of New Brunswick, Fredericton, New Brunswick, PO Box 45222, Canada E3B 6E2

Received (in Corvallis, OR, USA) 2nd December 1998, Accepted 16th February 1999

A new catalytic asymmetric one-carbon homologation strategy has been developed which employs a rhodium catalyzed asymmetric hydroboration followed by homologation with $LiCHCl_2$ and oxidation to generate 2-arylpropionic acids of high enantiomeric purity.

Asymmetric carbon–carbon bond forming reactions are among the most important transformations in organic synthesis.[1] Catalytic methods are the most efficient means to affect these reactions, since the source of chirality is also used in catalytic quantities. The asymmetric synthesis of 2-aryl substituted carboxylic acids is of particular importance since non-steroidal anti-inflammatory agents such as Ibuprofen™ and Naproxen™ are among this class of compounds. Furthermore, the positive medicinal effects of these pharmaceuticals are ascribed to only one of the enantiomeric forms.[2] State-of-the-art catalytic asymmetric C–C bond forming methods for the synthesis of 2-aryl substituted propionic acids include hydrocarbonylation techniques employing carbon monoxide.[3] The key step in these methods is the enantioselective addition of a transition metal hydride across an olefin, which is followed by C–C bond formation (carbonylation). It occurred to us that an alternative strategy would be to employ a catalytic asymmetric reaction to install the required stereocentre followed by a second, stereospecific C–C bond forming reaction (Scheme 1). This basic principle has been realized in our labs leading to a highly enantioselective synthesis of 2-arylpropionic acids with the aid of catalytic asymmetric hydroboration.[4]

The catalytic asymmetric hydroboration reaction occurs with essentially complete regiochemical control and extremely high enantiocontrol in the hydroboration of vinylarenes to give the corresponding chiral 2-aryl boronate esters.[4] Despite the success of this transformation, it has thus far been relegated to a method for the preparation of enantiomerically enriched aryl methyl alcohols,[4] and more recently extended to include the preparation of amines.[5]

Although the application of chiral borane species prepared using *stoichiometric* amounts of chiral materials in C–C bond forming reactions has been reported in the elegant work of Matteson[6] and Brown,[7] no such use of the catalytically synthesized catecholate **1** has been described. We report herein a new asymmetric hydroboration–homologation method in which vinyl arenes are converted into 2-arylpropionic acids using only catalytic quantities of chiral material [eqn. (1)].

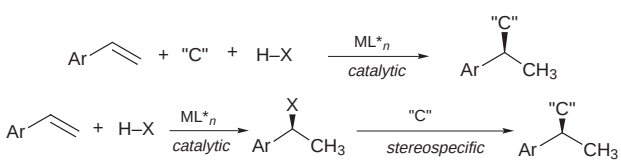

Scheme 1

† Presented in part: 80th Canadian Society for Chemistry conference, Whistler, B.C., June, 1998.

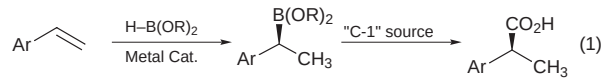

Several potential 'C-1' sources can be employed for the stereospecific C–C bond forming reaction. We first examined lithiated methylthiophenyl methyl ether,[7] but found the reaction to be low yielding with substrate **1** [eqn. (2)]. Transesterification of catechol boronate **1** to the corresponding pinacol boronate **3** prior to homologation gave **2** in higher yields, up to 75% isolated (as the hydrazone), but the highly capricious procedure requiring large quantities of $HgCl_2$ prompted us to consider alternative homologating reagents. Matteson has described the use of $LiCHCl_2$ in his homologation–Grignard addition strategy carried out on boronate esters prepared with stoichiometric amounts of chiral borane reagents.[6] Indeed $LiCHCl_2$ could be reliably prepared using Matteson's detailed procedure[6] and reacted with boronate ester **3** to yield, after oxidative workup, the homologation product **2** in good yield: 79% isolated as the alcohol after $BH_3{\cdot}SMe_2$ reduction, or 70% as the carboxylic acid after Lindgren oxidation [eqn. (3)].

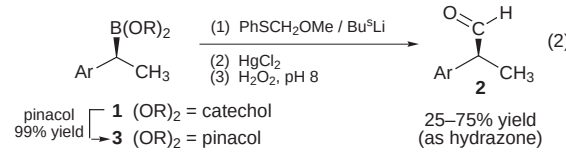

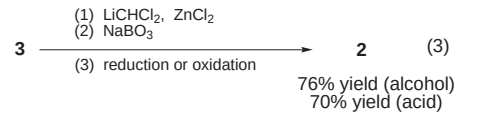

Having established a reliable homologation method, we then carried out the sequence under asymmetric conditions. Reaction of styrene with catechol borane in the presence of catalytic amounts of $[Rh(COD)_2]^+BF_4^-$ and (*S*)-BINAP[4] generated the boronate ester **1** asymmetrically. Conversion of boronate ester **1** to pinacolate **3** allowed us to isolate and purify this species by column chromatography. The enantioselectivity of the process was high (91% ee).‡ The purified material was then homologated with $LiCHCl_2$. Oxidation of the intermediate chloroboronate using Kabalka's procedure[8] yielded aldehyde **2**, which was further oxidized to the carboxylic acid under Pinnick-modified Lindgren conditions.[9] Analysis of this material by optical rotation and chiral GC§ showed that the homologation–oxidation had proceeded with some loss of enantiomeric purity, yielding the desired product in only 77% ee. This decrease in ee was determined by independent experiments to be occurring *via* the aldehyde. Thus direct oxidation of the intermediate chloroboronate to the acid under Lindgren conditions[10] was affected and yielded the desired product in a slightly reduced yield, but with complete retention of enantioselectivity [eqns. (4) and (5)].¶

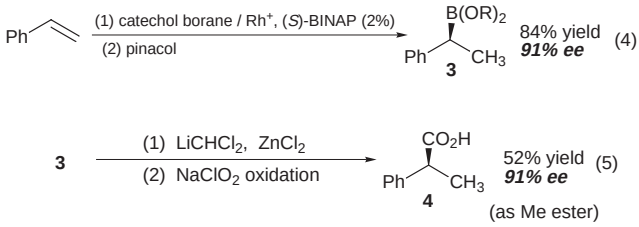

The slow addition of catechol borane as a solution in DME and maintenance of a low internal temperature were found to be crucial for achieving good enantioselectivities in our hands. (*R*)-BINAP gave slightly better enantioselectivities in the hydroboration, yielding **3** (*ent.*) in 95% ee (95% yield), which translated into 95% ee (45% yield) in the homologated carboxylic acid **4** (*ent.*).

The homologation method described herein is, to the best of our knowledge, the first use of chiral boronate esters prepared by *catalytic* hydroboration in a carbon–carbon bond forming reaction. With our method, the high regioselectivity observed in the catalytic asymmetric hydroboration is transferred to the subsequent C–C bond forming process, and the enantioselectivity is completely retained, offering a useful alternative to catalytic asymmetric hydrocarbonylation strategies. We are currently examining the application of this carbon monoxide-free hydrocarboxylation to more complex systems, and will report these results in due course.

The Natural Sciences and Engineering Research Council of Canada (NSERC) is gratefully acknowledged for support of this research in terms of research grants to C. M. C. and a PGS-A scholarship to A. C. C. We thank Professors David Magee, Steven Westcott and Donald Matteson for helpful discussions.

Notes and references

‡ Determined by oxidizing a small portion of the boronate ester, and subjecting the resulting alcohol to chiral gas chromatography: Column = 2,3-di-*O*-acetyl-6-*O*-*tert*-butyldimethylsilyl-β-cyclodextrin, (Suppelco, BETA DEX-225) 30 m, 0.25 mm diameter, 0.25 μm thickness, He carrier, 12.5 psi head pressure, 1.15 ml min^{-1} flow, FID detection. Retention time (t_R) = 44.6 (*R*) and 46.0 min (*S*) @ 70 °C for 5 min, then increase 1 °C per min to 150 °C for 30 min.

§ Column and conditions as above, **4**: (converted to Me ester by treatment with CH_2N_2) 154.1 (*S*) and 155.0 (*R*) min @ 50 °C for 100 min, then ramp at 1 °C per min to 160 °C.

¶ We thank a reviewer for pointing out this oxidation technique. The following procedure (styrene) is representative.

Hydroboration: In a flame dried round-bottomed flask, $[Rh(COD)_2]^+BF_4^-$ (32.4 mg, 0.078 mmol) and (*S*)-(−)-BINAP (54.8 mg, 0.088 mmol) were mixed. Dried, deoxygenated DME was added (4 ml) and the suspension stirred for 30 min. Styrene, previously distilled, was filtered through a plug of alumina and added to the mixture (0.46 ml, 4.0 mmol), which was then cooled to −66 °C. Catechol borane (0.5 ml, 4.7 mmol, distilled) was added as a solution in 2 ml DME dropwise over 45 min. During the addition, the internal temp did not exceed −66 °C. The solution was kept between −67 and −66 °C for 4 h. Pinacol (recrystallised and dried, 1.0121 g, 8.56 mmol) was added and the solution warmed slowly to room temperature overnight. Flash chromatography (silica gel, 24 : 1 hexane–EtOAc) yielded 761.4 mg (82%) of **3**. Enantioselectivity was determined to be 91% ee by oxidizing a small portion of this material under the conditions described in ref. 4, and analyzing the resulting material by chiral GC.

Homologation: this was carried out using $LiCHCl_2$ (1.25 mmol) generated by the slow addition of Bu^nLi (0.8 ml of a 1.57 M solution in hexane, 1.25 mmol) to a mixture of THF (6.5 ml) and CH_2Cl_2 (0.67 ml, 10 mmol) at −100 °C in a 95% EtOH–liq. N_2 bath. The clear colourless solution was stirred at −100 °C for 10 min before the rapid addition of boronate ester **3** (246 mg, 1.06 mmol) as a solution in 2 ml THF. $ZnCl_2$ (1.1 ml of a 1.0 M solution in Et_2O, 1.1 mmol) was then added. The reaction was left to warm to room temperature overnight. After this time, the volatiles were removed under a vigorous flow of N_2. The residue was quenched with 5 ml of sat. aq. NH_4Cl, extracted with light petroleum (4 × 20 ml), dried over $MgSO_4$, filtered and concentrated *in vacuo*. NMR analysis of the material thus obtained (283 mg, 95% crude yield) indicated no starting material remained, and only the chloroboronate product was present. This material was then oxidized to the acid directly following the procedure in ref. 9, (48 h reaction time were necessary). Purification of acid **4** was affected by an acid–base extraction, followed by methylation with CH_2N_2 and flash chromatography (7 : 1 hexane–EtOAc) giving the methyl ester of **4** in 52% yield (91% ee).

1 I. Ojima, *Catalytic Asymmetric Synthesis*, VCH, New York, 1993.
2 J. P. Rieu, A. Boucherle, H. Cousse and G. Mouzin, *Tetrahedron*, 1986, **42**, 4095.
3 H. Alper and N. Hamel, *J. Am. Chem. Soc.*, 1990, **112**, 2803; N. Sakai, S. Mano, K. Nozaki and H. Takaya, *J. Am. Chem. Soc.*, 1993, **115**, 7033.
4 T. Hayashi, Y. Matsumoto and Y. Ito, *J. Am. Chem. Soc.*, 1989, **111**, 3426; J. M. Brown, D. E. Hulmes and T. P. Layzell, *J. Chem. Soc., Chem. Commun.*, 1993, 1673.
5 E. Fernandez, M. W. Hooper, F. I. Knight and J. M. Brown, *Chem. Commun.*, 1997, 173.
6 D. S. Matteson, K. M. Sadhu and M. L. Peterson, *J. Am. Chem. Soc.*, 1986, **108**, 810.
7 H. C. Brown, I. Imai, M. C. Desai and B. Singaram, *J. Am. Chem. Soc.*, 1985, **107**, 4980.
8 G. W. Kabalka, T. M. Shoup and N. M. Goudgaon, *J. Org. Chem.*, 1989, **54**, 5930.
9 B. S. Bal, W. E. Childers and H. W. Pinnick, *Tetrahedron*, 1981, **37**, 2091.
10 D. S. Matteson and E. C. Beedle, *Tetrahedron Lett.*, 1987, **28**, 4499.

Communication 8/09435G

Defluorinative silylation toward a selective preparation of α-trimethylsilyl-α,α-difluoroacetates from trifluoroacetates

Kenji Uneyama* and Go Mizutani

Department of Applied Chemistry, Faculty of Engineering, Okayama University, Okayama 700-8530, Japan. E-mail: uneyamak@cc.okayama-u.ac.jp

Received (in Cambridge, UK) 18th January 1999, Accepted 2nd March 1999

Electrochemical reduction of *n*-hexyl trifluoroacetate 1a in MeCN, involving Bu_4NBr, TMSCl, and Et_3N using an H-type divided cell equipped with carbon plate as an anode and lead plate as a cathode at 50 °C, provided *n*-hexyl α-trimethylsilyl-α,α-difluoroacetate 2a in 62% yield, which is a promising precursor of an alkoxycarbonyldifluoromethyl carbanion equivalent and can be alkylated at the α-carbon by fluoride ion catalysis.

Difluoromethylene compounds have become one of the most important synthetic targets because of their unique biological activity.[1] Among the various difluorinated building blocks, difluoroketene silyl acetals **3** have often been employed for syntheses of difluorinated β-amino-β-hydroxy esters and β-ethoxycarbonyldifluoromethyl-β-lactams under mild conditions.[2] However, they are unstable in the presence of moisture[3] and zinc salts, so that they must be employed mostly *in situ* soon after their generation by Reformatsky reaction of halodifluoroacetates, and are utilized for alkylation in Lewis acid catalyzed carbon–carbon bond formation at the difluoromethylene carbon. Here we describe a first selective preparation of α-trimethylsilyl-α,α-difluoroacetates **2**,[4,5] a stable and isolable alternative of **3**, by electrochemical reductive defluorination[6] of trifluoroacetates, which are more readily available than halodifluoroacetates, and its fluoride ion catalyzed selective alkylation at the α-carbon [eqn. (1)].[7]

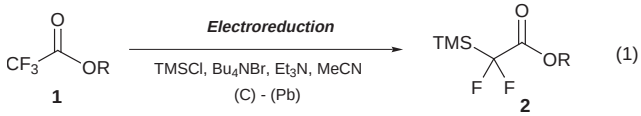

(1)

Electrochemical reduction of *n*-hexyl trifluoroacetate was conducted in MeCN involving Bu_4NBr, Et_3N and TMSCl using an H-type divided cell (with a sintered glass filter) equipped with carbon plate as an anode and lead plate as a cathode at 50 °C.† The product selectivity was found to be remarkably dependent on both reaction temperature and the concentration of TMSCl. At 50 °C the desired α-silylated acetate **2** was formed selectively in the presence of an excess of TMSCl (4 equiv.). On the other hand, a mixture of **2** and ketene silyl acetal **3** was formed at 0 °C in the presence of an excess of TMSCl (Table 1). Two-electron reduction followed by defluorination leads to the formation of the β,β-difluoro enolate which is trapped with TMSCl to give **3** as the kinetic product. *C*-Silylated product **2**[8,9] was the thermodynamic product since ketene silyl acetal **3** was found to be transformed to **2** under the electrolysis conditions at 50 °C. Meanwhile, formation of Claisen condensation product **4** was accompanied by **2** in the presence of only 1 equiv. of TMSCl. The selective formation of **2** was observed even in ethyl and *tert*-butyl esters [R = Et (47%), and Bu^t (58%)].

Table 1 Electrochemical preparation of **2**, **3** and **4**[a]

Entry	R	TMSCl/ equiv.[b]	*T*/°C	Yield(%)[c] **2**	**3**	**4**
1	n-C_6H_{13}	4	50	62 (68)	0	< 1
2	Bu^t	4	50	58 (68)	0	< 1
3	Et	4	50	47 (65)	0	< 1
4	n-C_6H_{13}	4	0	41	(18)	< 1
5	Et	1	0	< 5	0	(21)[d]

[a] *Reagents and conditions:* **1** (5 mmol), TMSCl (20 mmol), Et_3N (20 mmol), Bu_4NBr (12 mmol), in MeCN (70 ml), 80 mA cm^{-2}, 2 F mol^{-1}. [b] Relative to **1**, [c] Isolated yield (yield in parenthesis obtained by ^{19}F NMR). [d] **1** was recovered in 33%.

Fluoride ion catalyzed generation of the alkoxycarbonyldifluoromethyl carbanion and its alkylation were performed with benzyl bromide (64%), benzoyl chloride (60%) and benzaldehyde (82%), respectively (Scheme 1). This alkylation under basic conditions[9] is an alternative to Lewis acid catalyzed alkylation of ketene silyl acetals **3**.[2]

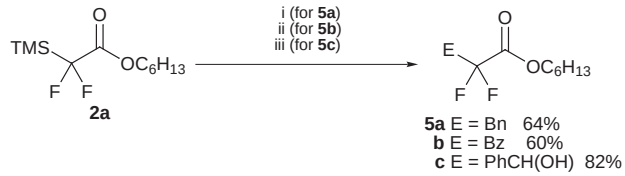

Scheme 1 *Reagents and conditions:* i, PhCHO (3.0 mmol), TBAF (1.0 mmol), THF, −78 °C, 1 h; ii, BnBr (1.0 mmol), KF (1.2 mmol), CuI (1.5 mmol), DMF, 80 °C, 5 h; iii, BzCl (3.0 mmol), KF (2.0 mmol), CuI (1.5 mmol), DMF, 80 °C, 10 h.

We are grateful to the Ministry of Education, Science, Sports and Culture of Japan for financial support (No. 09305058) and the SC-NMR Laboratory of Okayama University for ^{19}F NMR analysis.

Notes and references

† *Typical procedure* for **2a**: the electroreductive defluorination of *n*-hexyl trifluoroacetate **1a** (5 mmol) was carried out using a Pb cathode (2 × 5 cm^2) and a carbon anode in anhydrous MeCN (70 ml) containing Bu_4NBr (12 mmol), Et_3N (20 mmol) and TMSCl (20 mmol) in an H-type divided cell. A constant current of 80 mA was passed at 50 °C under an argon atmosphere until **1a** was consumed (2 F mol^{-1}). *Selected data* for **2a**: colorless oil, bp 80 °C (2 mmHg) (bath temperature) (62%); ν_{max}(neat)/cm^{-1} 1756 (C=O); δ_H($CDCl_3$, 200 MHz) 0.23 (s, 9 H), 0.89 (t, 3 H, *J* 6.6), 1.30–1.41 (m, 6 H), 1.62–1.72 (m, 2 H), 4.23 (t, 2 H, *J* 6.8); δ_F($CDCl_3$, 188 MHz, C_6F_6 as an internal standard) 38.7 (s, 2 F); δ_C($CDCl_3$, 50 MHz) 4.9, 13.9, 22.5, 25.4, 28.4, 31.3, 66.2, 121.0 (t, J_{CF} 269, CF_2), 166.3 (t, J_{CF} 26, C=O); *m/z* (GC/MS) 168 (M − C_6H_{12}), 152 (M − OC_6H_{12}), 73 (M − $CF_2CO_2C_6H_{13}$) (Found: C, 52.04; H, 8.99. Calc.: C, 52.35; H, 8.79%).

1 I. Ojima, J. R. McCarthy and J. T. Welch, *Biochemical Frontiers of Fluorine Chemistry*, ACS, Washington, 1996.
2 O. Kitagawa, T. Taguchi and Y. Kobayashi, *Tetrahedron Lett.*, 1988, **29**, 1803; O. Kitagawa, A. Hashimoto, Y. Kobayashi and T. Taguchi, *Chem. Lett.*, 1990, 1307.
3 K. Iseki, Y. Kuroki, D. Asada, M. Takahashi, S. Kishimoto and Y. Kobayashi, *Tetrahedron*, 1997, **53**, 10 271.
4 *Novel Trends in Electroorganic Synthesis*, ed. S. Torii, Springer Verlag, Tokyo, 1998, p. 299.
5 J. C. Easdon, PhD Thesis, University of Iowa, 1987; J. A. Weigel, *J. Org. Chem.*, 1997, **62,** 6108.
6 K. Uneyama, K. Maeda, T. Kato and T. Katagiri, *Tetrahedron Lett.*, 1998, **39,** 3741; K. Uneyama and T. Kato, *Tetrahedron Lett.*, 1998, **39,** 587.
7 M. Rajaonah, M. H. Rock, J-P. Begue, D. Bonnet-Delpon, S. Condon and J-Y. Nedelec, *Tetrahedron Lett.*, 1998, **39,** 3137.
8 B. I. Martynov, A. A. Stepanov and D. V. Griffiths, *Tetrahedron Lett.*, 1998, **54,** 257.
9 G. K. S. Prakash and A. K. Yudin, *Chem. Rev.*, 1997, 757 and references cited therein.

Communication 9/00455F

Lithium templated synthesis of catenanes: efficient synthesis of doubly interlocked [2]-catenanes

Christiane Dietrich-Buchecker and Jean-Pierre Sauvage*

Laboratoire de Chimie Organo-Minérale, CNRS UMR 7513, Université Louis Pasteur, Institut Le Bel, 4 rue Blaise Pascal, F-67070 Strasbourg, France. E-mail: sauvage@chimie.u-strasbg.fr

Received (in Basel, Switzerland) 21st December 1998, Accepted 8th February 1999

Li^+ (3 equiv.) is used as an assembling centre to generate a double-stranded helical complex from two linear coordinating fragments, each containing three 1,10-phenanthroline units and bearing terminal olefins at their ends; ruthenium-catalyzed ring-closing metathesis on the helical precursor leads to a 4-crossing [2]-catenane in 30% yield, making the procedure reasonably preparative.

The synthesis of interlocking rings[1,2] and molecular knots has undergone spectacular progress in the course of the last 15 years due to the development of templated strategies.[3–5] Copper(I) has been used extensively as an assembling and templating centre,[3] but a few examples based on other transition metals [Ru(II) or Co(II)] have also been reported.[6,7]

To the best of our knowledge, alkali or alkaline-earth cations have never been utilized. We now report that Li^+ is also well adapted to the formation of a double-stranded helical complex used as a precursor, and, in a subsequent reaction, to the synthesis of a doubly interlocked catenane.

Helical transition metal complexes ('helicates') constitute an important field of research in relation with so-called 'self-assembly' processes. Although known for more than two decades,[8] it is only recently that transition metal incorporating helices have been made deliberately and the properties of these multinuclear species studied.[9–11] A double stranded helical complex containing two Na^+ ions has been characterized by ^1H NMR spectroscopy.[12] Li^+ is known to display relatively strong affinity for ligands of the aromatic polyimines family.[13] In the present work, Li^+ turned out to be very well adapted to the formation of a trinuclear double helix, which surprisingly appeared sufficiently robust to resist the cyclization conditions.

The general strategy for preparing a 4-crossing [2]-catenane is shown in Scheme 1. It is based on two key reactions: (i) formation of a double-stranded helical precursor from 2 equivalents of a molecular string which incorporates three chelating units, and 3 equivalents of the templating metal; the string-like fragment bears olefinic functions attached at the ends of flexible fragments; (ii) the ring closing metathesis (RCM) reaction leading to the catenate.

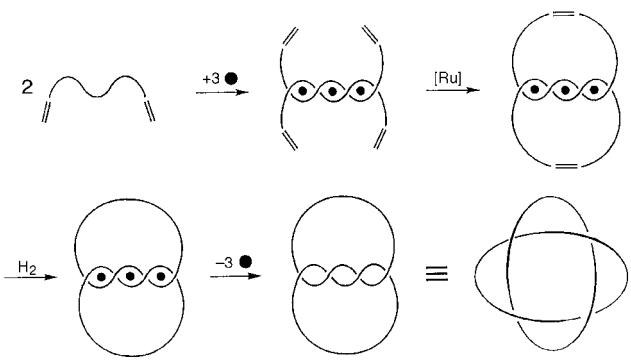

Scheme 1 General strategy for the preparation of 4-crossing [2]-catenanes.

In previous work, we could prepare small amounts of a 4-crossing [2]-catenane. Unfortunately, the yield was so poor (1.8%) that we could only characterize the compound by ^1H NMR and mass spectrometry (ES-MS and FAB-MS).[14] The modified strategy we describe now leads to dramatic improvement, affording the new doubly interlocked catenane in 30% yield. The main factors which are responsible for the much more preparative procedure of the present approach are (i) the quantitative formation of the three-lithium ion double-stranded helical precursor and (ii) the very mild and efficient RCM reaction,[15] as already used in previous work for making [2]-catenanes[16] or molecular trefoil knots.[17]

The various compounds prepared as well as the reactions leading to the target molecule are shown in Scheme 2.

The tris-chelating ligand **3** could be prepared in 11% yield from the monosubstituted phenanthrolines **1**[18] and **2**[19] in a multistep reaction shown in Scheme 2. Ligand **4** obtained

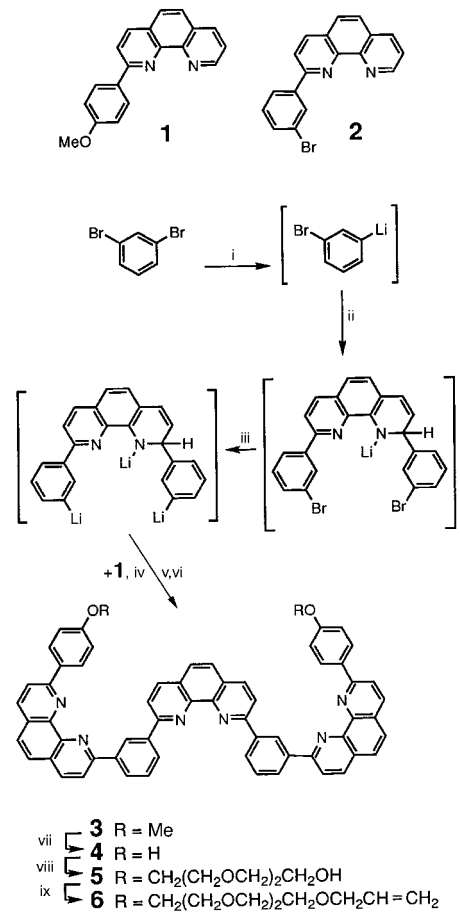

Scheme 2 *Reagents and conditions*: i, Bu^nLi, Et_2O, 2 °C; ii, **2** in THF, 0 °C; iii, Bu^tLi (4 equiv.), −78 °C; iv, **1** (2.5 equiv.) in THF, 10 °C; v, H_2O, 0 °C; vi MnO_2, excess; vii, HCl, pyridine, 210 °C; viii, Cs_2CO_3, DMF, 75 °C, $ClCH_2(CH_2OCH_2)_2CH_2OH$ (excess); ix, NaH, THF reflux, $BrCH_2CH{=}CH_2$ (excess).

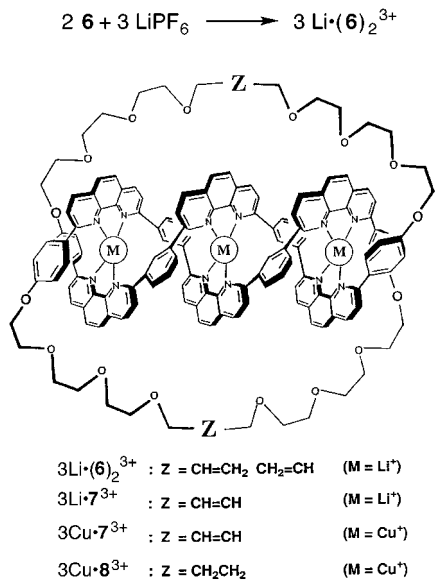

Fig. 1 Double stranded helix formation and cyclisation.

quantitatively after demethylation of **3** by HCl–pyridine,[20] was converted to diol **5** in 87% yield by reaction with 2-[2-(2-chloroethoxy)ethoxy]ethanol in DMF at 75 °C in the presence of Cs_2CO_3. **5** led to **6** in 88% yield after formation of the dialcoholate with NaH and subsequent reaction with an excess of allyl bromide in refluxing THF.

The tris-lithium helical precursor $3Li\cdot(\mathbf{6})_2^{3+}$ was formed quantitatively by addition of $LiPF_6$ in MeOH to a solution of **6** in CH_2Cl_2 at room temperature (Fig. 1). To avoid competitive protonation solid Li_2CO_3 was subsequently added to the solution until it was weakly basic. The double helix $3Li\cdot(\mathbf{6})_2^{3+}$, fully characterized by ^{1}H NMR and ESI-MS, was stable enough to survive the mild RCM conditions (0.05 mol equiv. of Grubbs catalyst $[RuCl_2\{P(C_6H_{11})_3\}_2(=CHPh)]$). The double cyclization could be monitored by ^{1}H NMR spectroscopy in the alkenic region. The unsuccessful attempt to separate the pure tris-lithium doubly interlocked [2]-catenate $3Li\cdot\mathbf{7}^{3+}$ from the oligomers arising from the intermolecular metathesis reaction led us to exchange Li^+ with Cu^+. This exchange was slow and required heating at 60 °C of a $3Li\cdot\mathbf{7}^{3+}$ acetonitrile solution in the presence of a large excess of $[Cu(MeCN)_4]PF_6$ for several days. Subsequent chromatography afforded the catenate $3Cu\cdot\mathbf{7}^{3+}$ in 30% yield. The cyclic alkenes remaining in $3Cu\cdot\mathbf{7}^{3+}$, originally present as a mixture of *cis* and *trans* isomers were later reduced by catalytic hydrogenation in EtOH–CH_2Cl_2 (1 : 1) with Pd/C affording $3Cu\cdot\mathbf{8}^{3+}$ quantitatively.

The unexpected stability of $3Li\cdot(\mathbf{6})_2^{3+}$ as well as the difficulty encountered to exchange the three lithium cations by copper(I) in $3Li\cdot\mathbf{7}^{3+}$, both reflect tight, highly entwined molecular structures.

Further evidence for the doubly interlocked topology of $3Cu\cdot\mathbf{8}^{3+}$ was obtained after its demetallation (excess KCN in refluxing MeCN) which led quantitatively to the free ligand **9** characterized by very broad and poorly resolved signals of its ^{1}H NMR spectrum : slow restricted molecular motions are clearly related to a topology which implies large mutual crowding between the rings. The FAB-MS of **9** confirms fully our assumption relative to a catenated structure characterized by peaks at *m/z* 2406, corresponding to the ion (**9** + Na^+) and *m/z* 1213.7, 1191.7 corresponding to the ions (**9**/2 + Na^+) and (**9**/2 + H^+), respectively. The two latter signals appear as monocharged species and thus can only originate from the cleavage of one ring followed by fast unthreading of the linear fragment produced.

In conclusion, RCM turned out to be again a surprisingly efficient reaction for preparing interlocking rings such as the present 4-crossing [2]-catenane, converting an exceedingly low yield synthesis, as reported a few years ago,[14] into a preparative procedure. The properties of the new ligand **9** and of its complexes are now under investigation.

Notes and references

1 G. Schill, in *Catenanes, Rotaxanes and Knots*, Academic Press, New York, 1971.
2 H. L. Frisch and E. Wasserman, *J. Am. Chem. Soc.*, 1961, **83**, 3789.
3 C. O. Dietrich-Buchecker, J.-P. Sauvage and J.-P. Kintzinger, *Tetrahedron Lett.*, 1983, **24**, 5095; J.-C. Chambron, C. O. Dietrich-Buchecker and J.-P. Sauvage, in *Comprehensive Supramolecular Chemistry*, Pergamon, 1996, vol. 9, p. 43.
4 P. R. Ashton, T. T. Goodnow, A. E. Kaifer, M. V. Redington, A. M. Z. Slavin, N. Spencer, J. F. Stoddart, C. Vicent and D. J. Williams, *Angew. Chem., Int. Ed. Engl.*, 1989, **28**, 1396; D. B. Amabilino, F. M. Raymo and J. F. Stoddart, in *Comprehensive Supramolecular Chemistry*, Pergamon, 1996, vol. 9, p. 85.
5 C. A. Hunter, *J. Am. Chem. Soc.*, 1992, **114**, 5303; F. Vögtle, S. Meier and R. Hoss, *Angew. Chem.*, 1992, **104**, 1628.
6 J.-P. Sauvage and M. Ward, *Inorg. Chem.*, 1991, **30**, 3869; J.-M. Kern, J.-P. Sauvage, G. Bidan, M. Billon and B. Divisia-Blohorn, *Adv. Mater.*, 1996, **8**, 580.
7 M. Fujita, F. Ibukuro, K. Yamaguchi and K. Ogura, *J. Am. Chem. Soc.*, 1995, **117**, 4175; C. Piguet, G. Bernardinelli, A. F. Williams and B. Bocquet, *Angew. Chem., Int. Ed. Engl.*, 1995, **34**, 582.
8 J. H. Fuhrhop, G. Struckmeier and U. Thewalt, *J. Am. Chem. Soc.*, 1976, **98**, 278.
9 J. M. Lehn, A. Rigault, J. Siegel, J. Harrowfield, B. Chevrier and D. Moras, *Proc. Natl. Acad. Sci. USA*, 1987, **84**, 2565; P. N. W. Baxter, in *Comprehensive Supramolecular Chemistry*, Pergamon, 1996, vol. 9, p. 165.
10 E. C. Constable, M. G. B. Drew and M. D. Ward, *J. Chem. Soc., Chem. Commun.*, 1987, 1600; E. C. Constable, in *Comprehensive Supramolecular Chemistry*, Pergamon, 1996, vol. 9, p. 213.
11 A. F. Williams, C. Piguet and G. Bernardinelli, *Angew. Chem., Int. Ed. Engl.*, 1991, **30**, 1490.
12 T. W. Bell and H. Jousselin, *Nature*, 1994, **367**, 441.
13 U. Olsher, R. M. Izatt, J. S. Bradshaw and N. K. Dalley, *Chem. Rev.*, 1991, **91**, 137; H. Sugihara, J.-P. Collin and K. Hiratani, *Chem. Lett.*, 1994, 397; S. Ogawa and S. Tsuchiya, *Chem. Lett.*, 1996, 709.
14 J.-F. Nierengarten, C. O. Dietrich-Buchecker and J.-P. Sauvage, *J. Am. Chem. Soc.*, 1994, **116**, 375; C. O. Dietrich-Buchecker, E. Leize, J.-F. Nierengarten, A. Van Dorsselaer and J.-P. Sauvage, *J. Chem. Soc., Chem. Commun.*, 1994, 2257.
15 R. H. Grubbs, S. J. Miller and G. C. Fu, *Acc. Chem. Res.*, 1995, **28**, 446; R. H. Grubbs and S. Chang, *Tetrahedron*, 1998, **54**,4413.
16 B. Mohr, M. Weck, J.-P. Sauvage and R. H. Grubbs, *Angew. Chem., Int. Ed. Engl.*, 1997, **36**, 1308.
17 C. O. Dietrich-Buchecker, G. Rapenne and J.-P. Sauvage, *Chem. Commun.*, 1997, 2053.
18 C. O. Dietrich-Buchecker, J.-F. Nierengarten, J.-P. Sauvage, N. Armaroli, V. Balzani and L. De Cola, *J. Am. Chem. Soc.*, 1993, **115**, 11237.
19 J. J. Eisch and R. B. King, in *Organometallic Synthesis*, Academic Press, 1981, vol. 2, p. 93.
20 T. J. Curphey, E. J. Hoffman and C. McDonald, *Chem. Ind.*, 1967, 1138.

Communication 8/09885I

Synthesis of a C_{60}-oligophenylenevinylene hybrid and its incorporation in a photovoltaic device

Jean-François Nierengarten,*[a] Jean-François Eckert,[a] Jean-François Nicoud,[a] Lahoussine Ouali,[b] Victor Krasnikov[b] and Georges Hadziioannou*[b]

[a] *Groupe des Matériaux Organiques, Institut de Physique et Chimie des Matériaux de Strasbourg, Université Louis Pasteur and CNRS, 23 rue du Loess, 67037 Strasbourg, France. E-mail: niereng@michelangelo.u-strasbg.fr*

[b] *Department of Polymer Chemistry and Materials Science Centre, University of Groningen, Nijenborgh 4, 9747 AG Groningen, The Netherlands*

Received (in Cambridge, UK) 1st February 1999, Accepted 3rd March 1999

A fulleropyrrolidine derivative bearing an oligophenylenevinylene substituent has been prepared by 1,3-dipolar cycloaddition of an azomethine ylide to C_{60} and incorporated in a photovoltaic device.

In light of its unusual electrochemical and electronic properties, the fullerene C_{60} is an attractive functional group for supramolecular assemblies and new advanced materials.[1] For example, photovoltaic devices using thin films of interpenetrating bicontinuous networks of C_{60} derivative and a number of conjugated polymers such as polyphenylenevinylene or polythiophene have been demonstrated to show promise for large-area photodetectors and solar cells.[2] In this class of devices the network provides the spatially distributed interfaces necessary for efficient exciton dissociation into electrons and holes, and pathways for their subsequent collection at opposite electrodes. Therefore the film morphology is of crucial importance for the device performance. Usually the donor and acceptor molecules are incompatible and tend to strong and uncontrolled phase separation. An alternative approach to create the bicontinuous network is based on chemically connected donor–acceptor molecules. Recent developments in the functionalisation of fullerenes allows the preparation of covalent C_{60} derivatives bearing electro- and/or photo-active substituents.[3] Some of those systems provide entry into intramolecular processes such as photoinduced charge separation, therefore they appear as potential candidates for the preparation of photovoltaic cells. In this context, we now report the preparation of the fullerene–oligophenylenevinylene hybrid **1** and its utilisation for the construction of a solar energy conversion system.

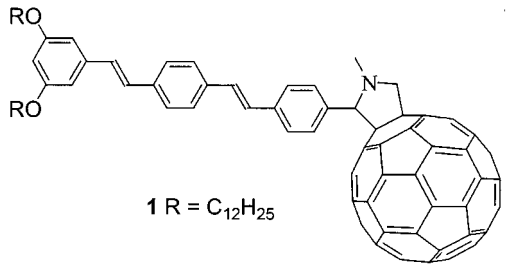

The synthesis of compound **1** is depicted in Scheme 1. The *E*-stilbene **2** was prepared from 4-methylstyrene and 4-bromobenzaldehyde **3** under Heck conditions with $Pd(OAc)_2$ as catalyst in toluene–Et_3N in the presence of tri-*o*-tolylphosphine.

Treatment of **2** with 2,2-dimethylpropane-1,3-diol in refluxing benzene in the presence of a catalytic amount of *p*-toluenesulfonic acid (*p*-TsOH) gave **4** in 95% yield. Compound **4** could also be prepared from **3** as follows: protection[4] (2,2-dimethyl-1,3-propanediol, C_6H_6, *p*-TsOH cat.), subsequent treatment with Bu^{t}Li in THF followed by quenching with DMF and reaction of the resulting **5** with (4-methylbenzyl)triphenylphosphonium chloride under Wittig conditions. The parent stilbene was thus obtained in 70% yield as an *E* : *Z* isomer mixture in a 55 : 45 ratio. However, the *Z* isomer could be easily isomerized to the *E* form by treatment with iodine in refluxing toluene. Oxidation of alcohol **6**[5] with MnO_2 in CH_2Cl_2 followed by condensation of the resulting benzaldehyde **7** with aniline in

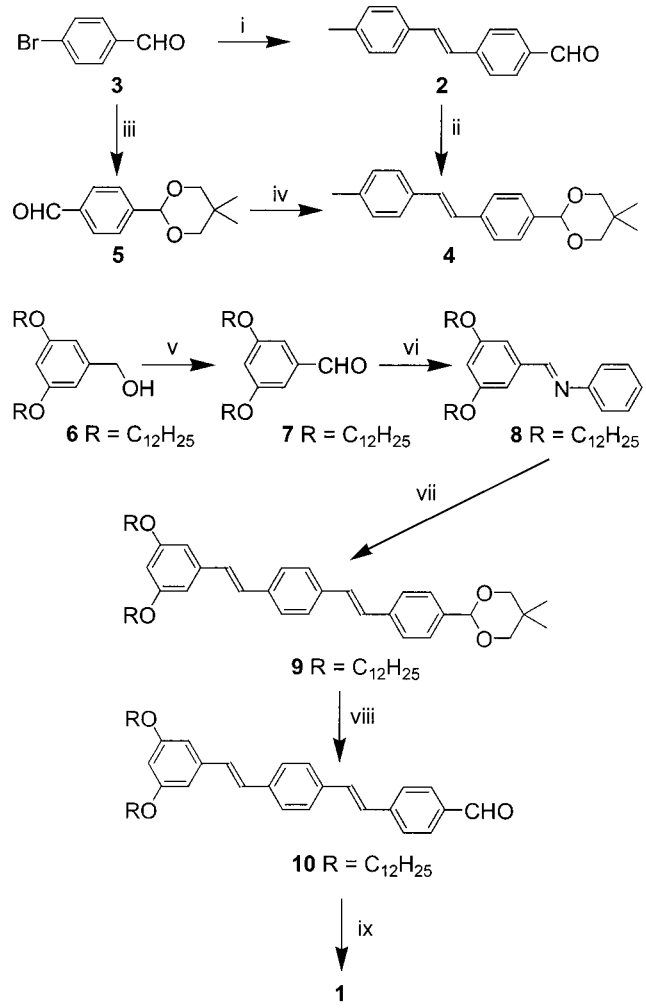

Scheme 1 *Reagents and conditions*: i, 4-methylstyrene, $Pd(OAc)_2$, tri-*o*-tolylphosphine, Et_3N, toluene, reflux, 48 h, 55%; ii, 2,2-dimethylpropane-1,3-diol, C_6H_6, *p*-TsOH cat., reflux, Dean–Stark trap, 24 h, 95%; iii, 2,2-dimethylpropane-1,3-diol, C_6H_6, *p*-TsOH cat., reflux, Dean–Stark trap, 48 h, then Bu^{t}Li, THF, −78 °C, 1 h, then DMF, −78 °C to room temp., 1 h, 85%; iv, (4-methylbenzyl)triphenylphosphonium chloride, Bu^{t}OK, EtOH, room temp., 2 h then I_2, toluene, reflux, 12 h, 70%; v, MnO_2, CH_2Cl_2, 1 h, 89%; vi, aniline, C_6H_6, reflux, Dean–Stark trap, 24 h, 90%; vii, **4**, Bu^{t}OK, DMF, 80 °C, 2 h, 74%; viii, TFA, CH_2Cl_2, H_2O, room temp., 4 h, 96%; ix, C_{60}, sarcosine, toluene, reflux, 16 h, 43%.

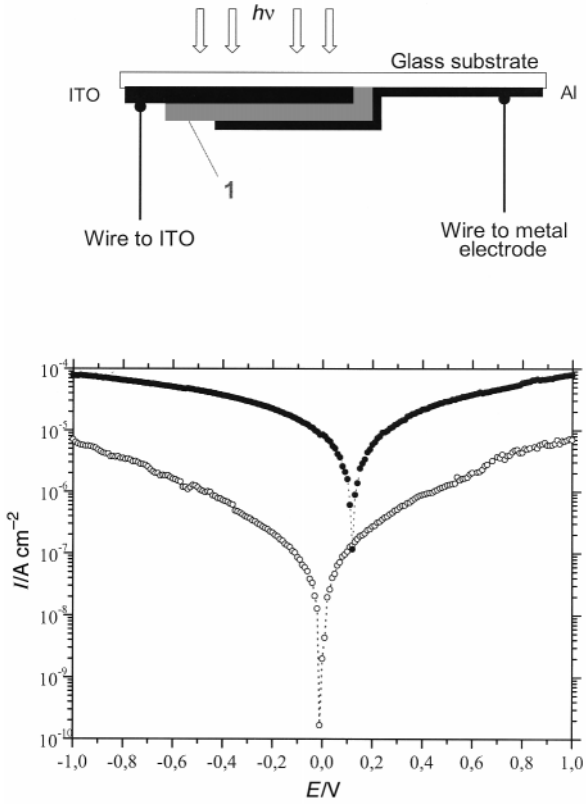

Fig. 1 Top: structure of the photovoltaic cell. Bottom: current–voltage characteristics of the ITO/C_{60}–oligophenylenevinylene/Al device in the dark (○) and under 5 mW cm^{-2} illumination (400 nm) (●).

refluxing benzene afforded **8** in an overall 80% yield. Benzaldimine **8** was subjected to the Siegrist reaction[6] with stilbene **4** to give protected trimer **9** in 74% yield. Treatment of **9** with CF_3CO_2H in CH_2Cl_2–H_2O (1 : 1) afforded aldehyde **10** in 96% yield. The functionalisation of C_{60} was based on the 1,3-dipolar cycloaddition[7] of the azomethine ylide generated *in situ* from **10**. The reaction of C_{60} with **10** in the presence of an excess of *N*-methylglycine (sarcosine) in refluxing toluene afforded fulleropyrrolidine **1** in 43% yield (or 62% based on the non-recovered C_{60}). All of the spectroscopic studies and elemental analysis results were consistent with the proposed molecular structures.† The UV–VIS spectrum of **1** corresponds to the sum of the spectra of its two components and shows the characteristic absorptions of a fulleropyrrolidine derivative at 254, 430 and 702 nm as well as the diagnostic oligophenylene-vinylene band at 363 nm indicating that there are no significant interactions between the two chromophores in the ground state. Preliminary luminescence measurements show a strong quenching of the oligophenylenevinylene fluorescence in **1**. Charge transfer is expected to occur and compound **1** appears as a potential candidate for the preparation of a photovoltaic cell. The device structure is schematically depicted in Fig. 1. The C_{60}-oligophenylenevinylene films were spin cast, on a glass substrate coated with indium–tin oxide (ITO), from a 4 wt% chloroform solution. The Al electrode was vacuum evaporated on the films to a thickness of 100 nm. Typical current–voltage curves (using ITO as positively and Al as negatively biased electrodes) measured under dark and under light (400 nm, 5 mW cm^{-2}) are presented in Fig. 1. Under the light the device shows clear photovoltaic behaviour with an open-circuit voltage of *ca.* 0.2 V and a short-circuit current density of 10 μA cm^{-2} corresponding to a collecting efficiency of 1%. Although we do not know the exact reason of the high dark current under reverse bias, we believe it leads to the relatively low collection efficiency and open-circuit voltage.

We have shown that photovoltaic cells can be prepared with a fullerene–oligophenylenevinylene conjugate. The device efficiency is not yet optimised and further improvements could be expected by utilisation of new fullerene derivatives with a stronger absorption in the visible range.

This work was supported by the CNRS and by a post-doctoral fellowship from The Netherlands Organization for Scientific Research to L. O. We further thank L. Oswald for technical help.

Notes and references

† *Selected spectroscopic data for* **1**: UV–VIS $\lambda_{max}(CH_2Cl_2)$/nm 254 (89 800), 363 (63 200), 386 (sh, 38 800), 430 (4700), 702 (340); ^{1}H NMR ($CDCl_3$, 400 MHz) δ 0.87 (t, *J* 5.5, 6H), 1.26–1.31 (m, 36H), 1.78 (m, 4H), 2.83 (s, 3H), 3.96 (t, *J* 5, 4H), 4.25 (d, *J* 9.5, 1H), 4.94 (s, 1H), 5.00 (d, *J* 9.5, 1H), 6.38 (t, *J* 1.5, 1H), 6.65 (d, *J* 1.5, 2H), 7.04 (AB, *J* 17, 2H), 7.12 (AB, *J* 17, 2H), 7.48 (s, 4H), 7.61 (d, *J* 8, 2H), 7.82 (br, 2H); ^{13}C NMR ($CDCl_3$, 100 MHz) δ 14.15, 22.71, 26.11, 29.34, 29.44, 29.63, 29.66, 29.69, 31.93, 40.05, 68.10, 69.06, 70.00, 83.35, 101.03, 105.17, 126.85, 126.90, 128.12, 128.54, 128.71, 128.86, 129.68, 135.77, 135.89, 136.43, 136.55, 136.60, 136.71, 136.82, 137.44, 139.15, 139.56, 139.89, 140.14, 141.52, 141.67, 141.84, 141.91, 141.95, 142.02, 142.05, 142.10, 142.15, 142.23, 142.27. 142.54, 142.66, 142.98, 143.13, 144.37, 144.58, 144.69, 145.14, 145.28, 145.52, 145.74, 145.92, 146.05, 146.10, 146.17, 146.27, 146.30, 146.46, 146.71, 147.28, 153.37, 153.98, 156.20, 160.50; FAB-MS: *m/z* 1426.8 (MH^+). Anal calc. for $C_{109}H_{71}O_2N$: C 91.76, H 5.02, N 0.98; found: C 91.27, H 5.09, N 1.07%.

1 A. Hirsch, *Adv. Mater.*, 1993, **5**, 859; F. Diederich and C. Thilgen, *Science*, 1996, **271**, 317; M. Prato, *J. Mater. Chem.*, 1997, **7**, 1097; L. Echegoyen and L. E. Echegoyen, *Acc. Chem. Res.*, 1998, **31**, 593; F. Diederich and M. Gomez-Lopez, *Chimia*, 1998, **52**, 551.

2 N. S. Sariciftci, L. Smilowitz, A. J. Heeger and F. Wudl, *Science*, 1992, **258**, 1474; N. S. Sariciftci, D. Braun, C. Zhang, V. Srdanov, A. J. Heeger, G. Stucky and F. Wudl, *Appl. Phys. Lett.*, 1993, **62**, 585; R. A. J. Janssen, M. P. T. Christiaans, K. Pakbaz, D. Moses, J. C. Hummelen and N. S. Sariciftci, *J. Chem. Phys.*, 1995, **102**, 2628; R. A. J. Jansen, J. C. Hummelen, K. Lee, K. Pakbaz, N. S. Sariciftci, A. J. Heeger and F. Wudl, *J. Chem. Phys.*, 1995, **103**, 788; G. Yu, J. Gao, J. C. Hummelen, F. Wudl and A. J. Heeger, *Science*, 1995, **270**, 1789; B. Kraabel, J. C. Hummelen, D. Vacar, D. Moses, N. S. Sariciftci, A. J. Heeger and F. Wudl. *J. Chem. Phys.*, 1996, **104**, 4267; L. S. Roman, M. R. Andersson, T. Yohannes and O. Inganäs, *Adv. Mater.*, 1997, **9**, 1164.

3 S. I. Khan, A. M. Olivier, M. N. Paddon-Row and Y. Rubin, *J. Am. Chem. Soc.*, 1993, **115**, 4919; R. M. Williams, J. M. Zwier and J. W. Verhoeven, *J. Am. Chem. Soc.*, 1995, **117**, 4093; D. Armspach, E. C. Constable, F. Diederich, C. E. Housecroft and J.-F. Nierengarten, *Chem. Commun.*, 1996, 2009; H. Imahori and Y. Sakata, *Adv. Mater.*, 1997, **9**, 537; N. Armaroli, F. Diederich, C. O. Dietrich-Buchecker, L. Flamigni, G. Marconi, J.-F. Nierengarten and J.-P. Sauvage, *Chem. Eur. J.*, 1998, **4**, 406; N. Martin, L. Sanchez, B. Illescas and I. Perez, *Chem. Rev.*, 1998, **98**, 2527; F. Effenberger and G. Grube, *Synthesis*, 1998, 1372; S. Llacay, J. Veciana, J. Vidal-Gancedo, J. L. Bourdelande, R. Gonzalez-Moreno and C. Rovira, *J. Org. Chem.*, 1998, **63**, 5201; J. M. Lawson, A. M. Olivier, D. F. Rotherfluh, Y.-Z. An, G. A. Ellis, M. G. Ranasinghe, S. I. Khan, A. G. Franz, P. S. Ganapathi, M. J. Shephard, M. N. Paddon-Row and Y. Rubin, *J. Org. Chem.*, 1996, **61**, 5032; R. M. Williams, M. Koeberg, J. M. Lawson, Y.-Z. An, Y. Rubin, M. N. Padden-Row and J. W. Verhoeven, *J. Org. Chem.*, 1996, **61**, 5055.

4 N. Solladié, J.-C. Chambron, C. O. Dietrich-Buchecker and J.-P. Sauvage, *Angew. Chem., Int. Ed. Engl.*, 1996, **35**, 906.

5 J.-F. Nierengarten and J.-F. Nicoud, *Tetrahedron Lett.*, 1997, **38**, 7737.

6 G. Zerban and H. Meier, *Z. Naturforcsh. Teil B*, 1993, **48**, 171.

7 M. Prato and M. Maggini, *Acc. Chem. Res.*, 1998, **31**, 519 and references therein.

Communication 9/00829B

New optically active polyarylene vinylenes: control of chromophore separation by binaphthyl units

Rafael Gómez, José L. Segura and Nazario Martín*

Departamento de Química Orgánica, Facultad de Ciencias Químicas, Universidad Complutense, E-28040-Madrid, Spain. E-mail: nazmar@eucmax.sim.ucm.es

Received (in Liverpool, UK) 1st December 1998, Accepted 25th February 1999

New optically active copolymers containing binaphthyl units to control the conjugation length of the emitting chromophores show intense photoluminescence and high electron affinity.

The design of tailor-made π-conjugated polymers has been a subject of intensive research during the last decade due to their potential applications as novel materials for optoelectronics[1–5] given that they combine the optical and electronic properties of semiconductors with the processing advantages and mechanical properties of polymers.

The HOMO–LUMO gap in semiconducting polymers is roughly determined by the extent of π-delocalization along the backbone, the so-called effective conjugation length, which is responsible for the emitting properties of these materials. Introduction of non-conjugated segments into conjugated polymer backbones results in confinement of π-electrons in the conjugated fragment. Thus, the conjugation length of conjugated–non-conjugated multiblock copolymers can be effectively tailored by choice of the appropriate chromophores and spacers. Here we use functionalized chiral binaphthyl monomers as the non-conjugated spacer in conjugated–non-conjugated polymers **1**–**3** (Fig. 1).

Binaphthyl derivatives are optically active materials, their chirality being derived from the restricted rotation of the two naphthalene rings. The angle between the rings ranges from 60 and 120° and therefore, conjugation between the two naphthalene units is minimal.[6] Thus, the conjugated system in polymer containing binaphthyl units is confined to the region between two binaphthyl units [Fig. 1(*a*)].[7,8] The structure of these block-copolymers can be schematically represented as in Fig. 1(*b*) with consecutive conjugated systems linked to each other in a non-coplanar way.

In order to obtain processible polymeric materials, long alkoxy chains have been introduced as substituents on the monomeric units. Especially interesting is the presence of CN groups on the vinylene bridges of poly(arylenevinylenes), which is known to result in an increase in the electron affinity of polymeric materials for light emitting diodes (LEDs) with air stable electrodes.[9] The preparation of this prototype main chain chiral, cyano-containing binaphthyl-based copolymers was carried out using the Knoevenagel condensation[9] of appropriately functionalized binaphthyl (**4**, **5**) and naphthalene (**6**, **7**) monomers. Polymer **1** was obtained by reaction of the new bis(cyanomethyl)-substituted binaphthyl (**4**) with dialdehyde **5**. When **4** was reacted with 1,5-bis(hexyloxy)naphthalene-2,6-dicarbaldehyde (**7**)[10] under analogous conditions, polymer **2** was obtained. Reaction of binaphthyl dialdehyde (**5**) with 2,6-bis-(cyanomethyl)-1,5-bis(hexyloxy)naphthalene (**6**)[10] afforded polymer **3**.

Polymers **1**–**3** were obtained as orange solids in good yields (90, 80 and 75% respectively) with optical HOMO–LUMO onsets of 2.53 eV for **2**, 2.64 eV for **3** and 2.76 eV for **1**, measured *via* their UV-Vis absorption spectra (in CH_2Cl_2 solution). Gel permeation chromatography (GPC) against polystyrene revealed a weight average (M_w) of *ca.* 164 000 and a number average (M_n) of 22 000 (polydispersity (pd) = 7.62) for polymer **1**. Polymer **2** had the lowest mass (M_w = 15 300 and M_n = 9400, pd = 1.62). Polymer **3** presented M_w = 27 500 and M_n = 12 200 (pd = 2.27). Polymers were fully characterized using ^{1}H NMR, ^{13}C NMR, FTIR, and UV-Vis measurements. The infrared spectra displayed the characteristic CN stretching frequency at around 2212 cm^{-1} for the three polymers. ^{1}H NMR measurements exhibit the characteristic singlet of the vinylene proton at around δ 8.1 together with the expected signals of the naphthalene units and the alkoxy chains.†

Polymers were synthesized by using enantiomerically pure (*S*)-binaphthyl derivatives (**4**, **5**) and therefore main chain chiral polymers have been obtained. The observed optical rotations ($[\alpha]_D$) are 305 (*c* 0.2, $CHCl_3$) for (*S*)-**1**, 832 (*c* 1.3, $CHCl_3$) for (*S*)-**2** and 220 (*c* 0.7, $CHCl_3$) for (*S*)-**3**. Thus, these polymers rotate the plane of polarized light in the opposite direction to the binaphthyl dicyanomethyl-substituted species (*S*)-**4**, {$[\alpha]_D$ −34

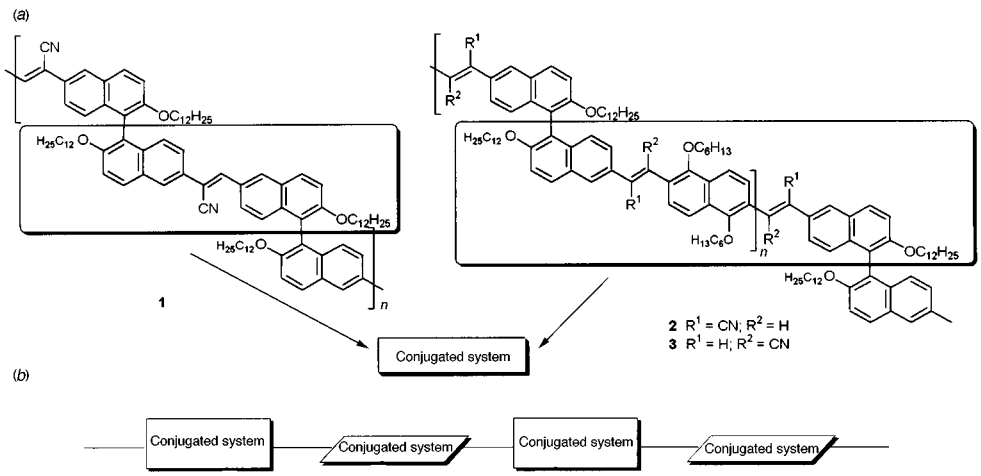

Fig. 1 (*a*) New block co-polymers showing the conjugated systems between binaphthyl units and (*b*) schematic representation of the polymers.

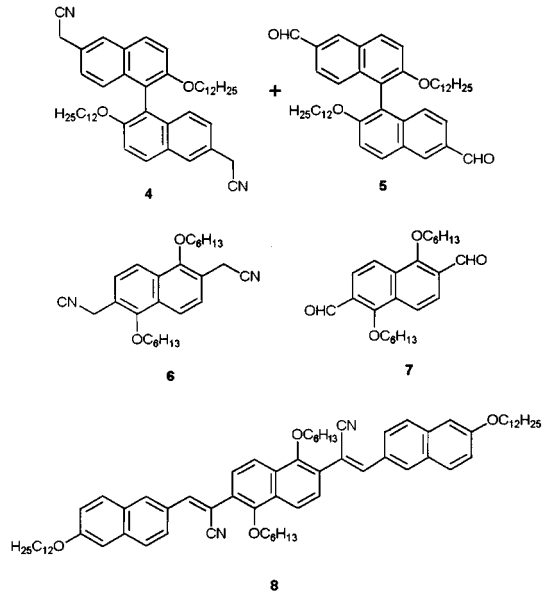

(*c* 0.6, $CHCl_3$)} and in the same direction as the binaphthyldicarbaldehyde (*S*)-**5** {$[\alpha]_D$ 56 (*c* 0.7, $CHCl_3$)}.

Cyclic voltammetry studies of polymers **1**–**3** were carried out in CH_2Cl_2 at room temperature using Bu_4NClO_4 as supporting electrolyte (0.3 mg ml^{-1}, SCE reference electrode and glassy carbon as the working electrode). It was found that all the polymers are oxidized at potentials above 1.2 V (*vs.* SCE) which is high compared with other conjugated polymers (0.6–1.0 V).[11] On the other hand, all the polymers were found to be reducible at potentials around −1.5 V (*vs.* SCE). The relatively good acceptor ability of these polymers can be ascribed to the presence of the cyanovinylene moieties on the conjugated system. As it was previously stated, high electron affinity materials are of special interest for the manufacture of LEDs providing that they can be used in combination with air stable electrodes, thus increasing device life time.[9]

The absorption maximum of these polymers increases from **3** (λ_{max} 378 nm) to **1** (λ_{max} 382 nm) to **2** (λ_{max} 422 nm). These polymers emit strong blue–green light under an UV lamp. The fluorescence spectrum of **1** shows emission maxima at λ_{emi} 475 nm when excited at 382 nm. The fluorescence spectrum of **2** displays λ_{emi} 496 nm when excited at 422 nm and **3** exhibits an emission maxima of λ_{emi} 485 nm when excited at 378 nm. Two factors may be considered in order to rationalize the observed absorption and emission data. First, there is the extension of the conjugated system, which for polymer **1** comprises two naphthalene units linked by a cyanovinylene group and for polymers **2** and **3** includes three naphthalene units linked by two cyanovinylene moieties. Second, there is the steric hindrance of the hexyloxy substituents with respect to the cyano groups in polymer **3** which may cause torsion of the chain, reducing the planarity of the backbone and therefore decreasing the degree of conjugation.[12] Thus, the more red-shifted absorption and fluorescence values, which may be correlated to a longer effective conjugation length, are observed for polymer **2** which has three naphthalene units conjugated through two cyanovinylene bridges and does not have alkoxy substituents in positions adjacent to the cyano groups. In polymer **3** the absorption and emission values are blue shifted in comparison with polymer **2**, probably as a consequence of the already mentioned steric hindrance. The blue shift of the absorption and emission in polymer **1** with respect to polymer **2** may be rationalized in terms of a shorter conjugated system.

In order to ascertain that the conjugated system in the new polymers is really confined to the region between the two binaphthyl moieties (Fig. 1), we have determined by semi-empirical calculations (PM3) the angle of rotation between the two naphthyl moieties of binaphthyl in a model compound constituted by the conjugated system of **3** end-capped by two naphthyl groups. The found values (85.7 and 92.1°) strongly suggest the lack of conjugation. Furthermore, we have synthesized compound **8**, which is the repetitive conjugated unit of polymer **3** (Fig. 1) in order to determine its UV-Vis spectrum. The data obtained (λ_{max} 380 nm) are in full agreement with that obtained for the related polymer **3** (λ_{max} 378 nm), showing the same onset value.

In summary, new optically active block copolymers containing binaphthyl units have been synthesized. They show an intense photoluminescence and a high electron affinity and therefore they are promising candidates for the fabrication of light emitting diodes. The main chain chiral character of these polymers may enable the observation of circularly polarized photo- and electroluminescence, which has not so far been reported.[13] Finally, a remarkable aspect of this contribution is that it might provide an effective approach to the synthesis of polymeric luminescent materials in which the emissive colors can be effectively tailored by reacting different appropriately functionalized fluorophores with binaphthyl monomers *via* Knoevenagel condensation polymerization.

This work has been supported by the Universidad Complutense de Madrid (Project PR49/98-7805) and DGICYT (Project PB95-0428-CO2). We are also indebted to Dr G. Orellana for the Photoluminescence measurements, Dr J. San Román and A. Gallardo for GPC measurements, and to Centro de Espectroscopía de la UCM.

Notes and references

† Polymers **1**–**3** were characterized on the basis of the FTIR, ^1H and ^{13}C NMR analyses for which satisfactory results were obtained. *Selected data* for **2**: ν_{max}(KBr)/cm^{-1} 3060, 2855, 2214, 1682, 1621, 1593, 1038, 937, 762, 697, 603, 496; δ_H($CDCl_3$, 300 MHz) 8.44 (d, 2H, *J* 9), 8.30 (s, 2 H, =CH or Ar), 8.18 (s, 2H, Ar or =CH), 8.07 (d, 2H, *J* 9), 8.00 (d, 2H, *J* 8.8), 7.61 (d, 2H, *J* 9.2), 7.51 (d, 2H, *J* 9.2), 7.26 (d, 2H, *J* 8.8), 4.03 (m, 8H, OCH_2), 1.9 (m, 4H, CH_2), 1.5 (m, 4H, CH_2), 1.4–0.9 (m, 48H, CH_2), 0.8 (m, 12H, CH_2); δ_C($CDCl_3$, 75 MHz) 155.9, 155.6, 135.0, 134.2, 130.2, 129.3, 128.8, 126.7, 126.3, 125.0, 124.8, 122.4, 119.8, 119.1, 118.1, 117.5, 116.1, 112.6, 77.1, 69.4, 31.8, 31.6, 30.3, 29.7, 29.6, 29.5, 29.3, 29.2, 29.1, 25.9, 25.6, 22.6, 22.5, 14.0, 13.9.

1 J. L. Segura, *Acta Polym.*, 1998, **49**, 319.
2 A. Kraft, A. C. Grimsdale and A. B. Holmes, *Angew. Chem., Int. Ed.*, 1998, **37**, 402.
3 F. Hide, M. A. Díaz-García, B. J. Schwartz and A. J. Heeger, *Acc. Chem. Res.*, 1997, **30**, 430.
4 N. C. Greenham and R. H. Friend, *Solid State Phys.*, 1995, **49**, 1.
5 *Handbook of Conducting Polymers*, ed. T. A. Skotheim, R. L. Elsenbaumer and J. R. Reynolds, 2nd edn., Marcel Dekker, New York, 1998.
6 S. F. Mason, *Molecular Optical Activity and the Chiral Discriminations*, Cambridge University Press, New York, 1982, p. 72.
7 L. Pu, *Acta Polym.*, 1997, **48**, 116; L. Pu, *Chem. Rev.*, 1998, **98**, 2405.
8 K. Y. Musick, Q.-S. Hu and L. Pu, *Macromolecules*, 1998, **31**, 2933.
9 N. C. Greenham, S. C. Moratti, D. D. C. Bradley, R. H. Friend and A. B. Holmes, *Nature*, 1993, **365**, 628; S. C. Moratti, R. Cervini, A. B. Holmes, D. R. Baigent, R. H. Friend, N. C. Greenham, J. Grúner and P. J. Hamer, *Synth. Met.*, 1995, **71**, 2117.
10 M. Hanack, J. L. Segura and H. Spreitzer, *Adv. Mater.*, 1996, **8**, 663.
11 S. C. Moratti, D. D. C. Bradley, R. Cervini, R. H. Friend, N. C. Greenham and A. B. Holmes, *SPIE Proc.*, 1994, **2144**, 108.
12 J. L. Segura, N. Martín and M. Hanack, *Eur. J. Org. Chem.*, 1999, 643.
13 B. M. V. Langenveld-Voss, R. A. J. Janssen, M. P. T. Christiaans, S. C. J. Meskers, H. P. J. M. Dekkers and E. W. Meijer, *J. Am. Chem. Soc.*, 1996, **118**, 4908.

Communication 8/09405E

Quantitative evaluation of steric effects for π-facial stereoselection: π-plane-divided accessible space

Shuji Tomoda* and Takatoshi Senju

Department of Life Sciences, Graduate School of Arts and Sciences, The University of Tokyo at Komaba, Meguro, Tokyo 153-8902, Japan. E-mail: tomoda@selen.c.u.-tokyo.ac.jp

Received (in Cambridge, UK) 28th January 1999, Accepted 26th February 1999

A simple method for quantitative evaluation of steric effects in π-facial stereoselection has been described.

Steric effects, defined as the exchange repulsion term between reactant molecules according to the Salem–Klopman equation,[1] often play a key role in stereochemical control of organic reactions. It is, however, commonly used only as a qualitative term. Nevertheless highly practical asymmetric syntheses have been designed through intuitive estimation of steric effects based on the size of substituents, such as *A* values[2] or van der Waals radii.[3] It is however often difficult to predict steric effects in π-facial selection[4] intuitively, in particular for substrates having complex substituents around the π-bond. A simple quantitative parameter of π-facial steric effects should provide a convenient means to gain clearer and more effective perception in designing organic syntheses. Herein we describe the first method that is useful for predicting π-facial steric effects for common organic unsaturated substrates.

The new method focuses on the three-dimensional space outside the van der Waals surface of a reactant molecule.[5] It is based on the simple assumption that the volume of the outer (exterior) space nearest to a reaction center should contain steric information of the reactant (substrate), since this volume precisely corresponds to the three-dimensional space available for a reagent to access the reaction center of the substrate. The exterior volume is calculated for the two faces of the π-plane separately. Fig. 1 illustrates the definition of the π-plane-divided accessible space (PDAS) as a reasonable quantitative measure of π-facial steric effects using formaldehyde as an example. The molecular surface is defined as an assembly of spherical atoms having the appropriate van der Waals radii.[3] Integration of exterior three-dimensional space for the PDAS of the carbonyl carbon is performed according to the following conditions. If a three-dimensional point P(*x*, *y*, *z*) outside the repulsive surface is the nearest to the surface of the carbonyl carbon (a reaction center on the *xz* plane) [*i.e.* if the distance between P and the van der Waals surface of the carbonyl carbon (d_C) is the shortest compared with the distances from P to the other atomic surfaces (two d_H and one d_O)] and if the point is located above the carbonyl plane ($y > 0$), the space at this point is assigned to the above-space of the carbonyl carbon. The integration (summation) of such points is defined as the PDAS of the carbonyl carbon for the above-plane. For the sake of convenience, spatial integration is limited to 5 au (2.65 Å) from the molecular surface, where extension of an electronic wave function is negligible beyond this limit. In general, the carbonyl plane is defined as the plane which includes the two sp^2 atoms of the π-bond and which is parallel with the vector connecting the two atoms at the α-positions. The basic concept of the PDAS definition is readily extended to other π-facial steric effects in compounds containing a general double bond other than a carbonyl. The calculation procedure usually begins with structure optimization at the HF/6-31G(d) level using GAUSSIAN 94.[6] PDAS calculation is then performed according to the three-dimensional lattice method with a unit lattice volume of 0.008 au^3 (1.18×10^{-3} Å^3). The method has been successfully applied to a variety of unsaturated substrates. A few examples, for which facial stereoselection has been previously explained without invoking steric effects, will be described.

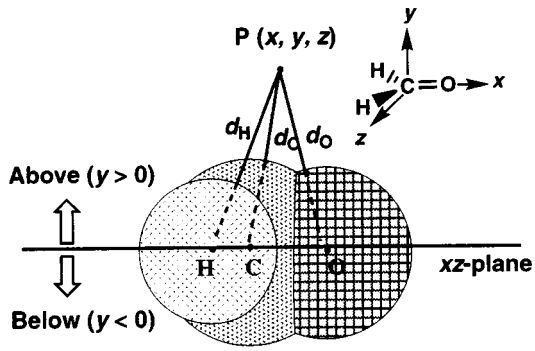

Fig. 1 Definition of π-plane-divided accessible space (PDAS) for the case of formaldehyde.

Table 1 collects the PDAS data of four cyclic ketones (**1**–**4**) along with two cyclohexanones for comparison. The *ax*-face of cyclohexanone (19.4 au^3) is indeed more hindered than the *eq*-face (47.2 au^3), as it is for *tert*-butylcyclohexanone.[7] The stereochemistries of these two and other alkyl-substituted cyclohexanones have been successfully rationalized with the EFOE model (exterior frontier orbital extension model)[8] and are apparently orbital-controlled. The stereochemical reversal observed for 4-*eq*-phenyl-1,3-dioxan-5-one (**1**)[9] and its sulfur analog (**2**)[10] has been the subject of intense investigation.[11,12] Not only the nearly constant stereoselectivity irrespective of the bulkiness of the Grignard reagent employed (RMgI; R = Me, Et, Pr^i),[9,10] but also the PDAS values for **1** and **2** clearly indicate that steric effects should be mainly responsible for the face selection of the heterocyclic ketones. Exclusive attack of $LiEt_3BH$ from the *ax*-face of 2-*ax*-methyl-3-*eq*-phenyl-5-*eq*-methoxypyran-4-one **3**[4,13] can also be explained by the substantially reduced PDAS value in the *eq*-face (13.8 au^3) compared to the *ax*-face (22.4 au^3). As seen in Table 1, exclusive equatorial hydride attack at 2-*eq*, 7-*eq*-dimethyl **4**[14] can be readily rationalized by severe steric hindrance in the *ax*-face where the PDAS value is only 5.5 au^3. In all these examples, the peculiar stereochemical behavior can be ex-

Table 1 π-Plane-divided accessible space (PDAS) for the carbonyl carbon of cyclic ketones and their observed π-facial stereoselectivity in nucleophilic additions[a]

Compound	PDAS/au^3 *ax*	PDAS/au^3 *eq*	Observed *ax*:*eq*
Cyclohexanone	19.4	47.2	—
4-eq-*tert*-butylcyclohexanone	19.6	46.7	86:14[b]
1	67.6	26.5	94–98:2–6[cd]
2	17.9	55.4	7–15:85–93[cd]
3	22.4	13.8	100:0[e]
4	5.5	36.4	0:100[c]

[a] HF/6-31G(d). [b] $NaBH_4$. [c] $LiAlH_4$. [d] RMgI (R = Me, Et, Pr^i. [e] $LiEt_3BH$.

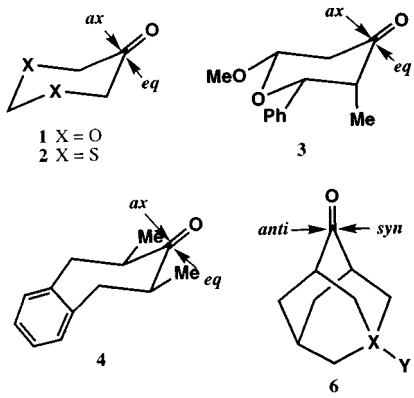

plained simply using ground-state conformations without resorting to transition state effects.[11,15]

Another intriguing example is the 3-substituted cyclohexanone system **5**. A plot of the PDAS values for the *ax*-face of **5** (*ax*-PDAS)[16] against facial stereoselectivity [ln(*ax*/*eq*)] for the reaction of **5** with MeLi reported previously by Cieplak[17,18] for eight substituents indicated an excellent linear correlation (r^2 = 0.95), strongly suggesting that the conformations of **5** are sensitive to the electronic properties of these substituents. Four major explanations have appeared to date to rationalize the enhancement of *ax*-attack in the cyclohexanone system carrying an electron-withdrawing substituent at C3 relative to 4-*tert*-butylcyclohexanone.[12*a*,17–20] Our PDAS calculations clearly indicate that subtle ground-state conformational changes in the cyclohexanone moiety caused by an equatorial substituent at C3 are most likely to be responsible for the observed trend of facial selection of this system.

5-Substituted adamantan-2-ones **6** (X = C or N; Y = substituent) have been regarded as sterically unnbiased systems, where both π-faces are assumed to be sterically equivalent.[21] The parent adamantan-2-one is less reactive with hydride than cyclohexanone,[22] despite the theoretical observation that the transition state antiperiplanar effects are much greater than those in cyclohexanone.[23] Table 2 collects the PDAS data of **6**.[6] The PDAS values of adamantan-2-one are both 11.1 au^3. This is much smaller than the PDAS value for the *ax*-face of cyclohexanone (19.4 au^3), suggesting that adamantan-2-one is *much more sterically demanding* than cyclohexanone. This in turn suggests that subtle changes in steric environment around the carbonyl of **6** may cause significant variation in π-facial stereoselection. The data in Table 2 exhibits a good correlation between the facial stereoselectivity (*anti* : *syn*) and the facial difference in the PDAS value [ω = PDAS(*syn*) − PDAS(*anti*)] (r^2 = 0.68). Among 16 substituents examined, those which pefer *anti*-selectivity are limited to two bulky substituents ($SiMe_3$ and $SnMe_3$; $\omega < 0$). This strongly indicates that in the adamantan-2-one system, where facial differences in frontier orbital extension are marginal, subtle steric effects may be especially important for facial stereoselection in agreement with the recent report by Gung.[24]

Table 2 π-Plane-divided accessible space (PDAS) of 5-substituted adamantan-2-ones **6**[a]

		PDAS/au^3			
X	Y	*anti*	*syn*	ω[b]/au^3	Observed[c] anti : syn
C	H	11.1	11.1	0.0	50 : 50
C	Me	10.7	11.2	0.5	—
C	Bu^t	11.1	10.7	−0.4	50 : 50[d]
C	Ph	10.7	11.9	1.2	42 : 58
C	F	10.3	12.7	2.4	38 : 62
C	Cl	10.5	12.5	2.0	41 : 59
C	Br[e]	10.6	11.8	1.2	41 : 59
C	I[f]	10.9	11.5	0.6	36 : 64
C	OH	10.9	11.2	0.3	43 : 57
C	NH_2	10.3	11.7	1.4	34 : 66
C	CO_2Me	10.4	11.6	1.2	39 : 61
C	CF_3	10.4	11.6	1.2	41 : 59
C	$SiMe_3$	11.3	10.6	−0.7	55 : 45
C	$SnMe_3$[f]	11.8	10.5	−1.3	56.5 : 43.5
N	—	10.2	11.5	1.3	38 : 62
N^+	Me	10.3	12.4	1.1	12 : 88
N^+	O^-	9.6	13.7	4.1	4 : 96

[a] HF/6-31G(d) unless otherwise noted. [b] ω = PDAS(*syn*) − PDAS(*anti*). [c] $NaBH_4$ in Pr^{i}OH or MeOH unless otherwise noted (ref. 21). [d] $LiAlH_4$ in Et_2O. [e] Huzinaga's 43321/4321/311(d) basis set for Br with 6-31(d) basis sets for C and H were used at the HF. [f] HF/3-21G*.

The Ministry of Education, Science, Sports and Culture is gratefully acknowledged for financial support through Grants-in Aid of Scientific Research (Project Nos. 09440215 and 09239207; Priority Area).

Notes and references

1 G. Klopman, *J. Am. Chem. Soc.*, 1968, **90**, 223; L. Salem, *J. Am. Chem. Soc.*, 1968, **90**, 543; I. Fleming, *Frontier Orbitals and Organic Chemical Reactions*, Wiley, London, 1977.
2 E. L. Eliel, S. H. Wilen and L. N. Mander, *Stereochemistry of Organic Compounds*, Wiley, New York, 1994, p. 695.
3 A. Bondi, *J. Phys. Chem.*, 1964, **68**, 441.
4 B. W. Gung, *Tetrahedron*, 1996, **52**, 5263.
5 K. Ohno, S. Matsumoto and Y. Harada, *J. Chem. Phys.*, 1984, **81**, 4447.
6 GAUSSIAN 94 (Revision D.1 and E.2), Gaussian, Inc., Pittsburgh, PA, 1997. For compounds containing I or Sn, the 3-21G* basis set was employed. For bromides, Huzinaga's 43321/4321/311(d) basis set was used for Br with 6-31G(d) basis sets for C and H.
7 D. C. Wigfield and D. J. Phelps, *J. Am. Chem. Soc.*, 1974, **94**, 543.
8 S. Tomoda and T. Senju, *Tetrahedron*, 1997, **53**, 9057.
9 J. C. Jochims, Y. Kobayashi and E. Skrzelewski, *Tetrahedron Lett.*, 1974, 571.
10 Y. Kobayashi, J. Lambrecht, J. C. Jochims and U. Burkert, *Chem. Ber.*, 1978, **111**, 3442.
11 A. S. Cieplak, *J. Am. Chem. Soc.*, 1981, **103**, 4540.
12 (*a*) Y.-D. Wu, K. N. Houk and M. N. Padden-Row, *Angew. Chem., Int. Ed. Engl.*, 1992, **31**, 1019; (*b*) Y.-D. Wu and K. N. Houk, *J. Am. Chem. Soc.*, 1987, **109**, 908.
13 S. Danishefsky and M. E. Langer, *J. Am. Chem. Soc.*, 1985, **50**, 3674.
14 D. Mukherjee, Y.-D. Wu, F. R. Fronczek and K. N. Houk, *J. Am. Chem. Soc.*, 1988, **110**, 3328.
15 M. Chérest, H. Felkin and N. Prudent, *Tetrahedron Lett.*, 1968, 2199; Y.-D. Wu and K. N. Houk, *J. Am. Chem. Soc.*, 1987, **109**, 908.
16 Equatorial orientation of a substituent at C3 is assumed for PDAS calculation of **5**.
17 C. R. Johnson, B. D. Tait and A. S. Cieplak, *J. Am. Chem. Soc.*, 1987, **109**, 5875.
18 A. S. Cieplak, B. D. Tait and C. R. Johnson, *J. Am. Chem. Soc.*, 1989, **111**, 8447.
19 Y. Amarendra, K. Yenkatesan, B. Ganguly, J. Chandrasekhar, F. A. Khan and G. Mehta, *Tetrahedron Lett.*, 1992, **33**, 3072.
20 G. Frenking, K. F. Kohler and M. T. Reez, *Angew. Chem., Int. Ed. Engl.*, 1991, **30**, 1146.
21 C. D. Jones, M. Kaselj, R. N. Salvatore and W. J. le Noble, *J. Org. Chem.*, 1998, **63**, 2758; H. Li and W. J. le Noble, *Tetrahedron Lett.*, 1990, **31**, 4391; M. Xie and W. J. le Noble, *J. Org. Chem.*, 1989, **54**, 3836; C. K. Cheung, L. T. Tseng, M.-H. Lin, S. Srivastava and W. J. le Noble, *J. Am. Chem. Soc.*, 1986, **108**, 1598; J. M. Hahn and W. J. le Noble, *J. Am. Chem. Soc.*, 1992, **114**, 1916; J. Lau, E. M. Gonikberg, J. Hung and W. J. le Noble, *J. Am. Chem. Soc.*, 1995, **117**, 11 421; M. Kaseij, E. M. Gonikberg and W. J. le Noble, *J. Org. Chem.*, 1998, **63**, 3218.
22 P. Geneste, G. Lamaty, C. Moreau and J.-P. Roque, *Tetrahedron Lett.*, 1970, **57**, 5011.
23 S. Tomoda and T. Senju, *Chem.Commun.*, 1999, in the press.
24 B. W. Gung and M. A. Wolf, *J. Org. Chem.*, 1996, **61**, 232.

Communication 9/00764D

ChemComm

Towards mechanically linked polyrotaxanes by sequential deprotection–coupling steps of bifunctional rotaxanes

Michel P. L. Werts, Maarten van den Boogaard, Georges Hadziioannou and Gerasimos M. Tsivgoulis*

Department of Polymer Chemistry and Materials Science Centre, University of Groningen, Nijenborgh 4, 9747 AG Groningen, The Netherlands. E-mail: g.tsivgoulis@chem.rug.nl

Received (in Liverpool, UK) 2nd February 1999, Accepted 25th February 1999

The monomer rotaxane 13, bearing two protected functional groups, is used to obtain a dimer, following a new approach of sequential deprotection–coupling steps which can lead to mechanically linked polyrotaxanes.

Rotaxanes and catenanes as well as their polymer derivatives appear increasingly in the literature. In the field of polymers, a number of fascinating polyrotaxane structures have been presented.[1] It has been shown that the properties of these compounds are in many cases very different compared to the 'naked' polymers.[2]

In the vast majority of the compounds synthesized so far, a covalently connected polymer backbone is surrounded by 'cyclic' molecules, or alternatively, rotaxane subunits are connected to the polymer backbone as side groups.[1,2] The very attractive concept of synthesizing oligomers and/or polymers where the repeating units are connected to each other in a non-covalent way was proposed some years ago,[3] but progress towards this aim has been achieved only very recently.[4–6] Such polymers and/or oligomers with non-covalent connections are expected to give materials with new rheological and mechanical properties. Until now, this research has mainly been focused on polycatenanes.[4] Reports on mechanically linked polyrotaxanes have only described small assemblies[5] and polypseudorotaxanes.[6]

Here we present the synthesis of a new mechanically linked dimer rotaxane, where the repeating units are connected by non-covalent bonds. The synthesis is based on a new step-by-step approach consisting of sequential deprotection–coupling steps that can lead to well defined oligomers. A bisfunctionalized rotaxane is used as the starting monomer. The dimer synthesis and some preliminary studies are presented.

The rotaxane structure used as monomer (compound **13** on Scheme 1) is based on dialkoxybenzene units with a cyclophane containing two 4,4′-bipyridinium groups. Similar types of systems have been studied extensively by the group of Stoddart.[7]

The synthesis of polyrotaxanes and polycatenanes has proven to be quite challenging. In the step-by-step approach, presented in Scheme 2, the initial monomer rotaxane **13** was designed to fulfil a number of requirements: (a) introduction of functional units so that polymerization is possible, (b) protection of these functional units for a step-by-step synthesis and (c) minimization of electronic and/or steric problems.

The positions of the two functional groups in the rotaxane were chosen in such a way that a dimerization and/or polymerization reaction could lead to oligomers with the repeating units connected non-covalently (Schemes 1 and 2). These groups are a phenol and a carboxylic acid. In general, between these two groups, a high-yield coupling reaction (esterification) can take place in only one synthetic step. This is important in order to minimize the number of reaction steps that involve the rotaxane molecule.

Although a number of protective groups are available for sequential removal, in our case the choice decreased significantly since selective deprotection of both groups is needed. In addition, the various sensitive groups in the rotaxane structure **13** should be inert to the deprotection conditions. This compound contains an ester bond and a bis(4,4′-bipyridinium) cyclophane derivative, which both show very limited stability in

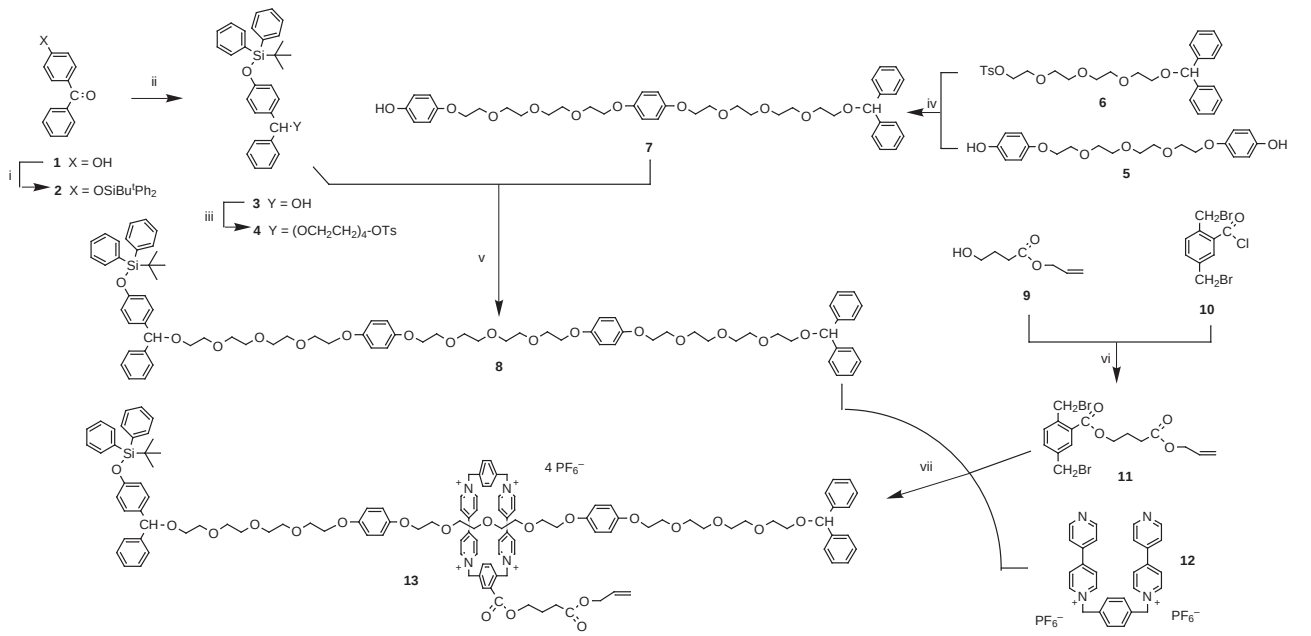

Scheme 1 Synthesis of the bisprotected monomer **13**. *Reagents and conditions*: i, TBDPSCl, Et_3N, DMAP, Py, THF (71%); ii, $NaBH_4$, THF (79%); iii, NaH, $Ts(OCH_2CH_2)_4OTs$, THF (65%); iv, K_2CO_3, DMF (58%); v, NaH, THF (38%); vi, Pr^i_2EtN, CH_2Cl_2 (49%); vii, CH_3CN, $AgPF_6$ (4.8%).

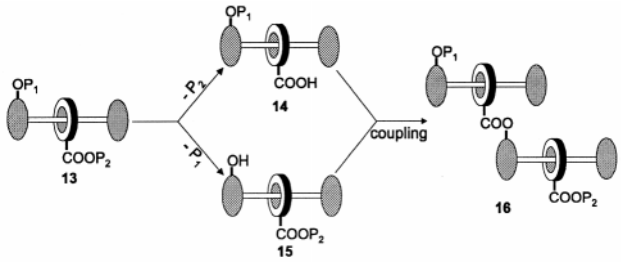

Scheme 2 Schematic representation of the synthesis of the bisprotected dimer **16**.

alkaline pH. Furthermore, the two blocking groups are of the diphenylmethyl ether type and are unstable in acidic conditions. The hindered TBDPS protective group appears to be a good protective group for the phenol unit. It is stable under a variety of basic and acidic conditions[8] (necessary in steps ii, iii and v in the rotaxane synthesis), while it can be removed specifically with fluoride anions under very mild conditions. In the carboxylic acid case, our initial attempts were focused on the tetrahydropyranyl (THP) group. Unfortunately, despite encouraging results obtained with model compounds, it was found that this group was too labile, and was removed during simple work-up operations of the rotaxane **13**. In contrast, the allyl group was found to be suitable. The allyl ester bond is stable during steps vi and vii (Scheme 1) as well as during the reactions used in the synthesis of oligomers. At the same time, it can be selectively removed in the presence of other ester bonds by Pd catalysts under mild conditions.

The last point in the design of rotaxane **13** concerns the reactivity of the carboxylic acid group. It has been reported[9] that a carboxylic group directly connected to the bis(4,4′-bipyridinium) cyclophane is not active towards esterification. In preliminary experiments we found similar behaviour. Therefore, in molecule **13** the protected carboxylic group was moved to a position that is not in close proximity to the tetracationic cyclophane.

The synthesis of the rotaxane **13** was accomplished by reacting **8**, **11** and **12** in the presence of excess of $AgPF_6$ in 4.8% yield.† The low yield may be attributed[5] to the steric hindrance of the carboxylic ester group of **11**. Despite this low yield, at the end of the reaction most of the unreacted compound **8** can be recovered and used again in step vii. Compounds **5**, **6**, **10** and **12** were obtained according to literature procedures while molecule **9** was accessed by ring opening of γ-butyrolactone with allyl alcohol under acidic conditions. The procedures followed for the synthesis of molecule **8** are delineated in Scheme 1.

Selective deprotection of the two functional groups in two different batches was the first step towards the synthesis of the dimer. Thus, rotaxane **14** contained a free carboxylic acid group obtained by deprotection of **13** with $Pd(PPh_3)_4$, while rotaxane **15** contained a free phenol group, obtained by deprotection of **13** with Bu_4NF. In the last step, esterification (DCC/Py) between the acid **14** and the alcohol **15** gave the dimer **16** in a 30–40% yield. This compound also contains a protected phenol and a protected carboxylic acid, like the monomer **13**. Therefore, longer derivatives (tetramer, octamer *etc.*) can be obtained by sequential deprotection–esterification steps.

Both the monomer **13** and the dimer **16** were characterized by MALDI-TOF mass spectrometry and ^{1}H NMR and UV-VIS absorption spectroscopy. The ^{1}H NMR spectra of **13** and **16** in CD_3COCD_3 are consistent with the assigned structures.

The hexafluorophosphate salts of the rotaxanes **13** and **16** are red solids, insoluble in H_2O but soluble in acetone, CH_3CN and CH_2Cl_2. Also, they are insoluble in solvents of lower polarity such as Et_2O, $CHCl_3$ and hexane. The UV-VIS spectra of both **13** and **16** in CH_3CN and in CH_2Cl_2 show two absorption maxima; an intense peak at 265 nm and a very weak peak at 480 nm. The last one corresponds to the charge transfer interaction known in rotaxanes of similar structure.[10]

The MALDI-TOF mass spectrum of **16** with 2,5-dihydroxybenzoic acid as matrix [Fig. 1(*b*)] shows four peaks at 4303, 4159, 4015 and 3869 mass units (mu), corresponding to the ions $[M - 4PF_6]^+$, $[M - 5PF_6]^+$, $[M - 6PF_6]^+$ and $[M - 7PF_6]^+$, respectively. The peaks at lower masses can be easily identified as fragments of the molecular ion. By using 5-methoxysalicylic acid instead of 2,5-dihydroxybenzoic acid as matrix, a different series of ions can be identified $[M - 2PF_6]^+$, $[M - 3PF_6]^+$, $[M - 4PF_6]^+$ and $[M - 5PF_6]^+$. Similar results were found for the monomer **13**. The three peaks at 2299, 2154 and 2009 mass units (mu) correspond to the ions $[M - 2PF_6]^+$, $[M - 3PF_6]^+$ and $[M - 4PF_6]^+$, respectively [Fig. 1(*a*)].

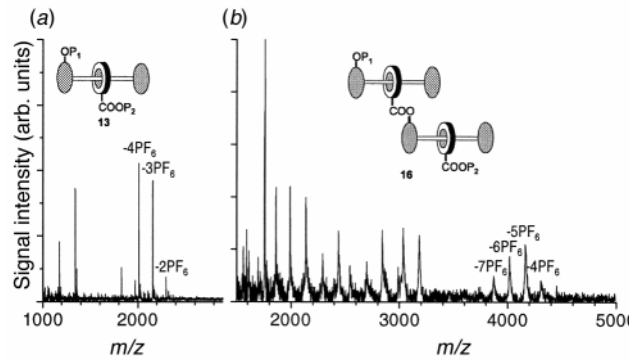

Fig. 1 MALDI-TOF spectra in 2,5-dihydroxybenzoic acid matrix: (*a*) monomer **13**, (*b*) dimer **16**.

In conclusion, we were able to synthesize the monomer rotaxane **13**, which bears two protected functional groups and can give oligomers in a controlled way for the first time, by sequential deprotection–coupling steps. Coupling between derivatives of **13** gives a dimer **16** which can be used for the synthesis of longer rotaxanes by applying the same approach. The connection of the repeating units in the dimer **16** provides a new way to obtain polyrotaxanes based on non-covalent bonds. Synthesis and study of the rheological properties of longer oligorotaxanes based on monomer **13** are in progress.

We are grateful to B. Kwant for help in the synthetic work and to Dr A. Kievit for his advice concerning MALDI-TOF spectrometry. This work was financially supported by the Netherlands Foundation for Chemical Research (NWO-CW).

Notes and references

† All new compounds have been characterized by mass and ^{1}H-NMR spectroscopy.

1 *Large ring molecules*, ed. J. A. Semlyen, Wiley-Interscience, New York, 1996, pp. 155–263.
2 H. W. Gibson and H. Marand, *Adv. Mater.*, 1993, **5**, 11.
3 J. A. Preece and J. F. Stoddart, *Macromol. Symp.*, 1995, **98**, 527.
4 For example: R. Jäger and F. Vögtle, *Angew. Chem., Int. Ed. Engl.*, 1997, **36**, 930; C. Hamers, F. M. Raymo and J. F. Stoddart, *Eur. J. Org. Chem.*, 1998, 2109; S. Shimada, K. Ishikawa and N. Tamaoki, *Acta Chem. Scand.*, 1998, **52**, 374.
5 T. Dünnwald, R. Jäger and F. Vögtle, *Chem. Eur. J.*, 1997, **3**, 2043; N. Tamaoki and S. Shimada, *Acta Chem. Scand.*, 1997, **51**, 1138.
6 N. Yamaguchi, D. S. Nagvekar and H. W. Gibson, *Angew. Chem., Int. Ed. Engl.*, 1998, **37**, 2361; P. R. Ashton, I. Baxter, S. J. Cantrill, M. C. T. Fyte, P. T. Glink, J. F. Stoddart, A. J. P. White and D. J. Williams, *Angew. Chem., Int. Ed. Engl.*, 1998, **37**, 1294; P. R. Ashton, I. W. Parsons, F. M. Raymo, J. F. Stoddart, A. J. P. White, D. J. Williams and R. Wolf, *Angew. Chem., Int. Ed. Engl.*, 1998, **37**, 1913.
7 V. Balzani, M. Gomez-Lopez and J. F. Stoddart, *Acc. Chem. Res.*, 1998, **31**, 405 and references therein.
8 *Protective Groups in Organic Synthesis*, ed. T. W. Greene, Wiley-Interscience, New York, 1981, pp. 47–48.
9 S. Menzer, A. J. P. White, D. J. Williams, M. Belohradsky, C. Hamers, F. M. Raymo, A. N. Shipway and J. F. Stoddart, *Macromolecules*, 1998, **31**, 295.
10 R. Ballardini, V. Balzani, M. T. Gandolfi, L. Prodi, M. Venturi, D. Philp, H. G. Ricketts and J. F. Stoddart, *Angew. Chem., Int. Ed. Engl.*, 1993, **32**, 1301.

Communication 9/00914K

Synthesis and photophysical properties of a diporphyrin–fullerene triad

Koichi Tamaki,[a] Hiroshi Imahori,*[a] Yoshinobu Nishimura,[b] Iwao Yamazaki*[b] and Yoshiteru Sakata*[a]

[a] *The Institute of Scientific and Industrial Research, Osaka University, Mihoga-oka, Ibaraki, Osaka 567-0047, Japan. E-mail: imahori@sanken.osaka-u.ac.jp; sakata@sanken.osaka-u.ac.jp*

[b] *Department of Molecular Chemistry, Graduate School of Engineering, Hokkaido University, Sapporo 060-8628, Japan. E-mail: yamiw@eng.hokudai.ac.jp*

Received (in Cambridge, UK) 6th January 1999, Accepted 2nd March 1999

A novel covalently-linked diporphyrin–C_{60} triad has been prepared by 1,3-cycloaddition of C_{60} with a diporphyrin.

Fullerenes have fascinated many researchers during the last decade because of the large size and spherical shape of their delocalized π-electron system with high symmetry.[1] In particular, the unique three-dimensional structures of fullerenes make them a good candidate as an electron acceptor (A). As such, a number of donor (D)–fullerene dyads have been prepared.[2,3] We and other groups have found that C_{60} accelerates photoinduced charge separation (CS) and retards charge recombination (CR) in donor-linked C_{60} dyads. The peculiar effect of C_{60} in electron transfer (ET) is quite similar to the situation in photosynthetic multistep ET, and therefore we were encouraged to design fullerene-containing multicomponent systems as artificial photosynthetic models. There are several reports of triads and a pentad, such as D–S (sensitizer)–C_{60},[4] S–A–C_{60},[5] and S–$(C_{60})_n$ (n = 2,4)[6–11] systems. However, to the best of our knowledge, no reports concerning S–S′–C_{60} systems have appeared so far. Here we report the synthesis and photophysical properties of diporphyrin–C_{60} triad **1**.

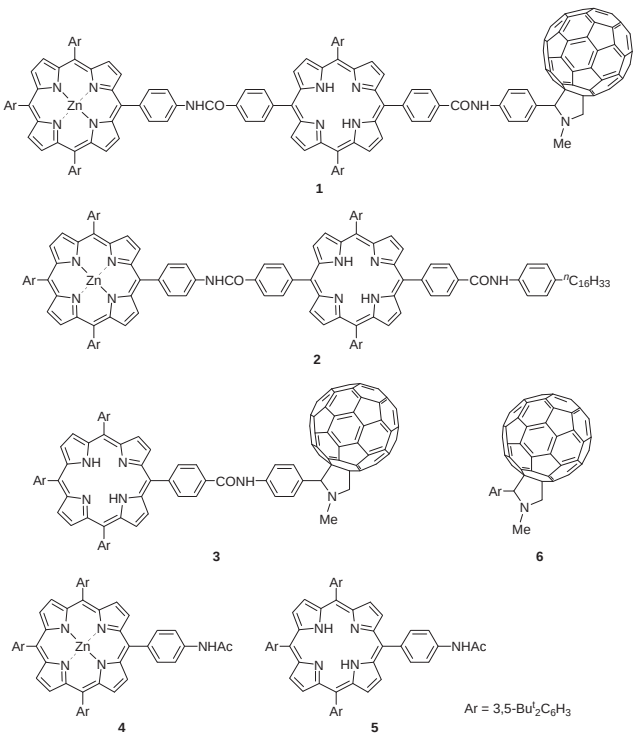

The synthesis of **1** is shown in Scheme 1. The key features involve selective insertion of a zinc atom into the diporphyrin and its protection from the demetallation. Therefore, after the insertion all the procedures were carried out under neutral or basic conditions. Free base porphyrin carboxylic diacid **7** was converted to the corresponding bis(acid chloride) **8** by treatment with $SOCl_2$. Cross-condensation of **8** with zinc amino porphyrin **9** and 4-*tert*-butyldimethylsiloxymethylaniline **10** in benzene in the presence of pyridine afforded a mixture of porphyrins. The desired diporphyrin **11** was isolated in 34% yield by tedious chromatographic separation. Removal of the TBDMS group in **11** with Bu_4NF gave **12**, which was oxidized using activated MnO_2 to yield **13**. The triad **1** was obtained by 1,3-dipolar cycloaddition using **13**, *N*-methylglycine and C_{60} in toluene in 79% yield.[12] Diporphyrin **2** was synthesized from **8**, **9** and 4-hexadecylaniline by a similar method. The reference compounds **3**–**6** were also prepared. Their structures were verified by spectroscopic analyses including ^{1}H NMR and MALDI-TOF mass spectra.†

The absorption spectrum of **1** in THF was almost a linear combination of the spectra of **4**, **5** and **6**, indicating no significant interactions among the three chromophores in the ground state. Absorption due to the two porphyrin chromophores is much stronger than that of C_{60}. The redox potentials of **1**–**6** were measured by differential pulse voltammetry in CH_2Cl_2 using 0.1 M Bu_4NPF_6 as supporting electrolyte. The potentials of **1** (−1.52, −1.14, +0.29, +0.54 V *vs*. Fc/Fc$^+$) can be roughly explained by the sum of **4**, **5** and **6** (**4**: +0.25 V; **5**: +0.43 V; **6**: −1.54, −1.15 V *vs*. Fc/Fc$^+$), implying weak electronic coupling among the three moieties.

Fig. 1 shows steady-state fluorescence spectra of **1**, **2**, **4** and **5** in THF with excitation at 426 nm. The zinc porphyrin **4** exhibits emission maxima at 604 and 657 nm, while the free base porphyrin **5** displays maxima at 652 and 719 nm. The emission of **2** is almost the same as that of **5**, with no appreciable emission from the zinc porphyrin, which is in good agreement with the results in a similar diporphyrin system.[13] Considering that both the porphyrins in **2** absorb at 426 nm, it is suggested that efficient singlet–singlet energy transfer (EN) occurs from the first excited singlet state of a zinc porphyrin (^{1}ZnP*) to a free

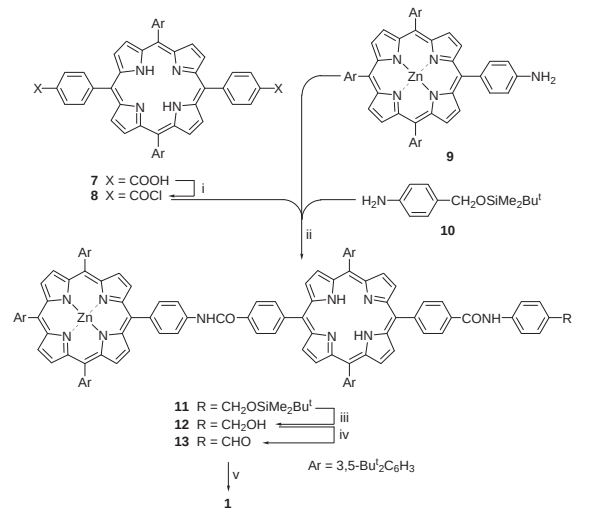

Scheme 1 *Reagents and conditions*: i, $SOCl_2$, pyridine, benzene, reflux; ii, pyridine, benzene, 34% (2 steps); iii, TBAF, THF, 81%; iv, activated MnO_2, $CHCl_3$, 78%; v, C_{60}, $MeNHCH_2CO_2H$, toluene, reflux, 79%.

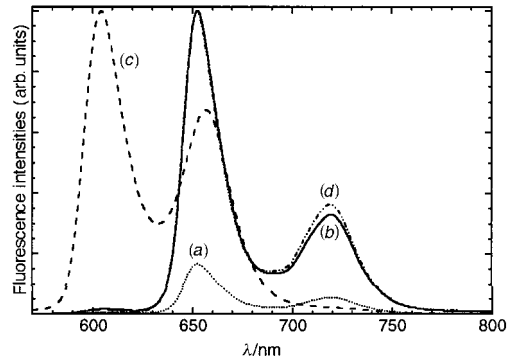

Fig. 1 Fluorescence spectra of (*a*) **1** and (*b*) **2** (2.0×10^{-6} M) in THF with excitation at 426 nm. The normalized spectra of (*c*) **4** and (*d*) **5** are shown as a comparison.

base porphyrin (H_2P). The emission of **1** was quenched strongly as compared with that of **2** when excited at 426 nm under the same concentration (relative intensity: 0.17). No apparent C_{60} emission (λ_{max} = 720 nm) could be detected.‡ Similar quenching behavior was seen for **3** *vs.* **5** (relative intensity: 0.19). These results show the rapid quenching of the excited singlet state of the porphyrin by the C_{60} in **1**.

Preliminary photophysical experiments of **1** and **2** in THF were carried out using a picosecond single photon counting technique with excitation at 422 nm, where both the porphyrins absorb, and monitoring at 655 and 720 nm, where the emission is due to both the porphyrins, and the free base porphyrin and the C_{60}, respectively. Fluorescence decay of **2** at 655 nm was analyzed by two exponential decays with time constants of 44 ps (A = 0.19) and 9.9 ns (A = 0.81). In contrast, the emission at 720 nm was fitted by a rise with a time constant of 44 ps and a decay with a time constant of 9.9 ns (A = 1.00) which agrees well with the fluorescence lifetime (9.8 ns) of **5** in THF. The matching of the time constants between the decay and the rise in **2** strongly supports the efficient EN from ^{1}ZnP* to H_2P in THF. Based on the results together with the fluorescence lifetime of **4** (2.0 ns) in THF, we can calculate the rate constant of EN to be 2.2×10^{10} s^{-1}. The component with the longer lifetime (9.9 ns) monitored at 655 and 720 nm can be assigned reasonably to the emission from the free base porphyrin. Similar results were obtained in **1**, except that a component corresponding to the longer lifetime showed a decreased time constant of 1.7 ns, which is consistent with the fluorescence lifetime of **3** (1.4 ns) in THF. The shorter time constant (τ = 1.7 ns, A = 1.00) of **1** due to the free base porphyrin, compared with that (9.9 ns) of **2**, indicates the photoinduced ET[4] or partial charge-transfer (CT) from ^1H_2P* to C_{60}[14] as shown in Fig. 2.§ These results suggest that initial photoinduced EN from ^{1}ZnP* to H_2P and subsequent CS or CT from $^1H_2P^*$ to C_{60} may take place in **1**.¶

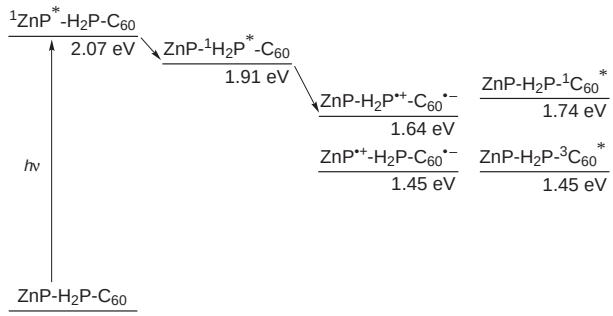

Fig. 2 Plausible reaction scheme and energy diagram for **1** in THF.

In conclusion, a diporphyrin–C_{60} triad has been prepared for the first time. Although our interpretation of the quenching mechanism is consistent with the results obtained by the fluorescence lifetime measurements, further details must wait transient absorption experiments, which are in progress.

This work was supported by Grants-in-Aid for COE Research and Scientific Research on the Priority Area of Electrochemistry of Ordered Interfaces (No. 10131246 to H. I.) and the Priority Area of Creation of Delocalized Conjugated Electronic Systems (No. 10146103 to Y. S.), and for the Encouragement of Young Scientists (No. 09740471 to H. I.) from the Ministry of Education, Science, Sports and Culture, Japan. Y. S. thanks the Mitsubishi Foundation for financial support. K. T. is the recipient of a Grant-in-Aid for JSPS Fellows (No. 81801).

Notes and references

† *Selected data* for **1**: δ_H(270 MHz; $CDCl_3$) −2.84 (s, 2H), 1.53 (s, 90H), 2.67 (br s, 3H), 3.67 (br s, 1H), 4.31 (br s, 1H), 4.50 (br s, 1H), 7.61 (br s, 2H), 7.79 (s, 3H), 7.81 (s, 2H), 7.96 (d, *J* 8, 2H), 8.04 (s, 4H), 8.09 (s, 6H), 8.20–8.31 (m, 8H), 8.42 (d, *J* 8, 2H), 8.48 (d, *J* 8, 2H), 8.70 (br s, 2H), 8.77 (d, *J* 4, 2H), 8.88–8.90 (m, 6H) and 9.01–9.03 (m, 8H); *m*/*z* (MALDI-TOF; positive mode) 2794 ($M+H^+$); (MALDI-TOF; negative mode) 721 (C_{60}^-); λ_{max} (THF)/nm 350 (sh), 361 (sh), 404 (sh), 420 (sh), 427, 485, 516, 555, 597, 649 and 704.

‡ In the steady-state fluorescence experiments it was quite difficult to discriminate the emissions from the free base porphyrin and the C_{60} because of overlapping at 700–750 nm as well as the weak fluorescence from the mono-functionalized C_{60}.

§ We cannot rule out the possibility that there are other competitive pathways, where EN from ^1H_2P* takes place to populate $^1C_{60}$*, followed by ET from the porphyrin to $^1C_{60}$* to produce $H_2P^{\cdot+}$–$C_{60}^{\cdot-}$, or equilibration with ^1H_2P* energetically and/or by intersystem crossing from $^1C_{60}$* to $^3C_{60}$*.

¶ Based on the energy level diagram in THF, a charge-shift might occur from ZnP to $H_2P^{\cdot+}$ in the ZnP–$H_2P^{\cdot+}$–$C_{60}^{\cdot-}$ state, leading to the production of ZnP$^{\cdot+}$–H_2P–$C_{60}^{\cdot-}$.

1 M. S. Dresselhaus, G. Dresselhaus and P. C. Eklund, *Science of Fullerenes and Carbon Nanotubes*, Academic Press, San Diego, 1996.
2 H. Imahori and Y. Sakata, *Adv. Mater.*, 1997, **9**, 537.
3 N. Martín, L. Sánchez, B. Illescas and I. Pérez, *Chem. Rev.*, 1998, **98**, 2527.
4 P. A. Liddell, D. Kuciauskas, J. P. Sumida, B. Nash, D. Nguyen, A. L. Moore, T. A. Moore and D. Gust, *J. Am. Chem. Soc.*, 1997, **119**, 1400.
5 H. Imahori, K. Yamada, M. Hasegawa, S. Taniguchi, T. Okada and Y. Sakata, *Angew. Chem., Int. Ed. Engl.*, 1997, **36**, 2626.
6 K. Dürr, S. Fiedler, T. Linßen, A. Hirsch and M. Hanack, *Chem. Ber.*, 1997, **130**, 1375.
7 N. Armaroli, F. Diederich, C. O. Dietrich-Buchecker, L. Flamigni, G. Marconi, J.-F. Nierengarten and J.-P. Sauvage, *Chem. Eur. J.*, 1998, **4**, 406.
8 D. Armspach, E. C. Constable, F. Diederich, C. E. Housecroft and J.-F. Nierengarten, *Chem. Eur. J.*, 1998, **4**, 723.
9 S. Higashida, H. Imahori, T. Kaneda and Y. Sakata, *Chem. Lett.*, 1998, 605.
10 J.-F. Nierengarten, L. Oswald and J.-F. Nicoud, *Chem. Commun.*, 1998, 1545.
11 J.-F. Nierengarten, C. Schall and J.-F. Nicoud, *Angew. Chem., Int. Ed. Engl.*, 1998, **37**, 1934.
12 M. Maggini, G. Scorrano and M. Prato, *J. Am. Chem. Soc.*, 1993, **115**, 9798.
13 D. Gust, T. A. Moore, A. L. Moore, F. Gao, D. Luttrull, J. M. DeGraziano, X. C. Ma, L. R. Makings, S.-J. Lee, T. T. Trier, E. Bittersmann, G. R. Seely, S. Woodward, R. V. Bensasson, M. Rougée, F. C. D. Schryver and M. V. der Auweraer, *J. Am. Chem. Soc.*, 1991, **113**, 3638.
14 H. Imahori, S. Ozawa, K. Ushida, M. Takahashi, T. Azuma, A. Ajavakom, T. Akiyama, M. Hasegawa, S. Taniguchi, T. Okada and Y. Sakata, *Bull. Chem. Soc. Jpn.*, in the press.

Communication 9/00176J

Reaction of (*Z*)-1-bromoalk-1-enyldialkylboranes with DMSO: regio- and stereo-selective formation of internal (*E*)-alkenyl bromides

Masayuki Hoshi,* Hideyuki Tanaka, Kazuya Shirakawa and Akira Arase

Department of Applied and Environmental Chemistry, Kitami Institute of Technology, 165 Koen-cho, Kitami 090-8507, Japan. E-mail: HOSHI-Masayuki/chem@king.cc.kitami-it.ac.jp

Received (in Cambridge, UK) 25th January 1999, Accepted 2nd March 1999

Treatment of (*Z*)-1-bromoalk-1-enyldialkylboranes 1 with DMSO results in 1,2-migration of an alkyl group from the boron to the α-carbon without elimination of bromine to give internal (*E*)-alkenyl bromides 2 with excellent stereoselectivity (> 99%).

(*Z*)-1-Haloalk-1-enylboranes, which can be prepared by hydroboration of 1-haloalk-1-ynes with borane derivatives, are versatile and potential precursors of alkenes.[1] For example, the reaction of (*Z*)-1-haloalk-1-enyldialkylboranes with MeONa followed by protonolysis with carboxylic acids offers regio- and stereo-selective syntheses of internal (*E*)-alkenes where one of the alkyl groups on the boron atom is introduced into the α-alkenyl carbon atom with elimination of a halogen atom [eqn. (1)].[2] This strategy could be applied to the synthesis of

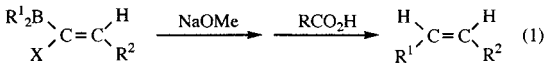

(1)

prostaglandin analogues.[3] On the other hand, we reported that a similar alkyl group migration was performed without elimination of the halogen atom by treatment of (*Z*)-1-haloalk-1-enyldialkylboranes, whose alkyl groups were derived from a relatively hindered alkene, with lead(IV) acetate or (diacetoxyiodo)benzene giving internal (*Z*)-alkenyl halides in a highly stereoselective manner (95–98% for *Z*) [eqn. (2)].[4] Ster-

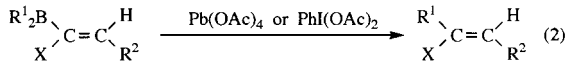

(2)

eodefined alkenyl halides are important substrates, especially as coupling partners of transition metal mediated cross-coupling reactions to give alkenyl units stereoselectively.[5] For example, (11*Z*)-retinal[6] and rapamycin[7] were synthesized using the above coupling reaction. In these reactions the purity of the haloalkene is important. This prompted us to investigate the alkyl group transfer reaction in the hope of obtaining highly pure internal alkenyl halides. We report here a new type of synthesis of internal (*E*)-alkenyl bromides **2** from (*Z*)-1-bromoalk-1-enyldialkylboranes **1** with excellent stereoselectivity (> 99%), on which DMSO has a decisive influence.

The reactions of **1** with DMSO were carried out under reaction conditions optimised using (*Z*)-1-bromohex-1-enyldicyclohexylborane **1a** as a typical substrate. Thus, **1a** was treated with 2 equiv. of DMSO in $ClCH_2CH_2Cl$ at 0 °C to room temperature for 18 h (Scheme 1). After work-up† (*E*)-1-bromo-1-cyclohexylhex-1-ene **2a**‡ was obtained in 73% yield and in > 99% isomeric purity (entry 1, in Table 1). The stereochemistry of **2a** was assigned the *E* configuration by comparing GC and ^1H and ^{13}C NMR analyses of **3a** (Scheme 2)

Table 1 Reaction of (*Z*)-1-bromoalk-1-enyldialkylboranes **1** with DMSO[a]

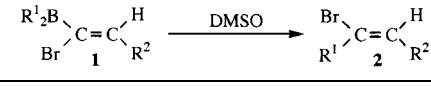

Entry	R^1	R^2	Product	Yield (%)
1	Cyclohexyl	Bu	**2a**	73
2	Hexyl[b]	Bu	**2b**	69
3	Pr(Me)$CHCH_2$[b]	Bu	**2c**	70
4	$Bu^tCH_2CH_2$[b]	Bu	**2d**	70
5	Cyclopentyl[b]	Bu	**2e**	68
6	Cyclohexyl	Ph	**2f**	59
7	Hexyl[b]	Ph	**2g**	45
8	Hexyl[b]	Bu^t	**2h**	28
9	Cyclohexyl	$(CH_2)_2CH_2Cl$	**2i**	60

[a] Reactions were carried out in $ClCH_2CH_2Cl$ using 2 equiv. of DMSO unless otherwise noted. [b] Reactions were carried out in CCl_4.

with those of an authentic sample prepared according to the literature.[8]

The above example demonstrates that the relatively hindered alkyl group on the boron atom is introduced to the alkenyl moiety of **2** as one of the alkyl substituents in a regio-and stereoselective manner. We next explored the reaction of **1**, which was prepared using a variety of dialkylboranes derived from less hindered alkenes through hydroboration with $BH_2Br{\cdot}SMe_2$,[9] followed by hydridation with $LiAlH_4$.[10] For example, (*Z*)-1-bromohex-1-enyldihexylborane **1b** reacted with DMSO under similar conditions§ to afford isomerically pure (*E*)-6-bromododec-5-ene **2b**¶ in 69% yield (entry 2).

In all cases listed in Table 1, internal (*E*)-alkenyl bromides **2** were obtained in > 99% isomeric purity. Accordingly, the present reaction can be applied not only to the cases of relatively hindered dialkylboranes (entries 1, 6 and 9) but also to the cases of less hindered dialkylboranes (entries 2–5, 7 and 8), demonstrating that a wide variety of compounds **2** can be formed using this strategy.

A plausible mechanism for the formation of internal (*E*)-alkenyl bromides **2** is shown in Scheme 3. It was observed that the yields of **2** depended considerably on the solvent employed. In addition, the addition of an equimolar amount of pyridine, a more polar compound than THF, to **1** inhibited completely the present reaction. These results suggest that the reaction is initiated by nucleophilic attack of DMSO. It appears that a concerted reaction, which involves the transfer of a methyl group from sulfur to oxygen and the concomitant formation of methylthio cation, occurs through two-electron oxidation. Then electrophilic addition of the methylthio cation to the carbon–carbon double bond followed by 1,2-migration of an alkyl group from boron to the α-carbon would take place to form intermediate **A**. Finally, intermediate **A** would undergo *trans*-

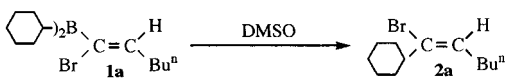

Scheme 1

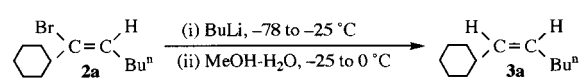

Scheme 2

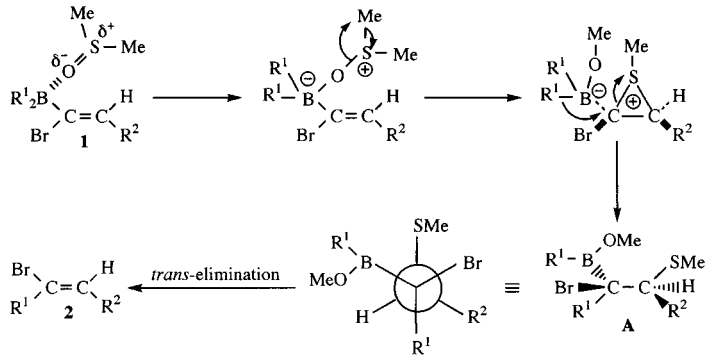

Scheme 3

elimination of an alkylmethoxyboryl group and a methylthio group‖ to yield **2**. In the case of entry 8, the large steric hindrance between R^1 and R^2 could be responsible for the low yield of (*E*)-4-bromo-2,2-dimethyldec-3-ene **2h**.

In summary, we have demonstrated that a variety of compounds **1** react with DMSO to provide the corresponding species **2** in > 99% isomeric purity, and thus both substituents (R^1 and R^2) in **2** can be selected from a wide range of possible groups. It should be noted that the present reaction is carried out under mild and essentially neutral conditions. Further studies on the application of this strategy to different types of species **1** with varying functionality and a similar nucleophilic attack on **1** are now in progress.

Notes and references

† For work-up of the reaction mixture the use of sodium perborate was effective.

‡ *Selected data* for **2a**: δ_H(200 MHz, $CDCl_3$) 0.90 (m, 3H), 1.10–1.88 (m, 14H), 1.98–2.18 (m, 2H), 2.35–2.55 (m, 1H), 5.78 (t, *J* 7.6, 1H); δ_C(50 MHz, $CDCl_3$) 13.8, 22.1, 25.6, 25.8 (2C), 29.1, 31.5, 31.6 (2C), 41.5, 130.9, 133.3; υ_{max}(film)/cm^{-1} 2929, 2854, 1637, 1450, 1377, 893, 648; *m*/*z* (EI) 246 (M^+, 22%), 244 (M^+, 21), 165 (32), 123 (17), 109 (100), 95 (67), 81 (48), 67 (63), 55 (51).

§ After preparation of **1b**, THF was removed under reduced pressure. The residue was extracted with CCl_4 under Ar atmosphere in order to separate **1b** from $LiAlBr_4$, and the extracts were transferred into another flask through a simple filter packed with glass wool.

¶ *Selected data* for **2b**: δ_H(200 MHz, $CDCl_3$) 0.79–1.04 (m, 6H), 1.18–1.62 (m, 12H), 1.90–2.04 (m, 2H), 2.41 (t, *J* 7.2, 2H), 5.84 (t, *J* 7.6, 1H); δ_C(50 MHz, $CDCl_3$) 13.8, 14.0, 22.1, 22.6, 28.0, 28.2, 29.2, 31.4, 31.6, 35.4, 125.9, 132.4; υ_{max}(film)/cm^{-1} 2956, 2927, 2858, 1645, 1463, 1379, 842, 727, 646; *m*/*z* (EI) 248 (M^+, 18%), 246 (M^+, 17), 122 (12), 120 (12), 111 (28), 97 (72), 83 (43), 81 (45), 69 (82), 67 (42), 55 (100).

‖ After hydrolysis of the reaction mixture, there is a characteristic odour of mercaptan.

1 For example, see A. Pelter, K. Smith and H. C. Brown, *Borane Reagents*, Academic Press, London, 1988; D. S. Matteson, *Stereodirected Synthesis with Organoboranes*, Springer, Berlin, 1995.

2 G. Zweifel and H. Arzoumanian, *J. Am. Chem. Soc.*, 1967, **89**, 5086; G. Zweifel, R. P. Fisher, J. T. Snow and C. C. Whitney, *J. Am. Chem. Soc.*, 1971, **93**, 6309; E. Negishi, J.-J. Katz and H. C. Brown, *Synthesis*, 1972, 555.

3 E. J. Corey and T. Ravindranathan, *J. Am. Chem. Soc.*, 1972, **94**, 4013.

4 Y. Masuda, A. Arase and A. Suzuki, *Chem. Lett.*, 1978, 665; *Bull. Chem. Soc. Jpn.*, 1980, **53**, 1652.

5 For example, see J. Tsuji, *Palladium Reagents and Catalysts*, Wiley, Chichester, 1995; N. Miyaura and A. Suzuki, *Chem. Rev.*, 1995, **95**, 2457.

6 J. Uenishi, R. Kawahama, O. Yonemitsu, A. Wada and M. Ito, *Angew. Chem., Int. Ed.*, 1998, **37**, 320.

7 K. C. Nicolaou, T. K. Chakraborty, A. D. Piscopio, N. Minowa and P. Bertinato, *J. Am. Chem. Soc.*, 1993, **115**, 4419.

8 G. Zweifel, H. Arzoumanian and C. C. Whitney, *J. Am. Chem. Soc.*, 1967, **89**, 3652.

9 H. C. Brown, N. Ravindran and S. U. Kulkarni, *J. Org. Chem.*, 1979, **44**, 2417.

10 H. C. Brown and S. U. Kulkarni, *J. Organomet. Chem.*, 1981, **218**, 299.

Communication 9/00652D

The biomimetic oxidation of dieldrin using polyhalogenated metalloporphyrins

Fumio Hino and David Dolphin*

Department of Chemistry, University of British Columbia, 2036 Main Mall, Vancouver, B.C., Canada V6T 1Z1. E-mail: ddolphin@qlt-pdt.com

Received (in Corvallis, OR, USA) 19th November 1998, Accepted 4th January 1999

Biomimetic oxidation of dieldrin produces the same metabolites as generated *in vivo*, which suggest a 'radical oxygen-rebound' mechanism.

Dieldrin **1**, like other insecticides, accumulates in the food chain and its use, as with other organochlorinated materials such as DDT, has been banned in many countries. Dieldrin accumulates principally in adipose tissue and is only slowly metabolized. Even though it has not been used in North America for more than two decades[1] it is, to this day, still found in the food chain. In the laboratory it was found that one year after injection of dieldrin only ~50% of the material had been metabolized and excreted, while half the dose was still retained by rabbits.[2] Some of the less interesting dieldrin metabolites arose from opening of the epoxide ring, but one particular metabolite, the intramolecularly bridged pentachloro ketone **6**, allowed for some very interesting speculation as to its mechanism of formation. McKinney *et al.* suggested[3] that the other principle mammalian metabolite, *syn*-9-hydroxydieldrin **3**, might be an intermediate in the formation of **6**, but they eventually considered this unlikely since feeding of **3** to a rat produced no pentachloro ketone in its liver, where it is known to accumulate. It was suggested, in 1975,[4] that a common intermediate, the species containing a radical at C-9 (**2**, Scheme 1), could account for the formation of both **3** and **6**; this suggestion is consistent with Groves' oxygen-rebound mechanism for the hydroxylation of alkanes by cytochrome P-450 which was formulated in 1976.[5,6]

We have been unsuccessful in oxidizing dieldrin using isolated liver microsomes, due principally to its solubility properties and the destruction of microsomes under forcing conditions. We also failed in oxidizing dieldrin using metalloporphyrins derived from tetrakis(2,6-dichlorophenyl)porphyrin as biomimetic catalysts since dieldrin is quite recalcitrant towards oxidation and the porphyrin catalysts were destroyed before sufficient substrate oxidation could occur.

Recently, however, new highly halogenated porphyrins containing eight halogen atoms on the porphyrin periphery have been reported and these third generation catalysts (**10**, **11**) are showing exciting potential as biomimetic and industrial catalysts.[7] The oxidizing power of these catalysts and the turnover numbers that they exhibit are extraordinary, and both the iron and manganese complexes **10** and **11** effectively oxidize dieldrin to give the same products (**3**, **6**) as those previously identified from mammalian metabolism studies.

We have examined a number of cooxidants in addition to those shown in Table 1 and found that Oxone ($KHSO_5$) and H_2O_2 caused considerable destruction of catalyst and, at best, gave only a trace of oxidized dieldrin. On the other hand, surprisingly good yields of **3** and **6** were observed using hypochlorite, iodosylbenzene (PhIO) and alkyl hydroperoxides in mixed aqueous/organic solvents; small amounts of the ketone **7** were also seen when the reaction was carried out in only organic solvents. Ketone **7** arises from the over-oxidation of **3**; when **3** was treated with **10a** and PhIO, **7** was isolated from the reaction in 24% yield. Similar overoxidation of an initially formed alcohol regularly occurs with these P-450 mimics, but the extent of overoxidation can be often controlled by choice of catalyst, cooxidant and reaction conditions.[11]

The general concensus is that the majority of P-450 mediated hydroxylations proceed *via* radical rearrangements. Radical rearrangements have been well-documented in P-450 biochemistry[6] and 'radical clocks' have been used to measure the rate of the rebound process.[12] Thus bicyclo[2.1.0]pentane gave a 7:1 mixture of *endo*-2-hydroxybicyclo[2.1.0]pentane and cyclopent-3-en-1-ol when oxidized by rat liver microsomes.[13] The bicyclo[2.1.0]pentan-2-yl radical rearranges to the cyclopent-3-en-1-yl radical with a rate constant of 2.4×10^9 s^{-1}.[14]

In addition, Groves *et al.*[15] have shown that when a chiral iron porphyrin hydroxylated ethylbenzene, the differences observed between the *pro-R* and *pro-S* hydrogen atoms were best explained *via* radical intermediates. Nevertheless, Newcomb, Hollenberg and their colleagues[16] have recently concluded, from their studies on a hypersensitive cyclopropyl radical probe, that ring opening of a cyclopropylmethyl radical is unreasonable in their system and that a cationic species is

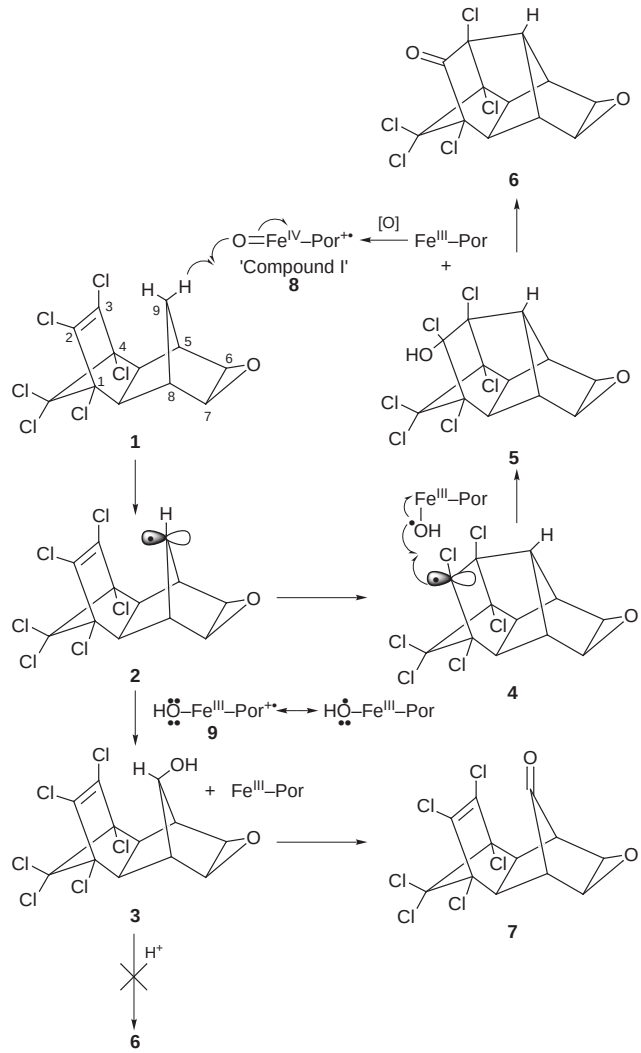

Scheme 1

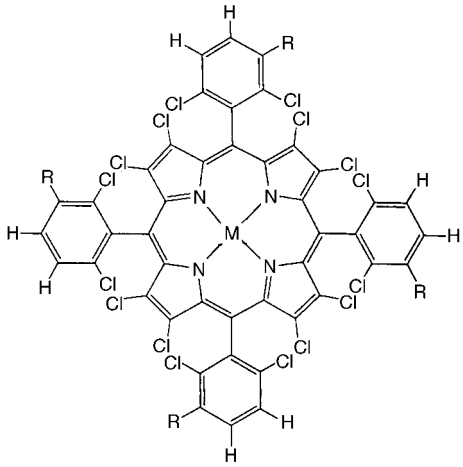

10 R = H, M = Fe
11a R = SO_3H, M = Fe
11b R = SO_3H, M = Mn

Table 1 Oxidation of dieldrin (ref. 8)

Catalyst	Co-oxidant	Solvent[a]	Product (%)[b] 6	3	7	1	Ratio 6/(3 + 7)
10	NaOCl	C	3	7	2	65	0.33
10	NaOCl	D	12	5	trace	73	2.4
10	Bu^tOOH	C	16	25	4	47	0.64
10	Bu^tOOH	D	36	19	trace	30	1.9
11a	NaOCl	A	24	5	—	63	19
11a	NaOCl	B	31	3	—	51	10
11a	PhIO	B	6	trace	trace	70	
11a	Bu^tOOH	A	38	14	—	30	2.7
11a	Bu^tOOH	B	43	12	—	32	3.6
11b	NaOCl	A	12	3	—	77	4
11b	NaOCl	B	15	8	—	60	1.9
11b	PhIO	A	8	trace	—	81	
11b	PhIO	B	11	trace	—	80	
11b	Bu^tOOH	A	31	10	—	40	3.1
11b	Bu^tOOH	B	41	8	—	36	5.1
Fenton[c]	H_2O_2	MeCN	8	13	—	18	0.6

[a] A: H_2O–CH_2Cl_2–MeOH = 2 : 10 : 30. B: pH 2 buffer–CH_2Cl_2–MeOH = 2 : 10 : 30. C: CH_2Cl_2. D: CH_2Cl_2–MeOH = 1 : 1. [b] Ref. 9. [c] Ref. 10.

intermediate in the rearrangements. In order to best accommodate their observations they suggest that the active oxidant in P-450 hydroxylations might be an iron–H_2O_2 complex and that the first species formed in the hydroxylation reaction is a protonated alcohol formed by 'OH^+' insertion into a C–H bond and that any subsequent rearrangements occur *via* solvolysis.

The question then arises as to how the principal oxidation product **6** is generated. Metabolic studies suggest that **6** does not derive from **3** and we have found no acid catalyzed reactions of **3** which generated **6**. Moreover, carbonium ion intermediates on the highly chlorinated 'perchlorocyclopentadiene ring' seem unlikely. Radical intermediates, however, would be consistent with the oxygen-rebound mechanism proposed by Groves and a radical at C-2 would be stabilized by the chlorine atom. Indeed, the P-450 mediated oxidation of dieldrin and the parallel biomimetic studies described here add further support to the oxygen-rebound mechanism and the intermediacy of substrate radicals where, as shown in Scheme 1, an initial hydrogen atom abstraction from C-9 by 'Compound I' (the common intermediate in these oxidations, $O{=}Fe^{IV+\cdot}$ **8**) would generate the substrate radical **2** and a heme intermediate **9** which can be formulated as an hydroxyl radical coordinated to (and stabilized by) the ferric iron. Intermediate **2** can then react at C-9 to give the alcohol **3** (and the ferric porphyrin ready for another catalytic cycle) or rearrange to the more stable tertiary radical at C-2 (**4**) where transfer of an hydroxyl radical from iron followed by loss of HCl would generate **6**.

The fact that we have been unable to bring about the acid catalyzed conversion of **3** → **6** does not preclude cationic intermediates in the P-450 metalated hydroxylation of dieldrin. Nevertheless, we conclude that the present study favors radical intermediates in the biomimetic oxidation of dieldrin and by analogy in the enzymatic reaction as well. Perhaps we should not be too surprised in either this case or that of Newcomb and Hollenberg *et al*. that electronically stacking a particular substrate may impose different reaction pathways for P-450-mediated hydroxylations.

As shown previously[7] these highly chlorinated metalloporphyrins can accurately mimic the cytochromes P-450. Not only can the production of natural metabolites be mimicked (and presumably predicted) but milligram (and even larger if required) amounts of such metabolites can be produced at the bench.

We thank the Canadian Natural Sciences and Engineering Research Council of Canada and Meiji Pharmaceutical University, Tokyo, Japan.

Notes and references

1 G. D. Bellward, R. J. Norstrom, P. W. Whitehead, J. E. Elliot, S. M. Bandiera, C. Dwonschak, T. Chang, S. Forbes, B. Cadario, L. E. Hart and K. M. Cheng. *J. Toxicol. Environ. Health*, 1990, **30**, 33.
2 F. Korte and H. Arent. *Life Sci*., 1965, **4**, 2017.
3 J. D. McKinney, H. B. Mathews and N. K. Wilson, *Tetrahedron Lett.*,, 1973, **21**, 1895; J. D. McKinney, S. M. DePaul Palaszek, H. B. Mathews and M. H. Behandale, in *Pesticides in the Environment. A Continuing Controversy*, ed. W. B. Deichmann, Intercontinental Medical Book Corp., New York, 1973, p. 103.
4 *Foreign Compound Metabolism Vol. 3, A Specialist Periodical Report*, Senior Reporter D. E. Hathway, The Chemical Society, London, 1975, p. 404.
5 J. T. Groves and G. A. McClusky, *J. Am. Chem. Soc*., 1976, **98**, 859; J. T. Groves, G. A. McClusky, R. E. White and M. J. Coon, *Biochem. Biophys. Res. Commun*., 1988, **81**, 154.
6 J. T. Groves and Y.-Z. Han, *Models and Mechanisms of Cytochrome P-450 Action*, in *Cytochrome P-450*, 2nd edn., ed. P. Ortiz de Montellano, 1995, pp. 1–45.
7 D. Dolphin, T. Traylor and L.Y. Xie, *Acc. Chem. Res*., 1997, **30**, 251.
8 The cooxidant (0.66 mmol) was added with stirring, at room temperature, in ten equal portions every 30 min to a solution of the porphyrin catalyst (0.032 mmol) in 10 ml of solvent (A, B, or C). An hour after the last addition of cooxidant the mixture was poured onto water (50 ml) and CH_2Cl_2 (50 ml). After separation the aqueous phase was extracted with CH_2Cl_2 (2 × 20 ml). The combined organic phases were dried over $MgSO_4$, filtered and concentrated to 1 ml which was applied to a thick layer silica TLC plate and developed with light petroleum–EtOAc (5 : 1).
9 The isolated products had identical NMR and IR spectra to authentic samples.
10 A solution of dieldrin (0.26 mmol) and $Fe(ClO_4)_2$ (0.1 mmol) in MeCN (5 ml) was flushed with argon, H_2O_2 (0.1 mmol) in MeCN (0.5 ml) was slowly added over 15 min and the solution was then allowed to stand at room temperature for 1 h. The mixture was then extracted with CH_2Cl_2 (2 × 20 ml) and the products separated by TLC.
11 D. Mansuy, *Coord. Chem. Rev*., 1993, **125**, 129.
12 P. R. Ortiz de Montellano, *Oxygen Activation and Reactivity in Cytochrome P-450*, 2nd edn., ed. P. R. Ortiz de Montellano, Plenum, New York, 1995.
13 P. R. Ortiz de Montellano and R. A. Stearns, *J. Am. Chem. Soc*., 1987, **109**, 3415.
14 V. W. Bowry and K. V. Ingold, *J. Am. Chem. Soc*., 1991, **113**, 5699.
15 J. T. Groves and P. Viski, *J. Am. Chem. Soc*., 1989, **111**, 8537.
16 M. Newcomb, M.-H. Le Tadic-Biadatti, D. L. Chestney, E. S. Roberts and P. F. Hollenberg, *J. Am. Chem. Soc*., 1995, **117**, 12 085; P. H. Toy, B. Dhanabalasingham, M. Newcomb, I. H. Hanna and P. F. Hollenberg, *J. Org. Chem*., 1997, **62**, 9114; M. Newcomb, M.-H. Le Tadic-Biadatti, D. A. Putt and P. F. Hollenberg. *J. Am. Chem. Soc*., 1995, **117**, 3312.

Communication 8/09080G

Self-assembly of novel trimers using dipyrromethene ligands

Alison Thompson, Steven J. Rettig† and David Dolphin*

Department of Chemistry, University of British Columbia, 2036 Main Mall, Vancouver, B.C., Canada V6T 1Z1

Received (in Corvallis, OR, USA) 23rd November 1998, Accepted 25th January 1999

Ligands comprising two dipyrromethene units linked at the β-position have been used to prepare trimeric complexes with Zn^{II} and Co^{II}; the structure of the Zn^{II} complex is confirmed by X-ray analysis.

The self-assembly of supramolecular structures by complexation chemistry utilizing metal ions and suitable ligands is one approach to new structures with unusual and interesting properties.[1] Three-dimensional inorganic arrays have been forthcoming, giving helicates,[2] grids,[3] cages,[4] ladders[5] and rings,[6] through the coordination chemistry of polybipyridine ligands and transition metal ions. Multi-porphyrin structures have also been reported.[7] Dipyrromethenes, the building blocks of porphyrins, are themselves interesting ligands for supramolecular coordination chemistry and we have been able to rationally design new architectures through self-assembly of these ligands and transition metal ions.

Metal complexes generated from polybipyridine ligands[2–7] are rendered neutral by the use of counter-ions. This may give rise to problematic isolation procedures, or induce disorder in the solid state. Our efforts in this field are aimed towards the preparation of uncharged supramolecular architectures, in which counter-ions are not required. The dipyrromethene unit **1** is a useful ligand in metal chelation,[8] as it is a monoanionic ligand and the pyrrolic moieties are coplanar. Indeed, preliminary investigations in our group have shown that dipyrromethene units linked at the α-position can be used to generate helical complexes.[9] We sought to design ligands comprising linked dipyrromethene binding units, with which to construct neutral three-dimensional structures, including grids and ladders.

When a solution of $Zn(OAc)_2$ and NaOAc in MeOH was added to a solution of **2**[10]‡ in $CHCl_3$ a single complex **3** was formed in high yield.§ EI mass spectroscopy showed the molecular mass of the product to be 1468, which corresponds to the trimeric complex with a ligand : metal ratio of 3 : 3. The X-ray structure¶ of the trinuclear complex (Fig. 1) shows that it crystallizes in a triangular fashion, with the ligands linking the three metal centers overlapping, in a progressive manner: in each ligand, one dipyrromethene binding unit lies above the averaged plane of the molecule, whilst the other dipyrromethene unit lies below the averaged plane. The distances between the three metal centers are 9.27, 9.34 and 9.36 Å. Each metal center has distorted tetrahedral geometry in order to permit the triangular arrangement. Selected N–Zn–N angles are shown in Fig. 1. The six planar dipyrromethene sub-units lie at 63.6, 85.6 and 68.7° to their partner dipyrromethene unit within the same ligand.

Similarly, **2** was reacted with $Co(OAc)_2$ to give the corresponding cobalt trimer, with molecular mass of 1449, again in high yield. Several reaction conditions were applied to these preparations including temperature variations (−10 °C to reflux in MeOH) and different lengths of addition period (metal salts added in one portion, to over 24 h). In each and every case, the same trimers were formed in high yield, suggesting them to be both the kinetic and thermodynamic products.

Continuing with the theme of pyrroles linked at the β-position, we subjected several hydrobromide salts **4**–**8** with varying hydrocarbon spacer lengths (n = 3, 4, 6, 8, 12) between the β-positions[10] to standard complexation reactions with $Zn(OAc)_2$. Complexation was almost quantitative for each ligand. Table 1 shows that as the length of the hydrocarbon chain between the pyrrole moiety increases, so formation of the

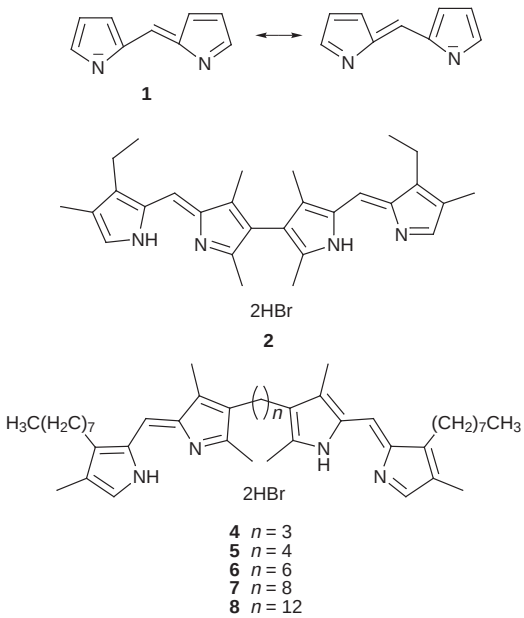

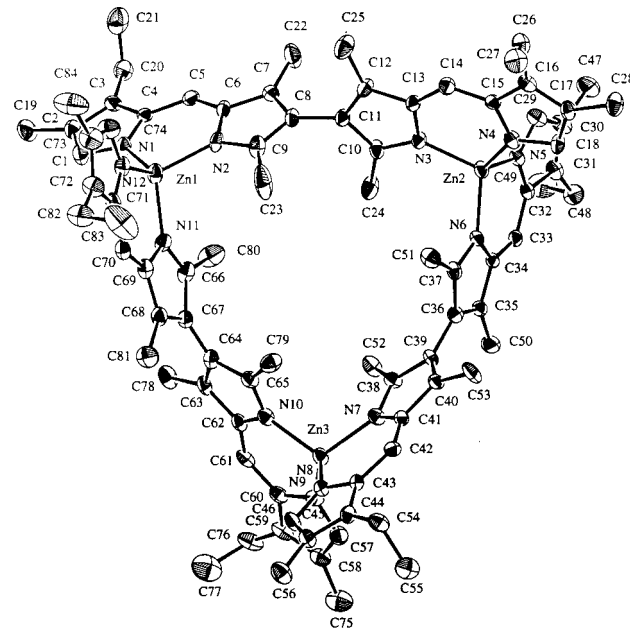

Fig. 1 X-Ray structure of **3** (hydrogen atoms and 2 $CHCl_3$ molecules of crystallization are omitted for clarity). Selected bond angles (°): N(1)–Zn(1)–N(2) 95.5(2), N(1)–Zn(1)–N(12) 116.4(2), N(1)–Zn(1)–N(11) 119.7(2), N(2)–Zn(1)–N(11) 111.3(2), N(2)–Zn(1)–N(12) 119.7(2), N(11)–Zn(1)–N(12) 96.0(2).

† Deceased October 27, 1998.

Table 1 Oligomeric ratios of metal complexes

Salt	*n*	Monomer : dimer : trimer[a]
2	0	0 : 0 : 1
4	3	0 : 1 : trace
5	4	0 : 1 : trace
6	6	1 : 1 : trace
7	8	1 : trace : trace
8	12	1 : 0 : 0

[a] Traces of higher oligomers were also observed for ligands **4**, **5** and **6**.

monomer dominates, as determined by MALDI spectroscopy. Molecular modeling[11] rationalizes this, as the longer spacer length allows the dipyrromethene units to fold back against each other, thus fulfilling the tetrahedral geometry requirements for binding to the metal ion. In the case of the ligand derived from salt **2** (n = 0) this folding is clearly not allowed and the trimer is formed. For **4** and **5** (n = 3 and 4, respectively) the spacer chain length permits sufficient folding for the corresponding dimers to be formed, but when n = 6 or greater, folding is sufficient to allow the monomer to form. However, MALDI spectroscopy showed small amounts of higher order complexes (trimers–hexamers) to be present in each case. Variation of reaction conditions did not alter the oligomeric ratio of products.

In summary, we have demonstrated the usefulness of linked dipyrromethene ligands in the self-assembled preparation of uncharged novel architectures. The properties of the trimeric complexes will be reported at a later date. Current work is focussed towards the construction of novel grids, ladders and supramolecular helicates using dipyrromethene ligands.

This work was supported by the Natural Sciences and Engineering Council of Canada.

Notes and references

‡ *Selected data for* **2**: mp > 230 °C (decomp.); $\lambda_{max}(CH_2Cl_2)$/nm 506; δ_H(200 MHz; $CDCl_3$) 1.23 (3H, t, *J* 7, C*H*$_3$), 2.13 (3H, s, C*H*$_3$), 2.20 (3H, s, C*H*$_3$), 2.58 (3H, s, C*H*$_3$), 2.72 (2H, q, *J* 7, C*H*$_2$), 7.72 (1H, s, C*H*), 13.40 (1H, br s, N*H*), 13.60 (1H, br s, N*H*); δ_H[200 MHz; $(CD_3)_2CO$] 1.24 (3H, t, *J* 7, C*H*$_3$), 2.18 (3H, s, C*H*$_3$), 2.37 (3H, s, C*H*$_3$), 2.89 (2H, q, *J* 7, C*H*$_2$CH$_3$), 7.67 (1H, s, C*H*), 7.78 (1H, s, C*H*), 8.12 (1H, br s, N*H*); δ_C(75 MHz; $CDCl_3$) 9.79 (*C*H$_3$), 11.02 (*C*H$_3$), 13.49 (*C*H$_3$), 16.03 (*C*H$_3$), 18.32 (*C*H$_2$), 121.06, 121.82 (*C*H), 125.02, 126.92, 127.29, 142.47 (*C*H), 145.03, 149.41, 155.63; *m/z* EI 426 [(M^+ − 2HBr) 55%], 411 (74, M − 2HBr − Me), 397 (48, M − 2HBr − Et), 213 [3, $(M - 2HBr)^{2+}$], 94 (100) (Found: M^+ − 2HBr, 426.2778. $C_{28}H_{34}N_4$ requires 426.2784).

§ *Experimental*: a solution of $Zn(OAc)_2$ (105 mg, 0.476 mmol) and $Na(OAc)_2$ (65 mg, 0.476 mmol) in MEOH (2 cm^3) was added to a solution of ligand **2** (56 mg, 0.095 mmol) in $CHCl_3$ (2 cm^3) and the reaction mixture stirred at room temperature for 4 h. The solvents were removed *in vacuo* and the resulting solid dissolved in $CHCl_3$ (10 cm^3) and filtered through a short plug of Celite. The solution was then washed with water (3 × 10 cm^3), dried over $MgSO_4$ and the solvent removed *in vacuo* to give **3** (40 mg, 86%) as a green metallic solid, R_f (3 : 1 hexane : CH_2Cl_2) 0.4; mp > 230 °C (decomp.); $\lambda_{max}(CH_2Cl_2)$/nm 522; δ_C(75 MHz; $CDCl_3$) 10.21 (*C*H$_3$), 11.12 (*C*H$_3$), 14.44 (*C*H$_3$), 16.65 (*C*H$_3$), 18.22 (*C*H$_2$), 122.78 (*C*H), 123.33, 123.93, 136.23, 136.95, 140.32, 142.58, 147.22 (*C*H), 159.10; *m/z* EI 1468 (M^+, 100%), 734 (50, M^{2+}), 490 (3, M^{3+}) (Found: M^+, 1468.5752. $C_{84}H_{96}N_{12}{}^{64}Zn_2{}^{68}Zn$ requires 1468.5791).

¶ *Crystal data* for **3**: $C_{84}H_{96}N_{12}Zn_3 \cdot 2CHCl_3$, M = 1708.66, triclinic, space group $P\bar{1}$ (No. 2), a = 14.251(3), b = 18.7667(9), c = 19.684(2) Å, α = 63.2582(11), β = 80.2531(15), γ = 68.169(2)°, U = 4364.1(8) Å3, Z = 2, D_c = 1.300 g cm^{-3}. Rigaku AFC7/ADSC Quantum 1 CCD diffractometer, T = 180 K, graphite-monochromated Mo-Kα radiation, λ = 0.71069 Å, $2\theta_{max}$ = 50.4°, 35289 reflections measured, 15359 unique (R_{int} = 0.051). The final unit-cell parameters were obtained by least-squares using 20163 reflections with 2θ = 4.0–50.4°. Data were corrected for Lorentz polarisation and absorption (multi-scan including decay and scaling, relative correction factors 0.89–1.00). The structure was solved by the Patterson method. One $CHCl_3$ molecule was modeled as (3 : 1) two-fold disordered; the carbon atom associated with the minor component could not be located and was not included in the model. Non-hydrogen atoms [except Cl(9)] were refined with anisotropic thermal parameters and hydrogen atoms were fixed in calculated positions with C–H = 0.98 Å. The refinement converged at R [F, 7705 reflections having $I \geqslant 3\sigma(I)$] = 0.062 and R_w (F^2, all 15359 unique reflections) = 0.129. Calculations were performed using the *teXsan* structure analysis package (Molecular Structure Corporation, 1985-1997). CCDC 182/1158.

1 D. Philp and J. F. Stoddart, *Angew. Chem.*, 1996, **108**, 1242; D. Philp and J. F. Stoddart, *Angew. Chem., Int. Ed. Engl.*, 1996, **35**, 1155; J.-M. Lehn, *Supramolecular Chemistry Concepts and Perspectives*, VCH, Weinheim, 1995; D. S. Lawrence, T. Jiang and M. Levett, *Chem. Rev.*, 1996, **95**, 2229; P. N. W. Baxter, *Comprehensive Supramolecular Chemistry*, ed. J. L. Atwood, J. E. D. Davis, D. D. MacNicol and F. Vögtle, Pergamon, Oxford, 1996, ch. 6; M. Fujita, *Comprehensive Supramolecular Chemistry*, ed. J. L. Atwood, J. E. D. Davis, D. D. MacNicol and F. Vögtle, Pergamon, Oxford, 1996, ch. 7.

2 B. Hasenknopf, J.-M. Lehn, G. Baum and D. Fenske, *Proc. Natl. Acad. Sci. U.S.A.*, 1996, **93**, 1397; C. Piguet, G. Bernardinelli and G. Hopfgartner, *Chem. Rev.*, 1997, **97**, 2005; D.-P. Funeriu, Y.-B. He, H.-J. Bister and J.-M. Lehn, *Bull. Soc. Chim. Fr.*, 1996, **133**, 673.

3 P. N. W. Baxter, J.-M. Lehn, J. Fischer and M.-T. Youinou, *Angew. Chem., Int. Ed. Engl.*, 1994, **33**, 2284; I. Weissbuch, P. N. W. Baxter, S. Cohen, H. Cohen, K. Kjaer, P. B. Howes, J. Als-Nielsen, G. S. Hanan, U. S. Schubert, J.-M. Lehn, L. Leiserowitz and M. Lahav, *J. Am. Chem. Soc.*, 1998, **120**, 4850.

4 P. N. W. Baxter, J.-M. Lehn, A. De Cian and J. Fischer, *Angew. Chem.*, 1993, **105**, 92; P. Baxter, J.-M. Lehn, A. DeCian and J. Fischer, *Angew. Chem., Int. Ed. Engl.*, 1993, **32**, 69; M. Fujita, S.-Y. Yu, T. Kusukawa, H. Funaki, K. Ogura and K. Yamaguchi, *Angew. Chem., Int. Ed.*, 1998, **37**, 2082.

5 P. N. W. Baxter, G. S. Hanan and J.-M. Lehn, *Chem. Commun.*, 1996, 2019.

6 D. P. Funeriu, J.-M. Lehn, G. Baum and D. Fenske, *Chem. Eur.*, 1997, **3**, 99; B. Hasenknopf, J.-M. Lehn, G. Baum, B. O. Kneisel and D. Fenske, *Angew. Chem., Int. Ed. Engl.*, 1996, **35**, 1838.

7 R. K. Kumar, S. Balasubramanian and I. Goldberg, *Inorg. Chem.*, 1998, **37**, 541; P. J. Stang, J. Fan and B. Olenyuk, *Chem. Commun.*, 1997, 1453.

8 C. Bruckner, Y. Zhang, S. J. Rettig and D. Dolphin, *Inorg. Chim. Acta*, 1997, **263**, 279; J. E. Fergusson and C. A. Ramsay, *J. Chem. Soc.*, 1965, 5222; M. Elder and B. R. Penfold, *J. Chem. Soc. (A)*, 1969, 2556.

9 Y. Zhang, A. Thompson, S. J. Rettig and D. Dolphin, *J. Am. Chem. Soc.*, 1998, **120**, 13 537.

10 J. B. I. Paine and D. Dolphin, *Can. J. Chem.*, 1978, **56**, 1710.

11 HyperChem Release 5.01 MM+ force field optimized by Polak-Ribiere.

Communication 8/09192G

Highly electrophilic lanthanide complexes containing fluorinated amido ligands: multiple Ln···F interactions, agostic interactions and η⁶-arene coordination

Damon R. Click, Brian L. Scott and John G. Watkin*

Chemical Science and Technology Division, Mail Stop J514, Los Alamos National Laboratory, Los Alamos, New Mexico, 87545. E-mail: jwatkin@lanl.gov

Received (in Bloomington, IN, USA) 26th November 1998, Accepted 15th January 1999

Highly fluorinated amido ligands have been employed as supporting ligands for homoleptic lanthanide complexes; X-ray diffraction studies reveal multiple Ln···F interactions and a rare example of an η⁶-bound toluene solvent molecule.

The chemistry of the transition metals coordinated by mono-, di- and tri-amido ligands has recently generated a considerable amount of interest, due to many interesting observations of catalytic activity,[1] small molecule activation[2] and unusual coordination modes of neutral ligands.[3] A number of these studies have involved amido ligands which have electron-withdrawing fluorinated phenyl groups directly attached to nitrogen.[4] Lanthanide amido complexes[5] are also experiencing renewed attention, due in part to the emergence of this class of compounds as effective catalysts[6] and their use as source molecules for rare-earth doping of semiconducting materials.[7] We are currently interested in the chemistry of highly electrophilic metal amido complexes as potential catalysts for olefin polymerization. We report here the results of a structural study of lanthanide metals (Ln = Nd, Sm) coordinated by a series of highly electron-withdrawing amido ligands: $-NH(C_6F_5)$,$-N(SiMe_3)(C_6F_5)$ and $-N(C_6F_5)_2$.

Reaction of $Sm[N(SiMe_3)_2]_3$ **1**[8] with 3 equiv. of pentafluoroaniline in toluene leads to the formation of a pale yellow solution. Removal of solvent, followed by dissolution of the solid in THF and low-temperature crystallization, allows isolation of the thf adduct $[Sm(NHC_6F_5)_3(thf)_3]$ **2** in 58% yield.† An X-ray diffraction study‡ revealed a highly distorted nine-coordinate geometry about the metal center (Fig. 1), which may best be described as a distorted capped square antiprism in which F(18) caps the face defined by N(1), N(3), O(2) and O(3). Sm–N distances to the amido ligands are 2.352(5), 2.360(5) and 2.371(5) Å while Sm–O distances to the thf ligands lie in the range 2.444(4)–2.502(4) Å. The Sm–N distances are found to be very similar to those observed for the terminal arylamido ligands in the anionic samarium complex $[Sm(\mu\text{-}NHC_6H_3Me_2\text{-}2,6)(NHC_6H_3Me_2\text{-}2,6)_3]_2^{2-}$, which average 2.354(9) Å.[5b] Three relatively weak Sm···F interactions[9] of 2.847(4), 2.870(3) and 2.876(3) Å are made by an *ortho*-fluorine substituent of each $-NH(C_6F_5)$ ligand. A hydrogen-bonding network with F···H distances of 2.688 Å and N–H–F angles of 163.8° is observed within the extended three-dimensional structure of **2**, which may explain the low solubility of the complex in non-polar solvents. In addition, intermolecular π-stacking of the arene rings[10] with interplanar contacts of 3.227 Å is observed.

Reaction of **1** with 3 equiv. of *N*-trimethylsilylpentafluoroaniline in toluene allowed the isolation of the base-free homoleptic complex $Sm[N(SiMe_3)(C_6F_5)]_3$ **3**. Single crystal X-ray diffraction‡ revealed an unusual trigonal planar SmN_3 skeleton (planar to within 0.01 Å), with *six* additional secondary contacts with ligand substituents (Fig. 2). Three short Sm···F interactions of 2.561(6), 2.566(5) and 2.587(6) Å with *ortho*-fluorine substituents from each $-N(SiMe_3)(C_6F_5)$ ligand, and three agostic interactions [Sm–C 3.058(11), 3.148(10) and 3.142(10) Å] with trimethylsilyl groups complete the overall nine-coordinate, tricapped trigonal prismatic geometry about the metal center. Sm–N–C_{ipso} and Sm–N–Si angles are almost equal for each amido ligand [*e.g.* Sm(1)–N(3)–C(19) 119.9(6), Sm(1)–N(3)–Si(3) 113.3(4)°], unlike the situation encountered in the related neodymium complex $Nd[N(C_6H_5)(SiMe_3)]_3(THF)$,[11] in which significant Nd–C_{ipso} and Nd–C_{ortho} interactions cause the Nd–N–C_{ipso} angles (110.2° av.) to be much more acute than Nd–N–Si angles (134.1° av.). In common with many similar interactions between $-SiMe_3$ groups and an f-element metal center, no solid-state IR or solution NMR evidence (*e.g.* lowered C–H stretching frequency) was found for

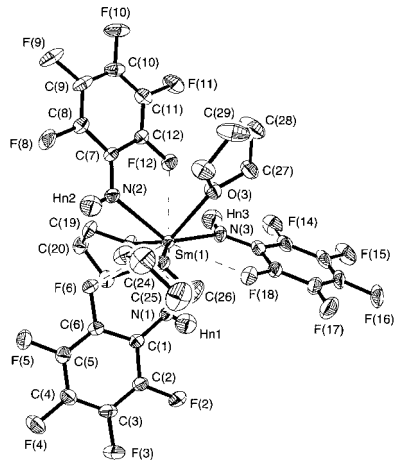

Fig. 1 ORTEP view (30% probability ellipsoids) of the molecular structure of $[Sm(NHC_6F_5)_3(thf)_3].thf$ **2**. Selected bond distances (Å): Sm(1)–N(1) 2.360(5), Sm(1)–N(2) 2.371(5), Sm(1)–N(3) 2.352(5), Sm(1)–O(1) 2.444(4), Sm(1)–O(2) 2.500(4), Sm(1)–O(3) 2.502(4), Sm(1)–F(6) 2.876(3), Sm(1)–F(12) 2.870(3), Sm(1)–F(18) 2.847(4).

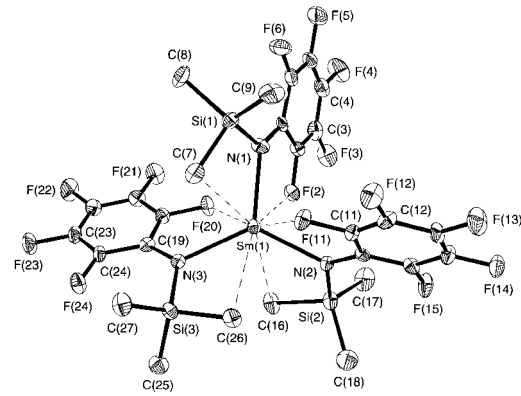

Fig. 2 ORTEP view (30% probability ellipsoids) of the molecular structure of $Sm[N(SiMe_3)(C_6F_5)]_3$ **3**. Selected bond distances (Å): Sm(1)–N(1) 2.329(8), Sm(1)–N(2) 2.330(7), Sm(1)–N(3) 2.362(8),Sm(1)–F(2) 2.566(5),Sm(1)-F(11) 2.587(6), Sm(1)–F(20) 2.561(6), Sm(1)–C(7) 3.058(11), Sm(1)–C(16) 3.148(10), Sm(1)–C(26) 3.142(10).

these 'agostic' interactions. ^{19}F NMR spectra of **3** (room temperature, toluene-d_8) reveal a 2 : 2 : 1 pattern for the *ortho*-, *meta*- and *para*-fluorine substituents. The resonances for the *para*- and *meta*-fluorines are sharp, whereas the *ortho* resonance is broadened almost into the baseline due to interaction with the paramagnetic samarium metal center. The observation of equivalent *ortho*- and *meta*-F resonances indicates rapid rotation about the N–C_{ipso} bond on the NMR timescale (indicative of a weak C–F···Sm interaction). No significant changes in the ^{19}F spectrum were observed upon cooling the sample. Reaction of **3** with stoichiometric quantities of Lewis bases such as thf results in the formation of adducts with reduced numbers of Sm···F–C and Sm···Me–Si interactions (*e.g.* structurally characterized Sm[N(C_6F_5)($SiMe_3$)]$_3$(thf)[12] displays two Sm···F–C and one Sm···Me–Si interaction).

Reaction of Nd[N($SiMe_3$)$_2$]$_3$ **4**[8] with 3 equiv. of decafluorodiphenylamine, [(C_6F_5)$_2$NH],[13] in toluene followed by crystallization from the same solvent leads to isolation of (η-C_6H_5Me)Nd[N(C_6F_5)$_2$]$_3$ **5** in good yield. An X-ray diffraction study‡ revealed a distorted three-legged piano-stool geometry about the metal center (Fig. 3). Nd–N distances to the amido ligands are 2.362(6), 2.392(7) and 2.397(7) Å, which is somewhat longer than those previously observed in neodymium amido complexes (*e.g.* 2.309 Å (av.) in Nd[N(C_6H_5)($SiMe_3$)]$_3$(thf),[11] 2.309(8) Å in Nd($NHC_6H_3Pr^i_2$-2,6)$_3$(thf)$_3$,[5b] and 2.270(2) Å in NdCl[N($SiMe_3$)($C_6H_3Pr^i_2$-2,6)]$_2$(thf)[11]]. Three significant Nd···F interactions of 2.572(5), 2.616(5) and 2.696(5) and one weak Nd···F interaction of 2.940(5) Å are also observed within the structure. The toluene ligand is bound in a rather asymmetric manner, with Nd–C distances lying in the range 2.98(2)– 3.324(13) Å. Although a number of lanthanide complexes exhibiting η^6-arene interactions have been described in the literature,[14] the majority of these interactions occur *via* intra- or inter-molecular ligand chelation. The only lanthanide complexes which have previously been shown to bind aromatic solvent molecules are of the class (η-arene)Ln(η^2-AlX_4)$_3$ (Ln = La, Nd, Sm, Er; X = Cl, Br).[15] We do note, however, that the Nd–C bond distances in **5** are somewhat longer than those found in the neodymium complex (η-C_6H_6)Ln(η^2-$AlCl_4$)$_3$ (2.93 Å (av.)],[15c] presumably indicative of a somewhat weaker Ln–arene interaction in the present case. Complexes such as **5** may also be considered as models for cationic Group 4 metallocene and related bis-amido olefin polymerization systems which have been found to bind toluene and other aromatic solvent, often to the detriment of catalytic activity.[16]

In conclusion, we have shown that fluorinated amido ligands may be used to support highly electrophilic lanthanide metal centers, which enter into multiple secondary interactions with C–F, C–H and C–C bonds of both ligands and solvent.

This work was performed under the auspices of the Laboratory Directed Research and Development Program. We acknowledge Dr. David L. Clark for providing funding to D. R. C. and Dr. Wayde V. Konze for experimental assistance. Los Alamos National Laboratory is operated by the University of California for the U.S. Department of Energy under Contract W-7405-ENG-36.

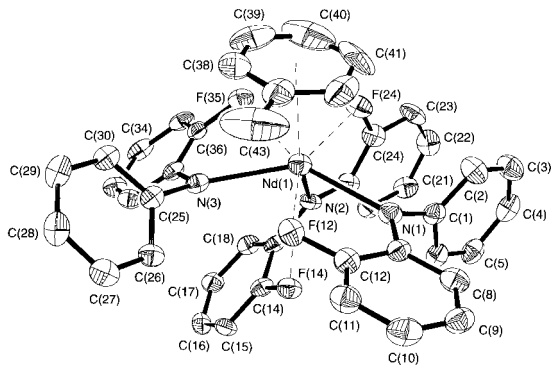

Fig. 3 ORTEP view (30% probability ellipsoids) of the molecular structure of (ηC_6H_5Me)Nd[N(C_6F_5)$_2$]$_3$ **5**. For clarity, only the fluorine atoms making Nd···F contacts are shown. Selected bond distances (Å): Nd(1)–N(1) 2.397(7), Nd(1)–N(2) 2.392(7), Nd(1)–N(3) 2.362(6), Nd(1)–F(12) 2.572(5), Nd(1)–F(24) 2.616(5), Nd(1)–F(35) 2.696(5), Nd(1)–F(14) 2.940(5), Nd(1)–C(41) 2.982(13), Nd(1)–C(40) 2.98(2), Nd(1)–C(42) 3.103(10), Nd(1)–C(39) 3.167(13), Nd(1)–C(37) 3.313(10), Nd(1)–C(38) 3.324(13).

Notes and references

† Experimental details for the preparation and characterization of **2**, **3**, and **5** are provided as electronic supplementary information (http//www.rsc.org/suppdata/cc/1999/633).

‡ *Crystallography*: in all X-ray diffraction studies, data were collected on a Siemens P4/PC diffractometer with Mo-Kα radiation (λ = 0.71069 Å). Patterson techniques were used to locate the lanthanide metal and the majority of all other atoms in the molecule. Subsequent Fourier synthesis gave the remaining light atom positions. Hydrogen atoms were refined using the riding model in the HFIX facility in SHELXL 93. CCDC 182/1182. See http://www.rsc.org/suppdata//cc/1999/633/ for crystallographic files in .cif format.

Crystal data: **2**·0.5thf: $C_{32}H_{35}F_{15}N_3O_{3.5}Sm$, M = 952.98, triclinic, space group $P\bar{1}$, a = 10.745(1), b = 10.773(1), c = 18.216(2) Å, α = 98.42(1), β = 95.81(1), γ = 114.02(1), V = 1874.8 Å^3, Z = 2, T = 203 K, μ = 16.79 cm^{-1}. The N–H hydrogens were located from the difference map and refined with free coordinates and fixed isotropic temperature factors (0.08 Å^2). The atoms of the solvent thf were refined isotropically at 1/2 occupancy. The final refinement (7673 reflections collected, 6535 independent) included anisotropic thermal parameters on all non-hydrogen atoms (except for atoms of the solvent thf) and converged to $R1$ = 0.0404 and $wR2$ = 0.1165.

3: $C_{27}H_{27}F_{15}N_3Si_3Sm$, M = 913.14, triclinic, space group $P\bar{1}$, a = 10.196(4), b = 10.868(4), c = 16.461(7) Å, α = 94.96(1), β = 107.33(1), γ = 95.26(1), V = 1721.4(12) Å^3, Z = 2, T = 198 K, μ = 19.16 cm^{-1}. The final refinement (5381 reflections collected, 4479 independent) included anisotropic temperature factors on all non-hydrogen atoms and converged to $R1$ = 0.0556 and $WR2$ = 0.1341.

5·C_6H_5Me: $C_{50}H_{16}F_{30}N_3Nd$, M = 1372.90, monoclinic, space group $P2_1/c$, a = 22.964(4), b = 8.712(2), c = 24.927(4) Å, β = 107.47(1), V = 4757 Å^3, Z = 4, T = 198 K, μ = 12.52 cm^{-1}. The final refinement (7834 reflections collected, 6217 independent) included anisotropic thermal parameters on all non-hydrogen atoms and converged to $R1$ = 0.0577 and wR_2 = 0.1015.

1 J. D. Scollard, D. H. McConville, N. C. Payne and J. J. Vittal, *Macromolecules*, 1996, **29**, 5241; R. Baumann, W. M. Davis and R. R. Schrock, *J. Am. Chem. Soc.*, 1997, **119**, 3830.
2 A. R. Johnson, W. M. Davis, C. C. Cummins, S. Serron, S. P. Nolan, D. G. Musaev and K. Morokuma, *J. Am. Chem. Soc.*, 1998, **120**, 2071.
3 A. L. Odom, P. L. Arnold and C. C. Cummins, *J. Am. Chem. Soc.*, 1998, **120**, 5836; P. Roussel and P. Scott, *J. Am. Chem. Soc.*, 1998, **120**, 1070.
4 C. Rosenberger, R. R. Schrock and W. M. Davis, *Inorg. Chem.*, 1997, **36**, 123; H. Memmler, U. Kauper, L. H. Gade, I. J. Scowen and M. McPartlin, *Chem. Commun.*, 1996, 1751.
5 Review article: R. Anwander, *Top. Curr. Chem.*, 1996, **179**, 33. See also: (*a*) R. K. Minhas, Y. Ma, J-I. Song and S. Gambarotta, *Inorg. Chem.*, 1996, **35**, 1866; (*b*) W. J. Evans, M. A. Ansari, J. W. Ziller and S. I. Khan, *Inorg. Chem.*, 1996, **35**, 5435.
6 H. Sasai, S. Arai and M. Shibasaki, *J. Org. Chem.*, 1994, **59**, 2661.
7 O. Just, A. C. Greenwald and W. S. Rees, Jr., *Mater. Res. Soc. Symp. Proc.*, 1996, **415**, 111.
8 D. C. Bradley, J. S. Ghotra and F. A. Hart, *J. Chem. Soc., Dalton Trans.*, 1973, 1021.
9 Examples of M···F interactions: H. Memmler, K. Walsh, L.H. Gade and J. W. Lauher, *Inorg. Chem.*, 1995, **34**, 4062; A. R. Siedle, R. A. Newmark, W. M. Lamanna and J. C. Huffman, *Organometallics*, 1993, **12**, 1491.
10 C. A. Hunter, X-J. Lu, G. M. Kapteijn and G. van Koten, *J. Chem. Soc., Faraday Trans.*, 1995, **91**, 2009.
11 H. Schumann, J. Winterfeld, E. C. E. Rosenthal, H. Hemling and L. Esser, *Z. Anorg. Allg. Chem.*, 1995, **621**, 122.
12 D. R. Click, B. L. Scott and J. G. Watkin, unpublished results.
13 R. Koppang, *Acta Chem. Scand.*, 1971, **25**, 3067.
14 G. B. Deacon and Q. Shen, *J. Organomet. Chem.*, 1996, **511**, 1.
15 See, for example: (*a*) F. A. Cotton and W. Schwotzer, *J. Am. Chem. Soc.*, 1986, **108**, 4657; (*b*) H. Liang, Q. Shen, J. Guan and Y. Lin, *J. Organomet. Chem.*, 1994, **474**, 113; (*c*) B. Fan, Q. Shen and Y. Lin, *J. Organomet. Chem.*, 1989, **377**, 51.
16 J. D. Scollard and D. H. McConville, *J. Am. Chem. Soc.*, 1996, **118**, 10 008.

Communication 8/09275C

ChemComm

A noncovalently linked, dynamic fullerene porphyrin dyad. Efficient formation of long-lived charge separated states through complex dissociation

Tatiana Da Ros,[a] Maurizio Prato,*[a] Dirk Guldi,*[b] Enzo Alessio,[c] Marco Ruzzi[d] and Luigi Pasimeni*[d]

[a] *Dipartimento di Scienze Farmaceutiche, Università di Trieste, Piazzale Europa, 1, 34127 Trieste, Italy E-mail: prato@univ.trieste.it*
[b] *Radiation Laboratory, University of Notre Dame, Notre Dame, IN 46656, USA*
[c] *Dipartimento di Scienze Chimiche, Università di Trieste, Italy*
[d] *Dipartimento di Chimica Fisica, Università di Padova, Italy*

Received (in Cambridge, UK) 25th January 1999, Accepted 3rd March 1999

Photoexcitation of a Zn–tetraphenyl porphyrin–fullerene complex leads to electron-transfer with very long lifetimes of the charge-separated pairs.

Photoactive supramolecular systems, in which a donor and an acceptor moieties are non-covalently linked, are particularly appealing either as models for natural photosynthesis and for the conversion of light into electric current.[1–3] In essence, a rapid photoinduced electron-transfer (ET) should be followed by a diffusional splitting of the charge-separated radical pair, thus mimicking a key step in photosynthesis. Here, we describe the assembly of a rigidly connected dyad, in which a zinc tetraphenyl porphyrin [Zn(TPP)] is non-covalently linked to a C_{60} fullerene derivative *via* axial pyridine coordination to the metal.[4–6] Information associated with the photoprocesses has been achieved by optical spectroscopy, in full agreement with time-resolved EPR spectroscopy.

Ligand **2** (Scheme 1) was prepared by azomethine ylide cycloaddition to C_{60},[7,8] using sarcosine and 4-pyridine aldehyde as the starting materials.[9] Semiempirical (PM3) minimization gives 4.5 Å for edge-to-edge distance between the chromophores or 9.5 Å for center-to-center distance.

The absorption spectrum of Zn(TPP) (**1**) was measured at increasing concentrations of fullerene ligand **2** in different solvents. In non-coordinating solvents, such as toluene and dichloromethane, the spectra reveal a noticeable red-shift of the two Q-bands (in CH_2Cl_2: 548 → 559 nm; 588 → 598 nm), as well as a minor broadening of the Soret band. This effect is commonly attributed to the formation of pyridine-Zn(TPP) complexes.[10] In contrast, a similar addition of methanofullerene **4** or pyrrolidine **5** does not affect the porphyrin ground state absorption and, accordingly, the spectra of **1** and the respective fullerene derivative become virtually superimposable. In the more polar and coordinating solvents THF and benzonitrile, no dependence was observed of the spectral features of **1** from fullerene **2** concentrations, indicating a competition in the coordination of Zn between the fullerenic pyridine and the solvent. The ^{1}H NMR spectrum of a 1 : 1 mixture (3×10^{-3} M) of **1** and **2** in $CDCl_3$ shows that the pyridine 2-protons are shifted to δ 3.6 (from δ 8.7 in pure **2**), confirming that coordination of the Zn metal occurs through the pyridine nitrogen and not the pyrrolidine nitrogen, leading to **3** (Scheme 1).

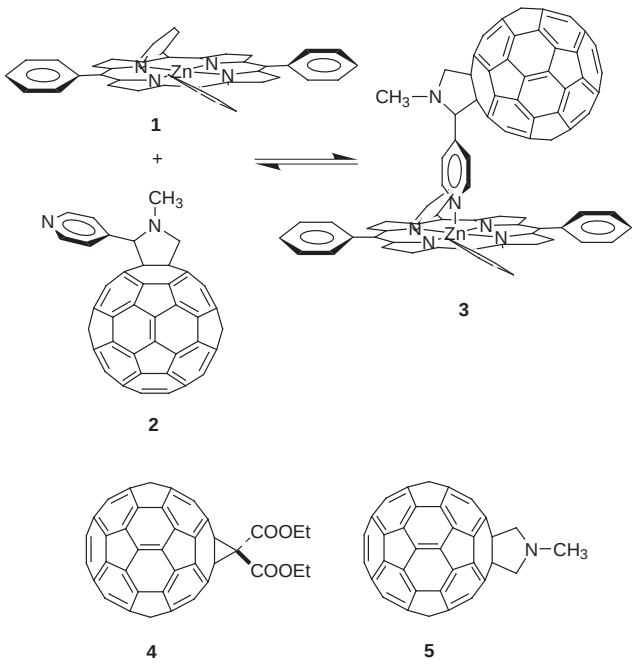

Scheme 1

Zn(TPP) displays a high lying (2.06 eV) and strongly emitting (Φ = 0.04) singlet excited state, $^1(\pi$–$\pi^*)$ Zn(TPP).[11] However, substantially lower emission yields were noticed upon excitation of (**1** + **2** ⇌ **3**) in solution relative to the Zn(TPP) reference. The emission quantum yields of the $^1(\pi$–$\pi^*)$ ZnTPP (**1**) (1.0×10^{-5} M) strongly decreased with progressing fullerene ligand **2** concentrations. Toluene and dichloromethane solutions of **1**, in the presence of 1.3×10^{-5} M **2**, gave rise to quantum yields (Φ) of 0.0156 and 0.0152, respectively. These values refer to kinetics much faster than diffusion, thus pointing toward intramolecular processes.

Time-resolved photolysis was carried out to complement the steady-state experiments and to characterize the resulting photoproducts. Irradiation into the porphyrin Q-bands yielded the characteristic $^1(\pi$–$\pi^*)$ Zn(TPP) absorptions, which decayed (τ = 2.5 ns), in the absence of any fullerene ligand **2**, into the energetically lower lying $^3(\pi$–$\pi^*)$ Zn(TPP) state (1.53 eV). A systematic addition of fullerene ligand **2** led to a substantial reduction of the singlet state lifetime. More importantly, the $^1(\pi$–$\pi^*)$ Zn(TPP) transforms into a new product with broad absorption features between 600 and 800 nm, which is a known characteristic for a one-electron oxidized porphyrin, [Zn(TPP)$^{\cdot+}$]. In addition, the charge-separated radical pair was unequivocally identified *via* the NIR-fingerprint absorption of ($C_{60}^{\cdot-}$) at 1010 nm.

While the insufficient polarity of toluene prevents an appreciable stabilization of the radical pair, in moderately polar dichloromethane a lifetime of 8.6 μs was measured. In contrast, parallel experiments using **4** or **5** instead of **2** did not result in any measurable ($C_{60}^{\cdot-}$)/[Zn(TPP)$^{\cdot+}$] absorptions.

In benzonitrile and THF, differential absorption changes in the NIR reveal the participation of two components in the formation of the ($C_{60}^{\cdot-}$). The faster process clearly evolves from an intramolecular ET process, while the slower one involves intermolecular quenching of the lower lying $^3(\pi$–$\pi^*)$ Zn(TPP) state. For the bimolecular quenching reaction a rate constant of 1.7×10^{10} dm^3 mol^{-1} s^{-1} was resolved. Kinetic

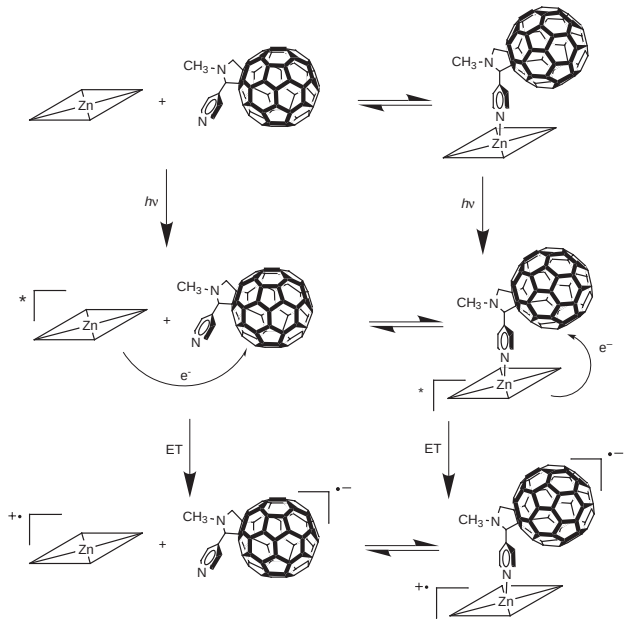

Scheme 2

analysis of the 1010 nm transient absorption ($C_{60}^{\bullet-}$) gives rise to a remarkable lifetime of the separated radical pair in deoxygenated benzonitrile of several hundred microseconds.

According to the above results, two different pathways can be envisioned for the ET processes (Scheme 2). The excitation of the porphyrin chromophore is followed by fast intramolecular ET inside the complex (right-hand pathway in Scheme 2). Alternatively, the free porphyrin is excited, undergoing intermolecular ET when the acceptor molecules approach closely enough during the molecular diffusion (left hand side pathway in Scheme 2). The former process is likely to occur in all solvents. However, in coordinating media, the solvent can displace **2** from the Zn metal, thus making intermolecular ET more effective. This latter ET process is slow enough to allow the excited porphyrin to convert from the singlet to triplet state by ISC.

Experiments performed by time resolved EPR (TREPR) fully support the mechanisms proposed in Scheme 2. The TREPR spectrum of (**1** + **2** ⇌ **3**) dissolved in THF (1×10^{-4} M) and detected at 180 K with 1 μs delay from the laser pulse is shown in Fig. 1. The spectrum consists of a broad signal superimposed to a narrow derivative-like EPR signal, displaying A/E spin polarization pattern (A and E mean absorption and emission), that is assigned to the singlet-born spin correlated radical pair (SCRP),[12,13] arising here from the CS state ($C_{60}^{\bullet-}$)/[Zn(TPP)$^{\bullet+}$] inside the complex and generated by intramolecular electron transfer. The spin system responsible for the narrow signal is described as two unpaired electrons weakly coupled by small spin exchange and electron–electron dipolar interactions, characterized by *J* and *D* constants, respectively. The spectrum is given by two doublets of lines with antiphase spin polarization pattern.[12] In our case, the low-field doublet is centered at the *g* value of ZnTPP$^{\bullet+}$ radical cation (2.0026)[14] and the high-field doublet at the *g* value of $C_{60}^{\bullet-}$ radical anion (1.9986).[15] The effect of the unresolved hyperfine interaction is taken into account by a linewidth contribution to the spectrum lines. Estimated linewidths are 1 and 0.1 mT for $C_{60}^{\bullet-}$ and Zn(TPP)$^{\bullet+}$, respectively.[14,15] Since Zn(TPP)$^{\bullet+}$ radical cation has a large inhomogeneous linewidth, while that of the fullerene (with little hyperfine interaction due to protons) is much smaller, the doublet due to the porphyrin radical cation is practically undetectable in the spectrum. Experimental and calculated spectra due to ($C_{60}^{\bullet-}$)/[Zn(TPP)$^{\bullet+}$] singlet-born SCRP are shown in Fig. 1.

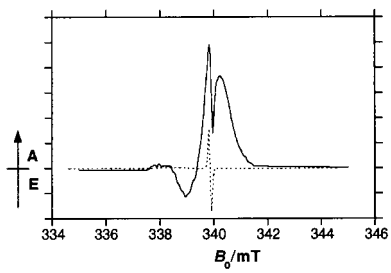

Fig. 1 TREPR spectrum (solid line) observed 1 μs after the laser pulse excitation of (**1** + **2** ⇌ **3**) dissolved in THF at 180 K. A Lambda Physik LPX 100 XeCl excimer laser (λ = 308 nm, 10 mJ pulse^{-1}) fed a Rhodamin G6 dye laser with emitting light at 581 nm (pulse duration 20 ns). The signal was taken directly from the microwave preamplifier immediately after the detection diode and fed into a EG&G Boxcar Averager mod. 162 equipped with a mod. 164 plug-in. It was operative with an integration window of 50 ns. Positive and negative signals indicate absorptive (A) and emissive (E) polarizations, respectively. Microwave frequency: $\omega/2\pi$ = 9.5256 GHz. Microwave field: B_1 = 0.023 mT.

The broad spectrum of Fig. 1 is attributed to the triplet-born radical ion pair[16] that is generated by intermolecular electron transfer between unlinked Zn(TPP)$^{\bullet+}$ cation and $C_{60}^{\bullet-}$ anion mediated by solvent molecules and stabilized by Coulomb attraction. Details on the spectrum simulation will be reported elsewhere. The separation between the outermost lines amounts to 2|*D*|, where *D* represents the dipolar coupling constants. If the classical expression of the point dipole model is used for *D*, from the measured value of $D = -1.72$ mT the estimated center-to-center distance of 11.7 Å between cation and anion is obtained.

The narrow transient signal detected at 339.9 mT was fitted by a single exponential function with decay time constant of 12 μs, this value being in good agreement with that measured by optical methods (11 μs, 1×10^{-5} M in THF).

This work was supported in part by the Office of Basic Energy Sciences of the US Dept. of Energy, by MURST (Italy), by CNR through the program 'Materiali Innovativi (legge 95/95)' and the European Commission (DG XII) through Brite-Euram III Contract BRPR-CT97-0564. This is contribution No. NDRL-4070 from the Notre Dame Radiation Laboratory.

Notes and references

1 J. L. Sessler, B. Wang, S. L. Springs and C. T. Brown, in *Comprehensive Supramolecular Chemistry*, ed. J. L. Atwood, J. E. D. Davies, D. D. MacNicol, F. Vögtle and Y. Murakami, Pergamon, Oxford, UK, 1996, p. 311.
2 T. Hayashi and H. Ogoshi, *Chem. Soc. Rev.*, 1997, **26**, 355.
3 M. D. Ward, *Chem. Soc. Rev.*, 1997, **26**, 365.
4 The use of donors and acceptors interacting through metal coordination was first reported by Sanders and coworkers: C. Hunter, J. Sanders, G. Beddard and S. Evans, *J. Chem. Soc., Chem. Commun.*, 1989, 1765.
5 J. Otsuki, K. Harada, K. Toyama, Y. Hirose, K. Araki, M. Seno, K. Takatera and T. Watanabe, *Chem. Commun.*, 1998, 1515.
6 N. Armaroli, F. Diederich, L. Echegoyen, T. Habicher, L. Flamigni, G. Marconi and J.-F. Nierengarten, *New J. Chem.*, 1999, 77.
7 M. Maggini, G. Scorrano and M. Prato, *J. Am. Chem. Soc.*, 1993, **115**, 9798.
8 M. Prato and M. Maggini, *Acc. Chem. Res.*, 1998, **31**, 519.
9 M. Prato, M. Maggini, C. Giacometti, G. Scorrano, G. Sandonà and G. Farnia, *Tetrahedron*, 1996, **52**, 5221.
10 J. Fujisawa, K. Ishii, Y. Ohba, S. Yamauchi, M. Fuhs and K. Möbius, *J. Phys. Chem. A*, 1997, **101**, 5869.
11 S. L. Murov, I. Carmichael and G. L. Hug, *Handbook of Photochemistry*, Marcel Dekker, New York, 1993.
12 C. D. Buckley, D. A. Hunter, P. J. Hore and K. A. McLauchlan, *Chem. Phys. Lett.*, 1987, **135**, 307.
13 J. R. Norris, A. L. Morris, M. C. Thurnauer and J. J. Tang, *J. Chem. Phys.*, 1990, **92**, 4239.
14 J. Fajer, D. C. Borg, A. Forman, D. Dolphin and R. H. Felton, *J. Am. Chem. Soc.*, 1970, **92**, 3451.
15 D. Carbonera, M. Di Valentin, C. Corvaja, G. Agostini, G. Giacometti, P. A. Liddell, D. Kuciauskas, A. L. Moore, T. A. Moore and D. Gust, *J. Am. Chem. Soc.*, 1998, **120**, 4398.
16 J. Schlüpmann, K. M. Salikhov, M. Plato, P. Jägermann, F. Leudzian and K. Möbius, *Appl. Magn. Reson.*, 1991, **2**, 117.

Communication 9/00645A

Bis(ferrocenyl)porphyrins. Compounds with strong long-range metal–metal coupling†

Peter D. W. Boyd,[b] Anthony K. Burrell,*[a] Wayne M. Campbell,[a] Paul A. Cocks,[c] Keith C. Gordon,[c] Geoffrey B. Jameson,[a] David L. Officer*[a] and Zhongde Zhao[b]

[a] *IFS - Chemistry, Massey University, Private Bag 11222, Palmerston North, New Zealand. E-mail: A.K.Burrell@massey.ac.nz*
[b] *Chemistry Department, The University of Auckland, Auckland, New Zealand*
[c] *Chemistry Department, University of Otago, PO Box 56, Dunedin, New Zealand*

Received (in Cambridge, UK) 26th January 1999, Accepted 4th March 1999

The condensation of a dipyrromethane with ferrocene aldehyde leads to a single atropisomer of α,α-5,15-bis(ferrocenyl)-2,8,12,18-tetrabutyl-3,7,13,17-tetramethylporphyrin 1; electrochemistry of 1 and Ni-1 reveals two consecutive ferrocene-based one-electron oxidation waves, which are separated by 0.19 and 0.41 V, respectively.

Discrete systems in which remote sites are electronically coupled have exciting possibilities for applications in molecular electronic devices.[1] However, despite much effort, particularly with compounds containing two connected ferrocene moieties,[2] useful devices have not yet been forthcoming. This is primarily because communication between the electronic (especially the redox) states at the two sites decreases rapidly with distance. Recent studies have identified a combination of factors that influence communication between connected ferrocene moieties, including the type of connection,[2] the length of the connector[3] and the orientation of the two ferrocenes.[4] Here, we report the synthesis, structure and properties of a bis(ferrocenyl)porphyrin **1** in which these factors are synergistically combined to give unprecedented strong coupling between the ferrocene moieties.

Porphyrin **1**‡ is formed in a classical condensation reaction between ferrocene aldehyde and a tetraalkyl dipyrromethane. The insertion of nickel gives Ni-**1**.§ To our surprise, compound **1** is formed as a single isomer in high yield (58%), with both ferrocenyl groups in a *syn* (or α,α-atropisomer) configuration with respect to the porphyrin macrocycle. The *anti* product, the α,β-atropisomer, is not observed. CPK-model studies indicate that the porphyrinogen conformation which leads to the α,α-isomer is the least sterically congested and thereby the most accessible to chemical oxidation to form **1**. This preference has not been observed previously and is a direct result of the unique steric requirements of the ferrocenyl moiety. Upon oxidation of the porphyrinogen, the methyl groups in the β-pyrrolic positions offer sufficient steric hindrance to prevent any isomerisation.

The geometry was confirmed by single-crystal structure determinations of **1**¶ [Fig. 1(a)] and its nickel(II)-substituted derivative Ni-**1**¶ [Fig. 1(b)]. The large steric bulk of the ferrocenyl moiety at opposite *meso* positions, clashing with the β-methyl substituents, not only prevents rotation of the ferrocenyl moiety but leads to a strongly ruffled porphyrin core. However, comparison of **1** and Ni-**1** reveals that the ferrocenyl moieties are not rigidly locked in a single conformation. Indeed the conformational disorder shown by Ni-**1** in the *solid state* provided further indication of the restricted conformational flexibility of the ferrocene groups, relevant to solution-state conformational flexibility and to the distinctive electrochemistry shown by these compounds.

The electrochemistry of **1** and Ni-**1** [Fig. 2(d)] shows two consecutive ferrocene-based one-electron oxidation waves

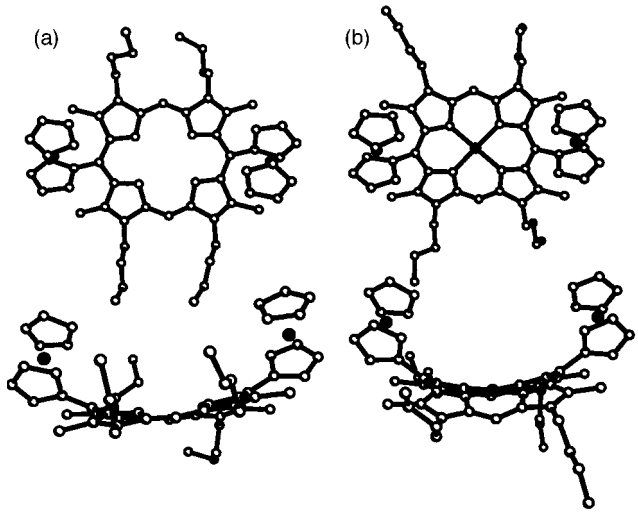

Fig. 1 Molecular structures of **1** (a) and the major conformation of Ni-**1** (b). The top view looking down on the porphyrin plane, showing the twist of the ferrocenyl moieties; the bottom view is side-on to the porphyrin plane, showing the distortions of the porphyrin ring.

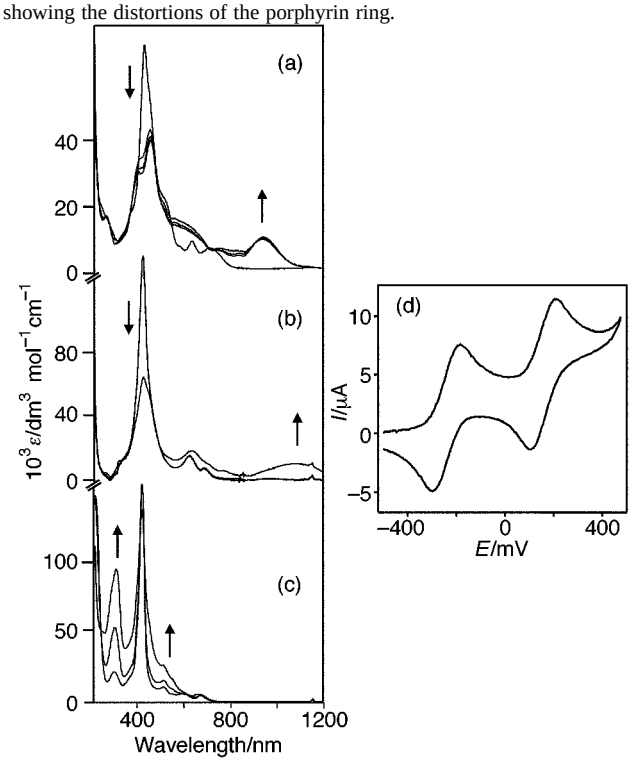

Fig. 2 Spectro-electrochemical UV–VIS spectra of Na-**1** (a), **1** (b) and **3** (c); arrows indicate direction of change in peaks during oxidation. (d) Cyclic voltammogram of Ni-**1** in CH_2Cl_2 at room temperature, $E°$/ *versus* Fc/Fc$^+$.

† The authors would like to dedicate this paper to Professor Warren R. Roper on the occasion of his 60th birthday.

separated by 190 and 410 mV, respectively. Spectroelectrochemical UV–VIS studies of **1** and Ni-**1** reveal that both show the growth of an absorption at 1080 and 946 nm, respectively [Fig. 2(a) and (b)], with single electron oxidation. These are assigned as intravalence charge-transfer (IVCT) bands. Further oxidation leads to depletion of these features. The behaviour of **1** and Ni-**1** may be contrasted to that of the sterically less congested reference compound **3**.‖ This compound shows a single two-electron ferrocene oxidation[7] and no near-IR absorption when oxidised [Fig. 2(c)]. From the separation of oxidation waves in **1** and Ni-**1** a conproportionation constant (K_c) of 1.6×10^3 for **1** and 8.5×10^6 for Ni-**1** is calculated,[6] indicating strong coupling of the ferrocene moieties. The small bandwidth of the IVCT band for the Ni-**1**$^+$ complex ($\Delta\nu_{\frac{1}{2}} = 1400$ cm^{-1}) suggests that it is a class III (highly localised) mixed-valence species,[7] consistent with the large value of K_c. For **1**, $\Delta\nu_{\frac{1}{2}} = 2600$ cm^{-1}, suggesting a class II/III behaviour.[6]

For **1** and Ni-**1** the coupling between ferrocene units, at a separation of > 10 Å, is remarkably high. Biferrocene shows an oxidation-wave peak splitting of only 330 mV where the ferrocenyl irons are < 5.4 Å distant,[8] and **3**, where a ferrocene–ferrocene distance of at least 10 Å can be estimated, has no observable coupling. Such strong coupling between the two ferrocenes was largely unexpected, as the related 5,10,15,20-tetraferrocenylporphyrin **2** and 5,15-diferrocenyl-10,20-di-*p*-tolylporphyrin **3**[9] display no such coupling. These porphyrins, however, lack substituents at the β-pyrrolic positions, and the ferrocenyl moieties are free to rotate, as evidenced by ^{1}H NMR spectroscopy.

A density functional calculation,** seeking to establish a basis for the origin of differences between **2**, **3** and **1** (and Ni-**1**), was carried out on the monocation **1**$^+$. The singly occupied HOMO in this system is delocalised over both ferrocene moieties and is composed of ferrocene (xy, $x^2 - y^2$, e_{2g}) Fe d orbitals and the porphyrin a_{2u} π molecular orbital. The separation between the positive and negative combination of these orbitals has been proposed to be related to the strength of coupling between ferrocene centres in mixed-valence systems.[3,10] In this case the difference in energy for the alpha spin orbitals is *ca.* 0.1 eV. This strong coupling appears to be the result of extensive mixing of both ferrocenyl molecular orbital systems with that of the porphyrin connector π system, as is apparent in the diminished intensity of the Soret band at 410 nm for **1** and Ni-**1** but not **3** upon oxidation.

The low symmetry of **1** and Ni-**1** (at best C_{2v}), the possibility of extensive vibronic coupling as a result of the restricted rotational flexibility of the ferrocenyl groups propagating into distortions of the porphyrin core, and the molecular dipole created by the α,α-atropisomer are all possible factors that may underpin the strong coupling. A thorough study of this system will be made in order to determine (i) the factors that lead to the very strong coupling and (ii) the extent to which this communication between two ferrocenyl moieties can be modified and exploited. For now, these results show for the first time in diferrocenylporphyrin systems that strong coupling can be created between remote centres using the porphyrin core as a connector.

We are grateful to The Public Good Science Fund (MAU602 and MAU809), the University of Auckland Research Committee and the Marsden Fund of New Zealand (UOA613) for support of this work and to Dr Cliff Rickard and The University of Auckland for X-ray data collection.

Notes and References

‡ Electrochemical data, CH_2Cl_2 solution, at room temperature, $E^{0\prime}$ *vs.* Fc/Fc$^+$ (peak separation/mV; I_A/I_c): −0.27 (120, 1.0), −0.08 (100; 1.0).

§ Electrochemical data, CH_2Cl_2 solution, at room temperature, $E^{0\prime}$ *versus* Fc/Fc$^+$ (peak separation/mV; I_A/I_c): −0.24 (110; 1.0), 0.17 (100; 1.0).

¶ *Crystal data*: **1**·CH_2Cl_2: $C_{61}H_{72}Cl_2Fe_2N_4$, M_r = 1043.83, triclinic, space group $P\bar{1}$, a = 13.722(3), b = 14.908(3), c = 15.368(3) Å, α = 73.49(3), β = 87.40(3), γ = 62.68(3)°, V = 2664.6(9) Å^3, Z = 2, D_c = 1.301 Mg m^{-3}, μ = 0.688 mm^{-1}, Enraf-Nonius CAD-4 diffractometer, Mo-Kα radiation (λ = 0.71073 Å), red crystal (0.11 × 0.11 × 0.31 mm), data collection range 4.0–40.0°, $0 \leqslant h \leqslant 13$, $-12 \leqslant k \leqslant 14$, $-14 \leqslant l \leqslant 14$, reflections collected 5249, unique 4967 [R_{int} = 0.0896]. The structure was solved by direct methods and refined by a full-matrix least-squares procedures to give final residuals of GOF = 0.987, parameters = 623, R_1 = 0.0586 [2219 data with $I > 2\sigma(I)$], wR_2 = 0.1645 (all data). The largest residual electron densities were 0.568 and −0.438 e Å^{-3}.

Ni-**1**·0.25H_2O: $NiC_{60}H_{68}Fe_2N_4O_{0.25}$, M_r = 1019.78, tetragonal, space group $I4_1/a$, a = 28.5339(2), c = 24.6067(1) Å, V = 20034.4(2) Å^3, Z = 16, D_c = 1.352 Mg m^{-3}, μ = 0.988 mm^{-1}, Seimens Smart diffractometer, Mo-Kα radiation (λ = 0.71073 Å), red crystal (0.10 × 0.09 × 0.28 mm), data collection range 16–46.5°, $-21 \leqslant h \leqslant 22$, $-27 \leqslant k \leqslant 31$, $0 \leqslant l \leqslant 27$, unique reflections 6852. Two distinct conformations are apparent. Thus, bond distances, bond angles and planarity associated with the substituted pyrrolic and ferrocenyl moieties were restrained to common values for the chemically approximately equivalent parameters, while permitting conformational flexibility at the *meso* positions, utilising the features of SHELXL-96 (G. M. Sheldrick SHELXL-96. Institut für Anorganische Chemie der Universität Göttingen, Germany, 1997) final values conform closely to expected values (J. L. Hoard, in *Porphyrins and Metalloporphyrins*, ed. K. M. Smith, Elsevier, Amsterdam, 1975, ch. 8) and the Ni is properly centred in the porphyrin hole for each conformation with relative occupancies of 0.684(5) and 0.316. Final values of residuals: GOF = 1.066, R_1 [4023 data with $F > 4\sigma(F)$] = 0.0805, wR_2 (all data) = 0.2036 for a model described by 1193 variable parameters and 3511 restraints on geometry and thermal motion. The largest residual electron densities were 0.356 and −0.335 e Å^{-3}.

CCDC 182/1186. See http://www.rsc.org/suppdata/cc/1999/637/ for crystallographic files in .cif format.

‖ 5,15-Diferrocenyl-10,20-ditolylporphyrin **3**, was prepared from tolyl dipyrromethane and ferrocene aldehyde using standard methods (F. Li, K. Yang, J. S. Tyhonas, K. A. MacCrum and J. S. Lindsey, *Tetrahedron*, 1997, **53**, 12339).

** A density functional calculation of the electronic structure of the singly oxidised **1**$^+$ was performed using the Amsterdam Density Functional program (ADF 2.3.0, Theoretical Chemistry, Vrije Universiteit, Amsterdam (E. J. Baerends, D. E. Ellis and P. Ros, *Chem. Phys.*, 1973, **2**, 41; G. te Velde and E. J. Baerends, *J. Comput. Phys.*, 1992, **99**, 84). The molecular geometry used in the calculation was taken from the X-ray crystal structure of **1**, with butyl substituents replaced by methyl groups. Double-ξ Slater-type basis sets were used for C(2s, 2p), N(2s, 2p) and H(1s) augmented by a single 3d polarisation function. A triple-ξ basis set was used for Fe (3s, 3p, 3d, 4s). The inner electron configurations were assigned to the core and were treated using the frozen core approximation. The calculation was spin unrestricted and used the local density approximation (S. H. Vosko, L. Wilk and M. Nusair, *Can. J. Phys.*, 1980, **58**, 1200) with non-local corrections for exchange (A. D. Becke, *Phys. Rev. A*, 1988, **38**, 3098) and with nonlocal corrections for correlation (C. Lee, W. Yang and R. G. Parr, *Phys. Rev. B*, 1988, **37**, 785).

1 A. J. Bard, *Pure Appl. Chem*., 1971, **25**, 379; R. M. Metzger and C. A. Panetta, *New J. Chem*., 1991, **15**, 209.
2 L. M. Tolbert, X. Zhao, Y. Ding and L. A. Bottomley, *J. Am. Chem. Soc*., 1995, **117**, 12 891.
3 A.-C. Ribou, J.-P. Launay, A. L. Sachtleben, H. Li and C. W. Spangler, *Inorg. Chem*., 1996, **35**, 3755.
4 C. Patoux, C. Coudret, J.-P. Launay, C. Joachim and A. Gourdon, *Inorg. Chem*., 1997, **36**, 5037.
5 J. L. Sessler, M. R. Johnson, S. E. Creager, J. C. Fettinger and J. A. Ibers, *J. Am. Chem. Soc*., 1990, **112**, 9310.
6 C. Creutz, *Prog. Inorg. Chem*., 1983, **30**, 1; S. Barlow and D. O'Hare, *Chem. Rev*., 1997, **97**, 637.
7 A. R. Rezvani, C. E. B. Evans and R. J. Crutchley, *Inorg. Chem*., 1995, **34**, 4600.
8 W. H. Morrison, S. Krogsrud and D. N. Hendrickson, *Inorg. Chem*., 1973, **12**, 1998.
9 N. L. Loim, N. V. Abromova and V. I. Sokolov, *Mendeleev Commun*., 1996, 46.
10 M. D. Newton, *Chem. Rev*., 1991, **91**, 767; C. Joachim, J.-P. Launay and S. Woitellier, *Chem. Phys*., 1990, **147**, 131; S. Larsson, *J. Am. Chem. Soc*., 1981, **103**, 4034; P. Siddarth and R. A. Marcus *J. Phys. Chem*., 1990, **94**, 2985; C. Patoux, J.-P. Launay, M. Beley, S. Chodorowski-Kimmes, J.-P. Collin, S. James and J.-P. Sauvage, *J. Am. Chem. Soc*., 1998, **120**, 3717.

Communication 9/00691E

ChemComm

Controlled synthesis of heterotetranuclear complexes

Paul E. Kruger, Frederic Launay and Vickie McKee*

Chemistry Department, Queen's University, Belfast, UK BT9 5AG. E-mail: v.mckee@qub.ac.uk

Received (in Basel, Switzerland) 18th January 1999, Accepted 1st March 1999

Template synthesis of a macrocyclic complex containing two copper(II) ions and two vacant coordination sites permits controlled access to a heterotetranuclear $Cu^{II}_2Ni^{II}_2$ complex without scrambling of the metal ions.

Heteronuclear complexes of the dinucleating 'Robson-type' macrocycles[1] have been known for many years.[2] Most commonly, these complexes are synthesised using ligands with dissimilar binding sites in either the final macrocyclic product or in a key non-cyclic intermediate in a stepwise synthesis. Here, we report a route for the controlled synthesis of heterotetranuclear complexes of a macrocycle with four identical binding sites.

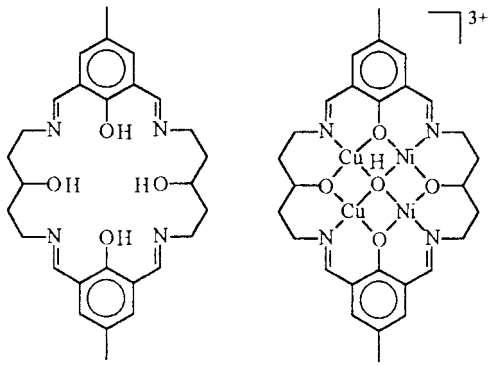

H_4L^1 $[Cu_2Ni_2(L^1)OH]^{3+}$

Previous work using the ligand H_4L^1 has established the template formation of planar tetracopper(II)[3,4] and tetranickel(II)[5] complexes. The metal ions are separated by *ca.* 3 Å and interact through phenoxo and alkoxo bridges as well as through a central μ_4-OH ion. In tetracopper(II) complexes, the central μ_4-hydroxo moiety can be replaced by two 1,1-azido ligands to yield $[Cu_4(\mu\text{-}N_3)_2(L^2)(N_3)_2]\cdot 2MeOH$.[4] The geometry of the tetracopper(II) array is only slightly modified to allow the azide bridges to lie one on either side of the macrocyclic plane. Incorporation of a larger bridge might be expected to force the copper ions apart, disrupting the planarity of the complex.

Schiff-base condensation of 2,6-diformyl-4-methylphenol (dfmp) and 1,5-diamino-3-hydroxypentane (dahp) in the presence of $Cu(BF_4)_2\cdot 6H_2O$ and pyrazole (Hpyr) (mole ratios dfmp : dahp : Cu^{2+} : Hpyr = 1 : 1 : 2 : 1) in 1 : 1 methanol–ethanol, yielded a green powder. On recrystallisation by diethyl ether diffusion from acetonitrile containing excess pyrazole, two crystalline macrocyclic products were obtained. The major component (*ca.* 80%) consists of red–green dichroic crystals of formula $[Cu_2(\mu\text{-pyr})(H_3L^1)](BF_4)_2\cdot MeCN$ (**1**·MeCN), a minor amount (*ca.* 5%) of a dark green complex, $[Cu_4(\mu\text{-pyr})_2(L^1)](BF_4)_2$ **2** was also isolated. Both complexes have been characterised by single crystal structure analysis.†

The cation of complex **1**, $[Cu_2(\mu\text{-pyr})(H_3L^1)]^{2+}$, is a dicopper complex in which the copper ions are bridged by an alkoxo oxygen (O2) and a pyrazolate ion (Fig. 1). It can be viewed as resulting from the previously characterised $[Cu_4(L^n)(OH)]^{3+}$ core by loss of two copper ions and replacement of the central hydroxide by pyrazolate. The macrocyclic ligand is only monodeprotonated but, as observed in related systems,[6–8] the phenolic protons have transferred to the non-coordinated imine groups; these protons were located in the structure refinement. The cation thus has two vacant (if protonated) coordination sites, somewhat blocked by the presence of the pyrazolate ligand. The geometry at each copper ion shows a tetrahedral distortion from square planar which is necessary to accommodate the two-atom bridge. The Cu···Cu distance of 3.246(1) Å is somewhat shorter than the values found in other dicopper systems linked by the same two bridges (3.34–3.30 Å).[9,10] A marked twist in the saturated section of the macrocycle is similar to that observed in a non-cyclic structure with the same donor set[10] and is therefore likely to be imposed by the bridges rather than the cyclic nature of the ligand. Intermolecular π–π stacking involving both the macrocyclic π-systems is evident (interplanar distances 3.4–3.6 Å), as an intramolecular H–π interaction where the alcohol proton lies directly over the centre of the pyrazolate ring (H–ring centroid 2.18 Å). There are no significant interactions involving the acetonitrile solvate or BF_4^- anions.

The tetranuclear cation of **2** (Fig. 2) sits on a centre of inversion; bridging pyrazolate groups lie above and below the plane of the macrocycle, each linking a pair of copper ions which are also bridged by an alkoxo group. The mean planes of the pyrazolate ions are parallel, one on either side of the macrocycle, and are inclined at 46.4(2)° to the plane of the eight macrocyclic donors. The Cu(1)···Cu(2) and Cu(1)···Cu(1A) distances are 3.254(2) and 3.133(1) Å respectively, compared to 2.953(1) and 3.000(1) Å in the $[Cu_4(L^1)(OH)](NO_3)_3\cdot 3H_2O$ complex.[3] The copper ions are essentially four-coordinate, although Cu(2) interacts weakly [2.515(6) Å] with a fluorine atom of BF_4^-. Each pair of copper ions is displaced from the plane of the macrocyclic donors towards the coordinated

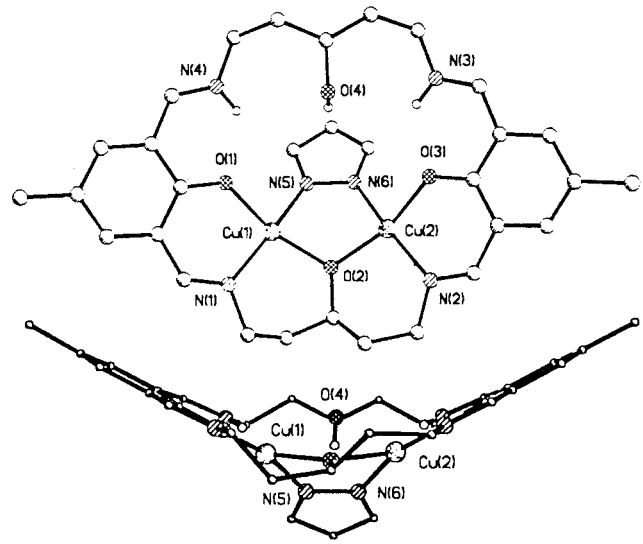

Fig. 1 Perspective views of the $[Cu_2(\mu\text{-pyr})(H_3L^1)]^{2+}$ cation; hydrogen atoms are omitted except for those bonded to oxygen or nitrogen atoms. Selected distances (Å) and angles (°): Cu(1)···Cu(2) 3.246(1), Cu(1)–O(1) 1.921(4), Cu(1)–N(1) 1.939(5), Cu(1)–O(2) 1.930(4), Cu(1)–N(5) 1.943(5), Cu(2)–O(3) 1.938(4), Cu(2)–N(2) 1.950(5), Cu(2)–O(2) 1.933(4), Cu(2)–N(6) 1.960(5); Cu(1)–O(2)–Cu(2) 114.4(2), Cu(1)–N(5)–N(6) 119.5(4), Cu(2)–N(6)–N(5) 118.3(4).

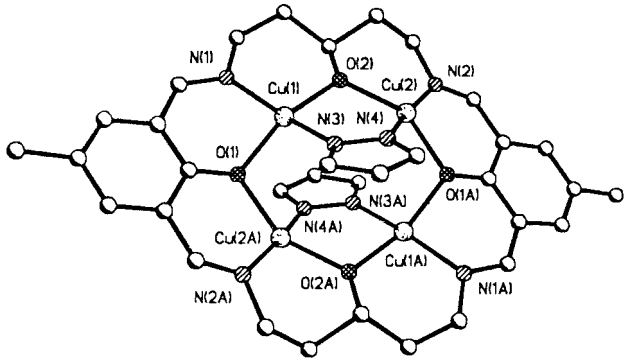

Fig. 2 Perspective view of the $[Cu_4(\mu\text{-pyr})_2(L^1)]^{3+}$ cation. Selected distances (Å) and angles (°): Cu(1)···Cu(2) 3.255(1), Cu(1)–Cu(2A) 3.133(1), Cu(1)–O(1) 1.949(5), Cu(1)–N(1) 1.945(7), Cu(1)–O(2) 1.918(6), Cu(1)–N(3) 1.954(6), Cu(2)–O(1A) 1.973(5), Cu(2)–N(2) 1.942(7), Cu(2)–O(2) 1.950(5), Cu(2)–N(4) 1.945(7); Cu(1)–O(1)–Cu(2A) 106.1(3), Cu(1)–O(2)–Cu(2) 114.6(2), Cu(1)–N(3)–N(4) 119.9(5), Cu(2)–N(4)–N(3) 118.4(5).

pyrazolate ligand and this arrangement causes the coordination geometry at copper to be substantially distorted towards tetrahedral. The resulting steric stress probably responsible for the formation of **1**, where the coordination geometry is more relaxed, as the major product.

Attempts to prepare a pure sample of the dinuclear complex **1**, using a ligand : Cu ratio of 1 : 2 rather than 1 : 4, have not proved successful to date. FAB and IR data are consistent with the suggestion that the initial green product contains the same complex as the crystals of **1** but recrystallised samples always contain a small amount of the tetranuclear complex **2**, suggesting an equilibration between **1** and **2** in solution. Clean samples of the tetranuclear complex can be obtained by treatment of $[Cu_4(L^1)(OH)](BF_4)_3$ with an excess of pyrazole in acetonitrile. In the solid state the two complexes can be distinguished from their IR spectra; **1** shows the expected split imine stretch (1637 and 1657 cm^{-1}) whereas **2** shows a single band at 1631 cm^{-1}. FAB mass spectra of the two complexes are also distinctly different; that of the initial green product shows peaks consistent with a dicopper complex **1**, while complex **2** clearly shows peaks due to tetracopper species.‡

In an attempt to fill the two vacant coordination sites of complex **1**, the crude dicopper complex was treated with an excess of nickel(II) acetate in 1 : 1 methanol–acetonitrile and refluxed overnight. The resulting green complex **3** was characterised from its FAB spectrum (Fig. 3). The spectrum is remarkably simple, showing only two significant clusters centered at *m/z* 807 and 748 which are assigned to $\{[Cu_2Ni_2(L^1)(OH)(MeCO_2)]^{2+}-H^+\}$ and $\{[Cu_2Ni_2(L^1)(OH)]^{+}-2H^+\}$ respectively; the isotope patterns in the

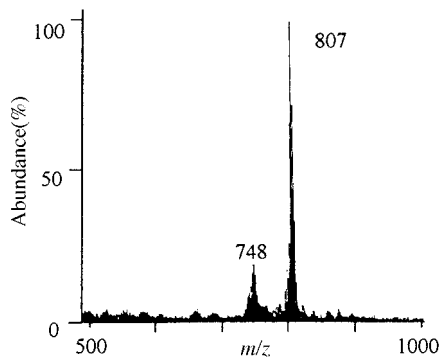

Fig. 3 FAB (SIMS) spectrum of the heterotetranuclear complex $[Cu_2Ni_2(L^1)(OH)(MeCO_2)](BF_4)_2$.

clusters match those predicted.[11] Notably, there are no peaks attributable to scrambled tetranuclear complexes (*e.g.* containing Cu_4, $CuNi_3$, Cu_3Ni or Ni_4 cores) or to unreacted complex **1**. The absence of metal ion scrambling in the FAB, together with the marked preference of tetranickel(II) complexes for bridging acetate groups,[5,12] suggests the structure shown in the scheme, with the addition of an acetate bridge linking the nickel ions is likely to be correct, *i.e.* $[Cu_2Ni_2(L^1)(OH)(MeCO_2)](BF_4)_2$.

This work was supported by EPSRC grant GR/J73773, we are also grateful to the EPSRC Mass Spectrometry Service for FAB (LSIMS) spectra and to QUB for the award of a postgraduate studentship (to F. L.).

Notes and references

† *Crystal data:* both data sets were collected ($4 < 2\theta < 50°$) using Mo-Kα radiation (λ = 0.71073 Å) at 153(2) K, corrected for Lorentz, polarisation and absorption effects. The structures were solved by direct methods[13] and refined by full-matrix least squares on F^2.[14]

1·MeCN: $[Cu_2(\mu\text{-pyr})(H_3L^1)](BF_4)_2\cdot MeCN$, $C_{33}H_{41}B_2Cu_2F_8N_7O_4$, red block, 0.55 × 0.30 × 0.12 mm, monoclinic, a = 8.059(2), b = 21.760(4), c = 21.431(2) Å, β = 98.50(1)°, U = 3717(1)) $Å^{-3}$, space group $P2_1/c$, Z = 4, μ = 1.233 mm^{-1}, $F(000)$ = 1840. 7596 reflections, 6524 independent (R_{int} = 0.0476). Non-hydrogen atoms were refined with anisotropic thermal parameters. Hydrogen atoms bonded to oxygen and nitrogen were initially located from difference maps but all hydrogen atoms were then inserted at calculated positions. Refinement converged with $wR2$ = 0.1497, GOF = 1.012 (all data) and conventional $R1$ = 0.0591 (2σ data).

2 $[Cu_4(\mu\text{-pyr})_2(L^1)](BF_4)_2$, $C_{34}H_{38}B_2Cu_4F_8N_8O_4$, green plate, 0.37 × 0.30 × 0.05 mm, monoclinic, a = 8.446(1), b = 25.567(3), c = 9.034(1) Å, β = 96.23(1)°, U = 1939.3(4) $Å^{-3}$, space group $P2_1/c$, Z = 2, μ = 1.799 mm^{-1}, $F(000)$ = 1056. 3444 reflections, 3233 independent (R_{int} = 0.0743). Non-hydrogen atoms were refined with anisotropic thermal parameters, except for the minor component of a disorder in the saturated part of the macrocycle, and hydrogen atoms were inserted at calculated positions. Refinement converged with $wR2$ = 0.1465, GOF = 1.037 (all data) and conventional $R1$ = 0.0665 (2σ data). CCDC 182/1180. See http://www.rsc.org/suppdata/cc/1999/639/ for crystallographic files in .cif format.

‡ For the crude dicopper complex the main signals are clusters around the following masses (rel. abundance, assignment): 654 (100%, $[Cu_2(H_3L^1)(H_2O)_2]^+$); 616 (70%, $[Cu_2(H_3L^1)]^+$); 635 (20%, $[Cu_2(H_3L^1)(H_2O)]^+$). For the tetracopper complex: 963 (30%, $[Cu_4(L^1)(pyr)_2(BF_4)]^+$); 876 (100%, $[Cu_4(L^1)(pyr)_2]^+$); 895 (60%, $[Cu_4(L^1)(pyr)_2(H_2O)]^+$).

1 N. H. Pilkington and R. Robson, *Aust. J. Chem.*, 1970, **23**, 2225.
2 See for example: R. R. Gagné, C. L. Spiro, T. J. Smith, C. A. Hamann, W.R.Thies and A. K. Shiemke, *J. Am. Chem. Soc.*, 1981, **103**, 4073; S. Ohtsuka, M. Kodera, K. Motoda, M. Ohba and H. Okawa, *J. Chem. Soc., Dalton Trans.*, 1995, 2599; T. Aono, H. Wada, Y. Aratake, N. Matsumoto, H. Okawa and Y. Matsuda, *J. Chem. Soc., Dalton Trans.*, 1996, 25; S. Mohanta, K. N. Nanda, L. K. Thompson, U. Florke and K. Nag, *Inorg. Chem.*, 1998, **37**, 1465.
3 V. McKee and S. S. Tandon, *J. Chem. Soc., Chem. Commun.*, 1988, 385.
4 V. McKee and S. S. Tandon, *J. Chem. Soc., Dalton Trans.*, 1991, 221.
5 J. E. Metcalfe, Ph.D. thesis, Queen's University, 1998.
6 S. S. Tandon and V. McKee, *J. Chem. Soc., Dalton Trans.*, 1988, 19.
7 M. G. B. Drew, O. W. Howarth, G. G. Morgan and J. Nelson, *J. Chem. Soc., Dalton Trans.*, 1994, 3149.
8 M. G. B. Drew, C. J. Harding, V. McKee, G. G. Morgan, and J. Nelson, *J. Chem. Soc., Chem. Commun.*, 1995, 1035.
9 H. Adams, N. A. Bailey, D. E. Fenton, R. Moody and J. M. Latour, *Inorg. Chim. Acta*, 1987, **135**, L1.
10 Y. Nishida and S. Kida, *Inorg. Chem.*, 1988, **27**, 447.
11 J. J. Manura and D. J. Manura, *Isotope Distribution Calculator*, SIS, 1996 *(http:/www.sisweb.com/mstools.htm)*.
12 P. E. Kruger and V. McKee, *Chem. Commun.*, 1997, 1341.
13 G. M. Sheldrick, *Acta Crystallogr., Sect. A*, 1990, **46**, 467.
14 G. M. Sheldrick, SHELXL-97, University of Göttingen, 1997.

Paper 9/00500E

Electrochemistry of quaternary ammonium binaphthyl salts

Andrew P. Abbott,*[a] Cherie S. M. Cheung,[a] Gillian R. Lonergan,[a] Irena G. Stará,[b] Ivo Starý*[b] and Pavel Kočovský*[a]

[a] *Department of Chemistry, University of Leicester, Leicester, UK LE1 7RH. E-mail: apa1@le.ac.uk*
[b] *Institute of Organic Chemistry and Biochemistry, AVČR, Flemingovo 2, 16610 Prague 6, Czech Republic*

Received (in Liverpool, UK) 12th January 1999, Accepted 25th February 1999

The redox behaviour of the binaphthyl unit in quaternary ammonium salts with an appended crown ether (3) is dramatically affected by the presence of metal cations and this effect can be used as an analytical tool to detect micromolar concentrations of alkali metal ions.

Axially chiral 2,2′-disubstituted 1,1′-binaphthyls, such as BINOL **1**,[1] have been utilised as a scaffold to construct a fascinating array of molecules, ranging from chiral ligands applied in asymmetric, metal-catalysed reactions[2,3] to complex supramolecular structures employed in molecular recognition studies.[4–6] The binaphthyl skeleton itself is normally viewed as an inert, robust block, whose activity is confined to occasional racemization; very little is known of its actual chemistry.

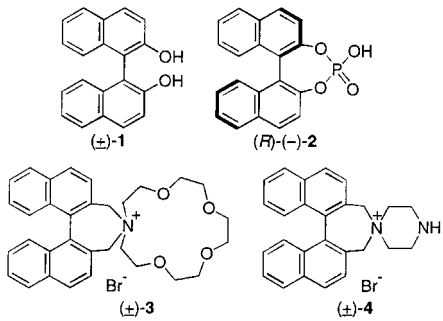

Shoute has recently studied the pulse radiolysis of BINOL hydrogen phosphate **2** in aqueous solutions (at pH 9.5, where **2** is dissociated).[7] Using time-resolved absorption spectroscopy, he has been able to show that the initially generated radical anion ($\mathbf{2}^- + e^- \rightarrow {}^{-\bullet}\mathbf{2}^-$) either undergoes an acid-catalysed protonation (${}^{-\bullet}\mathbf{2}^- + H^+ \rightarrow {}^{\bullet}\mathbf{H2}^-$) or transfers an electron to organic molecules present in the solution.[7] Since the protonation of radical anions is generally known to be slowed down by electron-withdrawing groups,[8] we became interested in the electrochemical generation of radical species from tetraalkylammonium binaphthyl salts, as a continuation of our efforts to develop new chiral ligands and electrochemical sensors.[9–11] Herein, we disclose preliminary results of the elucidation of the redox properties of novel quaternary aza-crown ether salt **3** and show how this molecule can be used in an electrochemical sensor for alkali metal cations in solution.

The quaternary ammonium aza-crown ether (±)-**3** was prepared from (±)-2,2′-bis(bromomethyl)-1,1′-binaphthyl[12] and the commercially available 1-aza-15-crown-5 (20 °C, overnight; 55%) in analogy to the published procedure.† Fig. 1 shows a cyclic voltammogram of a 2×10^{-3} mol dm^{-3} solution of **3** in MeCN containing 0.1 mol dm^{-3} $TBABF_4$ on a pyrolytic graphite (PG) electrode which gave a quasi-reversible response with ΔE_p = 129 mV. The electron transfer process was also found to be reversible on a Hg/Au amalgam electrode but was significantly less reversible on Pt, Au, Fe and Ag electrodes.

A quasi-reversible process on the PG electrode was also observed when the crown ether unit was replaced with a piperazine ring, as in (±)-**4**.[13] By contrast, reduction of (±)-**1**, carried out under the same conditions, showed an irreversible process, suggesting that the relative stability of **3** and **4** originates in the presence of the N^+ group. The addition of 20 μmol dm^{-3} of HCl (aq) to a solution of **3** in MeCN caused the current for the re-oxidation of the radical species to decrease dramatically.

The radical species generated from **3** (and from its congener **4**) must be stable in the order of minutes to allow quasi reversible responses to be observed with slow scan rate voltammograms (ν = 10 mV s^{-1}). To demonstrate the increased stability of the $ArCH_2N^+$ system, the visible spectrum of **3** was measured during a bulk electrolysis experiment. Fig. 2 shows the spectrum of **3** in the electrolyte solution described above as a function of time following the application of a constant current density of 50 μA cm^{-2} to a PG rod electrode. The growth of a peak at 410 nm is consistent with the formation of a binaphthyl radical species analogous to that observed by Shoute[7] for **2** (*vide supra*). This peak disappeared following the addition of 20 μmol dm^{-3} of HCl (aq), suggesting a chemical reaction which must clearly be an irreversible process that would account for the loss of the reverse peak in Fig. 1 following the acidification of the solution.

The mechanism of stabilisation of the binaphthyl system in **3** by the N^+ group is intriguing. Whereas in conjugated systems the effect of an electron-withdrawing group[8] can easily be understood, in **3** the electron-withdrawing N^+ is insulated from the aromatic ring by the benzylic CH_2 group, so that direct conjugation is precluded. However, molecular modelling shows that the twisted-chair conformation of the dihydroazepine ring in **3** renders the CH_2–N^+ σ-bond almost perpendicular to the aromatic system (Fig. 3). Hence, this conformation is ideally predestined to allow a donation from the aromatic π-system to the low-lying σ* orbital of the C–N^+ bond, so that a stabilisation (similar to that observed with the 'normally' conjugated systems) can be anticipated.

The effect of the quaternary ammonium group of **3** can, *a priori*, be modified by complexation of the crown ether moiety with a metal cation. Note that the positive charge on nitrogen in **3** can be assumed to be partly stabilised either by interaction with a lone pair of one of the oxygen atoms or, more likely, *via*

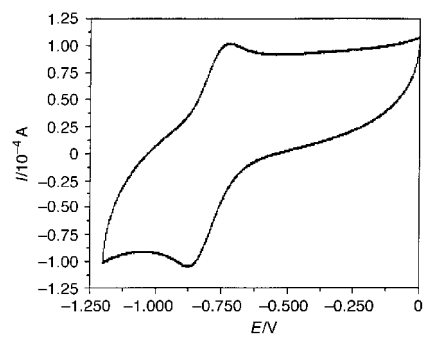

Fig. 1 Cyclic voltammogram of a 2×10^{-3} mol dm^{-3} solution of (±)-**3** in MeCN containing $TBABF_4$ (0.1 mol dm^{-3}) on a pyrolytic graphite (PG) electrode (sweep rate = 0.1 V s^{-1}). Potentials *vs.* SCE.

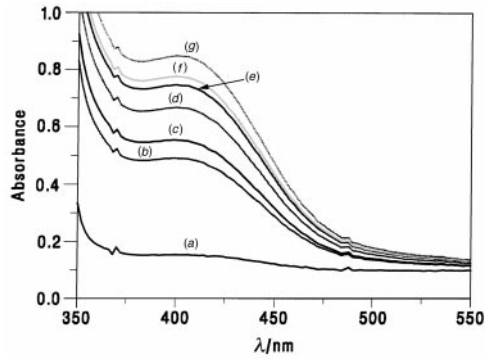

Fig. 2 Visible spectrum of (±)-**3** in the electrolyte solution described in Fig. 1 as a function of time following the application of a constant current density of 50 μA cm^{-2} to a PG rod electrode: (*a*) 0, (*b*) 1, (*c*) 2, (*d*) 3, (*e*) 4, (*f*) 5 and (*g*) 6 min.

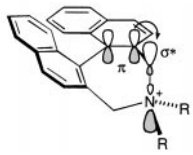

Fig. 3 Stereoelectronic effects in **3**.

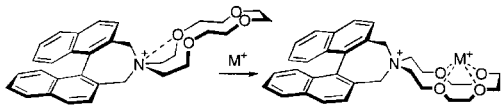

Scheme 1

the Cieplak effect.[14] Complexation of **3** with the metal cation (**3** → **5**; Scheme 1) should engage the latter, Lewis basic oxygen, leaving N$^+$ with a higher effective charge. To address this issue, the electrochemical experiments were repeated in the presence of $LiClO_4$ and $NaClO_4$, respectively. Fig. 4 shows that the peak current for the cathodic process decreases linearly as the concentration of Li$^+$ increases. Since the redox potentials of both processes are unaffected by the addition of Li$^+$, it can be concluded that the irreversible transformation of **3** is precluded by Li$^+$ binding. The decrease in current must result from the effective decrease in the concentration of unbound **3**. These results appear to be in agreement with the original hypothesis of increasing stabilisation of the binaphthyl system by enhancement of the neighbouring charge.

Fig. 4 also shows the effect of Na$^+$ on the cathodic current for the reduction of **3**. It can be seen that the current decreases more rapidly upon addition of Na$^+$ to the solution. This effect presumably results from the greater binding constant for Na$^+$ over Li$^+$ with the 1-aza-15-crown-5 unit.[15] However, because the reduction current has fallen to effectively zero with the addition of 0.5 equiv. of Na$^+$, it is likely that the Na$^+$ ion complexes with two crown ether molecules. Complementary

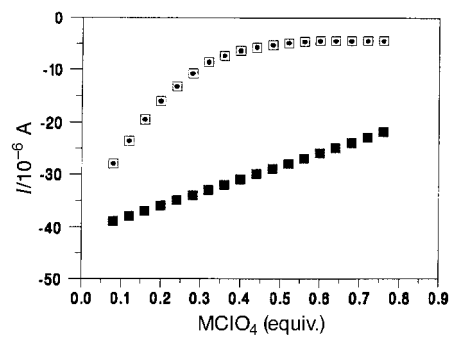

Fig. 4 Peak current for the reduction of (±)-**3** (5 × 10^{-3} mol dm^{-3}) in MeCN following the addition of $NaClO_4$ and $LiClO_4$ to the solution: (■) M = Li and ⊡ M = Na.

results were obtained with 1-aza-12-crown-4, a lower homologue of **3** which exhibited higher affinity to Li$^+$.

The observed response to the presence of Li$^+$ or Na$^+$ suggests that these systems can be potentially utilised as sensors for detecting alkali metal cations and, perhaps, of other cationic species. While there are numerous electrochemical, alkali metal sensors based on crown ethers,[16–18] most of them are potentiometric, relying on a change in energy of the electroactive moiety which tends to limit their sensitivity. As Fig. 4 clearly shows, a solution of **3** can detect the concentrations of Na$^+$ below 10 μmol dm^{-3}. Presumably, further tailoring the aza-crown ether cavity could generate molecules specific for other cations.

In conclusion, we have demonstrated for the first time that the radical species, generated electrochemically from a quaternary ammonium binaphthyl salt such as **3**, is relatively stable in non-acidic media. Since binding a cation to the appended crown ether moiety dramatically affects the redox behaviour of the binaphthyl unit, this novel class of binaphthyl crown ethers may be developed into very sensitive electrochemical sensors specific to alkali metal cations at micromolar concentrations which are beyond reach of the crown ether-based devices currently available.

This work was supported by the University of Leicester, the Grant Agency of the Czech Republic (Reg. No 203/96/0288) and the Academy of Sciences of the Czech Republic.

Notes and references

† *Synthesis* of (±)-**3**. A solution of (±)-2,2′-di(bromomethyl)-1,1′-binaphthyl[12] (500 mg, 1.14 mmol) and 1-aza-15-crown-5 (523 mg, 2.38 mmol) in benzene (5 ml) was left at ambient temperature overnight. The precipitate was filtered off and washed with benzene and the crude product was recrystallized from boiling distilled water (44 ml). The crystalline product was collected by suction and dried in a desiccator to afford pure (±)-**3** (359 mg, 55%): mp 268–271 °C (decomp.); ν_{max}(KBr)/cm^{-1} 2995, 2981, 2956, 2887, 2854, 1130, 1123, 1112, 1092; δ_H(200 MHz, DMSO-d_6) 3.52–3.72 (m, CH_2O, 16 H), 3.78–4.19 (m, CH_2N^+, 4 H), 3.92 (d, *J* 13.0, 2 H, ArCH_2), 4.85 (d, *J* 13.0, 2 H, ArCH_2), 7.27–8.35 (m, 12 H, arom); *m*/*z* (FAB MS) (3 : 1 thioglycerol–glycerol matrix) 498 (M − Br)$^+$, 470, 322, 308, 281, 279, 266, 265, 252 (Calc. for $C_{32}H_{36}BrNO_4$: C, 66.43; H, 6.27; N, 2.49. Found: C, 66.22; H, 6.27; N, 2.29%).

1 E. L. Eliel and S. H. Wilen, *Stereochemistry of Organic Compounds*, Wiley, New York, 1994.
2 C. Rosini, L. Franzini, A. Raffaelli and P. Salvadori, *Synthesis*, 1992, 503.
3 R. Noyori, *Asymmetric Catalysis in Organic Synthesis*, Wiley, New York, 1994.
4 J. Chao and D. J. Cram, *J. Am. Chem. Soc.*, 1976, **98**, 1015.
5 J. K. Judice and D. J. Cram, *J. Am. Chem. Soc.*, 1991, **113**, 2791.
6 J.-M. Lehn, *Supramolecular Chemistry*, Verlag Chemie, Weinheim, 1995.
7 L. C. T. Shoute, *J. Phys. Chem. A*, 1997, **101**, 5535.
8 A. J. Birch and G. Subbarao, in *Advances in Organic Chemistry, Methods and Results*, ed. E. C. Taylor, Wiley-Interscience, New York, 1972, p. 1.
9 M. Smrčina, M. Lorenc, V. Hanuš, P. Sedmera and P. Kočovský, *J. Org. Chem.*, 1992, **57**, 1917.
10 M. Smrčina, J. Poláková, Š. Vyskočil and P. Kočovský, *J. Org. Chem.*, 1993, **58**, 4543.
11 M. Smrčina, Š. Vyskočil, J. Polívková, J. Poláková, J. Sejbal, V. Hanuš, M. Polášek, H. Verrier and P. Kočovský, *Tetrahedron: Asymmetry*, 1997, **8**, 537.
12 D. M. Hall and E. E. Turner, *J. Chem. Soc.*, 1955, 1242.
13 For the preparation of **4**, see: I. G. Stará, I. Starý and J. Závada, *J. Org. Chem.*, 1992, **57**, 6966.
14 A. S. Cieplak, *J. Am. Chem. Soc.*, 1981, **103**, 4540.
15 A. D'Aprano, M. Salomon and V. Mauro, *J. Solution Chem.*, 1995, **24**, 685
16 P. D. Beer and K. Y. Wilde, *Polyhedron*, 1996, **15**, 775.
17 Z. Chem, A. J. Pilgrim and P. D. Beer, *J. Chem. Soc., Faraday Trans.*, 1995, **91**, 4331.
18 H. K. Youssoufi, M. Hmyene, F. Garnier and D. Delabouglise, *J. Chem. Soc., Chem. Commun.*, 1993, 1550.

Communication 9/00386J

Characterisation of a dodecanuclear chromium(III) cage with an $S = 6$ ground state

Frank E. Mabbs,[b] Eric J. L. McInnes,[b] Mark Murrie,[a] Simon Parsons,[a] Graham M. Smith,[d] Chick C. Wilson[c] and Richard E. P. Winpenny*[a]

[a] *Department of Chemistry, The University of Edinburgh, West Mains Road, Edinburgh, UK EH9 3JJ. E-mail: repw01@holyrood.ed.ac.uk*
[b] *EPSRC c.w.-EPR Centre, Department of Chemistry, The University of Manchester, Manchester, UK M13 9PL*
[c] *ISIS Department, CLRC Rutherford Appleton Laboratory, Chilton, Didcot, Oxon, UK OX11 0QX*
[d] *School of Physics and Astronomy, University of St. Andrews, North Haugh, St. Andrews, Fife, UK KY16 9SS*

Received (in Basel, Switzerland) 4th January 1999, Accepted 25th February 1999

Neutron diffraction, magnetic susceptibility and EPR spectroscopic studies of a dodecanuclear chromium cage are reported which show the molecule has an $S = 6$ spin ground state; this is the highest spin ground state known for a cage of this metal.

Research on high nuclearity paramagnetic cages has recently led to the discovery of single molecule magnets,[1–4] *i.e.* complexes which show hysteresis in magnetisation *versus* external field response which is of a molecular origin. The initial discovery was in a dodecanuclear mixed-valent manganese(III)/(IV) cage stabilised by carboxylate ligands.[1] Our interest in the area led us to examine a report of a mixed valent chromium cage,[5] of formula $[Cr_{12}O_{12}(O_2CBu^t)_{15}]$, where many of the features of the Mn_{12} single molecule magnets are present, at least in principle.

The synthesis is unusual, but straightforward. Reaction of $Cr(NO_3)_3{\cdot}9H_2O$ (0.050 mol) with $K(O_2CBu^t)$ (0.178 mol) in H_2O (500 cm^3) at *ca.* 80 °C gives a blue precipitate (90% yield) which is soluble in several organic solvents. Heating this precipitate at 400 °C under a stream of N_2 for 1 h eliminates HO_2CBu^t, yielding a dark green solid which analyses well for $[Cr_{12}O_{12-x}(OH)_x(O_2CBu^t)_{15}]$; electrospray mass spectrometry† of a CH_2Cl_2–MeOH solution of this solid indicates that the only significant species present in solution is $[Cr_{12}O_{12-x}(OH)_x(O_2CBu^t)_{15}]$. The yield of this compound is 77%. Very large green crystals could be grown by slow evaporation of an *n*-propanol solution of this material.

Initially we performed an X-ray structure determination of these crystals,‡ which revealed a dodecanuclear chromium cage, based on a centred-pentacapped-trigonal prism (Fig. 1). The complex has crystallographic D_3 symmetry, with the central Cr [Cr(1)] at the junction of the C_3 and C_2 axes, the Cr atoms [Cr(2) and symmetry equivalents (s.e.)] capping the triangular faces on the C_3 axis, and the Cr centres [Cr(3) and s.e.] capping the rectangular faces on the C_2 axes of the cage. Only the Cr atoms [Cr(4) and s.e.] at the vertices of the trigonal prism are in general positions. The cage is held together by μ_4-oxides [O(1) and s.e.], which bridge between the central Cr site, and one each of the vertex, triangular face-capping and rectangular face-capping sites; six μ_3-oxygens [O(2) and s.e.], which each bridge between two vertex sites and a cap on a rectangular face, and fifteen O_2CBu^t groups, which each bridge a Cr···Cr vector in a 1,3-bridging mode. Examination of the structure revealed that all Cr sites had similar bond lengths and angles; there was no sign of mixed valency which would lead to a charge imbalance if the apparent formula of $[Cr_{12}O_{12}(O_2CBu^t)_{15}]$ is correct. We therefore examined the alternative explanation, that some of the bridging oxide units were protonated, by performing a single crystal neutron diffraction study.‡

The presence of O_2CBu^t as the carboxylate ligand is not ideal for a neutron study, especially as all the methyl groups are disordered. However, the study unambiguously shows the presence of a half-weight hydrogen atom attached to the μ_3-O-atoms [O(2) and s.e.]. The formula should therefore be corrected to $[Cr_{12}(O)_9(OH)_3(O_2CBu^t)_{15}]$ **1**, and all Cr sites are Cr(III).

The magnetic properties of the cage remain interesting. Susceptibility studies§ reveal a double maxima in the $\chi_M T$ *vs.* T plot (where χ_M is the molar susceptibility) (Fig. 2). The low temperature maximum, at *ca.* 10 K, has a value of 21.6 cm^3 K mol^{-1}, consistent with an $S = 6$ ground state (χ_M calculated for $g = 1.99$ is 20.8 cm^3 K mol^{-1}), and the presence of the higher temperature maximum suggests a complicated ordering of the higher energy spin states. The complexity of the structure makes modelling this behaviour difficult, however further characterisation of the spin ground state comes from multifrequency EPR studies. At low temperature, and all frequencies studied (24, 34, 90, 180 GHz), a complex multiplet is observed (Fig. 3). The 90 GHz spectrum in Fig. 3(b) can be simulated¶ with the spin-Hamiltonian parameters: $S = 6$, $g_{zz} = 1.965$, $g_{xx} = g_{yy} = 1.960$, $D = +0.088$ cm^{-1}, $E = 0$ (where D and E are the axial and rhombic zero-field splitting parameters respectively) [Fig. 3(c)]. Simulations with other values for S result in significantly poorer fits with the experimental spectra. It is unusual to

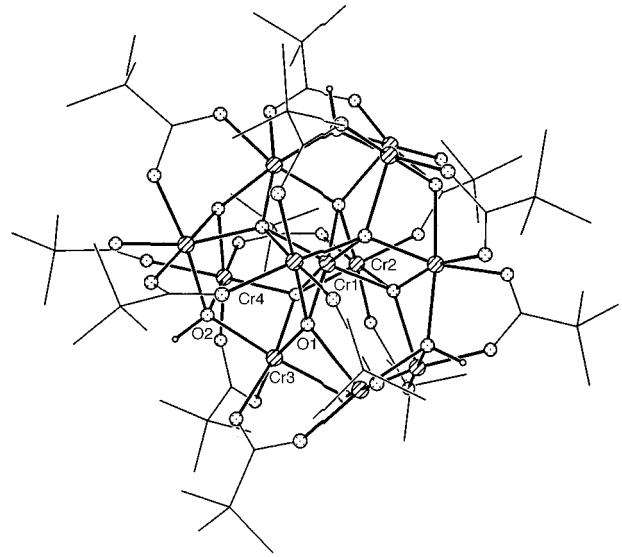

Fig. 1 The structure of **1**. Bond lengths (Å): Cr(1)–O(1) 1.980, Cr(2)–O(1) 1.994, Cr(2)–O(1B) 1.982, Cr(3)–O(1) 2.022, Cr(3)–O(2) 1.971, Cr(3)–O(1C) 1.988, Cr(4)–O(1) 1.987, Cr(4)–O(2) 1.971–1.978, Cr(4)–O(carboxylate) 1.93–1.959 (av. esd. 0.003). Bond angle (°) ranges: *cis* at Cr(1) 81.46–102.4, *trans* at Cr(1) 174.38, *cis* at Cr(2) 80.77–99.14, *trans* at Cr(2) 176.78, *cis* at Cr(3) 76.96–98.94, *trans* at Cr(3) 167.47–174.2, *cis* at Cr(4) 78.5–102.75, *trans* at Cr(4) 165.3–179.39 (av. esd. 0.7). (Cr atoms, shaded; O atoms, regular dots; C atoms shown as lines).

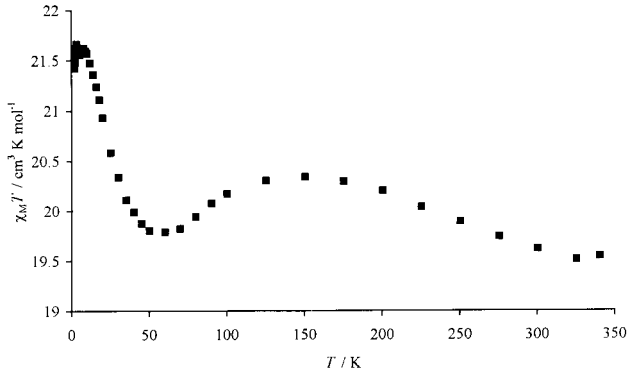

Fig. 2 Plot of $\chi_M T$ *vs.* T for **1**, measured with a 1000 G field.

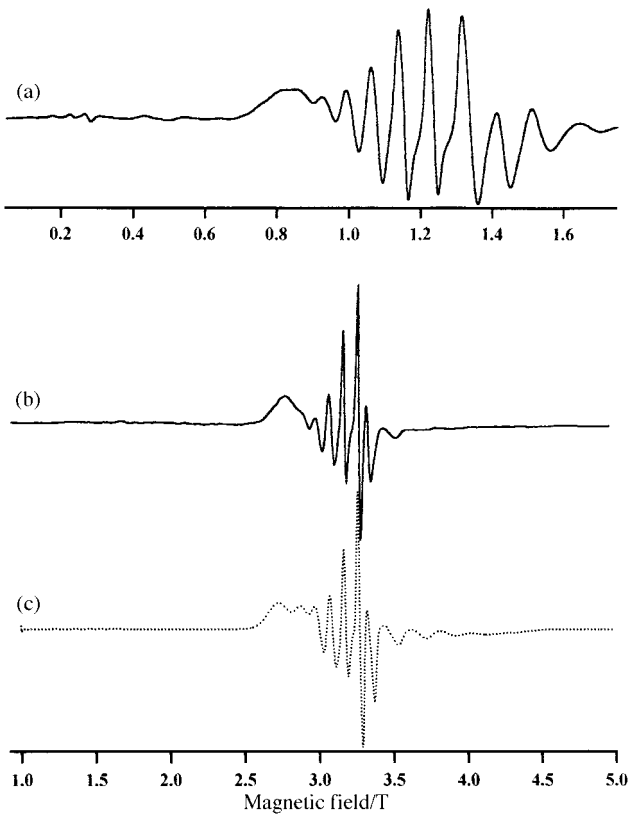

Fig. 3 EPR spectra of a powdered sample of **1** at (a) 34.11 GHz and 10 K, (b) 89.21 GHz and 5 K, (c) simulation of the 89.21 GHz spectrum using parameters given in the text.

observe such detail in spectra of high spin state cages.[9] The sign of D was determined by examining depopulation effects in spectra recorded at 180 GHz, between 20 and 2.8 K.

The cage is therefore the highest spin Cr cage known. Unfortunately the sign of D indicates that it will not be a single molecule magnet. Further studies of the cage will include a polarised neutron study which we hope will give the spin structure of the ground state of the cage directly.

We thank the EPSRC(UK) for funding for a diffractometer, SQUID susceptometer, an electrospray mass spectrometer, EPR spectrometers, access to ISIS and for Fellowships (to E. J. L. M and M. M.), and for an Advanced Research Fellowship (to G. M. S.).

Notes and references

† Electrospray mass spectra were obtained on a Finnegan LCQ spectrometer with the sample dissolved in CH_2Cl_2 which was added to MeOH prior to injection into the spectrometer.

‡ *Crystal data* for $C_{75}H_{138}Cr_{12}O_{42}\cdot 4.5H_2O\cdot C_3H_8O$ **1**: rhombohedral, space group $R32$, a = 18.3867(11), c = 36.034(6) Å, V = 10550(2) Å^3, M = 2477.0, Z = 3 (the molecule lies on a 32 site), T = 150.0(2) K, $R1$ = 0.0649. Data collection, structure solution and refinement were performed using programs DIRDIF[6] and SHELXL-97.[7] Neutron data were collected at 150 ± 1 K on the SXD instrument at the ISIS spallation neutron source using the time-of-flight Laue diffraction method.[8] The intensities of 5093 observed reflections were extracted and reduced to structure factors using standard SXD procedures,[8] which gave a merged data set comprising 1048 unique reflections. CCDC 182/1183.

§ Variable-temperature magnetic measurements on **1** in the region 1.8–325 K were made using a SQUID magnetometer (Quantum Design) with samples sealed in gelatine capsules. A diamagnetic correction for the sample holder was applied to the data.

¶ The simulation requires the line-width of the 2S allowed transitions to vary with the M_s states according to a power series $\Delta B = A + BM_s + CM_s^2$. The spectra were fitted with A = 400 G for z and 270 G for xy lines, B = 0 and C = 50 G.

1 R. Sessoli, H.-L. Tsai, A. R. Schake, S. Wang, J. B. Vincent, K. Folting, D. Gatteschi, G. Christou and D. N. Hendrickson, *J. Am. Chem. Soc.*, 1993, **115**, 1804; R. Sessoli, D. Gatteschi, A. Caneschi and M. A. Novak, *Nature*, 1993, **365**, 141.
2 S. M. J. Aubin, M. W. Wemple, D. M. Adams, H.-L. Tsai, G. Christou and D. N. Hendrickson, *J. Am. Chem. Soc.*, 1996, **118**, 7746.
3 C. Sangregorio, T. Ohm, C. Paulsen, R. Sessoli and D. Gatteschi, *Phys. Rev. Lett.*, 1997, **78**, 4645.
4 Z. Sun, C. M. Grant, S. L. Castro, D. N. Hendrickson and G. Christou, *Chem. Commun.*, 1998, 721.
5 A. S. Batsanov, G. A. Timko, Y. T. Struchkov, N. V. Gérbéléu and K. M. Indrichan, *Koord. Khim.*, 1991, **17**, 662.
6 P. T. Beurskens, G. Beurskens, W. P. Bosman, R. de Gelder, S. Garcia-Granda, R. O. Gould, R. Israel and J. M. M. Smits, DIRDIF-96 program system, University Crystallography Laboratory, University of Nijmegen, 1996.
7 G. M. Sheldrick, University of Göttingen, 1997.
8 C. C. Wilson, *J. Mol. Struct.*, 1997, **405**, 207.
9 A.-L. Barra, L.-C. Brunel, D. Gatteschi, L. Pardi and R. Sessoli, *Acc. Chem. Res.*, 1998, **31**, 460.

Communication 9/00023B

Improvement of the enantioselectivity in the enantioselective hydrogenation of ethyl pyruvate by addition of achiral tertiary amines

József L. Margitfalvi, Emilia Tálas and Mihály Hegedûs

Institute of Chemistry, Chemical Research Center, Hungarian Academy of Sciences, 1025 Budapest Pusztaszeri út 59-67, Hungary. E-mail: joemarg@cric.chemres.hu

Received (in Liverpool, UK) 25th January 1999, Accepted 24th February 1999

In the asymmetric hydrogenation of ethyl pyruvate over the catalyst system cinchonidine–Pt/Al_2O_3 the enantioselectivity was significantly improved by addition of different achiral tertiary amines to the reaction mixture, however the effect appeared to be strongly solvent and concentration dependent.

The hydrogenation of α-keto esters and related compounds over cinchonidine–Pt/Al_2O_3 catalyst is of great scientific interest.[1] In these heterogeneous catalytic asymmetric hydrogenation reactions the enantioselectivity (ee) (ee = ([*R*] − [*S*])/([*R*] + [*S*])) appeared to be strongly solvent dependent.[2] In different solvents the ee increased in the following order: alcohols (ee = 0.70–0.75) < hydrocarbons (ee = 0.80–0.85) < acetic acid (ee = 0.92–0.95%).[2] In all solvents the ee depended strongly on the concentration of the modifier.[1,2] This effect was studied in detail in ref. 2, however neither the chemistry nor the surface phenomena responsible for the observed strong solvent effect could be explained. One of the most interesting observations is that in acetic acid (AcOH) ten times less cinchonidine is needed to obtain the maximum ee value than in toluene.[2]

We have also shown that the addition of small amounts of AcOH is sufficient to increase the ee value.[3] For instance, in EtOH at [AcOH] = 5 M the ee increased to 0.91 compared to 0.73 in its absence. In toluene, under similar conditions, the ee increased to 0.93 compared to 0.81 in its absence. Consequently, the above ee values were very close to those obtained in pure AcOH. However, it should be mentioned that the use of AcOH requires corrosion resistant stainless steel autoclaves and accessories, this fact strongly hinders its general use in academic research. Therefore, any new approach resulting in an increase in enantioselectivity in the absence of AcOH will be of great scientific and practical interest.

In this contribution we report that the addition of achiral tertiary amines (ACTAs) to the reaction mixture containing cinchonidine, substrate, solvent (*e.g.* toluene) and catalyst significantly increases both the rate and the enantioselectivity of the given asymmetric hydrogenation reaction. It is known that when the hydrogenation of ethyl pyruvate is carried out in the presence of ACTAs, *e.g.* triethylamine (TEA), quinuclidine (QN), pronounced rate acceleration is observed without asymmetric induction.[4–6] However, the rate acceleration was much less than in the presence of cinchona alkaloids.

In this study the modifier, either cinchonidine alone or its mixture with achiral tertiary amines, was injected by high pressure hydrogen at $t = 0$ into the reactor containing the catalyst, the substrate and toluene as solvent. Pseudo first order rate constants describing the kinetics for the first 6–10 min (k_1) and 10–40 min (k_2) were used to evaluate the effect of ACTAs. Details of the experimental method and the kinetic approach can be found elsewhere.[3,7,8]

Reaction kinetic data and enantioselectivities obtained in a series of experiments carried out at 20 °C either in the presence or absence of ACTAs are summarized in Table 1, while Fig. 1 shows the corresponding enantioselectivity *vs.* conversion dependencies. In these experiments the ACTAs : cinchonidine (CD) ratio was five and almost full conversion ($x < 0.99$) was achieved within 90 min. Thus, the addition of ACTAs did not result in any decrease in the rate of hydrogenation, moreover, as emerges from the data given in Table 1, the addition of ACTAs led to a considerable increase in both rate constants k_1 and k_2. The rate acceleration increased in the following order: TEA < DABCO < QN.

The enantioselectivity *vs.* conversion dependencies show a monotonic increase type. This form of ee–conversion dependency has been observed by different authors.[2,3,7–10] In the absence of ACTAs the enantioselectivity *vs.* conversion dependency passes through a maximum and decreases slightly above 0.5 conversion giving a final ee value (ee_{end}) around 0.71. Similar behaviour had been observed in our earlier work when $[CD]_0 < 5 \times 10^{-5}$ M.[3,8,11] Analogous results were obtained when TEA was added, however in this case both the ee_{max} and ee_{end} values increased quite substantially (see Table 1). The addition of quinuclidine or DABCO altered the character of the enantioselectivity *vs.* conversion dependency as the monotonic increase in ee was maintained up to 0.99 conversion. This type

Table 1 Influence of different achiral tertiary amines on the enantioselective hydrogenation of ethyl pyruvate in the presence of the cinchonidine–Pt/Al_2O_3 catalyst system[a]

ACTA	k_1/min^{-1}	k_2/min^{-1}	ee_{max}
—	0.0352	0.0465	0.750 (0.714)[b]
TEA[c]	0.0407	0.0676	0.841 (0.793)[b]
DABCO	0.0886	0.1588	0.915[b]
QN[c]	0.1289	0.1645	0.898[b]
QN[c]	0.1297	0.1757	0.909[b]

[a] Solvent: toluene; T = 20 °C; hydrogen pressure = 50 bar; $[Etpy]_0$ = 1.0 M (batch No. 1), $[CD]_0 = 1.2 \times 10^{-5}$ M, $[ACTA]_0 = 1.2 \times 10^{-5}$ M. Catalyst: 5 wt% Pt on Al_2O_3 (Engelhard, E4759), dispersion = 22%, amount = 0.125 g. [b] Measured at the end of reaction. [c] TEA = triethylamine, QN = quinuclidine.

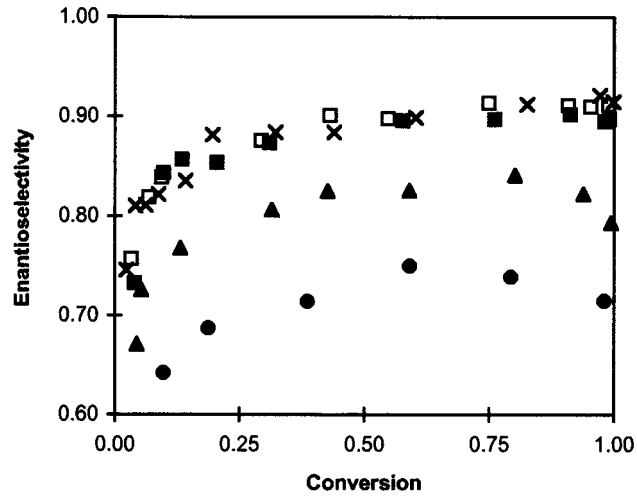

Fig. 1 Enantioselectivity *vs.* conversion obtained in the presence of different ACTAs. Experimental details and abbreviations are given in Table 1. (●) No ACTA, (▲) TEA, (X) DABCO, (■) and (□) QN.

Table 2 Influence of the concentration of quinuclidine (QN) on the enantioselective hydrogenation of ethyl pyruvate in the presence of the cinchonidine–Pt/Al_2O_3 catalyst system[a]

[QN]/M	k_1/min^{-1}	k_2/min^{-1}	ee[b]
0.0	0.0254	0.0065	0.775
1.2×10^{-6}	0.0273	0.0156	0.782
6.0×10^{-6}	0.0601	0.0932	0.910
1.2×10^{-5}	0.0832	0.1346	0.926
6.0×10^{-5}	0.1267	0.0371	0.936
1.2×10^{-4}	0.1219	n.m.[c]	0.946

[a] Solvent: toluene; T = 10 °C; hydrogen pressure = 50 bar; amount of catalyst = 0.125 g; $[Etpy]_0$ = 1.0 M (batch No. 1); $[CD]_0 = 1.2 \times 10^{-5}$ M. [b] Measured at the end of reaction. [c] n.m. = not measurable.

Table 3 Influence of the concentration of cinchonidine (CD) on the enantioselective hydrogenation of ethyl pyruvate in the presence of the cinchonidine–Pt/Al_2O_3 catalyst system[a]

Concentration of [CD]/M	k_1/min^{-1}	k_2/min^{-1}	ee_{max}[b]
0.0	0.0050	—	—
1.4×10^{-6}	0.0147	0.0109	0.216 (0.054)
6.8×10^{-6}	0.0273	0.0271	0.560 (0.334)
1.2×10^{-5}	0.0371	0.0413	0.646 (0.621)
3.4×10^{-5}	0.0823	0.1270	0.868
1.2×10^{-4}	0.1123	n.m.[c]	0.870

[a] Solvent: toluene; T = 20 °C; hydrogen pressure = 50 bar; amount of catalyst = 0.125 g; $[Etpy]_0$ = 1.0 M (batch No. 2). [b] Measured at the end of reaction. [c] n.m. = not measurable.

of enantioselectivity *vs.* conversion dependency was obtained[3,8,11] when $[CD]_0 > 5 \times 10^{-5}$ M. There was no measurable difference between quinuclidine or DABCO, however, the phenomena was well reproducible (see Table 1 and Fig. 1). In conclusion, results given in Table 1 and Fig. 1 precisely demonstrate that in the presence of ACTAs the final enantioselectivity (ee_{end}) increases from 0.71–0.72 to 0.91. This increase in enantioselectivity is considered to be a very pronounced selectivity improvement. Note that in toluene the highest ee value was 0.87 which was measured at $[CD]_0 = 6 \times 10^{-4}$ M. Similar ee values were reported in ref. 2. As emerges from data given in Fig. 1 the ability of ACTAs to increase the enantioselectivity increased in the following order TEA < DABCO = QN, *i.e.* the increase in ee is of a similar order as the rate acceleration effect. However, no measurable effect was induced by achiral tertiary amines when the concentration of CD increased to 10^{-4} M.

Analogous results were obtained in a series of experiments carried out at 10 °C. In these experiments quinuclidine was used as the ACTA and its concentration was varied. Related kinetic data and enantioselectivities are summarized in Table 2, which shows that the influence of ACTAs is strongly concentration dependent. These experiments indicate that the addition of quinuclidine (QN) in the given concentration range increases both the rate of the hydrogenation (rate constants k_1 and k_2) and the enantioselectivity. In these experiments, due to the decrease in the temperature, very high enantioselectivities were obtained. Table 2 shows the influence of ACTAs is already very pronounced at ACTA : CD = 0.5. The increase in the QN concentration resulted in a further increase in the k_1, k_2 and ee_{max} values. The increase in the rate constant k_1 and ee_{max} is gradual and levels off at ACTA : CD = 5–10, while the rate constant k_2 passes through a maximum. The enantioselectivities obtained in this series of experiments (ee_{max} = 0.93–0.94) are the highest values that have ever been obtained in this reaction in the absence of AcOH.

When EtOH was used as solvent no increase in ee was observed in the 10^{-5}–10^{-4} M concentration range of CD and at ACTA : CD = 1–5. No effect was observed in other alcohols, such as methanol or propanol. All of these results strongly indicate that the recognized effect induced by ACTAs depends on (i) the type of solvent used, (ii) the concentration of achiral tertiary amines, and (iii) the concentration of cinchonidine. Note that the observed effect appears at a very low concentration of cinchonidine (1.2×10^{-5} M), *i.e.* in the concentration range characteristic of enzyme catalytic reactions.

The observed increase of both the rate of hydrogenation and the enantioselectivity upon addition of ACTAs strongly resembles the influence of the initial concentration of cinchonidine on the kinetics and enantioselectivity.[2,3,8,11] Results obtained in this study indicated that addition of ACTAs would increase the amount of cinchonidine involved in the enantioselective hydrogenation. The above suggestion is strongly supported by results attained at difference concentrations of CD, but in the absence of ACTA. These results are summarized in Table 3. As emerges from the data in Tables 2 and 3, the increase in the concentration of both CD and ACTA resulted in similar changes in the reaction kinetics: (i) an increase of k_1, k_2 and ee_{max} values and (ii) alteration of the form of the enantioselectivity–conversion dependencies (see Fig. 1 in this paper and Fig. 2 in ref. 11).

The absence of any effect of ACTAs both at high concentrations of cinchonidine and in EtOH strongly resembles the solute–solute (alkaloid–alkaloid) interactions observed in the case of different dihydroquinines ((+)-DHQN and (−)-DHQN).[12] The (+)-alkaloid–(−)-alkaloid interaction was greatly reduced when an alcohol was used as solvent.[12] We propose that the alkaloid–alkaloid (cinchonidine–cinchonidine) interaction is not favourable for the given catalytic reaction as it reduces the amount of 'free alkaloid' required for asymmetric induction. It should be mentioned that in crystallographic form cinchonidine is stabilized by two hydrogen bonds between the OH group and the quinuclidine nitrogen,[13] consequently cinchonidine exists in the form of a cyclic 'dimer'. Based on the above literature analogy[12] we suggest that in the presence of ACTAs a new type of solute–solute interaction (*e.g.*, alkaloid–ACTA interaction) appears provided the concentration of the alkaloid is low and the solvent is not an alcohol. Due to the above interaction the amount of 'free alkaloid' required for asymmetric induction increases. Further studies are in progress in our laboratory to elucidate the character of interactions involved in the phenomena observed.

The partial financial support of OTKA (grants T023317, T025732) is greatly acknowledged.

Notes and references

1 H. U. Blaser, H. P. Jalett, M. Müller and M. Studer, *Catal. Today*, 1997, **37**, 441 and refs. cited therein.
2 H. U. Blaser, M. Garland and H. P. Jallett, *J. Catal.*, 1993, **144**, 569.
3 J. L. Margitfalvi and M. Hegedûs, *J. Mol. Catal. A*, 1996, **107**, 281.
4 J. L. Margitfalvi and M. Hegedûs, *J. Catal.*, 1995, **156**, 175.
5 H. U. Blaser, H. P. Jalett, D. M. Monti, J. F. Reber and J. T. Wehrli, *Stud. Surf. Sci Catal.*, 1988, **41**, 153.
6 G. Bond, P. A. Meheux, A. Ibbotson and P. B. Wells, *Catal. Today*, 1991, **10**, 371.
7 J. L. Margitfalvi, B. Minder, E. Tálas, L. Botz and A. Baiker, in *New Frontiers in Catalysis*, ed. L. Guczi, F. Solymosi and P. Tétényi, Proc. 10th Int. Cong. Catal., Budapest, July 1992, Elsevier, Amsterdam, 1993, p. 2471.
8 J. L. Margitfalvi, M. Hegedûs and E. Tfirst, *Stud. Surf. Sci. Catal.* (11th International Congress on Catalysis), 1996, **101**, 241.
9 R. A. Augustine and S. K. Tanielyan, *J. Mol. Catal. A: Chem.*, 1996, **112**, 93.
10 J. Wang, Y. Sun, C. LeBlond, R. N. Landau and D. G. Blackmond, *J. Catal.*, 1996, **161**, 752.
11 J. L. Margitfalvi, E. Tfirst, M. Hegedûs and E. Tálas, *Catalysis of Organic Reactions*, ed. Frank E. Herkes, Marcel Dekker, New York, 1998, vol. 75, p. 531.
12 T. Williams, R. G. Pitcher, P. Bommer, J. Gutzwiller and M. Uskovic, *J. Am. Chem. Soc.*, 1969, **91**, 1870.
13 B. J. Oleksyn, *Acta Crystallogr., Sect. B*, 1982, **38**, 1832.

Communication 9/00681H

Strong optical limiting (OL) capability of the two-dimensional network cluster polymer $[MoS_4Cu_6I_4(py)_4]_n$

Hongwei Hou,*[a] Yaoting Fan,[a] Chenxia Du,[a] Yu Zhu,[a] Wenling Wang,[a] Xinquan Xin,*[b] Michael K. M. Low,[c] Wei Ji*[c] and How Ghee Ang*[c]

[a] *Department of Chemistry, Zhengzhou University, Zhengzhou 450052, Henan, PR China. E-mail: houhongw@hotmail.com*

[b] *Department of Chemistry, Nanjing University, Nanjing 210093, Jiangsu, PR China*

[c] *Departments of Physics and Chemistry, National University of Singapore, 10 Kent Ridge Crescent, Singapore 119260, Singapore*

Received (in Cambridge, UK) 19th January 1999, Accepted 3rd March 1999

The two-dimensional network compound $[MoS_4Cu_6I_4(py)_4]_n$ is the first example of a cluster polymer showing very large optical limiting effects; its nonlinear absorptive index α_2 and nonlinear refractive value n_2 are 1.5×10^{-9} m W^{-1} and -2.5×10^{-17} m^2 W^{-1}, respectively, in 6.5×10^{-5} mol dm^{-3} DMSO solution; the optical limiting threshold was determined to be 0.6 J cm^{-2}, which is about three times better than that of C_{60}.

Research into optical limiting (OL) materials has become increasingly intensive because of their potential applications in the protection of optical sensors from high-intensity laser beams. Thus the design and synthesis of new materials with large optical limiting capability represents an active field in modern chemistry, physics, and materials science.[1,2] Our research interest focuses on cluster compounds. Although many clusters show strong nonlinear optical (NLO) absorptive and NLO refractive properties, only the clusters $[NBu_4]_2[MoOS_3Cu_3BrCl_2]$, $[NBu_4]_2[MoOS_3(CuSCN)_3]$, $[NBu_4]_3[MS_4M'_3BrX_3]$ (M = Mo, W; M′ = Cu, Ag; X = Cl, Br, I), $[NBu_4]_3[MoOS_3Cu_3BrI_3]$, $[WS_4Cu_4(SCN)_2(py)_6]$, $[Mo_2Ag_4S_8(PPh_3)_4]$ and $[NEt_4]_4[Mo_2O_2S_6Cu_6Br_2I_4]$ exhibit large optical limiting effects.[3–10] The limiting thresholds of $[NBu_4]_3[MS_4M'_3BrX_3]$, $[WS_4Cu_4(SCN)_2(py)_6]$ and $[Mo_2Ag_4S_8(PPh_3)_4]$ were measured to be 0.6, 0.3 and 0.1 J cm^{-2}, respectively. These data are comparable to those of phthalocyanine derivations and better than that observed in C_{60}.[1,11]

The complex $[MoS_4Cu_6I_4(py)_4]_n$ is one of *ca.* 20 cluster polymers. While $[NBu_4N][MS_4Tl]$ (M = Mo, W) have strong NLO absorptive and NLO refractive properties,[12,13] they do not exhibit optical limiting effects. $[MoS_4Cu_6I_4(Py)_4]_n$ is the first cluster polymer to show strong optical limiting effects.

The polymer $[MoS_4Cu_6I_4(py)_4]_n$ was prepared by the reaction of $(NEt_4)_2MoS_4$, CuI and cyanopyridine with pyridine in MeCN solution. The crystal structure of $[MoS_4Cu_6I_4(py)_4]_n$, together with some bond parameters, is shown in Fig. 1.†

The basic structural unit of the polymer $[MoS_4Cu_6I_4(py)_4]_n$ may be regarded as an octahedron, in which MoS_4 is enveloped by six copper atoms. The same Mo–S bond lengths [2.268(3) Å] and similar S–Mo–S bond angles [108.6(1)–109.92(6)°] reveal that the structure of the central MoS_4 core is close to that of the $[MoS_4]^{2-}$ tetrahedron. Each S atom acts as a tetradentate ligand binding with three Cu atoms and one Mo atom. There are two types of copper atoms in the Cu_6 octahedron, two axial Cu(2) atoms and four equatorial Cu(1) atoms. The distance Cu(2)–Mo is not equal to Cu(1)–Mo, while several Cu–Mo–Cu bond angles are inequivalent. Thus, six Cu atoms form a distorted octahedron. Cu(2) atoms each coordinate with two S atoms and one terminal I(2) atom, and exhibit triangular planar geometry. Cu(1) atoms bind with two S atoms, one μ-I(1) atom and one N from py, and adopts a distorted tetrahedral geometry. Each $[MoS_4Cu_6I_4(py)_4]$ unit forms four Cu(1)–I(1)–Cu(1) bridges with four $[MoS_4Cu_6I_4(py)_4]$ units leading to the two-dimensional network structure.

Two shoulder peaks at 300 and 410 nm are observed in the electronic spectrum of $[MoS_4Cu_6I_4(py)_4]_n$. The polymer has a relatively low linear absorption in the visible and near IR region. Z-scan data indicate that the polymer exhibits both strong NLO absorption and NLO refraction (self-defocusing effects), which were measured as described in ref. 13.

It should be pointed out that both excited state population (and absorption) and two-photon absorption can be responsible for the measured NLO effect.[14] Fig. 2 shows typical Z-scan measurements of the polymer in DMSO solution without the aperture. The open circles are the experimental data, and the solid curves are the theoretical fit by using Z-scan theory described in ref. 13. It is obvious that the theoretical curves qualitatively reproduce well the general pattern of the observed experimental data. This fact suggests an effectively third-order characteristic for the experimentally detected NLO effects. The

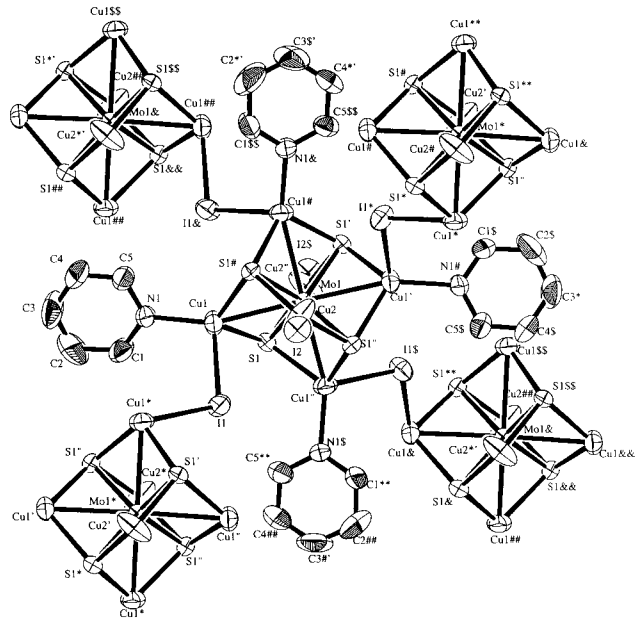

Fig. 1 The crystal structure of $[MoS_4Cu_6I_4(py)_4]_n$. Selected bond lengths (Å) and angles (°): Mo(1)–S(1) 2.268(3), Mo(1)–Cu(1) 2.684(2), Mo(1)–Cu(2) 2.653(2), I(1)–Cu(1) 2.784(2), I(2)–Cu(2) 2.455(2), Cu(1)–N(1) 1.995(10); S(1)–Mo(1)–S(1)′ 108.6(1), S(1)′–Mo(1)–S(1)″ 109.92(6), Cu(1)–Mo(1)–Cu(1)′ 168.80(7), Cu(1)–Mo(1)–Cu(2) 84.40(4), Cu(1)–Mo(1)–Cu(1)# 90.55(1), Cu(1)–Mo(1)–Cu(2)″ 95.60(4), Cu(1)–Mo(1)–S(1) 55.49(9), Cu(1)–Mo(1)–S(1)′ 117.19(9), Cu(2)–Mo(1)–S(1)′ 125.72(6), Cu(2)–Mo(1)–S(1)″ 54.28(6), I(1)–Cu(1)–S(1) 94.87(9), I(2)–Cu(2)–S(1)″ 125.82(7), I(2)–Cu(2)–Mo(1) 180.0, Mo(1)–S(1)–Cu(1) 71.33(9).

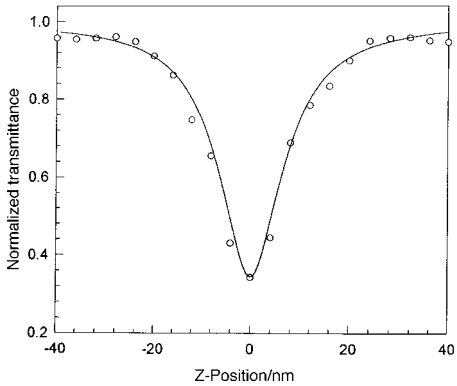

Fig. 2 Z-scan data showing NLO absorption of $[MoS_4Cu_6I_4(py)_4]_n$.

effective nonlinear absorptive index α_2 is 1.5×10^{-9} m W^{-1} in 6.5×10^{-5} mol dm^{-3} DMSO solution. The data is comparable to those of $[Mo_2Ag_4S_8(PPh_3)_4]$ and $[W_2Ag_4S_8(AsPh_3)_4]$ which have the largest α_2 values known, and superior to those of other inorganic clusters.

The Z-scan data measured with the aperture are depicted in Fig. 3. The data show that the polymer $[MoS_4Cu_6I_4(py)_4]_n$ has a negative sign for the refractive nonlinearity, which gives rise to self-defocusing behavior. A reasonably good fit between the experimental data and the theoretical curves described in ref. 13 was obtained. The effective third-order NLO absorptive index n_2 is -2.5×10^{-17} m^2 W^{-1}. The polymer is composed of octahedral structural units $[MoS_4Cu_6I_4(py)_4]$ and its NLO refractive behavior differs from that of cluster polymers $\{[NBu_4][MS_4Tl]\}_n$ (M = Mo, W), which consist of dinuclear structural units $[MS_4Tl]$ and exhibit strong self-focusing effects. However, twin nest-shaped clusters consisting of two nest-shaped structural units have the same NLO refractive properties as $[MoS_4Cu_6I_4(py)_4]_n$, with strong self-defocusing behavior.

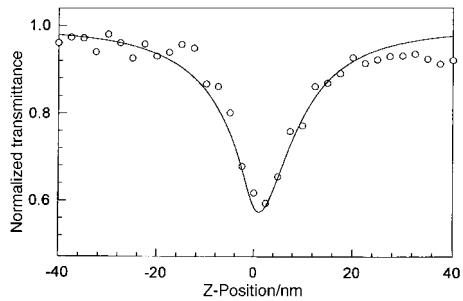

Fig. 3 Z-scan data showing NLO refraction of $[MoS_4Cu_6I_4(py)_4]_n$.

We also observed that the polymer possesses large optical limiting (OL) effects because of its very strong NLO absorption (α_2 value is the largest for any known inorganic cluster). The measurement of the transmitted pulse energy was conducted with a full collection of the transmitted pulse, and no aperture was used. The OL capability utilizing only the NLO absorption is demonstrated in Fig. 4 (open circles). The solid curves in Fig. 4 are from the theoretical model described in ref. 14. It is manifest that the observed OL effect arises as a direct consequence of the ionization recombination process. The light energy transmitted starts to deviate from Beer's law as the input light fluence reaches *ca.* 0.3 J cm^{-2}, and the solution become increasely less transparent as the incident fluence rises. The limiting threshold, which is defined as the incident fluence at which the actual transmittance falls to 50% of the corresponding linear transmittance, is 0.6 J cm^{-2} in DMSO solution. This value is three times better than that of C_{60}. These results clearly

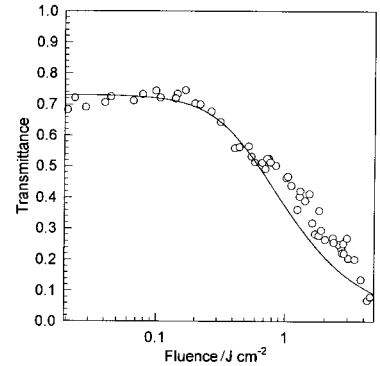

Fig. 4 Dependence of the transmitted energy at 532 nm of a DMSO solution of $[MoS_4Cu_6I_4(py)_4]_n$ on the incident light fluence. Beating rate: single shot (5 s interval).

indicate that the cluster polymer exhibits strong NLO properties and *also* a large OL capability. The properties should make the polymer a very promising candidate for broad-band OL application.

The authors acknowledge financial support from the National Natural Science Foundation of China, Zhengzhou University of China, National University of Singapore and Defence Science Organisation of Singapore.

Notes and references

† *Crystal data*: $C_{20}H_{20}N_4S_4I_4Cu_6Mo$, M = 1429.48, tetragonal, space group $I\bar{4}2d$ (no. 122), a = 14.814(3), c = 15.712(5) Å, V = 3447.75 $Å^3$, Z = 4, D_c = 2.75 g cm^{-1}, $F(000)$ = 2640.00, μ (Mo-Kα) = 78.3 cm^{-1}, $2\theta_{max}$ = 55.0°. All measurements were made on a Rigaku RAXIS-IV image plate area detector. A total of 1012 reflections were collected. The data were corrected for Lorentz and polarization effects. The structure was solved by direct methods and expanded using Fourier techniques. The final cycle of full-matrix least-squares refinement was based on 853 observed reflections [($I > 2.00\sigma(I)$] and 91 variable parameters and converged with R = 0.043 and R_w = 0.042. All calculations were performed using the teXsan crystallographic software package of Molecular Structure Corporation (1985 and 1992). CCDC 182/1183. See http://www.rsc.org/suppdata/cc/1999/647/ for crystallographic files in .cif format.

1 J. W. Perry, K. Mandour, I.-Y. S. Lee, X.-L. Wu, P. V. Bedworth, C.-T. Chen, D. Ng, S. R. Marder, P. Miles, T. Wada, M. Tian and H. Sasabe, *Science*, 1996, **273**, 1533.
2 R. Signorini, M. Zerbetto, M. Meneghetti, R. Bozio, M. Maggini, C. D. Faveri, M. Prato and G. Scorrano, *Chem. Commun.*, 1996, 1891.
3 H. W. Hou, X. R. Ye, X. Q. Xin. J. Liu, M. Q. Chen and S. Shi, *Chem. Mater.*, 1995, **7**, 472.
4 S. Shi, W. Ji, W. Xie, T. C. Chong, H. C. Zeng, J. P. Lang and X. Q. Xin, *Mater. Chem. Phys.*, 1995, **39**, 298.
5 S. Shi, W. Ji, S. H. Tang, J. P. Lang and X. Q. Xin, *J. Am. Chem. Soc.*, 1994, **116**, 3615.
6 S. Shi, W. Ji, J. P. Lang and X. Q. Xin, *J. Phys. Chem.*, 1994, **98**, 3570.
7 P. E. Hoggard, H. W. Hou, X. Q. Xin and S. Shi, *Chem. Mater.*, 1996, **8**, 2218.
8 M. K. M. Low, H. W. Hou, H. G. Zheng, W. T. Wong, G. X. Jin, X. Q. Xin and W. Ji, *Chem. Commun.*, 1998, 505.
9 W. Ji, S. Shi, H. J. Du, P. Ge, S. H. Tang and X. Q. Xin, *J. Phys. Chem.*, 1995, **99**, 17 297.
10 H. W. Hou, X. Q. Xin. J. Liu, M. Q. Chen and S. Shi, *J. Chem. Soc., Dalton Trans.*, 1994, 3211.
11 L. W. Tutt and A. Kost, *Nature*, 1992, **356**, 224.
12 J. P. Lang, K. Tatsumi, H. Kawaguchi, J. M. Lu, P. Ge, W. Ji and S. Shi, *Inorg. Chem.*, 1996, **35**, 7924.
13 B. Sheik-Bahae, A. A. Said, T. H. Wei, D. J. Hagan and E. W. Van Stryland, *IEEE J. Quantum Electron*, 1990, **26**, 760.
14 W. Ji, H. J. Du and S. Shi, *J. Opt. Soc. Am.*, 1995, **12**, 876.

Communication 9/00518H

Polyazacyclophanes containing biphenyl fragments

M. Isabel Burguete,[a] Pilar Diaz,[b] Enrique García-España,*[b] Santiago V. Luis,*[a] Juan F. Miravet,[a] Manuel Querol,[a] and J. A. Ramirez[b]

[a] *Department of Inorganic and Organic Chemistry, University Jaume I, E-12080 Castellón, Spain. E-mail: luiss@qio.uji.es*

[b] *Department of Inorganic Chemistry, University of Valencia, 46100 Burjassot, Spain*

Received (in Cambridge, UK) 21st December 1998, Accepted 2nd March 1999

Polyaza[*n*]cyclophanes containing the 2,2′-biphenyl subunit are prepared in good yields by reaction of the corresponding pertosylated polyamine and 2,2′-bis(bromomethyl)biphenyl in basic media followed by detosylation with Na/Hg; the dynamic behaviour of those receptors is clearly affected by their interaction with different cationic and anionic guests.

Macrocyclic receptors containing biphenyl subunits represent a very interesting class of hosts because of their dynamic properties provided by the presence of the biphenyl moiety. A clear example of the interest of this kind of compound is the work of Rebek in the development of simple allosteric systems.[1] Most work in this area has been directed towards the preparation of the all-oxygen macrocycles,[2] and only rarely has the synthesis of compounds in which some of the oxygen atoms have been substituted by nitrogen been reported.[3,4] However, our recent work on polyaza[*n*]cyclophanes[5] suggested to us that biphenyl polyaza macrocycles could represent a very interesting target as they combine the coordination trends of polyazacyclophanes with the dynamic properties of biphenyl crown ethers, giving rise to better regulated systems when supramolecular assemblies and catalytic properties are considered. Here we report on the first synthesis of such macrocyclic receptors and on preliminary results on their coordination properties that confirm their very interesting behaviour.

Synthesis of the expected macrocyclic receptors was carried out using a Richman–Atkins procedure optimized by us for the preparation of polyaza[*n*]cyclophanes (Scheme 1).[5a]

Cyclization of pertosylated polyamines **2** with **1** was performed very efficiently in 60–70% yield for **3c** and **3d** using MeCN as the solvent and K_2CO_3 as the base, without the need of high dilution conditions. Lower yields were obtained for the smaller macrocycles **3a** and **3b** due to the simultaneous formation of dimeric cyclic species **5** and **6**.[4] Detosylation was best carried out with Na/Hg,[5a] very good yields (*ca.* 70–80%) were obtained for the crude products. Chromatographic purification afforded the pure compounds in *ca.* 40% yield.

The dynamic properties of these systems are clearly seen in their ^{1}H NMR spectra, in particular when benzylic C–H signals are considered. In general, benzylic protons in compounds **4**, at 200 MHz in $CDCl_3$ at room temperature, appear as AB systems, in agreement with the presence of the slow equilibrium shown in Scheme 2.

Coalescence of the AB benzylic peaks occurs at not very high temperatures for the larger macrocycles, and variable temperature experiments allowed, for instance, us to determine for

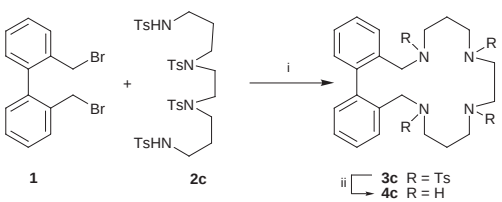

1 2c

Scheme 1 *Reagents and conditions*: i, K_2CO_3, MeCN; ii, Na/Hg, THF–MeOH.

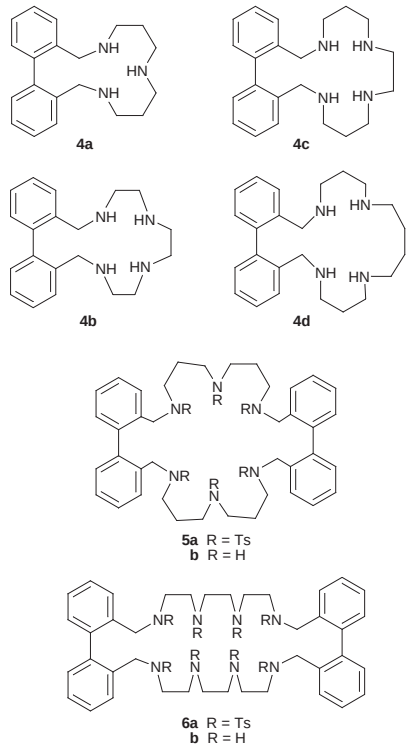

4c a coalescence temperature of 22 °C with $\Delta G = 14.5 \pm 0.3$ kcal mol^{-1}.

Blocking of the interconversion can be easily achieved by protonation of the nitrogen atoms, as indicated by the observation of the benzylic protons as two well-defined AB doublets. Protonation of compounds **4** could be followed by potentiometry and NMR techniques and showed similar trends to those found for related polyaza[*n*]cyclophanes.[5a] The observed separation of the two benzyl doublets is dependent on the pH. For **4c**, $\Delta\delta$ values at 300 MHz and room temperature vary from 41 Hz at pH 11 to 69 Hz at pH 2. Obviously interconversion of the two rotamers has to proceed through a coplanar disposition of the aromatic rings in which electrostatic repulsions are maximized, in particular when the protonated benzylic nitrogen atoms are considered.

These compounds seem to present a more versatile coordination chemistry than their simple polyaza[*n*]paracyclophane analogues, and this can be ascribed to the dynamic behaviour of

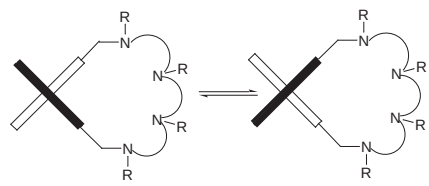

Scheme 2

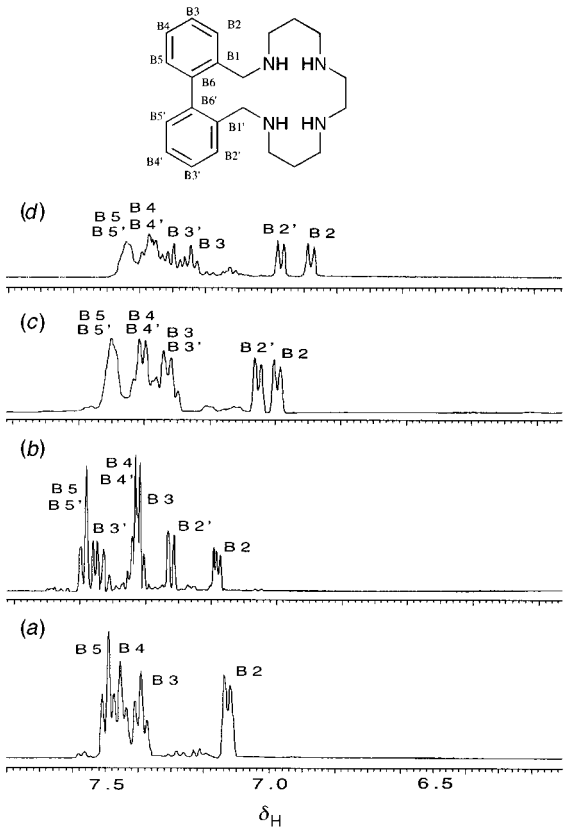

Fig. 1 ^{1}H NMR spectra (D_2O) (aromatic region): (*a*) **4c** at acidic pH, (*b*) **4c**·Pd^{2+} at basic pH, (*c*) **4c**·ATP at acidic pH, (*d*) **4c**·ATP at basic pH.

the biphenyl spacer. Thus, for instance, while coordination of **4c** to Cu^{2+} gives rise to a $[CuL]^{2+}$ complex with a stability constant of 18.7 logarithmic units, the related $[ZnL]^{2+}$ complex presents a constant of only 8.7 logarithmic units, strongly suggesting that the strength of the coordinative bonds formed tunes the conformation of the receptor. In the case of Cu^{2+} all the N donors would be participating in the recognition of the metal ion, while for Zn^{2+} just three out of the four N donors would be involved. These results are further supported by the presence in the Zn^{2+}·**4c** system of a hydroxylated species as well as by the large constant found for the protonation of the $[ZnL]^{2+}$ complex.† This behaviour is clearly dependent on the nature of the polynitrogenated bridge, which plays a very important role in determining the dynamic properties of the biphenyl moiety.‡

A particular situation is found when $PdCl_4^{2-}$ is used as the guest. The ^{1}H and ^{13}C NMR spectra at basic pH show that Pd^{2+} is coordinated to only three of the nitrogen atoms, introducing a high degree of rigidity in the macrocyclic framework. Thus, the ^{13}C NMR spectrum shows twelve signals for the aromatic carbons and ten for the aliphatic ones, denoting a complete loss of symmetry. On the other hand, while one of the benzylic signals appears with a chemical shift similar to that of the non-protonated free ligand, the other one is shifted downfield more than 6 ppm. Similar trends are observed in the ^{1}H NMR spectrum, all the hydrogen atoms being magnetically non-equivalent [see Fig. 1(*b*) for the aromatic region].

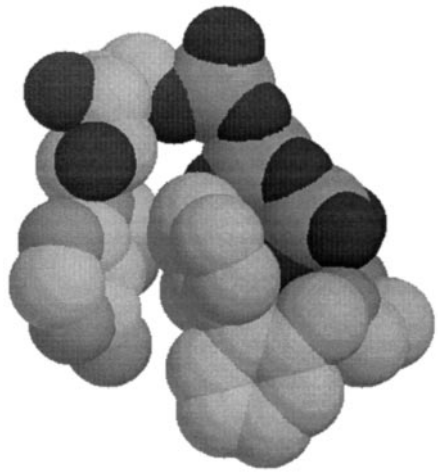

Fig. 2 CPK model of the calculated structure for the interaction of protonated **4c** and ATP (AMBER*, MACROMODEL® 5.0 package). GB/SA solvation model for water has been considered.

These receptors also strongly interact with anionic guests such as ATP.§ In this case a complete loss of symmetry is only observed for the aromatic region in the ^{1}H NMR spectrum [see Fig. 1(*c*) and 1(*d*)]. For **4c** four triplets and four doublets are observed in that region. These spectral features suggest a structure of the adduct in which the adenosine fragment of the ATP is located above the biphenyl moiety, freezing the rotation of and making non-equivalent both aromatic rings. These kinds of structures are also suggested by molecular mechanics calculations (see Fig. 2).

Additional work is being carried out in order to fully understand these interactions and to develop novel supramolecular systems based on these structures.

Financial support was provided by the CICYT (PB96-0792-C02) and Generalitat Valenciana (GV-D-CN-09-140-96). M. Querol and P. Díaz are indebted to Bancaja and CYCIT for predoctoral grants.

Notes and References

† Protonation constants of **4c** determined in 0.15 mol dm^{-3} $NaClO_4$ at 298.1 K are as follows: $\log K_{HL}$ = 9.91(2), $\log K_{H_2L}$ = 8.85(3), $\log K_{H_3L}$ = 6.55(3), $\log K_{H_4L}$ = 4.05(5). Stability constants for the formation of Cu^{2+} complexes with **4c**; $\log K_{CuI/Cu.L}$ = 18.66(3), $\log K_{CuHL/CuL.H}$ = 4.10(3). Stability constants for the formation of Zn^{2+} complexes with **4c**; $\log K_{ZnI/Zn.L}$ = 8.70(2) $\log K_{ZnHL/ZnL.H}$ = 6.91(3), $\log K_{ZnL(OH)/ZnL.H_2O}$ = −9.33(3). The degrees of protonation of receptor and substrate have been estimated taking into account their basicity constants.

‡ Stability constants for the formation of Cu^{2+} complexes with **4b** and **4d** are: $\log K_{CuI/Cu.L}$ = 23.19(7) and $\log K_{CuL/u.L}$ = 10.18(4).

§ Interaction of **4c** with ATP in 0.15 mol dm^{-3} $NaClO_4$ at 298.1 K gives rise to adduct species with AH_jL (j = 2 to 6) (A = ATP^{4-}, L = **4c**) with stability constants: $LH_4 + H_2A = H_6LA$, $\log K$ = 6.01(4). $LH_4 + HA = H_5LA$, $\log K$ = 6.30(4), $LH_3 + HA = H_4LA$, $\log K$ = 5.41(4), $LH_2 + HA = H_3LA$, $\log K$ = 5.55(4) and $LH_2 + A = H_2LA$, $\log K$ = 4.17(3).

1 J. Rebek, R. W. Wattley, T. Costello, R. Gadwood and L. Marshall, *J. Am. Chem. Soc.*, 1980, **102**, 7398; J. Rebek, *Acc. Chem. Res.*, 1984, **17**, 258; F. Gaviña, S. V. Luis, A. M. Costero, M. I. Burguete and J. Rebek, *J. Am. Chem. Soc.*, 1988, **110**, 7140; S. V. Luis, M. I. Burguete, F. Gaviña, A. M. Costero and J. Rebek, *Bioorg. Med. Chem. Lett.*, 1991, **1**, 87.

2 S. P. Artz and D. J. Cram, *J. Am. Chem. Soc.*, 1984, **106**, 2160; R. C. Helgerson, G. R. Weisman, J. L. Toner, T. L. Tarnowski, Y. Chao, J. M. Mayer and D. J. Cram, *J. Am. Chem. Soc.*, 1979, **101**, 4928; R. C. Helgerson, T. L. Tarnowski and D. J. Cram, *J. Org. Chem.*, 1979, **44**, 2538; V. M. L. J. Aarts, P. D. J. Grootenhuis, D. N. Reinhoudt, A. Czech, B. P. Czech, and R. Bartsch, *Recl. Trav. Chim. Pays-Bas*, 1988, **107**, 94; D. N. Reinhoudt, F. de Joy and M. van de Vondervoot, *Tetrahedron*, 1981, **37**, 1985; *Tetrahedron*, 1981, **37**, 1753; H. Kohama, M. Yoshinaga and K. Ishizu, *Bull. Chem. Soc. Jpn.*, 1980, **53**, 3707; K. Brandt, I. Powolik, M. Siwy, T. Kupka, R, A. Shaw, D. B. Davies and R. A. Bartsch, *J. Am. Chem. Soc.*, 1996, **118**, 4496; *J. Am. Chem. Soc.*, 1997, **119**, 12 432.

3 D. P. J. Pearson, S. J. Leigh and I. O. Sutherland, *J. Chem. Soc. Perkin Trans. 1*, 1979, 3113; A. M. Costero, C. Andreu, R. Martínez-Máñez, J. Soto, L. E. Ochando and J. M. Amigó, *Tetrahedron*, 1997, 8159.

4 Y. Nagao, T. Miyasaka, K. Seno and E. Fujita, *Heterocycles*, 1981, **15**, 1037.

5 (*a*) A. Bencini, M. I. Burguete, E. García-España, S. V. Luis, J. F. Miravet and C. Soriano, *J. Org. Chem.*, 1993, **58**, 4749; M. I. Burguete, B. Escuder, J. C. Frias, E. García-España, S. V. Luis and J. F. Miravet, *J. Org. Chem.*, 1998, 63, 1810; (*b*) J. Aguilar, E. García-España, J. A. Guerrero, S. V. Luis, J. M. Llinares, J. F. Miravet, J. A. Ramírez and C. Soriano, *J. Chem. Soc., Chem. Commun.*, 1995, 2237; M. I. Burguete, E. García-España, S. V. Luis, J. F. Miravet, L. Payá, M. Querol and C. Soriano, *Chem. Commun.*, 1998, 1823.

Communication 8/09912J

ChemComm

A three-component coupling protocol for the synthesis of substituted hexahydropyrrolo[3,2-*c*]quinolines

Robert A. Batey,* Paul D. Simoncic, Denny Lin, Robert P. Smyj and Alan J. Lough†

Department of Chemistry, University of Toronto, Toronto, Ontario, Canada M5S 3H6.
E-mail: rbatey@alchemy.chem.utoronto.ca

Received (in Corvallis, OR, USA) 7th December 1998, Accepted 10th February 1999

One pot reaction of anilines, benzaldehydes and 2-pyrrolines under lanthanide triflate catalysis affords substituted hexahydropyrrolo[3,2-*c*]quinolines in good to excellent yields.

Multi-component coupling reactions are of growing interest in synthetic organic chemistry, because of their applications in combinatorial chemistry.[1] Those reactions that provide access to novel heterocyclic structures are particularly useful, because of the importance of heterocycles as scaffolds in pharmaceutical development. However, there are relatively few examples of such reactions, and a need exists to expand the repertoire of multi-component coupling methods leading to heterocycles. Accordingly, we now report a versatile one-pot synthesis of substituted hexahydropyrrolo[3,2-*c*]quinolines utilizing a Lewis acid promoted three component coupling reaction.[2]

We have become interested in hexahydropyrrolo[3,2-*c*]quinolines because of the recent isolation of the alkaloids martinelline **1** and martinellic acid **2** from the roots of the

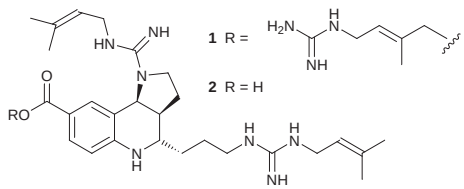

Amazonian plant *Martinella iquitosensis*.[3] These compounds are the first natural products containing a hexahydropyrrolo[3,2-*c*]quinoline core structure. Tetrahydroquinolines and 4-aminoquinolines, of which **1** is an example, are found in a number of pharmaceutically active compounds.[4] Indeed, martinelline has antibiotic activity, affinity for several G-protein coupled receptors, and was the first example of a naturally occurring non-peptidic bradykinin receptor antagonist.[3,5] The core structure is thus of pharmaceutical interest, with the potential for functionalization of the rigid heterocyclic scaffold and/or the two differentiated amine groups.

Although there are several reports of the synthesis of pyrrolo[3,2-*c*]quinolines, these usually require a number of steps, proceed in modest yields, and do not give compounds at the same oxidation state as **1**.[6] We envisaged a highly convergent route, involving a three-component coupling reaction of anilines **3**, benzaldehydes **4**, and the *N*-substituted 2-pyrroline **5**, for the synthesis of differentially substituted analogs **6** (Scheme 1). The *in situ* formed imine generated upon condensation of **3** and **4** can act as a diene, in a formal hetero-Diels–Alder reaction with the electron-rich dienophile **5**.[7] This approach is analogous to the formation of 4-alkoxytetrahydroquinolines, such as the $BF_3{\cdot}OEt_2$ and $EtAlCl_2$ promoted reaction of 2,3-dihydrofuran and the imine formed between aniline and benzaldehyde.[8] Recent findings by Kobayashi have shown that lanthanide triflates[9] will similarly catalyze the reaction of cyclopentadiene or dihydrofuran with *in situ* formed imines derived from anilines and aldehydes.[10]

Endocyclic enamine derivatives such as **5**[11] have not previously been employed in these reactions, and we were delighted to find that lanthanide triflates catalyze their addition (Table 1). Treatment of PhCHO (1.4 equiv.), $PhNH_2$ (1.4 equiv.) and **5** with $Dy(OTf)_3$ (0.07 equiv.) afforded **6a**‡ in 91% yield as an approximately 1 : 1 mixture of readily separable *endo* and *exo* diastereomers, where H3a and H4 have a *cis* and *trans* relationship respectively.[12] The reaction is remarkably facile, and because of the air and water stability of the catalyst, the reaction requires no special precautions. There is little effect on the choice of lanthanide triflate catalyst on the outcome of the reaction, although $Dy(OTf)_3$ gives marginally better yields. Deprotection of the BnO_2C group in the adducts is readily achieved by hydrogenolysis with Pearlman's catalyst. For example, deprotection of the *endo* and *exo* diastereomers of **6a** occurs in 87 and 98% yield, respectively.

The mechanism for the three component coupling reaction presumably involves complexation of the *in situ* formed imine by the lanthanide triflate catalyst, promoting stepwise nucleophilic addition of the electron-rich 2-pyrroline **5** (*i.e.* formation of the C3a–C4 bond), followed by electrophilic aromatic substitution of the aniline ring by the incipient *N*-acyl iminium ion intermediate (*i.e.* formation of the C9a–C9b bond). The initial addition step thus controls the diastereoselectivity of the reaction. The diastereoselectivity is strongly solvent dependent (Table 2). Although there is relatively little effect using dry solvents, a significant change in diastereoselectivity in favor of the *endo* product was observed using water as a co-solvent (entries 6–8, Table 2). The use of THF–water (4 : 1) as solvent results in an enhancement of the de to 92%, but occurs in lower yields (entry 8, Table 2). The origin of the enhanced diastereoselectivity is unclear, but the hydrophobic effect[13] would presumably favor the more compact transition state leading to the *endo* products.

Interestingly, we have found that in the absence of an aldehyde, anilines **3** will couple with *two equivalents* of endocyclic enamines such as **5**. For example, treatment of methyl 4-aminobenzoate with **5** gave **7** in excellent yield as mainly the *endo* diastereomer (Scheme 2).[14] Deprotection of **7** proceeded smoothly with Pearlman's catalyst to yield the free amine **8** in 88% yield as an 85 : 15 mixture of diastereomers in favour of the *endo* product (Scheme 2). The formation of **7** is the first example of a coupling of this type, and presumably occurs *via* the imine formed on condensation of the aniline with the *in situ* hydrolysis product of **5**. This imine may also form directly

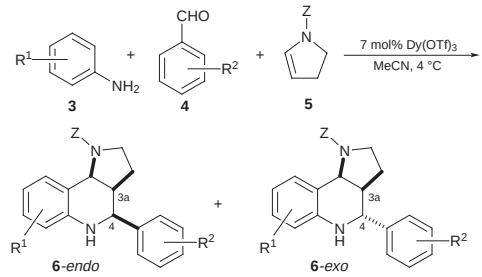

Scheme 1

† To whom correspondence concerning crystal data should be addressed.

Table 1 Synthesis of substituted hexahydropyrrolo[3,2-*c*]quinolines **6**[a,b]

	Compound	R^1	R^2	R^3	R^4	R^5	Yield (%)	*endo* : *exo*
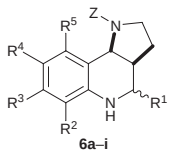	**6a**	Ph	H	H	H	H	91	51 : 49
	6b	3,4-$Cl_2C_6H_3$	H	H	H	H	93	57 : 43
	6c	4-$MeOC_6H_4$	H	H	H	H	84	50 : 50
	6d	2-MeC_6H_4	H	H	H	H	96	42 : 58
	6e	4-$O_2NC_6H_4$	H	H	H	H	96	53 : 47
	6f	Ph	H	H	MeO_2C	H	61	50 : 50
	6g	3,4-$Cl_2C_6H_3$	Cl	H	Cl	Cl	47	40 : 60
	6h	3,4-$Cl_2C_6H_3$	H	O_2N	H	H	65	55 : 45
	6i	3,4-$Cl_2C_6H_3$	–N=CHCH=CH–		H	H	78	63 : 37

6a–i

[a] *Conditions*: **5** (1.0 equiv.), **3** (1.4 equiv.), **4** (1.4 equiv.), $Dy(OTf)_3$ (7 mol%), MeCN, 4 °C, 16 h. [b] Yields are for chromatographically pure material, and diastereomeric ratios are based upon NMR analysis of the crude products.

Table 2 Solvent effects on the diastereoselectivity of the formation of **6a**

Entry	Solvent[a]	Dr (*endo* : *exo*)[b]	Yield (%)[c]
1	MeCN	51 : 49	91
2	CH_2Cl_2	54 : 46	72
3	$MeNO_2$	45 : 55	86
4	DMF	70 : 30	35[d]
5	CF_3CH_2OH	45 : 55	73
6	MeCN–H_2O (9 : 1)	65 : 35	55
7	DMF/H_2O (4 : 1)	97 : 3	26
8	THF–H_2O (4 : 1)	96 : 4	47

[a] *Conditions*: [**5**] = 0.14 M, **3a** (1.4 equiv.), **4a** (1.4 equiv.), $Dy(OTf)_3$ (7 mol%), 4 °C, 16 h. [b] Diastereomeric ratios are based upon NMR analysis of the crude products. [c] Yields are for chromatographically purified material. [d] Material isolated was 95% pure by ^{1}H NMR analysis.

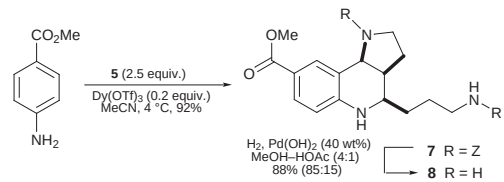

Scheme 2

via addition of aniline to protonated **5**, followed by ring-opening. The structural similarities of **7** with **1** may indicate an analogous process occurs in the biosynthesis of martinelline.

In summary, a convergent method for the synthesis of hexahydropyrrolo[3,2-*c*]quinolines has been established, using a lanthanide triflate catalysed three-component coupling reaction. Further studies towards control of the diastereoselectivity of this process for the synthesis of **1**, and other multi-component coupling reactions of endocyclic enamine derivatives, will be reported in due course.

We thank Astra Pharma Inc. and the Natural Sciences and Engineering Research Council of Canada (NSERC) for financial support of this work. P. D. S. thanks the NSERC for a Postgraduate Scholarship. We thank Dr A. B. Young for mass spectroscopic assistance.

Notes and references

‡ The synthesis of **6a** is representative. To a solution of $Dy(OTf)_3$ (32 mg, 0.05 mmol) in MeCN (2.0 ml) at 4 °C was added PhCHO (100 µl, 0.98 mmol) and $PhNH_2$ (89 µl, 0.98 mmol) in MeCN (1.0 ml) *via* cannula. After stirring for 5 min, a solution of **5** (108 mg, 0.705 mmol) in MeCN (1.0 ml) was added *via* cannula. The reaction was stirred under N_2 for 16 h at 4 °C. The reaction was quenched with H_2O and extracted with CH_2Cl_2 (3 × 30 ml). The combined organic extracts were washed with brine, dried, concentrated *in vacuo* and filtered through a plug of silica gel. The crude products were purified *via* flash chromatography (silica gel, EtOAc–hexanes, CH_2Cl_2 or CH_2Cl_2–MeOH) to yield the two separable diastereomers. Ratios of diastereomers were determied *via* ^{1}H NMR analysis of the crude mixtures.

1 R. W. Armstrong, A. P. Combs, P. A. Tempest, S. D. Brown and T. A. Keating, *Acc. Chem. Res.*, 1996, **29**, 123; A. Nefzi, J. M. Ostresh and R. A. Houghten, *Chem. Rev.*, 1997, **97**, 449.
2 Presented in part at the 15th International Symposium on Synthesis in Organic Chemistry of the Royal Society of Chemistry, Oxford, UK, July 1997; paper P47, and at the 79th Canadian Society for Chemistry Conference, St. John's, Newfoundland, June 1996.
3 K. M. Witherup, R. W. Ransom, A. C. Graham, A. M. Bernard, M. J. Salvatore, W. C. Lumma, P. S. Anderson, S. M. Pitzenberger and S. L.Varga, *J. Am. Chem. Soc.*, 1995, **117**, 6682.
4 A. R. Katritzky, S. Rachwal and B. Rachwal, *Tetrahedron*, 1996, **52**, 15 031.
5 Bradykinin (BK) is an endogenous nonapeptide, and BK antagonists have potential for the treatment of chronic inflammatory conditions, shock, pain, rhinitis and asthma: J. M. Hall, *Gen. Pharmacol.*, 1997, **28**, 1.
6 S. S. Kim, H. G. Cheon, S. K. Kang, E. K. Yum and J. K. Choi, *Heterocycles*, 1998, **48**, 221; T. C. T. Ho and K. Jones, *Tetrahedron*, 1997, **53**, 8287; M. K. Gurjar, S. Pal and A. V. R. Rao, *Heterocycles*, 1997, **45**, 231; K. K. Park and H. Rapoport, *J. Heterocycl. Chem.*, 1992, **29**, 1031; T. H. Brown, R. J. Ife, D. J. Keeling, S. M. Laing, C. A. Leech, M. E. Parsons, C. A. Price, D. R. Reavill and K. J. Wiggall, *J. Med. Chem.*, 1990, **33**, 527.
7 For reviews on hetero-Diels–Alder reactions: D. L. Boger, in *Comprehensive Organic Synthesis*, ed. B. M. Trost, I. Fleming and L. A. Paquette, Pergamon, Oxford, 1991, vol. 5, p. 451; S. M. Weinreb, in *Comprehensive Organic Synthesis*, ed. B. M. Trost, I. Fleming and L. A. Paquette, Pergamon, Oxford, 1991, vol. 5, p. 401.
8 For the first examples of this type of cycloaddition reaction, see: L. S. Povarov, *Russ. Chem. Rev.*, 1967, **36**, 656. See also: T. Kametani, H. Furuyama, Y. Fukuoka, H. Takeda, Y. Suzuki and T. Honda, *J. Heterocycl. Chem.*, 1986, **23**, 185; T. Kametani, H. Takeda, Y. Suzuki and T. Honda, *Synth.Commun.*, 1985, **15**, 499. For a detailed mechanistic discussion: V. Lucchini, M. Prato, G. Scorrano, M. Stivanello and G. Valle, *J. Chem. Soc., Perkin Trans. 2*, 1992, 259.
9 T. Imamoto, *Lanthanides in Organic Synthesis*, Academic Press, London, 1994; G. A. Molander, *Chem. Rev.*, 1992, **92**, 29.
10 S. Kobayashi, H. Ishitani and S. Nagayama, *Chem. Lett.*, 1995, 423; *Synthesis*, 1995, 1195; Y. Makioka, T. Shindo, Y. Taniguchi, K. Takaki and Y. Fujiwara, *Synthesis*, 1995, 801; S. Kobayashi and S. Nagayama, *J. Am. Chem. Soc.*, 1996, **118**, 8977.
11 G. A. Kraus and K. Neuenschwander, *J. Org. Chem.*, 1981, **46**, 4791; Y. Nomura, K. Ogawa, Y. Takeuchi and S. Tomoda, *Chem. Lett.*, 1977, 693.
12 The ^{1}H NMR spectra of the *endo* and *exo* products are easily distinguished, and correlate well along the series **6a-i**. The *endo* and *exo* stereochemistry was determined unambiguously by crystal structure determinations of **6f**-*endo* and **6g**-*exo*. *Crystal data* for **6f**-*endo*: $C_{27}H_{26}N_2O_4$, M = 442.50, orthorhombic, $P2_12_12$, a = 11.0687(14), b = 25.113(3), c = 7.8901(8) Å, V = 2193.2(5) Å^3, Z = 4, T = 173(2) K, D_c = 1.340 Mg m^{-3}, μ = 0.090 mm^{-1}, 3622 reflections collected, 3622 independent reflections, $R1$ = 0.0426, $R2$ = 0.1042. For **6g**-*exo*: $C_{25}H_{19}Cl_5N_2O_2$, M = 556.67, monoclinic, $P2_1/c$, a = 12.4852(8), b = 20.673(2), c + 19.5393(14) Å, β = 105.48(2)°, V = 4860.4(6) Å^3, Z = 8, T = 293(2) K, D_c = 1.521 Mg m^{-3}, μ = 0.624 mm^{-1}, 21842 reflections collected, 6312 independent reflections, $R1$ = 0.0528, $wR2$ = 0.1333. CCDC 182/1171.
13 C.-J. Li and T.-H. Chan, *Organic Reactions in Aqueous Media*, Wiley, New York, 1997.
14 Attempted three-component coupling of simple aliphatic aldehydes such as pentanal with **5** and an aniline does not result in the formation of aldehyde derived adducts, but instead leads to the formation of **7**.

Communication 8/09614G

New chemoenzymatic approach to glyco-lipopolymers: practical preparation of functionally active galactose–poly(ethylene glycol)–distearoylphosphatidic acid (Gal–PEG–DSPA) conjugate

Samuel Zalipsky,* Nasreen Mullah, Andrew Dibble and Terrence Flaherty

SEQUUS Pharmaceuticals, Inc., 960 Hamilton Court, Menlo Park, CA94025, USA. E-mail: samuelz@sequus.com

Received (in Corvallis, OR, USA) 11th January 1999, Accepted 24th January 1999

A practical approach to galactose–PEG–distearoylphosphatidic acid (DSPA) retaining full lectin binding, involves glycosylation of monobenzyl ether–PEG, suitable protection of the sugar hydroxy groups, debenzylation, followed by enzymatic transphosphatidylation with phosphatidylcholine and final deprotection.

The ability of poly(ethylene glycol) (PEG) conjugates of lipids, usually phosphatidylethanolamine (PE),[1] to increase systemic circulation and concomitantly decrease uptake of micelles or liposomes by the reticuloendothelial system is well recognized and routinely used. To combine this useful property with a ligand specific targeting, we and others introduced a series of ligand–PEG–lipid conjugates and their liposomes.[2] Among the ligands used in this capacity are antibodies, and fragments thereof, peptides, vitamins, and carbohydrates. The latter group of ligands is particularly promising. These are small and very polar molecules of low immunogenicity. There are a host of useful carbohydrate–receptor interactions suitable for utilization in PEG-grafted liposomes.[3] These ligands, even when individually of only weak binding affinity, maximize the targeting ability through a multivalent array presentation on the surface of a liposome. Saccharide–PEG–lipid conjugates are rather challenging synthetic targets. There are only a few examples of their preparation.[4–6] Here we describe a new chemoenzymatic approach to these constructs. The method is exemplified by the preparation of galactose–PEG–DSPA, which in its liposomal formulation exhibits substantial lectin-binding activity. This conjugate is potentially suitable for targeting liposomes to the asialoglycoprotein receptors expressed on liver hepatocytes.[7]

The synthetic pathways employed in this study are summarized in Scheme 1. Initially we explored preparation of PEG-yl–β-D-galactopyranoside (Gal–PEG). Enzymatic galactosylation of monobenzyl ether PEG (BnO–PEG–OH)[8] of molecular weight 2000 Da utilizing β-galactosidase proceeded well under modified conditions described by Matsushima *et al.*[9] resulting in formation of β-Gal*p*–O–PEG–OBn in 25% isolated yield. We also explored a two step chemical approach to the same product utilizing first iodonium ion promoted thioglycoside-mediated attachment of the peracetylated Gal*p* moiety,[10] followed by deacetylation. Although longer, this approach yielded galactosylated PEG derivatives in essentially quantitative yield. β-Glycosides were exclusively formed from both the enzymatic and chemical methods (Fig. 1a).

Recently we developed a new method for the preparation of phosphatidyl–PEG by an enzymatic process utilizing phospholipase D and distearoyl phosphatidylcholine.[11] To apply this reaction to Gal–O–PEG–OBn, the benzyl group had to be removed and the primary hydroxy group at C-6 of the galactose moiety had to be suitably protected.[12] Silylation with excess of TBDMS-Cl in presence of the DMAP provided the desired monoprotected saccharide along with several oversilylated products. Oversilylation had no bearing on the final outcome of the synthesis. Removal of the benzyl ether from the other terminal of the PEG chain proceeded quantitatively under catalytic transfer hydrogenation conditions with Pd/C and ammonium formate in MeOH.[13] Enzymatic elaboration of the distearoylphosphatidyl moiety proceeded smoothly in CCl_4–acetate buffer, pH 5.6, in 50% yield, and finally silyl groups

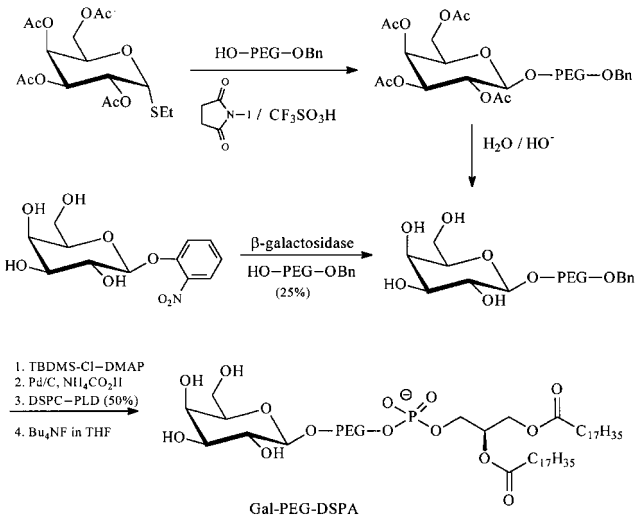

Scheme 1 Reaction pathways used in this study. Yields of the transformations shown were quantitative unless indicated in parentheses (PEG ≡ –(CH_2CH_2O)$_{44}$–CH_2CH_2–).

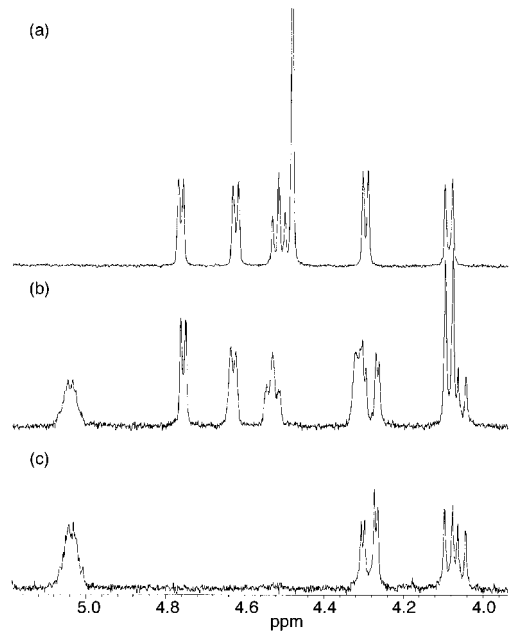

Fig. 1 ^{1}H-NMR (360 MHz, d_6-DMSO) spectra of (a) Gal–PEG–OBn, (b) Gal–PEG–DSPA, and (c) MeO–PEG–DSPA. Only the region 3.8–6 ppm containing the characteristic signals of the sugar and glycerophospho moieties is shown. Characteristic peaks of stearoyl (t 0.84, s 1.24, m 1.50, m 2.24 ppm in b and c only) and PEG (s 3.5 ppm) residues were present.

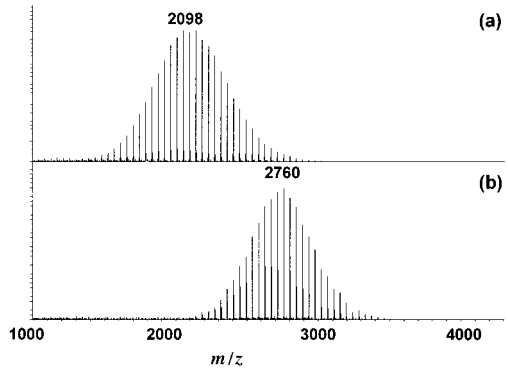

Fig. 2 MALDI-TOFMS of (a) Gal–PEG–OBn and (b) Gal–PEG–DSPA. Spectra were acquired on a PHI-EVANS MALDI triple electrostatic TOFMS analyzer using a 337 nm (600 ps pulse width) desorption laser, and gentisic acid as the matrix material.

were cleanly removed by fluoridolysis to provide Gal–PEG–DSPA. Fig. 1 illustrates the ^{1}H-NMR spectra of β-Gal*p*–O–PEG–OBn (a), β-Gal*p*–O-PEG–DSPA (b), and for comparison MeO–PEG–DSPA (c). The presence of a H-1 signal (d, 4.08 ppm, $J_{1,2}$ = 7.2 Hz) of the β-linked Gal residue as well as an additional primary and three secondary hydroxy groups is clearly seen. The final product also produced the characteristic signals of a glycerophospholipid moiety (dd at 4.1 and 4.3 ppm, as well as m at 5.1 ppm), the first two signals overlapping with the anomeric hydrogen and another secondary OH peak. Further corroboration of the structure of the glycosylated conjugates was obtained by matrix-assisted laser desorption ionization-time of flight mass spectrometry (MALDI-TOF MS) (Fig. 2). Single-modal distributions of signals equally spaced at 44 Da intervals of the ethylene oxide repeating unit of PEG are clearly visible. Average molecular weights of the galactosylated PEG derivatives were in accordance with the expected values.

To ascertain the functional activity of Gal–PEG–DSPA, the conjugate was incorporated at 0, 1, and 5 mol% into egg-phosphatidylcholine large unilamellar vesicles. Interaction of the liposomes with *Ricinus communis* lectin (RCA-I) was monitored turbidometrically as illustrated in Fig. 3. It was observed that the lectin caused agglutination of the liposomes, which was more intense with a higher content of Gal–PEG–DSPA. The agglutination process could be inhibited by Gal–PEG–OBn; however, a 10-fold excess over liposome-bound Gal was required to achieve 50% inhibition. Complete inhibition was observed at 25-fold excess of the competitor. Similar experiments with lactose acting as a competitor showed that it was approximately 5-fold more effective at inhibiting agglutination than Gal–PEG–OBn (data not shown). Thus the multivalent liposome was binding more avidly than either one of the two monovalent competitors. It is interesting that the presence of MeO–PEG_{2000}–DSPA conjugate in the same lipid vesicles greatly inhibited agglutination. We previously observed a similar inhibitory effect on the binding of folate–PEG–liposomes to folate receptor-bearing cells.[14] It is pertinent to note that our findings do not support observations of Shimada *et al.*[5] They prepared Gal–PEG–lipids containing acyl glycosidic linkages and PEG tethers of different lengths, and reported that only liposomal preparations of the conjugates with decaethylene oxide spacer, and no longer, were agglutinated with RCA lectin.

We developed a practical method for the preparation of glyco-lipopolymers of the type Gal–PEG–DSPA. Lectin binding activity of the galactopyranoside moiety was well preserved, although it was inhibited if substantial amounts of MeO-PEG-lipid was included in the same liposomes. Monovalent

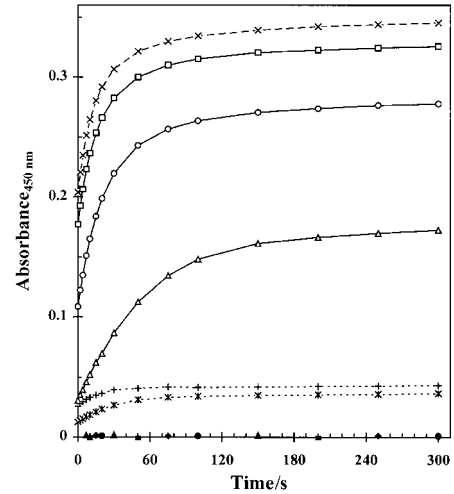

Fig. 3 Turbidometric measurements of RCA-I (50 μg ml^{-1}) mediated agglutination of Gal–PEG–DSPA containing liposomes (0.5 mM total lipid; 120–130 nm mean particle size). Liposomes containing 5 mol% Gal–PEG–DSPA (×), 5 mol% Gal–PEG–DSPA and 5 mol% MeO-PEG-DSPA (+), 1 mol% Gal–PEG–DSPA (✻), 1 mol% Gal–PEG–DSPA and 5 mol% MeO–PEG–DSPA (▲), without any PEG-lipids (●), 5 mol% MeO–PEG–DSPA (◆). Agglutination of liposomes containing 5 mol% Gal–PEG–DSPA in presence of Gal–PEG–OBn at 25 (□), 125 (○), 250 (△) and 625 μM (■).

Gal–PEG was more than one order of magnitude weaker at binding to the lectin than liposomal Gal–PEG–DSPA, suggesting that multivalent presentation of the carbohydrate moiety results in more effective binding.

Notes and references

1 S. Zalipsky, in *Stealth Liposomes*, ed. D. Lasic and F. Martin, Boca Raton, FL, 1995, pp. 93–102, and refs. cited therein.
2 S. Zalipsky, J. Gittelman, N. Mullah, M. M. Qazen and J. A. Harding, in *Targeting of Drugs 6: Strategies for Stealth Therapeutic Systems*, ed. G. Gregoriadis, New York, 1998, pp. 131–138, and refs. cited therein.
3 H.-J. Gabius, *Angew. Chem., Int. Ed. Engl.*, 1988, **27**, 1267, and refs. cited therein.
4 S. A. DeFrees, L. Phillips, L. Guo and S. Zalipsky, *J. Am. Chem. Soc.*, 1996, **118**, 6104.
5 K. Shimada, J. A. A. M. Kamps, J. Regts, K. Ikeda, T. Shiozawa, S. Hirota and G. L. Scherphof, *Biochim. Biophys. Acta*, 1997, **1326**, 329.
6 S. Zalipsky, N. Mullah, J. A. Harding, J. Gittelman, L. Guo and S. A. DeFrees, *Bioconjugate Chem.*, 1997, **8**, 111.
7 G. Ashwell and J. Harford, *Ann. Rev. Biochem.*, 1982, **51**, 531, and refs. cited therein.
8 J. M. Harris, M. R. Sedaghat-Herati, P. J. Sather, D. E. Brooks and T. M. Fyles, in *Poly(ethylene glycol) Chemistry: Biotechnical and biomedical applications*, ed. J. M. Harris, New York, 1992, pp. 371–381.
9 S. Matsushima, H. Kubokawa and K. Toshima, *Makromol. Chem. Rapid Commun.*, 1993, **14**, 55.
10 G. H. Veeneman, S. H. van Leeuwen and J. H. van Boom, *Tetrahedron Lett.*, 1990, **31**, 1331.
11 S. Zalipsky, unpublished results.
12 P. Wang, M. Schuster, Y.-F. Wang and C.-H. Wong, *J. Am. Chem. Soc.*, 1993, **115**, 10487.
13 M. K. Anwer and A. F. Spatola, *Synthesis*, 1980, 929.
14 A. Gabizon, A. Horowitz, D. Goren, D. Tzemach, F. Mandelbaum-Shavit, M. Qazen and S. Zalipsky, *Bioconjugate Chem.*, 1999, **10**, 289.

Paper 9/00355J

ChemComm

Efficient thermochemical alkane dehydrogenation and isomerization catalyzed by an iridium pincer complex

Fuchen Liu and Alan S. Goldman*

Department of Chemistry, Rutgers University, Piscataway, NJ 08854-8087, USA.
E-mail: goldman@rutchem.rutgers.edu

Received (in Bloomington, IN, USA) 22nd January 1999, Accepted 9th February 1999

(i-^{Pr}PCP)IrH$_2$ is found to be a remarkably effective solution-phase catalyst for the 'acceptorless' thermochemical dehydrogenation of cycloalkanes (and isomerization in the case of cyclodecane), and the first such catalyst reported to effect the dehydrogenation of *n*-alkanes.

Alkanes are the world's most abundant organic resource, yet methods for their conversion to useful chemicals remain extremely limited. Alkenes, by contrast, are probably the single most useful and versatile class of feedstock for commodity-scale organic chemical syntheses. Methods for the dehydrogenation of alkanes to give alkenes are therefore of great interest.[1]

In general, the yields and selectivity afforded by heterogeneous alkane dehydrogenation catalysts are very low.[1] Soluble transition metal complexes, however, have held promise in this respect since the early 1980s when Crabtree and Felkin reported the development of catalysts for transfer-dehydrogenation.[2]

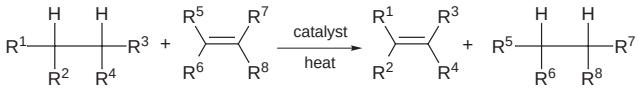

The initially reported catalysts suffered from ligand degradation which severely limited turnover numbers; systems were later developed that afforded much higher turnover numbers;[3] of these, the most important in the context of the present work was the 'pincer' complex, ($^{t\text{-Bu}}$PCP)IrH$_2$ [**1**; $^{t\text{-Bu}}$PCP = 2,5-C$_6$H$_3$(CH$_2$PBu$^t_2$]].[4]

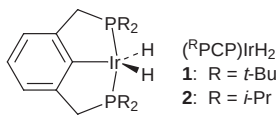

(^{R}PCP)IrH$_2$
1: R = *t*-Bu
2: R = *i*-Pr

Recently [eqn. (1)] it was reported that refluxing alkane solutions of **1** resulted in dehydrogenation with evolution of dihydrogen; no sacrificial hydrogen acceptor was required.[5] Although this was by far the most efficient catalyst to date for such 'acceptorless' dehydrogenation,[6,7] the observed rates were still fairly low by the standards of practical catalytic systems.

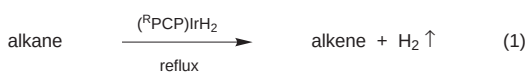

To a significant extent, the pincer geometry 'holds back' the phosphinoalkyl groups such that they are further removed from the metal, and the molecule is sterically less congested, relative to a hypothetical analogous complex of monodentate ligands [*e.g.* Ir(PR$_2$Me)$_2$(Ph)H$_2$]. Nevertheless, Milstein and coworkers recently reported that H_2 adds to the carbonyl complex ($^{i\text{-Pr}}$PCP)Ir(CO)[8] whereas, in contrast, we find that the $^{t\text{-Bu}}$PCP analog undergoes no observable addition of H_2 (800 Torr). Thus in spite of the 'pincer effect' the *tert*-butyl groups are apparently still bulky enough to inhibit H_2 addition; this led us to suspect that alkyl hydrides and other presumed intermediates of a dehydrogenation cycle may be even more sterically disfavored by the *tert*-butyl groups. Accordingly we synthesized† and investigated the $^{i\text{-Pr}}$PCP analog of **1**, *i.e.* ($^{i\text{-Pr}}$PCP)IrH$_2$ (**2**).

Vigorously refluxing (151 °C) a cyclooctane solution of **2** (1.0 mM) leads to the formation of 47 mM cyclooctene (47 turnovers) after 30 min. The reaction rate subsequently levelled off; 105 mM cyclooctene was present after 15 h. This initial dehydrogenation rate (>94 turnover h^{-1}) may be compared with 11 turnover h^{-1} resulting from cyclooctane dehydrogenation catalyzed by **1** under similar conditions,[5] and 1.41 turnover h^{-1} reported for IrH$_2$(O$_2$CCF$_3$)(PCy$_3$)$_2$.[7]

Cyclodecane, with a reflux temperature of 201 °C, undergoes dehydrogenation at a much greater rate than cyclooctane: for example *460 turnovers cyclodecene* are obtained after 1 h of reflux, (*cis*:*trans* ratio of 4.6:1; see Table 1). This compares, for example, with 170 turnover after 4 h obtained from the use of catalyst **1**.[5] The isopropyl derivative **2** is thus an extremely efficient catalyst for acceptorless dehydrogenation of cycloalkanes, yielding turnover rates a full order of magnitude greater than the *tert*-butyl derivative.

The dehydrogenation enthalpy of cyclooctane, and probably that of cyclodecane as well, is anomalously low.[9–12]‡ Accordingly, with *n*-alkanes, the $^{t\text{-Bu}}$PCP catalyst **1** gave no observable yields of acceptorless dehydrogenation product.§ By contrast, **2** is able to catalyze the acceptorless dehydrogenation of *n*-alkanes, though the efficiency is less than that with cyclodecane. Refluxing an *n*-undecane solution of **2** (1.0 mM; 196 °C) yields 35.4 mM undecenes, as a mixture of internal isomers (not fully characterized), after 0.5 h. Unfortunately, the yield quickly levelled off and after 1 and 45 h the respective concentrations of undecenes were 42.3 and 44.1 mM. This represents the first report of a homogenous catalytic system for the dehydrogenation of *n*-alkanes.

To determine whether product concentrations level off due to catalyst decomposition or product inhibition, we allowed an *n*-decane solution of **2** to reflux (174 °C) until the decene concentration reached a constant value.§ Volatiles (decenes and decane) were then removed and fresh *n*-decane was added; upon refluxing, the kinetics of decene production were identical to those of the initial run indicating that the catalyst did not decompose. This result is similar to that obtained previously for **1**-catalyzed dehydrogenation of cyclooctane.[5] In the case of *n*-alkanes, however, the removal of product, if sufficiently rapid, could have an additional and very significant benefit. When *n*-alkane dehydrogenation is conducted (at 150 °C) using *a*

Table 1. Dehydrogenation and isomerization of cyclodecane catalyzed by **2**[a]

t/h	*cis*-Cyclodecene	*trans*-Cyclodecene	*cis*-DEC[b]	*trans*-DEC
1	378	82	16	10
4	619	145	38	59
8	692	163	42	79
20	700	163	43	81

[a] Refluxing cyclodecane; 1.0 mM **2**; values are turnover numbers (equal to concentration/mM). [b] DEC = diethylcyclohexane.

sacrificial acceptor, the major kinetic product is the terminal (α) olefin which then undergoes isomerization to the more stable internal olefins.[13] Presumably the same kinetic product is formed in the absence of an acceptor but isomerization is much more rapid relative to dehydrogenation; accordingly, added dec-1-ene is rapidly isomerized (> 99% in 2.5 min) in refluxing *n*–undecane. Thus, efficient dynamic removal of product from the mixture might lead not only to high turnover numbers, but also to high regioselectivity for α-olefins in the case of *n*-alkanes.

Returning to the **2**-catalyzed dehydrogenation of cyclodecane, two intriguing products other than *cis*- and *trans*-cyclodecene are observed to accumulate in significant concentration (by GC and GC–MS); GC–MS and ^{1}H NMR data indicate them to be diethylcyclohexanes (DEC). When *cis*- and *trans*-1,2-DEC were independently generated by the hydrogenation of 1,2-diethylbenzene; ^{1}H NMR, GC and GC–MS data were in complete agreement with those of the cyclodecane reaction products.

The unprecedented isomerization of cyclodecane to *cis*- and *trans*-1,2-DEC might seem to suggest the involvement of a cyclodecane C–C bond activation step. It is difficult, however, to envisage such a mechanism that would account for the selectivity of this ring-contraction. Furthermore, the formation of DEC's appeared to be a secondary reaction since the ratio of the DEC's to cyclodecenes significantly increased with time (Table 1). This leads us to propose, for the overall isomerization reaction, the mechanism of Scheme 1 which receives strong additional support from the following observations:

(i) A mixture of **2** (1.0 mM) and cyclodecene (200 mM) in *n*-undecane solvent was refluxed (196 °C). After 30 min, 4.2 mM diethylcyclohexane had appeared (*ca*. 2 : 1 *trans* : *cis*);¶ in addition, *ca*. 50% of the cyclodecene had been transfer-hydrogenated to cyclodecane (with commensurate formation of undecenes), while 98 mM cyclodecene remained. This rate of DEC formation (8.4 turnover h^{-1}; 149 mM time-averaged concentration of cyclodecene) is proportional to the time-averaged concentration of cyclodecene present in the reactions that began with cyclodecane only; *i.e.* this result is entirely consistent with the DEC being derived from cyclodecene (not directly from cyclodecane).

(ii) *trans*,*trans*-1,5-cyclodecadiene has been reported to undergo a thermal Cope rearrangement to give *trans*-1,2-divinylcyclohexane.[14]‖ Extrapolating the rate data to 201 °C gives a rate of 1.2 s^{-1},[14]** which is clearly consistent with Scheme 1 and the lack of build-up of observable quantities of the cyclodiene. Presumably, cyclodecadienes other than the 1,5-isomers are initially formed and these undergo isomerization to the 1,5-diene which then undergoes rearrangement.

(iii) Since divinylcyclohexane is not formed in an observable quantity, the mechanism of Scheme 1 requires that this intermediate is rapidly hydrogenated under the reaction conditions. Accordingly, when a cyclodecane solution of **2** (1.0 mM) and added vinylcyclohexane (100 mM) was refluxed, after only 10 min 100% conversion to ethylcyclohexane was observed.

In summary, we describe the first homogeneous catalyst system to dehydrogenate alkanes at rates that might be considered suitable for a practical and useful system. It would appear that efficient removal of the olefin product, by either physical or chemical means, might lead to dramatically increased yields and even regioselectivity. The formation of DEC represents a novel example of catalytic alkane functionalization proceeding *via* dehydrogenation and a secondary olefin reaction.

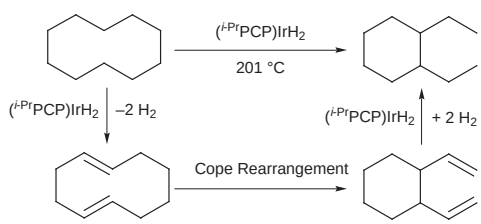

Scheme 1

Support by the Division of Chemical Sciences, BES, OER, US Department of Energy is gratefully acknowledged. We thank Johnson-Matthey for a generous loan of iridium.

Notes and references

† The protonated $^{i\text{-Pr}}$PCP ligand was synthesized according to Milstein[8] and reacted with [Ir(cyclooctene)$_2$Cl] in refluxing toluene for 3 days. The resulting ($^{i\text{-Pr}}$PCP)IrHCl was isolated and converted to ($^{i\text{-Pr}}$PCP)IrH$_2$ using the procedure previously reported for ($^{t\text{-Bu}}$PCP)IrH$_2$.[4]

‡ The dehydrogenation enthalpy of cyclooctane is *ca.* 23.8(5) kcal mol^{-1} as determined by either direct measurement of hydrogenation or on the basis of enthalpies of formation.[9,10] The value for cyclodecane is less certain. Based on available data for enthalpies of formation it would appear to be rather high, at least 30 and 33 kcal mol^{-1} for formation of *cis*- and *trans*-cyclodecene respectively.[9–11] However, direct hydrogenation measurements yield values of −20.7(1) and −24.0(9) kcal mol^{-1}, respectively, in acetic acid solvent.[12] Enthalpies of other cycloalkene hydrogenations in acetic acid, determined by the same workers, are *ca*. 1.3 kcal mol^{-1} less negative than reliable values in hydrocarbon solvent.[9,12] Thus, 22 and 25 kcal mol^{-1} are probably the best estimates for the dehydrogenation of cyclodecane to give *cis*- and *trans*-cyclodecene respectively.

§ An attempt to dehydrogenate *n*-decane using catalyst **1** gave no detectable decene. It is difficult to set an upper limit on the amount of decene produced since as many as eight major isomers could be formed. Nevertheless, the reaction of *n*-decane catalyzed by **2**, unlike that of **1**, gave very easily detectable decene GC peaks indicating total concentrations of 14.4 and 16.1 mM after 0.5 and 5 h respectively.

¶ Both our dehydrogenations and our independent synthesis gave mixtures of the two DEC's; we are unable to assign their respective stereochemistry with high confidence. However, the ratio changes with time during the cyclodecane dehydrogenation and we tentatively assign the product that relatively increases in concentration as the more stable *trans*-DEC.

‖ The product of the uncatalyzed reaction of 1,5-*trans*,*trans*-cyclodecadiene is exclusively the *trans*-DEC isomer in contrast with our observation of a mixture of *trans* and *cis*. However, MOPAC calculations indicate that the 1,5-*cis*,*trans*-cyclodecadiene is the more stable diene; molecular modeling suggests that this isomer would yield *cis*-1,2-diethylcyclohexane. Furthermore, Cope rearrangements can be metal-catalyzed which might represent another pathway leading to the *cis* isomer.

** The measured rates (40–90 °C) give the following activation parameters: $\Delta H^{\ddagger}$ = 24.32 kcal mol^{-1}; $\Delta S^{\ddagger}$ = −7.81 cal mol^{-1} K^{-1}.[14]

1 P. N. Rylander, in *Ullmann's Encyclopedia of Industrial Chemistry*, ed. B. Elvers, J. F. Rounsaville and G. Schulz VCH Verlagsgesellschaft, Weinheim, 1989, p. 494.
2 D. Baudry, M. Ephritikine, H. Felkin and R. Holmes-Smith, *J. Chem. Soc., Chem. Commun.*, 1983, **788**; M. J. Burk, R. H. Crabtree, C. P. Parnell and R. J. Uriarte, *Organometallics*, 1984, **3**, 816.
3 J. A. Maguire and A. S. Goldman, *J. Am. Chem. Soc.*, 1991, **113**, 6706.
4 M. Gupta, C. Hagen, R. J. Flesher, W. C. Kaska and C. M. Jensen, *Chem. Commun.*, 1996, 2083; M. Gupta, C. Hagen, W. C. Kaska, R. E. Cramer and C. M. Jensen, *J. Am. Chem. Soc.*, 1997, **119**, 840.
5 W. Xu, G. P. Rosini, M. Gupta, C. M. Jensen, W. C. Kaska, K. Krogh-Jespersen and A. S. Goldman, *Chem. Commun.*, 1997, 2273.
6 T. Fujii, Y. Higashino and Y. Saito, *J. Chem. Soc., Dalton. Trans.*, 1993, 517.
7 T. Aoki and R. H. Crabtree, *Organometallics*, 1993, **12**, 294.
8 B. Rybtchinski, A. Vigalok, Y. Bendavid and D. Milstein, *Organometallics*, 1997, **16**, 3786.
9 NIST Standard Reference Database Number 69, 1996, http://webbook.nist.gov/chemistry/
10 D. R. Stull, E. F. Westrum and G. C. Sinke, *The Chemical Thermodynamics of Organic Compounds*, Robert E. Kreiger Publishing, Malabar, FL, 1987.
11 J. B. Pedley and J. Rylance, *Computer Analysed Thermochemical Data: Organic and Organometallic Compounds*, University of Sussex, Brighton, UK, 1977.
12 R. B. Turner and W. R. Meador, *J. Am. Chem. Soc.*, 1957, **79**, 4133.
13 F. Liu, E. B. Pak, B. Singh, C. M. Jensen and A. S. Goldman, *J. Am. Chem. Soc.*, in press.
14 P. S. Wharton and D. W. Johnson, *J. Org. Chem.*, 1973, **38**, 4117.

Communication 9/00631A

ChemComm

Investigation of restricted backbone conformations as an explanation for the exceptional thermal stabilities of duplexes involving LNA (Locked Nucleic Acid):† synthesis and evaluation of abasic LNA

Lisbet Kværnø and Jesper Wengel*

Center for Synthetic Bioorganic Chemistry, Department of Chemistry, University of Copenhagen, Universitetsparken 5, DK-2100 Copenhagen, Denmark. E-mail: wengel@kiku.dk

Received (in Cambridge, UK) 18th January 1999, Accepted 25th January 1999

In order to investigate the structural basis of the unique hybridization properties of LNA (Locked Nucleic Acid), an abasic LNA monomer (a 1-deoxy-2-*O*,4-*C*-methylene-D-ribofuranose derivative) was synthesized and evaluated with respect to influence on duplex stability, showing that effects mediated *via* the nucleobase are pivotal for the properties of LNA.

In recent years much attention in the search for effective antisense oligonucleotides has been focused on the synthesis of conformationally restricted analogues, stimulated by the promise of entropically advantageous duplex formation.[1,2] So far,

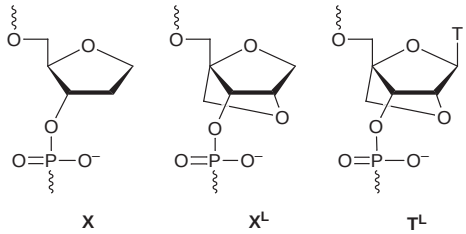

X **X^{L}** **T^{L}**

LNA (Locked Nucleic Acid, thymine monomer **T^{L}**) is showing the most promising properties,[3–7,†] *e.g.* unprecedented thermal stabilities towards complementary DNA and RNA (ΔT_m/modification = +3 to +9 °C), stability towards 3′-exonucleolytic degradation, efficient automated oligomerization and good aqueous solubility. As an attempt to investigate the structural elements of LNA responsible for the remarkably enhanced duplex stabilities we have synthesized and evaluated the hydridization properties of oligonucleotides containing the novel abasic LNA monomer **X^{L}** in comparison with unmodified reference sequences, sequences containing the abasic DNA monomer **X**, and sequences containing thymine LNA monomer **T^{L}**.

The 4-*C*-hydroxymethylfuranose **1** was converted in two steps to the anomeric methyl furanosides **2** (Scheme 1).[8] As previously reported, treatment of **2** with NaH induced cyclization to give furanosides **3** which after hydrolysis afforded the monocyclic aldehyde.[8] Reduction of this aldehyde with $NaBH_4$ proceeded smoothly to give the novel diol **4** in 84% yield (from **2**). Selective tosylation of the primary hydroxy group followed by treatment with NaH afforded the bicyclic skeleton of abasic LNA whereafter hydrogenolysis to give diol **5**,‡ dimethoxytritylation and phosphitylation yielded the phosphoramidite building block **6** suitable for oligonucleotide synthesis. Except for prolonged coupling times (8 min compared with standard 1 min), normal coupling conditions were used for amidite **6** on an automated DNA synthesizer. The stepwise coupling yield was approximately 99% as was also obtained for both the unmodified DNA and RNA phosphoramidites as well as for the commercially available amidite leading to the abasic DNA monomer **X**.

In nucleic acids the conformation of the furanose ring is decisive for the type of duplex formed. The pentofuranose moieties in RNA normally exist in an N-type conformation leading to A-type duplexes, while an S-type conformation as generally seen in DNA leads to B-type duplexes. Also the dihedral phosphate backbone angle C4′–C3′–O3′–P (denoted ε^{t} and ε^{-} for *trans* and *gauche*, respectively[9]) and the furanose conformation have been shown to be interdependent for monomeric nucleotides or single stranded oligonucleotides.[9–12] Thus, for dinucleotides an N-type conformation strongly favours the ε^{t} dihedral angle while a mixture of ε^{t} and ε^{-} is seen for S-type conformations.[9] Studies of ethyl phosphate mononucleotides which mimic dinucleotides with total elimination of base–base stacking interactions likewise show an interdependency between the N/S and $\varepsilon^{t}/\varepsilon^{-}$ equilibria for ethyl ribonucleotides while these two equilibria seem to be independent for ethyl 2′-deoxyribonucleotides.[10–12] The rigid structure of an LNA monomer which restricts the furanose ring to the N-type conformation[3,4,13] is therefore expected to influence the local phosphate backbone fluctuations by quenching the $\varepsilon^{t}/\varepsilon^{-}$ equilibrium.

The question under investigation here is whether the abasic LNA monomer **X^{L}**, which is anticipated to display the same fixed furanose and restricted backbone conformations as the parent LNA monomers (*e.g.* monomer **T^{L}**) but with the exclusion of base–base stacking interactions, induces an increased duplex stability relative to the abasic DNA monomer **X** comparable to the one obtained for the parent LNA monomers relative to the DNA monomers. In this respect, the modified 9- and 13-mer oligodeoxyribonucleotides and oligo-

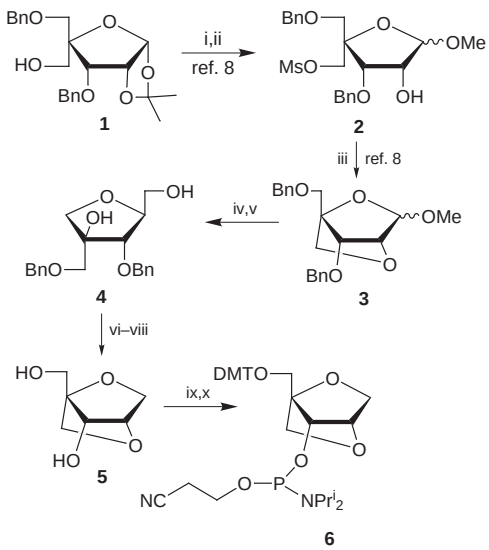

Scheme 1 *Reagents and conditions:* i, MsCl, pyridine; ii, 20% HCl, MeOH–H_2O (7 : 1), iii, NaH, DMF; iv, 80% AcOH; v, $NaBH_4$, MeOH, 84% for 3 steps; vi, TsCl, pyridine, 71%; vii, NaH, DMF, 82%; viii, H_2, Pd/C, 80%; ix, DMTCl, pyridine, 73%; x, $NC(CH_2)_2OP(Cl)NPr^{i}_2$, $EtNPr^{i}_2$, CH_2Cl_2, 62%.

Table 1 Sequences synthesized and T_m values towards fully complementary DNA sequences[a]

Entry	Sequence	Y	T_m/°C
1	5′-d(GTGA-**Y**-ATGC)	T	27
2		**T**^{L}	35
3		**X**	[b]
4		**X**^{L}	[b]
5	5′-r(GUGA-**Y**-AUGC)	U	27
6		**T**^{L}	38
7		**X**^{L}	~3
8	5′-d(CAGTGA-**Y**-ATGCGA)	T	48
9		**T**^{L}	53
10		**X**	27
11		**X**^{L}	27
12	5′-r(CAGUGA-**Y**-AUGCGA)	U	46
13		**T**^{L}	53
14		**X**	29
15		**X**^{L}	29

[a] T_m values measured as the maximum of the first derivative of the melting curve (A_{260} *vs.* temperature) recorded in medium salt buffer (10 mM $NaHPO_4$, 100 mM NaCl, 0.1 mM EDTA, pH 7.0) using 1.5 mM concentrations of the two complementary strands (assuming identical extinction coefficients for T and **T**^{L} and for the different monomeric nucleotides whether present in LNA, the unmodified references or the strands containing an abasic monomer). A = adenosine monomer, C = cytidine monomer, G = guanosine monomer, U = uridine monomer, T = thymidine monomer, **X** = abasic DNA monomer, **X**^{L} = abasic LNA monomer, **T**^{L} = LNA thymine monomer. Oligo-2′-deoxynucleotide sequences are depicted as d(sequence) and oligoribonucleotide sequences as r(sequence). [b] No T_m detected.

ribonucleotides depicted in Table 1 were synthesized§ and their hybridization to fully complementary oligodeoxyribonucleotide sequences [5′-d(GCATATCAC) and 5′-d(TCGCATATCACTG)] was studied. For each oligonucleotide sequence, the melting temperature (T_m value) for the unmodified reference was compared with the T_m values for the analogues containing either one LNA thymine monomer (**T**^{L}), one abasic DNA monomer (**X**) or one abasic LNA monomer (**X**^{L}). The effect of a single LNA monomer on the thermal stability, which hitherto has not been reported, is profound, with ΔT_m values of +8 and +5 °C for deoxy-LNA† (entries 2 and 9, **T**^{L} compared to a thymidine monomer) and +11 and +7 °C for ribo-LNA† (entries 6 and 13, **T**^{L} compared to a uridine monomer¶). In analogy with previously reported data,[14] we observed a detrimental effect of the abasic DNA monomer **X** on the thermal stability (entries 3, 10 and 14, ΔT_m values < -17 °C). The T_m values obtained for the abasic LNA monomer **X**^{L} (entries 4, 7, 11 and 15) were identical to those obtained for **X**. Thus, despite the very large stabilizing effect induced by incorporation of one LNA monomer **T**^{L} instead of a thymidine monomer, no effect resulted from the exchange of the abasic DNA monomer **X** with the abasic LNA monomer **X**^{L}.

NMR investigations[13] on single stranded LNA and LNA:DNA duplexes have shown that LNA monomers induce a shift towars an N-type conformation in neighboring unmodified monomers. Quenched backbone torsions and/or improved nucleobase stacking are possible explanations for this conformational effect. Since the structural difference for both pairs examined herein (**T**^{L} *vs.* T and **X**^{L} *vs.* **X**) is an oxymethylene bridge linking the 2(′)- and the 4(′)-carbon atoms the thermal denaturation studies have shown that conformational restrictions of the pentofuranose and backbone alone are not sufficient to induce an effect. We therefore conclude that the nucleobase is essential as a mediator of the conformational changes.

The Danish Natural Science Research Council, The Danish Technical Research Council and Exiqon A/S are thanked for financial support. Ms Britta M. Dahl is thanked for oligonucleotide synthesis and Dr Carl Erik Olsen is thanked for recording MALDI mass spectra.

Notes and references

† We have defined LNA as an oligonucleotide containing one or more 2′-*O*,4′-*C* methylene linked bicyclic ribonucleoside LNA monomers. Deoxy-LNA consists of 2′-deoxynucleotide and LNA monomers, while ribo-LNA consists of ribonucleotide and LNA monomers (see ref. 3–5).

‡ *Selected data* for **5**: δ_H (CD_3OD) 4.74 (2 H, br s, OH), 4.01 and 4.04 (2 H, 2 s, H-2, H-3), 3.85 (1 H, d, *J* 8.0, H-4'a), 3.85 (1 H, d, *J* 8.0, H-1a), 3.75 (1 H, d, *J* 7.9, H-4'b), 3.74 (1 H, d, *J* 8.2, H-1b), 3.68 (2 H, d, *J* 2.7, H-5), assignment of H-1 and H-4′ signals may be interchanged; δ_C (CD_3OD) 86.28 (C-4), 78.72, 72.54, 72.38 and 71.21 (C-1, C-2, C-3, C-4′), 57.68 (C-5); *m/z* (FAB^+) 147 $[M + H]^+$.

§ MALDI mass data $[M\text{-}H^-]^-$: 5′-d(GTGA-**X**-ATGC) 2630, calc. 2628; 5'-d(GTGA-**X**^{L}-ATGC) 2657, calc. 2656; 5′-r(GUGA-**X**^{L}-AUGC) 2759, calc. 2755; 5′-d(CAGTGA-**X**-ATGCGA) 3874, calc. 3873; 5′-d(CAGTGA-**X**^{L}-ATGCGA) 3901, calc. 3901; 5′-r(CAGUGA-**X**-AUGCGA) 4037, calc. 4036; 5′-r(CAGUGA-**X**^{L}-AUGCGA) 4068, calc. 4064.

¶ We have previously shown for the identical 9-mer sequence that a 'U-LNA monomer' and a 'T-LNA monomer' induce identical T_m values (see ref. 4).

1 P. Herdewijn, *Liebigs Ann. Chem.*, 1996, 1337.
2 E. T. Kool, *Chem. Rev.*, 1997, **97**, 1473.
3 S. K. Singh, P. Nielsen, A. A. Koshkin and J. Wengel, *Chem. Commun.*, 1998, 455.
4 A. A. Koshkin, S. K. Singh, P. Nielsen, V. K. Rajwanshi, R. Kumar, M. Meldgaard, C. E. Olsen and J. Wengel, *Tetrahedron*, 1998, **54**, 3607.
5 S. K. Singh and J. Wengel, *Chem. Commun.*, 1998, 1247.
6 S. Obika, D. Nanbu, Y. Hari, J. Andoh, K. Morio, T. Doi and T. Imanishi, *Tetrahedron Lett.*, 1998, **39**, 5401.
7 A. A. Koshkin, P. Nielsen, M. Meldgaard, V. K. Rajwanshi, S. K. Singh and J. Wengel, *J. Am. Chem. Soc.*, 1998, **120**, 13252.
8 P. Nielsen and J. Wengel, *Chem. Commun.*, 1998, 2645.
9 P. P. Lankhorst, C. A. G. Haasnoot, C. Erkelens, H. P. Westerink, G. A. van der Marel, J. H. van Boom and C. Altona, *Nucleic Acids Res.*, 1985, **13**, 927.
10 C. Thibaudeau and J. Chattopadhyaya, *Nucleosides Nucleotides*, 1998, **17**, 1589.
11 J. Plavec, C. Thibaudeau, G. Viswanadham, C. Sund and J. Chattopadhyaya, *J. Chem. Soc., Chem. Commun.*, 1994, 781.
12 J. Plavec, C. Thibaudeau, G. Viswanadham, C. Sund, A. Sandström and J. Chattopadhyaya, *Tetrahedron*, 1995, **51**, 11775.
13 M. Petersen, C. B. Nielsen, K. E. Nielsen, G. A. Jensen, K. Bondesgaard, S. K. Singh, V. K. Rajwanshi, A. A. Koshkin, B. M. Dahl, J. Wengel and J. P. Jacobsen, submitted for publication in *Biochemistry*.
14 A. Millican, G. A. Mock, M. A. Chauncey, T. P. Patel, M. A. W. Eaton, J. Gunning, S. D. Cutbush, S. Neidle and J. Mann, *Nucleic Acids Res.*, 1984, **12**, 7435.

Communication 9/00458K

Synthesis and X-ray crystal structure of [Na(18-crown-6)][U(Cp*)$_2$(SBu^t)(S)], the first f-element compound containing a metal–sulfur double bond

Lionel Ventelon,[a] Christophe Lescop,[a] Thérèse Arliguie,[a] Pascal C. Leverd,[b] Monique Lance,[b] Martine Nierlich[b] and Michel Ephritikhine*[a]

[a] *Laboratoire de Chimie de l'Uranium, Service de Chimie Moléculaire, CNRS URA 331, CEA Saclay, 91191 Gif sur Yvette, France. E-mail: ephri@nanga.saclay.cea.fr*

[b] *Laboratoire de Cristallochimie, Service de Chimie Moléculaire, CNRS URA 331, CEA Saclay, 91191 Gif sur Yvette, France.*

Received (in Cambridge, UK) 18th January 1999, Accepted 5th March 1999

The C–S bond cleavage of a thiolate ligand of [U(Cp*)$_2$(SBu^t)$_2$] was induced by treatment with Na(Hg) and the title compound was isolated after addition of 18-crown-6; the crystal structure exhibited the unsupported U–S–Na linkage of the molecular complex, with a U–S bond distance of 2.462(2) Å.

In the course of our studies of uranium complexes with sulfur ligands, we were interested in preparing a molecular compound with a U=S double bond. Such a sulfide of a f-element has not been described so far, whereas transition metal sulfides have received much attention in recent years because of their rich coordination chemistry and their relevance in bioinorganic systems and industrial catalytic processes.[1] A classical route to early transition metal sulfide groups is C–S bond cleavage of coordinated aliphatic thiolate ligands; this reaction is in fact a relatively common decomposition pathway for *tert*-butyl thiolate complexes.[2–5] However, the propensity of sulfides to bridge metal atoms is a serious obstacle in the synthesis of complexes containing M=S multiple bonds,[2,3] and the current formation of clusters has to be avoided by the presence of sterically demanding ligands, as recently demonstrated with pentamethylcyclopentadienyl derivatives of group IV and V metals.[4,5] From these considerations, we decided to examine thiolate C–S bond cleavage in the complexes [U(Cp*)$_2$(SR)$_2$] (R = Pr^i, **1** and Bu^t, **2**). Here we present the synthesis and X-ray crystal structure of [Na(18-crown-6)][U(Cp*)$_2$(SBu^t)(S)] **4**, isolated from the reduction of **2**; the results provide new information about the influence of the metal oxidation state on the cleavage of the thiolate C–S bond.

The uranium(IV) bisthiolate compounds **1** and **2** were simply synthesized by treating [U(Cp*)$_2$Cl$_2$] with a slight excess of NaSR in thf and were isolated as dark red microcrystals in 79 and 85% yield respectively.[6] Compounds **1** and **2** were quite stable in thf or benzene solution and in the solid state. Reduction of **1** (211 mg) with 2% Na(Hg) (369 mg) in the presence of 18-crown-6 (85.5 mg) in thf (100 ml) led to the formation of [Na(18-crown-6)][U(Cp*)$_2$(SPr^i)$_2$] **3** (Scheme 1); the reaction mixture was stirred for 24 h at 20 °C and after filtration and evaporation, the green microcrystals of **3** were washed with pentane and dried under vacuum (243 mg, 80%). The ^{1}H NMR signals of **3** are broader (30–50 Hz) than those of **1** (10–20 Hz) and are characteristic of a U(III) compound. After the triscyclopentadienyl derivative Na[U(Cp)$_3$(SR)],[7] **3** is a new example of a uranium(III) thiolate.

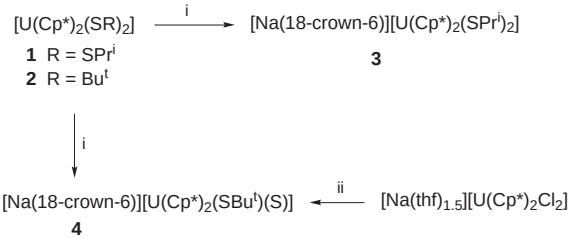

Scheme 1 *Reagents and conditions*: i, Na(Hg), 18-crown-6; ii, NaSBu^t,18-crown-6. All reactions in thf at 20 °C.

Treatment of **2** with sodium amalgam did not afford the corresponding U(III) anionic complex but readily gave a new product which contained, from the NMR spectrum, two Cp* ligands for only one SBu^t group; the narrow resonances indicated that this complex was in the +4 oxidation state. Concomitant formation of isobutylene and isobutane, detected by GLC, suggested that the likely intermediate [U(Cp*)$_2$(SBu^t)$_2$]$^-$ was oxidized into [U(Cp*)$_2$(SBu^t)(S)]$^-$ by facile homolytic C–S bond cleavage of a SBu^t ligand. The same complex was alternatively prepared by reaction of [Na(thf)$_{1.5}$][U(Cp*)$_2$Cl$_2$] (560 mg) and NaSBu^t (313 mg) in thf (50 ml); here again, isobutylene and isobutane evolved. After stirring for 18 h at 20 °C, the red solution was filtered and evaporated and the ochre powder extracted in pentane (482 mg, 95%). In the presence of 18-crown-6, red needles of **4** were obtained from thf-pentane (521 mg, 77%). Complexes **1**–**4** were characterized by elemental analyses (C, H, S) and ^{1}H NMR spectroscopy.†

The crystal structure of **4**, shown in Fig. 1 together with selected data,‡ first revealed the unsupported U–S–Na linkage of the molecular compound. Such heterobimetallics with a single sulfur bridge are very rare, being limited to Ta–M (M = Cr, Mo, W),[8] Re–Ru[9] and Zr–W[10] complexes. However, the most interesting feature of the structure is the U–S distances of the sulfide ligand [2.477(2) and 2.462(2) Å in the two independent molecules] which are shorter than those of the

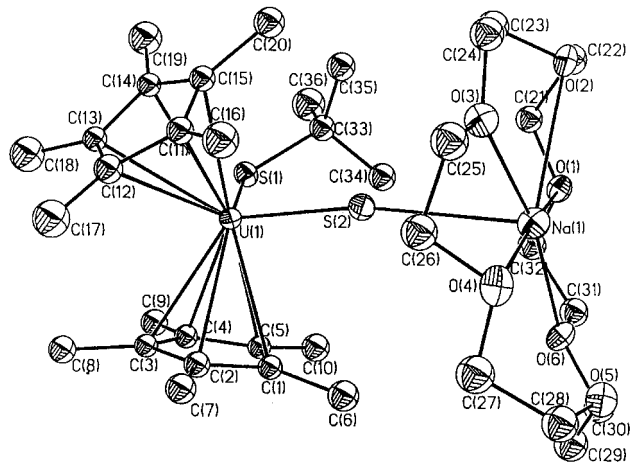

Fig. 1 X-Ray crystal structure of one of the two independent molecules of [Na(18-crown-6)][U(Cp*)$_2$(SBu^t)(S)] with thermal ellipsoids at the 20% probability level. Selected bond distances (Å) and angles (°) : U(1)–S(1) 2.744(2), U(1)–S(2) 2.477(2), Na(1)–S(2) 3.135(4), S(1)–U(1)–S(2) 101.71(7), U(1)–S(2)–Na(1) 168.7(1).

thiolate group [2.744(2) and 2.712(2) Å]. In fact, these are shorter than the shortest U–S distances previously reported, 2.57(2) Å in $[U_3(S)(SBu^t)_{10}]$[2] and 2.60(1) Å in $[\{U(Cp)_3\}_2(\mu\text{-}S)]$,[11] and is consistent with a formal U=S double bond. Thus, **4** ought to be viewed as the adduct of the terminal sulfide $[U(Cp^*)_2(SBu^t)(S)]^-$ to $[Na(18\text{-crown-}6)]^+$. Among the aforementioned compounds which contain an unsupported M–S–M′ linkage, such a dative coordination of a sulfur lone pair of the Ta=S double bond has been encountered in $[Ta(Cp^*)_2(H)(\mu\text{-}S)W(CO)_5]$[8] while the other complexes exhibit single metal–sulfur bonds. In the few adducts of transition metal terminal sulfides with alkali metal ions, such as $[Ti(Cp^*)(OR)(\mu\text{-}S)(\mu\text{-}Cl)Li(thf)_2]$[4] and $[Li_2(thf)_2(Cp^*)TaS_3]$,[5] the metal centres are linked by at least two bridging ligands. The Na–S bond distance and geometrical parameters of the $U(Cp^*)_2$ moiety are unexceptional; steric interactions between the two bulky bridged fragments would explain the large U–S–Na angle [168.7(1) and 174.3(1)°].

Finally, it is worth noting that **2** was stable towards thiolate C–S bond cleavage unless it was reduced by Na(Hg); this fact is in contradiction with previous indications that this reaction would be facilitated by a highly oxidized, electrophilic metal centre.[3] Our results thus give a new insight into the influence of the metal oxidation state on the activation and rupture of thiolate C–S bonds, which is of great importance in catalytic desulfurization processes.

Notes and references

† *Characterising data*. ^{1}H NMR (200 MHz, 30 °C in $[^2H_6]$benzene for **1** and **2** and $[^2H_8]$thf for **3** and **4**). **1**, δ 11.8 (30H, s, Cp*), −18.1 (12H, s, Me), −33.7 (2H, s, CH); **2**, δ 12.2 (30H, s, Cp*), −17.7 (18H, s, Bu^t); **3**, δ 3.8 (24H, s, 18-crown-6), −4.2 (30H, s, Cp*), −6.0 (2H, s, CH), −10.3 (12H, s, Me); **4**, δ 4.5 (24H, s, 18-crown-6), 2.3 (30H, s, Cp*), −17.2 (9H, s, Bu^t). Elemental analyses (calculated values in parentheses). **1**: C, 47.25(47.4); H, 6.85(6.75); S, 9.45(9.75). **2**: C, 48.7(48.95); H, 6.9(7.05); S, 9.15(9.35). **3**: C, 48.0(48.25); H, 7.1(7.25); S, 6.95(6.8). **4**: C, 46.9(47.15); H, 6.8(6.9); S, 6.75(7.0%).

‡ *Crystal data* for $[Na(18\text{-crown-}6)][U(Cp^*)_2(SBu^t)(S)]$: $C_{36}H_{63}NaO_6S_2U$, monoclinic, space group $P2_1/c$, a = 19.174(4), b = 18.548(4), c = 23.132(5) Å, β = 103.31(3)°, V = 8005(3) Å^3, Z = 8, D_c = 1.522 g cm^{-3}, Mo-Kα radiation (λ = 0.71073 Å), μ = 4.210 mm^{-1}, F(000) = 3696, total reflections = 31073, independent reflections = 8203, data/parameter ratio = 8142/808, R_1 = 0.0334 ,wR_2 = 0.0748, GOF = 1.071, residuals based on $I > 2\sigma(I)$. Diffraction collection was carried out on an Enraf-Nonius diffractometer equipped with a CCD detector at 123 K. Data were corrected for Lorentz-polarization effects but not for absorption. The structure was solved by the heavy-atom method and refined by full-matrix least squares on F^2 . There are two independent but similar molecules in the unit cell. A disorder was found on one half of the 18-crown-6 ether of the molecule containing U(2). This disorder is made of two distinct positions that were assigned a 0.5 occupancy factor; they share two carbon atoms which were given an occupancy factor of 1. All non-H atoms were considered anisotropic except those of the disordered half of the crown-ether. H atoms were introduced at calculated positions and constrained to ride on their parent C atoms with displacement parameters of 1.2(CH_2) or 1.5(CH_3) times that of the parent atom. All calculations were performed on an O2 Silicon Graphics Station with the SHELTX package.[13] CCDC 182/1188. See http://www.rsc.org/suppdata/cc/1999/659/ for crystallographic files in .cif format.

1 E. I. Steifel and K. Matasumoto, *Transition Metal Sulfur Chemistry, Biological and Industrial Significance*, American Chemical Society, Washington, DC, 1996.
2 P. C. Leverd, M. Lance, J. Vigner, M. Nierlich and M. Ephritikhine, *J. Chem. Soc., Dalton Trans*., 1995, 237.
3 W. E. Piers, L. Koch, D. S. Ridge, L. R. MacGillivray and M. Zaworotko, *Organometallics*, 1992, **11**, 3148.
4 A. V. Firth, E. Witt and D. W. Stephan, *Organometallics*, 1998, **17**, 3716.
5 H. Kawaguchi and K. Tatsumi, *Organometallics*, 1997, **16**, 307; K. Tatsumi,Y. Inoue, H. Kawaguchi, M. Kohsaka, A. Nakamura, R. E. Cramer,W. VanDoorne, G. J. Taogoshi and P. N. Richmann, *Organometallics*, 1993,**12**, 352.
6 C. Lescop, T. Arliguie, M. Lance, M. Nierlich and M. Ephritikhine, *J. Organomet. Chem*., in the press.
7 P. C. Leverd, M. Ephritikhine, M. Lance, J. Vigner and M. Nierlich, *J. Organomet. Chem*., 1996, **507**, 229.
8 H. Brunner, S. Challet, M. M. Kubicki, J. C. Leblanc, C. Moïse, F. Volpato and J. Wachter, *Organometallics*, 1995, **14**, 3623.
9 M. A. Massa, T. B. Rauchfuss and S. R. Wilson, *Inorg. Chem*., 1991, **30**, 4667.
10 J. A. Kovacs and R. G. Bergman, *J. Am. Chem. Soc*., 1989, **111**, 1131.
11 J. G. Brennan, R. A. Andersen and A. Zalkin, *Inorg. Chem*., 1986, **25**, 1761.
12 SHELTX: Sheldrick Program for the Refinement of Crystal Structures, 1993, University of Göttingen, Germany.

Communication 9/00466A

One- and two-step [2 + 2] cycloaddition reactions of group 4 imides with the phosphaalkyne Bu^{t}CP. Crystal and molecular structures of [Zr(η^5-C_5H_5)$_2$(PCBu^{t}NC$_6$H$_3$Me$_2$-2,6)] and [TiCl$_2$(P$_2$C$_2$Bu$^t_2$NBu^t)(py)] (py) = pyridine)

F. Geoffrey N. Cloke,*[a] Peter B. Hitchcock,[a] John F. Nixon,*[a] D. James Wilson[a] and Philip Mountford[b]

[a] *School of Chemistry, Physics and Environmental Science, University of Sussex, Brighton, Sussex, UK BN1 9QJ. E-mail: J.Nixon@sussex.ac.uk*

[b] *Inorganic Chemistry Laboratory, South Parks Road, Oxford, UK OX1 3QR*

Received (in Cambridge, UK) 25th January 1999, Accepted 4th March 1999

The structures of novel complexes resulting from one- and two-step [2 + 2] cycloaddition reactions of four group 4 imides with the phosphaalkyne Bu^{t}CP are described.

Regitz and coworkers[1] have recently reported novel reactions of the phosphaalkyne Bu^{t}CP with vanadium(v) imido complexes to afford either 3-aza-1,2,4,6-tetraphosphaquadricyclanes **B** or 1,3,5-triphosphabenzenes **A**, the products critically depending on reaction conditions (Scheme 1). They proposed a mechanism for the formation of **A** and **B** which involves an initial [2 + 2] cycloaddition step of the vanadium imide with the phosphaalkyne, but no metal containing complexes have been characterised.

In order to better understand this interesting type of reaction, we now describe the first fully structurally characterised complexes of Zr(IV) and Ti(IV) resulting from one- and two-step [2 + 2] cycloaddition reactions of Bu^{t}CP with '[Zr(η^5-C_5H_5)$_2$(NC$_6$H$_3$Me$_2$-2,6)]' **1**[2] and [TiCl$_2$(NBu^t)(py)$_3$] **2**[3,4] respectively. In addition we report the NMR spectroscopically characterised [2 + 2] phosphaalkyne adducts of '[Zr(η^5-C_5H_5)$_2$(NBu^t)]' **3**[2], and [Ti{(SiMe$_3$)N[CH$_2$CH$_2$N(SiMe$_3$)$_2$]}(NBu^t)(py)][5] **4**.

Treatment of the transient imide complex **1** (prepared from the thermolysis of [Zr(η^5-C_5H_5)$_2$(NHC$_6$H$_3$Me$_2$-2,6)$_2$])[2] with an excess of Bu^{t}CP in toluene at 100 °C for 48 h yielded the orange crystalline complex [Zr(η^5-C_5H_5)$_2$(PCBu^{t}NC$_6$H$_3$Me$_2$-2,6)] **5** in 45% yield.† A single crystal X-ray diffraction study on **5**‡ established that its molecular structure (Fig. 1) contains the four membered planar metallacycle ($\Sigma_{\text{internal angles}}$ = 360 °C) resulting from the [2 + 2] phosphaalkyne–imide cycloaddition, in which the phosphorus is bonded to the nitrogen of the imide function, consistent with the bond polarity of the unsaturated reactive sites. This geometry is similar to that observed for the addition of internal alkynes to **1**.[2] The Zr–N–C(6) bond angle in **5** (147.8°) is typical of double bond character of the metal–nitrogen linkage. A similar adduct [Zr(C_5H_5)$_2$(PCBu^{t}NBu^t)] **6** can also be prepared from '[Zr(η^5-C_5H_5)$_2$(NBu^t)]' (generated *in situ* by thermolysis of [Zr(η^5-C_5H_5)$_2$(NHBu^t)$_2$])[2], as determined by NMR spectroscopy.§

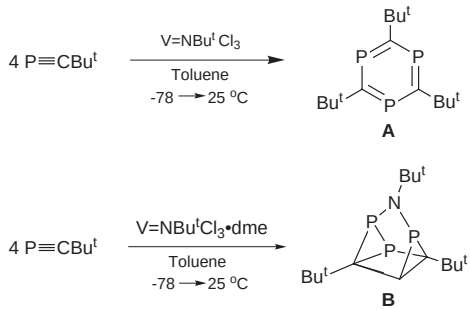

Scheme 1

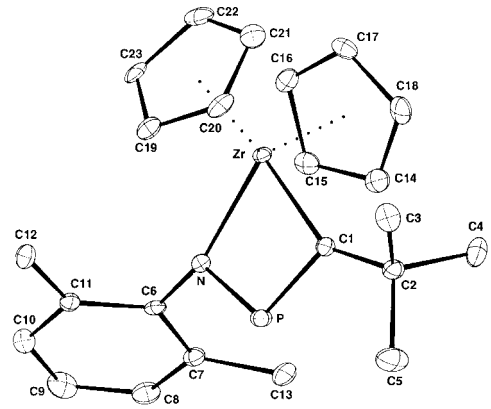

Fig. 1 Molecular structure of [(C_5H_5)$_2$Zr(PCBu^{t}NC$_6$H$_3$Me$_2$-2.6)] **5**. Selected distances (Å) and angles (°): Zr–N 2.101(4), P–N 1.729(4), P–C(1) 1.692(5), Zr–C(1) 2.188(5); Zr–N–P 91.0(2), C(1)–P–N 102.8(2), P–C(1)–Zr 89.1(2), N(1)–Zr–C(1) 77.1(2)°. Displacement elipsoids are shown at 50% probability level.

The investigation of this type of addition was subsequently extended to the sterically encumbered titanium imide **4**. Treatment of **4** with an excess of Bu^{t}CP at room temperature in toluene, yielded an orange oil after work up. NMR spectroscopic data were found to be very similar to that of **5** indicative of formation of the [2 + 2] cycloadduct [Ti{N(SiMe$_3$)[CH$_2$CH$_2$N(SiMe$_3$)]$_2$}(PCBu^{t}NBu^t)] **7**¶ (Scheme 2).

Since the reactivity presumably results from release of steric strain, complex **2** was reacted with an excess of Bu^{t}CP in toluene at 55 °C for 72 h to yield the dark-red crystalline complex [TiCl$_2$(P$_2$C$_2$Bu$^t_2$NBu^t)(py)] **8** (61% yield).‖** The corresponding pyridine free complex [TiCl$_2$(P$_2$C$_2$Bu$^t_2$NBu^t)] **8a** can be obtained (25%) by subliming **8** *in vacuo* at 110 °C. A single crystal X-ray diffraction study was carried out on **8**‡ and its molecular structure, (Fig. 2), reveals a TiC$_2$P$_2$N core in which the Ti(IV) centre is in an unsymmetrical environment resulting from being capped by a puckered 1,3-diphosphacyclobutadiene unit, whose P(1) atom is σ-bonded to the nitrogen of the imide function [interplanar angle between C(1)P(2)C(2) and C(1)P(1)P(2), 23.3°]. One representation of the bonding to the Ti centre involves an η^3-interaction with the 2-phosphaallyl fragment of the C$_2$P$_2$ ring which is augmented by interaction

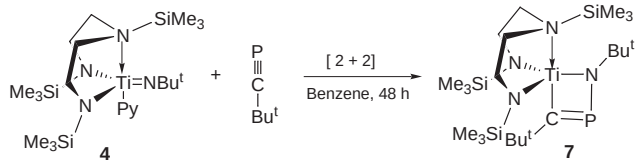

Scheme 2

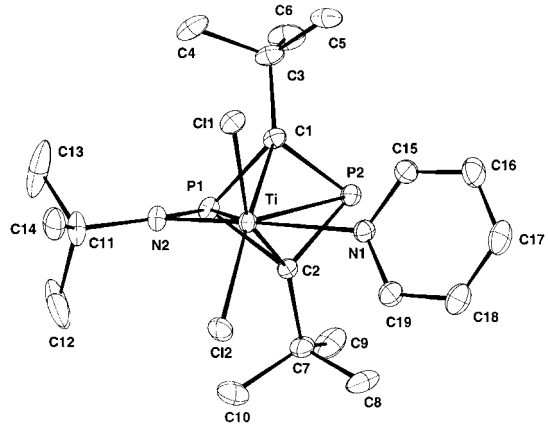

Fig. 2 Molecular structure of [Ti{NBu^{t}PCBu^{t}PCBu^t}Cl_2(py)]**8**. Selected distances (Å) and angles (°): P(1)–N(2) 1.727(2), Ti–N(2) 1.880(2), P1–C(1) 1.825(2), P(2)–C(1) 1.735(2), P(2)–C(2) 1.768(2), C(2)–P(1) 1.847(2), Ti–N(1) 2.394(2), Ti–P(2) 2.784(2), Ti–C(2) 2.221(2), Ti–P(1) 2.442(1), Ti–C(1) 2.439(2); Ti–N(2)–C(11) 148.31(14), Cl(2)–Ti–Cl(1) 109.57(2), C(2)–P(1)–C(1) 80.86(8), C(1)–P(2)–C(2) 85.65(8). Displacement ellipsoids are shown at 50% probability level.

with the N, two Cl ions, P lone pair and the pyridine. As expected the Ti–N(2) bond length [1.880(2) Å] in **8** is considerably elongated when compared with the starting imide complex **2** [1.705(3) Å] and the Ti–N(pyridine) bond length [2.394(2) Å] is very long. The Ti–N–C(α) bond angle in **8** (148.3°) is typical for a metal–nitrogen double bond.

Although no reaction intermediates have been spectroscopically characterised, the formation of the TiC_2P_2N core in **8** is presumed to proceed by sequential [2 + 2] cycloaddition of Bu^{t}CP with (i) the titanium–nitrogen double bond and (ii) the resulting P=C double bond (Scheme 3).

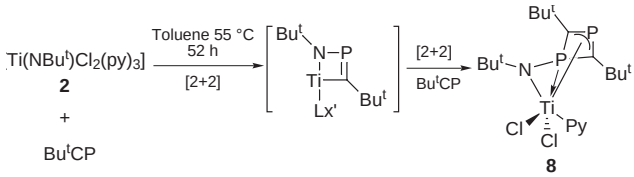

Scheme 3

Interestingly, the course of the reactions involving complexes of type **2** is also affected by the nature of the imido N-substituent. Thus treatment of [Ti(NR)Cl_2(py)$_3$] (R = Ph, *p*-MeC_6H_4, *p*-$NO_2C_6H_4$ or Pr^i) with Bu^{t}CP gave the previously unknown 1,2,4-azadiphospholes $P_2C_2Bu^t_2NR$. The molecular structure of $P_2C_2Bu^t_2NPh$ has been determined and this new class of heteroaromatic ring systems will be the subject of a separate publication.[6] The range of products obtained with different metal and N-substituents indicates the possibility for a rich and diverse derivative chemistry.

Philip Mountford is the Royal Society of Chemistry Sir Edward Frankland Fellow for 1998–9.

Notes and references

† **5**: NMR (d_6-benzene, 295 K), ^{1}H δ 7.16, 7.09 (m, 3H, C_6H_3), 5.69 [(s, 10H, C_5H_5)], 2.28 [s , 6H, $C_6H_3(CH_3)_2$], 1.52 [s, 9H, PCC(CH$_3$)$_3$] ^{31}P{^{1}H} δ 81.7. EI-MS *m/z* (%): 439 (20) [M]$^+$, 339 (100) [M − PCCMe$_3$]$^+$. Elemental analysis: Calc. for $C_{23}H_{28}NPZr$; C, 62.69; H, 6.40, N, 3.18. Found: C, 62.41; H, 6.37, N, 3.12%.

‡ *Crystal data*: **5**: $C_{23}H_{28}NPZr$, M = 440.6, monoclinic space group $P2_1/c$, a = 11.622(3), b = 21.830(8), c = 8.389(4) Å, β = 107.01(3), U = 2035.3(13) Å^3, Z = 4, D_c = 1.44 Mg m^{-3}, crystal dimensions 0.40 × 0.30 × 0.02 mm, T = 173(2) K, Mo-Kα, radiation λ = 0.71073 Å. Data were collected on an Enraf-Nonius CAD4 diffractometer and of the total 3811 reflections measured, 3563 unique (R_{int} = 0.042). Refinement on F^2, $wR2$ = 0.138 (all data), $R1$ = 0.048 [for 2651 reflections with $I > 2\sigma(I)$].

7: $C_{19}H_{32}Cl_2N_2P_2Ti$, M = 469.2, monoclinic, space group $P2_1/n$, a = 12.728 (2), b = 12.170(1), c = 15.596(1) Å, β = 97.5(1)°, U = 2395.1(5) Å^3, Z = 4, D_c = 1.3 Mg m^{-3}, T = 173(2) K, Mo-Kα, radiation λ = 0.71073 Å. Data were collected on an Enraf-Nonius CAD4 diffractometer and of the total 7242 reflections measured, 6969 unique (R_{int} = 0.017). Refinement on F^2, $wR2$ = 0.095 (all data), $R1$ = 0.040 [for 5271 reflections with $I > 2\sigma(I)$]. CCDC 182/1184. See http:/www rsc.org/suppdata/cc/1999/661/ for crystallographic files in .cif format.

§ **6**: NMR (d_6-benzene, 295 K), ^{1}H δ 5.68 (s, 10H, C_5H_5), 1.31 [s , 9H, NC(CH$_3$)], 1.52 [s, 9H, PCC(CH$_3$)$_3$]. ^{31}P{^{1}H} δ 64.1. EI-MS *m/z* (%): 391 (30) [M]$^+$, 376 (20) [M − Me]$^+$, 276 (55) [M − Me − PCCMe$_3$]$^+$.

¶ **7**: NMR (d_6-benzene, 295 K), ^{1}H δ 4.12, 3.8, 2.81 (3 × m, 8H, CH_2CH_2), 1.5 [s, 9H, NC(CH$_3$)], 1.48 [s, 9H, PC(CH$_3$)], 0.2 (s, 9H, NSiMe$_3$), 0.09 (s, 18H, NSiMe$_3$). ^{13}C{^{1}H δ53.7, 51.6 (CH_2CH_2), 35.2 [d, NC(*C*H$_3$), $^3J_{PC}$ 12.2 Hz], 34.4 [d, PCC(*C*H$_3$)$_3$, $^3J_{PC}$ 8 Hz] 2.5 [SiC(*C*H$_3$)], 0.2 [SiC(*C*H$_3$)]. ^{31}P{^{1}H} δ209.4. EI-MS *m/z* (%): 536 (20) [M]$^+$, 436 (45) [M − (PCBu^t)]$^+$. The oily nature of this compound precluded satisfactory microanalysis.

‖ **8**: NMR (d_6-benzene, 295 K), ^{1}H δ 9.5, 6.78, 6.53 (m, 5H, NC_5H_5), 1.46 [s, 9H, NC(CH$_3$)$_3$], 1.32, 1.30 [s × 2, 18H, PC(CH$_3$)$_3$]. ^{13}C{^{1}H} (d_8-toluene, 295 K): 198.3 (dd, PCP, $^1J_{PC}$ 61.95, $^2J_{PC}$ 29.9 Hz), 151.1, 123.2 (m, NC_5H_5), 68.89 [d, N*C*(CH$_3$)$_3$, $^2J_{PC}$ 8.10 Hz], 41.33 [pseudo-t, {PC*C*(CH$_3$)$_3$}$_2$, $^2J_{PC}$ 6.50 Hz], 33.96 [pseudo-t, {PCC(*C*H$_3$)$_3$}$_2$, $^3J_{PC}$ 4.97 Hz], 32.37 [d, NC(*C*H$_3$)$_3$, $^3J_{PC}$ 6.03 Hz]. ^{31}P{^{1}H} (d_6-benzene, 295 K) δ 296.5, −139.5 (d × 2, $^2J_{PP}$ 40.5 Hz). EI-MS *m/z* (%): 465 (85) [M]$^+$, 389 (10) [M − py]$^+$, 333 (12) [M − Py −Bu^t)]$^+$.

** Similarly [Ti(η^8-C_8H_8)(NBu^t)] readily reacted with Bu^{t}CP in toluene at room temp. to afford, after recrystallisation from pentane, dark brown crystals of [Ti(η^8-C_8H_8)($P_2C_2Bu^t_2NBu^t$)] **9** in 71% yield. Although not shown here, the molecular structure of **9** has also recently been obtained and reveals a common TiC_2P_2N core comfirming its structural significance for this type of reaction.

1 F. Tabellion, A. Nachbauer, S. Leininger, C. Peters and M. Regitz, *Angew. Chem., Int. Ed.*, 1998, **37**, 1233.
2 P. A. Walsh, A. M. Baranger and R. G. Bergman, *J. Am. Chem. Soc.*, 1992, **114**, 1708.
3 For a review of titanium imido chemistry, see: P. Mountford, *Chem. Commun*., 1997, 2127 and references therein (Feature Article).
4 A J. Blake, P. E. Collier, S. C. Dunn, W.-S. Li, P. Mountford and O. V. Shishkin, *J. Chem Soc., Dalton Trans.*, 1997, 1549.
5 P. Mountford and F. G. N. Cloke, unpublished work.
6 A. J. Blake, S. C. Dunn, J. C. Green, N. M. Jones, A G. Moody and P. Mountford, *Chem. Commun*., 1998, 1235.
7 F. G. N. Cloke, P. B. Hitchcock, J. F. Nixon, L. Nyulaszi, M. Regitz and D. J. Wilson, unpublished work.

Communication 9/00648F

Typeset and printed by Black Bear Press Limited, Cambridge, England

Medicinal chemistry with fullerenes and fullerene derivatives

Tatiana Da Ros and Maurizio Prato*

Dipartimento di Scienze Farmaceutiche, Università di Trieste, Piazzale Europa 1, 34127 Trieste, Italy. E-mail: prato@univ.trieste.it

Received (in Cambridge, UK) 4th December 1998, Accepted 8th February 1999

The study of the biological applications of fullerenes has attracted increasing attention despite the low solubility of the carbon spheres in physiological media. The organic functionalisation of fullerenes has helped solubilisation by covalent attachment of hydrophilic appendages. Therefore, recently synthesised fullerene derivatives reach satisfactory concentrations in water. However, the tendency of the fullerenes to form clusters is enhanced in polar media, where better solubilisation can be achieved by means of multiple functionalisation or using micellar systems. Once homogeneously dissolved, the fullerenes and fullerene derivatives exhibit an interesting range of biological activities, especially promising in the field of photodynamic therapy, HIV, neuroprotection and apoptosis.

The fullerenes, a class of spheroidally shaped molecules made exclusively of carbon atoms, were observed for the first time in 1985[1] and isolated in bulk in 1990.[2] Since then, many research groups have been eagerly looking for practical applications of these novel materials.[3] Their interesting features are at the edge of different scientific disciplines, ranging from non-linear optical properties to superconductivity. Also in the biological field the fullerenes have had a strong impact, as it was discovered that functionalised fullerenes can be used in photodynamic therapy[4] or as inhibitors of the HIV-1 protease.[5,6] However, the general excitement was not followed by a comparable outburst of results. The main reason for the slow progress in this field is generally attributed to the total absence of solubility in aqueous media, a problem that has hampered systematic testing. On the other hand, it is clear that size, hydrophobicity, three-dimensionality and electronic effects make the fullerenes very appealing subjects in medicinal chemistry.[7] For instance, it can be easily conceived that the spheroidal shape of fullerenes is potentially accommodated inside hydrophobic regions of enzymes or cells, with biological applications in different fields.

Two excellent reviews cover the main achievements in the biological application of fullerenes up to 1996.[8,9] In this article, we will provide a general overview of the current state of the art of the medicinal chemistry of fullerenes, with particular emphasis on one hand on the most recent and promising general applicative aspects and on the other hand to our own achievements in this field.

Tatiana Da Ros was born in Palmanova, Italy, in 1969. She received her Laurea degree in Pharmaceutical Chemistry from the University of Trieste in 1995 working with Professor Marco De Amici (magna cum laude). *She then took her PhD in 1999, under the supervision of Professor Maurizio Prato, her dissertation dealing with the biological properties of water-soluble fullerene derivatives. She has a research contract with the University of Trieste and is currently working in the Department of Pharmaceutical Sciences.*

Maurizio Prato took his Laurea degree in Chemistry in Padova in 1978, under the supervision of Professor Gianfranco Scorrano. He then joined the Faculty of Science and the Organic Chemistry Department at the University of Padova. He moved to the University of Trieste in 1992, where he is currently Associate Professor of Organic Chemistry. He spent sabbatical terms at Yale University in 1986–1987 (with Professor Samuel J. Danishefsky) and at the University of California, Santa Barbara in 1991–1992 (with Professor Fred Wudl). He received the Federchimica Prize in 1995. His current research interests focus mainly on functionalised fullerenes for applications in materials science and medicinal chemistry.

Solubility

There have been several attempts to overcome the natural repulsion of fullerenes for water. The most widely used methodologies are: (a) encapsulation or microencapsulation in special carriers; (b) suspension with the help of co-solvents; (c) chemical functionalisation for the introduction of solubilising appendages.

Encapsulation

It has long been known that [60]fullerene can be solubilised in water in the form of complexes with cyclodextrins[10,11] or calixarenes.[12,13] More concentrated solutions (up to 4.1×10^{-5} M) can be achieved using polyvinylpyrrolidone (PVP)[14] or artificial membranes like Triton X-100, DODAB (dimethyldioctadecylammonium bromide), DHP (dihexadecyl hydrogen phosphate) or lecithin.[15,16] Colloidal systems are formed with ammonium halides such as cetyltrimethylammonium bromide or sodium dodecyl sulfate.[17] Also co-polymers such as polyphenyl quinoline/polystyrene form self-assemblying systems with well-organised structures.[18] Incorporation of [60]fullerene and photoactive [60]fullerene derivatives in liposomes suggests that a photoexcited fullerene is capable of initiating a redox cycle that has cytochrome *c* and ubiquinone as mediators.[19]

The combination of fullerenes and lipid membranes has led to very interesting results. Lipid bilayers are dynamically mobile structures, partially ordered and of biopharmaceutical interest for covering biocompatible surfaces or for the controlled release of drugs. Hexakis adducts of [60]fullerene with an octahedral pattern, functionalised with C_{12} or C_{18} chains, have allowed the formation of lipid systems with multilamellar vesicles of dipalmitoyl-*sn*-glycero-3-phosphatidylcholine.[20]

Suspensions

Suspensions of fullerenes can be prepared from saturated benzene solutions poured into THF. The resulting mixture is

added dropwise to acetone, and then water is slowly added. A yellow suspension is formed, and the solvents are evaporated to a final known volume of water.[21]

Soluble fullerene derivatives

So far, several fullerene derivatives relatively soluble in water or aqueous mixtures have been synthesised. Fullerenols or fullerols **1**,[22] for instance, are very soluble in water, and even though their structures are not well-defined, a lot of biological studies have been carried out (see below). Water soluble polymers, covalently attached to [60]fullerene, are also easily dissolved in water.[23] Well-defined compounds solubilised in water media include **2**–**5**. Among these, compound **4** reaches a maximum concentration of 1.5×10^{-5} M in H_2O–DMSO 9 : 1.[24] The record for water solubility among monofunctionalised fullerenes so far is to be attributed to dendrimer **5**, whose solubilty in water is 34 mg ml^{-1} at pH 7.4 and an outstanding 254 mg ml^{-1} at pH 10.[25]

In conclusion, when a hydrophilic appendage is covalently attached to [60]fullerene, solubilisation in aqueous solvents is ensured. However, addition of only one solubilizing chain appears insufficient to avoid clustering. The hydrophobic carbon spheres will stick together, leaving the hydrophilic chains on the outside of the aggregate.[26,27] More importantly, formation of clusters decreases the lifetime of the excited triplet state by 2–3 orders of magnitude,[28,29] thus affecting the potential of fullerenes in photodynamic therapy (see below). The degree of aggregation can be monitored by UV–VIS spectrophotometry, pulse radiolysis or light-scattering. Clustering seems to cause broadening of the absorption bands with decrease of absorption coefficients and loss of structural features.[16,26,30,31] To avoid aggregation of the fullerene spheres, either calixarenes or cyclodextrins can be used, or surfactants.[16,29] However, the presence of bulky functionalities, able to shield the fullerene spheroid from water, produces sufficiently homogeneous solutions. Dendrimer **5** shows an almost ideal behavior, with formation of very small aggregates whose size decreases with increasing pH.[25]

Multiple functionalisation can also be helpful. By means of controlled additions it is possible to place polar groups around the fullerene spheroid. It appears that bis-functionalisation is sufficient to avoid clustering in reasonably dilute solutions.[27] However, the radical quenching ability and the singlet oxygen production of the multiple adducts may depend on the number of addends. To test this, the reaction of OH• with a series of functionalised fullerenes was studied.[32] It was found that the reaction rates decrease with an increasing number of additions, fast reactions occurring with bisadducts and much slower reactions with fullerenols.[32] On the other hand, singlet oxygen production was found to be independent of the nature of the addends, but it did decrease with an increasing number of saturated double bonds on the spheroid.[33]

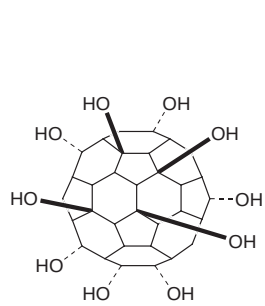

1

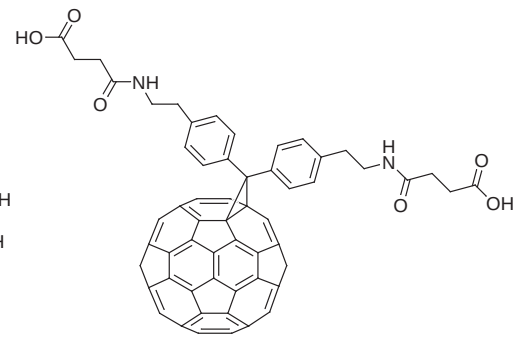

2

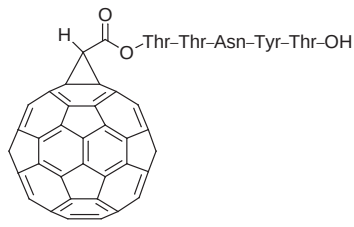

3

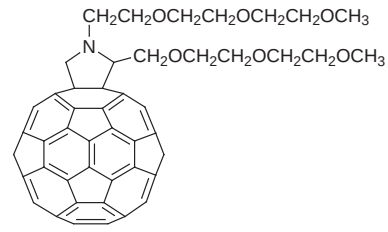

4

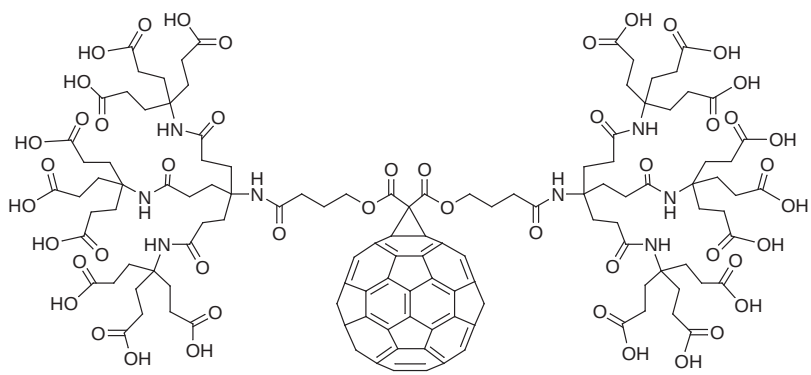

5

Fullerenic amino acids and peptides

Fullerene-based amino acids (*e.g.* **6**–**9**) have been synthesised by several groups.[34–42] The main objective of these studies is the potential incorporation of these non-natural amino acids in natural peptides and proteins.

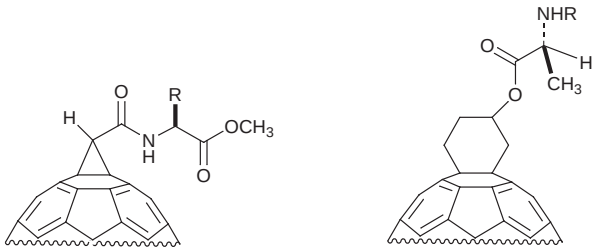

6

7

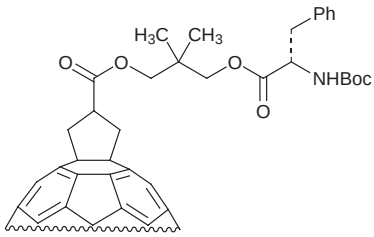

8

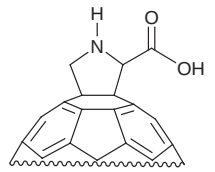

9

Fulleroproline **9** (abbreviated to Fpr using the three-letter code for amino acids), probably the biggest unnatural amino acid,[43] features a proline ring fused with the 6,6 ring junction of [60]fullerene.[37,44] Fpr forms peptides both at the amine and the carboxylic acid ends leading to di- and tri-peptides.[44–46] However, Fpr is usually prepared in racemic form, such that two diastereoisomers are formed when this amino acid is coupled with chiral amino acids. This problem can be overcome by using diastereoselective additions, starting with chiral components.[44,47] Alternatively, the diasteromeric mixtures can be separated by column chromatography or by preparative HPLC. In all cases, enantiopure fulleroprolines can be obtained.[44] Their absolute configuration can be easily established by means of circular dichroism. In all CD spectra of fulleroproline derivatives and peptides, a sharp maximum at about 428 nm was always observed. The sign of this Cotton effect is diagnostic for the determination of the absolute configuration of the chiral C^{α} atom in fulleroproline: a positive maximum is indicative of *R* configuration, whereas the *S* isomer gives rise to a negative maximum.[44]

Naturally encoded proline stands alone in the α-amino acid panorama, as it plays a central role in directing polypeptide folding and in providing conformational rigidifying effects to Pro-containing compounds.[48] Two conformational features contribute to the peculiarity of proline: (1) the propensity to induce a β-turn conformation and (2) the relatively slow rotation around the C–N tertiary amide bond, which results in *trans–cis* isomerism. Both aspects have been examined in fulleroproline peptides. A conformational study in solution has shown that the heterochiral -L-Fpr-D-Ala- sequence is mostly folded in a type-II β-turn conformation, in analogy with the known behavior of the -L-Pro-D-Ala- parent sequence.[45] On the other hand, it was found that the activation parameters for *trans–cis* isomerism in Ac-Fpr-OBu^t are very different from the model Ac-Pro-OBu^t. A difference of *ca*. 7 kcal mol^{-1} in the activation enthalpy makes the conformational interconversion much faster in the fullerene derivative.[46] This was attributed to a low level of availability of the nitrogen lone pair for carbonyl conjugation in fulleroproline.[46] In fact, the nitrogen in pyrrolidine and proline derivatives of [60]fullerene is much less basic than in the corresponding, non-fullerenic, amines.[49]

The ability of some representative hydrolytic enzymes to induce modifications in a series of fulleroprolines was tested with the aim of resolving racemic mixtures and also to obtain detailed structural information on the nature of the interaction.[50] Preliminary results show that, among the many enzymes tested, only lipase B from *Candida antarctica* (CALB) and lipoprotein lipase from *Pseudomonas specie* (LPL) were able to catalyse the acylation of fullerene derivatives, the former being more efficient (Scheme 1). However, even with these active enzymes, no reaction was observed when the functional group to be transformed is close to the fullerene spheroid (Scheme 1).

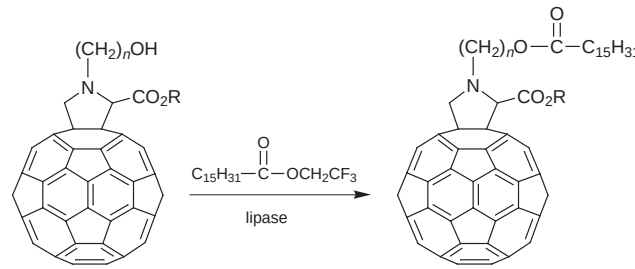

10

n = 2, 3

11

Scheme 1

Relatively fast reactions and modest enantioselectivities (up to 45% ee) were observed for reaction centers spatially distant from the carbon sphere. These results seem to indicate that the [60]fullerene spheroid encumbers the productive fitting of the substrate either in the acyl- or alcohol-binding sites when the reaction center is close to the fullerene spheroid. This may also be due to the fact that [60]fullerene derivatives, owing to their size, cannot be easily accommodated inside the lipase active site. However, it looks as though the [60]fullerene spheroid is able to establish hydrophobic interactions with more superficial regions of the enzyme, while the proline moiety approaches the active site cavity of the lipase and the hydroxy group interacts with the catalytic triad.[50]

Other examples of fullerene–peptide conjugates have been reported. The first fulleropeptide reported contained a sequence of five hydrophobic amino acids.[51] On the basis of spectroscopic data, it was concluded that the conjugate possesses the properties of both [60]fullerene and peptide. The secondary structure adopted by the new peptide in solution was found to be the 3_{10}-helix[52] rather than the α-helix, owing to the high AIB content.[51] In a next step, the synthesis of a fullerene–peptide conjugate involving a series of highly hydrophilic amino acids was studied (**3**). The compound is reasonably soluble in water and exhibits interesting biological properties in terms of monocyte chemotaxis and anti-HIV activity (*vide infra*).[53]

More complex peptides such as alamethicin[54] and proteins such as azurin[55] have been covalently attached to [60]fullerene. IgG antibodies have been produced for the first time using [60]fullerene–bovine thyroglobulin conjugates, which could be used in very sensitive immunological procedures.[56]

Given the complexity of the biological systems, a quick way to establish potential interactions of fullerenes with enzymes and proteins would be of great help in preliminary screenings. To this aim, a stationary phase for HPLC was functionalised using a fulleroproline derivative, which, through a silicon alkoxide end group, ensures the chemical linking of the fullerene to the silica matrix (Scheme 2).[57]

The new phase is suitable for analysis in aqueous media, which represents a real practical advantage: tests of interactions of physiological solutions with fullerenes are possible without necessarily solubilizing the carbon cages in water. As a test of efficiency, a series of small peptides containing hydrophobic cavities, simulating a biological environment, was selectively recognised. Peptides characterised by electron-rich hydro-

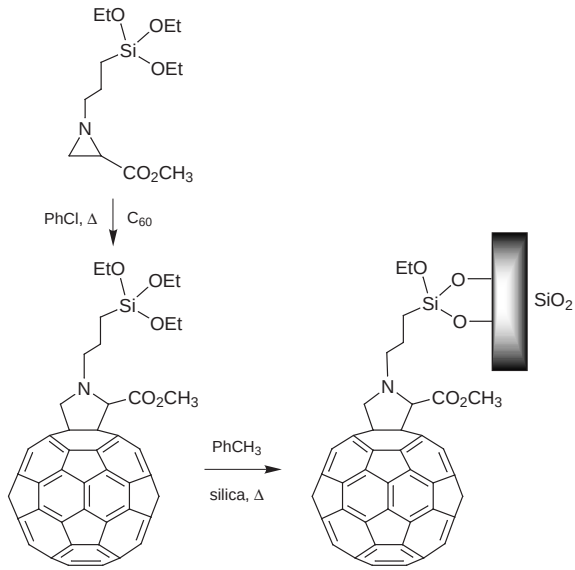

Scheme 2

phobic clefts, thus giving rise to favourable interactions, were more strongly retained in the chromatographic runs.[57]

Toxicity studies

The absorption, distribution and excretion of fullerenes, together with their potential toxicity, are of fundamental importance in any biological evaluation and, accordingly, have been studied in detail using either unmodified [60]fullerene and water-soluble fullerene derivatives.

Unmodified [60]fullerene

A water suspension of ^{14}C-labelled [60]fullerene was added to a culture medium in which immortalised human keratinocytes were grown. [60]Fullerene was associated to the cells in a way dependent of time, such that after six hours about 50% of radioactivity was captured by keratinocytes.[21] No effects of [60]fullerene on the proliferation rate of keratinocytes and fibroblasts was observed, since no variations were detected on thymidine incorporation. *In vivo* tests, performed on Swiss mice and using a dispersion of micronised [60]fullerene in water containing surfactants, did not give any lethal effect, toxicity, or growth inhibition. The accumulation of [60]fullerene in fat-storing cells, in which the retinoid concentration is very high, led to an unusual metabolic path.[58] [60]Fullerene reacted *via* Diels–Alder addition, producing vitamin A derivatives. It was also found that [60]fullerene can be phagocytised by human leukocytes[59] and monocytes.[60] However, the associated usual increase of interleukin IL-1β release was not observed. This effect is not clear but it seems to be correlated with the lack of inflammatory response observed after [60]fullerene administration in Swiss mice.[61]

Hemolysis tests performed on sheep-red blood cells showed no effects of a [60]fullerene–PVP suspension.[14] The same suspension was used to study chondrogenesis in cells. Whereas PVP exhibits cytotoxicity, weakly increases chondrogenesis and decreases cell proliferation, the presence of [60]fullerene specifically increases the differentiation of LB cells (rat limb bud cells). The fullerene could then be incorporated in the endoplasmic reticulum and could promote the synthesis of proteoglycan with a mechanism similar to that known for other substances.[62] Damaging effects *in vitro* have been found in mouse MB cells (midbrain cells), since [60]fullerene decreases cell differentiation and proliferation. Embryos of pregnant mice treated *in vivo* with fullerene died with deformations: [60]fullerene was incorporated through maternal flux producing heavy disfunctions to the embryo morphogenesis.[63]

Fullerene derivatives

Pyrrolidinium salt **12** was synthesised using ^{14}C-labelled [60]fullerene.[64] It was possible to see that, after intravenous administration, the compound was rapidly adsorbed and accumulated by the liver. Only 9% of **12** was in the blood one

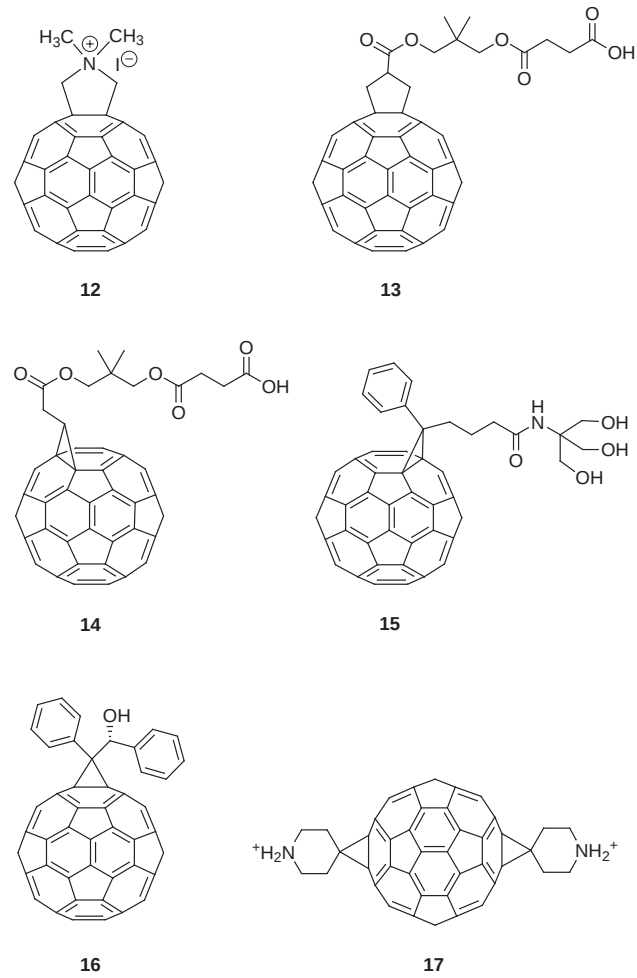

12 **13** **14** **15** **16** **17**

minute after application, a percentage reduced to 1.5% after 2 h. After five days, 95% of the compound was accumulated in the liver, whereas no traces were found in urine or feces.[64] Partially similar results were found for derivative **13**, differences from **12** probably arising from different hydrophobicities.[65] Oral administration of labelled **13** gave only a trace of radioactivity in the liver after 6 h, whereas 97% was excreted in 48 h, with traces in urine. Intravenous administration was followed by quick localisation in the liver with slow excretion (5.4% in the feces after 160 h). Compound **14** exhibited relative acute toxicity on ddY female mice, when administered intraperitoneally in concentrations of 200–500 mg kg^{-1}, with 5–10% weight loss, but full survival rate after a week.[65] Succinic derivative **2** (15 mg kg^{-1}) was injected intravenously in mice.[66] In this case, 99% was found to bind plasmatic proteins with fast distribution and slow excretion, with accumulation in the liver. Administration of higher doses (25 mg kg^{-1}) led to shortness of breath and death after five minutes.

Toxicity studies of fullerenols carried out intraperitoneally on male ICR mice and Sprague–Dawley rats showed that DL_{50} is 1.2 g kg^{-1} (confidence limits 0.5–2.4 g kg^{-1}). *In vivo* studies suggested that fullerenols can suppress the microsomial enzyme levels and decrease the activities of P450-dependent monooxygenase. These compounds can also inhibit mitochondrial

Mg^{2+}-ATPase activity, in a way that is dependent on fullerenol concentration, with an IC_{50} of 7.1 ± 0.3 μM. It was suggested that fullerenols can behave as artificial electron acceptors, thus decreasing the flux of reducing equivalents from NADPH to oxidase through NADPH-cytochrome P450 reductase.[67]

DNA cleavage and photodynamic therapy

The ground state absorption spectrum of [60]fullerene is characterised by intense absorptions in the UV region with weaker bands extending throughout the visible region up to 700 nm. Upon irradiation, [60]fullerene is excited to a short-lived singlet state (lifetime ≈ 1.3 ns), which converts almost quantitatively into a longer-lived triplet state (lifetime = 50–100 μs). The triplet state transfers energy very efficiently to molecular oxygen, generating singlet oxygen with almost unitary yield.[68] The triplet lifetime is fundamental for photoactivity in cells, whose viscosity is much higher than fluid solutions. In fact, it was suggested that only triplet states with lifetimes longer than 100 μs have enough cytotoxic potential.[69] Compound **14**, which has a triplet lifetime of 40 μs, was not active up to 50 μM concentrations, whereas at higher concentrations inhibited cell growth even in the absence of light.[69] The strongly oxidative properties typical of singlet oxygen are therefore considered to be responsible for a series of biological activities exhibited by fullerene solutions. In fact, the damaging effects are usually inhibited by the presence of singlet oxygen quenchers.

Supercoiled pBR322 DNA, incubated with compound **13** and irradiated by visible light, was cleaved with moderate efficiency.[4] Also membranes of cells grown on the surface of unmodified [60]fullerene were heavily damaged by photoirradiation.[70,71] Immobilised DNA on a monolayer containing [60]fullerene was cleaved.[72] DNA cleavage was improved when an acridine moiety was attached to [60]fullerene, most probably owing to the known affinity of acridine for DNA double helix.[73]

Usually, DNA cleavage occurs selectively at guanine (G) residues, but without differentiation among the various G sites.[4] Specific G residues can be recognised utilizing more complex conjugates. A [60]fullerene derivative, conjugated with 14 deoxynucleotides, was synthesised and found to possess high affinity for both single and double stranded DNA.[74] The observed increased reactivity at specific G sites was tentatively attributed to the action of singlet oxygen. A similar study by Rubin, Foote and collaborators was also reported.[75] A comparison between two identical deoxyoligonucleotide residues linked to [60]fullerene and eosin, respectively, showed a clear difference in that the latter was much less selective, cleaving a number of different G sites. The fullerene derivative gave a marked preference for the cleavage of a specific G site, namely that closest to the fullerene spheroid. The authors concluded that the cleavage cannot be attributed to the activity of singlet oxygen, an easily diffusing species whose action should be wider, but most probably is to be ascribed to a direct electron-transfer between guanosine and excited fullerene.

A direct consequence of DNA cleavage is the observed cytotoxicity of fullerene derivatives. *In vitro* tests performed on tumoral HeLa S3 cells using compound **13** confirmed that cytotoxic activity is present only in the case of irradiation.[4]

Another case of antitumoral activity was observed by Tabata *et al*.[23] Local irradiation of mice affected by fibrosarcoma and treated with a functionalised [60]fullerene derivative gave not only reduction of the tumor mass but also tumor necrosis without skin damage. It was noted that [60]fullerene accumulates in tumoral tissues not for a specific tropism, but, essentially, because of the excellent vascular permeability and the relatively immature lymphatic system of the tumoral tissues.[23]

It has also been shown that [60]fullerene deactivated enveloped viruses (Togaviridae and Rhabdoviridae) owing to the production of singlet oxygen. The deactivation was oxygen-dependent and the efficacy was maintained even in the presence of proteins.[76]

Enzymatic inhibition and anti-HIV activity

Fullerene derivatives (**13** and **14**) exhibited inhibition of cysteine (papain and cathepsin) and serine (trypsin, plasmin, trombine) proteinases.[4,9] The mechanism of action is not yet well understood, but the hydrophobicity and the electrophilicity of the fullerene spheroid seem to be responsible for inhibition.

The active site of the HIV-1 Protease (HIVP) is a quasi-spherical hydrophobic cavity, whose diameter is about 10 Å. On its surface, two amino acid residues, aspartate 25 and aspartate 125, catalyse the hydrolysis of the substrate. On the basis of molecular modeling, Friedman *et al*. were the first to recognise that the [60]fullerene spheroid can be almost perfectly accommodated inside the hydrophobic site.[5] If the interactions are sufficiently strong, inhibition of the catalytic activity of HIVP is to be expected. *In vitro* studies, performed using a 'first generation' water soluble fullerene derivative (**2**), confirmed that inhibition of acutely and cronically affected peripheral blood mononuclear cells (PBMC) indeed occurred with an EC_{50} of 7 μM.[6,77] In addition, no cytotoxic effect was recorded on non-infected PBMC. Although HIVP inhibitors currently considered for therapy are active at nanomolar or even subnanomolar concentrations, the potential use of fullerene derivatives in this field should not be disregarded, because the recent advancements in the functionalisation chemistry of fullerenes can produce novel interesting candidates. For instance, derivatisation of the fullerene at specific positions with groups that may give electrostatic interactions with Asp 25 and 125 should increase the binding constant by up to three orders of magnitude.[5] A guideline for the preparation of more active fullerene derivatives was suggested based on an increase of desolvation of the hydrophobic cavity of the enzyme and the formation of stronger hydrophobic interactions. Inside the cavity, in fact, two symmetric hydrophobic channels are not occupied by **2** because of steric hindrance. The incorporation of appropriate apolar groups on the fullerene derivative might lead to occupancy of those channels with an increase of binding constants. Calculations carried out on derivatives **16** and **17** confirmed this hypothesis, with a binding constant for **16** about fifty times higher than for **2**.[78]

Other fullerene derivatives that have been solubilised and tested as HIVP inhibitors include **15**, **14** and water soluble peptide **3**.[53] Compound **15** showed an EC_{50} of 2.5 μM without any toxicity,[79] whereas the more active derivative **14** displayed a K_i value of 0.32 μM.[9]

An extensive study of anti-HIVP activity was performed using a variety of functionalised [60]fullerene derivatives. For three of these compounds, an EC_{50} in the range of 0. 9–2.9 μM was observed.[80]

Neuroprotective properties

Many neurodegenerative diseases originate from excess production of superoxide and nitric oxide radicals, whose origin may be due to overexcitation of glutamic acid receptors. It has been shown that compounds that act as radical sponges reduce, though not completely, neuronal death. [60]Fullerene, owing to its antioxidant properties and high reactivity toward free radicals, shows promising behavior in this field.[81] Two derivatives of trisaddition of malonic units to [60]fullerene, **18** and **19**,[82] are highly soluble in water and are excellent radical scavengers. *In vitro* experiments using cultures of neocortical cells showed a dose-dependent decrease of neuronal death, with

derivative **18** being more active than **19**.[83] Compound **18** increases also the lifetime of cells deprived of oxygen and glucose, without antagonism between **18** and NMDA (*N*-methyl-D-aspartate) receptors. Daily administration of **18** (15 mg kg^{-1}) to G93A SOD1 G_1 mice, used as models of amyotrophic lateral sclerosis, led to an increase of lifetime of about ten days with respect to control animals.[83]

Superoxide radical quenching was also observed in a bis-malonic acid derivative of [60]fullerene.[84]

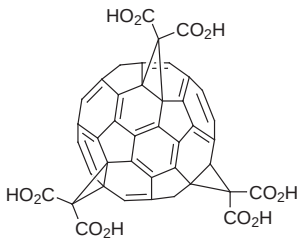

18

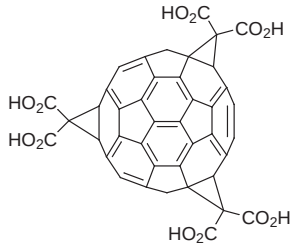

19

Antiapoptotic activity

Serum depletion induces apoptosis associated with an increase of production of free radicals. The same isomers **18** and **19** have been shown to possess antiapoptotic activity. Apoptosis due to amyloyl peptide $A\beta_{1\text{-}42}$ was also inhibited by the same fullerene derivatives.[83] In a strictly connected work, the effects of trisadducts **18** and **19** on apoptosis induced by ceramide were evaluated. In this case isomer **19** is more active.[85]

A study carried out again utilizing derivatives **18** and **19** among other antioxidant agents showed that only the fullerene derivatives inhibit apoptosis of human hepatoma Hep3B cells, induced by transforming growth factor β (TGF-β).[86] The mechanism of action is supposed to be indirect because all other actions induced by TGF-β remain unaltered.

Antibacterial activity

In preliminary tests, water soluble fullerene derivative **4** was found to be active against a variety of microorganisms. Different species of bacteria and different fungal strains were killed in a slightly modified agar diffusion test: two strains, clinical isolates CA1 and Z11, of *Candida albicans*, a fastidious pathogenic eukariote; strain ATCC 6633 of *Bacillus subtilis*, a spore-forming, Gram positive bacterium; strain AB1153 of *Escherichia coli*, a Gram negative enteric bacterium; a clinical isolate, strain 261/6 of *Mycobacterium avium*, an acid fast, emerging pathogen resistant to most antimicrobial drugs. In the latter case, 70% inhibition was observed with a concentration of 26 μg ml^{-1}, whereas complete inhibition was achieved with concentrations 10 times higher.[24]

Miscellaneous uses

Broncoconstriction induced by exsanguination in guinea-pigs was limited by fullerenols, without significant alteration of respiratory functions.[87] Fullerenols could be used in the perfusion of kidneys before transplantation, as they decreased infiltration of inflammatory cells and inhibited tubular swelling and necrosis.[88] Fullerenols were also investigated as anti-proliferative agents in arteriosclerosis, because they inhibited transduction signals.[89]

Macroscopic quantities of endohedral metallofullerenes containing Gd, Ho, Y, Ce were synthesised, in which, upon neutron activation, the inside metals become radioactive, but are still isolated from the outside world by the presence of the carbon cage. As a matter of fact, this novel class of fullerenes might be useful in nuclear medicine, with potential use as radiotracers or radiopharmaceuticals.[90]

Fullerenes can also be used for analytical purposes. Modelling studies have shown that it is possible to form a salt in which the anion is a DNA phosphate and the cation is a pyrrolidinium salt of [60]fullerene. This hybrid nanoarchitecture would be easily detected with transmission electron microscopy, since the fullerene moiety confers the necessary electron density to these complexes.[91]

Conclusions and perspectives

The impact of fullerenes and fullerene derivatives in biology will be substantiated only if their toxicity is found to be sufficiently low. Preliminary toxicological studies have shown that these novel compounds are not carcinogenic when applied on skin. Although [60]fullerene is incorporated inside cells, it does not seem to affect the proliferation rate of keratinocytes, fibroblasts or leucocytes. Studies of acute, subacute and chronic toxicity at reasonable dosing have so far given negative results. However, dose-dependent toxicity has been observed, whereas administration to pregnant mice gave rise to genetic malformations. Different toxicity levels have also been found for different derivatives.

On the other hand, once the problems of solubilisation and clustering are completely solved, and their toxicity fully tested, the fullerenes will probably find extended use in biology. In fact, owing to their ability of cleaving DNA, these carbon spheres appear promising candidates for use in diagnostics, photodynamic therapy, and as useful photoprobes in the study of genetic transcription. As radical scavengers, the fullerenes are to be considered neuroprotectors in neurodegenerative diseases and in the inhibition of apoptosis. The peculiar geometrical shape makes [60]fullerene an ideal inhibitor of HIV protease, especially if additional stabilising interactions, besides hydrophobic affinity, can be obtained.[5]

Maybe the phrase 'medicinal chemistry' used for the title of this Article is a bit premature for this young field. But we hope that this work will attract organic and medicinal chemists, as well as pharmacologists and biologists. Only their combined efforts will help create the new field of the medicinal chemistry of fullerenes.

Notes and references

1 H. W. Kroto, J. R. Heath, S. C. O'Brien, R. F. Curl and R. E. Smalley, *Nature*, 1985, **318**, 162.
2 W. Krätschmer, L. D. Lamb, K. Fostiropoulos and D. R. Huffman, *Nature*, 1990, **347**, 354.
3 M. Prato, *J. Mater. Chem.*, 1997, **7**, 1097.
4 H. Tokuyama, S. Yamago, E. Nakamura, T. Shiraki and Y. Sugiura, *J. Am. Chem. Soc.*, 1993, **115**, 7918.
5 S. H. Friedman, D. L. DeCamp, R. P. Sijbesma, G. Srdanov, F. Wudl and G. L. Kenyon, *J. Am. Chem. Soc.*, 1993, **115**, 6506.
6 R. Sijbesma, G. Srdanov, F. Wudl, J. A. Castoro, C. Wilkins, S. H. Friedman, D. L. DeCamp and G. L. Kenyon, *J. Am. Chem. Soc.*, 1993, **115**, 6510.
7 *Comprehensive Medicinal Chemistry*, ed. C. Hansch, P. G. Sammes and J. B. Taylor, Pergamon, Oxford, 1990, vol. 4.
8 A. W. Jensen, S. R. Wilson and D. I. Schuster, *Bioorg. Med. Chem.*, 1996, **4**, 767.
9 E. Nakamura, H. Tokuyama, S. Yamago, T. Shiraki and Y. Sugiura, *Bull. Chem. Soc. Jpn.*, 1996, **69**, 2143.
10 T. Andersson, K. Nilsson, M. Sundahl, G. Westman and O. Wennerström, *J. Chem. Soc., Chem. Commun.*, 1992, 604.
11 T. Braun, *Fullerene Sci. Technol.*, 1997, **5**, 615.
12 J. L. Atwood, G. A. Koutsantonis and C. L. Raston, *Nature*, 1994, **368**, 229.
13 S. Shinkai and A. Ikeda, *Gazz. Chim. Ital.*, 1997, **127**, 657.
14 Y. N. Yamakoshi, T. Yagami, K. Fukuhara, S. Sueyoshi and N. Miyata, *J. Chem. Soc., Chem. Commun.*, 1994, 517.
15 H. Hungerbühler, D. M. Guldi and K.-D. Asmus, *J. Am. Chem. Soc.*, 1993, **115**, 3386.
16 R. V. Bensasson, E. Bienvenue, M. Dellinger, S. Leach and P. Seta, *J. Phys. Chem.*, 1994, **98**, 3492.

17 N. O. Mchedlov-Petrossyan, V. K. Klochkov and G. V. Andrievsky, *J. Chem. Soc., Faraday Trans.*, 1997, **93**, 4343.
18 S. A. Jenekhe and X. L. Chen, *Science*, 1998, **279**, 1903.
19 R. M. Williams, W. Crielaard, K. J. Hellingwerf and J. W. Verhoeven, *Recl. Trav. Chim. Pays-Bas*, 1996, **115**, 72.
20 M. Hetzer, S. Bayerl, X. Camps, O. Vostrowsky, A. Hirsch and T. M. Bayerl, *Adv. Mater.*, 1997, **9**, 913.
21 W. A. Scrivens, J. M. Tour, K. E. Creek and L. Pirisi, *J. Am. Chem. Soc.*, 1994, **116**, 4517.
22 L. Y. Chiang, J. B. Bhonsle, L. Wang, S. F. Shu, T. M. Chang and J. R. Hwu, *Tetrahedron*, 1996, **52**, 4963.
23 Y. Tabata, Y. Murakami and Y. Ikada, *Fullerene Sci. Technol.*, 1997, **5**, 989.
24 T. Da Ros, M. Prato, F. Novello, M. Maggini and E. Banfi, *J. Org. Chem.*, 1996, **61**, 9070.
25 M. Brettreich and A. Hirsch, *Tetrahedron Lett.*, 1998, **39**, 2731.
26 D. M. Guldi, H. Hungerbülher and K.-D. Asmus, *J. Phys. Chem.*, 1995, **99**, 13 487.
27 D. M. Guldi, *Res. Chem. Intermed.*, 1997, **23**, 653.
28 J. Eastoe, E. Crooks, A. Beeby and R. Heenan, *Chem. Phys. Lett.*, 1995, **245**, 571.
29 D. M. Guldi, *J. Phys. Chem. A*, 1997, **101**, 3895.
30 J. Eastoe, E. R. Crooks, A. Beeby and R. K. Heenan, *Chem. Phys. Lett.*, 1995, **245**, 571.
31 I. Lamparth and A. Hirsch, *J. Chem. Soc., Chem. Commun.*, 1994, 1727.
32 D. M. Guldi and K.-D. Asmus, *Radiat. Phys. Chem.*, in the press.
33 T. Hamano, K. Okuda, T. Mashino, M. Hirobe, K. Arakane, A. Ryu, S. Mashiko and T. Nagano, *Chem. Commun.*, 1997, 21.
34 Y.-Z. An, J. L. Anderson and Y. Rubin, *J. Org. Chem.*, 1993, **58**, 4799.
35 L. Isaacs and F. Diederich, *Helv. Chim. Acta*, 1993, **76**, 2454.
36 S. Yamago, H. Tokuyama, E. Nakamura, M. Prato and F. Wudl, *J. Org. Chem.*, 1993, **58**, 4796.
37 M. Maggini, G. Scorrano, A. Bianco, C. Toniolo, R. P. Sijbesma, F. Wudl and M. Prato, *J. Chem. Soc., Chem. Commun.*, 1994, 305.
38 A. Skiebe and A. Hirsch, *J. Chem. Soc., Chem. Commun.*, 1994, 335.
39 N. Wang, J. Li, D. Zhu and T. H. Chan, *Tetrahedron Lett.*, 1995, **36**, 431.
40 l. Gan, D. Zhou, C. Luo, H. Tan, C. Huang, M. Lü, J. Pan and Y. Wu, *J. Org. Chem.*, 1996, **61**, 1954.
41 M. E. Vol'pin, E. M. Belavtseva, V. S. Romanova, A. I. Lapshin, L. I. Aref'eva and Z. N. Parnes, *Mendeleev Commun.*, 1995, 129.
42 M. E. Vol'pin, Z. N. Parnes and V. S. Romanova, *Russ. Chem. Bull.*, 1998, **47**, 1021.
43 A. B. Holmes and G. R. Stephenson, *Chem. Ind.*, 1994, 303.
44 A. Bianco, M. Maggini, G. Scorrano, C. Toniolo, G. Marconi, C. Villani and M. Prato, *J. Am. Chem. Soc.*, 1996, **118**, 4072.
45 A. Bianco, T. Bertolini, M. Crisma, G. Valle, C. Toniolo, M. Maggini, G. Scorrano and M. Prato, *J. Peptide Res.*, 1997, **50**, 159.
46 A. Bianco, V. Lucchini, M. Maggini, M. Prato, G. Scorrano and C. Toniolo, *J. Peptide Sci.*, 1998, **4**, 364.
47 F. Novello, M. Prato, T. Da Ros, M. De Amici, A. Bianco, C. Toniolo and M. Maggini, *Chem. Commun.*, 1996, 903.
48 A. Yaron and F. Naidor, *C. R. C. Crit. Rev. Biochem.*, 1993, **28**, 31.
49 M. Prato and M. Maggini, *Acc. Chem. Res.*, 1998, **31**, 519.
50 S. Schergna, T. Da Ros, P. Linda, C. Ebert, L. Gardossi and M. Prato, *Tetrahedron Lett.*, 1998, **39**, 7791.
51 M. Prato, A. Bianco, M. Maggini, G. Scorrano, C. Toniolo and F. Wudl, *J. Org. Chem.*, 1993, **58**, 5578.
52 C. Toniolo and E. Benedetti, *TIBS*, 1991, **16**, 350.
53 C. Toniolo, A. Bianco, M. Maggini, G. Scorrano, M. Prato, M. Marastoni, R. Tomatis, S. Spisani, G. Palù and E. D. Blair, *J. Med. Chem.*, 1994, **37**, 4558.
54 T. Redemann, C. Kempter, H.-G. Ihlenfeld, I. Lamparth, A. Skiebe, S. Meder, A. Hirsch, G. Boheim and G. Jung, *Peptides*, 1996, 747.
55 A. Kurz, C. Halliwell, J. Davis, A. Hill and G. Canters, *Chem. Commun.*, 1998, 433.
56 B.-X. Chen, S. R. Wilson, M. Das, D. J. Coughlin and B. F. Erlanger, *Proc. Natl. Acad. Sci. U.S.A.*, 1998, **95**, 10 809.
57 A. Bianco, F. Gasparrini, M. Maggini, D. Misiti, A. Polese, M. Prato, G. Scorrano, C. Toniolo and C. Villani, *J. Am. Chem. Soc.*, 1997, **119**, 7550.
58 F. Moussa, S. Roux, M. Pressac, E. Génin, M. Hadchouel, F. Trivin, A. Rassat, R. Céolin and H. Szwarc, *New J. Chem.*, 1998, 989.
59 F. Moussa, P. Chretien, P. Dubois, L. Chuniaud, M. Dessante, F. Trivin, P.-Y. Sizaret, V. Agafonov, R. Céolin, H. Szwarc, V. Greugny, C. Fabre and A. Rassat, *Fullerene Sci. Technol.*, 1995, **3**, 333.
60 F. Moussa, P. Chrétien, M. Pressac, F. Trivin, H. Szwarc and R. Céolin, *Fullerene Sci. Technol.*, 1997, **5**, 503.
61 F. Moussa, F. Trivin, R. Céolin, M. Hadchouel, P.-Y. Sizaret, V. Greugny, C. Fabre, A. Rassat and H. Szwarc, *Fullerene Sci. Technol.*, 1996, **4**, 21.
62 T. Tsuchiya, Y. N. Yamakoshi and N. Miyata, *Biochem. Biophys. Res. Commun.*, 1995, **206**, 885.
63 T. Tsuchiya, I. Oguri, Y. N. Yamakoshi and N. Miyata, *FEBS Lett.*, 1996, **393**, 139.
64 R. Bullard-Dillard, K. E. Creek, W. A. Scrivens and J. M. Tour, *Bioorg. Chem.*, 1996, **24**, 376.
65 S. Yamago, H. Tokuyama, E. Nakamura, K. Kikuchi, S. Kananishi, K. Sueki, H. Nakahara, S. Enomoto and F. Ambe, *Chem. Biol.*, 1995, **2**, 385.
66 P. Rajagopalan, F. Wudl, R. F. Schinazi and F. D. Boudinot, *Antimicrob. Agents Chemother.*, 1996, **40**, 2262.
67 T. H. Ueng, J. J. Kang, H. W. Wang, Y. W. Cheng and L. Y. Chiang, *Toxicol. Lett.*, 1997, **93**, 29.
68 C. S. Foote, *Top. Curr. Chem.*, 1994, **169**, 347.
69 K. Irie, Y. Nakamura, H. Ohigashi, H. Tokuyama, S. Yamago and E. Nakamura, *Biosci. Biotechnol. Biochem.*, 1996, **60**, 1359.
70 R. C. Richmond and U. J. Gibson, in *Recent Advances in the Chemistry and Physics of Fullerenes and Related Materials*, ed. K. M. Kadish and R. S. Ruoff, The Electrochemical Society Inc., Pennington, NJ, USA, 1995, p. 684.
71 See also: J. Kamat, T. Devasagayam, K. Priyadarsini, H. Mohan and J. Mittal, *Chem.-Biol. Interact.*, 1998, **114**, 145.
72 N. Higashi, T. Inoue and M. Niwa, *Chem. Commun.*, 1997, 1507.
73 Y. N. Yamakoshi, T. Yagami, S. Sueyoshi and N. Miyata, *J. Org. Chem.*, 1996, **61**, 7236.
74 A. Boutorine, H. Tokuyama, M. Takasugi, H. Isobe, E. Nakamura and C. Hélène, *Angew. Chem., Int. Ed. Engl.*, 1994, **33**, 2462.
75 Y.-Z. An, C.-H. B. Chen, J. L. Anderson, D. S. Sigman, C. S. Foote and Y. Rubin, *Tetrahedron*, 1996, **52**, 5179.
76 F. Kasermann and C. Kempf, *Antiviral Res.*, 1997, **34**, 65.
77 R. F. Schinazi, R. P. Sijbesma, G. Srdanov, C. L. Hill and F. Wudl, *Antimicrob. Agents Chemother.*, 1993, **37**, 1707.
78 S. H. Friedman, P. S. Ganapathi, Y. Rubin and G. L. Kenyon, *J. Med. Chem.*, 1998, **41**, 2424.
79 R. F. Schinazi, C. Bellavia, R. Gonzalez, C. L. Hill and F. Wuld, in *Recent Advances in the Chemistry and Physics of Fullerenes and Related Materials*, ed. K. M. Kadish and R. S. Ruoff, The Electrochemical Society Inc., Pennington, NJ, 1995.
80 D. I. Schuster, S. R. Wilson and R. F. Schinazi, *Bioorg. Med. Chem. Lett.*, 1996, **6**, 1253.
81 R. Pellicciari, G. Costantino, M. Marinozzi and B. Natalini, *Farmaco*, 1998, **53**, 255.
82 A. Hirsch, I. Lamparth and H. R. Karfunkel, *Angew. Chem., Int. Ed. Engl.*, 1994, **33**, 437.
83 L. L. Dugan, D. M. Turetsky, C. Du, D. Lobner, M. Wheeler, C. R. Almli, C. K.-F. Shen, T.-Y. Luh, D. W. Choi and T.-S. Lin, *Proc. Natl. Acad. Sci. U.S.A.*, 1997, **94**, 9434.
84 K. Okuda, T. Mashino and M. Hirobe, *Bioorg. Med. Chem. Lett.*, 1996, **6**, 539.
85 S.-C. Hsu, C.-C. Wu, T.-Y. Luh, C.-K. Chou, S.-H. Han and M.-Z. Lai, *Blood*, 1998, **91**, 2658.
86 Y. L. Huang, C. K. Shen, T. Y. Luh, H. C. Yang, K. C. Hwang and C. K. Chou, *Eur. J. Biochem.*, 1998, **254**, 38.
87 Y. L. Lai and L. Y. Chiang, *J. Auton. Pharmacol.*, 1997, **17**, 229.
88 S. C. Chueh, M. K. Lai, S. C. Chen, L. Y. Chiang and W. C. Chen, *Transplant. Proc.*, 1997, **29**, 1313.
89 L.-H. Lu, Y.-T. Lee, H.-W. Chen, L. Y. Chiang and H.-C. Huang, *Br. J. Pharmacol.*, 1998, **123**, 1097.
90 D. W. Cagle, T. P. Thrash, M. Alford, L. P. F. Chibante, G. J. Ehrhardt and L. J. Wilson, *J. Am. Chem. Soc.*, 1996, **118**, 8043.
91 A. M. Cassell, W. A. Scrivens and J. M. Tour, *Angew. Chem., Int. Ed.*, 1998, **37**, 1528.

Paper 8/09495K

ChemComm

First example of opening and hydrogenation of 2,3-dihydrobenzo[*b*]thiophene to 2-ethylthiophenol assisted by a soluble metal complex

Claudio Bianchini,* Andrea Meli, Werner Oberhauser and Francesco Vizza

Istituto per lo Studio della Stereochimica ed Energetica dei Composti di Coordinazione, ISSECC-CNR, 50132 Firenze, Italy. E-mail: bianchin@fi.cnr.it

Received (in Cambridge, UK) 4th February 1999, Accepted 8th March 1999

Displacement of THF by dihydrobenzo[*b*]thiophene (DHBT) in [(triphos)Ir(H)$_2$(THF)]BPh$_4$ yields the η^1-*S*-DHBT adduct [(triphos)Ir(H)$_2$(η^1-DHBT)]BPh$_4$ which reacts in THF at room temperature with KOBu^t to give the neutral 2-vinylthiophenolate derivative (triphos)Ir(H)$_2${η^1-*o*-S(C$_6$H$_4$)CH=CH$_2$} *via* C$_2$–S bond cleavage; the latter compound is hydrogenated under mild conditions (2 bar H$_2$, 80 °C) to the 2-ethylthiophenolate derivative (triphos)-Ir(H)$_2${*o*-S(C$_6$H$_4$)Et} and under harsh conditions (30 bar H$_2$, 160 °C) to free 2-ethylthiophenol and (triphos)IrH$_3$.

The hydrodesulfurization (HDS) of thiophenic molecules occurring in the course of the hydrotreating catalysis of petroleum feedstocks is a complex process whose mechanism is still quite speculative.[1] As is outlined in Scheme 1 for the model substrate benzo[*b*]thiophene (BT), the hydrogenation of thiophenes over heterogeneous catalysts may lead to the formation of hydrocarbons and H_2S *via* two principal mechanisms.

Kinetic studies at elevated H_2 pressures suggest that the reactions go through hydrogenated intermediates (Scheme 1, path a), especially with higher analogs of thiophene such as BT in which the electron density is less localized on the sulfur atom.[2] The prehydrogenation path has never been confirmed by the homogeneous modeling studies which are all consistent with the alternative hydrogenolysis route (Scheme 1, path b).[3]

The present paper constitutes a preliminary account of the first example of opening and hydrogenation of 2,3-dihydrobenzo[*b*]thiophene (DHBT) to 2-ethylthiophenol (ETP) assisted by a transition metal complex. C–S bond cleavage of tetrahydrothiophene (THT) has previously been found to occur on polymetallic species.[4,5] Notably, the C–S bond cleavage of THT in $Cl_3W(\mu\text{-THT})WCl_3$ was obtained by reaction with a nucleophile that remains attached to the C_2 carbon atom.[4]

The iridium complex [(triphos)Ir(H)$_2$(η^1-DHBT)]BPh$_4$ **2** has been synthesized by adding a slight excess of DHBT to a tetrahydrofuran (THF) solution of [(triphos)Ir(H)$_2$(THF)]BPh$_4$[6] **1** [triphos = MeC(CH$_2$PPh$_2$)$_3$].† At room temperature, the reaction is quantitative even in THF as DHBT is a much better ligand than THF. Very few η^1-DHBT complexes have been reported,[7] but their existence has frequently been claimed in homogeneous and heterogeneous catalytic hydrogenation cycles of BT.[1,2,3,7]

As shown in Scheme 2, the reaction of the η^1-S-DHBT adduct **2** in THF with an equivalent amount of KOBu^t at room temperature,[8] followed by treatment with a high pressure of H_2 at 160 °C yields the hydrogenolysis product ETP and converts all the iridium precursor to the trihydride (triphos)IrH$_3$ **3**.[9] The overall process was studied *in situ* by multinuclear NMR spectroscopy in THF-d$_8$ using a sapphire high-pressure NMR tube, initially under nitrogen and then under H_2.[3] The strong base has been found to transform the DHBT ligand in **2** into a 2-vinylthiophenolate group yielding the neutral complex (triphos)Ir(H)$_2${η^1-*o*-S(C$_6$H$_4$)CH=CH$_2$} **4**.† The tube was then pressurized with 2 bar of H_2. No reaction occurred at room temperature. Only at 80 °C, the ^{1}H NMR spectrum showed the signals of the vinyl hydrogens of **4** to decrease in intensity and the ^{31}P NMR spectrum showed the appearance of a new AM_2 spin system. Within 15 h at 80 °C, all **4** converted to the known 2-ethylthiophenolate derivative (triphos)Ir(H)$_2${*o*-S(C$_6$H$_4$)Et} **5**.[10] Both **4** and **5** were isolated in the solid state by simply scaling up the NMR conditions. The hydrogen pressure in the tube was increased to 30 bar and the temperature was raised to 160 °C to observe a further chemical transformation: free 2-ethylthiophenol was formed quantitatively (^{1}H NMR, GCMS)[3d] together with the known trihydride (triphos)IrH$_3$ **3**.[9]

The opening of the DHBT ligand by KOBu^t most likely occurs *via* an E_2 elimination as shown in Scheme 3(a).[11] Indeed, an E_2 elimination mechanism has been proposed to account for the hydrodesulfurization (HDS) of DHBT over the surface of real heterogeneous catalysts [Scheme 3(b)].[12]

The Ministero dell'Ambiente of Italy (contract PR1/C) is gratefully acknowledged for financial support.

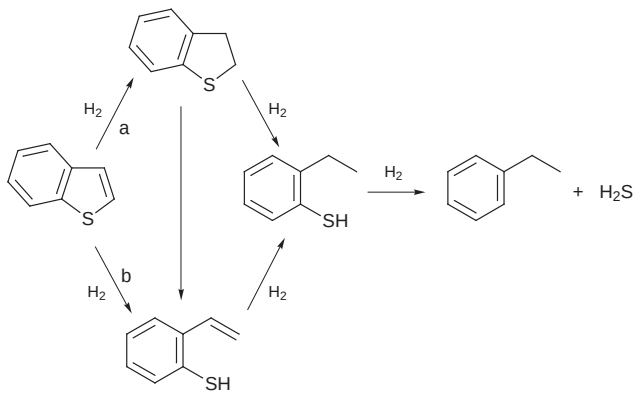

Scheme 1 Principal mechanisms proposed for the HDS of benzo[*b*]thiophene over heterogeneous catalysts.

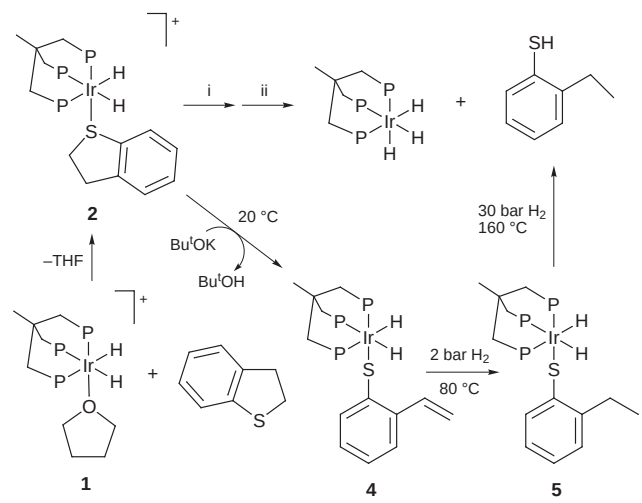

Scheme 2 *Reagents and conditions*: i, Bu^{t}OK, 20 °C; ii, 30 bar H_2, 160 °C.

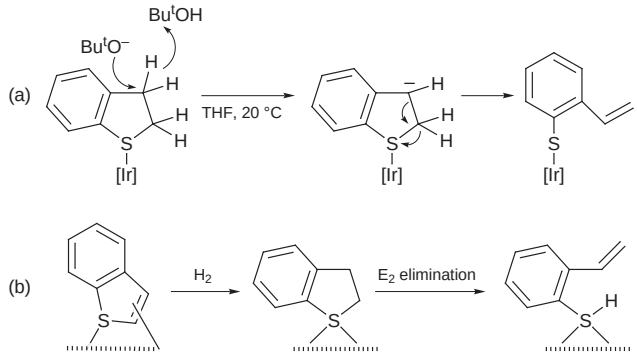

Scheme 3 [Ir] = (triphos)Ir(H)$_2$.

Notes and references

† Satisfactory elemental analysis was obtained for all new compounds that were isolated as off-white microcrystals. *Selected spectroscopic data* for **2**: ^{31}P{^{1}H} NMR (THF-d$_8$, 81.01 MHz) δ −2.4 (t, P$_A$), −15.8 (d, P$_M$), J(P$_A$P$_M$) 17.8; ^{1}H NMR (THF-d$_8$, 200.13 MHz) δ 3.52 (m, DHBT), −9.35 (second-order dm, Ir–H); IR (Nujol mull) ν_{IrH}/cm^{-1} 2074s.

For **4**: ^{31}P{^{1}H} NMR (THF-d$_8$, 81.01 MHz) δ −0.5 (t, P$_A$), −25.4 (d, P$_M$), J(P$_A$P$_M$) 13.6; ^{1}H NMR (THF-d$_8$, 200.13 MHz) δ 7.8 (masked, C*H*=CH$_c$H$_t$), 5.55 (dd, CH=CH$_c$*H*$_t$), 5.02 (dd, CH=C*H*$_c$H$_t$), −8.82 (second-order dm, Ir–H), J(HH$_c$) 11.0, J(HH$_t$) 17.6, J(H$_c$H$_t$) 2.2; IR (Nujol mull) ν_{IrH}/cm^{-1} 2055s.

1 H. Topsøe, B. S. Clausen and F. E. Massoth, *Hydrotreating Catalysis*, Springer-Verlag, Berlin, 1996.

2 G. H. Singhal, R. L. Espino and J. E. Sobel, *J. Catal.*, 1981, **67**, 446; P. Pokorny and M. Zdrazyl, *Collect. Czech. Chem. Commun.*, 1981, **46**, 2185.

3 C. Bianchini and A. Meli, *Acc. Chem. Res.*, 1998, **31**, 109; C. Bianchini, A. Meli, S. Moneti and F. Vizza, *Organometallics*, 1998, **17**, 2636; C. Bianchini, A. Meli, V. Patinec, V. Sernau and F. Vizza, *J. Am. Chem. Soc.*, 1997, **119**, 4945; C. Bianchini, V. Herrera, M. V. Jiménez, A. Meli, R. A. Sánchez-Delgado and F. Vizza, *J. Am. Chem. Soc.*, 1995, **117**, 8567; A. Iretskii, H. Adams, J. J. Garcia, G. Picazo and P. M. Maitlis, *Chem. Commun.*, 1998, 61; J. J. Garcia, B. E. Mann, H. Adams, N. A. Bailey and P. M. Maitlis, *J. Am. Chem. Soc.*, 1995, **117**, 2179.

4 P. M. Boorman, X. Gao, J. F. Fait and M. Parvez, *Inorg. Chem.*, 1991, **30**, 3886.

5 R. D. Adams, M. P. Pompeo, W. Wu and J. H. Yamamoto, *J. Am. Chem. Soc.*, 1993, **115**, 8207.

6 C. Bianchini, K. G. Caulton, T. J. Johnson, A. Meli, M. Peruzzini and F. Vizza, *Organometallics*, 1995, **14**, 933.

7 V. Herrera, A. Fuentes, M. Rosales, R. A. Sánchez-Delgado, C. Bianchini, A. Meli and F. Vizza, *Organometallics*, 1997, **16**, 2465.

8 In a blank experiment, a sample of DHBT in THF was treated with KOBu^t. The mixture was stirred for 6 h at room temperature but no reaction occurred.

9 P. Janser, L. M. Venanzi and F. Bachechi, *J. Organomet. Chem.*, 1985, **296**, 229.

10 C. Bianchini, A. Meli, M. Peruzzini, F. Vizza, S. Moneti, V. Herrera and R. A. Sánchez-Delgado, *J. Am. Chem. Soc.*, 1994, **116**, 4370.

11 J. March, *Advanced Organic Chemistry*, John Wiley and Sons, New York, 1985, p. 873.

12 M. D. Curtis and S. H. Druker, *J. Am. Chem. Soc.*, 1997, **119**, 1027.

Communication 9/00959K

Nanosized zeolite crystals—convenient control of crystal size distribution by confined space synthesis

Claus Madsen[a,b] and Claus J. H. Jacobsen*[b]

[a] *Inter-disciplinary Research Center for Catalysis (ICAT), Department of Chemistry, Building 207, Technical University of Denmark, 2800 Lyngby, Denmark*

[b] *Haldor Topsøe Research Laboratories, Nymøllevej 55, 2800 Lyngby, Denmark. E-mail: chj@topsoe.dk*

Received (in Cambridge, UK) 15th February 1999, Accepted 2nd March 1999

Confined space synthesis is a novel method in zeolite synthesis, which allows preparation of nanosized ZSM-5 crystals with a controlled crystal size distribution.

Traditional methods of zeolite synthesis typically involve crystallization from a gel or a clear solution under hydrothermal conditions.[1] Much work has been focused on preparation of large zeolite crystals suitable, *e.g.* for single crystal X-ray diffraction studies. Key factors in controlling the crystal size and morphology have been systematically studied.[2] In shape-selective zeolite catalysis improved selectivity is often found with larger crystals.[3] However, in many other catalytic reactions it appears favourable to use very small zeolite crystals since mass transfer limitations are of less importance. Furthermore, deactivation has in several cases been shown to proceed slower on small crystals due to their larger specific external area.[4] In the literature, some synthesis methods yielding small zeolite crystals have been reported.[5] However, none of these methods allow an easy control of the crystal size and the resulting crystal size distributions appear to be very dependent on the exact experimental conditions. Furthermore, isolation of the small zeolite crystals is not simple due to the colloidal properties of these materials. Therefore, we have attempted a novel method for the preparation of nanosized zeolite crystals. In contrast to other methods, it is possible to tailor-make zeolite crystal size distribution and recovery of the zeolite is simple. The synthesis method involves crystallization of the zeolite within the mesopore system of an inert support material. By use of carbon as the inert support material easy recovery of the zeolite is possible by controlled pyrolysis of the carbon.

Two different carbon black materials, Black Pearls 700 (BP700) and Black Pearls 2000 (BP2000) (supplied by Carbot Corp.) were used in the experiments. The carbon black was dried at 150 °C for 24 h prior to use. All other reagents, tetraethylorthosilicate (TEOS, 98 wt%), tetrapropylammonium hydroxide (TPAOH, 40 wt%), ethanol (EtOH, 99 wt%), sodium hydroxide (NaOH, 97 wt%), aluminium isopropoxide [Al(OPr^i)$_3$, 98 wt%] and distilled water, were used as received.

In a typical recipe, 20 g of carbon black was impregnated to incipient wetness with a clear solution of TPAOH, H_2O, NaOH, EtOH and optionally aluminium isopropoxide. Ethanol was evaporated at room-temperature and subsequently the carbon black was impregnated with TEOS yielding *ca.* 10 and 38 wt% SiO_2 in BP700 and BP2000, respectively. The composition of the synthesis gel (molar basis) was

$$x\ Al_2O_3 : 9\ TPA_2O : 0.15\ Na_2O : 50\ SiO_2 : 390\ H_2O : 200\ EtOH,$$
$$0 \leqslant x \leqslant \tfrac{1}{2}$$

After ageing for 3 h at room temperature the impregnated carbon black was transferred to a porcelain cup, introduced into a stainless steel autoclave containing enough water to produce saturated steam and heated in an oven at 180 °C for 48 h.

After cooling the autoclave to room temperature the product was suspended in water, filtered by suction, resuspended in water, and filtered again. This was repeated four times and finally the product was washed with 99% ethanol and dried at 110 °C for 3 h. The carbon black was removed by pyrolysis in a muffle furnace at 550 °C for 6 h. Three different zeolite samples were prepared using the reported method.

X-Ray powder diagrams were recorded by slow scanning on a Phillips vertical goniometer equipped with a θ-compensating divergence slit and a diffracted beam graphite monochromator utilizing Cu-Kα radiation. Crystal sizes were calculated from the two most intense diffraction peaks (2θ at 23.1 and 23.72° corresponding to the 501 and 151 reflections, respectively) by XRPD line broadening using the Scherrer equation. Transmission electron micrographs were obtained with a Philips EM430 (300 kV).

The ZSM-5 crystals are grown inside the pore structure of the carbon black support materials. Table 1 gives details of the pore structure of the two carbon blacks obtained from N_2 adsorption and desorption isotherms. The significantly larger pore volume of BP2000 compared with BP700 accounts for the higher SiO_2 content after impregnation. It is also seen that the average pore radius of the BP2000 is about twice as large as for BP700.

Fig. 1 illustrates the X-ray powder diagrams obtained after the zeolite synthesis and pyrolysis of the carbon black. It is seen that the sample contains highly crystalline ZSM-5 with an apparently small crystal size as judged from the diffraction line width. Table 2 gives details of crystal sizes determined using the Scherrer equation where crystal sizes of the ZSM-5 prior to and after removal of the carbon support by pyrolysis are provided. Apparently, some growth results from the removal of the carbon black, but this is within within the experimental uncertainty of the crystal size determination using the Scherrer equation.

The transmission electron micrograph of SZ† shown in Fig. 2 provides independent support for the formation of very small

Table 1 Selected properties of carbon black material

Support	d_{pore}[a]/nm	Pore volume[a]/mg g^{-1}	Surface area[a]/m^2 g^{-1}
Carbon Black Pearls, BP700	21.2	0.73	170
Carbon Black Pearls, BP2000	45.6	4.5	520

[a] BJH method (desorption).

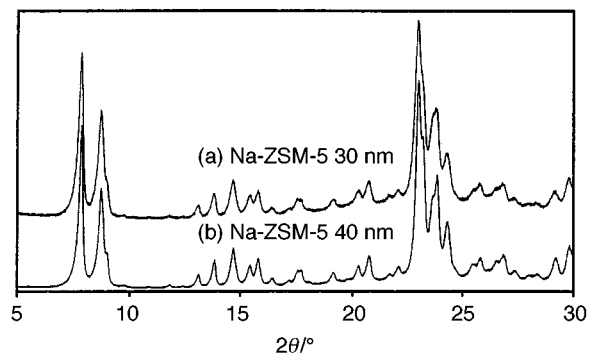

Fig. 1 XRPD of (a) SZ50† and (b) LZ100†. Carbon black removed by pyrolysis at 550 °C.

Table 2 Crystal sizes L_{501} and L_{151} determined by the Scherrer equation of ZSM-5 zeolites prepared by confined space synthesis. Calcination of ZSM-5 causes a phase transition[6,7]

Sample	Support	Si/Al	L_{501}/nm	L_{151}/nm
SZ	BP700	∞	20.3	16.0
SZ†[a]			37.4	25.8
SZ50	BP700	50	19.1	15.5
SZ50†[a]			29.4	31.2
LZ100	BP2000	100	48.4	67.1
LZ100†[a]			45.0	33.9

[a] Carbon black removed by pyrolysis at 550 °C.

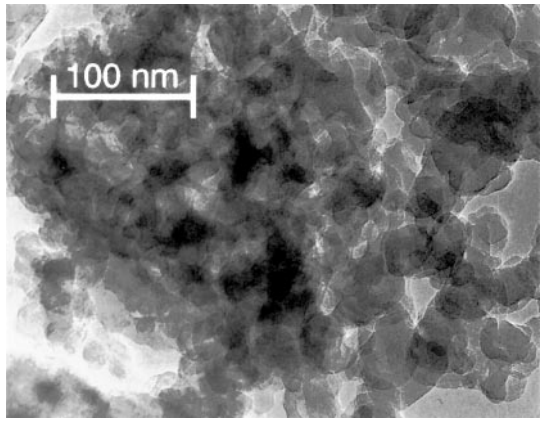

Fig. 2 Transmission electron micrograph of ZSM-5 crystals (SZ†) prepared by confined space synthesis.

zeolite crystals. From this figure it can also be seen that most crystals are in the range 8–30 nm and very little intergrowth is observed.

Sample SZ† has a total BET surface area of 412.4 $m^2\ g^{-1}$ with an external surface area of 185.0 $m^2\ g^{-1}$. The t-plot method (de Boer) of the SZ material revealed a bimodal pore size distribution. In addition to the pore volume inside the ZSM-5 crystals the material had an additional pore volume of 0.58 ml g^{-1} with an average pore radius of 15 nm. This mesopore system resulting from the packing of nanosized ZSM-5 crystals seems to provide excellent possibilities for diffusion of reactants and products, which is of significant importance in heterogeneous catalysis.

The ZSM-5 crystals synthesised using the confined space synthesis have sizes as low as 8 nm. To our knowledge this is the smallest crystal size of highly crystalline ZSM-5 reported so far. Jacobs *et al*.[8] reported the existence of X-ray amorphous ZSM-5, which contained crystals of <8 nm size in an amorphous matrix of silica. Camblor *et al*.[9] were able to synthesize zeolite beta with a crystal size as low as 10 nm determined by TEM. However, the crystal sizes depended strongly on the content of aluminium in the synthesis gel.

By use of the confined space synthesis it is possible to tailor-make zeolites with a given crystal size distribution and also to prepare very small zeolite crystals. Currently, studies are in progress to determine the minimum size of crystalline ZSM-5 crystals that can be prepared by the reported method. Furthermore, other zeolites and zeotypes are being prepared by confined space synthesis.

We would like to thank Iver Schmidt for helpful discussions and Poul Lenvig for obtaining the transmission electron micrographs.

Notes and references

1 See, for example: R. M. Barrer, *Hydrothermal Chemistry of Zeolites*, Academic Press, London, 1982, pp. 186–250; P. A. Jacobs and J. A. Martens, *Stud. Surf. Sci. Catal.*, 1987, **33**, 1 and references therein.
2 See, for example: L. D. Rollman and E. W. Valyocsik, *US Pat.*, 4 205 052, 1980, Mobil Oil Corp.; J. P. Verduyen, *Eur. Pat. Appl.*, 219.354, 1986, Exxon Co.
3 S. M. Csicsery, *Zeolites*, 1984, **4**, 202; K. Beschmann and L. Riekert, *J. Catal.*, 1993, **141**, 548.
4 S. B. Pu and T. Inui, *Zeolites*, 1996, **17**, 334; M. Yamamura, K. Chaki, T. Wakatsuki, H. Okado and K. Fujimoto, *Zeolites*, 1994, **14**, 643.
5 F. D. Renzo, *Catal. Today*, 1998, **41**, 37 and references therein; N. B. Castagnola and P. K. Dutta, *J. Phys. Chem. B*, 1998, **102**, 1696; A. E. Persson, B. J. Schoeman, J. Sterte and J.-E. Ottersted, *Zeolites*, 1995, **15**, 611; W. J. Ambs, *US Pat.*, 4 372 931, 1983; B. J. Schoeman, J. Sterte and J. E. Otterstedt, *J. Chem. Soc., Chem. Commun.*, 1993, 994; M. A. Camblor, A. Corma, A. Mifsud, J. Pérez-Pariente and S. Valencia, *Stud. Surf. Sci. Catal.*, 1997, **105**, 341.
6 H. van Koningsveld, H. van Bekkum and J. C. Jansen, *Acta. Crystallogr., Sect. B*, 1987, **43**, 127.
7 H. van Koningsveld, J. C. Jansen and H. van Bekkum, *Zeolites*, 1990, **10**, 235.
8 P. A. Jacobs, E. G. Derouane and J. Weitkamp, *J. Chem. Soc., Chem. Commun.*, 1981, 591.
9 M. A. Camblor, A. Corma and S. Valencia, *Microporous Mesoporous Mater.*, 1998, **25**, 59.

Communication 9/01228A

Anion pore structure through packing of molecular triangles

Ralf-Dieter Schnebeck, Eva Freisinger and Bernhard Lippert*

Fachbereich Chemie, Universität Dortmund, D-44221 Dortmund, Germany. E-mail: lippert@pop.uni-dortmund.de

Received (in Basel, Switzerland) 4th February 1999, Accepted 24th February 1999

A molecular triangle, generated from [(en)Pd(2,2′-bpz-N^1,$N^{1'}$)]$^{2+}$ and *trans*-$(NH_3)_2Pt^{II}$, encapsulates a ClO_4^- and aggregates in the solid state in such a way as to form long channels containing a string of anions.

The thermodynamically preferred product of the reaction between $[(en)Pd(H_2O)_2]^{2+}$ and 2,2′-bipyrazine (2,2′-bpz) is the mononuclear chelate [(en)Pd(2,2′-bpz-N^1,$N^{1'}$)]$^{2+}$ **1**.[1] By contrast, $[(en)Pt(H_2O)_2]^{2+}$ forms the kinetic product, triangular [{(en)Pt(2,2′-bpz-N^4,$N^{4'}$)}$_3$]$^{6+}$ **2** (Scheme 1).[1] Both **1** and **2** bind additional metal electrophiles *via* the still available N^4 (**1**) and N^1 (**2**) sites, respectively, to give hexanuclear molecular cups [after reacting **1** with additional $(en)Pd^{II}$ or **2** with $(en)M^{II}$ (M = Pt or Pd)[2,3]], or a flat triangle upon reaction of **1** with *trans*-$(NH_3)_2Pt^{II}$, as demonstrated here.

The compound isolated† and structurally characterised‡ proved to be [{(en)Pd}$_{2.5}$(2,2′-bpz)$_3$]{$(NH_3)_2$Pt}$_3$]$(ClO_4)_6$-$(NO_3)_5$·5H_2O **3** (Fig. 1), a molecular triangle of C_2 symmetry with one of the Pd corners [enPd(2)] having a 50% occupancy only.

Both the Pd_3 and Pt_3 triangles are close to equilateral, with Pd–Pd distances of 13.5 Å and Pt–Pt distances of 7.6–7.7 Å. As a consequence of the incompatibility of the bite angle at Pd (*ca.* 80°) and the 60° angles of the triangle, the Pt atoms are not centred on the sides of Pd_3 but lie outside the sides of these by *ca.* 0.5 Å, with Pt–Pd–Pt angles of *ca.* 69°. Triangle **3** differs from **2** in that the bpz ligands in **3** are, unlike in **2**, essentially coplanar with all metal ions. A single ClO_4^- anion is encapsulated in the centre of the cation, bearing some similarity with the situation in a recently described Co_8 compound.[4] Pairs of triangles approach each other *via* the half-occupied Pd(2) positions [ideally separated by 4.363(8) Å] and are propeller-twisted by *ca.* 50°.

The packing of the cations of **3** is such that they are approximately parallel oriented, yet by 180° rotation the triangles form a stair, which is inclined by *ca.* 60° and has treads separated by *ca.* 6.1 Å (Fig. 2). In the interior of this stair, a channel is formed (Fig. 3), which hosts one ClO_4^- per subunit. This situation is in a way reminiscent of self-assembling ion channels that generate pore structures,[5] however, there are also differences: the interaction between the layered triangles is

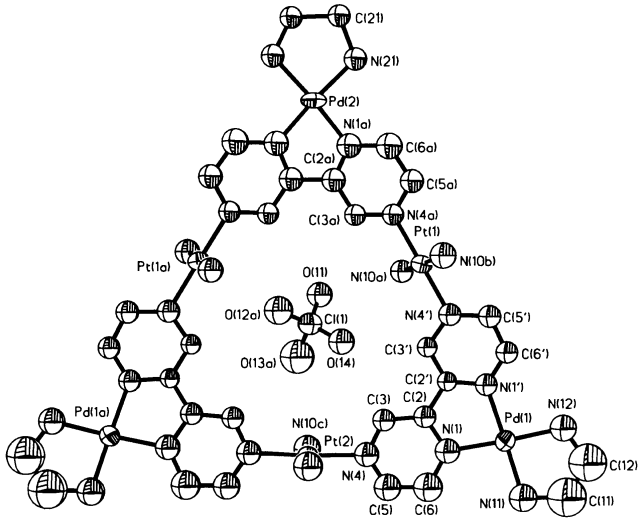

Fig. 1 Crystal structure of cation **3** with encapsulated ClO_4^-. Note that (en)Pd(2) has a 50% occupancy only. Relevant distances (Å) and angles (°): Pt(1)–N(4′) 1.97(2), Pt(1)–N(10b) 1.98(2), Pt(1)–N(10a) 2.00(2), Pt(1)–N(4a) 2.00(2), Pt(2)–N(10c) 2.02(2), Pt(2)–N(10c)#1 2.02(2), Pt(2)–N(4) 2.01(2), Pt(2)–N(4)#1 2.01(2), Pd(1)–N(1) 2.02(2), Pd(1)–N(1′) 2.03(2), Pd(2)–N(1a) 2.00(2), Pd(2)–N(1a)#1 2.00(2), N(10b)–Pt(1)–N(10a) 179.0(7), N(4′)–Pt(1)–N(4a) 178.7(6), N(10c)–Pt(2)–N(10c)#1 179.7(10), N(4)–Pt(2)–N(4)#1 177.1(11), N(1)–Pd(1)–N(1′) 80.5(7), N(1a)–Pd(2)–N(1a)#1 80.4(11).

neither *via* direct stacking, the NH_3 ligands of the three Pt^{II} ions are roughly perpendicular to the triangle plane, thereby preventing stacking of the bpz rings, nor by direct H bonding between the layers, as seen in nanotubes generated by cyclic peptides, for example.[6] Rather NO_3^- anions and water molecules, sandwiched between adjacent triangles, act as a 'glue' between the positively charged triangles, reinforced by ClO_4^- anions at the periphery of the triangles, all of which are involved in multiple H bonding interactions with NH_3 and en ligands.

The inner cavity within **3**, across diagonal C(3)H proton sites, is 6.24–6.42 Å wide. The ClO_4^- is located in such a

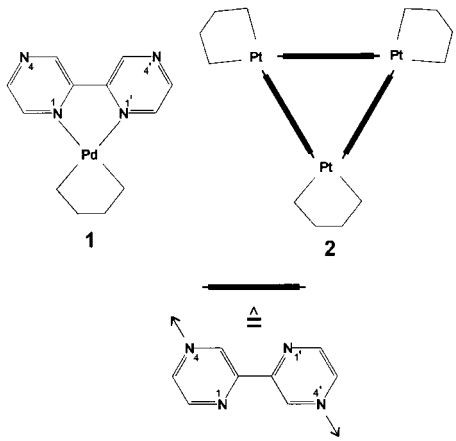

Scheme 1

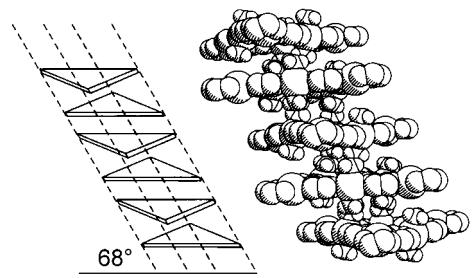

Fig. 2 Schematic representation and space filling of the layered triangles forming a 'stair'. Two NO_3^- anions and two H_2O molecules are layered between adjacent triangles and form multiple H bonds between each other and the Pt-NH_3 groups (not shown). At the periphery ClO_4^- anions interact *via* H bonds with NH_2 groups of Pd(en) entities as well as Pt–NH_3 groups (not shown), thereby generating a very compact structure that resembles a pipe rather than a stair.

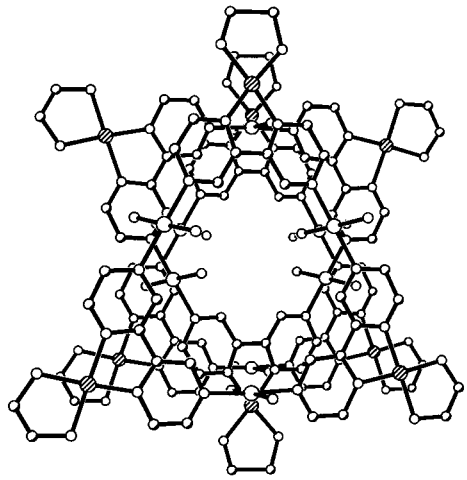

Fig. 3 View along the central channel formed by cations of **3** with ClO_4^- anions omitted. The molecular triangles are not perpendicular to the view but rather inclined by *ca*. 68°.

manner that Cl resides in the plane of the triangle, whereas the oxygen atoms lie pairwise above and below this plane and are clearly disordered. It appears that the oxygen atoms can weakly H bond to both the heterocyclic C(3)H protons [distances: $O_3ClO\cdots C(3)$ 3.02(4)–3.40(4) Å; angles: $O_3Cl–O\cdots H(3)$ 100.8(17)–128.4(19)°] and to the NH_3 protons of the Pt ions (distances: $O_3ClO\cdots H$ 2.6(1)–2.8(1) Å; angles: $O_3Cl–O\cdots H$ 168.8(21)–168.81(21)°], hence simultaneously to both hydrophobic and hydrophilic areas within the channel.

The ^1H NMR spectrum of **3** in D_2O, (pH* = 3.3) confirms the presence of more than a single species in solution. Spectra recorded within 2 h after dissolving crystals of **3** are dominated by three intense resonances in the aromatic region, namely at δ 10.62 (s, H3,H3′), 9.70 (s, w = 14 Hz, H5,H5′), and 8.99 (d, ^3J 3.7 Hz, H6,H6′) which are assigned to the Pd_3Pt_3 species. In addition, there is a large number (> 15) of minor resonances. For the Pd_2Pt_3 species nine sets of aromatic proton resonances are to be expected, each having an intensity of one third of the intensity of the resonances of Pd_3Pt_3. The ^{195}Pt NMR spectrum confirms also the presence of at least two species with PtN_4 coordination (δ −2449 and −2500, *ca*. 3 : 1). The larger number of observable resonances and also the time-dependent changes in the spectrum (resonances due to Pd_3Pt_3 decrease with time) strongly point toward the existence of more species than just Pd_3Pt_3 and Pd_2Pt_3 in solution, possibly $PdPt_3$ is present. There are two ways to simplify the spectrum: first, addition of $[(en)Pd(D_2O)_2]^{2+}$ to a solution of **3** leads to an increase in the intensities of the three resonances assigned to Pd_3Pt_3 with some of the minor resonances, however, still detectable. The relative intensities of the ^{195}Pt NMR resonances are now *ca*. 10 : 1. Second, addition of excess NaCl to an aqueous solution of **3** causes rapid precipitation of yellow $(en)PdCl_2$ and formation of a new major species with three intense sets of resonances at δ 10.20 (s), 9.28 (d, ^3J 3.2 Hz) and 9.18 (br, d), with some additional minor resonances still observable. The major component is tentatively assigned as a Pt_3 species. We have been as yet unable to isolate this compound and to prepare it directly from 2,2′-bpz and *trans*-$(NH_3)_2Pt^{II}$.

In summary, compound **3** is unique in that it (i) combines structural features of 'molecular triangles' which commonly have metal entities either at the corners[1,9] or at the centres of the sides[10] and in addition (ii) crystallises in a fashion that is reminiscent of an anion channel comprised of identical subunits.

This work was supported by the Fonds der Chemischen Industrie.

Notes and references

† $[\{(en)Pd\}_{2.5}(2,2'\text{-bpz})_3\{(NH_3)_2Pt\}_3](ClO_4)_6(NO_3)_5\cdot 5H_2O$ **3** was obtained in two steps. (a) *trans*-$(NH_3)_2PtCl_2$ (57.5 mg, 0.192 mmol) was suspended in water (10 ml), $AgNO_3$ (63.4 mg, 0.373 mmol) added, and the mixture stirred for three days at 45 °C. The mixture was cooled and AgCl removed by filtration. (b) $[(en)Pd(2,2'\text{-bpz})](ClO_4)_2$ (100 mg, 0.191 mmol) was added to the filtrate and the reaction mixture stirred for three days at 45 °C. Red–yellow **3** was obtained in 35% yield after 7 days at 4 °C. Satisfactory elemental analysis for $C_{29}H_{66}O_{44}N_{28}Cl_6Pd_{2.5}Pt_3$: Anal. Calc. for **3**: C = 13.5, H = 2.8, N = 15.2. Found C = 13.6, H = 2.5, N = 14.9%.

‡ *Crystal data* for **3**: M = 1287.53, orthorhombic, space group *Ccca*, a = 31.616(6), b = 35.691(7), c = 13.355(3) Å, U = 15069.9(53) Å^3, Z = 16, D_c = 2.270 g cm^{-3}, μ = 6.462 mm^{-1} (Mo-Kα, λ = 0.71069 Å), F(000) = 9912, T = 293(2) K. Enraf-Nonius-CAD4 diffractometer, crystal size 0.38 × 0.06 × 0.06 mm, 20205 reflections measured, 5555 unique (R_{int} = 0.1895), 2086 observed reflections with $F_0 > 4\sigma(F_0)$, R_1 = 0.0613, wR_2 = 0.1308 (observed data), S = 1.177. The structure was solved by the Patterson method[7] and refined using least-squares.[8] The crystals were of poor quality but showed no decay during measurements. Some of the anions and water molecules are disordered, *e.g.* one perchlorate and two nitrate anions in the crystallographic unit are only half occupied, respectively. Only a few atoms are refined anisotropically, because of the poor data to parameter ratio. CCDC 182/1179. See http://www.rsc.org/suppdata/cc/1999/675 for crystallographic files in .cif format.

1 R.-D. Schnebeck, L. Randaccio, E. Zangrando and B. Lippert, *Angew. Chem.*, 1998, **110**, 128; *Angew. Chem., Int. Ed.*, 1998, **37**, 119.
2 R.-D. Schnebeck, E. Freisinger and B. Lippert, *Angew. Chem.*, 1999, **111**, 235; *Angew. Chem., Int. Ed.*, 1999, **38**, 168.
3 R.-D. Schnebeck, E. Freisinger, F. Glahé and B. Lippert, to be submitted.
4 P. L. Jones, K. J. Byrom, J. C. Jeffery, J. A. McCleverty and M. D. Ward, *Chem. Commun.*, 1997, 1361.
5 J.-M. Lehn, *Supramolecular Chemistry: Concepts and Perspectives*, VCH, Weinheim, 1995.
6 J. D. Hartgerink, T. D. Clark and M. R. Ghadiri, *Chem. Eur. J.*, 1998, **4**, 1367.
7 SHELXS-86: G. M. Sheldrick, *Acta Crystallogr., Sect. A*, 1990, **46**, 467.
8 G. M. Sheldrick, SHELXL-93, Program for crystal structure refinement, University of Göttingen, Germany, 1993.
9 M. Fujita, O. Sasaki, T. Mitsuhashi, T. Fujita, J. Yazaki, K. Yamaguchi and K. Ogura, *Chem. Commun.*, 1996, 1535.
10 R. G. Raptis and J. P. Fackler, Jr, *Inorg. Chem.*, 1979, **18**, 658; H. H. Murray, R. G. Raptis and J. P. Fackler, Jr, *Inorg. Chem.*, 1988, **27**, 26.

Communication 9/00964G

A novel screening method for combinatorial chemistry for low affinity interactions

Naoki Sugimoto,* Hideki Kazuta, Jin Zou and Daisuke Miyoshi

Department of Chemistry, Faculty of Science, Konan University, 8-9-1 Okamoto, Higashinada-ku, Kobe 658-8501, Japan. E-mail: sugimoto@konan-u.ac.jp

Received (in Cambridge, UK) 20th November 1998, Accepted 4th March 1999

A novel screening method for combinatorial chemistry was developed by utilizing the high binding affinity of the avidin–biotin complex (K_a = 10^{15} M^{-1}), making possible the efficient detection of low affinity interactions between tryptophan and pentapeptides.

Combinatorial chemistry has attracted enormous attention because it can greatly facilitate the drug discovery process.[1,2] It is also an extremely powerful tool in the biotechnology of peptides[3,4] and nucleic acids. In nucleic acid research, this technology (*in vitro* selection) has been employed for finding small ribozymes and recently its reaction mechanism has been elucidated.[5,6] In the field of peptides, several screening methods have been employed using labeled target compounds such as colored dyes,[7] fluorescent dyes,[8] magnetic beads[9] and radioisotopes such as [γ-^{32}P].[10] However, many difficulties have been encountered in the selection of short peptides for a small target with low affinity. In particular, the above screening methods were not successful in extracting tryptophan (Trp) selective peptides from the pentapeptide library.

In this study, we developed a novel screening method utilizing the formation of the avidin–biotin complex, which has a large binding constant of 10^{15} M^{-1}. This screening method made possible the effective detection of low affinity interactions between tryptophan and pentapeptides. Trp was chosen as a target molecule since it is known to play a key role in biological processes, such as the functional peptide that recognizes porphyrin *via* a sandwiching interaction[11] and the *Trp* repressor in which binding Trp enhances DNA affinity as an allosteric effector.[12] Therefore, we have attempted the selection of short peptides that would recognize Trp from a combinatorial library to establish a general model system of low affinity interactions.

The random synthetic pentapeptide library was constructed by the 'split synthesis approach' as previously described.[1,2]† Nineteen natural L-amino acids were used, excluding cysteine to avoid intramolecular cyclization or intermolecular disulfide formation. The library theoretically contains about 2.5 million pentapeptide sequences. Biotin and a hydrophilic linker {biotinyl-ε-aminocaproic acid *N*-hydroxysuccinimide and [2-(2-*tert*-butoxycarbonylaminoethoxy)ethoxy]acetic acid (Boc-AEEA-OH)} were covalently attached to Trp. The introduction of a hydrophilic linker was performed to avoid aggregation of target molecules and such a linker is also effective in raising the activity of the avidin–biotin interaction because its affinity increases with linker length.‡ Moreover, the interactions of individual compounds on both sides of the linker can be treated independently by its introduction.

Our new approach is a novel screening method utilizing the avidin–biotin interaction in two steps. The first step of this screening method is mixing of the pentapeptide library and biotinylated Trp with the hydrophilic linker (BTHL) in an empty column, by gently shaking for 16 h and then washing the library beads.§ There may exist three binding modes between the pentapeptide library and BTHL during this step. These are between the pentapeptide library and the Trp site (W) [Scheme 1(*a*)], the biotin site (B) [Scheme 1(*b*)], and the linker site (L) [Scheme 1(*c*)] of BTHL, respectively. It is also possible that there may be no interaction between pentapeptide library and BTHL. The only desirable binding mode is between the pentapeptide library and W; the other cases must be eliminated. The second step is the addition of fluorescein labeled streptoavidin (FLS) to the library containing BTHL. The solution was gently shaken for 30 min and the library beads were washed with buffer solution to eliminate nonspecific interactions.¶ The concentration of added FLS was evaluated according to the amount of interacting target molecule, whose concentration was determined by UV absorbance of tryptophan in aqueous solution, using an extinction coefficient of 5500 cm^{-1} M^{-1}. Only the desirable interaction in the first step (formation of the W–library complex) will be able to form the avidin–biotin complex preferentially upon FLS addition. The other undesirable interactions, the B–library or L–library complexes, were eliminated since the binding constant of avidin–biotin complex formation (10^{15} M^{-1}) is much larger than those with other sites of BTHL, including W. Furthermore, the activity of the avidin–biotin interaction increases with the linker length of biotin. By regulating the concentration of added FLS, the case of no interaction in the first step can also be eliminated.

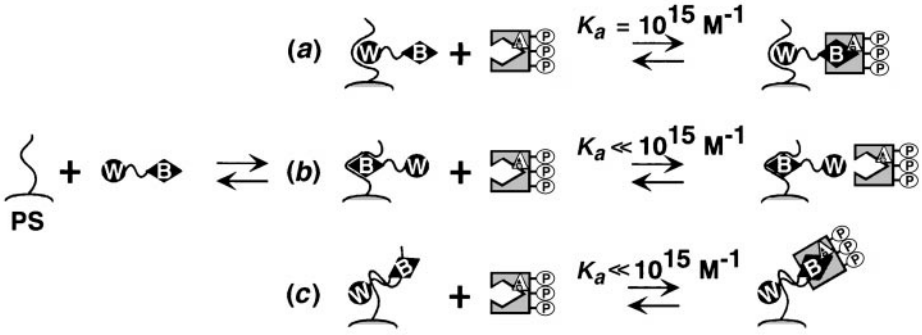

Scheme 1 Schematic drawing of the new selection method using the avidin–biotin interaction: Trp, biotin, avidin (streptoavidin), and the probe (fluorescein) are designated by W, B, A and P, respectively. Schemes (*a*), (*b*) and (*c*) show interactions of the pentapeptide library with W, B and L (linker), respectively. The pentapeptide library theoretically contains 2 480 000 pentapeptide sequences. PS designates PEG-PS resin which contains poly(ethylene glycol)-grafted polystyrene.

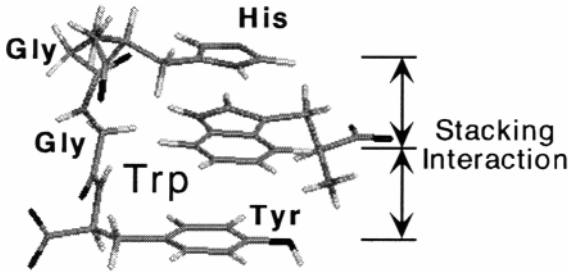

Fig. 1 Structure of the (His-Gly-Gly-Tyr) + Trp complex drawn *via* molecular modeling calculation using QUANTA 96/CHARMm 23.2. The energy of the complex was minimized by the Newton–Raphson method with an adopted basis set. Dynamic simulation of the energy-minimized structure was performed to obtain various conformations as initial coordinates for the calculation. The VERLET algorithm with a time step of 1 fs was used in the dynamic simulation. The system was heated from 0 to 1000 K for the conformational search in the MD simulation. All calculations were performed by running IRIX 5.3 on a Silicon Graphics Indigo2 workstation.

The library beads were subsequently poured carefully onto a plate. By exposing the pentapeptide library beads on the plate to UV light, only the beads which contain the avidin–biotin complex between FLS and TLB are able to generate fluorescence light. As a result, fluorescent beads (positive for the target molecule) were observed in the 2.5 million pentapeptide library. The fluorescent beads which contain the pentapeptide selective for Trp (target molecule) were physically removed from the library and subsequently microsequenced by protein sequencer. A total of ten pentapeptide sequences from the library were determined.

A consensus sequence of the selected peptides is Tyr/His-Gly-Gly-Tyr or His-Pro-Gly-His. The binding behavior of tryptophan with the peptide (Glu-His-Gly-Gly-Tyr) immobilized on the resin was analysed by a Langmuir isotherm. The binding constant was approximately 1.2×10^3 M^{-1} at room temperature. The consensus sequence has aromatic residues (His and Tyr) at the *i* and *i* + 3 positions, and a glycine residue at the *i* + 2 position in the motif can induce a β-turn structure.[13,14] When the motif forms the β-turn structure, two aromatic residues may orient in the same side to produce the sandwiching interaction with Trp between the two aromatic residues possible. To estimate the detailed interaction of the motif peptide (His-Gly-Gly-Tyr) with Trp, energy minimization calculations were performed using QUANTA 96/CHARMm 23.2. The result shows that the motif peptide may form a β-turn structure and the (His-Gly-Gly-Tyr) + Trp complex forms a stacking interaction between the two aromatic residues (His and Tyr) and Trp *via* the sandwiching interaction shown in Fig. 1. It was suggested that the motif peptide specifically recognizes Trp *via* the β-turn motif.

We thank Professor Fu-Ming Chen, Tennessee State University, for a critical reading of the manuscript and helpful comments. This work was supported in part by Grants-in-Aid from the Ministry of Education, Science Sports and Culture, Japan, and a Grant from the 'Research for the Future' Program of the Japan Society for the Promotion of Science.

Notes and references

† A split synthesis approach was carried out with standard peptide synthesis methods on solid phase with fluorenylmethoxycarbonyl (Fmoc) chemistry. Coupling was initiated by the addition of four-fold molar excess concentration of HATU and an eight-fold molar excess concentration of Pr^i_2NEt. The coupling reaction was driven to completion with a four-fold molar excess of Fmoc amino acids and monitored by the standard ninhydrin test. Occasionally, double coupling was needed. The resin was first divided into 19 aliquots of poly(ethylene glycol)-grafted polystyrene (PEG-PS) × HCl which has a hydrophilic linker (PEG) and was chosen as a solid phase support.

‡ Biotinyl-ε-aminocaproic acid *N*-hydroxysuccinimide and Boc-AEEA-OH were purchased from Calbiochem-Novabiochem Corporation and PerSeptive Biosystems, respectively. The coupling was carried out with *tert*-butoxycarbonyl (Boc) solid phase synthesis methods.

§ All experiments were conducted in buffer including 100 mM NaCl, 10 mM Na_2HPO_4 and 1 mM Na_2EDTA (pH 7.0) at room temperature in a same empty column.

¶ The composition of fluorescein labeled streptoavidin is F/S (molar) = 4.6 where F and S indicate fluorescein and streptoavidin, respectively. It was purchased from Vector Laboratories.

1 K. S. Lam, S. E. Salmon, E. M. Hersh, V. J. Hruby, W. M. Kazmierski and R. J. Knapp, *Nature*, 1991, **354**, 82.
2 R. A. Houghten, C. Pinilla, S. E. Blondelle, J. R. Appel, C. T. Dooley and J. H. Cuervo, *Nature*, 1991, **354**, 84.
3 N. Sugimoto and S. Nakano, *Chem. Commun.*, 1997, 2125.
4 N. Sugimoto and S. Nakano, *Bull. Chem. Soc. Jpn.*, 1998, **71**, 2205.
5 T. Ohmichi and N. Sugimoto, *Biochemistry*, 1997, **36**, 3514.
6 N. Sugimoto, T. Toda and T. Ohmichi, *Chem. Commun.*, 1998, 1533.
7 R. Boyce, G. Li, H. P. Nestler, T. Suenaga and W. C. Still, *J. Am. Chem. Soc.*, 1994, **116**, 7955.
8 H. Wennemers and W. C. Still, *Tetrahedron Lett.*, 1994, **35**, 6413.
9 S. Sasaki, M. Takagi, Y. Tanaka and M. Maeda, *Tetrahedron Lett.*, 1996, **37**, 85.
10 J. Wu, Q. N. Ma and K. S. Lam, *Biochemistry*, 1994, **33**, 14825.
11 N. Sugimoto and S. Nakano , *Chem. Lett.*, 1997, 939.
12 R. W. Schevitz, Z. Otwinowski, A. Joachimiak, C. L. Lawson and P. B. Sigler, *Nature*, 1985, **317**, 782.
13 C. M. Venkatachalam, *Biopolymers*, 1968, **6**, 1425.
14 T. Yamada, M. Nakao, T. Miyazawa, S. Kuwata, M. Sugiura, Y. In and T. Ishida, *Biopolymers*, 1993, **33**, 813.

Communication 8/09090D

Synthesis of the first gold complex with a central μ_4-selenido ligand

Silvia Canales,[a] Olga Crespo,[a] M. Concepción Gimeno,[a] Peter G. Jones[b] and Antonio Laguna*[a]

[a] *Departamento de Química Inorgánica, Instituto de Ciencia de Materiales de Aragón, Universidad de Zaragoza-CSIC, E-50009 Zaragoza, Spain. E-mail: alaguna@posta.unizar.es*

[b] *Institut für Anorganische und Analytische Chemie der Technischen Universität, Postfach 3329, D-38023 Braunschweig, Germany*

Received (in Basel, Switzerland) 15th December 1998, Accepted 4th March 1999

The first gold complex, $[Se(AuPPh_3)_4](CF_3SO_3)_2$, with a μ_4-selenido ligand has been prepared; the crystal structure reveals a square pyramidal geometry with short gold–gold interactions.

The chemistry of complexes in which a main-group element is surrounded by several (phosphino)gold fragments was pioneered by Schmidbaur *et al.*,[1] who prepared fascinating hypercoordinated species of the type $[C(AuPR_3)_5]^+$, $[C(AuPR_3)_6]^{2+}$, $[N(AuPR_3)_5]^{2+}$, $[P(AuPR_3)_5]^{2+}$ and $[P(AuPR_3)_6]^{2+}$.[2–6] Many of these heteroatom-centered complexes are electron-deficient, and gold–gold interactions provide a significant contribution to their stability. Such interactions between formally closed-shell (d^{10}) metal centres have been termed 'aurophilic attractions'[1] and their origin is still a matter of controversy;[7] Pyykkö *et al.* have presented theoretical evidence that these attractions are mainly correlation effects, strengthened by relativistic effects.[8–10]

Although the chemistry of the carbon-, nitrogen-, phosphorus- or arsenic-centered complexes was developed rapidly, the corresponding chalcogen-centered derivatives are still being studied. Recently the μ_4-sulfido[11] or μ_4-oxido[12] gold species were reported and shown to possess square pyramidal (apical sulfur) or tetrahedral geometry (central oxygen), respectively. Our previous work in the area of sulfur-centered complexes involved examples of gold(I) or gold(III) derivatives[13–17] with a μ_3- or μ_4-sulfur ligand. Selenium-centered compounds are limited to the species $[Se(AuPPh_3)_2]$ and $[Se(AuPPh_3)_3]PF_6$;[18–20] here we report the synthesis and structural characterisation of the first μ_4-selenido gold derivative.

The reaction of $[Se(AuPPh_3)_2]$ with 2 equiv. of $[Au(CF_3SO_3)(PPh_3)]$ in dichloromethane affords a solution from which the colourless air- and moisture-stable solid $[Se(AuPPh_3)_4](CF_3SO_3)_2$ **1** can be isolated.† Complex **1** behaves as a 1:2 electrolyte in acetone solution. The $^{31}P\{^1H\}$ NMR spectrum shows only one signal corresponding to a unique phosphorus environment, shifted to high field in comparison with the starting material (δ 4) or the trinuclear compound $[Se(AuPPh_3)_3](CF_3SO_3)$ (δ 1.3). In the liquid secondary positive-ion mass spectrum the monocationic peak $[Se(AuPPh_3)_4]^+$ appears at *m/z* 1915 (35%).

Crystals of **1** suitable for X-ray structure analysis were obtained from dichloromethane–heptane.‡ Compound **1** crystallises with two molecules of dichloromethane and is isostructural with the analogous sulfido compound $[S(AuPPh_3)_4](SO_3F_3)_2$[11] and its cation (Fig. 1) is also similar to that of $[As(AuPPh_3)_4]BF_4$.[21] It possesses a tetragonal pyramidal framework, with the selenium atom occupying the apical position. The Au atoms are not exactly coplanar, but arranged in a flattened butterfly form with a hinge angle of 27° about the Au1···Au2 diagonal; their deviations from the best Au_4 plane are ±0.27 Å, and that of the Se atom is 1.4 Å. The $SeAu_4$ core should be regarded as electron-deficient, considering the selenido ligand to serve as a six-electron donor. Therefore it still possesses a lone pair of electrons in the apical position, which means that further coordination of gold around the selenium atom is conceivable.

Complex **1** may be compared with the above-mentioned trinuclear selenide or the tetranuclear sulfide derivatives; observed differences are essentially as expected. The Au–Se–Au angles, which range from 70.45(4) to 72.59(4)° in **1**, are smaller than those in $[Se(AuPPh_3)_3]PF_6$ [77.7(1)–80.0(1)°][19] or the corresponding S–Au–S angles in the isostructural $[S(AuPPh_3)_4](CF_3SO_3)_2$ [73.5(2)–75.6(2)°]. This difference may be associated with the presence of more diffuse 3p orbitals in the selenium derivative, allowing smaller angles, and/or a

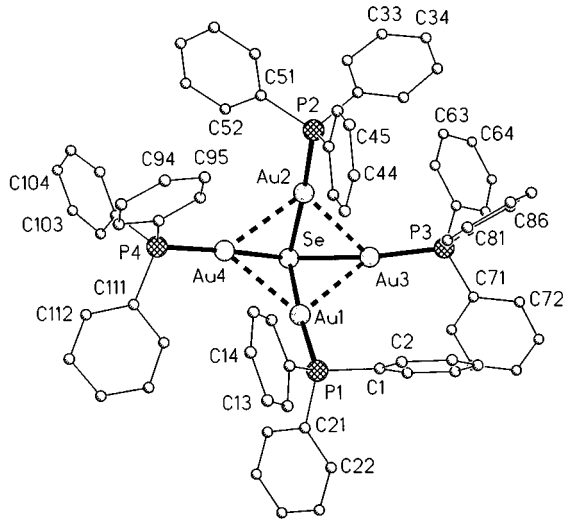

Fig. 1 The structure of the cation of complex **1** in the crystal. Hydrogen atoms have been omitted for clarity; radii are arbitrary.

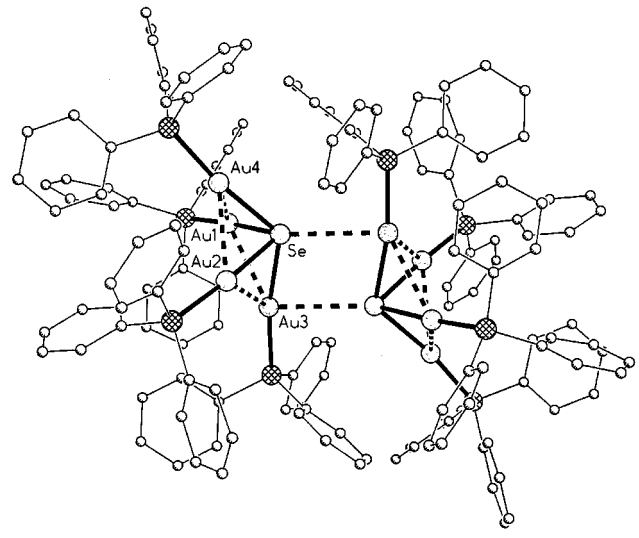

Fig. 2 Association of two cations of **1** in the crystal. The $CF_3SO_3^-$ ions and the CH_2Cl_2 molecules have been omitted.

greater electron repulsion of the lone pair of electrons. The Au–Se distances, 2.4654(13)–2.5347(14) Å, in **1** are longer than in $[Se(AuPPh_3)_3]^+$ [2.425(2)–2.451(2) Å] or (than Au–S) in $[S(AuPPh_3)_4]^{2+}$ [2.362(5)–2.429(5) Å]. Gold–gold distances between adjacent gold atoms in the pyramid base are short, 2.8959(8) to 2.9605(8) Å [the diagonal distances are 3.6 Å for Au(1)···Au(2) and 4.5 Å for Au(3)···Au(4)]. These contacts are longer than those found in the tetranuclear sulfide derivative, 2.883(2)–2.938(2) Å. The Au–P bond lengths in **1** [2.265(3)–2.282(3) Å] lie in the expected range for two-coordinate gold(I) complexes and are very similar to those found in $[Se(AuPPh_3)_3]PF_6$ [2.257(6)–2.283(5) Å].

The cations of **1** are paired across symmetry centres to form loose dimers (Fig. 2), the shorter intermolecular distances being Se···Au3′ 3.248 Å and Au3···Au3′ 4.45 Å.

This work was supported by the DGES (PB-97-1010-C02-01), the Caja de Ahorros de la Inmaculada (CB4/98) and the Fonds der Chemischen Industrie.

Notes and references

† *Preparation*: $[Au(CF_3SO_3)(PPh_3)]$ (0.2 mmol, 0.121 g) was added to a solution of $[Se(AuPPh_3)_2]$ (0.1 mmol, 0.100 g) in dichloromethane (20 mL) and the mixture was stirred for 30 min and then the solvent removed under vacuum to *ca.* 5 mL. Addition of diethyl ether (10 mL) gave complex **1** as a white solid. Yield 81%. (Found: C, 39.45; H, 2.60; S, 2.70. Calc. for $C_{74}H_{60}Au_4F_6O_6P_4S_2Se$; C, 39.0; H, 2.7; S, 2.8%). Λ_M = 165 Ω^{-1} cm^2 mol^{-1}. NMR: $^{31}P\{^1H\}$ (121 MHz, $CDCl_3$, reference 85% H_3PO_4), δ 31.0 (s); ^1H (300 MHz, $CDCl_3$, reference $SiMe_4$), δ 7.3–7.5 (m, Ph). Mass spectrum (LSIMS+): *m/z* 1915 ($[Se(AuPPh_3)_4]^+$, 35%).

‡ *Crystal data* for **1**·$2CH_2Cl_2$: $C_{74}H_{60}Au_4F_6O_6P_4S_2Se{\cdot}2CH_2Cl_2$, M_r = 2383.90, monoclinic, space group $P2_1/n$, a = 16.410(2), b = 23.353(3), c = 20.352(2) Å, β = 91.593(8)°, V = 7796.4(17) Å^3, Z = 4, D_c = 2.031 Mg m^{-3}, μ(Mo-Kα) = 8.31 mm^{-1}, F(000) = 4528, Siemens P4 diffractometer, λ(Mo-Kα) = 0.71073 Å, T = −100 °C. A colourless tablet 0.20 × 0.20 × 0.15 mm was used to collect 11096 intensities to $2\theta_{max}$ = 46°, of which after absorption corrections (transmission 0.685–0.873) 10820 were unique (R_{int} 0.0499). Scan type: ω. The structure was solved by direct methods and subjected to anisotropic refinement on F^2 (program SHELXL-97, G. M. Sheldrick, University of Göttingen). H atoms were included using a riding model. The final $wR(F^2)$ was 0.0536 for 10820 reflections, 928 parameters and 1206 restraints (to local ring symmetry and light atom displacement factors), conventional $R(F)$ = 0.0386, $S(F^2)$ = 0.743, max. $\Delta\rho$ 0.84 e Å^{-3}.

CCDC 182/1190. See http://www.rsc.org/suppdata/cc/1999/679/ for crystallographic files in .cif format.

1 H. Schmidbaur, *Gold Bull.*, 1990, **23**, 11; *Interdisc. Sci. Rev.*, 1992, **17**, 213; *Pure Appl. Chem.*, 1993, **65**, 691; *Chem. Soc. Rev.*, 1995, **24**, 391.
2 F. Scherbaum, A. Grohmann, G. Müller and H. Schmidbaur, *Angew. Chem., Int. Ed. Engl.*, 1989, **28**, 463.
3 F. Scherbaum, A. Grohmann, B. Huber, C. Krüger and H. Schmidbaur, *Angew. Chem., Int. Ed. Engl.*, 1988, **27**, 1544.
4 A. Grohmann, J. Riede and H. Schmidbaur, *Nature*, 1990, **345**, 140.
5 H. Schmidbaur, G. Weidenhiller and O. Steigelmann, *Angew. Chem., Int. Ed. Engl.*, 1991, **30**, 433; R. E. Bachman and H. Schmidbaur, *Inorg. Chem.*, 1996, **35**, 1399.
6 E. Zeller and H. Schmidbaur, *J. Chem. Soc., Chem. Commun.*, 1993, 69.
7 N. Kaltsoyannis, *J. Chem. Soc., Dalton Trans.*, 1997, 1.
8 J. Li and P. Pyykkö, *Chem. Phys. Lett.*, 1992, **197**, 586.
9 P. Pyykkö, J. Li and N. Runeberg, *Chem. Phys. Lett.*, 1994, **218**, 133.
10 P. Pyykkö, *Chem. Rev.*, 1997, **97**, 597.
11 F. Canales, M. C. Gimeno, P. G. Jones and A. Laguna, *Angew. Chem., Int. Ed. Engl.*, 1994, **33**, 769.
12 H. Schmidbaur, S. Hofreiter and M. Paul, *Nature*, 1995, **377**, 503.
13 F. Canales, M. C. Gimeno, A. Laguna and M. D. Villacampa, *Inorg. Chim. Acta*, 1996, **244**, 95.
14 F. Canales, M. C. Gimeno, A. Laguna and P. G. Jones, *J. Am. Chem. Soc.*, 1996, **118**, 4839.
15 F. Canales, M. C. Gimeno, A. Laguna and P. G. Jones, *Organometallics*, 1996, **15**, 3412.
16 M. J. Calhorda, F. Canales, M. C. Gimeno, J. Jiménez, P. G. Jones, A. Laguna and L. F. Veiros, *Organometallics*, 1997, **17**, 3837.
17 F. Canales, S. Canales, O. Crespo, M. C. Gimeno, P. G. Jones and A. Laguna, *Organometallics*, 1998, **17**, 1617.
18 H. Schmidbaur, F. Franke and J. Eberlein, *Chem. Z.*, 1975, **99**, 91.
19 C. Lensch, P. G. Jones and G. M. Sheldrick, *Z. Naturforsch., Teil B*, 1982, **37**, 944.
20 P. G. Jones and C. Thöne, *Chem. Ber.*, 1991, **124**, 2725.
21 E. Zeller, H. Beruda, A. Kolb, P. Bissinger and H. Schmidbaur, *Nature*, 1991, **352**, 141.

Communication 8/09739I

Conformationally flexible calix[4]arene chromoionophores: optical transduction of soft metal ion complexation by cation–π interactions

Niels J. van der Veen, Richard J. M. Egberink, Johan F. J. Engbersen, Frank J. C. M. van Veggel and David N. Reinhoudt*

Laboratory of Supramolecular Chemistry and Technology and MESA Research Institute, Faculty of Chemical Technology, University of Twente, 7500 AE, Enschede, The Netherlands. E-mail: d.n.reinhoudt@ct.utwente.nl

Received (in Liverpool, UK) 4th January 1999, Accepted 8th March 1999

Soft metal ions like Pb^{2+}, Cd^{2+}, and Cu^{2+} form partial-cone complexes with a flexible calix[4]arene chromoionophore in which cation–π interactions cause a bathochromic shift of the UV/Vis absorption maximum.

Calix[4]arenes have been extensively used as selective ligands for a wide range of metal ions in selective transport,[1] potentiometric[2] and optical[3] sensors. Recently, they are also being used as building blocks for chromoionophores.[4] The conformation of the calix[4]arene moiety determines the size and geometry of the ligand and therefore has a significant influence on the selectivity.[5] In the partial-cone and 1,3-alternate conformations cation–π interactions between metal ion and the ligand's benzene rings play an important role.[6] Usually, the conformation of these ligands is *fixed* in the synthesis.[7] However, Bartsch *et al.* have shown that conformationally *flexible* calix[4]arene ionophores are selective for heavy metal ions like Pb^{2+} and Hg^{2+}.[8] We are currently studying the application of chromoionophores in integrated optical waveguide sensors selective for heavy metal ions. For this application it is desirable that the chromoionophores have a high selectivity for heavy metal ions over alkali metal ions and that complexation leads to a bathochromic shift of the absorption maximum. The calix[4]arene-based chromoionophores with substantial changes in their absorption spectra published thus far respond to alkali metal ions or Ca^{2+} and are based on the interaction of the complexed ion with a hard donor heteroatom of the chromophore.[9]

Here we report that conformationally flexible chromoionophore **1** is highly selective for Pb^{2+} over Na^+ and shows a

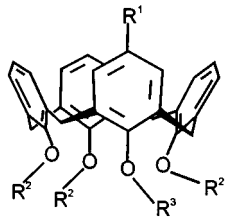

1 $R^1 = N_2C_6H_4NO_2$, $R^2 = OCH_2C(O)N(CH_3)_2$, $R^3 = OCH_3$
2 $R^1 = N_2C_6H_4NO_2$, $R^2 = OCH_2C(O)N(CH_3)_2$, $R^3 = OC_3H_7$
3 $R^1 = H$, $R^2 = OCH_2C(O)N(CH_3)_2$, $R^3 = OH$
4 $R^1 = H$, $R^2 = OCH_2C(O)N(CH_3)_2$, $R^3 = OCH_3$

bathochromic shift of λ_{max} upon complexation of *soft* metal ions. The bathochromic shift does *not* occur when alkali metal ions are complexed. Complexation of either Pb^{2+} or Na^+ by the conformationally fixed analogue **2** leads to a *hypsochromic* shift. Chromoionophores **1** and **2** were synthesized† from calix[4]arene **3**[10] by diazonium coupling with *p*-nitroaniline, followed by alkylation at the lower rim with MeI or PrI, respectively. Reference compound **4** was prepared in two steps from the parent calix[4]arene, *viz.* monomethylation at the lower rim followed by introduction of the (*N*,*N*-dimethylaminocarbonyl)methoxy functionalities on the three remaining hydroxy groups.

It is well known that a methoxy substituent at the lower rim is not sufficiently bulky to fix the conformation of chromoionophore **1**, which can attain both the cone and the partial-cone conformation.[11] When a metal ion is complexed, the ligand will occupy the conformation optimal for the complexation of that particular metal ion. The UV/Vis absorption spectra in Fig. 1 show that complexation of Pb^{2+} ions by either **1** or **2** leads to shifts of λ_{max} in opposite directions. This is caused by the different conformations of the two complexes, involving two principally different modes of metal–chromophore interaction.

Compound **1** binds Pb^{2+} in the partial-cone conformation because in this geometry the metal ion interacts favorably with the π-surface of the chromophore,[12] leading to a 14 nm bathochromic shift of λ_{max} (Fig. 1). A Pb^{2+} ion complexed in chromoionophore **2**, fixed in the cone conformation, interacts with the methoxy oxygen atom lone-pair rather than with the chromophores' π-surface, resulting in a 22 nm hypsochromic shift. Na^+ prefers hard donor atoms, *i.e.* oxygen, and is therefore complexed by chromoionophore **1** in the cone conformation, causing a 4 nm hypsochromic shift of λ_{max}. This shift is small compared to the 22 nm hypsochromic shift of **2** upon Na^+ complexation, because **1** binds Na^+ only weakly.

^{13}C NMR spectroscopy proved that ionophore **4** complexes Na^+ and Pb^{2+} in different conformations.‡ These studies could

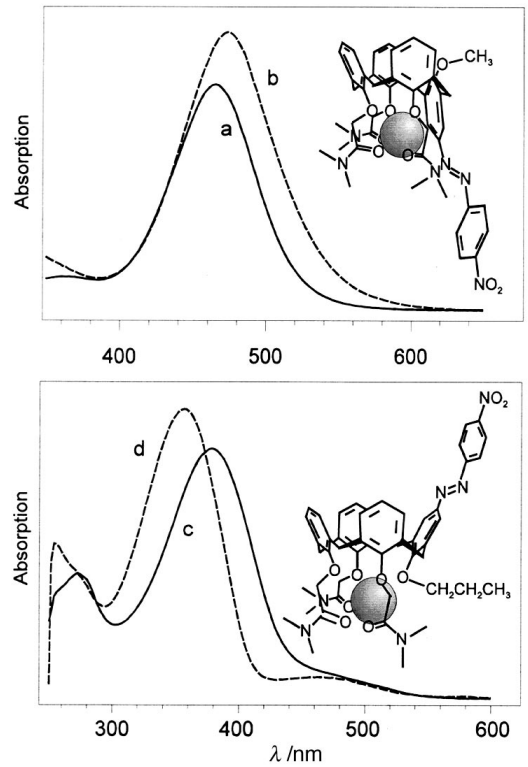

Fig. 1 UV/Vis absorption spectra of (a) **1**, (b) **1**·Pb^{2+}, (c) **2** and (d) **2**·Pb in CH_2Cl_2, with the proposed structures of the complexes.

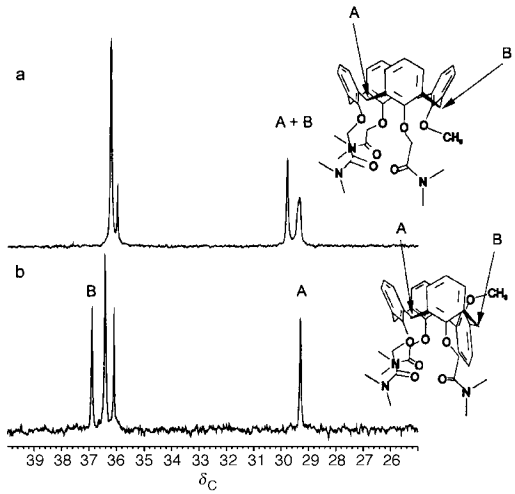

Fig. 2 ^{13}C NMR spectra (δ 40–25) of the complexes (a) **4**·Na^+ and (b) **4**·Pb^{2+}.

not be performed with **1** because of the low solubilities of its complexes. In the absence of metal ions, the NMR spectra of ionophore **4** show broad signals because of the equilibrium between cone and partial-cone conformation. When metal perchlorate salts are added, the signals sharpen into one set that can be attributed to a single conformation. For Na^+ this is the cone conformation, which can be determined from the ^{13}C NMR spectrum of the complex shown in Fig. 2: the methylene carbon atoms bridging the aromatic rings appear at δ 29.30 and 29.11, typical resonances for cone calix[4]arenes.[13] The Pb^{2+} complex has the partial-cone conformation, which can be determined from the two different chemical shifts of the bridging methylene carbon atoms at δ 36.90 and 29.31. The aromatic region of the ^{1}H NMR spectrum is consistent with a quasi-C_{4v} symmetry axis of the Na^+ complex, since all protons *para* with respect to the lower rim oxygen coincide, as do all *meta* protons. The more complex spectrum of the Pb^{2+} complex is typical for the partial-cone conformation.

The results of solution experiments in MeCN (Table 1) show that chromoionophore **1** exhibits bathochromic shifts upon complexation of different metal ions. Soft metal ions with high charges cause the largest shifts, with a maximum shift of 20 nm for Cu^{2+}. Under the same conditions, the alkali metal ions cause no, and alkaline-earth metal ions small, optical responses.

The complexation behavior of **1** shows that conformational flexibility can bias the selectivity of calix[4]arene chromoionophores towards soft heavy metal ions. Addition of 10 equiv. of $Pb(ClO_4)_2$ to a solution of **1** and a *thousand-fold excess* of $NaClO_4$ in MeCN leads to complete formation of the Pb^{2+} complex. This selectivity for Pb^{2+} over Na^+ should find its origin in the conformational flexibility, since ligating amides are generally used in Na^+-selective receptors. In fixed cone ligands, soft donating thioamide groups are necessary to obtain selectivity for Pb^{2+}.[14]

In conclusion, we have found a new type of optical transduction of soft metal ion complexation *via* a bathochromic shift of the absorption maximum due to side-on metal–chromophore interactions, unique to the partial-cone conformation of chromoionophore **1**. The selectivity for Pb^{2+} over Na^+ is due to the different preferential conformations of complexation by **1**. Our current research is aimed at improving the selectivity and sensitivity of flexible chromoionophores.

We thank the Technology Foundation (STW), the Technical Science Branch of the Netherlands Organization for Scientific Research (NWO), for financial support.

Table 1 Optical response of **1** (10^{-5} M) to different metal perchlorate salts (10^{-4} M) in MeCN. The samples were prepared by mixing equal volumes of stock solutions of **1** and the metal perchlorate salts. Reported values signify bathochromic shifts

Metal ion	$\Delta\lambda_{max}$/nm	Metal ion	$\Delta\lambda_{max}$/nm	Metal ion	$\Delta\lambda_{max}$/nm
Li^+	0	Ca^{2+}	8	Cd^{2+}	12
Na^+	0	Sr^{2+}	6	Pb^{2+}	14
Cs^+	0	Ba^{2+}	4	Ga^{3+}	2
Ag^+	0	Cu^{2+}	20	Ce^{3+}	16

Notes and references

† All compounds reported were characterized by ^{1}H NMR analysis, melting point, elemental analysis and FAB mass spectrometry.

‡ *Selected data* for **3**·$NaClO_4$: δ_H(300 MHz, CD_3CN) 7.34–7.28 (m, 8H, ArH-*m*), 6.98–6.89 (m, 4H, ArH-*p*), 4.84 and 4.13 [AB q, 4H, *J* 14.4, OCH_2C(O)], 4.52 [s, 2H, OCH_2C(O)], 4.38 and 4.31 (AB q, 4H, *J* 12.0, ArCH_2Ar), 3.89 (s, 3H, OCH_3), 3.43 and 3.30 (AB q, 4H, *J* 12.0, ArCH_2Ar), 3.02 (s, 6H, NCH_3), 2.91 (s, 3H, NCH_3), 2.81 (s, 3H, NCH_3), 2.79 (s, 6H, NCH_3); δ_C 167.8, 167.4 (C=O), 154.2, 152.6, 151.6 (ArC–O), 135.3, 134.9, 134.7, 134.3 (ArC-*o*), 128.7, 128.6, 128.4 (ArC-*m*), 125.5, 125.3, 124.8 (ArC-*p*), 74.9, 74.5 (OCH_2), 64.2 (OCH_3), 35.1, 35.0, 34.7 (NCH_3), 29.3, 29.1 ($ArCH_2Ar$). For **3**·$Pb(ClO_4)_2$: δ_H 7.47 (d, 2H, *J* 7.8, ArH-*m*), 7.45 (d, 2H, *J* 7.8, ArH-*m*), 7.34 (t, 1H, *J* 7.8, ArH-*p*), 7.32 (d, 2H, *J* 7.8, ArH-*m*), 7.19 (d, 2H, *J* 7.8, ArH-*m*), 7.14 (t, 1H, *J* 7.8, ArH-*p*), 7.00 (t, 2H, *J* 7.8, ArH-*p*), 4.90 and 4.78 [AB q, 4H, *J* 14.7, OCH_2C(O)], 4.63 [s, 2H, OCH_2C(O)], 4.35 and 3.55 (AB q, 4H, *J* 12.6, ArCH_2Ar), 3.98 (s, 4H, ArCH_2Ar), 3.31 (s, 3H, OCH_3), 3.05 (s, 6H, NCH_3), 3.05 (s, 3H, NCH_3), 2.95 (s, 6H, NCH_3), 2.91 (s, 3H, NCH_3); δ_C 173.3, 171.3 (C=O), 159.7, 152.5, 151.4 (ArC–O), 137.8, 136.4, 136.1, 134.7 (ArC-*o*), 132.9, 130.5, 130.3, 130.3 (ArC-*m*), 127.5, 126.7, 125.7 (ArC-*p*), 74.5, 74.0, (OCH_2), 58.3 (OCH_3), 36.4, 36.1 (NCH_3), 36.9, 29.3 ($ArCH_2Ar$).

1 W. F. Nijenhuis, E. G. Buitenhuis, F. de Jong, E. J. R. Sudhölter and D. N. Reinhoudt, *J. Am. Chem. Soc.*, 1991, **113**, 7963; E. G. Reichwein-Buitenhuis, H. C. Visser, F. de Jong and D. N. Reinhoudt, *J. Am. Chem. Soc.*, 1995, **117**, 3913; D. M. Rudkevich, J. D. Mercer-Chalmers, W. Verboom, R. Ungaro, F. de Jong and D. N. Reinhoudt, *J. Am. Chem. Soc.*, 1995, **117**, 6124.
2 P. L. H. M. Cobben, R. J. M. Egberink, J. G. Bomer, P. Bergveld, W. Verboom and D. N. Reinhoudt, *J. Am. Chem. Soc.*, 1992, **114**, 10 573; D. N. Reinhoudt, *Sensors Actuators B*, 1992, **6**, 179.
3 B. Bühlmann, E. Pretsch and E. Bakker, *Chem. Rev.*, 1998, **98**, 1593.
4 V. Böhmer, *Angew. Chem., Int. Ed. Engl.*, 1995, **34**, 713; A. Ikeda and S. Shinkai, *Chem. Rev.*, 1997, **97**, 1713.
5 A. Casnati, A. Pochini, R. Ungaro, F. Ugozzoli, F. Arnaud, S. Fanni, M.-J. Schwing, R. J. M. Egberink, F. de Jong and D. N. Reinhoudt, *J. Am. Chem. Soc.*, 1995, **117**, 2767; A. Casnati, A. Pochini, R. Ungaro, C. Bocchi, F. Ugozzoli, R. J. M. Egberink, H. Struijk, R. Lugtenberg, F. de Jong and D. N. Reinhoudt, *Chem. Eur. J.*, 1996, **2**, 436.
6 F. Inokuchi, Y. Miyahara, T. Inazu and S. Shinkai, *Angew. Chem., Int. Ed. Engl.*, 1995, **34**, 1364; X. Delaigue, M. W. Hosseini, N. Kyritsakas, A. De Cian and J. Fischer, *J. Chem. Soc., Chem. Commun.*, 1995, 609.
7 P. J. Dijkstra, J. A. J. Brunink, K.-E. Bugge, D. N. Reinhoudt, S. Harkema, R. Ungaro, F. Ugozzoli and E. Ghidini, *J. Am. Chem. Soc.*, 1989, **111**, 7567; E. Ghidini, F. Ungozzoli, R. Ungaro, S. Harkema, A. Abu El-Fadl and D. N. Reinhoudt, *J. Am. Chem. Soc.*, 1990, **112**, 6979.
8 G. G. Talanova, H.-S. Hwang, V. S. Talanov and R. A. Bartsch, *Chem. Commun.*, 1998, 419; G. G. Talanova, H.-S. Hwang, V. S. Talanov and R. A. Bartsch, *Chem. Commun.*, 1998, 1329.
9 Y. Kubo, S. Tokita, Y. Kojima, Y. T. Osano and T. Matsuzaki, *J. Org. Chem.*, 1996, **61**, 3758; D. Diamond and M. A. McKervey, *Chem. Soc. Rev.*, 1996, 15; H. Mohindra Chawla and K. Srinivas, *J. Org. Chem.*, 1996, **61**, 8464; J. L. M. Gordon, V. Böhmer and W. Vogt, *Tetrahedron Lett.*, 1995, **36**, 2445; M. McCarrick, S. J. Harris and D. Diamond, *J. Mater. Chem.*, 1994, **4**, 217; H. Shimizu, K. Iwamoto, K. Fujimoto and S. Shinkai, *Chem. Lett.*, 1991, 2147.
10 R. J. W. Lugtenberg, PhD Thesis, University of Twente, 1997.
11 C. D. Gutsche, B. Dhawan, J. A. Levine, K. H. No and L. J. Bauer, *Tetrahedron*, 1983, **39**, 409.
12 J. C. Ma and D. A. Dougherty, *Chem. Rev.*, 1997, **97**, 1303.
13 C. Jaime, J. de Mendoza, P. Prados, P. M. Nieto and C. Sánchez, *J. Org. Chem.*, 1991, **56**, 3372.
14 R. J. W. Lugtenberg, R. J. M. Egberink, J. F. J. Engbersen and D. N. Reinhoudt, *J. Chem. Soc., Perkin Trans. 2*, 1997, 1353.

Communication 9/00077A

ChemComm

The synthesis of α-amino-γ-substituted adipic acids: stereoelectronic effects during the 1,4-addition of organocuprates to methyl *N-tert*-butoxy-6-oxo-1,2,3,6-tetrahydropyridine-2-carboxylate

Mireille Muller, Angèle Schoenfelder, Bruno Didier, André Mann* and Camille-Georges Wermuth

Laboratoire de Pharmacochimie de la Communication Cellulaire, ERS 655, Faculté de Pharmacie, 74, route du Rhin, BP 24, F-67401 Illkirch Cedex, France. E-mail: andre.mann@pharma.u-strasbg.fr

Received (in Liverpool, UK) 26th November 1998, Accepted 4th March 1999

The α,β-unsaturated lactam 3 was submitted to 1,4-addition of organocuprate reagents R_2CuLiI_2 (R = Me, Bu or Ph) to provide the 4-substituted compounds 5a–c, 6a–c as a mixture of diastereomers; these intermediates were then transformed into the corresponding α-amino-γ-substituted adipic acids 7a–c, 8a–c.

The synthesis of modified and unnatural amino acids is a source of constant inspiration in organic chemistry.[1–3] In recent years glutamic acid, a major neurotransmitter in the mammalian brain, has received considerable attention from chemists involved in neurosciences.[4,5] During earlier studies on modified glutamates, we and others have found that the γ-substituted analogues of structure **1** are invaluable tools for the pharmacological exploration of excitatory amino acid receptors.[6,7] Interestingly it was found that the biological activity of such derivatives was largely confined to the 2*S*,4*S* diastereomers. For structure–activity studies devoted to this class of amino acids, we decided to synthesize compounds of type **2** in which the distal carboxylate is moved an additional methylene unit away from the α-amino acid group compared with **1**, generating γ-substituted α-amino adipic acids (Adi). As earlier observations have already demonstrated that Adi itself possesses good affinity for the glutamate receptors,[8] the introduction of different substituents on the Adi backbone may contribute to a better knowledge of steric demands at the receptor level.[9] Our goal was to employ an enantiospecific and diastereoselective synthesis which would provide analogues **2** in which the C-2 and C-4 substituents have the correct configuration for high biological activity. Since we have previously prepared modified glutamic acids using a conjugate addition of organocopper reagents,[10] we therefore proposed to submit compound **3** to a similar sequence, in the expectation that the presence of the C-2 carboxylate would provide facial selectivity.[11,12] We report herein our observations on the diastereoselectivity obtained in the 1,4-addition of organocuprate reagents to the α,β-unsaturated lactam **3**.

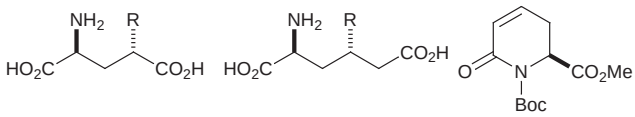

1 **2** **3**

The starting compound **3** was obtained from (*S*)-lysine in enantiomerically pure form *via* piperidone **4**, following literature reports.[13–15] The unsaturation was introduced by a sequence involving selenation and oxidative elimination, as decribed for the preparation of the corresponding benzyl ester (Scheme 1).[15] Since lactam **3** is potentially prone to nucleophilic attack, we were pleased to find that the reaction of this substrate in Et_2O with different organocuprates gave the expected adducts as mixtures of *cis/trans* diastereomers (**5a–c** and **6a–c**) in acceptable yields, and in moderate to good stereoselectivity.† Examination of the ^1H NMR (200 MHz) spectra of the crude mixtures revealed that each diastereomer has a well resolved signal (dd) between δ 4.5–4.8 for the hydrogen attached at C-2. Surprisingly, in analyzing these signals for the **5a**/**6a**, **5b**/**6b** and **5c**/**6c** mixtures, we observed that the intensity for the upfield signal (*trans* diastereomer) increases at the expense of the corresponding downfield one (*cis* diastereomer). These results indicate a change in the *cis* : *trans* ratio related to the structure of the transfered substituent. After purification, the pattern of the H-5ax proton was identified in each diastereomer as a doublet of doublets (B part of an ABX spin sytem) in which largest *J* value (around 17 Hz), corresponds to the geminal coupling H-5ax/H5eq. The smaller *J* value (around 11 Hz) arises from to the coupling between H-5ax and H-4, and these were of comparable value in all the compounds (**5a–c** and **6a–c**), consistent with an axial disposition of the proton at C-4. As a consequence the Me, Bu or Ph substituents attached at C-4 have an equatorial disposition in each diastereomer. For the protons attached at C-2 in **5a** and **6a** two sets of coupling constants were measured: J = 10 and 6 Hz, and J = 4 and 2 Hz, repectively. From these data it was clear that in the analogues **5a–c** the carboxylate adopts an equatorial disposition (large J values = axial orientation of the proton at C-2) whilst in contrast for derivatives **6a–c** the carboxylate has

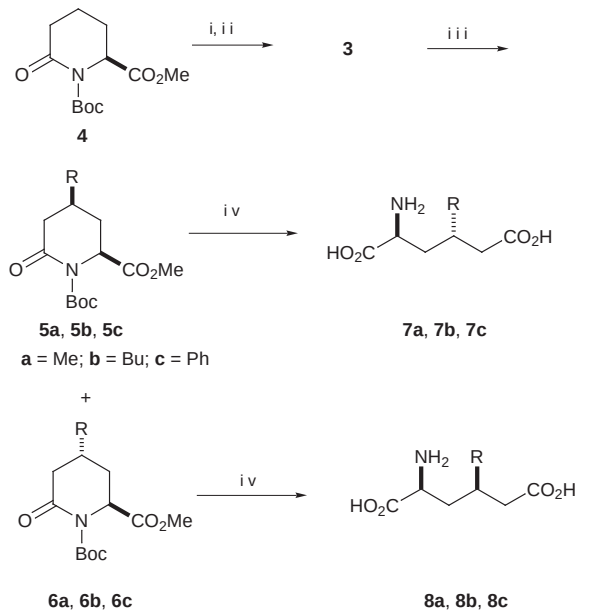

Scheme 1 *Reagents and conditions*: i, LiHMDS (1.1 equiv.), PhSeCl (1. 2 equiv.), THF −78 °C, 2 h (78%); ii, MCPBA (2 equiv.), CH_2Cl_2, 25 °C, 12 h (72%); iii, for **5a**/**6a**: MeLi (2 equiv.), CuI (1 equiv.), Et_2O, −78 °C, 2 h, **5a** (68%) and **6a** (9%); for **5b**/**6b**: BuLi (2 equiv.), CuI (1 equiv.), −78 °C, 2 h , **5b** (35%) and **6b** (33%); for **5c**/**6c**: PhLi (2 equiv.), CuI (1 equiv.), Et_2O, −78 °C, 2 h , **6c** (48%); HCl in AcOH, reflux, 3 h (from 45 to 80%).

an axial orientation (small *J* values = equatorial orientation of the proton at C-2). These data are consistent with a chair conformation for all of the isolated compounds, in which the products **5a–c** have the substituents in a 1,3-*cis* arrangement, and **6a**–**c** in a 1,3-*trans* arrangement. In order to explain these findings, we performed calculations on lactam **3** (MOPAC out of SYBYL 6.3) which demonstrated that the conformer having the carboxylate at C-2 in an axial disposition is, by far, more stable (5 kcal mol^{-1}) than the corresponding equatorial conformer‡ (Scheme 1). This result is the obvious consequence of a strong $A^{1,3}$ strain between the carboxylate at C-2 and the Boc group on the nitrogen atom.[16] Based on these calculations and several literature reports on the stereoelectronic effects during conjugated addition in related α,β-unsaturated cyclohexanones or 2,3-dihydro-4-pyridones,[17,18] a strong axial bias was expected to operate during the addition of nucleophilic reagents to lactam **3**. Therefore one should observe the preferential formation of the *cis* adducts (**5a**–**c**) at the expense of the corresponding *trans* epimers (**6a**–**c**). Indeed for the smallest substituent (R = Me) an appreciable diastereoselectivity in favor of the *cis* adduct was observed (**5a** : **6a** = 5 : 1). However when the steric demand of the organocuprate was increased (R = Bu), the facial selectivity was lost (**5b** : **6b** = 1 : 1) or, for still bulkier groups (R = Ph) the facial steroselectivity was reversed, and the *trans* diastereomer was the only one detected (**5c** : **6c** = 1 : 30). Allinger has discussed a closely related example involving the 1,4-addition of Grignard reagents to 5-methylcyclohex-2-enone,[19] in which the importance of the conformation of the conjugated enolate (chair or boat) produced by parallel or anti-parallel attack was considered. As the carboxylate function in **3** is assumed to be axial, the major pathway for the reaction with Me_2CuLi_2I was *via* an anti-parallel attack to give the transient enolate of **5a.** This intermediate possesses a low energy chair-like conformation (TS chair), in spite of the 1,3-diaxial interaction between the carboxylate and the incoming methyl group. When the nucleophile is larger, such as in Bu_2CuLi_2I (**5b**/**6b**) or Ph_2CuLi_2I (**5c**/**6c**), the reaction pathway *via* parallel attack takes place preferentially due to a competing strong 1,3-diaxial interaction between the carboxylate and the bulky incoming nucleophile. This gives a transient, boat-like (TS boat) enolate, which collapses to the *trans* chair conformer. The final transformation of **5a**–**c** and **6a–c** into the desired substituted adipic acids was realized under hydrolytic conditions and the amino acids **7a,b** and **8a**–**c** were obtained as crystalline hydrochlorides.§

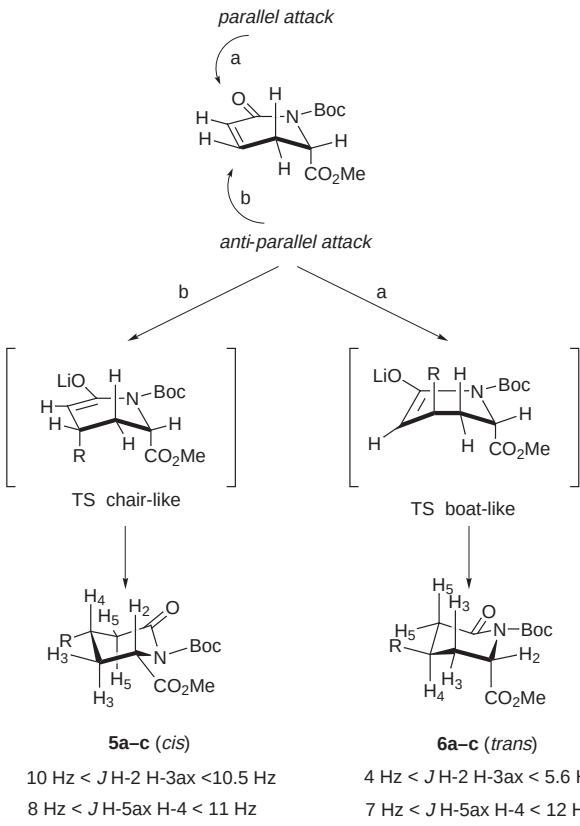

Scheme 2 Possible transition states and recorded values for coupling constants.

In conclusion, the diastereoselectivity observed for the conjugate addition of organocuprates to cyclic enamide **3** could be controlled by an appropriate choice of the transferable nucleophilic reagent. The significant $A^{1,3}$ strain inherent to the ring system and the size of the nucleophile are probably the key factors responsible for the diastereoselectivity observed in this conjugate addition reaction. Our findings demonstrate that α,β-unsaturated species **3** is an excellent substrate for the preparation of enantiomerically pure (2*S*,4*S*)- or (2*S*,4*R*)-2-amino-4-substituted adipic acids.

We thank Dr Jacques Royer (Gif sur Yvette, France) and Professor Maurizio Taddei (Sassari, Italy) for valuable discussions.

Notes and references

† *Selected data* for **5a**: mp 60 °C; R_f 0.30 (hexanes–Et_2O = 5 : 5); $[\alpha]_D$ −66.2 (*c* 5, $CHCl_3$); δ_H(200 MHz, 30 °C) 4.51 (dd, *J* 10.2 and 6.2, 1 H), 3.74 (s, 3 H), 2.62 (dt, *J* 17 and 2.4, 1 H), 2.30 (m, 1 H), 2.10 (dd, *J* 17 and 10, 1 H), 2.15 (m, 1 H), 1.53 (m, 1 H),1.48 (s, 9 H), 1.02 (d, *J* 6, 3 H); δ_C(50 MHz) 172.1, 170.1, 151.9, 83.6, 58.6, 52.3, 42.7, 34.1, 28.3, 27.7, 26.3, 20.7. (Calc. for $C_{13}H_{21}NO_5$: C, 57.54; H, 7.80; N, 5.16. Found: C, 57.3; H, 7.9; N, 5.2%). For **6a**: oil; R_f 0.35 (hexanes–Et_2O = 6 : 5); $[\alpha]_D$ +20.1 (*c* 2, $CHCl_3$, 30 °C); δ_H(200 MHz) 4.71 (dd, *J* 4 and 1.8, 1 H), 3.80 (s, 3 H), 2.66 (ddd, *J* 16.3, 3.2 and 1.4, 1 H), 2.21 (dd, *J* 9.1, 4 and 1.4, 1 H), 2.09 (dd, *J* 16.3 and 9.6, 1 H), 1.96 (m, 1 H), 1.73 (m, 1 H), 1.51 (s, 9 H), 1.01 (d, *J* 4.2, 3 H); δ_C(50 MHz) 172.2, 169.9, 152.2, 83.6, 58.3, 52.6, 42.8, 33.5, 29.7, 27.9, 25.1, 21.1. (Calc. for $C_{13}H_{21}NO_5$: C, 57.54; H, 7.80; N, 5.16. Found: C, 57.6; H, 7.6; N, 5.1%).

‡ In compound **3**, the recorded coupling constant (dd, *J* 4.5) is consistant with an axial orientation of the carboxylate.

§ *Preparation* of **7a**: Lactam **5a** (96 mg, 0.35 mmol) was heated at reflux for 2 h in a mixture of concentrated HCl (2 ml) and AcOH (4 ml). The mixture was concentrated *in vacuo* and triturated with Et_2O, to provide a solid which was filtered to yield **7a** (60 mg, 81%) as a hygroscopic solid; mp 178 °C; $[\alpha]_D$ −79 (*c* 1, MeOH); *m/z* (FAB) 176 ($M + H^+$). For **8a**: mp 196 °C; $[\alpha]_D$ +26 (*c* = 1.8, MeOH); *m/z* (FAB) 176 ($M + H^+$).

1 F. J. Sardina and H. Rapoport, *Chem. Rev*., 1996, **96**, 1825.
2 R. O. Duthaler, *Tetrahedron*, 1994, **50**, 1539.
3 J. Jurczak and A. Golebiowski, *Chem. Rev*., 1989, **89**, 149.
4 M. G. Moloney, *Nat. Prod. Rep.*, 1998, 205.
5 T. Knöpfel, R. Kuhn and A. Allgeier, *J. Med. Chem.*, 1995, **38**, 1417.
6 C. G. Wermuth, A. Mann, A. Schoenfelder, R. A. Wright, B. G. Johnson, J. P. Burnett, N.G. Mayne and D. D. Schoepp, *J. Med. Chem.*, 1996, **39**, 814.
7 Z.-Q. Gu, X.-F.Lin and D. P. Hesson, *Bioorg. Med. Chem. Lett.*, 1995, **5**, 1973.
8 R. H. Evans, A. A. Francis and J. C. Watkins, *Brain Res.*, 1978, **148**, 536.
9 J. Ezquerra, C. Pedregal, A. Escribano, M. C. Carreno and J. L. G. Ruano, *Tetrahedron Lett*., 1995, **36**, 3247.
10 I. Jako, P. Uiber, A. Mann, C. G. Wermuth, T. Boulanger, B. Norberg, G. Evrard and F. Durant, *J. Org. Chem*., 1991, **56**, 5729.
11 N. Krause and A. Gerold, *Angew. Chem., Int. Ed. Engl.*, 1997, **36**, 186.
12 P. Perlmutter, in *Conjugate Addition Reactions in Organic Synthesis*, Pergamon, Oxford, 1992, pp. 137–197 and references cited therein.
13 S. A. Hermitage and M. G. Moloney, *Tetrahedron*: *Asymmetry*, 1994, **5**, 1463.
14 C. E. Davies, T. D. Heightman, S. A. Hermitage and M. G. Moloney, *Synth. Commun*., 1996, **26**, 687.
15 P. J. Murray and I. D. Starkey, *Tetrahedron Lett.*, 1996, **37**, 1875.
16 R. W. Hoffmann, *Chem. Rev*., 1989, **89**, 1841.
17 P. Deslongchamp, in *Stereoelectronic Effects in Organic Chemistry*, Pergamon, Oxford, 1983, p. 209.
18 J. D. Brown, M. A. Foley and D. L. Comins, *J. Am. Chem. Soc*., 1988, **110**, 7445.
19 N. L. Allinger and C. K. Riew, *Tetrahedron Lett.*, 1966, **7**, 1269.

Communication 8/09274F

Magnesium fluoride as a catalytic support in hydrodechlorination of CCl_2F_2 (CFC-12)

A. Malinowski,[a] W. Juszczyk,[a] J. Pielaszek,[a] M. Bonarowska,[a] M. Wojciechowska[b] and Z. Karpiński*[a]

[a] *Institute of Physical Chemistry, Polish Academy of Sciences, Kasprzaka 44/52, PL-01224 Warszawa, Poland. E-mail: zk@ichf.edu.pl*

[b] *Faculty of Chemistry, A. Mickiewicz University, Grunwaldzka 6, PL-60780 Poznań, Poland*

Received (in Liverpool, UK) 26th January 1999, Accepted 9th March 1999

Magnesium fluoride-supported palladium and ruthenium appear to be useful catalysts in the reaction of CCl_2F_2 (CFC-12) hydrodechlorination; after doping Pd/MgF_2 with gold the selectivity for CH_2F_2 increased from ~70 to almost 90%.

The need to replace environmentally detrimental chlorofluorocarbons (CFCs) by benign hydrochlorofluorocarbons (HCFCs) and hydrofluorocarbons (HFCs) has resulted in considerable interest in catalytic hydrodechlorination of CFCs.[1] It is obvious from the patent literature that there is much activity in the development of new catalysts capable of very selective chlorine removal from a CFC molecule, *i.e.* avoiding undesired hydrodefluorination. Although this can be achieved with the use of heterogeneous catalysts containing such transition metals as iridium, ruthenium and, especially, palladium,[2] nevertheless the formation of over-dehalogenated products still presents a major concern. The role of a support (active carbon[3] and AlF_3[4] are reported most often in the patent literature) appears important; however, for this class of reaction one must also consider modifying the catalyst by doping the active phase (preferably palladium) with other elements.[5,6]

This report presents preliminary results obtained for MgF_2-supported Pd and Ru catalysts. Several metal fluorides have exhibited interesting properties as carriers for palladium (AlF_3, ZrF_4, TiF_3[4,7,8]), but MgF_2 has not been tested yet. In addition, MgO, as a support in hydrodechlorination,[9] is not resistant to the highly corrosive conditions of this reaction which results from considerable evolution of HCl, which can transform the support into $MgCl_2$. Similarly, by analogy to the catalytic behaviour of alumina-supported catalysts,[7,8] due to inevitable (albeit undesired) formation of HF during CFCs hydrodehalogenation, MgO is (at least partly) transformed into magnesium fluoride, which when located at a metal/support interface might favorably modify the electronic state of the metal particles.[7,8] All these facts and speculations have encouraged us to investigate this area.

The MgF_2-supported Pd, Pd–Au, Ru and Ru–Au catalysts were prepared by impregnation of MgF_2 (obtained in the reaction of $MgCO_3$ with aqueous solution of HF[10]) with appropriate metal salts. X-Ray diffraction (XRD) examination of MgF_2 (BET surface area 43 $m^2\ g^{-1}$, Barrett–Joyner–Halenda average pore size 20 nm, micropore volume 0.22 $cm^3\ g^{-1}$) showed a rutile structure. The reaction of CF_2Cl_2 with dihydrogen was conducted in a glass flow system. The experimental procedure and reaction conditions have been reported elsewhere.[11] Turnover frequencies (TOFs) were calculated on the basis of metal loadings and dispersions (from chemisorption measurements) and are shown in Table 1.

Our results indicate that MgF_2-supported palladium-based catalysts exhibit interesting properties in CCl_2F_2 hydrodechlorination. The first positive point is that CHF_3 is not produced by these catalysts, as often happens on catalysts capable of Cl/F exchange. Secondly, the time-on-stream behaviour (Fig. 1) shows an initial increase in activity, which appears to be stable during the next 17 hours. Thirdly, the selectivity towards CH_2F_2 production is reasonably high (> 70%), resembling the catalytic behaviour of AlF_3-supported palladium catalysts.[7] It can be speculated as others[7,8] have done, that the Lewis acidity of MgF_2, as in the case of AlF_3, decreases electron density in neighbouring Pd sites. In effect, electron-deficient Pd species bind :CF_2 carbene radicals (commonly accepted intermediate species[2,7,8,12]) less strongly, so a hydrogenative desorption of these radicals distinctly prevails over

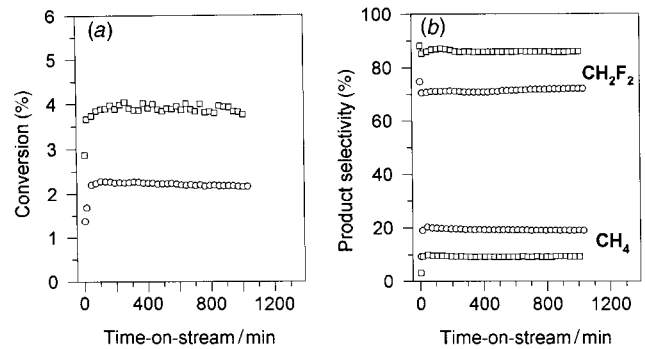

Fig. 1 Time-on-stream behaviour of 2 wt% Pd/MgF_2 (0.121 g, circles) and Pd–Au/MgF_2 (0.201 g, squares) catalysts in CCl_2F_2 hydrodechlorination. (*a*) Overall conversion, (*b*) selectivities to CH_4 and CH_2F_2.

Table 1 Hydrodechlorination of CCl_2F_2 on Pd/MgF_2, Pd–Au/MgF_2, Ru/MgF_2 and Ru–Au/MgF_2 catalysts: steady-state turnover frequencies (TOFs), product selectivities and apparent activation energies (E_as). Reaction temperature 453 K, H_2–CCl_2F_2 ratio 10 : 1.

	Selectivity[a] (%)							
Catalyst	CH_4	CH_2F_2	$CClF_3$	$CHClF_2$	C_2H_6	$C_2H_4F_2$	TOF/s^{-1}	E_a/kJ mol^{-1}
Pd/MgF_2[b]	19.0	72.0	—	8.5	0.2	—	0.0765	61.0 ± 0.4
Pd–Au/MgF_2[b]	9.3	86.0	0.4	3.8	0.1	—	0.0820	61.8 ± 1.0
Ru/MgF_2[b]	67.5	7.0	—	19.2	3.8	2.5	0.0053	60.3 ± 0.3
Ru–Au/MgF_2[b]	56.4	12.9	3.4	21.7	3.2	1.9	0.0160	54.1 ± 2.5

[a] Minor products (*e.g.* CH_3Cl, Σ% < 0.5%). [b] 2 wt% Pd/MgF_2 (metal dispersion, H/Pd = 0.02_3); 3.5 wt% $Pd_{0.7}Au_{0.3}/MgF_2$ (H/Pd = 0.02); 2.4 wt% Ru/MgF_2 (CO/Ru = 0.20); 2 wt% $Ru_{0.75}Au_{0.25}/MgF_2$ (CO/Ru = 0.03_2). Subscripts in chemical formulae denote atomic fractions.

hydrodefluorination. Interestingly enough, the selectivity for CH_2F_2 increases with Au doping: from ~72% for the Pd/MgF_2 to 86% for the $Pd–Au/MgF_2$ (Fig. 1 and Table 1).

As expected, preliminary XRD data manifest a substantial degree of Pd–Au mixing in the MgF_2-supported catalyst after reduction. Two Pd–Au solid solutions are present: $Pd_{0.81}Au_{0.19}$ and $Pd_{0.4}Au_{0.6}$ (indexes denote atomic fractions). This significant alloying concerns both reduced as well as spent $Pd–Au/MgF_2$ catalyst. XRD profiles obtained with used Pd–Au catalyst are somewhat complicated because large amounts of carbon (originating from CCl_2F_2) are incorporated into the Pd-based phase.[11,12] Since a Pd–C solution has a lattice parameter ($a_{PdC_{0.13}}$ = 0.399 nm[13,14]) larger than Pd (a_{Pd} = 0.3890 nm), it is difficult to assess whether an increase in the lattice parameter of Pd is due to Au (a_{Au} = 0.4078 nm) or C incorporation. In order to estimate to what extent Pd diffraction lines are affected by carbon dissolution and alloying with Au further studies are underway in our laboratory. This issue seems important, because, as is expected, a close contact between Pd and Au is essential for obtaining higher selectivity towards CH_2F_2. The Pd–Ag/graphite catalyst tested in CFC-12 hydrodechlorination by Coq *et al.*[15] showed selectivity for CH_2F_2 to be similar to that of the Pd/graphite catalyst. Such a result can be interpreted by an apparent absence of Pd–Ag interaction in the catalyst and, indeed, their XRD study of Pd–Ag/graphite showed no formation of Pd–Ag solid solution.

The Ru/MgF_2 catalyst showed rather low selectivity to CH_2F_2 (Table 1), but the selectivity to $CHClF_2$ was higher than in the case of Pd/MgF_2, in a qualitative agreement with Wiersma *et al.*[2] Again, doping with gold increased the selectivity towards partial hydrodechlorination (CH_2F_2 + $CHClF_2$) at the cost of CH_4 formation.

In conclusion, we have shown fair to respectable selectivities towards partial hydrodehalogenation of CCl_2F_2 over Pd, Pd–Au, Ru and Ru–Au catalysts supported on MgF_2. Our results indicate that the presence of gold in the catalyst is beneficial for selectivity variations. Studies are in progress to prepare new Pd–Au and Ru–Au catalysts (with different gold contents), supported on MgF_2 and active carbon.

Footnotes and references

1 Z. Ainbinder, L. E. Manzer and M. J. Nappa, in *Handbook of Heterogeneous Catalysis*, ed. G. Ertl, H. Knözinger and J. Weitkamp, VCH, Weinheim, 1997, vol. 4, p. 1677.
2 A. Wiersma, E. J. A. X. van de Sandt, M. A. Hollander, H. van Bekkum, M. Makkee and J. A. Moulijn, *J. Catal.*, 1998, **177**, 29.
3 For example, J. I. Darragh, UK Patent 1980, 1578933; V. N. M. Rao, US Patent 1992, 5136113.
4 For example, S. C. Kellner and V. N. M. Rao, US Patent 1989, 4873381.
5 R. Onishi, I. Suzuki and M. Ichikawa, *Chem. Lett.*, 1991, 841; R. Onishi, W.-L. Wang and M. Ichikawa, *Appl. Catal. A: Gen.*, 1994, **113**, 29.
6 V. N. M. Rao, US Patent 1995, 5447896; S. Morikawa, S. Samejima, M. Yositake and S. Tatematsu, Eur. Patent 1989, 0 347830 A2.
7 B. Coq, J.-M. Cognion, F. Figuéras and D. Tournigant, *J. Catal.*, 1993, **141**, 21.
8 B. Coq, F. Figuéras, S. Hub and D. Tournigant, *J. Phys. Chem.*, 1995, **99**, 11 159.
9 H. C. Choi, S. H. Choi, O. B. Yang, J. S. Lee, K. H. Lee and Y. G. Kim, *J. Catal.*, 1996, **161**, 790.
10 J. Haber and M. Wojciechowska, *J. Catal.*, 1988, **110**, 23.
11 W. Juszczyk, A. Malinowski and Z. Karpiński, *Appl. Catal. A: Gen.*, 1998, **166**, 311.
12 E. J. A. X. van de Sandt, A. Wiersma, M. Makkee, H. van Bekkum and J. A. Moulijn, *Catal. Today*, 1997, **35**, 163.
13 J. Stachurski and A. Frąckiewicz, *J. Less-Common Metals*, 1985, **108**, 249.
14 S. B. Ziemecki, G. A. Jones, D. G. Swartzfager, R. L. Harlow and J. Faber, Jr., *J. Am. Chem. Soc.*, 1985, **107**, 4547.
15 B. Coq, S. Hub, F. Figuéras and D. Tournigant, *Appl. Catal. A: Gen.*, 1993, **101**, 41.

Communication 9/00731H

ChemComm

Flexibility of the Cu(110)–O structure in the presence of pyridine

A. F. Carley, P. R. Davies,* R. V. Jones, G. U. Kulkarni† and M. W. Roberts

Department of Chemistry, Cardiff University, PO Box 912, Cardiff, UK CF1 3TB. E-mail: daviespr@cf.ac.uk

Received (in Cambridge, UK) 15th February 1999, Accepted 9th March 1999

The presence of pyridine is shown by STM to have a profound effect on the structure of a Cu(110)–O surface; the spacing within the < 100 > directed Cu–O chains is unchanged at 3.6 Å but there is an increase in the spacing between the chains from 5.1 to 7.7 Å; the flexibility of the Cu(110)–O structure is emphasised by the observation that the change in structure is reversible when the pyridine is thermally desorbed.

Surface reactions are often discussed in the context of stable structures. However, work in Cardiff over the last 15 years has shown[1–4] that this neglects much of the interesting chemistry that goes on before the stable structures are formed. Furthermore, even when stable structures have been formed they can still be sensitive to weakly adsorbed species and this may have consequences for the chemistry that can occur at the surface.

Here, we return to the adsorption of pyridine at preoxidised copper surfaces, a system which we have previously studied[5] with XPS and HREELS. We reported that at clean Cu(111) surfaces pyridine desorbs completely below 240 K but that at preoxidised surfaces it is stable to 380 K. The HREELS data indicated that in the absence of preadsorbed oxygen, pyridine physisorbs with its ring plane parallel to the surface whereas in the presence of oxygen the orientation is different, with the ring plane perpendicular to the surface. There was also strong evidence for the formation of an N–O bond. The direct interaction between the oxygen and the nitrogen was confirmed by the XPS spectra which showed a shift of the O1s peak upwards in binding energy. The XPS also showed that the maximum concentration of pyridine adsorbed at the Cu(111)-O surface corresponded to approximately one-fifth of the pre-adsorbed oxygen concentration.

Here, we investigate the pyridine–oxygen interaction at the Cu(110) plane where in contrast to Cu(111)[6] there is extensive surface reconstruction[7,8] with the oxygen being incorporated into added copper–oxygen chains orientated in the < 100 > direction.

XPS and STM data were acquired on a combined STM/XPS instrument designed and built by Omicron Vacuum Physik. The sample was sputtered clean using argon at an energy of 0.6 kV and subsequently annealed at *ca.* 750 K for 30 min. Surface cleanliness was confirmed by XPS and the purity of the gases tested with *in situ* mass spectrometry.

Initial oxidation of the Cu(110) surface leads to the formation of copper–oxygen added rows, orientated in the < 100 > direction. The O–O spacing along the row is *ca.* 3.6 Å whilst the inter-row spacing is 5.1 Å giving an overall (2 × 1) unit cell. This well known structure was used to check the calibration of the STM measurements. Fig. 1(a) shows a section of a Cu(110) surface with several small islands of added oxygen–copper rows after exposure of the surface to dioxygen giving a surface coverage of approximately one-third of saturation. The (2 × 1) unit cell can be clearly made out in the image and more faintly the substrate rows that run in the $< 1\bar{1}0 >$ direction. The islands in Fig. 1(a) were stable over several scans and our experience from all of our work on this surface is that oxygen islands of this size are completely stable at room temperature and in the *absence*[9] of any other adsorbates.

Exposure of this surface to 1 L‡ of pyridine results in an increase in the spacing between the Cu–O chains to *ca.* 7.7 Å (three times the copper lattice dimensions), Fig. 1(b), but it is clear from the STM images that the structure within the chains maintains its original spacing. Quantification of the XPS data shows a ratio of 1:0.8 between the surface oxygen concentration and the pyridine molecule concentration. The copper substrate

† Permanent address: Chemistry and Physics of Materials Unit, Jawaharlal Nehru Centre for Advanced Scientific Research, Jakkur (PO) Bangalore −560064, India.

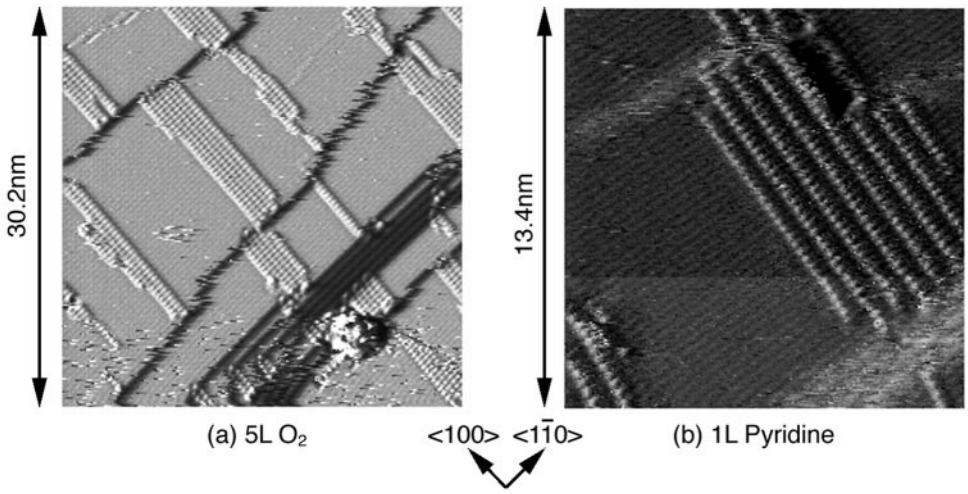

Fig. 1 The effect of pyridine on preadsorbed oxygen at a Cu(110) surface. (a) Cu(110) surface after exposure to 5 L O_2 at 290 K. The added Cu–O rows are *ca.* 5.1 Å apart and are orientated in the < 100 > direction giving a (2 × 1) structure. Imaging conditions: sample bias = −0.94 V, current = 3.1 nA. (b) Close up view of a section from (a) after exposure to pyridine at room temperature, the inter-row spacing is now 7.7 Å but the maxima within the rows are still spaced at 3.6 Å. Imaging conditions: sample bias = −0.12 V, current = 3.1 nA.

structure is very clearly resolved in STM images taken under these conditions, possibly because of the adsorption of pyridine molecules on to the imaging tip. One can see that the brightest features in the restructured chains are exactly in line with the bright rows visible on the substrate. In the original (2 × 1)O structure, the copper rows line up with the positions of the oxygen atoms in the copper–oxygen chains,[7,8] Fig. 2(a). We would expect these features in the restructured chains to be the sites where pyridine is adsorbed and therefore the image adds further weight to the earlier XPS and HREELS evidence from Cu(111) that the pyridine interacts directly with the oxygen atoms within the chains. This is also consistent with the structure of pyridine *N*-oxide.

On heating the surface to *ca*. 380 K for 40 minutes the structures orientated in the <100> direction revert to the interchain separation of 5.1 Å typical of the (2 × 1) oxygen structure.

We deduce that the pyridine molecules adsorb on the Cu–O chains at the oxygen sites and are responsible for forcing the rows apart. The reason for the increase in the inter-row spacing can be understood when one considers that the internal structure along the rows retains its 3.6 Å spacing. The pyridine molecule is *ca*. 5 Å in diameter and the XPS shows close to a 1 : 1 pyridine/oxygen ratio. This implies that the pyridine ring must be orientated perpendicular to the surface with its plane lying in the $<1\bar{1}0>$ direction, in other words at right angles to the direction of the Cu–O chain, Fig. 2(b). Because of the diameter of the ring, steric hindrance would prevent pyridine adsorption on adjacent rows. It seems however, that the formation of the pyridine–oxygen complex provides sufficient energy to break up the existing structure forcing the chains apart and thereby enabling further pyridine adsorption.

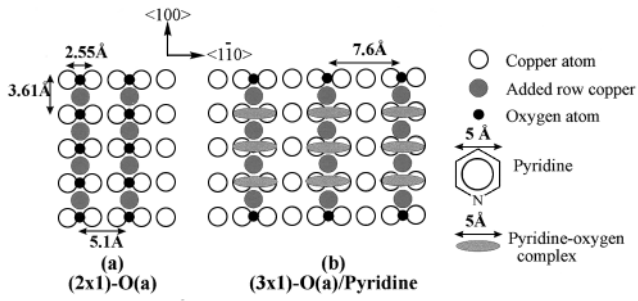

Fig. 2 (a) Structure of the (2 × 1)O(a) added row reconstruction on Cu(110); (b) proposed structure for pyridine adsorbed at the preoxidised Cu(110) surface.

Comparing the adsorption of the pyridine at the (111) and (110) surfaces we note that five times as much pyridine will adsorb onto the surface of the latter. We believe this is due to the flexibility of the particular structure formed by oxygen on Cu(110) in which the oxygen atoms are present in the added chains which are capable of moving over the surface with a low energy cost.[9] In contrast, the adsorbed state of oxygen on Cu(111) involves no large scale reconstruction[6] and the oxygen atoms are embedded within the substrate lattice effectively immobilising them.

The relevance of the observations here to the reactivity of a surface in the presence of a 'co-adsorbate' is obvious. They show that even weakly adsorbed species may influence the structure of the surface in such a way as to increase (or decrease) the availability of adsorption and reaction sites at the surface. Clearly, this must cast doubt on conclusions reached about reaction mechanisms based on structures observed in the absence of other reactants.

We are grateful to EPSRC for their generous support of this research.

Notes and references

‡ 1 L = 10^{-6} Torr s.

1 A. F. Carley, A. Chambers, P. R. Davies, G. G. Mariotti, R. Kurian and M. W. Roberts, *Faraday Discuss.*, 1996, **105**, 225.
2 M. W. Roberts, *Surf. Sci.*, 1994, **300**, 769.
3 C. T. Au and M. W. Roberts, *J. Chem. Soc., Faraday Trans. 1*, 1987, **83**, 2047.
4 M. W. Roberts, *Chem. Soc. Rev.*, 1996, **25**, 437.
5 P. R. Davies and N. Shukla, *Surf. Sci.*, 1995, **322**, 8.
6 F. Jensen, F. Besenbacher and I. Stensgaard, *Surf. Sci.*, 1992, **270**, 400.
7 J. Wintterlin, R. Schuster, D. J. Coulman, G. Ertl and R. J. Behm, *J. Vac. Sci. Technol. B*, 1991, **9**, 902.
8 F. Jensen, F. Besenbacher, E. Laesgaard and I. Stensgaard, *Phys. Rev. B. Condens. Matter*, 1990, **41**, 10233.
9 A. F. Carley, P. R. Davies, G. U. Kulkarni and M. W. Roberts, *Catal. Lett.*, 1999, in press.

Communication 9/01221D

ChemComm

The facile synthesis of α-aryl-α-hydroxy esters *via* one-pot vicarious nucleophilic substitution and oxidation

Nicholas J. Lawrence,* Olivier Lamarche† and Nabil Thurrab‡

Department of Chemistry, UMIST, PO Box 88, Manchester, UK M60 1QD. E-mail: n.lawrence@umist.ac.uk

Received (in Liverpool, UK) 4th February 1999, Accepted 1st March 1999

The anion produced by the vicarious nucleophilic substitution reaction of nitroarenes and α-chloro esters is hydroxylated by the action of air and benzaldehyde, thereby producing α-hydroxy esters.

The recently developed process of vicarious nucleophilic substitution (VNS), pioneered by Makosza and co-workers,[1,2] offers a selective mild method for the controlled substitution of hydrogen atoms of aromatic systems. As part of our contribution to the study of the VNS reaction we have developed[3] a one-pot coupling reaction of three components (a nitroarene, a stabilised carbanion derived from **1** and an electrophilic species E^+) for the construction of nitroarenes **4** bearing an adjacent quaternary chiral centre, as illustrated in Scheme 1.[4,5] This process first involves a VNS reaction between the nitroarene and the carbanion to give the intermediate anion **3** *via* loss of HX from the σ-adduct **2**. This post-VNS anion is sufficiently nucleophilic to be quenched *in situ* with a variety of electrophiles E^+ to give the *para*-functionalised nitroarene **4**.

During the study of the reaction of the post-VNS anion **3** with aldehydes, we serendipitously discovered a process for the synthesis of α-aryl-α-hydroxy esters. When the anion **3a** (R = Me), derived from ethyl 2-chloropropionate **1a**, was reacted with benzaldehyde we did not observe the formation of an aldol product. However on one occasion, when air was inadvertently introduced into the reaction flask, we obtained the hydroxy ester **5a** in approximately 50% yield. A careful study of the reaction revealed that the yield could be increased to 66% when 3 equiv. of the ester is used with respect to nitrobenzene (Scheme 2).§ In most of these reactions a small amount (5–10%) of *p*-nitroacetophenone was also produced. It was clear that both benzaldehyde and air were required in the reaction. In the absence of air, the only product obtained upon work up (**4**, R = Me, *E* = H) arose from protonation of the anion **3**. The reaction of the post-VNS anion **3a** with air in the absence of benzaldehyde gave a mixture of α-hydroxy ester **5a** and ketone *p*-nitroacetophenone in near equal proportions. We then applied this intriguing one-pot VNS–hydroxylation process to the reaction of ethyl 2-chlorobutanoate **1b** with nitrobenzene and obtained the ester **5b**. This ester was also obtained in 40% yield when the post-VNS anion was prepared *via* direct deprotonation (NaH, DMF) of ethyl 2-(*p*-nitrophenyl)butanoate followed by oxidation with air and benzaldehyde. In this case the ester was accompanied by 2-(*p*-nitrophenyl)propiophenone (8%) and the diester **6b** (10% as 1 : 1 mixture of *racemic* : *meso* stereoisomers). As confirmation of its structure, the diester **6b** was obtained in 89% yield (*racemic* : *meso* 1 : 1) by treatment of the post-VNS anion **3b** with iodine (Scheme 2).[6] Since such an oxidative coupling is thought to occur *via* a mechanism involving single electron transfer,[5] this reaction also sheds light on the mechanism of the hydroxylation reaction (*vide supra*). Reaction of ethyl α-chlorophenylacetate with nitrobenzene gave ethyl benzoylformate in 35% yield when the VNS reaction was performed at 0 °C for 1 h and 25 °C for 1.5 h; the product presumably arising from direct oxidation of the anion of **1c**. The hydroxy ester **5c** was obtained, albeit in low yield, when nitrobenzene was used in excess (1.5 equiv.) and a longer period of time was used for the VNS reaction (0 °C for 1 h and 25 °C for 3 h). It seems that the enolate derived from **1c** is insufficiently nucleophilic to react efficiently with nitrobenzene. We then applied the hydroxylation reaction to other nitroarenes (Table 1).

Reaction of ethyl 2-chlorobutanoate **1b** with *o*- and *m*-chloronitrobenzenes (entries 1 and 2) and two nitro-substituted pyridines (entries 3 and 4) gave the hydroxy ester products in which the VNS nucleophile has added *para* to the nitro group, as determined from their ^{1}H NMR spectra.¶ The product from 2-nitrothiophene with ethyl 2-chloropropionate **1a** (entry 5) is the 5-substituted hydroxy ester **5e**, as determined from its ^{1}H nmr spectrum.¶ A pair of doublets were observed at δ 7.05 and 7.80 with a coupling constant of 4.3 Hz corresponding to signals from H-3 and H-4 (expected coupling constants:[7] $J_{3,4}$ 3.45–4.35 Hz and $J_{4,5}$ 4.90–5.80 Hz). At low temperature (−33 °C, NH_3, KOH), 2-nitrothiophene is attacked by a variety VNS nucleophiles predominantly at the 3-position.[8] However, as the nucleophile **1a** provides a tertiary anion, it is not surprising that at room temperature the 5-substituted isomer is the exclusive product. It should be noted that oxidation of nitrobenzylic carbanions (made by deprotonation of products of VNS reaction) to aldehydes and ketones has been reported.[9]

The oxidation of enolates by oxygen is, of course, not without precedent. For example, Wasserman and Lipshutz have shown

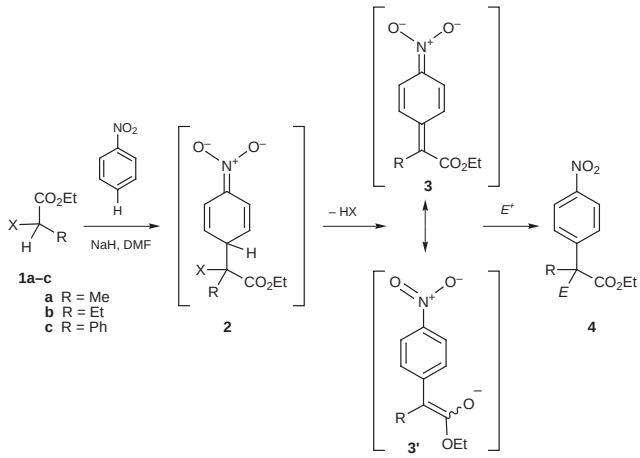

Scheme 1

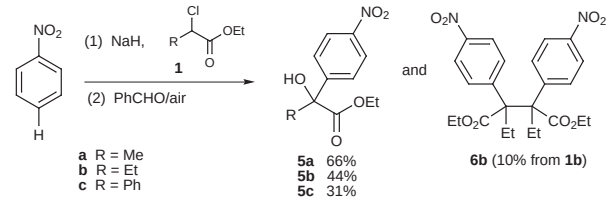

Scheme 2

† Undergraduate research assistant from the Ecole Nationale Supérieure de Synthèses, de Procédés, et d'Ingénierie Chimiques d'Aix-Marseille.
‡ MSc candidate from the University of Al Azhar, Gaza, Palastine.

Table 1 Reaction of nitroarenes to give hydroxy esters

Entry	Nitroarene	Ester	Product	Yield (%)
1		**1b**	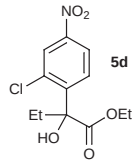 **5d**	53
2		**1b**	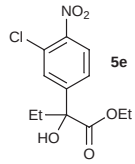 **5e**	62
3	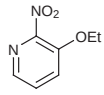	**1b**	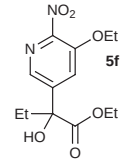 **5f**	52
4		**1b**	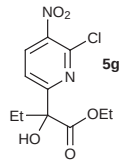 **5g**	50
5	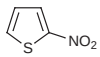	**1a**	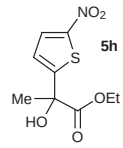 **5h**	44

that lithium enolates of esters react with molecular oxygen to give α-hydroxy esters (after reduction of the first formed peroxide with sodium sulfite).[10] A similar procedure lacking the reductive work-up gives the α-hydroperoxy acids from carboxylic acids.[11] The post-VNS hydroxylation we observe is possibly occurring *via* initial oxidation of the anion **3**, *via* single electron transfer, to a radical which combines with an oxygen radical anion to give peroxide **7** which is trapped by benzaldehyde to give species **8** (Scheme 3). Finally a 1,3-hydride shift gives the alkoxide **8**.[12] Clearly the formation of products such as **6** indicate a mechanism involving radicals. We found that the enolate of **1c**, generated by reaction of sodium hydride, in the absence of nitrobenzene, does not react with oxygen. This suggests that the nitro group also plays a role in the oxidation process, in addition to activating the arene to attack by the VNS nucleophile and stabilising the anion **3**. This is in agreement with the finding of Russel and Bemis[13] that nitrobenzene acts as a single eletron transfer catalyst in the oxidation of stabilised

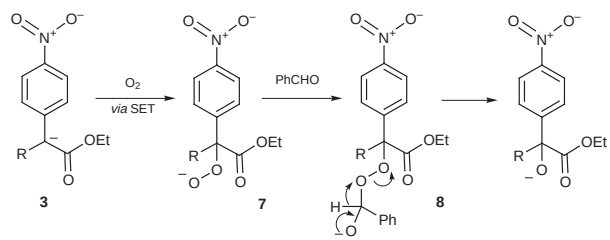

Scheme 3

benzylic anions to peroxides. In summary, we have developed an intriguing one-pot VNS–hydroxylation reaction using inexpensive reagents that lead to novel α-aryl-α-hydroxy esters.

We thank the University of Al Azhar, Palastine and ENSSPICAM (Marseille) for financial support to N. T. and O. L. respectively and the EPSRC for Research Grants (GR/L52246: NMR spectrometer; GR/L84391: chromatographic equipment).

Notes and references

§ To a stirred slurry of NaH (0.74 g of a 60% dispersion in oil, 18.5 mmol) in dry DMF (10 cm^3) at 0 °C was added dropwise solution of ethyl 2-chloropropionate **1a** (1.68 g, 12.33 mmol) and nitrobenzene (0.76 g, 6.16 mmol) in dry DMF (10 cm^3). The deep blue–purple reaction mixture was stirred at 0 °C for 60 min and room temperature for 2 h. Benzaldehyde (0.98 g, 9.25 mmol) was added and the reaction mixture stirred at room temperature under an atmosphere of dry air for 24 h. The resulting brown mixture was poured onto a slurry of ice and hydrochloric acid (1 M, 20 cm^3) and extracted with $CHCl_3$ (3 × 20 cm^3). The solvent (DMF and $CHCl_3$) was removed from the combined extracts *in vacuo*. $CHCl_3$ (75 cm^3) was added to the residue. This solution was washed with water (5 × 75 cm^3) and aq. $NaHCO_3$ (5 × 75 cm^3), dried ($MgSO_4$) and evaporated *in vacuo*. The residue was purified by chromatography to give the hydroxy ester **5a**.

¶ *Selected data* for **5d**: δ_H(300 MHz, $CDCl_3$) δ_H 1.25 (3H, t, *J* 7.15, OCH_2CH_3), 1.85 (3H, s, CH_3), 3.75 (1H, s, OH), 4.25 (2H, q, *J* 7.15, OCH_2CH_3), 7.84 (1H, d, *J* 8.7, H-6′), 8.15, (1H, dd, *J* 8.7 and 2.3, H-5′) and 8.23 (1H, d, *J* 2.3, H-3′). For **5e**: δ_H 0.90 (3H, t, *J* 7.4, CH_2CH_3), 1.30 (3H, t, *J* 7.2, OCH_2CH_3), 1.98 (1H, dq, *J* 14.7 and 7.4, $CH_aH_bCH_3$), 2.20 (1H, dq, *J* 14.7 and 7.4, $CH_aH_bCH_3$), 3.95 (1H, s, OH), 4.19–4.38 (2H, m, OCH_2CH_3), 7.67 (1H, d, *J* 8.6 and 1.9, H-6′), 7.85 (1H, d, *J* 8.6, H-5′) and 7.87 (1H, d, *J* 1.9, H-2′). For **5f**: δ_H 0.92 (3H, t, *J* 7.4, CH_2CH_3), 1.32 (3H, t, *J* 7.2, $CO_2CH_2CH_3$), 1.45 (3H, *J* 6.9, OCH_2CH_3), 2.01 (1H, dq, *J* 14.7 and 7.4, $CH_aH_bCH_3$), 2.23 (1H, dq, *J* 14.7 and 7.4, $CH_aH_bCH_3$), 3.97 (1H, s, OH), 4.18–4.40 (4H, m, 2 × OCH_2CH_3), 7.85 (1H, d, *J* 1.8, H-4′) and 8.30 (1H, d, *J* 1.8, H-6′). For **5g**: δ_H 0.95 (3H, t, *J* 7.4 Hz, CH_2CH_3), 1.28 (3H, t, *J* 7.2, OCH_2CH_3), 2.02 (1 H, dq, *J* 14.7 and 7.4, $CH_aH_bCH_3$), 2.37 (1H, dq, *J* 14.7 and 7.4, $CH_aH_bCH_3$), 4.20–4.32 (2H, m, OCH_2CH_3), 4.35 (1H, s, OH), 7.78 (1H, d, *J* 8.3, H-5′) and 8.25 (1H, d, *J* 8.3, H-4′). For **5h**: δ_H 1.35 (3H, t, *J* 7.15, OCH_2CH_3), 1.80 (3H, s, CH_3), 4.24 (1H, s, OH), 4.26–4.40 (2H, m, CH_2CH_3), 7.05 (1H, d, *J* 4.3, 3′-H) and 7.80 (1H, *J* 4.3, 4′-H).

1 O. N. Chupakhin, V. N. Charushin and H. C. van der Plas, *Nucleophilic Aromatic Substitution of Hydrogen*, Academic Press Inc., London, 1994. For reviews of aromatic vicarious nucleophilic substitution, see M. Makosza, *Chimia*, 1994, **48**, 499; M. Makosza and J. Winiarski, *Acc. Chem. Res.*, 1987, **20**, 282; M. Makosza, *Synthesis*, 1991, 103; M. Makosza and A. Kwast, *J. Phys. Org. Chem.*, 1998, **11**, 341; and ref. 2.

2 M. Makosza and K. Wojciechowski, *Liebigs Ann./Recl.*, 1997, 1805.

3 N. J. Lawrence, J. Liddle and D. A. Jackson, *Tetrahedron Lett.*, 1995, **36**, 8477.

4 N. J. Lawrence, J. Liddle and D. A. Jackson, *Synlett*, 1996, 55; S. M. Bushell, J. P. Crump, N. J. Lawrence and G. Pineau, *Tetrahedron*, 1998, **54**, 2269.

5 M. D. Drew, N. J. Lawrence, D. A. Jackson, J. Liddle and R. G. Pritchard, *Chem. Commun.*, 1997, 189.

6 T. Langer, M. Illich and G. Helmchen, *Tetrahedron Lett.*, 1995, **36**, 4409.

7 S. Gronwitz, *Adv. Heterocycl. Chem.*, 1963, **1**, 1.

8 M. Makosza and E. Kwast, *Tetrahedron*, 1995, **51**, 8339.

9 K. Wojciechowski, *Synth. Commun.*, 1997, **27**, 135; J.-P. Wulf, K. K. Sienkiewicz, M. Makosza and E. Schmitz, *Leibigs Ann. Chem.*, 1991, 537. Also see ref. 2.

10 H. H. Wasserman and B. H. Lipshutz, *Tetrahedron Lett.*, 1975, 1731.

11 D. A. Konen, L. S. Silbert and P. E. Pfeffer, *J. Org. Chem.*, 1975, **40**, 3253.

12 We did not try to isolate the benzoic acid which would be produced by the proposed mechanism. We intentionally performed a base wash as part of the work−up to remove any acidic by-products. We will report further on the mechanism in due course.

13 G. A. Russell and A. G. Bemis, *J. Am. Chem. Soc.*, 1966, **88**, 5491.

Communication 9/00986H

Montmorillonite-mediated hetero-Diels–Alder reaction of alkenes and *o*-quinomethanes generated *in situ* by dehydration of *o*-hydroxybenzyl alcohols

Kazuhiro Chiba,* Tetsuya Hirano, Yoshikazu Kitano and Masahiro Tada

Laboratory of Bio-organic Chemistry, Tokyo University of Agriculture and Technology, 3-5-8 Saiwai-cho, Fuchu, Tokyo 183-8503, Japan. E-mail: chiba@cc.tuat.ac.jp

Received (in Cambridge, UK) 25th January 1999, Accepted 9th March 1999

The intermolecular hetero-Diels–Alder reaction of *in situ*-generated *o*-quinomethanes and unactivated alkenes has been accomplished through a wet montmorillonite catalyst in a $LiClO_4$–$MeNO_2$ solution to give good yields of varied chromane skeletons.

o-Quinomethanes play an important role as the heterodiene in the construction of a wide variety of chromane skeletons *via* hetero-Diels–Alder reaction with alkenes (Scheme 1). The generation and cycloaddition of *o*-quinomethanes has been extensively investigated, including pyrolysis of *o*-hydroxybenzyl alcohols,[1] one-electron oxidation of *o*-substituted phenols,[2] desilylation of an *o*-hydroxybenzyl alcohol disilyl ether,[3] and dehydrogenation of allylphenols with DDQ.[4] However, as the *o*-quinomethanes are generally very unstable, they must be trapped by highly active, electron-rich alkenes, by intramolecular reactions, or under high-temperature conditions. Furthermore, by-products of the homo-Diels–Alder reaction, Michael addition, or Friedel–Crafts reaction of *o*-quinomethanes have also often been obtained with desired products (Scheme 2).[5] On the other hand, it has been proposed that many natural products can be generated *via* the intermolecular cycloaddition of *o*-quinomethanes and aliphatic alkenes.[6] Biogenetically, it has been proposed that *o*-quinomethanes are produced by the dehydration of the corresponding *o*-hydroxybenzyl alcohols or benzylic oxidation of the corresponding *o*-cresol derivatives.[7] Biomimetic mild reaction media in which *o*-quinomethanes are generated and trapped efficiently by unactivated aliphatic alkenes have therefore been sought. Recently, we performed the intermolecular hetero-Diels–Alder reaction of electrochemically generated electon-rich *o*-quinomethanes and unactivated aliphatic alkenes to construct some natural product skeletons, but the *o*-quinomethanes were limited to stable ones possessing electron-donating groups (Scheme 3). Accordingly we have further investigated the biomimetic facile method for the generation and cycloaddition reaction of *o*-quinomethanes, and found that a catalytic amount of wet montmorillonite in a $LiClO_4$–$MeNO_2$ solution efficiently

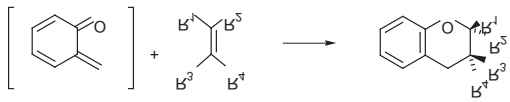

Scheme 1

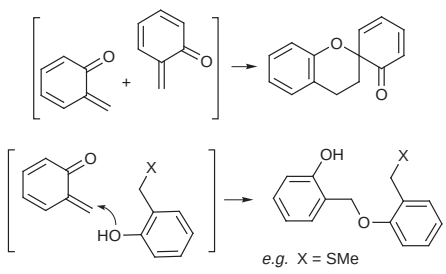

Scheme 2

generated *o*-quinomethanes by the dehydration of the corresponding *o*-hydroxybenzyl alcohol. The reaction media showed a remarkable acceleration property in the generation and intermolecular cycloaddition of the unstable *o*-quinomethanes with varies unactivated alkenes.

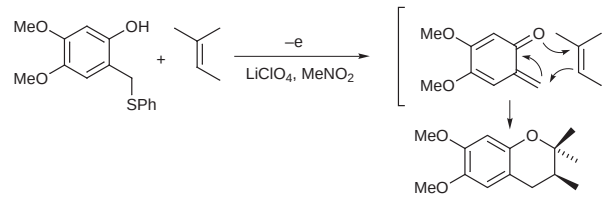

Scheme 3

Under the usual dehydration conditions of benzyl alcohols using Lewis acids or Brønsted acids, salicyl alcohol and 2-methylbut-2-ene **3** gave the corresponding cycloadducts **10** and **11** in very low yields (Table 1). On the other hand, a catalytic amount of dry montmorillonite K 10 in $MeNO_2$ gave the desired cycloadducts in 26.8%, and the addition of $LiClO_4$ effectively increased the yield to 54.8%. Furthermore, the reaction proceeded to give **10** and **11** (6 : 1) almost quantitatively by using wet montmorillonite K 10 in the presence of $LiClO_4$ in $MeNO_2$ at ambient temperature. The wet montmorillonite did not work well in other solvents, even in the presence of $LiClO_4$. Accordingly, the targeted reactions with varied alkenes were performed in $MeNO_2$ in the presence of an *o*-hydroxybenzyl alcohol, wet montmorillonite, and $LiClO_4$ at ambient temperature.† Styrenes gave excellent yields of the corresponding flavanes, while unactivated aliphatic alkenes simply gave chromanes and spirochromanes in good yields (Table 2). Some products were obtained due to skeleton rearrangement of the alkene moieties (Scheme 4).

In the present reaction media, the dehydration reaction may be accelerated on the wide surface of montmorillonite, and the

Table 1 Effect of catalysts and reaction media on the cycloaddition of **3** and *o*-quinomethane generated by the dehydration of salicyl alcohol **1**[a]

Solvent	Catalyst	Additive	Yield (%)
CH_2Cl_2	$TiCl_4$[b]	none	12.7
CH_2Cl_2	BF_3/Et_2O[b]	none	13.7
CH_2Cl_2	$ZnCl_2$[b]	none	1.8
CH_2Cl_2	MsOH[b]	none	17.1
CH_2Cl_2	P_2O_5[b]	none	10.6
MeCN	wet mont.[c]	$LiClO_4$[e]	12.1
Et_2O	wet mont.	$LiClO_4$	trace
CH_2Cl_2	wet mont.	$LiClO_4$	trace
$MeNO_2$	wet mont.	none	15.8
$MeNO_2$	dry mont.[d]	none	26.8
$MeNO_2$	dry mont.	$LiClO_4$	54.8
$MeNO_2$	wet mont.	$LiClO_4$	> 99

[a] 20 mg of **1** and 3 equiv. of **3** were dissolved in 2.0 ml of solvent. [b] 1.5 equiv. of catalyst was added. [c] 20 mg of montmorillonite and 36 mg of water were added to 2 ml of solvent. [d] 20 mg of montmorillonite was added to 2.0 ml of solvent. [e] 200 mg of $LiClO_4$.

Table 2 Montmorillonite-mediated cycloaddition of *o*-quinomethanes and alkenes[a]

Substrate	Alkene	Products	Yield (%)
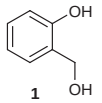 **1**	 **3**	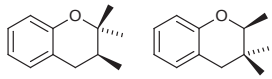 **10** **11** (**10**:**11**=6:1)	>99
1	 **4**	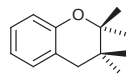 **12**	>99
1	 **5**	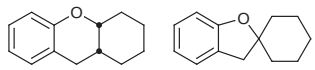 **13** **14** (**13**:**14**=2:1)	>99
1	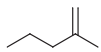 **6**	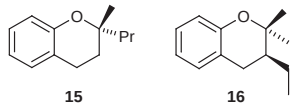 **15** **16** (**15**:**16**=4:1)	85

Substrate	Alkene	Products	Yield (%)
1	 **7**	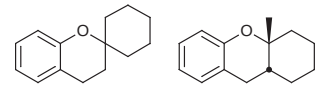 **17** **18** (**17**:**18**=1.7:1)	78
1	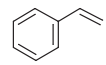 **8**	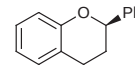 **19**	94
1	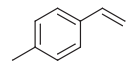 **9**	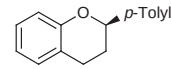 **20**	>99
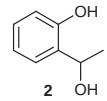 **2**	**4**	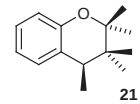 **21**	76
2	**8**	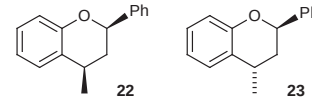 **22** **23** (**22**:**23**=2:1)	79

[a] 2-Hydroxybenzyl alcohol (20 mg) and 3 equiv. of alkene were dispersed in 2.0 ml of 0.1 M $LiClO_4$–$MeNO_2$ in the presence of 20 mg of montmorillonite and 36 mg of water. The reaction mixture was allowed to stand at ambient temperature for 48 h.

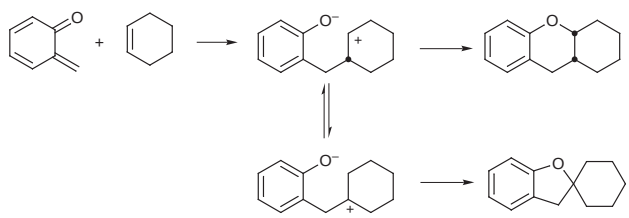

Scheme 4

addition of water might regulate the acidic decomposition and polymerization of starting materials. $LiClO_4$ is expected to stabilize the *in situ*-generated zwitterion, which is an equivalent of the *o*-quinomethane (Scheme 5). Furthermore, the products are easily extracted from the reaction media with *n*-hexane, and the catalytic solvent system can be reused many times. Employing the hetero-Diels–Alder reaction of *o*-quinomethanes in $LiClO_4$–$MeNO_2$ mediated by wet montmorillonite K 10 is applicable to the formation of a variety of chromanes. In these cases involving unsubstituted, unstable *o*-quinomethanes, the cycloaddition reactions with unactivated alkenes proceeded smoothly to give cycloadducts, including those which are difficult to obtain in high yields *via* other methods.

This work was supported by a Grant-in-Aid for Scientific Research on Priority Areas (No. 283, 'Innovative Synthetic Reactions') from the Ministry of Education, Science, Sports and Culture, Japan.

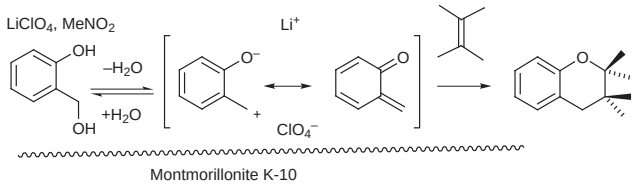

Scheme 5

Notes and references

† *General procedure:* Montmorillonite K 10 (Aldrich) and water were dispersed in 5 ml of $MeNO_2$, and salicyl alcohol **1** (25 mg), styrene **8** (63 mg) and $LiClO_4$ (50 mg) were dissolved in the solution. The reaction mixture was allowed to stand at ambient temperture for 48 h under air atmosphere. After the reaction was completed, products were extracted with *n*-hexane. The *n*-hexane was removed *in vacuo* after drying with Mg_2SO_4, and the residue was then separated by silica gel column chromatography (*n*-hexane–AcOEt) to give the cycloadduct **19** in 94% yield.

1 T. Katada, S. Eguchi, T. Esaki and S. Sasaki, *J. Chem. Soc., Perkin Trans. 1*, 1984, 2649; S. K. Paknikar, K. P. Fondekar and R. Mayer, *Natl. Prod. Lett.*, 1996, **8**, 253.
2 D. A. Bolon, *J. Org. Chem.*, 1970, **35**, 3666; O. L. Chapman, M. R. Engel, J. P. Springer and J. C. Cardy, *J. Am. Chem. Soc.*, 1971, **93**, 6696; M. Cornia, L. Merlini and A. Zanarotti, *Gazz. Chim. Ital.*, 1977, **107**, 299.
3 J. P. Marino and S. L. Dax, *J. Org. Chem.*, 1984, **49**, 3672,
4 G. Cardillo, M. Orena, G. Porzi and S. Sandri, *J. Chem. Soc., Chem. Commun.*, 1979, 836; W. K. Anderson, E. J. LaVoie and P. G. Whitkop, *J. Org. Chem.*, 1974, **39**, 881.
5 Y.-L. Mao and Y. Boekelheide, *Proc. Natl. Acad. Sci. U.S.A.*, 1980, **77**, 1732; T. Inoue, S. Inoue and K. Sato, *Bull. Chem. Soc. Jpn.*, 1990, **63**, 1062; T. Inoue, S. Inoue and K. Sato, *Bull. Chem. Soc. Jpn.*, 1990, **63**, 1647.
6 H. Weenen and M. H. H. Nkunya, *J. Org. Chem.*, 1990, **55**, 5107; V. S. Parmar, O. D. Tyagi, A. Malhotra, S. K. Singh, K. S. Bisht and R. Jain, *Nat. Prod. Rep.*, 1994, 219.
7 E. L. Ghisalberti, *Phytochemistry*, 1996, **41**, 7.
8 K. Chiba, J. Sonoyama and M. Tada, *J. Chem. Soc., Chem. Commun.*, 1995, 1381; K. Chiba, J. Sonoyama and M. Tada, *J. Chem. Soc., Perkin Trans. 1*, 1996, 1435; K. Chiba, T. Arakawa and M. Tada, *Chem. Commun.*, 1996, 1763; K. Chiba, T. Arakawa and M. Tada, *J. Chem. Soc., Perkin Trans. 1*, 1998, **17**, 2939; K. Chiba, Y. Yamaguchi and M. Tada, *Terahedron Lett.*, 1998, **39**, 9035.

Communication 9/00657E

ChemComm

Covalently attached multilayer assemblies of diazo-resins and porphyrins

Junqi Sun, Zhiqiang Wang, Yipeng Sun, Xi Zhang* and Jiacong Shen

Key Lab of Supramolecular Structure and Spectroscopy, Department of Chemistry, Jilin University, Changchun, 130023, PR China. E-mail: xi@mail.jlu.edu.cn

Received (in Cambridge, UK) 2nd December 1998, Accepted 10th March 1999

Construction of highly stable covalently attached multilayer films containing porphyrins was achieved by UV irradiation of ionic self-assembled multilayer films of diazo-resins (DAR) and tetrasodium 5,10,15,20-tetraphenyl-21H,23H-porphine-P,P′,P″,P‴-tetrasulfonic acid ($tpps_4$).

Layered construction of porphyrins into organized systems has increasingly gained in importance due to its potential application in various disciplines ranging from voltaics, electrochromics to nonlinear optics. Many strategies have been exploited to fulfill this purpose, including Langmuir–Blodgett,[1] self-assembly[2] and electropolymerization techniques.[3] Recently, ourselves and others have developed a new method to fabricate porphyrin multilayer films based on electrostatic interactions as the driving force.[4] This technique has proven to be a rapid and experimentally very simple way to fabricate porphyrin containing films. However, porphyrin films fabricated by this technique are not robust enough and can be etched by solvents which limits applications in an extended range. Here we introduce a new method to fabricate covalently attached multilayer films containing porphyrins by UV photoreacting diazonium and sulfonate groups at the interface. This method combines the simplicity of the ionic self-assembly technique and the high stability of the covalently attached multilayer films. Thus it promises to be a very efficient method to prepare highly stable multilayer films containing porphyrins.

Diazo-resin (DAR) was kindly provided by Prof. Weixiao Cao (College of Chemistry and Molecular Engineering, Peking University, Beijing), and its synthesis has been reported previously.[5] The porphyrin $tpps_4$ was synthesized according to the literature.[6] A freshly cleaned quartz slide was first modified with a layer of (3-mercaptopropyl)trimethoxysilane (MPTS) from benzene, after which terminal –SH functional groups at the exposed surface were oxidized by 30% H_2O_2–HOAc *in situ* into sulfonic acid groups.[7] The sulfonic acid covered quartz slide was then alternately immersed in aqueous solutions of DAR (1.5 mg ml^{-1}) and $tpps_4$ (0.2 mg ml^{-1}) for 20 min, with an intermediate water washing and N_2 drying. Multilayer films can be formed by repeating the above step in a cyclic fashion. The above deposition process was conducted in the dark. Finally, irradiating the multilayer films with UV light for a given time is required to convert the ionic interaction of neighboring layers into covalent bonds.

UV–VIS spectroscopy was used to follow the fabrication process. Fig. 1(a) shows the UV–VIS absorption spectra of eight bilayers of DAR/$tpps_4$ assembled on a quartz slide. The absorbance at 380 nm is attributed to the π–π* transition of the diazonium group, while the absorbance at 426 nm corresponds to the Soret band of porphyrin. It was found that the absorbances at 380 and 426 nm increase linearly with the number of layers, which demonstrates a progressive deposition process. UV–VIS spectroscopy also indicates that the Soret band of the porphyrin in the DAR/$tpps_4$ multilayer films is red-shifted by *ca*. 12 nm compared with that in solution, which is a consequence of formation of aggregates of chromophores in the films.

Owing to the well known photoreaction of diazonium and sulfonate groups, the above assembled films containing eight bilayers of DAR/$tpps_4$ were irradiated with a 30 W medium power mercury lamp at a distance of 20 cm. Fig. 1 shows the changes in UV–VIS spectra of the films with different irradiation times, from which, we can clearly see that the absorbance at 380 nm decreases dramatically due to the decomposition of the diazonium group, concomitantly, the absorbance at 290 nm increases gradually. Throughout the experiment, we found that the decomposition proceeded completely within 30 min. It was also found that at the same time the absorbance of the Soret band of $tpps_4$ decreases gradually with no change in peak position or shape. This decrease is caused by the decrease of the contribution of diazonium groups at this wavelength. The fact that the peak position and shape of the Soret band of $tpps_4$ did not change shows that no or few conformational changes took place during the reaction, which was consistent with the result of polarized UV–VIS spectroscopy.

We compared the stability of the multilayer films before and after UV irradiation by immersing the corresponding films into a ternary mixture of H_2O–DMF–$ZnCl_2$ (3 : 5 : 2, w/w/w). This ternary system was chosen because of the high solubility of the DAR/$tpps_4$ complex in it compared to other solutions, such as aqueous $ZnCl_2$ DMF, chloroform, *etc*. The UV–VIS spectra showed that before UV irradiation treatment, almost all the porphyrin and most of DAR can be dissolved after 5 min of immersion as seen the large decrease of the absorbance at 426 and 380 nm. However, for the UV irradiated films, the spectrum after immersion scarcely decreased showing that < 10% of the films dissolved. Thus the stability of the irradiated films was substantially improved.

From the change of the stability of the multilayer films before and after UV irradiation, it is proposed that a photoreaction takes place between the diazonium groups of DAR and sulfonate groups of $tpps_4$. As for the general reaction mechanism,[8] it is thought that DAR is first converted into its phenyl cationic form after release N_2 upon UV irradiation. Then an S_N1 type of nuclear displacement by sulfonate occurs as shown in Scheme 1. The fact that the photoreaction changes the

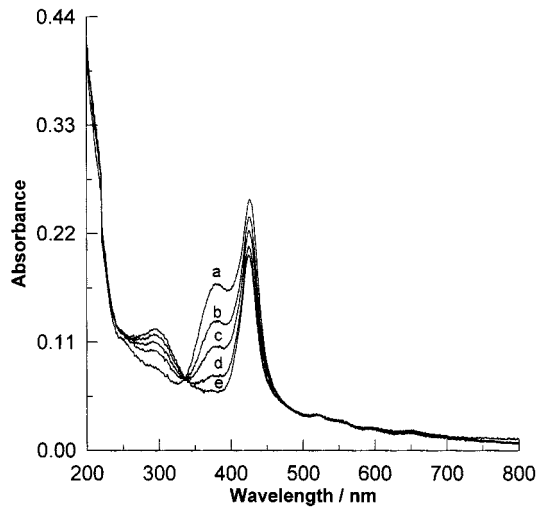

Fig. 1 UV–VIS absorption spectra of eight bilayers of DAR/$tpps_4$ upon irradiation with UV light for (a) 0, (b) 2, (c) 4, (d) 8 and (e) 15 min.

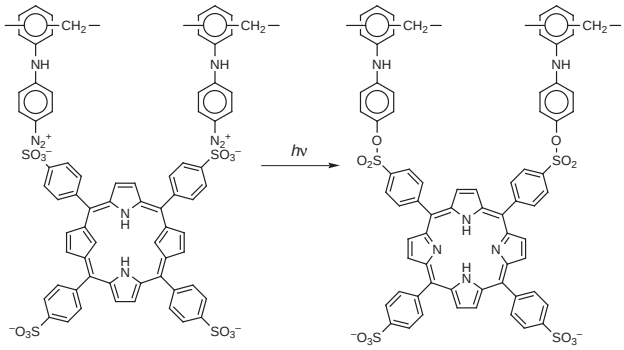

Scheme 1 Photoreaction of DAR and $tpps_4$ in one bilayer.

interactions not only between the neighboring layers, but also the first layer of DAR and the modified substrate from ionic to covalent is likely to be responsible for the improvement of the stability of the irradiated films.

The photoreaction of diazonium and sulfonate groups in multilayer films was further confirmed by IR spectroscopy. Three absorption peaks at 2220, 2163 and 1177 cm^{-1} are observed in the IR spectra of an 18-bilayer film of DAR/$tpps_4$ assembled on CaF_2 substrate [modified by cationic poly-(diallyldimethyl ammonium chloride)] before UV irradiation. The first two originate from the stretching of $-CN_2$ and that at 1177 cm^{-1} from symmetric stretching of $-SO_3^-$. After UV irradiation, the absorptions at 2220 and 2163 cm^{-1} disappeared completely, indicating decomposition of the diazonium group. Meanwhile, a new absorption at 1170 cm^{-1} appeared which corresponds to the symmetric stretching of the sulfonate coupled with the phenyl group. In layer-by-layer multilayer films, the photoreaction should be facilitated to some extent by the close proximity of the diazonium and sulfonate groups. However, it is very difficult to determine the extent of reaction of diazonium with sulfonate groups. Further efforts to solve this problem are in progress.

Polarized UV–VIS spectroscopy was used to study the orientation of the planar porphyrin in the multilayer films before and after photoreaction. In both cases, no detectable changes were found when the multilayer films were examined at normal incidence using polarized light with its electric vector parallel or perpendicular to the plane of incidence, indicating that no in-plane anisotropy exists. When the film was examined at 30° incidence under the similar process, an obvious change of the spectra could be observed both before and after UV irradiation as shown in Fig. 2. We can calculate the orientation angle of the porphyrin plane by using the method described previously by us.[4] Herein, we presume the optical indices of the films before and after UV irradiation are the same and have a value of 1.5. The angle between the normal line of plane *x* and the substrate, *i.e.* θ, calculated before and after UV irradiation films is 53 and 49°. In other words, the oriented angle between the plane and horizon of the substrate are 53 and 49°, respectively, which

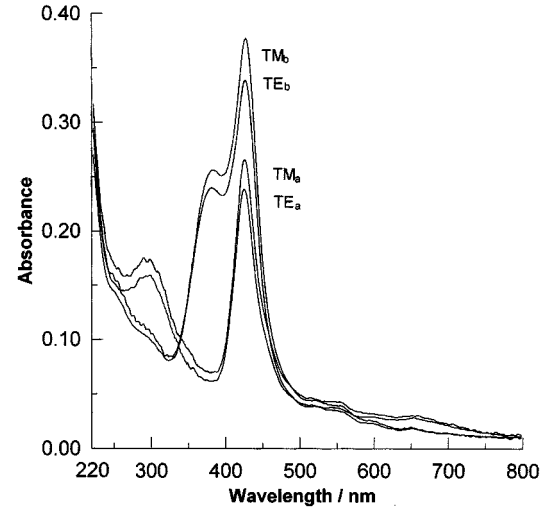

Fig. 2 Polarized UV–VIS spectra of a 12-bilayer DAR/$tpps_4$ film before (TE_b and TM_b) and after (TE_a and TM_a) UV irradiation for TE and TM polarisations. Incident angle = 30°.

show little conformational change of the porphyrin in multilayer films before and after UV irradiation.

In conclusion, a new method to fabricate covalently attached multilayers of porphyrin has been developed exploiting the ionic self-assembly technique and post UV-irradiation photoreaction of the diazonium and sulfonate groups in the multilayer assemblies. This technique is a simple but efficient method to prepare highly stable porphyrin-containing multilayer films.

This work was supported by National Natural Science Foundation of China.

Notes and references

1 H. Chou, C. T. Chen, K. F. Stork, P. W. Bohn and K. S. Suslick, *J. Phys. Chem*., 1994, **98**, 383.
2 S. B. Ungashe, W. L. Wilson, H. E. Katz, G. R. Scheller and T. M. Putvinski, *J. Am. Chem. Soc*., 1992, **114**, 8717.
3 N. L. Jaeger, R. Lehmkuhl, D. Schlettwein and D. Wöhrle, *J. Electrochem. Soc*., 1994, **141**, 1735.
4 X. Zhang, M. L. Gao, X. X. Kong, Y. P. Sun and J. C. Shen, *J. Chem. Soc., Chem. Commun*., 1994, 1055; K. Ariga, Y. Lvov and T. Kunitake, *J. Am. Chem. Soc*., 1997, **119**, 2224.
5 H. Luo, B. X. Yang, L. Yang and W. X. Cao, *Makrolmol. Rapid Commun*., 1998, **19**, 291.
6 E. B. Fleischer, J. M. Palmer, T. S. Srivastava and A. Chattergee, *J. Am. Chem. Soc*., 1971, **93**, 3162.
7 D. Huang., Z. D. Xiao, J. H. Gu, N. P. Huang and C. W. Yuan, *Thin Solid Films*, 1997, **305**, 110.
8 B. S. Furniss, A. J. Hannaford, P. W. G. Smith and A. R. Tatchell. *Textbook of Practical Organic Chemistry*, Longman Scientific & Technical, London, 5th edn, 1989, p. 922.

Communication 8/09419E

Insertion of a metal-bound nitrogen atom into a disulfide (S–S) bond. Synthesis and characterisation of $[Co^{III}L_2]ClO_4$ [HL = di(2-pyridylthio)amine]

Hiroaki Nakayama,[a] Keith Prout,[b] H. Allen O. Hill[b] and Dipankar Datta*[c]

[a] *Laboratory of Chemistry, Kagawa Nutrition College, Chiyoda, Sakado, Saitama 350-02, Japan*
[b] *Inorganic Chemistry Laboratory, University of Oxford, South Parks Road, Oxford, UK OX1 3QR*
[c] *Department of Inorganic Chemistry, Indian Association for the Cultivation of Science, Calcutta 700 032, India. E-mail: icdd@mahendra.iacs.res.in*

Received (in Cambridge, UK) 22nd February 1999, Accepted 10th March 1999

Reaction of *cis*-$[Co^{III}(NH_3)_4(H_2O)_2](ClO_4)_3$ with 2,2′-dithiodipyridine (2,2′-DTDP) in nearly equimolar proportion generates $[Co^{III}L_2]ClO_4$ where HL (H = dissociable proton) is di(2-pyridylthio)amine, resulting in an unprecedented insertion of a coordinated ammine N into the S–S bond of 2,2′-DTDP.

Reactions of a disulfide bond (S–S) are of much biological importance.[1] This bond usually undergoes reductive cleavage giving rise to sulfur radicals, thiols/thioethers or thiolate anions.[1] Herein we describe a novel reaction of the disulfide bond.

Reaction of *cis*-$[Co^{III}(NH_3)_4(H_2O)_2](ClO_4)_3$ with 2,2′-dithiodipyridine (2,2′-DTDP) leads to the isolation of diamagnetic $[Co^{III}L_2]ClO_4$ **1** [HL = di(2-pyridylthio)amine ≡ HN{(2-C_5H_4N)S}$_2$] [eqn. (1)].

cis-$[Co^{III}(NH_3)_4(H_2O)_2](ClO_4)_3$ + 2 (2,2′-DTDP)

↓

$Co^{III}[N\{(2\text{-}C_5H_4N)S\}_2]_2 \bullet ClO_4$ + 2 NH_4ClO_4 (1)

1

In this reaction, two coordinated ammine N atoms are inserted into the S–S bonds of two molecules of 2,2′-DTDP, *i.e.* two of the three hydrogen atoms of two coordinated ammine nitrogens are replaced by the sulfur atoms of 2,2′-DTDP and the remaining hydrogen atom of each of the two disulfur substituted amino nitrogens dissociate as protons resulting in two L^- units. Though eqn. (1) suggests a 1 : 2 reaction stoichiometry between the metal and 2,2′-DTDP, the optimum yield of **1** is obtained by reacting almost equimolar amounts of the cobalt tetraammine complex and 2,2′-DTDP.†

The structure of **1** as determined by X-ray crystallography‡ is shown in Fig. 1. The cobalt atom lies at the center of a distorted but centric octahedron of six N (four pyridyl and two amide) atoms. Interestingly, each L^- fragment does not span a meridian but caps a face of the octahedron. If a Co–N(amide) bond is placed along the *y*-axis, then the two pyridyl rings of the L^- moiety lie quite close to the *xy* and *yz* planes, and one of the two sulfur atoms lies in the *xy* plane and the other in the *yz* plane. The average bond length of Co–N(pyridyl) is 1.963 Å and that of Co–N(amide) is 1.951 Å. The amide N is pyramidal with valence angles in the range 111.5(2)–112.0(2)° which are slightly larger than the ideal tetrahedral angle of 109.5°.

X-Ray photoelectron spectra of **1** show normal[2] binding energies: 62 (Co 3p), 164 (S 2p), 227 (S 2s), 284 (C 1s), 398 (N 1s), 533 (O 1s), 782 (Co 2p) and 929 eV (Co 2s). The absence of the spin multiplicity splitting in Co 3p confirms diamagnetism of the complex.[2] A broadening of the linewidth was observed at the lower binding energy side in the N 1s signal. This is possibly due to the difference in the binding energies of pyridyl N (401 eV) and dithioamide N (399 eV).

^{1}H and ^{13}C NMR spectral data for **1** in $(CD_3)_2SO$ are given in Table 1 together with their assignments. The two pyridyl rings become equivalent in solution, though they are not so in the crystal. The doublet signals are assigned to H4 and H1, while triplet signals are assigned to H2 and H3; these assignments are confirmed by 2D NMR. The ^{13}C signals are assigned considering the ^{1}H signals and the electron withdrawing effect of S on the C1 (or C6) atom. For ready comparison, ^{1}H and ^{13}C NMR data for 2,2′-DTDP are also given in Table 1.[3]

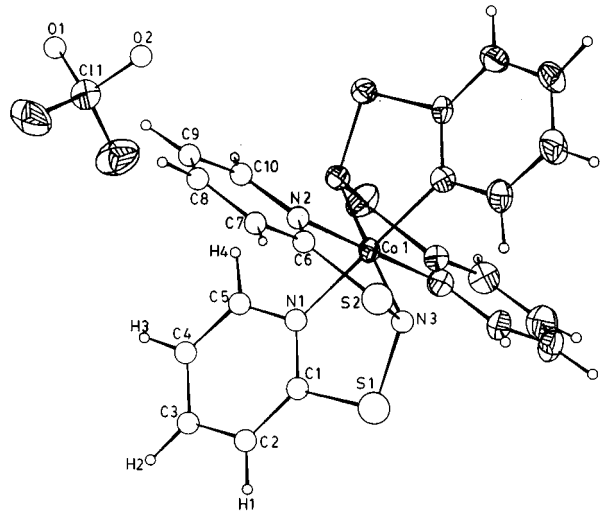

Fig. 1 X-Ray crystal structure of **1**. Selected bond distances (Å) and angles (°): Co1–N1 1.960(3), Co1–N2 1.966(3), Co1–N3 1.951(3), S1–N3 1.711(3), S2–N3 1.718(3), S1–C1 1.747(4), S2–C6 1.742(4); N1–Co1–N2 86.1(1), N1–Co1–N3 88.2(1), N2–Co1–N3 87.9(1), S1–N3–S2 111.5(2), Co1–N3–S1 111.6(2), Co1–N3–S2 112.0(2), N3–S1–C1 100.6(2), N3–S2–C6 101.0(2).

The known complexes of 2,2′-DTDP can be divided into two classes. In one class, metal complexes are formed after reductive cleavage of the S–S bond of 2,2′-DTDP. In such cases, 2-pyridylthiolato complexes are generated with four membered M–N–C–S chelate rings[4] or unidentate thiolato moieties.[4,5] The other class consists of metal complexes of 2,2′-DTDP itself in which the ligand can act in an N,N-bidentate,[6,7]

Table 1 ^{1}H and ^{13}C NMR spectral data for **1** and 2,2′-DTDP in $(CD_3)_2SO$ (δ in ppm from TMS)[a]

	H4	H2	H3	H1	
1	9.13	7.68	7.28	7.47	
2,2′-DTDP	8.4	7.6	7.1	7.2	
	C1	C5	C3	C4	C2
1	177.31	153.24	138.73	118.47	122.04
2,2′-DTDP	158.85	149.45	137.26	119.62	121.02

[a] The atom labelling scheme for **1** is shown in Fig. 1 and similar labelling applies to 2,2′-DTDP; Spectral data for 2,2′-DTDP are taken from ref. 3.

N,S-bidentate[7] or N-unidentate[7] mode. In the N,N-bidentate mode, it can act as a bridging ligand giving rise to polymeric species.[8] Our present complex belongs to a new class of complex of 2,2′-DTDP where a donor atom is inserted into the S–S bond. Such insertion of an atom into an S–S bond in the absence or presence of a metal is, to our knowledge, hitherto unknown.

H. N. thanks the Kagawa Nutrition College, Japan and the Japan Private School Promotion Foundation for support on an outside studies program. Thanks are also due to Dr M. Koizumi, Central Research Laboratory of Mitsubishi Materials Co., Omiya, Saitama, Japan for helping with the X-ray photoelectron spectra and to Dr T. Ekita, Tosoh Co., Ayase, Kanagawa, Japan for helping with the NMR spectra.

Notes and references

† 4.6 g (10 mmol) of *cis*-[$Co^{III}(NH_3)_4(H_2O)_2$](ClO_4)$_3$, synthesised by a reported procedure,[9] and 2.8 g (13 mmol) of 2,2′-DTDP was dissolved in 12 ml of DMF and heated at 100 °C for 1 h. Within 30 min of heating, a shiny dark compound started to separate. The reaction mixture was cooled to room temp. and 6 ml of ethyl acetate was added dropwise with stirring. The precipitate was allowed to settle for 15 min. It was filtered, washed first with 15 ml of DMF–ethylacetate (1 : 2) and then with ethyl acetate, and was dried in air. The crude product was recrystallised from DMF–ethyl acetate. Yield, 1.2 g (20%). Colour: shining brown. Anal. Found (calc.): Co, 9.33(9.41); C, 38.14(38.29); H, 2.42(2.57); N, 13.50(13.40)%. Diamagnetic. Single crystals were grown by direct diffusion of ethyl acetate into a dilute DMF solution of **1**.

‡ *Crystal data* for $CoC_{20}N_6S_4H_{16}O_4Cl$ **1**: M_w = 626.86, monoclinic, space group *C*2/*c*, a = 21.049(3), b = 12.603(2), c = 9.523(2) Å, β = 97.39(4)°, U = 2505.3 Å^3, Z = 4, D_c = 1.662 g cm^{-3}. The data were collected on a CAD-4 diffractometer with Cu-Kα radiation (λ = 1.54178 Å) at 295 K. Absorption correction: empirical T_{min} = 0.7082, T_{max} = 1.6595. The crystal structure was solved by direct methods (SHELXS) and refined by full matrix least squares methods with first isotropic then anisotropic displacement parameters. The hydrogen atoms were located from difference electron density function after the isotropic refinement and placed geometrically, and their isotropic displacement parameters were refined. R = 0.0524 (R_w = 0.0632) for 1908 observed reflections with $F > 3\sigma(F)$. CRYSTALS[10] was used for calculations and CAMERON[11] for diagrams. CCDC 182/1194.

1 U. Ermler, W. Grabarse, S. Shima, M. Goubeaud and R. K. Thauer, *Science*, 1997, **278**, 1457.
2 K. Siegbahn, C. Nordling, G. Johansson, J. Hedman, P. F. Heden, K. Hamrin, U. Gelius, T. Bergmerk, L. O. Werne, R. Manne and Y. Baker, *ESCA Applied to Free Molecules*, North-Holland, Amsterdam, 1969.
3 C. J. Pouchert and J. R. Cambell, *The Aldrich Library of NMR Spectra*, Aldrich Chemical Co., Inc., Milwaukee, WI, 1974.
4 M. Kita, K. Yamanari and Y. Shimura, *Bull. Chem. Soc. Jpn.*, 1989, **62**, 3081.
5 E. C. Constable and P. R. Raithby, *J. Chem. Soc., Dalton Trans.*, 1987, 2281.
6 M. Keeton and A. B. P. Lever, *Inorg. Chem.*, 1971, **10**, 47.
7 M. M. Kadooka, L. G. Warner and K. Seff, *J. Am. Chem. Soc.*, 1976, **98**, 7569.
8 M. M. Kadooka, E. Hilti, L. G. Warner and K. Seff, *Inorg. Chem.*, 1976, **15**, 1186.
9 F. Basolo and R. K. Murmann, *Inorg. Synth.*, 1953, **4**, 171.
10 D. J. Watkin, J. R. Carruthers and P. W. Betteridge, *CRYSTALS User Guide*, Chemical Crystallography Laboratory, Oxford, 1985; J. R. Carruthers and D. J. Watkin, *Acta Crystallogr., Sect. A*, 1979, **35**, 698; D. T. Cromer and J. T. Weber, in *International Tables for X-ray Crystallography*, ed. J. A. Ibers and W. C. Hamilton, Kynoch Press, Birmingham, 1974, vol. 4.
11 L. J. Pearce, K. Prout and D. J. Watkin, *CAMERON User Guide*, Chemical Crystallography Laboratory, Oxford, 1994; N. Walker and D. Stuart, *Acta Crystallogr., Sect. A*, 1983, **39**, 158.

Communication 9/01442J

Formation of 2-phenylethanol from styrene in the presence of zeolites and UV irradiation

Markus Steilemann,[a] John N. Armor[b] and Wolfgang F. Hölderich*[a]

[a] *Department of Chemical Technology and Heterogeneous Catalysis, University of Technology RWTH Aachen, Worringerweg 1, D-52072 Aachen, Germany. E-mail: hoelderich@rwth-aachen.de*
[b] *Air Products and Chemicals, Inc., 7201 Hamilton Boulevard, Allentown, PA 181951501, USA*

Received (in Cambridge, UK) 14th December 1998, Accepted 9th March 1999

2-Phenylethanol is formed *via* an *in situ* multistep reaction by irradiation of styrene in the presence of silica–alumina compounds such as zeolites in aqueous and methanolic systems; the first step is presumably an oxidation.

The formation of anti-Markovnikov compounds by direct functionalization of olefins is of great interest for technical and synthetic applications. The Brown hydroboration–oxidation provides a useful tool to obtain the interesting products, but unfortunately this method is accompanied by disadvantages for its commercial application.[1–3] It is known that anti-Markovnikov addition can be achieved by the use of photosensitizers under photochemical reaction conditions, involving radical cations as intermediates.[4,5] It is also well known that zeolites are excellent hosts for photochemical reactions.[6–8] We tried to replace these photosensitizers by zeolites due to their known properties for the generation and stabilization of organic radicals adsorbed on their surface. Here we present some unexpected results pointing to an unusual combination of photochemical and thermal processes.

With regard to the work of Yates and Arnold we choose styrene as a model substance for our investigation.[9] By using EPR and UV spectroscopy we were able to show the formation of styrene radical cations on an H-ZSM-5 zeolite. The formation of this radical cation occurs, either in non-irradiated or in irradiated samples, equally as well in aqueous as in organic slurries of the zeolite with styrene. For the reaction we used the following reaction conditions: a 450 W mercury medium pressure lamp from Ace Glass, Inc., and quartz tube reactors with a magnetic stirrer placed beside the immersion lamp, while the reaction mixture is cooled by a centered cooling finger. In this reactor a mixture of typically 15 g water, 2 mmol styrene and 3 g of the zeolite was placed and irradiated for a period of 24 h at room temperature. After the reaction the mixture was centrifuged, the zeolite was separated and the fluid phase was extracted with Et_2O, then dried with Na_2SO_4 and, after evaporation of the solvent, analysed by gas chromatography. Instead of the zeolite a commercially available silica–alumina, Aldrich 34, 335–8 and CdS, ZnS and ZnO were used in other experiments. A 30 W D_2 lamp from Heraeus was also used as the irradiation source. In all cases the conversion was higher than 99%. In water the selectivity for 2-phenylethanol was 0.06% for H-ZSM-5 and 0.04% for SiO_2–Al_2O_3; for CdS, ZnS, ZnO or SiO_2 it was not detectable. But for H-ZSM-5 in MeOH the selectivity for 2-phenylethanol rises to 19.4%; methoxystyrene was not detected. Therefore we do not believe MeOH participates directly in this reaction and we regard this result as a proof for our proposed reaction mechanism (discussed below). Other by-products such as olefins, oligomers or alkylated styrene compounds were also not observed.

Although in the case of water as reaction medium the selectivity is negligible and more than 90% of the styrene reacts to form polymeric products, we tried to determine if direct addition of water in the anti-Markovnikov direction is the reason for the formation of 2-phenylethanol. By mass spectroscopy and cross checking experiments with the identified products, we identified the substances acting as intermediates in the reaction. Styrene is oxidized. This step is proved to be made possible by light below $\lambda \leqslant 290$ nm and we suspect the formation of superoxide radical anions and their reaction with styrene or the styrene radical cations. In the absence of the zeolite or silica–alumina under otherwise identical conditions no styrene oxide is found, but benzaldehyde is formed because of singlet oxygen formation. In the following step phenylacetaldehyde is formed *via* thermally or photochemically induced rearrangement of styrene oxide. The next steps are not clearly identified: possibly a decarbonylation and the formation of benzyl radicals take place, followed by a further reaction with formaldehyde or MeOH to give the corresponding alcohol. This could explain the drastically increased selectivity in the presence of MeOH. Nevertheless, the MeOH could act as an electron-donating reductant adsorbed on the surface. In this case the zeolite and the silica–alumina would show photo-semiconducting properties. A two-electron reduction of the phenylacetaldehyde would take place leading to 2-phenylethanol by *in situ* protonation. The assumed reaction steps are shown in Fig. 1.

The use of the deuterium lamp in our experiments increased the selectivity for 2-phenylethanol to 0.5% in aqueous systems. Due to the shorter reaction time of 6 h instead of 24 h in these experiments, the much lower overall irradiation energy, the specific spectra of both lamps and the absorption spectra of the organic and inorganic compounds, we assume the required wavelength to run the reaction to be *ca.* 210 nm. Although the spectra of styrene adsorbed on the zeolite shows a new broad absorption at $\lambda \approx 550$ nm, this absorption is not required for the reaction, as experiments with Pyrex reactors show. Other spectra with MeOH- or water-loaded zeolites showed no differences in the range $\lambda \leqslant 290$ nm that could be assigned to the creation of special electronic states too. Therefore we expect

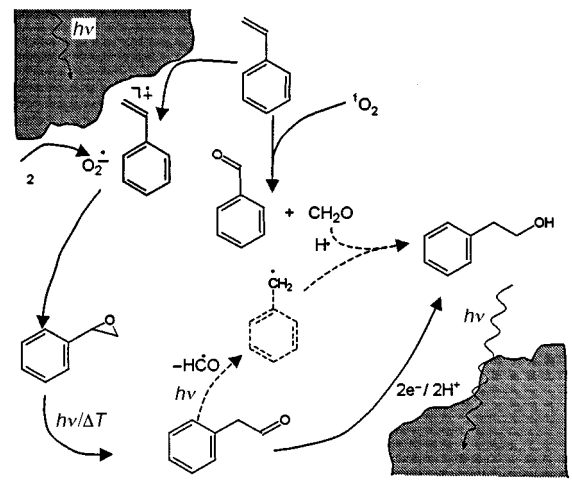

Fig. 1 Assumed reaction scheme for the formation of 2-phenylethanol from styrene.

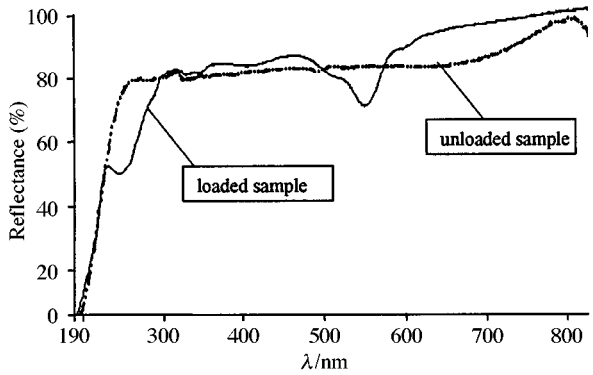

Fig. 2 UV–VIS reflectance spectra of the styrene loaded and unloaded zeolite H-ZSM-5.

the reaction to take place by direct excitation of the zeolite or the silica–alumina. Judging from the recorded spectra this is only possible by irradiation at $\lambda \leqslant 210$ nm. The spectra of preadsorbed styrene and without preadsorbtion of styrene are shown in Fig. 2. Experiments to obtain more reliable information and to run the reaction more selectively using UV lasers are planned. These would also enable us to carry out the kinetic studies which are currently lacking.

In conclusion, this is the first time, to the best of our knowledge, that the formation of 2-phenylethanol has occurred *via* the assumed reaction scheme, *i.e.* by a combination of the assumed thermal and photochemical steps *via* irradiation of styrene in the presence of silica–alumina and H-ZSM-5.

Furthermore, the substantial selectivity for the anti-Markovnikov product 2-phenylethanol under irradiation in the presence of H-ZSM-5 and MeOH is reported here for the first time.

Notes and references

1 H. C. Brown and B. C. Shubba Rao, *J. Am. Chem. Soc.*, 1956, **78**, 2582.
2 H. C. Brown, *J. Am. Chem. Soc.*, 1959, **81**, 6423.
3 H. C. Brown and G. Zweifel, *J. Am. Chem. Soc.*, 1961, **83**, 2544.
4 Y. Shigemitsu and D. R. Arnold, *Chem. Commun.*, 1975, 407.
5 R. A. Neunteufel and D. R. Arnold, *J. Am. Chem. Soc.*, 1973, **95**, 4080.
6 H. Yamashita, N. Sato, M. Ampo, T. Mamajima, M. Hada and H. Namatsuji, *Stud. Surf. Sci. Catal., Prog. Zeolite Mater.*, 1997, **105**, 1141.
7 H. Frei, F. Blatter and H. Sun, *Chem. Technol.*, 1996, **26**, 24.
8 N. J. Turro and V. Ramamurthy, *J. Inclusion Phenom. Mol. Recognit.*, 1995, **21**, 239.
9 K. Yates and J. McEwen, *J. Am. Chem. Soc.*, 1987, **109**, 580.

Communication 8/09705D

Capillarity and silver nanowire formation observed in single walled carbon nanotubes

Jeremy Sloan,[ab] David M. Wright,[ab] Hee-Gweon Woo,[c] Sam Bailey,[a] Gareth Brown,[a] Andrew P. E. York,[a] Karl S. Coleman,[a] John L. Hutchison[b] and Malcolm L. H. Green[a]

[a] *Inorganic Chemistry Laboratory, University of Oxford, South Parks Road, Oxford, UK OX1 3QR. E-mail: malcolm.green@chem.ox.ac.uk*
[b] *Department of Materials, University of Oxford, Parks Road, Oxford, UK OX1 3PH*
[c] *Chonnam National University, 300 Yongbong-Dong, Puk-Ku, Kwangju, 500-757, Korea*

Received (in Cambridge, UK) 26th February 1999, Accepted 10th March 1999

Single walled carbon nanotubes (SWNTs) exhibit similar capillarity properties to those exhibited by multiple walled carbon nanotubes (MWNTs); SWNTs, previously filled in low yield (*ca.* 2%) by solution chemistry techniques, can be filled in high yield (up to *ca.* 50%) by the liquid phase method; compositions from the KCl–UCl_4 and AgCl–AgBr systems were used to fill SWNTs without causing them significant chemical or thermal damage; in the case of the latter, exposure to light or an electron beam resulted in the partial photolytic reduction of SWNT incorporated silver halides to continuous metallic silver 'nanowires' within the capillaries.

It has been demonstrated that molten media such as PbO_x, V_2O_5 and MoO_3 can fill MWNTs by capillary action.[1–3] This ability of such materials to be so incorporated depends on three characteristics of the filling materials: (i) they must 'wet' the capillaries and have surface tensions below a threshold value in the range 100–200 mN m^{-1};[4] (ii) their overall melting temperature must be low enough to preclude thermal damage to the MWNT capillaries; and (iii) they must not attack MWNTs chemically. A modification to the capillary method has extended both the range and complexity of materials available for filling of MWNTs by capillarity.[5] This technique is based on the deposition of either eutectic or non-eutectic components from a mixed metal salt system. Here, we show how the melting properties of the KCl–UCl_4[6] eutectic melting system [Fig. 1(a)] and also those of the AgCl–AgBr[7] solid solution [Fig. 1(b)] system can be used to introduce continuous fillings of solid phase materials into SWNTs. The filling yield obtained from these liquid phases and mixtures greatly exceeds that obtained previously by the solution-deposition filling technique.[8]

The conditions for preparing SWNTs filled with compositions from the KCl-UCl_4 and AgCl–AgBr systems were established from surface tension/composition data (Tables 1 and 2)[9] and the phase relations depicted in Fig. 1(a) and (b). The SWNTs used in this study were prepared according to the high yield catalytic arc synthesis method reported by Journet *et al.*[10] A structural representation and HRTEM lattice image of an empty 'kinked' unfilled SWNT obtained by the catalytic method are shown in Fig. 2(a) and (b), respectively. All of the halide mixtures were ground and weighed under dry box conditions, and in the case of the silver halide mixtures, exposure to light was minimised. The halide samples were ground together with SWNTs and sealed under vacuum in silica quartz ampoules. The ampoules were passed at 3 cm min^{-1} through a 30 cm three-zone tube furnace with a temperature gradient spanning 300 °C and held for 30 min. at a maximum temperature of *ca.* 100 °C higher than the liquidus or melting temperature of the filling material [see Fig. 1(a) and (b)]. The resultant mixture was then furnace cooled for 3 h to room temperature. The filled specimens were characterised by high resolution transmission electron microscopy (HRTEM) and energy dispersive X-ray spectroscopy (EDX).

In the case of the KCl–UCl_4 system, the pure end component UCl_4 apparently attacked the SWNTs and no filling was observed. In addition, the KCl end member was found to be too

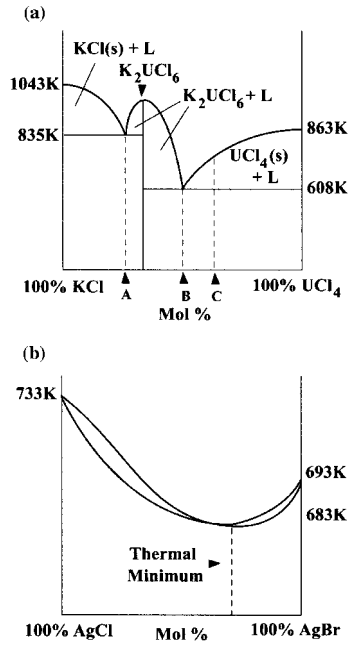

Fig. 1 (a) KCl–UCl_4 pseudobinary eutectic melting system. Compositions A, B and C were used to fill SWNTs. (b) Diagram showing the melting properties of the AgCl–AgBr solid solution system. AgCl, AgBr and the thermal minimum ($AgCl_{0.2}Br_{0.8}$) were used to fill SWNTs.

Table 1 Melting temperatures and surface tensions of compositions used to fill SWNTs in the KCl-UCl_4 system [see also Fig. 1(a)]

Composition [see Fig. (1b)]	KCl–UCl_4 (mol %)	Filling temperature/K	Surface tension/mN m^{-1}
KCl	100	1143	93.13
A	73.2 : 26.8	935	64.98
B	50 : 50	700	54.00
C	39.33 : 60.67	842	50.54
UCl_4	0 : 100	963	26.8

Table 2 Melting temperatures and surface tensions of compositions used to fill SWNTs in the AgCl–AgBr system [see also Fig. 1(b)]

Composition	Filling temperature/K	Surface tension/mN m^{-1}
AgCl	833	173.08
AgBr	800	151.3
$AgBr_{0.2}Cl_{0.8}$	783	154.4

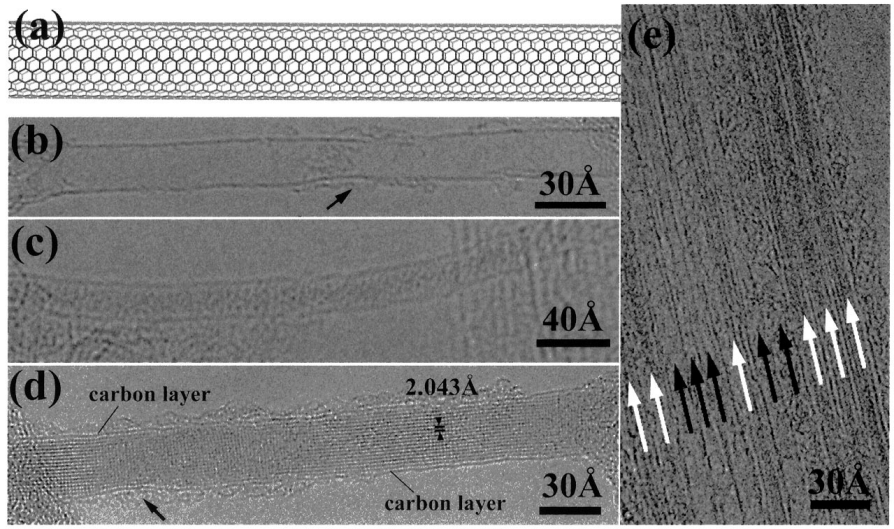

Fig. 2 (a) Schematic structural representation of a SWNT. (b) HRTEM image showing an empty SWNT. The defect region near the centre (arrowed) is possibly caused by the incorporation of non-six-membered rings into the graphene wall. (c) SWNT continuously filled with a KCl–UCl_4 eutectic mixture [composition A, Fig. 1(a)]. (d) Wide capillary SWNT continuously filled with Ag metal formed by capillary insertion of AgCl followed by photolytic decomposition. The indicated *d*-spacings correspond to the (020) lattice planes of Ag metal. Note 'kink' causing distortion in the Ag microstructure [*cf.* Fig. (b)]. (e) Showing high yield incorporation of AgBr into an SWNT bundle. Filled SWNTs are indicated by light arrows; unfilled SWNTs by dark arrows.

beam sensitive to be directly observed at room temperature *via* HRTEM. However, the three lower melting compositions A, B and C [Fig. 1(a)] were able to wet and fill the SWNTs without causing them significant damage. For composition A, corresponding to one of two eutectics in the KCl-UCl_4 system [see Fig. 1(a)], an amorphous homogenous product of composition $(KCl)_x(UCl_4)_y$ (with $x/y \approx 3:1$) was obtained inside SWNTs. Fig. 2(c), shows a HRTEM micrograph of a discrete (10,10) SWNT continuously filled with the $(KCl)_x(UCl_4)_y$ eutectic mixture. Fillings obtained with compositions B and C (not shown) were found to be either crystalline or polycrystalline.

For the AgCl–AgBr system, the melting range was both lower and narrower than for the KCl–UCl_4 system [see Fig. 1(b)]. An important difference was that both end components were able to fill SWNTs without damaging them. The filling yields for the various compositions were found to be $AgCl_{0.2}Br_{0.8} \geqslant AgBr > AgCl$ with approaching 50% filling for the highest yield specimen and *ca.* 20% for the lowest. A difficulty with directly observing the SWNT incorporated products in these kinds of experiments by HRTEM was that the silver halides are both light and electron beam sensitive. However, in the case of SWNTs with lower diameters, phototolytic reduction was apparently retarded and EDX showed that SWNT bundles incorporated with either of the two silver halides still contained both the metal and the respective halogen. For wide bore SWNTs, this was not the case and several were observed with pure Ag filling. Figure 2(d) shows a HRTEM image of a large diameter [≈ 38 Å; *ca.* (28,28) nanotube] SWNT completely filled with 17 layers of silver metal. The initial filling medium in this case was AgCl. A noticeable 'kink' in the SWNT (arrowed), possibly originating from defects present in the original SWNT [*cf.* Fig. 2(b)], causes a corresponding distortion in the incorporated crystal. The *d*-spacing of the material, measured relative to nearby 3.4 Å (0002) graphene fringes (not shown) was measured to be 2.04 ± 0.05 Å, which corresponds to the (200) *d*-spacing of Ag metal and not to the corresponding (020) *d*-spacing in AgCl (2.775 Å), which has a similar $Fm\bar{3}m$ cubic unit cell.[11] Fast Fourier transforms (FFTs) calculated from the lattice image of the incorporated crystal (not shown) also indicated that the Ag wire was veiwed close to a [100] projection and that the (020) lattice fringes belonged to this projection. Fig. 2(e) shows a HRTEM micrograph of the product of a high yield SWNT filling with AgBr within a bundle of (10,10) SWNTs. The paths of empty and filled SWNTs are indicated by dark and light arrows, respectively, and the difference in contrast between the empty and filled SWNTs is clearly visible. Several bundles similar to those illustrated in Fig. 2(e). were observed in this specimen with up to 50% of similarly filled SWNTs.

An important aspect of this work concerns the mechanism of opening of the SWNTs. Previously, we stated that SWNTs could be opened by gently refluxing in HCl.[8] However, none of the filling experiments described in this communication required a separate opening step which indicates that either one is unnecessary (*i.e.* the SWNTs are already open at at least one end) or that the fullerenic end caps of SWNTs are selectively attacked by the molten media during the filling process.

In conclusion, we have demonstrated a simple and reproducible method for the continuous filling of the capillaries of SWNTs in high yield with a variety of materials, thereby showing that these types of nanotubes exhibit similar wetting and capillarity properties to MWNTs. The advantages of using SWNTs over MWNTs in these types of filling experiments is that the former are relatively much more uniform and defect free structures in comparison to the latter and their composite properties will be correspondingly more uniform. The physical properties of the composite materials formed by the methods decribed here are expected to be considerably modified with respect to those of unfilled SWNTs.

Notes and references

1 P. M. Ajayan and S. Iijima, *Nature*, 1993, **361**, 333.
2 P. M. Ajayan, O. Stephan, P. Redlich and C. Colliex, *Nature*, 1995, **375**, 564.
3 Y. K. Chen, S. C. Tsang and M. L. H. Green, *Chem. Commun.*, 1996, 2489.
4 T. W. Ebbesen, *J. Phys. Chem. Solids*, 1996, **57**, 951.
5 J. Sloan, J. Cook, M. Zweifka-Sibley, M. L. H. Green and J. L. Hutchison, *J. Solid State Chem.*, 1998, **140**, 83.
6 V. N. Desyatnik and S. P. Raspopin, *Russ. J. Inorg. Chem.*, 1975, **20**, 780.
7 V. V. Grozentskii, V. D. Zhuravlev, G. A. Kitaev and L. B. Zhukov, *Russ. J. Inorg. Chem.*, 1985, **30**, 582.
8 J. Sloan, J. Hammer, M. Zweifka-Sibley and M. L. H. Green, *Chem. Commun.*, 1998, 347.
9 G. J. Janz, *J. Phys. Chem. Ref. Data*, 1998, **17**, 129.
10 C. Journet, W. K. Maser, P. Bernier, A. Loiseau, M. Lamy, M. L. de la Chappelle, S. Lefrant, P. Derniard, R. Lee and J. E. Fisher, *Nature*, 1997, **388**, 756.
11 Lin-gun Liu and W. A. Bassett, *J. Appl. Phys.*, 1973, **44**, 1475.

Communication 9/01572H

ChemComm

Diastereo- and enantioselective synthesis of 2,8-dioxabicyclo[3.3.0]octan-3-one derivatives

Dieter Enders,* Juan Vázquez and Gerhard Raabe

Institut für Organische Chemie, Rheinisch-Westfälische Technische Hochschule, Professor-Pirlet-Straße 1, D-52074 Aachen, Germany. E-mail: enders@rwth-aachen.de

Received (in Liverpool, UK) 8th December 1998, Accepted 11th March 1999

An efficient asymmetric synthesis of 4-substituted (1*S*,4*S*,5*R*)-2,8-dioxabicyclo[3.3.0]octan-3-one derivatives (de ⩾98%, ee = 80– > 98%) in good overall yields is reported by a stepwise Michael addition–α-alkylation and subsequent hydrolytic domino reaction protocol employing formaldehyde SAMP-hydrazone as a neutral formyl anion equivalent and 5,6-dihydro-2*H*-pyran-2-one as a Michael acceptor.

Many insect antifeedant clerodanes, such as clerodin (R = H) and caryoptin (R = OAc) **A** or mycotoxins like aflatoxin B_1 **B**,

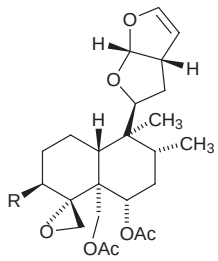

A

clerodin (R = H)
caryoptin (R = OAc)

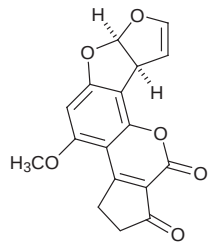

B

aflatoxin B_1

contain furo[2,3-*b*]furan moieties in various oxidation levels.[1] Although many synthetic methods for accessing such furofurans have been reported during the last decade,[2] there is still a need for enantioselective procedures suitable for structural variations and, for instance, their incorporation into the clerodane framework. Since it has been reported that this and other clerodane subunits may be crucial for insect antifeedant activity,[3,4] the development of novel asymmetric syntheses is an important goal in this context.

We describe here the asymmetric synthesis of diastereomerically pure and highly enantiomerically enriched derivates of the title perhydrofuro[2,3-*b*]furan lactone system based on the Michael addition of formaldehyde SAMP-hydrazone[5] **1** to 5,6-dihydro-2*H*-pyran-2-one **2** as the key step (Scheme 1).[6] The 1,4-adduct **3** was obtained under Lewis acid activation with TBDMSOTf (1.2 equiv.) in acceptable yield (54%) and good diastereomeric excess (de = 80%). Because the mixture of diastereoisomers of **3** was only separable by HPLC on chiral stationary phase, this mixture was directly used in the subsequent deprotonation–α-alkylations. The use of LDA at −78 °C, followed by addition of HMPA and finally the requisite alkylating agent afforded the 4-substituted lactone hydrazones **4** in good to excellent yields (67–90%) and diastereomeric excesses (de = 80– > 98%). The *trans* configuration of the disubstituted lactones **4** was determined by ^{1}H NMR spectroscopy through the *trans*-diaxial coupling constants (9.5–10.7 Hz) of the protons at the new stereogenic centres. This was confirmed by NOE experiments on compound **4b** (R = Me).† The absolute configuration of the minor diastereoisomer (*R*,*R*)-**4b** was determined by X-ray structure analysis,‡ the absolute configuration of the major diastereoisomer therefore being (3*S*,4*R*). Fortunately, in some cases the diastereoisomers of the lactone hydrazones **4** are separable by flash chromatography (**4b**) or by HPLC (**4c**,**d**) and it was possible to use the diastereomerically enriched hydrazones in the following key step.

Thus, the asymmetric Michael addition of **1** to pent-2-enolide **2** and subsequent α-alkylations enabled us to synthesize the appropriate precursors with the desired carbon skeleton for the formation of the title compounds. Finally, a domino reaction was initiated by acidic hydrolysis in a two-phase system and afforded the desired furofuran lactones derivatives **5**[7] in excellent yields (87–98%) and stereoisomeric purity (de ⩾ 98%, ee = 80–98%) (Table 1). Only in the case of the unsubstituted compound **5a** is the yield lower probably due to its sensitivity under the reaction conditions. The final cascade

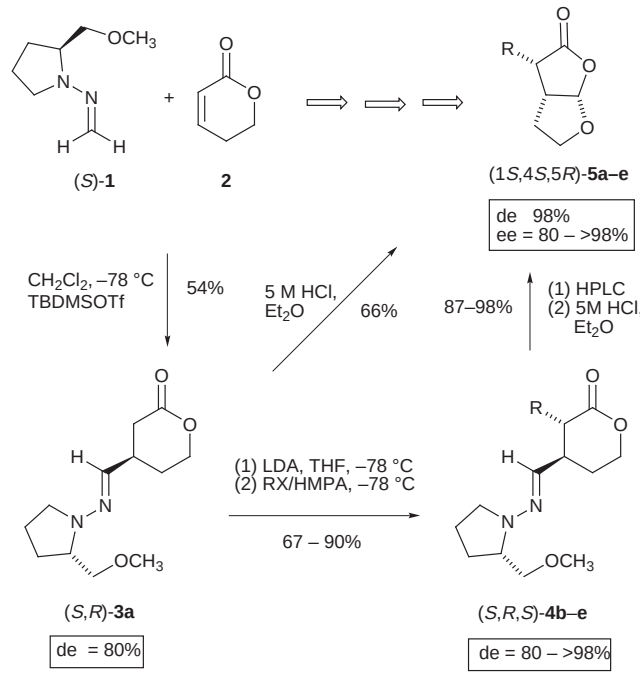

Scheme 1

Table 1 Asymmetric synthesis of (1*S*,5*R*)-2,8-dioxabicyclo[3.3.0]octan-3-one derivatives

5	R	Yield[a] (%)	Mp[b]/°C	$[\alpha]_D^{RT}$ (*c*, $CHCl_3$)	Ee[c] (%)
a	H	66	oil	+29.5 (0.96)	85
b	Me	98 (75)[d]	78–80	+49.8 (0.95)	80 (> 98)[d]
c	Pr^n	97	oil	+76.8 (0.80)	88
d	Allyl	87	52–54	+75.6 (0.80)	> 98
e	Bn	90	oil	+104.4 (0.91)	80

[a] Yield after flash chromatography. [b] Uncorrected, measured on a Büchi apparatus. [c] Determined by GC on chiral stationary phases. [d] Figures in parentheses indicate values after recrystallization of the final product.

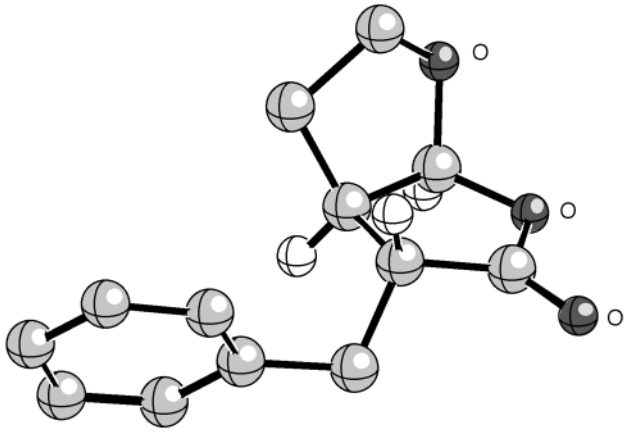

Fig. 1 X-Ray structure of furofuran lactone (1*S*,4*R*,5*R*)-**5e**.

steps involve the cleavage of the hydrazone moiety, opening of the lactone ring and, finally, formation of the furofuran lactone system through the corresponding hemiacetal intermediate.

The relative configuration of the perhydrofurofuran lactones **5** was confirmed by NOE experiments on (1*S*,4*S*,5*R*)-**5e**§ and the absolute configuration of this compound was determined by X-ray structure analysis of its minor diastereoisomer (1*S*,4*R*,5*R*)-**5e**, which was separable from the major one by HPLC (Fig. 1).¶ Assuming uniform reactions pathways, the absolute configuration of **5a**–**d** were assigned by analogy with **5e**.

The enantiomeric purity of all compounds was determined by GC on chiral stationary phases indicating the absence of racemization during our procedure. Some of the substituted derivatives of (1*S*,5*R*)-2,8-dioxabicyclo[3.3.0]octan-3-one **5a** were solids and enabled us to increase the ee of the final furofuran lactones by simple recrystallization.

The bicyclic lactone acetal **5a**, which constitutes a valuable chiral building block for the synthesis of clerodane derivatives, could be easily transformed to the alcohol and to the 2,3-dihydrofurofuran[8] derivatives widely encountered in the clerodane family.

In conclusion, our new procedure *via* asymmetric Michael addition of formaldehyde SAMP-hydrazone to pent-2-enolide followed by α-alkylations, and subsequent cleavage of the hydrazones using acidic hydrolysis in a two-phase system affords the desired 4-substituted furofuran lactone derivatives in acceptable overall yields (32–47%) and high diastereo- and enantiomeric purity (de ⩾98%, ee = 80–98%). In addition, pentenolides with different substituents in position 6 could allow access to a library of potential insect antifeedants. The extension of this methodology is currently under study in our laboratory.

This work was supported by the Deutsche Forschungsgemeinschaft (Leibniz Prize, Sonderforschungsbereich 380) and the Fonds der Chemischen Industrie. We thank the Ministerio de Educación y Cultura for a postdoctoral fellowship to J. V. We also thank Degussa AG, BASF AG, Bayer AG and Hoechst AG for the donation of chemicals.

Notes and references

† Representative NOE data for **4b**: $CH_3 \rightarrow H_4$ 10.2%, $CH_3 \rightarrow H_3$ 16.5%, $H_3 \rightarrow H_{6eq}$ 2.8%, $H_3 \rightarrow H_{5ax}$ 2.2%.

‡ The crystal structure of (2′*S*, 3*R*, 4*R*)-**4b** will be part of our full paper on this chemistry: D. Enders, J. Vázquez and G. Raabe, manuscript in preparation.

§ Representative NOE data for (1*S*,4*S*,5*R*)-**5e**: $H_1 \rightarrow H_5$ 4.2%, $H_1 \rightarrow H_4$ 1.3%, $H_4 \rightarrow H_5$ 3.1%, $H_5 \rightarrow H_6$ 3.9%.

¶ *Crystal data* for (1*S*,4*R*,5*R*)-**5e:** $C_{13}H_{14}O_3$, orthorhombic, a = 6.250(3), b = 9.353(1), c = 19.655(2) Å, V = 1149.0 Å^3, $P2_12_12_1$, Z = 4, μ = 6.9 cm^{-1}, no absorption correction, T = 298 K, 2378 independent and 1351 observed $I > 2\sigma(I)$] reflections, 145 parameters in final least-squares full-matrix refinement on F, terminating at R = 0.053 (R_w = 0.033, $w = \sigma^{-2}$), a goodness of fit of 1.677, and a residual electron density of −0.22/+0.24 e Å^{-3}. Refinement of the Flack parameter (ref. 9) to determine the absolute configuration of the minor isomer (1*S*,4*R*,5*R*)-**5e** resulted in a value of X = 0.01(68) for the structure shown in Fig. 1. The authors recognize that due to the high standard uncertainty the diffraction results alone do not definitely fix the absolute configuration, which, however is determined based on the X-ray structures of several hydrazone precursors, such as (2′*S*,3*R*,4*R*)-**4b** (see note ‡). CCDC 182/1195. Crystallographic data are available in CIF format from the RSC web site, see: http://www.rsc.org/suppdata/cc/1999/701/

1 For reviews see: T.A. van Beeck and Ae. de Groot, *Recl. Trav. Chim. Pays-Bas*, 1986, **105**, 513; A. T. Merritt and S. V. Ley, *Nat. Prod. Rep*., 1992, 243.
2 F. Petit and R. Furstoss, *Synthesis*, 1995, 1517; H. Bouchard, J. Soulié and J. Y. Lallemand, *Tetrahedron Lett*., 1991, **32**, 2621; J. Vader, H. Sengers and Ae. de Groot, *Tetrahedron*, 1989, **45**, 2131 and references cited therein.
3 Y. Kojima and N. Kato, *Agric. Biol. Chem*., 1980, **44**, 855.
4 S. V. Ley, N. S. Simpkins and A. J. Whittle, *J. Chem. Soc., Chem. Commun*., 1981, 1001.
5 H. Eichenauer, Dissertation, University of Giessen, 1980.
6 D. Enders and J. Vázquez, submitted. For a short review on nucleophilic formylations and cyanations with **1** see: D. Enders, M. Bolkenius, J. Vázquez, J.-M. Lassaletta and R. Fernández, *J. Prakt. Chem., Chem. Ztg.*, 1998, **340**, 281.
7 *Typical procedure*: To a cooled (0 °C) solution of hydrazone **4** (1 mmol) in Et_2O (20 ml) was added 5 M HCl (4 ml), and the mixture was vigorously stirred until TLC indicated total consumption of the starting material (*ca.* 20 min). The aqueous layer was extracted with CH_2Cl_2 (3 times). The combined organic layers were neutralized ($NaHCO_3$, 0.1 g), dried ($MgSO_4$) and concentrated. The resulting residue was purified by flash chromatography.
8 M. Pezechk, A. P. Brunetiere and J. Y. Lallemand, *Tetrahedron Lett*., 1986, **27**, 3715; A. P. Brunetiere and J. Y. Lallemand, *Tetrahedron Lett*., 1988, **29**, 179; J. C. Anderson, S. V. Ley, D. Santafianos and R. N. Sheppard, *Tetrahedron*, 1991, **47**, 6813.
9 H. D. Flack, *Acta Crystallogr., Sect. A*, 1983, **39**, 876; G. Bernardinelli and H. D. Flack, *Acta Crystallogr., Sect. A*, 1985, **41**, 500.

Communication 8/09611B

Decapitation of dihydroporphyrazinediol derivatives: synthesis and X-ray structure of a novel seco-porphyrazine

Hanlin Nie,[a] Charlotte L. Stern,[a] Anthony G. M. Barrett*[b] and Brian M. Hoffman[a]

[a] *Department of Chemistry, Northwestern University, Evanston, Illinois 60208, USA. E-mail: bmh@nwu.edu*
[b] *Department of Chemistry, Imperial College of Science, Technology and Medicine, London, UK SW7 2AY*

Received (in Cambridge, UK) 20th January 1999, Accepted 4th March 1999

The dihydroporphyrazinediol 8, which was prepared by Linstead macrocyclisation of 2,5-diiminopyrrolidine with 3,4-bis(4-*tert*-butylphenyl)pyrroline-2,5-diimine, followed by TFA demetallation and OsO_4 tetroxide mediated dihydroxylation, underwent reaction with $Ni(OAc)_2$ at 100 °C in the presence of air to give the novel seco-porphyrazine 10, the structure of which was established by an X-ray crystallographic study.

Recently, we described the synthesis of seco-porphyrazines **1a**–**d** by the peripheral oxidations of porphyrazines. Subsequent to our report, several related seco-chlorins have been described, and we have shown that porphyrazine **1d** (M = Zn) sensitises the formation of singlet oxygen with the remarkable overall quantum yield of $\phi_\Delta = 0.54$. In a continuation of our efforts to develop porphyrazines peripherally functionalised for metal bindings and porphyrazines with strong absorptions at wavelengths above 700 nm for biomedical applications, we have prepared porphyrazine *cis*-diols **8** *and* **9** *via* the OsO_4 mediated dihydroxylation of porphyrazines **6** and **7**, respectively. Surprisingly, reaction of diol **8** with $Ni(OAc)_2$ in air at 100 °C did not give any nickel(II) porphyrazinediol **9**. Instead, this procedure gave a mixture of products including a red pigment with much lower polarity than the porphyrazine diols **8** or **9**. Herein, we report the full characterisation of novel compound **10** a new type of seco-porphyrazine ring system generated by the loss of the two β-carbons of a pyrrole.

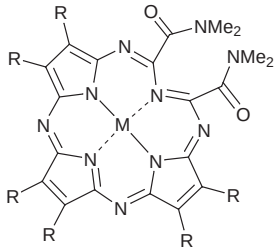

1a M = 2H, R = -NMe_2
b M = Zn, R = -NMe_2
c M = 2H, R = Pr
d M = Zn, R = Pr

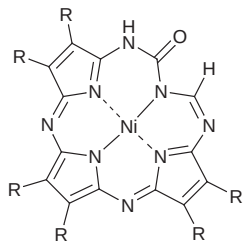

10

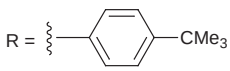

2,5-Diiminopyrrolidine **2** was co-macrocyclised with 3,4-bis(4-*tert*-butylphenyl)pyrroline-2,5-diimine **3** using $Mg(OBu)_2$ in BuOH at reflux (Scheme 1). The products contained both the unsymmetrical porphyrazine **5**† and symmetrical porphyrazine **4**, which were separated by chromatography. Demetallation of **5** by treatment with TFA gave the free base porphyrazine **6**. In a typical cyclisation, reaction of **2** with 3.5 equiv. of **3** ultimately led to porphyrazine **6** with an overall yield of 17% following demetallation. Subsequent reaction of **6** with $Ni(OAc)_2$ at 100 °C in PhCl–DMF (3 : 1) under N_2 resulted in the formation of nickel complex **7** (98% yield). Finally, OsO_4 mediated dihydroxylation of **6** and **7** gave dihydroporphyrazinediol **8** (69% yield) and the nickel(II) dihydroporphyrazinediol **9** (65% yield), respectively. Subsequent reflux of a solution of diol **8** with $Ni(OAc)_2$ in $CHCl_3$–MeOH (3 : 1) under nitrogen also gave the nickel diol **9** (90%).

The parent porphyrazine **6** showed a UV-visible absorption spectrum with two well separated Q-bands at λ_{max} 587 and 655 nm; porphyrazine 7 showed a typical metalloporphyrazine absorption spectrum, with a strong Q-band at 615 nm (Fig. 1) whereas the *cis*-diols **8** and **9** displayed different optical spectra from those observed for the related chlorins, 2,3-*vic*-dihydroxy *meso*-tetraphenylchlorins, with strong absorptions at λ_{max} 730 and 702 nm for porphyrazines **8** and **9**, respectively.

Reaction of porphyrazine **8** with 10 equiv. of $Ni(OAc)_2$ at 100 °C in PhCl–DMF (3 : 1) that had been only partially deaerated gave a mixture of products, including a new red pigment, denoted **10**, which was obtained with higher yields when porphyrazinediol **9** was reacted in air under similar conditions (Scheme 1). This pigment,‡ which was less polar

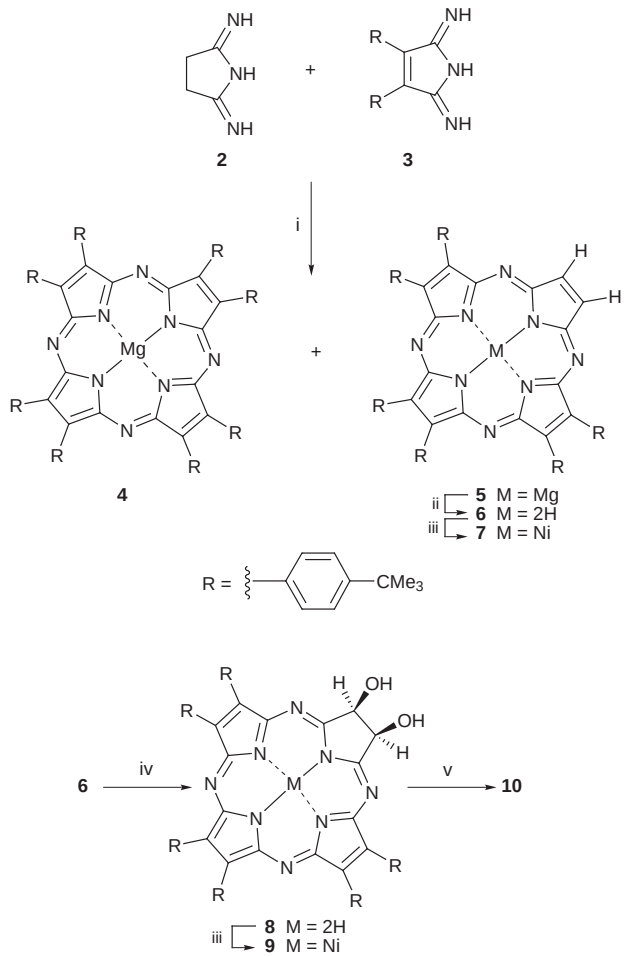

Scheme 1 *Reagents and conditions*: i, $Mg(OBu)_2$, BuOH, reflux; ii, TFA, then NH_4OH (17% from **2**); iii, $Ni(OAc)_2$, MeOH–$CHCl_3$, N_2, reflux (98%); iv, OsO_4, CH_2Cl_2–pyridine, then H_2S (69%); v, $Ni(OAc)_2$, DMF–PhCl, air, 100 °C (40%).

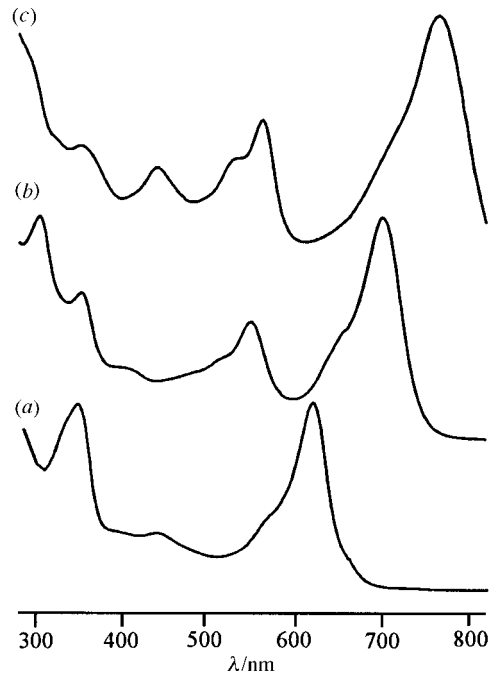

Fig. 1 UV-visible spectra of porphyrazines (*a*) **7** and (*b*) **9**, and (*c*) seco-porphyrazine **10**.

than the diols, was obtained in 40% yield after chromatography (silica, CH_2Cl_2–hexanes 4 : 1). Its UV-visible spectrum (Fig. 1) showed an unusual strong absorption band at λ_{max} 768 nm, which is red shifted by 66 nm compared to that of porphyrazinediol **9**.

Slow diffusion of MeOH into a $CHCl_3$ solution of **10** yielded single crystals suitable for X-ray crystallographic study,§ which (Fig. 2) unequivocally established the structure of the red pigment as seco-porphyrazine **10**. Spectroscopic measurements confirm the tautomeric form shown for **10**. Both ^{1}H and ^{13}C NMR spectra showed that the compound lacks the C_{2v} symmetry of the porphyrazine diols, and FAB$^+$ MS measurement was consistent with the composition of $C_{74}H_{80}N_8NiO$. The IR spectrum displayed a medium intensity band at ν_{max} 3380 cm^{-1} and a strong band at ν_{max} 1674 cm^{-1} which are consistent with the urea-like functionality on the ring of **10**, and ^{1}H NMR analysis showed the expected exchangeable proton signal at δ 9.45.

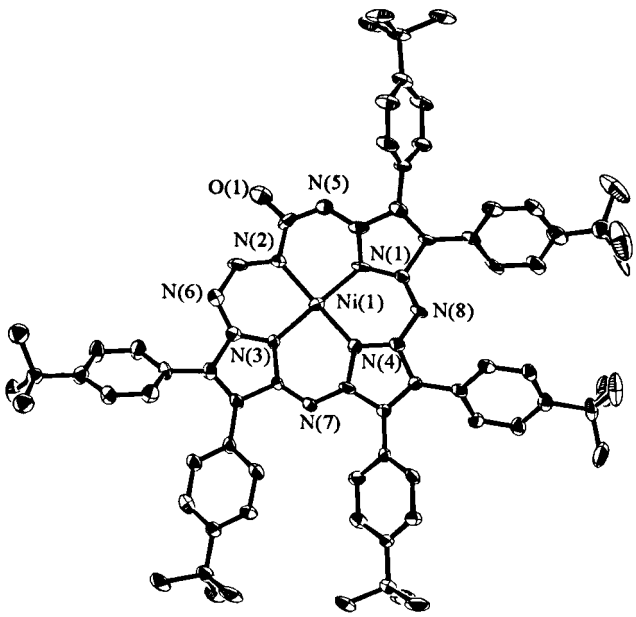

Fig. 2 X-Ray crystal structure of seco-porphyrazine **10**.

Compound **10** represents a novel macrocyclic ring system, which may result from the nickel-mediated air oxidation of the *cis*-diol unit and subsequent double loss of CO_2. Alternatively the mechanism may involve dehydration and subsequent cycloaddition of singlet oxygen, decarboxylation and deformylation. The methodology described above offers the opportunity for synthesis of the same type of heterocycles with other internal metal ions and different peripheral substituents for biomedical applications, and this investigation is in progress.

This work was supported by the National Science Foundation [CHE9727590 (B. M. H. and A. G. M. B.)], DMR {9523228 (B. M. H.)], the Materials Research Laboratory of Northwestern University, the EPSRC, Glaxo Wellcome *via* endowment support (A. G. M. B.), the Wolfson Foundation (A. G. M. B.) and NATO.

Notes and references

† All new compounds were characterised by ^{1}H and ^{13}C NMR, MS, IR and UV-visible spectroscopy, microanalysis and cyclic voltammetry; in all cases the spectroscopic data were consistent with the assigned structures.

‡ *Selected data* for **10**: mp > 320 °C; TLC 0.37 (silica, CH_2Cl_2–hexanes 4 : 1); ν_{max}/cm^{-1} 3380, 2962, 1674, 1598, 1549, 1363, 1266, 1104, 986, 838, 750, 565; $\lambda_{max}(CH_2Cl_2)$/nm (log ε) 352 (4.40), 440 (4.32), 532 (4.33), 562 (4.44), 768 (4.65); δ_H(300 MHz, $CDCl_3$) 10.25 (s, 1H), 9.45 (s, 1H, exch. D_2O), 7.83 (d, *J* 8.4, 2H), 7.79 (d, *J* 8.4, 2H), 7.72 (d, *J* 8.4, 2H), 7.68 (d, *J* 8.7, 2H), 7.65 (d, *J* 8.4, 2H), 7.58 (d, *J* 8.1, 2H), 7.47 (d, *J* 8.4, 2H), 7.40 (d, *J* 8.4, 2H), 7.39 (d, *J* 8.4, 2H), 7.38 (d, *J* 8.7, 2H), 7.34 (d, *J* 8.4, 2H), 7.30 (d, *J* 8.7, 2H), 1.44 (s, 9H), 1.43 (s, 18H), 1.40 (s, 9H), 1.39 (s, 9H), 1.35 (s, 9H); δ_C(100 MHz, $CDCl_3$) 159.1, 153.4, 152.9, 152.8, 152.1, 151.8, 150.7, 150.6, 148.2, 146.5, 144.7, 144.5, 144.0, 143.2, 139.6, 139.5, 137.6, 132.8, 132.7, 132.6, 132.5, 132.0, 131.8, 131.6, 131.0, 130.5, 130.4, 129.6, 128.8, 128.8, 128.0, 126.2, 125.9, 125.8, 125.6, 36.0, 35.8, 35.7, 35.7, 32.68, 32.66, 32.5, 32.5, 32.4; *m/z* (FAB$^+$) 1156 (M$^+$); $E_{1/2}$/V (*vs.* Fc$^+$/Fc) 0.81, 0.45, −1.03 (E_{pc}), −1.07 (E_{pc}) (Calc. for $C_{74}H_{80}N_8NiO$: C, 76.87; H, 6.97; N, 9.69. Found: C, 76.57; H, 6.96; N, 9.67%).

§ *Crystal data* for **10**: $C_{78}N_8OH_{84}NiCl_{12}$, *M* = 1633.70, triclinic, *a* = 14.923(1), *b* = 16.310(1), *c* = 17.626(1) Å, α = 82.070(1), β = 71.520(1), γ = 80.380(1)°, *V* = 3995.0(4) Å^3, *T* = −120 °C, space group $P\bar{1}$ (#2), *Z* = 2, D_c = 1.355 g cm^{-3}, μ(Mo-Kα) = 6.92 cm^{-1}, *F*(000) = 1692.00. Data were collected on a CCD plate area detector with graphite monochromated Mo-Kα radiation. The structure was solved by direct methods and refined by the full-matrix least-squares technique to give *R*1 = 0.10 and *wR*2 = 0.192 for 28117 independent observed reflections among 36794 measured reflections. The structure contains two disordered *tert*-butyl groups on the macrocycle and four disordered $CHCl_3$ solvent molecules. The non-hydrogen atoms on the macrocycle were refined anisotropically except for C25, C45, C47 and C48 on the disordered *tert*-butyl groups; for the solvent, Cl1–C9 were refined anisotropically and C10–C12, isotropically, while the remaining chlorine and carbon atoms were fixed. CCDC 182/1189. Crystal data is available in CIF format from the RSC web site, see: http://www.rsc.org/suppdata/cc/1999/703/

1 N. S. Mani, L. S. Beall, A. J. P. White, D. J. Williams, A. G. M. Barrett and B. M. Hoffman, *J. Chem. Soc., Chem. Commun.*, 1994, 1943.
2 A. G. Montalban, S. J. Lange, L. S. Beall, N. S. Mani, D. J. Williams, A. J. P. White, A. G. M. Barrett and B. M. Hoffman, *J. Org. Chem.*, 1997, **62**, 9284.
3 K. R. Adams, R. Bonnett, P. J. Burke, A. Salgado and M. A. Vallés, *J. Chem. Soc., Perkin Trans. 1*, 1997, 1769.
4 C. Brückner, S. J. Rettig and D. Dolphin, *J. Org. Chem.*, 1998, **63**, 2094.
5 A. G. Montalban, H. G. Meunier, R. Ostler, A. G. M. Barrett, B. M. Hoffman and G. Rumbles, *J. Phys. Chem.*, in the press.
6 E. D. Sternberg, D. Dolphin and C. Brückner, *Tetrahedron*, 1998, **54**, 4151.
7 *Photodynamic Theory: Basic Principles and Clinical Applications*, ed. B. W. Henderson and T. J. Dougherty, Marcel Dekker, New York, 1992.
8 J. A. Elvidge and R. P. Linsted, *J. Chem. Soc.*, 1954, 442.
9 T. F. Baumann, A. G. M. Barrett and B. M. Hoffman, *Inorg. Chem.*, 1997, **36**, 5661.
10 H. Fischer and H. Eckoldt, *Liebigs Ann. Chem.*, 1940, **543**, 138.
11 C. Brückner and D. Dolphin, *Tetrahedron Lett.*, 1995, **36**, 3295.

Communication 9/00555B

ChemComm

Synthesis and structures of neutral and cationic β-diketiminatoaluminium methyls†

Frédéric Coslédan, Peter B. Hitchcock and Michael F. Lappert*

The Chemistry Laboratory, University of Sussex, Brighton, UK BN1 9QJ. E-mail: m.f.lappert@sussex.ac.uk

Received (in Basel, Switzerland) 4th January 1999, Accepted 25th February 1999

Trimethylaluminium with the β-diketimine H(LL) yields the aluminium complex [Al(LL)Me$_2$], from which the salts [Al(LL)Me(thf)][BMe(C$_6$F$_5$)$_3$]·0.5thf and [Al(LL)Me(OEt$_2$)][B(C$_6$F$_5$)$_4$]·0.5Et$_2$O have been prepared, and crystallographically characterised.

There is much current interest in bi- or tri-dentate nitrogen-centered spectator ligands, which often are a component of electrophilic metal alkyl catalysts for olefin polymerisation or related reactions. Emphasis has been on Ti^{IV}, Zr^{IV}, Fe^{II}, Co^{II}, Ni^{II} or Pd^{II} complexes.[1] Attention is also now turning to Al compounds, triggered by the disclosure of Coles and Jordan in 1997 that certain cationic amidinatoaluminium methyls **A**–**C** are active catalysts for polymerisation of ethylene [**A** > **B** or **C**; LL = Bu^{t}C(NPr^i)$_2$ in **A** or **B**, but MeC(NPr^i)$_2$ in **C**];[2] as are compounds **D** (R = H, Ar = C$_6$H$_3$Pr$^i_2$-2,6 or C$_6$H$_2$Me$_3$-2,4,6; or, the least active, R = Me, Ar = C$_6$H$_3$Pr$^i_2$-2,6)[3] and **E** (LL = **G**),[4] while the X-ray-characterised **F** only showed only trace activity.[4]

[Al(LL)Me][B(C$_6$F$_5$)$_4$] **A**

[{Al(LL)Me}$_2$(μ-Me)][BMe(C$_6$F$_5$)$_3$] **B**

[$^+$Al(LL)(Me)…MeB$^-$(C$_6$F$_5$)$_3$] **C**

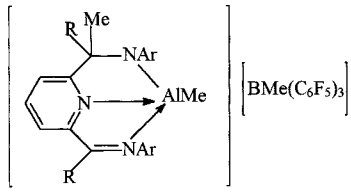

D

[Al(LL)R][B(C$_6$F$_5$)$_4$] **E** (R = Et or Bu^t)

[{Al(LL)Me}$_2$(μ-Pr^i)][B(C$_6$F$_5$)$_4$] **F**

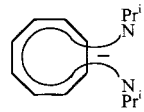

G

Nitrogen-centered, bidentate, monoanionic, four-electron spectator ligands [LL]$^-$ which form four-coordinate aluminium dimethyls [Al(LL)Me$_2$] are the amidinates [LL = RC(NR′)$_2$],[2,5] guanidinates [LL = R$_2$NC(NR′)$_2$ or **H**],[6] aminotroponimate **G**[4,7] and the β-diketinimates **I**;[8] the thioureido complex [Al{N(Ad)C(Me)S}Me$_2$] is a close relative (Ad = adamantyl).[9]

Tridentate, monoanionic ligands, such as those in **D**[2] or [R(H)N(CH$_2$)$_2$N(Me)(CH$_2$)$_2$NR] (R = Me or SiMe$_3$)[10] have yielded five-coordinate AlMe$_2$ complexes. The diketiminatoaluminium compounds [Al(LL)Me$_2$] (LL = **I**, R = C$_6$H$_4$Me-4) failed to furnish an isolable cationic complex with B(C$_6$F$_5$)$_3$.[8] The related compounds [Al(LL)R′$_2$] (LL = **I** with R = C$_6$H$_3$Pr$^i_2$-2,6 and R′ = Et or Bu^i) with [Ph$_3$C][B(C$_6$F$_5$)$_4$] and (for R′ = Et) then PhNMe$_2$ gave [Al(LL)Et(NMe$_2$Ph)][B(C$_6$F$_5$)$_4$] or [Al(LL)Bu^i][B(C$_6$F$_5$)$_4$] (structures based on ^{1}H and ^{13}C NMR spectral data).[11]

† No reprints available.

We now report the synthesis and structures of the crystalline β-diketiminatoaluminium compounds [Al(LL)Me$_2$] **1**, [Al(LL)Me(thf)][BMe(C$_6$F$_5$)$_3$] **2** and [Al(LL)Me(OEt$_2$)][B(C$_6$F$_5$)$_4$] **3**, and of some related complexes based on the spectator ligand **J**.[12] Compounds **2** and **3** are the first X-ray-characterised, mononuclear, four-coordinate, cationic aluminium methyls. Preliminary experiments, to be reported in details elsewhere, show that **3** catalyses the conversion of MMA to syndiotactic PMMA of low polydispersity.

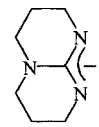

H

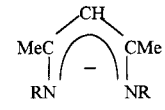

I (R = C$_6$H$_3$Pr$^i_2$ or C$_6$H$_4$Me-4)

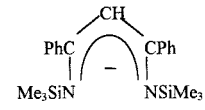

J

The β-diketiminatoaluminium dimethyl **1** was obtained (Scheme 1, step i) by addition of trimethylaluminium to an equivalent portion of the β-diketimine H(LL) (LL = **J**).[12] Treatment of **1** in diethyl ether with tris(pentafluorophenyl)borane in pentane and addition of thf yielded (Scheme 1, step ii) the cationic methylaluminium tris(pentafluorophenyl)methylborate **2**. When the same procedure was carried out, but omitting addition of thf, a sticky orange product, tentatively formulated as impure **4** (on the basis of the ^{11}B NMR spectral signal at δ −16.85; *cf.* δ −16.7 (**2**), −19.1 (**3**) and −19.0 (**4**), was obtained (Scheme 1, step iv). From equivalent portions of **1** and *N*,*N*-dimethylanilinium tetrakis(pentafluorophenyl)borate in toluene at ambient temperature and successive removal of toluene, washing with pentane, dissolution of the residue in diethyl ether and crystallisation the cationic methylaluminium salt **3** (Scheme 1, step iii) was isolated. In a similar NMR spectroscopic experiment in C$_6$D$_6$ rather than toluene, but without addition of Et$_2$O, quantitative formation of the related salt **5** is inferred (step v of Scheme 1).

The new, pale yellow, highly air-sensitive, readily benzene-soluble, crystalline compounds **1**–**3** gave satisfactory analyses, NMR solution spectra (to be reported in the full paper) and single crystal X-ray diffraction data. The EI-MS data showed the highest *m/z* peak corresponded to [M − Me]$^+$ for **1** and [B(C$_6$F$_5$)$_3$]$^+$ for **2**.

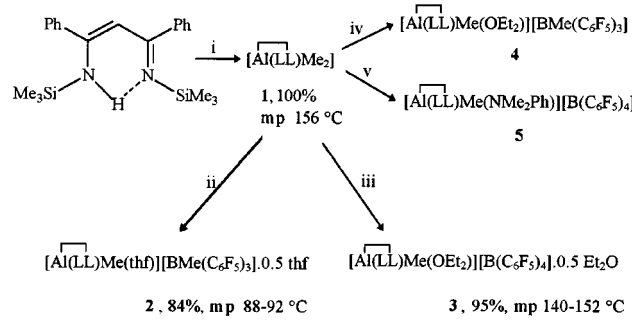

Scheme 1 Synthesis of neutral and cationic, four-coordinate β-diketiminatoaluminium methyls. *Reagents and conditions*: i, AlMe$_3$ in C$_6$H$_{14}$, C$_5$H$_{12}$, −78 °C; ii, B(C$_6$F$_5$)$_3$ in C$_5$H$_{12}$, Et$_2$O, −78 °C, then thf at 20 °C; iii, [NHMe$_2$Ph][B(C$_6$F$_5$)$_4$], PhMe, 20 °C; iv, [NHMe$_2$Ph][B(C$_6$F$_5$)$_4$] in C$_6$D$_6$.

Table 1 Selected geometric parameters for crystalline β-diketinimatoaluminium methyls

Compound	Property				
	av. Al–C/Å	av. Al–N/Å	C–Al–C′/°	N–Al–N′/°	Deviation (Å) of Al and CH from NC···C′N′ plane
[Al(LL)Me$_2$][8] (LL=**I**, R=C$_6$H$_3$Pr$^i_2$-2,6)	1.964(3)	1.928(2)	115.4(2)	96.18(9)	0.33, —
[Al(LL)Me$_2$][8] (LL=**I**, R=C$_6$H$_4$Me-4)	1.958(4)	1.906(3)	117.4(1)	94.72(14)	0.72, —
1	1.959(5)	1.921(4)	111.3(2)	97.1(2)	0.95, 0.12
2	1.868(4)	1.941(5)	—	100.8(2)	0.75, 0.13
3	1.872(4)	1.951(5)	—	102.6(2)	0.78, 0.13

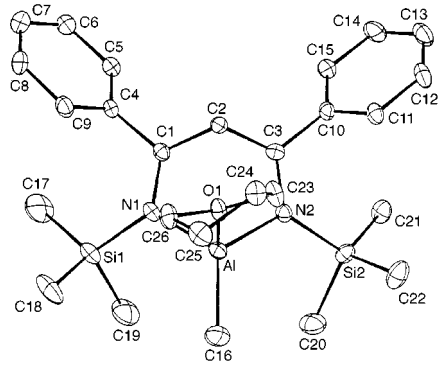

Fig. 1 Molecular structure of **2** with selected bond distances (Å) and angles (°) (see also Table 1). Cation: av. Si–N 1.787(3), Al–O(1) 1.875(3); N(2)–Al–C(16) 123.2(2), N(1)–Al–C(16) 122.9(2), av. N–Al–O 100.0(2), C–Al–O 103.4(2). Anion: B–C(27) 1.635(6), av. B–C(aryl) 1.656(6); C(28)–B–C(34) 104.4(3), C(28)–B–C(40) 112.2(3), C(28)–B–C(27) 114.7(3).

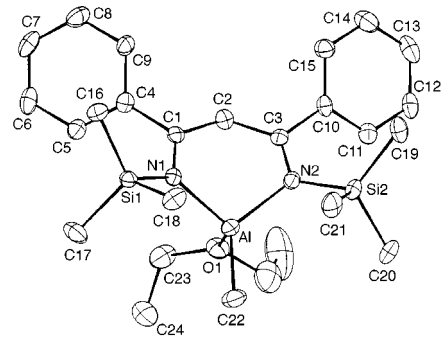

Fig. 2 Molecular structure of **3** with selected bond distances (Å) and angles (°) (see also Table 1). Cation av. Si–N 1.801(4), Al–O(1) 1.887(4); N(2)–Al–C(22) 123.7(2), N(1)–Al–C(22) 122.8(2), av. N–Al–O 101.6(2), C–Al–O 102.3(2). Anion av. B–C 1.653(4); C(27)–B–C(33) 113.5(4), C(27)–B–C(39) 113.8(4), C(27)–B–C(45) 102.4(4).

The molecular geometry of crystalline **1** (details to be published in the full paper) and the two compounds [Al(LL)Me$_2$] (LL = **I**)[8] are closely similar, Table 1. The AlNCCCN fragment in **1** has the boat conformation, as previously found *inter alia* in [Li(LL)]$_2$ and Sn(LL)Me$_3$,[12] although sometimes this β-diketiminatometal moiety is planar, as in [Co(LL)$_2$][13] (LL = **J**).

The molecular structures of the cations of the crystalline salts **2** and **3** are illustrated in Fig. 1 (**2**) and 2 (**3**); the anions will be described in the full paper. The four-coordinate aluminium atom in each cation has a distorted monopyramidal (TMP) geometry, with a similar distortion from tetrahedral to TMP. The Al–C distances are significantly shorter in each cation than in the neutral precursor **1**, but the Al–N bonds are slightly longer due to the widening of the N–Al–N′ angle in **2** or **3** compared with **1**, Table 1. The remaining geometric parameters of the β-diketiminato ligand are very similar in **1**–**3**. The sum of the angles at each nitrogen atom (of **1**–**3**) is close to 360°. There is no evidence of significant cation–anion interaction; the anion structures are unexceptional.[14]

The NMR spectra of compounds **1**–**3** in C$_6$D$_6$ (**1** and **3**) or CDCl$_3$ (**2**) indicate that the solution structures of **1**–**3** are identical to those in the crystal, except that in **1** there is only one ^{1}H or ^{13}C(^{1}H) signal for the two methyl groups, indicating that they undergo fast exchange.

The present results demonstrate once again [*e.g.*[15] the monomeric [Ce(LL)$_2$Cl] (LL = **J**)] that the β-diketiminato ligand **J** is exceptionally sterically demanding, having allowed us to prepare the well separated ion pairs in **2** and **3**; reactivity and catalytic studies are in hand. This ligand can be fine-tuned by varying the substituents in its skeleton.

We thank EPSRC for support.

Notes and references

‡ *Crystallographic data* for **1**/**2**/**3**: C$_{23}$H$_{35}$AlN$_2$Si$_2$/C$_{45}$H$_{43}$AlBF$_{15}$N$_2$OSi$_2$·0.5(C$_4$H$_{10}$O)/C$_{50}$H$_{42}$AlBF$_{20}$N$_2$OSi$_2$·0.5(C$_4$H$_{10}$O), M = 422.69/1043.8/1197.9, triclinic for all, space group $P\bar{1}$ for all, a = 6.335(2)/12.016(3)/13.503(5), b = 12.139(3)/13.439(5)/14.557(11), c = 17.103(4)/16.409(7)/15.403(7) Å, α = 78.55(2)/99.44(3)/69.39(5), β = 79.90(3)/91.80(3)/88.02(3), γ = 74.84(3)/108.31(7)/74.04°, U = 1233.6(6)/2472(2)/2718(3) Å^3, Z = 2/2/2, λ(Mo-Kα) = 0.71073 Å, μ = 0.19/0.19/0.19 mm^{-1}. Data were collected at 173(2) K on an Enraf Nonius CAD4 diffractometer in the ω–2θ mode for the range of 2 < θ < 25°. Final residuals for 4338/8664/9546 independent reflections were wR_2 = 0.235/0.201/0.214 and for the 3026/5806/6098 with $I > 2\sigma(I)$, R_1 = 0.079/0.053/0.067. CCDC 182/1181. See http://www.rsc.org/suppdata/cc/1999/705/ for crystallographic files in .cif format.

1 Selected references: J. D. Scollard, D. H. McConville and J. Vittal, *Macromolecules*, 1996, **29**, 5241; B. L. Small, M. S. Brookhart and A. M. A. Bennett, *J. Am. Chem. Soc.*, 1998, **120**, 4049; G. J. Britovskek, V. C. Gibson, B. S. Kimberley, P. J. Maddox, S. J. McTavish, G. A. Solan, A. J. P. White and D. J. Williams, *Chem. Commun.*, 1998, 849 and references therein.

2 M. P. Coles and R. F. Jordan, *J. Am. Chem. Soc.*, 1997, **119**, 8125.

3 M. Bruce, V. C. Gibson, C. Redshaw, G. A. Solan, A. J. P. White and D. J. Williams, *Chem. Commun.*, 1998, 2523.

4 E. Ihara, V. G. Young and R. F. Jordan, *J. Am. Chem. Soc.*, 1998, **120**, 8277.

5 D. Kottmair-Maieron, R. Lechler and J. Weidlein, *Z. Anorg. Allg. Chem.*, 1991, **593**, 111; R. Lechler, H.-D. Hausen and J. Weidlein, *J. Organomet. Chem.*, 1989, **359**, 1; M. P. Coles, D. C. Swenson, R. F. Jordan and V. G. Young, *Organometallics*, 1997, **16**, 5183.

6 S. L. Aeilts, M. P. Coles, D. C. Swenson, R. F. Jordan and V. G. Young, *Organometallics*, 1998, **17**, 3265.

7 H. V. R. Dias, W. Jin and R. E. Ratcliff, *Inorg. Chem.*, 1995, **34**, 6100.

8 B. Qian, D. L. Ward and M. R. Smith, *Organometallics*, 1998, **17**, 3070.

9 M. P. Coles, D. C. Swenson, R. F. Jordan and V. G. Young, *Organometallics*, 1998, **17**, 4042.

10 N. Emig, H. Nguyen, H. Krautscheid, R. Réau, J.-B. Cazaux and G. Bertrand, *Organometallics*, 1998, **17**, 3599.

11 C. E. Radzewich, M. P. Coles and R. F. Jordan, *J. Am. Chem. Soc.*, 1998, **120**, 9384.

12 P. B. Hitchcock, M. F. Lappert and D.-S. Liu, *J. Chem. Soc., Chem. Commun.*, 1994, 1699.

13 M. F. Lappert and D.-S. Liu, *J. Organomet. Chem.*, 1995, **500**, 203.

14 *Cf.* Y.-X. Chen, M. V. Metz, L. Li, C. L. Stern and T. J. Marks, *J. Am. Chem. Soc.*, 1998, **120**, 6287 and references therein.

15 P. B. Hitchcock, M. F. Lappert and S. Tian, *J. Chem. Soc., Dalton Trans.*, 1997, 1945.

Communication 9/00003H

Phase transitions in disordered solids *via* hybrid Monte Carlo: the orthorhombic to cubic phase transition in $(Mg,Mn)SiO_3$ perovskite

John A. Purton,[ab]† Neil L. Allan*[a] and Jon D. Blundy[b]

[a] *School of Chemistry, University of Bristol, Cantock's Close, Bristol, UK BS8 1TS. E-mail: n.l.allan@bristol.ac.uk*
[b] *CETSEI, Department of Geology, University of Bristol, Wills Memorial Building, Bristol, UK BS8 1RJ*

Received (in Cambridge, UK) 11th January 1999, Accepted 9th March 1999

We show how a novel hybrid Monte Carlo simulation technique can be used to investigate the influence of high impurity or defect concentrations on phase transitions; impurity cations can have a much larger effect than that expected from a mean-field treatment or linear interpolation between end-member compounds.

We report a novel computational methodology for determining the phase stability of disordered inorganic materials and solid solutions. The motivation for this work is twofold. Firstly, although calculations have provided considerable insight into the thermodynamic and structural aspects of materials,[1] most have been limited to the study of solids with periodic, ordered structures. Secondly, a detailed understanding of the thermodynamics and phase stability of disordered solids is crucial for many areas of mineralogy and solid-state chemistry. For example, minerals often contain a large number of minor and trace element impurities, possibly disordered over several crystallographic sites, which may have dramatic effects on physical and chemical behavior and phase stability.

Supercell or *point* defect calculations have traditionally been used to investigate impurities in solid state materials. The clear limitations of these methods for systems with an appreciable impurity or defect content exclude studies of many naturally occurring minerals and ceramics of industrial importance. Accordingly, the principal objective of this work is to show how a modified hybrid Monte Carlo (HMC) technique can be used to study the effect of disorder on phase transitions in ionic solids and minerals. The HMC technique permits an efficient sampling of different configurations, takes explicit account both of ionic relaxation near impurity ions and thermal effects, and is readily extended to different ensembles. Our methods do not involve the use of an approximate parameterised Hamiltonian since the parameterisation of, for example, an Ising-type Hamiltonian becomes increasingly difficult beyond binary or pseudobinary mixtures and can average out local effects due to ion clustering and association. Moreover, such methods cannot readily be extended to include the effects of lattice vibrations and pressure.

Most Earth materials are solid solutions rather than pure end-members and an understanding of the effect of trace components is essential. Many properties of the deep Earth, such as electrical conductivity,[2] phase changes[3] and rheology are profoundly altered by the presence of impurities at concentrations of a few wt%, or less. The magnesium-rich silicate perovskite is thought to be the major constituent of the Earth's lower mantle and an understanding of its thermodynamic and physical behaviour is crucial for a wide range of geophysical and geochemical problems such as the convection and chemical differentiation of the mantle. Previous work[4] used constant-pressure molecular dynamics (MD) to demonstrate that at pressures above 10 GPa, orthorhombic $MgSiO_3$ undergoes a temperature induced phase transition to a cubic phase prior to melting, whereas at lower pressures the orthorhombic phase melts without any change of solid phase. The size difference between Mn^{2+} and Mg^{2+} is such that Mn–Mg mixing in silicates is expected to be quite non-ideal[5] and so here we investigate the effect of Mn, a minor element constituent of the Earth's mantle, on the high pressure orthorhombic–cubic phase transition. The potential model used within this study has been discussed previously;[6] we have employed the ionic model assigning charges of +1.2 for Mg and Mn, –1.2 for O and +2.4 for Si, and used the set of short-range potential parameters discussed in ref. 3.

The HMC approach we have developed is related to that used in the modelling of polymers and biomolecules.[7–9] The technique has been applied recently to such problems as the enthalpies of mixing of binary oxides[10] and non-convergent ordering of cations in olivine,[11] but not thus far to phase transitions. During one HMC cycle, one of three options is chosen at random, with equal probability. The first of these is a short NVE molecular dynamics (MD) simulation consisting of 15 steps and with a timestep of 1.5 fs. The length and timestep were chosen so as to allow efficient sampling of the different configurations. The last configuration is accepted or rejected by comparing its energy with the energy of the starting configuration and using the standard Metropolis algorithm.[12] If the last configuration is rejected, the original configuration is included in the statistical averaging of thermodynamic properties. In the second, which is only applicable to the solid solution, a short MD run follows a random exchange of Mg and Mn ions. Again, the difference in energy between the previous configuration and that immediately after the MD simulation is used in the Metropolis algorithm. At the start of each MD run, velocities are chosen anew at random from a Maxwellian distribution. The third option is a random change of the volume/shape of the box,[13] which again is accepted or rejected using the Metropolis algorithm. Enthalpy and structural data were averaged over a period of 50 000 cycles, prior to which an equilibration period of 50 000 cycles was undertaken. Results presented here are for a simulation cell containing 540 ions ($3 \times 3 \times 3$ unit cells).

For $MgSiO_3$ we obtain very similar results using HMC to those of the MD study of Matsui and Price[4] with a calculated transition temperature of 3900 K at 20 GPa from the orthorhombic to the cubic phase. Fig. 1 shows the calculated variation of the lattice parameters for $Mg_{0.6}Mn_{0.4}SiO_3$ which shows that this compound also undergoes a similar phase transition at this pressure. From the calculated transition temperatures at 20 GPa for $Mg_xMn_{1-x}SiO_3$ (Fig. 2) as a function of composition *x*, it is clear that a linear extrapolation between the two end members, is a very poor approximation. For example, the phase transition for $Mg_{0.6}Mn_{0.4}SiO_3$ is at a much lower temperature (2500 ± 50 K) than the value of almost 3000 K predicted by a simple linear interpolation of transition temperature *vs.* composition. In this context it is worth noting that, unlike the transition temperature, the calculated volume as a function of composition displays only a small positive deviation from Vegards' law, since the *a* lattice parameter itself has a positive and the *b* and *c* lattice parameters a negative deviation. We have been unable to find any experimental data for comparison. An orthorhombic–cubic transition at high

† Present address: CLRC, Daresbury Laboratory, Warrington, Cheshire WA4 4AD, UK.

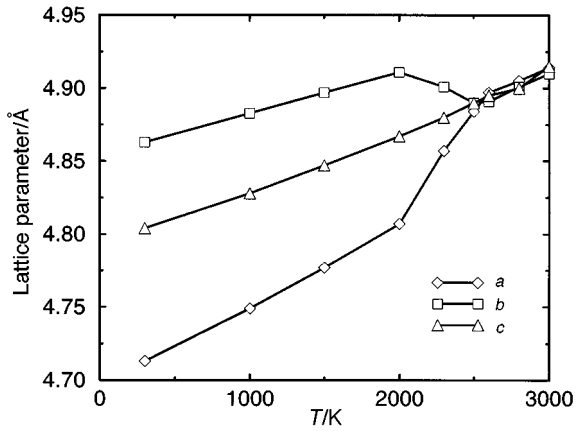

Fig. 1 Lattice parameters (Å) *vs.* T(K) at 20 GPa for $Mg_{0.6}Mn_{0.4}SiO_3$.

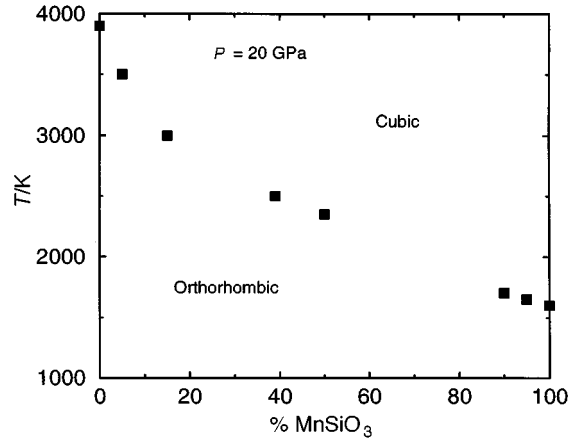

Fig. 2 Calculated orthorhombic–cubic transition temperature (K) at 20 GPa *vs.* composition.

pressure by the analogous compound (Mg,Fe)SiO_3, for which experimental evidence is currently contradictory,[14] would have important implications for the thermodynamic and compositional modelling of the Earth's mantle since thermodynamic data is often extrapolated from low pressures and temperatures and from the end-member compositions.

In summary, the HMC technique removes major limitations of the existing methods for the simulation of phase transitions in disordered solids, which restrict considerably the contact between experiment and theory. The methodology is general and readily applicable to a wide range of real rather than model, undefective systems. It is essential to take explicit account of ionic relaxation in each of the configurations without any averaging out of local effects. We envisage that that our new approach will add significantly to our understanding of the behaviour of complex systems at the atomic level, providing an important link between the microscopic and macroscopic behaviour of ceramics and minerals, and hope the present study will prompt new experimental investigations of the effects of trace impurities on high-pressure phase transitions.

This work was supported by NERC grants GR3/09772 and GR9/02621 and EPSRC grant GR/L31340.

Notes and references

1 *Computer Modelling in Inorganic Crystallography*, ed. C. R. A. Catlow Academic Press, SanDiego–London, 1997.
2 J. Brodholt, *Am. Mineral.*, 1997, **82**, 1049.
3 G. H. Gudfinnsson and B. J. Wood, *Am. Mineral.*, 1998, **83**, 1037.
4 M. Matsui and G. D. Price, *Nature*, 1991, **351**, 735.
5 For example, B. J. Wood, R. T. Hackler and D. P. Dobson, *Contrib. Miner. Petrol.*, 1994, **115**, 438.
6 C. R. A. Catlow and G. D. Price, *Nature*, 1990, **347**, 243 and references therein.
7 S. Duane, A. D. Kennedy, B. J. Pendleton and D. Roweth, *Phys. Lett. B*, 1987, **195**, 216.
8 B. Mehlig, D. W. Heermann and B. M. Forrest, *Phys. Rev. B*, 1992, **45**, 679.
9 M. E. Clamp, P. G. Baker, C. J. Stirling and A. Brass, *J. Comput. Chem.*, 1994, **15**, 838.
10 J. A. Purton, J. D. Blundy, M. B. Taylor, G. D. Barrera and N. L. Allan, *Chem. Commun.*, 1998, 627.
11 J. A. Purton, G. D. Barrera, N. L. Allan and J. D. Blundy, *J. Phys. Chem. B*, 1998, **102**, 5202.
12 N. Metropolis, A. W. Rosenbluth, M. N. Rosenbluth, A. H. Teller and E. Teller, *J. Chem. Phys.*, 1951, **21**, 1087.
13 Q. Wang, J. K. Johnson and J. Q. Broughton, *Mol. Phys.*, 1996, **89**, 1105.
14 For example, E. Knittle and R. Jeanloz, *Science*, 1987, **235**, 668; C. Meade. H. K. Mao and J. Hu, *Science*, 1995, **268**, 1743. The second paper suggests that a possible reason for the failure of the authors of the first paper to observe an orthorhombic–cubic phase transition is the reversibility of the transition on quenching to room temperature conditions.

Communication 9/00303G

Catalytic reaction of methane with $CBrF_3$

Kai Li,[a] Eric Kennedy,*[a] Bogdan Dlugogorski[a] and Russell Howe[b]

[a] *Department of Chemical Engineering, University of Newcastle, Callaghan, NSW 2308, Australia. E-mail: cgek@cc.newcastle.edu.au*
[b] *School of Chemistry, University of New South Wales, Sydney, NSW 2052, Australia*

Received (in Cambridge, UK) 4th February 1999, Accepted 10th March 1999

The catalytic reaction of CH_4 with $CBrF_3$ over Co, Cu and Mn ZSM-5 zeolites is described; major products (at low temperatures) are those expected for simple hydrodebromination: CH_3Br and CHF_3.

The hydrodehalogenation reaction of chlorofluorocarbons (CFCs) and bromofluorocarbons or bromochlorofluorocarbons (halons) are potentially important reactions for both disposal of ozone depleting chemicals and production of hydrofluorocarbon replacements. Previous work in this area has focussed on reactions of CFCs with hydrogen over supported palladium catalysts.[1–12] Little attention has been paid to the corresponding hydrodebromination of halons. Here we describe for the first time the catalytic reaction of halon 1301 ($CBrF_3$) with methane over transition metal exchanged ZSM-5 zeolites. This novel catalytic reaction offers potential new routes to hydrofluorocarbons using methane as the hydrogen source.

Cobalt, copper and manganese exchanged ZSM-5 zeolites were prepared from a commercial ZSM-5 (PQ, Si/Al = 25), and charged into an alumina plug flow microreactor. Reactant gas stream (CH_4–$CBrF_3$–N_2 = 1 : 1 : 10) was flowed over the catalyst at a GHSV of 3500 h^{-1}, and products were analyzed by on-line gas chromatography after passing through a caustic scrubber.

Fig. 1 shows typical $CBrF_3$ conversions *versus* time on stream over four different zeolite catalysts at 873 K. Also shown is the corresponding conversion in the homogeneous reaction, as reported elsewhere.[13] The gas phase reaction between CH_4 and $CBrF_3$ begins at *ca.* 800 K, and increases dramatically above 900 K. A striking feature of the reaction in the presence of zeolite catalysts is the initial high conversion of $CBrF_3$ which then falls to a steady state value. Our preliminary investigations of this breakthrough period suggest reaction of $CBrF_3$ with the zeolite which generates the active phase for the hydrodehalogenation reaction. ^{27}Al MAS NMR measurements show that framework tetrahedral aluminium in the zeolite is completely transformed into an as yet unidentified form, although XRD analysis shows no change in the zeolite structure. In the case of HZSM-5, the steady state conversion approaches that found in the absence of catalyst. For the transition metal exchanged zeolites, however, there is a very evident influence of catalyst on the steady state conversion. It is important to note that zeolite crystallinity is fully retained during this reaction, even after 36 h on stream.

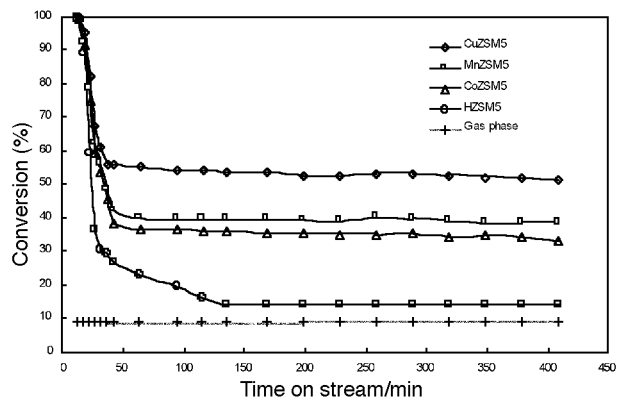

Fig. 1 Conversion of $CBrF_3$ *versus* time on stream at 873 K over various catalysts.

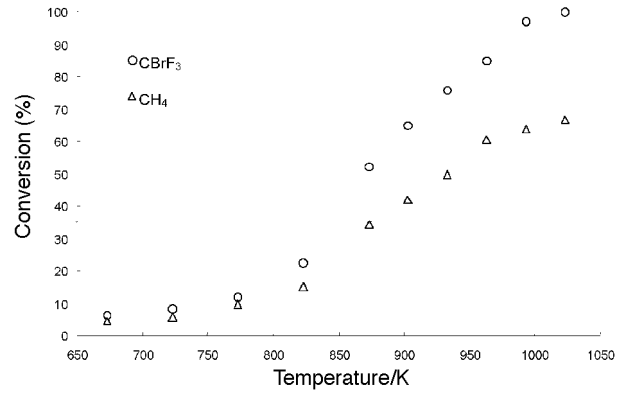

Fig. 2 Steady state conversion of $CBrF_3$ and CH_4 *versus* temperature over MnZSM-5.

Fig. 2 plots the steady state $CBrF_3$ and CH_4 conversions *versus* reaction temperature over MnZSM-5; similar profiles were measured for the other transition metal zeolites. The $CBrF_3$ conversion exceeds that of CH_4 at all temperatures, suggesting that the reaction pathway is more complex than that predicted for the simple 1:1 stoichiometry of reaction (1):

$$CBrF_3 + CH_4 \rightarrow CH_3Br + CHF_3 \quad (1)$$

In separate experiments, we have noted that $CBrF_3$ undergoes pyrolysis reactions over the same catalysts, producing C_2F_6 and Br_2,[14] and C_2F_6 was detected as a minor product also in the reactions with methane. The major reaction products detected in the reactions with methane at lower temperatures are those expected from reaction (1), as illustrated in Fig. 3. Above 873 K, however, the yield of CH_3Br declines, and other reaction products appear, (notably hydrocarbons C_2H_4 and C_2H_2), due to further reaction of CH_3Br. Other products identified include $C_2H_2F_2$, C_2H_3Br, CH_2BrF, and trace (less than 5 ppm) quantities of $C_2HBr_2F_3$, CH_2Br_2, C_2F_6, $C_2H_3F_3$, C_6H_5Br and H_2. Mass balances for all reactions were generally better than ±

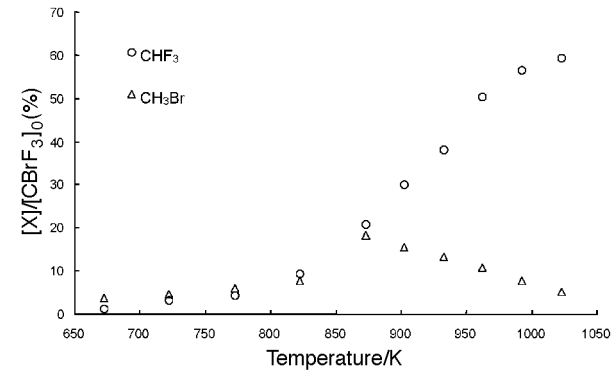

Fig. 3 Steady state conversion of $CBrF_3$ to major products CHF_3 and CH_3Br *versus* temperature over MnZSM-5.

3% and usually ± 1%, and suggest any as-yet unidentified species represent only a small fraction of reaction products.

The reaction mechanisms involved in this intriguing chemistry are not yet clear. The high initial conversions of $CBrF_3$, and the results of preliminary characterization experiments on catalysts exposed to $CBrF_3$ plus CH_4 or $CBrF_3$ alone for short periods[14] suggest that initial reaction of $CBrF_3$ with fresh catalysts generates the catalytically active species. The high reaction selectivity (at low temperatures) may result from the selective cleavage of C–Br bonds in preference to C–F bonds in $CBrF_3$, and reflects the lower relative strength of the C–Br bond (295 kJ mol^{-1})[15] compared with C–F bonds (*ca*. 460 kJ mol^{-1}, estimated from analogous F–CF_2Cl bond strength) in CF_3Br. Low temperature cleavage of C–Br would occur before evidence of C–F bond cleavage, leaving the CF_3 moiety intact.

Further work is needed to optimize catalysts, identify active sites and determine reaction pathways. At present we are also investigating the reactions of CFCs and other halocarbons with methane. The results presented here offer a new route for methane utilization in the disposal and upgrading of ozone depleting materials.

This work has been supported by the Australian Research Council.

Notes and references

1 C. Gervasutti, L. Marangoni and W. Marra, *J. Fluorine Chem*., 1981/82, **19**, 1.
2 B. Coq, J.-M. Cognion, F. Figuras and D. Tournigant, *J. Catal.*, 1993, **141**, 21.
3 B. Coq, F. Figuras, S. Hub and D. Tournigant, *J. Phys. Chem.* 1995, **99**, 11 159.
4 A. Wiersma, E. J. A. X. van de Sandt, M. Makkee, C. P. Luteijn, H. van Bekkum and J. A. Moulijn, *Catal. Today*, 1996, **27**, 257.
5 E. J. A. X. van de Sandt, A. Wiersma, M. Makkee, H. van Bekkum and J. A. Moulijn, *Catal. Today*, 1997, **35**, 163.
6 E. J. A. X. van de Sandt, A. Wiersma, M. Makkee, H. van Bekkum and J. A. Moulijn, Appl. Catal. A, 1997, **155**, 59.
7 Z. Karpinski, K. Early and J. L. d'Itri, *J. Catal.*, 1996, **164**, 378.
8 W. Juszczyk, A. Malinowski and Z. Karpinski, *Appl. Catal. A*, 1998, **166**, 311.
9 B. Coq, S. Hub, F. Figuras and D. Tournigant, *Appl. Catal. A*, 1993, **101**, 41.
10 R. Onishi, I. Suzuki and M. Ichikawa, *Chem. Lett.*, 1991, 841.
11 R. Onishi, W. L. Wang and M. Ichikawa, *Appl. Catal. A*, 1994, **113**, 29.
12 A. Malinowski, W. Juszczyk, M. Bonarowska, J. Pielaszek and Z. Karpinski, *J. Catal.*, 1998, **177**, 153.
13 K. Li, E. Kennedy, B. Dlugogorski and B. Moghtaderi, *Proceedings of 25th Australian and New Zealand Chemical Engineering Conference, CHEMECA 97*, Rotorua, New Zealand, 1997, p. SF4a.
14 K. Li, F. Oghanna, E. M. Kennedy, B. Z. Dlugogorski, A. Fazeli, S. Thomson and R. F. Howe, to be published.
15 *Handbook of Chemistry and Physics*, ed. R. C. Weast and M. J. Astle, CRC Press, Boca Raton, FL, 63rd edn., 1982, F-199, Table 3.

Communication 9/00972H

Syntheses of mixed-metal $M_2Ti_2S_4$ cubane-type sulfido clusters (M = Ru, Rh, Ir, Cu) from a dinuclear organometallic thiotitanate anion

Takashi Amemiya, Shigeki Kuwata and Masanobu Hidai*

Department of Chemistry and Biotechnology, Graduate School of Engineering, The University of Tokyo, Hongo, Bunkyo-ku, Tokyo 113-8656, Japan. E-mail: hidai@chembio.t.u-tokyo.ac.jp

Received (in Cambridge, UK) 5th February 1999, Accepted 8th March 1999

The dinuclear organometallic thiotitanate anion $[(CpTiS)_2(\mu\text{-}S)_2]^{2-}$ reacted with $[Cp^*Ru(\mu_3\text{-}Cl)]_4$, $[(cod)M(\mu\text{-}Cl)]_2$ (M = Rh, Ir) and $[Cu(\mu_3\text{-}Cl)(PPh_3)]_4$ to afford the early–late heterobimetallic cubane-type sulfido clusters $[(CpTi)_2(Cp^*Ru)_2(\mu_3\text{-}S)_4]$, $[(CpTi)_2\{M(cod)\}_2(\mu_3\text{-}S)_4]$ and $[(CpTi)_2\{Cu(PPh_3)\}_2(\mu_3\text{-}S)_4]$, respectively.

Mixed-metal sulfido clusters have been the subject of much attention owing to their possible relevance to biological and industrial catalysis.[1] Thiometalate anions such as $[MS_4]^{2-}$ (M = Mo, W) are now recognized as versatile building blocks for the syntheses of such clusters.[2] Recently organometallic thiometalates, which contain both hydrocarbyl and sulfido ligands, have often been employed to this end because of their solublity in organic solvents and facility for the NMR study.[3] However, employment of polynuclear organometallic thiometalates as precursors for syntheses of heterometallic clusters remains undeveloped[4] compared with uncharged metal–sulfur aggregates with hydrocarbyl ligands.[5] As to group 4 metals, thiometalate species themselves are quite rare.[6] Kubas and coworkers have recently prepared the organometallic thiotitanate salt $[Na_4(thf)_8][\{(CpTiS)_2(\mu\text{-}S)_2\}_2]$ **2** from $[Cp_2Ti(SH)_2]$ **1** and an equimolar amount of sodium hydride.[7] Since the Ti_2S_4 framework in **2** may be regarded as a part of the cubane-type metal–sulfur core, it is expected to incorporate heterometals into the two missing vertices to afford mixed-metal cubane-type sulfido clusters. Indeed, more prevalent group 6 metal–sulfur aggregates with similar M_2S_4 frameworks are known to form a variety of mixed-metal cubane-type clusters in such a manner.[8,9] In our ongoing effort to develop the syntheses and reactivities of cubane-type sulfido clusters,[9–11] we have found that **2** reacts with late transition metal complexes to give a series of mixed-metal cubane-type sulfido clusters containing titanium.

Because of the low stability of **2**, we used **2** for further reactions without its isolation. To the dark green solution of **2** in THF was added $[(cod)M(\mu\text{-}Cl)]_2$ (M = Rh, Ir) in a Ti : M ratio of 1 : 1, and the mixture was stirred for 3 h at room temperature. The resultant dark brown suspension was evaporated *in vacuo* and extracted with benzene. Subsequent recrystallization from dichloromethane–ethanol afforded the mixed-metal cubane-type sulfido clusters $[(CpTi)_2\{M(cod)\}_2(\mu_3\text{-}S)_4]$ (**3**, M = Rh; **4**, M = Ir) in moderate yield [eqn. (1)].† The ^1H NMR spectra of **3** and **4** show the presence of both Cp and cod ligands in a ratio of 1 : 1. The heterobimetallic cubane type structure has further been confirmed by the X-ray analysis for **3** (Fig. 1).‡ The structure of **3** closely resembles that of the related ruthenium cluster $[(CpTi)_2(Cp^*Ru)_2(\mu_3\text{-}S)_4]$ **5**, which we have recently prepared through a different synthetic route.[11] The Ti–Ti distance of 3.051(2) Å is comparable to that in **5** [3.060(1) Å].[11] The four Ti–Rh distances [2.927(1)–3.056(1) Å] are consistent with the Rh→Ti dative bond, which is observed in the thiolato-bridged heterobimetallic complex $[CpTi(\mu\text{-}SCH_2CH_2CH_2S)_2Rh(nbd)]$ (nbd = norbornadiene) with a Ti–Rh distance of 2.915(2) Å.[12] The long Rh–Rh distance in **3** [3.575(1) Å] precludes the presence of the metal–metal bond. Very recently, Oro and coworkers have prepared the related titanium–rhodium sulfido clusters $[CpTi(\mu_3\text{-}S)_3\{Rh(tfbb)\}_3]$[13] (tfbb = tetrafluorobenzobarrelene) and $[(CpTi)_2\{Rh(CO)\}_2\{Rh(CO)[P(OPh)_3]\}_2(\mu_4\text{-}O)(\mu_3\text{-}S)_4]$[14] by the reaction of **1** with $[(diene)Rh(\mu\text{-}OMe)]_2$.

To delineate the synthetic versatility of the dinuclear organometallic thiotitanate **2** we have further investigated the reaction of **2** with various heterometal complexes. As expected, treatment of **2** with $[Cp^*Ru(\mu_3\text{-}Cl)]_4$ resulted in the formation of the known titanium–ruthenium heterobimetallic cubane-type sulfido cluster **5** in 49% yield; furthermore, **2** also reacted with $[Cu(\mu_3\text{-}Cl)(PPh_3)]_4$ to give the novel titanium–copper cluster $[(CpTi)_2\{Cu(PPh_3)\}_2(\mu_3\text{-}S)_4]$ **6** (Scheme 1). The molecular structure of **6** has unequivocally been determined by the X-ray analysis (Fig. 2).‡ Each Ti atom adopts a three-legged piano stool geometry, whilst each Cu atom has a tetrahedral geometry. The short Ti–Cu distances of 2.8093(9)–2.833(1) Å suggest the dative interaction between the d^{10} copper centre and the d^0 titanium centre. Related Cu→Ti dative bonds are found in thiolato-bridged heterobimetallic complexes such as $[Cp_2Ti(\mu\text{-}SMe)_2Cu(NCMe)_2][PF_6]$ [2.847(2) Å].[15] In contrast, the Cu–Cu

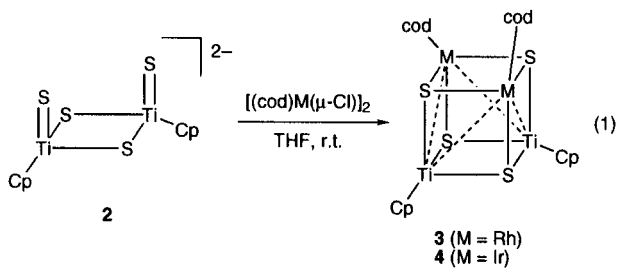

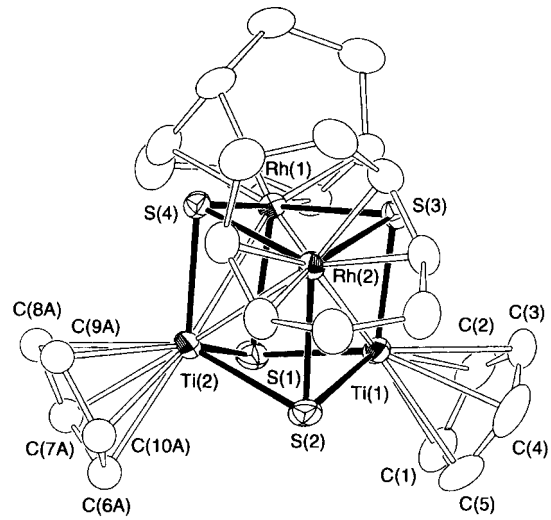

Fig. 1 Molecular structure of **3**. One of the cyclopentadienyl groups [C(6)–C(10)] was found in two disordered positions and refined as rigid groups with the occupancies of 60 and 40%. The minor component as well as all hydrogen atoms is omitted for clarity. Selected interatomic distances (Å): Ti(1)–Ti(2) 3.051(2), Ti(1)–Rh(1) 2.927(1), Ti(1)–Rh(2) 3.056(1), Ti(2)–Rh(1) 3.007(1), Ti(2)–Rh(2) 2.940(1), Rh(1)–Rh(2) 3.575(1).

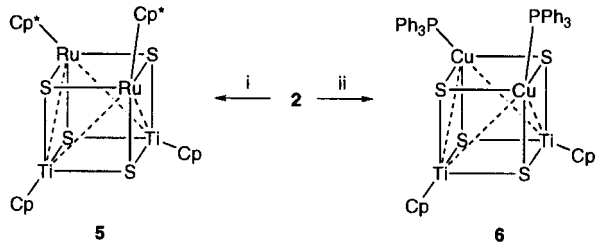

Scheme 1 *Reagents*: i, $[Cp^*Ru(\mu_3\text{-}Cl)]_4$; ii, $[Cu(\mu_3\text{-}Cl)(PPh_3)]_4$.

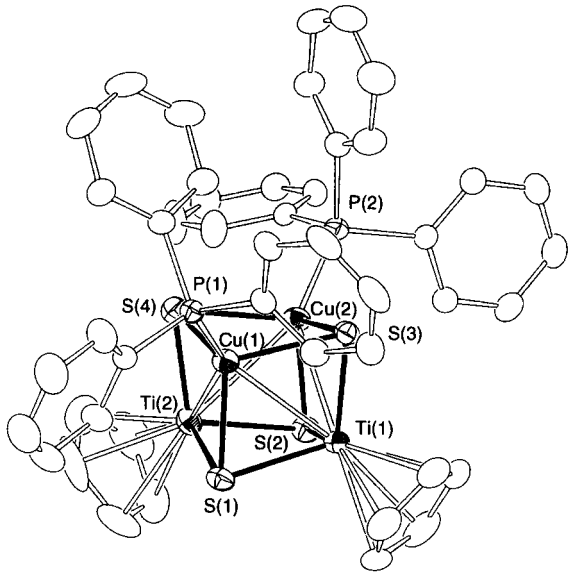

Fig. 2 Molecular structure of **6**. Hydrogen atoms are omitted for clarity. Selected interatomic distances (Å): Ti(1)–Ti(2) 3.178(1), Ti(1)–Cu(1) 2.8093(9), Ti(1)–Cu(2) 2.8306(9), Ti(2)–Cu(1) 2.8155(9), Ti(2)–Cu(2) 2.833(1), Cu(1)–Cu(2) 2.878(1).

distance in **6** [2.878(1) Å] falls in the range of those observed in Cu^I clusters which contain little direct metal–metal interaction according to theoretical calculations (2.60–3.26 Å);[16] however, the closed-shell interactions between the d^{10} metal centres remain debatable.[17] The Ti–Ti distance [3.178(1) Å] is comparable to the nonbonding Ti^{IV}–Ti^{IV} contact in the parent complex **2** [3.174(1) Å].[7]

Mixed-metal sulfido clusters containing group 4 metals are still scarce compared with those of group 6 and 8 metals.[18] The present study has demonstrated that the dinuclear organometallic thiotitanate **2** serves as a useful precursor to early–late heterobimetallic cubane-type sulfido clusters containing titanium. Further studies on syntheses of heterobimetallic clusters from **2** as well as the reactivities of **3**–**6** are now under way.

This work was supported by a Grant-in-Aid for Specially Promoted Research (09102004) from the Ministry of Education, Science, Sports, and Culture of Japan.

Notes and references

† **3**: Yield 61%. $\delta_H(C_6D_6)$ 5.83 (s, 10H, C_5H_5), 3.72–3.57, 2.51–2.32, 1.94–1.80 (m, 8H each, C_8H_{12}). **4**: Yield 57%. $\delta_H(C_6D_6)$ 5.72 (s, 10H, C_5H_5), 3.40–3.26, 2.37–2.15, 1.97–1.74 (m, 8H each, C_8H_{12}).

‡ *Crystal data*: for **3**: $C_{26}H_{34}Rh_2S_4Ti_2$, M = 776.41, monoclinic, space group $C2/c$, a = 26.410(5), b = 15.468(4), c = 15.683(4) Å, β = 119.47(2)°, U = 5577(2) Å^3, Z = 8, T = 297 K, μ(Mo-Kα) = 20.27 cm^{-1}, R = 0.037 and R_w = 0.037 for 277 variables and 4638 unique reflections [$I > 3.0\sigma(I)$]. For **6**: $C_{46}H_{40}Cu_2P_2S_4Ti_2$, M = 1005.90, monoclinic, space group $C2/c$, a = 25.876(3), b = 11.435(4), c = 31.271(4) Å, β = 105.849(9)°, U = 8900(3) Å^3, Z = 8, T = 297 K, μ(Mo-Kα) = 15.80 cm^{-1}, R = 0.040 and R_w = 0.035 for 505 variables and 5450 unique reflections [$I > 3.0\sigma(I)$]. CCDC 182/1187. See http://www.rsc.org/suppdata/cc/1999/711 for crystallographic files in .cif format.

§ Yield 32%. $\delta_H(C_6D_6)$ 7.90–6.94 (m, 30H, PPh_3), 6.39 (s, 10H, C_5H_5).

1 *Transition Metal Sulfur Chemistry*, ed. E. I. Stiefel and K. Matsumoto, American Chemical Society, Washington, 1996.
2 A. Müller, E. Diemann, R. Jostes and H. Bögge, *Angew. Chem., Int. Ed. Engl.*, 1981, **20**, 934; Y. Mizobe, M. Hosomizu, Y. Kubota and M. Hidai, *J. Organomet. Chem.*, 1996, **507**, 179; J. Guo, T. Sheng, W. Zhang, X. Wu, P. Lin, Q. Wang and J. Lu, *Inorg. Chem.*, 1998, **37**, 3689.
3 J.-P. Lang, H. Kawaguchi and K. Tatsumi, *J. Organomet. Chem.*, 1998, **569**, 109 and references therein.
4 D. Seyferth, R. S. Henderson and L.-C. Song, *Organometallics*, 1982, **1**, 125.
5 J. Wachter, *Angew. Chem., Int. Ed. Engl.*, 1989, **28**, 1613; M. A. Mansour, M. D. Curtis and J. W. Kampf, *Organometallics*, 1997, **16**, 275; Z. Tang, Y. Nomura, S. Kuwata, Y. Ishii, Y. Mizobe and M. Hidai, *Inorg. Chem.*, 1998, **37**, 4909; M. Yuki, M. Okazaki, S. Inomata and H. Ogino, *Angew. Chem., Int. Ed.*, 1998, **37**, 2126.
6 V. Krug, G. Koellner and U. Müller, *Z. Naturforsch., Teil B*, 1988, **43**, 1501.
7 P. J. Lundmark, G. J. Kubas and B. L. Scott, *Organometallics*, 1996, **15**, 3631.
8 T. R. Halbert, S. A. Cohen and E. I. Stiefel, *Organometallics*, 1985, **4**, 1689; N. Zhu, Y. Zheng and X. Wu, *J. Chem. Soc., Chem. Commun.*, 1990, 780.
9 T. Ikada, S. Kuwata, Y. Mizobe and M. Hidai, *Inorg. Chem.*, 1998, **37**, 5793; T. Ikada, S. Kuwata, Y. Mizobe and M. Hidai, *Inorg. Chem.*, 1999, **38**, 64.
10 T. Murata, Y. Mizobe, H. Gao, Y. Ishii, T. Wakabayashi, F. Nakano, T. Tanase, S. Yano, M. Hidai, I. Echizen, H. Nanikawa and S. Motomura, *J. Am. Chem. Soc.*, 1994, **116**, 3389.
11 S. Kuwata and M. Hidai, *Chem. Lett.*, 1998, 885; S. Kabashima, S. Kuwata and M. Hidai, submitted.
12 T. T. Nadasdi and D. W. Stephan, *Inorg. Chem.*, 1994, **33**, 1532.
13 R. Atencio, M. A. Casado, M. A. Ciriano, F. J. Lahoz, J. J. Pérez-Torrente, A. Tiripicchio and L. A. Oro, *J. Organomet. Chem.*, 1996, **514**, 103.
14 M. A. Casado, M. A. Ciriano, A. J. Edwards, F. J. Lahoz, J. J. Pérez-Torrente and L. A. Oro, *Organometallics*, 1998, **17**, 3414.
15 T. A. Wark and D. W. Stephan, *Inorg. Chem.*, 1990, **29**, 1731.
16 S. P. Abraham, A. G. Samuelson and J. Chandrasekhar, *Inorg. Chem.*, 1993, **32**, 6107.
17 J.-M. Poblet and M. Bénard, *Chem. Commun.*, 1998, 1179 and references therein.
18 I. Dance and K. Fisher, *Prog. Inorg. Chem.*, 1994, **41**, 637; T. Saito, in *Early Transition Metal Clusters with π-Donor Ligands*, ed. M. H. Chisholm, VCH, New York, 1995, p. 63.

Communication 9/01002E

One-pot stereoselective synthesis of tricyclic γ-lactones from 2-methoxyfuran and 2-methoxyphenols

Polisetti Dharma Rao, Chien-Hsing Chen and Chun-Chen Liao*

Department of Chemistry, National Tsing Hua University, Hsinchu, Taiwan 300. E-mail: ccliao@faculty.nthu.edu.tw

Received (in Cambridge, UK) 16th February 1999, Accepted 10th March 1999

A one-pot synthesis of the title compounds is achieved *via* highly facile Diels–Alder reactions of 2-methoxyfuran with masked *o*-benzoquinones.

The butyrolactone moiety features in a large number of natural products which exhibit interesting and useful biological activities.[1] Moreover, the butyrolactone moiety is an immediate precursor of the α-methylene-γ-butyrolactone substructure which also features in many pharmacologically important natural products.[1,2] During the synthesis of natural products, construction of a β,γ-fused butyrolactone skeleton is generally achieved in a linear fashion using various precursors that contribute at least two carbons to the butyrolactone moiety.[2,3] In contrast, there are no efficient methods that can directly and stereoselectively introduce a β,γ-fused butyrolactone unit into a carbocycle in an intermolecular reaction using a four-carbon unit.[4] In this regard, the intermolecular Diels–Alder reactions of 5-alk-1-enylfuran-2(3*H*)-one with maleic anhydride, vinyl sulfones and α-chloroacrylonitrile and intramolecular cycloaddition reactions of 5-alkadienylfuran-2(5*H*)-one are noteworthy.[5]

Masked *o*-benzoquinones (MOBs) are a type of cyclohexa-2,4-dienones with a high propensity to dimerize.[6] Our laboratory has succeeded in developing efficient procedures for their generation and in identifying their immense synthetic potential especially as dienes in Diels–Alder reactions. Their inter- and intra-molecular Diels–Alder reactions have been shown to be quite useful in the synthesis of various polysubstituted cyclohexanes, *cis*-decalins, bicyclo[2.2.2]octenones, bicyclo[4.2.2]-decenones, linear and angular triquinanes.[7,8] Although furans have been widely used as dienes in Diels–Alder reactions,[9] their dienophilic behavior was observed only in a few specially activated cases.[10] Recently we have clearly shown that furan as well as some of its derivatives can function efficiently as dienophiles in their Diels–Alder reactions with selected MOBs.[11] It occurred to us that if 2-alkoxyfurans can also function as dienophiles, the reactions would provide an easy means for the direct and stereoselective synthesis of β,γ-fused butyrolactones. Accordingly, Diels–Alder reactions of 2-methoxyfuran with several MOBs were examined. We herein report that 2-methoxyfuran reacts as a dienophile with MOBs **1a–l** generated from 2-methoxyphenols **2a–l** to provide an easy access to highly functionalized tricyclic γ-lactones **3a–l** in excellent yields (Scheme 1, Table 1).

Addition of 2-methoxyfuran to a freshly prepared MOB **1** in MeOH at 0 °C (Method A) or gradual addition of (diacetoxy)-iodobenzene (DAIB) to a mixture of 2-methoxyphenol **2** and 2-methoxyfuran in MeOH at room temperature (Method B) affords ortho esters of the type **5**. These cyclic ortho esters, which should have resulted from the addition of MeOH to the initially formed cyclic ketene acetals **4**, are not stable to purification by column chromatography and are not characterized. Instead they were hydrolyzed to afford the tricyclic lactones **3a–l** in excellent yields.[12] The reactions of MOBs **1a–c** produced considerable amounts of dimers when they were generated in the absence of 2-methoxyfuran. Consequently, phenols **2a–c** were oxidized in the presence of 2-methoxyfuran to suppress dimerization.

The gross structures of all the lactones were determined by their IR, ^{1}H and ^{13}C NMR, DEPT, low- and high-resolution mass spectral analyses. All these lactones provided satisfactory elemental analyses. The ^{1}H NMR (400 MHz) spectra of the crude reaction mixtures showed the formation of a single lactone in every case indicating the high regio- and stereoselectivity of the initial cycloaddition reactions. The regiochemistry of these cycloaddition reactions was determined by ^{1}H–^{1}H decoupling NMR experiments on the corresponding lactones in each case and is in agreement with our earlier results.[11]

The assigned stereochemistry of the lactones was deduced from the observed long-range coupling between vinylic hydrogens and the nearest ring junction hydrogens in all the cases where vinylic hydrogens exist. In the cases of **3h** and **3j**, it was assigned as shown by analogy with our earlier results where the

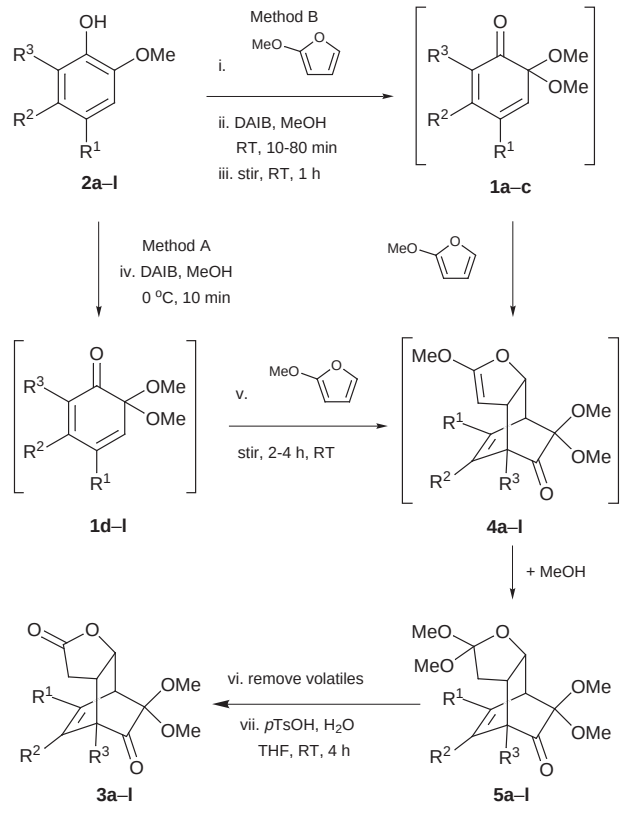

For **1–5**

a: $R^1 = R^2 = R^3 = H$
b: $R^1 = R^2 = H$, $R^3 = Me$
c: $R^1 = CO_2Me$, $R^2 = H$, $R^3 = OMe$
d: $R^1 = CO_2Me$, $R^2 = R^3 = H$
e: $R^1 = COMe$, $R^2 = H$, $R^3 = H$
f: $R^1 = R^3 = H$, $R^2 = CO_2Me$
g: $R^1 = Me$, $R^2 = R^3 = H$
h: $R^1 = Me$, $R^2 = Br$, $R^3 = H$
i: $R^1 = R^3 = H$, $R^2 = Me$
j: $R^1 = Br$, $R^2 = Me$, $R^3 = H$
k: $R^1 = Br$, $R^2 = H$, $R^3 = Me$
l: R^1 = 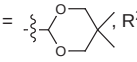 , $R^2 = R^3 = H$

Scheme 1

Table 1 Synthesis of tricyclic γ-lactones

Entry	Phenol	MOB	Method[a]	Lactone/ Yield (%)[b]
1	**2a**	**1a**	B	**3a**/80
2	**2b**	**1b**	B[c]	**3b**/44[d]
3	**2c**	**1c**	B	**3c**/80
4	**2d**	**1d**	A	**3d**/89
5	**2e**	**1e**	A	**3e**/90
6	**2f**	**1f**	A	**3f**/86
7	**2g**	**1g**	A	**3g**/88
8	**2h**	**1h**	A	**3h**/94
9	**2i**	**1i**	A	**3i**/78
10	**2j**	**1j**	A	**3j**/95
11	**2k**	**1k**	A	**3k**/93
12	**2l**	**1l**	A	**3l**/90

[a] See ref. 12. [b] Yields are of isolated lactones and are not optimized. [c] DAIB was added during 80 min. [d] Dimer of **1b** was also produced in 30% yield.

anti configuration of furan moiety to the keto group was confirmed by X-ray diffraction analysis.[11] The fact that in all the cases the *endo* adducts were produced exclusively shows that these cycloaddition reactions obey all the ground rules of Diels–Alder reactions.[13]

It is important to mention that 2-methoxyfuran was earlier shown to act as dienophile in its high pressure cycloaddition reactions with tropone albeit with moderate efficiency and poor stereoselectivity.[14] On the other hand, 2-alkoxy- and 2-silyloxyfurans have been often used as dienes and nucleophiles.[9,15] Interestingly, 2-methoxyfuran underwent facile cycloaddition with MOBs bearing electron-withdrawing as well as electron-donating substituents unlike other furan derivatives which reacted with only MOBs bearing electron-withdrawing substituents in our earlier studies.[11]

In conclusion, the present reactions make use of readily available 2-methoxyfuran and 2-methoxyphenols and produce highly complex and potentially useful multifunctional molecules in excellent yields *via* a simple one-pot process. Most importantly, these reactions resulted in the development of a novel and efficient methodology for the direct and stereoselective introduction of a β,γ-fused γ-butyrolactone moiety using 2-methoxyfuran as a masked but-3-enolide.

We thank National Science Council (NSC) of the Republic of China for financial support to our research. P. D. R. thanks NSC for a postdoctoral fellowship.

Notes and references

1 G. R. Pettit, G. M. Grag and R. H. Ode, *Biosynthetic Products for Cancer Therapy*, Plenum, New York, 1977–1979, vol. I-III.

2 P. A. Grieco, Synthesis, 1975, 67; H. M. R. Hoffman and J. Rabe, *Angew. Chem., Int. Ed. Engl.*, 1985, **24**, 94; N. Petragnani, H. M. C. Ferraz and G. Silva, *Synthesis*, 1986, 157.

3 I. Collins, *Contemp. Org. Synth.*, 1997, **4**, 281 and 1996, **3**, 295; C. H. Heathcock, S. L. Graham, M. C. Pirrung, F. Plavac and C. T. White, in *The Total Synthesis of Natural Products*, ed. J. ApSimon, Wiley-Interscience, New York, 1982, vol. 5; G. V. Boyd, in *The Chemistry of Acid Derivatives*, *The Chemistry of Functional Groups*, ed. S. Patai, Wiley, Chichester, 1979, vol. 1, p. 491 and 1992, vol. 2, p 597; J. F. Wolfe and M. A. Ogliaruso, in *The Chemistry of Acid Derivatives*, *The Chemistry of Functional Groups*, ed. S. Patai, Wiley, Chichester, 1979, vol. 1, p. 1063 and refs. cited therein.

4 M. A. Brimble and R. J. Elliot, *Tetrahedron*, 1997, 53, 7715; C. Camiletti, L. Poletti and C. Trombini, *Tetrahedron: Asymmetry*, 1996, **7**, 1059 and refs. cited therein.

5 C. Alexandre, C. Bertho, B. Tabti and F. Rouessac, *Tetrahedron*, 1991, **47**, 5481; S. D. Burke, D. R. Magnin, J. A. Oplinger, J. P. Baker and A. Abdelmagid, *Tetrahedron Lett.*, 1984, **25**, 19; D. Craig, *Chem. Soc. Rev.*, 1987, **16**, 187 and refs. cited therein.

6 G. Andersson and P. Berntsson, *Acta Chem. Scand., Ser. B*, 1975, **29**, 948.

7 For reactions of MOBs as dienes, see: D.-S. Hsu, P. D. Rao and C.-C. Liao, *Chem. Commun.*, 1998, 1795; P. D. Rao, C.-H. Chen and C.-C. Liao, *Chem. Commun.*, 1998, 155; P.-Y. Hsu, Y.-C. Lee and C.-C. Liao, *Tetrahedron Lett.*, 1998, **39**, 659; W.-C. Liu and C.-C. Liao, *Synlett*, 1998, 912; P.-Y. Hsiu and C.-C. Liao, *Chem. Commun.*, 1997, 1085; R. Carlini, K. Higgs, C. Older and S. Randhawa, *J. Org. Chem.*, 1997, **62**, 2330; C.-S. Chu, C.-C. Liao and P. D. Rao, *Chem. Commun.*, 1996, 1537 and refs. cited therein.

8 For some other recent applications of MOBs, see: R. S. Coleman and E. B. Grant, *J. Am. Chem. Soc.*, 1995, **117**, 10 889; K. S. Feldman and S. M. Ensel, *J. Am. Chem. Soc.*, 1994, **116**, 3357; A. S. Mitchell and R. A. Russell, *Tetrahedron Lett.*, 1993, **34**, 545; M. G. Banwell and M. P. Collis, *J. Chem. Soc., Chem. Commun.*, 1991, 1343 and refs. cited therein.

9 C. O. Kappe, S. S. Murphree and A. Padwa, *Tetrahedron*, 1997, **42**, 14 179.

10 E. Wenkert, P. D. R. Moeller and S. R. Piettre, *J. Am. Chem. Soc.*, 1988, **110**, 7188; M. E. Jung, L. J. Street and Y. Usui, *J. Am. Chem. Soc.*, 1986, **108**, 6810; M. S. Raasch, *J. Org. Chem.*, 1980, **45**, 867.

11 C.-H. Chen, P. D. Rao, C.-C. Liao, *J. Am. Chem. Soc.*, 1998, **120**, 13254.

12 Method A: *General procedure for 2-methoxyphenols* **2d-l**: A solution of phenol **2** (1 mM) in MeOH (10 mL) was cooled to 0 °C and DAIB (1.1 mM) was added as solid in one portion. After 10 min of stirring at 0 °C, 2-methoxyfuran (5 mM) was added and the cooling bath was removed. The reaction mixture was stirred at room temperature for 2–4 h (2 h for **2d–f** and 4 h for **2g–l**) and then MeOH and other volatile materials were removed under reduced pressure. The residue was dissolved in THF and *p*-TsOH (100 mg) and water (3 drops) were added. The resulting solution was stirred for 4 h at room temperature and the volatiles were then removed under reduced pressure. The residue was purified by column chromatography on silica gel using 40% ethyl acetate in hexanes as eluent to obtain lactone **3** as a colorless solid. Method B: *General procedure for 2-methoxyphenols* **2a-c**: To a mixture of 2-methoxyphenol (1 mM) and 2-methoxyfuran (5 mM) in MeOH (4 mL) was added a solution of DAIB (1.2 mM) in MeOH (6 mL) during a period of time (10 min for **2a** and **2c** and 80 min for **2b**) using a syringe pump at room temperature. After stirring for a further 1 h, MeOH and other volatile materials were removed under reduced pressure and the residue was subjected to hydrolysis as described in method A.

13 I. Flemming, *Frontier Orbitals and Organic Chemical Reactions*, Wiley, Chichester, 1978.

14 S. Sugiyama, T. Tsuda and A. Mori, *Chem. Lett.*, 1986, 1315; S. Sugiyama, T. Tsuda and A. Mori, H. Takeshita, M. Kodama, *Bull. Chem. Soc. Jpn.*, 1987, **60**, 3633.

15 G. Casiraghi and G. Rassu, *Synthesis*, 1995, 607; K. Oda and M. Machida, *J. Chem. Soc., Chem. Commun.*, 1994, 1477.

Communication 9/01267B

Catalytic asymmetric reaction of lithium ester enolates with imines

Kiyoshi Tomioka,*[a] Hiroki Fujieda,[b] Satoko Hayashi,[b] Mostafa Ahmed Hussein,[a] Takeshi Kambara,[a] Yumiko Nomura,[c] Motomu Kanai,[c] and Kenji Koga[c]

[a] *Graduate School of Pharmaceutical Sciences, Kyoto University, Sakyo-ku, Kyoto 606-8501, Japan. E-mail: tomioka@pharm.kyoto-u.ac.jp*
[b] *ISIR, Osaka University, Mihogaoka, Ibaraki, Osaka 567-0047, Japan*
[c] *Graduate School of Pharmaceutical Sciences, The University of Tokyo, Hongo, Bunkyo-ku, Tokyo 113-0033, Japan*

Received (in Cambridge, UK) 22nd February 1999, Accepted 11th March 1999

An external chiral tridentate amino diether ligand 7 catalyzed the condensation reaction of a lithium ester enolate 2 with an imine 3 to give the enantiomerically enriched β-lactam 4 in high yield.

Condensation of a lithium ester enolate with an imine is the established synthetic methodology for β-lactams.[1] Although the asymmetric reaction has been developed using chiral enolates or chiral imines,[2] the asymmetric reaction of achiral lithium ester enolates with prochiral imines in the presence of an external chiral controller is undeveloped.[3,4] We have reported that a ternary complex reagent, constituted from a lithium enolate, chiral diether **1** and an achiral lithium amide, enables the asymmetric condensation of the lithium ester enolate with the imine.[5] However, this methodology lacks generality because strong lithium amides cause undesirable side reactions such as deprotonation and nucleophilic attack. During continuing efforts directed towards the development of simple catalytic reactions which use lithium enolates and catalytic amounts of chiral ligands as a nucleophile and a catalyst, we found that 5–20 mol% of a tridentate amino diether ligand catalyzed asymmetric condensation of lithium ester enolates with imines to afford β-lactams in high ee. The efficiency of the reaction is crucially governed by the structural features of the ligand.

At the beginning of studies, we examined the catalytic activity of chiral diether **1** and found that condensation of 2.2 equiv. of lithium ester enolate **2**, generated from pentan-3-yl 2-methylpropanoate and LDA, with imine **3a** (R = Ph, PMP = 4-$MeOC_6H_4$) in the presence of 5 mol% of **1** in toluene at 0 °C for 7 h gave (*S*)-**4a** (R = Ph) quantitatively in 40% ee (Scheme 1).[6] It was a logical extension to examine the catalytic activity of amino ether ligand **5** because the dimethylamino group of **5** would coordinate to lithium and enhance the reactivity of the lithium enolate more efficiently than the methoxy group of **1** does.[7] As expected, the reaction was catalyzed by 5 mol% of **5** more efficiently at −20 °C for 3 h to afford **4a** quantitatively in 49% ee. Encouraged by these results, we examined the reaction in the presence of a tridentate amino diether ligand **6** which had been found to be a good ligand for the asymmetric Michael reaction of lithium thiophenoxide.[8] Although the reaction was completed within 1 h at −20 °C, the selectivity was not satisfactory, affording **4a** in only 47% ee even if 2.6 equiv. of **6** were used. However, we were pleased to find that a stoichiometric amount of amino diether **7**,[8] bearing a methoxyethoxy group in place of the methoxyphenoxy group of **6**, gave **4a** quantitatively in 91% ee after 1 h at −20 °C. Catalytic reactions using 10 and 5 mol% of **7** at −20 °C for 1.5 h gave **4a** quantitatively in 88 and 84% ees, respectively. Recrystallization of **4a** of 84% ee from Pr^i_2O gave optically pure **4a** in 75% overall yield. The chiral ligand **1** was recovered quantitatively for reuse.

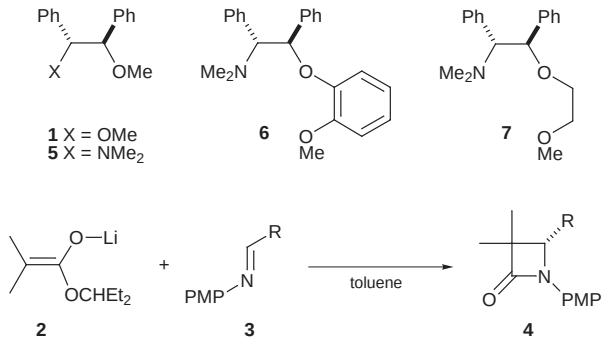

Scheme 1

The efficiency of the catalytic reaction was examined in the presence of 20 mol% of **7** using imines **3a-f** having aryl, vinyl and alkyl groups as shown in Table 1. The arylimines were converted to **4a-d** in 90–84% ee. The imine **3e** bearing a vinyl group also gave **4e** in 82% ee, whereas alkylimine **3f** was converted to **4f** in a lower 65% ee.

Table 1 The asymmetric condensation of **2** with **3** giving **4** catalyzed by **7**[a]

Entry	3	R	*t*/h	Yield (%)	Ee (%)[b]
1	**a**	Ph	1.5	99	89
2	**b**	PMP	3.5	99	90
3	**c**	1-Naphthyl	1.5	99	84
4	**d**	2-Naphthyl	2.5	99	88
5	**e**	CMe=CHPh	5	90	82
6	**f**	CH_2CH_2Ph	0.5	99	65

[a] Reaction was carried out using 20 mol% of **1** in toluene at −20 °C. [b] The ee was determined *via* chiral stationary phase HPLC using Daicel Chiralcel OD or OD-H, Pr^iOH–hexane (1 : 100). The absolute configuration was determined according to the reported procedure (ref. 5).

Although the enantioselectivity is not extremely high, we believe that the catalytic asymmetric reaction demonstrated here provides a promising approach to efficient catalytic carbon–carbon bond forming reactions.

We gratefully acknowledge financial support from the Japan Society for Promotion of Science (RFTF-96P00302), the Ministry of Education, Science, Sports and Culture, and the Science and Technology Agency, Japan.

Notes and references

1 For reviews, see: D. J. Hart and D.-C. Ha, *Chem. Rev.*, 1989, **89**, 1447; E. F. Kleinman, in *Comprehensive Organic Synthesis*, ed. C. H. Heathcock, Pergamon, Oxford, 1991, vol. 2, ch. 4.1.

2 For representative examples, see: C. Baldoli and P. D. Buttero, *J. Chem. Soc., Chem. Commun.*, 1991, 982; H. Fujioka, T. Yamanaka, N. Matsunaga, M. Fujii and Y. Kita, *Synlett*, 1992, 35; I. Ojima, Y. H. Park, C. M. Sun, T. Brigaud and M. Zhao, *Tetrahedron Lett.*, 1992, **33**, 5737; K. Hattori, M. Miyata and H. Yamamoto, *J. Am. Chem. Soc.*, 1992, **115**, 1151; F. A. Davis, P. Zhou and G. V. Reddy, *J. Org. Chem.*, 1994, **59**, 3243; M. Shimizu, Y. Teramoto and T. Fujisawa, *Tetrahedron Lett.*, 1995, **36**, 729; R. N. Warrener, L. Liu and R. A. Russell, *Chem. Commun.*, 1997, 2173.

3 The recent situation with respect to the external ligand-controlled asymmetric reaction of organolithiums with imines has been summa-

rized: S. E. Denmark and O. J.-C. Nicaise, *Chem. Commun.*, 1996, 999; D. Enders and U. Reinhold, *Tetrahedron: Asymmetry*, 1997, **8**, 1895.
4 Catalytic asymmetric addition of silyl enol ethers has been reported. H. Ishitani, M. Ueno and S. Kobayashi, *J. Am. Chem. Soc.*, 1997, **119**, 7153; E. Hagiwara, A. Fujii and M. Sodeoka, *J. Am. Chem. Soc.*, 1998, **120**, 2474; D. Ferraris, B. Young, T. Duddling and T. Lectka, *J. Am. Chem. Soc.*, 1998, **120**, 4548.
5 H. Fujieda, M. Kanai, T. Kambara, A. Iida and K. Tomioka, *J. Am. Chem. Soc.*, 1997, **119**, 2060; T. Kambara, M. A. Hussein, H. Fujieda, A. Iida and K. Tomioka, *Tetrahedron Lett.*, 1998, **39**, 9055.
6 The absolute configuration and ee were determined according to the reported procedure (ref. 5).
7 However, 1,2-bis(dimethylamino)-1,2-diphenylethane was not a satisfactory ligand for the asymmetric conjugate addition reaction of organolithiums with unsaturated imines: M. Shindo, K. Koga and K. Tomioka, *J. Org. Chem.*, 1998, **63**, 9351.
8 K. Tomioka, M. Okuda, K. Nishimura, S. Manabe, M. Kanai, Y. Nagaoka and K. Koga, *Tetrahedron Lett.*, 1998, **39**, 2141.

Communication 9/01424A

ChemComm

Biosynthesis of isoprenoids in *Escherichia coli*: stereochemistry of the reaction catalyzed by isopentenyl diphosphate : dimethylallyl diphosphate isomerase

Aquiles E. Leyes, Jonathan A. Baker, Frederick M. Hahn and C. Dale Poulter*

Department of Chemistry, 300 South 1400 East, Henry Eyring Building, University of Utah, Salt Lake City, UT 84112, USA. E-mail: poulter@chemistry.chem.utah.edu

Received (in Corvallis, OR, USA) 22nd January 1999, Accepted 25th February 1999

The interconversion of isopentenyl diphosphate (IPP) and dimethylallyl diphosphate (DMAPP) catalyzed by *E. coli* and *S. pombe* IPP isomerase proceeds with removal of the *pro-R* proton at C2 of IPP and addition of a water-derived proton to the *re* face of the C2–C3 double bond in DMAPP; this is the same stereochemistry observed for *S. cerevisiae* and rat liver enzymes.

The isomerization of isopentenyl diphosphate (IPP)† to dimethylallyl diphosphate (DMAPP) is a key activation step in the biosynthesis of isoprenoid compounds by the mevalonate pathway.[1] In eukaryotes and yeast, IPP isomerase catalyzes an antarafacial [1.3] transposition of hydrogen by a proton addition–elimination mechanism. For IPP→DMAPP, the *pro-R* proton at C2 of IPP is removed, while for DMAPP→IPP a proton from water is delivered to the *re* face of the C2–C3 double bond.

Many bacteria, including *E. coli*, and plant chloroplasts synthesize isoprenoids from 1-deoxy-D-xylulose by a non-mevalonate pathway.[2] In experiments where 3-deutero-1-deoxy-D-xylulose was fed to *E. coli* cultures, deuterium was found exclusively at the C2 position of the ω-isoprene unit of the ubiquinone-8 side chain.[3] These results are in contrast to the biosynthesis of isoprenoids in yeast and rat liver by the mevalonate pathway, where the *pro-R* proton is removed both in the isomerization and chain elongation reactions.[1] In an attempt to reconcile these observations we have determined the stereochemistry at C2 for IPP→DMAPP and DMAPP→IPP using recombinant *E. coli* enzyme.[4]

The experiment to determine the stereochemistry for IPP→DMAPP is outlined in Scheme 1. A 2 mg (6.7 μmol) sample of (*R*)-2-deuteroisopentenyl diphosphate {(*R*)-[2-^{2}H]-IPP} was incubated with 0.02 units of recombinant *E. coli* IPP isomerase and 1 unit of avian FPP synthase (FPS)[5] in a 20 mM BHDA buffer (pH 7.0) containing 1 mM $MgCl_2$, 50 mM KCl, and 0.5 mM DTT, at 37 °C. After 5 h, diethanolamine buffer (0.5 M), pH 10.5, 0.5 mM $ZnCl_2$, and 100 units of calf intestinal alkaline phosphatase were added. Incubation was continued for 8 h, after which time the samples were extracted with *tert*-butyl methyl ether. Farnesol, synthesized enzymatically from (*R*)-[2-^{2}H]-IPP, was analyzed by GC/MS. A parallel set of reactions was run using recombinant *Schizosaccharomyces pombe* IPP isomerase[6] as a control. Electron impact mass spectra for the enzymatically synthesized farnesol samples were similar to that from an authentic sample of unlabeled alcohol. An intense peak was seen at *m/z* 69 (100%) for the $C_5H_9^+$ fragment from the ω-isoprene unit. Thus, little of the deuterium originally at C2 in [2-^{2}H]-IPP was incorporated into the portion of farnesol arising from DMAPP. Chemical ionization (CH_4) mass spectra for enzymatic and unlabeled farnesol gave peaks at *m/z* 223 (1–3%, $[M + 1]^+$) and 205 (18%, $[M + 1 - H_2O]^+$). In addition, the enzymatic samples had small peaks at *m/z* 224 ([224]/[223] = 0.3) and 206 ([206]/[205] = 0.4), consistent with a small amount (~10%) of (*S*)-[2-^{2}H]-IPP in the sample. As shown in Scheme 1, the lack of deuterium incorporation in the ω-isoprene unit of farnesol indicates that the *pro-R* methylene hydrogen is preferentially removed from IPP by both *E. coli* and *S. pombe* IPP isomerases during isomerization to DMAPP.

Scheme 2 outlines a complementary set of experiments to determine the stereochemistry at C2 in the DMAPP→IPP direction. DMAPP (6 mg, 20 μmol) was incubated for 4 h with 0.6 units of IPP isomerase in a deuterated buffer[7] (pD 7.0).‡ The isomerization was rendered irreversible by adding geranyl diphosphate (GPP) (18 mg, 42 μmol) and FPP synthase (6.4 units) to the mixture so that newly formed [2-^{2}H]-IPP was immediately converted to FPP. FPP synthesized from the coupled reactions was purified by reversed phase HPLC on a C18 Magellan column§ and analyzed by ^{1}H NMR spectroscopy. As illustrated in Fig. 1, the low field region of the spectrum showed peaks at δ 4.52, 5.24 and 5.52 corresponding to protons at C1, C6/C10 and C2, respectively. The ratio of the intensities for the resonances at δ 4.52 and 5.52 (5.52/4.52 = 2.1) demonstrates that deuterium from the buffer was not incorporated at C2 of FPP. A portion of the sample was hydrolyzed with alkaline phosphatase as described previously, and analyzed by GC/MS (CI, CH_4). Samples of enzymatic and authentic unlabeled farnesol gave identical spectra. Eukaryotic FPP synthases remove the *pro-R* hydrogen from IPP during

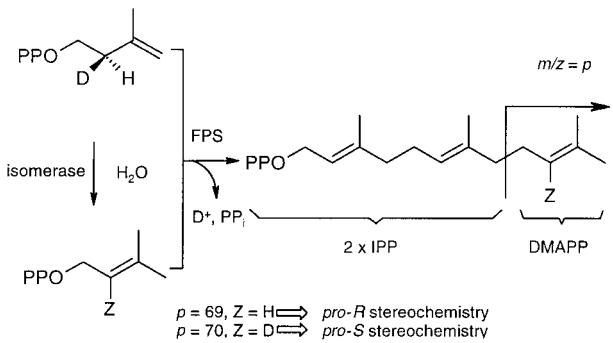

Scheme 1

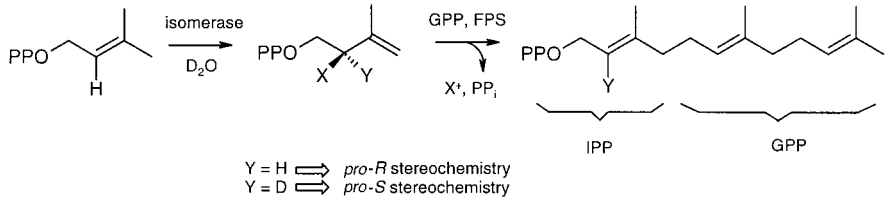

Scheme 2

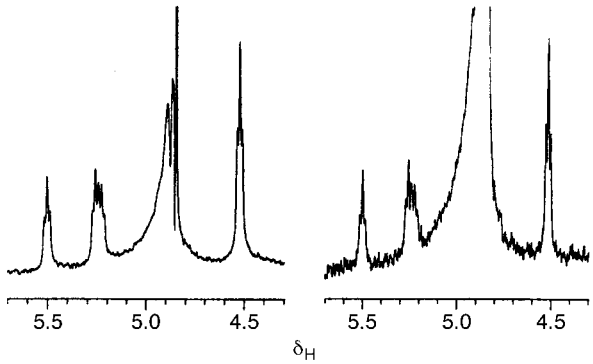

Fig. 1 500 MHz ^{1}H NMR spectra of enzymatically produced FPP in D_2O, low field region. Left: *S. pombe* isomerase reaction. Right: *E. coli* isomerase reaction. Signal at δ 5.52 corresponds to vinylic proton at C2. Solvent peak (δ 4.85) was presaturated before pulsing.

chain elongation. The absence of label in FPP therefore requires synthesis of (*R*)-2-deuteroisopentenyl diphosphate by addition of a deuterium to the *re* face of DMAPP and subsequent loss of deuterium during chain elongation.

Our data show that the stereochemistry at C2 for the reactions catalyzed by *E. coli* IPP isomerase is the same as the eukaryotic isomerases—the *pro-R* proton is removed during IPP→DMAPP and a proton is added to the *re* face of the double bond during DMAPP→IPP. These findings have interesting implications in light of the recently reported labeling studies in *E. coli* with deoxy-D-xylulose.[3] If (*S*)-[2-^{2}H]-IPP is produced from 3-deutero-1-deoxy-D-xylulose, the stereochemistry of chain elongation by *E. coli* FPP synthase must be different than its eukaryotic relatives. However, if the (*R*)-enantiomer of [2-^{2}H]-IPP is formed, the molecule of DMAPP incorporated into the ω-position of the ubiquinone side chain cannot be synthesized from IPP by the action of the *E. coli* isomerase we have characterized. Perhaps *E. coli* has another as yet unidentified IPP isomerase with the opposite stereospecificity. Alternatively, there is no *a priori* requirement that IPP be synthesized before DMAPP by the non-mevalonate pathway, and both diphosphates might be synthesized simultaneously from a common precursor. In this scenario, the *E. coli* isomerase would not be a required enzyme for isoprenoid biosynthesis but it would allow the cell to balance the concentrations of IPP and DMAPP during periods of active metabolism to optimize their utilization.

This work was supported by NIH grant GM 25521.

Notes and references

† Abbreviations used: BHDA = bicyclo[2.2.1]hept-5-ene-2,3-dicarboxylic acid; DMAPP = dimethylallyl diphosphate; FPP = farnesyl diphosphate; FPS = farnesyl diphosphate synthase; GPP = geranyl diphosphate; [2-^{2}H]-IPP = 2-deuteroisopentenyl diphosphate; IPP = isopentenyl diphosphate.

‡ Reaction conditions were as described for IPP→DMAPP, except that the buffer was deuterated.

§ Elution conditions: 0.7 ml min^{-1}, isocratic 20% MeCN-80% 25 mM NH_4HCO_3 for 7 min, then linear gradient to 100% MeCN in 20 min.

1 K. Clifford, J. W. Cornforth, R. Mallaby and G. T. Phillips, *J. Chem. Soc., Chem. Commun.*, 1971, 1599; J. W. Cornforth, R. H. Cornforth, G. Popjak and I. Y. Gore, *Biochemistry*, 1958, **69**, 146; J. W. Cornforth, R. H. Cornforth, C. Donninger and G. Popjak, *Proc. R. Soc. London, Ser. B*, 1966, **163**, 492. G. Popjak, D. S. Goodman, J. W. Cornforth, R. H. Cornforth and R. Ryhage, *Biochem. Biophys. Res. Commun.*, 1961, **4**, 138. G. Popjak, D. S. Goodman, J. W. Cornforth, R. H. Cornforth and R. Ryhage, *J. Biol. Chem.*, 1961, **236**, 1934. For a review, see C. D. Poulter and H. C. Rilling, in *Biosynthesis of Isoprenoid Compounds*, ed. J. W. Porter and S. L. Porter, Wiley, New York, 1981, vol. 1, p.161.

2 G. A. Sprenger, U. Schorken, T. Wiegert, S. Grolle, A. A. Graaf, S. V. Taylar, T. P. Begley, S. Bringer-Meyer and H. Sahm, *Proc. Natl. Acad. Sci. U.S.A.*, 1998, **94**, 12957; L. M. Lois, N. Campos, S. R. Putra, K. Danielsen, M. Rohmer and A. Boronat, *Proc. Natl. Acad. Sci. U.S.A.*, 1998, **95**, 2105. For a review, see W. Eisenreich, M. Schwarz, A. Cartayrade, D. Arigoni, M. H. Zenk and A. Bacher, *Chem. Biol.*, 1998, **5**, 221.

3 J.-L. Giner, B. Jaun and D. Arigoni, *Chem. Commun.*, 1998, 1857.

4 F. M. Hahn, J. A. Baker and C. D. Poulter, *J. Bacteriol.*, 1996, **178**, 619. The cloning and characterization of the *E. coli* isomerase has been submitted for publication elsewhere.

5 L. C. Tarshis, M. Yan, C. D. Poulter and J. C. Sacchettini, *Biochemistry*, 1994, **33**, 10871.

6 F. M. Hahn and C. D. Poulter, *J. Biol. Chem.*, 1995, **270**, 11298.

7 I. P. Street, D. J. Christensen and C. D. Poulter, *J. Am. Chem. Soc.*, 1990, **112**, 8577.

Communication 9/00621D

The self-assembly and spontaneous resolution of a hydrogen-bonded helix

Tyler B. Norsten, Robert McDonald and Neil R. Branda*

Department of Chemistry, University of Alberta, Edmonton, Alberta, Canada T6G 2G2. E-mail: neil.branda@ualberta.ca

Received (in Columbia, MO, USA) 2nd November 1998, Accepted 9th February 1999

Although geometrically similar at the single-molecule level, the crystal structures of 2,2′-dipyrrolyl ketone and its synthetic precursor, 2,2′-dipyrrolyl thioketone, vary greatly at the supramolecular level: the ketone self-assembles *via* hydrogen bonding into supramolecular helices accompanied by a spontaneous resolution process to generate homochiral crystals, whereas the thioketone assembles into non-helical and racemic crystals composed of layers of alternating enantiomers held together by weak interactions.

The ability to encode molecules with well-defined non-covalent binding motifs, such as hydrogen bond sites, is critical in order to create predictable and useful solid-state supramolecular architectures of nanoscale dimensions.[1] During the synthesis of C_2-symmetric porphyrins, we prepared 2,2′-dipyrrolyl ketone **1**

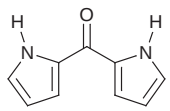

1

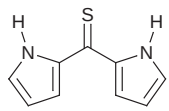

2

as previously described.[2] This simple molecule contains a high degree of encoded molecular recognition functionality. Of the twelve non-hydrogen atoms, three possess complementary hydrogen bond sites: two amine (N–H) donors and two carbonyl (C=O) lone pair acceptors. Additionally, the steric crowding of the C3 and C7 hydrogen atoms† on the two pyrrole rings forces the molecule into a twisted conformation. It was anticipated that the combination of these molecular features would translate into a helical supramolecular array held together by intermolecular N–H···O=C hydrogen bonds.[3]

We present here the crystal structures‡ of ketone **1** and its synthetic precursor, thioketone **2**. Single crystals of the ketone were obtained by layering a $CHCl_3$ solution of **1** with hexane. Ketone **1** self-assembles *via* hydrogen bonding into supramolecular helices, accompanied by a spontaneous resolution process to generate homochiral crystals. Interestingly, the sulfur analogue thioketone **2** crystallizes, under the same conditions, into a non-helical racemate.

Crystalline 2,2′-dipyrrolyl ketone **1** adopts a conformation in which both amine (N–H) groups point in the same direction as the ketone's carbonyl group [Fig. 1(*a*)]. Solution-state studies of the electric dipole moment of **1** attribute this conformational preference to the existence of intramolecular hydrogen bonding between the two N–H hydrogen atoms and the lone pair electrons of the carbonyl oxygen.[4] As expected, the crystal structure shows that the steric crowding of the C3 and C7 hydrogen atoms on the pyrrole rings does force the molecule to adopt a slightly twisted conformation. The result of these two effects is a convergent but non-coplanar self-complementary hydrogen bond surface. It is this spatial positioning of the molecular recognition sites that influences the self-assembly process in terms of the resulting supramolecular topology.

Ketone **1** crystal packs into supramolecular hydrogen bonded helices that extend indefinitely throughout the crystal lattice (Fig. 2). It is this extended network of strong N–H···O

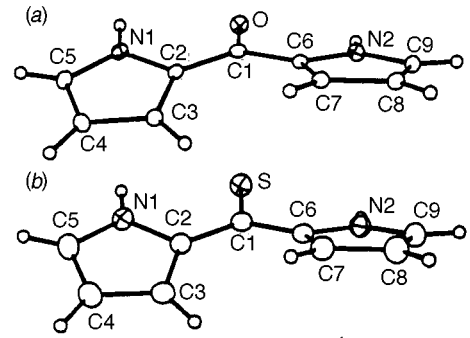

Fig. 1 Perspective view of (*a*) ketone **1** and (*b*) thioketone **2** showing the atom labeling schemes.

intermolecular hydrogen bonds (2.86 Å in length)§ that drives the formation of the helix between adjacent stacked columns of the ketone (Fig. 3). The dipyrrole building blocks are compressed within each of these columns so as to maximize favorable intermolecular π–π stacking interactions.¶ The path of the helix can easily be traced by following the hydrogen bonds counterclockwise around the two-fold screw axis of the helix (dashed lines in Fig. 3). Only one of the N–H groups is involved in intermolecular hydrogen bonding while the other N–H acts as a spectator. Two units of the ketone combine to make up a single turn of the helix generating a helical pitch of 5.9 Å.

At the molecular level, the crystal contains a single enantiomer of the ketone. This local chirality translates throughout the crystal into the formation of only left-handed (*Λ*)

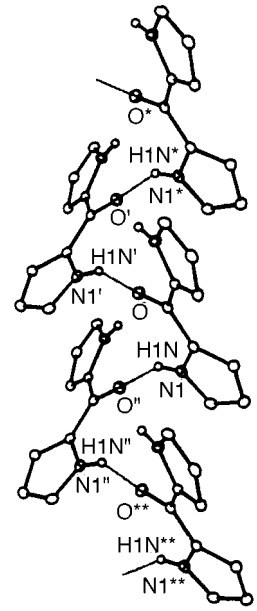

Fig. 2 View illustrating intermolecular hydrogen-bonded interactions between adjacent molecules within the helix. Carbon-bound hydrogen atoms have been omitted for clarity.

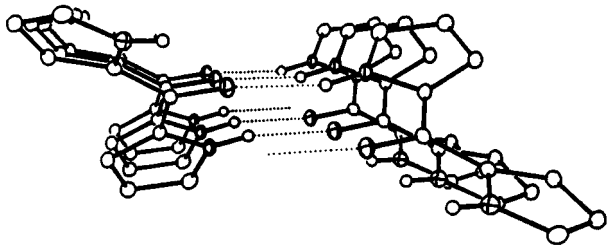

Fig. 3 Crystal packing diagram of ketone **1** viewed down the screw axis of an isolated helix. Intermolecular hydrogen bonds between stacked columns of molecular units are illustrated as dashed lines.

helices at the supramolecular level. There clearly must exist an auto-resolution process that is in effect during crystallization, whereby the pre-assembled helices *communicate* with the neighboring helices during the packing of the crystal lattice. Such chiral resolution processes are of interest because of their implications in the origin of homochirality.[5] Although only one crystal was sampled, we are assuming there exists an equal amount of crystals of both handedness in the bulk solid-state mixture.

At the molecular level, the geometry of thioketone **2** is virtually identical to that of the ketone. The only difference is a slightly increased interplanar angle (31.9°) presumably due to the larger sulfur atom, which forces the N–H groups slightly further out of coplanarity [Fig. 1(*b*)]. A significant difference is seen, however, at the supramolecular level, where a non-helical racemic crystal is generated falling into the achiral space group *Pbca*. The thioketone packs into antiparallel layers of opposing enantiomers. These layers appear to be held together by very weak interactions between the amine hydrogen and the sulfur atom of adjacent but offset enantiomers (dashed lines in Fig. 4) about which an inversion center is created. It is not clear whether these interactions can be rigidly defined as hydrogen bonds as the NH···S distance is close to the sum of the van der Waal's radii of these atoms.‖ It is clear that the replacement of the strong hydrogen bond acceptor (the carbonyl oxygen atom) with a weaker acceptor (the sulfur atom)[6] has a great effect on the supramolecular architecture. We attribute this to the change in the driving force for crystal packing from strong hydrogen bonds in the case of ketone **1** to weaker van der Waal's interactions in the case of thioketone **2**.

We have shown here that although the geometries of both ketone **1** and thioketone **2** are virtually identical at the molecular level, they vary greatly in their supramolecular topologies.[7] Where ketone **1** packs primarily *via* strong hydrogen-bonding interactions into helical arrays, the crystal packing of the thioketone **2** seems to be driven mainly by weaker interactions. The hydrogen-bonded network of ketone **1** results in a helical architecture that may play a role in the resulting auto-resolution. The effects of varying recrystallization conditions such as solvent, temperature and the presence of seed crystals are currently being investigated. This body of work demonstrates how the appropriate tailoring of prefabricated molecular components can lead to interesting supramolecular structures. Great care must be taken when choosing the molecular recognition constituents as the solid-state architecture is clearly governed by their attributes.

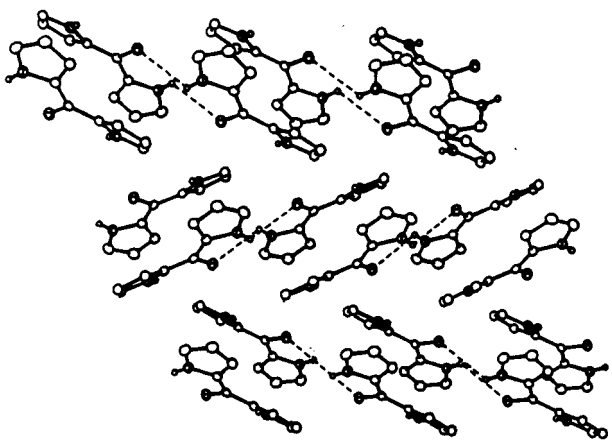

Fig. 4 Cross-section of the crystal packing diagram of thioketone **2** illustrating the herringbone arrangement of stacked antiparallel layers. Carbon-bound hydrogen atoms have been omitted for clarity. Dashed lines represent weak N–H···S contacts between offset enantiomers.

We are grateful to Dr Daniel Frankel (Nonius Co., Bohemia, New York 11716) and Scott Lovell (University of Washington, Seattle, Washington 98195-1700) for the X-ray crystallographic data collection of ketone **1**. Financial support for this work was provided by the Natural Sciences and Engineering Research Council of Canada.

Notes and references

† The numbers refer to the atom labelling scheme in Fig. 1(*a*).

‡ *Crystal data* for **1**: $C_9H_8N_2O$, M = 160.17, orthorhombic, space group $P_12_12_12_1$, (No. 19), a = 5.919 (1), b = 8.569 (1), c = 14.959 (1) Å, V = 758.7 (2) Å^3, T = −100 °C, Z = 4, μ = 0.095 mm^{-1}, number of reflections and independent reflections = 4159, $R_1(F)$ = 0.0594 [$F^2 \geq 2\sigma(F^2)$], wR_2 (F^2) = 0.1249 (all data). The absolute configuration of **1** was determined by refinement of the Flack parameter. For **2**: $C_9H_8N_2S$, M = 176.23, orthorhombic, space group *Pbca* (No. 61), a = 7.2510 (2), b = 13.8734(4), c = 16.4273 (4) Å, V = 1675.31 (8) Å^3, T = −60 °C, Z = 8, μ = 2.927 mm^{-1}, number of reflections = 2169, number of independent reflections = 1113, $R_1(F)$ = 0.0391 [$F^2 \geq 2\sigma(F^2)$], wR_2 (F) = 0.1019 (all data). In both cases, the amine hydrogen atoms were placed in calculated positions. CCDC 182/1178. Crystallographic data in CIF format are available from the RSC web site, see: http://www.rsc.org/suppdata/cc/1999/719/

¶ The shortest distance between stacked π-systems is 3.45 Å in the crystal. The aromatic pyrrole rings appear to be arranged so as to maximize offset π–π stacking.

§ The hydrogen bond length refers to the center-to-center distance between the carbonyl oxygen and N–H nitrogen obtained directly from the crystal structure.

‖ The N···S distance between antiparallel dimers is 3.50 Å which is close to the sum of the van der Waals' radii of sulfur and nitrogen (3.4 Å).

1 D. S. Lawrence, T. Jiang and M. Levett, *Chem. Rev.*, 1995, **95**, 2229; J.-M. Lehn, *Supramolecular Chemistry*, VCH, Weinheim, Germany, 1995.

2 J. A. de Groot, J. H. Koek and J. Lugtenburg, *Recl. Trav. Chim. Pays-Bas*, 1981, **100**, 405.

3 For examples of supramolecular helices, see: S. Hanessian, M. Simard and S. Roelens, *J. Am. Chem. Soc*., 1995, **117**, 7630; T. Gulik-Krzywicki, C. Fouquey and J.-M. Lehn, *Proc. Natl. Acad. Sci. U.S.A.*, 1993, **90**, 163; S. Geib, C. Vincent, E. Fan and A. D. Hamilton, *Angew. Chem., Int. Ed. Engl.*, 1993, **32**, 119; S. Sun, J. F. Britten, C. N. Cow, C. F. Matta and P. H. M. Harrison, *Can. J. Chem.*, 1998, **76**, 301; A. E. Rowan and R. J. M. Nolte, *Angew. Chem., Int. Ed.*, 1998, **37**, 63.

4 H. Lumbroso, C. Liegeois, G. C. Pappalardo and C. G. Andrieu, *J. Mol. Struct.*, 1984, **112**, 85; for an example of the solid state structure of a monopyrrolyl ketone, see: W. S. Sheldrick and W. Becker, *Acta Crystallogr., Sect. B*, 1978, **34**, 2929.

5 M. Suárez, N. Branda, J.-M. Lehn, A. Decian and J. Fischer, *Helv. Chim. Acta*, 1998, **81**,1; for a general discussion of non-chiral molecules packing into chiral crystals, see: J. Jacques, A. Collet and S. H. Wilen, *Enantiomers, Racemates and Resolution*, Wiley Interscience, New York, 1981; for other examples of hydrogen bond directed resolution in the solid state, see: H. Koshima, E. Hayashi, T. Matsuura, K. Tanaka, F. Toda, M. Kato and M. Kiguchi, *Tetrahedron Lett.*, 1997, **38**, 5009; L. Leiserowitz and M. Weinstein, *Acta Crystallogr., Sect. B*, 1975, **31**, 1463 and references cited therein.

6 V. R. Pedireddi, S. Chatterjee, A. Ranganathan and C. N. R. Rao, *J. Am. Chem. Soc.*, 1997, **119**, 10867; C. E. Bugg and U. Thewalt, *J. Am. Chem. Soc.*, 1970, **92**, 7441.

7 For a similar comparison of urea and thiourea, see: D. Mullen, *Acta Crystallogr., Sect. B*, 1982, **38**, 2620 and refs. therein.

Communication 8/08638I

ChemComm

Esterase catalysed enantioselective ring closure

C. Vivienne Barker,[a] Stewart R. Korn,[b] Michael Monteith[b] and Michael I. Page*[a]

[a] *Department of Chemical and Biological Sciences, University of Huddersfield, Queensgate, Huddersfield, UK HD1 3DH. E-mail: m.i.page@hud.ac.uk*

[b] *Zeneca, PO Box A38, Leeds Road, Huddersfield, UK HD2 1FF*

Received (in Liverpool, UK) 11th February 1999, Accepted 9th March 1999

Porcine liver esterase catalyses the reaction of γ-amino esters in water to give a mixture of the corresponding γ-lactam and the hydrolysis product, deacylation of the acyl enzyme intermediate by ring closure occurs with a high enantioselectivity giving an ee of 90% for the formation of (*S*)-5-phenyl-2-pyrrolidone from racemic ethyl 4-phenyl-4-aminobutanoate.

Enzymes which catalyse reactions in discrete steps by, for example, the formation of a covalently modified enzyme intermediate, have the potential to exhibit their chirality in at least two steps—formation and breakdown of the intermediate. Esterase enzymes catalyse the hydrolysis of esters through the intermediate formation of an acyl enzyme[1] but generally exhibit little significant enantioselectivity with racemic esters with chiral centres in either the alcohol or carboxylic acid residues.[2] Acyl enzyme intermediates potentially can be trapped not only by external nucleophiles but also intramolecularly to form cyclic products. This ring closure may be favoured over hydrolysis either because of the entropy effect[3] and/or because it is enzyme catalysed.

In the absence of enzymes, the intermolecular aminolysis of esters occurs readily only with reactive amines or with activated esters with good leaving groups,[3] or those with electron-withdrawing substituents in the acyl group.[4] Intramolecular lactam formation from amino esters occurs more easily but is normally hydroxide ion catalysed and requires high pH.[5] In aqueous solution, amide or lactam formation occurs in competition with hydrolysis which is also usually hydroxide ion catalysed and so the ratio of aminolysis to hydrolysis is dependent on the pK_a of the amino ester and the pH. By contrast, enzyme catalysed hydrolysis of esters can occur under mild conditions near neutrality. The esterase catalysed reaction of γ-amino esters generates an acyl–enzyme intermediate which could be trapped by the amino group to form a γ-lactam rather than the hydrolysis product (Scheme 1).[6]

Although the stereoselective enzymatic acylation of alcohols is well established, the enzymatic resolution of amines is less common.[7] The ring closure reaction offers a potential method of enantioselective cyclisation as it occurs at the enzyme surface, even though the first acylation step shows little or no selectivity.[2] A problem with such reactions is that it may be expected that the amino group would be protonated at neutral pH and therefore the enzyme reaction would be sensitive to pH and the pK_a of the aminium ion of the amino ester.

In the absence of enzyme, the reaction of ethyl 4-aminobutanoate in aqueous solution gives both hydrolysis and ring closed products. The ratio of 4-aminobutanoic acid to 2-pyrrolidone depends on the pH, buffer type and buffer concentration. For example, at pH 9.0 and 30 °C, no γ-lactam is formed, whereas at pH 10.0 and 12.0, 16 and 100% of the product is 2-pyrrolidone, respectively. At pHs above the pK_a of 9.9, the amount of lactam formed increases because the rate of lactamisation is given by eqn. (1), where RNH_2 and RN^+H_3 are the unprotonated and protonated forms of the γ-amino ester,

$$\text{Rate} = k_{OH}(RNH_2)(OH^-) = \frac{k_{OH}K_a}{K_w}(RNH_3^+)(OH^-)^2 \quad (1)$$

respectively, and K_a is its dissociation constant. Consequently, the rate of lactamisation is second-order in hydroxide ion at pHs below its pK_a and the rate of ring closure falls off rapidly with decreasing pH.

Likewise it was anticipated that the amount of lactam formed in the enzyme catalysed reaction and the extent of catalysis would be critically dependent on the pH and the pK_a of the amino ester. The degradation of ethyl 4-aminobutanoate in water is catalysed very effectively by pig liver esterase, with an apparent first order rate constant which shows a first order dependence on enzyme concentration. At pH 9.0, 30 °C and an enzyme concentration of 1.2×10^{-7} mol dm^{-3}, the rate of reaction is increased 360-fold over the non-enzyme catalysed reaction under the same conditions. Whereas there is no γ-lactam formed at this pH in the absence of enzyme, in its presence 48% of the product is 2-pyrrolidone. The amount of γ-lactam formed is independent of enzyme concentration, as expected for the ring closure reaction taking place within the acyl–enzyme intermediate. The amount of ring closed product formed increases with pH ranging from 20% at pH 7 to 80% at pH 10.5. The logarithm of the second order rate constant for enzyme catalysed reaction (k_{cat}/K_m) has a unit positive slope with respect to pH from pH 7.0 to 9.5, but becomes pH independent above the pK_a of the substrate with a maximal value of k_{cat}/K_m of 1.33×10^6 dm^3 mol^{-1} s^{-1}. This suggests that the substrate for the esterase catalysed reaction of the amino esters is the unprotonated form of the substrate. Below pH 7 the rate of hydrolysis of *neutral* esters falls off very fast because enzyme activity is dependent on an unknown ionising group of pK_a 7 in its basic form.[8] Above pH 7, the rate of the esterase catalysed hydrolysis of *neutral* esters is pH independent.

Similar catalytic behaviour is seen with the degradation of racemic ethyl 4-phenyl-4-aminobutanoate **1** (Scheme 3, Nu = NH) but because the pK_a is reduced to 8.90 maximal catalytic activity is reached at a lower pH and very effective catalysis occurs with an enzyme concentration of 1.0×10^{-8} mol dm^{-3}. The second order rate constant, k_{cat}/K_m, is 1.78×10^6 dm^3 mol^{-1} s^{-1} at 30 °C. Not only is the γ-lactam formed in the presence of the enzyme but it is predominantly (> 95%) the *S* enantiomer as determined by GC on a β-cyclodextrin column. The enantiomeric excess for 5-phenyl-2-pyrrolidone is independent of pH and enzyme concentration. The enantiomeric excess of the hydrolysis product agrees with that predicted from the assumption that hydrolysis is not stereoselective, as found for the hydrolysis of substituted acyclic esters.[2] For example, at pH 9.0, 38% of the γ-lactam is formed from racemic ethyl 4-phenyl-4-aminobutanoate with 90% ee for the *S* enantiomer, which gives a calculated ee for the *R* amino acid of 56%. This agrees perfectly with the observed ratio of 22% (*S*) and 78% (*R*) for 4-phenyl-4-aminobutanoic acid as determined by chiral

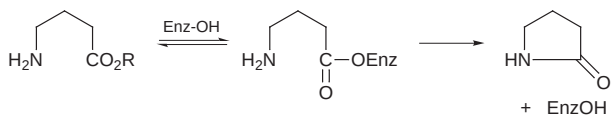

Scheme 1

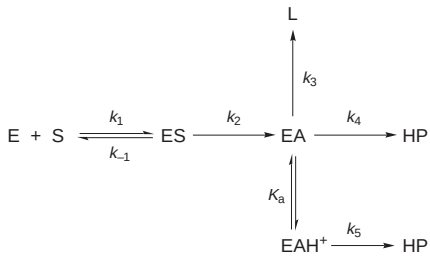

Scheme 2

HPLC (CHIROBIOTIC T250X 4.6 mm, teichoplanin coating eluting with 60 : 40 v/v EtOH–H_2O, t_R 11.5 and 13.2 min).

It is interesting to note that hydrolysis of the acyl enzyme appears to be non-selective whereas the intramolecular aminolysis to give the lactam is enantioselective. Deacylation of the acyl–enzyme is rate-limiting[2] and although the substrate for acylation of the esterase by amino esters is the neutral unprotonated amine, the same may not hold for deacylation. The dominant species at pHs below the pK_a of the amino acyl enzyme should be the protonated amine if the system is at thermodynamic equilibrium. However, the rate of hydrolysis–lactamisation could be faster than proton transfer to allow equilibrium with the pH environment. The unprotonated amino acyl enzyme (EA) must be the substrate for ring closure but not necessarily for hydrolysis (Scheme 2, where L and HP are the lactam and hydrolysis products, respectively). If the mechanism for hydrolysis and lactamisation occur through the same intermediate using the same catalytic apparatus of the enzyme then the ratio of lactam to amino acid product would be pH independent. If hydrolysis can occur through the protonated amine then the ratio of products should change with pH according to eqn. (2). The amount of lactam formed does increase with pH, as predicted by eqn. (2).

$$\frac{[\text{lactam}]}{[\text{hydrolysis}]} = \frac{k_3}{k_4 + k_5(\text{H}^+/K_a)} \qquad (2)$$

Previous work from our laboratory[2,9,10] has shown that the hydrolysis of γ-lactones catalysed by pig liver esterase occurs enantioselectively and the ring opening acylation step is selective (Scheme 3, Nu = O) whereas acylation of the acyclic hydroxy ester does not show selectivity during the hydrolysis mechanism.[9] The present results show that ring closure of γ-amino esters occurs enantioselectively (Scheme 3, Nu = NH)

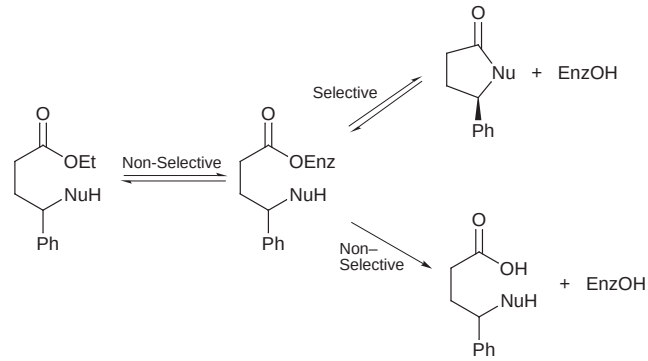

Scheme 3

and is therefore compatible with intramolecular attack of the amino group occurring from only one face of the acyl enzyme with some form of recognition for the amino group—perhaps involving the enzyme catalytic machinery used for deacylation—and a binding pocket for the phenyl group.

Chiral ring closure is less effective for other γ-substituted amino esters but pig liver esterase does also catalyse the formation of δ-lactams but not β- or ε-lactams, from their respective amino esters.

Notes and references

1 M. I. Page and A. Williams, *Organic and BioOrganic Mechanisms*, Longmans, London, 1997.
2 P. Barton, A. P. Laws and M. I. Page, *J. Chem. Soc., Perkin Trans. 2*, 1994, 2021.
3 A. C. Satterthwaite and W. P. Jencks, *J. Am. Chem. Soc.*, 1974, **96**, 7018.
4 Y. Pocker and E. Green, *J. Am. Chem. Soc.*, 1976, **98**, 6197.
5 A. J. Kirby, T. G. Mujahid and P. Camilleri, *J. Chem. Soc., Perkin Trans. 2*, 1979, 1610; T. C. Bruice and S. J. Benkovic, *J. Am. Chem. Soc.*, 1963, **85**, 1.
6 A. L. Gutman, E. Meyer, X. Yue and C. Abell, *Tetrahedron Lett.*, 1992, **33**, 3493.
7 S. Takayama, S. T. Lee, S.-C. Hung and C.-H. Wong, *Chem. Commun.*, 1999, 127.
8 D. Farb and W. P. Jencks, *Arch. Biochem. Biophys.*, 1980, **203**, 227.
9 P. Barton and M. I. Page, *J. Chem. Soc., Perkin Trans. 2*, 1993, 2317.
10 P. Barton and M. I. Page, *Tetrahedron*, 1992, **47**, 7731.

Communication 9/01204D

Hybrid organic–inorganic materials. Preparation and properties of dibenzo-18-crown-6 ether-bridged polysilsesquioxanes

Claude Chuit, Robert J. P. Corriu,* Géraud Dubois and Catherine Reyé

Laboratoire de Chimie Moleculaire et Organisation du Solide, UMR 5637 CNRS, Université de Montpellier II, Sciences et Techniques du Languedoc, Place E. Bataillon, F-34095 Montpellier Cedex 5, France.
E-mail: reye@crit.univ-montp2.fr

Received (in Cambridge, UK) 28th January 1999, Accepted 15th March 1999

The complexation of alkali metal cations (Na^+ and/or K^+) by organic–inorganic hybrid materials incorporating dibenzo-18-crown-6 ether moieties covalently linked to silica by two Si–C bonds is explained in terms of deformations of the crown ether moiety during the sol–gel process

Crown ethers[1] immobilised on organic or inorganic polymers,[2] have been widely used for the separation of alkali or alkaline earth metal ions. The use of silica as an inorganic polymer is interesting especially for ion chromatography[2] and as an ion transport membrane.[3,4] Crown ethers can be linked to the stationary phase either dynamically[5] (physically absorbed) or through a covalent bond. Up to now two methods have been used to chemically bond the crown ether to the silica framework. The first consists of anchoring either a crown ether to a chemically modified silica[6] or a silylated crown ether to silica.[7,8] The second method is the co-hydrolysis and co-polymerisation of a mixture of a crown ether bearing one hydrolysable $Si(OR)_3$ group with a tetraalkoxysilane[9] or an organotriethoxysilane[9–11] by using the sol–gel process.[12] In both cases, the crown ether is co-valently bound to the matrix by only one Si–C bond and it is located at the surface.[13,14] Recently, the sol–gel process has been used to prepare hybrid organic–inorganic materials by hydrolysis and polycondensation of organic molecules substituted by more than one hydrolysable $Si(OR)_3$ group.[15–17] It has been shown that in this case the organic units can be incorporated into the silica matrix. Furthermore, a short-range organisation has been found by means of chemical reactivity studies.[16,17]

We report here the preparation of the 4,4′(5′) mixture of the bisilylated 18-crown-6-ethers **1**, as well as its hydrolysis and polycondensation by the sol–gel process and the study of the binding ability of the resulting solid towards Na^+ and/or K^+.

Bisilylated crown ether **1** was prepared by reaction of triisopropyloxysilylmethylmagnesium chloride[18] with the commercial mixture of 4,4′(5′)-dibromo-18-crown-6.† Treatment of **1** with 1 equiv. of NaSCN or KSCN in EtOH gave the corresponding complexes **2** and **3** respectively in high yield (Scheme 1). Sol–gel polycondensation of **1**, **2** and **3** was performed at room temperature in THF solution (1 M for **1** and 0.5 M for **2** and **3**) in the presence of a stoichiometric amount of water (3 equiv.) and 10% of HCl as catalyst. The gel formation is very fast (< 5 min) for **2** and **3** but takes nearly 12 h for **1**. This large difference in gel times could be attributed to an increased rigidity for **2** and **3** compared to that of **1** and most probably to a partial protonation of the free oxygen atoms of the crown ether **1**, thus decreasing the catalytic activity of HCl. The gels were allowed to age for five days at room temperature and were powdered and washed twice with ethanol followed by diethyl ether and dried at 120 °C under vacuum (20 mm Hg) for 12 h. From ^{29}Si CP MAS NMR spectroscopy it was shown that the xerogels **X1**, **X2**[Na] and **X3**[K} all display one major resonance centred at δ −62 (substructure T^2 [C–Si(OR)-$(OSi)_2$]). Thus, in spite of different gel times the degrees of polycondensation lie in the same range. The specific surface areas of these three xerogels, determined by adsorption–desorption of N_2 (BET), were found to be very low (< 10 m^2 g^{-1}). Furthermore, during the sol–gel polymerisation of **2** and **3**, 95% of Na^+ cations and 96% of K^+ cations were retained within the xerogel (as measured by elemental analysis) which indicates that the conformation of the crown-ether moiety was not distorted during the sol–gel process.

The xerogel **X1** was treated with 1 equiv. of NaSCN or KSCN in EtOH for 12 h at room temperature or under reflux. The amount of non-complexed cations was measured by flame spectrophotometry after filtration of the solid followed by washing with EtOH until no more salt was recovered, and then evaporation of the solvent, and solubilisation of the remaining alkali metal salt in water. From these data the amount of cations incorporated into **X1** was inferred (Table 1). Further confirmation of the complexation of Na^+ and K^+ cations into **X1** was given by IR spectroscopy (DRIFT). Indeed, ν(C≡N) frequencies of NaSCN and KSCN incorporated into **X1** appear respectively

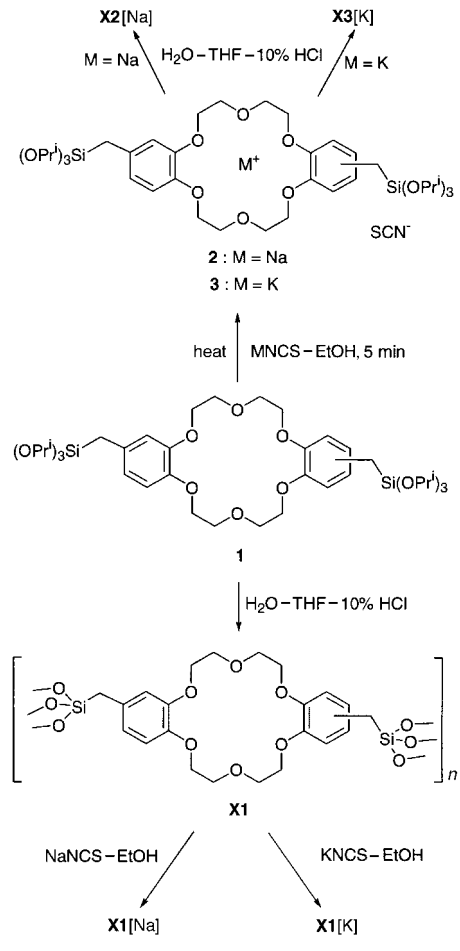

Scheme 1

Table 1 Yield (%) of alkali metal cations incorporated into xerogel **X1**

Salt	*T*/°C	%Na^+	%K^+
NaSCN	20	47[a], 47[b]	
	78	43[a], 46[b]	
KSCN	20		72[b], 73[b]
	78	12[b]	72[a], 76[b]
NaSCN–KSCN (1 : 1)[c]	78	10[b]	74[a], 76[b]

[a] Measured by flame spectrophotometry. [b] Measured by microanalysis. [c] Competitive experiments.

at 2068 and 2059 cm^{-1} (2073 and 2024 cm^{-1} for NaSCN and at 2042 and 2004 cm^{-1} for KSCN). The formation of the Na^+ complex was also shown by solid state ^{23}Na NMR spectroscopy. The ^{23}Na NMR spectrum of **X1**[Na] displays one broad signal centred at δ −25 (δ −10.6 for NaSCN under the same conditions). The poor yield (43–47%) of complexation of Na^+ cations into **X1** could be due to the rigidity of the crown ether moiety bound to the inorganic matrix, rigidity which did not allow the crown ether to adopt the more favorable conformation for the Na^+ complexation.

Competition experiments from a 1 : 1 mixture of NaSCN and KSCN in EtOH were likewise investigated using the same method of titration by flame spectrophotometry (Table 1). About 10% of the crown-ether moieties are able to complex Na^+ in the presence of K^+. As about 45% of the crown-ether moieties are able to complex Na^+ in the absence of K^+, we can conclude that about 35% of the complexing sites are able to complex both ions but should be more specific for K^+. If we compare the results of the competition experiments with those for the complexation of K^+, we can infer that about 40% (75 − 35) of the crown ether moieties are specific for K^+. Thus from the overall results it appears that the crown-ether sites are of three types: (1) specific for Na^+ (*ca.* 10%), (2) able to complex both ions but more specifically K^+ (*ca.* 35%) and (3) specific for K^+ (*ca.* 40%). One explanation could be that during the sol–gel process the crown ether undergoes steric constraints which distort the rings giving rise, in the xerogel, to sites which are specific for the complexation of Na^+ and/or K^+. Furthermore from the competition experiments, it appears that 85–90% of the crown ether moieties are accessible to the salts, though the crown-ether moieties are most probably located in the core of the solid in contrast to the case of crown-ether grafted to silica.[6–8] In order to analyse the surface composition of these materials, TOF-SIMS investigations[14] are currently in progress.

Notes and references

† *Experimental procedure*. A mixture of 80.4 ml (579 mmol) of a THF solution of $(Pr^iO)_3SiCH_2MgCl$,[18] 10 g (19.2 mmol) of 4,4′(5′)-dibromo-18-crown-6, and 630 mg (1.16 mmol) of $(PPh_3)_2NiCl_2$ in THF (200 ml) was heated under reflux for 48 h. The THF was removed under vacuum and 150 ml of ether was added to precipitate the salts. After filtration and removal of ether under vacuum, 35.4 g of the $MgCl_2$–crown ether complex was obtained as a brown oil. Decomplexation was accomplished by heating the complex in 200 ml of MeOH under reflux overnight. MeOH was removed under vacuum and 150 ml of pentane was added. A precipitate was formed which was filtered and washed with pentane (3 × 50 ml). Evaporation of pentane gave 17.6 g of a yellow oil which was purified by chromatography to give 6 g (7.52 mmol, 39%) of **1** as a white oil.

NMR ($CDCl_3$): ^1H, δ 1.07 (d, 36H, d, CH_3), 2.02 (s, 4H, CH_2Si), 3.93 (m, 8H CH_2O), 4.07 (m, 14H, CH_2O + CH), 6.66–7.02 (m, 6H, aryl); ^{13}C, δ 21.15 (CH_2Si), 25.9 (CH_3), 65.6 (CH), 69.2, 69.7, 70.45, 70.52, 70.63 (CH_2O), 114.55, 114.67, 115.38, 115.49, 121.96 (CH aryl), 131.8, 146.4, 148.96 (C aryl); ^{29}Si, δ −54.8. Satisfactory elemental analyses (C, H, Si) were obtained.

1 J. C. Pedersen, *J. Am. Chem. Soc.*, 1967, **89**, 7017.
2 M. Takagi and H. Nakamura, *J. Coord. Chem.*, 1986, **15**, 53.
3 J. C. Galvan, P. Aranda, J. M. Amarilla, B. Casal and E. Ruiz-Hitzky, *J. Mater. Chem.*, 1993, **3**, 687.
4 P. Lacan, C. Guizard, P. Le Gall, D. Wettling and L. Cot, *J. Membr. Sci.*, 1995, **100**, 99.
5 K. Kimura, E. Hayata and T. Shono, *J. Chem. Soc., Chem. Commun.*, 1984, 271.
6 T. G. Waddell and D. E. Leyden, *J. Org. Chem.*, 1981, **46**, 2406.
7 J. S. Bradshaw, R. L. Bruening, K. E. Krakowiak, B. J. Tarbet, M. L. Bruening, R. M. Izatt and J. J. Christensen, *J. Chem. Soc., Chem. Commun.*, 1988, 812.
8 C. W. McDaniel, J. S. Bradshaw, K. E. Krakowiak, R. M. Izatt, P. B. Savage, B. J. Tarbet and R. L. Bruening, *J. Heterocycl. Chem.*, 1989, **26**, 413.
9 M. Barboiu, C. Luca, C. Guizard, N. Hovnanian, L. Cot and G. Popescu, *J. Membr. Sci.*, 1997, **129**, 197.
10 P. Aranda, A. Jiménez-Morales, J. C. Galvan, B. Casal and E. Ruiz-Hitzky, *J. Mater. Chem.*, 1995, **5**, 817.
11 K. Kimara, T. Sunagawa and M. Yokoyama, *Chem. Commun.*, 1996, 745.
12 C. J. Brinker and G. W. Cherer, *Sol–Gel Science*, Academic Press, London, 1990; L. L. Hench and J. K. West, *Chem. Rev.*, 1990, **90**, 33.
13 U. Schubert, N. Hüsing and A. Lorenz, *Chem. Mater.*, 1995, **7**, 2010.
14 G. Cerveau, R. J. P. Corriu, J. Dabosi, J. L. Aubagnac, R. Combarieu and Y. de Puydt, *J. Mater. Chem.*, 1998, **8**, 1761.
15 D. A. Loy and K. J. Shea, *Chem. Rev.*, 1995, **95**, 1431.
16 R. J. P. Corriu and D. Leclercq, *Angew. Chem., Int. Ed. Engl.*, 1996, **35**, 1421; R. Corriu, *Polyhedron*, 1998, **17**, 925; R. Corriu, *C. R. Acad. Sci. Sér. IIc*, 1998, 83.
17 G. Cerveau, R. J. P. Corriu and C. Lepeytre, *Chem. Mater.*, 1997, **9**, 2561.
18 D. J. Brondani, R. J. P. Corriu, S. El Ayoubi, J. J. E. Moreau and M. Wong Chi Man, *J. Organomet. Chem.*, 1993, **451**, C1.

Communication 9/00767I

Novel supported uranium oxide catalysts for NO_x abatement

Steve D. Pollington,[a]† Adam F. Lee,*[a] Tina L. Overton,[a] Patrick J. Sears,[a] Peter B. Wells,*[a] Sarah E. Hawley,[b] Ian D. Hudson,[b] Darren F. Lee*[b] and Victoria Ruddock[b]

[a] *Department of Chemistry, University of Hull, Hull, UK HU6 7RX. E-mail: P.B.Wells@chem.hull.ac.uk*
[b] *R + T BNFL plc. Springfields, Salwick, Preston, Lancashire, UK PR4 OXJ*

Received (in Oxford, UK) 29th January 1999, Accepted 10th March 1999

The catalytic reduction of NO has been studied over novel supported uranium oxide catalysts which exhibit comparable activity and selectivity to that of conventional supported Pt catalysts and for which *in situ* XRD identifies the active phase to be UO_x ($2 < x < 2.25$).

Emissions of NO and higher nitrogen oxides (NO_x) are the subject of stringent legislation as a result of their adverse environmental impact.[1] An effective method of reducing such emissions is to employ catalytic systems such as the three-way catalyst, currently installed in automotive vehicles, and selective catalytic reduction (SCR) of NO_x by ammonia in stationary sources. Selectivity is a key issue since catalysts can reduce NO_x to undesirable nitrous oxide (N_2O) instead of nitrogen. Nitrous oxide is now recognised as a contributor to the destruction of ozone in the stratosphere and has a high Greenhouse coefficient. Despite intensive research over many years few catalyst systems have been developed which exhibit both the desired levels of activity, selectivity and stability, together with high poison tolerances.

The potential of uranium oxides as catalytic materials has been reviewed by Collette *et al.*[2] Uranium is an actinide element and, with six valence electrons, is similar to chromium, molybdenum and tungsten. The ability to attain high coordination numbers makes for a promising catalytic material and indeed uranium has been used in applications such as Fischer–Tropsch synthesis, dehydrogenation and oxidation (ref. 2 and references therein). More recently, uranium oxides have been identified as candidates for the destruction of volatile organic compounds.[3,4] Uranium is reported to be a uniquely effective promoter of rhodium and platinum in three-way catalysts in the presence of high sulfur levels.[5–7] This study identifies uranium oxide derived catalysts for the selective reduction of nitric oxide.

Reactions were performed in a single-pass, fixed-bed microreactor. The reactor comprised a 10 mm i.d. silica tube located inside a Carbolite MTF furnace. Gas-flow rates were independently regulated by three mass-flow controllers (Hastings and MKS). An in-line filter (2 μm) was located downstream of the reactor to contain UO_x dust particles. On-line analysis of reactant and product gas streams was performed using a Perkin-Elmer 8410 TCD gas chromatograph with a Carboxen 1000 (60/80 mesh) column. Quoted conversions are ±3% and selectivities are ±5%. The catalyst charge, of between 0.5 and 4 g (250–500 μm particle size), was supported inside the reactor on a silica wool bed. The catalyst temperature was read from an external thermocouple located adjacent to the catalyst bed. The feed gases used in this study included NO (99%), CO (99.99%) and He (99%). A constant GHSV of 2300 h^{-1} (total gas flow rate of 70 ml min^{-1}) was employed in all experiments, using a 4% NO and 4% CO mixture with He balance. Before reaction, samples were heated to temperature under He (30 ml min^{-1}) before introducing reactants. *In situ* XRD spectra were acquired at BNFL Springfields using a Philips Expert MPD diffractometer and Cu-Kα radiation in conjunction with an Antonparr XRK cell equipped with Brooks mass-flow controllers. The scan range was 2θ = 5–50° in increments of 0.05°. Single point BET (N_2) surface areas were determined by standard N_2 adsorption for samples degassed at 200 °C.

Alumina supported catalysts were synthesised from solutions of uranium(VI) dinitrate hexahydrate, $UO_2(NO_3)_2{\cdot}6H_2O$ (Strem Chemicals 99.8%) as follows. First, $UO_2(NO_3)_2{\cdot}6H_2O$ (containing *ca.* 0.2% ^{235}U) was dissolved in water to produce a 1.1 M solution (pH = 2). A known quantity of the support was dried and subsequently impregnated with the $UO_2(NO_3)_2{\cdot}6H_2O$ solution by the incipient wetness method. Finally, samples were dried for 24 h at 100 °C prior to calcination under flowing air for 3 h at either 450 or 800 °C. The support used was γ-Al_2O_3 (Alumina C, Degussa), with catalysts designated as UO_x(450 or 800). A third catalytic formulation, $UO_x(H_2)$, was obtained by reducing the 800 °C calcined sample under flowing hydrogen for 10 h at 523 °C as described by Madhavaram *et al.*[8] The nominal uranium oxide loadings (based on oxide stoichiometries discussed below) ranged between 26 and 29 wt%. Comparative experiments were also conducted with uranium(V,VI) oxide (U_3O_8 99.8%), and a conventional 5 wt% Pt/Al_2O_3 Type 94 catalyst from Johnson Matthey. Before reaction, samples were heated under He (30 ml min^{-1}) to 450 °C for 1 h and cooled to reaction temperature. Steady-state was achieved and results obtained after > 1 h reaction.

In the absence of a reductant, the uranium-oxide catalysts, and the alumina support, were each inactive for direct NO decomposition at temperatures below 1000 °C. In contrast, following the introduction of CO the light-off curves shown in Fig. 1 were obtained. For simplicity, only results for the most active bulk UO_x phase, which we have identified as U_3O_8, are included. The catalytic performance of the $UO_x(H_2)$ and UO_x(800) samples was indistinguishable, and hence only results for the UO_x(800) catalyst are shown.

The most striking aspect of the light-off curves is the substantial promotional effect of supporting uranium oxides on high surface area oxide supports. The temperature for 50% NO conversion (T_{50}) is decreased by up to 300 °C following UO_x

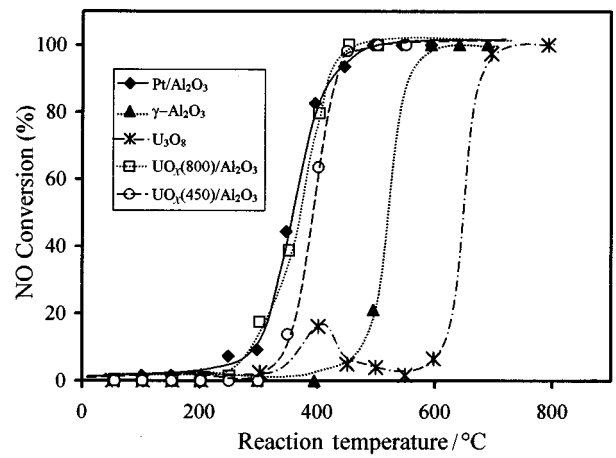

Fig. 1 Effect of temperature on catalyst activity for NO reduction.

† Present address: Johnson Matthey Technology Centre, Sonning Common, Reading, UK.

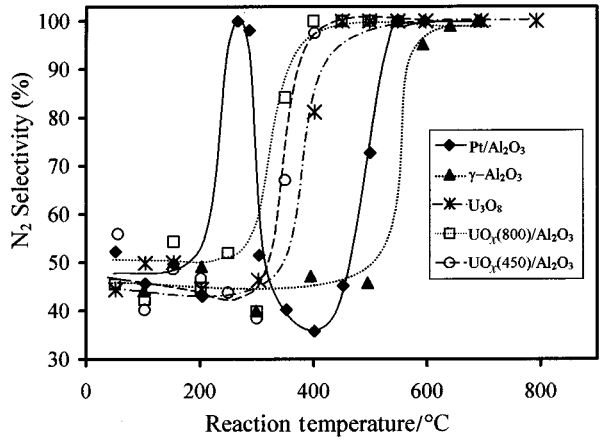

Fig. 2 Effect of temperature on catalyst selectivity towards N_2.

Table 1 BET surface areas for fresh and post light-off catalyst samples[a]

Sample	Surface area[b]/m^2 g^{-1} (±5 %)
5% Pt/Al_2O_3 (fresh)	144
5% Pt/Al_2O_3 (post reaction)	137
UO_x(800) (fresh)	52
UO_x(800) (post reaction)	54
UO_x(450) (fresh)	57
UO_x(450) (post reaction)	57

[a] *Reaction conditions*: 4% NO + 4% CO, balance He; T_{react} = 25–1000 °C. [b] ±5%.

dispersion on alumina; indeed bulk U_3O_8 is less active for NO reduction than the alumina support. T_{50} values for the supported UO_x/Al_2O_3 catalysts appear relatively insensitive to precalcination temperature, although higher temperature calcination does produce the most active uranium catalyst. Remarkably these supported catalysts exhibit T_{50} values essentially identical to those of a commercial Pt/Al_2O_3 NO_x-reduction catalyst. The best uranium-derived catalyst, UO_x(800) lights off at *ca.* 250 °C, attaining 100% NO conversion above 400 °C. Light-off was accompanied in all cases by small, sustained exotherms of *ca.* 5–10 °C.

Over all the uranium catalysts the initial low temperature reduction of NO produced predominantly N_2O as the major product. With increasing reaction temperature and thus NO conversion, the selectivities of all bulk and supported uranium catalysts rise rapidly, with 100% selectivity towards N_2 achieved above 400 °C (Fig. 2). The temperature-dependent selectivity of the Pt/Al_2O_3 catalyst differs markedly from those of the uranium catalysts. Selectivity towards N_2 rises to a sharp maximum just before catalyst light off, albeit at low conversions, before gradually returning to zero at at *ca.* 400 °C. The selectivity recovers at higher temperatures with only N_2 formed above 500 °C, although at these temperatures the alumina support is itself active and selective for NO reduction to N_2.

Preliminary lifetime studies (> 24 h on-stream) show that the supported UO_x catalysts exhibit both high thermal stability and high sulfur tolerance. Indeed steady state NO conversion remains *ca.* 60% after 140 h reaction at 375 °C in the absence of SO_2, and at similar levels for > 17 h after the introduction of 1000 ppm SO_2 into the reaction stream at 550 °C, conditions which strongly poison the commercial Pt/Al_2O_3 catalyst. The N_2 BET surface areas of the fresh and spent supported UO_x catalysts are *ca.* 50 m^2 g^{-1} for reaction temperatures up to 1000 °C, above which the alumina support itself begins to sinter (Table 1).

The supported UO_x catalysts underwent colour changes during use in the reactor. The UO_x(800) sample turned from green to brown, while the UO_x(450) sample changed from orange to brown. Comparison with the colours of bulk uranium oxides suggests that these changes are associated with catalyst reduction from U_3O_8-like and UO_3-like phases respectively to a UO_2-like phase under reaction conditions. This interpretation is supported by *in situ* XRD measurements (Fig. 3) on the UO_x(450) and UO_x(800) sample. For both catalysts a phase transformation occurs between 375 and 400 °C associated with the disappearance of reflections at 2θ 21.4, 26.02 and 33.94° characteristic of stoichiometric U_3O_8, and the emergence of new peaks at 2θ 28.37 and 32.9° characteristic of stoichiometric UO_2. This transformation is complete above 400 °C for the UO_x(800) catalyst; however, for the UO_x(450) catalyst calcined at lower temperature a mixture of U_3O_8 and UO_2 phases coexists even after reaction at 525 °C. The $UO_x(H_2)$ sample remained brown for the duration of the experiments and the *in situ* XRD data exhibited diffraction lines at 2θ 28.37 and 32.9°, characteristic of stoichiometric U_4O_9, which did not change for the duration of the experiment. No such colour or phase changes are observed following identical thermal treatments under inert atmospheres for any sample. These results suggest the existence of a common active phase of stoichiometry UO_x ($2 < x < 2.25$) within the supported UO_x catalysts.

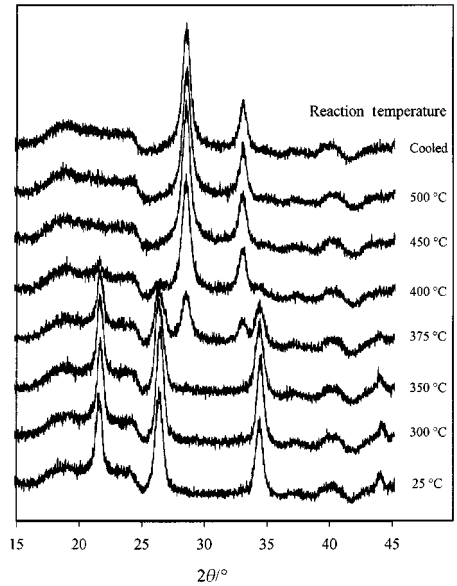

Fig. 3 *In situ* X-ray diffractograms for UO_x(800) as a function of temperature under standard reaction conditions.

P. B. W., A. F. L., T. L. O. and S. D. P. thank BNFL Springfields for financial assistance.

Notes and references

1 J. N. Armor, *Catal. Today*, 1995, **26**, 99.
2 H. Collete, V. Dereminee-Mathieu, Z. Gabelica, J. B. Nagy, E. G. Derouane and J. J. Verbist, *J. Chem. Soc., Faraday Trans. 2*, 1987, **83**, 1263.
3 G. J. Hutchings, C. S. Heneghan, I. D. Hudson and S. H. Taylor; in *Heterogeneous Hydrocarbon Oxidation*, ed. B. K. Warren and S. E. Oyama, *ACS Symp. Ser.*, 1996, p. 58.
4 G. J. Hutchings, C. S. Heneghan, I. D. Hudson and S. H. Taylor, *Nature*, 1996, **384**, 341.
5 F. Nakajima, M. Takeuchi, S. Matsuda, S. Uno, T. Mori, Y. Watanabe and M. Imanari, *US Pat.* 4085193, 1978.
6 G. C. Joy, *US Pat.*, 4232542, 1982.
7 G. Mabilon, D. Durand, P. Courty and M. Priget, *US Pat.* 5051392, 1991.
8 H. Madhavaram, P. Buchanan and H. Idriss, *J. Vac. Sci. Technol. A*, 1997, **15**, 1685.

Communication 9/00802K

ChemComm

Epoxidation of alkenes using dioxygen in the presence of an alcohol catalyzed by *N*-hydroxyphthalimide and hexafluoroacetone without any metal catalyst

Takahiro Iwahama, Satoshi Sakaguchi and Yasutaka Ishii*

Department of Applied Chemistry, Faculty of Engineering & High Technology Research Center, Kansai University, Suita, Osaka 564-8680, Japan. E-mail: ishii@ipcku.kansai-u.ac.jp

Received (in Cambridge, UK) 1st March 1999, Accepted 12th March 1999

A new approach for the epoxidation of alkenes using O_2 without any metal catalyst was developed; a variety of alkenes were epoxidized in a regio- and stereoselective manner with O_2 in the presence of benzhydrol catalyzed by *N*-hydroxyphthalimide and hexafluoroacetone.

From an economic and environmental viewpoint, the epoxidation of olefins with O_2 is valuable and particularly attractive. Therefore, much effort has been made to utilize O_2 for the epoxidation of olefins, especially using transition metals as catalysts.[1] However, few efficient catalytic aerobic oxidation systems are known that proceed under mild conditions and are amenable to the production of bulk and fine chemicals.[2] We have recently found a novel aerobic oxidation system of hydrocarbons *via* a radical process which employs *N*-hydroxyphthalimide (NHPI) as the catalyst under mild conditions.[3,4] Using this method, alcohols are also able to be oxidized with O_2 to ketones or carboxylic acids *via* the formation of α-hydroxy hydroperoxides.[5] To highlight the importance of this radical catalyst for aerobic oxidation, our efforts are now directed to a new approach for the epoxidation of alkenes using O_2 without any metal catalyst.

Our epoxidation involves a new strategy consisting of radical and ionic processes as key reactions, *i.e.* (i) *in situ* generation of H_2O_2 *via* α-hydroxy hydroperoxide **A** from an alcohol and O_2 assisted by NHPI, and (ii) the epoxidation of olefins by 2-hydroperoxyhexafluoropropan-2-ol **B** derived from the formed H_2O_2 and hexafluoroacetone (HFA) (Scheme 1).†

To optimize reaction conditions for the epoxidation of alkenes, oct-2-ene **1** was chosen as a model substrate and allowed to react under O_2 (1 atm) in the presence of alcohol **2** under the influence of catalytic amounts of NHPI and HFA (Table 1).‡

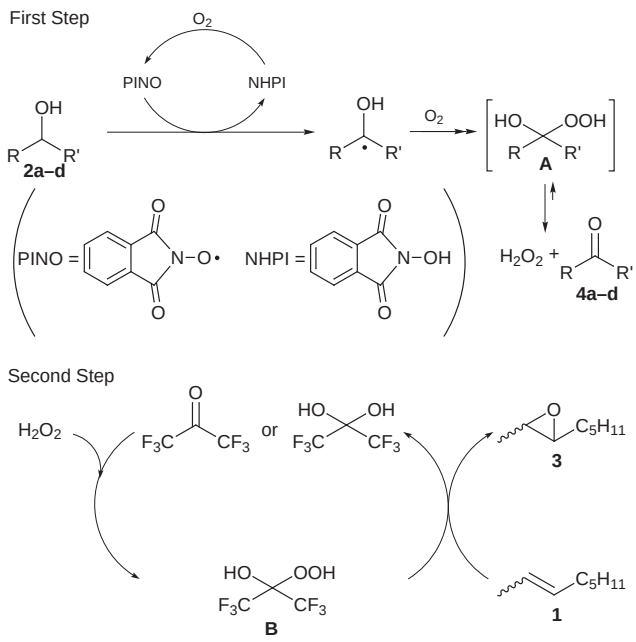

Scheme 1

The first variable examined was the alcohol used as the source of hydroperoxide (entries 1–4). It was proved that benzhydrol **2b** is the best source of hydroperoxide in the present epoxidation system. The use of propan-2-ol **2c** reduced the conversion and selectivity of **1** to **3**. It is believed that abstraction of the α-hydrogen from **2c** by phthalimide-*N*-oxyl (PINO), generated from NHPI and O_2, takes place in competition with abstraction of the allylic hydrogen of the olefin **1**.§ In an electrochemical oxidation using NHPI as the mediator, Masui *et al.* reported that the allylic oxidation of olefins occurs more easily than the dehydrogenation of alcohols, such as propan-2-ol and cyclohexanol, to ketones.[6] Hence, in epoxidations using an alcohol whose α-hydrogen is more easily abstracted than the allylic hydrogen of **1**, the epoxidation was expected to proceed more easily. Thus, the reaction of **1** using benzyl alcohol **2d** led to **3** with higher selectivity and conversion. HFA was also important to complete the epoxidation (entries 1, 5 and 6). An α-hydroxy hydroperoxide derived from 1,1,1-trifluoroacetone was inadequate to epoxidize **1** in satisfactory yield.

On the basis of these results, the aerobic epoxidation of various olefins using **2b** in the presence of catalytic amounts of NHPI and HFA was examined under selected reaction conditions (Table 2).

The epoxidation of *cis*- and *trans*-oct-2-enes proceeded smoothly in a stereospecific manner to form *cis*- and *trans*-2,3-epoxyoctanes, respectively, in high yields. It is noteworthy that the present system provides a stereospecific epoxidation route with O_2, since in the epoxidation of *cis* olefins using O_2 no such selectivity has been previously observed. Geranyl acetate and neryl acetate afforded the corresponding epoxides in which the double bonds remote from their acetoxy groups were epoxidized with high regioselectivities. Even terminal olefins, which are difficult to epoxidize compared with internal olefins, could be epoxidized by the present method. However, the epoxidation of cyclohexene led to cyclohexene oxide in

Table 1 Epoxidation of oct-2-ene **1** to 2,3-epoxyoctane **3** with O_2 in the presence of alcohols **2a–d** by NHPI and HFA[a]

		Conversion (%)		Yield (%)[b]	
Run	Alcohol	**1**	**2a–d**	**3**	**4a–d**
1	MePhCHOH **2a**	90	30	66 (73)	29 (97)
2[c]	Ph_2CHOH **2b**	94	36	85 (90)	33 (92)
3[d]	Pr^iOH **2c**	58	—	24 (42)	—
4	BnOH **2d**	84	27	60 (71)	20 (74)
5[e]	**2a**	7	34	3	32 (94)
6[f]	**2a**	8	34	4	33 (98)

[a] **1** (3 mmol) was allowed to react with O_2 (1 atm) in the presence of NHPI (10 mol%), HFA (HFA•$3H_2O$) (10 mol%) and **2** (15 mmol) in PhCN (6 ml) for 24 h. [b] Product yields were determined by GC analysis. Selectivity is in parentheses. [c] 18 h. [d] Conversion of **2c** and yield of **4c** were not determined. [e] In the absence of HFA. [f] 1,1,1-Trifluoroacetone was used instead of HFA.

Table 2 Epoxidation of various alkenes with O_2 catalyzed by NPHI and HFA in the presence of benzhydrol **2b**[a]

Entry	Substrate	*t*/h	Conversion (%)	Product	Yield (%)	Selectivity (%) (*trans* : *cis*)
1	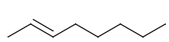	18	93	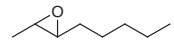	87	93 (>99:<1)
2 [b]		24	90		72	80 (>99:<1)
3	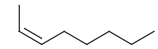	16	94	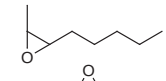	81	86 (98:2)
4	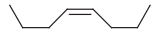	16	96		80	83 (99:1)
5	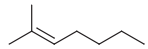	15	90	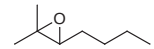	74	82
6	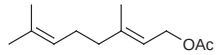	20	88	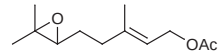	71	81
7	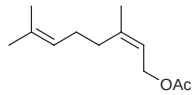	20	89	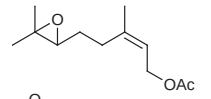	74	83
8 [c,d]	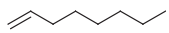	24	80	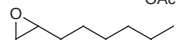	72	90
9 [d,e]	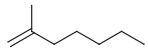	24	83	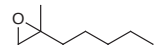	70	84
10 [d,f]		24	78		63	80
11 [d,e]	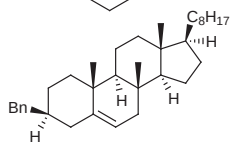	20	72	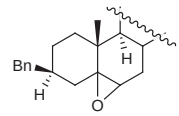	60	83 (75:25)

[a] Substrate (3 mmol) was allowed to react under dioxygen (1 atm) in the presence of NHPI (0.3 mmol), HFA (0.3 mmol) and **2b** (15 mmol) in PhCN (6 ml) at 80 °C. [b] **2a** was used in place of **2b**. [c] Reaction was carried out at 90 °C. [d] α,α,α-Trifluorotoluene was used as solvent. [e] NHPI (0.6 mmol) was used. [f] Cyclohex-2-en-1-one (8%), cyclohex-2-en-1-ol (2%) and cyclohexane-1,2-diol (1%) were obtained. [g] Ratio α : β.

somewhat lower yield because of concomitant formation of allylic oxidation products such as cyclohexenone (8%) and cyclohexenol (2%). Cholesteryl benzoate produced the 5,6-α-epoxide in preference to the 5,6-β-epoxide (α : β = 75 : 25), which is comparable to epoxidation by MCPBA.[7] In contrast, the same epoxidation using the aldehyde–O_2 system with an Ni complex is reported to give α : β = 31 : 69.[8]

We believe that the actual epoxidizing reagent **B** arises from HFA and H_2O_2 liberated from α-hydroxy hydroperoxides **A**.[9] In fact, ^{1}H NMR experiments show that treatment of **2a** with O_2 in the presence of NHPI in CD_3CN at 70 °C produced H_2O_2, but not α-hydroxy hydroperoxide.¶

In conclusion, we have developed the epoxidation of olefins by *in situ* generation of H_2O_2 from alcohols and O_2 under the influence of NHPI and HFA without any metal catalyst. This method provides an alternative route to the epoxidation of olefins by molecular oxygen in a stereospecific manner.

This work was partly supported by the Research for the Future program.

Notes and references

† 2-Hydroperoxyhexafluoropropan-2-ol is reported to be easily derived from HFA (or HFA hydrate) and H_2O_2: see R. P. Heggs and B. Ganem, *J. Am. Chem. Soc.*, 1979, **101**, 2484.

‡ *Typical procedure* for the epoxidation of **1**: A PhCN (6 ml) solution of **1** (3 mmol), NHPI (49 mg, 10 mol%), HFA•$3H_2O$ (66 mg, 10 mol%) and **2b** (15 mmol) was placed in a two–necked flask equipped with a balloon filled with O_2. The mixture was stirred at 80 °C for 18 h, and then extracted with Et_2O. The organic layer was dried over $MgSO_4$ and analyzed by GLC with an internal standard. The products were separated from the solvent under reduced pressure and purified by column chromatography on silica gel (*n*-hexane–AcOEt = 20 : 1) to give the corresponding epoxides.

§ In a previous paper, we reported that phthalimide-*N*-oxyl (PINO) is produced by exposing NHPI to O_2 at 80 °C in PhCN, see ref. 4.

¶ ^{1}H NMR analysis of the resulting reaction mixture indicates a broad peak at δ 8.8 attributed to the proton of H_2O_2 and protons assigned to the methyl groups of alcohol **2a** and ketone at δ 1.4 and δ 2.6, respectively, but no peaks corresponding to the α-hydroxy hydroperoxide were observed. In addition, an independent reaction of **2a** (5 mmol) with O_2 (1 atm) in the presence of NHPI (10 mol%) at 70 °C in MeCN (5 ml) gave H_2O_2 (1.6 mmol) and acetophenone (**4a**) (1.8 mmol).

1 S. Ito, K. Inoue and M. Matsumoto, *J. Am. Chem. Soc.*, 1982, **104**, 6450; F. P. Guengrich and T. L. Macdonald, *Acc. Chem. Res.*, 1984, **17**, 9; J. T. Groves and R. Quinn, *J. Am. Chem. Soc.*, 1985, **107**, 5790; I. Tabushi and M. Kodera, *J. Am. Chem. Soc.*, 1986, **108**, 1101; D. Mansuy, M. Fontecve and J.-F. Bartoli, *J. Chem. Soc., Chem. Commun.*, 1981, 874; D. H. Chin, G. N. La Mar and A. L. Balch, *J. Am. Chem. Soc.*, 1980, **102**, 1446; D. H. Chin, G. N. La Mar and A. L. Balch, *J. Am. Chem. Soc.*, **102**, 1980, 4344; J.-C. Marchon and R. Ramasseul, *Synthesis*, 1989, 389.

2 T. Mukaiyama, T. Takai, T. Yamada and O. Rhode, *Chem. Lett.*, 1990, 1661; S.-I. Murahashi, Y. Oda, T. Naota and N. Komiya, *J. Chem. Soc., Chem. Commun.*, 1993, 139; R. Neumann and M. Dahan, Nature, 1997, **388**, 24.

3 Y. Ishii, K. Nakayama, M. Takeno, S. Sakaguchi, T. Iwahama and Y. Nishiyama, *J. Org. Chem.*, 1995, **60**, 3934; Y. Yoshino, Y. Hayashi, T. Iwahama, S. Sakaguchi and Y. Ishii, *J. Org. Chem.*, 1997, **62**, 6810; T. Iwahama, K. Syojyo, S. Sakaguchi and Y. Ishii, *Org. Process Res. Dev.*, 1998, **2**, 255; S. Sakaguchi, T. Takase, T. Iwahama and Y. Ishii, *Chem. Commun.*, 1998, 2037.

4 Y. Ishii, T. Iwahama, S. Sakaguchi, K. Nakayama and Y. Nishiyama, *J. Org. Chem.*, 1996, **61**, 4520.

5 T. Iwahama, S. Sakaguchi, Y. Nishiyama and Y. Ishii, *Tetrahedron Lett.*, 1995, **36**. 6923.

6 C. Ueda, M. Nayama, H. Ohmori and M. Masui, *Chem. Pharm. Bull.*, 1987, **35**, 1372.

7 P. Brougham, M. S. Cooper, D. Cummersou, H. Heaney and N. Thompson, *Synthesis*, 1987, 1015.

8 T. Yamada, T. Takai, O. Rhode and T. Mukaiyama, *Bull. Chem. Soc. Jpn.*, 1991, **64**, 2109.

9 It is well-known that the α-hydroxy hydroperoxide easily gives H_2O_2 and a ketone, see W. T. Hess, *Kirk-Othmer Encyclopedia of Industrial Chemistry*, ed. J. I. Kroschwitz and M. Howe-Grant, 4th edn., Wiley, New York, 1995, vol. 13, pp. 976–977 and references cited therein.

Communication 9/01615E

ChemComm

A chemical synthesis of nicotinamide adenine dinucleotide (NAD^+)

Jaemoon Lee,* Hywyn Churchil, Woo-Baeg Choi, Joseph E. Lynch, F. E. Roberts, R. P. Volante and Paul J. Reider

Process Research, Merck Research Laboratories, PO Box 2000, Rahway, NJ 07065 USA. E-mail: jaemoon_lee@merck.com

Received (in Cambridge, UK) 18th February 1999, Accepted 10th March 1999

A practical synthesis of nicotinamide mononucleotide (β-NMN) and a high yield coupling with AMP-morpholidate that also provides NAD^+ in an efficient manner are reported.

The nicotinamide cofactors, NAD^+, $NADP^+$, NADH and NADPH, are useful in a variety of enzyme-catalyzed oxidation and reduction reactions in organic synthesis. In the course of bioconversion research in our laboratories, there was need for a reliable, practical synthesis of these cofactors. NAD^+ **1**, also known as Coenzyme 1, is currently manufactured by a yeast based fermentation process.[1] An early chemical synthesis of NAD^+ was reported by Todd *et al*.[2] In their approach, dicyclohexylcarbodiimide (DCC) was used for the coupling of adenosine monophosphate (AMP) and β-nicotinamide mononucleotide (β-NMN, **5**). In a semi-synthetic approach to NAD^+

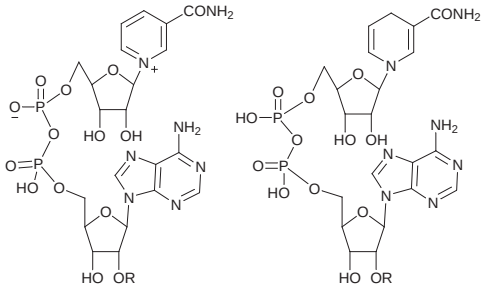

1 NAD^+, R = H
2 $NADP^+$, R = $PO(OH)_2$
3 NADH, R = H
4 NADPH, R = $PO(OH)_2$

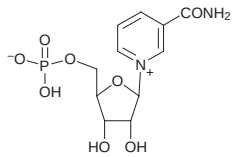

5 β-NMN

by Whitesides *et al*., β-NMN was reacted with adenosine triphosphate (ATP) using NAD pyrophosphorylase (NADPP) immobilized in a polyacrylamide gel.[3b] Since this condensation required a stoichiometric amount of ATP, a costly reagent, a method to generate ATP from AMP was developed. This required the use of several enzymes and associated reagents, such as acetyl phosphate, acetyl kinase, adenyl kinase, and NAD-pyrophosphorylase.[3b] We envisioned that AMP could be activated as a phosphoroamidate and would react with β-NMN or *vice versa*. For this purpose we first examined the existing methods for preparing β-NMN. The β-NMN synthesis reported by Todd *et al.*,[2,3] was improved by Mikhailopulo and co-workers in terms of β-selectivity in the *N*-glycosylation step using SO_2 as a solvent.[4]

We found, however, that the deprotection of tribenzoate **10** under the literature conditions (NH_3, MeOH) was not easily repeated on a large scale (Scheme 1). We observed substantial epimerization giving a *ca.* 2 : 1 β : α mixture of anomeric nucleosides **12**. After considerable effort to improve the deprotection of the tribenzoate, we decided to define a more suitable protecting group with the following requirements: (i) readily removable in the presence of the reactive anomeric pyridinium group; (ii) stable to the bromination conditions; and (iii) able to provide neighboring group participation during the glycosylation step. Nicotinamide triacetate **11** was identified as a potential candidate and was prepared as follows. Bromination of commercial tetra-*O*-acetyl-β-D-ribofuranose **7** with HBr in CH_2Cl_2 gave a 1.5 : 1 β : α mixture of anomeric bromides **9**. Condensation of **9** with nicotinamide in SO_2 at −10 °C followed by a crystallization from 5 : 1 acetone–Bu^{t}OMe afforded the desired β-nicotinamide mononucleoside **11** in 90% overall yield from **7**. We examined other solvents for the glycosylation step. Although a 3.3 : 1 (β : α) anomeric mixture was obtained in MeCN, the pure β-anomer was selectively crystallized in 65% yield from the reaction mixture (−15 °C). Although lower yielding, this procedure provides an alternative to SO_2.

Clean deprotection of tri-*O*-acetate **11** was elusive. A substantial amount of nucleoside cleavage at the glycosidic linkage was observed on treatment with methanolic ammonia. After several attempts, it was learned that the extent of cleavage was largely dependent on the initial concentration and the total amount of ammonia in the reaction mixture. Under the optimized conditions (3 equiv. of NH_3, 1 M in MeOH, −3 to −5 °C for 20 h), deacetylation followed by a crystallization (1 : 5 MeOH–acetone), gave a single β-nicotinamide nucleoside

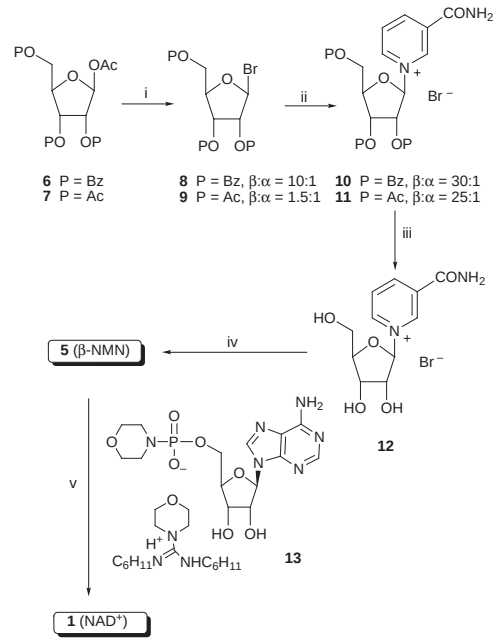

6 P = Bz
7 P = Ac
8 P = Bz, β:α = 10:1
9 P = Ac, β:α = 1.5:1
10 P = Bz, β:α = 30:1
11 P = Ac, β:α = 25:1
12
13

Scheme 1 *Reagents and conditions*: i, HBr (g), CH_2Cl_2; ii, nicotinamide, SO_2, −10 °C, 90% from **7**; iii, NH_3, MeOH, −5 °C, 20 h, 80%; iv, $POCl_3$ (4 equiv.), $PO(OMe)_3$, −5 to 0 °C, 7 h, 80%; v, $MnCl_2$–$MgSO_4$, $HCONH_2$, room temp., 16 h, 78% (58% isolated yield, > 99% purity).

bromide salt **12** as a crystalline solid in 80% isolated yield. It is noteworthy that, contrary to the previous report,[4] we found both **11** and **12** to be air-stable and non-hygroscopic solids.

The phosphorylation of the nicotinamide triol **12** has been reported in the literature using 1 equiv. of $POCl_3$ in $PO(OMe)_3$ with variable yield (35–64%).[4,5] Accordingly, we reexamined the reaction conditions and observed that reaction was very slow below −5 °C, while at > 5 °C a chlorination reaction was the favored pathway.[6,7] Thus the triol **12** was treated with 4.0 equiv. of $POCl_3$ in $PO(OMe)_3$ between −5 and 0 °C for 7 h to give the desired phosphorylated product in 90–92% yield (Scheme 1). Upon neutralization of the reaction mixture, the crude β-NMN **5** was separated from the reaction mixture by addition of MeCN–Et_2O (1 : 3). This crude product was further purified using resin chromatography to give the β-NMN in > 97% purity in 80% isolated yield.[8,9] Use of excess of $POCl_3$ (4 equiv.) at controlled temperature proved far superior to the more conventional stoichiometric amount of the reagent.

With β-NMN in hand, our attention turned to development of a practical method for pyrophosphate bond formation *en route* to NAD^+.[10] Conventional ways to make the pyrophosphate bonds include carbodiimide coupling,[2,11] the Michelson procedure,[12] and the Khorana–Moffatt procedure.[13] This last method, involving the coupling of a suitable salt of a sugar phosphate and a nucleotide phosphoromorpholidate, has been widely used for the synthesis of various sugar nucleotides.[13] However, the reaction between β-NMN and AMP-morpholidate[13*b*] (**13**) was attempted and gave NAD^+ in < 5% yield.[14] Our initial attempts using the AMP-imidazolidate,[15] triazolidate, or tetrazolidate, or to react AMP with β-NMN-imidazolidate[16] under the modified Khorana–Moffat conditions gave only low conversion to NAD^+ (formamide, 16 h to 6 days). We reasoned that this low reactivity of AMP-amidates might be due to the fact that β-NMN is an inner salt and is thus less nucleophilic. Under these conditions, a second dissociation of the phosphoric acid in the β-NMN, pK_a ~ 7, is probably not occurring to any significant extent. Accordingly, we attempted to activate the reaction using Lewis acid additives. The coupling between β-NMN and AMP-imidazolidate in the presence of $MnCl_2$–$4H_2O$ in formamide gave the desired NAD^+ in 25% yield after 16 h.[16] Further fine-tuning of the reaction conditions improved conversion up to 78% (HPLC assay yield). Typically, the reaction was carried out using 1.0 equiv. of AMP-morpholidate (**13**) with 1.1 equiv. of β-NMN (**5**) in 0.2 M solution of $MnCl_2$ (1.5 equiv.)[17] and $MgSO_4$ (2 equiv.) in formamide at room temperature for 16 h. Upon completion, the crude NAD^+ was precipitated from the reaction mixture with MeCN, and further purified by resin chromatography (Sephadex QAE A-25, elution with 0.25 M aq. $(NH_4)HCO_3$ solution; then Amberite XAD-16 with water–MeOH gradient at 5 °C)[18] followed by freeze-drying to give the NAD^+ as its ammonium salt with > 99% purity in 58% isolated yield.

The practical synthesis of NAD^+ outlined above has a number of noteworthy steps. The mild deacetylization procedure allowed isolation of the crystalline air stable nicotinamide nucleoside. Phosphorylation conditions were developed to provide β-NMN in 80% isolated yield. A new catalyzed pyrophosphate formation between β-NMN and AMP-morpholidate using a combination of $MnCl_2$ and $MgSO_4$ gave NAD^+ in 78% yield. An improved resin isolation process provided NAD^+ in 58% isolated yield.

We are grateful to Dr R. Czaja, Mr J. Bergan and Mr Bob Reamer for technical assistance.

Notes and references

1 *The Merck Index*, 6259, 11th edn., ed. S. Budavari, Merck, Rahway, NJ, 1989.

2 N. H. Hughes, G. W. Kenner and A. Todd, *J. Chem. Soc*., 1957, 3733; L. J. Haynes, N. H. Hughes, G. W. Kenner and A. Todd, *J. Chem. Soc*., 1957, 3727.

3 While β-NMN is commercially available, its high price ($508 per gram, Sigma 1997 catalog) and a lack of supply made large scale preparation of NAD^+ difficult. For other preparations of β-NMN, see D. R. Walt, V. M. Rios-Mercadillo, J. Auge and G. M. Whitesides, *J. Am. Chem. Soc*., 1980, **102**, 7806; D. R. Walt, M. A. Findeis, V. M. Rois-Mercadillo, J. Auge and G. M. Whitesides, *J. Am. Chem. Soc*., 1984, **106**, 234; G. M. Whitesides and D. R. Walt, US Pat. 4,411,995-A, 1983; R. Jeck, P. Heik and C. Woenckhaus, *FEBS Lett*., 1974, **42**, 161.

4 I. A. Mikhailopulo, T. I. Pricota, V. A. Timoshchuk and A. A. Akhrem, *Synthesis*, 1981, 387.

5 M. Yoshikawa, T. Kato and T. Takenishi, *Tetrahedron Lett.*, 1967, 5065; K. Imai, S. Fujii, K. Takanohashi, Y. Furukawa, T. Masuda and M. Honjo, *J. Org. Chem*., 1969, **34**, 1547.

6 In considering an efficient method for the synthesis of the pyrophosphate, we attempted to prepare the intermediate dichlorophosphate (phosphorodichloridate). Dichloridate was then treated *in situ* with AMP monosodium salt and triazole. However, no pyrophosphate bond formation was observed by ^{31}P NMR spectroscopy.

7 In an attempt to eliminate the bis-adduct formation, the reaction was also carried out using a 1 : 1 mixture of $POCl_3$–H_2O [*in situ* generation of $(HO)POCl_2$]; see M. Yoshikawa, T. Kato and T. Takenishi, *Bull. Chem. Soc. Jpn.*, 1969, 3505.

8 Chromatography on Dowex resin (two successive columns, 1X2 formate, 50WX8 H^+ form) followed by subsequent lyophilization of the aqueous fractions provided β-NMN in 80% yield, 97% purity (120 g scale). The two resin column isolation process proved to be operationally simple and the Dowex 50WX8 resin (H^+ form) served the dual purpose of purification and, more importantly, pH adjustment to provide the desired inner salt form of β-NMN.

9 The crude β-NMN was initially purified by a resin-free isolation [*i.e.* precipitation followed by treatment with activated carbon (Ecorsob-C, P-502-H)]. Although the process is simple, the yield for the next coupling reaction with AMP-morpholidate under the optimized condition was only moderate (it still required pH adjustment using H^+ cation resin). Alternatively, a direct resin chromatography using Dowex (50W X 8-100) resin column was developed (97% purity, eluted with 5% formic acid in water). However, this procedure required high resin loads with the product eluting in a large volume of water.

10 For examples of general pyrophosphate bond formation, see: A. F. Cook, M. J. Holman and A. L. Nussbaum, *J. Am. Chem. Soc*., 1969, **91**, 1522; K. Furusawa, M. Sekine and T. Hata, *J. Chem. Soc., Perkin Trans. 1,* 1976, 1711; F. Cramer and H. Schaller, *Chem. Ber*., 1961, **94**, 1634; V. J. Davisson, A. B. Woodside, T. R. Neal, K. E. Stremler, M. Muehlbacher and C. D. Poulter, *J. Org. Chem*., 1986, **51**, 4768; J. R. Falck, K. K. Reddy, J. Ye, M. Saady, C. Mioskowski, S. B. Shears, Z. Tan and S. Safrany, *J. Am. Chem. Soc*., 1995, **117**, 12172; V. Wittmann and C.-H. Wong, *J. Org. Chem*., 1997, **62**, 2144.

11 V. C. Bailey, J. K. Sethi, A. Galione and B. V. L. Potter, *Chem. Commun.*, 1997, 695.

12 A. M. Michelson, *Biochim. Biophys. Acta*, 1968, **91**, 1; H. Kim and B. E. Haley, *J. Biol. Chem.*, 1990, **265**, 3636.

13 (*a*) J. G. Moffat and H. G. Khorana, *J. Am. Chem. Soc*., 1959, **81**, 1265; (*b*) J. G. Moffat and H. G. Khorana, *J. Am. Chem. Soc*.,, 1961, **83**, 649; (*c*) E. S. Simon, S. Grabowski and G. M. Whitesides, *J. Org. Chem*., 1990, **55**, 1834.

14 L. M. Mel'nikova and V. M. Berezovkii, *Zh. Obshch. Khim*., 1970, **40**, 918.

15 R. Lohrmann and L. E. Orgel, *Tetrahedron*, 1978, **34**, 853.

16 B. C. F. Chu and L. E. Orgel, *Biochim. Biophys. Acta*, 1984, **782**, 103; M. Shimazu, K. Shinozuka and H. Sawai, *Tetrahedron Lett*., 1990, **31**, 235.

17 For a successful high yielding coupling reaction, reagents and the solvents were dried. A $MnCl_2$ solution was prepared by dissolution of the commercial tetrahydrate in formamide to give a 0.2 M stock solution. The solution was dried over 4 Å molecular sieves for several days prior to use. Typically the solution had 0.5 M H_2O content and was used for the reaction successfully. Use of commercial anhydrous $MnCl_2$ proved inferior.

18 Purification of NAD^+ using resin chromatography at room temperature resulted in partial decomposition of purified NAD^+ (5% purity loss). Therefore, the chromatography was carried out at 5 °C (110 g scale, > 99% purity).

Communication 8/09930H

The cyclization mechanism of squalene in hopene biosynthesis: the terminal methyl groups are critical to the correct folding of this substrate both for the formation of the five-membered E-ring and for the initiation of the polycyclization reaction†

Tsutomu Hoshino,*[ab] and Tomohiro Kondo[b]

[a] *Department of Applied Biological Chemistry, Faculty of Agriculture, and* [b] *Graduate School of Science and Technology, Niigata University, Ikarashi, Niigata 950-2181, Japan. E-mail: hoshitsu@agr.niigata-u.ac.jp*

Received (in Cambridge, UK) 18th February 1999, Accepted 10th March 1999

Incubations of C(23)-norsqualenes 5 and 6, lacking one of the two terminal methyl groups, with squalene-hopene cyclase gave unprecedented products 7 and 8 having a tetrahymanol skeleton together with a neohopane skeleton 12, strongly suggesting that the two geminal methyls of squalene 1 are critical to the formation of the five-membered E-ring in hopene biosynthesis and also are required to initiate the cyclization reactions of 1 into the pentacyclic triterpenes 2 and **3**.

The biocyclization of squalene **1** into hop-22(29)-ene **2** catalyzed by squalene-hopene cyclase [EC 5.4.99.-] (SHC) or into tetrahymanol **3**, by squalene-tetrahymanol cyclase [EC 5.4.99.-] (STC), is one of the most intricate biochemical reactions (Scheme 1).[1] Compound **4**, hopan-22-ol, is a minor by-product. The cyclization proceeds *via* precise enzymatic control to form the fused 6/6/6/6/5- or 6/6/6/6/6-ring system and nine new stereocenters. The polyene cyclization reaction of **1** is analogous to that of 2,3-oxidosqualene into lanosterol catalyzed by lanosterol synthase.[1] Recently, it has been proposed that a ring expansion process from the five- to the six-membered ring is involved in the D-ring formation of hopene biosynthesis, prior to the further cyclization (Scheme 1).[2a,b] Formation of the five-membered intermediate D-ring is consistent with the Markovnikov rule. The expansion process of the D-ring may also be responsible for tetrahymanol biosynthesis.[2c] Such a ring expansion reaction was also demonstrated for the oxidosqualene cyclization.[3] Computational energy calculations of the five- and six-membered intermediates have supported the feasibility of such a ring expansion process.[4] The structure of **2** differs from that of **3** only in the terminal E-ring, *i.e.* five- and six-membered rings for **2** and **3**, respectively. To gain insight into the different cyclization mechanism between SHC and STC, the substrate analogues **5** and **6**, lacking one of the two terminal methyls in squalene backbone **1**, were separately incubated with SHC or STC, resulting in the formation of **7**, **8** and **12** as SHC enzyme products, and **7** and **8** as STC products; SHC, despite responsibility for the formation of the five-membered E-ring, did produce a tetrahymanol skeleton having a six-membered E-ring. We show herein that the terminal methyl groups play a critical role for the determination of either five- or six-membered E-ring formation.

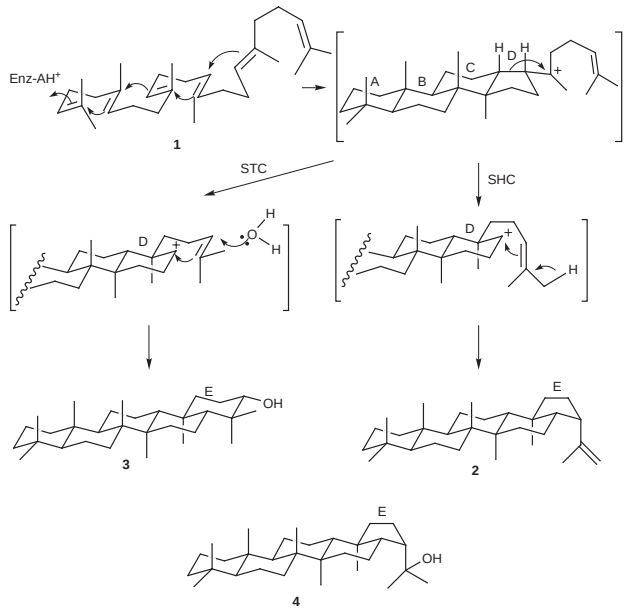

Scheme 1

The analogues **5** and **6** were synthesized as follows: (±)-2,3-oxidosqualene was treated with HIO_4 to give the C_{27}-aldehyde, which was then subjected to a Wittig reaction with $EtPPh_3Br$ in the presence of Bu^nLi in THF. The C(23)-norsqualenes **5** and **6** thus obtained were separated with a SiO_2 column (10% $AgNO_3$) with hexane; **6** followed by **5.** The 7 methyl signals of **5** in $CDCl_3$ were as follows: δ_H 1.66 [3H, s, (*E*)-CH_3C=] and 1.58 [18H, (*Z*)-CH_3C=], while those of **6** were: δ_H 1.66 [3H, s, (*E*)-CH_3C=], 1.61[3H, brd, *J* 5.8, (*E*)-CH_3C=], 1.58 [12H, s, (*Z*)-CH_3C=] and 1.57 [3H, s, (*Z*)-CH_3C=].[5]

Separate incubations of **5** and **6** with cell-free homogenates from the cloned *E. coli* harboring SHC under catalytic optimal conditions[6] afforded highly polar products **7** and **8**, respectively (Scheme 2). From the incubation mixtures of **5**, another product **12** was found together with some minor products, both of which had lower polarities than **7** on TLC. Separation of each product was performed using a SiO_2 column with hexane–EtOAc, but the minor products, present in negligible amounts, were inseparable even on $AgNO_3$–SiO_2 TLC. Isolation yields of **7** and **12** from **5** were 17 and 12%, respectively, while that of **8** from **6** was 16%; neither **12** nor the minor products were detected from **6** (Scheme 3), using the same quantities of the substrate and the cell-free extracts as for **5**.

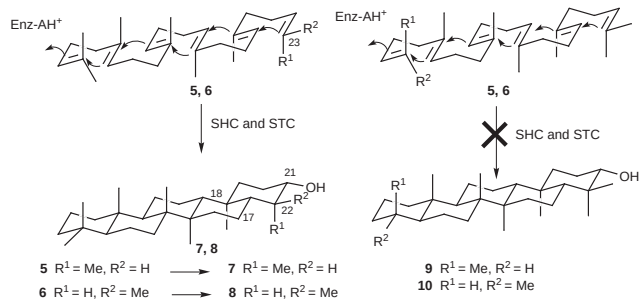

Scheme 2

† Details of orbital interactions and 2D NMR analyses for **7**, **8** and **12** are available from the RSC website, see: http://www.rsc.org/suppdata/cc/1999/731/

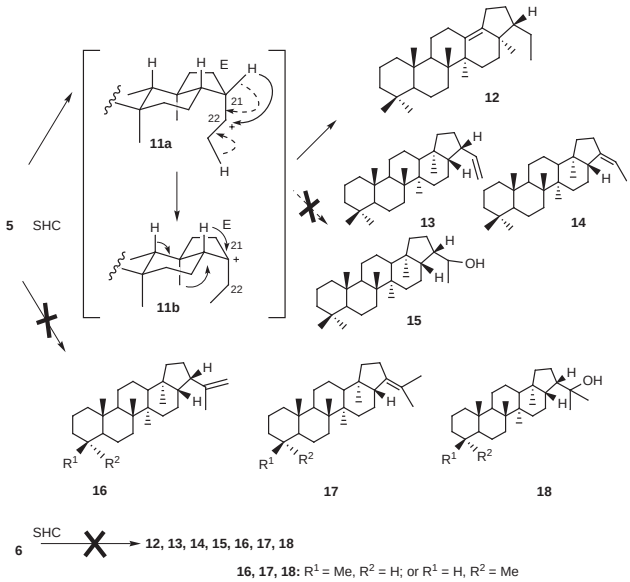

Scheme 3

Independent incubations of **5** and **6** with cell-free extracts from *Tetrahymena pyriformis* STC[7] also gave **7** and **8** (1 : 2.5 ratio), respectively. No other products were detected. The products with STC were indistinguishable from those with SHC *via* GC-MS.

The structures of highly polar compounds **7**[5] ($C_{29}H_{50}O$, EI-HRMS: *m/z* 414.3834; requires 414.3862) and **8**[5] ($C_{29}H_{50}O$, *m/z* 414.3854) were determined *via* NMR analysis. The signals at δ_C 74.1 and 76.7 in **7** and **8**, respectively, proved the involvement of a hydroxy group. Detailed analyses using 2D NMR revealed that **7** and **8** had a pentacyclic tetrahymanol skeleton possessing a chair conformation of the E-ring.[5] The hydroxy groups of both **7** and **8** were in the same equatorial orientation at the 21-position, but the arrangements of the methyl at the 22-position were different; axial for **7** by taking account of the coupling constants of H-21 [δ_H 3.69 (*ddd*, J = 11.2, 5.2, 5.2 Hz)] and equatorial for **8** owing to the *ddd* splitting of H-21 [δ_H 3.05 (J = 11.0, 11.0, 4.8 Hz)]. Product **12**[5] ($C_{29}H_{48}$, EI-HRMS: *m/z* 396.3722; requires 396.3756) did not have a hydroxy group. One of the 7 methyl groups appeared as a triplet (J = 7.6 Hz) and the other 6 methyls as singlets in the ^{1}H NMR spectrum, showing the presence of one ethyl group in **12**, and detailed analysis revealed a neohopene skeleton,[2a] but with a carbon skeleton of C_{29}.

Formation of the tetrahymanol skeleton by SHC has never been reported before, and also is quite interesting from the evolutionary aspect of squalene cyclases. The E-ring formation proceeded with complete stereoselectivity; the (23*Z*)-methyl group of **5** was axial, while the corresponding *E*-methyl of **6** was equatorial during the E-ring formation. The methyl orientations of each product from SHC agreed with those from STC (Scheme 2), and were consistent with the previous report that the (23*E*)-methyl of natural **1** was arranged in an equatorial orientation during the E-ring formation.[7a] The hydroxy groups of both **7** and **8** were introduced in the same equatorial disposition as a result of nucleophilic attack of a water molecule in an equatorial direction on the C-21 cation. The cyclization of the six-membered E-ring formation would be a concerted reaction under stereoelectronic control and explained in terms of HOMO–LUMO interactions.[8]

It is noticeable that **12** was produced only from **5**, and not from **6** (Scheme 3). This fact implicates that the (23*Z*)-methyl of **1** is more important than the (23*E*)-methyl for the formation of the hopanyl cation **11** with the 5-membered E-ring. However, the two terminal methyls would be necessary for the complete building of the five-membered E-ring, since the six-membered species **7** and **8** were produced in significant amounts when one of the two methyls was absent. Why was the tetrahymanol skeleton produced by the incubations of the norsqualene **5** and **6** with SHC? One plausible answer may be that the two geminal methyls strongly bind to SHC to acquire the desired conformation, shown in Scheme 1, during the formation of the five-membered E-ring, and the substrate affinity would become looser when one of the terminal methyls is absent, which would have led to the formation of a tetrahymanol skeleton under stereoelectronic control. The binding force of the *Z*-methyl to the SHC would be stronger than the corresponding *E*-methyl, because **12** was produced only from **5**, and not from **6**. The absence of **13** from **5**, although the hopanyl cation **11** has been produced, suggests that the migration of the hydride (1, 2-shift) must be fast compared with the two deprotonation reactions for the formations of **13** and **14**. This would be due to a greater stability of the tertiary C21-carbocation intermediate **11b** compared to the secondary C22-cation **11a**. The hopanol analogue **15** was also not found. At the present time, we cannot propose which terminal methyl of either the *Z*- or *E*-isomers of the natural **1** is responsible for the proton elimination when the double bond in **2** is introduced. Compounds **9**, **10**, **16**, **17** and **18** were also not detected in any reaction mixture from either SHC or STC, all of which are the presumed enzymic products based on the idea that the polycyclization could be initiated from the methyl-deficient part (Scheme 2 and 3). This finding strongly suggested that the two geminal methyls are indispensable for the initiation of polycyclizations by both STC and SHC, which is in contrast to the report that 2,3-*trans*-1′-norsqualene 2,3-oxide, lacking one methyl on the epoxide ring, was cyclized by the lanosterol synthase.[1,9]

This work was partly supported by a Grant-in-Aid to T.H. (No.0966011) from the Ministry of Education, Science and Culture, Japan.We are also indebted to Dr M. Takahashi, Tsukuba University, for the gift of *Tetrahymena pyriformis* (GL strain).

Notes and references

1 I. Abe, M. Rohmer and G. D. Prestwich, *Chem. Rev*., 1993, **93**, 2189.
2 (*a*) C. Pale-Grosdemange, C. Feil, M. Rohmer and K. Poralla, *Angew. Chem. Int. Ed.*, 1998, **37**, 2237; (*b*) T. Sato, T. Abe and T. Hoshino, *Chem. Commun.*, 1998, 2617; (*c*) I. Abe and M. Rohmer, *J. Chem. Soc., Chem. Commun*., 1991, 902.
3 E. J. Corey, S. C. Virgil, H. Cheng, C. H. Baker, S. P. T. Matsuda, V. Singh and S. Sarshar, *J. Am. Chem. Soc*., 1995, **117**, 11 819; E. J. Corey and H. Cheng, *Tetrahedron Lett.*, 1996, **37**, 2709; T. Hoshino and Y. Sakai, *Chem. Commun.*, 1998, 1591.
4 C. Jenson and W. L. Jorgensen *J. Am. Chem. Soc.*, 1997, **119**, 10 846.
5 Analyses of NMR data (^{1}H-^{1}H COSY 45, HOHAHA, NOESY, DEPT, HMQC and HMBC) unequivocally supported the structures of **5**, **6**, **7**, **8** and **12**.
6 T. Sato, Y. Kanai and T. Hoshino, *Biosci. Biotechnol. Biochem.*, 1998, **62**, 407.
7 (*a*) P. Bouvier, Y. Berger, M. Rohmer and G. Ourisson, *Eur. J. Biochem.*, 1980, **112**, 549; (*b*) M. Renoux and M. Rohmer, *Eur. J. Biochem.*, 1986, **155**, 125.
8 Given that a water molecule attacks in the axial direction, a more hindered interaction would occur between the LUMO at C17–C18 and the HOMO at C21–C22 due to constrained overlapping (carbon numbering shown in Scheme 2).
9 R. B. Clayton, E. E. van Tamelene and R. G. Nadeau, *J. Am. Chem. Soc*., 1968, **90**, 820.

Communication 9/01351B

Adsorptive separation of methylalumoxane by mesoporous molecular sieve MCM-41

Tsuneji Sano,* Keiko Doi, Hitoshi Hagimoto, Zhengbao Wang, Toshiya Uozumi and Kazuo Soga

School of Materials Science, Japan Advanced Institute of Science and Technology, Tatsunokuchi, Ishikawa 923-1292, Japan. E-mail: t-sano@jaist.ac.jp

Received (in Cambridge, UK) 4th January 1999, Accepted 17th March 1999

Separation of methylalumoxane (MAO) by adsorption on siliceous porous materials with different average pore diameters has been carried out; polymerization of ethylene was conducted with Cp_2ZrCl_2 using the separated MAO as cocatalyst, it was found that the MAO adsorbed on MCM-41 with average pore size of *ca*. 25 Å is very effective for ethylene polymerization.

Methylalumoxane (MAO) generated by controlled hydrolysis of trimethylaluminium (TMA) is known to be a changeable mixture of oligomers owing to the coexistence of TMA. Although several structures have been proposed for MAO such as rings, clathrates and linear or branched chains, the detailed structure of active MAO remains ambiguous because of the multiple equilibria being present in the solution.[1–3]

Recently, heterogenization of the alumoxane structure has been widely studied by using a variety of porous materials such as amorphous silica gel, zeolite or siliceous mesoporous materials MCM-41 as carriers.[4] However, no report concerning the adsorptive separation of MAO by such porous materials has been published. From such a viewpoint, we have attempted to separate MAO with the use of typical porous inorganic materials having different pore sizes and tested them towards ethylene polymerization. From those results, we propose here the potential use of mesoporous molecular sieve MCM-41 for the separation of active MAO.

MCM-41 has a regular array of uniform unidimensional pores where diameter can be controlled by altering the alkyl chain length of the surfactant.[5] Siliceous MCM-41(*n*) [*n*; chain length of 10, 16 and 22] were prepared from surfactants of decyltrimethylammonium bromide, hexadecyltrimethylammonium bromide and docosyltrimethylammonium chloride.[6,7] A silicalite of a MFI type was prepared under conventional hydrothermal synthesis conditions. Amorphous silica gels (average pore diameter : grade P6 = 137 Å, P10 = 293 Å) were donated by Fuji Silysia Co. To prevent the reaction between MAO and the surface hydroxy groups in the carriers, these materials were silylated by refluxing for 8 h with trimethylchlorosilane as a silylating agent. Characterization of these materials was conducted by X-ray diffraction (Rigaku RINT 2000), FTIR (JEOL JIR-7000) and nitrogen adsorption (Belsorp 28SA).

MAO was purified by drying the commercial MAO (from Tosoh Akuzo Co.) *in vacuo* in order to remove the free TMA. The amount of TMA left in the purified MAO was estimated to be *ca*. 8 wt% by ^{1}H NMR (Varian Gemini 300).[8] Separation of MAO from the silylated porous materials was conducted as follows : 0.7 g of each carrier was added to 10 mmol (based on Al) of MAO in toluene (10 ml) and the mixture was left to stand at room temperature for 5 h. The solid fraction was separated by filtration and washed 3 times with 20 ml toluene, followed by drying at room temperature under vacuum. The concentrations of Al in both solution and solid fractions were analyzed by inductively coupled plasma atomic emission spectroscopy (ICP, Seiko SPS7700) after decomposition of MAO with nitric acid. The concentrations of Zr were also analyzed by ICP.

Polymerization of ethylene was conducted at 40 °C for 10 min with Cp_2ZrCl_2 using the separated MAO as cocatalyst. The Al/Zr ratio in the feed was kept constant. Measured amounts of toluene and the separated MAO were introduced into a 300 ml glass reactor equipped with a mechanical stirrer at room temperature. After the reactor was heated to the polymerization temperature (40 °C), the MAO solution was saturated with ethylene. A given amount of Cp_2ZrCl_2 was then injected to initiate the polymerization reaction. Ethylene was continuously fed to the reactor to keep the pressure constant during polymerization. The polymerization reaction was terminated by adding acidified methanol (5 wt% HCl). The precipitated polymers were washed with fresh methanol and dried under vacuum at 60 °C for 6 h. The number-average molecular weight ($\overline{M}_n$) and molar mass distribution (MMD; $\overline{M}_w/\overline{M}_n$) of the polymers were measured at 145 °C by gel permeation chromatography (GPC; Senshu Scientific SSC7100) using *o*-dichlorobenzene as the solvent. The GPC was calibrated using polystyrene standards and the method of universal calibration.

The synthesized MCM-41(*n*) (specific BET surface area *ca*. 1000 $m^2\ g^{-1}$) and silicalite (382 $m^2\ g^{-1}$) had well defined structures, as demonstrated by their X-ray diffraction patterns. The loss of the 3740 cm^{-1} peak assigned to the isolated OH groups was observed in the FTIR spectra of the silylated materials. Although a slight reduction in the specific BET surface area and the pore size calculated by the Dollimore–Heal (D–H) method was observed for silylated materials, no structural degradation occurred. The amount of MAO adsorbed in the carrier strongly depended upon its pore diameter. MCM-41(10), MCM-41(16) and MCM-41(22) showed higher adsorption ability, while MAO was scarcely adsorbed by silicalite probably due to an insufficient pore size. The pore volume of the MAO-containing MCM-41(16) (0.495 $cm^3\ g^{-1}$) was reduced to *ca*. three fifths of its original value.

Fig. 1 shows the correlation between the pore size of porous materials and the activity of ethylene polymerization when MAO left in the liquid phase was used as cocatalyst. Activity is defined as the yield of polyethylene (PE) calculated from the

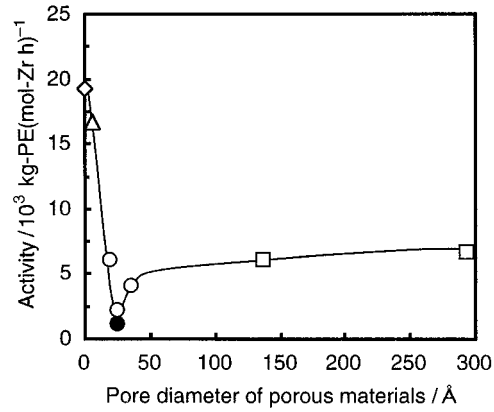

Fig. 1 Effect of pore diameter of porous materials on the initial activity of ethylene polymerization using the solution fraction. *Polymerization conditions*: T = 40 °C, Cp_2ZrCl_2 = 0.001 mmol, Al/Zr = 1000: (◇) ordinary MAO, (△) Silicalite, (○) MCM-41, (●) addition of TMA (1 mmol), (□) Silica gel.

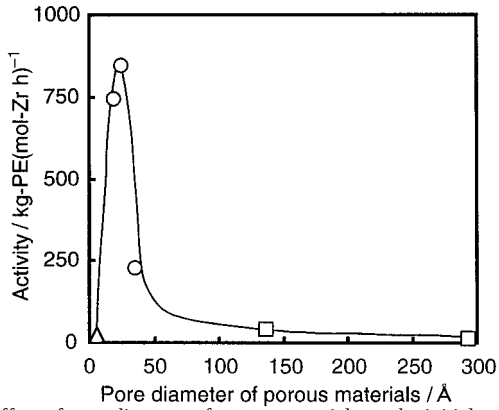

Fig. 2 Effect of pore diameter of porous materials on the initial activity of ethylene polymerization using the solid fraction. *Polymerization conditions*: T = 40 °C, Cp_2ZrCl_2 = 0.02 mmol, Al/Zr = 40: (△) Silicalite, (○) MCM-41, (□) Silica gel.

ethylene consumption at 10 min of the polymerization time. It was confirmed that the ethylene consumption measured by the flow meter agrees well with the polymer yield. The polymerization activity decreased drastically with increase in the pore diameter, and the minimum value was obtained at *ca*. 25 Å, suggesting that the MAO adsorbed on MCM-41 with an average pore size of *ca*. 25 Å is very effective for ethylene polymerization. Of course, we can not rule out a possibility that some factors other than the size of MAO affect the polymerization activity.

It is reported that some free TMA remains unremoved even when the MAO solution is dried under vacuum.[9,10] The residual TMA is considered to play an important role in the activation of metallocenes. Accordingly, it may be plausible to assume that such a marked decrease in the polymerization activity as observed in Fig. 1 is attributable to the reduction of free TMA. To clarify this point, ethylene polymerization was conducted by injecting additional TMA (1 mmol). The activity decreased slightly as shown in Fig. 1, indicating that the decrease in the activity is caused by some other factors.

Ethylene polymerization was then carried out using the solid fraction as cocatalyst. Prior to the polymerization, it was confirmed from the following experiments that the MAO once adsorbed in MCM-41(10), does not elute into the liquid phase during polymerization. The mixture of MAO-containing MCM-41(10) and Cp_2ZrCl_2 was brought into contact in toluene, and ethylene polymerization was conducted using the solution fraction as cocatalyst. However, only a trace amount of polymer was obtained. The degree of Al elution measured by elemental analysis of the solution fraction was *ca*. 1%. Fig. 2 shows the correlation between the pore size of porous materials and the polymerization activity, where the activity was evaluated on the basis of the amount of Cp_2ZrCl_2 occluded in the pores. The Al/Zr ratios in the solid were 70–90. In contrast to the results obtained by using the solution fraction (Fig. 1), the polymerization activity of the solid fraction was initially low and increased markedly, followed by a drastic decrease passing through a maximum value at *ca*. 25 Å. The result again supports the above assumption that the MAO adsorbed on MCM-41 with average pore size of *ca*. 25 Å is very effective for ethylene polymerization. Similar results have recently been reported by Van Looveren *et al*.[11] They studied the *in-situ* synthesis of MAO in the pores of MCM-41, and found that the $\{C_2H_4(1\text{-indenyl})_2\}Zr(CH_3)_2$ catalyst combined with the resulting MAO displays activity as high as the corresponding ordinary homogeneous catalyst system for ethylene–propylene co-oligomerization.

Table 1 Number-average molecular weight ($\overline{M}_n$) and molar mass distribution (MMD: $\overline{M}_w/\overline{M}_n$) of polyethylene obtained with various MAO materials.

Cocatalyst	Carrier	$10^{-3}\,\overline{M}_n$	$\overline{M}_w/\overline{M}_n$
MAO (solution fraction)	Silicalite	160	2.3
	MCM-41(10)	156	2.3
	MCM-41(16)	116	2.4
	MCM-41(22)	149	2.3
	Silica gel P6	178	2.1
	Silica gel P10	145	2.2
MAO (solid fraction)	MCM-41(10)	46	2.9
	MCM-41(16)	22	3.7
	MCM-41(22)	34	3.7
	Silica gel P6	7	6.6
Ordinary MAO		245	1.9

For reference, some analytical data of polyethylene obtained here are summarized in Table 1. The number-average molecular weights ($\overline{M}_n$) of polyethylene produced by the solution fraction are much higher as compared with those produced by the solid fraction. On the other hand, the molar mass distributions (MMD) of polyethylene produced by the solid fraction seem to be slightly broader. These results may suggest that the polymerization in MCM-41 is controlled by monomer (ethylene) diffusion through the pores which are sterically very crowded by MAO, Cp_2ZrCl_2 and produced polyethylene. A further study is now in progress to isolate the active MAO using the modified separation technology.

We thank Dr E. Kaji (Tosoh Akuzo Co.) for helpful discussions.

Notes and references

1 M. R. Mason, J. M. Smith, S. G. Bott and A. R. Barron, *J. Am. Chem. Soc*., 1993, **115**, 4971.
2 A. R. Barron, *Macromol. Symp*., 1995, **97**, 15.
3 H. Shin, *Macromol. Symp*., 1995, **97**, 27.
4 See for example; J. C. W. Chien and D. He, *J. Polym. Sci. Part A, Polym. Chem*., 1991, **29**, 1603; K. Soga and M. Kaminaka, *Macromol. Chem. Rapid. Commun*., 1992, **13**, 221; W. Kaminsky and F. Renner, *Macromol. Chem. Rapid. Commun*., 1993, **14**, 239; F. Ciardelli, A. Altomare, G. Counti, G. Arribas, B. Mendez and A. Ismayel, *Macromol. Chem. Macromol. Symp*., 1994, **80**, 29; T. Tudor and D. O'Hare, *Chem. Commun*., 1997, 603.
5 J. S. Beck, J. C. Vartuli, W. J. Roth, M. E. Leonowicz, C. T. Kresge, K. D. Schmitt, C. T-W. Chu, D. H. Olson, E. W. Sheppard, S. B. MacCullen, J. B. Higgins and J. L. Schlenker, *J. Am. Chem. Soc*., 1992, **114**, 10 834.
6 J. M. Kim. J. H. Kwak, S. Jun and R. Ryoo, *J. Phys. Chem*., 1995, **99**, 16 742.
7 S. Namba, A. Mochizuki and M. Kito, *Stud. Surf. Sci. Catal*., 1998, **117**, 257.
8 D. W. Imhoff, L. S. Simeral, S. A. Sangokoya and J. H. Peel, *Organometallics*, 1998, **17**, 1941.
9 W. Hagendorf, A. Harder and H. Sinn, *Macromol. Symp*., 1995, **97**, 127.
10 I. Tritto, M. C. Sacchi and S. Li, *Macromol. Chem. Rapid. Commun*., 1994, **15**, 217.
11 L. K. Van Looveren, D. F. Geysen, K. A. Vercruysse, B. H. Wouters, P. J. Grobet and P. A. Jacobs. *Angew. Chem., Int. Ed*., 1998, **37**, 517.

Communication 9/00030E

A ruthenium(II) *tris*(2,2′-bipyridine) derivative possessing a triplet lifetime of 42 μs

Anthony Harriman,* Muriel Hissler, Abderrahim Khatyr and Raymond Ziessel*

Laboratoire de Chimie, d'Electronique et de Photonique Molécu laires, Ecole Européenne de Chimie, Polymères et Matériaux, Université Louis Pasteur, UPRES-A 7008 au CNRS, 25 rue Becquerel, 67087 Strasbourg Cedex 2, France. E-mail: ziessel@chimie.u-strasbg.fr

Received (in Cambridge, UK) 4th February 1999, Accepted 11th March 1999

Grafting an ethynylated-pyrene moiety to a Ru(II) or Os(II) polypyridine complex perturbs the photophysical properties of the metal fragment and, when the relevant energy levels are properly balanced, provides a 115-fold prolongation of the triplet lifetime.

Ford and Rodgers[1] have described reversible triplet energy transfer between pyrene and a ruthenium(II) polypyridine complex attached *via* a flexible hydrocarbon chain. This strategy prolonged the triplet lifetime of the metal complex by a factor of *ca*. 11-fold; a feat confirmed by Sasse and coworkers[2,3] who achieved a 5-fold extension in triplet lifetime with a similar dyad. In seeking to design improved luminophores for specific analytical applications we note the following points: (i) conformational heterogeneity introduced by the flexible connector, or by direct attachment of the reactants,[4] would be avoided with a rigid spacer. (ii) The rates of forward and reverse triplet energy transfer would be increased with an acetylene group as connector.[5] Consequently, photoactive dyads have been synthesized (Scheme 1) wherein an ethynylated pyrene moiety is grafted onto an Ru(II) or Os(II) polypyridine complex† and the photophysical properties recorded.

The emission spectrum recorded for pyr-bpy-Os (Fig. 1) is characteristic[5] of an 'Os(bpy)' molecular fragment (bpy = 2,2′-bipyridine), allowing[6] the triplet energy (E_T) to be derived (Table 1). The emission quantum yield (Φ_L), peak maximum (λ_L) and lifetime (τ_L) remain as expected for an 'Os(bpy)' fragment while the transient absorption spectrum recorded after laser excitation (FWHM = 20 ps, λ = 532 nm) is entirely consistent[7] with the excited triplet state being localized on the metal complex (Fig. 2). Decay of the triplet absorption signal follows first-order kinetics, giving a lifetime (τ_T) similar to that measured by emission spectroscopy (Table 1). Laser spectroscopy shows that the pyrene triplet is not populated but, since the corrected emission excitation spectrum closely matches the absorption spectrum, photons absorbed by pyrene must be channelled quantitatively to the 'Os(bpy)' fragment. It appears, therefore, that the triplet state of the 'Os(bpy)' fragment lies at lower energy than the pyrene-like triplet state.[8]

Under identical conditions, the emission spectrum of pyr-bpy-Ru is characteristic of the 'Ru(bpy)' fragment (Fig. 1) but emission is exceptionally long-lived for such a species (Table 1). Both λ_L and Φ_L remain typical of a 'Ru(bpy)' fragment bearing an ethynylene group while the corrected excitation spectrum agrees well with the absorption spectrum. Control studies show the free ligand (*i.e.*, pyr-bpy) to be non-phosphorescent at rt. Analysis of the emission spectral profile[6] shows that the triplet energy of the 'Ru(bpy)' fragment greatly exceeds that of the corresponding 'Os(bpy)' fragment (Table 1). However, the transient absorption spectral profile (Fig. 2) is remarkably similar to that recorded for the pyrene unit in pyr-bpy and is unlike that of any 'Ru(bpy)'-based triplet. This pyrene-like triplet decays with the same lifetime as found for the 'Ru(bpy)'-like luminescence. These observations can be satis-

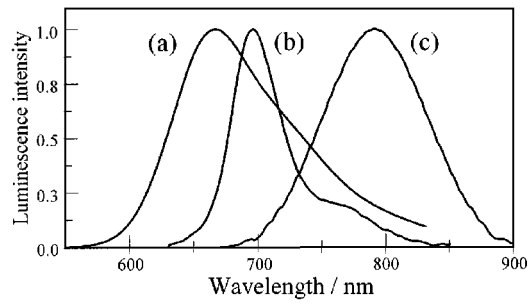

Fig. 1 Corrected luminescence spectra recorded for (a) pyr-bpy-Ru, (b) pyr-terpy-Ru and (c) pyr-bpy-Os in deoxygenated acetonitrile at 20 °C.

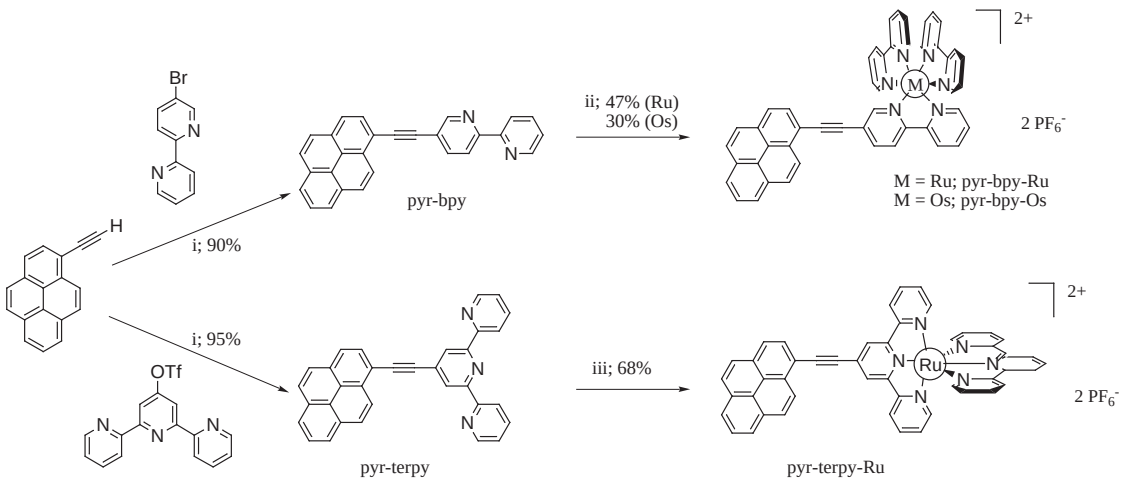

Scheme 1 *Reagents and conditions*: i, benzene, diisopropylamine, [$Pd^0(PPh_3)_4$] (6 mol %), 80 °C, 1 day; ii, *cis*-[$Ru(bpy)_2Cl_2$]·$2H_2O$ or *cis*-[$Os(bpy)_2Cl_2$], ethanol, 80 °C, 1 day, followed by anion metathesis; iii, [$Ru(terpy)(Me_2SO)Cl_2$], $AgBF_4$, methanol, 80 °C, 16 h.

Table 1 Photophysical properties measured for the various pyrene-containing molecular dyads in deoxygenated acetonitrile at 20 °C

Compound	λ_L/nm	Φ_L	τ_L/ns	τ_T/ns	E_T/kJ mol^{-1}	ΔE_{TT}/cm^{-1}	α	K	S
pyr-bpy-Ru	670	0.026	42 000	43 000	195	930	0.98	49	35
pyr-terpy-Ru	698	0.005	580	560	179	−390	0.13	0.15	1.2
pyr-bpy-Os	790	0.001	12	14	162	−1865	0	0	1.0

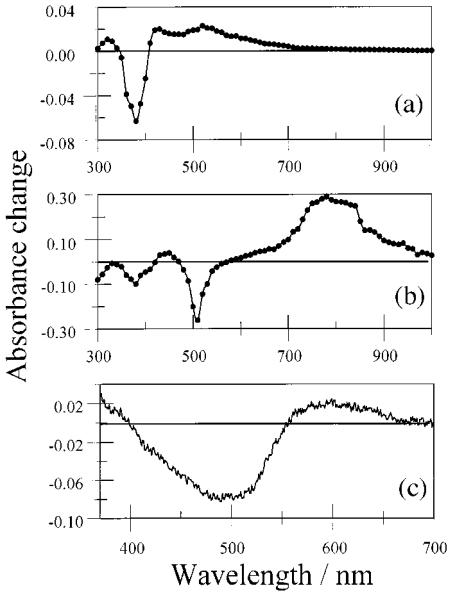

Fig. 2 Transient differential absorption spectra recorded for (a) pyr-bpy-Ru after 500 ns, (b) pyr-terpy-Ru after 100 ns, and (c) pyr-bpy-Os after 1 ns in deoxygenated acetonitrile at 20 °C following excitation with a 20-ps laser pulse at 532 nm.

factorily explained[1] in terms of the two triplet states being in thermal equilibrium at rt, with the balance favouring the pyrene-like triplet. In fact, comparing Φ_L measured for pyr-bpy-Ru with appropriate 'Ru(bpy)'-based reference compounds[5] lacking the pyrene substituent but possessing a similar radiative rate constant, allows the fraction (α) of pyrene-like triplets in the equilibrium distribution to be established at 0.98. On this basis, the energy of the pyrene-like triplet state must be *ca*. 184 kJ mol^{-1} since the equilibrium constant [K = $\alpha/(1-\alpha)$] is calculated to be *ca*. 49.

Confirmation of these energy gaps was sought by measuring the photophysical properties of pyr-terpy-Ru for which r.t. emission (Fig. 1) is characteristic[9] of the 'Ru(terpy)' fragment (terpy = 2,2′:6′,2″-terpyridine). The emission lifetime recorded for pyr-terpy-Ru is long for an ethynylated mononuclear 'Ru(terpy)' fragment (Table 1) whilst the transient absorption spectrum clearly contains important contributions associated with triplet-triplet transitions localized on the metal complex (Fig. 2). Spectral analysis indicates that the triplet energy of the 'Ru(terpy)' fragment in pyr-terpy-Ru is slightly lower than that derived for the pyrene-like triplet with the result that the triplet equilibrium distribution (K = 0.15; α = 0.13) lies in favour of the metal complex. Reversible energy transfer, therefore, provides only a minor stabilization for the triplet localized on the 'Ru(terpy)' fragment. It should be noted, however, that relative to the parent $[Ru(terpy)_2]^{2+}$ complex (Φ_L < 0.0002; τ_L = 0.56 ns), pyr-terpy-Ru is strongly luminescent at r.t.

Reversible triplet energy transfer[1–3] between the terminals in pyr-bpy-Ru serves to extend the triplet lifetime of the 'Ru(bpy)' fragment to 42 μs, which is well beyond the range of any related system. The equilibrium distribution is established within the 20 ps excitation pulse, indicating that both forward and reverse energy-transfer steps are rapid. The observed triplet lifetime is set by the inherent decay rate constants for individual triplets localized on pyrene (k_P) and 'Ru(bpy)' (k_R) and by the fractional contribution of each component [eqn. (1)]:

$$k_D = 1/\tau_T = \alpha k_P + (1 - \alpha)k_R \quad (1)$$

Here, α is determined by the energy gap (ΔE_{TT}) between the two triplets (Table 1) while k_P (= 7770 s^{-1}) is obtained by monitoring the triplet state of pyr-bpy under appropriate conditions. This allows k_R to be estimated from the experimental data and the derived value ($k_R = 8.4 \times 10^5$ s^{-1}) is seen to be comparable to decay rates measured for other ethynylated 'Ru(bpy)' fragments, where inherent triplet lifetimes tend to be slightly > 1 μs.[5] Furthermore, it now becomes possible to quantify the effect of the pyrene unit in terms of a stabilization factor ($S = k_R\tau_T$), which for pyr-bpy-Ru has a value of *ca*. 35 and is marginally greater than unity for pyr-terpy-Ru. For both compounds, however, S increases markedly when due allowance is made for the additional stabilization imposed by the ethynylene group. Thus, using k_R values appropriate[10] for simple 'Ru(bpy)' or 'Ru(terpy)' units having the same triplet energy as the metallo-fragments in pyr-bpy-Ru and pyr-terpy-Ru, respectively, gives revised S values of 115 and 10.‡ It is anticipated that this prolongation of the triplet lifetime will advance opportunities for employing the unique luminescence properties of 'Ru(bpy)'-based systems in sophisticated analytical or electro-chemiluminescent applications.

Notes and references

† Full synthetic details will be given elsewhere. All new compounds were authenticated by NMR, FTIR, MS and elemental analyses. *Selected data*: pyr-bpy-Ru, IR (KBr disc): 2195 cm^{-1} [ν(C≡C)];^{13}C{^{1}H} NMR ($CDCl_3$): δ 96.4 (C≡C), 90.7 (C≡C), MS (FAB$^+$, *m*-NBA): 939.0 $(M-PF_6)^+$; UV-VIS (MeCN) λ_{max}/nm (ε/dm^3 mol^{-1} cm^{-1}): 416 (45 200), 280 (118 300). pyr-bpy-Os, IR(KBr disc): 2195 cm^{-1} [ν (C≡C)] MS (FAB$^+$, *m*-NBA): 1029.0 (M − PF_6 + H)$^+$; UV-VIS (MeCN) λ_{max}/nm (ε/dm^3 mol^{-1} cm^{-1}): 408 (23 900), 284 (72 600). pyr-terpy-Ru, IR(KBr disc): 2192 cm^{-1} [ν(C≡C)]; ^{13}C{^{1}H} NMR (CD_3CN): δ 97.2 (C≡C), 93.1 (C≡C), MS (FAB$^+$, *m*-NBA): 937.2 $(M - PF_6)^+$; UV-VIS (MeCN) λ_{max}/nm, ε/dm^3 mol^{-1} cm^{-1}): 511 (44 800), 281 (53 200).

‡ For example, Cook *et al*.[10] list four $[Ru(bpy)_3]^{2+}$ analogues with emission maxima at 670 nm and for which the triplet lifetime is (0.36 ± 0.04) μs. Similarly, examination of the photophysical properties of $[Ru(terpy)_2]^{2+}$ complexes indicates that the triplet lifetime of a compound having an emission maximum at 698 nm should be (60 ± 15) ns.

1 W. E. Ford and M. A. J. Rodgers, *J. Phys. Chem*., 1992, **96**, 2917.
2 G. J. Wilson, W. H. F. Sasse and A. W.-H. Mau, *Chem. Phys. Lett*., 1996, **250**, 583.
3 G. J. Wilson, A. Launikonis, W. H. F. Sasse and A. W.-H. Mau, *J. Phys. Chem*., 1997, **101**, 4860.
4 J. A. Simon, S. L. Curry, R. H. Schmehl, T. R. Schatz, P. Piotrowiak, X. Jin and R. P. Thummel, *J. Am. Chem. Soc*., 1997, **119**, 11 012.
5 V. Grosshenny, A. Harriman, F. M. Romero and R. Ziessel, *J. Phys. Chem*. 1996, **100**, 17 472.
6 Z. Murtaza, A. P. Zipp, L. A. Worl, D. K. Graff, W. E. Jones Jr., W. D. Bates and T. J. Meyer, *J. Am. Chem. Soc*., 1991, **113**, 5113; Z. Murtaza, D. K. Graff, A. P. Zipp, L. A. Worl, W. E. Jones Jr., W. D. Bates and T. J. Meyer, *J. Phys. Chem*., 1994, **98**, 10 504.
7 A. El-ghayoury, A. Harriman, M. Hissler and R. Ziessel, *Coord. Chem. Rev*,. 1998, **178-180**, 1251.
8 M. Striles and L. J. Cline Love, *Anal. Chem*., 1980, **52**, 1559.
9 V. Grosshenny, A. Harriman and R. Ziessel, *Angew. Chem., Int. Ed. Engl*., 1995, **34**, 2705.
10 M. J. Cook, A. P. Lewis, G. S. G. McAuliffe, V. Skarda, A. J. Thompson, J. L. Glasper and D. J. Robbins, *J. Chem. Soc., Perkin Trans 2*., 1984, 1293.

Communication 9/00962K

ChemComm

Alkane-tetrathiol induced formation of remarkably stable self-assembled monolayer and polymer films containing electroactive tetrathiafulvalene moieties on metal electrodes

Hisashi Fujihara,* Hidetaka Nakai, Masakuni Yoshihara and Toshihisa Maeshima

Department of Applied Chemistry, Kinki University, Kowakae, Higashi-Osaka 577-8502, Japan.
E-mail: h-fuji@apch.kindai.ac.jp

Received (in Cambridge, UK) 4th February 1999, Accepted 16th March 1999

Remarkably stable self-assembled monolayer and polymer films composed of a new tetrathiafulvalenyl-tetrathiol have been formed on metal electrodes: this is a new class of surface modification by self-assembly and electrochemical polymerization using the same alkane-tetrathiol.

Self-assembled monolayer and polymer films on metal surfaces are the focus of intense investigation, because these films constitute an important strategy in the surface modification of electrodes.[1–4] The majority of self-assembled organosulfur monolayers studied consist of adsorbates which contain an alkyl chain with a surface-active sulfur group, such as alkane-*monothiols* and *n*-alkyl disulfides, however, such surface modification using alkane-*polythiols* has received much less attention. Meanwhile, the modification of electrodes with electroactive polymer films has been performed from the electrochemical polymerization of pyrrole and thiophene-based monomers which are the most commonly used materials.[4] We have now found that a new class of surface-modification reagent, tetrathiafulvalenyl alkane-tetrathiol **1**, gives remarkably stable self-assembled monolayers on a gold (Au) electrode and polymer films on a glassy carbon (GC) electrode. To our knowledge, this is the first example for the surface modification of metallic electrodes with the same adsorbate molecule by the self-assembly method and electropolymerization using the same starting material.

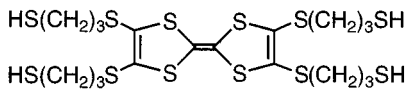

1

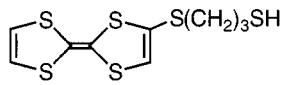

2

The immersion of a clean polycrystalline gold electrode in a solution of the new tetrathiol **1**[5] (1.0 mM in CH_2Cl_2, 40 °C, 24 h) resulted in the formation of a monolayer of tetrathiol **1**, which chemisorbed on the gold surface *via* thiolate–Au bonds. After extensive rinsing of the modified electrode, the voltammetric response in CH_2Cl_2 clearly exhibited anodic and cathodic waves characteristic of the reversible two-electron oxidation of the immobilized tetrathiafulvalene (TTF)-groups [Fig. 1(a)]. The potential ($E_{1/2}$) for the oxidation process was +0.35 and +0.66 V (*vs.* Ag/0.1 M $AgNO_3$). The potential difference between the anodic and cathodic peaks was 20 mV at v = 100 mV s^{-1}, and the peak current increased linearly with the scan rate. These two voltammetric features unequivocally indicate the surface-confined nature of the electroactive TTF groups. The surface coverage (Γ) of **1** on the Au electrode was found to be 1.6×10^{-10} mol cm^{-2}.

Tetrathiol-monolayer modified Au electrode allowed to stand at 0 V in CH_2Cl_2 or MeCN showed no diminution of the anodic peak current response over more than several weeks, showing that the molecular film is not readily stripped by non-aqueous solvents. The electrochemical stability of the monolayer of **1** on an Au electrode in CH_2Cl_2 was investigated by continuously cycling the potential. After 10 scans between −0.05 and +0.95 V, only 5% of the electroactivity is lost [Fig. 1(b)]. This finding indicates that the monolayer of tetrathiol **1** is stable in non-aqueous solvents.[6] Interestingly, the monolayer of the *tetrathiol* **1** was remarkably stable compared to the monolayer of the *monothiol* **2** on an Au electrode as evidenced from the repeated electrochemical cycling of those monolayers.

Normally, alkane-monothiols can not be polymerized by repeated anodic oxidations and none of the polymer film from monothiol **2** was formed upon repeated cyclic scanning of the potential.[7] However, tetrathiol **1** on repeated electrochemical oxidation showed intriguing results. The first scan of the cyclic voltammogram of tetrathiol **1** in CH_2Cl_2 + 0.1 M NBu_4PF_6 at a glassy carbon electrode exhibited the regular reversible waves corresponding to the TTF–$TTF^{\cdot+}$–TTF^{2+} system at $E_{1/2}$ = +0.34 and +0.67 V [Fig. 2(a)]. These two waves are followed by an irreversible oxidation peak at +0.90 V (E_p) which seems to correspond to oxidation of thiol groups. Surprisingly, repeated

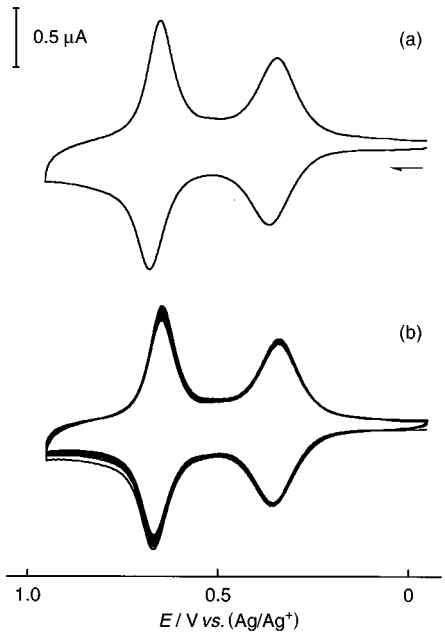

Fig. 1 Cyclic voltammograms for a monolayer of **1** adsorbed onto an Au electrode in 0.1 M NBu_4PF_6–CH_2Cl_2: (a) first scan; (b) multiple scans. Scan rate 100 mV s^{-1}.

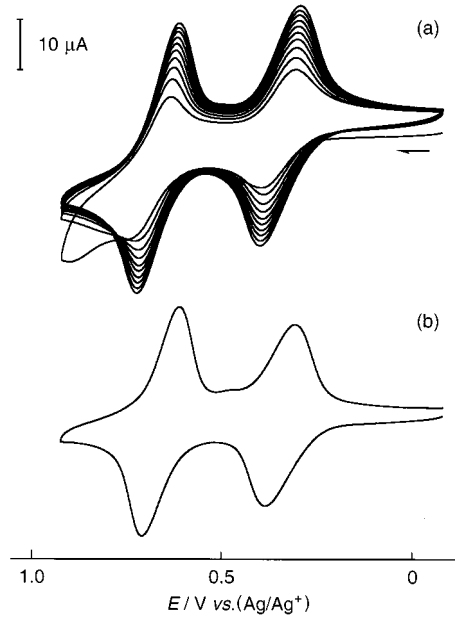

Fig. 2 (a) Oxidative electropolymerization of **1** (1 mM) by repeated potential scans on a GC electrode in 0.1 M NBu_4PF_6–CH_2Cl_2; scan rate 100 mV s^{-1}. (b) Cyclic voltammogram of a poly-TTF modified GC electrode in 0.1 M NBu_4PF_6–CH_2Cl_2; scan rate 100 mV s^{-1}.

scans over the −0.08 to +0.92 V range led to the growth of a polymer film on the electrode.[8] Evidence for this is given by the continuous increase in the peak intensity of the TTF–$TTF^{\cdot+}$–TTF^{2+} system. After 10 scans, the electrode was rinsed copiously with solvent and dipped into fresh CH_2Cl_2 solution. The cyclic voltammogram of the polymer–TTF modified electrode ($\Gamma = 1.0 \times 10^{-9}$ mol cm^{-2} after 10 cycles) is shown in Fig. 2(b).[9] The cyclic voltammogram of the polymer modified GC electrode displayed only two redox peaks corresponding to the TTF–$TTF^{\cdot+}$–TTF^{2+} system at $E_{1/2}$ = +0.34 and +0.66 V. This contrasts with the electropolymerization of pyrrole-substituted electroactive compounds which showed oxidation waves of both the pyrrole and the electroactive groups in the cyclic voltammogram. Many scans of the poly-TTF modified electrode can be performed without any change of the voltammetric wave. Thus, poly-TTF is readily formed as stable films on a GC electrode surface. This is a new type of controlled polymerization using alkane-polythiols.[10]

In summary, a monolayer of a new TTF-derivatized tetrathiol **1** on a gold electrode is more stable than that of monothiol **2** under electrochemical recycling. Tetrathiol **1** can be easily electropolymerized at moderate potential into highly stable poly-TTF films. Thus, alkane-tetrathiol **1** provides both remarkably stable monolayers and multilayers containing electroactive TTF moieties. Further work is currently in progress in this and related areas.

This work was supported in part by the Grant-in-Aid for Scientific Research No. 09239252 and No. 10133255 from the Ministry of Education, Science and Culture, Japan.

Notes and references

1 *Molecular Design of Electrode Surfaces*, ed. R. W. Murray, Wiley-Interscience, New York, 1992.
2 A. Ulman, *An Introduction to Ultrathin Organic Films*, Academic Press, Inc., Boston, MA, 1991.
3 L. H. Dubois and R. G. Nuzzo, *Annu. Rev. Phys. Chem.*, 1992, **43**, 437; A. Ulman, *Chem. Rev.*, 1996, **96**, 1533.
4 A. Deronzier and J. C. Moutet, *Acc. Chem. Res.*, 1989, **22**, 249; J. Roncali, *Chem. Rev.*, 1992, **92**, 711.
5 **1**: FTIR 2554 cm^{-1} (SH); ^{1}H NMR ($CDCl_3$) δ 1.39 (t, 4H, *J* 8.1 Hz, SH), 1.94 (q, 8H, *J* 6.8 Hz, CH_2), 2.69 (dt, 8H, *J* 8.1, 6.8 Hz, CH_2SH), 2.96 (t, 8H, *J* 6.8 Hz, SCH_2); ^{13}C NMR ($CDCl_3$) δ 23.0, 33.3, 34.5, 110.5, 127.9. Exact mass: calc. for $C_{18}H_{28}S_{12}$: 627.8840. Found: 627.8856. **2**: FTIR 2557 cm^{-1} (SH); ^{1}H NMR ($CDCl_3$) δ 1.37 (t, 1H, *J* 8.0 Hz, SH), 1.93 (q, 2H, *J* 7.0 Hz, CH_2), 2.65 (dt, 2H, *J* 8.0, 7.0 Hz, CH_2SH), 2.87 (t, 2H, *J* 7.0 Hz, SCH_2), 6.32 (s, 2H, C=CH), 6.37 (s, 1H, C=CH); ^{13}C NMR ($CDCl_3$) δ 22.9, 33.2, 34.0, 109.4, 112.9, 118.9, 119.0, 122.9, 126.6. MS, *m/z* 310 (M^+). The synthesis of **1**, **2** and related compounds will be reported elsewhere.
6 Most electrochemical studies of self-assembled monolayers carried out to date have used aqueous media. The properties of self-assembled monolayers in organic solvents have been discussed: K. A. Groat and S. E. Creager, *Langmuir*, 1993, **9**, 3668 and references therein.
7 The tetramethylsulfide of **1** did not polymerize upon repeated electrochemical oxidation. This result indicates that the tetrathiol needs to form polymer films for this to occur.
8 The polymerization may proceed *via* the formation of disulfide linkages upon oxidation of the thiol groups of **1**. Mechanistic studies for the electropolymerization of tetrathiol **1** are in progress.
9 The surface coverage of the polymer films on the electrode can be controlled by cycling times.
10 Although there have been numerous investigations into the electropolymerization of pyrrole- and thiophene-based monomers, the mechanism for the deposition of these films on electrode surfaces is not well defined.[4]

Communication 9/00960D

A simple route to multifunctional phosphide and amide donor sets; syntheses and structures of $[\{Bu^tPAs(NMe_2)_2\}K{\cdot}pmdeta]_2$ and $[\{CyNAs(NMe_2)_2K\}_2]_\infty$

Michael A. Beswick,*[a] Alan Bashall,[b] Alexander D. Hopkins,[a] Sara J. Kidd,[a] Yvonne G. Lawson,[a] Mary McPartlin,[b] Paul R. Raithby,[a] Alexander Rothenberger,[c] Dietmar Stalke[c] and Dominic S. Wright*[a]

[a] *Chemistry Department, University of Cambridge, Lensfield Road, Cambridge, UK CB2 1EW. E-mail: dsw1000@cus.cam.ac.uk*

[b] *School of Chemistry, University of North London, London, UK N7 8DB*

[c] *Institut für Anorganische Chemie, Universität Würzburg, Am Hubland, 97074 Würzburg, Germany*

Received (in Cambridge, UK) 15th February 1999, Accepted 10th March 1999

The syntheses of $[Bu^tPAs(NMe_2)_2K{\cdot}pmedta]_2$ 1 and $[\{CyNAs(NMe_2)_2K\}_2]_\infty$ 2 from the reactions of $[As(NMe_2)_3]$ with Bu^tPH_2 and $CyNH_2$, respectively, in the presence of potassiated bases exemplify a general approach to multifunctional secondary phosphide and amide anions containing variable sets of group 15 donor centres.

Studies of alkali metal phosphoramide (containing $[R_2PNR]^-$)[1] and related hydrazide (containing $[R_2NNR]^-$)[2] complexes have revealed a diverse range of structural types in the solid state for this important class of ligands, in which both the anionic and neutral N and P centres can coordinate the cations. However, to our knowledge the only analogous ligands containing other combinations of group 15 elements to be structurally characterised are $[Bu^t(H)PPBu^t]^{-3}$ and $[Bu^t_2AsAsBu^t]^-$.[4] We have recently synthesised new polydentate imido and phosphinidene anion ligand systems containing other group 15 elements, such as $[Sb(ER)_3]^{3-}$ (E = N, P),[5] and now report that a related methodology involving dimethylamido group 15 reagents gives the anions $[REAs(NMe_2)_2]^-$. These secondary phosphide and amide anions (related to simple phosphoramides and hydrazides) are a new class of highly functionalised donor ligands.

The reaction of $[As(NMe_2)_3]$ (1 equiv.) with Bu^tPH_2/$[Bu^tPHK]$ (1:1 equiv.) can be controlled, giving the stable complex $[\{Bu^tPAs(NMe_2)_2\}K{\cdot}pmdeta]_2$ **1** in the presence of pmdeta [= $(Me_2NCH_2CH_2)_2NMe$].† This outcome contrasts with the prolonged reactions between $[As(NMe_2)_3]$ and [Bu^t-PHLi] (1:3 equiv.) or $[Bu^tPHLi]/Bu^tPH_2$ (1:1:1 equiv.), which yield species containing the cyclic $[(Bu^tP\}_3As)^-$ anion.[6] The reaction producing **1** appears to involve an acid-catalysed process (Scheme 1), as is suggested by the isolation of the related amide complex $[\{CyNAs(NMe_2)_2K\}_2]_\infty$ **2** from the reaction of $[As(NMe_2)_3]$ with $CyNH_2$ in the presence of $[Pr^i_2NK]$ (1:1:1 equiv.) as the base.†

The X-ray structures of **1** (Fig. 1) and **2** (Fig. 2)‡ reveal that both species are composed of similar centrosymmetric K_2P_2 and K_2N_2 dimeric units in the solid state, in which two K^+ cations are bridged by the anionic P and N centres of their respective $[Bu^tPAs(NMe_2)_2]^-$ and $[CyNAs(NMe_2)_2]^-$ ligands. The K–P bond lengths in **1** [K(1)–P(1) 3.315(4), K(1)–P(1a) 3.462(3)Å] and K–N distances in **2** [K(1)–N(1) 2.893(6) to K(1)–N(1A) 2.780(7) Å] within these dimer units are similar to those found in the few structurally characterised K phosphide[3,7] and amide[8] complexes. The K^+ cation in each complex further interacts with one of the Me_2N groups [K(1)–N(5) 2.991(8) in **1**, K(1)–N(3) 2.852(7)Å in **2**] to form a four-membered chelate ring. Further aggregation of the dimeric units of **1** is prevented by coordination of the K^+ cations by pmdeta, resulting in a distorted octahedral geometry at the metal centres. However, the absence of Lewis base solvation in **2** leads to the association of the dimers, *via* the second Me_2N group of each [CyN-$As(NMe_2)_2]^-$ anion [K(1)–N(2B) 3.071(7) Å], giving a novel poymeric chain structure. This arrangement results in a distorted-tetrahedral geometry for the K^+ centres and in the formation of puckered centrosymmetric $[KNAsN]_2$ rings which link the K_2N_2 dimer units of **2** together. The low coordination number of the K^+ cations of **2** appears to be compensated for by extensive, relatively short[9] Cy α-C···K and Me C···K contacts [K(1)···C 3.26–3.48Å].

Comparison with other As–P[10] and As–N[11] bonded compounds reveals that the As–P and As–N bonds in **1** [As(1)–P(1) 2.260(3) Å] and **2** [As(1)–N(1) 1.782(7) Å] are at the lower end of the range of values observed for single bonds, and in **2** this bond is significantly shorter than the two As–NMe_2 bonds (mean 1.914 Å). It seems most likely that the relatively short As–P bond in **1** largely stems from the effect of polarisation, with the geometry about the anionic P centre in this complex giving no indication of any partial multiple bonding [*e.g.* C(14)–P(1)–As(1) 98.1(3)°]. However, the bond angle at the

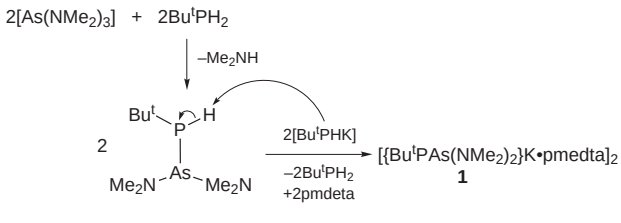

Scheme 1

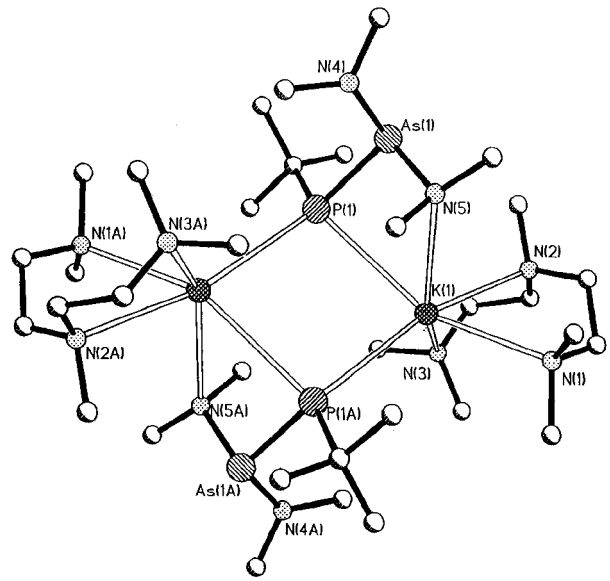

Fig. 1 Dimer structure of **1**. H atoms have been omitted for clarity. Selected bond lengths (Å) and angles (°): P(1)–K(1) 3.315(4), P(1A)–K(1) 3.462(3), N(5)–K(1) 2.991(8), mean N(1,2,3)–K 2.93, As(1)–P(1) 2.260(3), N(4)–As(1) 1.869(9), As(1)–N(5) 1.877(9), K(1)–P(1)–K(1A) 96.98(8), P(1)–K(1)–P(1A) 93.02(8), C(14)–P(1)–As(1) 98.1(3), P(1)–As(1)–N(4) 107.1(3), P(1)–As(1)–N(5) 97.7(2), N(4)–As(1)–N(5) 100.7(4), As(1)–N(5)–K(1) 101.9(3).

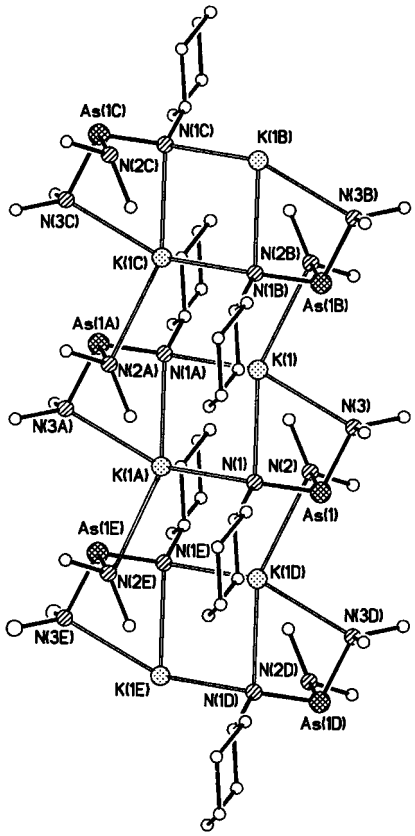

Fig. 2 Part of the infinite polymeric structure of **2** which runs along the *a*-axis of the unit cell. H atoms have been omitted for clarity. Selected bond lengths (Å) and angles (°): K(1)–N(1) 2.893(6), K(1)–N(1A) 2.780(7), K(1)–N(3) 2.852(7), K(1)–N(2B) 3.071(7), Cy α-C(–H) and Me C(–H) K(1)···C 3.26-3.48, As(1)–N(1) 1.782(7), As(1)–N(2) 1.894(7), As(1)–N(3) 1.935(6), K(1)–N(1)–K(1A) 87.9(2), N(1)–K(1)–N(1A) 92.1(2), C(1)–N(1)–As(1) 117.4(6), N(1)–As(1)–N(2) 98.9(3), N(1)–As(1)–N(3) 99.8(3), N(2)–As(1)–N(3), 97.5(3), As(1)–N(3)–K(1) 97.3(3).

anionic N centre in **2** [C(1)–N(1)–As(1) 117.4(6)°] may indicate that there is some contribution from p_π–d_π interaction, an effect which may be exacerbated by the elongation of the As–N bond involved in the chelate ring [As(1)–N(3) 1.935(6); *cf.* As(1)–N(2) 1.894(7)].

In conclusion, the synthetic route used in the preparation of **1** and **2** is potentially applicable to an extensive series of related group 15 anions. The $[Bu^tPAs(NMe_2)_2]^-$ and $[CyN\text{-}As(NMe_2)_2]^-$ anions **1** and **2** represent a unique set of readily accessible new ligands, containing combinations of group 15 elements within their frameworks (all of which being capable potentially of coordinating a metal centre). The structural studies of **1** and **2** provide the first indication of the coordination chemistry and structural trends in these species. The structure of **2** is particularly noteworthy, being composed of a polymer of dimers rather than having a more conventional ladder arrangment.[12]

We gratefully acknowledge the EPSRC (A. D. H., S. J. K., Y. G. L., M. McP.), the Leverhulme Trust (M. A. B.), Electron Industries (A. D. H.), the Gottleib Daimler- und Karl Benz-Stiftung (A. R.) and the ARC (D. S., D. S. W.) for financial support.

Notes and references

† *Syntheses* **1**: [Bu^tPHK] was prepared by the reaction of $PhCH_2K$ (0.78 g, 6.0 mmol) with Bu^tPH_2 (0.4 ml, 6.0 mmol) in hexane (10 ml)/thf (5 ml) under argon. After stirring the reaction at room temp. (30 min.) it was cooled (−78 °C) and a mixture of $[As(NMe_2)_3]$ (6.0 mmol, 2.4 ml, 2.5 mol dm^{-3} in hexane) and Bu^tPH_2 (0.4 ml, 6.0 mmol) in hexane (10 ml) [which had previously been stirred at room temp. (30 min.)] was added. Excess pmdeta (7.1 mmol, 1.5 ml) was added and the reaction was allowed to warm to room temperature. Removal of the solvent under vacuum and addition of hexane (17 ml) gave a precipitate. Addition of thf (5 ml) and gentle heating dissolved the solid. Storage at −30 °C gave colourless crystals of **1**. First batch yield 0.30g (11%). mp 121 °C (decomp. to a brown solid). ^{31}P NMR (MHz, +25 °C, d_8-thf, rel. to 80% H_3PO_4–D_2O), δ−5.91(s). Satisfactory elemental analyses (C,H,N,P) were obtained for **1**.

2: [Pr^i_2NK] (6.0 mmol) was prepared by the reaction of $PhCH_2K$ (0.78 g, 6.0 mmol) with Pr^i_2NH (0.85 ml, 6 mmol) in hexane (20 ml)–toluene (10 ml). After heating to reflux and stirring at room temp. (30 min.), a mixture of $[As(NMe_2)_3]$ (3.9 ml, 1.55 mmol dm^{-3} in hexane, 6.0 mmol) and $CyNH_2$ (0.69 ml, 6.0 mmol) in hexane (10 ml) [which had previously been heated to reflux and stirred at room temperature (30 min.)] was added. After stirring at room temperature (10 min.) a green solution was formed with a small amount of precipitate. Gentle heating dissolved the solid and storage at −30 °C (24 h) gave yellow crystals of **2**. First batch yield 0.14 g (8%). ^1H NMR (250 MHz, +25 °C, d_8-thf), δ 2.60 (s., 12H, Me_2N), *ca.* 3.3–1.0 (collection of overlapping mult., 11 H, Cy). Satisfactory elemental analyses (C,H,N) were obtained for **2**.

‡ *Crystal data*: **1**: $C_{34}H_{84}As_2K_2N_{10}P_2$, M = 923.09, monoclinic, space group $P2_1/n$, Z = 2, a = 14.014(3), b = 12.750(4), c = 15.014(3) Å, β = 105.48(3)°, U = 2585.4(10) Å^3, μ(Mo–Kα) = 1.547 mm^{-1}, T = 180(2) K. Of a total of 3473 data collected 3357 were independent (R_{int} = 0.098). An empirical absorption correction based on ψ-scans was used. The structure was solved by direct methods and refined by full-matrix least squares on F^2 to final values of $R1[F > 4\sigma(F)]$ = 0.075 and $wR2$ = 0.189 (all data).[13]

2: $C_{10}H_{23}AsKN_3$, M = 299.33, triclinic, space group $P\bar{1}$ (no. 2), Z = 2, a = 6.3524(13), b = 10.275(2), c = 10.957(2) Å, α = 91.31(3), β = 99.86(3), γ = 95.73(3)°, U = 693.5(2) Å^3, μ(Mo-Kα) = 2.728 mm^{-1}, T = 223(2) K. Of a total of 2427 data collected, 1880 were independent (R_{int} = 0.283). The structure was solved by the Patterson method and refined by full-matrix least squares on F^2 [13,14] to final values of $R1$ [$I > 2\sigma(I)$] = 0.0620, $wR2$ = 0.1970 (all data).

CCDC 182/1193. See http://www.rsc.org/suppdata/cc/1999/739/ for crystallographic files in .cif format.

1 M. T. Ashby and Z. Li, *Inorg. Chem.*, 1992, **31**, 1321; A. Müller, B. Neumüller, K. Deniche, J. Magull and D. Fenske, *Z. Anorg. Allg. Chem.*, 1997, **623**, 1306.
2 M. Metzler, H. Nöth and H. Sachdev, *Angew. Chem., Int. Ed. Engl.*, 1994, **33**, 1746; C. Dost, C. Jager, U. Klingebiel, C. Freire-Erdbrugger, R. Herbst-Irmer and M. Schafer, *Z. Naturforsch, Teil B*, 1995, **50B**, 76; B. Gemund, H. Nöth, H. Sachdev and M. Schmidt, *Chem. Ber.*, 1996, **129**, 1335.
3 M. A. Beswick, A. D. Hopkins, L. C. Kerr, M. E. G. Mosquera, J. S. Palmer, P. R. Raithby, A. Rothenberger, D. Stalke, A. Steiner, A. E. H. Wheatley and D. S. Wright, *Chem. Commun.*, 1998, 1527.
4 A. M. Arif, R. A. Jones and K. B. Kidd, *J. Chem. Soc., Chem. Commun.*, 1986, 1440.
5 M. A. Beswick, M. E. G. Mosquera and D. S. Wright, *J. Chem. Soc., Dalton Trans.*, 1998, 2437.
6 M. A. Beswick, N. Choi, A. D. Hopkins, M. McPartlin, M. E. G. Mosquera, P. R. Raithby, A. Rothenberger, D. Stalke. A. E. H. Wheatley and D. S. Wright, *Chem. Commun.*, 1998, 2485; M. A. Beswick, A. D. Hopkins and D. S. Wright, unpublished work.
7. G. W. Rabe, G. P. A. Yap and A. L. Rheingold, *Inorg. Chem.*, 1997, **36**, 1990.
8 See for example, A. M. Domingos and G. M. Sheldrick, *Acta Crystallogr., Sect. B*, 1974, **30**, 517; K. F. Tesh, T. P. Hanusa and J. C. Huffman, *Inorg. Chem.*, 1990, **29**, 1584; P. C. Andrews, D. R. Baker, R. E. Mulvey, P. A. O'Neil and W. Clegg, *Polyhedron*, 1991, **10**, 1839; F. M. Mackenzie, R. E. Mulvey, W. Clegg and L. Horsborough, *J. Am. Chem. Soc.*, 1996, **118**, 4721.
9 Typical values of 3.0–3.4 Å are observed in organopotassium complexes, see C. Schade and P. v. R. Schleyer, *Adv. Organomet. Chem.*, 1987, **27**, 169 and references therein.
10 For comparison, see: L. Weber, D. Bungardy, R. Boese and D. Blaser, *Chem. Ber.*, 1988, **121**, 1033; A. H. Cowley, J. E. Kilduff, J. G. Lasch, S. K. Mehrotra, N. C. Norman, M. Pakulski, B. R. Whittlesey and J. L. Atwood, *Inorg. Chem.*, 1984, **23**, 2582.
11 See; J. L. Atwood, A. H. Cowley, W. E. Hunter and S. K. Mehritra, *Inorg. Chem.*, 1982, **21**, 1354; R. Bohra, H. W. Roesky, M. Noltemeyer and G. M. Sheldrick, *Acta, Crystallogr., Sect. C*, 1984, **40**, 1150; J. Weiss and W. Einenhuth, *Z. Anorg. Allg. Chem.*, 1967, **350**, 9; M. G. Begley, D. B. Sowerby and R. J. Tillott, *J. Chem. Soc., Dalton Trans.*, 1974, 2527.
12 K. Gregory, P. v. R. Schleyer and R. Snaith, *Adv. Organomet. Chem.*, 1991, **37**, 47; R. E. Mulvey, *Chem. Soc. Rev.*, 1991, **20**, 167.
13 SHELXTL PC version 5.03, Siemens Analytical Instruments, Madison, WI, 1994.
14 N. Walker and D. Stuart, *Acta Crystallogr., Sect. A*, 1983, **39**, 158.

Communication 9/01222B

Ir-catalysed allylic substitution: mechanistic aspects and asymmetric synthesis with phosphorus amidites as ligands

Björn Bartels and Günter Helmchen*

Organisch-Chemisches Institut der Universität, Im Neuenheimer Feld 270, D-69120 Heidelberg, Germany. E-mail: en4@ix.urz.uni-heidelberg.de

Received (in Liverpool, UK) 29th January 1999, Accepted 16th March 1999

Ir-catalysed allylic alkylations of enantiomerically enriched monosubstituted allylic acetates proceed with up to 79% retention of configuration using $P(OPh)_3$ as ligand; further evidence supports the assumption of σ-allyl complexes as intermediates, and high regio- and enantioselectivity in asymmetric allylic alkylations of achiral or racemic substrates is achieved with phosphorus amidites as ligands.

The transition metal catalysed asymmetric allylic alkylation is a useful reaction in organic synthesis.[1] Over the last few years, research has been focused on finding catalysts which favour the formation of branched, chiral products **3** in the substitution of monosubstituted allylic substrates **1** or **2** (Scheme 1). With palladium complexes this is so far only possible for special cases.[2] With Mo- or W-based catalysts, so far only substrates with R = aryl gave high levels of both regio- and enantioselectivity.[3] Reactions with all these catalysts proceed *via* π-allyl complexes as intermediates which display fast π–σ–π-rearrangement. However, the substitutions catalysed by Fe- or Rh-complexes probably proceed *via* σ-allyl complexes which isomerise slowly so that almost complete chirality transfer occurs. As a consequence, even with achiral ligands, enantiomerically enriched products **3** are obtained in a double inversion process from enantiomerically enriched substrates **1**.[4]

Ir-catalysed allylic substitutions have so far been rarely studied. It was recently found that catalysts prepared by combining $[Ir(COD)Cl]_2$ with a strong π-acceptor ligand, *e.g.* triphenyl phosphite, *in situ* give rise to excellent regioselectivities in favour of the branched product **3** for both aryl and alkyl substituted allylic substrates.[5] We were able to achieve regioselectivity of 95 : 5 and enantioselectivity of 96:4 for aryl substituted substrate **2b** with phosphinooxazoline **5** as chiral ligand.[6]

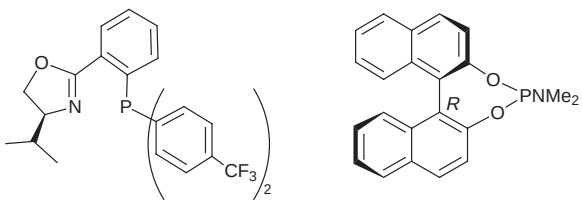

5

(*R*)-**6**

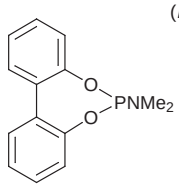

7

Extending this work, we have investigated the application of our catalyst to alkyl substituted allylic acetates. The reaction with substrate *rac*-**1a** using an *in situ* catalyst $[Ir(COD)Cl]_2$–**5** (24 h at 65°C) was found to be significantly slower than the reaction catalysed by $[Ir(COD)Cl]_2$–$P(OPh)_3$ or $[Ir(COD)Cl]_2$ without an additional ligand (*ca.* 3 h at room temperature) (*cf.* Table 1, entries 1,2,4). This observation led us to search for a suitable monodentate chiral ligand. Furthermore, the re-

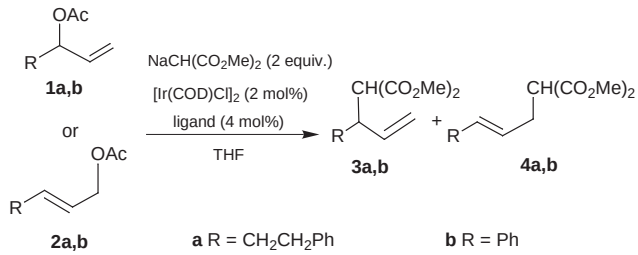

Scheme 1

Table 1 Allylic alkylation of acetates **1** and **2** catalysed by Ir^I complexes (reaction at 65 °C for 24 h with **5**, at room temperature for 3 h with all other ligands)[a]

Entry	Substrate	Ligand	Additive[b]	Yield[c] (%) **3** and **4**	Ratio **3** : **4**[d]	Ee (%)[d] of **3** (Configuration)
1	*rac*-**1a**	$P(OPh)_3$	—	99	95 : 5	—
2	*rac*-**1a**	—	—	66	89 : 11	—
3	*rac*-**1a**	PPh_3	—	—	—	—
4	*rac*-**1a**	**5**	—	99	95 : 5	8 (*S*)
5	**2a**	**5**	—	93	62 : 38	78 (*R*)
6	*rac*-**1b**	**5**		99	95 : 5	15 (*S*)
7	**2b**	**5**		99	95 : 5	91 (*R*)
8	(*R*)-**1b**[e]	$P(OPh)_3$	—	98	95 : 5	56 (*S*)
9	(*R*)-**1a**[f]	$P(OPh)_3$	—	97	95 : 5	51 (*R*)
10	(*R*)-**1a**[f]	$P(OPh)_3$	LiCl	71	93 : 7	49 (*R*)
11	*rac*-**1a**	(*R*)-**6**	—	92	98 : 2	69 (*R*)
12	**2a**	(*R*)-**6**	—	54	95 : 5	43 (*R*)
13	*rac*-**1b**	(*R*)-**6**	—	98	92 : 8	8 (*S*)
14	**2b**	(*R*)-**6**	—	99	98 : 2	37 (*R*)
15	*rac*-**1a**	(*R*)-**6**	LiF	99	> 99 : 1	58 (*R*)
16	*rac*-**1a**	(*R*)-**6**	LiCl	83	> 99 : 1	86 (*R*)
17	*rac*-**1a**	(*R*)-**6**	LiBr	69	98 : 2	83 (*R*)
18[g]	(*R*)-**1a**[h]	(*R*)-**6**	—	99	99 : 1	75 (*R*)
19	(*S*)-**1a**[i]	(*R*)-**6**	—	92	99 : 1	31 (*R*)
20	(*R*)-**1a**[h]	(*R*)-**6**	LiCl	99	99 : 1	93 (*R*)
21	(*S*)-**1a**[i]	(*R*)-**6**	LiCl	54	99 : 1	68 (*R*)
22	(*R*)-**1a**[f]	**7**	—	98	99 : 1	39 (*R*)
23	(*R*)-**1a**[f]	**7**	LiCl	61	71 : 29	32 (*R*)

[a] General procedure: A solution of $[Ir(COD)Cl]_2$ (6.7 mg, 0.01 mmol), substrate (0.5 mmol) and ligand (0.02 mmol) in dry THF (2 ml) under argon was treated with a solution of dimethyl 2-sodiomalonate in dry THF (0.5 M, 2 ml, 1.0 mmol). Water was added after stirring under the conditions stated. Extraction with Et_2O followed by flash chromatography (silica, light petroleum–EtOAc 97 : 3) gave mixtures of **3** and **4**. [b] Modification of the general procedure: Addition of 0.5 mmol of lithium halide before addition of the dimethyl 2-sodiomalonate solution. [c] Yield of isolated product. [d] Determined by HPLC on DAICEL CHIRACEL OJ column, length: 25 cm + 5 cm precolumn, flow: 0.5 ml min^{-1}, eluent: *n*-hexane–Pr^iOH (97 : 3), **3a**: $t_R(R)$ = 33 min, $t_R(S)$ = 42 min; **4a**: t_R = 50 min; **3b**: $t_R(S)$ = 53 min, $t_R(R)$ = 60 min; **4b**: t_R = 83 min. [e] 93.8% ee. [f] 90.8% ee. [g] Reaction time: 1 h. [h] 99.5% ee. [i] 96.4% ee.

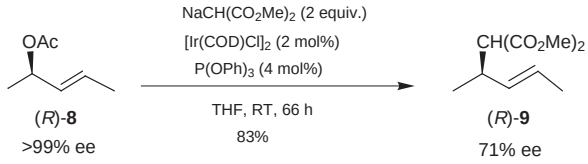

Scheme 2

gioselectivity (ratio of **3**:**4**) starting from achiral **2a** was low (**3**:**4** = 62:38) and the enantioselectivity high [(*R*)-**3a** of 78% ee], whereas with the regioisomeric racemic substrate **1a** it was just the opposite: the regioselectivity was high (**3**:**4** = 95:5) and the enantioselectivity low [(*S*)-**3a** of 8% ee] (entries 4–7). These results demonstrate that properties of allyl–Ir intermediates differ from those of allyl–Pd intermediates. As a rule, in Pd-catalysed allylic substitutions regioisomeric starting materials give rise to the same products; memory effects are known, but are small for bidentate ligands.[7]

For further clarification, the configurational stability of intermediary allyl–Ir complexes and the configurative course of the substitution were investigated. First, enantiomerically enriched **1a** and **1b** were alkylated using $P(OPh)_3$ as ligand.† Starting from (*R*)-**1a** of 91% ee the product (*R*)-**3a** was obtained with 51% ee with retention of configuration, *i.e.* 79% of the substrate had reacted with retention of configuration (entry 9). Similar results were achieved with the phenyl substituted substrate **1b** (entry 8).‡ Second, enantiomerically pure pent-3-en-2-yl acetate† [(*R*)-**8**] was reacted with dimethyl 2-sodiomalonate (Scheme 2); alkylation product (*R*)-**9** with 71% ee was formed.

As of now we cannot offer a conclusive explanation of our results. As a working hypothesis we assume that the Ir-catalysed reactions proceed, similar to the mechanism proposed for Rh-catalysed reactions,[4] by substitution of acetate to give σ-allyl–Ir complexes which further react with malonate again with inversion; the σ-complexes undergo slow racemisation (or epimerisation) *via* σ–π–σ-rearrangement or sigmatropic 1,3-rearrangement (Scheme 3).

The easily accessible phosphorus amidite **6**[8] was used as a monodentate chiral ligand (ratio Ir:**6** = 1:1). For all substrates this ligand is equivalent to $P(OPh)_3$ with respect to catalytic efficiency and regioselectivity (entries 11–14). Surprisingly, and in contrast to the results obtained with the bidentate ligand **5**, enantioselectivity induced by **6** was higher for the branched substrate *rac*-**1a** than for the linear substrate **2a**.

Reactions with added halide salts were investigated (entries 15-17) because a marked influence of halide ions on allylic substitution has been reported.[9] LiCl or LiBr indeed caused a marked increase of regio- and enantioselectivity, although also a small decrease of reactivity (entry 10). The effect of chloride was further studied for alkylations of (*R*)- and (*S*)-**1a** (entries 18–23). The reaction with the substrate–ligand combination (*R*)-**1a**–(*R*)-**6** was faster and more enantioselective (matched case) than with the combination (*S*)-**1a**–(*R*)-**6** (mismatched), yielding (*R*)-**3a** in both cases, *i.e.* control by the ligand is stronger than that by the substrate. The influence of the ligand is enhanced by addition of LiCl.

As the acetates **1** and **2** do not isomerise under the usual reaction conditions,§ it was of interest to explore a kinetic resolution. The result for the reaction of *rac*-**1a** with NaHC$(CO_2CH_3)_2$, catalysed by $[Ir(COD)Cl]_2$–(*R*)-**6,** is shown in Fig. 1. According to this plot, (*R*)-**1a** is consumed *ca.* 12 times faster than (*S*)-**1a**.[10] Consequently, the slower reacting acetate is

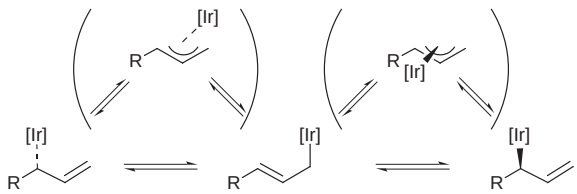

Scheme 3

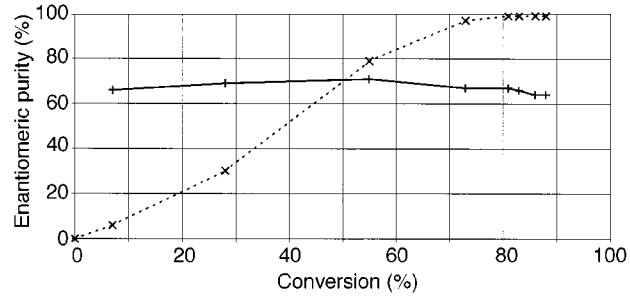

Fig. 1 Enantiomeric purity of (×) **1a** and (+) **3a** vs. conversion¶ for the reaction of (±)-**1a** with dimethyl 2-sodiomalonate catalysed by $[Ir(COD)Cl]_2$–(*R*)-**6**.

obtained in enantiomerically pure form beyond conversion of *ca*. 80%.

In conclusion, our results demonstrate that it is possible to achieve high levels of enantioselectivity in Ir-catalysed alkylations of monoalkylallyl acetates. Presently it is necessary to use racemic, branched substrates. Further progress will be achieved on the basis of detailed mechanistic investigations. It appears of particular importance to investigate the structure and dynamic properties of allyl–Ir complexes.

This work was supported by the Deutsche Forschungsgemeinschaft (SFB 247) and the Fonds der Chemischen Industrie. We thank Degussa AG for iridium salts.

Notes and references

† Enantiomerically enriched **1a** and **8** were prepared by enzyme (Novozym 435) catalysed esterification in vinyl acetate. (*R*)-**1b** was prepared from (*R*)-1-phenylprop-2-en-1-ol which was purchased from Fluka.

‡ Change of the descriptors in the starting material and product is a consequence of CIP priorities of substituents.

§ Isomerisation between **1a** and **2a** was not observed starting either from **1a** or from **2a** (reaction conditions: 2 mol% $[Ir(COD)Cl]_2$, 4 mol% $P(OPh)_3$, 2 equiv. NaOAc, 18 h, room temperature). For enantiomerically enriched **1a** (83% ee) a low degree of racemisation was obtained when the same reaction conditions were employed (70% ee).

¶ The degree of conversion was determined by HPLC.

1 B. M. Trost and D. L. Van Vranken, *Chem. Rev.*, 1996, **96**, 395; T. Hayashi, in *Catalytic Asymmetric Synthesis*, ed. I. Ojima, VCH, New York, 1993, p. 325.
2 R. Prétôt and A. Pfaltz, *Angew. Chem., Int. Ed.*, 1998, **37**, 323; T. Hayashi, K. Kishi, A. Yamamoto and Y. Ito, *Tetrahedron Lett.*, 1990, **31**, 1743; T. Hayashi, A. Ohno, S.-j. Lu, Y. Matsumoto, E. Fukuyo and K. Yanagi, *J. Am. Chem. Soc.*, 1994, **116**, 4221; T. Hayashi, M. Kawatsura and Y. Uozumi, *Chem. Commun.*, 1997, 561; B. M. Trost and F. D. Toste, *J. Am. Chem. Soc.*, 1998, **120**, 9074.
3 Mo: B. M. Trost and I. Hachiya, *J. Am. Chem. Soc.*, 1998, **120**, 1104; W: G. C. Lloyd-Jones and A. Pfaltz, *Angew. Chem., Int. Ed. Engl.*, 1995, **34**, 462.
4 Fe: Y. Xu and B. Zhou, *J. Org. Chem.*, 1987, **52**, 974; Rh: P. A. Evans and J. D. Nelson, *J. Am. Chem. Soc.*, 1998, **120**, 5581.
5 R. Takeuchi and M. Kashio, *Angew. Chem., Int. Ed. Engl.*, 1997, **36**, 263; R. Takeuchi and M. Kashio, *J. Am. Chem. Soc.*, 1998, **120**, 8647.
6 J. P. Janssen and G. Helmchen, *Tetrahedron Lett.*, 1997, **38**, 8025.
7 T. Hayashi, M. Kawatsura and Y. Uozumi, *J. Am. Chem. Soc.*, 1998, **120**, 1681; G. C. Lloyd-Jones and S. C. Stephen, *Chem. Eur. J.*, 1998, **4**, 2539; B. M. Trost and R. C. Bunt, *J. Am. Chem. Soc.*, 1996, **118**, 235; B. M. Trost, M. G. Morgan and G. A. O'Doherty, *J. Am. Chem. Soc.*, 1995, **117**, 9662.
8 B. L. Feringa, M. Pineschi, L. A. Arnold, R. Imbos and A. H. M. de Vries, *Angew. Chem., Int. Ed. Engl.*, 1997, **36**, 2620.
9 U. Burckhardt, M. Baumann and A. Togni, *Tetrahedron: Asymmetry*, 1997, **8**, 155; M. Kawatsura, Y. Uozumi and T. Hayashi, *Chem. Commun.*, 1998, 217.
10 The relative rate was estimated by comparison with a published plot of conversion *vs.* ee of residual substrate for a kinetic resolution: V. S. Martin, S. S. Woodard, T. Katsuki, Y. Yamada, M. Ikeda and K. B. Sharpless, *J. Am. Chem. Soc.*, 1981, **103**, 6237.

Communication 9/00864K

ChemComm

Why is the antiviral nucleotide analogue 9-[2-(phosphonomethoxy)ethyl]adenine in its diphosphorylated form ($PMEApp^{4-}$) initially a better substrate for polymerases than (2′-deoxy)adenosine 5′-triphosphate ($dATP^{4-}$/ATP^{4-})? Considerations on the mechanism of nucleic acid polymerases

Helmut Sigel,*[a] Bin Song,[a] Claudia A. Blindauer,[a] Larisa E. Kapinos,[a] Fridrich Gregáň[b] and Nadja Prónayová[c]

[a] *Institute of Inorganic Chemistry, University of Basel, Spitalstrasse 51, CH-4056 Basel, Switzerland. E-mail: sigel@ubaclu.unibas.ch*
[b] *Faculty of Pharmacy, Comenius University, Kalinčiaková 8, 83232 Bratislava, Slovakia*
[c] *Faculty of Chemistry, Slovak University of Technology, Radlinskeho 9, 81237 Bratislava, Slovakia*

Received (in Basel, Switzerland) 15th February 1999, Accepted 4th March 1999

The observation that the antivirally active PMEA in its diphosphorylated form ($PMEApp^{4-}$) is initially a better substrate for polymerases than $dATP^{4-}$ (ATP^{4-}) can be rationalized by (i) the increased basicity of the phosphonyl group (compared to a phosphoryl group) and (ii) the participation of the ether O atom of $PMEApp^{4-}$ in metal ion binding; both effects together favor M^{2+} binding at the α group and thus its nucleophilic attack.

Since adenosine 5′-triphosphate is at the crossroad of many metabolic processes, the search for analogues which can be employed as therapeutic agents is long-standing.[1] A promising attempt is presently focusing on 9-[2-(phosphonomethoxy)-ethyl]adenine (PMEA) and related derivatives,[1,2] which can be considered as acyclic analogues of adenosine 5′-monophosphate (AMP^{2-}; Fig. 1)[3] as well as of its 2′-deoxy or 2′,3′-dideoxy derivatives. PMEA shows antiviral properties and is active, after its diphosphorylation by kinases,[4] against a variety of DNA viruses and retroviruses (*e.g.* human immunodeficiency viruses; HIV).[1,4]

The triphosphate analogue ($PMEApp^{4-}$) is recognized by nucleic acid polymerases as substrate and incorporated in the growing nucleic acid chain, which is then terminated due to the lack of a 3′-hydroxy group, which is present in the parent adenosine 5′-triphosphate (ATP^{4-}) and 2′-deoxyadenosine 5′-triphosphate ($dATP^{4-}$) nucleotides.[4,5] Indeed, $PMEApp^{4-}$ is initially an excellent substrate, *e.g.* for reverse transcriptases, which are effectively inhibited even in the presence of a 20-fold excess of $dATP^{4-}$; similar observations have been made for other DNA polymerases.[6] Why are $PMEApp^{4-}$ and its relatives excellent substrates for polymerases? We are suggesting below that this is due to the special metal ion-binding properties of these nucleoside 5′-triphosphate (NTP) analogues.

Kinetic studies of the M^{2+}-promoted dephosphorylation of ATP^{4-} and other triphosphates have shown[7] that in the most reactive species one metal ion is coordinated to the α,β-phosphate groups and one to the terminal γ-phosphate group. This transphosphorylation mechanism was recently confirmed in biological systems by an X-ray structural study of *Escherichia coli* phosphoenolpyruvate carboxykinase.[8] The mentioned

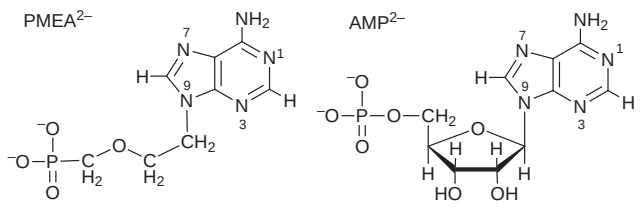

Fig. 1 $PMEA^{2-}$ in comparison to AMP^{2-} which is depicted in its dominating *anti* conformation; the structure of $PMEA^{2-}$ is analogous.[3]

kinetic studies[7] have also led to the conclusion that the two activating metal ions 'may interact not only in a M(α,β)–M(γ)-like way but that a M(α)–M(β,γ) coordination can also be enforced (by an enzyme) and this would then lead to a reactive species ready for the transfer of . . . a nucleoside monophosphate' unit.[7a] Indeed, X-ray studies of nucleic acid polymerases have confirmed that two metal ions are involved in this process and corresponding mechanisms were proposed.[9]

The crucial step in the polymerase mechanism indicated above is to force a metal ion into the α position of the triphosphate chain[7] of an NTP^{4-}. Hence, one might suspect that $PMEApp^{4-}$, being initially an excellent substrate, has in this respect an advantage over $dATP^{4-}$ or ATP^{4-}. Indeed, methylphosphonate is somewhat more basic than methyl phosphate; this follows from the release of the primary proton from the twofold protonated species which occurs with $pK^{H}_{CH_3P(O)(OH)_2}$ = 2.10 ± 0.03 (ref. 10) and $pK^{H}_{CH_3OP(O)(OH)_2}$ = 1.1 ± 0.2,[11] respectively. This increased basicity of a phosphonyl compared to a phosphoryl group should favor metal ion binding.

To verify the above assumption, we compared for Mg^{2+}, Mn^{2+} and Zn^{2+} (M^{2+}) the metal ion-binding properties of methyl phosphonylphosphate, $CH_3–P(O)_2^{-}–O–PO_3^{2-}$ ($MePP^{3-}$),[12,13] with those of methyl diphosphate and other diphosphate monoesters, $R–OP(O)_2^{-}–O–PO_3^{2-}$ ($R–DP^{3-}$), where R is a noncoordinating residue. The results summarized in Fig. 2, where the logarithms of the measured stability constants are plotted in dependence on the pK_a values of $H(R–DP)^{2-}$ or $H(MePP)^{2-}$, show that the $Mg(MePP)^{-}$ and $Mn(MePP)^{-}$ complexes are somewhat more stable than is expected on the basis of the basicity of the terminal phosphate group of $MePP^{3-}$. The stability increases, which correspond to the vertical broken lines seen in Fig. 2, are $\log \Delta_{Mg(MePP)}$ = 0.08 ± 0.04 and $\log \Delta_{Mn(MePP)}$ = 0.16 ± 0.04; not shown in Fig. 2 is $\log \Delta_{Zn(MePP)}$ = 0.16 ± 0.04.[14] Hence, the higher basicity of a phosphonyl unit, compared to that of a phosphoryl group, leads to an increased complex stability!

In the present context one must also mention that the ether oxygen of $PMEA^{2-}$ (see Fig. 1) participates in M^{2+} binding[15,16] which gives rise to the following intramolecular equilibrium:

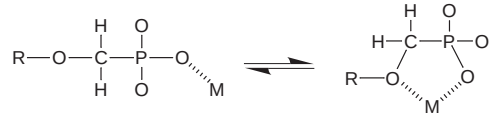

Of course, the formation of the indicated five-membered chelate is also reflected in an increased complex stability (based on log *K versus* pK_a correlation lines)[16] which amounts for the M(PMEA) complexes[15a] of Mg^{2+}, Mn^{2+} and Zn^{2+} to $\log \Delta_{Mg(PMEA)}$ = 0.16 ± 0.05, $\log \Delta_{Mn(PMEA)}$ = 0.21±0.08, and log

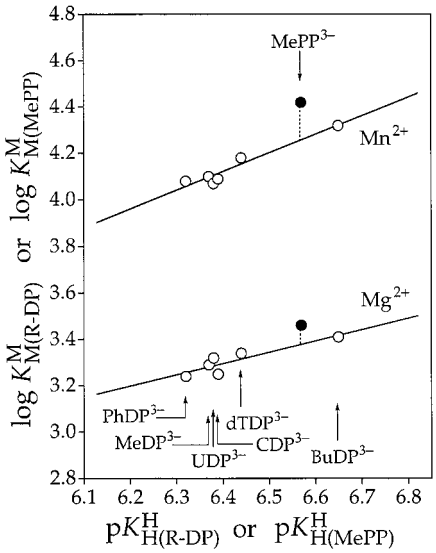

Fig. 2 Comparison of the stabilities of the Mg(MePP)$^{-}$ and Mn(MePP)$^{-}$ complexes (●) with those of the corresponding M^{2+} complexes formed with diphosphate monoesters (R–DP^{3-}) (○) based on the relationship between log $K^{M}_{M(R-DP)}$ and p$K^{H}_{H(R-DP)}$, for the Mg^{2+} and Mn^{2+} 1:1 complexes of phenyl diphosphate (PhDP^{3-}), methyl diphosphate (MeDP^{3-}), uridine 5′-diphosphate (UDP^{3-}), cytidine 5′-diphosphate (CDP^{3-}), thymidine [= 1-(2′-deoxy-β-D-ribofuranosyl)thymine] 5′-diphosphate (dTDP^{3-}), and *n*-butyl diphosphate (BuDP^{3-}) (from left to right). The least-squares lines are drawn through the indicated six data sets; the corresponding straight-line equations are listed in Table 4 of ref. 13(*b*). The equilibrium constants for the M^{2+}–MePP systems are given in footnote 13(*a*). All plotted values refer to aqueous solution at 25 °C and I = 0.1 M ($NaNO_3$).

$\Delta_{Zn(PMEA)}$ = 0.30 ± 0.10,[17] respectively; the corresponding formation degrees of the five-membered chelates are 31(±8), 38(±11), and 50(±12)%, respectively.[15a]

The above mentioned two effects, *i.e.* the increased basicity of the phosphonyl group and the participation[15c] of the ether oxygen in metal ion binding, favor the coordination of a second metal ion at the α group which occurs under the 'guidance' of the enzyme.[7,9] The binding of both metal ions to PMEApp^{4-} is depicted in Fig. 3 in comparison to the situation in ATP^{4-}. Of course, a higher formation degree of the structurally correct M_2(PMEApp) species will also facilitate the nucleophilic attack

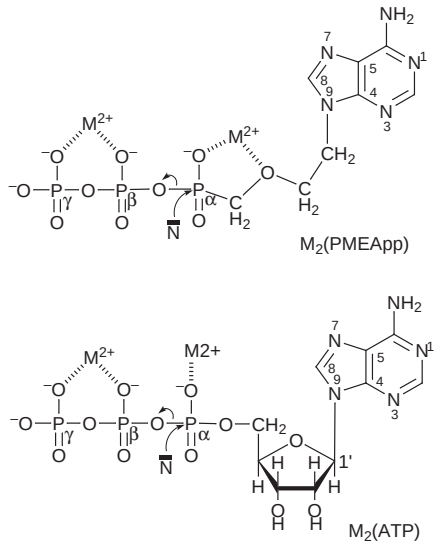

Fig. 3 Structures of the M_2(PMEApp) and M_2(ATP) intermediates ready for the attack of a nucleophile (N) and on their way to the transition state in nucleic acid polymerases. Metal ion binding to the α group is favored with PMEApp^{4-} (top) due to the formation of the five-membered chelate involving the ether oxygen atom as well as by the enhanced basicity of the α-phosphonyl group. Both divalent metal ions (usually Mg^{2+}) are anchored to amino acid-side chains (see, *e.g.* ref. 9) of the protein. Of course, the adenine residue can also be replaced by other nucleobase moieties.

at the α group and thus favor the transfer of the phosphonyl unit with its nucleobase residue in the polymerase-catalyzed reaction and its incorporation into the growing nucleic acid chain and thus, the termination of the latter. The above given mechanistic considerations are further confirmed by the repeated observation that the ether oxygen of PMEA^{2-} and of its (phosphonomethoxy)ethyl relatives is important for obtaining a biological effect:[1,6] its omission or replacement leads to a reduction or even loss of the antiviral activity.[18]

To conclude, in the search for new antivirally active nucleotide analogues the above gained insight should be kept in mind that favored metal ion-binding properties of the α-group are important for obtaining a high biological activity of the nucleotide analogues.

The assistance of Mrs Rita Baumbusch in the preparation of this manuscript and research grants from the Swiss National Science Foundation, the Swiss Federal Office for Education & Science (COST D8) and the Novartis Foundation (formerly Ciba-Geigy-Jubilee Foundation) are gratefully acknowledged.

Notes and references

1 See, *e.g.:* A. Holý, in *Advances in Antiviral Drug Design*, ed. E. De Clercq, JAI Press, Greenwich, CN, 1993, pp. 179–231.
2 C.-C. Tsai, K. E. Follis, A. Sabo, T. W. Beck, R. F. Grant, N. Bischofberger, R. E. Benveniste and R. Black, *Science*, 1995**, 270**, 1197.
3 C. A. Blindauer, A. Holý, H. Dvořáková and H. Sigel, *J. Chem. Soc., Perkin Trans. 2* 1997, 2353.
4 J. Balzarini, Z. Hao, P. Herdewijn, D. G. Johns and E. De Clercq, *Proc. Natl. Acad. Sci. USA*, 1991, **88**, 1499.
5 P. Kramata, I. Votruba, B. Otová and A. Holý, *Mol. Pharmacol.*, 1996, **49**, 1005.
6 A. Holý, I. Votruba, A. Merta, J. Černý , J. Veselý, J. Vlach, K. Šedivá, I. Rosenberg, M. Otmar, H. Hřebabecký, M. Trávnirček, V. Vonka, R. Snoeck and E. De Clercq, *Antiviral Res.*, 1990, **13**, 295.
7 (*a*) H. Sigel, F. Hofstetter, R. B. Martin, R. M. Milburn, V. Scheller-Krattiger and K. H. Scheller, *J. Am. Chem. Soc.*, 1984, **106**, 7935; (*b*) H. Sigel, *Coord. Chem. Rev.* 1990, **100**, 453; (*c*) ATP and Mg^{2+} in early evolution, see: H. Sigel, *Inorg. Chim. Acta* 1992, **198**–**200**, 1.
8 L. W. Tari, A. Matte, H. Goldie and L. T. J. Delbaere, *Nature Struct. Biol.*, 1997, **4**, 990.
9 For example: H. Pelletier, M. R. Sawaya, W. Wolfle, S. H. Wilson and J. Kraut, *Biochemistry*, 1996, **35**, 12 762; H. Pelletier, *Science*, 1994, **266**, 2025; T. A. Steitz, *Nature*, 1998, **391**, 231.
10 H. Sigel, C. P. Da Costa, B. Song and F. Gregáň, submitted for publication.
11 A. Saha, N. Saha, L.-n. Ji, J. Zhao, F. Gregáň, S. A. A. Sajadi, B. Song and H. Sigel, *J. Biol. Inorg. Chem.*, 1996, **1**, 231.
12 (*a*) The trisodium methyl phosphonylphosphate (IUPAC name: phosphoric methylphosphonic monoanhydride trisodium salt) was prepared in Bratislava similarly as described recently for alkyl diphosphate esters;[12b] further details are given in ref. 12*c*. All the other reagents were the same as used previously;[11,12c] (*b*) F. Gregáň, V. Kettmann, P. Novomeský and E. Mišiková, *Boll. Chim. Farm*, 1996, **135**, 229; (*c*) B. Song, S. A. A. Sajadi, F. Gregán, N. Prónayová and H. Sigel, *Inorg. Chim. Acta* 1998, **273**, 101.
13 (*a*) The equilibrium constants were determined as described.[12c,13b] The values are p$K^{H}_{H(MePP)}$ = 6.57 ± 0.02,[12c] log$K^{Mg}_{Mg(MePP)}$ = 3.46 ± 0.03, log $K^{Mn}_{Mn(MePP)}$ = 4.42 ± 0.02, and log $K^{Zn}_{Zn(MePP)}$ = 4.46 ± 0.03 (aqueous solution; 25 °C; I = 0.1 M, $NaNO_3$) (the error limits given are three times the standard error of the mean value); (*b*) S. A. A. Sajadi, B. Song, F. Gregáň and H. Sigel, *Inorg. Chem.* 1999, **38**, 439.
14 Similar stability increases were observed for the MePP^{3-} complexes of Co^{2+} (log $\Delta_{Co(MePP)}$ = 0.15 ± 0.06), Cu^{2+} (log $\Delta_{Cu(MePP)}$ = 0.17 ± 0.06), and Cd^{2+} (log $\Delta_{Cd(MePP)}$ = 0.17 ± 0.04); details to be published.
15 (*a*) H. Sigel, D. Chen, N. A. Corfù, F. Gregáň, A. Holý and M. Strašák, *Helv. Chim. Acta* 1992, **75**, 2634; (*b*) C. A. Blindauer, A. Holý, H. Dvořáková and H. Sigel, *J. Biol. Inorg. Chem.*, 1998, **3**, 423.
16 (*a*) H. Sigel, *Coord. Chem. Rev.*, 1995, **144**, 287; (*b*) H. Sigel, *J. Indian Chem. Soc.*, 1997, **74**, 261 (P. Ray Award Lecture).
17 Estimated value; see ref. 15*a*.
18 It may be added that PMEApp is a *poorer* substrate than ATP for ATPases[4] and this agrees with the above conclusions because for ATPases, like for kinases,[7,8] a M(α,β)–M(γ)-like coordination is desirable. Clearly, M(α,β) binding of M^{2+} will be somewhat inhibited by the five-membered chelate formed with the α group and the ether O atom.

Communication 9/01233H

Unprecedented nitrosyl-bridged double-A-frame triplatinum complexes, $[Pt_3(\mu\text{-triphosphine})_2(\mu\text{-NO})_2(RNC)_2](BF_4)_4$

Tomoaki Tanase,*[a] Makiko Hamaguchi,[a] Rowshan Ara Begum,[a] Shigenobu Yano[a] and Yasuhiro Yamamoto[b]

[a] *Department of Chemistry, Faculty of Science, Nara Women's University, Kitauoya-higashi-machi, Nara 630-8285 Japan*

[b] *Department of Chemistry Faculty of Science, Toho University, Miyama 2-2-1, Funabashi, Chiba 274-5076 Japan*

Received (in Cambridge, UK) 11th January 1999, Accepted 22nd March 1999

Reaction of linear triplatinum complexes, *linear*-$[Pt_3(\mu\text{-dpmp})_2(RNC)_2](PF_6)_2$ 1, with an excess of $[NO][BF_4]$ afforded an unprecedented nitrosyl-bridged double-A-frame triplatinum complexes, $[Pt_3(\mu\text{-dpmp})_2(\mu\text{-NO})_2(RNC)_2](BF_4)_4$ [2a: R = 2,6-xylyl; 2b: R = 2,4,6-mesityl, dpmp = bis(diphenylphosphinomethyl)phenylphosphine], which were characterized by X-ray crystallographic analysis and extended Hückel MO calculations.

Metal–metal bonded small-size transition-metal clusters have attracted increasing attention, since they could be minimal models for the surface of heterogeneous catalysts and have the potential to promote new homogeneous reactions which are not established by mononuclear centers.[1] We have recently reported a new strategic synthetic route to homo- and hetero-trimetallic clusters with Pt_2M cluster cores by using a tridentate phosphine ligand, bis(diphenylphosphinomethyl)phenylphosphine (dpmp).[2–5] In particular, we have demonstrated the synthesis and characterization of linearly ordered, side-by-side triplatinum complex, *linear*-$[Pt_3(\mu\text{-dpmp})_2(RNC)_2](PF_6)_2$ [**1a**: R = xylyl (Xyl)], which could be regarded as an indispensably important expansion of the well known chemistry on dppm-bridged diplatinum complexes, where dppm = bis(diphenylphosphino)methane. Complex **1a** was also shown to react with H^+, electron-deficient alkynes, and *p*-nitrophenyl isocyanide, affording asymmetrical A-frame triplatinum clusters bridged by hydride and the organic molecules, where only one Pt–Pt bond breaking took place even treated with an excess amount of reagents.[6] In the present report, we have examined the reaction of **1** [R = Xyl, mesityl (Mes)] with $[NO][BF_4]$ and have successfully isolated and characterized unprecedented nitrosyl-bridged double-A-frame triplantinum complexes, $[Pt_3(\mu\text{-dpmp})_2(\mu\text{-NO})_2(RNC)_2](BF_4)_4$. The reaction involves a novel, simultaneous three-center oxidative addition on linearly ordered triplatinum core supported by the tridentate phosphine ligands.

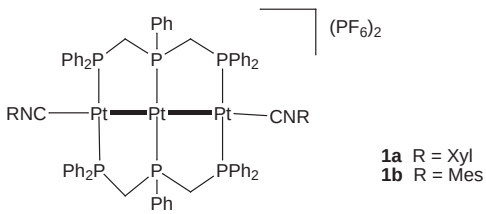

1a R = Xyl
1b R = Mes

Reaction of **1a** with an excess of $[NO][BF_4]$ yielded pale green crystals formulated as $[Pt_3(\mu\text{-dpmp})_2(\mu\text{-NO})_2(XylNC)_2](BF_4)_4$ **2a** (yield 66%).† Similar reaction of **1b** also gave $[Pt_3(\mu\text{-dpmp})_2(\mu\text{-NO})_2(MesNC)_2](BF_4)_4$ **2b** in 68% yield. The IR spectra of **2** indicated the presence of terminal isocyanide ligands at 2206 (**2a**), 2205 cm^{-1} (**2b**) and nitrosyl units at 1514 (**2a**), 1513 cm^{-1} (**2b**), the latter corresponding to the values for N–O triple bond rather than double bond. The detailed structure of **2a** was determined by an X-ray crystallographic analysis and an ORTEP plot for the complex cation is illustrated in Fig. 1.‡ The complex cation has a crystallographically imposed inversion center on the central platinum (Pt2) and consists of three platinum atoms linearly supported by two dpmp ligands. The Pt–Pt separation of 3.0962(4) Å, indicating the absence of a Pt–Pt bond, is shorter than those for the A-frame diplatinum complexes with dppm ligands, *e.g.* $[Pt_2Cl_2(\mu\text{-NO})(\mu\text{-dppm})_2]BPh_4$ **3a** (3.246 Å),[7a] $[Pt_2Cl_2(\mu\text{-NO})(\mu\text{-dppm})_2]BF_4$ **3b** (3.186 Å),[7b] $[Pt_2Cl_2(\mu\text{-CH}_2)(\mu\text{-dppm})_2]$ (3.151 Å),[8] and is comparable to that of $[Pt_2Cl_2(\mu\text{-CS}_2)(\mu\text{-dppm})_2]$ (3.094 Å).[9] Two nitrosyl groups are inserted into the two Pt–Pt bonds of **2a** with an almost symmetrical manner, Pt1–N1 2.020(6) Å, Pt2–N1 2.019(6) Å, Pt1–N1–Pt2 100.1(3)°, Pt1–N1–O1 125.9(6)°, Pt2–N1–O1 133.2(6)°, resulted in a double-A-frame trimetallic structure. This is the first structurally characterized example of nitrosyl-bridged double-A-frame trinuclear clusters on the basis of analysis of the Cambridge Crystallographic Structure Database. The N–O bond lengths is 1.09(1) Å,§ which corresponds to values for a neutral N–O triple bond rather than an N–O double bond,[10] and is in accord with the IR data. This nitrosyl-bridging structure is quite different from that of **3** which involves an NO^- unit with an N–O bond length of 1.20(2) Å.[7,8] From the X-ray crystal structure, the present reaction can be regarded as a novel three-center oxidative addition proceeding on a linear triplatinum center, which involves an apparent two electron transfer from the triplatinum core to two NO^+ ions.

Structurally characterized nitrosyl-bridged diplatinum complexes are extremely rare, with the two complexes **3** being the sole example, probably owing to the low-lying LUMO and small HOMO–LUMO gap as Hoffmann predicted theoretically on the basis of extended Hückel MO calculations.[11] In order to elucidate the electronic structure of **2**, we have carried out EHMO calculations on a model compound $[Pt_3(\mu\text{-}$

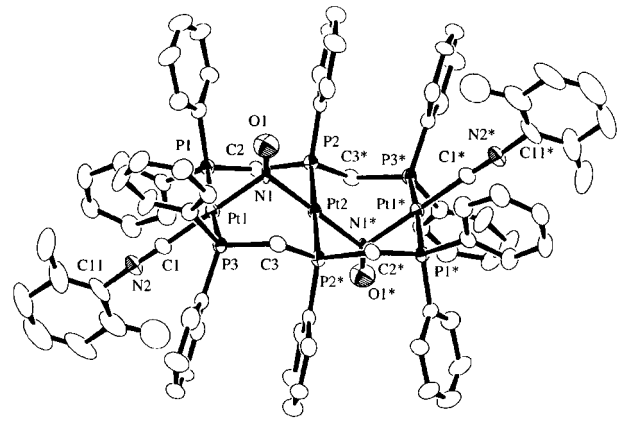

Fig. 1 ORTEP diagram for the complex cation of **2a**. Selected distances (Å) and angles (°): Pt1···Pt2 3.0962(4), Pt1–P1 2.358(2), Pt1–P3 2.343(2), Pt1–N1 2.020(6), Pt1–C1 1.923(8), Pt2–P2 2.321(2), Pt2–N1 2.019(6), O1–N1 1.09(1), N2–C1 1.14(1); N1–Pt1–C1 176.1(2), N1–Pt2–N1* 180.0, Pt1–N1–Pt2 100.1(3), Pt1–N1–O1 125.9(6), Pt2–N1–O1 133.2(6), Pt1–C1–N2 175.7(7).

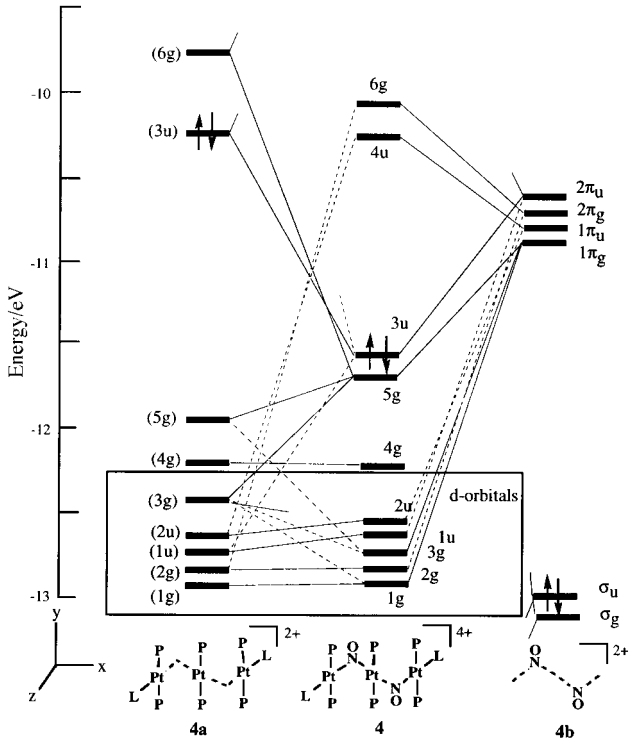

Fig. 2 MO interaction diagram for $[Pt_3(\mu\text{-}NO)_2(PH_3)_6(CNH)_2]^{4+}$ **4** (C_i), in terms of the fragments $[Pt_3(PH_3)_6(CNH)_2]^{2+}$ **4a** and $[NO)_2]^{2+}$ **4b**; P = PH_3, L = CNH.

$NO)_2(PH_3)_6(CNH)_2]^{4+}$ **4** (C_i), the ideal coordinates being derived from simplification of the crystal structure of **2a**.[12–15] An interaction diagram for **4** in terms of the fragments $[Pt_3(PH_3)_6(CNH)_2]^{2+}$ **4a** and $[(NO)_2]^{2+}$ **4b** is shown in Fig. 2.[16] The triplatinum system of **1** has a Pt–Pt σ-bonding orbital (HOMO) and σ-antibonding orbital (LUMO) at higher and lower energy levels, respectively, than the corresponding σ_{Pt-Pt} and σ^*_{Pt-Pt} orbitals of the diplatinum model.[2] The decrease of the σ–σ* energy gap causes the HOMO (3u) and LUMO (6g) of **4a** to match well with the low-laying π* orbitals of **4b** ($2\pi_u$ and $1\pi_g$), generating two significant bonding interactions, 3u (−11.61 eV) and 5g (−11.62 eV) orbitals of **4**. These two bonding orbitals should be responsible for partial electron transfer from the Pt_3^{2+} core to the two bridging NO^+ groups and stabilize the double-A-frame structure. There is no bonding overlap between the central and terminal Pt atoms as expected from the crystal structure. When CO groups are used instead of NO^+, the high-lying π* orbitals of CO groups do not match with the σ and σ* orbitals of the Pt_3^{2+} core and the corresponding 3u (−10.62 eV) and 5g (−11.34 eV) orbitals are destabilized at higher energy levels, consistent with our failure to obtain $[Pt_3(\mu\text{-dpmp})_2(\mu\text{-CO})_2(RNC)_2]^{2+}$ from the reaction of **1** with CO.

The present results could provide useful information in relation to metal-surface mimetic chemistry or fine organometallic cluster chemistry. We are now attempting to explore the reactivity of complex **2**, involving transformation of bridging NO groups to nitrogen-containing organic compounds.

This work was partly supported by Grants-in-Aid for Scientific Research from the Ministry of Education, Science, Sports, and Culture of Japan.

Notes and references

† To a 20 ml dichloromethane solution containing 100 mg of *linear*-$[Pt_3(\mu\text{-dpmp})_2(XylNC)_2](PF_6)_2$ was added 27 mg of $[NO][BF_4]$. The reaction solution was stirred at room temp. for 3 h during which it changed from orange to pale green. The solution was concentrated to *ca.* 3 ml and was kept in a refrigerator to afford block-shaped plae green crystals of $[Pt_3(\mu\text{-dpmp})_2(\mu\text{-NO})_2(XylNC)_2](BF_4)_4\cdot CH_2Cl_2$ (**2a**$\cdot CH_2Cl_2$) in 66% yield. Anal. Calc. for $C_{83}H_{78}O_2N_4P_6B_4F_{16}Cl_2Pt_3$: C, 42.51; H, 3.83; N, 1.84. Found: C, 42.37; H, 3.34; N, 2.38%. A similar procedure using *linear*-$[Pt_3(\mu\text{-dpmp})_2(MesNC)_2](PF_6)_2$ **1b** (43 mg) afforded pale green crystals of $[Pt_3(\mu\text{-dpmp})_2(\mu\text{-NO})_2(MesNC)_2](BF_4)_4\cdot 2CH_2Cl_2$ (**2b**$\cdot 2CH_2Cl_2$) in 68% yield. Anal. Calc. for $C_{86}H_{84}O_2N_4P_6B_4F_{16}Cl_4Pt_3$: C, 41.89; H, 3.43; N, 2.27. Found: C, 42.02; H, 3.45; N, 1.80%. Complex **1b** was prepared by the reaction of **1a** with MesNC and was characterized by X-ray crystallography, which will be reported elsewhere.

‡ *Crystal data*: **2a**$\cdot CH_2Cl_2\cdot 3H_2O$ ($C_{83}H_{84}N_4O_5P_6B_4F_{16}Cl_2Pt_3$, M_r = 2406.83, T = −116 °C, monoclinic, space group $P2_1/c$, a = 12.873(4), b = 29.350(6), c = 14.826(4) Å, β = 110.49(3)°, V = 5246(2) Å^3, Z = 2. A pale green block-shaped crystal was fixed on the top of a glass fiber with Paraton N oil. 9211 reflections ($4 < 2\theta < 50°$) were measured on a Rigaku AFC7R diffractometer with graphite monochromated Mo-Kα radiation. The structure was solved by direct methods using the program SIR92 and was refined to R = 0.058, R_w = 0.072, and GOF = 2.53 for 6842 independent reflections with $I > 3\sigma(I)$. CCDC 182/1201. See http://www.rsc.org/suppdata/cc/1999/745/ for crystallographic files in .cif format.

§ It should be noted that the Pt–N and N–O bond lengths derived from the X-ray crystallography might involve relatively large errors on the basis of flat (N1) and large (O1) thermal motions of the NO unit, the former seemingly resulting from the influence of highly scattering Pt Atoms.

1 A. L. Balch, *Prog. Inorg. Chem.*, 1994, **41**, 239 and references therein; R. J. Puddephatt, L. Manojlovic-Muir and K. W. Muir, *Polyhedron*, 1990, **9**, 2767 and references therein.
2 T. Tanase, H. Ukaji, H. Takahata, H. Toda, T. Igoshi and Y. Yamamoto, *Organometallics*, 1998, **17**, 196.
3 T. Tanase, H. Takahata, M. Hasegawa and Y. Yamamoto, *J. Organomet. Chem.*, 1997, **545**/**546**, 531.
4 T. Tanase, H. Toda and Y. Yamamoto, *Inorg. Chem.*, 1997, **36**, 1571.
5 T. Tanase, H. Toda, K. Kobayashi and Y. Yamamoto, *Organometallics*, 1996, **15**, 5272.
6 T. Tanase, H. Ukaji, T. Igoshi and Y. Yamamoto, *Inorg. Chem.*, 1996, **14**, 4114.
7 (*a*) F. Neve, M. Ghedini, A. Tirpicchio and F. Ugozzoli, *Organometallics*, 1992, **11**, 795; (*b*) M. Ghedini, F. Neve, C. Mealli, A. Tirpicchio and F. Ugozzoli, *Inorg. Chim. Acta*, 1990, **178**, 5.
8 K. A. Azam, A. A. Frew, B. R. Lloyd, L. Manojlovic-Muir, K. W. Muir and R. J. Puddephatt, *Organometallics*, 1985, **4**, 1400.
9 T. S. Cameron, P. A. Gardner and K. R. Grundy, *J. Organomet. Chem.*, 1981, **212**, C19.
10 J. H. Enemark and R. D. Feltham, *Coord. Chem. Rev.*, 1974, **13**, 339.
11 D. M. Hoffman and R. Hoffmann, *Inorg. Chem.*, 1981, **20**, 3543.
12 R. Hoffman, *J. Chem. Phys.*, 1963, **39**, 1397.
13 R. Hoffmann and W. N. Lipscomb, *J. Chem. Phys.*, 1962, **36**, 2179.
14 R. Hoffmann and W. N. Lipscomb, *J. Chem. Phys.*, 1962, **36**, 3489.
15 J. H. Ammeter, H.-B. Burgi, J. C. Thibeault and R. Hoffmann, *J. Am. Chem. Soc.*, 1978, **100**, 3686.
16 C. Mealli and D. Prosterpio, *J. Chem. Educ.*, 1990, **67**, 399.

Communication 9/00302I

Fatigue resistant properties of photochromic dithienylethenes: by-product formation

Masahiro Irie,* Thorsten Lifka, Kingo Uchida, Seiya Kobatake and Yuriko Shindo

Department of Chemistry and Biochemistry, Graduate School of Engineering, Kyushu University, and CREST, Japan Science and Technology Corporation, Hakozaki 6-10-1, Higashi-ku, Fukuoka 812-8581, Japan.
E-mail: irie@cstf.kyushu-u.ac.jp

Received (in Cambridge, UK) 2nd December 1998, Accepted 12th March 1999

Beside normal cyclization/ring-opening photochromic reactions, a side reaction to produce a photostable by-product took place when 1,2-bis(2-methyl-5-phenyl-3-thienyl)perfluorocyclopentene was irradiated in deaerated hexane with ultraviolet light.

Light-induced reversible isomerization between two forms having different absorption spectra is referred to photochromism, and compounds capable of these reactions are called photochromic compounds. Various types of photochromic compounds, such as spiropyrans, spirooxazines, fulgides and diarylethenes, have been so far developed[1] in an attempt to apply the compounds to optoelectronic devices,[2,3] such as optical memory, photo-optical switching and displays. Among the compounds, diarylethenes with heterocyclic aryl groups are the most promising photochromic compounds for these applications, because of their fatigue-resistant and thermally-irreversible properties.[4] Although diarylethenes with benzothiophene aryl groups undergo fatigue-resistant photochromic reactions (more than 10 000 coloration/decoloration cycles)[5–7] without any destruction of their structures, some diarylethenes with thiophene rings cease their photochromic cycles in less than several hundred cycles even in the absence of oxygen.[6–9] To know the reason why the thiophene derivatives are easily damaged by photoirradiation, we compared the fatigue-resistant properties of dithienylethenes **1** and **2**.[10,11]

Compound **1**[10] has methyl groups at the 4 and 4′ positions of the thiophene rings, while compound **2**[11]† has no methyl groups at these positions. The cyclization quantum yield of **2a** (Φ = 0.68) is larger than that of **1a** (Φ = 0.46),[10] while the ring-opening quantum yields are similar (Φ = 0.013 and 0.015, respectively).

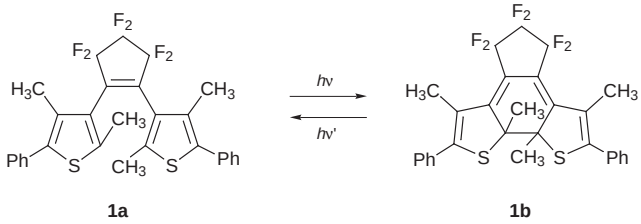

1a **1b**

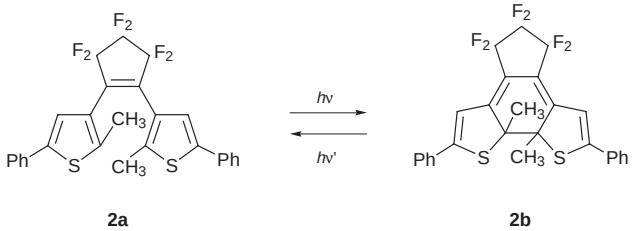

2a **2b**

Fig. 1 shows the fatigue resistant behavior of the two compounds in hexane in the absence of oxygen. The absorbance of the two compounds at 313 nm was normalised. In each cycle **1a** and **2a** were converted to **1b** and **2b**, respectively, to give 80% of the photostationary states by irradiation with 313 nm light, and both closed-ring forms, **1b** and **2b**, were completely bleached by irradiation with > 440 nm light. The absorbances of the bleached samples were plotted in Fig. 1. The absorbance of **1a** (λ_{max} 268 nm) remained almost constant even after 800 cycles, while the absorbance of **2a** (λ_{max} 276 nm) gradually declined. At the same time a photostable violet product with an absorption maximum at 547 nm was formed. As can be seen in Fig. 1 the formation process of the by-product coincides with a decrease of the open-ring form **2a**. The saturation tendency after 200 cycles is ascribed to the overlapping of the strong absorption of the by-product at 313 nm (see Fig. 2). In the case of **1** no such colored photoproduct was detected. In the presence of oxygen both **1** and **2** readily decomposed in less than 500 cycles. The decomposition is due to the formation of oxidized products.[7]

The stable photoproduct could be isolated by HPLC (silica gel column, hexane) and was found by elementary analysis and molecular mass determination to be isomeric with compound **2a**. Fig. 2 shows the absorption spectrum of the by-product **3** along with those of **2a** and **2b**. The absorption maximum of the by-product slightly shifted to shorter wavelength and its ε value

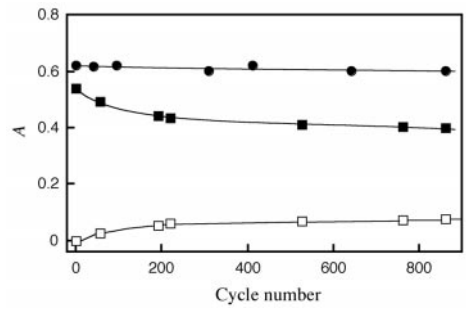

Fig. 1 Fatigue resistant properties of **1** and **2** in deaerated hexane. Absorbances of **1a** (●) and **2a** (■) were plotted after irradiation with visible light. The visible absorbance at 547 nm (□), which still remained after visible irradiation of a hexane solution containing **2**, was also plotted.

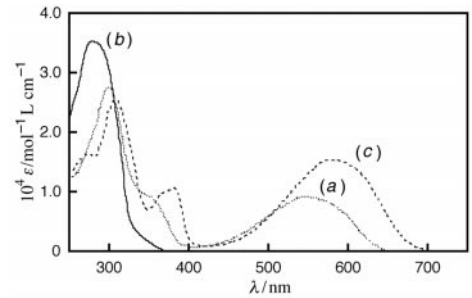

Fig. 2 Absorption spectrum of the (*a*) by-product **3** along with those of (*b*) **2a** and (*c*) **2b** in hexane.

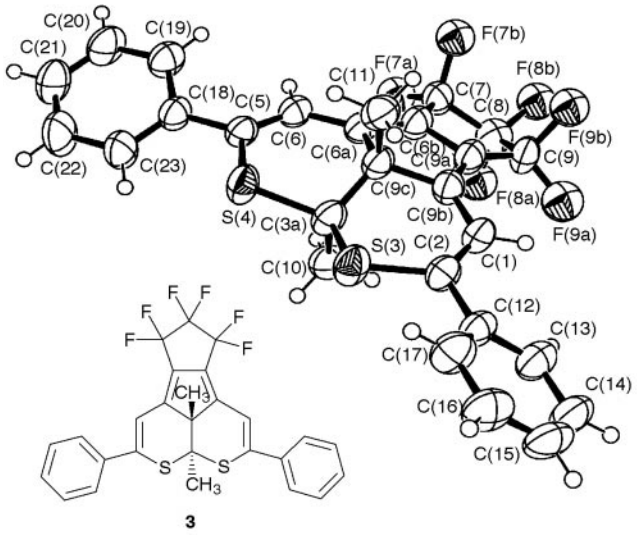

Fig. 3 ORTEP view of by-product **3** (50% probability thermal ellipsoids) and its chemical structure. The fluorinated cyclopentane ring was disordered. Only the major structure is illustrated for clarity.

in the visible region was 60% of the closed-ring form.The structure of the by-product could not be determined conclusively by NMR spectroscopy,‡ but was established by X-ray crystallographic analysis of a single crystal (mp 131 °C) from MeOH–hexane.§

Fig. 3 shows the molecular structure of by-product **3**. The thiophene rings no longer exist, having formed a condensed system with two six-membered heterocyclic rings. The polyene structure is similar to the closed-ring form **2b**. This is the reason why the by-product has a similar absorption spectrum. Although the formation mechanism of the by-product has not yet been revealed, the by-product was more efficiently produced from **2b** by ultraviolet irradiation.

Compound **2** underwent photochromism even in the crystalline phase. It is worthwhile to note that the by-product **3** formation was not observed in the crystalline phase. The fatigue resistant characteristics of crystalline **2a** were examined by alternate irradiation with ultraviolet (313 nm) and visible ($\lambda > 440$ nm) light. Any appreciable increase in the visible absorption was not observed for the crystal even after 2000 coloration–decoloration cycles. The transmittance of the crystal decreased to around 80% of the fresh crystal after 10 000 cycles, but the decrease is mainly due to an increasing roughness of the crystal surface and not due to by-product formation.

Notes and references

† *Selected data* for **2a**: 140 °C; δ_H(200 MHz) 7.30–7.75 (m, 10H, CH of Ph), 7.28 (s, 2H, CH of thiophene), 1.97 (s, 6H, Me); δ_C(125 MHz) 142.2, 141.1, 133.3, 109.8 (8C, Cq), 128.9, 127.8, 125.6 (10C, CH of Ph), 122.4 (2C, CH of thiophene), 14.5 (2C, Me); *m/z* 520 (M^+, 64%), 505 (100), 490, 472, 385, 121, 77. (Calc. for $C_{27}H_{18}F_6S_2$: C, 62.30; H, 3.49. Found: C, 62.66; H, 3.72%).

‡ *Selected data* for **3**: mp 131 °C; δ_H(200 MHz) 7.36–7.51 (m, 10H, CH of Ph), 6.50 (s, 2H, H at C1/C6), 2.78 (s, 3H, Me at C3a), 2.75 (s, 3H, Me at C9c); δ_C(125 MHz) 144.8 (2C, C2/C5), 144.5 (2C, C6a, C9b), 137.3 (2C, ipso-C of Ph), 130.3 (2C, *p*-C of Ph), 128.7 (4C, *m*-C of Ph), 126.0 (4C, *o*-C of Ph), 123.1 (2C, C6b/C9a), 115.5 (1C, C8), 112.5 (2C, C1/C6), 112.4 (2C, C7/C9), 65.8 (1C, C3a), 59.6 (1C, C9c), 28.2 (1C, Me at C3a), 22.9 (1C, Me at C9c); *m/z* 520 (M^+, 63%), 505 (100), 490, 385, 121, 77 (Calc. for $C_{27}H_{18}F_6S_2$: C, 62.30; H, 3.49. Found: C, 62.64; H 3.72%).

§ *Crystal data* for **3**: $C_{27}H_{18}F_6S_2$, T = 293(2) K, M = 520.56, triclinic, space group $P\bar{1}$, a = 11.565(3), b = 11.827(3), c = 10.206(2) Å α = 95.45(2), β = 100.68(2), γ = 60.12(2)°, V = 1189.4(5) Å^3, Z = 2, μ = 2.584 mm^{-1}, 4741 measured, 4506 independent reflections, of which 2932 were considered as observed [$I > 2\sigma(I)$]. Final $R1$ = 0.0778, $wR2$ = 0.2121. CCDC 182/1196. Crystallographic data are available in .cif format from the RSC web site, see: http://www.rsc.org/suppdata/cc/1999/747/

1 G. H. Brown, in *Photochromism*, Wiley-Interscience, New York, 1971; H. Dürr and H. Bouas-Laurent, in *Photochromism. Molecules and Systems*, Elsevier, Amsterdam, 1990.
2 C. B. McArdle, in *Applied Photochromic Polymer Systems*, Blackie, Glasgow, 1992.
3 M. Irie, in *Photo-Reactive Materials for Ultrahigh Density Optical Memory*, Elsevier, Amsterdam, 1994.
4 M. Irie and K. Uchida, *Bull. Chem. Soc. Jpn.*, 1998, **71**, 985.
5 K. Uchida, Y. Nakayama and M. Irie, *Bull. Chem. Soc. Jpn.*, 1990, **63**, 1311.
6 M. Hanazawa, R. Sumiya, Y. Horikawa and M. Irie, *J. Chem. Soc., Chem Commun.*, 1992, 206.
7 H. Taniguchi, A. Shinpo, T. Okazaki, F. Matsui and M. Irie, *Nippon Kagaku Kaishi*, 1992, 1138; *Chem. Abstr.*, 1993, **118**, 59154m.
8 Ref. 3, pp. 1–12.
9 M. Irie, *Pure Appl. Chem.*, 1996, **68**, 1367.
10 M. Irie, K. Sakemura, M. Okinaka and K. Uchida, *J. Org. Chem.*, 1995, **60**, 8305.
11 **2a** was prepared by a similar method as used for **1a**. See also S. H. Kawai, S. L. Gilat, R. Ponsinet and J.-M. Lehn, *Chem. Eur. J.*, 1995, **1**, 285.

Communication 8/09410A

ChemComm

Synthesis of the functionalised core of neoliacinic acid

J. Stephen Clark,*[a] Alexander G. Dossetter,[a] Alexander J. Blake,[a] Wan-Sheung Li[a] and William G. Whittingham[b]

[a] *School of Chemistry, University of Nottingham, University Park, Nottingham, UK NG7 2RD. E-mail: j.s.clark@nottingham.ac.uk*

[b] *ZENECA Agrochemicals, Jealott's Hill Research Station, University Park, Bracknell, Berkshire, UK RG42 6ET*

Received (in Cambridge, UK) 3rd March 1999, Accepted 18th March 1999

An advanced intermediate in the synthesis of neoliacinic acid has been prepared, and the structure and relative stereochemistry have been confirmed by X-ray crystallography.

The highly oxidised sesquiterpene neoliacinic acid **1** was isolated from leaves of the plant *Neolitsea acciculata* Koidz in 1987,[1] and is a member of a burgeoning family of bioactive ether-bridged germacranolides. These compounds have been isolated from a variety of plants worldwide; other representative examples are the lactone **2**[2] and the anti-bacterial compound tanargyrolide **3**.[3] Neoliacinic acid **1**[1] is thought to possess cytotoxic activity in common with a structurally related compound, neoliacine, which was isolated from the same plant.[4]

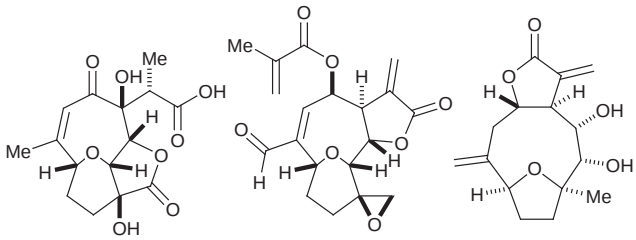

1 neoliacinic acid **2** **3** tanargyrolide

The unusual ether-bridged tricyclic framework of neoliacinic acid **1** coupled with the dense array of oxygen-containing functionality and the number of contiguous stereogenic centres present a formidable challenge to contemporary methods for ring construction and stereocontrol. Recently, we disclosed a powerful new strategy for the synthesis of neoliacinic acid, in which the required ring system was constructed using a carbenoid C–H insertion reaction in conjunction with tandem oxonium ylide generation and rearrangement.[5] We now report the exploitation of this reaction sequence for the construction of an advanced precursor of neoliacinic acid, the structure of which has been confirmed by X-ray crystallography.

Preparation of the required side chain from commercially available methyl (*R*)-3-hydroxy-2-methylpropionate was undertaken first (Scheme 1). Protection of the hydroxy group as the TIPS ether and reaction of the ester with an excess of the organocerium reagent prepared from $TMSCH_2MgCl$ and $CeCl_3$[6] afforded the allylic silane **4** resulting from double Grignard addition and *in situ* Peterson elimination of the intermediate β-hydroxy disilane.[6,7] The allylic silane **4** was then converted to the allylic bromide **5** by treatment with pyrrolidone hydrotribromide.[8,9] This reagent was used to deliver the precise amount of bromine required, circumventing the problem of over-bromination that was encountered when molecular bromine was employed for the transformation.

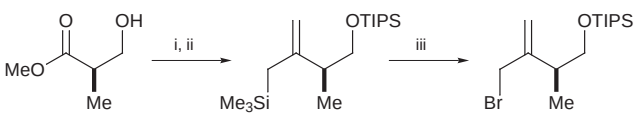

4 **5**

Scheme 1 *Reagents and conditions*: i, Pr^i_3SiCl (1 equiv.), imidazole (2 equiv.), DMF, rt (99%); ii, $TMSCH_2MgCl$ (3 equiv.), $CeCl_3$ (3 equiv.), THF, −70 °C→rt (98%); iii, pyrrolidone hydrotribromide (1 equiv.), pyridine, THF, –10 °C→rt (97%).

Assembly of the cyclisation precursor **11** commenced with (*R*)-isopropylideneglyceraldehyde, which was readily prepared from D-mannitol in two steps using standard literature methods (Scheme 2).[10] Chelation-controlled addition of the organocopper reagent prepared from reaction of CuI with *p*-$MeOC_6H_4CH_2O(CH_2)_3MgBr$ afforded the alcohol **6** in good yield as a 10:1 mixture of diastereoisomers.[11] Alkylation of the alcohol **6** with the allylic bromide **5** under standard ether coupling conditions, followed by acid-promoted removal of the acetonide and periodate cleavage of the resulting 1,2-diol provided the aldehyde **7** in good yield. Subsequent oxidation of

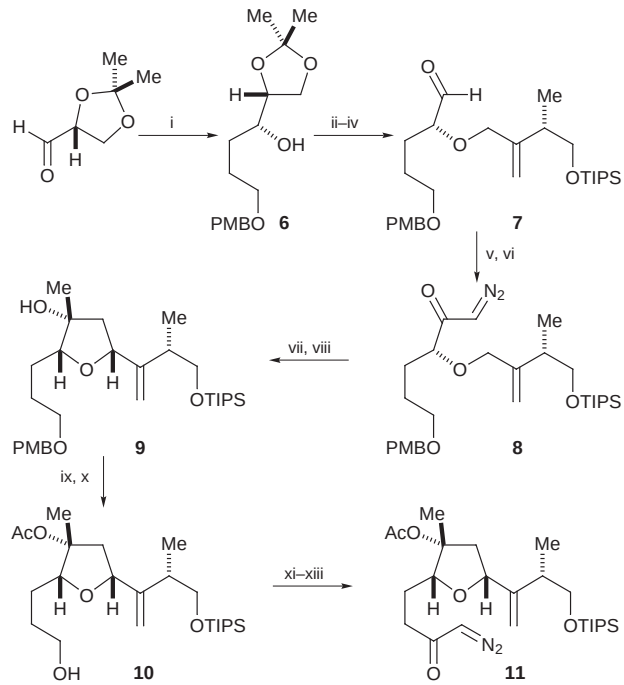

Scheme 2 *Reagents and conditions*: i, *p*-$MeOC_6H_4CH_2O(CH_2)_3MgBr$, CuI, DMS, THF, −78 °C→rt (81%, 10:1 mixture of diastereoisomers); ii,NaH, THF, rt→reflux, then **5**, THF, rt→reflux (90%); iii, PPTS (0.2 equiv.), $HO(CH_2)_2OH$–THF–CH_2Cl_2 (2 : 1 : 1), reflux; iv, $NaIO_4$ (4 equiv.), THF–H_2O (95%, 2 steps); v, PDC (3.5 equiv.), DMF, rt; vi, Bu^iOCOCl (1 equiv.), Et_3N, Et_2O, rt then CH_2N_2, Et_2O, rt (82%, 2 steps); vii, $Rh_2(HNCOCF_3)_4$ (1 mol%), CH_2Cl_2, rt; viii, $AlMe_3$ (3 equiv.), CH_2Cl_2, −78→5 °C (60%, 2 steps); ix, Ac_2O (3 equiv.), DMAP (3 equiv.), CH_2Cl_2, reflux (74%); x, DDQ (1.5 equiv.), CH_2Cl_2–H_2O, rt (94%); xi, PDC (3.5 equiv.), DMF, rt; xii, NaOMe (1 equiv.), MeOH, rt; xiii $(COCl)_2$, C_6H_6, rt, then CH_2N_2, Et_2O, rt (47%, 3 steps).

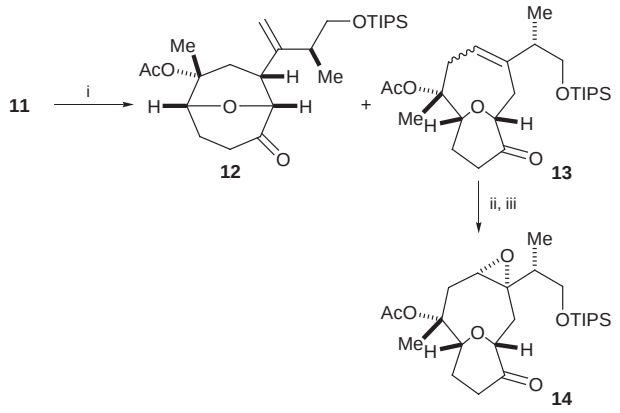

Scheme 3 *Reagents and conditions*: i, $Cu(hfacac)_2$ (2 mol%), CH_2Cl_2, reflux (**12** 7%, **13** 61%); ii,AIBN, EtSH, C_6H_6, reflux (81%); iii, MCPBA (1.5 equiv.), CH_2Cl_2, reflux (95%).

the aldehyde to afford the carboxylic acid was effected using PDC. The acid was then converted into a mixed anhydride, and this was treated with an excess of CH_2N_2 to give the α-diazo ketone **8**. Exposure of this α-diazo ketone to $Rh_2(HNCOCF_3)_4$[12] in CH_2Cl_2 resulted in formation of a reactive carbenoid that underwent intramolecular C–H insertion adjacent to the ether oxygen[13] to give the required cyclic ether, as a diastereomeric mixture (~7:1, *cis*:*trans*), along with some of the product arising from competitive intramolecular alkene cyclopropanation. Separation of the products was not performed at this stage, and the mixture was treated directly with $AlMe_3$.[5,14] This delivered the required alcohol **9** (60% yield from the α-diazo ketone **8**), which was easily separated from all other products and stereoisomers by chromatography. Standard protocols were then used to acetylate the tertiary hydroxy group and remove the *p*-methoxybenzyl protecting group, and oxidation of the free primary hydroxy group to the carboxylic acid was then performed using PDC. The synthesis of the α-diazo ketone **11** was completed by conversion of the sodium salt of the carboxylic acid to the corresponding acid chloride and treatment of this compound with an excess of CH_2N_2.

The pivotal cyclisation reaction was effected using analogous conditions to those employed in our model study (Scheme 3).[5] Treatment of the α-diazo ketone **11** with copper(II) hexafluoroacetylacetonate [Cu(hfacac)$_2$] in CH_2Cl_2 at reflux afforded the bridged bicyclic ether **13** in 61% yield as a 3:2 mixture of *Z* and *E* isomers along with the compound **12** (7% yield) arising from a [1,2]-shift of the intermediate oxonium ylide.[15] It is noteworthy that a mixture of alkene isomers was obtained upon rearrangement of the putative oxonium ylide intermediate, in contrast with the model reaction which provided the *E* isomer exclusively.[5] Isolation of the [1,2]-shift product[15] was also significant because analogous products were not isolated from model cyclisation reactions.[5]

The mixture of isomers was then subjected to isomerisation under radical conditions[16] to give the thermodynamically favoured *Z* alkene, which was then treated with MCPBA to afford the solid epoxide **14**.† Recrystallisation provided crystals that were suitable for X-ray analysis (Fig. 1),‡ and the structure and relative stereochemistry of the epoxide **14** were confirmed by this method.

We have prepared an advanced intermediate **14** in the synthesis of neoliacinic acid **1**, which possesses the skeleton found in the natural product and most of the oxygen-containing functionality. Completion of the synthesis by elaboration of this highly functionalised intermediate is in progress, and the results of this work will be reported in due course.

We thank the EPSRC for support, and the award of a CASE studentship (to A. G. D.) and a postdoctoral fellowship (to W.-S. L.).

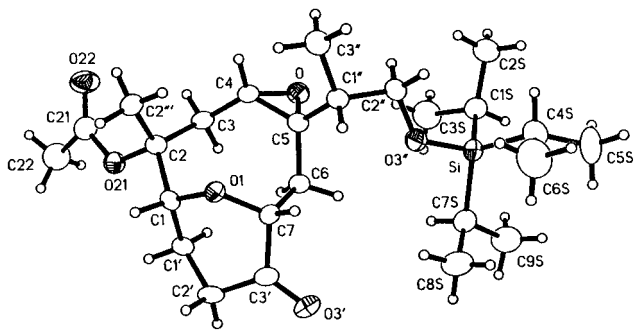

Fig. 1 X-Ray crystal structure of the epoxide **14.**

Notes and references

† *Selected data* for **14**: mp 84–86 °C; $[\alpha]_D^{24}$ −11.9 (*c* 0.426 in $CHCl_3$); $\nu_{max}(CHCl_3)/cm^{-1}$ 2867, 1731, 1459, 1371, 1321, 1085; δ_H(500 MHz; $CDCl_3$) 0.95 (3H, d, *J* 7.0, CHC*H*$_3$), 0.98–1.11 (21H, m, {[C*H*$_3$]$_2$C*H*}$_3$Si), 1.32 (1H, 't', *J* 14.2, O=CCHC*H*$_2$), 1.66 (1H, dd, *J* 9.8, 14.2, C*H*$_2$CH{O}C), 1.82 (3H, s, CC*H*$_3$), 1.84–1.88 (1H, m, C*H*$_2$CH$_2$C=O), 1.90–1.95 (1H, m, C*H*CH$_3$), 1.98 (3H, s, O=CC*H*$_3$), 2.09–2.15 (1H, m, C*H*$_2$CH$_2$C=O), 2.47–2.58 (2H, m, C*H*$_2$C=O), 2.65 (1H, dd, *J* 5.0, 14.4, O=CCHC*H*$_2$), 2.74 (1H, dd, *J* 5.3, 14.2, C*H*$_2$CH{O}C), 3.12 (1H, dd, *J* 5.3, 9.8, CH$_2$C*H*{O}C), 3.51 (1H, dd, *J* 6.7, 9.8, OC*H*$_2$Si), 3.83 (1H, dd, *J* 5.8, 9.8, OC*H*$_2$Si), 4.26 (1H, dd, *J* 5.0, 14.0, O=CC*H*O), 4.46 (1H, dd, *J* 6.1, 12.2, CH$_2$C*H*O); δ_C(126 MHz; $CDCl_3$) 12.3 (d), 13.3 (q), 18.4 (q), 20.3(t), 22.4 (q), 22.7 (q), 33.8 (t), 35.5 (t), 37.1 (t), 39.4 (d), 57.2 (d), 62.7 (s), 66.0 (t), 76.8(d), 77.4 (d), 83.3 (s), 170.0 (s), 210.9 (s); *m*/*z* (FAB) 274 (M^+,100%) (Found: $[M+H]^+$ 469.2966. $C_{25}H_{45}0_6Si$ requires *M*, 469.2985).

‡ *Crystal data* for **14**: $C_{25}H_{44}O_6Si$, *M* = 468.69, orthorhombic, *a* = 8.638(5), *b* = 9.693(9), *c* = 32.149(16)Å, *V* = 2692(3)Å^3, *T* = 150(2)K, space group $P2_12_12_1$ (No. 19), *Z* = 4, μ(Mo-*K*α) = 0.122mm^{-1}, 5535 reflections measured, 5481 unique (R_{int} = 0.023) which were retained in all calculations. The final wR_2 was 0.117 [all data] and R_1 was 0.0506 [4688 $F \geqslant 4\sigma(F)$]. Crystals were grown over a period of 7 d at ambient temperature from a solution in Et_2O into which *n*-hexane had been diffused. The structure was solved by direct methods and refined by full-matrix least-squares on F^2. The Flack absolute structure parameter refined to 0.00(8), confirming the chirality shown. CCDC 182/1200. Crystallographic data are available in CIF format from the RSC web site, see: http://www.rsc.org/suppdata/cc/1999/749/

1 D. Takaoka, H. Nozaki and M. Nakayama, *J. Chem. Soc., Chem. Commun.*, 1987, 1861.
2 J. Jakupovic, V. Castro and F. Bohlmann, *Phytochemistry*, 1987, **26**, 2011.
3 N. Gören, J. Jakupovic and S. Topal, *Phytochemistry*, 1990, **29**, 1467.
4 H. Nozaki, M. Hiroi, D. Takaoka and M. Nakayama, *J. Chem. Soc., Chem. Commun.*, 1983, 1107.
5 J. S. Clark, A. G. Dossetter and W. G. Whittingham, *Tetrahedron Lett.*, 1996, **37**, 5605.
6 B. A. Narayanan and W. H. Bunnelle, *Tetrahedron Lett.*, 1987, **28**, 6261; T. V. Lee, J.A. Channon, C. Cregg, J. R. Porter, F. S. Roden and H. T.-L. Yeoh, *Tetrahedron*, 1989, **45**, 5877.
7 T. J. Mickelson, J. L. Koviach and C. J. Forsyth, *J. Org. Chem.*, 1996, **61**, 9617.
8 D. Grafstein, *J. Am. Chem. Soc.*, 1955, **77**, 6650.
9 D. V. C. Awang and S. Wolfe, *Can. J. Chem.*, 1969, **47**, 706.
10 D. Y. Jackson, *Synth. Commun.*, 1988, **18**, 337.
11 F. Sato, Y. Kobayashi, O. Takahashi, T. Chiba, Y. Takeda and M. Kusakabe, *J. Chem. Soc., Chem. Commun.*, 1985, 1636.
12 A. M. Dennis, J. D. Korp, I. Bernal, R. A. Howard and J. L. Bear, *Inorg. Chem.*, 1983, **22**, 1522.
13 J. Adams, M.-A. Poupart, L. Grenier, C. Schaller, N. Ouimet and R. Frenette, *Tetrahedron Lett.*, 1989, **30**, 1749.
14 For examples of the stereoselective addition of $AlMe_3$ to cyclic ketones, see: E. C. Ashby and J. T. Laemmle, *Chem. Rev.*, 1975, **75**, 521; K. C. Nicolaou, M. E. Duggan and C.-K. Hwang, *J. Am. Chem. Soc.*, 1989, **111**, 6666.
15 For examples of the synthesis of bicyclic ethers by [1,2]-shifts of oxonium ylides generated from carbenoids, see: F. G. West, T. H. Eberlein and R. W. Tester, *J. Chem. Soc., Perkin Trans. 1*, 1993, 2857.
16 R. Annunziata, M. Cinquini, F. Cozzi, C. Gennari and L. Raimondi, *J. Org. Chem.*, 1987, **52**, 4674.

Communication 9/01711I

The influence of pressure and temperature on the crystal structure of acetone

David R. Allan,[a] Stewart J. Clark,[b] Richard M. Ibberson,[c] Simon Parsons,[d] Colin R. Pulham[d] and Lindsay Sawyer[e]

[a] *Department of Physics and Astronomy, The University of Edinburgh, King's Buildings, West Mains Road, Edinburgh, Scotland, UK EH9 3JZ*
[b] *Department of Physics, University of Durham, South Road, Durham, UK DH1 3LE*
[c] *ISIS Facility, Rutherford Appleton Laboratory, Chilton, Didcot, Oxfordshire, UK OX11 0QX*
[d] *Department of Chemistry, The University of Edinburgh, King's Buildings, West Mains Road, Edinburgh, Scotland, UK EH9 3JJ. E-mail: s.parsons@ed.ac.uk*
[e] *Structural Biochemistry Group, ICMB, The University of Edinburgh, Michael Swann Building, King's Buildings, West Mains Road, Edinburgh, Scotland, UK EH9 3JR*

Received (in Cambridge, UK) 20th January 1999, Accepted 16th March 1999

Dipolar carbonyl–carbonyl contacts generally occur in one of three motifs, and all are exhibited in the X-ray crystal structures of two phases of acetone derived at 15 kBar and at 150 K; a neutron powder-diffraction study at 5 K and an X-ray diffraction study at 110 K reveal strengthened CH···O as well as CO···CO electrostatic contacts which appear to explain the unusual thermodynamic properties of acetone, the nature of which have remained a mystery since 1929.

One motive for performing crystallographic studies on very simple systems is that they can reveal structural motifs that are applicable to whole classes of compound. Though there are few compounds so familiar in the laboratory as acetone, little is known about its structure in the solid state. We now describe five crystal structures of acetone determined at high pressure and at low temperature. The two distinct phases characterised in this study exhibit all three of the archetypal packing motifs identified in an important recent survey of dipolar carbonyl–

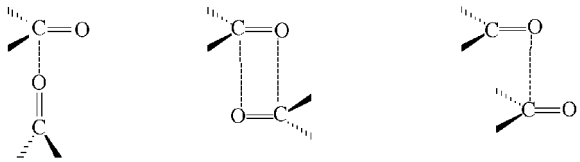

carbonyl interactions.[1] The identification of more than eighty 'highly unsatisfied' main-chain H-bond acceptors in protein structures[2] reflects the likely structural significance of dipolar interactions in biological macromolecules,[3] and the results described here are relevant to identifying and modelling these contacts. We have also been able to suggest a solution to a long-standing question about the thermodynamic properties of crystalline acetone.[4,5]

A sample of acetone was solidified at room temperature under pressure and a single crystal obtained by the methods described in ref. 6. X-Ray diffraction data were collected at 15 kBar (at room temperature), and structure solution† revealed a C-centred orthorhombic phase composed of layers of acetone molecules disposed along the *c*-axis. The layers consist of molecules stacked along the [010] direction, in which each molecule is involved in four C···O contacts formed in a sheared-parallel motif (Type III, Fig. 1) with a C=O···C=O distance of 3.365(2) Å, which is slightly shorter than the median for this type of interaction (3.45 Å).[1]

An orthorhombic C-centred phase can also be obtained by cooling the liquid slowly through the melting point at ambient pressure. A data set acquired at 165 K showed this to be essentially isostructural with the high pressure phase, except that the cell dimensions increase by between 4 and 7%.‡ This phase is metastable and decomposes after a few hours to the primitive phase described below. The shortest 'Type III' C=O···C=O distance is 3.587(3) Å, and in the context of other, similar, interactions examined in ref. 1 this contact is of marginal significance. Since there do not appear to be any other notable contacts, this may explain the instability of this phase.

During the course of this study this metastable phase was observed only twice, and the precise conditions which promote its formation are as yet unclear, although it seems to decompose more quickly the lower the temperature. All other low-temperature crystallisations yielded a stable, primitive orthorhombic phase.§ Once again, the crystal structure (determined at 150 K) consists of layers of molecules stacked along the *c*-axis, which is approximately twice as long as in the high pressure phase because neighbouring layers are crystallographically independent. The arrangement of molecules in the layers is quite different from that observed at high pressure. In one layer [Fig. 2(*a*)] pairs of molecules interact in antiparallel fashion ['Type II', C···O 3.300(3) Å], with each pair forming perpendicular 'Type I' contacts to neighbouring molecules [C···O 3.491(3) Å]. The other layers [Fig. 2(b)] consist of chains of molecules interacting only *via* the perpendicular motif [C···O 3.458(3) Å]; the closest C to O distance between the chains is 3.74 Å.

Calorimetric studies on crystalline acetone show a broad peak in the heat capacity *vs*. temperature curve centred around 127 K. The origin of this behaviour has remained an unresolved issue since it was first observed in 1929,[4] although the entropy change suggested that it was not associated with an order–disorder transition or rotations of the methyl groups.[5] Neutron powder diffraction patterns were measured for acetone between 5 and 140 K, and at all temperatures these patterns could be indexed on primitive orthorhombic unit cells similar to that given in

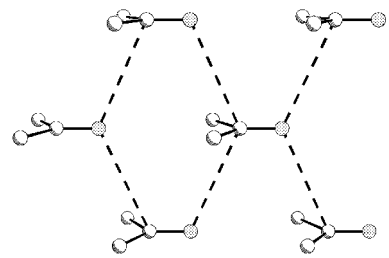

Fig. 1 Skew-parallel (Type III) C=O···C=O intermolecular interactions in the crystal structure of acetone at 15 kBar. H-atoms are disordered and omitted for clarity.

footnote §, although the cell dimensions changed rapidly and anisotropically with temperature. The crystal structure could not be resolved in the original neutron study, and so a firm statement regarding the structural nature of the heat capacity behaviour was not possible.[5]

We have refined the structure of acetone against the neutron powder data set collected at 5 K¶ to reveal C–H···O contacts of 2.336(6) and 2.479(5) Å respectively formed between and within the chains of molecules shown in Fig. 2(*b*); the angles at the donor H-atoms are 154.9(3) and 133.4(3)°. The dipolar contacts are also shorter at 5 K, and details are given in the figure captions. Although O···H distances derived from X-ray and neutron diffraction experiments are difficult to compare directly, at 150 K only one C–H···O contact (2.51 Å, where the C–H distance has been 'normalised' to 1.08 Å) falls within the sum of the van der Waals radii of O and H (2.60 Å).

It seemed plausible that the variation of heat capacity with temperature is associated with the strengthening of electrostatic C=O···C=O and CH···O contacts. This was confirmed in a variable-temperature X-ray structure determination study which at 110 K§ shows three contacts 'locking-in' with significantly shortened distances: the CH···O contact between the chains in Fig. 2(*b*) has an X-ray CH···O distance of 2.511(12) Å, compared to 2.618(13) Å at 150 K; the CH···O contact within the chains shortens from 2.71(2) to 2.604(18) Å, and the Type I (perpendicular) C=O···C=O interaction between the molecules in Fig. 2(*a*) shortens from 3.491(4) to 3.417(4) Å. The cell dimensions derived in this single crystal study are somewhat different from those obtained in the variable temperature neutron powder-diffraction study. It is important to emphasise that the heat capacity transition is very broad, occurring over a range of some 60 K, and varies with the thermal history of the sample.[5] Structural parameters observed in a particular run of experiments may well therefore exhibit effects which are sample-specific.

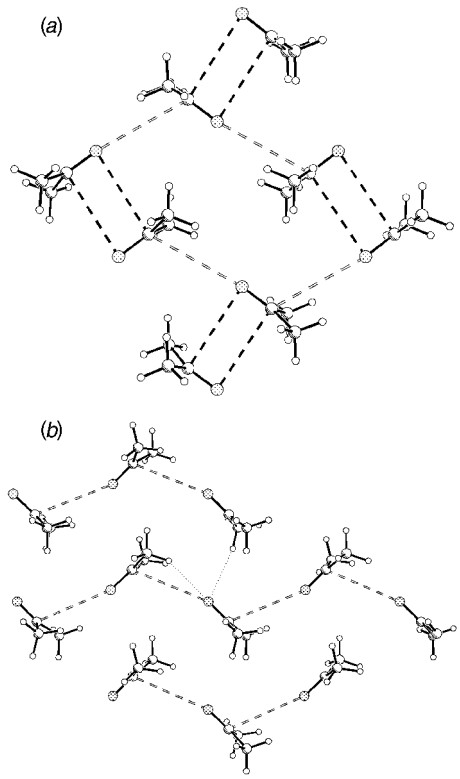

Fig. 2 The stable primitive orthorhombic phase of acetone at 150 K. (*a*) Layers containing perpendicular and antiparallel carbonyl interactions. The C···O distances at 5 K were 3.368(4) and 3.231(5) Å, respectively. (*b*) Layers comprised of strands of acetone molecules interacting *via* the perpendicular motif [Type I, 3.391(4) Å at 5 K]. Also shown (dotted lines) are C–H···O contacts that assume importance at 5 K.

A series of *ab initio* density functional calculations was performed with the aim of modelling the enthapy derived experimentally for this phase transition (259 J mol^{-1}).‖ Since the systems are periodic, an unbiased plane wave basis set was used to express the electronic wavefunction to alleviate the convergence problems of traditional quantum chemistry basis sets.[7] On minimising the total energy of the systems, the energy difference between the phases is 215 J mol^{-1}. This is below the experimental value because total energy calculations measure the absolute difference in the local energy minima of the two phases, and do not take dynamics into account.

We thank Mr Hugh Vass for technical assistance and the EPSRC for support.

Notes and references

All structures were solved by direct methods (ref. 8) and refined with Shelxl (ref. 9); *R* factors were between 5 and 6%.

† *Crystal data* for acetone at 15 kBar: C_2H_6O, M = 58.04, orthorhombic, a = 6.1219(11), b = 5.2029(10), c = 10.244(3) Å, *Cmcm*, Z = 4. The methyl groups are rotationally disordered about the C–C axis.

‡ *Crystal data* for the metastable C-centred orthorhombic low-temperature phase of acetone: a = 6.514(4) , b = 5.4159(18), c = 10.756(5) Å, U = 379.5(3) Å^3, T = 165 K, *Cmcm*. The H-atoms are ordered and were located in a difference map and refined freely.

§ *Crystal data* for the stable orthorhombic low-temperature phase of acetone: a = 8.873(3), b = 8.000(4), c = 22.027(7) Å, U = 1563.5(10) Å^{-3}, T = 150 K, *Pbca*, Z = 16, H-atom positional parameters were refined subject C–H and H–H similarity restraints. Cell dimensions at 110 K: a = 9.172(8), b = 7.761(8), c = 21.66(2) Å, U = 1542(3) Å^3.

¶ Time-of-flight diffraction data were recorded on the High Resolution Powder Diffractometer (ref. 10) at the ISIS spallation neutron source at 5 K over a time-of-flight range of 30 to 230 ms corresponding to a *d*-spacing range of 0.6 to 4.6 Å. a = 9.16686(1), b = 7.53231(1), c = 21.24861(5) Å. The structure was refined without constraints using the Rietveld method (ref. 11, 12) and using the 150 K structure as the starting model (space group *Pbca*). Only the D atoms were refined anisotropically. R_E = 1.64%, R_P = 3.03%, R_{wP} = 3.84%, χ^2 = 5.48 for 5948 observations and 162 basic variables. CCDC 182/1197. Crystallographic data are available in CIF format from the RSC web site, see: http://www.rsc.org/suppdata/cc/1999/751/

‖ The calculations were performed using the CASTEP density functional code (ref. 13). A generalised gradient approximation (ref. 14) was used to describe the exchange and correlation energy, requiring a plane wave basis set of 1.5 million functions for convergence. The *ab initio* forces on the atoms and stresses on the unit cell were used to perform an energy minimisation of the structure using a pre-conditioned conjugate gradients routine (note that these calculations refer to systems at zero-pressure and so the quantity minimised was the total energy of the system U). During the relaxation no symmetry constraints were applied; symmetry-breaking was not observed.

1 F. H. Allen, C. A. Baalham, J. P. M. Lommerse and P. R. Raithby, *Acta Crystallogr.*, 1998, **B54**, 320.
2 I. K. McDonald and J. M. Thornton, *J. Mol. Biol*., 1994, **238**, 777.
3 P. H. McCallum, R. Poet and E. J. Milner-White, *J. Mol. Biol*., 1995, **248**, 361 and 374.
4 K. K. Kelley, *J. Am. Chem. Soc*., 1929, **51**, 1145.
5 R. M. Ibberson, W. I. F. David, O. Yamamuro, Y. Miyoshi, T. Matuso and H. Suga, *J. Phys. Chem.*, 1992, **99**, 14 167.
6 W. L. Vos, L. W. Finger, R. J. Hemley and H. K. Mao, *Phys. Rev. Lett.*, 1993, **71**, 3150.
7 D. R. Allan, S. J. Clark, M. J. P. Brugmans, G. J. Ackland and W. L. Vos, *Phys. Rev. B*, 1998, **58**, 11 809.
8 A. Altomare, M. C. Burla, M. Camalli, G. Cascarano, C. Giacovazzo, A. Guagliardi and G. Polidori, *J. Appl. Crystallogr*., 1994, **27**, 435.
9 G. M. Sheldrick, Shelxl-97, University of Göttingen, 1997.
10 R. M. Ibberson, W. I. F. David and K. S. Knight, Rutherford Appleton Laboratory Report, RAL-92-031, 1992.
11 H. M. Rietveld, *J. Appl. Crystallogr*., 1969, **2**, 65.
12 W. I. F. David, R. M. Ibberson and J. C. Matthewman, Rutherford Appleton Laboratory Report, RAL-92-032, 1992.
13 M. C. Payne, M. P. Teter, D. C. Allan and T. A. Arias, *Rev. Mod. Phys*., 1992, **64**, 1045.
14 J. P. Perdew and Y. Wang, *Phys. Rev*., 1992, **B46**, 6671.

Communication 9/00558G

ChemComm

Structural distortions and the insulator to metal transition in $NiCr_{2-x}V_xS_4$

Anthony V. Powell* and Paz Vaqueiro

Department of Chemistry, Heriot-Watt University, Edinburgh, UK EH14 4AS. E-mail: a.v.powell@hw.ac.uk

Received (in Oxford, UK) 20th January 1999, Accepted 18th March 1999

The insulator to metal transition in $NiCr_{2-x}V_xS_4$ is accompanied by a structural distortion which results in the formation of zigzag chains of cations within the $(Cr,V)S_2$ layer.

The insulator to metal (ITM) transition[1,2] is of fundamental importance in condensed-matter science and encompasses phenomena as diverse as metallization processes in stars and size-induced transitions in microscopic metal particles.[3] From a chemical perspective, materials which lie close to the metal–insulator divide are of immense interest owing to the unique properties which they frequently exhibit and the opportunities afforded to tailor such properties using chemical control. For example, high temperature superconductivity in the cuprates[4] and the exceptional magnetotransport properties of mixed-manganese oxides[5] are two phenomena which appear to be linked to the proximity of these materials to the metal–insulator boundary.

Our investigations have been directed towards mixed-metal sulfides which lie in this important region of the electronic phase diagram, and have focused on materials which adopt the monoclinic Cr_3S_4 structure. This consists[6] of hexagonally close-packed sulfide layers, between alternate pairs of which, all of the octahedral sites are occupied by cations, giving rise to a unit of stoichiometry CrS_2. Half-occupancy, in an ordered manner, of the remaining octahedral sites between CrS_2 units, leads to a two-dimensional superstructure, with dimensions related to those of the primitive hexagonal unit cell (a_h) by $\sqrt{3}a_h \times a_h$. Progressive substitution of chromium by either divalent vanadium[7] or nickel[8] has been used to effect changes to the physical properties of metallic Cr_3S_4 and the contrasting electronic and magnetic properties of the two resulting non-stoichiometric series, $A_xCr_{3-x}S_4$ (A = V, Ni; $0 \leqslant x \leqslant 1$), may be correlated with differing cation distributions.[8,9]

This investigation has recently been extended to study the effect of chemical substitution within the MS_2 layers, through preparation of mixed-metal sulfides of general formula $NiCr_{2-x}V_xS_4$ ($0 \leqslant x \leqslant 2$). As the end-member phase $NiCr_2S_4$ is a semiconducting ferrimagnet[10] (T_c = 180 K) whilst NiV_2S_4 appears to be a metallic paramagnet,[11] an ITM transition would be expected in the non-stoichiometric series $NiCr_{2-x}V_xS_4$. The rigid-band model, which successfully accounts for the electronic properties of the stoichiometric end-member phases,[12] predicts all non-stoichiometric materials to be metallic, owing to holes in the t_{2g}-derived band. Here, we report that a critical level of substitution is required before the ITM transition occurs, and that this transition is accompanied by a structural distortion of the MS_2 unit which results in zigzag chains of octahedrally coordinated cations in the fully occupied layer.

All materials were prepared by conventional high temperature techniques. Initial characterisation by analytical electron microscopy, thermogravimetry and powder X-ray diffraction demonstrated that single-phase Cr_3S_4-type materials, with compositions in good agreement with nominal stoichiometries, were produced across the entire series. Transport properties, determined by the four-probe DC technique, clearly indicate semiconducting behaviour in the compositional range $0 \leqslant x \leqslant 0.5$ and metallic behaviour in the range $0.8 \leqslant x \leqslant 2.0$. However, for $NiCr_{1.4}V_{0.6}S_4$, $\rho(T)$ is almost temperature independent down to *ca*. 40 K, below which a slight increase in resistivity is observed leading to ambiguity over the sign of $d\rho/dT$ for materials in the composition range $0.5 < x < 0.8$. This may be the result of the influence of grain boundary resistances arising from the polycrystalline nature of the materials. Nevertheless, it leads to an uncertainty of no more than ±0.15 in the location of the ITM transition. Magnetic susceptibility data suggest that materials with $0 \leqslant x \leqslant 0.6$ exhibit long-range magnetic order. This has been confirmed by low temperature neutron diffraction. Conversely, materials with $0.6 < x \leqslant 2.0$ are paramagnetic, with evidence for spin-glass behaviour at low temperatures. Representative transport and magnetic data for materials in the semiconducting and metallic regions are presented in Fig 1.

Detailed structural studies were carried out by Rietveld analysis using a combination of powder X-ray diffraction and powder neutron diffraction, undertaken at the high-flux reactor, ILL Grenoble. Structural refinements, full details of which will be presented in due course, proceeded smoothly with weighted residuals of 4–7%. In addition to confirming solid-solution behaviour across the whole series, data demonstrate that in the

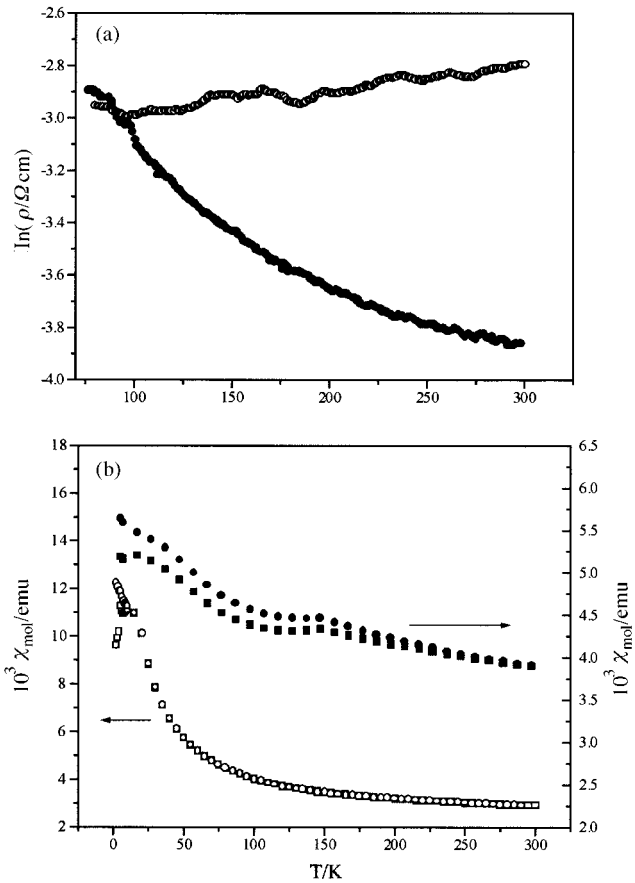

Fig. 1 (a) Resistivity data and (b) magnetic susceptibility data for $NiCrVS_4$ (open points) and $NiCr_{1.6}V_{0.4}S_4$ (solid points). Zero-field-cooled and field-cooled magnetic susceptibilities are denoted by squares and circles respectively.

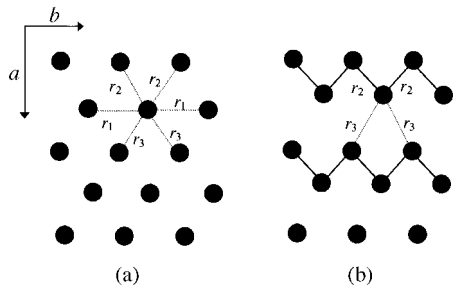

Fig. 2 (a) The pseudo hexagonal arrangement of cations in the MS_2 layer in materials with $x \leqslant 0.4$ and (b) the zigzag chains of cations in materials with $x > 0.4$.

non-stoichiometric materials, vanadium substitution occurs exclusively at sites in the fully occupied (MS_2) layer. There was no evidence of ordering of vanadium and chromium cations in the MS_2 layer.

Examination of cation–cation separations reveals that despite the solid-solution behaviour of $NiCr_{2-x}V_xS_4$, vanadium doping induces structural changes in the fully occupied layer, in the region of composition where the change from a magnetically ordered semiconductor to a paramagnetic metal is observed. The geometry of this layer in $NiCr_2S_4$ is shown in Fig. 2(a). Each cation has two neighbours at *ca.* 3.4 Å (r_1) resulting from lattice translation along the *b*-axis, two at a comparatively short distance (r_2) of *ca.* 3.2 Å and two at a slightly greater separation (r_3) of *ca.* 3.6 Å, giving six nearest neighbours in a pseudo-hexagonal arrangement within the layer. Although at low levels of vanadium doping this geometry is little perturbed, above x = 0.4, r_2 begins to decrease and r_3 increase whilst r_1 shows little change across the entire compositional range. Significantly, between x = 0.6 and 0.8, the decrease in r_2 is sufficient to bring it below the critical distance (R_c = 3.09–3.12 Å) proposed by Goodenough[13] for itinerant electron behaviour as a result of direct cation–cation interaction. These changes in cation–cation separations are manifested in an abrupt increase in the ratio r_3/r_2 at compositions with $x > 0.4$ (Fig. 3). This increase corresponds to a change from the pseudo-hexagonal symmetry of the fully occupied layer in $NiCr_2S_4$ to an arrangement in which there are zigzag chains of cations directed parallel to the *b*-axis [Fig. 2(b)]. The separation between cations within the chains (r_2) is considerably shorter than the shortest inter-chain (r_3) distance. These distances are *ca.* 2.9 and *ca.* 3.8 Å respectively, in NiV_2S_4.

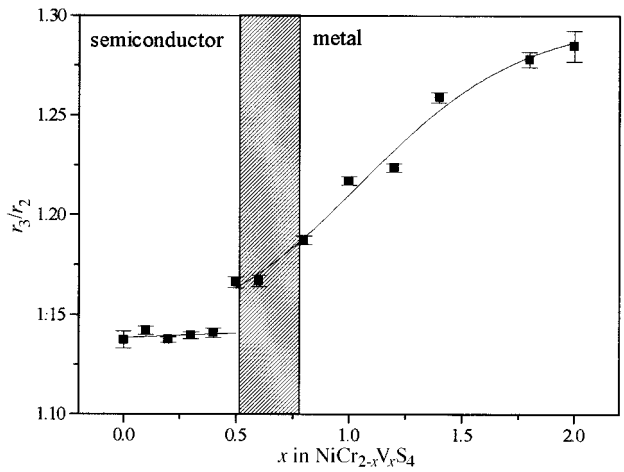

Fig. 3 Correlation between the compositional dependence of the degree of structural distortion within the MS_2 layer and electronic properties. Compositions for which there is ambiguity over the sign of $d\rho/dT$ are indicated by the shaded region.

The data presented here suggest that, contrary to predictions based on changing electron populations, the substitution of Cr^{III} d^3 by V^{III} d^2 is itself insufficient to induce metallization through the introduction of holes into the t_{2g}-derived band. This is a limitation of the approximations of the rigid-band model which ignores the effect of distortions on band structure or changes to band width as substitution proceeds. Using the extended Hückel method, Canadell *et al.*[14] have performed band structure calculations for a series of stoichiometric mixed-metal sulfides containing the MS_2 structural unit. Describing the MS_2 unit in terms of edge-sharing M_2S_6 double octahedral chains, the effect on band structure of distortions which give rise to metal clustering within the MS_2 layer, was investigated. The results demonstrate that when d^2 ions are present in this layer, strong cation–cation interactions within M_2X_6 chains lead to pronounced dispersion of one component of the t_{2g}-derived band and metallic behaviour pertains. The accompanying distortion of the ideal hexagonal array of cations corresponds to a structure in which zigzag clustering of the type depicted in Fig. 2(b) is present. Conversely, calculations reveal that when the t_{2g} manifold is half-filled as in AMo_2S_4, a Peierls distortion within individual M_2S_6 chains gives rise to a diamond clustering within the MS_2 layer and opens a band gap, resulting in semiconducting behaviour. Interestingly, despite the half-filled t_{2g} band, no metal clustering has been observed in materials of the form ACr_2S_4 (A = V, Cr, Ni). This has been attributed to the effects of electron localisation,[14] consistent with the more contracted orbitals of chromium compared to those of molybdenum [R_c(Mo) = 3.97 Å]. With increasing vanadium content in the series, $NiCr_{2-x}V_xS_4$, semiconducting behaviour persists until above some critical composition ($x \approx 0.4$), the MS_2 layer begins to distort resulting in the formation of chains of cations in which the intrachain cation–cation separation becomes lower than the critical distance for direct cation–cation orbital interaction. Of the three components of the t_{2g}-derived band, that in the chain direction, which is predominantly of $d_{x^2-y^2}$ character, shows pronounced dispersion, resulting in metallic behaviour.

The authors wish to thank The Leverhulme Trust for a research fellowship for P. V. The assistance of Dr C. Ritter, ILL, Grenoble, with the collection of neutron diffraction data is gratefully acknowledged.

Notes and references

1 N. F. Mott, *Metal–Insulator Transitions*, Taylor and Francis, 2nd edn., London, 1990.
2 P. P. Edwards, R. L. Johnston, C. N. R. Rao, D. P. Tunstall and F. Hensel, *Philos. Trans. R. Soc. London Ser. A*, 1998, **356**, 5.
3 P. P. Edwards, T. V. Ramakrishnan and C. N. R. Rao, in *Metal–Insulator Transitions Revisited*, ed. P. P. Edwards and C. N. R. Rao, Taylor and Francis, London, 1995, p. xv.
4 P. P. Edwards, T. V. Ramakrishnan and C. N. R. Rao, *J. Phys. Chem.*, 1995, **99**, 5228.
5 C. N. R. Rao, A. K. Cheetham and R. Mahesh, *Chem. Mater.*, 1996, **8**, 2421.
6 F. Jellinek, *Acta. Crystallogr.*, 1957, **10**, 620.
7 A. V. Powell and S. Oestreich, *J. Mater. Chem.*, 1996, **6**, 807.
8 D. C. Colgan and A. V. Powell, *J. Mater. Chem.*, 1997, **7**, 2433.
9 D. C. Colgan and A. V. Powell, *J. Mater. Chem.*, 1996, **6**, 1579.
10 A. V. Powell, D. C. Colgan and C. Ritter, *J. Solid State Chem.*, 1997, **134**, 110.
11 A. V. Powell, D. C. Colgan and P. Vaqueiro, *J. Mater. Chem.*, 1999, **9**, 485.
12 S. L. Holt, R. J. Bouchard and A. Wold, *J. Phys. Chem. Solids*, 1966, **27**, 755.
13 J. B. Goodenough, *Magnetism and the Chemical Bond*, Wiley, New York, 1963, ch. III.
14 E. Canadell, A. LeBeuze, M. Abdelaziz El Khalifa, R. Chevrel and M. H. Whangbo, *J. Am. Chem. Soc.*, 1989, **111**, 3778.

Communication 9/00561G

A crystalline carbene–silylene adduct 1,2-$C_6H_4[N(R)]_2C$-$Si[N(R)]_2C_6H_4$-1,2 (R = CH_2Bu^t); synthesis, structure and bonding in model compounds†

W. Marco Boesveld,[ab] Barbara Gehrhus,[a] Peter B. Hitchcock,[a] Michael F. Lappert*[a] and Paul von Ragué Schleyer[b]

[a] *The Chemistry Laboratory, University of Sussex, Brighton, UK BN1 9QJ. E-mail: M.F. Lappert@sussex.ac.uk*
[b] *Computer Chemistry Center, Universität Erlangen-Nürnberg, Henkestrasse 42, D-91504, Erlangen, Germany*

Received (in Basel, Switzerland) 28th January 1999, Accepted 17th March 1999

The red–brown, crystalline carbene–silylene adduct, 1,2-$C_6H_4[N(R)]_2C$-$Si[N(R)]_2C_6H_4$-1,2 (R = CH_2Bu^t) 4, was obtained from its factors, the carbene 3 and silylene 1, or from $Ni\{C[N(R)]_2C_6H_4$-1,2$\}_2$ and 1; the X-ray structure of 4 shows a long C–Si bond [2.162(5) Å] and NMR spectral data indicate significant C^+–Si^- bond polarity, features consistent with DFT calculations at the B3LYP/6-311+G level on $[(CH)_2(NH)_2]C$–$Si[(NH)_2(CH)_2]$, $(H_2N)_2C$–$Si(NH_2)_2$ or even $[(CH)_2(NH)_2]C$–SiH_2 and $(H_2N)_2C$–SiH_2, but not H_2C=$Si(NH_2)_2$ or H_2C=$Si[(NH)_2(CH)_2]$.**

Recently we reported on the coordination chemistry of the stable silylene $Si[N(CH_2Bu^t)]_2C_6H_4$-1,2 **1** [abbreviated as Si(NN)]. The crystalline, diamagnetic complexes [Ni(PPh$_3$)-{Si(NN)}$_3$], [Ni{Si(NN)}$_4$] or *trans*-[Pt{Si(NN)Cl}$_2$-{Si(NN)}$_2$] were obtained from **1** and [$NiCl_2(PPh_3)_2$], [Ni(cod)$_2$] or [$PtCl_2(PPh_3)_2$].[1] An attempt to synthesise a mixed carbene(silylene)–nickel complex was the starting point of the present investigation.

The new bis(carbene)nickel(0) complex **2** {obtained from [Ni(cod)$_2$] and the carbene **3** (*cf.* ref. 2)} afforded the crystalline carbene-silylene adduct **4** in good yield, accompanied by a deposit of Ni; an intermediate may have been a transient Ni{C(NN)}{Si(NN)} complex. Compound **4** was also prepared directly from its factors **1** and **3**. Compound **3** was synthesised from the thiourea **5** and C_8K at ambient temperature (*cf.* ref. 3). These data are summarised in Scheme 1.

Each of the new compounds **2**–**5** gave satisfactory microanalytical and NMR spectroscopic data. The $^{13}C\{^1H\}$ and $^{29}Si\{^1H\}$ NMR spectral signals for **4** in [$^2H]_8$toluene or [$^2H]_6$benzene at ambient temperature were at *ca.* 15 ppm lower frequency compared to the values in the free carbene **3**, δ_C 231.6, or silylene **1**, δ_{Si} 96.9.[4] However, these chemical shifts for **4** rose in frequency with increasing temperature, steadily approaching those for **3** and **1**, indicative of a dissociative equilibrium: **4** ⇄ **1** + **3**. Nonetheless, the EI mass spectrum of **4** at 70 eV showed the molecular ion $[\mathbf{4}]^+$ at *m/z* 532 as the highest peak present in substantial abundance (46%).

Crystalline **4** is a monomer, Fig. 1.‡ There is a long central bond of 2.162(5) Å between the three-coordinate C and Si atoms, the carbon atom being in an almost planar but the silicon in a pyramidal environment: the sum of the angles at C(1) being 351.4° and at Si 291.6°. This may be compared with the C=Si bond length in the silenes $Ad(Me_3SiO)C{=}Si(SiMe_3)_2$ [1.764(3) Å, twist angle 14.6°][5] and $Bu^t_2(Me)Si(Me_3Si)C{=}SiMe_2$ [1.702(5) Å, twist angle 1.6°][6] having the essentially planar double bond geometry; the sum of the three angles at Si or C is 360°. In **4**, the fold angles are 28° at C(1) and 77° at Si. There is significant torsion of the N_2CSiN_2 skeleton as evident by the dihedral angles N(1)–C(1)–Si–N(4) of 75° and N(2)–C(1)–Si–N(3) of 128.1°. We infer that the CSi bond in **4** is dipolar, with the silicon being the negative end of the dipole, a C=Si double bond being ruled out. This conclusion is supported by DFT calculations on model compounds (see below), as well as by analogy with suggestions on the nature of the di(amino)-carbene–tin(II) and –germanium(II) complexes **6**,[7] **7**,[8] and **8**.[9]

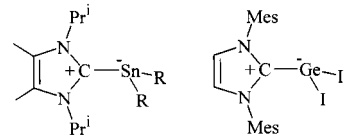

6 R = $C_6H_2Pr^i_3$-2,4,6 **8**
7 R = Cl

The silylene M[N(Bu^t)(CH$_2$)$_2$NBu^t] (M = Si) failed to react with the carbene (M = C), germylene (M = Ge) or CO.[10] By contrast, **1** not only forms the adduct **4** with **3**, but also reacts with the heavier group 14 carbene analogues M′[$N(SiMe_3)_2]_2$ (M′ = Ge, Sn or Pb),[11] although we now report that it did not react with CO in supercritical xenon at > 20 atm at 25 °C.[12]

Density functional calculations[13] were performed on the parent silene $H_2C{=}SiH_2$ **9** and derivatives X_2CSiY_2 **10**–**15** (X_2

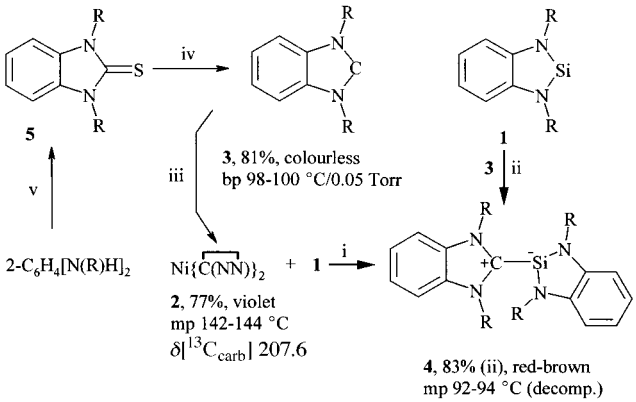

Scheme 1 Synthesis of the carbene-silylene adduct **4** and compounds **2**, **3** and **5** (R = CH_2Bu^t). *Reagents and conditions* (at *ca.* 20 °C): i or ii, C_6H_6; iii, [Ni(cod)$_2$], C_6H_6; iv, 2 C_8K, thf; v, $C(S)Cl_2$, 2 NEt_3.

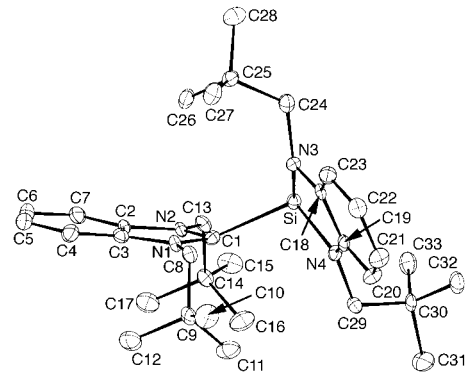

Fig. 1 Molecular structure of **4**. Selected bond lengths (Å) and angles (°): Si–C(1) 2.162(5), C(1)–N(1) 1.362(5), C(1)–N(2) 1.362(5), Si–N(3) 1.791(4), Si–N(4) 1.790(4), N(1)–C(1)–N(2) 105.6(4), N(3)–Si–N(4) 87.5(2).

and Y_2 are hydrogens or nitrogen functions, Table 1). The structures, illustrated by **9**, **10**, **12** and **15** in Fig. 2, separate into two distinct groups. The model compounds $H_2C{=}SiY_2$ **9**–**11** all have CSi double bonds with distances near 1.70 Å, planar or nearly planar geometries and large association energies. The second group, **12**–**15**, like **4**, have longer SiC distances (1.93–2.02 Å, compared with 1.885 Å in $H_3C{-}SiH_3$),[14] strongly pyramidal geometries at silicon, and weaker association energies.

The dramatic structural changes produced by substituting the hydrogens at carbon by amino groups are clarified by natural bond order analysis. The N–C–N unit delocalises the positive charge on carbon. The polarities of **12**–**15** are reversed (*cf.* **9** and **10**) and the SiY_2 moieties are negative (Fig. 2). The π-delocalisation causes amino groups on carbon, but not on silicon, to be co-planar (or nearly so). The silicon substituents bond through the silicon p orbitals at angles approaching 90°.

The association energies for the model compounds **9**–**15** (Table 1) are highly revealing. These are based on the energies of the process $X_2C{:} + {:}SiY_2 \rightarrow X_2CSiY_2$ [using the $:CH_2$ ($^1A_1$) energy for uniformity as the other carbenes and silylenes are ground state singlets]. The association energies vary remarkably, from 116.5 kcal mol^{-1} for the parent silene **9** to only 3.2 kcal mol^{-1} for **15**, the model closest to **4**. These energies reflect the changes in carbene and silylene stability due to their substituents. The C=Si bond in the parent silene **9** is weakened markedly by NH_2 substitution, much more on C than on Si. The effects on C and Si are roughly additive. The aromaticity conferred by the five-membered Si[$(NH)_2(CH)_2$] ring in **11** (*vs.* **10**) has a much greater effect on lowering the association energy than that due to the C[$(NH)_2(CH)_2$] ring in **13** (*vs.* **12**).[15]

The structures of **4** and **12**–**15** can best be considered as donor–acceptor complexes in which the carbene lone pair interacts with the formally vacant silicon p orbital, as suggested for the H_2Si–CO complex which also has pronounced pyramidalisation at silicon.[16] The polarisation of the parent silene **9** is reversed by amino substitution at the carbon and the SiY_2 moiety assumes anionic character. The lowering of the association energy in **12**–**15** also results in longer CSi separations. The difference between the CSi distance in **15** (2.02 Å) from that in **4** (2.16 Å) is not significant in view of the weakness of these complexes. The computed torsion barrier for **15** is only 1 kcal mol^{-1} and, like **4**, has a significantly twisted energy minimum.

In a full paper, we shall report on the synthesis and structures of the heavier group 14 analogues of the carbene–silylene complex **4**.

We thank EPSRC, the European Union, [especially for fellowships for B. G. (EPSRC) and W. M. B. (HCM, category 20)] and the Fonds der Chemischen Industrie for support.

Table 1 Carbene–silylene association energies[a]

			r_{CSi}/Å	$-\Delta H_0$/ kcal mol^{-1}
9	$H_2C{=}SiH_2$	C_{2v}	1.708	116.5
10	$H_2C{=}Si(NH_2)_2$	C_2	1.699	89.3
11	$H_2C{=}Si[(NH)_2(CH)_2]$	C_{2v}	1.698	74.7
12	$(H_2N)_2C{-}SiH_2$	C_s	1.934	47.6
13	$[(CH)_2(HN)_2]C{-}SiH_2$	C_s	1.927	46.4
14	$(H_2N)_2C{-}Si(NH_2)_2$	C_s	1.960	15.8
15	$[(CH)_2(HN)_2]C{-}Si[(NH)_2(CH)_2]$	C_1	2.024	3.2

[a] B3LYP/6-311+G(d, p) optimised data, with zero-point energy obtained at B3LYP/6-31G* scaled by 0.96 for $-\Delta H_0$ (1 kcal = 4.182 kJ).

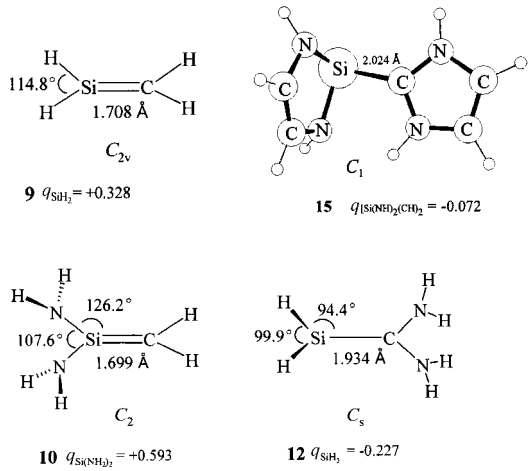

Fig. 2 Optimized structures at B3LYP/6-311+G** level for silenes **9**, **10**, **12** and **15** (Mulliken charges are given).

Notes and references

† No reprints available.

‡ *Crystal data for* **4**: $C_{33}H_{52}N_4Si$, M = 532.9, monoclinic, space group $P2_1/n$ (no. 14), a = 10.212(4), b = 16.231(5), c = 19.776(8) Å, β = 101.73(3)°, U = 3209(2) Å^3, Z = 4, D_c = 1.10 g cm^{-3}, μ(Mo-Kα) = 0.1 mm^{-1}, T = 173(2) K, Final residuals were R_1 = 0.075 for the 3093 reflections with $I > 2\sigma(I)$ and wR_2 = 0.198 for all reflections. Intensities were measured in the ω–2θ mode in the range $2 < \theta < 25°$ on an Enraf-Nonius CAD4 diffractometer. Full-matrix least-squares refinement, on all F^2, with SHELXL-93, H atoms in riding mode and non-H atoms anisotropic. CCDC 182/1199. See http://www.rsc.org/.suppdata/cc/755/ for crystallographic files in .cif format.

1 B. Gehrhus, P. B. Hitchcock, M. F. Lappert and H. Maciejewski, *Organometallics*, 1998 , **17**, 5599.
2 For Ni{CN(R)$(CH)_2$NR}$_2$ from [Ni(cod)$_2$] and a carbene (R = $C_6H_2Me_3$-2,4,6), see: A. J. Arduengo, S. F. Gamper, J. C. Calabrese and F. Davidson, *J. Am. Chem. Soc.*, 1994, **116**, 4391.
3 For CN(R)$(CH)_2$NR from the appropriate thiourea and K in refluxing thf (R = Me, Et, Pr^i), see: N. Kuhn and T. Kratz, *Synthesis*, 1993, 561; for R = Bu^t, see: M. K. Denk, A. Thadani, K. Hatano and A. J. Lough, *Angew. Chem., Int. Ed. Engl.*, 1997, **36**, 2607.
4 B. Gehrhus, P. B. Hitchcock, M. F. Lappert, J. Heinicke, R. Boese and D. Bläser, *J. Organomet. Chem.*, 1996, **521**, 211.
5 A. G. Brook, S. C. Nyburg, F. Abdesaken, B. Gutekunst, G. Gutekunst, R. K. M. R. Kallury, Y. C. Poon, Y.-M. Chang and W. Wong-Ng, *J. Am. Chem. Soc.*, 1982, **104**, 5667.
6 N. Wiberg, G. Wagner, J. Riede and G. Müller, *Organometallics*, 1987, **6**, 32.
7 A. Schäfer, M. Weidenbruch, W. Saak and S. Pohl, *J. Chem. Soc., Chem. Commun.*, 1995, 1157.
8 N. Kuhn, T. Kratz, D. Bläser and R. Boese, *Chem. Ber.*, 1995, **128**, 245.
9 A. J. Arduengo, H. V. R. Dias, J. C. Calabrese and F. Davidson, *Inorg. Chem.*, 1993, **32**, 1541.
10 M. K. Denk, K. Hatano and A. J. Lough, *Eur. J. Inorg. Chem.*, 1998, 1067.
11 B. Gehrhus, P. B. Hitchcock and M. F. Lappert, *Angew. Chem., Int. Ed. Engl.*, 1997, **36**, 2514; C. Drost, B. Gehrhus, P. B. Hitchcock and M. F. Lappert, *Chem. Commun.*, 1997, 1845.
12 A ^{13}C NMR spectroscopic experiment, for which we thank Dr. G. A. Lawless.
13 Calculations were performed using GAUSSIAN 94, Revision B.1, M. J. Frisch *et al.*, Gaussian Inc., Pittsburgh, PA, 1995. Structures of **9**–**15** were optimized at the RB3LYP/6-311+G** level and established to be a minimum by frequency calculation at B3LYP/6-31G*.
14 T. Müller, W. Ziche and N. Auner, (ch. 16 and P. P. Gaspar and R. West, (ch. 43 in *The Chemistry of Organic Silicon Compounds*, ed. Z. Rappoport and Y. Apeloig, New York, vol. 2, 1998.
15 For aromaticity in carbenes and silylenes, see: S. G. Urquhart, A. P. Hitchcock, J. F. Lehmann and M. Denk, *Organometallics*, 1998, **17**, 2352; R. West, J. J. Buffy, M. Haaf, T. Müller, B. Gehrhus, M. F. Lappert and Y. Apeloig, *J. Am.Chem. Soc.*, 1998, **120**, 1639; C. Boehme and G. Frenking, *J. Am. Chem. Soc.*, 1996, **118**, 2039.
16 T. P. Hamilton and H. F. Schaefer, *J. Chem. Phys.*, 1989, **90**, 1031.

Communication 9/00784I

ChemComm
FEATURE ARTICLE

MOVPE Mechanisms from studies of specially designed and labelled precursors

David J. Cole-Hamilton

School of Chemistry, University of St. Andrews, St. Andrews, Fife, Scotland, UK KY16 9ST. E-mail: djc@st-and.ac.uk

Received (in Cambridge, UK) 5th January 1999, Accepted 5th February 1999

Studies of the reaction or decomposition products of precursors for metal organic vapour phase epitaxy (MOVPE) do not always give enough information to allow the unequivocal determination of decomposition or growth mechanisms. By studying deuterium labelled precursors in the presence or absence of their protio analogues, other precursors and/or He, H_2, D_2 or by studying precursors carrying substituents that are designed to give different products if different mechanisms operate, it is possible to draw more definitive conclusions.

Using these studies coupled with semi-empirical molecular orbital calculations, it is shown that primary arsines decompose by reductive elimination of H_2 followed by β-abstraction (Bu^tAsH_2) or reaction with the parent arsine to form RAsH·, which undergoes reductive elimination (PhAsH·), β-abstraction (Bu^tAsH·) or As–C bond cleavage (Bu^tAsH·). Hex-5-enylarsine has been used to show that adduct formation is not important during growth of GaAs.

For group 16 dialkyls (R_2E, E = S, Se or Te), the predominant decomposition mechanism is homolytic E–C bond cleavage. Subsequent reactions involve abstraction of H from the β-position of the intact R_2E to give alkane, two molecules of alkene E and H· (E = Te or Se). For E = Te, H· does not react significantly with Pr^i_2Te, but for Bu^t_2Se a short chain-reaction is initiated by H·. The importance of free radicals is confirmed by studies of (but-2-enyl)$_2$Te, (hex-5-enyl)$_2$E (E = S, Se, Te), (pent-5-enyl)$_2$Te and (hex-5-enyl)SH, as well as of secondary and tertiary analogues. Reactions of the labelled and designed group 16 precursors with Me_2M (M = Cd or Zn) are also discussed.

Introduction

Semiconductors are the major components of the computer age. Elemental semiconductors such as silicon from Group 14 have found use in applications from transistors and computers through to solar energy converters, but they have the limitation that the band-gap is fixed so that the wavelengths they can absorb or emit cannot be varied over a wide range. Compound semiconductors, which are made up from elements of Groups 13 and 15, 12 and 16 or sometimes 13 and 16, on the other hand, have a variety of different band gaps which cover the whole electromagnetic spectrum from the IR (InSb) through to the UV (ZnS).[1] Using three or four of these elements, *e.g.* $Cd_xHg_{1-x}Te$ or $Ga_xIn_{1-x}As_yP_{1-y}$, the band gap within one materials system can be varied over a wide range. In addition, the mobility of electrons within some of these materials can be an order of magnitude higher than in silicon.

For the elemental semiconductors, large single crystals can be grown and cleaved to make the required electronic devices, but the growth of large single crystals of the compound materials has proved highly problematical. Since only a thin film of the semiconductor is usually required for the fabrication of devices, the most important methods to have been developed to surmount this problem involve the growth of thin layers of the desired semiconductor on a single crystal of another, using the ordered array of the substrate atoms to align those of the growing layer. A variety of methods has been devised for doing this, but one of the most important is metal organic vapour phase epitaxy (MOVPE).[1,2] In this approach, highly purified volatile compounds of the elements to be incorporated into the semiconductor are passed over the heated substrate where they decompose to give the thin film. The composition of the growing layer can be controlled by regulation of the gas phase composition and dopants can be included by incorporating extra precursor streams. The technique has proved highly versatile and is now production technology for a variety of semiconductor devices, many of which contain up to 100 layers of different but controlled composition.[2]

The earliest examples of semiconductor growth by MOVPE involved metal alkyls (usually MMe_n) for the Group 12 or 13 precursors and hydrides (EH_n) for the Group 15 or 16 elements.[3,4] In most cases these systems worked well and in some they continue to be used in production.[1] These compounds are, however, highly reactive and often toxic materials[5] so there have been developments in recent years particularly towards the use of different precursors for the Group 15 and 16 precursors. Most of these involve the replacement of the hydrides by compounds that contain one or more alkyl or amide groups and hence the chemistry leading to the semiconductor film becomes more complex and has the potential to incorporate extraneous elements into the growing layer such as carbon or nitrogen, which have detrimental effects on the electronic properties.[6] There is thus a considerable interest in understanding the processes that occur during the growth of layers from these precursors so as to be able to improve on their design.

Various groups have used surface science techniques to study the species present on the surface during growth,[7,8] but often these studies have been carried out under high vacuum and there can be no certainty that the interesting results obtained correlate with what occurs under growth conditions (generally *ca.* 1 atm).

David Cole-Hamilton received his training in Organometallic Chemistry with Dr T. A. Stephenson (Edinburgh) and Professor Sir Geoffrey Wilkinson (Imperial College). He was on the staff at Liverpool, where Professor A. K. Holliday introduced him to Dr J. B. Mullin (MOD) and the design of MOVPE precursors, before taking up the Irvine Chair of Chemistry in St. Andrews. His work is in the area of organometallic compounds applied to homogeneous catalysis and problems in Materials Chemistry. Some of his work on the production of highly purified metal alkyls has been commercialised through Epichem Ltd (Founded 1983). He was the first Sir Edward Frankland Fellow of the RSC (1984–5) and won the Corday Morgan medal and prize in 1983. In 1998 he won the RSC Industrial award for Organometallic Chemistry sponsored by Monsanto.

Furthermore, in addition to reactions on the surface, gas phase processes may be occurring of which surface techniques remain ignorant. Gas phase reactions may also determine the nature of the surface species. Kinetic studies have been carried out under real growth conditions and certain conclusions have been drawn on the basis of product analyses (usually using mass spectrometry, gas chromatography–mass spectrometry (GCMS)[9] or FTIR[10] studies). These have given valuable insight, although without quantitative calibration, they are of limited value and, as will be demonstrated, they do not always lead to the appropriate conclusions.

Our approach has been to design precursors which are as similar as possible to those that are used in the growth process, but which, as a result of the products they form, give definitive information about the way in which they decomposed or reacted. We have used two main approaches. The first involves the use of deuterium labelling whilst the second involves the design of special 'reporter ligands', whose reaction products give information on the mechanisms involved in their formation. Product analyses are carried out using multinuclear NMR spectroscopy or GCMS and in some cases these experimental studies are backed up by theoretical calculations. In this article, we discuss our work on gallium arsenide and on II–VI (12–16) semiconductors involving Zn, Cd, Hg, S, Se or Te.

Gallium arsenide

Gallium arsenide was originally grown from Me_3Ga and AsH_3[3] and some commercial processes still use these precursors extensively.[2] However, AsH_3 is a highly toxic gas and is usually supplied in high pressure cylinders diluted with hydrogen. The risks associated with the possible rupture of one of these cylinders or their ancilliary equipment, either in use or during transport, led to a search for alternative arsenic precursors. The main ones to be introduced were the primary arsines, Bu^tAsH_2 and $PhAsH_2$, of which Bu^tAsH_2 is now the precursor of choice. These compounds are not intrinsically very much less toxic than AsH_3,[5] but being liquids, they are generally supplied in small metal containers and a spillage is not catastrophic—it simply requires evacuation of the area until the arsenic compound has evaporated and dissipated.

The various first steps in the decomposition mechanisms for Bu^tAsH_2 are shown in Fig. 1. They are, reductive elimination of Bu^tH or H_2, β-H abstraction to give AsH_3 and 2-methylpropane or homolytic cleavage of the As–C or As–H bond. At the time when we started to work in this area, some elegant studies had been performed that showed that both 2-methylpropene and 2-methylpropane were products.[11,12] All of these only considered that mechanisms that involved loss of the As–C bond, by reductive elimination of 2-methylpropane, by homolytic fission of the As–C bond or by β-H abstraction, were likely to be important since literature values of the bond enthalpies are much higher for As–H than for As–C.[13]

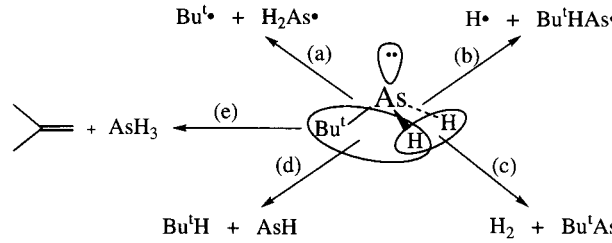

Fig. 1 Possible first steps in the decomposition of Bu^tAsH_2. (a) As–C bond cleavage; (b) As–H bond cleavage; (c) reductive elimination of H_2; (d) reductive elimination of Bu^tH; (e) β-elimination.

We opted to study[13–15] $PhAsH_2$ since one of the pathways (β-H abstraction) is not available. The organic product from its decomposition is benzene and this could arise from As–C bond cleavage or from reductive elimination. To test which of these was operative, we studied the decomposition of (*o*-tolyl)AsD_2, reasoning that reductive elimination would only give toluene deuteriated in the *ortho* position, whereas homolytic fission would give the *o*-tolyl radical which would either abstract D to give toluene deuteriated in the *ortho*-position or would isomerise to the allylic stabilised benzyl radical which would abstract D to give toluene deuteriated in the methyl group.

Decomposition of *o*-tolylAsD_2 produced toluene with D in the *ortho*-position, but also in the methyl group. Surprisingly, however, we observed that the methyl group contained 0, 1, 2 or 3 D atoms. This could not easily be explained by any of the mechanisms that had previously been suggested so we carried out calculations in the PM3 system on the various possible first steps in the decomposition, including those which involved As–H bond cleavage. These showed that, at the temperatures involved, loss of H_2 was both kinetically and thermodynamically the most favoured option.[15] We also showed that reductive elimination of toluene from (*o*-toly)AsH· had a very similar free energy of activation to tautomerism to give the stabilised benzyl radical, $H_2AsC_6CH_2$·; a pathway that could account for multiple D incorporation into the methyl group. This led us to propose that the decomposition of (*o*-tolyl)AsH_2 occurred as shown in Fig. 2, with (*o*-tolyl)As reacting with (*o*-tolyl)AsH_2 to give (*o*-tolyl)AsH· from which the final products were generated. Calculations suggested that a very similar sequence of reactions accounted for the decomposition of Bu^tAsH_2 except that β-H abstraction in Bu^tAs, formed by loss of H_2, competed with the bimolecular reaction to produce Bu^tAsH·.[15]

One of the other controversies surrounding the growth of GaAs by MOVPE concerned whether or not adducts of the form [Me_3Ga·AsR_3] (R = H, alkyl or aryl) were involved in the growth process. There is no doubt that these form at room temperature and below, but at 600–700 °C entropy may ensure that their existence is at best fleeting. We probed this by studying the model primary alkyl arsine, (hex-5-enyl)-AsH_2.[15–18] We selected the hex-5-enyl group originally as a

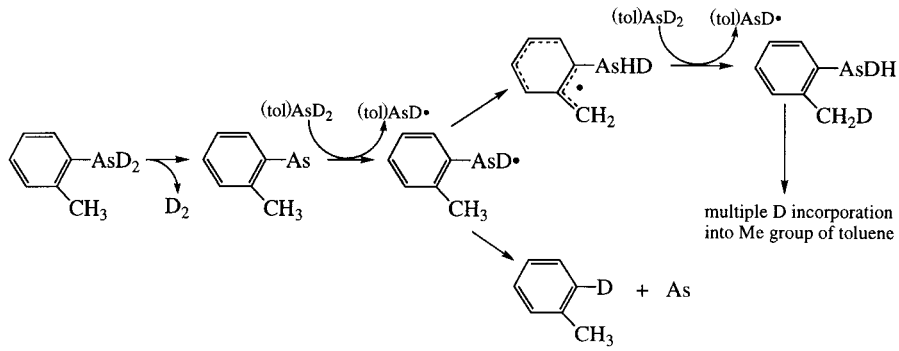

Fig. 2 Proposed mechanism for the decomposition of (*o*-tolyl)AsD_2.

probe for the decomposition mechanism of primary arsines since, if hex-5-enyl radicals are formed at any stage by As–C cleavage, they will cyclise to cyclopentylmethyl or cyclohexyl radicals.[19,20] Non-radical processes will, on the other hand, give straight chain products. The decomposition of (hex-5-enyl)-AsH_2 on its own produces hex-1-ene as the major hydrocarbon product,[16,17] showing that free alkyl radicals are not produced, as confirmed by the decomposition of (*o*-tolyl)AsD_2 and the calculations on Bu^tAsH_2 (see above). When (hex-5-enyl)arsine was reacted with Me_3Ga in the liquid phase at low temperature, we were able to identify the adduct, [$Me_3Ga{\cdot}As(hex)H_2$] which decomposed on heating, giving off methane, to produce [$Me_2GaAs(hex)H]_3$ then [$MeGaAs(hex)]_n$. Heating the polymer produced GaAs together with methane and methylene-cyclopentene. The last product shows that the final step involves As–C and Ga–C bond cleavage to give Me· and hex-5-enyl radicals, which cyclise to cyclopentylmethyl radicals and react with Me· to give the observed products (see Fig. 3). The different products obtained from the decomposition of [(hex-5-enyl)AsH_2] in the presence or absence of Me_3Ga allow us to determine whether the gas phase reaction involved adduct formation or not, by analysing the products from the gas-phase reaction of Me_3Ga with [(hex-5-enyl)AsH_2]. In practice, we obtained[16,17] a product distribution that is extremely similar to that obtained from [(hex-5-enyl)AsH_2] alone along with methane and unreacted Me_3Ga, confirming that adduct formation is not significant in the gas-phase—at least in this system.

II–VI Compounds

$Cd_xHg_{1-x}Te$, ZnSe, ZnS

Cadmium mercury telluride is the main semiconductor used for IR detectors and emitters. It is also of importance for long range transmission over fibre optic cables made from fluoride glasses. Hydrogen telluride is not sufficiently stable for use in MOVPE[4] so dialkyl- or diallyl-tellurium compounds have generally been employed together with Me_2Cd and elemental mercury.

Diallyltellurium [bis(prop-2-enyl)tellurium] decomposes to give hexa-1,5-diene and tellurium.[21] These products could be produced by reductive elimination or by Te–C bond cleavage to give prop-2-enyl radicals which combine to give the observed product. In order to test which of these mechanisms is operating, we studied[22] the decomposition of [bis(but-2-enyl)tellurium] since reductive elimination should give only octa-2,6-diene (as *Z,Z, E,Z* and *Z,E* isomers) whilst formation of butenyl radicals followed by radical coupling should give these products together with 2,4-dimethylhexa-1,5-diene and *Z*- and *E*-3-methylhepta-1,5-diene. In practice, we observed that all the products were observed (Fig. 4) in similar ratios to those obtained from bis(but-2-enyl)zinc, which is known to decompose by a free radical mechanism.[23] Furthermore, at partial conversion there was no evidence for isomerisation of the starting material to bis(1-methylpropenyl)tellurium, ruling out the reductive elimination mechanism.

The main tellurium precursors that have been employed are dialkyltelluriums, especially Pr^i_2Te. To probe the decomposition mechanisms of this kind of alkyl in the presence or absence of Me_2Cd and/or Hg, we have studied the decomposition of bis(hex-5-enyl)tellurium,[24,25] bis(pent-4-enyl)tellurium[24] and of Pr^i_2Te labelled with deuterium.[26]

The model studies in the gas phase showed that a mixture of straight chain and cyclic products was obtained from bis(hex-5-enyl)tellurium indicating that Te–C bond cleavage was certainly important (Fig. 5), but not giving detailed information about subsequent steps in the decomposition. In the liquid phase, bis(hex-5-enyl)tellurium produced linear and cyclic hydrocarbons, but also (cyclopentylmethyl)(hex-5-enyl)tellurium and bis(cyclopentylmethyl)tellurium. Both of these products suggest that the dialkyltellurium undergoes homolytic fission of the Te–C bond and that the free carbon based radical (after cyclisation in this case) reacts back with intact bis(hex-5-enyl)tellurium, eliminating a further hex-5-enyl radical.[24,25] Using bis(pent-5-enyl)tellurium in the liquid or gas phase, we obtain pent-1-ene and penta-1,4-diene together with 2-methyltelluracyclopentane. The last product shows that once Te–C bond cleavage has occurred, the RTe· formed in this case is sufficiently stable to undergo internal cyclisation to the telluracyclopentylmethyl radical which then picks up H·.

These reactions clearly show that Te–C bond cleavage is important, but they involve primary alkyls which differ from those generally employed in growth. We, therefore, studied d[14]-

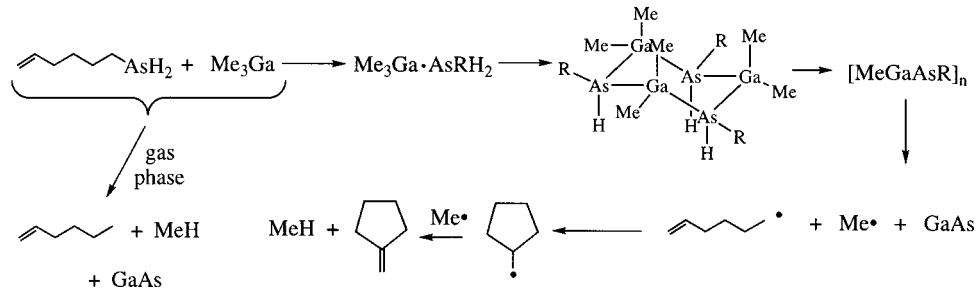

Fig. 3 Reactions occurring during the codecomposition of Me_3Ga with (hex-5-enyl)AsH_2 in the liquid or gas phases (R = hex-5-enyl).

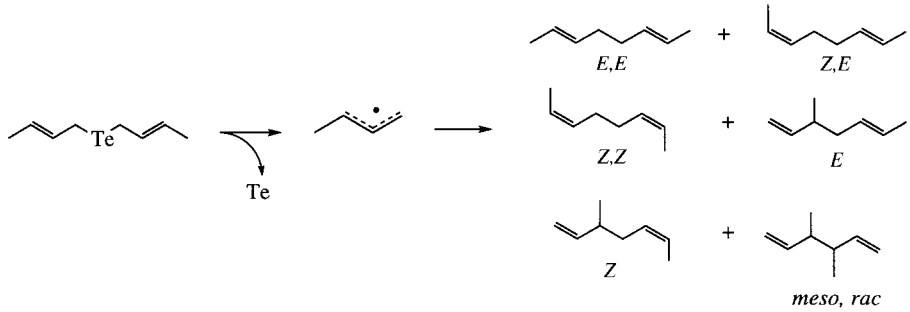

Fig. 4 Proposed mechanism of decomposition of (prop-2-enyl)$_2$Te.

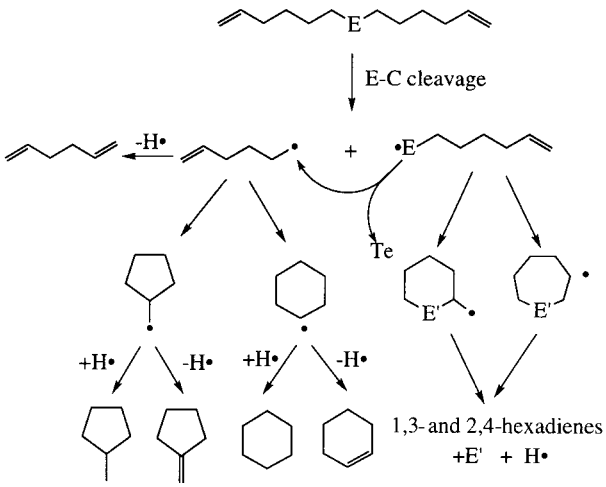

Fig. 5 Proposed mechanism of decomposition of (hex-5-enyl)$_2$E (E = S, Se or Te; E′ = S or Se).

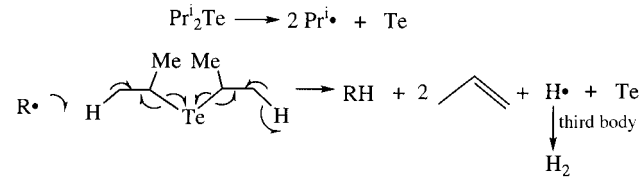

Fig. 6 Proposed major pathway for the decomposition of Pr$^i_2$Te [R = Pr^i or Me (from Me_2Cd)].

labelled Pr$^i_2$Te to investigate the pathways open to a real precursor.[26] The organic products from decomposition of unlabelled Pr$^i_2$Te are propene and propane (2 : 1) together with small amounts of 2,3-dimethylbutane, much less than would be expected from gas phase reactions of Pr^i· with one another.[27] The various possible processes for decomposition of a compound of this type are similar to those shown in Fig. 1 but involve reductive elimination to give 2,3-dimethylbutane, β-H abstraction or Te–C bond cleavage.

Codecomposition of d^0- and d^{14}-Pr$^i_2$Te gives a mixture of d^0, d^1, d^7 and d^8 propane (1.7 : 1 : 1.5 : 1) together with d^0 and d^6-propene. This strongly suggests that Te–C bond cleavage occurs rather than β-H abstraction followed by competing β-H abstraction and reductive elimination, which might be expected to give only d^0- and d^8-propane together with d^0- and d^6-propene. Care must be exercised here, however, since exchange of [C_3H_7TeH] with [C_3D_7TeD] is expected to occur to give [C_3H_7TeD] and [C_3D_7TeH] from which reductive elimination would give d^1- and d^7-propane. Careful analysis of the product ratios does allow us to distinguish between the two pathways, however, since it can be shown that the expected ratio for the β-H elimination-scrambling-reduction elimination process should be approximately 1 : 1 : 1 : 1 for d^0, d^1, d^7 and d^8-propane (given the *ca.* 1 : 1 ratio of C_3H_7 : C_3D_7 observed in the products) whereas kinetic isotope effects should make d^0 and d^7 the major products from a free radical process, as is observed. The fact that the d^0 : d^1 ratio (1.7) is very similar to d^7 : d^8 (1.5) is consistent with a free radical mechanism with k_H/k_D for H abstraction being *ca.* 1.6. Further support for the free radical processes arises from the fact that we have trapped free alkyl radicals and observed them by EPR spectroscopy during the liquid phase decomposition of simple tellurium alkyls such as Pr$^i_2$Te.[28,29]

For Pr$^i_2$Te, carrying out the decomposition in hydrogen increases the amount of propane relative to propene formed and decomposition of d^{14}-Pr$^i_2$Te in hydrogen produces some C_3D_7H (d^7 : d^8 ≈ 1 : 1) confirming that Pr^i· is formed and reacts with H_2. To explain the 2 : 1 ratio of propane : propene obtained in the decomposition of Pr$^i_2$Te in helium, we have proposed that Pr^i· formed from homolytic fission of the Te–C bond abstracts H· from intact Pr$^i_2$Te initiating a 'cascade' reaction that leads to 2-methylpropane, 2 × 2-methylpropene, Te and H· (Fig. 6).

Recently we have obtained further support for mechanisms of this kind from studies of Bu^{t}Se,[30–32] a precursor that has recently found favour because H_2Se leads to severe problems associated with prereactions if used with R_2M (R = Me or Et, M = Zn or Cd) to grow MSe,[33] as well as to passivation of N dopants, probably as N–H.[34] We have shown that the prereactions involve cluster growth in the gas phase leading to nucleation as nanoparticles[35–37] and have developed this chemistry into a method for synthesising polymer–nanoparticle composites of these important materials.[38–40] The replacement of H_2E (E = S or Se) by Bu^{t}EH has been partially successful in eliminating the prereaction,[41,42] although we have recently shown that a different prereaction occurs to give [Bu^{t}EMR]$_5$ which, in turn decompose on heating to give nanoparticles of ME.[43]

Bu$^t_2$Se completely removes the problem of prereaction and may reduce the problem of N–H passivation. Previous studies had suggested, on rather limited evidence, that β-H elimination might be important.[10,44] We have used both deuterium labelling and designed precursors to study the decomposition of bis-(tertiaryalkyl)selenium compounds and find that a radical mechanism is the only one that explains all of the data. The key observations from the gas phase pyrolysis of Bu$^t_2$Se in He, H_2 or D_2 in the presence or absence of d^{18}-Bu$^t_2$Se are: (i) 2-methylpropene and 2-methylpropane are formed in a 10 : 1 ratio; (ii) neither Bu^{t}SeH nor H_2S are observed, although they would be stable under the decomposition conditions; (iii) the temperature profiles of the decomposition and the 2-methylpropene : 2-methylpropane ratio are essentially the same in H_2 or He; (iv) decomposition of d^{18}-Bu$^t_2$Se in H_2 produces C_4D_9H and C_4D_{10} (ratio 2.6 : 1); (v) co-decomposition of d^0- and d^{18}-Bu$^t_2$Se produces d^0, d^1, d^9 and d^{10} 2-methylpropane in the ratio 2.29 : 1 : 2.86 : 1.2.[31,32] The failure to observe 2,2,3,3-tetramethylbutane, Bu^{t}SeH or H_2Se effectively rules out reductive elimination or β-H abstraction.

The failure to observe 2,2,3,3-tetramethylbutane together with the observation that the 2-methylpropane : 2-methylpropene ratio ≠ 1 might also indicate that the products cannot be formed from reactions of Bu^t·. However, at temperatures above 290 °C, the loss of H· from Bu^t· becomes competitive with disproportionation and combination and the proportions of both 2-methylpropane and 2,2,3,3-tetramethylbutane fall as the temperature rises.[45] This complication does not arise in the studies of Pr$^i_2$Te since these were carried out at 370 °C, whilst the loss of H· from Pr^i· is not significant below 400 °C.[27] Although the close similarity of the 2-methylpropene : 2-methylpropane ratio formed from Bu$^t_2$Se in He and H_2 suggests no involvement of the carrier gas, the formation of C_4D_9H from the decomposition of d^{18}-Bu$^t_2$Se in H_2 shows that the carrier gas can be involved.

A mechanism that would rationalise all of these observations is similar to that shown in Fig. 6 for Pr$^i_2$Te, with R· being Bu^t· or H·. In helium Se–C bond cleavage leads to Bu^t· and Bu^{t}Se· which immediately decomposes Se and a second Bu^t·. Bu^t· then abstracts H· from Bu$^t_2$Se (the highest concentration species available) to give 2-methylpropane, 2 × 2-methylpropene, Se and H· (as for Pr$^i_2$Te, see above). H· then starts a chain reaction by abstracting H· from Bu$^t_2$Se. In H_2, Bu^t· can abstract H· from intact Bu$^t_2$Se or from H_2. Either way, the product ratio will be unaffected since H· continues the chain. For Pr$^i_2$Te, the 2 : 1 ratio of 2-methylpropene : 2-methylpropane and the increase in the proportion of 2-methylpropane in hydrogen over that obtained in helium suggests that H· does not abstract H· from intact Pr$^i_2$Te in this case. Calculations have shown, however that the concerted reaction similar to that shown in Fig. 6 may not occur for Bu$^t_2$Se, at least in the gas phase, because both $Se_{(g)}$ and H· are high energy species, but rather that it occurs in a

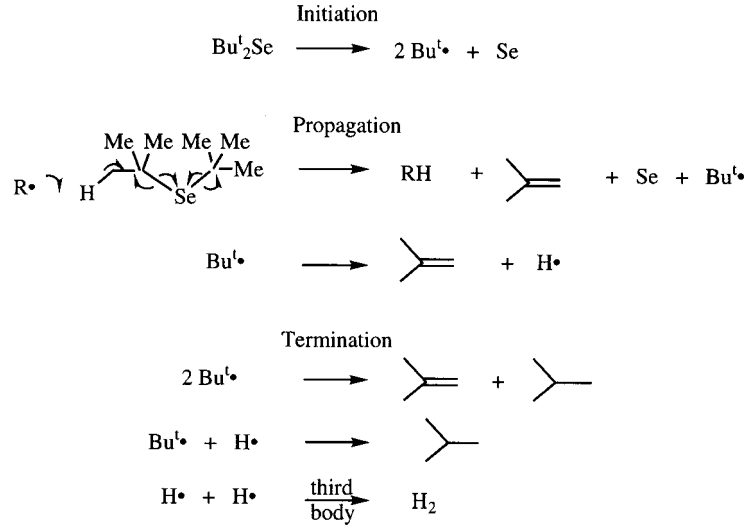

Fig. 7 Proposed mechanism for the decomposition or reaction of Bu^t_2Se [R = Bu^t·, Me· (from Me_2Zn) or H· (from decomposition of Bu^t· or from Bu^t· + H_2)].

stepwise manner (Fig. 7). This is very likely because H· loss from Bu^t· is important at these temperatures.[45] Using published and calculated activation parameters, it is possible to model all the observed results using this sequential mechanism.[32]

A sequence of reactions similar to that shown in Fig. 7, but with HS· as the chain carrier, accounts for the decomposition of Bu^tSH and it is sobering to note that this mechanism was first proposed nearly 50 years ago on the basis of careful kinetic measurements![46]

Me_2M (M = Cd or Zn) both undergo homolytic cleavage of the M–C bond, but in the absence of any other reagent the radicals recombine and the decomposition temperature is very high. In the presence of Bu^t_2Se[31,32] or Pr^i_2Te,[26] the methyl radicals abstract H·, in the case of Me_2Zn and Bu^t_2Se to initiate a chain reaction similar to that shown in Fig. 6, but with all the species except the hydrocarbons adsorbed on the surface of ZnSe. This reaction becomes accessible if surface bound, rather than free, Se and H· are formed. Surface bound H· carries the chain so that methane and 2-methylpropene are the major products. For Me_2Cd and Pr^i_2Te, similar reactions occur but radical coupling to give 2-methylpropene (Me· + Pr^i·), ethane (Me· + Me·) and 2,3-dimethylbutane (Pr^i· + Pr^i·) are also important. In this case, it is believed that Me· reacts with Pr^i_2Te by H abstraction, but also by addition to give $MeTePr^i_2$· from which Pr^i· is released, enhancing the flux of Pr^i· and forming $MeTePr^i$, which is an observed product and leads on to Me_2Te *via* Me_2Te_2.[26] Similar reactions have led us to show that $MeTe^tBu$[47] and MeTe(allyl)[48] are not good tellurium precursors because, although Te–C bond cleavage occurs at low temperature, Me_2Te is very stable so that their ability to release tellurium at low temperature is limited. Interestingly, we do not see evidence for addition of Me· to Bu^t_2E' (E′ = S or Se), presumably for steric reasons (bigger alkyl group, smaller chalcogenide). We do, however, observe small amounts of 2-methylpropane if the Me_2Zn and Bu^t_2Se are copyrolysed in hydrogen. In D_2, the 2-methylpropane is predominantly $C_4H_8D_2$ whereas Me_2Zn and d^{18}-Bu^tSe in H_2 give $C_4D_9H_2$, showing that the 2-methylpropane is a secondary product formed from the hydrogenation of 2-methylpropene, presumably catalysed by ZnSe.[31,32]

Photochemically at room temperature, Bu^t_2Se decomposes to give 2-methylpropene and 2-methylpropane (1 : 1) together with small amounts of 3,4-dimethylbutane and $Bu^t_2Se_2$. Co-photolysis of d^0- and d^{18}-Bu^t_2Se gives the same products (2-methylpropane is d^0, d^1, d^9 and d^{10}) together with d^9-Bu^t_2Se, suggesting that Bu^tSe· is stable at this temperature and that radical–radical reactions dominate. The $Bu^t_2Se_2$ is d^0 and d^{18} (no d^9 is formed) so it is formed by a concerted reaction between Bu^t_2Se and Se.[31,32]

We have also used 'reporter groups' to probe the decomposition of R_2E' and RE′H (E′ = S or Se), based on the ideas elaborated above for hex-5-enyl groups[25] but extending them to include secondary (1-methylhex-5-enyl) and tertiary (1,1-dimethylhex-5-enyl) groups.[49]

For $(hex\text{-}5\text{-}enyl)_2E'$, 50% of the products are cyclic whilst the other 50% are hexa-1,3- or -2,4-dienes. As shown in Fig. 5, the cyclic products arise from E′–C bond cleavage followed by cyclisation of the formed hex-5-enyl radicals and we have concluded that the hexadienes arise from cyclisation of (hex-5-enyl)E′· to give a six- or seven-membered ring from which the dienes are produced by an unknown mechanism.[25] Abstraction of H from intact $(hex\text{-}5\text{-}enyl)_2E'$ by cyclohexyl or cyclopentyl methyl radicals, analogous to the reactions proposed for the decomposition of Bu^t_2Se or Pr^i_2Te, does not appear to be important since we largely see cyclohexene and methylenecyclopentene from *loss* of H· from the radicals. This may be rationalised because the primary alkyl groups have only a small number of β-H atoms available for abstraction. The presence of primary alkyl groups and/or the ability of (hex-5-enyl)E′· to cyclise might also explain the stability of (hex-5-enyl)E·, the similarity in the product distribution for E′ = S or Se and the high decomposition temperature of these alkyls. Reducing the number of β-H atoms reduces the probability of reaction between (hex-5-enyl)E′· and $(hex\text{-}5\text{-}enyl)_2E'$ and radical radical reactions must then become more important, thus also contributing to the higher decomposition temperatures. For (hex-5-enyl)SH, the majority of the products are the hexa-2,3- and -3,4-dienes suggesting that, in this case, S–H bond cleavage is important.

Using a similar approach but designing the hexenyl group so that it has a tertiary C atom attached to the chalcogenide, *i.e.* 1,1-dimethyhex-5-enyl (hex′), the dialkyl compounds are too involatile for gas phase studies, but we have studied the decomposition of MeE(hex′) (E = Se or Te).[49] In both cases the major hydrocarbon products are unsaturated cyclic hydrocarbons, with smaller amounts of 2-methylhepta-1,6- and -1,5-diene. (These products are more important for E = Se.) The cyclic hydrocarbons mainly contain six-membered rings, but some of them do not contain the expected geminal dimethyl group. We assume that these are secondary products caused by rearrangements at the high temperatures involved in this study. For the tellurium compound, products in which the cyclised radicals add back to MeTe· are also observed together with Me_2Te_2 and Me_2Te. The Se containing products are Me_2Se_2, Me_2Se and MeSeH. All the hydrocarbon products can be rationalised by a decomposition mechanism involving E–C

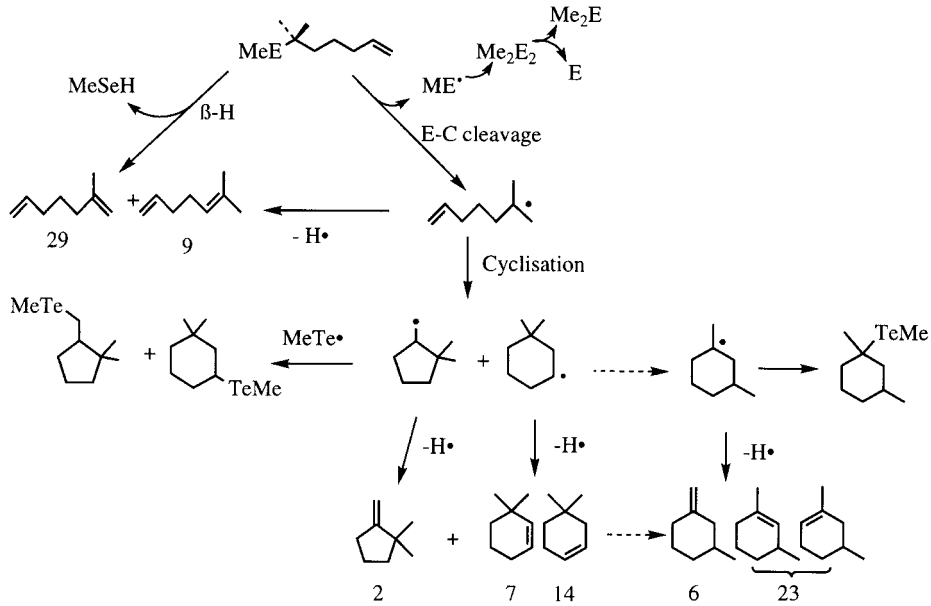

Fig. 8 Proposed mechanism for the decomposition of (1,1-dimethylhex-5-enyl)MeE (E = Se or Te). The dashed arrows indicate tentative rearrangements. Numbers shown are % of hydrocarbon products for E = Se at 450 °C in He (10% of an unknown product was also observed). For E = Te, the ratios are similar, except that much less of the straight chain products are observed indicating that β-H elimination is not important for E = Te.

cleavage followed by loss of H· from the 2-methylhept-6-en-2-yl radical before or after cyclisation (Fig. 8). However, the larger amounts of straight chain products obtained when E = Se and the observation of MeSeH show that in this case, β-H abstraction is a competing process, although its importance decreases as the temperature is raised. There is no evidence for abstraction of H from intact MeE(hex′) by any of the radicals since this would lead to saturated cyclic or monounsaturated straight chain products. None are observed. This is presumably because H· loss from these bulky radicals is expected to be dominant at the high temperatures of this study, by analogy with the reactivity of Bu^{t}·.[45]

Conclusions

Labelled and specially designed analogues of precursors are capable of giving high quality information about the processes that occur during MOVPE reactions. For primary arsines, these studies together with semi-empirical calculations show that reductive elimination of H_2 is the first step and that gas-phase adducts are not important in the reaction chemistry. For Group 16 precursors, homolytic cleavage of the C–E bond (E = S, Se or Te) occurs and detailed product analyses, especially when using labelled precursors give mechanistic details about susbequent steps in the reactions. These types of studies allow new precursors with better properties for *e.g.* low temperature growth to be designed.[50]

Acknowledgements

I thank all the authors whose names appear in the list of references, but especially Doug Foster, a fine experimentalist and constant source of ideas; Brian Mullin and Janet Hails (DERA) with whom I have had countless fruitful discussions and who (Janet Hails) did many painstaking GCMS studies and Chris Glidewell and Nick Maung who have underpinned our wilder speculations by careful calculations. I am also indebted to the funding agencies, DERA and EPSRC and their pregenitors without whose help this work would not have been possible.

Notes and references

1 P. Zanella, G. Rossetto, F. Ossola, M. Porchia and J. O. Williams, *Chem. Mater.*, 1991, **3**, 225.
2 *Metal Organic Vapour Phase Epitaxy 1996*, ed. J. B. Mullin, *J. Cryst. Growth*, 1997, **104**, and references therein.
3 H. M. Manasevit, *Appl. Phys. Lett.*, 1968, **12**, 156.
4 H. M. Manasevit and W. I. Simpson, *J. Electrochem. Soc.*, 1971, **118**, 644.
5 R. M. Lum and J. K. Klingert, *J. Cryst. Growth*, 1991, **107**, 290.
6 D. J. Cole-Hamilton, *Chem. Br.*, 1990, **26**, 852.
7 M. E. Pemble, in *Mechanisms of Reactions of Organometallic Compounds with Surfaces*, ed. D. J. Cole-Hamilton and J. O. Williams, Plenum, New York, 1989, p. 145.
8 J. S. Foord, C. L. French, C. L. Levoguer, G. J. Davies and P. J. Skevington, *Semiconduct. Sci. Technol.*, 1993, **8**, 959.
9 J. E. Hails, *Adv. Mater. Opt. Electron.*, 1994, **3**, 151.
10 G. H. Fan, N. Maung, T. L. Ng, P. F. Heelis, J. O. Williams, A. C. Wright, D. F. Foster and D. J. Cole-Hamilton *J. Cryst. Growth*, 1997, **170**, 485.
11 S. H. Li, C. A. Larsen, N. I. Buchan, G. B. Stringfellow, W. P. Kosar and D. W. Brown, *J. Appl. Phys.*, 1989, **65**, 5161 and references therein.
12 R. H. Marking, W. L. Gladfelter and K. F. Jensen, *Chem. Mater.*, 1990, **2**, 499.
13 D. F. Foster, C. Glidewell and D. J. Cole-Hamilton, *Appl. Phys. Lett.*, 1993, **63**, 57.
14 D. F. Foster, C. Glidewell and D. J. Cole-Hamilton, *J. Electron. Mater.*, 1994, **23**, 69.
15 D. F. Foster, C. Glidewell, G. R. Woolley and D. J. Cole-Hamilton, *J. Electron. Mater.*, 1995, **24**, 1731.
16 D. F. Foster, C. Glidewell and D. J. Cole-Hamilton, *Appl. Phys. Lett.*, 1993, **63**, 214.
17 D. F. Foster, C. Glidewell, D. J. Cole-Hamilton, I. M. Povey, R. D. Hoare and M. E. Pemble, *J. Cryst. Growth*, 1995, **145**, 104.
18 R. D. Hoare, M. E. Pemble, I. M. Povey, J. O. Williams, D. F. Foster, C. Glidewell and D. J. Cole-Hamilton, *J. Cryst. Growth*, 1994, **137**, 347.
19 D. Griller and K. U. Ingold, *Acc. Chem. Res.*, 1980, **13**, 137.
20 A. S. Gordon and S. R. Smith, *J. Phys. Chem.*, 1962, **66**, 521.
21 J. E. Hails, I. Girling and D. R. Stern, *Mater. Res. Soc. Symp. Proc.*, 1991, **204**, 155.
22 J. Stevenson, W. Bell, J. Ferry, D. J. Cole-Hamilton and J. E. Hails, *J. Organomet. Chem.*, 1993, **449**, 141.
23 H. Lemkuhl, I. Döring and H. Nehr, *J. Organomet. Chem.*, 1981, **221**, 7.
24 W. Bell, E. A. D. McQueen, J. C. Walton, D. F. Foster and D. J. Cole-Hamilton, *J. Cryst. Growth*, 1992, **117**, 58.
25 D. F. Foster, W. Bell, J. Stevenson, D. J. Cole-Hamilton and J. E. Hails, *J. Cryst. Growth*, 1994, **145**, 520.
26 W. Bell, J. Stevenson, D. J. Cole-Hamilton and J. E. Hails, *Polyhedron*, 1994, **13**, 1253.
27 J. A. Kerr and A. F. Trotman-Dickenson, *Trans. Faraday Soc.*, 1969, **55**, 921.

28 W. Bell, D. J. Cole-Hamilton, P. N. Culshaw, A. E. D. McQueen, D. V. Shenai-Khatkhate, J. C. Walton and J. E. Hails, *J. Organomet. Chem.*, 1992, **430**, 43.
29 A. E. D. McQueen, P. N. Culshaw, J. C. Walton, D. V. Shenai-Khatkhate, D. J. Cole-Hamilton and J. B. Mullin, *J. Cryst. Growth*, 1991, **107**, 325.
30 D. F. Foster, N. L. Pickett and D. J. Cole-Hamilton, *Silicon, Phosphorus Sulfur*, 1998.
31 N. L. Pickett, D. F. Foster and D. J. Cole-Hamilton, *Proc. Electrochem. Soc. Conf.*, 1998, in press.
32 N. L. Pickett, D. F. Foster, D. Ellis, N. Maung, J. E. Hails and D. J. Cole-Hamilton, *J. Mater. Chem.*, to be submitted.
33 P. J. Wright, B. Cockayne, P. J. Parbrook, P. E. Oliver and A. C. Jones, *J. Cryst. Growth*, 1991, **108**, 525 and references therein.
34 A. Kamata, M. Mitsuhashi and H. Fujita, *Appl. Phys. Lett.*, 1993, **63**, 3353.
35 N. L. Pickett, D. F. Foster and D. J. Cole-Hamilton, *J. Mater. Chem.*, 1996, **6**, 507.
36 N. L. Pickett, D. F. Foster and D. J. Cole-Hamilton, *J. Cryst. Growth*, 1997, **170**, 476.
37 N. L. Pickett, F. G. Riddell, D. F. Foster, D. J. Cole-Hamilton and J. R. Fryer, *J. Mater. Chem.*, 1997, **7**, 1855.
38 X. Li, J. R. Fryer and D. J. Cole-Hamilton, *J. Chem. Soc., Chem. Commun.*, 1994, 1715.
39 S. W. Haggata, X. Li, D. J. Cole-Hamilton and J. R. Fryer, *J. Mater. Chem.*, 1996, **6**, 1771.
40 S. W. Haggata, D. J. Cole-Hamilton and J. R. Fryer, *J. Mater. Chem.*, 1997, **7**, 1969.
41 D. N. Armitage, H. M. Yates, J. O. Williams, D. J. Cole-Hamilton and I. L. J. Patterson, *Adv. Mater. Opt. Electron.*, 1992, **1**, 43.
42 D. F. Foster, I. L. J. Patterson, L. D. James, D. J. Cole-Hamilton, D. N. Armitage, H. M. Yates, A. C. Wright and J. O. Williams, *Adv. Mater. Opt. Electron.*, 1994, **3**, 163.
43 N. L. Pickett, S. Lawson, W. G. Thomas, F. G. Riddell, D. F. Foster, D. J. Cole-Hamilton and J. R. Fryer, *J. Mater. Chem.*, 1998, **8**, 2769.
44 W. S. Kuhn, R. Helbing, B. Qu'Hen and O. Gorochov, *J. Cryst. Growth*, 1995, **146**, 580.
45 R. N. Birrell and A. F. Trotman-Dickenson, *J. Chem. Soc.*, 1960, 4218.
46 C. G. Thompson, R. A. Meyer and J. S. Ball, *J. Am. Chem. Soc.*, 1952, **74**, 3284.
47 J. E. Hails, D. J. Cole-Hamilton and W. Bell, *J. Cryst. Growth*, 1994, **145**, 596.
48 J. E. Hails, D. J. Cole-Hamilton and A. E. D. McQueen, *J. Cryst. Growth*, 1998, **183**, 594.
49 D. F. Foster, J. E. Hails and D. J. Cole-Hamilton, unpublished observations.
50 W. Bell, J. Stevenson, J. E. Hails, D. Ellis and D. J. Cole-Hamilton, unpublished observations.

Paper 9/00115H

ChemComm

Morphosynthesis of macrocellular mesoporous silicate foams

Stephen A. Bagshaw

Advanced Materials Group, Industrial Research Limited, PO Box 31-310, Lower Hutt, New Zealand.
E-mail: s.bagshaw@irl.cri.nz

Received (in Cambridge, UK) 23rd February 1999, Accepted 23rd March 1999

Silicate macroskeletons which have both templated mesoporosity and open-cell macrovoid structures have been prepared in monolithic form at near ambient temperatures from continuous metastable foams of non-ionic alkylpolyethylene oxide surfactants under aqueous, neutral pH reaction conditions.

The controlled synthesis of inorganic frameworks exhibiting very large pores and complex macroscale forms is an area of intense scientific and technological effort for potential applications in catalysis, molecular sieving and biomaterials.[1] Assemblies of both charged and uncharged amphiphilic molecules are known to interact with inorganic precursors to form complex architectures in the inorganic phase.[2,3] However, void size control of such porous compositions has generally been restricted to the micro- and meso-scales between 0.3 and 30 nm diameter.[4,5] Recent work by the groups of Ozin, Stucky and Mann have produced materials that display porosity and morphology on the supermeso- and macro-scales.[6–8] Ozin reported the morphosynthesis of SBA-2 materials into complex rod, disc, swirl and top shapes,[6] while Stucky described the templating and shaping of supermesoporous oxides.[7] The morphosynthesis of silica and calciferous materials displaying open skeletal frameworks have been reported by Mann and coworkers.[8] The voids created by the amorphous silica, calcium phosphate or carbonate skeletons are of the order of micrometres and thus begin to approach structures with void dimensions and compositions desirable for bioceramic applications.[9] Possible technological drawbacks of these materials are that they are obtained as precipitated particles, the solid phases are non-porous and that they are synthesised in frozen, complex bicontinuous microemulsions over long reaction times. The use of biliquid foam structures to prepare transition metal oxide films from super-saturated precursor solutions has also been reported.[10] Ceramic foams of various metal oxide compositions are well known in industrial applications and are generally prepared by slurry coating a ceramic powder, for example alumina and zirconia, onto the surface of a fibrous polymer support which is then removed through calcination.

In an effort to simplify the microemulsion synthesis system and to produce materials with larger macrovoids, we replaced the unstable biliquid microemulsion with a metastable surfactant foam system. This was with the goal of replicating, in an inorganic silica phase, the three dimensional macrostructured foam under ambient and benign reaction conditions. Here we describe the sol–gel synthesis of novel silica and metallosilicate materials that exhibit both open macroporous skeletal networks of amorphous silica and templated mesoporosity within the solid skeleton. These novel macrostructured mesoporous silica foam materials, which we label MMSF, are formed directly from tetraethoxyorthosilicate (TEOS) or TEOS plus a basic metal salt, solubilised within the water-rich film of an alkylpolyethylene oxide (PEO) based nonionic surfactant foam.[11] The reaction conditions are almost identical to those previously reported for [Si]- and [M]-MSU-X mesostructure syntheses.†[12,13] The appearance of these products suggests that void size control over length scales[14] of differing orders of magnitude can be achieved in a single, simple synthesis medium. The MMSFs have added novelty over most existing macrostructured materials in that they can be formed in monolithic shapes with, in principle, no limit to their dimensions.

X-Ray diffraction (XRD) patterns‡ of the hydrothermally treated and calcined MMSFs (Fig. 1) exhibit single peak d_{100} reflections at low angle. No higher angle reflections and hence long-range symmetry were indicated, suggesting that the solid part of the MMSF material is amorphous with a regular repeating pore motif. The single reflection XRD patterns are identical to those obtained from [M]-MSU-X mesostructures and thus suggest that a pore structure exists that is similar to the three dimensional disordered worm-like pore arrays exhibited by [M]-MSU-X materials.[13–15] Nitrogen sorption isotherms‡ of hydrothermally treated/calcined monolithic samples indicate the presence of well defined large mesopores. The adsorption branch displays a strong capillary condensation step indicative of mesopores with well defined diameters (Fig. 2) while the desorption branch exhibits some hysteresis as a result of the high partial pressure of adsorption. We therefore conclude that the solid silicate phase that makes up the MMSF material, is itself mesoporous and furthermore, the analytical data indicate that the solid skeleton of MMSF is at the mesoscopic level, identical to hydrothermally treated [M]-MSU-X powders[15] exhibiting surface areas between 800 and 900 $m^2\ g^{-1}$, pore volumes of *ca.* 1.0 mL g^{-1} and pore diameters between 20 and 40 nm depending upon template dimensions, synthesis temperatures and length of hydrothermal treatment. Optical photographs‡ of sections of MMSF monoliths display the macrovoid nature of the MMSF materials that distinguish them from exisiting [M]-MSU-X materials which are produced only as powders. These images suggest that a true macrostructured skeletal material is assembled from both skeleton-like silica filaments or struts [Fig. 3] and surface-like structures and not agglomerations of silica particles. The open-cell nature of the MMSF was demonstrated by the absorption of a brightly

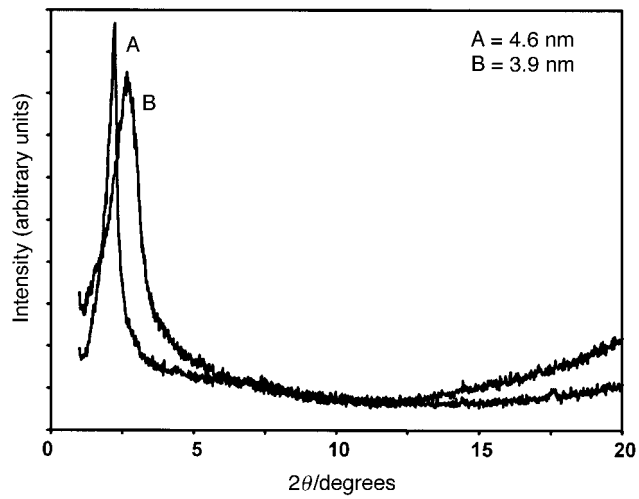

Fig. 1 XRD patterns of a representative macrostructured mesoporous silica foam MMSF prepared from Triton N-101 surfactant. (A) after hydrothermal treatment for 72 h, (B) hydrothermally treated and calcined at 600 °C 4 h in air.

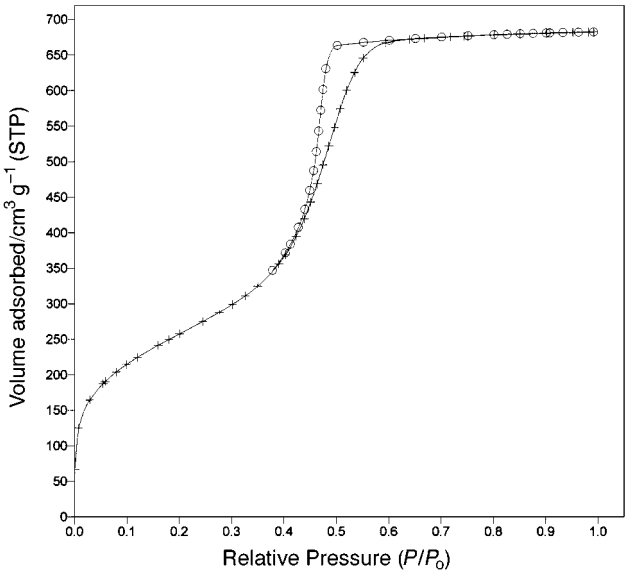

Fig. 2 Nitrogen sorption isotherms of MMSF after hydrothermal treatment and calcination; (+) adsorption, (○) desorption.

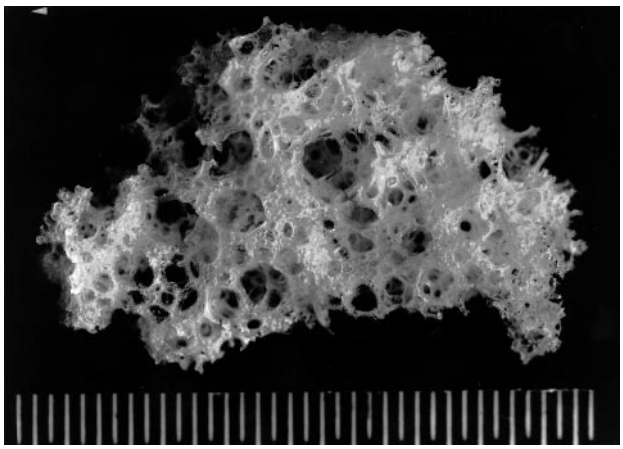

Fig. 3 Optical photograph of hydrothermally treated and calcined MMSF exhibiting macrocellular form. Scale divisions are 0.5 mm.

coloured aqueous dye solution into a monolithic sample *via* capillary action. The photographs presented indicate that the macrovoids range in diameter from hundreds of microns to 1–2 mm, the smaller end of this scale being ideal for application in artificial bioceramic bone implant technologies.[9] Currently the MMSF materials are brittle and exhibit only limited fracture resistance. Improvement of the compressive and tensile strengths is being pursued.

A perhaps surprisingly simple mechanism of formation of the MMSFs is proposed. Minimum surface spherical bubbles make up the surfactant foam, their diameters being determined by the rate and mode of agitation of the surfactant emulsion. Upon TEOS addition, the water immiscible $Si(OC_2H_4)_4$ monomers are progressively solubilised through hydrogen bonding between the surfactant PEO head-group of micelle structures and the alkoxide species. The PEO micellar corona solvates the TEOS monomers, transports them throughout the foam film and the strong H-bonding therein induces polarisation of the Si–OR bond and subsequent hydrolysis and condensation.[12] In the initial stages of reaction the rate of film drainage is high and no stable foam results. As hydrolysis and condensation of the TEOS proceed, the viscosity within the foam film increases and drainage from the film slows, allowing a stable, interconnected open cell foam to be maintained.[16]

The synthesis route described here is very simple, low cost, environmentally benign and able to be modified in many ways so that varied product engineering is possible. Development of the MMSF structures, compositions and physical properties is continuing. The author thanks Industrial Research Ltd. for funding through the Non-Specific Output Fund as part of a contract with the New Zealand Foundation for Research, Science and Technology.

Notes and references

† *Experimental*: in a typical MMSF synthesis, TEOS is added to a dilute 5–10 wt% solution of a non-toxic, inexpensive non-ionic surfactant (*e.g.* Triton N-101 nonyl-PEO_{10}), at 24–30 °C and at neutral pH. Metallosilicate analogues may be prepared by adding a basic metal salt solution [*e.g.* $Al_2(SO_4)_3$, $TiOSO_4$, $ZrOCl_2$, $VOSO_4$] to the TEOS, before addition to the surfactant emulsion. This causes pre-hydrolysis of the TEOS and formation of water soluble Si–O–M units.[14] In the step that separates [M]-MSU-X synthesis from MMSF synthesis, the surfactant/TEOS emulsion is then stirred rapidly at 750–1000 rpm with a magnetic stirrer whose length is 60–75% of the width of the reaction vessel thereby creating turbulence within the vessel. Hydrolysis of the TEOS is catalysed by hydrogen bonding with the PEO[13] surfactant headgroup. As this hydrolysis proceeds spherical bubbles aggregate to form an organic/inorganic composite foam which adopts the dimensions of the reaction vessel. After 16–24 h, stirring is arrested and the foam composite is allowed to age under static conditions for 24–48 h. The solid foam monolith that results may then be removed from the vessel and dried, taking care to avoid cracking caused by drying too quickly. The as-prepared MMSFs may then be hydrothermally treated at 100–150 °C and/or calcined at 450 °C for 4 h in air to yield an inorganic silicate foam. Calcination without hydrothermal treatment invariably induces cracking in the MMSF monoliths. Hydrothermal treatment[15] improves the cross-linking within the amorphous silica, the mesopore diameters and also the fracture resisitance. MMSF yields are typically 80–90% in Si while the remainder of the SiO_2 is retrieved as precipitated templated [M]-MSU-X. Foam bubble sizes and hence final macrovoid dimensions may be modified by changing the turbulence within the reaction vessel. This can be achieved by moderation of the stirring speed or by substituting different shaped magnetic stirrer followers and is the subject of continued investigation.

‡ *Characterisation*: XRD patterns were measured on a Philips PW 1700 series APD diffractometer equipped with an automatic variable divergence slit and Co-Kα radiation (λ = 0.179026 nm). Nitrogen sorption isotherms were obtained with a Micromeritics ASAP 2010 sorptometer at −196 °C. Surface areas were calculated using the BET model while pore size distributions were calculated using the BJH model. Optical photographs were obtained with a Nikon Multiphot type A camera equipped with a 65 mm Macro Nikkor lens using incident lighting and T-Max 100 black and white film.

1 S. Mann and G. A. Ozin, *Nature*, 1996, **273**, 768.
2 C. T. Kresge, M. E. Leonowicz, W. J. Roth, J. C. Vartuli and J. S. Beck, *Nature*, 1992, **359**, 710.
3 C. G. Guizard, A. C. Julbe and A. Ayral, *J. Mater. Chem.*, 1999, **9**, 55.
4 D. W. Breck, *Zeolite Molecular Sieves*, J. W. Wiley and Sons, New York, 1974.
5 A. Corma, *Chem. Rev.* 1997, **97**, 2373.
6 H. Yang, N. Coombs and G. A. Ozin, *Nature*, 1997, **386**, 692.
7 P. Yang, T. Deng, D. Zhao, P. Feng, D. Pine, B. F. Chmelka, G. M. Whitesides and G. D. Stucky, *Science*, 1998, **282**, 2244.
8 S. D. Sims, D. Walsh and S. Mann, *Adv. Mater.*, 1998, **10**, 151.
9 *An Introduction to Bioceramics*, ed. L. L. Hench and J. Wilson, Advanced Series in Ceramics Vol 1., World Scientific, Singapore, vol. 1, 1993.
10 S. Mann, S. L. Burkett, S. A. Davis, C. E. Fowler, N. H. Mendelson, S. D. Sims, D. Walsh and N. T. Wilton, *Chem. Mater.*, 1997, **9**, 2300.
11 M. R. Porter, *Handbook of Surfactants*, Chapman and Hall, New York, 2nd edn., 1994.
12 S. A. Bagshaw, T. Kemmitt and N. B. Milestone, *Microporous Mesoporous Mater.*, 1998, **22**, 419.
13 S. A. Bagshaw, E. Prouzet and T. J. Pinnavaia, *Science*, 1995, **269**, 1242.
14 P. Schmidt-Winkel, W. W. Lukens Jr., D. Zhao, P. Yang, B. F. Chemlka and G. D. Stucky, *J. Am. Chem. Soc.*, 1999, **121**, 254.
15 S. A. Bagshaw, *Chem. Commun.*, 1999, **271**.
16 P. Boltenhagen and N. Pittet, *Europhys. Letts.*, 1998, **41**, 571.

Communication 9/01480B

A heterodinuclear macrocyclic complex containing both nickel(II) and palladium(II) ions

Przemysław Starynowicz and Jerzy Lisowski*

Department of Chemistry, University of Wrocław, 14 F. Joliot-Curie, 50-383 Wrocław, Poland.
E-mail: jurekl@wchuwr.chem.uni.wroc.pl

Received (in Cambridge, UK) 4th Febuary 1999, Accepted 16th March 1999

The first heterodinuclear macrocyclic Schiff base complex containing both first- and second row transition metal ions, $[NiPdL](ClO_4)_2\cdot 3MeCN$ has been synthesised and characterised by spectroscopic methods; the X-ray structure of this complex and its mononuclear precursor are reported.

The first macrocyclic dinuclear complexes $[M_2L]^{2+}$ {where H_2L is the macrocyclic Schiff base ligand (Fig. 1) 11,23-dimethyl-3,7,15,19-tetraazatricyclo[19.3.1.1^{19,13}]hexacosa-2,7,9,11,13(26),14,19,21(25),22,24-decaene-25,26-diol and $M^1 = M^2 = Mn^{2+}$, Fe^{2+}, Co^{2+}, Ni^{2+}, Cu^{2+} ord Zn^{2+}} were synthesised in a direct template 2+2 condensation of 2,6-diformyl-4-methylphenol and 1,3-diaminopropane by Robson and Pilkington[1] and by Okawa and Kida[2] in a stepwise synthesis. More recently, the first examples of homodinuclear complexes of the ligand L^{2-} with second- and third-row transition metal ions have been reported.[3]

Apart from homodinuclear complexes, the analogous heterodinuclear ($M^1 \neq M^2$) complexes have also been synthesised in stepwise syntheses starting from non-cyclic precursors.[4] This synthetic strategy often utilises the difference in the coordination preferences of the two metal ions by using two different diamine fragments in the left and right side of the macrocyclic system. Both homo- and hetero-dinuclear complexes of L^{2-} and related ligands have proved to be very useful in studying magnetic coupling phenomena, mimicking bimetalic metalloenzymes, investigating mixed-valence systems *etc.*,[4–6]

Here, we report the synthesis, spectroscopic characterisation and X-ray crystal structure of the mixed nickel(II)–palladium(II) complex $[NiPdL](ClO_4)_2\cdot 3MeCN$. To the best of our knowledge this is the first example of a heterodinuclear macrocyclic complex containing both first- and second-row transition metal ions. We present also the X-ray crystal structure of the mononuclear complex $[Ni(H_2L](ClO_4)_2\cdot 2MeOH$[1] which is the precursor in the synthesis of the mixed $Ni^{II}Pd^{II}$ complex and other heterodinuclear complexes.[7]

The starting complex $[Ni(H_2L)](ClO_4)_2\cdot H_2O$ was obtained as described in ref. 1. $[NiPdL](ClO_4)_2\cdot 3MeCN$† was obtained by reacting $[NiH_2L](ClO_4)_2\cdot H_2O$ with palladium(II) acetate in acetonitrile, in a similar fashion to related heterodinuclear complexes containing two first row metal ions[7]. This synthetic strategy is remarkably simple compared to the stepwise syntheses of related heterodinuclear macrocyclic complexes. Moreover, our attempts to obtain the $[NiPdL]^{2+}$ complex in alternative stepwise syntheses starting from the non-cyclic *N*,*N*′-propylenebis(3-formyl-5-methylsalicylideneaminato)-nickel(II) or -palladium(II) complexes, although while leading to the desired heterodinuclear systems as judged from spectroscopic data, have not yielded pure products so far.

^{1}H NMR and electrospray MS spectra confirm the heterodinuclear nature of the obtained complex and show that no scrambling of metal ions takes place during the synthesis. The ESMS of $[NiPdL](ClO_4)_2\cdot 3MeCN$ shows signals with a maximum at *m/z* 667.3 corresponding to $[NiPdL](ClO_4)^+$ and at *m/z* 282.9 corresponding to $[NiPdL]^{2+}$. The large isotropic shifts observed for the ^{1}H NMR spectra of $[NiPdL](ClO_4)_2\cdot 3MeCN$ in D_2O or CD_3OD solutions are in accord with the presence of high-spin Ni^{II}. The signal assignment was based on the intensity, expected shift values, linewidth analysis and comparison with the spectra[7] of $[Ni(H_2L)](ClO_4)_2\cdot H_2O$ and $[Ni_2L]Cl_2\cdot 2H_2O$. Protons **a**, **b**, **d**, **e**, **h** and **i** resonate at δ −6.17, 119.2, 9.77, 3.06, 6.32 and 2.75, respectively (see Fig. 1 for labelling scheme). The signals at δ 24.34 and 11.55 correspond to positions **f** and **g** or *vice versa*, while the signal of proton **c**, expected in the region δ 250–450 region, is too broad to be

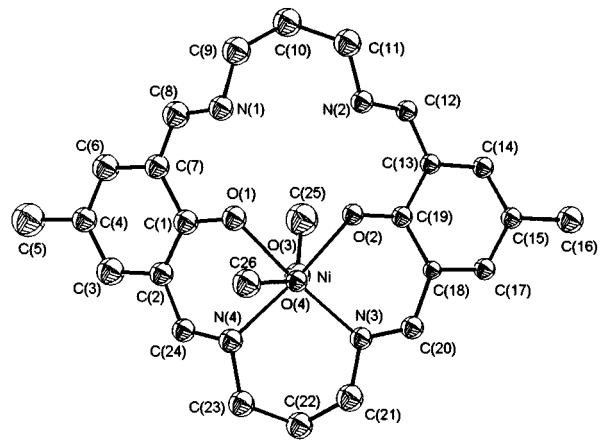

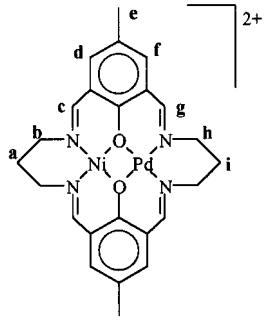

Fig. 1 The labelling scheme of the ligand L^{2-} in the $[NiPdL]^{2+}$ complex (axial ligands omitted).

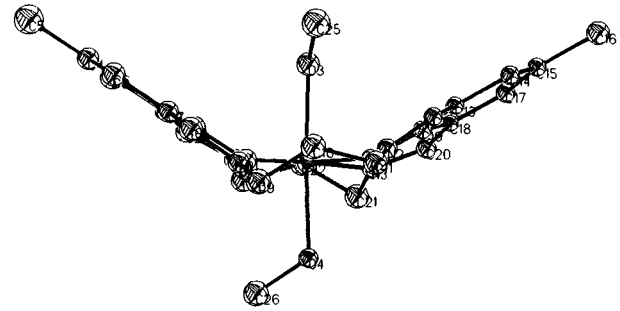

Fig. 2 Top and side view of the $[Ni(H_2L)(MeOH)_2]^{2+}$ complex cation together with atom labels.

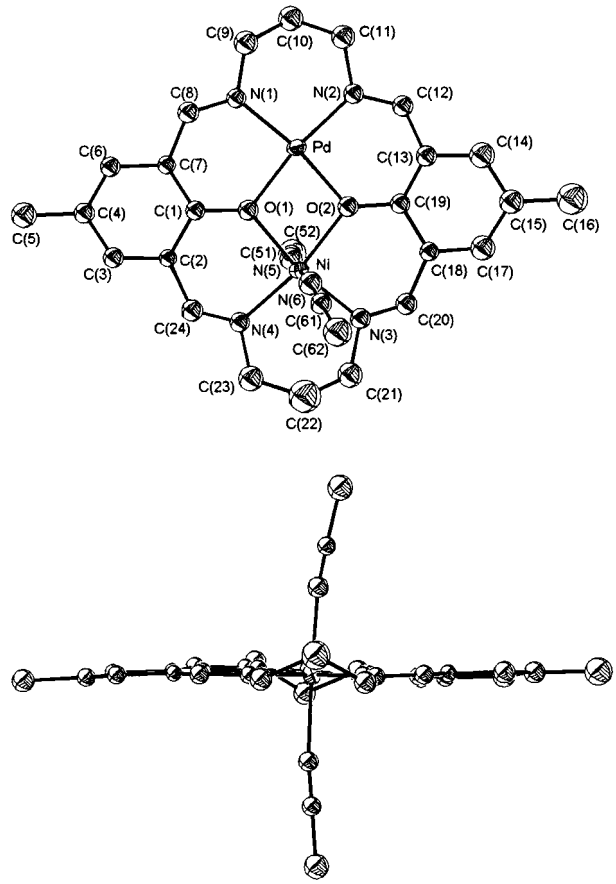

Fig. 3 Top and side view of the $[NiPdL(MeCN)_2]^{2+}$ complex cation together with atom labels.

detected. As expected, the protons that are three or four bonds away from the paramagnetic Ni^{II} ion exhibit relatively large isotropic shifts. On the other hand the protons that belong to the methyl group and the Pd^{II}-complexed side of the ligand experience smaller isotropic shifts due to less effective spin delocalisation.

Crystals of $[Ni(H_2L)](ClO_4)_2\cdot 2MeOH$ were obtained by diffusion of diethyl ether into methanol solution of $[Ni(H_2L)](ClO_4)_2\cdot H_2O$ and crystals of $[NiPdL](ClO_4)_2\cdot 3MeCN$ were grown from acetonitrile.‡ The complex cation in $[Ni(H_2L)](ClO_4)_2\cdot 2MeOH$ (Fig. 2) is composed of the macrocyclic ligand bonded to Ni^{II} with four of its ligating atoms [two O and two N atoms; Ni–O(1) 2.013(11), Ni–N(3) 2.017(13), Ni–O(2) 2.022(10), Ni–N(4) 2.040(13) Å]. The two remaining coordination sites of Ni^{II} are occupied by two methanol molecules [Ni–O(4) 2.101(10), Ni–O(3) 2.156(11) Å], leading to a slightly distorted octahedron around the metal ion. In $[NiPdL](ClO_4)_2\cdot 3MeCN$ the macrocyclic ligand binds two metal ions, Ni^{II} and Pd^{II} (Fig. 3). Both phenyl oxygen atoms, unlike in the case of $[Ni(H_2L)](ClO_4)_2\cdot 2MeOH$, are deprotonated. The octahedral coordination of Ni^{II} cation is completed by two acetonitrile molecules [Ni–N(4) 2.002(15), Ni–N(3) 2.003(14), Ni–O(2) 2.035(12), Ni–O(1) 2.037(11), Ni–N(5) 2.09(2), Ni–N(6) 2.10(2) Å], whereas the Pd^{II}) environment forms a slightly distorted square [Pd-N(1) 1.990(14), Pd-O(2) 1.997(11), Pd-N(2) 2.000(13), Pd-O(1) 2.012(11) Å]. The presence of Pd^{II} changes the overall conformation of the macrocycle. In $[NiPdL](ClO_4)_2\cdot 3MeCN$ the ligand adopts a planar conformation similar to that observed in other crystallographically characterised $[M_2L]^{n+}$ complexes.[3a,6] The angle between two flat fragments of the ligand [C(1)C(2)C(3)C(4)C(5)C(6)C(7)C(8)C(24)O(1)N(1)N(4) and C(12)C(13)C(14)C(15)C(16)C(17)C(18)C(19)C(20)O(2)N(2)-N(3)] is 177.4°. In contrast, in $Ni(H_2L)](ClO_4)_2\cdot 2MeH$ (Fig. 3) the ligand is considerably bent with the above mentioned planes forming the angle of 115.9°. However, this bending of the ligand is not as profound as that observed in the completely bent conformation of the protonated free ligand[3a] (phenyl rings almost parallel).

In principle, the unique combination of macrocyclic environment and different reactivities of the first- and second-row metal complexes may lead to new catalytic systems. Presently we are investigating the catalytic properties of $[NiPdL](ClO_4)_2\cdot 3MeCN$ and related complexes.

This work was supported by KBN grant 3 T09A 071 12.

Notes and references

† The complex has been characterised by elemental analysis, IR and UV-VIS spectroscopy

‡ *Crystal data:* the crystals chosen for the data collection were placed in Lindemann glass capillaries and then mounted on a Kuma KM4 diffractometer. The intensities of three standards were monitored every 100 reflections. During measurement both crystals partially decomposed. The final loss of intensity was 57% for $[NiPdL](ClO_4)_2\cdot 3MeCN$ and 79% for $[Ni(H_2L)](ClO_4)_2\cdot 2MeOH$. The structures were solved using Patterson methods with SHELXS-86, and then refined with SHELXL-93. The C-bonded hydrogen atoms were placed in geometrically calculated positions. As both crystals were poor scatterers, and the data/parameters ratios were unfavourable, the anisotropic thermal vibration parameters were applied to metal and chlorine atoms only, the other atoms being refined isotropically. The temperature factors for H atoms were set as 1.2 times the factors of the C atoms to which the relevant H atoms were bonded. For $[NiPdL](ClO_4)_2\cdot 3MeCN$ it was found that the oxygen atoms of the perchlorate anions and a part of the solvent (acetonitrile) molecules were disordered. The respective site occupation factors were assumed to be 0.5. a)

$[Ni(H_2L)](ClO_4)_2\cdot 2MeOH$: $C_{26}H_{36}Cl_2N_4NiO_{12}$, M = 726.20, triclinic, $P\bar{1}$, a = 9.789(2), b = 11.737(2), c = 14.795(3) Å, α = 92.05(3), β = 99.19(3), γ = 107.00(3)°, V = 1598.6(5) Å^3, Z = 2, T = 293(2) K, μ = 0.840 mm^{-1}, number of reflections measured = 2270, number of observed reflections [$I \geqslant 3\sigma(I)$] = 1466, $R(F)$ = 0.0707, $R_w(F^2)$ = 0.1352.

$[NiPdL](ClO_4)_2\cdot 3MeCN$: $C_{30}H_{35}Cl_2N_7NiO_{10}Pd$, M = 889.66, monoclinic, $P2_1/c$, a = 16.627(3), b = 19.701(4), c = 10.951(2) Å, β = 91.35(3)°, V = 3586.2(12) Å^3, Z = 4, T = 293(2) K, μ = 1.239 mm^{-1}, number of reflections measured = 3308, number of reflections observed [$I \geqslant 3\sigma(I)$] = 1837, $R(F)$ = 0.0673, $R_w(F^2)$ = 0.1243.

CCDC 182/1198. See http://www.rsc.org/suppdata/cc/1999/769/ for crystallographic files in .cif format.

1 N. H. Pilkington and R. Robson, *Aust. J. Chem.*, 1970, **23**, 2225.
2 H. Okawa and S. Kida, *Bull. Chem. Soc. Jpn.*, 1972, **45**, 1759.
3 (*a*) A. J. Atkins, A. J. Blake and M. Schröder, *J. Chem. Soc., Chem. Commun.*, 1993, 353; (*b*) A. J. Atkins, D. Black, A. J. Blake, A. Marin-Becerra, L. Ruiz-Ramirez and M. Schröder, *Chem. Commun.*, 1996, 457.
4 See, for example: R. R. Gagne, C. L. Spiro, T. J. Smith, C. A. Hamann, W. R. Thies and A. K. Shiemke, *J. Am. Chem. Soc.*, 1981, **103**, 4073; H. Okawa, J. Nishio, M. Ohba, M. Tadakoro, N. Matsumoto, M. Koikawa, S. Kida and D. E. Fenton, *Inorg. Chem.*, 1993, **32**, 2949; M. Yonemura, Y. Matsumura, H. Furutachi, M. Ohba, H. Okawa and D. E. Fenton, *Inorg. Chem.*, 1997, **36**, 2711; H. Furutachi and H. Okawa, *Inorg. Chem.*, 1997, **36**, 3911, J. Lisowski and P. Starynowicz, *Inorg. Chem.*, 1999, **38**, 1351.
5 H.-R. Chang, S. K. Larsen, P. D. W. Boyd, C. G. Pierpont and D. N. Hendrickson, *J. Am. Chem. Soc.*, 1988, **110**, 4565; D. G. McCollum, G. P. A. Yap, A. R. Rheingold and B. Bosnich, *J. Am. Chem. Soc.*, 1996, **118**, 1365.
6 B. F. Hoskins, R. Robson and G. A. Williams, *Inorg. Chim. Acta*, 1976, **16**, 121; L. K. Thompson, S. K. Mandal, S. T. Tandon, J. N. Bridson and M. K. Park, *Inorg. Chem.*, 1996, **35**, 3117; A. Asokan, B. Varghese, A. Caneschi and P. T. Manoharan, *Inorg. Chem.*, 1998, **37**, 228.
7 J. Lisowski, *Inorg. Chim. Acta*, 1999, **285**, 233.

Communication 9/00969H

ChemComm

The insertion of alkylgallium(I) groups [Ga–C(SiMe$_3$)$_3$] into P–P bonds of P$_4$: formation of a P$_4$(GaR)$_3$ cage

Werner Uhl* and Maike Benter

Fachbereich Chemie, Universität, Postfach 2503, D-26111 Oldenburg, Germany.
E-mail: Uhl@chemie.uni-oldenburg.de

Received (in Basel, Switzerland) 25th January 1999, Accepted 8th March 1999

The tetrahedral gallium(I) compound Ga$_4$[C(SiMe$_3$)$_3$]$_4$ 1 reacted with white phosphorus by the threefold insertion of its monovalent gallium atoms into P–P bonds of the P$_4$ tetrahedron with formation of a novel P$_4$(GaR)$_3$ cage possessing a structure similar to P$_4$S$_3$.

Recently, we succeeded in synthesizing the first known alkylgallium(I) compound (**1**), which in the solid state adopted the tetrahedral structure Ga$_4$[C(SiMe$_3$)$_3$]$_4$, but dissociated into monomeric GaR fragments in dilute solutions.[1] Compound **1** is available now in a high yield by the reduction of the corresponding alkyltrichlorogallate with Rieke magnesium,[2] and shows a remarkable and unprecedented chemical reactivity similar to the up to now more intensively investigated indium analogue In$_4$[C(SiMe$_3$)$_3$]$_4$.[3] The chalcogens sulfur, selenium and tellurium gave heterocubane type molecules,[4] the insertion of a GaR fragment into one P–P bond of tri(*tert*-butyl)cyclotriphosphane was observed,[5] and the monomers are able to replace carbonyl groups in transition metal carbonyl complexes to yield novel transition metal gallium compounds.[5] The reaction of **1** with white phosphorus is reported here.

Tetragallane(4) **1** and P$_4$ reacted slowly in boiling *n*-hexane to yield yellow crystals of the novel trigallium tetraphosphorus compound **2** in a yield of 52%. The formation of **2** can be described by the insertion of three monomeric GaR fragments into three of the six P–P bonds of the P$_4$ tetrahedron. A similar reaction has not been observed before. The cyclopentadienylaluminium(I) derivative (AlCp*)$_4$ gave the electron deficient cage compound (AlCp*)$_6$P$_4$, which consists of two face-sharing heterocubanes with two opposite corners unoccupied.[6] The indium analogue of **1** yielded another product probably containing four indium atoms and only one phosphorus atom, which, however, could not, as yet, be characterized completely. As expected, singlets were observed for the SiMe$_3$ groups in the ^{1}H and ^{13}C NMR spectra of **2**, and the resonance of the α carbon atoms attached to gallium (δ 27.8) was in the characteristic range of compounds containing coordinatively unsaturated tricoordinated gallium atoms. Two resonances were detected in the ^{31}P NMR spectrum at δ −202.8 and −521.9. The first is in the expected range and splits into a doublet due to the coupling with the phosphorus atom at the apex of the cage. It was assigned to the P$_3$ group, of which each member is further coordinated by only one gallium atom. The apical phosphorus atom attached to three gallium atoms showed a quite unusual chemical shift to a very high field and gave a quartet caused by the coupling to the equivalent phosphorus atoms of the P$_3$ ring. To the best of our knowledge, similar high field shifts have been observed for only very few compounds such as P$_4$ itself (δ −488), tin(II) derivatives (SnPR)$_x$ and BaSn$_3$P$_4$R$_4$ (up to δ −529).[7]

The molecular structure of the Ga$_3$P$_4$ cage (Fig. 1) contains a homocycle of three phosphorus atoms, of which each is further attached to one gallium atom. The fourth phosphorus atom resides at the apex of the cage and is pyramidally coordinated by three gallium atoms, which are coordinatively unsaturated and bind to one carbon atom and two phosphorus atoms in an ideal planar arrangement (Ga2 due to its special position on a crystallographic mirror plane, Ga1: sum of angles 360.0°). The structure is, thus, quite similar to the structures of [P$_7$]$^{3-}$ or P$_4$S$_3$,[8] which have, however, electronically saturated atoms in the bridging positions. The Ga–P distances to the single phosphorus atom P1 (234.2 pm) are little shorter than those to the P$_3$ ring (237.2 pm), which may be caused by the higher negative charge at P1 and a stronger ionic contribution to its bonds. All Ga–P bonds are in the lower range usually observed for organogallium phosphides, in which generally the phosphorus atoms are further attached to alkyl groups as in heterocubane type molecules (RGaPR)$_4$.[9] The P–P distances (218.1 pm, average) are in the usual range and only a little shorter than in

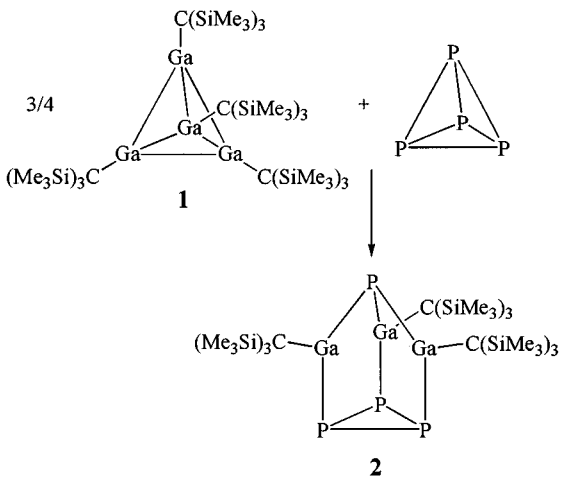

Scheme 1

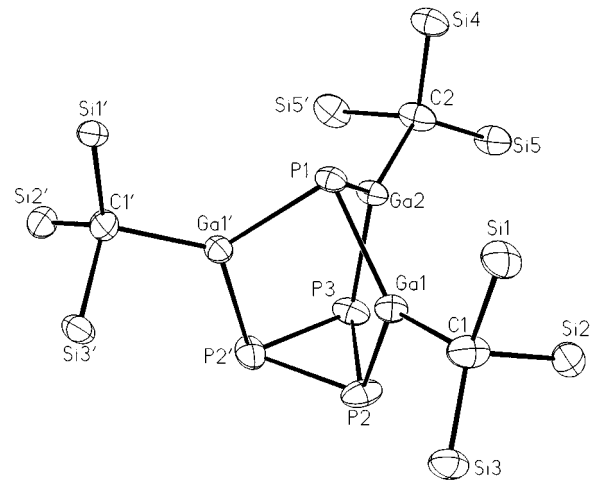

Fig. 1 Molecular structure of **2**. Selected bond lengths (pm) and angles (°): P1–Ga1 234.2(1), P1–Ga2 234.2(2), P2–Ga1 236.9(2), P3–Ga2 237.8(2), P2–P2′ 217.8(3), P2–P3 218.3(2), Ga1–C1 197.5(5), Ga2–C2 198.1(7); Ga1–P1–Ga1′ 86.43(6), Ga1–P1–Ga2 85.91(5), Ga1–P2–P2′ 102.54(4), Ga1–P2–P3 102.20(8), Ga2–P3–P2 102.33(7), P2′–P2–P3 60.08(5), P2–P3–P2′ 59.8(1), P1–Ga1–P2 113.76(5), P1–Ga2–P3 113.53(7).

P_4. The cage geometry forces the Ga atoms to approach to a distance of 319.7 pm on average, which is much shorter than the sum of the van der Waals radii (380 pm),[10] but longer than the Ga–Ga separation in the Ga_4 tetrahedron of **1** (268.8 pm).[1] These structural parameters suggest the treatment of **2** with a strong reducing agent in order to transfer electron density to the unsaturated gallium atoms and to obtain a delocalized σ bond in the cage. The Ga–C bonds (197.7 pm) are much shortened compared to those of the starting compound **1** (208 pm). The shortening is more pronounced than observed previously, and even in heterocubanes with the more electronegative chalcogen atoms longer distances were observed.[4] Several reasons may account for this observation such as the increase of oxidation state of the Ga atoms from +1 in **1** to +3 in compound **2**, the lower steric strain in the molecule and the low coordination number of the Ga atoms with an increased s character of the Ga–C bond.

We are grateful to the Deutschen Forschungsgemeinschaft and the Fonds der Chemischen Industrie for generous financial support.

Notes and references

† A solution of compound **1** (469 mg, 0.390 mmol, small excess) in 40 ml of *n*-hexane (dried over *n*-butyllithium) was added under argon to 56 mg of white phosphorus (0.452 mmol). The mixture was refluxed for 14 h, and the color changed from red to orange. After cooling, filtration and evaporation the product was recrystallized from toluene or cyclopentane (20/ −30 °C). Yield: 240 mg (52%, based on P_4); yellow, air-sensitive crystals (decomp. 215 °C). ^{1}H NMR (300 MHz, C_6D_6): δ 0.42. ^{13}C NMR (75.5 MHz, C_6D_6): δ 27.8 (GaC), 6.7 ($SiMe_3$). ^{31}P NMR (202 MHz, C_6D_6): δ −202.8 (d), −521.9 (q, $^2J_{PP}$ 31 Hz). IR (paraffin, cm^{-1}): 1304w, 1260m (δCH_3); 1169vs, 1157vw, 1117vw, 1078w, 1045m; (pentane) 856vs, 783w, 721m (ρCH_3); 675w, 654w, 627w (νSiC); 521w, 463w (νGaC), 380vw (δSiC). UV–VIS (hexane): λ_{max} (log ε) = 225 (sh, 3.7), 255 (3.9), 295 (sh, 3.5), 380 nm (3.0). Molar mass (cryoscopically in benzene): obs. 980, calc. 1027.8 g mol^{-1}.

‡ *Crystal data*: single crystals from cyclopentane; not evacuated; handled in perflourinated polyether; four solvent molecules each formula unit; $C_{30}H_{81}Ga_3P_4Si_9 \cdot 4C_5H_{10}$; orthorhombic; space group *Pnma* (no. 62), a = 13.132(3), b = 32.368(6), c = 17.233(3) pm, U = 7325(3) Å^3, Z = 4, D_c = 1.186 g cm^{-3}, crystal dimensions 0.5 × 0.4 × 0.2 mm, T = 213 K; μ(Mo-Kα) = 1.359 mm^{-1}; STOE IPDS diffractometer; 266 exposures, $\Delta\varphi$ = 0.7°, $-16 \leqslant h \leqslant 16$, $-39 \leqslant k \leqslant 39$, $-21 \leqslant l \leqslant 21$; 7293 independent reflections; 4973 reflections with $F > 4\sigma(F)$; structure solved by direct methods and refined with all independent structure factors based on F^2;[11] 414 parameters; $R1$ = 0.058; $wR2$ = 0.165; max., min. residual electron density 1.437 (near the disordered silyl group at Si5A), −0.611 e Å^{-3}. The molecule is located on a crystallographic mirror plane with the atoms P1, P3, Ga2, C2, Si4 and C41 on special positions. All $C(SiMe_3)_3$ groups were statistically disordered, their atoms were refined by restrictions of bond lengths and angles. CCDC 182/1192. See http://www.rsc.org/suppdata/cc/1999/771/ for crystallographic files in .cif format.

1 W. Uhl, W. Hiller, M. Layh and W. Schwarz, *Angew. Chem.*, 1992, **104**, 1378; *Angew. Chem., Int. Ed. Engl.*, 1992, **31**, 1364.
2 W. Uhl and A. Jantschak, *J. Organomet. Chem.*, 1998, **555**, 263.
3 W. Uhl, R. Graupner, M. Layh and U. Schüz, *J. Organomet. Chem.*, 1995, **493**, C1.
4 W. Uhl, M. Benter, W. Saak and P. G. Jones, *Z. Anorg. Allg. Chem.*, 1998, **624**, 1622.
5 W. Uhl, M. Benter and M. Prött, unpublished work.
6 C. Dohmeier, H. Schnöckel, C. Robl, U. Schneider and R. Ahlrichs, *Angew. Chem.*, 1994, **106**, 225; *Angew. Chem., Int. Ed. Engl.*, 1994, **33**, 199.
7 M. Driess, S. Martin, K. Merz, V. Pintchouk, H. Pritzkow, H. Grützmacher and M. Kaupp, *Angew. Chem.*, 1997, **109**, 1982; *Angew. Chem., Int. Ed. Engl.*, 1997, **36**, 1894; M. Westerhausen, M. Krofta, N. Wiberg, W. Ponekwar, H. Nöth and A. Pfitzner, *Z. Naturforsch., Teil B*, 1998, **53**, 1489.
8 D. Weber, C. Mujica and H. G. von Schnering, *Angew. Chem.*, 1982, **94**, 869; *Angew. Chem., Int. Ed. Engl.*, 1982, **21**, 863; H. Hönle and H. G. von Schnering, *Angew. Chem.*, 1986, **98**, 370; *Angew. Chem., Int. Ed. Engl.*, 1986, **25**, 352; Y. C. Leung, J. Waser, S. van Houten, A. Vos, G. A. Wiegers and E. H. Wiebenga, *Acta Crystallogr.*, 1957, **10**, 574.
9 K. Niedick and B. Neumüller, *Z. Anorg. Allg. Chem.*, 1995, **621**, 889.
10 J. E. Huheey, E. A. Keiter and R. L. Keiter, *Inorganic Chemistry*, Harper Collins, 1993.
11 SHELXTL-Plus REL. 4.1, Siemens Analytical X-RAY Instruments Inc., Madison, WI, 1990; G. M. Sheldrick SHELXL-93, Program for the Refinement of Structures, Universität Göttingen, 1993.

Communication 9/00670B

The isolated iron–molybdenum cofactor of nitrogenase catalyses hydrogen evolution at high potential

Thierry Le Gall, Saad K. Ibrahim, Carol A. Gormal, Barry E. Smith and Christopher J. Pickett*

Nitrogen Fixation Laboratory, John Innes Centre, Norwich Research Park, Norwich, UK NR4 7UH. E-mail: chris.pickett@bbsrc.ac.uk

Received (in Cambridge, UK) 1st March 1999, Accepted 23rd March 1999

The isolated cofactor of nitrogenase FeMoco catalyses hydrogen evolution at the high potential associated with the FeMoco$^{ox/semi\text{-}red}$ couple ($E°$ = −280 mV *vs.* NHE , $C_6F_5S^-$ ligated form); analysis of the current–potential dependence of the catalysis suggests a mechanism involving rate-determining loss of H_2 from an FeMoco(H)$_2$ ^{red} intermediate (k = 3 s^{-1}); the relatively slow kinetics of this step may be related to an obligatory role for hydridic intermediates in substrate reductions by nitrogenase.

Catalysis of proton reduction to dihydrogen is an intrinsic property of the nitrogenase system. In the absence of molecular nitrogen (or other reducible substrates) turnover of the enzyme results in hydrogen evolution which is believed to be associated with successive 1e/1H$^+$ transfers to the resting-state redox level of the molybdenum–iron protein.[1] The centre within this protein at which proton reduction takes place is almost certainly[2] the {$MoFe_7S_9$}-cluster which has been shown to have the structure depicted in Scheme 1 when the protein is in the resting-state.[3] Disruption of the protein ligation of the cluster allows extraction into *N*-methylformamide (NMF) of a cofactor (FeMoco) which reactivates mutant apo-protein.[4] Spectroscopic, analytical and other evidence indicate that FeMoco retains the structure of the protein bound {$MoFe_7S_9$}-cluster but with the histidine ligand replaced by coordination of a solvent molecule to Mo and the cysteinyl ligand at the capping Fe replaced by an anion, probably *N*-methylformamidate.[5] Herein we show that FeMoco is capable of electrocatalysing the reduction of protons to dihydrogen at high potential, a process which may directly relate to the enzymic catalysis.

FeMoco was extracted into an NMF–phosphate buffer solution from molybdenum–iron protein that had been isolated from *Klebsiella pneumoniae* using minor modifications of the method described earlier.[6] It was derivatised by pentafluorothiophenolate (PfpS$^-$) ligation at the capping tetrahedral Fe atom,[7] and studied in the oxidised, EPR-silent, form which we shall refer to as {(PfpS)FeMoco}^{ox}. Cyclic voltammetry of {(PfpS)FeMoco}^{ox} showed that the cofactor undergoes a well defined, reversible, diffusion-controlled, single-electron reduction to give {(PfpS)FeMoco}$^{semi\text{-}red}$. This directly parallels earlier observations by Schultz, Newton and coworkers on the thiophenolate derivatised form of the cofactor.[8]

However, pentafluorothiophenol can function both as a ligand to FeMoco and as a source of protons. The pK_a(H_2O) for PfpSH (2.68) is considerably lower than that for PhSH (6.43) and we would expect that this greater acidity of PfpSH also pertains in the NMF system. Fig. 1 shows the effect of increasing [PfpSH]$_{total}$ on the cyclic voltammetry of the {(PfpS)FeMoco}$^{ox/semi\text{-}red}$ couple.† The peak current, I_p^{red}, is enhanced and the reversibility of the system decreased as the concentration of the acid is increased. Fast potential scan-rates (v) restore some reversibility to the system whereas at low v, the current response approaches that expected for a catalytic substrate reduction with the magnitude of I_p^{red} independent of v.

Controlled potential electrolysis of the cofactor (0.5 μmol) was performed at $E_{applied}$ = −550 mV *vs.* SCE (*ca.* −320 mV *vs.* NHE) in a sealed electrochemical cell in the presence of 60 mM of [PfpSH]$_{total}$. The gas-space was sampled after the passage of 4.3 μmol of electrons. Gas chromatographic analysis confirmed the formation of dihydrogen (1.84 μmol, 85%, *ca.* 9 turnovers). An enzyme reconstitution assay[4] of a sample of the catholyte after electrolysis showed that the cofactor was still fully active, *i.e.* the structural integrity of the cofactor was retained.

Fig. 2 shows a plot of I_p^{red} *vs.* [PfpSH]$_{total}$ together with the calculated response based on the mechanism proposed in Scheme 1. At low [PfpSH]$_{total}$ the phosphate buffer neutralises protons and there is little enhancement of I_p^{red}; above [PfpSH]$_{total}$ *ca.* 40 mM the current increases as the semi-

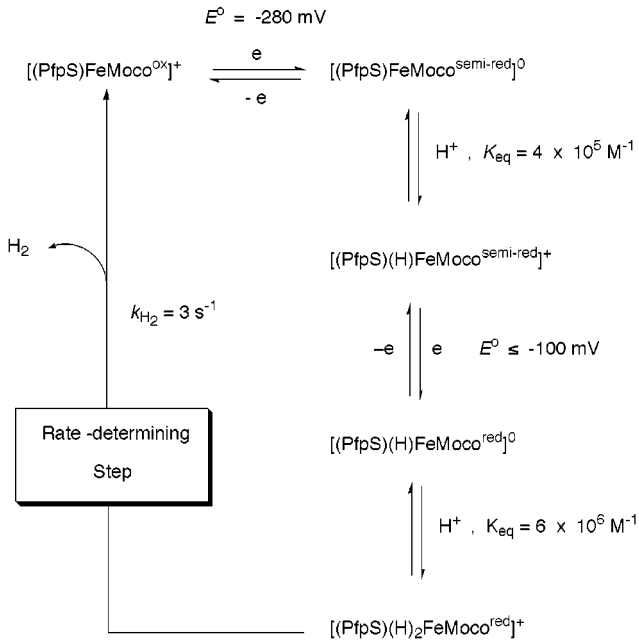

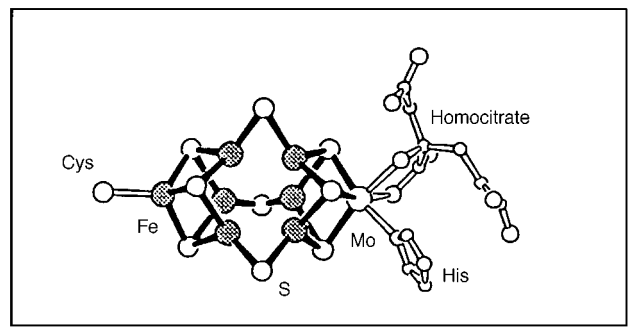

Scheme 1 Mechanism and key constants for hydrogen evolution catalysed by extracted FeMoco. [PfpSFeMoco^{ox}] is assigned an *arbitrary* net charge of 1+ to clarify proton/electron counting. The potentials are quoted *vs.* NHE which is taken to be 242 mV positive of SCE in the NMF electrolyte.[8] The box shows the structure of Femoco bound within the protein in the semi-reduced resting state.[3]

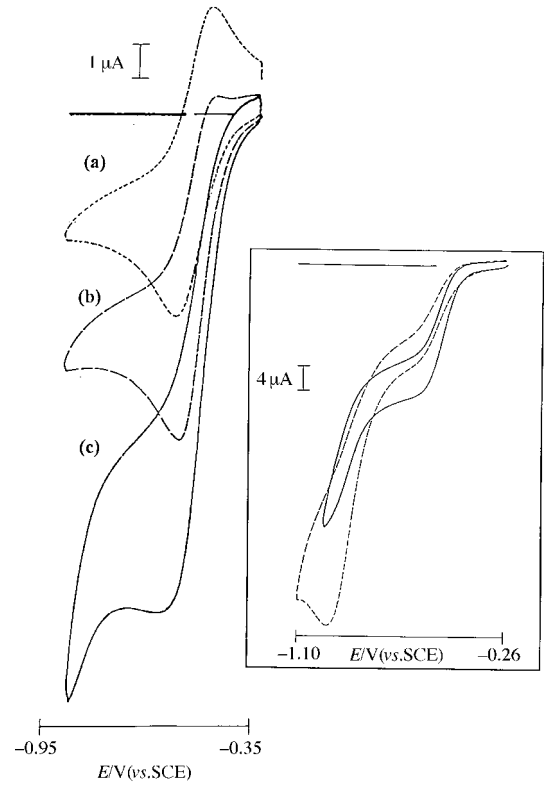

Fig. 1 Effect of adding PfpSH on the cyclic voltammetry of the {(PfpS)FeMoco}$^{ox/semi\text{-}red}$ system. *Conditions*: 1.3 mM FeMoco extract in NMF containing sodium hydrogen phosphate, *ca.* 40 mM; potential scan-rate = 20 mV s^{-1} at a vitreous carbon working electrode of area 0.0707 cm^2; SCE reference and platinum secondary electrodes were employed. Nominal concentration of PfpSH (a) 30 mM (b) 60 mM and (c) 75 mM. Inset: effect of cyanide ($[Et_4N]CN$, 2 equiv.) on the catalytic wave, $[PfpSH]_{total}$ = 135 mM; (—) before addition of cyanide; (- - -) after addition of 2 equiv. CN^-. Note the enhanced reduction of free proton at the more negative potential in the presence of cyanide.

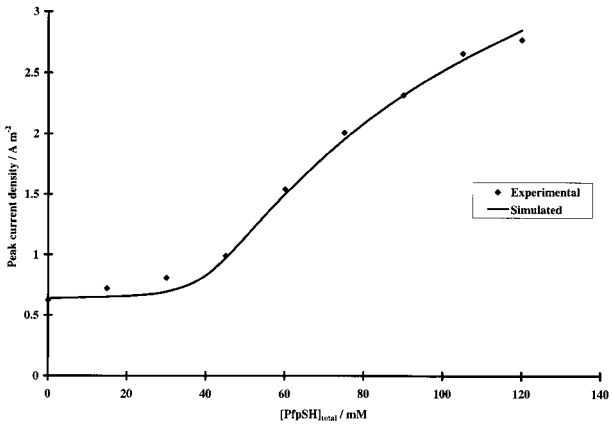

Fig. 2 Plot of I_p^{red} *vs.* $[PfpSH]_{total}$. The points are experimental data, the solid line is the simulated response based upon the mechanism shown in Scheme 1. For the simulation all protonation steps were assumed to be diffusion-controlled; the acid dissociation constant of PfpSH in NMF was taken as 2×10^{-7}; the diffusion coefficient of FeMoco^{ox} used in the simulation was independently measured as 1.65×10^{-6} cm^2 s^{-1} at 293 K; full details of the simulation are supplied as supplementary material (http://www.rsc.org/suppdata/1999/cc/773).

reduced cofactor protonates and is engaged in the catalytic cycle.‡ The rate-determining step in the mechanism involves the irreversible loss of dihydrogen from an hydridic intermediate, {(PfpS)FeMoco$(H)_2$}^{red}; the first-order rate constant (k_{H_2}) for this step is estimated to be 3 s^{-1} at 293 K (Scheme 1).

Accessing reduced states of the cofactor at high potential by protonation may well be essential for the binding of molecular nitrogen, or other substrates, within the enzyme.[1,9] Oxidation by fast release of molecular hydrogen from such states cannot be conducive to efficient catalysis, *viz.* nitrogenase is a 'poor' hydrogenase. The observation that reduced states of isolated FeMoco can be accessed at high potential and that re-oxidation by dihydrogen loss involves a kinetically slow step may be closely linked to the behaviour of the enzyme.

A key feature of hydrogen evolution by nitrogenase is its inhibition by cyanide which is presumed to bind to the iron–molybdenum cluster and decreases electron flux to this centre.[1] Remarkably we also find that cyanide decreases catalytic reduction of protons by isolated cofactor. Fig. 1 (inset) shows the effect of cyanide (2 equiv.) on the catalytic wave. This wave is suppressed and that for direct reduction of proton at the electrode is enhanced. Detailed studies of the electrochemistry of FeMoco in the presence of cyanide, which will be reported elsewhere, show that ligation of this inhibitor to the cofactor shifts the potential of the FeMoco$^{ox/semi\text{-}red}$ couple to a more negative value. This presumably accounts for suppression of electron flux at high potential in both the isolated cofactor and the enzyme system.

In conclusion, we are now beginning to see that the extracted cofactor can engage in electron-transfer chemistry which has some of the attributes of the whole enzyme system : catalytic hydrogen evolution which is kinetically slow and cyanide inhibition of the catalysis. Other parallels are also emerging, for example we have observed the capacity of the cofactor to bind carbon monoxide when the system turns over.[10] In addition, there are reports that acetylene can be catalytically reduced by amalgam reductants in the presence of FeMoco.[11] It is not excessively speculative to suggest that, by suitable modification, it may be possible to achieve the binding and reduction of molecular nitrogen by isolated FeMoco.

We thank the BBSRC and the John Innes Foundation for supporting this work and Dr R. A. Henderson for helpful comments.

Notes and references

† $[PfpSH]_{total}$ is the concentration of the added thiol if it were undissociated. It corresponds to $[PfpSH]_{total}$ = {[PfpSH] + [$PfpS^-$]}.
‡ The equilibrium constant for protonation of {(PfpS)FeMoco}$^{semi\text{-}red}$ is very similar to that determined for the unmodified cofactor in a related system.[12]

1 B. K. Burgess and D. J. Lowe, *Chem. Rev.*, 1996, **96**, 2983.
2 T. R. Hawkes, P. A. McLean and B. E. Smith, *Biochem. J.*, 1984, **217**, 317.
3 J. B. Howard and D. C. Rees, *Chem. Rev.*, 1996, **96**, 2965 and references therein.
4 V. K. Shah, W. Brill, *Proc. Natl. Acad. Sci. USA*, 1977, **74**, 3249; B. E. Smith, *Molybdenum Chemistry of Biological Significance*, ed. W. E. Newton and S. Otsuka, Plenum Press, New York, 1980, pp. 179–190.
5 S.-S. Yang, W.-H. Pan, G. D. Friesen, B. K. Burgess, J. L. Corbin, E. I. Stiefel and W. E. Newton, *J. Biol. Chem.*, 1982, **257**, 8042; M. A. Walters, S. K. Chapman and W. H. Orme-Johnson, *Polyhedron*, 1986, **5**, 561.
6 A. J. M. Richards, D. J. Lowe, R. L. Richards, A. J. Thomson and B. E. Smith, *Biochem. J.*, 1994, **297**, 373 and references therein.
7 S. D. Conradson, B. K. Burgess, W. E. Newton, A. Di Cicco, Z. Y. Wu, C. R. Natoli, B. Hedman and K. O. Hodgson, *Proc. Natl. Acad. Sci. USA*, 1994, **91**, 1290; I. Harvey, R. W. Strange, R. Schneider, C. A. Gormal, C. D. Garner, S. S. Hasnain, R. L. Richards and B. E. Smith, *Inorg. Chim. Acta*, 1998, **275**–**276**, 150.
8 F. A. Schultz, S. F. Gheller, B. K. Burgess, S. Lough and W. E. Newton, *J. Am. Chem. Soc.*, 1985, **107**, 5364; F. A. Schultz, B. J. Feldman, S. F. Gheller and W. E. Newton, *Inorg. Chim. Acta.*, 1990, **170**, 115.
9 C. J. Pickett, *J. Biol. Inorg. Chem.*, 1996, **1,** 606.
10 S. P. Best, C. A. Gormal, S. K. Ibrahim, B. E. Smith, K. Vincent and C. J. Pickett, *Chem. Commun.*, 1999, submitted.
11 T. A. Bazhenova, M. A. Bazhenova, S. A. Mironova, G. N. Petrova, A. K. Shilova, N. I. Shuvalova and A. E. Shilov, *Inorg. Chim. Acta*, 1998, **270**, 221; T. A. Bazhenova, M. A. Bazhenova, G. N. Petrova, A. K. Shilova and A. E. Shilov, *Russ. Chem. Bull.*, 1998, **47**, 861.
12 K. L. C. Grönberg, C. A. Gormal, B. E. Smith and R. A. Henderson, *Chem. Commun.*, 1997, 713.

Communication 9/01608B

A new multicomponent reaction of nitro compounds with isocyanides

Paul Dumestre, Laurent El Kaim* and Ariane Grégoire

Laboratoire Réacteur et Processus, Ecole Nationale Superieure de Techniques Avancées, 75015 Paris, France. E-mail: elkaim@ensta.fr

Received (in Liverpool, UK) 4th February 1999, Accepted 16th March 1999

The first multicomponent reaction between nitro compounds, isocyanides and acylating agents is described, providing an original route to α-oximinoamides.

α-Oximinoamides form a class of compounds with useful pharmaceutical applications as shown by the structures of cephalosporin **1** and β-lactamase inhibitor **2**.[1] Following our efforts towards finding new applications of isocyanides in synthesis,[2] we wish to report a straightforward synthesis of α-oximinoamides by the interaction of isocyanides with nitro compounds.

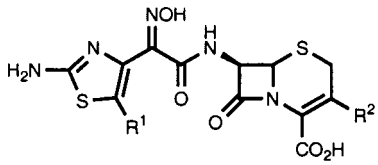

1

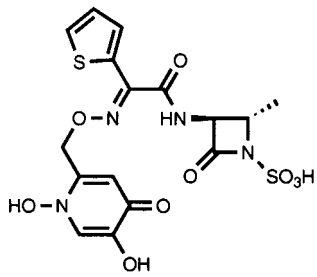

2

Most applications of nitro compounds in synthesis take advantage of easy proton abstraction under basic conditions to form nitronate anions followed by coupling with an electrophile.[3] Nucleophilic attack by carbon nucleophiles on the carbon of the nitro group are more rare. Water adds to nitro compounds following their conversion into the tautomeric nitronic acids, leading to their efficient transformation into ketones and aldehydes (Nef reaction).[4] The extension of the Nef reaction to carbon nucleophiles has probably been hampered by the reported instability of nitronic acid derivatives.[5] Besides some useful [3 + 2] cycloaddition of nitronates under acid catalysis,[6] this approach has been mainly exploited by Seebach *et al.*, giving average to good yields of ketoximes from primary nitro compounds and alkyllithiums.[7]

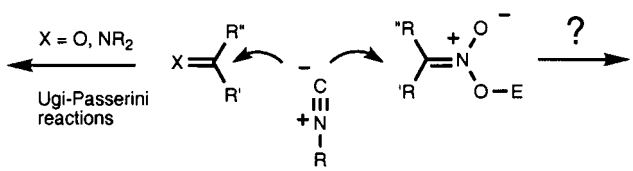

Scheme 1 Nucleophilic attack of isocyanides on carbonyl derivatives.

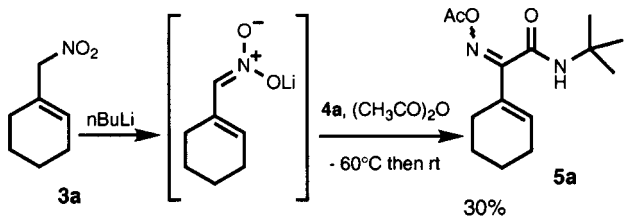

Scheme 2 Addition of *tert*-butyl isocyanide **4a** on the nitronate derived from **3a**.

Table 1 Products isolated after isocyanide addition to nitro compounds[a]

Starting nitro and isocyano compounds	Product (yield, time)
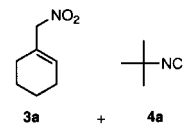 **3a** + **4a**	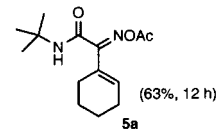 (63%, 12 h) **5a**
 **3b** + **4a**	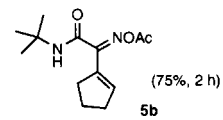 (75%, 2 h) **5b**
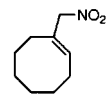 **3c** + **4a**	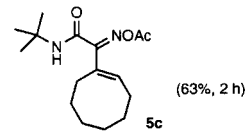 (63%, 2 h) **5c**
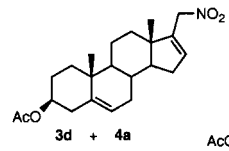 **3d** + **4a**	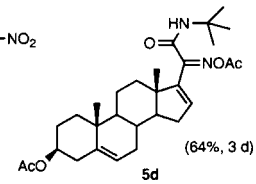 (64%, 3 d) **5d**
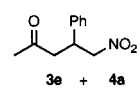 **3e** + **4a**	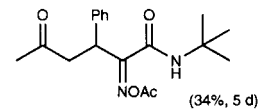 (34%, 5 d) **5e**
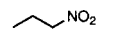 **3f** + **4a**	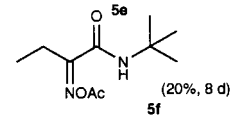 (20%, 8 d) **5f**
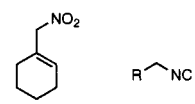 **3a** + **4b** R = CO_2Et **4c** R = 4-MeOPh	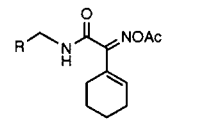 **5g** R = CO_2Et (30%, 2 d) **5h** R = 4-MeOPh (51%, 24 h)
 **3b** + **4b**	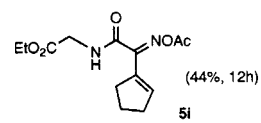 (44%, 12h) **5i**

[a] Ref. 11.

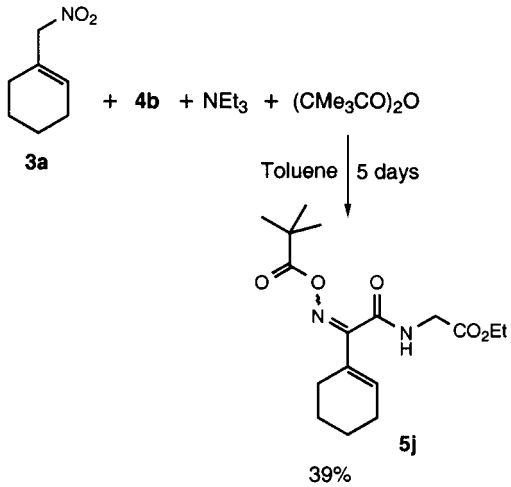

Scheme 3 Addition of isocyanide **4a** to nitro derivative **3a** under pivalic anhydride activation.

The Ugi–Passerini reactions[8] exploit the nucleophilic properties of isocyanides towards carbonyl derivatives; a similar reaction can be envisaged with nitronic acids as shown in Scheme 1.

Keeping in mind the sensitivity of nitronic acid derivatives and their ability to form nitrile oxides,[5] we first examined and reported[9] the behaviour of isocyanides in the presence of NEt_3, primary nitro compounds and butyl isocyanate under conditions propicious for nitrile oxide formation. Under such conditions, the primary nitro compound is cleanly converted into a nitrile by oxygen transfer to the isocyanide.

To avoid nitrile oxide formation, we decided to generate the *O*-acyl nitronate at low temperatures in the presence of the isocyanide by analogy to the addition of organometallics to silyl and acyl nitronate.[7,10] Preliminary experiments were encouraging as a 30% yield of the α-oximinoamide **5a** was obtained after reaction of nitro derivative **3a** with butyllithium, acetic acid anhydride and *tert*-butyl isocyanide **4a** (Scheme 2). However all our attempts to raise this yield through changes in reactants, temperature and order of addition did not meet with success.

Our problems may stem from the ambiphilic nature of nitronic acid derivatives which may compete as nucleophiles with the isocyanide; a slow generation of the reactive *O*-acyl nitronate in the presence of the isocyanide could alleviate this problem. In our conversion of nitro compounds into nitriles,[9] fast dimerisation of nitrile oxide was suppressed under such conditions: slow generation of nitrile oxide through nitronate formation using a tertiary amine in toluene. Indeed, a remarkable increase in yield (63%) was observed when a solution of nitro compound **3a** (1 M), NEt_3 (1.1 equiv.), acetic acid anhydride (1.1 equiv.) and isocyanide **4a** was left to react at room temperature for a few hours. Various nitro compounds **3** and isocyanides **4** were tested in this new multicomponent reaction, giving moderate to good yields of α-acyloximinoamide **5** (Table 1).

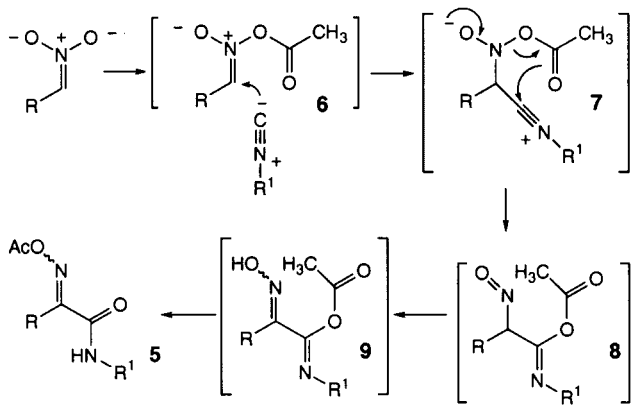

Scheme 4 Possible mechanism for the formation of amides **5**.

As observed for nitrile formation, best yields were obtained with allylic nitro derivatives prone to easy base deprotonation. For aliphatic nitro compounds, the yield can however be raised by a proper selection of the reagents, the formation of **5f** was thus enhanced up to 60% yield by changing from NEt_3 to the more basic DBU. The synthetic potential of this reaction can easily be extended by a change in the starting carboxylic acid (Scheme 3). A significant decrease in yield was observed with isocyanides possessing electron withdrawing groups. Even though yields are modest, it represents nevertheless a very straightforward preparation of complex dipeptide analogues **5g**, **5i** and **5j**. A possible mechanism for this new reaction is depicted in Scheme 4. The acid-base equilibrium between the nitro compound and its nitronate conjugate base is slowly displaced with acetic acid anhydride to give the *O*-acyl nitronate **6**. The latter, though highly unstable at room temperature, is trapped by the isocyanide to give the putative species **7**–**9** through nitroso formation and acylation of the tautomeric oxime.

In conclusion, we have disclosed in this study, the first three-component reaction involving the addition of isocyanides to nitro compounds. This reaction enables a fast preparation of complex peptide analogues from readily available nitro derivatives; it could find application in total synthesis as well as in combinatorial chemistry. Efforts to increase the yield by a proper selection of reagents and solvents are under way in our group.

Notes and references

1 D. T. W. Chu, *Annual Reports in Medical Chemistry Vol 33*, ed. J. A. Bristol, Academic Press, San Diego, 1998, pp. 141–150.
2 C. Buron, L. El Kaïm and A. Uslu, *Tetrahedron Lett.*, 1997, **38**, 8027; L. El Kaïm and E. Pinot-Périgord, *Tetrahedron*, 1998, **54**, 3799.
3 E. Breuer, *The Chemistry of Amino, Nitroso and Nitro Compounds and their derivatives*, ed. S. Patai, Wiley, New York, 1982.
4 H. W. Pinnick, *The Nef Reaction, Organic Reaction Vol 38*, ed. L. A. Paquette, Wiley, 1990, p. 659.
5 K. B. G. Torsell, *Nitrile Oxides, Nitrones, and Nitronates in Organic Synthesis*, VCH, Weinheim, 1988; M. Cherest and X. Lusinchi, *Tetrahedron*, 1986, **42**, 3825.
6 A. McKillop and R. J. Kobylecki, *Tetrahedron*, 1974, **30**, 1365.
7 E. W. Colvin, A. D. Robertson, D. Seebach and A. K. Beck, *J. Chem. Soc., Chem. Commun.*, 1981, 952.
8 I. Ugi, *Isonitrile Chemistry*, Academic Press, New York, 1971.
9 L. El Kaïm and A. Gacon, *Tetrahedron Lett.*, 1997, **38**, 3391.
10 T. Fujisawa, Y. Kurita and T. Sato, *Chem. Lett.*, 1993, 1537.

11 A typical experimental procedure is as follows: to a solution of nitro compound (2 mmol) in toluene (2 ml) were added NEt_3 (2.2 mmol), acetic anhydride (2.2 mmol) and isocyanide (3 mmol). The reaction was stirred at room temperature under an inert atmosphere until completion (a few hours to a few days for aliphatic nitro compounds); evaporation of the solvent and chromatography on silica finally furnished the desired product.

Communication 9/00987F

1,4-Dithiin annelated with bicyclo[2.2.2]octene units: experimental and theoretical evidence for the aromaticity in 1,4-dithiin dication

Tohru Nishinaga, Atsushi Wakamiya and Koichi Komatsu*

Institute for Chemical Research, Kyoto University, Uji, Kyoto 611-0011, Japan. E-mail: komatsu@scl.kyoto-u.ac.jp

Received (in Cambridge, UK) 15th February 1999, Accepted 16th March 1999

1,4-Dithiin dication annelated with bicyclo[2.2.2]octene units was generated by the two-electron oxidation of the neutral dithiin and found to be aromatic based on the results of NMR measurements and theoretical calculations.

Although there have been a considerable number of studies on cationic π-conjugated systems containing sulfur atom(s), surprisingly little is known on the dicationic species of 1,4-dithiin,[1] and the spectroscopically characterized derivative is limited only to the expanded π-system of 2,3,7,8-tetramethoxythianthrene dication (**1**$^{2+}$). The ^{1}H NMR spectra of this dication showed broad signals at room temperature[2] while the $\Delta m = 2$ transition was observed by EPR at low temperature.[3] From the EPR experiments, it was concluded that this dication is ground state triplet and the energy gap between the singlet and triplet states is < 1 kcal mol^{-1}.[3] These results are consistent with the X-ray structure of **1**$^{2+}$($SbCl_6^-$)$_2$, in which it was interpreted that this dication is divided into two cyanine subunits with each π-delocalization more favored than the cyclic π-conjugation as a whole.[4]

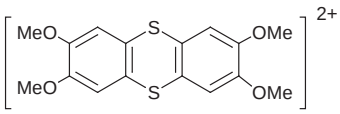

1^{2+}

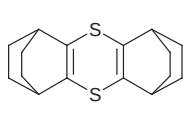

2

Is the triplet state of non-expanded 1,4-dithiin dication itself also more stable than the singlet state which might have an aromatic stabilization? Here, is given the first experimental and theoretical evidence for the presence of aromaticity in a derivative of 1,4-dithiin dication, *i.e.* 1,4-dithiin dication **2**$^{2+}$ annelated with bicyclo[2.2.2]octene units. The annelation of this bicyclic unit has been shown to be quite effective for the stabilization of the radical cation[5] and dication[6] of cyclooctatetraene, which is isoelectronic to 1,4-dithiin. Also the electronic structures of the singlet and triplet states are compared between the dications of parent 1,4-dithiin **3** and thianthrene **4** for better understanding of the electronic properties of these species.

For the synthesis of 1,4-dithiin derivative **2**,† the method of Nakayama *et al.*[7] was employed. Thus, 3-bromobicyclo[2.2.2]octan-2-one, synthesized from 2-bromobicyclo[2.2.2]octene by the same method for the chloro derivative,[8] was allowed to react with Na_2S to give bis(3-oxobicyclo[2.2.2]oct-2-yl) sulfide (63%). The reaction of this sulfide with Lawesson's reagent[9] afforded **2** in 63% yield.

Cyclic voltammetry of **2** in CH_2Cl_2 at −78 °C under vacuum using a Pt wire as a pseudo-reference electrode showed two reversible oxidation waves at +0.00‡ and +0.82 V§ *vs.* Fc/Fc^+ (Fig. 1), indicating that both the radical cation and dication of **2** are stable under these conditions. In comparison with the oxidation potential of tetramethoxythianthrene **1** (E^1 = +0.58, E^2 = +0.83 V *vs.* Fc/Fc^+, calibrated from the potential *vs.* Ag/Ag^+ in acetonitrile),[2]¶ the first oxidation potential of **2** is remarkably lowered owing to the inductive and σ–π conjugative effects of bicyclo[2.2.2]octene units. On the other hand, the difference between the first and second oxidation potentials of

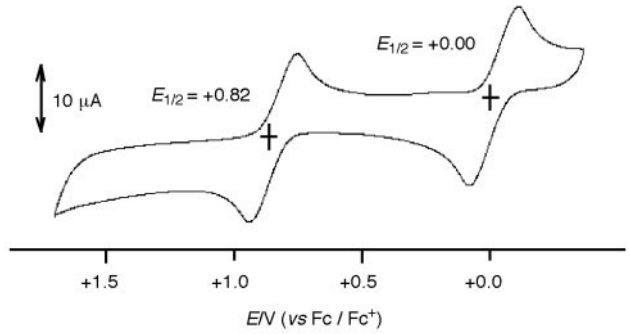

Fig. 1 Cyclic voltammogram of **2** in CH_2Cl_2 containing NBu_4ClO_4 (0.1 M) at −78 °C under vacuum; scan rate, 0.1 V s^{-1}.

2 is larger than that of **1**, suggesting that there is a larger Coulombic repulsion in dication **2**$^{2+}$ than in **1**$^{2+}$.

The reaction of **2** with an excess of SbF_5 in CD_2Cl_2 at ambient temperature gave an orange solution, which exhibited ^{1}H and ^{13}C NMR signals at considerably low field compared with the neutral dithiin (Table 1). The observed chemical shifts for this orange solution were in fair agreement with the calculated values for **2**$^{2+}$ (GIAO/HF/6-31+G*//B3LYP/6-31G*), giving a strong support to the formation of dication **2**$^{2+}$. The signal of bridgehead protons which are located in the plane of the dithiin's π-system exhibited a marked downfield shift of 2 ppm as compared with that of neutral **2**. This clearly indicates the presence of a diamagnetic ring current in the dicationic dithiin ring and the aromatic character in this 6π-electronic system. The value of nucleus independent chemical shift (NICS)[10] of **2**$^{2+}$ was calculated to be −8.8 (GIAO/HF/6-31+G*//B3LYP/6-31G*), which also supports the aromaticity in this dication.

The optimized structures obtained theoretically at the B3LYP/6-31G* level for neutral and dicationic species **2** and **2**$^{2+}$ are shown in Fig. 2. As two electrons are removed from **2**, the C–S single bonds in the dithiin ring are shortened and the C=C double bonds elongated, with the conformational change from boat to planar structures. Such changes in the bond length and conformation can be rationalized by the enhanced cyclic π delocalization for **2**$^{2+}$ again supporting the presence of the aromaticity in the 1,4-dithiin dication.

Table 1 ^{1}H and ^{13}C NMR chemical shifts for **2** and **2**$^{2+}$

	δ_H			δ_C		
Compound		CH	CH_2	C=C	CH	CH_2
2	Obs.[a]	2.46	1.53 (8H) 1.33 (8H)	128.4	38.1	26.2
2^{2+}	Obs.[a]	4.48	2.47 (8H) 1.86 (8H)	180.0	43.0	25.1
	Calc.[b]	4.18	2.84 (*anti*) 1.66 (syn)	197.0	38.7	22.2

[a] In CD_2Cl_2. [b] GIAO/HF/6-31+G*//B3LYP/6-31G*.

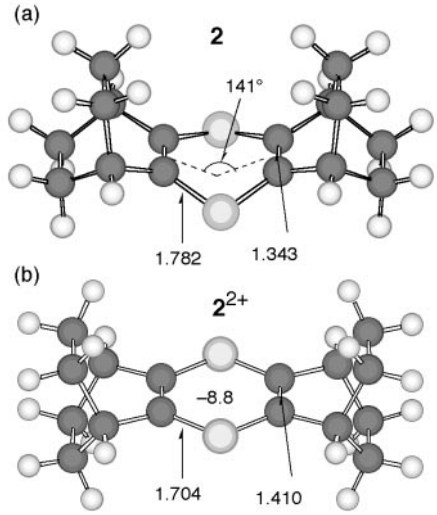

Fig. 2 Calculated structures of (a) **2** and (b) $\mathbf{2}^{2+}$ at the B3LYP/6-31G* level. Selected bond lengths (Å), a bending angle of **2**, and a NICS value (ppm) of $\mathbf{2}^{2+}$ are included.

The ^{1}H NMR spectrum of dication $\mathbf{2}^{2+}$ showed no line broadening and the triplet state did not seem to mix to the singlet state in contrast to the case of $\mathbf{1}^{2+}$. In order to gain further insight with regard to these results, the difference in energy between the singlet (s) and triplet (t) states for the parent 1,4-dithiin dication $\mathbf{3}^{2+}$ and for the thianthrene dication $\mathbf{4}^{2+}$ were calculated (B3LYP/6-31G*), together with their NICS values (GIAO/HF/6-31+G*//B3LYP/6-31G*). The calculated results are shown in Fig. 3, together with the resonance formulae for $\mathbf{4}^{2+}$. As to the dication $\mathbf{3}^{2+}$, the singlet state $\mathbf{3}^{2+}$(s) was shown to be more stable than the triplet state $\mathbf{3}^{2+}$(t) by 54.1 kcal mol^{-1}, with a significant difference in the NICS value, *i.e.* −8.5 for $\mathbf{3}^{2+}$(s) and 5.1 for $\mathbf{3}^{2+}$(t). Similarly the singlet state $\mathbf{4}^{2+}$(s) was found to be more stable than the triplet state $\mathbf{4}^{2+}$(t), with the NICS value in the dithiin ring calculated to be −9.6 for $\mathbf{4}^{2+}$(s) and 1.8 for $\mathbf{4}^{2+}$(t), but the energy gap between the singlet and triplet states was smaller (11.2 kcal mol^{-1}). In the resonance structures, the canonical formulae of $\mathbf{4}^{2+}$(t) involve the extended π-conjugation for each of the radical cation parts as compared with $\mathbf{3}^{2+}$(t) and the retention of some aromaticity in the benzene ring (NICS value, −5.2). Thus it is concluded that, owing to further substitution with methoxy groups at appropriate positions, the triplet ground state has been attained for $\mathbf{1}^{2+}$ while $\mathbf{2}^{2+}$ with electron-donating σ-frameworks is exhibiting the singlet-state aromaticity.

The present work is supported by a Grant-in-Aid for Scientific Research on Priority Areas (A) (No. 10146101) from the Ministry of Education, Science, Sports and Culture, Japan. Computation time was provided by the Super Computer Laboratory, Institute for Chemical Research, Kyoto University.

Notes and references

† *Synthesis* of **2**: An ethanol solution (10 ml) of 3-bromobicyclo[2.2.2]octan-2-one (1.31 g) and $Na_2S{\cdot}9H_2O$ (0.83 g) was refluxed for 50 min. After usual work-up and separation using GPC, bis(3-oxobicyclo[2.2.2]oct-2-yl) sulfide (0.57 g) was obtained as a colorless solid. This sulfide (0.48 g) was allowed to react with Lawesson's reagent (1.46 g) in toluene (18 ml) at reflux temperature for 3 h to give **2** as a crude product. Flash chromatography over alumina eluted with hexane–benzene (10 : 1) afforded **2** (0.30 g, 63%) as yellow crystals. **2**: mp 190 °C (decomp.). Anal. Calc. for $C_{16}H_{20}S_2$: C, 69.51; H, 7.29. Found: C, 69.35; H, 7.20%.

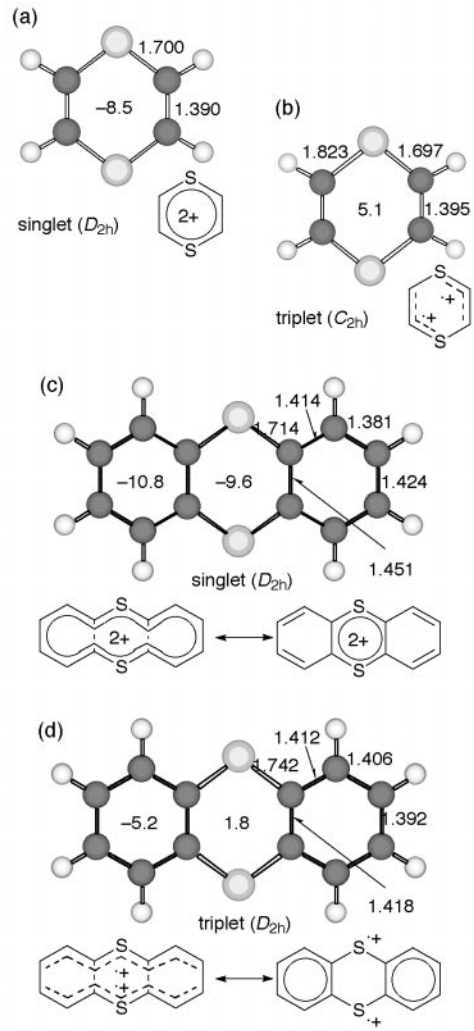

Fig. 3 Calculated structures of (a) $\mathbf{3}^{2+}$(s), (b) $\mathbf{3}^{2+}$(t), (c) $\mathbf{4}^{2+}$(s) and (d) $\mathbf{4}^{2+}$(t) at the B3LYP/6-31G* level and their resonance formulae. Selected bond lengths (Å) and NICS values (ppm) are included.

‡ E_{pa} +0.09, E_{pc} –0.09 V.
§ E_{pa} +0.91, E_{pc} +0.73 V.
¶ For the results of electrochemical studies on 1,4-dithiins, see ref. 1 and references cited therein.

1 G. Klar, in *Methods of Organic Chemistry*, ed. E. Schaumann, Thieme, Stuttgart, 1997, vol. E9a, pp 250–407.
2 R. S. Glass, W. J. Britt, W. N. Miller and G. S. Wilson, *J. Am. Chem. Soc.*, 1973, **95**, 2375.
3 I. B. Goldberg, H. R. Crowe, G. S. Wilson and R. S. Glass, *J. Phys. Chem.*, 1976, **80**, 988.
4 H. Bock, A. Rauschenbach, K. Ruppert and Z. Havlas, *Angew. Chem., Int. Ed. Engl.*, 1991, **30**, 714.
5 T. Nishinaga, K. Komatsu, N. Sugita, H. J. Lindner and J. Richter, *J. Am. Chem. Soc.*, 1993, **115**, 11 642.
6 T. Nishinaga, K. Komatsu and N. Sugita, *J. Chem. Soc., Chem. Commun.*, 1994, 2319.
7 J. Nakayama, H. Motoyama, H. Machida, M. Shimomura and M. Hoshino, *Heterocycles*, 1984, **22**, 1527.
8 R. N. McDonald and R. N. Steppel, *J. Org. Chem.*, 1970, **35**, 1250.
9 B. S. Pederson, S. Scheibye, N. H. Nilsson and L.-O. Lawesson, *Bull. Chem. Soc. Belg.*, 1978, **87**, 223.
10 P. v. R. Schleyer, C. Maerker, A. Dransfeld, H. Jiao and N. J. R. v. E. Hommes, *J. Am. Chem. Soc.*, 1996, **118**, 6317.

Communication 9/01216H

ChemComm

Ti/ITQ-2, a new material highly active and selective for the epoxidation of olefins with organic hydroperoxides

Avelino Corma,* Urbano Díaz, Vicente Fornés, José L. Jordá, Marcelo Domine and Fernando Rey

Instituto de Tecnología Química, UPV-CSIC, Universidad Politécnica de Valencia, Avda. de los Naranjos s/n, 46022 Valencia, Spain. E-mail: acorma@itq.upv.es

Received (in Cambridge, UK) 28th January 1999, Accepted 23rd March 1999

Materials containing highly accessible and well ordered titanium sites prepared by grafting titanocene on ITQ-2 material are excellent catalysts for epoxidation of olefins, yielding high conversions and selectivities to the desired epoxides.

In recent years Ti containing molecular sieves, which are able to catalyze the selective oxidation of hydrocarbons using peroxides as oxidants, have been developed.[1] In this way, Ti-silicalite and Ti-beta are able to carry out successfully the epoxidation of olefins using H_2O_2,[2,3] while Ti-MCM-41 materials, incorporating the Ti, either by one-step synthesis or by post-synthesis, are active and selective catalysts to perform the epoxidation of olefins using organic hydroperoxides.[4–7] A successful Ti/MCM-41 catalyst was obtained when a titanocene was grafted on the surface of a MCM-41,[7] opening the possibility for preparing highly accessible and isolated Ti sites on a very high surface area silica. However, this material still presents some drawbacks related with the stability of the material and the formation of Ti–O–Ti linkages owing to the closeness of the silanol groups. Then, in order to design new Ti grafted solid catalysts, it would be highly desirable to start with a highly stable material with a high surface area accessible to reactants, and containing a well defined distribution of silanol groups on which Ti species can be grafted. Such characteristics coincide with those of the large or extralarge pore Ti-zeolites. Unfortunately, the Ti-zeolites prepared up to now are not successful epoxidation catalysts when reactants with large molecular diameters are involved.[5] Looking for new structures which combine the benefits of the mesoporous and zeolitic materials, we have recently obtained a new material denoted as ITQ-2,[8] which is prepared by delaminating the precursor of the pure siliceous MWW polymorph (ITQ-1).[9] ITQ-2, consists of very thin silica layers of 2.5 nm height with an extremely high and well defined (> 700 m^2 g^{-1}) external surface. As shown in Fig. 1, an hexagonal array of 'cups' of 0.7×0.7 nm penetrate into these layers from each side of the sheet. The structure of this layer is completed by a double 6-ring window which connects the bottom of the cup to the bottom of another cup located at the other side of the layer. In between the cups, *i.e.* inside the sheet, runs a smooth 10-membered ring (10 MR) channel system. Moreover the external surface formed by the array of cups has an important population of silanol groups which are located in specific positions as corresponding to the lamellar precursor of the MWW structure.[10] Such highly accessible well defined silanols are clear candidates to anchor Ti precursors, which can lead to highly dispersed and stable Ti catalytic active sites. This approach has been pursued by first preparing the pure silica layered precursor as follows: 6.164 g of hexamethyleneimine (HMI) and 1.88 g of NaCl were dissolved in 131.40 g of a 0.38 M solution of trimethyladamantamonium hydroxide (TMAdaOH). 37.56 g of H_2O and 12.02 g of SiO_2 (Aerosil 200) were added to the above solution, and a gel was obtained with the following composition: $1SiO_2 : 0.25$ TMAdaOH : 0.31 HMI : 0.1 NaCl : 44 H_2O

The resultant gel was mechanically stirred for 90 min at room temperature. Crystallisation of the lamellar precursor was performed at 150 °C over 5 days at 60 rpm. The material which was filtered off and dried at 100 °C for 12 hours, shows an XRD pattern characteristic of the laminar precursor of the MWW structure.[9,10]

The purely siliceous ITQ-2 was prepared from the lamellar precursor following a previously described procedure[8] and the resultant material shows a BET surface area of 800 m^2 g^{-1}.

Ti was grafted on the surface of the pure silica ITQ-2, by the procedure illustrated in Fig. 1:[7] 10 g of ITQ-2 was dehydrated at 300 °C at 10^{-3} Torr over 2 h. Then, a solution containing an appropriate amount of titanocene dichloride in 90.0 g of $CHCl_3$ was added. The suspension was stirred for 1 h at room temperature under an inert atmosphere. Subsequently, triethylamine dissolved in 10 g of $CHCl_3$ giving a ratio $NEt_3/TiCp_2Cl_2 = 1$ was added and the suspension changed from orange–red to yellow–orange indicating a change of coordination around the Ti atoms. The solids were recovered by filtration and after prolonged washing with CH_2Cl_2, calcination at 540 °C for 1 h

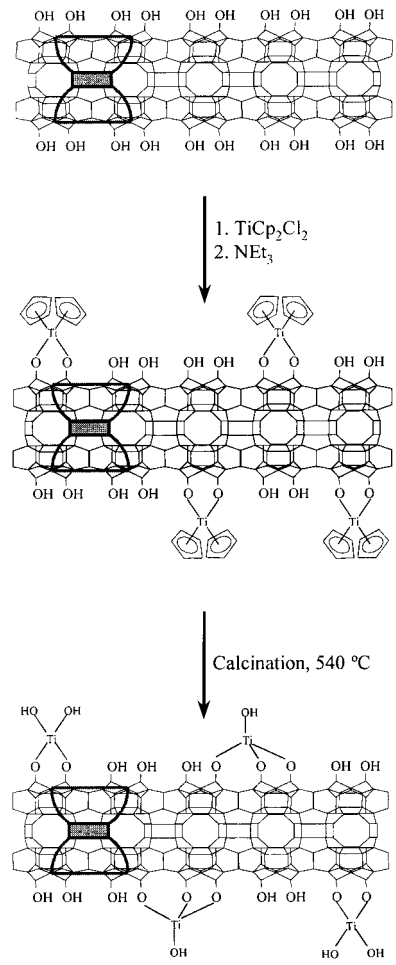

Fig. 1 Schematic grafting of titanocene on the ITQ-2 surface.

Table 1 Cyclohexene conversion and selectivity after 120 min reaction time, and initial rate of reaction for Ti containing samples

Sample	Conversion (%)	Selectivity (%)	r_c/mol g_{cat}^{-1} h^{-1}	r_c/mol mol_{Ti}^{-1} min^{-1}
0.125%TiO_2/ITQ-2	71.7	98.3	0.044	46.9
0.25%TiO_2/ITQ-2	75.1	97.8	0.047	25.0
0.5%TiO_2/ITQ-2	70.8	95.4	0.049	13.1
1%TiO_2/ITQ-2	68.2	91.6	0.045	7.5
0.125%TiO_2/ITQ-2/sil.	73.4	99.4	0.049	64.7
1%TiO_2/ITQ-2/sil.	85.3	99.0	0.070	11.7
Ti/MCM-41[a,7]			0.18	2.1
TiO_2-SiO_2 co-gel[b,18]			0.50	3.3

[a] TBHP/cyclohexene = 1.2, 8 wt% cyclohexene in $CHCl_3$; reaction temperature = 40 °C. [b] Using cumene hydroperoxide (CHP) as oxidant (12 wt% in cumene). Cyclohexene/CHP = 4, 4 wt% of catalyst, reaction temperature = 60 °C.

in N_2 and then 6 h in air was carried out in order to remove all the organics. The resultant materials (Ti/ITQ-2) have the same textural and structural characteristics as ITQ-2, and present in their UV–VIS spectrum only a narrow band located below 220 nm assigned to the formation of monomeric Ti^{IV} species.[11,12] The presence of monomeric Ti species has been further established by the presence of a very intense pre-edge peak in the XANES spectrum of the dehydrated Ti/ITQ-2 sample with an intensity of 0.74, close to the intensities found for Ti-zeolites possessing Ti isomorphically substituted in the framework,[13,14] and higher than those reported for Ti-MCM-41[15,16] and Ti grafted on MCM-41.[15,16,7] This is clear evidence for the presence of Ti linked through O bridges to the siliceous ITQ-2 framework, in the absence of polymeric species of titanium.

Ti/ITQ-2 (295 mg) was used as a catalyst for epoxidation of cyclohexene (4.648 g) with *tert*-butyl hydroperoxide (TBHP) (cyclohexene/TBHP = 4.0) at 60 °C. Results are given in Table 1 where it is evident that the activity and selectivity of all the Ti/ITQ-2 materials to the epoxide are excellent. It is clear that the selectivity to the epoxide decreases as the Ti content increases. This is an indication of the presence of some weak acid sites which are responsible for the opening of the epoxide ring to form the corresponding glycols. Recently, we have reported that the presence of glycols in the reaction medium deactivates the catalysts.[17] The selectivity to the epoxide can be improved, and therefore the formation of glycols reduced, by modifying the adsorption properties of the Ti/ITQ-2 catalysts by silylation. This can be done by contacting 10 g of dehydrated Ti/ITQ-2 with a solution of 6.33 g of $SiMe_3Cl$ in 90 g of $CHCl_3$, and subsequently with a solution of 4.27 g of NEt_3 in 10 g of $CHCl_3$. The catalytic performance of two silylated Ti/ITQ-2 catalysts containing different loadings of Ti is also given in Table 1 where a strong improvement in the activity and selectivity is observed. Also, it is noticeable that Ti/ITQ-2 containing 1 wt% TiO_2 shows a higher activity and similar selectivity to a 0.125 wt% TiO_2 catalyst, indicating that when no deactivation occurs, the higher the Ti content, the higher the catalytic activity.

In order to obtain comparative estimates of the catalytic performances of the different Ti/ITQ-2 catalysts, Table 1 lists catalytic conversion of cyclohexene and the selectivity to the corresponding peroxide. Also, the turnover number and the kinetic rate obtained on Ti/ITQ-2 is compared to literature values for other Ti-containing catalysts (Ti grafted on MCM-41 and Ti mesoporous materials obtained by a co-gel procedure).[18] Ti/ITQ-2 shows the best performance per Ti atom.

However, as important as the activity and selectivity of the catalysts are their stability towards Ti leaching. In order to study this, we have recycled the Ti-ITQ-2 silylated catalysts (METIQ-2) (1wt% TiO_2) three times, and the conversion obtained remained practically the same indicating the good stability of this catalyst.

Financial support by the Spanish MAT97-1016-CO2-01 and MAT97-1207-CO3-01 is gratefully acknowledged. J. L. Jordá thanks the M.E.C. and M. E. Domine thanks the M.E.A. for their doctoral fellowships.

Notes and references

1 B. Notari, *Adv. Catal.*, 1996, **41**, 253.
2 M. Tamarasso, C. Perego and B. Notari, *US Pat.*, 4 410 501, 1983.
3 M. A. Camblor, A. Corma, A. Martínez and J. Pérez-Pariente, *J. Chem. Soc., Chem. Commun.*, 1992, 589.
4 A. Corma, M. T. Navarro and J. Pérez-Pariente, *J. Chem. Soc., Chem. Commun.*, 1994, 47.
5 A. Corma, *Chem. Rev.*, 1997, **97**, 2373.
6 T. Blasco, A. Corma, M. T. Navarro and J. Pérez-Pariente, *J. Catal.*, 1996, **156**, 65.
7 T. Maschmeyer, F. Rey, G. Sankar and J. M. Thomas, *Nature*, 1995, **278**, 159.
8 A. Corma, V. Fornés, S. B. Pergher, Th. L. M. Maesen and J. G. Buglass, *Nature*, 1998, **396**, 353.
9 M. A. Camblor, C. Corell, A. Corma, M. J. Díaz-Cabañas, S. Nicolopoulos, J. M. González-Calbet and M. Vallet-Regí, *Chem. Mater.*, 1996, **8**, 2415.
10 R. Millini, G. Perego, W. O. Parker Jr., G. Bellussi and L. Carluccio, *Microporous Mater.*, 1995 **4**, 221; L. Puppe and J. Weisser, *US Pat.*, 4 439 409, 1984.
11 L. Marchese, E. Gianotti, T. Maschmeyer, G. Martra, S. Coluccia and J. M. Thomas, *Nuovo Cimento Soc. Ital. Fis. D.*, 1997, **11**, 1707.
12 L. Marchese, T. Maschmeyer, E. Gianotti, S. Coluccia and J. M. Thomas, *J. Phys. Chem. B*, 1997, **101**, 8836.
13 T. Blasco, M. A. Camblor, A. Corma and J. Perez-Pariente, *J. Am. Chem. Soc.*, 1993, **115**, 11 806; T. Blasco, M. A. Camblor, A. Corma, P. Esteve, J. M. Guil, A. Martinez, J. A. Perdigon-Melon and S. Valencia, *J. Phys. Chem. B*, 1998, **102**, 75.
14 S. Bordiga, S. Coluccia, C. Lamberti, L. Marchese, A. Zecchina, F. Boscherini, F. Buffa, F. Genoni and G. Leofanti, *J. Phys. Chem.*, 1994, **98**, 4125.
15 T. Blasco, A. Corma, M. T. Navarro and J. Pérez-Pariente, *J. Catal.*, 1995, **156**, 65; F. Rey, G. Sankar, T. Maschmeyer, J. M. Thomas, R. G. Bell and G. N. Greaves, *Top. Catal.*, 1996, **3**, 121.
16 W. Zhang, M. Froeba, J. Wang, P. T. Tanev, J. Wong and T. J. Pinnavaia, *J. Am. Chem. Soc.*, 1996, **118**, 9164.
17 A. Corma, M. Domine, J. A. Gaona, J. L. Jordá, M. T. Navarro, F. Rey, J. Pérez-Pariente, J. Tsuji , B. McCulloch and L. T. Nemeth, *Chem. Commun.*, 1998, 2211.
18 D. C. M. Dutoit, M. Schneider, R. Hutter and A. Baiker, *J. Catal.*, 1996, **161**, 651.

Communication 9/00763F

Smectic liquid-crystalline physical gels. Anisotropic self-aggregation of hydrogen-bonded molecules in layered structures

Norihiro Mizoshita,[a] Takaaki Kutsuna,[a] Kenji Hanabusa[b] and Takashi Kato*[a]

[a] *Department of Chemistry and Biotechnology, Graduate School of Engineering, The University of Tokyo, Hongo, Bunkyo-ku, Tokyo 113-8656, Japan. E-mail: kato@chiral.t.u-tokyo.ac.jp*

[b] *Department of Functional Polymer Science, Faculty of Textile Science and Technology, Shinshu University, Ueda, Nagano 386-8567, Japan*

Received (in Cambridge, UK) 8th February 1999, Accepted 23rd March 1999

Smectic liquid-crystalline states have been successfully gelled by low molecular weight hydrogen-bonded molecules and anisotropic fibrous aggregates of the gelling agents are obtained when the sol–gel transition occurs within the smectic temperature range.

In recent years, a number of low molecular weight compounds have been found to gel various organic solvents.[1] The self-aggregation of the gelling agents through intermolecular interactions, such as hydrogen bonding, leads to the formation of solid fibrous networks in organic solvents. Recently, we have shown that nematic liquid crystals can be gelled by these hydrogen-bonded compounds.[2] Faster electro-optic responses of nematic materials induced by this physical gelation have been achieved in twisted nematic cells.[3] These mixtures of liquid crystals and gelling agents show three thermoreversible states: isotropic liquid, isotropic gel, and liquid-crystalline gel.[2,3] In these cases, the aggregation of the gelling agent occurs in the isotropic state of mesogenic molecules on cooling the sample from the isotropic liquid, which results in the formation of random networks of dispersed fibres. The liquid-crystalline gel is obtained at the transition of the isotropic state to the liquid-crystalline state of mesogenic solvents.

Smectic liquid crystals have higher molecular order which leads to potential applications in functional devices.[4] We expect that the molecular self-organization in smectic mesomorphic order leads to the fabrication of smectic gels, which are a new type of anisotropic material.

Here, we report the anisotropic aggregation of a hydrogen-bonded compound in a smectic molecular structure and the gelation of a smectic liquid crystal. A commercially available ferroelectric liquid crystal, SCE8 (Hoechst), which is a mixture of low molecular weight compounds, was used as a smectic material. On cooling, SCE8 exhibits isotropic–nematic, nematic–smectic A, smectic A–chiral smectic C phase transitions at 102, 78 and 58 °C, respectively. Amino acid derivative **1**, which is able to gel various organic solvents and nematic liquid crystals by the formation of intermolecular hydrogen bonds,[5] was chosen as the gelling agent.

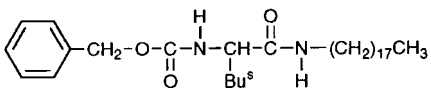

1

When the gelling agent was added to SCE8 and then cooled to room temperature, **1** effectively gelled the smectic liquid-crystalline state. Fig. 1 shows the phase transition behavior of a mixture of SCE8 and **1** as a function of the concentration (wt%) of **1** on cooling. In this system, the sol–gel transition occurs within the range of smectic A and chiral smectic C phases. In the gelation process of SCE8 with **1**, the growth of fibrous network aggregates of **1** and the microphase separation in the polydomain of the smectic liquid-crystalline state have been observed under a polarizing optical microscope.

In order to control the aggregation process of **1** in the smectic liquid-crystalline state, a mixture of SCE8 and **1** was placed between polyimide-coated glass substrates, which had been rubbed in the parallel direction. The mixture was then heated to an isotropic state, and slowly cooled to the required temperature. The formation of fibrous solids ordered in one direction was formed in the smectic liquid-crystalline medium. A polarized photomicrograph of the mixture of SCE8 and **1** containing 1.0 wt% of **1** in a parallel rubbed cell is shown in Fig. 2(*a*). Interestingly, the growing direction of the fibres is perpendicular to the rubbing direction, *i.e.* to the direction of the long axis of the liquid-crystalline molecular order. The scanning electron micrograph (SEM) in Fig. 2(*b*) represents the directional ordering of the bundles of the fibres.† FTIR measurements of the mixture of SCE8 and the anisotropic fibre of **1** in the parallel rubbed cell showed that the absorbance of the amide bond of **1** at 3294 cm^{-1} (N–H stretch) and 1647 cm^{-1} (C=O stretch) was at a maximum value when the polarized light was perpendicular to the molecular orientation of liquid-crystalline molecules, whereas the minimum absorbance was observed when the polarized light was parallel to the long axis of the liquid crystal.‡ These results suggest that compound **1** forms an anisotropic aggregation structure as shown schematically in Fig. 3.

In contrast to the results of the SCE8 mixture, for covalently bonded polymers that are formed in liquid crystals,[6] the direction of the fibre is parallel to the molecular axis of the anisotropic solvents. For the formation of hydrogen-bonded aggregates of compound **1**, the compound is also aligned in the direction of the molecular axis of SCE8 and thereby the hydrogen bonding chains develop in the direction perpendicular to the molecular long axis between the smectic molecular layers.

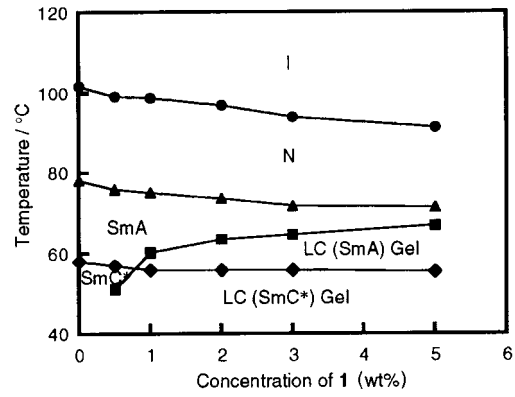

Fig. 1 Phase behavior of a mixture of SCE8 and **1** on cooling. I: isotropic; N: nematic; SmA: smectic A; SmC*: chiral smectic C; LC: liquid-crystalline.

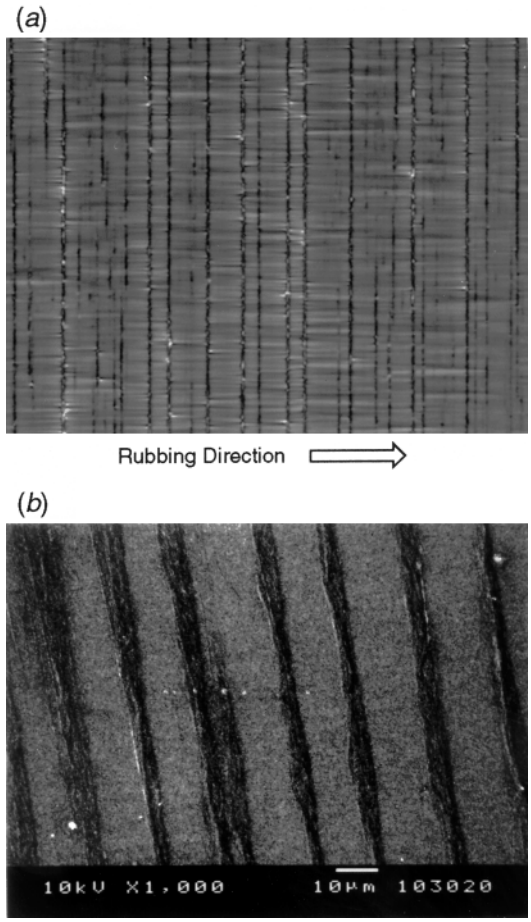

Fig. 2 (*a*) Optical polarized photomicrograph of a mixture of SCE8 and **1** (1.0 wt%) at 60 °C in a parallel rubbed cell; (*b*) SEM image of oriented fibres made of **1** after the extraction of SCE8.

Up until now, although molecular self-aggregation in isotropic solvents has been extensively studied, no attention had been paid to molecular assembly in anisotropic solvents. The present results show a controlled molecular aggregation in anisotropic solvents, which is a new class of self-assembly.

The composite materials of covalently bonded polymers and ferroelectric liquid crystals are studied for potential electro-optic systems.[7] The smectic liquid-crystalline gel reported here is a new material, which is a molecular composite consisting of a molecular aggregate and a smectic solvent. It offers potential applications in dynamically functional molecular materials.

Notes and references

† For SEM observation, samples in the cells were prepared by immersing the liquid-crystalline materials in hexane for two days to remove the liquid-crystalline solvent and finally drying at room temperature.

‡ For polarized FTIR measurements, sample cells were prepared by using BaF_2 substrates instead of glass cells.

1 T. Tachibana, T. Mori and K. Hori, *Bull. Chem. Soc. Jpn.*, 1980, **53**, 1714; K. Hanabusa, T. Miki, Y. Taguchi, T. Koyama and H. Shirai, *J. Chem. Soc., Chem. Commun.*, 1993, 1382; L. Lu and R. G. Weiss, *Langmuir*, 1995, **11**, 3630; R. J. H. Hafkamp, B. P. A. Kokke, I. M. Danke, H. P. M. Geurts, A. E. Rowan, M. C. Feiters and R. J. M. Nolte, *Chem. Commun.*, 1997, 545; A. Aggeli, M. Bell, N. Boden, J. N. Keen, P. F. Knowles, T. C. B. McLeish, M. Pitkeathly and S. E. Radford, *Nature*, 1997, **386**, 259; E. J. de Vries and R. M. Kellogg, *J. Chem. Soc., Chem. Commun.*, 1993, 238; S. W. Jeong, K. Murata and S. Shinkai, *Supramol. Sci.*, 1996, **3**, 83.

2 T. Kato, T. Kutsuna, K. Hanabusa and M. Ukon, *Adv. Mater.*, 1998, **10**, 606; T. Kato, G. Kondo and K. Hanabusa, *Chem. Lett.*, 1998, 193.

3 N. Mizoshita, K. Hanabusa and T. Kato, *Adv. Mater.*, in press.

4 G. W. Gray and J. W. Goodby, *Smectic Liquid Crystals*, Leonard Hill, London, 1984; J. W. Goodby, R. Blinc, N. A. Clark, S. T. Lagerwall, M. A. Osipov, S. A. Pikin, T. Sakurai, K. Yoshino and B. Zeks, *Ferroelectric Liquid Crystals: Principles, Properties and Applications*, Gordon and Breach, Philadelphia, 1991.

5 K. Hanabusa, R. Tanaka, M. Suzuki, M. Kimura and H. Shirai, *Adv. Mater.*, 1997, **9**, 1095; K. Hanabusa and H. Shirai, *Kobunshi Ronbunshu*, 1998, **55**, 585.

6 K. Araya, A. Mukoh, T. Narahara and H. Shirakawa, *Chem. Lett.*, 1984, 1141; K. Akagi, S. Katayama, H. Shirakawa, K. Araya, A. Mukoh and T. Narahara, *Synth. Met.*, 1987, **17**, 241.

7 R. A. M. Hikmet and M. Michielsen, *Adv. Mater.*, 1995, **7**, 300; C. A. Guymon, L. A. Dougan, P. J. Martens, N. A. Clark, D. M. Walba and C. N. Bowman, *Chem. Mater.*, 1998, **10**, 2378; J. W. Goodby, personal communication.

Communication 9/01035A

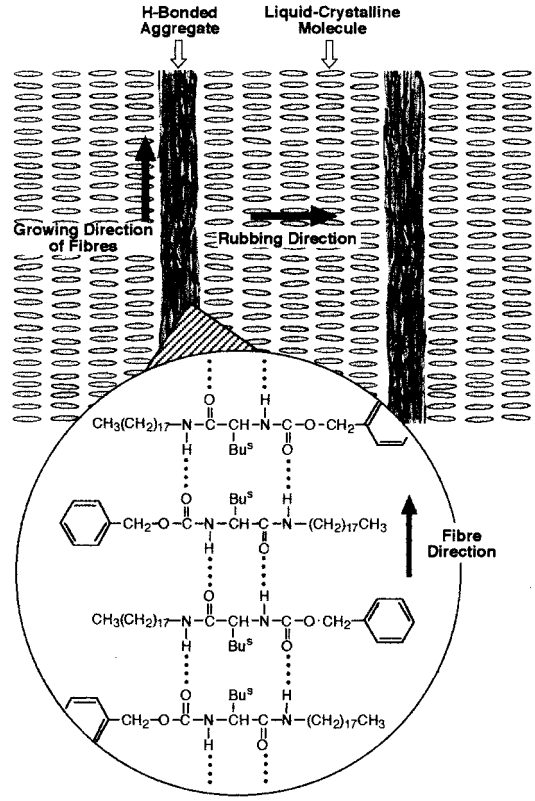

Fig. 3 Schematic representation of the anisotropic aggregation structure of **1** in a smectic liquid crystal.

A new class of single-molecule magnets: mixed-valent $[Mn_4(O_2CMe)_2(Hpdm)_6][ClO_4]_2$ with an $S = 8$ ground state

Euan K. Brechin,[a] Jae Yoo,[b] Motohiro Nakano,[b] John C. Huffman,[a] David N. Hendrickson*[b] and George Christou*[a]

[a] *Department of Chemistry and Molecular Structure Center, Indiana University, Bloomington, IN 47405-4001, USA. E-mail: christou@indiana.edu*

[b] *Department of Chemistry-0358, University of California at San Diego, La Jolla, CA 92093-0358, USA. E-mail: dhendrickson@ucsd.edu*

Received (in Cambridge, UK) 9th February 1999, Accepted 25th March 1999

The reaction of pyridine-2,6-dimethanol (H_2pdm) with $[Mn_3O(O_2CMe)_6(py)_3][ClO_4]$ gives the $2Mn^{II}$, $2Mn^{III}$ title compound 1, which has an $S = 8$ ground state and displays strong out-of-phase signals in ac susceptibility studies that establish 1 as a new class of single-molecule magnet.

The study of molecules with unusually large numbers of unpaired electrons has taken on added impetus in recent years as this area has been identified as the source of a new magnetic phenomenon of relevance to the magnetic materials arena, *i.e.* the ability of molecules below a critical temperature to function as magnetizable magnets.[1–10] Samples of such molecules thus function as collections of extremely small magnetic particles and ones that are of a uniform size distribution in contrast to metal oxide particles (or other magnetic materials) of nanoscale dimensions, which are prepared as a range of particle sizes. To date, $[Mn_{12}O_{12}(O_2CR)_{16}(H_2O)_4]$ ($S = 10$),[1–5] $[Mn_{12}O_{12}(O_2CR)_{16}(H_2O)_4]^-$ salts ($S = 19/2$),[6] $[Mn_4O_3X(O_2CMe)_3(dbm)_3]$ ($S = 9/2$; dbm is the anion of dibenzoylmethane),[7,8] $[Fe_8O_2(OH)_{12}(tacn)_6]^{8+}$ (tacn = 1,4,7-triazacyclononane) salts ($S = 10$)[9] and $[V_4O_2(O_2CR)_7(L–L)_2]^z$ ($S = 3$; L–L = 2,2′-bipyridine, pyridine-2-carboxylate anion)[10] are the most well studied examples. A convenient way of detecting the slow magnetic relaxation (reorientation of the magnetic moment or magnetization vector) of a single-molecule magnet (SMM) is by the appearance of an out-of-phase signal (χ_M'') in ac susceptibility studies showing that the relaxation is too slow to keep up with the oscillating field. We herein report access to a new class of Mn-based SMMs with an $S = 8$ ground state and a strong χ_M'' signal, representing an important new addition to this small family of molecules.

The potentially tridentate chelating ligand pyridine-2,6-dimethanol(H_2pdm), or 2,6-bis(hydroxymethyl)pyridine has been little employed[11,12] in metal chemistry but offers interesting possibilities for transition metal cluster chemistry. Reaction of H_2pdm with $[Mn_3O(O_2CMe)_6(py)_3][ClO_4]$ in a 3 : 1 molar ratio in CH_2Cl_2 gives a red–brown solution from which $[Mn_4(O_2CMe)_2(Hpdm)_6][ClO_4]_2$ **1** precipitates within 24 h. The solid can be recrystallized in *ca.* 50% total yield after three days from a MeCN/Et_2O layering. Diffusion of Et_2O directly into an MeCN reaction solution also gives **1** but in only 15% yield after one week. The centrosymmetric cation of **1**†‡ (Fig. 1) consists of a planar, mixed-valence Mn_4 rhombus with Mn(1) and Mn(2) assigned as being Mn^{III} and Mn^{II}, respectively, on the basis of bond valence sum calculations and the presence at Mn(1) of a Jahn–Teller elongation axis [O(17)–Mn(1)–N(30)], as expected for high-spin Mn^{III}. All ligands are thus only mono-deprotonated (*i.e.* Hpdm) as found for this group previously.[11] Two Mn_3 triangular faces are each bridged by a μ_3-oxygen [O(17)] from a bidentate, chelating Hpdm whose protonated [O(23)] is unbound. Two of the remaining groups are also bidentate, with O(27) bridging Mn(1) and Mn(2′) and O(33) not ligated, but the remaining two Hpdm groups are tridentate with protonated O(13) terminally coordinated and O(7) bridging Mn(1) and Mn(2). Two bridging $MeCO_2^-$ groups complete the ligation. The Mn^{II} metal atoms Mn(2) are thus seven-coordinate with distorted pentagonal bipyramidal geometry, whereas Mn(1) is distorted octahedral. There is an intramolecular hydrogen bond between O(13) and O(23) [2.852(9) Å]. The cation of **1** is the first example of the (H)pdm ligand in a bridging mode and suggests that other clusters might be accessible with this versatile ligand.

Solid-state dc magnetization measurements were performed on **1** in the range 5.0–300 K. The effective magnetic moment (μ_{eff}) slowly increases from 10.5 μ_B at 300 K to 12.8 μ_B at 15.0 K, and then decreases to 11.3 μ_B at 5.0 K, suggesting the complex to have a high spin ground state; the low-temperature decrease is assigned to zero-field splitting (ZFS) and Zeeman effects. Owing to the low symmetry of the cation of **1**, it is not possible to use the Kambe approach to fit the μ_{eff} *vs.* T data with the three requisite J values. In order to determine the ground state, therefore, magnetization data were collected in the temperature and magnetic field ranges 2.00–4.00 K and 20.0–50.0 kG (2–5 T) (Fig. 2). Fitting of these data, assuming only the ground state is populated at $T \leqslant 4.00$ K, gave $S = 8$, $g = 1.85(3)$ and $D = -0.25(3)$ cm^{-1}, where D is the axial ZFS parameter. Thus, **1** is a new example of a species with an unusually large spin.

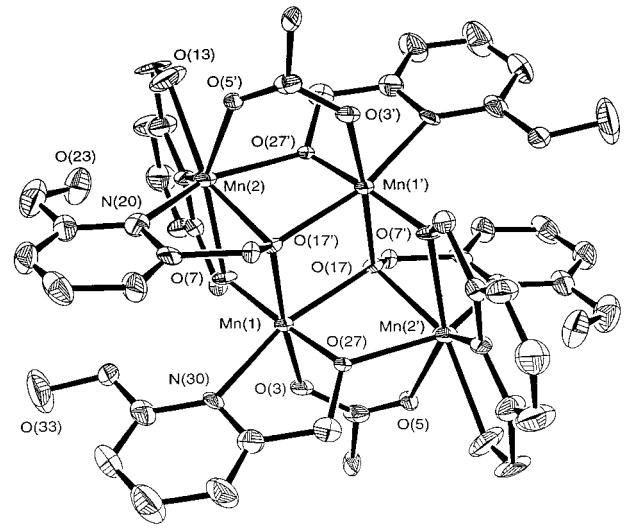

Fig. 1 ORTEP plot with 50% probability ellipsoids of the cation of **1**. Selected interatomic distances (Å) and angles (°): Mn(1)···Mn(1′) 3.253(2), Mn(1)···Mn(2) 3.351(2), Mn(1)···Mn(2′) 3.284(2), Mn(1)–O(7) 1.879(5), Mn(1)–O(17′) 1.967(4), Mn(1)–O(17) 2.264(4), Mn(1)–O(27) 1.873(5), Mn(2)–O(7) 2.271(4), Mn(2)–O(17) 2.300(5), Mn(2)–O(27′) 2.227(4); Mn(1)–O(17)–Mn(1′) 100.27(17), Mn(1)–O(17′)–Mn(2) 103.24(20), Mn(1′)–O(17′)–Mn(2) 92.03(16), Mn(1)–O(7)–Mn(2) 107.30(23), Mn(1′)–O(27′)–Mn(2) 106.13(22).

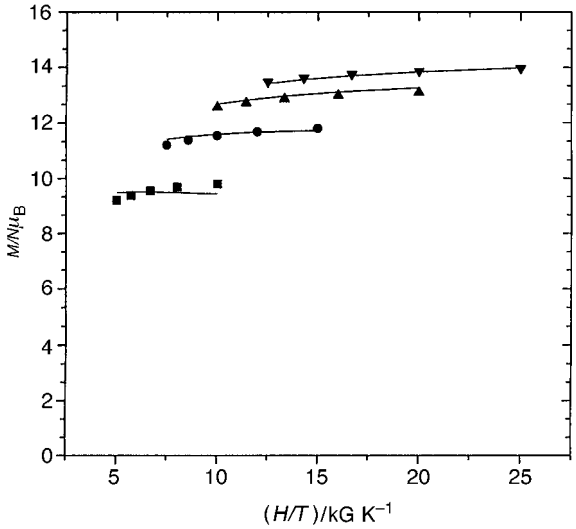

Fig. 2 Plot of reduced magnetization *vs.* *H/T* for complex **1**. The solid lines are fits of the data to an $S = 8$ state with $g = 1.85$ and $D = -0.25$ cm^{-1}. Data were measured at 20 (■), 30 (●), 40 (▲) and 50 kG (▼).

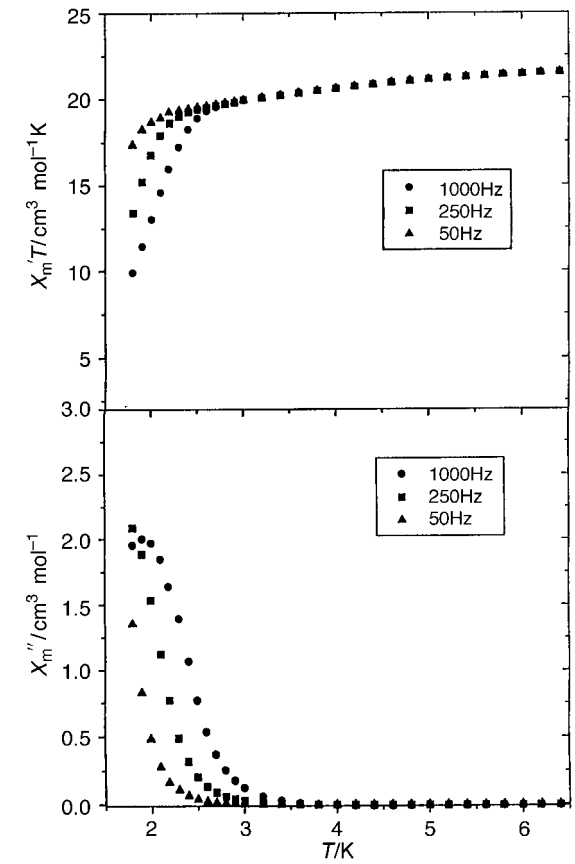

Fig. 3 Plots of the in-phase (χ_M') signal as $\chi_M'T$ and out-of-phase (χ_M'') signal in ac susceptibility studies *vs.* temperature in a 1 G field oscillating at the indicated frequencies.

Complex **1** appeared a good candidate for ac susceptibility studies to determine if it displays the slow magnetization relaxation characteristic of a single-molecule magnet; data were thus collected in the range 1.8–6.4 K range in a 1 G ac field oscillating at 50–1000 Hz. The barrier to thermally activated magnetization relaxation is $S^2|D|$ for an integer spin system, which is 16 cm^{-1} for $S = 8$ and $D = -0.25$ cm^{-1}, a value that is significant compared with thermal energy at low temperature. Indeed, the in-phase $\chi_M'T$ signal (Fig. 3) shows a frequency-dependent decrease at $T < 3.5$ K indicative of the onset of slow relaxation, and this was confirmed by the appearance of an out-of-phase (χ_M'') signal showing that **1** cannot relax fast enough at these temperatures to keep in phase with the oscillating field. The χ_M'' signal is strong, with a peak evident at *ca.* 2 K at a 1000 Hz ac frequency; the peak position corresponds to the temperature at which the relaxation rate is equal to the ac oscillation frequency. A preliminary analysis of the χ_M'' data indicates that the barrier for magnetization relaxation is 12(2) cm^{-1}, in keeping with the presence of magnetization tunnelling. Complex **1** is only the third structural type to show such a strong χ_M'' signal with a peak at $T \geqslant 2$ K, the others being the complexes $[Mn_{12}O_{12}(O_2CR)_{16}(H_2O)_4]^{0,-}$ and $[Mn_4O_3X(O_2C\text{-}Me)_3(dbm)_3]$, and this indicates **1** to be a particularly welcome new addition to this small but growing class of molecules. It also emphasizes that oxide (O^{2-}) bridged clusters are not the sole source of the SMM family of complexes. Efforts are in progress to fit the μ_{eff} *vs.* T data for **1** by a matrix diagonalization approach to determine the individual pairwise exchange interactions, as well as extending studies to $T < 1.8$ K to investigate the degree of hysteresis exhibited by **1**.

This work was supported by the National Science Foundation.

Notes and references

† The complex analysed satisfactorily (C, H, N) as solvent-free. Crystals were kept in contact with mother liquor to avoid solvent loss and were crystallographically identified as **1**·2MeCN.*x*Et$_2$O.

‡ *Crystal data*: $C_{50}H_{60}Cl_2Mn_4N_8O_{24}$ (excl. solv.), $M_r = 1447.75$, triclinic, space group $P\bar{1}$ $a = 11.914(3)$, $b = 15.342(4)$, $c = 9.660(3)$ Å, $\alpha = 104.58(1)$, $\beta = 93.42(1)$, $\gamma = 106.06(1)°$, $U = 1626(3)$ Å^3, $Z = 1$, $T = 105$ K. Residuals R and R_w were 0.0871 and 0.0679, respectively, from refinement on F using 3038 unique data with $F > 2.33\sigma(F)$. The solv group(s) comprised a total of seven peaks (of occupancy *ca.* 50%) assigned to a badly disordered Et$_2$O molecule. CCDC 182/1203. See http://www.rsc.org/suppdata/cc/1999/783/ for crystallographic files in .cif format.

1 R. Sessoli, H.-L. Tsai, A. R. Schake, S. Wang, J. B. Vincent, K. Folting, D. Gatteschi, G. Christou and D. N. Hendrickson, *J. Am. Chem. Soc.*, 1993, **115**, 1804.

2 R. Sessoli, D. Gatteschi, A. Caneschi and M. A. Novak, *Nature*,1993, **365**, 141.

3 J. Tejada, R. F. Ziolo and X. X. Zhang, *Chem. Mater.*, 1996, **8**, 1784; L. Thomas, F. Lionti, R. Ballau, D. Gatteschi, R. Sessoli and B. Barbara, *Nature*, 1996, **383**, 145.

4 J. R. Friedman, M. P. Sarachik, J. M. Hernandez, X. X. Zhang, J. Tejada, E. Molins and R. Ziolo, *J. Appl. Phys.*, 1997, **81**, 3978.

5 D. Ruiz, Z. Sun, B. Albela, K. Folting, J. Ribas, G. Christou and D. N. Hendrickson, *Angew. Chem., Int. Ed. Engl.*, 1998, **37**, 300.

6 H. J. Eppley, H.-L. Tsai, N. de Vries, K. Folting, G. Christou and D. N. Hendrickson, *J. Am. Chem. Soc.*, 1995, **117**, 301.

7 S. M. J. Aubin, M. W. Wemple, D. M. Adams, H.-L. Tsai, G. Christou and D. N. Hendrickson, *J. Am. Chem. Soc.*, 1996, **118**, 7746.

8 S. M. J. Aubin, N. R. Dilley, L. Pardi, J. Krzystek, M. W. Wemple, L.-C. Brunel, M. B. Maple, G. Christou and D. N. Hendrickson, *J. Am. Chem. Soc.*, 1998, **120**, 4991.

9 C. Sangregorio, T. Ohm, C. Paulsen, R. Sessoli and D. Gatteschi, *Phys. Rev. Lett.*, 1997, **78**, 4645.

10 S. L. Castro, Z. Sun, C. M. Grant, J. C. Bollinger, D. N. Hendrickson and G. Christou, *J. Am. Chem. Soc.*, 1998, **120**, 2977.

11 F. D. Rochon, R. Melanson and P.-C. Kong, *Inorg. Chim. Acta*, 1997, **254**, 303; T. I. A. Gerber, J. Bruwer, G. Bandoli, J. Perils and J. G. H. du Preez, *J. Chem. Soc., Dalton Trans.*, 1995, 2189.

12 J. M. Berg and R. H. Holm, *Inorg. Chem.*, 1983, **22**, 1768.

Communication 9/01106D

ChemComm

Flavins as modular and amphiphilic probes of silica microenvironments

Michael D. Greaves, Robert Deans, Trent H. Galow and Vincent M. Rotello*

Department of Chemistry, University of Massachusetts, Amherst, Massachusetts 01003, USA.
E-mail: rotello@chem.umass.edu

Received (in Columbia, MO, USA) 21st October 1998, Accepted 16th March 1999

The amphiphilic and solvochromatic characteristics of flavins are utilized as a non-invasive polarity sensor for silica-based media.

Zeolites, molecular sieves and other porous media are crucial components in catalysis and separation technology.[1,2] In these systems, surface structure is a key determinant of performance. To determine surface and pore polarities, both silicas[3] and sol–gels[4] have been doped with various dyes. These dyes have generally relied upon large hydrophobic aromatic groups, with charged functionality as the sensing element. This creates the potential for perturbation of local environments through both dopant size and functionality.[5]

N^{10}-isobutyl flavin **1** (Fig. 1) and flavin mononucleotide (FMN) **2** possess isoalloxazine units with highly solvochromic S_0–S_2 transitions: λ_{max} (FMN) **2** occurs at 374 nm in aqueous media and 358 nm in ethanolic solution,[6] while λ_{max} (**1**) occurs at 349 nm in chloroform and 335 nm in carbon tetrachloride.[7] The amphiphilicity of the heterocyclic flavin nucleus plays two key roles in microenvironment sensing. First, it allows solubilization without aggregation[8] in virtually any solvent using non-interfering sidechains at the N^{10} position. Second, it provides a non-invasive probe for the characterization of dynamic media. We report here the application of flavins **1** and **2** as solvochromic probes of silicate microenvironments.

In initial investigations, we explored the environment of silica gel environment. Flavin **1** in chloroform has a λ_{max} of 349 nm (Fig. 2). When commercial grade silica gel[9] was soaked with a chloroform solution of **1** (providing an approximate matching of refractive index), the λ_{max} shifted to 374 nm, indicating the flavin was responding as expected to the polar surface of the silica gel.

In further studies, we used flavin to probe the polarity of 'MCM-type' silicates. The final preparation of these porous silica materials involves calcination at high temperatures in which the polar Si–OH functionalities on the interior silica surface revert to Si–O–Si *via* dehydration.[10] When a non-calcined, templated silica material[11] was soaked with a chloroform solution of **1**, the λ_{max} (S_0–S_2) was 374 nm. This indicates that the surface was highly polar with surface functionality consisting primarily of Si–OH groups. However, the λ_{max} occurred at 349 nm with a calcined MCM-41 type material,[12] confirming no interaction between the flavin and the interior surface (Fig. 2). This is consistent with the low surface density (8–27%) of silanols present in calcined MCM-41.[13]

With the ability of flavin to sense polarity in preformed, static environments established, we next explored the application of this sensing methodology to dynamic systems. Previous studies had seen relatively minor changes in polarity in silicate matrices during their formation *via* the sol–gel process, a result that could arise from 'templating' effects by the sensing molecule. To explore polarity changes in these systems, flavin silicate sols were prepared by the addition of aqueous solutions of flavin **2** to tetramethylorthosilicate. After sonication, homogeneous and transparent yellow sols were obtained which subsequently solidified yielding the flavin **2** functionalized sol–gels. In these gels, the flavin provides a direct probe the polarity of the microenvironment within the developing sol–gel silicate. In the sol phase, the λ_{max} of flavin **2** occurred at 374 nm, confirming the essentially aqueous nature of the sol–gel at preparation. Polarity changes indicative of a two-step transformation were observed. During the initial stages of gelation a large decrease in polarity was observed, arising from release of methanol during orthosilicate hydrolysis. After this initial phase, the λ_{max} moved steadily to shorter wavelengths, reaching a limiting value of 360 nm (Fig. 3). This slower process can be attributed to the decrease in silanol concentration during the formation of the silicate matrix.

When these methanol-rich sol–gels were allowed to dry under ambient conditions, the λ_{max} shifted to longer wavelengths, reaching a final value of 370 nm (Fig. 3). This red shift arises from the diffusion of methanol out of the silicate matrix, resulting in shrinkage of the silicate structure.[14] Constricting the region surrounding the flavin. In consequence, the polar Si–OH functionalities of the silicate matrices interact with the immobilized flavin, creating a microenvironment slightly less polar than water.[15]

In conclusion, we have shown flavins nucleus to be extremely capable microenvironmental probes of silicate-based media. The amphiphilicity and solvochromicity of the isoalloxazine nucleus, coupled with its non-invasive nature, make these

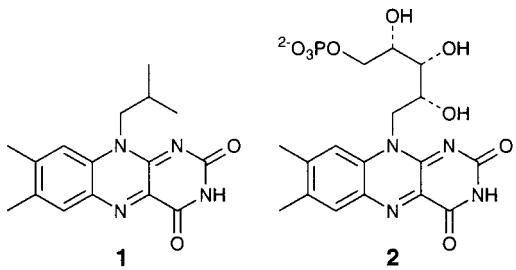

Fig. 1 N^{10}-*iso*butyl flavin **1** and flavin mononucleotide (FMN) **2**.

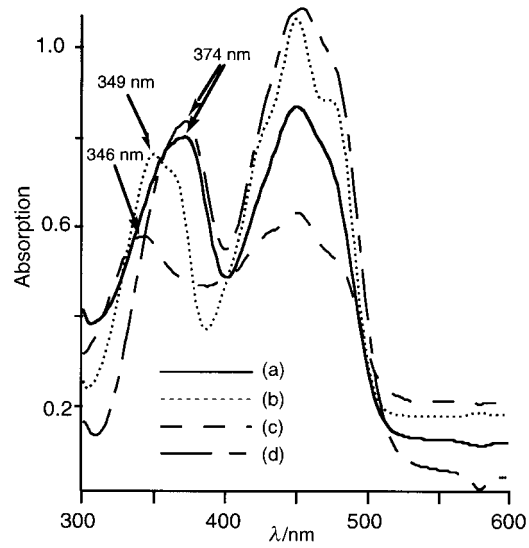

Fig. 2 UV–VIS spectra of **1** in (a) silica–$CHCl_3$ suspension; (b) $CHCl_3$; (c) MCM-41–$CHCl_3$ slurry; (d) non-calcined MCM–$CHCl_3$ slurry ([**1**] = 7.0×10^{-5} M).

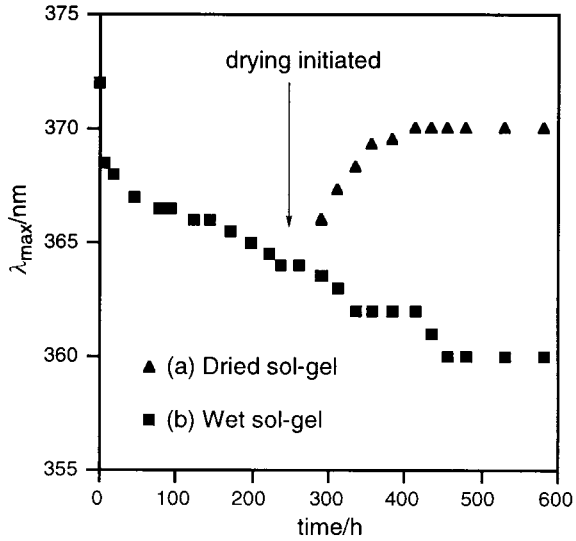

Fig. 3 Plot of λ_{max} for the S_0–S_2 transition of **2** as a function of sol–gel formation.

systems effective probes of polarity for both static and dynamic systems.

We would like to thank a referee for helpful suggestions. This research was supported by the National Science Foundation (CHE-9703466). V. R. acknowledges support from the Alfred P. Sloan Foundation, Research Corporation, and the Camille and Henry Dreyfus Foundation.

Notes and references

1 For reviews, see: M. E. Davis, *Acc. Chem. Res.*, 1993, **26**, 111; P. T. Tanev and T. J. Pinnavaia, *Access in Nanoporous Materials*, Plenum Press, New York, 1995, pp. 13–28.

2 C. T. Kresge, M. E. Leonowicz, W. J. Roth, J. C. Vartuli and J. S. Beck, *Nature*, 1992, **359**, 710; J. S. Beck, J. C. Vartuli, W. J. Roth, M. E. Leonowicz, C. T. Kresge, K. D. Schmitt, C. T.-W. Chu, D. H. Olson, E. W. Sheppard, S. B. McCullen, J. B. Higgins and J. L. Schlenker, *J. Am. Chem. Soc.*, 1992, **114**, 10 834; J. C. Vartuli, C. T. Kresge, M. E. Leonowicz, A. S. Chu, S. B. McCullen, I. D. Johnson and E. W. Sheppard, *Chem. Mater.*, 1994, **6**, 2070; S. Schacht, Q. Huo, I. G. Voigt-Martin, G. D. Stucky and F. Schüth, *Science*, 1996, **273**, 768; P. T. Tanev, Y. Liang and T. J. Pinnavaia, *J. Am. Chem. Soc.*, 1997, **119**, 8616; K. M. McGrath, D. M. Dabbs, N. Yao, I. A. Aksay and S. M. Gruner, *Science*, 1997, **277**, 552.

3 S. J. Tavener, J. H. Clark, G. W. Gray, P. A. Heath and D. J. MacQuarrie, *Chem. Commun.*, 1997, 1147; S. Spange, A. Reuter and E. Vilsmeier, *Colloid Polym. Sci.*, 1996, **274**, 59; M. Kosmulski, *J. Colloid Interface Sci.*, 1996, **179**, 128; Z. Li and S. C. Rutan, *Anal. Chim. Acta*, 1995, **312**, 127; C. G. Flowers, S. Lindley and J. E. Leffler, *Tetrahedron Lett.*, 1984, **25**, 4997.

4 U. Narang, J. D. Jordan, F. V. Bright and P. N. Prasad, *J. Phys. Chem.*, 1994, **98**, 8101; F. Nishida, J. M. McKiernan, B. Dunn, J. I. Zink, C. J. Brinker and A. J. Burd, *J. Am. Ceram. Soc.*, 1995, **78**, 1640; L. M. Ilharco, A. M. Santos, M. J. Silva and J. M. G. Martinho, *Langmuir*, 1995, **11**, 2419. For reviews, see: D. Avnir, *Acc. Chem. Res.*, 1995, **28**, 328; B. Dunn and J. I. Zink, *Chem. Mater.*, 1997, **9**, 2280.

5 R. C. Chambers, Y.Haruvy and M. A. Fox, *Chem. Mater.*, 1994, **6**, 1351.

6 For a detailed UV–VIS investigation of solvent effects on flavins bearing ribose functionalities in the N^{10} position, see: J. Koziol, *Photochem. Photobiol.*, 1966, **5**, 41.

7 For detailed UV–VIS studies of solvent effects on flavin moieties bearing an alkyl functional group in the N^{10} position, see: H. A. Harbury, K. F. LaNoue, P. A. Loach and R. M. Amick; *Proc. Natl. Acad. Sci. USA*, 1959, **45**, 1708; P. F. Heelis, *Chem. Soc. Rev.*, 1982, **11**, 15; J. Koziol, *Photochem. Photobiol.*, 1969, **9**, 45.

8 UV–VIS dilution studies of isobutylflavin **1** in $CHCl_3$ and EtOH, and FMN **2** in H_2O demonstrated that no aggregation took place for the concentrations used in these studies.

9 EM Science Silica Gel 60: 0.040–0.063 mm particle size, 0.71–0.78 mL g^{-1} pore volume and 490 m^2 g^{-1} surface area (BET). Silica gel was suspended in chloroform for these experiments to minimize light scattering *via* refractive index matching during UV–VIS measurements.

10 C.-Y. Chen, S. L. Burkett, H.-X. Li and M. E. Davis, *Microporous Mater.*, 1993, **2**, 27.

11 The procedure for the preparation of this material was derived from: D. J. MacQuarrie, *Chem. Commun.*, 1996, 1961.

12 The sample the MCM-41 was kindly provided by Professor M. Tsapatsis.

13 C.-Y. Chen, H.-X. Li and M. E. Davis, *Microporous Mater.*, 1993, **2**, 17; B. P. Feuston and J. B. Higgins, *J. Phys. Chem.*, 1994, **98**, 4459.

14 U. Narang, R. Wang, P. N. Prasad and F. V. Bright, *J. Phys. Chem.*, 1994, **98**, 17.

15 The polarity determined using FMN is similar, but higher than that found by previous researchers. This can be attributed to the hydrophobicity of the probes used in these studies: D. Avnir, D. Levy and R. Reisfeld, *J. Phys. Chem.*, 1984, **88**, 5956; K. Matsui and T. Nakazawa, *Bull. Chem. Soc. Jpn.*, 1990, **63**, 11.

Communication 8/08194H

$[Mo^{V}_{2}Mo^{VI}_{6}V^{IV}_{8}O_{40}(PO_4)]^{5-}$: the first polyanion with a tetra-capped Keggin structure

Yan Xu,* Hao-Guo Zhu, Hu Cai and Xiao-Zeng You*

Coordination Chemistry Institute, State Key Laboratory of Coordination Chemistry, Nanjing University, Nanjing, 210093 P. R. China. E-mail: SKLC@uju.edu.cn

Received (in Cambridge, UK) 3rd February 1999, Accepted 24th March 1999

The new mixed Mo/V heteropoly compound $[Ni(C_2N_2H_8)_3]_2Na[Mo^{V}_{2}Mo^{VI}_{6}V^{IV}_{8}O_{40}(PO_4)]\cdot H_2O$ with a tetra-capping Keggin structure has been synthesized hydrothermally and its structure determined by X-ray diffraction

There is considerable current interest in polyoxometalates containing Keggin moieties from both fundamental and practical points of view.[1,2] They are capable of being fine-tuned at the molecular level to promote a variety of applications ranging from catalysis to medicinal use.[3–7] To our knowledge, in contrast to an extensive literature on Keggin and transition metal substituted Keggin species, structural information relating to capped Keggin structures is very limited due to the lack of good quality single crystals, and only bi- and mono-capped Keggin derivatives are structurally known.[8–18] It has been recently demonstrated that the hydrothermal technique is well suited for the preparation and crystal growth of mixed Mo/V heteropoly compounds.[16–18] Here, we report the application of this technique to an Mo/V system which has resulted in the formation of $[Ni(C_2N_2H_8)_3]_2Na[Mo^{V}_{2}Mo^{VI}_{6}V^{IV}_{8}O_{40}(PO)_4].H_2O$ **1**, the first mixed Mo/V tetra-capped Keggin structure heteropoly compound to be structurally characterised.

Compound **1** was prepared hydrothermally from a mixture of NH_4VO_3, $Ni(OAc)_2$, Na_2MoO_4, en, H_3PO_3 and H_2O heated to 160 °C for six days.† The IR spectrum of **1** exhibited a complex pattern of bands at 1060, 940, 920, 720 and 650 cm^{-1}, ascribed to ν(P–O), ν(M=O), ν(M–O–M) (M = V or Mo), respectively. A novel discrete polyanion $[Mo^{V}_{2}Mo^{VI}_{6}V^{IV}_{8}O_{40}(PO)_4]^{5-}$, counter ions Na^+, $[Ni(C_2N_2H_8)_3]^{2+}$ and lattice water molecules were revealed by X-ray analysis.‡ The polyanion $[Mo^{V}_{2}Mo^{VI}_{6}V^{IV}_{8}O_{40}(PO_4)]^{5-}$ (Fig. 1) is based on the well known Keggin structure of $[XM_{12}O_{40}]^{n-}$ with four additional five-coordinated terminal VO^{2+} units, which include V(3) and its symmetry-related partner V(4) and V(5). The polyanion lies on a crystallographic twofold axis at *x*, 0, 0.25 which passes through P, V(4) and V(5), and it is disordered. The cluster anion contains a central P^{5+} in an almost regular tetrahedral environment of PO_4 with P–O distances in the range 1.514(7)–1.518(6) Å, and bond angles of 108.5(4)–110.3(4)°.

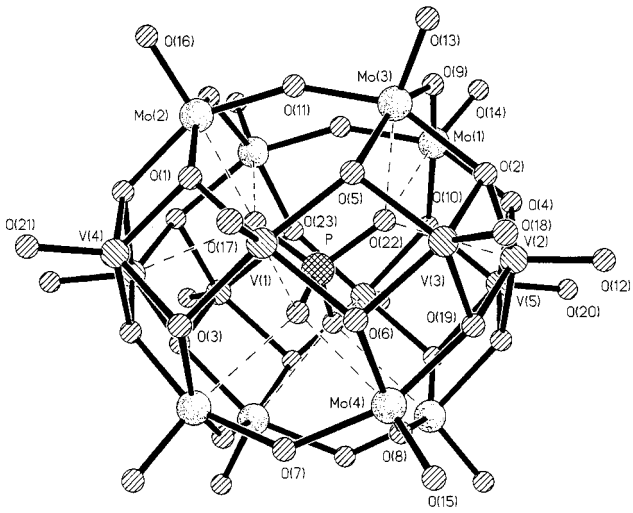

Fig. 1 Ball-and-stick representation of the structure of the polyanion $[Mo^{V}_{2}Mo^{VI}_{6}V^{IV}_{8}O_{40}(PO_4)]^{5-}$ in **1**

The number of Mo sites revealed by X-ray analysis is consistent with the result of elemental analysis§ which gave an average ratio Mo/V of 1.0. While all the Mo atoms have a distorted octahedral environment, vanadium displays two different coordination environments square pyramidal and distorted octahedral. The Mo–O and V–O bond lengths are in the range 1.661(9)–2.543(5) and 1.589(8)–2.562(7) Å, respectively, comparable to those found in capping-Keggin structures. As shown in Fig. 1, the unusual feature of compound **1** is that the V=O units cap four of the six available four coordinate sites on the surface of the $[Mo^{V}_{2}Mo^{VI}_{6}V^{IV}_{4}O_{40}(PO_4)]^{13-}$ Keggin anion so as to produce a structure in which the vanadium atoms form a central belt, and each trimetallic group of $[Mo^{V}_{2}Mo^{VI}_{6}V^{IV}_{4}O_{40}(PO_4)]^{13-}$ (Keggin part) contains one V and two Mo atoms. The Mo_4 rings (each one-electron-reduced) are bonded above and below this V_8 belt. To the best of our knowledge, such a tetra-capped Keggin structural polyanion has not been previously observed in other heteropoly compounds. Only a Ni^{2+} signal was evident (g = 2.07) in the room temperature EPR spectra, the lack of signals for Mo^{5+} and V^{4+} indicating that the 10 electrons of the polyanion are delocalised. The assignment of oxidation states for the vanadium and molybdenum atoms are consistent with their coordination geometries and are confirmed by valence sum calculations[19] which gives the values for Mo(1), Mo(2), Mo(3) and Mo(4) of 5.45, 6.007, 5.656 and 5.870, while the calculated valence sum for V(1), V(2), V(3), V(4) and V(5) are 3.901, 4.180, 4.103, 4.501 and 3.685, respectively. The average value for calculated oxidation state of Mo and V are 5.746 and 4.074, consistent with the formula of **1**. The Ni^{2+} cations are coordinated by three ethylene diamine ligands with Ni–N distances in the range 1.999(4)–2.208(7) Å.

This research was supported by the National Foundation of China and Key Project of the Ministry of Science and Technology.

Notes and references

† A mixture of NH_4VO_3 (0.40 g), $Ni(OAc)_2$(0.40 g), Na_2MoO_4 (0.8 g), en (2 ml) and H_2O (10 ml) ratio was neutralized to pH = 6.0 with 50% phosphorous acid. It was then sealed in a 15 cm^{-3} Teflon-lined reactor, which was heated to 160 °C for six days. After cooling to room temperture, black needle crystals were isolated (0.4 g, 48% based on Mo).

‡ *Crystal data* for **1**: tetragonal, space group $P4_322$, $a = b$ = 15.829(2) c = 28.712(6) Å, v = 7194(2) $Å^3$, Z = 4. A black needle crystal with dimension of 0.22 × 0.16 × 0.14 mm was mounted on a glass fiber. Data were collected on Siemens P4 four-circle diffractometer at 20 °C in the range $3.64 < 2\theta < 23.05°$ using the ω scan technique. A total of 12486 reflections was collected of which 8353 with $I > 2\sigma(I_0)$ were used. An empirical absorption correction was applied. The structure was solved by direct methods and refined using SHELX86 and SHELXL93 programs. The occupancy factor of major conformation [Mo(1)–Mo(4), V(1)–V(3),

O(91)–O(19)] is 0.8564(6). The metal atoms and P atom were refined anisotropically, and the remaining non-metal atoms were refined isotropically. Structure solution and refinement based on 5046 reflections with $I > 2\sigma(I_0)$ and 382 parameters gave $R(R_w) = 0.0765$ (0.1987). CCDC 182/1204. See http://www.rsc.org/suppdata/cc/1999/787/ for crystallographic files in .cif format.

§ Anal. Calc. for $Mo_8Ni_2V_8NaPO_{45}C_{12}N_{12}H_{50}$: Mo, 31.28; V, 16.80; Ni, 4.83; P, 1.28; Na, 0.95; C, 5.93; N, 6.91; H, 2.02. Found: Mo, 29.60; V, 16.24; Ni, 4.98; P, 1.36; Na, 1.10; C, 5.79; N, 6.71; H, 2.16%.

1 G. M. Brown, M. R. Noe-Spirlet, W. R. Busing and H. A. Levy, *Acta Crystallogr., Sect. B*, 1977, **33**, 1038.
2 H. T. Jr. Evans, *Perspect. Struct. Chem.*, 1971, **4**, 1.
3 M. T. Pope, *Heteropoly and Isopoly Oxometalates*, Springer-Verlag, Berlin, 1983.
4 V. W. Day and W. G. Klemperer, *Science*, 1985, **228**, 533.
5 M. T. Pope and A. Muller, *Angew. Chem., Int. Ed. Engl.*, 1991, **30**, 34.
6 M. T. Pope and A. Muller, *Polyoxometalates: From Platonic Solids to Anti-Retroviral Activity*, Kluwer Academic Publishers, Dordrecht, The Netherlands, 1994.
7 C. L. Hill and C. M. Prosser-McCartha, *Coord. Chem. Rev.*, 1995, **143**, 407.
8 D. Hou, S. K. Hagen and C. L. Hill, *J. Chem. Soc., Chem. Commun.*, 1993, 426.
9 R. Kato, A. Kobayaski and Y. Sasaki, *J. Am. Chem. Soc.*, 1980, **102**, 6572.
10 M. I. Khan, J. Zubieta and P. Toscano, *Inorg. Chim. Acta*, 1992, **193**, 17.
11 M. I. Khan, Q. Chen and J. Zubieta, *Inorg. Chim. Acta*, 1993, **212**, 199.
12 M. I. Khan, Q. Chen and J. Zubieta, *Inorg. Chem.*, 1993, **32**, 2924.
13 G. Q. Huang, S. W. Zhang, Y. G. Wei and M. C. Shao, *Polyhedron*, 1993, **12**, 1483.
14 A. Muller, M. Koop, P. Schiffels and H. Bogge, *Chem. Commun.*, 1997, 1715.
15 A. Seling, I. Anderson, L. Petterssin, C. M. Schramm, S. L. Downey and J. H. Grate, *Inorg. Chem.*, 1994, **33**, 3141.
16 Y. Zhang, R. C. Haushalter and A. Clearfield, *J. Chem. Soc., Chem. Commun.*, 1995, 1149.
17 L. Q. Chen and C. L. Hill, *Inorg. Chem.*, 1996, **35**, 2403.
18 Y. Xu, J. Q. Xu, G. Y. Yang, T. G. Wang, Y. Xing, Y. H. Ling and H. Q. Jia, *Polyhedron*, 1998, **17**, 2441.
19 M. O'Keeffe and A. Navrotsky, *Structure and Bonding in Crystals*, Academic Press, New York, 1981.

Communication 9/00928K

ChemComm

Stabilities of cooperatively formed cyclic pseudorotaxane dimers

Nori Yamaguchi and Harry W. Gibson*

Department of Chemistry, Virginia Polytechnic Institute and State University, Blacksburg, Virginia, USA. E-mail: hwgibson@vt.edu

Received (in Cambridge, UK) 8th February 1999, Accepted 24th March 1999

Systematic analysis of the stabilities of cyclic pseudorotaxane dimers formed between complimentary homoditopic molecules demonstrates that cooperative cyclic dimerization can be minimized by increasing the length of one component *via* an aliphatic spacer.

Recently, we reported preparation of supramolecular linear polymer **5b** (Scheme 1) with up to 9.1 repeat units in which monomeric homoditopic molecules **1** and **2b** containing

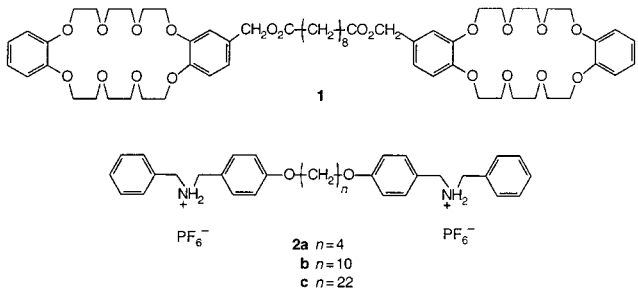

dibenzo-24-crown-8 (DB24C8) and dibenzylammonium hexafluorophosphate moieties, respectively, are linked non-covalently *via* pseudorotaxane complexes in equimolar concentrated solutions (> 1.0 M in CD_3COCD_3–$CDCl_3$, 1 : 1 v/v at 295 K).[1]

Unsurprisingly, cyclic dimer **4b** (Scheme 1) was preferentially formed in equimolar dilute solutions ($< 1.0 \times 10^{-3}$ M in CD_3COCD_3–$CDCl_3$, 1 : 1 v/v at 295 K) as observed in other cases.[2–6] In pursuit of more efficient construction of supramolecular polymers **5**, we speculated that by mismatching the lengths of the aliphatic spacer units in the homoditopic molecules (*e.g.* **1** and **2**),† the equilibrium process may be reversed to favor linear extension (*e.g.* **3** and then to **5**) even in dilute conditions largely due to a greater steric penalty associated with the corresponding cyclic dimer complex (*e.g.* **4**).‡ Here, we investigate the stabilities of cyclic and linear dimer complexes based on complementary homoditopic molecules whose spacer segments were varied systematically.

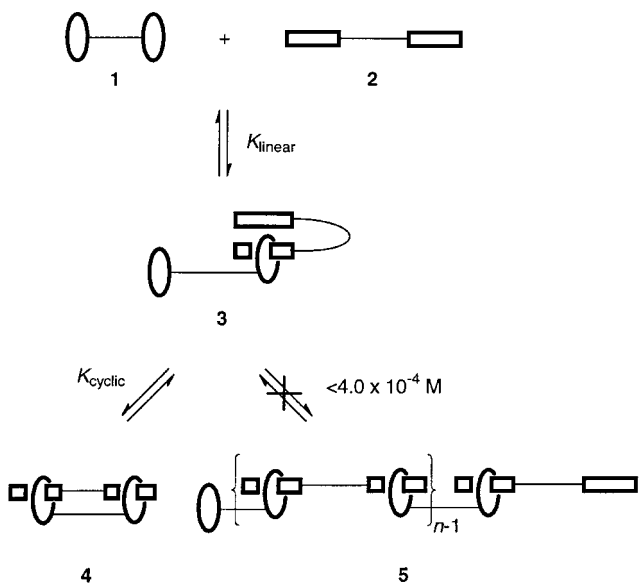

Scheme 1 Cartoon illustrations of formation of the linear dimer complex **3** and cyclic dimer complex **4** from homoditopic molecules **1** and **2** in substantially dilute conditions.

The ^{1}H NMR spectra of dilute equimolar solutions of **1** and **2** [Fig. 1(*a*)–(*c*)] revealed four sets of N-CH_2 signals corresponding to (i) uncomplexed moieties of the ditopic guest molecule [H(**2**)$_u$], (ii) complexed moieties in cyclic dimer [H(**4**)], and (iii) complexed and (iv) uncomplexed moieties in the linear dimer [H(**3**)$_c$ and H(**3**)$_u$, respectively] on the basis of slow exchange on the NMR time scale.§ Integration of H(**3**)$_c$ and H(**3**)$_u$ gave a ratio of 1:1 for each solution,¶ indicating that the signals assigned to H(**3**)$_c$ and H(**3**)$_u$ arise from the same species.

The signal assignments were properly made based on our previous investigation[1] and the ^{1}H NMR spectrum [Fig. 1(*d*)] of a dilute solution of DB24C8 and **2b** which exhibited three sets of N-CH_2 signals corresponding to uncomplexed ammonium salt moieties of **2b** [H(**2b**)$_u$]‖ and complexed and uncomplexed ammonium salt moieties of **6b** [H(**6b**)$_c$ and H(**6b**)$_u$, respectively].** The signals for H(**6b**)$_c$ and H(**6b**)$_u$ were integrated to be 1 : 1; thus complex **6b** was exclusively formed, confirming that the two signals assigned to **6b** (and to **3**) arise from the same species. The considerable downfield chemical shift observed for H(**6b**)$_u$ with respect to H(**2b**)$_u$ in Fig.1(*d*) ($\Delta\delta$ = 0.17 ppm) is presumably a consequence of interaction(s) between the pseudorotaxane and free ammonium salt moieties in **6b** (and by analogy in **3**); *e.g.* 'intramolecular' π-stacking between a benzo ring of complexed DB24C8 and the terminal phenyl ring of the free ammonium salt moiety achieved by folding of the flexible aliphatic spacer, as illustrated in Scheme 2.†† These spectroscopic observations allowed us to conclude that the signals in the region of δ 4.35 to 4.45 in Fig. 1(*a*)–(*c*) correspond to H(**3**)$_u$, and that only **3** and **4** exist and cyclic or linear oligomers **5** are not present in detectable amounts in these dilute solutions.

Since the concentrations of each species (**1**, **2**, **3** and **4**) at equilibrium are readily known, one can estimate the association

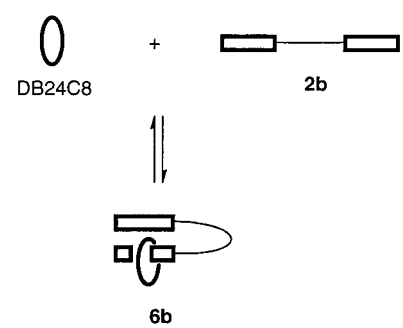

Scheme 2 Cartoon illustrations of formation of the 1 : 1 dimer complex **6b** from DB24C8 and homoditopic molecule **2b** in substantially dilute conditions.

Table 1 Association constants (K_{linear}) at 295 K and enthalpy and entropy for linear dimerization in CD_3COCD_3–$CDCl_3$ (1 : 1, v/v)[a]

Complex	K_{linear}/M^{-1}	ΔH_1/kcal mol^{-1}	ΔS_1/cal mol^{-1} K^{-1}
3a	(1.3 ± 0.3) × 10^3	−8.0 ± 0.6	−13 ± 1
3b	(3.7 ± 0.7) × 10^3	−11 ± 2	−20 ± 3
3c	(5.2 ± 0.6) × 10^3	−10 ± 3	−23 ± 7

[a] ± values represent standard deviations.

Table 2 Association constants (K_{cyclic}) at 295 K and enthalpy and entropy for cyclic dimerization in CD_3COCD_3–$CDCl_3$ (1 : 1, v/v)[a]

Complex	K_{cyclic}/M^{-1}	ΔH_c/kcal mol^{-1}	ΔS_c/cal mol^{-1} K^{-1}
4a	2.5 ± 0.4	−8.6 ± 1.0	−27 ± 2
4b	1.7 ± 0.3	−3.7 ± 0.1	−12 ± 1
4c	0.62 ± 0.03	−2.1 ± 0.6	−8.1 ± 0.4

[a] ± values represent standard deviations.

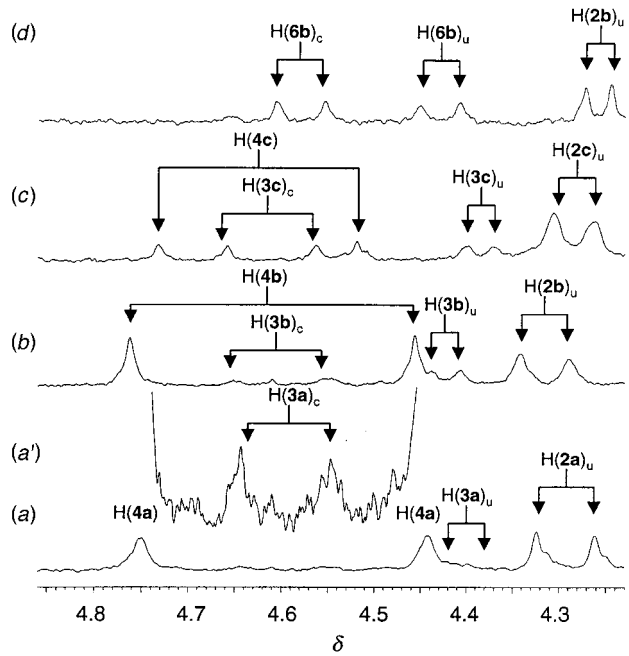

Fig. 1 The stacked ^{1}H NMR spectra of equimolar solutions of (*a*) **1** and **2a**, (*b*) **1** and **2b**, and (*c*) **1** and **2c** (4.0 × 10^{-4} M each) and (*d*) a solution of DB24C8 and **2b** (8.0 × 10^{-4}/4.0 × 10^{-4} M) at 295 K (400 MHz, CD_3COCD_3–$CDCl_3$, 1 : 1, v/v). A vertically enlarged version of the spectrum in Fig. 1(*a*) (δ 4.45-4.75) is shown in Fig. 1(*a*′). In Fig. 1(*a*)–(*c*) the four sets of signals are assigned for the benzylic protons of the ammonium salt units in **2** (uncomplexed, u), **3** (complexed end, c, and uncomplexed end, u) and **4**. In Fig. 1(*d*) the three sets of signals are assigned for the benzylic protons of the ammonium salt units in **2b** (uncomplexed, u) and **6b** (complexed end, c, and uncomplexed end, u).

constants (K_{linear} and K_{cyclic}); the results at 295 K are summarized in Tables 1 and 2 with ΔH and ΔS values.‡‡

K_{linear} (Table 1) varies systematically, increasing as the length of the aliphatic spacer increases (from **3a** to **3c**). Note that ΔH_1 and ΔS_1 become more negative from **3a** to **3b**, but the values for **3b** and **3c** are essentially identical. This observation is consistent with more effective stabilization of **3b** and **3c** relative to **3a** by 'intracomplex' interaction between the threaded crown ether and the non-threaded ammonium salt moiety; as shown by CPK models the longer spacers in the latter two species allow more effective interaction.

Similarly, K_{cyclic} (Table 2) varies systematically, decreasing as the length of the aliphatic spacer increases (from **4a** to **4c**). ΔH_c and ΔS_c also become less negative as the spacer length increases, the most dramatic change taking place from **4a** to **4b**. These observations are consistent with two factors: (i) limited stabilization of precursor **3a** by intracomplex interaction and (ii) the increasing end-to-end distance of the linear precursors **3**.

As we anticipated, K_{cyclic} for **4c** was reduced, almost three-fold, compared to that for **4b**. Most importantly, the K_{linear}/K_{cyclic} value, which should be regarded as a critical parameter for the efficiency of linear extension to **5**, obtained for **3c**/**4c** (8.4 × 10^3 M^{-1}) clearly stands out, showing nearly a 16-fold improvement with respect to that of **3a**/**4a** (5.2 × 10^2 M^{-1}).

Our present results, contrary to our initial speculation, indicate that the steric penalty associated with **4** may not be as important as the end-to-end distance of **3** in terms of shifting the equilibrium over to the linear dimer complex. Nevertheless, purposely increasing the length of the spacer in one component successfully reversed the equilibrium of **3** and **4** toward **3**. Our preliminary investigation of construction of a supramolecular polymer using **1** and **2c** as building components has revealed an improved linear extension in **5c** at lower concentrations relative to using **1** and **2b**. We will report these results in detail in a forthcoming publication.

Footnotes and references

† All compounds were characterized by ^{1}H NMR spectroscopy, FAB mass spectrometry, and elemental analysis.

‡ Similar observations, though qualitative in nature, were reported for complexation of ditopic aromatic guests with biscyclophanes in water (ref. 6).

§ Slow exchange was also reported for the complexation of Bn-NH_2^+–Bn·PF_6^- and DB24C8 in solution (ref. 7).

¶ The ^{1}H NMR spectra of three sets of each solution were recorded with at least 50 min of acquisition time for determination of ratios of the H(**3**)$_c$ and H(**3**)$_u$ signals. Each spectrum was enlarged vertically (thus the signals of interest were detectable from the baselines; *e.g.* Fig. 1(*a*′) shows a vertically enlarged version of the spectrum in Fig. 1(*a*) from δ 4.45 to 4.75) and the signals were integrated using a deconvolution technique. Ratios of the H(**3**)$_c$ and H(**3**)$_u$ signals were determined within experimental errors (*ca.* 5%).

‖ The downfield chemical shift ($\Delta\delta$ = 0.05 ppm) observed for H(**2b**)$_u$ in Fig. 1(*b*) compared to that in Fig. 1(*d*) is attributed to the increased ratio of PF_6^- relative to uncomplexed ammonium salt moieties of **2b**. To demonstrate this phenomenon experimentally, a solution of DB24C8 and **2b** (8.0 × 10^{-4}/4.0 × 10^{-4} M in CD_3COCD_3–$CDCl_3$, 1 : 1 v/v) was mixed with solutions of $Bu_4N^+PF_6^-$ (from 4.0 × 10^{-4} to 16 × 10^{-4} M in the same solvent system) and the ^{1}H NMR spectra were taken at 295 K. A gradual downfield chemical shift for H(**2b**)$_u$ was observed as the PF_6^- concentration was increased, validating the hypothesis.

** Many different conformations existing at the pseudorotaxane complexation site of **6b** contribute to the broadening of the H(**6b**)$_c$ and H(**6b**)$_u$ signals since the signals are time averaged.

†† In the crystal structure of the pseudorotaxane from DB24C8 and Bn–NH_2^+–Bn·PF_6^- (ref. 7) one of the benzo rings π-stacks with one of the phenyl rings. The other electron rich benzo ring is uncomplexed.

‡‡ Variable-temperature ^{1}H NMR spectroscopy was performed in the range 285–313 K. Plots of $R\ln K_{linear}$ and $R\ln K_{cyclic}$ *versus* 1/*T* yielded straight lines (R > 0.97) from which ΔH and ΔS values for linear and cyclic dimerization were obtained.

1 N. Yamaguchi and H. W. Gibson, *Angew. Chem., Int. Ed.*, 1999, **38**, 143.
2 J. Rebek, Jr., *Angew. Chem., Int. Ed. Engl.*, 1990, **29**, 245.
3 E. Fan, S. A. Van Arman, S. Kincaid and A. D. Hamilton, *J. Am. Chem. Soc.*, 1993, **115**, 369.
4 A. P. Bisson, F. J. Carver, C. A. Hunter and J. P. Waltho, *J. Am. Chem. Soc.*, 1994, **116**, 10 292; A. P. Bisson and C. A. Hunter, *Chem. Commun.*, 1996, 1723.
5 J. Sartorius and H.-J. Schneider, *Chem. Eur. J.*, 1996, **2**, 1446; F. Eblinger and H.-J. Schneider, *Angew. Chem., Int. Ed.*, 1998, **37**, 826.
6 C.-F. Lai, K. Odashima and K. Koga, *Tetrahedron Lett.*, 1985, **26**, 5179.
7 P. R. Ashton, P. J. Campbell, E. J. T. Chrystal, P. T. Glink, S. Menzer, D. Philp, N. Spencer, J. F. Stoddart, P. A. Tasker and D. J. Williams, *Angew. Chem., Int. Ed. Engl.*, 1995, **34**, 1865.

Communication 9/01044K

ChemComm

Odd–even effect in optically active poly(3,4-dialkoxythiophene)

Elena Ramos Lermo, Bea M. W. Langeveld-Voss, René A. J. Janssen and E. W. Meijer*

Laboratory of Macromolecular and Organic Chemistry, Eindhoven University of Technology, PO Box 513, 5600 MB Eindhoven, The Netherlands. E-mail: tgtobm@chem.tue.nl

Received (in Cambridge, UK) 12th March 1999, Accepted 23rd March 1999

An odd–even effect is observed in the CD spectra of a homologous series of aggregated optically active poly(3,4-dialkoxythiophene)s, suggesting a helical packing of polymer chains into chiral superstructures, similar to that of the cholesteric liquid crystalline phase.

Polythiophenes attract considerable interest for their incorporation as active elements into electronic and electro-optical devices.[1] The optical and electronic properties of polythiophenes are dependent on the chemical structure[2] as well as on the intrachain and interchain structural organisation.[3] Control over the chemical structure has improved dramatically since synthetic routes towards well-defined substituted polythiophenes have become available.[2] The three-dimensional structure of the macromolecules in solution and the morphology in the solid state are influenced to a great extent by solvent and temperature.[4]

Novel insights into the organisation process of substituted polythiophenes have been obtained from well-defined polymers carrying optically active β-substituents.[5] Although in solution or in the melt no optical activity is observed for the π–π* transition of these chiral polythiophenes, they exhibit a strong bisignate circular dichroism (CD) effect associated with the main-chain absorption in the aggregated or solid state, consisting of a positive and a negative signal of comparable intensity. The presence of a CD effect shows that the chirality of the side chains induces optical activity in the polythiophene main chains. The parallel occurrence of aggregation and optical activity, as well as studies on bis(oligothiophene) model compounds,[6] indicate that the bisignate CD effect originates *via* exciton coupling from adjacent polythiophene chains in chiral superstructures. The sign of the experimental CD effects in the model compounds is in accordance with the prediction from exciton theory for the relative orientation of the two oligothiophene moieties in these models.[6] This suggests that in optically active polythiophenes, chiral packing of polythiophene chains occurs, comparable to the organisation processes in cholesteric liquid crystals. However, a complete understanding of the organisation process and the induction of chirality is lacking.

For some cholesteric liquid crystalline compounds an empirical relation between the helical ordering of the constituent molecules in the mesophase and the chirality in the flexible chain has been established by Gray and McDonnell.[7] According to these Sol-Rel, Sed-Rod alternation rules, the rotation of plane polarised light through a helical mesophase, clockwise (+, dextro) or counterclockwise (–, laevo), depends on the absolute configuration of the chiral centre (*S* or *R*) and its distance to the rigid mesogenic core (odd or even number of atoms). By definition the dextro-rotation is produced from a left handed helix, while the laevo-rotation originates from a right handed helical organisation. The rules are also applicable to other liquid crystalline mesophases, like helicoidal smectics,[8] and a similar odd–even alternation effect has even been observed for helical poly(isocyanides) with mesogenic substituents.[9] Here we show that the alternation rules are applicable to aggregated optically active poly(3,4-dialkoxythiophene)s.

In order to investigate the effect of distance between the stereocentre in the side chain and the polymer main chain, a series of poly(3,4-dialkoxythiophene)s **2**–**7** (Fig. 1) containing

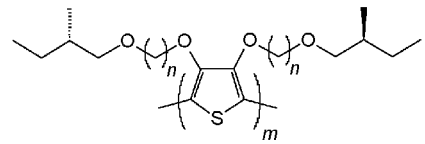

2 (*n*=2) – **7** (*n*=7)

Fig. 1 Optically active poly(3,4-dialkoxythiophene)s **2**–**7**.

increasing lengths of alkoxy spacers has been synthesised. For the synthesis the tosylate of commercially available (*S*)-2-methylbutanol is coupled once to the spacers ethane-1,2-diol through to heptane-1,7-diol. The resulting optically active alcohols are introduced at the β-positions of thiophene by transetherification of 3,4-dimethoxythiophene.[10] Polymerisation is accomplished by chemical oxidation using anhydrous iron(III) chloride.[11] The crude poly(3,4-dialkoxythiophene)s are dedoped by precipitation in MeOH–25% ammonia (v/v, 5/1). Further purification *via* Soxhlet extractions using MeOH–25% ammonia (v/v, 5/1) and hexane, and isolation *via* Soxhlet extraction with $CHCl_3$ gives pristine **2**–**7**. ^1H and ^{13}C NMR spectroscopy reveal the desired 2,5-polymerization without any observable irregularities.†

Microcrystalline aggregates of **2**–**7** are readily formed in poor solvents, *e.g.* decan-1-ol and pentan-1-ol.‡ The UV–Vis spectra of the microaggregates of **2**–**7** exhibit vibronic fine structure, indicative of intrachain and interchain order, with a 0–0 transition at *ca.* 610 nm, *i.e.* considerably red-shifted compared to the spectra of the polymers in good solvents (*e.g.* $CHCl_3$).[5b,c] The CD spectra of these ordered aggregates alternate in sign with an odd or even number of atoms in the spacer (Fig. 2).§

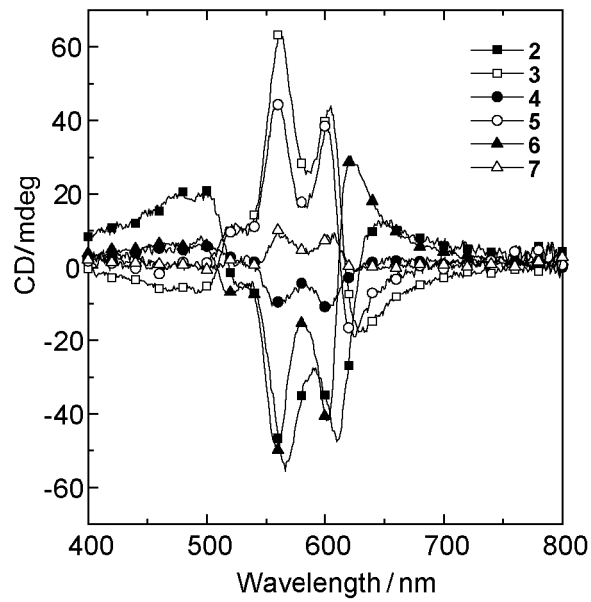

Fig. 2 CD spectra of **2**–**7** in decan-1-ol at room temperature. The spectra are normalised to unit absorbance at λ_{max}.

It is tempting to interpret the sign of the CD effect of these poly(3,4-dialkoxythiophene)s in terms of supermolecular helicity. Exciton theory and model studies predict that, for the π–π* transition of helically ordered aggregates of poly(3,4-dialkoxythiophene)s, a positive CD signal at the high wavelength implies a right-handed organisation of the chains in the aggregates, *i.e.* laevo in liquid crystal terminology. When the CD signal at the 0-0 transition (*ca*. 610 nm) is taken to represent the sign of the low-energy component of the couplet, it is found that **2**–**7** follow the Sol-Rel, Sed-Rod alternation rules that were originally developed for cholesteric liquid crystals. Polymer **6**, for example, has an *S* configuration at the stereocentre, 10 atoms (even) from the rigid part to the stereocentre, and is organised according to a left-handed helix (dextro) because of a negative CD signal at 605 nm.

While the CD spectra of **2**–**7** are indeed reminiscent of exciton coupling, the spectra fail to represent the characteristic exciton couplet, consisting of two peaks of equal intensity and opposite sign,[6] and integration of the CD spectrum over the π–π* band does not yield zero. These are clear indications that the CD spectra do not represent simple exciton couplets. Therefore, the explanation of the CD effect in terms of an interaction between chains in a helical fashion, providing the exciton coupled CD (bisignate), has to be augmented with a helical conformation for the individual polymer chains resulting in an intrinsic CD (monosignate).

The CD spectra of **2**–**7** in Fig. 2 are normalised to unit absorbance and clearly differ in intensity. Similar to a decreasing pitch observed in liquid crystals with increasing distance between the stereocentre and mesogenic core,[7] it can be expected that the influence of the optical activity in the side chain on the chiral organisation within the aggregates decreases with the number of atoms in the spacer. However it was extremely difficult to verify this expectation, because the magnitude of the CD effect is influenced by batch-dependent characteristics like the molecular weight and polydispersity,[12] and on subtle changes in sample preparation conditions, *i.e.* polymer concentration, temperature, and time of aggregation.¶

In conclusion, we have shown that in a homologous series of poly(3,4-dialkoxythiophene)s **2**–**7** with increasing lengths of spacers in β-substituents, the sign of the induced optical activity in the π–π* transition alternates with the parity of the number of atoms in the spacer when the polymers are in an aggregated phase. This effect is similar to alternation effects observed in helical liquid crystals and suggests that the CD effect associated with the π–π* transition arises from a similar chiral organisation of the polythiophene main chains. When the CD signal at the first vibronic transition is used to predict the sense of helicity *via* exciton theory, it is found that the alternation of CD signal in polythiophenes is consistent with the Sol-Rel, Sed-Rod alternation rules that were originally developed for cholesteric liquid crystals.‖

We would like to thank the EU for support for E. R. L. (Marie Curie Fellowship) and Philips Research BMWLV.

Notes and references

† The polymerisation conditions were varied for the amount of oxidising agent (2–4 equiv.) and the reaction time (4–16 h) but have not been optimised for each monomer. The final polymers differ significantly in molecular weight M_n and polydispersity D as determined by SEC measurements in THF, relative to polystyrene standards. M_n (D) varies between 10 kg mol^{-1} (3.3) for **2** and 62 kg mol^{-1} (4.7) for **5**. The work-up procedure of **4** repeatedly gave problems in the dedoping step and results presented for **4** should be regarded as tentative.

‡ Microaggregate formation in decan-1-ol was achieved by adding a small quantity of the polymer to decan-1-ol, warming until the polymers dissolved completely, and slow cooling to room temperature. Solutions in pentan-1-ol were prepared by adding a drop of a concentrated solution of **2**–**7** in $CHCl_3$ to pentan-1-ol.

§ Similar CD spectra with alternating sign have been obtained for thin films of polymers **3** and **5**–**7** on glass substrates when spin coated from $CHCl_3$ solution. For polymer **3** this involved an annealing step at 150 ºC for 2 h to reach the thermodynamically most stable form of aggregation, while **4** did not show good film formation.

¶ The shape and sign of the CD spectra are usually not affected by these parameters.

‖ Poly{3,4-bis[(*S*)-2-methylbutoxy]thiophene}[5b,c] also follows the Sol-Rel, Sed-Rod alternation rules (*S*, odd, CD at 610 nm is positive and hence laevo), whereas poly{2,5-bis[(*S*)-2-methylbutoxy]-1,4-phenylenevinylene} shows an opposite behaviour (*S*, odd, CD at 575 nm is negative and hence dextro).[13]

1 J. Roncali, *Chem. Rev*., 1992, **92**, 711; *Handbook of Organic Conductive Molecules and Polymers*, ed. H. S. Nalwa, Wiley, New York, 1997, vols. 1–4; W. J. Feast, J. Tsibouklis, K. L. Pouwer, L. Groenendaal and E. W. Meijer, *Polymer*, 1996, **37**, 5017; *Handbook of Conducting Polymers*, 2nd edn., ed. T. A. Skotheim, R. L. Elsenbaumer and J. R. Reynolds, Marcel Dekker, New York, 1998.

2 For a review on the chemistry of polythiophene, see: R. D. McCullough, *Adv. Mater*., 1998, **10**, 93.

3 S. Son, A. Dodabalapur, A. J. Lovinger and M. E. Galivin, *Science*, 1995, **269**, 376.

4 S. D. D. V. Rughooputh, S. Hotta, A. J. Heeger and F. Wudl, *J. Polym. Sci., B: Polym. Phys.*, 1987, **25**, 1071.

5 (*a*) M. M. Bouman, E. E. Havinga, R. A. J. Janssen and E. W. Meijer, *Mol. Cryst. Liq. Cryst.*, 1994, **256**, 439; (*b*) B. M. W. Langeveld-Voss, R. A. J. Janssen, M. P. T. Christiaans, S. C. J. Meskers, H. P. J. M. Dekkers and E. W. Meijer, *J. Am. Chem. Soc*., 1996, **118**, 4908; (*c*) B. M. W. Langeveld-Voss, E. Peeters, R. A. J. Janssen and E. W. Meijer, *Synth. Met*., 1997, **84**, 611.

6 B. M. W. Langeveld-Voss, D. Beljonne, Z. Shuai, R. A. J. Janssen, S. C. J. Meskers, E. W. Meijer and J. L. Brédas, *Adv. Mater*., 1998, **10**, 1343.

7 G. W. Gray and D. G. McDonnell, *Mol. Cryst. Liq. Cryst.*, 1977, **34**, 211.

8 J. W. Goodby, *Science*, 1986, **231**, 350; J. W. Goodby, in *Handbook of Liquid Crystals*, ed. J. W. Goodby, G. W. Gray, H.-W. Spiess and V. Vill, Wiley-VCH, Weinheim, 1998, vol. 1.

9 E. Ramos, J. Bosch, J. L. Serrano, T. Sierra and J. Veciana, *J. Am. Chem. Soc*., 1996, **118**, 4703; D. B. Amabilino, E. Ramos, J.-L. Serrano and J. Veciana, *Adv. Mater*., 1998, **10**, 1001; D. B. Amabilino, E. Ramos, J.-L. Serrano, T. Sierra and J. Veciana, *J. Am. Chem. Soc.*, 1998, **120**, 9126.

10 F. Goldoni, B. M. W. Langeveld-Voss and E. W. Meijer, *Synth. Commun*., 1998, **28**, 2237.

11 R.-I. Sugimoto, S. Takeda, H. B. Gu and K. Yoshino, *Chem. Express*, 1986, **1**, 635.

12 B. M. W. Langeveld-Voss, R. J. M. Waterval, R. A. J. Janssen and E. W. Meijer, *Macromolecules*, 1999, **32**, 227.

13 E. Peeters, M. P. T. Christiaans, R. A. J. Janssen, H. F. M. Schoo, H. P. J. M. Dekkers and E. W. Meijer, *J. Am. Chem. Soc*., 1997, **119**, 9909.

Communication 9/01960J

Double intramolecular Diels–Alder reaction of α,β-unsaturated hydrazones: a new route to 2,2′-bipyridines

Nicholas Bushby,[a] Christopher J. Moody,*[ab] David A. Riddick[b] and Ian R. Waldron[c]

[a] *School of Chemistry, University of Exeter, Stocker Road, Exeter, UK EX4 4QD. E-mail: c.j.moody@ex.ac.uk*
[b] *Department of Chemistry, Loughborough University, Loughborough, Leicestershire, UK LE11 3TU*
[c] *Zeneca Pharmaceuticals, Hurdsfield Industrial Estate, Macclesfield, UK SK10 2NA*

Received (in Liverpool, UK) 26th February 1999, Accepted 15th March 1999

Heating the 1,3-diynyl bis-α,β-unsaturated hydrazones 3, 6 and 10 results in double intramolecular Diels–Alder reaction of the 1-azadienes, and after aromatisation by loss of dimethylamine, the formation of bipyridines 11–14.

In the 110 years since its first preparation, 2,2′-bipyridine has been extensively used as a ligand in organometallic chemistry.[1] Indeed 2,2′-bipyridine is one of the best known, and most effective bidentate ligands for a range of metals, and in recent years chiral bipyridine ligands have found wide use in asymmetric synthesis.[2] We now report a new route to 2,2′-bipyridines based on the double intramolecular Diels–Alder reaction of 1,3-diynyl bis-α,β-unsaturated hydrazones (Scheme 1).

The preparation of 6-membered ring heterocyclic compounds by the hetero Diels–Alder reaction is now a common tactic in organic synthesis,[3] and the use of azadienes as components in such reactions is established.[4] One useful route to pyridine derivatives is the Diels–Alder reaction of α,β-unsaturated hydrazones with various dienophiles, and since the pioneering work of Ghosez,[5] these 1-azadienes have been used in both inter- and intra-molecular Diels–Alder approaches to pyridine derivatives.[6–8] The intramolecular Diels–Alder (IMDA) reaction of α,β-unsaturated hydrazones with alkynes, first reported in 1988,[8] is a particularly attractive route to annelated pyridines since the initial Diels–Alder adduct readily aromatises by loss of dimethylamine. Therefore we decided to adapt this procedure to the direct synthesis of annelated bipyridines by the simple incorporation of an oxidative homocoupling step giving a 1,3-diyne which would then undergo the desired double IMDA reaction (Scheme 1).

The substrates for the double IMDA reactions were prepared by straightforward routes (Schemes 2–4). The first route involved the alkylation of salicylaldehyde with propargyl chloride (prop-2-ynyl chloride) to give the corresponding aldehyde **1**. Subsequent homologation of the aldehyde with either α,α-bis(trimethylsilyl)-*N*-*tert*-butylacetaldimine,[9] or with acetylmethylenetriphenylphosphorane gave the α,β-unsaturated aldehydes and ketones **2**. Hydrazone formation followed by Glaser–Eglinton coupling with copper(II) acetate[10] then gave the first substrates **3** for the double IMDA reaction (Scheme 2).

The IMDA substrate **6** was prepared from the known hydrazone **4**[11] by propargylation, and oxidative homocoupling of the alkyne (Scheme 3).

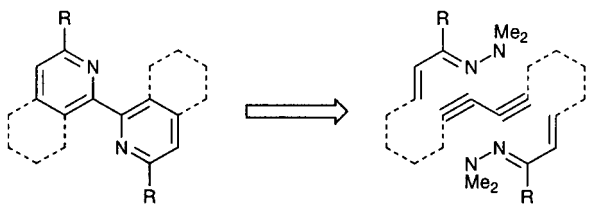

Scheme 1 (Alkynes drawn non-linear for clarity.)

The final substrate investigated was derived from hex-5-ynol **7**, the homocoupling of the terminal acetylene being carried out first (Scheme 4). Thus Glaser–Eglinton coupling of the alkyne gave the corresponding 1,3-diyne **8**; oxidation to the corresponding aldehyde **9** was achieved using *o*-iodylbenzoic acid (IBX) in DMSO.[12] The hydrazone **10** was prepared directly by reaction of **9** with diethoxyphosphonoethanal *N*,*N*-dimethylhydrazone.[8]

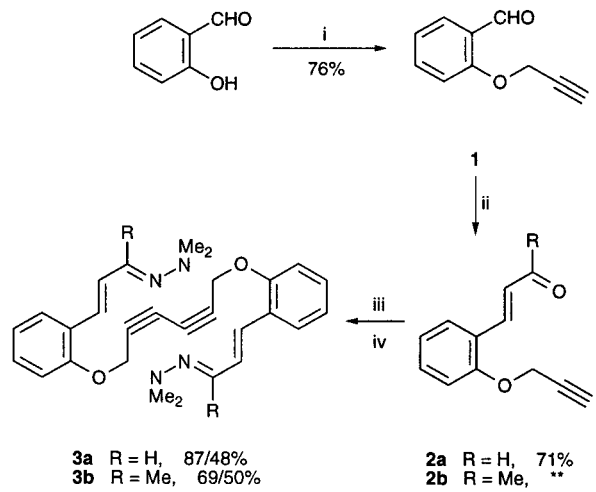

Scheme 2 *Reagents and conditions*: i, $HC{\equiv}CCH_2Cl$, K_2CO_3, EtOH; ii, (R = H) *t*-BuN=CHCH(TMS)$_2$, $ZnBr_2$, THF, followed by aq. $ZnCl_2$; ** (R = Me) prepared from salicylaldehyde by reaction with $Ph_3P{=}CHCOMe$ (91%), followed by $HC{\equiv}CCH_2Cl$, K_2CO_3, EtOH (76%); iii, Me_2NNH_2, $MgSO_4$, CH_2Cl_2; iv, Cu(OAc)$_2$, pyridine, MeOH, ether.

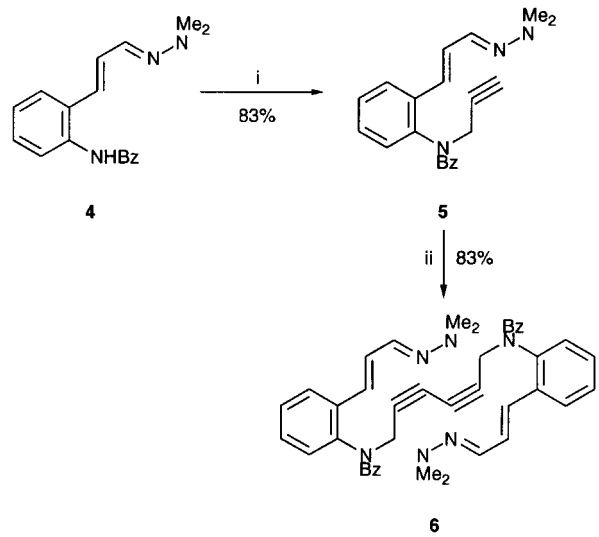

Scheme 3 *Reagents and conditions*: i, $HC{\equiv}CCH_2Cl$, KH, DMF; ii, Cu(OAc)$_2$, pyridine, MeOH, ether.

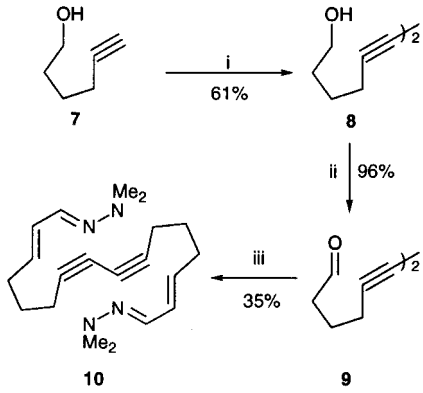

Scheme 4 *Reagents and conditions*: i, $Cu(OAc)_2$, pyridine, MeOH, ether; ii, IBX, DMSO; iii, $(EtO)_2POCH_2CH{=}NNMe_2$, BuLi, THF.

With a range of substrates in hand, the key double IMDA reactions were carried out. Heating the 1,3-diyne bis-hydrazone **3a** in boiling xylene gave the desired annelated 2,2′-bipyridine as the only isolable product (yield of crude material 60–87%), though considerable losses occurred in purification. The substrate **3b** derived from the α,β-unsaturated ketone was much less satisfactory in the double IMDA reaction; azadiene **3b** gave only 17% of a bipyridine after prolonged heating in mesitylene, though the product was isolated as the mono-oxidation product, the monolactone **12** formed by oxidation at the 5-position of one

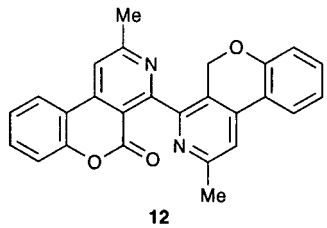

12

of the benzopyrano[3,4-*c*]pyridine rings. The *N*-benzoyl compound **6**, a nitrogen analogue of **3a**, underwent smooth double IMDA on heating in xylene to give, after loss of dimethylamine, the 4,4′-bi(benzo[*c*][2,7]naphthyridine) **13** in 68% yield. Finally in the series where the azadiene fragment is connected to the alkyne dienophile by a simple alkyl chain, substrate **10** readily underwent the desired double IMDA reaction in boiling xylene to give the 1,1′-bi(cyclopenta[*c*]pyridine) **14** in good yield (Scheme 5).

We thank the EPSRC for support of this work, and the EPSRC and Zeneca Pharmaceuticals for a CASE Award (D. A. R.).

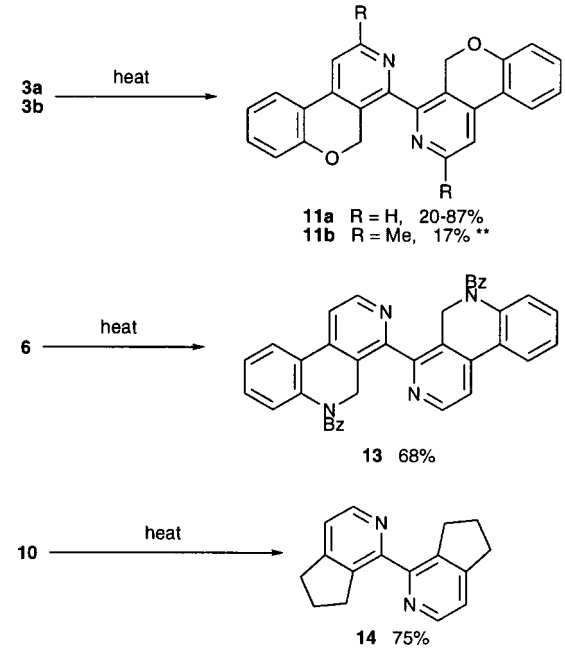

Scheme 5 (** Isolated as an oxidation product, the monolactone **12** formed by oxidation at the 5-position of one of the benzopyrano[3,4-*c*]pyridine rings.)

Notes and references

1 E. C. Constable and P. J. Steel, *Coord. Chem. Rev.*, 1989, **93**, 205.
2 C. Botteghi, G. Chelucci, G. Chessa, G. Delogu, S. Gladiali and F. Soccolini, *J. Organomet. Chem.*, 1986, **304**, 217; C. Bolm, M. Zehnder and D. Bur, *Angew. Chem., Int. Ed. Engl.*, 1990, **29**, 205; C. Bolm, M. Ewald, M. Zehnder and M. A. Neuburger, *Chem. Ber.*, 1992, **125**, 453; C. Bolm, M. Ewald, M. Felder and G. Schlingloff, *Chem. Ber.*, 1992, **125**, 1169; G. Chelucci and F. Soccolini, *Tetrahedron: Asymmetry*, 1992, **3**, 1235; P. Hayoz and A. V. Zelewsky, *Tetrahedron Lett.*, 1992, **33**, 5165; K. Ito, S. Tabuchi and T. Katsuki, *Synlett*, 1992, 575; K. Ito and T. Katsuki, *Tetrahedron Lett.*, 1993, **34**, 2661; K. Ito and T. Katsuki, *Synlett*, 1993, 638; H. Nishiyama, S. Yamaguchi, S.-B. Park and K. Itoh, *Tetrahedron: Asymmetry*, 1993, **4**, 143; H. L. Kwong, W. S. Lee, H. F. Ng, W. H. Chiu and W. T. Wong, *J. Chem. Soc., Dalton Trans.*, 1998, 1043; G. Chelucci, G. A. Pinna and A. Saba, *Tetrahedron: Asymmetry*, 1998, **9**, 531.
3 D. L. Boger and S. M. Weinreb, *Hetero Diels–Alder Methodology in Organic Synthesis*, Academic Press, New York, 1987; L. F. Tietze and G. Kettschau, *Top. Curr. Chem.*, 1997, **189**, 1.
4 J. Barluenga and M. Tomas, *Adv. Heterocycl. Chem.*, 1993, **57**, 1.
5 B. Serckx-Poncin, A. M. Hesbain-Frisque and L. Ghosez, *Tetrahedron Lett.*, 1982, **23**, 3261; R. Beaudegnies and L. Ghosez, *Tetrahedron: Asymmetry*, 1994, **5**, 557; R. Tamion, C. Mineur and L. Ghosez, *Tetrahedron Lett.*, 1995, **36**, 8977.
6 E. Gómez-Bengoa and A. M. Echavarren, *J. Org. Chem.*, 1991, **56**, 3497; Y. Kitahara and A. Kubo, *Heterocycles*, 1992, **34**, 1089; P. Nebois, H. Fillion, L. Benameur, B. Fenet and J. L. Luche, *Tetrahedron*, 1993, **49**, 9767; P. Nebois, O. Cherkaoui, L. Benameur, H. Fillion and B. Fenet, *Tetrahedron*, 1994, **50**, 8457; S. Levesque and P. Brassard, *Heterocycles*, 1994, **38**, 2205; L. Chaker, F. Pautet and H. Fillion, *Heterocycles*, 1995, **41**, 1169; J. M. Perez, C. Avendano and J. C. Menendez, *Tetrahedron*, 1995, **51**, 6573; M. D. Blanco, M. A. Alonso, C. Avendano and J. C. Menendez, *Tetrahedron*, 1996, **52**, 5933; R. A. Tapia, C. Quintanar and J. A. Valderrama, *Heterocycles*, 1996, **43**, 447; Y. Kitahara, F. Tamura, M. Nishimura and A. Kubo, *Tetrahedron*, 1998, **54**, 8421.
7 S. J. Allcock, T. L. Gilchrist and F. D. King, *Tetrahedron Lett.*, 1991, **32**, 125; S. J. Allcock, T. L. Gilchrist, S. J. Shuttleworth and F. D. King, *Tetrahedron*, 1991, **47**, 10 053.
8 R. E. Dolle, W. P. Armstrong, A. N. Shaw and R. Novelli, *Tetrahedron Lett.*, 1988, **29**, 6349.
9 M. Bellassoued and A. Majidi, *J. Org. Chem.*, 1993, **58**, 2517.
10 G. Eglinton and W. McCrae, *Adv. Org. Chem.*, 1963, **4**, 225.
11 A. M. Echavarren, *J. Org. Chem.*, 1990, **55**, 4255.
12 M. Frigerio and M. Santagostino, *Tetrahedron Lett.*, 1994, **35**, 8019.

Communication 9/01641D

A new calix[4]arene-based fluorescent sensor for sodium ion

I. Leray,[a] F. O'Reilly,[b]† J.-L. Habib Jiwan,[b] J.-Ph. Soumillion[b] and B. Valeur*[ac]

[a] *Laboratoire de Photophysique et Photochimie Supramoléculaires et Macromoléculaires (CNRS UMR 8531), Département de Chimie, ENS-Cachan, 61 Av. du Président Wilson, F-94235 Cachan cedex, France. E-mail: valeur@cnam.fr*

[b] *Laboratoire de Photochimie et Chimie Organique Physique, Université catholique de Louvain, 1 Place Louis Pasteur, B-1348 Louvain-la-Neuve, Belgium*

[c] *Laboratoire de Chimie Générale, Conservatoire National des Arts et Métiers, 292 rue Saint-Martin, F-75141 Paris Cedex 3, France*

Received (in Basel, Switzerland) 4th January 1999, Accepted 8th March 1999

A new calix[4]arene with three ester groups and an appended naphthalenic fluorophore has been synthesized; investigation of its photophysical and complexing properties towards alkali and alkaline-earth metal ions reveals a high selectivity for Na^+ in water–ethanol mixtures.

Considerable effort is being devoted to the design of a fluorescent sensor for metal ions.[1–4] Progress has still to be made in relation to the selectivity exhibited towards a given ion. Calixarenes with appropriate appended groups are good candidates because they have been shown to be highly specific ligands[5] and their potential applications as sensing agents have received increasing interest.[6] In particular, several calixarene-based fluorescent sensors have already been designed.[7]

In the present work, a novel calix[4]arene containing three ester groups and an appended naphthalenic fluorophore is described. Calix[4]arene tetraesters have been previously shown to be of interest as complexing agents of alkali metal ions.[8] In view of our previous studies on crowned-coumarin sensors, based on cation-enhancement of photoinduced charge transfer,[9] we have chosen as a fluorophore 6-acyl-2-methoxynaphthalene (AMN) which includes an electron-donating substituent (methoxy group) conjugated to an electron-withdrawing substituent (carbonyl group). It undergoes intramolecular charge transfer upon excitation and is thus expected to be environmentally sensitive. As for crowned coumarins, the fluorophore is linked to calix[4]arene so that the carbonyl group participates in the complexation process (Scheme 1). Consequently, cation binding results in the enhancement of photoinduced charge transfer with concomitant marked changes of photophysical characteristics.

Calix[4]arene **2**‡ was prepared in three steps. 6-Choroacyl-2-methoxynaphthalene was obtained by Friedel–Craft acylation between methoxynaphthalene and chloroacetyl chloride in nitrobenzene.[10] 4-*tert*-Butylcalix[4]arene was mono-alkylated using 2 equiv. of 6-chloroacyl-2-methoxynaphthalene and 2 equiv. of $KHCO_3$ in acetone. The remaining three phenolic groups were later functionnalized using 4 equiv. of ethyl bromoacetate and 2 equiv. of K_2CO_3 in acetone.[8] The cone conformation was confirmed by NMR.[11]

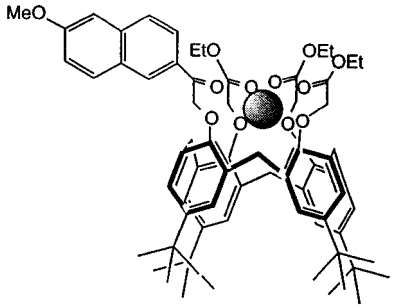

Scheme 1

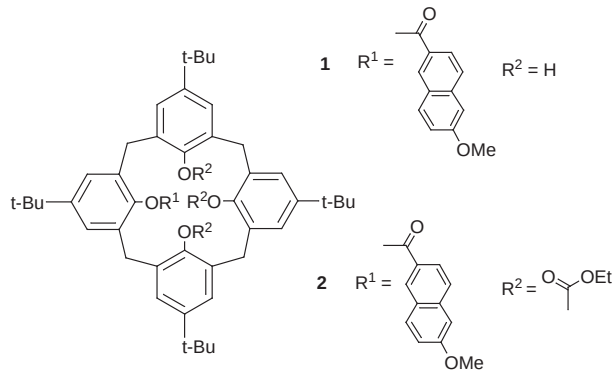

The effects upon addition of Li^+, Na^+, K^+, Mg^{2+} and Ca^{2+} perchlorates to **2** were first examined in acetonitrile solution. The absorption and fluorescence spectra of **2** and its complexes with Li^+, Na^+, K^+ and Ca^{2+} are shown in Fig. 1 and 2, respectively. The spectra of the Mg^{2+} complex are not shown because full complexation was still not achieved upon addition of $Mg(ClO_4)_2$ at a concentration of 0.04 M. An increase in the molar absorption coefficients together with red shifts of the absorption and emission spectra are observed upon cation binding, as expected from the cation-induced enhancement of the electron-withdrawing character of the carbonyl; the higher the charge density of the cation, the larger the observed effects. The red shifts of the emission spectrum are 45 and 61 nm upon complexation of Na^+ and Ca^{2+}, respectively.

Moreover, the fluorescence quantum yield, which is very low for **2** (1.24×10^{-3}), drastically increases upon cation binding (*e.g.* 0.68 for Ca^{2+}). The enhancement factors are 16, 35, 250, 550, for K^+, Na^+, Li^+, Ca^{2+}, respectively, again following the trend in charge density. Such an enhancement can be tentatively explained in terms of the relative locations of the singlet $\pi\pi^*$ and $n\pi^*$ states. For a ketone like **2**, some $n\pi^*$ character is expected for the lowest excited singlet state.[12] This results in an efficient intersystem crossing to the triplet state and consequently a low fluorescence quantum yield. In the presence of cation which strongly interacts with the lone pair of the carbonyl group, the $n\pi^*$ state is likely to be shifted to higher energy so that the lowest excited state becomes $\pi\pi^*$.

In ethanol, we first note that the fluorescence quantum yield of **2** is 2.5×10^{-3}, *i.e.* 2 times larger than in acetonitrile. This solvent dependency of the quantum yield, which increases with increasing solvent polarity, supports the existence of a low lying $n\pi^*$ state in the absence of a cation. The cation-induced photophysical changes in ethanol follow the same trends as in acetonitrile, but they were found to be weaker upon addition of Li^+, Mg^{2+} and Ca^{2+} and subsequently it was impossible to measure the spectral characteristics and the fluorescence quantum yields of the relevant complexes in this solvent. The fluorescence quantum yield increases by a factor of 15 and 38 upon binding of K^+ and Na^+, respectively.

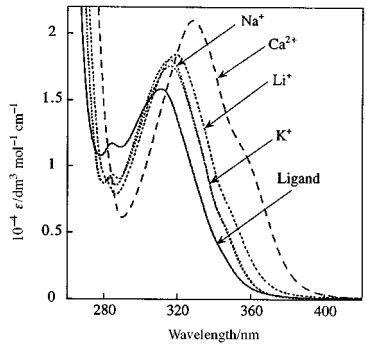

Fig. 1 Absorption spectra of ligand **2** and its complexes in acetonitrile.

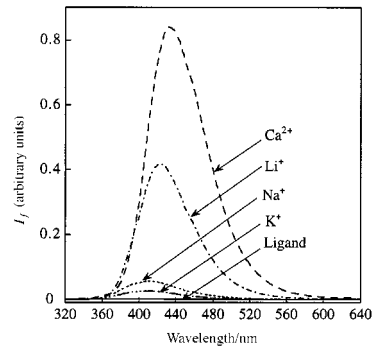

Fig. 2 Corrected fluorescence spectra of ligand **2** and its complexes in acetonitrile. Excitation wavelength 320 nm.

Table 1 Stability constants of the complexes of **3** in acetonitrile, ethanol and ethanol–water mixtures

Solvent	Cation	logβ
MeCN	Li^+	6.32 ± 0.07[a]
	Na^+	6.28 ± 0.06[a]
	K^+	4.74 ± 0.03[a]
	Mg^{2+}	2.06 ± 0.04[a]
	Ca^{2+}	5.30 ± 0.06[a]
EtOH	Li^+	0.9 ± 0.08[a]
	Na^+	14.3[b]
	K^+	2.87 ± 0.03[a]
	Mg^{2+}	1.82 ± 0.06[a]
	Ca^{2+}	1.25 ± 0.03[a]
EtOH–H_2O (80 : 20 v/v)	Na^+	3.87 ± 0.05[a]
	K^+	1.17 ± 0.05[a]
EtOH–H_2O (60 : 40 v/v)	Na^+	3.04 ± 0.07[a]
	K^+	0[a] (β = 0.75 ± 0.3)

[a] 1 : 1 stoichiometry for the complex. [b] 1.2 stoichiometry, log K_{11} = 4.6 ± 0.1 (M + L ⇌ ML), log K_{12} = 9.7 ± 0.1 (ML + L ⇌ ML_2), β = $K_{11}K_{12}$.

We then examined the stability of the complexes and their selectivity. The stability constants of the complexes in acetonitrile, ethanol and water/ethanol mixtures are reported in Table 1. In acetonitrile, the values of the stability constants are consistent with those previously reported for the analogous tetraethyl *p-tert*-butylcalix[4]arene tetraacetate and tetraphenyl *p-tert*-butylcalix[4]arene tetraketone.[8] As expected, the stability of the complexes is lower in ethanol. In the case of Na^+, the titration curve could not be satisfactorily fitted under the assumption of a 1 : 1 complex. Careful analysis of the evolution of the absorption spectra revealed that a 2 : 1 complex and a 1 : 1 complex with sodium were successively formed upon addition of Na^+.§

We then studied the ion-response of **2** in the presence of water since in most applications the metal ions to be detected are in aqueous solutions. Although, **2** is not soluble in water, this is not considered to be a drawback as our eventual aim is to design an optical-fibre device in which **2** will be immobilized in a polymer or sol–gel film. Furthermore, insolubility in water is preferable so as to minimize leakage. Meanwhile, in order to test the response of **2** in aqueous environments, we measured the stability constants in ethanol–water mixtures. The maximum water content which facilitates sufficient solubility of **2** is 40% by volume. Values are reported in Table 1. It is worth noting, that, in the presence of water, the 2 : 1 complex with Na^+ is no longer observed. The stability constant decreases as the water content increases, as expected, but it appears to level off. It is remarkable that the stability constant of the Na^+ complex in ethanol–water (60 : 40 v/v) is *ca.* 1300; this is suitable for measuring sodium ion concentrations in the mmolar range. In the same ethanol–water mixture, the stability constant of the K^+ complex is *ca.* 1. Therefore, selectivity Na^+/K^+ (expressed by the ratio of the stability constants) is *ca.* 1300. Moreover, it should be emphasized that the other cations used in this study (Li^+, Mg^{2+} and Ca^{2+}) have negligible effects. Finally, it is remarkable that the fluorescence quantum yield of the sodium complex in ethanol–water (60 : 40 v/v) is 0.11, *i.e.* 30 times larger than that of the free ligand.

The next step of this investigation will be the synthesis of calix[4]arenes with four appended chromophores along the same design principles. The molar absorption coefficient will therefore be four times larger and additional cation-induced photophysical effects are expected.

We acknowledge Ania Chaouanne for assistance with the spectroscopy measurements. The Belgian FNRS and French CNRS institutions are thanked for financial support. J. L. H. J. is a 'Chercheur qualifie' from the FNRS.

Notes and references

† Present address: Laboratoire de Canaux Ioniques et Signalisation, Département de Biologie Moléculaire et Structurale, CEA-Grenoble, 17 rue des Martyrs, 38054 Grenoble, France.

‡ The typical experimental procedures for **1** and **2** will be reported elsewhere together with elemental analysis and NMR data.

§ The constants of the successive equilibria K_{11} and K_{12} were determined using the Specfit software version 211 (Spectrum Software Associates).

1 B. Valeur, in *Topics in Fluorescence Spectroscopy, Volume 4: Probe Design and Chemical Sensing*, ed. J. R. Lakowicz, Plenum Press, New York, 1994, p. 21.
2 *Chemosensors of Ion and Molecule Recognition*, ed. J.-P. Desvergne and A. W. Czarnik, NATO ASI series, Kluwer Academic, Dordrecht, 1997.
3 A. P. de Silva, H. Q. N. Gunaratne, T. Gunnlaugsson, A. J. M. Huxley, C. P. McCoy, J. T. Rademacher and T. E. Rice, *Chem. Rev.*, 1997, **97**, 1515.
4 L. Fabbrizzi and A. Poggi, *Chem. Soc. Rev.*, 1995, **24**, 197.
5 V. Böhmer, *Angew. Chem., Int. Ed. Engl.*, 1995, **34**, 713; A. Ikeda and S. Shinkai, *Chem. Rev.*, 1997, **97**, 1713.
6 D. Diamond and M. A. McKervey, *Chem. Soc. Rev.*, 1996, 16.
7 I. Aoki, H. Kawabata, K. Nakashima and S. Shinkai, *J. Chem. Soc., Chem. Commun.*, 1991, 1771; T. Jin, K. Ichikawa and T. Koyama, *J. Chem. Soc., Chem. Commun.*, 1992, 499; I. Aoki, T. Sakaki and S. Shinkai, *J. Chem. Soc., Chem. Commun.*, 1992, 730; C. Perez-Jimenez, S. Harris and D. Diamond, *J. Chem. Soc., Chem. Commun.*, 1993, 480; F. Unob, Z. Asfari and J. Vicens, *Tetrahedron Lett.*, 1998, **39**, 2951.
8 F. Arnaud-Neu, E. M. Collins, M. Deasy, G. Ferguson, S. J. Harris, B. Kultner, A. J. Lough, M. A. McKervey, E. Marques, B. L. Ruhl, M. J. Schwing-Weil and E. M. Seward, *J. Am. Chem. Soc.*, 1989, **111**, 8681.
9 J. Bourson, J. Pouget and B. Valeur, *J. Phys. Chem.*, 1993, **97**, 4552; J.-L. Habib-Jiwan, C. Branger, J.-Ph. Soumillion and B. Valeur, *J. Photochem. Photobiol. A: Chem.*, 1998, **116**, 127.
10 M. Balo, F. Fernadez, C. Gonzalez, E. Lens and C. Lopez, *J. Chem. Res. (S)*, 1993, 132.
11 C. D. Gutsche, *Calixarenes*, in *Monographs in Supramolecular Chemistry*, ed. J. F. Stoddart, Royal Society of Chemistry, Cambridge vol. 1, 1989.
12 R. Nurmukhametov, L. Mileshina and D. Shigorin, *Opt. Spectrosc.*, 1967, **23**, 404.

Communication 9/00020H

Synthesis of a novel C2/C2′-*exo* unsaturated pyrrolobenzodiazepine cross-linking agent with remarkable DNA binding affinity and cytotoxicity

Stephen J. Gregson,[a] Philip W. Howard,*[a] Terence C. Jenkins,[b] Lloyd R. Kelland[c] and David E. Thurston*[a]

[a] *CRC Gene Targeted Drug Design Research Group, School of Pharmacy and Biomedical Sciences, University of Portsmouth, St Michael's Building, White Swan Road, Portsmouth, Hants, UK PO1 2DT. E-mail: david.thurston@port.ac.uk*

[b] *School of Chemical and Life Sciences, University of Greenwich, Wellington St., Woolwich, London, UK SE18 6PF*

[c] *CRC Centre for Cancer Therapeutics, Institute for Cancer Research, Clifton Avenue, Sutton, Surrey, UK SM2 5PX*

Received (in Liverpool, UK) 16th December 1998, Accepted 1st March 1999

A C2/C2′-*exo* unsaturated pyrrolobenzodiazepine dimer 1 has been synthesised which is cytotoxic at the picomolar level and has remarkable covalent DNA binding affinity, raising the melting temperature of duplex-form calf thymus DNA by 34 °C after 18 h incubation.

There is presently interest in low molecular weight ligands that can interact with nucleic acids in a sequence-selective manner. Such agents have potential use in the validation of DNA sequences as potential therapeutic targets, in the therapy of genetic-based diseases (*e.g.* cancer[1,2]), and in the development of diagnostic agents. The pyrrolo[2,1-*c*][1,4]benzodiazepines (PBDs) are a family of antitumour antibiotics derived from various *Streptomyces* species that exert their biological activity by interacting with DNA in a sequence-selective fashion, forming a covalent bond between their electrophilic C11-position and the exocyclic C2-NH_2 group of a guanine base in the minor groove of DNA.[3] Recently, it has been demonstrated that PBDs can inhibit both endonuclease activity[4] and *in vitro* transcription[5] in a highly sequence-selective manner.

Although the parent PBDs span approximately three base pairs with a preference for purine–guanine–purine (*e.g.* AGA) sequences, a series of C-ring-unsubstituted C8-diyldioxy ether-linked PBD dimers have been synthesised (*e.g.* DSB-120 **4**) that

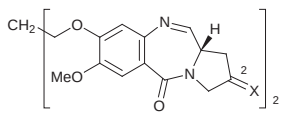

1 X = CH_2
4 X = H,H

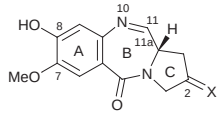

2 X = H, H
3 X = CHMe

span approximately six base pairs of DNA and have enhanced sequence selectivity (*e.g.* purine-GATC-pyrimidine for DSB-120).[6,7] The sub-micromolar cytotoxicity of DSB-120 has been attributed to its ability to irreversibly cross-link DNA *via* guanine residues on opposite strands.[8] In an attempt to further extend base-pair span and recognition behaviour, we have investigated the inclusion of C2/C2′ substituents that should follow the contour of the host minor groove. Here, we report a novel synthesis of SJG-136 **1**, a C2/C2′*exo*-methylene analogue of DSB-120. This molecule has exquisite cytotoxicity in the picomolar region (*i.e.* IC_{50} = 0.000024 μM) in the cisplatin-resistant A2780cis human ovarian carcinoma cell line, some 9000-fold more potent than DSB-120 (IC_{50} = 0.21 μM). Furthermore, SJG-136 raises the melting temperature of calf thymus (CT) DNA by a record value of 33.6 °C after 18 h incubation at a [PBD] : [DNA] ratio of 1 : 5.

Synthesis of the target molecule was initially approached using the thioacetal method of Thurston and co-workers.[9,10] However, this had to be abandoned due to the unwanted addition of EtSH across the C4-*exo*-methylene of intermediates of type **11** during attempted thioacetal formation. Instead, synthesis of **1** was achieved by employing the B-ring cyclisation strategy first reported by Fukuyama and co-workers[11] (Scheme 1). Commercially available *trans*-4-hydroxy-L-proline **5** was initially *N*-protected as carbamate **6** in 87% yield.[12] Following esterification in disappointing yield (43%) using catalytic H_2SO_4 in refluxing MeOH, the resulting ester **7** was reduced with $LiBH_4$ to give diol **8** in quantitative yield. Selective silylation of the primary alcohol (**8** → **9**) was achieved using DBU as a silyl transfer agent. Disilylated product and unreacted diol were removed by column chromatography to provide the TBDMS ether **9** in 52% yield. Oxidation to the ketone **10** was achieved using either the Swern reaction or tetrapropylammonium perruthenate (TPAP) in the presence of NMO and 4 Å molecular sieves, both methods producing **10** in almost quantitative yield. The key C4 (*pro*-C2/C2′) unsaturation was introduced by performing a Wittig reaction on **10** to afford the olefin **11** in 87% yield. Initial attempts to deprotect **11** using

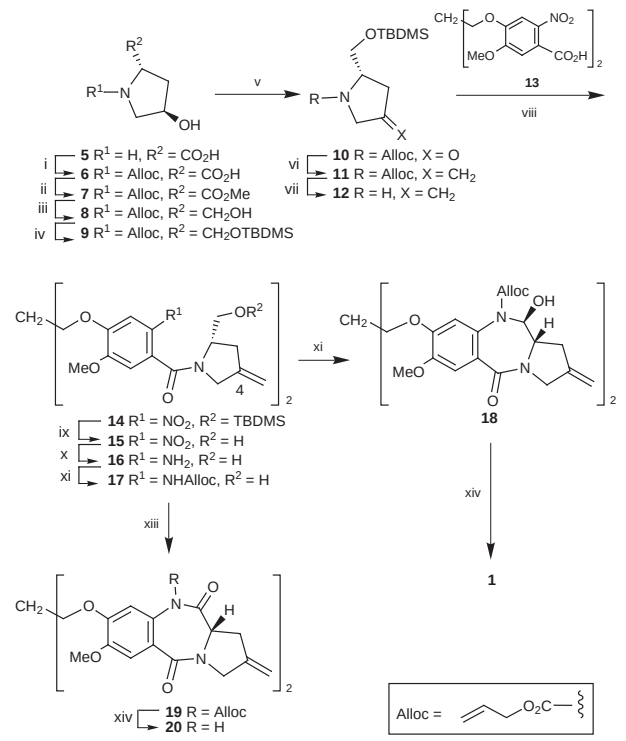

Scheme 1 *Reagents and conditions*: i, Alloc-Cl, aq. NaOH, THF, 0 °C, 87%; ii, MeOH, H_2SO_4, Δ, 43%; iii, $LiBH_4$, THF, 0 °C, 99%; iv, TBDMS-Cl, Et_3N, DBU, CH_2Cl_2, 52%; v, TPAP, NMO, 4 Å molecular sieves, CH_2Cl_2, MeCN, 92% or $(COCl)_2$, DMSO, Et_3N, CH_2Cl_2, −70 °C, 95%; vi, Ph_3PCH_3Br, $KOBu^t$, THF, 0 °C, 87%; vii, Bu_3SnH, $Pd(PPh_3)_2Cl_2$, H_2O, CH_2Cl_2, 77%; viii, $(COCl)_2$, DMF, THF, then **12**, Et_3N, H_2O, 0 °C, 74%; ix, TBAF, THF, 0 °C, 94%; x, $SnCl_2.2H_2O$, MeOH, Δ, 61%; xi, Alloc-Cl, pyridine, CH_2Cl_2, 0 °C, 50%; xii, TPAP, NMO, 4 Å molecular sieves, CH_2Cl_2, MeCN, 32%; xiii, $(COCl)_2$, DMSO, Et_3N, CH_2Cl_2, −45 °C, 51%; xiv, $Pd(PPh_3)_4$, PPh_3, pyrrolidine, CH_2Cl_2, MeCN, 0 °C, 77% for **1** and 43% for **20**.

$PPh_3/Pd(PPh_3)_4$ in the presence of a suitable allyl scavenger (*e.g.* pyrrolidine, dimedone, 2-ethylhexanoic acid)[13,14] were unsuccessful. Eventually, the Alloc group was cleaved by palladium-catalysed hydrostannolysis[15] with Bu_3SnH to provide the amine **12** in 77% yield.

The known PBD dimer core **13**[6,7] was converted to the corresponding acid chloride, and coupled to **12** to furnish the bis(nitro amide) **14** in 74% yield. The TBDMS protecting groups were removed rapidly and selectively under mild conditions using TBAF in THF to produce the bis(nitro alcohol) **15** in 94% yield. Reduction of the nitro groups while retaining the C4/C4′ unsaturation intact was achieved in 61% yield by employing $SnCl_2 \cdot 2H_2O$ in refluxing MeOH. The resulting *bis*-aniline **16** was Alloc-protected at the *pro*-N10/N10′ positions (**17**), before subjecting it to Swern conditions in order to bring about oxidative cyclisation to give the bis-N10-protected product **18**. Unfortunately, **18** was prone to over-oxidation and only the tetralactam **19** was obtained under these conditions. However, oxidation with TPAP, NMO and 4 Å molecular sieves afforded the required **18** in 32% yield with no contaminating tetralactam. Deprotection of **18** with $Pd(PPh_3)_4$, PPh_3 and pyrrolidine[13] afforded the novel PBD dimer **1** in 77% yield. Treatment of **19** under identical conditions afforded **20**, the first example of a PBD dimer tetralactam, in 43% yield.

The C2/C2′-methylene groups of **1** were clearly visible in the ^{1}H NMR (broad singlets at δ 5.17 and 5.20) and ^{13}C NMR (δ 109.4) spectra.† Similarly, the diagnostic N10-C11/N10′-C11′ imine signals could be observed at δ 7.68 (d, J 4.4 Hz) and δ 162.6, respectively. FAB MS gave parent ions at 665 and 773, corresponding to single and double thioglycerol addition adducts, respectively. In addition, the observed $[\alpha]_D^{21}$ value of +357.7 (*c* 0.07, $CHCl_3$) compared favourably with that for DSB-120[7] ($[\alpha]_D^{23}$ +330 (*c* = 0.6, $CHCl_3$)], confirming that the C11a/C11a′ stereochemistry crucial for DNA interaction had been maintained throughout the synthesis.

The data presented in Table 1 show that SJG-136 **1** is the most potent DNA-stabilising agent known to date according to this particular assay.[16] For a 1 : 5 molar ratio of [PBD] : [DNA], the PBD dimer elevates the helix melting temperature of CT DNA by an unprecedented 33.6 °C after incubation for 18 h at 37 °C. Under identical conditions, the C-ring-unsubstituted dimer DSB-120 **4** provides a ΔT_m of 15.1 °C, demonstrating the extraordinary effect of introducing C2/C2′-unsaturation. In common with other PBD dimers, **1** exerts most of its effect upon the GC-rich or high temperature regions of the DNA melting curves. In a similar fashion to DSB-120, it provides some 60–80% of its stabilising effect without prior incubation, suggesting a kinetic effect in the reactivity profile. However, the comparative ΔT_m curves show that, on a concentration basis alone, SJG-136 is ≥10-fold more effective than DSB-120. Even at a [PBD] : [DNA] molar ratio of 1 : 100, SJG-136 effects significantly better DNA binding affinity than the monomer tomaymycin **3** at a 1 : 5 molar ratio (see Table 1).

Table 1 Thermal denaturation with calf thymus DNA[a] at a [PBD] : [DNA] molar ratio of 1 : 5[b] and *in vitro*[c] cytotoxicity data in the A2780 and A2780cisR cell lines for SJG-136 **1** and DSB-120 **4**

	Induced ΔT_m/°C[a,b,d] after incubation at 37 °C for			IC_{50}/μM[c]		
Compound	0 h	4 h	18 h	A2780	A2780cisR	RF[e]
SJG-136 **1**	25.7	31.9	33.6	0.0000225	0.000024	1.1
DSB-120 **4**	10.2	13.1	15.1	0.0072	0.21	29.2
Cisplatin	—	—	—	0.265	8.4	32

[a] For CT-DNA at pH 7.00 ± 0.01, T_m = 67.83 ± 0.06 °C (mean value from 30 separate determinations). All ΔT_m values ± 0.1–0.2 °C. [b] For a 1 : 5 molar ratio of [ligand] : [DNA], where CT DNA concentration = 100 μM in aqueous buffer [10 mM sodium phosphate + 1 mM EDTA, pH 7.00 ± 0.01]. [c] Dose of PBD required to inhibit cell growth by 50% compared with PBD-free controls. The cells were incubated with the compounds for 96 h at 37 °C. [d] For comparative purposes: ΔT_m of tomaymycin **3** = 0.97, 2.38 and 2.56 °C at 0, 4 and 18 h, respectively. [e] RF is the resistance factor (IC_{50} resistant/parent).

Representative cytotoxicity data for SJG-136 in the human ovarian carcinoma cell line A2780 and its cisplatin-resistant subline A2780cisR are shown in Table 1, together with data for DSB-120 and cisplatin for comparison. Relative to the parental line, the A2780cisR subline is known to have elevated GSH levels, an increased level of repair of DNA–cisplatin adducts, and a decreased ability to uptake cisplatin.[17] The IC_{50} value for **1** in the A2780 cell line is only 23 pM, representing a 320-fold increase in cytotoxicity compared to DSB-120 (IC_{50} = 7.2 nM). Interestingly, whereas DSB-120 has a reduced potency towards A2780cisR (IC_{50} = 0.21 μM), SJG-136 is almost 9000-fold more potent in this cell line with a similar IC_{50} value (24 μM) to that in the parent cells, giving a Resistance Factor of 1.1. The fact that DSB-120 and cisplatin give RF values of 29.2 and 32, respectively, for this pair of cell lines suggests that SJG-136 may have potential in cisplatin-refractory disease.

In summary, the synthesis of SJG-136 **1** reported here demonstrates the importance of C2/C2′-*exo*-unsaturation in enhancing the DNA-binding affinity and cytotoxicity of the PBD dimers, and in overcoming cisplatin resistance. The sequence selectivity and cross-linking ability of **1** will be reported elsewhere.

We thank the CRC for providing financial support (Programme Grant SP1938/0401 to DET) and Jane Rimington for help with manuscript preparation.

Notes and references

† *Selected data* for **1**: δ_H(270 MHz, $CDCl_3$) 7.68 (d, 2H, *J* 4.4, H11/H11′), 7.49 (s, 2H, H6/H6′), 6.85 (s, 2H, H9/H9′), 5.20 and 5.17 (2 × br s, 4H, H12/H12′), 4.46–4.19 (m, 8H, H3/H3′ and H13/H13′), 3.93 (s, 6H, 2 × OCH_3 at C7/C7′), 3.89–3.80 (m, 2H, H11a/H11a′), 3.12 (dd, 2H, J_1 = 16.2, J_2 8.6, H1b/H1b′), 2.94 (d, 2H, *J* 16.3, H1a/H1a′), 2.45–2.38 (m, 2H, 2 × H14); *m/z* (FAB) 773 ([M + H + 2 × thioglycerol]$^{\cdot+}$, 3%), 665 ([M + H + thioglycerol]$^{\cdot+}$, 7), 557 ([M + H]$^{\cdot+}$, 9), 464 (3), 279 (12), 257 (5), 201 (5), 185 (43), 166 (6), 149 (12), 93 (100); ν_{max}(Nujol)/cm^{-1} 3600–3100 (br), 2923, 2849, 1599, 1511, 1458, 1435, 1391, 1277, 1228, 1054, 1011, 870, 804, 761, 739; $[\alpha]_D^{21}$ + 357.7 (*c* 0.07, $CHCl_3$).

1 S. Neidle, M. S. Puvvada and D. E. Thurston, *Eur. J. Cancer*, 1994, **30A**, 567.
2 S. Neidle and D. E. Thurston, *New Targets for Cancer Chemotherapy*, ed. D. J. Kerr and P. Workman, CRC Press, London, 1994, p. 159.
3 D. E. Thurston, in *Molecular Aspects of Anticancer Drug–DNA Interactions*, ed. S. Neidle and M. J. Waring, Macmillan, London, 1993, p. 54.
4 M. S. Puvvada, J. A. Hartley, T. C. Jenkins and D. E. Thurston, *Nucleic Acids Res.*, 1993, **21**, 3671.
5 M. S. Puvvada, J. A. Hartley, I. Gibson, P. Stephenson, T. C. Jenkins and D. E. Thurston, *Biochemistry*, 1997, **36**, 2478.
6 D. S. Bose, A. S. Thompson, J. Ching, J. A. Hartley, M. D. Berardini, T. C. Jenkins, S. Neidle, L. H. Hurley and D. E. Thurston, *J. Am. Chem. Soc.*, 1992, **114**, 4939.
7 D. E. Thurston, D. S. Bose, A. S. Thompson, P. W. Howard, A. Leoni, S. J. Croker, T. C. Jenkins, S. Neidle, J. A. Hartley and L. H. Hurley, *J. Org. Chem.*, 1996, **61**, 8141.
8 T. C. Jenkins, L. H. Hurley, S. Neidle and D. E. Thurston, *J. Med. Chem.*, 1994, **37**, 4529.
9 D. R. Langley and D. E. Thurston, *J. Org. Chem.*, 1987, **52**, 91.
10 D. E. Thurston and D. S. Bose, *Chem. Rev.*, 1994, **94**, 433.
11 T. Fukuyama, G. Liu, S. D. Linton, S.-C. Lin and H. Nishino, *Tetrahedron Lett.*, 1993, **34**, 2577.
12 M. Murata, T. Chiba and A. Yamada, *Eur. Pat. Appl.* 89102859.9; Publication No. 0-330-108-A1; Filing date: 18 Feb. 1989.
13 R. Deziel, *Tetrahedron Lett.*, 1987, **28**, 4371.
14 S. F. Martin and C. L. Campbell, *J. Org. Chem.*, 1988, **53**, 3184; H. Kunz and C. Unverzagt, *Angew. Chem., Int. Ed. Engl.*, 1984, **23**, 436.
15 O. Dangles, F. Guibé, G. Balavoine, S. Lavielle and A. Marquet, *J. Org. Chem.*, 1987, **52**, 4984.
16 G. B. Jones, C. L. Davey, T. C. Jenkins, A. Kamal, G. G. Kneale, S. Neidle, G. D. Webster and D. E. Thurston, *Anti-Cancer Drug Des.*, 1990, **5**, 249.
17 M. Smellie, L. R. Kelland, D. E. Thurston, R. L. Souhami and J. A. Hartley, *Br. J. Cancer*, 1994, **70**, 48.

Communication 8/09791G

ChemComm

Bathochromicity of Michler's ketone upon coordination with lanthanide(III) β-diketonates enables efficient sensitisation of Eu^{3+} for luminescence under visible light excitation†

Martinus H. V. Werts, Marcel A. Duin, Johannes W. Hofstraat and Jan W. Verhoeven*

Laboratory of Organic Chemistry, University of Amsterdam, Nieuwe Achtergracht 129, NL-1018 WS Amsterdam, The Netherlands. E-mail: jwv@org.chem.uva.nl

Received (in Exeter, UK) 15th March 1999, Accepted 23rd March 1999

The electronic absorption of Michler's ketone (MK) and related push–pull sensitisers undergoes a strong red shift upon coordination with lanthanide(III) β-diketonates, which enables unprecedently efficient sensitisation of Eu^{3+} luminescence for excitation at long wavelengths extending well into the visible region to above 450 nm.

The design of photoluminescent lanthanide complexes continues to be an active area of research,[1,2] mainly because such complexes may be useful for application in fluorescent probes, and for the conversion and amplification of light. The long lifetimes of the excited states of the lanthanide ions are an advantage in these applications, and so is the spectral purity of their light emission. The ligands in luminescent lanthanide complexes contain, besides chelating groups, one or more sensitising chromophores ('antennae') which are needed to overcome the excitation bottleneck formed by the inherently small absorption cross sections of the lanthanide ions. The chromophores absorb the light and consecutively transfer the energy to the lanthanide ion.[3] Bearing in mind possible applications, it would be most advantageous to have antenna chromophores that absorb significantly at wavelengths longer than 400 nm and then transfer the excitation energy efficiently and irreversibly to the ion. However, for luminescent Eu^{3+} and Tb^{3+} complexes, the excitation window appears to be limited to the near-UV due to the energetic constraints posed by the photophysics of sensitised lanthanide luminescence.[4] Eu^{3+} complexes containing chromophores that absorb at wavelengths longer than 400 nm have been reported, but the overall luminescence quantum yields of these systems are generally low, because energy transfer is inefficient due to back energy transfer processes. For example, mixed complexes of certain β-diketonates and *o*-phenanthroline display absorption bands in the region 380–400 nm, but show luminescence quantum yields upon ligand excitation of 10^{-4} to 2×10^{-3}.[5] Also in a series of Eu^{3+} Schiff base complexes studied recently,[6] the quantum yield drops dramatically as the absorption maximum of the ligand approaches the visible region. In our ongoing search for improved antenna chromophores for lanthanide ions, experiments aimed at observing intermolecular energy transfer between organic chromophores and lanthanide chelates in organic solvents yielded surprising results.

When colourless solutions of Michler's ketone [4,4′-bis(*N*,*N*-dimethylamino)benzophenone] and $Eu(fod)_3$ [europium tris(6,6,7,7,8,8,8-heptafluoro-2,2-dimethyloctane-3,5-dione)] in benzene (both 1 mM) are mixed, a yellow colour develops instantaneously. Moreover, a red glow emerges from the solution under daylight illumination. The emission spectrum (Fig. 1) demonstrates that this red glow is europium(III) luminescence: the sharp peaks are characteristic of lanthanide ion emission, Eu^{3+} usually having its most intense emission around 615 nm.[7] The corresponding excitation spectrum is in accordance with the observation that this luminescence can be excited by visible light. It extends well beyond 450 nm (λ_{max} 414 nm). The quantum yield was found to be 0.17 in aerated solution and 0.20 after deoxygenation by four freeze-pump-thaw cycles (excitation at 420 nm, using quinine bisulfate in 1 M H_2SO_4 as a reference[8]).

Michler's ketone and $Eu(fod)_3$ apparently form a ground-state complex under the experimental conditions, most likely by interaction of the electron rich carbonyl group with the positively charged Eu^{3+} ion. Such interactions are already well known from the use of lanthanide diketonates as NMR shift reagents,[9,10] and in fact coordination of certain aliphatic substrates to $Eu(fod)_3$ have been found to enhance its luminescence quantum yield.[11] Never before, however, has it been reported that complexation of chromophores to lanthanide β-diketonates yields efficient luminescent Eu^{3+} complexes that absorb visible light. The new absorption band is probably due to a bathochromic shift of the first singlet–singlet transition of Michler's ketone occurring upon complexation. This π–π* transition possesses charge-transfer character: in the process of excitation, electron density is moved towards the carbonyl group making the transition solvatochromic.[12] Thus, it is quite likely that the transition energy is largely affected by the presence of the lanthanide ion.

Upon closer inspection, the coordination of MK to lanthanide β-diketonates was found to occur only in non-coordinating solvents. Also, water molecules can compete with MK for free coordination sites on the lanthanide ion. Therefore, all reagents and solvents were dried before use. MK was purified according to a literature procedure.[13]

The complex formation of MK with $Eu(fod)_3$ in benzene can be monitored using UV-VIS absorption spectroscopy. The absorption band of the complex resides at longer wavelengths, where MK and $Eu(fod)_3$ themselves do not absorb. Fig. 2 shows a titration experiment, in which small amounts of a $Eu(fod)_3$ stock solution are added to a solution of MK. It clearly shows 1 : 1 complex formation of MK with $Eu(fod)_3$. Analysis of the titration data yields the formation constant for the MK–$Eu(fod)_3$ complex in benzene, $\log K = 4.85$. The extinction coefficient at 414 nm, the absorption maximum, was found to be 3.04×10^4 M^{-1} cm^{-1}.

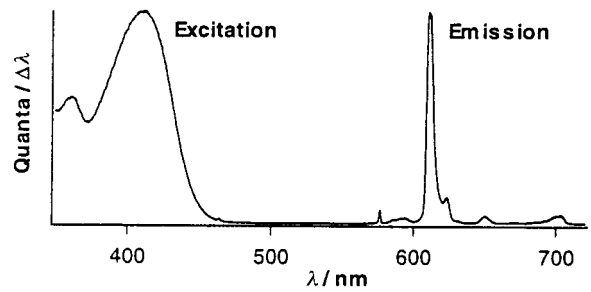

Fig. 1 Corrected luminescence excitation (λ_{em} = 612 nm) and emission (λ_{exc} = 450 nm) spectra of a solution of 10^{-5} M Michler's ketone and 10^{-4} M $Eu(fod)_3$ in benzene.

† Supplementary data outlining the analysis methodology used and giving additional spectra are available from the RSC web site, see: http://www.rsc.org/suppdata/cc/1999/799/

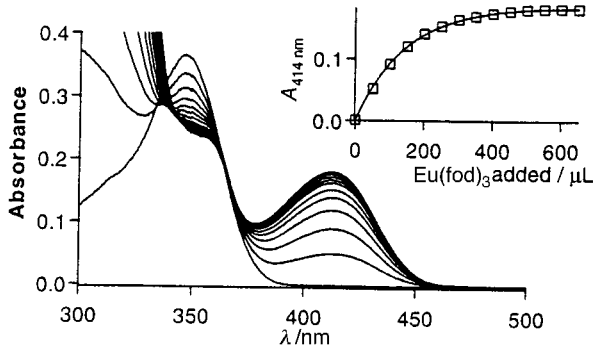

Fig. 2 UV–VIS titration of a solution of Michler's ketone in benzene with $Eu(fod)_3$. To 2.5 ml of a 10^{-5}M solution of MK in benzene, a $Eu(fod)_3$ solution (5×10^{-4} M in benzene) is added in steps of 50 μl. The inset shows formation of the complex by means of its absorption at 414nm as a function of the amount of $Eu(fod)_3$ solution added. The solid line is the theoretical curve for a 1 : 1 complex with log K = 4.85 and $\varepsilon_{max} = 3.04 \times 10^4$ M^{-1} cm^{-1}. The dilution has been taken into account.

The same bathochromic shift of the MK absorption as the one induced by $Eu(fod)_3$ is also observed with other lanthanides. Addition of $Yb(fod)_3$, $Er(fod)_3$, $Gd(fod)_3$ or $Pr(fod)_3$ to MK in benzene produces in all cases the same 414 nm absorption band. This reflects the electrostatic nature of the interaction: all lanthanide ions carry a 3+ charge and the distance between the ion and the MK is equal in all complexes. They will therefore have the same effect on the electronic energy levels of the chromophore. Obviously, the red glow is only observed with $Eu(fod)_3$.

Although the induced 'optical shifts' are the same for different $Ln(fod)_3$ species, the shifts of the MK ^{1}H nuclear magnetic resonances induced by these complexes are entirely different, which clearly shows that the effects have different origins (electrostatic *vs.* magnetic). For example, $Eu(fod)_3$ causes a downfield shift whereas $Pr(fod)_3$ shifts the resonances upfield. The protons closest to the carbonyl group are affected most, and the protons on the dimethylamino groups are relatively unaffected. This supports our view that the MK interacts with the lanthanide diketonate through its carbonyl group.

The sensitisation pathway in luminescent lanthanide complexes generally consists of excitation of the antenna chromophore into its singlet state, subsequent intersystem crossing of the antenna to its triplet state and energy transfer from the antenna triplet to the lanthanide ion,[14] implying that the triplet energy must be sufficiently high. In view of the unprecedented observation of efficiently sensitised Eu^{3+} luminescence upon excitation with visible light the singlet–triplet gap of the coordinated MK must be exceptionally small compared to other organic chromophores used until now as sensitisers or (less likely) another mechanism such as the electron transfer mechanism proposed by Horrocks *et al.*[15] must be involved.

The Gd^{3+} β-diketonates provide a way to study the triplet state energy of the coordinated MK. Having no electronic energy levels below 32000 cm^{-1} (310 nm), Gd^{3+} can not accept any energy from MK, but as mentioned above, it induces the same optical shift and eventually enhances singlet–triplet and triplet–singlet transitions in MK by its heavy atom effect. As a result in deoxygenated benzene, even at room temperature, phosphorescence of MK–$Gd(fod)_3$ is observed (excitation at 410 nm), as a broad band peaking at 540 nm. From the emission spectrum of MK–$Gd(fod)_3$ in methylcyclohexane glass at 77 K, the triplet energy of the coordinated MK is estimated to be 19600 cm^{-1}, which is indeed sufficient to efficiently populate the $^5D_0$ luminescent state of Eu^{3+} (17500 cm^{-1}), possibly *via* energy transfer to the $^5D_1$ state (19000 cm^{-1}) and subsequent relaxation to $^5D_0$.[16] The triplet energy of free MK is around 23000 cm^{-1}.[13] These results clearly point to the occurrence of the 'usual' triplet pathway in the sensitisation of Eu^{3+} by MK without resort to more exotic mechanisms. The crucial point is that the very small singlet–triplet gap of MK is fully retained upon coordination *via* its carbonyl oxygen to the lanthanide but that at the same time these energy levels are significantly lowered because the coordination stabilises the very polar excited states involved.

The effect of variation of β-diketonates was investigated as well. In benzene, the maximum of the absorption band varies from 398 nm for MK–$Eu(dpm)_3$ (dpm = 2,2,6,6-tetramethylheptane-3,5-dionate) *via* 414 nm for MK–$Eu(fod)_3$ to 430 nm for MK–$Eu(hfa)_3$ (hfa = 1,1,1,5,5,5-hexafluoropentane-2,4-dionate). We tentatively attribute this to a variation of the distance between the MK chromophore and the lanthanide ion in the complexes due to steric hindrance by the β-diketonate ligand. Unlike MK–$Eu(dpm)_3$ and MK–$Eu(fod)_3$ (both having 0.20 quantum yield in deoxygenated benzene), the sensitised luminescence quantum yield of MK–$Eu(hfa)_3$ is very low (6.2×10^{-5} in deoxygenated benzene). This is probably a result of too low a triplet energy of the antenna chromophore. The phosphorescence spectrum of MK–$Gd(hfa)_3$ (methylcyclohexane, 77 K) reveals a triplet energy of about 18800 cm^{-1}, which means that back energy transfer processes from Eu^{3+} to the coordinated MK might readily occur at room temperature.

In conclusion, lanthanide β-diketonates have been found to form complexes with the carbonyl containing 'push–pull' chromophore Michler's ketone. This interaction brings about a bathochromic shift in the optical absorption spectum of this chromophore. We note that this 'optical shift' effect is more general. In preliminary experiments, we also found bathochromic shifts in the dyes Nile Red and Phenol Blue induced by $Ln(fod)_3$.[17] A remarkable feature of the 'optically shifted', visible light absorbing MK chromophore is that it efficiently sensitises Eu^{3+} luminescence, which is an interesting property, *e.g.* for application as a luminescent label in time-resolved fluorescence microscopy, since visible light is less harmful to biological tissue than ultraviolet. A challenge in this respect is the development of more stable, water soluble complexes. This aspect and more details of the interesting photophysics of MK–$Eu(fod)_3$ and related complexes are currently under investigation.

Notes and references

1 D. Parker and J. A. G. Williams, *J. Chem. Soc., Dalton Trans.*, 1996, 3613.
2 M. Elbanowski and B. Makowska, *J. Photochem. Photobiol. A*, 1996, **99**, 85.
3 S. I. Weissman, *J. Chem. Phys.*, 1942, **10**, 214.
4 F. J. Steemers, W. Verboom, D. N. Reinhoudt, E. B. Van der Tol and J. W. Verhoeven, *J. Am. Chem. Soc.*, 1995, **117**, 9408.
5 J.-C. G. Bunzli, E. Moret, V. Foiret, K. J. Schenk, W. Mingzhao and J. Linpei, *J. Alloys Compd.*, 1994, **207**, 107.
6 R. D. Archer, H. Chen and L. C. Thompson, *Inorg. Chem.*, 1998, **37**, 2089.
7 Especially in Eu^{3+} β-diketonates, this so-called hypersensitive $^5D_0 \rightarrow {}^7F_2$ transition is usually very intense. See *e.g.* L. R. Melby, N. J. Rose, E. Abramson and J. C. Caris, *J. Am. Chem. Soc.*, 1964, **86**, 5117.
8 D. F. Eaton, *J. Photochem. Photobiol. B*, 1988, **2**, 523.
9 B. C. Mayo, *Chem. Soc. Rev.*, 1973, **2**, 49.
10 A. F. Cockerill, G. L. O. Davies, R. C. Harden and D. M. Rackham, *Chem. Rev.*, 1973, **73**, 553.
11 H. G. Brittain, *Inorg. Chem.*, 1980, **19**, 640.
12 E. J. J. Groenen and W. N. Koelman, *J. Chem. Soc., Faraday Trans. 2*, 1979, **75**, 58.
13 D. I. Schuster, M. D. Goldstein and P. Bane, *J. Am. Chem. Soc.*, 1977, **99**, 187.
14 G. A. Crosby, R. E. Whan and R. M. Alire, *J. Chem. Phys.*, 1961, **34**, 743.
15 W. D. Horrocks, Jr., J. P. Bolender, W. D. Smith and R. M. Supkowski, *J. Am. Chem. Soc.*, 1997, **119**, 5972.
16 Indeed, a weak $^5D_1 \rightarrow {}^7F_0$ emission is observed at 530 nm upon excitation of MK–$Eu(fod)_3$ at 420 nm.
17 A solution of Nile Red in benzene turns blue when solid $Ln(fod)_3$ is added. Moreover, the complexed Nile Red efficiently sensitises the near-infrared luminescence of erbium(III) and ytterbium(III).

Communication 9/02035G

ChemComm

Photochemistry of bicyclo[2.2.2]octenones: an uncommon oxidative decarbonylation

Tsung-Ho Lee, Polisetti Dharma Rao and Chun-Chen Liao*

Department of Chemistry, National Tsing Hua Univesity, Hsinchu, Taiwan 30043. E-mail: ccliao@faculty.nthu.edu.tw

Received (in Cambridge, UK) 11th February 1999, Accepted 16th March 1999

Several substituted 3,3-dialkoxy-5-methoxycarbonylbicyclo[2.2.2]oct-5-en-2-ones underwent unusual oxidative decarbonylation to produce polysubstituted cyclohexenes upon direct irradiation and usual ODPM rearrangement under sensitized conditions. A plausible mechanism for the oxidative decarbonylation is also given.

Bicyclo[2.2.2]octenones, with an embedded β,γ-unsaturated carbonyl chromophore, are rich with photochemistry.[1] They are known to undergo a variety of photochemical reactions such as decarbonylation, ketene extrusion, 1,3-acyl shift and most importantly the 1,2-acyl shift, also known as oxa-di-π-methane (ODPM) rearrangement, depending on reaction conditions, substrate structure and the wavelength of the incident light.[1] Apart from the ODPM rearrangement, and the 1,3-acyl shift,[2–4] other reactions of bicyclo[2.2.2]octenones or β,γ-unsaturated ketones in general have been considered as undesirable side reactions and received little attention.[5] This may be due to the fact that these fragmentation reactions were observed only when the desired ODPM rearrangement or 1,3-acyl shift are inefficient processes for the given substrate or when the substrate undergoes reactions in indescrete modes. Furthermore, these reactions appear to be more structure dependent and selectively affecting them may not always be possible. Apparently, the synthetic potential of decarbonylation has remained unexplored apart from a few cases.

We have been interested in this area of research for sometime and we have already employed the ODPM rearrangement reactions of bicyclo[2.2.2]octenones in the synthesis of iridoids and both angular and linear triquinanes.[6,7] In continuation of our efforts towards exploitation of the synthetic potential of bicyclo[2.2.2]octenones,[8] a study of the photochemical reactions of compounds **1** and **2** was contemplated. We now report that direct irradiation of bicyclo[2.2.2]octenones **1** and **2** in benzene results in the production of stereochemically pure polysubstituted cyclohexenes and under sensitized conditions **1** and **2** yield the usual ODPM rearrangement products in fair yields as one of the major isolable products (Schemes 1 and 2). To the best of our knowledge such formation of cyclohexenes *via* photochemical oxidative decarbonylation of bicyclo[2.2.2]octenones is unprecedented.

Accordingly the required bicyclo[2.2.2]octenones **1a–d** were prepared *via* intermolecular Diels–Alder reactions of methyl acrylate, methyl methacrylate and vinyl acetate with masked *o*-benzoquinone generated *in situ* by the oxidation of methyl vanillate using diacetoxyiodobenzene in MeOH. Compounds **2a-d** were prepared *via* intramolecular Diels–Alder reactions of masked *o*-benzoquinones generated by the oxidation of methyl vanillate in presence of allyl alcohol, crotyl alcohol, cinnamyl alcohol and homoallyl alcohol in CH_2Cl_2 using the procedure developed in our laboratory.[9] Direct irradiation of compounds **1a–d** in benzene (1% w/v) using light of wavelength centered at 300 nm in a Rayonet reactor for about 8 h furnished cyclohexenes **3a–d** in 41–43% yield along with ODPM rearrangement products **4a–d** in about 8–12% yield. However, irradiation of **1a–d** in acetone for 3 h produced the expected ODPM rearrangement products **4a–d** in 51–77% yield along with 2–12% of **3a–d** (Scheme 1).

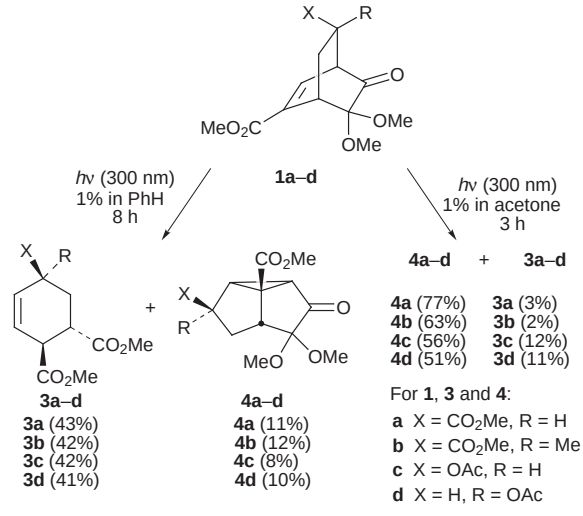

Scheme 1

On the other hand, irradiation of **2a** in benzene provided the expected cyclohexene **5a** and the corresponding lactone **6a** in a total yield of 68%. No ODPM rearrangement product could be observed. In contrast, **2b** provided both decarbonylated products **5b** and **6b** as well as ODPM rearrangement product **7b**. Both **5a** and **5b** could be transformed into **6a** and **6b** respectively by treatment with silica gel in EtOAc. The reaction mixtures obtained upon irradiation of **2c** and **2d** in benzene could not be separated into individual compounds. However, irradiation of **2a–d** in acetone furnished the expected ODPM rearrangement products **7a–d** in good yields (Scheme 2).

All the new compounds were thoroughly charecterized *via* their IR, ^{1}H (400 MHz) and ^{13}C NMR, DEPT, low and high resolution mass spectral analyses. The relative stereochemistry of compounds **3a**, **4b**, **6b** and **7c** was unambiguosly established with the aid of ^{1}H-^{1}H COSY and NOESY spectra. The stereochemical assignments of their analogues were based on analogy and coupling constants.

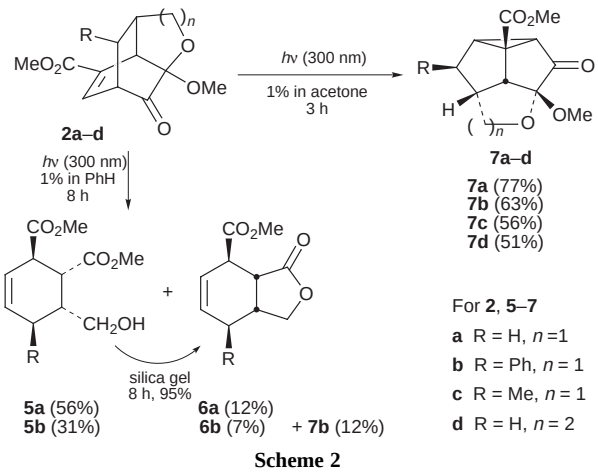

Scheme 2

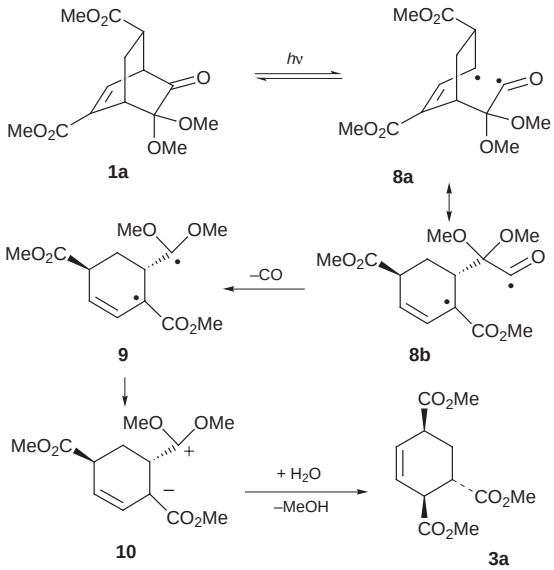

Scheme 3

The following mechanism is believed to be responsible for the formation of cyclohexenes upon direct irradiation of compounds **1** and **2** (Scheme 3). The initial Norrish type I α-cleavage of the C_1-C_2 bond results in the diradical species **8**.[10] The diradical **8**, instead of undergoing 1,3-acyl shift to provide the cyclobutanone derivative **11**, undergoes decarbonylation to

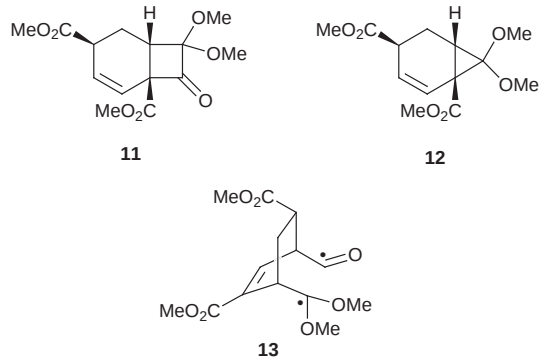

result in the relatively more stable diradical **9**. The diradical **9** fails to cyclize to provide the cyclopropane derivative **12**, and instead results in the zwitterion **10**, which upon stereoselective abstraction of a proton from the traces of water present in benzene followed by hydrolysis provides **3a**. An alternative pathway for the formation of **11** *via* the diradical **13**, which in turn could result from C_2–C_3 bond cleavage, cannot be ruled out. The intermediacy of the zwitterion gained support from the formation of the orthoester **14** as the sole isolable product when compound **1a** was irradiated in MeOH at 300 nm (Scheme 4).

The fact that both **11** and **12** were not observed indicates that the recyclization, prior to decarbonylation (1,3-shift) or fol-

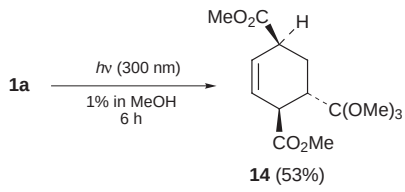

Scheme 4

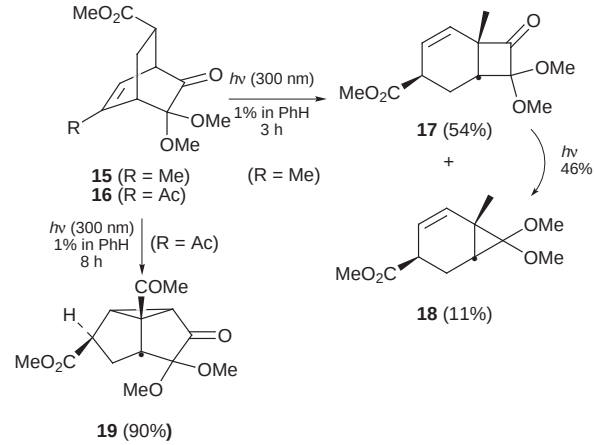

Scheme 5

lowed by decarbonylation, is constrained probably by electronic factors. The stability of the zwitterion **10** appears to be the driving force for the preferential decarbonylation against formation of strained cyclobutanone **11** or cyclopropane **12**. In order to verify this hypothesis, compound **15** (R = Me) was irradiated under identical conditions to obtain both 1,3-acyl shift product **17** and cyclopropane **18**. On the other hand, irradiation of **16** in benzene at 300 nm furnished ODPM rearrangement product **19** in 90% yield (Scheme 5). Obviously, the C-5 ester group is responsible for prevention of 1,3-acyl shift and formation of cyclopropane.

Nevertheless, these reactions provide an easy access to stereochemically defined polysubstituted cyclohexenes and tricyclo[3.3.0.$0^{2,8}$]octanones of established synthetic potential. Furthermore the starting materials are obtained from inexpensive aromatic compounds in excellent yields. In conclusion the present study has unravelled previously unknown photochemical behavior of a type of bicyclo[2.2.2]octenones.

We thank the National Science Council (NSC) of the Republic of China for financial support. P. D. R. thanks NSC for a post-doctoral fellowship.

Notes and references

1 K. N. Houk, *Chem. Rev.*, 1976, **76**, 1; D. I. Schuster, in *Rearrangements in Ground and Excited States*, ed. P. de Mayo, Academic Press, New York, 1980, vol. 3, p. 167.
2 H. E. Zimmerman and D. Armesto, *Chem. Rev.*, 1996, **96**, 3065 and references cited therein.
3 M. Demuth and K. Schaffner, *Angew. Chem., Int. Ed. Engl.*, 1982, **21**, 820.
4 V. Singh and M. Porinchu, *J. Chem. Soc., Chem. Commun.*, 1993, 134.
5 S. Katayama, H. Hiramatsu, K. Aoe and M. Yamauchi, *J. Chem. Soc., Perkin Trans. 1*, 1997, 561.
6 C.-C. Liao and C.-P. Wei, *Tetrahedron Lett.*, 1989, **30**, 2255.
7 J.-T. Hwang and C.-C. Liao, *Tetrahedron Lett.*, 1991, **32**, 6583; D.-S. Hsu, P. D. Rao and C.-C. Liao, *Chem. Commun.*, 1998, 1795.
8 C.-S. Chu, C.-C. Liao and P. D. Rao, *Chem. Commun.*, 1996, 1537; T.-H. Lee, C.-C. Liao and W.-C. Liu, *Tetrahedron Lett.*, 1996, **37**, 5897; T.-H. Lee and C.-C. Liao, *Tetrahedron Lett.*, 1996, **37**, 6869; P.-Y. Hsiu, Y.-C. Lee and C.-C. Liao, *Tetrahedron Lett.*, 1998, **39**, 659; W.-C. Liu and C.-C. Liao, *Chem. Commun.*, 1999, 117.
9 C.-S. Chu, T.-H. Lee and C.-C. Liao, *Synlett*, 1994, 635.
10 C. Bohne, in *CRC Handbook of Organic Photochemistry and Photobiology*, ed. W. M. Horspool and P.-S. Song, CRC Press, New York, 1995, p. 416.

Communication 9/01182J

Porphodimethylidenes from porphyrin-fused 3-sulfolenes—versatile porphyrin dienes for cycloadditions

Maxwell J. Gunter,*[a] Hesheng Tang[a] and Ronald N. Warrener[b]

[a] *Division of Chemistry, University of New England, Armidale, NSW 2351, Australia. E-mail: mgunter@metz.une.edu.au*

[b] *Centre for Molecular Architecture, Central Queensland University, Rockhampton, Queensland 4702, Australia*

Received (in Cambridge, UK) 22nd February 1999, Accepted 26th March 1999

A porphyrin with a β-fused 3-sulfolene on one of the pyrroles acts as a porphodimethylidene precusor which can be used for a variety of Diels–Alder cycloaddition reactions.

The need for molecular assemblies that will match the increasingly sophisticated design demands of supramolecular chemistry has been the motive for the production of modular components that can be assembled readily and predictably. This is especially so for custom-designed porphyrins which can be utilised in an impressive variety of systems.[1]

For some applications it has been necessary to constrain rotational freedom of the porphyrin nucleus within the assembly, and this has most effectively been achieved by a 1,2-linkage at adjacent β-pyrrole positions. Hence the construction of many rigid porphyrin-containing systems has commonly utilised Schiff base formation with preformed porphyrin diamines or diones.[2] However, the Diels–Alder reaction is a classic cycloaddition reaction which leads to fused ring systems and is ideally suited to the construction of well-defined molecular assemblies with limited flexibilities.

There have been few reports of Diels–Alder chemistry involving porphyrins and related macrocycles. Of these, several have used β-vinyl porphyrins as the diene,[3] and a related tetramethine-bridged porphyrin has also been shown to undergo cycloaddition reactions.[4] Alternatively, tetraaryl porphyrins have been used as dienophiles, giving a mixture of products with reactive dienes under forcing conditions,[5] and Diels-Alder methodology has been used in the construction of benzoporphyrins.[6] More recently, *N*-substituted β-fused pyrroloporphyrins have been used as dienes for certain cycloaddition reactions.[7] We have shown that cycloaddition reactions provide an excellent method for geometric control in certain made-to-order rigid assemblies which incorporate porphyrins.[8]

Aromatic fused 3-sulfolenes have been used as precursors for highly reactive *o*-quinodimethanes.[9] Thermal extrusion of sulfur dioxide from the sulfolenes is usually performed in the presence of a dienophile so that the quinodimethane is trapped as a Diels–Alder adduct.[10] While *N*-substituted pyrrole-fused 3-sulfolenes have been used as a source of annelated pyrroles,[11] some of which have been subsequently used in the synthesis of pyrroloporphyrins[12] and symmetrical tetra-substituted porphyrins,[6] reported here is the first example to the best of our knowledge of a porphyrin with a β-fused sulfolene that allows subsequent chemistry at only *one* of the pyrroles. This is a key precusor for a range of cycloadducts resulting from Diels–Alder reaction of the intermediate porphodimethylidene which is formed by elimination of sulfur dioxide under mild conditions.

The pyrrole-fused 3-sulfolene **1** was prepared by a modification of the Barton–Zard reaction[13] using benzyl isocyanoacetate and 3-phenylsulfonyl-2,5-dihydrothiophene 1,1-dioxide (Scheme 1),[14] in an analogous manner to that for the corresponding ethyl ester reported by Vicente *et al*.[6] Hydrogenolysis (H_2, 10% Pd–C) and oxidative iodination (I_3^-, room temperature, 2 h) to give **2** followed by reduction (H_2, 10% Pd–C, NaOAc, 3 atm) produced **3**. Condensation (Montmorillonite clay, CH_2Cl_2, room temperature, 10 h) with benzyl 5-acetoxymethyl-4-ethyl-3-methylpyrrole-2-carboxylate resulted in the tripyrrane **4**, which was subsequently hydrogenolysed and subjected to a '3 + 1' porphyrin synthesis[15] with pyrrole-2,5-dicarbaldehyde (TFA, CH_2Cl_2, room temperature, 2 h, followed by DDQ, 1 h) to form the desired porphyrin **5**.†

While **5** is indefinitely stable at ambient temperatures, on heating above 80 °C it readily loses SO_2 to form the reactive porphodimethylidene **6**. Although it was not possible to isolate **6**, it could be trapped as Diels–Alder adducts in the presence of suitable dienophiles. In the absence of a dienophile and at moderate temperatures (80–110 °C, toluene) it cleanly produced the dimer **7**.

Compound **7** is analogous to the previously identified dimeric product formed from *o*-quinodimethane itself,[9] and its structure was established from its ^{1}H NMR spectrum and mass spectrum [*m/z* 841.5 $(M + H)^+$]. In particular the NMR spectrum (C_6D_6) showed a clear lack of simple symmetry, and individual

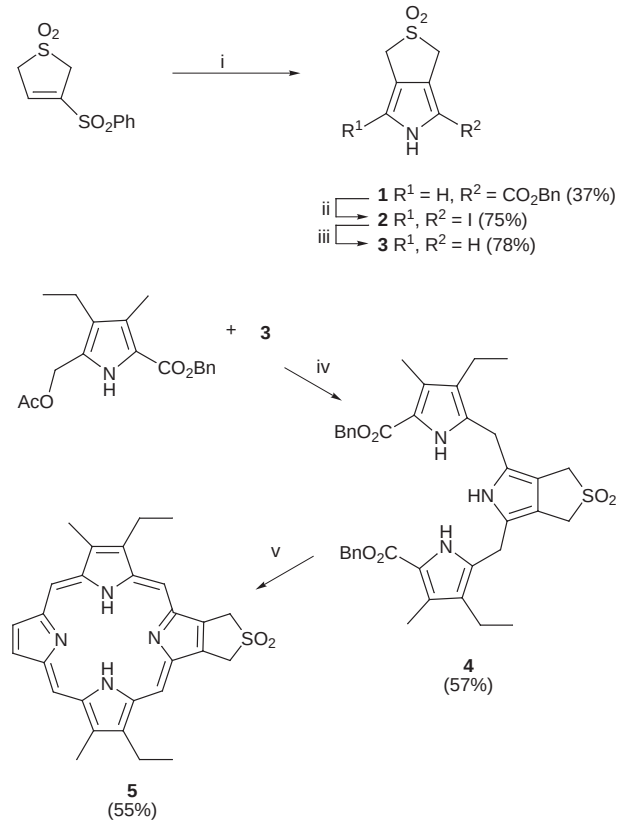

Scheme 1 *Reagents and conditions*: i, $NCCH_2CO_2Bn$, KOBu^t, THF, −15–25 °C, 2 h; ii, H_2, Pd–C (10%), 3 atm, 7 h, room temp., then I_2, KI(aq. EtOH), 5 h, room temp.; iii H_2, Pd–C (10%), NaOAc, 3 atm, 22 h, room temp.; iv, Montmorillonite clay K-10, CH_2Cl_2, N_2, 10 h, room temp.; v, H_2, Pd–C (10%), 3 atm, 3 h, then pyrrole-2,5-dicarbaldehyde, TFA, CH_2Cl_2, 2 h, then DDQ, 1 h, room temp.

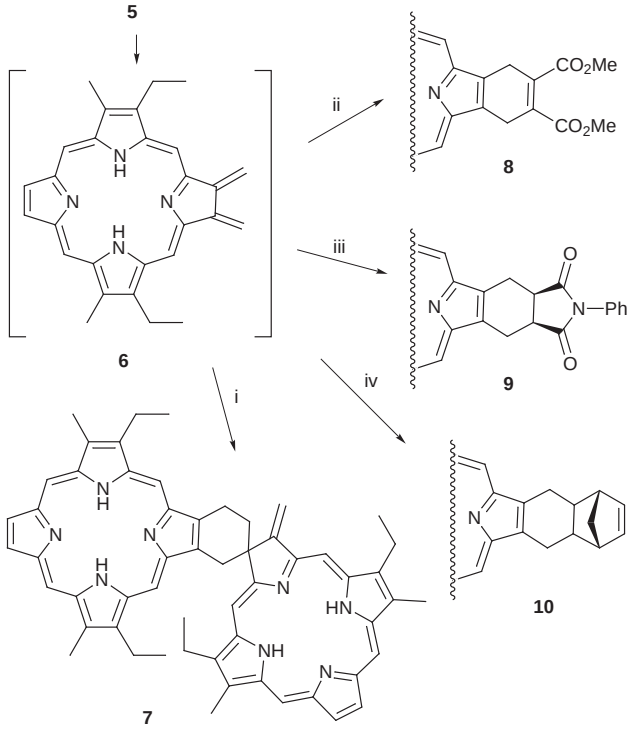

Scheme 2 *Reagents and conditions*: i, Δ, toluene, 80–110 °C, 2 h; ii, $MeO_2CC{\equiv}CCO_2Me$, Δ, toluene, 110 °C, 4.5 h; iii, *N*-phenylmaleimide, Δ, 85 °C, 3 h; iv, norbornadiene, Δ, 80 °C, 2 h.

resonances for each of the substituents on the porphyrin and chlorin rings.† For example, there are four distinct ethyl and methyl resonances, two AB quartets for the β-pyrrole protons, eight singlets for the *meso*-protons, and two NH singlets at high field. The exocyclic methylene is defined by two singlets (δ 6.16 and 6.95) significantly deshielded by the neighbouring porphyrin while the deshielded single bridging methylene is a clear AB quartet at δ 5.18 and 5.56. The remaining ethylene of the spiro-linked cyclohexene bridge is a series of complex multiplets at δ 3.05, 3.34 and 4.68. The UV-visible spectrum of **7** is a composite of both porphyrin and chlorin-type rings and not surprisingly shows little evidence of electronic communication between the linked macrocycles.

On heating **5** in toluene at 80–110 °C in the presence of various dienophiles shown in Scheme 2, the corresponding Diels–Alder adducts were isolated in good yields (65–95%).† The C_{2_v} symmetry of each is clear from the ^{1}H NMR spectra. In the case of **10**, only a single stereoisomer was isolated, and both a lack of vicinal H, H-coupling and no significant shielding of the ethylenic protons indicates it to be the *exo*-product (molecular modelling indicates a close proximity of the ethylenic protons to the shielding region of the porphyrin in the *endo*-isomer, although the environments of the bridge methylenes are little different in either isomer). Each of these suggests considerable potential as building blocks for higher level structures. For example **8** can be utilised in further cycloaddition reactions using its activated double bond, **9** *via* a variety of associated *N*-substituted derivatives can provide a single attachment point on a *meso*-unsubstituted porphyrin, and the formation of **10** indicates the possibility for more elaborate architectures. Although these few reactions demonstrate the utility of **5**, its potential is clearly much more extensive and can now be explored.

This research was supported by the Australian Research Council.

Notes and references

† *Selected data* for **5**: δ_H($CDCl_3$) −4.0 [2H, br s, NH], 1.84 [6H, t, CH_2CH_3], 3.70 [6H, s, CH_3], 4.12 [4H, q, CH_2CH_3], 5.67 [4H, s, CH_2], 9.38 [2H, s, pyrrole β-H], 9.87 [2H, s, *meso*-H], 10.21 [2H, s, *meso*-H]; λ_{max}($CHCl_3$)/nm 392, 502, 539, 561; ν_{max}/cm^{-1} 1216(S=O); *m/z* (FAB) 485.20074 (M^+ + 1). For **7**: δ_H(300 MHz, C_6D_6, dashed (′) numbering for chlorin ring) −1.62 [2H, br s, N′H], −2.76 [2H, s, NH], 0.82 [3H, t, C(7′)CH_2CH_3], 1.67 [3H, t, C(18′)CH_2CH_3], 1.76 [3H, t, C(13)CH_2CH_3], 1.95 [3H, t, C(2)CH_2CH_3], 2.93 [3H, s, C(8′)CH_3], 3.28 [3H, s, C(17′)CH_3], 3.34 [3H, s, C(12)CH_3], 3.48 [3H, s, C(3)CH_3], 2.83 [2H, m, C(7′)CH_2CH_3], 3.05 [1H, m, C(22′)CH_2], 3.34 [1H, m, C(22′)CH_2], 3.84 [4H, m, C(18′, 13)CH_2CH_3], 4.11 [2H, m, C(2)CH_2CH_3], 4.68 [2H, m, C(21)CH_2CH_2], 5.18 [1H, d, *J* 21, C(23) CH_2], 5.56 [1H, d, *J* 21, C(23) CH_2], 6.16 [1H, s, C(3′)=CH_2], 6.95 [1H, s, C(3′)=CH_2], 9.21 [1H, d, C(7)H], 9.23 [1H, d, C(12′)H], 9.45 [1H, d, C(8)H], 9.46 [1H, d, C(13′)H], 9.50. 9.75, 9.80, 9.87, 10.20, 10.27, 10.38, 10.48 [1H each, s, *meso*-H′s]; *m/z* (FAB) 841.47036 (M^{+}+1). For **8**: δ_H($CDCl_3$) −4.01 [2H, br s, NH], 1.86 [6H, t, CH_2CH_3], 3.68 [6H, s, CH_3], 4.08 [6H, s, OCH_3], 4.12 [4H, q, CH_2CH_3], 5.10 [4H, s, CH_2], 9.36 [2H, s, pyrrole β-H], 9.93 [2H, s, *meso*-H], 10.17 [2H, s, *meso*-H]; *m/z* (EI) 562.25886 (M^+). For **9**: δ_H($CDCl_3$) −3.95 [2H, br s, NH], 1.88 [6H, t, CH_2CH_3], 3.68 [6H, s, CH_3], 4.15 [6H, m, CH_2CH_3, CH], 4.30, 4.36 [2H, m, CH_2], 4.84 [2H, d, CH_2′], 6.86 [2H, m, Ar–H], 7.10 [3H, m, Ar–H], 9.38 [2H, s, pyrrole β-H], 10.11 [2H, s, *meso*-H], 10.19 [2H, s, *meso*-H]; *m/z* (EI) 593.27971 (M^+). For **10**: δ_H($CDCl_3$) −3.90 [2H, br s, NH], 1.84 [6H, t, CH_2CH_3], 1.86 [1H, d, *J* 10, CH_2], 2.35 [1H, d, *J* 10, CH_2], 2.57 2H, m, CH], 3.13 [2H, s, CH], 3.45 [2H, dd, CH_2], 3.64 [6H, s, CH_3], 4.12 [4H, q, CH_2CH_3], 4.69 [2H, dd, CH_2], 6.38 [2H, s, =CH], 9.40 [2H, s, pyrrole β-H], 10.09 [2H, s, *meso*-H], 10.18 [2H, s, *meso*-H].

1 See, for example *Comprehensive Supramolecular Chemistry*, ed. J. L. Atwood, J. E. D. Davies, D. D. MacNicol and F. Vogtle, Elsevier, Oxford, 1996, vol. 2, 4, 5, 6, 9, 10.

2 M. J. Crossley, L. G. King, I. A. Newsom and C. S. Sheehan, *J. Chem. Soc., Perkin Trans. 1*, 1996, 2675; M. J. Crossley and J. K. Prashar, *Tetrahedron Lett.*, 1997, **38**, 6751; M. J. Crossley, L. J. Govenlock and J. K. Prashar, *J. Chem. Soc., Chem. Commun.*, 1995, 2379; M. J. Crossley, P. L. Burn, S. J. Langford and J. K. Prashar, *J. Chem. Soc., Chem. Commun.*, 1995, 1921; E. J. Atkinson, A. M. Oliver and M. N. Paddon-Row, *Tetrahedron Lett.*, 1993, **34**, 6147; P. T. Gulyas, S. J. Langford, N. L. Lokan, M. G. Ranasinghe and M. N. Paddon-Row, *J. Org. Chem.*, 1997, **62**, 3038; K. A. Jolliffe, T. D. M. Bell, K. P. Ghiggino, S. J. Langford and M. N. Paddon-Row, *Angew. Chem., Int. Ed.*, 1998, **37**, 916.

3 M. A. F. Faustino, M. G. P. M. S. Neves, M. G. H. Vicente, A. M. S. Silva and J. A. S. Cavaleiro, *Tetrahedron Lett.*, 1996, **37**, 3569; S. Kai and M. Suzuki, *Tetrahedron Lett.*, 1996, **37**, 5931; G. Zheng, A. N. Kozyrev, T. J. Dougherty, K. M. Smith and R. K. Pandey, *Chem. Lett.*, 1996, 1119.

4 P. A. Liddell, L. J. Demanche, S. Li, A. N. Macpherson, R. A. Nieman, A. L. Moore, T. A. Moore and D. Gust, *Tetrahedron Lett.*, 1994, **35**, 995.

5 A. C. Tomé, P. S. S. Lacerda, M. G. P. M. S. Neves and J. A. S. Cavaleiro, *Chem. Commun.*, 1997, 1199.

6 S. Ito, T. Murashima and N. Ono, *J. Chem. Soc., Perkin Trans. 1*, 1997, 3161; S. Ito, T. Murashima, H. Uno and N. Ono, *Chem. Commun.*, 1998, 1661; M. G. H. Vicente, A. C. Tomé, A. Walter and J. A. S. Cavaleiro, *Tetrahedron Lett.*, 1997, **38**, 3639.

7 S. Knapp, J. Vasudevan, T. J. Emge, B. H. Arison, J. A. Potenza and H. J. Schugar, *Angew. Chem., Int. Ed.*, 1998, **37**, 2368.

8 R. N. Warrener, A. C. Schultz, M. R. Johnston and M. J. Gunter, *J. Org. Chem.*, 1999, in press; R. N. Warrener, M. R. Johnston and M. J. Gunter, *Synlett*, 1998, 593; R. N. Warrener, M. R. Johnston, A. C. Schultz, M. Golic, M. A. Houghton, M. J. Gunter and R. A. Russell, *Synlett*, 1998, 590.

9 J. L. Charlton and M. M. Alauddin, *Tetrahedron* (*Tetrahedron Report No. 220*), 1987, **43**, 2873; T.-S. Chou, *Rev. Heteroatom Chem.*, 1993, **8**, 65.

10 H.-C. Chen and T.-S. Chou, *Tetrahedron*, 1998, **54**, 12 609.

11 K. Ando, M. Kankake, T. Suzuki and H. Takayama, *Synlett*, 1994, 741.

12 M. G. H. Vicente, M. T. Cancilla, C. B. Lebrilla and K. M. Smith, *Chem. Commun.*, 1998, 2355.

13 D. Barton and S. Zard, *J. Chem. Soc., Chem. Commun.*, 1985, 1098; D. Barton, J. Kertvagoret and S. Zard, *Tetrahedron*, 1990, **46**, 7587; D. P. Arnold, L. Burgess-Dean, J. Hubbard and M. A. Rahman, *Aust. J. Chem.*, 1994, **47**, 969.

14 P. Hopkins and P. Fuchs, *J. Org. Chem.*, 1978, **43**, 1208; S.-S. Chou and C. M. Sun, *Tetrahedron Lett.*, 1990, **31**, 1035.

15 T. D. Lash, *Chem. Eur. J.*, 1996, **2**, 1197.

Communication 9/01446B

The iron-mediated intramolecular addition of carboxylates to conjugated dienes

Ming-Chang P. Yeh,* Li-Wen Chuang, Ya-Sheng Hsieh and Ming-Shan Tsai

Department of Chemistry, National Taiwan Normal University, 88 Sec. 4, Ding-Jou Road, Taipei, Taiwan, Republic of China. E-mail: cheyeh@scc.ntnu.edu.tw

Received (in Cambridge, UK) 1st March 1999, Accepted 25th March 1999

Treatment of carboxylic acid functionalized (η^4-diene)-$Fe(CO)_3$ complexes with 3.0 equiv. of $NOBF_4$ in the presence of Et_3N generates γ- and δ-lactones containing an α,β-unsaturated aldehyde or oxime functionality after NO^+ insertion.

Nucleophilic additions to conjugated dienes coordinated to a transition metal have attracted considerable interest in organic synthesis.[1] Transition metals, such as molybdenum, palladium or iron, have been used to activate dienes towards nucleophilic additions. The (η^4-cyclohexa-1,3-diene)$MoCp(CO)_2$ cations underwent reaction with a variety of carbon nucleophiles at the terminal position of the diene ligand to produce neutral (π-allyl)molybdenum complexes. Hydride abstractions from these complexes regenerated cationic diene complexes which again underwent intermolecular nucleophilic attack from the face opposite the metal, resulting in overall 1,3-stereocontrol in the six-membered ring.[2] With a pendant carboxylic acid group, neutral (π-allyl)molybdenum complexes underwent intramolecular addition with carboxylates by conversion of the neutral species to the cationic nitrosyl intermediates (exchange of neutral CO for NO^+) to afford γ- and δ-lactone derivatives.[3] In the palladium-catalyzed oxidation of conjugated dienes, two nucleophiles were added in a regio- and stereoselective manner across the diene. Nucleophiles that could be used in the overall 1,4-addition included carboxylates, amides, alcohols, and halides.[4] Conjugated dienes could also be activated towards nucleophilic additions by the $Fe(CO)_3$ moiety. The intermolecular addition of reactive ester or cyano stabilized carbanions to diene–iron complexes under CO afforded cyclopentanoids after acid quenching.[5] Recently, we have extended this chemistry into an intramolecular variant. Thus, sequential additions of carboester functionalized zinc–copper organometallics to (η^5-pentadienyl)$Fe(CO)_3$ cations furnished bicyclo[3.3.0]octanones or trisubstituted cyclopentanecarboxylic acid derivatives depending on the quenching process.[6] However, nucleophiles that could be used to add at the diene ligand of $Fe(CO)_3$ complexes have been restricted to stabilized carbanions. It would be of great synthetic interest to extend these regio- and stereoselective additions to other nucleophiles, such as oxygen and nitrogen nucleophiles. Here we report, for the first time, on the intramolecular addition of carboxylates to conjugated dienes by conversion of neutral (η^4-diene)$Fe(CO)_3$ complexes to the cationic nitrosyl intermediates (exchange of neutral CO and NO^+). The addition proceeded regiospecifically to form γ- and δ-lactones with an α,β-unsaturated aldehyde or oxime functionality after NO^+ insertion.

The starting acid complexes **1**–**3** were prepared in two steps according to literature procedures.[6,7] Addition of carboester functionalized zinc–copper reagents to the corresponding (η^5-dienyl)$Fe(CO)_3$ cationic salts followed by hydrolysis of the residue with KOH in MeOH–THF–H_2O at 30 °C produced complexes **1**–**3** as the major products in good yields (70–90%). Finally, our intramolecular addition involved the addition of an MeCN solution of $NOBF_4$ (3.0 equiv.) to **1a** in MeCN at 0 °C under nitrogen and then addition of Et_3N (2.0 equiv.). The addition was carried out for 30 min at 0 °C followed by workup with saturated aqueous NH_4Cl and CH_2Cl_2 extraction. After purification by flash column chromatography on silica gel and distillation under reduced pressure, γ-lactone **4**† bearing an α,β-unsaturated aldehyde at the γ-position of the ring was obtained as the major product in 60% yield (entry 1, Table 1). Under the same reaction conditions, intramolecular cyclization of **1b** with an additional methyl group at the terminal position of the diene ligand afforded γ-lactone **5** with an α,β-unsaturated oxime at the γ-position of the ring in 64% yield (entry 2, Table 1). The formation of **4** and **5** may result from NO^+ insertion. However, it is important to mention that the intramolecular addition of carboxylates to (η^3-allyl)$MoCp(CO)(NO)$ cations to give γ and δ-lactones did not involve NO^+ insertion.[3] A mechanism for generation of **4** and **5** is suggested in Scheme 1. Addition of $NOBF_4$ to complexes **1a**,**b** may produce the cationic species **10**. Deprotonation of **10** with Et_3N gave carboxylate **11**, with attack exclusively at the terminal position of the diene ligand to

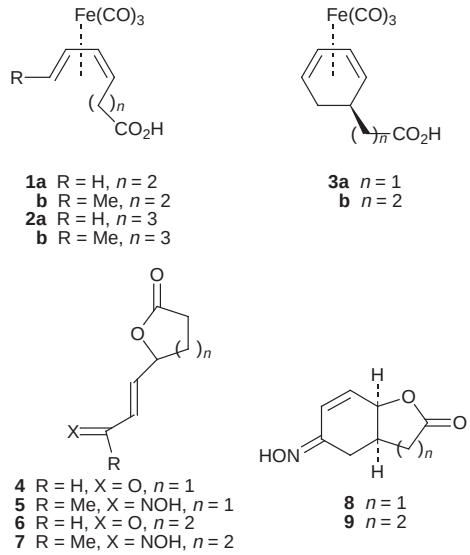

1a R = H, *n* = 2
b R = Me, *n* = 2
2a R = H, *n* = 3
b R = Me, *n* = 3

3a *n* = 1
b *n* = 2

4 R = H, X = O, *n* = 1
5 R = Me, X = NOH, *n* = 1
6 R = H, X = O, *n* = 2
7 R = Me, X = NOH, *n* = 2

8 *n* = 1
9 *n* = 2

Table 1 Intramolecular additions of carboxylates to (η^4-Diene)$Fe(CO)_3$ complexes

Entry	Starting complex	Product	Yield (%)[a]
1	**1a**	**4**	60
2	**1b**	**5**	64
3	**2a**	**6**	55
4	**2b**	**7**	53
5	**3a**	**8**	50
6	**3b**	**9**	53

[a] All products were purified by flash column chromatography on silica gel and distillation under reduced pressure and have been fully characterized by ^1H and ^{13}C NMR, IR, mass and high resolution mass spectra.

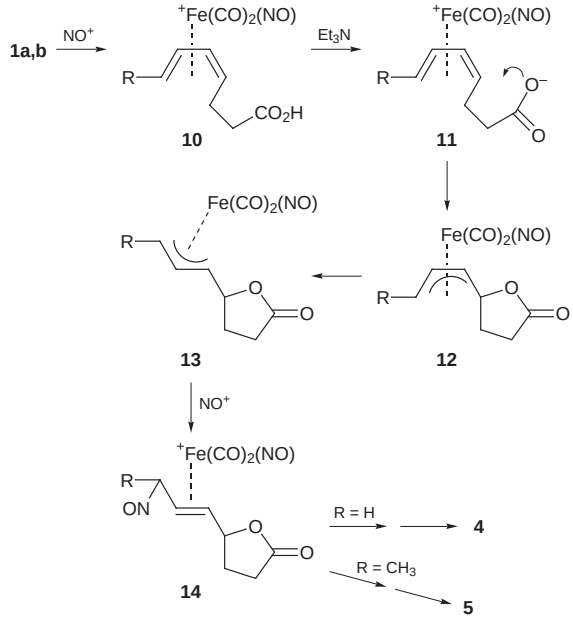

Scheme 1 Proposed reaction pathway for the formation of lactones **4** and **5**.

produce the postulated neutral (π-allyl)$Fe(CO)_2(NO)$ intermediate **12**. *Syn/anti* isomerization of **12** *via* π-allyl/σ-allyl interconversion of the allyl ligand produced **13**.[8] Intermediate **13** may undergo nitrosyl migration with an additional NO^+ to give **14**. However, neutral complexes, such as (η^3-allyl)$Fe(CO)_2NO$, underwent internal CO (rather than NO^+) insertion upon treatment with 1,2-bis(diphenylphosphino)ethane to give an iron acyl intermediate. Quenching the iron acyl intermediate with I_2/EtOH produced a β,γ-unsaturated carboxylic ester.[9] Thus, it is reasonable to suggest that complex (η^3-allyl)$Fe(CO)_2NO$ **13** may undergo nitrosyl insertion with an excess of $NOBF_4$ (3.0 equiv. of NO^+) to produce **14**. The primary nitroso compound (R = H) hydrolyzed to **4**, while the secondary nitroso derivative (R = CH_3) underwent nitroso–oxime tautomerization to produce **5** after aqueous workup and flash column chromatograph of the residue.

Increasing the tether length by one with complexes **2a** and **2b** (entries 3 and 4, Table 1) also allowed intramolecular cyclisation to provide δ-lactones **6** (55%) and **7** (53%), respectively, as the only product in each case. The results are consistent with complexes **1a** and **1b**. Thus, the substrate with an additional methyl group at the diene ligand, **2b**, produced lactone **7** with an α,β-unsaturated oxime functionality at the δ-position of the ring, while complex **2a** generated δ-lactone **6** bearing an α,β-unsaturated aldehyde functionality. However, preliminary attempts to prepare β- and ω-lactones were unsuccessful. No cyclization has been observed for acid complexes **15** and **16**.

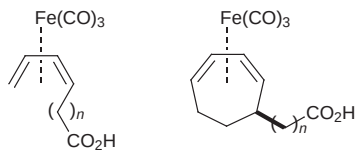

15 $n = 1$ **16** $n = 4$ **17** $n = 1$ **18** $n = 2$

Using the same methodology, we are able to construct fused bicyclic lactones **8** and **9** *via* intramolecular addition of carboxylates to cyclic diene–iron complexes **3a** and **3b**, respectively. Fused bicyclic lactones **8**† (50%) and **9** (64%) bearing an α,β-unsaturated oxime functionality were obtained as the only diastereoisomer in each case. The *cis*-stereochemistry at the ring juncture in lactones **8** and **9** was fixed by *anti* addition of carboxylates at the terminal position of the diene ligands and ^1H NMR studies provided evidence supporting the structure assignments. The coupling constants of 5.3 and 4.8 Hz, respectively, of the adjacent fused protons in **8** and **9** demand *cis*-fused bicyclic skeletons. These values are consistent with the couling constants observed for the *cis* fused bicyclo γ- and δ-lactones reported in the literature.[8] Rigorous proof of the structure of **8** was further accomplished by X-ray diffraction analysis.‡ Although the iron-mediated intramolecular cyclisation works well for the formation of fused bicyclic lactones **8** and **9** from (η^4-cyclohexa-1,3-diene)-$Fe(CO)_3$ acid complexes, attempts to obtain fused bicyclo γ- and δ-lactones from intramolecular cyclisation of (η^4-cyclohepta-1,3-diene)$Fe(CO)_3$ acid complexes **17** and **18** have thus far failed.

We thank the National Science Council of the Republic of China for the financial support.

Notes and references

† *Selected data* for **4**: $\delta_H(CDCl_3)$ 9.63 (1H, d, *J* 7.3), 6.80 (1H, dd, *J* 15.6, 4.4), 6.37 (1H, dd, *J* 15.6, 7.3), 5.21 (1H, m), 2.61 (3H, m) and 2.05 (1H, m); $\delta_C(CDCl_3)$ 192.2, 175.6, 150.9, 131.8, 77.5 and 27.8; $\nu_{max}(CH_2Cl_2)/cm^{-1}$ 3040w, 3012w, 2959w, 2928, 2872, 1779m, 1732m, 1603m, 1460w, 1375w, 1236w, 1198w, 1113w and 1045m; *m*/*z* (EI) 140 (M^+, 48%), 123 (38), 111 (42), 98 (29), 95 (47), 85 (43), 81 (82), 70 (13), 67 (25), 56 (23) and 55 (57); HRMS: calc. for $C_7H_8O_3$ 140.0437, found 140.0471.

‡ *Crystal data* for **8**: $C_8H_9NO_3$, M = 167.16, monoclinic, a = 9.535(2), b = 7.052(1), c = 12.691(3) Å, U = 791.4(3) Å^3, T = 298 K, space group $P2_1/c$, Z = 4, μ(Mo-Kα) = 0.71073 mm^{-1}, 2395 reflections measured, 2298 unique (R_{int} = 0.012), which were used in all calculations. The final $wR(F^2)$ was 0.078 (all data). Single crystals of compound **8** were recrystallised from hexane–EtOAc. The structure was solved using direct methods and refined by full-matrix least-squares on F^2. CCDC 182/1211. See http://www.rsc.org/suppdata/cc/1999/805/ for crystallographic files in .cif format.

1 J. E. Bäckvall, in *Advances in Metal-Organic Chemistry*, ed. L. S. Liebeskind, JAI, London, 1989, vol. 1, p. 135; L. S. Hegedus, *Tetrahedron*, 1984, **40**, 2415; B. M. Trost, *Angew. Chem., Int. Ed. Engl.*, 1989, **28**, 1173.

2 J. W. Faller, H. H. Murray, D. L. White and K. H. Chao, *Organometallics*, 1983, **2**, 400; A. J. Pearson, M. N. I. Kahn, J. C. Clardy and H. Ciu-Heng, *J. Am. Chem. Soc.*, 1985, **107**, 2748; A. J. Pearson and M. N. I. Kahn, *Tetrahedron Lett.*, 1985, **26**, 1407; S. Hansson, J. F. Miller and L. S. Liebeskind, *J. Am. Chem. Soc.*, 1990, **112**, 9660.

3 A. J. Pearson, S. Mallik, R. Mortezaei, M. W. D. Perry, D. J. Shively, Jr. and W. J. Youngs, *J. Am. Chem. Soc.*, 1990, **112**, 8034; A. J. Pearson and M. N. I. Kahn, *Tetrahedron Lett.*, 1984, **25**, 3507; M. C. P. Yeh, C. J. Tsou, C. N. Chuang and H. C. Lin, *J. Chem. Soc., Chem. Commun.*, 1992, 890.

4 J. E. Bäckvall, J. E. Nyström and R. E. Nordberg, *J. Am. Chem. Soc.*, 1985, **107**, 3676; J. E. Bäckvall, S. E. Byström and R. E. Nordberg, *J. Org. Chem.*, 1984, **49**, 4619; J. E. Bäckvall and J. O. Vågberg, *J. Org. Chem.*, 1988, **53**, 5695; J. E. Bäckvall, P. G. Andersson and J. O. Vågberg, *Tetrahedron Lett.*, 1989, **30**, 137; J. E. Bäckvall, *Pure Appl. Chem.*, 1992, **64**, 429; J. E. Bäckvall, and P. G. Andersson, *J. Am. Chem. Soc.*, 1990, **112**, 3683; 1992, **114**, 6374.

5 M. F. Semmelhack and J. W. Herndon, *Organometallics*, 1983, **2**, 363; M. F. Semmelhack, J. W. Herndon and J. K. Liu, *Organometallics*, 1983, **2**, 1885; M. F. Semmelhack, J. W. Herndon and J. P. Springer, *J. Am. Chem. Soc.*, 1983, **15**, 2497; M. F. Semmelhack and H. T. M. Le, *J. Am. Chem. Soc.*, 1984, **106**, 2715; M. F. Semmelhack and J. W. Herndon, *J. Organomet. Chem.*, 1984, **265**, C15; M. F. Semmelhack and H. T. M. Le, *J. Am. Chem. Soc.*, 1985, **107**, 1455; M. C. P. Yeh, K. K. Kang and C. C. Hwu, *J. Chin. Chem. Soc.*, 1991, **38**, 475.

6 M. C. P. Yeh, B. A. Sheu, H. W. Fu, S. I. Tau and L. W. Chuang, *J. Am. Chem. Soc.*, 1993, **115**, 5941; M. C. P. Yeh, L. W. Chuang, C. C. Hwu, J. M. Sheu and L. C. Row, *Organometallics*, 1995, **14**, 3396; M. C. P. Yeh and L. W. Chuang, *J. Org. Chem.*, 1995, **61**, 3874.

7 M. C. P. Yeh, L. W. Chuang, S. C. Chang, M. L. Lai and C. C. Chou, *Organometallics*, 1997, **16**, 4435.

8 J. K. Becconsall and S. J. O'Brien, *J. Chem. Soc., Chem. Commun.*, 1966, 302; P. Corradini, G. Maglio, A. Musco and G. Paiaro, *J. Chem. Soc., Chem. Commun.*, 1966, 618.

9 S. Nakanishi, T. Yamamoto, N. Furukawa and Y. Otsuji, *Synthesis*, 1994, 609.

Communication 9/01628G

Realisation of highly stereoselective dihydroxylation of a cyclopentene in the synthesis of (−)-aristeromycin

Yuko Tokoro and Yuichi Kobayashi*

Department of Biomolecular Engineering, Tokyo Institute of Technology, 4259 Nagatsuta-cho, Midori-ku, Yokohama 226-8501, Japan. E-mail: ykobayas@bio.titech.ac.jp

Received (in Cambridge, UK) 8th March 1999, Accepted 23rd March 1999

A 2-furyl group was used as a synthetic equivalent of the CH_2OH at the 4′ position of aristeromycin, and dihydroxylation of the cyclopentene possessing the furyl group proceeded highly stereoselectively to produce the key diol for the synthesis of (−)-aristeromycin.

Aristeromycin **1** is a carbocyclic analogue of adenosine and its unique biological properties and structure have attracted considerable interest among organic chemists. Total syntheses of **1** have been reported and are summarised in several reviews.[1] In order to improve or use the biological properties of **1**, analogues of **1** have also been synthesised. Among these syntheses, the strategy of utilizing the monoacetate of *cis* cyclopent-4-ene-1,3-diol (*i.e.* **2**)† as the starting material, which

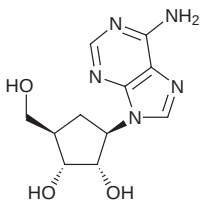

1

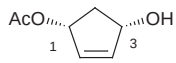

2

was originally reported by Deardorff,[2] is attractive especially in that (i) both enantiomers are readily available[3] and (ii) installation of the substituents onto the cyclopentene ring of **2** simply accomplishes a synthesis of **1**. Several groups have published syntheses of **1** along this line, and the efficiency in installing the nitrogen-containing moiety and "CH_2OH" group has also been improved.[4] The stereoselectivity of the dihydroxylation, however, still remains at low levels.[2,4,5] Recently, an explanation for the low selectivity of the dihydroxylation was proposed by Katagiri.[6] Namely, the cyclopentene possessing the requisite 'CH_2OR' group at the 4′ position (aristeromycin numbering) and a heteroatom at the 1′ position adopts minor and major conformers, and the dihydroxylation of the latter inevitably produces a mixture of stereoisomeric diols. Therefore, a new approach, whereby dihydroxylation would take place stereoselectively, is required in order to use the convenient monoacetate **2** as a starting material for **1**.

Recently, we reported a nickel-catalysed coupling reaction of **2** and lithium borates **3**, where aryl, furyl and alkenyl groups (R) on the borates can be transferred onto **2** (eqn. 1).[7] This reaction proceeds stereo- and regio-selectively to furnish *trans* 1,4-products **4**, for the first time, as the major products. These groups (R) are all candidates for 'CH_2OR' and are bigger than 'CH_2OR'. Consequently, even in the *undesired* conformer of the cyclopentene possessing such a group (R) and a nitrogen atom at the 4′ and 1′ positions, respectively, the approach from the β-face would be prevented more effectively than that with CH_2OR as the R group. Our proposal is illustrated in Fig. 1. To examine the above idea, we chose the furyl group (R = 2-furyl) as a 'CH_2OR' precursor and succeeded in the stereoselective synthesis of acetonide **11**. Hydrolysis of **11** to aristeromycin has already been established.[4b,8] In addition, **11** is an important starting compound for the synthesis of analogues and supermolecules containing aristeromycin.[9]

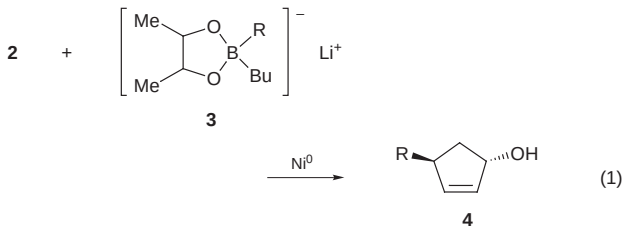

The synthetic route is summarised in Scheme 1. The cyclopentenol **4a** was prepared from (1*R*)-acetate **2** (> 95% ee)[3c] and lithium 2-furylborate **3** (R = 2-furyl). Reaction of **4a** with $(PhO)_2P(O)N_3$[10] proceeded selectively to afford **5**‡ as the sole product. The key dihydroxylation was examined under various conditions and the results are summarised in Table 1. A 4 : 1 ratio of the desired product **6** and the stereoisomer **12** was obtained in good yield when the reaction was carried out at room temperature (entry 1). Although the ratio was definitely higher than previously reported ones, it was still low from a synthetic point of view. Fortunately, reaction at lower temperature (0 °C) resulted in a substantially higher ratio of 14 : 1 (entry 2). Since the observed coupling constant between Ha and Hc of **5** (J_{ac} = 5.4 Hz) indicates that **5** does take both the desired and undesired conformers according to Katagiri,[6] it is clear that the observed high stereoselectivity is provided by the furyl group. Use of acetone as solvent slightly decreased the ratio (entry 3). Double diastereoselectivity between chiral **5** and the Sharpless reagent (AD-mix-α or –β),[11] was also examined. Unfortunately, better selectivity (*i.e.* ratio of **6** to **12**) was not attained (entries 4 and 5). A reagent lacking the chiral ligand for AD-mix resulted in a similar ratio (entry 6).[12]

Since separation of the diols **6** and **12** by chromatography was not an easy task due to their similar mobility on TLC, the mixture was transformed into the corresponding acetonides **7** and **13**, which were easily separated by chromatography. The furyl group of **7** was then transformed into a CO_2Me group by oxidation using $NaIO_4$ and $RuCl_3$ catalyst followed by esterification with CH_2N_2 to afford **8** in 80% yield. Treatment of **8** with $LiAlH_4$ effected reduction of the ester and the azide

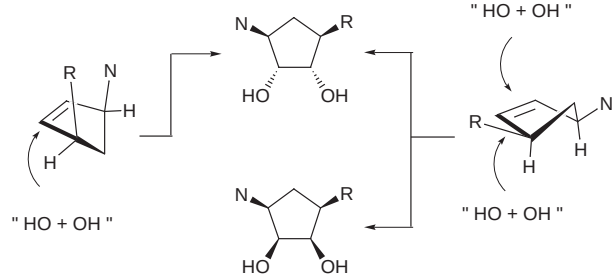

Fig. 1 Desired (left) and undesired (right) conformers for dihydroxylation.

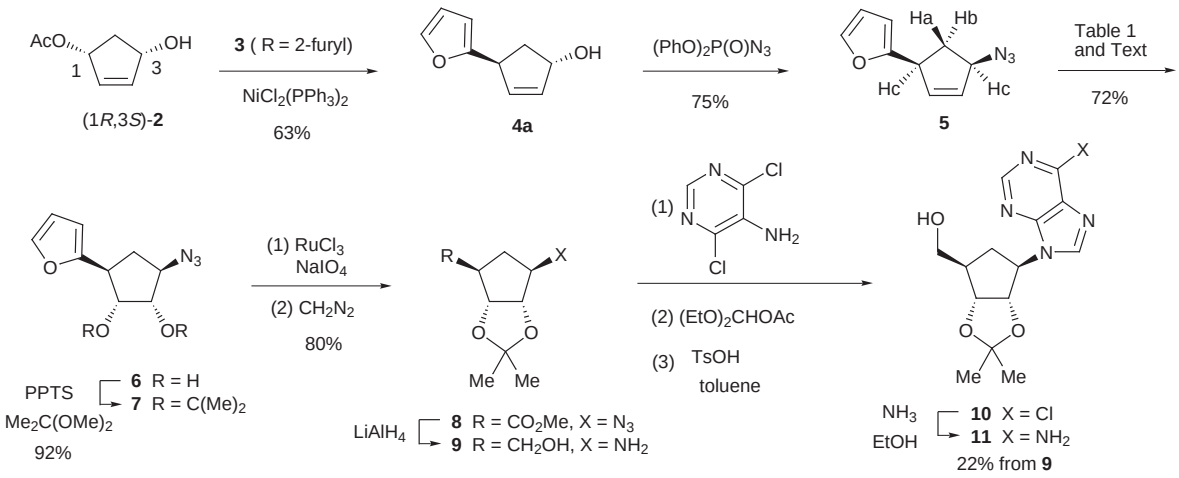

Scheme 1

Table 1 Dihydroxylation of **5**

Entry	Reagent	Conditions	Ratio[a] **6**:**12**	Yield (%)[b]
1	OsO_4,[c] NMO	MeCN–Bu^{t}OH–H_2O (4:1:1), room temp., 16 h	4:1	71
2	OsO_4,[c] NMO	MeCN–THF–Bu^{t}OH–H_2O (4:2:1:1), 0 °C, 7 h	14:1	72
3	OsO_4,[c] NMO	Acetone–THF–H_2O (8:4:1), 0 °C, 7 h	11:1	65
4	AD-mix-α	Bu^{t}OH–H_2O (1:1), 0 °C, 24 h	3:1	—[d]
5	AD-mix-β	Bu^{t}OH–H_2O (1:1), 0 °C, 24 h	6:1	34
6	OsO_4,[e] $K_3Fe(CN)_6$, K_2CO_3	Bu^{t}OH–H_2O (1:1), 0 °C→ room temp., 24 h	4:1	—[d]

[a] Ratios were determined by ^{1}H NMR. [b] Isolated yields. [c] 3 mol%. [d] Not determined. [e] 1.25 mol%.

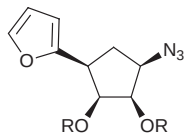

12 R = H
13 R = C(Me)$_2$

groups to afford **9**. The amino group of **9** was converted to a chloropurine moiety using the standard procedure. Finally, reaction of **10** with NH_3 gave the acetonide of aristeromycin **11**, whose ^{1}H NMR (300 MHz) spectrum was fully coincident with the reported data.[13] Use of EtOH for this transformation proved to be better than the standard solvent of MeOH since NH_3–MeOH gave the corresponding methoxide as a by-product. The deprotection of **11** to aristeromycin has already been published.[8]

Since high stereoselection in the dihydroxylation was achieved using the furyl group, it is possible that an aryl or alkenyl group may control the dihydroxylation and that such a group, after being installed onto the cyclopentene ring, can be transformed by taking advantage of their reactivity into various polyoxygenated side chains at the 4' position. These modifications are important for the next generation of carbocyclic sugars.

We thank to Toyo Kasei Kogyo Co. Ltd. for a generous supply of $(PhO)_2P(O)N_3$.

Notes and references

† For convenience, one enantiomer is shown.

‡ *Selected data* for **5**: δ_H(300 MHz, $CDCl_3$) 1.93 (dt, *J* 14, 5.4, 1H), 2.76 (dt, *J* 14, 8.3, 1H), 3.92–4.00 (m, 1H), 4.41–4.49 (m, 1H), 5.91 (dt, *J* 5.7, 2.4, 1H), 6.04–6.10 (m, 2H), 6.30 (dd, *J* 3.0, 1.8, 1H), 7.34 (d, *J* 2, 1H).

1 Reviews: M. T. Crimmins, *Tetrahedron*, 1998, **54**, 9229; L. Agrofoglio, E. Suhas, A. Farese, R. Condom, S. R. Challand, R. A. Earl and R. Guedji, *Tetrahedron*, 1994, **50**, 10 611; A. D. Borthwick and K. Biggadike, *Tetrahedron*, 1992, **48**, 571; D. M. Huryn and M. Okabe, *Chem. Rev*., 1992, **92**, 1745.

2 D. R. Deardorff. K. A. Savin, C. J. Justman, Z. E. Karanjawala, J. E. Sheppeck, II, D. C. Hager and N. Aydin, *J. Org. Chem*., 1996, **61**, 3616.

3 (1*R*,3*S*)-**2**: (*a*) K. Laumen and M. P. Schneider, *J. Chem. Soc., Chem. Commun*., 1986, 1298; (*b*) D. R. Deardorff, A. J. Matthews, D. S. McMeekin and C. L. Craney, *Tetrahedron Lett*., 1986, **27**, 1255; (*c*) T. Sugai and K. Mori, *Synthesis*, 1988, 19. (1*S*,3*R*)-**2**: (*d*) Y.-F. Wang, C.-S. Chen, G. Girdaukas and C. J. Sih, *J. Am. Chem. Soc*., 1984, **106**, 3695; (*e*) K. Laumen and M. Schneider, *Tetrahedron Lett*., 1984, **25**, 5875.

4 (*a*) R. Vince and S. Daluge, *J. Org. Chem*., 1980, **45**, 531; (*b*) B. M. Trost, G.-H. Kuo and T. Benneche, *J. Am. Chem. Soc*., 1988, **110**, 621; (*c*) E. A. Saville-Stones, S. D. Lindell, N. S. Jennings, J. C. Head and M. J. Ford, *J. Chem. Soc., Perkin Trans. 1*, 1991, 2603; (*d*) S. M. Roberts and K. A. Shoberu, *J. Chem. Soc., Perkin Trans. 1*, 1991, 2605; (*e*) B. M. Trost, L. Li and S. D. Guile, *J. Am. Chem. Soc*., 1992, **114**, 8745; (*f*) E. A. Saville-Stones, R. M. Turner, S. D. Lindell, N. S. Jennings, J. C. Head and D. S. Carver, *Tetrahedron*, 1994, **50**, 6695; (*g*) F. Burlina, A. Favre, J.-L. Fourrey and M. Thomas, *Bioorg. Med. Chem. Lett*., 1997, **7**, 247.

5 R. Csuk and P. Dörr, *Tetrahedron*, 1995, **51**, 5789.

6 N. Katagiri, Y. Ito, K. Kitano, A. Toyota and C. Kaneko, *Chem. Pharm. Bull*., 1994, **42**, 2653.

7 Y. Kobayashi, E. Takahisa and S. B. Usmani, *Tetrahedron Lett*., 1998, **39**, 597; S. B. Usmani, E. Takahisa and Y. Kobayashi, *Tetrahedron Lett*., 1998, **39**, 601.

8 A. Holý, *Collect. Czech. Chem. Commun*., 1976, **41**, 2096; A. K. Saksena, *Tetrahedron Lett*., 1980, **21**, 133; G. V. B. Madhavan and J. C. Martin, *J. Org. Chem*., 1986, **51**, 1287.

9 E. M. Peterson, J. Brownell and R. Vince, *J. Med. Chem*., 1992, **35**, 3991; D. P. Matthews, M. L. Edwards, S. Mehdi, J. R. Koehl, J. A. Wolos and J. R. McCarthy, *Bioorg. Med. Chem. Lett*., 1993, **3**, 165; W. B. Lott, A. M. Chagovetz and C. B. Grissom, *J. Am. Chem. Soc*., 1995, **117**, 12 194; S. F. Wnuk, C.-S. Yuan, R. T. Borchardt and M. J. Robins, *Nucleosides Nucleotides*, 1998, **17**, 99.

10 A. S. Thompson, G. R. Humphrey, A. M. DeMarco, D. J. Mathre and E. J. J. Grabowski, *J. Org. Chem*., 1993, **58**, 5886.

11 K. B. Sharpless, W. Amberg, Y. L. Bennani, G. A. Crispino, J. Hartung, K.-S. Jeong, H.-L. Kwong, K. Morikawa, Z.-M. Wang, D. Xu and X.-L. Zhang, *J. Org. Chem*., 1992, **57**, 2768; H. C. Kolb, M. S. VanNieuwenhze and K. B. Sharpless, *Chem. Rev*., 1994, **94**, 2483.

12 M. Minato, K. Yamamoto and J. Tsuji, *J. Org. Chem*., 1990, **55**, 766.

13 Y. F. Shealy and J. D. Clayton, *J. Am. Chem. Soc*., 1969, **91**, 3075.

Communication 9/01819K

ChemComm

Synthesis of the macrocyclic core of sanglifehrin A

K. C. Nicolaou* Takashi Ohshima, Fiona Murphy, Sofia Barluenga, Jinyou Xu and Nicolas Winssinger

Department of Chemistry and The Skaggs Institute for Chemical Biology, The Scripps Research Institute, 10550 North Torrey Pines Road, La Jolla, California 92037, USA and Department of Chemistry and Biochemistry, University of California, San Diego, 9500 Gilman Drive, La Jolla, California 92093, USA. E-mail: kcn@scripps.edu

Received (in Cambridge, UK) 5th February 1999, Accepted 24th March 1999

The synthesis of the macrocyclic core of sanglifehrin A, a newly discovered natural product, is described.

Sanglifehrin A[1] **1** is a newly discovered natural product with impressive biological properties, including cyclophilin binding,

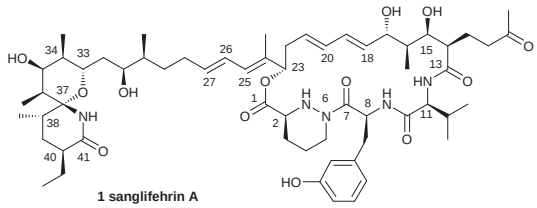

immunosuppressive activity and inhibition of both B-cell and T-cell proliferation.[1] Isolated from the fermentation broths of an unidentified species of Actinomycetes by a team of scientists at Novartis, this substance possesses a novel molecular architecture whose main domains are a [5.5] spirolactam moiety and a 22-membered macrocycle featuring a number of novel functionalities. Here we report construction of the macrocyclic system of sanglifehrin A in which the diene segment at C23 has been judiciously replaced by a hydrogen substituent for the purpose of this model study (compound **2**, Scheme 1).

From the many disconnections one can envision for the construction of macrocycle **2**, we chose the strategy based on the intramolecular Stille coupling,[2] (Scheme 1). This approach requires the preparation of a precursor carrying the C21–C20 vinyl iodide and C18–C19 vinyl stannane functionalities for the cyclization process under the catalytic influence of palladium(0). Disconnection of the indicated NH–CO linkage led to building blocks **3** and **4**, which became our first subtargets.

The synthesis of the C13–C19 vinyl stannane fragment **4** is summarized in Scheme 2. Thus, the α,β-unsaturated ester **5**[3] was converted to its TIPS ether **6** (95% yield) and thence reduced with DIBAL-H (87% yield) to afford allylic alcohol **7**. The MCPBA-mediated epoxidation of **7** proceeded stereoselectively to afford epoxide **8** in 100% yield (β:α epoxide ratio *ca.* 6:1). Regioselective epoxide opening[4] of **8** by

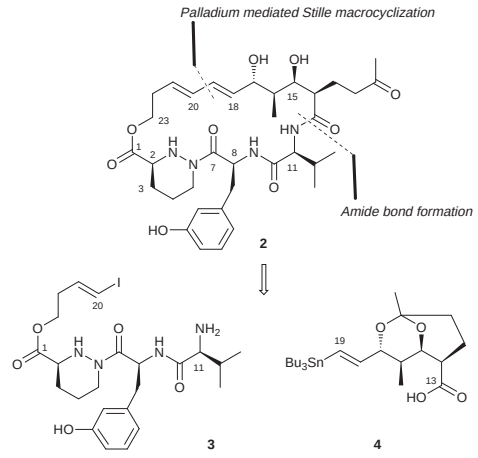

Scheme 1 Retrosynthetic analysis of sanglifehrin model system **2**.

CH_2=$CHCH_2CH_2MgBr$[5] in the presence of CuI furnished diol **9** (80% yield), whose selective protection as a pivaloate ester proceeded smoothly (95% yield) to afford monopivaloate **10**. Desilylation of **10** with TBAF provided **11** (81% yield) which was subjected to Wacker oxidation[6] and internal ketalization to furnish **12** in 88% overall yield *via* the corresponding dihydroxy ketone. Sequential hydrogenolysis of the benzyl ether group from **12**, tetrapropylammonium perruthenate (TPAP)–NMO[7] oxidation of the resulting alcohol (83% for two steps), and reaction with $(MeCO)C(=N_2)PO(OMe)_2$[8] in the presence of K_2CO_3 led to terminal alkyne **14** (98%) *via* aldehyde **13**. Regio- and stereoselective addition of Bu_3SnH to acetylenic compound **14** proceeded in the presence of catalytic amounts of $PdCl_2(PhCN)_2$, P(*o*-Tol)$_3$ and Pr^i_2NEt to afford vinyl stannane **15** in 79% yield (regioselectivity > 20:1). The latter (**15**) was oxidised in high yield to carboxylic acid **4** by sequential treatment with TPAP–NMO and $NaClO_2$ (NaH_2PO_4, 2-methylbut-2-ene) and was judged to be of sufficient purity after work-up to be used as such in the subsequent coupling with amide **3**.

The second required fragment, compound **3**, was synthesized according to Scheme 3. Thus, coupling of *m*-hydroxybenzaldehyde **16** with phosphonate **17**[9] in the presence of DBU proceeded smoothly to afford olefinic product **18** in geometrically pure form (90% yield). The asymmetric hydrogenation of **18** was carried out in the presence of [SS-Et-DuP-Rh]$^+$TfO$^-$ catalyst[10] and was followed by hydrogenolysis of the Cbz group

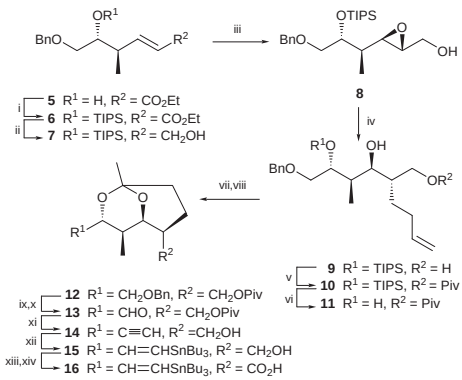

Scheme 2 *Reagents and conditons:* i, TIPSC (2 equiv.), imidazole (3 equiv.), DMF, 60 °C, 24 h, 95%; ii, DIBAL-H (3 equiv.), CH_2Cl_2, −78 °C, 2 H, 87%; iii MCPBA (1.5 equiv.), CH_2Cl_2 −25 °C, 100%, β:α epoxide ratio *ca.* 6:1; iv, H_2C=$CHCH_2CH_2MgBr$ (5 equiv.), CuI (1 equiv.) Et_2O–THF (1:1), −40 → −20 °C, 18 h, 80%; v, PivCl (25 equiv.), pyridine (50 equiv.), 25 °C, 24 h, 95%; vi, TBAF (2 equiv.), THF, 25 °C, 1 h, 81%; vii, $PdCl_2$ (0.1 equiv.), benzoquinone (1.5 equiv.), DMF–H_2O (7:1), 25 °C, 3 h; viii, TsOH·H_2O (0.05 equiv.), benzene, reflux, 88% for two steps; ix, H_2, 10% Pd/C (0.1 equiv.), EtOH, 25 °C, 1 h; x, TPAP (0.05 equiv.), NMO (3 equiv.), 4 Å MS, CH_2Cl_2, 25 °C, 20 min, 83% for two steps; xi, $MeCOC(=N_2)PO(OMe)_2$ (5.0 equiv.), K_2CO_3 (5 equiv.), MeOH, 0 → 25 °C, 13 h; then K_2CO_3 (5 equiv.), 25 °C, 24 h, 98%; xii, Bu^n_3SnH (4 equiv.), $PdCl_2(PhCN)_2$ (0.3 equiv.), P(*o*-Tol)$_3$ (0.6 equiv.), Pr^i_2NEt (4.0 equiv.), CH_2Cl_2 −20 °C, 1 h, 79%; xiii, TPAP (0.05 equiv.), NMO (3.0 equiv.), 4 Å MS, CH_2Cl_2, 25 °C, 15 min; xiv, $NaClO_2$ (6.0 equiv.), NaH_2PO_4 (2. equiv.), 2-methybut-2-ene (10 equiv.), THF–Bu^tOH–H_2O (1:5:1), 25 °C, 15 min.

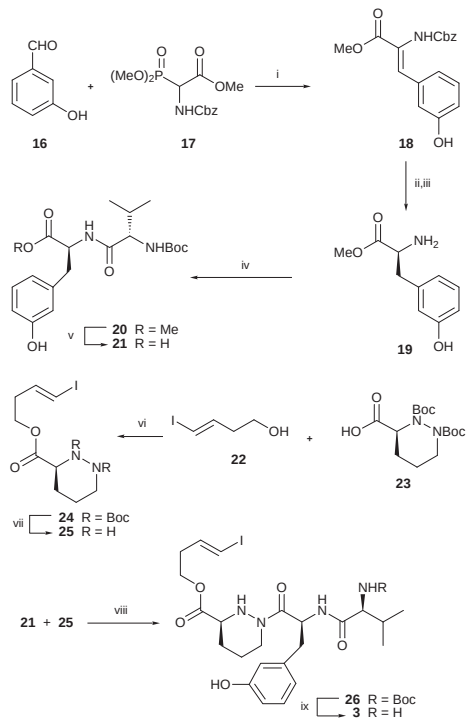

Scheme 3 *Reagents and conditions:* i, DBU (2 equiv.), CH_2Cl_2, 25 °C, 2 h, 90%; ii, [(*S*,*S*)-Et-DuP-Rh]$^+$TfO$^-$ (0.7 mol%), 60 psi, 96 h, 98% ee, 90%; iii, H_2, 10% Pd/C, MeOH, 25 °C, 12 h, 96%; iv EDC (3 equiv.), HOAt (3 equiv.), CH_2Cl_2, 0 → 25 °C, 3 h, 78%; v, LiOH (2 equiv.), THF–H_2O (3 : 1), 0 → 25 °C, 1.5 h, 89%; vi, EDC (2 equiv.), 4-pyrolidinopyridine (0.1 equiv.), Pr$^i_2$NEt (1 equiv.), CH_2Cl_2, 0 → 25 °C, 80%; vii, TFA–CH_2Cl_2 (1 : 1), 0 → 25 °C, 2 h, viii, HOAt (1 equiv.), Pr$^i_2$NEt (3 equiv.), EDC (1.2 equiv.), CH_2Cl_2, 0 → 25 °C, 3.5 h, 66% for two steps; ix, TFA–CH_2Cl_2 (1 : 1), 0 → 25 °C, 2 h.

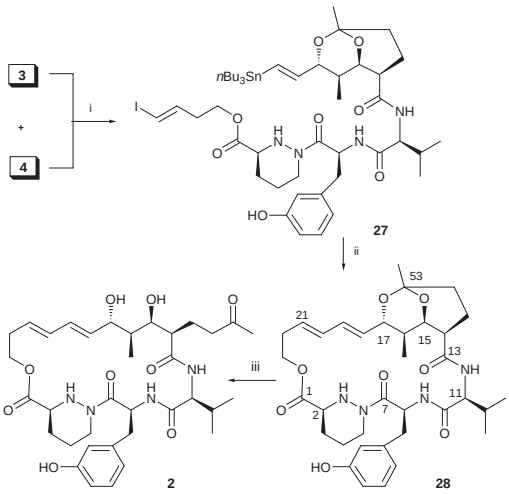

Scheme 4 *Reagents and conditions:* i, HATU (1 equiv.) Pr$^i_2$NEt (4 equiv.) DMF, 0 → 25 °C, 10 h, 51% over three steps from **15**; ii, $Pd_2(dba)_3$·$CHCl_3$ (0.15 equiv.), $AsPh_3$ (0.6 equiv.), Pr$^i_2$NEt (10 equiv.), DMF, 25 °C, 3 h, 40%; iii, 0.8 M H_2SO_4, THF–H_2O (4 : 1), 25 °C, 10 h.

(H_2, 10% Pd/C), furnishing amino acid derivative **19** in 98% *ee* and 96% yield. Coupling of **19** with the Boc derivative of valine, facilitated by 1-(3-dimethylaminopropyl)-3-ethylcarbodümide hydrochloride (EDC) and 1-hydroxy-7-azabenzotriazole (HOAt)[11] gave peptide **20** in 78% yield. The next step involved mild hydrolysis of the methyl ester group of **20** (LiOH, THF : H_2O) to afford the carboxylic acid **21** (89% yield), whose coupling with piperazic acid derivative **25** (EDC, HOAt) led to product **26** (66% yield from **25**). Compound **25** was prepared by coupling of fragments **22**[12] and **23**[13] (80% yield), followed by TFA-induced removal of the Boc groups. Liberation of the amino group from **26** furnished segment **3** in high yield which was used directly in the coupling with acid **4**.

Union of fragments **3** and **4** proceeded smoothly in the presence of *o*-(7-azabenzotriazol-1-yl)-*N*,*N*,*N*′,*N*′-tetramethyluronium hexofluorophosphate (HATU),[11] furnishing the cyclisation precursor **27** (51% over three steps from **15** *vs*. 58% over two steps from **3**), whose cyclisation was realized upon exposure to $Pd_2(dba)_3$ and $AsPh_3$[14] in DMF at room temperature affording compound **28**† (40% yield). Acidic rupture of the internal ketal **3** furnished the sanglifehrin model system **2** as part of a three component mixture presumably due to the formation of two diastereomeric six-membered ring lactols[1a] [HMRS (FAB) calc. for $C_{35}H_{50}N_4O_9$ (M+Cs): 803.2632, found 803.2606].

The described chemistry demonstrates the feasibility of an intramolecular Stille coupling approach to sanglifehrin's macrocyclic skeleton and paves the way for a total synthesis of this novel natural product. A solid phase version of this strategy may also be envisioned, as can the application of the developed technology to combinatorial sanglifehrin libraries for biological screening.

We thank Dr D. H. Huang and Dr G. Siuzdak for NMR and mass spectroscopic assistance. This work was financially supported by the NIH (USA), The Skaggs Institute for Chemical Biology, and grants from Pfizer, Schering Plough, Hoffmann La Roche, Merck, Dupont, and Parke-Davis.

Notes and references

† *Selected data* for **28**: R_f = 0.30 (silica, EtOAc-hexane, 1 : 1) $[\alpha]_D^{23}$ +45 (*c* 0.35, $CHCl_3$); ν_{max}(neat)/cm^{-1} 3332, 2919, 1713, 1660, 1644, 1530, 1454, 1351, 1126, 2093, 1044; δ_H(600 MHz, $CDCl_3$, sanglifehrin numbering) 7.53 (brs, 1 H, 9), 7.07 (t, *J* 7.5, 1 H, ArH), 6.78–6.71 (m, 1 H, ArH), 6.74 (d, *J* 7.5, 1 H, ArH), 6.69 (s, 1 H, ArOH), 6.62 (d, *J* 7.5, 1 H, ArH), 6.47 (brd, *J* 9.2, 1H, 12), 6.34 (dd, *J* 15.2, 10.4, 1 H, 19), 6.17 (dd, *J* 15.1, 10.4 , 1 H, 20), 5.87 (ddd, *J* 15.1, 7.5, 7.0, 1 H, 21), 5.63–5.58 (m, 1 H, 8), 5.22 (dd, *J* 15.2, 7.8, 1 H, 18), 4.66 (dd, *J* 10.7, 7.8, 1 H, 17), 4.51–4.46 (m, 2 H, 5 and 11), 4.42 (m, 1 H, 15), 4.22 (m, 1 H, 23), 4.16 (m, 1 H, 23'), 3.57 (td, *J* 11.9, 3.0, 1 H, 2), 3.16–3.12 (m, 1 H, 14), 2.74 (m, 2 H, 58), 2.57 (brd, *J* 11.9, 1 H, NH), 2.53–2.46 (m, 5 H, 5', 22 and 51), 2.17 (dd, *J* 13.8, 5.7, 1 H, 52), 2.05–1.98 (m, 3 H, 3, 16 and 55), 1.93–1.87 (m, 1 H, 52'), 1.83 (brd, *J* 12.8, 1 H, 4), 1.69 (m, 1 H, 4'), 1.35 (s, 3 H, 54), 1.31 (m, 1 H, 3'), 1.03 (d, *J* 6.7, 3 H, 56 or 57), 0.96 (d, *J* 6.7, 3 H, 56 or 57), 0.37 (d, *J* 7.3, 3 H, 50); δ_c (150 MHz, $CDCl_3$) 172.8 (CO), 172.0 (CO), 170.8 (CO), 170.5 (CO), 156.8 (C), 137.2 (CH), 136.1 (C), 132.2 (CH), 130.4 (CH), 129.7 (CH), 128.7 (CH), 121.3 (CH), 116.0 (CH), 114.6 (CH), 95.8 (C), 81.0 (CH), 73.2 (CH), 65.2 (CH_2), 58.5 (CH), 58.1 (CH), 50.0 (CH), 43.8 (CH), 41.8 (CH_2), 38.7 (CH), 34.0 (CH_2), 30.8 (CH_3), 29.7 (CH_2), 29.3 (CH_2), 29.0 (CH_2), 27.8 (CH), 27.2 (CH_2), 22.8 (CH_2), 19.3 (CH_3), 18.5 (CH_3), 13.7 (CH_3); HRMS (FAB) calc. for $C_{35}H_{48}NaN_4O_8$ (M+Na$^+$): 675.3370, found 675.3356.

1 (*a*) T. Fehr, L. Oberer, V Quesniaux Ryffel, J-J. Sanglier, W. Schuler and R. Sedrani, PCT Int. Appl., WO 9702285 A1 970123, 1997, Sandoz Ltd., Switzerland; (*b*) R. Banteli, B. Ivan, P. Hall and R. Metternich, *Tetrahedron Lett.*, 1999, **40**, 2109; (*c*) *Chem. Abstr.*, 1997, **126**, 170491y.
2 J. K. Stille, *Angew. Chem., Int. Ed. Engl.*, 1986, **25**, 508; K. C. Nicolaou, T. K. Chakraborty, A. D. Piscopio, N. Minowa and P. Bertinato, *J. Am. Chem. Soc.*, 1993, **115**, 4419; D. A. Entwistle, S. I. Jordan, M. Montgomery and G. Pattenden, *Synthesis*, 1998, 603.
3 M. Miyashita, M. Hoshino and A. Yoshikoshi. *J. Org. Chem.*, 1991, **56**, 6483.
4 M. A. Tius and A. H. Fauq, *J. Org. Chem.*, 1983, **48**, 4131.
5 D. J. Patel, C. L. Hamilton and J. D. Roberts, *J. Am. Chem. Soc.*, 1965, **87**, 5144.
6 J. Tsuji, in *Comprehensive Organic Synthesis*, ed. B. M. Trost and I. Fleming, Pergamon, New York, 1991, Vol. 7, p. 449.
7 W. P. Griffith and S. V. Ley, *Aldrichim. Acta*, 1990, **23**, 13.
8 S. Ohira, *Synth. Commun.*, 1989, **19**, 561.
9 U. Schmidt, H. Griesser, V. Leitenberger, A. Lieberknecht, R. Mangold, R. Meyer and B. Reidl, *Synthesis*, 1992, 487.
10 M. J. Burk, O. E. Feaster, W. A. Nugent and R. L. Harlow, *J. Am. Chem. Soc.*, 1993, **115**, 10 125.
11 L. A. Carpino, *J. Am. Chem. Soc.*, 1993, **115**, 4397.
12 K. C. Nicolaou,, N. A. Stylianides and J. Y. Ramphal, *J. Chem. Soc., Perkin Trans. 1*, 1989, 2131.
13 K. J. Hale, O. Cai, V. Delisser, V., S. Manaviazar, S. A. Peak, G. S. Bhatia, T. C. Collins and H. Jogiya, *Tetrahedron*, 1996, **52**, 1047.
14 V. Farina and B. Krishnan, *J. Am. Chem. Soc.*, 1993, **115**, 9585.

Communication 9/01008D

The first highly diastereo- and enantioselective polymeric catalyst for the 1,3-cycloaddition reaction of nitrones with alkenes

Klaus B. Simonsen,[a] Karl Anker Jørgensen,*[a] Qiao-Sheng Hu[b] and Lin Pu*[b]

[a] *Center for Metal Catalyzed Reactions, Department of Chemistry, Aarhus University, DK-8000 Aarhus C, Denmark. E-mail: kaj@kemi.aau.dk*

[b] *Department of Chemistry, University of Virginia, Charlottesville, VA 22901, USA. E-mail: lp6n@virginia.edu*

Received (in Cambridge, UK) 17th February 1999, Accepted 11th March 1999

A highly diastereo- and enantioselective 1,3-dipolar cycloaddition reaction of nitrones with alkenes catalyzed by chiral polybinaphthyl Lewis acids has been developed giving isoxazolidines with up to 99% ee; the chiral polymer ligand shows almost identical stereoselectivity to its monomeric version but has the advantage of easy recovery and reuse, and this work further demonstrates that a rigid and sterically regular polymer chain can be used to preserve the catalytic properties of monomeric catalysts.

The potential of polymer-based catalysts, compared to the traditional monomeric catalysts, has stimulated the development of new polymeric chiral Lewis acid catalysts for asymmetric catalysis.[1] Easy recovery of the reusable catalyst/ligand and an often simplified purification procedure are among the obvious advantages of this class of catalysts. Furthermore, these catalysts may lead to the development of enantioselective continuous reactions by means of flow reactors or flow membrane reactors.

Two entries have been used to prepare chiral polymeric catalysts: (i) the traditional approach, where a chiral monomeric ligand is attached to a polymer support, often resulting in a marked decrease in selectivity when compared to the monomeric ligand,[1] and (ii) systems in which the optically active monomer is a part of a polymer backbone. Recently, optically active polymeric ligands of the latter type, based on a binaphthol (BINOL) backbone, have been developed,[1c,2] and shown the ability, in combination with a Lewis acid, to catalyse the addition of Et_2Zn to aldehydes[3] and a hetero-Diels–Alder reaction with high enantioselectivity.[4]

The asymmetric 1,3-dipolar cycloaddition (1,3-DC) reaction between nitrones and alkenes has been studied extensively recently because of the importance of the isoxazolidines formed.[5] The development of catalytic enantioselective 1,3-DC reactions has mainly involved electron-deficient alkenes reacting with various types of nitrones,[6] whereas only a few examples of catalytic enantioselective cycloaddition reaction of nitrones, activated by chiral Lewis acid complexes, with electron-rich alkenes are known.[7]

Here we report the first example of a polymer-catalyzed highly diastereo- and enantioselective 1,3-DC reaction. In this study, the reaction of *N*-phenyl nitrones **1** with vinyl ethers **2** gives the *exo*-diastereomer of the isoxazolidines **3** catalyzed by the polymeric ligand (*R*)-**4**, as well as the monomeric counterpart-ligands (*R*)-**6**, in combination with $AlMe_3$ as the Lewis acid [(eqn. (1)]. To the best of our knowledge only one example of a

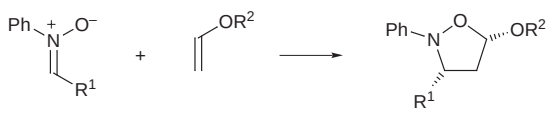

1 **2** *exo*-**3** (1)

1,3-DC reaction for nitrones with electron-deficient alkenes catalyzed by a polymeric catalyst, based on solid supported Ti-TADDOLates, has been reported and with varying diastereoselectivity (52–86% de), but with only modest enantioselectivity (< 56% ee).[8]

The active polymeric chiral aluminium catalysts were prepared *in situ* by addition of a solution of $AlMe_3$ in hexane to

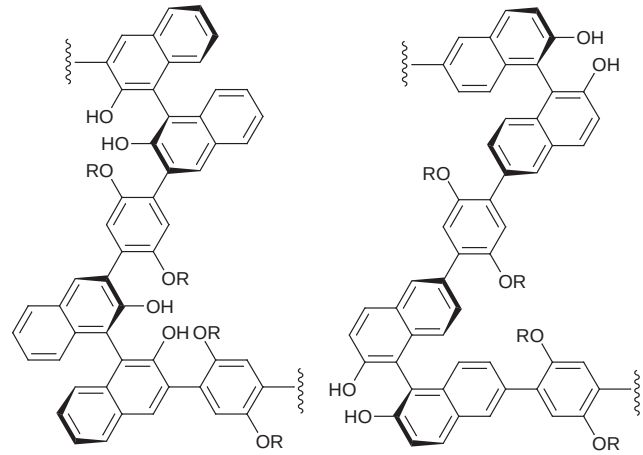

(*R*)-**4** R = C_6H_{13} (*R*)-**5** R = C_6H_{13}

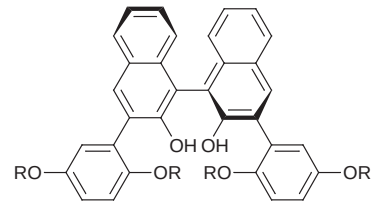

(*R*)-**6** R = C_6H_{13}

a solution of the polymer (*R*)-**4** (20 mol%) in CH_2Cl_2 (1 mL). The solution was allowed to stand for 1 h before diphenyl nitrone **1a** and ethyl vinyl ether **2a** were added in an 1:2.5 ratio. Complete conversion of **1a** was observed after 2 h whereupon the catalysts were hydrolyzed and precipitated by addition of MeOH (1–2 mL).[9] The polymeric ligand was precipitated and isolated by centrifugation and the clear solution was removed by decantation and evaporated to give isoxazolidine *exo*-**3a** in nearly quantitative isolated yield (97%) as an enantiopure compound (99% ee) and with very high diastereoselectivity (> 96% de). The purity of the reaction without any form of purification is notable as a ^1H NMR spectrum of the crude product after evaporation only gives signals consistant with *exo*-**3a**. When the reaction was tested with 10 mol% catalyst, a slight decrease in enantioselectivity was observed, but due to the fact that the polymeric ligand can be recycled (*vide infra*) with only moderate degeneration the use of 20 mol% is reasonable.

The use of the 6,6′ linked polymeric catalyst (*S*)-**5**–AlMe (20 mol%) on the same substrates resulted in a 75 : 25 *exo* : *endo* ratio of **3a** and a significant decrease in enantioselectivity (23%

Table 1 1,3-Dipolar cycloaddition reaction of nitrones **1a**,**b** with vinyl ethers **2a**–**c** catalyzed by the polymer catalyst (*R*)-**4**-AlMe (20 mol%)

Entry	**1**	R^1	**2**	R^2	**3**	Yield[a] (%)	*Exo* : *endo*[b]	Ee *exo*[c] (%)
1	**1a**	Ph	**2a**	Et	**3a**	97	> 98 : < 2	99
2[d]	**1a**	Ph	**2a**	Et	**3a**	80	> 98 : < 2	94
3	**1a**	Ph	**2b**	Bu^t	**3b**	86	> 98 : < 2	95
4	**1a**	Ph	**2c**	Bn	**3c**	72	> 98 : < 2	93
5	**1b**	*p*-Tolyl	**5b**	Bu^t	**3d**	77	> 98 : < 2	94

[a] Isolated yield. [b] Determined by ^{1}H NMR. [c] Determined by HPLC using a Daicel Chiralcel OD column. [d] 10 mol%.

ee). Despite this low selectivity, this result is better than the reaction using the (*S*)-1,1′-bi-2-naphthol-derived catalyst which gives the same diastereoselectivity, but less than 5% ee.[7c] The catalytically active species for the (S)-1,1′-bi-2-naphthol-based aluminium catalyst may not be monomeric, but rather may be an aggregate.

The polymeric catalyst (*R*)-**4**–AlMe was applied to the 1,3-DC reaction of different nitrones **1a**,**b** with vinyl ethers **2a**–**c**. Generally, *exo*-**3a**–**d** were isolated in very high yield, diastereoselectivity and ee (Table 1, entries 1–5).

The polymeric ligand (*R*)-**4** has been isolated and reused successfully in at least four consecutive reactions of nitrone **1a** with ethyl vinyl ether **2a**, as shown in Fig. 1. Both the yield and ee of *exo*-**3a** showed only slight decreases after the catalyst had been reused four times. The reason for the slight decrease is probably that the reactions are performed on a small scale and that a small part of the catalyst is lost when recovered. However, after four cycles the catalyst still gives *exo*-**3a** in 88% yield and with 90% ee.

It is often observed that the traditional polymeric catalysts give lower ee's than their monomeric counterparts. Therefore, the reaction was carried out with the monomeric 3,3'-bis(2,5-dihexyloxyphenyl)-BINOL (*R*)-**6** as the ligand. When (*R*)-**6**, in combination with $AlMe_3$ (10 mol%) was used as the catalyst, the 1,3-DC reaction between nitrone **1a** and ethyl vinyl ether **2a** showed complete conversion after 1 h with the same high selectivities as found using the polymeric catalyst (Table 2, entry 1). Similar selectivities were also found when the reaction was carried out in the presence of 10 mol% of the catalyst at 0 °C (entry 2) and in toluene (entry 3). This ligand system proved to be quite general. When the same conditions were used for reaction of the nitrones **1a**–**c** with the vinyl ethers **2a**,**b**, the isoxazolidines exo-**3a**–**g** were isolated in good yield (76–93%), very high *endo* : *exo* ratio (96% de) and chiral induction (93% ee) (Table 2, entries 4–8).

The present work on the use of the poly-BINOL–AlMe catalyst represents the first chiral polymer catalyzed highly regio-, diastereo- and enantioselective 1,3-dipolar cycloaddition reaction of nitrones with alkenes. The chiral polymeric ligand can be easily recovered, and after multiple recycling, the

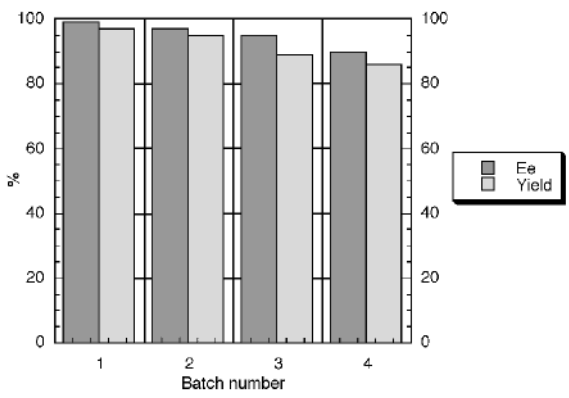

Fig. 1 Isolated yield and ee for formation of *exo*-**3a** using the regenerated polymer (*R*)-**4**-AlMe (20 mol%) in CH_2Cl_2 at room temperature for 12 h. The polymer was precipitated with MeOH and isolated by centrifugation.

Table 2 1,3-Dipolar cycloaddition reactions of aromatic nitrones **1a**–**c** with vinyl ethers **2a**,**b** catalyzed by (*R*)-**6**-AlMe (10 mol%)

Entry	**1**	R^1	**2**	R^2	**3**	Yield[a] (%)	*Exo* : *endo*[b]	Ee *exo*[c] (%)
1	**1a**	Ph	**2a**	Et	**3a**	93	> 98 : < 2	99
2[d]	**1a**	Ph	**2a**	Et	**3a**	83	> 98 : < 2	99
3[d,e]	**1a**	Ph	**2a**	Et	**3a**	76	> 98 : < 2	99
4	**1b**	*p*-Tolyl	**2a**	Et	**3d**	76	> 98 : < 2	94
5	**1c**	*p*-ClC_6H_4	**2a**	Et	**3e**	85	> 98 : < 2	95
6	**1a**	Ph	**2b**	Bu^t	**3b**	89	> 98 : < 2	95
7	**1b**	*p*-Tolyl	**2b**	Bu^t	**3f**	85	98 : 2	93
8	**1c**	*p*-ClC_6H_4	**2b**	Bu^t	**3g**	82	> 98 : < 2	93

[a] Isolated yield. [b] Determined by ^{1}H NMR. [c] Determined by HPLC using a Daicel Chiralcel OD column. [d] 0 °C. [e] Solvent = toluene.

polybinaphthyl ligand still maintains most of its original catalytic properties. Unlike many traditional polymer catalysts, the rigid and sterically regular binaphthyl polymer (*R*)-**4** shows almost the same high stereoselectivity as its monomeric version. This demonstrates that a rigid and sterically constrained polymer backbone can be used to preserve the steric and electronic environment of monomeric catalysts, and thus to preserve their catalytic properties.

This work was made possible by a grant from The Danish National Research Foundation. Q. S. H. and L. P. acknowledge the partial support of the US National Science Foundation (DMR-9529805).

Notes and references

1 (*a*) S. Itsuno, *Polymeric Materials Encyclopedia; Synthesis, Properties and Applications*, ed. J. C. Salamone, CRC Press, Boca Raton FL, 1996, vol 10, p 8078; (*b*) E. C. Blossey and W. T. Ford, *Comprehensive Polymer Science. The Synthesis, Characterization, Reactions and Applications of Polymers*, ed. G. Allen and J. C. Bevington, Pergamon, New York, 1989, vol. 6, p. 81; (*c*) L. Pu, *Chem. Rev.*, 1998, **98**, 2405.

2 Q.-S. Hu, X.-F. Zheng and L. Pu, *J. Org. Chem.*, 1996, **61**, 5200; Q.-S. Hu, D. Vitharana, X.-F. Zheng, C. Wu, C. M. S. Kwan and L. Pu, *J. Org. Chem.*, 1996, **61**, 8370.

3 See *e.g.*: W.-S. Huang, Q.-S. Hu, X.-F. Zheng, J. Anderson and L. Pu, *J. Am. Chem. Soc.*, 1997, **119**, 4313; Q.-S. Hu, W.-S. Huang, D. Vitharana, X.-F. Zheng and L. Pu, *J. Am. Chem. Soc.*, 1997, **119**, 12 454; Q.-S. Hu, W.-S. Huang and L. Pu, *J. Org. Chem.*, 1998, **63**, 2798.

4 M. Johannsen, K. A. Jørgensen, X.-F. Zheng, Q.-S. Hu and L. Pu, *J. Org. Chem.*, 1999, **64**, 299.

5 For reviews see: K. V. Gothelf and K. A. Jørgensen, *Chem. Rev.*, 1998, **98**, 863; M. Frederickson, *Tetrahedron*, 1997, **53**, 403.

6 See *e.g.*: K. V. Gothelf and K. A. Jørgensen, *J. Org. Chem.*, 1994, **59**, 5687; K. V. Gothelf, I. Thomsen and K. A. Jørgensen, *J. Am. Chem. Soc.*, 1996, **118**, 59; K. V. Gothelf, R. G. Hazell and K. A. Jørgensen, *J. Org. Chem.*, 1996, **61**, 346; K. B. Jensen, K. V. Gothelf, R. G. Hazell and K. A. Jørgensen, *J. Org. Chem.*, 1997, **62**, 2471; K. B. Jensen, K. V. Gothelf and K. A. Jørgensen, *Helv. Chim. Acta*, 1997, **80**, 2039; S. Murahashi, Y. Imada, M. Kohno and T. Kawakami, *Synlett*, 1993, 395; S. Kobayashi and M. Kawamura, *J. Am. Chem. Soc.*, 1998, **120**, 5840; S. Kanemasa, T. Tsuruoka and H. Yamamoto, *Tetrahedron Lett.*, 1995, **36**, 5019; S. Kanemasa, Y. Oderaotoshi, J. Tanaka and E. Wada, *J. Am. Chem. Soc.*, 1998, **120**, 12 355.

7 See *e.g.*: (*a*) J.-P. G. Seerden, A. W. A. Scholte op Reimer and H. W. Scheeren, *Tetrahedron Lett.*, 1994, **35**, 4419; (*b*) J.-P. G. Seerden, M. M. M. Boeren and H. W. Scheeren, *Tetrahedron*, 1997, **53**, 11 843; (*c*) K. B. Simonsen, P. Bayón, R. G. Hazell, K. V. Gothelf and K. A. Jørgensen, *J. Am. Chem. Soc.*, 1999, in the press.

8 D. Seebach, R. E. Marti and T. Hintermann, *Helv. Chim. Acta*, 1996, **79**, 1710.

9 Experimental procedure. The appropriate ligand (0.02 mmol) was placed in a 5 mL Schlenk flask flushed three times with N_2, and CH_2Cl_2 (1 mL) was added with a syringe. To this solution was added a 2 M solution of $AlMe_3$ in heptane (10 mL, 0.02 mmol). The solution was stirred for 1 h and the nitrone (0.2 mmol) and vinyl ether (0.5 mmol) were added. After the appropriate reaction time, the reaction was quenched with MeOH (1 mL) and the ligand was isolated by centrifugation. The clear solution was evaporated to give the single diasteromer of *exo*-**3** as a pure product (TLC, ^{1}H and ^{13}C NMR).

Communication 9/01316D

Unprecedented μ-1,2,3κ*S*:4,5κ*N* coordination mode of the thiocyanate anion in two new double salts of silver(I), $AgSCN·2AgNO_3$ and $AgSCN·AgClO_4$

Guo-Cong Guo and Thomas C. W. Mak*

Department of Chemistry, The Chinese University of Hong Kong, Shatin, New Territories, Hong Kong, China. E-mail: tcwmak@cuhk.edu.hk

Received (in Cambridge, UK) 9th March 1999, Accepted 31st March 1999

The double salts $AgSCN·2AgNO_3$ and $AgSCN·AgClO_4$ both feature an unprecedented μ_5-1,2,3κ*S*:4,5κ*N* coordination mode of the thiocyanate ligand, which generates a two- or three-dimensional network according to the relative coordinating capability of the co-existing nitrate or perchlorate anion.

With the advent of supramolecular chemistry, the coordination concept as applied to metal ions has been extended to polyatomic species such as neutral molecules, organic cations, and anions of various types.[1] In the design of polynuclear metal complexes[2] and the crystal engineering of coordination networks,[3] the possible coordination modes of anionic ligands have to be considered in the synthetic strategy. In this context, it is of interest to determine the highest ligation number[4] (HLN) of simple inorganic polyatomic anions, namely the largest number of coordination bonds that a particular anion can form with neighboring metal centers in its complexes. For example, the HLN of the μ_6-carbonato group in the hexanuclear oxovanadium(IV) cluster $[(VO)_6(CO_3)_4(OH)_9]^{5+}$ is six.[5]

The group 11 metal(I) ions, each having a spherical d^{10} electronic configuration, can in principle serve as ideal probes for obtaining the HLN of small inorganic anions. The synthesis of suitable complexes for such investigations is favored by the tendency of the monovalent coinage metal ions to form aggregates through homoatomic d^{10}–d^{10} interactions.[6,7] Furthermore, silver(I) has distinct advantages over the other members of the coinage triad, as copper (I) is easily oxidized to the +2 oxidation state, and gold(I) has a strong tendency to adopt linear digonal coordination geometry and is also susceptible to disproportionation into Au(III) and Au(0). Our recent studies on the crystal structures of double salts of silver have shown that the cyanide ion has a HLN of four in $3AgCN·2AgF·3H_2O$,[8] and the azide ion has a HLN of six in $AgN_3·2AgNO_3$.[9]

The coordination modes of the ambident thiocyanate ligand[10] in their metal complexes exhibit considerable diversity (Fig. 1), and modes **F**, **H** and **K** are hitherto unknown.[11] Thus far the maximum coordinating capacity of SCN^- involves the formation of two coordination bonds by its nitrogen atom, or three coordination bonds by its sulfur atom, but not simultaneously. Here, we report two novel double salts $AgSCN·2AgNO_3$ **1** and $AgSCN·AgClO_4$ **2**† in which the thiocyanate group exhibits an unprecedented μ_5-1,2,3κ*S*:4,5κ*N* coordination mode **K** with a HLN of five.

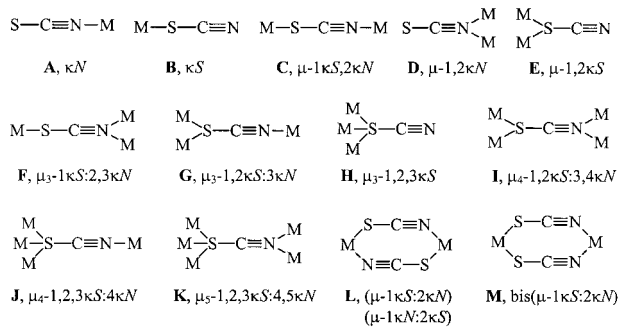

Fig. 1 Possible coordination modes of the thiocyanate ligand.

The crystal structures‡ of both **1** and **2** feature a common centrosymmetric, nearly planar eight-membered $(AgSCN)_2$ ring that has angularly distorted hexagonal geometry, which can be regarded as a basic architectural unit for constructing the coordination network. In each planar heterocycle, there are two 'substituent' silver atoms bonded to each sulfur atom and one 'substituent' silver atom bonded to each nitrogen atom, as shown in Fig. 2. To our knowledge the nearly planar $(AgSCN)_2$ ring moiety with six additional silver atoms attached to it and the resulting μ_5-1,2,3κ*S*:4,5κ*N* coordination mode of the thiocyanate ligand are both unprecedented.

In the crystal structure of **1**, the basic architectural units share the S-bonded 'substituent' silver atoms of type Ag2 and Ag3 along the $[1\bar{1}0]$ and [110] directions to generate a corrugated layer (Fig. 3), with the nitrate anions located between adjacent layers. One of the two independent NO_3^- anions functions as a tightly bridged ligand to silver atoms of type Ag1 and Ag4 [average Ag–O 2.445(3) Å], and the other as a loosely bridged one to silver atoms of type Ag2 and Ag4 [average Ag–O

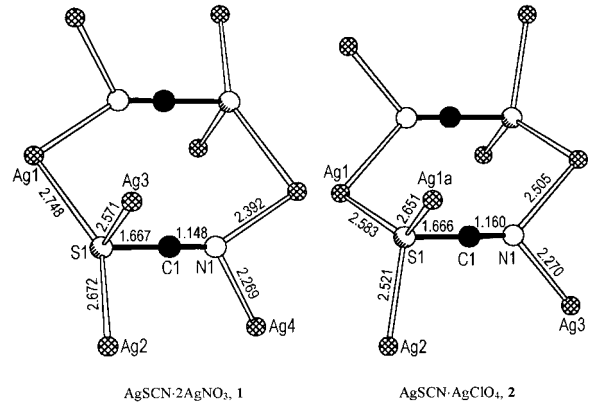

$AgSCN·2AgNO_3$, **1** $AgSCN·AgClO_4$, **2**

Fig. 2 Basic architectural units in **1** and **2**, each consisting of a nearly planar eight-membered $(AgSCN)_2$ ring with six 'substituent' silver atoms.

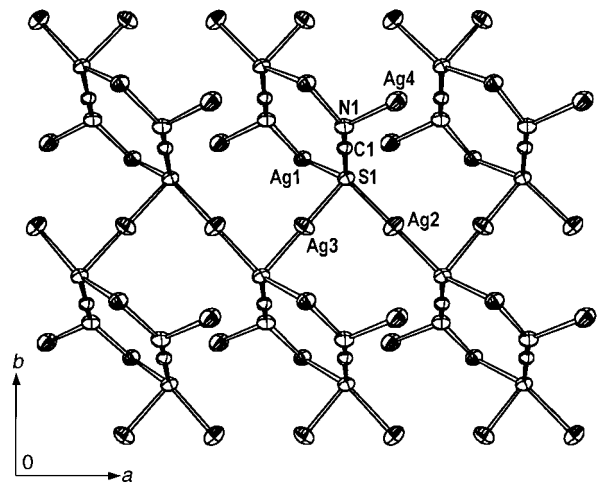

Fig. 3 Corrugated layer formed by linkage of basic architectural units in **1**. The interlayer NO_3^- ligands have been omitted for clarity.

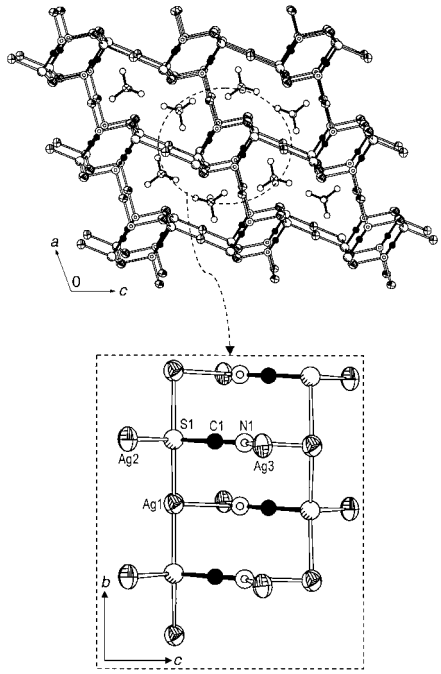

Fig. 4 Crystal structure of **2** viewed along the *b* direction (top), and a hexagonal channel viewed along the *a* direction showing it as a ladder-like chain of fused $(SCN)_2$ rings.

2.579(4) Å], thus linking adjacent layers along the *c* direction into a three-dimensional framework. Interestingly, there co-exist four kinds of coordination modes of silver atoms in **1**, namely linear coordination for type Ag3 atoms at $\bar{1}$ [Ag3–S1 2.571(1) Å], nearly coplanar triangular coordination for type Ag1 atoms [Ag1–N1 2.392(4), Ag1–O2 2.479(3), Ag1–S1 2.748(2) Å, sum of bond angles at Ag1 358.5°], distorted square coordination for type Ag2 atoms at $\bar{1}$ [Ag2–O6 2.566(4), Ag2–S1 2.672(1) Å] and distorted tetrahedral coordination for type Ag4 atoms [Ag4–N1 2.269(4), Ag4–O3 2.411(3) Ag4–O5 2.591(4), Ag4–S1 2.861(2) Å].

In the crystal structure of **2**, fusion of the basic architectural units along the *b* direction generates a ladder-like chain, which takes the appearance of a hexagonal column when viewed in the *b* direction (Fig. 4). The hexagonal columns are connected by sharing the S-bonded Ag2 atoms (site symmetry 2) along the *c* direction and the N-bonded Ag3 atoms (site symmetry $\bar{1}$) along the *a* direction to form a three-dimensional channel-type network, as shown in Fig. 4. The perchlorate anions are stacked as a double column within each channel. In contrast to the nitrate anions in **1**, the perchlorate anions in **2** do not directly bond to silver atoms, leading to lower coordination numbers, namely linear coordination for type Ag2 [Ag2–S1 2.521(2) Å] and Ag3 [Ag3–N1 2.270(6) Å] atoms, and trigonal pyramidal coordination for the type Ag1 atom [Ag1–S1 2.583(2) and 2.651(2), Ag1–N1 2.505(6) Å].

The sulfur and nitrogen atoms of the thiocyanate unit in both **1** and **2** are asymmetrically bonded to silver atoms. The Ag–S and Ag–N distances are significantly longer than those found in AgSCN [Ag–S 2.428(11), Ag–N 2.223(28) Å],[12] respectively, but still fall within the range found in many transition metal thiocyanate complexes.[13] The thiocyanate units in both **1** and **2** are essentially linear. The S–C and C≡N distances of the thiocyanate ligands in **1** [S–C 1.669(4), C–N 1.148(5) Å] and **2** [S–C 1.666(2), C–N 1.160(3) Å] are in good agreement with those found in AgSCN [S–C 1.64(3), C–N 1.19(7) Å][12] and many transition metal thiocyanates.[11] In contrast to AgSCN, in which the cations and anions are arranged alternately to form an infinite zigzag chain such that each silver atom is only bound to one nitrogen and one sulfur atom,[12] the thiocyanate unit bridges five silver atoms in both double salts **1** and **2** to form two- and three-dimensional networks, respectively, resulting in a variety of coordination environments around individual silver atoms.

This work is supported by Hong Kong Research Grants Council Earmarked Grant CUHK 4022/98P and Direct Grant A/C 2060129 of The Chinese University of Hong Kong.

Notes and references

† *Synthesis*: AgSCN was prepared by mixing aqueous solutions of ammonium thiocyanate and silver nitrate at room temperature. The white precipitate was filtered, washed several times with de-ionized water, and temporarily stored in wet form in the dark.

Synthesis of $AgSCN{\cdot}2AgNO_3$ **1**: wet AgSCN was added to 2 mL of a concentrated MeCN solution of $AgNO_3$ (*ca.* 40%) with stirring until saturated at 40 °C. The excess amount of AgSCN was filtered off, and the solution was placed into a desiccator charged with P_2O_5. In the course of two days colorless crystals of $AgSCN{\cdot}2AgNO_3$ were obtained in nearly quantitative yield. The compound is stable when immersed in its mother liquor; it is hygroscopic and slowly decomposes in air.

Synthesis of $AgSCN{\cdot}AgClO_4$ **2**: the above procedure was repeated using EtOH and silver perchlorate instead of MeCN and silver nitrate, respectively. The distinct difference between the two preparations is that the filtrate of **2** turned from colorless to pale purple and the cyrstals of **2** are pale purple.

‡ *Crystal data*: **1**: colorless prism, Siemens P4/PC diffractometer, Mo-Kα radiation (λ = 0.71073 Å), 2275 unique reflections (R_{int} = 0.0247), 1423 of which with $I > 2\sigma(I)$ were considered as observed, triclinic, space group $P\bar{1}$ (no. 2), Z = 2, D_c = 4.256 g cm^{-3}, a = 6.569(5), b = 7.732(1), c = 8.031(2) Å, α = 104.09(1), β = 93.94(4), γ = 90.04(3)°, V = 394.6(3) Å^3, μ = 76.41 cm^{-1}, $R1$ = 0.0394, GOF = 0.990.

2: pale purple plate, Rigaku RAXIS IIC diffractometer, Mo-Kα radiation (λ = 0.710 73 Å), 1086 unique reflections (R_{int} = 0.0862), 1032 of which with $I > 2\sigma(I)$ were considered as observed, Monoclinic, space group $C2/c$ (No. 15), Z = 8, D_c = 3.958 g cm^{-3}, a = 15.294(4), b = 4.766(1), c = 18.278(4) Å,β = 109.89(2)°, V = 1252.7(5) Å^3, μ = 69.55 cm^{-1}, $R1$ = 0.0642, GOF = 1.116. The structures of **1** and **2** were solved by the direct method (SHELXS-86) and refined by full-matrix least squares on F^2 using the Siemens SHELXTL-93 (PC Version) package of crystallographic software. All non-hydrogen atoms were refined with anisotropic thermal parameters. Results of the crystal structure determination (CSD-410622 and 410623) have been deposited at the Fachinformationszentrum Karlsruhe, D-76344, Eggenstein-Leopoldshafen, Germany (fax: (+49)7247-808-666; e-mail: crysdata@fiz-karlsruhe.de). CCDC 182/1206. See http://www.rsc.org/suppdata/cc/1999/813/ for crystallographic files in .cif format.

1 *Supramolecular Chemistry of Anions*, ed. A. Bianchi, K. Bowman-James and E. Garcia-España, Wiley–VCH, New York, 1996; P. D. Beer and D. K. Smith, *Prog. Inorg. Chem.*, 1997, **46**, 1; A. Clearfield, *Prog. Inorg. Chem.*, 1998, **47**, 371; J.-M. Lehn, *Angew. Chem., Int. Ed. Engl.*, 1988, **27**, 89.
2 P. J. Stang, *Chem. Eur. J.*, 1998, **4**, 19; P. J. Zapf, R. C. Haushalter and J. Zubieta, *Chem. Commun.*, 1997, 321; M. Fujita, *Chem. Soc. Rev.*, 1998, **27**, 417.
3 S. R. Batten and R. Robson, *Angew. Chem. Int. Ed.*, 1998, **37**, 1460; K. R. Dunbar and R. A. Heintz, *Prog. Inorg. Chem.*, 1997, **45**, 283.
4 The term 'ligation number' is used here in preference to 'coordination number' which generally to refers to the number of ligand around an atomic center, normally a metal ion.
5 T. C. W. Mak, P.-J. Li, C.-M. Zheng and K.-Y. Huang, *J. Chem. Soc., Chem. Commun.*, 1986, 1597.
6 M. Jansen, *Angew. Chem. Int. Ed. Engl.*, 1987, **26**, 1098; M. Jansen and C. Linke, *Angew. Chem., Int. Ed. Engl.*, 1992, **31**, 653.
7 H. Schmidbaur, *Chem. Soc. Rev.*, 1995, 391.
8 G. C. Guo and T. C. W. Mak, *Angew. Chem., Int. Ed. Engl.*, 1998, **37**, 3183.
9 G. C. Guo and T. C. W. Mak, *Angew. Chem., Int. Ed.*, 1998, **37**, 3268.
10 R. G. Pearson, *J. Am. Chem. Soc.*, 1963, **85**, 3533; R. G. Pearson, *J. Chem. Educ.*, 1968, **45**, 643; M. K. Kroeger and R. S. Drago, *J. Am. Chem. Soc.*, 1981, **103**, 3250.
11 A. M. Golub, H. Kohler and V. V. Skopenko, in *Chemistry of Pseudohalides*, ed. R. J. H. Clark, Elsevier, New York, 1986, p. 239; M. Kabešová, R. Boca, M. Melník, D. Valìgura and M. Dunaj-Jurco, *Coord. Chem. Rev.*, 1995, **140**, 115.
12 I. Lindqvist, *Acta Crystallogr.*, 1957, **10**, 29.
13 N. K. Mills and A. H. White, *J. Chem. Soc., Dalton Trans.*, 1984, 229; H. Krautscheid, N. Emig, N. Klaassen and P. Seringer, *J. Chem. Soc., Dalton Trans.*, 1998, 3071.

Communication 9/01876J

ChemComm

Possible intermediates in the selective catalytic reduction of NO_x: differences in the reactivity of nitro-compounds and *tert*-butyl nitrite over γ-Al_2O_3

Virginie Zuzaniuk,* Frederic C. Meunier*† and Julian R. H. Ross

Centre for Environmental Research, University of Limerick, National Technological Park, Limerick, Ireland. E-mail: virginie.zuzaniuk@ul.ie

Received (in Liverpool, UK) 19th January 1999, Accepted 24th March 1999

Nitromethane decomposes over alumina to give various surface species such as isocyanates and its oxidation by O_2 yields significant amounts of ammonia; on the other hand, *tert*-butyl nitrite decomposes to give only surface nitrate species and mostly oxides of nitrogen are formed by reaction with O_2.

Several authors have suggested that the selective catalytic reduction (SCR) of nitrogen oxides by hydrocarbons proceeds *via* organic nitro or nitrite intermediates over various catalysts such as promoted ZSM5[1–3] or Pt/SiO_2.[4] For the latter material, Tanaka *et al.* reported that the oxidation of both nitromethane and *n*-butyl nitrite gave products similar to those of the SCR of NO_x.[4] The gas phase decomposition and oxidation of nitromethane and its reactivity have previously been studied in connection with the NO_x-SCR over different catalysts such as Co-ZSM5, H-ZSM5, Na-ZSM5, SiO_2 or Al_2O_3.[5,6] The adsorption of this molecule on Al_2O_3, one of the most active single metal oxides for SCR reactions, has also been studied by Yamaguchi.[7] While organic nitro or nitrite species have not usually been differentiated in their involvement in the SCR reaction, our present work reports significant differences in the adsorption and reaction/oxidation of nitromethane and *tert*-butyl nitrite over Al_2O_3. These differences stress the need to consider differently the role of these compounds in the modelling of SCR reactions over alumina.

The catalytic experiments were carried out in a quartz flow microreactor (4 mm internal diameter) using 200 mg of Al_2O_3 (Alcan AA400, 150 $m^2\ g^{-1}$) previously calcined for 6 h at 973 K . The reactant gases used were O_2 (BOC 99%) and Ar (Air Products, high purity grade). Nitromethane (Fluka, puriss $\geqslant$ 99.0%) and *tert*-butyl nitrite (Fluka, assay $\geqslant$ 90%) were fed using a saturator flushed by the O_2 stream, which was then added to the Ar stream. The total rate of flow was 100 $cm^3\ min^{-1}$ with 1.5% O_2 in the gas mixture. The saturator was kept at room temperature and at 273 K for the experiments using nitromethane and *tert*-butyl nitrite, respectively. The products of reaction were analysed using a gas-cell (Foxboro®) fitted in a FTIR spectrophotometer (Nicolet 550®), 64 scans with a resolution of 1 cm^{-1} were usually collected. The diffuse reflectance FTIR measurements (DRIFTS) were carried out *in situ* using a finely ground sample (*ca.* 30 mg) of Al_2O_3 and the spectra were recorded after 128 scans at a resolution of 2 cm^{-1}. The catalytic experiments and the *in situ* measurements were both carried out at 573 K under steady state conditions. The nitromethane and *tert*-butyl nitrite were pre-adsorbed on the Al_2O_3 at room temperature for the *in situ* DRIFTS experiments.

Fig. 1(a) shows the DRIFT spectrum of the species formed from the adsorption of nitromethane on Al_2O_3 at room temperature and subsequently heated to 573 K in argon alone. The bands at 1376 cm^{-1} ($\nu^{sym}{}_{OCO}$), 1393 cm^{-1} (δ_{CH}), 1598 cm^{-1} ($\nu^{a}{}_{OCO}$), 2902 cm^{-1} (ν_{CH}) and 3003 cm^{-1} (combination band $\nu^{a}{}_{OCO} + \delta_{CH}$) can be assigned to a formate species; the vibration mode to which each band corresponds is given in parentheses.[8,9] The small band at 2092 cm^{-1} could be characteristic of a linearly adsorbed cyanide whereas the major band at 2228 cm^{-1} could be characteristic of an (inorganic) isocyanate group, a bridged cyanide or a nitrile species.[9,10] The adsorption of HCN on our Al_2O_3 showed in the spectral region 2000–2300 cm^{-1}, only a band at 2092 cm^{-1} whereas a band at 2228 cm^{-1} was observed when cyclohexyl isocyanate was adsorbed. Additional experiments have shown that the band at 2228 cm^{-1} derived from nitromethane was readily displaced by water at 573 K and NH_3 was observed in the gas phase. This high reactivity with water suggests that this band should be assigned to an isocyanate species rather than to a cyanide/nitrile species which are significantly less reactive towards water.[11,12] Other peaks were detected at 1447, 1681 and 3390 cm^{-1} which could tentatively be assigned to the ν_{NCO}, ν_{CO} and ν_{NH} of carbamic acid (NH_2CO_2H), respectively. Similar DRIFTS spectra to that observed with nitromethane were obtained with several other nitro compounds: nitroethane, 2-nitropropane and nitrobutane.

The DRIFT spectrum obtained from the adsorption of *tert*-butyl nitrite on Al_2O_3 at room temperature followed by heating to 573 K in Ar alone [Fig. 1(b)] was markedly different from that obtained using nitromethane. Only nitrate species, with characteristic bands at 1258, 1306 and 1554 cm^{-1}, were detected. Separate adsorption experiments over the same Al_2O_3 sample using NO, NO_2 and O_2 showed that the bands at 1258 and 1554 cm^{-1} were coupled, whereas the band at 1306 cm^{-1} was coupled with a band at 1580 cm^{-1}. This latter could not be observed here because it overlapped with the band at 1554 cm^{-1}. According to the literature, these bands correspond to two different types of bidentate nitrate species.[9] Some CH vibrations were also observed following the pre-adsorption of

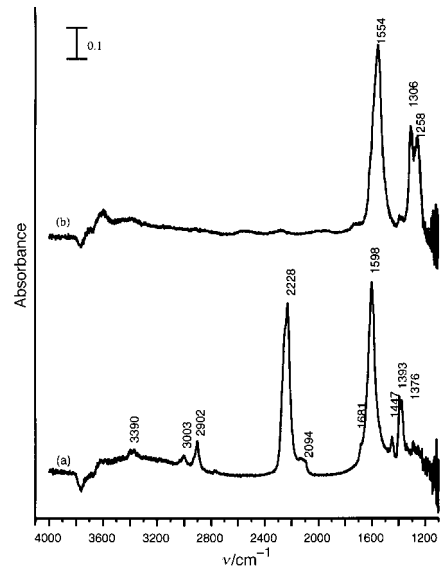

Fig. 1 DRIFT spectra at 573 K in argon of Al_2O_3 following pre-adsorption of (a) nitromethane and (b) *tert*-butyl nitrite at room temperature.

† Present address: Technische Universität München, Germany D-85747. E-mail: meunier@thor.tech.chemie.tu-muenchen.de

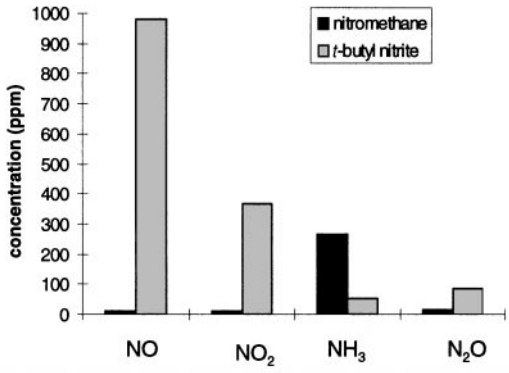

Fig. 2 Distribution of the products of reaction in the oxidation of nitromethane and *tert*-butyl nitrite at 573 K over Al_2O_3. Feed: 1.5% O_2 + 405 ppm nitromethane or 1700 ppm *tert*-butyl nitrite in Ar. Total flow 100 $cm^3\ min^{-1}$.

the *tert*-butyl nitrite at room temperature. However, these CH bands were readily displaced with increasing temperature (under argon) and only the ad-NO_x species bands remained on the sample surface at 573 K. Details of these experiments will be given in a subsequent paper.

Fig. 2 shows the distributions of the main products of the oxidation of nitromethane and *tert*-butyl nitrite over alumina: NO, NO_2, N_2O and NH_3 were detected in both cases. Traces of HCN (not quantified) were also detected during oxidation of nitromethane and *tert*-butyl nitrite. Any N_2 formed could not be detected as it is inactive in the IR. The oxidation of nitromethane yielded a significant proportion (267 ppm) of NH_3, but NO (12 ppm), NO_2 (10 ppm) and N_2O (14 ppm) were formed only in much lower concentrations. In contrast, the oxidation of *tert*-butyl nitrite yielded oxides of nitrogen (*i.e.* NO: 983 ppm, NO_2: 366 ppm and N_2O: 87 ppm) as the main products of reaction whereas only traces of NH_3 (51 ppm) were observed.

The formation of NH_3 from the oxidation of nitromethane can be explained by the following reaction mechanism [eqn. (1)]:[5,6,12,13]

$$MeNO_2 \longrightarrow HNCO_{(ads)} + H_2O \longrightarrow NH_2CO_2H_{(ads)} \longrightarrow CO_2 + NH_3 \quad (1)$$

The formation of the isocyanate species from the nitro-compound is believed to occur through the dehydration of the enol tautomer of nitromethane followed by isomerisation of the corresponding nitrile *N*-oxide. The intermediacy of carbamic acid in eqn. (1) is supported by the observation by DRIFTS of IR bands at 1448, 1681 and 3390 cm^{-1} which are compatible with its molecular structure. The reaction between the surface isocyanate species ($HNCO_{ads}$) and H_2O is probably fast enough on the Al_2O_3 surface to prevent the release of isocyanic acid (HNCO) to the gas phase, as no HNCO was detected during the catalytic oxidation experiment.

As described above, the adsorption of *tert*-butyl nitrite on Al_2O_3 gave rise to nitrate surface species [Fig. 1(b)], and so the formation of NO and NO_2 during the oxidation of this molecule was easily understandable. It has previously been reported that NO and NO_2 were formed in TPD experiments of nitrate species adsorbed on various catalysts.[14]

As has been often suggested,[1–3] organic nitro and organic nitrite compounds might both be intermediate species in the SCR of NO_x by hydrocarbons since their oxidation products were similar to those obtained in this reaction. However, the present work shows that their reactivity was quite different on alumina and hence that any reaction scheme for the SCR reaction must associate with them a specific role. This is of particular importance with regards to some recent results from our laboratory[15] which indicate that the formation of organo-nitrogen compounds may be a crucial step in the C_3H_6-SCR of NO over alumina. Among other reactions, it would be quite understandable if any ammonia (or, for that matter, any primary amine from which ammonia could be derived) formed from the decomposition of a nitro-type compound were to react with the NO_2 formed from the decomposition of a nitrite-type compound to yield N_2 as in a typical ammonia-SCR process.

Part of this work was funded by the European Community, through the Environment and Climate Programme, Contract ENV4-CT97-0658 and by Forbairt, Contract SC/1997/519.

Notes and references

1 C. Yokoyama and M. Misono, *J. Catal.*, 1994, **150**, 9.
2 N. W Hayes, R. W. Joyner and E. S. Shpiro, *Appl. Catal. B: Environ.*, 1996, **8**, 343.
3 G. Centi, A. Galli and S. Perathoner, *J. Chem. Soc., Faraday Trans.*, 1996, **94**, 5129.
4 T. Tanaka, T. Okuhara and M. Misono, *Appl. Catal. B: Environ.*, 1994, **4**, L1.
5 A. D. Cowan, N. W. Cant, B. S. Haynes and P. F. Nelson, *J. Catal.*, 1998, **176**, 329.
6 N. W Cant, A. D Cowan, A. Doughty, B. S. Haynes and P. F. Nelson, *Catal. Lett.*, 1997, **46**, 207.
7 M. Yamaguchi, *J. Chem. Soc., Faraday Trans.*, 1997, **93**, 3581.
8 G. Busca, J. Lamotte, J. C. Lavalley and V. Lorenzelli, *J. Am. Chem. Soc.*, 1987, **109**, 5197.
9 K. Nakamoto, *Infrared and Raman Spectra of Inorganic and Coordination Compounds*, Wiley-Interscience, 4th edn., 1986.
10 N. B. Colthup, L. H. Daly and S. E. Wiberley, *Introduction to Infrared and Raman Spectroscopy*, Academic Press, Boston, MA, 1990, pp. 448–449.
11 N. W. Hayes, W. Grünert, G. J. Hutchings, R. J. Joyner and E. S. Shpiro, *J. Chem. Soc., Chem. Commun.*, 1994, 531.
12 A. Obuchi, C. Wögenbauer, R. Köppel and A. Baiker, *Appl. Cat. B*, 1998, **19**, 9.
13 E. A. Lombardo, G. A. Sill, J. L. d'Itri and W. K. Hall, *J. Catal.*, 1998, **173**, 440.
14 V. A. Sadykov, S. L. Baron, V. A. Matyshak, G. M. Alikina, R. V. Bunina, A. Ya. Rozovskii, V. V. Lunin, E. V. Lunina, A. N. Ivanova and S. A. Veniaminov, *Catal. Lett.*, 1996, **37**, 157.
15 F. C. Meunier, J. P. Breen and J. R. H. Ross, *Chem. Commun.*, 1999, 259.

Communication 9/00548J

ChemComm

Short and efficient enantioselective total synthesis of angucyclinone type antibiotics (+)-rubiginone B_2 and (+)-ochromycinone

M. Carmen Carreño,* Antonio Urbano and Claudio Di Vitta†

Departamento de Química Orgánica (C-I), Universidad Autónoma, Cantoblanco, 28049-Madrid, Spain. E-mail: carmen.carrenno@uam.es

Received (in Liverpool, UK) 26th February 1999, Accepted 15th March 1999

The enantioselective total synthesis of antibiotics rubiginone B_2 and ochromycinone is achieved from enantiopure (*S*)-5-methoxy-2-(*p*-tolylsulfinyl)-1,4-naphthoquinone and a racemic vinylcyclohexene through a short sequence involving a tandem Diels–Alder reaction–sulfoxide elimination process with simultaneous kinetic resolution of the racemic diene, followed by controlled aromatization and functional group deprotection.

Ochromycinone and rubiginone B_2, first isolated respectively by Bowie[1] and Oka,[2] are components of the anguciclinone family, a growing class of natural products with remarkable antibiotic activity and cytotoxicity.[3] The major components of this family show a benz[*a*]anthracene framework of decaketide origin[4] bearing a methyl group at C-3 and an oxygen function at C-1. The 3*S* absolute configuration is also a common characteristic of C-3 non-oxygenated angucyclinones. The main structural differences are found in the aromatic or hydroaromatic nature of the A and/or B rings. The regioselective construction of the angularly fused tetracyclic skeleton has been achieved applying several methods which are summarized in a recent review article.[5] The most general strategy employed is based on the Diels–Alder reaction between a substituted naphthoquinone and a vinylcyclohexene. While several efficient total syntheses have focused on the racemic forms, access to the isolated optically active species remains a problem. The asymmetric syntheses of antibiotics (+)-SF 2315A and urdamycinone B were reported by Sulikowski[6] who used an asymmetric Diels–Alder reaction with an appropriately functionalized chiral diene obtained from (−)-quinic acid as the key step. A second Diels–Alder approach was described by Larsen[7] who achieved the total syntheses of antibiotics (+)-emycin A and (+)-ochromycinone by using a chiral catalyst in the cycloaddition step which allowed the kinetic resolution of the diene partner in a single operation. Finally, chromatographic separation of the diastereoisomeric mixture resulting in the cycloaddition between a *C*-glycosyl juglone and a racemic vinylcyclohexene has also allowed the asymmetric synthesis of urdamycinone B.[8,9] In spite of the structural similarities between (+)-ochromycinone and (+)-rubiginone B_2 (ochromycinone methyl ether), to the best of our knowledge, the latter has never been synthesized in an optically active form.

Our previous work devoted to the use of enantiopure (*S*)-2-(*p*-tolylsulfinyl)-1,4-quinones as dienophiles[10] had shown a high ability of the sulfoxide to control the regiochemistry, *endo*-selectivity and π-facial diastereoselectivity of their Diels–Alder cycloadditions with a wide range of cyclic and acyclic dienes. We established the tandem Diels–Alder reaction–pyrolytic sulfoxide elimination as a general one-pot strategy to enantiomerically pure polycyclic dihydroquinones. More recently,[11,12] we envisaged the ability of the sulfinyl group to promote a double induction in the cycloaddition process leading to the efficient kinetic resolution of differently substituted chiral racemic vinylcyclohexenes.[11] The high facial selectivity achieved was explained by invoking the favored transition state indicated in Scheme 1. This strategy provided a diastereoselective entry into the tetracyclic framework of angucyclinones.[12] To account for this, we reasoned that cycloaddition of a methoxy substituted sulfinylnaphthoquinone such as **1** would provide a short and convergent asymmetric entry into the angucyclinone family. Here we report the application of this novel methodology for the total synthesis of natural antibiotics (+)-rubiginone B_2 and (+)-ochromycinone.

Our approach to an immediate tetracyclic precursor to both natural products is outlined in Scheme 1. We selected the TBDMS protected derivative of *trans*-3-hydroxy-5-methyl-1-vinylcyclohexene **2** as starting material since our previous studies had shown that free OH was less efficient in the *anti/syn* discrimination of the cycloaddition transition states.[11,12] Diene **2** was synthesized from *cis*-3-hydroxy-5-methyl-1-vinylcyclohexene through a Mitsunobu inversion of C-3 followed by protection of the OH group.[11] Thus, cycloaddition of enantiopure (*S*)-5-methoxy-2-(*p*-tolylsulfinyl)-1,4-naphthoquinone (+)-**1**[13] with two equivalents of chiral racemic *trans*-3-[(*tert*-butyldimethylsilyl)oxy]-5-methyl-1-vinylcyclohexene **2** af-

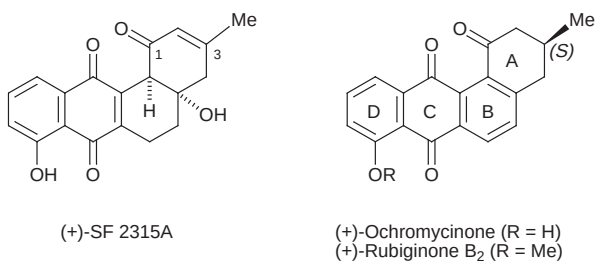

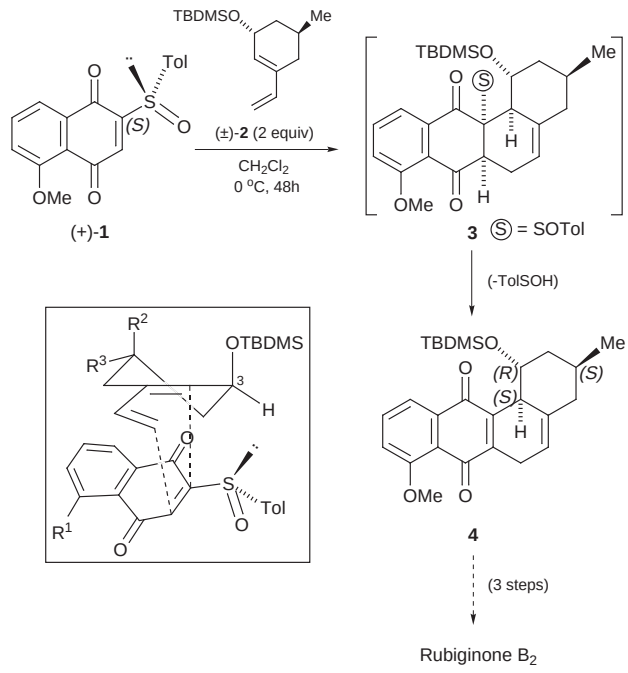

Scheme 1

† On leave from Instituto de Química da Universidade de São Paulo, Brazil.

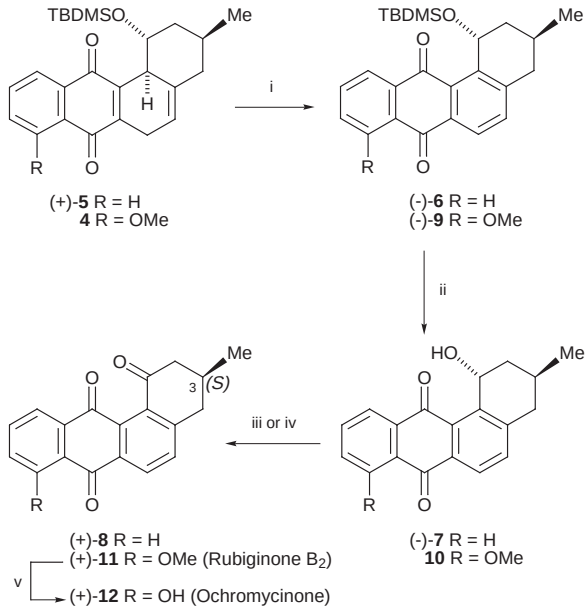

Scheme 2 *Reagents and conditions*: i, DBU, CH_2Cl_2, 0 °C, 2 h, 81% from **5**, 58% from **1** for two steps; ii, 40% aq. HF, CH_3CN, rt, 1 h, 52% from **6**; iii, air, *hv*, CH_2Cl_2, rt, 2 h, 70% from **7**, 48% from **9** for two steps; iv, PCC, CH_2Cl_2, rt, 8 h, 74% from **7**; v, $AlCl_3$, CH_2Cl_2, rt, 20 h, 86%.

forded the 1,4-dihydroquinone derivative **4**, after pyrolytic elimination of the sulfoxide in the initially formed adduct **3** which occurred spontaneously even at 0 °C. The formation of **4** as a single regioisomer and *anti* diastereoisomer revealed a high efficiency of the sulfinylquinone **1** in controlling both the regioselectivity and diastereoselectivity of the cycloaddition step. Transformation of **4** into rubiginone B_2 only required three steps: aromatization of the B ring, deprotection of the OTBDMS group and further oxidation of the benzylic alcohol function. Unfortunately, compound **4** was not stable enough to be isolated pure due to its easy decomposition. We thus turned our attention to the more stable demethoxy analogue (+)-**5** (Scheme 2), which had been obtained in the reaction between (*S*)-2-(*p*-tolylsulfinyl)-1,4-naphthoquinone and diene (±)-**2**.[11]

Upon treatment with DBU,[14] partial aromatization of compound **5** proceeded rapidly to give the benz[*a*]anthraquinone (−)-**6** in 81% yield (Scheme 2). The OTBDMS protecting group of **6** was removed by treatment with 40% aqueous HF in CH_3CN[15] to provide alcohol (−)-**7** in 52% yield. The oxidation of **7** into the 8-deoxyangucyclinone (+)-**8** was carried out in 70% yield following a photooxygenation process,[16] in which a CH_2Cl_2 solution of **7** was exposed to daylight. This transformation could also be achieved by using a PCC oxidation (74% yield). The optical rotation of **8** was $[\alpha]_D^{20}$ +97 (*c* 0.5, $CHCl_3$), in accordance with those of natural angucyclinones rubiginone B_2[2] and ochromycinone,[1] suggesting the correct *S* absolute configuration at C-3, the only stereocenter present in the molecule. From a ^{1}H-NMR study an 80% ee was determined for (+)-**8** using $Pr(hfc)_3$ as chiral lanthanide shift reagent,‡ showing that no racemization had occurred during the reaction sequence outlined in Scheme 2, which started from derivative (+)-**5** (ee = 80%).

The natural products **11** and **12** were then synthesized following a similar reaction sequence (Scheme 2). Thus, after cycloaddition between (+)-**1** and (±)-**2** (Scheme 1), the crude reaction mixture containing compound **4** was aromatized into benz[*a*]anthraquinone (−)-**9** by treatment with DBU at 0 °C. Derivative **9** could thus be obtained in 58% yield for the one-pot three steps cycloaddition–sulfoxide elimination–aromatization process from (+)-**1**. Further deprotective treatment of OTBDMS derivative **9** with 40% aqueous HF in CH_3CN gave rise to the very unstable alcohol **10** which, without isolation, was oxidized in the presence of air and daylight to the corresponding ketone **11** in 48% yield from **9** for the one-pot two step desilylation–oxydation sequence. Synthetic **11** {$[\alpha]_D^{20}$ +62 (*c* 0.5, $CHCl_3$), 80% ee} was shown to be identical in all physical and spectroscopic properties to the natural (+)-rubiginone B_2 {$[\alpha]_D^{20}$ +78 (*c* 0.5, $CHCl_3$)}.[2] Finally, demethylation of rubiginone B_2 (+)-**11** was achieved in 86% yield by using $AlCl_3$ in CH_2Cl_2 at room temperature, to afford the hydroxy derivative **12** {$[\alpha]_D^{20}$ +163 (*c* 0.05, CH_2Cl_2), 80% ee} which was identical in all physical and spectroscopic data[14] to the natural (+)-ochromycinone {$[\alpha]_D^{20}$ +204.5 (*c* 0.05, CH_2Cl_2)}.[1] The analoguous rotary power of synthetic and natural products confirmed the (3*S*) configuration of the former as well as the (1*R*,3*S*,12b*S*) configuration for intermediate **5** which resulted in the cycloaddition process shown in Scheme 1. On this basis, a transition state similar to that indicated in Scheme 1 explains the major formation of the observed diastereoisomer.

In summary, we have reported a short enantioselective synthesis of the angucyclinone antibiotics rubiginone B_2 and ochromycinone, based on the asymmetric Diels–Alder reaction between the enantiopure methoxy substituted 2-(*p*-tolylsulfinyl)-1,4-naphthoquinone (+)-**1** and the racemic chiral vinylcyclohexene (±)-**2**, through the efficient kinetic resolution of the diene partner and the spontaneous sulfoxide elimination which recovers the quinone skeleton in a single step. The total synthesis of natural derivative (+)-**11** was thus achieved in a two-pot four step procedure starting from (+)-**1** with 80% ee and 28% overall yield. Ochromycinone (+)-**12** was obtained from (+)-**11** after an additional demethylation step with the same optical purity and 25% overall yield.

We thank DGICYT (PB95-0174) for financial support and FAPESP for a post-doctoral fellowship to C. D. V.

Notes and references

‡ The racemic derivative **8** necessary for such evaluation was prepared from racemic sulfinylnaphthoquinone **1**.

1 J. H. Bowie and A. W. Johnson, *Tetrahedron Lett.*, 1967, 1449.
2 M. Oka, H. Kamei, Y. Hamagishi, K. Tomita, T. Miyaki, M. Konishi and T. Oki, *J. Antibiot.*, 1990, **43**, 967.
3 R. H. Thomson, in *Naturally Occurring Quinones IV*, 4th edn., Blackie Academic & Professional, London, 1996; J. Rohr and R. Thiericke, *Nat. Prod. Rep.*, 1992, **9**, 103; M. Ogasawara, M. Hasegawa, Y. Hamagishi, H. Kamei and T. Oki, *J. Antibiot.*, 1992, **45**, 129.
4 S. J. Gould, X. C. Cheng and C. Melville, *J. Am. Chem. Soc.*, 1994, **116**, 1800 and refs. cited therein.
5 K. Krohn and J. Rohr, *Top. Curr. Chem.*, 1997, **188**, 128. For other recent references, see: D. S. Larsen and M. D. O'Shea, *J. Org. Chem.*, 1996, **61**, 5681; K. Krohn, N. Böker, U. Flörke and C. Freund, *J. Org. Chem.*, 1997, **62**, 2350.
6 K. Kim and G. Sulikowski, *Angew. Chem., Int. Ed. Engl.*, 1995, **34**, 2396; V. A. Boyd and G. Sulikowski, *J. Am. Chem. Soc.*, 1995, **117**, 8472.
7 D. S. Larsen, M. D. O'Shea and S. Brooker, *Chem. Commun.*, 1996, 203.
8 G. Matsuo, Y. Miki, M. Nakata, S. Matsumura and K. Toshima, *Chem. Commun.*, 1996, 225.
9 Based on a polyketide condensation, (−)-urdamycinone B had been synthesized in the first example of the asymmetric synthesis of an angucyclinone: M. Yamaguchi, T. Okuma, A. Horiguchi, C. Ikeura and T. Minami, *J. Org. Chem.*, 1992, **57**, 1647.
10 For an overview of our work, see: M. C. Carreño, *Chem. Rev.*, 1995, **95**, 1717. For more recent references, see: M. C. Carreño, J. L. García Ruano, M. A. Toledo, A. Urbano, V. Stefani, C. Z. Remor and J. Fischer, *J. Org. Chem.*, 1996, **61**, 503; M. C. Carreño, R. Hernández-Sánchez, J. Mahugo and A. Urbano, *J. Org. Chem.*, 1999, **64**, 1387.
11 M. C. Carreño, A. Urbano and C. Di Vitta, *J. Org. Chem.*, 1998, **63**, 8320.
12 M. C. Carreño, A. Urbano and J. Fischer, *Angew. Chem., Int. Ed. Engl.*, 1997, **36**, 1621.
13 M. C. Carreño, J. L. García Ruano and A. Urbano, *Synthesis*, 1992, 651.
14 D. S. Larsen and M. D. O'Shea, *J. Chem. Soc., Perkin Trans. 1*, 1995, 1019.
15 B. H. Lipshutz and D. F. Harvey, *Synth. Commun.*, 1982, **12**, 267.
16 K. Krohn, F. Ballwanz and W. Baltus, *Liebigs Ann. Chem.*, 1993, 911; K. Krohn, K. Khanbabaee, U. Flörke, P. G. Jones and A. Chrapkowski, *Liebigs Ann. Chem.*, 1994, 471.

Communication 9/01642B

Towards hydrocarbon analogues of the porphyrins: synthesis and spectroscopic characterization of the first dicarbaporphyrin†

Timothy D. Lash,* Jennifer L. Romanic, Michael J. Hayes and John D. Spence

Department of Chemistry, Illinois State University, Normal, Illinois 61790-4160, U.S.A. E-mail: tdlash@ilstu.edu

Received (in Corvallis, OR, USA) 8th December 1999, Accepted 5th March 1999

Condensation of 3,4-diethylpyrrole with 1,3-diformylindane in the presence of catalytic HBr afforded, following oxidation with $FeCl_3$, the first example of a dicarbaporphyrin in moderate yield; this novel bridged annulene system retains a strong diamagnetic ring current in ^{1}H NMR spectroscopy as well as a porphyrin-like UV–VIS spectrum.

The nature of aromaticity in porphyrins and related structures has been the subject of much debate,[1] although these systems are commonly described as bridged diaza[18]annulenes.[2] This description also helps to explain the properties of synthetic porphyrinoids such as porphyrin isomers[3] and expanded porphyrins.[4] Nonetheless, the nitrogen atoms clearly play an important role in the spectroscopic and chemical properties of Nature's [18]annulenes. In earlier studies, the replacement of pyrrole subunits with furan and/or thiophene rings was explored.[3,5] While the resulting porphyrin analogues had substantially modified properties they retained the aromatic characteristics that are associated with the tetrapyrrolic structures. However, it has only been very recently that porphyrin analogues with carbocyclic rings replacing one of the pyrrolic moieties have been reported.[6–9] These include oxybenziporphyrin (**1**),[6] tropiporphyrin,[7] carbaporphyrins (*e.g.* **2**)[8] and carbachlorins.[9] It is noteworthy that all of these structures show powerful diamagnetic ring currents by ^{1}H NMR where the internal CHs resonate near $\delta -7$ and the external *meso*-protons mostly appear downfield between δ 9 and 10.[6–9] Although the substitution of one nitrogen by a carbon atom does not significantly disrupt the aromaticity of these macrocycles, it remains less than clear whether hydrocarbon porphyrinoids such as **3** would similarly retain porphyrin-like aromatic properties. While at the present time the characteristics of the tetracarbaporphyrin system **3** remain open to speculation, we now report the next step towards this hypothetical system.

During our earlier work on the synthesis of carbaporphyrins **2**,[8] we reacted the diformylindene intermediate **4** with diethylpyrrole **5** in the presence of TFA in CH_2Cl_2 (Scheme 1). Following neutralization, a nonpolar orange–brown band was collected from column chromatography on alumina that appeared to correspond to the dicarbaporphyrin **6**. The yield for this chemistry was very low (< 0.1%), but this is perhaps not surprising as the relatively high oxidation level of **4** must require that some type of reduction takes place in order to generate the aromatic porphyrinoid **6**. While these observations demonstrated that syntheses of dicarbaporphyrins are achievable, the methodology was not suitable for synthesizing more than trace amounts of material.

Given our recent successes in utilizing aliphatic dialdehydes in the synthesis of carbachlorins,[9] diformylindane **7** was considered to be a better choice for these investigations. This previously unknown compound was synthesized in two steps from norbornadiene derivative **8**[10] (Scheme 2). Oxidation of **8** with $KMnO_4$ afforded the diol **9** in 45% yield, and subsequent

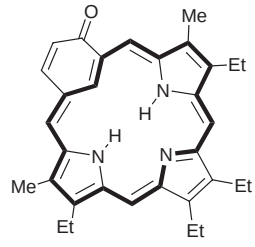

1

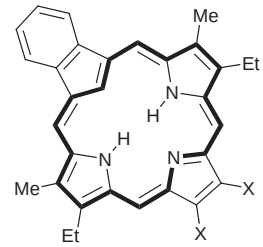

2a X = Et
b X–X = $(CH_2)_4$

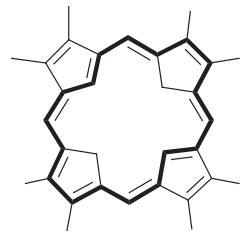

3

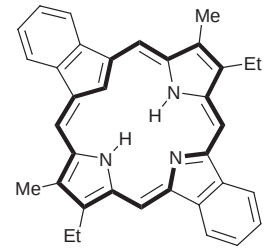

10

reaction with $NaIO_4$ afforded the required dialdehyde **7** as a pale yellow oil (quantitative). Condensation of **7** with diethylpyrrole **5** in the presence of TFA in CH_2Cl_2, followed by oxidation with 0.52 equiv. of DDQ, afforded the dicarbaporphyrin in low yields. Some improvement was observed when HBr was used as the acid catalyst, although the yields were still generally only approximately 1–2%. However, superior results (4.0–7.8%) were obtained when the DDQ oxidation was replaced by a brief treatment with aqueous $FeCl_3$. In this procedure, the acidic CH_2Cl_2 solution was washed successively with water, 0.1% $FeCl_3$ solution, water and saturated $NaHCO_3$. The crude material was chromatographed on Grade III neutral alumina eluting with CH_2Cl_2, and the colored fractions combined and further chromatographed on Grade I alumina. The first orange–brown band was evaporated and recrystallized from $CHCl_3$–MeOH to give the new porphyrinoid as dull purple crystals.‡

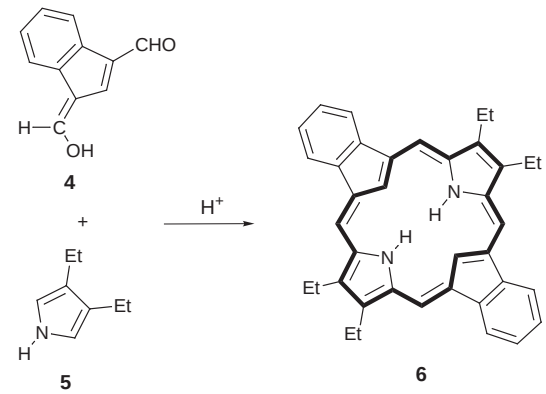

Scheme 1

† Part 15 of the series 'Conjugated Macrocycles Related to the Porphyrins'. Part 14: M. J. Hayes, J. D. Spence and T. D. Lash, *Chem. Commun.*, 1998, 2409.

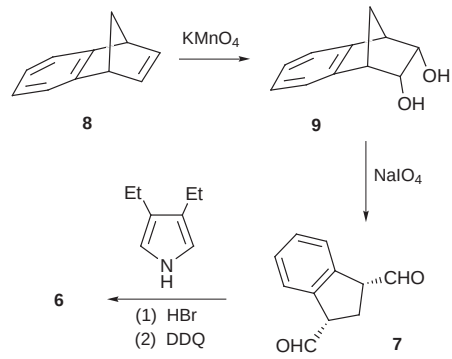

Scheme 2

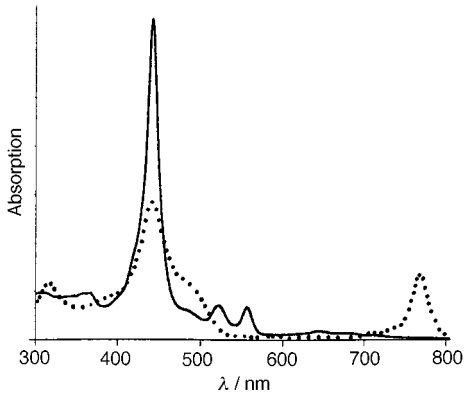

Fig. 1 UV–VIS spectra of dicarbaporphyrin **6**: free base in $CHCl_3$ (bold line); monocation **11** in 0.1% TFA–$CHCl_3$ (dotted line).

Solutions of the dicarbaporphyrin proved to be unstable, even in the absence of light, producing unidentified green materials. As a precaution, all manipulations were carried out with low ambient lighting and the columns, flasks and separatory funnels were covered with aluminium foil to limit photodegradation. In crystalline form, dicarbaporphyrin **6** appears to be reasonably stable and can be stored indefinitely.

Dicarbaporphyrin **6** was only sparingly soluble in $CDCl_3$, and this led to some problems in obtaining quality proton NMR spectra for this species. Trace impurities, together with the instability problems, led to the presence of small impurity peaks but otherwise the data were in full agreement with the proposed structure. Owing to the high level of symmetry in **6**, all four *meso*-protons are equivalent and resonate at δ 9.8. In addition, the internal CH protons appeared upfield at δ −5.7, while the NHs were noted at δ −4.8. It is evident that this species possesses a strong diamagnetic ring current and this supports the formulation of **6** as a bridged annulene structure with porphyrinoid aromaticity. A dibenzomonocarbaporphyrin **10** has also been prepared by dehydrogenation of **2b** with DDQ in refluxing toluene, and this structurally similar compound provides some useful comparisons. For the ^{1}H NMR spectra of carbaporphyrin **10** in $CDCl_3$, the external *meso*-protons appeared at δ 10.04 and 10.06, while the internal CH resonated at δ −6.6 and the NHs were observed near δ −4. These data indicate that the macrocyclic ring current is slightly greater in **10** compared to **6**, possibly due to the more crowded cavity in the latter which contains four hydrogens, compared to three in the former, and this factor may perturb that planarity of the structure. Further evidence for the porphyrin-like nature of **6** comes from the UV–VIS spectrum in $CHCl_3$ (Fig. 1) which shows a strong Soret band at 442 nm, together with a series of Q absorptions between 500 and 700 nm. EI mass spectrometry shows a strong molecular ion at *m/z* 520 and a small amount of benzylic fragmentation together with doubly charged ions of 25–30% the intensity of the base peak.

When small amounts of TFA were added, the brown solution turned green due to C-protonation to give the related cation **11**

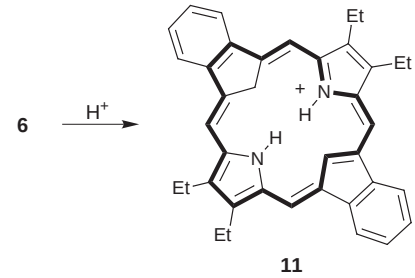

Scheme 3

(Scheme 3). Although 0.1% TFA–$CHCl_3$ was sufficient to fully protonate the dicarbaporphyrin, further protonation to a dication was not observed even in 50% TFA–$CHCl_3$. The UV–VIS spectrum for **11** was radically altered (Fig. 1), showing a broadened Soret band of much lower intensity together with a strong absorption in the far red near 760 nm (Fig. 1). The proton NMR spectrum for **6** in TFA-$CDCl_3$ confirmed the presence of a strong aromatic ring current, although the lower symmetry of structure **11** resulted in a larger number of resonances; two 2H singlets were noted for the *meso*-protons near δ 10, while the upfield region showed the internal CH_2 at δ −4.3, the remaining CH at δ −3.3 and the two NHs near δ −1. The two benzo units also displayed surprisingly different chemical shifts and one of the 2H multiplets was shifted downfield to δ 9.7. These data are consistent with a benzo[18]annulene formulation for **11** where the C-protonated indene unit directs 18π-electron delocalization through one of the fused benzene rings.

The synthesis of the first dicarbaporphyrin represents an important step forward and allows us to set our sights on still further modified porphyrin analogs such as the tetracarbaporphyrin system **3**, a structure that must now be considered to be the Holy Grail in this research area. However, the marked decrease in stability of the dicarbaporphyrin system may not bode well for these investigations.

This work was supported by the National Science Foundation under Grant No. CHE-9732054, the Camille and Henry Dreyfus Scholar/Fellow Program and the Donors of the Petroleum Research Fund, administered by the American Chemical Society.

Notes and references

‡ *Selected data* for **6**: mp > 300 °C; λ_{max}($CHCl_3$)/nm ($\log_{10}\varepsilon$) 442 (5.29), 522 (4.28), 556 (4.29), 643 (3.66); λ_{max}(0.1% TFA–$CHCl_3$)/nm ($\log_{10}\varepsilon$) 439 (4.96), 581 (3.71), 629 (3.62), 697 (3.88), 766 (4.67); δ_H(400 MHz, $CDCl_3$) −5.68 (2H, br s), −4.82 (2H, br s), 1.83 (12H, t, *J* 7.5), 3.97 (8H, q, *J* 7.5), 7.74 (4H, m), 8.76 (4H, m), 9.79 (4H, s); δ_H(400 MHz, TFA–$CDCl_3$) −4.34 (2H, br s), −3.30 (1H, br s), −0.95 (2H, br s), 1.66–1.71 (12H, m), 3.79–3.86 (8H, m), 7.72–7.75 (2H, m), 8.55–8.59 (4H, m), 9.72–9.75 (2H, m), 10.02 (2H, s), 10.35 (2H, s); δ_C(TFA–$CDCl_3$) 17.30, 17.80, 19.13, 19.52, 33.01, 105.68, 113.14, 120.86, 123.15, 123.55, 127.97, 131.30, 135.53, 136.44, 137.87, 140.13, 141.73, 142.24, 143.06, 143.73; HRMS: Calc. for $C_{38}H_{36}N_2$: 520.28785. Found: 520.28783. Calc. for $C_{38}H_{36}N_2.^1/_2H_2O$: C, 86.16; H, 7.04; N, 5.29. Found: C, 86.12; H, 6.68; N, 4.50%).

1 *E.g.* M. K. Cyranski, T. M. Krygowski, M. Wisiorowski, N. J. R. van E. Hommes and P. von R. Schleyer, *Angew. Chem., Int. Ed.*, 1998, **37**, 177.
2 E. Vogel, W. Haas, B. Knipp, J. Lex and H. Schmickler, *Angew. Chem., Int. Ed. Engl.*, 1988, **27**, 406; T. D. Lash and S. T. Chaney, *Chem. Eur. J.*, 1996, **2**, 944.
3 E. Vogel, *J. Heterocycl. Chem.*, 1996, **33**, 1461.
4 J. Ayub and D. Dolphin, *Chem. Rev.*, 1997, **97**, 2267.
5 M. J. Broadhurst, R. Grigg and A. W. Johnson, *J. Chem. Soc. (C)*, 1971, 3681.
6 T. D. Lash, *Angew. Chem., Int. Ed. Engl.*, 1995, **34**, 2533.
7 T. D. Lash and S. T. Chaney, *Tetrahedron Lett.*, 1996, **37**, 8825.
8 T. D. Lash and M. J. Hayes, *Angew. Chem., Int. Ed. Engl.*, 1997, **36**, 840; T. D. Lash, *Chem. Commun.*, 1998, 1683.
9 M. J. Hayes and T. D. Lash, *Chem. Eur. J.*, 1998, **4**, 508.
10 T. F. Mich, E. J. Nienhouse, T. E. Farina and J. J. Tufariello, *J. Chem. Educ.*, 1968, **45**, 272.

Communication 8/09639B

ChemComm

Methyltrioxorhenium-catalysed epoxidation of alkenes in trifluoroethanol

Michiel C. A. van Vliet, Isabel W. C. E. Arends and R. A. Sheldon*

Laboratory for Organic Chemistry and Catalysis, Delft University of Technology, Julianalaan 136, 2628 BL Delft, The Netherlands. E-mail: secretariat-ock@stm.tudelft.nl

Received (in Cambridge, UK) 17th March 1999, Accepted 30th March 1999

The well known methyltrioxorhenium-catalysed epoxidation of alkenes with aqueous H_2O_2 is significantly improved by conducting the epoxidation in trifluoroethanol; excellent reaction rates and yields can be obtained for a variety of (terminal) alkenes with only 0.1 mol% of catalyst.

Catalytic epoxidation of alkenes with aqueous H_2O_2 has been extensively studied in the last two decades.[1] Rhenium-based systems are especially interesting because rhenium, in contrast to many other transition metals, does not catalyse the facile decomposition of H_2O_2.[2]

The discovery of the catalytic activity of methyltrioxorhenium ($MeReO_3$; MTO) by Herrmann and co-workers[3] marks a turning point in the use of rhenium compounds as catalysts for epoxidations with H_2O_2. This catalyst proved to be very active in epoxidation with anhydrous H_2O_2 in Bu^{t}OH. The main disadvantage, however, was the low selectivity when acid sensitive epoxides were formed. The high acidity of MTO–H_2O_2 caused hydrolysis and further degradation of the epoxide. This drawback could be partly circumvented by adding basic ligands (*e.g.* bipyridine) to the catalyst, but not without decreasing the activity of the catalyst.[4]

A major improvement in the MTO catalysed epoxidation was achieved by Sharpless and co-workers.[5] They discovered that a large excess of pyridine relative to the catalyst ($>10:1$) actually improved the activity of the catalyst while maintaining the high selectivity. An important feature of this new system was the possibility of using commercially available aqueous H_2O_2 as the oxidant. This discovery boosted interest in MTO research and shortly afterwards new improvements were achieved by the Sharpless and Herrmann groups.[6,7] The best results up to now were reported with pyrazole (pyrazole : MTO ratio of 24 : 1) as the basic ligand and CH_2Cl_2 as solvent.[7]

During our research on catalytic epoxidation with inorganic rhenium compounds as the catalyst, we found that trifluoroethanol was an excellent solvent for epoxidations with aqueous H_2O_2.[8] We subsequently found that a major improvement could be achieved when this solvent was used in the MTO system.

Fig. 1 shows the catalytic epoxidation of hex-1-ene. The results using 0.5 mol% MTO, 10 mol% pyrazole and 2 equiv. 30% H_2O_2 in CH_2Cl_2 are comparable to those reported by Herrmann and co-workers (95% conversion in 8 h; curve A). The use of 0.1 mol% MTO resulted in a much slower reaction and complete conversion of the alkene could not be reached in 24 h (curve B). The use of 60% H_2O_2 showed a slightly increased rate, but again complete conversion was not reached in 24 h (curve C).

A marked increase in the rate was observed, however, when the same catalyst and ligand were used in trifluoroethanol. This increase was observed both with 30% H_2O_2 (curve D) and more pronounced with 60% H_2O_2 (curve E). The rate was comparable to that observed with five times as much MTO in CH_2Cl_2 and complete conversion of the alkene with high selectivity to the epoxide could be reached within 24 h. With 5 mol% of pyrazole the rate was even slightly higher and a 95% yield of epoxide could be obtained in 5 h (curve F). The use of pyridine or 3-cyanopyridine resulted in slower rates, in analogy with the CH_2Cl_2 based system.

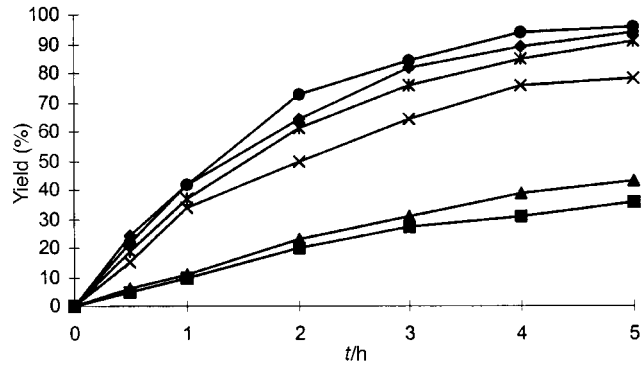

Fig. 1 Epoxidation of hex-1-ene by various catalytic systems. Conditions: 10 mmol hex-1-ene, 1 mmol Bu_2O (internal standard), $MeReO_3$, pyrazole, 20 mmol H_2O_2 and 5 ml of solvent. Reaction at room temperature. Analysis by GC. (◆) Curve A: 0.5 mol% MTO, 10 mol% pyrazole, 30% H_2O_2 in CH_2Cl_2. (■) Curve B: 0.1 mol% MTO, 10 mol% pyrazole, 30% H_2O_2 in CH_2Cl_2. (▲ Curve C: 0.1 mol% MTO, 10 mol% pyrazole, 60% H_2O_2 in CH_2Cl_2. (×) Curve D: 0.1 mol% MTO, 10 mol% pyrazole, 30% H_2O_2 in trifluoroethanol. (*) Curve E: 0.1 mol% MTO, 10 mol% pyrazole, 60% H_2O_2 in trifluoroethanol. (●) Curve F: 0.1 mol% MTO, 5 mol% pyrazole, 60% H_2O_2 in trifluoroethanol.

The high rates in trifluoroethanol are in agreement with earlier observation by Sharpless and co-workers, who found that polar, non-coordinating solvents showed the highest rates.[5] Despite its alcoholic nature, trifluoroethanol is a non-coordinating solvent owing to the strong electron-withdrawing effect of the trifluoromethyl group. The trifluoromethyl group also prevents the oxidation of the alcohol group, rendering this primary alcohol relatively stable towards oxidation.

Based on these results we tested a number of terminal alkenes in the MTO catalysed epoxidation in trifluoroethanol (Table 1). In most cases complete conversion was observed within 24 h

Table 1 Epoxidation of terminal alkenes catalysed by MTO in trifluoroethanol[a]

Alkene	*t*/h	Yield (%)
Hex-1-ene	6	95
	21	>99
Hept-1-ene	21	>99
Oct-1-ene	21	>99
Non-1-ene	21	>99
Dec-1-ene	21	97
Vinylcyclohexane	21	>99
Styrene	2	82[b]
3-Phenylpropene	21	97
4-Phenylbut-1-ene	21	>99

[a] Conditions: 10 mmol alkene, 1 mmol Bu_2O (internal standard), 0.010 mmol $MeReO_3$ (0.1 mol%), 0.5 mmol pyrazole, 20 mmol 60% H_2O_2 and 5 ml trifluoroethanol. Stirring at room temperature, analysis by GC. [b] Phenylethane-1,2-diol and benzaldehyde were also detected.

Table 2 Epoxidation of internal alkenes catalysed by MTO in trifluoroethanol[a]

Alkene	*t*/h	Yield (%)
Cyclohexene	0.5	> 99
Cycloheptene	1	> 99
Cyclooctene	1	> 99
1-Methylcyclohexene	0.5	> 99
Methylenecyclohexane	1	99
Indene	1	65[b]
2-Methylhept-1-ene	1.5	98
2-Methylhept-2-ene	1	99

[a] Conditions:1 mmol Bu_2O (internal standard), 0.010 mmol $MeReO_3$ (0.1 mol%), 1 mmol pyrazole and 20 mmol 60% H_2O_2 were dissolved in 5 ml trifluoroethanol. The stirred mixture was cooled in an ice bath to *ca.* 5 °C. The alkene (10 mmol) was then added dropwise in 20–30 min. The mixture was warmed to room temperature and analysed by GC. [b] Several hydrolysis products were also detected.

with 0.1 mol% of catalyst. The epoxide was formed with high selectivity and no noticeable by-products were observed. The only notable exception was styrene. Its very sensitive epoxide was partly decomposed to phenylethane-1,2-diol and benzaldehyde. The yield, however, is comparable to the best results claimed by Sharpless and co-workers.[6] These high turnovers obtained for terminal alkenes are unprecedented and can only be approached by the recently improved manganese triazonane catalyst.[9]

The high turnovers could also be obtained in the oxidation of the more reactive internal alkenes. However, the reaction was in several cases too fast, resulting in the decomposition of the catalyst and incomplete conversion of the alkene. When appropriate cooling was applied, no catalyst decomposition was observed. A better procedure was to add the substrate slowly (*ca.* 20 to 30 min) to the ice-cooled reaction mixture. In most cases the reaction was complete within minutes after the addition of the last portion of alkene. The presence of the active catalyst, even after 1000 turnovers, was indicated by the intense yellow colour of the peroxo complex. The results for some internal alkenes are shown in Table 2. Most epoxides give > 99% yield of epoxide, except indene. Indene oxide is known to be very sensitive towards hydrolysis. The homogeneous reaction mixture with water present in the same phase as the epoxide results in decomposition of the product. The two-phase system with CH_2Cl_2 generally gives higher yields, because the water and epoxide are present in separate phases. This behaviour is known for other catalytic systems as well.[10] Most other epoxides, however, are stable enough to resist hydrolysis in a monophasic system.

The catalyst is still active after 1000 turnovers, and 2500 turnovers could be obtained by slow addition of alkene to the reaction mixture. At a substrate to catalyst ratio of 2000 complete conversion was reached within 1 h with cyclohexene. At a substrate to catalyst ratio of 3000 the catalyst decomposed and only 90% conversion could be reached. These high turnovers require very careful addition of the alkene. A slightly faster addition of the alkene than the optimum addition rate causes the reaction mixture to warm up, resulting in complete loss of catalytic activity.

One disadvantage of the present catalytic system is the high polarity of the reaction medium. Very apolar alkenes (C_{12} or higher alkenes and stilbenes) do not dissolve in the reaction medium, and are therefore not epoxidised. In other cases (the experiments of Table 1 and 2) the alkene does not dissolve completely at the beginning of the reaction. During the course of the reaction the medium becomes homogeneous due to the formation of polar, soluble epoxide. The time required for a homogeneous reaction mixture depends on the polarity of the alkene and ranges from 1 h for hex-1-ene to 6 h for dec-1-ene. The more reactive internal alkenes give a homogeneous reaction mixture within minutes after the addition.

In summary, the use of MTO–pyrazole in trifluoroethanol allows for the highly selective epoxidation of a variety of olefins with 30–60% aqueous H_2O_2 at low (0.1 mol%) catalyst loading. The methodology should have wide applicability in organic synthesis.

Notes and references

1 G. Strukul and R.A. Michelin, *J. Chem. Soc., Chem. Commun.*, 1984, 1538; C. Venturello and R. D'Aloisio, *J. Org. Chem.*, 1988, **53**, 1553; Y. Ishii, K. Yamawaki, T. Ura, H. Yamada, T. Yoshida and M. Ogawa, *J. Org. Chem.*, 1988, **53**, 3587; K. Sato, M. Aoki, M. Ogawa, T. Hashimoto and R. Noyori, *J. Org. Chem.*, 1996, **61**, 8310; T. Kamiyama, M. Inoue, H. Kashiwagi and S. Enomoto, *Bull. Chem. Soc. Jpn.*, 1990, **63**, 1559; P. L. Anelli, S. Banfi, F. Montanari and S. Quici, *J. Chem. Soc., Chem. Commun.*, 1989, 779; D. de Vos and T. Bein, *Chem. Commun.*, 1996, 917; M. G. Clerici and P. Ingallina, *J. Catal.*, 1993, **140**, 71.

2 M. Rüsch, gen. Klaas, Thesis RWTH Aachen, 1993.

3 W. A. Herrmann, R. W. Fischer and D. W. Marz, *Angew. Chem.*, 1991, **103**, 1706; W. A. Herrmann, D. W. Marz, W. Wagner, J. G. Kuchler, G. Weichselbaumer and R. W. Fischer, *Ger. Pat.*, 3902357, 1989 to Hoechst AG.

4 W. A. Herrmann, R. W. Fischer, M. U. Rauch and W. Scherer, *J. Mol. Catal.*, 1994, **86**, 221.

5 J. Rudolph, K. L. Reddy, J. P. Chiang and K. B. Sharpless, *J. Am. Chem. Soc.*, 1997, **119**, 6189.

6 C. Copéret, H. Adolfsson and K. B. Sharpless, *Chem. Commun.*, 1997, 1565.

7 W. A. Herrmann, R. M. Kratzer, H. Ding, W. R. Thiel and H. Glas, *J. Organomet. Chem.*, 1998, **555**, 293.

8 M. C. A. van Vliet, I. W. C. E. Arends and R.A. Sheldon, manuscript in preparation.

9 D. E. de Vos, B. F. Sels, M. Reynaers, Y. V. Subba Rao and P. Jacobs, *Tetrahedron Lett.*, 1998, **39**, 3221.

10 K. Sato, M. Aoki, M. Ogawa, T. Hashimoto, D. Panyella and R. Noyori, *Bull. Chem. Soc. Jpn.*, 1997, **70**, 905.

Communication 9/02133G

ChemComm

Non-peptidic liposome-fusion compounds at acidic pH

Yoshikatsu Ogawa,[a] Takenori Tomohiro,[a] Yoshimitsu Yamazaki,[b] Masato Kodaka*[a] and Hiroaki Okuno[a]

[a] *Biomolecules Department, National Institute of Bioscience and Human-Technology, Higashi 1-1, Tsukuba, Ibaraki 305-8566, Japan. E-mail: kodaka@nibh.go.jp*

[b] *Biosignaling Department, National Institute of Bioscience and Human-Technology, Higashi 1-1, Tsukuba, Ibaraki 305-8566, Japan*

Received (in Cambridge, UK) 22nd February 1999, Accepted 19th March 1999

Liposomes including aspartic acid-derived artificial lipids (ADL) with various carboxy alkyl chains as head groups (ADL*n*; *n* indicates the number of the methylene groups, *n* = 2,4,6,8,10,12) are prepared, in which ADL6 and ADL8 liposomes induce remarkably high lipid-mixing in the acidic region.

For the last decade, liposomes have been exploited predominantly as potent carriers of various polar materials into cells.[1–4] We show here that artificial lipids with simple structures can induce pH-dependent membrane fusion in a manner similar to authentic fusion inducers such as the Spike protein of the influenza virus.[5–7] Homologous artificial lipids (ADL*n*; *n* = 2, 4, 6, 8, 10, 12) were designed and synthesized according to Scheme 1.† These lipids are composed of three fundamental parts: (A) two long alkyl chains in the tail part, which can be anchored to the hydrophobic region of lipid bilayer, (B) a polar moiety composed of two aspartic acid residues in the central part, (C) a terminal carboxylic acid group as a pH-dependent trigger for liposome fusion. Part (C) composed of the carboxy group and the alkyl chain was designed so that its polarity could be controlled by pH, depending upon whether the carboxy group is protonated or deprotonated. Since the pK_a was expected to be 4.6–4.8, in view of the pK_a of an ordinary carboxy group, part (C) was expected to behave as a hydrophobic protrusion on the lipid membrane like fusion peptides[8] at acidic pH. The time course of fusion % of liposomes composed of ADL*n* (5–20 mol%) and egg phosphatidylcholine (Egg PC, Avanti Polar Lipids, Inc., special grade) was measured from the efficiency of the fluorescence resonance energy transfer (FRET) between *N*-(7-nitro-2,1,3-benzoxadiazol-4-yl)phosphatidylethanolamine (NBD-PE) and lissamine rhodamine B sulfonyl phosphatidylethanolamine (Rh-PE).[9,10]‡ The fusion % was calculated from eqn. (1),

$$\text{Fusion \%} = 100[F(t)-F(0)]/[F(\text{Triton})-F(0)] \qquad (1)$$

where $F(0)$, $F(t)$ and F(Triton) signify the fluorescence intensity at 530 nm (λ_{ex} = 480 nm) before adding citric acid, at time t, and after the collapsing of liposomes by Triton X-100, respectively. Fusion % after 5 min reaction at pH 4 is depicted in Fig. 1 ([ADL*n*] = 5, 10, 15, 20 mol%). As expected, very high liposome fusion was observed in some liposomes, which suggests that the carboxy group in the head part can act as a trigger in the fusion. It should be noted here that there are optimal lengths of the methylene group in the head group between 6 and 10, with ADL6 (20 mol%) showing especially high fusion % (*ca.* 40%). It was also confirmed that at neutral pH the liposome fusion was scarcely observed for any of the lipids, at least within 1 h. The pH dependence of the fusion % for ADL6 and ADL8 is shown in Fig. 2 together with the control experiment where liposomes are composed of only Egg PC without ADL*n*. The fusion in the presence of ADL6 or ADL8 was significantly accelerated below *ca.* pH 5 due to the protonation of the carboxy group, while that of the control liposome gave low fusion % between pH 3.6 and 7.2. In contrast to ADL6, ADL8 and ADL10, the lipids with shorter or longer chains, ADL2, ADL4 and ADL12, did not induce remarkable fusion even at acidic pH.

In most fusion inducers such as the Spike protein of the influenza virus, the hydrophobic fusion peptide is hidden at neutral pH. At acidic pH, however, it protrudes from the membrane surface and is incorporated into another membrane. Consequently these membranes are close together, resulting in membrane fusion. The carboxylic acid with a long alkyl chain, which is protonated at low pH, seems an appropriate hydrophobic group to mimic fusion peptides as a simple fusion inducer. Fig. 2 clearly suggests that the protonation of the terminal carboxylate of ADL*n* is the trigger of liposome fusion and Fig. 1 suggests that there is an optimal hydrophobicity

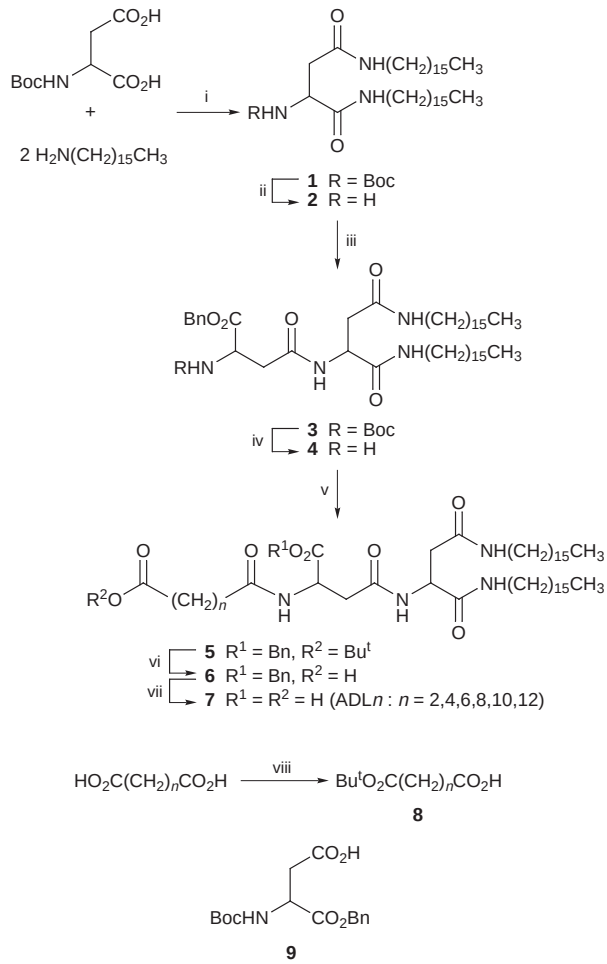

Scheme 1 Synthetic route to ADL*n*: i, HOBt, TBTU, DMAP; ii, TFA; iii, **9**, HOBt, EDC, DMAP; iv, TFA; v, **8**, HOBt, TBTU, DMAP; vi, TFA; vii, H_2/Pd-C; viii, Bu^{t}OH, EDC, DMAP. EDC = 1-(3-dimethylaminopropyl)-3-ethylcarbodiimide hydrochloride, HOBt = 1-hydroxybenzotriazole, TBTU = *O*-(1*H*-benzotriazol-1-yl)-*N*,*N*,*N*′,*N*′-tetramethyluronium tetrafluoroborate.

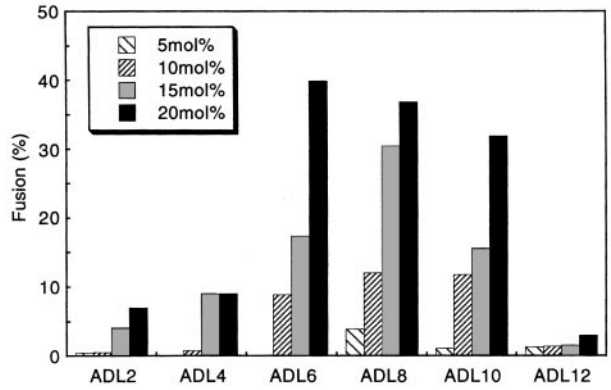

Fig. 1 Dependence of fusion % after 5 min reaction upon alkyl chain lengths of head groups of ADL*n*; pH 4.0, 37 °C; composition (mol%) of ADL*n* in liposomes is described inside the figure.

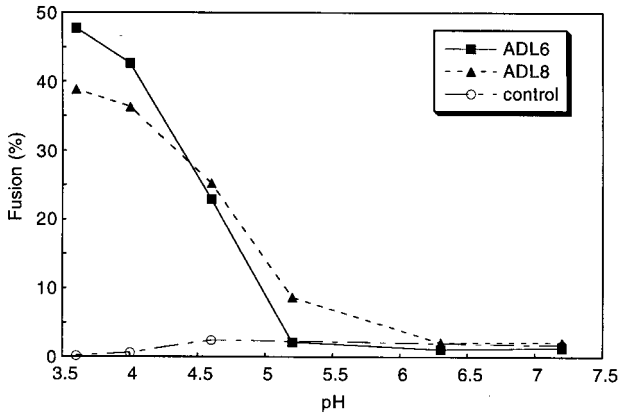

Fig. 2 pH profile of fusion % after 5 min reaction at 37 °C; [ADL*n*] = 20 mol%.

between ADL6 and ADL10. The reason for the very poor ability of ADL12 to induce liposome fusion may be that its alkyl chain in the head part is too long and too hydrophobic to remain in an outer aqueous phase and, consequently, ADL12 may be embedded in the membrane even at neutral pH. In contrast, the head alkyl chains of ADL2 and ADL4 are considered too short and too hydrophilic to migrate to another membrane, which may also result in low fusion %.

Notes and references

† All new lipids were fully characterized by ^{1}H NMR and mass spectroscopy and elemental analysis as follows. ADL2: δ_H(270 MHz, $CDCl_3$ and CD_3OD) 4.76 (t, 1H, CH, *J* 5.5), 4.62 (t, 1H, CH, *J* 5.9), 3.10–3.22 (m, 4H, 2NHCH_2), 2.78 (d, 2H, CH(COOH)CH_2, *J* 5.6), 2.46–2.73 (m, 6H, CHCH_2 and (CH_2)$_2$CO), 1.48 (br s, 4H, 2NHCH$_2$CH_2), 1.27 (br s, 52H, 2(CH_2)$_{13}$CH$_3$), 0.89 (t, 6H, 2CH2CH_3, *J* 6.4). Anal. Calcd for $C_{44}H_{82}N_4O_8$·0.7CF_3COOH: C, 62.32; H, 9.53; N, 6.40. Found: C, 62.00; H, 9.41; N, 6.16. FAB MS calcd: 795.6 (M + H$^+$). Found: 796. ADL4: δ_H(270 MHz, $CDCl_3$ and CD_3OD); 4.76 (t, 1H, CH, *J* 5.8), 4.64 (t, 1H, CH, *J* 6.1), 3.11–3.22 (m, 4H, 2NHCH_2), 2.79 (dd, 1H, CHCH_AH$_B$, *J* 5.9 and 15.7), 2.74 (dd, 1H, CHCH$_A$$H_B$, *J* 6.6 and 15.7), 2.64 (dd, 1H, CHCH_AH$_B$, *J* 5.9 and 15.2), 2.54 (dd, 1H, CHCH$_A$$H_B$, *J* 6.3 and 15.2), 2.33 (t, 2H, CH$_2$CH_2CO, *J* 6.9), 2.27 (t, 2H, CH2CH_2CO, *J* 7.3), 1.67 (m, 4H, 2CH_2CH$_2$CO), 1.48 (m, 4H, 2NHCH$_2$CH_2), 1.27 (br s, 52H, 2(CH_2)$_{13}$CH$_3$), 0.89 (t, 6H, 2CH$_2$CH_3, *J* 6.6). Anal. Calcd for $C_{44}H_{82}N_4O_8$·0.5CF_3COOH: C, 64.13; H, 9.91; N, 6.37. Found: C, 63.83; H, 9.83; N, 6.13%. FAB MS calcd: 823.7 (M + H$^+$). Found: 824. ADL6: δ_H(270 MHz, $CDCl_3$ and CD_3OD) 4.75 (t, 1H, CH, *J* 5.6), 4.64 (t, 1H, CH, *J* 6.1), 3.10–3.22 (m, 4H, 2NHCH_2), 2.78 (dd, 1H, CHCH_AH$_B$, *J* 5.8 and 15.3), 2.75 (dd, 1H, CHCH$_A$$H_B$, *J* 5.8 and 15.3), 2.63 (dd, 1H, CHCH_AH$_B$, *J* 5.9 and 15.0), 2.53 (dd, 1H, CHCH$_A$$H_B$, *J* 6.3 and 15.0), 2.30 (t, 2H, CH$_2$CH_2CO, *J* 7.4), 2.24 (t, 2H, CH$_2$CH_2CO, *J* 7.9), 1.62 (m, 4H, 2CH_2CH$_2$CO), 1.48 (m, 4H, 2NHCH$_2$CH_2), 1.33 (m, 4H, (CH_2)$_2$CH$_2$CH$_2$CO), 1.26 (br s, 52H, 2(CH_2)$_{13}$CH$_3$), 0.89 (t, 6H, 2CH$_2$CH_3, *J* 6.8). Anal. Calcd for $C_{48}H_{90}N_4O_8$: C, 67.73; H, 10.66; N, 6.58. Found: C, 67.60; H, 10.69; N, 6.40%. FAB MS calcd: 851.7 (M + H$^+$). Found: 852. ADL8: δ_H(270 MHz, $CDCl_3$ and CD_3OD) 4.76 (t, 1H, CH, *J* 5.6), 4.64 (t, 1H, CH, *J* 5.9), 3.10–3.22 (m, 4H, 2NHCH_2), 2.79 (dd, 1H, CHCH_AH$_B$, *J* 5.6 and 15.2), 2.75 (dd, 1H, CHCH$_A$$H_B$, *J* 5.6 and 15.2), 2.64 (dd, 1H, CHCH_AH$_B$, *J* 5.9 and 14.6), 2.53 (dd, 1H, CHCH$_A$$H_B$, *J* 6.3 and 14.6), 2.29 (t, 2H, CH$_2$CH_2CO, *J* 7.6), 2.23 (t, 2H, CH$_2$CH_2CO, *J* 8.3), 1.61 (m, 4H, 2CH_2CH$_2$CO), 1.48 (m, 4H, 2NHCH$_2$CH_2), 1.32 (m, 8H, (CH_2)$_4$CH$_2$CH$_2$CO), 1.26 (br s, 52H, 2(CH_2)$_{13}$CH$_3$), 0.88 (t, 6H, 2CH$_2$CH_3, *J* 6.6). Anal. Calcd for $C_{50}H_{94}N_4O_8$: C, 68.29; H, 10.78; N, 6.37. Found: C, 68.26; H, 10.78; N, 6.21%. FAB MS calcd: 879.7 (M + H$^+$), Found: 880. ADL10: δ_H(270 MHz, $CDCl_3$ and CD_3OD) 4.76 (t, 1H, CH, *J* 5.6), 4.63 (t, 1H, CH, *J* 5.9), 3.10–3.24 (m, 4H, 2NHCH_2), 2.74–2.84 (m, 2H, CHCH_2CO), 2.64 (dd, 1H, CHCH_AH$_B$, *J* 5.9 and 14.7), 2.52 (dd, 1H, CHCH$_A$$H_B$, *J* 5.9 and 14.7), 2.29 (t, 2H, CH$_2$CH_2CO, *J* 7.2), 2.23 (t, 2H, CH$_2$CH_2CO, *J* 8.6), 1.61 (m, 4H, 2CH_2CH$_2$CO), 1.48 (m, 4H, 2NHCH$_2$CH_2), 1.29 (br s, 12H, (CH_2)$_6$CH$_2$CH$_2$CH$_2$CO), 1.26 (br s, 52H, 2(CH_2)$_{13}$CH$_3$), 0.88 (t, 6H, 2CH$_2$CH$_3$, *J* 6.4). Anal. Calcd for $C_{52}H_{98}N_4O_8$·H$_2$O: C, 67.49; H, 10.89; N, 6.05. Found: C, 67.85; H, 10.77; N, 5.84%. FAB MS calcd: 907.7 (M + H$^+$), Found: 908. ADL12: δ_H(270 MHz, $CDCl_3$ and CD_3OD) 4.76 (t, 1H, CH, *J* 5.6), 4.63 (t, 1H, CH, *J* 6.1), 3.10–3.22 (m, 4H, 2NHCH_2), 2.70–2.84 (m, 2H, CHCH_2), 2.63 (dd, 1H, CHCH_AH$_B$, *J* 5.8 and 14.9), 2.52 (dd, 1H, CHCH$_A$$H_B$, *J* 6.3 and 14.9), 2.29 (t, 2H, CH$_2$CH_2CO, *J* 7.4), 2.23 (t, 2H, CH2CH_2CO, *J* 8.6), 1.62 (m, 4H, 2CH_2CH$_2$CO), 1.48 (m, 4H, 2NHCH$_2$CH_2), 1.26 (br s, 68H, (CH_2)$_8$CH$_2$CH$_2$CO and 2(CH_2)$_{13}$CH_3), 0.88 (t, 6H, 2CH$_2$CH_3, *J* 6.4). Anal. Calcd for $C_{54}H_{102}N_4O_8$·H$_2$O: C, 68.03; H, 10.99; N, 5.88. Found: C, 68.52; H, 10.83; N, 5.67%. FAB MS calcd: 935.8 (M + H$^+$), Found: 936.

‡ Egg PC was dissolved in $CHCl_3$–MeOH (3 : 1, v/v) with various amounts of ADL*n* for fusion liposome (Fusion-Lip), and with 0.5 mol% of NBD-PE and 0.5 mol% of Rh-PE for fluorescence-labeled liposome (Label-Lip). Lipid solutions were dried under a N_2 gas stream followed by the removal of residual solvent under high vacuum for 3 h. The resulting lipid films were hydrated by vortex-mixing with HEPES buffer (10 mM HEPES, 100 mM NaCl, pH 7.2) to make multilamellar vesicles (MLVs). MLVs were sonicated at 65 °C for 5 min by a probe-type sonicator and the resulting clear suspension (SUVs) was used in the experiments. After Fusion-Lip and Label-Lip (10:1, v/v) were mixed at 37 °C the lipid mixing assay was started by adding the necessary amount of citric acid (0.4 M) to adjust the pH.

1 C.-Y. Wang and L. Huang, *Biochemistry*, 1989, **28**, 9508.
2 C.-Y. Wang and L. Huang, *Proc. Natl. Acad. Sci. U.S.A.*, 1987, **84**, 7851.
3 C. Ropert, M. Lavignon, C. Dubernet, P. Couvreur and C. Malvy, *Biochem. Biophys. Res. Commun.*, 1992,1**83**, 879.
4 G. Zhang, V. Gurtu, T. H. Smith, P. Nelson and S. R. Kain, *Biochem. Biophys. Res. Commun.*, 1997, **236**, 126.
5 S. A. Tatulian and L. K. Tamm, *J. Mol. Biol.*, 1996, **260**, 312.
6 P. A. Bullough, F. M. Hughson, J. J. Skehel and D. C. Wiley, *Nature*, 1994, **371**, 37.
7 I. A. Wilson, J. J. Skehel and D. C. Wiley, *Nature*, 1981, **289**, 366.
8 R. A. Parente, S. Nir and F. C. Szoka, Jr., *J. Biol. Chem.*,1988, **263**, 4724.
9 D. K. Struck, D. Hoekstra and R. E. Pagano, *Biochemistry*, 1981, **20**, 4093.
10 A. L. Bailey and P. R. Cullis, *Biochemistry*, 1997, **36**, 1628.

Communication 9/01419E

Highly *trans*-selective intramolecular pinacol coupling of dials catalyzed by bulky Cp_2TiPh

Yoshihiko Yamamoto, Reiko Hattori and Kenji Itoh*

Department of Applied Chemistry and Department of Molecular Design and Engineering, Graduate School of Engineering, Nagoya University, Chikusa, Nagoya 464-8603, Japan. E-mail: itohk@apchem.nagoya-u.ac.jp

Received (in Cambridge, UK) 18th March 1999, Accepted 29th March 1999

$Cp_2Ti(Ph)Cl$ in the presence of Me_3SiCl and Zn provides an effective pinacol coupling catalyst for aromatic and aliphatic aldehydes.

Chiral 1,2-diols have found extensive use as asymmetric ligands for catalytic asymmetric reactions[1] and as chiral auxiliaries for diastereoselective transformation of carbonyl substrates.[2] Such valuable diols are commonly obtained by the resolution of racemic products prepared from a wide variety of aldehydes *via threo*-selective pinacol coupling.[3] Pinacol coupling has also been employed as a key step in the construction of highly important natural and artificial compounds.[3] For these purposes, stoichiometric reactions have so far been employed, however, catalytic methods are highly desirable as a metal-atom-economical and practical entry to the above 1,2-diols. From this point of view, some catalytic methods have been developed,[4] but few of them have been applied to the intramolecular coupling of dials.[4g] This is partly because the intramolecular pinacol coupling of dials is often accompanied by side reactions such as intramolecular aldol condensation. With this in mind, we developed the $Cp_2Ti(Ph)Cl$-catalyzed intramolecular pinacol coupling of dials, which gave cyclic 1,2-diols in moderate to good yields with excellent *trans*-selectivity under mild conditions (Scheme 1).

Cp_2TiCl has received much attention as an excellent single-electron reductant in organic synthesis.[5] In this context, Teuben *et al.* have reported the Cp_2TiPh-mediated reductive coupling of benzonitrile leading to benzil,[6] and recently we have found that the same titanium(III) reagent reacted with γ- and δ-ketonitriles to give α-hydroxycycloalkanones as reductive cyclization products in good yield.[7] The importance of the Ti^{III}–Ph σ-bond is obvious from the fact that the parent Cp_2TiCl was not effective for the above two reductive transformations. The phenyltitanium(III) reagent was readily prepared *in situ via* reduction of Cp_2TiCl_2 with Pr^iMgCl followed by the addition of PhMgBr.[6,7] The same reactive species may alternatively be generated by reducing $Cp_2Ti(Ph)Cl$[8] with Zn powder.[9] Given this fact, $Cp_2Ti(Ph)Cl$ should catalyze pinacol coupling reactions in the presence of a stoichiometric amount of Zn. In fact, stoichiometric reaction using equimolar amounts of $Cp_2Ti(Ph)Cl$ and Zn promoted the desired reductive coupling of benzaldehyde **1a** to give hydrobenzoin **2a** in 99% yield with a diastereoselectivity of *threo* : *erythoro* = 84 : 16. We carried out the catalyzed reaction as follows; a THF (5 ml) solution of **1a** (3 mmol) and Me_3SiCl (1.5 equiv.) was added to a mixture of 3 mol% $Cp_2Ti(Ph)Cl$ and Zn (1 equiv.) in THF (20 ml) and the mixture was stirred for 70 min at ambient temperature. Usual work-up gave **2a** in 88% yield with a diastereomeric ratio of *threo* : *erythro* = 71 : 29 (Scheme 2). In the absence of the titanium catalyst, **2a** was obtained in only 7% yield (*threo* : *erythro* = 50 : 50) along with the reduced product benzyl alcohol (13%).[10] The complete loss of diastereoselectivity demonstrated the importance of the titanocene catalyst. In addition to the aromatic aldehyde, less reactive aliphatic aldehyde **1b** was converted into the corresponding diol **2b** in good yield, although its *threo*-selectivity was lower than **2a**. These results demonstrate that $Cp_2Ti(Ph)Cl$ is an efficient catalyst for the pinacol coupling of both aromatic and aliphatic aldehydes.

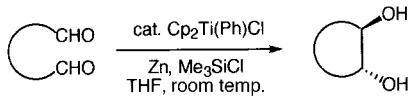

Scheme 1

On the basis of the above results, we applied our new catalytic system to the intramolecular reductive coupling of dials (Table 1). In the presence of 6 mol% $Cp_2Ti(Ph)Cl$, the acid sensitive 1,5-dial **3a** was reduced at ambient temperature over 38 h to afford the desired diol **4a** in 40% yield with excellent *trans*-selectivity (*trans* : *cis* = 99 : 1). It is noteworthy that this high diastereoselectivity is in striking contrast to the *cis*-selectivity observed in the known methods using stoichiometric amounts of SmI_2[11] or $TiCl_3(THF)_3$–Bu^tOH catalyst.[4g] In a similar manner, 10 mol% of the catalyst transformed 1,6-diol **3b** into *trans*-cyclohexanediol **4b** in a higher yield (65%). Moreover, 1,6-dial **3c** having a bulky Bu^t group at the 3-position gave only a single stereoisomer **4c** in 52% yield. The relative

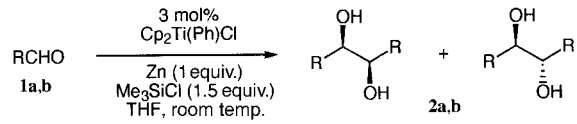

2a R = Ph, 0.12 M, 70 min, 88% (*threo* : *erythro* = 71 : 29)
2b R = CH_2CH_2Ph, 0.2 M, 18 h, 80% (*threo* : *erythro* = 64 : 36)

Scheme 2

Table 1 Intramolecular pinacol coupling of dials **3a–d** using $Cp_2Ti(Ph)Cl$–Zn–Me_3SiCl[a]

Dial	Catalyst/ mol%	*t*/h	Diol	Yield[b] (%)	*trans* : *cis*[c]
 **3a**	6	38	 **4a**	40%	99 : 1
 **3b**	10	14	 **4b**	65%	99 : 1
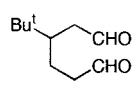 **3c**	10	14	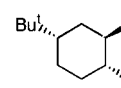 **4c**	52%	single isomer
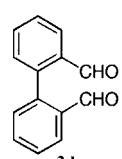 **3d**	6	14	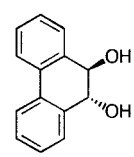 **4d**	70%	91 : 9

[a] Conditions: $Cp_2Ti(Ph)Cl$, Zn (1 equiv.), Me_3SiCl (1.5 equiv), THF (0.05 M), room temp. [b] Isolated yields. [c] Ratios determined by ^1H NMR analysis of isolated products.

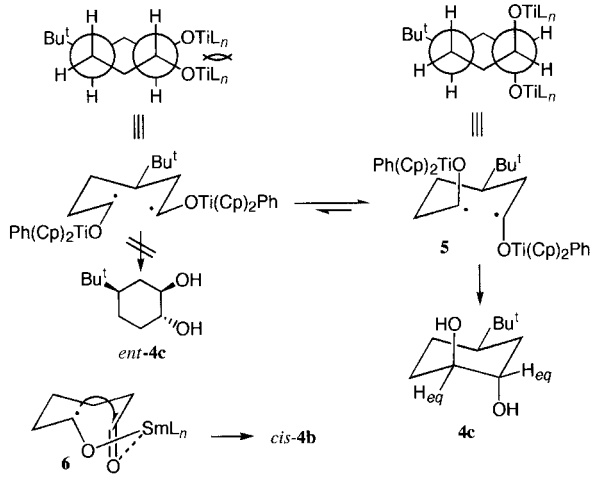

Fig. 1 Mechanism of stereoselection.

configurations of all three stereogenic centers in **4c** were completely controlled. The stereochemistry of **4c** was determined by comparison of its spectral data with those previously reported.[12] In the ^{1}H NMR spectrum, the methyne protons α to the hydroxy groups have no H_{ax}–H_{ax} or H_{ax}–H_{eq} coupling with coupling constants over 10 Hz, indicating that both are constrained to occupy the equatorial positions. Among the four isomers, **4c** is the only one having no axial methyne proton α to the hydroxy groups, as shown in Fig. 1. In addition, the ^{13}C NMR spectrum of **4c** and its melting point are in good agreement with reported data.[12]

These results clearly indicate that the bulky Ti^{IV} fragment surrounded by two cyclopentadienyl and one phenyl ligands cannot coordinate to the other carbonyl terminus, and cyclization must proceed *via* diradical intermediates such as **5**, in which two bulky Cp_2(Ph)TiO moieties occupy axial positions in order to reduce steric repulsion (Fig. 1). This is in contrast to the intramolecular coupling of **3b** promoted by SmI_2 affording *cis*-products *via* chelated intermediates such as **6**.[11]

In addition to the aliphatic dials, a biphenylic dial **3d** was converted into a tricyclic diol **4d**[13] in good yield (70%) with high *trans*-selectivity (*trans* : *cis* = 91 : 9).

In conclusion, we have demonstrated that Cp_2Ti(Ph)Cl is an effective pinacol coupling catalyst for both aromatic and aliphatic aldehydes in the presence of Me_3SiCl and Zn. The catalytic intramolecular pinacol coupling of dials afforded cyclic *trans*-1,2-diols with excellent *trans*-selectivities of *trans* : *cis* = > 90 : 10, indicative of non-chelation intermediates being involved in the present reductive cyclization. These results are in striking contrast to reported *cis*-selective methods.

We gratefully acknowledge financial support (09750947 and 09305059) from the Ministry of Education, Science Sports and Culture, Japan.

Notes and references

1 J. Seyden-Penne, *Chiral Auxiliaries and Ligands in Asymmetric Synthesis*, Wiley, New York, 1995.
2 H.-J. Altenbach, *Chiral Cyclic Acetals in Synthesis*, in *Organic Synthesis Highlights*, ed. J. Mulzer, H.-J. Altenbach, M. Braun, K. Krohn and H.-U. Reissig, Wiley, Weinheim, 1991, p. 19.
3 For recent review of pinacol coupling, see: R. G. Dushin, in *Comprehensive Organometallic Chemistry II*, ed. L. S. Hegedus, Pergamon, Oxford, 1995, vol. 12, p. 1071; G. M. Robertson, in *Comprehensive Organic Synthesis I*, ed. B. M. Trost, Pergamon, New York, 1991, vol. 3, p. 563; A. Fürstner and B. Bogdanovic, *Angew. Chem., Int. Ed. Engl.*, 1996, **35**, 2443.
4 Samarium-catalyzed reactions: (*a*) E. Léonard, E. Dunach and J. Périchon, *J. Chem. Soc., Chem. Commun.*, 1989, 276; (*b*) R. Nomura, T. Matsuno and T. Endo, *J. Am. Chem. Soc.*, 1996, **118**, 11666. Titanium-catalyzed reactions: (*c*) A. Gansäuer, *Chem. Commun.*, 1997, 457; (*d*) A. Gansäuer, *Synlett*, 1997, 363; (*e*) A. Gansäuer and D. Bauer, *J. Org. Chem.*, 1998, **63**, 2070; (*f*) T. Hirao, B. Hatano, M. Asahara, Y. Muguruma and A. Ogawa, *Tetrahedron Lett.*, 1998, **39**, 5247; (*g*) T. A. Lipski, M. A. Hilfiker and S. G. Nelson, *J. Org. Chem.*, 1997, **62**, 4566; (*h*) M. Bandini, P. G. Cozzi, S. Morganti and A. Umani-Ronchi, *Tetrahedron Lett.*, 1999, **40**, 1997. Vanadium-catalyzed reactions: (*i*) T. Hirao, T. Hasegawa, Y. Muguruma and I. Ikeda, *J. Org. Chem.*, 1996, **61**, 366; (*j*) T. Hirao, M. Asahara, Y. Muguruma and A. Ogawa, *J. Org. Chem.*, 1998, **63**, 2812. Chromium-catalyzed reactions: (*k*) A. Svatos and W. Boland, *Synlett*, 1998, 549.
5 Y. Hanada and J. Inanaga, *Tetrahedron Lett.*, 1987, **28**, 5717; R. Schobert, *Angew. Chem., Int. Ed. Engl.*, 1988, **27**, 855; W. A. Nugent and T. V. RajanBabu, *J. Am. Chem. Soc.*, 1988, **110**, 8561; T. V. RajanBabu and W. A. Nugent, *J. Am. Chem. Soc.*, 1989, **111**, 4525; T. V. RajanBabu, W. A. Nugent and M. S. Beattie, *J. Am. Chem. Soc.*, 1990, **112**, 6408; M. C. Barden and J. Schwartz, *J. Am. Chem. Soc.*, 1996, **118**, 5484; R. P. Spencer and J. Schwartz, *J. Org. Chem.*, 1997, **62**, 4204; J. S. Yadav and D. Srinivas, *Chem. Lett.*, 1997, 905; T. K. Chakraborty and S. Dutta, *J. Chem. Soc., Perkin Trans. 1*, 1997, 1257; A. Gansäuer, *Synlett*, 1998, 549.
6 E. J. M. de Boer and J. H. Teuben, *J. Organomet. Chem.*, 1977, **140**, 41; E. J. M. de Boer and J. H. Teuben, *J. Organomet. Chem.*, 1978, **153**, 53.
7 Y. Yamamoto, D. Matsumi and K. Itoh, *Chem. Commun.*, 1998, 875.
8 J. A. Waters and G. A. Mortimer, *J. Organomet. Chem.*, 1970, **22**, 417.
9 T. Chivers and E. D. Ibrahim, *J. Organomet. Chem.*, 1972, **46**, 313.
10 For the reductive coupling of benzaldehyde with Zn, see: J.-H. So, M.-K. Park and P. Boudjouk, *J. Org. Chem.*, 1988, **53**, 5871.
11 J. L. Chiara, W. Cabri and S. Hanessian, *Tetrahedron Lett.*, 1991, **32**, 1125.
12 R. W. Trainor, G. B. Deacon, W. R. Jackson and N. Giunta, *Aust. J. Chem.*, 1992, **45**, 1265.
13 D. A. Lewis and R. N. Armstrong, *Biochemistry*, 1983, **22**, 6297.

Communication 9/02154J

Unusual redox-type addition of nitroalkanes on the C_{60} surface

Masatomi Ohno,* Arihiro Yashiro, Yohei Tsunenishi and Shoji Eguchi

Department of Molecular Design and Engineering, Graduate School of Engineering, Nagoya University, Chikusa, Nagoya 464-8603, Japan. E-mail: ohno@apchem.nagoya-u.ac.jp

Received (in Cambridge, UK) 2nd March 1999, Accepted 30th March 1999

Nitroethanes underwent base-catalyzed addition to C_{60} to give 2-hydroxy-1,2-dihydrofulleryl ketoximes by way of a unique intramolecular redox process, which is not observed in normal alkenes.

Usual base-catalyzed reaction of nitroalkanes with electron-deficient alkenes is known to proceed in a 1,4-addition manner to give γ-nitro-functionalized products [eqn. (1)].[1] While fullerenes possess similar reactivity with nucleophilic reagents because of their low LUMO level,[2] this reaction with C_{60} was found to proceed with a different addition pattern to give β-hydroxy oxime products [eqn. (2)].

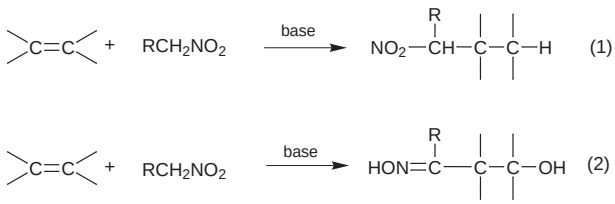

This result is not observed with standard alkenes and is ascribable to the specific nature of the double bonds on the C_{60} surface. So far, remarkable oxidative (cyclo)additions of C_{60} have been recorded in nucleophilic cyclization of 1,2-diamines,[3] photoinduced cyclization of Et_3N,[4] F-promoted cyclopropanation of a silyl enol ether,[5] 1,4-bisaddition of Grignard reagents,[6,7] and 1,2-bisaddition of alkoxy anions.[8] In our studies on heterocyclization of C_{60}, base-catalyzed oxidative [3+2]cycloaddition of β-dicarbonyl compounds has also been shown to give dihydrofuran-fused C_{60} derivatives [eqn. (3)].[9] Likewise,

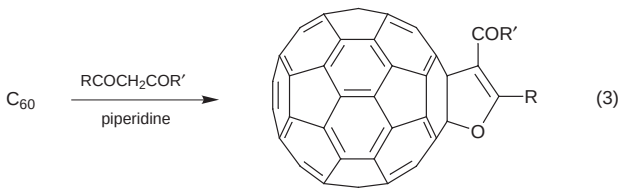

ambiphilic nitroalkanes could undergo an analogous addition but instead lead to the formation of a 1,2-bifunctionalized hydroxy oxime derivative as a result of an intramolecular redox process, which is reported here with a proposed mechanism.

Previously, nitromethane **1a** was demonstrated to react with C_{60} in the presence of Et_3N and TMSCl to give the parent *N*-silyloxyisoxazolidine **3a** as the result of 1,3-dipolar cycloaddition of the *in situ* formed *N*-silyloxynitrone; a following acid-catalyzed elimination reaction gave isoxazoline **4a** (Scheme 1).[10] The same reaction conditions in the absence of the silylating reagent were anticipated to allow the oxidative [3+2]cycloaddition as observed in β-dicarbonyl compounds, but this did not take place. Despite this failure, homologous nitroethane **1b** could be reacted smoothly with C_{60} at room temperature for 2 h by employing excess reagents (20 equiv.), and a brown product was obtained after silica gel chromatography (toluene). Unexpectedly, the FAB mass spectrum included a molecular ion peak at *m/z* 795 (exact sum of molecular weights of C_{60} + $C_2H_5NO_2$), which revealed that the product was certainly a 1 : 1 adduct but not an oxidative cycloadduct (M^+ must be reduced by 2 amu). Nevertheless, the IR (KBr) and UV–VIS (dioxane) spectra showed absorptions at 527 cm^{-1} and 428 nm, respectively, which are characteristics of a C_{60} derivative arising from 1 : 1 addition at a 6,6 junction. The ^1H NMR signals were observed at δ 2.83 (3 H), 4.20 (1 H), and 6.45 (1 H), all as singlet peaks, with the integrations of the last two decreased by addition of D_2O, implying the existence of OH groups but no methylene or methine groups in the molecule. The ^{13}C NMR signals were observed at δ 14.95, 83.58, 99.59, 135.65–149.86 (52 lines),† and 156.53. The first three peaks and next low field aromatic peaks were assignable to sp^3

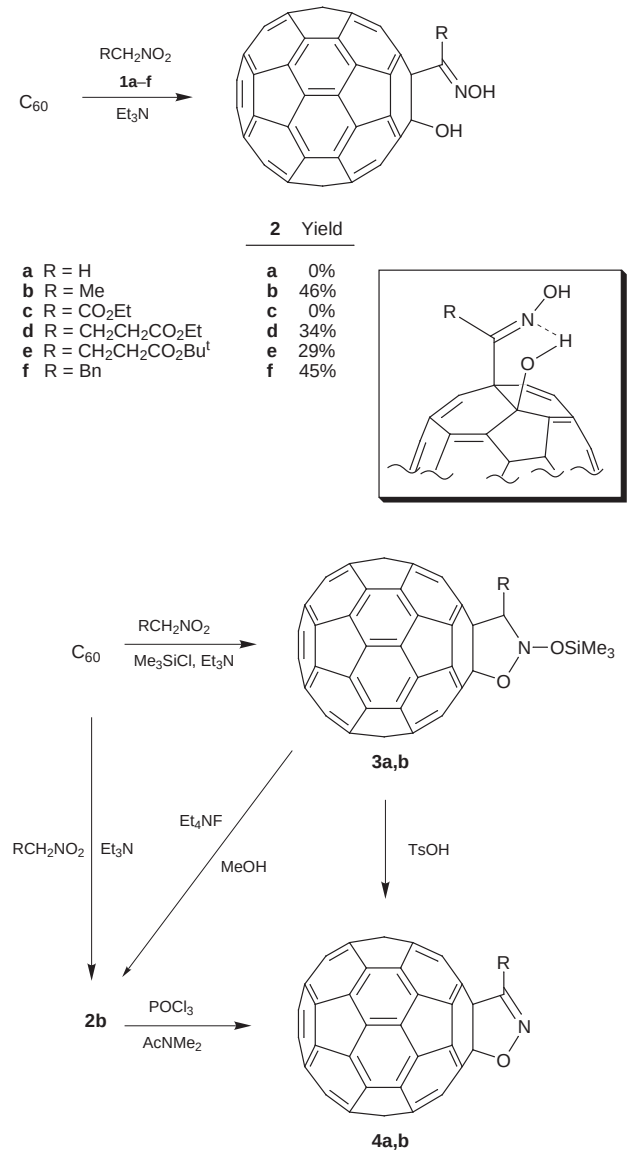

Scheme 1

carbons due to methyl and junction carbons and spherical sp^2 carbons, respectively; the total 52 lines due to C_{60}, seemingly, suggested no molecular symmetry. The last peak might be due to a C=N moiety. These data were difficult to completely assign. Consequently, the suggestion that an intramolecular redox process may split the nitro group to give nitroso (tautomeric oxime) and hydroxy groups, as shown below, prompted us to determine the structure *via* an independent synthesis. Recently, Hassner reported that β-hydroxy ketoximes were obtained by the fluoride-induced ring cleavage of *N*-silyloxyisoxazolidines derived from 1,3-dipolar cycloaddition reaction of *N*-silyloxy-nitrones.[11] This method was applied to the chemistry of C_{60}. Thus, C_{60} was allowed to react with **1b** in the presence of Et_3N and TMSCl,[10] and the prepared **3b** was successively treated with Et_4NF in MeOH at −20 °C for 1 h to give the ring-cleaved product, 2-hydroxy-1,2-dihydrofulleryl methyl ketoxime **2b**. As a result, the HPLC retention time and spectral data of this authentic sample were consistent with those of the addition product obtained from the base-catalyzed reaction with **1b**. This identification was supported by chemical conversion of the product into isoxazoline **4b** by cyclodehydration with $POCl_3$ and $AcNMe_2$. Intuitively, the confirmed β-hydroxy oxime structure might have C_s symmetricity, but this was not supported by the ^{13}C NMR data; however, the spectrally observed lack of symmetry could be explained by considering a boat-like form (as shown in Scheme 1) composed of an intramolecular hydrogen-bond between the oxime and hydroxy groups. In fact PM3 calculations suggested that a coplanar hydrogen-bonded structure was much less stable than the boat-like one. From a synthetic point of view, the above new 1,2-bifunctionalization of C_{60} can be applied to nitroethanes but not to nitromethanes. Whereas the similar reaction with ethyl nitroacetate **1c** was unsuccessful, those with ethyl and *tert*-butyl 4-nitrobutanoates **1d**,**e** and β-nitroethylbenzene **1f** under the same conditions lead to the formation of the corresponding bifunctionalized **4d**–**f** in moderate yields (Scheme 1).

As a clue to understanding the mechanism of the above unusual addition reaction, it is considered likely that a nitro group can essentially serve as an oxygen donor (*i.e.* reduction to a nitroso group), a β-hydrogen to this group being necessary for the reaction to occur. Since the use of active methylene compounds in oxidative [3+2]cycloadditions has precedent from our previous work,[9a] a formal intramolecular redox process is proposed as follows (Scheme 2). First, addition of a nitronate anion at the carbon site to a double bond on C_{60} is followed by 1,5-hydrogen shift and subsequent addition at the oxygen site to give an isoxazoline *N*-oxide intermediate (**i** → **ii** → **iii**; this resembles the foregoing reaction with β-dicarbonyl compounds[9]). Second, two hydrogens migrate to a fused isoxazoline ring *via* tautomerization from a nitrone form to a *N*-hydroxyenamine species (this step requires the β-H); abstraction of an acidic hydrogen on the core by the enamine is followed by a 1,4-hydrogen shift and subsequent hydride attack on an iminium cation (**iii** → **iv** → **v** → **vi**). This sequence is regarded as an intramolecular redox process. Finally, eliminative ring cleavage to a nitroso alcohol intermediate and subsequent tautomerization gives the product β-hydroxy ketoxime (**vi** → **vii** → **viii**).

In conclusion, nitroethanes were shown to undergo redox-type addition to a double bond of C_{60} under base-catalyzed conditions to give 2-hydroxy-1,2-dihydrofulleryl ketoximes. The mode of addition as seen in this reaction is quite unique, compared with normal electron-deficient alkenes which simply act as a Michael acceptor in the common nucleophilic reaction of nitroalkanes. While some previous oxidative additions to C_{60} were reported to occur with C_{60} itself as an oxidant,[4b,8a] in this case, a nitro group played such a part intramolecularly. This pattern is peculiar in fullerene chemistry and provides a new methodology for its bifunctionalization.

This work was partly supported by a Grant-in-Aid for Scientific Research on Priority Area (A) (No. 10146101) from the Ministry of Education, Science, Sports and Culture, Japan.

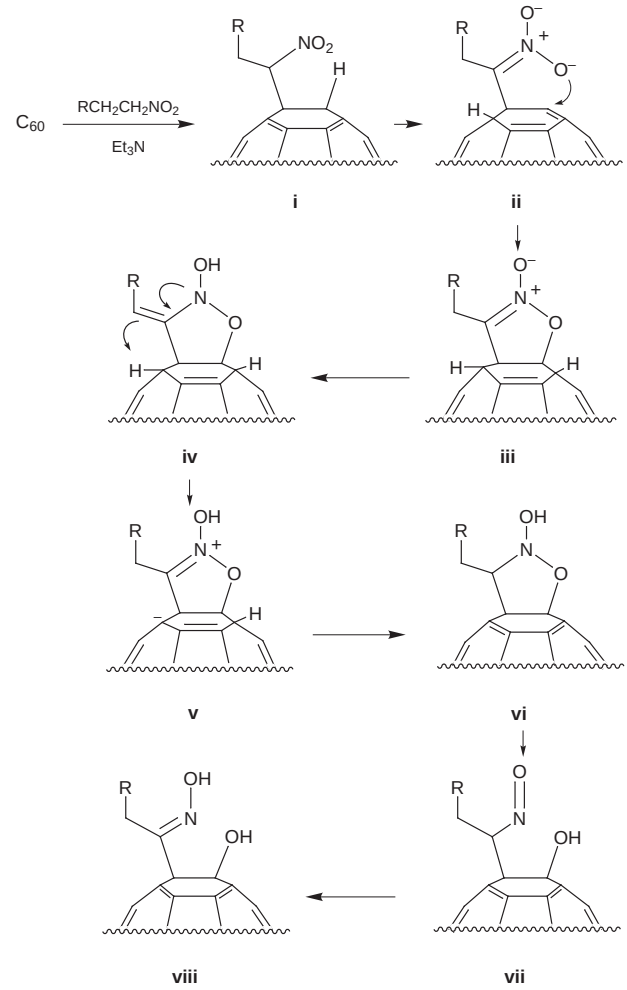

Scheme 2

Notes and references

† The ^{13}C NMR signals due to C_{60} sp^2 carbons (52 lines) were 135.65, 136.55, 137.15, 138.46, 139.77, 141.41, 141.60, 141.76, 142.10, 142.59, 142.79, 142.86, 143.08, 143.30, 143.44, 143.61, 143.82, 143.87, 143.96, 144.32, 144.50, 144.58, 144.63, 144.65, 144.75, 144.79, 144.94, 145.03, 145.11, 145.23, 145.24, 145.54, 145.56, 145.65, 145.98, 146.18, 146.50, 146.59, 146.67, 146.93, 147.07, 147.26, 147.39, 147.44, 147.75, 148.16, 148.42, 149.08, 149.49, 149.57, 149.73 and 149.86.

1 H. H. Baer and L. Urbas, *The Chemistry of Nitro and Nitroso Groups*, part 2, ed. H. Feuer, Wiley, New York, 1970, p. 75.
2 A. Hirsch, *Synthesis*, 1995, 895.
3 K.-D. Kampe, N. Egger and M. Vogel, *Angew. Chem., Int. Ed. Engl.*, 1993, **32**, 1174; K.-D. Kampe and N. Egger, *Liebigs Ann.*, 1995, 115.
4 (*a*) G. E. Lawson, A. Kitaygorodskiy, B. Ma, C. E. Bunker and Y.-P. Sun, *J. Chem. Soc., Chem. Commun.*, 1995, 2225; (*b*) K.-F. Liou and C.-H. Cheng, *Chem. Commun.*, 1996, 1423.
5 L.-H. Shu, G.-W. Wang, S.-H. Wu and H.-M. Wu, *J. Chem. Soc., Chem. Commun.*, 1995, 367.
6 H. Nagashima, H. Terasaki, E. Kimura, K. Nakajima and K. Itoh, *J. Org. Chem.*, 1994, **59**, 1246.
7 M. Sawamura, H. Iikura and E. Nakamura, *J. Am. Chem. Soc.*, 1996, **118**, 12 850; M. Sawamura, H. Iikura, A. Hirai and E. Nakamura, *J. Am. Chem. Soc.*, 1998, **120**, 8285.
8 (*a*) S. Fukuzumi, I. Nakanishi, J. Maruta, T. Yorisue, T. Suenobu, S. Itoh, R. Arakawa and K. M. Kadish, *J. Am. Chem. Soc.*, 1998, **120**, 6673; (*b*) For the case of benzyloxy anion with air, see: G.-W. Wang, L.-H. Shu, S.-H. Wu, H.-M. Wu and X.-F. Lao, *J. Chem. Soc., Chem. Commun.*, 1995, 1071.
9 (*a*) M. Ohno, A. Yashiro and S. Eguchi, *Chem. Commun.*, 1996, 291; (*b*) for the case of photochemical cycloaddition, see: A. W. Jensen, A. Khong, M. Saunders, S. R. Wilson and D. I. Schuster, *J. Am. Chem. Soc.*, 1997, **119**, 7303.
10 M. Ohno, A. Yashiro and S. Eguchi, *Synlett*, 1996, 815.
11 L. Gottlieb and A. Hassner, *J. Org. Chem.*, 1995, **60**, 3759.

Communication 9/01664C

New catalysts for the aerobic selective oxidation of hydrocarbons: Mn(III)- and Co(III)-containing molecular sieves for the epoxidation of alkenes

Robert Raja, Gopinathan Sankar and John Meurig Thomas

Davy Faraday Laboratory, The Royal Institution of Great Britain, 21 Albemarle Street, London, UK W1X 4BS. E-mail: robert@ri.ac.uk

Received (in Liverpool, UK) 9th February 1999, Accepted 16th March 1999

Co(III) or Mn(III) ions that replace some 4 atom% of Al(III) sites in microporous aluminophosphate number 36 (AlPO-36) function as catalytically active centres for the production from benzaldehyde of acylperoxy radicals: these, in turn, in dry air (30 bar) convert cyclohexene, pinene, limonene and styrene to their corresponding epoxides and diols.

Replacing stoichiometric oxidants such as $KMnO_4$, Ag_2O and CrO_3 by less environmentally damaging ones is self-evidently a sensible chemical strategy. Doing so catalytically, with alkyl-hydroperoxides or hydrogen peroxide as the oxidants, is an even better one: but best of all would be to develop[1] catalysts that selectively oxidise hydrocarbons using either dioxygen or air under mild conditions. In this communication we describe two related heterogeneous catalysts that efficiently epoxidise alkenes using molecular oxygen and sacrificial aldehydes, under conditions that mirror those of Mukaiyama *et al*.,[2] who used homogeneous (transition-metal-based) catalysts.

By extending our earlier work on the design of redox molecular sieve catalysts for the aerobic terminal oxidation of linear alkanes,[3] for the selective oxidation of cyclohexane[4] (to cyclohexanone and cyclohexanol) and for the Baeyer–Villiger oxidation of ketones to lactones,[5] we have achieved good conversions and selectivities for the epoxidation of cyclohexene and other alkenes using framework-substituted metal ions (M) in microporous aluminium phosphate, MAlPO-36 (M = Mn or Co), catalysts.

Details of the synthesis (and structure) of the Mn(II)- and Co(II)-containing AlPO-36 molecular sieves have been reported previously.[4,6] Briefly, the Mn(II) (or Co(II)) ion is introduced to the template-containing precursor gel from which small crystals of phase-pure product appear. Upon calcination in O_2 at *ca.* 550 °C, the organic template (tripropylamine) is entirely gasified, leaving the oval-shaped cages (6.5 × 7.5 Å) of the resulting catalyst empty. X-Ray absorption spectroscopy shows[7] that after calcination in O_2, some 50% of the Mn(II) (or Co(II)) originally present (isomorphously substituting for Al(III)) are converted to the Mn(III) (Co(III)) oxidation state, but that all these transition-metal ions remain securely in tetrahedral co-ordination within the microporous AlPO framework.[8] Others[9–12] have also shown that Co(II) ions in framework sites may be raised to the Co(III) state without loss of structural integrity of the AlPO framework.

In a typical experiment, 0.25 g of catalyst, 35 g of the alkene and an alkene–benzaldehyde (mole) ratio of 1 : 3 are used. The reaction mixture is loaded into a stainless steel, high-pressure catalytic reactor (Cambridge Reactor Design), lined with polyether ether ketone (PEEK), and equipped with a mechanical stirrer and liquid sampling value. Dry air is pressurised into the reaction vessel (30 bar), and the reactor heated typically for 8 h at a temperature of 323 K. The results are summarised in Table 1, and Fig. 1 shows a typical kinetic plot. Results obtained with comparable larger-pore (MAlPO-5) and smaller-pore (MAlPO-18) redox molecular sieve catalysts, the shapes of which are 7.3 × 7.3 Å and 3.8 × 3.8 Å respectively, are also tabulated. Note that conversions are consistently higher for both the MnAlPO-36 and CoAlPO-36 catalysts compared with those of their larger-pore (AlPO-5) analogues. Almost certainly, the reasons for the superior performance of the MAlPO-36 catalyst is because a greater fraction (*ca.* 0.5 compared with 0.25) of the Mn (or Co) can be raised to the +3 oxidation state,[7] which (see below) is the root cause of catalytic activity. Significantly MgAlPO-36 is totally inactive: there is no redox ion in the framework of the micropores in this case, and hence there is no

Table 1 Catalytic aerobic partial oxidation of alkenes[a]

Substrate	Catalyst	*t*/h	Conv. (%)	Product selectivity (%) Epoxide	Diol	Others
Cyclohexene	CoAlPO-36	8	54	69	27	4[b]
	CoAlPO-5	8	47	74	15	11[b]
	MnAlPO-36	8	62	77	19	5[b]
	MnAlPO-5	8	44	77	13	10[b]
	MgAlPO-36	8		No reaction		
α-(+)-Pinene	CoAlPO-36	8	54	84	—	16[c]
	CoAlPO-5	8	32	55	—	46[c]
	MnAlPO-36	8	59	91	—	9[c]
	MnAlPO-5	8	42	66	—	34[c]
(*R*)-(+)-Limonene	CoAlPO-36	8	46	78	—	23[d]
	CoAlPO-5	8	28	39	—	61[d]
	MnAlPO-36	8	51	87	—	13[d]
	MnAlPO-5	8	30	51	—	49[d]
Styrene	CoAlPO-36	4	46	34	59	8[e]
	MnAlPO-36	4	55	27	61	12[e]
	MnAlPO-5	4	32	49	60	1[e]
Hex-1-ene[f]	CoAlPO-18	24	37	87	—	13
	MnAlPO-18	24	43	91	—	9

[a] Reaction conditions: *T* = 323 K; 30 bar, dry air; 35 g substrate; substrate–benzaldehyde mole ratio 1 : 3; solid catalyst 0.25 g. [b] Mainly cyclohex-2-en-1-ol and cyclohex-2-en-1-one. [c] Verbenol and verbenone. [d] Carveol, carvone and *trans*-carveyl acetate. [e] 1-Phenylethane-1,2-diol. [f] Hexanal was used instead of benzaldehyde.

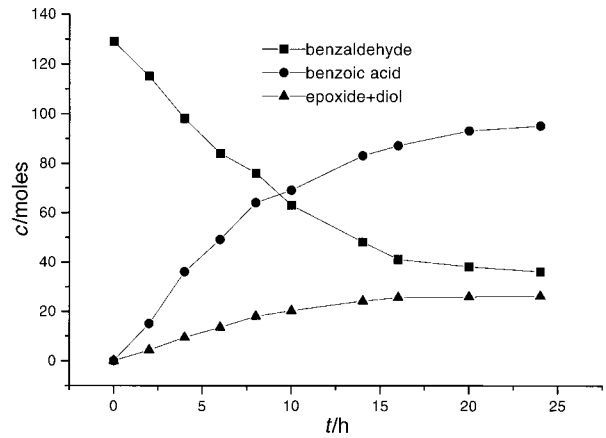

Fig. 1 Typical conversion plot for the selective oxidation of cyclohexene using CoAlPO-36 catalyst in the presence of air and benzaldehyde (conditions as in Table 1).

PhCHO + Mn(III)	⟶	PhCO• + H^+ + Mn(II)	(1)
PhCO• + O_2	⟶	PhCOOO•	(2)
PhCOOO• + PhCHO	⟶	PhCOOOH + PhCO•	(3)
PhCOOOH + PhCHO	⟶	2PhCOOH	(4)
PhCOOO• + C_6H_{10}	⟶	$C_6H_{10}O$ + PhCOO•	(5)
PhCOOOH + C_6H_{10}	⟶	$C_6H_{10}O$ + PhCOOH	(6)
PhCOO• + PhCHO	⟶	PhCOOH + PhCO•	(7)
PhCOOOH + Mn(II)	⟶	PhCOO• + OH^- + Mn(III)	(8)

Scheme 1

means of initiating the free-radical reactions leading to epoxidation.

Benzaldehyde molecules may freely enter the large (*ca.* 650 $m^2\ g^{-1}$) internal surfaces of both MAlPO-36 and MAlPO-5 catalysts, thereby generating[11,13] first PhCO· and then the PhCOOO· radicals which, from the sequence of steps shown in Scheme 1, lead to the formation of benzoic acid and cyclohexene oxide. In this sequence, reaction (5) is known[14] to proceed much faster than reaction (6). This free-radical based epoxidation of cyclohexene (and the other alkenes listed in Table 1) is mechanistically quite distinct from the radical-free epoxidation of alkenes[15–17] using alkyl hydroperoxides and titanosilicate catalysts.

Other aldehydes may also be used as sacrificial oxidants provided they are small enough to gain access to the active sites situated at the inner surface of the molecular sieve catalyst. Benzaldehyde is itself too large to enter Mn (or Co)-AlPO-18, but hexanal is not. Although it diffuses less rapidly into the MAlPO-18 structure than benzaldehyde does in AlPO-36, it nevertheless functions efficiently in epoxidising hex-1-ene.

The experimental conditions chosen for this study—the concentration of catalytically active redox ions at the inner surface of the molecular sieve (arbitrarily set at 4 atom%), the ratio of reactants, the amount of catalyst, temperature, pressure, *etc.*—have not been optimised for maximal conversion and selectivity. There is considerable scope for achieving improvements in catalytic performance. Note also that under the reaction conditions employed here, the framework-substituted transition-metal-ions are not leached out during use. When the solid catalyst is removed by filtration and the reactants returned into the reactor no epoxidation ensues under the conditions given in Table 1.

We thank the EPSRC, UK for financial support (rolling grant to J. M. T.), the Royal Commission for the Exhibition of 1851 for a Research Fellowship to R. R., and Professors J. M. van Hooff and R. A. van Santen for sending us a copy of H. F. W. J. van Breukelen's Eindhoven thesis, 1998.

Notes and references

1 C. Bolm, G. Schlingloff and K. Weickhardt, *Angew. Chem., Int. Ed. Engl.*, 1994, **33**, 1848.
2 T. Yamada, T. Takai, O. Rhode and T. Mukaiyama, *Chem. Lett.*, 1991, 1.
3 R. Raja and J. M. Thomas, *Chem. Commun.*, 1998, 1841.
4 G. Sankar, R. Raja and J. M. Thomas, *Catal. Lett.*,1998, **55**, 15.
5 R. Raja, J. M. Thomas and G. Sankar, *Chem. Commun.*, 1999, 525.
6 P. A. Wright, S. Natarajan, J. M. Thomas, R. G. Bell, P. L. Gai-Boyes, R. H. Jones and J. Chen, *Angew. Chem., Int. Ed. Engl.*, 1992, **31**, 1472.
7 P. A. Barrett, G. Sankar, C. R. A. Catlow and J. M. Thomas, *J. Phys. Chem.*, 1996, **100**, 8977.
8 J. M. Thomas, R. Raja, G. Sankar and R. G. Bell, *Nature*, 1999, **398**, 227.
9 B. Kraushaar-Czarnetzki, W. G. M. Hoogeroorst, R. R. Andrea, C. A. Ameis and W. H. J. Stork, *J. Chem. Soc., Faraday Trans.*, 1991, **87**, 891.
10 L. E. Iton, I. Choi, J. A. Desjardins and V. A. Moroni, *Zeolites*, 1989, **9**, 535.
11 H. F. W. J. van Breukelen, M. E. Gerritsen, V. M. Ummels, J. S. Broens and J. H. C. van Hooff, *Stud. Surf. Sci. Catal.*, 1996, **105**, 1029.
12 M. P. J. Peeters, M. Basio and P. Leijten, *Appl. Catal. A: Gen.*, 1994, **118**, 51.
13 T. C. Chou and C. C. Lee, *Ind. Eng. Chem., Fundam.*, 1985, **24**, 32.
14 S. A. Maslov and E. A. Blyumberg, *Russ. Chem. Rev.*, 1976, **45**, 155.
15 G. Sankar, F. Rey, J. M. Thomas, G. N. Greaves, A. Corma, B. R. Dobson and A. J. Dent, *J. Chem. Soc., Chem. Commun.*, 1994, 2279.
16 R. D. Oldroyd, J. M. Thomas, T. Maschmeyer, P. A. MacFaul, D. W. Snelgrove, K. U. Ingold and D. D. M. Wayner, *Angew. Chem., Int. Ed. Engl.*, 1996, **35**, 2787.
17 R. Murugavel and H. W. Roesky, *Angew. Chem., Int. Ed. Engl.*, 1997, **36**, 477.

Communication 9/01127G

ChemComm

Photolytic induction of the asymmetric catalytic complexation of prochiral cyclohexa-1,3-dienes by the tricarbonyliron fragment[1]

Hans-Joachim Knölker,* Holger Hermann and Daniela Herzberg

Institut für Organische Chemie, Universität Karlsruhe, Richard-Willstätter-Allee, 76131 Karlsruhe, Germany. E-mail: knoe@ochhades.chemie.uni-karlsruhe.de

Received (in Liverpool, UK) 11th March 1999, Accepted 24th March 1999

Photolytic induction of the asymmetric catalytic complexation of prochiral cyclohexa-1,3-dienes by the tricarbonyliron fragment using a camphor-derived azadiene catalyst provides the corresponding tricarbonyliron complexes quantitatively in up to 86% ee.

Asymmetric catalysis provides the most efficient access to enantiopure compounds for organic synthesis starting from achiral precursors because only catalytic amounts of the chiral auxiliary are required.[2] We recently reported a novel method of asymmetric catalysis which transforms prochiral dienes into their planar-chiral tricarbonyl(η⁴-diene)iron complexes. Tricarbonyl(η⁴-diene)iron complexes have found numerous applications to stereoselective organic synthesis.[3] Therefore, a simple and versatile access to the chiral complexes in enantiomerically pure form would open up new routes for enantioselective synthesis. We now report that the asymmetric catalytic complexation of prochiral cyclohexa-1,3-dienes proceeds much more efficiently by photolytic induction.

The reaction of dienes with tricarbonyliron transfer reagents provides a much better access to the corresponding iron complexes than direct complexation with pentacarbonyliron.[4] Enantioselective complexations of prochiral 1,3-dienes were achieved with moderate enantioselectivity using chiral tricarbonyl(η⁴-1-oxadiene)iron complexes as transfer reagents.[5] Recently we introduced (η⁴-1-azadiene)tricarbonyliron complexes as a novel class of tricarbonyliron transfer reagents.[6] Moreover, the 1-azadienes represent highly efficient catalysts for the catalytic complexation of dienes with pentacarbonyliron.[7] Most noteworthy using chiral 1-azadienes an asymmetric catalytic complexation of prochiral cyclohexa-1,3-dienes was achieved.[8] The highest asymmetric inductions were obtained by using chiral catalysts which have a fixed s-*cis* conformation of the 1-azadiene moiety. These 1-azadiene catalysts are easily prepared by aldol condensation of a chiral cyclic ketone with *p*-methoxybenzaldehyde and subsequent imine formation with *p*-anisidine. Thus, (1*R*)-(+)- and (1*S*)-(−)-camphor were transformed to (*R*)-**1** and (*S*)-**1**, (1*R*)-(+)-nopinone to (*R*)-**2**, and (+)-estrone methyl ether to (−)-**3** [$[\alpha]_D^{20}$ −318.1 (*c* 0.53, $CHCl_3$)]. The catalyst (*R*)-**4** was prepared by imine condensation of *o*-anisidine with (1*R*)-(−)-myrtenal.

Catalyst **1** showed the highest enantioselectivity in the asymmetric catalytic complexation of 1-methoxycyclohexa-1,3-diene **5a** which was performed in benzene at reflux with exposure to daylight. An extensive reinvestigation of the asymmetric catalytic complexation of **5a** using catalyst (*R*)-**1** revealed two important aspects (Table 1). First, the result is strongly dependent on the amount of catalyst applied. Higher turnovers and asymmetric inductions are obtained at higher concentrations of the catalyst (*R*)-**1**. Second, the asymmetric catalysis is influenced by light, perhaps due to a photolytically induced loss of a carbon monoxide ligand (compare our proposed mechanism).[7b,8c] In the dark the reaction proceeds much more slowly and using catalytic amounts of (*R*)-**1** also the ee of the product is lower in the absence of light. After reaction for 7 d with exclusion of light in the presence of 4 equiv. of (*R*)-**1** the asymmetric complexation of **5a** provides a result (99% yield, 88% ee of the *S* enantiomer) which is comparable with respect to yield and ee to the corresponding outcome obtained in the presence of daylight after 2 d.

Based on the experimental observations described above, we hoped to exploit the photolytic induction of the asymmetric complexation in order to achieve a quantitative reaction with high asymmetric induction (> 85% ee) by using only catalytic amounts of the chiral 1-azadienes with shorter reaction times. Therefore, we investigated the asymmetric catalytic complexation of **5a** with pentacarbonyliron in benzene at reflux on irradiation with a 10 W halogen lamp using the catalysts (*R*)-**1** to (*R*)-**4** (Scheme 1, Table 2). The ee values were determined accurately *via* separation of the two enantiomers by chiral HPLC on a cyclodextrin column.[9] To avoid the formation of hexacarbonyldiiron clusters,[7b,8c] the excess of pentacarbonyliron was reduced to 1.5 equiv. based on the diene. A blank experiment (complexation without catalyst) demonstrated that photolytic induction in contrast to the solely thermal conditions promotes also the uncatalyzed complexation, which leads to the formation of racemic product (compare also the two blank experiments in Table 1). However, the catalytic complexation proceeds much faster and therefore, this pathway predominates. The camphor-derived catalyst **1** proved to be the best for the photolytically induced asymmetric catalytic complexation and

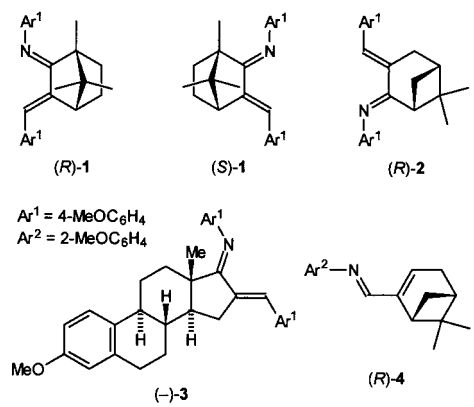

Table 1 Asymmetric catalytic complexation of **5a** with catalyst (*R*)-**1**: variation of the reaction conditions[a]

(*R*)-**1**/equiv.	$Fe(CO)_5$/ equiv.	Conditions	Yield (%)	Ee (%)[b]
0.0	4.0	2 d, daylight	26	—
0.125	4.0	2 d, daylight	62	56 (*S*)
0.25	4.0	2 d, daylight	66	73 (*S*)
0.25	4.0	12 d, daylight	99	73 (*S*)
0.50	4.0	2 d, daylight	87	80 (*S*)
1.0	4.0	2 d, daylight	94	83 (*S*)
2.0	4.0	2 d, daylight	98	86 (*S*)
4.0	4.0	2 d, daylight	96	89 (*S*)
0.0	4.0	9 d, dark	2	—
0.25	4.0	2 d, dark	3	53 (*S*)
0.25	4.0	14 d, dark	14	56 (*S*)
4.0	4.0	7 d, dark	99	88 (*S*)

[a] *Reaction conditions*: **5a**, (*R*)-**1**, $Fe(CO)_5$, C_6H_6, 80 °C. [b] Ee determined by chiral HPLC (absolute configuration) (ref. 9).

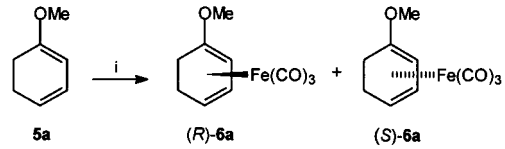

5a (*R*)-6a (*S*)-6a

Scheme 1 *Reagents and conditions*: i, $Fe(CO)_5$ (1.5 equiv.), catalyst (0.25 equiv.), benzene, 80 °C, *hν* (10 W halogen lamp, 12 V).

Table 2 Photolytically induced asymmetric catalytic complexation of **5a** with $Fe(CO)_5$ to give **6a**: variation of the catalyst[a]

Catalyst	*t*/d	Yield (%)	Ee (%)[b]	$[\alpha]_D^{20}(c)$[c]
—	1	20	0	—
(*R*)-**4**	2	98	39 (*R*)	−54.0 (1.02)
(−)-**3**	2	94	57 (*R*)	−83.5 (0.97)
(*R*)-**2**	5	92	59 (*S*)	+87.4 (0.96)
(*S*)-**1**	1	99	85 (*R*)	−127.3 (1.00)
(*R*)-**1**	1	97	86 (*S*)	+130.0 (1.09)

[a] All reactions were performed using 0.25 equiv. of catalyst, 1.5 equiv. of $Fe(CO)_5$ and a 10 W halogen lamp (12 V) in benzene at 80 °C. [b] Ee determined by chiral HPLC (absolute configuration) (ref. 9). [c] Specific rotation in $CHCl_3$ (concentration).

led to a quantitative complexation within only one day. Using the 1-azadiene (*R*)-**1** complex (*S*)-**6a** was obtained in 86% ee (Fig. 1) and (*S*)-**1** provided complex (*R*)-**6a** in 85% ee.† The previous procedure for asymmetric catalytic complexation using the same catalyst afforded complex **6a** quantitatively after a reaction time of 12 days and with 73% ee of either enantiomer.[8c] Also for the other catalysts application of the photolytic induction led to a significant increase of the asymmetric induction compared to the result of the thermally induced catalytic complexation.

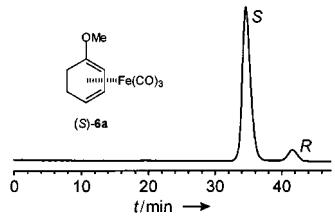

Fig. 1 Chiral HPLC on a permethylated β-cyclodextrin column of complex **6a** with 86% ee of the (*S*)-(+) enantiomer.

We investigated the photolytic induction of the asymmetric catalytic complexation for a series of prochiral cyclohexa-1,3-dienes **5** using the chiral catalysts (*R*)-**1** and (*S*)-**1** (Scheme 2, Table 3). Quantitative yields should be available in all cases simply by extension of the reaction time. However, further optimization was not executed because at this stage of our studies we were primarily interested in the enantioselectivity of the reaction. The asymmetric induction for the catalytic complexation of **5b**,**c** and **e** was in the range of 70–80% ee. Complex **6d**, a potential precursor for discorhabdin alkaloids,[10] was obtained in 50% ee for either enantiomer. The photolytically induced asymmetric catalytic complexation of **5f** with pentacarbonyliron using the catalysts (*R*)-**1** and (*S*)-**1** provided only 42% ee for either enantiomer of the corresponding tricarbonyliron complex. In this case however, the estrone-

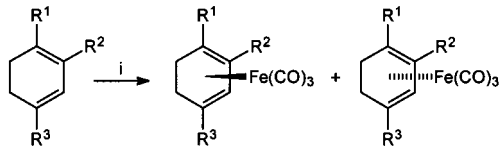

5a–e 5f (*R*)-6a–e (*S*)-6f (*S*)-6a–e (*R*)-6f

Scheme 2 *Reagents and conditions*: i, $Fe(CO)_5$ (1.5 equiv.), (*R*)-**1** or (*S*)-**1** (0.25 equiv.) respectively, C_6H_6, 80 °C, *hν* (10 W halogen lamp, 12 V).

Table 3 Photolytically induced asymmetric catalytic complexation of the prochiral cyclohexa-1,3-dienes **5** with $Fe(CO)_5$ to give **6** using the camphor-derived azadiene catalysts (*R*)-**1** and (*S*)-**1** [a]

					(*R*)-**1**/(*S*)-**1**	
5	R^1	R^2	R^3	*t*/d	Yield (%)	Ee (%)[b]
a	OMe	H	H	1	97/99	86 (*S*)/85 (*R*)
b	OPr^i	H	H	3	78/82	79 (+)/81 (−)
c	OMe	H	Me	2	86/81	72 (*S*)/73 (*R*)
d	OMe	H	CH_2CO_2Me	2	93/89	50 (*S*)/50 (*R*)
e	H	CO_2Me	H	1	90/87	76 (−)/74 (+)
f	CO_2Me	H	H	1	81/77	42 (−)/42 (+)

[a] All reactions were performed using 0.25 equiv. of catalyst, 1.5 equiv. of $Fe(CO)_5$ and a 10 W halogen lamp (12 V) in benzene at 80 °C. [b] Ee determined by chiral HPLC (absolute configuration or, respectively, direction for rotation of the plane of polarized light) (ref. 9).

derived catalyst (−)-**3** was superior and afforded after 2 d complex **6f** in 87% yield and 57% ee of the (+)-enantiomer.

This work was supported by the Deutsche Forschungsgemeinschaft (Kn 240/5-3) and the Fonds der Chemischen Industrie. We are grateful to the Schering AG, Berlin, for a generous gift of estrone methyl ether and to the BASF AG, Ludwigshafen, for a supply of pentacarbonyliron.

Notes and references

† Photolytically induced asymmetric catalytic complexation of **5a**: The 1-azadiene (*R*)-**1** or (*S*)-**1** (188 mg, 0.50 mmol) was added to a solution of 1-methoxycyclohexa-1,3-diene **5a** (220 mg, 2.00 mmol) and pentacarbonyliron (395 μl, 588 mg, 3.00 mmol) in anhydrous, degassed benzene (30 ml) under an argon atmosphere. The solution was heated at reflux for 24 h and irradiated with a 10 W halogen lamp (Osram 64415S, 12 V) positioned about 20 cm from the flask. Evaporation of the solvent and flash chromatography (pentane) of the residue on silica gel afforded (*S*)-**6a** (484 mg, 97%) [$[\alpha]_D^{20}$ +130.0 (*c* 1.09, $CHCl_3$)], or respectively, (*R*)-**6a** (497 mg, 99%) [$[\alpha]_D^{20}$ −127.3 (*c* 1.00, $CHCl_3$)] as yellow oils.

1 Part 52 of Transition Metal Complexes in Organic Synthesis. Part 51: H.-J. Knölker, E. Baum, H. Goesmann and R. Klauss, *Angew. Chem*., 1999, **111**, in the press.
2 *Catalytic Asymmetric Synthesis*, ed. I. Ojima, VCH, Weinheim, 1993.
3 A. J. Pearson, *Iron Compounds in Organic Synthesis*, Academic Press, London, 1994, ch. 4 and 5; R. Grée and J.-P. Lellouche, in *Advances in Metal-Organic Chemistry*, ed. L. S. Liebeskind, JAI Press, Greenwich (CT), 1995, vol. 4, p. 129; H.-J. Knölker, in *Transition Metals for Organic Synthesis*, ed. M. Beller and C. Bolm, Wiley-VCH, Weinheim, 1998, vol. 1, ch. 3.13; H.-J. Knölker, *Chem. Soc. Rev*., 1999, **28**, in the press.
4 J. A. S. Howell, B. F. G. Johnson, P. L. Josty and J. Lewis, *J. Organomet. Chem*., 1972, **39**, 329; M. Brookhart and G. O. Nelson, *J. Organomet. Chem*., 1979, **164**, 193; H. Fleckner, F.-W. Grevels and D. Hess, *J. Am. Chem. Soc*., 1984, **106**, 2027; H.-J. Knölker, in *Encyclopedia of Reagents for Organic Synthesis*, ed. L. A. Paquette, Wiley, Chichester, 1995, vol. 1, p. 333.
5 A. J. Birch, W. D. Raverty and G. R. Stephenson, *Organometallics*, 1984, **3**, 1075.
6 H.-J. Knölker and P. Gonser, *Synlett*, 1992, 517; H.-J. Knölker, G. Baum, N. Foitzik, H. Goesmann, P. Gonser, P. G. Jones and H. Röttele, *Eur. J. Inorg. Chem*., 1998, 993.
7 (*a*) H.-J. Knölker, P. Gonser and P. G. Jones, *Synlett*, 1994, 405; (*b*) H.-J. Knölker, E. Baum, P. Gonser, G. Rohde and H. Röttele, *Organometallics*, 1998, **17**, 3916.
8 (*a*) H.-J. Knölker, G. Baum and P. Gonser, *Tetrahedron Lett*., 1995, **36**, 8191; (*b*) H.-J. Knölker and H. Hermann, *Angew. Chem*., 1996, **108**, 363; *Angew. Chem., Int. Ed. Engl*., 1996, **35**, 341; (*c*) H.-J. Knölker, H. Goesmann, H. Hermann, D. Herzberg and G. Rohde, *Synlett*, 1999, 421; (*d*) H.-J. Knölker and D. Herzberg, *Tetrahedron Lett.*, 1999, **40**, 3547.
9 H.-J. Knölker, P. Gonser and T. Koegler, *Tetrahedron Lett*., 1996, **37**, 2405.
10 N. B. Perry, J. W. Blunt, M. H. G. Munro, T. Higa and R. Sakai, *J. Org. Chem*., 1988, **53**, 4127; H.-J. Knölker and K. Hartmann, *Synlett*, 1991, 428.

Communication 9/01472A

'Zeofen', a user-friendly oxidizing reagent

Majid M. Heravi,* Dariush Ajami, Kuoumars Aghapoor and Mitra Ghassemzadeh

Chemistry and Chemical Engineering Research Center of Iran, PO Box 14335-186, Tehran, Iran.
E-mail: ccerci@neda.net

Received (in Cambridge, UK) 4th January 1999, Accepted 26th March 1999

A variety of alcohols are oxidized to the corresponding carbonyl compounds in excellent yields by zeofen under classical heating and microwave irradiation in solventless system.

Oxidation of alcohols to carbonyl compounds is a fundamental transformation in organic synthesis and, because of its significant role, the development of newer methods is attracting much current interest[1–4] in spite of the availability of numerous methods reported in the literature.[5,6] The use of heavy metals and peracids is very common.[7,8] However, a drawback of such oxidants and their use in multistage organic synthesis in spite of their power is their lack of selectivity. For instance, over-oxidation of aldehydes to carboxylic acids[9] and degradation of unsaturated substrates are often unavoidable side reactions.[10] In addition to their lack of selectivity, oxidants based on chromium[11] and manganese[12] are corrosive, irritants and toxic.[13]

In view of economic, practical and recent environmental demands,[14] we saw significant advantage in using a non-toxic and inexpensive metal salts such as iron(III) nitrate. Some early success in the use of clayfen for oxidation of alcohols[15] supported this idea.

Reagents impregnated on mineral supports have gained popularity in organic synthesis because of their selectivity and ease of manipulation.[16,17] Recently we reported the use of zeolite catalyzed[18] and microwave enhanced chemical reactions[19] on organic solid supports.[20] We report here a facile oxidation of alcohols to carbonyl compounds using zeofen [short for zeolite HZSM-5 supported iron(III) nitrate] in CH_2Cl_2 at room temperature and under microwave irradiation in a solventless system.

To prepare zeofen, $Fe(NO_3)_3.9H_2O$ (0.80 g, 2 mmol) and a weight equivalent of HZSM-5 zeolite[21] were crushed together so as to form an intimate mixture (zeofen). This new reagent can be stored in a dark brown bottle and is stable without suffering from the problem of slow decomposition that clayfen does.[22] In a typical reaction 1–1.2 equiv. of zeofen was added to a stirring solution of an alcohol in dry CH_2Cl_2 at room temperature. After the completion of the reactions (monitored by TLC) the reagent was filtered off and washed with CH_2Cl_2. Evaporation of solvent gave the corresponding carbonyl compounds. It should be pointed out that in the absence of zeolite, the reaction was sluggish and even at reflux temperature a considerable amount of starting material was recovered unchanged. Different types of alcohols were converted to their corresponding carbonyl compounds by this procedure in high yields. The results are presented in Table 1.

Although there has been growing interest in applying microwave dielecteric heating to accelerate organic reactions,[23] oxidation reactions are less often considered as candidates for microwave irradiation due to their unsafe and uncontrollable experimental conditions.[24] It has been shown that polar reactants adsorbed on the surface of solid supports absorb microwaves.[25] In connection with our interest in using microwaves to increase the rates of reactions,[19] we have investigated the above oxidation under microwave irradiation. The oxidation reactions were carried out simply by mixing 1–1.2 equiv. of zeofen with 1 equiv. of an alcohol in a beaker under microwave irradiation (900 W) for 2 min. For example, benzyl alcohol was oxidized to benzaldehyde in almost quantitative yields after 10 s. It is noteworthy to mention that in the absence of zeolite, the reaction was slow and, more seriously, molten ferric nitrate and/or its degradation product(s) adhered to the walls of the reaction vessel, forming an intractable solid mass which made the isolation of carbonyl compounds difficult and led to erratic results. Indeed when iron(III) nitrate was used without zeolite the conversion of benzyl alcohol to benzaldehyde was only 50% under conditions otherwise similar to those described above. Clearly zeolite aided the reproducibility and high activity of iron(III) nitrate. To assess the generality of this oxidation a variety of alcohols were reacted under these conditions, which yielded the corresponding carbonyl compounds in excellent yields. Table 2 summarizes the data for oxidation of alcohols under microwave irradiation in a solventless system.

In conclusion, zeofen can be easily prepared from inexpensive and non-toxic materials and serves as an excellent oxidizing agent for various types of alcohols at room tem-

Table 1 Oxidation of alcohols to carbonyl compounds by zeofen in CH_2Cl_2[a]

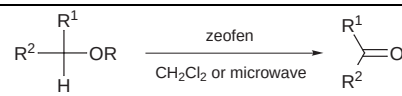

	Alcohol	*t*/min	Product	Yield[b] (%)
1	$PhCH_2OH$	20	PhCHO	99 (90)
2	$4\text{-}MeC_6H_4CH_2OH$	20	$4\text{-}MeC_6H_4CHO$	93 (88)[c]
3	$2\text{-}NO_2\text{-}5\text{-}MeC_6H_3CH_2OH$	20	$2\text{-}NO_2\text{-}5\text{-}MeC_6H_3CHO$	92 (85)[c]
4	(DL)-PhCH(Me)OH	30	PhCO(Me)	89 (80)
5	Ph_2CHOH	40	Ph_2CO	90 (82)
6	$PhCH{=}CHCH_2OH$	40	PhCH=CHCHO	77 (67)
7	$PhCH_2CH(Ph)OH$	40	$PhCH_2COPh$	91 (88)
8	Cyclohexanol	60	cyclohexanone	82 (78)[c]
9	2-Methylcyclohexanol	60	2-methylcyclohexanone	85 (76)[c]
10	(−)-Menthol	60	menthone	85 (78)

[a] Reaction using 1–1.2 equiv. of zeofen in CH_2Cl_2. The physical data of the isolated products are in agreement with those of authentic samples. [b] Yields are based on GLC analysis. Figures in parenthesis are yields of isolated products. [c] Yields based on isolation of the 2,4-DNPH derivative.

Table 2 Oxidation of alcohols using zeofen under microwave irradiation in a solventless system[a]

	Alcohol	*t*/s	Product	Yield[b] (%)
1	$PhCH_2OH$	10	PhCHO	99 (92)
2	4-$MeC_6H_4CH_2OH$	20	4-MeC_6H_4CHO	97 (88)[c]
3	2-NO_2-5-$MeC_6H_3CH_2OH$	20	2-NO_2-5-MeC_6H_3CHO	95 (82)[c]
4	(DL)-PhCH(Me)OH	30	PhCO(Me)	90 (82)
5	Ph_2CHOH	20	Ph_2CO	92 (80)
6	$PhCH{=}CHCH_2OH$	60	PhCH=CHCHO	81 (87)
7	$PhCH_2CH(Ph)OH$	60	$PhCH_2COPh$	91 (88)
8	Cyclohexanol	120	cyclohexanone	85 (81)[c]
9	2-Methylcyclohexanol	120	2-methylcyclohexanone	84 (78)[c]
10	(−)-Menthol	120	menthone	88 (80)

[a] Reaction using 1–1.2 equiv. of zeofen under microwave irradiation in a solventless system. The physical data of the isolated products were in agreement with those of authentic samples. [b] Yields are based on GLC analysis. Figures in parentheses are yields of isolated products. [c] Yields based on isolation of the 2,4-DNPH derivative.

perature in solvent and under solvent-free conditions using a house-hold microwave oven. Solvent-free microwave irradiation has an advantage over conventional heating, offering a practical and environmentally benign protocol, decreasing reaction time and in some cases giving cleaner reactions and easier work up.

Research supported by the National Research Council of Iran (NRCI) as a National Research project under grant number 3708.

Notes and references

1 I. Delaude and P. Lazlo, *J. Org. Chem.*, 1996, **61**, 6360.
2 R. S. Varma, R. K. Saini and R. Dahuja, *Tetrahedron Lett.*, 1997, **38**, 7823.
3 G. Sh. Zhang, Cr. Z. Shi, M. F. Chen and K. Cai, *Synth. Commun.*, 1997, **27**, 3691.
4 R. S. Varma and R. K. Saini, *Tetrahedron Lett.*, 1998, **39**, 1481.
5 *Comprehensive Organic Synthesis* (*Oxidation*), ed. B. M. Trost, Pergamon, New York, 1991, vol. 7.
6 A. J. Fatiadi, in *Organic Synthesis by Oxidation with Metal Compounds*, ed. W. J. Mijs and C. R. H. I. de Jonge, Plenum, New York, 1986, pp. 119–260.
7 J. Einhorn, C. Einhorn, F. Ralajczak and J. L. Piere, *J. Org. Chem.*, 1996, **61**, 7452.
8 J. Mazart, A. N. Ait Aijou and S. Ait-Mohand, *Tetrahedron Lett.*, 1994, **39**, 1989.
9 M. M. Heravi, D. Ajami and K. Tabar-Hydar, *Monatsh. Chem.*, 1998, **129**, 1305.
10 M. M. Heravi, D. Ajami, K. Tabar-Hydar and M. M. Mojtahedi, *J. Chem. Res.* (*S*), 1998, 620.
11 B. J. Page and G. W. Loar, in *Kirk-Othmer Encyclopedia of Chemical Technology*, 4th edn., Wiley, New York, 1998, vol. 6, pp. 263–311.
12 A. H. Reidies, in *Kirk-Othmer Encyclopedia of Chemical Technology*, 3rd edn., Wiley, New York, 1981, vol. 14, pp. 844–895.
13 *Chromium in the Natural and Human Environments*, ed. J. O. Nriagn and E. Nieboer, Wiley, New York, 1988.
14 *Chemistry of Waste Minimization*, ed. J. H. Clark, Chapman and Hall, London, 1995.
15 R. S. Varma and R. Dehija, *Tetrahedron Lett.*, 1997, **38**, 2043.
16 A. McKillop and D. W. Young, *Synthesis*, 1979, 401 and 481.
17 M. Balogh and P. Lazlo, *Organic Chemistry using Clays*, Springer Verlag, Berlin, 1993.
18 M. M. Heravi, M. Tajbakhsh, S. Y. Beheshtiha and H. A. Oskooie, *Indian J. Heterocyclic Chem.*, 1996, **6**, 143; M. M. Heravi, H. A. Oskooie and M. Mafi, *Synth. Commun.*, 1997, **27**, 1725; M. M. Heravi, M. Tajbakhsh and B. Mohajerani, *Synth. Commun.*, 1999, **29**, 135.
19 M. M. Heravi, K. Aghapoor, M. A. Nooshabadi and M. M. Mojtahedi, *Monatsh. Chem.*, 1997, **128**, 1143; K. Aghapoor, M. M. Heravi and M. A. Nooshabadi, 1998, **37B**, 84.
20 M. M. Heravi, R. Kiakoojori and K. Tabar-Hydar, *J. Chem. Res.*, 1998, 656; M. M. Heravi, D. Ajami and K. Tabar-Hydar, *Synth. Commun.*, 1999, **29**, 163; M. M. Heravi, D. Ajami, M. M. Mojtahedi and M. Ghassemzadeh, *Tetrahedron Lett.*, 1999, **40**, 561.
21 HZSM-5 zeolite was prepared by calcination of NH_4ZSM5 zeolite at 500 °C for 8 h. Si : Al = 40 : 1 and pore diameters are 5.1 × 55 Å. We are grateful to Dr A. R. Garakani for a gift of zeolite.
22 A. Cornilis and P. Lazlo, *Synthesis*, 1985, 909.
23 R. A. Abramovitch, *Org. Prep. Proced. Int.*, 1991, **23**, 683; S. Cadadick, *Tetrahedron*, 1995, **51**, 10 403; C. R. Strauss and R. W. Trainer, *Aust. J. Chem.*, 1995, **48**, 1665.
24 R. Gedye, F. Smith, K. Weslaway, A. Humera, L. Baldisera and L. R. Laberge, *Tetrahedron Lett.*, 1986, **26**, 279.
25 R. S. Varma, R. Dahija and R. K. Saini, *Tetrahedron Lett.*, 1997, **38**, 7029 and references from this group cited therein.

Communication 9/00087I

ChemComm

A new germanium based linker for solid phase synthesis of aromatic compounds

Alan C. Spivey,*[a] Christopher M. Diaper[a] and Andrew J. Rudge[b]

[a] *University of Sheffield, Brook Hill, Sheffield, Yorkshire, UK S3 7HF. E-mail: a.c.spivey@sheffield.ac.uk*
[b] *Pfizer Central Research, Sandwich, Kent, UK CT13 9NJ*

Received (in Liverpool, UK) 2nd February 1999, Accepted 22nd March 1999

An efficient three-step synthesis of germyl linker precursor 4 is described which enables a simple two step immobilisation of lithiated aromatics to Argogel™ polymer; cleavage from the polymer support *via ipso*-degermylation with TFA, ICl, Br_2 and NCS provides protio-, iodo-, bromo- and chloroaryls, respectively.

The development of new linkers for the immobilisation of organic compounds on functionalised polymer supports is an area of current interest.[1] The immobilisation of aromatics has commanded particular importance as compounds of this type are pervasive constituents of pharmaceuticals. Protecting-group linker strategies are suitable for this purpose provided that the functional group unmasked on cleavage is required in the target molecules. If not, then a traceless linker (*e.g.* arylsilane based) can be employed.[2] Arylsilane cleavage is generally achieved *via* acidolytic or basic fluoridolytic *ipso*-protodesilylation,[3] or by electrophilic *ipso*-halodesilylation using Br_2 or ICl to release aryl bromides and iodides respectively.[4] The ability to employ a range of electrophiles for cleavage is desirable for library preparation as diversity is introduced on release into solution.

We were interested in devising a new aryl linker susceptible to cleavage by an increased range of electrophiles and to this end the work of Vasella[5] on trimethylgermane protection of alkynes drew our attention. Vasella has noted that relative to the corresponding alkynylsilanes, alkynylgermanes are more readily cleaved by electrophiles (due to the more powerful β-effect of germanium)[6] and additionally display enhanced stability towards bases and nucleophiles. These properties combined with the low toxicity of aryl- and alkylgermane compounds suggested to us that an arylgermane-based linker might provide a useful addition to the current repertoire of traceless linkers.

During the course of our studies Ellman,[7] in response to the low reactivity of an electron deficient arylsilane bound benzodiazepine library towards acidolytic cleavage, reported the first arylgermane linker. Ellman demonstrated that his arylgermane linker was more readily cleaved by electrophiles (TFA, Br_2) than the corresponding arylsilane linker and that his linker was compatible with a range of transformations associated with the introduction and manipulation of a diverse array of functional groups. In the light of this pioneering 'proof of concept' our efforts focussed on the development of a more economic arylgermane linker as Ellman's linker synthesis relied on Me_2GeCl_2 for introduction of the germanium. This compound is expensive and is difficult to prepare from $GeCl_4$ (the cheapest commercial source of germanium).

One interesting facet of germanium chemistry is the coordination and insertion reactions associated with dihalogermylenes.[8] We opted to exploit this chemistry in the preparation of our arylgermane linker. Thus, known dichlorogermylene–1,4-dioxane complex, $GeCl_2.C_4H_8O_2$ **1**, was synthesised in one step from $GeCl_4$ by reduction with tetramethyldisiloxane (TMDS) in refluxing dioxane (Scheme 1). This reaction routinely provides 70–90% isolated yields of this stable crystalline complex on a preparative scale.[9]

Various dichlorogermylene complexes have been reported to undergo thermally induced insertion into C–Cl bonds.[10] We found that the dioxane complex **1** inserts cleanly into the homobenzylic C–Cl bond of 4-(2-chloroethyl)phenol **2**.† Simply heating the two components in a Carius tube with a minimum amount of dioxane furnished trichlorogermane **3** in 91% yield. Exhaustive methylation by refluxing with an excess of MeMgBr then furnished trimethylgermane linker precursor **4**‡ in 82% yield[11] (Scheme 2).

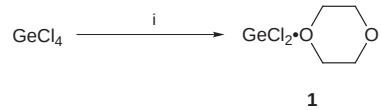

1

Scheme 1 *Reagents and conditions*: i, TMDS, 1,4-dioxane, 3 h, 100 °C.

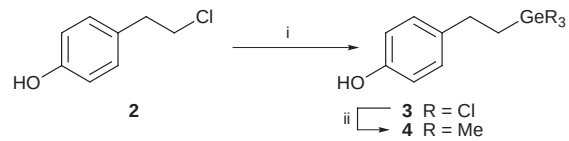

Scheme 2 *Reagents and conditions*: i, $GeCl_2.C_4H_8O_2$ **1**, 1,4-dioxane, 16 h, 140 °C (91%); ii, MeMgBr, Et_2O, toluene, 16 h, 110 °C (82%).

We envisaged that immobilisation of an aromatic compound onto a hydroxy functionalised polymer support could be achieved in a simple two step procedure using trimethylgermane linker precursor **4**. This would involve selective monohalodemethylation and *in situ* arylation with the appropriate aryl organometallic species (→ **I**, Scheme 3) followed by Mitsunobu coupling of the resulting phenolic dimethylarylgermane to the polymer support (→ **II**, Scheme 3).

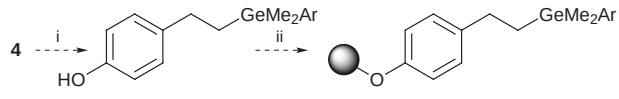

I **II**

Scheme 3 Two step immobilisation strategy: i, mono-halodemethylation and *in situ* arylation with aryl organometallic; ii, Mitsunobu coupling to resin.

To exemplify this protocol we report here the immobilisation of two aromatic systems: 4-(4′-methoxy)biphenyl and 4-acetophenone. The former was chosen as this biphenyl would provide a stringent test system on which to assess electrophilic cleavage by virtue of having an electron rich aryl group susceptible itself to competitive electrophilic aromatic substitution. The latter was chosen as acetophenone provides a versatile functional handle for library construction.

Butyltrimethylgermane (Me_3BuGe) has been shown to undergo selective mono-chlorodemethylation to give chlorobutyldimethylgermane ($Me_2BuGeCl$) upon treatment with $SnCl_4$.[12] We were able to replicate this exquisite chemoselectivity with our linker precursor **4**. Thus treatment with $SnCl_4$ in $MeNO_2$ gave chlorodimethylgermane **5** quantitatively (Scheme 4).

Arylation of **5** was accomplished by refluxing overnight in toluene–THF with the appropriate aryllithium reagent.[13] The 4-litho-4′methoxybiphenyl and dioxolane protected 4-lithioacetophenone, used to prepare arylgermanes **6a** and **6b**

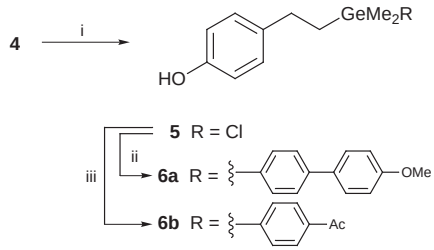

Scheme 4 *Reagents and conditions*: i, $SnCl_4$, $MeNO_2$, 16 h, 50 °C (100%); ii, 4-bromo-4′-methoxybiphenyl, BuLi, hexane, THF, toluene, 16 h, 110 °C [**6a** (82%)]; iii, (a) 2-(4-bromophenyl)-2-methyl-1,3-dioxolane, BuLi, THF, toluene, 16 h, 110 °C, (b) PPTS, acetone, H_2O, 48 h, 67 °C [**6b** (84% from **5**)].

respectively, were made from the corresponding bromides by standard lithium–halogen exchange at −78 °C. Dioxolane deprotection was accomplished using PPTS in acetone–H_2O (Scheme 4).

Tsunoda's modified Mitsunobu redox system of *N*,*N*,*N*′,*N*′-tetramethylazodicarboxamide (TMAD)–PBu_3 was found to effect efficient coupling of arylgermanes **6a** and **6b** to ethoxyethanol to give model systems **7a** and **7b** respectively.[14] Ethoxyethanol was selected as a solution phase 'surrogate' for PEG based Argogel™.§ Use of a solution phase model for development of appropriate Mitsunobu coupling conditions was vindicated when these optimised conditions were employed without modification for the efficient loading of arylgermanes **6a** and **6b** to Argogel™. Thus following successive washing of the polymer with DMF, EtOH, THF, Et_2O and CH_2Cl_2 the aryl functionalised polymers **8a** and **8b** were obtained with loading levels of 0.47 and 0.43 mmol g^{-1}¶ respectively (Scheme 5).

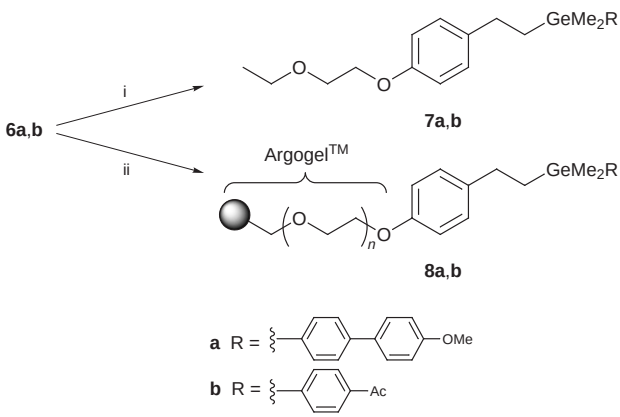

Scheme 5 *Reagents and conditions*: i, $EtOCH_2CH_2OH$, TMAD, PBu_3, PhH, room temp. 16 h [**7a** (98%), **7b** (87%)]; ii, Argogel™, TMAD, PBu_3, PhH, room temp., 16 h (**8a**, **8b**, see text).

Electrophilic cleavage conditions were optimised initially using solution phase biarylgermane model system **7a**. It was pleasing to find that treatment with TFA, ICl and Br_2 at room temperature led to quantitative cleavage of the aryl–germanium bond, yielding the protio-, iodo- and bromobiaryl products **9**, **10** and **11** respectively. Furthermore, chlorobiaryl **12** could also be obtained cleanly using NCS (or Dichloramine-T) in refluxing THF. There were no traces of products resulting from competitive electrophilic substitution in the anisole ring. Minimal optimisation was required to translate this success to cleavage from Argogel™. Thus when employing functionalised resin **8a**, monitoring release of the biaryl products into solution by analytical HPLC of the *crude* washings revealed all these protocols to proceed cleanly and quantitatively (Fig. 1). The identity of the released biaryls **9**, **10**, **11** and **12** were confirmed in each case by co-injection with authentic samples.

To conclude, we have developed an efficient three step synthesis of germyl linker precursor **4** (from inexpensive $GeCl_4$) and demonstrated that this compound can be employed in a simple two step immobilisation of lithiated aromatics to Argogel™ polymer. Clean release from the polymer by electrophilic *ipso*-degermylation affords either protio-, iodo-, bromo- or chloroaryls, depending on the electrophile employed.

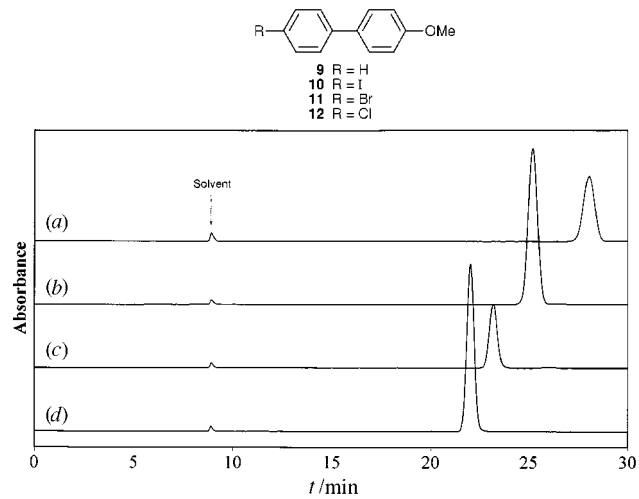

Fig. 1 HPLC traces of biaryls cleaved from Argogel™. [Column: Hichrom spherisorb-S5W (25 × 0.8 cm), eluting with 80 : 20 hexane–$CHCl_3$, 1.0 ml min^{-1}]. *Reagents and conditions*: (*a*) TFA room temp., 16 h (→ **9**); (*b*) ICl, CH_2Cl_2, room temp., 30 min (→ **10**); (*c*) NCS, THF, 67 °C, 14 h (→ **12**); (*d*) Br_2, CH_2Cl_2, room temp., 2 h (→ **11**).

We are currently preparing a library of aryl containing compounds using functionalised polymer **8b** and extending the range of electrophiles able to effect cleavage of the aryl–germanium bond.

Grateful acknowledgement is made to Pfizer for financial support of this work.

Notes and references

† 4-(2-Chloroethyl)phenol is readily prepared in 90% yield from commercially available 4-(2-hydroxyethyl)phenol by heating in concentrated HCl (ref. 15).

‡ Now commercially available from AFChemPharm Ltd., Unit B31-14, Manor Development Centre, 40 Alison Crescent, Sheffield, UK S2 1AS.

§ Commercial Argogel™ (nominal loading level 0.49 mmol g^{-1}) was selected as the polymer support due to its non-benzylic hydroxy functionalisation and favourable characteristics for high resolution MAS ^1H NMR.

¶ As determined by mass balance (of introduction and subsequent cleavage). Polymers **8a** and **8b** were also characterised by solid state MAS ^1H NMR.

1 B. B. Backes and J. A. Ellman, *Curr. Opin. Chem. Biol.*, 1997, **1**, 86.
2 Y. Hu, J. A. Porco, J. W. Labadie, O. W. Gooding and B. M. Trost, *J. Org. Chem.*, 1998, **63**, 4518 and references therein.
3 C. J. Eaborn, *J. Organomet. Chem.*, 1975, **100**, 43.
4 Y. Han, S. D. Walker and R. N. Young, *Tetrahedron Lett.*, 1996, **37**, 2703.
5 A. Vasella and C. Cai, *Helv. Chim. Acta*, 1996, **79**, 255.
6 C. Dallaire and M. A. Brook, *Organometallics*, 1990, **9**, 2873.
7 M. J. Plunkett and J. A. Ellman, *J. Org. Chem.*, 1997, **62**, 2885.
8 J. Satge, M. Massol and P. Riviere, *J. Organomet. Chem.*, 1973, **56**, 1.
9 V. F. Mironov and T. K. Gar, *J. Gen. Chem. USSR* (*Engl. Transl.*), 1975, **45**, 94.
10 S. P. Kolesnikov, B. L. Perl'mutter and O. M. Nefedov, *Dokl. Chem.* (*Engl. Transl.*), 1970, **196**, 85.
11 M. Lesbre, P. Mazerolles and J. Satge, *The Organic Compounds of Germanium*, ed. D. Seyferth, Wiley, 1973.
12 E. J. Bulten and W. Drenth, *J. Organomet. Chem.*, 1973, **61**, 179.
13 C. Eaborn and K. C. Pande, *J. Chem. Soc.*, 1960, 3200.
14 T. Tsunoda, J. Otsuka, Y. Yamamiya and S. Ito, *Chem. Lett.*, 1994, 539.
15 F. Ehrlich and P. Pistchimuka, *Chem. Ber.*, 1912, **45**, 2428.

Communication 9/00915I

The synthesis and crystal structure of the first metal-bound stannatrane complex $Os(Sn[OCH_2CH_2]_3N)(\eta^2\text{-}S_2CNMe_2)(CO)(PPh_3)_2$: structural comparisons with the analogous silatrane complex $Os(Si[OCH_2CH_2]_3N)(\eta^2\text{-}S_2CNMe_2)(CO)(PPh_3)_2$

Clifton E. F. Rickard, Warren R. Roper,* Timothy J. Woodman and L. James Wright*

Department of Chemistry, The University of Auckland, Private Bag 92019, Auckland, New Zealand.
E-mail: w.roper@aukland.ac.nz

Received (in Cambridge, UK) 22nd February 1999, Accepted 29th March 1999

The first metal substituted stannatrane, $Os(Sn[OCH_2CH_2]_3N)(\eta^2\text{-}S_2CNMe_2)(CO)(PPh_3)_2$, has been synthesised by reaction between triethanolamine and the triiodostannyl osmium complex $Os(SnI_3)(\eta^2\text{-}S_2CNMe_2)(CO)(PPh_3)_2$: the transannular Sn–N distance of 2.422(4) Å indicates a bonding interaction which is not seen in the corresponding silatranyl complex $Os(Si[OCH_2CH_2]_3N)(\eta^2\text{-}S_2CNMe_2)(CO)(PPh_3)_2$ which has an Si–N distance of 3.176(6) Å.

Silatranes, cyclic organosilicon ethers of tris(2-oxyalkyl)amine, have been the subject of intense study since their discovery in 1961.[1] Perhaps the most intriguing aspect of these hypervalent silicon compounds is the nature of the silicon–nitrogen interaction and the variation in the transannular Si–N distance as a function of change in the axial silicon substituent.[2–5] Although many structurally characterised examples of silatranes have been reported,[6] only two bear metal atoms as axial substituents, and both of these feature strikingly long Si–N distances.[7,8] In contrast to silatranes, reports of the analogous tin compounds, stannatranes, are sparse, with only two crystallographically characterised examples.[9,10] Our recent work has focused on the synthesis of trihalostannyl osmium complexes because these complexes are amenable to further derivatisation at the tin centre. Here, we report the synthesis and structural characterisation of the first metal-substituted stannatrane, $Os(Sn[OCH_2CH_2]_3N)(\eta^2\text{-}S_2CNMe_2)(CO)(PPh_3)_2$, which is formed by a ligand reaction of the triiodostannyl osmium complex, $Os(SnI_3)(\eta^2\text{-}S_2CNMe_2)(CO)(PPh_3)_2$, with triethanolamine. In order to compare the properties of stannatranyl and silatranyl ligands, particularly with respect to the transannular interaction, the structure of the analagous silatranyl complex, $Os(Si[OCH_2CH_2]_3N)(\eta^2\text{-}S_2CNMe_2)(CO)(PPh_3)_2$, has also been determined.

The coordinatively unsaturated complex, $Os(SnMe_3)Cl(CO)(PPh_3)_2$ **1**,[11] may be converted easily to the six coordinate dithiocarbamate complex, $Os(SnMe_3)(\eta^2\text{-}S_2CNMe_2)(CO)(PPh_3)_2$ **2**, by treatment with NaS_2CNMe_2 at 0 °C (Scheme 1). Reaction of **2** with an excess of tin(IV) iodide in benzene provides $Os(SnMeI_2)(\eta^2\text{-}S_2CNMe_2)(CO)(PPh_3)_2$ **3** in high yield. Although such redistribution reactions are common for R_xSnX_{4-x} systems we believe this represents the first example of such a reaction for a metal stannyl complex. All attempts to remove the last methyl substituent with an excess of SnI_4 failed, even at elevated temperatures. However, treatment of **3** with one equivalent of I_2 in dichloromethane smoothly cleaves the remaining Sn–Me bond to yield yellow $Os(SnI_3)(\eta^2\text{-}S_2CNMe_2)(CO)(PPh_3)_2$ **4**. It should be noted here that direct addition of I_2 to **2** results mainly in the cleavage of the osmium–tin bond.

Treatment of **4** with an excess of triethanolamine in benzene over 30 min provides the colourless, air stable, stannatranyl compound, $Os(Sn[OCH_2CH_2]_3N)(\eta^2\text{-}S_2CNMe_2)(CO)(PPh_3)_2$ **5**, in good yield.† A single crystal X-ray structure determination of this product has been carried out‡ and the molecular structure is depicted in Fig. 1.

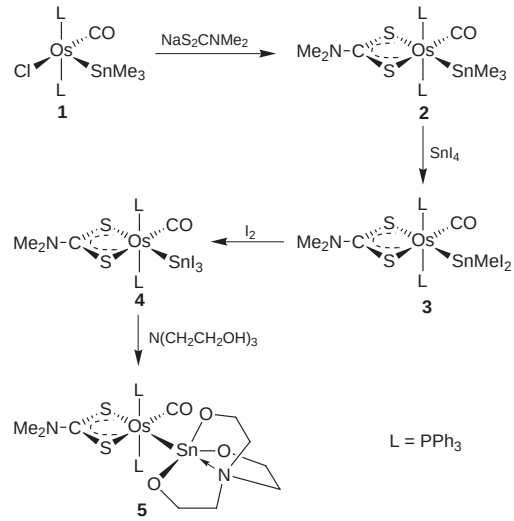

Scheme 1

The geometry about the osmium centre can be best described as distorted octahedral with the main cause of distortion arising from the necessarily constricted bite angle of the dithiocarbamate ligand. The Os–Sn bond distance of 2.6119(3) Å is at the low end of the range of previously reported values the mean of which is 2.721 Å.[12] The most arresting aspect of the structure lies in the stannatranyl moiety where the Sn–N distance of 2.422(4)Å is only slightly longer than those found in

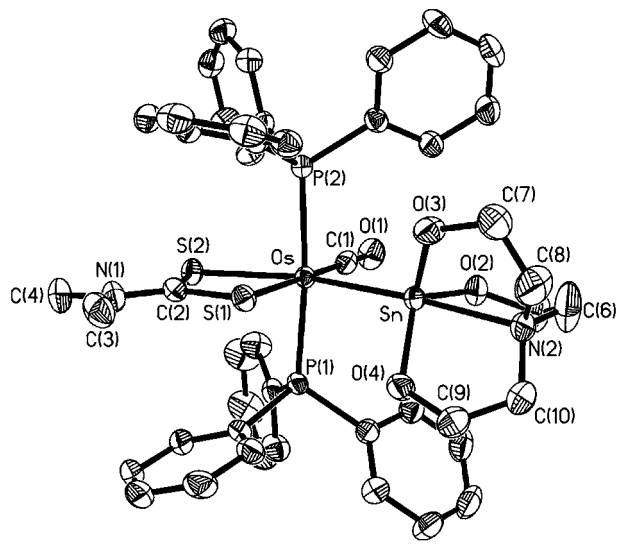

Fig. 1 Crystal structure of **5**. Selected bond lengths (Å) and angles (°): Os–Sn 2.6119(3), Sn–N(2) 2.422(4), C(8)–N(2)–C(6) 110.8(6), C(10)–N(2)–C(6) 114.4(5), C(10)–N(2)–C(8) 114.0(5), Sn–Os–S(2) 160.62(3).

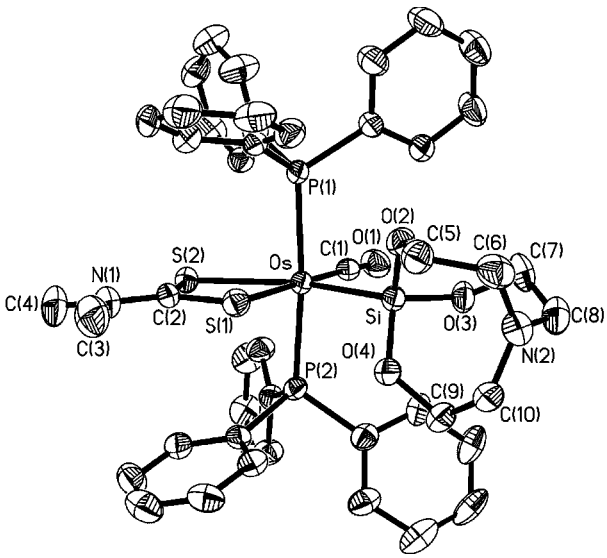

Fig. 2 Crystal structure of **6**. Selected bond lengths (Å) and angles (°): Os–Si 2.3783(17), Si–N(2) 3.176(6), C(8)–N(2)–C(6) 120.3(6), C(10)–N(2)–C(6) 120.0(6), C(10)–N(2)–C(8) 118.6(7), Si–Os–S(2) 154.98(6).

$[MeSn(OCH_2CH_2)_3N]_3$ [2.28(1) Å][9] or $Bu^tSn(OCH_2CH_2)_3N$ (2.324 Å).[10] However, is still considerably shorter than the sum of the van der Waals radii, and must surely constitute a significant interaction. The tin atom displays a very distorted trigonal bipyramidal arrangement, with the osmium and nitrogen atoms axial, and the oxygen atoms equatorial. The tin lies out of a plane taken through O(2), O(3) and O(4) by 0.533(2) Å in the direction of the osmium atom. The geometry at the nitrogen can be seen as tetrahedral, with the nitrogen atom lying out of the plane defined by C(8), C(6) and C(10) by 0.388(5) Å towards osmium.

In order to compare the structural features of this stannatrane with the corresponding silatrane, $Os(Si[OCH_2CH_2]_3N)(\eta^2\text{-}S_2CNMe_2)(CO)(PPh_3)_2$ **6** was prepared in high yield by the addition of NaS_2CNMe_2 to $Os(Si[OCH_2CH_2]_3N)Cl(CO)(PPh_3)_2$.[8] Crystals were grown from dichloromethane–ethanol and a single crystal diffraction study performed.‡ The structure of **6** is shown in Fig. 2, along with selected bond lengths and angles. It is immediately apparent that the silatrane moiety has a very different cage geometry. In this case the Si–N distance is 3.176(6) Å, whereas typical silatrane structures feature values in the range 2.00–2.26 Å. The Si–N distance in **6** is even longer than the distances found in either $Os(Si[OCH_2CH_2]_3N)Cl(CO)(PPh_3)_2$ [3.000(7) Å][8] or *trans*-$Pt(Si\{OCH_2CH_2\}_3N)Cl(CO)(PMe_2Ph)_2$ [2.89(1) Å].[7] The bonds about the nitrogen atom are almost perfectly trigonal planar with the sum of angles at N being 358.9°. The nitrogen atom is displaced 0.088(7) Å from the plane defined by C(6), C(8) and C(10) in the direction away from the metal atom. The silicon atom has approximately tetrahedral geometry. The geometry about the osmium atom does not differ markedly from that found in compound **5**, except that the Os–S(2) distance is significantly longer for **6** [2.5431(15) Å] compared to the corresponding distance in compound **5** [2.4805(10) Å]. This disparity is presumably a reflection of a greater *trans* influence exerted by the silicon atom over that of the tin atom.

The structural comparison of these two analogous metal substituted atrane systems reveals marked differences. Whereas the stannatrane retains the Sn–N interaction to a large extent, in the silatrane the Si–N interaction is almost totally absent. This is most likely a reflection on the greater ability of tin to form hypervalent compounds when compared to silicon.

T. J. W. is grateful to the Royal Society for the award of a Post Doctoral Fellowship.

Notes and references

† *Synthesis and selected data for* $Os(Sn[OCH_2CH_2]_3N)(\eta^2\text{-}S_2CNMe_2)(CO)(PPh_3)_2$ **5**: triethanolamine (1.10 g, 1.09 mmol) was added dropwise to a chilled (0 °C) and stirred solution of $Os(SnI_3)(\eta^2\text{-}S_2CNMe_2)(CO)(PPh_3)_2$ (0.195 g, 0.143 mmol) in deoxygenated dichloromethane (40 cm³). The solution was stirred for 1 h, during which time the yellow colour faded completely. The organic layer was washed with water (3 × 25 cm³) and filtered. Addition of ethanol (20 cm³) and reduction of solvent volume *in vacuo* to 5 cm³ produced a white precipitate which was collected by filtration. Recrystallisation from dichloromethane–ethanol provided **5** in 76% yield. ν_{max}(KBr)/cm^{-1}: 1896 (CO), 1535, 1155 (dithiocarbamate); δ_H($CDCl_3$, 400.133 MHz, 300 K) 1.89 (s, 3H, NCH_3), 2.23 (t, 6H, *J* 5.34 Hz, NCH_2), 2.31 (s, 3H, NCH_3), 3.28 (t, *J* 5.34 Hz, 6H, OCH_2), 7.25–7.95 (m, 30H, PhH); δ_C($CDCl_3$, 100.623 MHz, 300 K) 35.80 (S_2CNMe_2), 36.42 (S_2CNMe_2), 53.30 [$Sn(OCH_2CH_2)_3N$, ^3J(SnC) 34.2 Hz), 57.39 [$Sn(OCH_2CH_2)_3N$, ^2J(SnC) 42.4 Hz], 126.76 (*o*-PPh_3), 128.67 (*p*-PPh_3), 129.78 (*ipso*-PPh_3), 135.27 (*m*-PPh_3), 185.61 [t, *C*O, ^2J(PC) 22.0 Hz], 210.59 (S_2CNMe_2); $\delta_{^{119}Sn}$[$CDCl_3$–$CHCl_3$ (1 : 3) 149.144 MHz, 300 K] −513.4 [t, ^2J(SnP) 193.86 Hz]; Calc. for $C_{46}H_{48}N_2O_4P_2S_2OsSn\cdot 2CH_2Cl_2$: C, 47.72; H, 4.22; N, 2.39. Found: C, 47.54; H, 4.29; N, 2.35%.

‡ *Crystal data*: $Os(Sn[OCH_2CH_2]_3N)(\eta^2\text{-}S_2CNMe_2)(CO)(PPh_3)_2\cdot 2CH_2Cl_2$ **5**: Crystals were grown from dichloromethane–ethanol. $C_{48}H_{52}Cl_4N_2O_4P_2S_2OsSn$, *M* = 1295.65, monoclinic, space group $P2_1/c$, *a* = 12.45670(10), *b* = 19.2826(2), *c* = 21.7933(2) Å, *β* = 100.76(1)°, *U* = 5142.61(8) Å³, *F*(000) = 2560, D_c = 1.673 g cm^{-3}, *Z* = 4, *μ*(Mo-K*α*, *λ* = 0.71073 Å) = 3.349 mm^{-1}. Intensity data were collected to a *θ* limit of 27.51° on a Siemens 'SMART' diffractometer[13] at 203(2) K and corrected for absorption.[14] The structure was solved from Patterson and heavy-atom electron density maps[15] and refined by full-matrix least squares analysis on F^2 employing SHELXL97.[16] All non-hydrogen atoms were allowed to assume anisotropic motion. Hydrogen atoms were placed in calculated positions and refined using a riding model. Refinement converged to 0.0354 (R_w = 0.0982) for 10018 reflections for which $I > 2\sigma(I)$.

$Os(Si[OCH_2CH_2]_3N)(\eta^2\text{-}S_2CNMe_2)(CO)(PPh_3)_2$ **6**: Crystals were grown from dichloromethane–ethanol. $C_{46}H_{48}N_2O_4P_2S_2OsSi$, *M* = 1037.21, orthorhombic, space group $Pca2_1/c$, *a* = 19.939(2), *b* = 9.94490(10), *c* = 22.2254(2) Å, *U* = 4401.56(7) Å³, *F*(000) = 2088, D_c = 1.565 g cm^{-3}, *Z* = 4, *μ*(Mo-K*α*, *λ* = 0.71073 Å) = 3.137 mm^{-1}. Intensity data were collected to a *θ* limit of 27.49° on a Siemens 'SMART' diffractometer[12] at 203(2) K and corrected for absorption.[13] Structure solution as above. Refinement converged to 0.0346 (R_w = 0.0762) for 8353 reflections for which $I > 2\sigma(I)$.

CCDC 182/1207. See http://rsc.org/suppdata/cc/1999/837/ for crystallographic files in .cif format.

1 C. L. Frye, G. E. Vogel and J. A. Hall, *J. Am. Chem. Soc*., 1961, **83**, 996.
2 See, for example: J. G. Verkade, *Acc. Chem. Res*., 1993, **26**, 483; M. G. Voronkov, V. M. Dyakov and S. V. Kirpichenko, *J. Organomet. Chem*., 1982, **233**, 1; S. N. Tandura, M. G. Voronkov and N. V. Alekseev, *Top. Curr. Chem*., 1986, **131**, 99; C. Chuit, R. J. Corriu, C. Reye and J. C. Young, *Chem. Rev*., 1993, **93**, 1371.
3 A. Haaland, *Angew. Chem., Int. Ed. Engl*., 1989, **28**, 992.
4 M. S. Gordon, M. T. Carrol, J. H. Jensen, L. P. Davis, L. W. Burggraf and R. M. Guidry, *Organometallics*, 1991, **10**, 2657.
5 M. W. Schmidt, T. L. Windus and M. S. Gordon, *J. Am. Chem. Soc*., 1995, **117**, 7480.
6 A search of the Cambridge Structural Database produced 70 examples of silatranes.
7 C. Eaborn, K. J. Odell, A. Pidcock and G. R. Scollary, *J. Chem. Soc., Chem. Commun*., 1976, 317.
8 M. T. Attar-Bashi, C. E. F. Rickard, W. R. Roper, L. J. Wright and S. D. Woodgate, *Organometallics*, 1998, **17**, 504.
9 R. G. Swisher, R. O. Day and R. R. Holmes, *Inorg. Chem*., 1983, **22**, 3692.
10 M. Dräger, quoted in K. Jurkschat, A. Tzschach, J. Meunier-Piret and M. Van Meerssche, *J. Organomet. Chem*., 1985, **290**, 285.
11 P. R. Craig, K. R. Flower, W. R. Roper and L. J. Wright, *Inorg. Chim. Acta*, 1995, **240**, 285.
12 Cambridge Crystallographic Database, mean of 53 observations on 22 individual compounds is 2.721 Å with sample standard deviation of 0.072 Å.
13 SMART and SAINT, Siemens Analytical Instruments Inc., Madison, WI, USA, 1994.
14 R. H. Blessing, *Acta Crystallogr., Sect. A*, 1995, **51**, 33.
15 G. M. Sheldrick, SHELXS-97, Program for the Solution of Crystal Structures, Universität Göttingen, Germany, 1990; SHELXTL, Siemens Analytical Instruments Inc., Madison, WI, USA, 1994.
16 G. M. Sheldrick, SHELXS-97, Program for the Solution of Crystal Structures, Universität Göttingen, Germany, 1997.

Communication 9/01408J

α-Diazo ketone self-assembled monolayer modified electrode: a proposed photoreactive template for electrode derivatisation

Glorija J. Jocys and Mark S. Workentin*

Department of Chemistry, The University of Western Ontario, London, Ontario Canada N6A 5B7. E-mail: mworkent@julian.uwo.ca

Received (in Corvallis, OR, USA) 14th January 1999, Accepted 22nd March 1999

A gold electrode modified with an α-diazo ketone has been prepared and its photo-Wolff chemistry investigated in the presence of MeOH as a ketene trap; results suggest that these modified electrodes are a potential photoreactive template for surface modifications.

Modification of electrode surfaces with monolayers of organic substrates *via* self-assembly continues to be an area of active investigation. In particular, there are a great number of studies whose goals are to prepare electrode surfaces modified with the appropriate organic functionality at the interface to provide the site for molecular recognition or modulation of electronic factors for a sensing action.[1,2] Despite the power of photochemistry to provide careful control of surface modifications of organic functionality through photo-patterning techniques, this approach remains relatively unexplored considering the enormous amount of work in the area of self-assembly of organic substrates on metals. Examples of the types of photoreactions of substrates on gold surfaces that have been reported include photoextrusion of nitrogen from aryl azide,[3] *E–Z* photoisomerisation of stilbenes[4] and azo compounds[5] and other photochromic materials,[5] and photodimerization reactions.[6]

Our approach is to employ the photochemistry of α-diazocarbonyl compounds to serve as a photoreactive template for further surface modifications. Compounds containing an α-diazo ketone functionality are known to produce a ketene intermediate, *via* the photo-Wolff rearrangement, upon photoexcitation and loss of nitrogen [eqn. (1)]. The resulting ketenes

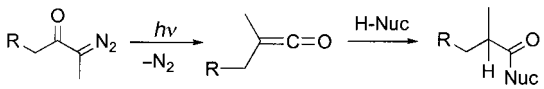

(1)

are known to react with a wide range of nucleophiles to form a variety of functional groups. Simple examples include water, alcohol and amine nucleophiles to form carboxylic acids, esters and amides, respectively. Owing to their wide-ranging reactivity, α-diazocarbonyl compounds[7] and ketenes[8] have been extensively used in solution phase synthetic strategies. Of particular interest to us is extending this chemistry to provide a template for ways to derivatize selectively the monolayer surface with a variety of nucleophile substrates. Here we report the first example of an α-diazo ketone functionality incorporated into the interface of a self-assembled monolayer on a gold electrode. As proof of concept that this modified surface has potential as a template for photo-Wolff chemistry, we have photolysed this novel surface in the presence of MeOH as the nucleophile to form an ester derivatized surface.

The α-diazo ketone monolayer precursor, 2-diazo-13-mercaptotridecan-3-one **1**, was synthesized in four steps

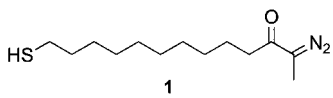

1

from 11-bromoundecanoic acid. First, the acid was converted into its acid chloride by refluxing in $SOCl_2$. This was followed by diazotisation of the acid chloride using $MeCHN_2$ to form 13-bromo-2-diazotridecan-3-one. The latter was thioesterified with AcSK to form $AcS(CH_2)_{10}C(O)C(N_2)Me$. Finally, the thioester was hydrolysed to the thiol with methanolic K_2CO_3 and then purified by repeated column chromatography to yield analytically pure **1**, in 10% overall yield. The structure of **1** was confirmed by ^1H and ^{13}C NMR, infrared and mass spectroscopy.[9] For latter comparison the transmission IR of **1** taken as a thin film on a NaCl plate is shown in Fig. 1(*c*).

Monolayers of **1** on gold (Au-**1**) were prepared by immersion of clean Au[10] in a 50 mM deareated EtOH solution of **1** for 1–96 h. The homogeneity of the monolayer was examined qualitatively using cyclic voltammetry, by monitoring the reversible $Fe^{2+/3+}$ redox chemistry of $Fe(CN)_6^{3-}$ in aqueous solution above the Au-**1** derivatized electrodes. On average soaking times of 16 h resulted in a overall current decrease of greater than 10^3 [*i.e.* no detectable $Fe(CN)_6^{3-}/Fe(CN)_6^{4-}$ redox activity] compared to the bare gold electrode (no further current reduction was observed on samples soaked for up to 4 days). This overall current decrease and the observed cyclic voltammograms of the blocked gold electrodes are similar to those published for other organic thiol self-assembled monolayer systems on Au using the same redox probe.[6,10] A grazing angle infrared spectrum of an Au-**1** substrate prepared in a similar manner is shown in Fig. 1(*a*). Note that the spectral features compare well to the transmission IR spectrum of the same compound measured as a thin film on NaCl [Fig. 1(*c*)]. Diagnostic absorptions are listed in Table 1; also listed for comparison are the absorptions for a thin film of **1**. In particular we note that the characteristic methylene symmetric and asymmetric stretching frequencies and intensities are similar to other densely packed, well-ordered Au-alkyl monolayers of similar length.[11] Also diagnostic are the C=N=N asymmetric and C=O stretching absorptions at 2086 and 1698/1646 cm^{-1}, respectively.[12] The C=O absorption appears to be split into two in Au-**1**. This may be due to (i) a solid state correlation effect,[13]

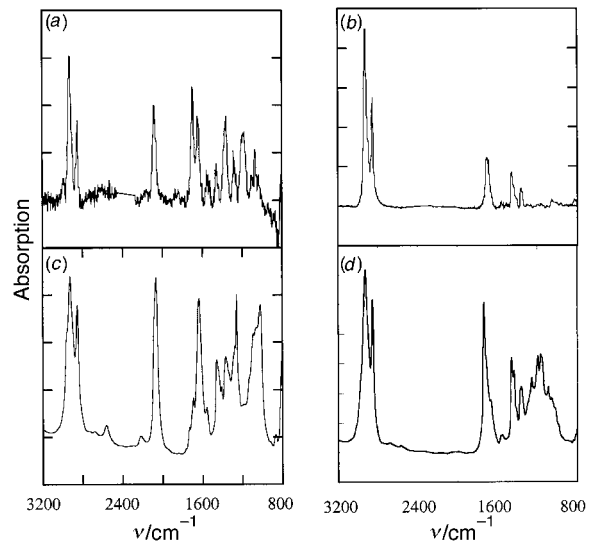

Fig. 1 Grazing angle fourier transform infrared spectra of (*a*) Au-**1** and (*b*) Au-**2** on gold and absorption FTIR of (*c*) **1** and (*d*) **2** as neat thin film samples on NaCl plates. Note: in the spectrum of Au-**1** the absorptions due to CO_2 have been deleted for clarity.

Table 1 Diagnostic infrared assignments for Au-**1** and **1** prior to and after irradiation in MeOH (Au-**2** and **2**)

Assignment, mode[a]	ν/cm^{-1} Au-**1**	**1**	Assignment, mode	ν/cm^{-1} Au-**2**	**2**
CH_2, asymmetric (d−)	**2926**	**2926**	**CH_2, asymmetric (d−)**	**2924**	**2926**
CH_2, symmetric (d+)	**2854**	**2854**	**CH_2, symmetric (d+)**	**2856**	**2854**
S–H, stretch (weak)		2565			2567
C=N=N, asymmetric, o.o.p.	**2086**	**2068**			
C=O stretch, conjugated	**1646 (1698)**[c]	**1639**	**C=O stretch (ester)**	**1710**	**1739**
CH bend (CH_2, scissor)[b]	1457	1459	CH bend (CH_2, scissor)	1458	1463
			O–CH_3 deformation[b]		1435
CH bend (CH_2, i.p.)	1362	1371	CH bend (CH_2, i.p.)	1363	1363
	1288	1261	C(CO)–O asymmetric[b]		1262
C–O carbonyl and/or CH_2 twist[b]	1179		C–O carbonyl and/or CH_2 twist[b]		1198
			C(CO)–O symmetric[b]		1168

[a] Assignments are based on similar systems and from ref. 12. [b] Tentative assignment, since multiple modes are possible in this region. [c] See text.

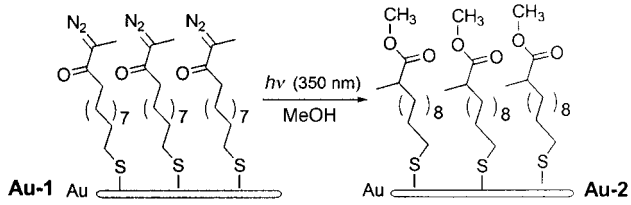

Scheme 1

suggesting that even the groups at the interface are well ordered, (ii) different rotational isomers of the O=C–C(N2) (*i.e.* s-*cis* and s-*trans*) that become more prevalent in the densely packed monolayer compared to **1**, or (iii) the rotational restrictions may lead to some decrease in the conjugation due to steric interactions in the densely packed monolayer.

Au-**1** samples above were irradiated in a nitrogen saturated MeOH solution at 350 nm using a medium pressure Hg-lamp with appropriate filters. A grazing angle IR spectrum of the Au-substrate after complete photolysis is shown in Fig. 1(*b*) and characteristic absorptions are listed in Table 1. Note the complete absence of the C=N=N asymmetric stretch; the appearance of the IR spectrum measured at intermediate times shows gradual loss of the characteristic C=N=N absorption concomitant with a change in the spectral region of the carbonyl absorption. The new C=O absorption is shifted to slightly higher energy consistent with that for a CH_2–C(O)–OMe ester.[13] The intensity of the C=O absorption of the ester is somewhat reduced compared to the thin film; we assign this tentatively to an orientation effect, where the C=O mode is aligned roughly parallel to the metal surface. The relative intensities of the absorptions due to the methylene groups of the long chain tether in the irradiated sample compared to those of Au-**1** before irradiation do not vary, indicating that under the photolysis conditions the monolayer remains intact and relatively ordered. After irradiation the same extent of electrochemical blocking of the $Fe(CN)_6^{3-}/Fe(CN)_6^{4-}$ redox probe also remained.

Fig. 1(*d*) shows an infrared spectrum of the corresponding thiol ester, methyl 12-mercapto-2-methyldodecanoate **2** synthesized from solution phase photochemical trapping of the ketene derived from photolysis of **1** in MeOH. Its spectrum compares favorably with the spectrum of photolysed Au-**1** [Fig. 1(*b*)]. In the solution phase photochemistry of **1** in MeOH using 350 nm irradiation, over 98% of the product isolated after complete photolysis was **2**, formed from MeOH trapping of the ketene intermediate. Based on this, we propose the photochemical modification of Au-**1** to Au-**2** as shown in Scheme 1. Under the conditions outlined no evidence was found for 'intra'-monolayer reactivity between a ketene and a neighbouring C=O or between two ketene moieties.[14]

These results suggest that Au-**1** is a potential photoreactive template for derivatisation of the self-assembled monolayer. Because of the absorption characteristics of the C(=N_2)C=O moiety, the photoinitiated Wolff rearrangement and ketene chemistry can be activated with comparatively long wavelengths of light in the presence of a large number of organic trapping agents that absorb at much higher energy and are transparent in the region where we irradiate. We believe that this particular feature makes the use of the photo-Wolff a powerful technology for synthetic modifications. The generality of this photochemistry for surface modifications, and photopatterning, and the limitations of this important technology are currently being investigated by extending the studies to other ketene trapping nucleophilic reagents.

We thank the Natural Sciences and Engineering Research Council of Canada (NSERC) and The University of Western Ontario (ADF) for financial support and Dr Danial Wayner at the National Research Council of Canada for use of the GAIR facilities. G. J. thanks NSERC for a PGS scholarship.

Notes and references

1 For a general introduction to self-assembled monolayers see: A. Ulman, *Chem. Rev.*, 1996, **96**, 1533.
2 See for example: K. Motecharei and D. C. Myles, *J. Am. Chem. Soc.*, 1998, **120**, 7328 and references cited therein; R. M. Crooks and A. J. Ricco, *Acc. Chem Res.*, 1998, **31**, 219.
3 L. F. Rozsnyai and M. S. Wrighton, *J. Am. Chem. Soc.*, 1994, **116**, 5993; E. W. Wollman, D. Kang, C. D. Frisbie, I. M. Lorkovic and M. S. Wrighton, *J. Am. Chem. Soc.*, 1994, **116**, 4395.
4 M. O. Wolf and M. A. Fox, *J. Am. Chem. Soc.*, 1995, **117**, 1845.
5 See for example: I. Willner, A. Doron and E. Katz, *J. Phys. Org. Chem.*, 1998, **11**, 546 and references cited therein.
6 M. O. Wolf and M. A. Fox, *Langmuir*, 1996, **12**, 955; T. Kim, K. C. Chan and R. M. Crooks, *J. Am. Chem. Soc.*, 1997, **119**, 189; M. A. Fox and M. D. Wooten, *Langmuir*, 1997, **13**, 7099; W. Li, V. Lynch, H. Thompson and M. A. Fox, *J. Am. Chem. Soc.*, 1997, **119**, 7211.
7 T. Ye and M. A. McKervey, *Chem. Rev.*, 1994, **94**, 1091.
8 T. Tidwell, *Ketenes*, Wiley, New York, 1995.
9 *Selected data* for **1**: δ_H($CDCl_3$, 300 MHz) 2.49 (2H, q), 2.43 (2H, t), 1.92 (3H, s), 1.52–1.64 (4H, m), 1.20–1.36 (12H, m); δ_C($CDCl_3$, 75 MHz) 195.0, 62.0, 37.8, 34.0, 29.4, 29.3, 29.2, 29.0, 28.3, 24.9, 24.6, 8.1.
10 H. O. Finklea, D. A. Snider, J. Fedyk, E. Sabatani, Y. Gafni and I. Rubinstein, *Langmuir*, 1993, **9**, 3660; C. E. D. Chidsey and D. N. Loiacono, *Langmuir*, 1990, **6**, 682.
11 M. D. Porter, T. B. Bright, D. L. Allara and C. E. D. Chidsey *J. Am. Chem. Soc.*, 1987, **109**, 3559.
12 D. Lin-Vien, N. B. Colthrup, W. G. Flately and J. G. Grasselli, *The Handbook of Infrared and Raman Characteristic Frequencies of Organic Molecules*, Academic Press, Boston, 1991.
13 J. R. Ferraro and K. Nakamoto, *Introductory Raman Spectroscopy*, Academic Press,, Boston, 1994. We rule out Fermi resonance as a possible contributor since no absorptions are observed at ν/2.
14 Such reactivity would produce a β-lactone or unsaturated β-lactone, respectively, with characteristic absorptions at 1830 cm^{-1} (ref. 13).

Communication 9/00497A

The designed 'self-assembly' of a three-dimensional molecule containing six quadruply-bonded Mo_2^{4+} units

F. Albert Cotton,*[a] Lee M. Daniels,[a] Chun Lin[a] and Carlos A. Murillo*[ab]

[a] *Laboratory for Molecular Structure and Bonding, Department of Chemistry, PO Box 30012, TexasA&M University, College Station, TX 77842-3012. E-mail: cotton@tamu.edu*

[b] *Departamento de Química, Universidad de Costa Rica, Ciudad Universitaria, Costa Rica. E-mail: murillo@tamu.edu*

Received (in Bloomington, IN, USA) 10th March 1999, Accepted 15th March 1999

Reaction of 1,3,5-tricarboxylatobenzene (trimesic acid) with $[Mo_2(DAniF)_2(MeCN)_4][BF_4]_2$ (DAniF = *N*,*N*′-di-*p*-anisylformamidinate) leads to the quantitative formation of a large tetrahedral molecule containing four triply-bridging $C_6H_3(CO_2)_3$ (trimesic acid trianion) groups and six $Mo_2(DAniF)_2$ units; the structure has been determined by X-ray crystallography.

Since the early 1990s there has been a lot of research activity directed toward the synthesis of nanosize polynuclear coordination compounds having two or more metal atoms assembled by suitable ligands into dinuclear (linear), trinuclear (triangular), and tetranuclear (square) molecules. Until very recently all of the reported work was done with building blocks consisting of single metal atoms associated with a few ligands (*e.g.* $[Pd(en)]^{2+}$, $[Pt(Ph_2PCH_2CH_2CH_2PPh_2)]^{2+}$, *etc.*) and these were linked by linear bidentate ligands such as 4,4′-dipyridine.[1]

Recently, in keeping with Chisholm's assertion[2] ('Anything one can do, two can do, too—and it's more interesting'), we have been developing this kind of chemistry with dimetal units, M_2^{n+}, where M = Mo, Rh, W, Ir, and others.[3] The metal-containing building blocks that we use are entities such as $[Mo_2(DAniF)_3]^+$ and $[Rh_2(DAniF)_2]^{2+}$, in which the remaining coordination sites are occupied by the easily displaced ligand, acetonitrile. In this way we have created molecules of the types shown in Scheme 1, where the dinuclear metal units are symbolized by the nicked circles and the linkers are dicarboxylate dianions, symbolized by the heavy double arrows. These linkers can be enormously varied; a few examples are shown in Scheme 2. In this way we have achieved results topologically equivalent to many of those obtained by using single metal centers. All these results, however, have been in the realm of one- or two-dimensional arrays. What about three-dimensional assemblages?

In the realm of single-metal compounds, although imaginative projections of what might be doable in three dimensions have not been lacking,[1a,b] relatively few actual syntheses have been reported,[4–9] and only a few three-dimensional assemblages have been confirmed by X-ray crystallography. Two[4] contain a tetrahedral array of four iron atoms, two others a set of six copper or silver atoms.[5] Fujita *et al.* have characterized an assembly of six metal atoms (Pd) connected by four trifunctional linkers[6] and another Pd compound has also been characterized crystallographically.

The molecule reported here was obtained in the so-called 'self-assembly' manner, but by design.† The key to this synthesis was, as in other cases,[6–9] the use of a trifunctional linker that imparts threefold symmetry to the assemblage.

The molecular structure is shown in Fig. 1.‡ The centroids of the four six-membered rings define a tetrahedron and the centroids of the six Mo_2^{4+} units define an octahedron. The overall idealized symmetry is T_d, but crystallographically there is only a single twofold axis that bisects the bonds between the atoms Mo(4), Mo(4A) and Mo(3), Mo(3A). The ^1H NMR spectrum is consistent with this high symmetry; it shows only one resonance for all of the 12 aromatic protons on the $C_6H_3(CO_2)_3^{3-}$ linkers and the signals for the twelve *N*,*N*′-di-*p*-anisylformamidinate ligands show them to be equivalent. Refinement of the structure presented some challenge, due to disorder in many of the peripheral anisyl groups and some disorder of the dimetal units spanning the two-fold axis. Disorder was also present at several of the 20 different sites containing interstitial acetonitrile and dichloromethane. The most prominent instance of CH_2Cl_2 is a disordered 'ball' of the solvent located directly in the center of the metal-complex cage. Careful modeling and judicious use of restraints allowed successful refinement of the whole model.

Cyclic and differential pulse voltammetries show three distinct reversible oxidation steps at $E_{1/2}$ of 268, 330 and 370 mV *vs.* the Ag/AgCl couple.§ Based on DPV, the ratio of the number of electrons involved in these steps is 1:1:1, respectively. Using $Mo_2[(m\text{-}CF_3C_6H_4N)_2CH]_4$ as a standard, these have been assigned as one-electron oxidation steps.

In closing, we make two observations. In the preparation of several of the previously reported three-dimensional assemblages, the use of a template or guest was said to be essential[8] or at least preferred. In the present case this is not so. We are not unmindful, however that the cavity in our molecule is well suited to being occupied by a variety of medium size entities, *inter alia*, N_2 and the noble gases.

We also note that while this type of chemistry has often been characterized[7] as using 'metal atoms to control self-assembly of

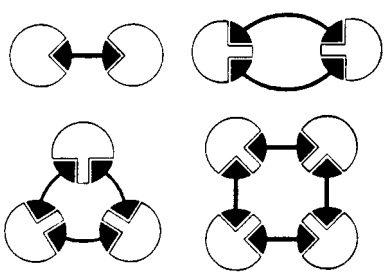

Scheme 1

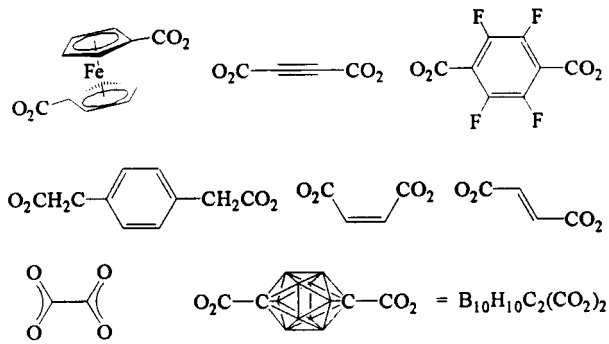

Scheme 2

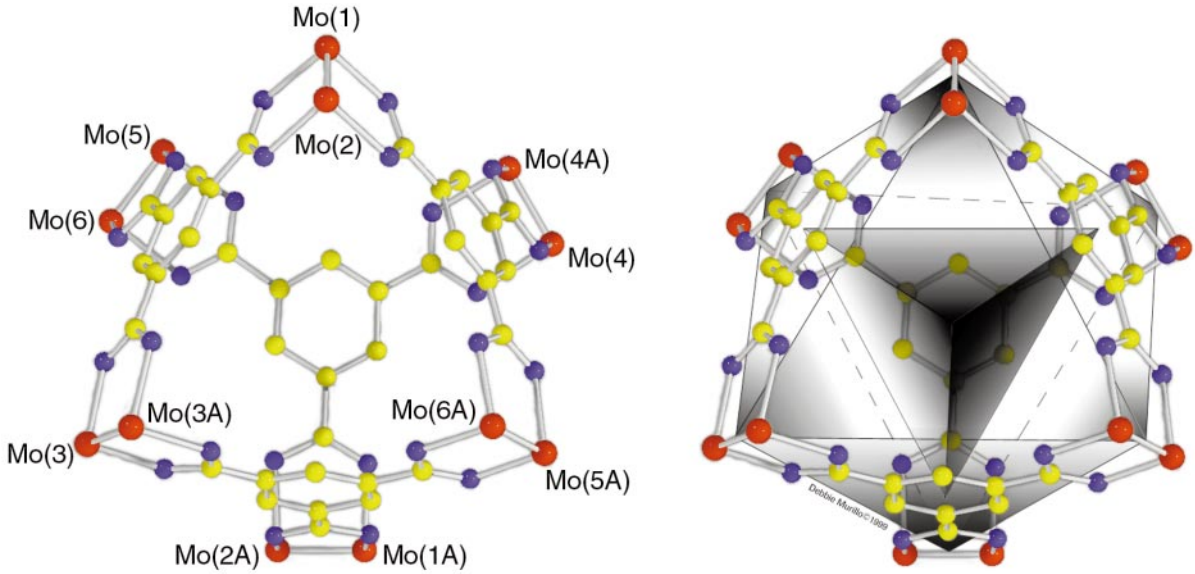

Fig. 1 The core of the molecular structure of $[Mo_2(DAniF)_2]_6[\mu_3\text{-}C_6H_3(CO_2)_3]_4$. The two DAniF anions attached to each quadruply bonded Mo_2^{4+} units and the interstitial solvent molecules have been omitted for clarity. The left view shows the atom labelling scheme. Selected bond distances (Å) are Mo(1)–Mo(2) 2.099(2), Mo(3)–Mo(3A) 2.098(2), Mo(4)–Mo(4A) 2.104(5), Mo(5)–Mo(6) 2.098[4]; Mo–N (av) 2.10[1]; Mo–O (av) 2.20[2]. The right drawing emphasizes the pseudo-octahedral distribution of the Mo_2^{4+} units. A cut of the octahedron shows the tetrahedral cavity; the apices are located at the center of the rings of the trimesate anions.

multicomponent supramolecular structures' this seems to us a one-sided view of the matter. The synthesis reported here, as well as several by Fujita and others, seem better characterized as using a suitably chosen linker to control the 'self-assembly'.

We thank the National Science Foundation for financial support and Debbie Murillo for the artwork in Fig. 1.

Notes and references

Note added in proof: The use of trimesic acid to form a similar structure was very recently reported by others: S. S.-Y. Chui, S. M.-F. Lo, J. P. H. Charmant, A. G. Orpen and I. D. Williams, *Science*, 1999, **283**, 1148.

† To a stirred solution of $[Mo_2(DAniF)_2(MeCN)_4][BF_4]_2$ (312 mg, 0.30 mmol) in 30 mL of MeCN was added $[NBu_4]_3[1,3,5\text{-}C_6H_3(CO_2)_3]$ (187 mg, 0.20 mmol) in 20 mL of MeCN. An immediate reaction took place with the formation of a bright red precipitate, which was collected, washed several times with MeCN, and dried. The crude product was extracted with CH_2Cl_2 (3 × 5 mL). Acetonitrile was then carefully layered on top. Bright red crystals were collected after about two weeks. The yield was essentially quantitative. ^{1}H NMR δ (ppm, in CD_2Cl_2) 9.39 (s, 12H, aromatic of trimesate), 8.52 (s, 12H, –NC*H*N–), 6.62 (dd, 96H, aromatic of formamidinate), 3.67 (s, 72H, –OCH_3).

‡ *Crystal data* for $[Mo_2(DAniF)_2]_6[C_6H_3(CO_2)_3]_4\cdot 22.1MeCN\cdot 2.3CH_2Cl_2$: $C_{262.5}H_{262.9}Cl_{4.6}Mo_{12}N_{46.1}O_{48}$, M = 6145.84, monoclinic, space group $C2/c$, a = 29.825(3), b = 27.377(2), c = 38.248(3), β = 112.71(1)°, V = 28809(4) Å^3, Z = 4, μ(Mo-Kα) = 0.622 mm^{-1}. Data were collected at 173(2) K. The structure, refined on F^2, converged for 13285 unique reflections and 1190 parameters to give $R1(F)$ = 0.098 and $wR2(F^2)$ = 0.217 with a goodness-of-fit of 1.073. CCDC 182/1205. See http://www.rsc.org/suppdata/cc/1999/841/ for crystallographic files in .cif format.

§ For detailed experimental conditions, see ref 3.

1 The already extensive literature may be accessed *via* the following review articles: (*a*) P. J. Stang and B. Olenyuk, *Acc. Chem. Res*., 1997, **30**, 502; (*b*) B. Olenyuk, A. Fechtenkötter and P. J. Stang, *J.Chem. Soc., Dalton Trans*., 1998, 1707; (*c*) M. Fujita, *Chem. Soc. Rev*., 1998, 417.
2 M. H. Chisholm, *ACS Symp. Ser*., 1981, **155**, 17.
3 (*a*) F. A. Cotton, C. Lin and C. A. Murillo, *J. Chem. Soc.*, *Dalton Trans*., 1998, 3151; (*b*) F. A. Cotton, L. M. Daniels, C. Lin and C. A. Murillo, *J. Am. Chem. Soc*., 1999, **121**, in press.
4 R. W. Saalfrank, R. Burak, A. Breit, D. Stalke, R. Herbst-Immer, J. Daub, M. Brosh, E. Bill, M.Müthe and A. X. Trautwein, *Angew. Chem., Int. Ed. Engl*., 1994, **33**, 1621.
5 P. Baxter, J.-M. Lehn and A. DeCian, *Angew. Chem., Int. Ed. Engl*., 1993, **32**, 69.
6 M. Fujita, D. Oguro, M. Miyazawa, H. Oka, K. Yamaquchi and K. Ogura, *Nature* (*London*), 1995, **378**, 469.
7 C. M. Hartshorn and P. J. Steel, *Chem. Commun*., 1997, 541.
8 M. Fujita, S. Nagao and K. Ogura, *J. Am. Chem. Soc*., 1995, **117**, 1649.
9 P. J. Stang, B. Olenyuk, D. C. Muddiman and R. D. Smith, *Organometallics*, 1997, **16**, 3094.

Communication 9/01645G

Side chain selective binding of *N*-acetyl-α-amino acid carboxylates by a 2-(guanidiniocarbonyl)pyrrole receptor in aqueous solvents

Carsten Schmuck

Institute of Organic Chemistry, University of Cologne, Greinstrasse 4, 50939 Cologne, Germany. E-mail: carsten.schmuck@uni-koeln.de

Received (in Liverpool, UK) 9th February 1999, Accepted 23rd March 1999

2-(Guanidiniocarbonyl)pyrrole 1 binds *N*-acetyl-α-amino acid carboxylates in 40% H_2O–DMSO with binding constants ranging from K = 360 to 1700 mol^{-1} depending on the structure of the amino acid side chain.

The development of artificial receptors for the selective molecular recognition of a given substrate is still a challenging task, especially in polar solvents.[1] A large number of host systems for hydrophobic solvents (mostly $CHCl_3$) have been described.[2] However, for the design of biosensors or the targeting of cellular molecules, like peptide hormones, neurotransmitters or carbohydrates, $CHCl_3$ is not the solvent of choice. There are only very few examples of artificial receptors that function in more 'natural' solvents like DMSO, MeOH or even water.[3] As the polarity of the surrounding solvent increases, the strength of hydrogen bonds and electrostatic interactions, mainly used for molecular recognition, decreases rapidly, due to the competitive solvation of donor and acceptor sites by the solvent.

Herein we describe a new class of receptor molecules for the binding of carboxylates in aqueous media. Our idea was to improve the binding affinity of guanidinium cations, well known for the complexation of oxo anions in organic solvents such as $CHCl_3$ or MeCN,[4] by adding additional binding sites. To serve this purpose, we chose substituted 2-(guanidiniocarbonyl)-1*H*-pyrroles. The pyrrole NH as well as suitable donor sites in the side chain should be able to hydrogen bond to the bound carboxylate in addition to ion pairing with the guanidinium unit. For the selective binding of *N*-acetyl-α-amino acid or peptide carboxylates[3,5] these primary interactions to the backbone can

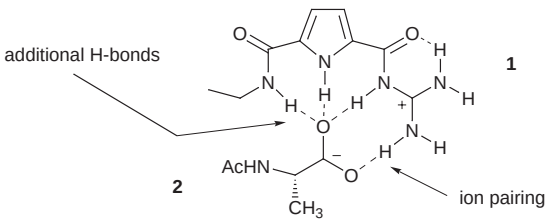

provide the necessary binding energy even in polar solvents. Additonal interactions of the amino acid side chain with the receptor could then be used to achieve selectivity of the recognition process.[1b,6] By variation of this general theme (*e.g.* by combinatorial methods), a new class of receptor molecules should be accessible whose binding properties and selectivity can be tuned deliberately. We wish to demonstrate the usefulness of this general design by reporting the binding properties of a first example: the [5-(*N*-ethylcarbamoyl)-1*H*-pyrrol-2-ylcarbonyl]guanidinium cation **1**. The synthesis of **1** is shown in Scheme 1.

As anticipated, addition of **1** to a solution of *N*-acetyl-L-alanine carboxylate **2** in DMSO caused significant complexation induced shifts of the various protons of **2** in the ^{1}H NMR spectrum. Actually, at millimolar concentrations, the binding is so strong that a NMR titration in [$^2H_6$]DMSO just showed a linear increase of the shift changes until a molar ratio of 1 : 1 was

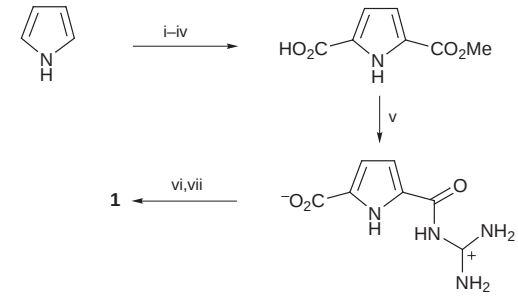

Scheme 1 *Reagents and conditions*: i, Cl_3CCOCl, Et_2O, reflux, 30 min, 85%; ii, NaOMe (0.1 equiv.), MeOH, room temp. 30 min, 63%; iii, $POCl_3$, DMF, CH_2Cl_2, 0 °C → reflux, 63%; iv, $KMnO_4$, acetone–H_2O (1 : 1), 40 °C, 30 min, 75%; v, guanidinium chloride (5 equiv.), NaOMe (5 equiv.), MeOH, reflux, 12 h, 72%; vi, $(COCl)_2$ (1.1 equiv.), DMF (cat.), CH_2Cl_2, reflux 2 h; vii, $EtNH_3Cl$, Et_3N, 68% over both steps.

reached, clearly proving the 1 : 1 binding stoichiometry.[7] Therefore NMR binding studies with various *N*-acetyl-α-amino acid carboxylates were performed in 40% water in DMSO (at higher concentrations of water the solubility of the receptor was too limited). The binding constants were calculated from the observed shift changes of the amide NH of the carboxylates (or of the α-CH in the case of acetate) using nonlinear least-squares fitting with a 1 : 1 association model (Fig. 1).[8]

As shown in Table 1, receptor **1** strongly binds carboxylates with binding constants up to $K \approx 2800$ mol^{-1}. These association constants are much larger than with the parent *N*-acetyl guanidinium cation, which, for example, binds **2** with K = 50 mol^{-1} (compared to K = 770 mol^{-1} for the binding of **2** by **1**). Obviously, as hoped for, the binding affinity of guanidinium cations for carboxylates can be significantly improved by additional hydrogen bonding donors in the receptor. Furthermore, the recognition process is selective for the amino acid side chain: phenylalanine is bound much stronger than alanine or lysine.

According to molecular modelling calculations† the general binding scheme for all carboxylates is the same: the guanidin-

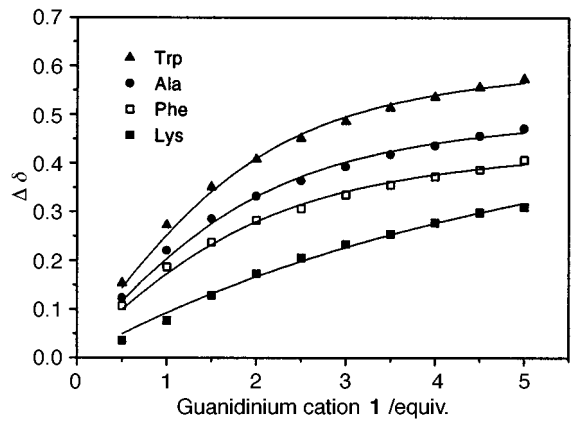

Fig. 1 NMR titration curves of **1** with various carboxylates in 40% water–[$^2H_6$]DMSO.

Table 1 Binding constants of **1** with various carboxylates[a]

Carboxylate	Solvent	K^b/mol^{-1}	$-\Delta G$/kJ mol^{-1}
Ac-L-Ala	DMSO	$>10^6$	
Ac-L-Ala	H_2O–DMSO	770	16.5
Ac-L-Phe	H_2O–DMSO	1700	18.4
Ac-L-Trp	H_2O–DMSO	810	16.6
Ac-L-Lys	H_2O–DMSO	360	14.6
Acetate	H_2O–DMSO	2790	19.7

[a] Measured by NMR titration, each one with 10 measurements at 25 °C; [carboxylate] = 1 mM in [$^2H_6$]DMSO or 40% H_2O–[$^2H_6$]DMSO. [b] Error limit in K < ± 5%.

ium cation forms an ion pair with the carboxylate which is simultaneously hydrogen bonded by both the pyrrole and the amide NH.[9] Acetate shows the highest binding constant with **1** because there are no unfavorable steric interactions with the receptor. The carboxylate group and the receptor binding sites are completely coplanar allowing maximum interaction. In the case of the amino acid carboxylates, the steric bulk of the *N*-acetyl group forces the carboxylate out of the plane of the receptor, thereby decreasing the binding affinity. The differences in complex stability among the various amino acids result from secondary interactions of the side chains with the receptor. The methyl group of alanine points away from the receptor molecule so that there are neither any stabilizing nor destabilizing interactions. In the case of phenylalanine the aromatic ring π-stacks with the acylguanidinium unit of **1** (Fig. 2). This cation–π interaction further stabilizes the complex.[10] Hence, the association constant for the binding of phenylalanine is more than two times larger than for the binding of alanine.

The indole ring of tryptophan is probably too large to effectively π-stack with the acylguanidinium unit. The positively charged ammonium group in lysine decreases the binding affinity relative to alanine due to unfavorable electrostatic interactions with the positively charged guanidinium group.

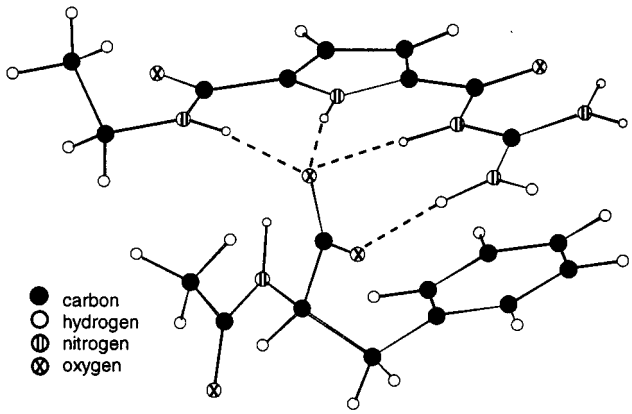

Fig. 2 Structure of **1** with *N*-acetylphenylalanine in water derived from molecular modelling. Intermolecular hydrogen bonds are shown as broken lines.

It is noteworthy that, even in 40% water–DMSO, this simple receptor **1** already shows a level of amino acid selectivity which is in the same range as described for other much more complex receptors in $CHCl_3$.[1b,2a,6] We hope that even greater selectivity including enantioselectivity can be achieved by variation of the substituent at the pyrrole ring.

Financial support for this work by the Fonds der Chemischen Industrie is gratefully acknowledged. The author thanks Professor Albrecht Berkessel (Cologne) for his generous support and helpful discussions.

Notes and references:

† Monte Carlo conformational searches with energy optimization using the Amber* force field and water GB/SA solvation as implemented in Macromodel ver. 6.0 (ref. 11).

1 (*a*) J.-M. Lehn, *Supramolecular Chemistry*; *Concepts and Perspectives*, VCH, Weinheim 1995; H. Dugas, *Bioorganic Chemistry, A Chemical Approach to Enzyme Action*, Springer Verlag, New York, 1996; see also (*b*) W. C. Still, *Acc. Chem. Res.*, 1996, **29**, 155.
2 (*a*) T. H. Webb and C. S. Wilcox, *Chem. Soc. Rev.*, 1993, 383; see also (*b*) *Chem. Rev.*, 1997, **97**, vol 5, special issue 'Molecular Recognition'.
3 For examples of peptide recognition in aqueous media see: A. Hossain, and H.-J. Schneider, *J. Am. Chem. Soc.*, 1998, **120**, 11 208; R. Breslow, Z. Yang, R. Ching, G. Trojandt and F. Odobel, *J. Am. Chem. Soc.* 1998, **120**, 3536; M. Davies, M. Bonnant, F. Guillier, J. D. Kilburn and M. Bradley, *J. Org. Chem.*, 1998, **63**, 8696; M. W. Peczuh, A. D. Hamilton, J. Sanchez-Qesada, J. deMendoza, T. Haak and E. Giralt, *J. Am. Chem. Soc.*, 1997, **119**, 9327.
4 Recent review articles: F. P. Schmidtchen, M. Berger, *Chem. Rev.*, 1997, **97**, 1609; A. Bianchi, K. Bowman-James and E. García-España, *Supramolecular Chemistry of Anions*, Wiley-VCH, New York, 1997; A. Galán and J. deMendoza, *Top. Curr. Chem.* 1995, **175**.
5 For a leading reference on general amino acid recognition, see: J. L. Sessler and A. Andrievsky, *Chem. Eur. J.*, 1998, **4**, 159 and references cited therein.
6 Side chain selective amino acid recognition in $CDCl_3$: J. Dowden, P. D. Edwards and J. D. Kilburn, *Tetrahedron Lett.*, 1997, **38**, 1095; C. P. Waymark, J. D. Kilburn and I. Gillies, *Tetrahedron Lett.*, 1995, **36**, 3051; S. S. Flack and J. D. Kilburn, *Tetrahedron Lett.*, 1995, **36**, 3409.
7 K. A. Connors, *Binding Constants*, Wiley, New York, 1987.
8 C. S. Wilcox, in *Frontiers in Supramolecular Chemistry and Photochemistry*, ed. H. J. Schneider and H. Dürr), VCH, Weinheim, 1990.
9 In accordance with this scheme, in the ^{1}H NMR spectrum one observes downfield shifts of all those receptor NHs, which participate in the proposed binding (up to 4 ppm in [$^2H_6$]DMSO). According to molecular dynamics calculations, the receptor conformation necessary for this type of binding is only 1 kJ mol^{-1} less stable than the energy minimum conformation in water (compared to 14 kJ mol^{-1} in $CHCl_3$).
10 T. H. Schrader, *Tetrahedron Lett.*, 1998, **39**, 517; D. A. Dougherty, *Science*, 1996, **271**, 163 and references cited therein.
11 F. Mohamadi, N. G. J. Richards, W. C. Guida, R. Liskamp, M. Lipton, C. Caufiled, G. Chang, T. Hendrickson and W. C. Still, *J. Comput. Chem.*, 1990, **11**, 440.

Communication 9/01126I

Catalytic dechlorination of aromatic chlorides using Grignard reagents in the presence of $(C_5H_5)_2TiCl_2$

Ryuichiro Hara, Kimihiko Sato, Wen-Hua Sun and Tamotsu Takahashi*

Catalysis Research Center and Graduate School of Pharmaceutical Sciences, Hokkaido University, Sapporo 060-0811, Japan and CREST, Science and Technology Corporation (JST), Sapporo 060-0811, Japan. E-mail: tamotsu@cat.hokudai.ac.jp

Received (in Cambridge, UK) 3rd March 1999, Accepted 30th March 1999

Dechlorination of aromatic chlorides was efficiently performed with alkyl Grignard reagents in the presence of a catalytic amount of $(C_5H_5)_2TiCl_2$.

Dehalogenation of organic halides is a fundamental subject in organic chemistry.[1] Therefore, diverse methods and a variety of reagents have been developed. The reactivity order of halogens is, in most cases, I > Br > Cl ⩾ F, and that of halogen-containing substrates is allylic ≈ benzylic > aliphatic > aromatic. It is thus suggested that dechlorination of aromatic chlorides cannot readily be achieved,[2] and the development of methodology for such remains to be studied. In addition to the synthetic usefulness of the reaction, recently evolving ecological demands for dechlorination of pollutant perchlorinated compounds[3] strongly motivated us toward this subject.[4]

We have recently published a report that $(C_5H_5)_2ZrCl_2$ catalyzed the efficient and selective debromination or deiodination reactions of aromatic halides using alkylmagnesium reagents.[5] However, this reaction did not proceed at a significant level for chloro derivatives. During the course of our study on the dechlorination reactions of aromatic chlorides, we found that titanocene dichloride catalyzed the reduction of aromatic chlorides when used with appropriate alkylmagnesium reagents [eqn. (1)].

$$\mathrm{Ar{-}Cl} \xrightarrow[\text{THF, room temp.}]{\text{RMgBr, } Cp_2TiCl_2 \text{ (cat.)}} \mathrm{Ar{-}H} \qquad (1)$$

Colomer and Corriu reported early in 1974 that Pr^iMgBr–$(C_5H_5)_2TiCl_2$ reacted with various organic bromides and iodides in Et_2O to give the dehalogenated products.[6] They suggested, however, that their system was not applicable to aromatic chlorides.

The use of THF as a solvent was found to dramatically improve the reactivity of the titanium-catalyzed dehalogenation reaction. A typical reaction procedure is as follows: To a solution of an aromatic chloride (1.0 mmol) and $(C_5H_5)_2TiCl_2$ (0.1 mmol, 0.1 equiv. with respect to the substrate) in THF (2.5 ml) was added BuMgCl (1.0 M solution in THF, 3.0 mmol, 3 equiv. at −78 °C. The reaction mixture was stirred at ambient temperature for several hours and the products were detected by GC and NMR.

Dechlorination of 4-chloroanisole was carried out using various Grignard reagents (Table 1). As expected, MeMgBr did not reduce 4-chloroanisole. The reaction with PhMgBr, which has an aromatic β-hydrogen, did not proceed. Bu^tCH_2MgBr which has γ- rather than β-hydrogens, gave a yield which did not exceed the amount of catalyst used. The reaction with Bu^tMgBr or EtMgBr gave moderate yields while the reactions with PrMgBr, Pr^iMgBr, Bu^iMgBr or BuMgCl gave high yields. Thus, the difference in reactivity may be due to both the β- and γ-hydrogens and their steric factors.

Table 2 shows the results of dechlorination of various aromatic chlorides. Chloroanisoles were reduced to anisole over varied reaction times (entries 2–4). Chloronaphthalenes were reduced within 30 min (entries 5 and 6). The hydroxy group of 4-chlorophenol was deprotonated by an additional equimolar amount of Grignard reagent and the reaction then proceeded (entry 7).

When 2,4-dichloroanisole was treated with a catalytic amount of $(C_5H_5)_2TiCl_2$ (0.2 mmol) and 6 equiv. of BuMgCl, the 2,4-dichloroanisole was completely consumed within 1 h. Anisole was obtained in 66% yield after 24 h, and 24% of 4-chloroanisole and 10% of 2-chloroanisole remained. Addition of 9 equiv. of BuMgCl did not significantly improve this situation.

Interestingly, when a combination of 1.0 equiv. of $(C_5H_5)_2TiCl_2$ and 2.0 equiv. of BuMgCl was used for the

Table 1 Assessment of Grignard reagents and solvents in the $(C_5H_5)_2TiCl_2$-catalyzed dechlorination of 4-chloroanisole[a]

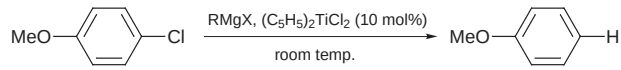

Entry	RMgX	Solvent	Yield (%)[b]	Recovered *p*-chloroanisole (%)[b]
1	MeMgBr	THF	0	100
2	EtMgBr	THF	59	34
3	PrMgBr	THF	91	5
4	Pr^iMgBr	THF	93	0
5	BuMgCl	THF	95	0
6	BuMgCl	Et_2O	59	35
7	BuMgCl	hexane	53	38
8	Bu^iMgBr	THF	42	52
9	Bu^tMgBr	THF	81	17
10	Isopentyl MgBr	THF	83	15
11	Neopentyl MgBr	THF	5	90

[a] The typical reaction conditions: 4-chloroanisole (1 mmol), alkylmagnesium reagent (3 mmol), $(C_5H_5)_2TiCl_2$ (0.1 mmol), room temperature, 48 h. [b] Yields were determined by GC.

Table 2 Results of $(C_5H_5)_2TiCl_2$-catalyzed dechlorination reaction[a]

Entry	Aromatic chloride	*t*/h	Yield (%)[b]	Recovered aromatic chlorides (%)[b]
1	PhCl	48	74[c]	12
2	2-Chloroanisole	6	99	0
3	3-Chloroanisole	48	80	12
4	4-Chloroanisole	48	95	0
5	1-Chloronaphthalene	0.5	> 99	0
6	2-Chloronaphthalene	0.5	> 99	0
7[d]	4-Chlorophenol	3	> 99[c]	0
8[e]	2,4-Dichloroanisole	24	*f*	*f*

[a] The typical reaction conditions: BuMgCl (3 equiv.), $(C_5H_5)_2TiCl_2$ (0.1 equiv.), room temperature. [b] Unless otherwise noted, yields were determined by GC. [c] Yield was determined by NMR. [d] BuMgCl (4 equiv.). [e] BuMgCl (6 equiv.), $(C_5H_5)_2TiCl_2$ (0.2 equiv.). [f] Yield of anisole: 66%; 2-ClC_6H_4OMe: 10%; 4-ClC_6H_4OMe: 24%; 2,4-$Cl_2C_6H_3OMe$: 0%.

stoichiometric reaction of 1-chloronaphthalene, we obtained only 10% of naphthalene after 1 h and 11% after 3 h. This is in sharp contrast to the fast reaction under catalytic conditions (see Table 2, entry 5) and the stoichiometric reduction of bromobenzene by $(C_5H_5)_2ZrBu_2$.[5] Addition of an additional 1.0 equiv. of BuMgCl promoted the reaction to afford 43% of the reduction product after 1 h. This suggests that the actual catalyst in the reaction is formed only when an excess of Grignard reagent is present, and the species is not solely $(C_5H_5)_2TiBu$ or $(C_5H_5)_2Ti–H$, which are thought to be formed in various hydrogenation reactions.[7]

The reduction of alkyl chlorides was also attempted under similar conditions. However, for example, 1-chlorooctane was reduced to octane in a moderate yield of 64% where isomers of octenes as by-products were detected. This may be due to the formation of an octyltitanium species followed by β-hydrogen elimination.

The reaction mechanism is not clear yet for our specific case although several possibilities in similar reactions have been discussed.[6] The plausible intermediates are (i) $(C_5H_5)_2Ti^{III}–H$,[8] which may transfer hydride through a four-membered transition state, (ii) a hydridomagnesium species,[9] and (iii) direct β-hydride transfer from an alkyl substituent on titanium metal.

In conclusion, aromatic chlorides were successfully dechlorinated by alkylmagnesium reagents in the presence of a catalytic amount of $(C_5H_5)_2TiCl_2$, where the corresponding bromides and iodides were also dehalogenated. The choice of solvent was found to be important. Our investigation on this subject is still progressing to widen the scope and to clarify the mechanism.

Notes and references

1 For general discussions of reduction of aryl halides, see: M. Hudlicky, in *Comprehensive Organic Synthesis*, ed. B. M. Trost and I. Fleming, Pergamon, Oxford, 1991, vol. 8, pp. 895; A. R. Pinder, *Synthesis*, 1980, 425.

2 Successful dechlorination reactions have appeared in a few articles. Monodehalogenation of 1,2,4,5-tetrachlorobenzene by $NaBH_4$ and $(C_5H_5)_2TiCl_2$ catalyst in DMA at 85 °C: Y. Liu and J. Schwartz, *Tetrahedron*, 1995, **51**, 4471; $NaBH_4$ and palladium catalyst: T. R. Bosin, M. G. Raymond and A. R. Buckpitt, *Tetrahedron Lett.*, 1973, **47**, 4699; palladium-catalyzed hydrodehalogenation reaction: P. N. Pandey and L. Purkayastha, *Synthesis*, 1982, 876.

3 R. A. Hites, *Acc. Chem. Res.*, 1990, **23**, 194.

4 M. Takada, *Chem. Chem. Ind.* (*Kagaku to Kogyo*), 1998, 1870 and references therein.

5 R. Hara, W.-H. Sun and T. Takahashi, *Chem. Lett.*, 1998, 1251.

6 E. Colomer and R. Corriu, *J. Organomet. Chem.*, 1974, **82**, 367.

7 Y. Qian, G. Li and Y. Huang, *J. Mol. Catal.*, 1989, **54**, L19; M. A. Djadchenko, K. K. Pivnitsky, J. Spanig and H. Schick, *J. Organomet. Chem.*, 1991, **401**, 1.

8 G. D. Cooper and H. L. Finkbeiner, *J. Org. Chem.*, 1962, **27**, 1493; H. L. Finkbeiner and G. D. Cooper, *J. Org. Chem.*, 1962, **27**, 3395; H. A. Martin and F. Jellinek, *J. Organomet. Chem.*, 1966, **6**, 293; H. A. Martin and F. J. Jellinek, *J. Organomet. Chem.*, 1968, **12**, 149; H. Felkin and G. Swierczewski, *Tetrahedron*, 1975, **31**, 2735; F. Sato, H. Ishikawa and M. Sato, *Tetrahedron Lett.*, 1980, **21**, 365.

9 The reactivity of the μ-H bimetallic complex of titanium and aluminium is well known: A. I. Sizov, I. V. Molodnitskaya, B. M. Bulychev, E. V. Evdokimova, G. L. Soloveichik, A. I. Gusev, E. B. Chuklanova and V. I. Andrianov, *J. Organomet. Chem.*, 1987, **335**, 323.

Communication 9/01705D

Synthesis and base-induced epimerization of *cis,cis,cis,trans*-tribenzo[5.5.5.6]fenestranes

Björn Bredenkötter,[a] Dieter Barth[a] and Dietmar Kuck*[ab]

[a] *Fakultät für Chemie, Universität Bielefeld, Universitätsstraße 25, D-33615 Bielefeld, Germany. E-mail: dietmar.kuck@uni-bielefeld.de*

[b] *Fachbereich Chemie und Chemietechnik, Universität-Gesamthochschule Paderborn, Warburger Straße 100, D-33098 Paderborn, Germany*

Received (in Liverpool, UK) 11th March 1999, Accepted 26th March 1999

Strained *cis,cis,cis,trans*-tribenzo[5.5.5.6]fenestranes are accessible in good yield by two-fold cyclodehydration of *cis*-2,6-diphenylspiro[cyclohexane-1,2′-indane]-1′,3′-diols and the particularly high acidity of their 'inverted' benzylic bridgehead C–H bonds, causing facile epimerization to the more stable all-*cis*-tribenzo[5.5.5.6]fenestranes, is shown.

Strained stereoisomers of all-*cis*-[*m.n.o.p*]fenestranes have been of particular interest with respect to the quest for planar tetracoordinate carbon.[1–3] While extensive computational work has been published on strain and geometry of stereoisomeric fenestranes,[3a–c,4–6] only a few small-ring congeners bearing a single *trans*-fused pair of rings together with three *cis*-annelated ones, *i.e.* the *cis,cis,cis,trans*-fenestranes, are known by experiment.[7–9] Fenestranes bearing more than one *trans* junction have remained unknown to-date,[3,10] and even normal-ring fenestranes containing the *cis,cis,cis,trans* skeleton have only recently been realized in a single case.[11] Herein we report the first synthesis of a *cis,cis,cis,trans*-tribenzo[5.5.5.6]fenestrane **2** and some of its derivatives, and demonstrate the ease and some mechanistic details of its epimerization to the corresponding all-*cis* stabilomers.

Benzoannelated all-*cis*-[5.5.5.6]- and all-*cis*-[5.5.5.5]-fenestranes have been synthesized by two-fold cyclodehydration of the stereochemically suitable *trans*-2,6-diarylspiro[cyclohexane-1,2′-indane]-1′,3′-diols.[12,13] In these tandem cyclization reactions, the *trans* orientation of the two aryl groups translates directly into the all-*cis* stereochemistry of the fenestrane nucleus. Surprisingly, and contra-intuitively, we found that, under similar conditions, isomeric *cis*-diarylspirodiols such as **1** and **3**,[14] which are readily accessible from the corresponding spirotriketones,[15,16] undergo two-fold cyclization as well, giving the corresponding *cis,cis,cis,trans*-[5.5.5.6]fenestranes, such as **2** and **4**,† in good yields (Scheme 1). Force-field and semi-empirical MO calculations (MM+ and PM3, respectively) suggest that *cis,cis,cis,trans*-[5.5.5.6]fenestranes are, by *ca*. 10 kcalmol^{-1}, more strained than the all-*cis* isomers,[3a] in agreement with previous estimates on alicyclic analogues,[4,6] and that one of the unbridged bond angles of the fenestrane nucleus is also considerably increased.‡ Moreover, the cyclohexane ring adopts a boat conformation in the most stable conformer of **2** and **4**.[14]

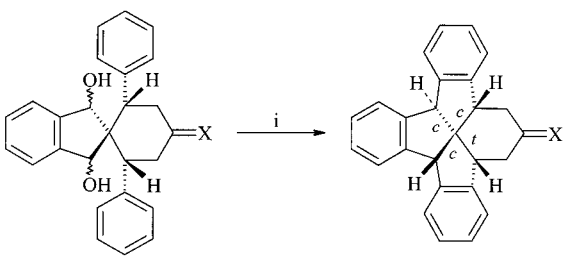

1 X = H, H
3 X = OCH_2CH_2O
2 X = H, H
4 X = O

Scheme 1 *Reagents and conditions*: i, H_3PO_4, toluene, Δ; **1** → **2**, 24 h, 82%; **3** → **4**, 15 h, 87%.

Reduction of fenestranone **4** under Wolff–Kishner–Huang–Minlon conditions, as well as reduction of its hydrazone with KOBu^t in DMSO at 20 °C and even Raney nickel-catalyzed hydrogenolysis of thioacetal **6**,[14] all resulted in the formation of the all-*cis* hydrocarbon **5** instead of **2** (Scheme 2). Obviously, the basic conditions used are sufficiently harsh to induce epimerization by a deprotonation–reprotonation sequence. In contrast, radical-induced desulfurization of **6** using Bu_3SnH and AIBN afforded retention of configuration at the 'inverted' bridgehead during reduction, giving the *cis,cis,cis,trans*-tribenzo[5.5.5.6]fenestrane **2** in good yield. These results suggest that C–H acidity at the strained fenestrane nucleus is the origin of epimerization, irrespective of the presence of a functional group at C(14).

In fact, independent experiments carried out with fenestranes **2** and **5** under essentially the same conditions used for reduction of **4** and its hydrazone revealed that base-induced epimerization occurs with high selectivity by deprotonation at the 'inverted' bridgehead (C-15a). Thus, treatment of all-*cis*-fenestrane **5** with KOBu^t in [$^2H_6$]DMSO gave rise to complete H/D exchange at the benzhydrylic bridgeheads to generate **5b**, whereas the *cis,cis,cis,trans* isomer **2** underwent complete epimerization with concomitant incorporation of three deuterium atoms at the benzhydrylic and one of the benzylic positions to yield **5c**

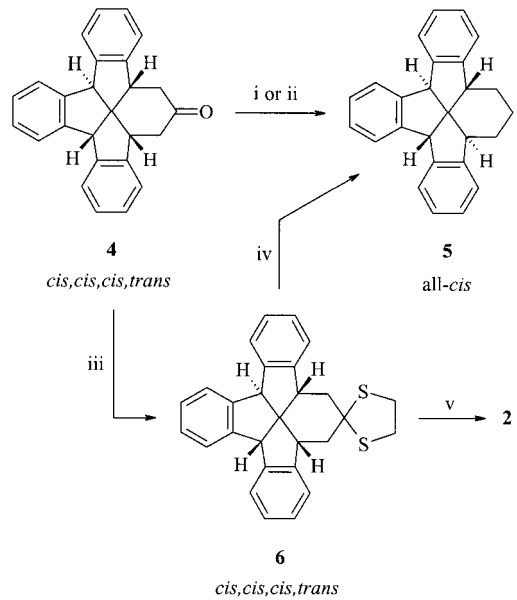

Scheme 2 *Reagents and conditions*: i, $N_2H_4{\cdot}H_2O$, KOH, diethylene glycol, 120 → 180 °C, 73%; ii, (a) $N_2H_4{\cdot}H_2O$, EtOH, Δ, 92%, (b) KOBu^t, DMSO, 20 °C, 80%; iii, $(CH_2SH)_2$, $BF_3{\cdot}Et_2O$, AcOH, 20 °C, 95%; iv, Raney-Ni (W2, 'neutral'), 1,4-dioxane, Δ, 80%; v, Bu_3SnH, AIBN, benzene, Δ, 87%.

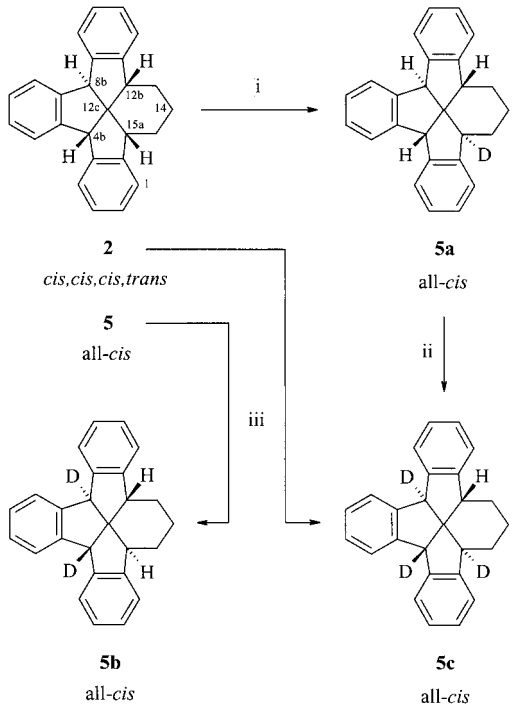

Scheme 3 *Reagents and conditions*: i, KOD, [*O*,*O*′-$^2H_2$]diethylene glycol, 180 °C, 3 h; ii, KOD, [*O*,*O*′-$^2H_2$]diethylene glycol, 240 °C, > 4 h; iii, KOBu^t, [$^2H_6$]DMSO, 20 °C, 15 h; > 90% in both cases.

(Scheme 3, paths iii). Moreover, use of KOD in *O*,*O*′-dideuterated diethylene glycol revealed that the C(15a)–H bond of **2** is far more acidic than the benzhydrylic C–H bonds in both **2** and **5**. When heated to 180 °C for 3 h, the *cis*,*cis*,*cis*,*trans* isomer **2** was partially epimerized (path i) to give a mixture consisting exclusively of monodeuterated all-*cis*-fenestrane **5a** and unlabelled starting material ([**5a**]:[**2**] ≈ 46:54 by ^{1}H NMR). Only prolongated heating at 240 °C effected relatively slow incorporation of deuterium into the benzhydrylic bridgeheads of **5a** to eventually give **5c** (path ii).

The results clearly show that benzoannelated *cis*,*cis*,*cis*,*trans*-[5.5.5.6]fenestranes are easily accessible by directed synthesis, in spite of the considerable increase of strain in the tetracyclic framework, but that the additional strain also induces facile base-induced epimerization of the 'inverted' bridgehead to give the more stable all-*cis* isomers. This sheds some light on the extraordinary challenge to synthesize benzoannelated *cis*,*cis*,*cis*,*trans*-[5.5.5.5]fenestranes.[3a]

We are grateful to the Deutsche Forschungsgemeinschaft and the Fonds der Chemischen Industrie for financial support.

Notes and references

† *Selected data* for **2**: mp 222–223 °C; δ_H($CDCl_3$, 500 MHz) 7.41–7.45 (m, 2 H), 7.00-7.20 (m, 10 H), 4.43 (s, 2 H), 3.79–3.82 (m, 2 H), 2.32–2.37 (m, 1 H), 2.21–2.24 (m, 1 H), 1.68–1.71 (m, 1 H), 1.53–1.59 (m, 2 H), 1.00–1.09 (m, 1 H); δ_C($CDCl_3$, 125.8 MHz) 146.6 (s), 146.3 (s), 145.9 (s), 144.8 (s), 144.7 (s), 143.8 (s), 126.9 (d), 126.8 (d), 126.7 (d), 126.6 (d), 126.4 (d), 126.2 (d), 125.1 (d), 124.6 (d), 124.5 (d), 123.2 (d), 122.8 (d), 120.9 (d), 66.8 (s, *centro*-C), 59.7 (d), 56.4 (d), 47.0 (d), 45.3 (d), 28.1 (t), 18.3 (t), 15.4 (t); *m*/*z* (EI, 70 eV) 334 (100, M$^{\bullet+}$), 305 (34), 291 (34), 257 (24). For **4**: mp 293–297 °C; δ_H($CDCl_3$, 500 MHz) 7.47–7.50 (m, 1 H), 7.38–7.41 (m, 1 H), 7.02–7.21 (m, 10 H), 4.58 (s, 1 H), 4.43 (s, 1 H), 4.28 (dd, ^3J 3.4, ^3J 14.6, 1 H), 4.28 (d, *J* 5.1, 1 H), 3.38 (dd, ^3J 6.2, ^2J 15.1, 1 H), 2.94 (dd, ^3J 3.6, ^2J 18.6, 1 H), 2.70 (dd, ^3J 1.8, ^2J 15.1, 1 H), 2.27 (dd, ^3J 14.8, ^2J 18.6, 1 H); δ_C($CDCl_3$, 125.8 MHz) 211.2 (s), 145.6 (s), 145.0 (s), 144.7 (s), 143.9 (s), 143.7 (s), 141.0 (s), 127.9 (d), 127.8 (d), 127.2 (d), 127.1 (d), 127.0 (d), 126.6 (d), 125.6 (d), 125.1 (d), 124.5 (d), 123.3 (d), 123.2 (d), 121.0 (d), 67.2 (s, *centro*-C), 58.7 (d), 56.7 (d), 47.1 (d), 47.0 (t), 44.3 (d), 37.8 (t); *m*/*z* (EI, 70 eV) 348 (100, M$^{\bullet+}$), 305 (37), 290 (39).

‡ Increase of strain in the *cis*,*cis*,*cis*,*trans*-hydrocarbon, as calculated by MM+ (PM3): $\Delta E_{strain} = \Delta H_f(\mathbf{2}) - \Delta H_f(\mathbf{5}) = 9.1$ (10.4) kcal mol^{-1}; bond angles calculated for **2**: C(4b)–C(12c)–C(12b) = 118.7° (120.0°), C(8b)–C(12c)–C(C15a) = 115.8° (116.5°).

1 H. J. Monkhorst, *J. Chem. Soc., Chem. Commun.*, 1968, 1111; R. Hoffmann, R. W. Alder and C. F. Wilcox, Jr., *J. Am. Chem. Soc.*, 1970, **92**, 4992; R. Hoffmann, *Pure Appl. Chem.*, 1971, **28**, 181; K. B. Wiberg, G. B. Ellison and J. J. Wendelowski, *J. Am. Chem. Soc.*, 1976, **98**, 1212; J. B. Collins, J. D. Hill, E. D. Jemmis, Y. Apeloig, P. v. R. Schleyer and J. A. Pople, *J. Am. Chem. Soc.*, 1976, **98**, 5419.
2 Most recent work concerning this topic: D. Röttger and G. Erker, *Angew. Chem., Int. Ed. Engl.*, 1997, **36**, 812; J. E. Lyons, D. R. Rasmussen, M. P. McGrath, R. H. Nobes and L. Radom, *Angew. Chem., Int. Ed. Engl.*, 1994, **33**, 1667 and literature cited therein.
3 Reviews on fenestrane chemistry: (*a*) D. Kuck, in *Advances in Theoretically Interesting Molecules*, ed. R. P. Thummel, JAI Press, Greenwich, CT, 1998, vol. 4, p. 81f; (*b*) M. Thommen and R. Keese, *Synlett*, 1997, 231; (*c*) W. Luef and R. Keese, in *Advances in Strain in Organic Chemistry*, ed. B. Halton, JAI Press, Greenwich, CT, 1993, vol. 3, p. 229f; (*d*) W. C. Agosta, in *The Chemistry of Alkanes and Cycloalkanes*, ed. S. Patai and Z. Rappoport, Wiley, New York, 1992, p. 927f; (*e*) A. K. Gupta, X. Fu, J. P. Snyder and J. M. Cook, *Tetrahedron* 1991, **47**, 3665; (*f*) K. Krohn, in *Organic Synthesis Highlights*, ed. J. Mulzer, H.-J. Altenbach, M. Braun, K. Krohn and H.-U. Reissig, VCH, Weinheim, 1991, p. 121f; (*g*) B. R. Venepalli and W. C. Agosta, *Chem. Rev.*, 1987, **87**, 399; (*h*) R. Keese, in *Organic Synthesis: Modern Trends*, ed. O. Chizhov, Blackwell, Oxford, 1987, p. 43f; (*i*) R. Keese, *Nach. Chem. Tech. Lab.*, 1982, **30**, 844.
4 W. L. Luef and R. Keese, *Helv. Chim. Acta*, 1987, **70**, 543.
5 P. Gund and T. M. Gund, *J. Am. Chem. Soc.*, 1981, **103**, 4458.
6 G. Kubiak, X. Fu, A. K. Gupta and J. M. Cook, *Tetrahedron Lett.*, 1990, **31**, 4285.
7 R. Keese, *Angew. Chem., Int. Ed. Engl.*, 1992, **31**, 344; D. Hirschi, W. Luef, P. Gerber and R. Keese, *Helv. Chim. Acta*, 1992, **75**, 1897; J. Wang, M. Thommen and R. Keese, *Acta Crystallogr., Sect. C*, 1996, **52**, 2311; M. Thommen, R. Keese and M. Förtsch, *Acta Crystallogr., Sect. C*, 1996, **52**, 2051.
8 P. A. Grieco, E. B. Brandes, S. McCann and J. D. Clark, *J. Org. Chem.*, 1989, **54**, 5849.
9 W. A. Smit, S. M. Buhanjuk, S. O. Simonyan, A. S. Shashkov, Y. T. Stuchkov, A. I. Yanovsky, R. Caple, A. S. Gybin, L. G. Anderson and J. A. Whiteford, *Tetrahedron Lett.*, 1991, **32**, 2105.
10 M. Luyten and R. Keese, *Tetrahedron*, 1986, **42**, 1687.
11 P. A. Wender, T. M. Dore and M. A. DeLong, *Tetrahedron Lett.*, 1996, **37**, 7687; P. A. Wender, M. A. DeLong and F. C. Wireko, *Acta Crystallogr., Sect. C*, 1997, **53**, 954.
12 D. Kuck, *Chem. Ber.*, 1994, **127**, 409; D. Kuck and H. Bögge, *J. Am. Chem. Soc.*, 1986, **108**, 8107.
13 D. Kuck, *Synlett*, 1996, 949; D. Kuck, *Top. Curr. Chem.*, 1998, **196**, 167.
14 B. Bredenkötter, U. Flörke and D. Kuck, to be published.
15 I. Ya. Shternberga and Y. F. Freimanis, *J. Org. Chem. USSR (Engl. Transl.)*, 1968, **4**, 1044; Yu. Yu. Popelis, V. A. Pestunovich, I. Y. Shternberga and Ya. F. Freimanis, *J. Org. Chem. USSR (Engl. Transl.)*, 1972, **8**, 1907.
16 W. Ten Hoeve and H. Wynberg, *J. Org. Chem.*, 1979, **44**, 1508.

Communication 9/02024/A

N-(2,4-Dinitrophenyl)-2-phenylfulleropyrrolidine: an electroactive organofullerene dyad

Gollapalli R. Deviprasad, Muhammad S. Rahman and Francis D'Souza*

Department of Chemistry, Wichita State University, Wichita, KS 67260-0051, USA.
E-mail: dsouza@wsuhub.uc.twsu.edu

Received (in Corvallis, OR, USA) 12th February 1999, Accepted 22nd March 1999

Using Sanger's method, an electroactive organofullerene dyad, *N*-(2,4-dinitrophenyl)-2-phenylfulleropyrrolidine, is synthesized and its spectral and electrochemical characterization is reported.

Studies on C_{60}-based electroactive organofullerene dyads[1] are of current interest due to the interesting electronic and optical properties they display. Such electroactive fullerenes are considered to be useful in the development of molecular electronic devices[2] and non-linear optical materials[3] as well as in the design of artificial photosynthetic systems.[4,5] Two types of electroactive organofullerene dyads are known, namely, (i) C_{60} covalently linked to a donor entity (C_{60}–Donor type dyads) and (ii) C_{60} bearing an electron-deficient entity (C_{60}–Acceptor type dyads). A number of studies have reported electroactive fullerene dyads of the former type, while only a few systems of the latter type are known in the literature,[1] even though the potential for such double electron acceptor systems as precursors for the formation of multichromophoric systems with well-defined gradient of redox potentials has been realized.[5]

Among the different types of electron deficient compounds that could be utilized to form C_{60}–Acceptor dyads, nitroaromatic compounds are one of the attractive candidates. This is because the reduction potential of this acceptor molecule can be easily tuned by choosing appropriate numbers of nitro groups and other substituents on the aromatic ring.[6] However, no nitroaromatic acceptor molecule-linked fullerene dyad is known to date, although several donor–acceptor type molecules involving nitroaromatic compounds are known in the literature.[7] This has been achieved in the present study where we report the first synthesis and electrochemical characterization of a nitroarene appended fullerene dyad.

The strategy adopted for the synthesis of nitroarene appended fullerene is shown in Scheme 1. This involves the initial synthesis of 2-phenylfulleropyrrolidine **1**[8] followed by treatment with 1-fluoro-2,4-dinitrobenzene in the presence of NaH according to Sanger's reaction.[9] The secondary nitrogen on the pyrrolidine ring reacts with 1-fluoro-2,4-dinitrobenzene to yield the desired *N*-(2,4-dinitrophenyl)-2-phenylfulleropyrrolidine **2**.† The molecular integrity of the newly synthesized compound is established from mass, UV–visible and ^{1}H NMR spectroscopy. In addition to the fullerene absorption bands, the UV–visible spectrum of the product in hexane exhibited an absorption band at 274 nm indicating the presence of the dinitrophenyl entity.[6] It is also observed that the proton resonance peaks of the *N*-dinitrophenyl entity are shielded by *ca.* 0.5 ppm as compared to the peaks of the starting material, 1-fluoro-2,4-dinitrobenzene, while the protons of the 2-phenylpyrrolidine group experienced a small deshielding upon forming the *N*-(2,4-dinitrophenyl)-2-phenylfulleropyrrolidine (Fig. 1).

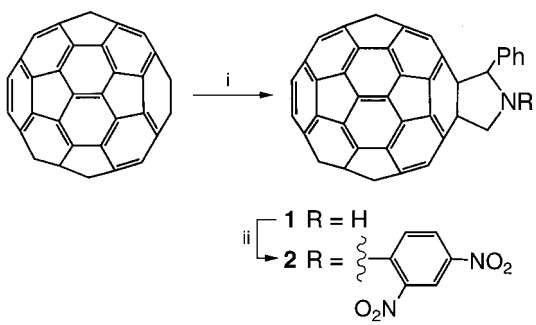

Scheme 1

The redox behavior of the newly synthesized compound has been investigated using cyclic voltammetry.‡ Fig. 2 shows the cyclic voltammograms of 2-phenylfulleropyrrolidine and *N*-(2,4-dinitrophenyl)-2-phenylfulleropyrrolidine in PhCN with 0.1 M Bu_4NPF_6. In the investigated solvent, the first three reductions of 2-phenylfulleropyrrolidine are found to be reversible one-electron processes with an anodic to cathodic peak separation, ΔE of *ca.* 80 mV. These processes are located at $E_{1/2}$ = −1.05, −1.48 and −2.01 V *vs.* Fc/Fc$^+$, respectively, and are negatively shifted by 120 to 190 mV compared to the corresponding electroreductions of C_{60} (Table 1). The redox behavior of *N*-(2,4-dinitrophenyl)-2-phenylfulleropyrrolidine is found to be more complicated due to the overlapping reductions of the dinitrophenyl entity [Fig. 2(*b*)]. Only the first reduction process is reversible and is located at $E_{1/2}$ = −1.01 V *vs.* Fc/Fc$^+$. Spectroelectrochemical studies have indicated that this reduction occurs at the C_{60} macrocycle resulting in the formation of a C_{60} anion radical. The observed positive shift of 40 mV for the first reduction of *N*-(2,4-dinitrophenyl)-2-phenylfulleropyrrolidine as compared to the first reduction of the starting material, 2-phenylfulleropyrrolidine, indicates small electronic interactions between the C_{60} and dinitrobenzene entities, consistent with the ^{1}H NMR results discussed above.

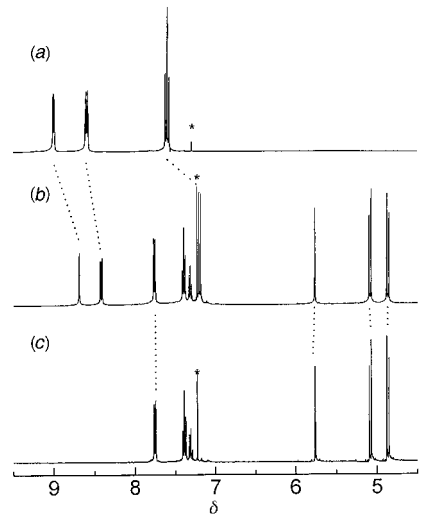

Fig. 1 ^{1}H NMR spectrum of (*a*) 1-fluoro-2,4-dinitrobenzene, (*b*) *N*-(2,4-dinitrophenyl)-2-phenylfulleropyrrolidine and (*c*) 2-phenylfulleropyrrolidine, in CS_2–$CDCl_3$ (1 : 1).

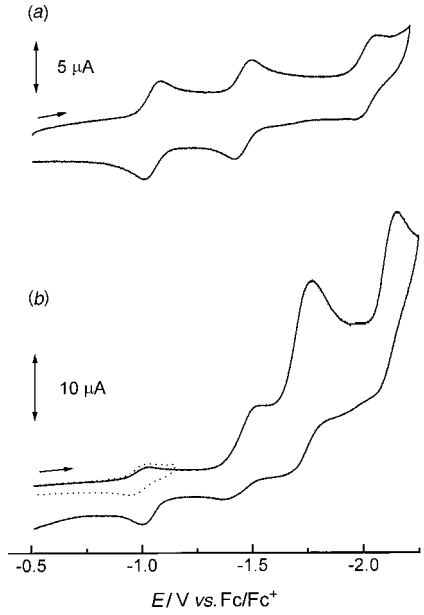

Fig. 2 Cyclic voltammogram of (*a*) 2-phenylfulleropyrrolidine and (*b*) *N*-(2,4-dinitrophenyl)-2-phenylfulleropyrrolidine in PhCN with 0.1 M Bu_4NPF_6. Scan rate = 100 mV s^{-1}.

Table 1 Half-wave potentials for the reduction of C_{60} and fulleropyrrolidine derivatives in PhCN with 0.1 M Bu_4NPF_6

	E/V *vs.* Fc/Fc^+		
Compound	1st	2nd	3rd
C_{60}	−0.92	−1.34	−1.83
2-phenylfulleropyrrolidine	−1.05	−1.48	−2.01
N-Dinitrophenyl-2-phenylfulleropyrrolidine[a]	−1.01		

[a] Additional peaks corresponding to the reduction of C_{60} and the dinitrobenzene entities are observed. See Fig. 2 and text for details.

The first reduction of the appended dinitrophenyl entity is found to be irreversible and is located at E_{pc} = −1.56 V *vs.* Fc/Fc^+, that is, the potential where the second reduction of C_{60} occurs. Control experiments performed by using a model compound, 1-morpholino-2,4-dinitrobenzene, synthesized by reacting morpholine and 1-fluoro-2,4-dinitrobenzene, confirmed the reduction of the dinitrophenyl entity in this potential range. When the potential is scanned to more negative potentials, additional reductions of the C_{60} and the dinitrophenyl entities are also observed. A comparison between the potentials corresponding to the first reduction of C_{60} and the first reduction of dinitrophenyl entities in the synthesized compound reveal a large potential separation of nearly 500 mV.

In summary, we are able to synthesize an *N*-dinitrobenzene-appended fulleropyrrolidine *via* Sanger's reaction using a simple one step procedure. The electrochemical and spectroelectrochemical results indicate that the reduction of C_{60} in the newly synthesized compound is easier by 40 mV than the starting fulleropyrrolidine. Both ^1H NMR and the cyclic voltammetric results indicate the existence of weak interactions between the C_{60} and dinitrophenyl entities in the synthesized compound. Owing to a potential separation of nearly 500 mV between the first reductions of the C_{60} and dinitrobenzene entities in the synthesized compound, utilization of this dyad as a precursor for developing multichromophoric supramolecular systems is envisioned.

The authors thank the donors of the Petroleum Research Fund, administered by the American Chemical Society, for support of this work.

Notes and references

† To a solution of 2-phenylfulleropyrrolidine (22.5 mg) in dry THF (15 ml), NaH (2 mg) was added and the resulting suspension was stirred. After the evolution of hydrogen had ceased, 1-fluoro-2,4-dinitrobenzene (20 μl) was added and the solution was stirred for another 6 h. At the end, water (1 ml) was added and the solution was evaporated under reduced pressure. The crude product was adsorbed on silica and separated on a silica gel column using 1 : 1 toluene–hexane as eluent (68% yield). Negative ion electrospray mass spectrum of the product in either a toluene or MeOH matrix revealed peaks at *m*/*z* 963.7 and 838.2 corresponding to the molecular ion minus nitro and dinitrobenzene units respectively. A control experiment performed using ^{19}F NMR of the product revealed the complete absence of the fluorine resonance peak that was present in the starting material, 1-fluoro-2,4-dinitrobenzene, at δ 221.5 (C_6F_6 at δ 166); $\delta_H[CS_2$–$CDCl_3$ (1 : 1) 8.69 (s, 1H, dinitrophenyl-H), 8.42 (m, 1H, dinitrophenyl-H), 7.76 (d, 1H, phenyl-H), 7.39 (m, 2H, phenyl-H), 7.31 (m, 2H, phenyl-H), 7.19 (d, 1H, dinitrophenyl-H), 5.77 (s, 1H, pyrrolidine-H), 5.09 (d, 1H, pyrrolidine-H), 4.87 (d, 1H, pyrrolidine-H); λ_{max}(hexane)/nm 429, 307(sh), 274, 252, 213.

‡ Cyclic voltammograms were obtained on a EG & G Model 263 A potentiostat using a three-electrode system. A glassy carbon electrode was used as the working electrode. A platinum wire served as the counter electrode, while a Ag/AgCl electrode was used as the reference electrode. All the potentials are referenced against an internal Fc/Fc^+ redox couple. Analysis of the peak current and peak potentials from the voltammetric data was carried out using EG&G M270 electrochemical software. All the experiments were carried at 22 ± 1 °C.

1 For a recent review on C_{60}-based electroactive organofullerenes, see, N. Martin, L. Sanchez, B. Illescas and I. Perez, *Chem. Rev*., 1998, **96**, 2527.
2 *Introduction to Molecular Electronics*, ed. M. C. Petty, M. R. Bryce and D. Bloor, OUP, New York, 1995; *Molecular Electronic-Science and Technologie*, ed. A. Aviram, Engineering Foundation, New York, 1989.
3 M. S. Nalwa, *Adv. Mater*., 1993, **5**, 341; N. J. Long, *Angew. Chem., Int. Ed. Engl*., 1995, **34**, 21; P. N. Prasad and D. J. Williams, *Introduction to Nonlinear Optical Effects in Molecules and Polymers*, Wiley, New York, 1991.
4 *Photoinduced Electron Transfer*, ed. M. A. Fox and M. Chanon, Elsevier, Amsterdam, 1988; H. A. Staab, A. Feurer and R. Hauck, *Angew. Chem., Int. Ed. Engl*., 1994, **33**, 2428.
5 M. R. Roest, J. W. Verhoever, W. Schuddeboon, J. M. Warman, J. M. Lawson and M. N. Paddon-Row, *J. Am. Chem. Soc*., 1996, **118**, 1762; J. M. Lawson, D. C. Craig, A. M. Oliver and M. N. Paddon-Row, *Tetrahedron*, 1995, **51**, 3841; P. A. Liddell, D. Kuciauskas, J. P. Sumida, B. Nash, D. Nguyen, A. L. Moore, T. A. Moore and D. Gust, *J. Am. Chem. Soc*. 1997, **119**, 1400; H. Imahori, K. Yamada, M. Hasegawa, S. Taniguchi, T. Okada and Y. Sakata, *Angew. Chem., Int. Ed. Engl*. 1997, **36**, 2626.
6 P. R. Droupadi and V. Krishnan, *Photochem. Photobiol*., 1984, **37**, 329; P. R. Droupadi and V. Krishnan, *Biochem. Biophys. Acta*, 1987, **894**, 284.
7 J. S. Connolly and J. R. Bolton, in *Photoinduced Electron Transfer*, ed. M. A. Fox and M. Chanon, Part D, Elsevier, Amsterdam, 1988.
8 F. D'Souza, G. R. Deviprasad, M. S. Rahman and J.-p. Choi, *Inorg. Chem*., 1999, **38**, in the press.
9 F. Sanger, *Biochem. J*., 1945, **39**, 507; *Vogel's Textbook of Practical Organic Chemistry*, ed. B. S. Furniss, A. J. Hannaford, P. W. G. Smith and A. R. Tatchell, 5 edn., Wiley, New York, 1989, p. 1279.

Communication 9/01224I

In situ energy dispersive EXAFS (EDE) of low loaded $Pt(acac)_2/H_I\ SiO_2$ catalyst precursors on a timescale of seconds and below

Steven G. Fiddy,[a] Mark A. Newton,[a] Andrew J. Dent,[b] Guiseppe Salvini,[b] Judith M. Corker,[a] Sandra Turin,[a] Tom Campbell[a] and John Evans[a]

[a] *Department of Chemistry, The University of Southampton, Highfield, Southampton, UK SO17 1BJ*
[b] *CLRC Daresbury, Warrington, UK WA4 4AD*

Received (in Cambridge, UK) 3rd February 1999, Accepted 29th March 1999

We demonstrate second and sub-second time resolved energy dispersive EXAFS (EDE) for *in situ* interrogation of phase changes in a supported metal catalyst precursor [(≤5 wt%) $Pt(acac)_2/H_I\ SiO_2$] during thermal decomposition and reduction; the formation of Pt particles is radically altered by the presence H_2, in both kinetic and structural senses.

Extended X-ray absorbtion fine structure (EXAFS) has long been a frontline technique in the determination of local structure and has found widespread application. However, the predominant *modus operandi* is rooted in the interrogation of the steady state, due to the stepwise progression of the monochromator through the energy window of interest. Quick EXAFS (QuEXAFS)[1] allows relatively rapid data acquisition *via* the optimisation of this monochromator movement: EXAFS spectra from supported metal catalysts can be collected on a timescale of > 20–30 s though timescales of > 1 min are more common,[2–5] in one case Cu K-edge XANES has been collected in *ca.* 3 s.[6]

EDE (or DEXAFS) utilises an (ideally) elliptically bent monochromator to produce a focused beam containing the required spread of X-ray energies. The EXAFS experiment may therefore be achieved with *no* subsequent monochromator movement.[7] In the present case a four point bending mechanism[8] is used to minimise aberations and produce an extremely small spot size. The speed of data acquisition is therefore limited only by the time required to achieve acceptable statistics. However, simultaneous illumination of the sample with a range of X-ray energies requires extreme spatial homogeneity of the sample. In the case of heterogeneous catalysts, these uniformity requirements have resulted in the predominate use of QuEXAFS[1–6] or pressed disk samples.[7,8b,9] Using this latter approach, EDE has been used on heterogeneous systems on a time scale of (at best) 30 s.[8b,9] Pressed disks present problems in terms of non-uniform gas distribution within the disk,[10a] and possible degradation of the support material structure.[10b,11] We present a methodology that allows fast, high quality, EDE measurements to be made with a sample presentation much more in keeping with catalytic testing.

The mesoporous silicas ($H_I\ SiO_2$), prepared following the procedure previously described,[12] were impregnated with $Pt(acac)_2$ from dry toluene. The $Pt(acac)_2/(H_I\ SiO_2)$ catalyst precursors were then sieved to a particle size of *ca.* 100 μm and packed into a flow microreactor based upon thin walled quartz tubes (*ca.* 2 mm o.d; 0.1 mm wall thickness). A second tube, the reference for the EDE experiment, was packed in the same manner with unloaded mesoporous silica ($H_I\ SiO_2$). This approach is similar to that demonstrated by Clausen *et al.*[2] although the increased diameter of the quartz tube used, allows the insertion of a 0.25 mm, mineral insulated, type K thermocouple directly into the sample. The samples were reacted under flowing N_2 or 10% H_2–90% N_2 gas using a linear sample heating ramp of 4 K min^{-1}. Gases are passed over the catalyst beds under mass flow control.

Fig. 1 shows Pt L_{III} edge EXAFS spectra obtained from $Pt(acac)_2/(H_I\ SiO_2)$ catalyst precursors. Spectrum (a) was obtained from a standard EXAFS experiment (*ca.* 1 h). Spectra (b)–(f) are EDE† obtained for a range of collection times (as indicated). Spectrum (f) is that derived from a 1 wt% $Pt/H_I\ SiO_2$ sample in 21 s. The Pt L_{III}-edge EXAFS-derived‡ structural parameters are summarised in Table 1.

Clearly, good quality EXAFS analysis (one or two coordination shells) can be obtained using this approach down to sub-second acquisition times (at 5 wt%). Analysis of the data obtained in 0.05 s leads to inconsistent structural parameters making it unsuitable for detailed EXAFS analysis. This data is suitable for determination of spectral change in the XANES region. The 1 wt% Pt case represents the current dilution limit of this approach and a reasonable quality of data can be achieved in *ca.* 21 s.

Fig. 2 shows phase corrected Fourier transforms derived from temperature dependent EDE spectra recorded at 8 s acquisition time (scan time 80 ms; 100 scans) for the reduction of a 5 wt% Pt sample under 8 ml min^{-1} 10% H_2–90% N_2 gas. The $Pt(acac)_2$ collapses to form Pt particles over an extremely narrow temperature region (*ca.* 15 K) indicative of some form of autocatalytic kinetics. In the temperature region shown these particles show little evidence of any subsequent increase in size.

Fig. 3 shows the variation in Pt–O and Pt–Pt coordination obtained from such EDE experiments for the following cases: 5 wt% Pt sample thermally decomposed as above in H_2–N_2 (a) and N_2 (c) mixtures; and a 1 wt% Pt sample reduced in H_2–N_2 (b). The particles resulting from the thermal decomposition of this catalyst precursor in pure N_2, and the kinetics of their production, are radically different to those produced *via* reduction in the H_2–N_2 mixture. The degree of particle agglomeration attained after the low *Z* coordination has been removed is significantly different between the case where H_2 is present and where only N_2 is used: with the latter case resulting in significantly smaller Pt particles. The persistence of low *Z* (C/O) coordination in the decomposition of this catalyst precursor therefore has considerable ramifications for the size of the particulate Pt formed.

In summary we have demonstrated that good quality, *in situ*, Pt L_{III} edge EDE can be obtained from low loaded heterogeneous samples on a time scale of seconds and below. The

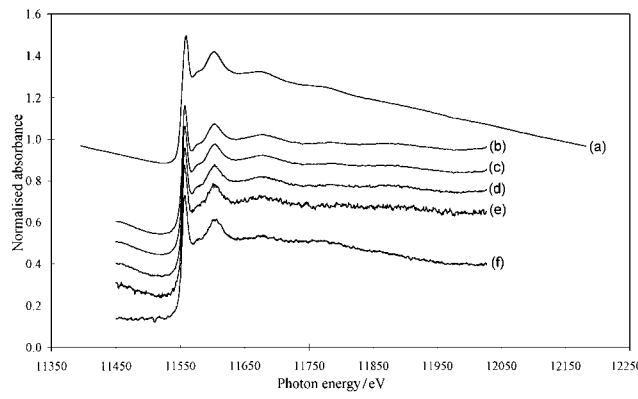

Fig 1 The Pt L_{III}-edge absorption spectra of as-synthesised 5wt%$Pt(acac)_2/H_I\ SiO_2$ catalysts showing (a) the conventional EXAFS data obtained over 1 h. Also shown is the equivalent EDE data obtained in (b) 50 s, (c) 5 s, (d) 0.5 s and (e) 0.05 s on Station 9.3. Spectra (f) shows the EDE data obtained in 21 s for a 1 wt% Pt $Pt(acac)_2/H_I\ SiO_2$ catalyst.

Table 1 Structural and statistical parameters derived from the analysis of the EDE and EXAFS spectra shown in Fig. 1. (a) Δk = 2–12 Å^{-1}, (b)–(f) Δk = 2–10 Å^{-1}. The *R* factors = $(\int [\chi^T - \chi^E]k^3dk/[\chi^E]k^3dk) \times 100\%$ where χ^T and χ^E are the theoretical and experimental EXAFS and *k* is the photoelectron wave vector; the Debye–Waller factor = $2\sigma^2$, where σ is the root mean square internuclear separation. Values in parentheses are statistical errors generated in EXCURVE (see footnote [b])

Sample	Shell	CN[a]	*r*/Å[b]	1.5% error in *r*[b]	$2\sigma^2$/Å^2 [b]	*R*-factor (%)
(a) 5%Pt(acac)$_2$/H$_I$ SiO$_2$	O	4.0(0.2)	1.991(2)	0.030	0.005(2)	24.4
(Station 7.1, AQ = 1 h)	C	4.0(0.3)	2.934(5)	0.044	0.004(3)	
	O	2.0(0.4)	3.104(9)	0.046	0.004(6)	
	C	2.0(0.4)	3.270(12)	0.049	0.005(6)	
(b) 5%Pt(acac)$_2$/H$_I$ SiO$_2$	O	4.0(0.5)	1.982(6)	0.030	0.010(3)	42.8
(Station 9.3 AQ = 50 s)	C	4.0(1.0)	2.838(10)	0.043	0.002(4)	
(c) 5%Pt(acac)$_2$/H$_I$ SiO$_2$	O	4.0(0.6)	1.981(7)	0.030	0.011(4)	49.6
(Station 9.3 AQ = 5 s)	C	4.0(1.1)	2.824(12)	0.042	0.003(8)	
(d) 5%Pt(acac)$_2$/H$_I$ SiO$_2$	O	4.0(0.9)	1.964(15)	0.030	0.012(5)	61.5
(Station 9.3 AQ = 0.5 s)						
(f) 1%Pt(acac)$_2$/ H$_I$ SiO$_2$	O	4.0(0.8)	1.988(8)	0.030	0.004(2)	70.2
(Station 9.3 AQ = 21 s)						

[a] CN = Coordination number. [b] In accordance with previous studies[16] we note that the true errors in bond lengths are likely to be of the order of 1.5% (as indicated); those for the coordination numbers *ca.* 20%. The variation of Debye–Waller factors the EDE may be due to some inhomogeneity in the sample or in the quartz tubes.

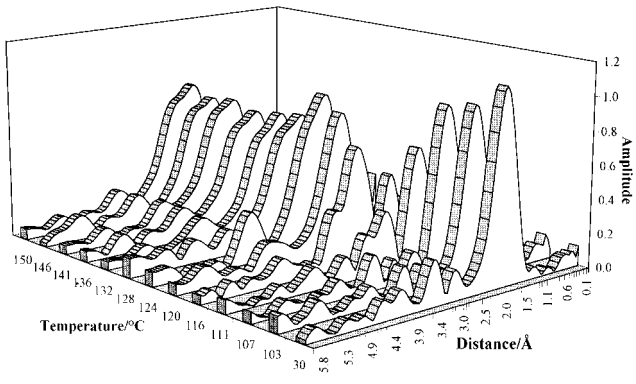

Fig 2 Fourier transforms, phase-shift corrected for oxygen, from EDE spectra derived from the reduction of 5 wt%Pt(acac)$_2$/H$_I$ SiO$_2$ catalysts in 10% H$_2$ in N$_2$ as a function of reduction temperature [heating rate 4 K min^{-1} acquisition time 8 s (scan time 80 ms; 100 scans)].

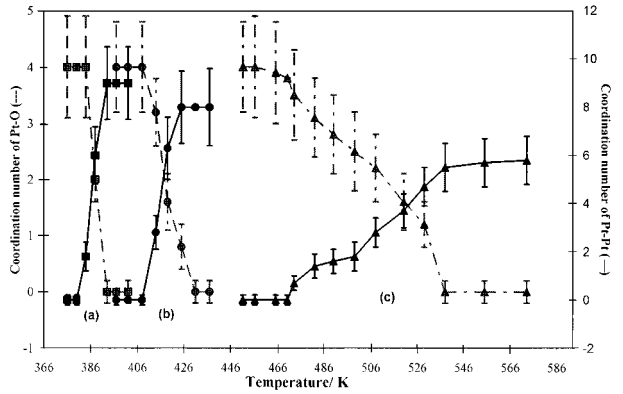

Fig. 3 The variation of Pt–O and Pt–Pt coordination number during the temperature programmed decomposition/reduction of (a) 5 wt%Pt(acac)$_2$/H$_I$ SiO$_2$ catalysts under 10% H$_2$ in N$_2$, (b) 1 wt%Pt(acac)$_2$/H$_I$ SiO$_2$ catalysts under 10% H$_2$ in N$_2$ and (c) 5 wt%Pt(acac)$_2$/H$_I$ SiO$_2$ catalysts under N$_2$.

approach described can be applied on timescales that allow detailed interrogation of the fluxion in supported catalyst phases under non-steady state conditions.

We acknowledge the EPSRC for funding of this project; BNFL and BP for postgraduate awards to T. C. and S. T.; CLRC Daresbury for access to facilities; Dr Fred Mosselmans (DL) and Dr John Couves (BP) for useful discussions; and the technical skills of John James, Mike Caplin, and Bruce Hancock.

Notes and references

† EDE experiments were recorded in transmission using a low noise, highly linear, photodiode array (Hamamatsu S4874).[8c]

‡ Normal X-ray absorption spectra were recorded (in transmission mode) on Station 7.1 at the Daresbury Laboratory operating at 2 GeV. All data reduction was carried out using PAXAS,[14] with the spherical wave analysis performed using EXCURV98.[15,16]

1 R. Frahm, *Nucl. Instrum. Methods A*, 1988, **270**, 578.
2 B. S. Clausen, L. Grabaek, G. Steffensen, P. L. Hansen and H. Topsoe, *Catal. Lett.*, 1993, **20**, 23.
3 D. Hecht, R. Frahm and H. H. Strehblow, *J. Phys. Chem.*, 1996, **100**, 10 831; N. Hilbrandt, R. Frahm and M. Martin, *J. Phys. IV*, 1997, **7**, 727.
4 G. Sankar, J. M. Thomas, F. Rey and G. N. Greaves, *J. Chem. Soc., Chem. Commun.*, 1995, 2549.
5 F. Cimini and R. Prins, *J. Phys. Chem. B*, 1997, **101**, 5277.
6 J. Als-Nielsen, G. Grubel, and B. S. Clausen, *Nucl. Instrum. Methods B*, 1995, **97**, 522.
7 J. W. Couves, J. M. Thomas, D. Waller, T. H. Jones, A. J. Dent, G. E. Derbyshire and G. N. Greaves, *Nature*, 1991, **354**, 465; R. P. Phizackerly, Z. V. Rek, G. V. Stephenson, S. Conradson, K. O. Hodgson, T Matsushita and H. Oyanagi, *J. Appl, Phys*., 1983, 16, 161.
8 For instance: (*a*) P. G. Allen, S. D. Conradson and J. E. Penner-Hahn, *Appl. Crystallogr.*, 1993, **26**, 172: (*b*) M. Hagelstein, C. Ferrero, U. Hatje, T. Ressler and W. Metz, *J. Synchrotron Radiat*., 1995, **2**, 174: (*c*) D. Bogg, A. J. Dent, G. E. Derbyshire, R. C. Farrow, C. A. Ramsdale and G. Salvini, *Nucl. Instrum. Methods A*, 1997, **392**, 461; (*d*) A. Dent, J. Evans, M. Newton, J. Corker, A. Russell, M. B. Abdul Rahman, S. Fiddy, R. Matthew, R. Farrow and G. Salvini, *J. Synchrotron Radiat*., in press.
9 For instance: J. W. Couves, J. M. Thomas, C. R. A. Catlow, G. N. Greaves, G. Baker and A. J. Dent, *J. Phys. Chem., 1990*, **94**, 6517: G. Sankar, J. M. Thomas, D. Waller, J. W. Couves, C. R. A. Catlow and G. N. Greaves, *J. Phys. Chem.*, 1992, **96**, 7485; T. Ressler, M. Hagelstein, U. Hatje and W. Metz, *J. Phys. Chem. B*, 1997, **101**, 6680.
10 (*a*) J. L. Van der Venne, J. P. M. Rindt and G. J. M. M. Coenen, *J. Colloid. Interface Sci*., 1990, **74**, 287; (*b*) W. C. Conner, E. L. Weist, T. Ito and J. Fraissard, *J. Phys. Chem.*, 1989, **93**, 4138.
11 V. Y. Gusev, X. B. Feng, Z. Bu, G. L. Haller and J. A. O'Brien, *J. Phys. Chem*., 1996, 100, 1985 [for structural degradation due to compression in mesopurous SiO$_2$ (MCM 41)].
12 G. Attard, J. C. Clyde and C. G. Göltner, *Nature*, 1995, **378**, 366.
13 N. Binsted, PAXAS Programme for the analysis of X-ray absorption spectra, University of Southampton, 1988.
14 S. J. Gurman, N. Binsted and I. Ross, *J. Phys. Chem.*, 1984, **17**, 143; 1986, **19**, 1845.
15 N. Binsted, EXCURV98, CCLRC Daresbury Laboratory computer programme, 1998.
16 For instance, J. M. Corker, J. Evans, H. Leach and W. Levason, *J. Chem. Soc., Chem. Commun.*, 1989, 181.

Communication 9/00923J

Metallation-induced migration of phosphorus from nitrogen to carbon in 1-oxo-2,8-diphenyl-2,5,8-triaza-1λ^5-phosphabicyclo[3.3.0]octane: unusual bonding parameters of the double migration product

Susan A. Bourne,[c] Zhengjie He,[a] Tomasz A. Modro*[a] and Petrus H. Van Rooyen[b]

[a] *Centre for Heteroatom Chemistry, Department of Chemistry, University of Pretoria, Pretoria 0002, South Africa. E-mail: tamodro@scientia.up.ac.za*
[b] *Department of Chemistry, University of Pretoria, Pretoria 0002, South Africa*
[c] *Department of Chemistry, University of Cape Town, Rondebosch 7700, South Africa*

Received (in Cambridge, UK) 9th March 1999, Accepted 31st March 1999

The title compound undergoes lithiation-induced rearrangement, first to a bicyclic phosphonic diamide, and next to a bicyclic phosphinic amide; for the latter product an unusually long phosphoryl bond was observed.

Recently we reported the regioselective cleavage of one P–N bond in the title compound **1** leading to either the eight-membered (2,5,8-triaza-1λ^5-phosphacyclooctane) or the five-membered (1,3,2λ^5-diazaphospholidine) monocyclic product.[1] We present here another transformation of substrate **1** induced by treatment with BuLi. We reported before the LDA-induced migration of phosphorus from nitrogen to aromatic carbon for simple phosphoric *N*-phenylamides,[2] but for **1** the reaction, involving a bicyclic substrate, leads to the formation of new bicyclic systems. Because of the presence of two N–Ph groups in **1**, lithiation can induce single or double N → C migration of the P atom, leading to the bicyclic phosphonic diamide **2** or the bicyclic, symmetrical phosphinic amide **3**, depending on the excess of BuLi.† The product of single migration **2** can be also converted to **3** upon further treatment with BuLi (Scheme 1). The structures of products **2** and **3** were deduced from their NMR (^{31}P, ^{1}H, ^{13}C) spectra, but the unambiguous structural evidence was obtained from the crystal structures of both products (Figs. 1 and 2).‡ Since the crystal structure of **1** was determined before,[3] we could compare the molecular parameters of all three bicyclic compounds. The comparison revealed some interesting structural changes that take place at the phosphorus centre during the transformation **1** → **2** → **3** leading to some unusual bonding parameters of the phosphoryl function in the final product **3** (Table 1). The P–C bond distance in **2** has a typical value,§ but for **3** the differences in the P–C distances within each of the crystallographically independent molecules are worth noting as they lead to the effective loss of the molecular symmetry for **3**. The P–N bond distances in all three compounds are typical for the amides of P^{IV} acids,[5] with the possible exception of the unusually long bond in one of the two molecules of **3**. Dramatic variations have however been

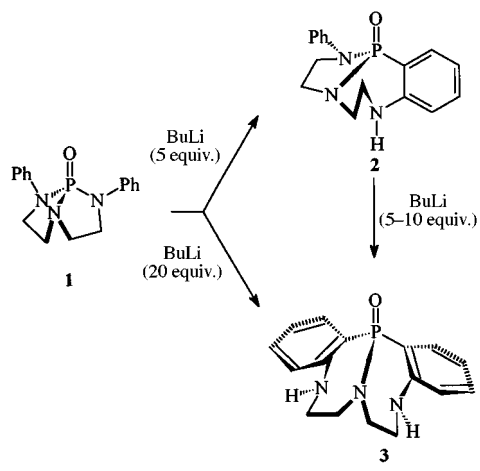

Scheme 1

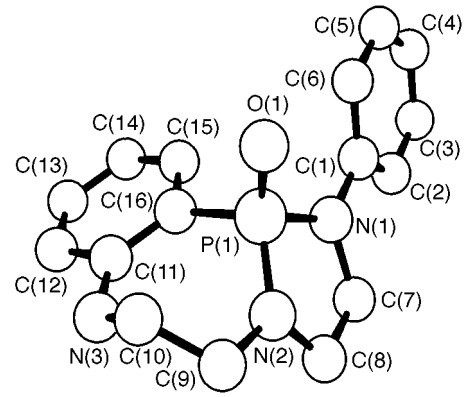

Fig. 1 ORTEP[11] plot of the structure of **2**.

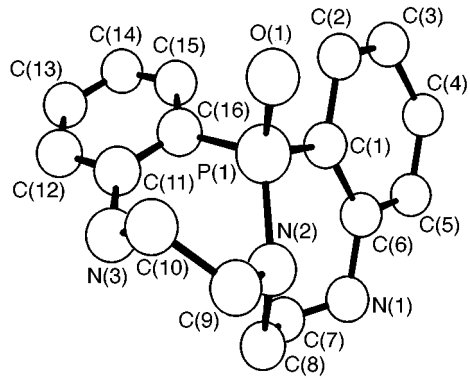

Fig. 2 ORTEP[11] plot of the structure of **3**.

Table 1 Structural data for amides **1**–**3**

Compound	P=O/Å	P–N/Å	P–C/Å
1[a]	1.437(5)	1.653(6) 1.661(6) 1.676(6)	
2	1.479(2)	1.675(2)[b] 1.630(3)[c]	1.816(3)
3	1.641(3)[d] 1.578(3)[d]	1.785(4)[d] 1.664(4)[d]	1.608(4)[e] 1.750(4)[e] 1.607(4)[e] 1.959(5)[e]

[a] Taken from ref. 3. [b] P–N(Ph) bond. [c] P–N(CH$_2$)$_2$ bond. [d] For two crystallographically independent molecules. [e] Each pair for one of the two crystallographically independent molecules.

observed within the series **1**, **2**, **3** for the distance parameter of the phosphoryl group. It is well known that the P–O bond distance in the phosphoryl function is insensitive to its molecular environment or external effects; for example, although the P=O group can accept up to three hydrogen bonds, its length seems to be little affected.[6] The average P=O bond length in phosphates is given as 1.462 Å, with the extreme range of 1.38–1.56 Å observed for 82 compounds studied.[7] The phosphoryl group in **1** represents a typical, average case of the P=O bond distance. The rearrangement to the structure **2** results in some increase of the P=O bond length, but still within the typical range. It is, however, the 7/7-membered fused ring system **3**, in which a dramatic elongation of the P=O bond takes place. In fact, the values of 1.578 and 1.641 Å locate the function within the typical range for a *single* P–O bond (1.56–1.64 Å[7]), thus indicate the dipolar resonance notation, P^{+}–O^{-}. Since **3** belongs to the class of *N*,*N*-disubstituted diarylphosphinic amides, it could be compared with the simplest analogue $Ph_2P(O)NMe_2$. The P=O bond distance in the latter was determined as 1.47 Å;[8] for **3** the average value is 0.14 Å greater, indicating *ca.* 10% elongation of the phosphoryl bond. A Cambridge Crystallographic Data File search revealed the distribution of the P=O bond distances for phosphinic amides [C(C)P(O)N structural unit, 44 structures], as shown in Fig. 3, showing that the P=O distance in **3** lies beyond the usual range, particularly in view of the fact that the few cases with the P=O distance greater than 1.49 Å concern complexes with Lewis acids, *i.e.* when a decrease in the P=O bond order is expected. The elongation of the P–O distance in **3** is not a consequence of any unusual 'back donation' effect of the amide nitrogen, as there is not only no shortening of the P–N bond in **3**, but the amide bond is slightly longer than the typical value for the related systems. The change in the nature of the P=O bond in **3** was confirmed by IR spectroscopy. The characteristic bands for the P=O stretching vibrations occur in the range of 1200–1400 cm^{-1}.[9] For **1** the ν_{PO} = 1234 cm^{-1}, similar to that of 1209 cm^{-1} reported for HMPA.[9] The change of **1** to **2** is followed by a bathochromic shift to ν_{PO} = 1185 cm^{-1}; for **3** the absorption occurs at 1162 cm^{-1}, beyond the usual range for the phosphoryl compounds and approaching the range typical for a single P–O bond stretching vibration.

In the solid state the molecules of **3** are interconnected *via* a network of hydrogen bonds between the phosphoryl oxygens and the N–H amine functions. Because of the packing pattern, there are three types of N–H···O=P bonds, each characterized by the following values of the N···O distance and the N–H···O angle: (i) 2.495(6) Å, 163(4)°; (ii) 3.478(6) Å, 167(3)°; (iii) 2.866(5) Å, 175(5)°. Those values are similar to the parameters observed for other phosphoric amides,[5] and do not indicate any particularly strong bonding that might be responsible for the unusually long P–O distance. It seems therefore that the observed bonding parameters are a consequence of the specific steric effects operating in the highly rigid skeleton of the molecule. This in turn suggested that the reactivity of the amide bond in **3** should differ from that observed for simple phosphinic amides, as well as from the reactivity of the precursors **2** and **1**. The reactivity of **3** is currently being studied in our laboratory.

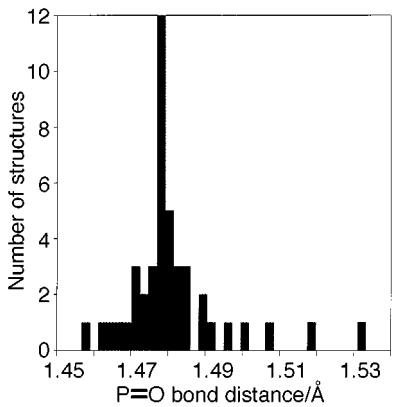

Fig. 3 Distribution of the P=O bond distances in phosphinic amides.[12]

Notes and references

† BuLi-induced rearrangement of **1**: A solution of **1** (0.60 g, 2.0 mmol) in anhydrous THF (100 ml) was cooled to −78 °C under an atmosphere of dry nitrogen. The required amount of BuLi (1.6 M solution in hexane) was added by means of a syringe with stirring and cooling. The solution was stirred at −78 °C for 1 h, warmed to room temperature and stirred for the required period. MeOH (1–2 ml) was added, followed by $CHCl_3$ (200 ml), and the solution was washed with water, dried (Na_2SO_4) and evaporated under reduced pressure. The crude product was purified by column chromatography (SiO_2, $CHCl_3$–acetone, 1 : 1). *Selected data* for **2** (prepared using BuLi (5 equiv.), 2 h of stirring at room temp., 0.51 g, 85%): mp 236.4–237.7 °C (from THF); δ_H(300 MHz, $CDCl_3$) 3.05–3.25 (2H, m), 3.40–3.68 (4H, m), 3.70–3.82 (1H, m), 3.96 (1H, m), 4.32 (1H, br s), 6.55–6.64 (2H, m), 7.00 (1H, t, *J* 6.8), 7.09 (1H, t, *J* 6.7), 7.29 (3H, m), 7.43 (2H, d, *J* 6.4); δ_C(CD_3OD) 47.1 (s), 48.2 (d, *J* 9.1), 49.5 (d, *J* 10.3), 52.8 (d, *J* 6.3), 120.2 (s), 120.4 (s), 120.7 (s), 120.8 (d, *J* 11.6), 124.9 (s), 131.9 (s), 132.4 (d, *J* 7.6), 134.2 (s), 146.3 (d, *J* 6.3), 154.4 (d, *J* 7.8); δ_P($CDCl_3$) 23.7 (Found: C, 64.61; H, 6.17; N, 14.08. $C_{16}H_{18}N_3OP$ requires: C, 64.21; H, 6.06; N, 14.04%). For **3** (prepared using BuLi (20 equiv.), 10 h of stirring at room temp., 0.30 g, 50%): mp 253.6–254.3° (decomp.); δ_H($CDCl_3$) 3.12 (2H, m), 3.41 (2H, m), 3.63 (4H, m), 4.06 (2H, br s), 6.67 (2H, dd, *J* 5.4, 1.0), 6.83 (2H, dd, *J* 5.5, 1.1), 7.23 (2H, m), 7.41 (2H, ddd, *J* 14.3, 7.7, 1.6); δ_C(CD_3OD) 49.6 (s), 56.4 (d, *J* 3.6), 121.1 (s), 121.3 (s), 121.4 (d, *J* 9.8), 135.1 (s), 135.8 (d, *J* 9.3), 155.0 (d, *J* 5.0); δ_P($CDCl_3$) 33.1 (Found: C, 64.28; H, 6.06; N, 13.81%).

‡ *Crystal data* for **2**: $C_{16}H_{18}N_3OP$, *M* = 299.30, monoclinic, space group $P2_1/n$ (No. 14), *a* = 8.201 (3), *b* = 9.054 (2), *c* = 20.266 (2) Å, β = 91.65 (2)°, *U* = 1504 (1) $Å^3$, *F*(000) = 632, λ(Mo-Kα) = 0.7107 Å, μ(Mo-Kα) = 0.185 mm^{-1}, *T* = 295 (1) K, *Z* = 4, D_c = 1.32 g cm^{-3}, 4659 reflections measured on a diffractometer in the range $3 \leqslant \theta \leqslant 30°$, ($R_{int}$ = 0.018). The structure was solved by different methods and refinement, based on F^2, was by full-matric least-squares methods (ref. 10) to *R*1 = 0.078, *wR*2 = 0.183, $w = 1/[\sigma^2(F_o^2) + (0.0584P)^2 + 0.8458P]$ where $P = (F_o^2 + 2F_c^2)/3'$ for 194 parameters using 2899 unique reflections with $I > 2\sigma(I)$. For **3**: $C_{16}H_{18}N_3OP$, *M* = 299.30, monoclinic, space group $P2_1/n$ (No. 14), *a* = 13.959 (30), *b* = 13.773 (2), *c* = 16.077 (4) Å, β = 113.44 (3)°, *U* = 2836 (1) $Å^3$, *F*(000) = 1264, λ(Mo-Kα) = 0.7107 Å, μ(Mo-Kα) = 0.196 mm^{-1}, *T* = 293 (2) K, *Z* = 8, D_c = 1.402 g cm^{-3}. Data were collected on a diffractometer in the range $1 \leqslant \theta \leqslant 30°$ (5169 reflections). The structure was solved by direct methods and refinement (ref. 10), based on F^2, was by full-matrix least-squares to *R*1 = 0.060, *wR*2 = 0.146, $w = 1/[\sigma^2(F_o^2) + (0.0916P)^2]$ where $P = [\max(F_o^2,0) + 2F_c^2]/3$ for 416 parameters using 2479 unique reflections with $I > 2\sigma(I)$. There are two independent molecules in the asymmetric unit. CCDC 182/1208. Crystallographic data are available in .cif format from the RSC website, see http://www.rsc.org/suppdata/cc/1999/853/

§ Emsley and Hall reported the value of 1.84 Å as average P–C bond length (ref. 4).

1 X. Y. Mbianda, T. A. Modro and P. H. van Rooyen, *Chem. Commun.*, 1998, 741.
2 A. M. Jardine, S. M. Vather and T. A. Modro, *J. Org. Chem.*, 1988, **53**, 3983.
3 S. A. Bourne, X. Y. Mbianda, T. A. Modro, L. R. Nassimbeni and H. Wan, *J. Chem. Soc., Perkin Trans. 2*, 1998, 83.
4 J. Emsley and D. Hall, *The Chemistry of Phosphorus*, Harper and Row, London, 1976, p. 34.
5 M. P. du Plessis, T. A. Modro and L. R. Nassimbeni, *J. Org. Chem.*, 1982, **47**, 2313.
6 D. E. C. Corbridge, *Phosphorus. An outline of its chemistry, biochemistry and technology*, 4th edn., Elsevier, Amsterdam, 1990, p. 963.
7 D. E. C. Corbridge, *The Structural Chemistry of Phosphorus*, Elsevier, Amsterdam, 1974, p. 262.
8 M. U. Haque and C. N. Caughlan, *J. Chem. Soc., Chem. Commun.*, 1966, 921.
9 R. A. Nyquist and W. J. Potts, in *Analytical Chemistry of Phosphorus Compounds*, ed. M. Halmann, Wiley-Interscience, New York, 1972, p. 205.
10 G. M. Sheldrick, SHELX-97: Programs for crystal structure analysis, University of Göttingen, Germany, 1997.
11 C. K. Johnson, ORTEP, Report ORNL-3794, Oak Ridge National Laboratory, Tennessee, USA, 1965.
12 F. H. Allen and O. Kennard, *Chem. Des. Automat. News*, 1993, **8**, 31.

Communication 9/01877H

ChemComm

A simple entry towards novel bi- and tricyclic *N*-oxy-β-lactams by high pressure promoted tandem [4 + 2]/[3 + 2] cycloadditions of enol ethers and β-nitrostyrene

George J. Kuster,[a] Faysal Kalmoua,[a] Rene de Gelder[b] and Hans W. Scheeren*[a]

[a] *Department of Organic Chemistry, NSR Center for Molecular Structure, Design and Synthesis, University of Nijmegen, Toernooiveld, 6525 ED Nijmegen, The Netherlands. E-mail: jsch@sci.kun.nl*

[b] *Department of Inorganic Chemistry, NSR Center for Molecular Structure, Design and Synthesis, University of Nijmegen, Toernooiveld, 6525 ED Nijmegen, The Netherlands*

Received (in Liverpool, UK) 23rd February 1999, Accepted 11th March 1999

A high pressure promoted tandem [4 + 2]/[3 + 2] cycloaddition of β-nitrostyrene with a variety of enol ethers followed by a base catalysed rearrangement provided a novel class of di- and tricyclic *N*-oxy-β-lactam compounds.

Since the discovery of heteroatom activated β-lactams several reports mention the unique properties of this class of compound which show potential antibacterial activity. The biological activity of *N*-oxy-β-lactams has been attributed to electronic activation of the azetidinone ring. The oxygen atom directly attached to the ring makes the β-lactam more susceptible to nucleophilic attack than the corresponding *N*-alkyl-β-lactams.[1] Although polycyclic *N*-oxy-β-lactams can be considered as attractive targets in the search for new antibiotics only a few articles describing their synthesis have been reported.[2,3]

Here we describe a stereoselective route towards novel di- and tricyclic heteroatom activated β-lactams **1** from easily accessible building blocks such as enol ethers and β-nitrostyrene. The bi- and tricyclic *N*-oxo-β-lactams described are new compounds strongly resembling the biologically active bicyclic oxamazins.[2,4]

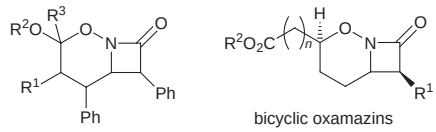

1a R^1 = H, R^2 = Et, R^3 = H
b R^1 = H, R^2 = PMB, R^3 = H
c R^1–R^3 = $(CH_2)_4$, R^2 = Me
d R^1–R^2 = $(CH_2)_2$, R^3 = H

Recently, we reported the one-pot three-component tandem [4 + 2]/[3 + 2] cycloaddition of nitroalkenes, enol ethers and mono-substituted electron-poor alkenes (Scheme 1).[5] The powerful effect of high pressure resulted in the formation of the nitroso-acetals **2** without the need of stoichiometric amounts of Lewis acid catalysts as reported by Denmark and Seebach.[6,7] Furthermore it is reported that 1,2-disubstituted olefins are unreactive under Lewis acid conditions at ambient pressure in this type of tandem [4 + 2]/[3 + 2] cycloaddition.[7] This stimulated us to study the reactivity of 1,2-disubstituted olefins under high pressure conditions.

Here we report the high pressure promoted tandem cycloaddition of enol ethers and β-nitrostyrene in which β-nitrostyrene reacts both as heterodiene and 1,2-disubstituted dipolarophile. In general, the tandem cycloaddition of the enol ether with an excess of β-nitrostyrene (4 equiv.) resulted in the formation of regioisomers **3** and **4** (Scheme 2). β-Nitrostyrene first reacts as an electron-poor diene in an inverse electron demand Diels–Alder reaction with an electron-rich enol ether and thereafter as an electron-poor dipolarophile with the *in situ* formed mono-adduct in a 1,3-dipolar cycloaddition. The reaction was studied with mono-substituted and cyclic enol ethers.

Surprisingly the main regioisomer **3** was converted in one step into β-lactam **1** during purification on silica gel using an eluent containing Et_3N, pointing to a base catalysed rearrangement (Scheme 2). This was further confirmed by stirring the crude reaction mixture in CH_2Cl_2 with a catalytic amount of Et_3N. In this way the same mixture of products was obtained. In agreement with these results it is suggested that first the acidic proton adjacent to the nitro group is removed by the base followed by N–O bond cleavage and elimination of nitrite (Scheme 2).[8] Table 1 shows the regioisomeric ratios of cycloadducts **1a**–**d** in the crude reaction mixture (measured by ^{1}H NMR).

The stereochemistry of the cycloadducts has been elucidated by high field 2D-NOESY ^{1}H NMR experiments. It was found that the [4 + 2] cycloaddition proceeded with complete regio- and *endo*-selectivity while the [3 + 2] cycloaddition proceeded with variable regioselectivity and with moderate *exo*-selectivity. However β-lactam **1** was formed after a completely *endo*-selective [4 + 2] and *exo*-selective [3 + 2] cycloaddition.

The stereochemistry of the cycloadducts is discussed on the basis of a representative example (entry 2, Table 1). The main product **7** and regioisomers **5a**† and **6** (Scheme 3) were detected by NMR analysis of the crude reaction mixture in a 7 : 2 : 1 ratio. After purification, β-lactam **1b**‡ and nitroso-acetals **5b** and **6** were isolated in a 7 : 2 : 1 ratio, indicating a complete conversion of **7** to **1b** and **5a** to **5b**. Product **5b** is the NO_2 epimer of the *endo*[4 + 2]-*anti-endo*[3 + 2]-isomer **5a** and product **6** is the

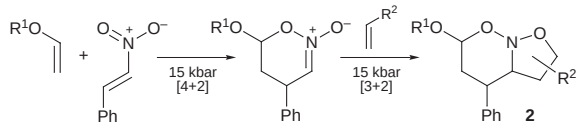

Scheme 1

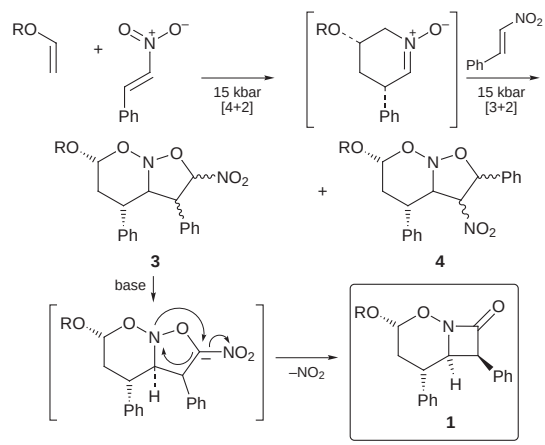

Scheme 2

Table 1 Synthesis of *N*-oxy-β-lactams **1a–d**

Entry		Ratio **3** : **4**	Yield (%)[a]	β-Lactam (%)[b]
1	**1a**	6 : 4	63	38
2	**1b**	7 : 3	87	61
3	**1c**	7 : 3	90	63
4	**1d**	3 : 7	68	20

[a] Combined yield of β-lactam **1** and regioisomer **4**. [b] Chemical yield of β-lactam after purification.

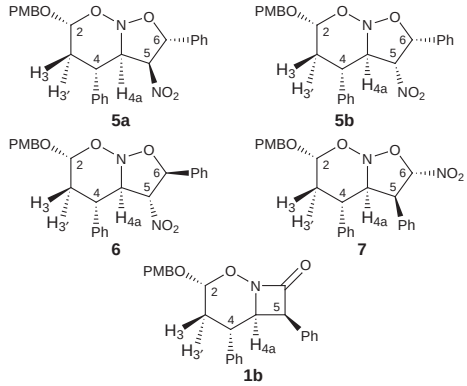

Scheme 3

endo[4 + 2]-*anti*-*exo*[3 + 2]-isomer.[9] Some crystals of compound **7** were obtained from the crude reaction mixture and the structure of **7** was assigned by 2D-NMR as depicted in Scheme 3. The C-5 epimer of β-lactam **1b** was not detected. NOE contact between H-4a and H-5 of **1b** indicate a *cis* configuration for these protons. The formation of regioisomers **5b** and **6** however proceeded with less selectivity (**5b** : **6** = 2 : 1). NOE-contacts between H-2 and H-3, H-3 and H-4, and H-2 and H-4 indicate a chair-like conformation of the 6-membered ring formed after the *endo*-selective hetero Diels–Alder reaction. These NOE contacts were observed for both regioisomers **5b**, **6** and β-lactam **1b**. X-Ray analysis of compound **1b** confirmed the configuration of the 6-membered ring. In all cases the attack of β-nitrostyrene in the [3 + 2] dipolar cycloaddition was *anti* (with respect to the phenyl group) since a *trans* relationship between H-4a and H-4 was found in the cycloadducts.

The formation of regioisomer **7** is rather unexpected since literature data concerning the 1,3-dipolar cycloaddition of nitrones and olefins with unequally electron-withdrawing groups such as nitro and phenyl substituents predict opposite regioselectivity (*e.g.* **5** and **6**).[10] AM1 calculations predict a HOMO-dipole controlled formation of regioisomers **5** and **6**.[11] The experimental regioisomeric outcome could be explained on the basis of charge distribution between dipole and dipolarophile obtained through AM1 calculations which is in agreement with calculations reported by Baskaran *et al.*[12,13]

1-Phenyl-2-nitropropene and *p*-methoxybenzyl vinyl ether reacted stereoselectively to give *endo* [4 + 2] adduct **9**. This mono-adduct failed to react with another molecule of 1-phenyl-2-nitropropene (15 kbar, 50 °C, 48 h) probably because of steric hindrance but it reacted completely regio- and stereoselectively with β-nitrostyrene in accordance with the predicted regioselectivity towards bicyclic nitroso-acetal **10**[13] (Scheme 4).

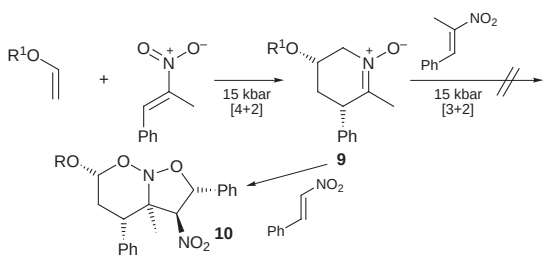

Scheme 4

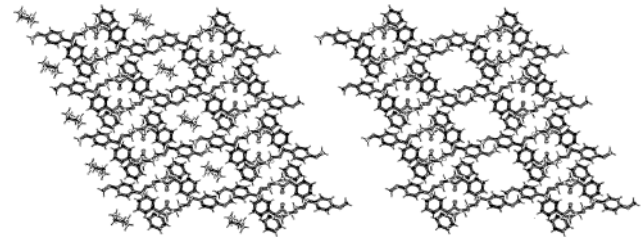

Fig. 1 2D depiction of the X-ray structure of β-lactam **1b** with (left) and without (right) cyclohexane.

Interestingly the X-ray structure of **1b** showed parallel oriented channels with aromatic walls holding cyclohexane molecules present in the solvent from which the compound was crystallised (Fig. 1). It seems that **1b** acts as an organic zeolite since complete selectivity for the inclusion of cyclohexane was found after crystallisation from *n*-hexane–CH_2Cl_2 (*n*-hexane contains 3–10% cyclohexane by GC analysis). The zeolite properties of this compound are under investigation (*e.g.* inclusion of other solvents or chiral compounds).

We gratefully acknowledge the support of NWO-CW and Solvay Pharmaceuticals.

Notes and references

† *Crystal data* for **5a**: $C_{26}H_{26}N_2O_6$, M = 462.49, triclinic, a = 8.9646(6), b = 9.4791(8), c = 14.7752(4) Å, α = 95.628(5), β = 100.8151(5), γ = 103.968(6)°, U = 1183.00(12) Å^3, T = 293 K, $P\bar{1}$, Z = 2, μ(Cu-Kα) = 0.765 mm^{-1}, 4780 reflections, 4471 unique (R_{int} = 0.0072) which were used in all calculations. The final $wR(F^2)$ was 0.1169 (all data).
‡ *Crystal data* for **1b**: $C_{26}H_{25}NO_4$, M = 415.49, monoclinic, a = 18.7886(4), b = 7.41628(19), c = 19.3640(3) Å, β = 116.2092(16)°, U = 2420.80(8) Å^3, T = 208 K, $P2_1/a$, Z = 4, μ(Cu-Kα) = 0.664 mm^{-1}, 4736 reflections, 4583 unique (R_{int} = 0.0257) which were used in all calculations. The final $wR(F^2)$ was 0.1367 (all data). CCDC 1202. See http://www.rsc.org/suppdata/cc/1999/855/ for crystallographic data in .cif format.

1 M. Gosh and M. J. Miller, *Tetrahedron*, 1996, **52**, 4225.
2 S. R. Woulfe and M. J. Miller, *Tetrahedron Lett.*, 1984, **25**, 3293; D. Kronenthal, P. Kuester and W. H. Koster, 1986, USP 4574153; *Chem. Abstr.*, 1986, **105**, 60477.
3 Overview of multicyclic β-lactams (not heteroatom activated): C. Niu, T. Pettersson and M. J. Miller, *J. Org. Chem.*, 1996, **61**, 1014 and refs. cited therein.
4 Representative experimental procedure for high pressure promoted tandem cycloaddition: 1 mmol of enol ether and 4 mmol of nitrostyrene were dissolved in CH_2Cl_2 and placed in a Teflon tube (7.5 mL) which was transferred in the high pressure apparatus (R. W. M. Aben and J. W. Scheeren, *J. Org. Chem.*, 1987, **52**, 365. After application of 15 kbar for 17 h (room temperature), the β-lactam was isolated from the reaction mixture by column chromatography using silica gel 60 and EtOAc–hexane (1 : 4) containing 1% Et_3N as eluent.
5 R. M. Uittenboogaard, J.-P. G. Seerden and J. W. Scheeren, *Tetrahedron*, 1997, **34**, 11 929.
6 S. E. Denmark and A. Thorarensen, *Chem. Rev.*, 1996, **96**, 137.
7 M. A. Brook and D. Seebach, *Can. J. Chem.*, 1987, **65**, 836.
8 A similar transformation has been reported by Padwa *et al.* A. Padwa, K. F. Koehler and A. Rodriguez, *J. Org. Chem.*, 1984, **49**, 282.
9 Compound **5a** was isolated from the crude reaction mixture by crystallisation from CH_2Cl_2–hexane. X-Ray analysis confirmed the configuration assigned by 2D-NOESY analysis. Product **5b** is formed *via* a base-promoted epimerisation of **5a**.
10 Review: D. C. Black, R. F. Crozier and V. C. Davis, *Synthesis*, 1975, 205; M. Joucla, D. Gree and J. Hamelin, *Tetrahedron*, 1973, **29**, 2315; Nour El-Din and Ahmed Moukhtar, *Bull. Chem. Soc. Jpn.*, 1986, 59, **4**, 1239.
11 MOPAC QCPE program no. 455 version 6.0 was used for AM1 calculations. M. J. S. Dewar, E. G. Z. Zoebisch, E. F. Healy and J. J. P. Stewart, *J. Am. Chem. Soc.*, 1985, **107**, 3902.
12 S. Baskaran, C. Baskaran, Pradeep J. Nadkarni and Girish K. Trivedi, *Tetrahedron*, 1997, **53**, 7057.
13 Further investigations concerning the regioselectivity of the [3 + 2] cycloadditions are in progress.

Communication 9/01505A

Typeset and printed by Black Bear Press Limited, Cambridge, England

Poly(ferrocenylsilanes): novel organometallic plastics

Ian Manners

Department of Chemistry, University of Toronto, 80 St. George St., Toronto M5S 3H6, Ontario, Canada.
E-mail: imanners@alchemy.chem.utoronto.ca

Received (in Cambridge, UK) 24th December 1998, Accepted 5th February 1999

Poly(ferrocenylsilanes) are a novel class of transition metal-containing macromolecules with a backbone that consists of alternating ferrocene and organosilane units. High molecular weight examples of these interesting materials were first prepared several years ago by thermal ring-opening polymerization (ROP) of silicon-bridged [1]ferrocenophanes ([1]silaferrocenophanes). This Feature Article discusses current knowledge of the properties of these readily available and processable organometallic polymers together with recent developments made possible by the discovery of living anionic and transition metal-catalyzed ROP routes. These methodologies have provided ambient temperature access to poly(ferrocenylsilanes) with molecular weight control and also to well defined architectures such as block copolymers. The latter materials self-assemble in the solid state to form ordered arrays of nanoscale redox-active organometallic domains and in solution form well defined supramolecular organometallic polymer aggregates such as spheres, cylinders, and more complex architectures.

Introduction

Whereas the synthetic scope and technological achievements of organic polymer science are remarkably impressive, the corresponding macromolecular chemistry of inorganic elements is at a much more primitive stage of development.[1] This is particularly the case for transition metal-based polymers which would be expected to possess a range of interesting and potentially useful physical and/or catalytic properties.[1,2] Nevertheless, synthetic breakthroughs, which have occurred sporadically over the last 10–15 years and at a more rapid pace recently, have provided access to a range of fascinating new materials.[1–5] Rigid rod poly(metallaynes) such as **1** and **2** provide an excellent illustration of the potential of this area.[4] These polymers, of which the first examples were reported at the end of the 1970s, possess novel conjugated backbones, and in several cases interesting physical properties such as lyotropic liquid crystallinity and third-order non-linear optical properties have been established.[1,4,6]

Much of the early pioneering work in transition metal-based polymer science in the 1950s and 1960s targeted poly(metallocenes).[7] Such efforts were encouraged by the remarkable stability and unusual properties of monomeric and dimeric metallocenes which were discovered by the fundamental, exploratory chemistry conducted during this period.[8] However, most of the attempted polymer syntheses utilized polycondensation reactions where either the difunctional monomeric precursors were impure or the coupling chemistry was not clean. For such step growth processes this guaranteed the generation of poorly defined, low molecular weight oligomeric materials (M_n < *ca.* 3000) of correspondingly low processability.[9] In addition, many of the resulting products were insoluble and poorly characterized.[9]

In 1992 our group reported the discovery of a thermal ring-opening polymerization (ROP) route to high molecular weight poly(ferrocenylsilanes) **4**, a novel class of poly(ferrocenes), from strained cyclic, silicon-bridged [1]ferrocenophane ([1]-silaferrocenophane) precursors (**3**).[10] This chain growth synthetic approach permitted access to very high molecular weight polymers with weight average molecular weights (M_w) and number average molecular weights (M_n) of the order of M_w = 10^5–10^6 and M_n > 10^5.[10–15] We have subsequently expanded this ROP methodology to a range of analogous strained monomers which contain other bridging elements and transition metals or different π-hydrocarbon rings.[15,16] In this article we

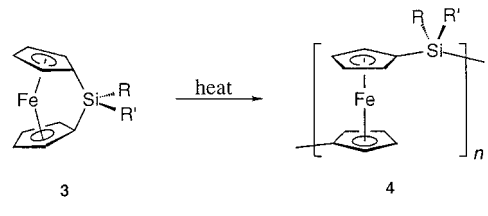

3 4

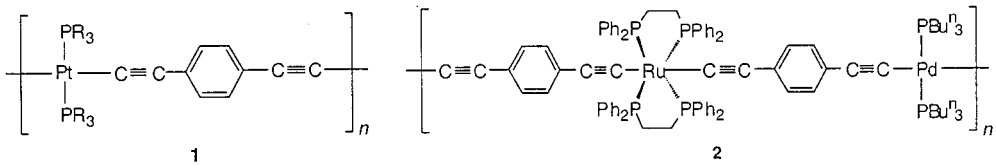

1 2

Professor Ian Manners is Professor of Chemistry in the Department of Chemistry, University of Toronto, Canada. He was born in London, England, in 1961 and received his BSc and PhD (with Professor Neil Connelly) from the University of Bristol in 1982 and 1985, respectively. From 1986–87 he was a Royal Society European Postdoctoral Fellow at the RWTH, Aachen (with Professor Peter Paetzold) and from 1988–90 he worked as a Research Associate (with Professor Harry R. Allcock) at the Pennsylvania State University, USA. He joined the Faculty at Toronto as an Assistant Professor in 1990. Manners' research interests focus on both the fundamental and applied aspects of the chemistry of rings, chains, and macromolecules based on main group or transition elements. He has received several awards and these include an E. W. R. Steacie Fellowship from Canada (1997–99), a Corday-Morgan Medal from the Royal Society (1997), an Alfred P. Sloan Fellowship from the USA (1994–98), and a University of Toronto Faculty of Arts and Science Outstanding Teaching Award (1993).

review progress specifically made on poly(ferrocenylsilanes) which have been particularly well studied since the initial ROP discovery. In particular we discuss some new directions arising from the development of more controlled polymerization methods which allow access to block copolymers. These have provided avenues to self-assembled, supramolecular organometallic polymer architectures.

Synthesis and properties of poly(ferrocenylsilanes)

[1]Silaferrocenophane monomers **3** are readily available on a substantial (>100 g) laboratory scale from the reaction of dilithioferrocene–tetramethylethylenediamine ($fcLi_2$·TMEDA) with dichloroorganosilanes $RR'SiCl_2$.[17] The first example of these species, the phenylated derivative **3** (R = R′ = Ph), was prepared by Osborn and Whiteley at the University of Exeter in the mid 1970s.[18] The cyclopentadienyl ligands present in [1]silaferrocenophanes are appreciably tilted with respect to one another by 16–21° which is indicative of the presence of appreciable ring strain which has been estimated to be *ca.* 60–80 kJ mol^{-1}.[16,19] Spirocyclic [1]silaferrocenophanes such as **5** are

5

also readily accessible.[18,20] The molecular structures of two typical [1]silaferrocenophanes polymerised in our group are shown in Fig. 1.[20,21]

Since the initial ROP discovery a wide range of silicon-bridge [1]ferrocenophanes **3** with either symmetrically or unsymmetrically alkyl- or aryl-substituted silicon atoms have been prepared and polymerized to afford high molecular weight poly(ferrocenylsilanes) **4**.[15] Substituents such as hydrogen, chlorine, trifluoropropyl, norbornenyl and ferrocenyl groups have also been introduced (Table 1).[15,22,23] Very recently, we have found a facile route to the first poly(ferrocenylsilanes)

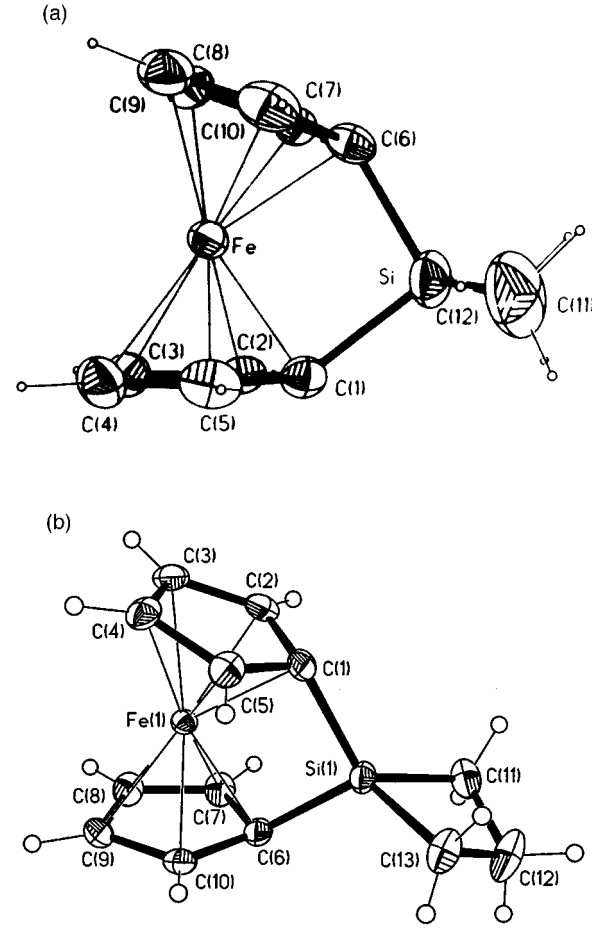

Fig. 1 Molecular structure of (a) silicon-bridged [1]ferrocenophane **3** (R = R′ = Me) and (b) spirocyclic [1]silaferrocenophane **5** determined by X-ray diffraction.

with alkoxy, aryloxy, and amino substituents at silicon.[24] These stable materials (**8** and **10**, respectively) are accessible *via* the ROP of similarly substituted [1]silaferrocenophane precursors (**7** and **9**) which can be accessed *via* nucleophilic substitution

Table 1 Thermal transition and GPC molecular weight data[a] for selected poly(ferrocenylsilanes)[15,22–24]

Polymer	R/OR	R′/OR	$T_g(T_m)$[b]/°C	M_n[a]	PDI[c]
4	H	H	16 (165)	—[e]	—[e]
4	Me	Me	33 (122–143)	3.4×10^5	1.5
4	Et	Et	22 (108)	4.8×10^5	1.6
4	Pr^n	Pr^n	24 (98)	8.5×10^4	2.7
4	Bu^n	Bu^n	3 (116, 129)	3.4×10^5	2.6
4	*n*-C_5H_{11}	*n*-C_5H_{11}	−11 (80–105)	3.0×10^5	1.6
4	*n*-C_6H_{13}	*n*-C_6H_{13}	−26	7.6×10^4	1.5
4	Me	H	9 (87, 102)	4.2×10^5	2.0
4	Me	$CH_2CH_2CF_3$	59	8.1×10^5	3.3
4	Me	$CH{=}CH_2$	28	7.7×10^4	2.1
4	Me	*n*-$C_{18}H_{37}$	1 (16)	5.6×10^5	2.5
4	Me	Ph	54	1.5×10^5	2.0
4	Me	Fc[d]	99	7.1×10^4	2.3
4	Me	5-Norbornyl	81	1.1×10^5	1.5
8	OMe	OMe	19	1.5×10^5	1.9
8	OEt	OEt	0	3.8×10^5	2.1
8	OCH_2CF_3	OCH_2CF_3	16	2.2×10^5	1.2
8	OBu	OBu	−43	3.9×10^5	2.1
8	OC_6H_{13}	OC_6H_{13}	−51	0.9×10^5	2.4
8	$O(CH_2)_{11}Me$	$O(CH_2)_{11}Me$	(−30)	1.9×10^5	2.5
8	$O(CH_2)_{17}Me$	$O(CH_2)_{17}Me$	(32)	2.3×10^5	2.2
8	OPh	OPh	54	2.3×10^5	2.0
8	$OC_6H_4Bu^t$-*p*	$OC_6H_4Bu^t$-*p*	89	1.9×10^5	1.9
8	OC_6H_4Ph-*p*	OC_6H_4Ph-*p*	97	5.4×10^4	2.4

[a] GPC data obtained from the analysis of THF polymer solutions which contained 0.1% $[Bu_4N][Br]$ and molecular weight values are relative to polystyrene standards. Although in this case GPC provides only molecular weight estimates absolute determinations of M_w by static light scattering for several polymers have indicated that GPC underestimates the real values by a factor of two (see ref. 15) [b] DSC data collected at a heating rate of at 10 °C min^{-1}. [c] PDI = M_w/M_n. [d] Fc = $(\eta\text{-}C_5H_4)Fe(\eta\text{-}C_5H_5)$. [e] Insoluble polymer.

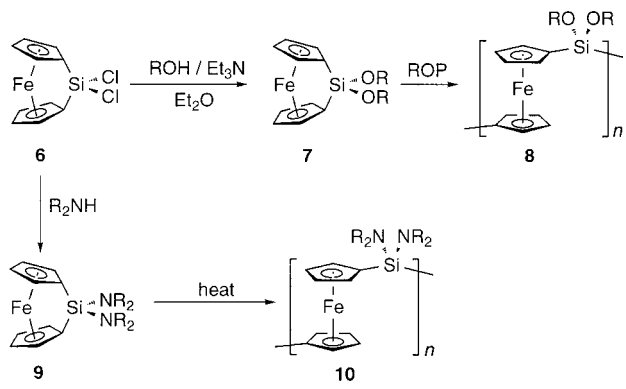

Scheme 1

reactions on the $SiCl_2$-bridged [1]ferrocenophane **6** (Scheme 1). The latter species is easily prepared in high yield *via* the reaction of $fcLi_2$·TMEDA with $SiCl_4$.

Because of their novel backbone of alternating ferrocene and organosilane units it is interesting to consider how the poly(ferrocenylsilane) chains pack together in the solid state and the possible chain conformations that might exist.[25] Another important feature of these polymers is their glass transition temperature (T_g) which reflects, at least to a certain degree, the conformational flexibility present. Regular packing in the solid state (*i.e.* crystallization) is possible for many symmetrically substituted derivatives.[15,25] For example, the prototypical poly(ferrocenylsilane), the dimethyl derivative **4** (R = R′ = Me), is an amber, film-forming thermoplastic [Fig. 2(a)] which possesses melt transitions (T_m) in the range 122–143 °C.[15,25,26] Crystals on the surface of aged polymer films can be observed by atomic force microscopy [Fig. 2(b)].[27] This material possesses a T_g at 33 °C, which is remarkably low for a polymer with a bulky unit such as ferrocene in the main chain. The ability of the iron atom in ferrocene to act as a freely rotating 'molecular ball-bearing' probably plays a key role in generating the observed conformational flexibility. The manner in which these polymer chains pack in the solid state for this polymer has attracted significant interest and has been examined by detailed conformational calculations and X-ray structural studies of well defined oligomers by O'Hare and coworkers and ourselves, respectively.[28,29]

Poly(ferrocenyldimethylsilane) [**4** (R = R′ = Me)] can be melt-processed into shapes above 150 °C [Fig. 2(c)] and can be used to prepare crystalline, nanoscale fibers (diameter < 1.5 μm) by electrospinning in which an electric potential is used to produce an ejected jet from a solution of the polymer in THF which subsequently stretches, splays, and dries. The nanofibers of different thickness show different colours due to interference effects similar to those in soap bubbles [Fig. 2(d)].[30]

Like the dimethyl material, other symmetrically substituted poly(ferrocenylsilanes) with short (C_2–C_5) alkyl chains at silicon will also crystallize and similar melting behavior is observed (Table 1). In contrast to the poly(ferrocenylsilanes) with shorter C_2–C_5 alkyl chains, the *n*-hexyl analogue **4** (R = R′ = *n*-hexyl) is an amber, gummy amorphous material with a T_g of −26 °C. Alkoxy-substituted poly(ferrocenylsilanes) such as **8** (OR = *n*-hexyloxy) are also amorphous and possess T_g values down to −51 °C. Poly(ferrocenylsilanes) with longer alkoxy side chains [*e.g.* **8** (OR = *n*-octadecyloxy)] have been found to crystallize and form lamellar structures with interdigitated side groups.[24]

In addition to their morphological behavior, considerable effort has also been directed towards investigating and understanding the physical properties of the resulting poly(ferrocenylsilane) materials the vast majority of which are soluble in organic solvents despite their very high molecular weights. Cyclic voltammetric studies of poly(ferrocenylsilanes) generally show the presence of two reversible oxidation waves spaced by *ca.* 0.25 V in a 1 : 1 ratio providing clear evidence for the existence of interactions between the iron atoms.[15] The proposal that initial oxidation occurs at alternating iron sites along the main chain followed by oxidation of those remaining at a higher potential has been supported by recent detailed work on individual members of a series of model oligomers with between two and nine ferrocene units.[29] Comparisons of the behavior of poly(ferrocenylsilanes) with analogous polymers suggest that the metal–metal interactions are mediated by the silicon spacer.[31] Poly(ferrocenylsilanes) also possess interesting hole transport properties and partial oxidation leads to a 10^{10} increase in electrical conductivity up to semiconductor values (*ca.* 10^{-3}–10^{-4} S cm^{-1}).[32] Thin films of the polymers are attracting attention as, for example, chemomechanical sensors, electrochromic materials, electrode mediators, and variable refractive-index materials.[33–36] The polymers also have interesting potential as precursors to ceramic materials. Thus, heating to 500–1000 °C can yield magnetic ceramics containing α-Fe crystallites. In several cases the ceramic yield is > 90% and allows the formation of ceramic monoliths with shapes defined by that of the processable polymeric precursor.[37] Oxidation of poly(ferrocenylsilanes) has been reported[38] to yield materials which display spin alignment, albeit at low temperatures although other studies have not reproduced these results.[39]

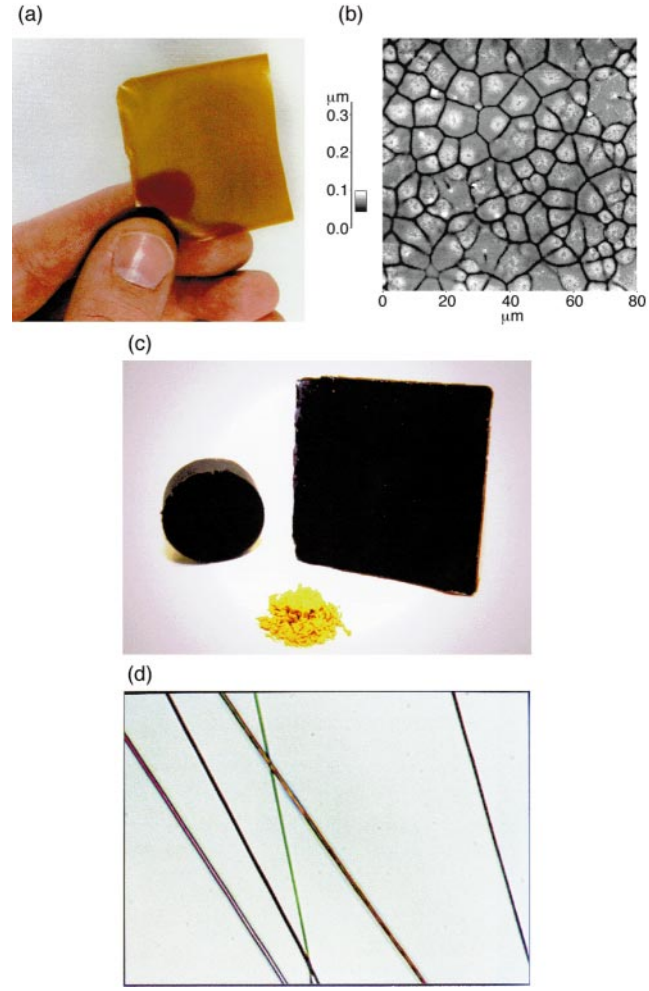

Fig. 2 Poly(ferrocenyldimethylsilane) **4** (R = R′ = Me): (a) a solvent-cast film, (b) surface crystals grown on a thin film after 3 months observed by atomic force microscopy, (c) melt-processed fabricated shapes, (d) electrospun fibers. Figures (b) and (d) are courtesy of Nina Sheller and Mark D. Foster and Zhihao Chen, Hao Fong, Darrell H. Reneker, and Mark D. Foster, respectively, of the Institute of Polymer Science at the University of Akron, USA.

Very recently, controlled crosslinking of poly(ferrocenylsilanes) has been achieved to yield solvent swellable, redox-active gels. The crosslinking can be controlled by using specific amounts of the spirocyclic [1]ferrocenophane **5** (Fig. 1) in the polymerization mixtures.[20]

Functionalization of poly(ferrocenylsilanes) has been achieved by several methods (Scheme 2).[23,40] For example,

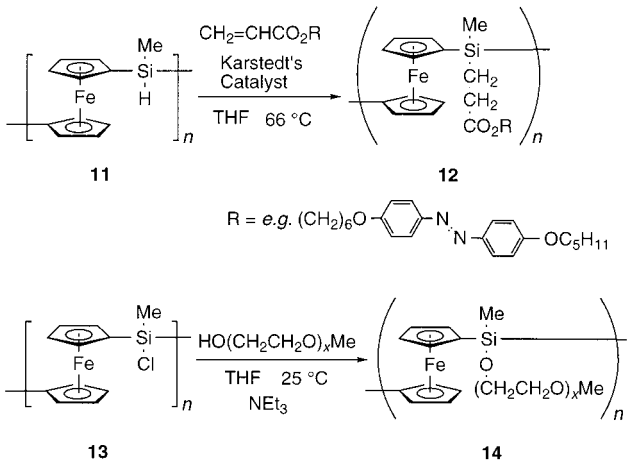

11 **12** **13** **14**

Scheme 2

ROP of [1]silaferrocenophane **4** (R = Me, R′ = H) with a Si–H functionality affords **11** which undergoes metal-catalyzed hydrosilylation reactions. This methodology has been recently used to prepare thermotropic liquid crystalline poly(ferrocenylsilanes) such as **12**. To illustrate another approach, ROP of **4** (R = Me, R′ = Cl) followed by substitution of Si–Cl bonds present in poly(ferrocenylsilane) **13**, permits access to water soluble poly(ferrocenylsilanes) such as **14** ($x \sim 7$).

Living anionic ROP of silicon-bridged [1]ferrocenophanes

Thermal copolymerization can be used to prepare random copolymers from mixtures of different silicon-bridged [1]ferrocenophanes and also copolymers of ferrocenophanes with other monomers such as cyclic silanes and silicon-bridged bis(benzene)chromium complexes.[32,41] However, thermal ROP of metallocenophanes at elevated temperatures leads to virtually no control over molecular weight and the molecular weight distribution is broad with polydispersity indices (PDI = M_w/M_n) of *ca.* 1.5–2.5. In 1994 we showed that highly purified silicon-bridged [1]ferrocenophanes undergo living anionic ROP at 25 °C using initiators such as Bu^nLi in THF.[42] This has permitted the synthesis of poly(ferrocenylsilanes) **15** (E = H) with controlled molecular weights and narrow molecular weight distributions (polydispersities < 1.3) and has also allowed the preparation of end-functionalized polymers **15** (E ≠ H) and the first block copolymers (*e.g.* **16** and **17**) containing skeletal transition metal atoms (Scheme 3).[43]

Logical further developments of this chemistry include the extension to other organic (and inorganic) monomers to access other poly(ferrocene) multiblock systems. Moreover, the ability to functionalize chain ends should allow the development of end-functionalized, redox-active polymers for surface (*e.g.* electrode) attachment, *etc.*[11,43]

Transition metal catalyzed ROP of [1]ferrocenophanes

Transition metal-catalyzed ROP of silicon-bridged [1]ferrocenophanes, which also occurs in solution at room temperature,

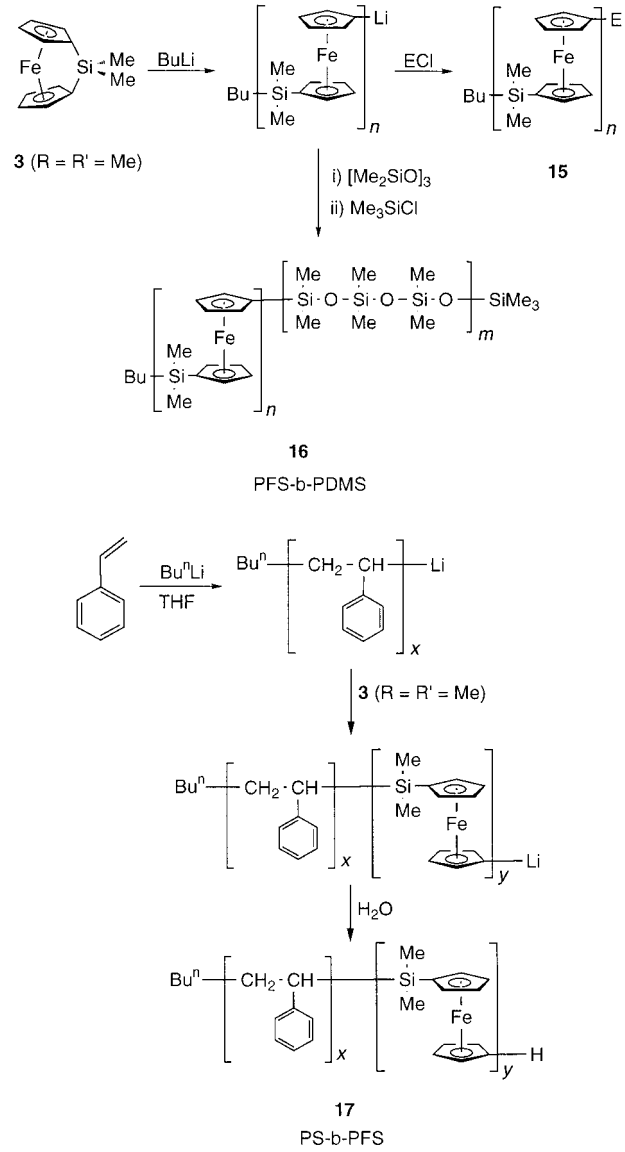

Scheme 3

has also been reported using Pt^{II}, Pt^0, Rh^I, and Pd^{II} pre-catalysts.[44,45] Significant understanding of the mechanism of these transition metal-catalyzed reactions has also been forthcoming and a possible mechanism is shown in Scheme 4.[9]

The initial step is believed to be insertion of the transition metal into the strained Cp–Si bond. Indeed, species such as **18** have been prepared from exactly this type of reaction [in the case of **18** from **3** (R = R′ = Me) and Pt(1,5-cod)$_2$] and function as ROP precatalysts.[46]

Transition metal catalyzed ROP is a mild method which does not require monomer with an exceptional degree of purity and has now been developed to the stage where considerable control over poly(metallocene) architectures is possible.[47,48] For example, [1]silaferrocenophanes with different cyclopentadienyl rings (**19**) undergo transition metal catalyzed ROP to yield the regioregular, crystalline poly(ferrocenylsilane) **20** whereas thermal ROP affords a regioirregular amorphous material **21** (Scheme 5).

Addition of sources of Si–H bonds such as Et_3SiH to the polymerization mixture allows molecular weight control (Fig. 3). The process is believed to occur *via* competition of the Si–H bond and the strained Si–C bond of the [1]ferrocenophane for oxidative addition at the metal center. Addition of the Si–H bond followed by reductive elimination affords the Et_3Si–fc and Si–H terminated product (**22**).

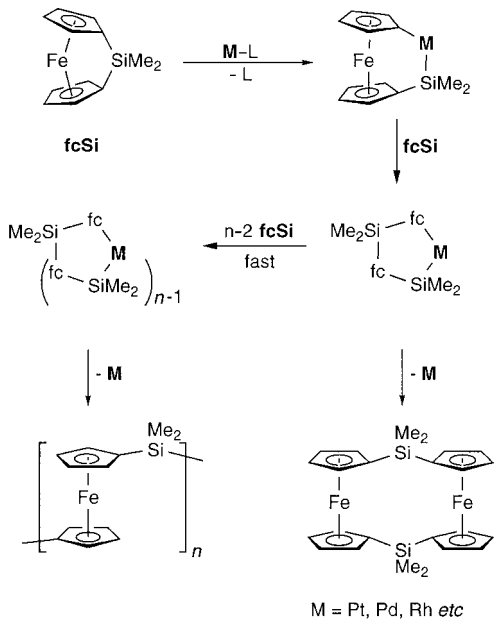

Scheme 4

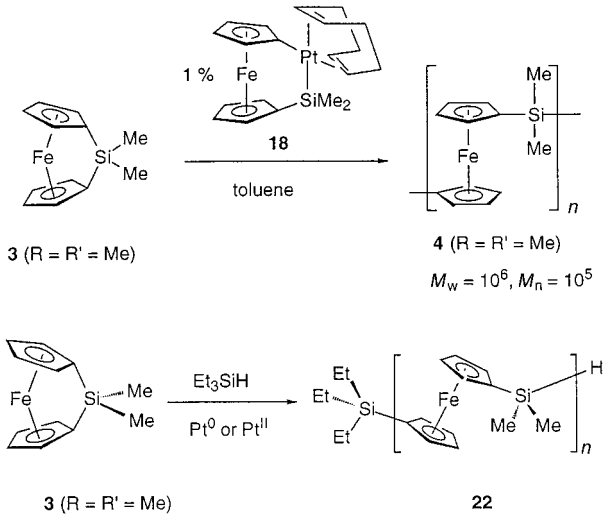

If polysiloxanes with Si–H groups as substituents or as terminii are used in place of Et_3SiH then graft (**23**) or block (**24**) copolymers can be prepared. Moreover, the use of cyclic tetrasiloxanes as sources of the Si–H functionalities allows the preparation of novel poly(ferrocenes) (**25**) with star architectures with a cyclosiloxane core (Scheme 6). The remarkable convenience by which complex organometallic polymer architectures can be constructed compensates for the broader polydispersities (M_w/M_n = 1.4–1.8) compared to materials prepared *via* anionic polymerization (M_w/M_n < 1.3).

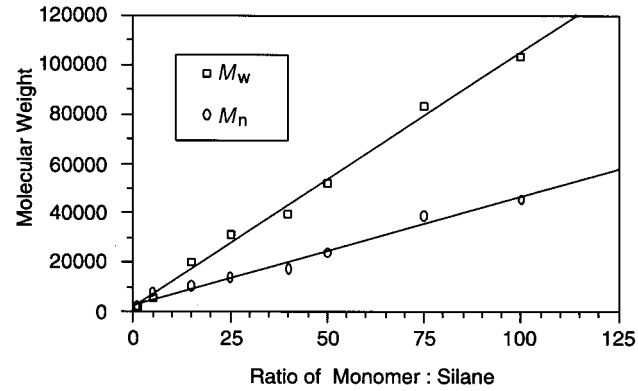

Fig. 3 Plot of M_w and M_n *vs.* ratio of monomer **3** (R = R′ = Me): Et_3SiH demonstrating molecular weight control (using Karstedt's catalyst in toluene).

Applications of ring-opened poly(ferrocenes) in the preparation of magnetic nanostructures

As mentioned above, poly(ferrocenylsilanes) function as preceramic polymers and have been shown to yield interesting ferromagnetic ceramic composites at 500–1000 °C which contain Fe particles in a SiC/C matrix.[37] The use of such involatile but processable polymeric precursors to ceramics is potentially an attractive way of circumventing the difficulty of processing ceramic materials into desired shapes. In collaboration with the group of Ozin at Toronto we have recently explored the pyrolysis of poly(ferrocenylsilanes) within the channels of the mesoporous silica MCM-41 with the aim of accessing nanostructured magnetic ceramic materials (Fig. 4).[49]

The monomer **3** (R = R′ = Me) can be sublimed into the hexagonal mesopores at room temperature. The resulting intercalated material was characterized by solid state ^{13}C and ^{29}Si NMR and by X-ray powder diffraction. ROP can then be induced by heating the resulting material at 200 °C, a process that was followed similarly and also by DSC which showed a ROP exotherm. Heating to 900 °C generates black, nanostructured magnetic ceramic products which can be visualized in the 30 Å channels by transmission electron microscopy (TEM) (Fig. 5). These materials were also characterized by X-ray diffraction, which showed the presence of small α-Fe nanoclusters with dimensions 20 ± 5 Å.[49] Studies of the

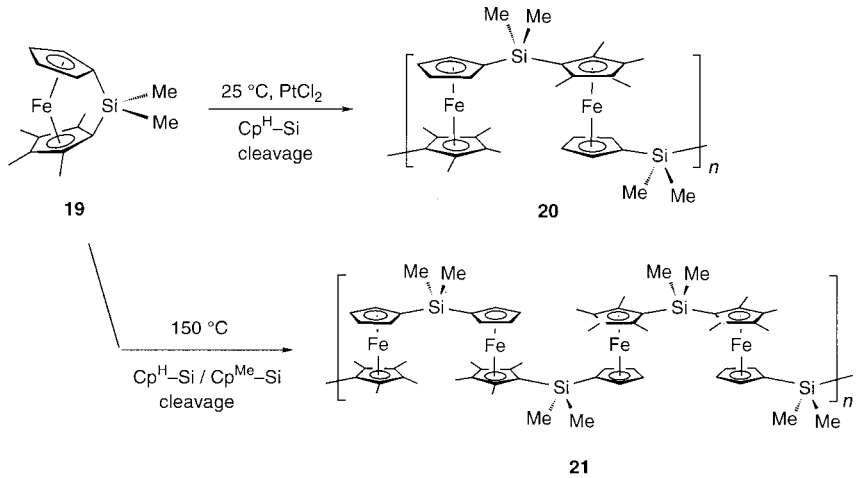

Scheme 5

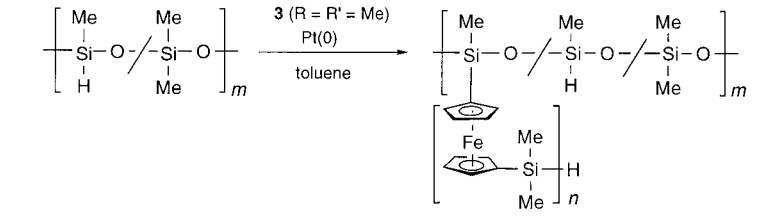

23

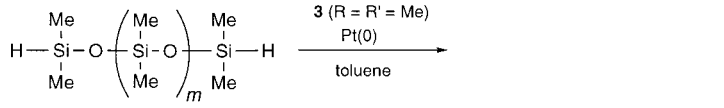

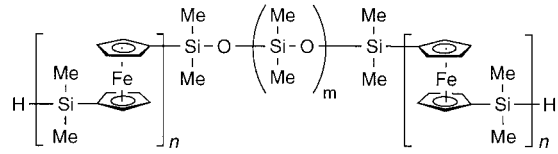

24

PFS-b-PDMS-b-PFS

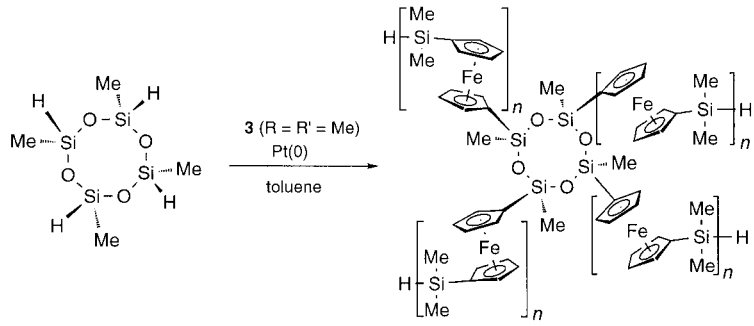

25

Scheme 6

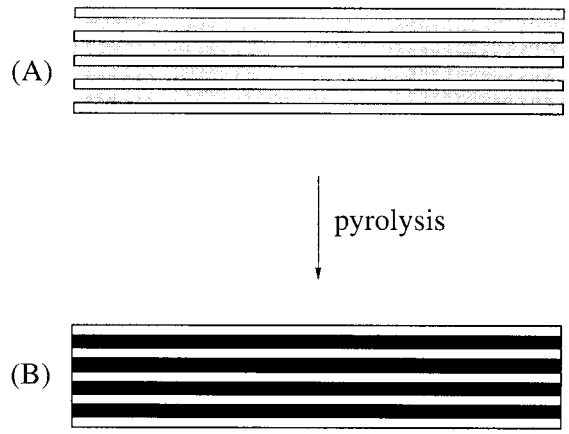

Fig. 4 Formation of nanostructured magnetic composites (B) *via* the pyrolysis of nanoscale cylinders of a poly(ferrocenylsilane) within the pores of mesoporous silica (MCM-41) (A).

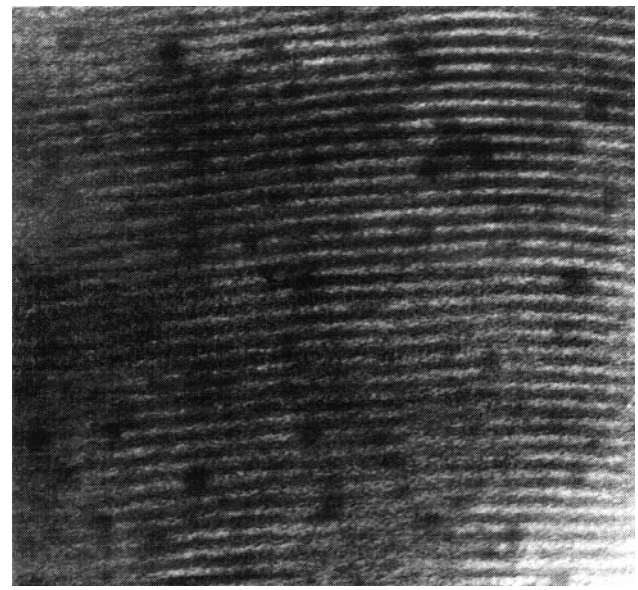

Fig. 5 Transmission electron micrograph perpendicular to the 30 Å channels of MCM-41 showing the incorporation of ceramics derived from the pyrolysis of poly(ferrocenylsilane) **4** (R = R′ = Me) in the mesopores at 900 °C.

magnetic properties of the composites confirmed that the materials are superparamagnetic rather than ferromagnetic which is consistent with the small sizes of the iron particles and the consequent, facile thermally induced reorientation of the magnetic domains at room temperature.

Self-assembly of poly(ferrocene) block copolymers: supramolecular organometallic polymer chemistry

Poly(ferrocene) block copolymers in which the blocks are immiscible (which is generally the case) would be expected to self-assemble to form phase separated domains in the solid state or to form micellar aggregates in selective solvents for one of the blocks.[50] This would allow the generation of unique supramolecular organometallic polymer architectures.

Based on the classical behavior of organic block copolymers, in the solid state poly(ferrocene) diblock copolymers should

form domains such as spheres, cylinders (or their anti-structures), double diamonds or gyroids, or lamellae. The preferred domain structure would be expected to be controlled by the ratio of the blocks, their degree of incompatibility (as defined by the Flory–Huggins interaction parameter χ), and the overall molecular weight of the block copolymer.[50] We reported the first studies in this area using differential scanning calorimetry (DSC) and TEM in 1996.[43] In the case of PS-b-PFS (**17**) detailed studies confirm that spherical, cylindrical, and lamellar domains are formed by using the expected block ratio variations [see, for example, Fig. 6(a) and (b)[27,51]] and also indicate that the PS-b-PFS materials possess phase behavior

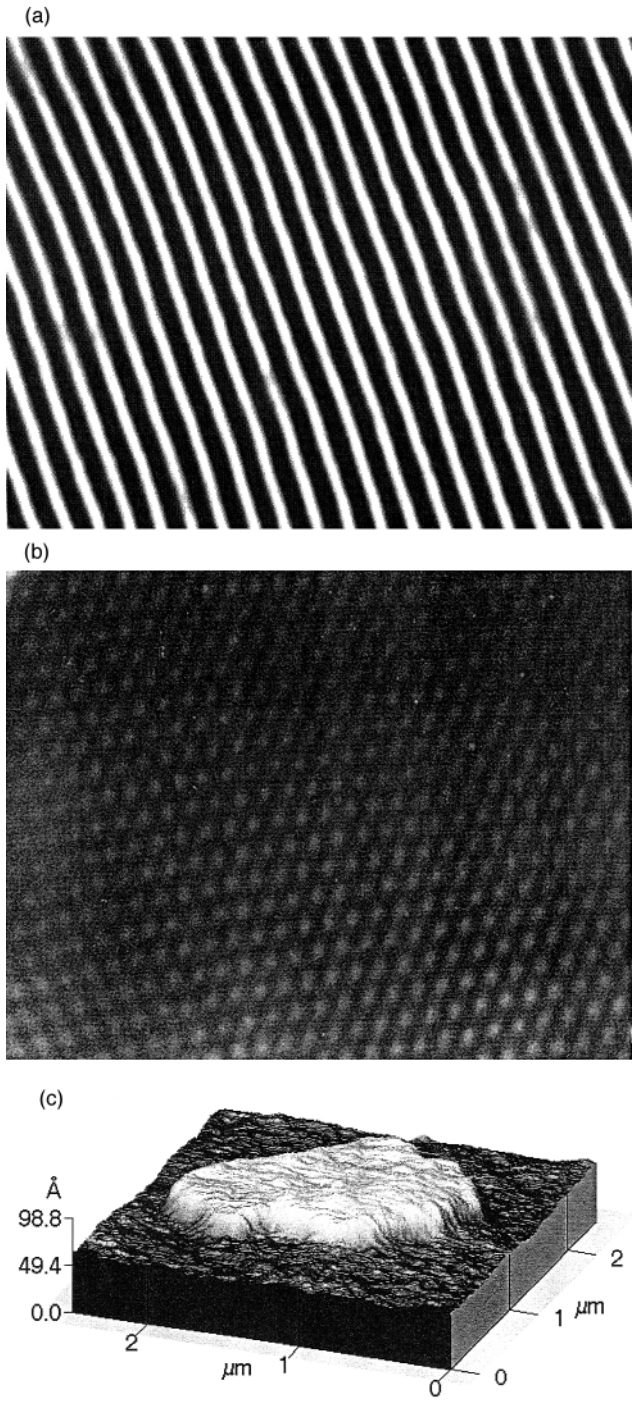

Fig. 6 Transmission electron micrographs of thin films of PS-b-PFS showing (a) lamellar morphology formed by a block copolymer with approximately equal block lengths, (b) ordered cylinders (end-on) of PS in a PFS matrix formed by a block copolymer with a 0.74 : 1.00 block ratio, (c) an AFM image showing crystals protruding from the surface of an annealed film. In TEM images (a) and (b) no staining agent was used and the PFS domains are dark and the PS domains light.

which is complicated by the presence of the crystallizable PFS block.[27,43,51–53] The crystallization is illustrated by the observation of 3D topological features on films of PS–b–PFS using atomic force microscopy (AFM) which shows elevated PFS crystallites [Fig. 6(c)].[27]

The self-assembly of poly(ferrocene) block copolymers in selective solvents for one block would also be anticipated based on studies of organic block copolymers. In the case of organic materials most studies have led to the identification of spherical structures with a core of the more insoluble polymer within a corona formed by the more soluble block. Only comparatively recently have non-spherical structures become more common.[54]

In collaboration with the group of Winnik at Toronto we have studied, for example, PS-b-PFS materials with a short PFS block (PS : PFS ratio 9 : 1). Films of these materials phase separate into spheres of PFS in a PS matrix and, in acetone, which is a selective solvent for low molecular weight PS, spherical micelles with an organometallic PFS core within a PS corona have been characterized.[51]

Recently, we have shown that interesting architectures can be generated *via* the solution aggregation of PFS-b-PDMS block copolymers (**16**) with long polysiloxane blocks (PFS : PDMS ratio = 1 : 6). Simply dissolving the amber, tacky block copolymer in warm hexanes leads to the formation of cylindrical, wormlike micelles with a PFS core and a corona of PDMS (Fig. 7).[55]

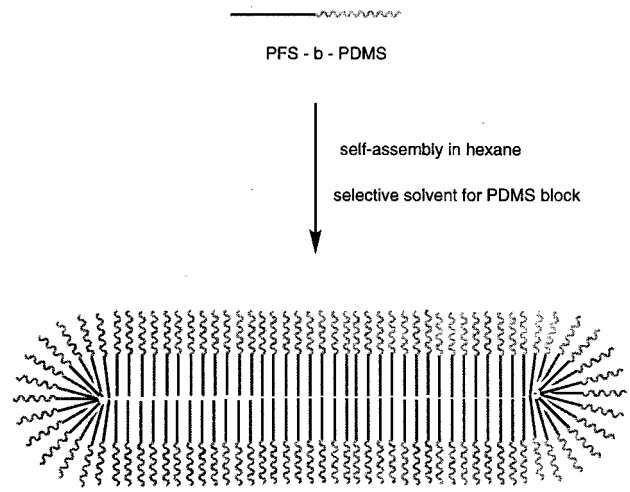

Fig. 7 Self-assembly of PFS-b-PDMS into cylindrical micelles in hexane.

These structures maintain their structural integrity in the solid state and the 20 nm iron-rich cores can be readily visualized by TEM which uses electron density differences to obtain contrast [see Fig. 8(a)]. AFM, on the other hand, allows both the core and corona to be imaged. The cylinders show considerable stability in solution and are unchanged in size after heating to 80 °C, However, ultrasonication of samples of the cylindrical micelles leads to a shortening as indicated by light scattering studies and by TEM [Fig. 8(b)].[55]

These cylinders formed in hexane consist of a wire-like core of semiconducting poly(ferrocenylsilane) surrounded by a sheath or corona of insulating poly(dimethylsiloxane) and are of interest as semiconducting nanowires (Fig. 9). Pyrolysis of such structures, particularly if crosslinked, offers the possibility of generating magnetic wire-like structures with a silica coating.

Recently we have prepared amphiphilic poly(ferrocenylsilane) diblock copolymers with N-methylated poly(vinylpyridine) (PVP) and poly(ethylene oxide) (PEO) and these materials, PVP-b-PFS and PFS-b-PEO, are soluble in water as long as the organic block is sufficiently long. Transition metal catalyzed ROP also provides very convenient access to block copolymers. The PFS-b-PDMS-b-PFS triblock materials (**24**) self-assemble in hexanes to yield a variety of remarkable

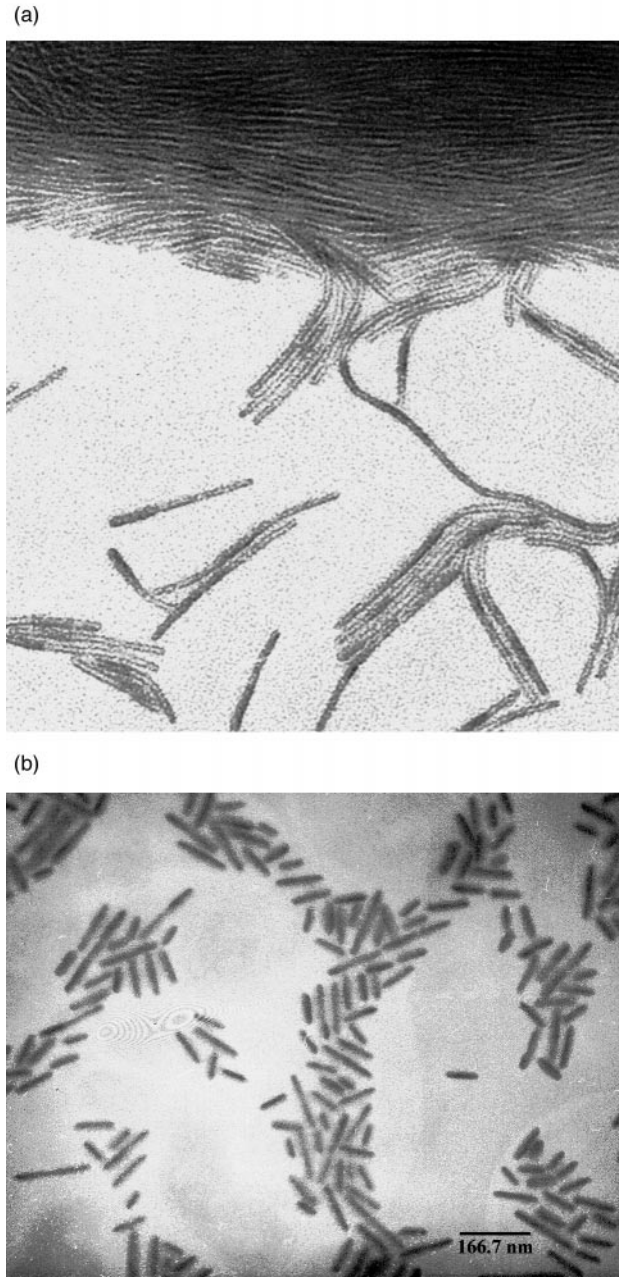

Fig. 8 Transmission electron micrograph of PFS-b-PDMS micelles aerosol-sprayed from a dilute solution in hexanes onto a thin carbon film supported on mica (no staining agent was used); (a) shows a region where the individual cylinders are starting to pack to form a 2D film as well as isolated cylinders; (b) shows the smaller cylinders that are formed after ultrasonication for 2 h (60 W).

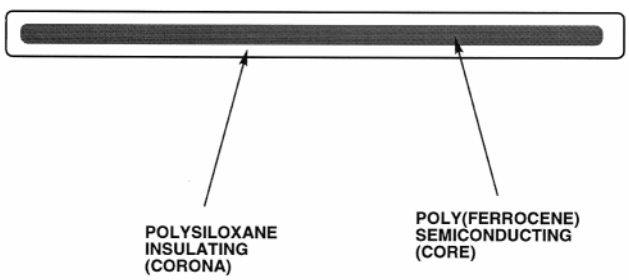

Fig. 9 Structure of cylindrical micelles of PFS-b-PDMS in hexanes.

architectures. In several systems morphologies such as vesicles and compound micelles in addition to spheres and cylinders have been identified.

Future opportunities exist for the generation of highly ordered, periodic structures which could be selectively oxidized (chemically or electrochemically, *e.g.* by using scanning probe microscope tips) to give materials with interesting properties. For example, the controlled orientation of nanoscale block copolymer cylindrical, or lamellar domains (*e.g.* at surfaces) might allow charge transport in certain directions. Of particular interest is an extension of the ideas that have been previously developed (and described above) for the synthesis of magnetic nanostructures *via* the pyrolysis of poly(ferrocene)/MCM-41 composites to ordered, phase-separated block copolymer structures. Thus, nanoscale poly(ferrocene) domains may allow the generation of ordered arrays of magnetic spheres, magnetic multilayers *etc*, *via* oxidation or pyrolysis (*e.g.* using lasers). Selective ablation of blocks (*e.g.* using plasmas) may also provide a methodology for defining patterns.[56] Research work on many of these ideas and others is ongoing in our group, in many cases in collaboration with other researchers.[11,43,51]

Summary

ROP of [1]silaferrocenophanes has permitted facile access to poly(ferrocenylsilane) homopolymers, a novel class of processable organometallic materials which have been found to possess a range of interesting physical properties. Living anionic and transition metal catalyzed ROP have allowed the preparation of materials with controlled molecular weights and architectures, *e.g.* block copolymers. Self-assembly of poly(ferrocenylsilane) block copolymers in the solid state or in solution yields well defined supramolecular, nanoscale organometallic architectures. Future work will be directed in particular towards further exploration of the properties of poly(ferrocenylsilane) homopolymers and understanding the self-assembly of block copolymers. In addition, applications in a variety of intriguing areas such as, for example, nanostructured magnetic materials, sensors, and charge-transport materials, and redox-active gels, will also be explored.

Acknowledgements

I would like to thank my exceptionally motivated and talented students who have performed most of the research described in this article and whose names are cited in the references. I also thank the funding agencies that have supported our research. I have had the privilege to collaborate with a variety of scientists with respect to some of the work described in this article, namely Mark Foster (Akron, USA) and Julius Vancso (initially at Toronto and now at Twente, the Netherlands) (morphology of homopolymers and block copolymers), John Sheridan (Rutgers University) (Transition Metal Catalyzed ROP), and Geoffrey Ozin and Mitchell A. Winnik of our Department (organometallic and magnetic nanostructures). I am also extremely grateful to the Alfred P. Sloan Foundation for a Research Fellowship (1994–98), the Natural Science and Engineering Research Council of Canada (NSERC) for an E. W. R. Steacie Fellowship (1997–1999), and the University of Toronto for a McLean Fellowship (1997–2003).

Notes and references

1 I. Manners, *Angew. Chem., Int. Ed. Engl.*, 1996, **35**, 1602; P. Nguyen, P. Gómez-Elipe and I. Manners, *Chem. Rev.*, 1999, in press.

2 F. Ciardelli, E. Tsuchida and D. Wöhrle, *Macromolecule–Metal Complexes*, Springer, Berlin 1996; C. U. Pittman, Jr., C. E. Carraher, M. Zeldin, J. E. Sheats and B. M. Culbertson, *Metal-Containing Polymeric Materials*, Plenum, New York, 1996.

3 Some recent examples: S. S. Zhu and T. M. Swager, *J. Am. Chem. Soc.*, 1997, **119**, 12 568; S. Kelch and M. Rehahn, *Macromolecules*, 1997, **30**, 6185; M. Altman and U. H. F. Bunz, *Angew. Chem., Int. Ed. Engl.*, 1995, **34**, 569; S. C. Tenhaeff and D. R. Tyler, *J. Chem. Soc., Chem. Commun.*, 1989, 1459; R. Bayer, T. Pöhlmann and O. Nuyken, *Makromol. Chem. Rapid Commun.*, 1993, **14**, 359; M. Rosenblum, H. M. Nugent, K.-S. Jang, M. M. Labes, W. Cahalane, P. Klemarczyk and W. M. Reiff, *Macromolecules*, 1995, **28**, 6330; H. Chen and R. D. Archer, *Macromolecules*, 1995, **28**, 1609.

4 N. Hagihara, K. Sonogashira and S. Takahashi, *Adv. Polym. Sci.*, 1981, **41**, 149; O. Lavastre, M. Even, P. H. Dixneuf, A. Pacreau and J. P. Vairon, *Organometallics*, 1996, **15**, 184.
5 M. Younis, A. Köhler, S. Cron, N. Chawdhury, M. Mandhary, M. S. Khan, J. Lewis, N. J. Long, R. H. Friend and P. R. Raithby, *Angew. Chem., Int. Ed.*, 1998, **37**, 3036; M. H. Chisholm, *Angew. Chem., Int. Ed. Engl.*, 1991, **30**, 673; H. B. Fyfe, M. Mlekuz, D. Zargarian, N. J. Taylor and T. B. Marder, *J. Chem. Soc., Chem. Commun.*, 1991, 188; S. J. Davies, B. F. G. Johnson, M. S. Khan and J. Lewis, *J. Chem. Soc., Chem. Commun.*, 1991, 187; K. C. Sturge, A. D. Hunter, R. McDonald and B. D. Santarsiero, *Organometallics*, 1992, **11**, 3056; M. J. Irwin, G. Jia, N. C. Payne and R. J. Puddephatt, *Organometallics*, 1996, **15**, 51; A. E. Dray, F. Wittmann, R. H. Friend, A. M. Donald, M. S. Kahn, J. Lewis and B. F. G. Johnson, *Synth. Met.*, 1991, **41**–**43**, 871; R. J. Puddephatt, *Chem. Commun.*, 1998, 1055.
6 N. J. Long, *Angew. Chem., Int. Ed. Engl.*, 1994, **33**, 1752.
7 E. W. Neuse and H. J. Rosenburg, *J. Macromol. Sci.*, 1970, **C4**, 1.
8 For overviews of the novel properties of ferrocenes, see: *Ferrocenes*, ed. A. Togni and T. Hayashi, VCH Publishers, New York, 1995; R. Deschenaux and J. W. Goodby, in *Ferrocenes*, ed. A.Togni and T. Hayashi, VCH Publishers, New York, 1995, pp. 471–495; *Inorganic Materials*, ed. D. W. Bruce and D. O'Hare, John Wiley and Sons, Toronto, 1992; S. Barlow and D. O'Hare, *Chem. Rev.*, 1997, **97**, 637.
9 I. Manners, *Polyhedron*, 1996, **15**, 4311.
10 D. A. Foucher, B. Z. Tang and I. Manners, *J. Am. Chem. Soc.*, 1992, **114**, 6246.
11 I. Manners, *Can. J. Chem.*, 1998, **76**, 371. This review includes a personal account of the initial ROP discovery.
12 A few months prior to the publication of ref. 10, Rauchfuss and coworkers reported an atom-abstraction ROP route to poly(ferrocenes) with disulfido spacers. See: P. F. Brandt and T. B. Rauchfuss, *J. Am. Chem. Soc.*, 1992, **114**, 1926. For other, recent ROP routes to poly(ferrocenes) see, C. E. Stanton, T. R. Lee, R. H. Grubbs, N. S. Lewis, J. K. Pudelski, M. R. Callstrom, M. S. Erickson and M. L. McLaughlin, *Macromolecules*, 1995, **28**, 8713; R. W. Heo, F. B. Somoza and T. R. Lee, *J. Am. Chem. Soc.*, 1998, **120**, 1621; M. A. Buretea and T. D. Tilley, *Organometallics*, 1997, **16**, 1507.
13 For the first example of well characterized, high molecular weight poly(ferrocenes) prepared *via* a condensation route, see: W. J. Patterson, S. P. McManus and C. U. Pittman, *J. Polym. Sci. A*, 1974, **12**, 837.
14 For condensation routes to impure, partially characterized, low molecular weight (M_n < 7000) poly(ferrocenylsilanes) see: H. Rosenberg, M. D. Rausch, *US Pat.*, 3 060 215, 1962; H. Rosenberg, *US Pat.*, 3 426 053, 1969; for a discussion of related work including an unsuccessful attempt to induce the anionic ROP of a phosphorus-bridged [1]ferrocenophane in 1982, see ref. 11.
15 I. Manners, *Adv. Organomet. Chem.*, 1995, **37**, 131.
16 For an overview of different strained metallocenophane monomers, see: M. Herberhold, *Angew. Chem., Int. Ed. Engl.*, 1995, **34**, 1837; R. Rulkens, D. P. Gates, J. K. Pudelski, D. Balaishis, D. F. McIntosh, A. J. Lough and I. Manners, *J. Am. Chem. Soc.*, 1997, **119**, 10 976.
17 Y. Ni, I. Manners, J. B. Sheridan and R. T. O. Oakley, *J. Chem. Ed.*, 1998, **75**, 766.
18 A. G. Osborne and R. H. Whiteley, *J. Organomet. Chem.*, 1975, **101**, C27.
19 H. Stoeckli-Evans, A. G. Osborne and R. H. Whiteley, *Helv. Chim. Acta*, 1976, **59**, 2402; A. G. Osborne, R. H. Whiteley and R. E. Meads, *J. Organomet. Chem.*, 1980, **193**, 345; A. B. Fischer, J. B. Kinney, R. H. Staley and M. S. Wrighton, *J. Am. Chem. Soc.*, 1979, **101**, 6501.
20 M. J. MacLachlan, A. J. Lough and I. Manners, *Macromolecules*, 1996, **29**, 8562; M. J. MacLachlan, A. J. Lough, W. E. Geiger and I. Manners, *Organometallics*, 1998, **17**, 1873.
21 W. Finckh, R. Ziembinski, B. Z. Tang, D. A. Foucher, D. B. Zamble, A. Lough and I. Manners, *Organometallics*, 1993, **12**, 823.
22 J. K. Pudelski, R. Rulkens, D. A. Foucher, A. J. Lough, P. M. Macdonald and I. Manners, *Macromolecules*, 1995, **28**, 7301.
23 D. L. Zechel, K. C. Hultzsch, R. Rulkens, D. Balaishis, Y. Ni, K. J. Pudelski, A. J. Lough and I. Manners, *Organometallics*, 1996, **15**, 1972.
24 P. Nguyen, G. Stojcevic, K. Kulbaba, M. MacLachlan, X. H. Liu, A. J. Lough and I. Manners, *Macromolecules*, 1998, **31**, 5977.
25 I. Manners, *Adv. Mater.*, 1994, **6**, 68.
26 J. Rasburn, R. Petersen, T. Jahr, R. Rulkens, I. Manners and G. J. Vancso, *Chem. Mater.*, 1995, **7**, 871.
27 N. Sheller, W. Li, M. D. Foster, D. Balaishis, I. Manners, L. Guo and R. J. P. Quirk, *Polym. Prepr.* (*Am. Chem. Soc., Div. Polym. Chem.*), 1998, **39**, 1204; W. Li, N. Sheller, M. D. Foster, I. Manners, B. Annis and J. S. Lin, *Polymer*, 1999, in press.
28 S. Barlow, A. L. Rohl, S. Shi, C. M. Freeman and D. O'Hare, *J. Am. Chem. Soc.*, 1996, **118**, 7578.
29 R. Rulkens, A. J. Lough, I. Manners, S. R. Lovelace, C. Grant, and W. E. Geiger, *J. Am. Chem. Soc.*, 1996, **118**, 12 683.
30 D. H. Reneker and I. Chun, *Nanotechnology*, 1996, **7**, 216.
31 F. Jäkle, R. Rulkens, G. Zech, D. A. Foucher, A. J. Lough and I. Manners, *Chem. Eur. J.*, 1998, **4**, 2117.
32 R. Rulkens, R. Resendes, A. Verma, I. Manners, K. Murti, E. Fossum, P. Miller and K. Matyjaszewski, *Macromolecules*, 1997, **30**, 8165.
33 D. A. Foucher, R. Ziembinski, R. Rulkens, J. M. Nelson and I. Manners, in *Inorganic and Organometallic Polymers II*, ed. P. Wisian-Neilson, H. R. Allcock and K. J. Wynne, American Chemical Society, Washington, DC, 1994, ACS Symposium Series 572.
34 H. Yim, M. D. Foster, D. Balaishis and I. Manners, *Langmuir*, 1998, **14**, 3921.
35 M. T. Nguyen, A. F. Diaz, V. V. Dement'ev and K. H. Pannell, *Chem. Mater.*, 1994, **6**, 952.
36 K. H. Pannell and J. Robillard, *US Pat.*, 308856, 1994.
37 B.-Z. Tang, R. Petersen, D. A. Foucher, A. J. Lough, N. Coombs, R. Sodhi and I. Manners, *J. Chem. Soc., Chem. Commun.*, 1993, **6**, 523; R. Petersen, D. A. Foucher, B.-Z. Tang, A. J. Lough, N. P. Raju, J. E. Greedan and I. Manners, *Chem. Mater.*, 1995, **7**, 2045.
38 M. Hmyene, A. Yasser, M. Escorne, A. Percheron-Guegan and F. Garnier, *Adv. Mater.*, 1994, **6**, 564.
39 J. M. Nelson, P. Nguyen, R. Petersen, H. Rengel, P. M. Macdonald, A. J. Lough, I. Manners, N. P. Raju, J. E. Greedan, S. Barlow and D. O'Hare, *Chem. Eur. J.*, 1997, **3**, 573.
40 X.-H. Liu, D. W. Bruce and I. Manners, *Chem. Commun.*, 1997, 289.
41 K. C. Hultzsch, J. M. Nelson, A. J. Lough and I. Manners, *Organometallics*, 1995, **14**, 5496.
42 R. Rulkens, Y. Ni and I. Manners, *J. Am. Chem. Soc.*, 1994, **116**, 12 121.
43 Y. Ni, R. Rulkens and I. Manners, *J. Am. Chem. Soc.*, 1996, **118**, 4102.
44 Y. Ni, R. Rulkens, J. K. Pudelski and I. Manners, *Macromol. Rapid Commun.*, 1995, **16**, 637.
45 N. P. Reddy, H. Yamashita and M. Tanaka, *J. Chem. Soc., Chem. Commun.*, 1995, 2263.
46 J. B. Sheridan, K. Temple, A. J. Lough and I. Manners, *J. Chem. Soc., Dalton Trans.*, 1997, 711.
47 P. Gómez-Elipe, P. M. Macdonald and I. Manners, *Angew. Chem., Int. Ed. Engl.*, 1997, **36**, 762.
48 P. Gómez-Elipe, R. Resendes, P. M. Macdonald and I. Manners, *J. Am. Chem. Soc.*, 1998, **120**, 8348.
49 M. J. MacLachlan, P. Aroca, N. Coombs, I. Manners and G. A. Ozin, *Adv. Mater.*, 1998, **10**, 144.
50 F. S. Bates, *Science*, 1991, **251**, 898; S. Förster and M. Antonietti, *Adv. Mater.*, 1998, **10**, 195.
51 J. Massey, K. N. Power, M. A. Winnik and I. Manners, *Adv. Mater.*, 1998, **10**, 1559.
52 I. Manners, *Can. J. Chem.*, 1998, **76**, 378.
53 R. G. H. Lammertink, D. J. Versteeg, M. A. Hempenius and G. J. Vancso, *J. Polym. Sci. Part A: Polym. Chem.*, 1998, **36**, 2147.
54 For recent work on non-spherical micellar aggregates of organic block copolymers in solution see, for example, C. Price, *Pure Appl. Chem.*, 1983, **55**, 1563; M. Antonietti, S. Heinz, M. Schimdt and C. Rosenauer, *Macromolecules*, 1994, **27**, 3276; L. Zhang and A. Eisenberg, *Science*, 1995, **268**, 1728; L. Zhang, K. Yu and A. Eisenberg, *Science*, 1996, **272**, 1777; J. P. Spatz, S. Mößmer and M. Möller, *Angew. Chem., Int. Ed. Engl.*, 1996, **35**, 1510.
55 J. Massey, K. N. Power, I. Manners and M. A. Winnik, *J. Am. Chem. Soc.*, 1998, **120**, 9533.
56 J. P. Spatz, S. Mößmer, M. Möller, T. Herzog, A. Plettl and P. Ziemann, *J. Luminesc.*, 1998, **76**/**77**, 168.

Paper 8/10043H

Novel highly ordered Langmuir–Blodgett films of regioregular poly(3-substituted thiophene)

Keiko Ochiai,[ab] Masahiro Rikukawa*[ab] and Kohei Sanui[ab]

[a] *Department of Chemistry, Sophia University, 7-1 Kioi-cho, Chiyoda-ku, Tokyo 102-8554, Japan. E-mail: m-rikuka@hoffman.cc.sophia.ac.jp*

[b] *CREST, Japan Science and Technology Corporation (JST), 4-1-8 Hon-cho, Kawaguchi, Saitama, 332-0012, Japan*

Received (in Cambridge, UK) 1st March 1999, Accepted 7th March 1999

Langmuir–Blodgett films have been fabricated from a regioregular poly(thiophene) derivative by the vertical dipping method while still maintaining the high self-organization associated with the regioregularity of the polymer.

A great deal of progress has been made towards the molecular engineering of conducting polymers that allow us to control nanoscopic structure and that possess exceptional properties. Many of the important advances in this area have centered on the synthesis of structurally homogeneous materials.[1,2] Most notably, the recent development of regioregular conducting polymers based on 3-substituted poly(thiophenes) has heralded a new direction for molecular engineering research.[3–6] These regiochemical arrangements provide an opportunity to understand structure–property relationships in conducting polymers with enhanced electrical and optical properties. It has been recognized that electrical and optical properties based on conjugated systems strongly depend on their nano-structural organization, which can be controlled by the introduction of functional groups and regioregularity. To date, however, only conventional solution casting and spin-coating methods, which offer very little control over molecular order and organization of the polymer, have been utilized to process the novel regioregular polymers. We have recently shown that it is possible to fabricate Langmuir–Blodgett (LB) thin films from mixed monolayers containing stearic acid and regioregular poly(3-alkylthiophenes).[7–9] This novel approach results in well-defined and controllable molecular architectures with desirable optical and electrical properties. We now report further work aimed at fabricating highly ordered LB films of regioregular poly(3-{2-[(*S*)-2-methylbutoxy]ethyl}thiophene) [P(S)MBET] without stearic acid as an amphiphilic molecule. The influence of regioregularity on LB manipulation and solid state structure is also discussed by comparing the monolayers of regioregular and regiorandom P(S)MBET.

The regioregular poly(thiophene) derivative, head-to-tail poly(3-{2-[(*S*)-2-methylbutoxy]ethyl}thiophene) [*HT*-P(S)MBET], was synthesized according to the modified Rieke method.[3] *HT*-P(S)MBET was an optically active polymer with > 93%e head-to-tail linkages, as determined from NMR data.[10] Regiorandom P(S)MBET [*R*-P(S)MBET] with 54% head-to-tail linkages was also prepared by the same catalytic polymerization with $Pd(PPh_3)_4$. *HT*-P(S)MBET used in this study had $M_w = 2.15 \times 10^4$, $M_n = 1.56 \times 10^4$ and $M_w/M_n = 1.38$, while *R*-P(S)MBET had $M_w = 2.05 \times 10^4$, $M_n = 1.02 \times 10^4$, and $M_w/M_n = 2.02$. Since the transfer ratios and the collapse pressures of the monolayer increased with decreasing temperature, LB monolayer and multilayer thin films were fabricated using a Lauda film balance at 10 °C. Monolayers were spread from $CHCl_3$ solutions on a purified aqueous subphase.[11,12]

In order to manipulate soluble conducting polymers into LB films, it is normally necessary to utilize amphiphilic molecules that are capable of forming monolayers at the air–water interface of an LB trough. Thus, poly(3-alkylthiophenes) cannot be formed directly into monolayers owing to the lack of a strong dipole. For example, the spreading of a $CHCl_3$ solution containing poly(3-hexylthiophene) onto the air–water interface of an LB trough simply results in the formation of aggregated islands of the polymer which only exhibit a surface pressure when they are forced together into a very small molecular area. Regioregular poly(3-hexylthiophene) also shows similar phenomena even if the higher regioregularity provides a more coplanar structure of thiophene rings and leads to higher rigidity in the monolayers. Highly ordered LB films of regioregular and regiorandom poly(3-alkylthiophenes) can be easily fabricated by mixing the polymer with suitable portions of an amphiphilic molecule such as stearic acid.[7–9]

HT-P(S)MBET and *R*-P(S)MBET were spread from a $CHCl_3$ solution on the water surface to measure the π–*A* isotherms at 10 °C. (Fig. 1). *HT*-P(S)MBET monolayers exhibit a stable condensed solid phase with a phase transition at about 18 mN m^{-1}. It is of interest that both the π-*A* isotherms show a relatively steep rise at a large molecular area. The area per molecule of *HT*-P(S)MBET was estimated to be 17 Å^2 per polymer repeat unit, which was larger than that for head-to-tail poly(3-hexylthiophene) (*HT*-PHT) (about 8 Å^2).[7–9] According to the CPK model, 17 Å^2 corresponds with the cross section of the thiophene ring of *HT*-P(S)MBET. As the most probable molecular orientation, the coplanar poly(thiophene) backbones float on the water surface and the side chains on one side of the zigzag formation orient toward the water phase. In contrast, the monolayer of *R*-(S)MBET shows a larger molecular area (19 Å^2) and lower collapsed pressure (10 mN m^{-1}), indicating that *R*-P(S)MBET molecules randomly orient and the monolayer is relatively unstable compared with *HT*-P(S)MBET. These results clearly demonstrate that the methylbutoxyethyl groups of P(S)MBET provide suitable dipoles for forming monolayers

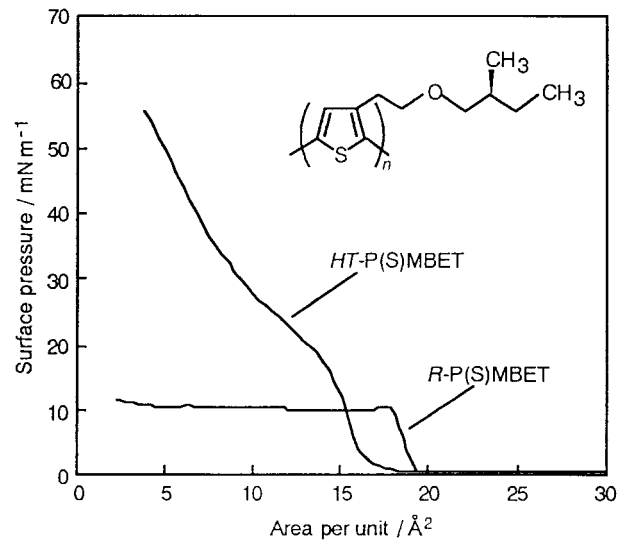

Fig. 1 Surface pressure–area isotherms of *HT*-P(S)MBET and *R*-P(S)MBET monolayers at 10 °C.

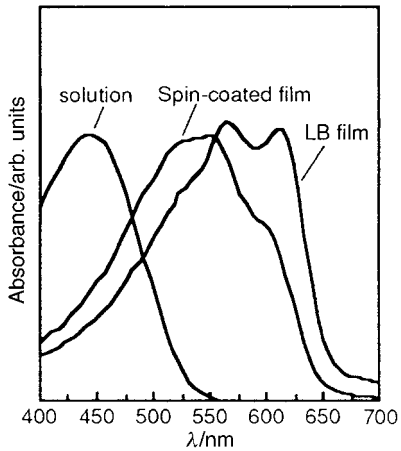

Fig. 2 UV–VIS spectra of *HT*-P(S)MBET in $CHCl_3$, an *HT*-P(S)MBET spin-coated film, and an *HT*-P(S)MBET LB film.

on the air–water interface. We further found that the higher regioregularity gives self-organized structures and induces rigid and coplanar main-chain structures that are capable of forming stable condensed solid monolayers at the air–water interface.

The *HT*-P(S)MBET LB films can be produced by the standard Langmuir–Blodgett vertical dipping method. Optical absorption measurements made on stepped films as a function of the number of layers deposited indicate that the *HT*-P(S)MBET is transferred reproducibly into the multilayer films, while multilayer thin films could not fabricated from *R*-P(S)MBET monolayers on the air–water interface due to the instability of the condensed monolayers. As shown in Fig. 2, the maximal absorption of the *HT*-P(S)MBET LB film shows lower π–π^* transition energy than that of the spin-coated film, while the intensity of the shoulder for the LB film at the longer wavelength around 610 nm is relatively stronger than that of the spin-coated film. These spectra also indicate that *HT*-P(S)MBET molecules in the LB films have a more planar conformation with longer conjugation length compared with the spin-coated films of *HT*-P(S)MBET. Further, it is found from the polarized UV-VIS absorption spectra that *HT*-P(S)MBET molecules in the LB films are oriented parallel to the plane of the substrate and have a tendency to orient along the dipping direction. In practice E_p/E_s was about 1.5, where E_p and E_s were the absorbances of light polarized with the electric vector parallel and perpendicular respectively to the direction of dipping of the substrate. Thus, the LB technique provides molecular control over the regioregular polymers to form better-organized structures that exhibit more planar conformations with low band-gaps and with anisotropic orientations of polymer chains.

The X-ray diffraction pattern of an *HT*-P(S)MBET LB film is shown in Fig. 3. The presence of at least three Bragg diffraction peaks clearly demonstrates that we have formed a well-defined layered structure with a repeat distance of around 18 Å, which is identical to the interlayer *d*-spacing of well-organized lamellar structure for *HT*-P(S)MBET spin-coated films. These results suggest that *HT*-P(S)MBET molecules in the LB films maintain the high self-organization associated with the regio-regularity and adopting a crystalline, self-organized lamellar morphology with three dimensional ordering of the polymer chains such as is observed for regioregular poly(3-alkyl-thiophene) cast films. Ultrathin films with lamellar morphology artificially built up were produced for the first time.

3-Substituted poly(thiophenes) with regioregular structures are expected to be highly ordered and therefore to exhibit improved electrical and optical properties. These highly-

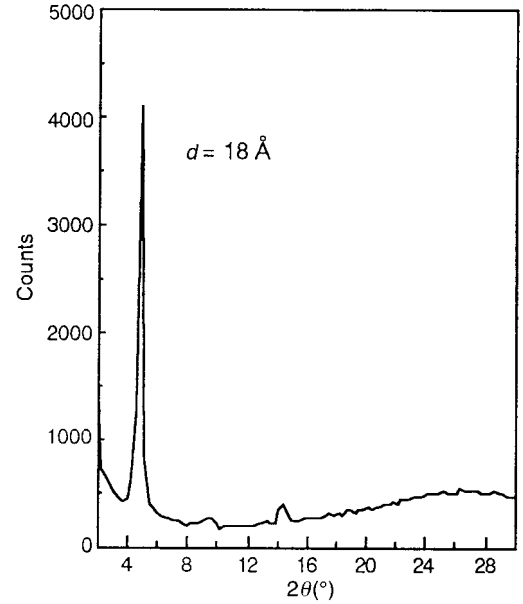

Fig. 3 X-Ray diffraction pattern of an LB film (10 layers) of *HT*-P(S)MBET.

ordered LB films are readily doped with oxidizing agents such as nitrosyl hexafluorophosphate and ferric chloride to produce electrically conductive multilayer thin films. To date, we have been able to reach in-plane conductivity of about 1-5 S cm^{-1}, which is 10^4- to 10^5-fold higher than *R*-P(S)MBET spin-coated films. Our films also exhibit highly anisotropic behavior in electrical conductivity to the dipping direction. In addition, preliminary results have shown that these LB films exhibit enhanced optical nonlinear susceptibility $\chi^{(3)}$.

In summary, we have presented a method for the synthesis and thin film formation of regioregular P(S)MBET, which results in a large improvement in electrical and optical properties. We believe that the introduction of regioregularity and suitable functional groups results in better molecular organization and this in turn results in the excellent optical and electrical properties of these interesting materials.

Notes and references

1 N. Basescu, Z.-X. Liu, D. Moses, A. Heeger, H. Naarmann and N. Theophilou, *Nature*, 1987, **327**, 403.
2 D. L. Gin, V. P. Conticello and R. H. Grubbs, *J. Am. Chem. Soc.*, 1992, **114**, 3167.
3 T.-A. Chen, X. Wu and R. D. Rieke, *J. Am. Chem. Soc.*, 1995, **117**, 233.
4 T.-A. Chen and R. D. Rieke, *Synth. Met.*, 1993, **60**, 175.
5 R. D. McCullough, R. D. Lowe, M. Jayaraman and D. L. Anderson, *J. Org. Chem.*, 1993, **58**, 904.
6 R. D. McCullough and R. D. Lowe, *J. Chem. Soc., Chem. Commun.*, 1992, 70.
7 M. Rikukawa, M. Nakagawa, H. Abe, K. Sanui and N. Ogata, *Thin Solid Films*, 1996, **284**–**285**, 636.
8 M. Rikukawa, M. Nakagawa, H. Abe, K. Ishida, K. Sanui and N. Ogata, *Thin Solid Films*,1996, **273**, 240.
9 M. Rikukawa, M. Nakagawa, Y. Tabuchi, K. Sanui and N. Ogata, *Synth. Met.*, 1997, **84**, 233.
10 M. Sato and H. Morii, *Macromolecules*,1991, **24**, 1196.
11 K. Ochiai, Y. Tabuchi, M. Rikukawa, K. Sanui and N. Ogata, *Thin Solid Films*, 1998, **327**–**329**, 454.
12 S. Kishino, Y. Ueno, K. Ochiai, M. Rikukawa, K. Sanui, T. Kobayashi, H. Kunugita and K. Ema, *Phys. Rev. B*, 1998, **58**, 430.

Communication 9/01617A

Luminescent molecular wires with 2,5-thiophenediyl spacers linking {Ru(terpy)$_2$} units

Edwin C. Constable,*[a] Catherine E. Housecroft,[a] Emma R. Schofield,[a] Susana Encinas,[b] Nicola Armaroli,[b] Francesco Barigelletti,*[b] Lucia Flamigni,*[b] Egbert Figgemeier[c] and Johannes G. Vos[c]

[a] *Institut für Anorganische Chemie, Spitalstrasse 51, CH-4056 Basel, Switzerland. E-mail: constable@ubaclu.unibas.ch*
[b] *Istituto FRAE-CNR, Via P. Gobetti 101, I-40129 Bologna, Italy*
[c] *Inorganic Chemistry Research Centre, School of Chemical Sciences, Dublin City University, Dublin 9, Ireland*

Received (in Cambridge, UK) 22nd January 1999, Accepted 7th April 1999

Whereas {Ru(terpy)$_2$}$^{2+}$ salts are essentially non-luminescent in fluid solution luminescent molecular wires with {Ru(bpy)$_3$}$^{2+}$-like activity result when these units are connected by 2,5-thiophenediyl spacers.

Multinuclear oligopyridine complexes are important in metallosupramolecular chemistry and species such as rods or wires,[1] helicates[2] and dendrimers[3] are well established.[4,5] The investigation of photoinduced energy- and electron-transfer in geometrically well defined polynuclear systems allows the electronic and nuclear factors governing these processes to be investigated.[6–8] The exploitation of the spectroscopic (particularly luminescence) properties of transition metal–oligopyridine complexes for ion-sensing,[4,5,9] light-harvesting or energy-collection using high-nuclearity dendrimers is of intense current interest.[6] The {Ru(terpy)$_2$}$^{2+}$ chromophore is often employed in such assemblies[10] even though its luminescence properties are poor (room temperature, MeCN solution: $\phi \approx 10^{-5}$, $\tau \leqslant 0.3 \times 10^{-9}$ s[10,11]) in comparison to {Ru(bpy)$_3$}$^{2+}$. Substituents on the terpy ligand significantly improve the luminescence properties[6,8,10,12] and we now describe a new ligand in which a 2,5-thiophenediyl spacer[13] connecting {Ru(terpy)$_2$}-chromophores modifies the properties such that di- and tri-nuclear complexes exhibit {Ru(bpy)$_3$}$^{2+}$-like luminescence.

The new dinucleating ligand **1** was prepared in a two step process from 2-acetylpyridine and thiophene-2,5-dicarbaldehyde in *ca.* 30% yield as a white solid.† The reaction of [Ru(terpy)Cl$_3$] with a stoichiometric amount of **1** in EtOH containing *N*-ethylmorpholine (NEM) gave the mononuclear *ligand-complex* [(terpy)Ru(**1**)]$^{2+}$ isolated as a red PF_6^- salt in 60% yield [MALDI-TOF MS: *m/z* 1024 (M − PF_6), 879 (M − 2PF_6)]. All ruthenium complexes were purified by chromatography over SiO_2 using MeCN–H_2O–saturated aqueous KNO_3 mixtures as the mobile phase. The direct reaction of 3 equivalents of [Ru(terpy)Cl$_3$] with **1** in ethanol containing NEM gave the dinuclear complex [(terpy)Ru(**1**)Ru(terpy)][PF_6]$_4$ [95%, MALDI-TOF MS: *m/z* 1362 (M − 3PF_6), 1212 (M − 4PF_6)] together with [(terpy)Ru(**1**)][PF_6]$_2$ (39%). The trinuclear complex [(terpy)Ru(**1**)Ru(**1**)Ru(terpy)][PF_6]$_6$ was obtained in 48% yield from the reaction of the ligand-complex [(terpy)Ru(**1**)][PF_6]$_2$ with $RuCl_3 \cdot 3H_2O$ in $HOCH_2CH_2OH$ containing NEM in a 600 W microwave oven. All of the complexes are electrochemically active, but in their cyclic voltammograms (MeCN, Fc/Fc$^+$ reference) exhibit only a single Ru(II)/Ru(III) process {[(terpy)Ru(**1**)][PF_6]$_2$ and [(terpy)Ru(**1**)Ru(**1**)Ru(terpy)][PF_6]$_6$ +0.87 V, [(terpy)Ru(**1**)Ru(terpy)][PF_6]$_4$ +0.88 V}. Preliminary structural data for the complex [(terpy)Ru(**1**)Ru(terpy)][PF_6]$_2$[NO_3]$_2$ indicate a planar bridging ligand and a Ru···Ru distance of 14.4 Å.[14]

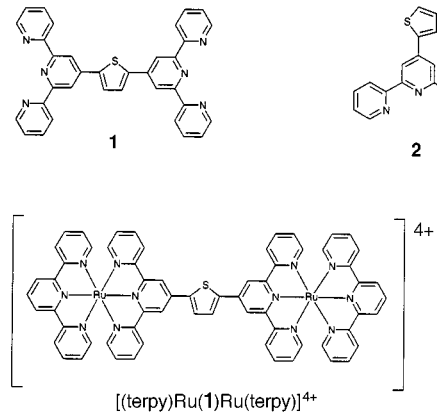

Table 1 lists room temperature absorption and luminescence data for MeCN solutions of the dinuclear and trinuclear complexes, together with those for mononuclear reference

Table 1 Spectroscopic and photophysical parameters[a]

	Absorption		Luminescence		
	λ_{max}^{abs}/nm	(10^{-4} ε/dm^3 mol^{-1} cm^{-1})	λ_{max}^{em}/nm[b]	τ/ns	10^4 ϕ[c]
[Ru(bpy)$_3$][PF_6]$_2$	288(7.7)	452(1.5)	615	170	160
[Ru(terpy)$_2$][PF_6]$_2$[d]	306(7.2)	490(2.8)	*ca.* 640	0.25	⩽0.3
[(terpy)Ru(**2**)][PF_6]$_2$	307(6.5)	486(2.4)	664	5.9	0.53
[Ru(**2**)$_2$][PF_6]$_2$	316(5.5)	498(2.9)	664	8.5	0.88
[(terpy)Ru(**1**)Ru(terpy)][PF_6]$_4$	307(10.6)	517(5.8)	738	340	6.9
[(terpy)Ru(**1**)Ru(**1**)Ru(terpy)][PF_6]$_6$	308(15.1)	532(10.8)	736	330	6.8

[a] Room temperature, air-equilibrated acetonitrile solvent. [b] Band maxima for uncorrected spectra. [c] Luminescence efficiency obtained from corrected spectra. [d] Refs. 10 and 11.

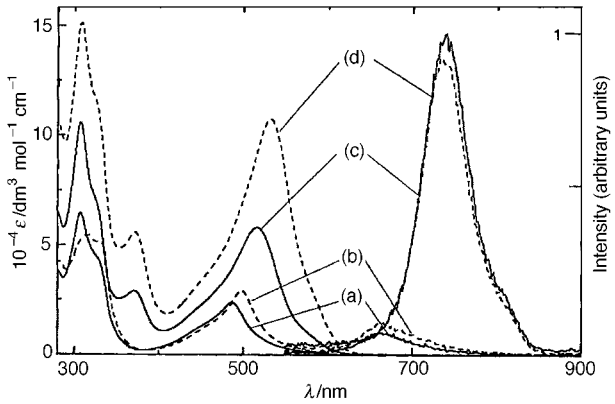

Fig. 1 Absorption and luminescence spectra of the ruthenium complexes: (a) [(terpy)Ru(**2**)][PF_6]$_2$, (b) [Ru(**2**)$_2$][PF_6]$_2$, (c) [(terpy)Ru(**1**(terpy)][PF_6]$_4$ and (d) [(terpy)Ru(**1**)Ru(**1**)(terpy)][PF_6]$_6$; excitation was at 480 nm.

complexes;‡ absorption and luminescence spectra of the complexes are presented in Fig. 1.§ All of the complexes display intense UV absorption bands (306–316 nm, ε = 5–15 10^4 dm^3 mol^{-1} cm^{-1}) and less intense bands in the visible region (485–532 nm, ε = 2.4–11 10^4 dm^3 mol^{-1} cm^{-1}). The former bands are due to ligand centered (^{1}LC) transitions and those in the visible are due to metal-to-ligand charge-transfer (^{1}MLCT).[6,10] For the mononuclear model complexes [(terpy)-Ru(**2**)][PF_6]$_2$ and [Ru(**2**)$_2$][PF_6]$_2$ the 2-thienyl group causes significant changes in the band maximum and minor changes of the band intensity with respect to [Ru(terpy)$_2$][PF_6]$_2$ (Table 1). In contrast, on passing from mononuclear [(terpy)Ru(**2**)][PF_6]$_2$ to the di- and tri-nuclear species, the band associated with the lowest lying ^{1}MLCT transition moves sequentially to longer wavelengths with a concomitant increase in ε (Table 1). This behaviour is consistent with the increasing numbers of {Ru-(terpy)$_2$}$^{2+}$ chromophores and may indicate that the 2,5-thiophenediyl spacer allows some intermetal electronic communication, allowing a stablisation of the MLCT levels through electronic and electrostatic effects.[8,15] The polynuclear complexes also exhibit a band at *ca.* 360 nm not present in the mononuclear compound; we are currently investigating the origin of this band which could arise from CT or LF states.

The excited states responsible for the luminescence are formally triplet Ru → terpy CT levels[10] and the luminescence maxima in Table 1 are consistent with their sequential stabilisation on passing from the mono- to the di- and tri-nuclear complexes (Table 1). What is remarkable is that for the polynuclear species the luminescence lifetime and efficiency increase by two and one order of magnitude, respectively, with respect to the mononuclear complexes. This effect is presumably related to the stabilisation of the cluster of ^{3}MLCT levels responsible for the luminescence leading to a large energy gap between these and the upper lying ^{3}MC levels which offer very effective pathways for non-radiative processes.[15]

The 2,5-thiophenediyl linker is chemically inert, in contrast to polyalkyne spacers, and offers new possibilities for building up high-nuclearity luminescent {Ru(terpy)$_2$}$^{2+}$-based molecular wires with photochemical properties akin to those of {Ru(bpy)$_3$} derivatives. Work is in progress to prepare and study mixed Ru(II)/Os(II) heteropolynuclear species where photoinduced RuOs energy transfer may allow a detailed understanding of the properties of the 2,5-thiophenediyl spacers.

We should like to thank the Schweizerischer Nationalfonds zur Förderung der wissenschaftlichen Forschung (E. C. C., C. E. H.), the University of Basel (E. C. C., C. E. H.), the European Community (J. G. V., E. F., T. M. R. contract no. CT96-0076 and S. E., F. B. contract no. 980226) for support. This paper is dedicated to Professor John A. Osborn on the occasion of his 60th birthday.

Notes and references

† **1**: δ_H($CDCl_3$) 8.76 (4H, d, H^{6A}), 8.75 (4H, s, H^{3B}), 8.65 (4H, d, *J* 8.3 Hz, H^{3A}), 7.87 (4H, dt, *J* 7.8, 1.8 Hz, H^{4A}), 7.84 (2H, s, $H^{3C,4C}$), 7.36 (4H, m, H^{5A}); δ_C($CDCl_3$) 156.2, 155.9, 149.2, 143.2, 142.8, 136.9, 126.9, 124.0, 121.3, 116.9; *m/z* 546.1628 (high resolution: calc. for $C_{34}H_{22}N_6S$, 546.1627).

‡ Full details of ligand **2** and its complexes will be reported later.

§ Absorption and luminescence spectra of dilute solutions (10^{-5} M) in MeCN were recorded with a PE Lambda 5 spectrophotometer and with a Spex Fluorolog II spectrofluorimeter (λ_{exc} = 480 nm) respectively. Uncorrected luminescence band maxima (±2 nm) are quoted. Corrected band maxima and luminescence quantum efficiencies (±20%) were determined using the procedure described in ref. 15. Luminescence lifetimes (±8%) were obtained with IBH single-photon counting equipment or with a picosecond fluorescence spectrometer based on a ND : YAG laser (Continuum PY62-10) and a Hamamatsu C1587 streak camera.[15]

1 See, for example: E. C. Constable, in *Electronic materials: the oligomer approach*, ed. K. Müllen and G. Wegner, Wiley-VCH, Weinheim, 1998, p. 273.
2 E. C. Constable, in *Comprehensive Supramolecular Chemistry*, ed. J.-M. Lehn, Pergamon, Oxford, 1996, vol. 9, p. 213; C. Piguet, G. Bernardinelli and G. Hopfgartner, *Chem. Rev.*, 1997, **97**, 2005.
3 V. Balzani, S. Campagna, G. Denti, A. Juris, S. Serroni and M. Venturi, *Acc. Chem. Res.*, 1998, **31**, 26; E. C. Constable, *Chem. Commun.*, 1997, 1073.
4 J.-M. Lehn, *Supramolecular Chemistry*, VCH, Weinheim, 1995.
5 *Transition Metals in Supramolecular Chemistry*, ed. L. Fabbrizzi and A. Poggi, Kluwer, Dordrecht, 1994.
6 V. Balzani, A. Juris, M. Venturi, S. Campagna and S. Serroni, *Chem. Rev.*, 1996, **96**, 759.
7 F. Barigelletti, L. Flamigni, J.-P. Collin and J.-P. Sauvage, *Chem. Commun.*, 1997, 333.
8 A. Harriman and R. Ziessel, *Chem. Commun.*, 1996, 1707.
9 A. P. de Silva, H. Q. N. Gunaratne, T. Gunnlaugsson, A. J. M. Huxley, C. P. McCoy, J. Rademacher and T. E. Rice, *Chem. Rev.*, 1997, **97**, 1515.
10 J.-P. Sauvage, J.-P. Collin, J.-C. Chambron, S. Guillerez, C. Coudret, V. Balzani, F. Barigelletti, L. De Cola and L. Flamigni, *Chem. Rev.*, 1994, **94**, 993.
11 J. R. Winkler, T. L. Netzel, C. Creutz and N. Sutin, *J. Am. Chem. Soc.*, 1987, **109**, 2381.
12 M. Maestri, N. Armaroli, V. Balzani, E. C. Constable and A. M. W. Cargill Thompson, *Inorg. Chem.*, 1995, **34**, 2759; E. C. Constable, A. M. W. Cargill Thompson, N. Armaroli, V. Balzani and M. Maestri, *Polyhedron*, 1992, **11**, 2707.
13 Other examples of the use of thiophenediyl spacers include: M. S. Vollmer, F. Würthner, F. Effenberger, P. Emele, D. U. Meyer, T. Stümpfig, H. Port and H. C. Wolf, *Chem. Eur. J.*, 1998, **4**, 260; P. N. Taylor, A. P. Wylie, J.Huuskonen and H. L. Anderson, *Angew. Chem.*, Int. Ed., 1998, **37**, 986.
14 G. Baum, E. C. Constable, D. Fenske, C. E. Housecroft and E. Schofield, unpublished results.
15 L. Hammarström, F. Barigelletti, L. Flamigni, M. T. Indelli, N. Armaroli, G. Calogero, M. Guardigli, A. Sour, J.-P. Collin and J.-P. Sauvage, *J. Phys. Chem. A*, 1997, **101**, 9061.

Communication 9/00617F

ChemComm

Tetrahedral bipyridyl copper(I) complexes: a new class of non-dipolar chromophore for nonlinear optics

Thierry Renouard,[a] Hubert Le Bozec,*[a] Sophie Brasselet,[b] Isabelle Ledoux[b] and Joseph Zyss[b]

[a] *Laboratoire de Chimie de Coordination et Catalyse, UMR 6509 CNRS-Université de Rennes 1, Campus de Beaulieu, 35042 Rennes Cedex, France. E-mail: lebozec@univ-rennes.fr*

[b] *ENS Cachan, Laboratoire de Photonique Quantique et Moléculaire, 61 avenue du Président Wilson, 94235 Cachan, France*

Received (in Oxford, UK) 12th March 1999, Accepted 9th April 1999

The synthesis of 4,4′-bis(dialkylaminostyryl)-6,6′-dimethyl-2,2′-bipyridine ligands is described; the corresponding tetrahedral bis(bipyridyl) copper(I) complexes have been prepared, and their second-order nonlinear optical properties determined by harmonic light scattering (HLS) at 1.34 μm; these new octupolar complexes exhibit large molecular hyperpolarisabilities *β*.

A new concept of octupolar non-linearities of two- and three-dimensional (2D and 3D) molecules has recently been proposed and has opened new perspectives in elaboration of efficient nonlinear optical materials.[1] Research on octupolar structures has mainly focused on organic chromophores with threefold symmetry such as 1,3,5-triamino-2,4,6-trinitrobenzene and related derivatives,[2] crystal violet,[3] trisubstituted amines[2,4] and cyanine salts.[2,5] The first examples of nondipolar tetrahedral organotin,[6] phosphonium[7] and biphenyl[8] chromophores have recently been investigated. Organotransition metal complexes also offer many possibilities for the design of 3D non-centrosymmetric octupolar molecules owing to the large diversity of metals, ligands and geometries. Thus, nonlinearities of tris(bipyridine) ruthenium(II) complexes has been demonstrated[9,10] and we have recently reported the enhanced molecular hyperpolarisability β of octahedral ruthenium(II) complexes possessing three bipyridine ligands substituted in 4,4′-positions by *p*-dialkylaminostyryl groups.[11] In the course of our study of nondipolar complexes for NLO, we have been interested in the generation of metal complexes displaying tetrahedral coordination geometries. Copper(I)–bipyridine or –phenanthroline complexes with substituents α to the nitrogen atoms are known to give stable tetrahedral molecules of D_{2d} symmetry[12] and such complexes have been widely used to prepare molecular architectures such as catenates and knots,[13] helicates[14] and polymers.[15] Using this approach, we sought to design 4,4′-dialkenyl-6,6′-dimethyl-2,2′-bipyridines in which the alkenyl fragments bear π-donor groups. Here we describe the synthesis of such ligands and we show that the corresponding copper(I) complexes represent a new class of nondipolar NLO organometallic chromophore combining good transparency and large nonlinearity.

The new ligands **2a** and **2b** were prepared by a controlled functionalisation of the 4,4′-positions of 4,4′,6,6′-tetramethyl-2,2′-bipyridine **1**: dilithiation of **1** with LDA at −20 °C followed by reaction with 2 equiv. of *p*-dibutylaminobenzaldehyde afforded the corresponding dialcohol, and subsequent dehydration with pyridinium toluene-*p*-sulfonate (PTPS) in boiling toluene yielded exclusively **2a** in 75% overall yield. Ligand **2b** was prepared analogously as described for **2a** (Scheme 1). The observation of a strong NOE (10%) between the methyl groups at $C^{6,6'}$ and the $H^{5,5'}$ protons clearly established the regioselectivity of the reaction. In their UV–VIS spectra, **2a**,**b** show typical bands at *ca.* 390 nm ($\varepsilon \approx 50\,000$ dm^3 mol^{-1} cm^{-1}) which are assigned to intramolecular charge-transfer transitions.[16]

Copper(I) complexes were obtained upon treatment of the ligands **2a**,**b** (2 equiv.) with $[Cu(MeCN)_4]PF_6$ (1 equiv.) in dichloromethane solution (Fig. 1). The red complexes **3a**,**b** were isolated in nearly quantitative yield and their structures were demonstrated by FAB-MS and ^{1}H NMR spectroscopy. In the ^{1}H NMR spectra, the methyl groups in the 6,6′ positions are characteristically shifted upfield by 0.45 ppm with respect to the free ligands, and according to the strong vicinal coupling constants of the olefinic protons ($J_{HH} \approx 16$ Hz) no detectable *E/Z* isomerization of the alkenyl fragments is observed. The UV–VIS spectra recorded in dichloromethane are dominated by intense intraligand charge-transfer bands ($\lambda_{ILCT} \approx 420$ nm, $\varepsilon \approx$ 80 000 dm^3 mol^{-1} cm^{-1}) which are 30–40 nm red-shifted upon complexation. It is noteworthy that the bis(bipyridyl)copper(I) derivatives **3a**,**b** have a considerably blue-shifted ILCT band when compared to the corresponding tris(bipyridyl)ruthenium(II) complexes ($\lambda_{ILCT} \approx 515$ nm),[11] which is of crucial importance for second-harmonic generation. The MLCT transi-

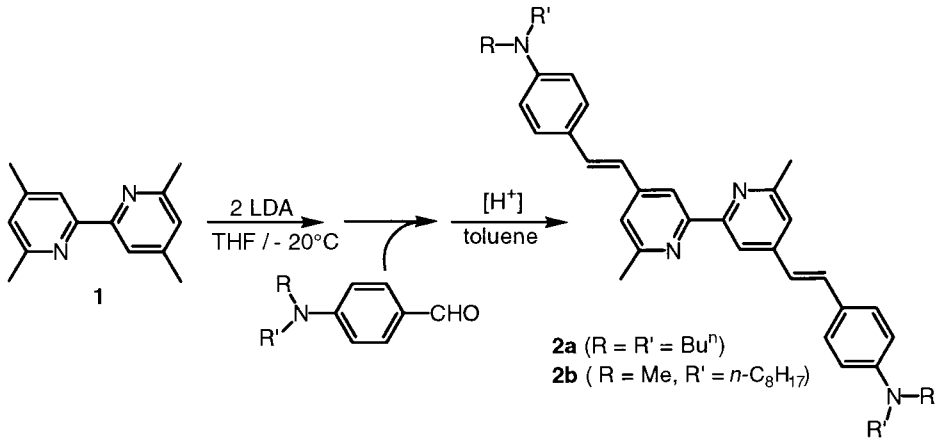

Scheme 1

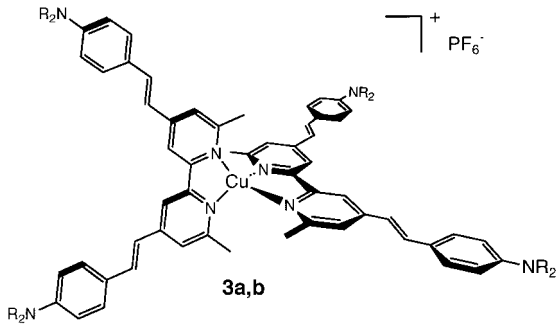

3a,b

Fig. 1

tion [$Cu^{I} \rightarrow \pi^*$(bpy)] is typically observed at *ca.* 480 nm with relatively smaller absorption coefficients and can be discerned in the spectra as a shoulder of the more intense ILCT band.

As EFISH experiment is precluded for nondipolar and/or ionic molecules like **3**, the molecular hyperpolarisability β was measured by means of the harmonic light scattering technique (HLS).[17] The experiments were performed in chloroform at a fundamental wavelength of 1.34 μm, generated by a Q-switched, mode-locked Nd:YAG laser providing subnanosecond pulse train at 10 Hz repetition rate. The T_d (or D_2) symmetry reduces the nonlinear microscopic coefficient to only one non-vanishing term, β_{xyz}, which can be easily deduced from the following relation: $<\beta^2_{HLS}> = 4/7\ \beta^2_{xyz}$. The experimentally determined $<\beta^2>^{1/2}$, the static $<\beta_0>^{1/2}$, deduced from $<\beta^2>$ using a degenerate three-level dispersion model valid in the case of purely octupolar molecules,[18] and the corresponding β_{xyz} coefficients for **3a**,**b** are given in Table 1.

Table 1 Linear[a] and nonlinear[b] optical data

Complex	λ/nm (ε/dm^3 mol^{-1} cm^{-1})	10^{30} β_{HLS}/esu	10^{30} β_{HLS}^0/esu	10^{30} β_{xyz}/esu	10^{30} β_{xyz}^0/esu
3a	424(83300) 484(sh)	144	78	190	103
3b	420(73800) 475(sh)	128	70	169	93

[a] In CH_2Cl_2. [b] HLS measurements in $CHCl_3$ at 1.34 μm. The error in the measurements is estimated to be ±10%.

Results show that chromophores **3a** and **3b** exhibit microscopic optical nonlinearities which are larger than those of recently reported tetrahedral molecules such as the tetrakis(dibutylaminoazobenzenephosphonium)chromophore [λ_{max} = 511 nm; $\beta_{HLS}^0 = 56.7 \times 10^{-30}$ esu].[7] Dibutylaminophenyl is slightly more efficient than the methyl(octyl)aminophenyl donor group, a trend that have already been observed for octahedral trisbipyridyl ruthenium(II) complexes bearing the same dialkylaminophenyl groups.[11] Compared to these latter complexes, the copper(I) derivatives **3** have lower β_{HLS} values. At first glance, this may be due to the presence of four *vs.* six donor groups and to the less efficient acceptor strength of Cu^+ *vs.* Ru^{2+} metallic ion. A more pronounced blue-shift of the absorption maximum is observed in the copper complexes, and the higher energy of the ILCT excited state also contributes to this observed decrease of β as compared to the octupolar ruthenium species.

To summarize, we have synthesized and investigated a new class of nondipolar NLO complexes showing good transparency/efficiency trade-off. Work towards the incorporation of such chromophores into macromolecular architectures are under progress.

Notes and references

1 J. Zyss, *Nonlinear Opt.*, 1991, **1**, 3; *J. Chem. Phys.*, 1993, **98**, 6583; J. Zyss and I. Ledoux, *Chem. Rev.*, 1994, **94**, 77.

2 I. Ledoux, J. Zyss, J. S. Siegel, J. Brienne and J. M. Lehn, *Chem. Phys. Lett.*, 1990, **172**, 440; T. Verbiest, K. Clays, C. Semyr, J. Wolff, D. Reihoudt and A. Persoons, *J. Am. Chem. Soc.*, 1994, **116**, 9320; J. L. Bredas, F. Meyers, B. M. Pierce and J. Zyss, *J. Am. Chem. Soc.*, 1992, **114**, 4928; R. Wortmann, C. Glana, P. Krämer, R. Matschiner, J. J. Wolff, S. Kraft, B. Treptow, E. Barbu, D. Längle and G. Göltz, *Chem. Eur. J.*, 1997, **3**, 1765.

3 J. Zyss, T. Chauvan, C. Dhenaut and I. Ledoux, *Chem. Phys.*, 1993, **177**, 281.

4 S. Stadler, Ch. Bräuchle, S. Brandl and R. Gompper, *Chem. Mater.*, 1996, **8**, 414.

5 S. Stadler, Ch. Bräuchle, S. Brandl and R. Gompper, *Chem. Mater.*, 1996, **8**, 676.

6 M. Lequan, C. Branger, J. Simon, T. Thami, E. Chauchard and A. Persoons, *Adv. Mater.*, 1994, **6**, 851.

7 C. Lambert, E. Schmälzlin, K. Meerholz and C. Bräuchle, *Chem. Eur. J.*, 1998, **4**, 512.

8 M. Blanchard-Desce, J.-B. Baudin, O. Ruel, L. Julien, S. Brasselet and J. Zyss, *Opt. Mater.*, 1997, **6**, 276.

9 J. Zyss, C. Dhenaut, T. Chauvan and I. Ledoux, *Chem. Phys. Lett.*, 1993, **206**, 409.

10 I. D. Morrison, R. G. Denning, W. M. Laidlaw and M. A. Stammers, *Rev. Sci. Instrum.*, 1996, **67**, 1445.

11 C. Dhenaut, I. Ledoux, I. F. W. Samuel, J. Zyss, M. Bourgault and H. Le Bozec, *Nature*, 1996, **374**, 339; Owing to possible two-photon excited luminescence,[10] the reported hyperpolarisabilities were overestimated and new measurements gave $<\beta^2>^{1/2}$ as ≈ 800–1000 × 10^{-30} esu: S. Brasselet, C. Dhenaut, I. Ledoux and J. Zyss, unpublished results.

12 P. J. Burke, K. Henrick and D. R. McMillin, *Inorg. Chem.*, 1982, **21**, 1881; D. A. Bardwell, J. C. Jeffery, C. A. Otter and M. D. Ward, *Polyhedron*, 1996, **15**, 191.

13 J.-P. Sauvage, *Acc. Chem. Res.*, 1990, **23**, 319; C. O. Dietrich-Bucheker and J.-P. Sauvage, *Chem. Rev.*, 1987, **87**, 795; C. O. Dietrich-Bucheker, J. F. Nierengarten, J.-P. Sauvage, N. Armaroli and L. De Cola, *J. Am. Chem. Soc.*, 1993, **115**, 11 237; C. O. Dietrich-Bucheker, J.-P. Sauvage, A. De Cian and J. Fischer, *J. Chem. Soc., Chem. Commun.*, 1994, 2231.

14 J.-M. Lehn, A. Rigault, J. Siegel, J. Harrowfield, B. Chevrier and D. Mores, *Proc. Natl. Acad. Sci. USA*, 1987, **84**, 2565; J. M. Lehn and A. Rigault, *Angew. Chem., Int. Ed.*, 1998, **27**, 1095; M. T. Youinou, R. Ziessel and J.-M. Lehn, *Inorg. Chem.*, 1991, **30**, 2144; G. Baum, E. C. Constable, D. Fenske, C. E. Housecroft and T. Kulke, *Chem. Commun.*, 1999, 195.

15 W. Velten and M. Rehahn, *Chem. Commun.*, 1996, 2639.

16 M. Bourgault, T. Renouard, B. Lognoné, C. Mountassir and H. Le Bozec, *Can. J. Chem.*, 1997, **75**, 318.

17 R. W. Terhune, P. D. Maker and C. M. Savage, *Phys. Rev. Lett.*, 1965, **61**, 681.

18 M. Joffre, D. Yaron, R. J. Silbey and J. Zyss, *J. Chem. Phys.*, 1992, **97**, 5607.

Communication 9/01972C

ChemComm

Supramolecular templated synthesis of platinum-supported silica

María Ángeles Aramendía, Victoriano Borau, César Jiménez,* José María Marinas and Francisco José Romero*

Department of Organic Chemistry, Faculty of Sciences, University of Córdoba, Avda. San Alberto Magno s/n, E-14004 Córdoba, Spain. E-mail: qo2rosaf@uco.es

Received (in Cambridge, UK) 10th March 1999, Accepted 7th April 1999

The incorporation of Pt onto MSU-1 mesoporous silica by direct inclusion of various precursors in a synthesis gel containing a structure-directing non-ionic surfactant was studied.

The M41S family of mesoporous molecular sieves has aroused enormous interest ever since these materials started to be used as sorbents, catalysts and supports[1] of high thermal stability, pore size uniformity and surface area. Individual noble metals including Pd[2] and Pt,[3,4] and combinations such as Cu–Ru,[5] have been supported on MCM-41 to prepare catalysts that are active in various processes. The metal is incorporated onto the support either by incipient wetness impregnation, ion exchange or direct introduction of platinum during the synthesis of MCM-41. This last procedure ensures uniform dispersion of platinum on the support, with particle sizes in the region of 6 nm that vary with the particular precursor used.[4]

Mesoporous metal oxides, designated MSU-X, can be obtained by assembling electrically neutral polyethylene oxide surfactants and neutral inorganic precursors.[6,7] These surfactants promote framework assembly through hydrogen bonding between the hydrophilic $(EO)_n$ segments and the silanol groups of the neutral inorganic precursor. These materials exhibit wormhole structures that lack regular channel packing order; however, they possess uniform channel diameters over a range comparable to M41S materials. The low cost and ready biodegradation of the surfactant are two major advantages of this synthetic procedure.

Controlled synthesis of colloidal platinum nanoparticles has been accomplished by altering the ratio of the concentration of a capping material (sodium polyacrylate) to that of Pt^{2+} ions.[8] Also, nanostructured mesoporous platinum has been synthesized by using a lyotropic liquid-crystalline phase as reaction medium.[9] This porous material possesses a high surface area, which is of great interest with a view to its catalytic application.

This paper reports the synthesis of platinum nanoparticles supported on mesoporous silica by use of the surfactant Tergitol 15-S-12 $[Me(CH_2)_{14}O(OCH_2CH_2)_{12}OH]$ as structure-directing agent.

Unsupported mesostructured silica (solid MSU-1) was synthesized following procedures similar to those reported elsewhere.[6] Platinum-supported silicas were obtained by supplying the starting mixture with 1 mol % Pt (relative to Si), using $(NH_4)_2PtCl_4$, H_2PtCl_6 and $(NH_3)_4PtCl_2$ as precursor salts, which produced the solids denoted MSU-1-1, MSU-1-2 and MSU-1-3, respectively.† A Tergitol 15-S-12 solution (0.1 mol l^{-1}), under stirring, was supplied with the platinum salt at 298 K. Then, TEOS was added and stirring was continued for a further 24 h. The TEOS–Pt–surfactant–H_2O mole proportion in the mixture was 10 : 0.1 : 1 : 560. The mixture was allowed to age for 72 h and the resulting powder was filtered, washed with distilled water and air-dried. Finally, the solid was calcined at 873 K in the air for 3 h.

Solids were characterized by powder X-ray diffraction (XRD), thermogravimetric analysis (TGA), N_2 sorptometry, elemental analysis (for Pt), transmission electron microscopy (TEM), temperature programmed reduction (TPR) and hydrogen chemisorption.

As a rule, the XRD patterns obtained (Fig. 1) exhibited a low angle peak (d_{100}), with a *d*-spacing between 37 and 66 Å (Table 1). The second-order peaks obtained at higher incidence angles were broad and short. These are typical of mesostructured materials with a sponge-like or worm-like pore channel structure, which are devoid of any regular long-range order, as expected for materials assembled using neutral or non-ionic surfactants. All the solids studied were calcined at 873 K in order to ensure removal of the surfactant, which was confirmed by TGA (*e.g.* solid MSU-1-1 exhibited a total weight loss of 52% as a result). In every case, the low angle d_{100} peak was

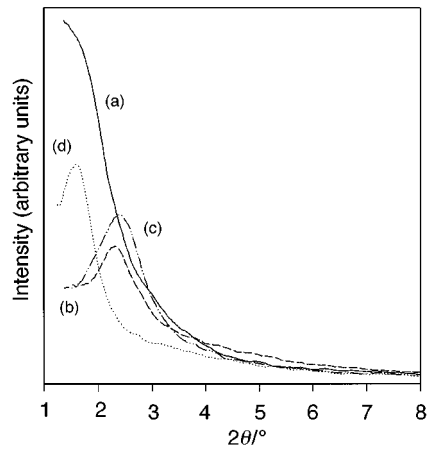

Fig. 1 Powder XRD patterns for solids MSU-1 (*a*), MSU-1-1 (*b*), MSU-1-2 (*c*) and MSU-1-3 (*d*), all calcined at 873 K.

Table 1 Physicochemical properties of Pt-supported and unsupported MSU-1 mesoporous silica

Solid	d_{100} lattice spacing[a]/Å	d_{100} lattice spacing[b]/Å	BET surface area/$m^2\ g^{-1}$	Pore volume/ml g^{-1}	BJH pore size/Å	Pt content (wt%)
MSU-1	—	55	644	0.96	37	—
MSU-1-1	41	38	851	0.42	19	2.08
MSU-1-2	43	37	606	0.30	19	0.36
MSU-1-3	66	56	707	0.87	38	0.23

[a] As synthesized. [b] Calcined in air at 873 K for 3 h.

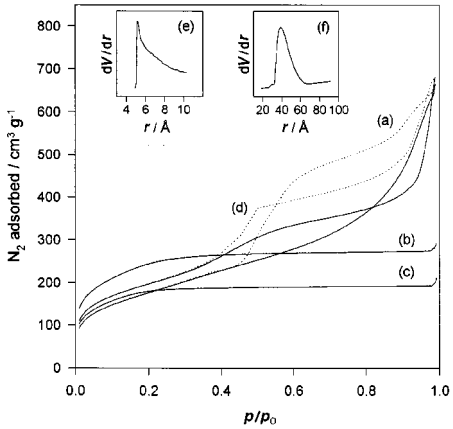

Fig. 2 N_2 adsorption (solid line) and desorption (dotted line) isotherms for calcined MSU-1 (*a*), MSU-1-1 (*b*), MSU-1-2 (*c*) and MSU-1-3 (*d*). Insets: Horvath–Kawazoe pore diameter (*r*) distribution of MSU-1-1 (*e*) and BJH pore diameter distribution of MSU-1 (*f*).

shifted to a higher angle upon calcination, thus indicating gradual contraction of *d*-spacings in the lattice upon removal of the surfactant.

Table 1 also gives the surface areas, pore diameters and pore volumes of the solids. As can be seen, all possess a high specific surface area (>600 m^2 g^{-1}). The N_2 adsorption–desorption isotherms are of type IV (*i.e.* typical of mesoporous solids) for MSU-1 and MSU-1-3 (Fig. 2), pore size in which varies over narrow ranges (35–50 and 32–42 Å), with type H2 and type H4 hysteresis cycles, respectively.[10] Also, MSU-1-1 and MSU-1-2 exhibit a type I isotherm, with the step at a relative pressure around 0.2. Nitrogen isotherms of this kind are typical of pores with sizes in between the micro and meso ranges.[11] The micropore distribution in solid MSU-1-1 as determined by the Horvath–Kawazoe method[12] confirms the presence of pores in this size range, most of size about 7 Å (Fig. 2).

Table 1 lists the Pt content in each solid. As can be seen, the amount of Pt incorporated into the silica was only significant (50% of the amount added) when $(NH_4)_2PtCl_4$ was used as precursor. A temperature programmed reduction (TPR) run for solid MSU-1-1 revealed that virtually the whole deposited metal was present as Pt^0, so the metal ion was reduced during the solid synthesis and calcination, which is consistent with previous findings in MCM-41 as support.[4] Chemisorption tests revealed solid MSU-1-1 to be able to adsorb 60 and 19 μl of H_2 at room temperature and 673 K, respectively; this results in a metal dispersion of 32%, with a metal surface area of 80 m^2 g_{metal}^{-1} and an average particle diameter of 43 Å, all consistent with the TEM results. Fig. 3 shows the particle size distribution as

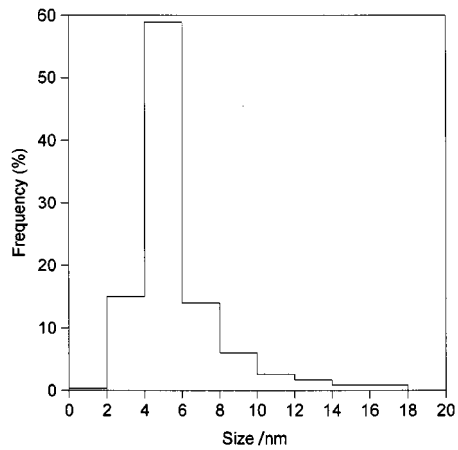

Fig. 3 Size distribution of platinum particles in solid MSU-1-1.

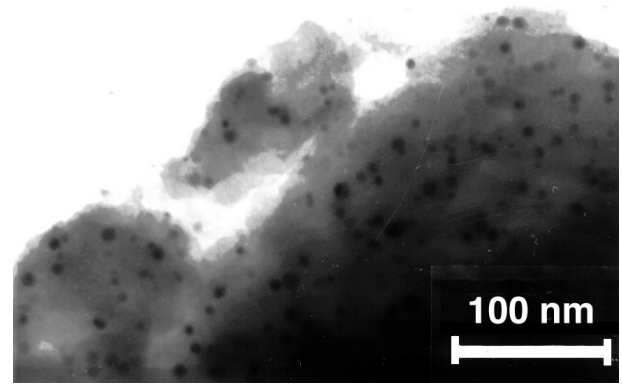

Fig. 4 TEM image of calcined MSU-1-1.

determined by this technique and Fig. 4 shows a typical TEM image.

In summary, our results suggest that platinum nanoparticles can be supported onto mesostructured silica by using a non-ionic surfactant assembly involving direct incorporation *via* the synthesis gel. Other experimental variables such as the surfactant used, temperature, concentrations, solvent extraction of the surfactant, *etc.*, can be altered as required. One of the most salient advantages of this procedure is that it allows the incorporation of metal nanoparticles into other mesoporous metal oxides that are inaccessible by electrostatic templating routes, simply by hydrolysing the corresponding alkoxides (*e.g.* titania or tin oxide). These materials can be used as, for example, catalysts, and also in optical, electronic and magnetic devices.

The authors would like to thank Spain's DGES, Ministry of Education and Culture, for funding this research within the framework of Project PB97-0446, and Junta de Andalucía for additional financial support.

Notes and references

† *Typical procedure:* solid MSU-1-1 was obtained by adding 10 ml of tetraethylorthosilicate (TEOS) over a solution containing 0.171 g of $(NH_4)_2PtCl_4$ in 46 mL of 0.1 mol l^{-1} Tergitol 15-S-12 at room temperature. After 24 h under stirring, the suspension was allowed to stand for 3 days and the solid was filtered off, air-dried and calcined at 873 K for 3 h.

1 C. T. Kresge, M. E. Leonowicz, W. J. Roth, J. C. Vartuli and J. S. Beck, *Nature*, 1992, **359**, 710.
2 C. A. Koh, R. Nooney and S. Tahir, *Catal. Lett.*, 1997, **47**, 199.
3 A. Corma, A. Martínez and V. Martínez-Soria, *J. Catal.*, 1997, **169**, 480.
4 U. Junges, W. Jacobs, I. Voigt-Martin, B. Krutzsch and F. Schüth, *J. Chem. Soc., Chem. Commun.*, 1995, 2283.
5 D. S. Shephard, T. Maschmeyer, G. Sankar, J. M. Thomas, D. Ozkaya, B. F. G. Johnson, R. Raja, R. D. Oldroyd and R. G. Bell, *Chem. Eur. J.*, 1998, **4**, 1214.
6 S. A. Bagshaw, E. Prouzet and T. J. Pinnavaia, *Science*, 1995, **269**, 1242.
7 E. Prouzet and T. J. Pinnavaia, *Angew. Chem., Int. Ed. Engl.*, 1997, **36**, 516.
8 T. S. Ahmadi, Z. L. Wang, T. C. Green, A. Henglein and M. A. El-Sayed, *Science*, 1996, **272**, 1924.
9 G. S. Attard, C. G. Göltner, J. M. Corker, S. Henke and R. H. Templer, *Angew. Chem., Int. Ed. Engl.*, 1997, **36**, 1315.
10 K. S. W. Sing, D. H. Everett, R. A. W. Haul, L. Moscou, R. A. Pierotti, J. Rouquérol and T. Siemieniewska, *Pure Appl. Chem.*, 1985, **57**, 603.
11 U. Ciesla, S. Schacht, G. D. Stucky, K. K. Unger and F. Schüth, *Angew. Chem., Int. Ed. Engl.*, 1996, **35**, 541.
12 G. Horvath and K. Kawazoe, *J. Chem. Eng. Jpn.*, 1983, **16**, 470.

Communication 9/01924C

ChemComm

Isolation and crystal structure of a novel dinuclear nickel(II) O-bound sulfinate from the oxidation of 2,2′-bipyridine-1,2-benzenedithiolatonickel(II)

T. Matthew Cocker and Robert E. Bachman*

Department of Chemistry, Box 571227, Georgetown University, Washington, D.C., 20057-1227, USA. E-mail: bachman@gusun.georgetown.edu.

Received (in Bloomington, IN, USA) 22nd January 1999, Accepted 30th March 1999

The first example of an O-bound sulfinate diimine nickel(II) complex has been isolated from the partial oxidation of Ni(bpy)(bdt) 1 (bpy = 2,2′-bipyridine, bdt = 1,2-benzenedithiolate), and characterized by X-ray crystallography and ESI-MS.

Since the first report by Miller and Dance in 1973, mixed dithiolene-α-diimine complexes of group 10 metals have received considerable attention because of their many unique physical properties, which include multiple accessible redox states, intense colors and non-linear optical behavior.[1] While complexes of this type have been reported for all three metals, particular attention has been focused on the heaviest (Pt^{II}) and the lightest (Ni^{II}) members of the group. In the former case this attention is the result of the unique optoelectronic properties of the systems.[2] In the latter case, the interest has been focused on the potential of these complexes to act as models for biological systems such as nickel-containing CO-dehydrogenase.[3,4] Investigations into the oxidation chemistry of nickel(II) diamine dithiolates have produced several compounds including monosulfenates [RS–M–SOR], disulfenates [M–$(SOR)_2$], monosulfinates [RS–M–SO_2R], disulfinates [M–$(SO_2R)_2$], and mixed sulfinate–sulfenate [ROS–M–SO_2R] complexes.[5] Recently, Henderson *et al*. reported the first process in which a Ni–S bond is oxidatively cleaved to yield an O-bound disulfonate [M–$(SO_3R)_2$].[6] However, to date no examples of O-bound sulfinates have been reported. We report herein the isolation and X-ray structure of an unusual dinuclear nickel(II) complex which contains the first example of an O-bound sulfinate diimine nickel(II) complex (**2**), as well as an additional example of a disulfonate diimine nickel(II) complex **3**.

During a UV–VIS study of Ni(bpy)(bdt) **1** (bpy = 2,2′-bipyridine, bdt = 1,2-benzenedithiolate) in DMF, we observed that solutions of **1** slowly changed color from purple to orange. While the initial spectrum contains a broad absorption between 500 and 600 nm, characteristic of complexes such as **1**, this band disappears and is replaced by a new absorption peak at 874 nm. Slow evaporation of this solution yielded a small amount of orange X-ray quality crystals. The X-ray crystal structure of these crystals was determined and is shown in Fig. 1.†

The solid material was found to be a co-crystal of both the monosulfinate $(bpy)_2$Ni(bdtO_2)Ni(bdt) **2a** and the disulfinate $(bpy)_2$Ni(bdtO_4)Ni(bdt) **2b** in an approximate 60:40 ratio. ESI-MS of the crystalline material yielded molecular ions for both **2a** and **2b** with appropriate relative intensities.[7] All attempts to prepare **2** in a rational fashion using a chemical oxidant, such as H_2O_2, produced only **3** (Fig. 2) regardless of the stoichiometry.†

The Ni–N distances in **2** and **3** (2.05–2.08 Å) are both similar to those observed for the related compound $(bpy)_2(PhS)_2$-Ni^{II}·D_2O (2.08–2.10 Å).[8] As expected, the Ni(1)–O bond distance in **2** (2.104(5) Å) is longer than the Ni–O bonds in complex **3** (2.05-2.06 Å) and is also longer than the Ni–O bonds in [(3-thia-1,5-diaminopentane *S*-oxide)$_2$Ni]$^{2+}$ (2.07–2.09 Å)[9] and the Ni–OH_2 bond [2.084(1) Å] in [Ni(dsodm)-$(H_2O)_2$]·$2H_2O$ (dsodm = [$(O_3SCH_2CH_2)MeNCH_2CH_2N$-$Me(CH_2CH_2SO_3)$]).[6] This difference is most likely the result of the stronger donor ability of the bpy ligands in **2**. The Ni–O bonds in **3** [2.060(3) Å and 2.054(3) Å]) are also slightly longer than the Ni–sulfonato bonds in [Ni(dsodm)$(H_2O)_2$]·$2H_2O$ [2.044(1) Å], again probably due to the more electron-rich nickel in **3**.[6] The Ni–S bond lengths observed for **2** are 2.13–2.17 Å for the square planar Ni(2) and 2.499(3) Å for the octahedral Ni(1). The former are similar to those observed for other four-coordinate systems such as **1** (2.14–2.15 Å) and Ni(bdt)$_2^{2-}$ (2.17–2.18 Å).[10,11] Interestingly the Ni–S bond length in **2** and other four-coordinate Ni-sulfinates are not significantly affected by the oxidation state of the sulfur.[5] The Ni–S bond length for the octahedral Ni in **2** is similar to that in $(bpy)_2(PhS)_2Ni^{II}$·D_2O [2.445(2) Å].[8]

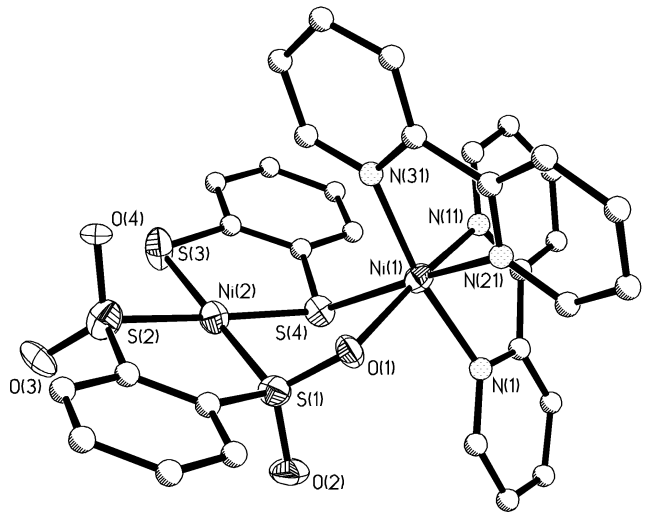

Fig. 1 Diagram showing the sulfinate complex **2a,b** with the significant atoms shown with displacement ellipsoids at 50% probability and the remaining atoms shown as spheres of arbitrary radius. The hydrogen atoms have been omitted for clarity. Selected bond distances (Å) and angles (°): Ni(1)-N 2.05-2.07, Ni(1)-O(1) 2.104(5), Ni(1)-S(4) 2.499(3), Ni(2)-S(1) 2.127(3), Ni(2)-S(2) 2.156(3), Ni(2)-S(3) 2.166(3), Ni(2)-S(4) 2.154(3), S(1)-O(1) 1.490(6), S(1)-O(2) 1.472(6); O(1)-S(1)-Ni(2) 111.8(3), Ni(2)-S(4)-Ni(1) 101.85(10), S(1)-O(1)-Ni(1) 122.8(4).

While the exact origin of **2** is still uncertain, it can be seen from **3** that the complete oxidation of **1** to **3** involves both rupture of the Ni–S bonds and the exchange of ligands. While the fate of the other nickel thiolate fragment in conversion of **1** to **3** remains unknown, the observed ligand disproportionation allows for a rationalization for the formation of **2** (Scheme 1).

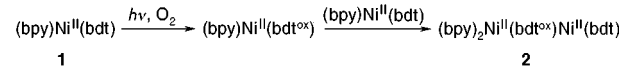

Scheme 1 A rationalization of the formation of **2** from **1** *via* a 'partial' disproportionation.

Under the ambient conditions present in the spectrometer, a small amount of **1** was converted into the mono or disulfinate form (**1^{ox}**) which then begins to undergo a disproportionation process with an unoxidized molecule of **1**. The decreased solubility of **2**, in relation to **1** or **1^{ox}**, leads to this 'intermediate'

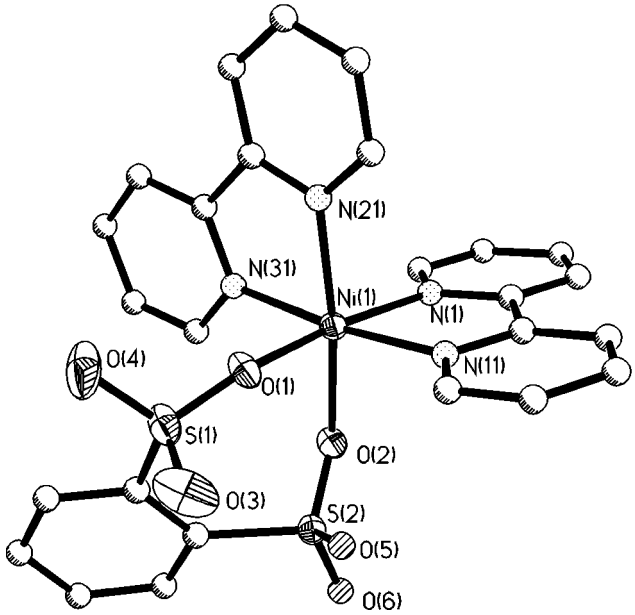

Fig. 2 Diagram showing the sulfonate complex **3**·0.5dmf with the significant atoms shown with displacement ellipsoids at 50% probability and the remaining atoms shown as spheres of arbitrary radius. The DMF molecule and the hydrogen atoms have been omitted for clarity. Selected bond distances (Å) and angles (°): Ni(1)–O(1) 2.060(3), Ni(1)–O(2) 2.054(3), Ni(1)–N 2.06–2.08, S(1)–O(1) 1.452(3), S(1)–O(3) 1.452(4), S(1)–O(4) 1.420(4), S(2)–O(2) 1.485(3), S(2)–O(5) 1.436(3), S(2)–O(6) 1.446(3); O(2)–Ni(1)–O(1) 90.97(12), S(1)–O(1)–Ni(1) 151.98(19), S(2)–O(2)–Ni(1) 128.38(16).

in the disproportionation process being 'trapped' by precipitation, producing the observed result. We are currently pursuing a rationale synthesis of **2a,b** and attempting to resolve the outstanding mechanistic questions related to the formation of both **2** and **3**.

This work was supported by Georgetown University and the donors of the Petroleum Research Fund, administered by the ACS. The purchase of the X-ray diffractometer was made possible by a grant from the National Science Foundation (CHE-9115394). The authors wish to acknowledge Professor J. T. Davis at University of Maryland, College Park for ESI-MS analysis.

Notes and references

† *Crystal data*: **2**: crystals of **2** were obtained by evaporation of a DMF solution used in a UV–VIS study at room temperature. $C_{32}H_{24}N_4Ni_2O_{2.83}S_4$, M = 755.45; monoclinic, $P2_1/n$, a = 11.5407(3), b = 16.9821(4), c = 16.7013(4) Å, β = 106.9880(10)°, V = 3130.39(13) Å^3, Z = 4, D_c = 1.603 g cm^{-3}, μ = 1.511 mm^{-1}. All data were collected on a Bruker-AXS SMART CCD system at −100 °C. A small orange plate of **2** (0.04 × 0.16 × 0.16 mm) was mounted on a glass fiber using epoxy. The data were collected as described elsewhere[12] to provide a complete sphere of data to 0.75 Å ($2\theta_{max}$ = 56.62°) yielding 25633 data. Final unit cell parameters were calculated using 5720 reflections culled from the entire data set. The data were corrected for Lorentz and polarization effects and an absorption correction was applied on the basis of equivalent reflection measurements using Blessing's method as incorporated into the program SADABS.[13]

Owing to their poor quality, the data were truncated on the basis of intensity statistics at a resolution of 0.85 Å ($2\theta_{max}$ = 49.42°) to yield a final data set of 19526 reflections (5340 unique, R_{int} = 0.2091). The structure was solved using direct methods and refined against F^2 by full-matrix least-squares methods using the programs in SHELXTL and SHELX-97.[14] All non-hydrogen atoms were refined anisotropically, while hydrogen atoms were refined isotropically. The oxygen atoms O(3) and O(4) were refined to 40% site occupancy and then held fixed at this value. The final refinement converged with residuals of wR_2 = 0.2125 (all data), $R_1(F)$ = 0.0785 [$I > 2\sigma(I)$], and GOF = 0.998. Significant bond lengths and angles are given in Fig 1.

3·0.5 dmf; crystals of **3**·0.5 dmf were obtained by treatment of **1** with H_2O_2 in DMF followed by slow evaporation of the solution at room temperature. $C_{27.50}H_{20}N_{4.50}NiO_{6.50}S_2$, M = 640.31; triclinic, $P\bar{1}$, a = 9.31350(10), b = 12.5526(2), c = 12.7451(2) Å, α = 96.0170(10), β = 101.8868(3), γ = 110.0760(10)°, V = 1344.26(3) Å^3, Z = 2, D_c = 1.582 g cm^{-3}, μ = 0.932 mm^{-1}. A small colorless plate of **3**·0.5 dmf (0.02 × 0.10 × 0.16 mm) was mounted on a glass fiber using epoxy and the data were collected as above to yield 11300 reflections (6302 unique, R_{int} = 0.0599). Final unit cell parameters were calculated using 5378 reflections culled from the entire data set. The dmf molecule was found to be disordered over the inversion center and was modeled as three separately oriented molecules with a total combined occupancy of 0.5. The final refinement converged with residuals of wR_2 = 0.1340 (all data), $R_1(F)$ = 0.0691 [$I > 2\sigma(I)$], and GOF = 1.066. Significant bond lengths and angles are given in Fig 2.

CCDC 182/1210. See http://www.rsc.org/suppdata/cc/1999/875/ for crystallographic files in .cif format.

1 T. R. Miller and I. G. Dance, *J. Am. Chem. Soc.*, 1973, **95**, 6970.
2 S. D. Cummings, L.-T. Cheng and R. Eisenberg, *Chem. Mater.*, 1997, **9**, 440 and references therein.
3 J. A. Bellefeuille, C. A. Grapperhaus, R. M. Buonomo, J. H. Reibenspies and M. Y. Darensbourg, *Organometallics*, 1998, **17**, 4813 and references therein.
4 S. A. Mirza, R. O. Day and M. J. Maroney, *Inorg. Chem.*, 1996, **35**, 1992.
5 C. A. Grapperhaus and M. Y. Darensbourg, *Acc. Chem. Res.*, 1998, **31**, 451.
6 R. K. Henderson, E. Bouwman, A. L. Spek and J. Reedijk, *Inorg. Chem.*, 1997, **36**, 4616.
7 All attempts to repeat this synthesis have so far proven unsuccessful. Solutions of **1** in dmf exposed to incandescent light and sunlight have yielded crystals of **1**.
8 K. Osakada, T. Yamamoto and A. Yamamoto, *Acta Crystallogr., Sect. C*, 1984, **40**, 85.
9 A. Löwe, R. Mattes and K. Wasielewski, *Z. Anorg. Allg. Chem.*, 1993, **619**, 905.
10 T. M. Cocker and R. E. Bachman, in preparation.
11 D. Sellmann, S. Fünfgelder, F. Knoch and M. Moll, *Z. Naturforsch., Teil B*, 1991, **46**, 1601.
12 R. E. Bachman and D. F. Andretta, *Inorg. Chem.*, 1998, **37**, 5657.
13 R. H. Blessing, *Acta Crystallogr., Sect. A*, 1995, **51**, 33; G. M. Sheldrick, SADABS, 1996, Universität Göttingen, Göttingen, Germany.
14 SHELXTL-PC, Vers. 5.10; 1998, Bruker-Analytical X-Ray Services; Madison, WI; G. M. Sheldrick, SHELX-97, 1997, Universität Göttingen, Göttingen, Germany.

Communication 9/00673G

ChemComm

Hybrid organic–inorganic, hexa-arm dendrimers based on an Mo_6Cl_8 core

Christopher B. Gorman,* Wendy Y. Su, Hongwei Jiang, Christopher M. Watson and Paul Boyle

Box 8204, Department of Chemistry, North Carolina State University, Raleigh, NC 27695, USA. E-mail: Chris_Gorman@ncsu.edu

Received (in Bloomington, IN, USA) 25th February 1999, Accepted 6th April 1999

Dendrons with focal phenoxide groups were shown to substitute for triflate or methoxide ligands around an Mo_6Cl_8 core to form molecules of the form $Mo_6(\mu_3\text{-}Cl)_8(OR)_6$ where R = dendrons with zero to two hyperbranches, respectively; these molecules represent a new type of metal cluster core dendrimer with six arms and high symmetry.

Metals and inorganic clusters have served several roles in the construction of dendrimer structures.[1] These include acting as the linking elements, the peripheral elements and as the core element of dendrimers. When used as cores, metals and inorganic clusters have several documented functions.[1] They can be used as reporters of the interior environment of these molecules by virtue of their luminescent, electrochemical or magnetic properties. They can take advantage of the microenvironment of the dendrimer in catalysis applications. Moreover, they can utilize the dendrimer to control electron transfer.[2,3]

To these ends and others, a variety of metal and metal cluster core dendrimers have been prepared. These include dendrimers with porphyrin,[4–8] iron–sulfur,[2] metal tris-bipyridine[9] and octasilsesquioxane[10,11] cores. All of these syntheses rely on either a core that is tolerant of organic coupling reactions or a core that can undergo some type of ligand exchange to substitute dendritic ligands for smaller ligands. The ligand exchange route to dendrimers can be particularly attractive. In the iron–sulfur core dendrimers discussed above, ligand exchange of a bulky aliphatic thiol for a focally substituted aromatic thiol dendron resulted in virtually quantitative synthesis of molecules with molecular weights of up to 22 kD.[2]

Here we report that ligand exchange reactions around a metal cluster core of the form Mo_6Cl_8 can be employed to form molecules of the form $Mo_6(\mu_3\text{-}Cl)_8(OR)_6$ (R = dendrons with 0–2 hyperbranches), respectively. These six arm, pseudo-octahedral core dendrimers represent one of the first examples of this type.[12] The replacement of both methoxy by other alkoxy ligands[13–16] and of triflate by other alkoxy or carboxy ligands[17,18] at the corner positions of these clusters have been reported. Here, the use of such reactions in the synthesis of new hybrid organic–inorganic macromolecules is illustrated.

The first and second generation ligands (**L1** and **L2**) used to prepare the six-arm dendrimers were prepared by reacting the previously reported[19] focally substituted dendron mesylates (mesylate = OSO_2CH_3) with mono-methoxymethyl hydroquinone followed by deprotection of the methoxymethyl group (Scheme 1). Molecules **G0**, **G1** and **G2** (named corresponding to the generation of dendrimer they represent) were prepared by ligand exchange with either triflate-capped $[n\text{Bu}_4\text{N}]_2[\text{Mo}_6$-

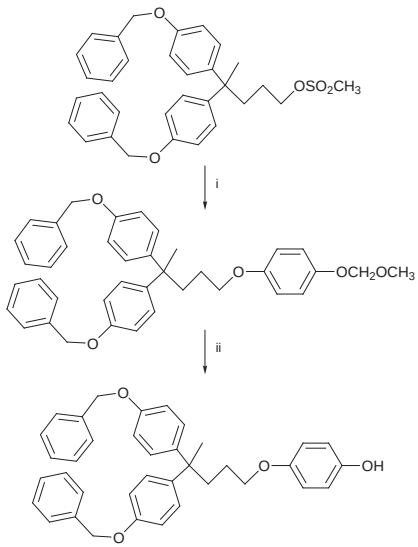

Scheme 1 Preparation of focally-substituted phenol dendrons. Sequence is shown for the preparation of **L1**. Preparation of **L2** is performed in an identical fashion. *Reagents and conditions*: i, HOC_6H_4OMOM (1 equiv.), K_2CO_3 (6 equiv.), 18-crown-6 (0.2 equiv.), dry acetone, reflux 60 h; ii, MeOH–THF–HCl, reflux overnight.

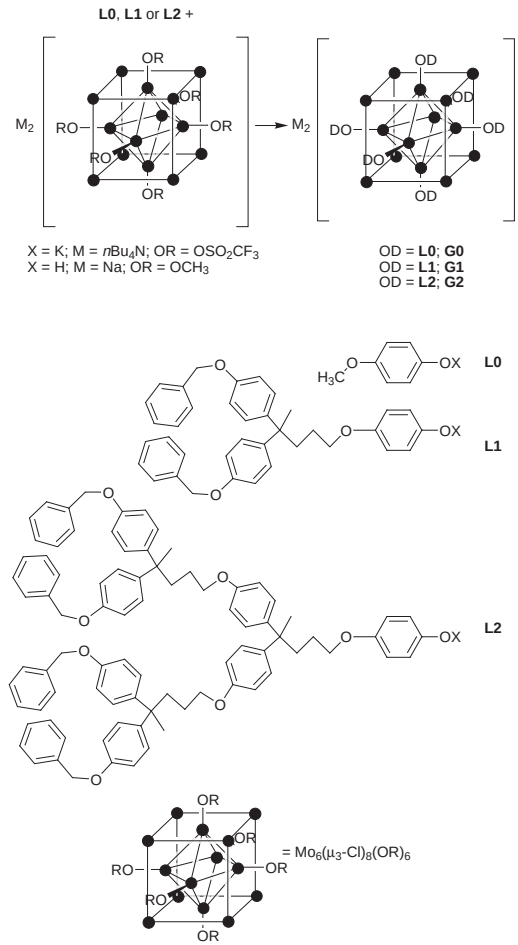

Scheme 2 Preparation of dendrimers. *Reagents and conditions* for $[n\text{Bu}_4\text{N}]_2\mathbf{G}x$ (x = 0, 1, 2): 10 equiv. $\mathbf{L}x$ (x = 0, 1 2), excess KH, THF, r.t., N_2, 30 min then $[n\text{Bu}_4\text{N}]_2\text{Mo}_6\text{Cl}_8(\text{OSO}_2\text{CF}_3)_6$, THF, r.t., N_2 overnight, ppt $KOSO_2CF_3$, washing with toluene, filter and ppt product washed with Et_2O. *Reagents and conditions for* $\text{Na}_2\mathbf{G}x$ (x = 0, 1, 2): 10 equiv. $\mathbf{L}x$ (x = 0, 1, 2), $\text{Na}_2\text{Mo}_6\text{Cl}_8(\text{OMe})_6$, MeOH–toluene or MeOH–1,2-dichlorobenzene, 80–90 °C, overnight, N_2, Et_2O ppt.

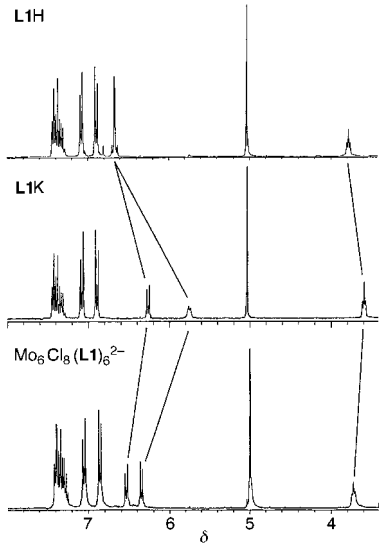

Fig. 1 Series of ^{1}H NMR spectra illustrating the distinct shifts in the resonances of the focal aromatic ring protons upon deprotonation and attachment to the cluster. Rapid exchange was ruled out by adding excess ligand and observing two distinct sets of peaks.

$Cl_8(OSO_2CF_3)_6]$[17] or methoxy-capped $Na_2[Mo_6Cl_8(OMe)_6]$[20] clusters (Scheme 2).

Deprotonation and subsequent reaction of a slight excess of ligand with the triflate-capped cluster resulted in complete exchange in the case of the $[n\text{Bu}_4\text{N}]_2$**G0** and $[n\text{Bu}_4\text{N}]_2$**G1** molecules.[21] This series of reactions is nicely illustrated by the series of ^{1}H NMR spectra shown in Fig. 1. Complete precipitation of potassium triflate coproduct was found to be essential as this reaction was determined to be reversible. NMR samples of pure **G1** in THF-d^8 were found to undergo ligand loss when a few equivalents of potassium triflate were added to this solution. Moreover, only partial exchange was observed when **L2** was employed as evidenced by broad ^{1}H NMR signals of the multiple, overlapping, partially substituted species. These two latter features limited the utility of this reaction in our hands.

Using a modification of conditions reported in the literature,[13–16,22] reaction of the ligands **L0**, **L1** and **L2** with $Na_2[Mo_6Cl_8(OCH_3)_6]$ resulted in complete exchange for all molecules prepared. In the case of Na_2**G0**, a 98% yield of an analytically pure product was obtained, and crystals suitable for X-ray structure determination were obtained (Fig. 2).[23] Bond lengths and angles similar to those reported for related Mo_6Cl_8-core structures were found (*e.g.* Mo–Cl 2.48–2.50 Å, Mo–O 2.04–2.09 Å).[13,16,24]

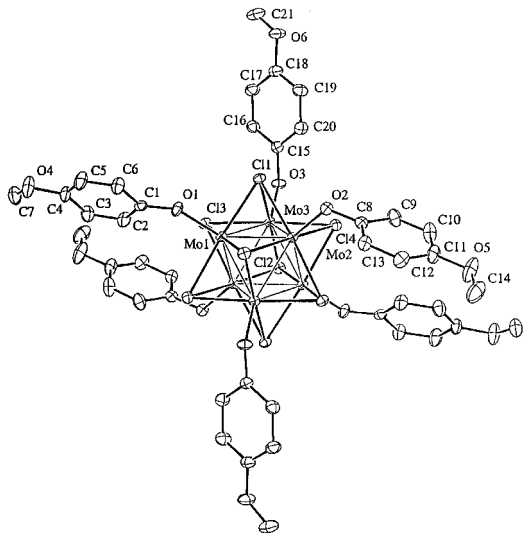

Fig. 2 The molecular structure of Na_2**G0.**

Dendrimers were characterized by NMR and mass spectrometry (MS). We found electrospray MS to be most convenient as a strong parent ion signal could be obtained. The charge on the clusters as well as perhaps their hydrophobicity[25] were probably beneficial factors in the success of these characterization experiments.

In conclusion, it has been shown that high-symmetry metal cluster cores can be used in the preparation of hybrid organic–inorganic dendrimers. In the case of an Mo_6Cl_8 core, the choice of ligand exchange reaction was found to be important to the success of making higher molecular weight dendrimers.

This research was supported by the Air Force Office of Scientific Research MURI program in Nanoscale Chemistry and by the National Science Foundation (CAREER Award, DMR-9600138). Mass spectra were obtained at the Mass Spectrometry Laboratory for Biotechnology. Partial funding for the Facility is from NSF grant 94-2.

Notes and references

1 C. B. Gorman, *Adv. Mater.*, 1998, **10**, 295.
2 C. B. Gorman, B. L. Parkhurst, K.-Y. Chen and W. Y. Su, *J. Am. Chem. Soc.*, 1997, **119**, 1141.
3 C. B. Gorman, *Adv. Mater.*, 1997, **9**, 1117.
4 P. Bhyrappa, J. K. Young, J. S. Moore and K. S. Suslick, *J. Am. Chem. Soc.*, 1996, **118**, 5708.
5 J. P. Collman, L. Fu, A. Zingg and F. Diederich, *Chem. Commun.*, 1997, 193.
6 P. J. Dandliker, F. Diederich, M. Gross, C. B. Knobler, A. Louati and E. M. Sanford, *Angew. Chem., Int. Ed. Engl.*, 1994, **33**, 1739.
7 P. J. Dandliker, F. Diederich, J.-P. Gisselbrecht, A. Louati and M. Gross, *Angew. Chem. Int., Ed. Engl.*, 1995, **34**, 2725.
8 D.-L. Jiang and T. Aida, *Chem. Commun.*, 1996, 1523..
9 J. Issberner, F. Vögtle, L. De Cola and V. Balzani, *Chem. Eur. J.*, 1997, **3**, 706.
10 B. Hong, T. P. S. Thoms, H. J. Murfee and M. J. Lebrun, *Inorg. Chem.*, 1997, **36**, 6146.
11 F. J. Feher and K. D. Wyndham, *Chem. Commun.*, 1998, 323.
12 Use of a Re_6Se_8 core has also recently been reported: Z. Zheng and R. Wang, *217th American Chemical Society Meeting*, Anaheim, CA, March 1999, Paper INOR563.
13 N. Prokopuk and D. F. Shriver, *Inorg. Chem.*, 1997, **36**, 5609.
14 P. Nannelli and B. P. Block, *Inorg. Chem.*, 1969, **8**, 1767.
15 P. Nannelli and B. P. Block, *Inorg. Chem.*, 1968, **7**, 2423-2426
16 N. Perchenek and A. Simon, *Z. Anorg. Allg. Chem.*, 1993, **619**, 103.
17 D. H. Johnston, D. C. Gaswick, M. C. Lonergan, C. L. Stern and D. F. Shriver, *Inorg. Chem.*, 1992, **31**, 1869.
18 J. H. Golden, H. Deng, F. J. DiSalvo, J. M. J. Fréchet and P. M. Thompson, *Science*, 1995, **268**, 1463.
19 K.-Y. Chen and C. B. Gorman, *J. Org. Chem.*, 1996, **61**, 9229.
20 P. Nannelli and B. P. Block, *Inorg. Synth.*, 1971, **13**, 99.
21 For experimental details see http://www.rsc.org/suppdata/cc/1999/877/
22 To a suspension of $Na_2[Mo_6Cl_8(OMe)_6]$ (80 mg, 0.073 mmol) in a solution of **L***x* (x = 1, 2) (0.47 mmol) in 1,2-dichlorobenzene (3 ml), 3 ml of anhydrous methanol was added with stirring. The resulting mixture became clear immediately, and was further stirred overnight under a partial vacuum of 100 mTorr. This allowed solvents and by-product methanol to be removed slowly, and a yellow solid remained. The residue was dissolved into 4 ml of toluene, and filtered under nitrogen to remove the unreacted starting cluster, and then 10 ml of Et_2O was added to the filtrate. The precipitate was collected and washed with Et_2O. The product was further purified by precipitation from toluene–Et_2O several times (yield: 92% for **G1**). Molecule **G0** was prepared similarly except that DMF was substituted for 1.2-dichlorobenzene.
23 *Crystal data* for $Mo_6Cl_8C_{60}H_{79}O_{16.5}Na_2$ (Na**G0**·4THF·2Et$_2$O): M = 1969.50, monoclinic, space group $C2/c$, a = 22.9666(19), b = 18.1932(18), c = 18.1761(19) Å, U = 7509.8(12) Å^3, T = 148 K, Z = 4, μ = 1.33 mm^{-1}, 8106 reflections measured, 6108 of which had intensities > 1.0 $\sigma(I)$ and were considered observed. The structure was refined using full matrix least squares based on F. The final R and R_w were 0.036 and 0.041 respectively. CCDC 182/1218. See: http://www.rsc.org/suppdata/cc/1999/877/ for crystallographic files in .cif format.
24 M. H. Chisholm, J. A. Heppert and J. C. Huffman, *Polyhedron*, 1984, **3**, 475.
25 C. G. Enke, *Anal. Chem.*, 1997, **69**, 4885.

Communication 9/01590F

ChemComm

Synthesis and X-ray structure of the first 1,3,2,4-diazaphosphaaluminetidine

Stephan Schulz,* Tillmann Bauer and Martin Nieger

Institut für Anorganische Chemie der Universität Bonn, Gerhard-Domagk-Str. 1, D-53121 Bonn, Germany. E-mail: stephan@ac4010se.chemie.uni-bonn.de

Received (in Basel, Switzerland) 3rd March 1999, Accepted 2nd April 1999

Dehydrogenation reaction between $AlH_3{\leftarrow}NMe_3$ and $Bu^tP[N(H)Bu^t]_2$ leads to $Bu^tP(NBu^t)_2AlH{\leftarrow}NMe_3$, the first neutral 1,3,2,4-diazaphosphaaluminetidine.

Four-membered heterocycles $RP(\mu\text{-}NR')_2ER''_x$ (E = main group element) have been studied extensively during the last two decades. Several neutral 1,3,2σ³λ³-diazaphosphatedines (type 1)[1] and 1,3,2σ⁴λ⁵-diazaphosphonatatedines (type 2)[2] have been synthesised and structurally characterised.

Type 1

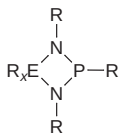

R_xE = RB,[1a] CO,[1b] R_2Si,[1c] RP,[1d] RAs,[1e] SO_2[1f]

Type 2

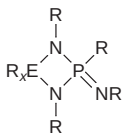

R_xE = RB,[2a] R_2Si,[1c, 2b] RP[2c]

Type 3

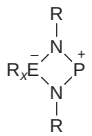

R_xE = R_2Al,[2b, 3a] R_2Ga[3b]

Type 4

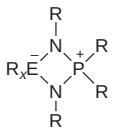

R_xE = R_2Al,[3a, 4a, 4b] R_2Ga,[4a, 4c] R_2In[4a]

We became interested in the synthesis of neutral 1,3,2σ³λ³-diazaphosphatedines containing an element of group 13 due to the lack of structural information. Although 1,3,2,4-diazaphosphaboretidines $RP(\mu\text{-}NR')_2BR''$, synthesised by reactions of (a) aminoiminophosphanes $RN{=}P{-}NR_2'$ with BX_3 (X = Cl, Br),[1a,4] (b) dilithiated bis(amino)phosphanes $RP(NR'Li)_2$ with dichloroboranes $RBCl_2$,[1a] (c) iminoboranes $RN{=}BR'$ with dichlorophosphanes $RPCl_2$,[1a,3] (d) iminoboranes with aminoiminophosphanes,[1a,2] (e) aminoiminoboranes with PCl_3,[1a,3] and (f) aminoiminoboranes with aminoiminophosphanes,[1a,5] have been known for several years, to our knowledge, their solid state structures have not been determined. Investigations concerning the synthesis of 1,3,2,4-diazaphosphatidines of higher homologues of group 13 were not successful, because reactions (a) and (b) using Al, Ga or In compounds lead to zwitterionic complexes (type 3,[3] or 4[4]) and the analogous starting compounds for reactions (c)–(f), imino-alanes, -gallanes and -indanes $RN{=}ER'$ (E = Al, Ga, In), are, as yet, unknown.

We now report the synthesis and structural characterisation of the first neutral 1,3,2,4- diazaphosphaaluminatidine by a dehydrogenation reaction. $Bu^tP[N(H)Bu^t]_2$ was added to $AlH_3{\leftarrow}NMe_3$, which immediately led to gas evolution. The resulting viscous solid was subsequently heated to 115 °C until the gas evolution stopped. Cooling to room temperature led to a light yellow solid, which was dissolved in pentane and stored at −30 °C. Colourless crystalline **1** was obtained and characterised by ^1H, ^{13}C and ^{31}P NMR, IR and mass spectroscopy as well as single crystal X-ray analysis.‡

The ^1H NMR spectrum shows a doublet for the Bu^tP group and a singlet for the Bu^tN moieties, indicating that the two Bu^tN groups are equivalent. The ^{31}P NMR spectrum shows a singlet at δ 121.2, comparable to that (δ 126.6) found in $MeP(\mu\text{-}NBu^t)_2BMe$.[1a] The Al–H resonance was not observed in the ^1H NMR spectrum probably owing to broadening,[5] but the IR spectrum displays a typical Al–H stretching absorption band at 1793 cm^{-1}.

Crystals of **1** suitable for a single crystal X-ray structure determination were grown in pentane at −30 °C. The geometry at the P atom is pyramidal with an endocyclic N1–P1–N2 bond angle of 89.6° (Fig. 1). The average P–N bond length [1.732(2) Å] is comparable to those found in $(Bu^tN)Bu^tP(\mu\text{-}NBu^t)_2BBu^t$ [171.0(2) Å],[2a] $RP(\mu\text{-}NBu^t)_2SiMe_2$ [174.1(3) Å][1c] and $(Me_3Si)_2NP(\mu\text{-}NR')_2SiBu^t_2$ [176.9(2) Å][6] and reveals the absence of any double-bond character within the PN_2 fragment. The Al atom shows a distorted tetrahedral environment with an endocyclic N1–Al1–N2 bond angle of 83.3°. The average Al–N bond length within the non-planar ring [1.836(2) Å] is comparable to Al–N compounds with four-coordinate Al centers bound to three-coordinate N atoms.[7] The zwitterionic complexes $P(\mu\text{-}NAr)_2AlMe_2$ (Ar = $C_6H_2Bu^t_3$-2,4,6),[3a,4] $P(\mu\text{-}NSiMe_3)AlCl_2$[3a] (type 3) and $[(Ph_2P)NPPh_2N(SiMe_3)AlMe_2]$[4b] (type 4) show significantly shorter P–N [average of 1.617(4), 1.614(6) and 1.613(1) Å, respectively] and longer Al–N bond lengths [average of 1.977(4), 1.890(6) and 1.947(2) Å,

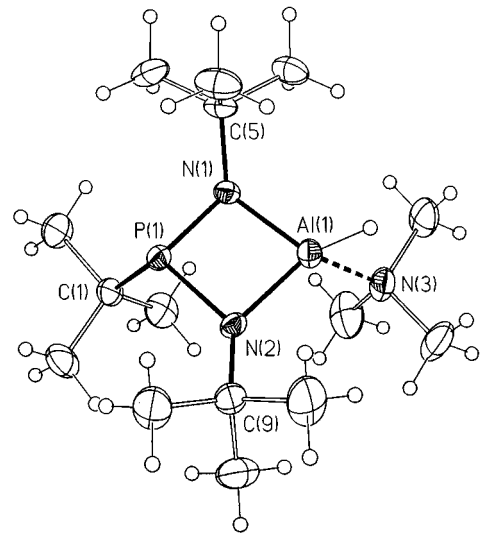

Fig. 1 The molecular structure of **1** (50% thermal ellipsoids). Selected bond lengths (Å) and angles (°): C(1)–P(1) 1.902(2), P(1)–N(1) 1.732(2), P(1)–N(2) 1.732(1), Al(1)–N(1) 1.846(2), Al(1)–N(2) 1.826(2), Al(1)–N(3) 2.028(2), Al(1)–H(1) 1.478(5); N(1)–P(1)–N(2) 89.6(1), C(1)–P(1)–N(1) 105.0(1), C(1)–P(1)–N(2) 106.3(1), N(1)–Al(1)–N(2) 83.3(1), N(1)–Al(1)–N(3) 118.2(1), N(2)–Al(1)–N(3) 116.2(1), C(5)–N(1)–Al(1) 123.3(1), C(5)–N(1)–P(1) 120.7(1), C(9)–N(2)–P(1) 126.4(1), C(9)–N(2)–Al(1) 131.8(1), H(1)–Al(1)–N(1) 122.9(7), H(1)–Al(1)–N(2) 121.3(7), H(1)–Al(1)–N(3) 96.8(8).

respectively], while coordination of a Lewis base to a complex of type 3 as shown in $P(\mu\text{-}NSiMe_3)_2AlCl_2\cdot$quinuclidine[8] leads to comparable Al–N [average 1.855(10) Å] and less shortened P–N bond lengths [average of 1.673(10) Å]. The Al–H bond length [1.478(5) Å] and the terminal Al–N bond length [2.028(2) Å] in **1** are within the expected range.[5]

This work was supported by the DFG, Fonds der Chemischen Industrie and the Bundesministerium für Bildung, Wissenschaft, Forschung und Technologie (BMBF). S. Schulz gratefully thanks Professor E. Niecke for financial support.

Notes and references

† **1**: mp 112 °C; yield 73%; NMR data: ^{1}H (C_6D_6, 25 °C) δ 1.20 (d, $^3J_{PH}$ 10.3 Hz, 9H, Bu^{t}P), 1.57 (d, $^4J_{PH}$ 0.7 Hz, 18H, Bu^{t}N), 1.99 (s, 9H, NMe_3); ^{13}C (C_6D_6, 25 °C) δ 27.99 (d, $^2J_{PC}$ 18.3 Hz, *Me*$_3$CP), 33.93 (d, $^1J_{PC}$ 45.4 Hz, Me$_3$*C*P), 35.56 (d, $^3J_{PC}$ 8.8 Hz, *Me*$_3$CN), 48.12 (s, NMe_3), 51.35 (d, $^2J_{PC}$ 17.2 Hz, Me$_3$*C*N); ^{31}P (C_6D_6, 25 °C) δ 121.2; IR (Nujol) ν/cm^{-1} 1793 (Al–H), 1205, 1007, 802, 736, 630, 577 cm^{-1}; EI-MS (20 eV, 150 °C) *m/z* (%): 317 (5) M^+, 258 (15) $[M - NMe_3]^+$, 201 (100) $[M - NMe_3 - Bu^t]^+$.

‡ *Crystal data* for **1**: $C_{15}H_{37}AlN_3P$, M = 317.4, orthorhombic, space group *Pbca* (no. 61), a = 12.8335(4), b = 16.7315(5), c = 18.6500(6) Å, V = 4004.6(2) Å^3, Z = 8, D_c = 1.053 g cm^{-3}, μ(Mo-Kα) = 0.178 mm^{-1}, F(000) = 1408, 48091 reflections measured (4824 unique), R [$I > 2\sigma(I)$] = 0.050, *wR2* (all data) = 0.15357, GOF = 1.004 for 184 parameters and two restraints. Data were collected on a Nonius Kappa-CCD diffractometer using Mo-Kα radiation (λ = 0.71073 Å). The structure was solved by direct methods (SHELXS-97)[9] and refined by full-matrix least squares on F^2. All non-hydrogen atoms were refined anisotropically and hydrogen atoms by a riding model (SHELXL-97).[10] CCDC 182/1214. See http://www.rsc.org/suppdata/cc/1999/879/ for crystallographic files in .cif format.

1 (*a*) W. Jacksties, H. Nöth and W. Storch, *Chem. Ber*., 1985, **118**, 2030; P. Paetzold, C. von Plotho, E. Niecke and R. Rüger, *Chem. Ber*., 1983, **116**, 1678; K.-H. van Bonn, P. Schreyer, P. Paetzold and R. Boese, *Chem. Ber*., 1988, **121**, 1045; E. Niecke and W. Bitter, *Angew. Chem.*, 1975, **87**, 34; *Angew. Chem., Int. Ed. Engl*., 1975, **14**, 56; U. Wietelmann, *PhD Thesis*, 1986, München; (*b*) J. Breker and R. Schmutzler, *Chem. Ber*., 1990, **123**, 1307; (*c*) O. J. Scherer, M. Püttmann, C. Krüger and G. Wolmershäuser, *Chem. Ber*., 1982, **115**, 2076; W. Bitter and E. Niecke, *Chem. Ber*., 1976, **109**, 415; U. Klingebiel, *Chem. Ber*., 1978, **111**, 2735; (*d*) E. Niecke, W. Flick and S. Pohl, *Angew. Chem.*, 1976, **88**, 305; *Angew. Chem., Int. Ed. Engl*,. 1976, **15**, 309; E. Niecke, A. Nickloweit-Lüke and R. Rüger, *Phosphorus Sulfur*, 1981, **12**, 213; O. J. Scherer, *Chem. Ber*., 1976, **109**, 2996; (*e*) O. J. Scherer, *Z. Naturforsch. Teil B*, 1976, **31**, 142; (*f*) A. H. Cowley, S. K. Mehrota and H. W. Roesky, *Inorg. Chem*., 1981, **20**, 712.

2 (*a*) D. Gudat, E. Niecke, M. Nieger and P. Paetzold, *Chem. Ber*., 1988, **121**, 565; (*b*) R. Kröher, PhD Thesis, 1978, Göttingen; (*c*) R. Appel and M. Halstenberg, *J. Organomet. Chem*., 1975, **99**, C25.

3 (*a*) E. Niecke and R. Kröher, *Angew. Chem.*, 1976, **88**, 758; *Angew. Chem., Int. Ed. Engl.*, 1976, **15**, 692; S. Pohl, *Chem. Ber*., 1979, **112**, 3159; S. Pohl, *Z. Naturforsch., Teil B*, 1977, **32**, 1342; P. B. Hitchcock, H. A. Jasim, M. F. Lappert and H. D. Williams, *J. Chem. Soc., Chem. Commun*., 1986, 1634; (*b*) R. Oberdörfer, M. Nieger and E. Niecke, *Chem. Ber*., 1994, **127**, 2397.

4 (*a*) H. Schmidbaur, K. Schwirten and H.-H. Pickel, *Chem. Ber*., 1969, **102**, 564; (b) P. Braunstein, R. Hasselbring and D. Stalke, *New J. Chem*., 1996, **20**, 337; (*c*) R. Oberdörfer, PhD Thesis, 1993, Bonn.

5 See for example: C. Jones, G. A. Koutsantonis and C. L. Raston, *Polyhedron*, 1993, **12**, 1829; M. G. Gardiner and C. L. Raston, *Coord. Chem. Rev*., 1997, **166**, 1.

6 J. Niesmann, U. Klingebiel, S. Rudolph, R. Herbst-Irmer and M. Noltemeyer, *J. Organomet. Chem*., 1996, **515**, 43.

7 B. Qian, D. L. Ward and M. R. Smith, III, *Organometallics*, 1998, **17**, 3070; S. L. Aeilts, M. P. Coles, D. C. Swenson and R. F. Jordan, *Organometallics*, 1998, **17**, 3265.

8 N. Burford, P. Losier, P. K. Bakshi and T. S. Cameron, *J. Chem. Soc., Chem. Commun*., 1996, 307.

9 G. M. Sheldrick SHELXS-90/96, Program for Structure Solution, *Acta Crystallogr., Sect. A*, 1990, **46**, 467.

10 G. M. Sheldrick SHELXL-97, Program for Crystal Structure Refinement, Universität Göttingen, 1997.

Communication 9/01556F

ChemComm

The crystal structures of glycylglycine and glycine complexes of *cis,cis*-1,3,5-triaminocyclohexane–copper(II) as reaction intermediates of metal-promoted peptide hydrolysis

Xiang Shi Tan,[a] Yuki Fujii,*[a] Tsuyoshi Sato,[a] Yoshiharu Nakano[a] and Morio Yashiro[b]

[a] *Department of Chemistry, Faculty of Science, Ibaraki University, Bunkyo 2-1-1, Mito 310-8512, Japan. E-mail: yuki@mito.ipc.ibaraki.ac.jp*

[b] *Department of Chemistry and Biotechnology, Graduate School of Engineering, The University of Tokyo, Hongo, Bunkyo-ku, Tokyo 113-8656, Japan*

Received (in Cambridge, UK) 26th February 1999, Accepted 6th April 1999

The glycylglycine and glycine complexes of *cis,cis*-1,3,5-triaminocyclohexane–copper(II), model reaction intermediates of peptide hydrolysis by Cu^{II}–triamine complexes, have been synthesized and characterized by X-ray crystallography.

There has been great interest in designing artificial metallopeptidases that hydrolyze unactivated amides under mild conditions.[1,2] Up to now a variety of metal complexes of Cu^{II},[1,3] Zn^{II},[3c,d] Ni^{II},[3c,d] Pd^{II},[4] Co^{III}[2,5] and Ce^{IV}[6] have been used to study the hydrolysis of amides. Recently Burstyn and coworker[1] reported the discovery that a macrocyclic copper(II) complex, Cu[9]aneN_3, can hydrolyze both the unactivated dipeptide glycylglycine and proteins at near physiological pH. Although no reaction mechanism has been shown for Cu[9]aneN_3, in such a reaction, the activation of the carbonyl group of the amide by the metal centre seems to play an important role, and it is necessary to get information about the reaction intermediate to advance the hydrolysis reaction. We have been studying some copper(II)–triamine complexes which effectively promote the hydrolytic cleavage of phage DNA,[7] as well as peptide bonds. To understand the mechanism of the hydrolytic reaction of peptides by Cu^{II}–triamine complexes, we present here the crystal structures of glycylglycine and glycine complexes of *cis,cis*-1,3,5-triaminocyclohexane–copper(II) as model reaction intermediates.

We have investigated the hydrolysis of peptide with *cis,cis*-1,3,5-triaminocyclohexane–copper(II) complex[7] **1** by HPLC and found that glycylglycine is hydrolyzed to glycine when incubated with **1**.† The hydrolysis of glycylglycine (Gly-Gly) (2 mM) to glycine (Gly) with **1** (2 mM) at 70 °C and pH 8.1 ± 0.1 (50 mM HEPES) is *ca.* 18% for 24 h, which is similar to that of Cu[9]aneN_3, and the conversion is dependent on metal complex concentration, reaction time and solution pH.

The tetraphenylborate salts of $[Cu(tach)(gly\text{-}gly)]^+$ **2** and $[Cu(tach)(gly)]^+$ **3** (tach = *cis,cis*-1,3,5-triaminocyclohexane, gly = glycine anion, gly-gly = glycylglycine anion) were synthesized by stirring a mixture of $CuSO_4.5H_2O$ (1 mmol), tach (1 mmol) and Gly-Gly (1 mmol) for **2** or Gly (1 mmol) for **3** in MeOH–water at pH 8 (in the presence of $NaBPh_4$) in 40% yield for **2** and 60% yield for **3**, respectively. Blue crystals of the two complexes were grown by slow evaporation of a MeOH–water solution and the structures were characterized by X-ray crystallography.‡

The crystal structures (Figs. 1 and 2) of complexes **2** and **3** both show a five co-ordinate copper centre ligated to the three face capping nitrogens of the tach ligand. In each case the copper co-ordination geometry is square pyramidal distorted along the apical Cu(1)–N(3) bond with a distance of 2.232(3) Å in **2** and 2.152(6) Å in **3**. The other Cu–N distances, Cu(1)–N(1) and Cu(1)–N(2), are 1.990(3) and 2.015(2) Å in **2** and 2.019(6) and 2.042(6) Å in **3**, respectively, as in other copper-tach complexes.[8] The peptide (gly-gly) is coordinated through the terminal NH_2 group and the carbonyl oxygen atom from the same glycine residue. The carbonyl oxygen atom O(1) is here prefered to the peptide nitrogen N(5) as a metal binding site at pHs where the amide proton is not dissociated, as in the tripeptide complexes of $Cu(gly\text{-}gly\text{-}gly)^+$,[9] $Cu(gly\text{-}leu\text{-}tyr)^+$,[10] and $Zn(gly\text{-}gly\text{-}gly)^+$,[11] or the Co^{III}–tetraamine complex of the glycylglycine *O*-ethyl ester.[12] This mode of co-ordination accounts for the ease of hydrolysis of the dipeptide. The positively charged copper(II) ion renders the carbonyl carbon atom C(8) more susceptible to nucleophilic reagents (OH^-) and the peptide chelate ring is not required to break for hydrolysis to occur, so the NH_2-terminal glycine remains attached to the Cu(tach) residue to form [glycinato–copper(II)–tach] complex

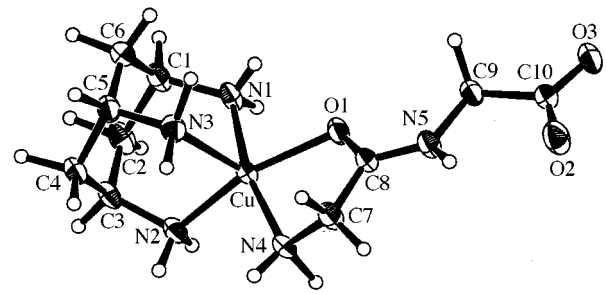

Fig. 1 ORTEP plot with 30% probability thermal ellipsoids showing the structure of the cation of **2**. Selected bond distances (Å) and angles (°): Cu–N(1) 1.990(3), Cu–N(2) 2.015(2), Cu–N(3) 2.232(3), Cu–N(4) 2.017(3), Cu–O(1) 2.039(2), O(1)–Cu–N(1) 89.38(9), O(1)–Cu–N(2) 162.32(10), O(1)–Cu–N(3) 104.52(9), O(1)–Cu–N(4) 80.32(9), N(1)–Cu–N(2) 92.61(9), N(1)–Cu–N(3) 91.5(1), N(1)–Cu–N(4) 167.49, N(2)–Cu–N(3) 93.00(9), N(2)–Cu–N(4) 95.09(9), N(3)–Cu–N(4) 97.9(1).

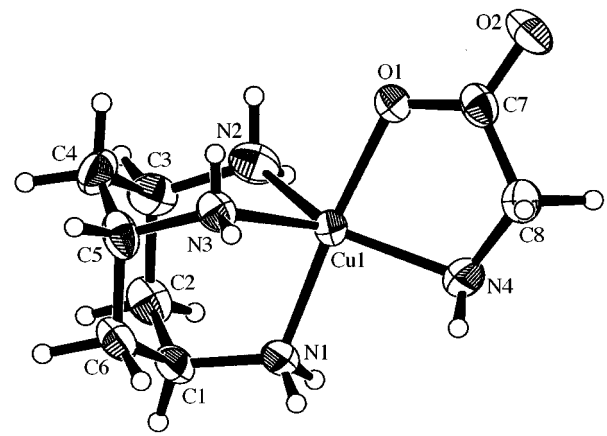

Fig. 2 ORTEP plot with 30% probability thermal ellipsoids showing the structure of the cation of **3**. Selected bond distances (Å) and angles (°): Cu–O(1) 1.974(4), Cu–N(1) 2.019(6), Cu–N(2) 2.042(6), Cu–N(3) 2.152(6), Cu–N(4) 2.007(6), O(1)–Cu–N(1) 173.6(2), O(1)–Cu–N(2) 87.5(2), O(1)–Cu–N(3) 97.0(2), O(1)–Cu–N(4) 82.6(2), N(1)–Cu–N(2), 92.8(3), N(1)–Cu–N(3) 89.4(2), N(1)–Cu–N(4) 93.2(2), N(2)–Cu–N(3) 92.7(2), N(2)–Cu–N(4) 141.4(2), N(3)–Cu–N(4) 125.5(2).

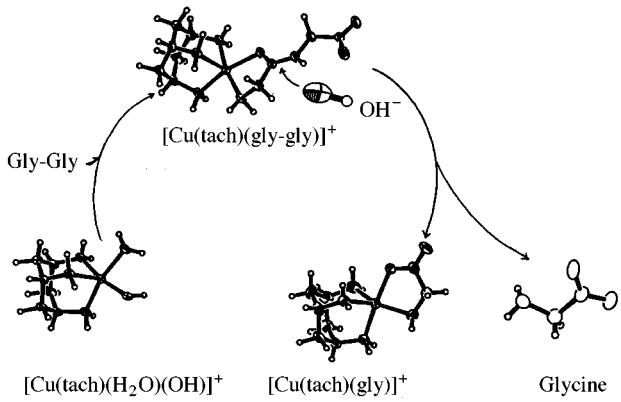

Scheme 1

ion, as shown in Fig. 2. Thus the complex cation of **2**, $[Cu(tach)(gly\text{-}gly)]^+$, is an intermediate of the hydrolysis of the N-terminal peptide bond promoted by Cu^{II}–triamine complex, and is clear evidence for the activation of the C=O group by the metal centre.

On the basis of the intermediate structure a reasonable mechanism may be postulated for the peptide hydrolysis at near physiological pH, as shown in Scheme 1. The initial step involves the rapid replacement of the water molecule by the N-terminal amino group of the peptide, which becomes chelated to the copper(II) ion. The carbonyl group is then activated to attack by external OH^-. The mechanism is supported by the fact that the rate of hydrolysis increases with increasing hydroxide concentration.§

Experiments to prove this mechanism *via* solution chemistry studies and kinetic measurements of the hydrolysis of peptides by Cu^{II}–triamine complexes are presently being conducted.

The support of this work by a JSPS postdoctoral fellowship to X. S. T. from the Japan Society for the Promotion of Science (No. P97370) and by a Grant-in-Aid for Science Research (No. 09440224) from the Ministry of Education, Science, Sports and Culture of Japan is gratefully acknowledged.

Notes and references

† Glycylglycine (2 mM) was dissolved in water and incubated with **1** (2 mM) at pH 8.1 ± 0.1 (50 mM HEPES) and 70 °C for 24 h. Samples were analyzed in a JASCO Model FP-920 Intelligent Fluorescence Detector.

‡ *Crystal data* for **2**: $C_{35}H_{46}N_5O_4BCu$, M = 675.14, triclinic, space group $P\bar{1}$, a = 10.238(4), b = 18.026(7), c = 10.065(3) Å, α = 92.29(3), β = 113.71(3), γ = 101.13(3)°, U = 1654(1) Å^3, λ = 0.71069 Å, Z = 2, D_c = 1.355 g cm^{-3}, μ = 0.707 mm^{-1}, 7778 reflections measured, 5756 observed [$I > 3.00\ \sigma(I)$]. Solution by direct methods with SIR92, expanded using Fourier Techniques with DIRDIF94. Full-matrix least-square refinement on F with all non-hydrogen atoms anistropic and hydrogens included but not refined. Final R and Rw values on observed data were 0.050 and 0.051.

For **3**: $C_{32}H_{39}N_4O_2BCu$, M = 586.04, orthorhombic, space group $P2_12_12_1$, a = 9.879(2), b = 30.374(9), c = 9.769(2) Å, U = 2931(1) Å^3, λ = 0.71069 Å, Z = 4, D_c = 1.328 g cm^{-3}, μ = 0.781 mm^{-1}. 3808 reflections measured, 2857 observed [$I > 3.00\ \sigma(I)$]. Solution methods and refinements as for **2**. Final R and Rw values on observed data were 0.052 and 0.051. CCDC 182/1212. See http://www.rsc.org/suppdata/cc/1999/881/ for crystallographic files in .cif format.

§ The pH dependency is independent on the pK_a curve of $[Cu(tach)(H_2O)_2]^{2+}$ [ref. 7(*b*)], indicating that the attack of internal coordinated OH^- can be neglected.

1 E. L. Hegg and J. N. Burstyn, *J. Am. Chem. Soc.*, 1995, **117**, 7015.
2 B. K. Takasaki, J. H. Kim, E. Rubin and J. Chin, *J. Am. Chem. Soc.*, 1993, **115**, 1157.
3 (*a*) K. V. Reddy, A. R. Jacobson, J. I. Kung and L. M. Sayre, *Inorg. Chem.*, 1991, **30**, 3520; (*b*) L. M. Sayre, K. V. Reddy, A. R. Jacobson and W. Tang, *Inorg. Chem.*, 1992, **31**, 935; (*c*) T. H. Fife and T. J. Przystas, *J. Am. Chem. Soc.*, 1986, **108**, 4631; (*d*) J. T. Groves and R. R. Chambers, Jr., *J. Am. Chem. Soc.*, 1984, **106**, 630; (*e*) B. F. Duerr and A. W. Czarnik, *J. Chem. Soc., Chem. Commun.*, 1990, 1707; (*f*) J. Chin, V. Jubian and K. Mrejen, *J. Chem. Soc., Chem. Commun.*, 1990, 1326; (*g*) L. Meriwether and F. H. Westheimer, *J. Am. Chem. Soc.*, 1956, **78**, 5119; (*h*) W. A. Connor, M. M. Jones and D. L. Tuleen, *Inorg. Chem.*, 1965, **4**, 1129.
4 I. E. Burgeson and N. M. Kostic, *Inorg. Chem.*, 1991, **30**, 4299; L. Zhu and N. M. Kostic, *J. Am. Chem. Soc.*, 1993, **115**, 4566; L. Zhu, L. Qin, T. N. Parac and N. M. Kostic, *J. Am. Chem. Soc.*, 1994, **116**, 5218.
5 D. A. Buckingham, G. S. Binney, C. R. Clark, B. Garnham and J. Simpson, *Inorg. Chem.*, 1985, **24**, 135.
6 M. Yashiro, T. Takarada, S. Miyama and M. Komiyama, *J. Chem. Soc., Chem. Commun.*, 1994, 1757.
7 T. Itoh, H. Hisada, T. Sumiya, M. Hosono, Y. Usui and Y. Fujii, *Chem. Commun.*, 1997, 677; T. Itoh, H. Hisada, Y. Usui and Y. Fujii, *Inorg. Chem. Acta*, 1998, **238**, 51.
8 L. Cronin, B. Greener, S. P. Foxon, S. L. Health and P. H. Walton, *Inorg. Chem.*, 1997, **36**, 2594.
9 H. C. Freeman, G. Robinson and J. C. Schoone, *Acta Crystallogr.*, 1964, **17**, 719.
10 W. A. Franks and D. van der Helm, *Acta Crystallogr., Sect. B*, 1971, **27**, 1299.
11 D. van der Helm and H. B. Nicholas, Jr., *Acta Crystallogr., Sect. B*, 1970, **26**, 1858.
12 D. A. Buckingham, P. A. Marzilli, I. E. Maxwell, W. T. Dwyer, A. M. Sargeson, M. Fehlman and H. C. Freeman, *J. Chem. Soc., Chem. Commun.*, 1968, 488.

Communication 9/01569H

ChemComm

Microreactors for elemental fluorine

Richard D. Chambers and Robert C. H. Spink

University of Durham, Department of Chemistry, South Road, Durham, UK DH1 3LE.
E-mail: r.d.chambers@durham.ac.uk.

Received (in Liverpool, UK) 18th January 1999, Accepted 29th March 1999

A microreactor has been designed for use with elemental fluorine, both for selective fluorination and for perfluorination of organic compounds.

Interest in the use of elemental fluorine directly, for the synthesis of fluorine-containing organic compounds, has increased dramatically in the last few years,[1–3] but scale-up will always present problems of safe handling and temperature control, for some of the most exothermic reactions in organic chemistry.

There is currently much interest in the development of microreactors for chemical processing,[4] because the benefits would include arithmetic scale-up from the performance of a single reactor to a theoretically unlimited number. Also, in principle, this scale-up could be achieved by the techniques of the electronics industry.

Microreactors have considerable attraction for application to direct fluorination processes because there is (i) a small inventory of fluorine in the reaction zone, (ii) opportunity for good mixing and temperature control, and (iii) simple scale-up. However, prior to this work, there was little knowledge available on the practicability of this approach.

After much development, we have now designed a simple micro-reactor, fabricated from a block of nickel (or copper), from which we have cut a groove as the micro-reactor; the design is indicated in Fig. 1, where the seal is provided by a block of polychlorotrifluoroethene, which also enables direct viewing of the reaction zone. Reactants and solvent were injected *via* a syringe and syringe-pump, while fluorine in nitrogen was introduced directly from a small cylinder *via* a mass-flow controller. Using this technique, all of the liquid–gas mixing that we carried out proceeded *via cylindrical flow* (the term is intended to indicate that the liquid forms an outer cylinder, coating the reactor surface, with the gas flowing through the centre) as opposed to *slug flow* (alternate slugs of liquid and gas), which might have been anticipated. Indeed, the former provides enormous advantages in that it provides very large surface to volume ratios for the liquid phase, which is highly beneficial for efficient reaction over a short distance in the reactor. There is also excellent mixing and very effective opportunities for heat control, through the cooling channels indicated. Furthermore, a surprisingly large through-put for such a small channel is possible, *e.g.* 0.5–5 ml h^{-1} have been used routinely.

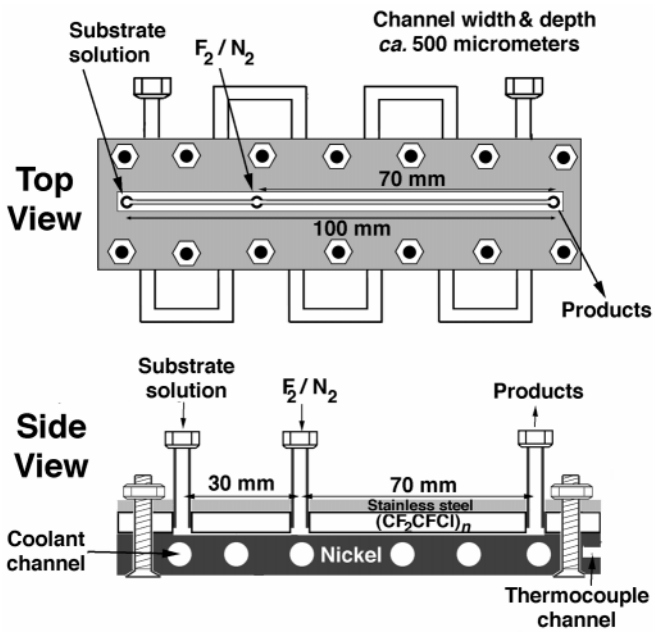

Fig. 1 Microreactor top and side view.

Products were trapped out in a half inch diameter FEP tube, cooled by either a salt–ice bath or an acetone–carbon dioxide slush bath. Residual gases were scrubbed in a soda-lime tower and any dissolved hydrogen fluoride was removed by either adding sodium fluoride to the product mixture or washing with water.

Using this system, we have successfully carried out various selective fluorinations, as shown in Schemes 1 and 2. Sulfur pentafluoride derivatives are of considerable interest[5] and

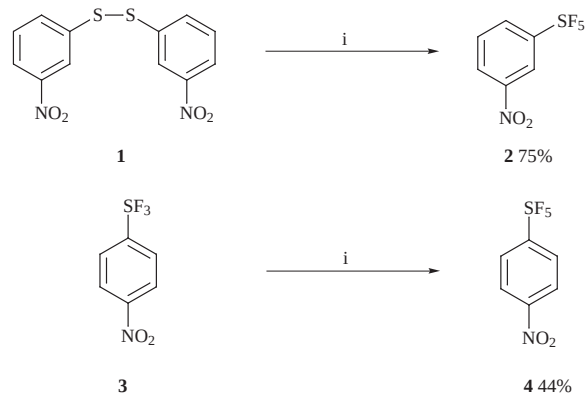

Scheme 1 *Reagents and conditions*: i, MeCN (5 ml h^{-1}), 10% F_2 in N_2 (10 ml min^{-1}), room temp.

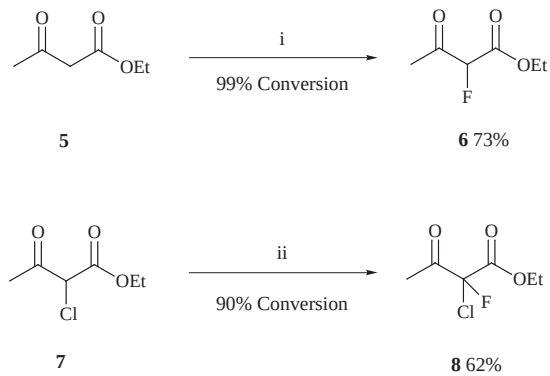

Scheme 2 *Reagents and conditions*: i, 10% F_2 in N_2 (10 ml min^{-1}), 5 °C, HCO_2H (0.5 ml h^{-1}); ii, 10% F_2 in N_2 (10 ml min^{-1}), 5 °C, HCO_2H (0.25 ml h^{-1}).

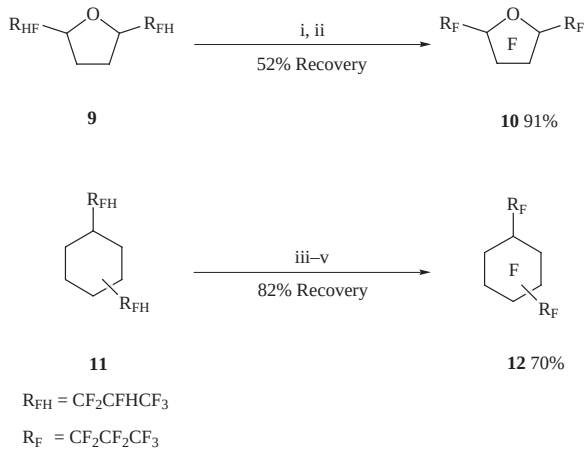

Scheme 3 *Reagents and conditions*: i, 0.5 ml h^{-1}, 50% F_2 in N_2 (15 ml min^{-1}), room temp.; ii, 0.5 ml h^{-1}, 50% F_2 in N_2 (15 ml min^{-1}), room temp. then 280 °C; iii, 0.5 ml h^{-1}, 20% F_2 in N_2 (20 ml min^{-1}), room temp.; iv, 0.5 ml h^{-1}, 50% F_2 in N_2 (10 ml min^{-1}), room temp. then 50 °C; v, 0.5 ml h^{-1}, 50% F_2 in N_2 (15 ml min^{-1}) room temp. then 280 °C.

fluorination can be achieved directly from the di(*m*-nitrophenyl) disluphide **1**. However, for the *p*-nitro system **3**, due to its very low solubility in MeCN, preliminary fluorination (in bulk) to produce soluble trifluorides was performed and then the more difficult fluorination to pentafluorides was carried out in the microreactor.

Fluorination of β-dicarbonyl compounds proceeded with high efficiency and, moreover, these reactions demonstrated clearly a catalytic effect by the fluorinated metal surface. Fluorination is usually limited by either the concentration of enol, at equilibrium, or the rate constant for forming the enol. However, while bulk fluorination of ethyl 2-chloroacetoacetate **7** gives only low conversion to **8**,[6] the flow system is clearly efficient and the fluorinated metal surface obviously promotes the formation of enol.

We have also demonstrated that the technique can be used for *perfluorination*. In this case, however, we need an additional heated stage to complete the reaction and this is connected simply to the outlet of the reactor. Results are shown in Scheme 3 and there is no reason why these otherwise hazardous procedures could not be scaled up with safety. Traditionally, cobalt trifluoride (obtained using elemental fluorine) is used in industry to perfluorinate hydrocarbons, but for some of the examples shown here, the temperature required for perfluorination with elemental fluorine is significantly lower than that required for perfluorination using cobalt trifluoride.[7]

These experiments illustrate the significant potential for this approach to the use of elemental fluorine, both in the laboratory and at the industrial scale.

We acknowledge financial support from BNFL.

Notes and references

1 J. Hutchinson and G. Sandford, *Top. Curr. Chem.*, 1997, **193**, 1.
2 S. Rozen, *Acc. Chem. Res.*, 1996, **21**, 307.
3 S. T. Purrington, B. S. Kagen and T. B. Patrick, *Chem. Rev.*, 1986, **86**, 997.
4 A. Green, *Chem. Ind. (London)*, 1998, 168.
5 WO 9705,106 (*Chem. Abstr.*, 1997, **126**, 199340)
6 R. D. Chambers, M. P. Greenhall and J. Hutchinson, *Tetrahedron*, 1996, **52**, 1.
7 R. D. Chambers, B. Grievson, F. G. Drakesmith and R. L. Powell, *J. Fluorine Chem.*, 1985, **29**, 323.

Communication 9/01473J

Transition metal labels on peptide nucleic acid (PNA) monomers

Alexandra Hess and Nils Metzler-Nolte*

Max-Planck-Institut für Strahlenchemie, Stiftstraße 34–36, D-45470 Mülheim/Ruhr, Germany.
E-mail: nils@mpi-muelheim.mpg.de

Received (in Basel, Switzerland) 25th February 1999, Accepted 2nd April 1999

The synthesis, spectroscopic properties (including Mössbauer and electrochemistry) and self-association characteristics of thymine peptide nucleic acid (T–PNA) monomers with covalently linked transition metal markers are described.

Peptide nucleic acids (PNA) constitute a relatively young class of DNA analogues[1] for studies in structural biology[2–5] and applications in antisense-antigene technology.[6] PNA consists of a pseudopeptide backbone, to which the nucleobases are attached through a methylene-carbonyl spacer.[7,8] Among the favourable properties of PNA in the form introduced by Nielsen and Burchardt are high binding affinity to single- and double-stranded DNA with the formation of duplex and triplex helices and an increased hydrolytic stability compared to analogous DNA strands. For analytical purposes in molecular biology, however, PNA lacks a unique spectroscopic handle. Consequently, it would be highly desirable to have PNA attached to an independent and sensitive spectroscopic probe. To this end we have synthesized two organometallic PNA hybrids, namely ferrocene–PNA for electrochemical detection and (benzene)-chromiumtricarbonyl–PNA in which the carbonyl groups provide a sensitive probe for IR detection. Also, we present here the first synthesis and spectroscopic properties of a bipyridyl–ruthenium PNA derivative. Ruthenium derivatives of oligonucleotides have become invaluable tools for the study of electron transfer in DNA.

Ferrocene carboxylic acid thymine-PNA methyl ester (Fc–(T–PNA)–OMe, **1**) was originally prepared by the reaction of ferrocene carboxylic acid chloride, prepared *in situ* from ferrocene carboxylic acid and oxalylic chloride in CH_2Cl_2 solution, with thymine–PNA methyl ester H_2N–(T–PNA)–OMe (Scheme 1). For the synthesis of benzoic acid chromium-tricarbonyl thymine–PNA methyl ester (Cr–(T–PNA)–OMe, **2**), a HBTU (*O*-(1*H*-benzotriazol-1-yl)-*N*,*N*,*N*′,*N*′-tetramethyluronium hexafluorophosphate) mediated coupling between benzoic acid chromium tricarbonyl and H_2N–(T–PNA)–OMe was used.† After work-up, both compounds are obtained in 80 and 60% yield, respectively, as analytically pure yellow solids. Deeply orange–red coloured bis(bipyridyl) (4-methyl-4′-carboxylic acid bipyridyl) ruthenium(II) thymine–PNA methyl ester (Ru–(T–PNA)–OMe, **3**) was obtained by reaction of HBTU-activated $[(bpy)_2Ru(4\text{-Me-bpy-}4'\text{-}CO_2H)]^{2+}$ with H_2N–(T–PNA)–OMe and purified by chromatography on silica.

All metal–PNA hybrids exhibit characteristic NMR spectra which are essentially a combination of their components.‡ As an indication of a successful coupling, however, the signal of the newly introduced amide proton can be observed in aprotic solvents. There is a distinct solvent dependence of this resonance [for **1**: δ 7.24 in $CDCl_3$, δ 7.9 in $(CD_3)_2SO$] which is attributed to the formation of hydrogen bonds with the $(CD_3)_2SO$ solvent. On the other hand, the ^{15}N NMR resonance of the attached nitrogen atom, which can be detected by 2D indirect detection techniques [**1**: δ_N −276 in $CDCl_3$, δ_N −274 in $(CD_3)_2SO$ $^1J_{NH}$ = 90 Hz], remains almost unperturbed.[9] The existence of two isomers denoted major (ma) and minor (mi) in PNA monomers[7,10] and oligomers[11] is well documented. These isomers are also observed in **1**–**3** and we have used the good solubility and stability of the ferrocene derivative **1** in different solvents to shed further light on the nature of the two conformers. First, there is a distinct solvent dependence of the ma/mi ratio as shown in the ^1H NMR spectra of **1**. If all intermolecular hydrogen bonds are broken in CD_3OD solvent in favor of PNA–solvent interactions, the ma/mi ratio is 65 : 35. Changing to an aprotic solvent infers a further stabilisation of the ma isomer, possibly due to hydrogen bonding [ma/mi = 71 : 29 in $(CD_3)_2SO$, ma/mi = 79 : 21 in $CDCl_3$). Coalescence of all ma/mi signal pairs was observed by ^1H NMR spectroscopy in $(CD_3)_2SO$ between 40 and 100 °C. From these data a rotation barrier of 75 ± 0.5 kJ mol^{-1} is calculated, consistent with rotation about the tertiary amide bond.[7,10] There is also a distinct concentration dependence of some ^1H NMR signals of **1** in $CDCl_3$ (Fig. 1). Over a concentration range of 0.375–0.0027 mol l^{-1} the NH proton of the pyrimidine ring (a) shifts 1.5 ppm to higher field, consistent with the accepted model of T–T self association.[12,13] However, while the positions of most other signals remain almost constant and the

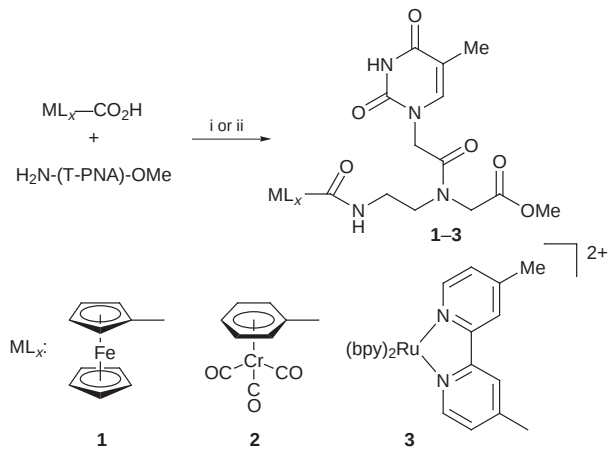

Scheme 1 Synthesis metal–PNA conjugates. *Reagents and conditions*: i, $(COCl)_2$, CH_2Cl_2 then NEt_3, THF (**1**), (ii) HBTU, MeCN (**2** and **3**, see Experimental).

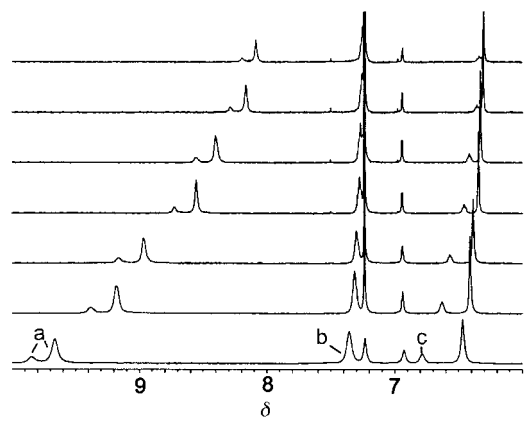

Fig. 1 ^1H NMR spectra of **1** at different concentrations between 375 mmol l^{-1} (bottom trace) and 2.7 mmol l^{-1} (top trace) in $CDCl_3$ at 27 °C. Marked signals are thymine NH(both isomers, a), amide NH (ma, b) and amide NH (mi, c).

FcCON*H* proton of the ma isomer (b) moves < 0.1 ppm, the amide proton signal of the mi isomer (c) shifts also by 0.5 ppm. This suggests that an additional intermolecular interaction, which may be impossible in the ma isomer on steric grounds, might stabilize the mi isomer.§

In the chromium derivative **2**, which is generally less soluble in organic solvents than **1**, the ma/mi ration is 25 : 10 in $(CD_3)_2SO$. In the IR spectrum of **2**, the two strongest bands occur at 1973 and 1898 cm^{-1} and can be assigned to the A and E modes of the $Cr(CO)_3$ moiety. Jaouen and coworkers have used the very strong bands of organometallic carbonyl compounds for the detection of biogenic amines with excellent sensitivity.[14,15] In an elegant application, this carbonyl metallo immuno assays (CMIA), has been applied to study the binding of polyclonal antibodies to cortisol and testosterone.[16]

To confirm the possibility of electrochemical detection of metal–PNA hybrids the ferrocene and ruthenium derivatives **1** and **3** were investigated by cyclic voltammetry. **1** can be reversibly oxidized at a potential of +169 mV *vs.* Fc/Fc^+ (CH_2Cl_2 solution with 0.1 mol l^{-1} NBu_4PF_6) a potential which can be easily achieved in a biological environment without destruction of the biological matrix.[17,18] For **3**, a reversible one-electron oxidation occurs at 897 mV *vs.* Fc/Fc^+, consistent with a Ru^{II}/Ru^{III} redox couple. Ligand centred redox waves were observed at −1.63, −1.90 and −2.15 V. The optical spectrum of **3** exhibits several overlapping bands around 450–430 nm which are assigned to metal-to-ligand charge transfer transitions (MLCT),[19] while two weak bands at 359 and 327 nm result from metal centred transitions and mostly ligand centred π–π* transitions are observed around 290 nm.[20] We have also recorded a ^{57}Fe Mössbauer spectrum for **1**. The isomer shift (0.52 mm s^{-1}) and quadrupole splitting (2.32 mm s^{-1}) are very similar to the value for ferrocene (0.53 mm s^{-1} and 2.37 mm s^{-1}),21 suggesting that there is little influence of the overall solid state structure of **1** on the electric field gradient of the iron nucleus.

We have reported the straightforward synthesis and full characterization of transition metal derivatives of T–PNA monomers and we are confident that this chemistry can be extended to PNA oligomers. As shown in this communication, these new compounds show unique spectroscopic features which in principle permit their sensitive detection even in complex biological matrices such as intact cells. Encouraged by these results, we are further developing the chemistry of metal–PNA hybrids towards applications in structural biology and antisense / antigene technology.

The authors are grateful to Professor. K. Wieghardt for his support of our work.

Notes and references

† *Typical experimental procedure using* HBTU: to a solution of 1 mmol of the transition metal complex in MeCN was added 1 equiv. of HBTU and NEt_3. After stirring for 15 min. (15 h for **3**) brine was added, the solution extracted with EtOAc ($MeNO_2$ for **3**), and the organic phase washed with 2 M HCl, water, aq. $NaHCO_3$, and water, dried over $MgSO_4$ and the solvent removed to yield the desired metal–PNA hybrid.

‡ *Spectroscopic data*: NMR spectra (500 MHz or 400 MHz for ^1H) in $CDCl_3$ (**1**), $(CD_3)SO$ (**2**, **3**), ma/mi where observed, all signals are s except when stated otherwise. **1**: δ_H 8.2/8.08 (1H, NH_T), 7.24/6.32 (br, 1H, NH), 6.8/6.3 (1H, C=CH), 4.76/4.62 (app. t, 2H, Cp), 4.39 (2H, CH_2), 4.39/4.30 (app. t, 2H, Cp), 4.23/4.17 (5H, Cp), 4.04 (2H, CH_2), 3.81/3.78 (3H, OCH_3), 3.54 (m, 4H, CH_2CH_2), 1.88/1.71 (3H, $CH_{3,\,T}$). δ_C 171.3 (CO_2Me), 170.7 (Cp-*C*O), 167.4 (CO), 164.5 (CO_T), 164.4 (CO_T), 151.3 (*C*=CH), 141.0 (C=*C*H), 75.4 ($Cp_{quat.}$), 70.8 (Cp), 68.2 (Cp), 69.8 (5C, Cp), 52.9 (OCH_3), 49.1 (CH_2), 48.3 (CH_2), 48.1, 37.4 (CH_2CH_2), 12.1 ($CH_{3,\,T}$). δ_N −273 (CONH), −269, −253 ($N_{1,\,T}$), −225 ($N_{3,\,T}$). IR (KBr): 1671 br cm^{-1}, UV-VIS [λ/nm (ε/l $mol^{-1}cm^{-1}$] 440 (156), 266 (25028). MS (EI, 70 eV): *m/z* 510 (100%, $M^{+\cdot}$), 445 (25%, M − Cp). **2**: δ_H 11.25 (NH_T), 8.65 / 8.45 (NH), 7.3 / 7.2 (s, 1H, C=CH), 6.2/6.1 (2H), 5.8 (1H), 5.8/5.7 (2H, CH_{Ar}), 4.69/4.48 (CH_2), 4.35/4.1 (CH_2), 3.7/3.6 (OCH_3), 3.4/3.3 (CH_2CH_2), 1.7 ($CH_{3,\,T}$). δ_C 232.7 [$Cr(CO)_3$], 170.0 (CO_2Me), 167.4, 164.3 (both CON), 150.9 (*C*=CH), 142.1 (C=*C*H), 98.0 ($C_{Ar,\,quat}$), 96.3, 94.0, 93.2 (all CH_{Ar}), 51.8 (OCH_3), 47.8, 47.7 (both CH_2), 46.5, 37.0 (CH_2CH_2), 11.9 ($CH_{3,\,T}$). IR (KBr): 1973 vs, 1898 vs, 1648 br cm^{-1}. MS (ESI^+, MeOH): *m/z* 561 (M + Na^+), 425 [M − $Cr(CO)_3$ + Na^+]. **3**: δ_H 11.2 (NH_T), 9.15/8.9 (br, NH), 9.05/8.95 (s), 8.82, 8.76/8.65 (s), 8.16, 7.87, 7.75, 7.72, 7.56, 7.52, 7.40 (all bpy), 7.30/7.2 (C=CH), 4.71/4.48 (2H, CH_2), 4.38/4.13 (2H, CH_2), 3.68/3.61 (3H, OCH_3), 3.58 (4H, CH_2CH_2), 2.53 ($CH_{3,\,bpy}$) 1.69/1.59 (3H, $CH_{3,\,T}$). δ_C 170 (CO_2Me), 169/167.5 (CO), 165 (CO_T), 152 (*C*=CH), 143 (C=*C*H), 120–160 (bpy), 52 (OCH_3), 48.5/49.2 (CH_2), 48.8 (CH_2), 47, 38 (CH_2-CH_2), 21.2 ($CH_{3,\,bpy}$), 12.4 ($CH_{3,\,T}$). UV–VIS [λ/nm, (ε/l $mol^{-1}cm^{-1}$) 455 (14 000), 290 (57 000). MS (ESI^+, Me_2CO): 1053 (M − PF_6^-).

§ Further investigations on the self association and A–T base pairing properties of transition metal PNA compounds are in progress in our group and will be reported comprehensively in due course.

1 P. E. Nielsen, M. Egholm, R. H. Berg and O. Buchardt, *Science*, 1991, **254**, 1497.
2 M. Egholm, O. Buchardt, L. Christensen, C. Behrens, S. M. Freier, D. A. Driver, R. H. Berg, S. K. Kim, B. Norden and P. E. Nielsen, *Nature*, 1993, **365**, 566.
3 P. Wittung, P. E. Nielsen, O. Buchardt, M. Egholm and B. Nordén, *Nature*, 1994, **368**, 561.
4 P. E. Nielsen and G. Haaima, *Chem. Soc. Rev*., 1997, **96**, 73.
5 P. E. Nielsen, *Pure Appl. Chem.*, 1998, **70**, 105.
6 L. Good and P. E. Nielsen, *Nature Biotechnol.*, 1998, **16**, 355.
7 K. L. Dueholm, M. Engholm, C. Behrens, L. Christensen, H. F. Hansen, T. Vulpius, P. K. H., R. H. Berg, P. E. Nielsen and O. Buchardt, *J. Org. Chem.*, 1994, **59**, 5767.
8 E. Uhlmann, A. Peyman, G. Breipohl and D. W. Will, *Angew. Chem.*, 1998, **110**, 2954, *Angew. Chem. Int. Ed.*, 1998, **37**, 2796.
9 M. Witanowski, L. Stefaniak and G. A. Webb, *Ann. Rep. NMR Spectrosc.*, 1993, **25**, 1.
10 S.-M. Chen, V. Mohan, J. S. Kiely, M. C. Griffith and R. H. Griffey, *Tetrahedron Lett.*, 1994, **35**, 5105.
11 M. Eriksson and P. E. Nielsen, *Quart. Rev. Biophys.*, 1996, **29**, 369.
12 W. Saenger, *Principles of Nucleic Acid Structure*, Springer, New York, 1984.
13 H. Iwahashi and Y. Kyogoku, *J. Am. Chem. Soc.*, 1977, **99**, 7761.
14 G. Jaouen, A. Vessières and I. S. Butler, *Acc. Chem. Res.*, 1993, **26**, 361.
15 M. Salmain, A. Vessières, P. Brossier, I. S. Butler and G. Jaouen, *J. Immunol. Methods*, 1992, **148**, 65.
16 V. Philomin, A. Vessiéres, M. Gruselle and G. Jaouen, *Bioconjugate Chem.*, 1993, **4**, 419.
17 H. Eckert and M. Koller, *J. Liq. Chromatogr.*, 1990, **13**, 3399.
18 T. Ihara, M. Nakayama, M. Murata, K. Nakano and M. Maeda, *Chem. Commun.*, 1997, 1609.
19 P. Lincoln, A. Broo and B. Nordén, *J. Am. Chem. Soc.*, 1996, **118**, 2644.
20 K. Kalyanasundaram, *Coord. Chem. Rev.*, 1982, **46**, 159.
21 N. N. Greenwood and T. C. Gibb, *Mössbauer Spectroscopy*, Chapman and Hall, London, 1971.

Communication 9/01561B

ChemComm

The *ansa*-effect in permethyltantalocene chemistry: a [Me_2Si] *ansa* bridge promotes olefin-insertion and reductive-elimination reactions for [$Me_2Si(C_5Me_4)_2$]Ta(η^2-C_2H_4)H and [$Me_2Si(C_5Me_4)_2$]TaH_3

Jun Ho Shin and Gerard Parkin*

Department of Chemistry, Columbia University, New York, New York 10027, USA.
E-mail: parkin@chem.columbia.edu

Received (in Bloomington, IN, USA) 1st February 1999, Accepted 31st March 1999

The *ansa*-effect, as it applies to tantalocene chemistry, has been investigated by a comparison of the chemistry of [$Me_2Si(C_5Me_4)_2$]TaH_3 and [$Me_2Si(C_5Me_4)_2$]Ta(η^2-C_2H_4)H with their permethyltantalocene counterparts; these studies demonstrate that incorporation of the [Me_2Si] *ansa* bridge substantially enhances the rates of both reductive elimination of H_2 and ethylene-insertion into a Ta–H bond.

The ability of an *ansa* bridge to modify the chemistry of a metallocene system has recently found important applications. For example, the stereoregularity of polymers obtained using metallocene catalysts is influenced considerably by the presence of such bridges.[1] The majority of studies on *ansa*-metallocene complexes, however, has principally been concerned with identifying the manner in which the *ansa*-bridge effects a product distribution, with relatively little attention having been given to defining, and quantifying, its effect on fundamental organometallic transformations.[2] Here, we describe quantitative aspects of the *ansa*-effect as it applies to two of the most important reactions in organometallic chemistry, namely olefin-insertion and reductive-elimination.

By comparison with unsubstituted tantalocene complexes, Cp_2TaX_n, their permethylated counterparts $Cp^*_2TaX_n$ (Cp^* = η^5-C_5Me_5) have provided a most valuable system for studying a variety of elementary organometallic transformations.[3] An investigation of the chemistry of the corresponding permethylated *ansa*-tantalocene complexes [$Me_2Si(C_5Me_4)_2$]TaX_n should, therefore, allow for a quantitative evaluation of the influence of an *ansa* bridge on elementary transformations at a tantalum center. Single atom bridged *ansa*-tantalocene complexes are, however, most uncommon. For example, the only structurally characterized *ansa*-tantalocene complexes with η^5,η^5-coordination listed in the Cambridge Structural Database[4] are the imido derivatives, [$Me_2C(C_5H_4)_2$]Ta(NBu^t)Cl[5] and [$Me_2C(C_5H_4)_2$]Ta[$N(C_6H_3Pr^i_2)$]Cl.[6,7] In view of the large number of *ansa*-metallocene complexes of Ti, Zr, and Hf, the paucity of studies in *ansa*-tantalocene chemistry may be a reflection of synthetic difficulties in obtaining the requisite compounds; indeed, even the literature synthesis of $Cp^*_2TaCl_2$[8] is considerably more complicated than those of the Group 4 analogues, $Cp^*_2MCl_2$ (M = Ti, Zr, Hf). It is, therefore, noteworthy that we have been able to access the *ansa* bridged {[$Me_2Si(C_5Me_4)_2$]Ta} system. Specifically, the trihydride complex [$Me_2Si(C_5Me_4)_2$]TaH_3 may be obtained *via* reaction of $TaCl_5$ with [$Me_2Si(C_5Me_4)_2$]$(SnBu^n_3)_2$,[9] followed by treatment with $LiAlH_4$ (Scheme 1).

[$Me_2Si(C_5Me_4)_2$]TaH_3 is a convenient precursor to other derivatives, including the ethylene and carbonyl complexes, [$Me_2Si(C_5Me_4)_2$]Ta(η^2-C_2H_4)H and [$Me_2Si(C_5Me_4)_2$]Ta(CO)H (Scheme 1). While the pentamethylcyclopentadienyl analogues, $Cp^*_2Ta(\eta^2$-$C_2H_4)H$ and $Cp^*_2Ta(CO)H$, have likewise been prepared from $Cp^*_2TaH_3$,[8] an important distinction between the two systems resides with the conditions required to effect reaction. For example, [$Me_2Si(C_5Me_4)_2$]Ta(η^2-C_2H_4)H is readily obtained over a period of hours at 80 °C, whereas the literature synthesis of the pentamethylcyclopentadienyl analogue requires prolonged heating for 10 days at 140 °C.[8] A more detailed comparison indicates that the *ansa* complex [$Me_2Si(C_5Me_4)_2$]TaH_3 reacts with C_2H_4 *ca.* 4000 times faster than does $Cp^*_2TaH_3$ under identical conditions.[10] Likewise, (i) the reaction of [$Me_2Si(C_5Me_4)_2$]TaH_3 with CO and (ii) H/D exchange with D_2 are also enhanced over the corresponding reactions of $Cp^*_2TaH_3$. These comparisons clearly demonstrate that the [Me_2Si] *ansa* bridge strongly promotes reductive elimination of H_2 in this system, a most notable result because a completely opposite effect is observed in a related tungsten system. Specifically, Green and coworkers demonstrated that the [Me_2C] *ansa* bridge in [$Me_2C(C_5H_4)_2$]W(R)H totally inhibits reductive elimination of alkane, an observation that was rationalized in terms of the *ansa* bridge preventing adoption of the parallel ring geometry favored for a tungstenocene intermediate.[11] The tantalum systems, however, do not require a parallel ring geometry since both monohydride intermediates, {[$Me_2Si(C_5Me_4)_2$]TaH} and [Cp^*_2TaH], are expected to have a bent sandwich structure.[12] Other factors are, therefore, responsible for dictating the influence of the [Me_2Si] *ansa* bridge on reductive elimination reactions in tantalocene complexes. One possible explanation is associated with the notion that the [Me_2Si] *ansa* bridge reduces the electron donating capability of the attached cyclopentadienyl groups (*vide infra*).[2b,13] As such, the Ta(V) trihydride would be stabilized with respect to the Ta(III) monohydride intermediate to a lesser degree for the *ansa* system than that for the unbridged system and so their interconversion would be more facile.

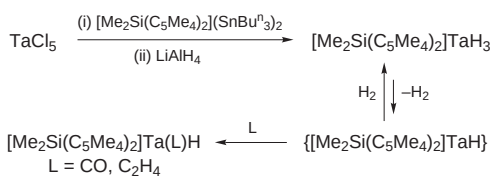

Scheme 1

Dynamic NMR spectroscopic studies (line broadening and magnetization transfer) indicate that the ethylene hydride complex [$Me_2Si(C_5Me_4)_2$]Ta(η^2-C_2H_4)H is in rapid equilibrium with its ethyl tautomer {[$Me_2Si(C_5Me_4)_2$]$TaCH_2CH_3$} (Scheme 2).[14] Significantly, the [Me_2Si] *ansa* bridge also enhances the rate of ethylene insertion in [$Me_2Si(C_5Me_4)_2$]-Ta(η^2-C_2H_4)H by a factor of *ca.* 760 (at 100 °C)[15] over that for its non-bridged counterpart, $Cp^*_2Ta(\eta^2$-$C_2H_4)H$.[16] As with the reductive elimination reactions described above, it is likely that the origin of the effect on the olefin insertion reaction is also attributable to an electronic influence resulting from the reduced electron donating properties of the *ansa* bridged ligand. Indeed, a similar argument has been made by Bercaw to rationalize the observation that olefin insertion within $Cp_2M(\eta^2$-$C_2H_4)H$ is more facile than that within $Cp^*_2M(\eta^2$-$C_2H_4)H$ (M = Nb, Ta).[3b]

In addition to olefin insertion, the barrier to 'inversion',[17] *i.e.* the combined barrier to cleaving any potential agostic interaction, passing the alkyl group through the center of the wedge, and rotating about a M–C bond (Scheme 2), is of most relevance

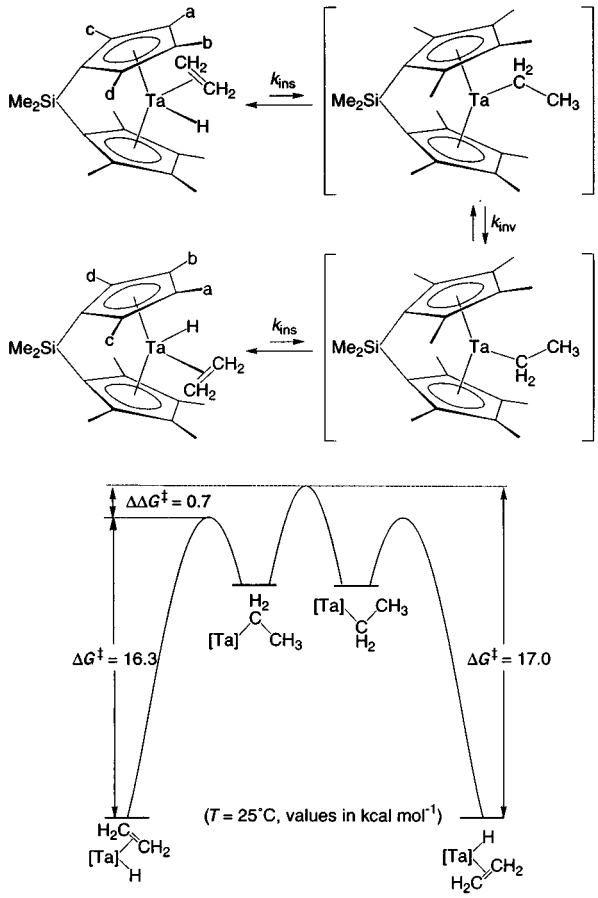

Scheme 2

to the use of metallocene derivatives as polymerization catalysts. Specifically, depending on the catalyst system, the polymer stereochemistry will depend critically on the relative rates of such 'inversion' and olefin insertion.[18] While it is not possible to study inversion within $Cp^*_2Ta(\eta^2\text{-}C_2H_4)H$ because of the lack of a suitable diagnostic technique, it is possible to detect the occurrence of this process for the *ansa* analogue $[Me_2Si(C_5Me_4)_2]Ta(\eta^2\text{-}C_2H_4)H$ by virtue of the diasterotopic methyl substituents of the $[Me_2Si(C_5Me_4)_2]$ ligand. In particular, the barrier for ethylene–hydride site interchange within $[Me_2Si(C_5Me_4)_2]Ta(\eta^2\text{-}C_2H_4)H$ may be conveniently measured by monitoring exchange of the aforementioned diasterotopic methyl substituents (a ↔ b and c ↔ d) by using ^{1}H NMR spectroscopy. These experiments indicate that there is indeed an additional barrier required to effect 'inversion' in this system. The additional barrier ($\triangle\triangle G^{\ddagger}$) is, however, modest, with a value of only *ca.* 0.7 kcal mol^{-1} at 25 °C (Scheme 2), corresponding to a factor of *ca.* 4 in rate constant.[15]

Spectroscopic studies are in accord with the notion that the $[Me_2Si]$ *ansa* bridge causes a reduction in the electron density at the tantalum centers in $\{[Me_2Si(C_5Me_4)_2]Ta\}$ complexes as compared with their $[Cp^*_2Ta]$ counterparts. Thus, the ν(CO) stretch of $[Me_2Si(C_5Me_4)_2]Ta(CO)H$ (1887 cm^{-1}) in pentane is substantially greater than that of $Cp^*_2Ta(CO)H$ (1868 cm^{-1}). X-Ray diffraction studies[19] suggest that these spectroscopic differences are a result of the $[Me_2Si]$ *ansa* bridge displacing the cyclopentadienyl groups from their preferred positions with respect to tantalum. For example, the Cp_{cent}–Ta–Cp_{cent} angle in $[Me_2Si(C_5Me_4)_2]Ta(CO)H$ [139.7°] is significantly reduced from that in $Cp^*_2TaH_3$ [148.3°].[20] More importantly, the angle between the ring normals in $[Me_2Si(C_5Me_4)_2]Ta(CO)H$ [131.3°] is reduced to an even greater extent, so that the ring normals lose coincidence with the Ta–Cp_{cent} vectors and there is an increase in the asymmetry of the Ta–Cp interactions.[21] The binding mode thus approaches η^3,η^3-coordination and thereby reduces the electron density transferred to the metal center.

We thank the U.S. Department of Energy, Office of Basic Energy Sciences (#DE-FG02-93ER14339) for support of this research and Dr Peter Desrosiers (Symyx Technologies) for valuable technical assistance.

Notes and references

1 H. H. Brintzinger, D. Fischer, R. Mülhaupt, B. Rieger and R. M. Waymouth, *Angew. Chem., Int. Ed. Engl.*, 1995, **34**, 1143.

2 For leading reports describing differences in the chemistry of *ansa* and non-*ansa* systems, see: (*a*) S. L. J. Conway, T. Dijkstra, L. H. Doerrer, J. C. Green, M. L. H. Green and A. H. H. Stephens, *J. Chem. Soc., Dalton Trans.*, 1998, 2689; (*b*) H. Lee, P. J. Desrosiers, I. Guzei, A. L. Rheingold and G. Parkin, *J. Am. Chem. Soc.*, 1998, **120**, 3255; (*c*) J. C. Green, *Chem. Soc. Rev.*, 1998, **27**, 263.

3 See, for example: (*a*) G. Parkin, E. Bunel, B. J. Burger, M. S. Trimmer, A. van Asselt and J. E. Bercaw, *J. Mol. Catal.*, 1987, **41**, 21; (*b*) B. J. Burger, B. D. Santarsiero, M. S. Trimmer and J. E. Bercaw, *J. Am. Chem. Soc.*, 1988, **110**, 3134; (*c*) V. C. Gibson, G. Parkin and J. E. Bercaw, *Organometallics*, 1991, **10**, 220.

4 CSD Version 5.16. *3D Search and Research Using the Cambridge Structural Database*; F. H. Allen and O. Kennard, *Chem. Des. Automat. News*, 1993, **8**(1), 1, 31–37.

5 N. J. Bailey, J. A. Cooper, H. Gailus, M. L. H. Green, J. T. James and M. A. Leech, *J. Chem. Soc., Dalton Trans.*, 1997, 3579.

6 W. A. Herrmann, W. Baratta and E. Herdtweck, *J. Organomet. Chem.*, 1997, **541**, 445.

7 *Ansa*-niobocene and tantalocene complexes with asymmetric η^5,η^1-coordination,[a,b] *e.g.* $[Me_2C(C_5H_4)_2]Ta[N(C_6H_3Pr^i_2)]NMe_2$, and η^5,η^2-coordination, $\{(Me_2Si)_2(\eta^5\text{-}C_5H_2Bu^t)(\eta^2\text{-}C_5HPr^i_2)\}TaMe_3$,[c] are also known: (*a*) A. N. Chernega, M. L. H. Green and A. G. Suárez, *Can. J. Chem.*, 1995, **73**, 1157; (*b*) W. A. Herrmann, W. Baratta and E. Herdtweck, *Angew. Chem., Int. Ed. Engl.*, 1996, **35**, 1951; (*c*) P. Chirik and J. E. Bercaw, personal communication.

8 V. C. Gibson, J. E. Bercaw, W. J. Bruton, Jr. and R. D. Sanner, *Organometallics*, 1986, **5**, 976.

9 $[Me_2Si(C_5Me_4)_2](SnBu^n_3)_2$ is generated *via* reaction of $[Me_2Si(C_5Me_4)_2]Li_2$ with Bu^n_3SnCl.

10 Rate constants for reaction with C_2H_4 at 90 °C: $[Me_2Si(C_5Me_4)_2]TaH_3$ [9.8(9) × 10^{-4} s^{-1}], $Cp^*_2TaH_3$ [2.5(2) × 10^{-7} s^{-1}]. Rate constants for reaction with CO at 90 °C: $[Me_2Si(C_5Me_4)_2]TaH_3$ [6.1(6) × 10^{-4} s^{-1}], $Cp^*_2TaH_3$ [2.2(2) × 10^{-7} s^{-1}].

11 L. Labella, A. Chernega and M. L. H. Green, *J. Chem. Soc., Dalton Trans.*, 1995, 395; J. C. Green and C. N. Jardine, *J. Chem. Soc., Dalton Trans.*, 1998, 1057; see also ref. 2(*a*).

12 J. W. Lauher and R. Hoffmann, *J. Am. Chem. Soc.*, 1976, **98**, 1729.

13 V. Varga, J. Hiller, R. Gyepes, M. Polasek, P. Sedmera, U. Thewalt and K. Mach, *J. Organomet. Chem.*, 1997, **538**, 63; C. S. Bajgur, W. R. Tikkanen and J. L. Petersen, *Inorg. Chem.*, 1985, **24**, 2539.

14 As has been noted previously, exchange processes of this type do not require the participation of a 16-electron alkyl complexes, but may occur *via* an 18-electron agostic alkyl species.

15 For ethylene insertion, $\Delta H^{\ddagger}$ = 15.49(33) kcal mol^{-1} and $\Delta S^{\ddagger}$ = −2.60(10) cal mol^{-1} K^{-1} corresponding to k_{ins} = 1.83 × 10^3 s^{-1} and $\Delta G^{\ddagger}$ = 16.44 kcal mol^{-1} at 100 °C. For inversion, $\Delta H^{\ddagger}$ = 17.96(24) kcal mol^{-1} and $\Delta S^{\ddagger}$ = 3.3(8) cal mol^{-1} K^{-1}.

16 Data for $Cp^*_2Ta(\eta^2\text{-}C_2H_4)H$ at 100 °C: k_{ins} = 2.4 s^{-1}; $\Delta G^{\ddagger}$ = 21.3 kcal mol^{-1}. See ref. 3(*b*).

17 The term 'inversion' in this sense is being used to refer to ethylene–hydride site (or alkyl–vacancy) interchange. Since the molecule is not chiral, it is not intended to refer to enantiomer interconversion.

18 See, for example: C. P. Casey, M. A. Fagan and S. L. Hallenbeck, *Organometallics*, 1998, **17**, 287 and references therein.

19 See supplementary data for the structures of $[Me_2Si(C_5Me_4)_2]Ta(CO)H$, $[Me_2Si(C_5Me_4)_2]Ta(\eta^2\text{-}C_2H_4)H$, and $Cp^*_2TaH_3$. The C_2H_4 and hydride ligands of $[Me_2Si(C_5Me_4)_2]Ta(\eta^2\text{-}C_2H_4)H$ are statistically disordered about a crystallographic mirror plane that lies in the Cp_{cent}–Ta–Cp_{cent} plane. CCDC 182/1209. See http://www.rsc.org/suppdata/cc/1999/887/ for crystallographic files in .cif format.

20 Cp_{cent}–Ta–Cp_{cent} = 148.3°; Cp_{norm}/Cp_{norm} = 148.2°.

21 Individual Ta–C_{Cp} bond lengths for $[Me_2Si(C_5Me_4)_2]Ta(CO)H$ range from 2.32 Å to 2.45 Å. The difference between the Cp_{cent}–Ta–Cp_{cent} angle and the angle between the ring normals is 8.2° for $[Me_2Si(C_5Me_4)_2]Ta(CO)H$, but only 0.1° for $Cp^*_2TaH_3$.

Communication 9/00895K

Kinetic and mechanistic examination of $NBu_4[IrH_2(CO)_2I_2]$ and $NBu_4[RhH_2(CO)_2I_2]$ *via para*-hydrogen enhanced NMR spectroscopy

Sarah K. Hasnip,[a] Simon B. Duckett,*[a] Diana R. Taylor,[b] Graham K. Barlow[b] and Mike J. Taylor[b]

[a] *Department of Chemistry,University of York, Heslington, York, UK YO10 5DD. E-mail: sbd3@york.ac.uk*
[b] *BP Chemicals, BP Chemicals Limited, Salt End, Hull, UK HU12 8DS*

Received (in Cambridge, UK) 4th February 1999, Accepted 12th April 1999

***para*-Hydrogen enhanced NMR signals are used to show that $NBu_4[M(CO)_2I_2]$ (M = Rh, Ir) add hydrogen to form NBu_4-{*all-cis*-$[M(H)_2(CO)_2I_2]$} which for M = Ir undergoes H_2 elimination in a step where $\Delta H^{\ddagger}$ 106 ± 10 kJ mol^{-1} and $\Delta S^{\ddagger}$ 60 ± 6 J K^{-1} mol^{-1} while showing a rich substitution chemistry with PPh_3 that leads to both charged and neutral products *via* square pyramidal $Ir(H)_2(CO)_2I$.**

When transition metal complexes are reacted with *para*-hydrogen (*p*-H_2) the size of the detectable NMR signatures of many hydride reaction products are dramatically enhanced owing to the generation of non-Boltzmann spin populations.[1–4] This phenomenon provides sufficient sensitivity to facilitate the observation of intermediates in catalytic reactions, species in minor reaction pathways such as $RhH_2(PMe_3)_2I_2Rh(PMe_3)(CO)$ and minor constituents in equilibria, for example *all-cis*-$[Ru(PMe_3)_2(CO)_2(H)_2]$.[5] Here we examine the reactivity of $NBu_4[M(CO)_2I_2]$ (M = Ir, Rh) towards hydrogen. While these complexes are known to react with MeI to form $NBu_4[MI_3Me(CO)_2]$, and play a substantial role in acetic acid generation, their reactivity towards hydrogen, a substrate also present in this process, is far less well understood.[6] We show that two isomers of $NBu_4[IrH_2(CO)_2I_2]$ are formed upon H_2 addition to $NBu_4[Ir(CO)_2I_2]$, and report for the first time kinetic and thermodynamic parameters for H_2 elimination from a *p*-H_2 enhanced dihydride. The lability of the ligand sphere of the *all-cis* isomer is further explored by employing PPh_3 as a vacant coordination site scavenger.

When a 0.1 mM solution of $NBu_4[Ir(CO)_2I_2]$ **1** in benzene-d_6 is monitored by ^{1}H NMR spectroscopy at 295 K while under 3 atm of *p*-H_2 substantial signals arise from a previously undetected complex at δ −9.13 and −13.30 [Fig. 1(a)].† These resonances are assigned to the hydride ligands H_a and H_b of **3a**, and their chemical shifts indicate they are *trans* to carbonyl and iodide respectively.† The two carbonyl resonances of **3a** were detected at δ 167.2 and 160.9 by a ^{1}H–^{13}C HMQC experiment, and when a sample containing **1** and *p*-H_2 was monitored with an excess of NBu_4I present the product signal intensities were unchanged. This information suggests that **3a** corresponds to the *all-cis* isomer of $NBu_4[Ir(H)_2(CO)_2I_2]$ **3a** as shown in eqn. (1).

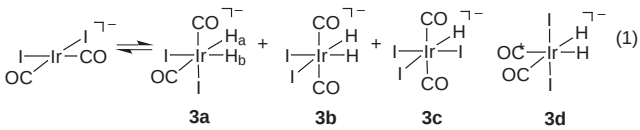

(1)

Weak hydride resonances attributable to species **3b** and **3c** of eqn. (1) were also observed in the ^{1}H NMR spectra.[7] Resonances attributable to **3a** are also observable in methanol-d_4 and acetic acid-d_4. We further note, that **3a** is only visible with *p*-H_2, and that isomer **3d** is not seen even when ^{13}CO labelled **1** is employed. Additionally, when the sample is left under H_2 at room temperature, the resonance for **3c** disappears leaving **3b** as the only detectable hydride containing species.

The mechanism of generation of these species requires further comment since concerted H_2 addition to NBu_4*{cis*-$[Ir(CO)_2I_2]$} should only yield **3a**. We therefore investigated the dynamic behaviour of **3a** using gradient-assisted EXSY spectroscopy. This revealed that at 323 K **3a** undergoes simple reductive elimination to form free H_2, which at temperatures beyond 350 K is complicated by both *intermolecular* hydride interchange and *intramolecular* exchange into **3b**. Under these conditions, addition of an excess of free NBu_4I, such that the solution is saturated, results in a 5% increase in the rate of H_2 loss and suppression of the intermolecular and intramolecular exchange peaks. In view of this we can state that H_2 loss occurs from **3a** rather than the 16-electron complex $[Ir(H)_2(CO)_2I]$. Analysis of the exchange peak intensity as a function of mixing time allowed the rate of H_2 elimination from **3a** to be determined; at 325 K this corresponds to 0.17 s^{-1}. Monitoring this process as a function of reaction temperature enabled the activation parameters $\Delta H^{\ddagger}$ 106 ± 10 kJ mol^{-1} and $\Delta S^{\ddagger}$ 60 ± 6 J K^{-1}mol^{-1} to be calculated.

Importantly, when a 0.1 mM solution of the rhodium analogue **2** is warmed with *p*-H_2 to 350 K and monitored by ^{1}H NMR spectroscopy [Fig 1(b)] two rhodium coupled hydride resonances are observed at δ −9.75 (J_{RhH} 17.3, J_{HH} −4 Hz) and −14.15 (J_{RhH} 16.5 Hz) which are consistent with the formation of the previously unseen species NBu_4*{all-cis*-$[RhH_2(CO)_2(I)_2]$}. Clearly the extent to which NBu_4*{all-*

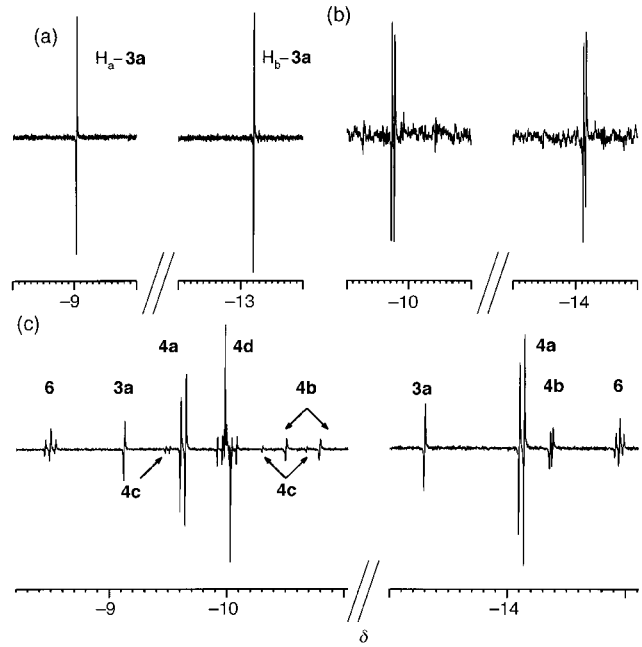

Fig. 1 (a) ^{1}H NMR spectrum (400 MHz, 295 K) of a 0.1 mM solution of **1** in benzene-d_6 under 3 atm of *p*-H_2. The antiphase resonances arise from the parahydrogen enhanced hydride resonances in the *all-cis* isomer of $NBu_4[Ir(H)_2(CO)_2I_2]$, **3a**. (b) ^{1}H NMR spectrum (400 MHz, 350 K) of a 0.1 mM solution of **2** in benzene-d_6 under 3 atm of *p*-H_2 showing resonances due to the *all-cis* isomer of $[Rh(H)_2I_2(CO)_2]$. (c) ^{1}H NMR spectrum (400 MHz, 295 K) of a 0.1 mM solution of **1** in benzene-d_6 under 3 atm of *p*-H_2, in the presence of 0.1 mM of PPh_3 with resonance assignments indicated.

cis[$RhH_2(CO)_2(I)_2$]} forms is much lower than that of **3a**, and the temperatures required to observe it are at least 60 K higher.

The observation of intramolecular and intermolecular exchange pathways indicated that the substitution reactivity of **3a** was worthy of examination. We therefore monitored benzene-d_6 solutions containing **1**, *p*-H_2 and PPh_3 (< 2 equivalents). A typical ^1H spectrum is shown in [Fig. 1(c)]. The new mononuclear products, identified by ^1H–^1H COSY, ^1H–^{31}P and ^1H–^{13}C HMQC techniques, correspond to four isomeric forms of $IrH_2(CO)_2(PPh_3)I$, three isomers of $NBu_4[IrH_2(CO)(PPh_3)I_2]$, and $IrH_2(CO)(PPh_3)_2I$ with *trans* phosphines are shown below.† Surprisingly, when $NBu_4[Rh(CO)_2I_2]$ **2**, *p*-H_2 and PPh_3 were examined at 350 K no new dihydride products were detected.

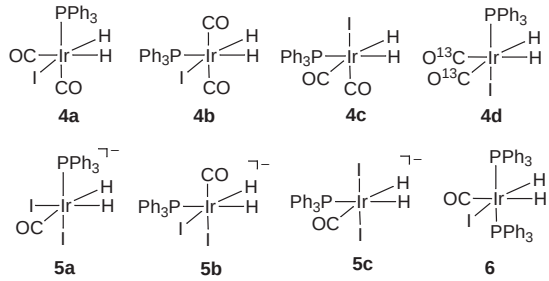

When samples containing **1**, PPh_3 and H_2 were monitored by EXSY spectroscopy at 295 K the signals observed for each hydride of **3a** connected to both hydride resonances of **4b** *via* cross peaks arising from chemical exchange. Examination of the intensity of these peaks indicated that interconversion of **3a** to **4b** places **3a**-H_a *trans* to phosphine in **4b** more often than *trans* to iodide; this process is suppressed upon addition of NBu_4I. As expected, the reverse situation is true when cross peaks from H_b-**3a** are considered and the difference in intensity between the corresponding hydride cross peaks falls as the temperature rises. This information suggests that **4b** forms from **3a** *via* a process involving iodide loss to yield an intermediate with inequivalent hydrides which undergoes rearrangement to form the square pyramidal intermediate $IrH_2(I)(CO)_2$ with *trans* carbonyls. Coordination of phosphine then generates **4b**, or iodide **3b**, as shown in Scheme 1. Furthermore, while the two hydride ligands of $IrH_2(I)(CO)_2$ are inequivalent they must be able to interchange their positions on the same time scale as phosphine coordination. Significantly, weaker cross peaks, connect the hydride resonances of **4b** to **3a** which indicates that they are in equilibrium.

The only other exchange peaks visible in the hydride region of the spectrum at 350 K connect the hydride resonances of **4c** to those of **4b**. This interconversion process occurs with a twofold preference for placing the hydride ligand of **4c** that was *trans* to phosphine *trans* to iodide in the product, **4b**. While both phosphine and CO loss from **4c** are possible in the first step, the data suggests CO loss is more likely since different intermediates to those shown in Scheme 1 are required to account for the dramatically different hydride exchange preferences seen in the two interconversion processes. This second reaction therefore most likely involves square pyramidal $Ir(H)_2(I)(CO)(PPh_3)$.

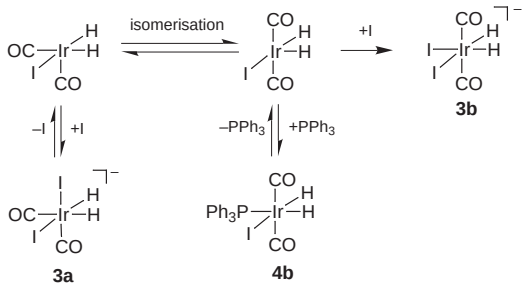

Scheme 1

Here, we have shown that *p*-H_2 derived spectral amplification can be used to examine the hydrogen addition chemistry of both $NBu_4[IrI_2(CO)_2]$ and $NBu_4[RhI_2(CO)_2]$. Products not previously observed have been characterised, and for the first time activation parameters have been determined for H_2 elimination from a *p*-H_2 enhanced product. Additionally, a new series of iridium dihydrides containing phosphine and carbonyl ligands have been characterised, and the intermediates, $IrH_2(I)(CO)_2$ and $Ir(H)_2(I)(CO)(PPh_3)$, involved in their formation shown to be square pyramidal.

Financial support from the EPSRC (Spectrometer and S.K.H.), BP Chemicals (CASE award S.K.H.), the Royal Society, NATO and Bruker UK, and discussions with Dr C. Sleigh, Professor R. Eisenberg, Profesor R. N. Perutz, Dr P. Dyson and Dr R. J. Mawby are gratefully acknowledged.

Notes and references

† *Selected spectroscopic data* in C_6D_6 at 295 K unless otherwise indicated with 400.13 MHz (^1H), 161.45 MHz (^{31}P) and 100.2 MHz (^{13}C). **3a**: ^1H δ −9.13 [H_a, *J*(HH) −4.4, *J*($H^{13}CO$) 58.4, 6.5 Hz], δ −13.30 [H_b, *J*(HH) −4.5, *J*($H^{13}CO$) 4.5 Hz], ^{13}C δ 167.2 (CO_a), 160.9 [CO_b, *J*(CC) 11.8 Hz]. **3b**: ^1H δ −15.40 [*J*($H^{13}CO$) 5.6 Hz}], ^{13}C δ 171.6 (CO). **3c**: ^1H δ −10.94 [*J*($H^{13}CO$) 2.9 Hz], ^{13}C δ 155.1 (CO). **4a**: ^1H δ 7.73 (*o*-phenyl H of P), −9.63 [H, *J*(PH) 17.0, *J*(^{13}COH) 44.9, 5.6, *J*(HH) −4.3 Hz], −14.12 [H, *J*(PH) 16.4, *J*(^{13}COH) 4.5, *J*(HH) −4.3 Hz], ^{31}P δ 0.2 (P, s), ^{13}C δ 164.3 [CO_a, *J*(PC) 118 Hz], 167.5 (CO_b). **4b**: ^1H δ −10.65 [H, *J*(PH) 115.6, *J*(^{13}COH) 4.0, *J*(HH) −4.7 Hz], −14.37 [H, *J*(PH) 8.8, *J*(^{13}COH) 4.0, *J*(HH) −4.7 Hz], ^{31}P δ −10.9 (P, s), ^{13}C δ 168.4 [CO, *J*(PC) 9 Hz]. **4c**: (*T* = 350 K) ^1H δ −9.62 [H, *J*(PH) 14.7, *J*(^{13}COH) 50.7, 3, *J*(HH) −3.5 Hz], −10.65 [H, *J*(PH) 151.1, *J*(HH) −3.5 Hz}, ^{31}P δ −16.3 (P, s), ^{13}C δ 164.3 [CO, *J*(PC) 118 Hz]. **4d**: (*T* = 350 K) ^1H δ −10.00 [H, *J*(PH) 17.1, *J*(^{13}COH) 45, 12 *J*(HH) −5.3 Hz], ^{31}P δ 3.7 (P, s), ^{13}C δ 166.1 [CO, *J*(PC) 18.8 Hz]. **5a** ^1H δ −8.13 [H, *J*(PH) 20.9, *J*(HH) −4.6 Hz], −16.45 [H, *J*(PH) 12.6, *J*(HH) −4.6 Hz], ^{31}P δ −18.1 (P, s). **5b** ^1H δ −10.20 [H, *J*(PH) 170.5, *J*(HH) −5.6 Hz], −14.80 [H, *J*(PH) 8.5, *J*(HH) −5.6 Hz], ^{31}P −14.5 (P, s). **5c** ^1H δ −9.89 [H, *J*(PH) 17.3, *J*(HH) −1.8 Hz], −10.60 [H, *J*(PH) 122.1, *J*(HH) −2.6 Hz], ^{31}P δ 3.00 (P, s). **6**: ^1H δ 8.02 (*o*-phenyl H of P), −8.49 {H, *J*(PH) 17.0, *J*(^{13}COH) 42.6, *J*(HH) −4.4 Hz], δ −14.95 [H, *J*(PH) 13.8, *J*(^{13}COH) 4, *J*(HH) −4.4 Hz], ^{31}P δ 6.1 (P, s), ^{13}C δ 175.4 [CO, *J*(PC) 8 Hz].

1 C. R. Bowers and D. P. Weitekamp. *J. Am. Chem. Soc.*, 1987, **109**, 5541.
2 R. Eisenberg. *Acc. Chem. Res.*, 1991, **24**, 110.
3 J. N. Atterer and J. Bargon. *Prog. Nucl. Magn. Reson. Spectrosc.*, 1997, **31**, 293.
4 C. J. Sleigh and S. B. Duckett. *Prog. Nucl. Magn. Reson. Spectrosc.*, 1999, **34**, 71.
5 S. B. Duckett, C. L. Newell and R. Eisenberg. *J. Am. Chem. Soc*., 1994, **116**, 10548; S. B. Duckett and R. Eisenberg. *J. Am. Chem. Soc*., 1993, **115**, 5292; S. B. Duckett, R. J. Mawby and M. G. Partridge. *Chem. Commun*., 1996, 383; P. D. Morran, S. A. Colebrooke, S. B. Duckett, J. A. B. Lohmann and R. Eisenberg. *J. Chem. Soc., Dalton. Trans*., 1998, 3363.
6 P. M. Maitlis, A. Haynes, G. J. Sunley and M. J. Howard, *J. Chem. Soc., Dalton Trans*., 1996, 2187.
7 When ^{13}CO labelled **1** is used both these resonances are split into a triplet. The hydride resonance attributable to **3c** is observed when HI is added to **1.**

Communication 9/00961B

ChemComm

A new mineralomimetic $Cd(CN)_2$ host framework which is intermediate between H- and L-cristobalite-like frameworks

Takafumi Kitazawa*

Department of Chemistry, Faculty of Science, Toho University, Miyama, Funabashi, Chiba 274-8510, Japan.
E-mail:kitazawa@chem.sci.toho-u.ac.jp

Received (in Cambridge, UK) 1st March 1999, Accepted 7th April 1999

The three-dimensional $Cd(CN)_2$ clathrate enclathrating the CH_2BrCH_2Br molecule produces a new mineralomimetic $Cd(CN)_2$ host framework (space group $I4_1/amd$) which is intermediate between H-cristobalite- (space group Fd-3m) and L-cristobalite-like species (space group $P4_12_12$).

In natural crystalline SiO_2 minerals, the SiO_4^{4-} tetrahedra are linked so that every oxygen atom is shared between two tetrahedra, giving the composition SiO_2. Likewise, the mineralomimetic $Cd(CN)_2$ host frameworks in the $Cd(CN)_2{\cdot}n$G clathrates are topologically similar to the polymorphic forms of SiO_2.[1–5] The nature of the $Cd(CN)_2$ host frameworks depends on guest molecules. The H-cristobalite, L-cristobalite and H-tridymite-like hosts of $Cd(CN)_2$ were obtained using guest molecules of different properties, sizes, shapes and symmetries. For example, $CHCl_2CHCl_2$,[2,3] $CHCl_2CH_2Cl$[4] and Bu_2O[4] produce an H-cristobalite-like $Cd(CN)_2$ host framework (Fd-3m), an L-cristobalite-like species ($P4_12_12$) and an H-tridymite-like species ($P6_3/mmc$), respectively. Selecting guest molecules provides new mineralomimetic $Cd(CN)_2$ host frameworks with a body-centered tetragonal $I4_1/amd$ lattice which is intermediate between the H-cristobalite-like species (space group Fd-3m) and the L-cristobalite-like species (space group $P4_12_12$).

In nature, H-cristobalite is the high-temperature polymorph of SiO_2, existing above 1743 K. However, H-cristobalite (cubic space group Fd-3m) metastably exists up to above 540 K, where it experiences a rapid and reversible inversion to L-cristobalite (tetragonal space group $P4_12_12$).[6] A crystallograhic comparison between the two structures has been reported.[7] To the best of my knowlege, the cristobalite structure which is intermediate between H-cristobalite (Fd-3m) and L-cristobalite ($P4_12_12$) has not previously been obtained and/or found. From a crystallographic view point, an intermediate structure with a tetragonal space group $I4_1/amd$ is possible.

The new mineralomimetic framework of $Cd(CN)_2$ between the H and L-cristobalite-like types has been obtained using CH_2BrCH_2Br as guest. Treating an equimolar aqueous solution of $CdCl_2{\cdot}2.5H_2O$ and $K_2[Cd(CN)_4]$ with 1,2-dibromoethane gives colourless tetragonal crystals of $Cd(CN)_2{\cdot}CH_2BrCH_2Br$. The IR spectrum indicates that the conformation of CH_2BrCH_2Br in $Cd(CN)_2$ is *trans* (1184, 594 cm^{-1}), based on the neat CH_2BrCH_2Br data.[8]

The X-ray single crystal determination† (Fig. 1) shows that the topological properties of the host framework in $Cd(CN)_2{\cdot}CH_2BrCH_2Br$ are intermediate between those of H- and L-cristobalite. For example, $Cd(CN)_2{\cdot}CMe_4$[3] and $Cd(CN)_2{\cdot}Pr^iBr$[4] contain mineralomimetic $Cd(CN)_2$ frameworks analogous to H- and L-cristobalite SiO_2, respectively: $Cd(CN)_2{\cdot}CMe_4$, space group Fd-3m, a = 12.757(2) Å, Z = 8; $Cd(CN)_2{\cdot}Pr^iBr$, $P4_12_12$, a = 9.124(1), c = 11.335(3) Å, Z = 4, while the new mineralomimetic $Cd(CN)_2{\cdot}CH_2BrCH_2Br$ crystalizes in the body-center tetragonal $I4_1/amd$ with lattice parameters, a = 8.116(5), c = 14.721(5) Å, Z = 4. Like the H- and L-cristobalite-like $Cd(CN)_2$ framework structures, the host framework of the present inclusion compound is composed of individual tetrahedral units linked to four neighboring tetrahedra by Cd–CN–Cd linkages. However, the new mineralominetic $Cd(CN)_2$ host framework in $Cd(CN)_2{\cdot}CH_2BrCH_2Br$ does not topologically correspond to natural SiO_2 structures. Clearly, there is a large difference in the scale and orientation of the tetrahedra between the $Cd(CN)_2$ and SiO_2 structures, since organic guest species must be accommodated in the adamantane-like cavity. The Cd–CN–Cd distance is *ca.* 5.5 Å and the Cd–CN–Cd angle is 180°, whereas the Si–O–Si distance is *ca.* 3.2 Å and the Si–O–Si bond angle is more flexible.

As shown in Fig. 2, the adamantane-like cavity in the new $Cd(CN)_2{\cdot}CH_2BrCH_2Br$ clathrate is occupied by the guest CH_2BrCH_2Br molecule, like the H- and L-cristobalite-like cadmium cyanide clathrates. However, the accommodation mode of CH_2BrCH_2Br is completely different from that of the guest molecules in the H- and L-cristobalike-like clathrates. The shape, size and conformation of CH_2BrCH_2Br is associated with forming the $I4_1/amd$ $Cd(CN)_2$ host framework. The orientation of the guest CH_2BrCH_2Br molecules is along the c axis. The Br atom projects toward a branch consisting of one Cd atom and two cyanide groups in the adamantane-like cavity, while each methyl group of CMe_4 in H-cristobalite-like $Cd(CN)_2{\cdot}CMe_4$ projects toward a tripod consisting of one Cd atom and three cyano groups,[3] and the two methyl groups of Pr^iBr in the L-cristobalite-like $Cd(CN)_2{\cdot}Pr^iBr$ project towards two tripods.[4] The guest CH_2BrCH_2Br as a template allows the new mineralomimetic $Cd(CN)_2$ host framework, which can be obtained by expanding the c axis and depressing the a and b axes in the H-cristobalite-like Fd-3m host framework. The insertion into the branch induces an expansion of the host framework along the c axis. The affinity of the guest molecules in the polymeric host framework varies depending on the

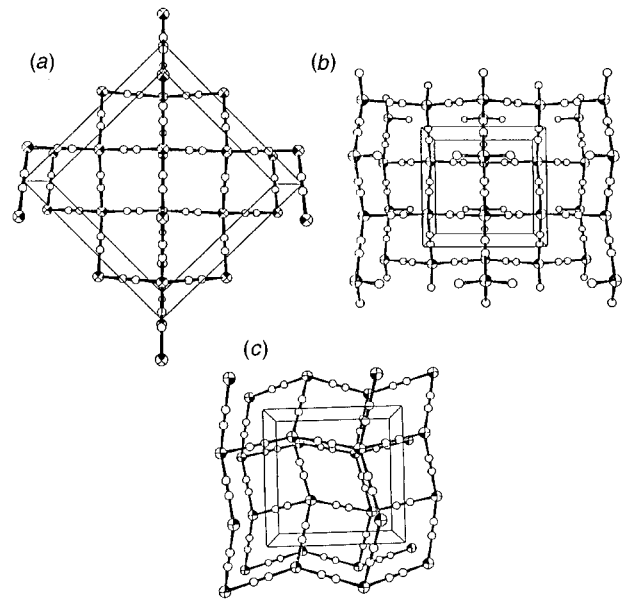

Fig. 1 The cristobalite-like $Cd(CN)_2$ host framework structures along the c axis. Guest molecules are omitted. (*a*) The H-cristobalite-like Fd-3m type, *e.g.* $Cd(CN)_2{\cdot}CMe_4$. (*b*) The new mineralomimetic $I4_1/amd$ type, $Cd(CN)_2{\cdot}CH_2BrCH_2Br$. (*c*) The L-cristobalite-like $P4_12_12$ type, *e.g.* $Cd(CN)_2{\cdot}Pr^iBr$.

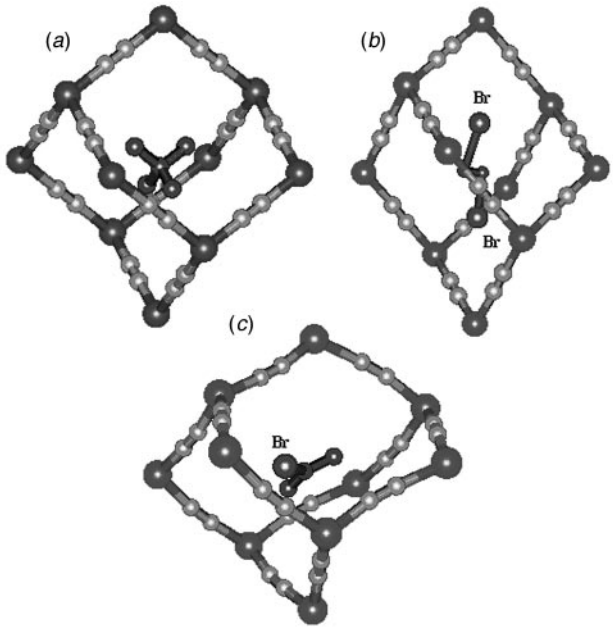

Fig. 2 The adamantane-like cavities of the $Cd(CN)_2$·G clathrates. (*a*) The cavity of the H-cristobalite-like $Cd(CN)_2$·CMe_4 clathrate. (*b*) The cavity of the new mineralomimetic $I4_1/amd$ type, $Cd(CN)_2$·CH_2BrCH_2Br clathrate. Since the C atoms of the CH_2BrCH_2Br are highly disordered, one possible conformation is shown. (*c*) The cavity of the L-cristobalite-like $Cd(CN)_2$·Pr^iBr.

proprieties of the guest molecules. The guest structure serves as a template for the solid host lattice.

These results indicate that the cadmium cyanide host is flexible depending on the guest molecules. To the best of my knowledge, a SiO_2 structure topologically similar to the host in $Cd(CN)_2$·CH_2BrCH_2Br has not been previously found. The new mineralomimetic $Cd(CN)_2$ host framework with a $I4_1/amd$ space group has implications for the natural and/or synthetic SiO_2 systems. The formation of the mineralomimetic $I4_1/amd$ $Cd(CN)_2$ host structure suggests the formation of $I4_1/amd$ type SiO_2 under special conditions. This new cadmium cyanide clathrate may be of significant interest as a crystalline model compound for studies of the transformation of SiO_2 and nanoscale control of host frameworks.

Notes and references

† *Crystal data*: $Cd(CN)_2$·CH_2BrCH_2Br, M = 352.31, $I4_1/amd$ (No. 141), a = 8.116(5), c = 14.721(5) Å, U = 969.7(9) Å^3, Z = 4, D_x = 2.41 g cm^{-3}, μ(Mo-Kα) = 10.423 mm^{-1}; 322 reflections observed, 2 restrains and 18 parameters refined: R = 0.0629 [$I > 2\sigma(I)$], goodness of fit (gof) = 1.056. The collection of X-ray diffraction intensity data was carried out on a Rigaku AFC5S diffractometer (Mo-Kα: λ = 0.71069 Å) at 180 K. The structure was solved using the TEXSAN software package installed on the diffractometer system and refined by full-matrix least-squares methods with the program SHELXL-93. After refinement of the host lattice $Cd(CN)_2$, the difference map suggested that the guest CH_2BrCH_2Br molecules displayed considerable positional disorder due to the large thermal motion and pseudo-symmetry associated with the space group. All non-hydrogen atoms were refined anisotropically. Hydrogen atoms have not been located. Since disorder in the orientation of the cyanide group between tetrahedral Cd atoms has been found by solid state ^{113}Cd NMR spectroscopy in $Cd(CN)_2$ host–guest materials (ref. 9), all the relevant C and N atoms were assumed to have 50% probability of being C and N. CCDC 182/1217. See http://www.rsc.org/suppdata/cc/1999/891/ for crystallographic files in .cif format.

1 T. Iwamoto, *Supramolecular Chemistry in Cyanometallate Systems*, in Comprehensive Supramolecular Chemistry, vol. 6, ed. D. D. MacNicol, F. Toda and R. Bishop, Pergamon, Oxford, 1996, ch. 19, pp. 643–690.
2 T. Kitazawa, S. Nishikiori, R. Kuroda and T. Iwamoto, *Chem. Lett*., 1988, 1729.
3 T. Kitazawa, S. Nishikiori, R. Kuroda and T. Iwamoto, *J. Chem. Soc., Dalton Trans*., 1994, 1029.
4 T. Kitazawa, T. Kikuyama, M. Takeda and T. Iwamoto, *J. Chem. Soc., Dalton Trans*., 1995, 3715.
5 T. Kitazawa, *J. Mater. Chem*., 1998, **8**, 671.
6 N. N. Greenwood and A. Earnshaw, *Chemistry of the Elements*, Pergamon, Oxford, 1984, pp. 393–395.
7 H. Arnord, *International Tables for Crystallography*, ed. Theo Hahn, Kluwer, Dordrech, 1989, vol.A, section 5.5., pp. 74–75.
8 P. K. Bose, D. O. Henderson, C. S. Ewing and P. L. Polavarasu, *J. Phys. Chem*., 1989, **93**, 5070.
9 S. Nishikiori, C. I. Ratcliffe and J. A. Ripmeester, *J. Am. Chem. Soc*., 1992, **114**, 8590.

Communication 9/01613I

ChemComm

Novel concise ring closure leading to bridged ten-membered ring compounds

Hiroshi Fujishima, Hiroshi Takeshita, Masahiro Toyota and Masataka Ihara*

Graduate School of Pharmaceutical Sciences, Tohoku University, Aobayama, Sendai, 980–8578, Japan. E–mail: mihara@mail.pharm.tohoku.ac.jp

Received (in Cambridge, UK) 19th February 1999, Accepted 12th April 1999

An unusual TBAF-mediated intramolecular cyclisation of diallylsilane derivatives 3 and 12 provided bicyclo[6.2.2]-dodecanes 5 and 13 in good yields.

The taxol derivatives have attracted the attention of synthetic chemists due to their novel mode of action and the complexity of their structures.[1] So far, several groups have achieved the total synthesis of taxol[2] and numerous synthetic methods have

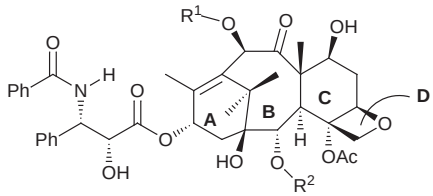

Taxol R^1 = Ac, R^2 = Bz
Taxotere R^1 = H, R^2 = Boc

been developed for the construction of the key bicyclic (BC ring) system. However, assembly of the eight-membered ring (B ring) needs multiple steps owing to its highly oxygenated structural features and, therefore, the establishment of a novel and concise route is highly desirable. In order to achieve an efficient construction of the B ring framework, we have been studying various intramolecular cyclisations.[3] In particular, cyclisation reactions employing allylsilanes[4,5] attracted our attention. During our investigations, we found that an unusual cyclisation took place when the diallylsilanes **3** and **12** were treated with TBAF, leading to the formation of the bridged ten-membered ring compounds **5** and **13**, respectively. Herein we describe the outcome of this novel TBAF-promoted cyclisation and the structural determination of the cyclised products.

The synthesis of substrate **3** is summarized in Scheme 1. The alcohol **1**[3a] was treated with BuLi and TMSCl in the presence of TMEDA to give the *C*- and *O*-silylated product, which was reacted with 2 M H_2SO_4 to furnish the diallylsilane **2** as a mixture of diastereoisomers (diastereoselection 3 : 1). Oxidation of **2** with a catalytic amount of tetrapropylammonium perruthenate (TPAP) and NMO[6] in CH_2Cl_2 afforded the desired aldehyde **3**.

First of all, **3** was subjected to the Hosomi–Sakurai reaction[4] in the presence of Lewis acids,[7] that is, the solution of material in solvent was treated with 1.1–3.0 equiv. of Lewis acid. Contrary to our expectations, reactions with $TiCl_4$ or $BF_3{\cdot}OEt_2$ did not provide the cyclised compound **4**, but brought about rapid decomposition of **3** (Table 1; entries 1 and 2); with $LiBF_4$ and HF·Py, compound **3** was recovered (entries 3 and 4). However, the α-carbon of the allylsilane moiety of **3** added as a nucleophile to the aldehyde in the presence of TBAF yielding the bicyclic products **5**[8] in fair to good yield (entries 5–8). It is important to note that this reaction proceeds with a catalytic amount of TBAF (0.05 equiv.) at room temperature for 1 h to afford **5** in 47% yield (entry 5). Moreover, the addition of 4 Å molecular sieves gave the best result and **4** was obtained in 79% yield (entry 7). The ten-membered structure (the so-called dihydro[6]paracyclophane) of **5**, obtained as a single isomer,

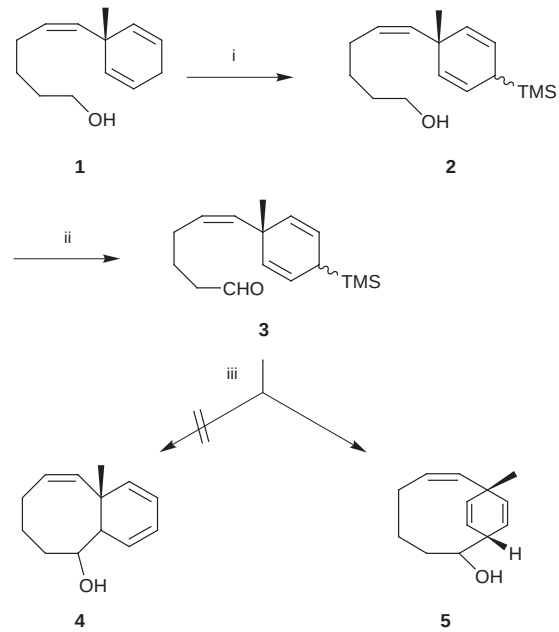

Scheme 1 *Reagents and conditions*: i, BuLi, TMSCl, TMEDA, THF, 0 °C, then 2 M H_2SO_4 (93%); ii, 20 mol% TPAP, NMO, 4 Å molecular sieves, CH_2Cl_2, rt (71%); iii, see Table 1.

was suggested by the absence of absorptions due to the conjugated diene in the UV spectrum.

The cyclisation of the substituted material **12** was next investigated under the same conditions as above. The assembly of **12** is depicted in Scheme 2. The coupling reaction of the aldehyde **6**[9] and the vinyl iodide **7**[10] with 2.2 equiv. of Bu^{t}Li afforded the alcohol **8** in 84% yield. Methylation of **8** followed by desilylation of **9** gave the alcohol **10**. Upon treatment of **10** as above, the diallylsilanes **11** were obtained as a mixture of diastereoisomers (diastereoselection 13 : 1). Oxidation of **11** with TPAP as above afforded the aldehyde **12**, which was converted into the bridged ten-membered ring products **13**[11] as a 14 : 1 mixture of two diastereoisomers with 1.1 equiv. of TBAF at room temperature in 66% yield.

The structure of the product **13** was determined by X-ray analysis (Fig. 1), after its conversion into the ketone **14**[12]

Table 1 Reactions of **3** with various Lewis acids or TBAF

Entry	Reagent (equiv.)	Solvent	*T*/°C	*t*/h	Yield(%)[a]
1	$TiCl_4$ (1.1)	CH_2Cl_2	−78	1.0	0
2	$BF_3{\cdot}OEt_2$ (1.5)	CH_2Cl_2	−78 → 0	4.0	0
3	$LiBF_4$ (1.1)	THF	0 → rt	7.0	0
4	HF·Py (1.1)	THF	0 → rt	7.0	0
5	TBAF[b] (0.05)	THF	rt	1.0	47
6	TBAF[b] (1.0)	THF	rt	0.7	44
7	TBAF[b,c] (3.0)	THF	rt	0.3	79
8	TBAF[b,c] (3.0)	MeCN	rt	1.0	38

[a] Isolated yield. [b] 1.0 M THF solution was used. [c] 4 Å molecular sieves were added.

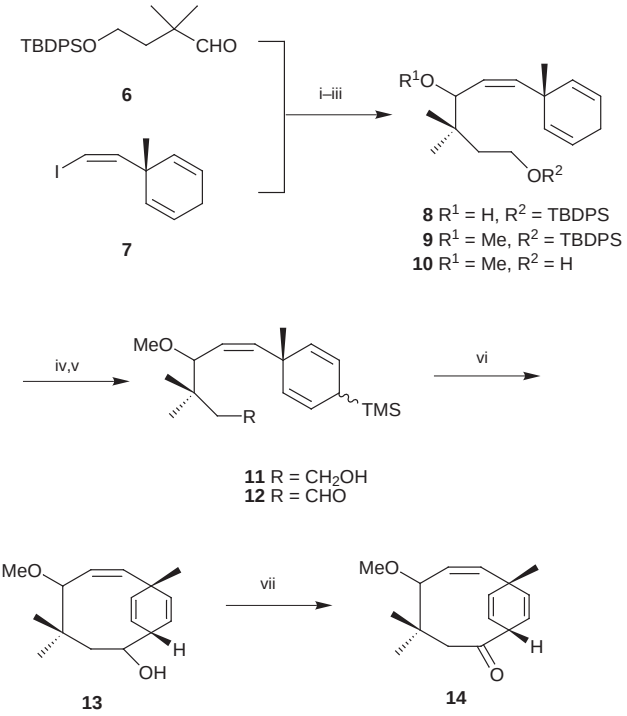

Scheme 2 *Reagents and conditions*: i, Bu^t Li, THF, −78 °C (84%); ii, MeI, NaH, DMF, 0 °C → rt (96%); iii, TBAF, THF, rt (94%); iv, BuLi, TMSCl, TMEDA, THF, 0 °C, then 10% $KHSO_4$ (94%); v, 20 mol% TPAP, NMO, 4 Å molecular sieves, CH_2Cl_2, rt (77%), vi, TBAF, THF, rt (66%); vii, 20 mol% TPAP, NMO, 4 Å molecular sieves, CH_2Cl_2, rt (95%).

obtained as a single stereoisomer. It is well documented by Birch that cyclopentadienyl anions react in the middle position.[13]

In summary, the Hosomi–Sakurai type reaction of **3** and **12** possessing the diallylsilane moiety afforded the bicyclic compounds **5** and **13** under mild conditions. We thank Dr C. Kabuto, Instrumental Analysis Center, Faculty of Science, Tohoku University, for the X-ray analysis of **14**.

Notes and references

1 For review: G. I. George, T. T. Chen, I. Ojima and D. M. Vyas, *Taxane Anticancer Agents*, American Cancer Society, San Diego. 1995.

2 For a recent total synthesis: K. Morihara, R. Hara, S. Kawahara, T. Nishimori, N. Nakamura, H. Kusama and I. Kuwajima, *J. Am. Chem. Soc.*, 1998, **120**, 12980 and references therein.

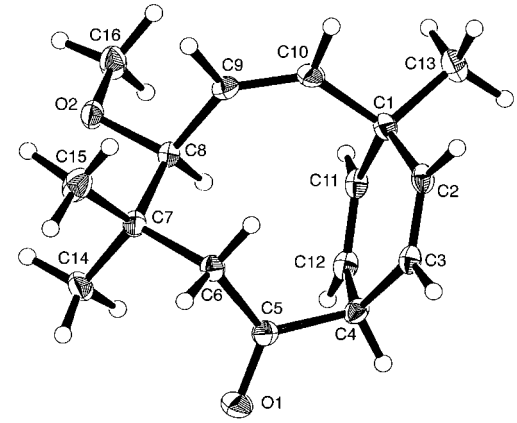

Fig. 1 Molecular structure of **14**.

3 (*a*) M. Ihara, S. Suzuki, Y. Tokunaga, H. Takeshita and K. Fukumoto, *Chem. Commun*., 1996, 1801; (*b*) M. Ihara, S. Suzuki, Y. Tokunaga and K. Fukumoto, *J. Chem. Soc*., *Perkin Trans. 1*, 1995, 2881.

4 A. Hosomi and H. Sakurai, *Tetrahedron Lett*., 1976, 1295.

5 G. Majetich, D. Lowery and V. Khetani, *Tetrahedron Lett*., 1990, **31**, 51.

6 S. V. Ley, J. Norman, W. P. Griffith and S. P Marsden, *Synthesis*, 1994, 639.

7 $EtAlCl_2$, $AlCl_3$, $SnCl_4$ and TBDMSOTf were also investigated in these reactions, however, neither **4** nor **5** was obtained.

8 *Selected data* for **5**: δ_H(300 MHz, $CDCl_3$) 1.17 (s, 3H), 1.35–1.59 (m, 4H), 1.84–1.99 (m, 2H), 2.90–3.01 (m, 1H), 3.11 (dt, *J* 4.8, 3.2, 1H), 3.79 (dd, *J* 8.8, 3.2, 1H), 5.25 (ddd, *J* 11.6, 9.2, 7.6, 1H), 5.31 (d, *J* 11.6 Hz), 5.71 (ddd, *J* 9.6, 5.2, 1.6 Hz), 5.81 (dd, *J* 9.6, 1.6 Hz), 5.83–5.92 (m, 2H); δ_C (75 MHz, $CDCl_3$) 137.3, 137.2, 136.0, 128.7, 126.0, 123.8, 77.6, 44.5, 40.0, 31.1, 29.6, 25.9, 25.6.

9 D. D. Sternbach and C. L. Ensinger, *J. Org. Chem*., 1990, **55**, 2725.

10 D. Seyferth, J. K. Heeren, G. Singh, S. O. Grim and W. B. Hughes, *J. Organomet. Chem*., 1966, **5**, 267; G. Stork and K. Zhao, *Tetrahedron Lett*., 1989, **30**, 2173.

11 *Selected data* for **13**: δ_H(300 MHz, $CDCl_3$): 0.79 (s, 3H), 0.93–0.99 (m, 4H), 1.21 (s, 3H), 1.40–1.60 (br s, 1H), 1.98 (dd, *J* 15.0, 8.8 Hz), 3.08–3.13 (m, 1H), 3.20 and 3.25 (each s, 2.8H and 0.2H), 3.99 (dd, *J* 8.8, 2.2 Hz), 4.67 (dd, *J* 9.2, 1.1 Hz), 5.09 (dd, *J* 12.5, 9.2 Hz), 5.52 (dd, *J* 12.5, 1.1 Hz), 5.70–5.90 (m, 4H); *m*/*z* 230 ($M^+ - 18$).

12 *Crystal data* for **14**: $C_{16}H_{22}O_2$, plates, mp 34–35 °C, triclinic, $P\bar{1}$, a = 7.641(1), b = 15.890(3), c = 6.3477(9) Å, α = 96.66(1), β = 109.31(1), γ = 99.48(1)°, V = 705.3(2) Å^3, Z = 2, μ = 0.75 cm^{-1}, D_c = 1.169 g cm^{-3}, $F000$ = 272, T = 150 K, R, Rw = 0.039, 0.038 for 2302 absorption–corrected reflections with $I > 3.10\ \sigma(I)$. CCDC 182/1220. see http://www.rsc.org/suppdata/cc/1999/893/ for crystallographic files in .cif format.

13 A. D. Birch, A. L. Hinde and L. Radom, *J. Am. Chem. Soc.*, 1981, **103**, 284 and references therein.

Communication 9/01392J

Photocatalytic oxidation of trichloroethylene using TiO_2 coated optical microfibers

Charles V. Rice and Daniel Raftery*

Department of Chemistry, H.C. Brown Laboratory, Purdue University, West Lafayette, Indiana 47907, USA. E-mail: raftery@chem.purdue.edu

Received (in Bloomington, IN, USA) 21st December 1998, Accepted 9th April 1999

TiO_2 particles have been attached to optical microfibers to allow the irradiation of the interior of a powdered photocatalyst, and the UV initiated photocatalytic oxidation of trichloroethylene was followed using ^{13}C solid-state NMR.

The photocatalytic activity and surface chemistry of TiO_2 is currently of significant interest owing to its use in light harvesting[1] and pollutant remediation applications.[2] Much is known about TiO_2 photocatalysis at the liquid/solid interface whereas the gas/solid interface is less well understood.[3] A variety of experimental techniques have been applied to study the surface photochemistry of TiO_2, including GC–MS,[4] IR[5] and XPS.[6] We have shown that solid-state nuclear magnetic resonance (SSNMR) spectroscopy can provide information about the identity and nature of surface-bound and gas-phase species during *in situ* photocatalytic reactions.[7] Owing to the light scattering characteristics of TiO_2, it is best to disperse the catalyst as a thin film to expose the particles in a homogeneous fashion. However, the outer portions of TiO_2 powders packed inside the SSNMR rotor will either scatter or absorb most of the incoming photons and create dark regions within the interior of the sample. Reactants in these dark regions will not participate in the photochemical reaction, producing long-lived species and complicating the interpretation of results. Our laboratory has previously circumvented this problem by supporting monolayer TiO_2 films on porous Vycor glass. This reduces scattering and can be successfully used to follow the photoreactions with SSNMR.[7] Here, we report a different approach which allows UV light to penetrate the interior of a powdered sample and creates an opportunity to use SSNMR to study the photocatalytic surface chemistry on TiO_2 powders.

TiO_2 powders can be supported on glass plates,[8] rods,[9] beads,[10] meshes[11] and large diameter optical fibers.[12] However, these supports are impractical for use in SSNMR experiments. Thus, we utilized microscopic quartz optical fibers to deliver the UV photons to the interior of the sample. The optical microfibers can be tightly packed inside the SSNMR rotor and the incident photons can be directed towards either the ends of the fibers or perpendicular to their long axis. The photochemical behavior of the coated fibers was evaluated by monitoring the conversion of trichloroethylene (TCE), an important environmental contaminant, into several intermediates and final products.

The quartz microfibers (Quartzel Fiber®, 9 μm diameter, Quartz Products Company) were supplied as a roving with each strand composed of 4800 individual fibers. Approximately 20 sections of the roving (each 15 cm long) were placed in a test tube (2.5 cm OD, 30 cm long) and calcined at 400 °C to remove the polyimide cladding. The fibers were allowed to cool, bound together at one end with copper wire and dipped into an aqueous suspension of TiO_2 similar to that used by Nazeeruddin *et al.*[13] The suspension was prepared by adding 4 ml of water to 10 g of TiO_2 powder (Degussa P-25, surface area 55 $m^2\ g^{-1}$, 70% anatase) in a ceramic mortar. A thick paste was formed by grinding the mixture and adding 800 μl of pentane-2,4-dione to promote dispersion of the particles. The paste was diluted by the slow addition of 16 ml of water while grinding. To allow the suspension to cover the fibers evenly, 200 μl of a detergent (Triton X-100, Aldrich) was added.

After dipping the fibers, they were heated at 500 °C for 30 min, cooled to room temperature and rinsed under flowing water to remove excess TiO_2. The dipcoating, heating, and rinsing procedure was repeated 2 additional times. It was found that the surface area of the coated fibers could be increased further by allowing the coated fibers to dry, then dipping them into a 20% solution of titanium isopropyl alcohol (Aldrich) in anhydrous isopropyl alcohol (Aldrich) and calcining at 500 °C for 3 h. After cooling, the fibers were rinsed a final time and dried. Assuming even coverage of the fibers, gravimetric analysis indicated that the TiO_2 layer is *ca.* 0.5 μm thick.

In a typical experiment, *ca.* 40 000 coated microfibers (estimated by weight) were gathered into a bundle and inserted into a Teflon tube (4.5 mm ID, Small Products Company). A 1 cm section of the fiber-filled tube was cut, held at the opening of a standard 5 mm NMR tube (Norell) and a glass rod used to push the fiber bundle into the bottom of the NMR tube. After attachment to a vacuum manifold, the fibers were calcined at 400 °C to remove any remaining organic material, cooled to room temperature and exposed to humid air for 12 h to rehydrate the surface. The NMR tube was reattached to the manifold and heated at 150 °C under vacuum (10^{-4} Torr) for 2 h to remove excess water. The tube was then cooled to 77 K for the addition of per-^{13}C trichloroethylene (Cambridge Isotopes) and oxygen. The sample was isolated from the manifold by flame sealing. The gas pressure of the reagents in the tube at room temperature is estimated to be 1–2 atm.

NMR analysis was performed on a 300 MHz Varian Unity Plus NMR spectrometer with a home built, double resonance optical magic angle spinning (MAS) probe which has been described previously.[7] A 300 W Xe arc lamp (ILC Technology) was used as the light source and a dichroic mirror (Oriel Corp.) was used to limit the light to 350–450 nm. Irradiation of the sample in the end-on configuration was performed outside the magnet while the side irradiation experiments were performed *in situ* as described previously.[7]

The proton decoupled ^{13}C MAS NMR spectra collected during the photocatalysis of 48 μmol of TCE in the presence of 96 μmol of O_2 are shown in Fig. 1. The sample was irradiated in the end-on configuration. Each spectrum represents an average of 256 transients obtained with a recycle time of 4 s. Spectra taken after various irradiation times show the formation and decomposition of reaction intermediates which have been identified by comparison with reported ^{13}C chemical shift data. As can be seen in the Fig. 1, dichloroacetyl chloride (DCAC, $Cl_2CHCOCl$, doublets at δ 70 and 167), dichloroacetic acid (Cl_2CHCO_2H, doublets at δ 63 and 167) oxalyl chloride (ClCOCOCl, δ159), phosgene (CCl_2O, adsorbed, δ143 and gas phase, δ 139), trichloroacetaldehyde (CCl_3CHO, doublets at δ 93 and 177) and carbon dioxide (δ 123) are formed during the reaction. The major products are phosgene and CO_2 with small quantities dichloroacetic acid and trichloroacetaldehyde remaining at the end of the reaction.

Although these results demonstrate the photocatalytic behavior of the coated optical fibers, the question as to whether the

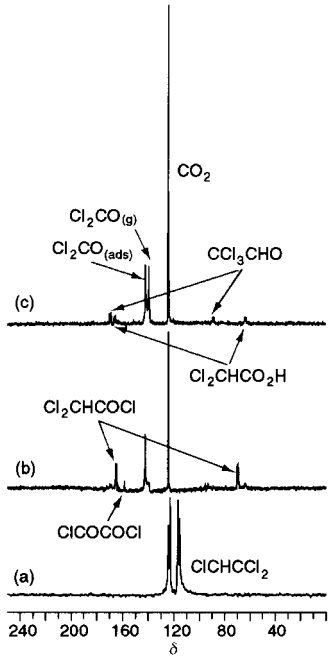

Fig. 1 Proton-decoupled ^{13}C MAS NMR spectra obtained during the photooxidation of 48 μmol of TCE and 96 μmol of O_2 on the TiO_2 coated optical fibers irradiated in the end-on configuration for (a) 0, (b) 30 and (c) 150 min. The spinning rate was 3 kHz.

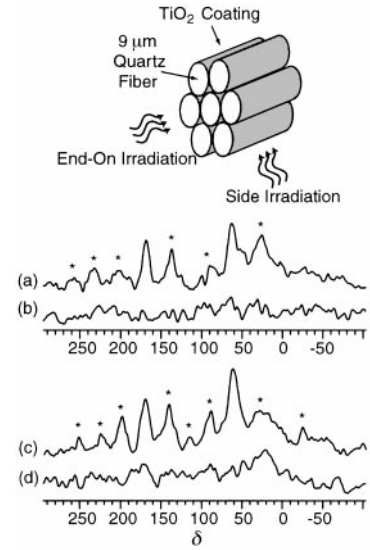

Fig. 2 ^{13}C proton-decoupled CP MAS spectra of chemisorbed dichloroacetate collected with ^{1}H–^{13}C cross polarization (contact time = 3 ms): (a) before end-on irradiation; (b) after end-on irradiation for 120 min; (c) before side irradiation; (d) after side irradiation for 150 min. The spinning rate was 3.0 kHz and asterisks denote spinning sidebands.

light is penetrating to the interior of the sample remained. This issue was explored by monitoring the formation and degradation of DCAC, which is known to chemisorb to the TiO_2 surface by reaction with hydroxyl groups to form dichloroacetate. The degradation of dichloroacetate requires additional UV photons, and thus its persistance under continued irradiation indicates the presence of dark regions within the sample.[7] In the case of the TiO_2-coated optical fibers, the concentration of dichloroacetate was maximized by stopping the photocatalysis of TCE after 30 min (when the DCAC concentration was highest) and storing the sample in the dark for several days to allow the DCAC to react with the surface hydroxyl groups. The sample was then broken open and evacuated to remove all non-surface bound species. Oxygen was reintroduced and the sample flame sealed. Fig. 2 shows the ^{13}C NMR spectrum taken using cross polarization (CP) and MAS conditions. Surface bound dichloroacetate has two isotropic peaks (δ 64 and 177) as well as a number of spinning sidebands. Subsequent irradiation of this sample in the end-on configuration shows the loss of the acetate signal [Fig. 2(b)] indicating that light is indeed reaching the interior of the sample. The experiment was repeated with the light directed towards the side of the sample and the degradation of the acetate [Fig. 2(c), (d)] was also observed, although the rate was slower. At this time, the mechanism for light transmission to the interior of the sample is not known. It is likely that the photons propagate down the microfibers, and that side irradiation is successful because the TiO_2 layer is not thick enough to absorb all of the photons.[14] Alternatively, it may be that the coated microfibers are able to create void spaces within the powder allowing the light to propagate between the particles which may also explain the success of side irradiation. Future experiments are planned to explore this issue further.

In summary, we have demonstrated that supporting TiO_2 powders on optical microfibers decreases light scattering, permitting study of the surface photochemistry with SSNMR. Efforts are currently underway to expand this methodology to other photochemical systems where light scattering is problematic, such as zeolite photochemistry.[15]

This work was supported by the National Science Foundation (CHE 97-33188 CAREER Award), the Petroleum Research Fund administered by the American Chemical Society and the AT&T/Lucent Technologies Industrial Ecology Program. C. V. R. thanks the Purdue Research Foundation for a fellowship.

Notes and references

1 U. Bach, D. Lupo, P. Comte, J. E. Moser, F. Weissortel, J. Salbeck, H. Spreitzer and M. Gratzel, *Nature*, 1998, **395**, 583; J. Hagen, W. Schaffrath, P. Otschik, R. Fink, A. Bacher, H. W. Schmidt and D. Haarer, *Synth. Met.*, 1997, **89**, 215; B. O'Regan and M. Gratzel, *Nature*, 1991, **353**, 737.
2 D. F. Ollis, E. Pelizzeti and N. Serpone, *Photocatalysis Fundamentals and Applications*, John Wiley and Sons, New York, 1989.
3 M. A. Fox and M. T. Dulay, *Chem. Rev.*, 1993, **93**, 341; A. L. Linsebigler, G. Lu and J. T. Yates Jr., *Chem. Rev.*, 1995, **95**, 735; A. Hagfeldt and M. Gratzel, *Chem. Rev.*, 1995, **95**, 49; M. R. Hoffmann, S. T. Martin, W. Choi and D. W. Bahnemann, *Chem. Rev.*, 1995, **95**, 69.
4 M. R. Nimlos, W. A. Jacoby, D. M. Blake and T. A. Milne, *Environ. Sci. Technol.*, 1993, **27**, 732; Y. Luo and D. F. Ollis, *J. Catal.*, 1996, **163**, 1.
5 J. Fan and J. T. Yates Jr., *J. Am. Chem. Soc.*, 1996, **118**, 4686; M. D. Driessen, A. L. Goodman, T. M. Miller, G. A. Zaharias and V. H. Grassian, *J. Phys. Chem. B.*, 1998, **102**, 549.
6 S. A. Larson and J. L. Falconer, *Appl. Catal. B: Environ.*, 1994, **4**, 325.
7 S.-J. Hwang, C. Petucci and D. Raftery, *J. Am. Chem. Soc.*, 1997, **119**, 7877; 1998, **120**, 4388; S.-J. Hwang and D. Raftery, *Catal. Today*, 1999, **49**, 353.
8 H. Tada and M. Tanaka, *Langmuir*, 1997, **13**, 360; P. Wyness, J. F. Klausner, D. Y. Goswami and K. S. Schanze, *J. Sol. Energy Eng.*, 1994, **116**, 2.
9 K. Hofstadler, R. Bauer, S. Novalic and G. Heisler, *Environ. Sci. Technol.*, 1994, **28**, 670.
10 H. Al-Ekabi and N. Serpone, *J. Phys. Chem.*, 1988, **92**, 5726.
11 C. Shifu, Z. Mengyue and T. Yaowu, *Microchem. J.*, 1996, **54**, 54; V. Brezova, A. Blazkova, L. Karpinsky, J. Groskova, B. Havlinova, V. Jorik and M. Ceppan, *J. Photochem. Photobiol. A*, 1997, **109**, 177.
12 N. J. Peill and M. R. Hoffmann, *Environ. Sci. Technol.*, 1995, **29**, 2974; N. J. Peill and M. R. Hoffmann, *Environ. Sci. Technol.*, 1996, **30**, 2806; N. J. Peill and M. R. Hoffman, *J. Sol. Energy Eng.* 1997, **119**, 229.
13 M. K. Nazeeruddin, A. Kay, I. Rodicio, R. Humphry-Baker, E. Muller, P. Liska, N. Vlachopoulos and M. Gratzel, *J. Am. Chem. Soc.*, 1993, **115**, 6382.
14 H. Tada and H. Honda, *J. Electrochem. Soc.*, 1995, **142**, 3438.
15 N. J. Turro, A. L. Buchachenko and V. F. Tarasov, *Acc. Chem. Res.*, 1995, **28**, 69.

Communication 8/09770G

Polar crystals with one-dimensional arrays from achiral components: crystal structures of 2 : 2 complexes of dibenzo-18-crown-6–imidazolium and pyrazolium perchlorates

Sari Kiviniemi,[a] Atte Sillanpää,[a] Maija Nissinen,[b] Kari Rissanen,*[b] Markku T. Lämsä[a] and Jouni Pursiainen*[a]

[a] *Department of Chemistry, University of Oulo, PO Box 3000, FIN-90401 Oulu, Finland. E-mail: jouni.pursiainen@oulu.fi*
[b] *Department of Chemistry, University of Jyväskylä, PO Box 35, FIN-40351 Jyväskylä, Finland. E-mail: kari.rissanen@jyu.fi*

Received (in Cambridge, UK) 15th March 1999, Accepted 12th April 1999

Biologically important planar five-ring aromatic bases as their imidazolium and pyrazolium cations form crystalline 2 : 2 complexes with dibenzo-18-crown-6, creating one-dimensional arrays in a polar crystal lattice.

Supramolecular complexation, where the main binding force is π-stacking or charge-transfer interaction between two aromatic units, has recently attracted increasing attention.[1] These interactions have been utilised for example in the preparation of catenanes and rotaxanes and their precursor complexes.[2] Carbocations such as tropylium ion also form supramolecular complexes, where the charge-transfer interaction is the dominant binding force.[3] The biologically important nitrogen-containing heterocycle imidazole and its isomer pyrazole form planar five-membered organic cations when treated with the proper acid. The cations are bis-functional and can interact with crown ether type host structures both by hydrogen bonding to the ether oxygen atoms and/or by charge-transfer interactions to the electron rich phenyl rings of the crown ether.[4] In this work we have prepared and characterised such complexes and found out that dibenzo-18-crown-6 (DB18C6) complexes form polar crystal lattices with very interesting structural features.

The DB18C6·imidazolium complex **6**† is much more stable (NMR titration in CD_3CN solution, Table 1) than the corresponding π–π tropylium complex (5.6 dm^3 mol^{-1}),[3] indicating additional H-bonding in the former compound. For the imidazolium perchlorate the highest stability constant was measured for 18-crown-6 (18C6) owing to the H-bonding to the ether oxygen atoms. The stability constants for the benzo and dibenzo crown ethers were, however, nearly 50% lower. This implies a competing complexation behaviour between H-bonding and π-stacking/charge-transfer interactions for the imidazolium complex. The stability constant of DB24C8 was close to the corresponding value of tropylium cation[3] (10.2 dm^3 mol^{-1}) and manifests complexation predominantly *via* π–π interactions. The aromatic ring in the crown ether decreases electron density in the adjacent oxygen atoms, which seems to result in higher stability of the 18C6·imidazolium complex. The stability constant of the DB18C6·pyrazolium complex **7** is much higher than that for the DB18C6·imidazolium complex. This can be rationalised by the suitable stereochemistry of two simultaneously-acting intracomplex (Scheme 1) hydrogen bonds.

Table 1 Stability constants and limiting shifts for the interaction of crown ethers with imidazolium and pyrazolium ions in CD_3CN at 303 K

Host	K_a/dm^3 mol^{-1}	$\Delta\delta_C$/ppm	$r^{2\,a}$
Imidazolium perchlorate			
DB24C8	8 ± 1	0.36 ± 0.04	0.993
DB18C6	27 ± 5	0.50 ± 0.06	0.977
B18C6	25 ± 1	0.62 ± 0.01	0.999
18C6	40 ± 1	0.563 ± 0.004	0.999
Pyrazolium perchlorate			
DB18C6	113 ± 6	0.197 ± 0.003 (H-3,5)	0.995
	65 ± 1	0.463 ± 0.004 (H-4)	0.999

[a] Regression correlation for Benesi–Hildebrandt plot.

In the crystalline state,‡ however, the structures of **6** and **7** are surprisingly similar. In both cases the complexes crystallised out in an acentric monoclinic space group (*Cc*) due to a spontaneous resolution. The crown ether offers two interaction sites, a structurally minor site that is formed by the OCH_2CH_2O chains of the crown and a structurally major site situated between the phenyl rings. These two sites, both capable of inclusion of a planar guest, have a 90° angle towards each other and are facing opposite directions (Fig. 1). The simultaneous inclusion of a guest into the both sites during the packing creates a one-dimensional array of host–guest complexes with a 90° turn between the adjacent DB18C6 molecules.

Although formally complexes are 1 : 1 complexes in solution, the crystal packing can only be described as a 2 : 2 complex. The

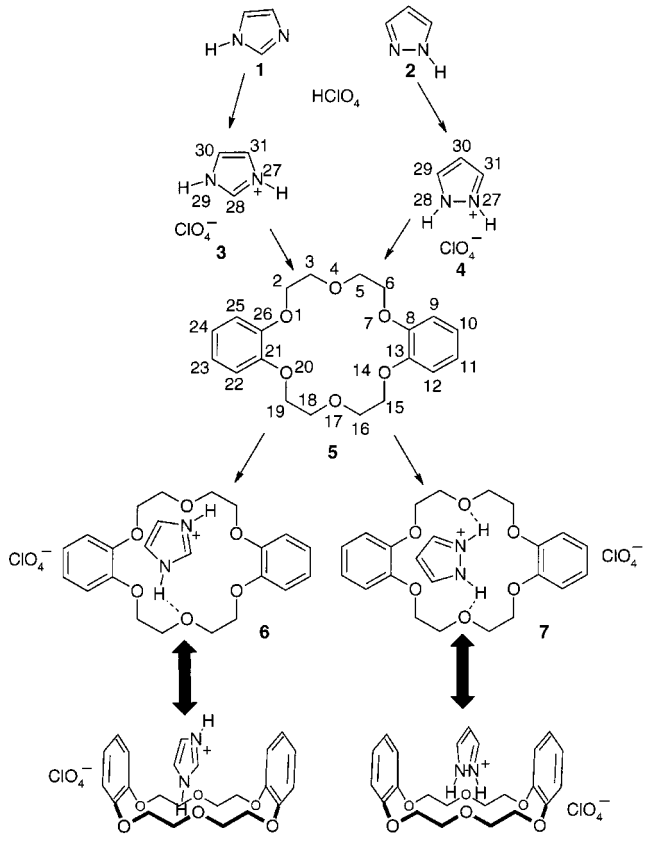

Scheme 1

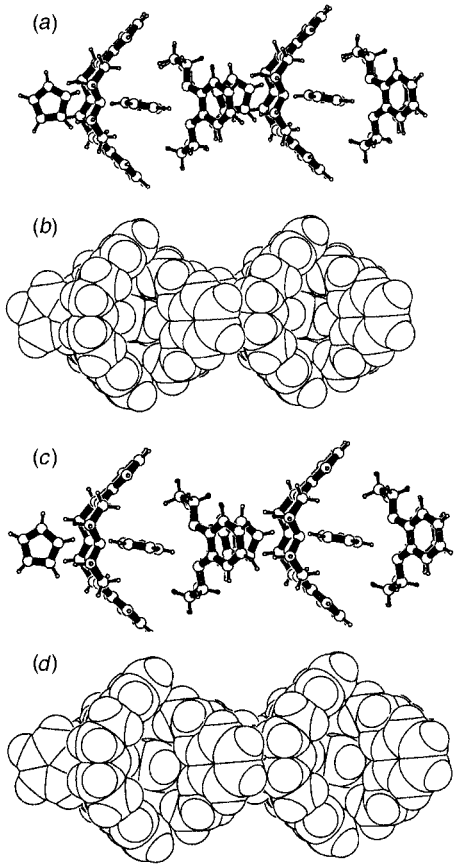

Fig. 1 PLATON (ref. 8) plot for the packing of complexes **6** and **7** into one-dimensional arrays. Four adjacent complexes are shown as ball-and-stick and VDW presentations: (*a*) and (*b*) for **6** and (*c*) and (*d*) for **7**.

polarity of the crystal is caused by the interaction of the adjacent one-dimensional arrays. The arrays all pack in the same direction, thus creating a polar axis in the crystal lattice. The existence of the H-bonding and the weak charge transfer interaction is evident for both structures. The imidazolium cation in **6** has one intracomplex H-bond to the major site of its host [N27···O4 = 2.823(7), H27···O4 = 1.99(9) Å and angle 148(7)°] and two weaker intercomplex H-bonds to the minor site of the adjacent host [N29···O1′ = 3.022(7), H27···O1′ = 2.28(8) Å and angle 132(6)°; N29···O20′ = 3.048(7), H27···O20′ = 2.19(8) Å and angle 144(6)°]. The distance between the centroids of the cation and the nearest phenyl ring is 4.12(1) Å, indicating a weak charge-transfer interaction. The pyrazolium cation in **7** is more strongly bound into the major site of its host by two H-bonds [N27···O17 = 2.71(1), H27···O17 = 1.88 Å and angle 155(1)°; N28···O4 = 2.79(1), H28···O14 = 1.91(12) Å and angle 174(1)°]. The charge-transfer interaction is similar to that in complex **6** [distance between closest centroids is 4.04(1) Å]. The interaction in complex **7** to the minor site of the adjacent host is much weaker (H···O′ distances vary from 2.59 to 3.45 Å) than in the case of complex **6**. The adjacent guests inside the arrays of **6** and **7** are surprising close to each other, the non-bonded contact distance between the closest adjacent H-atoms are 2.82 Å for **6** (H31···H29′) and 2.83 and 2.96 Å for **7** (H30···H27′ and H30···H28′, respectively).

The structures presented here are interesting from the crystal engineering[5] and supramolecular technology[6] points of view. This type of tightly packed one-dimensional molecular arry could form a matrix for (photo)chemical reactions leading to advanced molecular wires and similar new materials. The close proximity of the guests inside the array is a feature not frequently encountered in crystal lattices and could, with the use of larger crown ethers and functionalised guests, lead to new tailor-made polymers or polyrotaxanes.

Notes and references

† *Synthesis and characterisation*: The imidazolium and pyrazolium salts were prepared according to a published procedure (ref. 7). The complexes were prepared by mixing equimolar amounts of the above salt and DB18C6 MeCN solutions. The complexes **6** and **7** precipitated soon after mixing of the components or after addition of anhydrous Et_2O.

Selected data for **6**: 54%, mp 215–220 °C; *m/z* (FAB, NBA matrix) 429 [DB18C6·$C_3N_2H_5$ − ClO_4]$^+$; δ_H(200 MHz, CD_3CN, 25 °C) 3.8 (m, OCH_2, 8H), 4.1 (m, OCH_2, 8H), 6.9 (s, aryl, 8H) 7.4 (d, imidazolium, 2H), 8.8 (t, imidazolium, 1H) ($C_{23}N_2H_{29}ClO_{10}$ (528.93): calc. C, 52.23; H, 5.53; N, 5.30; found C, 52.70; H, 5.50; N, 5.31%). For **7**: 62%, mp 210–215 °C; *m/z* (FAB, NBA matrix) 429 [DB18C6·$C_3N_2H_5$ − ClO_4]$^+$; δ_H(200 MHz, CD_3CN, 25 °C) 3.9 (m, OCH_2, 8H), 4.1 (m, OCH_2, 8H), 6.6 (t, pyrazolium, 1H), 6.9 (s, aryl, 8H), 8.1 (d, pyrazolium, 2H) ($C_{23}N_2H_{29}ClO_{10}$ (528.93): calc. C, 52.23; H, 5.53; N, 5.30; found C, 52.14; H, 5.10; N, 5.36%).

‡ The data were recorded with Enraf-Nonius CAD4 (**6**) or Kappa CCD (**7**) diffractometers using graphite monochromatised Mo-Kα radiation [λ(Mo-Kα) = 0.71073 Å]. The data was processed with Denzo-SMN ver. 0.93.0 (Z. Otwinowski and W. Minor, *Processing of X-ray Diffraction Data Collected in Oscillation Mode*, in *Methods in Enzymology, Vol. 276, Macromolecular Crystallography, Part A*, ed. C. W. Carter, Jr. and R. M. Sweet, Academic Press, 1997, pp. 307–326). The structures were solved by direct methods [SHELXS-97 (G. M. Sheldrick, *Acta Crystallogr.*, 1990, **A46**, 467] and refinements, based on F^2, were made by full-matrix least-squares techniques [SHELXL-97 (G. M. Sheldrick, SHELXL-97—A program for crystal structure refinement, 1997, University of Göettingen, Germany)]. H-atoms calculated and refined as riding atoms, absolute structure could not be reliably determined. *Crystal data* for **6**: colourless, 0.20 × 0.20 × 0.40 mm, $C_2H_{24}O_6{\cdot}C_3H_5N_2{}^+ClO_4{}^-$, from MeCN, M_r = 528.93, monoclinic, space group *Cc* (no. 9), a = 17.802(4), b = 14.225(4), c = 12.199(3) Å, β = 129.34(2)°, V = 2394(1) Å^3, F(000) = 1112, T = 173.0 ± 0.1 K, Z = 4, D_c = 1.467 g cm^{-3}, 2184 reflections were recorded in the range 2.06 ⩽ θ ⩽ 24.97° (h: 0 → 21, k: 0 → 16, l: −14 → 11). Reflections were corrected for Lorentz polarisation effects and the ψ-scan method was used for absorption correction [μ(Mo-Kα) = 0.221 mm^{-1}, maximum transmission 0.9571 and minimum transmission 0.9167]. The final residuals were $R1$ = 0.0433 and $wR2$ = 0.1201 for 1887 unique data with $I > 2\sigma(I)$ and $R1$ = 0.0596, $wR2$ = 0.1259 for all data and for 325 parameters: $w = 1/[\sigma^2(F_o^2) + (0.0405P)^2 + 7.62P]$, where P [Max (F_o^2, 0) + 2 F_c^2]/3 and GooF = 1.193. The final difference map displayed no electron density higher than 0.24 e Å^{-3}. For **7**: colourless, 0.15 × 0.20 × 0.45 mm, $C_{20}H_{24}O_6{\cdot}C_3H_5N_2{}^+ClO_4{}^-$, from MeCN, M_r = 528.93, monoclinic, space group *Cc* (no. 9), a = 17.804(1), b = 14.131(1), c = 12.317(1) Å, β = 129.00(1)°, V = 2408.1(3) Å^3, F(000) = 1112, T = 173.0 ± 0.1 K, Z = 4, D_c = 1.459 g cm^{-3}, 2828 reflections were recorded in the range 2.94 ⩽ θ ⩽ 27.87° (h: 0 → 23, k: 0 → 18, 1: −16 → 12). Reflections were corrected for Lorentz polarisation effects and no absorption correction was applied. [μ(Mo-Kα) = 0.220 mm^{-1}). The final residuals were $R1$ = 0.0887 and $wR2$ = 0.2290 for 1953 unique data with $I > 2\sigma(I)$ and $R1$ = 0.1319, $wR2$ = 0.2536 for all data and for 326 parameters: $w = 1/[\sigma^2(F_o^2) + (0.0588P)^2 + 10.71P]$ where P = [Max (F_o^2, 0) + 2F_c^2]/3 and GooF = 1.125. The final difference map displayed no electron density higher than 0.78 e Å^{-3}. CCDC 182/1221. See http://www.rsc.org/suppdata/cc/1999/897/ for crystallographic files in .cif format.

1 J. C. Ma and D. A. Dougherty, *Chem. Rev.*, 1997, **97**, 1303.
2 D. B. Amabilino, F. M. Raymo and J. F. Stoddart, *Comprehensive Supramolecular Chemistry*, ed. J. L. Atwood, J. E. D. Davies, D. D. MacNicol and F. Vögtle, Elsevier, Amsterdam, 1996, vol. 9, pp. 86–127.
3 M. Lämsä, T. Suorsa, J. Pursianen, J. Huuskonen and K. Rissanen, *Chem. Commun.*, 1996, 14 443; M. Lämsä, J. Pursianen, K. Rissanen and J. Huuskonen, *Acta Chem. Scand.*, 1998, **52**, 563.
4 B. Stolwijk, E. J. R. Sudhölter, D.N. Reinhoudt, J. van Eerden and S. Harkema, *J. Org. Chem.*, 1989, **54**, 1000; J. Rebek, B. Askew, M. Killoran, D. Nemeth and F.-T. Lin, *J. Am. Chem. Soc.*, 1987, **109**, 2426.
5 *Comprehensive Supramolecular Chemistry*, ed. J. L. Atwood, J. E. D. Davies, D. D. MacNicol and F. Vögtle, Elsevier, Amsterdam, 1996, vol. 6.
6 *Comprehensive Supramolecular Chemistry*, ed. J. L. Atwood, J. E. D. Davies, D. D. MacNicol and F. Vögtle, Elsevier, Amsterdam, 1996, vol. 9.
7 A. R. Katritzky, Yu-Kun Yang, B. Gabrielsen and J. Marquet, *J. Chem. Soc., Perkin Trans. 2*, 1984, 857.
8 PLATON, A Multipurpose Crystallographic Tool, A. L. Spek, Utrecht University, Utrecht, The Netherlands, 1998.

Communication 9/02014D

ChemComm

Solid-state electrogenerated chemiluminescence in sol–gel derived monoliths

Maryanne M. Collinson* and Skylar A. Martin†

Department of Chemistry, 111 Willard Hall, Kansas State University, Manhattan, KS 66506-3701, USA. E-mail: mmc@ksu.edu

Received (in Bloomington, IN, USA) 11th February 1999, Accepted 29th March 1999

Stable solid-state electrogenerated chemiluminescence has been achieved by trapping the chemiluminescent precursors, ruthenium(II) tris(bipyridine) and tripropylamine, in a porous silicate host matrix prepared by the sol–gel process and exciting them electrochemically *via* an immobilized microelectrode assembly.

The development of new technology and methods for the fabrication of large area emissive panels and displays with low operating voltages is important in the electro-optics industry. Conjugated polymers (*i.e.* the organic semiconductors) have received considerable attention due to the ease at which they can be prepared, processed, and modified.[1–2] To a lesser extent, electrogenerated chemiluminescence[3] (ECL) based materials have also been investigated. These materials hold considerable promise because the ECL can be generated with relatively low voltage bias and with reasonably high efficiency.

To date, several approaches to solid-state ECL have been investigated. Abruna and Bard initially showed in the 1980s that ECL can be observed from electropolymerized films of $Ru(vbpy)_3^{2+}$ (vbpy = 4-vinyl-4′-methyl-2,2′ bipyridyl) on platinum electrodes in acetonitrile *via* sequential oxidation and reduction of the immobilized redox centers.[4] Similar results have also since been observed with chemiluminescence or conjugated polymers prepared from diphenylanthracene and polyphenylenevinylene derivatives.[5,6] More recently, solid-state ECL has been observed from poly$[RuL_3]^{2+}$ (L = vbpy or ester substituted bipyridine) films prepared on interdigitated array electrodes or in a sandwich type arrangement.[7,8] Light emission results from the reaction between RuL_3^{+} and the RuL_3^{3+} states formed *via* independent control of the potentials of the closely spaced electrodes.[7,8] When fixed concentration gradients are established in the film, the system gives rise to ECL in the *absence of solvent*.[7,8] In related work, Rubner and coworkers have also noted solid-state ECL from ruthenium derivatives trapped in an ionic polymer or bound to the polymer framework and sandwiched between two electrodes.[9]

In this work, an entirely different approach has been taken to generate ECL in the absence of solution. Ruthenium(II) tris(bipyridine) [$Ru(bpy)_3^{2+}$] and tripropylamine (TPA) have been encapsulated, along with a microelectrode assembly, in a porous, solid host prepared *via* the sol–gel approach.[10,11] This ECL system was chosen because it allows the luminescence to be generated at a relatively *low* potential bias in an *aqueous* environment.[12,13] The known immunity of the $Ru(bpy)_3^{2+}$–TPA system to water will likely improve the long term stability of the ECL. In this system, emission results when the TPA amine radical formed upon reduction of $Ru(bpy)_3^{3+}$ or *via* direct electrode oxidation reacts with another $Ru(bpy)_3^{2+}$ or additional $Ru(bpy)_3^{3+}$ to form $[Ru(bpy)_3^{2+}]^*$ which then decays to produce orange emission centered at 610 nm.[12,13] The original $Ru(bpy)_3^{2+}$ species is regenerated during the reaction, albeit with consumption of TPA.[12,13] In contrast to previous studies[4–7,9] where the ECL decayed on the timescale of seconds to tens of minutes and often required an inert atmosphere, this approach yields stable emission for over *two hours* under room conditions.

† Current address: Department of Chemistry, Truman State University, Kirksville, Missouri 63501, USA.

In these experiments, the silica sol was prepared by mixing tetramethoxysilane (Aldrich, 98%) with water and 0.1 M hydrochloric acid followed by rapid stirring for at least 2 h. The hydrolyzed sol was doped with $[Ru(bpy)_3]Cl_2$ (Aldrich) and stirred for 45–90 min. A 2 mL aliquot of the doped sol was pipetted in a silanized glass vial[14] housing the microelectrode assembly.[15] 1 mL of TPA (Aldrich, 99%) in pH 7.0, 0.1 M phosphate buffer was then added to the sol and the resultant solution quickly mixed. The gel was aged for 2–3 days and dried for 1–2 days at a relative humidity of 60–70% by exposing a small hole (*ca.* 2 mm diameter.) in the cap to the atmosphere. Very little shrinkage ($< 10\%$) in volume was observed. The solid-state electrochemical cell was placed in a dark box *ca.* 3.5 cm from the photocathode of a Hammamatsu 4632 photomultiplier tube and the data collected with a multichannel scaler (photon counter, EGG Ortec T-914). Either a Pine AFRDE5 bipotentiostat or a BAS 100 potentiostat was used to apply the excitation waveform (linear sweep or potential step).

Fig. 1(a) shows cyclic voltammograms (CVs) of gel-encapsulated $Ru(bpy)_3^{2+}$ at a 13 μm radius Pt ultramicroelectrode acquired at 10 mV s^{-1} (solid line). In the absence of TPA, the voltammograms are steady state in nature and superimposed on a relatively large rising background from solvent oxidation. As the sweep rate is increased (up to 10 V s^{-1}), the

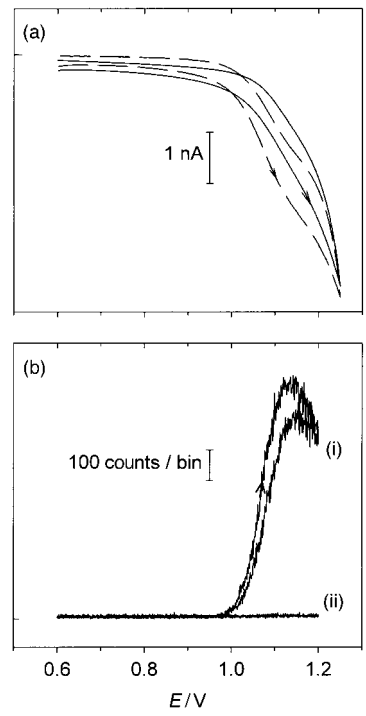

Fig. 1 (a) Cyclic voltammograms of gel-encapsulated $Ru(bpy)_3^{2+}$ (solid line) and gel encapsulated $Ru(bpy)_3^{2+}$ and TPA (dashed line) at a 13 μm radius Pt microdisk electrode. Scan rate: 10 mV s^{-1}. (b) Corresponding intensity–potential curves for gel-encapsulated $Ru(bpy)_3^{2+}$ (i) and gel-encapsulated $Ru(bpy)_3^{2+}$ + TPA (ii). Precursor concentrations in the sol: 10 mM $Ru(bpy)_3^{2+}$ or 10 mM $Ru(bpy)_3^{2+}$ + 10 mM TPA. Bin size = 100 ms.

voltammograms become more peak shaped in appearance due to the onset of planar diffusion (data not shown).[16,17] A half-wave potential ($E_{1/2}$) of *ca.* 1.1 V was estimated from the voltammograms acquired at 100–1000 mV s^{-1}. This value is consistent with that previously measured for both solution and gel-encapsulated $Ru(bpy)_3^{2+}$.[18] In the presence of TPA, the oxidation current for gel-entrapped $Ru(bpy)_3^{2+}$ increases consistent with the oxidative–reduction mechanism for $Ru(bpy)_3^{2+}$ ECL [Fig. 1(a)], dashed line). The relatively facile nature at which gel-entrapped $Ru(bpy)_3^{2+}$ and TPA can diffuse in the gel and be oxidized at the electrode surface is evident in the shapes of the voltammograms acquired at 10–1000 mV s^{-1} and the resultant luminescence. Although the gel is macroscopically rigid, it is microscopically porous and hydrated.[19,20] Prior work has shown the diffusion coefficients of redox molecules trapped with these solids during the initial stages of drying to be nearly identical to values measured in solution (10^{-6} cm^2 s^{-1}).[19,20]

Corresponding ECL-potential curves for these materials are shown in Fig. 1(b). In the absence of either TPA or $Ru(bpy)_3^{2+}$, no significant ECL emission can be observed at the Pt microdisk electrode. Only when both reagents are present can the ECL be observed. The onset of luminescence is contiguous with the oxidation of gel-encapsulated $Ru(bpy)_3^{2+}$ and TPA and peaks near 1.15 V. It is not fully understood at the present time why the ECL intensity becomes lower as the electrode potential is scanned significantly past $E_{1/2}$, but it may be related to quenching, solvent oxidation products or concentration polarization.

The long term stability of the ECL at the ultramicroelectrode was evaluated by repetitively cycling the electrode potential for > 30 min and also by stepping the electrode potential to a near diffusion controlled value for 2 h. The results are shown in Fig. 2. As can be seen, the light intensity is remarkably stable upon repetitive potential cycling at 10 mV s^{-1}. The ECL is typically *ca.* 5–20% lower on the first potential scan relative to subsequent cycles where near constant emission is observed. Fig. 2(b) shows the ECL emission at a 13-μm Pt microdisk electrode following a potential step from 0.6 to 1.15 V. The luminescence increases nearly immediately upon application of the potential step where it then remains at a near constant level for the duration of the experiment. Typically, < 15% drop in intensity is observed over 2 h.

The enhanced stability of the ECL can be attributed not only to the small size of the electrode which results in a decreased consumption of TPA, but also to the steady state or quasi-steady state flux of reagents to the electrode surface.[16,17] For an ultramicroelectrode, the dimensions of the diffusion layer greatly exceed that of the electrode in a relatively short period of time (*e.g.* seconds).[16,17] Because a greater population of TPA molecules are then able to diffuse to the electrode from the increased volume around the electrode, steady state is reached quickly.[16,17] Since the electrode area is very small (10^{-6} cm^2), very little TPA is consumed during the experiment (*i.e.* theoretically calculated to be ≪0.01% for a 2 h time period). Similar results were also observed using microband electrodes.

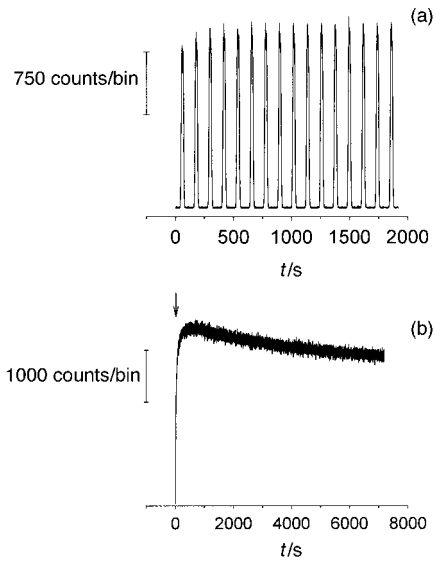

Fig. 2 Intensity–time transients during 16 repetitive potential cycles from 0.6 to 1.2 V at 10 mV s^{-1} (a) and following a potential step from 0.6 to 1.15 V (b) for gel-encapsulated $Ru(bpy)_3^{2+}$ + tripropylamine at a 13-μm radius Pt microdisk electrode. Precursor concentration in the sol: 10 mM $Ru(bpy)_3^{2+}$ + 5 mM tripropylamine. Bin size: 0.2 s (a) and 1 s (b).

In summary, the use of ultramicroelectrodes for the generation of ECL reagents in a solid host results in remarkably stable light emission under room conditions. At a microdisk electrode, the ECL remains at a near constant level upon application of a relatively low potential for time periods in excess of 2 h. One of the most promising aspects of this work is that it provides a relatively simple approach for the generation of light without the use of excess solvent, flowing streams, stringent solution conditions, or inert atmosphere. Different emission wavelengths can likely be achieved through variations in the gel-encapsulated precursor molecules. Likewise, optimization of precursor concentrations, the porosity of the host, and the electrode geometry and size, should result in greater emission intensities. Future work will be directed toward these investigations.

We gratefully acknowledge support of this work by the National Science Foundation through the NSF CAREER Award Program (CHE-9624813) and the Research Experiences for Undergraduates Program (CHE-9732103). We also like to thank Dr Rajendra Makote for useful discussions concerning the experiments and Dr Jon Howell from BAS for the trigger output modification to the BAS 100.

Notes and references

1 P. L. Burns, A. B. Holmes, A. Kraft, D. D. C. Bradley, A. R. Brown, R. H. Friend and R. W Gymer, *Nature*, 1992, **356**, 47.
2 Z. Bao, Z. Peng, M. E. Galvin and E. A Chandross, *Chem. Mater*, 1998, **10**, 1201.
3 L. R. Faulkner and A. J. Bard, in *Electroanalytical Chemistry*, ed. A. J. Bard, Marcel Dekker, New York, 1977, vol 10, pp. 1–95.
4 H. D. Abruna and A. J. Bard, *J. Am. Chem. Soc.*, 1982, **104**, 2641.
5 M. M. Richter, F.-R. F. Fan, F. Klavetter, A. J. Heeger and A. J. Bard, *Chem. Phys. Lett.*, 1994, **226**, 115.
6 F.-R. F. Fan, A. Mau and A. J. Bard, *Chem. Phys. Lett.*, 1985, **116**, 400.
7 K. M. Maness, R. H. Terrill, T. J. Meyer, R. W. Murray and R. M Wightman, *J. Am. Chem. Soc.*, 1996, **118**, 10 609.
8 C. M. Elliott, F. Pichot, C. J. Bloom and L. S. Rider, *J. Am. Chem. Soc.*, 1998, **120**, 6781.
9 (a) A. Wu, J. Lee and M. F. Rubner, *Thin Solid Films*, 1998, **327**–**329**, 663; (b) C. H. Lyons, E. D. Abbas, J.-K. Lee and M. F. Rubner, *J. Am. Chem. Soc*. 1998, **120**, 12100.
10 D. Avnir, *Acc. Chem. Res.*, 1995, **28**, 328.
11 J. Brinker and G. Scherer, *Sol–Gel Science*, Academic Press, New York, 1989.
12 W.-Y. Lee, *Mikrochim. Acta*, 1997, **127**, 19.
13 J. K. Leland and M. J Powell, *J. Electrochem. Soc.*, 1990, **137**, 3127.
14 The glass vials were silanized with chlorotrimethylsilane.
15 The microelectrode assembly consisted of a working electrode (*i.e.* a Pt microwire sealed in glass) and a reference electrode (silver chloride coated silver wire) sealed in a Nylon cap.
16 C. Amatore, in *Physical Electrochemistry, Principles, Methods, and Applications*, ed. I. Rubinstein, Marcel Dekker, Inc, New York, 1995, pp. 131–208.
17 R. M. Wightman and D. O Wipf, *Electroanalytical Chemistry*, ed. A. J. Bard, Marcel Dekker, New York, 1989, vol 15.
18 M. M. Collinson, C. G. Rausch and A. Voigt, *Langmuir*, 1997, **13**, 7245 and references therein.
19 M. M. Collinson, P. Zambrano, H. Wang and J. Taussig, *Langmuir*, 1998, **15**, 662.
20 P. Audebert, P. Griesmar, P. Hapiot and C. Sanchez, *J. Mater. Chem.*, 1992, **2**, 1293.

Communication 9/01185D

Bis(phospha-adamantyl)alkanes: a new class of very bulky diphosphines

Victoria Gee, A. Guy Orpen, Hirihattaya Phetmung, Paul G. Pringle* and Robert I. Pugh

School of Chemistry, University of Bristol, Cantock's Close, Bristol, UK BS8 1TS. E-mail: paul.pringle@bristol.ac.uk

Received (in Cambridge, UK) 26th March 1999, Accepted 12th April 1999

Adamantane-like cages are formed when $H_2P(CH_2)_nPH_2$ (n = 2 or 3) react with acetylacetone or trifluoroacetylacetone and the crystal structures of the dichloropalladium(II) complexes of the C_3-diphosphine ligands show that their cone angles are much larger than $Bu^t_2P(CH_2)_3PBu^t_2$; a diphospha-adamantane derived from o-$C_6H_4(PH_2)_2$ is also described.

Bulky alkyl diphosphines of the type $R_2P(CH_2)_nPR_2$, (n = 1–5, R = Bu^t, Pr^i or Cy) have been at the heart of many key developments in transition metal chemistry over the last 25 years[1–7] including the stabilisation of unusual oxidation states and low coordination numbers,[1,2] formation of agostic alkyls, activation of C–H and C–C bonds,[3,4] and preparation of polyhydride complexes.[1,3,5] Recently bulky alkyl diphosphine complexes of palladium have attracted attention as carbonylation catalysts[6] and as catalysts for the Heck reaction.[7] We report here a simple route to a new class of very bulky alkyl diphosphines which are air-stable.

It has been reported that PH_3 reacts with acetylacetone[8] or trifluoroacetylacetone[9] to give adamantane-like cage secondary phosphines although no coordination chemistry of these ligands has been reported. This prompted us to attempt the synthesis of bis(phospha-adamantyl)alkanes from diprimary phosphines. Thus $H_2P(CH_2)_3PH_2$ was reacted with acetylacetone in the presence of HCl and this gave an air-stable, crystalline product which was identified as a mixture of the diastereomeric phospha-adamantane diphosphines **1a** and **1b** [eqn. (1)] on the

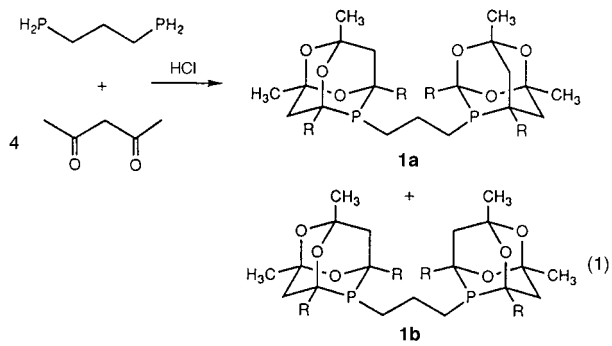

(1)

basis of elemental analysis, mass spectrometry, ^{31}P and ^{1}H NMR spectroscopy. The $^{31}P\{^{1}H\}$ NMR spectrum of the product in $CDCl_3$ showed two singlets at −31.0 and −30.2 ppm in the ratio of *ca.* 1 : 1, consistent with the presence of *rac* (**1a**) and *meso* (**1b**) diastereoisomers. Addition of MeOH to a CH_2Cl_2 solution of the mixture of ligands **1a** and **1b** leads to selective crystallisation of the *rac* isomer **1a**; in this way samples of **1a** and **1b** in purity of > 95% are readily obtained.

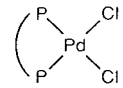

2a diphosphine = **1a** **2b** diphosphine = **1b**
6a diphosphine = **3a** **6b** diphosphine = **3b**
7a diphosphine = **4a** **7b** diphosphine = **4b**
8a diphosphine = **5a** **8b** diphosphine = **5b**

The dichloropalladium(II) chelates **2a** and **2b** were made by treatment of $[PdCl_2(NCPh)_2]$ with **1a** and **1b** respectively and the crystal structure of **2a**, as determined by X-ray crystallography,† is illustrated in Fig. 1. The bulk of the phospha-adamantane diphosphines is evident and the estimated cone angle[10] is 173° (*cf.* 155° for $Bu^t_2PCH_2CH_2CH_2PBu^t_2$ in its $PtCl_2$ complex[11]); furthermore there is no possibility of

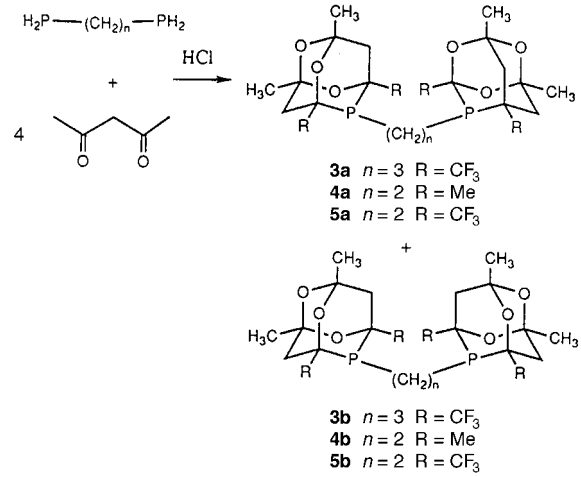

(2)

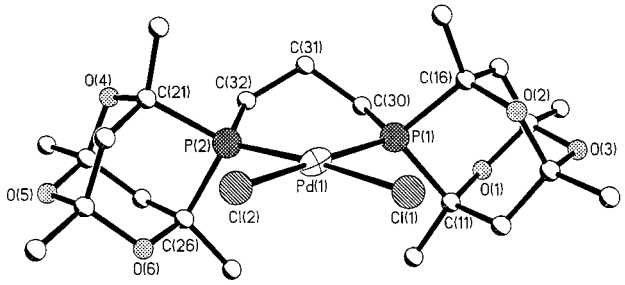

Fig. 1 Molecular structure of **2a** with all hydrogen atoms omitted for clarity.

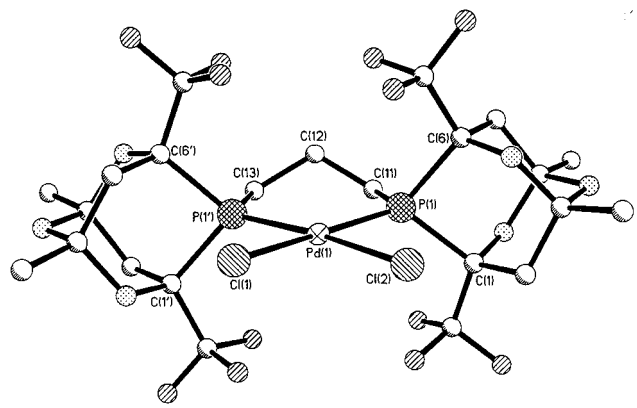

Fig. 2 Molecular structure of **6a** with all hydrogen atoms omitted for clarity. Primed atoms are related by non-crystallographic mirror symmetry.

reduction of the bulk of this ligand by intermeshing. The most unusual aspect of the geometry is the long intra-cage P–C distances and small C–P–C angles (Fig. 1). The electronic consequences of this geometric distortion at phosphorus on the metal–phosphine bond and its chemistry is currently under investigation. Methoxycarbonylation of alkenes catalysed by derivatives of **2a** and **2b** has recently been reported.[12]

The condensation reaction shown in eqn. (1) can be generalised to other diphosphines and other acetylacetones [eqn. (2)]. Hence the ligands **3**–**5a**,**b** have been made in high yield as mixtures of diastereoisomers using the appropriate $H_2P(CH_2)_nPH_2$ and 1,3-diketone. Preliminary results show that the corresponding dichloropalladium chelates **6**–**8a**,**b** can be made and the crystal structure of **6a** (Fig. 2)† reveals the great steric bulk of the coordinated diphosphine **3a**, with an estimated cone angle of 192°.

A different type of product was obtained when 1,2-diphosphinobenzene was added to acetylacetone in the presence of HCl. The structure of the product was assigned to the diphospha-adamantane **9** on the basis of the symmetry of its ^{1}H, ^{13}C{^{1}H} and ^{31}P{^{1}H} NMR spectra and the structure was confirmed by X-ray crystallography.† The diphosphine **9** reacts with [AuCl(tht)] to give the binuclear gold(I) complex **10** which has also been characterised by X-ray crystallography (Fig. 3).†

The mechanism for the formation of the monophospha-adamantanes has been previously discussed[9] and a mechanism for the formation of the diphospha-adamantane cage **9** is suggested in Scheme 1. The rigidity of the phenylene backbone promotes the formation of **9** because the pendant PH_2 group in **A** is held in close proximity to the electrophilic carbon thus facilitating the ring closure step ii.

We have shown that diphosphines featuring very bulky, rigid, phospha-adamantane cages are readily accessible in one step from primary diphosphines. The extension of this work to other diprimary phosphines and other 1,3-diketones is being explored alongside investigation of the coordination chemistry and applications of these remarkable ligands. We thank EPSRC, Albright and Wilson and Shell International for supporting this work and Johnson Matthey for a loan of palladium compounds.

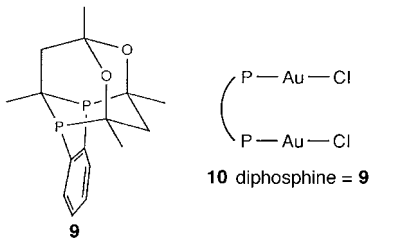

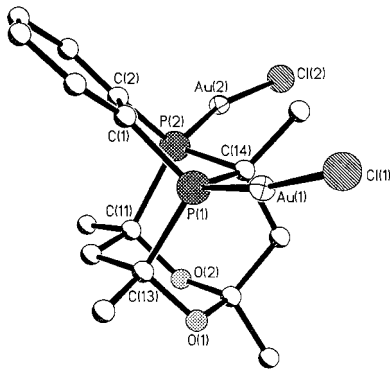

Fig. 3 Structure of **10** with all hydrogen atoms omitted for clarity.

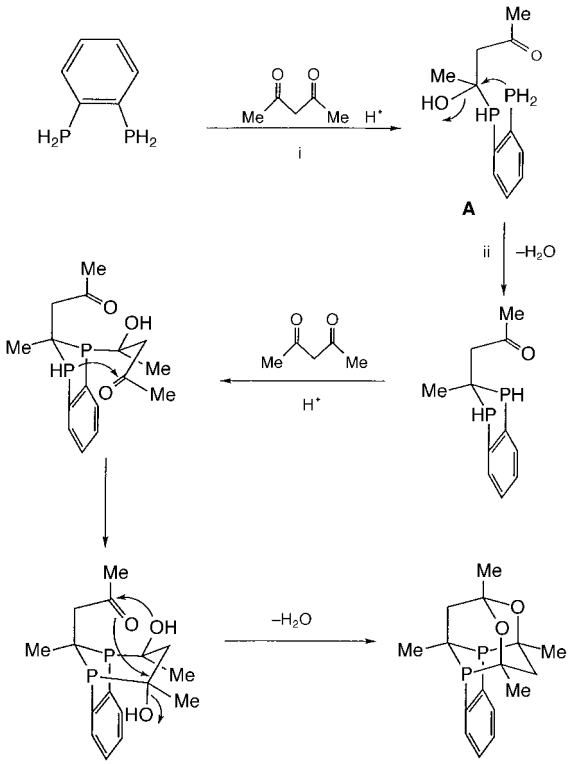

Scheme 1 Suggested mechanism for the formation of the diphospha-adamantane **6**.

Notes and references

† Crystal structures were determined from data collected on a Siemens SMART diffractometer for $2.0 < \theta < 27.5°$ (λ = 0.71073 Å), at 173 K. The structures were solved by direct and Fourier methods and refined by least-squares against all unique F^2 data corrected for absorption. *Crystal data*: for **2a**: $C_{23}H_{38}Cl_2O_6P_2Pd$, M = 649.8, monoclinic, space group $P2_1/c$ (no. 14), a = 13.402(5), b = 14.735(3), c = 14.150(3) Å, β = 103.48(2)°, V = 2717.3(13) Å^3, Z = 4, μ = 1.033 mm^{-1}, 6219 unique data, $R1$ = 0.059. For **3a**·$CHCl_3$: $C_{24}H_{27}Cl_5F_{12}O_6P_2Pd$, M = 985.05, monoclinic, space group Cc (no. 9), a = 13.142(2), b = 11.987(2), c = 22.167(3) Å, β = 102.419(8)°, V = 3410.4(9) Å^3, Z = 4, μ = 1.135 mm^{-1}, 7771 unique data, $R1$ = 0.026. For **9**: $C_{16}H_{20}O_2P_2$, M = 306.26, orthorhombic, space group *Pnma* (no. 62), a = 17.491(3), b = 12.133(2), c = 7.347(2) Å, V = 1559.1(6) Å^3, Z = 4, μ = 0.277 mm^{-1}, 1882 unique data, $R1$ = 0.047. For **10**: $C_{16}H_{20}Au_2Cl_2O_2P_2$, M = 771.1, triclinic, space group $P\bar{1}$ (no. 2), a = 7.934(2)(3), b = 8.2681(12), c = 15.118(2) Å, α = 85.449(13), β = 87.77(2), γ = 76.846(12)°, V = 962.4(3) Å^3, Z = 2, μ = 15.68 mm^{-1}, 4343 unique data, $R1$ = 0.020. CCDC 182/1219. See http://www.rsc.org/suppdata/cc/1999/901/ for crystallographic files in .cif format.

1 B. L. Shaw, *J. Organomet. Chem.*, 1980, **200**, 307 and references therein; C. Crocker, R. J. Errington, R. Markham, C. J. Moulton, K. J. Odell and B. L. Shaw, *J. Am. Chem. Soc.*, 1980, **102**, 4373; B. L. Shaw, *Adv. Chem.*, 1982, **196**, 101 and references therein; R. J. Errington and B. L. Shaw, *J. Organomet. Chem.*, 1982, **238**, 319.
2 P. Leoni, M. Pasquali, L. Fadini, A. Albinati, P. Hofmann and M. Metz, *J. Am. Chem. Soc.*, 1997, **119**, 8625.
3 L. Mole, J. L. Spencer, S. A. Litster, A. D. Redhouse, N. Carr and A. G. Orpen, *J. Chem. Soc., Dalton Trans.*, 1996, 2315 and references therein.
4 B. Rybtchinski, A. Vigalok, Y. Ben-David and D. Milstein, *J. Am. Chem. Soc.*, 1996, **118**, 12, 406.
5 T. H. Tulip, T. Yamagata, T. Yoshida, R. D. Wilson, J. A. Ibers and S. Otsuka, *Inorg. Chem.*, 1979, **18**, 2239.
6 E. Drent and E. Kragtwijk, *Eur. Pat.*, EP 495548, 1992 (to Shell); R. P. Tooze, G. R. Eastham, K. Whiston and X. L. Wang, *World Pat.*, 96/19434, 1996 (to ICI).
7 M. Ohff, A. Ohff, M. E. van der Boom and D. Milstein, *J. Am. Chem. Soc.*, 1997, **119**, 11, 687.
8 M. Epstein and S. A. Buckler, *J. Am. Chem. Soc.*, 1961, **83**, 3279.
9 G. Bekiaris, E. Lork, W. Offermann and G.-V. Röschenthaler, *Chem. Ber.*, 1997, **130**, 1547.
10 C. A. Tolman, *Chem. Rev.*, 1977, **77**, 313.
11 M. Harada, Y. Kai, N. Yasuoka and N. Kasai, *Bull. Chem. Soc. Jpn.*, 1979, **52**, 390.
12 P. H. M. Budzelaar, E. Drent and P. G. Pringle, *Eur. Pat.*, 97 302 079, 1996 (to Shell).

Communication 9/02434D

ChemComm

Theoretical evidence of a feasible concerted *antara–antara* cycloaddition

José I. García*, José A. Mayoral and Luis Salvatella*

Departamento de Química Orgánica, Instituto de Ciencia de Materiales de Aragón, Facultad de Ciencias, Universidad de Zaragoza-C.S.I.C. Pedro Cerbuna, 12, E-50009 Zaragoza, Spain. E-mail: jig@posta.unizar.es

Received (in Liverpool, UK) 8th March 1999, Accepted 7th April 1999

For the first time it is demonstrated, based on theoretical considerations, that concerted *antara–antara* cycloadditions are chemically possible, and even easy to observe for molecules with the appropriate geometry.

Since the discovery of the Diels–Alder reaction in 1928,[1] cycloadditions[2] have become very useful tools in organic synthesis.[3] One of the main features of these reactions is that they frequently follow concerted mechanisms, which accounts for the stereospecificities observed. Many aspects of cycloaddition reactions have been explained by means of the Woodward–Hoffmann rules.[4] According to these rules, two types of reactivity can be considered for each of the reactants involved: *supra* (if newly forming sigma bonds are situated on the same face of the π-system) and *antara* (if these bonds are situated on opposite faces). Since concerted cycloadditions involving more than two reactive systems seem to be very unlikely,[5] cycloadditions can thus be classified as *supra–supra*, *supra–antara* and *antara–antara*. It is worth mentioning that each of these possibilities would lead to compounds with different stereochemistries.

The *supra–supra* mechanism is involved in most of these reactions, for example Diels–Alder[6] and 1,3-dipolar cycloaddition reactions.[7] On the other hand, the *supra–antara* pathway is much less common[8] and it has recently been disregarded for the ketene + cyclopentadiene reaction,[9] which was, up until then, considered a typical example from theoretical considerations. Theoretical calculations on the ethylene dimerization reaction indicate that the concerted mechanism is not favoured.[10] Finally, to the best of our knowledge, the concerted *antara–antara* cycloaddition mechanism has never been invoked for any chemical reaction to date.

The Woodward–Hoffmann rules predict that *antara–antara* cycloadditions are allowed in the same cases as the *supra–supra* ones, *i.e.* thermal reactions involving $2n + 2$ π electrons and photochemical reactions involving $2n$ π electrons. Competition with the *supra–supra* mechanism could explain the lack of experimental evidence for the occurrence of *antara–antara* cycloadditions, the latter being generally disfavoured because of the molecular distortion necessary to obtain the adequate geometrical requirements in the transition states (TSs). However, the question remains; are concerted *antara–antara* cycloadditions really impossible from an experiment point of view?

In our search for chemical systems for which this kind of mechanism was plausible, we considered the [6 + 4] cycloadditions as a good starting point, given that the combination of triene + diene may offer the flexibility required for an *antara–antara* approach. Thus, the reaction between *cis* hexa-1,3,5-triene and buta-1,3-diene was chosen as a model example, and, using Density Functional Theory calculations,[11] we were able to build a template for the corresponding *antara–antara* TS. Examination of this structure suggested to us that the simplest way to obtain a chemical system able to give a cycloaddition through a concerted *antara–antara* mechanism would consist of freezing the spatial arrangement of the atoms in the corresponding transition structure. This action would diminish the contribution of the reactive distortion to the activation barrier. With this aim in mind we designed the molecule

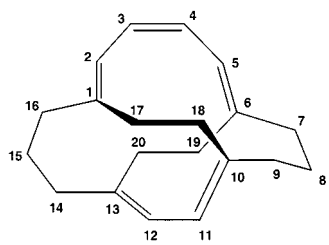

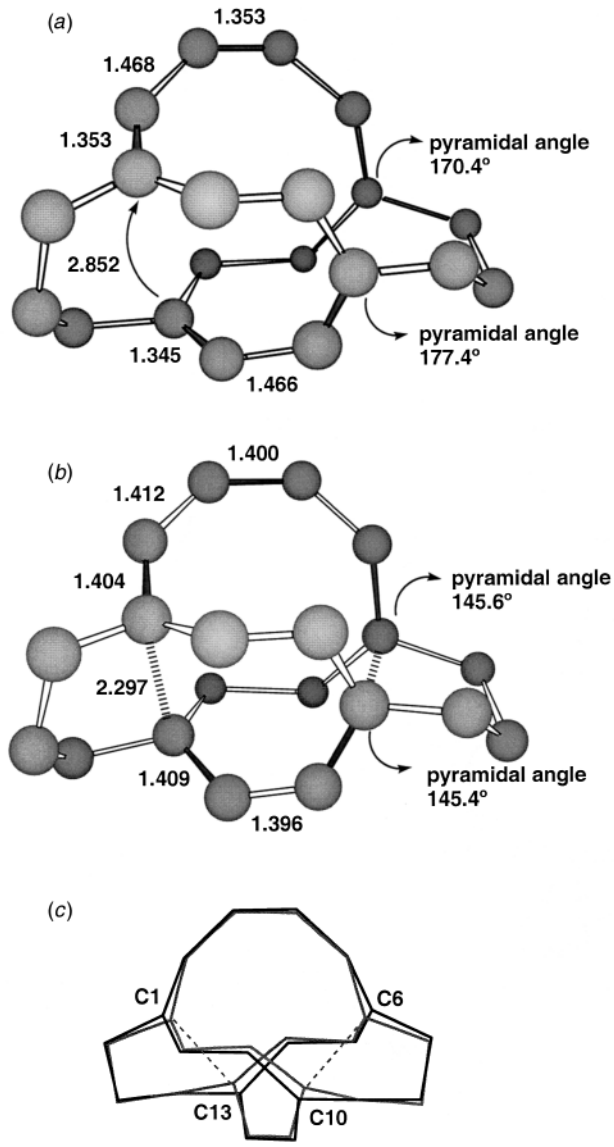

Fig. 1 Some calculated [at the B3LYP/6-31G(d) level] geometrical features of (*a*) antarene and (*b*) the corresponding TS for the *antara–antara* [6 + 4] cycloaddition, and (*c*) a superimposition of the two structures. Hydrogen atoms are omitted for clarity.

Table 1 Relative energies, enthalpies, free energies and entropies of the structures involved in the *antara–antara* [6 + 4] cycloaddition of antarene, calculated at the HF/6-31G(d) and B3LYP/6-31G(d)[a] theoretical levels

Level	Structures	ΔE_0/kcal mol^{-1}	ΔH_{298}/kcal mol^{-1}	ΔG_{298}/kcal mol^{-1}	ΔS_{298}/cal mol^{-1} K^{-1}
HF/6-31G(d)	Reactant	0.0	0.0	0.0	0.0
	TS	49.7	47.4	48.5	−3.8
	Adduct	−29.0	−27.9	−26.1	−6.2
B3LYP/6-31G(d)	Reactant	0.0	0.0	0.0	—
	TS	16.0	13.7	14.9	—
	Adduct	−23.6	−22.6	−20.7	—

[a] Using the frequencies HF/6-31G(d) for thermochemical data.

(1*Z*,3*Z*,5*Z*,10*Z*,12*Z*)-tricyclo[8.6.2.2^{6,13}]icosa-1,3,5,10,12-pentaene, hereafter referred to as 'antarene'.

Fig. 1(*a*) shows some geometrical parameters of this molecule, calculated at the B3LYP/6-31G(d) theory level. As can be seen, antarene consists of the hexatriene and butadiene moieties, linked by two trimethylene and two ethylene bridges in such a manner that the *antara–antara* disposition of the reactive parts of the molecule are strongly enforced. The transition structure of the intramolecular [$_\pi 6_a + {}_\pi 4_a$] cycloaddition of antarene could be found at the B3LYP/6-31G(d) level[16] [Fig. 1(*b*)]. This transition structure shows C_2 symmetry, corresponding to a concerted and synchronous process with newly forming bond lengths of 2.297 Å.

Relative energies for the structures involved (Table 1) show that the reaction is exothermic (22.6 kcal mol^{-1}) and presents a low barrier of activation (16.0 kcal mol^{-1}). Since the geometrical constraints of antarene are assumed to make other competitive reactions very difficult, one can deduce that antarene must react through a concerted *antara–antara* cycloaddition mechanism. Fig. 1(*c*) also illustrates this point, showing that the only noticeable geometrical difference between antarene and the transition structure is the displacement of the carbon atoms involved in the formation of the new signma bonds, caused by the change of hybridization from sp^2 to sp^3. As a consequence of the rigidity of the structure, and of the small degree of atomic reorganization along the reaction path, the activation entropy is as low as −3.8 cal mol^{-1} K^{-1}. In fact, the free activation energy is so low (*ca.* 15 kcal mol^{-1}) that one can deduce that antarene should not be very stable in solution at room temperature!

Antara–antara cycloadditions, whose feasibility we have demonstrated for the first time from theoretical considerations, open the door to the synthesis of medium-sized and macropolycycles with unique stereochemical features, and hence to new compounds with different properties.

Notes and references

1 J. A. Berson, *Tetrahedron*, 1992, **48**, 3.
2 R. Huisgen, *Angew. Chem.*, 1968, **80**, 329; *Angew. Chem., Int. Ed. Engl.*, 1968, **7**, 321.
3 W. Carruthers, *Cycloaddition Reactions in Organic Synthesis*, Pergamon, Oxford, 1990.
4 R. B. Woodward and R. Hoffmann, *Angew. Chem.*, 1969, **81**, 797; *Angew. Chem., Int. Ed. Engl.*, 1969, **8**, 781; *The Conservation of Orbital Symmetry*, Verlag Chemie, Weinheim, 1970.
5 K. N. Houk, Y. Li and J. D. Evanseck, *Angew. Chem.*, 1992, **104**, 711; *Angew. Chem., Int. Ed. Engl.*, 1992, **31**, 682.
6 J. Sauer and R. Sustmann, *Angew. Chem.*, 1980, **92**, 773; *Angew. Chem., Int. Ed. Engl.*, 1980, **19**, 779.
7 A. Padwa, *1,3-Dipolar Cycloaddition Chemistry, Vol. 2*, Wiley, New York, 1984.
8 H. Hart, T. Miyashi, D. N. Buchanan and S. Sasson, *J. Am. Chem. Soc.*, 1974, **96**, 4857.
9 S. Yamabe, T. Dai, T. Minato, T. Machiguchi and T. Hasegawa, *J. Am. Chem. Soc.*, 1996, **118**, 6518.
10 F. Bernardi, A. Bottoni, M. A. Robb, H. B. Schlegel and G. Tonachini, *J. Am. Chem. Soc.*, 1985, **107**, 2260.
11 Calculations were carried out by means of the Gaussian 94 package (ref. 12) using the Hartree–Fock and Density Functional Theory [through the B3LYP hybrid functional (ref. 13)] levels and the 6-31G(d) basis set (ref. 14). B3LYP/6-31G(d) calculations are known to perform well as regards cycloaddition reactions (ref. 15). The nature of all stationary points (reactants, transition structures and adducts) was tested by means of frequency calculations, which also served to calculate the thermodynamic parameters of the reactions considered.
12 Gaussian 94 (Revision C.2), M. J. Frisch, G. W. Trucks, H. B. Schlegel, P. M. W. Gill, B. G. Johnson, M. A. Robb, J. R. Cheeseman, T. A. Keith, G. A. Petersson, J. A. Montgomery, K. Raghavachari, M. A. Al-Latham, V. G. Zakrzewski, J. V. Ortiz, J. B. Foresman, J. Cioslowski, B. B. Stefanov, A. Nanayakura, M. Challacombe, C. Y. Peng, P. Y. Ayala, W. Chen, M. W. Wong, J. L. Andrés, E. S. Replogle, R. Gomperts, R. L. Martin, D. J. Fox, J. S. Binkley, D. J. Defrees, J. Baker, J. J. P. Stewart, M. Head-Gordon, C. González and J. A. Pople, Gaussian Inc., Pittsburgh, PA, 1995.
13 A. D. Becke, *J. Chem. Phys.*, 1993, **98**, 5648; C. Lee, W. Yang and R. Parr, *Phys. Rev. B*, 1988, **37**, 785.
14 W. J. Hehre, R. Ditchfield and J. A. Pople, *J. Chem. Phys.*, 1972, **56**, 2257.
15 O. Wiest and K. N. Houk, *Top. Curr. Chem.*, 1996, **183**, 1; V. Barone and R. Arnaud, *Chem. Phys. Lett.*, 1996, **251**, 393; V. Barone, R. Arnaud, P. Y. Chavant and Y. Vallée, *J. Org. Chem.*, 1996, **61**, 5121; E. Goldstein, B. Beno and K. N. Houk, *J. Am. Chem. Soc.*, 1996, **118**, 6036; K. N. Houk, B. R. Beno, M. Nendel, K. Black, H. Y. Yoo, S. Wilsey and J. K. Lee, *J. Mol. Struct. (THEOCHEM)*, 1997, **398**, 169; B. S. Jursic, *J. Org. Chem.*, 1997, **62**, 3046; O. Wiest, D. C. Montiel and K. N. Houk, *J. Phys. Chem. A*, 1997, **101**, 8378; J. Liu, S. Niwayama, Y. You and K. N. Houk, *J. Org. Chem.*, 1998, **63**, 1064; J. I. García, V. Martínez-Merino, J. A. Mayoral and L. Salvatella, *J. Am. Chem. Soc.*, 1998, **120**, 2415.
16 The transition structure search was performed without any geometrical constraint at the HF/6-31G(d) and B3LYP/6-31G(d) levels, leading to very similar geometries. The nature of the transition structure was fully characterized by the presence of only one imaginary frequency, correponding to the symmetric stretching of the four atoms involved in the formation of the sigma bonds. Frequency calculations were only carried out at the HF/6-31G(d) level, due to the size of the system.

Communication 9/01922G

Cyclic alkynes–electronic behaviour as a function of ring strain

Rik R. Tykwinski

Department of Chemistry, University of Alberta, Edmonton, Alberta, Canada T6G 2G2. E-mail: rik.tykwinski@ualberta.ca

Received (in Corvallis, OR, USA) 2nd February 1999, Accepted 2nd April 1999

UV/Vis spectroscopic analysis of a series of cross-conjugated enediyne macrocycles as a function of increasing ring strain and planarity shows little effect on the electronic absorptions of the macrocycles, despite an obvious rehybridization of the alkylidene carbon atoms as evidenced by ^{13}C NMR spectroscopy.

Conjugated organic compounds have considerable potential as materials for electronics and photonics.[1] We are interested in the electronic characteristics of cross-conjugated oligomers

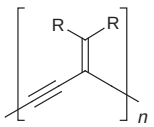

1

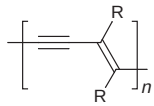

2

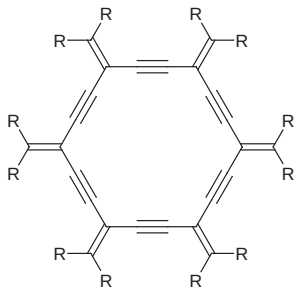

3

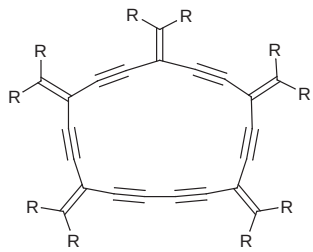

4

such as *iso*-polydiacetylenes (*iso*-PDAs, **1**)[2] and the comparison of their properties to the more prevalently studied compounds, *e.g*. polydiacetylenes **2**, that contain linear conjugation.[3] In the course of investigating the effects of cross conjugation in the cyclic analogues of **1**, namely radialenes **3** and **4**,[4] it became necessary to evaluate the influence of ring strain on the electronic absorption behavior of these molecules.[5–11] Reported herein is the synthesis of a novel series of cross-conjugated, enyne macrocycles[4,12–14] (cyclic expanded dendralenes)[15] and their UV/Vis absorption characteristics as a function of ring strain and planarity.

The macrocyclic enynes **8a**–**c** were constructed as outlined in Scheme 1. Vinyl triflate **5** (2.2 equiv.)[16] was coupled with the commercially available diynes **6a**,**b** and **6c**[17] in DMF in the presence of Et_2NH, CuI and $Pd(PPh_3)_4$.[2] The coupling process proceeded rapidly at room temperature as monitored by TLC, and column chromatography (silica gel, hexanes–CH_2Cl_2 20:1) afforded fair yields of tethered enediynes **7a**–**c**.† Compounds **7a-c** were protodesilylated with K_2CO_3 in MeOH–THF (1 : 1) for 2–3 h to afford the terminal alkynes. The desilylation was essentially quantitative, and (following aqueous work-up) the products were immediately carried on to the next step. Oxidative acetylenic coupling of the respective terminal alkynes of **7a**–**c** was conducted in CH_2Cl_2 (*ca*. 0.001 M) in the presence of CuI and TMEDA.[18] Under these relatively dilute conditions, the coupling reactions were complete in *ca*. 4–5 h. Macrocycles **8a**–**c** were isolated in modest yields as white solids by column chromatography (SiO_2, hexanes–CH_2Cl_2 4:1).‡ Oligomers resulting from intermolecular oxidative coupling of the acetylenic precursors were observed as the major side-products. Unfortunately, this intermolecular coupling process effectively competed with intramolecular cyclization despite the use of increasingly dilute reaction conditions. The isolated macrocycles are thermally stable, and even the highly strained **8a** was stable as a crystalline solid to well above 100 °C. Under ambient conditions in the presence of oxygen, all cycles slowly decompose over a period of days. They can, however, be stored under refrigeration for months with minimal decomposition.

The structure of the most strained cyclic dendralene **8a** was confirmed by X-ray crystallographic analysis of a single crystal grown by diffusion of MeOH into a $CHCl_3$ solution at 4 °C.§ An ORTEP drawing of **8a** is shown in Fig. 1, and, interestingly, it shows that in the solid state this molecule is not C_2 symmetrical as might be expected. Whereas all of the alkyne moieties are strained, with angles much smaller than an ideal 180°, the angles of enediyne segment C(4)–C(5)–C(6)–C(7)–C(8) bear the majority of this strain with C(4)–C(5)–C(6) bent to just over 160°. The conjugated enyne portion of macrocycle **8a** is only slightly twisted from planarity, with a torsion angle between C(14)–C(13) • • • C(7)–C(8) of 3°. The enediyne bond angles C(14)–C(1)–C(2) and C(5)–C(6)–C(7) at *ca*. 111 and 108° are both smaller than the analogous angles of an acyclic *iso*-PDA at *ca*. 115°.[2] Despite the strained nature of macrocycle **8a**, there are no anomalous bond lengths when compared to the *iso*-PDA. The crystal structure of **8a** provides a quite remarkable example of the significant ability of packing forces to distort molecular structure in the solid state as compared to solution.¶

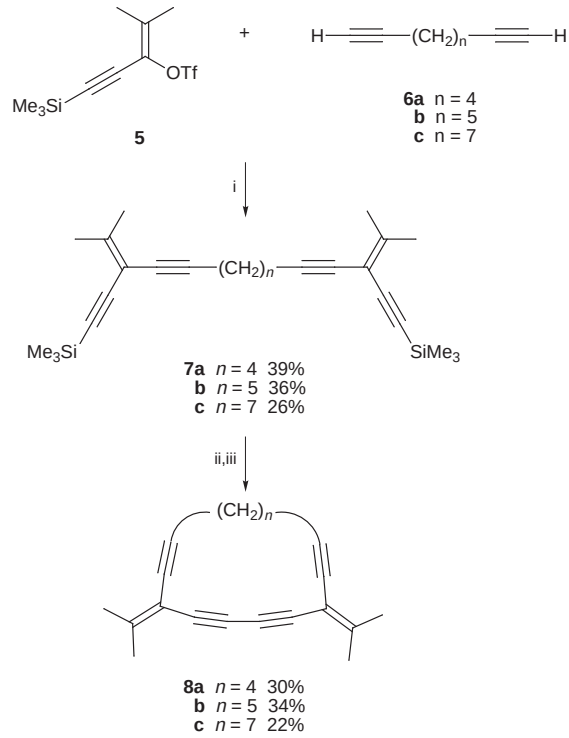

Scheme 1 *Reagents and conditions*: i, $Pd(PPh_3)_4$, CuI, Et_2NH, DMF, rt; ii, K_2CO_3, MeOH–THF; iii, CuI, TMEDA, O_2, CH_2Cl_2.

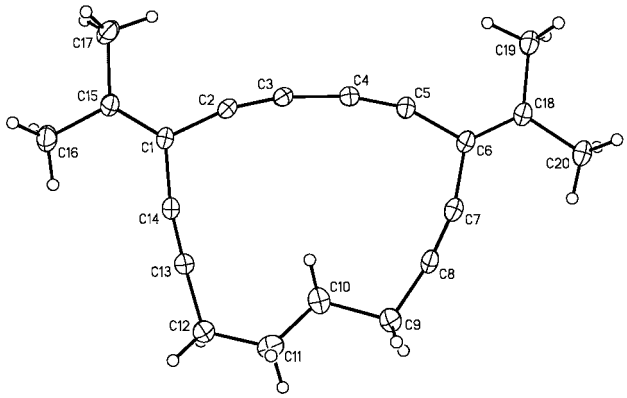

Fig. 1 X-Ray crystal structure of **8a**. Selected bond lengths (Å) and angles (°): C(1)–C(2) 1.439(5), C(2)–C(3) 1.196(5), C(3)–C(4) 1.378(5), C(4)–C(5) 1.207(5), C(5)–C(6) 1.433(5), C(6)–C(7) 1.444(6), C(7)–C(8) 1.188(5), C(13)–C(14) 1.180(5), C(1)–C(15) 1.337(5), C(6)–C(18) 1.341(5); C(1)–C(2)–C(3) 166.5(4), C(2)–C(3)–C(4) 169.0(4), C(3)–C(4)–C(5) 168.3(4), C(4)–C(5)–C(6) 161.6(4), C(5)–C(6)–C(7) 108.4(3), C(6)–C(7)–C(8) 165.4(4), C(7)–C(8)–C(9) 170.5(4), C(12)–C(13)–C(14) 176.6(5), C(1)–C(13)–C(14) 171.0(4), C(2)–C(1)–C(14) 110.9(3).

The ^{1}H and ^{13}C NMR spectra of macrocycles **8a-c** are completely consistent with their macrocyclic structures. Particularly interesting are the shifts of the alkylidene carbons. As the size of the macrocycle is decreased from 17 to 15 to 14 carbons in **8c**, **8b** and **8a**, respectively, a consistent shift is observed for the ^{13}C resonances of the olefinic carbons. The ^{13}C resonance of the endocyclic vinylidene carbon of **8c**, representing that of an unstrained system, is found at δ 82, whereas the analogous ^{13}C resonances of **8b** and **8a** are deshielded to δ 88 and 90, respectively. These shifts likely result from rehybridization effects as bond angle deformation imparts greater p character to the σ-bonds of the ring and, consequently, more s character to the olefin. The chemical shifts of the exocyclic vinylidene carbons, affected to a lesser extent, are consistently shifted upfield from δ 151 in **8c** to δ 149 and 147 for **8b** and **8a**, respectively. These ^{13}C resonances clearly reflect the expected rehybridization of the ring carbons as a function of decreased bond angles and increased ring strain.[12,19]

The UV/Vis spectra of the new macrocycles **8a-c** were examined to determine if the varied hybridization of the ring carbons affected the electronic absorption characteristics. In addition, the increased rigidity and enforced planarity as the ring size is decreased could also influence the respective electronic absorptions as observed previously for radialenes.[20] Unexpectedly, the electronic absorption spectra for **8a-c** (Fig. 2) show no variation in energy of the lowest energy electronic absorptions. These absorptions, presumably arising from the linearly conjugated dienediyne segment of each macrocycle, are observed at virtually identical values of 290, 309 and 329 nm. The absorption peaks do, however, gradually broaden as the ring size, and hence flexibility, is increased from 14 to 15 to 17 carbons. The absence of electronic absorption changes between *e.g.* **8a** and **8c** also suggests little or no contribution to π-electron delocalization *via* homoconjugation, as might be

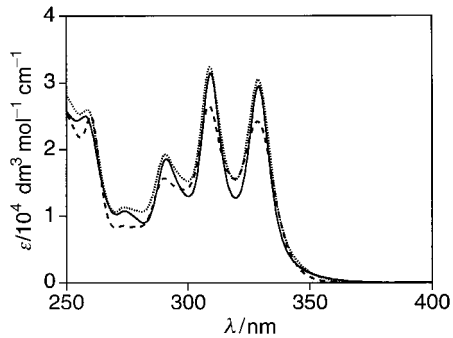

Fig. 2 Electronic absorption spectra in $CHCl_3$ comparing cyclic alkynes **8a** (———), **8b** (• • • • •) and **8c** (– – – – –).

anticipated from the constricted ring size that forces the in-plane acetylenic sp orbitals to closer spatial proximity.[21]

The syntheses of more strained derivatives of **8** (n = 2, 3) are currently being pursued, as is the analogous series of macrocycles containing the ene-yne-ene segment of **3**. Together, these additional analogues will further detail the influence of ring strain on π-electron delocalization.

This work was supported by a Gen-Science Endowment from the University of Alberta and by NSERC of Canada. I thank Dr R. McDonald for the X-ray structural determination of **8a**.

Notes and references

† The purity and structures of all new compounds were confirmed by ^{1}H and ^{13}C NMR, IR, UV, MS and either EA or HRMS.

‡ *Selected data* for **8a**: white solid, mp 129–130 °C; ν(solid)/cm^{-1} 2905, 2214, 2192, 2118, 1618, 1334; δ_H(300 MHz, $CDCl_3$) 2.35 (4 H, m), 1.91 (6 H, s), 1.89 (6 H, s), 1.74 (4 H, AA'BB'); δ_C(75.5 MHz, $CDCl_3$) 146.9, 102.8, 94.6, 90.4, 80.7, 80.0, 29.2, 22.9, 22.2, 19.9; λ_{max} ($CHCl_3$)/nm (ε/dm^3 mol^{-1} cm^{-1}) 329 (29 500), 309 (31 500), 290 (18 600), 275 (10 700), 258 (25 000) [Calc. for ($C_{20}H_{20}$): 260.1565. Found 260.1564]. For **8b**: white solid, mp 168 °C; ν(solid)/cm^{-1} 2905, 2215, 2130, 1617, 1349; δ_H(300 MHz, $CDCl_3$) 2.42 (4 H, t, J 5.6), 1.92 (6 H, s), 1.89 (6 H, s), 1.70 (2 H, m), 1.54 (4 H, m); δ_C(125 MHz, $CDCl_3$) 148.5, 102.2, 93.7, 88.4, 79.5, 78.2, 29.8, 28.9, 22.9, 22.2, 19.9; λ_{max}($CHCl_3$)/nm (ε/dm^3 mol^{-1} cm^{-1}) 329 (30 500), 309 (32 400), 291 (19 300), 275 (11 300), 259 (26 000) [Calc. for ($C_{21}H_{22}$): 274.1722. Found: 274.1726]. For **8c**: see ref. 4.

§ *Crystal data* for **8a**: $C_{20}H_{20}$, M = 260.4, monoclinic ,space group $P2_1/c$ (No. 14), D_c = 1.079 g cm^{-3}, Z = 4, a = 9.2119(8), b = 12.5305(12), c = 14.5747(10) Å, b = 107.744(7)°, V = 1602(2) Å^3, μ = 0.061 mm^{-1}. Final $R(F)$ = 0.076, $wR_2(F^2)$ = 0.20 for 185 variables and 2814 data with $F_o^2 \geq -3\sigma(F_o^2)$ (1399 observations [$F_o^2 \geq 2\sigma(F_o^2)$]. CCDC 182/1213. See http://www.rsc.org/suppdata/cc/1999/905/ for crystallographic files in .cif format.

¶ No evidence of symmetry distortion was observed in solution on the time scale of NMR analysis.

1 *Conjugated Polymers and Related Materials: The Interconnection of Chemical and Electronic Structure*, ed. W. R. Salaneck, I. Lundström and B. Rånby, OUP, Oxford, 1993.
2 Y. Zhao and R. R. Tykwinski, *J. Am. Chem. Soc.*, 1999, **121**, 458.
3 *Polydiacetylenes*, ed. D. Bloor and R. R. Chance, Martinus Nijhoff, Dordrecht, 1985.
4 S. Eisler and R. R. Tykwinski, *Angew. Chem.*, in the press.
5 W. Sander, *Angew. Chem., Int. Ed. Engl.*, 1994, **33**, 1455.
6 H. Meier, N. Hanold, T. Molz, H. J. Bissinger, H. Kolshorn, and J. Zountsas, *Tetrahedron*, 1986, **42**, 1711.
7 G. Maas and H. Hopf, in *The Chemistry of Dienes and Polyenes*, ed. Z. Rappoport, Wiley, Chichester, 1997, pp. 927–977.
8 A. Krebs and J. Wilke, *Top. Curr. Chem.*, 1983, **109**, 189.
9 R. Gleiter and W. Schäfer, in *The Chemistry of Triple-Bonded Functional Groups: Supplement C2*, ed. S. Patai, Wiley, Chichester, 1994, pp. 153–189.
10 R. Gleiter, *Angew. Chem., Int. Ed. Engl.*, 1992, **31**, 27.
11 R. Gleiter and R. Merger, in *Modern Acetylene Chemistry*, ed. P. J. Stang and F. Diederich, VCH, Weinheim, 1995, pp. 285–319.
12 J. Anthony, A. M. Boldi, C. Boudon, J.-P. Gisselbrecht, M. Gross, P. Seiler, C. B. Knobler and F. Diederich, *Helv. Chim. Acta*, 1995, **78**, 797.
13 R. Faust, F. Diederich, V. Gramlich and P. Seiler, *Chem. Eur. J.*, 1995, **1**, 111.
14 M. Schreiber, R. R. Tykwinski, F. Diederich, R. Spreiter, U. Gubler, C. Bosshard, I. Poberaj, P. Günter, C. Boudon, J.-P. Gisselbrecht, M. Gross, U. Jonas and H. Ringsdorf, *Adv. Mater.*, 1997, **9**, 339.
15 H. Hopf, *Angew. Chem., Int. Ed. Engl.*, 1984, **23**, 948.
16 P. J. Stang and T. E. Fisk, *Synthesis*, 1979, 438-440.
17 L. Brandsma, *Preparative Acetylenic Chemistry*, Elsevier, Amsterdam, 1988.
18 A. S. Hay, *J. Org. Chem.*, 1962, **27**, 3320.
19 H. N. C. Wong and F. Sondheimer, *Tetrahedron*, 1981, **37**, W99.
20 H. Hopf and G. Maas, *Angew. Chem., Int. Ed. Engl.*, 1992, **31**, 931.
21 A change in absorption energy as a result of angle deformation would also be expected for the in-plane π-system of the central butadiyne moiety of **8a-c**, as has been previously shown for cycloalkynes (ref. 8). Whereas absorptions are observed in the expected region of the butadiyne segment (*ca.* 250–275 nm) of **8a-c**, interpretation of shifts is, at this point, inconclusive. The expected absorption range of 250–275 nm is based on the lowest energy absorptions of known butadiyne derivatives, see: J. B. Armitage and M. C. Whiting, *J. Chem. Soc.*, 1952, 2005. I thank one of the reviewers for helpful suggestions.

Communication 9/00910H

Porphyrin derivatives as water-soluble receptors for peptides†

Mallena Sirish and Hans-Jörg Schneider*

FR 11.2 Organische Chemie der Universität des Saarlandes, D-66041 Saarbrücken, Germany. E-mail: ch12hs@rz.uni-sb.de

Received (in Cambridge, UK) 17th February 1999, Accepted 13th April 1999

The porphyrin–crown ether derivatives described here exhibit affinities to unprotected peptides of hitherto unknown magnitude in aqueous solution; the optical signal built-in to porphyrin receptors makes these applicable also to sensor techniques; the results can also form the basis of new catalytic systems, *e.g.* for the catalytic oxidation of peptides (such as tyrosinase models).

Porphyrins and their non-covalent interactions are of interest in view of their role in biological systems. They also can provide new artificial host compounds with a built-in optical sensor by their Soret bands, which are sensitive towards binding of many ligands. Porphyrin derivatives with positively charged substituents in the *meso*-position were shown earlier to interact with nucleotides and with DNA[1] as well as with many aromatic substrates[2] primarily *via* stacking between the aromatic units. We wanted to explore the use of modified porphyrins as peptide receptors, which unlike most artificial host compounds in this important class of compounds[3] work in protic solvents. The goal of selective peptide complexation in aqueous solution was approached only recently,[4] and still needs considerable progress until artificial receptors come close to the efficiency of biological systems. The present paper reports a new step in this direction, with binding constants of hitherto unkown magnitude for natural, unprotected peptides.[5]

We first carried out UV-visible titrations using the commercially available 5,10,15,20-tetrakis(4-methylpyridinium)porphyrin **1** with several *N*-benzyloxycarbonyl-protected amino acids and peptides, as unprotected amino acids and peptides showed no detectable binding. Addition of the Z derivatives (Z = benzyloxycarbonyl) resulted in a intensity reduction of the Soret band with a concomitant red shift of the band maximum. The change in absorbance values (ΔA), varied from 0.2 to 0.4, and the change in wavelength ($\Delta\lambda$) from 5 to 10 nm. Non-linear least-squares fitting of the observed absorbance changes obtained at several different wavelengths in the region 400–430 nm showed satisfactory fitting with a 1 : 1 association model. Similar behaviour was observed with a new porphyrin derivative **2** with one methyl benzoate and three 4-pyridinium substituents in the *meso* positions. This as well as two other derivatives with only two or one 4-pyridinium substituents (**3** and **4**) were synthesized analogous to literature procedures,[6] as it was hoped that partial displacement of the charged units might lead to more selective binding. Dilution experiments, however, made evident the fact that **3** and **4** aggregate severely in water in spite of the charges even at 10^{-6} M concentration, and were therefore unsuitable for binding studies.

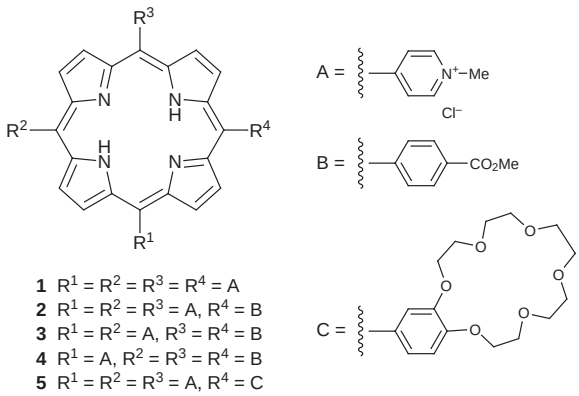

1 $R^1 = R^2 = R^3 = R^4 = A$
2 $R^1 = R^2 = R^3 = A$, $R^4 = B$
3 $R^1 = R^2 = A$, $R^3 = R^4 = B$
4 $R^1 = A$, $R^2 = R^3 = R^4 = B$
5 $R^1 = R^2 = R^3 = A$, $R^4 = C$

With host compounds **1** and **2** the log*K* values (2.9–3.7 M^{-1}, Table 1) show rather high affinities, in particular if a geometric fit is to be expected from the models. It is obvious that the binding strength with the protected peptides is generally larger for aromatic ligands, except in the case of Z-Asp, in line with previous findings.[1,2]

Considering the aqueous medium the affinities observed with **1** and **2** are promising, but unprotected peptides did not show any binding. The positive charge at the peptide NH_3 terminus will always destabilize complexes with **1** or **2**, which suggests the introduction of an additional binding site at the porphyrin ring in order to complex natural peptides. This was achieved by inserting a crown ether unit, which is known to complex primary ammonium groups. The synthesis of this porphyrin derivative **5** was carried out in acid medium using the classical Adler–Longo method.[7] Reaction of 4-formylbenzo-18-crown-6, pyridine-4-carbaldehyde and pyrrole in the presence of Ac_2O and refluxing propionic acid for 1.5 h gave a mixture of porphyrins which after purification on an alumina column and subsequent methylation yielded **5** in an overall yield of about 3%.

UV titrations with the new crown ether receptor **5** indeed showed with *unprotected* peptides binding constants (Table 2) which are even higher than those observed with the protected peptides necessary for the use of **1** and **2**. The fit to a 1 : 1 model was again satisfactory (Fig. 1), as long as the molar ratio of [peptide]/[**5**] did not exceed 200. At higher concentrations of the

Table 1 Logarithm of association constants of **1** and **2** with Z-amino acids and Z-peptides[a,b]

		1		**2**	
Entry	Amino acid/ peptide	log*K*	$\Delta\varepsilon/10^3$ dm^3 mol^{-1} cm^{-1}	log*K*	$\Delta\varepsilon/10^3$ dm^3 mol^{-1} cm^{-1}
1	Z-Ala	3.06	56.2	2.94	31.4
2	Z-Phe	2.91	75.0	3.29	44.8
3	Z-Tyr	2.93	80.4	3.39	47.5
4	Z-Trp	3.43	94.9	3.58	49.2
5	Z-Asp	3.73	63.9	3.69	48.2
6	Z-Ile	3.40	64.7	2.94	35.4
7	Z-Gly–Phe	3.17	44.8	3.38	50.6
8	Z-Ala–Trp	3.20	92.4	3.60	69.6

[a]Measured by UV-visible titration of **1** and **2** with Z-amino acids or Z-peptides at 25 °C. Titrations were carried out in 5 mM phosphate buffer, pH 6.9 ± 0.2 by adding concentrated stock solutions of Z-amino acid or Z-peptide ([Z-amino acid] or [Z-peptide] = 10 mM) containing *ca.* 5 μM of **1** or **2** to an equally concentrated solution of **1** or **2** in a 10 mm cuevette. Error limits: log*K* ±5%. [b] $\Delta\varepsilon$ changes at [ligand]/[host] = 200, the values agree within ±5% with the $\Delta\varepsilon$ from non-linear fit [ε (410 nm): **1**, 149300; **2**, 128 800, Error limits: ±5%).

† Supramolecular Chemistry, Part 86; Part 85: M. Alamgir Hossain and H.-J. Schneider, *Chem. Eur. J.*, 1998, in the press.

Table 2 Logarithm of association constants of **5**, with peptides[a,b]

Entry	Peptide	log*K*	$\Delta\varepsilon/10^3$ dm^3 mol^{-1} cm^{-1}
1	Gly–Gly	2.93	15.7
2	Gly–Phe	4.71	22.0
3	Phe–Gly	4.36	18.0
4	Ala–Phe	4.60	10.2
5	Asp–Phe	4.05	14.0
6	Phe–Phe	4.52	13.1
7	Gly–Gly–Gly	3.41	7.8
8	Gly–Gly–Phe	4.39	20.7
9	Gly–Phe–Gly	4.35	12.5
10	Phe–Gly–Gly	4.48	12.3
11	Gly–Gly–Trp	3.52	15.4
12	Trp–Gly–Gly	4.48	16.9
13	Gly–Gly–Gly–Gly	5.02	18.9

[a] See footnotes to Table 1. [b] ε (410 nm): **5**, 91200, Error limits: ±5%.

added peptide one observes a biphasic behaviour of the isotherm, indicating other binding modes. The complexation-induced absorption and wavelength changes were smaller than those with **1** and **2**, but in most cases sufficient for evaluation of *K*. Computer aided molecular modelling of the complex between **5** and Gly-Gly-Phe using energy minimization with the CHARMm force field established an essentially strain-free fit between the crown and $^+NH_3$ at one end, and between an adjacent 4-pyridinium unit and the COO^- groups at the other end, as well as stacking between the terminal phenyl ring and the porphyrin, with retention of most stable extended conformation of the peptide (Fig. 2). The two carboxylate oxygens of Gly–Gly–Phe are in van der Waals contact with the neighbouring pyridyl *ortho*-Hs [PheCO(1)···HC(pyridyl-*ortho*) = 2.52 Å] and the β-pyrrole carbon atom [PheCO(2)···C(β-pyrrole) 3.03 Å].

The data in Table 2 illustrate that the binding strength increases as a function of the peptide length and with the number of aromatic units in the amino acid side chains, as expected from stacking contributions. A force field-minimised structure of the complex between **5** and Phe–Gly–Gly did show stacking interactions between the porphyrin pyridyl group and the peptide phenyl ring, in addition to other non-covalent interactions. However, the extremely large association constants, such as $K = 10^5$ M^{-1} with tetraglycine, are obviously due to additional binding effects. Preliminary measurements with aliphatic amides, hampered by very small spectral changes,

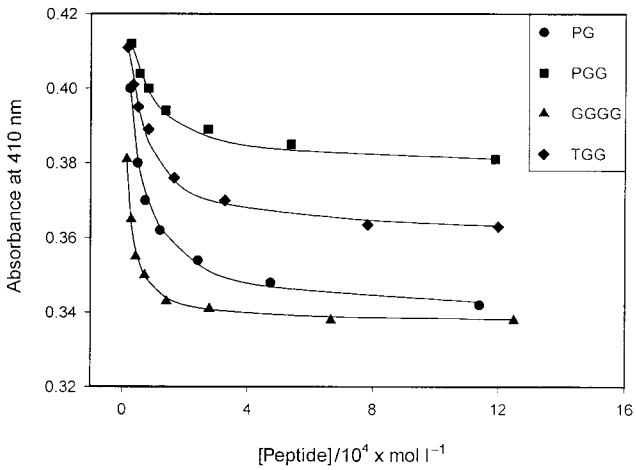

Fig. 1 UV-visible titration curves of porphyrin **5** with peptides (PG = Phe–Gly, PGG = Phe–Gly–Gly, GGGG = Gly–Gly–Gly–Gly, TGG = Trp–Gly–Gly).

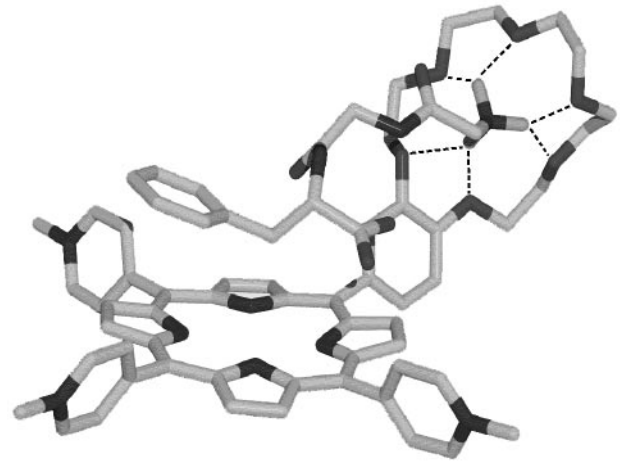

Fig. 2 A force field (CHARMm) optimized structure of porphyrin **5** with the peptide Gly–Gly–Phe. Hydrogens are omitted for clarity except those of peptide NH_3 . The phenyl group of Phe is not far from van der Waals contacts to the pyrrole (d_{av} = 3.95 Å); the NH_3 protons have distances of 1.90–2.05 Å to the crown ether oxygen; the carboxylate group comes close to neighbouring pyridyl protons with d_{av} = 3.0 Å.

suggest the amide function itself contributes significantly to the associations.

In conclusion, we have shown that porphyrins can associate with peptides with high affinities, if the charges are accommodated in a complementary fashion. The findings suggest new approaches to the design of peptide receptors and potentially also to supramolecular catalysts for peptide modification; they also shed light on possible interaction mechanisms in protein–porphyrin aggregations.[8]

Our work is supported by the Deutsche Forschungsgemeinschaft, Bonn, and the Fonds der Chemischen Industrie, Frankfurt. M. S. thanks the A. v. Humboldt foundation for a stipend.

Notes and references

1 G. Pratviel, J. Bernadou and B. Meunier, *Angew. Chem.*,1995, **107**, 819; *Angew. Chem., Int. Ed. Engl.*,1995, **34**, 746.
2 K. Kano, T. Hayakawa and S. Hashimoto, *Bull. Chem. Soc. Jpn.*, 1991, **64**, 778; H.-J. Schneider and M. Wang, *J. Org. Chem.*, 1994, **59**, 7464.
3 W. C. Still, *Acc. Chem. Res*., 1996, **29**, 155; R. Purrello, L. M. Scolaro, E. Bellacchio, S. Gurrieri and A. Romeo, *Inorg. Chem.*, 1998, **37**, 3647; For studies in $CHCl_3$, see T. Mizutani, T. Ema, T. Tomita, Y. Kuroda and H. Ogoshi, *J. Am. Chem. Soc.*, 1994, **116**, 4240; X. Huang, B. H. Rickman, B. Borhan, N. Berova and N. Nakanishi, *J. Am. Chem. Soc.*, 1998, **120**, 6185 and references therein.
4 (*a*) R. Breslow, Z. Yang, R. Ching, G. Tzrojandt and F. Odobel, *J. Am. Chem. Soc.*, 1998, **120**, 3536; (*b*) M. W. Peczuh, A. D. Hamilton, J. Sanchez-Qesada, J. de Mendoza, T. Haack and E. Giralt, *J. Am. Chem. Soc.*, 1997, **119**, 9327; (*c*) M. A. Hossain and H.-J. Schneider, *J. Am. Chem. Soc.*, 1998, **120**, 11 208. For highly selective peptide recognition on polymer surfaces with immobilized hosts see: (*d*) C.-T. Chen, H. Wagner and W. C. Still, *Science*, 1998, **279**, 851; (*e*) H. Hioki and W. C. Still, *J. Org. Chem.*, 1998, **63**, 904 and references cited therein.
5 Amino acids and peptides form complexes with 18-crown-6 with low to moderate constants, depending on the nature of the solvent medium (R. M. Izatt, P. Krystyna and J. S. Bradshaw *Chem. Rev.*, 1991, **97**, 1721). Typical log*K* values in MeOH for the association of Gly–Phe and Ala–Met with 18-crown-6 are 3.5 and l.75 M^{-1}, respectively (V. A. Bidzilya, L. P. Golovkova and K. B. Yatsimirski *J. Gen. Chem. USSR* (*Engl. Transl.*), 1986, **56**, 1251; *Zh. Obshch. Khim.*, 1986, **56**, 1412).
6 L. Ding, C. Casas, G. E. Moghadam and B. Meunier, *New. J. Chem.*, 1990, **14**, 421.
7 A. D. Adler, F. R. Longo, J. D. Finarelli, J. Goldmacher, J. Asour and L. Korsakoff, *J. Org. Chem.*, 1967, **32**, 476.
8 All new compounds showed satisfactory analytical data; the synthesis will be described elsewhere.

Communication 9/01325C

Formation of 2-oxa- or 2-azabicyclo[3.3.0]octa-3,7-diene by a novel tandem intramolecular photo-cyclization of 2,4,6-tris(phenylthio)hepta-2,4,6-trienal derivatives

Mitsuhiro Yoshimatsu,*[a] Satoshi Gotoh,[a] Genzoh Tanabe[b] and Osamu Muraoka[b]

[a] *Department of Chemistry, Faculty of Education, Gifu University, Yanagido, Gifu 501-1193, Japan. E-mail: yoshimae@gumail.cc.gifu-u.ac.jp*

[b] *Kinki University, Faculty of Pharmaceutical Sciences, 3-4-1, Kowakae, Higashi-osaka, Osaka 577-8502, Japan*

Received (in Cambridge, UK) 3rd March 1999, Accepted 12th March 1999

The photo-reactions of 2,4,6-tris(phenylthio)hepta-2,4,6-trienal 1 and its 2,4-dinitrophenylhydrazone 5 gave the 2-oxa- or 2-azabicyclo[3.3.0]octa-3,7-dienes 2 and 9, respectively, *via* a photo-induced intramolecular tandem cyclization reaction.

The Paterno–Büchi reaction has become increasingly familiar to chemists engaged in investigation of its mechanism or synthetic applications.[1] The widespread advances in this area of synthetic organic chemistry have led to convenient methodology for the preparation of the oxetane-containing biologically active materials.[2] Intramolecular photo-reactions of the vinyloxy ω-carbonyl compounds and their furan derivatives usually provides the fused oxetane ring compounds,[3] which lead to other useful compounds by successive transformations.[4]

Recently, we reported the tandem α-(thio)- or α-(seleno)-formylolefination reactions of the aldehydes.[5] Three cycles of the olefination process with pivalaldehyde stereoselectively afforded (2*E*, 4*E*, 6*E*)-8,8-dimethyl-2,4,6-tris(phenylthio)nona-2,4,6-trienal **1**, which contains three conjugated vinyl sufide moieties. This trienal **1** was found to be light-sensitive like the retinal chromophores.[6] This result prompted us to investigate the reactivities of the trienal under photo-irradiation conditions; surprisingly, a new ring system, oxabicyclo[3.3.0]octa-3,7-diene, was formed *via* an unusual photo-cyclization. Here we report the unprecedented intramolecular tandem cyclization reaction of trienal **1**.

Irradiation of an Ar saturated solution of **1** in MeCN (1.0×10^{-3} mol l^{-1}) using a 40 W fluorescent daylight lamp afforded (1*R**, 5*R**, 6*S**)-6-*tert*-butyl-1,4,7-tris(phenylthio)-2-oxabicyclo[3.3.0]octa-3,7-diene **2**[7] in 54% yield as shown in Scheme 1. The structure of **2** followed from the fact that the IR spectrum showed no carbonyl absorption, while the ^{1}H NMR spectrum showed two methine protons at δ 2.82 (t, *J* 2) and 3.40 (t, *J* 2) and two olefinic protons at δ 5.07 (s) and 6.50 (d, *J* 2). The stereochemistry of oxabicyclo compound **2** was determined as (1*R**, 5*R**, 6*S**) by single crystal X-ray analysis; the ORTEP drawing of **2** is shown in Fig. 1.[8] Furthermore, a few fundamental reactions of **2** were examined using oxidizing agents. MCPBA oxidation of **2** gave the corresponding sulfone **3** in 78% yield (Scheme 2). The reaction with Pd–C in toluene under reflux conditions afforded the ring-opened cyclopentadiene **4** in 40% yield. The structure of **4** was determined from the IR spectrum, which showed the carbonyl absorption at ν 1650 cm^{-1}, the ^{1}H NMR spectrum, which exhibited two doublets at δ 6.54 (d, *J* 7) (due to the olefinic proton) and 11.13 (d, *J* 7) (due to the aldehyde proton), and the mass spectrum, which showed a molecular ion peak ($C_{28}H_{22}OS$) at *m/z* 378. The stereochemistry of **4** was determined as *Z* by an NOE experiment. Irradiation of the *tert*-butyl protons at δ 1.22 increased the intensity of the olefinic proton at δ 6.54 (4%).

Next, we examined the photo-reaction of the trienal hydrazone **5**, irradiating at 400–500 nm in benzene to give 2-azabicyclo[3.3.0]octa-3,7-diene **6** in 41% yield (Scheme 3).[9]

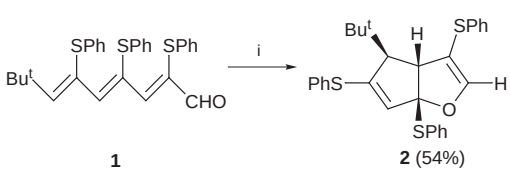

1 **2** (54%)

Scheme 1 *Reagents and conditions*: i, *hν* (500–600 nm), MeCN.

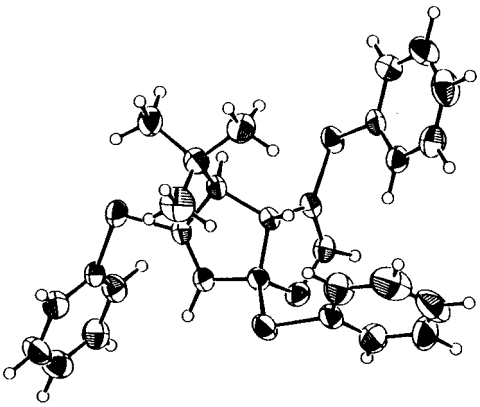

Scheme 2 *Reagents and conditions*: i, MCPBA, $ClCH_2CH_2Cl$; ii, Pd–C, toluene.

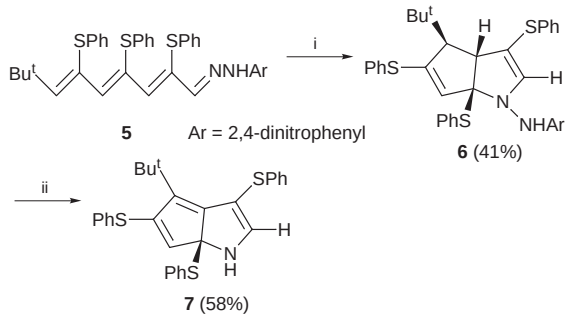

Scheme 3 *Reagents and conditions*: i, *hν* (400–500 nm), benzene; ii, AIBN, benzene, reflux.

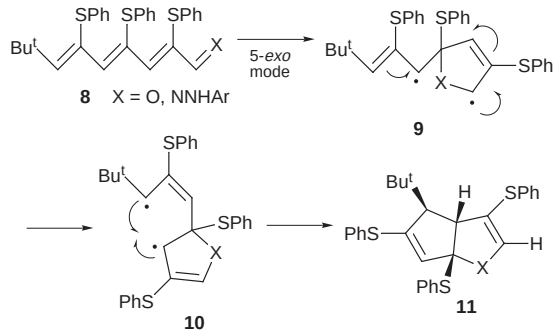

Scheme 4

Recently, we reported that the 2,4-dinitrophenylhydrazones reacted with AIBN and underwent dearylamination.[10] Treatment of the hydrazone **6** with AIBN in benzene afforded 2-azabicyclo[3.3.0]octa-3,5,7-triene **7** in good yield.

A plausible mechanism for formation of the photo-reaction products is shown in Scheme 4. Intermolecular [2 + 2] photocycloadditions have been intensively investigated and have indicated that the reaction intermediate is a flexible 1,4-biradical.[11] Our intramolecular cyclization would also proceed *via* triplet biradical intermediates and cyclize in 5-*exo* mode to give the 1,4-biradical **9**. Isomerization of **9** affords a 1,5-biradical **10**. Tandem cyclization leads to the bicyclo-[3.3.0]octa-3,7-diene **11**.

In conclusion, 2,4,6-tris(phenylthio)hepta-2,4,6-trienal derivatives are highly sensitive to light and their photo-reactions were found to afford the 2-oxa- or 2-azabicyclic compounds *via* a unique tandem cyclization reaction.

Notes and references

1 J. A. Porco and S. L. Schreiber, *Comprehensive Organic Synthesis*, ed. B. M. Trost, I. Fleming and L. A. Paquette, Pergamon, New York, 1991, vol. 5, p. 151.

2 S. S. Bhagwat, P. R. Hamann, W. C. Still, S. Bunting and F. A. Fitzpatrick, *J. Am. Chem. Soc.*, 1985, **107**, 6372; S. S. Bhagwat, P. R. Hamann, W. C. Still, S. Bunting and F. A. Fitzpatrick, *Nature*, 1985, **315**, 511; D. W. Norbeck and J. B. Kramer, *J. Am. Chem. Soc.*, 1988, **110**, 7217; Y. Kawahata, S. Takatsuto, N. Ikekawa, M. Murata and S. Omura, *Chem. Pharm. Bull.*, 1986, **34**, 3102.

3 M. Sakamoto, Y. Omote and H. Aoyama, *J. Org. Chem.*, 1984, **49**, 396; G. Pattenden and A. M. Birch, *J. Chem. Soc., Chem. Commun.*, 1980, 1195; M. J. Begley, A. M. Birch and G. Pattenden, *J. Chem. Soc., Chem. Commun.*, 1979, 235.

4 H. A. J. Carless, J. Beanland and S. Mwesigye-Kibonde, *Tetrahedron Lett.*, 1987, **28**, 5933; M Riediker and J. Schwartz, *J. Am. Chem. Soc.*, 1982, **104**, 5842; K. Maruyama and Y. Kubo, *J. Org. Chem.*, 1977, **42**, 3215; P. H. Mazzocchi, L. Klingler, M. Edwards, P. Wilson and D. Shook, *Tetrahedron Lett.*, 1983, **24**, 143.

5 M. Yoshimatsu, K. Oguri, K. Ikeda and S. Gotoh, *J. Org. Chem.*, 1998, **63**, 4475.

6 Q. Tan and K. Nakanishi, *J. Am. Chem. Soc.*, 1998, **120**, 12 357 and references cited therein.

7 *Selected data* for **2**: ν_{max}/cm^{-1} 1130 (ether); δ_H 0.91 (9H, s, Me × 3), 2.82 (1H, t, *J* 2, 6-H), 3.40 (1H, t, *J* 2, 5-H), 5.07 (1H, s, 8-H), 6.50 (1H, d, *J* 2, 3-H), 6.55–6.59 (2H, m, ArH), 7.01–7.07 (3H, m, ArH), 7.36–7.42 (5H, m, ArH), 7.46–7.51 (3H, m, ArH), 7.60–7.62 (2H, m, ArH); δ_C 28.60 (q × 3), 34.54 (s), 54.53 (d), 64.28 (d), 107.23 (s), 107.77 (s), 123.29 (d), 125.03 (d × 2), 126.16 (d), 128.89 (d × 2), 129.00 (d), 129.07 (d), 129.15 (d × 2), 129.57 (d × 2), 131.19 (s × 2), 132.13 (s), 132.46 (d × 2), 135.95 (d × 2), 150.10 (d), 150.65 (s); *m/z* 488 (M^+) (Calc. for $C_{29}H_{28}OS_3$; C, 71.27; H, 5.77. Found: C, 71.12; H, 5.77%).

8 *Crystal data* for **2**: $C_{29}H_{28}OS_3$ *M* = 488.72, monoclinic, *a* = 9.007(2), *b* = 26.879(6), *c* = 10.945(2) Å, β = 99.34(2)°, *V* = 2614.7(9) Å^3, *T* = 298 K, space group $P2_1/n$, *Z* = 4, μ(Cu-Kα) = 2.728 mm^{-1}, D_c = 1.214 Mg m^{-3}, 4284 reflections collected (Rigaku AFC5R diffractometer) of which 4096 were unique (R_{int} = 0.030) and 2720 were observed [$I > 3.00\sigma(I)$]. Solved by direct methods (MITHRIL90 and DIRDIF) and refined by full-matrix least-squares (teXsan) on *F* of all unique data to *R* = 0.056 (observed data), wR = 0.070 (all data). CCDC 182/1222. See http://www.rsc.org/suppdata/cc/1999/909/ for crystallograpic files in .cif format.

9 *Selected data* for **6**: ν_{max}/cm^{-1} 3330 (NH), 1620, 1340 (NO_2); δ_H 1.28 (9H, s, Me × 3), 4.47 (1H, s, 6-H), 6.29 (1H, s, 8-H), 6.47 (1H, s, 5-H), 6.57 (1H, s, 3-H), 6.74 (1H, d, *J* 10, ArH), 7.07–7.40 (15H, m, ArH), 8.13 (1H, dd, *J* 2 and 10 ArH), 9.02 (1H, br d, *J* 2, ArH), 10.06 (1H, s, NH); δ_C 30.39 (q × 3), 33.85 (s), 67.58 (d), 101.02 (s), 114.20 (d), 121.73 (s), 123.65 (d), 123.71 (d), 125.69 (d), 126.19 (d), 126.42 (d), 126.66 (d × 2), 128.23 (d), 128.45 (d × 2), 128.98 (d), 129.24 (d), 129.30 (d), 129.58 (s), 130.52 (d), 130.82 (s), 132.17 (d × 2), 132.74 (s), 133.92 (d), 133.98 (d), 134.08 (s), 138.33 (s), 138.68 (s), 140.31 (d), 147.70 (s), 152.78 (d); *m/z* 429 [$M^+ - (Bu^t + (O_2N)_2C_6H_3NH)$] (Calc. for $C_{35}H_{32}N_4O_4S_3$: C, 62.85; H, 4.82; N, 8.38. Found: C, 62.71; H, 5.23; N, 7.96%).

10 M. Yoshimatsu, S. Gotoh, K. Ikeda and M. Komori, *J. Org. Chem.*, 1998, **63**, 6619.

11 A. G. Griesbeck, S. Buhr, M. Fiege, H. Schmickler and J. Lex, *J. Org. Chem.*, 1998, **63**, 3847.

Communication 9/01707K

Helical chirality control in zinc bilinone dimers

Shigeyuki Yagi,[a] Noriaki Sakai,[b] Ryuhei Yamada,[a] Hiroshi Takahashi,[b] Tadashi Mizutani,*[b] Toru Takagishi,[a] Susumu Kitagawa[b] and Hisanobu Ogoshi[c]

[a] *Department of Applied Materials Science, Osaka Prefecture University, Gakuen-cho, Sakai, Osaka 599-8531 Japan*
[b] *Department of Synthetic Chemistry and Biological Chemistry, Graduate School of Engineering, Kyoto University, Yoshida, Sakyo-ku, Kyoto, 606-8501 Japan. E-mail: mizutani@sbchem.kyoto-u.ac.jp*
[c] *Fukui National College of Technology, Geshi, Sabae, Fukui 916-0064 Japan*

Received (in Cambridge, UK) 19th March 1999, Accepted 16th April 1999

Helical chirality of zinc bilinone is completely regulated by dimerizing bilinone units through a chiral cyclohexane spacer.

Zinc bilinone (ZnBL) is a helical molecule[1,2] with the low energetic barrier between the *P*- and *M*-helix conformers leading to rapid racemisation at room temperature.[3] Upon complexation with chiral amino acid esters and amines, the racemisation equilibrium is driven to a preferred enantiomer, implying the possible use of zinc bilinones as a framework for a chiral receptor.[4] For this purpose, however, the conformational flexibility of zinc bilinones should be limited. As an approach to rigidly fix the helical chiral conformation, we report here the synthesis of ZnBL dimers and complete control of the chirality by use of a rigid chiral spacer. Two ZnBL frameworks that are assembled *via* a chiral *trans*-cyclohexane-1,2-dioxy spacer gave a homochiral structure exclusively.

The bilinone dimer **1** was synthesized by a nucleophilic ring-opening reaction of oxoniaporphyrin by an alkoxide generated *in situ* from optically active *trans*-(*R*,*R*)- or (*S*,*S*)-1,2-cyclohexanediol, followed by zinc insertion using zinc(II) acetate.[5–7] The total yield of **1** from the oxoniaporphyrin was 35–46%. The

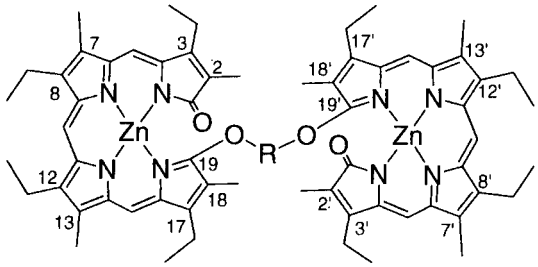

1a ; R = 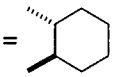 **1b** ; R = 

2 ; R = 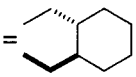

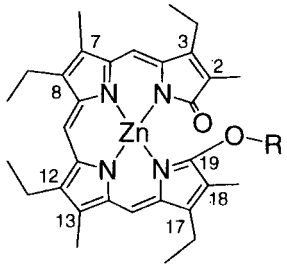

3 ; R = 

4 ; R = Me

structure of dimer **1** was confirmed by ^{1}H and ^{13}C NMR, UV–VIS, high resolution mass spectrometry and elemental analysis. Full assignments of all the protons and carbons were achieved by ^{1}H–^{1}H COSY, ROESY, and ^{1}H–^{13}C HSQC spectra. In the ^{1}H NMR spectrum of **1**, each bilinone moiety is magnetically equivalent, indicating that **1** adopts a C_2 symmetric conformation.

Circular dichroism spectra of **1**, **2** and **3** are shown in Fig. 1. The signs of the Cotton effects show that the *P*-helix conformation is more abundant than that of the *M*-helix in **1a**, and *vice versa* in **1b**.[8–11] The Cotton effects observed for **2** were much smaller than those for **1** or for the ZnBL monomer **3** bearing a chiral auxiliary. Previously we found that the magnitude of Cotton effects of ZnBL derivatives is directly in proportion to the efficiency of helical chirality induction.[4,12,13] Therefore, these CD spectral studies revealed that the helical chirality induction in **1** is much more effective than in **2** and **3**.

Variable-temperature ^{1}H NMR and CD studies offered more conclusive evidence for chiral induction in **1**: one set of the signals [Fig. 2(a)] was observed in the ^{1}H NMR spectrum over the temperature range 288–198 K. UV–VIS and CD spectra showed small changes upon cooling from 288 to 198 K: a 2 nm blue shift and a 9 nm red shift in the higher energy band and the lower energy band respectively, in the UV–VIS while CD spectra suggested a minor conformational equilibrium, but indicative of no changes in distribution among (*P*,*P*)-, (*P*,*M*)- and (*M*,*M*)-conformers. In contrast to this observation, monomeric ZnBL **3**, exhibited a drastic change in the CD intensity upon cooling from 288 to 223 K ($\Delta\varepsilon_{405}$ = −65.2 dm^3 mol^{-1} cm^{-1} at 288 K, $\Delta\varepsilon_{402}$ = −88.2 dm^3 mol^{-1} cm^{-1} at 223 K), where the diastereomeric excesses of the helical structure were 51 and 72%, respectively. All these results indicate that both ZnBL moieties of **1a** exclusively adopt the (*P*)-conformation.

In the ^{1}H NMR spectra of a more flexible dimer **2**, three sets of signals were observed in the region of the methine protons and the methylene protons adjacent to the oxygens, which were

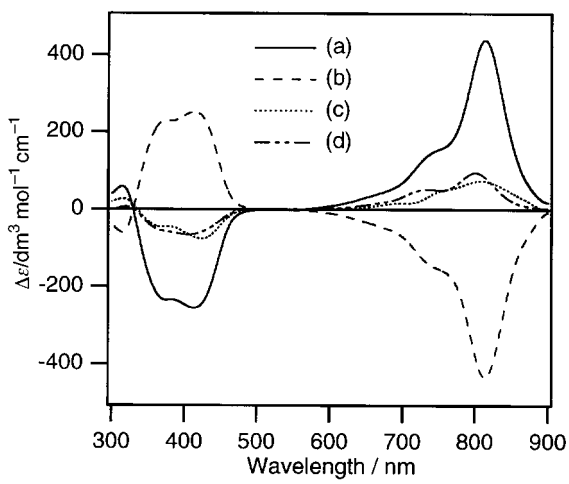

Fig. 1 Circular dichroism (CD) spectra of (a) **1a** (1.97×10^{-5} M), (b) **1b** (1.53×10^{-5} M), (c) **2** (1.99×10^{-5} M) and (d) **3** (3.68×10^{-5} M) in CH_2Cl_2 at 288 K.

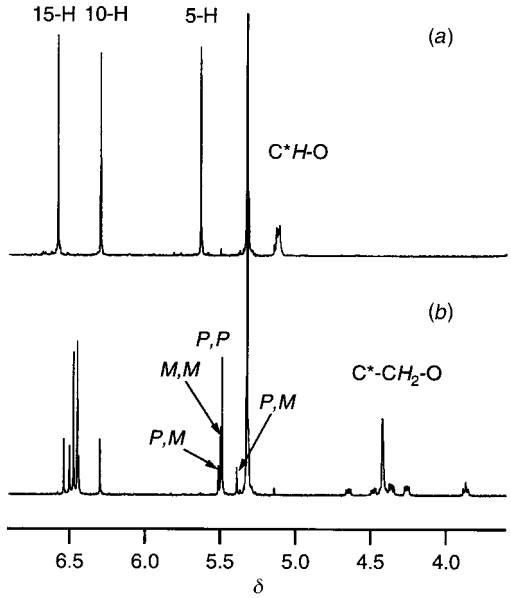

Fig. 2 Expanded region of ^{1}H NMR spectra of (a) **1a** and (b) **2** in CD_2Cl_2 at 288 K. [**1a**] = 2.57 mM and [**2**] = 2.50 mM.

ascribed to (*P*,*P*)-, (*P*,*M*)- and (*M*,*M*)-conformers, respectively [Fig. 2(b)]. The ratio of these three isomers determined by the signal integrations of the 5-H proton was (*PP*) : (*MM*) : (*PM*) = 51 : 27 : 22, indicating that homochiral conformers are preferred over *M*-helix, with a 24% excess of the *P*-helix of ZnBL. Therefore, extra methylene groups in **2** led to larger rotational freedom and less efficient helical chirality induction. It is noteworthy that, even in the flexible dimer **2**, homochiral conformers were preferred over the heterochiral one.

A further remarkable feature of **1** is that an anomalous upfield shift of one of the peripheral methyl groups was found in the ^{1}H NMR spectrum: the chemical shift of the 18-Me protons of **4** was observed at δ 1.72, whereas that of **1** was at δ 1.01. Other methyl protons appeared in a narrow region (δ 1.75, 2.01 and 2.07 for 2-, 7- and 13-methyl protons in **4**). This upfield shift is most likely caused by the proximity of the 18-methyl group of **1** to the ring current anisotropy of the other ZnBL. These NMR results and conformational search by force field/molecular orbital calculations afforded one of the possible conformers as shown in Fig. 3. In this conformation, the distance between the 18-Me carbon of ZnBL and the C-2′ carbon of the other ZnBL was 3.51 Å, indicating the van der Waals contact between the methyl group at the 18-Me and the A-ring pyrrole moiety of the other ZnBL. These van der Waals forces effectively fix the homochiral conformation.

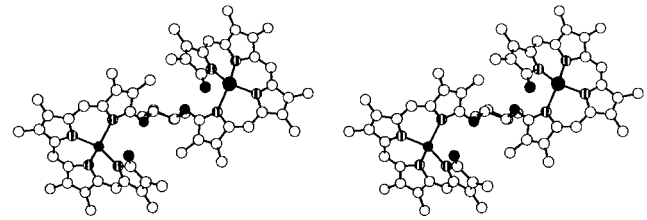

Fig. 3 Stereoview of one of the possible conformers of a model compound of **1a**, in which all the peripheral ethyl groups were replaced by methyl groups. All hydrogen atoms are omitted for clarify. The C_2 symmetric conformer was found by use of the grid conformational search program of Sybyl and the geometry was further optimized by MO calculations at the PM3 level (Spartan version 3).

Preliminary experiments showed that the (*P*,*P*)-conformer of **1a** was stable even in the presence of excess amounts of (*M*)-conformer-inducing L-amino acid esters.[4] Therefore, dimerization of the highly flexible framework of zinc bilinone led to the robust structure of **1**, which should be suitable as a framework of receptors.

Notes and references

1 J.-M. Lehn and A. Rigault, *Angew. Chem., Int. Ed. Engl.*, 1988, **27**, 1095.
2 C. Piguet, G. Bernardinelli and G.Hopfgartner, *Chem. Rev.*, 1997, **97**, 2005.
3 H. Falk, *The Chemistry of Linear Oligopyrroles and Bile Pigments*, Springer-Verlag, 1989.
4 T. Mizutani, S. Yagi, A. Honmaru and H. Ogoshi, *J. Am. Chem. Soc.*, 1996, **118**, 5318.
5 J. H. Fuhrhop, P. Krueger and W. S. Sheldrick, *Justus Liebigs Ann. Chem.*, 1977, 339.
6 J. H. Fuhrhop and P. Krueger, *Justus Liebigs Ann. Chem.*, 1977, 360.
7 R. Koerner, L. Latos-Grazynski and A. L. Balch, *J. Am. Chem. Soc.*, 1998, **120**, 9246.
8 M. J. Bulke, D. C. Pratt and A. Moscowitz, *Biochemistry*, 1972, **11**, 4025.
9 G. Blauer and G. Wagniere, *J. Am. Chem. Soc.*, 1975, **97**, 1949.
10 G. Wagniere and G. Blauer, *J. Am. Chem. Soc.*, 1976, **98**, 7806.
11 H. Scheer, H. Formanek and S. Schneider, *Photochem. Photobiol.*, 1982, **36**, 259.
12 T. Mizutani, S. Yagi, A. Honmaru, S. Murakami, M. Furusyo, T. Takagishi and H. Ogoshi, *J. Org. Chem.*, 1998, **63**, 8769.
13 T. Mizutani, S. Yagi, T. Morinaga, T. Nomura, T. Takagishi, S. Kitagawa and H. Ogoshi, *J. Am. Chem. Soc.*, 1999, **121**, 754.

Communication 9/02215E

First highly enantioselective allylic alkylations catalysed by platinum complexes

A. John Blacker,[a] Matthew L. Clark,[b] Michael S. Loft[c] and Jonathan M. J. Williams*[b]

[a] *Zeneca, Huddersfield Works, Leeds Road, Huddersfield, UK HD2 1FF*
[b] *Department of Chemistry, University of Bath, Claverton Down, Bath, UK BA2 7AY. E-mail: j.m.j.williams@bath.ac.uk*
[c] *Glaxo-Wellcome, DC1, Temple Hill, Dartford, UK DA1 5AH*

Received (in Liverpool, UK) 25th February 1999, Accepted 7th April 1999

Platinum complexes derived from phosphino-oxazolines are highly enantioselective catalysts for allylic alkylation reactions, but show different behaviour from related palladium complexes.

Transition metal catalysed allylic substitution reactions are classically carried out with palladium catalysts.[1] Although palladium often gives excellent results, the use of alternative metal catalysts has expanded the scope of the reaction considerably. Consequently, the study of different transition metals in this type of reaction is currently attracting considerable attention,[1,2] and there are recent reports on enantioselective allylic substitutions catalysed by iridium, [3] tungsten,[4] molybdenum[5] and nickel.[6] Reports on platinum catalysed allylic substitution reactions are extremely rare,[7] so we elected to study whether the different properties of platinum could expand the scope of this reaction still further.

Our initial studies have focused on the alkylation of diphenylpropenyl acetate with dimethyl sodiomalonate (Scheme 1). The chiral ligand **3** was chosen as it has been shown to be particularly suited to the palladium catalysed reaction.[8] As a starting point, we tested some readily available precursors in the presence of the chiral ligand. For example, 5 mol% of $(Ph_3P)_2Pt–(C_2H_4)$ in the presence of 10% of ligand **3** gave complete conversion to product at room temperature, but with low enantioselectivity (90% yield; 28% ee, 16 h, CH_2Cl_2, 20 °C).

We thought it likely that the PPh_3 present was competing with ligand **3**, and hence reducing the ee. We therefore felt that we needed to prepare a catalyst which would contain a single P,N ligand as the only phosphine present.

We had previously found that a combination of $(Ph_3P)_2PtCl_2$ and the reducing agent $NaBH(OMe)_3$ generates a Pt^0 complex which is an active catalyst (100% conversion: 16 h, 20 °C). We therefore chose to prepare the related complex **4**. This is readily accomplished by stirring the ligand and K_2PtCl_4 in refluxing MeCN (Scheme 2).

In contrast to the $(Ph_3P)_2PtCl_2/NaBH(OMe)_3$ system, a combination of complex **4** and $NaBH(OMe)_3$ does not catalyse the allylic alkylation of **1** at room temperature (Table 1, entry 1). However, after 30–50 h in refluxing THF, complete conversion into product is observed. It seems that complexes containing a bidentate P,N ligand make much less reactive catalysts when compared with complexes containing two phosphines. The ee of the products was high, but not as high as can be obtained with palladium.[8,9] If **4** is used in conjunction with 5% of ligand **3**, a small increase in ee was observed, whereas 10% added ligand

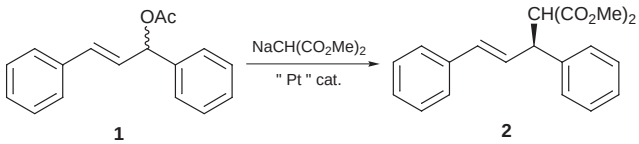

1 **2**

Scheme 1

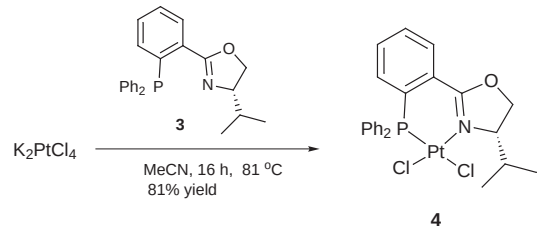

Scheme 2

gives significantly lower ee as shown in Table 1 (entries 4 and 5). If 5% PPh_3 is added, a highly reactive (but unselective) catalyst is generated (Table 1, entry 6). These results suggest that the P–Pt–N chelate ring is not stable in the presence of other ligands.

Despite early failures using the readily available tetrameric compound $[(C_3H_5)PtCl]_4$, **5**,[10] it was found that 1.25 mol% of **5** in combination with 5 mol% of ligand **3** catalysed the reaction. This system also requires reflux temperatures to obtain high yields of product. The highest ee (90%) was obtained at room temperature (Table 2, entry 1) and is reduced somewhat (entry 2) when the reaction is carried out at 65 °C. It should be noted that at high conversions, the ee of the starting acetate **1** had

Table 1 Enantioselective allylic alkylation of acetate **1** with complex **4** in the presence of 10% $NaBH(OMe)_3$[a]

Entry	Additive	*T*/°C	*t*/h	Conversion (%)[b] (% yield)	Ee (%) (config.)
1	—	20	20	—	—
2 [c]	—	65	90	48	77 (*S*)
3	—	65	44	65 (—)	77 (*S*)
4	**3** (5%)	65	35	100 (93)	83 (*S*)
5	**3** (10%)	65	44	100 (—)	61 (*S*)
6	PPh_3 (5%)	20	16	100 (91)	2 (*S*)

[a] All reactions carried out in THF, using 1.7 equiv. $NaCH(CO_2Me)_2$ as nucleophile. [b] Determined by HPLC using Daicel Chiralcel® OD column (hexane–Pr^{i}OH, 99 : 1) Configuration by comparison with known Pd catalysed products (ref. 8). [c] Reaction carried out in MeCN.

Table 2 Enantioselective allylic alkylation of acetate **1** using $[(C_3H_5)PtCl]_4$ in the presence of ligand **3**

Entry	**3** (%)	*T*/°C	*t*/h	Conversion (%) (% yield)	Ee (%) (config.)
1	5	20	72	25 (—)	90 (*S*)
2	5	65	48	81 (74)	84 (S)
3	10	20	24	32 (—)	86 (*S*)
4	10	65	44	100 (90)	57 (*S*)

[a] All reactions carried out in THF, using 1.7 equiv. $NaCH(CO_2Me)_2$ as nucleophile. [b] Determined by HPLC using Daicel Chiralcel® OD column (hexane/Pr^{i}OH 99 : 1). Configuration by comparison with known Pd catalysed products (ref. 8).

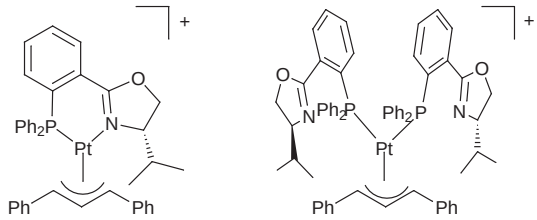

Fig. 1 Possible competing pathways in Pt catalysed allylic alkylation.

reached significant levels (73% ee). With this catalytic system, the presence of an increased amount of ligand is again detrimental to the enantioselectivity.

It seems clear that enantioselectivity and reactivity in the platinum catalysed reaction are much more sensitive to reaction conditions when compared with palladium. A possible explanation for this is that ligand **3** can be hemilabile when complexed to platinum. If this were the case, even to a small extent, it would be possible for the reaction to go *via* two competing pathways (Fig. 1). It is assumed that intermediate B would fail to give any significant level of enantiocontrol.

The platinum catalysed reaction had one more surprise in store for us, we tested the ligand (*R*,*R*)-chiraphos **6** in the catalytic reactions using tetramer **5** as our platinum source.

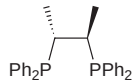

6

Bosnich and co-workers had previously found that, in the Pd catalysed reaction, this ligand does not give high enantioselectivity for substrate **1** (100% yield, 22% ee).[11] It was therefore interesting to find that at moderate conversion the product obtained had 95% ee. If the reaction was carried out at higher temperatures, moderate yields and somewhat lower enantioselectivity were obtained (Table 3, entry 2). The reaction was then tested using the palladium catalyst $[(C_3H_5)PdCl]_2$. In this instance we observed substantially higher enantioselectivity than was previously obtained (entry 3).

In conclusion, we have shown that several Pt complexes catalyse allylic alkylation with good enantioselectivity. Carefully controlled conditions are required in order to prevent loss of enantioselectivity by less selective pathways. This suggests that ligand **3** shows different coordination chemistry for platinum (compared with palladium). We are now trying to exploit the different properties of platinum to develop new asymmetric allylation reactions.

Table 3 Enantioselective allylic alkylation of acetate **1** in the presence of (*R*,*R*)-chiraphos[a]

Entry	Catalyst	*T*/°C	*t*/h	Conversion (%)[b]	Ee (%)[b] (config.)
1	5% $[(C_3H_5)PtCl]_4$	20	72	39	95 (S)
2	5% $[(C_3H_5)PtCl]_4$	56	67	57	74 (S)
3	5% $[(C_3H_5)PdCl]_2$	20	16	100	85 (S)

[a] All reactions carried out in THF, using 1.7 equiv. $NaCH(CO_2Me)_2$ as nucleophile. [b] Determined by HPLC using Daicel Chiralcel® OD column (hexane/Pr^{i}OH 99 : 1). Configuration by comparison with known Pd catalysed products (ref. 8).

We are grateful to the LINK asymmetric synthesis programme, Glaxo-Wellcome and Zeneca for financial support.

References

1 For reviews see C. G. Frost, J. Howarth and J. M. J. Williams, *Tetrahedron: Asymmetry*, 1992, **3**, 1089; B. M. Trost and D. L. Van Vranken, *Chem. Rev.*, 1996, **96**, 395.
2 Rhodium catalysis: P. A. Evans and J. D. Nelson, *J. Am. Chem. Soc.*, 1998, **120**, 5581; Iridium catalysis: R. Takeuchi and M. Kashio, *J. Am. Chem. Soc.*, 1998, **120**, 8647; Ruthenium catalysis: S. Zhang, T. Mitsudo, T. Kondo and Y. Watanabe, *J. Organomet. Chem.*, 1993, **450**, 197; Cobalt catalysis: J. Iqbal, M. Mukhopadhyay and A. K. Mandal, *Synlett*, 1996, 876; Molybdenum catalysis: A. V. Malkov, S. L. Davis, W. L. Mitchell and P. Kocovsky, *Tetrahedron Lett.*, 1997, **38**, 4899.
3 J. P. Janssen and G. Helmchen, *Tetrahedron Lett.*, 1997, **38**, 8025.
4 B. M. Trost and I. Hachiya, *J. Am. Chem. Soc.*, 1998, **120**, 1104.
5 G. C. Lloyd-Jones and A. Pfaltz, *Angew. Chem., Int. Ed. Engl.*, 1995, **34**, 462 and references therein.
6 N. Nomura and T. V. RajanBabu, *Tetrahedron Lett.*, 1997, **38**, 1713.
7 Pt catalysed allylic substitution: H. Kurosawa, *J. Chem. Soc., Dalton Trans.*, 1979, 939; J. M. Brown and J. E. MacIntyre, *J. Chem. Soc., Perkin Trans. 2*, 1985, 961.
8 J. M. J. Williams, *Synlett*, 1996, 705 and references therein.
9 Catalyst **4** was tested under a variety of conditions, but no improvement in ee was found. It should also be noted that to obtain the selectivities described here, it is important to use pure **4**, as crude material gives 50–60% ee.
10 J. Lucas, *Inorg. Synth.*, 1974, **15**, 79.
11 P. R. Aubern, P. B. MacKenzie and B. Bosnich, *J. Am. Chem. Soc.*, 1985, **107**, 2033.

Communication 9/01555H

Antineoplastic agents. Part 395.[1] Isolation and structure of agelagalastatin from the Papua New Guinea marine sponge *Agelas* sp.

George R. Pettit,* Jun-ping Xu, Diane E. Gingrich, Michael D. Williams, Dennis L. Doubek, Jean-Charles Chapuis and Jean M. Schmidt

Cancer Research Institute and Department of Chemistry, Arizona State University, Tempe, Arizona 85287-2404, USA

A human cancer cell line bioassay-directed investigation of the Western Pacific marine sponge *Agelas* sp. led to isolation of a trace (7.42×10^{-6}% yield) cancer cell growth inhibitor (lung NCI-H460 GI_{50} 0.77 μg m^{-1} to ovary OVCAR-3 GI_{50} 2.8 μg ml^{-1}) designated agelagalastatin 6; it is the first example of a natural product containing a digalactofuranosyl unit.

The marine porifera genus *Agelas* (class Demospongae, order Agelasida, family Agelasidae) has proven to be a rich source of new marine alkaloids[2] such as the cytotoxic (L1210 leukemia cell line) agelastatin A **1**[2a] and a series of glycosphingolipids[3]

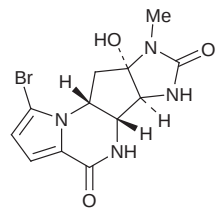

Agelastatin A **1**

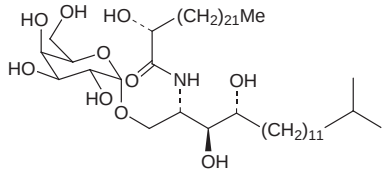

Agelasphin-9b **2**

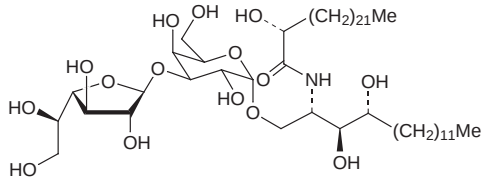

Longiside **3**

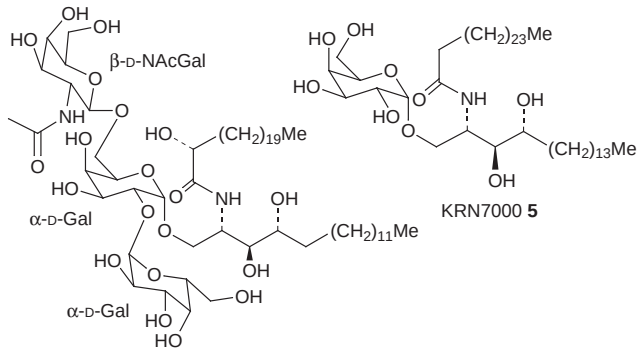

4

(*cf.* **2**,[3a], **3**,[3b], **4**[3c], **5**[3d]). Some (*e.g.* **2** and **5**) of these have shown immunomodulating activity,[2a,3d] and a structural modification **5**[3g] has been considered for preclinical development as an anticancer (murine melanoma B16 *in vivo* active) and non-specific immunostimulating agent.[3a,g] Because glycosphingolipids (cerebrosides) are vitally important in a variety of biochemical processes ranging from antigenic specificity to cell–cell signaling and modulation of the immune response, discovery of new naturally occurring cancer cell growth inhibitory compounds is clearly necessary. We now report the isolation and structural elucidation of the new glycosphingolipid agelagalastatin **6** from *Agelas* sp. that was initially evaluated during our 1980 expedition to the southeast coast of Papua New Guinea and recollected in 1983.

Agelas sp. (450 kg wet wt.) was extracted with MeOH and the alcohol-soluble portion was successively partitioned between 1 : 1 CH_2Cl_2–MeOH and water followed by n-hexane and 9 : 1 MeOH–water and finally CH_2Cl_2 and 3 : 2 MeOH–water. The resulting CH_2Cl_2-soluble fraction (630.5 g) was separated (directed by human cancer cell line bioassays) by a series of gel permeation and partition chromatographic procedures on Sephadex LH-20 columns with the series MeOH → n-hexane–CH_2Cl_2–MeOH (8 : 1 : 1) → n-hexane–Pr^iOH–MeOH (8 : 1 : 1) → n-hexane–toluene–acetone (1 : 4 : 4) as eluents to afford a fraction inhibitory to a selection of cancer cells. The bioactive fraction was treated with MeOH to selectively isolate the more soluble active constituent herein named agelagalastatin (**6**, 6.5 mg, 7.42×10^{-6}% yield). The residual fraction was dissolved in CH_2Cl_2–MeOH (1 : 1) and subsequently identified (by NMR spectral analysis) as a mixture of monogalactosyl ceramides[4,5] related to agelasphin-9b **2**.

Agelagalastatin **6** was obtained as a colorless amorphous powder: $[\alpha]_D$ + 59 (*c* 0.65, CH_3OH) which showed a molecular ion peak in the HRFABMS spectrum at *m*/*z* 1192.7859 $[M+Na]^+$ (calc. 1192.7910) corresponding to molecular formula $C_{60}H_{115}NO_{20}$. When a 5.2 mg specimen of agelagalastatin was subjected to acid hydrolysis (15 h at 70 °C) with 1 M HCl–MeOH (8 : 91) followed by acetylation, methyl α,β-D-galactopyranoside tetracetate (identical with an authentic sample) and the sphinganines (2*S*,3*S*,4*R*)-2-amino-15-methyl-1,3,4-trihydroxyhexadecane and (2*S*,3*S*,4*R*)-2-amino-16-methyl-1,3,4-hydroxyheptadecane were identified by physical and spectral data. The FABMS spectrum afforded three fragment ion peaks at *m*/*z* 1030.5 $(M + Na + H - Gal)^+$, 868.5 $(M + Na + H\text{-}2Gal)^+$ and 706.5 $(M + Na + H - 3Gal)^+$, suggesting the trisaccharide unit [Gal-Gal-Gal].

Interpretation of the ^1H–^1H COSY and TOCSY-NMR spectra led to assignment of the proton relay signals corresponding to five spin systems. The HMBC and ROESY 2D NMR experiments supplied definitive structural information regarding connections to the five spin systems and allowed a view of the overall structure. Detailed data from HMQC and HMBC spectra suggested the ceramide unit was composed of two spin systems, namely 4-hydroxysphinganine and an α-hydroxy ester. The latter was shown by mass spectral analysis of the preceding methanolysis products to be primarily a (2*R*)-hydroxypentacosanoate with about 20% of the corresponding homologous (2*R*)-hydroxytetracosanoate. Furthermore, the HMBC correlation peaks of C-1* with NH, H-2 and H-2* indicated that the two segments were linked together through an amide bond and all the chemical shifts shown by the ceramide units were reminiscent of those known for related compounds.[3]

The three anomeric proton signals appeared as doublets at δ 5.47 (H-1′), 5.78 (H-1″) and 5.61 (H-1‴) and were a useful starting point for establishing an additional three spin systems. The heteronuclear chemical shift correlation (HMQC) spectrum was used to assign relationships between protons and carbon in the three carbohydrate units A, B, and C. The ^{13}C NMR chemical shift data and the proton coupling constants measured by 2D *J* resolution experiments revealed the inner galactose (A) unit to be a D-galactopyranoside. From consideration of the *J*

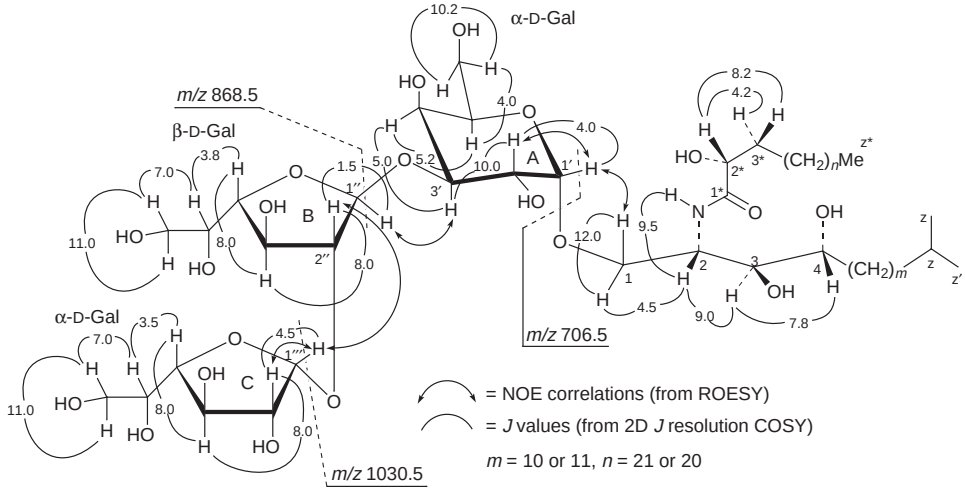

Fig. 1 NOE correlations and *J* values of agelagalastatin **6** (mass fragments include sodium).

value of the anomeric proton (H-1′, *J* 4.0 Hz) as well as the chemical shift of the corresponding carbon (C-1′, δ 101.31), the anomeric α-configuration was assigned. The HMBC correlations of H-1/C-1′ and H-1′/C-1 proved that the inner galactose segment (A) was directly connected with the C-1 ceramide hydroxy group by a glycosyl linkage.

Glycosylation shifts were observed at C-3′ (+8.42 ppm) and C-2′ (−2.36 ppm), along with HMBC correlations involving H-3′/C-1″ and H-1″/C-3′. Both results signified that C-3′ of galactose unit (A) was bonded through a glycoside link to the middle saccharide unit (B). The NOE correlation peaks of H-1/H-1′ and H-3′/H-1″ provided further evidence supporting two glycosyl linkages at two positions of the inner galactose section (A).

The two series of ^{13}C chemical shifts displayed by units B and C were both characteristic of a D-galactofuranoside.[6] Because of the five-membered ring, the ^{13}C chemical shifts of C-2″, C-3″ and C-4″ of unit B as well as those of C-2‴, C-3‴, and C-4‴ of unit C were significantly downfield compared with the corresponding data for D-galactopyranoside. Additional NMR data suggested that the two furanoside units (B and C) corresponded to 1,4-linked five-membered rings. Confirmatory evidence arose from the HMBC correlations of H-1″/C-4″, H-1‴C-4‴ and H-4‴/C-1‴, which exactly defined the furanosyl 1,4-linkages, and from 2D *J* resolution values attesting to the 2,3-diaxial (*J* 8.0 Hz) and 3,4-diaxial (*J* 8.0 Hz) relationships in the D-galactofuranoside (Fig. 1).

The chemical shifts of the anomeric carbons at δ 108.51 (C-1″) and 101.69 (C-1‴) together with the coupling constants of the anomeric protons (H-1″, *J* 1.5 Hz and H-1‴, *J* = 4.5 Hz) allowed the middle (B) and outer D-galactofuranosyl units (C) to be assigned β- and α-configurations,[6] respectively. Furthermore, the NOE relationship from H-1″ to H-3′ together with HMBC correlation between H-1″ and C-3′ showed the presence of a 1″–3′ glycosyl linkage between galactosyl sections A and B. The HMBC correlations of H-1‴/C-2″ and H-2″/C-1‴ combined with the NOE relationship of H-2″/H-1‴ indicated that the outer furanose unit (C) was joined to the C-2″ hydroxy group of the middle furanose (B). Thus, agelagalastatin was assigned structure **6** assuming that the overall stereochemistry and absolute configuration corresponds to that generally found for such glycosphingolipids.[3] To the best of our knowledge, agelagalastatin **6** is the first marine animal constituent found to possess a digalactofuranosyl unit.

Agelagalastatin **6** displayed significant *in vitro* activity against a portion of our minipanel (including brain SF-295, renal A498, colon KM20L2 and melanoma SK-MEL-5) of human cancer cell lines with GI_{50} values ranging from 0.77 μg ml^{-1} for lung NCI-H460 to 2.8 μg ml^{-1} for the ovarian OVCAR-3. Future research based on discovery of agelagalastatin will entail confirmation of the stereochemistry by total synthesis followed by detailed biological evaluation.

We thank the following for necessary financial assistance: Outstanding Investigator Grant CA 44344-01A1-09 and PHS Grant CA-16049-09-12 awarded by the Division of Cancer Treatment, National Cancer Institute, DHHS; the Fannie E. Rippel Foundation; the Arizona Disease Control Research Commission; the Robert B. Dalton Endowment Fund; Virginia Piper; Diane Cummings Halle (The Nathan Cummings Foundation); Lottie Flugel; Polly J. Trautman; John and Edith Reyno; the Fraternal Order of Eagles Art Ehrmann Cancer Fund; and the Ladies Auxiliary, VFW, Department of Arizona. In addition, we thank for other assistance the Government of Papua New Guinea (Andrew Richards and Navu Kwapena), Drs Daniel Brune, Ronald L. Cerny, Fiona Hogan and Yoshiaki Kamano; Mrs Betty J. Abbott, Mr Lee Williams and Ms Kim M. Weiss; the US National Science Foundation (NSF Grants CHE-8409644 and BBS-88-04992); and the NSF Regional Instrumentation Facility in Nebraska (Grant CHE-8620177).

Notes and references

1 Part 394: J. O. Carey, K. J. Posekany, J. E. de Vente, G. R. Pettit and D. K. Ways, *Blood*, 1996, **87**, 4316.
2 (*a*) M. D'Ambrosio, M. Ripamonti, C. Debitus, J. Waikedre and F. Pietra, *Helv. Chim. Acta*, 1996, **79**, 727; (*b*) F. Cafieri, E. Fattorusso, A. Mangoni and O. Taglialatela-Scafati, *Tetrahedron Lett.*, 1995, **36**, 7893; (*c*) C. Jiménez and P. Crews, *Tetrahedron Lett.*, 1995, **35**, 1375.
3 (*a*) T. Natori, M. Morita, K. Akimoto and Y. Koezuka, *Tetrahedron*, 1994, **50**, 2771; (*b*) F. Cafieri, E. Fattorusso, Y. Mahajnah and A. Mangoni, *Liebigs Ann. Chem.*, 1994, 1187; (*c*) V. Costantino, E. Fattorusso, A. Mangoni, M. Aknin and E. M. Gaydon, *Liebigs Ann. Chem.*, 1994, 1181; (*d*) V. Costantino, E. Fattorusso and A. Mangoni *Tetrahedron*, 1996, **52**, 1573; (*e*) F. Cafieri, E. Fattorusso A. Mangoni and O. Taglialetela-Scafati, *Liebigs Ann. Chem.*, 1995, 1477; (*f*) V. Costantino, E. Fattorusso and A. Mangoni, *Liebigs Ann. Chem.*, 1995, 1471; (*g*) M. Morita, K. Motoki, K. Akimoto, T. Natori, T. Sakai, E. Sawa, K. Yamaji, Y. Koezuka, E. Kobayashi and H. Fukushima, *J. Med. Chem.*, 1995, **38**, 2176; (*h*) F. Cafieri, E. Fattorusso, A. Mangoni and O. Taglialatela-Scafati, *Gazz. Chim. Ital.*, 1996, **126**, 711.
4 H. Y. Li, S. Matsunaga and N. Fusetani, *Tetrahedron*, 1995, **51**, 2273; W. Jin, K. Rinehart and E. A. Jares-Erijman, *J. Org. Chem.*, 1994, **59**, 144.
5 J. Shin and Y. Seo, *J. Nat. Prod.*, 1995, **58**, 948; I. Mancini, G. Guella, C. Debitus and F. Pietra, *Helv. Chim. Acta*, 1994, **77**, 51.
6 R. George and S. Ritchie, *Can. J. Chem.*, 1975, **53**, 1424.

Communication 9/02380A

A concise approach towards the synthesis of steganone analogues

Adrian Bradley,[a] William B. Motherwell*[a] and Feroze Ujjainwalla[b]

[a] *Department of Chemistry, Christopher Ingold Laboratories, University College London, 20 Gordon Street, London, UK WC1H 0AJ. E-mail: w.b.motherwell@ucl.ac.uk*

[b] *Department of Chemistry, Imperial College of Science, Technology and Medicine, South Kensington, London, UK SW7 2AY*

Received (in Cambridge, UK) 27th January 1999, Accepted 12th April 1999

The cobalt-mediated [2+2+2] cycloaddition of a tethered deca-1,9-diyne is used as a key step in a highly convergent route to steganone analogues.

Steganone **1** is one member of the family of four bisbenzocyclooctadiene lignan lactones isolated from the Ethiopean shrub *Steganotaenia araliciae* Hochst and characterised by Kupchan[1]

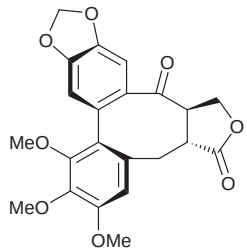

1

in 1973. These compounds have displayed significant activity *in vivo* against P-388 leukemia in mice and *in vitro* against cells derived from human carcinoma of the nasopharynx (KB). They act as spindle poisons and function by stabilising dimeric tubulin and thereby inhibiting formation of microtubules.[2] These intriguing structures, comprising an eight-membered ring fused to a biaryl moiety, are composed of three stereochemical elements, two deriving from the *trans*-fused γ-lactone, whilst the third is the stereogenic axis of the atropisomeric biaryl unit. Since its discovery, steganone **1** has proven to be a favoured target for sustained synthetic effort, and for more than two decades a wide variety of synthetic strategies have culminated in a number of total/formal syntheses.[3] Careful scrutiny of these approaches reveals striking parallels in retrosynthetic analysis, with no less than ten of the syntheses requiring a late stage installation of the *trans*-fused γ-lactone. Moreover, in every single instance to date some variant of a biaryl coupling reaction is used to forge the crucial carbon–carbon bond between the two aromatic rings.

Since the properties of steganone **1** itself are well known, our own objective in this area was to develop a highly convergent route which would be potentially amenable to the syntheses of a wide variety of differentially substituted aromatic analogues for use in structure–activity studies. To the best of our knowledge, only a single analogue of this type has thus far been reported.[4] As shown in Scheme 1, the key element of the present strategy involves the use of the tethered diyne **2** in a cobalt mediated [2+2+2] cycloaddition,[5] thereby enabling closure of the eight-membered carbocyclic ring with concomitant construction of a usefully functionalised northern aryl unit for further elaboration. We also envisaged that the required *trans* stereochemistry round the γ-lactone **2** would be derived by alkylation of the lactone enolate from **3** with the benzylic bromide **4** or congeners thereof which would allow yet further variation in aromatic functionality to be introduced at an antepenultimate stage.

In the event, as outlined in Scheme 2, it was possible to develop a concise and highly efficient route to multigram quantities of the required diyne **2**. Thus, the protected lactone **3** was readily prepared from racemic paraconic acid **5** *via* palladium-catalysed coupling of the derived acid chloride with $Me_3SiC{\equiv}CSnMe_3$ followed by ketalisation of the resultant ynone **6**, whilst the known benzylic alcohol[7] **7** was available from 3,4,5-trimethoxybenzaldehyde *via* a straightforward sequence involving iodination, borohydride reduction, and a second palladium catalysed coupling reaction of the resultant iodoarene with $Me_3SiC{\equiv}CH$. The transformation to the corresponding bromide **4** was then acheived using the PPh_3–CBr_4 protocol. The coupling reaction of the two fragments proceeded smoothly through prior generation of the lithium enolate of lactone **3** with LDA at −78 °C followed by alkylation with the benzylic bromide **4** at −35 °C to give **8** as a single diastereoisomer. Deprotection of the acetylenic groups then furnished the parent diyne **2**.

Our attention then focused on the crucial $CpCo(CO)_2$-mediated [2+2+2] cycloaddition step using diyne **2**, $Me_3SiC{\equiv}CSiMe_3$ as the third acetylenic component, and the standard irradiation conditions developed by Vollhardt.[5] To our consternation, initial experiments failed to yield any significant amounts of the desired biaryl **9**, and the beautifully crystalline orange material which could be isolated as a single diastereoisomer in up to 57% yield was shown by X-ray crystallography to be the cobaltacyclobutadiene complex **10** (Scheme 3). Although the formation of similar complexes has been previously observed[9] and is generally considered to arise when either co-ordination or insertion of the third alkyne component is problematic, it was nevertheless encouraging to note that the structure **10** confirmed both the viability of the eight-membered ring closure and also the *trans* stereochemistry around the γ-lactone. Gratifyingly however, whether *via* the intermediacy of the putative metallocyclopentadiene precursor to **10** or one of the other two possible candidates from reaction with Me_3-

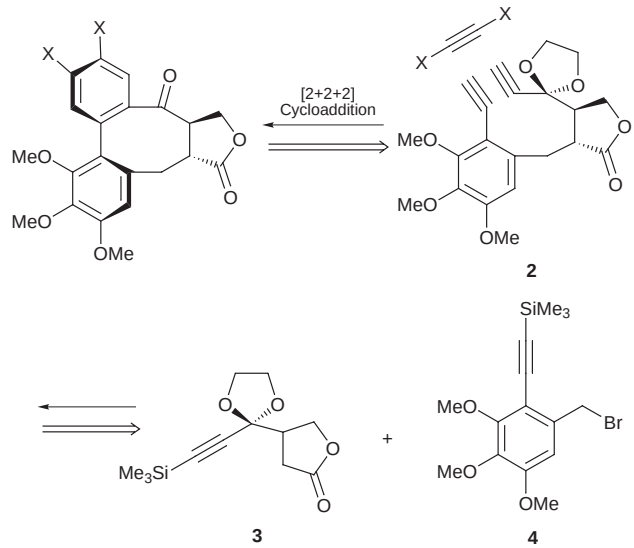

2 **3** **4**

Scheme 1

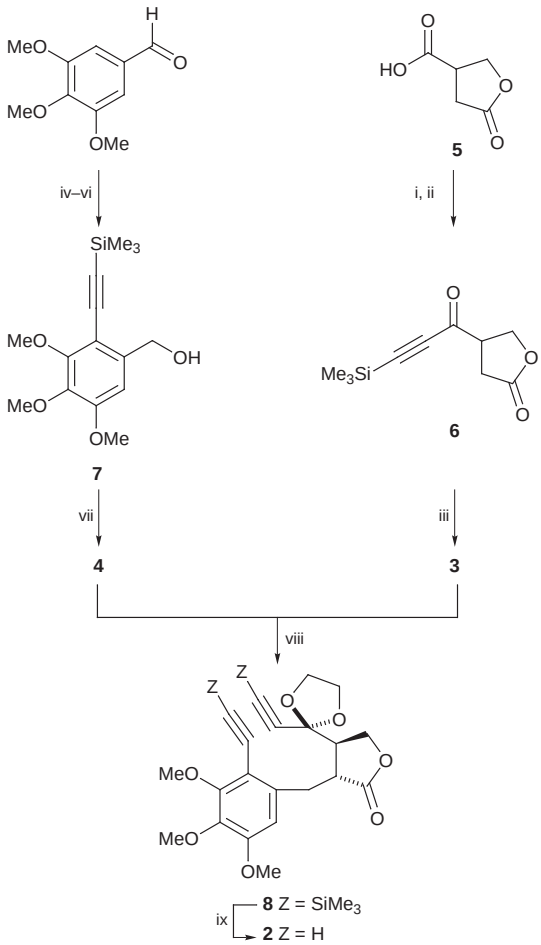

Scheme 2 *Reagents and conditions*: i, $(COCl)_2$, CH_2Cl_2, DMF (cat), room temp., 1 h; ii, $Me_3SiC{\equiv}CSnMe_3$, $Pd(PPh_3)_2Cl_2$, $ClCH_2CH_2Cl$, 50 °C, 16 h, 67% over 2 steps; iii, $HOCH_2CH_2OH$, PhH, PPTS (cat), reflux, 12 h, 87%; iv, I_2, AgO_2CCF_3, CH_2Cl_2, 20 °C, 12 h, quant.; v, $NaBH_4$, MeOH, −5 °C, 30 min, quant.; vi, $Me_3SiC{\equiv}CH$, $Pd(PPh_3)_2Cl_2$, CuI, Et_2NH, 50 °C, 2 h, 92%; vii, CBr_4, PPh_3, Et_2O, 24 h, 92%; viii, **4**, LDA, THF, −78 °C, 1 h, then add **3**, −35 °C, 1 h, 80%; ix, K_2CO_3, MeOH, 20 °C, 15 h, 95%.

$SiC{\equiv}CSiMe_3$, further variation in experimental conditions gave the desired biaryl **9** possessing the carbocyclic steganone core in 20% yield.

The structure of the indicated atropisomer of the biaryl **9**, which corresponds to the natural series, was established both by NOE experiments and also by deprotection of the ketal using wet formic acid which furnished the parent ketone **11** (ν_{max} 1674 cm^{-1}) in 54% yield (Scheme 3). Deprotection accompanied by selective mono- or di-protodesilylation could also be achieved in a single step by treatment of **9** with TFA either at room temperature or at reflux to afford the further steganone analogues **12** and **13** in 73 and 51% yield, respectively.

In summary, these preliminary results demonstrate the viability of using a tethered deca-1,9-diyne in a cobalt-mediated [2+2+2] cyclobenzannulation strategy for the construction of steganone analogues in a highly convergent manner. Within this framework, current studies are directed towards the use of further 2π addends and additional metal-based cyclotrimerisation reactions both for aromatic and heteroaromatic rings in order to further enhance the flexibility of this approach.

We thank the EPSRC and Zeneca Agrochemicals for the award of a CASE studentship to F. U., and University College London for the provision of a Provosts' studentship to A. B. We are also indebted to Professor D. Williams and Dr A. M. Z. Slawin for X-ray structural determination and the University of London Intercollegiate Research School (ULIRS) for mass spectral measurements. Finally, one of us (W. B. M.) wishes to acknowledge his personal debt of gratitude to the late Professor R. A. Raphael FRS, whose mastery of the Art of Organic Synthesis was matched only by his ability to encourage and to instil his love and enthusiasm for the subject in others.

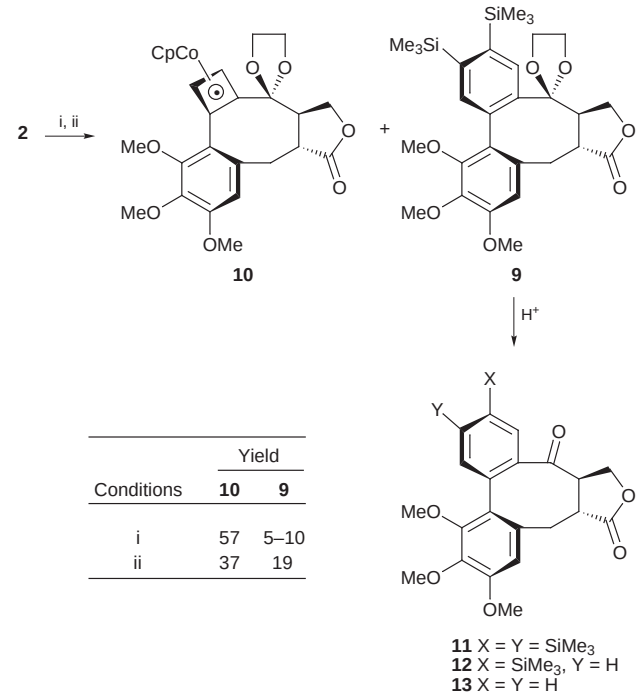

	Yield	
Conditions	**10**	**9**
i	57	5–10
ii	37	19

Scheme 3 *Reagents and conditions*: i, $Me_3SiC{\equiv}CSiMe_3$, $CpCo(CO)_2$, 50–65 °C, reflux, *hν*, addition of **2** in THF over 9 h; ii, $Me_3SiC{\equiv}CSiMe_3$, MeCN, reflux, *hν*, addition of **2** in THF over 9 h.

Notes and references

1 S. M. Kupchan, R. W. Britton, M. F. Ziegler, C. J. Gilmore, R. J. Restivo and R. Bryan, *J. Am. Chem. Soc.*, 1973, **95**, 1335
2 R. W. J. Wang, L. I. Rebbun and M. S. Kupchan, *Cancer Res.*, 1977, **37**, 3071.
3 N. S. Narasimhan and I. R. Aiden, *Tetrahedron Lett.*, 1988, **29**, 2987; N. S. Narasimhan and I. R. Aiden, *Indian J. Chem., Sect. B.*, 1993, **32B**, 211; A. I. Meyers, J. R. Flisak and R. A. Aitken, *J. Am. Chem. Soc.*, 1987, **109**, 5446; P. Magnus, J. Schultz and T. Gallagher, *J. Am. Chem. Soc.*, 1985, **107**, 4984; R. Dhal, J. P. Robin and E. Brown, *Tetrahedron* 1983, **39**, 2787; M. Mervic, Y. Ben-David and E. Ghera, *Tetrahedron Lett.*, 1981, **22**, 5091; F. E. Ziegler, I. C. Chliwner, K. W. Fowler, S. J. Kanfer, S. J. Kuo and N. D. Sinha, *J. Am. Chem. Soc.*, 1980, **102**, 790; E. Brown, R. Dhal and J. P. Robin, *Tetrahedron Lett.*, 1979, 733; E. R. Larson and R. A. Raphael, *Tetrahedron Lett.*, 1979, 5041; G. R. Krow, K. M. Damadoran, E. Michener, R. Wolf and J. Gaure, *J. Org. Chem.*, 1978, **43**, 3950; D. Becker, L. R. Hughes and R. A. Raphael, *J. Chem. Soc., Perkin Trans. 1*, 1977, 1674; L. R. Hughes and R. A. Raphael, *Tetrahedron Lett.*, 1976, 1543; A. S. Kende and L. S. Liebskind, *J. Am. Chem. Soc.*, 1976, **98**, 267; M. Uemura, A. Daimon and Y. Hayashi, *J. Chem. Soc., Chem. Commun.*, 1995, 1943.
4 D. Becker, L. R. Hughes and R. A. Raphael, *J. Chem. Soc., Chem. Commun.*, 1974, 430.
5 K. P. C.Vollhardt, *Angew. Chem., Int. Ed. Engl.*, 1984, **28**, 539.
6 J. F. Tocanne and C. Asselineau, *Bull. Chem. Soc. Fr.*, 1965, 3346.
7 M. E. Garst and B. J. McBride, *J. Org. Chem.*, 1989, **54**, 249.
8 F. Ujjainwalla, PhD thesis, University of London, 1993. We are grateful to Drs D. Williams and A. M. Z. Slawin for the crystal structure determination, which will be discussed in the full paper.
9 R. Gleiter, D. Kratz, M. L. Ziegler and B. Nuber, *Tetrahedron Lett.*, 1990, **31**, 6175; C.-A. Chang, J. A. King Jr. and K. P. C. Vollhardt, *J. Chem. Soc., Chem. Commun.*, 1981, 53; C.-A. Chang, C. G. Francisco, T. R. Gadek, J. A. King Jr., E. D. Sternberg and K. P. C. Vollhardt, in *Organic Synthesis Today and Tomorrow*, ed. B. M. Trost and C. R. Hutchinson, Pergamon, New York, 1981, 71; P. Phanasavath, C. Aubert and M. Malacria, *Tetrahedron Lett.*, 1998, **39**, 1561.

Communication 9/00743A

Trifluorovinylxenon(II) tetrafluoroborate

H.-J. Frohn*[a] and V. V. Bardin[b]

[a] *Fachgebiet Anorganische Chemie, Gerhard-Mercator-Universität Duisburg, Lotharstr. 1, D-47048 Duisburg, Germany. E-mail: frohn@uni-duisburg.de*

[b] *Institute of Organic Chemistry, Lotharstr. 1, 630090 Novosibirsk, Russia*

Received (in Basel, Switzerland) 18th February 1999, Accepted 2nd April 1999

The first acyclic alkenylxenon(II) compound, trifluorovinylxenon(II) tetrafluoroborate, was prepared from XeF_2 and trifluorovinylboron difluoride and characterized by ^{13}C, ^{19}F and ^{129}Xe NMR spectroscopy.

In 1993 we reported the first preparation of the cyclic alkenylxenon(II) compounds, (heptafluorocyclohexa-1,4-dien-1-yl)xenon(II) **1** and (nonafluorocyclohexen-1-yl)xenon(II) **2** hexafluoroarsenates by stepwise fluorine addition to $[C_6F_5Xe]^+[AsF_6]^-$ using XeF_2 in anhydrous HF (aHF).[1] Later (2-H-hexafluorocyclohexa-1,4-dien-1-yl)xenon(II) **3** and (2-H-octafluorocyclohexen-1-yl)xenon(II) **4** tetrafluoroborates[2] were obtained in a similar manner from (2,3,4,5-tetrafluorophenyl)xenon(II) tetrafluoroborate. Electrophilic oxygenation of $[C_6F_5Xe]^+[AsF_6]^-$ with XeF_2 and stoichiometric amounts of H_2O in HF gave (3-oxopentafluorocyclohexa-1,4-dien-1-yl)xenon(II) **5** and (3-oxo-4,5-epoxypentafluorocyclohexen-1-yl)xenon(II) **6** hexafluoroarsenates.[3]

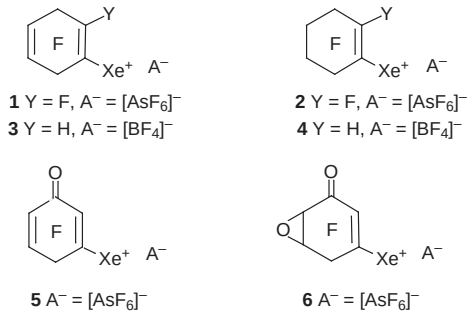

1 Y = F, A^- = $[AsF_6]^-$ **2** Y = F, A^- = $[AsF_6]^-$
3 Y = H, A^- = $[BF_4]^-$ **4** Y = H, A^- = $[BF_4]^-$

5 A^- = $[AsF_6]^-$ **6** A^- = $[AsF_6]^-$

All these synthetic routes to cyclic alkenylxenon(II) salts are based on the functionalization of arylxenon(II) salts and are restricted to the preparation of compounds with cyclohexadienyl- and cyclohexenyl-xenon(II) skeletons.

The topic of this paper is the elaboration of an alternative and new strategy and a more general approach to the synthesis of fluoroalkenylxenon(II) compounds: the reaction of XeF_2 with polyfluoroalkenylboron difluorides. When XeF_2 was reacted with trifluorovinylboron difluoride at −40 °C in CH_2Cl_2 the first acyclic alkenylxenon(II) salt, trifluorovinylxenon(II) tetrafluoroborate **7**,† was obtained in very good yield [eqn. (1)].

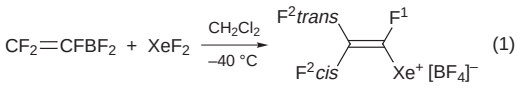

(1)

7

Salt **7** is a white solid which decomposes above *ca*. 0 °C. It is insoluble in CH_2Cl_2 but dissolves well in anhydrous HF (aHF), MeCN and EtCN. Its solution in aHF is stable at room temperature for some hours (monitored by ^{19}F NMR), whereas in MeCN (basic medium) **7** decomposes slowly above −20 °C and rapidly at room temperature with formation of xenon and some uncharacterized polyfluoroolefins.

The ^{19}F NMR spectrum[4] of the vinylxenon salt **7** in aHF (−30 °C) consists of resonances at δ −81.91 (F-2 *trans*) [^2J(F-2 *trans*)-(F-2 *cis*) 42 Hz, ^3J(F-2 *trans*)–(F-1) 105 Hz], −100.13 (F-2 *cis*) [^3J(F-2 *cis*)–(F-1) 126 Hz], −126.36 (F-1), −148.22 ($[BF_4]^-$, br) and HF at δ −190.83. All resonances of fluorine atoms bonded to carbon have ^{129}Xe satellites corresponding to the natural abundance of ^{129}Xe (I = 1/2) of 26.4%: ^3J(F-2 *cis*)-(^{129}Xe) 30 Hz, ^3J(F-2 *trans*)–(^{129}Xe) 146 Hz and ^2J(F-1)–(^{129}Xe) 248 Hz.

Resonances[4] of the carbon atoms C-1 and C-2 in the ^{19}F-decoupled ^{13}C NMR spectrum of **7** were located at δ 100.60 and 148.77, respectively and both displayed ^{129}Xe satellites: ^1J(C-1)–(^{129}Xe) 131 Hz and ^2J(C-2)–(^{129}Xe) 18 Hz. For comparison, the resonance of the carbon atom C-1 in the ^{13}C NMR spectrum of (nonafluorocyclohexen-1-yl)xenon(II) hexafluoroarsenate **2** in aHF (−10 °C) occurs at δ 96.28 and ^1J(C-1)–(^{129}Xe) is 114 Hz.[1]

The ^{129}Xe NMR spectrum[4] of compound **7** in aHF (−30 °C) displays a doublet of doublets of doublets at δ −3636.1($\Delta\nu_{1/2}$ = 13 Hz) [^2J(^{129}Xe)–(F-1) 248 Hz, ^3J(^{129}Xe)–(F-2 *cis*) 30 Hz, ^3J(^{129}Xe)–(F-2 *trans*) 146 Hz] (Fig. 1). This deshielding of the xenon atom in **7** is remarkable when compared to δ(^{129}Xe) values of the (polyfluorocycloalken-1-yl)xenon(II) compounds **1**–**6** (δ −3912.3, −3858.4, −3771.8, −3714.0, −3916.2 and −3900.3, respectively)[1–3] and is probably the result of a strong 'through-space' electronic interaction of the xenon atom with the geminal fluorine atom F-1. This consideration is also in agreement with the large value of ^2J(^{129}Xe)–(F-1), which is the largest of the the known coupling constants in organoxenon compounds.

The ^{19}F NMR spectrum of a solution of **7** in EtCN at −40 °C consists of resonances at δ −84.97 (F-2 *trans*) [^2J(F-2 *trans*)–(F-2 *cis*) 46 Hz, ^3J(F-2 *trans*)–(F-1) 90 Hz], −103.36 (F-2 *cis*) [^3J(F-2 *cis*)–(F-1) 124 Hz], −137.81 (F-1) and −149.59 ($[BF_4]^-$) [^3J(F-2 *cis*)–(^{129}Xe) 29 Hz, ^3J(F-2 *trans*)–(^{129}Xe) 139 Hz, ^2J(F-1)–(^{129}Xe) 191 Hz]. The ^{129}Xe NMR signal was located at δ −3510.6 [^2J(^{129}Xe)–(F-1) 197 Hz, ^3J(^{129}Xe)–(F-2

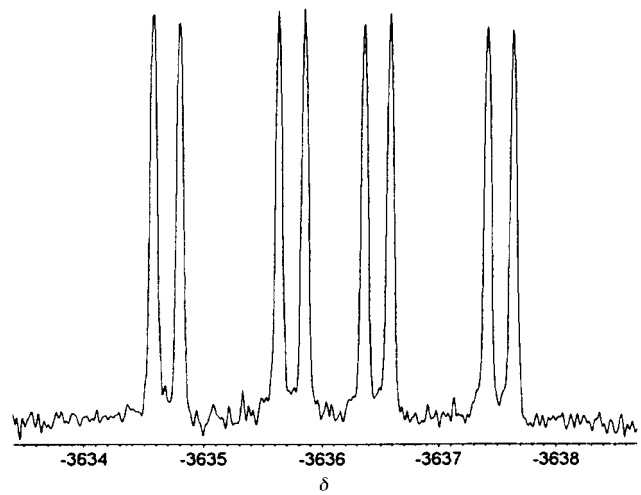

Fig. 1 ^{129}Xe NMR resonance of **7** (aHF, −30 °C, 5 mm glass tube with FEP inliner, measured on a Bruker DRX 500 spectrometer at 138.34 MHz; shift values relative to neat $XeOF_4$ at 24 °C.

cis) 27 Hz, $^3J(^{129}Xe)$–(F-2 *trans*) 136 Hz]. Cooling to −70 °C led to shielding of the fluorine atom F-1 and a decrease of ^2J(F-1)–(^{129}Xe) to 188 Hz resulting from a favoured cation–anion interaction over the cation–EtCN interaction:[5] δ −84.09 (F-2 *trans*) [^2J(F-2 *trans*)–(F-2 *cis*) 46 Hz, ^3J(F-2 *trans*)–(F-1) 88 Hz], −102.62 (F-2 *cis*) [^3J(F-2 *cis*)–(F-1) 123 Hz], −138.27 (F-1) and −150.31 ([BF_4]$^-$) [^3J(F-2 *cis*)–(^{129}Xe) 28 Hz, ^3J(F-2 *trans*)–(^{129}Xe) 136 Hz].

Chemical proof of the carbon–xenon bond and of the electrophilic nature of the vinylxenon(II) cation in **7** was obtained by conversion into trifluoroiodoethene with loss of Xe^0 when a solution of **7** in EtCN was treated with NaI in excess at ⩽−30 °C [eqn. (2)] (*cf.* ref. 6).

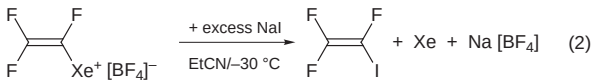

(2)

In summary, the trifluorovinylxenon cation is of great importance for preparative and theoretical chemistry because it is an unique precursor for the trifluorovinyl radical and cation.

We gratefully acknowledge Volkswagen Stiftung and Fonds der Chemischen Industrie for financial support.

Notes and references

† *Synthesis of trifluorovinylxenon*(II) *tetrafluoroborate* **7**: a solution of XeF_2 (1.83 mmol) in CH_2Cl_2 (15 ml) was cooled to −40 °C and added to a solution of trifluorovinylboron difluoride (1.54 mmol) in dichloromethane (10 ml) at −40 °C under a dry argon atmosphere. After stirring at −40 to −50 °C for 5 h the mother liquor was decanted and the residual product was washed and dried under vacuum to yield compound **7** (1.30 mmol, 85 %).

1 H.-J. Frohn and V. V. Bardin, *J. Chem. Soc., Chem. Commun.*, 1993, 1072.
2 H.-J. Frohn and V. V. Bardin, *Z. Naturforsch., Teil B*, 1998, **53**, 562.
3 H.-J. Frohn and V. V. Bardin, *Z. Naturforsch., Teil B*, 1996, **51**, 1011.
4 The NMR shift values are relative to CCl_3F (^{19}F), TMS (^{13}C) and $XeOF_4$ (^{129}Xe).
5 H.-J. Frohn, A. Klose, T. Schroer, G. Henkel, V. Buss, D. Opitz and R. Vahrenhorst, *Inorg. Chem.*, 1998, **37**, 4884.
6 H.-J. Frohn and V. V. Bardin, *Z. Anorg. Allg. Chem.*, 1996, **622**, 2031.

Communication 9/01380F

ChemComm

Zeolite-β grown epitaxially on SSZ-31 nanofibers

Sankar Nair,[a] Luis A. Villaescusa,[b] Miguel A. Camblor*[b] and Michael Tsapatsis*[a]

[a] *Department of Chemical Engineering, University of Massachusetts, Amherst MA 01003, USA. E-mail: tsapatsi@ecs.umass.edu*

[b] *Instituto de Tecnología Química (CSIC-UPV), Universidad Politécnica de Valencia, Avda. Los Naranjos s/n, 46071 Valencia, Spain. E-mail: macamblo@itq.upv.es*

Received (in Columbia, MO, USA) 31st December 1998, Accepted 31st March 1999

The synthesis and characterization of an epitaxial growth of zeolite β on SSZ-31 nanofibers is described, and a structural model of the interface between the two zeolites is proposed.

Zeolite crystals in the form of nanofibers have several potential catalytic applications, owing to the short diffusion lengths across these fibers and their low resistance to fluid flow (low pressure drop), as well as other advanced materials applications owing to the possibility of incorporating them in membrane, sensor or electronic devices. A few zeolites with one-dimensional (1-D) pore systems are known to crystallize in a needle-like morphology[1–3] with the channels running along the long axis of the particles. This raises the possibility of epitaxially growing other zeolitic structures on nanofibers of such 1-D pore zeolites. We report here, the first such epitaxial process, involving the growth of zeolite-β on nanofibers of the 1-D zeolite SSZ-31, and we propose a structural model for the interface between the two zeolites.

Zeolite-β is an industrially important large-pore material, widely used in catalytic and adsorption processes.[4,5] Previous syntheses of zeolite-β resulted in equiaxed particles that contain both the β polymorphs A and B. In this study, zeolite-β was synthesized as pure silica polymorph using 1,3,3,6,6-pentamethyl-6-azoniumbicyclo[3.2.1]octane cation as the organic structure-directing agent (SDA). This cation was synthesized by quaternization of the parent amine with an excess of MeI in CCl_3H, and was used in hydroxide form after anion exchange of the iodide.

For the zeolite synthesis, tetraethylorthosilicate (21.89 g) was hydrolysed in 35.02 g of an aqueous solution of the SDA in hydroxide form (1.49 mmol g^{-1}). The mixture was stirred, allowing evaporation of the ethanol produced in the hydrolysis. Further stirring for 3 h at room temperature allowed the evaporation of a total mass of 22.69 g (ethanol plus water). Then, HF (2.18 g, 48% aqueous solution) was added and the mixture was shaken till homogeneous. Hydrothermal crystallization of this mixture (final composition SiO_2 : 0.5 $C_{12}H_{24}NOH$: 0.5 HF : 9.9 H_2O) in rotating (60 rpm) Teflon-lined stainless steel autoclaves at 150 °C for 20 days produced a crystalline solid with an XRD pattern similar to that of zeolite-β.[6,7]

However, there were several facts suggesting that this material was not identical to zeolite-β and that it could also be related to zeolite SSZ-31. First, the XRD pattern shows some differences with the pattern of zeolite-β and some similarities with that of SSZ-31[3,8]. For instance, the shape of the first broad peak at low angle is more like that of the second peak in SSZ-31 rather than the first peak in zeolite-β. Also, the separation of the two main peaks in the range 2θ 20–22.5° of 1.20° is closer to that in SSZ-31 (1.28°) than in β (1.08°). Furthermore, the adsorption capacity of this material (0.13 cm^3 g^{-1}) calculated from the N_2 adsorption isotherm using the *t*-plot method, is intermediate between those of zeolites β (0.19 cm^3 g^{-1}) and SSZ-31 (0.08 cm^3 g^{-1}). Interestingly, when the final water : silica ratio in the above synthesis mixture composition was increased to 15, SSZ-31 was obtained (when the ratio was decreased to 7.5, ITQ-3[9] was the crystallization product). All these suggested that the synthesized solid could actually be an intergrowth of zeolites β and SSZ-31.

To characterize the synthesized crystals, transmission electron microscopy was performed with a JEOL 3010 microscope operating at 300 kV. A low-resolution TEM image shows that a significant number of crystals are nanofibers of length 1–2 μm, with radial outgrowths *ca.* 20 nm in radius [Fig. 1(a)]. A few fibers of length up to 5 μm have also been observed. A high-resolution TEM image [Fig. 1(b)] from the center of such a crystallite reveals that a nanofiber of zeolite SSZ-31 forms a 'backbone' (running along the centerline of the nanofiber) for epitaxial growth of zeolite-β. This is further corroborated by the presence of SSZ-31 nanofibers free of zeolite-β outgrowths. Complete channels of β (polymorph B) lie immediately above the β/SSZ-31 interface. Two SSZ-31 channels are observed, apparently running parallel to the second channel direction of zeolite-β. These observations suggest that the β/SSZ-31 interface contains composite 12-membered channels constructed from β and SSZ-31 'half-channels'. The SSZ-31 'backbone' is observed to be always three unit cells thick.

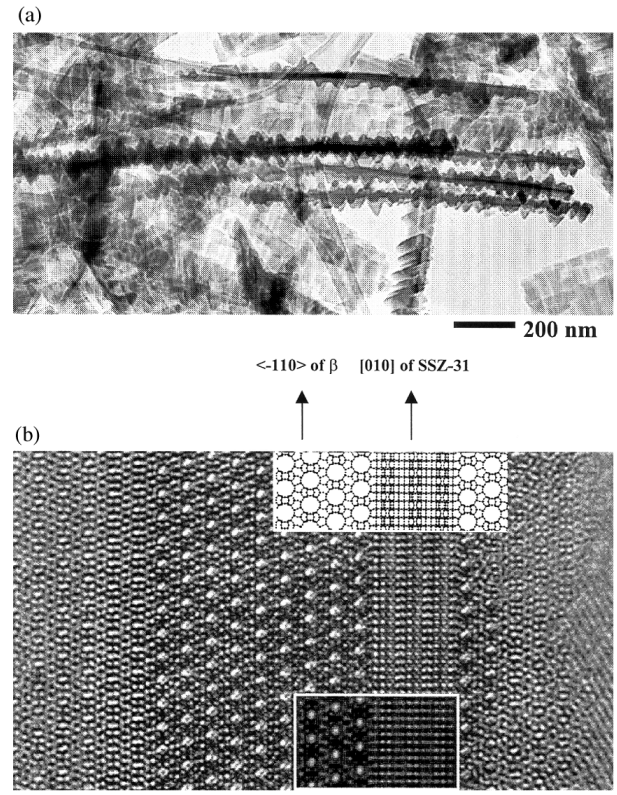

Fig. 1 (a) TEM image of synthesized crystals showing SSZ-31 nanofibers with epitaxial outgrowths of zeolite-β; (b) high-resolution TEM image of the epitaxial growth of zeolite-β on zeolite SSZ-31; model of the intergrowth (inset, upper); and TEM simulation of this model (inset, lower).

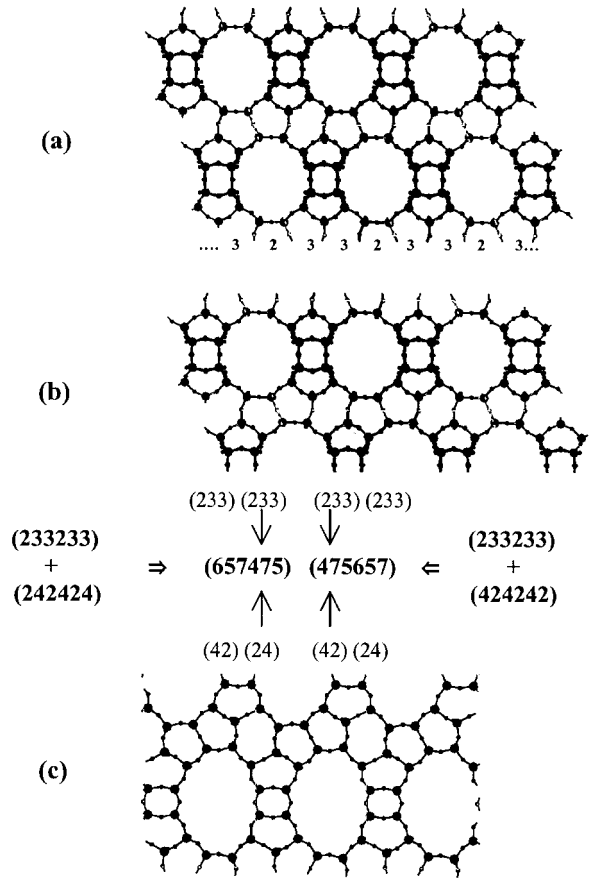

Fig. 2 (a) Projection of β structure along < 110 > showing the two- and three-membered ring fragments in a (233) sequence; (b) projection along < −110 > showing the half-channels. Each of the eight lowermost silicon atoms is a member of a (233) sequence running alongside a half-channel in the < −110 > direction; (c) projection of SSZ-31 polymorph B along [010] showing the half-channels. Each of the uppermost silicon atoms is a member of a (24) sequence running alongside the half-channel. These sequences are laterally shifted with respect to each other. The generation of the (657475) and (475657) sequences at the interface of zeolite-β with SSZ-31 polymorphs A–D is indicated.

To construct possible interfaces, it is first assumed that the 12-membered composite channels are comprised of six silicate tetrahedra derived from a β channel, and the remaining six tetrahedra from an SSZ-31 channel. We terminate the β structure at a plane parallel to the < −110 > channel direction, leaving six-membered half-channels in this direction and complete channels in the < 110 > direction. Fig. 2(a) shows a view of the β polymorph B along the < 110 > direction, and Fig. 2(b) shows a view along the < −110 > direction showing the half-channels. Since the β channels are enclosed by four-, five- and six-membered rings, the termination results in ring 'fragments' of two or three tetrahedra, which are visible at the bottom of Fig. 2(a). These fragments follow a periodic 2–3–3–2–3–3 . . . sequence (abbreviated to 233), as shown in the figure. At the interface plane, a β half-channel is therefore bounded by two identical 233 sequences (one on either side of the half-channel) propagating down the < −110 > channel direction, as indicated in Fig. 2(b). Similar termination of β polymorph A results in the same structure at the interface. Since β polymorph B is observed at the interface in Fig. 1(b), only this polymorph is considered in the following discussion.

There are eight polymorphs (A–H) of SSZ-31 with different connectivities down the [010] channel direction.[8] The SSZ-31 structure is similarly terminated by a plane parallel to the [010] direction, leaving six-membered half-channels. Fig. 2(c) shows the terminated structure of SSZ-31 polymorph B viewed along the [010] direction, indicating the half-channels. Inspection of this structure in the channel direction shows that the interface plane contains ring fragments of two or four tetrahedra, that form periodic (2–4–2–4–) chains (abbreviated to 24) running along the channel direction. However, these chains are laterally shifted with respect to each other, so that a two-membered fragment on one chain has as its neighbor, a four-membered fragment of the adjacent chain. The two sequences running alongside an SSZ-31 half-channel can be represented as (24) □ (42) for polymorphs A–D. The symbol □ indicates the half-channel as viewed down [010], with one sequence running along its left and right. Polymorphs E–H have adjacent (24) □ (26), and (26) □ (24) half-channels.

The epitaxy is achieved by bonding the half-channels of β and SSZ-31 (*via* oxygen atoms) to form 12-membered interfacial composite channels. The combination of the sequences of zeolite-β with the sequences of SSZ-31 polymorphs A–D results in closed rings following the periodic sequences (475657) ■ (657475); where the symbol ■ indicates the composite channel. Interfaces of β with SSZ-31 polymorphs E–H have two types of composite channels when viewed down the channel direction: (475657) ■ (495858), and (495858) ■ (475657). These channels are adjacent to each other at the interface. The interfaces therefore contain seven-membered rings, and even nine-membered rings in the case of epitaxial growths involving SSZ-31 polymorphs E–H. The two polymorphs of β together with the eight polymorphs of SSZ-31 lead to 16 possible epitaxial growths, with only two possible interfacial structures, (475657) and (495858), as shown above. Considering the unit cell dimensions of the two zeolites, the 2-D rectangular epitaxial unit cell at the interface would have dimensions of 25.2 Å in the SSZ-31 channel direction and 12.33 Å in the perpendicular β channel direction. Composite channels comprising unequal numbers of tetrahedra from each zeolite (*e.g.*, eight from β and four from SSZ-31) do not appear to be feasible due to non-matching bond positions on either side of the interface.

The epitaxy of β polymorph B on SSZ-31 polymorph B is simulated as described above, using the *Cerius*[2] Interface Builder. The resulting structure [Fig. 1(b), upper inset] is found to match the TEM image. In the TEM image, the two zeolite-β domains on either side of the SSZ-31 domain appear to be laterally shifted with respect to each other. The structural model proposed above accounts for this observation, since it allows the β structure to be shifted along the channel direction of SSZ-31. This shift is captured in the interface simulation, and appears in the upper inset of Fig. 1(b). A TEM simulation of the interface is also shown (lower inset), and it is seen to match the actual image. However, the information available from the TEM image appears insufficient to identify the SSZ-31 polymorph that is actually involved in the epitaxy. It is also possible that the synthesized sample contains intergrowths of zeolite-β and SSZ-31 in addition to the epitaxial regions that we observe.

S. N. and M. T. acknowledge funding from the NETI, the David and Lucile Packard Foundation, and the Camille and Henry Dreyfus Foundation. L. A. V. and M. A. C. are grateful to the Spanish CICYT (project MAT97-0723) for financial support.

Notes and references

1 C. C. Freyhardt, M. Tsapatsis, R. F. Lobo, K. J. Balkus and M. E. Davis, *Nature*, 1996, **381**, 295.
2 A. Araya and B. M. Lowe, *Zeolites*, 1984, **4**, 280.
3 R. F. Lobo, M. Tsapatsis, C. C. Freyhardt, I. Chan, C.-Y. Chen, S. I. Zones and M. E. Davis, *J. Am. Chem. Soc.*, 1997, **119**, 3732.
4 D. V. Jorgensen and C. R. Kennedy, *US Pat.*, 4714537, 1988.
5 D. M. Barthomeuf, *US Pat.*, 4584424, 1986.
6 J. M. Newsam, M. M. J. Treacy, W. T. Koetsier and C. B. de Gruyter, *Proc. R. Soc. London Ser. A*, 1988, **420**, 375.
7 M. A. Camblor, A. Corma, A. Mifsud and S. Valencia, *Chem. Commun.*, 1996, 2365.
8 S. I. Zones, T. V. Harris, A. Rainis and D. S. Santilli, *US Pat.*, 5106801, 1992.
9 M. A. Camblor, A. Corma, L. A. Villaescusa and P. A. Wright, *Angew. Chem., Int. Ed. Engl.*, 1997, **36**, 2659.

Communication 9/00538B

Unusual cyclopropanol formation from a β-silyl aldehyde

Ian Fleming* and Ajay K. Mandal

Department of Chemistry, Lensfield Road, Cambridge, UK CB2 1EW. E-mail: if10000@cam.ac.uk

Received (in Liverpool, UK) 9th March 1999, Accepted 6th April 1999

The hemiacetals 15 and 18 gave cyclopropanols 17 and 20 when treated with NaH in DMSO, showing that the silyl group has enhanced electrofugal powers because of the participation of the oxyanion.

The well known electrofugal power of a silyl group attached to carbon is enhanced when a nucleophilic atom coordinates to it. This unexceptionable statement is supported by much circumstantial evidence (Scheme 1). A silyl group can be removed more easily (**1** → **2**) by protodesilylation from a vinyl, or even an alkyl, carbon when an oxyanion is poised five atoms away.[1] More generally, a variety of electrophiles can be made to react with the incipient or actual carbanion nucleophile (**3** → **4**) if the carbon carrying the silyl group has an anion-stabilising group on it.[2] An oxyanion can also remove a silyl group in a 5-*endo-tet* sense to create a double bond (**5** → **6**).[3] And an oxyanion can push one of the other ligands off a silyl group in the sense (**7** → **8**) to make the R group into a carbon nucleophile.[4] We now report a case where the presence of an oxyanion makes a silyl group behave more like a stannyl group, in a reaction with precedent only with a 1,2-Brook rearrangement from an α-oxyanion rather than a γ-oxyanion.[5]

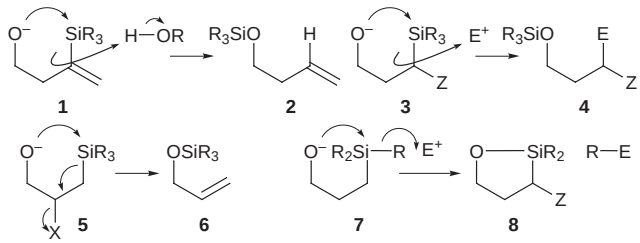

Scheme 1

β-Stannyl aldehydes and ketones[6] form cyclopropanols on treatment with Lewis acids (**9** → **10**) (Scheme 2), but β-silyl aldehydes and ketones are remarkably robust to acid and base, often being carried through many steps before being used as masked α,β-unsaturated carbonyl compounds,[7] or as masked β-hydroxy carbonyl compounds.[8] When they do react with Lewis or protic acids, they undergo rearrangements,[9] or intramolecular transfer of ligand from the silicon to the carbonyl group,[10] and we know of only one example where a cyclopropanol-forming pathway has been suggested.[11] In parallel with these observations, cyclopropane formation (**11** → **12**) is normal with γ stannyl carbocations and their precursors,[12] but is unusual with the corresponding silyl compounds,[13] for which rearrangement (**13** → **14**) is the normal pathway.[14]

The reaction we have now discovered occurred originally when we had been trying to carry out a Wittig reaction on the racemic hemiacetal **15**, prepared by DIBAL-H reduction of the corresponding lactone.[15] When we treated the hemiacetal **15** with NaH in DMSO at room temperature for 3 h, with or without methyltriphenylphosphonium iodide, we obtained only the cyclopropanol **17** (Scheme 3). We see this tin-like behaviour as having taken place because of the presence in the intermediate aldehyde of an oxyanion, which can coordinate to the silicon **16** (arrows), and make the pentacovalent silyl anion into a better electrofugal group. We were not able to assign the stereochemistry of the cyclopropanol **17** reliably from the ^{1}H NMR spectrum, it is assigned here by analogy, so we repeated the reaction with a marginally more simple analogue **18**, which similarly gave the cyclopropanol **20** (Scheme 3). COSY and NOE difference experiments on this compound allowed us to confirm the stereochemistry, which corresponds to inversion of configuration at the silicon-bearing carbon, exactly analogous to the inversion seen in reactions of the type **11** → **12** in the tin series. The stereochemistry at the C–OH carbon corresponds to that expected if the carbonyl group more or less eclipses the neighbouring hydrogen atom at the time of cyclopropane formation, which seems reasonable.

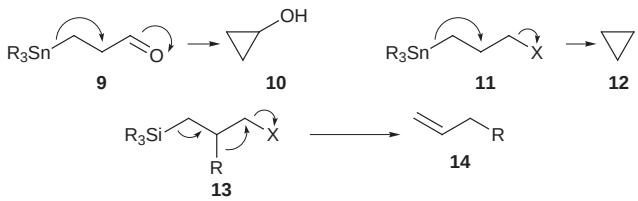

Scheme 2

If we left the hemiacetal **18** and NaH/DMSO at room temperature for 10 h instead of 3 h, we obtained a mixture of four hemiacetals, which gave a mixture of two lactones **21** and **22** on oxidation (Scheme 4). The hemiacetal precursor of the lactone **21** looks as though the original hemiacetal **18** had merely undergone a somewhat implausible protodesilylation, but the true pathway, by way of the cyclopropanol **20**, is revealed by the presence of the minor lactone **22**.

This observation may explain our failure to achieve cyclopropanol formation from the even more simple hemiacetal **23**, which gave only the product **24** of protodesilylation (Scheme 5), possibly directly in this case, but also possibly by way of a cyclopropanolate, which can be expected to open regioselectively by way of the benzyl anion.

The cyclopropanol formation is not a general reaction, for we found that the 2-methyl and 2-allyl groups in **15** and **18** appear to be necessary, not only for the determination of the stereochemistry of the reaction, but also for it to take place at all. The hemiacetal **25** gave no sign of a cyclopropanol, but gave instead a diene **26**, which we suggest has taken the course illustrated in Scheme 6, with the possibility that the final elimination step is actually preceded by a Mislow rearrangement.

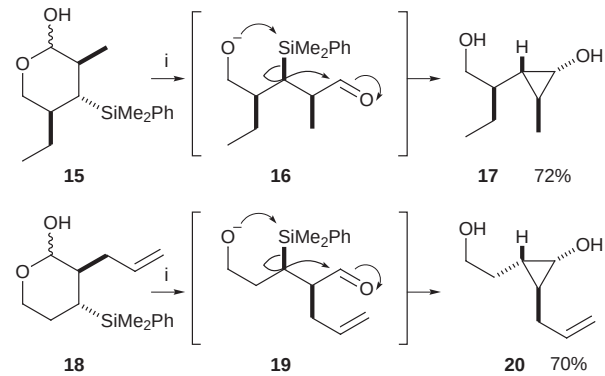

Scheme 3 *Reagents and conditions*: i, NaH, DMSO, rt, 3 h.

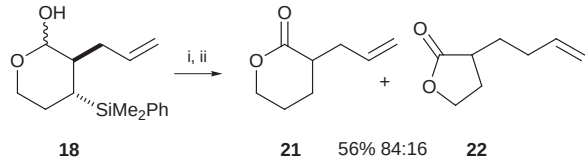

18 **21** 56% 84:16 **22**

Scheme 4 *Reagents and conditions*: i, NaH, DMSO, rt, 10 h; ii, PCC, CH_2Cl_2, rt, 2 h.

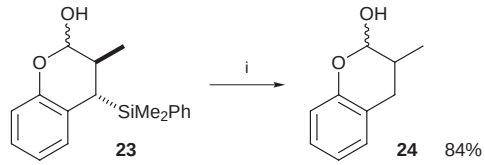

23 **24** 84%

Scheme 5 *Reagents and conditions*: i, NaH, DMSO, rt, 3 h.

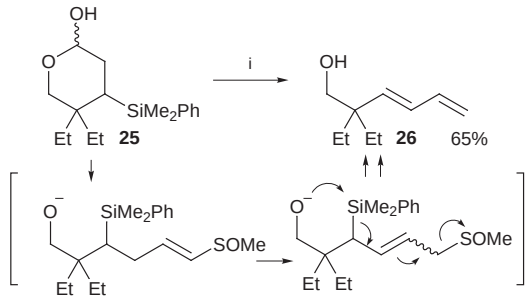

Scheme 6 *Reagents and conditions*: i, NaH, DMSO, rt, 3 h.

Perhaps most intriguing is the contrast between the reaction described here, *pushed* forward by nucleophilic activation **16**, and the reaction on a closely similar system **27** *pulled* forward by electrophilic activation.[10] In both cases, our plans for a synthesis of ebelactone-a were thwarted.

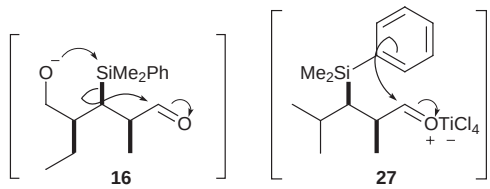

We thank the CVCP as managers of the ORS scheme and the managers of the Nehru Trust for support (A. K. M.).

Notes and references

1 S. Murata and I. Matsuda, *Synthesis*, 1978, 221; M. Isobe, M. Kitamura and T. Goto, *Tetrahedron Lett.*, 1980, 4727; A. G. Brook and J. J. Chrusciel, *Organometallics*, 1984, **3**, 1317; K. Yamamoto, T. Kimura and Y. Tomo, *Tetrahedron Lett.*, 1985, **26**, 4505; A. D. Kaye, G. Pattenden and S. M. Roberts, *Tetrahedron Lett.*, 1986, **27**, 2033; P. F. Hudrlik, P. E. Holmes and A. M. Hudrlik, *Tetrahedron Lett.*, 1988, **29**, 6395; E. Schaumann, A. Kirschning and F. Narjes, *J. Org. Chem.*, 1991, **56**, 717.

2 I. Fleming and C. D. Floyd, *J. Chem. Soc., Perkin Trans. 1*, 1981, 969; T. Takeda, K. Ando and T. Fujiwara, *Chem. Lett.*, 1983, 1285; E. Block, J.-A. Laffitte and V. Eswarakrishnan, *J. Org. Chem.*, 1986, **51**, 3428; P. L. Coe, A. S. Jones, A. Kumar and R. T. Walker, *Tetrahedron Lett.*, 1988, **29**, 835; E. Schaumann and C. Friese, *Tetrahedron Lett.*, 1989, **30**, 7033; T. Michel, A. Kirschning, C. Beier, N. Bräuer, E. Schaumann and G. Adiwidjaja, *Liebigs Ann. Chem.*, 1996, 1811; H. Shinokubo, K. Miura, K. Oshima and K. Utimoto, *Tetrahedron*, 1996, **52**, 503.

3 M. Ochiai, K. Sumi and E. Fujita, *Chem. Pharm. Bull, Jpn.*, 1984, **32**, 3686; M. Tsukamoto, H. Iio and T. Tokoroyama, *Tetrahedron Lett.*, 1987, **28**, 4561; H. Iio, A. Fujii, M. Ishii and T. Tokoroyama, *J. Chem. Soc., Chem. Commun.*, 1991, 1390; M. Franciotti, A. Mann and M. Taddei, *Tetrahedron Lett.*, 1991, **32**, 6783; A. Fujii, Y. Usuki, H. Iio and T. Tokoroyama, *Synlett*, 1994, 725.

4 C. Eaborn and F. M. S. Mahmoud, *J. Organomet. Chem.*, 1981, **209**, 13; W. Kirmse and F. Söllenböhmer, *J. Chem. Soc., Chem. Commun.*, 1989, 774; C. Eaborn and P. B. Hitchcock, *J. Chem. Soc., Perkin Trans. 2*, 1991, 1137; T. Harada, S. Imamaka, Y. Ohyama, Y. Matsuda and A. Oku, *Tetrahedron Lett.*, 1992, **33**, 5807; P. F. Hudrlik, Y. M. Abdallah and A. M. Hudrlik, *Tetrahedron Lett.*, 1992, **33**, 6743 and 6747; K. Takaku, H. Shinokubo and K. Oshima, *Tetrahedron Lett.*, 1998, **39**, 2575; Y. M. Hijii, P. F. Hudrlik and A. M. Hudrlik, *Chem. Commun.*, 1998, 1213. See also N. D. Hone, S. G. Davies, N. J. Devereux, S. L. Taylor and A. D. Baxter, *Tetrahedron Lett.*, 1998, **39**, 897.

5 K. Takeda, J. Nakatani, H. Nakamura, K. Sako, E. Yoshii and K. Yamaguchi, *Synlett*, 1993, 841.

6 T. Sato, M. Watanabe and E. Murayama, *Tetrahedron Lett.*, 1986, **27**, 1621; T. Sato, M. Watanabe, T. Watanabe, Y. Onoda and E. Murayama, *J. Org. Chem.*, 1988, **53**, 1894; T. Sato, T. Watanabe, T. Hayata and T. Tsukui, *J. Chem. Soc., Chem. Commun.*, 1989, 153; T. Sato, M. Hayashi and T. Hayata, *Tetrahedron*, 1992, **48**, 4099; J. Fujiwara, T. Yamamoto and T. Sato, *Chem. Lett.*, 1992, 1775; J. Fujiwara and T. Sato, *Bull. Chem. Soc. Jpn.*, 1993, **66**, 1258; M. Yamamoto, M. Nakazawa, K. Kishikawa and S. Kohmoto, *Chem. Commun.*, 1996, 2353.

7 I. Fleming and J. Goldhill, *J. Chem. Soc., Perkin Trans. 1*, 1980, 1493; I. Fleming and D. A. Perry, *Tetrahedron*, 1981, **37**, 4027; several papers from the Asaoka group reviewed in I. Fleming, A. Barbero and D. Walter, *Chem. Rev.*, 1997, **97**, 2063.

8 I. Fleming, *Chemtracts*: *Org. Chem.*, 1996, **9**, 1; G. R. Jones and Y. Landais, *Tetrahedron*, 1996, **37**, 7599; K. Tamao, *Adv. Silicon Chem.*, **3**, 1.

9 K. Tanino, K. Sato and I. Kuwajima, *Tetrahedron Lett.*, 1989, **30**, 6551.

10 S. C. Archibald and I. Fleming, *Tetrahedron Lett.*, 1993, **34**, 2387.

11 A. R. Katritzky, M. V. Voronkov and D. Toader, *J. Chem. Soc., Perkin Trans. 2*, 1998, 2515.

12 D. D. Davis and H. T. Johnson, *J. Am. Chem. Soc.*, 1974, **96**, 7576; D. D. Davis and R. H. Black, *J. Organomet. Chem.*, 1974, **82**, C−30; S. Teratake, *Chem. Lett.*, 1974, 1123; R. H. Fish and B. M. Broline, *J. Organomet. Chem.*, 1978, **159**, 255; D. C. McWilliam, T. R. Balasubramanian and H. G. Kuivila, *J. Am. Chem. Soc.*, 1978, **100**, 6407; I. Fleming and C. J. Urch, *J. Organomet. Chem.*, 1985, **285**, 173; C. R. Johnson and J. F. Kadow, *J. Org. Chem.*, 1987, **52**, 1493; L. Plamondon and J. D. Wuest, *J. Org. Chem.*, 1991, **56**, 2066 and 2076; T. Sato, T. Kikuchi, H. Tsujita, A. Kaetsu, N. Sootome, K. Nishida and E. Murayama, *Tetrahedron*, 1991, **47**, 3281; T. Sato and S. Nagatsuka, *Synlett*, 1995, 653; R. L. Beddoes, M. L. Lewis, P. Quayle, S. Johal, M. Atwood and D. Hurst, *Tetrahedron Lett.*, 1995, **36**, 471; S. Hanessian, U. Reinhold and S. Ninkovic, *Tetrahedron Lett.*, 1996, **37**, 8976; N. Isono and M. Mori, *J. Org. Chem.*, 1997, **62**, 7867; H. Wakamatsu, N. Isono and M. Mori, *J. Org. Chem.*, 1997, **62**, 8917; A. Krief and L. Provins, *Tetrahedron Lett.*, 1998, **39**, 2017. But for notable exceptions, see G. D. Hartman and T. G. Traylor, *J. Am. Chem. Soc.*, 1975, **97**, 6147; M. J. Goldstein and J. P. Barren *Helv. Chim. Acta*, 1986, **69**, 548.

13 V. J. Shiner, Jr., M. W. Ensinger and R. D. Rutkowske, *J. Am. Chem. Soc.*, 1987, **109**, 804; W. Kirmse and F. Söllenböhmer, *J. Am. Chem. Soc.*, 1989, **111**, 4127; V. J. Shiner, Jr., M. W. Ensinger and J. C. Huffman, *J. Am. Chem. Soc.*, 1989, **111**, 7199; J. Coope and V. J. Shiner, Jr., *J. Org. Chem.*, 1989, **54**, 4270; V. J. Shiner, Jr., M. W. Ensinger, G. S. Kriz and K. A. Halley, *J. Org. Chem.*, 1990, **55**, 653.

14 I. Fleming and J. P. Michael, *J. Chem. Soc., Perkin Trans. 1*, 1981, 1549; J. P. Michael, N. F. Blom and J. C. A. Boeyens, *J. Chem. Soc., Perkin Trans. 1*, 1984, 1739; I. Fleming, S. K. Patel and C. J. Urch, *J. Chem. Soc., Perkin Trans. 1*, 1989, 115; S. R. Wilson and A. Shedrinsky, *J. Org. Chem.*, 1982, **47**, 1983; S. R. Wilson, A. Shedrinsky and M. S. Haque, *Tetrahedron*, 1983, **39**, 895; W. R. Roush and T. E. D'Ambra, *J. Am. Chem. Soc.*, 1983, **105**, 1058; M. Hannaby and S. Warren, *Tetrahedron Lett.*, 1986, **27**, 765; M. Asaoka and H. Takei, *Tetrahedron Lett.*, 1987, **28**, 6343; K. Tanino, Y. Hatanaka and I. Kuwajima, *Chem. Lett.*, 1987, 385; W. Kirmse and F. Söllenböhmer, *Angew. Chem., Int. Ed. Engl.*, 1989, **28**, 1667; J. Coope, V. J. Shiner, Jr., and M. W. Ensinger, *J. Am. Chem. Soc.*, 1990, **112**, 2834; J. R. Hwu and J. M. Wetzel, *J. Org. Chem.*, 1992, **57**, 922; A. Yamazaki, I. Achiwa, K. Horikawa, M. Tsurubo and K. Achiwa, *Synlett*, 1997, 455; E. J. Corey and B. E. Roberts, *J. Am. Chem. Soc.*, 1997, **119**, 12425; I. Achiwa, A. Yamazaki and K. Achiwa, *Synlett*, 1998, 45; A. Nowak, O. Bolte and E. Schaumann, *Tetrahedron Lett.*, 1998, **39**, 529.

15 I. Fleming, N. L. Reddy, K. Takaki and A. C. Ware, *J. Chem. Soc., Chem. Commun.*, 1987, 1472.

Communication 9/01920K

Hydrazinolysis of Fischer-type oxacarbenes made efficient: a new and easy entry to alkyl and aryl hydrazinocarbene complexes

Emanuela Licandro,* Stefano Maiorana,* Antonio Papagni, Dario Perdicchia and Raffaella Manzotti

Dipartimento di Chimica Organica e Industriale, Università degli Studi di Milano, via C.Golgi, 19, I-20133 Milano, Italy. E-mail: maior@icil64.cilea.it

Received (in Liverpool, UK) 14th January 1999, Accepted 16th April 1999

Hydrazinolysis of the pentacarbonyl[alkyl- or aryl-(methoxy)carbene] complexes of W^0 and Cr^0 with both 1,1- and 1,2-disubstituted hydrazines affords the corresponding new hydrazinocarbenes 15–18, 21 and 22, and the presence of LiCl in the reaction medium greatly increases their yields.

We have recently achieved the first synthesis of a number of new pentacarbonyl and chelate hydrazino(alkyl)carbene complexes **1**–**3**.[1]

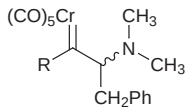

1 R = Me
2 R = Et, but-3-enyl

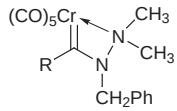

3 R = Et, but-3-enyl, Pr^i

The synthesis of **1**–**3** is of general applicability only when applied to 1-substituted hydrazides.[2] The hydrazinolysis of oxacarbenes was a highly appealing procedure, even if Fischer[3] reported that, for the reaction between the 1,1-dimethylhydrazine and the pentacarbonyl[methoxy(methyl)carbene]chromium(0), it was unsuccessful. However, the hydrazinolysis of oxacarbenes has more recently been shown to be possible in a few specific cases.[4,5]

We here report on the reactions between the 1,1-disubstituted hydrazines **5** and **7**–**10** and the methoxy(methyl)carbene tungsten(0) complex **11**, as well as those between the 1,2-dimethylhydrazine **12** and the methoxy(methyl)- and methoxy(phenyl)-carbene chromium(0) complexes **4** and **13**. The results of this study eventually revealed a new and efficient entry to alkyl- and aryl-(hydrazino)carbenes.

We initially reacted under nitrogen the 1,1-dimethylhydrazine **5** (1.1 mmol) with the tungsten complex **11** (1 mmol) in dry THF solution at −78 °C for 30 min, but even the use of tungsten only afforded the $(CO)_5W{\leftarrow}N{\equiv}C{-}Me$ complex **14** (Table 1). However, when we reacted the hydrazines **7**–**10** with **11** under the same conditions, we isolated a reaction mixture containing the (*Z*)-hydrazinocarbenes **15**–**18**† and variable amounts of the acetonitrile complex **14**; the yields are shown in Table 1.

Although the yields of hydrazinocarbenes **15**–**18** were not very high, this first set of results showed us that it was possible to use the simple procedure described above to prepare stable and isolable alkyl hydrazinocarbene complexes of tungsten. We therefore decided to look carefully at the possible mechanism of the hydrazinolysis reaction. The aim was to identify the factors potentially capable of differentiating the pathway leading to the acetonitrile complex **14** from that affording the target hydrazinocarbenes **15**–**18**.

According to Aumann,[4] during the hydrazinolysis of alkoxy(alkynyl)carbenes, the hydrazinocarbenes **15**–**18** are formed through the elimination of MeOH from the tetrahedral intermediate of the reaction, whereas product **14** arises from the breaking of the N–N bond with amine elimination. This latter process is a consequence of the proton shift from the α- to the β-nitrogen.

All of the attempts to prevent this proton shift, *i.e.* (i) by increasing steric hindrance around the β-nitrogen, (ii) by running the reactions in the presence of an excess of Et_3N as an external competing base and, (iii) by reducing the β-nitrogen lone pair availability by means of acylation, failed, and there was no improvement in the yields of the complexes **15**–**18**. Looking for an alternative way to minimize the undesirable β-nitrogen protonation, we considered a Lewis acid as a possible coordinating species capable of engaging the β-nitrogen lone pair without transforming this nitrogen into a good leaving group: Li^+ (as LiCl) appeared to be a suitable reagent for achieving this goal.

The results of the hydrazinolysis of complex **11** with the *N*-aminomorpholine **8** and *N*-amino-*trans*-2,6-dimethylmorpholine **9** in the presence of 2.2 equiv. of LiCl were surprisingly good, with the yields of complexes **16** and **17** being respectively double and eight times of those obtained in the absence of LiCl (Scheme 1).

The presence of LiCl also had a dramatic effect on the reaction times, which increased from 30 min to 5 h. We believe that this effect can be rationalized in terms of the formation of an aggregate in THF between LiCl and the hydrazines **8** and **9**,‡ in which the nucleophilic character of the hydrazines would be

Table 1 Reaction of **11** with various hydrazines[a]

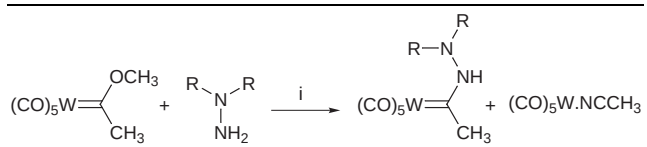

11 **5, 7–10** **15–18** **14**

Hydrazine	(*Z*)-Hydrazinocarbene **15**–**18** (% yield)	Yield of **14** (%)
5 	—	52
7 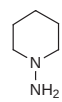	**15** (34)	42
8 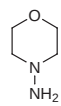	**16** (34)	50
9 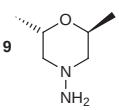	**17** (6)	74
10 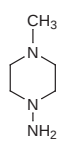	**18** (28)	41

[a] *Reagents and conditions*: i, THF, −78 °C, 30 min.

Table 2 Hydrazinolysis in the presence of LiCl

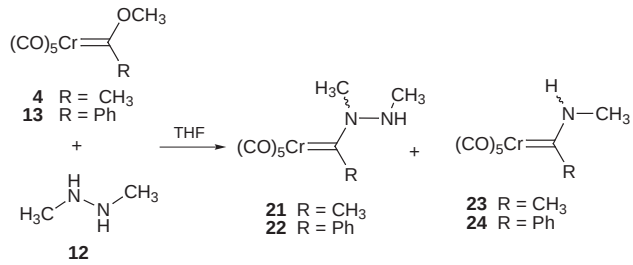

Complex	LiCl (equiv.)	*T*/°C	Time	Hydrazinocarbene (% yield, *E* : *Z*)	Aminocarbene (% yield)
4	—	−78	5 min	21 (18, 7 : 3)	23 (40)
4	2	−78 → −20	15 h	21 (73, 4 : 6)	23 (7)
13	—	−78	5 min	22 (30, 1 : 1)	24 (35)
13	2	−78 → −20	15 h	22 (80, 1.3 : 1)	23 (13)

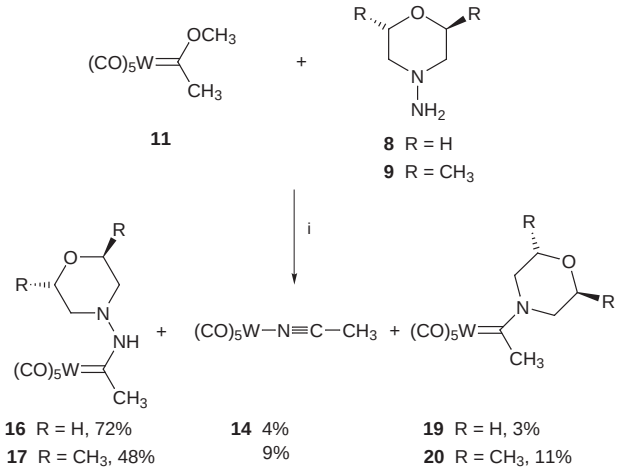

Scheme 1 *Reagents and conditions*: i, LiCl (2 equiv.), THF, −40 °C, 3 h.

reduced. As a result of the decrease in reaction rates, the amines produced in the N–N bond breaking step can compete with the hydrazine in the reaction with **11** affording the aminocarbenes **19** and **20** (Scheme 1).

Even in the presence of LiCl, only the (*Z*)-isomer of the hydrazinocarbenes **16** and **17** was formed. In a typical procedure, LiCl (0.0999 g, 2.47 mmol) was dissolved in anhydrous THF (3 ml) and hydrazine **8** (0.115 ml, 1.19 mmol.) was added under N_2 at the same temperature, thus generating a white slurry to which a 3 ml THF solution of **11** (0.412 g, 1.08 mmol.) was added dropwise over 5 min at −78 °C. After 2 h at −78 °C, the temperature was raised and kept at −40 °C for a further 3 h. Standard work-up followed by purification by flash chromatography [eluent: Et_2O–light petroleum (6 : 4) then Et_2O] gave the hydrazinocarbene **16**.§

The hydrazinolysis reaction was then extended to the 1,2-dimethylhydrazine **12** which was reacted with the chromium(0) carbenes **4** and **13** (Table 2). When the free hydrazine was used, the expected hydrazinocarbenes **21** (*E*/*Z* = 7 : 3) and **22** (*E*/*Z* = 1 : 1) were obtained in 18 and 30% yield respectively, as well as the methyl(amino)carbene complexes **23** and **24** (yields of 40 and 35%, respectively). Also in this case, the presence of 2 equiv. of LiCl in the reaction mixture greatly increased the yields of hydrazinocarbenes **21** and **22** (see Table 2), thus demonstrating a general and important effect of the presence of this salt in the reaction medium. The reaction was carried out starting from a commercially available dihydrochloride salt of the 1,2-dimethylhydrazine (0.328 g, 2.46 mmol) suspended in anhydrous THF (20 ml), and treated under nitrogen at 0 °C with a stoichiometric amount of Bu^nLi (1.4 M *n*-hexane solution, 3.5 ml, 4.92 mmol) (Table 2).

In conclusion, carbene complexes of tungsten(0) and chromium(0) **16**, **17**, **21** and **22** were synthesized in satisfactory to good yields by means of the hydrazinolysis reaction carried out in the presence of 2 equiv. of LiCl. It is likely that hydrazine/LiCl aggregates are involved as the reactive species. To the best of our knowledge, nothing has yet been reported in the literature concerning the use of stable aggregates between hydrazines and LiCl for synthetic purposes.[6]

We gratefully acknowledge joint financial support from M.U.R.S.T., Rome, and the University of Milan (National Project 'Stereoselezione in Sintesi Organica, Metodologie ed Applicazioni'). We also acknowledge the C.N.R. of Rome.

Notes and references

† Only the (*Z*)-rotamers were observed. The lack of isolation of any of the (*E*)-rotamers of **15**–**18** means that they are not formed at all or, if formed, they are unstable and immediately give the $W(CO)_5{\cdot}NCCH_3$ as postulated by Fischer (ref. 3).

‡ To a THF solution of LiCl (2 equiv.), the hydrazine **8** (1 equiv.) was added at room temperature. The resulting white solid was isolated and used for the hydrazinolysis of complex **11**, affording the hydrazino complex **16** in the same yield as that shown in Scheme 1 (72%). The structure of the above lithium aggregate is under investigation.

§ *Selected data* for (*Z*)-**16**: yellow solid, mp 112 °C (from CH_2Cl_2–pentane); ν_{max}(Nujol)/cm^{-1} 3161 (NH), 2060 (CO_{trans}) 1960–1880 (CO_{cis}); δ_H(300 MHz, $CDCl_3$) 2.92–3.03 (m, 7 H, Cr=CCH_3 + NCH_2), 3.87–3.92 (m, 4 H, OCH_2), 8.50 (br s, 1 H, NH); δ_C(75 MHz, $CDCl_3$) 42 (q, CH_3), 55 (t, NCH_2), 56.2 (t, CH_2), 65 (t, OCH_2) 198 (s, CO_{cis}), 204 (s, CO_{trans}), 253 (s, C=W); *m*/*z* (EI) 452 [M$^+$] (Calc. for $C_{11}H_{12}N_2O_6W$: C, 29.2, H, 2.7; N, 6.2%. Found, C, 29.50; H, 2.88; N, 6.07%). For (*E*)-**21**: light yellow solid, mp 79–80 °C (from CH_2Cl_2–pentane); ν_{max}(Nujol)/cm^{-1} 3334 (NH), 2054 (CO_{trans}), 1917–1803 (CO_{cis}); δ_H(300 MHz, $CDCl_3$) 2.71 (d, 3 H, *J* 6.2, NHCH_3) 2.78 (s, 3H, Cr=CCH_3), 3.96 (s, 3 H, Cr=CNCH_3), 4.36 (q, 1 H, *J* 6.2, N*H*CH_3); δ_C(75 MHz, $CDCl_3$) 36.2 (NHCH_3) 37.2 (Cr=C*C*H_3), 48.4 (NCH_3), 217.8 (s, 2CO_{cis}), 223.4 (s, CO_{trans}), 265.2 (s, C=Cr) (Calc. for $C_9H_{10}CrN_2O_5$: C, 38.86, H, 3.62, N, 10.07. Found: C, 38.93; H, 3.39; N, 9.95%). For (*Z*)-**21**: yellow solid, mp 95–96 °C (from EtOAc–pentane); ν_{max}(Nujol)/cm^{-1} 3321 (NH), 2054 (CO_{trans}), 1917–1803 (CO_{cis}), δ_H(300 MHz, $CDCl_3$) 2.61 (s, 3H, Cr=CCH_3), 2.82 (d, 3 H, *J* 6.3, NHCH_3), 3.41 (s, 3 H, Cr=CNCH_3), 6.10 (q, 1 H, *J* 6.3, N*H*CH_3); δ_C(75 MHz, $CDCl_3$) 36.7 (NHCH_3) 37.6 (Cr=C*C*H_3), 39.1 (NCH_3), 217.1 (s, 2CO_{cis}), 222.7 (s, CO_{trans}), 258.9 (s, C=Cr) (Calc. for $C_9H_{10}CrN_2O_5$: C, 38.86, H, 3.62; N, 10.07. Found: C, 38.79; H, 3.60; N, 10.26%).

1 E. Licandro, S. Maiorana, R. Manzotti, A. Papagni, D. Perdicchia, M. Pryce, A. Tiripicchio and M. Lanfranchi, *Chem. Commun.*, 1998, 383.
2 Results to be published.
3 E. O. Fischer and R. Aumann, *Chem. Ber.*, 1968, **101**, 963.
4 R. Aumann, B. Jasper and R. Fröhlich, *Organometallics*, 1995, **14**, 2447.
5 M. Iyota, L. Zhao and M. Matsuyama, *Chem. Lett.* , 1994, 777
6 M. A. Klochko and M. P. Mikhailova, *Zh. Neorgan. Khim.*, 1960, **5**, 2319.

Communication 9/00166B

ChemComm

A hydrogen-bonded cluster with 'onion-type' structure, encapsulated and induced by a spherical cluster shell: $[(H_2O)_n \subset Mo^{VI}_{72}Mo^{V}_{60}O_{372}(HCO_2)_{30}(H_2O)_{72}]^{42-}$

Achim Müller,* Vladimir P. Fedin,† Christoph Kuhlmann, Hartmut Bögge and Marc Schmidtmann

Fakultät für Chemie der Universität, Lehrstuhl für Anorganische Chemie I, Postfach 100131, D-33501 Bielefeld, Germany. E-mail: a.mueller@uni-bielefeld.de

Received (in Basel, Switzerland) 18th December 1998, Accepted 2nd April 1999

By reacting an aqueous solution of ammonium heptamolybdate with formic acid in the presence of hydrazinium sulfate at pH ≈ 4.2 the compound $(NH_4)_{42}[Mo^{VI}_{72}Mo^{V}_{60}O_{372}(HCO_2)_{30}(H_2O)_{72}]\cdot x HCO_2Na\cdot y H_2O$ 1 ($x \approx 30$, $y \approx 250$) with spherically shaped stable cluster anions is obtained; owing to the spherical shape of the cluster–shell template, the anion 1a (with the small 'nondisturbing' bidentate HCO_2^- ligand) exhibits a remarkable overall 'onion-type' structure, thereby revealing also a novel type of inclusion: a hydrogen-bonded cluster with 'onion-type' structure, which suggests interesting aspects for a new type of supramolecular chemistry.

Linking elementary building blocks in different ways in order to synthesize a large variety of different molecular constructions, in particular those of the nanoworld is still a formidable challenge for the inorganic chemist.[1] Recently we succeeded in developing a synthetic route for an inorganic superfullerene or a giant ball-shaped cluster anion.[2] Here we report on the synthesis of a new related compound **1** which shows a novel structural feature: an unusual hydrogen-bonded cluster of guest molecules encapsulated as a part of the overall 'onion-type' structure.

Compound **1** which crystallizes in the space group $R\bar{3}$ was synthesized by reducing an aqueous molybdate solution with hydrazinium sulfate in the presence of formic acid (pH ≈ 4.2).‡§ The spherical icosahedral cluster shell of the anion **1a** is built up by 12 $\{Mo_{11}\}$ fragments of the type $\{(Mo)Mo_5\}\{Mo^{V}_1\}_5$ with a central bipyramidal pentagonal $\{MoO_7\}$ unit (Fig.1). (Throughout, the oxidation state of the molybdenum center is only given if different from VI.) Each central $\{MoO_7\}$ unit is connected *via* edges to five $\{MoO_6\}$ octahedra which are linked in pairs to the five surrounding Mo^V atoms. Each of the latter is bonded to a Mo^V center of one of the five neighbouring $\{Mo_{11}\}$ fragments thus forming a $\{Mo^{V}_2\}$ unit. All oxygen atoms of the 132 $Mo–O_{term}$ groups lie on the surface of the ball-shaped cluster and accordingly the *trans*-orientated H_2O ligands of the 72 Mo centers as also the carboxylate ligands bonded to the $\{Mo^{V}_2\}$ groups point towards the center of the ball. To give an alternative description, the twelve $\{(Mo)Mo_5\}$ pentagons of **1a** are bridged *via* the 30 well known $\{Mo^{V}_2\}$ groups with Mo–Mo single bonds which themselves are stabilized by the bidentate carboxylate ligands. The corresponding formulation is $[\{(Mo)Mo_5O_{21}(H_2O)_6\}_{12}\{Mo^{V}_2O_4(HCO_2)\}_{30}]^{42-}$.

Most interestingly, the small carboxylate ligand used here allows a special type of organization of the encapsulated H_2O molecules resulting in a hydrogen-bonded cluster as guest system with an 'onion-type' structure[3] (see Fig. 2 with space filling representation). Six H_2O molecules with nearly trigonal antiprismatic ordering (in violet) form the innermost shell with a distance of *ca.* 3.5 Å from the (unoccupied) center of the 'onion'. The second shell (6.2–6.9 Å, highlighted as green spheres) is approximately close packed and contains *ca.* 35 H_2O molecules. The third shell (8.2–8.7 Å, shown as yellow spheres) contains a smaller number of H_2O molecules. This unusual arrangement which is induced by the spherical cluster shell spanned by the 132 molybdenum atoms is obviously only possible in the presence of the comparatively small formate ligands coordinating to the $\{Mo^{V}_2\}$ groups. This allows the H_2O molecules of the third shell to occupy positions between the bidentate ligands in the region of the 'pores'.

To evaluate the influence of the carboxylate ligands on the structure of the encapsulated molecules we also used other carboxylate ligands. The analogous reaction of sodium molybdate with monochloroacetic acid, for instance, led to the formation of a spherically shaped cluster anion and the related compound $(NH_4)_{42}[Mo^{VI}_{72}Mo^{V}_{60}O_{372}(ClCH_2CO_2)_{30}(H_2O)_{72}]\cdot x ClCH_2COONa\cdot y H_2O$ ($x \approx 15$, $y \approx 250$) which crystallizes in the space group $Fm\bar{3}$. However, due to the poor crystal quality and disorder problems we were unable to locate in detail the arrangement of guest molecules inside the cavity.¶ Interestingly, the spherical anion was possibly abundant in a solution investigated by Ostrowetsky in the early 1960s as the UV–VIS spectrum reported there is identical with that obtained by us.[4]

The high stability of **1** is remarkable and allows the development of a chemistry similar to that of the Keggin-ion type, for instance a new type of host–guest chemistry. In the

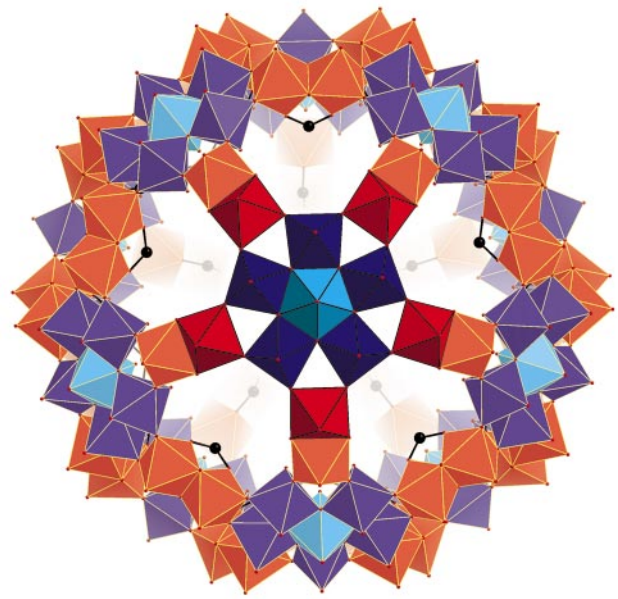

Fig. 1 Illustration of the structure of **1a** with perspective view along a fivefold symmetry axis highlighting a pentagonal $\{Mo_{11}\}$ unit owing to the structural complexity of the spherical shape shown in polyhedral representation. The five peripheral atoms of a $\{Mo_{11}\}$ unit are formed by the Mo centers of the five related $\{Mo^{V}_2O_4\}^{2+} = \{Mo^{V}_2\}$ groups attached to the $\{(Mo)Mo_5\}$ pentagons ($\{(Mo)Mo_5\}$ groups blue with the central MoO_7 bipyramids cyan; $\{Mo^{V}_2\}$ bridge red).

† On leave from the Institute of Inorganic Chemistry, Russian Academy of Sciences, pr. Lavrentjeva 3, Novosibirsk 630090, Russia.

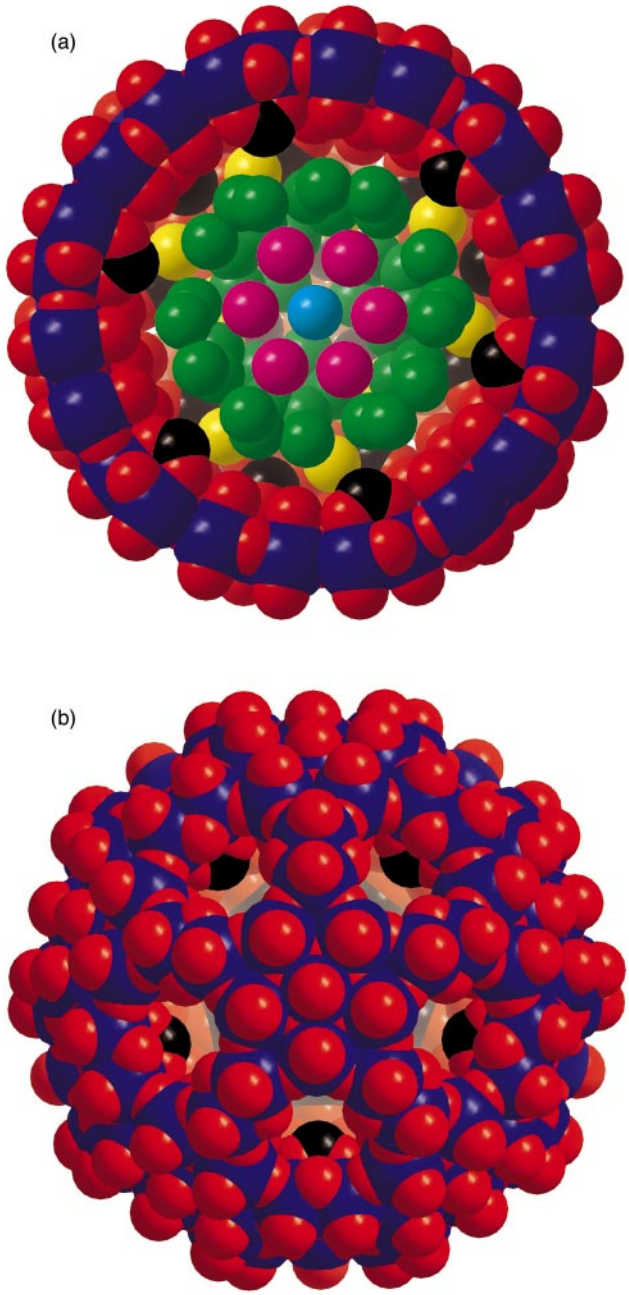

Fig. 2 Cross section through the equator of **1a** (shown in space filling representation) allowing a view into its cavity and highlighting the hydrogen-bonded cluster of the encapsulated H_2O molecules (only oxygen atoms are shown) (*a*). While the empty central region is marked by a light-blue circle, the different shells spanned by encapsulated H_2O molecules are represented by spheres with different colours: violet shell (radius *ca.* 3.5 Å), green shell (6.2–6.9 Å) and yellow shell (8.2–8.7 Å). Interestingly, the onion-like structure of the whole anion is completed by the three successive outer shells consisting of (1) that of the 72 H_2O and 30 formate ligands coordinated to molybdenum atoms and pointing into the cavity (*ca.* 10.5 Å), (2) that of the 132 molybdenum atoms (*ca.*13.1 Å) and (3) that of the terminal 132 oxygen atoms (*ca.* 14.7 Å) (molybdenum atoms blue, oxygen red, carbon black). For comparison, the whole spherical cluster anion is shown in space filling representation (*b*) (molybdenum atoms blue, oxygen red, carbon black).

present case it would be of special interest, theoretically, to study the influence of the outer spherical shell (including that with differently coordinated ligands) on the organization of the complementary inner-shells of hydrogen-bonded-type clusters, such as observed in compound **1**. The structures of the discrete $(H_2O)_n$-type clusters and related hydrogen-bonded aggregates are, of course, also interesting (see for instance ref. 5 and papers cited therein).

We acknowledge useful contributions from E. Krickemeyer and thank the Deutsche Forschungsgemeinschaft and the Fonds der Chemischen Industrie for financial support.

Notes and references

‡ *Synthesis of* $(NH_4)_{42}[Mo^{VI}_{72}Mo^{V}_{60}O_{372}(HCO_2)_{30}(H_2O)_{72}]\cdot xHCO_2Na\cdot yH_2O$ **1** ($x \approx 30$, $y \approx 250$): to a solution of NaOH (4.24 g), HCO_2H (5.00 ml; 98%) and $(NH_4)_6Mo_7O_{24}\cdot 4H_2O$ (5.30 g) in 50 ml of water, $N_2H_4\cdot H_2SO_4$ (0.76 g) was added under continuous stirring, resulting in a green–blue colouration of the reaction mixture. After 10 min the pH value of the solution was adjusted to 4.2 by adding 10% HCO_2H dropwise. The solution was kept at room temperature for 4 days. The red–brown crystals which precipitated were filtered off, washed with MeOH and dried at room temperature. Yield: 1.90 g (32%). Correct elemental analyses for C, H, N, Na and H_2O. IR (solid, KBr pellet, ν/cm^{-1}): 1618m [$\delta(H_2O)$], 1562s [$\nu_{as}(CO_2)$], 1401s [$\delta_{as}(NH_4^+)$], 1350w [$\nu_s(CO_2)$], 972s and 938w [ν(Mo=O)], 858m, 801vs, 727vs, 633w, 572s, 474w, 414w. FT-Raman [solid (λ = 1064 nm), ν/cm^{-1}]: 923m and 880s [ν(Mo=O)], 695w, 477w, 434w, 375s, 316 m, 255w, 123w. UV–VIS [H_2O, absorption, λ/nm (ε/dm^3 mol^{-1} cm^{-1})]: 450 (22000).

§ *Crystal data* for **1**: $C_{60}H_{872}Mo_{132}N_{42}Na_{30}O_{814}$, M = 28565.20, hexagonal, space group $R\bar{3}$, a = 32.4214(10), c = 73.249(3) Å, U = 66679.9(39) Å^3, Z = 3, D_c = 2.134 g cm^{-3}, μ = 1.93 mm^{-1}, F(000) = 41736.0, crystal size = 0.25 × 0.20 × 0.15 mm^3. Crystals of **1** were removed from the mother-liquor and immediately cooled to 183(2) K on a Bruker AXS SMART diffractometer (three circle goniometer with 1K CCD detector, Mo-Kα radiation, graphite monochromator). Hemisphere data collection in ω at 0.3° scan width in three runs with 606, 435 and 230 frames (φ = 0, 88 and 180°) at a detector distance of 5.00 cm. A total of 115045 reflections ($0.78 < \theta < 25.01°$) were collected of which 25930 unique reflections (R_{int} = 0.1066) were used. An empirical absorption correction using equivalent reflections was performed with the program SADABS. The structure was solved with the program SHELXS-97 and refined using SHELXL-97 to R = 0.0784 for 12308 reflections with $I > 2\sigma(I)$ (all programs from G. M. Sheldrick, University of Göttingen). Max./min. residual electron density 2.629 and −1.367 e Å^{-3} . CCDC 182/1216. See http://www.rsc.org/suppdata/cc/1999/927/ for crystallographic files in .cif format.

¶ *Synthesis of* $(NH_4)_{42}[Mo^{VI}_{72}Mo^{V}_{60}O_{372}(ClCH_2CO_2)_{30}(H_2O)_{72}]\cdot xClCH_2CO_2Na\cdot yH_2O$ ($x \approx 15$, $y \approx 250$). To a solution of NaOH (4.00 g), $ClCH_2CO_2H$ (9.45 g) and $Na_2MoO_4\cdot 2H_2O$ (5.00 g) in 50 ml of water, $N_2H_4\cdot H_2SO_4$ (0.610 g) was added under continuous stirring, resulting in a green–blue colouration of the reaction mixture. After 10 min the pH of the solution was adjusted to 4.2 by adding 20% $ClCH_2CO_2H$ dropwise and kept at room temperature for 4 days. H_2O (50 ml) and NH_4Cl (8.0 g) were subsequently added to the filtrate and the solution allowed to stand for a further 2 days. The red–brown crystals which precipitated were filtered off, washed with MeOH and dried at room temperature. Yield: 1.05 g (24%). Correct elemental analyses for C, H, N, Na and H_2O. IR (solid, KBr pellet, ν/cm^{-1}): 1758w, 1618sh [$\delta(H_2O)$], 1579s, [$\nu_{as}(CO_2)$], 1407s [$\delta_{as}(NH_4^+)$], (1259w, 1172w, 1085w), 969s and 938sh [ν(Mo=O)], 852m, 795s, 725s, 630w, 570s, 486w, 414w. FT-Raman [solid (λ 1064 nm), ν/cm^{-1}]: 942m and 873s [ν(Mo=O)], 465w, 437w, 373s, 316m, 251w, 212w, 132w. UV–VIS [H_2O, absorption, λ/nm (ε/dm^3 mol^{-1} cm^{-1})]: 452 (21000). *Crystal data*: $C_{90}Cl_{45}Mo_{132}N_{42}Na_{15}O_{784}$, M = 29726.32, cubic, space group $Fm\bar{3}$, a = 46.06 Å, U = 97703 Å^3, Z = 4, T = 173(2) K. The structure was not fully reported because of the poor crystal quality.

The figures were prepared with the program DIAMOND (K. Brandenburg, *Diamond—Informationssystem für Kristallstrukturen*, Crystal Impact GbR, Germany).

1 *Polyoxometalates: From Platonic Solids to Anti-Retroviral Activity*, ed. M. T. Pope and A. Müller, Kluwer, Dordrecht, 1994; M. T. Pope and A. Müller, *Angew. Chem., Int. Ed. Engl.*, 1991, **30**, 34; A. Müller, F. Peters, M. T. Pope and D. Gatteschi, *Chem. Rev.*, 1998, **98**, 239.
2 A. Müller, E. Krickemeyer, M. Schmidtmann, H. Bögge and F. Peters, *Angew. Chem., Int. Ed. Engl.*, 1998, **37**, 3360.
3 Compare with MS_2-based onion-type structures (M = Mo, W), *e.g.* R. Tenne, L. Margulis, M. Genut and G. Hodes, *Nature*, 1992, **360**, 444.
4 S. Ostrowetsky, *Bull. Soc. Chim. Fr.*, 1964, 1003; S. Ostrowetsky and P. Souchay, *Compt. Rend.*, 1960, **251**, 373.
5 M. R. Viant, J. D. Cruzan, D. D. Lucas, M. G. Brown, K. Liu and R. J. Saykally, *J. Phys. Chem. A*, 1997, **101**, 9032; R. Ludwig, F. Weinhold and T. C. Farrar, *J. Chem. Phys.*, 1997, **107**, 499.

Communication 8/09856E

ChemComm

Symmetric bis-benzimidazoles: new sequence-selective DNA-binding molecules

Stephen Neidle,*[a] John Mann,*[b] Emma L. Rayner,[a] Anne Baron,[b] Yaw Opoku-Boahen,[b] Ian J. Simpson,[a] Nicola J. Smith,[a] Keith R. Fox,[c] John A. Hartley[d] and Lloyd R. Kelland[e]

[a] *The CRC Biomolecular Structure Unit, The Institute of Cancer Research, Sutton, Surrey, UK SM2 5NG*
[b] *Department of Chemistry, University of Reading, Whiteknights Park, Reading UK RG6 6AD*
[c] *Division of Biochemistry and Molecular Biology, University of Southampton, Southampton, UK SO16 7PX*
[d] *CRC Drug-DNA Interactions Research Group, UCL Medical School, London, UK W1P 8BT*
[e] *CRC Centre for Cancer Therapeutics, The Institute of Cancer Research, Sutton, Surrey, UK SM2 5NG*

Received (in Liverpool, UK) 8th February 1999, Accepted 30th March 1999

A series of *bis*-benzimidazole compounds with a head-to-head orientation have been designed as sequence-specific DNA binders; crystallographic analysis of oligonucleotide complexes has been combined with DNase I footprinting to confirm that the predicted optimal site for the core bis-benzimidazole motif is the four-base-pair sequence 5′-AATT; this sequence specificity results in inhibition of transcription at A/T sites and may be responsible for the cytotoxic and antitumour effects shown by these head-to-head bis-benzimidazoles.

The minor groove of duplex DNA is the site of non-covalent interaction of a large number of anticancer drugs, antibiotics and antiviral agents,[1] which are believed to exert their action by competing with transcription factors[2] or architectural proteins,[3] such as E2F, TATA-box binding proteins or DNA topoisomerase I/II. The molecular basis of DNA recognition for a number of drugs in this super-family (notably distamycin, netropsin, berenil, pentamidine and Hoechst 33258) has been extensively studied, by crystallographic,[4] NMR[5] and footprinting methods.[6] These studies have shown that their AT preferences are a consequence of, in particular, (i) the sequence-dependent narrow width of the minor groove of B-form DNA, resulting in stabilisation by van der Waals interactions with the walls of the groove,[7] and (ii) their ability to form specific H-bonds with donor and acceptor atoms on the minor groove edge of A : T base pairs. These factors have been utilised in the design of molecules with altered and extended recognition properties, some of which are capable of sequence-specific gene regulation.[8]

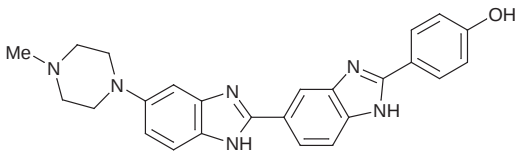

Hoechst 33258

We have previously reported crystallographic analyses of a number of oligonucleotide complexes with the head-to-tail bis-benzimidazole compound Hoechst 33258, and several of its derivatives,[9] including a tris-benzimidazole with an extended recognition site.[10] These have shown that each benzimidazole subunit interacts with two A : T base pairs by means of a pair of cross-strand H-bonds. The head-to-tail arrangement forces the site for each successive subunit to overlap the previous one by one base-pair (bp), so that each benzimidazole group in Hoechst 33258 and other head-to-tail analogues effectively recognises 1.5 A : T bps.

Molecular modelling, based on these structural studies, has suggested to us that the novel symmetric head-to-head benzimidazole arrangement could also effectively bind in the minor groove. This arrangement would extend the size of the *bis*-benzimidazole recognition site from three (in Hoechst 33258 and analogues) to four consecutive A:T bps, with distinctive cross-strand H-bonding involving each base pair. This arrangement thus extends the effective recognition of each benzimidazole sub-unit to two A:T bps. The modelling used the structures of the self-complementary duplex sequences d(CGCGAATTCGCG) and d(CGCAAATTTGCG), as found in several relevant drug complexes.[9,10] It suggested that the central 5'-AATT sequence would be an optimal site for the head-to-head motif and for maintenance of helical register with all four consecutive bps without necessitating significant DNA conformational change. An initial range of head-to-head bis-benzimidazoles have now been synthesised, and is reported here.

The highly convergent synthesis of these bis-benzimidazoles (Scheme 1) involves the condensation between the requisite 4-substitituted aryl aldehyde and 3,3′,4,4′-tetraaminobiphenyl **7**. The latter is commercially available, but is of variable quality, and we preferred to prepare it by the route shown. Thus, **1** and **2** were easily obtained from 4-methoxybenzaldehyde and 4-hydroxybenzaldehyde, respectively, while **3** was obtained from 4-(3-dimethylaminopropoxy)benzaldehyde prepared from 4-hydroxybenzaldehyde and 3-dimethylaminopropanol using a Mitsunobu reaction. In each instance the aryl aldehyde and 3,3′,4,4′-tetraaminobiphenyl were heated in nitrobenzene at 150 °C for 8–10 h to effect the condensation, and the yields of bis-benzimidazoles were typically 25–40% on the 10 mmol scale.

Crystallographic analyses have been undertaken on (i) the bis(hydroxyphenyl) compound **2** co-crystallised with the oligonucleotide sequence d(CGCGAATTCGCG), and (ii) its Me_2N derivative **3** with the sequence d(CGCAAATTTGCG). Both crystal structures[11] show a B-form DNA double helix with ligand bound in the A/T region of the minor groove [Fig. 1(*a*)]. They show H-bonding between all four central A : T bps and the benzimidazole subunits [Fig. 1(*b*)], in full accord with the modelling predictions. Each inner-facing ring nitrogen atom of

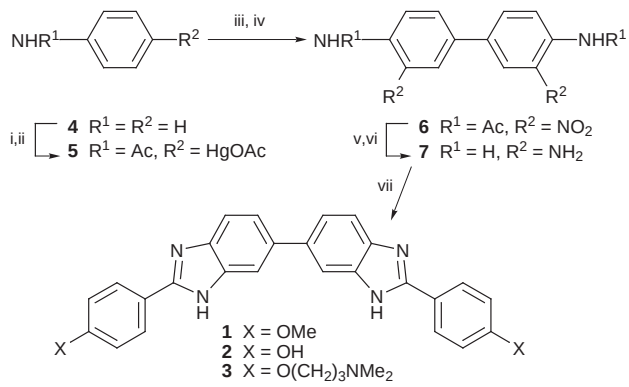

Scheme 1 *Reagents and conditions*: i, Ac_2O, AcOH; ii, $Hg(OAc)_2$, AcOH, $HClO_4$, *ca.* 20% (2 steps); iii, Cu, $PdCl_2$, Py; iv, HNO_3, AcOH, *ca.* 50% (2 steps); v, H_2SO_4; vi, Raney Ni, H_2, *ca.* 70% for 2 steps; vii, 4-XC_6H_4CHO [X+MeO (**1**), OH (**2**) or $Me_2N(CH_2)_3O$ (**3**)], $PhNO_2$, 150 °C.

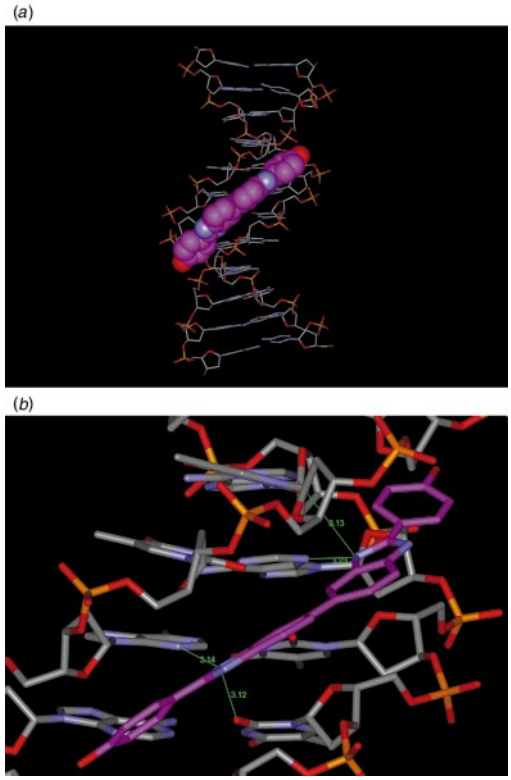

Fig. 1 Computer plots of the crystal structure of the complex of **2** with d(CGCGAATTCGCG): (*a*) shows the ligand, in space-filling mode, centrally bound in the minor groove of the 12-mer double helix, while (*b*) shows a detailed view of **2** and the H-bond contacts to A : T bp edges.

Table 1 Cytotoxicity of *bis*-benzimidazole compounds, for 96 h exposure in a panel of four ovarian cell lines (as $IC_{50}/\mu M$)

Compound	A2780	A2780-Pt^R	CH1	SKOV-3
1	13.5	5.1	3.8	16.5
2	4.3	2.7	1.05	16
3	0.235	0.115	0.24	0.375
Hoechst 33258	12.0	9.5	26.5	> 100

a benzimidazole ring H-bonds to a thymine O2 atom of one bp and an adenine N3 atom on the opposite strand of an adjacent one. It is notable that the absence of formal cationic charge in **2**, does not affect its sequence selectivity, suggesting that the role of charge is to modulate affinity rather than to determine sequence selectivity.

These preferences have also been observed in DNase I footprinting studies with a natural DNA fragment, which have shown that **2** and **3** both interact preferentially with some A/T sites. Compound **3** binds to AT sites between 7–10-fold better than **2**, and has an especially high affinity for the 5′-AATT site (30 nM). Quantitative footprinting data indicated that the order of preference is 5′-AATT > 5′-ATAT > 5′-TAAT > 5′-TATA ~ 5′-TTAA, similar to that previous determined for Hoechst 33258. The increased affinity of **3** relative to **2** does not affect its sequence selectivity. This enhanced binding strength may be a consequence of its cationic charge or its increased DNA site size, since the crystal structure of the complex with $d(CGCAAATTTGCG)_2$ shows it to cover 6 bps. The ability of the head-to-head bis-benzimidazoles to discriminate between the 136 possible tetranucleotide sequences may be further enhanced by flanking sequence preferences. These remain to be systematically explored. Whilst this paper was in preparation, a report has appeared which describes compound **2** and its interactions with tRNA.[12]

These new bis-benzimidazoles have been examined for potential cytotoxic effects in a group of ovarian carcinoma cell lines. Table 1 shows that all compounds are cytotoxic at the μM level, with activity significantly greater than that shown by Hoechst 33258. The Me_2N derivative **3** is over 10-fold more active than the others in three out of the four lines. **3** also shows significant activity in several ovarian lines in the NCI 60-cell line panel (to be published). The compound with least *in vitro* activity, the hydrophobic dimethoxy derivative **1**, has been examined in an *in vivo* tumour model with the ADJ/PC6 plasmacytoma, where it showed 44% tumour inhibition with ip administration. Compound **3** has been examined in an *in vitro* transcription assay. It effectively inhibits transcription at a number of A/T sites, consistent with the above data. In addition, compound **3** inhibited transcription at least 10-fold more efficiently than compound **2**, consistent with its increased cytoxicity. We speculate that the activity of **3** *in vitro* and *in vivo* may be related to its potent ability to specifically inhibit transcription at a small sub-set of A/T sites. The relatively low affinity of compound **3** for 5′-TATA sites suggests that it is less likely to block TATA-box binding proteins at the start of transcription.

This work has been supported by grants from the Cancer Research Campaign, the Royal Society of Chemistry (Adrien Albert Memorial Fund) and the Ghanaian Government.

Notes and references

1 C. Zimmer and U. Wähnert, *Prog. Biophys. Mol. Biol*., 1986, **47**, 31; P. B. Dervan, *Science*, 1986, **232**, 464.
2 See for example: J. J. Welch, F. J. Rauscher III and T. A. Beerman, *J. Biol. Chem*., 1994, **269**, 31 051; S.-Y. Chiang, J. C. Azizkhan and T. A. Beerman, *Biochemistry*, 1998, **37**, 3109.
3 For example: Z. Xu, T.-K. Li, J. S. Kim, E. J. LaVoie, K. J. Breslauer, L. F. Liu and D. S. Pilch, *Biochemistry*, 1998, **37**, 3558; J. S. Kim, Q. Sun, C. Yu, A. Liu, L. F. Liu and E. J. LaVoie, *Bioorg. Med. Chem*., 1998, **6**, 163.
4 S. Neidle, *Biopolymers*, 1997, **44**, 105.
5 A. Fede, A. Labhardt, W. Bannwarth and W. Leupin, *Biochemistry*, 1991, **30**, 11 377; J. A. Parkinson, S. E. Ebrahimi, J. H. McKie and K. T. Douglas, *Biochemistry*, 1994, **33**, 8442; C. E. Bostock-Smith, C. A. Laughton and M. S. Searle, *Nucleic Acids Res*., 1998, **26**, 1660.
6 K. D. Harshman and P. B. Dervan, *Nucleic Acids Res*., 1985, **13**, 4825; A. Abu-Daya, P. M. Brown and K. R. Fox, *Nucleic Acids Res*., 1995, **23**, 3385.
7 S. Neidle, *FEBS Lett.*, 1992, **298**, 97; A. Czarny, D. W. Boykin, A. A. Wood, C. M. Nunn, S. Neidle, M. Zhao and W. D. Wilson, *J. Am. Chem. Soc*., 1995, **117**, 4716.
8 J. M. Gottesfield, L. Neely, J. W. Trauger, E. E. Baird and P. B. Dervan, *Nature*, 1997, **387**, 205; S. White, J. W. Szewczyk, J. M. Turner, E. E. Baird and P. B. Dervan, *Nature*, 1998, **391**, 468; L. A. Dickinson, R. J. Gulizia, J. W. Trauger, E. E. Baird, D. M. Mosier, J. M. Gottesfield and P. B. Dervan, *Proc. Natl. Acad. Sci. U.S.A.*, 1998, **95**, 12 890.
9 N. Spink, D. G. Brown, J. V. Skelly and S. Neidle, *Nucleic Acids Res*., 1994, **22**, 1607; G. R. Clark, D. W. Boykin, A. Czarny and S. Neidle, *Nucleic Acids Res*., 1997, **25**, 1510.
10 G. R. Clark, E. J. Gray, S. Neidle, Y.-H. Li and W. Leupin, *Biochemistry*, 1996, **35**, 13 745.
11 Compound **2** was co-crystallised with d(CGCGAATTCGCG) (from Oswell DNA Service, Southampton) using the hanging-drop method at 286 K. Elongated prismatic crystals were obtained from a 1.5 mM solution of 1 in 50% w/w MPD, in a droplet containing 10 mM $MgCl_2$, 60 mM KCl, 0.75 mM DNA and 6 mM spermine, equilibrated against 30% w/w MPD. The crystals are orthorhombic, space group $P2_12_12_1$, with cell dimensions a = 25.46(2), b = 39.96(4) and c = 65.66(7) Å. Intensity data were collected from a flash-frozen crystal maintained at 100 K with a RAXIS-4 image plate detector, using Cu-Kα radiation from a rotating-anode generator and mirror-focussing optics. A total of 6380 unique reflections were obtained after merging Friedel equivalents (R_{merge} = 0.044) to a resolution of 1.8 Å. The structure was solved using molecular replacement, and refined with the SHELX-97 package. The final model included 174 water molecules, and had an R of 0.229 for 6157 reflections with $F > 4\sigma(F)$, and 23.2% for all data to 1.8 Å. R_{free} was 25.1%. Coordinates and reflection data have been deposited at the Nucleic Acid Database as entry no. dd0013. See http://www.rsc.org/suppdata/cc/1999/929/ for a 3D image in .pdb format.
12 E. V. Bichenkova, S. E. Sadat-Ebrahimi, A. N. Wilton, N. O'Toole, D. S. Marks and K. T. Douglas, *Nucleosides Nucleotides*, 1998, **17**, 1651.

Communication 9/01074B

Phosphonamidothioic acids as thiophosphonylating agents: stereochemistry of reactions of *N*-*tert*-butyl-*P*-phenylphosphonamidothioic acid with alcohols

Martin J. P. Harger* and Christopher Pater

Department of Chemistry, The University, Leicester, UK LE1 7RH

Received (in Liverpool, UK) 18th March 1999, Accepted 9th April 1999

Enantiopure PhP(S)(OH)NHBu^t reacts with alcohols in CH_2Cl_2 to give PhP(S)(OH)OR (R = Me, Pr^i, Bu^t); reaction is completely non-stereospecific with Bu^{t}OH and largely so with Pr^{i}OH and very low concentrations of MeOH, pointing to the involvement of a thiometaphosphonate (PhPOS) intermediate.

Early work on the synthesis of biologically important pyrophosphates and triphosphates made use of phosphoramidic acid monoesters **1** as phosphorylating agents (Scheme 1).[1] In

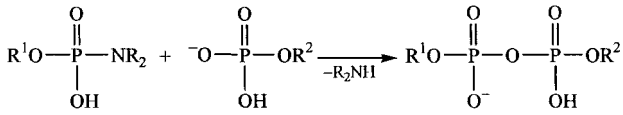

1 **2** **3**

Scheme 1

principle the phosphoryl transfer could involve a monomeric metaphosphate intermediate (R^1OPO_2) but the kinetics indicated rather a bimolecular reaction,[1,2] *i.e.* direct nucleophilic attack of the acceptor **2** to give the product **3**. More recently Jankowski and Quin[3] have found that phosphoramidic acid monoesters will also phosphorylate alcohols efficiently, even (or especially) when bimolecular reaction is impeded by steric factors in the donor and acceptor. For these reactions the kinetics,[3] including kinetic isotope effects,[4] appear to indicate the dominance of a unimolecular mechanism (Scheme 2; R^1 = Et, R = 1-adamantyl or mesityl), *i.e.* decomposition of the

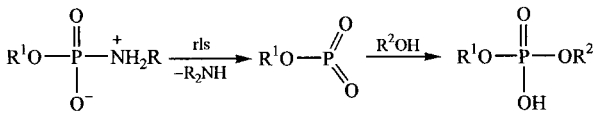

4 **5** **6**

Scheme 2

zwitterionic form **4** of the donor to release the monomeric metaphosphate **5** which is then trapped by the alcohol to give the product **6**. Moreover, the thiophosphorylation[5] of alcohols by phosphoramidothioic monoesters **7** and phosphonylation[6] by phosphonamidic acids **8** seem to be mechanistically similar.

It should be possible to distinguish between bimolecular and unimolecular mechanisms by examining the stereochemistry of reaction. A P=O donor compound (*e.g.* **1** or **8**) will not be chiral at phosphorus unless one of the oxygen (^{16}O) atoms is replaced by an isotope (^{18}O), but a P=S donor compound (*e.g.* **7** or **9**) is inherently chiral. We have therefore sought to obtain the phosphonamidothioic acid **9** as a single enantiomer and ascertain the stereochemistry of its reactions with alcohols.

Racemic phosphonamidothioic acid **9** was prepared from $PhPCl_2$ by a published procedure[7] and was resolved using α-methylbenzylamine. From the less soluble (Et_2O) of the diastereoisomeric salts formed with (*R*)-(+)-$PhMeCHNH_2$ the acid **9** was obtained as a single enantiomer (≥99%) after

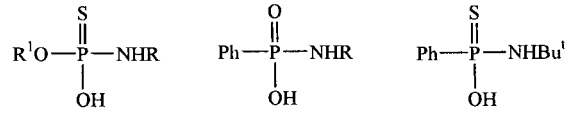

7 **8** **9**

recrystallisation (Et_2O–light petroleum), mp 82–83 °C (lit.,[7] 81.5–82.5 °C for the racemate); $[\alpha]_D$ + 21.7 (*c* 1.2 in CH_2Cl_2); salt with (*S*)-(−)-$PhMeCHNH_2$, $\delta_P(C_6D_6)$ 54.3; $\delta_H(C_6D_6)$ 1.22 (NBu^t) [addition of racemic **9** introduced new peaks at higher field, $\Delta\delta_P$ 2.1 ppm, $\Delta\delta_H$ 0.11 ppm].†

The reactions of the amidic acid (+)-**9** were examined at 30 °C as dilute solutions (0.02 mol dm^{-3}) in CH_2Cl_2 containing an excess (10 equiv.) of the appropriate alcohol (0.20 mol dm^{-3}). Reaction was halted at 50–60% completion (0.4–0.8 h) and the product **12** (Scheme 3) and unreacted substrate were isolated as a mixture of the free acids. This mixture was treated with (*S*)-(−)-$PhMeCHNH_2$ to form diastereoisomeric salts of the acids. Analysis by $^{31}P\{^1H\}$ NMR spectroscopy (C_6D_6 solution) revealed the diastereoisomer ratios for the salts and by implication the enantiomer ratios of the acids. In every case the unreacted substrate was found to be still a single enantiomer, showing that it is configurationally stable under the conditions of reaction. Any departures from enantiopurity in the products must therefore be a reflection of how they are formed from (+)-**9**.‡

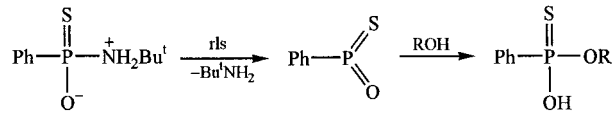

10 **11** **12**

Scheme 3

With MeOH the product **12** (R = Me) was obtained with one enantiomer in large excess (ee 76%) [salt: $\delta_P(C_6D_6)$ 72.8 and 72.5, ratio 88 : 12; $\delta_H(C_6D_6)$ 3.36 (major) and 3.35 (both d, J_{PH} 13.5, OMe)] but with Pr^{i}OH the excess of one of the enantiomers of **12** (R = Pr^i) was modest (ee 15%) [salt: δ_P 68.7 and 68.35, ratio 57.5 : 42.5; δ_H 1.34, 0.88 (major) and 1.32, 0.87 (all d, J_{HH} 6, OCH*Me*$_2$)] and with Bu^{t}OH the product **12** (R = Bu^t) was practically racemic [salt: δ_P 60.3 and 60.2; δ_H 1.47 and 1.46 (both s, OBu^t)].§ A reasonable explanation is that there are competing stereospecific and non-stereospecific pathways and that the relative importance of each is dependent on the identity of the alcohol nucleophile. Also, given the earlier mechanistic evidence, it seems likely that these pathways are bimolecular and unimolecular respectively.¶

The bimolecular pathway would presumably involve in-line attack [$S_N2(P)$] of the alcohol on the zwitterionic form **10** of the substrate, giving the product **12** with inversion of configuration at phosphorus.[8] Steric interactions in the five-coordinate transition state will be more severe with bulky alcohols and reaction by this pathway will be correspondingly less favourable. The unimolecular pathway would involve unassisted decomposition of the zwitterion **10** and liberation of the

thiometaphosphonate **11** (Scheme 3); this, being planar (trigonal) and open to attack at either face by the alcohol, will give the product **12** as the racemate. In this case, the alcohol does not bond to phosphorus in the rate-limiting step; the unimolecular pathway will therefore acquire increasing relative importance as the bimolecular pathway becomes less favourable, *i.e.* as the bulk of the alcohol nucleophile increases.

As a test of mechanistic duality the dependence of the stereochemistry of reaction on the concentration of the nucleophile was examined. With lower concentrations of alcohol the non-stereospecific unimolecular pathway should assume greater importance while higher concentrations should favour the stereospecific bimolecular pathway. In the event, reducing the concentration of MeOH or Pr^iOH to 0.05 mol dm^{-3} gave the product **12** with an enantiomer ratio of 70 : 30 (R = Me) or 51 : 49 (R = Pr^i) and increasing it to 0.80 mol dm^{-3} gave an enantiomer ratio of 98 : 2 (R = Me) or 58.5 : 14.5 (R = Pr^i). With Bu^tOH the product was practically racemic at all alcohol concentrations, implying a negligible contribution from stereospecific bimolecular reaction.§

In one case—the 0.20 mol dm^{-3} MeOH reaction—the dependence of the stereochemistry on the temperature was also examined. Relative to the reaction at 30 °C (enantiomer ratio of product **12**, 88 : 12), reducing the temperature increased the overall stereospecificity of reaction (enantiomer ratio 96 : 4 at 0 °C) and increasing the temperature reduced it (72 : 28 at 60 °C). This implies a more ordered transition state for the stereospecific pathway, consistent with it being of higher molecularity.

That the monomeric thiometaphosphonate **11** plays an important part in the reactions of **9** with alcohols seems certain, but the nature of the competing stereospecific process is less clear. It shows the characteristics expected of an associative $S_N2(P)$ reaction but so might a dissociative reaction if it involves preassociation of the substrate and nucleophile.[9] Then the nucleophile will already be in place when the zwitterion **10** decomposes and the thiometaphosphonate is formed. This may now be trapped stereoselectively, by attack of the alcohol on one face before the leaving group (H_2NBu^t) has diffused away from the other. The reactions of **9** with alcohols may therefore proceed *entirely via* the thiometaphosphonate, in a free (liberated) state or associated with the nucleophile. The stereochemistry observed with **9** does, we think, support the view of Jankowski and Quin that metaphosphate intermediates are involved in the reactions of related amidic acids with alcohols.

Notes and references

† The free amidic acid **9** begins to decompose as soon as it is dissolved in an aprotic solvent. All operations involving solutions of **9** were conducted with cooling and executed as rapidly as possile. The value of $[\alpha]_D$ must be considered approximate.

‡ The products **12** were isolated from reactions allowed to proceed to ⩾90% completion and were purified and characterised as their dicyclohexylammonium salts [^1H and ^{31}P NMR and IR spectroscopy; mass spectrometry (ES and −FAB) including accurate mass measurement].

§ The ^{31}P NMR signals for the diastereoisomeric salts of **12** (R = Bu^t) were not quite fully resolved and in this case the enantiomer ratio is not as precise (±2% in each component) as for **12** (R = Me) or **12** (R = Pr^i).

¶ With Pr^iOH and Bu^tOH the substrate **9** and product **12** (salts with $PhMeCHNH_2$) accounted for only ~90% of the $^{31}P\{^1H\}$ NMR spectrum. The most prominent of the minor peaks were doublets (J_{PP} 39 Hz) at *ca.* $\delta_P(C_6D_6)$ 67 and 62.5, most likely due to the pyrophosphonate $PhP(S)(O^-)OP(S)(NHBu^t)Ph$ [*m/z* (−ES) 384] resulting from reaction of **9** with itself instead of with the alcohol (*cf.* ref. 3, 5 and 6).

1 V. M. Clark, G. W. Kirby and A. Todd, *J. Chem. Soc.*, 1957, 1497; J. G. Moffatt and H. G. Khorana, *J. Am. Chem. Soc.*, 1961, **83**, 649; A. Todd, *Proc. Chem. Soc. London*, 1962, 199.

2 N. K. Hamer, *J. Chem. Soc.*, 1965, 46; V. M. Clark and S. G. Warren, *J. Chem. Soc.*, 1965, 5509.

3 L. D. Quin and S. Jankowski, *J. Org. Chem.*, 1994, **59**, 4402.

4 S. Jankowski, L. D. Quin, P. Paneth and M. H. O'Leary, *J. Am. Chem. Soc.*, 1994, **116**, 11675.

5 L. D. Quin, P. Hermann and S. Jankowski, *J. Org. Chem.*, 1996, **61**, 3944; S. Jankowski, L. D. Quin, P. Paneth and M. H. O'Leary, *J. Organomet. Chem.*, 1997, **529**, 23.

6 G. S. Quin, S. Jankowski and L. D. Quin, *Phosphorus Sulfur Silicon*, 1996, **115**, 93.

7 S. Freeman and M. J. P. Harger, *J. Chem. Soc., Perkin Trans. 2*, 1988, 81.

8 G. R. J. Thatcher and R. Kluger, *Adv. Phys. Org. Chem.*, 1989, **25**, 99.

9 W. P. Jencks, *Acc. Chem. Res.*, 1980, **13**, 161; *Chem. Soc. Rev.*, 1981, **10**, 345.

Communication 9/02222H

Designer clusters: synthesis and characterization of $Cp^*_2Rh_2Co_3(CO)_8B_3HCl$ ($Cp^* = \eta^5$-C_5Me_5)

Xinjian Lei, Maoyu Shang and Thomas P. Fehlner*

Department of Chemistry & Biochemistry, University of Notre Dame, Notre Dame, IN 46556, USA

Received (in Bloomington, IN, USA) 19th February 1999, Accepted 13th April 1999

Sigma bond metathesis of B–H in $Cp^*_2Rh_2B_3H_6Cl$ with Co–Co in $Co_2(CO)_8$ leads directly to the title compound.

Both B–H[1,2] and Si–H[3] bonds undergo σ-bond metathesis with the Co–Co bond in $Co_2(CO)_8$ as illustrated in eqns. (1a) and (1b).

$$2\ R_3SiH + Co_2(CO)_8 \rightarrow 2\ (CO)_4CoSiR_3 + H_2 \quad (1a)$$
$$2\ BH_3{\cdot}thf + Co_2(CO)_8 \rightarrow 2\ (CO)_4CoBH_2{\cdot}thf + H_2 \quad (1b)$$

For this reason, the formation of the unusual cluster, $Co_5(CO)_{14}B_2H$ **1**, from the reaction of $BH_3{\cdot}SMe_2$ and $Co_2(CO)_8$ was rationalized using σ-bond metathesis of the B–H bond as an essential feature of the cluster building reaction. [4,5] However, this metallaborane, and an intermediate compound, $Co_2(CO)_6B_2H_4$, were only isolated in low yields partly due to efficient competitive formation of $Co_4(CO)_{12}$. Hence, without confirmation this mechanism remains speculative. For this reason, we have sought support for such a cluster building route in alternative systems. Here, we report the rational synthesis of an analog of **1** formed in good yield from $(Cp^*Rh)_2B_3H_6Cl$ ($Cp^* = \eta^5$-C_5Me_5), which, in turn, is readily accessible from the reaction of $Cp^*_2Rh_2Cl_4$ and $BH_3{\cdot}thf$. [6,7] The postulated cluster building reaction is corroborated and the structure exhibited by **1** is verified as the preferred core geometry for the cluster electron count.

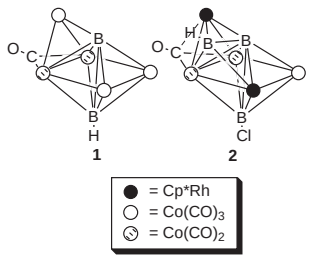

The reaction of $Cp^*_2Rh_2B_3H_6Cl$ and $Co_2(CO)_8$ under mild conditions gives $(Cp^*Rh)_2Co_3(CO)_8B_3HCl$ **2**, in 30% isolated yield.† The spectroscopic data are consistent with the molecular structure shown in Fig. 1 and derived from a solid state structure determination.‡ Comparison of **2** with **1** reveals the close structural relationship of these two clusters. Compound **1** was shown to be an unanticipated isomeric analog of a trigonal prismatic, boron centered M_6 90 cluster valence electron (cve) cluster.[5,8] Converting one M vertex of the M_6 cluster to BH leads to the observed 80 cve and the M *vs* B size mismatch leads to the isomeric structure observed. As shown in Scheme 1, **2** can be derived from a rectangular face-capped trigonal prismatic, boron centered M_7 102 cve cluster, *e.g.* $[HFe_7(CO)_{20}B]^{2-}$.[9] Just as with **1**, conversion of two M vertices to BH and BCl followed by rearrangement leads to the observed geometry. The predicted cve count is 82 as observed. The difference between the radial properties (size) of main group and transition metal fragments with similar frontier angular orbital properties and populations (isolobal) forces the unexpected isomeric structure observed for **1** and **2**.[10]

The origin of **2** from $Cp^*_2Rh_2B_3H_6Cl$ can be described with a small set of reasonable assumptions that allow the stoichiometric and geometric pathway to **2** *via* **3** to be traced out. We assume the B_3 fragment remains intact; the BH cluster bonds react with the cobalt reagent by σ-bond metathesis; CO loss from the cluster bound $Co(CO)_4$ fragment leads to insertion and consequent cluster expansion; and ML_x fragment rearrangement is facile.[11] The result is shown in Scheme 2. Reaction with $Co_2(CO)_8$ at room temperature leads to the formation of $Cp^*_2Rh_2Co(CO)_3B_3H_3Cl$ **3** (80%, Scheme 2) which has been fully characterized. [7] By itself **3** is stable at 60 °C; however, in the presence of $Co_2(CO)_8$ it is rapidly converted to **2**. Three repetitions of σ-bond methathesis plus insertion lead from reactant to product **2**. Of course the detailed nature of the insertion and rearrangement processes remains unclear, but the overall process is straightforward.

The use of $Co_2(CO)_8$ as a metal fragment source is well illustrated in cluster chemistry.[12] Evidence for a radical pathway was found for reactions of $Co_2(CO)_8$ with organome-

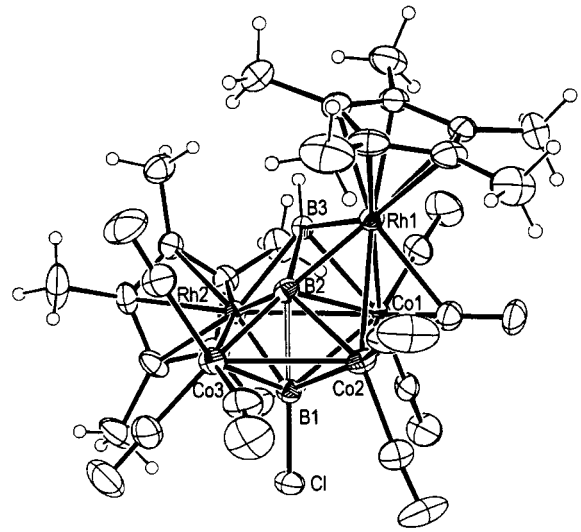

Fig. 1. Molecular structure of $Cp^*_2Rh_2Co_3(CO)_8B_3HCl$ **2**. Selected bond distances (Å) and angles (°): Rh1–Co1 2.5960(7), Rh1-Co2 2.5981(8), Rh2-Co3 2.7111(9), Rh2-Co1 2.7207(8), Co1-Co2 2.5157(10), Co2-Co3 2.6434(10), Rh1-B2 2.077(5), Rh1-B3 2.138(5), Rh1-C23, 2.297(5), Rh2-B2 2.056(5), Rh2-B1 2.066(5), Rh2-B3 2.103(5), Co1-C23 1.892(5), Co1-B3 2.161(5), Co1-B2 2.231(5), Co1-B1 2.299(5), Co2-C23 2.007(5), Co2-B2 2.082(5) Co2-B1 2.194(5), Co3-B2 1.984(5), Co3-B1 2.071(5), B1-B2 1.973(7), B2-B3 1.680(7), Cl-B1 1.831(5), B2-Rh1-B3 46.9(2), B3-Rh1-Co2 91.80(14), Co1-Rh1-Co2 57.94(2), B2-Rh2-B1 57.2(2), B2-Rh2-B3 47.6(2), B1-Rh2-B3 94.9(2), B2-Rh2-Co3 46.7(2), B3-Co1-B1 87.0(2), B2-Co1-B1 51.6(2), B3-Co1-Co2 93.54(14), B1-Co1-Rh1 97.94(13), Co2-Co1-Rh2 89.48(3), Rh1-Co1-Rh2 91.71(2), Co1-Co2-Co3 94.74(3), Rh1-Co2-Co3 93.69(3), Co2-Co3-Rh2 87.08(3).

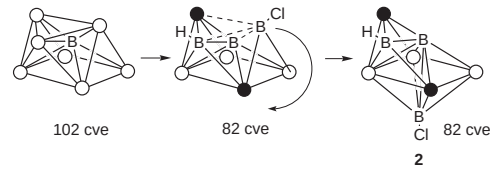

Scheme 1

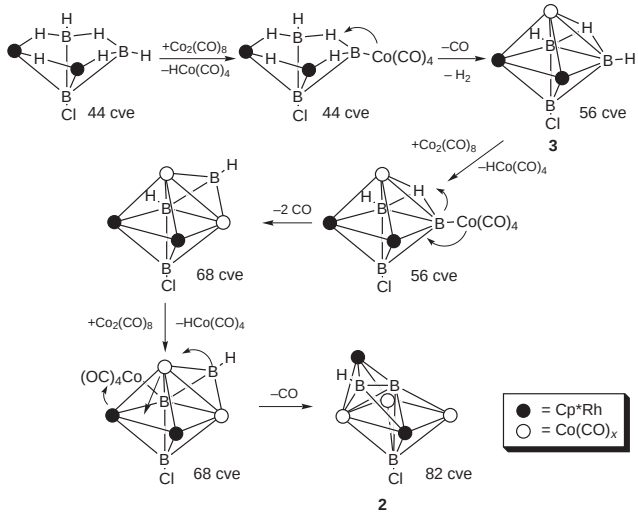

Scheme 2

tallic clusters resulting in metal fragment substitution or cluster expansion.[13,14] Presumably the cluster metal–metal bonding network is directly involved. The nature of the cluster building pathway observed here appears distinctly different. This is consistent with earlier work which demonstrates that BH bonds can interact directly with transition metal centers.[15–18] For example, the activity of exocluster B–H bonds towards metal addition has been utilized in promoting the addition of unsaturated organic substrates to borane cages.[19] Thus, even though we have no direct evidence for the cluster–$Co(CO)_4$ intermediates proposed in Scheme 2, their existence is reasonable.

The generous support of the National Science Foundation is gratefully acknowledged.

Notes and references

† *Experimental procedure:* a mixture of $Cp^*_2Rh_2B_3H_6Cl$ (0.14 g, 0.26 mmol) and $Co_2(CO)_8$ (0.25 g, 0.60 mmol) in 10 mL of hexane was heated to 60 °C for 1 h. Removal of insoluble black solids by filtration (Celite) was followed by column chromatography. After $Co_4(CO)_{12}$ was removed (hexane), elution with ether afforded a greenish brown solution which gave 0.075 g of **1** (31% based on Rh). MS (EI), P^+ = 946 (3B, 1Cl, 2Rh atoms, loss of 8 CO). Calc. for weighted average of isotopomers lying within the instrument resolution, *m*/*z* 946.8144, obs. 946.8180. NMR: ^{11}B(hexane, 22 °C), δ 90.9 (s, {^{1}H}, s, 1B), 92.0 (s, {^{1}H), s, 1B), 87.1 (d, J_{BH} 160 Hz, s, {^{1}H}, 1B); ^{1}H(C_6D_6, 22 °C), δ 10.22 (partially collapsed quartet, 1H, BH_t), 1.68 (s, 15H, C_5Me_5), 1.59 (s, 15H, C_5Me_5), IR(hexane, cm^{-1}): 2513w (B-H); 2058s, 2033s, 2016w, 1999m, 1986s, 1964w, 1880w, 1778w (CO). Anal. calc. for $C_{28}H_{31}O_8B_3Cl_1Co_3Rh_2$: C, 35.53, H, 3.30. Found: C, 35.60; H, 3.41%.

‡ *Crystal data:* **2**: black crystals, $C_{28}H_{31}O_8B_3Cl_1Co_3Rh_2$, triclinic, space group $P\bar{1}$, a = 9.498(2), b = 9.4931(13), c = 21.394(3) Å, α = 88.104(10), β = 77.308(14), γ = 62.825(11)°, V = 1669.1(4) Å^3, Z = 2, M = 946.02, D_c = 1.882 g cm^{-3}, μ = 2.553 mm^{-1}, Mo-Kα radiation, λ = 0.71073 Å, T = 293K, Enraf-Nonius CAD4, crystal size, 0.16 × 0.12 × 0.10 mm, $2\theta_{max}$ = 50°. Structure solution and refinement were performed on a PC by using the SHELXTL package (G. M. Sheldrick, Siemens Industrial Automation Inc. Madison, WI 1994); $R1$ = 0.0348, $wR2$ = 0.0821 for 4737 observed unique reflections [I > 2σ(I)] and $R1$ = 0.0475, $wR2$ = 0.0884 for all 5874 unique reflections including those with negative intensities. The maximum and minimum residual electron densities on the final difference Fourier map were 0.611 and −0.855 e Å^{-3}, respectively. CCDC 182/1230. See http://www.rsc.org/suppdata/cc1999/933/ for crystallographic files in .cif format.

1 J. D. Basil, A. A. Aradi, N. K. Bhattacharyya, N. P. Rath, C. Eigenbrot and T. P. Fehlner, *Inorg. Chem.*, 1990, **29**, 1260.
2 D. J. Elliot, C. J. Levy, R. J. Puddephatt, D. G. Holah, A. N. Hughes, V. R. Magnuson and I. M. Moser, *Inorg. Chem.*, 1990, **29**, 5014.
3 A. J. Chalk and J. F. Harrod, *J. Am. Chem. Soc.*, 1967, **89**, 1640.
4 C. S. Jun, T. P. Fehlner and A. L. Rheingold, *J. Am. Chem. Soc.*, 1993, **115**, 4393.
5 C.-S. Jun, J.-F. Halet, A. L. Rheingold and T. P. Fehlner, *Inorg. Chem.*, 1995, **34**, 2101.
6 X. Lei, M. Shang and T. P. Fehlner, *J. Am. Chem. Soc.*, 1998, **120**, 2686.
7 X. Lei, M. Shang and T. P. Fehlner, *J. Am. Chem. Soc.*, 1999, **121**, 1275.
8 D. M. P. Mingos and D. J. Wales, *Introduction to Cluster Chemistry*, Prentice Hall, New York, 1990.
9 A. Bandyopadhyay, M. Shang, C.-S. Jun and T. P. Fehlner, *Inorg. Chem.*, 1994, **33**, 3677.
10 D. M. P. Mingos, in *Inorganometallic Chemistry*, ed. T. P. Fehlner, Plenum, New York, 1992, p. 179.
11 R. D. Adams and S. Wang, *Inorg. Chem.*, 1985, **24**, 4447.
12 *The Chemistry of Metal Cluster Complexes*, ed. D. F. Shriver, H. D. Kaesz and R. D. Adams, VCH, New York, 1990.
13 C. P. Horwitz, E. M. Holt and D. F. Shriver, *Organometallics*, 1985, **4**, 1117.
14 J. A. Hriljac, P. N. Swepston and D. F. Shriver, *Organometallics*, 1985, **4**, 158.
15 M. R. Churchill, J. J. Hackbarth, A. Davison, D. D. Traficante and S. S. Wreford, *J. Am. Chem. Soc.*, 1974, **96**, 4041.
16 P. E. Behnken, D. C. Busby, M. S. Delaney, R. E. King III, C. W. Kreimendahl, T. B. Marder, J. J. Wilczynski and M. F Hawthorne, *J. Am. Chem. Soc.*, 1984, **106**, 7444.
17 D. D. Ellis, J. M. Farmer, J. M. Malget, D. F. Mullica and F. G. A. Stone, *Organometallics*, 1998, **17**, 5540.
18 S. A. Snow, M. Shimoi, C. D. Ostler, B. K. Thompson, G. Kodama and R. W. Parry, *Inorg. Chem.*, 1984, **23**, 511.
19 L. G. Sneddon, *Pure Appl. Chem.*, 1987, **59**, 837.

Communication 9/01491H

ChemComm

Photophysical properties of osmium(II) complexes with the novel 4′-*p*-phenylterpyridine-triarylpyridinium ligand

Philippe Lainé* and Edmond Amouyal

Molecular Photonics Group, Laboratoire de Physico-Chimie des Rayonnements, CNRS UMR 8610, Université Paris-Sud, Bâtiment 350, 91405 Orsay, France. E-mail: philippe.laine@lpcr.u-psud.fr

Received (in Basel, Switzerland) 14th February 1999, Accepted 11th April 1999

A new family of electron acceptor ligands complexed with osmium(II) and associated with appropriate electron donor subunits within heteroleptic compounds, results in multicomponent assemblies of potential interest for both synthetic chemistry and supramolecular photochemistry.

As part of our studies devoted to photochemical conversion of solar energy[1] we are interested in producing long-lived photoinduced charge separation (CS) states within inorganic supramolecular species. Determining criteria that govern intramolecular electron transfers (ET) in multicomponent systems (*i.e.* polyads) have already been addressed in previous work.[2,3] A representative composition for a polyad system devised for CS purposes consists of a linear disposition of peripheral electron donating (D) and withdrawing (A) groups borne by a central photosensitiser P in a *trans* configuration *e.g.* D–P–A (triad).[4] Spacers do play an important role in such constructions by providing the rigidity of the architecture and mediating the electronic coupling between the components. Regarding non-porphyrinic inorganic polyads, widespread strategy is to modulate the efficiency of A (and/or D) *vs.* intramolecular ET by varying the length and nature of saturated spacers; our approach hereby described is to preferably involve *intrinsically weak* electron acceptors *fairly strongly coupled* to P rather than the usual *good* acceptors *almost insulated* from P. The aim remains the same in both cases *i.e.* favour the formation of the CS state D^+–P–A^- by retarding the charge recombination (CR).

Based on hitherto established structural and energetic requirements, we have designed the new 4′-[4-*N*-(2,4,6-triarylpyridinio)phenyl]-2,2′:6′,2″-terpyridine ligand ($R^1{}_2R^2TP^+$-pterpy) depicted in Scheme 1. Related triphenylpyridinium derivatives are known to undergo charge transfer reactions when covalently linked to some donor groups as is the case for solvatochromic Reichardt's dyes like betaine 30,[5,6] the promoted electron being located on the pyridinium moiety. Our proposal is thus to replace the latter donor by a light-triggered electron donor, namely an inorganic chromophore (P) of the Ru/Os-bis(terpyridyl) type.

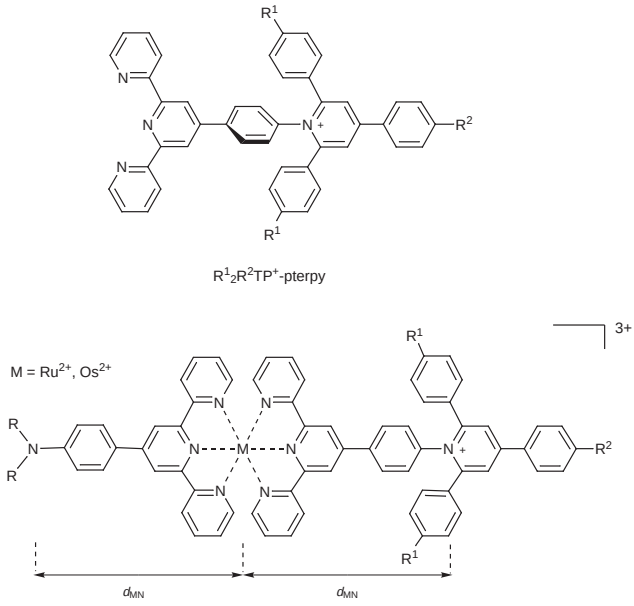

Scheme 1

It is noteworthy that $R^1{}_2R^2TP^+$-pterpy (A) specifically fits to polyad architectures where the electron-donating part (D) is built from 4′-(4-*N*,*N*-disubstituted-aminophenyl)terpy (R_2N-pterpy, R = alkyl, aryl). In such a structure, both pyridinio and amino nitrogen atoms are located at equal distance d_{MN} from the metal centre and connected to it with identical spacers (Scheme 1). From a topological viewpoint, the CS-state lifetime is expected to be increased in this particular arrangement that allows an optimal competition between the possible reductive quenching reactions of oxidised photosensitiser ($D–P^+–A^- \rightarrow D^+–P–A^-$ *vs.* $D–P^+–A^- \rightarrow D–P–A$). Another advantage of $R^1{}_2R^2TP^+$-pterpy ligands comes from the tuneable redox properties of the pyridinium moiety[5,7] the potential of which can be varied systematically by altering substituents R^1 and R^2.

These acceptor-modified terpyridyl ligands (A) are readily synthesised following a general convergent approach[8] consisting in separately preparing the triarylpyrylium salt and the amino derivative of the chelating polyimine which are subsequently reacted together to afford the target molecule in reasonable yield (*ca.* 60% *vs.* amine). The chemical variability of $R^1{}_2R^2TP^+$-pterpy actually stems from pyrylium precursors, the chemistry of which is very rich and also well documented from the synthetic viewpoint.[9] In addition, this route to pyridinium derivatives can be successfully applied to other oligopyridine molecules.[10] Typically, the first element of the ligand family ($R^1 = R^2 = H$), H_3TP^+-pterpy, is obtained by the reaction of 4′-*p*-aminophenyl-terpy ($Na_2S_2O_4$-reduced 4′-*p*-nitrophenyl-terpy) with a triphenylpyrylium cation (HSO_4^- salt, 1 equiv.) in refluxing EtOH for 6 h in the presence of anhydrous NaOAc. Regarding the electron-donor component, the model ligand used is 4′-*p*-dimethylaminophenyl-terpy (Me_2N-pterpy) synthesised following the classical method for *para*-substituted phenyl terpy.[11] Up to 12 Ru^{II} and Os^{II} complexes were then synthesised corresponding to the different combinations between the following three ligands: H_3TP^+-pterpy, Me_2N-pterpy and 4′-*p*-tolyl-terpy (tterpy); after standard work-up purification these compounds prepared as PF_6^- salts afforded microcrystalline powders which were fully characterised;† experimental details will be given elsewhere.[10*b*] Owing to their better emission properties at room temperature than that of analogous Ru^{II} complexes, preliminary photophysical results are given for the Os^{II} complexes only *i.e.* $[Os(tterpy)_2]^{2+}$ **1**, $[Os(Me_2N\text{-}pterpy)_2]^{2+}$ **2**, $[Os(pterpy\text{-}TPH_3^+)_2]^{4+}$ **3**, $[(Me_2N\text{-}pterpy)Os(tterpy)]^{2+}$ **4**, $[(tterpy)Os(pterpy\text{-}TPH_3^+)]^{3+}$ **5** and $[(Me_2N\text{-}pterpy)Os(pterpy\text{-}TPH_3^+)]^{3+}$ **6**. Properties of two H_3TP^+-pterpy complexes **5** and **6**, compared to that of **1** are more specifically discussed.

As illustrated in Fig. 1 for this series, the luminescence is shown to be gradually weakened when going from **1** to **6**. Compared to the reference chromophore **1** with an emission

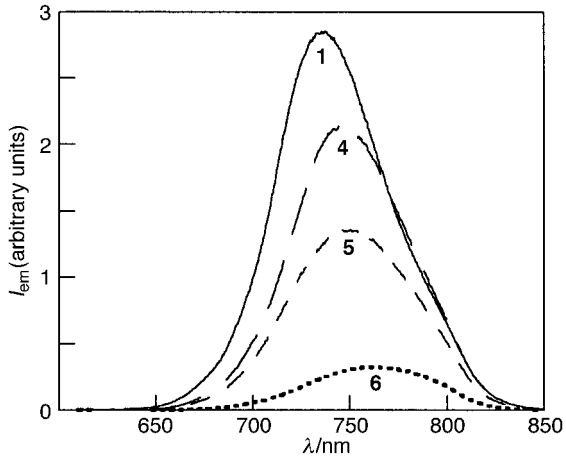

Fig. 1 Emission spectra of Os^{II} complexes in deaerated MeCN solutions at room temperature, measured in identical experimental conditions (in particular, same OD at $\lambda_{exc.}$ = 600 nm).

Table 1 Luminescence properties[a]

	λ_{max}[b]/nm	$10^2\Phi$[c]	I_{rel}[c,d](%)	τ[e]/ns
1	734	2.00	100	247
4	747	1.48	74.3	206
5	750	1.02	50.9	168
6	764	0.24	12.1	57

[a] Room temperature measurements; deaerated MeCN solutions. [b] Emission maxima for uncorrected spectra. [c] Luminescence quantum yields were determined relative to $[Os(bpy)_3]^{2+}$ (Φ_{em} = 5×10^{-3} in MeCN at 298 K).[12] [d] I_{rel} = 100 × [Φ_{em}(species)/Φ_{em}(**1**)]. [e] Determined by laser flash photolysis, λ_{exc} = 308 nm.[13]

quantum yield of 2.0×10^{-2}, ^{3}MLCT emission of the D–P–A triad **6** is *ca.* 90% quenched and lifetime shortened to 57 ns (Table 1).

Note that the contribution of the donor fragment to the quenching phenomenon should not be overestimated as revealed by I_{rel} values for **2** and **4**: 80.5 and 74.3%, respectively. A synergetic effect of electroactive subunits D and A upon emission is, however, clearly identified in the case of **6** when compared with luminescence properties of heteroleptic compounds **4** and **5**.

The rate constant k_Q for the bimolecular quenching reaction (1) of the excited state of the reference chromophore **1** (*P) by the model-acceptor species *N*-phenyl-2,4,6-triphenylpyridinium (p-TPH_3^+) was experimentally determined (Stern–Volmer plot). This k_Q value of *ca.* 6×10^7 dm^3 mol^{-1} s^{-1} (with τ_{em} of **1** = 247 ns) cannot account for the more efficient quenching process observed within the dyads and triad; therefore, the effective contribution of an *inter*-molecular ET to the quenching mechanism is negligible.

$$*[Os(tterpy)_2]^{2+} + p\text{-}TPH_3^+ \rightarrow [Os(tterpy)_2]^{3+} + p\text{-}TPH_3^{\bullet} \quad (1)$$

In addition, owing to photophysical properties of organic colourless D and A electroactive fragments (UV-absorbing) with respect to that of *P (NIR–VIS-emitting ^{3}MLCT state at *ca.* 740 nm), the above reported quenching effect cannot originate from energy transfer.

Further photophysical investigations at low temperature and picosecond time-scale are currently under way in order to elucidate whether the luminescence behaviour of this series results from effective *intra*-molecular ET or an alteration of the electronic properties of the complexes due to their inter-component coupling.[14]

The chemical variability provided by R^1 and R^2 (Scheme 1) allows the modulation of the electron withdrawing ability of the acceptor as well as leading to the opportunity to expand the structure along the C_2-axis (*via* R^2) in polyads such as D–P–A_1–A_2 (redox cascade). Hence, $R^1{}_2R^2TP^+$-pterpy is a promising candidate to perform sequential and vectorial long-range ET over extended rod-like rigid systems engineered for CS.

Helpful discussions with Dr Valérie Marvaud were much appreciated by P. L.

Notes and references

† All new compounds exhibited satisfactory elemental, spectroscopic (^{1}H and ^{13}C NMR), spectral (UV–VIS–NIR) and mass (ES-MS for **2**–**6** and CI-MS for H_3TP^+-pterpy) data.

Selected spectroscopic data for H_3TP^+-pterpy. δ_H (Bruker AC300, 300 MHz, $CDCl_3$): 8.65 (d, *J* 4.8 Hz, 2 H), 8.57 (d, *J* 7.9 Hz, 2H), 8.46 (s, 2 H), 8.15 (s, 2 H), 7.94 (d, *J* 8.0 Hz, 2 H), 7.83 (dd, *J* 7.9, 7.6 Hz, 2 H), 7.75 (d, *J* 8.7 Hz, 2 H), 7.62 (m, 4 H), 7.59 (d, *J* 8.7 Hz, 2 H), 7.54 (m, 3 H), 7.33 (dd, *J* 4.8 Hz, 2 H), 7.29 (m, 6 H). For **6**: δ_H(300 MHz, CD_3CN): 8.98 (s, 2 H), 8.81 (s, 2 H), 8.60 (d, *J* 8.0 Hz, 2 H), 8.57 (d, *J* 8.3 Hz, 2 H), 8.50 (s, 2 H), 8.17 (dd, *J* 7.8, 1.4 Hz, 2 H), 8.08 (d, *J* 8.9 Hz, 2 H), 7.98 (d, *J* 8.6 Hz, 2 H), 7.80 (m, 4 H), 7.73 (m, 3 H), 7.62 (d, *J* 8.6 Hz, 2 H), 7.54 (m, 4 H), 7.47 (m, 6 H), 7.34 (d, *J* 5.4 Hz, 2 H), 7.18 (d, *J* 5.0 Hz, 2 H), 7.12 (dd, *J* 7.3, 5.7 Hz, 2 H), 7.04 (d, *J* 8.8 Hz, 2 H), 7.03 (dd, *J* 5.9 Hz, 2 H), 3.15 (s, 6 H). For **6** ES-MS (modified NERMAG R10-10 quadrupole mass spectrometer, solvent: MeCN): *m/z* 1448 (^{190}Os) and 1450 (^{192}Os), [M − PF_6^-]$^+$; 652 [M − $2PF_6^-$]$^{2+}$; 386 [M − $3PF_6^-$]$^{3+}$.

Selected electrochemical data [differential pulse voltammetry, $E_{1/2}$/V *vs.* SSCE in freshly distilled MeCN/0.1 M $TBAPF_6$ at 298 K]. For **6**: $E(Os^{III/II})$ = +1.03 (rev.), $E(dma^{+/0})$ = +0.77 (rev.), $E(TP^{+/0})$ = −0.93 (rev.), $E(TP^{0/-1})$ = −1.01 (rev.), $E(terpy^{0/-1})$ = −1.24 (rev.).

1 E. Amouyal, in *Homogeneous Photocatalysis*, ed. M. Chanon, John Wiley, Chichester, 1997, ch. 8, 263; E. Amouyal, *Sol. Energy Mater. Sol. Cells*, 1995, **38**, 249.
2 V. Balzani and F. Scandola, *Supramolecular Photochemistry*, Ellis Horwood, Chichester, 1991.
3 J.-P. Sauvage, J.-P. Collin, J.-C. Chambron, S. Guillerez, C. Coudret, V. Balzani, F. Barigelletti, L. De Cola and L. Flamigni, *Chem. Rev*., 1994, **94**, 993; V. Balzani, A. Juris, M. Venturi, S. Campagna and S. Serroni, *Chem. Rev*., 1996, **96**, 759.
4 E. C. Constable, *Adv. Inorg. Chem. Radiochem*., 1986, **30**, 69; J.-P. Collin, S. Guillerez and J.-P. Sauvage, *J. Chem. Soc., Chem. Commun.*, 1989, 776; J.-P. Collin, S. Guillerez, J.-P. Sauvage, F. Barigelletti, L. de Cola, L. Flamigni and V. Balzani, *Inorg. Chem*., 1992, **31**, 4112.
5 C. Reichardt, *Chem. Rev.*, 1994, **94**, 2319.
6 P. Chen and T. J. Meyer, *Chem. Rev.*, 1998, **98**, 1439.
7 M. Martiny, E. Steckhan and T. Esch, *Chem. Ber*., 1993, **126**, 1671.
8 B. R. Osterby and R. D. McKelvey, *J. Chem. Educ*., 1996, **73**, 260.
9 A. T. Balaban, A. Dinculescu, G. N. Dorofeyenko, G. W. Fischer, A. V. Koblik, V. V. Mezheritskii and W. Schroth, in *Pyrylium Salts: Synthesis, Reactions and Physical Properties. Advances in Heterocyclic Chemistry*, ed. A. R. Katritzky, Academic Press, New York, 1982, Supplement 2.
10 (*a*) Work in progress; (*b*) manuscript in preparation.
11 W. Spahni and G. Calzaferri, *Helv. Chim. Acta*, 1984, **67**, 450.
12 E. M. Kober, J. V. Caspar, R. S. Lumpkin and T. J. Meyer, *J. Phys. Chem*., 1986, **90**, 3722.
13 E. Amouyal, M. Mouallem-Bahout and G. Calzaferri, *J. Phys. Chem*., 1991, **95**, 7641.
14 M. Maestri, N. Armaroli, V. Balzani, E. C. Constable and A. M. W. Cargill Thompson, *Inorg. Chem*., 1995, **34**, 2759.

Communication 9/01237K

Grinding of an organometallic crystalline material leads to quantitative formation of a hydrated polymorph

Dario Braga,*[a] Lucia Maini[a] and Fabrizia Grepioni*[b]

[a] *Department of Chemistry G. Ciamician, Via F. Selmi 2, University of Bologna, 40126 Bologna, Italy. E-mail: dbraga@ciam.unibo.it*

[b] *Department of Chemistry, Via Vienna 2, Universita' di Sassari, 07100 Sassari, Italy. E-mail: grepioni@ssmain.uniss.it*

Received (in Basel, Switzerland) 8th February 1999, Accepted 11th April 1999

The hydrated crystalline material $[(\eta^5\text{-}C_5H_5)_2Co]^+[(\eta^5\text{-}C_5H_4CO_2H)(\eta^5\text{-}C_5H_4CO_2)Fe]^-\cdot H_2O$ 3 is prepared by simply *grinding* either the crystalline powder 1 that precipitates from thf on reacting $[(\eta^5\text{-}C_5H_5)_2Co]$ with $[(\eta^5\text{-}C_5H_4CO_2H)_2Fe]$ or single crystals of $[(\eta^5\text{-}C_5H_5)_2Co]^+[(\eta^5\text{-}C_5H_4CO_2H)(\eta^5\text{-}C_5H_4CO_2)Fe]^-$ 2 obtained by recrystallization of 1 from nitromethane; on heating at 373K 3 loses water and reverts to the starting material 1.

Crystal engineering is a bridge between supramolecular and molecular materials chemistry and constitutes one of the most attractive research fields in modern structural chemistry.[1] Crystal-to-crystal transformations are of obvious interest.

Recently, we have begun to utilize organometallic building blocks to prepare crystalline materials to exploit the variable valence, spin and charge states of coordination complexes.[2] Exciting new results are being obtained, in particular when the crystalline products are investigated by a combination of different solid state techniques.[3]

Here we report the unusual behaviour of the crystalline material[2b] $[(\eta^5\text{-}C_5H_5)_2Co]^+[(\eta^5\text{-}C_5H_4CO_2H)(\eta^5\text{-}C_5H_4CO_2)Fe]^-$ **2**, previously synthesised together with the mixed-metal mixed-spin system $\{[(\eta^6\text{-}C_6H_6)_2Cr]^+\}_2\{[(\eta^5\text{-}C_5H_4CO_2H)(\eta^5\text{-}C_5H_4CO_2)Fe]_2[(\eta^5\text{-}C_5H_4CO_2H)_2Fe]^{2-}\}$.[4]

We have discovered that the hydrated *pseudo*-polymorph $[(\eta^5\text{-}C_5H_5)_2Co]^+[(\eta^5\text{-}C_5H_4CO_2H)(\eta^5\text{-}C_5H_4CO_2)Fe]^-\cdot H_2O$ **3** is obtained by *grinding* either the crystalline powder **1** that precipitates from thf on reacting $[(\eta^5\text{-}C_5H_5)_2Co]$ and $[(\eta^5\text{-}C_5H_4COOH)_2Fe]$ to prepare **2**,† or single crystals of **2** obtained by subsequent recrystallization of **1** from nitromethane or methanol.† Importantly, both **2** and **3** have been characterized by single crystal X-ray-diffraction, while powder diffractograms have been measured for **1** and **3** so that the relationship between reactant and product of this peculiar solid state transformation is known in detail.‡ The process is summarized in Scheme 1. The reverse process proceeds only from **3** → **1** as confirmed by thermal gravimetric analysis, which shows stoichiometric loss of water at *ca.* 373 K, and by powder X-ray diffraction, which shows the conversion into **1** of a sample of **3** heated for 2 h at 383 K under argon. Single crystals of **2** do not absorb water in the air, while crystalline **3**, once formed, behaves like any 'normal' crystalline salt, *i.e.* can be dissolved and recrystallized without further structural change.

The key structural features of **2** and **3** can be summarised as follows:

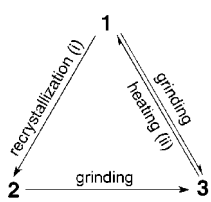

Scheme 1 *Reagents and conditions* i, from $MeNO_2$ or MeOH; ii, 383 K, 2 h, argon atmosphere.

(i) both **2** and **3** belong to the class of supramolecular salts (*supersalts*[2b]) in which the anions, obtained by deprotonation of the dicarboxylic acid $[(\eta^5\text{-}C_5H_4CO_2H)_2Fe]$, are self-assembled *via* O–H···O and/or O–H···O$^-$ hydrogen bonding interactions and are linked to the cobaltocenium cations $[(\eta^5\text{-}C_5H_5)_2Co]^+$ *via* a profusion of *charge assisted* $C\text{–}H^{\delta+}\cdots O^{\delta-}$ interactions.[5] For sake of clarity only the anionic backbones are compared in Fig. 1. Relevant hydrogen bonding parameters are given in the caption.

(ii) In **2** the $[(\eta^5\text{-}C_5H_4CO_2H)(\eta^5\text{-}C_5H_4CO_2)Fe]^-$ anions form chains with no cross-links, *viz.* a mono-dimensional network,[6] while in **3** the chains are *cross-linked* by water molecules inserted between $–CO_2$ groups, generating a two-dimensional network.

(iii) The ferrocene moieties in **2** and **3** not only show different ring conformations but have also different relative orientations along the chains.

Fig. 2 collects the evidence on the process depicted in Scheme 1 and compares the experimental (exp) X-ray powder diffractograms obtained for **1** and **3** with those calculated (calc) on the basis of the single-crystal structures for **2** and **3**. It can be seen that: (i) **1**(exp) ≠ **3** (exp) and **2** (calc), (ii) **3** (exp) ≠ **2** (calc), and (iii) **3** (exp) ≡ **3** (calc).

Although the effect of grinding samples for powder diffraction, as well as the possibility of monitoring solid state reactions

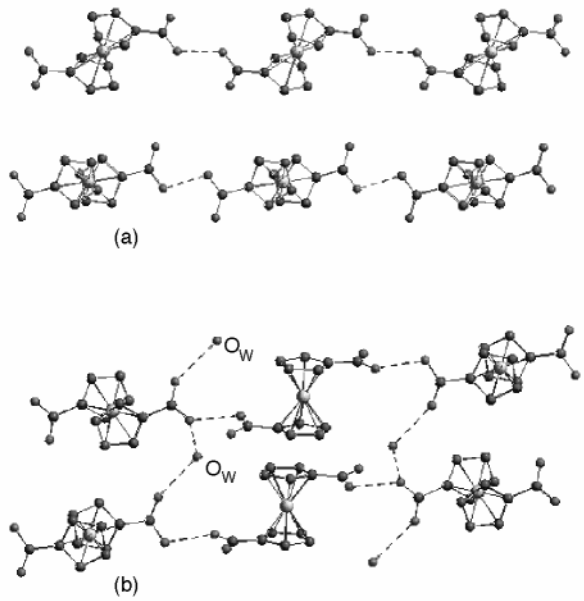

Fig. 1 Chains of O–H···O bonded $[(\eta^5\text{-}C_5H_4CO_2H)(\eta^5\text{-}C_5H_4CO_2)Fe]^-$ anions in **2** (a) and **3** (b). Note how the water molecules in **3** act as *cross-links* between the anionic chains. Hydrogen atoms are omitted for clarity. Relevant O···O separations within the hydrogen bonded systems are: **2** anion–anion 2.45(2), **3** anion–anion 2.49(2) and 2.52(2), anion–water 2.81(2), 2.73(2), 2.83(2) Å.

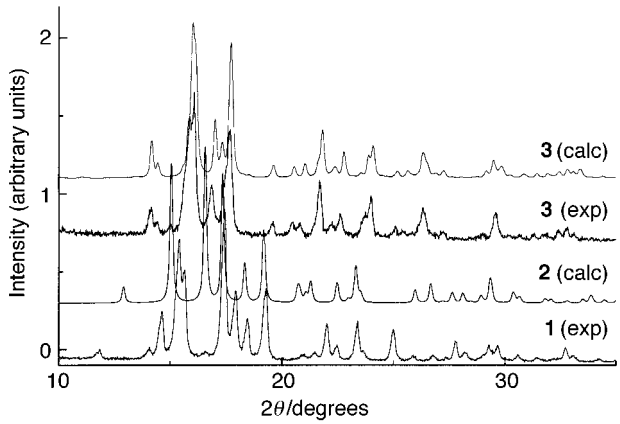

Fig. 2 Comparison between the experimental powder diffractograms of **1** (obtained from the reaction mixture in thf) and **3** (obtained by grinding crystalline **2**) and the diffractograms of **3** and **2** calculated on the basis of the experimental single-crystal structures. A colour version of this figure is shown in electronic form, see http://www.rsc.org/suppdata/cc/1999/937.

via powder diffraction, is well known,[7] what appears to be unprecedented in the case of the **1**, **2** → **3** transformations is the fact that water molecules can be inserted in stoichiometric ratio into a complex and highly organized crystal edifice without loss of crystallinity or (at least in the case of **2**) disruption of the anionic organization. The overall process is fully reproducible. The relationship between the structure of **1** and that of **2** remains unknown, though they are very likely two polymorphic modifications of the same anhydrous material.[8]

Although it is difficult (and somewhat 'unsafe') to model solid-to-solid transformations, *e.g.* between two thermodynamic free energy minima, it is still interesting to observe what is *preserved* and what is *changed* on passing from **2** to the *pseudo*-polymorph **3**. The anionic chain structure is maintained, together with the sequence of O–H···O interactions, while the distribution of cations, hence the distribution of weak C–H···O bonds, and the relative orientation of the ferrocene moieties along the chain change significantly. The former aspect reveals that the hydrogen bonded chain is a *structural determinant* which, together with inter-ion interactions, is responsible for crystal cohesion. Structural flexibility and the diffuse network of weak, less directional, interactions provide instead the necessary ion mobility and permeability to water molecules.

Two remarks to conclude this preliminary communication: (i) since the reaction products in crystal engineering are solids the utilization of powder diffraction is, sometimes, the only way to ascertain whether the whole solid material has the *same structure* as that characterized by single crystal X-ray diffraction.[9] Our findings are a *caveat* since a common method of sample preparation (powder grinding) may lead to dramatic solid state transformations.

(ii) Not less important is the notion that such crystal transformations may be quantitatively achieved by mechanical stress (and consequent thermal effect). Indeed this is something that may be exploited: work is in progress to ascertain whether other molecules with hydrogen bonding capacity similar to that of water may be used in solid state reactions with crystalline **2**.

We thank Dr Gianna Cojazzi for help with the thermal gravimetric analysis. Financial support from the University of Bologna—Project '*Innovative Materials*' and from MURST–Project '*Supramolecular Devices*' is acknowledged.

Notes and references

† [(η^5-C_5H_5)$_2$Co] and [(η^5-$C_5H_4CO_2H$)$_2$Fe] were purchased from Aldrich. For the preparation of crystalline **2** see ref. 4. Upon 1 : 1 reaction between [(η^5-$C_5H_4CO_2H$)$_2$Fe] (84 mg, 0.30 mmol) and [(η^5-C_5H_5)$_2$Co] (57 mg, 0.30 mmol) in 20 ml of anhydrous thf an orange powder precipitate **1** immediately formed. After 1 h, **1** was filtered and a portion was recrystallized overnight from nitromethane (or methanol), yielding air stable orange crystals of **2**. Grinding of the second portion of **1** to prepare a sample for powder diffraction led to formation of crystalline powder **3**, which on recrystallization from nitromethane gave single crystals of **3**. It is important to stress that, in the preparation of powder diffraction samples, we followed a conventional 'open-air' procedure. Grinding was performed manually for few minutes till a fine powder was obtained in order to avoid preferential orientation problems. If the grinding is done in a dry box, only partial hydration is observed and the powder spectrum is a mixture of those of **1** and **3**. This indicates that water for hydration comes both from ambient humidity and from surface wetting, this latter water is very difficult to remove.

‡ Powder X-ray diffraction measurements: Philips PW-1100 automated diffractometer, Cu-Kα radiation, monochromator graphite. Single crystal X-ray diffraction: CAD4 diffractometer, Oxford Cryostream liquid-N2 device, Mo-Kα radiation, monochromator graphite. Data were corrected for absorption by azimuthal scanning of high-χ reflections (min. and max. transmission 0.87 and 1.00). *Crystal data* for **3**: $C_{22}H_{21}CoFeO_5$, T = 223(2) K, M = 480.17, monoclinic, $P2_1/n$, a = 12.251(5), b = 17.276(6), c = 18.083(7) Å, β = 91.56(3), V = 3825.8(25) Å^3, Z = 8, F(000) = 1968, μ = 1.658 mm^{-1}, θ-range 3.0–25 °, 6933 reflections, 6710 independent, refinement on F^2 for 454 parameters, wR (F^2, all reflections) = 0.1495, R_1[I > 2σ(I)] = 0.0455. SHELXS-97[10a] and SHELXL97[10a] were used for structure solution and refinement based on F^2. The asymmetric unit contains two cations, one anion, two 'half' anions located on inversion centres, and two water molecules unit. The hydrogen bond pattern in **3** is more complex than in **2** and will be discussed in a full report. SCHAKAL97[10b] was used for the graphical representation of the results.

CCDC 182/1223. See http://www.rsc.org/suppdata/cc/1999/937/ for crystallographic files in .cif format.

1 See, for example: J.-M. Lehn, *Supramolecular Chemistry—Concepts and Perspectives*, VCH Weinheim, 1995; C. V. K. Sharma and R. D. Rogers, *Chem. Commun.*, 1999, 83; D. Braga and F. Grepioni, *Chem. Commun.*, 1996, 571; C. B. Aakeröy, *Acta Crystallogr., Sect. B*, 1997, **53**, 569; G. R. Desiraju, *Angew. Chem., Int. Ed. Engl.*, 1995, **34**, 2311; V. A. Russell, C. C. Evans, W. Li and M. D. Ward, *Science*, 1997, **276**, 575.

2 D. Braga, F. Grepioni and G. R. Desiraju, *Chem. Rev.*, 1998, **98**, 1375; D. Braga and F. Grepioni, *J. Chem. Soc., Dalton Trans.*, 1999, 1.

3 See for example: F. Grepioni, G. Cojazzi, S. M. Draper, N. Scully and D. Braga, *Organometallics*, 1998, **17**, 296; J. S. Miller and A. J. Epstein, *Chem. Commun.*, 1998, 1319; P. J. Fagan and M. D. Ward, *The Crystal as a Supramolecular Entity. Perspectives in Supramolecular Chemistry*, ed. G. R. Desiraju, Wiley, Chichester, 1996, vol. 2, p. 107; D. Braga, O. Benedi, L. Maini and F. Grepioni, *J. Chem. Soc., Dalton Trans.*, submitted.

4 D. Braga, L. Maini and F. Grepioni, *Angew. Chem., Int. Ed.*, 1998, **37**, 2240.

5 D. Braga, F. Grepioni, E. Tagliavini, J. J. Novoa and F. Mota, *New J. Chem.*, 1998, 755; D. Braga, F. Grepioni and J. J. Novoa, *Chem. Commun.*, 1998, 1959.

6 M. W. Hosseini and A. De Cian, *Chem. Commun.*, 1998, 727; G. Aullon, D. Bellamy, L. Brammer, E. A. Bruton, A. G. Orpen, *Chem. Commun.*, 1998, 653.

7 *Modern Powder Diffraction*, ed. B. L. Bish and J. E. Post, *Rev. Miner*, 1989, **20**, 19; N. Masciocchi and A. Sironi, *Chem. Commun.*, 1997, 4643.

8 J. D. Dunitz and J. Bernstein, *Acc. Chem. Res.*, 1995, **28**, 193.

9 C. B. Aakeröy and K. R. Seddon, *Chem. Soc. Rev.*, 1993, 397.

10 (*a*) G. M. Sheldrick, SHELXL97, *Program for Crystal Structure Determination*; University of Göttingen: Göttingen, Germany, **1997**; (*b*) E. Keller, SCHAKAL97, *Graphical Representation of Molecular Models*, University of Freiburg, Germany, 1997.

Communication 9/01078E

ChemComm

Drastic enhancement of the enantioselectivity of lipase-catalysed esterification in organic solvents by the addition of metal ions

Takashi Okamoto[a] and Shinichi Ueji*[b]

[a] *The Graduate School of Science and Technology, Kobe University, Nada, Kobe 657-8501, Japan*
[b] *Division of Natural Environment and Bioorganic Chemistry, Faculty of Human Development and Sciences, Kobe University, Nada, Kobe 657-8501, Japan. E-mail: ueji@natura.h.kobe-u.ac.jp*

Received (in Cambridge, UK) 22nd March 1999, Accepted 12th April 1999

By the addition of metal ion-containing water, a marked enhancement of the enantioselectivity for the lipase-catalysed esterification of 2-(4-substituted-phenoxy)propionic acids in Pr^i_2O was observed, the mechanism of which will be discussed briefly on the basis of the initial rate obtained for each enantiomer of the substrate.

Recently, much attention has been paid to lipase-catalysed enantioselective transformations in organic solvents, because lipases display broad substrate specificities with high enantioselectivities.[1] For this reason, organic chemists often use lipases for the synthesis of useful optically active compounds. One of the most important factors for lipase-catalysed reactions is the control of their enantioselectivites as a function of reaction conditions.[1]

Here, we report a new and a simple method for improving markedly the enantioselectivity of lipase-catalysed esterification of 2-(4-substituted-phenoxy)propionic acids **1**–**5** in Pr^i_2O as a model reaction by the addition of alkaline metal ion (*e.g.* LiCl)-containing water (Scheme 1). This is the first example of an alkaline metal ion enhancing the enantioselectivity of a lipase in organic solvents. Furthermore, the mechanism of the enhanced enantiorecognition will be discussed briefly utilising data on the initial rate obtained for each enantiomer of substrate **1** in the model reaction.

All the substrates used in the model reactions, racemic 2-(4-substituted-phenoxy)propionic acids, were prepared from ethyl 2-bromopropionate and the corresponding 4-substituted-phenols according to the known method.[2]

In a typical enzymatic reaction, the substrates **1**–**5** (0.36 mmol) and a three-fold molar excess of BuOH (1.08 mmol, 80 mg) were dissolved in 2 ml of Pr^i_2O. To the solution, a small amount of 2.4 M metal ion-containing water or water (0–0.75 vol%) was added followed by ultrasonic dispersion, and then powdered lipase MY or lipase AY from *Candida rugosa* (30 mg) was added. The suspension was shaken (170–200 strokes min^{-1}) at 37 °C until *ca.* 40% of the substrate was converted to the corresponding butyl ester. The enantiomeric ratio (*E* value) was calculated from the enantiomeric excess (ee) for the butyl ester produced, according to the literature.[3] The ee was measured by HPLC on a chiral column [Daicel Chiral Cel OK].

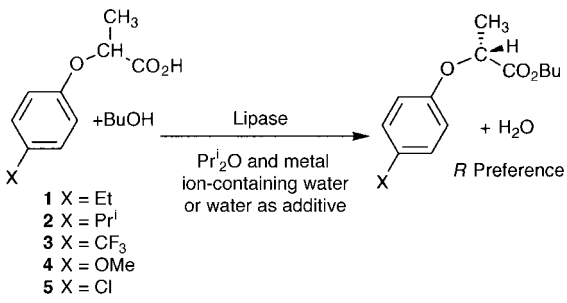

Scheme 1

For the model reaction (Scheme 1), the *R* enantiomer of the butyl ester were preferentially produced in all the substrates **1**–**5**. We investigated the behaviour of the lipase's enantioselectivity caused by the addition of a small amount of alkaline metal ion (LiCl, NaCl or KCl)-containing water or a small amount of water to the Pr^i_2O of the reaction medium. Fig. 1 shows the variation of the *E* value for the lipase MY-catalysed esterification of **1** at *ca.* 40% conversion as a function of the amount of each additive. As is seen in Fig. 1, when a small amount of the alkaline metal ion-containing water was added to the reaction medium, the enantioselectivity was found to be dramatically enhanced, as compared with addition of water alone or no additive. In particular, upon addition of 0.5 vol% of LiCl-containing water, lipase MY displayed the highest *E* value (*ca.* 200), which was 5 and 50 times larger than that for water alone or no additive, respectively. A drop in the *E* value, however, was produced by the addition of a large amount of the metal ion-containing water (see the bell-shaped plots in Fig. 1). This can be explained by assuming that an excess of water molecules hydrated to the ion in the reaction medium causes the hydrolysis (the reverse reaction) of the corresponding ester product of **1**, thus leading to the loss of enantioselectivity, probably because the sites of the lipase molecule associated with the water molecule are restricted. The same trend was also observed for water alone (Fig. 1). In fact, the ester product of **1** was subjct to hydrolysis in Pr^i_2O with water or LiCl-containing water of 0.75 vol% or above.†

In order to investigate the scope of this enhancement effect, the other substrate **2**–**5** with a wide variety substituents and the other enzyme lipase AY were submitted to the model reaction. From the data summarized in Table 1, the optimum additive conditions (0.5 vol% of LiCl-containing water) were found to produce dramatically increased enantioselectivity for all the substrates **1**–**5** and both lipases, although lipase AY differs from lipase MY in its catalytic features.[4]

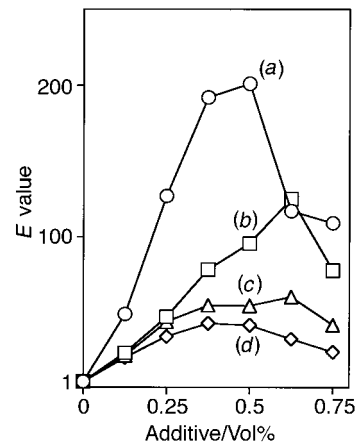

Fig. 1 The variation of the *E* value of lipase MY-catalysed esterification of **1** at *ca.* 40% conversion as a function of the amount of each additive: (*a*) LiCl, (*b*) NaCl, (*c*) KCl and (*d*) water.

Table 1 Enantioselectivity of lipase MY or AY-catalysed butyl esterifications of 2-(4-substituted-phenoxy)propionic acids under various additive conditions

	X	Lipase	Additive[a]	t/h	Conv. (%)	Ee (%)	*E*
1	Et	MY	A	120	25.0	52.3	3.8
			B	6	41.7	90.9	41
			C	16.5	39.5	98.1	201
2	Pr^i	MY	A	240	67.4	30.7	3.4
			B	12	43.5	84.1	22
			C	48	30.9	97.9	145
3	CF_3	MY	A	168	12.6	10.6	1.3
			B	24	40.8	74.6	11.4
			C	168	19.7	90.9	26.0
4	OMe	MY	A	168	6.65	17.8	1.5
			B	16	43.6	82.1	20
			C	168	33.9	92.8	43
5	Cl	MY	A	168	8.82	15.1	1.4
			B	24	38.1	61.4	6.0
			C	168	9.75	87.7	17
1	Et	AY	A	120	19.1	84.9	15
			B	24	43.9	84.7	24
			C	48	34.8	96.4	90
2	Pr^i	AY	A	200	5.5	53.8	3.4
			B	12	39.7	94.8	71
			C	120	37.1	97.9	170
3	CF_3	AY	A	168	1.93	11.6	1.3
			B	62	39.0	90.1	34
			C	168	26.3	95.1	56
4	OMe	AY	A	168	2.56	35.5	2.1
			B	62	48.8	82.7	25
			C	122	40.4	92.6	49
5	Cl	AY	A	168	2.89	17.9	1.4
			B	62	38.0	80.3	15
			C	168	33.9	87.1	23

[a] A: None; B: 0.5 vol% water; C: 0.5 vol% aq. LiCl (2.4 M).

It is known that a small amount of water improves the lipase's enantioselectivity in organic solvents, the origin of which is due to the enzyme's conformational flexibility arising from multiple hydrogen bond formation with water molecules.[5] This fact was also supported by solid-state NMR measurements as judged by tyrosyl ring motion in α-lytic protease.[6]

In order to gain an insight into the mechanism of the enhancement of the enantioselectivity by the metal ion and water, we investigated the initial rate for each enantiomer of **1** in the presence of the additives (Table 2). For addition of water alone, the initial rates for the *R* enantiomer (correctly reacting substrate) and the *S* enantiomer (incorrectly reacting substrate) were accelerated 37-fold and 12-fold, respectively, as compared with no additive conditions (see the relative ratio of the initial rate listed in Table 2). From the value of (relative ratio of V_R)/(relative ratio of V_S) = *ca.* 3 calculated from Table 2, the enhancement of the enantioselectivity was found to be mainly ascribed to the greater acceleration in the initial rate for the *R* enantiomer compared to that for the *S* enantiomer.

Table 2 The initial rate of the esterification for each enantiomer under the three conditions

Additive	V_R[b]	Relative ratio of V_R	V_S[b]	Relative ratio of V_S
None	9.0	1	0.56	1
Water (0.5 vol%)	340	37	6.9	12
LiCl (0.5 vol%)[a]	140	15	0.51	0.91

[a] The additive concentration was 2.4 M. [b] The V_R and V_S denote the initial rates of the *R* and *S* enantiomers, respectively, in nM s^{-1} (mg of protein)$^{-1}$.

In contrast, the addition of LiCl-containing water was found to bring about a slight inhibition (0.91-fold) of the initial rate for the *S* enantiomer, whereas that for the *R* enantiomer was accelerated (12-fold), as compared with the water alone additive (Table 2). Therefore, the larger value of (relative ratio of V_R)/(relative ratio of V_S) = *ca.* 18, arising from the reverse trend of each initial rate, is responsible for the significant enhancement of the lipase MY's enantioselectivity.

In conclusion, there is a difference in the mechanism of the enhancement of the lipase's enantioselectivity between the alkaline metal ion-containing water and water alone as the additive. Our method forms a useful tool to improve the enantioselectivity in lipase-catalysed reactions in organic solvents.

Notes and references

† For 0.75 vol% water of LiCl-containing water in Pr^i_2O *ca.* 20% of the butyl ester of **1** was hydrolyzed.

1 Bernardo Herradon, *J. Org. Chem.*, 1994, **59**, 2891; E. Santaniello, P. Ferraboschi, P. Grisenti and A. Manzocchi, *Chem. Rev.*, 1992, **92**, 1071; A. M. Klibanov, *Acc. Chem. Res.*, 1990, **23**, 114.
2 D. T. Witiak, C.-L. Ho, R. E. Hackney and W. E. Coner, *J. Med. Chem.*, 1968, **11**, 1086.
3 C.-S. Chen, Y. Fujimoto, G. Girdankas and C. J. Sih, *J. Am. Chem. Soc.*, 1982, **104**, 7294.
4 Y. Yasufuku and S. Ueji, *Bioorg. Chem.*, 1997, **25**, 88.
5 H. Kitaguchi, I. Toh and M. Ono, *Chem. Lett.*, 1990, 1203.
6 P. A. Buruke, R. G. Griffin and A. M. Klibanov, *Biotechnol. Bioeng.*, 1993, **42**, 87.

Communication 9/02255D

ChemComm

Stereochemical preference for heterochiral coupling controls selectivity in competitive peptide synthesis

David Birch,[a] Roger R. Hill,*[b] G. E. Jeffs[b] and Michael North[a]

[a] *Department of Chemistry, University of Wales, Bangor, Gwynedd, UK LL57 2UW*
[b] *Department of Chemistry, The Open University, Milton Keynes, UK MK7 6AA. E-mail: r.r.hill@open.ac.uk*

Received (in Cambridge, UK) 4th March 1999, Accepted 13th April 1999

Competitive activated couplings of *N*-phthaloyl amino acids with amino acid dimethylamides show little selectivity among substrates in respect of their sidechains, but a consistent and significant preference for heterochiral outcomes.

Spontaneous abiotic formation of peptides from amino acid derivatives is a topic of considerable interest within prebiotic chemistry,[1] peptide synthesis[2] and combinatorial chemistry.[3] Whilst non-random thermal condensations in amino acid mixtures are seen as routes to incipient informational biopolymers,[4] evidence for selectivity at lower temperatures is equivocal.[2,5] Moreover, we are unaware of any study that addresses the question of stereoselectivity in competitive reactions where epimerizing equilibration is not a factor. We have found that, in DCC/HOBt-mediated coupling of *N*-phthaloyl amino acids and amino acid dimethylamides, stereoselectivity not only is the dominant controlling factor but also favours reaction between substrates of opposite configuration. An explanation of this phenomenon implies that such selectivity could be more widely applicable, with potentially significant consequences.

N-Phthaloyl (Pth) and *N*,*N*-dimethylamido (DMA) derivatives were selected for convenient chromophorically-based detection and as an inert C-terminus, respectively. Competitive couplings were carried out mostly pair-wise, where one type of substrate had the opportunity to react with two of the other type of substrate, the latter usually present in considerable molar excess. In an illustrative procedure, a solution of Pth-L-phenylalanine 1-hydroxybenzotriazole (HOBt) ester (0.1 mmol) in CH_2Cl_2 (10 cm^3), prepared *in situ* from Pth-L-phenylalanine, HOBt (0.12 mmol) and DCC (0.12 mmol), was added to racemic phenylalanine dimethylamide hydrobromide (1.0 mmol) dissolved in CH_2Cl_2 (25 cm^3) and Et_3N (1.2 mmol).[6] The mixture was stirred for two days, the CH_2Cl_2 removed by evaporation, the residue taken up in the initial HPLC eluent (30% aq. MeCN) and a homogeneous sample analysed by the area ratio of peaks identified by standards[7] as the L,L- and D,L-diastereoisomers of the corresponding derivatized dipeptides.

The outcomes of 28 such competition experiments are summarised in Tables 1 and 2, results being averaged in the cases where experiments were repeated. Table 1 shows the consistent and significant preference for heterochiral couplings, irrespective of whether the excess reagent is the Pth component or the DMA component. In order to confirm that products resulted from kinetic rather than thermodynamic control, we allowed one experiment to proceed with 1 equiv. of the racemic DMA and found the ratio of diastereomers to be close to 1 : 1 at completion. Table 2 demonstrates that when a choice of amino acids is presented, selectivity additional to that of stereochemistry is only significant in respect of the preferred coupling with glycyl residues.

The presence of one reactant in significant excess allows the approximation that product ratios in competing reactions correspond with the ratio of rate constants. Thus, the rate of peptide bond formation in these reactions is largely independent of β-substitution but significantly and uniformly faster between amino acid derivatives of opposite configuration. Further confirmation of a substantial preference for heterochiral coupling was found in the outcome of reactions between equimolar racemic reagents. Thus, the percentages of heterochiral diastereoisomer in reactions between racemic Pth-alanine and racemic dimethylamides of alanine, valine and phenylalanine were 75.6, 89.3 and 87.9, respectively. More complex mixtures also behaved consistently. For example, reaction between 1 equiv. of Pth-L-phenylalanine and a mixture of 5 equiv. each of the dimethylamides of L-alanine, L-phenyl-

Table 1 Competition outcomes in reactions between Pth-L-X and racemic Y-DMA using DCC/HOBt coupling

X	Y	Initial [Y-DMA]/[Pth-L-X]	LD-dipeptide derivative[a] (%)
Ala	Ala	9.9	86
Ala	Ala	1.0	55
Ala	Ala	0.08[b]	85
Ala	Phe	7.0	92
Ala	Phe	18.0	90
Ala	Phe	45.0	85
Ala	Val	8.0	94
Phe	Phe	10.0	89
Phe	Phe	6.3	87
Phe	Phe	0.1[b]	75
Phe	Ala	7.5	90
Phe	Val	10.0	94
Val	Val	10.0	96
Val	Ala	10.0	95
Val	Phe	8.3	83

[a] Determined by integration of HPLC traces, typically at 220 nm using a 250 × 4.6 mm (ID) Phenomenex Luna C18 (2) column at 35 °C and a linear mobile phase gradient from 30 to 95% MeCN in water over 20 min. Error < ± 5%. [b] Racemic Pth-X and L-Y-DMA.

Table 2 Competition outcomes in reactions between Pth-X and equimolar mixtures of Y-DMA and Z-DMA using DCC/HOBt coupling.

X	Y	Z	Initial {[Y] + [Z]}/[X][b]	Final [XY]/[XZ][c]	% LD-dipeptide derivative[a] (%)
L-Ala	L-Ala	L-Phe	6.0	1.0	—
L-Ala	L-Ala	L-Phe	0.17	0.8	—
L-Ala	L-Ala	D-Phe	13.0	0.3	78
L-Ala	D-Ala	L-Phe	10.2	3.5	78
L-Ala	L-Ala	L-Val	10.0	1.4	—
L-Ala	L-Ala	D-Val	11.0	0.2	85
L-Ala	D-Ala	L-Val	10.0	9.0	90
Gly	Gly	L-Ala	9.3	2.7	—
Gly	Gly	L-Phe	8.1	7.3	—
Gly	Gly	L-Va	10.0	4.2	—
L-Phe	L-Phe	D-Val	10.0	0.07	93
L-Phe	L-Phe	L-Val	10.0	1.06	—
L-Phe	D-Phe	L-Val	10.0	7.3	88

[a] See Table 1. [b] {[Y-DMA] + [Z-DMA]}/[Pth-X]. [c] [PthXYDMA]/[PthXZDMA].

alanine and *racemic* valine gave a product mixture with a ratio 15 : 6 : 4(LL):75(LD), respectively.

The dominance of chirality over sidechain as an influence in these competitive reactions may be explained by considering the probable structure of the activated complex **1**, where it can

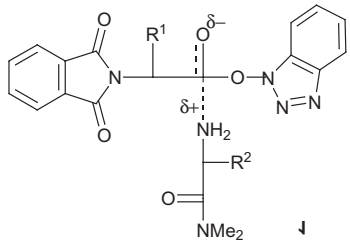

be seen that the two α-carbon atoms are separated by only two other atoms, whereas β-carbon atoms are more remote from potentially interacting centres. The consistent preference for a heterocyclic outcome is less readily anticipated, but would follow if **1** gained secondary stabilization by interactions between the terminal groups in a six-membered chair conformation, where the more favoured diequatorial disposition of sidechains would lead to the observed results (**2b**).

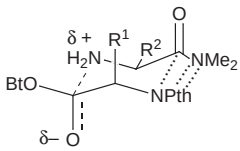

L, L
2a

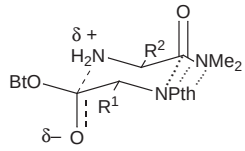

L, D
2b

If valid, this interpretation would suggest that the selectivity is largely independent of activating and terminal groups as long as the latter interact positively. (Similar independence has been noted in respect of amino acid selectivity in the reactions of different amino acids with the phosphoanhydrides of alanine and various nucleoside monophosphates; specificity was unaffected by alternative nucleosides.[8]) The results support Dose's contention that rate differences in condensations in amino acid mixtures would generally be too small to direct sidechain sequences,[5] but introduce the prospect that, in the absence of epimerization equilibria, such sequences in extendable systems would entail alternating configurations at C_α until interrupted by a glycyl residue. We are presently exploring the generality of this effect with other systems.

We thank Mrs J Burrage and Mr Eric Williams for technical assistance.

Notes and references

1 S. A. Kaufman, *The Origins of Order*, OUP, Oxford, 1993; B. M. Rode, *J. Phys. Chem*., 1992, **96**, 4170; A. Brack, *Origins Life*, 1987, **17**, 367; K. Dose, *Naturwissenschaften, 1983*, **70**, 378.
2 M. Mutter, *Int. J. Peptide Protein Res*., 1979, **13**, 274.
3 N. K. Terrett, *Combinatorial Chemistry*, OUP, Oxford, 1998; S. R. Wilson and A. W. Czarnik, *Combinatorial Chemistry*, Wiley, New York, 1997.
4 S. W. Fox and K. Dose, *Molecular Evolution and the Origin of Life*, Dekker, New York, 1974.
5 K. Dose, *Interdiscip. Sci. Rev*., 1988, **13**, 348.
6 M. Bodansky and A. Bodansky, *The Practice of Peptide Synthesis*, Springer-Verlag, Berlin, 1984.
7 Authentic standards for each coupling experiment were prepared by reaction between a single *N*-phthaloyl amino acid and a single amino acid dimethyl amide, and gave satisfactory spectroscopic and analytical data.
8 S. Tyagi and C. Pomamperuma, *J. Mol. Evol*., 1990, **30**, 391.

Communication 9/01730E

ChemComm

Low temperature selective methane activation to alkenes by a new hydrogen-accumulating system

M. V. Tsodikov,[a] Ye. V. Slivinskii,[a] V. P. Mordovin,[a] O. V. Bukhtenko,[a] G. Colón,[b] M. C. Hidalgo[b] and J. A. Navío*[b]

[a] *A.V. Topchiev Institute of Petrochemical Synthesis, Russian Academy of Sciences, 117912-Moscow, Leninskii prosp. 29, Russia*

[b] *Instituto de Ciencia de Materiales de Sevilla, Centro Mixto CSIC-Universidad de Sevilla and Dpto. de Química Inorgánica, Universidad de Sevilla, Avda. Américo Vespucio, s/n. 41092-Sevilla, Spain. E-mail: navio@cica.es*

Received (in Cambridge, UK) 22nd February 1999, Accepted 16th April 1999

A heterogeneous hydrogen-accumulating system containing porous titanium with 0.4 wt% Ni combined with high-purity titanium chips was tested for methane activation; methane conversion to C_1–C_4 hydrocarbons reached a value of *ca.* 20% over this material, working at 450 °C and 10 atm, after methane circulation across the system for 22 h; the split hydrogen was accumulated as TiH_2, being in solid solution with porous metallic titanium.

Methane is the principal constituent of natural gas, landfill gas or coalbed methane. It is also a by-product of oil refining and chemical processing. Many techniques have been developed for improving the industrial processes which convert methane into higher hydrocarbons, gasoline and olefins by both indirect and direct conversion processes.[1,2] However these industrial processes involve expensive separation steps and/or require the use of temperatures higher than 80 °C, with the subsequent consumption of energy.[1,2]

Direct methane conversion eliminates the need (and subsequently reduces the cost) for the syngas preparation step. However, since methane is a very stable molecule[2,3] its reactions generally have high activation energy and, once activated, it is difficult to stop the reaction from going further than desired.

On the other hand, the non-favourable thermodynamic parameters[4] for methane self-interaction reactions led us to predict that, without strong oxidants, it would be difficult to transform methane into higher homologues at moderate temperatures using conventional catalytic approaches. We presumed, however, that it should be possible to shift the equilibrium *via* the introduction of separate stages, including the formation of [CH_3*] and [CH_2*] intermediates using heterogeneous systems with dual activities: a high activity for C–H bond fission and simultaneous hydrogen-accumulating properties. The latter might lead to an increase in the probability of direct self-interactions between generated intermediates, giving higher hydrocarbon molecules by a route which has not been explored until now. The adsorption of H_2 on transition metals has been much studied.[5] At the same time the adsorption/reaction of hydrocarbons on metallic catalysts is a very well known topic,[5] with Ni metal having a capability for hydrogenolysis of C–C and steam reforming of CH_4.

With this goal in mind we used a heterogeneous system containing porous high purity titanium (99.6%) with 0.4 wt% Ni in the form of cylindrical pellets (10 mm long and 5 mm in diameter) (**I**) combined with titanium chips (**II**) also obtained from high purity titanium. The **I**:**II** ratio was 5.3. The composite was thermally activated at 850 °C *in vacuo* (10^{-5} torr) before being placed in a loop reactor with a total volume of 0.42 L in circulation mode with a flow rate of 5 L of gas per hour at 10 atm. It was shown by laser (ML-2) and scanning high temperature mass spectroscopy (VIMS MS-720) that vacuum treatment is sufficient to clean up the surface. Using 19 g of this catalytic material it was found that methane conversion reached around 20% after methane flow-circulation across the catalyst bed at a temperature of 450 °C for 22 h. This degree of conversion was constant even after 28 h of continuous flow-circulation, as experimental controls showed (Fig. 1). It should be mentioned that methane conversion into C_2 hydrocarbons was initiated at 330 °C. Table 1 summarises the composition of the methane conversion products. As can be seen, after methane flow-circulation for 1 h a conversion of about 4.5% was reached, yielding predominantly ethylene and ethane (92.9%). After prolonged reaction time an increase of C_2–C_4 olefins of around 70–75% was observed, 50–55% of which was ethylene. At this point, the level of hydrogen in the reaction volume was not more than 0.01% according to GC (LKhM-8MD and Biokhrom chromatographs) and MS (VIMS MS-7201) analyses.

Analysis by X-ray (DROM-3M, Cu-Kα) diffraction of the composition of the catalyst showed that, in addition to the reflections corresponding to the metal titanium phase [d = 2.24; 2.34; 2.55 A], titanium chips removed from the reactor under anaerobic conditions showed well-resolved intense reflections

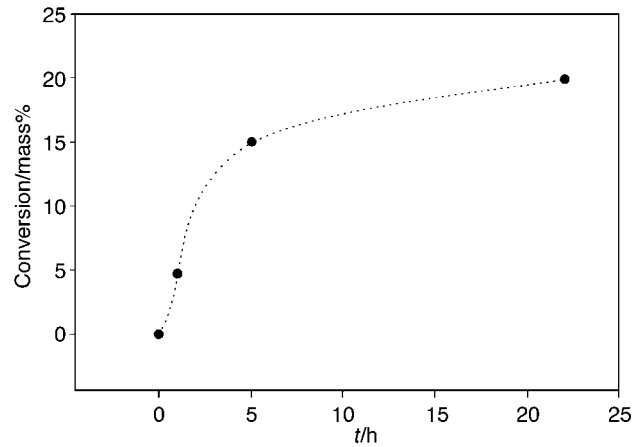

Fig. 1 Conversion of methane into products summarised in Table 1.

Table 1 Methane conversion and the composition of products from its transformation (T = 450 ºC, P = 10 atm)

Composition (% mass)	Composition (mass%)			
	1 h	5 h	22 h	28 h
CH_4	95.3	85.3	79.8	80.1
C_2H_4	2.5	8.2	10.0	10.8
C_2H_6	1.9	3.0	4.8	4.4
C_3H_6	0.1	2.5	3.1	2.1
C_3H_8	0.2	0.4	0.4	0.3
C_4H_8	< 0.1	0.4	1.3	1.7
C_4H_{10}	< 0.1	0.2	0.6	0.6

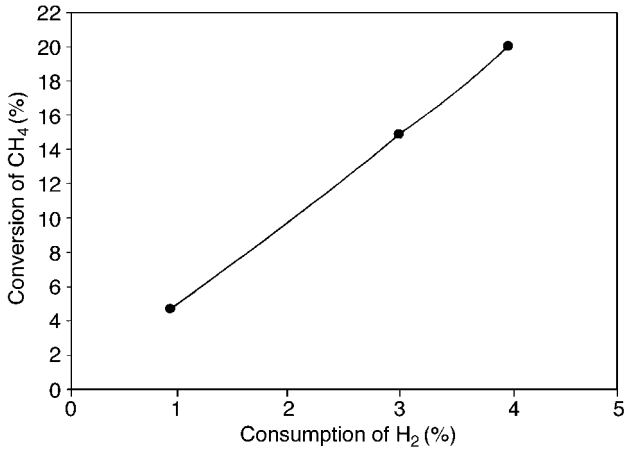

Fig. 2 Dependence of methane conversion on the quantity of hydrogen evolved and sorbed by the heterogeneous system.

due to a hydride phase (TiH_2) [d = 2.22; 2.31; 2.53 A]. At the same time, the reflections associated with the metal titanium phase shifted by only 0.45–0.47° (2θ) with respect to the starting system for the porous titanium. This evidence for the formation of a Ti–H interstitial solid solution during the decomposition of methane.

Fig. 2 shows that the increase in the methane conversion, in the range of operation, is proportional to the amount of hydrogen sorbed by the system, this being calculated on the basis of the stoichiometry of the reaction. This enables us to conclude that the removal of hydrogen from the reaction zone is, as expected, one of the main stages of the transformation of methane into higher products.

On the basis of the balance of the identified products, we may propose the pathways in eqns. (1)–(4) for the self-interaction reactions between the intermediates formed from methane activation.

$$2\ CH_4 \rightarrow 2\ [CH_2^*] - 4\ [H] \rightarrow C_2H_4 \quad (1)$$

$$2\ CH_4 \rightarrow 2\ [CH_3^*] - 2\ [H] \rightarrow C_2H_6 \quad (2)$$

$$3\ CH_4 \rightarrow 3\ [CH_2^*] - 6\ [H] \rightarrow C_3H_6 \quad (3)$$

$$3\ CH_4 \rightarrow [CH_2^*] + 2\ [CH_3^*] - 4\ [H] \rightarrow C_3H_6 \quad (4)$$

The C_4 fraction is probably a result of ethylene dimerization. We also propose that one of the limitations of this process is the coordination of CH_2^* intermediates to the surface metal centres. The interaction between closely coordinated [CH_2–M] species at the catalyst surface could be followed by their elimination leading to ethylene formation. In this way we can explain the high selectivity for C_2 alkene. In fact this tentative mechanism for the formation of olefins is in good accordance with the concepts of metal complex homogeneous catalysis.[6]

In any case our results indicate that C_2–C_3 species can be obtained by a single step, compared with direct or indirect processes which involve multi-steps such as the syngas and steam reactions. Of course, the problem of the hydrogen spillover to the titanium chips requires further study, which is now in progress.

Here we have reported a new finding which opens the way to selective low temperature methane conversion to important products by a new means using bifunctional hydrogen accumulating systems. At the same time the process offers the possibility of simultaneously obtaining high purity dihydrogen.

The authors acknowledge the Russian Science Foundation (Project 970332028a), NATO (Project ref. ENVIR.LG 971292) and DGICYT-Spain (Project PB96-1346) for supporting part of this work.

Notes and references

1 J. M. Fox, *Catal. Rev.-Sci. Eng.*, 1993, **35**, 169.
2 A. Ye. Shilov and G. B. Shulpin, in *Activation and Catalytic Reactions of Hydrocarbons*, ed. A. P. Purmal, Moscow, 1995, p. 399.
3 *Methane*, ed. F. A. Alekseev, Nedra, Moscow, 1978.
4 D. R. Stull, E. F. Westrum and G. C. Siuke, in *The Chemical Thermodynamics of Organic Compounds*, Wiley, New York, 1969.
5 J. H. Ross, in *Metal Catalysed Methanation and Steam Reforming*, in *Catalysis*, ed. G. C. Bond and G. Webb, The Royal Society of Chemistry, London, 1985, vol. 7, p. 1.
6 M. L. H. Green, *Organometallic Compounds*, in *The Transition Elements*, Methuen, London, vol. 2, 1968.

Communication 9/01439J

Typeset and printed by Black Bear Press Limited, Cambridge, England

Magnetic anisotropy in cyano-bridged bimetallic ferromagnets synthesized from the $[Mo(CN)_7]^{4-}$ precursor

Olivier Kahn,[a] Joulia Larionova[a] and Lahcène Ouahab[b]

[a] *Laboratoire des Sciences Moléculaires, Institut de Chimie de la Matière Condensée de Bordeaux, UPR CNRS No 9048, 33608 Pessac, France. E-mail: kahn@icmcb.u-bordeaux.fr*

[b] *Laboratoire de Chimie du Solide et Inorganique Moléculaire, UMR CNRS No 6511, Université de Rennes I, 350042 Rennes, France*

Received (in Cambridge, UK) 6th January 1999, Accepted 9th March 1999

The goal of this feature article is to introduce the dimension 'magnetic anisotropy' in the field of molecule-based magnets. For that, we have focused on three cyano-bridged $Mn^{II}Mo^{III}$ compounds synthesized from the $[Mo^{III}(CN)_7]^{4-}$ precursor. The pentagonal bipyramid structure of this precursor is not compatible with a cubic lattice, as found in the Prussian blue phases. In this precursor, Mo^{III} has a low-spin configuration, with a local spin $S_{Mo} = 1/2$, and a strongly anisotropic *g* tensor. Two of the compounds have a three-dimensional structure. Their formulas are $Mn_2(H_2O)_5Mo(CN)_7 \cdot nH_2O$, with $n = 4$ for the α phase, and $n = 4.75$ for the β phase. One of the compounds, of formula $K_2Mn_3(H_2O)_6[Mo(CN)_7]_2 \cdot 6H_2O$, has a two-dimensional structure, with K^+ cations and water molecules located between double-sheet layers. The compounds crystallize in the monoclinic system, and the lattice symmetries are very low. For the three compounds, we have succeeded in growing well shaped single crystals suitable for magnetic anisotropy measurements, and we have investigated the magnetic properties as follows: first, we have determined the magnetic axes by looking for the extremes of the magnetization in the three crystallographic planes *ab*, *bc*, and *ac*. Then, we have measured the temperature and field dependences of the magnetization in the dc mode along the three magnetic axes. These measurements have revealed the existence of several magnetically ordered phases for the three-dimensional compounds, and of field-induced spin reorientations for the three compounds. For the very first time in the field of molecular magnetism, we have been able to determine the magnetic phase diagram for each compound. We have obtained additional information from magnetic data recorded in the ac mode, with both zero and non-zero static fields. Finally, we have found that when the non-coordinated water molecules are released, the long-range magnetic ordering temperatures are shifted toward higher temperatures. Irrespective of the structural details, the Mo^{III}–C–N–Mn^{II} interaction has been found to be ferromagnetic. We have discussed this unexpected result, and proposed a mechanism accounting for this. We have also discussed the factors governing the magnetic anisotropy of the compounds.

Introduction

The first two molecular compounds exhibiting a spontaneous magnetization below a certain critical temperature, T_c, were described in 1986.[1,2] These reports have opened a new field of research, that of molecule-based magnets, and in the last decade quite a few new compounds of that kind have been synthesized.[3–19] What characterizes this field of research is its deeply multidisciplinary nature; it brings together synthetic organic, organometallic, and inorganic chemists along with theoreticians and physicists as well as material and life science people.

To a large extent, the field so far has been governed by the race toward high coercivity and/or high critical temperature. High coercivity means that the material has a pronounced memory effect. As a matter of fact, applying a weak magnetic field to a magnet results in a saturation magnetization aligned in the field direction. When the field is switched of, the magnetization does not disappear, but takes a value called remnant magnetization. The coercive field is the field which must be applied in the opposite direction to annul this remnant magnetization, *i.e.* to suppress the information associated with the remnant magnetization. Recently, a very hard molecule-based magnet was discovered. Its coercive field depends on the particle size; it may be as large as 25 kOe at 5 K. This compound contains three kinds of spin carriers, Co^{2+} and Cu^{2+} ions as well as radical cations. It structure is very peculiar; it consists of two perpendicular honeycomb like (or graphite like) networks which interpenetrate in such a way that each hexagon belonging to one of the networks is interlocked with a hexagon belonging to the perpendicular network.[20–22] The key factor of the huge coercivity is the presence of very anisotropic Co^{2+} ions in octahedral surroundings. The interlocking of the two networks also contributes to this coercivity.

High critical temperature obviously means that the magnetically ordered state is easily accessible. In that respect, T_c above room temperature is a must. This goal has been reached with a compound of formula $V^{II}_{0.42}V^{III}_{0.58}[Cr^{III}(CN)_6]_{0.86} \cdot 2.8H_2O$.[23] This compound belongs to the vast family of the Prussian blue like phases with the general formula $A_k[B(CN)_6]_l \cdot nH_2O$ where

Olivier Kahn was born in Paris (France). He received his PhD thesis from the University of Paris in 1969. He became Professor of Chemistry at the University of Paris South in 1975, and moved to the Institut de Chimie de la Matière Condensée de Bordeaux in 1995. He is presently Professor at the University of Bordeaux I, and Member of the Institut Universitaire de France. Olivier Kahn is a Fellow of the (French) Academy of Science and of other academies. His fields of research are molecular materials, molecular electronics, and molecular magnetism.

Joulia Larionova was born in Saint Petersburg (Russia). She received her PhD thesis from the University of Bordeaux I in 1998. She initiated the work on the anisotropy properties of molecule-based magnets and determined the first magnetic phase diagrams for this class of compounds during her PhD.

Lahcène Ouahab was born in Sétif (Algeria). He received his PhD thesis from the University of Rennes I in 1985. He is presently Director of Research at the Laboratoire de Chimie du Solide et Inorganique Moléculaire of the University of Rennes I, and leads the molecular materials group. His fields of research concern the synthesis, and the crystal chemistry of molecular materials, in particular charge transfer complexes, radical ion salts, and organic–inorganic hybrids.

A is a high spin metal ion and B a low spin one. The basic structure is faced-centered cubic with A–N–C–B linear linkages along three perpendicular directions. Alkaline cations may occupy A_4 or B_4 tetrahedral sites. For $k > 1$, some $B(CN)_6$ groups are missing, which creates a local breaking of the three-dimensional periodicity. These vacant sites are usually occupied by water molecules coordinated to the adjacent A site.[24,25] The magnetic interaction between nearest neighbor A and B ions may be antiferro- or ferromagnetic. In the former case, the local spins tend to align in an antiparallel way. When it is so, the compound below T_c is a ferrimagnet, provided that there is no exact cancellation of the A and B spin sublattices. This situation is by far the most frequent. In the latter case, the local spins tend to align in a parallel way, and below T_c the compound is a ferromagnet. One of the appealing aspects of the magnetic studies dealing with Prussian blue phases[26–30] resides in the fact that it is possible to predict the nature, and to estimate *a priori* the value of the critical temperature, using simple theoretical models based on the symmetry of the singly occupied orbitals.[31] This is due to the fact that the symmetry of both the A and B metal sites is strictly octahedral so that the e_g and t_{2g} orbitals do not mix. The design of the room temperature magnet mentioned above does not arise from serendipity, but was achieved in a rational way.[32] The cubic symmetry of the Prussian blue phases, however, has a cost. These compounds are structurally, and hence magnetically isotropic, and many interesting features associated with the structural and magnetic anisotropies cannot be observed. It may be noticed that nobody so far has succeeded in growing single crystals of Prussian blue phases suitable for detailed magnetic measurements. This situation is not too embarrassing as no anisotropy is expected, except perhaps a weak shape anisotropy for thin film samples. On the other hand, the thorough investigation of the properties of molecule-based magnets of low symmetry requires obviously well shaped single crystals.

The goal of this article is to emphasize the beauty and the richness of the phenomena arising from the low symmetry of molecule-based magnets. For that, we will focus on cyano-bridged bimetallic magnets synthesized from the $[Mo(CN)_7]^{4-}$ precursor. The choice of this precursor is motivated by three reasons: (i) as for the Prussian blue phases, the presence of cyano ligands can lead to extended lattices. (ii) These networks should be of low symmetry; as a matter of fact, the heptacoordination of the precursor is not compatible with a cubic symmetry. (iii) In $KNa_2[Mo(CN)_7]\cdot 2H_2O$, the Mo^{III} ion is in a low-spin pentagonal bipyramid environment. The orbitally degenerate ground state, $^2E''_1$, is split into two Kramers doublets by the spin–orbit coupling, and the ground Kramers doublet is strongly anisotropic.[33–35] In other words, the value of the magnetization when applying a magnetic field strongly depends on the orientation of this field with respect to the fivefold axis of the pentagonal bipyramid.

We will try to present this article in a tutorial way; we will report on the magnetic properties of three compounds, but each new concept in molecular magnetism will be introduced and discussed only once.

The three-dimensional compounds $Mn_2(H_2O)_5Mo(CN)_7\cdot nH_2O$, α and β phases

Crystal structure of the α phase

The slow diffusion of two aqueous solutions containing $K_4[Mo(CN)_7]\cdot 2H_2O$ and $[Mn(H_2O)_6](NO_3)_2$, respectively, affords two kinds of single crystals, with elongated plate (α phase) and prism (β phase) shapes.[36,37] The local environments of the metal sites are similar for both phases, but the three-dimensional organizations are different. There is one molybdenum site along with two manganese sites, denoted as Mn1 and Mn2, as shown in Fig. 1. The molybdenum atom is surrounded by seven –C–N–Mn linkages, four of them involving a Mn1 site and three of them a Mn2 site. The geometry may be described as a slightly distorted pentagonal bipyramid. Both Mn1 and Mn2 sites are in distorted octahedral surroundings. Mn1 is surrounded by four –N–C–Mo linkages and two water molecules in *cis* conformation. Mn2 is surrounded by three −N–C–Mo linkages and three water molecules in a *mer* conformation. The three-dimensional organization for the α phase may be described as follows: edge-sharing lozenge motifs $(MoCNMn1NC)_2$ form bent ladders running along the *a* direction. Each ladder is linked to four other ladders of the same kind along the [011] and [01 − 1] directions through cyano bridges. These ladders are further connected by the $Mn2(CN)_3(H_2O)_3$ groups. Mn2 is linked to a Mo site of one of the ladders and to two Mo sites of the adjacent ladder. The structure as a whole viewed along the *a* direction is represented in Fig. 2.

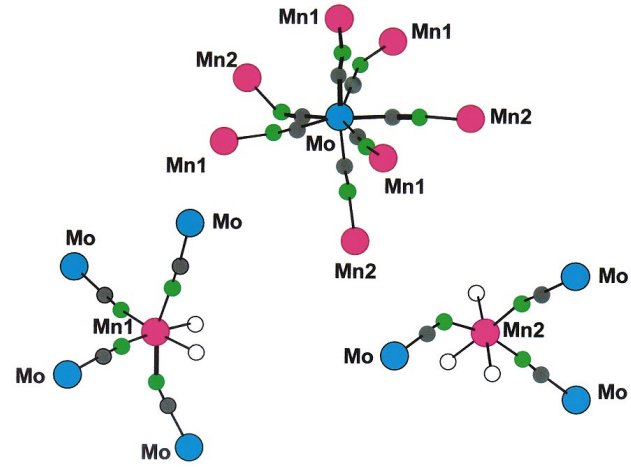

Fig. 1 Local structure of the molybdenum and manganese sites for $Mn_2(H_2O)_5Mo(CN)_7\cdot 4H_2O$ (α phase). The color code is the following: the manganese atoms are in red, the molybdenum atoms in blue, the carbon atoms in black, the nitrogen atoms in green, and the oxygen atoms (of water molecules) in white.

Magnetic properties of the α phase

We first checked that in the three crystallographic planes *ab*, *bc*, and *ac*, the extremes of the magnetization are obtained when the field is aligned along the *a*, *b* and *c** axes. Therefore, these axes are the magnetic axes of the compound. It may be noticed that the twofold axis of the monoclinic lattice, *b*, was necessarily one of the magnetic axes.[38] All the magnetic measurements were carried out on single crystals with the external field successively applied along these three axes. We first measured the temperature dependences of the magnetization, *M*, under a field of 5 Oe. The three curves are shown in Fig. 3. They reveal that the material is anisotropic, the magnetization along the easy magnetization axis, *b*, being about twice as large as along the *a* axis. Moreover, these curves exhibit a break with an inflexion point at $T_{1c} = 51$ K along with another anomaly, more visible along the *a* axis, at $T_{2c} = 43$ K. Very few magnetic anisotropy measurements on molecule-based magnets were performed so far.[3,39]

The most accurate technique to determine transition temperatures is the measure of the heat capacity as a function of temperature. In the present case, the heat capacity curve shows a λ peak at 51 K, but nothing is detected at 43 K (see Fig. 4). It follows that the compound presents two magnetic transitions, and the entropy change associated with that occurring at 51 K is much larger than the entropy change associated with that occurring at 43 K.

In order to obtain more insights on the magnetic anomaly detected at 43 K, visible essentially along the *a* direction, we measured the magnetization along this direction with an external field varying from 1 up to 100 Oe. The results are

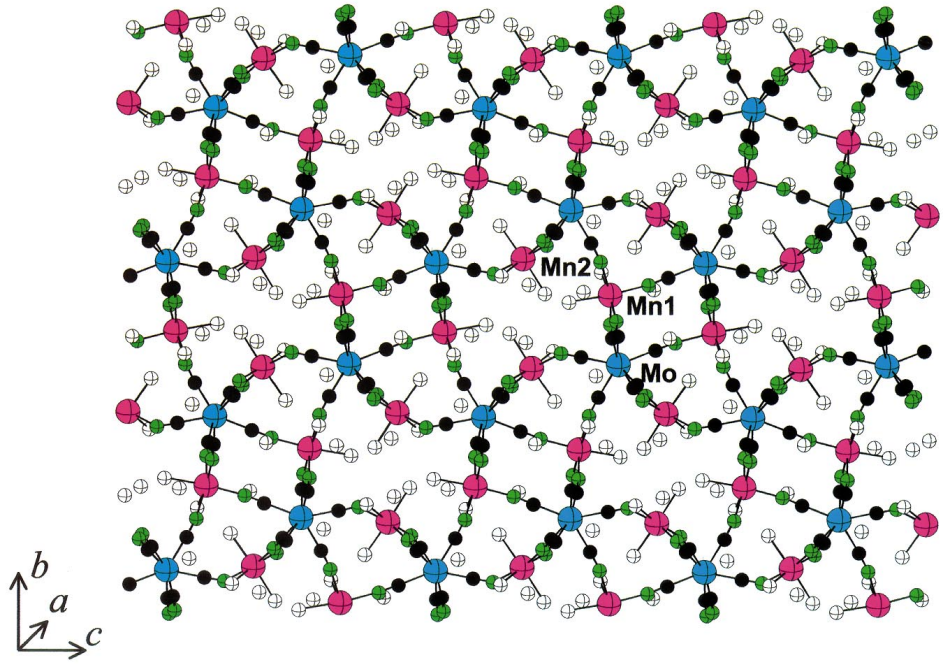

Fig. 2 Structure of the compound $Mn_2(H_2O)_5Mo(CN)_7{\cdot}4H_2O$ (α phase) viewed along the *a* direction.

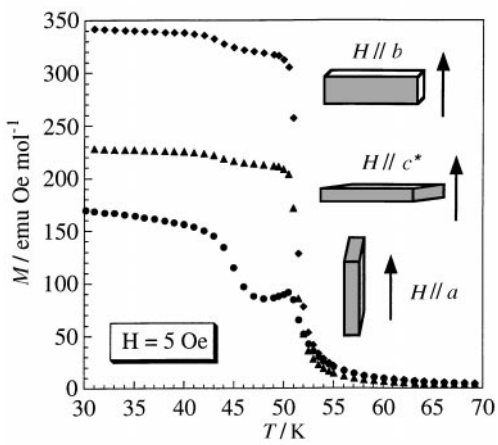

Fig. 3 Temperature dependences of the magnetization along the *a*, *b* and *c** directions, using an external field of 5 Oe, for $Mn_2(H_2O)_5Mo(CN)_7{\cdot}4H_2O$ (α phase).

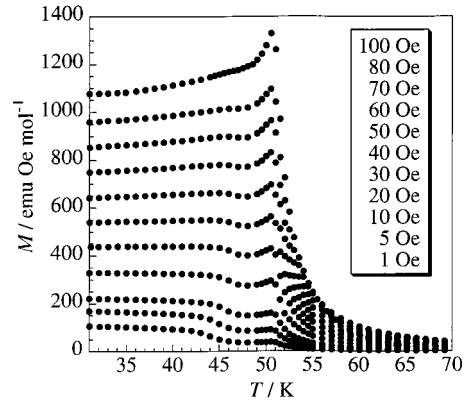

Fig. 5 Temperature dependences of the magnetization along the *a* direction, using different values of the external field, for $Mn_2(H_2O)_5Mo(CN)_7{\cdot}4H_2O$ (α phase).

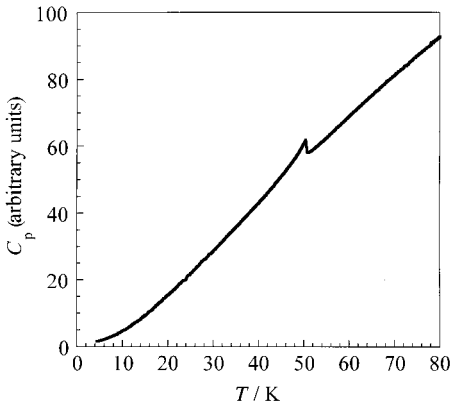

Fig. 4 Temperature dependence of the heat capacity for $Mn_2(H_2O)_5Mo(CN)_7{\cdot}4H_2O$ (α phase).

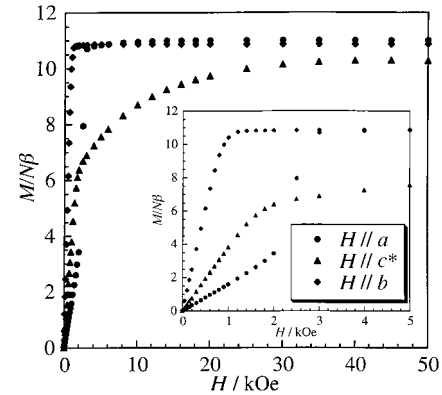

Fig. 6 Field dependences of the magnetization at 5 K along the *a*, *b* and *c** directions for $Mn_2(H_2O)_5Mo(CN)_7{\cdot}4H_2O$ (α phase).

displayed in Fig. 5. T_{2c} is shifted toward higher temperatures as the magnetic field increases, and eventually, for a field of *ca.* 100 Oe, merges with the transition at 51 K. For each field, T_{2c} was determined as the inflexion point of the $M = f(T)$ curve.

We then measured the field dependences of the magnetization at 5 K along the *a*, *b* and *c** directions (see Fig. 6). The curves are strictly identical when increasing and decreasing the field; the compound exhibits no coercivity. Along the easy magnetization direction, *b*, the saturation is reached with *ca.* 1 kOe. The saturation magnetization is found equal to 11 Nβ. This value corresponds exactly to what is expected for one $S_{Mo} = 1/2$ and two $S_{Mn} = 5/2$ local spins aligned along this direction. The interaction between adjacent Mo^{III} and Mn^{II} ions is ferromagnetic. Along the *c** direction, the magnetization increases progressively when applying the field, and even at 50 kOe the

saturation is not totally reached. Along the *a* direction, the *M versus H* curve is peculiar; it shows an inflexion point for a critical field, H_c, of about 2.2 kOe. We are faced with a field-induced spin reorientation phenomenon.[40–44]

Field-induced spin reorientation

Let us examine in more detail what happens when applying the field along the *a* axis. In zero field, the resulting moment of 11 Nβ is essentially aligned along *b*. When applying the field, first this moment hardly rotates from *b* to *a*, then for a critical value of the field the rotation becomes much easier. Finally, for a saturation value of the field, H_{sat}, the moment is aligned along *a*. The spin reorientation is a non-linear phenomenon. It is difficult to unhook the moment from the *b* axis. When the field is large enough, this unhooking is realized, and then a weak increase of the field induces a strong rotation until the moment is collinear with *a*. To determine the H_c and H_{sat} *versus T* curves, we measured the field dependence of the magnetization along *a* every 5 K in the 5–51 K range. The critical field at each temperature was determined as the field for which the d*M*/d*H* derivative is maximum. The saturation field at each temperature was determined as the weakest field for which the saturation is reached. The temperature dependences of H_c and H_{sat} for a field applied along the *a* axis are utilized to determine the magnetic phase diagram of the compound.

Magnetic phase diagram

From the magnetic data presented above, it is possible to plot the magnetic phase diagram of the compound when the field is applied along the *a* axis. This diagram shown in Fig. 7 presents

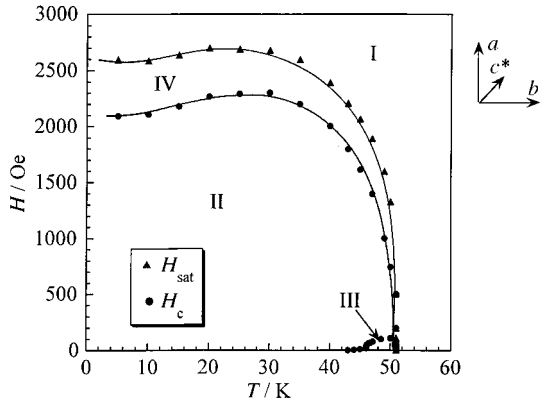

Fig. 7 Magnetic phase diagram for $Mn_2(H_2O)_5Mo(CN)_7{\cdot}4H_2O$ (α phase); the full lines are a guide to the eye.

four domains. Domain I is the paramagnetic domain in which the spins are either randomly oriented, or aligned along the field direction. Domains II and III are ferromagnetic domains in which the spins are essentially aligned along the *b* direction. Domain III is limited to the 43–51 K temperature range and the 0–100 Oe field range. Domain IV, finally, is limited by the $H_c = f(T)$ and $H_{sat} = f(T)$ curves, and corresponds to a mixed domain in which the spins may rotate easily from the *b* to the *a* direction. It is worth mentioning that the boundary between domains II and IV corresponds to a first-order transition, while that between domains I and IV corresponds to a second-order transition.

The question we are faced with is the difference between domains II and III. We have seen that the entropy variation associated with the transition between these two domains is very weak, and not detected in the heat capacity curve of Fig. 4. Therefore, the magnetic structures of these domains are similar to each other. The transition between these two domains, at 43 K in zero field, is more pronounced when applying the field along the *a* axis than along the other two magnetic axes. This strongly suggests that the main difference between domains II and III concerns the component of the resulting moment along *a*. Assuming that the magnetic symmetry of the low-temperature domain II is lower than that of the high-temperature domain III, we may suggest that domain III is a perfectly ferromagnetic domain with the magnetic moments aligned along *b* in zero field, and that a small canting occurs as *T* is lowered below 43 K, with a weak component of the resulting moment along *a*. If it was so, applying a field of 100 Oe along *a* would destabilize the perfectly ferromagnetic domain in favor of the weakly canted domain. Alternatively, the two domains might be weakly canted, with a component of the moment along *a*, the degree of canting being slightly more pronounced in domain II. Neutron diffraction studies should allow us to specify the differences between domains II and III.

A quick look on the β phase

The structure of the β phase is shown in Fig. 8. Each ladder made of edge-sharing lozenge motifs is surrounded only by two instead of four identical ladders. This phase again exhibits a ferromagnetic transition at T_c = 51 K. It is even more anisotropic than the α phase, and the magnetic phase diagram is even more complex, with several ferromagnetically ordered domains, and a spin reorientation domain.[45]

The partial dehydration of the α or β phase leads to the same compound which exhibits a long-range ferromagnetic ordering at 66 K along with a coercive field of 850 Oe at 5 K.

The two-dimensional compound $K_2Mn_3(H_2O)_6[Mo(CN)_7]_2{\cdot}6H_2O$

When the slow diffusion between aqueous solutions containing $K_4[Mo(CN)_7]{\cdot}2H_2O$ and $[Mn(H_2O)_6](NO_3)_2$, respectively, takes place in the presence of an excess of K^+ ions, a two-dimensional compound of formula $K_2Mn_3(H_2O)_6$-$[Mo(CN)_7]_2{\cdot}6H_2O$ is obtained.[46] The structure contains again a unique molybdenum site along with two manganese sites, denoted as Mn1 and Mn2, as shown in Fig. 9. The molybdenum atom is surrounded by six –C–N–Mn linkages and a terminal –C–N ligand. The geometry may be described as a strongly distorted pentagonal bipyramid, and both the Mo–C–N and C–N–Mn bridging angles deviate significantly from 180°. Both the Mn1 and Mn2 sites are surrounded by four –N–C–Mo linkages and two water molecules in *trans* conformation. The two-dimensional structure is made of anionic double-sheet layers parallel to the *bc* plane, and K^+ and non-coordinated water molecules situated between the layers, as shown in Fig. 10. Each sheet is a kind of grid in the *bc* plane made of edge-sharing lozenges $[MoCNMn2NC]_2$. Two parallel sheets of a layer are further connected by $Mn1(CN)_4(H_2O)_2$ units situated between the sheets. The thickness of a double-sheet layer is 8.042 Å, and that of the gap between two layers is 7.263 Å.

Magnetic phase diagram

We first checked that *a*, *b* and *c** were the magnetic axes of the compound, *b* being the easy magnetization axis, then we studied the temperature and field dependences of the magnetization along the three axes. No hysteresis was observed along *a* and *b*, while a narrow hysteresis, of *ca.* 125 Oe, was observed along *c** at 5 K. These measurements revealed that the compound exhibits a long range ferromagnetic ordering at T_c = 39 K, and that below T_c a field induced spin reorientation occurs along the *c** axis. We determined the critical and saturation fields every 5 K below T_c when applying the field along *c**. The H_c and H_{sat} *versus T* curves shown in Fig. 11 define the magnetic phase diagram for the compound when the magnetic field is applied along *c**. This diagram is simpler than that of Fig. 7. It presents only three domains. Domain I corresponds to the paramagnetic, or saturated paramagnetic domain. Domain II corresponds to

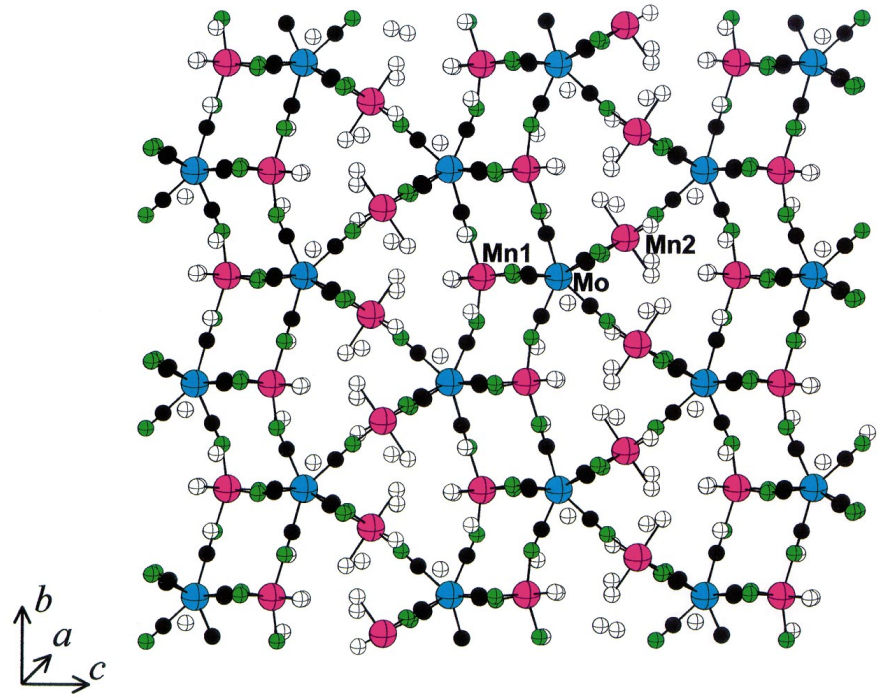

Fig. 8 Structure of the compound $Mn_2(H_2O)_5Mo(CN)_7{\cdot}4.75H_2O$ (β phase) viewed along the *a* direction.

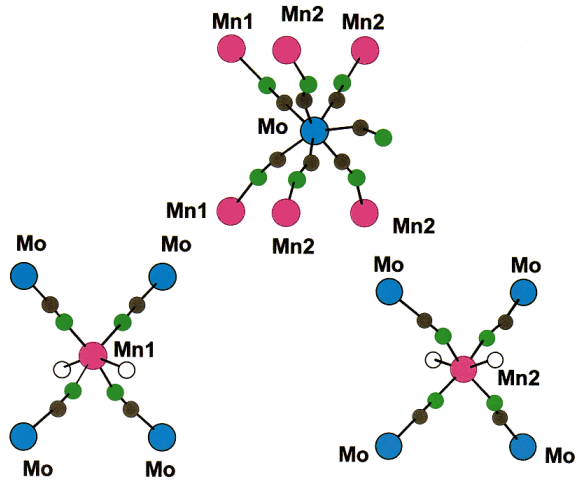

Fig. 9 Local structure of the molybdenum and manganese sites for $K_2Mn_3(H_2O)_6[Mo(CN)_7]_2{\cdot}6H_2O$. The color code is the same as for Fig. 1.

the ferromagnetically ordered domain in which the spins are essentially aligned along the *b* axis. Domain III, finally, is a spin-reorientation domain in which the spins rotate from the *b* to the *c** direction as the field increases from H_c to H_{sat}.

To complete this study, we also determined the temperature dependence of the spontaneous magnetization. For that, we studied the field dependence of the magnetization along the *b* axis every 5 K. Some curves are shown in Fig. 12 (top). At each temperature, the spontaneous magnetization, M_S, can be determined by extrapolating down to zero the $M = f(H)$ data obtained in the field range where the variation is linear. The temperature dependence of the spontaneous magnetization is represented in Fig. 12 (bottom). The spontaneous magnetization is equal to 17 $N\beta$ at absolute zero, decreases as the temperature increases, and vanishes at T_c = 39 K.

ac Magnetic measurements

So far, we only spoke of magnetic measurements recorded in the dc mode; *i.e.* with a static external field. Additional information can be obtained by working in the ac mode.[47] The magnetic field is then expressed as:

$$H = H_0 + h \exp(i\omega t)$$

where H_0 is the static field, which may be taken as zero, h is the amplitude of the oscillating field, ω the frequency, and t the time. The ac susceptibility, χ_{ac}, is then equal to dM/dH. The ac magnetic susceptibility is determined from its two components, the in-phase (or real) component, χ'_{ac}, and the out-of-phase (or imaginary) component, χ''_{ac}. The in-phase susceptibility is an initial susceptibility with the same phase as the oscillating field. The out-of-phase susceptibility characterizes the phase delay of the magnetization with respect to the oscillating field in the magnetically ordered phase.

We report here on two experiments in the ac mode. First, we measured the temperature dependences of the in-phase, χ'_{ac}, and out-of-phase, χ''_{ac}, magnetic susceptibilities under a zero static field. Along the three directions, the in-phase responses exhibit a break at T_c = 39 K. The χ'_{ac} values along the *b* axis below T_c are much higher than along the other two directions. The out-of-phase response along the *b* axis is zero down to 39 K, then presents an abrupt break as T is lowered below this temperature, and reaches a maximum around 34 K. Along the other two directions, χ''_{ac} is negligibly weak down to 2 K.

When the field is applied along the easy magnetization axis, *b*, both the displacement of the domain walls and the rotation of the magnetic moments contribute to the ac magnetic response. On the other hand, when the field is applied along a hard magnetization axis, only the rotation of the magnetic moments contributes to the ac response.[48] In the present case, the very high response along *b* as compared to the responses along *a* and *c** indicates that the domain walls move very easily, which is in line with the quasi absence of hysteresis in the $M = f(H)$ curves.

The second experiment consisted of measuring the field dependence of χ'_{ac} along the *c** axis every 5 K in the magnetically ordered phase. The results are displayed in Fig. 13. At each temperature, χ'_{ac} first increases as the field increases, reaches a maximum, then tends to zero at high field. The maximum of χ'_{ac} determines the critical field, H_c, and the extreme of the derivative $d\chi'_{ac}/dH$ determines the saturation field, H_{sat}. The $H_c = f(T)$ and $H_{sat} = f(T)$ curves deduced from this experiment are strictly similar to those shown in Fig. 11.

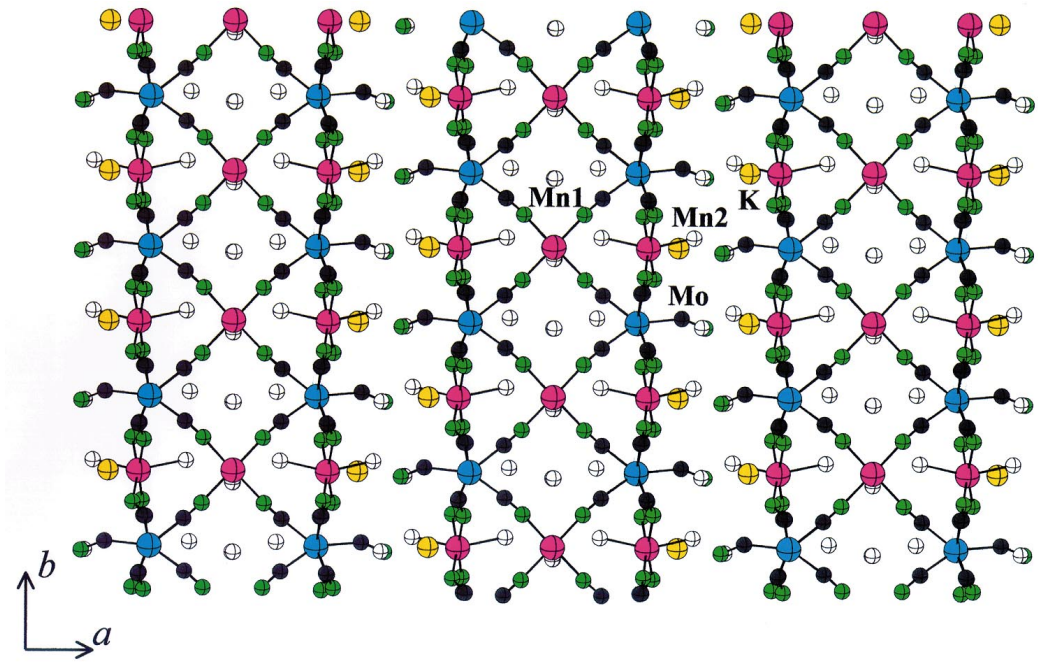

Fig. 10 Structure of the compound $K_2Mn_3(H_2O)_6[Mo(CN)_7]_2{\cdot}6H_2O$ in the *ab* plane. Potassium atoms are in yellow.

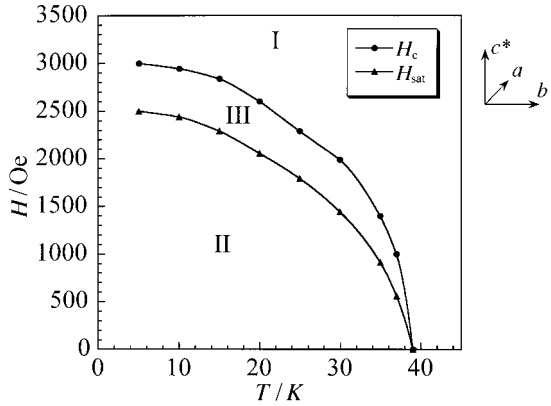

Fig. 11 Magnetic phase diagram for $K_2Mn_3(H_2O)_6[Mo(CN)_7]_2{\cdot}6H_2O$; the full lines are a guide to the eye.

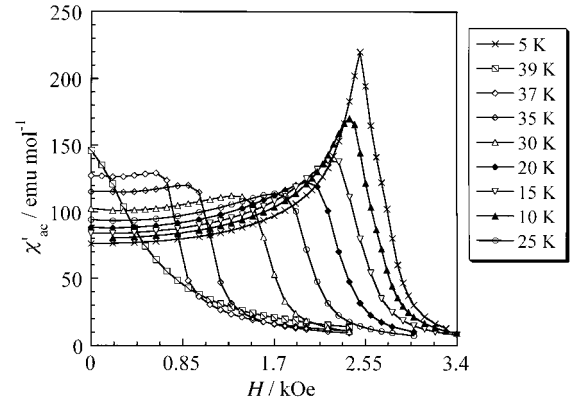

Fig. 13 Field dependences of the in-phase ac susceptibilities at different temperatures along the *c** axis for $K_2Mn_3(H_2O)_6[Mo(CN)_7]_2{\cdot}6H_2O$.

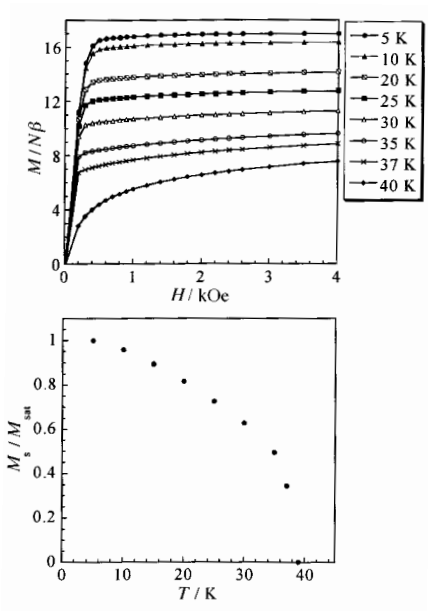

Fig. 12 (Top) Field dependences of the magnetization along the *b* axis at different temperatures for $K_2Mn_3(H_2O)_6[Mo(CN)_7]_2{\cdot}6H_2O$. (Bottom) Temperature dependence of the normalized spontaneous magnetization.

Modification of the magnetic properties through partial dehydration

The magnetic properties of $K_2Mn_3(H_2O)_6[Mo(CN)_7]_2{\cdot}6H_2O$ can be dramatically modified through partial dehydration. When the non-coordinated water molecules of a single crystal are released under vacuum, the external shape of the crystal is not modified. Magnetic measurements suggest that the crystallographic directions are retained. We then investigated the temperature dependences of the magnetization along these directions. The $M = f(T)$ curves along *b* and *c** are not distinguishable. After dehydration, the *bc* plane may be considered as an easy magnetization plane, even in low field. The spin reorientation is suppressed. Both in the *bc* plane and perpendicularly to this plane, the magnetization shows a break at T_c = 72 K, while the critical temperature for the non-dehydrated compound is 39 K. We measured the field dependences of the magnetization at 10 K both in the *bc** plane and along the *a* direction. The results are displayed in Fig. 14. In the easy magnetization plane, the saturation value of 17 $N\beta$ corresponding to the parallel alignment of all the spins is obtained under *ca.* 5.0 kOe. On the other hand, along the *a* axis, the saturation is not reached yet under 50 kOe. Magnetic hystereses are observed along both directions, with coercive fields of 1.3 kOe in the *bc* plane, and 0.55 kOe along *a*.

We can notice here that the Prussian blue phases are also hydrated. It would be interesting to see whether their partial dehydration also modifies their magnetic properties.

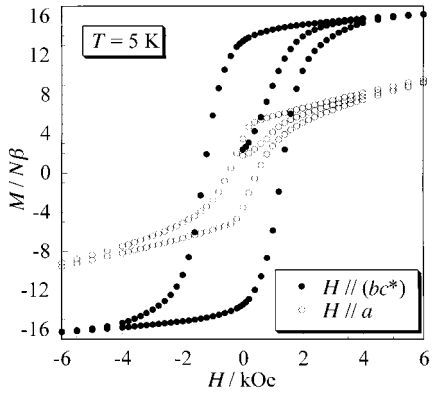

Fig. 14 Hysteresis loops in the *bc** plane and along the *a* axis at 10 K for a partially dehydrated crystal of $K_2Mn_3(H_2O)_6[Mo(CN)_7]_2{\cdot}6H_2O$.

Why is the Mo^{III}–C–N–Mn^{II} interaction ferromagnetic?

One of the striking features concerning the compounds described in this article is the ferromagnetic nature of the interaction between low-spin Mo^{III} and high-spin Mn^{II} ions through the cyano bridge. For several decades, quite a few studies have been devoted to the microscopic mechanisms of the interaction between spin carriers, more particularly to those of the mechanisms favoring a parallel alignment of the electron spins.[31,49] Three situations have been found to stabilize the parallel spin state, namely: (i) *the strict orthogonality of the magnetic orbitals*. Such a situation is achieved when all the singly occupied orbitals centered on a spin carrier (called also magnetic orbitals) are orthogonal (*i.e.* give a zero overlap integral) with all the singly occupied orbitals centered on the adjacent spin carrier. This situation of strict orthogonality of the magnetic orbitals is certainly the most efficient way to achieve a ferromagnetic interaction. (ii) *The electron transfer from a singly-occupied orbital on a site toward an empty orbital on an adjacent site, or from a doubly-occupied orbital on a site toward a singly-occupied orbital on an adjacent site*. This mechanism is probably less efficient than the previous one, and more difficult to control. (iii) *The interaction between a zone of negative spin density on a fragment and a zone of positive spin density on an adjacent fragment*. This mechanism, first suggested in the context of assemblies of organic radicals,[50] may apply for transition metal species as well.

We carefully examined the relevance of each of these mechanisms in the case of Mo^{III}–C–N–Mn^{II}. The strict orthogonality of the magnetic orbitals is not realized, and the absorption spectra of the compounds synthesized from the $[Mo(CN)_7]^{4-}$ precursor do not reveal any metal–metal charge transfer band of relatively low energy. Therefore, we are wondering whether the ferromagnetic interaction could arise from a close contact between negative and positive spin density zones.

The orbital energy diagram for low-spin Mo^{III} in pentagonal bipyramid symmetry (D_{5h}) is represented below.

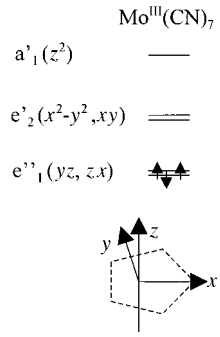

At the self consistent field (SCF) approximation, the e'_2 ($x^2 - y^2$, xy) and a'_1 (z^2) orbitals with a predominant 4d character are empty. It follows that at this approximation level, there is no spin density along both equatorial and axial Mo–C–N directions. It is now well established that such a view is oversimplified. The $^2E''_1$ SCF ground state may couple with SCF excited states of the same symmetry in which electrons have been promoted from the doubly-occupied and bonding e'_2 and a'_1 orbitals with a predominant cyano character to the empty and antibonding e'_2 and a'_1 orbitals with a predominant metal character. This configuration interaction gives rise to a negative spin density in the σ orbitals of the cyano ligands, along the Mo–C–N directions. This spin polarization effect has been experimentally observed in the hexacyanometallates involving 3d ions, such as $[Cr(CN)_6]^{3-}$ and $[Fe(CN)_6]^{3-}$, from polarized neutron diffraction experiments.[51,52]

The crucial point is that the stronger (*i.e.* the more covalent) the M–(CN) bond is, the more pronounced the spin polarization. Owing to the diffuseness of the 4d orbitals as compared to the 3d orbitals, the Mo^{III}–(CN) bond is significantly stronger than the Cr^{III}–(CN) or Fe^{III}–(CN) bond. It follows that the negative spin density along the Mo–C–N directions of the $Mo(CN)_7$ fragment might be particularly important. If it was so, the interaction between this negative spin density with a σ character and the σ singly occupied orbitals of Mn^{II} might favor the parallel alignment of the S_{Mo} and S_{Mn} spins.

If the interpretation above was correct, this would mean that the Mo^{III}–C–N–M interaction should be ferromagnetic for all M ions with unpaired electrons in σ (*i.e.* e_g in the case where M is in an octahedral environment) orbitals. All the data available so far confirm this idea.

What is the origin of the anisotropy?

Let us list the various factors affording magnetic anisotropy. We begin with the two local factors: the anisotropy of the ***g*** tensors and the zero-field splitting of the local spin states for the magnetic ions with a local spin higher than 1/2. In addition, there are several many-body (or collective) factors. These are: (i) the anisotropic interactions, resulting from the synergistic effect of the local spin–orbit coupling for an ion and the interaction between the excited states of this ion and the ground state of the adjacent ion; (ii) the antisymmetric interaction whose origin is similar to that of the anisotropic interaction, but in addition requires a low lattice symmetry; (iii) the dipolar interactions which may become important for lattices of low symmetry, and/or for high local spins (for instance $S_{Mn} = 5/2$); (iv) the shape anisotropy, finally, depending on the shape and size of the single crystals or particles utilized for the magnetic measurements.[38,53] Applying an external field H along the easy magnetization axis results in an internal field H_i related to H through:

$$H_i = H - NM$$

where N is the demagnetizing factor depending on the shape anisotropy, and NM the demagnetizing field. The field dependences of M shown in Fig. 6 are not corrected for the demagnetizing field.

Except when all the local spins are 1/2, the local zero-field splittings are usually more important than the anisotropic interactions. As for the antisymmetric interaction, it leads to spin canting, which may superimpose to both a ferromagnetic or an antiferromagnetic state. In this latter case, it gives rise to the phenomenon of weak ferromagnetism.[31]

What are the relevant factors in the case of the compounds described in this article? Mn^{II} in octahedral surroundings has a $^6A_1$ ground state, with a very weak zero-field splting. On the other hand, the ***g*** tensor for the $[Mo^{III}(CN)_7]$ chromophore is expected to be strongly anisotropic.[34] In other respects, the lattice symmetries are very low, even for the three-dimensional compounds. It follows that the two main anisotropy factors are the anisotropy of the ***g*** tensor for the $[Mo^{III}(CN)_7]$ chromophore along with the dipolar interactions. The spin reorientation might be due to a competition between these two factors. In zero (or low) external field, the ferromagnetically coupled local spins tend to align along the direction of the Mo–C–N–Mn–C–N

infinite linkages (for instance, the *b* axis for $Mn_2(H_2O)_5$-$Mo(CN)_7{\cdot}4H_2O$, α phase), which minimizes the dipolar energy. When the magnetic field reaches a certain value, the ***g*** anisotropy for Mo^{III} favors the spin alignment along another direction.

Conclusion

One of the peculiarities of molecular chemistry as compared to high-temperature solid state chemistry is that it usually affords species of low symmetry. In the field of molecule-based magnets, this low symmetry may lead to very interesting physical phenomena. Of course, the thorough investigation of these phenomena and their correct interpretation requires work on single crystals, which is time consuming and sometimes not trivial. However, accepting to do so may be very rewarding. To the best of our knowledge, the spin reorientation phenomenon had only been found so far for ferromagnetic intermetallic compounds, and not for insulating ferromagnets. In other respects, the magnetic phase diagrams of Fig. 7 and 11 are the very first for magnetic materials synthesized from molecular precursors.

The field of molecule-based magnets has many fascinating issues, such as strong coercivity, high critical temperature, processability, and photomagnetic effects.[54] The characterization of new phenomena arising from structural and magnetic anisotropies may be also considered as one of these issues.

Acknowledgements

This work was partly funded by the TMR Research Network ERBFMRXCT980181 of the European Union, entitled: Molecular Magnetism; from Materials toward Devices.

References

1 J. S. Miller, J. C. Calabrese, A. J. Epstein, R. W. Bigelow, J. H. Zang and W. M. Reiff, *J. Chem. Soc., Chem. Commun.*, 1986, 1026.
2 Y. Pei, M. Verdaguer, O. Kahn, J. Sletten and J.-P. Renard, *J. Am. Chem. Soc.*, 1986, **108**, 428.
3 J. S. Miller, J. C. Calabrese, H. Rommelman, S. R. Chittipedi, J. H. Zang, W. M. Reiff and A. J. Epstein, *J. Am. Chem. Soc.*, 1987, **109**, 769.
4 O. Kahn, Y. Pei, M. Verdaguer, J.-P. Renard and J. Sletten, *J. Am. Chem. Soc.*, 1988, **110**, 782.
5 A. Caneschi, D. Gatteschi, R. Sessoli and P. Rey, *Acc. Chem. Res.*, 1989, **22**, 392.
6 W. E. Broderick, J. A. Thompson, E. P. Day and B. M. Hoffman, *Science*, 1990, **249**, 410.
7 G. T. Yee, J. M. Manriquez, D. A. Dixon, R. S. McLean, D. M. Groski, R. B. Flippen, K. S. Narayan, A. J. Epstein and J. S. Miller, *Adv. Mater.*, 1991, **3**, 309.
8 Y. Nakazawa, M. Tamura, N. Shirakawa, D. Shiomi, M. Takahashi, M. Kinoshita and M. Ishikawa, *Phys. Rev. B*, 1992, **46**, 8906.
9 H. Tamaki, Z. J. Zhong, N. Matsumoto, S. Kida, S. Koikawa, S. Achiwa, Y. Hashimoto and H. Okawa, *J. Am. Chem. Soc.*, 1992, **114**, 6974.
10 R. Chiarelli, M. A. Nowak, A. Rassat and J.-L. Tholence, *Nature*, 1993, **363**, 147.
11 J. S. Miller and A. J. Epstein, *Angew. Chem., Int. Ed. Engl.*, 1994, **33**, 385.
12 D. Gatteschi, *Adv. Mater.*, 1994, **6**, 635.
13 K. Inoue and H. Iwamura, *J. Am. Chem. Soc.*, 1994, **116**, 3173.
14 S. Decurtins, H. W. Schmalle, H. R. Oswald, A. Linden, J. Ensling, P. Gütlich and A. Hauser, *Inorg. Chim. Acta*, 1994, **216**, 65.
15 S. Descurtins, H. W. Schmalle, P. Schneuwly, J. Ensling and P. Gütlich, *J. Am. Chem. Soc.*, 1994, **116**, 9521.
16 M. Ohba, N. Maruono and H. Okawa, *J. Am. Chem. Soc.*, 1994, **116**, 11566.
17 K. Inoue, T. Hayamizu, H. Iwamura, D. Hashizume and Y. Ohashi, *J. Am. Chem. Soc.*, 1996, **118**, 1803.
18 C. Mathonière, C. J. Nuttall, S. Carling and P. Day, *Inorg. Chem.*, 1996, **35**, 1201.
19 H. Iwamura, K. Inoue and N. Koga, *New J. Chem.*, 1998, **10**, 201.
20 H. O. Stumpf, L. Ouahab, Y. Pei, D. Grandjean and O. Kahn, *Science*, 1993, **261**, 447.
21 H. O. Stumpf, L. Ouahab, Y. Pei, P. Bergerat and O. Kahn, *J. Am. Chem. Soc.*, 1994, **116**, 3866.
22 M. G. F. Vaz, L. M. M. Pinheiro, H. O. Stumpf, A. F. C. Alcântara, S. Gohlen, L. Ouahab, O. Cador, C. Mathonière and O. Kahn, *Chem. Eur. J.*, in press.
23 S. Ferlay, T. Mallah, R. Ouahès, P. Veillet and M. Verdaguer, *Nature*, 1995, **378**, 701.
24 A. Ludi and H. Güdel, *Struct. Bonding* (*Berlin*), 1973, **14**, 1.
25 O. Kahn, *Adv. Inorg. Chem.*, 1995, **43**, 179.
26 D. Babel, *Comments Inorg. Chem.*, 1986, **5**, 285.
27 V. Gadet, T. Mallah, I. Castro and M. Verdaguer, *J. Am. Chem. Soc.*, 1992, **114**, 9213.
28 T. Mallah, S. Thiebaut, M. Verdaguer and P. Veillet, *Science*, 1993, **262**, 1554.
29 W. R. Entley and G. S. Girolami, *Inorg. Chem.*, 1994, **33**, 5165.
30 W. R. Entley and G. S. Girolami, *Science*, 1995, **268**, 397.
31 O. Kahn, *Molecular Magnetism*, VCH, New York, 1993.
32 O. Kahn, *Nature*, 1995, **378**, 667.
33 G. R. Rossman, F. D. Tsay and H. B. Gray, *Inorg. Chem.*, 1973, **12**, 824.
34 M. B. Hursthouse, K. M. A. Maijk, A. M. Soares, J. F. Gibson and W. P. Griffith, *Inorg. Chim. Acta*, 1980, **45**, L81.
35 R. C. Young, *J. Am. Chem. Soc.*, 1932, **54**, 1402.
36 J. Larionova, J. Sanchiz, S. Golhen, L. Ouahab and O. Kahn, *Chem. Commun.*, 1998, 953.
37 J. Larionova, R. Clérac, J. Sanchiz, O. Kahn, S. Golhen and L. Ouahab, *J. Am. Chem. Soc.*, 1998, **120**, 13088.
38 W. A. Wooster, *Tensor and Group Theory for the Physical Properties of Crystals*, Clarendon Press, Oxford, 1973.
39 A. K. Gregson and N. T. Noxon, *Inorg. Chem.*, 1982, **21**, 3464.
40 M. A. Salgueiro da Siva, J. M. Moreira, J. A. Mendes, V. S. Amaral, J. B. Sousa and S. B. Palmer, *J. Phys.: Condens. Mater.*, 1995, **7**, 9853.
41 B. Garcia-Landa, E. Tomey, D. Fruchart, D. Gignoux and R. Skolozdra, *J. Magn. Magn. Mater.*, 1996, **157–158**, 21.
42 W. A. Mendoza and S. A. Shaheen, *J. Appl. Phys.*, 1996, **79**, 6327.
43 G. Cao, S. McCall and J. E. Crow, *Phys. Rev. B*, 1997, **55**, R672.
44 X. C. Kou, M. Dahlgren, R. Grössinger and G. Wiesinger, *J. Appl. Phys.*, 1997, **81**, 4428.
45 J. Larionova, O. Kahn, S. Golhen, L. Ouahab and R. Clérac, *Inorg. Chem.*, in press.
46 J. Larionova, O. Kahn, S. Gohlen, L. Ouahab and R. Clérac, *J. Am. Chem. Soc.*, in press.
47 F. Palacio, F. J. Lazaro and A. J. Duyneveldt, *Mol. Cryst. Liq. Cryst.*, 1989, **176**, 289.
48 X. C. Kou, R. Grössinger, G. Hischer and H. R. Kirchmayr, *Phys. Rev. B*, 1996, **54**, 6421.
49 C. Kollmar and O. Kahn, *Acc. Chem. Res.*, 1993, **26**, 259.
50 H. M. McConnell, *J. Chem. Phys.*, 1963, **39**, 1910.
51 B. N. Figgis, J. B. Forsyth and P. A. Reynolds, *Inorg. Chem.*, 1987, **26**, 101.
52 B. N. Figgis, E. S. Kucharski and M. Vrtis, *J. Am. Chem. Soc.*, 1993, **115**, 176.
53 A. Bencini and D. Gatteschi, *EPR of Exchange Coupled Systems*, Springer-Verlag, Berlin, Germany, 1989.
54 O. Sato, T. Iyoda, A. Fujishima and K. Hashimoto, *Science*, 1996, **272**, 704.

Paper 9/00180H

Synthesis and reactivity of the osmium methylidene complex $[(C_5Me_5)Os(=CH_2)(dppm)][OTf]$

Julia L. Brumaghim and Gregory S. Girolami*

School of Chemical Sciences, University of Illinois at Urbana-Champaign, 600 South Mathews Avenue, Urbana, Illinois 61801. E-mail: girolami@scs.uiuc.edu

Received (in Bloomington, IN, USA) 26th February 1999, Accepted 12th April 1999

Treatment of the hydride complex $(C_5Me_5)Os(dppm)H$, [dppm = bis(diphenylphosphino)methane] with 2 equivalents of methyl trifluoromethanesulfonate (MeOTf) affords the methylidene complex $[(C_5Me_5)Os(=CH_2)(dppm)][OTf]$; the molecular structure and dynamic NMR behavior of this methylidene complex are described.

Transition metal alkylidenes have been of interest for the last 20 years owing to their role as intermediates in olefin metathesis[1–7] and Fischer–Tropsch[8] reactions. In most cases, the alkylidene ligand is substituted; in contrast, there are relatively few examples of the simplest alkylidene, a terminal methylidene ($=CH_2$) ligand. In 1975, Schrock described the first such complex, $Cp_2Ta(=CH_2)(CH_3)$,[9] and the number of complexes containing a terminal methylidene ligand has slowly grown since.[1,10–19]

Most terminal methylidene complexes have been synthesized by one of two routes: by abstraction of a hydride from a methyl group, or by abstraction of a proton from a cationic methyl compound.[13] We now describe the synthesis of an osmium methylidene complex from the reaction of an osmium hydride with methyl trifluoromethanesulfonate (MeOTf).

Treatment of $(C_5Me_5)Os(dppm)H$[20] with 2 equivalents of MeOTf in pentane at room temperature for 18 h affords a yellow powder, which has been identified as the new methylidene compound $[(C_5Me_5)Os(=CH_2)(dppm)][OTf]$ **1**.† The ^1H NMR spectrum of **1** at −30 °C shows that the two hydrogen atoms of the methylidene ligand are inequivalent. In the ^{13}C NMR spectrum of **1**, the methylidene carbon gives rise to a triplet at δ 261.9 (J_{CH} 144 Hz). The inequivalence of the hydrogen atoms is a result of the preferred orientation of the methylidene ligand, which places one hydrogen atom proximal to, and the other distal from, the C_5Me_5 ligand. The same orientation is seen for the methylidene ligands in other $[(C_5R_5)M(=CH_2)L_2]^{n+}$ complexes.[15,17,18]

As the temperature is raised, the methylidene signals in the ^1H NMR spectrum broaden and finally coalesce at 60 °C as rotation of the methylidene ligand around the Os=C bond becomes fast on the NMR time scale. The variable-temperature ^1H NMR line shapes and the simulations of the spectra are shown in Fig. 1. An Eyring plot showed that the activation parameters for rotation of the methylidene ligand in **1** are $\Delta H^{\ddagger}$ = 16.4 ± 0.5 kcal mol^{-1} and $\Delta S^{\ddagger}$ = 5.7 ± 1.5 cal mol^{-1} K^{-1}; the free energy of activation is 14.7 ± 0.5 kcal mol^{-1} at 25 °C.

The rotation barrier is a measure of how much the π bonding is weakened upon rotating the methylidene ligand by 90° about the M=C axis. Somewhat surprisingly, the activation entropies and enthalpies of rotation have never been measured for any terminal methylidene complex.[15,17,18] For four molecules, however the free energies of activation have been reported: 8.3 ± 0.1 kcal mol^{-1} at −85 °C for $[(C_5Me_5)W(=CH_2)(PPh_3)(CO)_2][AsF_6]$,[15] 9.0 ± 0.1 kcal mol^{-1} at −70 °C for $[(C_5Me_5)W(=CH_2)(PEt_3)(CO)_2][AsF_6]$,[15] 10.7 ± 0.2 kcal mol^{-1} at −28 °C for $[(C_5Me_5)Fe(=CH_2)(dppe)][BF_4]$,[18] and ≥ 19 kcal mol^{-1} at 114 °C for $[(C_5Me_5)Re(=CH_2)(NO)(PPh_3)][PF_6]$.[17]

An X-ray crystallographic study‡ of **1** revealed that the Os–C distance for the methylidene ligand is 1.926(9) Å (Fig. 2). This value is comparable to the M=C bond distances seen for other late transition metal methylidene complexes: 1.87(1) Å in $Ir(=CH_2)[N(SiMe_2CH_2PPh_2)_2]$,[11] 1.90(2) Å in $[(C_5Me_5)Re(=CH_2)(NO)\{P(OPh)_3\}]^+$,[17] and 1.92(1) Å in $Os(=CH_2)(PPh_3)(NO)Cl$.[14]

Like other cationic methylidene complexes,[14] the methylidene complex **1** is susceptible to attack by nucleophiles. Thus, treatment of **1** with $LiBH_4$ yields the corresponding methyl complex, $(C_5Me_5)Os(dppm)CH_3$.§

At least two mechanisms could account for the formation of **1** upon treatment of $(C_5Me_5)Os(dppm)H$ with MeOTf. In one mechanism [eqn. (1)], an osmium methyl/hydride intermediate is generated initially, and dihydrogen is lost to form **1**.

$$L_nOs{-}H \xrightarrow{CH_3^+} L_nOs^{+}(H)(CH_3) \xrightarrow{-H_2} L_nOs{=}CH_2^+ \quad (1)$$

In another mechanism [eqn. (2)], the osmium methyl/hydride intermediate undergoes reductive elimination of methane;

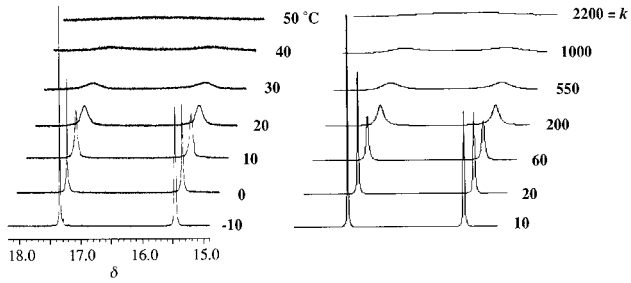

Fig. 1 Variable temperature 500 MHz ^1H NMR line shape for the methylidene protons in **1** (thf-d_8, left) and simulated spectra (right). Rate constants are given in s^{-1}.

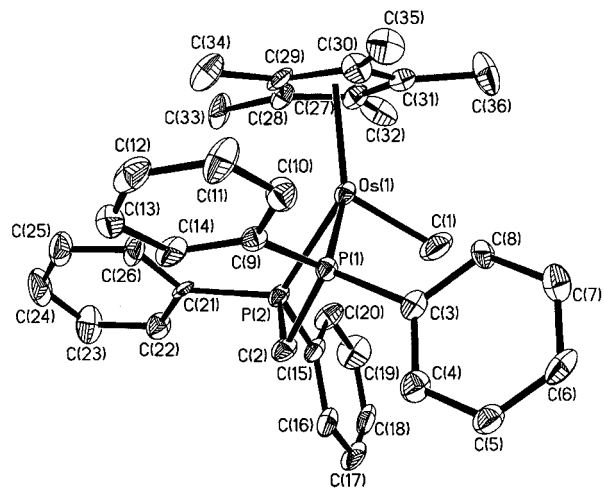

Fig. 2 Crystal structure of $[(C_5Me_5)Os(=CH_2)(dppm)][OTf]$, molecule 1; 35% probability density surfaces are shown. The hydrogen atoms and triflate anion are omitted for clarity.

attack by a second equivalent of MeOTf followed by loss of a proton affords **1**.

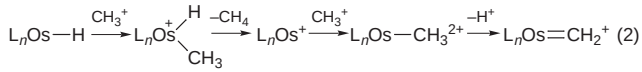

In both of these mechanisms, the first step is formation of an osmium methyl/hydride cation. This step has precedence in our study of the analogous $(C_5Me_5)Os(dmpm)H$ system [dmpm = bis(dimethylphosphino)methane].[21] The mechanism responsible for the formation of **1** was determined by following the reaction of $(C_5Me_5)Os(dppm)H$ with MeOTf in a sealed NMR tube. As judged by ^1H NMR spectroscopy, no dihydrogen is generated, but a peak attributable to methane (δ 0.11) grows in during the course of the reaction. On a preparatory scale, if $(C_5Me_5)Os(dppm)H$ and MeOTf are allowed to react for only 1 h in pentane, the triflate complex $(C_5Me_5)Os(dppm)OTf$ can be isolated.¶ Subsequent treatment of isolated samples of $(C_5Me_5)Os(dppm)OTf$ with additional MeOTf affords **1** in high yield. These results suggest that **1** is generated by the second of the two mechanisms shown above.

Further studies of these new osmium complexes are in progress.

We thank the Department of Energy (Grant DEFG02-96-ER45439) for support of this work, and the University of Illinois School of Chemical Sciences for a departmental fellowship to J. L. B. NMR spectra were collected on instruments in the Varian Oxford Instrument Center for Excellence at the University of Illinois at Urbana-Champaign; external funding for this instrumentation was obtained from the Keck Foundation, NIH, and NSF.

Notes and references

† *Selected spectroscopic data* for **1**: MS(FD); *m/z* 725[M^+]. ^1H NMR (thf-d_8, −30 °C): δ 15.49 (td, $^3J_{HP}$ 6.5, $^1J_{HH}$ 1.2 Hz, Os=CH_2), 17.36 (d, $^1J_{HH}$ 1.2 Hz, Os=CH_2). $^{13}C\{^1H\}$ NMR (CD_2Cl_2, −30 °C): δ 261.9 (s, Os=CH_2). ^{19}F NMR (thf-d_8, 25 °C): δ −80.0 (CF_3). $^{31}P\{^1H\}$ NMR (thf-d_8, 25 °C): δ −37.7 (s).

‡ *Crystal data* for **1** at 198 K: monoclinic, space group $P2_1/n$, with a = 11.5525(10), b = 50.217(4), c = 18.410(2) Å, β = 96.866(2)°, V = 10603(2) Å^3, Z = 12, R_1 (obs. data) = 0.0754, wR_2 (all data) = 0.2182 for 1078 parameters and 101 restraints refined against 18671 unique data. The crystal chosen was grown from diethyl ether by treating $(C_5Me_5)Os(dppm)H$ with MeOTf; we have not been able to grow crystals from other solvents. Under these conditions, the crystals obtained were a mixture of **1** with a second compound, the ethylene complex $[(C_5Me_5)Os(dppm)(C_2H_4)][OTf]$, which was evidently generated by alkyl exchange between the diethyl ether solvent and the MeOTf reagent. There are three molecules in the asymmetric unit, but one of these sites is occupied exclusively by the Os=CH_2 complex. The metric parameters discussed in the text are for this molecule. The presence of the ethylene complex in the sample was confirmed by NMR spectroscopy and by mass spectrometry. CCDC 182/1226.

§ *Selected spectroscopic data* for $(C_5Me_5)Os(dppm)Me$: MS(FD): *m/z* 726[M^+]. ^1H NMR (C_6D_6, 25 °C): δ 0.30 (t, J_{HP} 7.9 Hz, Os–CH_3). $^{13}C\{^1H\}$ NMR (C_6D_6, 25 °C): δ −26.8 (t, J_{CP} 8.6 Hz, Os–CH_3). $^{31}P\{^1H\}$ NMR (C_6D_6, 25 °C): δ −32.6 (s).

¶ *Selected spectroscopic data* for $(C_5Me_5)Os(dppm)(OTf)$: MS(FD): *m/z* 860[M^+]. ^{19}F NMR (C_6D_6, 25 °C): δ −80.0 (s, CF_3). $^{31}P\{^1H\}$ NMR (C_6D_6, 25 °C): δ −31.0 (s).

1 P. Schwab, R. H. Grubbs and J. W. Ziller, *J. Am. Chem. Soc.*, 1996, **118**, 100.
2 V. Dragutan, A. T. Balban and M. Dimonie, *Olefin Metathesis and Ring-Opening Polymerization of Cyclo-Olefins*, Wiley, New York, 1985.
3 W. J. Feast, *The Chemistry of the Metal Carbon Bond*, Wiley, New York, 1989, vol. 5.
4 R. H. Grubbs and W. Tumas, *Science*, 1989, **243**, 907.
5 K. J. Ivin, *Olefin Metathesis*, Academic Press, New York, 1983.
6 C. Pariya and K. N. Jayaprakash, *Coord. Chem. Rev.*, 1998, **168**, 1.
7 R. R. Schrock, *Acc. Chem. Res.*, 1990, **23**, 158.
8 H. Werner, A. Kletzin, P. W. Höhn, W. Knaup, M. L. Ziegler and O. Serhadli, *J. Organomet. Chem.*, 1986, **306**, 227.
9 R. R. Schrock, *J. Am. Chem. Soc.*, 1975, **97**, 6577.
10 A. K. Burrell, G. R. Clark, C. E. F. Rickard, W. R. Roper and A. H. Wright, *J. Chem. Soc., Dalton Trans.*, 1991, 609.
11 M. D. Fryzuk, X. Gao, K. Joshi, P. A. MacNeil and R. L. Massey, *J. Am. Chem. Soc.*, 1993, **115**, 10 581.
12 T. B. Gunnoe, P. S. White, J. L. Templeton and L. Casarrubios, *J. Am. Chem. Soc.*, 1997, **119**, 3171.
13 D. M. Heinekey and C. E. Radzewich, *Organometallics*, 1998, **17**, 51.
14 A. Hill, W. R. Roper, J. M. Waters and A. H. Wright, *J. Am. Chem. Soc.*, 1983, **105**, 5939.
15 S. E. Kegley, M. Brookhart and G. R. Husk, *Organometallics*, 1982, **1**, 760.
16 M. Oliván and K. G. Caulton, *J. Chem. Soc., Chem. Commun.*, 1997, 1733.
17 A. T. Patton, C. E. Strouse, C. B. Knobler and J. A. Gladysz, *J. Am. Chem. Soc.*, 1983, **105**, 5804.
18 C. Roger and C. Lapinte, *J. Chem. Soc., Chem. Commun.*, 1989, 1598.
19 L. G. Chamberlain, I. P. Rothwell and J. C. Huffman, *J. Am. Chem. Soc.*, 1986, **108**, 1502.
20 C. L. Gross and G. S. Girolami, *Organometallics*, 1996, **15**, 5359.
21 C. L. Gross and G. S. Girolami, *J. Am. Chem. Soc.*, 1998, **120**, 6605.

Communication 9/01644I

Selective synthesis of monohydrosilanes by the reactions of organoytterbium iodides with dihydrosilanes

Wu-Song Jin, Yoshikazu Makioka, Tsugio Kitamura and Yuzo Fujiwara*

Department of Chemistry and Biochemistry, Graduate School of Engineering, Kyushu University, 6-10-1 Hakozaki, Higashiku, Fukuoka 812-8581, Japan. E-mail: yfujitcf@mbox.nc.kyushu-u.ac.jp

Received (in Cambridge, UK) 22nd February 1999, Accepted 12th April 1999

Monohydrosilanes can be prepared selectively in high yields from the reaction of various aryl and alkyl iodides with ytterbium metal followed by the reaction with dihydrosilanes.

Recently, lanthanoid complexes with the pentamethylcyclopentadienyl ligand and its analogues have been reported to catalyze the hydrosilylation reactions of alkenes and alkynes, as well as cyclization/silylation and polymerization of silanes.[1,2] Marks and coworkers and others reported that the reactions of $Cp^*_2LnCH(SiMe_3)_2$ (Cp^* = C_5Me_5, Ln = La, Nd, Sm) with $PhSiH_3$ gave $CH_2(SiMe_3)_2$, while $Cp^*_2YMe(THF)$ converted $PhSiH_3$ to $PhMeSiH_2$.[2] However, applications of lanthanoid complexes to direct alkylation or arylation of silanes are still limited. Evans *et al.* reported the synthesis of divalent organolanthanoid σ-complexes (RLnI) from organic iodides and lanthanoid metals in THF.[3] We have explored the chemistry of RLnI and found some unique reactivity toward various electrophiles.[4] In our continuing study on the organolanthanoid chemistry, we have found that the monohydrosilanes can be prepared selectively from the reaction of excess divalent organoytterbium σ-complexes (RYbI) with dihydrosilanes [eqn. (1)]. Here, we report these results.

$$\mathrm{RI} + \mathrm{Yb} \xrightarrow[\mathrm{THF}]{} \mathrm{RYbI} \xrightarrow{\mathrm{R'R''SiH_2}} \mathrm{R'R''RSiH} \qquad (1)$$

First, we studied the reaction of various arylytterbium σ-complexes (ArYbI) with dihydrosilanes [eqn. (2)] and results are summarized in Table 1.

As shown in entry 1 in Table 1, when the reaction was carried out using an equimolar amount of iodobenzene **1a**, Yb metal and $MePhSiH_2$ **2a**, the monosilane **3a** was formed only in 64% yield. However, when the ratio of **1a** and Yb to **2a** was doubled, **3a** was obtained quantitatively (entry 2). Most of the substrates **1a**–**g** and **1i**–**m** (entries 2–15 and 17–26) reacted smoothly with ytterbium metal to produce arylytterbium iodides, and successive treatment with dihydrosilanes gave selectively monohydrosilanes **3a**–**g**, **3a′**–**g′** and **3i**–**m′** in high yields. For *o*-chloroiodobenzene **1h** (entry 16), many by-products were formed, and the isolation of the desired product **3h** was unsuccessful. Under the present conditions, arylytterbium iodides displayed high reactivity toward not only methylphenylsilane but also diphenylsilane. In addition, dimers of silanes were not formed in this reaction.[5]

On the other hand, different results were obtained in the reaction of aliphatic iodides [eqn. (3)] as shown in Table 2. Primary alkyl iodides such as 1-iodoethane, 1-iodoheptane and isobutyl iodides (**1n**–**p**) proceeded smoothly to afford monohydrosilanes **3n**–**p** in high yields (entries 15–17). By contrast, for bulky **1q**, the yield of **3q** was low (entry 4). In the reactions of secondary and tertiary iodides **1r**–**t**, the reaction proceeded slowly to give small amounts of the monosilanes **3r**–**t**. These results indicate that steric factors of the substrates plays an important role in the reaction. It seems curious that no reaction occurs with α-methoxy-substituted **1u** although Yb metal reacts with **1u** to form $(MeOCH_2)YbI$ (entry 8).

In similar reactions of Grignard reagents and organolithiums, the former give monosubstituted silanes in low yields even

Table 1 Reaction of arylytterbium(II) iodides with dihydrolsilane **2a** and **2a′**[a]

$$\underset{\mathbf{1}}{\mathrm{ArI}} + \mathrm{Yb} \xrightarrow[\mathrm{THF}]{} \xrightarrow[\text{room temp.}]{\substack{\mathrm{RPhSiH_2}\\ \mathbf{2a}\text{: R = Me}\\ \mathbf{2a'}\text{: R = Ph}}} \underset{\mathbf{3}}{\mathrm{ArRPhSiH}} \qquad (2)$$

Entry	Substrate	Ar	Dihydrosilane	*t*/h	Product	Yield(%)[b]
1	**1a**	Ph	**2a**	8	**3a**	64[c]
2		Ph	**2a**	2	**3a**	> 99
3			**2a′**	1	**3a′**	99
4	**1b**	*o*-$MeOC_6H_4$	**2a**	2	**3b**	97
5			**2a′**	8	**3b′**	96
6	**1c**	*m*-$MeOC_6H_4$	**2a**	1	**3c**	> 99
7			**2a′**	2	**3c′**	95
8	**1d**	*p*-$MeOC_6H_4$	**2a**	8	**3d**	93
9			**2a′**	4	**3d′**	78
10	**1e**	*o*-MeC_6H_4	**2a**	1	**3e**	99
11			**2a′**	2	**3e′**	> 99
12	**1f**	*m*-MeC_6H_4	**2a**	2	**3f**	> 99
13			**2a′**	1	**3f′**	> 99
14	**1g**	*p*-MeC_6H_4	**2a**	1	**3g**	> 99
15			**2a′**	2	**3g′**	98
16	**1h**	*o*-ClC_6H_4	**2a**	8	**3h**	—[d]
17	**1i**	*m*-ClC_6H_4	**2a**	4	**3i**	92
18			**2a′**	8	**3i′**	80
19	**1j**	*p*-ClC_6H_4	**2a**	2	**3j**	> 99
20			**2a′**	4	**3j′**	89
21	**1k**	*o*-$CF_3C_6H_4$	**2a**	8	**3k**	> 99
22			**2a′**	4	**3k′**	> 99
23	**1l**	α-Naphthyl	**2a**	2	**3l**	> 99
24			**2a′**	1	**3l′**	97
25	**1m**	2-Thienyl	**2a**	4	**3m**	> 99
26			**2a′**	4	**3m′**	> 99

[a] See footnote † for reaction conditions. [b] GC yield based on **2a** and **2a′**. [c] Yb:RI:$MePhSiH_2$ = 1:1:1 and unreacted $MePhSiH_2$ recovered. [d] Complex mixture obtained.

Table 2 Reaction of alkylytterbium(II) iodides with methylphenylsilane **2a**[a]

$$\underset{\mathbf{1}}{\mathrm{RI}} + \mathrm{Yb} \xrightarrow[\mathrm{THF}]{} \xrightarrow[\text{room temp.}]{\mathbf{2a}} \underset{\mathbf{3}}{\mathrm{RPhSiMeH}} \qquad (3)$$

Entry	Substrate	R	*t*/h	Product	Yield(%)[b]
1	**1n**	Et	8	**3n**	> 99
2	**1o**	*n*-C_7H_{15}	8	**3o**	89
3	**1p**	Bu^i	8	**3p**	> 99
4	**1q**	Bu^tCH_2	24	**3q**	50
5	**1r**	Pr^i	4	**3r**	10[c]
6	**1s**	$^cC_6H_{11}$	8	**3s**	18
7	**1t**	Bu^t	72	**3t**	Trace
8	**1u**	$MeOCH_2$	72	**3u**	—[d]

[a] See notes as to the other reaction conditions. [b] GC yield based on **2a**. [c] Isolated yield. [d] Methylphenylsilane recovered.

under refluxing conditions,[6] while the latter afford tetra-substituted silanes rather than monosubstituted silanes.[7] By contrast, the present reaction of organoytterbium iodides with dihydrosilanes proceeds smoothly under mild conditions and gives monosubstituted silanes exclusively. Thus this reaction should be a useful method for the synthesis of mono-hydrosilanes.

In conclusion, we have demonstrated that monohydrosilanes can be prepared selectively and conveniently from the reaction of dihydrosilanes with excess divalent organoytterbium σ-complexes under mild conditions.

The present work was supported in part by a Grant-in-Aid for Scientific Research on Priority Areas No. 283, 'Innovative Synthetic Reaction' from Monbusho. Y. M. gratefully acknowledges the Japan Society for the Promotion of Science for its financial support.

Notes and references

† *Typical reaction procedure*: Yb metal (173 mg, 1.0 mmol) was placed in a 50 ml Schlenk tube. Then, THF (4.0 ml) and *p*-iodoanisole (234 mg, 1.0 mmol) were successively added at 0 °C under argon and the mixture stirred for 30 min at this temperature to give a red–brown solution of the ArYbI complex. Then, methylphenylsilane (61 mg, 0.5 mmol) was added. The mixture was then heated to room temperature and stirred for 4 h. Usual workup followed by a silica gel column chromatography (*n*-hexane–benzene) gave *p*-anisylmethylphenylsilane **3d** in 79% (90 mg) yield. The GC yields were determined using *n*-tetradecane, *n*-nonadecane and *n*-eicosane for aromatic iodides, 1-iodonaphthalene and aliphatic ioidides, respectively, as an internal standard. Yields are based on dihydrosilanes.

1 T. Sakakura, H.-J. Lautenschlager and M. Tanaka, *J. Chem. Soc., Chem. Commun.*, 1991, 40; T. Kobayashi, T. Sakakura, T. Hayashi, M. Yumura and M. Tanaka, *Chem. Lett.*, 1992, 1157; S. Onozawa, T. Sakakura and M. Tanaka, *Tetrahedron Lett.*, 1994, **35**, 8177; G. A. Molander and W. H. Retsch, *Organometallics*, 1995, **14**, 4570; G. A. Molander and W. H. Retsch, *J. Am. Chem. Soc.*, 1997, **119**, 8817; G. A. Molander and E. D. Dowdy, *J. Org. Chem.*, 1998, **63**, 3386; G. A. Molander and C. P. Corrette, *Organometallics*, 1998, **17**, 5504.

2 C. M. Forsyth, S. P. Nolan and T. J. Marks, *Organometallics*, 1991, **10**, 2543; N. S. Radu and T. D. Tilley, *J. Am. Chem. Soc.*, 1992, **114**, 8293; P.-F. Fu, L. Brard, Y. Li and T. J. Marks, *J. Am. Chem. Soc.*, 1995, **117**, 7157; N. S. Radu, F. J. Hollander, T. D. Tilley and A. L. Rheingold, *Chem. Commun.*, 1996, 2459.

3 D. F. Evans, G. V. Fazakerley and R. F. Phillips, *Chem. Commun.*, 1970, 244; D. F. Evans, G. V. Fazakerley and R. F. Phillips, *J. Chem. Soc. A*, 1971, 1931.

4 T. Fukagawa, Y. Fujiwara, K. Yokoo and H. Taniguchi, *Chem. Lett.*, 1981, 1771; T. Fukagawa, Y. Fujiwara and H. Taniguchi, *Chem. Lett.*, 1982, 601; K. Yokoo, Y. Yamanaka, T. Fukagawa, H. Taniguchi and Y. Fujiwara, *Chem. Lett.*, 1983, 1301; K. Yokoo, Y. Fujiwara, T. Fukagawa and H. Taniguchi, *Polyhedron*, 1983, **2**, 1101; K. Yokoo, T. Fukagawa, Y. Yamanaka, H. Taniguchi and Y. Fujiwara, *J. Org. Chem.*, 1984, **49**, 3237; K. Yokoo, Y. Kijima, Y. Fujiwara and H. Taniguchi, *Chem. Lett.*, 1984, 1321; K. Yokoo, N. Mine, H. Taniguchi and Y. Fujiwara, *J. Organomet. Chem.*, 1985, **279**, C19; Z. Hou, N. Mine, Y. Fujiwara and H. Taniguchi, *J. Chem. Soc., Chem. Commun.*, 1985, 1700; N. Mine, Y. Fujiwara and H. Taniguchi, *Chem. Lett.*, 1986, 357; Z. Hou, H. Taniguchi and Y. Fujiwara, *Chem. Lett.*, 1987, 305; Z. Hou, Y. Fujiwara, T. Jintoku, N. Mine, K. Yokoo and H. Tanguchi, *J. Org. Chem.*, 1987, **52**, 3524.

5 Probably, the reaction would proceed *via* a four-centered transition state, which implies hydride transfer to ytterbium atom.

6 H. Gilman and E. A. Zuech, *J. Am. Chem. Soc.*, 1957, **79**, 4560.

7 W. H. Nebergall, *J. Am. Chem. Soc.*, 1950, **72**, 4702; J. S. Peake, W. H. Nebergall and Y. T. Chen, *J. Am. Chem. Soc.*, 1952, **74**, 1526.

Communication 9/01434I

Transparent colloidal solution of 2 nm ceria particles

Masashi Inoue,* Minoru Kimura and Tomoyuki Inui

Department of Energy and Hydrocarbon Chemistry, Graduate School of Engineering, Kyoto University, Yoshida, Kyoto 606-8501 Japan. E-mail: inoue@scl.kyoto-u.ac.jp

Received (in Cambridge, UK) 3rd February 1999, Accepted 20th April 1999

The reaction of cerium metal in 2-methoxyethanol at 200–250 °C yielded a transparent colloidal solution of ultrafine (2 nm size) ceria particles.

Hydrothermal oxidation of metals has been widely examined as a synthesis route for inorganic materials and various compounds having specific properties have been prepared.[1,2] Although it is known that some metals corrode in alcohols, oxidation of metals in alcohols has never been examined from the viewpoint of material synthesis until our recent report that the reaction of aluminium metal in alcohols at 250–300 °C yielded alkoxyalumoxanes.[3] As an extension, we applied this method to cerium metal and found that a transparent colloidal solution of ultrafine ceria particles was directly obtained by the reaction of cerium metal in 2-methoxyethanol at 200–300 °C.

Cerium metal chips [*ca.* 2.40 g; 0.2 mm × 3.5 mm × (3–5) mm] and 2-methoxyethanol (85 mL) were placed in a test tube, which was then set in an autoclave (200 mL). An additional 20 mL of 2-methoxyethanol was placed in the gap between the test tube and the autoclave wall. The autoclave was completely purged with nitrogen and heated to 250 °C at a rate of 2.3 °C min^{-1} and kept at that temperature for 2 h. After the assembly was cooled, the product mixture was centrifuged and yellow precipitates and a dark brown transparent solution were obtained. The XRD pattern of the precipitates showed characteristic peaks of ceria, and the crystallite size of the precipitates, calculated by the X-ray diffraction (XRD) line broadening technique, was > 100 nm. The precipitates are postulated to derive from the ceria surface layer of the cerium metal chips, because the properties of the precipitates were not altered by the reaction conditions.

Addition of distilled water to the transparent solution obtained as the supernatant after centrifugation of the product did not lead to any change except for dilution of the color of the solution. When the solution was kept standing for several weeks with gradual evaporation of the solvent, gelation took place liberating a small amount of a colorless supernatant, and the gel gradually shrank while remaining transparent. On the other hand, when the solution was kept in a closed bottle, it was stable for at least several months. Addition of salt solutions such as aqueous NaCl to the transparent solution immediately caused the formation of gelatinous precipitates.

Transmission electron microscopic observation of a specimen prepared by dipping a microgrid into the diluted solution followed by drying in air revealed that ultrafine particles of size 1.5–2 nm formed a thin film on the microgrid, which is believed to arise from agglomeration at the drying stage owing to the large surface energy of the particles. Electron diffraction of the film gave diffuse 111, 200, 220, 311 Debye–Scherrer rings of cubic ceria with the fluorite structure.[4] These results indicate that the dark brown transparent solution is a colloidal solution of ultrafine particles of ceria.

The colloidal particles were coagulated by addition of methanol and aqueous NH_3 to the colloidal solution. The use of NaCl solution was avoided because of possible effects of the remaining salt on the properties of the particles. The precipitates were separated from a slightly turbid supernatant by centrifugation, washed with methanol, and then air-dried. The yellow powder obtained exhibited fairly broad XRD peaks (Fig. 1);

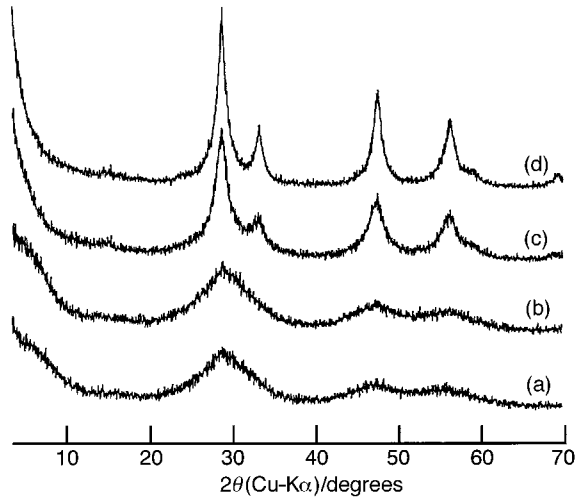

Fig. 1 XRD patterns of the powders collected from the colloidal solutions prepared by the reaction of cerium metal in 2-methoxyethanol at: (a) 200, (b) 250, (c) 280 and (d) 300 °C.

however, the peak positions were identical to the three strongest lines for cubic ceria. The crystallite size of the powder was calculated to be *ca.* 2 nm, which was essentially identical with the particle size observed by TEM, suggesting that each particle observed by TEM is a single crystal of ceria.

Various methods have been reported for the synthesis of ultrafine ceria particles.[5–13] However, as far as we are aware, the smallest particle size of ceria prepared so far is 2.6 nm, prepared by Masui *et al.*[12] using reversed micelles. Note that the reduction of particle size from 2.6 to 2 nm corresponds to the reduction of number of cerium atoms in a particle by a half and

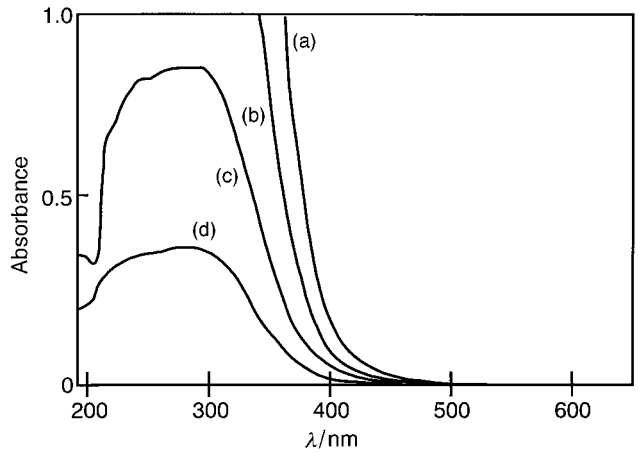

Fig. 2 Electronic spectra of the colloidal solution of ultrafine ceria particles. The original colloidal solution was obtained by the reaction of cerium metal in 2-methoxyethanol at 250 °C for 2 h, and the solution was diluted with 2-methoxyethanol to a concentration of (a) 0.172, (b) 0.086, (c) 0.043 and (d) 0.017 g L^{-1}.

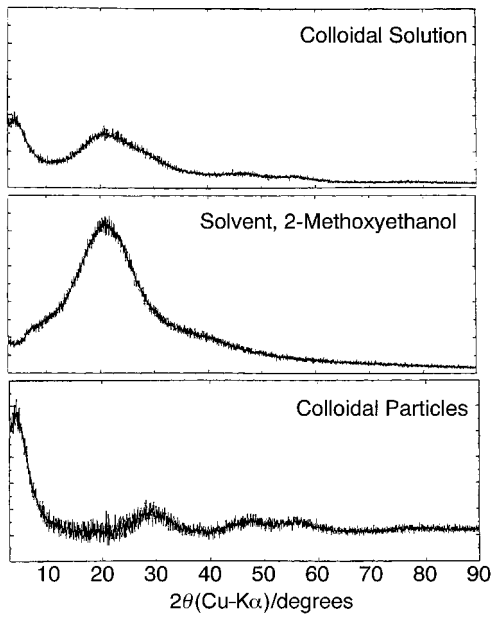

Fig. 3 XRD pattern of the ceria colloidal particles in the transparent solution (bottom) calculated by subtraction of the XRD pattern of the solvent, 2-methoxyethanol, (middle) from that of the colloidal solution (top). The XRD patterns were recorded on a Rigaku Rint-Ultima$^+$ diffractometer equipped with a θ–θ goniometer.

that a spherical ceria particle with a diameter of 2 nm contains only 100 cerium atoms.

The reaction proceeded at as low as 200 °C yielding a transparent solution, but the particle size of the ceria colloid was not decreased (Fig. 1). On the other hand, increase in the reaction temperature above 250 °C progressively increased the crystallite size of the ceria particles (8 nm by the reaction at 300 °C).

When the particles were calcined, the XRD peaks gradually sharpened, but no phases other than ceria were detected in the calcined samples. Crystal growth took place after calcination at 450 °C, *i.e.* at a much lower temperature than the lowest crystal growth temperature of 'reactive' 15.5 nm ceria powders prepared by the hydrazine method.[11]

Electronic spectra of the diluted colloidal solutions (Fig. 2) exhibited a strong absorption band at the UV region, whereas no absorption was detected above 500 nm. The observed absorbance followed Lambert–Beer's law, suggesting that the ultrafine ceria particles are well dispersed with no evidence for agglomeration under the concentrations of the UV measurement. The bandgap energies, E_i and E_d, for the ceria particles were calculated from these spectra to be 2.90 and 3.52 eV (1 eV $= 1.602 \times 10^{-19}$ J), respectively. These values were larger than those reported for the 2.6 nm ceria particles,[12] owing to the quantum size effect, although slightly larger values have been reported for ceria films.[14–16]

To ensure that the ultrafine ceria particles were not originated by any stages of the work-up process, XRD of the colloidal solutions was examined (Fig. 3). The XRD patterns of the colloidal particles, calculated by subtracting the XRD pattern of the solvent, 2-methoxyethanol, from that of the colloidal solutions, coincided with those for the particles obtained after coagulation. Therefore, it was concluded that the ultrafine ceria particles are actually present in the solution.

The present work was supported by a Grant-in-Aid for Scientific Research No. 09650922, from The Ministry of Education, Science, Sports and Culture, Japan. The authors also thank Dr T. Kubo of Osaka Application Laboratory, Rigaku Corporation for the XRD measurement of the colloidal solutions.

Notes and references

1 K. Torkar, H. Worel and H. Krischner, *Monatsh. Chem.*, 1960, **91**, 653: K. Torkar and H. Krischner, *ibid*., 1960, **91**, 658; 1960, **91**, 757; 1960, **91**, 764.
2 M. Yoshimura and S. Somiya, *Am. Ceram. Soc., Bull*., 1980, **59**, 246: H. Toraya, M. Yoshimura and S, Somiya, *J. Am. Ceram. Soc*., 1982, **65**, C-72.
3 M. Inoue, M. Kimura and T. Inui, *Proceedings of 9th Cimtec-World Ceramic Congress 'Ceramics: Getting into the 2000's'*, Part D, Ed. P. Vincenzini, Techna, Faenza, Italy, 1999, p. 593.
4 Joint Committee of Powder Diffraction Standards, Card No. 4-593.
5 Y. C. Zhou and M. N. Rahaman, *J. Mater. Res.*, 1993, **8**, 1680.
6 A. Tschöpe, W. Liu, M. Flytzani-Stephanopoulos and J. Y. Ying, *J. Catal*., 1995, **157**, 42.
7 Y. Zhou, R. J. Phillips and J. A. Switzer, *J. Am. Ceram. Soc*., 1995, **78**, 981.
8 W. Chengyun, Q. Yitai, X. Yi, W. Changsui, Y. Li and Z. Guiwen, *Meter. Sci. Eng. B*, 1996, **39**, 160.
9 J. Herrmann, C. Hoang-Van, L. Dibansa and R. Harivololona, *J. Catal.*, 1996, **159**, 361.
10 M. Hirano and E. Kato, *J. Am. Ceram. Soc*., 1996, **79**, 777.
11 S. Nakane, T. Tachi, M. Yoshinaka, K. Hirota and O. Yamaguchi, *J. Am. Ceram. Soc.*, 1997, **80**, 3221.
12 T. Masui, K. Fujiwara, K. Machida, G. Adachi, T. Sakata and H. Mori, *Chem. Mater*., 1997, **9**, 2197.
13 T. Masui, K. Machida, T. Sakata, H. Mori and G. Adachi, *J. Alloys Compd.*, 1997, **256**, 97.
14 C. A. Hogarth and Z. T. Al-Dhhan, *Phys. Status Solidi B*, 1986, **137**, K157.
15 K. B. Sundaram and P. Wahid, *Phys. Status Solidi B*, 1990, **161**, K63.
16 Z. C. Orel and B. Orel, *Phys. Status Solidi B*, 1994, **186**, K33.

Communication 9/00930B

Pyridine-based dendritic wedges with a specific metal ion coordination site and their palladium(II) complexes

Gavino Chessa,* Alberto Scrivanti, Luciano Canovese, Fabiano Visentin and Paolo Uguagliati

Dipartimento di Chimica, Università di Venezia, Calle Larga S. Marta, 2137, Venezia, Italy. E-mail: chessa@unive.it

Received (in Cambridge, UK) 28th January 1999, Accepted 19th April 1999

The 2,6-di(thiomethyl)pyridine sub-unit has been incorporated into pyridine-based dendritic structures providing a series of dendritic wedges, which readily form Pd^{II} complexes.

The incorporation of metal centres into a dendritic structure is a challenging idea aimed at generating materials with potentially useful features.[1–3] Numerous dendrimers, which contain coordination sites on the outer surface,[4] within the macrostructure throughout all layers,[5] and at the inner core[6] have been prepared. In contrast, except for scant coordination studies,[7] very little has been done about the construction of dendrimers with specific coordination centres within the dendritic wedges and their reaction with metal substrates. In particular, no report has yet appeared on the synthesis of dendrimers with a pyridine-based skeleton incorporating a specific coordination site for platinum-group metals.

As a preliminary study of the assembly of such dendrimers we report herein the synthesis of the pyridine-based dendrons **3**–**5** containing the 2,6-di(thiomethyl)pyridine sub-unit, which has been shown to form very stable Pd^{II} complexes.[8] The complexation of Pd^{II} with **3**–**5** to give metallodendrons **6**–**8** is also reported on.

Our approach to the synthesis of the dendrons **3**-**5** is based on a convergent strategy which implies the preparation of the dendritic fragments **I**–**III** as 4-hydroxo species[9] followed by attachment to the metal binding site **2b.** The key building block **2b** (Scheme 1) was prepared by coupling 2,6-bis(chloromethyl)-4-benzyloxypyridine **1**[9] with 4-mercaptobenzyl alcohol[10] (DMF, K_2CO_3, 18-crown-6, 70 °C). This reaction occurred with preferential formation of the thioether bond, providing the hydroxymethyl derivative **2a**. Subsequent chlorination ($SOCl_2$, 50 °C) followed by attachment of the diester **I** to the resulting chloride **2b**, gave **3** in 92% yield after purification by column chromatography (SiO_2, CH_2Cl_2–2% MeOH) (Scheme 2). Similarly, the reactions of **2b** with tetraester **II** and octaester **III** yielded the dendrons **4** and **5** (Scheme 2) in 85 and 51% yield, respectively.

The dendrons obtained were fully characterised by IR and NMR techniques as well as by matrix assisted laser desorption ionization mass spectrometry (MALDI-MS; dithranol 10 mg cm^{-3} acetone matrix). The reaction of the dendritic fragment **3** with $Pd(PhCN)_2Cl_2$ in CH_2Cl_2 at 25 °C (1 : 1 Pd/**3** molar ratio) gave a stable orange microcrystalline Pd^{II} complex **6** in 76% yield (Fig. 1). Direct evidence of a successful complexation at

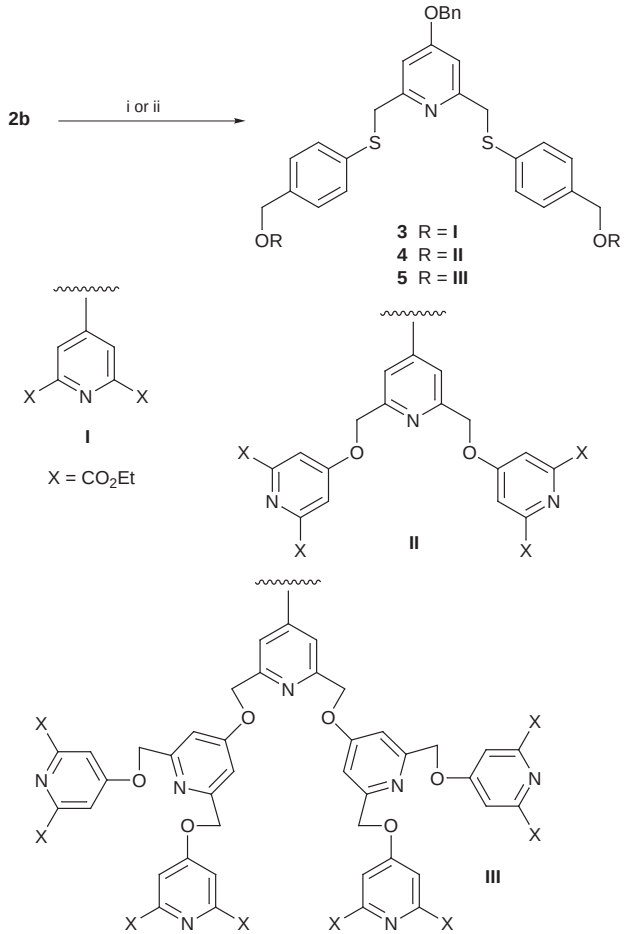

Scheme 2 *Reagents and conditions*: i, K_2CO_3, DMF, 70 °C, 24 h; ii, K_2CO_3, DMF, 60 °C, 48 h.

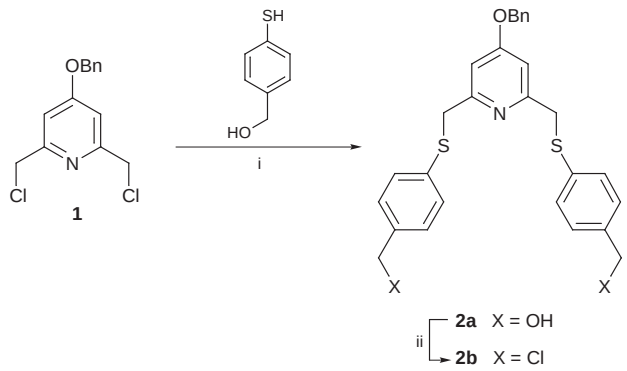

Scheme 1 *Reagents and conditions*: i, K_2CO_3, 18-crown-6, DMF, 70 °C, 24 h; ii, $SOCl_2$,50 °C, 4 h.

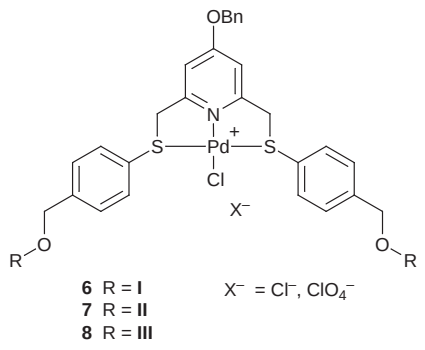

Fig. 1 Schematic representation of metallodendrons **6**–**8** (dendritic polypyridines of 0, 1, 2 generation).

the 2,6-di(thiomethyl)pyridine site is provided by the significant downfield shifts of the thiomethylene protons (1.2 ppm) and carbons (11.2 ppm) in the ^{1}H NMR and ^{13}C NMR spectra, respectively. The absence of the 3,5-pyridine protons peak at δ 6.87 further supports the complexation hypothesis. Moreover, the presence of the characteristic molecular peak at *m/z* 1074 ([**3**PdCl]$^+$) in the MALDI-TOF spectrum of **6** clearly indicates the formation of a 1:1 complex between Pd^{II} and **3**.

The complexation of Pd^{II} with the dendron **4** did not proceed smoothly under the same experimental conditions. The ^{1}H NMR spectrum of a $CDCl_3$ solution of complex **7**, isolated as its chloride salt, suggests the presence of an undesired product. A possible explanation for its formation is the competition of chloride ion as a nucleophile with other donor centres in the dendritic structure, namely the sulfur and nitrogen atoms of the 2,6-di(thiomethyl)pyridine sub-unit.[11] However, **7** was successfully purified by conversion into its yellow ClO_4^- salt, the ^{1}H NMR spectrum of which exhibits a pattern similar to those observed for **6**, furthermore the MALDI-TOF mass spectrum shows a parent ion at *m/z* 1792 coorresponding to [**4**PdCl]$^+$.

Extension of this finding to the reaction of **5** with Pd^{II} allowed us to obtain metallodendron **8**. As in the foregoing spectra, the resonances associated with the 2,6-di(thiomethyl)pyridine fragment are affected by complexation and lie at lower field than those of the uncoordinated domain. In particular, the CH_2S singlet, which is found at δ 4.21 in a uncoordinated ligand, shifts to δ 5.26 (br s) in a coordinated unit. Once again, the MALDI-TOF mass spectrum displaying the characteristic molecular peak at *m/z* 3225 ([**5**PdCl]$^+$) provides convincing evidence for the formulation of product **8**. Analytical data, ^{1}H, ^{13}C NMR and MALDI-TOF spectra of all species prepared are fully consistent with the proposed structures. In particular, for complex **8** the synthetic approach (1 : 1 Pd/**5** molar ratio and the ensuing 78% yield) and the presence of one single signal for the carboxylate ethyl protons (X = CO_2Et) strongly support the formulation of Fig. 1.

These results indicate that the presence of the 2,6-di(thiomethyl)pyridine sub-unit in dendritic wedges is particularly attractive for developing dendrimers with specifically localised metal centres. The physical properties of the metallodendrons **6**–**8** are now under extensive investigations. Of particular interest are the selectivity towards other transition metals and the influence of dendrimer framework on the metal-binding process.

We thank the MURST (Ministero per l' Università e la Ricerca Scientifica e Tecnologica) for financial support, Dr R. Seraglia (C.N.R. of Padova) for mass spectra, and Mrs L. Gemelli for technical assistance.

Notes and references

1 S. Serroni, G. Denti, S. Campagna, A. Juris, M. Ciano and V. Balzani, *Angew. Chem., Int. Ed. Engl.*, 1992, **31**, 1493; E. C. Constable, *Chem. Commun.*, 1997, 1073.
2 W. Knapen, A. W. van der Made, J. C. de Wilde, P. W. N. M. van Leeuwen, P. Wijkens, D. M. Grove and G. van Koten, *Nature*, 1994, **372**, 659; A. Miedaner, C. J. Curtis, R. M. Barkley and L. DuBois, *Inorg. Chem.*, 1994, **33**, 5482.
3 M. Albrecht, R. A. Gossage, A. L. Spek and G. van Koten, *Chem. Commun.*, 1998, 1003.
4 G. R. Newkome, F. Cardullo, E. C. Constable, C. N. Moorefield and A. M. W. Cargill Thompson, *J. Chem. Soc., Chem. Commun.*, 1993, 925; F. Moulines, L. Djakovitch, R. Boese, B. Gloaguen, W. Thiel, J.-L. Fillaut, M.-H. Delville and D. Astruc, *Angew. Chem., Int. Ed. Engl.*, 1993, **32**, 1075; B. Alonso, I. Cuadrado, M. Moran and J. Losada, *J. Chem. Soc., Chem. Commun.*, 1994, 2575; Y. H. Liao and J. R. Moss, *Organometallics*, 1995, **14**, 2130; D. Seyferth, T. Kugita, A. L. Rheingold and G. P. A. Yap, *Organometallics*, 1995, **14**, 5362; R. Deschenaux, E. Serrano and A.-M. Levelut, *Chem. Commun.*, 1997, 1577; C. F. Shu and H. M. Shen, *J. Mater. Chem.*, 1997, **7**, 47; M. Bardajì, M. Kustos, A. M. Caminade, J. P. Majoral and B. Chaudret, *Organometallics*, 1997, **16**, 403; J. L. Hoare, K. Lorenz, N. J. Hovestad, W. J. J. Smeets, A. L. Spek, A. J. Canty, H. Frey and G. van Koten, *Organometallics*, 1997, **16**, 4167.
5 W. T. S. Huck, F. C. J. M. van Veggel and D. N. Reinhoudt, *Angew. Chem., Int. Ed. Engl.*, 1996, **35**, 1213; S. Achar, J. J. Vittal and R. J. Puddephatt, *Organometallics*, 1996, **15**, 43; S. Serroni, A. Juris, M. Venturi, S. Campagna, I. R. Resino, G. Denti, A. Credi and V. Balzani, *J. Mater. Chem.*, 1997, **7**, 1227.
6 G. R. Newkome, R. Guther, C. N. Moorefield, F. Cardullo, L. Echegoyen, E. Perez-Cordero and H. Luftmann, *Angew. Chem., Int. Ed. Engl.*, 1995, **34**, 2023; P. J. Dandliker, F. Diederich, J.-P. Gisselbrecht, A. Louati and M. Gross, *Angew. Chem., Int. Ed. Engl.*, 1995, **34**, 2725; P. Bhyrappa, J. K. Young, J. Moore and K. S. Suslick, *J. Am. Chem. Soc.*, 1996, **118**, 5708; M. Kimura, K. Nakada, Y. Yamaguchi, K. Hanabusa, H. Shirai and N. Kobayashi, *Chem. Commun.*, 1997, 1215; J. Issberner, F. Vögtle, L. De Cola and V. Balzani., *Chem. Eur. J.*, 1997, **3**, 706.
7 U. Stebani, G. Lattermann, M. Wittemberg, and J. H. Wendorff, *Angew. Chem., Int. Ed. Engl.*, 1996, **35**, 1858; G. R. Newkome, J. Groβ, C. N. Moorefield and B. D. Woosley, *Chem. Commun.*, 1997, 515.
8 L. Canovese, G. Chessa, G. Marangoni, B. Pitteri, F. Visentin and P. Uguagliati, *Inorg. Chim. Acta*, 1991, **186**, 79.
9 G. Chessa and A. Scrivanti, *J. Chem. Soc., Perkin Trans. 1*, 1996, 307.
10 R. N. Young, J. Y. Gauthier and W. Coombs, *Tetrahedron Lett.*, 1984, **25**, 1753.
11 M. L. Tobe, *Comprehensive Coordination Chemistry*, ed. G. Wilkinson, R. D. Gillard and J. A. McCleverty, Pergamon, Oxford, 1987, vol. 1, p. 282.

Communication 9/00783K

Air-stable crystalline primary phosphines and germanes: synthesis and crystal structures of dibenzobarellenephosphine and tribenzobarellenegermane

Marcin Brynda,[a] Michel Geoffroy*[a] and Gérald Bernardinelli[b]

[a] *Département de Chimie Physique, 30 Quai Ernest Ansermet, 1211 Genève, Switzerland*
[b] *Laboratoire de Cristallographie, 24 Quai Ernest Ansermet, 1211 Genève, Switzerland.*
E-mail: geoffroy@sc2a.unige.ch

Received (in Basel, Switzerland) 9th February 1999, Accepted 13th April 1999

The syntheses of dibenzobarellenephosphine and tribenzobarellenegermane are described; at room temperature these primary phosphines and germanes form air-stable crystals whose structures are reported together with that of tribenzobarellenemethane.

Primary phosphines are generally air-sensitive liquid compounds. Most of the reported crystal structures with an RPH_2 moiety have therefore been determined on molecules where the phosphorus atom is coordinated to a metal atom.[1] The crystal structure of free primary phosphines could be obtained in only a very limited number of cases: (1) when the phosphorus atom is bound to a cumbersome protective aryl group ($Bu^t_3C_6H_2$),[2] to an iron dicyclopentadienyl group[3] or to a triptycyl moiety;[4] (2) after dimerisation of anthracenephosphine;[5] (3) after N-quaternisation of aminoalkylphosphines.[6] Recent results[7] indicated that benzo derivatives of barrelene were likely to lead to stable crystalline RPH_2 compounds; we have therefore taken advantage of this to attempt the synthesis of a primary phosphine which contains a double bond in the vicinity of the phosphorus atom. We report below the synthesis and the structure of the remarkably air-stable primary phosphine **1**. The synthesis of dibenzobarellenephosphine† is shown in Scheme 1.

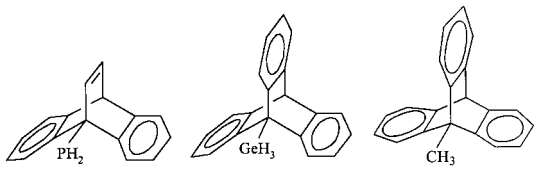

1 **2** **3**

In the solid state the dibenzobarellenephosphine **1**‡ is located on a mirror plane perpendicular to the *b* axis with P1, C7, C8, C9, C10, H8, H9 and H10 in special positions 4c. All hydrogen atoms have been observed and refined without constraint. No significant electronic density corresponding to a hydrogen site located in the *trans* position relative to the C7–C8 bond was observed, meaning that only one rotamer is present and that no free rotation of the phosphine around the C–P bond occurs at 180 K. The dihedral angle between the mean planes of the phenyl moieties is 113.8° (angle between the central ethylene bridge and a phenyl moiety = 123.1°).

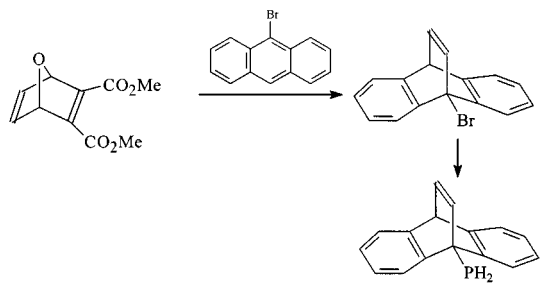

Scheme 1

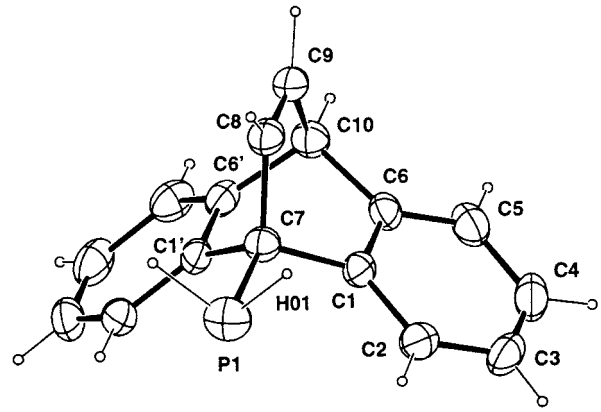

Fig. 1 Perspective view of **1**. Ellipsoids are represented with 40% probability. Selected bond distances (Å) and angles (°): P1–C7 1.859(4); C1–C6 1.402(4); C1–C7 1.536(4); C6–C10 1.522(4); C7–C8 1.539(6); C8–C9 1.314(7); C9–C10 1.520(6); P–H01 1.36(3); C1–C7–C8 105.5(2); C1–C7–C1′ 103.3(3); C1–C7–P1 113.2(2); C7–C8–C9 115.2(4); C8–C9–C10 114.1(4); C6–C10–C6′ 104.5(3); C6–C10–C9 106.1(2); H01–P–H01′ 93(2).

In the context of this study, we envisaged using benzobarellene derivatives to form a crystalline primary germane. Although less reactive than their silicon homologues, primary germanes are generally air-sensitive liquid (or gaseous) compounds at room temperature. As far as we know, the only crystal structure reported for $RGeH_3$ was obtained at 160 K on cyclopentadienyl germane, which melts at 200 K.[8] We report below the synthesis† (Scheme 2) and the crystal structure‡ of tribenzobarrelenegermane **2** which forms air-stable crystals with a melting point of 232 °C.

This compound is isostructural with tribenzobarellenemethane **3**,[9] whose structure,‡ to the best of our knowledge, has never been published. Both **2** and **3** show disordered structures. The molecules are located on 3-fold axes with C1, C8, Ge (resp. C9) and H8 atoms in special positions 6c of the space group $R\bar{3}$. The disorder consists of an inversion of the molecule approximately maintaining the position of the tribenzobarrelene skeleton and mainly affecting the germanium (resp. C9) atom. The refinement of such models fixing the sum of the occupations of the Ge (resp. C9) sites to 1 shows disorder ratios of 60.0(4)/40.0(4)% and 61.5(7)/38.5(7)% for **2** and **3** respectively. The relatively high values of the *R* factors and uncertainties obtained for **2** show that this compound is more affected than **3** by the disorder. Indeed, in the crystal packing,

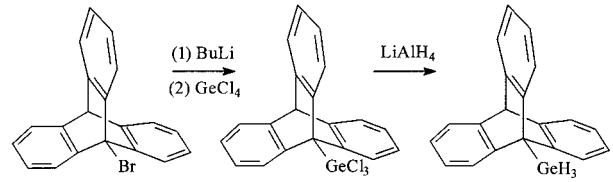

Scheme 2

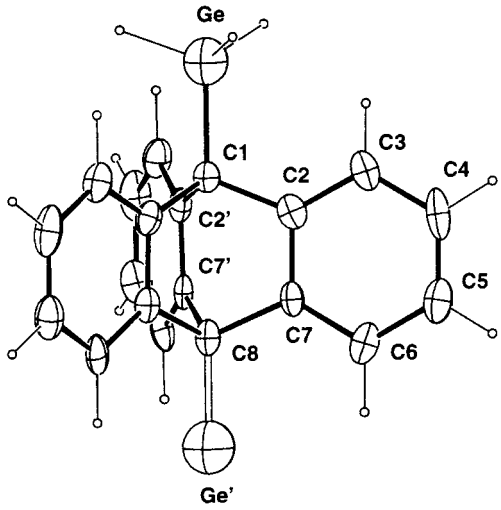

Fig. 2 Perspective view of **2**. Ellipsoids are represented with 40% probability. Selected bond distances (Å) and angles (°): C1–Ge 1.861(8); C1–Ge′ 1.77(1); Cl–C2 1.513(8); C7–C8 1.541(5); C2–C1–Ge 111.8(3); C7–C8–Ge′ 114.0(3); C2–C1–C2′ 107.1(5); C7–C8–C7′ 104.6(5) [for the isostructural **3** (Ge⇔C9): C1–C2 1.529(2); C1–C9 1.546(5); C1–C9′ 1.546(6), C7–C8 1.524(2); C2–C1–C2′ 105.0(1); C2–C1–C9 113.62(9); C7–C8–C9′ 113.07(8); C7–C8–C7′ 105.6(1)].

the shortest distances between two disordered sites of the Ge (resp. C9) atoms located along *c* axis (on both sides of a centre of inversion) are 1.557(7) and 2.065(8) Å for **2** and **3** respectively. It should be noted that a refinement of **2** in the noncentrosymmetric space group *R*3 leads to a final value of the Flack parameter[10] of $x = 0.47(28)$, large values of Δ/σ, non-positive values of $\|U_{ij}\|$ and a value of *R* of about 13%. These observations lead us to exclude the presence of a non-centrosymmetric, twinned and disordered structure as observed for the analogous tribenzobarrelenephosphine compound.[4]

EPR experiments on the dynamics of radicals produced from **1** and **2** are currently in progress.

We thank the Swiss National Science Foundation for financial support.

Notes and references

† *Syntheses*: All experiments were performed under dry N_2.

Bromodibenzobarellene was synthesized following a slight modification of the method reported by Mori *et al.* (ref. 11): 3.57 g (14 mmol) of 9-bromoanthracene and 3.48 g (17 mmol) of the furan–acetylene adduct in 20 ml of triglyme were sealed in a glass tube and placed in an autoclave. Very vigorous stirring was applied and the mixture was heated at 120 °C for 48 h and then at 200 °C for 24 h. The oily brown solution was washed with water (3 × 30 ml) to remove the solvent. After the usual work-up bromodibenzobarellene was separated by chromatography on silica gel using hexane–Et_2O (10 : 1) as eluant. The yellow powder was recrystallised from CH_2Cl_2–EtOH (68%): transparent crystals, mp 105 °C; δ_H($CDCl_3$, 200 MHz) 5.13 (dd, 1H), 7.05 (m, 6H), 7.26 (d, 2H), 7.71 (d, 2H); *m/z* (M^+), 282, 256, 203, 176, 150, 101, 75.

Dibenzobarellenephosphine: 4.9 ml of BuLi (1.6 M, hexane) were very slowly introduced, at −80 °C, into a solution containing 2 g (7.1 mmol) of bromodibenzobarellene dissolved in 30 ml of dry THF. After 10 min the temperature was slowly raised up to −60 °C. Then the solution was quickly cooled to −100 °C and 1.1 ml of PCl_3 (12.5 mmol) was added all at once; the solution was vigorously stirred for 30 min and gently refluxed for 1 h. The solution was then cooled in an ice bath and 0.53 g (14 mmol) of $LiAlH_4$ were carefully added. After refluxing for 2 h, the reaction was quenched with a few drops of HCl/H_2O and the residual phosphine was extracted with Et_2O (3 × 30 ml). The final product was purified by chromatography on silica gel using hexane–Et_2O (9 : 1) as eluant. Small, thin crystals were obtained directly from this solution (42%): mp 108 °C; δ_P($CDCl_3$, 80 MHz) 143.6 (t, J_{PH} 199); δ_H($CDCl_3$, 200 MHz) 3.55 (d, J_{PH} 200, 1H, PH), 5.13 (dd, 2H), 6.76 (ddd, 1H), 7.05 (m, 6H), 7.32 (m, 2H), 7.50 (m, 2H).

Tribenzobarellenegermane: 2 g (6.0 mmol) of bromotriptycene were dissolved in 30 ml of dry THF. Then 4.1 ml of BuLi (1.6 M hexane) were introduced very slowly into the solution during a few minutes at −78 °C. After 10 min the temperature was slowly raised up to 0 °C and then cooled quickly to −80 °C. 1.93 g of $GeCl_4$ (9.0 mmol) was added all at once and the solution was vigorously stirred. After 30 min a gentle reflux was applied during 1.5 h. The solution was cooled in an ice bath and 0.4 g (10.6 mmol) of $LiAlH_4$ was carefully added. After refluxing for 2 h the reaction was quenched with a few drops of HCl/H_2O and the residual germane was extracted with Et_2O (3 × 30 ml). The final product was purified *via* silica gel chromatography using hexane–Et_2O (9 : 1) as eluant. Small transparent crystals were obtained directly from this solution (35%), mp 232 °C; δ_H($CDCl_3$, 200 MHz) 2.37 (s, 3H), 4.44 (s, 1H), 6.96–7.04 (m, 6H), 7.33–7.42 (m, 6H); *m/z* 330 (M^+), 253, 226, 176, 126.

‡ *Crystal data* for **1**: $C_{16}H_{31}P$, $M = 236.3$; orthorhombic, *Pnma*, $Z = 4$, $a = 11.7836(5)$, $b = 14.3232(7)$, $c = 7.2002(5)$ Å, $V = 1215.2(1)$ Å^3, $T = 180$ K, $\mu = 1.753$ mm^{-1} for Cu-Kα radiation (*A** min., max. = 1.174, 1.585), $F_{000} = 496$, $D_c = 1.291$ g cm^{-3}, 1560 measured reflections, 780 unique reflections of which 665 were observable [$|F_o| > 4\sigma(F_o)$]. Full-matrix least-squares refinement based on *F* using weight of $1/[\sigma^2(F_o) + 0.0001(F_o^2)]$ gave final values $R = 0.038$, $\omega R = 0.037$ for 115 variables and 665 contributing reflections. Hydrogen atoms were observed and refined. For **2**: $C_{20}H_{16}Ge$, $M = 328.9$; trigonal, $R\bar{3}$, $Z = 6$, $a = 11.8154(7)$, $c = 17.7571(7)$ Å, $V = 2146.8(3)$ Å^3, $T = 200$ K, $\mu = 2.794$ mm^{-1} for Cu-Kα radiation (*A** min., max. = 1.661, 2.898), $F_{000} = 1008$, $D_c = 1.527$ g cm^{-3}, 1872 measured reflections, 593 unique reflections of which 563 were observables [$|F_o| > 4\sigma(F_o)$]. Full-matrix least-squares refinement based on *F* using weight of $1/\sigma^2(F_o)$ gave final values $R = 0.086$, $\omega R = 0.060$ for 69 variables and 563 contributing reflections. Hydrogen atoms were calculated. For **3**: $C_{21}H_{16}$, $M = 268.4$; trigonal, $R\bar{3}$, $Z = 6$, $a = 11.7919(7)$, $c = 17.5871(8)$ Å, $V = 2117.8(2)$ Å^3, $T = 170$ K, $\mu = 0.538$ mm^{-1} for Cu-Kα radiation (*A** min., max. = 1.083, 1.165), $F_{000} = 852$, $D_c = 1.263$ g cm^{-3}, 1985 measured reflections, 634 unique reflections of which 629 were observables [$|F_o| > 4\sigma(F_o)$]. Full-matrix least-squares refinement based on *F* using weight of $1/\sigma^2(F_o)$ gave final values $R = 0.038$, $\omega R = 0.036$ for 95 variables and 629 contributing reflections. Hydrogen atoms were observed and refined. CCDC 182/1228. See http://www.rsc.org/suppdata/cc/1999/961/ for crystallographic files in .cif format.

1 P. G. Jones, H. W. Roesky, H. Grutzmacher and G. M. Sheldrick, *Z. Naturforsch., Teil B*, 1985, **40**, 590; P. G. Edwards, J. S. Fleming, S. S. Liyanage, S. J. Coles and M. B. Hursthouse, *J. Chem. Soc., Dalton Trans.*, 1996, 1801; R. J. Batchelor, T. Birchall and R. Faggiani, *Can. J. Chem.*, 1985, **63**, 928; R. Felsberg, S. Blaurock, S. Jelonek, T. Gelbrich, R. Kirmse, A. Voigt and E. Hey-Hawkins, *Chem. Ber.*, 1997, **130**, 807; I. V. Kourkine, S. V. Maslennikov, R. Ditchfield, D. S. Glueck, G. P. A. Yap, L. M. Liable-Sands and A. L. Rheingold, *Inorg. Chem.*, 1998, **35**, 1996; D. S. Bohle, G. R. Clark, C. E. F. Rickard, W. R. Roper and W. B. Shepard, *J. Organomet. Chem.*, 1991, **402**, 375; B. D. Zwick, M. A. Dewey, D. A. Knight, W. E. Buhro, A. M. Arif and J. A. Gladysz, *Organometallics*, 1992, **11**, 2673, G. A. A. Hadi, K. Fromm, S. Blaurock, S. Jelonek and E. Hey-Hawkins, *Polyhedron*, 1997, **16**, 721.

2 R. A. Barlett, M. M. Olmstead, P. P. Power and G. A. Sigel, *Inorg. Chem.*, 1987, **26**, 1941.

3 N. J. Goodwin, W. Henderson and B. K. Nicholson, *Chem. Commun.*, 1997, 31.

4 G. Ramakrishnan, A. Jouaiti, M. Geoffroy and G. Bernardinelli, *J. Phys. Chem.*, 1996, **100**, 10 861.

5 L. Heuer, D. Schomburg and R. Schmutzler, *Chem. Ber.*, 1989, **122**, 1473.

6 D. J. Brauer, J. Fischer, S. Kuchen, K. P. Langhans and O. Stelzer, *Z. Naturforsch., Teil B*, 1994, **49**, 1511.

7 M. Brynda, T. Berclaz, M. Geoffroy, G. Ramakrishnan and G. Bernardinelli, *J. Phys. Chem.*, 1998, **102**, 8245.

8 M. J. Barrow, E. A. V. Ebsworth, M. M. Harding and D. W. H. Rankin, *J. Chem. Soc., Dalton Trans.*, 1980, 604.

9 F. Imashiro, T. Terao and A. Saika, *J. Am. Chem. Soc.*, 1979, **101**, 3762.

10 H. D. Flack, *Acta Crystallogr.*, 1983, **A39**, 876; G. Bernardinelli and H. D. Flack, *Acta Crystallogr.*, 1985, **A41**, 500.

11 G. R. Tian, S. Sugiyama, A. Mori and H. Takeshita, *Sogo Rikogaku Hokoku* (*Kyushu Daigaku Daigakuin*), 1988, **10**, 171 (*Chem. Abstr.*, 1990, **112**, 197798).

Communication 9/01083A

A Lewis acid dependent asymmetric Diels–Alder process in the cyclization of new chiral acrylamides with dienes

Doo Han Park, Sung Han Kim, Sam Min Kim, Jin Dong Kim and Yong Hae Kim*

Department of Chemistry, Korea Advanced Institute of Science & Technology, Taejon, 305-701, Korea. E-mail: kimyh@sorak.kaist.ac.kr

Received (in Cambridge, UK) 30th March 1999, Accepted 20th April 1999

Diels–Alder cycloadditions of chiral acrylamides with cyclopentadiene proceed with high diastereofacial selectivity, giving either *endo-R* to *endo-S* products depending of the Lewis acid used.

Lewis acid catalyzed addition of dienes to chiral acrylamides is a useful reaction because it provides one of the most effective methods for creating new chiral centers during the formation of six-membered rings.[1] Various types of chiral dienophiles such as chiral esters,[1] *N*-acyloxazole derivatives,[2] *N*-acylsultams,[3] acrylates[4] and acrylamides[5] have been developed. Metal coordination is important for diastereofacial selectivity in the asymmetric synthesis. Lewis acids have been used for chelate formation in Diels–Alder cyclizations to obtain high diastereofacial selectivities.[1–5] In general, the *S* form of the chiral dienophile (auxiliary) exclusively afford the *endo-R* adduct over the *endo-S* one, and the *R* form exclusively gives the *S* adduct over the *endo-R* one. Issues associated with this absolute stereochemical control depending upon Lewis acids and the structures of dienophiles provide an important challenge in the area of practical Diels–Alder reaction designs.[4a,5b]

In the hope of obtaining the opposite configuration of the *endo* adduct and understanding the mechanism, three different dienophiles **1**, **2** and **3** were prepared and reacted with dienes in the presence of various Lewis acids. Here we describe the intriguing results obtained during development of Lewis acid dependent stereocontrol toward both *endo-R* and *endo-S* configuration with high diastereofacial selectivity. In order to generalize the results, the requisite dienophiles **1**–**3** were synthesized from (*S*)-indoline-2-carboxylic acid.[6] They were purified and their optical purities (> 99.8% ee) were determined by HPLC (Daicel chiral OD column, Pr^{i}OH–n-hexane, 5 : 95). The preliminary studies involved reaction of **1**–**3** with **4** and **5**, as shown in Scheme 1.

Extremely high levels of asymmetric induction can be achieved in Diels–Alder cycloadditions of **1** or **3** with **4**; in contrast to other general dienophiles, **1** containing a carboxylate moiety reacts with **4** to give differently configured adducts depending on the Lewis acids employed; in the presence of $TiCl_4$, $Ti(OPr^i)_4$ or $SnCl_4$, **6a** was obtained as the major diastereomer (**6a** : **6b** = *endo-R* : *endo-S* = > 99 : 1; entries 4–6 in Table 1), but with $AlEt_2Cl$, $ZnCl_3$ or $BF_3{\cdot}Et_2O$ the opposite configuration of **6b** was obtained (**6a** : **6b** = 1 : > 99; entries

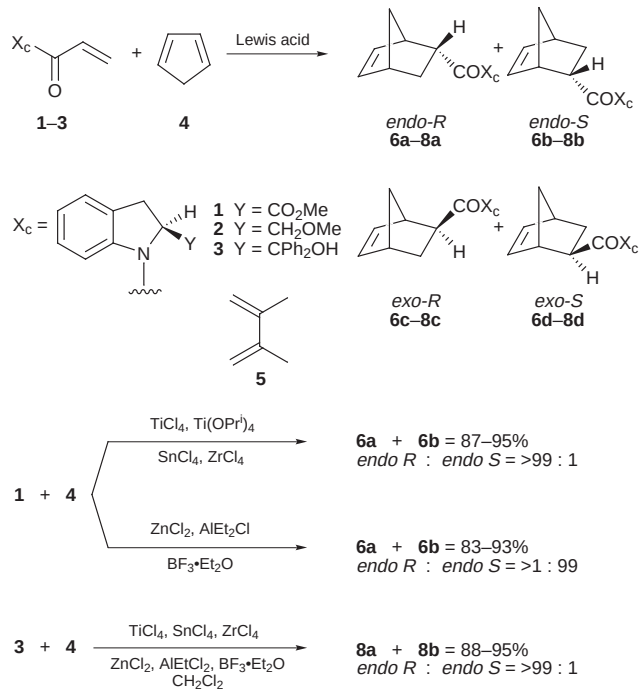

Scheme 1

Table 1 Assymetric Diels–Alder cycloaddition with **1** and **3**

Entry	Dienophile	Lewis acid	*T*/°C	*t*/h	Yield (%)[a]	*endo* : *exo*[b]	*endo*[b] ds	Config.[c]
1	**1**	Et_2AlCl	−78	10	95	90 : 10	> 99 : 1	*S*
2	**1**	$BF_3{\cdot}Et_2O$	−78	5	90	94 : 6	> 99 : 1	*S*
3	**1**	$ZnCl_2$	25	12	90	83 : 17	99 : 1	*S*
4	**1**	$TiCl_4$	0	10	92	65 : 5	99 : 1	*R*
5	**1**	$Ti(OPr^i)_4$	25	12	87	72 : 28	94 : 6	*R*
6	**1**	$SnCl_4$	−78	5	92	95 : 5	91 : 1	*R*
7	**3**	—	25	48	92	> 99 : 1	> 99 : 1	*R*
8	**3**	Et_2AlCl	−40	10	95	> 99 : 1	> 99 : 1	*R*
9	**3**	$AlCl_3$	−40	8	88	> 99 : 1	> 99 : 1	*R*
10	**3**	$BF_3{\cdot}Et_2O$	−78	5	91	> 99 : 1	> 99 : 1	*R*
11	**3**	$ZnCl_2$	25	12	90	> 99 : 1	> 99 : 1	*R*
12	**3**	$TiCl_4$	25	7	90	> 99 : 1	> 99 : 1	*R*
13	**3**	$Ti(OPr^i)_4$	25	15	89	> 99 : 1	> 99 : 1	*R*
14	**3**	$SnCl_4$	−78	10	91	98 : 2	98 : 2	*R*
15	**3**	$ZrCl_4$	−40	5	93	> 99 : 1	> 99 : 1	*R*
16	**2**	$EtAlCl_2$	−78	7	83	88 : 12	86 : 14	*S*
17	**2**	$TiCl_4$	−78	12	75	85 : 15	97 : 3	*R*

[a] Isolated yield. [b] Determined by HPLC analysis. (Chiral Column: Daicel OD). [c] Confirmed by $[\alpha]_D$ of iodolactone or norbonene-2-methanol.

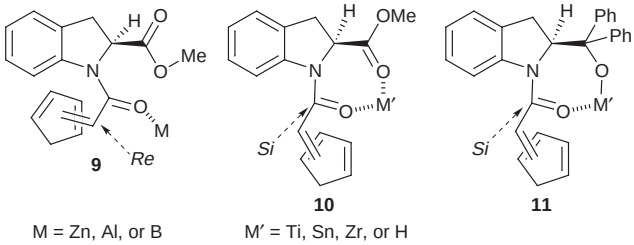

Fig 1 Possible intermediates in Diels–Alder reactions.

1–3 in Table 1). In the case of **2**, the same trend of **7b** was observed, but in a less diastereoselective manner than for **1** (entries 16 and 17). In particular, **3** containing a diphenyl-substituted tertiary alcohol moiety affords exceptionally high diastereofacial selectivities (**8a**:**8b** = >99:1, yield = >90%; entries 7–15) regardless of the natures of the Lewis acid. The *endo* configurations were readily ascertained by iodolactonization of **6a**–**8a** with I_2 in DMF.[5b] The *exo* compound cannot be lactonized under the same reaction conditions. The ratio of *endo-R* and *endo-S* was determined by HPLC with the crude **6a**–**8a** and **6b**–**8b** without purification.[7] The absolute configuration of **6a**, **7b** or **8a** was determined by reductive cleavage of **6a** to the known norbornene-2-methanol and subsequent comparison of $[\alpha]_D$ values.[8]

The differently configured adducts produced can be rationalized by the different intermediates formed between **1**–**3** and the metals of the Lewis acids. Compounds **1**–**3** react with **4** to favor formation of *endo-R* species **6a** or **8a** with $TiCl_4$, $Ti(OPr^i)_4$, $SnCl_4$ or $ZrCl_4$ probably *via* formation of seven-membered ring chelates with the acryloyl moiety of **10** or **11** having a *cisoid* conformation.[4a,5b] Helmechen and co-workers reported the first evidence of formation of a seven-membered ring chelate complex.[4a] It is noteworthy that even in the absence of any Lewis acid, **3** reacts with **4** to give an excellent chemical yield (92%) and high stereofacial selectivity (*endo*:*exo* = >99:1, *endo-R*:*endo-S* = >99:1; entry 9 in Table 1) at 25 °C after a long reaction time (24 h). The results can be attributed to the hydrogen-bond *cisoid* conformation intermediate **11** where the hydrogen acts as a Lewis acid. On the other hand, **1** or **2** prefer *endo-S* formation **6b** or **7b** with $ZnCl_2$, $AlEtCl_2$ or $BF_3{\cdot}Et_2O$, with high diastereofacial selectivity probably resulting from intermediate **9**, as shown in Fig. 1 In contrast to Ti or Sn Lewis acids, relatively weaker Lewis acids such as Zn, Al, or B may not form a seven-membered ring complex, instead forming a weak coordination with the amide carbonyl group (**9**).[4a,5b] In the case of Evans' model dienophile, an α,β-unsaturated *S*-oxazolidinone, the *endo-R* form was obtained[2a] and explained by formation of a six-membered ring intermediate with Et_2AlCl, which was clarified by a ^{13}C NMR study.[2c] However, in contrast to a significant chemical shift change[9a] in the **1**–$SnCl_4$ chelation complex **11**, ^{13}C NMR measurement of the **1**-Et_2AlCl mixture did not show significant changes in the chemical shifts for either of the amide or ester carbonyl peaks,[9b] *which can be explained by a weak coordination* (**9**) between **1** and Et_2AlCl. Species **1** and **3** also reacted with less reactive acrylic diene **5** at 25 °C to result in the same trend: for **1** with $TiCl_4$ the ratio of *endo R*:*endo S* was 97:3, while with $EtAlCl_2$ the ratio was reversed to 3:97, which is comparable to entry 1; for **3** with both $TiCl_4$ and Et_2AlCl, *endo R*:*endo S* = 97:3 and 94:6 respectively, which is comparable to entries 8 and 12.

In summary, asymmetric Diels–Alder cycloadditions of **1**, or **3** with **4** proceed with absolutely stereocontrolled diastereofacial selectivities in both *endo-S* and *endo-R* (up to >99% de) depending upon Lewis acids used and the structures of chiral dienophiles.

This work was supported by the Center for Biological Molecules, Korea Science and Engineering Foundation.

Notes and references

1 For reviews, see L. A. Paquett, *Asymmetric Synthesis*, ed. J. D. Morrison, Academic Press, New York, 1994, vol. 3; W. Oppolzer, *Angew. Chem., Int. Ed. Engl.*, 1984, **23**, 876; H. Waldmann, *Synthesis*, 1994, 535.

2 (*a*) D. A. Evans, K. T. Chapman and J. Bisaha, *J. Am. Chem. Soc.*, 1986, **110**, 1238 and references therein; (*b*) K. Kimura, K. Murata, K. Otsuka, T. Shizuka, M. Maratake and T. Kunieda, *Tetrahedron Lett.*, 1992, **33**, 4461; (*c*) S. Castellino and W. J. Dwight, *J. Am. Chem. Soc.*, 1993, **115**, 2986; (*d*) S. Castellino, *J. Org. Chem.*, 1990, **55**, 5197; (*e*) M. R. Banks, A. J. Blake, A. R. Brown, J. I. G. Cadosan, S. Gavr, I. Gosney, P. K. G. Hodgson and P. Thorburn, *Tetrahedron Lett.*, 1994, **35**, 489; (*f*) N. Hashimoto, T. Ishizuha and T. Kunieda, *Tetrahedron Lett.*, 1994, **35**, 721; (*g*) L. F. Tietze, C. Schneider and A. Montenbruck, *Angew. Chem., Int. Ed. Engl.*, 1994, **33**, 980.

3 W. Oppolzer, M. Wills, M. J. Kelly, M. Signer and J. Blagg, *Tetrahedron Lett.*, 1990, **35**, 5015; W. Oppolzer, *Pure Appl. Chem.*, 1990, **62**, 1241 and references therein; W. Oppolzer, C. Chapus, G. M. Dao, D. Reichlin and T. Godel, *Tetrahedron Lett.*, 1982, **23**, 4781; D. P. Curran, B. H. Kim, J. Daugherty and T. A. Heffner, *Tetrahedron Lett.*, 1988, **29**, 3555; W. Oppolzer, C. Chapuis and G. Bernardinelli, *Helv. Chim. Acta*, 1984, **67**, 1397.

4 (*a*) T. Poll, O. Metter and G. Helmechen, *Angew. Chem., Int. Ed. Engl.*, 1985, **24**, 112; (*b*) T. Poll, G. Helmechen and B. Bauer, *Tetrahedron Lett.*, 1984, **25**, 2191; (*c*) W. Choy, L. A. Reed, III and S. Masamune, *J. Org. Chem.*, 1983, **48**, 1137; (*d*) W. Oppolzer, C. Chapuis, G. M. Dao, D. Reichlin and J. T. Godel, *Tetrahedron Lett.*, 1982, **46**, 4781.

5 (*a*) Y. Kawanami, T. Katsuki and M. Yamaguchi, *Bull. Chem. Soc. Jpn.*, 1987, **60**, 4190; (*b*) H. Waldmann, *J. Org. Chem.*, 1988, **53**, 6133, *Tetrahedron Lett.*, 1989, **30**, 4227; (*c*) M. P. Buence, C. A. Cativiela and J. A. Magorall, *J. Org. Chem.*, 1991, **56**, 6551; (*d*) R. K. Boeckman, Jr., S. G. Nelson and M. D. Gaul, *J. Am. Chem. Soc.*, 1992, **114**, 2258.

6 Y. H. Kim, D. H. Park and I. S. Byun, *J. Org. Chem.*, 1993, **58**, 4511; Y. H. Kim, S. H. Kim and D. H. Park, *Tetrahedron Lett.*, 1993, **34**, 6063; (*c*) Y. H. Kim and J. Y. Choi, *Tetrahedron Lett.*, 1996, **37**, 5543.

7 In a typical experimental, a Lewis acid (1 mmol) was added to a solution of **1** (0.5 mmol) in CH_2Cl_2 (5 ml) under N_2. After stirring 10 min, **4** (5 mmol) was added. The reaction mixture was stirred while following the reaction by TLC, quenched with 1 M HCl solution, and then extracted with CH_2Cl_2 three times. The organic layer was dried over anhydrous $MgSO_4$ and concentrated *in vacuo*. The *endo* configurations were determined by the known iodolactonizations of **6a**–**8a** with I_2 in DMF [**8a** lactone: $[\alpha]_D$ −110.6 (*c* 1.0, $CHCl_3$)] [ref. 5(*b*)]. The ratio of *endo-R* and *endo-S* was determined by HPLC analysis using a chiral column (Daicel OD, Pr^iOH–n-hexane 1:9).

8 J. A. Berson, A. Remanick, S. Suzuki, D. R. Warnhoff and D. Willner, *J. Am. Chem. Soc.*, 1961, **83**, 3986; W. Krimse and R. Siegfried, *J. Am. Chem. Soc.*, 1983, **105**, 950.

9 (*a*) The ^{13}C NMR spectrum of the mixture of **6a** and $SnCl_4$ (1:1) was taken to show the significant chemical shift changes of the acrylamide carbonyl carbon (δ 163.8) and ester carbonyl carbon (δ 171.7) to δ 169.6 and 175.0, respectively, which support formation of a seven-membered ring complex between **6a** and $SnCl_4$. (*b*) In the case of **6a**–Et_2AlCl (1:2) no significant chemical shift changes for the two carbonyl carbons could be observed.

Communication 9/02535I

Metal-catalyzed transformation of D-glucal to optically active furan diol

Masahiko Hayashi,* Hirotoshi Kawabata and Kanako Yamada

Department of Chemistry, Faculty of Science, Yamaguchi University, Yamaguchi 753-8512, Japan.
E-mail: hayashi@po.cc.yamaguchi-u.ac.jp

Received (in Cambridge, UK) 29th March 1999, Accepted 19th April 1999

The treatment of D-glucal with a catalytic amount of $Sm(OTf)_3$ or $RuCl_2(PPh_3)_3$ in the presence of 1 equiv. of H_2O afforded optically active furan diol in good yield under mild conditions.

In 1975, Gonzales and co-workers reported the conversion of 3,4,6-tri-*O*-acetyl-D-glucal into 4,6-di-*O*-acetyl-2,3-dideoxy-*aldehydo*-D-erythro-*trans*-hex-2-enose in the presence of mercuric sulfate in 1,4-dioxane–sulfuric acid solution.[1,2] This mercuric ion-assisted acid glycal opening reacton has been applied to hexose and pentose derivatives to obtain acyclic α,β-unsaturated aldehydes. They also reported that the reaction of unprotected D-glucal under the same mercuric ion-assisted acidic conditions afforded optically active furan diol, 2-(D-*glycero*-1,2-dihydroxyethyl)furan. These transformations are very useful to obtain chiral building blocks, however, these reactions require acidic conditions. Therefore, the use of mild and neutral conditions to accomplish these transformations would be desirable, Here we report metal ion-catalyzed furan diol synthesis from D-glucal under mild conditions.

We recently reported the oxidation of the allylic alcohol moiety in D-glucal **1** by the aid of a catalytic amount of palladium complexes, which leads to the efficient synthesis of 1,5-anhydrohex-1-en-3-uloses.[3] During this study, we found that when the reactions were carried out in water, the formation of optically active furan diol **3** was observed (44% yield). The reaction in MeCN in the presence of water resulted in the formation of a mixture of furan diol **3**, oxidation product **4** and hydrogenated product **5**. These results promoted us to examine this transformation in detail. After examining several systems for the efficient conversion of **1** to furan diol **3**, we found that $RuCl_2(PPh_3)_3$ and $Sm(OTf)_3$ worked effectively to convert D-glucal to furan diol (Scheme 1). Some of the results obtained are summarized in Table 1. The treatment of D-glucal with 5–10 mol% of $RuCl_2(PPh_3)_3$ in the presence of 1 equiv. of H_2O afforded optically active furan diol in 64–70% yield. In the case of the reaction without H_2O, very slow dehydrogenation–hydrogenation to form **4** and **5** occured. Some rare-earth metal triflates also proved to be effective. Among the rare-earth metal triflates we examined, $Sm(OTf)_3$ exhibited the highest activity. The treatment of D-galactal **2** with 5 mol% of $Sm(OTf)_3$ afforded furan diol **3** with the same configuration. The reaction probably proceeds *via* nucleophilic attack of H_2O on glucal. Then opening of pyranose ring followed by cyclization to a five-membered ring and dehydration furnished the furan ring.

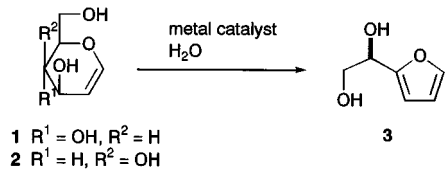

1 R^1 = OH, R^2 = H
2 R^1 = H, R^2 = OH

3

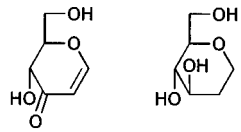

4 **5**

Scheme 1

A typical procedure is as follows: D-Glucal (204 mg, 0.356 mmol), MeCN (1.5 ml) and H_2O (0.03 ml) were placed under argon in an ampoule equipped with a magnetic stirring bar and a Young valve. After addition of $Sm(OTf)_3$ (44.8 mg, 0.07 mmol), the mixture was stirred for 40 min at 80 °C. The completion of the reaction was confirmed by TLC, then the mixture was poured into brine. Extracton with EtOAc (15 ml × 5) and concentration afforded the crude product, which was chromatographed on silica gel to give 2-(D-*glycerol*-1,2-dihydroxyethyl)furan **3** (131 mg, 70%) as a colorless oil {$[\alpha]_D$ +36.4 (*c* 1.2, $CHCl_3$) [lit.,[1] +38.0 (*c* 3.3, $CHCl_3$)]}.

The present method has the following advantages: (1) The reaction proceeds under neutral conditions, unlike the conventional mercuric ion-assisted acidic reaction; (2) highly toxic mercury can be replaced by less toxic metals; (3) operational simplicity—the direct derivatization of glycol to a protected species is possible.

Financial support from Monbusho (Grant-in-Aid for Scientific Research on Priority Areas, No. 706: Dynamic Control of Stereochemistry) is gratefully acknowledged.

Notes and references

1 F. Gonzales, S. Lesage and A. S. Perlin, *Carbohydr. Res.*, 1975, **42**, 267.
2 F. M. Dean, in *Advances in Heterocyclic Chemistry*, ed. by A. R. Katritzky, Academic Press, 1982, vol. 30, pp. 167–238; F. W.

Table 1 The conversion of D-glycals to furan glycol[a]

Entry	Glycal	Catalyst (mol%)	Solvent	H_2O/equiv.	Conditions		Yield[b] (%)
					T/°C	*t*/min	
1	**1**	$Pd(OAc)_2$ (5)	H_2O	—	80	30	44
2	**1**	$RuCl_2(PPh_3)_3$ (5)	C_6H_6	1	100	165	64
3	**1**	$RuCl_2(PPh_3)_3$ (10)	CH_2=CHOAc	1	100	45	70
4	**1**	$Sm(OTf)_3$ (5)	MeCN	1	80	40	70
5	**2**	$Sm(OTf)_3$ (5)	MeCN	1	80	50	60
6	**1**	$Yb(OTf)_3$, (5)	MeCN	1	80	50	51

[a] All reactions were carried out under argon atmosphere. [b] Isolated yield after silica gel column chromatography.

Lichtenthaler, in *Modern Synthetic Methods*, VCH, Basel, 1992, vol. 6; pp. 273–376; K. Walczak and E. B. Pedersen, *Synthesis*, 1991, 959; A. G. Tolstikov, N. V. Khakhalina and L. V. Spirikhin, *Synthesis*, 1988, 221; J. Wengel, J. Lau and E. B. Pedersen, *Synthesis*, 1989, 829.

3 M. Hayashi, K. Yamada and O. Arikita, *Tetrahedron Lett.*, 1999, **40**, 1171.

Communication 9/02510C

A four stranded β-sheet structure in a designed, synthetic polypeptide

Chittaranjan Das,[a] S. Raghothama[b] and P. Balaram*[a]

[a] *Molecular Biophysics Unit, Indian Institute of Science, Bangalore-560012, India. E-mail: pb@mbu.iisc.ernet.in*
[b] *Sophisticated Instrumentation Facility, Indian Institute of Science, Bangalore-560012, India*

Received (in Cambridge, UK) 29th March 1999, Accepted 20th April 1999

A designed four stranded β-sheet peptide has been constructed using three internal D-proline residues to nucleate β-hairpin formation.

De novo protein design provides a firm test of our understanding of the principles that govern the folding of polypeptide chains. The key element in this approach is the construction of synthetic peptide sequences which give rise to well characterized secondary and tertiary structures.[1] The choice of sequences is based on the propensities of specific sequences to adopt well defined local folds like helices, β-turns, and β-strands.[2] There has been considerable recent success in designing helical bundles [3] and mixed α/β models,[4] but attempts to design all β-sheet structures have been far fewer. β-Sheet formation has acquired a new dimension after the recognition that such structures are involved in the pathogenesis of Alzheimer's and prion diseases.[5] Two major difficulties have retarded the development of design approaches to β-sheets. (i) The intrinsic tendency of sheet-like structures to aggregate, leading to solubility problems, was indeed recognized in early studies of the β-sheet model betabellin.[1] (ii) The absence of well determined cross-strand amino acid preferences in protein β-sheets[6] limits rational design of sequences to facilitate long-range interactions. Recent success in development of soluble β-hairpin models has resulted from the recognition that nucleating β-turns of the appropriate stereochemistry (type I′ and type II′) can facilitate hairpin formation. The sequence choices at the turns have been limited to Asn-Gly and DPro-Gly; segments which have a strong tendency to adopt type I′/II′ conformations. This is a consequence of the stereochemical imperative that the $i + 1$ residue in type I′/ II′ β-turns must adopt local left-handed helical (α_L) conformations. While in DPro, pyrrolidine ring formation restricts the N–C$^\alpha$ torsion angle to the desired value of +60 ± 20°, Asn residues have the highest propensity to adopt α_L conformations, amongst the 20 protein amino acids.[7] DPro-Gly segments have been shown to be superior to Asn-Gly segments in stabilizing β-hairpins.[8] There have been several recent reports describing construction of three-stranded β-sheet structures soluble in both organic and aqueous media.[9] We describe here the unambiguous characterization of a four-stranded β-sheet structure in a designed 26 residue synthetic peptide (Beta-4, Fig 1).† Three internal DPro-Xxx sequences were positioned to nucleate type II′/I′ β-turn conformations. In the strands, a preponderance of β-branched residues (Ile, Val, Thr) was chosen to facilitate extended strand formation. Lys/Arg residues were introduced to promote solubility and reduce the chances of aggregation. The aromatic residues Phe/Tyr were positioned so as to permit observation of long-range side chain interactions as diagnostics for structure formation.

The CD spectrum of the peptide in water showed a negative band at *ca.* 213 nm. In MeOH and MeOH–water mixtures, there is considerable intensification of this negative CD band, a feature consistent with a β-sheet structure for the peptide Beta-4. The 500 MHz ^{1}H NMR spectrum for Beta-4 in MeOH was extremely well resolved, permitting sequence specific assignments using a combination of TOCSY and NOESY experiments. All proton resonances observed for the peptide Beta-4 were sharp and there was no appreciable concentration dependence of chemical shifts in the range of 3.2 to 0.1 mM, suggesting the absence of aggregation effects. Several C$^\alpha$H resonances were observed at low field positions, ≥4.6 ppm [T3 (4.60), I4 (4.87), K5 (4.85), I8 (4.74), T9 (4.87), F10 (5.00), A11 (4.96), V15 (4.61), L16 (5.04), F17 (5.10), A18 (4.94), T23 (4.75), Y25 (5.15)]. Furthermore, large values of vicinal coupling constants $J_{\alpha HNH} \geq 8.5$ Hz were observed for several NH resonances which could be accurately measured from resolution enhanced 1D experiments [J(Hz): T3 (8.9), I4 (9.4), K5 (8.6), F10 (9.4), A11 (9.0), T14 (9.0), A18 (8.5), V19 (8.6), K22 (8.8), L24 (8.7), Y25 (8.5)]. These parameters are consistent with a large number of residues in Beta-4 adopting β-strand conformations. NOE data provide definitive confirmation of the β-sheet structure in the peptide. For all residues in the strand segments the observed $C_i^\alpha HN_{i+1}H$ ($d_{\alpha n}$) NOE was appreciably more intense than the corresponding intraresidue $N_iHC_i^\alpha H$ ($d_{n\alpha}$) NOE. This is a characteristic of residues adopting (ϕ, ψ) values in the β-strand region. Observation of several key long-range NH–NH NOEs (T3-F10, K5-I8, A11-T14, V19-K22, and V15-R26) in the NOESY spectra of Beta-4 provide evidence for the proper registry of the β-strands, as shown in Fig.1. The location of the turn segments is confirmed

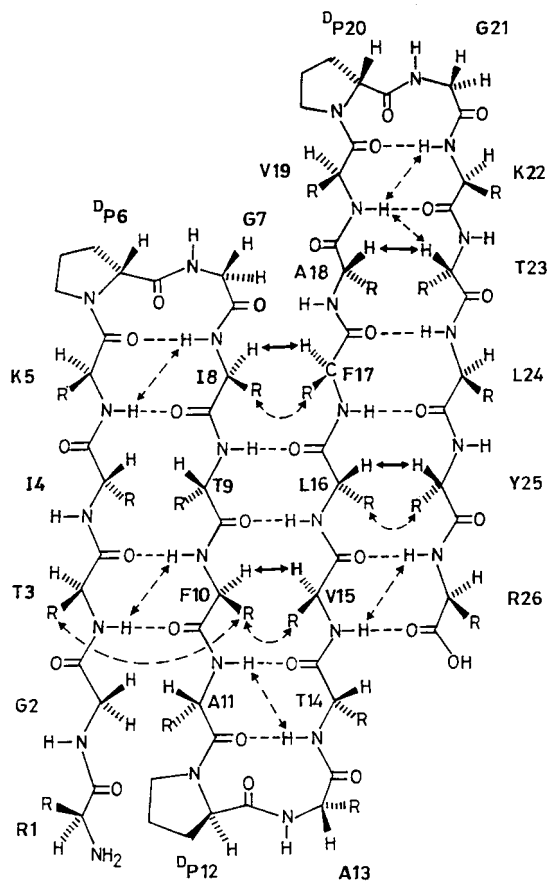

Fig. 1 Schematic representation of the target structure for the peptide Beta-4. A summary of some important long range NOEs observed for the peptide are indicated by arrows. Solid arrows indicate strong NOEs and broken arrows indicate weak NOEs.

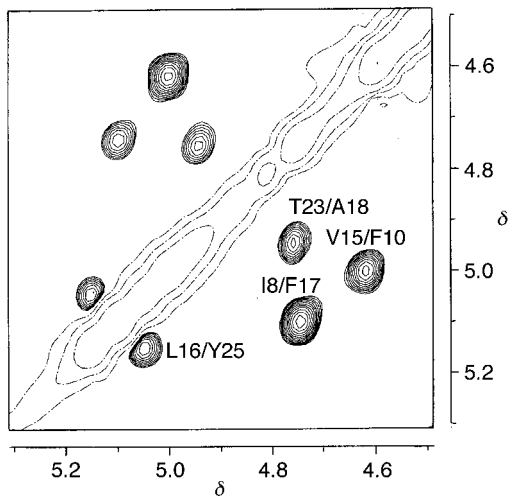

Fig. 2 Portion of the ROESY spectrum of Beta-4 in CD_3OD at 300 K, highlighting long-range $C^{\alpha}H$–$C^{\alpha}H$ NOEs.

by the observation of the sequential d_{NN} connectivities, G7-I8, A13-T14 and G21-K22. In all three turns the $i + 2$ residue must adopt local helical conformations in which these NOEs are expected. Fig. 2 shows an expanded view of the NOEs observed between $C^{\alpha}H$ protons. The observed cross-stranded interactions between I8-F17, F10-V15, A18-T23 and L16-Y25 provide clear support for the structure in Fig.1. The $d_{\alpha\alpha}$ NOE between I4 and T9 could not be detected due to overlap of these resonances with the residual OH resonance of the solvent. However, the proper registry of the two N-terminal strands is supported by the observation of both the expected cross-strand NH–NH NOEs (K5-I8 and T3-F10). Identification of several sidechain–sidechain NOEs between methyl resonances at high field and the aromatic resonances at low field provides strong evidence of compact structure of the peptide in solution. Most importantly, the NOEs observed between the aromatic protons of F10 and the methyl protons of V15 and T3 clearly support the alignment of the first three N-terminal strands. Inter-residue aromatic proton–methyl proton NOEs between I8-F17 and L16-Y25 are also clearly indicative of proper strand registry. Using a total of 100 observed NOEs, 11 dihedral angle constraints from *J* values, and 10 hydrogen bonding constraints obtained from H/D exchange data, structure calculations were performed using DYANA.[10] Fig. 3 shows a superposition of 12 calculated structures with a mean RMSD of 0.59 Å for all back bone atoms in the the well-ordered region of residues 3–25 and 1.32 Å for all heavy atoms in the same region of residues. In 50% MeOH–water most of the long range NOEs characteristic of the β-sheet structure are retained. Methyl resonances of I8 and V15 appear at extremely high field due to the shielding of aromatic rings of F10 and F17. This feature is characteristic of sidechain clustering in the β-sheet. In 50% MeOH–water both these resonances move to slightly lower field. In water these ring current effects are significantly reduced [I8 $C^{\gamma}H_3$ (0.40 ppm) in MeOH, (0.50 ppm) in 50% MeOH–water, (0.67 pm) in water]. In water, NOEs characteristic of the three β-turn segments are retained (NH–NH NOEs between G7-I8, A13-T14 and G21-K22). However, long range interstrand NOEs diagnostic of the β-sheet structure were abolished suggesting that solvent invasion disrupts the proper strand registry for β-sheet formation. Since cooperative cross-strand hydrogen bonding may be the dominant cementing force in β-sheets, competition from a strongly hydrogen bonding solvent like water may disrupt sheet formation unless the segment is sequestered in a relatively apolar environment. It is not surprising that β-sheets in proteins are often largely solvent inaccessible. The recent observation of completely solvent exposed β-sheet[11] holds promise for further refining of Beta-4 to provide additional stability for a sheet in a completely aqueous environment. Rational design of β-sheet structures will prove useful in understanding the forces of

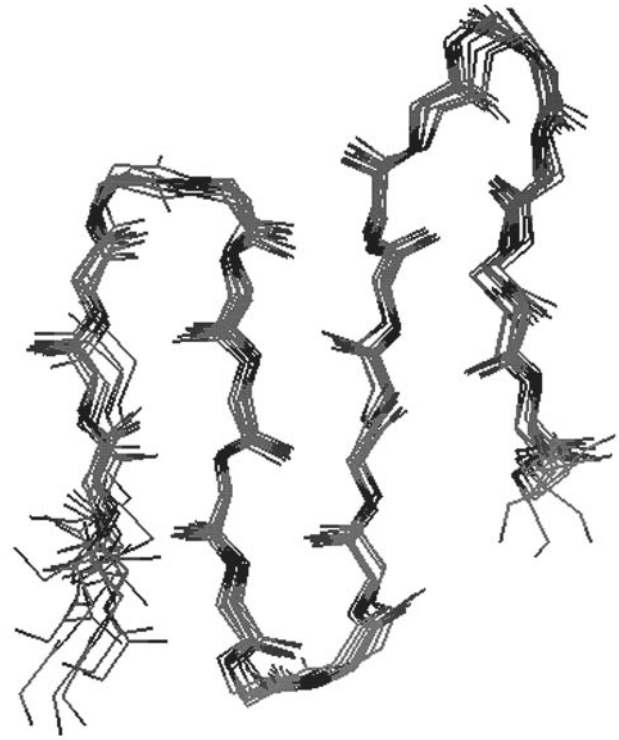

Fig. 3 Superposition of the best 12 structures of Beta-4 obtained from NMR restraints. Backbone traces illustrating the four-stranded β-sheet fold of the molecule are shown.

nucleation and structure propagation in addition to throwing light on the factors that determine the tendency of these structures to aggregate, a factor of particular importance in diseases caused by polypeptide precipitation.

Program support from the Department of Biotechnology to the Indian Institute of Science is gratefully acknowledged. The authors thank S. Kumar Singh and S. Madhusudan for help with structure calculations.

Notes and references

† The 26-residue peptide (Beta-4) was synthesized by standard solid-phase procedures based on Fmoc chemistry and purified by reverse phase HPLC (C18, 10μ) using MeCN–water (containing 0.1% TFA) gradients for elution. The peptide was characterized by its electrospray ionization mass spectrum (M observed 2775.10, M calculated 2775.30) and by complete assignment of the 500 MHz ^{1}H NMR spectrum. All NMR studies were carried out on a Bruker DRX 500 spectrometer.

1 S. F. Betz, D. P. Raleigh and W. F. DeGrado, *Curr. Opin. Struct. Biol.*, 1995, **5**, 457; J. S. Richardson, D. C. Richardson, N. B. Tweedy, K. M. Gernert, T. P. Quinn, M. H. Hecht, B. W. Erickson, Y. Yan, R. D. McClain, M. E. Donlan and M. C. Surles, *Biophys. J.*, 1992, **63**, 1186.
2 P. Y. Chou and G. D. Fasman, *Biochemistry*, 1974, **13**, 222.
3 R. B. Hill and W. F. DeGrado, *J. Am. Chem. Soc.*, 1998, **120**, 1138.
4 M. D. Struthers, R. P. Cheng and B. Imperiali, *Science*, 1996, **271**, 342; B. I. Dahiyat and S. L. Mayo, *Science*, 1997, **278**, 82.
5 J. W. Kelly, *Curr. Opin. Struct. Biol.*, 1996**, 6**, 11.
6 K. Gunasekaran, C. Ramakrishnan and P. Balaram, *Protein Eng.*, 1997, **10**, 1131.
7 J. S. Richardson, *Adv. Protein. Chem.*, 1981**, 34**, 167.
8 H. E. Stanger and S. H Gellman, *J. Am. Chem. Soc.*, 1998, **120**, 4236.
9 G. J. Sharman and M. S. Searle, *J. Am. Chem. Soc.*, 1998, **120**, 5291; C. Das, S. Raghothama and P. Balaram, *J. Am. Chem. Soc.*, 1998, **120**, 5812; H. L. Schenck and S. H. Gellman, *J. Am. Chem. Soc.*, 1998, **120**, 4869; T. Kortemme, M. R. Alvarado and L. Serrano, *Science*, 1998, **281**, 253.
10 P. Güntert, C. Mumenthaler and K. Wüthrich, *J. Mol. Biol.*, 1997, **273**, 283.
11 T. N. Pham, A. Koide and S. Koide, *Nat. Struct. Biol.*, 1998, **5**, 115.

Communication 9/02466B

First observation of excited triplet dimers with strong intramolecular interactions: planar binuclear phthalocyanines

Kazuyuki Ishii,[ac] Nagao Kobayashi,*[ab] Yasuhiro Higashi,[b] Tetsuo Osa,[b] Dominique Lelièvre,[d] Jacques Simon*[d] and Seigo Yamauchi*[c]

[a] *Department of Chemistry, Graduate School of Science,* [b] *Pharmaceutical Institute, and* [c] *Institute for Chemical Reaction Science, Tohoku University, Sendai 980-8578, Japan. E-mail: nagaok@mail.cc.tohoku.ac.jp*
[d] *ESPCI-CNRS Chimie et Electrochimie des Matériaux Moléculaires, 10 rue Vauquelin, 75231 Paris Cedex 05, France*

Received (in Cambridge, UK) 12th January 1999, Accepted 19th April 1999

Zero field splitting parameters of planar binuclear phthalocyanines in the lowest excited triplet state have been obtained by using a time-resolved EPR method to show a delocalization of excitation over two phthalocyanine units for a homodimer and a contribution from a charge transfer configuration for a heterodimer.

Phthalocyanine (Pc) and porphyrin (Pr) dimers have been intensively investigated as a model of photosynthetic reaction centers.[1] It has been an important objective to evaluate intramolecular interactions of these dimers in the excited state.[2]

Zero field splittings (ZFSs) of dimers in the lowest excited triplet (T_1) state, which can be obtained by EPR, are useful parameters for evaluating interactions between constituent units in dimers.[3] Although it is difficult to obtain this kind of information on Pc derivatives due to the lack of phosphorescence in the visible region and the short lifetime,[4] a time-resolved EPR (TREPR) technique has been shown to be useful for analyses of Pc derivatives,[5] and applied to several 'face-to-face' dimers having strong intramolecular interactions.[6] However, 'head-to-tail' dimers with strong interactions have not been observed in the T_1 state not only of Pc but also of Pr derivatives, while a charge transfer (CT) contribution in the T_1 state is observed for the photosynthetic reaction centers.[7] This originates from the fact that the interaction in the T_1 state is much smaller than that in the lowest excited singlet (S_1) state.

In this study, we have applied the TREPR method to two planar binuclear conjugated Pc derivatives **3** and **4**, in which two Pcs or one Pc and pyrazinoporphyrazine (Pyz) strongly interact with each other through a common benzene ring, and have succeeded in observing TREPR spectra in the T_1 state. The ZFSs of these dimers are compared with those of the corresponding monomers, and analyzed in terms of a delocalization of excitation over two units and a contribution of a CT configuration for homo- and hetero-dimers, respectively.

Pc derivatives have been reported by us previously.[8] A 1 : 1 mixture of toluene and $CHCl_3$ of spectral grade was used as solvent for the TREPR measurements. The concentrations of the samples were (0.5–1) $\times$ 10^{-3} M. All samples were deaerated by freeze-pump-thaw cycles. TREPR measurements and simulations of the T_1 spectra were carried out following the method already reported.[9,10] Molecular orbital (MO) calculations were performed for the deprotonated species under the Pariser–Parr–Pople (PPP) approximation.[11]

TREPR spectra of **1**, **3** and **4** observed at 20 K and 0.5 μs after laser excitation are shown in Fig. 1. ZFS parameters and intersystem crossing (ISC) ratios evaluated by spectral simulations are summarized in Table 1. The ISC from the S_1 state is selective to upper T_x and T_y sublevels for all Pc derivatives, where T_z is the lowest sublevel (z = an out of plane axis). This selectivity is consistent with those of metal-free porphyrins previously reported,[12] and is interpreted by contribution of

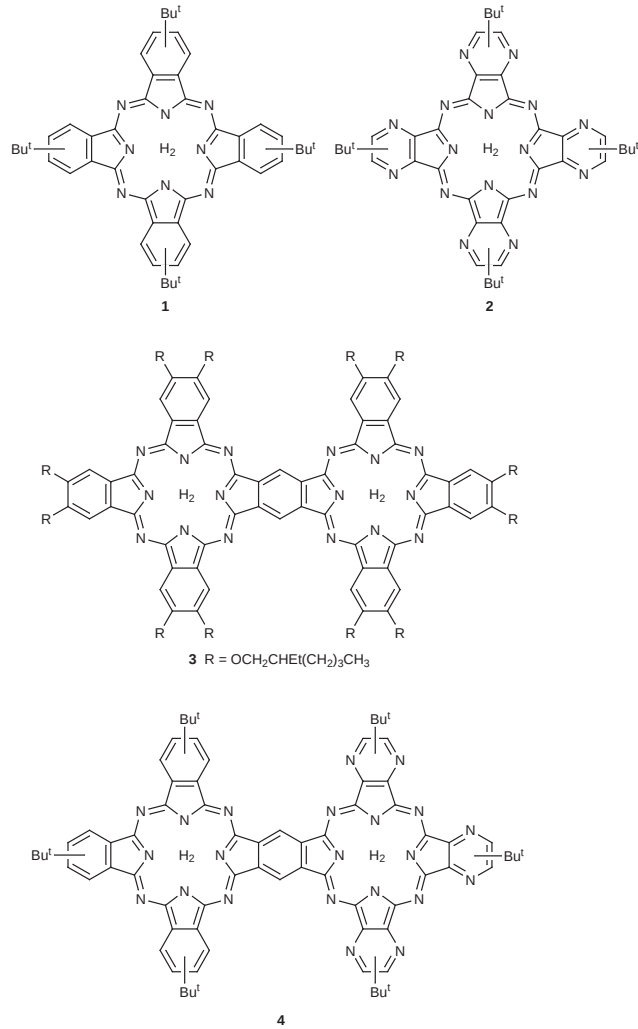

(n,π*), (σ,π*) and (π, σ*) configurations. These results indicate that the signs of the D (= $-3E_z/2$) values are positive for all Pc derivatives examined here.

It is found that the D value of **3** is much smaller than that of **1**. This decrease can be explained by a delocalization of excitation over two Pc units in the T_1 state. This is supported by a MO analysis of **3**, where the π-electrons of the HOMO and LUMO delocalize over two Pc units.[8,11] To allow a quantitative discussion, D values were calculated under a half-point charge approximation.[11,13,14] The results are summarized in Table 1, where the calculated D value (0.426 GHz) of **3** is smaller than that (0.605 GHz) of **1** in analogy with the experimental results.

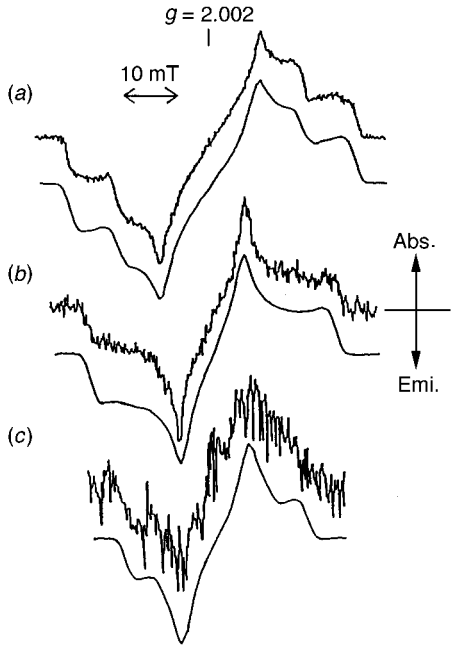

Fig. 1 TREPR spectra of (*a*) **1**, (*b*) **3** and (*c*) **4** with their simulations (lower line). These spectra were observed at 20 K and 0.5 μs after laser excitation.

Table 1 ZFS parameters and ISC ratio[a]

	D[b]/GHz	E/GHz	$P_x:P_y:P_z$	D_{calc}/GHz
1	0.758	0.070	0.46 : 0.54 : 0	0.605
2	0.900	0.080	0.47 : 0.53 : 0	0.673
3	0.645	0.105	0.35 : 0.65 : 0	0.426
4	0.480	0.040	0.4 : 0.6 : 0	0.422

[a] $D = -3E_z/2$, $E = |E_x - E_y|/2$ and P_i ($i = x, y$ and z) denotes anisotropic ISC. [b] Errors of D values are within 0.016 and 0.008 GHz for **4** and the other Pcs, respectively.

The D value (0.480 GHz) of **4** is the smallest in our Pc derivatives, and cannot be interpreted simply by the expansion of π delocalization in the T_1 state. Since the D value of **2** is larger than that of **1**, localization of excitation on the Pyz ring can be ruled out. The MO analyses of the monomers suggest that the HOMO (−7.49 eV) and LUMO (−3.74 eV) of **1** are higher than the HOMO (−7.98 eV) and LUMO (−4.02 eV) of **2**, respectively. In fact, the electron density on the Pc ring is larger than that on the Pyz ring for the HOMO of **4**, while it is smaller for the LUMO. Therefore, the small D of **4** originates from a contribution of a CT configuration between the Pc and Pyz systems. The calculated D value of **4** is smaller than that of **3** in accordance with the experimental trend.

In summary, planar and conjugated Pc dimers have been studied in terms of D values. The D value of **3** is smaller than that of **1** and can be explained by a delocalization of excitation over two Pc units in the T_1 state. The D value of **4** is further lowered and can be interpreted as the contribution of the CT configuration between the Pc and Pyz systems. The CT contribution to the D value is strikingly similar to the photosynthetic reaction center. To the best of our knowledge, 'head-to-tail' dimers with such strong T_1 interactions have not been reported in Pr and Pc derivatives to date. Therefore, these results are not only important as a model of the photosynthetic reaction center but also attractive in relation to the mechanism of electron and energy transfer in photonic devices.

This work was supported by a Grant-in-Aid for Scientific Research on Priority Area 'Nanoscale Magnetism and Transport' No. 10130202 and for Scientific Research No. 10740300 from the Ministry of Education, Science, Sports, and Culture, Japan, and the Mitsubishi Foundation.

Notes and references

1 J. Deisenhofer, O. Epp, K. Miki, R. Huber and H. Michel, *J. Mol. Biol.*, 1984, **180**, 385; J. Deisenhofer, O. Epp, K. Miki, R. Huber and H. Michel, *Nature*, 1985, **318**, 618.
2 M. Gouterman, D. Holten and E. Lieberman, *Chem. Phys.*, 1977, **25**, 139; A. Osuka and K. Maruyama, *J. Am. Chem. Soc.*, 1988, **110**, 4454; O. Bilsel, J. Rodriguez, D. Holten, G. S. Girolami, S. N. Milam and K. S. Suslick, *J. Am. Chem. Soc.*, 1990, **112**, 4075; N. Ishikawa, O. Ohno, Y. Kaizu and H. Kobayashi, *J. Phys. Chem.*, 1992, **96**, 8832; A. M. Brun, A. Harriman, V. Heitz and J.-P. Sauvage, *J. Am. Chem. Soc.*, 1991, **113**, 8657.
3 H. Stenlicht and H. M. McConnell, *J. Chem. Phys.*, 1961, **35**, 1793; H. Hayashi, S. Iwata and S. Nagakura, *J. Chem. Phys.*, 1969, **50**, 993; H. Hayashi and S. Nagakura, *Mol. Phys.*, 1970, **19**, 45.
4 P. S. Vincett, E. M. Voigt and K. E. Rieckoff, *J. Chem. Phys.*, 1971, **55**, 4131.
5 K. Akiyama, S. Tero-Kubota and Y. Ikegami, *Chem. Phys. Lett.*, 1991, **185**, 65.
6 R. Miyamoto, S. Yamauchi, N. Kobayashi, T. Osa, Y. Ohba and M. Iwaizumi, *Coord. Chem. Rev.*, 1994, **132**, 57; S. Yamauchi, H. Konami, K. Akiyama, M. Hatano and M. Iwaizumi, *Mol. Phys.*, 1994, **83**, 335; N. Kobayashi, M. Togashi, T. Osa, K. Ishii, S. Yamauchi and H. Hino, *J. Am. Chem. Soc.*, 1996, **118**, 1073.
7 J. R. Norris, D. E. Budil, P. Gast, C.-H. Chang, O. El-Kabbani and M. Schiffer, *Proc. Natl. Acad. Sci. U.S.A.*, 1989, **86**, 4335; J. R. Norris, T. J. DiMagno, A. Angerhofer, C.-H. Chang, O. El-Kabbani and M. Schiffer, *Jerusalem Symp. Quantum Chem. Biochem.*, 1990, **22**, 11.
8 D. Lelièvre, L. Bosio, J. Simon, J.-J. André and F. Bensebaa, *J. Am. Chem. Soc.*, 1992, **114**, 4475; N. Kobayashi, H. Lam, W. A. Nevin, P. Janda, C. C. Leznoff, T. Koyama, A. Monden and H. Shirai, *J. Am. Chem. Soc.*, 1994, **116**, 879; N. Kobayashi, Y. Higashi and T. Osa, *J. Chem. Soc., Chem. Commun.*, 1994, 1785.
9 K. Ishii, S. Yamauchi, Y. Ohba, M. Iwaizumi, I. Uchiyama, N. Hirota, K. Maruyama and A. Osuka, *J. Phys. Chem.*, 1994, **98**, 9431; K. Ishii, Y. Ohba, M. Iwaizumi and S. Yamauchi, *J. Phys. Chem.*, 1996, **100**, 3839.
10 K. Tominaga, S. Yamauchi and N. Hirota, *J. Phys. Chem.*, 1990, **94**, 4425.
11 N. Kobayashi and H. Konami, in *Phthalocyanines: Properties and Applications*, ed. C. C. Leznoff and A. B. P. Lever, VCH, New York, 1996, vol. IV, p. 343.
12 J. H. van der Waals, W. G. van Dorp and T. J. Schaafsma, in *The Porphyrins*, ed. D. Dolphin, Academic Press, New York, 1978, vol. IV, p. 257.
13 J. Higuchi, *J. Chem. Phys.*, 1963, **38**, 1237; S. Yamauchi, N. Hirota and J. Higuchi, *J. Phys. Chem.*, 1988, **92**, 2129.
14 The D values were evaluated using HOMO and LUMO calculated under the PPP approximation (ref. 11)

Communication 9/00347I

Homogeneous hydrogenation of aqueous hydrogen carbonate to formate under exceedingly mild conditions—a novel possibility of carbon dioxide activation†

Ferenc Joó,*[ab] Gábor Laurenczy*[c], Levente Nádasdi[bc] and János Elek[b]

[a] *Institute of Physical Chemistry and* [b] *Research Group of Homogeneous Catalysis of the Hungarian Academy of Sciences, L. Kossuth University, H-4010 Debrecen, PO Box 7, Hungary. E-mail: jooferenc@tigris.klte.hu*
[c] *Universitè de Lausanne, Institut de Chimie Minèrale et Analytique, CH-1015 Lausanne-Dorigny, Switzerland*

Received (in Cambridge, UK) 24th March 1999, Accepted 26th April 1999

Water soluble ruthenium(II)– and rhodium(I)–phosphine complexes catalyze the hydrogenation of aqueous HCO_3^- to HCO_2^- under mild conditions with turnover frequencies up to 262 TO h^{-1}.

Reduction of carbon dioxide into useful starting materials of organic synthesis is an aim of paramount importance both for economic and environmental reasons.[1] It is intriguing that while in the dark reactions of photosynthesis carbon dioxide reacts in an aqueous medium under very mild conditions, efficient synthetic systems usually require elevated temperatures and pressures to achieve reasonable reaction rates. In homogeneous systems, both in the liquid and in the supercritical state, several ruthenium complexes, such as $[RuCl_2(PMe_3)_4]$ **1** and $[RuCl_2(dppe)_2]$ **2** showed impressive catalytic activity in the reaction of CO_2, H_2 and $HNMe_2$ yielding dimethyl formamide.[2,3] Leitner *et al*.[4] investigated the hydrogenation of CO_2 in *aqueous solutions* with $[RhCl(tppts)_3]$ **3** as catalyst [tppts = tris(3-sulfonatophenyl)phosphine] which gave formate with initial reaction rates of 7260 h^{-1} at 81 °C and 1365 h^{-1} at 23 °C in the presence of $HNMe_2$ under 40 atm total pressure (CO_2/H_2 = 1). It is of interest that under identical conditions $[RuCl_2(tppts)_3]$ **4** showed[4] a TOF of only 6 h^{-1} (23 °C), and no formic acid was detected in aqueous solutions with **3** without an amine.

Water soluble phosphine complexes of platinum metals were introduced into the homogeneous catalysis scene by Joó and Beck[5] who also noted the interaction of CO_2 with $[HRuCl(tppms)_3]$ **5** (tppms = 3-sulfonatophenyldiphenylphosphine) in aqueous solution.[6] Recently it was established that formation of the water soluble hydrides of ruthenium(II), such as **5** $[H_2Ru(tppms)_4]$ **6** and $[HRuCl(tppms)_2]_2$ **7** from $[RuCl_2(tppms)_2]_2$, **8**, tppms and H_2, and their distribution in aqueous solution is strongly pH-dependent which leads to opposite selectivities in acidic and basic solutions during the biphasic hydrogenation of unsaturated aldehydes.[7] This prompted us to reinvestigate the hydrogenation of carbon dioxide and its derivatives in aqueous solutions catalyzed by water soluble platinum group metals phosphine complexes *as a function of pH*. In addition to $[RuCl_2(tppms)_2]_2$, $[RhCl(tppms)_3]$ **9** $[HRu(ac)(tppms)_3]$ **10**, *trans*-$[IrCl(CO)(tppms)_2]$ **11**, $[PdCl_2(tppms)_2]$ **12**, and complexes of 1,3,7-triaza-7-phosphaadamantane (pta), such as $[RuCl_2(pta)_4]$ **13** and $[RhCl(pta)_3]$ **14** were also studied.[8] Here we report that **8**–**10** and **13** catalyze the hydrogenation of CO_2 in aqueous solutions under mild conditions without the need of an amine additive.

When solutions of **8**, **9** and **13** were agitated under a CO_2–H_2 atmosphere (up to 80 atm total pressure) at 24 °C, small amounts of formic acid were detected by $^1H/^{13}C$ NMR with TOFs not exceeding 1.5 h^{-1} (Table 1). However, when the solvent was changed for 0.2–1.0 M $NaHCO_3$ a substantial increase in the catalytic activity was observed and TOFs reached 262 h^{-1} with **9** at 24 °C. Further increase of the pH decreased the rate of hydrogenation (entry 7). These data represent a significant improvement over previous results in that the turnover frequencies for Ru-based catalysts are among the highest obtained so far in aqueous solutions, moreover, the reductions do not require addition of an organic co-solvent or an amine or alcohol to stabilize the product. In contrast, no formate production took place with **11**, **12** and **14** under the conditions of entry 13. Instead, **12** yielded a dark brown precipitate while the originally yellow solutions of **11** and **14** became colorless; these reactions were not investigated in further detail. We note, however, that Pruchnik *et al*.[9] observed catalysis of the reverse water gas shift reaction in aqueous solution by $[Rh_2(ac)_4(H_2O)_2]$ + pta (Rh : pta = 1 : 3); no sign of CO formation in our system with **14** was detected.

Most of the experiments were done on the hydrogenation of aqueous $NaHCO_3$ solutions; the results are summarized in Table 1. No carbon containing products other than formate were

† Dedicated to Prof. Mihály T. Beck on the occasion of his 70th birthday.

Table 1 Reduction of CO_2 in aqueous systems at various pH catalyzed by water soluble Ru- and Rh-phosphine complexes‡

Entry	Catalyst	[P]/[M][a]	Base/solvent	$p(CO_2)$/atm	$p(H_2)$/atm	T/°C	t/h	TON	TOF/h^{-1} average
1	**8**	5	H_2O	20	60	24	14.5	21.6	1.49
2	**9**	6	H_2O	20	60	24	14.5	1.6	0.11
3	**13**	4	H_2O	20	60	24	13.5	3.2	0.24
4	**8**	4	1 M $NaHCO_3$	—	60	54	209	289	1.4 (47)[b]
5	**13**	4	1 M $NaHCO_3$	—	60	54	456	358	0.78 (4.5)[b]
6	**13**	4	1 M $NaHCO_3$	—	60	103	22.5	358	16 (49)[b]
7	**13**	4	0.2M $NaHCO_3$+0.8 M Na_2CO_3	—	60	54	286	75	0.26
8	**10**	6	1 M $NaHCO_3$	—	10	50	18	284	16
9	**8**	5	200 mg $CaCO_3$/2 ml H_2O[c]	20	60	24	14	372[d]	26.6
10	**9**	6	200 mg $CaCO_3$/2 ml H_2O[c]	20	60	24	14	262	18.7
11	**13**	4	200 mg $CaCO_3$/2 ml H_2O[c]	20	60	24	14	35	2.5
12	**8**	2	0.2 M $NaHCO_3$	—	10	50	4	0.04	0.01
13	**8**	4	0.2 M $NaHCO_3$	—	10	50	4	60	15
14	**8**	6	0.2 M $NaHCO_3$	—	10	50	4	60	15
15	**8**	4	0.2 M $NaHCO_3$ + 0.2 M KI	—	10	50	4	55	14
16	**9**	7	1 M $NaHCO_3$	5	35	24	2	524	262

[a] Total phosphorus to metal ratio; [M] = 2.0–2.5 mM. [b] Initial turnover frequencies in parentheses. [c] Suspensions. [d] 0.93 M HCO_2^- final solution.

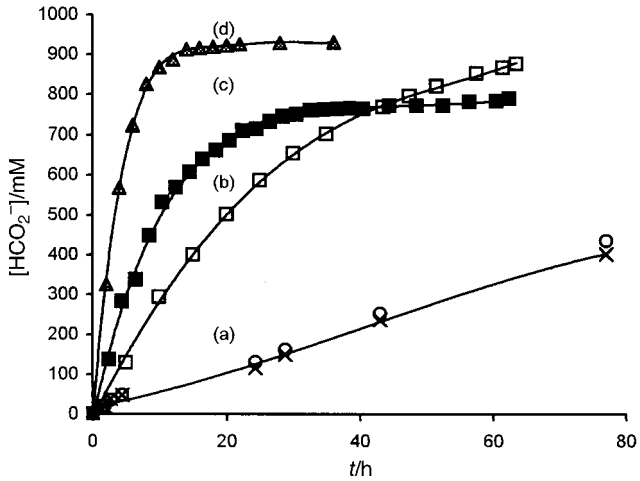

Fig. 1 Time course of formate production in reaction of HCO_3^- with H_2 catalyzed by $[RuCl_2(pta)_4]$ [(a), (b), (d)] and by $½[RuCl_2(tppms)_2]_2$ + 2 tppms (c) at 50 (c), 54 (a), 90 (b) and 103 °C (d) followed by ^1H [(a), –**x**–] or ^{13}C NMR (all other cases).

detected. With any of **8**–**10** and **13** the reactions started with no appreciable induction period (Fig. 1). Increase of the temperature from 54 to 103 °C caused an 11-fold increase of the initial rate of formate production with **13** (entries 5, 6). Despite the similarity[10] of pta to PMe_3, **13** proved considerably less active than **8**. However, the anionic ligand of the catalyst (precursor) had no significant influence: either **8** in the presence of NaI or **10** gave approximately the same rate as the unmodified **8** (entries 8, 13, 15). Both with **8** and **9** some excess of tppms proved beneficial for activity and catalyst stability—in fact **8** was almost completely inactive without added tppms; however, its catalytic activity was no further increased when the total tppms/Ru ratio exceeded 4 (entries 12–14). As expected, increase of the hydrogen pressure increased the rate of reduction with all catalysts. Conversely, while CO_2 in the gas phase was detrimental with **8** and **13**, it was essential for high reaction rates with **9** (although a much slower reaction still proceeded in its absence). The substrate bicarbonate can be produced *in situ* in the reaction of carbonates and CO_2. When a 2 ml aqueous suspension of 200 mg $CaCO_3$ was pressurized with CO_2 (20 atm) and H_2 (60 atm) and shaken in an NMR tube overnight at 24 °C with **8**, calcium formate was produced with TOF = 26.6 h^{-1}, the total TON reaching 372. Similar experiments with **9** and **13** yielded formate with TOF 18.7 and 2.5 h^{-1}, respectively (see also Table 1). The presence of $CaCO_3$ in these systems is highly beneficial, since under the same conditions CO_2 alone is reduced with TOF 1.49 (**8**), 0.11 (**9**), and 0.24 h^{-1} (**13**); the rate increase with **9** is more than 160-fold!

It is premature to speculate on detailed mechanisms of the hydrogenation of bicarbonate in these systems. It is known[7] that in aqueous KCl solutions, at the pH (8.3) corresponding to that of 1 M of $NaHCO_3$ solutions used in the present experiments, **8** + tppms + H_2 rapidly yields **6** in which the total P/Ru ratio is 4, found optimal for reductions here (entry 13). However, pH-static titrations (similar to those described in ref. 7) of **8** under H_2 in $NaHCO_3$ solutions containing an excess of tppms showed formation of only 0.4–0.6 mol H^+ for 1 mol Ru during the early phase of the reaction (instead of 2 mol required for **6**). This suggests a monohydride, possibly $[HRu(HCO_3)(tppms)_4]$ as a more likely intermediate. Both of these catalysts would account for the observed independence of the rate from the starting composition of the catalyst precursor. Assuming a constant catalyst composition in the pH range from 8.3 (1 M $NaHCO_3$) to 10.8 (0.2 M $NaHCO_3$ + 0.8 M Na_2CO_3) the lower reactivity of CO_3^{2-} (entry 7) is consistent with its known inferior tendency of oxygen exchange with H_2O compared to HCO_3^-.[11]

So far homogeneous catalytic hydrogenation of HCO_3^- in aqueous solutions has not been reported in the literature. Stalder *et al.*[12] used various heterogeneous Pd catalysts with a maximum TOF of 35 h^{-1} (Pd/C, 25 °C). Kudo *et al.*[13] studied in detail the reduction of CO_2 (40 atm) catalyzed by $PdCl_2$ in aqueous KOH at forcing conditions (106 atm H_2, 240 °C). In our opinion, based on the $CO_3^{2-}/HCO_3^-/H_2O$ equilibrium, all similar reactions using *aqueous* solutions or mixture of amines or carbonates under CO_2 pressure, in fact, may have utilized HCO_3^- as the real substrate in the catalytic cycle. This could also explain the beneficial effect of a small amount of H_2O on CO_2 reductions often observed[4b,14] in organic solvent systems.

This work was supported by the Hungarian National Research Foundation (OTKA T023997 and F 023159) and by the Office Fédéral de l'Education et de la Science, Suisse (OFES C98.0011 to G.L.). L. N. is grateful for an OFES fellowship, 1998/99. The loan of $RuCl_3.xH_2O$ by Johnson-Matthey PLC is gratefully acknowledged. This research is part of the collaboration within the COST Action D10 /0001 Working Group.

Notes and references

‡ Non-SI units: *p*/atm = 101.325 kPa; *T*/K = T/°C + 273.15. Ligands tppms, pta and their Rh, Ru and Ir complexes were prepared as described in refs 8–10. Hydrogenation experiments were carried out in well stirred, heavy walled glass tubes with 10 atm H_2 or in high pressure sapphire NMR tubes with 60 atm H_2 (pressures at room temperature) intensively shaken (300 min^{-1}) on top of a laboratory shaker. Formate concentration was determined by HPLC or the reaction mixture was analyzed *in situ* by ^1H and/or ^{13}C NMR spectroscopy (Bruker AC 200, AM 360, DRX 400) using ^{13}C-enriched (99%) $NaHCO_3$.

1 Most recent reviews: D. Walther, M. Ruben and S. Rau, *Coord. Chem. Rev*., 1999, **182**, 67; X. Yin and J. R. Moss, *Coord. Chem. Rev*., 1999, **181**, 27.
2 P. G. Jessop, T. Ikariya and R. Noyori, *Nature*, 1994, **368**, 231.
3 O. Kröcher, R. A Köppel and A. Baiker, *Chem. Commun*., 1997, 453.
4 (*a*) W. Leitner, *Angew. Chem*., 1995, **107**, 2391; *Angew. Chem., Int. Ed. Engl.*, 1995, **34**, 2207; (*b*) W. Leitner, E. Dinjus and F. Gassner, in *Aqueous-Phase Organometallic Catalysis*, ed. B. Cornils and W. A. Herrmann, Wiley-VCH, Weinheim, 1998, p. 486.
5 F. Joó and M. T. Beck, *Magy. Kém. Foly.*, 1973, **79**, 189; F. Joó, *Proc. 15th ICCC* (*Moscow, USSR, 1973*), p. 556.
6 F. Joó and M. T. Beck, *React. Kinet. Catal. Lett*., 1975, **2**, 257.
7 F. Joó, J. Kovács, A. Cs. Bényei and Á. Kathó, *Catal. Today*, 1998, **42**, 441.
8 (**8**, **10**): Z. Tóth, F. Joó and M. T. Beck, *Inorg. Chim. Acta.*, 1980, **42**, 153; (**9**, **11**): F. Joó, J. Kovács, Á. Kathó, A. C. Bényei, T. Decuir and D. J. Darensbourg, *Inorg. Synth.*, 1998, **32**, 1; (**12**): K.-C. Tin, N.-B. Wang, R.-X. Li, Y.-Z. Li and X.-J. Li, *J. Mol. Catal. A: Chem.*, 1998, **137**, 113; (**13**): D. J. Darensbourg, F. Joó, M. Kannisto and Á. Kathó, *Organometallics*, 1992, **11**, 1990; (**14**): F. Joó, L. Nádasdi, A. Cs. Bényei and D. J. Darensbourg, *J. Organomet. Chem*., 1996, **512**, 45.
9 F. P. Pruchnik, P. Smolenski and I. Raksa, *Pol. J. Chem*., 1995, **69**, 5.
10 J. R. Delerno, L. M. Trefonas, M. Y. Darensbourg and R. J. Majeste, *Inorg. Chem*., 1976, **15**, 816.
11 H. Gamsjäger and R. K. Murmann, in *Adv. Inorg. Bioinorg. Mech.*, 1983, **2**, 343.
12 C. J. Stalder, S. Chao, D. P. Summers and M. S. Wrighton, *J. Am. Chem. Soc*., 1983, **105**, 6318.
13 K. Kudo, N. Sugita and Y. Takezaki, *Nippon Kagaku Kaishi*, 1997, 302; *Chem. Abstr*., 1977, **86**, 178068s.
14 Y. Inoue, H. Izumida, Y. Sasaki and H. Hashimoto, *Chem. Lett*., 1976, 863.

Communication 9/02368B

ChemComm

Crystal structure of the microporous titanosilicate ETS-10 refined from single crystal X-ray diffraction data

Xiqu Wang and Allan J. Jacobson*

Department of Chemistry and Materials Research Science and Engineering Center, University of Houston, Houston, Texas 77204-5641. E-mail: ajjacob@uh.edu

Received (in Bloomington, IN, USA) 16th February 1999, Accepted 20th April 1999

ETS-10 crystals up to 45 μm in size have been synthesized at 240 °C under a pressure of 80 MPa and the structure refined from single crystal X-ray diffraction data.

Microporous titanosilicates have been of interest since the discovery of important catalytic properties in titanium silicalite-1 (TS-1) in oxidation and epoxidation reactions.[1] ETS-10 is a porous titanosilicate first reported by Kuznicki *et al.*[2,3] A large number of studies have been devoted to this material owing to its interesting chemical and physical properties.[3–18] A model for the structure of the ETS-10 framework was recently proposed by Anderson *et al*. based on a detailed HREM, NMR, powder XRD and structural modeling study.[5,6] The location of the extra-framework cations and the local environments of the framework cations have also been studied by NMR, XAS and computer modeling techniques.[7,12,17] However, to date, the small crystal size of samples of ETS-10 has prevented accurate structure refinement from single crystal data, in spite of efforts to improve the syntheses.[18] The positions of the extra-framework cation sites have not yet been determined experimentally from diffraction data.

We are investigating the possibility of improving the size and crystal quality of microporous materials by using synthesis temperatures and pressures that are higher than those usually employed (≤400 °C and ≤200 MPa). By using this approach, ETS-10 crystals as large as *ca.* 45 μm have been obtained and successfully used to obtain single crystal X-ray diffraction data and to subsequently refine the structure.

In a typical synthesis Na_2TiF_6 (0.208 g, 1 mmol) and TPABr (0.26 g, 1 mmol) were mixed with H_2O (2.2 ml). This mixture (0.36 ml) together with sodium silicate solution (0.72 ml, Aldrich, 14% NaOH, 27% SiO_2) and 1 M NaOH solution (0.2 ml) were sealed in a Teflon tube in air. The tube was inserted into a high pressure vessel and heated at 240 °C under an applied pressure of 80 MPa for 3 days using a LECO HR-1B-2 high pressure–high temperature system. The reaction vessel was then removed from the oven and cooled to room temperature in air. The product was washed with water, filtered and air dried. Well developed tetragonal platy crystals of ETS-10 with sizes up to *ca.* 45 μm were formed together with silicalite-1 and quartz. The yield is *ca.* 20%. All of the reflections characteristic of ETS-10 were identified in a X-ray powder diffraction pattern of the multiphase product. Composition analysis of the crystals with a JEOL 8600 electron microprobe gave the atomic ratio Ti : Si = 1.00 : 5.07 which is consistent with the formula $Na_2TiSi_5O_{13}$ reported in the literature[5] and which was confirmed by our structure refinement. For many crystallites, Na peaks were observed but diminished in intensity during the microprobe measurement probably owing to the instability of the crystals under the measurement conditions. A few crystals which did not show loss of intensity of the Na peak gave Na : Si ratios ≈ 2 : 5. ETS-10 is usually prepared from gel compositions containing both potassium and sodium cations. Synthesis in the presence of Na^+ alone, however, has been previously reported.[18]

A tetragonal body centered unit cell with a = 7.481(1) and c = 27.407(5) Å was derived from the single crystal data measured with CCD detector. Careful checking of all of the measured frames indicated that all observed reflections were consistent with this cell. This cell corresponds to that of the ordered polymorph A (see below) predicted by Anderson *et al.*[5,6] except that the a axis length is halved. The halving is expected because the electron diffraction patterns of ETS-10 reported in the literature show streaking of all reflections with h,k = odd indicative of a high degree of disorder along a.[5,6] The unit cell observed by the single crystal X-ray diffraction is a subcell of the true unit cell. Unfortunately, our samples are very sensitive to an electron beam and consequently efforts to measure their electron diffraction patterns were unsuccessful. The powder X-ray diffraction pattern of a sample from the same synthesis is consistent with a disordered structure and differs from the calculated patterns for ordered structure models.[6] The systematic extinctions in the measured X-ray reflections based on the subcell correspond to the space group $I4_1/amd$. A disordered structure model was successfully solved and refined with this symmetry, although the converged R factors of the refinements are moderately high because of the structural disorder and small crystal size.†

The refined framework structure is consistent with the structure model proposed by Anderson *et al.*[5] The TiO_6 octahedra share *trans* vertices to form TiO_5 infinite chains. These chains are each connected to two folded chains of $Si(2)O_4$ tetrahedra to form $[TiSi(2)_4O_{13}]$ columns through vertex sharing between the octahedra and tetrahedra. The columns are packed into layers parallel to the (001) plane with the columns in neighboring layers perpendicular to each other. The layers are interconnected by $Si(1)O_4$ tetrahedra which share all their vertices with the $Si(2)O_4$ tetrahedra to form a framework structure (Fig. 1, 2). In the disordered structure model based on the subcell, neighboring column positions cannot be occupied simultaneously because the resulting interatomic distances would be too short. The unoccupied column positions correspond to wide 12-ring channels. The occupancies of the column atoms [Ti, Si(2), O(3–5)] were refined to 0.50(1) and were fixed at 50% in the final refinements. Thus, each column belongs to a (001) layer that consists of parallel columns alternating with

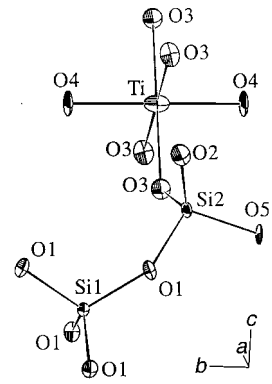

Fig. 1 Coordination environments of the Ti and Si atoms. Thermal ellipsoids are drawn with 50% probability. Bond lengths (Å): Si(1)–O(1) 1.612(7) (×4), Si(2)–O(3) 1.61(1), Si(2)–O(1) 1.615(7), Si(2)–O(5) 1.629(6), Si(2)–O(2) 1.698(4), Ti-O(4) 1.872(1) (×2), Ti–O(3) 1.99(1) (×4).

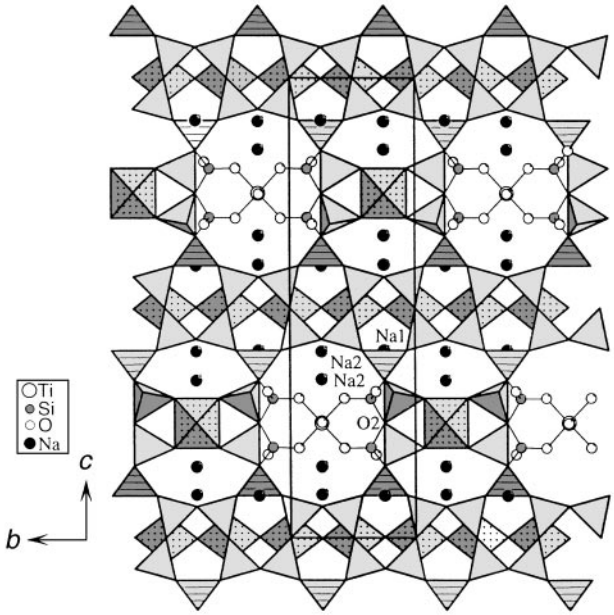

Fig. 2 Projection of the structure down (100). An ordered framework is represented with polyhedra. The $Si(1)O_4$ tetrahedra are hatched, the $Si(2)O_4$ are shaded and the TiO_6 octahedra are stippled. The non-framework Na cations are shown as filled circles.

12-ring channels. The O(2) site was found fully occupied because this site is located in the channel walls and is independent of the disorder. No disorder of the $Si(1)O_4$ tetrahedra was found in the refinements. As shown in Fig. 2, each $Si(1)O_4$ tetrahedron is connected to either a [100] $[TiSi(2)_4O_{13}]$ column plotted as ball-and-sticks or the one plotted as polyhedra. Since the neighboring (001) layers of columns are related by the 4_1 symmetry, there are four ways in which two neighboring layers are interconnected by the $Si(1)O_4$ tetrahedra to form an ordered double layer. Each of these ordered double layers may be considered as a stacking unit. Neighboring units can shift a half subcell along either [110] or [110] direction in order to form a framework. This gives rise to various stacking disorder possibilities. However, such stacking disorder does not cause blocking of the 12-ring channels. The hypothetical ordered polymorph A predicted by Anderson *et al.*[5,6] corresponds to simple ABAB… stacking. The structure model based on the subcell corresponds to fully disordered stacking.

The TiO_6 octahedron has site symmetry 2/*m* with the Ti–O bond lengths along the column axis (1.87 Å) being shorter than the others (1.99 Å). The $Si(1)O_4$ tetrahedron has site symmetry 4*m*2 with Si–O bond length 1.61 Å. The $Si(2)O_4$ tetrahedron with Si–O bond lengths 1.61–1.70 Å and O–Si–O angles 103.3–116.8° is apparently distorted but this may be a consequence of the disorder. The –O–Ti–O–Ti– backbones of the columns are nearly linear (O–Ti–O) 180°, (Ti–O–Ti) = 177.9°. The elongated thermal ellipsoids of the Ti and O(4) atoms suggest some Ti–O bond length alternation along the chain and some tilting of adjacent octahedra in the ordered structure, as predicted from previous studies.[13,17]

The sodium cations occupy two nonequivalent positions. Na(1) is located near the $Si(1)O_4$ tetrahedra and is coordinated to eight oxygen atoms at distances 2.50–2.99 Å. The occupancy of Na(1) was found, as expected, to be nearly equal to that of the column atoms. Na(2) is split into two equivalent positions 1.67 Å apart, each of which has five coordinating oxygen atoms at 2.57–2.62 Å all located on one side of the position. The nearest oxygen atom positions on the opposite side are > 3.6 Å away. The apparent one-sided coordination implies that there are disordered space-filling species such as H_2O molecules which complete the coordination sphere of Na(2), but which can not be located by the refinements because the electron density overlaps with those of the column atoms in the subcell. Substantial water loss (> 8%) below 200 °C has been reported for as-synthesized ETS-10 samples previously.[3] The splitting of the Na(2) site is related to the stacking disorder of the $[TiSi(2)_4O_{13}]$ columns.

In conclusion, we have employed a new synthesis approach to obtain ETS-10 crystals suitable for single crystal X-ray structure refinement. The structure refinement based on a disordered cell, confirms the previous structure model and provides details of the positions of both the framework atoms and extra-framework cations.

We thank the National Science Foundation (DMR9214804), the R. A. Welch Foundation for financial support. This work made use of MRSEC/TCSUH Shared Experimental Facilities supported by the National Science Foundation under Award Number DMR-9632667 and the Texas Center for Superconductivity at the University of Houston.

Notes and references

† *Crystal data*: space group $I4_1/amd$, a = 7.481(1), c = 27.407(5) Å, colorless plate, crystal size 0.045 × 0.045 × 0.01 mm. Mo-Kα radiation (λ = 0.71073 Å), μ = 1.1 mm^{-1}, $2\theta_{max}$ = 57°, $R(F)$ = 0.119/0.158 for 426 reflections with $[I > 2\sigma(I)]$ all 532 unique reflections and 52 variables.

Intensities were measured on a SMART platform diffractometer equipped with a 1K CCD area detector using graphite-monochromatized Mo-Kα radiation at 20 °C. A hemisphere of data (1271 frames at 5 cm detector distance) was collected using a narrow-frame method with scan widths of 0.30° in ω and an exposure time of 90 s frame^{-1}. The first 50 frames were remeasured at the end of data collection to monitor instrument and crystal stability, and the maximum correction applied on the intensities was < 1%. The data were integrated using the Brucker SAINT program, with the intensities corrected for Lorentz factor, polarization, air absorption, and absorption due to variation in the path length through the detector faceplate. The structure was solved with direct methods and refined using SHELXTL. All atom positions were refined anisotropically in the final refinements. Na(1) and Na(2) were fixed to have the same thermal parameters and a total occupancy of unity with a free occupancy ratio. CCDC 182/1236. See http://www.rsc.org/suppdata/cc/1999/973/ for crystallographic files in .cif format.

1 M. Taramasso, G. Perego and B. Notari, *US Pat.* 4410501, 1983.
2 S. M. Kuznicki, *US Pat.* 4853202, 1989.
3 S. M. Kuznicki, K. A. Thrush, F. M. Allen, S. M. Levine, M. M. Hamil, D. T. Hayhurst and M. Mansour, *Synth. Micopor. Mater.*, 1992, **1**, 427.
4 V. Valtchev and S. Mintova, *Zeolites*, 1994, **14**, 697.
5 M. W. Anderson, O. Terasaki, T. Ohsuna, P. J. O. Malley, A. Philippou, S. P. Mackay, A. Ferreira, J. Rocha and S. Lidin, *Nature*, 1994, **367**, 347.
6 M. W. Anderson, O. Terasaki, T. Ohsuna, P. J. O. Malley, A. Philippou, S. P. Mackay, A. Ferreira, J. Rocha and S. Lidin, *Philos. Mag. B*, 1995, **71**, 813.
7 R. J. Davis, Z. Liu, J. E. Tabora and W. S. Wieland, *Catal. Lett.*, 1995, **34**, 101.
8 R. Carli, C. L. Bianchi and V. Ragaini, *Catal. Lett.*, 1995, **33**, 49.
9 T. K. Das, A. J. Chandwadkar and S. Sivasanker, *J. Mol. Catal.*, 1996, **107**, 199.
10 X. Yang and R. E. Truitt, *J. Phys. Chem.*, 1996, **100**, 3713.
11 X. Liu and J. K. Thomas, *Chem. Commun.*, 1996, 1435.
12 M. E. Grillo and J. Carrazza, *J. Phys. Chem.*, 1996, **100**, 12 261.
13 G. Sankar, R. G. Bell, J. M. Thomas, M. W. Anderson, P. A. Wright and J. Rocha, *J. Phys. Chem.*, 1996, **100**, 449.
14 M. E. Grillo and J. Carrazza, *J. Phys. Chem.*, 1997, **101**, 6749.
15 E. Borello, C. Lamberti, S. Bordiga and C. O. Arean, *Appl. Phys. Lett.*, 1997, **71**, 2319.
16 T. K. Das, A. J. Chandwadkar and S. Sivasanker, *Catal. Lett.*, 1997, **44**, 113.
17 S. Ganapathy, T. K. Das, R. Vertrivel, S. S. Ray, T. Sen, S. Sivasanker, L. Delevoye, C. Fernandez and J. P. Amoureux, *J. Am. Chem. Soc.*, 1998, **120**, 4752.
18 J. Rocha, A. Ferreira, Z. Lin and M. W. Anderson, *Micropor. Mesopor. Mater.*, 1998, **23**, 253.

Communication 9/01280J

Apparent equilibrium shifts and hot-spot formation for catalytic reactions induced by microwave dielectric heating

Xunli Zhang, David O. Hayward and D. Michael P. Mingos*

Department of Chemistry, Imperial College of Science, Technology and Medicine, South Kensington, London, UK SW7 2AY. E-mail: d.mingos@ic.ac.uk

Received (in Cambridge, UK) 16th February 1999, Accepted 21st April 1999

Microwave dielectric heating of the gas phase decomposition of H_2S catalysed by metal sulfides on a γ-Al_2O_3 support results in significant apparent shifts in the equilibrium constant, which have been attributed to the development of hot-spots in the catalytic beds; X-ray diffraction and electron microscopy measurements have indicated the formation of hot-spots with dimensions of 90–1000 μm and which involve not only the active phase, but also the support.

The acceleration of heterogeneous catalytic processes under microwave dielectric heating conditions has attracted both academic and industrial interest.[1–5] The majority of systems studied involve a catalyst which preferentially absorbs the microwaves relative to the support material and the reasons for the observed rate enhancements have been the subject of some controversy. The measurement of temperature under conditions where there are strong electric fields is problematical, but may be overcome, for example, by using optical fibre technology. Such measurements are still only capable of providing average temperatures. Both differential coupling abilities of materials and distribution of electromagnetic fields may result in localized temperature distribution in catalytic beds, but the contribution of these effects is difficult to quantify. Stuerga and Gaillard [6,7] have given a thorough theoretical analysis which has conclusively demonstrated that specific athermal effects are implausible given the small energies associated with the microwave quanta and the classical nature of the heating phenomenon and have suggested that localized enhancements of the reaction rates may be responsible for non-isothermal and heterogeneous kinetic phenomena. The majority of the experimental studies on catalytic reactions under microwave conditions have dwelled on the kinetic aspects and noted that the rates of reaction and product distributions are more consistent with a temperature 300-400 K higher than that measured for the bulk of the catalyst bed. However, for supported metal catalysts, calculations[8,9] have shown that the rate of heat transfer at 1 atm gas pressure is so high that the formation of hot-spots localised at the catalytically active sites are implausible. Here we report significant circumstantial evidence for the formation of hot-spots in the microwave experiments and have demonstrated for the first time that these hot-spots are not localised exclusively on the active catalyst, but also involve the support material. We have also estimated the dimensions of these hot-spots.

The catalytic conversion of H_2S into hydrogen and sulfur, which is commercially important for the coal and petrochemical industry,[10,11] has recently been investigated in our laboratories using parallel microwave and conventional heating conditions. The experimental set-up is illustrated schematically in Fig. 1 and the reactions were performed under continuous flow conditions using quartz reactors. The temperature in the microwave cavity was monitored using an Accufibre optical fibre thermometer (Model 10 Luxtron) which had its tip at the centre of the catalyst sample, as shown. The microwaves were generated at 2.45 GHz using an Electro-Medical Supplies Ltd generator (0–200 W) and relayed by means of a co-axial cable to a tunable cylindrical microwave cavity placed around the reactor. The catalysts used for the study were either an impregnated catalyst based on molybdenum oxide on a γ-alumina support, which was sulfided by a pre-treatment using an H_2S–H_2 flow at atmospheric pressure for 2 h, or a mechanically mixed sample of MoS_2 and γ-alumina. The reaction products were analyzed using a quadrupole mass spectrometer (QMS-200D, European Spectrometry System).

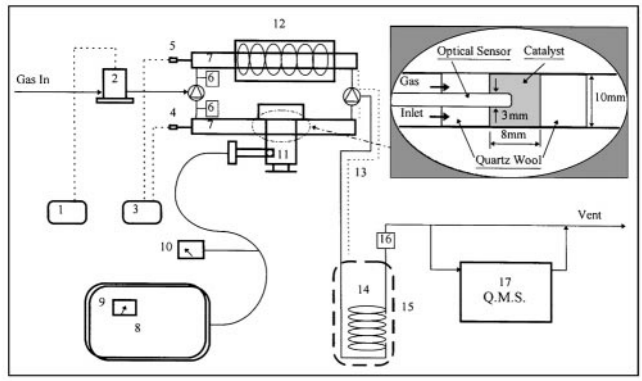

Fig. 1 Flow system for the H_2S decomposition. 1, Mass flow control unit; 2, mass flow controller; 3, temperature display; 4, optical sensor; 5, thermal couple; 6, pressure gauges; 7, quartz reactors; 8, microwave generator; 9, forward power meter; 10, reflected power meter; 11, microwave cavity; 12, conventional furnace; 13, heating tapes; 14, cold trap; 15, ice–water Dewar; 16, filter; 17, quadrupole mass spectrometer(QMS).

Fig. 2 compares the conversion efficiency for the decomposition of H_2S under microwave and conventional thermal conditions in the temperature range 500–1100 K for both the impregnated catalyst and the mechanical mixture of MoS_2 and γ-alumina (both 30% by weight MoS_2 on γ-alumina). Fig. 2 also illustrates the calculated equilibrium conversion efficiencies based on thermodynamic data of Kaliodas and Papayannakas.[12] It is noteworthy that for such an endothermic reaction the conversion efficiencies are relatively low and that for the conventional thermal reaction the experimental observed per-

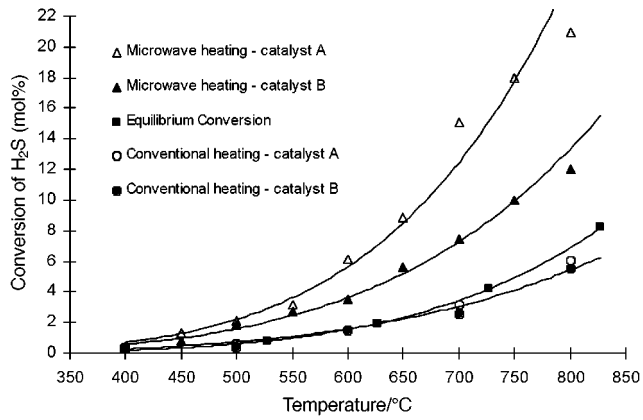

Fig. 2 H_2S conversion *vs.* temperature with mechanically mixed catalyst A and impregnated catalyst B

Table 1 Dielectric properties of the chemicals (25 °C, 2.45 GHz)

Chemical(s)	Dielectric constant, ε'	Dielectric loss, ε''	Dielectric loss tangent, tan δ
γ-Al_2O_3	2.678	0.01768	0.006604
MoS_2/γ-Al_2O_3 (impregnated)	2.971	0.2694	0.09068
$MoS_2+\gamma$-Al_2O_3 (mechanically mixed)	3.115	0.3162	0.1015
MoS_2	3.331	0.6410	0.1924

centage conversions are in good agreement with the equilibrium data. The basic reaction is given by eqn (1)

$$H_2S_{(g)} = H_{2(g)} + 1/2S_{2\,(g)} \quad (1)$$

with negligible production of other gaseous sulfur species.[12] Surprisingly, the conversion efficiency for the reaction which takes place in the microwave cavity is higher than that predicted on thermodynamic grounds. For the impregnated catalyst the percentage conversion at a temperature of 800 °C has risen from *ca*. 6.5% with conventional heating to 12% when microwaves are used. The effect is even greater for the mechanically produced catalyst, where the conversion efficiency has risen to 21% under microwave heating at 800 °C. We have concluded that these observations are not due to any athermal microwave effect, but rather that the selective features of microwave dielectric heating have induced an anisotropic temperature profile on the catalytic bed which is giving rise to 'apparent' shifts in the equilibrium constant for the reaction.

The dielectric measurements on MoS_2, the impregnated catalyst and the support materials, which are summarised in Table 1, clearly indicate that the catalysts are more 'lossy'[13] than the support materials and will initially preferentially absorb the microwave energy. The extent to which the heat is then transferred to the support has not previously been addressed. While the dielectric loss of γ-alumina is temperature dependent, particularly in the high temperature range, this temperature rise may be amplified to develop hot-spots. Such hot-spots could not only give rise to increased reaction rates, but also, if the residence times of the gases flowing over the catalyst are relatively long compared to the half-lives for the reaction, then they could create local shifts in equilibrium constant. To our knowledge attention has not been drawn previously to large equilibrium shift effects arising from this phenomenon.

We have argued that these 'apparent' equilibrium shift effects may be enhanced if the catalyst had a higher concentration of hot-spots, or had a higher temperature of hot-spots. Although, the maximum rate enhancements are achieved using a well dispersed catalyst with a high surface area, the hot-spot phenomenon is accentuated by having a poorly dispersed catalyst, such as that produced by mechanically mixing MoS_2 and γ-alumina.

Provided that the rate determining step for both forward and back reactions occurs between adsorbed species that are fully accommodated to the active catalyst temperature the equilibrium that is set-up will be characteristic of the hot-spot temperature and not the average temperature of the catalyst bed as a whole. By using this principle the hot-spot temperatures given in the second and third columns of Table 2 were calculated. The hot-spot temperatures for the impregnated and mechanically mixed catalysts are respectively *ca*. 100 and 200 °C higher than the temperature measured by the probe.

Table 2 Hot-spot temperatures calculated for impregnated catalyst and mechanical mixture of MoS_2 and γ-Al_2O_3

Probe temp./°C	Hot-spot temp./°C impregnated catalyst	Hot-spot temp./°C mechanically mixed catalyst
500	600	650
600	700	770
700	810	890
800	920	1010

X-Ray diffraction measurements on the catalyst before and after microwave heating have demonstrated some important differences compared with the parallel experiments done under thermal conditions. Firstly, some of the alumina undergoes a phase change from γ- to α-alumina—a transition which only occurs at temperatures above 1273 K.[14] It is noteworthy that the maximum average temperature recorded in the microwave experiments was 1073 K. The average crystallite size calculated from the peak widths of five intense peaks is 90 μm. Secondly, the molybdenum disulfide, which was initially evenly distributed as 150–170 μm amorphous particles (electron microscopy measurements), forms some hexagonal crystals during the microwave process. Since the melting point of MoS_2 is 1458 K, this is further evidence for the formation of hot-spots involving both the MoS_2 and the alumina support. The electron microscopy studies have also indicated that considerable migration of MoS_2 has occurred during the reaction since spheres as large as 1000 μm containing both Al_2O_3 and MoS_2 are formed. Surface area and size pore measurements have also confirmed that a considerable reorganisation has occurred and has resulted in a decrease in the surface area.

In summary, the preferential heating effects associated with microwave dielectric heating can give rise to hot-spots which result not only in rate enhancements, but also in apparent shifts in the equilibrium constant. These hot-spots probably are larger than 90 μm and may be as large as 1000 μm and have temperatures 100-200 K above that of the remainder of the bulk. The hot-spots also induce a considerable re-organisation of the catalyst under microwave conditions.

The selective nature of the dielectric heating effect cannot be reproduced easily using conventional heating methods. This phenomenon is not only interesting from an academic perspective because the results are initially counter-intuitive, but since it has the potential to increase the conversion efficiencies of reactions with low yields by an order of magnitude, whilst maintaining the same operating temperature as a conventionally heated reactor, it is not without commercial potential.

BP is thanked for endowing DMPM's Chair and EPSRC are thanked for financial support.

Notes and references

1 G. Bond and R. B. Moyes, in *Microwave Enhanced Chemistry*, ed. H. M. Kingston and S. J. Haswell, ACS Publications, Washington, 1997, p. 551 gives a review of the applications of microwaves in catalytic chemistry.
2 T. M. Thiebaut, G. Roussy, M. Medjram, L. Seyfield, F. Gasin and J. Maine, *J. Chem. Phys*., 1992, **89**, 1427.
3 G. Bond, R. B. Moyes and D. A. Whan, *Catal. Today*, 1993, **17**, 427.
4 G. Roussy, E. Marchal, J. M. Thiebaut, A. Kiennemann and G. Maire, *Fuel Process Technol*., 1997, **50**, 261.
5 G. Roussy, S. Hilaire, J. M. Thiebaut, G. Maire, F.Garin and S. Ringler, *Appl. Catal. A: Gen*., 1997, **156**, 167.
6 D. Stuerga and P. Gaillard, *Tetrahedron*, 1996, **52**, 5505.
7 D. A. C. Stuerga and P. J. Gaillard, *J. Microwave Power Electromagn. Energy*, 1996, **31**, 87; 101.
8 W. L. Perry, D. W. Cooke, J. D. Katz, and A. K. Datye, *Catal. Lett.*, 1997, **47**, 1.
9 J. R. Thomas, *Catal. Lett.*, 1997, **49**, 137.
10 V. E. Kaloidas and N. G. Papayannakas, *Ind. Eng. Chem. Res*., 1991, **30**, 345.
11 E. A. Fletcher, J. Noring and J. Murray, *Int. J. Hydrogen Energy*, 1984, **9**, 587.
12 V. E. Kaloidas and N. G. Papayannakas, *Int. J. Hydrogen Energy*, 1987, **12**, 403.
13 A. C. Metaxas and R. J. Meredith, *Industrial Microwave Heating*, Peter Peregrines Ltd, London, 1983.
14 Powder Diffraction Files, 'Inorganic Volume No. PD1S-10iRB, Joint Committee on Powder Diffraction Standards, Philadelphia, 1967' Card 10-425, American Society for Testing and Materials, PA.

Communication 9/01245A

Bathochromic or hypsochromic effects *via* the extension of conjugation: a study of stilbenoid squaraines

Herbert Meier,* Ralf Petermann and Jürgen Gerold

Institute of Organic Chemistry, University of Mainz, Duesbergweg 10-14, D-55099 Mainz, Germany. E-mail: hmeier@mail.uni-mainz.de

Received (in Liverpool, UK) 1st February 1999, Accepted 12th April 1999

In contrast to normal conjugated oligomers, the stilbenoid squaraines 3a–d do not show a convergence of VIS/NIR absorption due to the extension of conjugation; the observed bathochromic effect in the beginning of the series is followed by a hypsochromic effect; this result seems to be characteristic for stilbenoid compounds with donor–acceptor substitution.

Due to their special chromophore, squaraines (1,3-dicondensation products of squaric acid)[1,2] not only attract theoretical interest, they are also the molecular basis for numerous applications in materials science. Electrophotography,[1] optical data storage,[3] non linear optics[4,5] and conversion of solar energy[6] should be mentioned in this context.

Recently we succeeded in the preparation of symmetrical squaraines which bear stilbenyl substituents in the 1- and 3-positions.[7] Compared to 1,3-diarylsquaraines, the extended conjugation causes a dramatic bathochromic shift of the π–π* transition at long wavelengths.[7] This finding raised the question: is it possible to increase this effect by the stepwise addition of further stilbene building blocks? For this purpose we synthesized the squaraines **3a–d**[8] (Scheme 1) which are–with the exception of **3d**—reasonably soluble in $CHCl_3$.

The condensation of the resorcinols **1a–d** with squaric acid **2** was performed at the boiling point of an azeotropic mixture of toluene and n-butanol (10 : 3). The stilbenoid components **1b–d** were generated by the Wittig–Horner reaction (Scheme 2). The substituted aniline **4** was first transformed to the aldehyde **5b** which yielded the monostilbene **7c** *via* reaction with phosphonate **6**. Formylation led to aldehyde **5c** which gave in an analogous reaction sequence *via* **7d** the higher aldehyde **5d**. The aldehydes **5b–d** were subsequently transformed *via* reaction with **8** to the stilbenoid compounds **9b–d**. Deprotection with BBr_3 yielded the dihydroxy compounds **1b–d** which served as coupling components. The starting compound **1a** was obtained by N-alkylation and subsequent ether cleavage of 3,5-dimethoxyaniline.

Many examples of conjugated oligomers show that the long wavelength absorption approaches a limiting value with

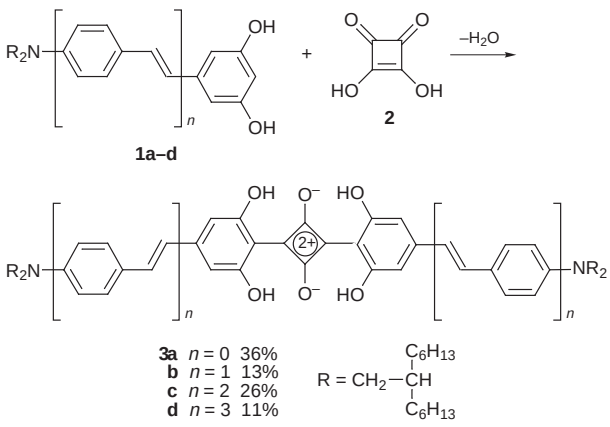

Scheme 1

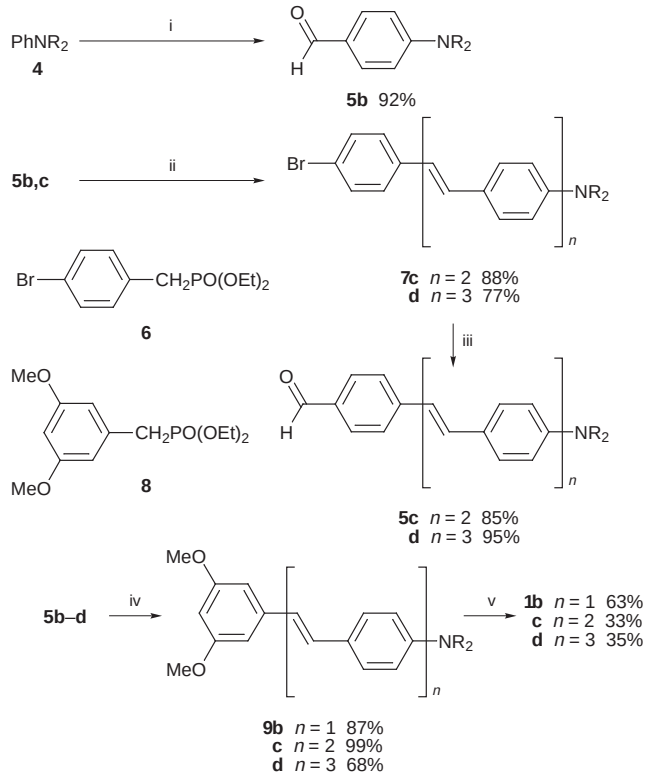

Scheme 2 *Reagents and conditions*: i, $POCl_3$, DMF; ii, **6**, Bu^{t}OK, DMF; iii, BuLi, DMF; iv, **8**, Bu^{t}OK, DMF; v, BBr_3, H_2O.

increasing number (*n*) of repeating units; we described recently this convergence behavior with the aid of exponential functions.[9] The convergence is used for the evaluation of the effective conjugation length (ECL). Surprisingly, the donor–acceptor substituted systems **3a–d** exhibit a totally different behavior. Fig. 1 demonstrates that the extension of the conjugation from **3a** to **3b** provokes a strong bathochromic effect. The shift $\Delta\lambda$ of the absorption maximum amounts to more than 250 nm and leads far into the NIR region. On going from **3b** to **3c** and finally to **3d** the λ_{max} value decreases again

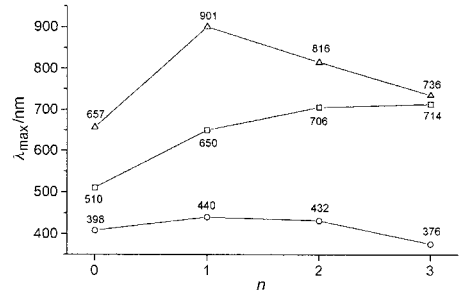

Fig. 1 Maxima of the long wavelength absorption of (△) **3a–d** (in $CHCl_3$), (□ **3a**$^+$–**d**$^+$ (in CF_3CO_2H) and (○) **10a–d** (in DMF).

Table 1 Long wavelength absorption of **3a–d** in $CHCl_3$

3	$\tilde{\nu}_{max}$/cm^{-1}	log ε	S/cm mol^{-1}
a	15221	5.602	2.42×10^8
b	11099	5.301	3.47×10^8
c	12255	5.041	3.62×10^8
d	13587	[a]	[a]

[a] The extremely low solubility of **3d** in $CHCl_3$ at ambient temperature does not permit an exact evaluation of ε and S; the limit of error for S of **3a–c** is ±5%.

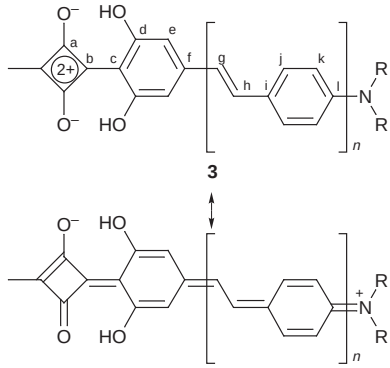

3

Scheme 3

Table 2 ^{13}C NMR data of **3b** compared to its components **1b** and **2** and compared to the deuteriated form **3**$^+$ (δ values in $CDCl_3$ and in CF_3CO_2D, respectively)

C Atom	δ_C (**1b**/**2**)	δ_C (**3b**)	$\Delta\delta$	δ_C (**3b**$^+$)	$\Delta\delta'$
a	189.5	182.0	−7.5	183.6	+1.6
b	189.5	167.1	−22.4	176.0	+8.9
c	101.4	110.2	+8.8	112.5	+2.3
d	156.8	162.5	+5.7	164.5	+2.0
e	105.7	107.0	+1.3	110.6	+3.6
f	141.2	154.1	+12.9	141.8	−12.3
g	123.0	121.9	−1.1	132.0	+10.1
h	129.8	137.8	+8.0	136.1	−1.7
i	124.1	123.2	−0.9	138.5	+15.3
j	127.7	129.8	+2.1	131.7	+1.9
k	112.6	112.6	0	123.9	+11.3
l	148.2	150.0	+1.8	156.1	+6.1
NCH_2	56.8	56.7	−0.1	67.5	+10.8

by 85 and 80 nm, respectively. Obviously the extended conjugation causes the hypsochromic effect. The intense absorption bands broaden in the series from **3a** (n = 0) to **3d** (n = 3). The absorption intensity S increases with growing extension of the chromophore (Table 1).

In order to judge whether this behavior is general or not in the series of push-pull substituted stilbenoid compounds, we made a comparison with the known compounds **10a–d**. Fig. 1 proves the principally analogous behavior of this series. However, the shifts $\Delta\lambda$[10] are considerably smaller than in the series **3a–d**. Probably the effect was not earlier detected due to the fact that the compounds **10a–d** were prepared by different groups.[11–13]

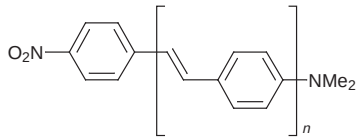

10a n = 0
b n = 1
c n = 2
d n = 3

The analysis of **3a–d** in TFA leads to the result normally observed for conjugated oligomers, namely to a monotonic increase of λ_{max} with growing number n. Protonation takes place at the terminal amino groups as ^{13}C NMR measurements prove (Scheme 3). Thus the donor–acceptor–donor character of **3a–d** is lost. The protonated series resembles the unsymmetrical cyanine and the protonated merocyanine dyes.[14,15]

Conjugation with delocalisation of charge can also be assessed *via* the ^{13}C NMR data. Table 2 shows a comparison of **3b** with its components **1b** and **2** (the correlation of the signals is based on normal and long-range ^{1}H,–^{13}C COSY measurements).

The $\Delta\delta$ values in Table 2 prove the low-field shift in the stilbene unit caused by bonding to the squaric acid. Besides the substitution position c, the alternating sequence d, f, h, j and l of carbon atoms is mainly affected. The central squaric acid unit induces positive partial charges in these positions. The protonation (deuteriation) on the nitrogen atom cancels the push-pull effect and causes strong low-field shifts, especially in the aniline building block. The $\Delta\delta'$ values indicate the differences in the chemical shifts between **3b** and **3b**$^+$.

In conclusion, the extension of the conjugation of chromophores does not always induce a bathochromic shift of the absorption. In a series of push-pull substituted systems like **3a–d** the initial strong red-shift is replaced for higher systems by a blue-shift. The distance between the donor and the acceptor groups has a decisive influence on the charge transfer transition.[16] We explain this using quinoid resonance structures, which become energetically unfavorable with growing number n, since more and more benzene rings are displaced by p-quinone rings (Scheme 3). Obviously this effect is contrary to the normal effect due to extension of conjugation; thus, a maximum of the bathochromic shift is observed in the series **3a–d**. The quantum chemical treatment[17] [MNDO and CNDO/S (S + DES CI)] of the electron transitions $S_0 \rightarrow S_1$ in squaraines localizes the charge transfer almost completely in the four-membered ring. The strong influence of the stilbene building blocks proves that this result is not valid; nevertheless, the squaraine chromophore remains a challenge for theoreticians.

Notes and references

1 K. Y. Law, *Chem. Rev.*, 1993, **93**, 449 and references therein.
2 A. H. Schmidt, in *Oxocarbons*, ed. R. West, Academic Press, New York, 1980, p. 185.
3 M. Emmelius, G. Pawlowski and H. W. Vollmann, *Angew. Chem.*, 1989, **101**, 1475; *Angew. Chem., Int. Ed. Engl.*, 1989, **28**, 1445.
4 C.-T. Chen, S. R. Marder and L. T. Cheng, *J. Chem. Soc., Chem. Commun.*, 1994, 259; *J. Am. Chem. Soc.*, 1994, **116**, 3117.
5 G. J. Ashwell, G. Gefferies, D. G. Hamilton, D. E. Lynch, M. P. S. Roberts, G. S. Bahra and C. R. Brown, *Nature*, 1995, **375**, 385.
6 R. O. Loutfy, C. K. Hsiao and P. M. Kazmaier, *Photogr. Sci. Eng.*, 1983, **27**, 5.
7 H. Meier and U. Dullweber, *J. Org. Chem.*, 1997, **62**, 4821.
8 *Selected data* for **3a**: mp 92 °C; $\delta_H(CDCl_3)$ 0.86 (t, 24 H, CH_3), 1.24 (m, 80 H, CH_2), 1.84 (m, 4 H, CH), 3.26 (d, 8 H, NCH_2), 5.79 (s, 4 H, arom. H), 10.94 (s, 4 H, OH). For **3b**: mp 169 °C; $\delta_H(CDCl_3)$ 0.86 (t, 24 H, CH_3), 1.24 (m, 80 H, CH_2), 1.82 (m, 4 H, CH), 3.23 (d, 8 H, NCH_2), 6.48 (s, 4 H, arom. H), 6.61/7.39 (AA′BB′, 8 H, arom. H), 6.70/7.31 (AB, ^3J 15.8, olefin H), 11.02 (s, 4 H, OH). For **3c**: mp 220–225 °C; $\delta_H(CDCl_2$–$CDCl_2$, 315 K) 0.83 (t, 24 H, CH_3), 1.20 (m, 80 H, CH_2), 1.75 (m, 4 H, CH), 3.10 (d, 8 H, NCH_2), 6.42 (s, 4 H, arom. H), 6.54/7.23 (AA′BB′, 8 H, arom. H), 6.70/6.96 (AB, ^3J 16.1, 4 H, olefin H), 6.74/7.18 (AB, ^3J15.8, 4 H, olefin H), 7.34/7.38 (AA′BB′, 8 H, arom. H), 10.88 (s, 4 H, OH). For **3d**: mp 245 °C (decomp.); $\delta_H(CDCl_2$–$CDCl_2$, 313 K) 0.84 (t, 24 H, CH_3), 1.20 (m, 80 H, CH_2), 1.73 (m, 4 H, CH), 3.29 (d, 8 H, NCH_2), 6.47 (s, 4 H, arom. H), 6.51 (m, 4 H, arom. H), 6.79–7.25 (m, 12 H, olefin H), 7.33–7.60 (m, 20 H, arom. H), 10.95 (br s, 4 H, OH).
9 H. Meier, U. Stalmach and H. Kolshorn, *Acta Polym.*, 1997, **48**, 379.
10 The $\Delta\tilde{\nu}$ values are in both series of comparable size.
11 C. Laurence, *J. Phys. Chem.*, 1994, **23**, 5807.
12 H. Grün and H. Görner, *J. Phys. Chem.*, 1989, **20**, 7144.
13 G. Manecke and S. Lüttke, *Chem. Ber.*, 1970, **103**, 700.
14 See also W. T. Simpson, *J. Am. Chem. Soc.*, 1951, **73**, 5359 and 5326.
15 P. Rys and H. Zollinger, *Farbstoffchemie*, Verlag Chemie, 1982, p. 91.
16 The enhanced polarity of the S_1 state compared to the ground state S_0 is proved by a pronounced positive solvatochromic effect; **3b** for example has an absorption maximum in cyclohexane at 840 and in CH_2Cl_2 at 911 nm.
17 R. W. Bigelow and H.-J. Freund, *Chem. Phys.*, 1986, **107**, 159.

Communication 9/00888H

$Ln_2Ti_2S_2O_5$ (Ln = Nd, Pr, Sm): a novel series of defective Ruddlesden–Popper phases

M. Goga, R. Seshadri, V. Ksenofontov, P. Gütlich and W. Tremel*

Institut für Anorganische Chemie und Analytische Chemie der Universität Mainz, Becherweg 24, D-55099 Mainz, Germany. E-mail: tremel@indigotrem1.chemie.uni-mainz.de

Received (in Cambridge, UK) 15th December 1998, Accepted 10th March 1999

The reaction of Nd_2S_2O, TiS_2 and S at 1000 °C and subsequent chemical transport with I_2 yields the new crystalline layered oxysulfide $Nd_2Ti_2S_2O_5$ that possesses a defective $Sr_3Ti_2O_7$ structure whose cuboctahedral sites within the double-perovskite layers are empty; $Nd_2Ti_2S_2O_5$ is paramagnetic and semiconducting; the synthesis of the isostructural compounds $Pr_2Ti_2S_2O_5$ and $Sm_2Ti_2S_2O_5$ is also reported.

Layered materials represent an active area of research owing to their interesting physical properties that include superconductivity[1] and charge density waves.[2] Important groups of layered compounds are bronzes $A_xM_yO_z$ (A = alkali, alkaline earth metals, lanthanides; M = Ti, V, Nb, Mo)[3] or early transition metal chalcogenides.[4] Surprisingly, chalcogenide analogues of bronzes are unknown; partial replacement of oxygen by chalcogen atoms leads to metal oxychalcogenides, a family of compounds that have received comparatively little attention so far. A number of rare-earth representatives have been reported, the simplest of them having compositions M_2O_2Q or $M_2O_2(Q_2)$ and $M_4O_4Q(Q_2)$ (Q = S, Se).[5] Most of them crystallize in layer structures where the oxide and chalcogenide ions form individual layers. We are generally interested in metallic layered materials close to the metal–semiconductor boundary that are composed of transition-metal oxide and/or transition-metal chalcogenide layers, where one of the components can act as a charge reservoir and the second electronically active component dictates the physical properties.[6] There is both experimental and theoretical evidence that a combination of the electronic properties of the individual layers may lead to materials with interesting electronic and magnetic properties;[7] therefore, a structural integration of these two types of layers represents a promising route to new electronic materials. The key problem in the design of new layered oxychalcogenides/oxypnictides is to achieve a large enough difference in the oxophilicity and chalcophilicity of the layer components that one metal is bonded to only one anion type and segregated layers (or stacks) with partial charge transfer are obtained. A combination of two metals with too similar oxo/chalcophilicity often leads to phase separation and the formation of ternary oxide and chalcogenide phases.

In the quest for new compounds with these properties we have investigated the quaternary Ln–M–O–Q phase systems (M = Ti, Nb, Mo, Mn, Fe; Q = S, Se); among others, we obtained the new layer compound $Nd_2Ti_2S_2O_5$ **1** whose synthesis, structure and properties are reported here. **1** was made by heating Nd_2S_2O, TiS_2 and S in a 1 : 1 : 1 ratio at 1000 °C. Single phase material was prepared using the following procedure: Nd_2S_2O, TiS_2 and S were mixed in a ratio 1 : 1 : 1, sealed in an evacuated quartz tube and fired at 1000 °C for one week. The corresponding Pr compound, $Pr_2Ti_2S_2O_5$ **2**, may be synthesized from the starting materials Pr_6O_{11}, TiS_2, Ti and S in a 1 : 2 : 2 : 3 ratio, $Sm_2Ti_2S_2O_5$ **3** was obtained by heating a 1 : 1 : 1 mixture of Sm_2O_3, TiO_2 and TiS_2 at 1000 °C for 1 week in a sealed quartz tube. The resulting powders are contaminated with small amounts of TiS_2 and rare earth oxysulfides. Single crystals of **1**–**3** were grown from the resulting powders by chemical transport (950 → 850 °C, 4 weeks) using iodine (3 mg cm^{-3}) as a transport agent. Red rectangular crystals of **1**, reddish brown crystals of **2** and brown–yellow platelets of **3** formed at the cold end of the tube.

A microprobe analysis by energy dispersive X-ray spectroscopy (EDX) performed in a Zeiss DSM 962/Philipps PSEM 500 scanning electron microscope (accelerating voltage 20 kV, accumulation time 1 min) equipped with a KEVEX energy dispersive spectroscopy detector indicated the presence of the elements Nd (Pr, Sm), Ti, S and O in an approximate 1 : 1 : 1 : 2 ratio in satisfactory agreement with the results of the structure determination.† The parent compouund $Nd_2Ti_2S_2O_5$ (Fig. 1) crystallizes in a defect Ruddlesden–Popper structure $Nd_2Ti_2(Q)_7$ of the $Sr_3Ti_2O_7$ type[8] and is structurally closely related to the high-T_c superconductors of the $La_2CaCu_2O_6$ type.[9] It is characterized by distorted double NdS rocksalt layers and defective double perovskite $Ti_2O_{10/2}S_2$ (=$Ti_2S_2O_5$) blocks intergrown along the *c* axis of the lattice. The perovskite $TiSO_2$ blocks contain the $TiSO_2$ octahedra linked at their corners with the twelve-coordinate site being empty. The Nd atoms in the NdS layers are eight-coordinate. The Nd–S bond length of 3.022(2) Å parallel to the *c* axis is significantly longer than the Nd–S distances of 2.855(1) Å in the *ab* plane. Furthermore, the Ti–S bond which is proximal to the NdS layer is, at 2.896(3) Å, extremely elongated and much longer than a typical Ti–S bond length, whereas the opposite Ti–O distance of 1.790(2) Å indicates significant double bond character and points to an effective 5 + 1 coordination of Ti. The Ti–O bond distances of 1.975(1) Å in the *ab* plane are in the expected distance range.

The magnetic behavior of **1** is determined by the f^3 configuration of the Nd atoms. The results of temperature dependent magnetic susceptibility measurements (Fig. 2) are

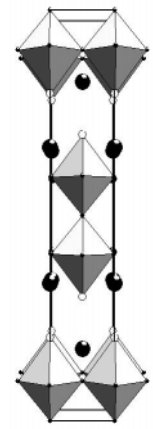

Fig. 1 Polyhedral view of the $Ln_2Ti_2S_2O_5$ structure along the *b* axis. The polyhedra represent the $TiSO_5$, large black circles the Ln atoms, open circles the S atoms, and small black circles the O atoms (selected distances [Å]: (Ln = Nd, Pr, Sm): Ln–O 2.496(3), 2.505(4), 2.474(3); Ln–S 2.855(1), 2.869(1), 2.834(1); 3.022(2), 3.025(3), 2.986(2), Ti–O(1) 1.975(2), 1.983(1), 1.961(1); Ti–O(2) 1.790(2), 1.796(2), 1.790(1); Ti–S 2.896(3), 2.881(3), 2.887(2)).

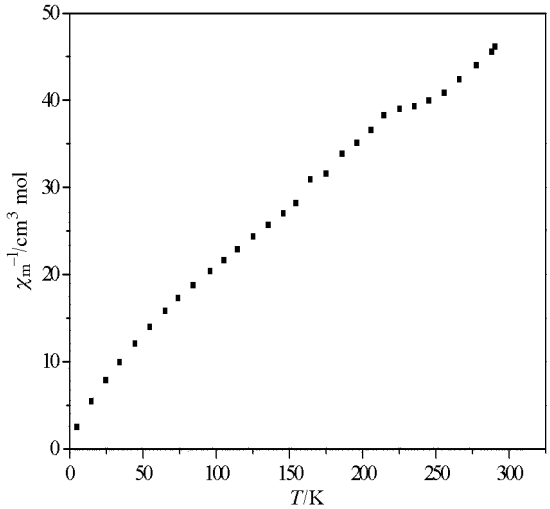

Fig. 2 Magnetic susceptibility χ_M *vs.* temperature plot for $Nd_2Ti_2S_2O_5$.

compatible with antiferromagnetically coupled Nd^{3+} centers with f^3 configuration as apparent from a room temperature magnetic moment of 10.04 μ_B (compared to a theoretical value of 14.48 μ_B for four independent Nd^{3+} centers). Above 260 K and below 175 K Curie–Weiss-type behavior is observed. The red color of $Nd_2Ti_2S_2O_5$ points to semiconducting behavior. This is in agreement with the results of LMTO-ASA calculations. The optical (diffuse reflectance) spectrum is characterized by a number of narrow bands that fall into the energy gap of 1.82 eV and can be assigned to transitions from the $^4I_{9/2}$ ground state to the excited $^4I_{11/2}$ $^4I_{13/2}$ $^4I_{15/2}$ (or $^4G_{5/2}$, $^4G_{7/2}$, $^2K_{13/2}$) states of the Nd^{3+} chromophore. The gap between filled and empty states in the LMTO-DOS is in reasonable agreement with the measured optical band gap obtained from the diffuse reflectance spectrum. In a similar fashion, it is possible to rationalize the diffuse reflectance spectra of **2** ($^3H_4$ ground state) and **3** ($^6H_{5/2}$ ground state).

The title compounds have several intriguing features, which are currently explored synthetically: (i) the R–P phases are the compounds for many high T_c superconductors and the layered manganites $Ln_{3-x}Sr_xMn_2O_7$[10] that exhibit large negative magnetoresistance effects. (ii) A series of presumably isostructural defective R–P phases $Ln_2Ti_2O_7$ (Ln = La, Nd, Sm, Gd) was reported recently by Gopalakrishnan and coworkers.[11] The materials were prepared by topotactic dehydration of $HLnTiO_4$[12] and considered metastable whereas the title compound was obtained from a high temperature reaction and should be therefore a thermodynamically stable phase. (iii) The replacement of oxide by *sulfide ions in the LnS layers* is counterintuitive as Ln is more chalcophilic than titanium. The sulfur substitution pattern can be rationalized by the amount of space accessible to the sulfide (compared to the oxide) anions through the less dense packing in the interlayer region. (iv) Electronic variation of the title compounds might be possible by cation intercalation into the unfilled voids in the LnS slab or metal substitution (*e.g.* group 5 metals for Ti).

We are indebted to the Bundesministerium für Forschung und Technologie (contract number DLR-2A523370-03N1023C1) and the Fonds der Chemischen Industrie for the financial support of this research and to Heraeus Quarzschmelze (Dr Höfer) for the donation of quartz tubes.

Notes and references

† *Crystal data*: $Nd_2Ti_2S_2O_5$ **1**: T = 25 °C: tetragonal, space group *I*4/*mmm* (no. 139), a = 3.849(1), c = 23.064(5) Å, V = 341.7(2) Å^3, Z = 2, λ = 0.71073 Å, D_c = 5.136 g cm^{-3}, μ(Mo-Kα) = 17.76 mm^{-1}, crystal block-like, dimensions 0.3 × 0.3 × 0.5 mm^3, $2\theta_{max}$ = 50°, data collected on a Nicolet P2$_1$ four circle diffractometer, number of reflections, 1902, unique data with $I > 4\sigma(I)$, 124, number of variables, 17. Structure solved and refined using the SHELX93 program system. A numerical absorption correction was applied to the data (min., max. transmission = 0.31, 0.49). Final R, R_w = 0.016, 0.042.

$Pr_2Ti_2S_2O_5$ **2**: T = 25 °C: tetragonal, space group *I*4/*mmm* (no. 139), a = 3.871(1), c = 23.036(5) Å, V = 345.2(2) Å^3, Z = 2, λ = 0.71073 Å, D_c = 5.020 g cm^{-3}, μ(Mo-Kα) = 16.66 mm^{-1}, crystal plate-like, dimensions 0.3 × 0.3 × 0.1 mm^3, $2\theta_{max}$ = 70°, data collected on a Nicolet P2$_1$ four circle diffractometer, number of reflections, 1782, unique data with $I > 4\sigma(I)$, 232, number of variables, 17. Structure solved and refined using the SHELXTL program system. A numerical absorption correction was applied to the data (min., max. transmission = 0.52, 0.99). Final R, R_w = 0.031, 0.070.

$Sm_2Ti_2S_2O_5$ **3**: T = 25 °C, tetragonal, space group *I*4/*mmm* (no. 139), a = 3.818(1), c = 22.952(5) Å, V = 334.6(2) Å^3, Z = 2, λ = 0.71073 Å, D_c = 5.366 g cm^{-3}, μ(Mo-Kα) = 20.17 mm^{-1}, crystal rod-like, dimensions 0.2 × 0.2 × 0.3 mm^3, $2\theta_{max}$ = 54°, data collected at 25° on a Nicolet P2$_1$ four circle diffractometer, number of reflections, 1066, unique data with $I > 4\sigma(I)$, 129, number of variables, 17. Structure solved and refined using the SHELXTL program system. A numerical absorption correction was applied to the data (min., max. transmission = 0.53, 0.78). Final R_1, wR_2 = 0.015, 0.035. CCDC 182/1191. See http://www.rsc.org/suppdata/cc/1999/979/ for crystallographic files in .cif format.

Note added in proof: After submission of this manuscript a paper describing the structure of $Sm_2Ti_2S_2O_5$ appeared; C. Boyer, C. Dendon and A. Meerschant, *C. R. Acad. Sci. Ser. 2*, 1999, 93.

1 A. W. Sleight, *Science*, 1988, **242**, 1519; R. Cava, *Science*, 1990, **247**, 656.
2 A. Meerschaut and J. Rouxel, in *Crystal Chemistry and Properties of Materials with Quasi-One-Dimensional Structures*, ed. J. Rouxel, D. Reidel Publishing Corporation, Dordrecht, 1986, p. 205.
3 M. Greenblatt, *Int. J. Mod. Phys. B*, 1993, **7**, 3937; G. Costenin, A. Leclaire, M. M. Borel, A. Grandin and B. Raveau, *Rev. Inorg. Chem.*, 1993, **13**, 77.
4 J. Rouxel and R. Brec, *Annu. Rev. Mater. Sci.*, 1986, **16**, 137; J. Rouxel and A. Meerschaut, in *Physics and Chemistry of Low-Dimensional Inorganic Conductors*, ed. C. Schlenker, Plenum Press, New York, 1996, p. 59.
5 J. Flahaut, in *Handbook on the Physics and Chemistry of Rare Earths*, ed. K. A. Gscheidner and L. Eyring, North-Holland, Amsterdam, 1979, vol. 4, p. 1.
6 J. K. Burdett, *Acc. Chem. Res.*, 1995, **28**, 227.
7 W. J. Zhu, P. H. Hor, A. J. Jacobson, G. Crisci, T. A. Albright, S.-H. Wang and T. Vogt, *J. Am. Chem. Soc.*, 1997, **119**, 12 398; S. L. Brock and S. M. Kauzlarich, *Inorg. Chem.*, 1994, **33**, 2491; *Incommensurate Sandwiched Layered Compounds*, ed. A. Meerschaut, Trans. Tech. Publications, Aedermannsdorf, 1994.
8 S. N. Ruddlesen and P. Popper, *Acta Crystallogr.*, 1958, **11**, 54.
9 R. J. Cava, B. Batlogg, R. B. van Dover, J. J. Krajewski, J. V. Wazczak, R. M. Fleming, R. F. Peck Jr., L. W. Rupp, P. Marsh, A. C. W. P. James and L. F. Schneemeyer, *Nature* (*London*), 1990, **345**, 602; A. Fuertes, X. Obradors and J. M. Navarro, *Physica C*, 1990, **170**, 153.
10 R. A. Mohan Ram, P. Ganguly and C. N. R. Rao, *J. Solid State Chem.*, 1987, **70**, 82; Y. Moritomo, A. Asimatsu, H. Kuwahara and Y. Tokura, *Nature* (*London*), 1996, **380**, 341; R. Seshadri, C. Martin, A. Maignan, M. Hervieu, B. Raveau and C. N. R. Rao, *J. Mater. Chem.*, 1996, **6**, 1585; P. D. Battle, M. A. Green, N. S. Laskey, J. E. Millburn, M. J. Rosseinsky, S. P. Sullivan and J. F. Vente, *Chem. Commun.*, 1996, 767; C. Felser, R. Seshadri, A. Leist and W. Tremel, *J. Mater. Chem.*, 1998, **8**, 787.
11 T. Thangadurai, G. N. Subbana and J. Gopalakrishnan, *Chem., Commun.*, 1998, 1299.
12 S. H. Bycon, J. J. Yoon and S. O. Lee, *J. Solid State Chem.*, 1996, **127**, 119.

Communication 8/09737B

ChemComm

Total synthesis of a keramamide

Jennifer A. Sowinski and Peter L. Toogood*

Willard H. Dow Laboratory, Department of Chemistry, University of Michigan, Ann Arbor, MI 48109-1055, USA. E-mail: peter.toogood@wl.com

Received (in Corvallis, OR, USA) 3rd March 1999, Accepted 15th April 1999

The first total synthesis of a molecule possessing the structure proposed for keramamide J is described, providing data indicating that the structure of this natural product should be re-examined.

Keramamide J (KJ; **1**)[1] is the simplest member of a class of *Theonella* natural products that collectively exhibit cytotoxic,[1–3] anti-fungal[4] and anti-oxidant activity.[5] To study the biological activities of these molecules, we required a general synthetic route that would be amenable to the synthesis of all members of this series.[4] Herein, we report our progress towards this goal, including the first total synthesis of a keramamide possessing structure **1**.

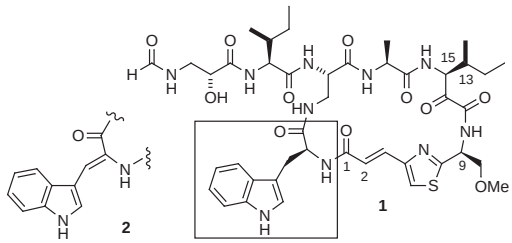

Our synthetic plan for constructing KJ is shown in Scheme 1.[6] A convergent route was devised, employing four fragments of comparable complexity (**3**–**6**). We decided to mask the electrophilic keto-amide moiety[7] as a protected α-hydroxy carbonyl group until the conclusion of the synthesis to avoid nucleophilic attack at this center. In addition, we elected to attempt ring closure between the amine of fragment **3** and the C-terminus of the alanine residue, which was anticipated to be less prone to epimerization than the tryptophan residue and easier to couple than the α-hydroxy acid. Late incorporation of side chain fragment **6** was selected to increase convergency and minimize potential side reactions during the critical macrocyclization reaction.

Thiazole **7**[8] was extended *via* reduction of the ester to an aldehyde and Wittig olefination to introduce the *E*-double bond (Scheme 2). Saponification of the ethyl ester, followed by coupling to L-tryptophan allyl ester provided fragment **4**. To obtain the hexanoic acid fragment **3**, enone **9** (Scheme 3) was

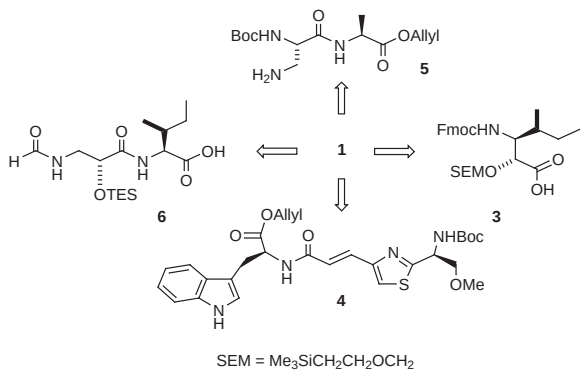

SEM = $Me_3SiCH_2CH_2OCH_2$

Scheme 1

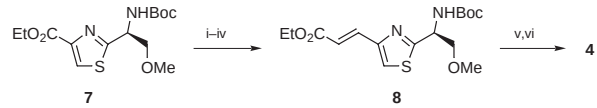

Scheme 2 *Reagents and conditions*: i, NaOH, MeOH; ii, BOP, Et_3N, HN(Me)OMe; iii, $LiAlH_4$; iv, $Ph_3P{=}CHCO_2Et$ (70% for 4 steps); v, NaOH, MeOH; vi, L-Trp-OAllyl, Ph_2POCl (68% for 2 steps).

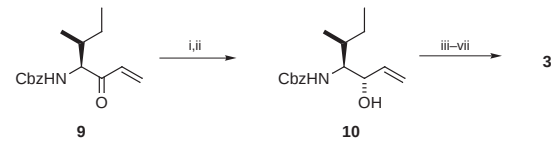

Scheme 3 *Reagents and conditions*: i, $NaBH_4$, $CeCl_3$; ii, separate (76% for 2 steps); iii, SEMCl, 2,6-lutidine; iv, O_3, DMS; v, $NaClO_2$, isobutene; vi, H_2, Pd/C; vii, FmocOSu, aq. $NaHCO_3$ (66% for 5 steps).

prepared from L-isoleucine *via* displacement of the corresponding Weinreb amide with vinyl magnesium bromide. Reduction of this enone with $NaBH_4$ under the Luche conditions[9] provided a 4 : 1 mixture of alcohols which could be separated by column chromatography. Protection of the major product (**10**)[10] as its (trimethylsilyl)ethoxymethyl (SEM) acetal, followed by a two step oxidation of the double bond, provided the carboxylic acid. Hydrogenolytic cleavage of the Cbz group and subsequent treatment with FmocOSu† gave compound **3**. Deprotection of fragment **4**, followed by condensation with acid **3**, gave the corresponding tripeptide in 77% yield (Scheme 4). Subsequent cleavage of the allyl ester and coupling to dipeptide **5** gave linear precursor to the KJ macrocycle **11**. Following deprotection of the C-terminus, and removal of the Fmoc group under standard conditions, macrocyclization proceeded smoothly to provide cyclic peptide **12** in 34–51% overall yields from intermediate **11**.

To prepare the KJ side chain, (*S*)-glycidol was oxidized to glycidic acid using $RuCl_3$ and $NaIO_4$,[11] then coupled with L-isoleucine methyl ester to give peptide **13** as a single diastereomer (Scheme 5). Attack of the oxirane by azide ion at

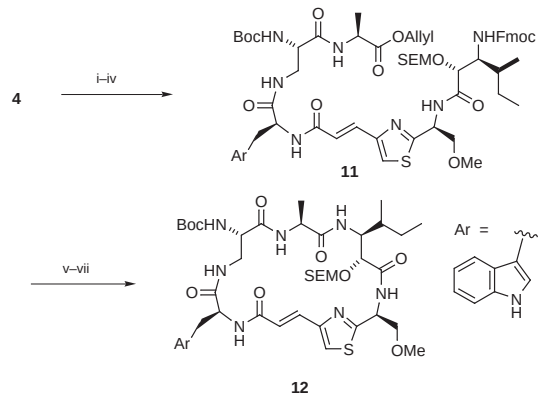

Scheme 4 *Reagents and conditions*: i, HCl, Et_2O; ii, **3**, DCC, HOBt, Pr^i_2EtN; iii, $Pd(PPh_3)_4$, dimedone; iv, **5**, DCC, HOBt, Pr^i_2EtN (56% for 4 steps); v, $Pd(PPh_3)_4$, dimedone; vi, Et_2NH; vii, $(PhO)_2PON_3$, $NaHCO_3$ (51% over 3 steps).

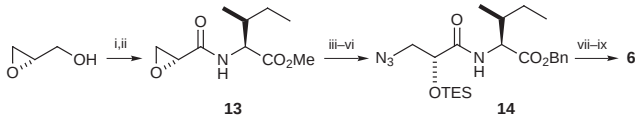

Scheme 5 *Reagents and conditions*: i, $RuCl_3$, $NaIO_4$; ii, L-Ile-OMe, DCC, HOBt (36% for 2 steps); iii, NaN_3, $MgSO_4$; iv, LiOH; v, $CsCO_3$, BnBr; vi, TESCl, imidazole (48% for 4 steps); vii, PPh_3, H_2O; viii, *p*-$O_2NC_6H_4$-OCHO; ix, H_2, Pd/C (79% for 3 steps).

the less substituted position, followed by transesterification and protection of the hydroxy function produced azido peptide **14**. Staudinger reduction of the azide to a primary amine,[12] followed by formylation with *p*-nitrophenyl formate and hydrogenolytic cleavage of the ester, provided fragment **6**.

Treatment of macrocycle **12** with HCl in Et_2O–MeOH–$CHCl_3$ deprotected the amine and secondary alcohol, and fragment **6** was attached using HATU† to produce alcohol **15** (Scheme 6).[13] Oxidation of the alcohol was performed under mild, non-acid conditions, using IBX† in DMSO.[14] Finally, removal of the TES group was achieved by stirring the peptide over Amberlite IR-120 suspended in EtOAc. Purification of the final product by silica gel chromatography followed by reversed-phase HPLC provided material that exhibits ^1H, ^{13}C, ^1H-^1H COSY and inverse detected ^1H–^{13}C HMQC NMR spectra consistent with the proposed structure **1**, and a high resolution mass spectrum corresponding to the expected molecular formula.

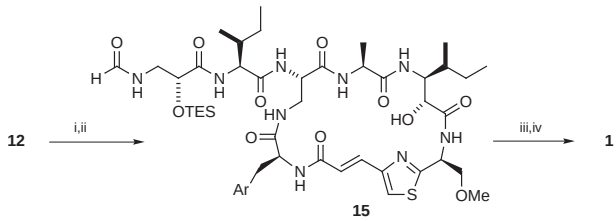

Scheme 6 *Reagents and conditions*: i, HCl, MeOH; ii, **6**, HATU, 2,4,6-collidine (48% for 2 steps); iii, IBX, DMSO; iv, Amberlite IR-120 (95% for 2 steps).

From the NMR data, it is apparent that our synthetic keramamide is not the same compound reported by Kobayashi and co-workers.[1,15] Comparison of the NMR spectra leads us to conclude that this synthetic keramamide and KJ are configurational isomers. In support of the assignment of structure **1** to the synthetic product, a very close correlation is observed between the spectral data for this compound and the data published for KF (**2**; Table 1), which differs only in the replacement of the tryptophan in structure **1** by *Z*-didehydrotryptophan. In particular, the ^1H and ^{13}C chemical shifts at C-9 and C-13 for these two compounds are in excellent agreement (^1H $\Delta\delta \leqslant 0.06$, ^{13}C $\Delta\delta \leqslant 1.3$ ppm). In contrast, the published data for KJ more closely resemble the data for keramamide G (KG) which is epimeric to KF at carbon-13.[1,16] We note that the degradation conditions used by Kobayashi to determine the absolute configuration at carbon-13 in KJ have been found previously to cause epimerization at this center in a closely related molecule and possibly could have been misleading.[3] Degradation of the synthetic keramamide under milder conditions using 30% H_2O_2 and 0.1 M NaOH (room temperature, overnight), followed by 6 M HCl (110 °C, 24 h), produced L-isoleucine containing less than 10% D-*allo*-isoleucine by chiral HPLC analysis, supporting assignment of the L-configuration to carbon-13 in the synthetic material.[17] Upon standing in aqueous solution, the synthetic material partially converted (~ 10%) to a new product possessing ^1H NMR resonances that match those observed for KJ, consistent with the notion that these two molecules differ at a single, epimerizable center.

Table 1 Selected ^1H and ^{13}C NMR resonances, and optical rotations published for keramamides F, G, J and observed for compound **1**

	δ_H		δ_C		
	H-9	H-13	C-9	C-13	$[\alpha]_D^{25}$ [a]
Keramamide G	4.81	5.49	53.7	56.7	+10.0
Keramamide J	4.75	5.49	53.7	56.1	+8.4
Compound **1**	5.31	5.19	51.4	61.0	−10.0
Keramamide F	5.33	5.25	51.7	59.7	−25

[a] Given in units of 10^{-1} degrees cm^2 g^{-1}.

Based on the preceding analysis, we conclude that our synthesis proceeded as intended to correctly provide a molecule possessing structure **1**. This work strongly indicates that the structure of KJ should be revised. However, since no natural KJ is presently available,[15] structural re-assignment will require either re-isolation or total synthesis of the correct structure.

This work was supported by NSF grant CHE-93221233, and by the donors to the Petroleum Research Fund, administered by the American Chemical Society.

Notes and references

† *Abbreviations*: HATU = *O*-(7-azabenzotriazol-1-yl)-1,1,3,3-tetramethyluronium hexafluorophosphate, IBX = 1-hydroxy-1,3-dihydro-1,2-benziodoxol-3-one 1-oxide, BOP = benzotriazol-1-yloxytris(dimethylamino)-phosphonium hexafluorophosphate, FmocOSu = *N*-(fluoren-9-ylmethoxycarbonyloxy)succinimide, HOBt = 1-hydroxybenzotriazole hydrate.

1 J. Kobayashi, F. Itagaki, H. Shigemori, T. Takao and Y. Shimonishi, *Tetrahedron*, 1995, **51**, 2525.
2 F. Itagaki, H. Shigemori, M. Ishibashi, T. Nakamura, T. Sasaki, and J. Kobayashi, *J. Am. Chem. Soc*., 1992, **57**, 5540.
3 N. Fusetani, T. Sugawara, S. Matsunaga and H. Hirota, *J. Am. Chem. Soc*. **1991**, **113**, 7811.
4 S. P. Gunasekara, S. A. Pomponi and P. J. McCarthy, *J. Nat. Prod*., 1994, **57**, 79.
5 J. Kobayashi, F. Itagaki, H. Shigemori, M. Ishibashi, K. Takahashi, M. Ogura, S. Nagasawa, T. Nakamura, H. Hirota, T. Ohta and S. Nozoe, *J. Am. Chem. Soc*., 1991, **113**, 7812.
6 Preliminary work on this synthesis has been published: J. A. Sowinski and P. L. Toogood, *Tetrahedron Lett*., **1995**, *36*, 67.
7 Examples of other ketoamide containing peptides see: N. Fusetani, S. Matsunaga, H. Matsumoto and Y. Y. Takebayashi, *J. Am. Chem. Soc*., 1990, **112**, 7053; M. Hagihara and S. L. Schreiber, *J. Am. Chem. Soc*., 1992, **114**, 6570; S. Toda, C. Kotake, T. Tsuno, Y. Narita, T. Yamasaki and M. Konishi, *J. Antibiot*., 1992, **45**, 1580; T. Aoyagi, M. Nagai, K. Ogawa, F. Kojima, M. Okada, T. Ikeda, M. Hamada and T. Takeuchi, *J. Antibiot.*, 1991, **44**, 949; M. Nagai, K. Ogawa, Y. Muraoka, H. Naganawa, T. Aoyagi and T. Takeuchi, *J. Antibiot*., 1991, **44**, 956.
8 J. A. Sowinski and P. L. Toogood, *J. Org. Chem*., 1996, **61**, 7671.
9 J.-L. Luche, *J. Am. Chem. Soc*., 1978, **100**, 2226; J.-L. Luche, L. Rodriguez-Hahn and P. J. Crabbé, *J. Chem. Soc., Chem. Commun*., 1978, 601.
10 The major product from this reduction was identified through its conversion to the corresponding oxazolidinone (NaH, DMF) and ^1H NMR spectral comparison with related literature compounds, See for example, T. Ibuka, H. Habashita, A. Otaka, N. Fujii, Y. Oguchi, T. Uyegara and Y. Yamamoto, *J. Org. Chem*., 1991, **56**, 4370.
11 C. H. Behrens and K. B. Sharpless, *J. Org. Chem*., 1985, **50**, 5696.
12 H. Staudinger and J. Meyer, *Helv. Chim. Acta*, 1919, **2**, 635; N. Knouzi, M. Voultier and R. Carrie, *Bull. Soc. Chim. Fr*., 1985, 815.
13 L. A. Carpino, *J. Am. Chem. Soc*., 1993, **115**, 4397; L. A. Carpino and A. El-Faham, *J. Org. Chem*., 1994, **59**, 695; L. A. Carpino, A. El-Faham, C. A. Minor and F. Albericio, *J. Chem. Soc., Chem. Commun*., 1994, 201; L. A. Carpino, A. El-Faham and F. Albericio, *Tetrahedron Lett*., 1994, **35**, 2279; L. A. Carpino and A. El-Faham, *J. Org. Chem*., 1995, **60**, 3561.
14 M. Frigerio, M. Santagostino, S. Sputore and G. Palmisano, *J. Org. Chem*., 1995, **60**, 7272.
15 Authentic samples of KJ and KF are not available. We thank Professor Kobayashi for providing a copy of the ^1H NMR spectrum for natural KJ.
16 Chemical degradation of KG converts the homo-Ile fragment to D-isoleucine indicating that KG possesses the (*R*) configuration at both C-13 and C-15.
17 A peak corresponding to L-alanine was also detected in this analysis, indicating that this residue did not epimerize during the cyclization reaction.

Communication 9/01928F

Metal–oxo cluster-supported transition metal complexes: hydrothermal synthesis and characterization of $[\{M(phen)_2\}_2(Mo_8O_{26})]$ (M = Ni or Co)

Ji-Qing Xu,*[ab] Ren-Zhang Wang,[a] Guo-Yu Yang,[a] Yong-Heng Xing,[a] Dong-Mei Li,[a] Wei-Ming Bu,[c] Ling Ye,[c] Yu-Guo Fan,[c] Guang-Di Yang,[c] Yan Xing,[d] Yong-Hua Lin[d] and Heng-Qing Jia[d]

[a] *Department of Chemistry, Jilin University, Changchun, Jilin 130023, PR China. E-mail: xjq@mail.jlu.edu.cn*
[b] *State Key Laboratory of Coordination Chemistry, Nanjing University, Nanjing, Jiangsu, 210093, China*
[c] *Key Laboratory for Supramolecular Structure and Spectroscopy, Jilin University, 130023, China*
[d] *Changhun Institute of Applied Chemistry, Chinese Academy of Sciences, Changchun, 130022, China*

Received (in Cambridge, UK) 25th January 1999, Accepted 19th April 1999

Two new metal–oxo supported transition metal complexes, $[\{M(phen)_2\}_2(Mo_8O_{26})]$ (M = Ni or Co; phen = 1,10-phenanthroline) are synthesized by a hydrothermal method and characterized by X-ray crystallography, showing that the octamolybdate possesses a novel unprecedented structure and that $[M(phen)_2]^{2+}$ units are covalently bonded to the $[Mo_8O_{26}]^{4-}$ cluster.

Metal–oxo cluster chemistry has been actively purchased owing to interest in the chemistry itself and its various applications in fields such as catalysis, electric conductivity, magnetism, nonlinear optical properties and medicine.[1] Recently, an important advance in metal oxide cluster chemistry has been study of polyoxoanion-supported inorganic or organometallic complexes. The syntheses and structures of complexes include $[\{Cu(4,4'\text{-bipy})\}_4(Mo_8O_{26})]$,[2] and $[\{Cu(en)_2\}_2(Mo_8O_{26})]$,[3] which possess infinite extended structures, $[\{Zn(2,2'\text{-bipy})_2\}_2(V_4O_{12})]$[4] and $[La(Mo_8O_{26})_2]^{5-}$,[5] which are molecular clusters; and organometallic compounds $[(CO)_3Mn(cis\text{-}Nb_2W_4O_{19})]^{3-}$,[6] and $[\{(\eta\text{-}C_5Me_5)Rh\}(Mo_{13}O_{40})]^{2+}$,[6] which have discrete cluster structures.

We report here the syntheses and characterization of octamolybdate-supported nickel– and cobalt–phenanthroline molecular clusters $[\{Ni(phen)_2\}_2(Mo_8O_{26})]$ **1** and $[\{Co(phen)_2\}_2(Mo_8O_{26})]$ **2**. To date, α-, β- and γ- isomers of octamolybdates have been crystallographically confirmed in several salts, and recently the δ-isomer in $[(\eta\text{-}C_5Me_5Rh)_2(\mu_2\text{-}SMe)_3]_4[Mo_8O_{26}]\cdot 2MeCN$[8] and $[\{Cu(4,4'\text{-bipy})\}_4(Mo_8O_{26})]$,[2] and ε-isomer in $[\{Ni(H_2O)_2(4,4'\text{-bipy})_2\}_2(Mo_8O_{26})]$[2] have also been characterized. The results of structure determination upon $[Mo_8O_{26}]^{4-}$ in both **1** and **2** indicates a novel unprecedented ξ-isomer structural form (Scheme1).

Compounds **1** and **2** were prepared hydrothermally from a mixture of MoO_3, H_2MoO_4, $Ni(OAc)_2\cdot 6H_2O$, 1,10-phenanthroline and H_2O in a mol ratio of 1.0: 1.0: 0.8: 1.6: 450, heated at 170 °C for three days. Purple block crystals of **1** were obtained in *ca*. 35% yield. While bright red tetragonal prismatic crystals of **2** were obtained under the same reaction conditions using $Co(OAc)_2\cdot 4H_2O$. Compounds **1** and **2** were characterized by elemental analyses,† spectroscopic (IR and UV-VIS)‡ and single-crystal X-ray structure analyses.§

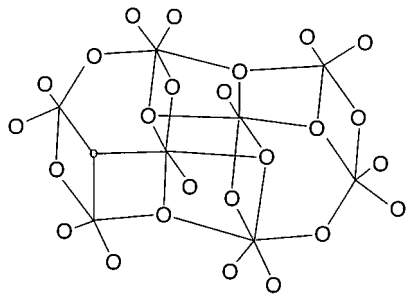

Scheme 1 The structure of ξ-$[Mo_8O_{26}]^{4-}$.

The crystal of **1** consists of discrete centrosymmetric heterometallic decanuclear clusters $[\{Ni(phen)_2\}_2(Mo_8O_{26})]$ (Fig. 1). The octamolybdate anion in **1** has a novel unprecedented structure mode denoted ξ- $[Mo_8O_{26}]^{4-}$ composed of a Mo_6O_6 ring capped on opposite faces by MoO_6 octahedra. The characteristic feature of this isomer is that the Mo_6O_6 ring contains two octahedral and four trigonal-bipyramidal Mo^{VI} atoms. In the ring, the linkage between any two MoO_5 trigonal bipyramids is edge-shared, while that between any MoO_6 octahedron and MoO_5 trigonal bipyramid is corner-shared. Each capping MoO_6 octahedron is linked to two MoO_6 octahedra and a trigonal bipyramid in the Mo_6O_6 ring by edge sharing and to another MoO_5 trigonal bipyramid of the ring by corner sharing. Two capping MoO_6 octahedra are attached to each other by edge sharing. The structural features of ξ-$[Mo_8O_{26}]^{4-}$ in **1** are different from those of the α-isomer consisting of six MoO_6 octahedra and two MoO_4 tetrahedra, the β-isomer consisting of eight edge-shared MoO_6 octahedra, the γ-isomer having six MoO_6 octahedra and two MoO_5 trigonal bipyramids, the δ-isomer composed of four MoO_6 octahedra and four MoO_4 tetrahedra[2,8] and the ε-isomer composed of six MoO_5 square pyramids and two MoO_6 octahedra.[2] The structure of the ξ- isomer also differs from that of (α–γ)- or (β–γ)-isomers proposed by Klemperer and Shum,[9] which, as yet has not been synthesized. Although the structure of proposed (α–γ)- or (β–γ)- isomers is also composed of four MoO_6 octahedra and four trigonal bipyramids as found in the ξ-isomer, their arrangement these isomers are different. In (α–γ)- or (β–γ)- isomers, the Mo_6O_6 ring contains four octahedral and two trigonal-bipyramidal Mo^{VI} atoms, and there are two edge-

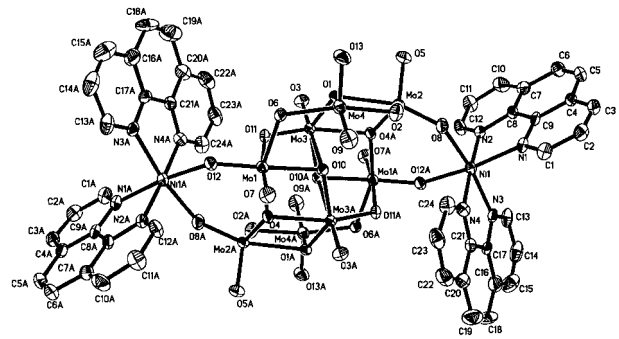

Fig. 1 Molecular drawing of **1** (50% displacement ellipsoids). Symmetry code: i −*x*, −*y*, −*z*. Selected bond lengths (Å): Mo(1)–O(7) 1.711(11), Mo(1)–O(6) 1.876(9), Mo(1)–O(12) 1.740(9), Mo(1)–O(4) 2.032(8), Mo(1)–O(10) 2.146(8), Mo(1)–O(11) 2.341(10), Mo(2)–O(5) 1.687(9), Mo(2)–O(8) 1.731(9), Mo(2)–O(2) 1.830(10), Mo(2)–O(4^i) 1.894(9), Mo(2)–O(1)2.244(8), Mo(3)–O(3)1.694(10), Mo(3)–O(11) 1.734(8), Mo(3)–O(1) 1.892(8), Mo(3)–O(10^i) 1.926(8), Mo(3)–O(4) 2.197(8), Mo(3)–O(10) 1.926(8), Mo(4)–O(13) 1.690(9), Mo(4)–O(9) 1.685(10), Mo(4)–O(2) 2.018(10), Mo(4)–O(6) 1.939(9), Mo(4)–O(1) 2.182(9), Ni(1)–O(8) 2.080(9), Ni(1)–O(12^i) 2.071(9).

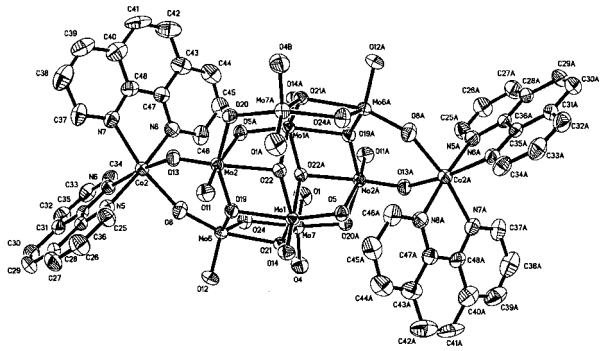

Fig. 2 Perspective drawing of one of the two crystallographically independent [{Co(phen)$_2$}$_2$(Mo$_8$O$_{26}$)] molecules in **2** (50% displacement ellipsoids). Symmetry code: i $-x + 2$, $-y + 2$, $-z$. Selected bond lengths (Å): Mo(1)–O(14) 1.688(3), Mo(1)–O(5) 1.740(3), Mo(1)–O(19) 2.190(3), Mo(1)–O(21) 1.897(3), Mo(1)–O(22) 1.911(3), Mo(1)–O(22^i) 2.504(3), Mo(2)–O(11) 1.688(3), Mo(2)–O(13) 1.736(3), Mo(2)–O(20) 1.866(3), Mo(2)–O(5^i) 2.337(3), Mo(2)–O(19) 2.024(3), Mo(2)–O(22) 2.149(3), Mo(6)–O(12) 1.696(3), Mo(6)–O(8) 1.733(3), Mo(6)–O(24) 1.831(4), Mo(6)–O(19) 1.900(3), Mo(6)–O(21) 2.236(3), Mo(7)–O(4) 1.693(4), Mo(7)–O(1) 1.685(4), Mo(7)–O(20^i) 1.947(3), Mo(7)–O(24) 2.002(4), Mo(7)–O(21) 2.159(3), Co(2)–O(8) 2.092(4), Co(2)–O(13) 2.107(4) (bond lengths in the other independent molecule are very close to the corresponding bonds above).

shared MoO_5 trigonal bipyramids in the cavity enclosed by polyhedra in the ring. More specifically, ξ-[Mo$_8$O$_{26}$]$^{4-}$ contains six O(μ_3), six O(μ_2) and fourteen O(t) atoms, while (α–γ)- or (β–γ)-[Mo$_8$O$_{26}$]$^{4-}$ contain two O(μ_4), two O(μ_3), eight O(μ_2) and fourteen O(t) atoms.

Each ξ-[Mo$_8$O$_{26}$]$^{4-}$ unit forms strong covalent interactions to two [Ni(phen)$_2$]$^{2+}$ units through terminal oxo groups of octahedral and trigonal-bipyramidal Mo sites in the Mo_6O_6 ring with Ni–O distances of 2.071(9) and 2.080(9) Å. Since the terminal oxo groups of fully oxidized polyoxomolybdate (all Mo sites in the VI oxidation state) are non-basic and unreactive, the formation of **1** reveals the oxophilicity of the [Ni(phen)$_2$]$^{2+}$ group and the structural flexibility of the octamolybdate core in adopting the ξ-structure. In the [Ni(phen)$_2$]$^{2-}$ unit, Ni is coordinated to four N donors of 1,10-phenanthroline ligands besides two terminal oxygen atoms of the octamolybdate cluster, forming a distorted octahedron with one relatively long Ni–N distance of 2.094(12) Å and three Ni–N distances in the range 2.055–2.065 Å. Compound **1** has three kinds of Mo–O bonds: 1.685(10)–1.711(11) Å for Mo–O(t), 1.731(9)–2.341(10) Å for Mo–O(μ_2) and 1.892(8)–2.244(8) Å for Mo–O(μ_3) bonds, respectively. The average Mo–O bond lengths of Mo(2), Mo(3) and Mo(4) are very similar (1.877–1.903 Å) whereas for Mo(1) Ni(phen)$_2$ this is longer (1.975 Å). It is found for Mo(2), Mo(3) and Mo(4) sites that Mo–O distances increase with increasing coordination number of oxygen (*i.e.* one < two < three), only for the Mo(1) site is this trend is not completely met, with Mo(1)–O(11)(μ_2)[2.341(10) Å] being obviously longer than Mo(1)–O(4)(μ_3) [2.042(8) Å] and Mo(1)–O(10) (μ_3)[2.146(8) Å], respectively.

There are two crystallographically independent [{Co(phen)$_2$}$_2$(Mo$_8$O$_{26}$)] molecules (Fig. 2) in the unit cell of **2** and both possess rigorous C_i symmetry in the solid state: their non-hydrogen atoms are symmetrically disposed about crystallographic inversion centers at (0,0,0) and (−1/2,1/2,−1/2), respectively. Both molecules contain a ξ-[Mo$_8$O$_{26}$]$^{4-}$ unit, with Mo–O(t) in the range 1.685(3)–1.696(3) Å [1.673(4)–1.690(4) Å second molecule]; Mo–O(μ_2) 1.733(3)–2.337(3) Å [1.734(3)–2.329(3) Å] and Mo–O(μ_3)1.897(3)–2.504(3) Å [1.903(3)–2.493(3) Å]. Average Mo–O bond lengths in molybdenum coordination polyhedra are as follows: for Mo atoms with coordination number of six, Mo(1)–O = 1.988 Å (av.) and Mo(2)–O = 1.967 Å (av.) [Mo(3)–O = 1.989 Å (av.) and Mo(4)–O = 1.964 Å (av)]; for Mo atoms with a coordination number of five, Mo(6)–O = 1.879 Å (av) and Mo(7)–O = 1.897 Å (av.) [Mo(5)–O = 1.881 Å (av.) and Mo(8)–O = 1.893 Å (av.)]. Thus average Mo–O bond lengths in five- and six-coordinated molybdenum polyhedra are very similar but the latter are significantly longer.

This work were supported by National Natural Science Foundation of China (No. 29671012 and No. 29733090) and The State Key Laboratory of coordination Chemistry.

Notes and references

† Anal: Calc. for **1** $C_{48}H_{32}N_8Ni_2Mo_8O_{26}$: C, 28.49; H, 1.58; N, 5.53; Ni, 5.83; Mo, 37.96. Found: C, 28.44; H, 1.52; N, 5.47; Ni, 5.76; Mo, 37.12%. Calc. for **2** $C_{48}H_{32}N_8Co_2Mo_8O_{26}$:C, 28.48; H, 1.58; N, 5.53; Co, 5.82; Mo, 37.95. Found: C, 28.24; H, 1.50; N, 5.23; Co, 5.78; Mo, 37.44%.

‡ *Spectroscopic data*: for **1**: IR (KBr pellet ν/cm^{-1}): Mo–O stretching region, 945, 885, 850, 705. UV–VIS (DMF solution), λ_{max} (ε/dm^3 mol^{-1} cm^{-1}): 322 (1.05×10^3), 340 (6.0×10^2), 585 (2.15×10^2).

For **2**: IR (KBr pellet ν/cm^{-1}): Mo–O stretching region, 960, 890, 850, 720. UV–VIS (DMF solution), λ_{max} (ε/dm^3 mol^{-1} cm^{-1}): 312 (1.1×10^3), 340 (1.3×10^3), 580 (2.06×10^2).

§ *Crystal data*: **1**: [{Ni(phen)$_2$}$_2$(Mo$_8$O$_{26}$)], M = 2021.76, monoclinic, space group $P2_1/n$, a = 12.952(2), b = 16.659(10), c = 13.956(12) Å, β = 106.273(8)°, V = 2890(5) Å^3, Z = 2, D_c = 2.323 g cm^{-3}, F(000) = 1952, T = 293 K. λ(Mo-Kα) = 0.71073 Å, θ range 1.90–26°. Bruker P4 four-circle diffractometer. ω-2θ scan. 5604 reflections are unique, 5604 reflections with $I > 2\sigma(I)$ were used in the refinement and the calculation of R_1 and wR_2. The last successful full-matrix least-squares refinement with anisotropic thermal parameters for all non-hydrogen atoms converged to R_1 = 0.0414, wR_2 = 0.0815. The positions of hydrogen atoms were calculated in ideal positions and not refined. The structure was solved by direct methods.

2: [{Co(phen)$_2$}$_2$(Mo$_8$O$_{26}$)], M = 2022.20, triclinic, space group $P\bar{1}$, a = 12.913(3), b = 14.021(3), c = 16.687(3) Å, α = 90.14(3), β = 90.13(3), γ = 106.26(3)°, V = 2900.4(10) Å^3, Z = 2, D_c = 2.316 g cm^{-3}, F(000) = 1948, T = 293 K. λ(Mo-Kα) = 0.71073 Å, θ range 1.51–23°. Bruker P4 four-circle diffractometer. ω–2θ scan. 8029 reflections are unique, 8029 reflections with $I > 2\sigma(I)$ were used in the refinement and the calculation of R_1 and wR_2. Least-squares refinement as above converged to R_1 = 0.026, wR_2 = 0.0615. Other details as above.

CCDC 182/1227.

1 *Polyoxometalates*, ed. C. L. Hill, *Chem. Rev.*, 1998, 98.
2 D. Hagrman, C. Zubita, D. J. Rose, J. Zubieta and R. C. Haushalter, *Angew. Chem., Int. Ed. Engl*., 1997, **36,** 873.
3 J. R. D. Debord, R. C. Haushalter, L. M. Meyer, D. J. Rose, P. J. Zapf and J. Zubieta, *Inorg. Chem. Acta*, 1997, **256**, 165.
4 Y. Zhang, P. J. Zappf, L. M. Meyer, R. C. Haushalter and J. Zubieta, *Inorg. Chem.*, 1997, **36**, 2159.
5 A. Kitamuura, T. Ozeki and A. Yagasaki, *Inorg. Chem*., 1997, **36**, 4285.
6 C. J. Besecher, V. W. Day, W. G. Klemperer and M. R. Thompson, *Inorg. Chem*., 1985, **24**, 44.
7 H. K. Chae, W. G. Klemperer, D. E. Paez Logo, V. W. Day and T. A Eberspacher, *Inorg. Chem*., 192, **31**, 3187
8 R. Xi, B. Wang, K. Isobe, T. Nishioka, K. Toriumi and Y. Ozawa, *Inorg. Chem*., 1994, **33**, 833.
9 W. G. Klemperer and W. Shum, *J. Am. Chem. Soc.*, 1976, **98**, 8281.

Communication 9/00643E

Palladium(II)-catalyzed oxidation of acrylate esters to acetals in supercritical carbon dioxide

Lanqi Jia, Huanfeng Jiang* and Jinheng Li

Guangzhou Institute of Chemistry, Chinese Academy of Sciences, PO Box 1122, Guangzhou 510650, China. E-mail: jhf@mail.gic.ac.cn

Received (in Cambridge, UK) 11th March 1999, Accepted 20th April 1999

The development of a new palladium(II)-catalyzed oxidation of methyl acrylate, affording methyl 3,3-dimethoxypropanoate in excellent conversion and selectivity in supercritical CO_2, is presented.

Alkyl 3,3-dialkoxypropanoates are important intermediates in organic synthesis and have been used to synthesize a variety of compounds, including coumarins,[1] porphyrins,[2] spermine metabolites[3] and loganin.[4] Previously reported methods for the preparation of alkyl 3,3-dialkoxypropanoates are not satisfactory, due to the high cost of the starting materials and the low overall yields of the process. The Pd^{II}-catalyzed oxidation of terminal olefins with water, which is well known as the Wacker reaction, produces methyl ketones.[5] A similar reaction of terminal olefins bearing electron-withdrawing groups upon treatment of alcohols catalyzed by Pd^{II} affords acetals at the terminal carbon in DME. High yields of methyl 3,3-dimethoxypropanoate (92%), however, were afforded only in the presence of HMPA. In the absence of HMPA the yield was only 46%.[6]

Using supercritical carbon dioxide ($scCO_2$) as a reaction solvent has been attracting extensive attention in recent years. First, CO_2 is inexpensive, nonflammable, nontoxic[7] and chemically inert under many conditions. $ScCO_2$, as an environmentally friendly reaction medium, may be a substitute for volatile and toxic organic solvents.[8] Secondly, $scCO_2$ possesses hybrid properties of both liquid and gas, to the advantage of some reactions involving gaseous reagents.[9] Control of the solvent density by variation of the temperature and pressure enables the solvent properties to be 'tuned' to reactants.[10] Finally, separating of CO_2 from the reaction mixture is energy-efficient and simple.

Organic reactions in $scCO_2$ have facilitated great progress in organometallic chemistry, particularly in homogeneous and heterogeneous catalysis. Several recent reports have shown that some interesting results are specifically associated with the use of $scCO_2$ as a reaction solvent.[11] Here we disclose our work on a Pd^{II}-catalyzed terminal olefin oxidation in $scCO_2$.‡ Our results show that Pd^{II}-catalyzed oxidation of methyl acrylate could be successfully processed in $scCO_2$ to give the dimethyl acetal as major product when an excess of MeOH was used (Scheme 1). Our previous experiments show that it is necessary to add an excess of MeOH to promote partial dissolution of the inorganic catalysts in $scCO_2$, since MeOH is miscible in $scCO_2$.[12]

The catalytic activity of $PdCl_2$ and $PdCl_2(MeCN)_2$ for oxidation of methyl acrylate were investigated. The reaction catalyzed by $PdCl_2$ were slightly faster than that by $PdCl_2(MeCN)_2$ (Table 1, entries 2 and 3).

It has been reported that CuCl was superior to $CuCl_2$ as the cocatalyst in the oxidation of acrylate esters.[13,6b] Interestingly, in our experiments carried out in $scCO_2$, 0.4 equiv. of $CuCl_2$ gave similar or even better results than the same amount of CuCl (Table 1, entries 8 and 9).

Hosokawa reported that the oxidation of methyl acrylate to the acetal was carried out at 50 °C in DME.[6] We found that the oxidation reaction could be completed at a lower temperature in $scCO_2$. In our experiment, the reaction afforded very good conversion and selectivity at 40 °C. The reaction was still smoothly accomplished at 27 °C, at which temperature CO_2 is a liquid, although the amount of byproducts increased slightly.

The CO_2 pressure had a great effect on the selectivity. The best results were obtained when the pressure of CO_2 was controlled between 12–13 MPa. As the pressure of CO_2 was reduced, the conversion and selectivity also declined. For example, the reaction gave **2** in a yield of only 75.8% and the

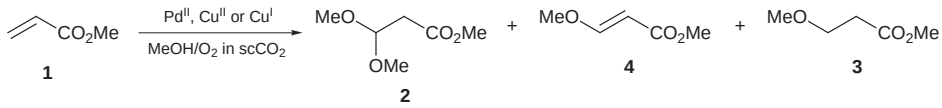

1 2 4 3

Scheme 1

Table 1 Oxidation reaction of methyl acrylate in $scCO_2$[a]

Entry	Catalyst	T/°C	P_{O_2}/MPa	P_{CO_2}/MPa	Conv.	Yield[b] (%) **2**	**3**	**4**	Selectivity for **2**[c] (%)
1	$PdCl_2(MeCN)_2$, CuCl[d]	50	0.1	13	99.0	81.1	3.5	8.8	86.8
2	$PdCl_2(MeCN)_2$, CuCl[d]	50	0.1	13	49.4	36.6	5.9	2.7	81.0
3	$PdCl_2$, $CuCl_2$[e]	50	0.1	13	71.0	42.9	6.6	3.1	81.6
4	$PdCl_2$, $CuCl_2$	50	0.1	13	98.5	82.7	4.0	3.5	91.7
5	$PdCl_2(MeCN)_2$, CuCl	40	0.1	12	93.0	82.4	2.8	3.0	93.4
6	$PdCl_2$, $CuCl_2$	27	0.1	12	93.0	75.0	5.1	2.9	90.3
7	$PdCl_2$, $CuCl_2$	40	0.1	9	92.0	75.8	2.8	3.4	92.4
8	$PdCl_2$, $CuCl_2$	40	0.5	13	99.1	87.9	1.6	2.5	95.5
9	$PdCl_2$, CuCl	40	0.5	13	99.7	86.3	1.5	4.5	93.5
10	$PdCl_2$, $CuCl_2$	40	1.0	12	99.4	91.7	1.2	2.0	96.6

[a] Methyl acrylate (5 mmol), MeOH (1 ml ≈ 24.7 mmol), $PdCl_2$ or $PdCl_2(MeCN)_2$ (3 mol%), CuCl or $CuCl_2$ (0.4 equiv.), 12 h. [b] By GC. [c] Selectivity = [**2**/(**2** + **3** + **4**)] × 100. [d] $PdCl_2(MeCN)_2$ (1 mol%), CuCl or $CuCl_2$ (2 mol%). [e] $CuCl_2$ (2 mol%).

amount of other unidentified products increased when 9 MPa CO_2 was charged in the autoclave.

The oxygen pressure also affected the conversion and selectivity. Lower oxygen pressure (0.1 MPa) gave satisfactory conversion but the selectivity to **2** was never higher than 93.4%. The best selectivity (over 96%) was obtained as the oxygen pressure was elevated to 1.0 MPa. Using ethyl acrylate as the substrate, the reaction affords similar results, and the further experiments are now in progress.

In summary, the oxidation reaction of methyl acrylate afforded the acetal in high conversion and selectivity at lower temperature when supercritical carbon dioxide instead of DME was used as the reaction medium without the presence of HMPA. The pressure of CO_2 and O_2 had a remarkable effect on the conversion and selectivity.

The authors are grateful to the National Natural Science Foundation of China for financial support of this work (29772036) and Dr Fanglü Huang for helpful discussions.

Notes and references

† Typical procedure: Reactions were carried out in a HF-25 autoclave. Pd^{II} catalyst (0.15 mmol, 3 mol%), $CuCl_2$ (4 mmol), MeOH (1 ml, 24.7 mmol) and acrylate ester (5 mmol) were added into a 25 ml autoclave in sequence. O_2 and then liquid CO_2 were pumped into the autoclave using a cooling pump to give the desired pressure. The autoclave was then put into an oil bath under magnetic stirring for the desired reaction time. After the reaction, the autoclave was allowed to cool to −30 °C. CO_2 was vented and the surplus was extracted with n-hexane. The extract was filtrated and condensed under reduced pressure. The product was analyzed using GC (quantitative analysis) and GC-MS, ^{1}H NMR ^{13}C NMR and IR analysis (identification of products).

1 D. G. Crosby and R. V. Berthold, *J. Org. Chem.*, 1962, **27**, 3083.
2 J. P. Collman, A. O. Chong, G. B. Jameson, R. T. Oakley, E. Rose, E. R. Schmittou and J. A. Ibers, *J. Am. Chem. Soc.*, 1981, **103**, 516.
3 M. Israel, E. C. Zoll, N. Muhammad and E. J. Modest, *J. Med. Chem.*, 1973, **16**, 1.
4 G. Büchi, J. A. Carlson, J. E. Powell, Jr. and L.-F. Tiztze, *J. Am. Chem. Soc.*, 1973, **95**, 504.
5 For a comprehensive review, see: J. Tsuji, *Synthesis*, 1984, 369.
6 (*a*) T. Hosokawa, S. Aoki and S.-I. Murahashi, *Synthesis*, 1992, 558; (*b*) T. Hosokawa, T. Ohta, S. Kanayama and S.-I. Murahashi, *Synthesis*, 1992, 558; (*b*) T. Hosokawa, T. Ohta, S. Kanayama and S.-I. Murahashi, *J. Org. Chem.*, 1987, **52**, 1758.
7 For discussions of the advantages of $scCO_2$, see T. Clifford and K. Bartle, *Chem. Ind.*, 1996, 449; M. Poliakoff and S. Howdle, *Chem. Ber.*, 1995, **31**, 118; H. Black, *Environ. Sci. Technol.*, 1996, **30**, 124A.
8 D. A. Morgenstern, R. M. LeLacheur, D. K. Morita, S. L. Borokowsky, S. Feng, G. H. Brown, L. Luan, M. F. Gross, M. J. Burk and W. Tumas, *ACS Symp. Ser.*, 1996, **626**, 132.
9 J. W. Rathke, R. J. Klinger and T. R. Krause, *Organometallics*, 1991, **10**, 1350; P. G. Jessop, T. Ikariya and R. Noyori, *Nature*, 1994, **368**, 231.
10 M. A. Carroll and A. B. Holmes, *Chem. Commun.*, 1998, 1395.
11 M. J. Burk, S. Feng, M. F. Gross and W. Tumas, *J. Am. Chem. Soc.*, 1995, **117**, 8277.
12 L. Jia, H. Jiang and J. Li, *Green Chem.*, 1999, 91.
13 J. Tsuji, H. Nagashima and H. Nemoto, *Org. Synth.*, 1984, **62**, 9.

Communication 9/01935I

ChemComm

A novel two-dimensional honeycomb-like bimetallic iron(III)–nickel(II) cyanide-bridged magnetic material $[Ni(cyclam)]_3[Fe(CN)_6]_2 \cdot nH_2O$ (cyclam = 1,4,8,11-tetraazacyclodecane)

Enrique Colacio,*[a] José M. Domínguez-Vera,[a] Mustapha Ghazi,[a] Raikko Kivekäs,[b] Francesc Lloret,*[c] José M. Moreno[a] and Helen Stoeckli-Evans[d]

[a] *Departamento de Química Inorgánica, Facultad de Ciencias, Universidad de Granada, E-18071, Spain. E-mail: ecolacio@goliat.ugr.es*
[b] *Department of Chemistry, Laboratory of Inorganic Chemistry, University of Helsinki, F-00014, Finland*
[c] *Departament de Química Inorgánica, Facultat de Química, Universitat de Valencia, Dr. Moliner 50, E-46100 Burjassot, Spain. E-mail: francisco.lloret@uv.es*
[d] *Institut de Chimie, Université de Neuchâtel, Avenue de Bellevaux 51, CH-200 Neuchàtel, Switzerland*

Received (in Cambridge, UK) 15th March 1999, Accepted 26th April 1999

The 2D honeycomb-like layered iron(III)–nickel(II) cyanide-bridged complex $[Ni(cyclam)]_3[Fe(CN)_6]_2 \cdot nH_2O$ exhibits ferromagnetic intralayer and antiferromagnetic interlayer interactions; above 3 K the magnetic properties are typical of a metamagnet with H_c = 5000 G, whereas below 3 K a canted structure is formed, leading to a long range ferromagnetic ordering.

Bimetallic assemblies with Prussian blue-like structure form a family of materials that exhibit spontaneous magnetization at T_c as high as 315 K,[1] and interesting electro-chemical, opto-electronic and magneto-optical properties.[2] The crystallization of Prussian blue analogues, however, is very difficult and it has been only quite recently that Kahn and coworkers[3] have succeeded in growing crystals of $[Mn_2(H_2O)_5Mo(CN)_7] \cdot nH_2O$ (α and β forms), which ferromagnetically order at 51 K.

One alternative route to bimetallic cyanide-bridged extended arrays is that of using hexacyanometalate building blocks with metal complexes containing polydentate ligands. This hybrid approach favours the crystallization and then their magneto-structural study. Depending on the nature of the building blocks different and fascinating extended network structures can be obtained, some of which are magnetically ordered.[4]

On reacting $[Ni(cyclam)]^{2+}$ and $[Fe(CN)_6]^{3-}$ in water using a 1 : 1 molar ratio the compound $[Ni(cyclam)]_3[Fe(CN)_6]_2 \cdot 12H_2O$ is obtained as a fine brown precipitate, however, by using a 1 : 10 molar ratio the complex $[Fe(cyclam)][Fe(CN)_6] \cdot 6H_2O$ is obtained.[5] Slow diffusion of two aqueous solutions of the reactants, into a U-tube containing silica gel, provided two kinds of well formed dark brown block-like single crystals of formula $[Ni(cyclam)]_3[Fe(CN)_6]_2 \cdot nH_2O$ (n = 12 and 22.5). X-ray analysis† reveals that both phases exhibit similar structures, which only differ in the number of water molecules (hereafter we shall discuss the results for n = 22.5, whose structure is more accurately determined). The structure consists of honeycomb-like layers (Fig. 1) and crystal water molecules that occupy the interlayer space. To form the layers, each $[Fe(CN)_6]^{3-}$ is coordinated to three $[Ni(cyclam)]^{2+}$ cations, at facial positions, through cyanide bridges, with Fe···Ni distances ranging from 5.037 to 5.202 Å, whereas each $[Ni(cyclam)]^{2+}$ cation is linked to two $[Fe(CN)_6]^{3-}$ units in *trans* positions. The *cis*-C–Fe–C angles are close to 90°, whereas the Fe–C distances are in the range 1.934(4)–1.954(4) Å. Ni^{II} ions, which are located on centres of symmetry, exhibit a *trans*-octahedral geometry; the nickel–cyanide nitrogen distances [2.123(3)–2.144(3) Å] being longer than the equatorial ones [2.059(4)–2.070(4) Å]. The Fe–C–N angles are close to linear and only vary in the small range 174.0(3)–179.1(3)°, whereas the Ni–N–C angles [165.4(3) and 154.9(3)°] deviate significantly from linearity. The layers are not planar but form an infinite staircase structure and align along the *a* axis with shortest interlayer separations of 7.688 Å, for Fe···Ni(2). This structure is similar to that reported for a hexacyanochromate(III) analogue.[4k]

The $\chi_M T$ *vs.* T plot per Fe_2Ni_3 unit (H = 50 G) is shown in Fig. 2.‡ On cooling, $\chi_M T$ increases reaching a maximum value of 15 $cm^3\ mol^{-1}\ K$ at 8 K, indicating a ferromagnetic interaction between Fe^{III} (t_{2g}^5) and Ni^{II} (e_g^2). The χ_M curve shows a maximum at *ca.* 8 K, for H < 5000 G, a clear indication of an antiferromagnetic interaction between the ferromagnetic sheets.

Below 6 K, $\chi_M T$ sharply increases again reaching a value of 60 $cm^3\ mol^{-1}\ K$ at 2 K, suggesting a canting of the local spins, which may arise from the local magnetic anisotropy of Ni^{II} and low-spin Fe^{III} ions. This phase transition is confirmed by ac susceptibility measurements which show an intense signal at 3 K. Above 3 K, the magnetic properties are typical of a metamagnet with a critical field H_c = 5000 G. For H < 5000 G,

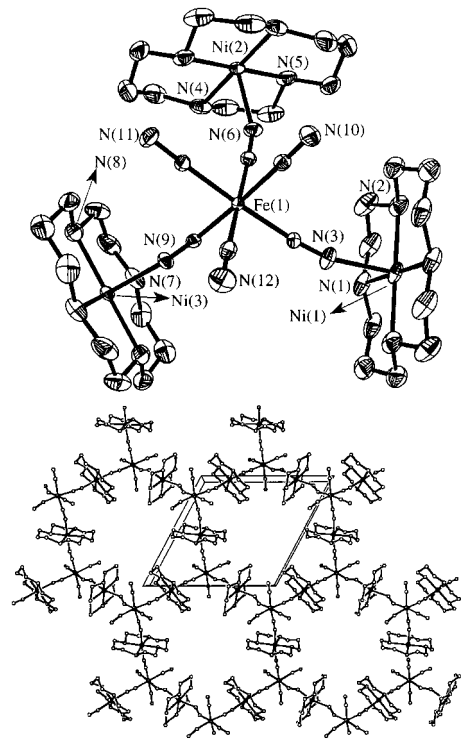

Fig. 1 Views of the asymmetric unit and 2D honeycomb-like layered. Water molecules are omitted for clarity.

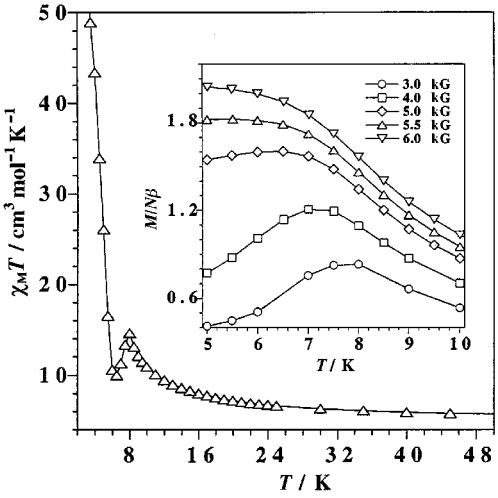

Fig. 2 $\chi_M T$ *vs.* T for H = 50 G. Inset: ($M/N\beta$) *vs.* T at various fields.

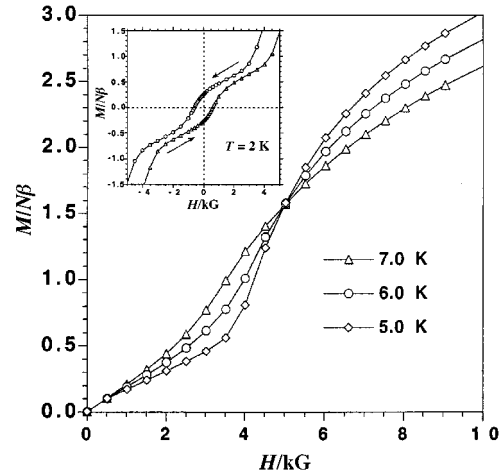

Fig. 3 ($M/N\beta$) *vs.* H at different temperatures. Inset: hysteresis loop at 2 K.

the ($M/N\beta$) *vs.* T curves (Fig. 2 inset) display a maximum which broadens as H is increased and finally disappears for $H > 5000$ G, demonstrating that a field-induced transition from an antiferro- to a ferro-magnetic ground state occurs. To confirm this metamagnetic behaviour, ($M/N\beta$) *vs.* H was measured at various temperatures (Fig. 3). As the temperature is lowered, the isotherms become increasingly sigmoidal and present a crossing point at *ca.* 5000 G, corresponding to H_c.

Below 3 K, a canted structure is formed. The magnetization curves present hysteresis loops with a remanent magnetization of 0.26 $N\beta$ and a coercive field of 600 G at 2 K (Fig. 3 inset). This canted structure is also broken when $H > 5000$ G, which is sufficient to overcome the intersheet interactions, responsible for the spin canting ground state. The chromium(III) analogue,[4k] does not exhibit any phase transition above 2 K.

This work was supported by the Spanish Dirección General de Investigación Científica y Técnica (projects PB97-0822 and PB97-1397), by the Junta of Andalucía and the TMR Programme from the European Union (Contract ERBFMRXCT98-0181).

Notes and references

† *Crystal structure analysis:* $[Ni(cyclam)]_3[Fe(CN)_6]_2\cdot 22.5H_2O$, $C_{42}H_{113}Fe_2N_{24}Ni_3O_{22.5}$, M_w = 1606.4, monoclinic, space group *A*2/*n*, *a* = 17.9384(12), *b* = 16.7894(12), *c* = 25.764(2) Å, β = 91.176(9)°, *V* = 7757.7(10) Å^3, *Z* = 4, D_c = 1.375 Mg m^{-3}, *F*(000) = 3396, μ = 1.157 mm^{-1}, *T* = 223(2) K, 0.50 × 0.50 × 0.40 mm, 7366 independent (R_{int} = 0.0497) with 4326 [$I > 2\sigma(I)$] observed data, *R*1 = 0.0457, *wR*2 = 0.1326. $[Ni(cyclam)]_3[Fe(CN)_6]_2\cdot 12H_2O$, $C_{42}H_{96}Fe_2N_{24}Ni_3O_{12}$, M_w = 1417.3, monoclinic, space group *C*2/*m*, *a* = 27.384(3), *b* = 14.3128(11), *c* = 8.4772(8) Å, β = 90.176(13)°, *V* = 3322.6(6) Å^3, *Z* = 2, D_c = 1.417 Mg m^{-3}, *F*(000) = 1496, μ = 1.330 mm^{-1}, *T* = 193(2) K, 0.25 × 0.20 × 0.20 mm, 3357 independent (R_{int} = 0.197) with 1571 [$I > 2\sigma(I)$] observed data, *R*1 = 0.0764 *wR*2 = 0.1840. Disordered macrocycle, atoms N21 and C21 (atoms A and B, were given an occupancy of 0.5 each). Graphite monochromatized Mo-Kα radiation, λ = 0.71073 Å, STOE Image Plate diffractometer. No absorption corrections. Solution by direct methods (SHELXS-97) and refinements on F^2 by full-matrix least squares. Non-hydrogen atoms were refined anisotropically, H-atoms in calculated positions as riding atoms, except those of the water molecules that were ignored. CCDC 182/1234. See http://www.rsc.org/suppdata/cc/1999/987/ for crystallographic files in .cif format

‡ Magnetic measurements were carried out on a SQUID-based sample magnetometer using a Quantum Design Model MPMS instrument.

1 M. Verdaguer, *Science*, 1996, **272**, 698; W. Entley and G. S. Girolami, *Science*, 1995, **268**, 397; O. Kahn, *Nature*, 1995, **378**, 667; S. Ferlay, T. Mallah, R. Ouahes, P. Veillet and M. Verdaguer, *Nature*, 1995, **378**, 701; E. Dujardin, S. Ferlay, X. Phan, C. Desplanches, C. Cartier dit Moulin, P. Sainctavit, F. Baudelet, E. Dartyge, P. Veillet and M. Verdaguer, *J. Am. Chem. Soc.*, 1998, **120**, 11 347.

2 K. R. Dumbar and R. A. Heintz, *Prog. Inorg. Chem.*, 1997, **45**, 283; O. Sato, T. Iyoda, A. Fujishina and K. Hashimoto, *Science*, 1996, **271**, 46; O. Sato, T. Iyoda, A. Fujishina and K. Hashimoto, *Science*, 1996, **272**, 704.

3 J. Larionova, R. Clerac, J. Sanchiz, O. Kahn, S. Golhen and L. Ouahab, *J. Am. Chem. Soc.*, 1998, **120**, 13 088.

4 (*a*) M. Ohba, H. Okawa, N. Fukita and Y. Hashimoto, *J. Am. Chem. Soc.*, 1997, **119**, 1011; (*b*) N. Fukita, M. Ohba, H. Okawa, K. Matsuda and H. Iwamura, *Inorg. Chem.*, 1998, **37**, 842 and references therein; (*c*) M. Ohba, N. Usuki, N. Fukita and H. Okawa, *Inorg. Chem.*, 1998, **37**, 3349 and references therein; (*d*) H. Miyasaka, N. Matsumoto, N. Re, E. Gallo and C. Floriani, *Inorg. Chem.*, 1997, **36**, 670; (*e*) H. Miyasaka, N. Matsumoto, H. Okawa, N. Re, E. Gallo and C. Floriani, *J. Am. Chem. Soc.*, 1996, **118**, 981; (*f*) N. Re, E. Gallo, C. Floriani, H. Miyasaka and N. Matsumoto, *Inorg. Chem.*, 1996, **35**, 6004; (*g*) H.-Z. Kou, D.-Z. Liao, P. Cheng, Z.-H. Jiang, S.-P. Yan, G. L. Wang, X.-K. Yao and H.-G. Wang, *J. Chem. Soc., Dalton Trans.*, 1997, 1503; (*h*) M. Salah El Fallah, E. Rentschler, A. Caneschi, R. Sessoli and D. Gatteschi, *Angew. Chem., Int. Ed. Engl.*, 1996, **35**, 9047; (*i*) T. Mallah, C. Auberger, M. Verdaguer and P. Veillet, *J. Chem. Soc., Chem. Commun.*, 1995, 61; (*j*) A. Scuiller, T. Mallah, M. Verdaguer, A. Nivorozkhin, J. Tholence and P. Veillet, *New J. Chem.*, 1996, **20**, 1; (*k*) S. Ferlay, T. Mallah, J. Vaisserman, F. Bartolomé, P. Veillet and M. Verdaguer, *Chem. Commum.*, 1996, 2481; (*m*) K. Van Langenberg, S. R. Batten, K. J. Berry, D. C. R. Hockless, B. Moubaraki and K. S. Murray, *Inorg. Chem.*, 1997, **36**, 5006; (*n*) N. Matsumoto, Y. Sunatsuki, H. Miyasaka, Y. Hashimoto, D. Luneau and J. P. Tuchagues, *Angew. Chem., Int. Ed.*, 1998, **38**, 171; (*o*) H.-Z. Kou, W.-M. Bu, D.-Z. Liao, Z.-H. Jiang, S.-P. Yan, Y.-G. Fan and G.-L. Wang, *J. Chem. Soc., Dalton. Trans.*, 1998, 4161; (*p*) J. Larionova, O. Kahn, S. Gohlen, L. Ouahab and R. Clerac, *J. Am. Chem. Soc.*, 1999, **121**, 3349.

5 E. Colacio, J. M. Domínguez-Vera, M. Ghazi, R. Kivekas, M. Klinga and J. M. Moreno, *Chem. Commum.*, 1998, 1071.

Communication 9/02041A

Antagonistic metal-directed inductions in catalytic asymmetric aziridination by manganese and iron tetramethylchiroporphyrins

Jean-Pierre Simonato,[a] Jacques Pécaut,[a] W. Robert Scheidt[b] and Jean-Claude Marchon*[a]

[a] *Laboratoire de Chimie de Coordination, Service de Chimie Inorganique et Biologique, Département de Recherche Fondamentale sur la Matière Condensée, CEA-Grenoble, 38054 Grenoble, France. E-mail: jcmarchon@cea.fr*
[b] *Department of Chemistry and Biochemistry, University of Notre Dame, Notre Dame, Indiana 46556, USA*

Received (in Basel, Switzerland) 25th February 1999, Accepted 11th April 1999

Catalytic asymmetric aziridination of styrene by [*N*-(*p*-toluenesulfonyl)imino]phenyliodinane was achieved by manganese and iron tetramethylchiroporphyrins; opposite enantioselectivities were obtained with the two metal centers, and possible mechanisms are proposed to explain this unexpected result.

Amongst atom- and group-transfer processes, including epoxidation[1] and cyclopropanation,[2] aziridination is probably the least studied reaction. However, transition metal catalysed aziridination of olefins has been a topic of increasing interest in the past five years.[3] Several atom-transfer catalysts have been found to induce olefin aziridination by [*N*-(*p*-toluenesulfonyl)-imino]phenyliodinane (PhINTS),[4] but generally they are only moderately efficient and the mechanisms of aziridination catalysis remain unclear. A number of chiral metalloporphyrins have been shown to catalyse the asymmetric epoxidation[1] and cyclopropanation[2] of olefins, but only one example of catalytic asymmetric aziridination of alkenes has been published up to now.[5] Metallochiroporphyrins are competent catalysts in the epoxidation of aromatic olefins,[6] thus it was tempting to assess their potential in catalytic nitrogen group transfer. Herein we report the catalytic activity of several metal complexes of tetramethylchiroporphyrin (TMCP) **1** in the asymmetric aziridination of styrene, and the opposite enantioselectivities induced by the iron(III) and manganese(III) centers.

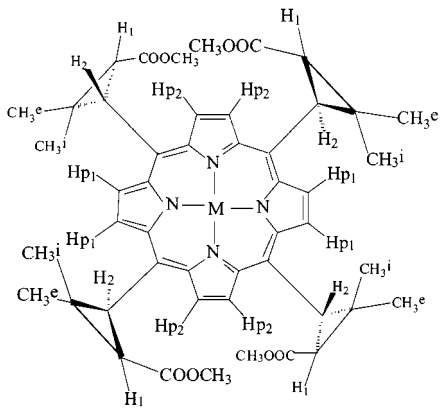

M = $Mn^{III}Cl$, $Fe^{III}Cl$, $Co^{III}Cl$, Ni^{II}, Cu^{II}, $Ru^{II}(CO)$, $Rh^{III}I$.

Initial experiments were carried out in order to probe the efficiency of various transition metals. Ni^{II}, Cu^{II}, Co^{III} and Rh^{III} were found to be inefficient and Ru^{II} nearly so [Ru(CO)(TMCP) led to 4% yield, 20% ee]. As anticipated from earlier work,[7] Mn^{III} and Fe^{III} are potent catalysts,[8] although the aziridine yields are only moderate (Table 1).[9] Unexpectedly, the iron(III) catalyst favours the synthesis of (+)-*N*-tosyl-2-phenylaziridine whereas the manganese(III) complex of the same TMCP chiral ligand preferentially leads to the (−) enantiomer. This result is reminiscent of the well documented opposite enantioface selection exhibited by (*R*)-BINAP–Rh^{I} and (*R*)-BINAP–Ru^{II} complexes in the asymmetric hydrogenation of *N*-acylaminoacrylic acids,[10] but to our knowledge this is the first demonstrated case of antagonistic metal-directed asymmetric inductions in a catalytic group-transfer process.

Table 1 Catalytic asymmetric aziridination of styrene with (TMCP) complexes[a]

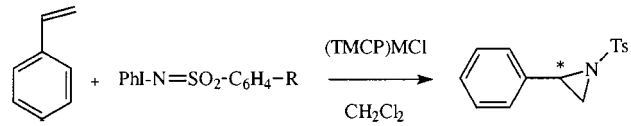

Entry	Substrate	M	R	Yield[b] (%)	% ee[c]
1	Styrene	Fe	Me	27	28 (+)
2	Styrene	Mn	Me	34	57 (−)
3	Styrene	Fe	OMe	27	n.d.[d]
4	Styrene	Mn	OMe	17	33 (−)
5	Dihydronaphthalene	Mn	Me	0	—
6	*cis*-Stilbene	Mn	Me	0	—

[a] *Reaction conditions*: (catalyst : $PhINSO_2Ar$: styrene = 1 : 50 : 500). [b] Isolated yields were based on the amount of $PhINSO_2Ar$ used. [c] Values of ee were determined by HPLC analysis (Whelk-O1 column), the sign corresponds to that of $[\alpha]_D$. [d] Not determined.

The X-ray structure of the MnCl(TMCP) catalyst was solved, and an ORTEP diagram is shown in Fig. 1. The complex exhibits a strong equatorial contraction, due to a highly ruffled macrocycle: the out of plane displacements of the C_{meso} atoms with respect to the 24-atom mean plane are *ca.* 0.73(1) Å. The average [Mn–Np] bond distance is short [1.974(2) Å] when compared to other manganese(III) porphyrins,[11] and especially to the very non-planar chloro[5,10,15,20-tetrakis(pentafluorophenyl)-2,3,7,8,12,13,17,18-octaphenylporphyrinato]manga-

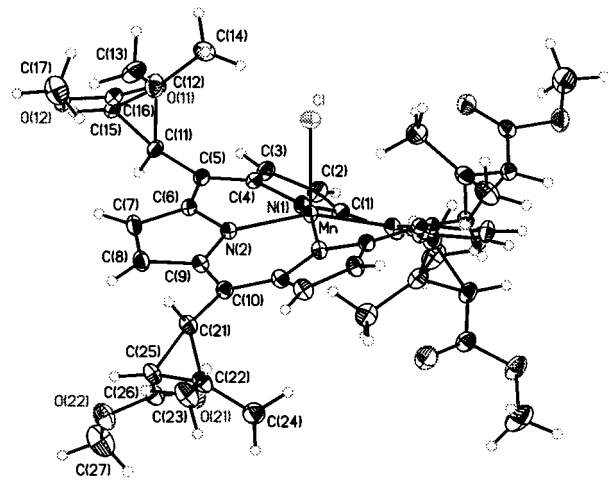

Fig. 1 ORTEP side view (30% probability) of **1** (M = MnCl). Selected bond lengths (Å): [Mn–Np] average 1.974(2), Mn–Cl 2.3475(9). Mn is displaced from the porphyrin mean plane towards Cl by 0.44(1) Å. The C_{meso} atoms are displaced alternatively up [+0.72(1) Å] and down [−0.74(1) Å] with respect to the 24-atom mean plane.

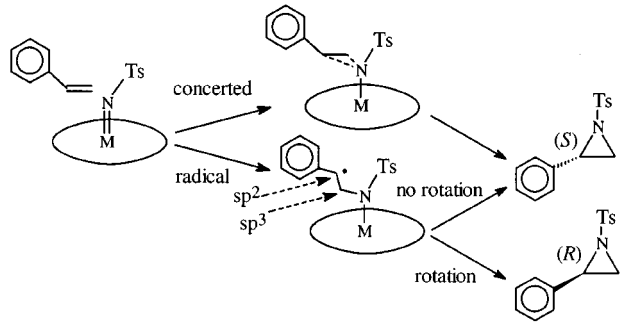

Scheme 1

nese(III) complex.[11d] The Mn–Cl bond distance [2.3475(9) Å] is similar to those observed for other chloromanganese(III) porphyrins.[11]

The MnCl(TMCP) complex is structurally very similar to FeCl(TMCP).[12] Hence, intermolecular steric interactions during the approach of the olefin towards the nitrenoid species are presumably similar for the two metal catalysts, implying that electronic effects are responsible for the observed opposite enantioselectivities. We speculate that each metal center favors one of two competing mechanisms (Scheme 1). The iron catalyst induces the preferential formation of the (+) enantiomer with the (*S*) absolute configuration[13] expected from steric exclusion during the side-on approach of the olefin in a concerted mechanism.[6b] In the case of the manganese catalyst, a radical intermediate which is sufficiently stable to allow an internal rearrangement can be invoked. Efforts towards a better understanding of these mechanisms and an extension of the scope of this catalytic system to other substrates are currently in progress.

Notes and references

† *Crystal data* for $C_{48}H_{52}N_4O_8MnCl\cdot CH_2Cl_2$: M = 988.25, tetragonal, a = b = 13.280(2), c = 26.529(5) Å, U = 4679.0(13) Å^3, T = 193(2) K, space group $P4_32_12$, Z = 4, μ(Mo-K) = 0.512 mm^{-1}, 22412 reflections measured, 4360 unique (R_{int} = 0.0494) which were used in all calculations. Final R indices [$I > 2\sigma(I)$], R = 0.0458, R_w = 0.1230, GOF = 1.034. CCDC 182/1224. See http://www.rsc.org/suppdata/cc/1999/989/ for crystallographic files in .cif format.

1 E. N. Jacobsen, *Catalytic Asymmetric Synthesis*, ed. I. Ojima, VCH, New York, 1993, p. 159.
2 M. P. Doyle, *Catalytic Asymmetric Synthesis*, ed. I. Ojima, VCH, New York, 1993, p. 63.
3 For a review, see: P. Müller, *Adv. Catal. Processes*, 1997, **2**, 113.
4 (*a*) D. A. Evans, M. M. Faul, M. T. Bilodeau, B. A. Anderson and D. M. Barnes, *J. Am. Chem. Soc.*, 1993, **115**, 5328; (*b*) D. A. Evans, M. M. Faul and M. T. Bilodeau, *J. Org. Chem.*, 1991, **56**, 6744; (*c*) D. A. Evans, M. M. Faul and M. T. Bilodeau, *J. Am. Chem. Soc.*, 1994, **116**, 2742; (*d*) Z. Li, K. R. Conser and E. N. Jacobsen, *J. Am. Chem. Soc.*, 1993, **115**, 5326; (*e*) K. Noda, N. Hosoaya, R. Irie, Y. Ito and T. Katsuki, *Synlett*, 1993, 469; (*f*) H. Nishikori and T. Katsuki, *Tetrahedron Lett.*, 1996, **37**, 9245; (*g*) P. Müller, C. Baud, Y. Jacquier, M. Moran and I. Nägeli, *J. Phys. Org. Chem.*, 1996, **9**, 341; (*h*) P. Müller, C. Baud and Y. Jacquier, *Tetrahedron*, 1996, **52**, 1543; (*i*) P. Müller, C. Baud and Y. Jacquier, *Can. J. Chem.*, 1998, **76**, 738; (*j*) A. M. Harm, J. G. Knight and G. Stemp, *Tetrahedron Lett.*, 1996, **37**, 6189; (*k*) D. Tanner, P. G. Andersson, A. Harden and P. Somfai, *Tetrahedron Lett.*, 1994, **35**, 4631.
5 T. S. Lai, H. L. Kwong, C. M. Che and S. M. Peng, *Chem. Commun.*, 1997, 2373.
6 (*a*) M. Veyrat, O. Maury, F. Faverjon, D. E. Over, R. Ramasseul, J. C. Marchon, I. Turowska-Tyrk and W. R. Scheidt, *Angew. Chem., Int. Ed. Engl.*, 1994, **33**, 220; (*b*) C. Pérollier, D.Sc. Thesis, Université de Grenoble, 1998.
7 (*a*) D. Mansuy, J. P. Mahy, A. Dureault, G. Bedi and P. Battioni, *J. Chem. Soc., Chem. Commun.*, 1984, 1161; (*b*) J. P. Mahy, G. Bedi, P. Battioni and D. Mansuy, *J. Chem. Soc., Perkin Trans. 2*, 1988, 1517.
8 The best yields were obtained with PhINTs. The nitro-substituted derivative *p*-$NO_2C_6H_4SO_2N$=IPh was unreactive, whereas the methoxy-substituted derivative *p*-$MeOC_6H_4SO_2N$=IPh increased the rate of aziridine formation. These observations suggest that electronic factors play a crucial role in the formation of the probable nitrenoid species. For similar notes and procedures for preparing the nitrene precursors, see: M. J. Södergren, D. A. Alonso, A. V. Bedekar and P. G. Andersson, *Tetrahedron Lett.*, 1997, **39**, 6897.
9 (*a*) We feel that formation of $TsNH_2$ is not entirely due to hydrolysis since experiments under highly anhydrous conditions did not lead to improved aziridine yields. We agree with P. Müller that the decomposition of the nitrene source must be competitive with the aziridination, and affords the sulfonamide after work-up;[4i] (*b*) In our case, addition of 4-phenylpyridine *N*-oxide resulted in lower yield and enantioselectivity with both catalysts.
10 H. Takaya, T. Ohta, R. Noyori, *Catalytic Asymmetric Synthesis*, ed. I. Ojima, VCH, New York, 1993, p. 1.
11 (*a*) A. Tulinsky and B. M. Chen, *J. Am. Chem. Soc.*, 1977, **99**, 3647; (*b*) P. Ochsenbein, D. Mandon, J. Fischer, R. Weiss, R. Austin, K. Jayaraj, A. Gold, J. Terner, E. Bill, M. Müther and A. X. Trautwein, *Angew. Chem., Int. Ed. Engl.*, 1993, **32**, 1437; (*c*) R. Guilard, S. Brandes, A. Tabard, N. Bouhmaida, C. Lecomte, P. Richard and J. M. Latour, *J. Am. Chem. Soc.*, 1994, **116**, 10 202; (*d*) R. Guilard, K. Perié, J. M. Barbe, D. J. Nurco, K. M. Smith, E. Van Caemelbecke and K. M. Kadish, *Inorg. Chem.*, 1998, **37**, 973.
12 M. Mazzanti, J. C. Marchon, J. Wojaczynski, S. Wolowiec, L. Latos-Grazynski, M. Shang and W. R. Scheidt, *Inorg. Chem.*, 1998, **37**, 2476.
13 The absolute configuration of (−)-(*R*)-2-phenyl-1-tosylaziridine has been demonstrated; A. Toshimitsu, H. Abe, C. Hirosawa and K. Tamao, *J. Chem. Soc., Perkin Trans. 1*, 1994, **23**, 3465.

Communication 9/01559K

ChemComm

Charge separation in a triosmium cluster zwitterion revealed by time-resolved microwave conductivity: first application of TRMC in organometallic chemistry

Jos Nijhoff,[a] František Hartl,[a] Derk J. Stufkens,*[a] Jacob J. Piet[b] and John M. Warman*[b]

[a] *Institute of Molecular Chemistry, Universiteit van Amsterdam, Nieuwe Achtergracht 166, 1018 WV Amsterdam, The Netherlands. E-mail: stufkens@anorg.chem.uva.nl*

[b] *Interfacultair Reactor Instituut, Technische Universiteit Delft, Mekelweg 15, 2629 JB Delft, The Netherlands. E-mail: warman@iri.tudelft.nl*

Received (in Cambridge, UK) 26th March 1999, Accepted 28th April 1999

The light-induced transformation of an $Os_3(CO)_{10}$(α-diimine) cluster into an intramolecularly stabilized zwitterion has been established with time-resolved microwave conductivity, this is the first application of this technique in organometallic chemistry.

Organometallic complexes that contain a metal–metal bond and an α-diimine ligand often undergo a homolytic cleavage of the metal–metal bond on visible excitation.[1,2] For instance, in non-coordinating solvents the complexes $(CO)_5MnMn(CO)_3$(α-diimine) produce the radicals $^{\bullet}Mn(CO)_5$ and $Mn(CO)_3$(α-diimine)$^{\bullet}$ which dimerize to give $Mn_2(CO)_{10}$ and $Mn_2(CO)_6$(α-diimine)$_2$.[3] In coordinating solvents, or in the presence of an N- or P-donor ligand (L), these complexes photodisproportionate into the ions $Mn(CO)_5^-$ and $Mn(CO)_3(L)$(α-diimine)$^+$.[4]

Recently, a similar behaviour was observed for the triangular clusters $Os_3(CO)_{10}$(α-diimine), the only difference being that instead of separate radicals and ions, biradicals and zwitterions are formed.[5] The biradicals $^{\bullet}Os(CO)_4$–$Os(CO)_4$–$Os(CO)_2$(α-diimine)$^{\bullet}$ are the primary photoproducts in weakly and non-coordinating solvents, and have been observed with nanosecond time-resolved absorption spectroscopy.[5] Again, zwitterions are only produced in the presence of a Lewis base (L) or upon irradiation of the cluster in a coordinating solvent. L transforms the biradical into the zwitterion $^-Os(CO)_4$–$Os(CO)_4$–$Os^+(CO)_2(L)$(α-diimine) by coordinating to the open site of the biradical. This process, which is schematically depicted in Scheme 1, has been established with nanosecond time-resolved absorption spectroscopy for the photoreaction of $Os_3(CO)_{10}$(Pr^i-AcPy) **1** [Pr^i-AcPy = $Me_2C(H)N{=}CMeC_5H_4N$) in THF in the presence of 0.5 M MeCN.[5] The lifetime of a biradical varies from a few nanoseconds to several microseconds depending on the α-diimine and the solvent; that of a zwitterion is a few seconds in acetonitrile and several minutes in pyridine.[5] Most biradicals and zwitterions regenerate their parent cluster.

Evidence for the dipolar character of the zwitterions has been obtained from ^{1}H NMR, UV–VIS and resonance Raman data, and from their reactivity,[5] but up to now these species could not be isolated and structurally characterized. The formation of such a transient dipolar species may, however, be established by time-resolved microwave conductivity (TRMC). This technique has often been applied to characterize the charge-separated D^+–A^- states of organic donor–acceptor systems.[6–8] To our knowledge, TRMC has, however, never been used to identify dipolar excited states and short-lived intermediates in organometallic chemistry. It is shown here that TRMC measurements, applied to a particular osmium cluster, establish the dipolar character of its zwitterionic product and provide an approximate value of its dipole moment. In a TRMC experiment a dilute solution of the compound of interest is placed in a microwave cavity and the change in conductivity of the solution during and after flash-photolysis is measured in the nanosecond to microsecond time domain.[7] The conductivity of the solvent itself must be very low. We therefore used cyclohexane and benzene for the TRMC experiments and, in conjunction with this, toluene for the IR and quantum yield studies. As the triosmium zwitterions are only formed in coordinating solvents or in the presence of a Lewis base, we prepared the cluster $Os_3(CO)_{10}\{Me_2N(CH_2)_3$-AcPy$\}$ **2**, in which the α-diimine bears a pendant sidearm that may act as such a base. The general procedure for the synthesis has been described in refs. 5 and 10.

Irradiation of **2** in toluene with the 514.5 nm line of an argon ion laser afforded a species with IR ν(CO) bands (2073vw, 1985vs, 1967s, 1921w, 1893w, 1870m, br cm^{-1}), which are very close in frequency to those of the zwitterion **1a** of $Os_3(CO)_{10}$(Pr^i-AcPy) **1** in pyridine (2071w, 1988vs, 1968vs, 1925w, 1898w, 1873m, br cm^{-1}).[5] Thus, the pendant $-(CH_2)_3NMe_2$ sidearm transforms the biradical photoproduct of **2** into the zwitterion $^-Os(CO)_4$–$Os(CO)_4$–$Os^+(CO)_2\{Me_2N$-$(CH_2)_3$-AcPy$\}$ **2a** (Scheme 1) which has a lifetime of *ca*. 5 s in

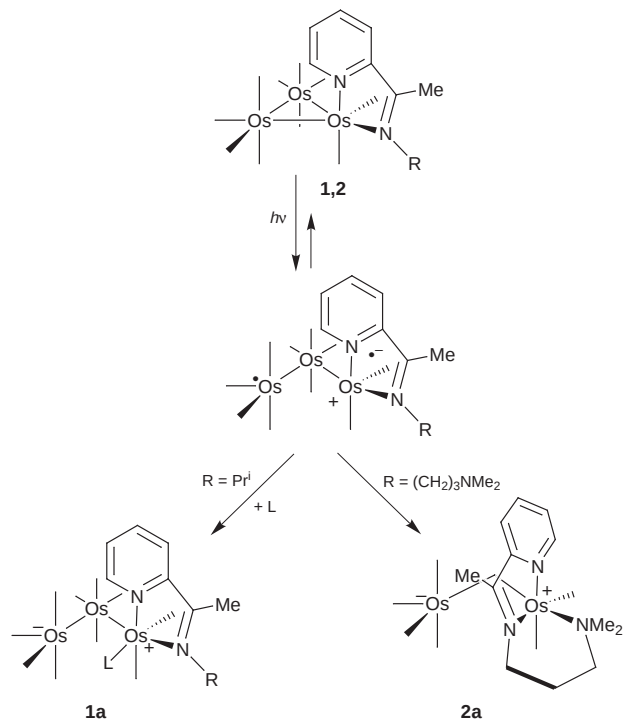

Scheme 1 General scheme for the formation of the zwitterions **1a** and **2a** on irradiation of **1** (R = Pr^i) and **2** [R = $(CH_2)_3NMe_2$], respectively. The primary photoproduct of the reaction is a biradical in which the unpaired electron at the $Os(CO)_2$(α-diimine) moiety (mainly) resides at the α-diimine ligand. This biradical transforms into a zwitterion by the attack of a strong Lewis base (L) (**1a**) or by the intramolecular coordination of a pendant sidearm (**2a**).

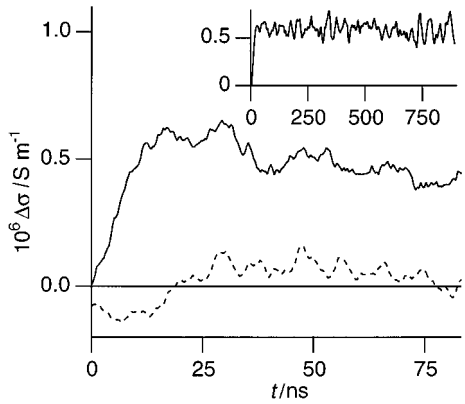

Fig. 1 Transient changes in the microwave conductivity (dielectric loss) of *ca*. 1×10^{-4} M solutions of **1** (dashed line) and **2** (full line) on 308 nm photoexcitation of cyclohexane solutions at room temperature. The inset shows the transient for **2** on a longer timescale.

toluene. As expected, the cluster **1** without such a sidearm did not produce a zwitterion in toluene.[5]

Cluster **2** therefore meets the requirement of the TRMC technique that the charge-separated species is formed in an apolar solvent. TRMC measurements were performed on **2** dissolved in both benzene and cyclohexane (absorbance per cm *ca*. 1.0 at 308 nm). For comparison a cyclohexane solution of **1**, which shows no evidence for zwitterion formation in apolar solvents,[5] was also studied. The solutions were placed in a microwave cavity (resonance frequency *ca*. 10 GHz) and were flash-photolysed using the 7 ns, 308 nm pulse from a Lumonics HyperEx 400 laser. The change in conductivity (dielectric loss) of the solutions, $\Delta\sigma$, was monitored as a change in the microwave power reflected by the cavity as described in detail previously.[7,9]

The TRMC transients found for solutions of **1** and **2** in cyclohexane are shown in Fig. 1. In agreement with the IR experiment no measureable change in the microwave conductivity, within the experimental noise, is observed for **1**. Cluster **2**, in contrast, shows a readily measureable conductivity transient which is already present within the laser pulse. The transient found for the benzene solution was similar in magnitude. The TRMC results therefore provide direct evidence for the formation of a photoproduct with a dipole moment larger than that of the ground state molecule, *i.e*. a zwitterionic state. The signal was found to decay little even on a timescale of microseconds, in agreement with the long lifetime of **2a** established in other experiments.

From the amplitude of the observed TRMC signal a value of 3.5×10^{10} D^2 s^{-1} was derived for the parameter $(\mu_*^2 - \mu_0^2)\phi_{308}/\theta_*$, in which μ_* and μ_0 are the dipole moments of **2a** and **2** respectively, ϕ_{308} the quantum yield for the formation of **2a** from **2** at 308 nm in an apolar solvent at 298 K, and θ_* the rotational relaxation time of the observed dipole. Since **2** has a close to spherical geometry, θ_*(= 190 ps) was estimated using the Stokes–Einstein relation taking 1.02×10^{-3} N s m^{-2} for the viscosity and 0.75 nm^3 for the molecular volume. The ground-state dipole moment μ_0 was determined by steady-state microwave conductivity measurements[9] at five different concentrations, and was found to be 6.0 ± 0.1 D.

The remaining parameter, ϕ_{308}, could not be determined from the transient absorption spectra since the quantum yield was too low and the differences in absorption between the cluster and the transient zwitterion were too small. It was therefore determined by a conventional steady-state experiment although the conditions (wavelength, temperature) were somewhat different from those used for the TRMC measurements. Thus, the back reaction of zwitterion **2a** to the parent cluster **2** was too fast to determine the quantum yield at room temperature. Besides, the 313 nm line of the Hg-lamp (closest in wavelength to the 308 nm line used for TRMC) was too weak. Because of this, ϕ was measured at different temperatures and wavelengths of excitation and these data were extrapolated to give a value of ϕ = 0.05 ± 0.02 at λ_{exc} = 308 nm and T = 298 K.†

Substitution of the above values of θ_*, μ_0 and ϕ_{308} in the expression $(\mu_*^2 - \mu_0^2)\phi_{308}/\theta_* = 3.5 \times 10^{10}$ D^2 s^{-1} results in a value of 13 ± 2 D for the dipole moment μ_* of **2a**. This value corresponds to a full charge separation over a distance of 2.7 ± 0.4 Å. The average covalent Os–Os distance is 2.88 Å in $Os_3(CO)_{10}(Pr^i\text{-DAB})$[11] and 2.87 Å in $Os_3(CO)_{10}$(bpy),[12] and the non-bonded distance in the η^2-imine bridged cluster $Os_3(CO)_{10}(Pr^c\text{-DAB})$ is 3.59 Å.[11] The range of the value derived from the TRMC measurements overlaps with that of the literature data but the calculated charge separation is rather small for two localised charges on the non-bonded osmium atoms.

This TRMC result confirms the zwitterionic character of the photoproduct of such an Os cluster when irradiated in the presence of a Lewis base, and even provides an approximate value of its dipole moment. To our knowledge this is the first application of this technique in organometallic chemistry. It may stimulate others to employ TRMC, not only for the characterization of transient intermediates of (photo)reactions, but in particular also for the characterization of charge transfer excited states. We emphasize again however that the method is only applicable for those compounds which are soluble in apolar solvents.

J. M. Ernsting is thanked for his assistance with the low temperature NMR experiments. This research has been financially supported by the Council for Chemical Sciences of the Netherlands Organization for Scientific Research (CW-NWO).

Supporting information: A table presenting IR, ^{1}H NMR and UV-VIS data for **1**, **2** and their zwitterions **1a** and **2a** and mass spectral data of **2** can be accessed electronically, see http://www.rsc.org/suppdata/cc/1999/991/

Notes and references

† First, ϕ was determined in toluene with 355 nm excitation between 203 and 223 K, where the zwitterion is thermally stable. Then the quantum yield was determined at 223 K for excitation wavelengths of 514.5, 488.0, 457.9 and 355 nm. The values of ϕ at this temperature were as follows: 0.026 (514.5 nm), 0.025 (488.0 nm), 0.026 (457.9 nm) and 0.024 (355 nm). Accordingly, ϕ_{308} at 223 K is estimated as 0.025 ± 0.001. Values of 0.022 and 0.019 were obtained on 355 nm excitation at 213 and 203 K, respectively. By extrapolation of these data a value of 0.05 ± 0.02 was obtained for ϕ_{308} at 298 K. The accuracy of this value is limited by the small temperature range that could be covered because of the thermal instability of the zwitterion **2a**.

1 J. C. Luong, R. A. Faltynek and M. S. Wrighton, *J. Am. Chem. Soc*., 1979, **101**, 1597; 1980, **102**, 7892.
2 D. J. Stufkens, M. P. Aarnts, J. Nijhoff, B. D. Rossenaar and A. Vlček, Jr., *Coord. Chem. Rev.*, 1998, **171**, 93 and references therein.
3 T. van der Graaf, D. J. Stufkens, A. Oskam and K. Goubitz, *Inorg. Chem*., 1991, **30**, 599.
4 T. van der Graaf, R. M. J. Hofstra, P. G. M. Schilder, M. Rijkhoff, D. J. Stufkens and J. G. M. van der Linden, *Organometallics*, 1991, **10**, 3668.
5 J. Nijhoff, M. J. Bakker, F. Hartl, D. J. Stufkens, W.-F. Fu and R. van Eldik, *Inorg. Chem*., 1998, **37**, 661.
6 J. M. Warman, M. P. de Haas, J. W. Verhoeven and M. N. Paddon-Row, *Adv. Chem. Phys*., 1999, **106**, 571.
7 M. P. de Haas and J. M. Warman, *Chem. Phys*., 1982, **73**, 35.
8 R. W. Fessenden, P. M. Carton, H. Shimamori and J. C. Sciano, *J. Phys. Chem*.,1982, **86**, 3803.
9 W. Schuddeboom, Ph.D. Thesis, Delft University of Technology, 1994.
10 J. Nijhoff, J. Fraanje, F. Hartl and D. J. Stufkens, submitted; J. Nijhoff, Ph.D. Thesis, University of Amsterdam, 1998.
11 R. Zoet, J. Jastrzebski G. van Koten, T. Mahabiersing, K. Vrieze, D. Heijdenrijk and C. H. Stam, *Organometallics*, 1988, **7**, 2108.
12 N. E. Leadbeater, J. Lewis, P. R. Raithby and G. N. Ward, *J. Chem. Soc., Dalton Trans.*, 1997, 2511.

Communication 9/02426C

Coordination compounds as building blocks: simple synthesis of Ru^{II}-containing amino acids and peptides

Dennis J. Hurley, Jeffrey R. Roppe and Yitzhak Tor*

Department of Chemistry and Biochemistry, University of California, San Diego, La Jolla, California 92093-0358, USA. E-mail: ytor@ucsd.edu

Received (in Corvallis, OR, USA) 15th February 1999, Accepted 12th April 1999

Ru^{II}-containing amino acids and short peptides are obtained in high yields *via* direct displacement reactions of $[(bpy)_2Ru(3\text{-bromo-}1,10\text{-phenanthroline})]^{2+}(PF_6^-)_2$ with amino acids and peptides that contain thiolate and phenolate nucleophiles.

Metal-containing amino acids and peptides are key components for the study of photo-induced energy– and electron–transfer processes,[1–3] as well as for the development of chemosensors and labeling reagents.[4,5] These organic–inorganic hybrid molecules have been constructed *via* three predominate approaches: (i) coordination of metal complexes to donor-containing natural amino acids (*e.g.* histidine),[6,7] (ii) conjugation of complexes to peptide termini,[2,3] and (iii) synthesis of chelator-containing amino acids followed by metal coordination.[8–12] These routes typically require the exposure of peptides to reactive metal precursors or necessitate the multistep synthesis of new amino acids. Although productive, these methods are elaborate and do not always provide full control over the final structure and absolute configuration at the metal center. Here we report a simple one-step synthesis of metal-containing amino acids and peptides *via* the direct reaction between nucleophile-containing amino acids (*e.g.* cysteine, tyrosine) and functionalized coordination compounds. Reactions of $[(bpy)_2Ru(3\text{-bromo-}1,10\text{-phenanthroline})]^{2+}(PF_6^-)_2$ **1** with free or *N*-protected amino acids, as well as short peptides, provide the Ru^{II}-containing amino acids in a single step with predetermined stereochemistry at the metal center.

We have previously reported that functionalized tris-chelate complexes (*e.g.* **1**) are excellent substrates for palladium-mediated cross-coupling reactions[13,14] and nucleophilic aromatic substitutions.[15] This unprecedented reactivity has been attributed to the increased electrophilicity of the 3-bromo-1,10-phenanthroline ring upon metal coordination.[15] Thus, when **1** is reacted with L-cysteine **2** in the presence of a weak base (*e.g.* Na_2CO_3) a smooth reaction takes place within 1–3 h giving the desired modified amino acid **4** in good yields (Scheme 1, Table 1).† Identical reaction conditions can be utilized to incorporate the octahedral complex into *N*-protected amino acids. Thus, reacting **1** and *N*-Boc-L-cysteine **3** in DMF–H_2O (1 : 1) at slightly elevated temperatures (45–55° C) affords the protected derivative **5**. Similarly, deprotonation of the phenolic side chain in *N*-Boc-L-tyrosine **6** followed by a reaction with **1** gives the expected metal-containing amino acid **7** (Scheme 2).

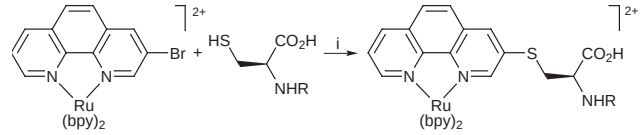

Scheme 1 *Reagents and conditions*: i, Na_2CO_3, H_2O–DMF (1 : 1), 55 °C, 1 h.

The compounds synthesized represent a novel family of photo- and redox-active Ru^{II}-containing amino acids. Their absorption spectra show intense bands in the UV region due to the overlapping π–π* transitions of the bipyridine and phenanthroline ligands (Table 1). The presence of a phenanthroline moiety with a heteroatom-containing substituent results in the appearance of lower energy bands between 320–350 nm (Table 1).[15] The tris-chelated Ru^{II} centers in **4**, **5** and **7** give rise to the typical visible metal to ligand charge transfer (MLCT) bands that are centered around 450 nm. Upon excitation at this wavelength, all the Ru^{II}-containing amino acids emit intensely at 600–615 nm (Table 1). Cyclic and square-wave voltammetry show the expected $Ru^{III/II}$ couple at $E_{1/2} \cong +1.0$ V *vs.* Ag/Ag+ (Table 1).‡

Mild substitution reaction conditions can be employed for the incorporation of octahedral Ru^{II} complexes into short peptides. Thus, reacting glutathione **8** (γ-L-glutamyl-L-cysteinylglycine)

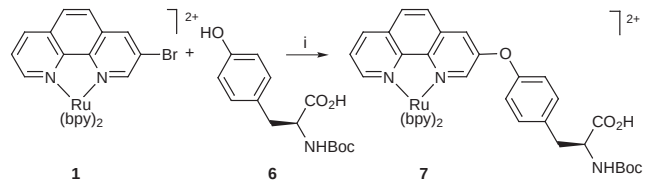

Scheme 2 *Reagents and conditions*: i, Na_2CO_3, H_2O–DMF (1 : 1), 55 °C, 1 h.

Table 1 Preparation, spectral and electrochemical data for metal-containing amino acids and peptides

Product	Yield (%)[a]	MS[b]	λ/nm (ε/10^4 M^{-1} cm^{-1})[c]	$E_{1/2}(Ru^{III/II})$[d]/V	λ_{em}[e]/nm
4	74–87	858.2 (M^+), 356.6 (M^{2+})	242 (4.3), 286 (7.5), 338 (1.7), 450 (1.5)	0.964	612
5	76–85	958 (M^+), 407 (M^{2+})	246 (4.1), 286 (6.9), 344 (1.8), 450 (1.5)	1.000	611
7	72	1018 (M^+), 436 (M^{2+})	234 (4.4), 286 (6.7), 320 (1.5), 446 (1.5)	0.992	601
9	58–63[f]	898.0 (MH^+), 449.5 (MH_2^{2+})	246 (4.0), 286 (7.1), 343 (1.6), 450 (1.4)	0.968	612
10	82–90	1043 (M^+)	246 (4.3), 286 (7.6), 344 (1.9), 448 (1.6)	0.996	614

[a] Isolated yields of chromatographed complexes. *N*-Boc protected derivatives were isolated as their PF_6^- salt. Unprotected derivatives were HPLC purified and isolated as the $CF_3CO_2^-$ salt. [b] Electrospray ionization mass spectra. [c] Measured in MeCN (for **5**, **7** and **10**) and MeOH (for **4**, **9**). [d] Measured in MeCN containing 0.1 M $Bu_4N^+PF_6^-$ *vs.* Ag/Ag^+. Under these conditions $E_{1/2}$ = 0.084 V for Fc/Fc^+. [e] Metal-centered emission taken in water upon excitation at 450 nm. [f] Individual yields for HPLC-purified products: **Δ,Λ-9** (60–63%), **Δ-9** (60%) and **Λ-9** (58%).

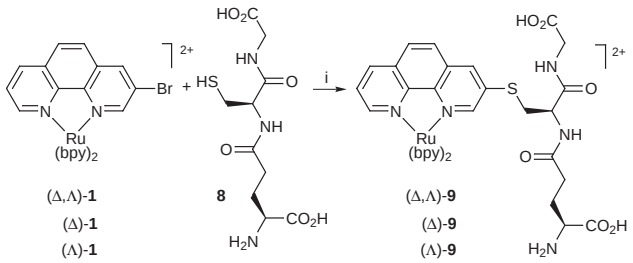

Scheme 3 *Reagents and conditions*: i, Na_2CO_3, H_2O–DMF (1 : 1), 65 °C, 1 h.

with the racemic complex **1** in a mixture of DMF–water gives the desired substituted peptide **9**, as a mixture of the two epimeric products (Scheme 3). The use of functionalized coordination compounds as building blocks permits the incorporation of coordination compounds with predetermined absolute configuration at the metal center.[16] Thus, reacting glutathione **8** with the enantiomerically-pure complexes **Λ-1** and **Δ-1** gives the diastereomerically-pure metal-containing peptides Λ-**9** and Δ-**9**, respectively (Scheme 3). The CD spectra of the various products clearly reveal the opposite absolute configuration at the two epimeric metal-containing peptides Λ-**9** and Δ-**9** (Fig. 1).[16]

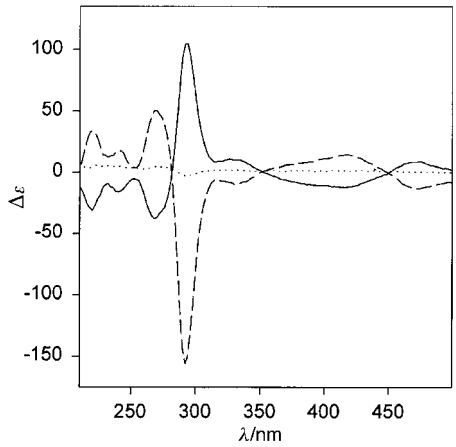

Fig. 1 CD spectra in MeOH of Λ-**9** (solid), Δ-**9** (dashed) and Λ,Δ-**9** (dotted).

Protected metal-containing amino acids such as **5** and **7** are useful building blocks for peptide synthesis. Their condensation with other suitably protected amino acids provides short metal-containing peptides. Thus the reaction of **5** with L-alanine methyl ester in the presence of benzotriazol-1-yloxytris(dimethylamino)phosphonium hexafluorophosphate ($BOPPF_6$), *N*-hydroxysuccinimide and DMAP proceeds rapidly at room temperature to give the fully protected dipeptide **10** in high yield (Scheme 4, Table 1). As is evident from the data presented in Table 1, the short metal-containing peptides **9** and **10** exhibit photophysical and electrochemical characteristics similar to their metal-containing precursors.

The direct incorporation of metal complexes into amino acids and peptides provides a facile new route for the synthesis of novel photo- and redox-active biomolecules. Modifying the side-chains of naturally-occurring amino acids places the polypyridine Ru^{II} complexes in close proximity to the peptide backbone. These derivatives are therefore useful building blocks for the study of photophysical processes in peptides and proteins. We are currently exploring these directions *via* the construction of metallated peptides with well-defined secondary structures.

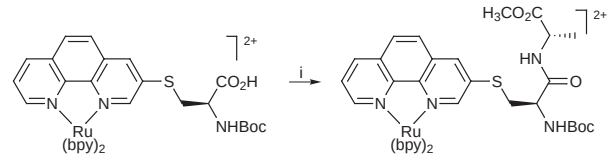

Scheme 4 *Reagents and conditions*: i, L–alanine methyl ester, $BOPPF_6$, *N*-hydroxysuccinimide, DMAP, DMF, 10 min at room temp.

We gratefully acknowledge the National Institutes of Health (GM58447) for financial support.

Notes and references

† Representative procedures: A solution of L-cysteine (20 mg, 0.13 mmol) and Na_2CO_3 (40 mg, 0.38 mmol) in degassed water (1 ml) is added to a degassed solution of **1** (40 mg, 0.042 mmol) in DMF (1 ml). The reaction mixture is kept at 55 °C for 1 h. It is then diluted with water (10 ml) and washed with CH_2Cl_2 (3 × 50 ml). The aqueous phase is evaporated to dryness and the dark red residue is HPLC-purified on a C8 semi-preparative reversed-phase column using 0.1% TFA in MeCN–0.1% TFA in H_2O (1 : 7.3) as eluent to afford **4** (34 mg, 87% yield) after lyophilization. The more lipophilic *N*-Boc protected metal-containing amino acids are chromatographed on silica gel using 0.5% saturated aq. KNO_3 in 10–15% H_2O in MeCN. In these cases the products contain a carboxylate anion as an internal counterion. The free carboxylic acid derivative can be obtained by dissolving the *N*-protected derivative in dilute aqueous HPF_6 followed by extraction into CH_2Cl_2.The organic phase is then dried (Na_2SO_4), filtered and evaporated to yield the desired product. All new compounds have been fully characterized by UV–VIS spectroscopy, ESI MS, IR and ^1H NMR as well as cyclic and squarewave voltammetry.

‡ The *N*-protected derivatives showed reversible cyclic voltammograms ($\Delta E_p \cong 60$–70 mV, $i_a \cong i_c$) while the free amines gave irreversible CV, and their $E_{1/2}$ values were determined using squarewave voltammetry.

1 D. S. Wuttke, H. B. Gray, S. L. Fisher and B. Imperiali, *J. Am. Chem. Soc.*, 1993, **115**, 8455.
2 T.-C. Tsai and I-J. Chang, *J. Am. Chem. Soc.*, 1998, **120**, 227.
3 A. B. Gretchikhine and M. Y. Ogawa, *J. Am. Chem. Soc.*, 1996, **118**, 1543.
4 A. Torrado and B. Imperiali, *J. Org. Chem.*, 1996, **61**, 8940.
5 For a recent review on organometallic amino acids and their applications, see: K. Severin, R. Bergs and W. Beck, *Angew. Chem., Int. Ed.*, 1998, **37**, 1634.
6 I-J. Chang, H. B. Gray and J. R. Winkler, *J. Am. Chem. Soc.*, 1991, **113**, 7056.
7 B. I. Dahiyat, T. J. Meade and S. L. Mayo, *Inorg. Chim. Acta*, 1996, **243**, 207.
8 B. Imperiali and S. L. Fisher, *J. Org. Chem.*, 1992, **57**, 757.
9 B. Imperiali and S. L. Fisher, *J. Am. Chem. Soc.*, 1991, **113**, 8527.
10 N. Nishino, T. Kato, T. Murata, H. Nakayama and T. Arai, *Chem. Lett.*, 1996, 49.
11 B. Geißer and R. Alsfasser, *Eur. J. Inorg. Chem.* 1998, 957.
12 R. Alsfasser and R. van Eldik, *Inorg. Chem.*, 1996, **35**, 628.
13 D. Tzalis and Y. Tor, *Chem. Commun.*, 1996, 1043.
14 P. J. Connors, Jr., D. Tzalis, A. L. Dunnick and Y. Tor, *Inorg. Chem.*, 1998, **37**, 1121.
15 D. Tzalis and Y. Tor, *Angew. Chem., Int. Ed. Engl.*, 1997, **36**, 2666.
16 D. Tzalis and Y. Tor, *J. Am. Chem. Soc.*, 1997, **118**, 852.

Communication 9/01272I

Metal dialkyl diselenophosphates:[1] a rare example of co-crystallization with clusters, $Ag_8(\mu_8\text{-}Se)[Se_2P(OPr^i)_2]_6$ and $Ag_6[Se_2P(OPr^i)_2]_6$, superimposing in a trigonal lattice†

C. W. Liu,*[a] Iu-Jie Shang,[a] Ju-Chung Wang[b] and Tai-Chiun Keng[b]

[a] *Department of Chemistry, Chung Yuan Christian University, Chung-Li, Taiwan 320, R. O. C. E-mail: chenwei@cchp01.cc.cycu.edu.tw*

[b] *Department of Chemistry, Soochow University, Taipei, Taiwan 111, R. O. C.*

Received (in Cambridge, UK) 26th March 1999, Accepted 28th April 1999

A remarkable co-crystallization in which two neutral clusters, $Ag_8(Se)[Se_2P(OPr^i)_2]_6$ and $Ag_6[Se_2P(OPr^i)_2]_6$, superimpose along the three-fold axis in the trigonal lattice and share a common $Ag_6[Se_2P(OPr^i)_2]_6$ unit, is reported.

Molecular cubic clusters encapsulating main-group elements are very rare[2] and they are particularly interesting from the general point of view of bonding.[3] Previously we reported the first discrete selenide-centered Cu^I cubic cluster containing diselenophosphate ligands (dsep), $\{Cu_8(\mu_8\text{-}Se)[Se_2P(OPr^i)_2]_6\}$.[4] To extend our research efforts in centered cubic cluster synthesis, herein, we report the synthesis of silver analogues and uncover an extremely rare example of co-crystallization, $Ag_8(Se)[Se_2P(OPr^i)_2]_6$ and $Ag_6[Se_2P(OPr^i)_2]_6$ share a common $Ag_6[Se_2P(OPr^i)_2]_6$ unit and have equal occupancies along the three-fold axis of the trigonal lattice. Co-crystallization of organic compounds is a common phenomenon[5] and recently it has been used to resolve the racemic 1,1′-bi-2-naphthol.[6] In organometallic chemistry many anion–cation pairs[7] as well as two neutral cluster molecules[8] in the same crystal have also been recognized. In inorganic compounds, two or three components can share the same metal core with minute differences in the composition of peripheral ligands. The most recent example is $[NEt_4]_2[(Mo_2O_2Se_6)_{0.20}(Mo_2O_2Se_7)_{0.18}(Mo_2O_2Se_8)_{0.62}]$, a dimeric molybdenum polyselenide containing a $Mo_2O_2(\mu\text{-}Se)_2$ core, reported by Mak and Guo.[9] To our knowledge, a co-crystallization as revealed in the superposition of Ag_8 and Ag_6 clusters which share a common $Ag_6[Se_2P(OPr^i)_2]_6$ unit is unprecedented.

Treatment of $NH_4Se_2P(OPr^i)_2$ (105 mg, 0.3 mmol) with $Ag(MeCN)_4PF_6$ (62.5 mg, 0.15 mmol) in CH_2Cl_2 (30 mL) at −50 °C resulted in a yellow solution after 12 h of stirring. After evaporation under vacuum, the residue was re-dissolved in 30 mL of hexanes from which a white precipitate was formed within a few minutes at ambient temperature (*ca.* 12% yield based on Ag). Upon dissolving the white precipitate in $CDCl_3$ a singlet at δ 72.7 (J_{PSe} = 654 Hz) flanked with selenium satellites was observed in the ^{31}P NMR spectrum while a doublet at δ 147 (J_{PSe} = 654 Hz) was observed in the ^{77}Se NMR spectrum.‡ These data implied that all dsep ligands are equivalent in solution. In order to understand the detailed structure of the isolated species, a single crystal X-ray diffraction analysis was undertaken and revealed a remarkable co-crystalline structure.§

The crystal structure of $\{Ag_8(\mu_8\text{-}Se)[Se_2P(OPr^i)_2]_6\}_{0.5}\{Ag_6[Se_2P(OPr^i)_2]_6\}_{0.5}$ contains $Ag_8(\mu_8\text{-}Se)[Se_2P(OPr^i)_2]_6$ and $Ag_6[Se_2P(OPr^i)_2]_6$ with equal occupancy, sharing the same $Ag_6[Se_2P(OPr^i)_2]_6$ unit. They are alternately distributed along the three-fold axis of the trigonal lattice. The thermal ellipsoid drawings (50% probability) of the octanuclear and hexanuclear silver clusters are depicted in Fig. 1 and 2, respectively. The six silver atoms of the latter form a slightly compressed octahedron with S_6 point group symmetry. This octahedron consists of two uncapped, equilateral triangles and six isosceles triangles in which each triangular face is bridged by a diselenophosphate ligand in a 'trimetallic triconnective'[10] (μ_2, μ_1) coordination mode. Silver–silver distances of 4.649(2) and 3.3578(8) Å within the isosceles triangles are observed in the hexanuclear silver cluster. Thus, the mean distance between the two uncapped Ag_3 triangles through which the three-fold axis passes is 2.0175 Å, whereas, that between two *trans* occupied Ag_3 planes is 3.3522 Å. Each silver atom of the octahedron is coordinated to three selenium atoms of three different ligands. The average Ag–Se(dsep) bond length is 2.6209(8) Å and Se–Ag–Se bond angles range from 115.80(2) to 122.62(3)°. In the octanuclear cluster, the eight silver atoms are arranged at the corners of an almost regular cube in which each square face of the cube is bridged by a dsep ligand exhibiting a 'tetrametallic tetraconnective'[10] (μ_2, μ_2) coordination mode. The coordination environment around each silver atom of the cube is very similar to that observed in the octahedron aside from the interaction to the central selenide anion. Hence two different bond lengths, 2.714(2) and 2.8675(6) Å, are observed between the central selenium atom and peripheral silver atoms so that a slightly compressed cube is observed along the three fold axis.

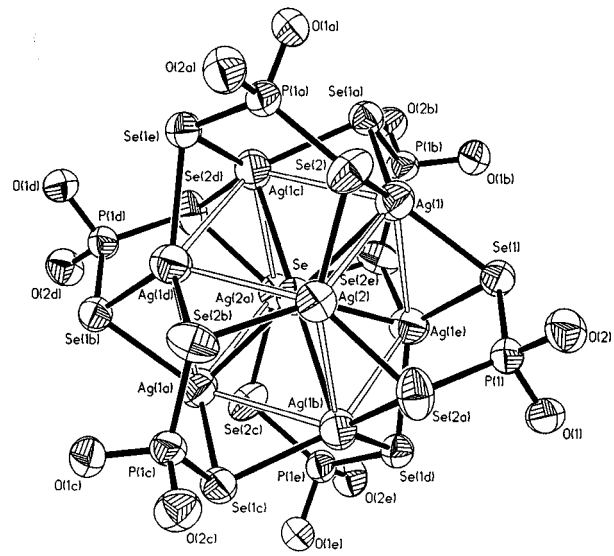

Fig. 1 Thermal ellipsoid drawing (50% probability) of $Ag_8(Se)[Se_2P(OPr^i)_2]_6$. The isopropyl groups are omitted for clarity. Selected bond lengths(Å) and angles(°): Se–Ag(2) 2.714(2), Se–Ag(1) 2.8675(5), Se(1)–Ag(1) 2.6236(8), Se(1)–Ag(1e) 2.6330(9), Se(2)–Ag(1) 2.6062(9), Se(2)–Ag(2) 2.5349(9), Ag(1)–Ag(2) 3.1800(12), Ag(1)–Ag(1e) 3.3578(8), Se(1)–P(1) 2.174(2), P(1)–O(1) 1.575(5), P(1)–O(2) 1.576(5); Ag(2a)–Se–Ag(1) 110.595(12), Ag(2)–Se–Ag(1) 69.403(12), Ag(1)–Ag(2)–Ag(1b) 93.94(4), Ag(1c)–Ag(1)–Ag(1e) 87.62(2), Ag(2)–Ag(1)–Ag(1c) 89.13(2).

† Dedicated to Professor John P. Fackler, Jr. on the occasion of his 65th birthday.

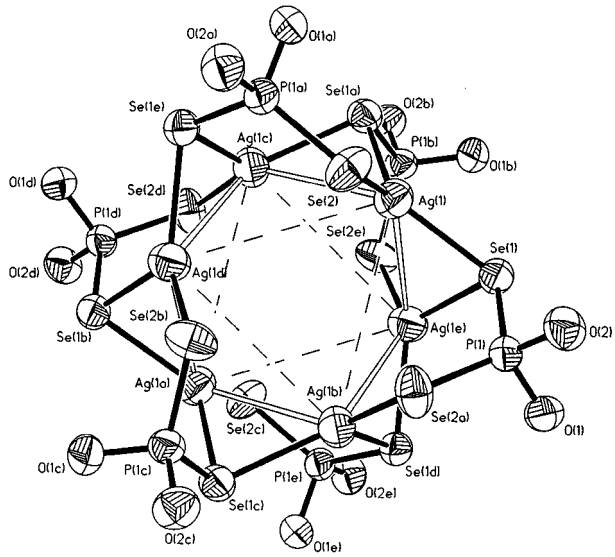

Fig. 2 Thermal ellipsoid drawing (50% probability) of $Ag_6[Se_2P(OPr^i)_2]_6$. The isopropyl groups are omitted for clarity. Selected bond lengths(Å) and angles(°): Ag(1)–Ag(1b) 4.649(2); Se(1)–Ag(1)–Se(2) 122.62(3), Se(1)–Ag(1)–Se(1a) 115.80(2), Se(2)–Ag(1)–Se(1a) 117.37(3), Se(1)–P(1)–Se(2a) 121.33(7).

Consequently a 0.1778 Å difference is seen in the Ag–Ag bond distances [3.3578(8) *vs*. 3.1800(12) Å]. The central selenide atom, in conjunction with the twelve selenium atoms of the ligands, forms a body-centered icosahedron. To our knowledge this geometry has never previously been observed in silver clusters.

An octahedral metal skeleton is commonly observed in hexanuclear silver clusters containing chalcogenide-donor ligands such as in $\{Ag_6(S_2CNPr^n_2)_6\}$,[11] $\{Ag_6[S(O)(CNPr^n)_2]_6\}$,[12] $\{Ag_6[S_2P(OPr^i)_2]_6\}$[13] and $[NMe_4]_6[Ag_6(i\text{-MNT})_6]$ [*i*-MNT = $S_2CC(CN)_2^{2-}$].[14] All six bridging sulfur atoms in these clusters are located on the two uncapped Ag_3 triangles while the terminally coordinated sulfur (or oxygen) atoms are in the belt positions of an octahedron.[13] Thus the Ag_6S_{12} (or $Ag_6S_6O_6$) core in these clusters has an idealized D_{3d} point group symmetry.[13] The S_6 point group symmetry found in the $Ag_6[Se_2P(OPr^i)_2]_6$ cluster results from the differences in bridging selenium atom positions in comparison with the bridging sulfur atom positions in $Ag_6[S_2P(OPr^i)_2]_6$.[13] On the other hand, an octanuclear silver cluster with cubic geometry is extremely rare. Examples prior to the title compound are $[Ag_8(i\text{-MNT})_6]^{4-}$,[15] and $[Ag_9(SCH_2CH_2S)_6]^{3-}$,[16] where a silver atom resides inside an extremely distorted Ag_8 cube. Furthermore, the title complex is the first discrete silver homocubane containing an encapsulated chalcogenide anion. Previously only one example[17] of a chloride-centered Ag_8 cuboidal structure was known found in the central portion of a mixed-valence, mixed-metal cluster $[Ag^I_8Ni^{II}_6\{SCMe_2CH(NH_2)CO_2\}_{12}Cl]^{5-}$.

Since the ligand bridging mode between Ag_8 and Ag_6 clusters is different, two chemical shifts should be observed in the ^{31}P NMR spectrum. Instead a single resonance flanked with selenium satellites is observed over the temperature range 300–180 K. Since the true bond connectivities are virtually identical for the phosphorus center in these two clusters and the spatial orientation magnetically is also virtually identical for all phosphorus positions, the chemical shifts are not expected to be very different. Although this possibility can not be ruled out, the fast ligand dissociation in solution or extreme lability of Ag–Se bond is the most likely reason for the single signal. This is further corroborated by the absence of one-bond coupling to $^{107/109}Ag$ nuclei of the title complex in the ^{77}Se NMR spectrum in which only a doublet arising from the coupling to ^{31}P nuclei is observed. In fact, it has been reported from multinuclear NMR studies that silver complexes of group 16 donor ligands are much more labile than their group 15 analogues in solution.[18]

We thank the National Science Council of Taiwan for support of this work.

Notes and references

‡ $^{31}P\{^1H\}$ NMR ($CDCl_3$), δ72.7(J_{SeP} 654 Hz); ^1H NMR ($CDCl_3$), δ 1.37 [d, 72H, $CH(CH_3)_2$], 4.88 [m, 12H, $CH(CH_3)_2$]; $^{77}Se\{^1H\}$ NMR ($CDCl_3$), δ 147 (J_{SeP} 654 Hz). Anal. Calc. for $C_{36}H_{84}Ag_7O_{12}P_6Se_{12.5}$: C, 16.40; H, 3.19. Found: C, 16.97; H, 3.16%.

§ *Crystal data*: $C_{36}H_{84}Ag_7O_{12}P_6Se_{12.5}$, $[(C_{36}H_{84}Ag_8O_{12}P_6Se_{13})_{0.5}\cdot(C_{36}H_{84}Ag_6O_{12}P_6Se_{12})_{0.5}]$, M = 2636.94; trigonal, space group $R\bar{3}$, a = 22.7866(12), b = 22.7866(12), c = 12.8738(9) Å , γ = 120°, V = 5788.9(6) Å^3, Z = 3, D_c = 2.269 Mg m^{-3}, $F(000)$ = 3720, μ = 7.800 mm^{-1}, T = 298(2) K.

The structure was solved by direct methods using the SHELXTL-PLUS software package,[19] and refined by full-matrix least squares on F^2. The site occupancies of Ag(2) and Se in special positions were initially set to unity. The U_{eq} of these two atoms are 0.128(1) and 0.118(2) which is nearly twice that of the averaged U_{eq} of other Ag and Se atoms. In addition, an unreasonably, high $wR2$ of 0.2996 was obtained. Therefore the site occupancy factors of Ag(2) and Se were tied and refined as a free variable. Final convergence resulted in site occupancies of 0.5. In addition, two carbon atoms of isopropyl groups were also found to be disordered and refined isotropically as an equal population model. Refinement converged to $R1 = 0.0382$ [$I > 2\sigma(I)$], $wR2 = 0.0992$ (all data) and GOF = 1.069 based on 114 variables and 2228 reflections. CCDC 182/1241. See http://www.rsc.org/suppdata/cc/1999/995/ for crystallographic files in .cif format.

1 See ref. 4 for preceeding paper.
2 C. W. Liu, R. T. Stubbs, R. J. Staples and J. P. Fackler, Jr. *J. Am. Chem. Soc*., 1995, **117**, 9778; Z. X. Huang, S. F. Lu, J. Q. Huang, D. M. Wu and J. L. Huang, *Jiegou Huaxue* (*J. Struct. Chem*.), 1991, **10**, 213; I. G. Dance, R. Garbutt and D. Craig, *Inorg. Chem*., 1987, **26**, 3732.
3 R. A. Wheeler, *J. Am. Chem. Soc*., 1990, **112**, 8737; E. Furet, A. L. Beuze, J.-F. Halet and J.-Y. Saillard, *J. Am. Chem. Soc*., 1995, **117**, 4936; B. Zouchoune, F. Ogliaro, J.-F. Halet, J.-Y. Saillard, J. R. Eveland and K. H. Whitmire, *Inorg. Chem*., 1998, **37**, 865.
4 C. W. Liu, H.-C. Chen, J.-C. Wang and T.-C. Keng, *Chem. Commun*., 1998, 1831.
5 A. I. Kitaigorodsky, in *Mixed Crystals*, ed. M. Cardona, Solid State Sciences, Springer-Verlag, Berlin, 1984, vol. 33; *Structure and Properties of Molecular Crystals*, ed. M. Pierrot, Elsevier, Amsterdam, 1990; G. R. Desiraju, *Crystal Engineering. The Design of Organic Solids*, Elsevier, Amsterdam, 1990.
6 M. Periasamy, L. Venkatraman and K. R. J. Thomas, *J. Org. Chem*., 1997, **62**, 4302.
7 D. Braga, F. Grepioni, P. Milne and E. Parisini, *J. Am. Chem. Soc*., 1993, **115**, 5115.
8 M. Maekawa, M. Munakata, T. Kuroda-Sowa and K. Hachiya, *Inorg. Chim. Acta*., 1995, **232**, 231; D. Braga, F. Grepioni, C. M. Martin, E. Parisini, P. J. Dyson and B. F. G. Johnson, *Organometallics*, 1994, **13**, 2170; P. W. Dyer, P. J. Dyson, S. L. James, P. Suman, J. E. Davies and C. M. Martin, *Chem. Commun*., 1998, 1375.
9 G.-C. Guo and T. C. W. Mak, *Inorg. Chem*., 1998, **37**, 6538.
10 I. Haiduc, D. B. Snowerby and S.-F. Lu, *Polyhedron*, 1995, **14**, 3389.
11 R. Hesse and L. Nilson, *Acta Chem. Scand*., 1969, **23**, 825.
12 P. Jennische and R. Hesse, *Acta Chem. Scand*., 1971, **25**, 423.
13 C. W. Liu, J. T. Pitts and J. P. Fackler, Jr., *Polyhedron*, 1997, **16**, 3899; J. P. Fackler, Jr., R. J. Staples, C. W. Liu, R. T. Stubbs, C. Lopez and J. T. Pitts, *Pure Appl. Chem*., 1998, **70**, 839.
14 H. Dietrich, W. Storck and G. Manecke, *J. Chem. Soc., Chem. Commun*., 1982, 1036; H. H. Zhang and X. F. Yu, *J. Struct. Chem*., 1987, **6**, 98.
15 P. J. M. W. L. Birker and G. C. Verschoor, *J. Chem. Soc., Chem. Commun*.,1981, 322.
16 G. Henkel, B. Krebs, P. Betz, H. Fietz and K. Saatkamp, *Angew. Chem., Int. Ed. Engl*., 1988, **27**, 1326.
17 P. J. M. W. L. Birker, J. Reedijk and G. C. Verschoor, *Inorg. Chem*., 1981, **20**, 2877.
18 J. R. Black, N. R. Champness, W. Levason and G. Reid, *J. Chem. Soc., Dalton Trans*., 1995, 3439.
19 SHELXTL-Plus 5.03. Siemens Analytical X-ray Instruments Inc., Karlsruhe, Germany, 1995.

Communication 9/02429H

Stabilization of selenium in zeolites: an anomalous X-ray scattering study

Andreas Goldbach,† Marie-Louise Saboungi,* Lennos Iton and David L. Price

Argonne National Laboratory, Argonne, Illinois 60439, USA. E-mail: mls@anl.gov

Received (in Columbia, MO, USA) 1st January 1999, Accepted 9th April 1999

The host–guest interactions in selenium/zeolite encapsulates are investigated with anomalous X-ray scattering (AXS) to rationalize the effects of the cation on the selenium incorporation.

The intriguing prospects of quantum confinement have stimulated many strategies to synthesize and investigate the properties of mesoscopic particles.[1] The encapsulation of semiconductor clusters within open-framework structures with large surface area like zeolites is particularly advantageous[2] since the zeolite itself can play the role of a solid support for these clusters, which is a prerequisite for prospective technical applications. Large arrays of quantum dots and wires with a narrow size distribution can be generated this way owing to the regular distribution of the cavities within the zeolite. The sorption of Se into molecular sieves is a typical example. Until now, studies of these systems[3–7] have focused mostly on the structure and electronic properties of the encapsulated Se. However, little is known about the host–guest interactions in these selenium/zeolite encapsulates and the question of the driving force for the easy sorption of elemental Se into the zeolite cages has not been addressed. We note that the synthesis and characteristics of these Se/zeolite composites are distinct from those of ultramarine pigments,[8] which are aluminosilicates with chalcogen radical anions trapped inside sodalite cages.

The sorption of elemental Se into zeolites is comparable to vaporization: the intermolecular bonds of the bulk material must be overcome to produce separate Se chains and rings inside the zeolite. The counter-cations, which counterbalance the negatively charged aluminosilica framework, are the anticipated binding sites and play a crucial role on the structure of the encapsulate as shown in our recent studies.[9–12] In particular, the Raman spectra of Se in a number of cation-exchanged Y zeolites show the formation of Se_8 rings and predominant Se chains[11,12] with the fraction of rings increasing along the series La-Y, Nd-Y, Ca-Y and Sr-Y. In the present work, we demonstrate that the counter-cations do not only act as structure directing agents but also contribute significantly to the stabilization of Se inside the zeolites.

A competition experiment was carried out in which La^{3+}-ion exchanged zeolite La-Y ($Na_3La_{21}Al_{56}Si_{136}O_{384}$) was loaded with 13.5 Se atoms per supercage (La-Y/13.5Se = $Se_{108}Na_3La_{21}Al_{56}Si_{136}O_{384}$), close to the maximum uptake.[10] A detailed description of the synthesis can be found elsewhere.[10,11] This composite was then sealed in an evacuated quartz tube together with Ca^{2+}-ion exchanged zeolite Ca-Y ($Na_{13}Ca_{21}Al_{56}Si_{136}O_{384}$), the two materials being separated by a frit. Upon heating to 350 °C, Se diffuses through the frit and is redistributed between the two zeolites. After a reaction time of 11 days, as indicated by color changes, Se was almost completely transferred to the Ca^{2+}-ion exchanged zeolite Y according to the net reaction:

$$\underset{\text{orange}}{0.9\ \text{La-Y/13.5Se}} + \underset{\text{white}}{\text{Ca-Y}} \rightarrow \underset{\text{gray–white}}{0.9\ \text{La-Y/0.8Se}} + \underset{\text{orange}}{\text{Ca-Y/11.5Se}} \quad (1)$$

(La-Y/0.8Se = $Se_6Na_3La_{21}Al_{56}Si_{136}O_{384}$, Ca-Y/11.5Se = $Se_{92}Na_{13}Ca_{21}Al_{56}Si_{136}O_{384}$). The Na, Al, Si, Ca, and La content were analyzed by atomic absorption spectroscopy (AAS). The Se uptake was determined from the weight balance (> 99%). The only difference between the two forms of zeolite is the number and location of the metal ions.[10,11] Rare-earth cations form oxygen bridged clusters inside the smaller sodalite cages (6.5 Å diameter), whose windows (1.4 Å wide) are too narrow to admit molecular Se structures. In contrast, alkaline-earth cations are found also in the large supercages (13 Å diameter, 7.5 Å windows) in close proximity to the Se encapsulates.[10,11]

Since the structure of the incorporated Se is disordered with respect to the zeolite framework, crystallography does not yield information about the Se–cation interactions. Instead, we employed anomalous X-ray scattering (AXS) that has been successfully used for the study of bulk disordered materials.[13] This method exploits the strong energy variation of the complex atomic scattering factor $f(Q,E) = f_0(Q) + f'(E) + if''(E)$ in the vicinity of an X-ray absorption edge. A differential structure factor $S_z(Q)$ associated with a particular element z can be obtained from the difference of two diffraction measurements performed with incident energies some ten and some hundred eV below the absorption edge.[14] The scattering factors of the other elements in the sample do not change significantly over such an energy range. The differential pair distribution function $T_z(r)$, which is obtained from $S_z(Q)$ *via* Fourier transformation, gives information about the average spatial environment about the z atoms.[14]

In the present study we determined $S_{Se}(Q)$ for two zeolites with Se loading similar to those of eqn. (1): La-Y/11.7Se and Ca-Y/12.8Se. (The samples used for the competition experiment were too small for the X-ray measurements. Since we are presenting a difference of two measurements, the result should not be sensitive to the actual Se loadings as long as they are reasonably high and of similar magnitude in the two samples). The diffraction patterns were measured at energies 20 eV and 300 eV below the K absorption edge of Se (12658 eV). Although the Se concentration is < 15 atom% in each compound, the quality of the $S_{Se}(Q)$ data (Fig. 1) is reasonably good. The two corresponding $T_{Se}(r)$ look similar (Fig. 2). The oscillations below 2 Å are due to truncation effects caused by the limited range of Q in the $S_{Se}(Q)$ data. The first real peak is centered at 2.34 ± 0.02 Å in both distribution functions: this distance is well within the range of intramolecular bond lengths observed for bulk Se forms: 2.33 Å (trigonal Se),[15] 2.37 Å (monoclinic Se)[16] and 2.35 Å (amorphous Se).[17] The number of next-nearest neighbors was determined from the area in the radial distribution function $T_{Se}(r)$ corresponding to these peaks. The extracted coordination number CN(1) = 2.2 ± 0.3 is consistent with the existence of either infinite chains or rings [both with CN(1) = 2.0] inside the zeolite pores, corroborating the conclusion of our earlier Raman spectroscopic studies.[11,12] The second peak is located between 3.0 and 4.3 Å in both $T_{Se}(r)$ functions. At least two different types of interaction contribute to it,[18] second-neighbor Se–Se interactions at a distance of 3.7 Å and Se–O (framework) interactions at a distance of 4 Å. From the first and second nearest Se–Se distances R_1 and R_2, a bond angle of $\phi = 104 \pm 2°$ can be deduced [$R_2 = R_1\sin(\phi/2)$] which again is in the range of values found in bulk Se forms.[18] In the region above 4.5 Å, the assignment of further interactions is impossible, but significant differences between the two sets of

† Present address: Fachbereich Physikalische Chemie, Philipps-Universität Marburg Hans-Meerwein-Str., 35032 Marburg/Lahn, Germany.

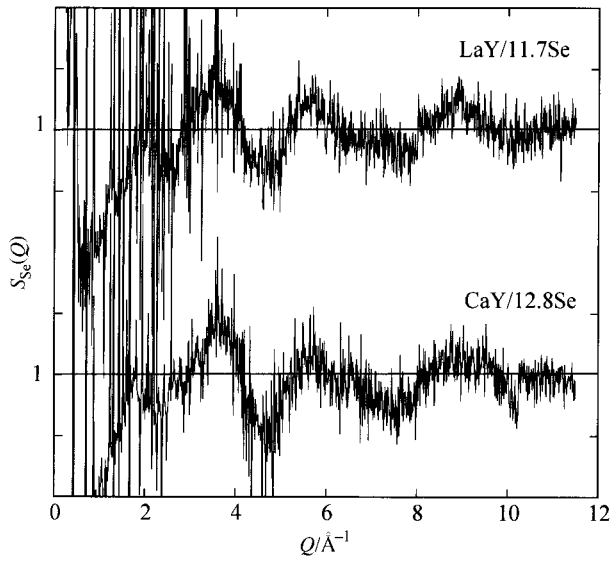

Fig. 1 Differential structure factors $S_{Se}(Q)$ of Ca-Y and La-Y loaded with 12.8 and 11.7 Se atoms per supercage, respectively, obtained from X-ray diffraction experiments at energies 20 and 300 eV below the K absorption edge of Se (12658 eV).

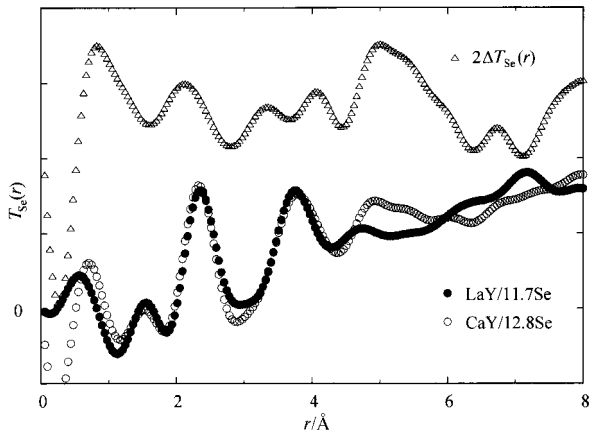

Fig. 2 Differential pair distribution functions $T_{Se}(r)$ of Ca-Y loaded with 12.8 Se atoms (open circles) and La-Y loaded with 11.7 Se atoms (filled circles) per supercage. The difference $\Delta T_{Se}(r)$ of the two $T_{Se}(r)$ functions is shown at the top: the peak around 5 Å is attributed to the Ca^{2+}–Se interaction, as discussed in the text.

$T_{Se}(r)$ functions in this region are noticeable and can be attributed to the Ca^{2+}–Se interaction, since, as discussed above, we believe that Se cation interactions exist in the Ca–Y zeolite and not in the La-Y zeolite. A corresponding peak emerges clearly around 5 Å in the difference $\Delta T_{Se}(r)$ of the two pair distribution functions (Fig. 2).

This long Ca^{2+}–Se distance is striking because it suggests a rather weak attraction. For comparison, the shortest possible Ca^{2+}–Se distance is given by the sum of the radii of Ca^{2+} (0.99 Å) and Se (1.17 Å). On the other hand, an interatomic distance of 2.965 Å is found in the ionic compound CaSe[19] where strong binding forces exist between Ca^{2+} and Se^{2-}. The attraction between Ca^{2+} and a neutral Se chain would be expected to be much weaker inside the zeolite. Probably, the geometrical requirements of both the zeolite framework and the Se chain prevent a close approach. The bond distances and angles of the zeolite encapsulated Se chains do not vary considerably from those found in bulk forms[18] and the dihedral angles are not expected to either. Thus, the short-range order appears to be rather robust and distortion of the Se chains towards the cations becomes unfavorable. Also, the Ca^{2+} ions in the supercage bind strongly to the anionic framework oxygen. In fact, the favorite Ca^{2+} site in the faujasite supercage is only slightly (0.3 Å) out of the plane of the sodalite windows.[20] Thus, they are not easily accessible for a fairly rigid Se chain. Furthermore, the electronic repulsion between the Se and the anionic framework oxygen prevents a close approach of the Se chain to the framework counteracting the weak attractive forces between Se and Ca^{2+}. On these considerations, the observed Ca^{2+}–Se distance of 5 Å appears reasonable. However, these attractive forces acting over this long range are still capable of stabilizing the Se chain significantly in the Ca-Y as opposed to the La-Y zeolite, as shown by the competition experiment described above.

In this work, we have shown that cations play an important role in the stabilization of Se in the pores of zeolites. The nature of the binding interactions has been investigated with AXS, which has allowed us to highlight the environment of the encapsulated Se with an atomic concentration of $< 15\%$: Se assumes a disordered arrangement within these porous materials. The attractive forces between the encapsulated Se and the zeolitic cations act over a surprisingly long distance of 5 Å.

We thank Drs D. E. Cox and Q. Zhu for valuable support and advice during the X-ray measurements. This work was supported by the US Department of Energy, Division of Materials Sciences, Office of Basic Energy Sciences, under Contract No. W-31-109-ENG-38. A. Goldbach gratefully acknowledges support by the Deutsche Forschungsgemeinschaft.

Notes and references

1 *Clusters and Colloids, From Theory to Application*, ed. G. Schmid, VCH, Weinheim, 1994.
2 G. A. Ozin, A. Kuperman and A. Stein, *Angew. Chem.*, 1989, **101**, 373.
3 V. N. Bogomolov, É. L. Lutsenko, V. P. Petranovskii and S. V. Kholodkevich, *JETP Lett.*, 1976, **23**, 482.
4 J. B. Parise, J. E. MacDougall, N. Herron, R. Farlee, A. W. Sleight, Y. Wang, T. Bein, K. Moller and L. M. Moroney, *Inorg. Chem.*, 1988, **27**, 221.
5 Y. Katayama, M. Yao, Y. Ajiro, M. Inui and H. Endo, *J. Phys. Soc. Jpn.*, 1989, **58**, 1811.
6 O. Terasaki, K. Yamakazi, J. M. Thomas, T. Oshuna, D. Watanabe, J. V. Sanders and J. C. Barry, *Nature*, 1987, **330**, 6143.
7 Z. K. Tang, M. M. T. Loy, T. Goto, J. Chen and R. Xu, *Solid State Commun.*, 1997, **10**, 333.
8 R. J. H. Clark, T. J. Dines and M. Kurmoo, *Inorg. Chem.*, 1983, **22**, 2766.
9 A. Goldbach, L. Iton, M. Grimsditch and M.-L. Saboungi, *J. Am. Chem. Soc.*, 1996, **118**, 2004.
10 A. Goldbach, M. Grimsditch, L. Iton and M.-L. Saboungi, *J. Phys. Chem. B*, 1997, **101**, 330.
11 A. Goldbach, L. Iton and M.-L. Saboungi, *Chem. Phys. Lett.*, 1997, **281**, 69.
12 A. Goldbach and M.-L. Saboungi, *Ber. Bunsen-Ges. Phys. Chem.*, 1997, **101**, 1660.
13 *Resonant Anomalous X-Ray Scattering*, ed. G. Materlik, C. J. Sparks and K. Fischer, Elsevier Science B.V., New York, 1994.
14 D. L. Price and M.-L. Saboungi, in *Local Structure from Diffraction*, ed. S. J. L. Billinge and M. F. Thorpe, Plenum, New York, 1998, pp. 23–33.
15 P. Cherin and P. Unger, *Inorg. Chem.*, 1967, **6**, 1589.
16 O. Foss and V. Janickis, *J. Chem. Soc., Dalton Trans.*, 1980, 624.
17 R. W. Johnson, D. L. Price, S. Susman, M. Arai, T. I. Morrison and G. K. Shenoy, *J. Non-Cryst. Solids*, 1986, **83**, 251.
18 P. Armand, M.-L. Saboungi, D. L. Price, L. Iton, C. Cramer and M. Grimsditch, *Phys. Rev. Lett.*, 1997, **71**, 2061.
19 I. Oftedal, *Z. Phys. Chem.*, 1927, **128**, 154.
20 Y. H. Yeom, S. B. Jang, Y. Kim, S. H. Song and K. Seff, *J. Phys. Chem. B*, 1997, **101**, 6914.

Communication 9/00253G

ChemComm

Novel supramolecular synthon in crystal engineering: ionic complexes of 4,4′-bipyridine and 1,2-bis(2-pyridyl)ethylene with 2,5-dichloro-3,6-dihydroxy-1,4-benzoquinone

Md. Badruz Zaman,*[ab] Masaaki Tomura[b] and Yoshiro Yamashita*[b]

[a] *Department of Applied Chemistry and Chemical Technology, University of Dhaka, Dhaka 1000, Bangladesh. E-mail: zaman@ims.ac.jp*

[b] *Institute for Molecular Science, Okazaki 444-8585, Japan. E-mail: yoshiro@ims.ac.jp*

Received (in Cambridge, UK) 23rd March 1999, Accepted 26th April 1999

4,4′-Bipyridine (BPY) and 1,2-bis(2-pyridyl)ethylene (2-PDE) form bifurcated hydrogen bonds with 2,5-dichloro-3,6-dihydroxy-1,4-benzoquinone (chloranilic acid, 2H-CLA) to afford [BPY-2H]$^{2+}$[CLA]$^{2-}$ 1 and [2-PDE-2H]$^{2+}$[CLA]$^{2-}$ 2; their crystal structures exhibit a new type supramolecular synthon and links as molecular chains and zigzag tapes, respectively.

Supramoleculer synthons establish the conceptual relationship between crystal engineering and organic synthesis. Most recently, a variety of supramolecular synthons have been drawn by Desiraju[1,2] to identify the design elements for intermolecular interactions in solid. These supramolecular synthons have allowed structural chemists, organic/inorganic chemists and crystallographers to utilize the new concepts of supramolecular strategy, target identification, and synthetic methodology as parts of successful crystal engineering.

Since benzoquinone-type molecules with dihydroxy groups undergo multi-stage deprotonation and protonation processes, it is interesting to use such molecules to form characteristic intermolecular hydrogen-bonded networks.[3] On the other hand, bidentate bridging ligands are widely used with inorganic compounds to construct stable supramolecular complexes with well-designed geometries and strictly controlled self-assembly.[4] Therefore, we reasoned that by combining bipyridinium-type molecules with organic counterparts, supramolecular assemblies would be formed which exhibited intermolecular interactions. With this in mind we have used bipyridines and centrosymmetric dihalodihydroxybenzoquinones to form hydrogen-bonded networks. Thus a new type of supramolecular synthon **IV** has been exploited to understand noncovalent donor–acceptor (DA) interactions in the design of new supramolecular architectures.

Although synthons affording three-center hydrogen bonds (**I** and **II**) have been well-documented as supramolecular patterns,[5,6] synthons involving two carbonyl groups are very rare. To the best of our knowledge, the only example of synthon **III** is a recent report with an amide structure,[2] and synthon **IV** is unknown. We now report the successful realization of our aim, with the synthesis and X-ray crystal structures of the complexes from diprotonated 4,4′-bipyridine ([BPY-2H]$^{2+}$) and 1,2-bis(2-pyridyl)ethylene ([2-PDE-2H]$^{2+}$) with a dianion of 2,5-dichloro-3,6-dihydroxy-1,4-benzoquinone (chloranilate, [CLA]$^{2-}$), both of which feature novel supramolecular synthon **IV**.

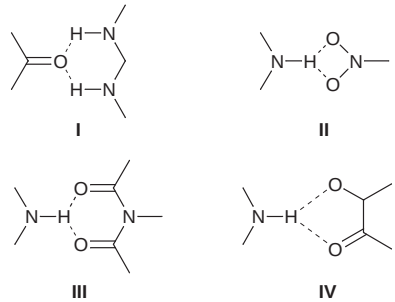

The complexes† were prepared by reacting BPY and 2-PDE with an equal amount of chloranilic acid (2H-CLA) in acetone and/or a mixture of acetone–MeOH. The single crystals grew by the diffusion method over a period of two days. The crystal structures‡ reveal that molecular complexes [BPY-2H]$^{2+}$[CLA]$^{2-}$ **1** and [2-PDE-2H]$^{2+}$[CLA]$^{2-}$ **2** are formed where proton transfer takes place. The component molecules are combined *via* three-centre hydrogen bonded interactions to build a linear molecular chain or a zigzag molecular tape. The structural views of the molecular chain for **1** and the molecular tape for **2** are shown in Fig. 1 and 2, respectively.

In both **1** and **2**, bifurcated interionic [N$^+$–H···O$^-$ and N$^+$–H···O] hydrogen bonds between the nitrogen atoms of the cations and the two oxygen atoms from the anion are observed. The different N···O (2.62–3.00 Å) distances§ are associated with strong and weak hydrogen bonding interactions.[5] The N···O distances are shorter than the mean distances observed for the hydrogen bonds between anilic acids and organic donors,[3,7] indicating the strength of the charged hydrogen bond interactions. The bond lengths in the anions, such as the double

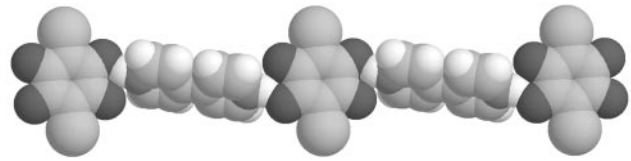

Fig. 1 View of the molecular chains of **1**.

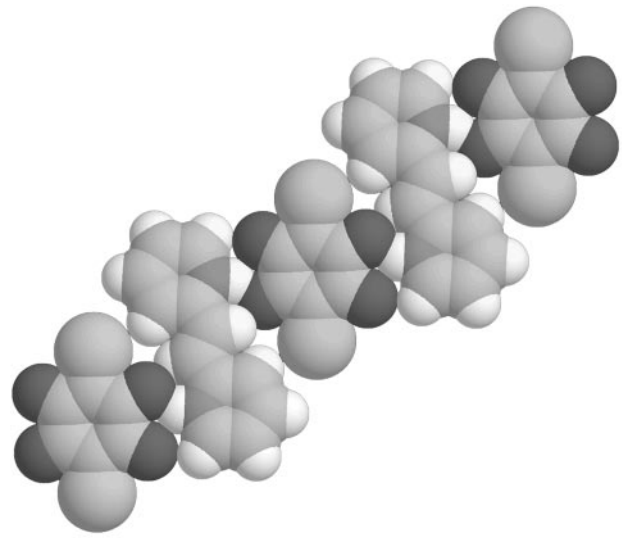

Fig. 2 View of the molecular tapes of **2**.

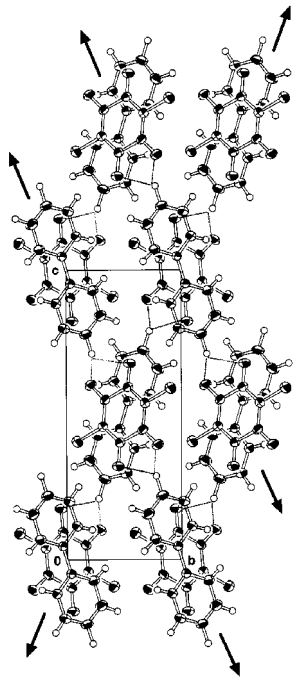

Fig. 3 Crystal packing of **1** viewed along the crystallographic *a* axis. This figure shows the cross-linked chains forming layers.

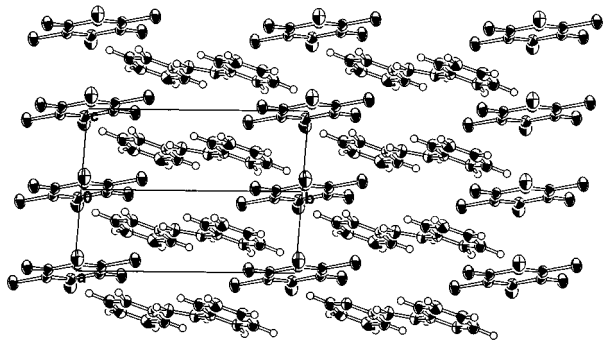

Fig. 4 Crystal packing of **2** viewed along the diagonal line of the *ac* plane. This shows the segregated stacking of the complex.

bonds (C=O, 1.235 Å for **1** and 1.238 Å for **2**) and the single bonds (C–O, 1.256 Å for **1** and 1.252 Å for **2**), are consistent with the molecular geometry of the chloranilate dianion.[7] The dihedral angles between the planes of the cations and anions are 65.8 and 23.6° for **1** and **2**, respectively.

In complex **1** one-dimensional molecular chains are observed toward the two cross diagonal lines within the *bc* plane. A view of such a two-directions cross-linked chain structure of complex **1** is shown in Fig. 3. Moreover, this structure reveals alternating DA-type pairs between the cation and anion molecules (the average distance and angle between the least-squares planes of the cation and anion are 3.42 Å and 3.8°) along the crystallographic *a* axis. Interestingly, complex **2** shows a segregated stacking assembly as DD- and AA-type pairs (Fig. 4), that is, no crossover association is observed in the tapes. The change of position of the nitrogen atoms in the ligands modifies the stacking arrangement though the supramolecular synthon pattern **IV** is unchanged. The *trans*-configuration of the linked ethylene group of the precursor 2-PDE seems to produce zigzag tape structure **2**.

This result not only describes a new supramolecular synthon motif but also highlights the molecules which will allow the design of further supramolecular architectures based on simple components. The present structures are the first examples; further studies in the field of crystal engineering will produce further enhancements, with the eventual creation of new supramolecular synthons and supramolecular architectures *via* investigation of geometrically and stoichiometrically matched donor and acceptor molecules.[8]

Notes and references

† *Selected data* for **1**: 98%, mp 228–230 °C (decomp.) (Calc. C, 47.90; H, 3.52; N, 6.98. Found: C, 47.30; H, 3.31; N, 6.86%). For **2**: 95%, mp 215–218 °C (decomp.) (Calc. C, 55.26; H, 3.09; N, 7.16. Found: C, 55.14; H, 2.84; N, 7.19%). Solid-state electronic spectra [22.9, 27.9, 36.4 $\times$ 10^3 cm^{-1} (for **1**) and 18.7, 30.3, 40.9 $\times$ 10^3 cm^{-1} (for **2**) are consistent with chloranilate dianions (ref. 9). The FT-IR spectra of **1** and **2** show similar broad bands around 2100 and 2600 cm^{-1} and an intense band around 3100 cm^{-1} (N^+H stretching vibration). This proves the intermolecular N^+–$H\cdots O^-$ and N^+–$H\cdots O$ hydrogen bonded system.

‡ *Crystal data* for **1**: $C_{16}H_{10}Cl_2N_2O_4$, M = 365.16, monoclinic, space group $P2_1/n$, a = 8.2377(7), b = 5.965(6), c = 15.089 (1) Å, β = 94.986(8)°, V = 738.7(1) $Å^3$, Z = 2, T = 293 K, μ(Cu-Kα) = 52.11 cm^{-1}, R_1 = 0.0366 and wR_2 = 0.0932 for 1265 data with $I > 2\sigma(I)$. For **2**: $C_{18}H_{12}Cl_2N_2O_4$, M = 391.21, triclinic, space group $P\bar{1}$, a = 9.855(1), b = 11.245(1), c = 3.9057(6) Å, α = 91.34(1)°, β = 99.69(1)°, γ = 111.702(8)°, V = 394.7(1) $Å^3$, Z = 1, T = 293 K, μ(Mo-Kα) = 4.40 cm^{-1}, R_1 = 0.033 and wR_2 = 0.034 for 1258 data with $I > 3\sigma(I)$. Non-hydrogen atoms were refined anisotopically and all hydrogen atoms were clearly localized in the Fourier maps and refined isotropically. CCDC 182/1235. See http://www.rsc.org/suppdata/cc/1999/999/ for crystallographic files in .cif format.

§ Intermolecular hydrogen bonds: for **1**: $N^+\cdots O^-$, 2.63 Å; $N^+H\cdots O^-$, 1.74 Å; $N^+\cdots O$, 3.00 Å; $N^+H\cdots O$, 2.26 Å; for **2**: $N^+\cdots O^-$, 2.62 Å; $N^+H\cdots O^-$, 1.73 Å; $N^+\cdots O$, 3.00 Å; $N^+H\cdots O$, 2.33 Å.

1 G. R. Desiraju, *Angew. Chem., Int. Ed. Engl.*, 1995, **34**, 2311; G. R. Desiraju, *Chem. Commun.*, 1997, 1475.

2 A. Nangia and G. R. Desiraju, *Top. Curr. Chem.*, 1998, **198**, 72.

3 M. B. Zaman, Y. Morita, J. Toyoda, H. Yamochi, G. Saito, N. Yoneyama, T. Enoki and K. Nakasuji, *Chem. Lett*., 1997, 729; H. Yamochi, S. Nakamura, G. Saito, M. B. Zaman, J. Toyoda, Y. Morita, K. Nakasuji and Y. Yamashita, *Synth. Met.*, 1998, in press.

4 M. A. Withersby, A. L. Blake, N. R. Champness, P. Hubberstey, W. S. Li and M. Schröder, *Angew. Chem., Int. Ed. Engl.*, 1997, **36**, 2327; C. V. K. Sharma and R. D. Rogers, *Chem. Commun.*, 1999, 83.

5 R. Thaimattam, D. S. Raddey, F. Xue, T. C. W. Mak, A. Nangia and G. R. Desiraju, *J. Chem. Soc., Perkin Trans. 2*, 1998, 1783.

6 M. C. Etter, Z. Urbánczyk-Lipkowska, M. Z-Ebrahimi and T. W. Panunto, *J. Am. Chem. Soc.*, 1990, **112**, 8415 and references therein; J. W. Chang, M. A. West, F. W. Fowler and J. W. Lauher, *J. Am. Chem. Soc.*, 1993, **115**, 5991; M. D. Hollingsworth, M. E. Brown, B. D. Santarsiero, J. C. Huffman and C. R. Goss, *Chem. Mater.*, 1994, **6**, 1227.

7 J. A. Kanters, A. Schouten, A. J. M. Duisenberg, T. Glowiak, Z. Malarski and L. Sobczyk and E. Greach, *Acta Crystallogr.*, 1991, **C47**, 2148; Z. G. Aliev, S. I. Kondrat'ev, L. O. Atovmyan, M. L. Khidekel and V. V. Karpov, *Bull. Acad. Sci. USSR*, 1981, **30**, 339.

8 M. L. Greer, B. J. McGee, R. D. Rogers and S. C. Blackstock, *Angew. Chem., Int. Ed. Engl.*, 1997, **36**, 1864; M. L. Greer and S. C. Blackstock, *Mol. Cryst. Liq. Cryst.*, 1998, **313**, 55.

9 S. Horiuch, H. Yamochi, G. Saito and K. Matsumoto, *Synth. Met.*, 1997 **86**, 1809.

Communication 9/02305D

The first catalytic, highly enantioselective hetero-Diels–Alder reaction of thiabutadienes

Takao Saito,* Kayoko Takekawa and Tatsuhisa Takahashi

Department of Chemistry, Faculty of Science, Science University of Tokyo, Kagurazaka, Shinjuku-ku, Tokyo 162, Japan. E-mail: tsaito@ch.kagu.sut.ac.jp

Received (in Cambridge, UK) 16th March 1999, Accepted 23rd April 1999

The catalytic, highly enantioselective hetero-Diels–Alder reactions of thiabutadienes using homochiral copper and nickel triflate and perchlorate bis(oxazoline) and bis(imine) complex catalysts to afford optically active dihydrothiopyrans are described for the first time.

The asymmetric hetero-Diels–Alder reaction is a powerful and versatile synthetic method and has a wide range of applications for the synthesis of not only optically active heterocycles as targets themselves but also useful compounds derived from them *via* further synthetic manipulation.[1] Despite its promising utility, however, the asymmetric hetero-Diels–Alder reaction of thiocarbonyl compounds has received much less attention and very few reports on the reaction have appeared so far.[2–4] Amongst the hitherto reported examples of asymmetric hetero-Diels–Alder reactions with thiabutadienes taking part as 4π-components, are diastereoselective methods that utilize chiral auxiliaries attached to either thiadienes or dienophiles for asymmetric induction.[3] To the best of our knowledge, the only report of an enantioselective thiadiene Diels–Alder reaction has been that recently presented by us.[4] Unfortunately, however, it required stoichiometric amounts of chiral Lewis acid to attain a high level of asymmetric induction (up to 95% ee). Therefore, our research has been focused on the development of chiral Lewis acid-induced catalytic thiadiene Diels–Alder cycloadditions giving dihydrothiopyrans with high enantiomeric excess. Here, we present for the first time the *catalytic*, highly enantioselective hetero-Diels–Alder reaction of thiabutadienes.

Prompted by the report by Ghosh and co-workers on the highly enantioselective carbo- and oxa-Diels–Alder reactions using bis(oxazoline) **4**–Lewis acid complexes as chiral catalysts,[5] we selected bis(oxazoline) **4** as the chiral catalyst ligand from among a variety of chiral bis(oxazoline) derivatives with a great deal of structural diversity employed in numerous asymmetric reactions.[6]

Initially, screening of Lewis acids used in combination with chiral ligand **4** was performed in the hetero-Diels–Alder reaction of thiabutadiene **1a** with dienophile **2** (Scheme 1) under various conditions,† and it was found that $Cu(OTf)_2$, $Cu(ClO_4)_2$, and $Ni(ClO_4)_2$ were the Lewis acids of choice in this reaction.‡ Some selected results are summarized in Table 1.

When the reaction was carried out at room temperature using 50 mol% $Ni(ClO_4)_2$–bis(oxazoline) **4** complex (run 3), cycloadduct **3a** was obtained in good yield (99%) with high enantiomeric excess (96%) of the *endo* adduct (3*S*, 4*S*),§ albeit with moderate *endo*:*exo* selectivity (76:24). It was found that at lower temperatures (−78 to 0 °C), the enantioselectivity was markedly decreased in the $Ni(ClO_4)_2$- and $Cu(OTf)_2$-catalyzed reactions (runs 1, 2, 5 and 6). The amount of the Ni^{II} catalyst could be reduced to 10 mol% while maintaining a good enantiomeric excess of 80% (run 4). The reaction using 100 mol% $Cu(OTf)_2$–**4** catalyst at room temperature (run 7) also afforded the cycloadduct **3a** in good yield (92%) with excellent enantioselectivity (98% ee). The high enantioselectivity (98% ee) was maintained in the presence of even catalytic amounts (10 mol%) of the catalyst (run 8). $Cu(ClO_4)_2$–**4** catalyst also induced good enantioselectivity (93 and 89% ee) with the use of only 5 mol% of the catalyst (runs 9 and 10).

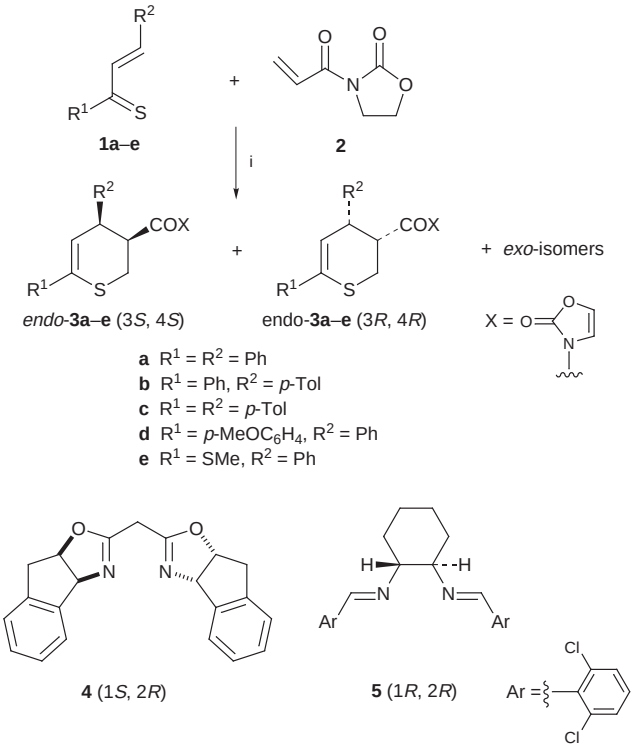

Scheme 1 *Reagent and conditions*: i, Lewis acid–bis(oxazoline) **4** or –bis(imine) **5**.

Table 1 Asymmetric hetero-Diels–Alder reaction of thiabutadiene **1a** (using precursor dimer D) with **2** in the presence of a chiral catalyst [Lewis acid-bis(oxazoline) **4** complex] to afford cycloadduct **3a**[a]

Run	Lewis acid (mol%)	*T*/°C[b]	Yield[c] (%)	*endo*:*exo*[d]	Ee (%) (*endo*)[e]
1	$Ni(ClO_4)_2$ (50)	−65	49[f]	79:21	1
2	$Ni(ClO_4)_2$ (50)	0	90	78:22	85
3	$Ni(ClO_4)_2$ (50)	rt	99	76:24	96
4	$Ni(ClO_4)_2$ (10)	rt	80	78:22	80
5	$Cu(OTf)_2$ (100)	−78	23[f]	77:23	1
6	$Cu(OTf)_2$ (100)	0	90	79:21	78
7	$Cu(OTf)_2$ (100)	rt	92	71:29	98
8	$Cu(OTf)_2$ (10)	rt	92	70:30	98
9	$Cu(ClO_4)_2$ (5)	rt	91	77:23	93
10	$Cu(ClO_4)_2$ (5)	0	92	78:22	89

[a] Reaction was carried out in CH_2Cl_2 for 1.5–7 h with a ratio of **1a**:**2**:catalyst (Lewis acid:**4** = 1.0:1.1) = 1.2:1.0:0.05–1.0. A dithiine-type dimer (D) of **1a** was used as the precursor. Concerning the dithiine-type (D) and thiopyran-type (T) dimers used in asymmetric hetero-Diels–Alder reactions, see our earlier report [ref. 3(*b*)]. [b] rt = room temperature. [c] Isolated yield. [d] Determined by ^1H NMR spectroscopy and HPLC analysis. [e] Determined by HPLC analysis. [f] Reaction was incomplete after 3 h.

Table 2 Asymmetric hetero-Diels–Alder reaction of thiabutadienes **1a–d** (using precursor dimer T) with **2** in the presence of a chiral catalyst [Lewis acid–bis(oxazoline) **4** complex] to afford cycloadducts **3a–d**[a]

Run	**1**, **3**	Lewis acid (mol %)	Yield[b] (%)	*endo* : *exo*[c]	Ee (%) (*endo*)[d]
1	**a**	$Ni(ClO_4)_2$ (50)	84	78 : 22	91
2	**a**	$Cu(OTf)_2$ (50)	62	60 : 40	80
3	**a**	$Cu(ClO_4)_2$ (10)	89	77 : 23	90
4	**a**	$Cu(ClO_4)_2$ (5)	84	78 : 22	86
5	**b**	$Cu(OTf)_2$ (50)	65	74 : 26	85
6	**b**	$Cu(ClO_4)_2$ (10)	88	64 : 36	81
7	**c**	$Cu(OTf)_2$ (50)	60	64 : 36	83
8	**d**	$Cu(OTf)_2$ (20)	66	71 : 29	96
9	**d**	$Cu(ClO_4)_2$ (10)	86	82 : 18	86

[a] Reaction was carried out in CH_2Cl_2 at room temperature for 3 h in a ratio of **1** : **2** : catalyst (Lewis acid : **4** = 1.0 : 1.1) = 1.2 : 1.0 : 0.05–0.5. A thiopyran-type dimer (T) of **1** was used as the precursor. [b] Isolated yield. Reaction was incomplete after 3 h. [c] Determined by ^{1}H NMR spectroscopy and HPLC analysis. [d] Determined by HPLC analysis.

The Cu^{II}– and Ni^{II}–**4** catalyzed reactions between thiabutadienes **1a–d** and **2** using the corresponding thiopyran-type dimers as the precursors of **1** were examined (Table 2). It was found that the reactions also proceeded efficiently at room temperature to show satisfactory enantioselectivities (96–80% ee). In the cases of **1a–c** using either $Ni(ClO_4)_2$ or $Cu(OTf)_2$, at least 50 mol% of the catalyst was needed to preserve the high enantioselectivities (> 80% ee) (runs 1, 2, 5 and 7), while 5–10 mol% $Cu(ClO_4)_2$–**4** catalyst efficiently catalyzed the reactions to give the high ees of the *endo* adducts (runs 3, 4, 6 and 9). It is noteworthy that the reaction with the *p*-methoxyphenyl-substituted thiabutadiene **1d** showed excellent enantioselectivity (96% ee) even with the use of 20 mol% $Cu(OTf)_2$–**4** catalyst (run 8).

Finally, α,β-unsaturated dithiocarboxylic ester **1e**, which can exist as a monomer, was subjected to a chiral Lewis acid-catalyzed hetero-Diels–Alder reaction and the results are summarized in Table 3. The observed enantioselectivity was found to be largely dependent on reaction temperature, the combination of the Lewis acid and the ligand (**4**/**5**), the amount used (stoichiometric or catalytic), and the presence or absence of an additive (molecular sieves). Namely, when the reactions were performed at room temperature in the presence of 100 or 20 mol% of the catalyst [$Ni(ClO_4)_2$–**4**] (runs 1 and 2), a cycloadduct **3e** was obtained in good to fair enantiomeric excess (89–82% ee). It is noteworthy that the use of a small amount (5 mol%) of $Cu(OTf)_2$–**4** catalyst in the reaction at room temperature gave cycloadduct **3e** in 74% yield with fair enantiomeric induction (74% ee) (run 3), whereas the reactions using 100 mol% of the catalyst at either room temperature, 0 or −78 °C) afforded none of the cycloadduct; only a decomposition reaction took place. By use of ligand **5** instead of **4** complexed with 100 mol% $Cu(OTf)_2$ at low temperature (−78 °C), almost complete enantioselectivity (> 99% ee) was obtained (run 4). Disappointingly, however, the enantioselectivity was reduced to only 10% ee in the presence of 20 mol% of the catalyst (run 5). It was exciting to eventually find that in the presence of 4 Å molecular sieves as an additive,¶ the catalytic process was completely restored without any reduction of the high enantiomeric excess (> 99%) when performed at −78 °C (runs 7 and 8) rather than at room temperature (run 6).‖

Table 3 Asymmetric hetero-Diels–Alder reaction of thiabutadiene **1e** with **2** in the presence of a chiral catalyst [Lewis acid–ligand **4**/**5** complex] to afford cycloadduct **3e**[a]

Run	Lewis acid (mol%)	Ligand	*T*/°C[b]	Yield[c] (%)	*endo* : *exo*[d]	Ee (%) (*endo*)[e]
1	$Ni(ClO_4)_2$ (100)	**4**	rt	53	78 : 22	89
2	$Ni(ClO_4)_2$ (20)	**4**	rt	55	70 : 30	82
3	$Cu(OTf)_2$ (5)	**4**	rt	74	65 : 35	74
4	$Cu(OTf)_2$ (100)	**5**	−78	95	89 : 11	> 99
5	$Cu(OTf)_2$ (20)	**5**	−78	78	85 : 15	10
6	$Cu(OTf)_2$ (10)[f]	**5**	rt	78	82 : 18	86
7	$Cu(OTf)_2$ (10)[f]	**5**	−78	70	86 : 14	> 99
8	$Cu(OTf)_2$ (5)[f]	**5**	−78	74	88 : 12	> 99

[a] Reaction was carried out in CH_2Cl_2 for 3–16 h in a ratio of **1e** : **2** : catalyst (Lewis acid : **4**/**5** = 1.0 : 1.1) = 1.2 : 1.0 : 0.05–1.0. [b] rt = room temperature. [c] Isolated yield. [d] Determined by ^{1}H NMR spectroscopy and HPLC analysis. [e] Determined by HPLC analysis. [f] In the presence of powdered 4 Å molecular sieves.

Notes and references

† For example, solvent effects on enantioselectivity were observed to a greater or lesser extent, and the presence of an additive such as powdered molecular sieves (4 Å) was found to effect almost no improvement in either ee or catalytic turnover in this cycloaddition.

‡ Some other Lewis acids used were found to be inferior to $Cu(OTf)_2$, $Cu(ClO_4)_2$ and $Ni(ClO_4)_2$: *e.g.* $Co(ClO_4)_2$ (50 mol%) 50% ee, $NiCl_2$–$6H_2O$ (100 mol%) 0% ee, $Mg(OTf)_2$ (100 mol%) 1% ee, $Mg(ClO_4)_2$ (100 mol%) 64% ee, and $Zn(OTf)_2$ (100 mol%) 5% ee.

§ The absolute configuration of the major *endo* isomer of **3a** was determined by comparison of its retention time by chiral HPLC analysis and specific rotation of its derived alcohol with those of authentic samples. (ref. 3, 4).

¶ In the presence of a dehydrating agent such as $Mg(SO_4)_2$ instead of 4 Å molecular sieves, only 40% ee was observed.

‖ Recently, a new aspect of the role of molecular sieves in metal-catalyzed asymmetric 1,3-dipolar cycloaddition reactions was reported by Jørgensen *et al.* (ref. 7). See also our earlier report (ref. 4).

1 L. F. Tietze and G. Kettshau, *Top. Curr. Chem.*, 1997, **189**, 1; S. Laschat, *Liebigs Ann. Chem.*, 1997, 1; H. Waldmann, *Synthesis*, 1994, 535; P. F. Vogt and M. J. Miller, *Tetrahedron*, 1998, **54**, 1317; J. Streith and A. Defoin, *Synthesis*, 1994, 1107; C. Kibayashi and S. Aoyagi, *Synlett*, 1995, 873 and references cited therein and in ref. 4.

2 For asymmetric hetero-Diels–Alder reaction with thiocarbonyl dienophiles: E. Vedjes, J. S. Stults and R. G. Wilde, *J. Am. Chem. Soc.*, 1988, **110**, 5452; G. W. Kirby and A. D. Sclare, *J. Chem. Soc., Perkin Trans. 1*, 1991, 2329; B. F. Bonini, G. Mazzanti, P. Zani and G. Maccagnani, *J. Chem. Soc., Chem. Commun.*, 1988, 365; T. Takahashi, N. Kurose and T. Koizumi, *Heterocycles*, 1993, **36**, 1601.

3 For asymmetric hetero-Diels–Alder reaction with thiabutadienes: (*a*) S. Motoki, T. Saito, T. Karakasa, H. Kato, T. Matsushita and S. Hayashibe, *J. Chem. Soc., Perkin Trans. 1*, 1991, 2281; (*b*) T. Saito, H. Fujii, S. Hayashibe, T. Matsushita, H. Kato and K. Kobayashi, *J. Chem. Soc., Perkin Trans. 1*, 1996, 1897; (*c*) T. Saito, T. Karakasa, H. Fujii, E. Furuno, H. Suda and K. Kobayashi, *J. Chem. Soc., Perkin Trans. 1*, 1994, 1359; (*d*) T. Saito, M. Kawamura and J. Nishimura, *Tetrahedron Lett.*, 1997, **38**, 3231; (*e*) T. Saito, H. Suda, M. Kawamura, J. Nishimura and A. Yamaya, *Tetrahedron Lett.*, 1997, **38**, 6035; (*f*) A. Marchand, D. Mauger, A. Guingant and J.-P. Pradère, *Tetrahedron: Asymmetry*, 1995, **6**, 853; (*g*) A. S. Bell, C. W. G. Fishwick and J. E. Reed, *Tetrahedron*, 1998, **54**, 3219.

4 T. Saito, K. Takekawa, J. Nishimura and M. Kawamura, *J. Chem. Soc., Perkin Trans. 1*, 1997, 2957.

5 A. K. Ghosh, P. Mathivanan and J. Cappiello, *Tetrahedron Lett.*, 1996, **37**, 3815; A. K. Ghosh, P. Mathivanan, J. Cappiello and K. Krishnan, *Tetrahedron: Asymmetry*, 1996, **7**, 2165. See also I. W. Davies, C. K. Senanayake, R. D. Larsen, T. R. Verhoeven and P. J. Reider, *Tetrahedron Lett.*, 1996, **37**, 1725.

6 A. K. Ghosh, P. Mathivanan and J. Cappiello, *Tetrahedron: Asymmetry*, 1998, **9**, 1.

7 K. V. Gothelf, R. G. Hazell and K. A. Jørgensen, *J. Org. Chem.*, 1998, **63**, 5483 and references cited therein.

Communication 9/02076D

ChemComm

Stereospecific rhenium catalyzed desulfurization of thiiranes

Josemon Jacob and James H. Espenson*

Ames Laboratory and Department of Chemistry, Iowa State University of Science and Technology, Ames, IA 50011, USA. E-mail: espenson@ameslab.gov

Received (in Bloomington, IN, USA) 3rd March 1999, Accepted 20th April 1999

Methyltrioxorhenium catalyzes the efficient and stereospecific desulfurization of thiiranes by triphenylphosphine at room temperature, moreso when MTO has been pretreated with hydrogen sulfide, with a Re^{V} species as the active form of the catalyst.

Desulfurization of thiiranes (episulfides) occurs thermally,[1] photochemically[2] and chemically.[3–11] One of the most widely used reactions of thiiranes is the stereospecific desulfurization by trivalent phosphorus compounds such as PPh_3.[4] These are very slow reactions, the rate constant for the reaction between PPh_3 and but-1-ene sulfide being $(0.9–1.8) \times 10^{-5}$ l mol^{-1} s^{-1} at 40 °C in different solvents. Recent studies of oxygen atom transfer[12–14] might be extended to sulfur atom transfer reactions, using organorhenium catalysts. Herein we report the results of our investigations.

Treatment of propylene sulfide with PPh_3 gave no direct reaction until catalytic amounts of $MeReO_3$ (MTO) were added.† Propylene was then formed, albeit quite slowly (Fig. 1) and only after a long induction period. The active catalyst, a Re^{V} species, from MTO and Ph_3P, is formed by a similar induction period.[15] Plausibly, an unspecified thiorhenium intermediate arises during that time.

Rhenium(v)[16] is proposed to be the active catalyst species here as well. Substitution of an oxygen atom on MTO by sulfur might perhaps eliminate the induction period, in that Re^{VII} transfers a sulfur atom to a phosphine faster than it does an oxygen atom. MTO exchanges oxygens with water[17,18] and could use H_2S to exchange one or more oxygen atoms with sulfur. As a test, H_2S was first bubbled through MTO in CD_3CN and the reaction repeated [eqn. (1)]. As predicted, the rate was significantly enhanced (Fig. 1).

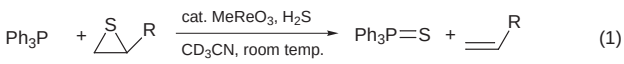

(1)

Removal of H_2S by bubbling argon through the reaction prior to the addition of the phosphine and episulfide did not diminish the reactivity.‡ The general reaction with episulfides[19,20] occurs efficiently on a 2 g scale at room temperature for many thiiranes

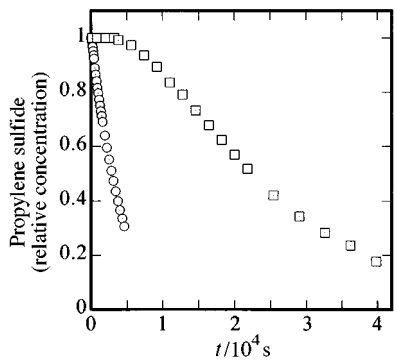

Fig. 1 Kinetics of the reaction of propylene sulfide with PPh_3 in the presence of MTO as followed by ^{1}H NMR: (□) no H_2S, [propylene sulfide] = 50 mM, [PPh_3] = 200 mM, [MTO] = 20 mM; (○) MTO solution (2 mM) rapidly pre-treated with H_2S, followed by an argon sparge, [propylene sulfide] = 100 mM, [PPh_3] = 200 mM.

(Table 1). This desulfurization process is tolerant of various functional groups. With both epoxy and episulfido groups (entry 10), only the episulfide undergoes atom transfer. Stereochemistry is retained completely, as indicated by entries 12 and 13.

In the absence of H_2S the reaction proceeds as shown in Scheme 1. H_2S alters the reaction by forming thiorhenium complexes in exchange processes [eqn. (2)]. Direct reaction

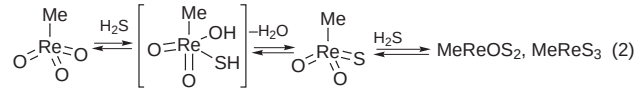

(2)

with H_2S yields Re_2S_7 from $KReO_4$ and MoS_3 from $(NH_4)_2MoO_4$.[21] The same components at elevated temperatures (> 450 °C) form reduced (Re^{V} and Mo^{IV}) sulfides.[22]

On bubbling H_2S through a solution of MTO in CD_3CN, a black solid separates out within a few minutes. It proved insoluble in all common organic solvents and in water, complicating its characterization. Excess H_2O_2 dissolved the black solid product, but the ^{1}H NMR chemical shift of the new species does not match that of the well-established diperoxo complex of MTO.

Our next approach was to prepare and study MTO complexes to establish the mechanism. Nitrogen donor ligands give well-documented complexes with MTO,[14] but complexes of MTO with phenanthroline, bipyridine and 8-hydroxyquinoline failed

Table 1 Yields obtained in the MTO-catalyzed desulfurization of thiiranes§

Entry	Substrate	Product	Time	Yield (%)
1			3 h	100
2			5 min	100
3			5 min	96
4			5 min	100
5			1 h	100
6			4 h	89
7			6 h	100
8			9 h	50
9			1 h	90
10			2 h	100
11			1 h	100
12			30 min	100
13			30 min	100

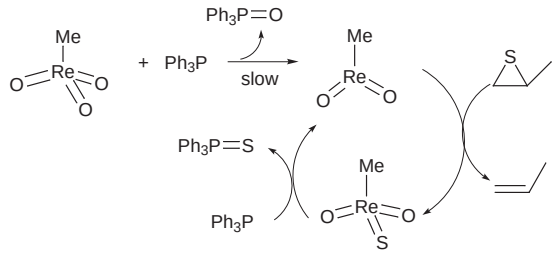

Scheme 1

to react with H_2S. Reaction with 2-mercaptomethylthiophenol[23,24] gave a new dimeric yellow rhenium(v) complex **D** [eqn. (3)], as reported earlier.[25]

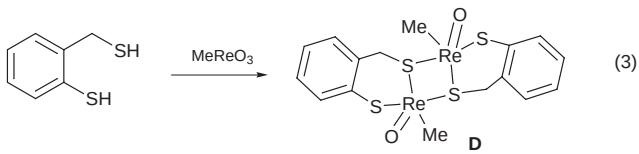

(3)

With **D** in hand it was possible to test the mechanism in Scheme 1, according to which 2 equiv. of episulfide should be desulfurized without phosphine. Fig. 2 shows the kinetics of an experiment with **D** and a four-fold excess of propylene sulfide. According to the amounts of material formed and remaining, **D** reacts with 2 equiv. of the thiirane, establishing rhenium(v) as the active catalyst. Furthermore, the reaction can be made catalytic in rhenium by the addition of PPh_3 and the use of much less **D** at the outset, although a longer time is required than with the use of the aforementioned MTO/H_2S procedure. The same rate of desulfurization as given by MTO/H_2S was achieved by bubbling H_2S through the dimer solution before the addition of the episulfide and phosphine (Fig. 2). Addition of H_2S changes the color of the solution from yellow to pink, consistent with conversion of the Re=O group of **D** to Re=S; the species responsible could not be isolated.

The question still remains, regarding the original MTO/H_2S system, of whether the reactions utilize a sulfur analogue of MTO or a rhenium(v) species that might have been formed in the system. The black solid obtained on reaction of MTO with H_2S is an oligomeric alkylrhenium sulfide. Transition metal sulfides, including high oxidation state rhenium sulfides, are known to oligomerize and some of them have been characterized. [26] When the black solid obtained on reaction with H_2S was treated with propylene sulfide, 4% desulfurization was observed in 2 h (starting with 5 mM MTO), suggesting the formation of at least some rhenium(v). The constitution of the major part was deduced by these experiments. First H_2S was bubbled through 20 mM MTO in CD_3CN until all the MTO had reacted (by ^{1}H NMR), the excess then being removed by an argon purge. Its reaction with successive 5 mM increments of PPh_3 was then monitored by ^{31}P NMR. Only Ph_3P=S was observed, and no PPh_3 detected, on addition of 15 mM PPh_3. Addition of a further 5 mM increment of PPh_3 showed very small amounts of PPh_3. Beyond that, more phosphine did not lead to more Ph_3P=S. These findings indicate the presence of a rhenium(VII) sulfide that easily transfers a sulfur atom to a phosphine to generate Re^V and phosphine sulfide. Most of product of the MTO/H_2S reaction exists as Re^{VII} on reaction with H_2S. On the basis of direct information, however, we cannot claim that another valence state, such as Re^{VI}, is not involved.

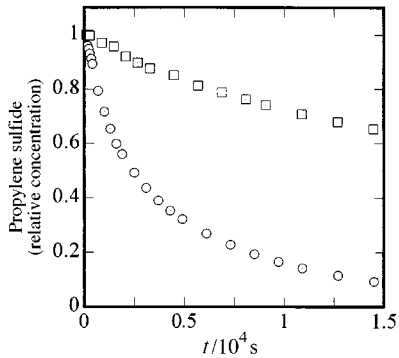

Fig. 2 Decrease in the concentration of propylene sulfide as followed ^{1}H NMR: (□) stoichiometric experiment, with [propylene sulfide] = 30 mM, [**D**] = 7.5 mM; (○) catalytic experiment, with [propylene sulfide] = 100 mM, [PPh_3] = 125 mM and [**D**] = 2 mM, at room temperature.

This is a novel catalytic system that effects the desulfurization of episulfides at ambient temperature and pressure. The reaction is stereospecific and tolerant to functional groups.

This research was supported by the U.S. Department of Energy, Office of Basic Energy Sciences, Division of Chemical Sciences, under contract W-7405-Eng-82.

Notes and references

† MTO, propylene sulfide and cyclohexene sulfide were purchased. The other episulfides were synthesized. NMR spectra were referenced to solvent peaks: δ 7.15 for C_6D_6 and δ 1.93 for CD_3CN.

‡ In a typical experiment, hydrogen sulfide was bubbled into 2 mM MTO in CD_3CN for about 5 min, as a black solid separated. The excess of H_2S was removed by sparging with argon, whereupon PPh_3 and the episulfide were added. The reaction was monitored by NMR, and yields obtained based on proton integration relative to the solvent or to an internal standard of Ph_3CH. The chemical shifts of the olefin products agreed well with reference data.

§ In a typical experiment, carried out at room temperature, H_2S was bubbled through a 2 mM MTO in CD_3CN for 5 min; excess H_2S was then removed by purging with argon. To this solution PPh_3 (125 mM) was added, followed by the thiirane (100 mM). The reaction was followed by ^{1}H NMR at 25 °C. The reaction also worked very well on a 2 g scale.

1 D. C. Dittmer, *Thiiranes and Thiirenes*, Pergamon, Oxford, 1984, vol. 7.
2 M. Torres, E. M. Lown, H. E. Gunning and O. P. Strausz, *Pure Appl. Chem.*, 1980, **52**, 1623.
3 P. Dybowski and Skowronska, *Synthesis*, 1991, 1134.
4 D. B. Denney and M. J. Boskin, *J. Am. Chem. Soc.*, 1960, **82**, 4736.
5 V. Calo, L. Lopez, A. Nacci and G. Mele, *Tetrahedron*, 1995, **51**, 8935.
6 B. M. Trost and S. D. Ziman, *J. Org. Chem*, 1973, **38**, 932.
7 S. Calet and H. Alper, *Tetrahedron Lett*, 1986, **27**, 3573.
8 V. Calo, L. Lopez, A. Mincuzzi and G. Pesce, *Synthesis*, 1976, 200.
9 P. S. Skell, K. J. Klabunde, J. H. Plonka, J. S. Roberts and D. L. Williams-Smith, *J. Am. Chem. Soc.*, 1973, **95**, 1547.
10 K. J. Klabunde and P. S. Skell, *J. Am. Chem. Soc.*, 1971, **93**, 3807.
11 J. K. Weseman, R. Williamson, J. L. Green and P. B. Shevlin, *J. Chem. Soc., Chem. Communun.*, 1973, 901.
12 J. H. Espenson and M. M. Abu-Omar, *Adv. Chem. Ser.*, 1997, **253**, 99.
13 J. H. Espenson, *Chem. Commun.*, 1999, 479.
14 C. C. Romão, F. E. Kühn and W. A. Herrmann, *Chem. Rev.*, 1997, **97**, 3197.
15 M. D. Eager and J. H. Espenson, *Inorg. Chem.*, 1999, in the press.
16 M. M. Abu-Omar, E. H. Appelman and J. H. Espenson, *Inorg. Chem.*, 1996, **35**, 7751.
17 W. A. Herrmann, *Angew. Chem., Int. Ed. Engl.*, 1988, **27**, 1297.
18 M. M. Abu-Omar, P. J. Hansen and J. H. Espenson, *J. Am. Chem. Soc.*, 1996, **118**, 4966.
19 F. G. Bordwell and H. M. Anderson, *J. Am. Chem. Soc.*, 1954, **75**, 4959.
20 M. Sander, *Chem. Rev.*, 1966, **66**, 297.
21 H. S. Broadbent, L. H. Slaugh and N. L. Jarvis, *J. Am. Chem. Soc*, 1954, **76**, 1519.
22 O. Weisser and S. Landa, *Sulphide Catalysts, Their Properties and Applications*, Pergamon, New York, 1973.
23 E. Klingsberg and A. M. Schreiber, *J. Am. Chem. Soc.*, 1962, **84**, 2941.
24 A. G. Hortman, A. J. Aron and A. K. Bhattacharya, *J. Org. Chem.*, 1978, **43**, 3374.
25 J. Jacob, I. A. Guzei and J. H. Espenson, *Inorg. Chem.*, 1999, **39**, 1040.
26 J. T. Goodman and T. B. Rauchfuss, *Inorg. Chem.*, 1998, **37**, 5040.

Communication 9/01708I

Total synthesis of (*S*)-espicufolin and absolute structure determinaton of espicufolin

Hidemitsu Uno,*[a] Katsuji Sakamoto,[a] Erina Honda[a] and Noboru Ono[b]

[a] *Advanced Instrumentation Center for Chemical Analysis, Ehime University, Bunkyo-cho 2-5, Matsuyama 790-8577, Japan. E-mail: uno@dpc.ehime-u.ac.jp*

[b] *Department of Chemistry, Faculty of Science, Ehime University, Bunkyo-cho 2-5, Matsuyama 790-8577, Japan*

Received (in Cambridge, UK) 1st March 1999, Accepted 13th April 1999

(*S*)-Espicufolin was synthesized from 1,4-dimethoxybenzene in 16 steps *via* an intramolecular acyl-transfer reaction as the key step; the absolute stereochemistry at the 14-position of natural espicufolin was determined to be *R*.

In the disease ischemia, L-glutamic acid in the brain is believed to play an important role as an excitatory neurotransmitter, increasing the level of powerful oxidants such as superoxide anion and oxygen radicals in the neuronal cells, which then cause neuronal cell death.[1] Neuronal cell-protecting compounds for such events have attracted increasing attention from scientists in many fields. In 1996, Seto *et al.* found a novel neuronal cell-protecting substance in the culture broth of *Streptomyces* sp. cu39 in the course of their screening for suppressors of glutamate toxicity using neuronal hybridoma N18-RE-105 cells and named it espicufolin (**1**, Fig. 1).[2] However, the action mechanism of espicufolin **1** was suggested not to relate to antioxidative activity, from an experiment involving buthionine sulfoximine toxicity.[2,3] From a structural viewpoint, espicufolin **1** has an anthraquinone skeleton fused with a γ-pyrone ring and one unknown stereogenic centre at the 14-position. Espicufolin **1** is considered as a new member of the pyranoanthraquinone family;[4] these compounds are also reported to show antitumor and antibiotic activity. Thus, we aimed to synthesize espicufolin **1** *via* a route which can be applied to the syntheses of other family members in addition to espicufolin analogues.

Since the regioselective Diels–Alder reaction of chloronaphthoquinone with 1-methoxycyclohexa-1,3-diene has been established as one of the most reliable methods for construction of anthraquinones bearing hydroxy groups, we required pyranonaphthoquinone **2**. First, we focussed on the preparation of the intermediate **2** from the readily available naphthol **3** (Scheme 1), which was obtained from 1,4-dimethoxybenzene in 22% yield (5 steps).[5] As attempts to introduce an acetyl group at the 2-position of **3** *via* a Friedel–Crafts reaction and a Fris rearrangement failed, probably due to steric encumbrance, we thought to utilise the neighbouring hydroxymethyl group at the 3-position. After selective acetylation of the primary hydroxy group of **3** (90%), iodination[6] of **6** was carried out in CH_2Cl_2 (0.2 mol l^{-1}) to give **5** regioselectively in 31% yield, in addition to a mixture of dimers (38%). The dimer formation was simply suppressed by using an increased volume of solvent (0.05 mol l^{-1}) to give **5** in 77% yield. Protection with a MOM group followed by saponification of the acetyl group afforded **7** in 77% yield. The alcohol **7** was condensed with (*S*)-4-methylhex-2-ynoic acid,[7] which was in turn prepared from commercially available (*S*)-2-methylbutan-1-ol according to a literature procedure,[8] by treatment with bis(2-oxo-1,3-oxazolidin-3-yl)-phosphinic chloride (BOPCl) and Et_3N to afford **8** in 97% yield.[9] By treatment of **8** with Bu^nLi at −78 °C, a smooth iodine–lithium exchange reaction followed by spontaneous intramolecular acyl transfer occurred to give 2-acylnaphthalene **9**† in almost quantitative (95%) yield as an equilibrium mixture

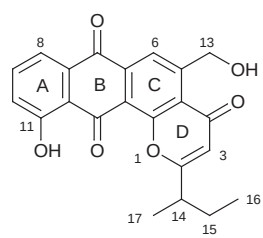

Fig. 1 Structure and numbering of espicufolin **1**.

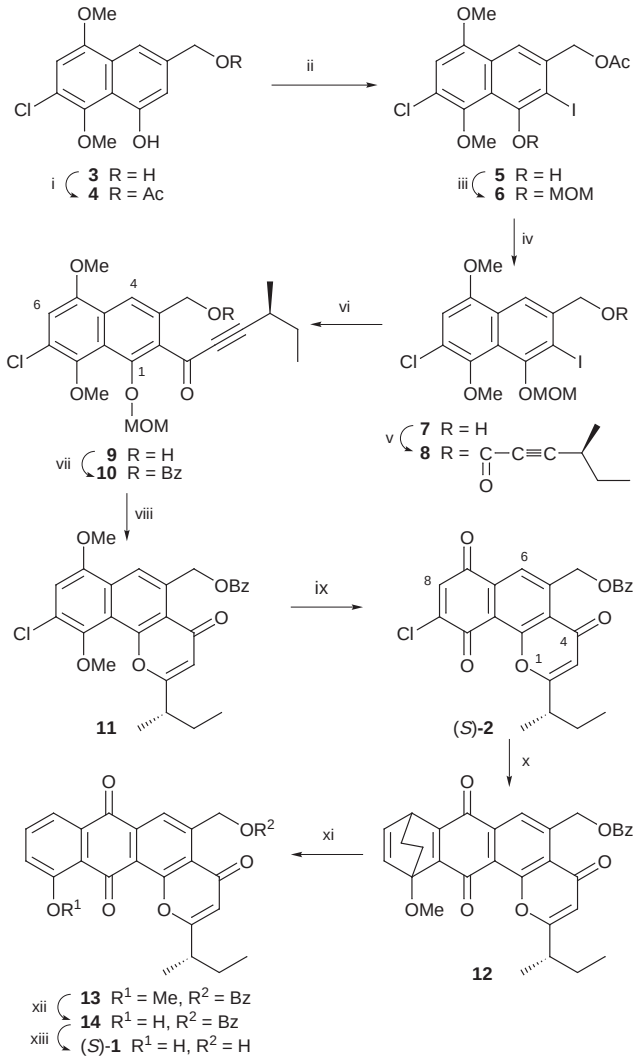

Scheme 1 *Reagents and conditions*: i, Ac_2O, $HClO_4$, CH_2Cl_2, rt; ii, I_2, *N*-methylmorpholine, CH_2Cl_2, rt; iii, NaH, MOMCl, DMF, rt; iv, NaOH, aq. THF–MeOH, rt; v, *S*-4-methylhex-2-ynoic acid, BOPCl, Et_3N, CH_2Cl_2, rt; vi, BuLi, THF, −78 °C; vii, BzCl, Py, rt; viii, HCl, aq. THF–Pr^iOH, reflux; ix, CAN, aq. MeCN, 0 °C; x, 1-methoxycyclohexa-1,3-diene, CH_2Cl_2, rt; xi, 140 °C, neat; xii, BBr_3, −78 °C; xiii, NaOH, aq. THF–MeOH, 0 °C.

with its hemiacetal form. This mixture was treated with BzCl in pyridine to give benzoate **10** in 87% yield. Removal of the MOM group from **10** under acidic conditions brought about simultaneous intramolecular cyclization forming desired γ-pyrone **11** (64%) predominantly; formation of any furanone compound could not be detected. This cyclization was formally thought to be a successful example of the *6-endo-dig* process, which usually competed the *5-exo-dig* ring closure giving furanones in the cases under basic conditions.[10] However, it is not clear at this moment if the allenic carbocation generated by protonation to the ynone carbonyl oxygen is directly attacked by the intramolecular phenolic oxygen or by water followed by dehydrative ring closure.[11] The γ-pyrone **11** was converted to the intermediate **2**† in 75% yield.

The one-pot method[5] of anthraquinone formation from naphthoquinones and 1-methoxycyclohexa-1,3-diene was applied for construction of the A ring of **1**. However, an intractable mixture was obtained due to decomposition probably by HCl. Thus, the Diels–Alder adduct from **2** and 1-methoxycyclohexa-1,3-diene was treated with pyridine to afford the diastereomeric quinone **12** in 77% yield. Heating **12** at 140 °C afforded anthraquinone **13** in good yield (74%). Demethylation of **13** with BBr_3 (75%) followed by saponification (69%) gave (*S*)-espicufolin, spectral and physical data† of which were identical to those previously reported, except for $[\alpha]_D$.[2] The value for synthetic (*S*)-**1** was $[\alpha]_D^{23}$ −11 (*c* 0.021, $CHCl_3$), whereas the authentic espicufolin kindly provided by Professor Seto was $[\alpha]_D^{23}$ +9.4 (*c* 0.020, $CHCl_3$). Therefore, the unknown stereochemistry at the 14-position can be assigned as *R*; our synthetic sample is an enantiomer of natural espicufolin. Espicufolin must therefore be synthesized starting from (*R*)-2-methylbutanol, which can be readily prepared by a literature procedure.[12]

We have achieved the synthesis of the enantiomer of neuronal cell-protecting espicufolin in 1.3% overall yield from 1,4-dimethoxybenzene in 15 steps. The absolute stereochemistry of espicufolin **1** is determined to be *R*.

Notes and references

† *Selected data* for **9**: pale yellow crystals, mp 92–93 °C; 6 : 1 mixture of keto and hemiacetal forms in $CDCl_3$ at ambient temperature; keto form: δ_H 1.03 (3H, t, *J* 7.3, H6′), 1.24 (3H, d, *J* 7.3, 4′-Me), 1.56 (2H, m, H5′), 2.63 (1H, m, H4′), 3.04 (1H, br t, *J* 6.4, OH), 3.58 (3H, s, OCH_2OMe), 3.84 (3H, s, 5- or 8-OMe), 3.95 (3H, s, 5- or 8-OMe), 4.71 (2H, d, *J* 6.4, CH_2OH), 5.10 (3H, s, OCH_2OMe), 6.83 (1H, s, H6) and 8.04 (1H, s, H4); δ_C 11.5 (C6′), 19.4 (4′-Me), 28.1 (C5′), 29.0 (C4′), 56.0 (OCH_2OMe), 58.1 (5- or 8-OMe), 61.6 (5- or 8-OMe), 63.6 (CH_2OH), 83.3 (C2′), 101.3 (C3′), 102.2 (OCH_2OMe), 107.8, 119.0, 122.3, 125.9, 128.0, 133.9, 136.2, 144.7, 151.4, 152.0 and 181.8 (C1′); hemiacetal form (1 : 1 diastereomeric mixture): δ_H 1.02 (3H both, t, *J* 7.3, H5′), 1.18 (3H of one diastereomer, d, *J* 7.3, 3′-Me), 1.19 (3H of another diastereomer, d, *J* 7.3, 3′-Me), 1.53 (2H, m, H4′), 2.49 (1H, m, H3′), 3.71 (3H of one diastereomer, s, OCH_2OMe), 3.72 (3H of another diastereomer, s, OCH_2OMe), 3.85 (3H both, s, 5- or 8-OMe), 3.96 (3H both, s, 5- or 8-OMe), 5.0–5.4 (5H, m, CH_2OH and OCH_2OMe), 6.81 (1H both, br s, H6) and 7.89 (1H both, br s, H4); δ_C(typical signals) 14.0 (C6′), 15.2 (C6′), 20.2 (4′-Me), 20.2 (4′-Me), 27.5 (C5′), 27.5 (C5′), 29.5 (C4′), 29.6 (C4′), 57.9, 61.5, 65.8, 71.2 (C3), 71.2 (C3), 79.8 (C1′), 89.3, 98.5, 101.4, 101.4, 102.2, 106.6, 111.3, 123.0, 124.8, 129.2, 135.1, 137.8, 137.8, 144.9 and 147.0; ν_{max}(KBr)/cm^{-1} 3456, 2200, 1650, 1334 and 1068. For **2**: yellow needles, mp 196–198 °C; δ_H($CDCl_3$) 0.98 (3H, t, *J* 7.3, H3′), 1.43 (3H, d, *J* 6.7, 1′-Me), 1.80 (1H, m, H2′), 1.96 (1H, m, H2′), 2.74 (1H, m, H1′), 6.16 (2H, s, CH_2OBz), 6.31 (1H, s, H3), 7.26 (1H, s, H8), 7.53 (2H, m, *m*-Bz), 7.64 (1H, m, *p*-Bz), 8.19 (2H, m, *o*-Bz) and 8.25 (1H, s, H6); δ_C($CDCl_3$) 11.7 (C3′), 17.9 (1′-Me), 27.3 (C2′), 40.5 (C1′), 65.3 (CH_2OBz), 111.1 (C3), 118.9 (C6), 125.1 (C4a or C10a), 128.6 (*m*-Ph), 129.6 (*i*-Ph), 129.8 (*o*-Ph), 133.4 (*p*-Ph or C8), 134.0 (*p*-Ph or C8), 134.6 (C6a), 147.3 (C5 or C9), 147.9 (C5 or C9), 155.8 (C10b), 166.0 (Ph*C*O), 173.6 (C2), 174.9 (C4), 178.7 (C10), 181.5 (C7) and one carbon (C4a or C10a) could not be identified; ν_{max}(KBr)/cm^{-1} 1716, 1680, 1651, 1267, 883 and 711. For **1**: orange needles, mp 185–187 °C (184–186 °C for natural espicufolin[2]); δ_H(DMSO-d_6) 0.93 (3H, t, *J* 7.3, H16), 1.38 (3H, d, *J* 6.8, H17), 1.75 (1H, m, H15), 1.92 (1H, m, H15), 2.78 (1H, m, H14), 5.16 (2H, t, *J* 4.8, H13) 5.56 (1H, t, *J* 4.8, 13-OH), 6.34 (1H, s, H3), 7.38 (1H, d, *J* 8.3, H10), 7.68 (1H, d, *J* 7.3, H8), 7.77 (1H, dd, *J* 8.3, 7.3, H9), 8.51 (1H, s, H6) and 12.6 (1H, s, 11-OH); δ_C(DMSO-d_6) 11.2 (C16), 17.3 (C17), 26.6 (C15), 39.2 (C14), 62.1 (C13), 110.3 (C3), 116.6 (C11a), 118.5 (C8), 118.7 (C6), 119.6 (C12a), 123.9 (C4a), 124.4 (C10), 132.0 (C7a), 135.9 (C6a), 136.4 (C9), 153.1 (C5), 155.5 (C12b), 161.2 (C11), 172.4 (C2), 178.1 (C4), 181.4 (C7) and 186.8 (C12); ν_{max}(KBr)/cm^{-1} 3473, 1676, 1647, 1583, 1460, 1272 and 1220; *m/z* (EI) (20 eV) 378 (100%), 349 (18), 320 (9.1) and 267 (21) (Calc. for $C_{22}H_{18}O_6$: 378.1103. Found: 378.1104).

1 D. W. Choi, *J. Neurosci.*, 1990, **10**, 2493; A. J. Grau, E. Berger, K.-L. Paul Sung and G. W. Schmid-Schönbein, *Stroke*, 1992, **23**, 33; K. Baker, C. B. Marcus, K. Huffman, H. Kruk, B. Malfroy and S. R. Doctrow, *J. Pharmacol. Exp. Ther.*, 1998, **284**, 215.
2 J.-S. Kim, K. Shin-ya, J. Eishima, K. Furihata and H. Seto, *J. Antibiot.*, 1996, **49**, 947.
3 J. T. Coyle and P. Puttfarcken, *Science*, 1993, **262**, 689.
4 R. H. Thomson, *Naturally Occurring Quinones III*, Chapman and Hall, London, 1987, p. 506.
5 J. L. Bloomer, K. W. Stagliano and J. A. Gazzillo, *J. Org. Chem.*, 1993, **58**, 7906.
6 C. A. Giza and R. L. Hinman, *J. Org. Chem.*, 1964, **29**, 1453.
7 L. Lardicci and L. Conti, *Atti Soc. Toscana Sci. Nat. Pisa, P.V. Mem., Ser. B*, 1962, **69**, 83; *Chem. Abstr.*, 1965, **63**, 9793h.
8 E. J. Corey and P. L. Fuchs, *Tetrahedron Lett.*, **1972**, 3769.
9 J. Diago-Mesequer, A. L. Palomo-Coll, J. R. Fernández-Lizarbe and A. Zugaza-Bilbao, *Synthesis*, 1980, 547.
10 K. Nakatani, A. Okamoto, M. Yamanuki and I. Saito, *J. Org. Chem.*, 1994, **59**, 4360; H. Garcia, S. Iborra, J. Primo and M. A. Miranda, *J. Org. Chem.*, 1986, **51**, 4432.
11 J. D. Hepworth, *Comprehensive Heterocyclic Chemistry*, ed. A. R. Katritzky and C. W. Rees, Pergamon, Oxford, 1984, vol. 3, ch. 2.24.3.4.
12 A. Ichihara, S. Miki, H. Kawagisi and S. Sakamura, *Tetrahedron Lett.*, 1989, **30**, 4551; D. A. Evans and J. M. Takacs, *Tetrahedron Lett.*, 1980, **21**, 4233.

Communication 9/01602C

Porphyrinatoerbium–crown ether conjugate for synergistic binding and chirality sensing of zwitterionic amino acids

Hiroshi Tsukube,*[a] Masatoshi Wada,[a] Satoshi Shinoda[a] and Hitoshi Tamiaki[b]

[a] *Department of Chemistry, Graduate School of Science, Osaka City University, Sugimoto, Sumiyoshi-ku, Osaka 558-8585, Japan. E-Mail: tsukube@sci.osaka-cu.ac.jp*

[b] *Department of Bioscience and Biotechnology, Faculty of Science and Engineering, Ritsumeikan University, Kusatsu, Shiga 525-8577, Japan*

Received (in Cambridge, UK) 15th April 1999, Accepted 26th April 1999

A porphyrinatoerbium–benzo-18-crown-6 conjugate offers efficient extraction and chirality sensing of amino acids under neutral conditions *via* synergistic binding of zwitterions.

Lanthanide complexes are widely employed as shift reagents in NMR spectroscopy,[1] catalysts in organic synthesis and biotechnology,[2] and probes for fluorescence/MRI sensing.[3] We recently demonstrated that lanthanide tris(β-diketonate)s and tetraphenylporphyrin complexes offered efficient extraction of unprotected amino acids under neutral pH conditions and also acted as circular dichroism (CD) probes capable of chirality sensing of the bound guests.[4,5] In these systems, the central lanthanide(III) ions were electrically neutralized by coordination from the diketonate and/or porphyrinate anions, with the additional CO_2^- group of the guest amino acids forming highly coordinated complexes.[4] Since zwitterionic amino acids are hydrophilic and bifunctional guests, more effective receptors should have multiple binding sites highly complementary to the NH_3^+ and CO_2^- sites of the guest. Thus, we designed a novel type of conjugate receptor for synergistic binding of zwitterionic amino acids in which a benzo-18-crown-6 moiety is covalently connected to the lanthanide porphyrin complex **1**–**3**. Because benzo-18-crown-6 coordinates to the NH_3^+ moiety and since lanthanide porphyrinate binds the CO_2^- moiety, these conjugates with two different kinds of binding sites within a molecule are expected to offer multiple binding of zwitterionic, chiral amino acids and sensitive CD probing of their chirality.[6]

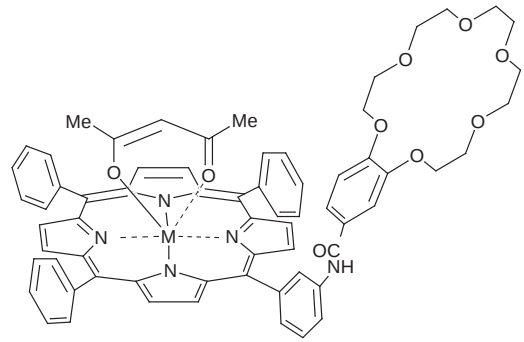

1 M = Er
2 M = Gd
3 M = Yb

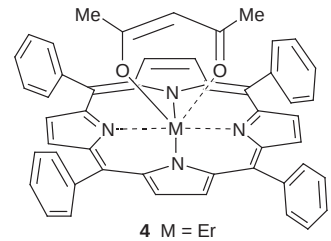

4 M = Er
5 M = Gd
6 M = Yb

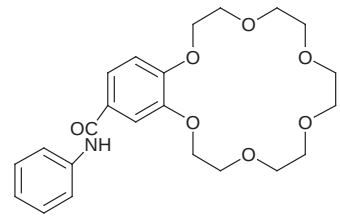

7

Conjugates **1**–**3** were prepared from lanthanide tris(acetylacetonate)s and the corresponding crowned porphyrin ligand,[7] which was derived from amino-substituted tetraphenylporphyrin and 4-chlorocarbonylbenzo-18-crown-6. Their receptor–probe abilities were characterized by liquid–liquid extraction of amino acids and subsequent CD measurements. The concentrations of the amino acids in the aqueous phases were determined, based on UV spectroscopy and/or amino acid analysis (ninhydrin colorimetry). Mixtures of lanthanide porphyrin complexes and benzo-18-crown-6 derivatives,[7,8] *i.e.* **4** + **7**, **5** + **7** or **6** + **7**, were also examined to compare the 'intermolecular' cooperativity of two different binding sites with the 'intramolecular' one.

Porphyrinatoerbium–crown ether conjugate **1** offered efficient extraction of several amino acids from neutral aqueous solution into CH_2Cl_2 solution (Fig. 1). Its extraction ability of tryptophan (Trp) (40%) is twice as high as those of **4** alone (18%) and the mixture **4** + **7** (18%). Although **4** and **7** have binding sites for CO_2^- and NH_3^+ groups respectively, the covalent connection between the two binding sites increased the extraction ability. In other words, bifunctional amino acids are believed to be cooperatively bound to the erbium center and 18-crown-6 ring of conjugate **1**. The extracted amount of Trp by conjugate **1** strongly depended on the pH of the aqueous solution, suggesting that the guest Trp was extracted in zwitterionic form: 13% (pH = 3.5) < 40% (pH = 5.7) ≃ 38% (pH = 8.1) > 28% (pH = 9.4) > 8% (pH = 10.1). When the concentration of Trp in the aqueous phase increased, the mole ratio of the extracted Trp to conjugate **1** increased and reached 0.9, suggesting 1 : 1 complexation. The organic phase was characterized using NMR spectroscopy after extraction experiments. The signals for the aliphatic protons of the extracted Trp disappeared in the presence of conjugate **1**, while those for the aromatic protons broadened but still appeared around 5.5–6.0 ppm. These observations support the suggestion that the extracted Trp locates near the erbium center and also above the porphyrin plane of conjugate **1**. This conjugate extracted a dipeptide as well as other amino acids more effectively than the mixture **4** + **7**: [extraction percentage by **1**]/[extraction percentage by **4** + **7**] = 40%/20% for tryptophanyl-glycine (Trp-Gly);

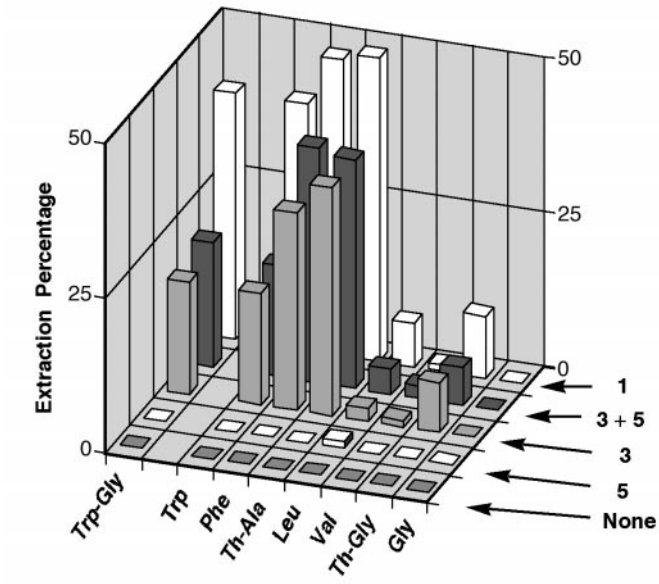

Fig. 1 Extraction of zwitterionic amino acids. Conditions: amino acid = 125 nmol, H_2O = 2.5 ml (pH = 5.9–6.2); receptor = 125 nmol, CH_2Cl_2 = 10 ml.

48%/38% for phenylalanine (Phe); 49%/37% for 3-(2-thienyl)-alanine (Th-Ala); 7%/4% for leucine (Leu); 10%/6% for (2-thienyl)glycine (Th-Gly).[9] In contrast, conjugates **2** and **3** containing gadolinium and ytterbium porphyrinates extracted Trp with comparable efficiencies to those with corresponding mixtures under the employed conditions: 39% for **2** and 34% for **5** + **7**; 14% for **3** and 10% for **6** + **7**. Thus, the nature of the lanthanide center is an important factor in designing effective conjugate receptors.

Conjugate **1** exhibited chirality-specific CD signals *via* complexation with chiral amino acids (Fig. 2). After extraction experiments with L-Trp, L-Phe, L-Th-Ala, L-Th-Gly and L-Leu guests, the resulting CH_2Cl_2 solutions gave the'reversed' S-shaped CD bands around the Soret band, while their D-isomers offered the S-shaped CD bands (Fig. 2). Their CD amplitudes ($[\theta$ at 1st $\lambda] - [\theta$ at 2nd $\lambda]/10^5$ deg cm^2 dmol^{-1}) were larger

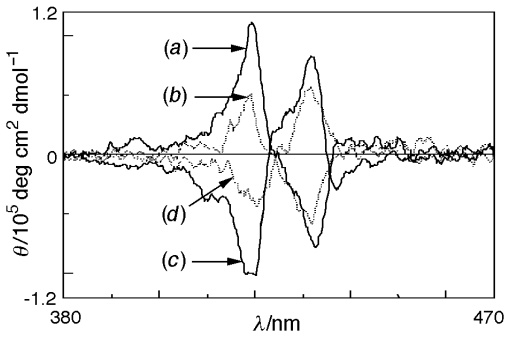

Fig. 2 CD spectra of conjugate **1** or mixture **4** + **7** in CH_2Cl_2 after shaking with an aqueous solution of L- or D-Trp. Conditions: see Fig. 1. (*a*) L-Trp·**1**, (*b*) L-Trp·**4** + **7**, (*c*) D-Trp·**1**, (*d*) D-Trp·**4** + **7**.

than those with **4** + **7**: **1** (1.9) > **4** + **7** (1.0) for L-Trp; **1** (1.8) > **4** + **7** (0.8) for L-Phe; **1** (2.3) > **4** + **7** (1.1) for L-Th-Ala; **1** (0.6) > **4** + **7** (0.5) for L-Leu; **1** (0.9) > **4** + **7** (0.4) for L-Th-Gly. Conjugate **1** was not only an effective extracting reagent of unprotected amino acids but also a sensitive CD probe for their chirality determination.

We have demonstrated that the effective cooperativity of porphyrinatoerbrium and 18-crown-6 ring promoted improved extraction of amino acids and sensitive CD probing of their chirality. A further hybridization of lanthanide complexes with receptor molecules provides promising possibilities in the development of effective sensing, transport and separation of multi-functional substrates of biological interest.

The authors are grateful to Ms M. Doe of the Analytical Center, Graduate School of Science, Osaka City University for determination of amino acid concentrations. This work was supported by a Grant-in-Aid for Scientific Research (No. 10440198) from the Ministry of Education, Science, Culture and Sports, Japan.

Notes and references

1 G. R. Sullivan, D. Ciavarella and H. S. Mosher, *J. Org. Chem.*, 1974, **39**, 2411; R. Hazama, K. Umakoshi, C. Kabuto, K. Kabuto and Y. Sasaki, *Chem. Commun*., 1996, 15.
2 M. Bednarski and S. Danishefsky, *J. Am. Chem. Soc.*, 1983, **105**, 3716; K. Mikami, M. Terada and T. Nakai, *J. Org. Chem.*, 1991, **56**, 5456.
3 V. Alexander, *Chem. Rev.*, 1995, **95**, 273.
4 H. Tsukube, S. Shinoda, J. Uenishi, T. Kanatani, H. Itoh, M. Shiode, T. Iwachido and O.Yonemitsu, *Inorg. Chem.*, 1998, **37**, 1585.
5 H. Tamiaki, N. Matsumoto and H. Tsukube, *Tetrahedron Lett.*, 1997, **38**, 4239.
6 Examples of crown ether conjugate receptors: M. T. Reetz, J. Huff, T. Rudolph, K. Tollner, A. Deege and R. Goddard, *J. Am. Chem. Soc.*, 1994, **116**, 11 588; P. D. Beer, M. G. B. Drew, R. J. Knubley and M. I. Ogden, *J. Chem. Soc., Dalton Trans.*, 1995, 3117; A. Metzger, K. Gloe, H. Stephan and F. P. Schmidtchen, *J. Org. Chem.*, 1996, **61**, 2051; M. F. Paugam, J. T. Bien, B. D. Smith, L. A. Chrisstoffels, F. Jong and D. N. Reinhoudt, *J. Am. Chem. Soc.*, 1996, **118**, 9820; A. P. Silva, H. Q. N. Gnaratne, C. Mcveigh, G. E. M. Maguire, P. R. S. Maxwell and E. O'Hanlon, *Chem. Commun*., 1996, 2191; I. S. Antipin, I. I. Stoikov, E. M. Pinkhassik, N. A. Fitseva, I. Stibor and A. I. Konovalov, *Tetrahedron Lett.*, 1998, **38**, 5865.
7 *Selected data* for crowned porphyrin ligand: mp 176–180 °C; *m/z* [FABMS (*m*-nitrobenzyl alcohol)] 990 (M + Na^+) (Calc. for $C_{61}H_{53}N_5O_7{\cdot}0.5H_2O$; C, 74.98; H, 5.57; N, 7.17. Found: C, 74.97; H, 5.45; N, 7.15%). For **1**: mp 249 °C (decomp.); *m/z* [FABMS (*m*-nitrobenzyl alcohol)] 1230 (M^+) (Calc. for $C_{66}H_{58}N_5O_9Er{\cdot}H_2O$; C, 63.39; H, 4.84; N, 560. Found: C, 63.33; H, 4.69; N, 5.80%). For **4**: mp > 300 °C; *m/z* (EIMS) 877 (M^+) (Calc. for $C_{49}H_{35}N_4O_2Er{\cdot}H_2O$; C, 65.60; H, 4.16; N, 6.25. Found: C, 65.69; H, 4.06; N, 6.52%). For **7**: mp 139–141 °C (Calc. for $C_{23}H_{29}NO_7{\cdot}H_2O$; C, 61.46; H, 6.95; N, 3.12. Found: C, 61.21; H, 6.98; N, 3.13%).
8 Synthesis of **4**–**6**: C. C.-P. Wong, *Inorg. Synth.*, 1983, **22**, 156.
9 The observed extraction efficiency was mostly dependent on the hydrophobicity of the guest amino acid. Octan-1-ol–water distribution co-efficients (log *D*) were determined at pH 5: Trp, −1.15; Phe, −1.44; Th-Ala, −1.50; Leu, −1.72; Val, −2.29; Th-Gly, −2.64; Gly, −3.02. See N. E. Tayar, R.-S. Tsai, P.-A. Carrupt and B. Testa, *J. Chem. Soc., Perkin Trans. 2*, 1992, 79 and ref. 4.

Communication 9/03024G

Diels–Alder trapping of an *o*-dinitroso intermediate in the 1-oxide/3-oxide interconversion of a 2,1,3-benzoxadiazole derivative

Muriel Sebban,[a] Régis Goumont,[a] Jean Claude Hallé,*[a] Jérome Marrot[b] and François Terrier*[a]

[a] *Laboratoire SIRCOB, UPRES A CNRS 8086, Bâtiment Lavoisier, Université de Versailles, 45, avenue des Etats-Unis, 78035 Versailles Cedex, France. E-mail: halle@chimie.uvsq.fr; terrier@chimie.uvsq.fr*

[b] *Institut Lavoisier, Laboratoire IREM, CNRS CO173, Université de Versailles, 45, avenue des Etats-Unis, 78035 Versailles Cedex, France*

Received (in Liverpool, UK) 16th March 1999, Accepted 21st April 1999

Convincing evidence is presented that the *o*-dinitroso intermediate involved in the exchange of the 1-oxide and 3-oxide tautomers of 6-nitro[2,1,3]oxadiazolo[4,5-*b*]pyridine 1-oxide 5 is the precursor of the Diels–Alder diadduct 7 isolated upon treatment of this compound with cyclohexadiene in $CHCl_3$.

The high susceptibility of the nitro-substituted 2,1,3-benzoxadiazoles to undergo covalent nucleophilic addition or substitution processes has attracted considerable attention over the two last decades, leading to numerous synthetic, analytical and biological applications.[1–8] A most significant finding has been, however, our recent discovery that the carbocyclic ring of these strongly electron-deficient heteroaromatics can also be involved in a variety of Diels–Alder type reactions.[9] As a prototype example, 4,6-dinitro-2,1,3-benzoxadiazole 1-oxide **1**

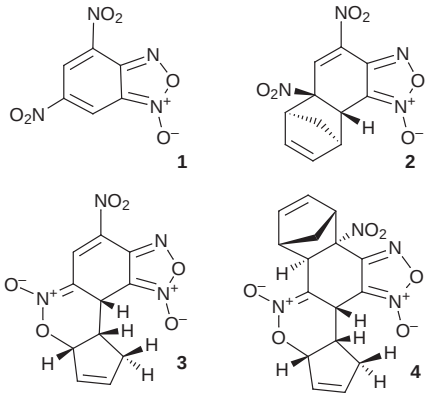

has been found to act as a dienophile in normal electron demand Diels–Alder (NEDDA) processes or as a heterodiene in inverse electron demand Diels–Alder (IEDDA) processes to give the monoadducts **2** and **3**, respectively, upon treatment with cyclopentadiene at −20 °C in $CHCl_3$. In the presence of excess cyclopentadiene at 0 °C, the IEDDA–NEDDA diadduct **4** is quantitatively formed with high stereoselectivity at the expense of **2** and **3**.[9]

Here we report our finding of another Diels–Alder reactivity pattern that we have identified in the reaction of 6-nitro[2,1,3]oxadiazolo[4,5-*b*]pyridine 1-oxide **5**[10] with cyclohexadiene. This new pattern provides convincing evidence in support of the long standing belief that the mechanism of the interconversion of the 1-oxide/3-oxide tautomers (Scheme 1) proceeds through formation of an *o*-dinitroso intermediate.[7,11,12] So far, it is only through photolysis of unsubstituted 2,1,3-benzoxadiazole and *o*-nitrophenyl azide in Ar matrices at 14 K that the existence of such an unstable species could be demonstrated by IR and UV spectroscopy.[13]

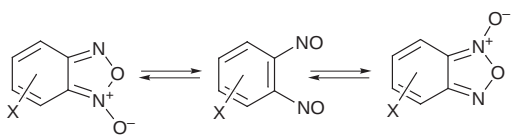

Scheme 1

Treatment of **5** with cyclohexa-1,3-diene (5 equiv.) in $CHCl_3$† affords a 2 : 1 mixture of two products which were readily separated by column chromatography and isolated as pale yellow solids. Although it has been obtained with a crystal of poor quality, the ORTEP view in Fig. 1 leaves no doubt that the major product is the diadduct **7**‡§ whose formation can only be accounted for in terms of two NEDDA processes, in which the N=O double bonds of the *o*-dinitroso intermediate **6** play the role of the dienophile contributors (Scheme 2). Such behaviour of N=O fragments is well known.[14] Based on a detailed analysis *via* COSY, HETCOR and *J* modulation experiments, the NMR data agree with the stereochemistry assigned to **7** in the solid state. The recovery of a pyridine ring on formation of **7** from **5** is supported by the disappearance in the ^{13}C NMR spectra of the

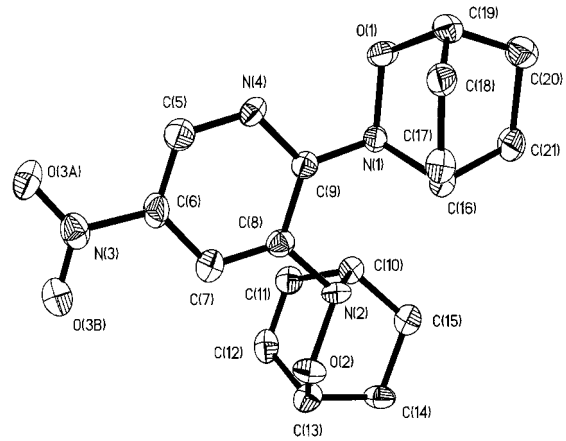

Fig. 1 ORTEP view of **7**, as derived from a partial structure solution (only one enantiomer is represented).

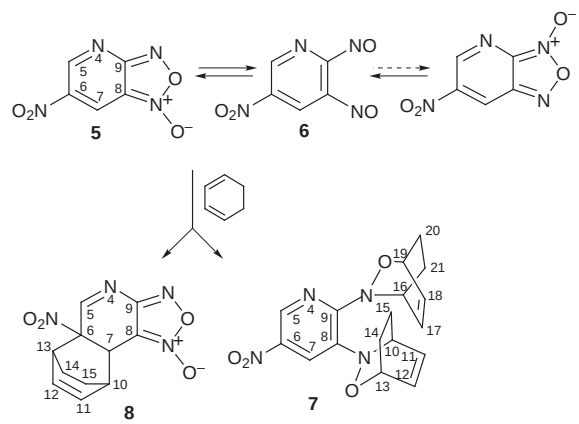

Scheme 2

resonance typical for the C_8 carbon of a 2,1,3-benzoxodiazole structure (δ_C 108.79 in **5**)[10,11] and its replacement by a resonance at δ_C 137.59 for **7**, a classical value for a pure aromatic carbon.

In view of the ^1H and ^{13}C NMR spectra also recorded in $CDCl_3$, the minor product can be formulated as the cycloadduct **8** in its racemic form. This adduct, which is not very stable in the solid state, results from a regioselective and diastereoselective NEDDA process involving the C_6–C_7 double bond of **5** as the dienophile contributor. It should be noted that the related *endo* cycloadduct **9** was recently isolated as the only product of the reaction of cyclopentadiene with 4-nitro-6-trifluoromethyl-2,1,3-benzoxadiazole.[15]

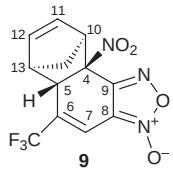

9

In the literature, many examples of 2,1,3-benzoxadiazole structures undergoing the tautomeric exchange shown in Scheme 1 have been reported,[10–12] but no firm Diels–Alder support for the transient formation of the postulated *o*-dinitroso intermediate along the reaction coordinate has been obtained so far. The isolation and characterization of the diadduct **7** *in a thermal process* is therefore of great relevance to the rearrangement shown in Scheme 1, especially because this equilibrium has been shown to be strongly shifted toward the 1-oxide tautomer in the case of the 6-nitro[2,1,3]oxadiazolo[4,5-*b*]-pyridine 1-oxide system.[10]

Notes and references

† *Synthetic procedure* for **7** and **8**: 1.3 ml of cyclohexa-1,3-diene (13.75 mmol) were added to a solution of 0.5 g of **5** (2.75 mmol) in $CHCl_3$. The solution turned rapidly orange.The mixture was maintained under stirring at room temperature for 2 d. Evaporation of $CHCl_3$ under reduced pressure gave a mixture of 7 and **8** as a red semi-solid (0.8 g). The product was purified by chromatography on silica gel using a gradient of EtOAc–pentane as eluent; **7** and **8** were obtained in a 2:1 ratio as yellow crystals.

‡ *Selected data* for **7**: δ_H(300.13 MHz, acetone-d_6) (1.40, 1.60 and 2.21 (m, H-14, H-15, H-20, H-21), 4.88 (dt, 2 H, H-10, H-16, *J* 1.47, 5.88), 5.06 (m, 1 H, H-13 or H-19), 5.67 (m, 1 H, H-13 or H-19), 6.01 (ddd, 1H, H-11 or H-17, *J* 1.47, 6.24, 7.71), 6.16 (ddd, 1H, H-11 or H-17, *J* 1.47, 6.24, 8.07), 6.62 (ddd, 1 H, H-12 or H-18, *J* 1.85, 5.88, 8.07), 6.74 (ddd, 1 H, H-12 or H-18, *J* 1.47, 5.88, 6.27), 7.88 (d, 1 H, H-7, J_{5-7} 2.58), 8.62 (d, 1 H, H-5); δ_C (75.47 MHz, acetone-d_6) 21.36, 21.82, 24.40 and 24.96 (C-14, C-15, C-20, C-21), 50.45 and 51.43 (C-10, C-16), 70.72 and 71.24 (C-13 , C-19), 121.41 (C 7), 129.91 and 130.35 (C-11, C-17), 132.95 and 133.27 (C-12, C-18), 137.59 (C 8), 138.20 (C 5), 140.78 (C 6), 156.52 (C 9); mp 147–150 °C; *m*/*z* (EI) 342 ($M^{+\cdot}$), 262 [$M - C_6H_8^{+\cdot}$]), 232 ($M - C_6H_8 - NO^{+\cdot}$]) (Found: C, 59.63; H, 5.43; N, 16.04 . $C_{17}H_{18}N_4O_4$ requires C, 59.65; H, 5.26; N, 16.37%). For **8**: δ_H(300.13 MHz, acetone-d_6) 1.15–1.60 (m, 4 H, H-14, H-15), 3.43 (dd, 1 H, H-10, J_{7-10} 2.94 , J_{10-11} 6.27), 4.07 (dd, 1 H, H-7 , J_{5-7} 1.83), 3.79 (m, 1 H, H-13), 6.35 (dd, 1 H, H-12, J_{11-12} 7.35), 6.65 (dd, 1 H, H-11), 8.48 (s, 1 H, H-5); δ_C (75.47 MHz, acetone-d_6) 19.00 and 20.36 (C-14, C-15), 30.54 (C-10), 35.62 (C-7), 38.41 (C-13), 91.38 (C-6), 102.15 (C-8), 130.95 (C-12), 136.51 (C-11), 157.26 (C-9), 166.95 (C-5); mp 185 °C; *m*/*z* (EI) 234 [$M + H_2O–NO_2^{+\cdot}$]), 216 ([$M - NO_2^{+\cdot}$]).

§ *Crystal data* for **7**: $C_{17}H_{18}N_4O_4$, M = 342.35, monoclinic, space group $P2_1/n$, a = 6.418(8), b = 10.010(11), c = 24.850(3) Å, β = 91.95(6)°, U = 1595(3) Å^3, Z = 4, D_c = 1.425 mg cm^{-3}, μ(Mo-Kα) = 1.04 cm^{-1}, λ = 0.71073 Å, graphite monochromator, crystal dimensions: 0.08 × 0.32 × 0.40 mm. The data were collected up to 2θ = 60° on a Siemens SMART three-circle diffractometer equipped with a bidimensional CCD detector. The poor quality of the data prevents the structure from being published in full.

1 F. Terrier, in *Nucleophilic Aromatic Displacement*, ed. H. Feuer, VCH, New York, 1991; F. Terrier, E. Kizilian, J. C. Hallé and E. Buncel, *J. Am. Chem. Soc.*, 1992, **114**, 1740.
2 E. Buncel, R. A. Manderville and J. M. Dust, *J. Chem. Soc., Perkin Trans. 2*, 1997, 1019 and numerous references therein.
3 W. P. Norris, R. J. Spear and R. W. Read, *Aust. J. Chem.*, 1989, **36**, 297.
4 J. Kund and H. J. Niclas, *Synth. Commun.*, 1993, **23**, 1569.
5 M. R. Crampton, L. C. Rabbit and F. Terrier, *Can. J. Chem.*, 1999, 77, in the press.
6 M. I. Evgen'yev, S. Y. Garmonov, I. I. Evgen'yeva and L. S. Gazizullina, *J. Anal. Chem.*, 1998, **53**, 57 and references therein.
7 A. Gasco and A. J. Boulton, *Adv. Heterocycl. Chem.*, 1981, **29**, 252 and references therein.
8 F. Terrier, E. Kizilian, J. C. Hallé, M. J. Pouet and E. Buncel, *J. Phys. Org. Chem.*, 1998, **11**, 707 and references therein.
9 J. C. Hallé, D. Vichard, M. J. Pouet and F. Terrier, *J. Org. Chem.*, 1997, **62**, 7178 ; D. Vichard, J. C. Hallé, B. Huguet, M. J. Pouet, D. Riou and F. Terrier, *Chem. Commun.*, 1998, 791 ; S. Pugnaud, D. Masure, J. C. Hallé and P. Chaquin, *J. Org. Chem.*, 1997, **62**, 8687 ; P. Sépulcri, R. Goumont, J. C. Hallé, D. Riou and F. Terrier, to be submitted.
10 C. K. Lowe-Ma, R. A. Nissan and W. S. Wilson, *J. Org. Chem.*, 1990, **55**, 3755.
11 R. K. Harris, A. R. Katritzky, S. Øksne, A. S. Bailey and G. Patterson, *J. Chem. Soc.*, 1963, 197 and references therein ; I. Yavari, R. E. Botto and J. D. Roberts, *J. Org. Chem.*, 1978, **43**, 2542; F. A. L. Anet and I. Yavari, *Org. Magn. Reson.*, 1976, **8**, 158; M. Witanowski, L. Stefaniak, S. Biernat and G. A. Webb, *Org. Magn. Reson.*, 1980, **14**, 365; F. B. Mallory, S. L. Manatt and C. S. Wood, *J. Am. Chem. Soc.*, 1965, **87**, 5433; M. J. Haddadin and C. H. Issidorides, *Tetrahedron Lett.*, 1965, **36**, 3253.
12 J. K. Gallos and E. Malamidou-Xenikaki, *Heterocycles*, 1994, **37**, 193; N. G. Argyropoulos, J. K. Gallos and D. N. Nicolaides, *Tetrahedron*, 1986, **42**, 3631; A. B. Bulacinski, E. F. V. Scriven and H. Suschitzky, *Tetrahedron Lett.*, 1975, 3577; J. W. McFarland, *J. Org. Chem.*, 1971, **36**, 1842.
13 I. R. Dunkin, M. A. Lynch, A. J. Boulton and N. Henderson, *J. Chem. Soc., Chem. Commun.*, 1991, 1178; S. Murata and H. Tomioka, *Chem. Lett.*, 1992, 57.
14 D. L. Boger and S. N. Weinreb, in *Hetero Diels–Alder Methodology in Organic synthesis*, Academic Press, New York, 1987, pp. 71–93.
15 P. Sépulcri, J. C. Hallé, R. Goumont, D. Riou and F. Terrier, unpublished results.

Communication 9/02170A

ChemComm

Direct NMR and luminescence observation of water exchange at cationic ytterbium and europium centres

Andrei S. Batsanov, Andrew Beeby, James I. Bruce, Judith A. K. Howard, Alan M. Kenwright and David Parker*

Department of Chemistry, University of Durham, South Road, Durham, UK DH1 3LE

Received (in Cambridge, UK) 22nd March 1999, Accepted 20th April 1999

Cationic chiral Yb and Eu tetra-amide complexes, have been studied by VT NMR, luminescence and crystallography: the rate of dissociation of water is about 500 times faster at Yb than at the square antiprismatic Eu centre.

Dissociative water exchange at lanthanide ion centres has traditionally been considered to be fast, with rates of oxygen exchange of the order of 5×10^6 s^{-1} at 298 K for related nine-coordinate anionic complexes.[1] This rate is much slower for neutral[2] and cationic complexes[3] and mean water exchange rates of 5×10^4 s^{-1} occur for cationic tetra-amide complexes of gadolinium. With the europium complexes of the achiral ligands **1**–**3**, two major diastereoisomeric species exist in

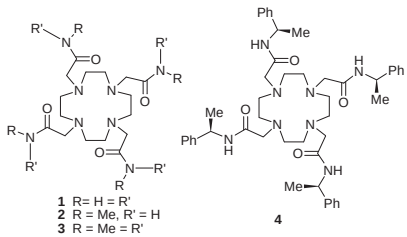

solution which interconvert by cooperative arm rotation (Δ/Λ conversion) and ring inversion (δ/λ exchange). For the corresponding complexes of the enantiopure ligand **4**, arm rotation is sterically inhibited and CD and NMR studies reveal that in D_2O and CD_3OD the complex exists as a single species, with average C_4 symmetry (⩾98%). Given that the rate of water exchange has now been shown to be markedly different for two isomers of the same complex[4] (twisted square antiprismatic *vs.* square-antiprismatic, Scheme 1), we set out to examine complexes[5] of the same ligand with Eu and Yb, which exist as different, single isomeric species in solution.

The solution and solid-state structures of [Eu.**4**]$^{3+}$$(CF_3SO_3)_3$ revealed[5] a square-antiprismatic geometry about the metal centre: an (*R*) configuration at the carbon stereocentre gave rise to a left-handed (Λ) helicity with a δ configuration in each of the NCCN chelate rings. At −40 °C in CD_3CN, a resonance due to a bound water molecule was observed at δ +84.3 for [Eu.**4**]$(CF_3SO_3)_3$ (250 MHz, 10 mM complex, 80 mM H_2O) which moved to lower frequency and broadened at higher temperatures. The bound water signal could still be observed (δ_H = 60, $\omega_{1/2}$ = 750 Hz) at 295 K, while the signal for unbound water (δ *ca.* +2.5) broadened further as the temperature was raised, reaching a coalescence around 328 K,

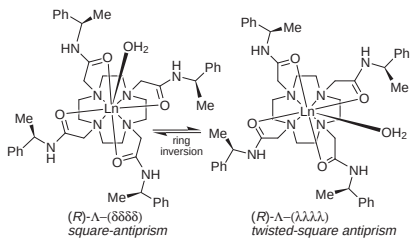

Scheme 1

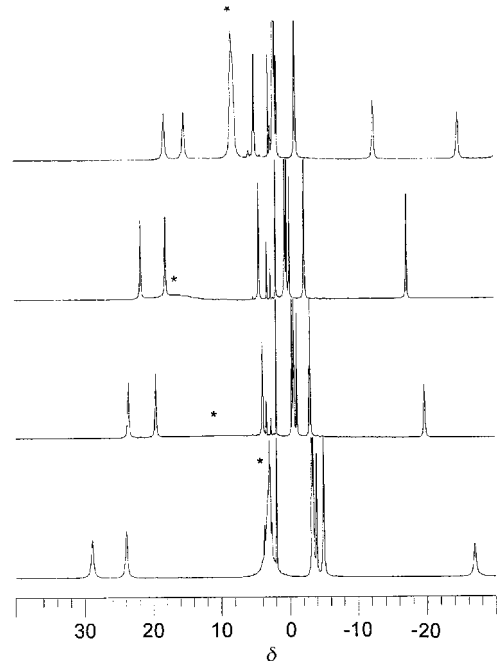

Fig. 1 Variable temperature 1H NMR spectra of [Yb.**4**(H_2O)][$CF_3SO_3)_3$ in CD_3CN (10 mM complex, 80 mM H_2O, 300 MHz) at 345, 293, 273 and 233 K, highlighting water exchange (H_2O = *).

before sharpening again at temperatures in excess of 330 K. Variable temperature saturation transfer experiments at 400 MHz, allowed the rate of water exchange in the range 260–280 K to be measured. Standard ln *k vs.* 1/*T* analysis revealed that the rate at 298 K was 3600 ± 800 s^{-1}, with $\Delta G^{\ddagger}$ = 50.3 ± 2.7 kJ mol^{-1}.

For [Yb.**4**][$CF_3(SO_3)_3$], ^{1}H NMR analysis (293 K, CD_3OD, 65.3 and 300 MHz) gave shifts for the ring axial protons of δ 108.0 and −35.5 (δ 20.5/16.8 for the related 'equatorial' pair). Proton NMR chemical shifts for Yb complexes are determined primarily by the dipolar contribution and the observed shift values for the (12)ane[N_4] ring protons are entirely consistent with those obtained for tetraphosphinate complexes of 1,4,7,10-tetraazacyclododecane,[6] which exist in solution only as a *twisted* square-antiprismatic isomer (Scheme 1). The ^{1}H NMR spectra recorded in CD_3CN at −40 °C, ([Yb.**4**] = 10 mM, $[H_2O]_{tot}$ = 90 mM, 65.3 MHz) revealed a broad resonance (2H, $\omega_{1/2}$ ≈ 2800 Hz) at δ 325 consistent with an Yb-bound water molecule. On raising the temperature to 238 K, this signal broadened further ($\omega_{1/2}$ ≈ 4000 Hz) and above 240 K, the resonance was too broad to be observed. The 'unbound' water signal resonated as a relatively sharp signal at temperatures in excess of 300 K. On lowering the temperature it broadened and shifted to higher frequency, with maximal line-broadening and positive shift (δ_{H_2O} 26) around 260 K (65.6 MHz), before the signal sharpened again and resonated at δ 6 at 233 K (slow-exchange limit). An independent VT NMR study at 300 MHz (Fig. 1) gave maximal exchange-broadening and positive shift

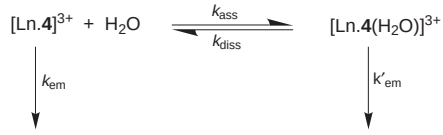

Scheme 2

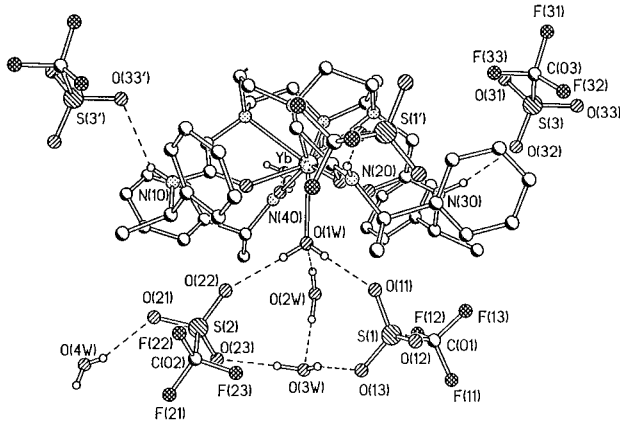

Fig. 2 View of the molecular structure of (*R*)-Λ-[Yb.**4**(H_2O)](CF_3SO_3)$_3$·3H_2O at 120 K, showing the hydrogen bonding of the inner and second sphere water molecules.

for the water signal at 283 K. Line-shape analysis for the water signal in the temperature range 293–343 K correcting for the predominant dipolar T^{-2} dependence of the chemical shift,[7] allowed the rate of water proton exchange to be measured ($\Delta\nu$ = 9.6 × 10^4 Hz at 233 K, 6.2 × 10^4 Hz at 283 K; $p^{Yb}_{H_2O}$ = 0.11, $p^{free}_{H_2O}$ = 0.89). At 298 K, the forward rate of association (Scheme 2) was 2.5 × 10^5 s^{-1}, and the rate of dissociation from ytterbium was 1.9 ± 0.7 × 10^6 s^{-1} with a free energy of activation of 34.6 ± 2.6 kJ mol^{-1}.

A single crystal X-ray diffraction analysis of (*R*)-[Yb.**4**(H_2O)]CF_3SO_3·3H_2O at 120 K revealed a nine-coordinate complex (Fig. 2)[8] with ligand Yb–N and Yb–O distances averaging 2.62 and 2.28 Å, some 0.08 Å longer than in the related europium complex.[4] The Yb–OH_2 distance of 2.44 Å was 0.01 Å longer than in the Eu analogue, but is similar to the only other Yb–water bond length reported for a nine-coordinate species.[10] The N–C–C–N and N–C–C–O torsional angles averaged +59.0 and −28.9°, consistent with a Λ(δδδδ) configuration. The twist of the N_4/O_4 planes about the C_4 axis was −39.7°, typical of a *regular* square-antiprismatic geometry at the metal centre. The selective crystallisation from water of this *minor* solution isomer at 293 K may seem surprising, but related square-antiprismatic complexes also crystallise preferentially.[9]

Luminescence from the $^2F_{5/2}$ and ^5D_o excited states of the Yb and Eu ions occurs on the micro- and milli-second timescale, respectively. The slowness of water exchange suggested that measurements of the rate constant for decay of the luminescent lanthanide excited state might allow simultaneous observation of decay from the shorter-lived nine-coordinate (Ln·OH_2) species (in which vibrational quenching to OH oscillators occurs) and from the eight-coordinate lanthanide species. The rate constant for decay of Yb luminescence in [Yb.**4**]$^{3+}$ was 1.6 × 10^5 s^{-1} at 295 K in D_2O, and a single exponential decay curve was observed. In H_2O, k_{obs} = 1.4 × 10^6 s^{-1} at 295 K, but bi-exponential decay was apparent at temperatures below 280 K. In D_2O there are no OH (or NH) oscillators available to quench the luminescence and a single exponential decay is observed: in H_2O the faster decay may be ascribed to the nine-coordinate monohydrated species, while the slower process occurs from the short-lived eight-coordinate intermediate. The rate of decay of europium emission from [Eu.**4**]$^{3+}$ was characterised by a single exponential decay profile, both in water (k_{H_2O} = 1.72 × 10^3 s^{-1}) and in dry acetonitrile (k_{MeCN} = 0.76 × 10^3 s^{-1} 293 K). The observed mono-exponential decay rate in MeCN increased as a function of added water and from a titration measuring k_{obs} as a function of added water concentration, the equilibrium constant for dissociation of water from the hydrated species was assessed to be K_d = 42 ±5 mM (298 K). Between −40 and 0 °C the rate of water exchange was sufficiently slow that independent (bi-exponential) decay was observed from the eight- and nine-coordinate species, under conditions where sufficient H_2O had been added to allow each species to be significantly populated. The proportion of the shorter-lived component (*i.e.* the species with water bound to Eu) in the bi-exponential decay increased as the temperature was lowered.

Taken together, this information is consistent with rate-limiting dissociative water exchange which occurs *ca.* 500 times faster at ambient temperature at Yb, in a twisted square-antiprismatic isomer, than at Eu in the related square-antiprismatic complex. The experiments also suggest that water (proton) exchange may be amenable to analysis by variable temperature luminescence measurements.

We thank EPSRC for support, and the Royal Society for a Leverhulme Trust Senior Research Fellowship (D. P.).

Notes and references

1 D. H. Powell, O. M. Ni Dhubhghaill, D. Pubanz, L. Helm, Y. S. Lebedev, W. Schlaepfer and A. E. Merbach, *J. Am. Chem. Soc.*, 1996, **118**, 9333.

2 G. Gonzàles, D. H. Powell, V. Tissierès and A. E. Merbach, *Inorg. Chem.*, 1994, **32**, 3844; D. Pubanz, G. Gonzalez, D. H. Powell and A. E. Merbach, *Inorg. Chem.*, 1995, **34**, 4457.

3 S. Aime, A. Barge, M. Botta, A. S. de Sousa and D. Parker, *J. Am. Chem. Soc.*, 1997, **119**, 4767.

4 R. S. Dickins, J. A. K. Howard, C. L. Maupin, J. M. Moloney, D. Parker, J. P. Riehl, G. Siligardi and J. A. G. Williams, *Chem. Eur. J.*, 1999, **5**, 1095.

5 S. Aime, A. Barge, M. Botta, A. S. De Sousa and D. Parker, *Angew. Chem. Int., Ed.*, 1998, **37**, 2673.

6 S. Aime, A. S. Batsanov, M. Botta, R. S. Dickins, S. Faulkner, C. E. Foster, A. Harrison, J. A. K. Howard, J. M. Moloney, T. J. Norman, D. Parker, L. Royle and J. A. G. Williams, *J. Chem. Soc., Dalton Trans.*, 1997, 3623.

7 The T^{-2} temperature dependence of the chemical shift of the bound water resonance (2.9 Å from Yb) is an approximation, as it assumes that the contact shift (varying as T^{-1}) is not significant. Earlier work has shown that a T^{-2} dependence represents a good approximation (valid to ±10%) for the dipolar term: B. McGarvey, *J. Magn. Reson.*, 1979, **33**, 445 and references therein. The most shifted axial ring proton (3.5 Å from the Yb centre), resonating at δ 108 at 293 K (CD_3OD), showed a T^{-2} dependence of its chemical shift.

8 Crystal data for $C_{46}H_{66}N_8O_5Yb(CF_3SO_3)_3.3H_2O$: M = 1509.29, monoclinic, space group $P2_1$; a = 14.390(1), b = 11.928(1), c = 19.300(1) Å; β = 102.67°, U = 3232.1(4) Å^3, D_c = 1.551 g cm^{-3}, λ(Mo-Kα) = 0.71073 Å, Z = 2, μ = 1.640 mm^{-1}. Data were collected on a SMART at 120(2) K. Refinement of 999 parameters by full matrix least squares on F^2 (SHELX96) converged at R = 0.021, wR_2 = 0.051 for 16442 observed reflections with $I > 2\sigma(I)$. The disordered phenyl ring in the structure was isotropically refined with two sets of partially occupied atoms. CCDC 182/1231. See http://www.rsc.org/suppdata/cc/1999/1011/ for crystallographic files in .cif format.

9 M. Woods, J. A. K. Howard, A. M. Kenwright, J. M. Moloney, D. Parker, M. Navet and O. Rousseau, *Chem. Commun.*, 1998, 1381.

10 I. N. Polyakova, T. A. Senina, T. N. Polynova and M. A. Porai-Koshits, *Koord. Khim.*, 1983, **9**, 1131: Yb–OH_2 = 2.41 Å.

Communication 9/02260K

ChemComm

Synthesis and luminescence behaviour of mixed-metal rhenium(I)–copper(I) and –silver(I) alkynyl complexes. X-Ray crystal structures of $[\{\eta^2\text{-Re(CO)}_3\text{(bpy)(C}\equiv\text{CPh)}\}_2\text{Cu}]\text{PF}_6$ and $[\{\eta^2\text{-Re(CO)}_3\text{(bpy)(C}\equiv\text{CPh)}\}_2\text{Ag}]\text{PF}_6$

Vivian Wing-Wah Yam,* Samuel Hung-Fai Chong, Keith Man-Chung Wong and Kung-Kai Cheung

Department of Chemistry, The University of Hong Kong, Pokfulam Road, Hong Kong SAR, People's Republic of China. E-mail: wwyam@hkucc.hku.hk

Received (in Cambridge, UK) 22nd March 1999, Accepted 28th April 1999

Two mixed-metal rhenium(I)–copper(I) and –silver(I) alkynyl complexes, $[\{\eta^2\text{-Re(CO)}_3\text{(bpy)(C}\equiv\text{CPh)}\}_2\text{Cu}]\text{PF}_6$ 1 and $[\{\eta^2\text{-Re(CO)}_3\text{(bpy)(C}\equiv\text{CPh)}\}_2\text{Ag}]\text{PF}_6$ 2, have been synthesized and shown to exhibit rich luminescence behaviour; the X-ray crystal structures of both complexes have also been determined.

There has been a rapidly growing interest in the chemical and physical properties of η^2-alkynyl-coordinated complexes.[1,2] Organometallic substituted alkynes $L_nMC{\equiv}CR$[3] exhibit a rich coordination chemistry with copper(I), silver(I) and gold(I) ions.[2] To the best of our knowledge, luminescence studies of π-bonded alkynyl complexes are rare[2f] despite numerous works on the luminescence behaviour of the σ-bonded counterparts have been reported.[4] With the recent reports on the successful isolation of acetylide-bridged rhenium(I) organometallics[1a,2b,e,5] and our recent efforts in incorporating metal-to-ligand charge transfer (MLCT) excited states into rhenium(I) acetylide units to make luminescent rigid-rod materials,[4d,6] we have extended our interest to utilize the luminescent alkynyl rhenium(I) complex, $\text{Re(CO)}_3\text{(bpy)(C}\equiv\text{CPh)}$, to function as an η^2-ligand towards Cu^{I} and Ag^{I}. Herein are reported the synthesis, structure and luminescence behaviour of two mixed-metal rhenium(I)–copper(I) and –silver(I) alkynyl complexes, $[\{\eta^2\text{-Re(CO)}_3\text{(bpy)(C}\equiv\text{CPh)}\}_2\text{Cu}]\text{PF}_6$ **1** and $[\{\eta^2\text{-Re(CO)}_3\text{(bpy)(C}\equiv\text{CPh)}\}_2\text{Ag}]\text{PF}_6$ **2**.

Reaction of $\text{Re(CO)}_3\text{(bpy)(C}\equiv\text{CPh)}$[6c] and $[\text{Cu(MeCN)}_4]\text{PF}_6$ in THF at room temperature in an inert atmosphere of nitrogen for 0.5 h afforded $[\{\eta^2\text{-Re(CO)}_3\text{(bpy)(C}\equiv\text{CPh)}\}_2\text{Cu}]\text{PF}_6$ **1**, which was isolated as yellow crystals after recrystallization from dichloromethane–*n*-hexane. Similarly, reaction of $\text{Re(CO)}_3\text{(bpy)(C}\equiv\text{CPh)}$ and $[\text{Ag(MeCN)}_4]\text{PF}_6$ in THF under similar conditions afforded $[\{\eta^2\text{-Re(CO)}_3\text{(bpy)(C}\equiv\text{CPh)}\}_2\text{Ag}]\text{PF}_6$ **2** as yellow crystals. The identities of both have been confirmed by satisfactory ^{1}H NMR spectroscopy, IR, positive ESI-MS, elemental analyses,† and X-ray crystallography.‡

Figs. 1 and 2 depict perspective drawings of the complex cations of **1** and **2**, respectively, with atomic numbering. The C≡C bond lengths are in the range 1.20(1)–1.23(1) Å in **1** and 1.199(8)–1.203(8) Å in **2**, which are slightly longer than that of their precursor complex $[\text{Re(CO)}_3\text{(bpy)(C}\equiv\text{CPh)}]$ of 1.199(9) Å.[6c] The bend-back angles (C–C–R) at the coordinated triple bond are 13.1(9)–18.2(9)° in **1** and 13.1(6)–14.4(6)° in **2** which are also larger than that of their precursor complex $[\text{Re(CO)}_3\text{(bpy)(C}\equiv\text{CPh)}]$ of 3.7(7)°.[6c] The interplanar angles between the MC≡C planes are 98.7 and 96.0° in the two independent molecules of **1** which is close to the expected 90° for a tetrahedrally coordinated Cu^{I} atom, and 149.0° in **2**. In addition, the bond weakening observed by IR spectroscopy of the C≡C triple bonds in **1** and **2** relative to the precursor complex (2083 cm^{-1}) further supports the π coordination mode of the alkynyl group to the d^{10} metal centres.

The electronic absorption spectra of **1** and **2** both show an intense absorption band at *ca.* 396 nm in dichloromethane solution. With reference to previous spectroscopic work on rhenium(I) diimine systems,[4d,6,7] the intense low energy absorption in the visible region is tentatively assigned as the $d_\pi(\text{Re}) \rightarrow \pi^*(\text{bpy})$ MLCT transition. The observation of the

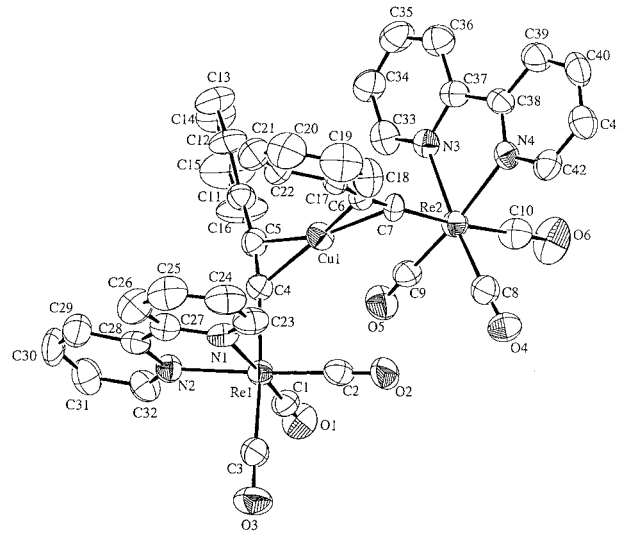

Fig. 1 Perspective drawing of the complex cation of **1** with atomic numbering. Hydrogen atoms have been omitted for clarity. Thermal ellipsoids were shown at the 40% probability level. Selected bond distances (Å) and bond angles (°): Re(1)–C(4) 2.139(8), C(11)–C(5) 1.46(1), C(4)–C(5) 1.23(1), C(4)–Cu(1) 1.997(8), C(5)–Cu(1) 2.093(8), C(6)–Cu(1) 2.076(8), C(7)–Cu(1) 2.004(7), C(6)–C(7) 1.20(1), C(17)–C(6) 1.47(1), Re(2)–C(7) 2.143(8), C(5)–C(4)–Re(1) 171.3(7), C(4)–C(5)–C(11) 166.9(9), C(6)–C(7)–Re(2) 178.4(7), C(7)–C(6)–C(17) 164.9(8).

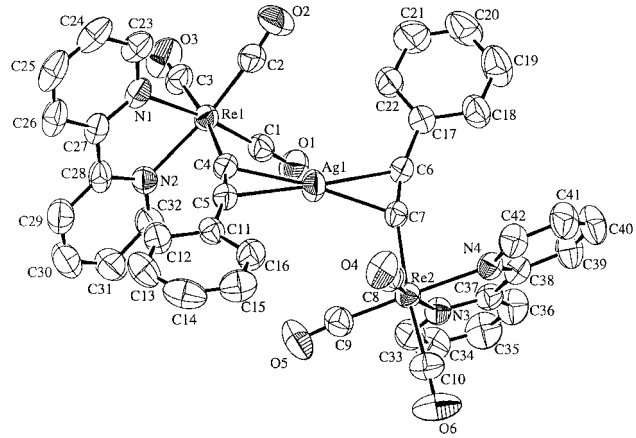

Fig. 2 Perspective drawing of the complex cation of **2** with atomic numbering. Hydrogen atoms have been omitted for clarity. Thermal ellipsoids were shown at the 40% probability level. Selected bond distances (Å) and bond angles (°): Re(1)–C(4) 2.159(6), C(11)–C(5) 1.444(8), C(4)–C(5) 1.203(8), C(4)–Ag(1) 2.257(6), C(5)–Ag(1) 2.378(6), C(6)–Ag(1) 2.382(6), C(7)–Ag(1) 2.244(6), C(6)–C(7) 1.199(8), C(17)–C(6) 1.477(8), Re(2)–C(7) 2.138(6), C(5)–C(4)–Re(1) 166.2(5), C(4)–C(5)–C(11) 166.9(6), C(6)–C(7)–Re(2) 165.9(5), C(7)–C(6)–C(17) 165.6(6).

MLCT absorption band at higher energy than that found in the related $Re(CO)_3(bpy)(C{\equiv}CPh)$ precursor, which absorbs at *ca.* 420 nm in dichloromethane, is supportive of a lower-lying $d_\pi(Re)$ orbital in **1** and **2**, resulted from the weaker π-donating ability of the acetylide ligand upon π-coordination to the d^{10} metal ions.

Excitation of **1** and **2** both in the solid state and in fluid solutions resulted in orange luminescence,† with emission lifetimes of 0.18 and 0.16 μs in dichloromethane solutions, respectively, which are attributed to the ^{3}MLCT phosphorescence. Similar to the absorption studies, the close resemblance of the MLCT emission energies of **1** and **2** is suggestive of the similar σ- and π-donating properties of the acetylide ligand upon coordination to Cu^I and Ag^I. It is also interesting that both **1** and **2** emit at higher energies than their precursor complex, *i.e.* the emission energies in CH_2Cl_2 follow the order: **1** (590 nm) ≅ **2** (600 nm) > $Re(CO)_3(bpy)(C{\equiv}CPh)$ (654 nm).[6c] The observation of a blue shift in emission energies on going from $Re(CO)_3(bpy)(C{\equiv}CPh)$ to **1** and **2** is in line with the assignment of a ^{3}MLCT [$d_\pi(Re) \rightarrow \pi^*(bpy)$] origin and disfavours the assignment of a ^{3}MLCT [$d_\pi(Re) \rightarrow \pi^*(C{\equiv}CPh)$] origin. Such a trend can be rationalized by the fact that the acetylide ligand would become a poorer electron donor upon coordination to Cu^I or Ag^I, and as a result, the energy of the Re d_π orbitals would be lowered, leading to a higher ^{3}MLCT emission energy.

V. W.-W. Y. acknowledges financial support from The University of Hong Kong, S. H.-F. C. the receipt of a postgraduate studentship, administered by The University of Hong Kong, and K. M.-C. W. the receipt of a research associateship supported by the Vice-Chancellor's Development Fund of The University of Hong Kong.

Notes and references

† **1**: ^{1}H NMR (300 MHz, acetone-d_6, 298 K, relative to $SiMe_4$): δ 6.80 (d, 2H, *J* 7.5 Hz, aryl H *meta* to ethynyl group), 7.15 (m, 3H, aryl H *ortho* and *para* to ethynyl group), 7.70 (t, 2H, *J* 7.2 Hz, bpy H), 8.30 (t, 2H, *J* 7.8 Hz, bpy H), 8.60 (d, 2H, *J* 8.2 Hz, bpy H), 9.15 (d, 2H, *J* 5.3 Hz, bpy H). IR (Nujol mull, cm^{-1}): 2029, 1999, 1932, 1911 ν(C≡O, C≡C). Positive ESI-MS: ion cluster at *m/z* 1119 $\{M\}^+$. UV–VIS [λ/nm (ε/dm^3 mol^{-1} cm^{-1})]: CH_2Cl_2, 246(28160), 288(29000), 396(6050). Emission [λ/nm (τ_o/μs)]: CH_2Cl_2 (298 K), 590 (0.18); solid (298 K), 550 (0.35); solid (77 K), 540; EtOH–MeOH glass (4 : 1 v/v) (77 K), 555. Found: C, 39.07, H, 2.07, N, 4.29. Calc. for **1**·0.5CH_2Cl_2: C, 39.17; H, 1.94, N, 4.31%. **2**: ^{1}H NMR (300 MHz, acetone-d_6, 298 K, relative to $SiMe_4$): δ 6.80 (d, 2H, *J* 7.2 Hz, aryl H *meta* to ethynyl group), 7.10 (m, 3H, aryl H *ortho* and *para* to ethynyl group), 7.60 (t, 2H, *J* 6.5 Hz, bpy H), 8.20 (t, 2H, *J* 7.4 Hz, bpy H), 8.55 (d, 2H, *J* 8.1 Hz, bpy H), 9.0 (d, 2H, *J* 5.5 Hz, bpy H). IR (Nujol mull, cm^{-1}): 2033, 2006, 1921, 1888 ν(C≡O, C≡C). Positive ESI-MS: ion cluster at *m/z* 1163 $\{M\}^+$. UV–VIS [λ/nm (ε/dm^3 mol^{-1} cm^{-1})]: CH_2Cl_2, 250(26890), 292(28240), 396(5930). Emission [λ/nm (τ_o/μs)]: CH_2Cl_2 (298 K), 600 (0.16); solid (298 K), 535 (< 0.1); solid (77 K), 533; EtOH–MeOH glass (4 : 1 v/v) (77 K), 540. Found: C, 38.53, H, 1.99, N, 4.28. Calc. for **2**: C, 38.44, H, 1.87, N, 4.26%.

‡ *Crystal data* for **1**: $[(C_{42}H_{26}N_4O_6CuRe_2)^+PF_6^-{\cdot}CH_2Cl_2]$, M = 1348.55, triclinic, space group $P\bar{1}$ (no. 2), a = 10.806(1), b = 17.408(2), c = 25.199(2) Å, α = 81.432(7), β = 82.688(7), γ = 88.139(7)°, V = 4648(1) $Å^3$, Z = 4, D_c = 1.927 g cm^{-3}, μ(Mo-Kα) = 58.74 cm^{-1}, F(000) = 2576, T = 301 K. One crystallographic asymmetric unit consists of two independent formula units. Convergence for 1111 variable parameters by least-squares refinement on F with $w = 4F_o^2/\sigma^2(F_o^2)$, where $\sigma^2(F_o^2) = [\sigma^2(I) + (0.036F_o^2)^2]$ for 10761 reflections with $I > 3\sigma(I)$ was reached at R = 0.032 and wR = 0.045 with a goodness-of-fit of 1.46. The F atoms in both PF_6 counter ions were refined isotropically.

For **2**: $[(C_{42}H_{26}N_4O_6AgRe_2)^+PF_6^-{\cdot}(CH_3)_2CO]$, M = 1366.02, triclinic, space group $P\bar{1}$ (no. 2), a = 11.485(1), b = 13.368(1), c = 17.259(1) Å, α = 102.048(6), β = 107.155(6), γ = 103.476(6)°, V = 2549.8(10) $Å^3$, Z = 2, D_c = 1.931 g cm^{-3}, μ(Mo-Kα) = 56.63 cm^{-1}, F(000) = 1304, T = 301 K. Convergence for 575 variable parameters by least-squares refinement on F with $w = 4F_o^2/\sigma^2(F_o^2)$, where $\sigma^2(F_o^2) = [\sigma^2(I) + (0.024F_o^2)^2]$ for 5957 reflections with $I > 3\sigma(I)$ was reached at R = 0.026 and wR = 0.034 with a goodness-of-fit of 1.33.

CCDC 182/1239. See http://www.rsc.org/suppdata/cc/1999/1013/ for crystallographic files in .cif format.

1 (*a*) T. Weidmann, V. Weinrich, B. Wagner, C. Robl and W. Beck, *Chem. Ber*., 1991, **124**, 1363; (*b*) H. Werner, P. Bachmann, M. Laubender and O. Gevert, *Eur. J. Inorg. Chem*., 1998, 1217; (*c*) V. Varga, J. Hiller, U. Thewalt, M. Polasek and K. Mach, *J. Organomet. Chem*., 1998, **553**, 15; (*d*) B. E. Woodworth, P. S. White and J. L. Templeton, *J. Am. Chem. Soc*., 1998, **120**, 9028.

2 (*a*) O. M. Abu Salah and M. I. Bruce, *J. Chem. Soc., Dalton Trans*., 1974, 2302; (*b*) H. Lang, K. Kohler and S. Blau, *Coord. Chem. Rev*., 1995, **143**, 113; (*c*) Y. Zhu, O. Clot, M. O. Wolf and G. P. A. Yap, *J. Am. Chem. Soc*., 1998, **120**, 1812; (*d*) C. Muller, J. A. Whiteford and P. J. Stang, *J. Am. Chem. Soc*., 1998, **120**, 9827; (*e*) S. Mihan, K. Sunkel and W. Beck, *Chem. Eur. J*., 1999, **5**, 745; (*f*) V. W. W. Yam, W. K. M. Fung and K. K. Cheung, *Angew. Chem., Int. Ed. Engl*., 1996, **35**, 1100.

3 J. Manna, K. D. John and M. D. Hopkins, *Adv. Organomet. Chem*., 1995, **38**, 79.

4 (*a*) V. W. W. Yam, S. W. K. Choi and K. K. Cheung, *Organometallics*, 1996, **15**, 1734; (*b*) V. W. W. Yam, W. K. M. Fung and K. K. Cheung, *Chem. Commun*., 1997, 963; (*c*) V. W. W. Yam, W. K. M. Fung, K. M. C. Wong, V. C. Y. Lau and K. K. Cheung, *Chem. Commun*., 1998, 777; (*d*) V. W. W. Yam, K. K. W. Lo and K. M. C. Wong, *J. Organomet. Chem*., 1999, **578**, 3.

5 (*a*) J. Heidrich, M. Steimann, M. Appel and W. Beck, *Organometallics*, 1990, **9**, 1296; (*b*) U. H. F. Bunz, *Angew. Chem., Int. Ed. Engl*., 1996, **35**, 969; (*c*) S. B. Falloon, W. Weng, A. M. Arif and J. A. Gladysz, *Organometallics*, 1997, **16**, 2008.

6 (*a*) V. W. W. Yam, V. C. Y. Lau and K. K. Cheung, *Organometallics*, 1995, **14**, 2749; (*b*) V. W. W. Yam, V. C. Y. Lau and K. K. Cheung, *Organometallics*, 1996, **15**, 1740; (*c*) K. M. C. Wong, Ph.D Thesis, The University of Hong Kong, 1998; (*d*) V. W. W. Yam, S. H. F. Chong and K. K. Cheung, *Chem. Commun*., 1998, 2121.

7 (*a*) M. S. Wrighton and D. L. Morse, *J. Am. Chem. Soc*., 1974, **96**, 998; (*b*) G. Tapolsky, R. Duesing and T. J. Meyer, *Inorg. Chem*., 1990, **29**, 2285; (*c*) J. K. Hino, L. D. Ciana, W. J. Dressick and B. P. Sullivan, *Inorg. Chem*., 1992, **31**, 1072.

Communication 9/02273B

Synthesis and molecular structure of vanadium(III) dithiolate complexes: a new class of alkene polymerization catalysts

Zofia Janas,[a] Lucjan B. Jerzykiewicz,[a] Raymond L. Richards[b] and Piotr Sobota*[a]

[a] *Faculty of Chemistry, University of Wrocław, 14 F.Joliot-Curie, 50-383 Wrocław, Poland. E-mail: plas@wchuwr.uni.wroc.pl*

[b] *Nitrogen Fixation Laboratory, John Innes Centre, Norwich Research Park, Norwich, UK NR4 7UH*

Received (in Basel, Switzerland) 3rd February 1999, Accepted 24th April 1999

The synthesis and catalytic activity in ethylene polymerization of new vanadium complexes of 2,2′-oxydiethanethiolate [$O(CH_2CH_2S)_2^{2-}$] are described; the complexes [V(μ-DIPP)$_2${$O(CH_2CH_2S)_2$}Li(MeCN)$_2$] and [V(DIPP)-{$O(CH_2CH_2S)_2$}(py)] [DIPP = ($OC_6H_3Pr^i_2$-2,6)$^-$] have been structurally characterized.

The synthetic development of well defined single-site vanadium catalysts for alkene polymerization is of extremely high industrial importance[1,2] because such catalysts are able to produce high molecular weight polymers with narrow molecular weight distribution as well as α-olefin copolymers with high α-olefin incorporation.[3,4] A recent trend has been the incorporation of sulfur-containing ligands: *e.g.* (TBP)$TiCl_2$/MAO catalyst [TBP = 2,2′-thiobis(6-*tert*-butyl-4-methylphenoxide, MAO = methylaluminoxane] was ten-fold more effective in ethylene polymerization than are metallocenes catalysts.[5,6] Moreover, it is well known that vanadium-based enzyme *nitrogenase* in which vanadium is thought to be bound to sulfur-, oxygen- and nitrogen-donor ligands is able to convert acetylene into ethylene and ethane.[7] These aspects of vanadium catalysis prompted us to prepare novel vanadium compounds with thiolate ligands such as 2,2′-oxydiethanethiolate [$O(CH_2CH_2S)_2^{2-}$] and study their reactions with alkenes, particularly their potential as precursors of new ethylene polymerization catalysts.

Studies of the oxidation state of active vanadium catalysts for ethylene polymerization by different investigators has led to the proposal that V^{III} and V^{II} represent the important oxidation states in the ethylene polymerization process.[8,9] Herein we report the synthesis, structural characterization and catalytic activity of the vanadium(III) heterodinuclear complexes [V(μ-DIPP)$_2${$O(CH_2CH_2S)_2$}Li(L)$_2$] **1**, **2** and the mononuclear complex [V(DIPP){$O(CH_2CH_2S)_2$}(py)] **3** [DIPP = (OC_6H_3-Pr^i_2-2,6)$^-$, py = C_5H_5N; L = THF **1** or MeCN **2**].

Dark pink [V(μ-DIPP)$_2${$O(CH_2CH_2S)_2$}Li(THF)$_2$] **1** was prepared by reaction of [V(μ-DIPP)$_2$(DIPP)$_2$Li(THF)][10] with an excess of $O(CH_2CH_2SH)_2$ in a mixture of hexane–THF [eqn. (1)].

$$[V(\mu\text{-DIPP})_2(DIPP)_2Li(THF)] + O(CH_2CH_2SH)_2 + L \rightarrow [V(\mu\text{-DIPP})_2\{O(CH_2CH_2S)_2\}Li(L)_2] + 2DIPPH \quad (1)$$

L = THF **1** or MeCN **2**

Recrystallization of **1** from MeCN gave new X-ray quality red crystals of [V(μ-DIPP)$_2${$O(CH_2CH_2S)_2$}Li(MeCN)$_2$] **2** [eqn. (1)]. Addition of pyridine to toluene solutions of compounds **1** and **2** breaks up the heterodinuclear structures forming the monomeric species [V(DIPP){$O(CH_2CH_2S)_2$}(py)] **3** in 85% yield (eqn. (2)].

Complex **3** can be also prepared but in lower yield (53%), by reaction of [V(DIPP)$_3$(py)$_2$][11] with 1 equiv. of $O(CH_2CH_2SH)_2$ in toluene. The temperature independent (80–293 K) magnetic moments of 2.6 and 2.7 μ_B per vanadium atom in **2** and **3** respectively, are consistent with non-interacting d^2 centres.

$$[V(\mu\text{-DIPP})_2\{O(CH_2CH_2S)_2\}Li(THF)_2] + py \rightarrow [V\{O(CH_2CH_2S)_2\}(DIPP)_3(py)] + Li(DIPP) + 2THF \quad (2)$$

3

The crystal structure of the heterodinuclear complex **2** is shown in Fig. 1.† Complex **2** contains a five-coordinate V^{III} center adopting a slightly distorted trigonal bipyramidal geometry. Two sulfur atoms from the $O(CH_2CH_2S)_2^{2-}$ ligand and an aryloxide oxygen O(21) of DIPP occupy the equatorial positions. The second aryloxide oxygen O(11) and the ether oxygen O(1) from the $O(CH_2CH_2S)_2^{2-}$ group fill the axial sites. Both aryloxide oxygen atoms are engaged in the bridging interaction to Li, inducing distortion from the ideal trigonal bipyramidal geometry. A similar double-bridged V(μ-DIPP)$_2$Li unit is present in the starting material [V(μ-DIPP)$_2$(DIPP)$_2$-Li(THF)]. The average V–S(thiolate) distance in **2** is 2.290(4) Å, within the range expected for V–S single bonds and comparable to other vanadium(III) thiolato complexes.[12–15]

The X-ray analysis of **3** reveals a mononuclear complex [V(DIPP){$O(CH_2CH_2S)_2$}(py)] with slightly distorted trigonal-bipyramidal coordination around the vanadium centre (Fig. 2).† The V–S and V–O(aryloxide) bond distances in the equatorial plane [V–S 2.2970(9), 2.2987(8) Å; V–O 1.8619(13) Å] do not differ significantly from those found in complex **2**. The V–N

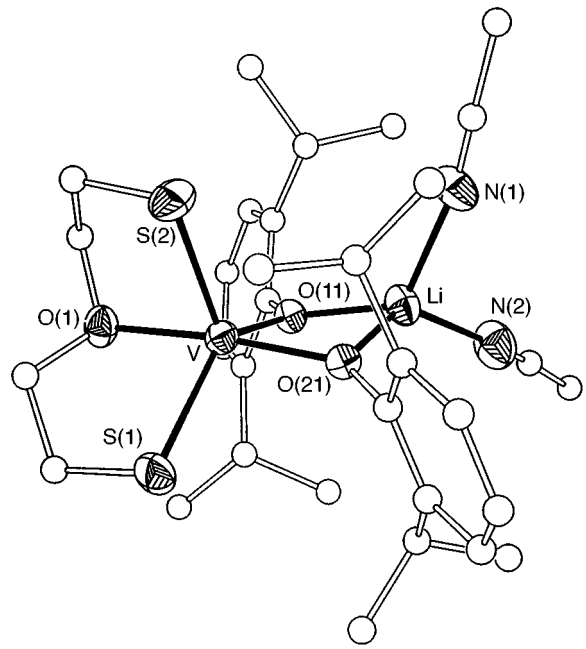

Fig. 1 The molecular structure of **2** (the displacement ellipsoids are drawn at the 30% probability level; the C bonded H atoms are excluded for clarity; the C atoms are represented by circles of arbitrary radii). Selected bond lengths (Å): V–S(1) 2.294(1), V–S(2) 2.286(2), V–O(1) 2.154(2), V–O(11) 1.917(2), V–O(21) 1.977(2), V–Li 2.830(5), Li–O(11) 1.942(6), Li(1)–O(21) 1.903(5), Li–N(1) 2.030(6), Li–N(2) 2.015(6).

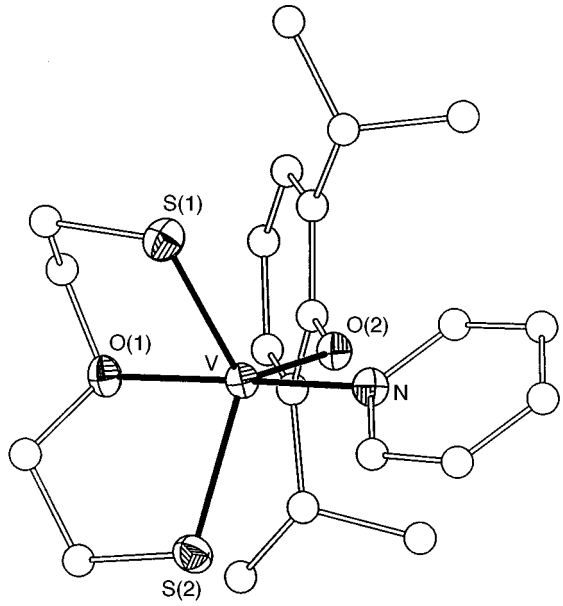

Fig. 2 The molecular structure of **3** (the displacement ellipsoids are drawn at the 30% probability level; the C bonded H atoms are excluded for clarity; the C atoms are represented by circles of arbitrary radii). Selected bond lengths (Å): V–S(1) 2.2970(9), V–S(2) 2.2987(8), V–O(1) 2.1195(14), V–O(2) 1.8619(13), V–N 2.1306(17).

Table 1 Polymerization[a] of ethylene with vanadium–$MgCl_2$–$AlEt_2Cl$ catalysts

Catalyst system	T/K	Productivity[b]/ kg(g V h)$^{-1}$	M_w/M_n	d/g cm^{-3}
1/$MgCl_2$/$AlEt_2Cl$	323	39	2.7	0.964
3/$MgCl_2$/$AlEt_2Cl$	323	20	3.8	0.961

[a] *Conditions:* $[V]_0$ = 0.02 mmol dm^{-3}, [Al] = 10 mmol dm^{-3}, Mg : V = 10, $P_{ethylene}$ = 0.6 MPa. [b] Mass in kg of polymer formed per g of vanadium atoms in 1 h.

distance is also near the values observed in the other V^{III}–pyridine complexes.[11]

Compounds **1** and **3**, in combination with $AlEt_2Cl$ and $MgCl_2$, are highly active towards ethylene polymerization.[16] Yields and polymer characterization data are listed in Table 1. The amount of polyethylene (PE) produced by the catalysts is comparable to the catalyst based on VCl_3.[17] The molecular weight distribution M_w/M_n of the PE obtained in the first catalytic system is < 3, and in the second one is > 3. These findings indicate that the polymerization process in **1**/$MgCl_2$/$AlEt_2Cl$ proceeds on a single vanadium site in a homogeneous system, however for **3**/$MgCl_2$/$AlEt_2Cl$ a heterogeneous system appears to operate. Hence, the catalytic activity of the **1**/$MgCl_2$/$AlEt_2Cl$ system is almost twice that of the **3**/$MgCl_2$/$AlEt_2Cl$ system.

To our knowledge complexes **1** and **3** represent the first examples of vanadium-thiolate catalyst precursors for ethylene polymerization. We suggest that the V{O(CH_2CH_2S)$_2$} moiety is maintained in the catalyst assembly and that the geometry of such catalytic species plays an important role in determining the reactivity. It is worth noting that vanadium catalysts are very important in ethylene–propylene rubber production.[18]

The authors thank the State Committee for Scientific Research for financial support of this work (Grant No. 3 T09A 131 15), and Dr Krzysztof Szczegot of the University of Opole for preliminary polymerization tests.

Notes and references

† *Crystal data for* **2** *and* **3**: The crystals were sealed in glass capillaries under a dinitrogen stream. Preliminary examination and data collections were carried out on a KUMA KM-4 four-circle diffractometer[19] using graphite-monochromated Mo-Kα radiation (0.71073 Å) with ω-2θ scan mode. The structures were solved by direct methods (SHELXS97)[20] and refined on F^2 by full-matrix least-squares (SHELXL97).[21] The carbon bonded H-atoms were included in calculated positions and refined using a riding model with isotropic displacement parameters equal to 1.2 U_{eq} of the attached C atom. *Crystal structure analyses*: **2**: $C_{32}H_{48}LiN_2O_3S_2V$, M = 630.72, monoclinic, space group $C2/c$, a = 27.297(5), b = 18.880(4), c = 17.444(3) Å, β = 126.76(3), U = 7203(2) Å^3, Z = 8, D_c = 1.163 Mg m^{-3}, μ = 0.422 mm^{-1}, F(000) = 2688. A total of 4086 reflections with $2\theta \leqslant 50°$ were collected, of which 3463 had $I \geqslant 2\sigma(I)$. Final residuals are R_1 = 0.0357, wR_2 = 0.1007 and GOF = 1.075 for 380 variables.

3: $C_{21}H_{30}NO_2S_2V$, M = 443.52, monoclinic, space group $P2_1/n$, a = 10.022(3), b = 12.156(4), c = 18.628(4) Å, β = 98.44(3)°, U = 2244.8(11) Å^3, Z = 4, D_c = 1.312, μ = 0.643 mm^{-1}, F(000) = 936. A total of 3526 reflections with $2\theta \leqslant 50°$ were collected, of which 3108 had $I \geqslant 2\sigma(I)$. Final residuals are R_1 = 0.0269, wR_2 = 0.0760 and GOF = 1.124 for 248 variables.

CCDC 182/1237. See http://www.rsc.org/suppdata/cc/1999/1015/ for crystallographic files in .cif format.

1 V. J. Murphy and H. Turner, *Organometallics*, 1997, **16**, 2495; F. J. Feher and J. F. Walzer, *Inorg. Chem.*, 1991, **30**, 1689; F. J. Feher, J. F. Walzer and R. L. Balnski, *J. Am. Chem. Soc.*, 1991, **113**, 3618; F. J. Feher and R. L. Balnski, *Organometallics*, 1993, **12**, 958; *J. Am. Chem. Soc.*, 1992, **114**, 5886.
2 S. Scheuer, J. Fischer and J. Kress, *Organometallics*, 1995, **14**, 2627.
3 W. L. Carrick, *J. Am. Chem. Soc.*, 1958, **80**, 6455; W. L. Carrick, R. W. Kluiber, E. F. Bonner, L. H. Wartman, F. M. Rugg and J. J. Smith, *J. Am. Chem. Soc.*, 1960, **82**, 3883; D. L. Christman, *J. Polym. Sci., Polym. Chem. Ed.*, 1972, **10**, 472; M. H. Lehr and C. J. Carmen, *Macromolecules*, 1969, **2**, 217; M. H. Lehr, *Macromolecules*, 1968, **1**, 178.
4 Y. Doi, N. Tokuhiro, M. Nunomura, H. Miyake and K. Soga, in *Transition Metals and Organometallics as Catalysts for Olefin Polymerization*, ed. W. Kaminsky and H. Sinn, Springer-Verlag, Berlin, 1998; V. E. Junghanns, V. A. Gumboldt and G. Bier, *Makromol. Chem.*, 1962, **58**, 18; V. A. Gumboldt, J. Helberg and G. Schleitzer, *Makromol. Chem.*, 1967, **101**, 229.
5 W. Kaminsky, *J. Chem. Soc., Dalton Trans.*, 1998, 1413; M. Bochmann, *J. Chem. Soc., Dalton Trans.*, 1996, 255.
6 T. Miyatake, K. Mizunuma and M. Kakugo, *Makromol. Chem., Macromol. Symp.*, 1993, **66**, 203; S. Fokken, T. P. Spaniol, H-C. Kang, W. Massa and J. Okuda, *Organometallics*, 1996, **15**, 5069.
7 See for example R. R. Eady and G. J. Leigh, *J. Chem. Soc., Dalton Trans.*, 1994, 2739 and refs. therein.
8 F. J. Karol, K. J. Cann and B. E. Wagner, in *Transition Metals and Organometallics as Catalysts for Olefin Polymerization*, ed. W. Kaminsky and H. Sinn, Springer, New York, 1988, pp. 149–161.
9 P. D. Smith, J. L Martin, J. C. Huffman, R. L Bansemer and K. G Caulton, *Inorg. Chem.*, 1985, **24**, 2997.
10 W. C. A. Wilisch, M. J. Scott and W. H. Armstrong, *Inorg. Chem.*, 1988, **27**, 4335.
11 S. Gambarotta, F. Van Bolhuis and M. Y. Chiang, *Inorg. Chem.*, 1987, **26**, 4303.
12 C. R. Randall and W. H. Armstrong, *J. Chem. Soc., Chem. Commun.*, 1988, 986.
13 S. C. Davies, D. L. Hughes, Z. Janas, L. B. Jerzykiewicz, R. L. Richards J. R. Sanders and P. Sobota, *Chem. Commun.*, 1997, 1261.
14 G. Henkel, B. Krebs and W. Schmidt, *Angew. Chem., Int. Ed. Engl.*, 1992, **31**, 1366.
15 R. W. Wiggins, J. C. Huffman and G. Christou, *J. Chem. Soc., Chem. Commun.*, 1983, 1313; D. Szeymies, B. Krebs and G. Henkel, *Angew. Chem., Int. Ed. Engl.*, 1983, **22**, 885; J. R. Dorfman and R. H. Holm, *Inorg. Chem.*, 1983, **22**, 3179.
16 In a typical test of ethylene homopolymerization the catalyst was prepared by milling a *n*-hexane slurry of [$MgCl_2$(THF)$_2$] with the vanadium compound and $AlEt_2Cl$ as the cocatalyst. In all cases studied an immediate exotherm indicated polymerization; reaction temperatures were kept at 323 K and pressure at 0.6 MPa. After 1 h the reactor was opened and the polymer was filtered off, washed with acidic methanol and water, and dried *in vacuo*.
17 K. J. Cann, D. L. Miles and F. J. Karol, *US. Pat.*, 4 670 526, 1987; X. Bai, *US Pat.*, 5 410 003, 1995.
18 F. J. Karol, *Macromol. Symp.*, 1996, **154**, 83.
19 Kuma Diffraction. Kuma KM4 software. User's Guide, version 6.1 Kuma Diffraction, Wrocław, Poland, 1996.
20 G. M. Sheldrick, *Acta Crystallogr., Sect. A*, 1990, 467.
21 G. M. Sheldrick, SHELXL97, Program for the Refinement of Crystal Structures, University of Göttingen, Germany, 1997.

Communication 9/00916G

Different fluoride anion sources and (trifluoromethyl)trimethylsilane: molecular structure of tris(dimethylamino)sulfonium bis(trifluoromethyl)trimethylsiliconate, the first isolated pentacoordinate silicon species with five Si–C bonds

Alexander Kolomeitsev,*[a] German Bissky,[b] Enno Lork,[b] Valery Movchun,[a] Eduard Rusanov,[a] Peer Kirsch[c] and Gerd-Volker Röschenthaler*[b]

[a] *Institute of Organic Chemistry, Ukrainian National Academy of Sciences, Murmanskaya 6, 253660 Kiev-94, Ukraine*

[b] *Institut für Anorganische und Physikalische Chemie, Universität Bremen, Leobener Strasse, D-28334 Bremen, Germany. E-mail: j18j@zfn.uni-bremen.de*

[c] *MERCK KGaA, Liquid Crystals Division, Frankfurter Strasse 250, Darmstadt 64293, Germany*

Received (in Cambridge, UK) 11th March 1999, Accepted 20th April 1999

(Trifluoromethyl)trimethylsilane, CF_3SiMe_3 reacts with $[(Me_2N)_3S]^+[Me_3SiF_2]^-$, Q^+F^- and $Q^+[HF_2]^-$ (Q^+ = Me_4N^+, $[(Me_2N)_3C]^+$, $[(Me_2N)_4P]^+$) at −70 to 50 °C to afford the first hypervalent silicon species, $[(CF_3)_2SiMe_3]^-$ with five Si–C bonds (stable in monoglyme up to −10 °C) as the main reactive species whose molecular structure was determined by X-ray crystallography.

One of the most useful reagents for anionic trifluoromethylation of different organic and organometallic electrophiles is (trifluoromethyl)trimethylsilane.[1,2] The instability of the corresponding lithium and magnesium counterparts (CF_3Li and CF_3MgX decompose even at −100 °C) and the reduced nucleophilicity of trifluoromethyl derivatives of zinc, cadmium and copper makes CF_3SiMe_3 indispensable in many cases.[3,4] For the generation of 'CF_3^-' in the presence of a catalytic[4] or stoichiometric[5] quantity of fluoride anion an intermediary hypervalent silicon species has not so far been found.[4,6a] This led to the conclusion[4] that the highly basic nature of the 'CF_3^-' anion together with the high propensity to eliminate α-fluoride renders the pentavalent CF_3 intermediate elusive. Investigation of the Me_3SiCF_3–$Me_4N^+F^-$ system in CD_3CN revealed Me_3SiF and CF_3D as the only reaction products.[4] Furthermore, if Me_3SiCF_3–$Me_4N^+F^-$ is reacted in MeCN the anion $[Me_3Si(CH_2CN)(F)]^-$ was found, but no CF_3 containing the hypervalent silicon derivative was found.[6b] It is noteworthy that the generation, structures and spectral properties and reactivities of fluorosiliconates $[R_nSiF_{5-n}]^-$ and $[R_nSiF_{6-n}]^{2-}$ (n = 1–3) have been extensively studied.[7] Despite the fact that fluorine directly bonded to hypervalent silicon has a stabilizing effect, no reports have appeared, to the best of our knowledge, describing their isolation and reliable characterization of $[(CF_3)_2SiF_3]^-$ and $[CF_3SiF_4]^-$ in the solid state.[8a] Lithium pentaphenylsiliconate was observed in solution at −80 °C.[8b] Investigation of species formed in the course of Me_3SiCF_3 interaction with fluoride ions is very important for designing selective high-yield trifluoromethylation procedures of synthetical and possible practical use.

Studying the Lewis acidic properties of $P(CF_3)_3$ we observed that a 1 : 2 : 1 mixture of $[(Me_2N)_3S]^+[Me_3SiF_2]^-$–$CF_3SiMe_3$–$P(CF_3)_3$ in THF yielded the stable acyclic phosphoranide, $[P(CF_3)_4]^-$ at −55 °C together with 5–10% $[P(CF_3)_3F]^-$ impurity.[9] However, if Me_4NF–CF_3SiMe_3(1 : 2–2.5), forming a clear solution at −60 °C in glyme was used and $P(CF_3)_3$ was added at −60 °C, analytically pure $[P(CF_3)_4]^-$ was obtained.[10] A trifluoromethylating species has been pre-generated, which we tried to elucidate by reacting CF_3SiMe_3 with a range of fluoride ion sources.

Here we report results obtained for CF_3SiMe_3 **1** reactions with $Q^+[Me_3SiF_2]^-$ **2a**,[11,12] Q^+F^-, **3b–d** and $Q^+HF_2^-$, **4b–d** [**a**: Q^+ = $(Me_2N)_3S^+$, **b**: Q^+ = Me_4N^+,[13] **c**: Q^+ = $[(Me_2N)_3C]^+$,[14] **d**: Q^+ = $[(Me_2N)_4P]^+$[15]).† When **1** was added to a suspension of **2a** or **3b–d** (2 : 1 ratio) in monoglyme at −50 °C or in THF at −78 °C, the solids were immediately dissolved to form a stable colourless solution of the siliconates, $Q^+[(CF_3)_2SiMe_3]^-$, **6a–d** in 95% yield (Scheme 1) with δ_F in the range −63.6 to −63.8, approximately 3.2–3.6 ppm downfield of the CF_3SiMe_3 resonance.‡§ After recrystallization of **6a** monitored by ^{19}F NMR spectroscopy only *one* species with δ_F −63.7 was present, namely $(Me_2N)_3S^+$ $[(CF_3)_2SiMe_3]^-$ **6a** the first isolated pentacoordinate silicon species having five Si–C binds, proven by single-crystal X-ray structural determination (Fig. 1).¶ The new compound is stable in the solid state upto 0 °C but decomposes exothermally at 0–5 °C with the formation of **2a**. The same reaction has been observed in monoglyme solution of **6b** at −30 °C with the quantitative formation of $Me_4N^+[F_2SiMe_3]^-$ **2b** proven by ^{19}F NMR and single-crystal X-ray diffraction.‖ The corresponding **6d** decomposes at −10–0 °C to give **2d**. Obviously, the size of the counter ion plays an important role in the thermal stability of $[(CF_3)_2SiMe_3]^-$.[8b] Expected reaction

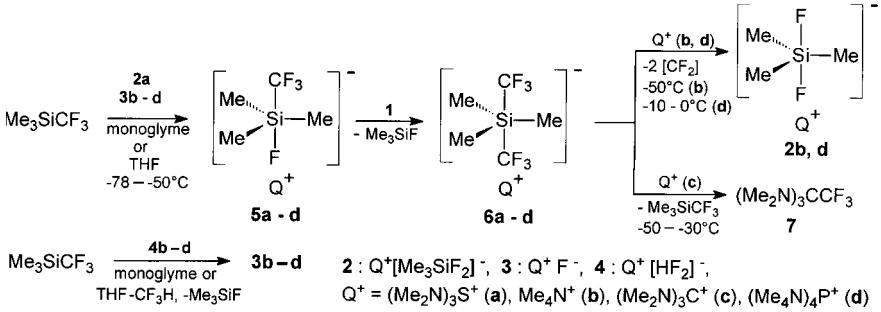

Scheme 1

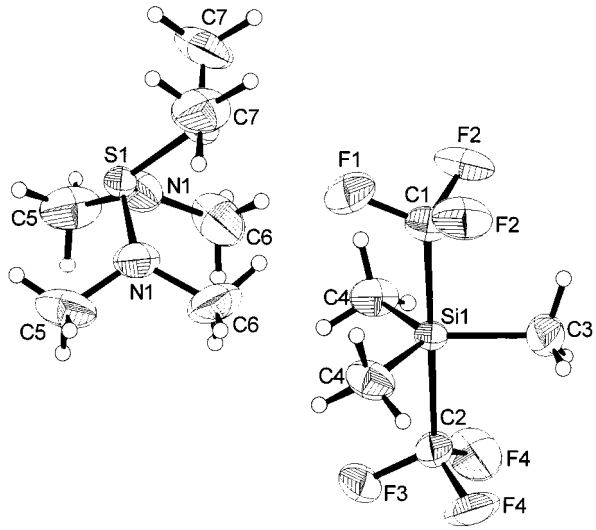

Fig. 1 Crystal structure of **6a** with thermal ellipsoids. Selected bond lengths (pm) and angles (°): Si(1)–C(1) 205.6(4), Si(1)–C(2) 206.2(4), Si(1)–C(3) 188.2(5), Si(1)–C(4) 188.6(3); C(3)–Si(1)–C(4) 120.85(12), C(3)–Si(1)–C(1) 91.0(2), C(3)–Si(1)–C(2) 89.6(2), C(1)–Si(1)–C(2) 179.40(19).

products[16] of difluorocarbene with monoglyme or THF were not detected. Addition of **1** to **3c** in THF at −80 °C afforded **6c** (δ_F −63.7) as the sole product, which upon warming to −50 °C gave slowly $(Me_2N)_3CCF_3$ **7** and **1** (Scheme 1), at −30 °C the formation of **7** proceeds much faster and was complete in 1 h along with gaseous Me_3SiF and CF_3H impurity.†† In the case of hydrogen difluorides and compound **1**, a 1 : 3 ratio has to be applied to convert **4b–d** at −80 °C into the fluorides **3b–d** under formation of CF_3H and Me_3SiF (Scheme 1) and subsequently **6b–d** are formed.

Probably the siliconates **5a–d** containing the $[(CF_3)Si(F)Me_3]^-$ anion were produced initially as intermediates releasing $[CF_3]^-$ to attack CF_3SiMe_3 yielding $[(CF_3)_2SiMe_3]^-$. So far, there is no direct spectroscopical observation of $[(CF_3)Si(F)Me_3]^-$, whereas the isoelectronic phosphorane, $(CF_3)P(F)Me_3$ could be isolated and fully characterized.[17]

The single crystal X-ray structure determination of **6a** showed almost ideal trigonal-bipyramidal geometry at silicon [C(1)–Si(1)–C(2) 179.40(19), C(3)–Si–C(1) 91.0(2) and C(3)–Si–C(4) 120.85(12)°] with a rather long[4] apical Si–C(1)F_3 bond [205.6(4)] and a considerably shorter equatorial Si–C(1)H_3 bond [188.2(5) pm] (*cf.* 187.4 pm in **2a**[12]). For the isoelectronic $(CF_3)_2PMe_3$ the same structure was found with shorter P–C distances[18] [P–CF_3 197.4(4) and P–CH_3 181.3(2) pm]. The geometry parameters of the cation $(Me_2N)_3S^+$ are similar to those investigated earlier.[12]

The use of the hypervalent trifluoromethylating silicon compounds for new carbon–carbon bond forming reactions and synthesis of trifluoromethylated phosphorus(v) derivatives is underway in our laboratories. The results of the study for CF_3SiF_3 and CF_3SiPh_3 interaction with the different fluoride anion sources including $(Et_2N)_3PF_2$ and Ph_3CF and reactions of $(Me_2N)_3CCF_3$ will be published in due course.

A. A. K. is grateful to the Deutsche Forschungsgemeinschaft for financial support. The generous gift of CF_3SiMe_3 by Bayer AG, Leverkusen (Germany) is gratefully acknowledged.

Notes and references

† All reactions were performed under nitrogen in carefully dried solvents. Compound **7** gave satisfactory elemental analysis. NMR spectra at 200.13 (^{1}H, TMS), 188.31 (^{19}F, $CClF_3$), 50.32 MHz (^{13}C, TMS) were recorded.

‡ *General procedure for* **6b–d**: to a solution of the corresponding fluoride **2a–d** (0.2 mmol) in monoglyme or THF (5 ml) has added 0.06 g (0.42 mmol) of **1**. The use of corresponding bifluorides gave the same products but the molar ratio of bifluoride to silane was 1 : 3 in this case. *Selected data for* **6b–d**: δ_F −63.67 (**6b**), −63.94 (**6c**), −63.82 (**6d**), −64.83 (**2b**), −64.75 (**2d**).

§ *Synthesis of* **6a**: to a solution of 0.41 g (1.49 mmol) **2a** in 5 ml monoglyme was condensed 0.45 g (3.13 mmol) **1** and the mixture stirred for 3 h at −55 °C, δ_F −64.04. Yield: 95%.

¶ *Crystal data* for **6a**: $C_{11}H_{27}F_6N_3SSi$, M = 375.51, monoclinic, space group $P2_1/m$, a = 769.8(2), b = 1132.1(2), c = 1135.6(2) Å, β 105.26(1)°, V = 0.9548(3) nm^3, Z = 2, D_c = 1.306 g cm^{-3}, λ(Mo-Kα) = 0.71073 Å. Siemens P4 m/v diffractometer, θ-2θ-scan type, 2.59 ⩽ θ ⩽ 24.99°, 173 K; 6512 reflections collected, 1775 independent reflections (R_{int} = 0.0672), full-matrix least-squares on F^2, goodness-of-fit (F^2) = 1.064, final R values [$I > 2\sigma(I)$]: $R1$ = 0.0476, $wR2$ = 0.1002, R values (all data): $R1$ = 0.0774, $wR2$ = 0·1157, extinction coefficient 0.0103(18), difference electron density: 0.264 and −0.244 e Å^3. CCDC 182/1232. See http://www.rsc.org/suppdata/cc/1999/1017/ for crystallographic files in .cif format.

‖ *Selected data* for **2b**: $\delta_F(CD_3CN, -30\ °C)$ −60.10; $\delta_H(CD_3CN, -30\ °C)$ −0.18 (s, Me_3Si), 3.10 (s, Me_4N^+). The geometry parameters, bond lengths and angles for the anion $[Me_3SiF_2]^-$ in **2b** are almost identical with those for **2a**[12] within the standard deviation.

†† *Selected data for* **7**: bp 166–170 °C (decomp.). δ_H 2.33 ($^5J_{FH}$ 1.23 Hz); δ_F −62.48; δ_C 127.35 (CF_3, $^1J_{CF}$ 305.6 Hz), 94.24 [$C(NMe_2)_3$], $^2J_{CF}$ 23.7 Hz), 39.36 (CH_3, $^4J_{CF}$ 2.3 Hz).

1 G. K. S. Prakash, R. Krishnamurti and G. A. Olah, *J. Am. Chem. Soc.*, 1989, **111**, 393.
2 I. Ruppert, K. K. Schlich and W. Volbach, *Tetrahedron Lett.*, 1984, **25**, 2195.
3 D. J. Burton and Z. Y. Yang, *Tetrahedron*, 1992, **48**, 189.
4 G. K. S. Prakash and A. K. Yudin, *Chem. Rev.*, 1997, **97**, 757.
5 (*a*) A. A. Kolomeitsev, V. N. Movchun and Yu. L. Yagupolskii, *Synthesis*, 1990, 1151; (*b*) A. A. Kolomeitsev, V. N. Movchun and Yu. L. Yagupolskii, W. Porwisiak and W. Dmowskii, *Tetrahedron Lett.*, 1992, **41**, 6191.
6 (*a*) C. R. J. P. Corriu, C. Reye and J. C. Young, *Chem. Rev.*, 1993, **93**, 1371; (*c*) R. Damrauer and J. A. Hankin, *Chem. Rev.*, 1995, **95**, 1145; (*b*) D. J. Adams, J. H. Clark, L. B. Hansen, V. C. Sanders and S. J. Tavener, *J. Fluorine Chem.*, 1998, **92**, 123.
7 (*a*) H. J. Frohn and V. V. Bardin, *J. Organomet. Chem.*, 1995, **501**, 155 and references cited therein; (*b*) A. S. Pilcher and P. DeShong, *J. Org. Chem.*, 1996, **61**, 6901.
8 (*a*) H. Beckers, H. Bürger and R. Eujen, *Z. Anorg. Allg. Chem.*, 1988, **563**, 39; (*b*) A. H. J. F. de Keijzer, F. J. J. de Kanter, M. Schakel, R. F. Schmitz and G. W. Klumpp, *Angew. Chem.*, 1996, **108**, 1183 and references therein.
9 Because of the high phosphorus affinity to fluorine, $[P(CF_3)_3F]^-$ even being treated with excess of Me_3SiCF_3 cannot be transformed quantitatively into $[P(CF_3)_4]^-$, *cf.* A. A. Kolomeitsev and G.-V. Röschenthaler, *12th ACS Winter Fluorine Conference*, St. Petersburg Beach, FL, USA, January 22–27, 1995, abstract 48.
10 A. A. Kolomeitsev, N. V. Pavlenko, A. B. Rozhenko, U. Dieckbreder, M. Görg and G.-V. Röschenthaler, *15th International Symposium on Fluorine Chemistry*, Vancouver, Canada, August 2–7, 1997, Abstract In (2) C-6.
11 W. J. Middleton, *US Pat.* N3, 940, 402, 1976.
12 D. A. Dixon, W. B. Farnham, W. Heilemann, R. Mews and M. Noltemeyer, *Heteroat. Chem.*, 1993, **4**, 287 and references therein.
13 A. A. Kolomeitsev, F. U. Seifert and G.-V. Röschenthaler, *J. Fluorine Chem.*, 1995, **71**, 47.
14 S. M. Igumnov, N. I. Delyagina and I. L. Knunyants, *Izv. Akad. Nauk SSSR, Ser. Khim.*, 1986, 1193 and references therein.
15 A. A. Kolomeitsev, N. V. Kirij, W. K. Appel, S. V. Pazenok, G.-V. Röschenthaler, *14th ACS Winter Fluorine Conference, St. Petersburg Beach*, January 17–22, 1999, abstract 37.
16 (*a*) R. Möckel, W. Tyrra and D. Naumann, *J. Fluorine Chem.*, 1995, **73**, 229 and references therein; (*b*) C.-M. Hu, F.-L. Qing and C.-X. Shen, *J. Chem. Soc., Perkin Trans. 1*, 1993, 335.
17 A. A. Kolomeitsev, Yu. L. Yagupolskij, A. Gentzsch, E. Lork and G.-V. Röschenthaler, *Phosphorus, Sulfur Silicon*, 1994, **92**, 179.
18 A. A. Kolomeitsev, U. Dieckbreder, M. Görg and G.-V. Röschenthaler, *Phosphorus Sulfur Silicon*, 1996, **109–110**, 597.

Communication 9/01953G

The isolated iron–molybdenum cofactor of nitrogenase binds carbon monoxide upon electrochemically accessing reduced states

Saad K. Ibrahim,[a] Kylie Vincent,[b] Carol A. Gormal,[a] Barry E. Smith,[a] Steven P. Best*[b] and Christopher J. Pickett*[a]

[a] *Nitrogen Fixation Laboratory, John Innes Centre, Norwich Research Park, Norwich, UK NR4 7UH. E-mail: chris.pickett@bbsrc.ac.uk*
[b] *School of Chemistry, University of Melbourne, Parkville, 3052 Victoria, Australia*

Received (in Cambridge, UK) 24th March 1999, Accepted 26th April 1999

The first spectroscopic evidence for the binding of a small gaseous molecule to the isolated iron molybdenum cofactor of nitrogenase (FeMoco) is presented: FTIR spectroelectrochemistry in a thin-layer cell shows that reduced FeMoco binds carbon monoxide and gives rise to ν(CO) stretches that are close to those observed during turnover of the enzyme.

The cofactor extract[1–3] in NMF was in the oxidised EPR-silent form, FeMoco^{ox}.† Cyclic voltammetry of FeMoco^{ox} at a vitreous carbon electrode is shown in Fig. 1. The primary reduction process [A in Fig. 1(a)] encompasses the one-electron reduction of the oxidised cofactor to the EPR-active (S = 3/2) FeMoco$^{semi\text{-}red}$ state, a process which involves reversible interconversion of redox isomers, as delineated earlier by Schultz *et al.*[4] The reduction of the semi-reduced state is observed as a poorly resolved irreversible process under argon or molecular nitrogen [B in Fig. 1(a)]. Whereas the primary process A is unperturbed by carbon monoxide, interaction with CO is evident by the resolution of process B into two successive reduction steps [C and D in Fig. 1(b)] and by the detection of two oxidisable species [E and F in Fig. 1(b)]. Purging the solution with argon or dinitrogen fully restores the response to that observed in the absence of CO. Importantly, an enzyme reconstitution assay[5] showed the cofactor to be fully active after exposure to CO for one hour.

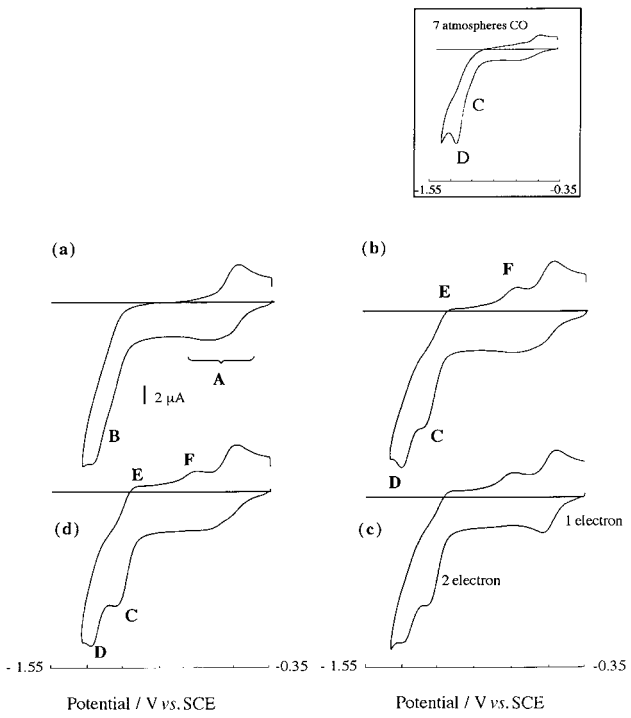

Fig. 1 (a) Cyclic voltammogram of FeMoco^{ox} (*ca.* 1.8 mM) in NMF recorded at a vitreous carbon electrode of area 0.071 cm^2 at 292 K under a dinitrogen atmosphere in a glove box operating at < 1 ppm O_2, the potential scan rate = 50 mV s^{-1}; (b) conditions as for (a) but saturated with CO at 1 atm; (c) conditions as for (b) after the addition of 1 equiv. of PhSH, the isomeric system A collapses to a single reversible one-electron process corresponding to thiolate ligation at the terminal Fe atom of the cofactor; (d) conditions as for (b) in the presence of 90 mM imidazole. Inset: cyclic voltammogram of FeMoco^{ox} recorded under CO at 720 KPa showing the increase in the height of peak D, conditions otherwise as for (b) except [FeMoco^{ox}] *ca.* 1 mM.

Variable scan-rate studies show that the intermediates detected at E and F are generated by the CO-dependent two-electron reduction process occurring at C. Process D involves further reduction and binding of CO. With increasing CO pressure, peak D increases in intensity and is shifted to more positive potentials; this is indicative of a rate-limiting interaction with CO, Fig. 1 (inset). Carbon monoxide is a powerful π-*acid* ligand, thus binding to the cofactor not unexpectedly promotes sequential two-electron transfer steps (processes C and D) *cf.* proton-coupled redox chemistry.[6]

Despite the nominal coordinatively unsaturated nature of the trigonal iron atoms of the Fe_7S_9Mo cluster in the protein and (presumably) in the isolated cofactor, neither the resting-state MoFe-protein nor the corresponding FeMoco$^{semi\text{-}red}$ state of the cofactor, interact measurably with CO. Turnover is necessary to observe MoFe-protein–CO interactions; accessing the FeMoco^{red} state is necessary to observe isolated cofactor interactions with CO, at least at pressures below 2016 kPa.

Since the cyclic voltammetry suggests that at least four electrons can be added overall to the FeMoco$^{semi\text{-}red}$ state under CO, it would not be surprising if redox chemistry associated with accessing low valent Fe and/or Mo states is involved.[7]

Direct spectroscopic evidence for the binding of carbon monoxide to reduced states of FeMoco is revealed by thin-layer FTIR spectroelectrochemistry[8] under moderate pressures (720 kPa) of CO at a highly polished vitreous carbon working electrode (2.6 mm diameter disc). Potential-dependent FTIR spectra obtained by reflectance through the thin solution layer (*ca.* 10–20 μm) are shown in Fig. 2. Two major bands develop at 1883 and 1922 cm^{-1} which we assign to terminally bound CO at reduced FeMoco states. Neither band appears under argon or dinitrogen, nor in a solution of the cofactor irreversibly damaged by exposure to air.

The band at 1883 cm^{-1} is the first to appear at high potential [compare Fig. 2(a)–(c)] and is therefore most likely associated with process C, that at 1922 cm^{-1} becomes dominant at lower potentials and is probably associated with process D [Fig. 1(b)]. Re-oxidation at E_{appl} −0.85 V *vs.* SCE selectively depletes the 1883 cm^{-1} band and gives rise to a strong new absorption at 1965 cm^{-1} and a weak band at 1999 cm^{-1} (data not shown). Re-oxidation at E_{appl} −0.45 V *vs.* SCE depletes both infrared bands. It is probable that these two oxidations are associated with processes E and F, respectively, Fig. 1(b).

Coordination of thiophenol at the terminal tetrahedral Fe atom and imidazole (Im) at the Mo atom provides a ligation environment for FeMoco akin to that of the cofactor in the

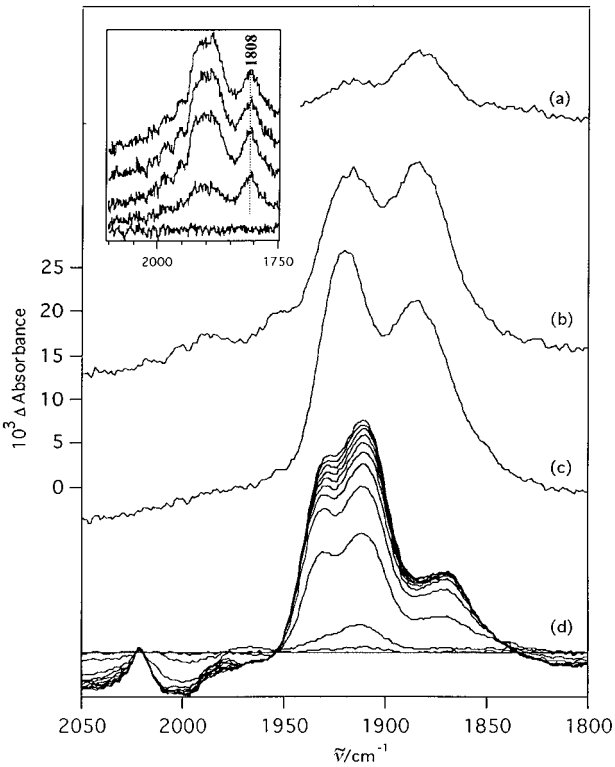

Fig. 2 Thin-layer FTIR spectroelectrochemistry of FeMoco at a highly polished vitreous carbon disc of area 0.053 cm^2 at ambient temperature. (a) Accumulated spectrum after electrolysis under CO at 720 KPa for 70 s at E_{appl} −1.05 V *vs.* SCE showing growth of bands centred on 1883 and 1922 cm^{-1}; (b) as for (a) but at E_{appl} −1.25 V *vs.* SCE; (c) as for (a) but at E_{appl} −1.45 V *vs.* SCE; (d) as for (c) showing the development of bands centred at 1870, 1910 and 1929 cm^{-1} when reduction is performed in the presence of thiophenol (*ca.* 100 mM) and imidazole (*ca.* 50 mM). Inset: development of spectra at low (pre-equibrium) concentrations of CO showing development of a band at 1808 cm^{-1}, the spectra were recorded at 12.4 s intervals.

enzyme.[1–3,9] Whereas FTIR spectra obtained in the presence of thiophenol are similar to those observed for the unmodified cofactor, the addition of imidazole has a substantial effect. This is shown by Fig. 2(d), the 1922 cm^{-1} band is split into two new bands which appear at 1910 and 1929 cm^{-1} and which develop at the same rate. This suggests that at least two CO molecules can be bound at the same cofactor molecule. Additionally, the band at 1883 cm^{-1} is shifted to 1870 cm^{-1}.

Cyclic voltammetry shows that ligation of thiophenolate collapses the redox isomerism of the FeMoco$^{ox/semi\text{-}red}$ system to that of a single reversible couple,[4] but does not otherwise perturb the voltammetry under CO [Fig. 1(c)], thus the terminal tetrahedral Fe-atom of the cofactor is unlikely to be a site at which CO binds. Imidazole does not change the form of the voltammetry under CO even at [Im] = 90 mM [Fig. 1(d)]. Evidently imidazole and CO do not compete for the same site at Mo, as is concordant with the spectroelectrochemistry.

George *et al.*[10] have recently reported that turnover of nitrogenase under CO at low partial pressure leads to the growth of a band at 1906 cm^{-1} which is replaced by an intense absorption near 1936 cm^{-1} at higher partial pressures of CO; weaker absorptions near 1958 and 1880 cm^{-1} also appear. The major bands we observe, particularly those obtained in the presence of imidazole and thiophenol, clearly fall in the spectral domain of CO interactions with the enzyme.

Hoffman and Hales[11] have proposed a model for CO interaction with the {Fe$_7$S$_9$Mo} cluster which is based on detailed isotopic EPR and ENDOR studies of the enzyme during turnover. At low [CO] they suggest the binding of CO in a bridging or semi-bridging fashion between two core Fe atoms; at high [CO] a second molecule then binds to one of these Fe atoms thereby opening the bridge and giving a species with two terminally bound CO ligands, one on each of the neighbouring Fe sites. *A priori* their data do not exclude CO binding at molybdenum nor the generation of EPR-active states produced by two- or four-electron reduction of the resting state MoFe-protein, *cf.* process C and D.

Whilst the major bands we observe for the cofactor are undoubtedly associated with terminally bound CO ligands,[12] at low [CO] a weak band at 1808 cm^{-1} precedes the growth of the 1883 and 1922 cm^{-1} absorptions, Fig. 2 (inset). This may arise from a bridging carbonyl intermediate, related to that proposed by Hoffman and Hales,[11] however a terminal CO stretch cannot be excluded.

In conclusion, direct studies of the isolated cofactor have certain advantages over studies on the whole enzyme system, notably the possibility of selectively accessing redox states; the exclusion of complications which might arise from the presence of the other metallo-sites within the MoFe- or Fe-proteins; and the opportunity to widely and systematically control both the co-ligand and the outer-sphere environment. The studies described herein take some first steps towards obtaining spectroscopic information on interactions of isolated FeMoco at redox levels not hitherto addressed, and which are complementary to studies of the whole enzyme system under turnover conditions.

We thank Glen Deacon (Monash) for providing IAB facilities, Steven Prawer for provision of machined vitreous carbon, Simon George, Graham Heath, Thierry LeGall, Ray Richards and Roger Thorneley for useful discussion. We thank the ARC and BBSRC for supporting this work and the Wilsmore Trust for funding a Visiting Fellowship (to C. J. P.).

Notes and references

† *Ca.* 1.8 mM FeMoco in NMF containing Na_2HPO_4 phosphate buffer (*ca.* 100 mM) and water (*ca.* 5% v/v). The NMF spectroscopic window is 2300–1720 cm^{-1}.

1 J. B. Howard and D. C. Rees, *Chem. Rev.*, 1996, **96**, 2965; B. K. Burgess and D. J. Lowe, *Chem. Rev.*, 1996, **96**, 2983.
2 B. K. Burgess, in *Molybdenum Enzymes*, ed. T. G. Spiro, J. Wiley and Sons, New York, 1985, vol. 7, pp. 161–220; T. R. Hawkes, P. A. McLean and B. E. Smith, *Biochem. J.*, 1984, **217**, 317.
3 B. K. Burgess, *Chem. Rev.*, 1990, **90**, 1377.
4 F. A. Schultz, S. F. Gheller, B. K. Burgess, S. Lough and W. E. Newton, *J. Am. Chem. Soc.*, 1985, **107**, 5364.
5 V. K. Shah and W. Brill, *Proc. Natl. Acad. Sci. USA*, 1977, **74**, 3249; B. E. Smith, in *Molybdenum Chemistry of Biological Significance*, ed. W. E. Newton and S. Otsuka, Plenum Press, New York and London, 1980, pp. 179–190.
6 B. A. Crichton, J. R. Dilworth, C. J. Pickett and J. Chatt, *J. Chem. Soc., Dalton Trans.*, 1981, 892; J. R. Dilworth, B. D. Neaves, C. J. Pickett, J. Chatt and J. Zubieta, *Inorg. Chem.*, 1983, 3524; F. T. Al Ani and C. J. Pickett, *J. Chem. Soc., Dalton Trans.*, 1988, 2329.
7 C. J. Pickett, *J. Biol. Inorg. Chem.*, 1996, **1**, 601 and references therein.
8 S. P. Best, S. A. Ciniawsky and D. G. Humphrey, *J. Chem. Soc., Dalton Trans.*, 1996, 2945; S. P. Best and A. B. Trucollo, *Electrochemistry, Crossing the Boundaries*, ed. D. M. Druskovich, RACI, Canberra, 1998, p. 15 (ISBN 187502678); C. G. Atwood, W. E. Geiger and T. E. Bitterwolf, *J. Electroanal. Chem.*, 1995, **397**, 279 and references therein.
9 S. D. Conradson, B. K. Burgess, W. E. Newton, A. Di Cicco, Z. Y. Wu, C. R. Natoli, B. Hedman and K. O. Hodgson, *Proc. Natl. Acad. Sci. USA*, 1994, **91**, 1290; I. Harvey, R. W. Strange, R. Schneider, C. A. Gormal, C. D. Garner, S. S. Hasnain, R. L. Richards and B. E. Smith, *Inorg. Chim. Acta*, 1998, **275–276**, 150.
10 S. J. George, G. A. Ashby, C. W. Wharton and R. N. F. Thorneley, *J. Am. Chem. Soc.*, 1997, **119**, 6450.
11 H.-I. Lee, L. M. Cameron, B. J. Hales and B. M. Hoffman, *J. Am. Chem. Soc.*, 1997, **119**, 10 121; H.-I. Lee, B. J. Hales and B. M. Hoffman, *J. Am. Chem. Soc.*, 1997, **119**, 11 395.
12 S. C. Davies, D. L. Hughes, R. L. Richards and J. R. Sanders, *Chem. Commun.*, 1998, 2699.

Communication 9/02371B

Triscyclopenta[*cd,fg,jk*]pyrene: another congener of the externally cyclopenta-fused pyrene series

Martin Sarobe,[a] Remco W. A. Havenith[ab] and Leonardus W. Jenneskens*[a]

[a] *Debye Institute, Department of Physical Organic Chemistry, Utrecht University, Padualaan 8, 3584 CH Utrecht, The Netherlands. E-mail: jennesk@chem.uu.nl*

[b] *Debye Institute, Theoretical Chemistry Group, Utrecht University, Padualaan 8, 3584 CH Utrecht, The Netherlands*

Received (in Liverpool, UK) 3rd March 1999, Accepted 23rd April 1999

Flash vacuum thermolysis of 1,3,6-tris(1-chloroethenyl)pyrene 5 between 900–950 °C gave the thermally labile triscyclopenta[*cd,fg,jk*]pyrene 1; in line with the 'conjugated circuits model' and supported by IGLO III//RHF/6-31G calculations, all hydrogen atoms of 1 are additionally shielded by 0.4–0.9 ppm (^{1}H NMR).

Flash vacuum thermolysis (FVT, 10^{-2} Torr, 1000 °C) of 1-(1-chloroethenyl)pyrene, *viz.* 'masked' 1-ethynylpyrene, quantitatively gave the ubiquitous and genotoxic combustion effluent cyclopenta[*cd*]pyrene **8** [mass recovery (MR) 90%].[1] This result supports the proposal[2] that ethynyl-substituted polycyclic aromatic hydrocarbons (E-PAH) play a pivotal role in the formation of externally cyclopenta-fused PAH (CP-PAH) effluents under high temperature conditions in the gas phase, *viz.* during combustion. Since 1-ethynylpyrene is thought to arise from C_2 and/or C_2H_2 addition to pyrene **7**,[3] we anticipated that multiple ethynyl-substituted pyrenes might be precursors for congeners of **8** containing multiple externally fused cyclopenteno units, that may represent hitherto unidentified combustion effluents. FVT of 1,6-, 1,8- and 1,3-bis(1-chloroethenyl)pyrene gave in reasonable to good yields dicyclopenta[*cd,jk*]- (**6a**), dicyclopenta[*cd,fg*]- (**6b**) and dicyclopenta[*cd,mn*]pyrene (**6c**), respectively,[4,5] which were all stable up to 1100 °C.† Subsequently, **6a–c** were indeed identified in flames as the three most abundant $C_{20}H_{10}$ CP-PAH combustion effluents.[6] Furthermore, it was shown that dicyclopenta-fusion topology markedly affects the electronic and magnetic properties of **6a-c**. Their gross ^{1}H NMR features, *i.e.* their average five- [$\delta(5)_{av}$] and six-membered ring [$\delta(6)_{av}$] ^{1}H chemical shifts, revealed that all hydrogen atoms of **6a,b** are 0.4–0.8 ppm more shielded than those of **6c** and **8** [$CDCl_3$; $\delta(5)_{av}/\delta(6)_{av}$: **6a**, 6.90/7.58, **6b**, 6.66/7.55, **6c**, 7.36/8.32 and **8**, 7.34/8.19].[4,5] These results were qualitatively rationalized using the obsolete ring perimeter model of Platt.[7] Whereas for **6a**,**b** two of the seven Kekulé resonance structures are anti-aromatic (16π-electron ring perimeter), similar anti-aromatic, ring perimeter resonance structures are unavailable for **6c** and **8**.[5,8] However Randić's conjugated circuits model,[9] which takes into account contributions of *all* possible [4*n*+2] and [4*n*] π-electron conjugated circuits, gives a better interpretation. It is readily shown that in the case of **6c** and **8** [4*n*] π-electron conjugated circuits are absent in their possible Kekulé resonance structures.

Here we report the synthesis of triscyclopenta[*cd,fg,jk*]pyrene **1** ($C_{22}H_{10}$) by FVT of 1,3,6-tris(1-chloroethenyl)pyrene **5**, *viz.* 'masked' 1,3,6-trisethynylpyrene **4** (Scheme 1),‡ and its salient spectroscopic properties. FVT (10^{-2} Torr, sublimation at 180 °C, rate 50 mg h^{-1}) of **5** (50 mg aliquots) was done at 800, 900, 950 and 1000 °C.§ In the 800 °C pyrolysate (MR 50%) the $C_{22}H_{10}$ (CP)-PAH **4** (30%),‡ the bisethynylcyclopenta[*cd*]pyrenes (**3a–c**, 20%) and traces of the ethynyldicyclopentapyrenes (**2a–c**) were identified [^{1}H NMR, GC-MS (Scheme 1)]. Surprisingly, the known $C_{20}H_{10}$, $C_{18}H_{10}$ and $C_{16}H_{10}$ (CP)-PAHs, 1,6-, 1,8- and 1,3-bisethynylpyrene (combined yield 20%),[4] 1-, 6- and 8-ethynylcyclopenta[*cd*]pyrene (combined yield 16%),[4] **6a–c** (1%),[4,5] **7** (7%) and **8** (5%),[1] respectively, were also found as side products (^{1}H NMR, GC-MS, GC-IR, HPLC). Hence, fragmentation reactions, *viz.* C_2 extrusions,[10] are competitive. At 900 °C (MR 20%) and 950 °C (MR 15%),§ instead of **4**, a novel compound (900 °C, 30% and 950 °C, 40%) was identified besides the fragmentation products

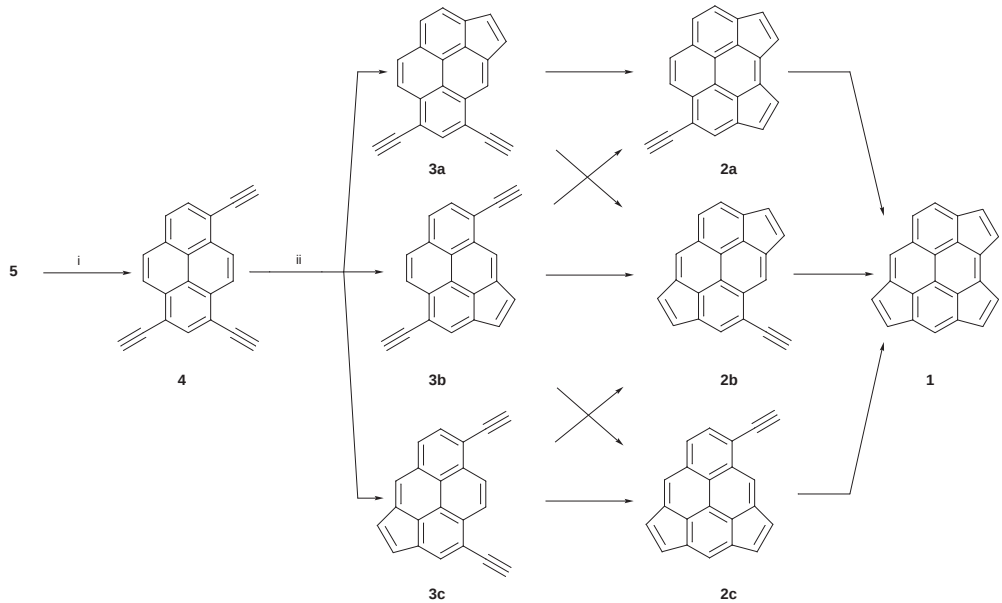

Scheme 1 *Conditions*: i, FVT (10^{-2} Torr, 800 °C); ii, FVT (10^{-2} Torr, 900 ≤ *T* < 1000 °C).

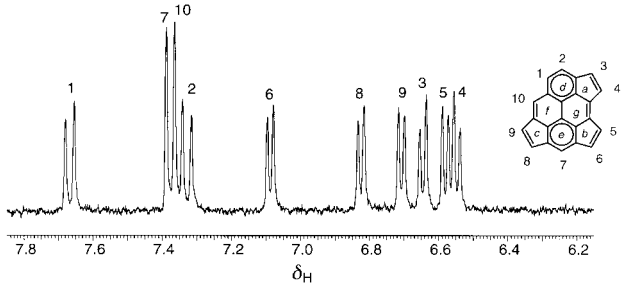

Fig. 1 ^{1}H NMR (300.13 MHz, acetone-d_6) spectrum of **1** (Table 1). See text for NICS(IGLO III//RHF/6-31G) (ref. 13) values *a–f*. Selected RHF/6-31G carbon–carbon bond lengths (in Å) (C_s): 1-2, 6a-7, 7-7a 1.41; 1-1a 1.40; 1a-10 1.48; 2-2a 1.39; 4a-5a 1.37; 9a-10, 1.36; 3-4, 5-6, 8-9 1.35; 2a-3, 4-4a, 5a-5, 6-6a, 7a-8, 9-9a 1.49 [*cf.* **7** (D_{2h}): 1-2, 1-1a, 1.39; 9-10, 1.34; 1a-10 1.44 and **8** (C_s): 1-2, 1-1a 1.40; 2-2a, 5a-6, 6-7, 7-8, 8-8a, 1.39; 2a-3 4-4a, 1.48; 3-4, 4a-5, 9-10 1.35; 5-5a 1.46; 8a-9, 1a-10, 1.45].

Table 1 δ_H (exp) *vs.* δ_H (IGLO) values of **1**

H atom[a]	δ_H(exp) [*J*/Hz][b]	δ_H (IGLO)[c]	$\Delta\delta$[d] (ppm)
1	7.67 [7.5]	8.35	0.68
2	7.33 [7.5]	7.87	0.54
3	6.65 [5.4]	7.32	0.67
4	6.54 [5.4]	7.23	0.69
5	6.58 [5.1]	7.28	0.70
6	7.09 [5.1]	7.77	0.68
7	7.39	8.03	0.64
8	6.82 [5.1]	7.51	0.69
9	6.71 [5.1]	7.24	0.53
10	7.36	7.99	0.63

[a] Fig. 1. [b] $^3J_{HH}$ coupling constants. [c] IGLO III//RHF/6-31G (ref. 12); Me_4Si at σ_H 32.1 or σ_C 196.1 ppm. [d] $\Delta\delta = \delta_H - \delta_H$(exp); mean deviation = 0.65 ppm.

(^{1}H NMR). Column chromatography (silica, *n*-hexane) of the 950 °C pyrolysate gave a pure sample (*ca.* 5 mg) that could be assigned to **1** [^{1}H, ^{13}C NMR, (HR)FAB-MS (Fig. 1)].¶ Whereas in the 950 °C pyrolysate besides **1** (40%) the $C_{20}H_{10}$ CP-PAH **6a**[4,5] (40%) is the other major product, the latter is the sole product upon FVT of **5** at 1000 °C [(MR *ca.* 10%) ^{1}H NMR, GC-MS]. In contrast with the prediction[11] that **1** represents a high temperature 'stabilomer', and the thermal stability of **6a-c**[4,5] and **8**,[1]† as well as their E-PAH precursors,[1,4] **1** and **4** are susceptible to fragmentation (C_2 extrusions[10]) under the FVT conditions.

The ^{1}H NMR chemical shifts of **1** resemble those of **6a**,**b** {Fig. 1 and Table 1 [$\delta(5)_{av}/\delta(6)_{av}$: **1** (acetone-$d_6$) 6.74/7.44, **6a** ($CDCl_3$) 6.90/7.58 and **6b** ($CDCl_3$) 6.66/7.55.[4,5]]}. This gives further credence to the applicability of the 'conjugated circuits model'.[9] Although **1** with its 17-carbon atom ring perimeter does not have any *closed shell* [4*n*] π-electron ring perimeter resonance structures, many [4*n*] (with n = 3, 4, 5) π-electron conjugated circuits can be distinguished in its available Kekulé resonance structures. Consequently, in analogy with **6a**–**b**, all its hydrogen atoms are 0.4–0.9 ppm more shielded than those of **6c** and **8** [$\delta(5)_{av}/\delta(6)_{av}$: **6c** ($CDCl_3$) 7.36/8.32[4,5] and **8** ($CDCl_3$) 7.34/8.19[1]]. This qualitative interpretation is further corroborated by *ab initio* calculations.

For **1** (C_s symmetry) a pyrene-like *ab initio* RHF/6-31G structure containing three cyclopenteno moieties with distinct sp^2–sp^2 carbon–carbon double (1.35 Å) and single (1.49 Å) bonds was obtained (Fig. 1). In addition, the IGLO III//RHF/6-31G[12] δ_H and δ_C chemical shifts of **1** were in good agreement with the experimental data (Table 1).¶ A comparison of the IGLO III//RHF/6-31G anisotropy of the diamagnetic magnetic susceptibility $\Delta\chi$ (= $\chi_{out\text{-}of\text{-}plane} - \chi_{in\text{-}plane}$)‖ of **1**, **7** and **8**, respectively, showed that **7** ($\Delta\chi$ −248.5 ppm cgs) and **8** ($\Delta\chi$ −267.2 ppm cgs) possess similar values. In contrast, $\Delta\chi$ of **1** (−206.5 ppm cgs) is substantially less negative due to changes of $\chi_{out\text{-}of\text{-}plane}$ and $\chi_{in\text{-}plane}$ (ratio $\chi_{out\text{-}of\text{-}plane}/\chi_{in\text{-}plane}$: **1**; −314.2/−107.7 = 2.9, **7**; −359.9/−92.7 = 3.9 and **8**; −333.7/−85.2 = 3.9). Hence, **1** will have a reduced ring current[12] leading to additional shielding of all hydrogen atoms. The magnetic properties of the individual rings of polycyclic **1** using the nucleus independent chemical shift criterion [NICS(I-GLO III//RHF/6-31G); 0.5 Å above each ring center[13]] reveal that the five-membered rings are anti-aromatic (*a*: 10.7, *b*: 4.8 and *c*: 5.3 ppm), the top/bottom six-membered rings are aromatic (*d*: −9.6 and *e*: −9.4 ppm) and the central ones are nearly non-aromatic [*f*: 1.3 and *g*: 0.5 ppm (Fig. 1)]. The NICS results indicate that **1**, like **7** and **8**,‖ is best represented by a Clar-type[14] structure. In going from **7** to **8** and finally **1**, the related NICS values of the five- (six-) membered rings become more positive (less negative); their anti-aromatic (aromatic) character increases (decreases).

Financial support [M. S. Basque Government (Beca de Formacion de Investigadores)], discussions with Dr J. H. van Lenthe (Utrecht University) and fruitful suggestions from a referee are acknowledged.

Notes and references

† At 1100 °C **6c** gave some **8** (16%) (ref. 4).

‡ Independent synthesis for **4**: Treatment of **5** with Na/NH_3 (l) (ref. 15) at −40 °C gave **4** (yield 40%). For **5**: Acetylation (3.5 equiv.) of **7** gave 1,3,6-trisacetylpyrene (ref. 16), which by treatment with PCl_5 (3.5 equiv. (ref. 1,4) gave **5** (overall yield 16%). Satisfactory analytical data [^{1}H, ^{13}C NMR, FT-IR, (HR)MS and/or EA] were found for **4** and **5**.

§ Only *ca.* 50% w/w of **5** sublimed into the hot zone, the remainder gave an intractable solid in the sample flask. At T ⩾ 900 °C carbonization became a competitive process. Pure **4** could not be sublimed into the hot zone; upon heating it gave an intractable solid.

¶ *Selected data* for **1**: δ_C(75.46 MHz, acetone-d_6) 139.1 (*C*H), 137.8 (*C*H), 135.3 (*C*H), 133.0 (*C*H), 130.6 (*C*H), 129.6 (*C*H), 126.9 (*C*H), 126.3 (*C*H), 124.6 (*C*H), 119.8 (*C*H), quaternary C not resolved; *m/z* (FAB-MS) 274 (**1**$^+$); (HRFAB-MS: calc. for $C_{22}H_{10}$ 274.0783, found 274.0750); λ_{max}(n-C_6H_{14})/nm (log ε) 550.0 (2.27), 485.0 (2.92), 455.0 (2.94), 420.5 (3.19), 397.0 (3.22), 338.5 (3.63), 297.5 (3.70), 240.0 (4.06), 205.0 (4.10); E_{tot} (a.u.) [RHF/6-31G (IGLO III//RHF/6-31G)] −838.595341 (−839.154631); δ_C(IGLO) 152.2, 148.9 (*C*H), 147.2, 145.8, 145.6 (*C*H), 145.5, 145.2, 144.7 (*C*H), 143.3, 140.8, 140.4, 140.2, 139.9, 139.1 (*C*H), 138.9 (*C*H), 136.9 (*C*H), 132.9 (*C*H), 132.6 (*C*H), 129.0, 128.5 (*C*H), 125.3 (*C*H), 122.7.

‖ $\chi_{out\text{-}of\text{-}plane} = \chi_{zz}$ and $\chi_{in\text{-}plane} = 0.5(\chi_{xx} + \chi_{yy})$ in ppm cgs; −/+ $\Delta\chi$ = dia-/para-magnetic (ref. 12). NICS(IGLO III//RHF/6-31G; 0.5 Å) (ref. 13) values: **7**, *d/e* −14.6 and *f/g* −5.5 ppm and **8**, *a* 2.0, *d* −13.2, *e* −13.4, *f* −4.9 and *g* −4.7 ppm.

1 M. Sarobe, J. W. Zwikker, J. D. Snoeijer, U. E. Wiersum and L. W. Jenneskens, *J. Chem. Soc., Chem. Commun.*, 1994, 89.
2 For a recent review: U. E. Wiersum and L. W. Jenneskens, in *Gas Phase Reactions in Organic Synthesis*, ed. Y. Vallée, Gordon and Breach, Amsterdam, The Netherlands, 1997, ch. 3, pp. 143–194.
3 H. Bockhorn, F. Fetting and H. W. Wenz, *Ber. Bunsenges. Phys. Chem.*, 1983, **87**, 1067 and references cited therein.
4 M. Sarobe, S. Flink, L. W. Jenneskens, B. L. A. van Poecke and J. W. Zwikker, *J. Chem. Soc., Chem. Commun.*, 1995, 2415.
5 L. T. Scott and A. Necula, *J. Org. Chem.*, 1996, **61**, 386.
6 A. L. Lafleur, J. B. Howard, K. Taghizadeh, E. F. Plummer, L. T. Scott, A. Necula and K. C. Swallow, *J. Phys. Chem.*, 1996, **100**, 17421 and references cited therein.
7 J. R. Platt, *J. Chem. Phys.*, 1954, **22**, 1448.
8 M. Kataoka, *Tetrahedron*, 1997, **53**, 12 875.
9 M. Randić, *Tetrahedron*, 1977, **33**, 1905 and references cited therein.
10 R. F. C. Brown, K. J. Coulston and F. W. Eastwood, *Tetrahedron Lett.*, 1996, **37**, 6819.
11 S. E. Stein and A. Fahr, *J. Phys. Chem.*, 1985, **89**, 3714.
12 U. E. Fleischer, W. Kutzelnigg, P. Lazzaretti and V. Mülhenkamp, *J. Am. Chem. Soc.*, 1994, **116**, 5298 and references cited therein.
13 P. von Rague Schleyer, C. Maerker, A. Dransfeld, H. Jiao and N. J. R. van Eikema Hommes, *J. Am. Chem. Soc.*, 1996, **118**, 6317.
14 E. Clar, in *Polycyclic Hydrocarbons*, Academic Press, London, 1964.
15 W. Ried and V.B. Saxema, *Angew. Chem.*, 1968, **80**, 366.
16 P. H. Gore, in *Friedel and Crafts and Related Reactions*, ed. G. A. Olah, Interscience, New York, vol. III, 1964, pp. 74–80.

Communication 9/01717H

Separation, isolation and characterisation of two minor isomers of the [84]fullerene C_{84}

Nikos Tagmatarchis,[a] Anthony G. Avent,[a] Kosmas Prassides,*[a] T. John S. Dennis[b] and Hisanori Shinohara*[b]

[a] *School of Chemistry, Physics and Environmental Science, University of Sussex, Falmer, Brighton, UK BN1 9QJ. E-mail: k.prassides@sussex.ac.uk*

[b] *Department of Chemistry, Nagoya University, Nagoya, 464-8602, Japan*

Received (in Oxford, UK) 3rd March 1999, Accepted 19th April 1999

The first successful separation and isolation from arc-burned soot of Gd-doped composite rods of a mixture (in an abundance ratio of 3 : 2) of two minor isomers of C_{84} with molecular symmetry D_{6h} and D_{3d}, and their characterisation by ^{13}C NMR and UV-VIS-NIR absorption spectroscopy, are described.

Following the discovery and isolation in pure form of macroscopic amounts of C_{60} and C_{70}, the presence of the so-called higher fullerenes (C_n, $n > 70$) was also identified in the soot obtained by the resistive heating of graphite under an inert atmosphere. Advances in the chromatographic separation of the higher fullerenes and their endohedrally-coordinated metal complexes have allowed the quantitative isolation and characterisation of certain higher fullerenes, even in isomer-pure form.[1] Examples of these include the molecular systems C_{76}, C_{78} and C_{84}, which have all been isolated quantitatively. While C_{76} exists as a single isomer with D_2 symmetry,[2] only three of the five possible isomers of C_{78} with isolated pentagons (IPR) and symmetry C_{2v}, C_{2v}', and D_3 have been studied.[3] The situation is even more complicated for the higher fullerene C_{84}. The C_{84} molecule can exist in 24 different structural isomers obeying the 'isolated pentagon rule'. However, two of the isomers with symmetry D_2 and D_{2d} (in the ratio 2 : 1) constitute the bulk of the material and these have been isolated and characterised in isomer-pure form by ^{13}C NMR and UV-VIS-NIR absorption spectroscopy.[4] The structural properties of the pristine [84]fullerene solid ($D_2 : D_{2d} \approx 2 : 1$) have also been reported as a function of temperature[5] together with the first results of the intercalation chemistry of both isomer-pure and mixed isomer solids with potassium.[6] In addition, the two dominant isomers have been separated chemically and the structure of the D_{2d} isomer has been determined by single crystal X-ray diffraction.[7] The structural solid state properties of the isomer-pure D_2 and D_{2d} C_{84} solids also exhibit a series of structural phase transitions on cooling.[8] An attempt to identify and characterise the major and minor isomers present in the main and tail HPLC fractions of C_{84} has been already reported in the literature.[9] However, the large number of lines (one hundred and fifty four) present in the ^{13}C NMR spectra has precluded reliable identification of isomers and correct assignment of the observed lines. Here we report the first successful isolation and characterisation of [84]fullerene comprising a mixture of only two of the minor isomers with symmetry D_{6h} and D_{3d}.

Fullerenes were produced by the dc arc discharge technique and extracted with CS_2 and pyridine. In the present experiments, we have used arc-burned soot of Gd-doped (0.8 wt%) composite rods. Similar experiments employing pure or Ca-doped graphite rods did not produce similar amounts of minor isomers of C_{84}, implying a catalytic effect for the Gd atoms in the early stage of the growth of these isomers. The separation of the C_{84} isomers was achieved by the technique of recycling HPLC using a Cosmosil 5PYE column and toluene as eluent (Fig. 1). Following recycling of the sample for 135 min, we succeeded in separating a fraction of minor isomers from the two major isomers of symmetry D_2 and D_{2d}. Further recycling of the fraction of the major isomers for an additional 70 min did not reveal the presence of other isomers of C_{84}.† Theoretical calculations[10] of the stability of C_{84} isomers predict that the most stable isomers after D_2 and D_{2d} should be those with symmetry (11)C_2, (16)C_s, (19)D_{3d} and (24)D_{6h}. From the above symmetries of the minor isomers, we expect in the ^{13}C NMR spectra the appearance of 42 ($\times$2 C), 43 (41 $\times$ 2 C + 2 $\times$ 1 C), 8 (6 $\times$ 12 C + 2 $\times$ 6 C) and 5 (3 $\times$ 12 C + 2 $\times$ 24 C) lines, respectively for each of these isomers.[11]

The ^{13}C NMR spectrum of our purified sample after accumulating 200 000 scans for ten days showed 13 single distinct lines (Fig. 2) which are attributed to a mixture of the D_{6h} and D_{3d} isomers of C_{84} in the ratio 3 : 2. The observed pattern can be classified as comprising of two groups of lines whose intensity ratio is almost in the ratio 2 : 1. The group of eight intense lines can be further divided into two subgroups, one with two lines (δ 139.50, 144.78) slightly more intense, assigned to the D_{6h} isomer, and one with the remaining six lines (δ 135.23, 139.41, 139.60, 139.64, 141.34, 147.49) with slightly lower intensity, assigned to the D_{3d} isomer, in an abundance ratio of 3 : 2. The group of five less intense lines can be also divided into two subgroups; three of them have slightly higher intensity than the other two and they can be assigned to the D_{6h} isomer (δ 135.70, 138.56, 148.14). The remaining two lines (δ 136.39, 147.81) are then assigned to the D_{3d} isomer.

We also measured the UV-VIS-NIR absorption spectrum (Fig. 3) of the purified sample of the mixture of the D_{6h} and D_{3d} isomers of C_{84}. The major features of the spectra appear at 492, 578, 649, 757 and 914 nm. The absorption dip near 750 nm in the spectrum accounts for the sample being of golden yellow colour in toluene.

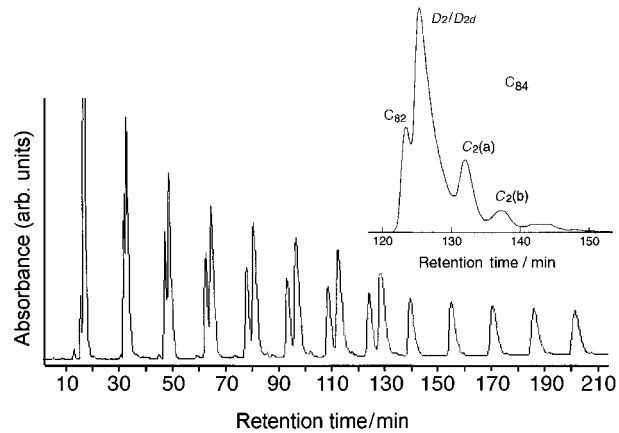

Fig. 1 HPLC profile of the second recycling phase, showing the separation of the mixture of the minor D_{6h} and D_{3d} isomers of C_{84} (second fraction with longer retention time) from its major D_2 and D_{2d} isomers (first fraction that elutes earlier). The second fraction was collected after 135 min and the first fraction was recycled for an additional 70 min. The inset shows part of an HPLC profile of the mixture obtained by using undoped graphite rods. The D_{6h} and D_{3d} isomers are absent and should have appeared between the major D_2/D_{2d} and C_2(a) isomers.

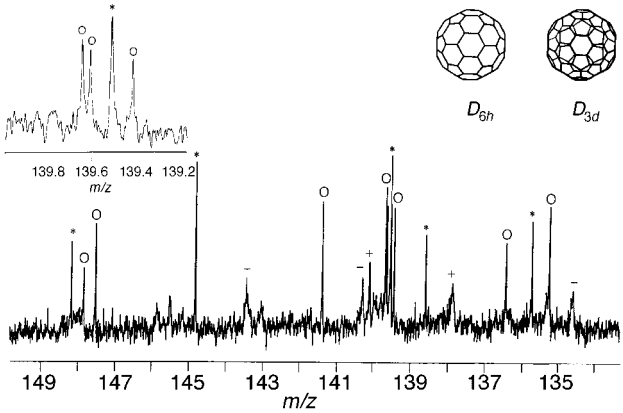

Fig. 2 ^{13}C NMR spectra [500 MHz, CS_2 solution with few drops of deuterated acetone as lock signal and $Cr(acac)_3$ as relaxant] of the purified mixture of the minor isomers D_{6h} (*) and D_{3d} (○) of C_{84}. Peaks labelled as (+) arise from the solvent (toluene) and other impurities. The region around δ139 is expanded for clarity. The inset shows the molecular structures of the two isomers.

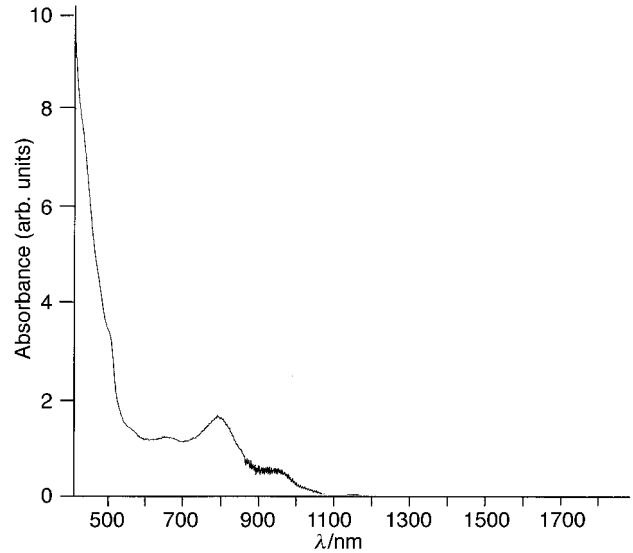

Fig. 3 UV-VIS-NIR absorption spectra of the purified mixture of the minor isomers D_{6h} and D_{3d} of C_{84}.

In conclusion, we have succeeded in separating, isolating and fully characterising by ^{13}C NMR spectroscopy a 3 : 2 mixture of the minor isomers D_{6h} and D_{3h} of the higher fullerene C_{84}.

N. T. thanks the European Union for the award of a Marie Curie Fellowship and Nagoya University for supporting his visit to Japan. Work in Nagoya is supported by the JSPS Future program for new Carbon Nanomaterials.

Notes and references

† *Note added at proof*: Further repeated HPLC recycling of the present sample results in the separation of an additional minor fraction, which is assigned to the C_2(a) isomer of C_{84} by comparison with earlier work (T. J. S. Dennis, T. Kai, T. Tomiyama, H. Shinohara, Y. Kobayashi, H. Ishiwatari, Y. Miyake, K. Kikuchi and Y. Achiba, to be published).

1 T. Kimura, T. Sugai, H. Shinohara, T. Goto, K. Tohji and I. Matsuoka, *Chem. Phys. Lett.*, 1995, **246**, 571.
2 R. Ettl, I. Chao, F. Diederich and R. L. Whetten, *Nature*, 1991, **353**, 149.
3 K. Kikuchi, N. Nakahara, T. Wakabayashi, S. Suzuki, H. Shiromaru, Y. Miyake, K. Saito, I. Ikemoto, M. Kainosho and Y. Achiba, *Nature*, 1992, **357**, 142.
4 T. J. S. Dennis, T. Kai, T. Tomiyama and H. Shinohara, *Chem. Commun.*, 1998, 619.
5 S. Margadonna, C. M. Brown, T. J. S. Dennis, A. Lappas, P. Pattison, K. Prassides and H. Shinohara, *Chem. Mater.*, 1998, **10**, 1742.
6 K. M. Allen, T. J. S. Dennis, M. J. Rosseinsky and H. Shinohara, *J. Am. Chem. Soc.*, 1998, **120**, 6681.
7 A. L. Balch, A. S. Kinwalla, J. W. Lee, B. C. Noll and M. M. Olmstead, *J. Am. Chem. Soc.*, 1998, **120**, 6681.
8 S. Margadonna, K. Prassides, A. N. Fitch, J. D. S. Dennis and H. Shinohara, unpublished results.
9 A. G. Avent, D. Dubois, A. Penicaud and R. Taylor, *J. Chem. Soc., Perkin Trans. 2*, 1997, 1907.
10 B. L. Zhang, C. Z. Wang and K. M. Ho, *J. Chem. Phys.*, 1992, **96**, 7183.
11 P. W. Fowler and D. E. Manolopoulos, *An Atlas of Fullerenes*, Clarendon Press, Oxford, 1995.

Communication 9/01709G

ChemComm

Asymmetric dihydroxylation route to a dipeptide isostere of a protease inhibitor: enantioselective synthesis of the core unit of ritonavir

Arun K. Ghosh,* Dongwoo Shin and Packiarajan Mathivanan

Department of Chemistry, University of Illinois at Chicago, 845 West Taylor Street, Chicago, Illinois 60607, USA. E-mail: arunghos@uic.edu

Received (in Corvallis, OR, USA) 29h March 1999, Accepted 22nd April 1999

An enantioselective synthesis of the dipeptide isostere of ritonavir has been accomplished utilizing Sharpless asymmetric hydroxylation as the key step.

The utility of dipeptide isosteres in the design and synthesis of potent and selective HIV protease inhibitors has been well documented.[1] A number of peptidomimetic protease inhibitors in combination with reverse transcriptase inhibitors have now been approved for treatment of AIDS, and early indications are very promising.[2, 3] Ritonavir **1** is one such protease inhibitor which is potent, selective and clinically effective.[2a] Ritonavir consists of a unique dipeptide mimic **2** evolved from structure-based design strategies (Fig. 1).[4] Most syntheses of the ritonavir isostere start with N-protected L-amino acids and are therefore limited to natural amino acid-derived substitutents.[5] Herein we report an enantioselective synthesis of the ritonavir isostere utilizing the Sharpless' catalytic asymmetric dihydroxylation reaction as the key step.

As illustrated in Scheme 1, γ,δ-unsaturated ester **4** was prepared by addition of vinyl magnesium bromide to phenylacetaldehyde **3**, followed by Claisen rearrangement of the resulting allylic alcohol with triethyl orthoacetate in the presence of propionic acid at 145 °C.[6] Ethyl ester **4** was converted to lactone **5** utilizing Sharpless protocol.[7] Thus, ester **4** was treated with AD-mix-β and $MeSO_2NH_2$ in a mixture (1 : 1) of Bu^tOH and H_2O at 0 °C for 36 h and the resulting hydroxy ester was lactonized in the presence of a catalytic amount of AcOH in refluxing toluene for 6 h. The desired hydroxy lactone **5** was obtained in 87% yield after silica gel chromatography [$[\alpha]_D^{23}$ −58, (*c* 1.81, $CHCl_3$)]. The hydroxy lactone **5** was transformed into protected amino lactone derivative **6** in the following three steps sequence: (1) formation of the mesylate with MsCl and Et_3N in the presence of a catalytic amount of DMAP; (2) displacement of the mesylate with NaN_3 in DMF at 90 °C and (3) catalytic hydrogenation of the resulting azide over 10% Pd/C in EtOAc in the presence of Boc_2O (overall 73% yield). The benzyl side chain at C-2 in isostere **2** was installed by a stereoselective alkylation of lactone derivative **6** as described previously.[8] Thus, generation of the enolate of lactone **6** with LiHMDS in THF at −78 °C, and subsequent reaction with BnI afforded the alkylated product **7** as a single diastereomer along with a small amount (4%) of dialkylated product. Alkylated lactone **7** was separated (70% yield) by silica gel chromatography. Saponification of lactone **7** by LiOH followed by protection of the resulting hydroxy acid with TBDMSCl, imidazole in DMF afforded the TBDMS protected acid derivative **8**.[5a] Curtius rearrangement of the acid **8** with $(PhO)_2PON_3$ and Et_3N in refluxing toluene followed by addition of BnOH as described previously provided the Z-

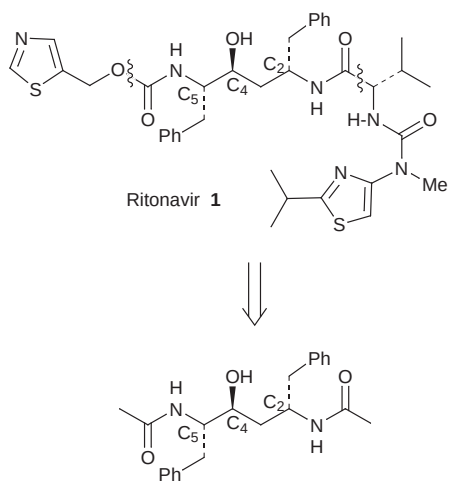

Fig. 1 Dipeptide mimetic of ritonavir **1**

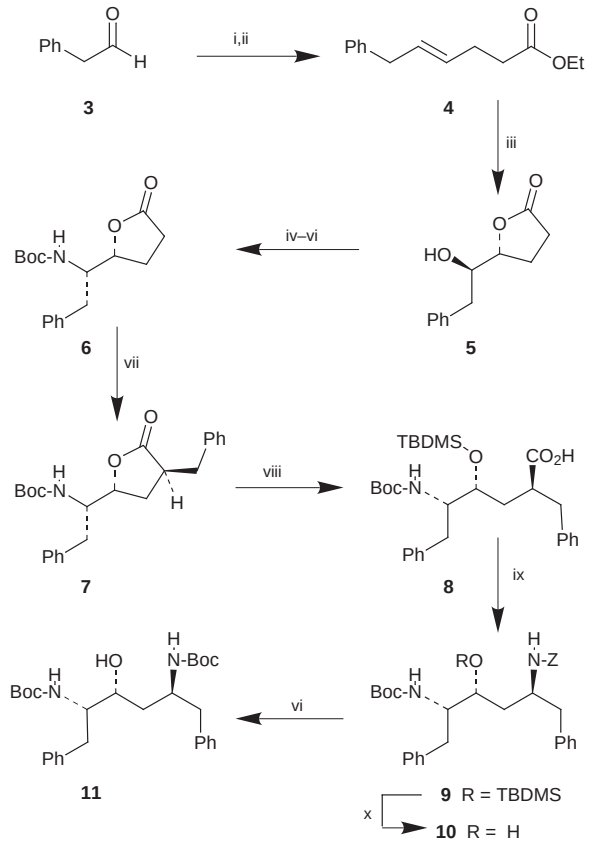

Scheme 1 *Reagents and conditions*: i, CH_2=$CHMgBr$, Et_2O, 0 °C, 57%; (ii) $MeC(OEt)_3$, $MeCH_2CO_2H$ (cat), 145 °C, 86%; (iii) AD-Mix-β, $MeSO_2NH_2$, Bu^tOH, H_2O, 0 °C, then PhMe, 115 °C, 87%; iv, MsCl, DMAP, Et_3N, CH_2Cl_2, 0 °C; v, NaN_3, DMF, 87%; vi, H_2, 10% Pd-C, Et_3N, Boc_2O, EtOAc, 23 °C, 84%; vii, LiHMDS, THF, BnI, −78 °C, 70%; viii, aq. LiOH, DME, 23 °C, H_3O^+, then imidazole, TBDMSCl, DMF, 23 °C, quant. ix, $(PhO)_2PON_3$, Et_3N, PhMe, then BnOH, 130 °C, 65%; x, TBAF, THF, 23 °C, 75%.

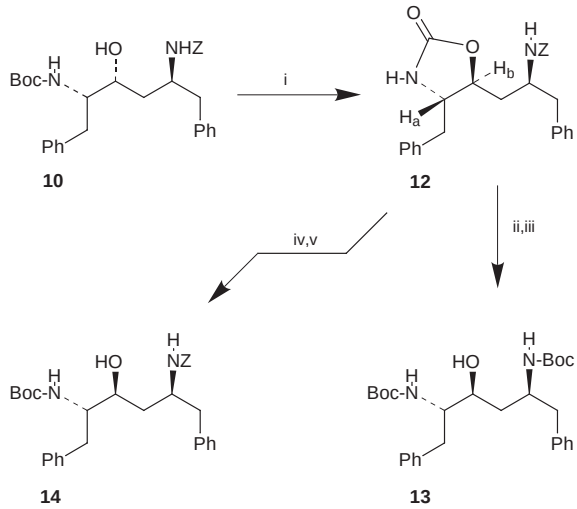

Scheme 2 *Reagents and conditions*: i, $SOCl_2$, THF, 23 °C, 73%; ii, KOH, EtOH–H_2O (1 : 1), 70 °C; iii, THF, Boc_2O, $NaHCO_3$, 23 °C, 52%; iv, Boc_2O, Et_3N, DMAP (cat), THF, 23 °C, 93%; v, Cs_2CO_3, Pr^iOH–MeOH (6 : 1), 23 °C, 60%.

derivative **9** (overall 65% yield from **7**).[9] Removal of the silyl group by treatment with TBAF in THF at 23 °C afforded the dipeptide isostere **10** with (4*R*)-configuration. Catalytic hydrogenation of **10** over 10% Pd/C in the presence of Boc_2O and Et_3N furnished the Boc derivative **11** in 72% yield after silica gel chromatography.

In the ritonavir isostere, the (4*S*)-configuration of the hydroxy group is known to be essential for effective enzyme inhibitory properties.[2a, 5, 10] Therefore, the C-4 hydroxy group stereochemistry was inverted as depicted in Scheme 2. Reaction of **10** with $SOCl_2$ in THF at 23 °C furnished the oxazolidinone **12** (73%). The vicinal coupling constant of oxazolidinone **12** is consistent with an *anti* stereochemical relationship (J_{AB} 4.8 Hz).[11] Treatment of the oxazolidinone **12** with KOH in EtOH–H_2O (1 : 1) resulted in the cleavage of the Z group and the oxazolidinone ring. Boc protection of the free amines afforded the biologically active dipeptide mimetic **13**. Differentially protected dipeptide mimic **14** was prepared by protection of oxazolidinone **12** with Boc_2O and Et_3N in the presence of a catalytic amount of DMAP in THF followed by selective cleavage of the oxazolidinone ring by treatment with Cs_2CO_3 in Pr^iOH–MeOH (6 : 1) at 23 °C for 6 h.[12] Consistent with the previous report, dipeptide mimic **11** with (4*R*)-hydroxy configuration has shown enzyme inhibitory potency (IC_{50} value) greater than 2 mM in the assay protocol developed by Toth and Marshall.[13, 14] Inversion of the C-4 hydroxy configuration of **10** resulted in derivatives **13** and **14** with inhibitory potencies of 118 nM and 75 nM respectively. Dipeptide isostere **14** has been previously converted to ritonavir and its derivatives.[2a]

In conclusion, we have developed an enantioselective synthesis of the core unit of ritonavir by utilizing Sharpless' catalytic asymmetric dihydroxylation reaction as the key step. The present route provides access to a diverse array of protease inhibitors containing designed functionalities. Synthesis and biological evaluation of novel protease inhibitors are currently in progress.

Financial support of this project was provided by the National Institutes of Health (GM 53386). We thank Ms Hanna Cho for the protease inhibition assay.

Notes and references

1 S. Thaisrivongs, *Annu. Rep. Med. Chem*., 1994, **29,** 133; P. L. Darke and J. R. Huff, *Advances in Pharmacology*, ed. J. T. August, M. W. Anders and F. Murad, Academic Press, San Diego, 1994, **25**, 399 and references cited therein.

2 (*a*) D. J. Kempf, K. C. Marsh, J. F. Denissen, E. McDonald, S. Vasavononda, C. A. Flentge, B. G. Green, L. Fino, C. H. Park, X.-P. Kong, N. E. Wideburg, A. Saldivar, L. Ruiz, W. M. Kati, H. L. Sham, T. Robins, K. D. Stewart, A. Hsu, J. J. Plattner, J. Leonard and D. Norbeck, *Proc. Natl. Acad. Sci. U.S.A.*, 1995, **92**, 2484; (*b*) J. P. Vacca, B. D. Dorsey, W. A. Schleif, R. B. Levin, S. L. McDaniel, P. L. Darke, J. Zugay, J. C. Quintero, O. M. Blahy, E. Roth, V. V. Sardana, A. J. Schlabach, P. I. Graham, J. H. Condra, L. Gotlib, M. K. Holloway, J. Lin, I-W. Chen, K. Vastag, D. Ostovic, P. S. Anderson, E. A. Emini and J. R. Huff, *Proc. Natl. Acad. Sci. U.S.A.*, 1994, **91,** 4096; (*c*) N. A. Roberts, J. A. Martin, D. Kinchington, A. V. Broadhurst, J. C. Craig, I. B. Duncan, S. A. Galpin, B. K. Handa, J. Kay, A. Krohn, R. W. Lambert, J. H. Merrett, J. S. Mills, K. E. B. Parkes, S. Redshaw, A. J. Ritchie, D. L. Taylor, G. J. Thomas and P. J. Machin, *Science*, 1990, **248**, 358 and references cited therein.

3 D. S. Stein, D. G. Fish, J. A. Bilello, S. L. Preston, G. L. Martineau and G. L. Drusano, *AIDS*, 1996, **10**, 485; J. M. Schapiro, M. A. Winters, F. Stewart, B. Efron, J. Norris, M. J. Kozal and T. C. Merigan, *Ann. Intern. Med.*, 1996, **124**, 1039 and references cited therein.

4 J. W. Erickson and S. W. Fesik, *Annu. Rep. Med. Chem*., 1992, **26**, 271 and references cited therein.

5 (*a*) A. K. Ghosh, S. P. McKee, W. J. Thompson, P. L. Darke and J. C. Zugay, *J. Org. Chem.*, 1993, **58**, 1025; (*b*) T. L. Stuk, A. R. Haight, D. Scarpetti, M. S. Allen, J. A. Menzia, T. A. Robbin, S. I. Parekh, D. C. Langridge, J.-H. Tien, R. J. Pariza and F. A. J. Kerdesky, *J. Org. Chem.*, 1994, **59**, 4040.

6 R. I. Trust and R. E. Ireland, *Org. Synth.*, 1988, **Coll. Vol. 6**, 606.

7 Z.-M. Wang, X.-L. Zhang, K. B. Sharpless, S. C. Sinha, A. Sinha-Bagchi and E. Keinan, *Tetrahedron Lett.*, 1992, **33**, 6407; K. B. Sharpless, W. Amberg, Y. L. Bennani, G. A. Crispino, J. Hartung, K. S. Jeong, H.-L. Kwong, K. Morikawa, Z.-M. Wang, D. Xu and X.-L. Zhang, *J. Org. Chem.*, 1992, **57**, 2768.

8 A. K. Ghosh and S. Fidanze, *J. Org. Chem.*, 1998, **63**, 6146; A. H. Fray, R. L. Kaye and E. F. Kleinman, *J. Org. Chem.*, 1986, **51**, 4828 and references therein.

9 T. Shioiri, K. Ninomiya and S. Yamada, *J. Am. Chem. Soc*., 1972, **94**, 6203; G. L. Grunewald and Q. Ye, *J. Org. Chem.*, 1988, **53**, 4021; A. K. Ghosh and W. Liu, *J. Org. Chem.*, 1996, **61**, 6175.

10 D. H. Rich, C.-Q. Sun, J. V. N. Prasad, A. Pathiasseril, M. V. Toth, G. R. Marshall, M. Clare, R. A. Mueller and K. Houseman, *J. Med. Chem.*, 1991, **34**, 1225.

11 D. J. Kempf, D. W. Norbeck, L. Codacovi, X. C. Wang, W. E. Kohlbrenner, N. E. Wideburg, D. A. Paul, M. F. Knigge, S. Vasavanonoda, A. Craig-Kennard, A. Saldivar, W. Rosenbrook Jr., J. J. Clement, J. J. Plattner and J. Erickson, *J. Med. Chem.*, 1990, **33**, 2687; A. K. Ghosh, S. P. McKee and W. J. Thompson, *Tetrahedron Lett.*, 1991, **32**, 5729.

12 T. Ishizuka and T. Kunieda, *Tetrahedron Lett*., 1987, **28**, 4185; H. Matsunaga, T. Ishizuka and T. Kunieda, *Tetrahedron*, 1997, **53**, 1275.

13 M. V. Toth and G. R. Marshall, *Int. J. Pept. Protein Res.* 1990, **36**, 544.

14 In-house prepared saquinavir [ref. 2(*c*)] exhibited an IC_{50} value of 1.6 nM in the same assay.

Communication 9/02518I

A new combination of donor and acceptor: bis(η⁶-benzene)chromium and hexafluorobenzene form a charge-transfer stacked crystal

Catherine J. Aspley,[a] Clive Boxwell,[a] Maria L. Buil,[a] Catherine L. Higgitt,[a] Conor Long[b] and Robin N. Perutz*[a]

[a] *Department of Chemistry, University of York, York, UK YO10 5DD. E-mail: rnp1@york.ac.uk*
[b] *Department of Chemistry, Dublin City University, Dublin, Ireland*

Received (in Oxford, UK) 3rd February 1999, Accepted 23rd April 1999

Bis(η⁶-benzene)chromium reacts with hexafluorobenzene to yield a red charge-transfer complex [Cr(η⁶-C_6H_6)$_2$•C_6F_6] which contains stacks of alternating donor and acceptor molecules with close inter- and intrastack contacts; in addition to the charge-transfer complex, formation of [Cr(η⁶-C_6H_6)$_2$]$^+$ is demonstrated by EPR and IR spectroscopy.

Non-covalent interactions have a major role in determining structures of molecular assemblies. The formation of stacks of donors alternating with acceptors can lead to special electronic and magnetic properties as in [Fe(η⁵-C_5Me_5)$_2$][TCNE] or [Fe(η⁶-$C_6Me_3H_3$)$_2$][$C_6(CN)_6$].[1,2] Stacking of aromatic rings (π-stacks) represents another motif, this time driven by quadrupolar interactions, *e.g.* in co-crystals of benzene and hexafluorobenzene.[3] Complex analogues of C_6H_6•C_6F_6 are attracting interest for their optoelectronic properties.[4,5] Bis(η⁶-benzene)chromium **1** has potential for both these types of interaction: it has featured as a donor in [Cr(η⁶-C_6H_6)$_2$][S_2O_6•2SO_2] and has been employed for crystal engineering.[6,7] Donor-acceptor (DA) complexes are also formed by **1** in [Cr(η⁶-C_6H_6)$_2$][TCNE] and [Cr(η⁶-$C_6Me_3H_3$)$_2$][TCNQ] but they are arranged in stacks of the type ⋯A_2DD⋯ or in chains.[8]

Several authors have proposed that an electron-transfer process precedes C–F bond activation of perfluoroalkanes and perfluoroarenes by transition metal complexes,[9–11] although experimental support for redox initiation is sparse. If this proposal is to be reconciled with the redox potentials, there must be either preassociation of the fluorocarbon and transition metal complex, or the products must be stabilised by rapid irreversible dissociation (*e.g.* $C_6F_6^-$ to C_6F_5 + F^-), or more likely both.[12] Crabtree *et al*. recently reported that [Fe(η⁵-C_5R_5)$_2$] (R = H or Me) associates with perfluoronaphthalene or perfluorophenanthrene in the solid state to form an irregular DA stack.[13] However, there was no optical evidence for a charge-transfer (CT) interaction. We report that **1** reacts with hexafluorobenzene to form a red CT complex in solution which crystallises as a donor–acceptor stack, and additionally that **1** undergoes one-electron oxidation by C_6F_6 to a limited extent.

When a large excess of dry hexafluorobenzene is condensed onto a freshly sublimed sample of **1** and thawed under argon, a claret-coloured solution is obtained from which crystals grow over several weeks at room temperature. The crystals have two habits, red–pink blocks and thin yellow plates, both of which are stable only in the mother liquor. An X-ray crystal structure of a red–pink crystal mounted in its mother liquor in a capillary at room temperature revealed it to be [Cr(η⁶-C_6H_6)$_2$•C_6F_6].† The structure contains face-to-face stacks of [Cr(η⁶-C_6H_6)$_2$] moieties alternating with C_6F_6 units at regular intervals of *ca*. 3.5 Å, a value similar to that in [Fe(η⁵-C_5Me_5)$_2$][TCNE].[2] The stacks lie approximately parallel to the body diagonal of the triclinic unit cell (Fig. 1) such that the benzene rings of the [Cr(η⁶-C_6H_6)$_2$] units eclipse the C_6F_6 rings in the same stack. The angle between the ring normals of the C_6F_6 and [Cr(η⁶-C_6H_6)$_2$] units is 5.9°. Each C_6F_6 lies approximately in line with one of the C_6H_6 rings in a neighbouring stack. The minimum C⋯C distance between C_6H_6 and C_6F_6 lies within a stack, while the minimum Cr⋯F distance lies between stacks (Fig. 2, Table 1). The regularly spaced DA stacks contrast with those of [Fe(η⁵-C_5Me_5)$_2$•$C_{14}F_{10}$][13] and [**1**][TCNE].[8]

We have also attempted to solve the structure of the thin yellow plates at −100 °C. Although the crystal did not diffract well, we found that the structure was little changed from that of the red–pink blocks. A compression along *b* and *c* led to a contraction of 1.9% in the minimum intrastack C⋯C distance and 3.7% in the minimum interstack Cr⋯F distance.

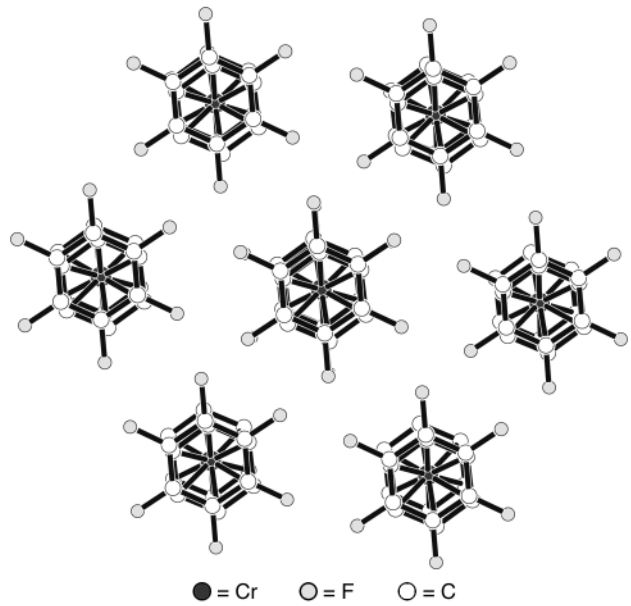

Fig. 1 Packing diagram for [Cr(η⁶-C_6H_6)$_2$•C_6F_6], viewed down the body diagonal of the triclinic cell (hydrogen atoms omitted).

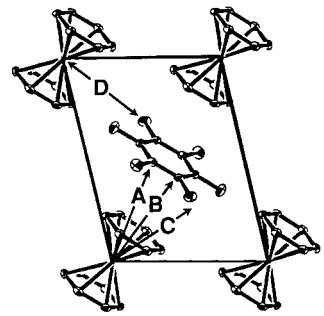

Fig. 2 ORTEP diagram (ref. 15) showing the key intra- and inter-stack spacings within the crystal structure of [Cr(η⁶-C_6H_6)$_2$•C_6F_6], viewed down the *c* axis. The hydrogen atoms are omitted for clarity. The average C–C and Cr–C bond lengths within a Cr(C_6H_6)$_2$ unit are 1.397 and 2.134 Å. For the C_6F_6 molecule, the C–C and C–F bond lengths average 1.365 and 1.341 Å.

Table 1 Minimum contact distances in the structure of [Cr(η⁶-C_6H_6)$_2$•C_6F_6]

Label[a]	Type of contact	Contact atoms	Distance/Å
A	Intrastack $C_6H_6\cdots C_6F_6$	*r*(C···C)	3.480(4)
B	Intrastack Cr···C_6F_6	*r*(Cr···C)	5.074(3)
C	Intrastack Cr···C_6F_6	*r*(Cr···F)	5.312(3)
D	Interstack Cr···C_6F_6	*r*(Cr···F)	4.490(2)

[a] labels A, B, C, D refer to Fig. 2.

When the reaction of **1** with C_6F_6 was carried out with higher concentrations of **1**, a fine yellow precipitate separated from the claret solution. A UV–VIS absorption spectrum of the solution, measured after filtering off the precipitate, showed an absorption at 503 nm and a shoulder at 390 nm.[16]‡ On freezing in liquid nitrogen, the claret solution turned to a yellow glass, but the claret colour returned on melting. The corresponding absorption maxima lie to longer wavelength (542, 414 nm) on reaction of [Cr(η⁶-1,4-$C_6H_4Me_2$)$_2$] with C_6F_6 and to shorter wavelength (424 nm)§ on reaction of **1** with C_6F_5H. These absorption bands are assigned to charge-transfer transitions of the complexes [Cr(η⁶-arene)$_2$•$C_6F_{6-n}H_n$] (n = 0, 1) which must be present in solution. Redox potentials suggest that the ground state of the complex will be close to the A•D description and the excited state close to A^+•D^-.¶

The solutions from reaction of **1** with C_6F_6 (whether dilute or more concentrated) gave a broad EPR signal at g = 1.987 consistent with formation of [Cr(η⁶-C_6H_6)$_2$]$^+$ **1**$^+$.[6] Solid-state EPR spectra of the yellow precipitate from reaction of **1** with C_6F_6 also revealed the presence of **1**$^+$ ($g_{||}$ = 2.002, $g_\perp$ = 1.983), while IR spectra showed characteristic bands of both **1** and **1**$^+$.[17] The presence of fluoride as a corresponding anion was revealed by its reaction with Me_3SiOTf yielding Me_3SiF.‖ In order to ascertain the proportion of **1** which is oxidised, we investigated the effect of addition of C_6F_6 to toluene solutions of **1**. A control sample of **1** in toluene showed only traces of **1**$^+$. On addition of 2 and 5 equiv. of C_6F_6, well-resolved resonances (A_H = 3.4 G) for **1**$^+$ were observed with intensities *ca*. 20 fold and 48 fold greater than the control, respectively. Comparison with the resonance of a standard solution of TEMPO (10^{-4} mol dm^{-3} in toluene) provided lower-limiting estimates that the solutions of **1** were 0.5 and 3.3% oxidised, respectively.** The extent of oxidation is appreciably higher than expected to arise from impurities in the hexafluorobenzene. The formation of [Cr(C_6H_6)$_2$]$^+$F$^-$ is reminiscent of the reaction of cobaltocene with perfluoroalkanes.[10]

These experiments lead to the following conclusions. (i) A donor–acceptor complex is formed between [Cr(η⁶-C_6H_6)$_2$] **1** and C_6F_6 with a long-wavelength absorption in solution, assigned to a CT transition between **1** and C_6F_6. (ii) The complex crystallises as [Cr(η⁶-C_6H_6)$_2$•C_6F_6] with a ···DADA··· stacked structure with close intra- and inter-stack contacts. The claret colour is observed in the larger crystals. The structure is probably stabilised by charge-transfer and π–π interactions. (iii) In addition to [Cr(η⁶-C_6H_6)$_2$•C_6F_6], salts including [Cr(η⁶-C_6H_6)$_2$]$^+$F— are formed in low conversion although half-wave potentials suggest that **1** is incapable of reducing C_6F_6.¶ (iv) The formation of the donor–acceptor complex and the oxidation of **1** provide support for related mechanisms for reactions of metal–hydride complexes with fluoroarenes.[11, 12]

We thank Dr T. Braun and Professors N. Connelly and W. E. Geiger for helpful discussions, the referees for helpful criticism, S. Foxon and Dr A. C. Whitwood for experimental help and the EPSRC and the European Commission for support.

Notes and references

† *Crystal data* for [Cr(η⁶-C_6H_6)$_2$•C_6F_6]: $C_{18}H_{12}CrF_6$, M = 394.28, red–pink blocks, triclinic, space group $P\bar{1}$, a = 7.3254(8), b = 9.2627(9), c = 6.6102(8) Å, α = 100.026(9), β = 112.327(8), γ = 97.532(9)°, V = 398.87(8) Å^3, Z = 1, T = 293(2) K, μ(Mo—Kα) = 0.778 mm^{-1}, F(000) = 198, 1477 reflections measured, 1401 unique (R_{int} = 0.040), 116 parameters. The crystal was mounted in a capillary in its mother liquor. The structure was solved by direct methods (SHELX) (ref. 14) and refined by full-matrix least-squares on F^2. Goodness of fit on F^2 1.083, final $R1$ [$I > 2\sigma(I)$] $R1$ = 0.0392, $wR2$ = 0.1027. CCDC 182/1238. See http://www.rsc.org/suppdata/cc/1999/1027/ for crystallographic files in .cif format.

‡ [Cr(C_6H_6)$_2$] is yellow–green with a weak band at 640 nm and an intense band at 320 nm. The corresponding cation exhibits weak bands in the near-IR region and a more intense band at 340 nm (ref. 16). The CT band of Cr(η⁶-C_6H_6)$_2$•SO_2 is observed at 540 nm (ref. 6).

§ The short-wavelength shoulder will overlap the bands of [Cr(η⁶-C_6H_6)$_2$] in C_6F_5H.

¶ The half-wave potentials of C_6F_6/$C_6F_6^-$ and [Cr(η⁶-C_6H_6)$_2$]$^+$/ [Cr(η⁶-C_6H_6)$_2$] are −2.55 and −0.68 V respectively *vs*. SCE. (ref. 18).

‖ Characterisation of the anion in the yellow precipitate was complicated by paramagnetic **1**$^+$. The precipitate was dissolved in CD_2Cl_2, Me_3SiOTf added and the volatiles condensed into an NMR tube. Me_3SiF was identified by the eight central lines of the decet at δ −157.96 (J_{HF} 7.6 Hz) in the ^{19}F NMR spectrum (ref. 19). A control experiment with C_6F_6, CD_2Cl_2 and Me_3SiOTf generated only traces of Me_3SiF.

** Complex **1** was freshly sublimed before use. Solutions in toluene (0.047 mol dm^{-3}) were made up in an argon-filled glove-box; C_6F_6 (99.9%), previously dried over molecular sieves and degassed by freeze-pump-thaw methods, was added in the box with a microsyringe. Typical impurities are C_6F_5Cl and $C_6F_5Cl_2$. Since the addition of C_6F_6 causes slight precipitation, the values of the percentage oxidation are lower limits.

1 J. S. Miller and A. J. Epstein, *Angew. Chem., Int. Ed. Engl.*, 1994, **33**, 385.
2 J. S. Miller, J. C. Calabrese, H. Rommelmann, S. R. Chittipeddi, J. H. Zhang, W. M. Reiff and A. J. Epstein, *J. Am. Chem. Soc.*, 1987, **109**, 769; M. D. Ward, *Organometallics*, 1987, **6**, 754; M. D. Ward and J. C. Calabrese, *Organometallics*, 1989, **8**, 593.
3 J. H. Williams, *Acc. Chem. Res.*, 1993, **26**, 593; A. P. Weat, S. Mecozzi and D. A. Dougherty, *J. Phys. Org. Chem.*, 1997, **10**, 347.
4 G. W. Coates, A. R. Dunn, L. M. Henling, J. W. Ziller, E. B. Lobkovsky and R. H. Grubbs, *J. Am. Chem. Soc.*, 1998, **120**, 3641.
5 P. Kirsch and K. Tarumi, *Angew. Chem., Int. Ed.*, 1998, **37**, 484.
6 C. Elschenbroich, R. Gondrum and W. Massa, *Angew. Chem., Int. Ed. Engl.*, 1985, **24**, 967.
7 D. Braga, A. L. Costa, F. Grepioni, L. Scaccianoce and E. Tagliavini, *Organometallics*, 1997, **16**, 2070.
8 J. S. Miller, D. M. O'Hare, A. Chakraborty and A. J. Epstein, *J. Am. Chem. Soc.*, 1989, **111**, 7853; D. O' Hare, M. D. Ward and J. S. Miller, *Chem. Mater.*, 1990, **2**, 758.
9 J. Burdeniuc and R. H. Crabtree, *J. Am. Chem. Soc.*, 1996, **118**, 2525; *Organometallics*, 1998, **17**, 1582.
10 B. K. Bennett, R. G. Harrison and T. G. Richmond, *J. Am. Chem. Soc.*, 1994, **116**, 11 165.
11 M. K. Whittlesey, R. N. Perutz and M. H. Moore, *Chem. Commun.*, 1996, 787.
12 B. L. Edelbach and W. D. Jones, *J. Am. Chem. Soc.*, 1997, **119**, 7734.
13 C. M. Beck, J. Burdeniuc, R. H. Crabtree, A. L. Rheingold and G. P. A. Yap, *Inorg. Chim. Acta*, 1998, **270**, 559.
14 G. M. Sheldrick, SHELXL 93, Program for the Refinement of Crystal Structures, University of Göttingen, 1995.
15 C. K. Johnson, ORTEP, Report ORNL-5138, Oak Ridge National Laboratory, Oak Ridge, TN, 1976.
16 K. D. Warren, *Struct. Bonding (Berlin)*, 1976, **27**, 45.
17 H. P. Fritz, W. Lüttke, H. Stammreich and R. Forneris, *Spectrochim. Acta*, 1961, **17**, 1068.
18 J. A. Marsella, A. G. Galicinski, A. M. Coughlin and G. P. Pez, *J. Org. Chem.*, 1992, **57**, 2856; D. Astruc, *Electron Transfer and Radical Processes in Transition Metal Chemistry*, VCH, Weinheim, 1995.
19 D. C. England, F. J. Weigart and J. C. Calabrese, *J. Org. Chem.*, 1984, **49**, 4816.

Communication 9/00919A

Long-lived [1.1.1.1]- and [2.2.1.1]-'Isopagodane' dications: novel 4C/2e σ-bishomoaromatic dications†

G. K. Surya Prakash,*[a] Klaus Weber,[ab] George A. Olah,*[a] Horst Prinzbach,*[b] Markus Wollenweber,[b] Markus Etzkorn,[b] Torsten Voss[b] and Rainer Herges*[c]

[a] *Donald P. and Katherine B. Loker Hydrocarbon Research Institute and Department of Chemistry, University of Southern California, Los Angeles, California 90089-1661, USA. E-mail: prakash@methyl.usc.edu*
[b] *Institut für Organische Chemie und Biochemie, Universität Freiburg, Albertstr. 21, D-79104 Freiburg, Germany*
[c] *Institut für Organische Chemie, TU Braunschweig, Hagenring 30, D-38106 Braunschweig, Germany*

Received (in Corvallis, OR, USA) 12th February 1999, Accepted 14th April 1999

The dications generated from [1.1.1.1] and [2.2.1.1]isopagodane in SbF_5–SO_2ClF solution at −78 °C are of σ-bishomoaromatic nature (4C/2e), very similar in geometry, yet chemically different in their properties.

The [1.1.1.1]pagodane (**A**, $m = n = 1$) and functionalized derivatives have received considerable attention as intermediates in the various synthetic routes to pentagonal dodecahedranes.[1] An important theoretical aspect is linked to the central, planar, peralkylated cyclobutane ring: Two-electron oxidations had allowed the experimental verification of σ-homoaromaticity in form of the respective 4C/2e dications.[2,3] In order to gain more insight into the limiting structural and energetic prerequisites of this intriguing phenomenon—and into the intermediate 'tight' and 'extended' radical cations[4]—structural variations of the pagodane skeleton have been made by homologation[5] and 90° rotation of the two molecular 'halves' to give the isopagodanes **B**.[6]

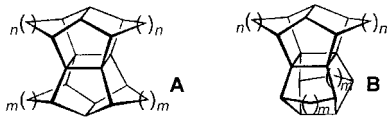

The [1.1.1.1]- and [2.2.1.1]-isopagodanes **1** and **6** had shown rather differing behaviour upon one-electron oxidation: the radical cation of **1** (Scheme 1) was only observable in a Freon matrix (−196 °C) and was identified as a tight species (**3**, a = 1.768 Å),[7] that from **6** was persistent in fluid solution (−40 °C, CH_2Cl_2) and existed, also in the Freon matrix, in an extended configuration (**9**, a = 2.512 Å). Under cyclic voltammetry (CV) conditions only for the latter a (reversible) two-electron oxidation wave (ECE) had been recorded.[8] Apparently the iso[1.1.1.1] skeleton does not allow the expansion of tight **3** into extended **4**. Here the question is addressed whether the σ-bishomoaromatic stabilization potentially arising from two-electron oxidation of **1** and **6** would be sufficient to enforce the skeletal changes which are necessary to make the respective cyclically delocalized 4C/2e dications observable.

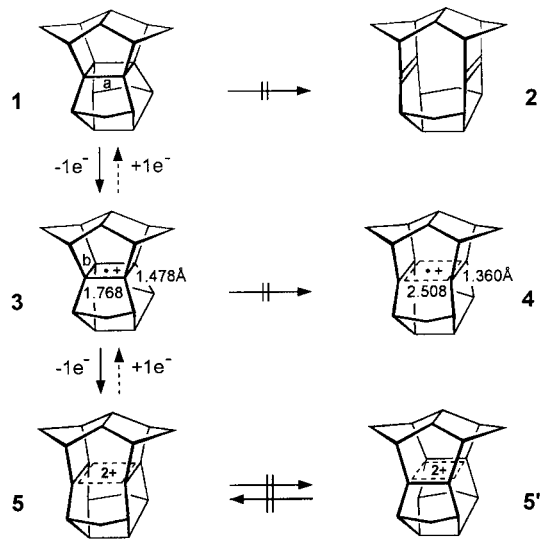

Scheme 1

Upon dissolution of **1** in SbF_5–SO_2ClF at −78 °C (dry ice–acetone bath) the initial dark green–blue color of the paramagnetic solution (**3**[7]) upon prolonged vortex stirring changed into the light yellow of the diamagnetic solution. The 75 MHz ^{13}C NMR spectrum[9] consisted of seven absorptions at δ_C 251.7 (s), 66.8 (d, $J_{C–H}$ 169), 66.5 (t, $J_{C–H}$ 139.6), 63.4 (d, $J_{C–H}$ 149.3), 51.2 (d, $J_{C–H}$ 163.0), 45.3 (d, $J_{C–H}$ 154.3) and 41.7 (t, $J_{C–H}$ 148.8), the 300 MHz ^1H NMR spectrum[9] of seven (two are overlapping) unresolved signals [δ_H 3.35 (br, 4H), 3.3 (br, 2H), 3.2 (br, 4H), 2.76 (br, 4H), 2.27 (br, 2H), 1.84 (br, 2H), 1.72 (br, 2H). Number and observed deshielding of carbons and protons relative to neutral **1**, in comparison with isomeric dication **15** (Fig. 1),[4] establish the C_{2v} symmetrical σ-bishomoaromatic structure **5** and exclude a rapid equilibration with degenerate **5′**. The lowering of the symmetry from D_{2d} of **1** to C_{2v} of **5** reflects distortion of the central carbon core from square to rectangular. Quenching the ion solution with cold MeOH (at −78 °C) induced two-electron reduction back to pagodane **1** (70% isolated) rather than to the much less stable diene **2** [ΔE_{rel} (**1**–**2**) = 14.68 kcal mol^{-1}, Fig. 2]. Particularly 1,4-bisaddition to give the bismethoxy ether was not observed (< 5%); in case of reference **15** the corresponding bisether had been the sole product.[2]

Exposure of **6** (Scheme 2) to similar oxidation conditions (−78 °C) produced the deep blue colour of the highly persistent extended radical cation **9**. Only after repeated vortex mixing at higher temperature (0 °C) the colour changed into pale yellow. The seven ^{13}C NMR signals of the diamagnetic solution at δ_C 238.5 (s), 67.0 (t, $J_{C–H}$ 142.9), 62.3 (d, $J_{C–H}$ 138.3), 48.0 (d, $J_{C–H}$ 148.8), 47.4 (d, $J_{C–H}$ 130.3) 43.5 (d, $J_{C–H}$ 150.2), 22.2 (t, $J_{C–H}$ 140.1) and the ^1H NMR signals (partially superimposed) at δ_H 3.26 (br, 6H), 2.88 (br, 6H), 2.66 (br, 4H), 2.08 (br d, 4H), 1.4 (br, 4H), 0.82 (br, 4H) are in line with the retention of C_{2V} symmetry in going from **6** to the σ-bishomoaromatic dication **10**. The formation of the same dication by the analogous oxidation of [2.2.1.1]isopagodadiene **7**[10] and the comparison with isomeric dication **16** (Fig. 1) provided additional confirmation. After quenching with MeOH (−78 °C) from a complex product mixture the dichlorodimethoxy- and chlorotrimethoxydienes **13** (two isomers) and **14** in the ratio ~1:2 were separated. Two-electron reduction to either **6** or **7** was not detected. A plausible explanation implies reduced *anti*-Bredt-

† Stable Carbocations, Part 309. For Part 308, see G. K. S. Prakash, V. P. Reddy, G. Rasul, J. Casanova and G. A. Olah, *J. Am. Chem. Soc.*, 1998, **120**, 13 362.

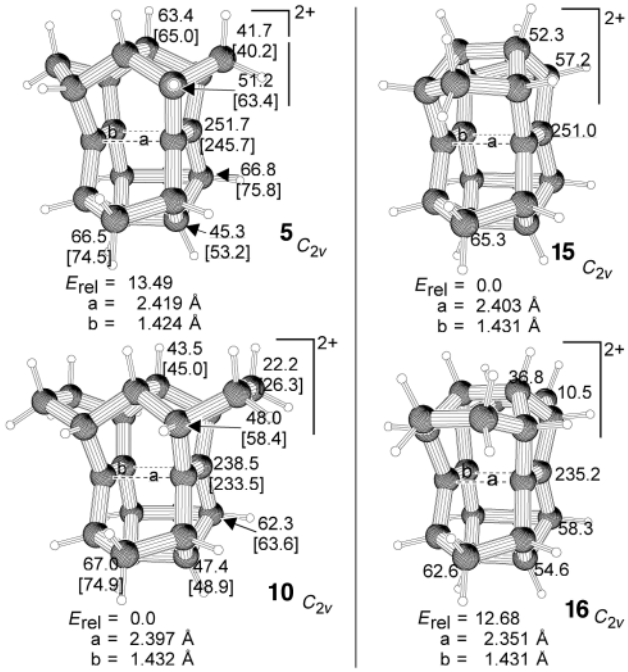

Fig. 1 B3LYP/6-31G* optimized structures, experimental and calculated (in brackets) ^{13}C NMR chemical shifts based on the DFT geometries and a GIAO B3LYP/6-31G* NMR calculation of the dications **3**, **10** (**15**, **16** as references); a and b denote DFT bond lengths; energies (E_{rel}) are given in kcal mol^{-1} and are relative to the more stable isomer.

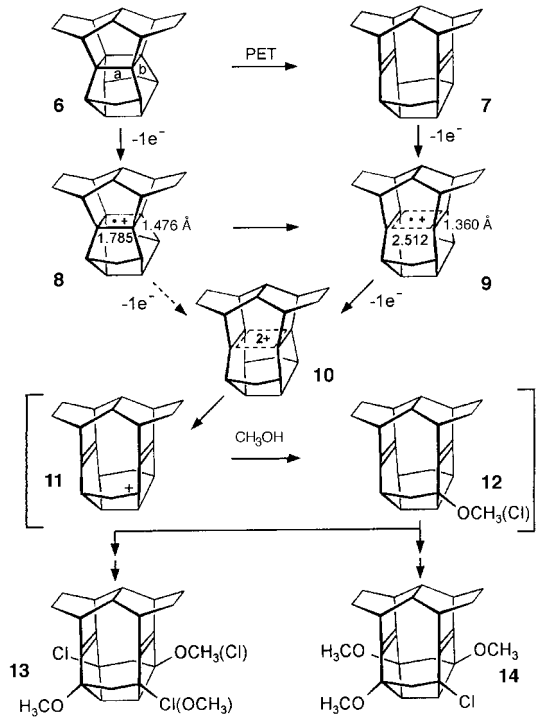

Scheme 2

protection in **10** opening up a sequence of deprotonation (*e.g.* **11**), nucleophilic addition (*e.g.* **12**) and reoxidation of the respective functionalized dienes.

GIAO[11] chemical shift calculations were performed based on the DFT calculated geometries. Calculated and observed chemical shifts agree within the error limit of the method. The ^{13}C shifts of the core carbons of **5** and **10** are very similar to those of the reference dications **15** and **16**; the ^{13}C NMR chemical shift additivity analysis[12] with total chemical shift differences of 910 and 905 ppm, respectively, amounts to more than 450 ppm deshielding per unit positive charge in both systems (*cf.* 460 ppm for **15**, 418 ppm for **16**).

According to *ab initio* calculations at the B3LYP/6-31G* level of theory[13] the dications **5** and **10** are of C_{2v} symmetry and the central C4 units have rectangular geometries very similar to the reference dications **15** and **16** (Fig. 1). As opposed to the hypersurface of the neutral species and the radical cations (tight isomers **3**, **8**; extended isomers **4**, **9**) there is only one minimum on both dicationic hypersurfaces. Evidently, σ-bishomoaromaticity provides the energy in dication **5** for the lengthening (shortening) of the a(b)-bonds by 0.651 (0.054) Å with respect to precursor **3** [by 0.857 (0.136) Å relative to **1**], in dication **10** for shortening (lengthening) by 0.115 (0.072) Å with respect to **9** [by 0.484 (0.092) Å relative to diene **7**].[14] The dications **5** and **10** (like **15** and **16**) can be viewed as frozen Woodward–Hoffmann allowed transition states of [1 + 1] cycloadditions of two ethylene radical cations with lengths of the a-bonds which are close to the mean values of the two isomers on the symmetry forbidden neutral [2+2] and radical cationic [2 + 1]cycloaddition energy hypersurfaces.

Support at USC by the Loker Hydrocarbon Research Institute and the National Science Foundation, at Freiburg and Braunschweig by the BASF AG, the Deutsche Forschungsgemeinschaft and the Fonds der Chemischen Industrie is gratefully acknowledged.

Notes and references

1 K. Scheumann, E. Sackers, M. Bertau, J. Leonhardt, D. Hunkler, H. Fritz, J. Wörth and H. Prinzbach, *J. Chem. Soc., Perkin Trans. 2*, 1998, 1195 and literature cited therein.

2 G. K. S. Prakash, V. V. Krishnamurthy, R. Herges, R. Bau, H. Yuan, G. A. Olah, W.-D. Fessner and H. Prinzbach, *J. Am. Chem. Soc.*, 1986, **108**, 836; G. K. S. Prakash, V. V. Krishnamurthy, R. Herges, R. Bau, H. Yuan, G. A. Olah, W.-D. Fessner and H. Prinzbach, *J. Am. Chem. Soc.*, 1988, **110**, 7764; G. K. S. Prakash, *New Carbocations and Dications*, in *Stable Carbocation Chemistry*, ed. G. K. S. Prakash and P. v. R. Schleyer, Wiley, N.Y., 1997, p. 137.

3 R. Herges, P. v. R. Schleyer, M. Schindler and W.-D. Fessner, *J. Am. Chem. Soc.*, 1991, **113**, 3649.

4 H. Prinzbach, G. Gescheidt, H.-D. Martin, R. Herges, J. Heinze, G. K. S. Prakash and G. A. Olah, *Pure Appl. Chem.*, 1995, **67**, 673; A. Trifunac, D. Werst, R. Herges, H. Neumann, H. Prinzbach and M. Etzkorn, *J. Am. Chem. Soc.*, 1996, **118**, 9444.

5 For the recent synthesis (and one-electron oxidation) of [2.2.2.2]iso pagodanes **A**/**B** ($m = n = 2$) see M. Etzkorn, F. Wahl, M. Keller, H. Prinzbach, F. Barbosa, V. Peron, G. Gescheidt, J. Heinze and R. Herges, *J. Org. Chem.*, 1998, **63**, 6080.

6 M. Wollenweber, R. Pinkos and H. Prinzbach, *Angew. Chem., Int. Ed. Engl.*, 1994, **33**, 117.

7 G. Gescheidt, R. Herges, H. Neumann, J. Heinze, M. Wollenweber, M. Etzkorn and H. Prinzbach, *Angew. Chem., Int. Ed. Engl.*, 1995, **34**, 1016.

8 H. Prinzbach, M. Wollenweber, R. Herges, H. Neumann, G. Gescheidt and R. Schmidlin, *J. Am. Chem. Soc.*, 1995, **117**, 1439.

9 Chemical shifts are referenced from external acetone-d_6 capillary signal (^{13}C shift from CD_3 septet at δ 29.8; ^1H shift from residual CHD_2 quintet at δ 2.09).

10 Pagodane **7**, not, however, **1**, underwent $2\sigma \rightarrow 2\pi$ isomerization (**8**) upon photosensitized electron transfer. M. Etzkorn, Dissertation, University of Freiburg, 1998; D. Heimbach, Diplomarbeit, 1995.

11 GIAO: R. McWeeny, *Phys. Rev.*, 1962, 1028; H. Hameka, *Mol. Phys.*, 1958, **1**, 203.

12 P. v. R. Schleyer, D. Lenoir, P. Mison, G. Liang, G. K. S. Prakash and G. A. Olah, *J. Am. Chem. Soc.*, 1980, **102**, 683. The sum of the ^{13}C NMR chemical shifts of the dications is compared with the sum of the ^{13}C NMR chemical shifts of the precursor isopagodanes.

13 GAUSSIAN 98, Revision B. M. I. Grisch, G. W. Grucks, M. Head-Gordon, P. M. W. Gill, M. W. Wong, I. B. Foresman, B. G. Johnson, H. B. Schlegel, M. A. Robb, E. S. Repogle, R. Gomperts, I. L. Andres, K. Raghavachari, I. S. Binkley, C. Gonzale, R. L. Martin, D. J. Fox, D. J. Defrees, J. Baker, J. J. P. Stewart and J. A. Pople, Gaussian, Inc., Pittsburgh PA, 1998.

14 *Cf.* the dimensions of 2.63/1.38 Å and of 2.50/1.42 Å for the recently described σ-bishomoaromatic N4/6e dianions and N4/2e dications: K. Exner, D. Hunkler, G. Gescheidt and H. Prinzbach, *Angew. Chem., Int. Ed.*, 1998, **37**, 1910; K. Exner, H. Prinzbach, G. Gescheidt, B. Großmann and J. Heinze, *J. Am. Chem. Soc.*, 1999, **121**, 1964.

Communication 9/01202H

Unexpected migration of the indenyl ligand in the reaction of alkynyl(η^5-indenyl)iron complexes with phosphanes and phosphites from iron to the alkynyl group

Helmut Fischer* and Peter A. Scheck

Fakultät für Chemie, Universität Konstanz, Fach M727, D-78457 Konstanz, Germany.
E-mail: hfischer@dg6.chemie.uni-konstanz.de

Received (in Cambridge, UK) 8th April 1999, Accepted 29th April 1999

Novel indenylvinylidene iron complexes are formed in the reaction of alkynyl(η^5-indenyl)iron complexes with phosphites and phosphanes in large excess by an intermolecular transfer of the indenyl ligand from iron to the C_β atom of the alkynyl ligand; mechanistic studies indicate that the reaction proceeds by a radical pathway.

Many associative substitution reactions of coordinatively saturated cyclopentadienyl and indenyl complexes have been documented.[1] These reactions have been interpreted as proceeding *via* an $\eta^5 \rightarrow \eta^3 \rightarrow \eta^5$ ring slippage.[2] The conversion of η^5- to isolable η^3- or even η^1-cyclopentadienyl or indenyl complexes has also been observed.[3] The cleavage of the cyclopentadienyl ligand as $[C_5H_5]^-$ from [(η^5-Cp)(CO)(NO)Re–Me] or *mer*-[(η^1-Cp)(NO)(PMe_3)$_3$Re–Me] in the reaction with PMe_3 in large excess to give ionic *trans*-[(NO)(PMe_3)$_4$Re–Me]$^+$[C_5H_5]$^-$ has also been described.[4] Finally, the loss of the indenyl ligand formally as a cation and the formation of [R_3P(Ind)]$^+$ in the reaction of [Cp(η^5-Ind)(CO)$_2$Mo]$^{2+}$ with PR_3 was recently proposed by Romão and coworkers.[5] We now report on (i) an unusual temperature-controlled product selectivity in the reaction of (alkynyl)(η^5-indenyl)iron complexes with phosphites and phosphanes, (ii) the novel transformation of (alkynyl)(η^5-indenyl)iron complexes into vinylidene complexes by reaction with PR_3, and (iii) the first evidence for the release of the indenyl ligand as a radical.

The alkynyl(dicarbonyl)(η^5-indenyl)iron complexes [(η^5-Ind)(CO)$_2$Fe–C≡CR] (R = Ph **1a**, C_6H_4Me-*p* **1b**, Me **1c**, $SiMe_3$ **1d** or C≡CBu^n **1e**) react in refluxing Bu_2O with a slight excess of $P(OMe)_3$ within a few minutes by substitution of $P(OMe)_3$ for one CO ligand to form a racemic mixture of [(η^5-Ind)(CO){$P(OMe)_3$}Fe–C≡CR] **2a**–**e**. However, when **1a**–**e** is heated in neat $P(OMe)_3$ for *ca.* 4 h at 70 °C, the complexes **2a**–**e** are formed in only minor amounts. The major products are the novel monocarbonyl-vinylidene complexes [CO{$P(OMe_3)_3$}-Fe=C=C(inden-1-yl)R] **3a**–**e** (Scheme 1).† The complexes **3a**–**e** are derived from **1a**–**e** by substitution of $P(OMe)_3$ for one CO ligand, addition of two more molecules of $P(OMe)_3$ and an unusual transfer of the indenyl group from iron to the C_β atom of the alkynyl ligand. Such a migration is without precedence. The migration is highly selective. In the reaction of **1e** with $P(OMe)_3$, in addition to **2e**, only the vinylidene complex **3e** is observed. The alternative butatrienylidene complex that would have been formed by migration of the indenyl ligand to the C_δ atom of the butadiynyl ligand could not be detected.

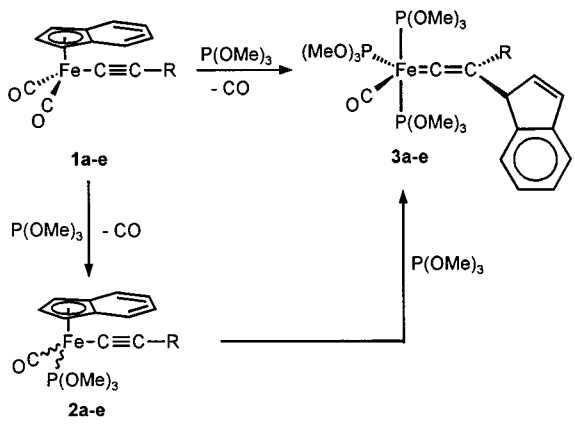

R = Ph (**a**), $C_6H_4CH_3$ (**b**), Me (**c**), $SiMe_3$ (**d**), C≡CBu^n (**e**)

Scheme 1

The product ratio **2a**–**e**:**3a**–**e** is strongly temperature dependent. With increasing temperature it is shifted towards the substitution product **2**. On prolonged heating at 70 °C in neat $P(OMe)_3$ the alkynyl complexes **2a**–**d** are also transformed into the vinylidene complexes **3a**–**d**.

When the nucleophilicity of the alkynyl C_β atom is changed by variation of its substituent (R = Me, C_6H_4OMe-*p*, C_6H_4Me-*p*, Ph, C_6H_4Br-*p*, $SiMe_3$) the product distribution and the reaction rate are only slightly influenced. Therefore, a bimolecular mechanism *via* a nucleophilic attack of the alkynyl C_β atom at an indenyl ligand is unlikely. In contrast, the steric requirements of the P-donors considerably influence the reaction rate and the product distribution. For instance, **1a** reacts significantly more slowly with $P(OEt)_3$ than with $P(OMe)_3$. When the even bulkier $P(OPr^i)_3$ or PPh_3 are employed in the reaction with **1a** no monocarbonyl-vinylidene complex analogous to **3a**–**e** is formed but rather a dicarbonyl-vinylidene complex [$(CO)_2(PR_3)_3$Fe=C=C(inden-1-yl)Ph] (R = OPr^i **4** or Ph **5** in addition to the substitution product [(η^5-Ind)-(CO)(PR_3)Fe–C≡CPh] (Scheme 2). The latter cannot be transformed into a vinylidene complex.

Labelling studies show that the Fe/C_β migration of the indenyl ligand proceeds by an intermolecular pathway. The reaction of a 1:1 mixture of undeuterated **1a** and [(η^5-1,3-$C_9H_5D_2$)$(CO)_2$Fe–C≡C–C_6D_5] ([D_7]-**1a**) with $P(OMe)_3$ at 70 °C affords [D_0]-, [D_2]-, [D_5]- and [D_7]-**3a** in a ≈ 1:1:1:1 ratio as determined by mass spectrometry.

In the reaction of **1a** with PPh_3, complex **5** is formed independent of whether the reaction is carried out in toluene, EtOH or EtOH–H_2O (20:1). Therefore, the formation of [C_7H_9]$^+$ and [$(CO)_2(PPh_3)_2$Fe–C≡CPh]$^-$ or of [C_7H_9]$^-$ and [$(CO)_2(PPh_3)_2$Fe–C≡CPh]$^+$ as intermediates is unlikely. Since [$(CO)_2(PPh_3)_2$Fe–C≡CPh]$^-$ and [C_7H_9]$^-$ are rapidly trapped in a large excess of EtOH–H_2O as [$(CO)_2(PPh_3)_2$Fe=C=C(H)Ph] and indene, respectively, complex **5** should not be formed.

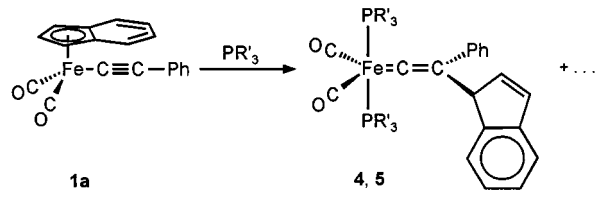

R′ = OPr^i (**4**), Ph (**5**)

Scheme 2

The most probable mechanism involves dissociation of the indenyl ligand as a radical and subsequent addition of $[C_7H_9]^{\cdot}$ to the alkynyl C_β atom of either $[(CO)(PR'_3)_3Fe–C{\equiv}CR]^{\cdot}$ or $[(CO)_2(PR'_3)_2Fe–C{\equiv}CR]^{\cdot}$. This mechanistic proposal is supported by two observations: (i) addition of the radical-scavenger galvinoxyl to the reaction mixture of **1a** and $P(OMe)_3$ efficiently inhibits the formation of **3a** but does not affect the formation of the substitution product **2a**; (ii) dimerization of the indenyl radical to give bisindenyl, $C_{14}H_{18}$, is preferentially observed when the addition of the indenyl radical to the alkynyl C_β atom is hindered by the sterically demanding mesityl (Mes) substituent. Then, only small amounts of the corresponding vinylidene complex, [CO{P(OMe)$_3$}$_3$Fe=C=C(inden-1-yl)Mes], are formed. In addition, small amounts of 1,4-bis-(mesityl)butadiyne are obtained. The butadiyne is presumably formed by decomposition of the 17-electron intermediate [CO{P(OMe)$_3$}$_3$Fe–C≡CMes].

The indenyl radical intermediates are very likely stabilized by addition to the phosphites or phosphanes which are present in the reaction mixture in a large excess. The reversible addition of radicals to PR_3 is well known.[6] The resulting phosphoranyl radical $[R_3P(Ind)]^{\cdot}$ would then act as a mediator. The assumption is supported by the following observation: when the *methyl*indenyl complex [(η^5-1-Me-Ind)(CO)$_2$Fe-C≡CPh] is treated with $P(OMe)_3$ in the presence of a mixture of $P(Ind)_3$ and $P(Ind)_2OMe$, both [CO{P(OMe)$_3$}$_3$Fe=C=C(1-Me-inden-1-yl)Ph] *and* [CO{P(OMe)$_3$}$_3$Fe=C=C(inden-1-yl)Ph] are formed in nearly equal amounts.

The results demonstrate a novel route to vinylidene complexes. Presumably, the transformation mode can also be extended to other complexes such as alkynyl(allyl) and alkynyl(fluorenyl) complexes. Based on previous results,[4,5] we initially assumed that the transformation most likely proceeds by an ionic pathway *via* either an indenyl anion or cation. However, all observations indicate a radical mechanism. Presumably, more organometallic reactions proceed by a radical mechanism than anticipated. There are some experimental hints that the proposed 17-electron intermediate is rather long-lived and can be intercepted also with other substrates. Recently, several other related 17-electron iron complexes $[(CO)_2(PR_3)_2FeX]$ (X = Br or I)[7] and [{P(CH$_2$CH$_2$PPh$_2$)$_3$}FeC≡CR][8] have been isolated and structurally characterized.

Financial support of this work by the Fonds der Chemischen Industrie is gratefully acknowledged.

Notes and references

† *Selected spectroscopic data*: IR (CH_2Cl_2): ν(CO): 1906 (**3a**), 1917 (**3b**), 1917 (**3c**), 1902 (**3d**), 1918 (**3e**), 1907, 1974 (**4**), 1896, 1962 cm^{-1} (**5**); ^{13}C NMR ($CDCl_3$, 0 °C): δ(Fe=C) 312.8 (q, *J* 42 Hz) (**3a**), 313.8 (q, *J* 42 Hz) (**3b**), 307.9 (q, *J* 42 Hz) (**3c**), 310.6 (q, *J* 41 Hz) (**3d**), 315.5 (q, *J* 41 Hz) (**3e**), 325.5 (t, *J* 63 Hz) (**4**), 325.2 (t, *J* 48 Hz) (**5**); ^{31}P NMR ($CDCl_3$): δ 177.54 (**3a**), 177.68 (**3b**), 178.93 (**3c**), 180.16 (**3d**), 175 (**3e**), 165.05 (**4**), 73.54 (**5**).

1 See, for example: J. A. S. Howell and P. M. Burkinshaw, *Chem. Rev.*, 1983, **83**, 557; F. Basolo, *Inorg. Chim. Acta*, 1985, **100**, 33; J. M. O'Connor and C. P. Casey, *Chem. Rev.*, 1987, **87**, 307; F. Basolo, *Polyhedron*, 1990, **9**, 1503.

2 A. J. Hart-Davis and R. J. Mawby, *J. Chem. Soc. A*, 1969, 2403.

3 See, for example: $\eta^5 \rightarrow \eta^3$: T. C. Forschner, A. R. Cutler and R. K. Kullnig, *Organometallics*, 1987, **6**, 889; $\eta^5 \rightarrow \eta^1$: H. Werner and A. Kühn, *Angew. Chem.*, 1979, **91**, 416; *Angew. Chem., Int. Ed. Engl.*, 1979, **91**, 447; C. P. Casey and W. D. Jones, *J. Am. Chem. Soc.*, 1980, **102**, 6154.

4 C. P. Casey, J. M. O'Connor and K. J. Haller, *J. Am. Chem. Soc.*, 1985, **107**, 1241.

5 C. A. Gamelas, E. Herdtweck, J. P. Lopes and C. C. Romão, *Organometallics*, 1999, **18**, 506.

6 See, for example: W. G. Bentrude, *Phosphorus Sulfur*, 1977, **3**, 109; B. P. Roberts, *Adv. Free Radical Chem.*, 1980, **6**, 225.

7 H. Kandler, C. Gauss, W. Bidell, S. Rosenberger, T. Bürgi, I. L. Eremenko, D. Veghini, O. Orama, P. Burger and H. Berke, *Chem. Eur. J.*, 1995, **1**, 541.

8 C. Bianchini, F. Laschi, D. Masi, F. M. Ottaviani, A. Pastor, M. Peruzzini, P. Zanello and F. Zanobini, *J. Am. Chem. Soc.*, 1993, **115**, 2723.

Communication 9/02785H

ChemComm

Novel η^1-alkynyl zirconium porphyrin complexes: synthesis and characterization of (por)Zr(η^1-C≡CR)$_3$Li(THF) [por = octaethylporphyrinato (oep) or tetraphenylporphyrinato dianion (tpp); R = Ph, SiMe$_3$]

Hee-Joon Kim, Sungkyung Jung, You-Moon Jeon, Dongmok Whang and Kimoon Kim*

National Creative Research Initiative Center for Smart Supramolecules and Department of Chemistry, Pohang University of Science and Technology, San 31 Hyojadong, Pohang 790-784, South Korea.
E-mail: kkim@postech.ac.kr

Received (in Cambridge, UK) 10th March 1999, Accepted 21st April 1999

Reaction of (por)ZrCl$_2$ [por = 2,3,7,8,12,13,17,18-octaethylporphyrinato dianion (oep) or 5,10,15,20-tetraphenylporphyrinato dianion (tpp)] with 3 equiv. of LiC≡CR (R = Ph and SiMe$_3$) produces novel alkynyl zirconium(IV) porphyrin complexes (por)Zr(η^1-C≡CR)$_3$Li(THF) in which three alkynyl ligands are coordinated to the zirconium center in a piano stool fashion and the Li$^+$ ion is bound to the pocket formed by three alkynyl ligands; treatment of (por)Zr(η^1-C≡CPh)$_3$Li(THF) with anhydrous HCl produces a C–C bond coupled product H$_2$C=CPh(C≡CPh) and HC≡CPh quantitatively.

Although early transition metal porphyrin complexes have received considerable attention in recent years,[1] the chemistry still remains in large part undeveloped. We[2] and others[3,4] have prepared organometallic zirconium porphyrin complexes and investigated their chemistry. As part of our work on organometallic zirconium porphyrin complexes, we are interested in alkynyl zirconium porphyrin complexes. Alkynyl metal complexes have been known to be involved in linear- and cyclooligomerization of terminal alkynes by various d-block[5] and f-block[6] metals. Alkynyl ligands σ-bonded to a metal center are also able to coordinate to other metal centers by using π-electrons of the C≡C groups. A variety of bridging fashions have been found in alkynyl bridged multinuclear complexes.[7] However, there are few transition metal alkynyl complexes containing three alkynyl ligands coordinated to a single metal center.[8] Here we report the synthesis and characterization of novel alkynyl zirconium porphyrin complexes. They are not only the first well-characterized alkynyl metalloporphyrin complexes[9] but also rare examples of trialkynyl transition metal complexes.

Alkynyl zirconium porphyrin complexes **1a**,**b**, **2a**,**b** were synthesized in high yields by the reactions of (por)ZrCl$_2$ with 3 equiv. of LiC≡CR.†

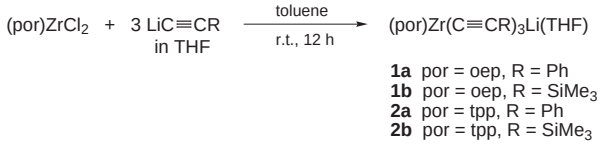

The ^{1}H NMR signals for the phenyl and the SiMe$_3$ protons of the alkynyl ligands coordinated to the (por)Zr moiety in **1a**–**2b** are shifted to higher field owing to the ring current of the porphyrin ligand. The diastereotopic methylene signals for the oep ligand in **1a** and **1b** indicates that the environments of the two sides of the porphyrin are different in these complexes. In addition, the significant upfield shift of the signals for one THF molecule implies that the THF molecule is located above the porphyrin ring current. The THF molecule is easily displaced by an excess of diethyl ether, as judged by NMR spectroscopy.

The structure of **1a** has been confirmed by X-ray crystallography (Fig. 1).‡ Three alkynyl groups are attached to the zirconium on one side of the (oep)Zr unit. The coordination geometry around the zirconium is best described as a 4 : 3 piano stool with the porphyrin occupying the square base. The Li$^+$ is coordinated by three C≡C bonds of the alkynyl ligands and one THF molecule in a pseudotetrahedral coordination geometry. The overall structure of **1a** is consistent with that in solution. The crystal structure of **1a** also suggests that the larger upfield shifted ^{1}H NMR signals for the THF molecule in **1a** than those in **1b** are due to the additional ring current of the three phenyl groups. The Zr–N bond distances range from 2.253(3) to 2.272(4) Å with an average value of 2.259(7) Å. The Zr atom is displaced 1.008 Å from the mean N$_4$ plane. The Zr–C bond distances in **1a** [2.305(10), 2.329(10) and 2.334(10) Å] are somewhat longer than those in (oep)Zr(CH$_2$SiMe$_3$)$_2$ [2.285(4), 2.289(4) Å],[3a] but shorter than those in (oep)ZrMe$_2$ [2.352(4), 2.334(4) Å].[3b] The Zr–C bond distances in **1a** are significantly longer than those in (C$_5$Me$_5$)$_2$Zr(C≡CPh)$_2$ [2.19(3), 2.21(3) Å],[10] which may be attributed to the large steric congestion caused by three alkynyl ligands in **1a**. However, the C≡C distances [1.210(12), 1.230(12) and 1.215(12) Å] in **1a** are similar to those in (C$_5$Me$_5$)$_2$Zr(C≡CPh)$_2$ [1.23(4) and 1.24 (4) Å]. The THF molecule is coordinated to the Li$^+$ along the Zr···Li axis (Zr···Li–O angle 175.8°) with a Li–O bond distance of 1.905(8) Å. The Zr···Li distance of 3.071(8) Å shows no direct interaction between two metal centers.

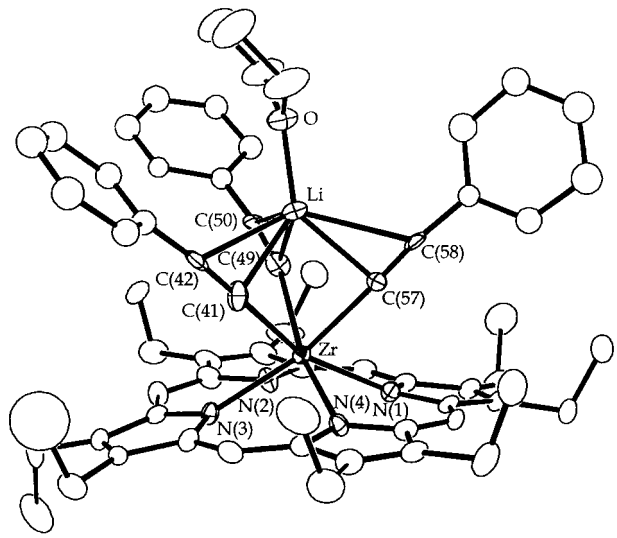

Fig. 1 Structure of (oep)Zr(η^1-C≡CPh)$_3$Li(THF) **1a**. Selected bond distances (Å) and angles (°): Zr–N(1) 2.254(4), Zr–N(2) 2.257(3), Zr–N(3) 2.272(4), Zr–N(4) 2.253(3), Zr–C(41) 2.334(10), Zr–C(49) 2.329(9), Zr–C(57) 2.305(10), Li–C(41) 2.212(12), Li–C(49) 2.240(12), Li–C(57) 2.227(12), Li–C(42) 2.611(12), Li–C(50) 2.676(12), Li–C(58) 2.590(12), C(41)–C(42) 1.210(12), C(49)–C(50) 1.230(12), C(57)–C(58) 1.215(12), Li–O 1.905(8), Zr···Li 3.071(8), C(41)–Zr–C(49) 77.2(3), C(49)–Zr–C(57) 78.3(3), C(41)–Zr–C(57) 76.8(3), Zr···Li–O 175.8.

Complexes **1a**–**2b** are highly sensitive to moisture similarly to other alkyl zirconium porphyrin complexes. Upon the addition of water, they are readily hydrolyzed to produce the corresponding acetylene HC≡CR and hydroxo-bridged dimeric zirconium porphyrins.[2b] On the other hand, treatment of **1a** with anhydrous HCl in C_6D_6 produces quantitatively a C–C bond coupled product H_2C=CPh(C≡CPh) and HC≡CPh along with (oep)$ZrCl_2$. In contrast, under the same conditions **1b** produces mainly the simple alkyne HC≡$CSiMe_3$ along with (*E*)-Me_3-SiCH=CHC≡$CSiMe_3$ as a minor product. The tpp analogs **2a** and **2b** show similar reactivities. It is not surprising that **1b** and **2b** exhibit different reactivity and regioselectivity from **1a** and **2a**. Such differences of the dimerization of terminal alkynes have been found in the literature,[5,6] which is believed to be due to the different electronic effect of the substituent on the alkyne. Negishi and coworkers reported similar reactivities of Li[$Cp_2Zr(C{\equiv}CPh)_3$] which is generated *in situ* from the reaction of Cp_2ZrCl_2 with 3 equiv. of LiC≡CPh.[11] Upon quenching Li[$Cp_2Zr(C{\equiv}CPh)_3$] with aqueous HCl, (*Z*)-PhCH=CHC≡CPh was produced as an isomerically pure compound. They proposed that C–C bond formation proceeds *via* a non-dissociative mechanism such as 1,2-migration of an alkynyl group. The mechanism of C–C bond formation in our case is still unclear, but the following observation is informative. Treatment of **1a** or **2a** with anhydrous HCl in the presence of an excess of HC≡CR (R = *p*-Tol, $SiMe_3$) produces only H_2C=CPh(C≡CPh) as a C–C bond coupled product without cross-coupled products such as H_2C=CPh(C≡CR) or H_2C=CR(C≡CPh). The result implies that C–C bond formation does not proceed *via* the dissociative pathway involving the reinsertion of free HC≡CPh into the Zr–C≡CPh, followed by protonolysis.

We have also attempted to synthesize the dialkynyl complexes (por)Zr$(C{\equiv}CR)_2$ using 2 equiv. of LiC≡CR, but the reaction afforded (por)Zr$(C{\equiv}CR)_3$Li(THF) as the major product. This is in sharp contrast to the zirconocene case in which stable dialkynyl complexes are isolated.[12] More electropositive metal centers of the Zr(por) unit compared to the Cp_2Zr moiety may account for their different reactivities.

In summary, we synthesized the novel trialkynyl zirconium porphyrin complexes (por)Zr(η^1-C≡CR)$_3$Li(THF). The porphyrin complexes show different reactivities compared to the analogous Cp_2 complex. Further studies on the mechanism of the enyne formation upon treatment of the alkynyl complexes with HCl as well as other reactivities of the alkynyl zirconium porphyrin complexes are underway. These complexes may be useful entries to a variety of bimetallic porphyrin complexes by replacing Li^+. Work along this line is also in progress.

We gratefully acknowledge support from the Korea Research Foundation (Non Directed Research Fund, 1996) and in part from Korea Science and Engineering Foundation through Center for Biofunctional Molecules.

Notes and references

† (oep)Zr(η^1-C≡CPh)$_3$Li(THF) **1a**: to a suspension of (oep)$ZrCl_2$ (0.280 g, 0.40 mmol) in toluene (*ca.* 30 mL) was slowly added a THF solution (*ca.* 3 mL) of LiC≡CPh (0.132 g, 1.22 mmol). The reaction mixture was stirred at room temp. for 12 h and then filtered. The solvent was removed under reduced pressure to give **1a** as a dark red solid in 92% yield. Analytically pure material was recrystallized from toluene–pentane. ^{1}H NMR (300 MHz, C_6D_6): δ 10.67 (s, 4H, *meso*-H), 6.78 (m, 9H, *m*-, *p*-Ph), 6.66 (d, 6H, *o*-Ph), 4.07 (m, 16H, CH_2CH_3), 2.14 (br s, 4H, α-THF), 1.89 (t, 24H, CH_2CH_3), 0.15 (br s, 4H, β-THF). IR (KBr, cm^{-1}): ν 2066 (C≡C). UV–VIS (toluene, nm): λ_{max} (log ε) 400 (5.24), 532 (4.31), 568 (4.58). MS (FAB): *m*/*z* 933 ([M − THF]H$^+$), 831 ([M − THF − C≡CPh]$^+$). Anal. Calc. for $C_{64}H_{67}N_4OLiZr$: C, 76.37; H, 6.72; N, 5.57. Found: C, 76.41; H, 6.36; N, 5.87%.

(oep)Zr(η^1-C≡$CSiMe_3$)$_3$Li(THF) **1b**: **1b** was synthesized from (oep)$ZrCl_2$ and LiC≡$CSiMe_3$ in 83% yield after recrystallization from pentane by the same procedure as for **1a**. ^{1}H NMR (300 MHz, C_6D_6): δ 10.55 (s, 4H, *meso*-H), 4.24 (m, 8H, CH_2CH_3), 3.98 (m, 8H, CH_2CH_3), 2.70 (br s, 4H, α-THF), 1.86 (t, 24H, CH_2CH_3), 0.72 (br s, 4H, β-THF), −0.18 [s, 27H, Si$(CH_3)_3$]. IR (KBr, cm^{-1}): ν 2010 (C≡C). UV–VIS (toluene, nm): λ_{max} (log ε) 400 (5.32), 532 (4.03), 568 (4.37). MS (FAB): *m*/*z* 921 ([M − THF]H$^+$), 823 ([M − THF − C≡$CSiMe_3$]$^+$). No satisfactory elemental analysis was obtained due to extreme air/moisture sensitivity.

Using the same procedure as for **1a** (tpp)Zr(η^1-C≡CPh)$_3$Li(THF) **2a** was synthesized from (tpp)$ZrCl_2$ and LiC≡CPh in 61% yield after recrystallization from toluene–pentane. Likewise, (tpp)Zr(η^1-C≡$CSiMe_3$)$_3$Li(THF) **2b** was synthesized from (tpp)$ZrCl_2$ and LiC≡$CSiMe_3$ in 72% yield after recrystallization. Full experimental data and descriptions of reactions as well as details of crystal data and structural refinement can be accessed electronically: see http://www.rsc.org/suppdata/cc/1999/1033.

‡ *Crystal data*: for **1a**: $C_{60}H_{59}N_4LiZr{\cdot}C_4H_8O$, *M* = 1006.38, monoclinic, *C*2/*c* (no. 15), *a* = 19.265(6), *b* = 19.952(3), *c* = 28.991(12) Å, β = 104.88(2)°, *U* = 10769(6) Å^3, *Z* = 8, μ(Mo-Kα) = 2.5 cm^{-1}, *T* = 188 K, Enraf-Nonius CAD4 diffractometer, Mo-Kα (λ = 0.71073 Å), anisotropic refinement for all nonhydrogen atoms (except for phenyl groups), final cycle of full matrix least squares refinement on F^2 with 6593 independent reflections and 705 variables (SHELXL-93), $R1$ [$I > 2\sigma(I)$] = 0.0535, $wR2$ (all data) = 0.1331, GOF = 1.039. CCDC 182/1233. See http://www.rsc.org/suppdata/cc/1999/1033/ for crystallographic files in .cif format.

1 H. Brand and J. Arnold, *Coord. Chem. Rev.*, 1995, **140**, 137.
2 (*a*) H.-J. Kim, D. Whang, K. Kim and Y. Do, *Inorg. Chem.*, 1993, **32**, 360; (*b*) H.-J. Kim, D. Whang, Y. Do and K. Kim, *Chem. Lett.*, 1993, 807; (*c*) S. Ryu, D. Whang, H.-J. Kim, K. Kim, M. Yoshida, K. Hashimoto and K. Tatsumi, *Inorg. Chem.*, 1997, **36**, 4607; (*d*) H.-J. Kim, S. Jung, Y.-M. Jeon, D. Whang and K. Kim, *Chem. Commun.*, 1997, 2201.
3 (*a*) H. Brand and J. Arnold, *J. Am. Chem. Soc.*, 1992, **114**, 2266; (*b*) H. Brand and J. Arnold, *Organometallics*, 1993, **12**, 3655; (*c*) J. Arnold, S. E. Johnson, C. B. Knobler and M. F. Hawthorne, *J. Am. Chem. Soc.*, 1994, **13**, 4469; (*d*) H. Brand, J. A. Capriotti and J. Arnold, *Organometallics*, 1994, **13**, 4469; (*e*) H. Brand and J. Arnold, *Angew. Chem., Int. Ed. Engl.*, 1994, **33**, 95.
4 K. Shibata, T. Aida and S. Inoue, *Tetrahedron Lett.*, 1992, **33**, 1077; K. Shibata, T. Aida and S. Inoue, *Chem. Lett.*, 1992, 1173.
5 C. S. Yi and N. Liu, *Organometallics*, 1996, **15**, 3968 and references therein.
6 H. J. Heeres, A. Heeres and J. H. Teuben, *Organometallics*, 1990, **9**, 1508; T. Straub, A. Haskel and M. S. Eisen, *J. Am. Chem. Soc.*, 1995, **117**, 6364.
7 R. Nast, *Coord. Chem. Rev.*, 1982, **47**, 89; S. Lotz, P. H. van Rooyen and R. Meyer, *Adv. Organomet. Chem.*, 1995, **37**, 219.
8 M. A. Putzer, B. Neumüller and K. Dehnicke, *Z. Anorg. Allg. Chem.*, 1997, **623**, 539; S. Tanaka, T. Yoshida, T. Adachi, T. Yoshida, K. Initsuka and K. Sonogashira, *Chem. Lett.*, 1994, 877.
9 Formation of an alkynyl lutetium porphyrin dimer has been reported. However, neither the dimeric nature nor the structure of the compound was confirmed: C. J. Schaverien and A. G. Orpen, *Inorg. Chem.*, 1991, **30**, 4968.
10 Z. Hou, T. L. Breen and D. W. Stephan, *Organometallics*, 1993, **12**, 3158.
11 K. Takagi, C. J. Rousset and E. Negishi, *J. Am. Chem. Soc.*, 1991, **113**, 1440.
12 G. Erker, W. Frömberg, R. Benn, R. Mynott, K. Angermund and C. Krüger, *Organometallics*, 1989, **8**, 911.

Communication 9/01923E

ChemComm

Assembling nanosized ring-shaped synthons to an anionic layer structure based on the synergetically induced functional complementarity of their surface-sites: $Na_{21}[Mo^{VI}_{126}Mo^{V}_{28}O_{462}H_{14}(H_2O)_{54}(H_2PO_2)_7]\cdot xH_2O$ ($x \approx 300$)

Achim Müller,* Samar K. Das, Hartmut Bögge, Christian Beugholt and Marc Schmidtmann

Fakultät für Chemie der Universität, D-33501 Bielefeld, Germany. E-mail: a.mueller@uni-bielefeld.de

Received (in Basel, Switzerland) 25th February 1999, Accepted 19th April 1999

The reaction of an aqueous solution of sodium molybdate with hypophosphorous (phosphinic) acid acting both as reducing agent and ligand at low pH values (≈ 1) results in the formation of nanosized ring-shaped cluster units which assemble to form layers of the compound $Na_{21}[Mo^{VI}_{126}Mo^{V}_{28}O_{462}H_{14}(H_2O)_{54}(H_2PO_2)_7]\cdot xH_2O$ 1 ($x \approx 300$); the assemblage is based on the synergetically induced functional complementarity of amphiphilic O=MoL (L = H_2O, $H_2PO_2^-$) groups and corresponds to the replacement of H_2O ligands of rings by related terminal Mo=O groups of other rings (and *vice versa*) the nucleophilicity of which is induced by coordinated $H_2PO_2^-$ ligands.

One of the great challenges of modern chemistry is to create multifunctional structures which have well defined cavities and surfaces with sites or areas of different reactivity by linking preorganized robust building blocks/synthons.[1,2] Here we report the synthesis of a related metal–oxide based electron-rich compound built up by nanosized ring-shaped cluster units using a type of crystal engineering.

If an aqueous acidified solution of Na_2MoO_4 is reduced with hypophosphorous acid (H_3PO_2) in the presence of a rather high electrolyte (salt) concentration, blue crystals of **1** precipitate after a few days.† Compound **1** was characterized by elemental analysis, thermogravimetric analysis (to determine the crystal water content), cerimetric titrations [for the determination of the (formal) number of the (28) Mo^V centres], bond valence sum (BVS) calculations (to determine the number and positions of H_2O ligands and OH groups as well as the number of Mo^V centres), [3] spectroscopic methods (IR, resonance-Raman, VIS–NIR) ‡ and single-crystal X-ray structure analysis.§

$Na_{21}[Mo^{VI}_{126}Mo^{V}_{28}O_{462}H_{14}(H_2O)_{54}(H_2PO_2)_7]\cdot xH_2O$ **1**
$\equiv Na_{21}$**1a**$\cdot xH_2O$ ($x \approx 300$)

The crystal structure of **1** (space group *Cmca*)§ shows the abundance of nanosized ring-shaped units (crystallographic site symmetry 2/*m*) which are linked through covalent Mo–O–Mo bonds to give a layered structure (Fig. 1). In the crystallographic *ac* plane, each cluster ring is surrounded by four rings such that the anionic layer structure **1a** with condensed ring-shaped units parallel to the *ac* plane results. The packing of these layers gives rise to nanosized channels (Fig. 1) with 'encapsulated' $H_2PO_2^-$ ligands, while 7 of the 14 $\{Mo_2\}$-type groups of the 'parent' layer system [with only H_2O ligands (see **2a**)] show the coordination of 7 bidentate $H_2PO_2^-$ ions (which are statistically distributed over the ring system but always with one ligand per bridge). Since the corresponding discrete (non–condensed) ring-shaped cluster with only H_2O ligands, which is known as the Na^+ salt, has the stoichiometry[4] $[\{(O)_2{=}Mo^{VI}(H_2O)(\mu_2\text{-}O)(H_2O)Mo^{VI} = (O)_2\}^{2+}{}_{14}\{Mo^{VI/V}{}_8O_{26}(\mu_3\text{-}O)_2H(H_2O)_3\text{-}Mo^{VI/V}\}^{3-}{}_{14}]^{14-}$ ($\equiv [\{Mo_2\}_{14}\{Mo_8\}_{14}\{Mo_1\}_{14}]^{14-}$) **2a**, the building-block description for the corresponding hypothetical discrete unit of **1a**, with 14 H_2O ligands replaced by 7 bidentate $H_2PO_2^-$ ligands, is $[\{(O)_2{=}Mo^{VI}(\mu_2\text{-}H_2PO_2^-)_{0.5}(\mu_2\text{-}O)(H_2O)\text{-}Mo^{VI} = (O)_2\}^{1.5+}{}_{14}\{Mo^{VI/V}ir8O_{26}(\mu_3\text{-}O)_2H(H_2O)_3\text{-}Mo^{VI/V}\}^{3-}{}_{14}]^{21-}$ **3a**.

It can be assumed that the formation of the ring system **1a** based on the reducing power of the hypophosphorous acid constitutes the initial step of the reaction considered here. This is a reasonable assumption as the characteristic spectrum of the

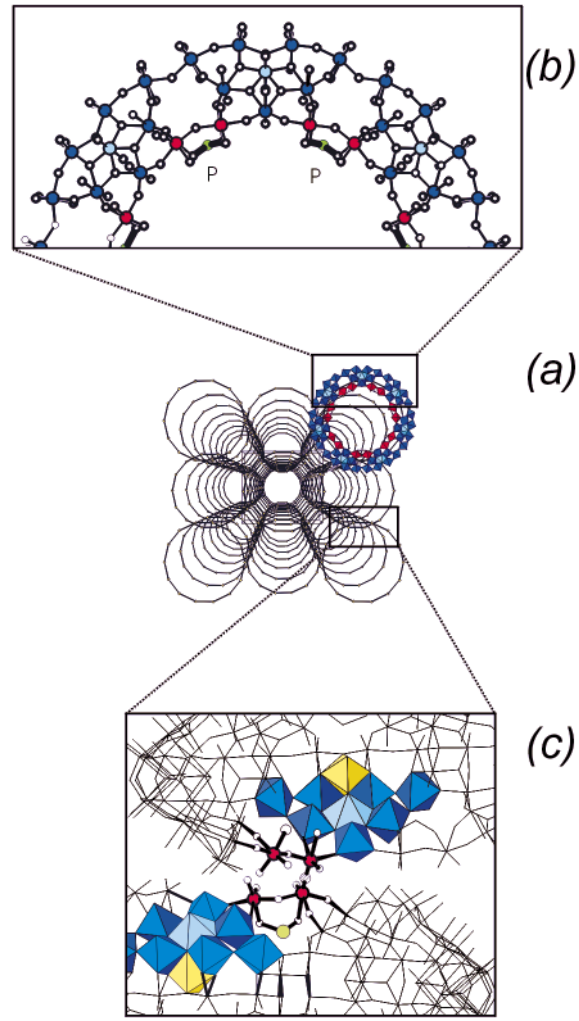

Fig. 1 (*a*) Perspective view of the cluster framework of **1** along the crystallographic *c* axis, showing the abundance of nanotubes and cavities. For clarity, only one complete ring (without the P ligands) is shown in polyhedral representation. With respect to the other rings, only the centres of the $\{Mo_1\}$ units are given and connected. (*b*) Ball-and-stick representation of the upper half of a ring segment showing the principal positions of the $H_2PO_2^-$ ligands. (*c*) Detailed view [perpendicular to (*a*) and (*b*)] of the bridging region between two cluster rings of **1** emphasizing one $\{Mo_8\}$, one $\{Mo_1\}$ unit (in polyhedral representation) as well as one $\{Mo_2\}^{2+}$ unit and one $H_2PO_2^-$ ligand (in ball-and-stick representation). The bridging (disordered) oxygen centre is depicted as a large hatched circle [colour code: $\{Mo_2\}$, red; $\{Mo_8\}$, blue (central MoO_7 pentagonal-bipyramid, light blue); $\{Mo_1\}$, yellow; P, green].

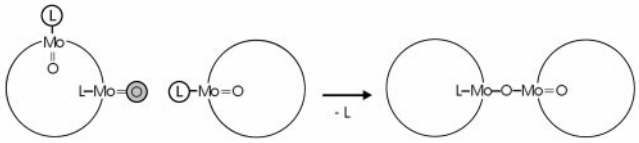

Fig. 2 Schematic presentation of the basic assembly principles of ring-shaped cluster units forming the layers of **1a** which are based on the synergetically induced functional complementarity of the $\{Mo_2\}$-type O=MoL (L = H_2O, $H_2PO_2^-$) sites of their surfaces: each precursor ring contains the corresponding virtual functional complementary O=Mo(H_2O) groups (becoming 'donors' due to the electron-donating $H_2PO_2^-$ replacing H_2O ligands and 'acceptors' without $H_2PO_2^-$ ligands).

discrete ring is observed after a few minutes, independent of the type of reducing agent used. The value accepted now for the charge of **1a** and all related compounds is in accord with the results of numerous Na analyses [4,5] and also with the analysis of the hydrogen-bond situation[5,6] in respect of the constant BVS values for the μ_3-O atoms of the equatorial (μ_3-O) · · · H · · · (μ_3-O) units.[4,5] Not only for the 'parent' system **2a** with only H_2O ligands but also for all known tetradecameric ring-shaped clusters without defects, the charge of 14− corresponds to the difference between the (formal) number of Mo^V centres and the number of protons at equatorial μ_3-O atoms.

The main difference between the discrete cluster **3a** and **1a** with the condensed clusters is that **1a** contains two $\{Mo_2\}$-type H_2O ligands less per formula unit. This is caused by the substitution of $\{Mo_2\}$-type H_2O ligands by terminal $\{Mo_2\}$-type Mo=O groups of neighbouring rings formally acting as ligands which results in the linkage of the rings (see formulae **2a** and **3a**). This means that each of the four connections of one ring unit corresponds to 0.5 H_2O molecules less per formula unit in **1a**. As the same $\{Mo_2\}$-type O=MoL group (L = H_2O, $H_2PO_2^-$) of the 'ring unit precursor' is involved in the present case, the linking procedure is based on a type of synergetically induced functional complementarity at the O=MoL sites of the cluster surfaces (see **2a** and **3a** as well as Fig. 2). In the crystal lattice the O=MoL groups are found for L = H_2O disordered in the sense that the O and L ligands can change their positions and the O=MoL group can thus act as 'donor' or 'acceptor'.

Because of the increased electron density (or the nucleophilicity/donor properties) of the considered Mo=O groups (when pointing to the outside of the ring), caused by the coordinated $H_2PO_2^-$ ligand, the related ring formally acts as a ligand due to a synergetic process resulting in the substitution of the H_2O ligand of a corresponding $\{Mo_2\}$-type Mo=O group of the adjacent ring which has no coordinated $H_2PO_2^-$ ligands (Fig. 2). In this context, it should be noted that in order to form the layer structure, not all H_2O ligands of the 14 $\{Mo_2\}$ groups have of course to be replaced by the abundant $H_2PO_2^-$ ligands.

The interesting aspects of this work are: (1) Giant robust ring-shaped building blocks can be linked together to form a well-defined layered network based on a type of crystal engineering, *i.e.* in this case based especially on the synergetically induced functional complementarity of relevant sites of the surfaces. (2) It is possible to place molecules/replace ligands at different sites of the surface of a giant cluster or within its cavity and subsequently change the properties of well defined regions of its surface (*e.g.* increase the nucleophilicity). (3) The investigation of reactions between molecules inside the cavity is in principle possible. (In this context, it is important to note that the system is metal–oxide based and electron rich, which allows activation of ligands.) The anion of the hypophosphorous acid, which is involved in each ring connection and coordinates as a bidentate ligand to the $\{Mo_2\}$ groups of **2a** by substituting two H_2O ligands of the 'parent' ring, can in principle be replaced by several other bidentate ligands, too.

We thank B. Hauptfleisch, C. Kuhlmann, F. Peters and Syed Q. N. Shah for their collaboration and Professor S. Sarkar (I.I.T. Kanpur, India) for helpful discussions. Financial support of the Deutsche Forschungsgemeinschaft and the Fonds der Chemischen Industrie is gratefully acknowledged.

Notes and references

† To a solution of $Na_2MoO_4{\cdot}2H_2O$ (3.04 g, 12.56 mmol) and NaCl (1.0 g, 17.11 mmol) in 25 mL of water which was acidified with 2.5 mL of hydrochloric acid (32%), hypophosphorous acid (0.2 mL, 50%, 1.93 mmol) was added as reducing agent. After stirring for 15 min under bubbling argon gas, the resulting solution was kept in a closed flask at room temperature. After 4 days the precipitated blue bipyramidal-shaped crystals were filtered, washed quickly with a small amount of cold water and dried at room temperature under argon. Yield: 0.38 g (16% based on Mo). (Note: the crystals should be separated out from the reaction mixture after 4 days, to avoid the coprecipitation of amorphous materials as after effect).

‡ *Selected data* for **1**: VIS–NIR (water) [λ_{max}/nm (ε/dm^3 mol^{-1} cm^{-1})]: 745 (1.59×10^5), 1070 (1.15×10^5). VIS/NIR (KBr pellet, in transmission) (λ_{max}/nm): 750 (IVCT), 1050 (IVCT). IR (KBr pellet, prepared under argon) (ν/cm^{-1}): 1616 m {$\delta(H_2O)$}, 1124w/1076vw/1039vw [$\tau(PH_2)$, $\gamma(PH_2)$, $\nu(PO_2)$], 991m/974m/910m {ν(M=O)}, 858m, 820sh, 740sh, 710sh, 631s, 558s, 482w. Resonance-Raman (KBr matrix, λ_e = 1064 nm) (ν/cm^{-1}): 806s, 535s, 462s, 325s, 215s. Anal. Calc. for $H_{736}Mo_{154}Na_{21}O_{830}P_7$ (*M* 29 496.23): Na, 1.6; Mo^V, 28; P, 0.73; crystal water (not coordinated), 18.3. Found: Na, 1.64; Mo^V, 28; P, 0.65; crystal water (not coordinated), 18.5% (thermogravimetry). The formal ε value of the layer is a rough measure for the number of Mo^V centres.

§ *Crystal data* for **1**: $H_{736}Mo_{154}Na_{21}O_{830}P_7$, *M* = 29 496.23, orthorhombic, space group *Cmca*, *a* = 50.075(3), *b* = 56.049(4), *c* = 30.302(2) Å; *U* = 85 048(10) Å^3, *Z* = 4, D_c = 2.304 g cm^{-3}, μ = 2.33 mm^{-1}, *F*(000) = 56720, crystal size = 0.30 x 0.30 x 0.15 mm^3. Crystals of **1** were taken directly out of the mother liquor and measured immediately (to prevent weathering through loss of water) at 183(2) K on a Bruker AXS SMART diffractometer (Mo-Kα radiation graphite monochromator). A total of 248 836 reflections ($1.53 < \theta < 26.99°$) were collected of which 46 660 unique reflections (R_{int} = 0.0983) were used. The structure was solved using the program SHELXS-97 and refined using the program SHELXL-97 to R = 0.0735 for 25 500 reflections with $I > 2\sigma(I)$. Further details of the crystal structure determination may be obtained from the Fachinformationszentrum Karlsruhe, D-76344 Eggenstein-Leopoldshafen, Germany, on quoting the depository number CSD 410795. CCDC 182/1228. See http://www.rsc.org/suppdata/cc/1999/1035/ for crystallographic files in .cif format.

1 *Multifunctional Inorganic Solids*, ed. C. A. C. Sequeira and M. J. Hudson, Kluwer, Dordrecht, 1993.
2 *Comprehensive Supramolecular Chemistry*, *Vol. 6*, *Solid-state Supramolecular Chemistry: Crystal Engineering* and *Vol. 7*, *Solid-state Supramolecular Chemistry: Two- and Three-dimensional Inorganic Networks*, ed. J. L. Atwood, J. E. D. Davies, D. D. MacNicol, F. Vögtle and J.-M. Lehn, Pergamon/Elsevier, Oxford, 1996.
3 I. D. Brown, in *Structure and Bonding in Crystals*, ed. M. O'Keeffe and A. Navrotsky, Academic Press, New York, 1981, vol. II, pp. 1–30.
4 (a) A. Müller, S. K. Das, V. P. Fedin, E. Krickemeyer, C. Beugholt, H. Bögge, M. Schmidtmann and B. Hauptfleisch, *Z. Anorg. Allg. Chem.*, 1999, **625**, in press; A. Müller, E. Krickemeyer, H. Bögge, M. Schmidtmann, C. Beugholt, S. K. Das and F. Peters, *Chem. Eur. J.*, 1999, **5**, 1496; (b) see also review: A. Müller, P. Kögerler and C. Kuhlmann, *Chem. Commun.*, in press.
5 A. Müller, M. Koop, H. Bögge, M. Schmidtmann and C. Beugholt, *Chem. Commun.*, 1998, 1501.
6 W. H. Baur, *Acta Crystallogr., Sect. B*, 1992, **48**, 745.

Communication 9/01562K

Peptide templated glycosidic bond formation: a new strategy for oligosaccharide synthesis†

Richard J. Tennant-Eyles,[a] Benjamin G. Davis[b] and Antony J. Fairbanks*[a]

[a] *Dyson Perrins Laboratory, Oxford University, South Parks Road, Oxford, UK OX1 3QY. E-mail: antony.fairbanks@chem.ox.ac.uk*

[b] *Department of Chemistry, University of Durham, Science Laboratories, South Road, Durham, UK DH1 3LE*

Received (in Liverpool, UK) 8th March 1999, Accepted 15th April 1999

Glycosidation reactions performed between glycosyl donors and acceptors covalently linked to a peptide template produced increased regio- and stereo-selectivities, which were dependent on the nature of the peptide, and which may be rationalised by simple molecular modelling.

Despite an enormous effort over the course of the last hundred years, the stereo- and regio-selective construction of glycosidic bonds remains an unsolved problem. Extremely significant advances have been made since Koenigs and Knorr disclosed their classic glycosidation methodology back at the beginning of the twentieth century,[1] and numerous excellent reviews on some of the most significant methodological developments exist.[2] However the ultimate goal for the synthetic chemist is the reduction of the synthesis of oligosaccharides to an automatable solid phase process, a feat which revolutionalised the synthesis of oligonucleotides and oligopeptides. We would therefore like to disclose our preliminary investigations into a completely novel approach to the construction of glycosidic linkages. Herein our strategy is to abandon the classical philosophy of the search for a 'general glycosidation reaction', and to attempt to use combinatorial techniques to search for separate synthetic solutions to the construction of each individual glycosidic bond.

The technique of molecular tethering, first introduced to glycosidation chemistry by Stork,[3] and also used by Hindsgaul[4] and Ogawa[5] amongst others, has proven to be an excellent approach for the synthesis of β-mannoside bonds. More recently, several groups have disclosed the use of more extended tethers for the stereo- and even regio-selective construction of glycosidic linkages.[6] As a solution to the problems of glycosidic bond formation we have combined the use of tethering, which displays great promise for the construction of particular glycosidic linkages, with a combinatorial approach. In theory this will allow us to search rapidly through libraries of tethers, screening their potential to promote the formation of particular glycosidic linkages in stereo- and regio-selective fashions.

Since we required tethers in which structural diversity can be readily introduced by solid phase synthesis, our initial investigations have focussed on peptides. Ultimately this may allow us to use existing automatable methodology for solid phase peptide synthesis for oligosaccharide construction. The question therefore is: can a peptide sequence, itself readily synthesizable quantitatively in an automated manner on the solid phase, be effectively translated into an oligosaccharide sequence?

We recently disclosed[7] the synthesis of the novel glycosyl amino acids **1**, **2** and **3**, wherein the sugar moieties are linked through the free OH-6 hydroxy to the β-carboxy of a suitably protected aspartic acid residue. We now disclose the results of several glycosidation reactions undertaken after linking glycosyl donor **1** and glycosyl acceptor **2** together *via* short peptide chains.

† Detailed NMR data are available for selected products, see http://www.rsc.org/suppdata/cc/1999/1037/

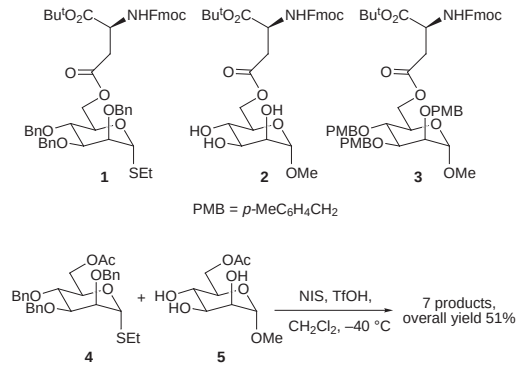

Scheme 1

Firstly, a control reaction of the protected thioglycosyl donor **4** with the triol **5** under standard conditions was investigated, and found to proceed in moderate yield but with extremely poor selectivity (Scheme 1). Of the seven products only two were found to be disaccharides, which were identified as the α(1-3) and β(1-3) linked materials **7** and **8** respectively. Four of the

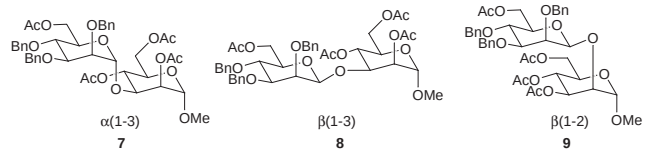

other products were found to be undesired trisaccharides, and the final material was simply the product of hydrolysis. Armed with the knowledge that the simple intermolecular reaction was particularly unselective we then undertook an investigation of several intramolecular reactions between the same acceptor and donor, when they were instead covalently linked to a peptide template.

Aspartate linked glycosyl donor **1** and acceptor **2** were elaborated to the oligopeptides **6a**–**g** using standard protecting group manipulations and EEDQ (2-ethoxy-1-ethoxycarbonyl-1,2-dihydroquinoline) mediated peptide coupling. Intramolecular glycosidation mediated by *N*-iodosuccinimide (NIS) and TfOH was then undertaken (Scheme 2). The resulting disaccharides were released from the peptide template by treatment with K_2CO_3 in MeOH, before complete acetylation and structural assignment. The results of this series of glycosidation reactions are summarised in Table 1.

Several points are worthy of comment. Firstly, the overall yields for the peptide templated glycosidation reactions are in all cases similar to those observed for the control reaction. Secondly, the absence of any trisaccharide products, in contrast to the control, is a clear indicator that all glycosidation is effected intramolecularly. Thirdly we were delighted to find that moderate levels of regio- and stereo-selectivity were achieved, and that the product distribution was dependent on the nature of the peptide template. It is clear that the α(1-3) **7** and

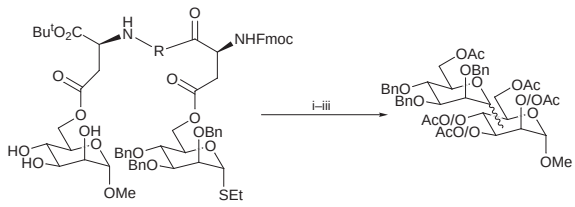

6a R = —
b R = Gly
c R = Ala
d R = Phe
e R = Asn
f R = Pro
g R = GlyGly

Scheme 2 *Reagents and conditions*: i, NIS, TfOH, −40 °C, CH_2Cl_2; ii, K_2CO_3, MeOH; iii, Ac_2O, pyridine.

Table 1 Results of peptide templated glycosidation reactions

Peptide[a]	Total yield[b] (%)	Major products and yields[b] (%)	Yields of acetylated disaccharides[c] (%)
Bu^{t}AspAspFmoc **6a**	59	α(1-3) 11	α(1-3) 60
		β(1-3) 23	β(1-3) 78
		β(1-2) 13	β(1-2) 54
Bu^{t}AspGlyAspFmoc **6b**	41	α(1-3) 21	α(1-3) 58
		β(1-3) 20	β(1-3) 77
Bu^{t}AspAlaAspFmoc **6c**	43	α(1-3) 20	α(1-3) 56
		β(1-3) 23	β(1-3) 59
Bu^{t}AspPheAspFmoc **6d**	44	α(1-3) 13	α(1-3) 58
		β(1-3) 18	β(1-3) 71
Bu^{t}AspAsnAspFmoc **6e**	43	β(1-3) 20	β(1-3) 63
Bu^{t}AspProAspFmoc **6f**	49	β(1-2) 16	β(1-2) 73
		β(1-3) 19	β(1-3) 62
		α(1-2) 14	α(1-2) 79
Bu^{t}AspGlyGlyAspFmoc **6g**	56	α(1-3) +	α(1-3) 30
		β(1-3) 56	β(1-3) 42

[a] Glycosyl donor linked *via* β ester to N-terminal aspartate, glycosyl acceptor linked *via* β ester to C-terminal asparate. [b] Minor or inseparable reaction products not identified. [c] Overall yield for cleavage from peptide backbone and subsequent acetylation.

β(1-3) **8** products dominate throughout, though the relative amount of these two isomers is variable. It would also seem that simple variation of the intermediate amino acid in the tripeptides from glycine (Gly) **6b** to alanine (Ala) **6c**, to phenylalanine (Phe) **6d** actually influences the outcome of the glycosidation reaction only slightly. However, with the use of proline (Pro) as the linking residue (**6f**) then a much higher degree of β selectivity is observed; β(1-2) linked disaccharide **9** now becomes a major product, together with the previously observed β(1-3) disaccharide **8**, and now none of the α(1-3) linked product **7** is formed. Moreover, increasing the length of the peptide by the addition of another Gly residue did not greatly alter the outcome (**6g**).

In order to begin to understand the dependence of product distribution upon peptide sequence we undertook some simple molecular modelling. Thus, a number of potential energy minima locations for a selection of these glycopeptides were probed by variation of the starting point through varying the torsional angles in the linker. This allowed us to probe a number of representative points at different relative orientations of the glycosyl acceptor ranging from the β face to the α face of the glycosyl donor. It was found that all of the modelled peptides AspGlyAsp, AspAlaAsp and AspPheAsp have minima in positions above both and α and β faces, *i.e.* there is little facial distinction, although the α face minima are typically slightly lower in energy. For example, Fig. 1(*a*) shows (hydrogen atoms omitted for clairty) the Bu^{t}AspGlyAspFmoc peptide system **6b** in which the glycosyl acceptor occupies a minimum above the α face of the glycosyl acceptor. In contrast the half chair conformation of the proline residue shown in Fig. 1(*b*) biases the AspProAsp model towards a β face energy minimum. This therefore suggests that the increased β selectivity observed for the AspProAsp peptide is a consequence of the conformation of this tether. In addition, changing identity of the intermediate amino acid from Gly to Ala or Phe changed the conformations of these minima only very slightly. This is consistent with the similar product distributions that were observed for these three peptide linkers. Finally, these simple models also provided a plausible explanation for the preponderance of (1-3)-linked disaccharide products; in all of the minimised models the 3-hydroxy of the acceptor is readily disposed to react with the anomeric centre of the donor.

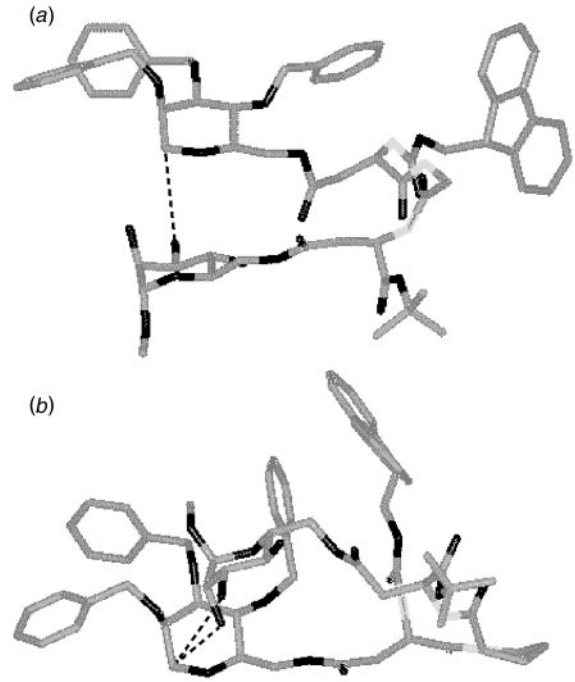

Fig. 1 Minimized structures of tripeptide-tethered systems illustrating the positions of O-2 and O-3 of the glycosyl acceptor relative to the anomeric centre of the glycosyl donor (hydrogens omitted for clarity): (*a*) Bu^{t}AspGlyAspFmoc **6b** and (*b*) Bu^{t}AspProAspFmoc **6f**.

In summary, we have successfully demonstrated for the first time that glycosidation reactions may be achieved between glycosyl donors and acceptors which are bound to a peptide template. In addition these reactions show enhanced, though at present modest, regio- and stereo-selectivities, the product distribution of which can be rationalised by simple molecular modelling. Further investigations in these areas are currently in progress and results will be published in due course.

We gratefully acknowledge financial support from the EPSRC (Quota award to R. J. T.-E.).

Notes and references

1 W. Koenigs and E. Knorr, *Chem. Ber.*, 1901, **34**, 957.
2 For some recent reviews and books see: K. Toshima and K. Tatsuta, *Chem. Rev.*, 1993, **93**, 1503; G.-J. Boons, *Tetrahedron*, 1996, **52**, 1095; *Modern Methods in Carbohydrate Synthesis*, ed. S. H. Khan and R. A. O'Neill, Harwood Academic, Amsterdam, 1996; *Preparative Carbohydrate Chemistry*, ed. S. Hanessian, Marcel Dekker, New York, 1997.
3 G. Stork and G. Kim, *J. Am. Chem. Soc.*, 1992, **114**, 1087.
4 F. Barresi and O. Hindsgaul, *Can. J. Chem.*, 1994, **72**, 1447; F. Barresi and O. Hindsgaul, *Synlett*, 1992, 759; F. Barresi and O. Hindsgaul, *J. Am. Chem. Soc.*, 1991, **113**, 9376.
5 Y. Ito, Y. Ohnishi, T. Ogawa and Y. Nakahara, *Synlett*, 1998, 1102; A. Dan, Y. Ito and T. Ogawa, *J. Org. Chem.*, 1995, **60**, 4680; Y. Ito and T. Ogawa, *Angew. Chem., Int. Ed. Engl.*, 1994, **33**, 1765.
6 T. Zeigler, G. Lemanski and A. Rakoczy, *Tetrahedron Lett.*, 1995, **36**, 8973; T. Zeigler and R. Lau, *Tetrahedron Lett.*, 1995, **36**, 1417; R. Lau, G. Schülle, U. Schwaneberg and T. Zeigler, *Liebigs Ann.*, 1995, 1475; H. Yamada, K. Imamura and T. Takahashi, *Tetrahedron Lett.*, 1997, **36**, 391; S. Valverde, A. M. Gómez, A. Hernández, B. Herradón and J. C. López, *J. Chem. Soc., Chem. Commun.*, 1995, 2005.
7 R. J. Tennant-Eyles and A. J. Fairbanks, *Tetrahedron : Asymmetry*, 1999, **10**, 391.

Communication 9/01916B

Biosynthesis of XR587 (streptopyrrole) in *Streptomyces rimosus* involves a novel carbon-to-nitrogen rearrangement of a proline-derived unit

Mairi E. Raggatt,[a] Thomas J. Simpson*[a] and Stephen K. Wrigley[b]

[a] *School of Chemistry, University of Bristol, Cantock's Close, Bristol, UK BS8 1TS. E-mail: tom.simpson@bristol.ac.uk*

[b] *TerraGen Discovery (UK) Ltd,† 545 Ipswich Road, Slough, Berkshire, UK SL1 4EQ*

Received (in Liverpool, UK) 7th April 1999, Accepted 22nd April 1999

Results from incorporation studies with ^{13}C-labelled acetate, propionate and proline establish a polyketide origin for the pyrrole-containing streptomycete metabolite, XR587, and are in accord with the formation of an amide bond *via* an unprecedented rearrangement of a proline-derived starter unit.

A pyrrole-containing metabolite, XR587, was isolated from a streptomycete strain (X10/78/978; NCIMB 40808) identified as *Streptomyces rimosus* during a screening programme for antibacterial agents.[1] The novel benzopyranopyrrole structure **1**

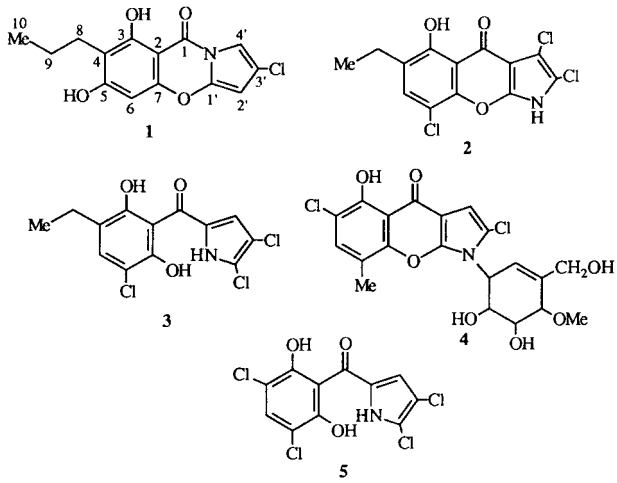

was deduced from spectroscopic studies and confirmed by X-ray crystallography. Recently, Breinholt and co-workers reported the isolation of a metabolite, streptopyrrole, from *Streptomyces armeniacus* whose structure is clearly identical to XR587.[2] Streptopyrrole was reported to display weak growth inhibitory activity against a range of fungi and bacteria.

A benzopyranopyrrole skeleton was first reported[3] for the metabolite TAN-876A **2** which is isolated along with the closely related TAN-876B **3**. The carbonyl group is, however, joined to the pyrrole unit at the β-position in **2**, and not through the nitrogen as in XR587. The pyralomycins isolated from *Microtetraspora spiralis* also contain a benzopyranopyrrole structure[4] and preliminary biosynthetic studies on the major metabolite, pyralomycin 1A **4**, indicated that the 2-ketopyrrole moiety is derived from proline although no mechanism for its formation was suggested.[5]

We initially proposed a biosynthetic pathway to XR587 in which the phenolic ring could be polyketide in origin and the pyrrole ring derived from proline. Oxidation of a propionate- (or possibly methionine-) derived methyl followed by amide formation (as indicated in Scheme 1) and subsequent oxidative modifications and chlorination would give XR587 by a pathway analogous to the biosynthesis of the mycotoxin, ochratoxin A **6**, which is formed *via* a similar polyketide linked to phenylalanine by an amide bond.[6] We now report the results of biosynthetic studies with ^{13}C-labelled precursors which show that XR587 is formed *via* two polyketide chains and a unique carbon-to-nitrogen rearrangement of proline.

The results of incorporation of [1,2-$^{13}C_2$]acetate, [1-^{13}C]propionate and [$^{13}C_5$]proline are summarised in Fig. 1 and Table 1.

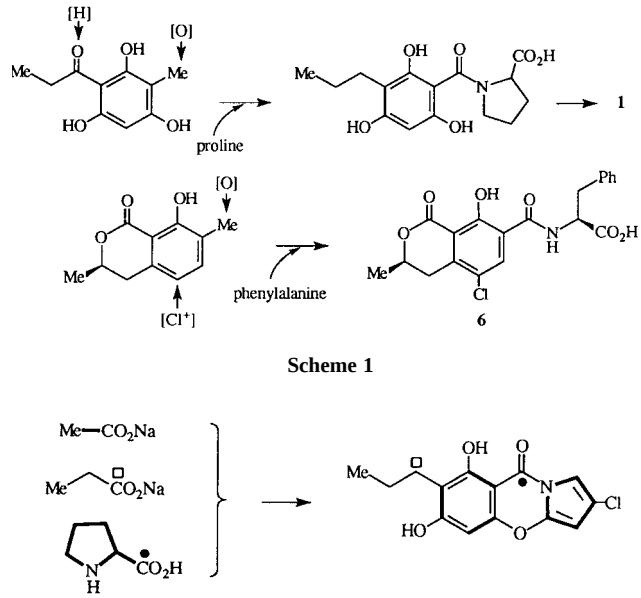

Scheme 1

Fig. 1 Labelling studies on XR587 **1**.

Table 1 ^{13}C–^{13}C couplings and enrichments observed in the ^{13}C NMR spectra of XR587 **1** enriched with ^{13}C-labelled precursors

		J/Hz		
Carbon	δ_C	[1,2-$^{13}C_2$]-Acetate	[$^{13}C_5$]-Proline[c]	[1-^{13}C]-Propionate enrichment(%)
1	159.8	—	5.5, 1.5	0.7
2	93.4	65.7[a]	—	—
3	161.1	65.6[a]	2.8	—
4	113.5	68.7[a]	—	—
5	165.5	68.6[a]	—	—
6	94.4	76.3[a]	—	—
7	154.9	74.8[a]	—	—
8	25.1	—	—	54
9	22.9	—	—	—
10	14.3	—	—	—
1′	142.6	—	89.5, 11.0, 8.5, 1.5	—
2′	91.0	—	89.5, 63.5, 2.8	—
3′	119.4	84.0[b]	83.5, 63.5, 11.0, 5.5	—
4′	105.1	83.9[b]	83.5, 8.5, 2.8	—

[a] 3.2% enrichment. [b] 1.0% enrichment. [c] 5.5% enrichment.

† Previously Xenova Discovery Ltd, 240 Bath Road, Slough, Berkshire, UK SL1 4EF.

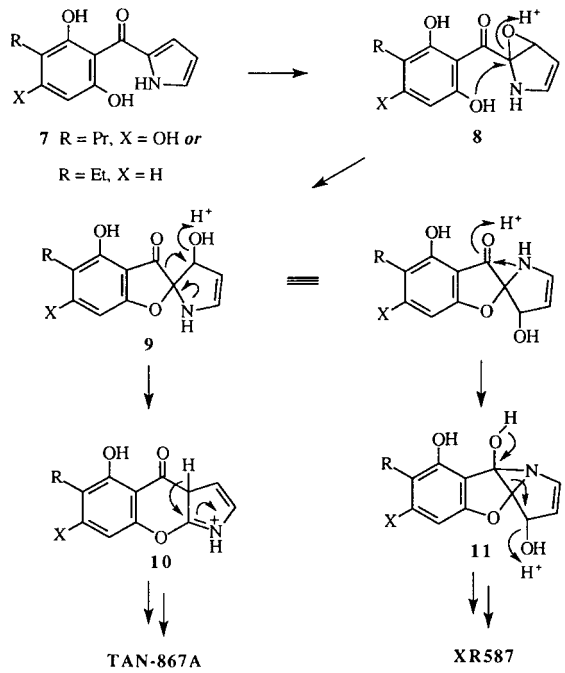

Scheme 2

The phenolic ring is derived from three intact acetate units arranged as shown in Fig. 1. The low level of labelling observed for carbons 3′ and 4′ is consistent with the derivation of the pyrrole ring from proline which itself is derived *via* α-ketoglutarate.[7] Similar low-level incorporation of acetate into the pyrrole ring of pyralomycin 1A was also observed by Kawamura *et al*.[5] An exceptionally high level of labelling from propionate (54%) was observed at C-8, and a very small amount of enrichment (< 1%) was observed at C-1. Although this low level of incorporation might have been indicative of enrichment of the C_1 pool, feeding ^{13}C-labelled methionine or formate failed to give any detectable enrichment of C-1, which implies that its derivation *via* the C_1 pool is unlikely. In fact, in several experiments, methionine was found to consistently inhibit the production of XR587. However, on feeding [$^{13}C_5$]proline, high levels of incorporation (average 5.5%) and ^{13}C–^{13}C couplings were observed at all positions in the pyrrole ring, confirming its derivation from proline. More surprisingly, the C-1 amide carbonyl was also enriched to a similar level and geminal and vicinal couplings were observed to C-1′ and C-3′ to prove that all five proline carbons are incorporated as an intact unit during the biosynthesis of XR587. Thus the original proposal for a polyketide origin for C-1 is firmly ruled out.

The pyrrolomycins, *e.g.* **5**, are pyrrole-containing metabolites of *Streptomyces fumanus* which have been shown to be derived *via* a tetraketide in which a proline-derived starter unit is extended with three acetates.[8] This, along with the reported derivation of pyralomycin 1A **4** from proline, one propionate and two acetates, and the co-occurrence of TAN-876A **2** and TAN-876B **3**, leads us to propose the pathway shown in Scheme 2 which rationalises the formation of the different benzopyranopyrrole metabolites *via* a pyrrole-polyketide intermediate **7**.

Conversion of **7** to the epoxide **8** followed by addition of the phenolic hydroxy group leads to the key spiro-intermediate **9**.‡ Subsequent loss of the hydroxy group after protonation or other activation, migration of the carbonyl bond to give the pyrrolinium intermediate **10**, and rearomatisation leads to the ketonic structure found in TAN-876A (and pyralomycins). Alternatively, addition of the pyrrolidine nitrogen to the ketonic carbonyl generates the aziridine **11** which rearranges as shown to generate the amide. To the best of our knowledge, this rearrangement of a proline-derived moiety is unprecedented.

The formation of the phenolic intermediate **7** requires comment. In the case of pyrrolomycin and pyralomycins, the corresponding intermediates may be formed from folding and condensation of a simple tetraketide intermediate which is presumably primed by the coenzyme-A thioester of pyrrole-2-carboxylate. However, the situation with XR587 is more complex. The single acetate labelling pattern observed in the phenolic ring is incompatible with a single-chain mechanism and makes the intermediacy of the phloroglucinol intermediates **12** or **13** (Scheme 3) unlikely, as there is ample precedent to suggest that the involvement of either of these symmetrical intermediates would lead to randomisation of acetate labelling of the ring.[9] Thus formation of **16** by acylation of **12** or **13** by pyrrole-2-carboxylate or propionate respectively is unlikely, and the remaining alternative requires condensation of separately formed triketide **14** and diketide **15** chains. Such two-chain mechanisms are rare but there is precedent in *e.g.* the biosynthesis of radicinin.[10]

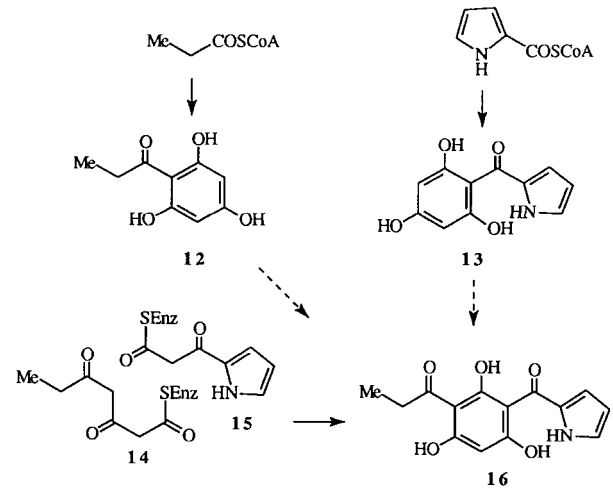

Scheme 3

Studies to provide further evidence for this pathway, and to establish *inter alia* the exact nature of the proline-derived starter unit, reduction of C-8 and the timing of the chlorination reactions, are in progress.

The EPSRC is thanked for a studentship (M. E. R.) and Drs Inês Chicarelli-Robinson, Carole McNicholas and Sally Trew for support and advice. Dr Martin Murray is thanked for his help with NMR experiments.

Notes and references

‡ An equally feasible alternative would involve the pyrrole nitrogen in the opening of the epoxide to give an iminium species, which would then be attacked by the phenolic hydroxy group.

1 E. Olsen, S. J. Trew, S. K. Wrigley, L. Pairet, M. A. Hayes, S. Martin and D. A. Kau, *Int. Pat.*, WO 98/25931.
2 J. Breinholt, H. Gürtler, A. Kjaer, S. E. Nielsen and C. E. Olsen, *Acta Chem. Scand.*, 1998, **52**, 1040.
3 Y. Funabashi, M. Takizawa, S. Tsubotani, S. Tanida and S. Harada, *Takeda Kenkyushosho*, 1992, **51**, 73; *Chem. Abstr.*, 1993, **118**, 55722x.
4 N. Kawamura, R. Sawa, Y. Takahashi, K. Issiki, T. Sawa, N. Kinoshita, H. Naganawa, M. Hamada and T. Takeuchi, *J. Antibiot*, 1995, **48**, 435.
5 N. Kawamura, R. Sawa, Y. Takahashi, T. Sawa, H. Naganawa and T. Takeuchi, *J. Antibiot.*, 1996, **49**, 657.
6 A. E. de Jesus, P. S. Steyn, R. Vleggaer and P. L. Wessels, *J. Chem. Soc., Perkin Trans. 1*, 1980, 52.
7 A. L. Lehninger, *Principles of Biochemistry*, Worth Publishers, 1982, pp. 450–451.
8 G. T. Carter, J. A. Nietsche, J. J. Goodman, M. J. Torrey, T. S. Dunne, M. M. Siegel and D. B. Borders, *J. Chem. Soc., Chem. Commun.*, 1989, 1271.
9 T. J. Simpson, *Top. Curr. Chem.*, 1997, **195**, 1.
10 B. Tal, G. Goldsby, B. A. Burke, A. J. Aasen and D. J. Robeson, *J. Chem. Soc., Perkin Trans. 1*, 1988, 1283.

Communication 9/02777G

ChemComm

Pd/C(en)-catalyzed regioselective hydrogenolysis of terminal epoxides to secondary alcohols

Hironao Sajiki, Kazuyuki Hattori and Kosaku Hirota*

Laboratory of Medicinal Chemistry, Gifu Pharmaceutical University, Mitahora-higashi, Gifu 502-8585, Japan. E-mail: hirota@gifu-pu.ac.jp

Received (in Cambridge, UK) 19th March 1999, Accepted 28th April 1999

Various terminal epoxides, such as 1,2-epoxyalkanes, glycidyl ethers and glycidol, were hydrogenolyzed to give secondary alcohols with high regioselectivity using a 10% Pd/C–ethylenediamine complex as a catalyst under entirely neutral conditions.

The reductive ring-opening reaction of epoxides, in particular terminal epoxides, to the corresponding alcohols is a transformation of considerable importance in organic synthesis[1] in connection with the recent progress in the development of practical and efficient methods for epoxidation of terminal olefins.[2] This important transformation has mainly been accomplished by stoichiometric metal hydride or dissolving metal reagents,[3] and such reductive cleavage with most reducing agents generally produces a large quantity of metal sludge. Industry in particular requires high yield, high selectivity, sufficient productivity, low cost, safety, operational simplicity, and environmental consciousness among other technical factors.[2a] In this context, the general advantages associated with heterogeneous catalysts for hydrogenolysis are convenient use and easy separation, production of no sludge and low cost. From investigation of the hydrogenolyses of 1,2-epoxyalkanes, it was found that while the primary alcohol is formed in greater quantity with a Ni catalyst, the secondary alcohol is predominant with a Pd catalyst.[4,5] However, the Pd catalysts have not been practically applicable since a substantial ratio of the reverse opening primary alcohol is obtained (*ca.* 35–15%) in most cases.[4,6] Some improvements were demonstrated by the combination of Pd/C with NaOH[4,7] or ammonium formate.[6] Although these few reports provide successful results, the basic or nucleophilic conditions (NaOH or ammonia provided from ammonium formate) often restrict their use.[7] Thus, there is a need for the development of novel hydrogenation catalysts that can provide high yields and selectivity as entirely heterogeneous catalysts under neutral conditions without any nucleophilic additives. We now disclose a very practical method that overcomes these serious problems.

Recently, we introduced a carbon-supported Pd–ethylenediamine complex [Pd/C(en)] as a catalyst of choice for general chemoselective hydrogenation of reducible functionalities such as olefin, acetylene, nitro, azide, aromatic bromine or benzyl ester moieties, in the presence of *O*-Bn or *N*-*Z* protective groups.[8] During the course of our studies aimed at developing the Pd/C(en) complexes[9] as catalysts for selective hydrogenation,[8,10] we found that 10% Pd/C(en), without any nucleophilic additives, promotes the regioselective reductive ring-opening of terminal epoxides to afford the corresponding secondary alcohols with high yields and selectivity.

Hydrogenolysis of a variety of terminal epoxides in the presence of 10% Pd/C(en) (10% of the weight of the substrate, *ca.* 2 mol% as Pd metal) as catalyst in MeOH at room temperature was carried out and the results are summarized in Table 1. For example, 1,2-epoxydecane was hydrogenolyzed using 10% Pd/C(en) under 5 atm of hydrogen pressure to afford decan-2-ol as the sole product in 81% yield, whereas employment of 10% Pd/C (Aldrich) under 1 or 5 atm hydrogen pressure resulted in the formation of a mixture of decan-2-ol and decan-1-ol (82 : 18 or 84 : 16, Table 1, entries 1–3). The 10% Pd/C(en)-catalyzed hydrogenolysis proceeded with complete regioselectivity, although the completion of the reaction required

Table 1 Regioselective hydrogenolysis of terminal epoxides using 10% Pd/C(en) catalyst[a]

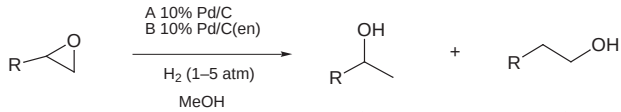

1 **2** **3**

Entry	Substrate	Catalyst	P_{H_2}/atm	*t*/h	Yield (%)[b]	Relative yield (%)[c] **2**	**3**
1	**1a** R = C_8H_{17}	A[d]	1	6	70	82	18
2	**1a** R = C_8H_{17}	A[d]	5[e]	3	72	84	16
3	**1a** R = C_8H_{17}	B	5[e]	24	81	100	ND[f]
4	**1b** R = Bu	B	5[e]	24	75	> 95	—[g]
5	**1c** R = $HO(CH_2)_8$	B	5[e]	32	94	> 95	—[g]
6	**1d** R = $PhCH_2CH_2$	B	5[e]	24	95	> 95	—[g]
7	**1e** R = $PhOCH_2$	B	1	24	95	100	ND[f]
8	**1f** R = XCH_2OCH_2[h]	B	1	24	99	100	ND[f]
9	**1g** R = $CyCH_2OCH_2$	B	1	66	79	100	ND[f]
10	**1h** R = $HOCH_2$	B	1	22	89	100	ND[f]
11[i]	**1g** R = 4-$ClC_6H_4OCH_2$	B	1	24	89	100[j]	ND[f,j]

[a] Unless otherwise specified, the reaction was carried out using 0.5 mmol of the substrate in methanol (1 ml) with 10% Pd/C(en) (10% of the weight of the substrate) under hydrogen atmosphere (1–5 atm) for the given reaction time. [b] Isolated yield. [c] Determined by ^{1}H NMR. [d] 10% Pd/C was purchased from Aldrich Co. [e] Reaction was performed using Ishii Medium Pressure Hydrogenator CHA-E. [f] Not detectable. [g] Trace (less than 5%). [h] X = 2,3-dihydro-1,4-benzodioxan-2-yl. [i] Reaction was performed in the presence of Et_3N (1.2 equiv. *vs.* substrate) to neutralize the resulting HCl. [j] Dechlorinated product.

higher hydrogen pressure (5 atm). 1,2-Epoxyhexane, 1,2-epoxydecan-10-ol and 1,2-epoxy-4-phenylbutane were similarly hydrogenolyzed (5 atm) with 10% Pd/C(en) to give the corresponding secondary alcohols in high yields (entries 4–6). The hydrogenolysis of glycidyl ethers and glycidol gave the corresponding secondary alcohols in high yields even under 1 atm hydrogen pressure without the formation of any detectable by-products, such as primary alcohols (entries 7–11). In the case of 4-chlorophenyl glycidyl ether, non-nucleophilic Et_3N (1.2 equiv.) was added to the reaction mixture as a base, which traps HCl generated during the reaction (entry 11). In this reaction the dechlorinated product, 1-phenoxypropan-2-ol, was obtained in 89% yield as the sole product.

The 10% Pd/C(en) catalyst is stable and retains high efficiency during consecutive catalytic cycles. The catalyst could be recovered almost quantitatively following simple filtration of the catalyst, washing with MeOH and Et_2O and drying, and it could be reused at least three times without any decrease in the yield and regioselectivity of the hydrogenolyzed product. One drawback of this method is the inapplicability encountered in the hydrogenolysis of styrene oxide (**1** R = Ph). Styrene oxide was converted to a 14 : 86 mixture of phenethyl alcohol (**3** R = Ph) and 1-phenylethylene glycol monomethyl ether **4**, which may be formed *via* Pd/C(en)-catalyzed regioselective solvolysis with MeOH.[11]

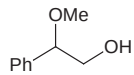

4

The exact role of the ethylenediamine of the 10% Pd/C(en) complex catalyst in facilitating the regioselective hydrogenolysis of terminal epoxides remains unclear. The catalytic activity of 10% Pd/C(en) to the reductive ring-opening reaction of terminal epoxides was lower than that of 10% Pd/C. It should be noted that higher regioselectivity was observed with the less active catalyst.

As described, the present 10% Pd/C(en)-catalyzed hydrogenolysis of terminal epoxides would provide a new catalytic method for regioselective synthesis of secondary alcohols under entirely neutral and heterogeneous reaction conditions.

Notes and references

1 F. A. Carey and R. J. Sundberg, *Advanced Organic Chemistry, Part B*, Plenum, New York, 1977; M. Bartok and K. L. Lang, *The Chemistry of Heterocyclic Compounds—Small Ring Heterocycles, Part 3*, ed. A. Weissberger and E. C. Taylor, Wiley, New York, 1985, p. 1 and references therein; R. Sreekumar, R. Padmakumar and P. Rugmini, *Tetrahedron Lett.*, 1998, **39**, 5151 and references therein.

2 (*a*) K. Sato, M. Aoki, M. Ogawa, T. Hashimoto and R. Noyori, *J. Org. Chem.*, 1996, **61**, 8310; (*b*) C. Coperet, H. Adolfsson and K. B. Sharpless, *Chem. Commun.*, 1997, 1565 and references therein.

3 Selected reviews: R. C. Larock, *Comprehensive Organic Transformations*, VCH, New York, 1989, p. 505; M. Hudlicky, *Reductions in Organic Chemistry*, 2nd edn., ACS, Washington, DC, 1996, p. 113.

4 For examples: M. S. Newman, G. Underwood and M. Renoll, *J. Am. Chem. Soc.*, 1949, 71, 3362; P. N. Rylander, *Catalytic Hydrogenation in Organic Synthesis*, Academic Press, New York, 1979, p. 260; P. N. Rylander, *Hydrogenation Methods*, Academic Press, New York, 1985, p. 137.

5 Besides the catalyst, the substrate also exerts a considerable effect on the regioselectivity (ref. 1 and 4), see also S. Torii, H. Okuno, S. Nakayasu and T. Kotani, *Chem. Lett.*, 1989, 1975.

6 P. S. Dragovic, T. J. Prins and R. Zhou, *J. Org. Chem.*,1995, **66**, 4922.

7 L. M. Schultze, H. H. Chapman, N. S. Louie, M. J. Postich, E. J. Prisbe, J. C. Rohloff and R. H. Yu, *Tetrahedron Lett.*, 1998, **39**, 1853.

8 H. Sajiki, K. Hattori and K. Hirota, *J. Org. Chem.*, 1998, **63**, 7990.

9 The preparation of 10% Pd/C(en) catalyst: (ref. 8): A suspension of 10% Pd/C (1.50 g, 1.40 mmol as Pd metal) and ethylenediamine (6.8 ml, 100.80 mmol) in MeOH (60 ml) under a rigorous argon atmosphere was stirred for 48 h at ambient temperature. The solid was filtered, washed vigorously with MeOH (20 ml × 5) and Et_2O (20 ml × 2), and dried under a vacuum pump at room temperature for 48 h to give the 10% Pd/C(en) (Found: C, 74.10; H, 2.64; N, 3.01%).

10 H. Sajiki, K. Hattori and K. Hirota, *J. Chem. Soc., Perkin Trans. 1*, 1998, 4043.

11 By use of EtOH instead of MeOH as a solvent, styrene oxide could also be converted to an 87 : 13 mixture of phenethyl alcohol (**3** R = Ph) and 1-phenylethylene glycol monoethyl ether.

Communication 9/02213I

Stereoselective hydrogenation reactions in chloroaluminate(III) ionic liquids: a new method for the reduction of aromatic compounds

Christopher J. Adams,[a] Martyn J. Earle[b] and Kenneth R. Seddon[b]

[a] *Institute of Applied Catalysis, PO Box 32, Prenton, Wirral, England, UK L43 5XT. E-mail: chris.adams@iac.org.uk*
[b] *School of Chemistry, The Queen's University of Belfast, Belfast, Northern Ireland, UK BT9 5AG. E-mail: k.seddon@qub.ac.uk; m.earle@qub.ac.uk*

Received (in Cambridge, UK) 15th February 1999, Accepted 19th April 1999

Stereoselective hydrogenation reactions in the ionic liquid system 1-ethyl-3-methylimidazolium chloride–$AlCl_3$ can be performed with excellent yields and selectivities, using electropositive metals and a proton source.

The hydrogenation of aromatic compounds can be achieved by a number of methods, including high pressure catalytic hydrogenation,[1] dissolving metal reductions,[2] and ionic hydrogenations with TFA and silanes.[3] Here, we report a new, highly stereoselective method for the reduction of carbocyclic aromatic compounds in chloroaluminate(III) ionic liquids at ambient temperatures.

Room temperature ionic liquids such as [emim]Cl–$AlCl_3$ (X = 0.67)[4] ([emim]$^+$ = 1-ethyl-3-methylimidazolium cation, see Fig. 1),† have been found to be excellent solvents for a number of reactions, such as the Friedel–Crafts reaction,[5] isomerisations,[6] polymerisation of alkenes such as refinery waste gas,[7] and catalytic hydrogenation reactions.[8,9]

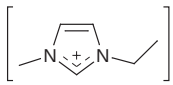

Fig. 1 Structure of the [emim]$^+$ cation.

When polycyclic aromatic compounds, such as anthracene, are dissolved in solvents containing dissolved aluminium(III) chloride, deeply coloured paramagnetic solutions are formed.[10] Authors such as Olah[11] have referred to these compounds as $AlCl_3$ π-complexes, but the precise structure and bonding of these complexes has yet to be elucidated.[10] It has also been observed that carbocyclic aromatic compounds are readily protonated in the [emim]Cl–$AlCl_3$ (X = 0.67) ionic liquid.[12] It was thus envisaged that the interaction of an electropositive metal with a protonated aromatic hydrocarbon would result in reduction of that compound. A preliminary investigation led to the observation that when moist air was introduced to a deep green solution of anthracene in [emim]Cl–$AlCl_3$ (X = 0.67), containing lithium metal, the green colour faded and 9,10-dihydroanthracene **1** was formed in 98% yield (Scheme 1).

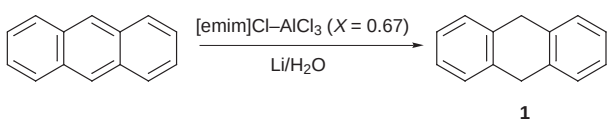

Scheme 1

Following on from this initial observation, a more detailed investigation was carried out with anthracene, pyrene and 9,10-dimethylanthracene, in order to examine the stereochemical outcome of this reaction. The results of this investigation are summarised in Table 1 and Schemes 2–4.

The partial reduction of anthracene and pyrene was achieved by using the ionic liquid [emim][HCl_2] as a proton source.[13] For complete reduction to the alicyclic products (**3** and **7**), anhydrous HCl gas was found be the most effective proton source. In general, this reaction was successful with electropositive metals (*e.g.* Na, Li, Mg, Al and Zn). The metal of choice was found to be aluminium, since the aluminium(III) chloride by-product of the reaction is precipitated and the composition of the ionic liquid remained largely unaffected. It should be noted that this reaction differs from other dissolving metal reductions, such as the Birch reduction,[2] in that products containing unconjugated double bonds are not observed.

Table 1 The reduction of aromatic compounds in [emim]Cl–$AlCl_3$ (X = 0.67) at 20 °C

Substrate	Metal	H^+ source	t/h	Products (% yield)
Anthracene	Al	[emim][HCl_2] (l)	24	**1** (25), **2** (25), **3** (25)
Anthracene	Zn	excess HCl (g)	6	**3** (90)
Pyrene	Li	[emim][HCl_2] (l)	1	**4** (2), **5** (18), **6** (20), **7** (25)
Pyrene	Al	excess HCl (g)	4	**7** (84)
9,10-Dimethyl-anthracene	Al	HCl (g)	0.5	**8** (81), **9** (14)

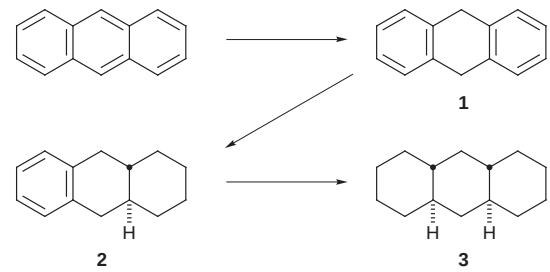

Scheme 2

The reduction of anthracene was found to proceed sequentially, as shown in Scheme 2. It should be noted that **2** and **3** are the thermodynamically most stable isomers.

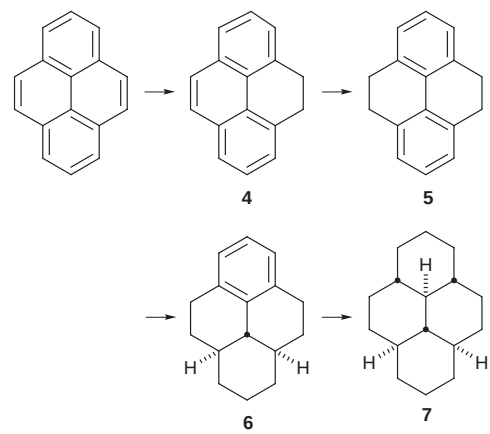

Scheme 3

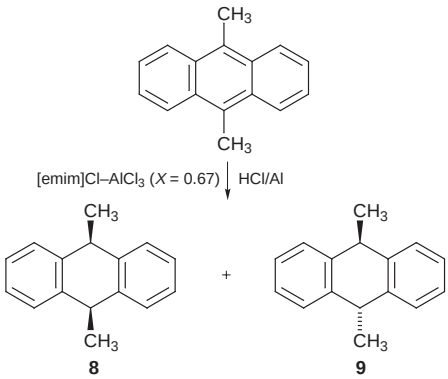

Scheme 4

The reduction of pyrene occurs in a similar manner to that of anthracene (see Scheme 3): the two most reactive bonds are reduced first. Again, the subsequent reduction gave rise to the thermodynamically most stable intermediate **6** and ultimately the product **7** as single diastereomers.[14] The structure of **7** was confirmed by X-ray crystallography[15] and was found to be identical to the published structure.[16]

The partial reduction of 9,10-dimethylanthracene (see Scheme 4) gave rise to two isomers (**8** and **9)** in a 6 : 1 ratio respectively. In contrast to the products from the reduction of pyrene and anthracene, the major product **8** was the *cis*-isomer and the minor product **9** was the *trans*-isomer. This difference from the behaviour of anthracene and pyrene can be explained by the enthalpies of formation of the two products **8** and **9**. The *cis*-isomer **8** is 16 kJ mol^{-1} more stable than the *trans*-isomer **9**.[17] Hence, as with the pyrene and anthracene reductions, the thermodynamic product predominates.

The reductions of simpler aromatic compounds such as benzene and naphthalene were found to behave in a more complex manner. In both these cases, the expected products [cyclohexane (2%) and decalin (15%, as a 5 : 1 *trans*- to *cis*-isomer mixture)] were obtained, but in low yields. In these two cases, polymerisation reactions occur in addition to reduction reactions. In the reduction of benzene, products such as phenylcyclohexane and bi(cyclohexyl) were detected, presumably from the Friedel–Crafts reaction between benzene and cyclohexene (a postulated intermediate in the reduction reaction): the major product was a non-volatile colourless oil—polycyclohexane—obtained in 70% yield.

In conclusion, reduction by a metal–acid combination in a chloroaluminate(III) ionic liquid provides an effective means of hydrogenating aromatic compounds in a highly selective manner. This contrasts with the catalytic hydrogenation of anthracene or pyrene, which requires high temperatures and pressures, and usually gives rise to isomeric mixtures.[1,18]

We are indebted to Unilever Research Laboratories, Port Sunlight for financial support, and the EPSRC and Royal Academy of Engineering for the award of a Clean Technology Fellowship (to K. R. S.).

Notes and references

† The composition of a tetrachloroaluminate(III) ionic liquid is best described by the apparent mole fraction of $AlCl_3$ {$X(AlCl_3)$} present. Ionic liquids with $X(AlCl_3) < 0.5$ contain an excess of Cl^- ions over $[Al_2Cl_7]^-$ ions, and are called 'basic'; those with $X(AlCl_3) > 0.5$ contain an excess of $[Al_2Cl_7]^-$ ions over Cl^-, and are called 'acidic'; melts with $X(AlCl_3) = 0.5$ are called 'neutral'.

1 K. Y. Sakanishi, M. S. Ohira, I. Mochida, H. Okazaki and M. H. Soeda, *Bull. Chem. Soc. Jpn.*, 1989, **62**, 3994; M. Yalpani and R. Koster, *Chem. Ber.*, 1990, **123**, 719.
2 A. A. Akhrem, I. G. Reshetova and Y. A. Titovin, *The Birch Reduction of Aromatic Compounds*, Plenum, New York, 1972.
3 D. N. Kursanov, Z. N. Parnes, M. I. Kalinkina and N. M. Lion, *Ionic Hydrogenation and Related Reactions*, A. N. Nesmeyov Institute of Organo Element Compounds, USSR Academy of Sciences, Moscow, 1985.
4 K. R. Seddon, in *Molten Salt Forum: Proceedings of 5th International Conference on Molten Salt Chemistry and Technology*, ed. H. Wendt, 1998, vol. 5–6, pp. 53–62.
5 C. J. Adams, M. J. Earle, G. Roberts and K. R. Seddon, *Chem. Commun.*, 1998, 2097.
6 Y. Chauvin, B. Gilbert and I. Guibard, *J. Chem. Soc., Chem. Commun*., 1990, 1715.
7 Y. Chauvin, A. Hirschauer and H. Olivier, *J. Mol. Catal.*, 1994, **92**, 155.
8 P. A. Z. Suarez, J. E. L. Dullius, S. Einloft, R. F. de Souza and J. Dupont, *Inorg. Chim. Acta*, 1997, **255**, 207.
9 P. J. Dyson, D. J. Ellis, D. G. Parker and T. Welton, *Chem. Commun*., 1999, 25.
10 P. Tarakeshwar, J. Y. Lee and K. S. Kim, *J. Phys. Chem. A*, 1998, **102**, 2253.
11 G. A. Olah, *Friedel-Crafts Chemistry*, Wiley-Interscience, New York, 1973.
12 G. P. Smith, A. S. Dworkin, R. M. Pagni and S. P. Zingg, *J. Am. Chem. Soc*., 1989, **111**, 525.
13 J. L. E. Campbell and K. E. Johnson, *Inorg. Chem*., 1993, **32**, 3809.
14 B. Kohne, K. Praefcke and G. Mann, *Chimia*, 1988, **42**, 139.
15 M. Nieuwenhuyzen, unpublished results, 1996.
16 J. P. Ding, R. Herbst, K. Praefcke, B. Kohne and W. Saenger, *Acta Crystallogr., Sect. B*, 1991, **47**, 739.
17 D. K. Dalling, K. W. Zlim, D. M. Grant, W. A. Heeschen, W. J. Horton and R. J. Pugmire, *J. Am. Chem. Soc.*, 1981, **103**, 4817.
18 D. K. Dalling and D. M. Grant, *J. Am. Chem. Soc.*, 1974, **96**, 1827.

Communication 9/01302D

ChemComm

Cyclodextrin-accelerated cleavage of phenyl esters: is it the 2-hydroxy or the 3-hydroxy that promotes the acyl transfer?

Makoto Fukudome, Yuji Okabe, De-Qi Yuan and Kahee Fujita*

Faculty of Pharmaceutical Sciences, Nagasaki University, 1-14 Bunkyo-machi, Nagasaki 852-8521, Japan. E-mail: fujita@net.nagasaki-u.ac.jp

Received (in Cambridge, UK) 17th March 1999, Accepted 28th April 1999

Both 2- and 3-monothiocyclodextrins have been synthesized and used in probing the mechanism of cyclodextrin-mediated cleavage of phenyl esters, showing that the 3-thiols are much more effective than the 2-thiols in promoting the acyl transfer.

Cyclodextrin-accelerated cleavage of phenyl esters is among the earliest examples of enzyme mimetic reactions.[1] Acylated cyclodextrins are usually the products and are difficult to recycle during the reaction. Although this reaction is not a catalytic one, it involves a rapid and reversible pre-binding of the substrate into the cyclodextrin cavity and subsequent acyl transfer to a cyclodextrin hydroxy group in the specifically arranged complex, in the same way that natural serine proteases bind their substrates and promote the transfer of an acyl group to a serine hydroxy group in the first enzymatic step.[2] Therefore, it provides an excellent model for better understanding enzyme action and has attracted a long-standing interest.[3] Some fundamental factors such as the effect of proximity,[4] binding of the substrate in the transition state,[5,6] geometric freedom needed for the entire reaction[7] and so forth have been elucidated, and very large rate-acceleration (up to 6 million-fold[4]) and good structural selectivity or enantioselectivity[8,9] have been obtained. However, the nucleophile in this reaction still remains to be determined. It is certain that the secondary hydroxy groups are engaged in the reaction, but there is no easy way to determine whether the 2-OH or 3-OH is the one to attack the ester first. Bender[10] suggested that the reaction involves the 3-OH group based on the observation that the 3-*O*-methylated derivative causes no rate-acceleration, while Breslow[8,11] believes that the reactive hydroxy group is the 2-OH by analogy with its greater reactivity toward methylation. Computer simulation[12] supports the 2-OH mechanism. Unfortunately, not enough experimental evidence for either mechanism has been obtained. We reason that adjusting the relative reactivity of the two positions can afford some insight into the mechanism. This idea is made practicable by our recent method[13] for selectively functionalizing the secondary face without significantly altering the conformation of cyclodextrin. Replacement of the secondary hydroxy group by a SH group has an interesting influence on the catalytic behaviour of cyclodextrins. Here we describe the preliminary results, which are striking and indicative of the 3-SH being preferred to the 2-SH as the nucleophile.

The syntheses of thiocyclodextrins **4**, **9** and **14** were carried out by nucleophilic ring-opening of cyclodextrin epoxides with BnSH followed by reduction with Na–NH_3 (l) (Scheme 1). The resultant thiols were converted to the corresponding dimers for easy storage. The nucleophilic ring-opening[14] of cyclodextrin mannoepoxide **1** was believed to exclusively result in the formation of a cyclodextrin derivative with a 3-functional altrose sub-unit which slightly distorts the cyclodextrin cavity.[15] We found that, with imidazole as nucleophile, the undistorted product with an imidazolyl group at C-2 of the glucoside unit can be obtained in addition to the distorted one.[13] This abnormal reaction actually occurs with various nucleophiles including BnSH, giving the undistorted cyclodextrin derivative with a functional group at C-2 of the glucoside unit as a minor product.[16] Though in very low yield, this method does afford the undistorted C-2 functional cyclodextrins which are otherwise inaccessible at present. Reaction of **1** with BnSH in DMF gave the undistorted cyclodextrin sulfide **3** in 6% yield in addition to **2** in 77% yield. The replacement of 3-OH was easily realized by the reaction of alloepoxides **6**[13,17,18] and **11** with BnSH which afforded the undistorted cyclodextrin sulfides **8** and **13** as main products. Reduction of the sulfides **3**, **8** and **13**

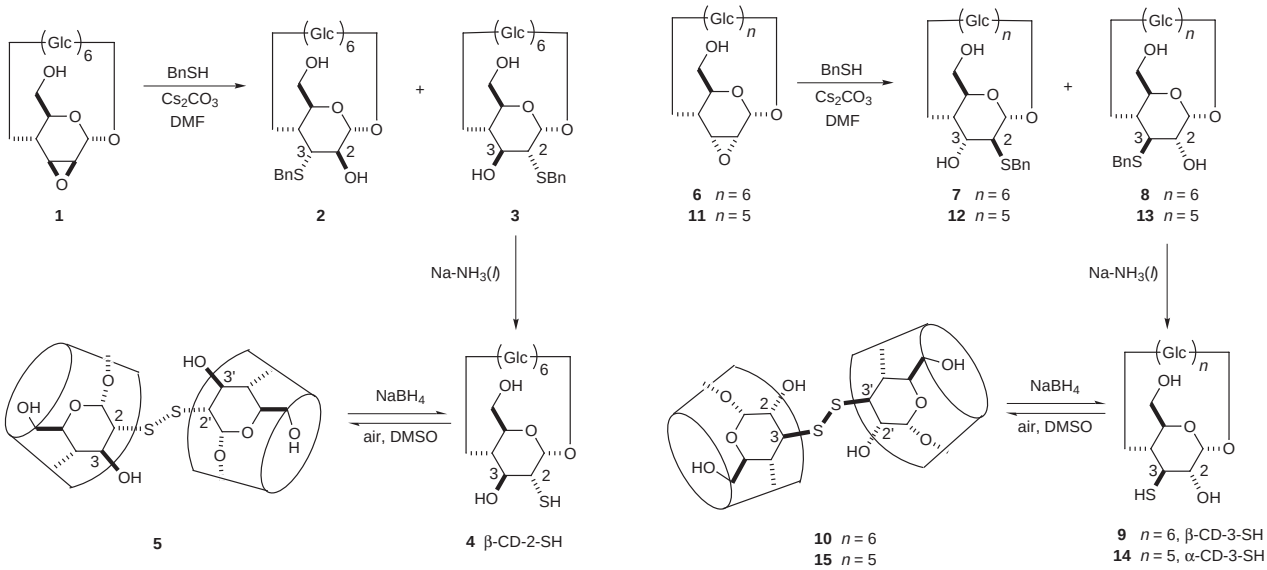

Scheme 1

Table 1 Kinetic parameters of the cleavage of nitrophenyl acetates by thiocyclodextrins at pH 9.0[a]

		p-Nitrophenyl acetate					*m*-Nitrophenyl acetate				
Catalyst	pK_a[b]	$k_{cat}/10^{-2}$ s^{-1}	$K_d/10^{-3}$ M	$(k_{cat}/k_{un})/10^2$	$(k_{cat}/K_d)/10$ M s^{-1}	$K_{TS}/10^{-4}$ M	$k_{cat}/10^{-2}$ s^{-1}	$K_d/10^{-3}$ M	$(k_{cat}/k_{un})/10^2$	$(k_{cat}K_d)/10$ M^{-1} s^{-1}	$K_{TS}/10^{-4}$ M
α-CD			10[c]	0.028[c]		36[c]	2.4	14	1.5	0.17	0.93
β-CD			7.8[c]	0.081[c]		9.6[c]	1.3	15	0.86	0.086	1.8
α-CD-3-SH	7.7	4.9	18	1.6	0.27	1.1	61	1.9	40	32	0.0049
β-CD-2-SH	7.5	0.80	12	0.26	0.068	4.5	0.4	7.0	0.26	0.058	2.7
β-CD-3-SH	7.7	15	7.6	5.0	2.0	0.15	4.5	3.2	2.9	1.4	0.11

[a] Reactions were carried out in a pH 9.0 standard buffer solution at 25 °C; the release of nitrophenols was monitored at 400 nm. Lineweaver–Burk treatment was applied to derive the k_{cat} and K_d values. [b] Determined by UV titration at 230 nm of the acidic solution of a cyclodextrin thiol with aq. NaOH. [c] Data at pH 11.7 from ref. 19.

with Na–NH_3 (l) gave the cyclodextrin thiols **4**, **9** and **14** which were further converted to the corresponding dimers **5**, **10** and **15** for storage.† The thiols were freshly regenerated with $NaBH_4$ just before use.

The free thiols show no obvious absorption above 215 nm while deprotonation of the thiol group generates a new absorption bond around 230 nm. Titrating the acidic solution of the thiols with aq. NaOH solution and following the absorption changes at 230 nm allows the determination of their pK_a values. As shown in Table 1, the three thiols **4**, **9** and **14** have pK_a values of 7.5, 7.7 and 7.7, respectively, very similar to each other. The behaviour of these thiols on cleavage of phenyl esters was investigated by following the absorption changes of the buffered aqueous solution of *m*-nitrophenyl acetate and its *p*-isomer, which are widely employed as substrates for serine protease mimics. The kinetic parameters of the thiocyclodextrin-mediated decomposition of nitrophenyl acetates at pH 9.0 are summarized in Table 1. β-CD-3-SH **9** significantly facilitates the reactions. It cleaves *p*- and *m*-nitrophenyl acetates 500 and 290 times faster than the buffer solution. Compared with β-cyclodextrin, β-CD-3-SH **9** is 62 times more effective towards *p*-nitrophenyl acetate and 3 times more effective towards the *m*-isomer. The result with β-CD-2-SH **4** is very different. This thiol shows a rate acceleration of 26 fold over the buffer solution in hydrolysing the *p*-nitrophenyl acetate, about 3 times that of β-CD. However, it hydrolyzes the *m*-isomer 3 times less effectively than β-cyclodextrin itself. As a result, β-CD-3-SH **9** is 10–20 times more effective than β-CD-2-SH **4** in promoting the acyl transfer of both substrates. Obviously the thiol group of both β-CD-2-SH **4** and β-CD-3-SH **9** is engaged in the reaction. The kinetic difference between them is most likely a reflection of their geometric specificity rather than their acidity difference since both thiols have similar pK_a values and should deprotonate almost to the same extent at pH 9.0. Only when SH is put in the right position with the correct conformation required to access the transition state can it significantly accelerate the reaction. This position appears to be C-3. Incorporation of SH at C-3 of α-cyclodextrin also gives striking results. α-CD-3-SH **14** accelerates the cleavage of *m*-nitrophenyl acetate by a factor of 4000, 25 times that of its *p*-isomer.

As suggested by the kinetic data in Table 1, the thiocyclodextrins decompose the nitrophenyl acetates in a pre-binding process, just in the same way that the native cyclodextrins do. All the thiocyclodextrins bind the ground state of *p*-nitrophenyl acetate ($1/K_d$) with a comparable strength which is not obviously different from that of native cyclodextrins. However, their transition state (TS) binding ($1/K_{TS}$) is quite different. β-CD-3-SH **9** binds the TS of *p*-nitrophenyl acetate 30 times tighter than its counterpart β-CD-2-SH **4**. Compared with the corresponding native cyclodextrins, β-CD-3-SH **9** and α-CD-3-SH **14** increase the TS binding by 64 and 33 fold, respectively, while β-CD-2-SH **4** does not significantly alter it. A similar result is also obtained in the case of *m*-nitrophenyl acetate. Replacement of one 3-OH of the cyclodextrins by SH greatly increases the TS binding of *m*-nitrophenyl acetate, whereas the replacement of one 2-OH by SH does not significantly change the binding of both ground state and TS. It is apparent that the 3-SH is preferred to the 2-SH as nucleophile in developing the transition state of the acyl transfer reaction of both substrates.

No significant conformational difference should exist between the modified cyclodextrins and the corresponding native ones except that one of the secondary hydroxy groups is replaced by SH. Though the S atom is larger than an O atom and would lead to an earlier TS for the acyl transfer, it appears that this replacement does not reverse the geometric preference of the ester cleavage for the 2- or 3-position. Thus the present research may supply a useful approach to evaluate the reactive group in the cyclodextrin-accelerated cleavage of phenyl esters.

We thank Japan Maize Products Co. Ltd. for a generous gift of cyclodextrins. D.-Q. Y. thanks the NSFC for projects 29632004 and 29772023 and the State Education Committee of China for project 380.

Notes and references

† All new compounds (**2**, **3**, **5**, **7**, **8**, **10**, **12**, **13** and **15**) were characterized *via* their FAB MS, ^1H and ^{13}C NMR spectra.

1 M. L. Bender and M. Komiyama, *Cyclodextrin Chemistry*, Springer, Berlin, 1978.
2 R. L. VanEtten, J. F. Sebastian, G. A. Clowes and M. L. Bender, *J. Am. Chem. Soc.*, 1967, **89**, 3242.
3 R. Breslow and S. D. Dong, *Chem. Rev.*, 1998, **98**, 1997.
4 R. Breslow, G. L. Trainor and A. Ueno, *J. Am. Chem. Soc.*, 1983, **105**, 2739.
5 W. J. le Noble, S. Srivastava, R. Breslow and G. Trainor, *J. Am. Chem. Soc.*, 1983, **105**, 2745.
6 O. S. Tee, *Adv. Phys. Org. Chem.*, 1994, **29**, 1.
7 R. Breslow and S. Chung, *Tetrahedron Lett.*, 1990, **31**, 631.
8 G. L. Trainor and R. Breslow, *J. Am. Chem. Soc.*, 1981, **103**, 154.
9 T. Beyrich, T. Jira and C. Beyer, *Chirality*, 1995, **7**, 560.
10 R. L. VanEtten, G. A. Clowes, J. F. Sebastian and M. L. Bender, *J. Am. Chem. Soc.*, 1967, **89**, 3253.
11 R. Breslow, M. F. Czarniecki, J. Emert and H. Hamaguchi, *J. Am. Chem. Soc.*, 1980, **102**, 762.
12 V. Luzhkov and J. Aqvist, *J. Am. Chem. Soc.*, 1998, **120**, 6131.
13 D.-Q. Yuan, K. Ohta and K. Fujita, *Chem. Commun.*, 1996, 821.
14 R. Breslow and A. W. Czarnik, *J. Am. Chem. Soc.*, 1983, **105**, 1390.
15 A. R. Kahn, P. Forgo, K. J. Stine and V. T. D'Souza, *Chem. Rev.*, 1998, **98**, 1977.
16 J. Yan, R. Watanabe, M. Yamaguchi, D.-Q. Yuan and K. Fujita, *Tetrahedron Lett.*, 1999, **40**, 1513.
17 W.-H. Chen, D.-Q. Yuan and K. Fujita, *Tetrahedron Lett.*, 1997, **38**, 4599.
18 D.-Q. Yuan, S. D. Dong and R. Breslow, *Tetrahedron Lett.*, 1998, **39**, 7673.
19 O. S. Tee, C. Mazza and X.-X. Du, *J. Org. Chem.*, 1990, **55**, 3603.

Communication 9/02123J

ChemComm

Dependence of the relaxivity and luminescence of gadolinium and europium amino-acid complexes on hydrogencarbonate and pH

Silvio Aime,*[a] Alessandro Barge,[a] Mauro Botta,[a] Judith A. K. Howard,[b] Ritu Kataky,[b] Mark P. Lowe,[b] Janet M. Moloney,[b] David Parker*[b] and Alvaro S. de Sousa[b]

[a] *Dipartimento di Chimica I.F.M., Universita degli Studi di Torino, 10125 Torino, Italy*
[b] *Department of Chemistry, University of Durham, South Road, Durham, UK DH1 3LE. E-mail: david.parker@durham.ac.uk*

Received (in Cambridge, UK) 22nd March 1999, Accepted 28th April 1999

Reversible binding of hydrogencarbonate to a chiral di-aqua lanthanide complex occurs in the pH range 6.5–8.5, limiting the measured relaxivity in the gadolinium complex and enhancing the metal-based emission in the europium analogue.

The behaviour of well defined lanthanide complexes is currently being explored in which the metal-based luminescence (Eu, Tb, Yb)[1] or relaxivity (Gd)[2,3] is a function of a defined biochemical parameter or set of variables, such as pH, $p(O_2)$ or anion concentration. Modulation of the luminescence or relaxivity of a given lanthanide complex may occur *via* ligand- or metal-based processes. Deprotonation of water molecules bound to the metal centre offers an effective means of reducing the relaxivity of cationic gadolinium complexes and pH-dependent behaviour has been demonstrated.[3] For luminescent complexes of europium and terbium, the removal of proximate OH oscillators increases both the lifetime and intensity of the metal-based emission,[4] as intramolecular vibrational quenching of the excited $^5D_0$ or $^5D_4$ state is significantly reduced.[5] Recent preliminary reports have suggested that the binding of hydrogencarbonate to a tri- or di-aqua metal centre may modulate the luminescence[4] (Eu, Tb) and the relaxivity[6] (Gd) of lanthanide complexes under ambient conditions. Such behaviour offers a means of studying both the concentration of HCO_3^- in solution and the pH in the ambient range *via* the H_2CO_3/HCO_3^- equilibrium (effective pK_a = 6.16, I = 0.1 mol dm^{-3}, 298 K).

With this in mind, a heptadentate ligand L^{1a} and two model octadentate analogues L^{2a} and L^{3a} have been prepared, and the luminescence and relaxivity of their Eu and Gd complexes studied as a function of pH in the presence or absence of HCO_3^-. Reaction of (*S*)-ethyl-*N*-2-chloroethanoylalanate with 1,4,7,10-tetraazacyclododecane (MeCN, Cs_2CO_3, 65 °C, 18 h, 1% KI) yielded the tetra-ester L^{2a}, and a similar reaction with the β-alanine analogue gave L^{3a} in 55% yield, after purification by column chromatography on neutral alumina. Under milder alkylation conditions (MeCN, $NaHCO_3$, 4 Å sieves, 48 h, 20 °C), the tri-ester L^{1a} was formed and purified on silica gel (CH_2Cl_2, 0→3% Pr^i_2NH). Reaction of the anhydrous $Ln(CF_3SO_3)_3$ salt with each of these ligands in boiling dry MeCN afforded the corresponding cationic esters, and controlled hydrolysis of the ester groups (20 °C, 24 h, 0.02 M NaOH) followed by cation exchange chromatography (Dowex 50 W H^+, eluent 0.5 M aq. ammonia) yielded the carboxylic acid complexes $[LnL^{2b}]^-NH_4^+$, $[LnL^{3b}]^-NH_4^+$ and $[LnL^{1b}]$. The complex $[EuL^{2a}]^{3+}$ crystallised as the hydrated hexafluorophosphate salt from aqueous solution and the crystal structure† revealed a regular mono-capped square-antiprismatic geometry about the europium ion. The NC–CN and NC–CO torsion angles averaged −58.9 and +28.6°, respectively consistent with a Δ(λλλλ) absolute configuration, as observed previously for related tetra-amides with an *S*-configuration at the stereogenic carbon centre.[7] Europium–ligand oxygen bond lengths averaged 2.405 Å [Eu–N(av) 2.642 Å] and the Eu–OH_2 bond length was 2.429(4) Å.

The kinetic stability of the gadolinium complexes was assessed by measuring the change in the water proton relaxation rate as a function of time in 2.5 M HNO_3 at 298 K. The half-lives for dissociation under these conditions were 639 h $[GdL^{2b}]^-$, 304 h $[GdL^{3b}]^-$ and 0.2 h $[GdL^{1b}]^-$. Such high stability to acid-catalysed dissociation has been observed previously for tetra-amide Gd complexes[9] and may be compared to a value of 4.5 h for $[Gd(dota)]^-$ (dota = 1,4,7,10-tetraazacyclododecane tetracetate). The corresponding europium complexes were stable in aqueous solution at 20 °C in the pH range 3–10 for several weeks.

Variable temperature ^{17}O NMR experiments with the Gd complexes of L^{1b}, L^{2b} and L^{3b} allowed the mean lifetime for water exchange to be estimated. At 298 K and pH 7, τ_m values of 8.31, 19.0 and 1.24 μs were measured for $[GdL^{2b}]^-$, $[GdL^{3b}]^-$ and $[GdL^{1b}]$ respectively which are sufficiently slow to limit the overall relaxivity of the two q = 1 complexes[9] [eqn. (1); $\tau_m > T_{1m}$, where R^{is}_{1p} is the inner sphere contribution to the

$$R^{is}_{1p} = \frac{C_{tot}q}{55.6\,(T_{1m} + \tau_m)} \quad (1)$$

measured relaxivity, τ_m is the mean water exchange rate, q is the number of bound water molecules, C_{tot} is the complex concentration (mM) and T_{1m} is the longitudinal relaxation time of the coordinated water protons]. Thus at 20 MHz, 298 K and pH 6, the measured proton relaxivity was 2.86 mM^{-1} s^{-1} for $[GdL^{2b}]^-$, 2.31 mM^{-1} s^{-1} ($[GdL^{3b}]^-$) and 7.21 mM^{-1} s^{-1} for $[GdL^{1b}]$. The pH dependence of the relaxivity of $[GdL^{2b}]^-$ and $[GdL^{3b}]^-$ (20 MHz, 298 K) was similar. In the pH range 5–8, the overall relaxivity is dominated by the outer sphere contribution, and at lower pH successive protonation of the carboxylate groups (pH 4.5–2.5) slightly enhanced the relaxiv-

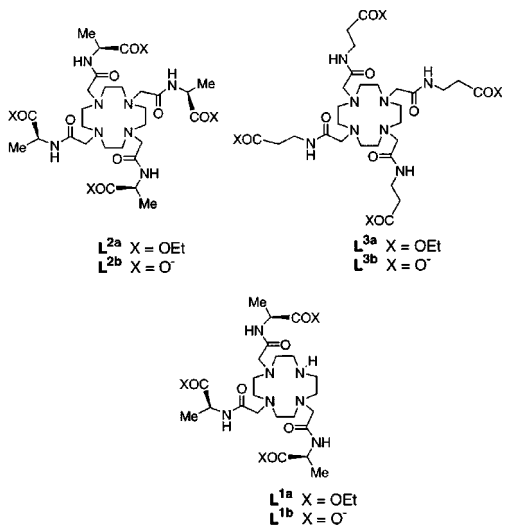

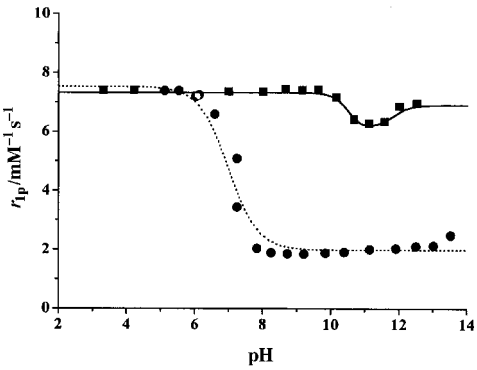

Fig. 1 pH Dependence of the relaxivity of [GdL^{1b}] (1 mM, 20 MHz, 298 K) in degassed aqueous solution (■), and in a saturated aqueous solution of $NaHCO_3$ (●). The solid and dotted lines show the fits to the experimental data.[11]

ity associated with prototropic exchange. At pH > 9, base-catalysed prototropic exchange occurs, involving the co-ordinated water molecule (pK_a = 9.3, measured potentiometrically, 298 K, I = 0.1 M NMe_4NO_3); at pH > 11, fast exchange of the amide NH protons is associated with even higher overall relaxivity values owing to an enhanced interaction with second-sphere waters, as suggested for related tetra-amide complexes.[8,11]

The relaxivity behaviour of [GdL^{1b}] differed markedly: in degassed solution (*i.e.* in the absence of dissolved CO_2 and [HCO_3^-]) the relaxivity in the pH range 2→10 was very similar to that observed for other q = 2 complexes . In aerated solution, and more clearly in a saturated aqueous solution of $NaHCO_3$, the relaxivity was very low in the pH range 8→12 (1.90 mM^{-1} s^{-1}), typical of a purely 'outer-sphere' contribution. As the pH tends towards 6, the [HCO_3^-] falls and the relaxivity increased markedly (Fig. 1).

With the corresponding europium complex, [EuL^{1b}], the rate constant for decay of the Eu luminescence was measured at pH/D = 3.80 to be 2.94 (H_2O) and 1.23 ms^{-1} (D_2O), and at a pH/D of 8.6 in the presence of a 40-fold excess of $NaHCO_3$ k_{H_2O} = 2.27, k_{D_2O} = 1.33 ms^{-1}. Such values are consistent with a reduction in the number of directly bound water molecules (q) and q values of 1.49 (pH 3.8) and 0.55 (pH 8.6) may be estimated.[5] The intensity (and lifetime) of the Eu-emission was only pH dependent in the presence of HCO_3^- and the intensity of the hypersensitive ΔJ = 2 band (λ_{em} = 618 nm) decreased by a factor of 9 as the pH fell to 6.5 (1 mM [EuL^{3b}], 40 mM $NaHCO_3$). A pH titration (Fig. 2) in a simulated background of physiological anions highlights the reduction in intensity of this band with pH. The ^{1}H NMR spectrum of [EuL^{1b}] at pD 3.8 (293 K) revealed a pattern of resonances characteristic of a square-antiprismatic coordination environment,[7,8,10] with the most shifted ring axial protons resonating at δ 24.9, 17.3, 14.8 and 12.0. At pD = 8.6, in the presence of a 40-fold excess of $NaHCO_3$, the spectrum changed dramatically and the four ring axial protons resonated at δ 11.0, 9.2, 7.7 and 6.2. In the absence of added $NaHCO_3$, no significant spectral changes occurred over the pD range 3–8.

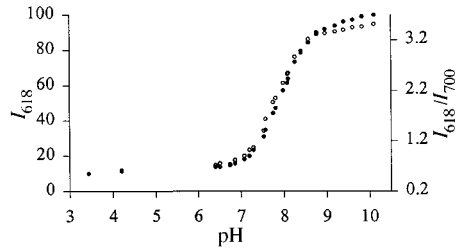

Fig. 2 pH Dependence of the europium luminescence of [EuL^{1b}] [1 mM, 298 K, 30 mM added $NaHCO_3$, 0.1 M NaCl, 2.3 mM lactate, 0.13 mM citrate, 0.9 mM hydrogenphosphate; λ_{em} = 618 nm (ΔJ = 2), and with the *ratio* of ΔJ = 2/ΔJ = 4 bands (open circles)].

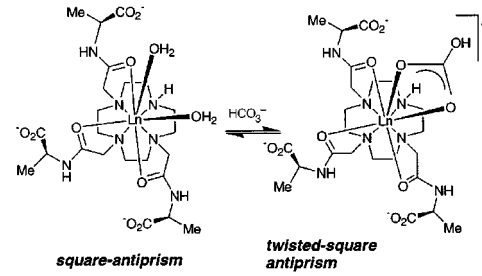

Scheme 1

Taken together the solution behaviour is consistent with reversible chelation of HCO_3^- at the lanthanide centre, displacing the bound water molecules. In the chelated ternary complex, the lanthanide ion adopts a twisted square-antiprismatic structure with a reduced helicity about the metal centre[4] (Scheme 1). The behaviour observed with these model complexes augurs well for the development of practicable relaxation and luminescent complexes that respond to pH and $pHCO_3$ changes in biological fluids under physiological conditions.

We thank EPSRC, BBSRC and the EU COST Action D-8 for support and the Royal Society for a Leverhulme Trust Senior Research Fellowship (D. P.).

Notes and references

† *Crystal data* for $C_{36}H_{70}EuF_{18}N_8O_{14.5}P_3$, M = 1433.87, orthorhombic, space group $P2_12_12_1$, a = 12.5731(4), b = 15.4085(5), c = 29.7563(10) Å, U = 5764.8(3) Å^3, D_c = 1.652 g cm^{-3}, λ(Mo-Kα) 0.71073 Å, Z = 4, μ = 1.294 mm^{-1}. Data were collected on a SMART at 150(2) K. Refinement of 786 parameters by full matrix least squares on F^2 (SHELX 96) converged at R = 0.049, wR_2 = 0.094 for 13218 reflections with $I > 2\sigma(I)$. CCDC 182/1240. See http://www.rsc.org/suppdata/cc/1999/1047/ for crystallographic files in .cif format.

1 D. Parker, P. K. Senanayake and J. A. G. Williams, *J. Chem. Soc., Perkin Trans. 2*, 1998, 2129; T. Gunnlaugsson and D. Parker, *Chem. Commun*., 1998, 511.

2 W. Li, S. E. Fraser and T. J. Meade, *J. Am. Chem. Soc*., 1999, **121**, 1413.

3 J. Hall, R. Häner, S. Aime, M. Botta, S. Faulkner, D. Parker and A. S. de Sousa, *New. J. Chem*., 1998, 627.

4 R. S. Dickins, T. Gunnlaugsson, D. Parker and R. D. Peacock, *Chem. Commun*., 1998, 1643.

5 A. Beeby, I. M. Clarkson, R. S. Dickins, S. Faulkner, D. Parker, L. Royle, A. S. deSousa, J. A. G. Williams and M. Woods, *J. Chem. Soc., Perkin Trans. 2*, 1999, 493 ; J. L. Kropp and M. W. Windsor, *J. Chem. Phys*., 1966, **45**, 761

6 L. Burai, V. Hietopelto, R. Király, E. Toth and E. Brücher, *Magn. Reson. Imag*., 1997, **38**, 146; B. László, Ph.D. Thesis, University of Debrecen, 1997.

7 R. S. Dickins, J. A. K. Howard, C. L. Maupin, J. M. Moloney, D. Parker, J. Riehl, G.Siligardi and J. A. G. Williams, *Chem. Eur. J*., 1999, **5**, 1095.

8 S. Aime, A. Barge, M. Botta, I. M. Clarkson, J. A. K. Howard, J. M. Moloney, D. Parker and A. S. deSousa, *J. Am. Chem. Soc*., 1999, **121**, in press; S. Amin, J. R. Morrow, C. H. Lake and M. R. Churchill, *Angew. Chem., Int. Ed. Engl*., 1994, **33**, 773

9 J. A. Peters, J. Huskens and D. J. Rabe, *Progr. NMR Spectrosc*., 1996, **28**, 283; S. Aime, M. Botta, M. Fasano and M. Terreno, *Chem. Soc. Rev*., 1998, **27**, 19.

10 S. Aime, M. Botta, G. Ermondi, F. Fedeli and F. Uggeri, *Inorg. Chem*., 1992, **31**, 1100; M. Woods, J. A. K. Howard, J. M. Moloney, M. Navet, D. Parker, M. Port and O. Rousseau, *Chem. Commun*., 1998, 1381.

11 Parameters for the fitting of the relaxivity/pH profiles, using T_{1m} data from NMRD profiles (0→100 MHz) and τ_m data from VT-^{17}O NMR measurements, gave, for example [Fig. 3, (○)]: q = 2, T_{1m} = 5 × 10^{-6} s, τ_m = 1.24 10^{-6} s, R^{os} = 1.99 ± 0.17 s^{-1} with an effective dissociation constant associated with bound HCO_3^- protonation of 6.99 ±0.05. Full details of the model used to analyse the pH dependence of related tetra-amide complexes are being published elsewhere.[9]

Communication 9/02238D

ChemComm
FEATURE ARTICLE

Organometallic chemistry on silicon surfaces: formation of functional monolayers bound through Si–C bonds

Jillian M. Buriak*

Department of Chemistry, 1393 Brown Laboratories, Purdue University, West Lafayette, IN 47907-1393, USA. E-mail: buriak@purdue.edu

Received (in Cambridge, UK) 5th January 1999, Accepted 8th March 1999

Silicon chips form the backbone of modern computing and yet until recently, the surface chemistry of this technologically essential material has remained relatively unexplored. As the size of devices on silicon wafers shrink (towards gigascale integration), the surface characteristics play increasingly crucial roles in the proper functioning of the device since the ratio of surface atoms/bulk escalates. While surface oxide has served thus far as the main passivation route, there is strong interest in precisely tailoring the interface properties, not only for microelectronics, but other applications including sensors, MEMS and biologically active surfaces. As a result, organometallic and organic chemistry has become essential for the synthesis of functional, modifiable monolayers, bound to non-oxidized silicon surfaces through silicon–carbon bonds. The latest approaches towards preparation of monolayers through Si–C bonds on both flat and photoluminescent porous silicon are described. Wet chemical techniques, accessible to most organometallic/organic chemists are highlighted, but recent developments using UHV conditions also receive attention.

Introduction

Silicon is clearly the most technologically important material utilized today owing to its ubiquitous role in microelectronic computing. With few exceptions, all microprocessor chips in electronic products are based upon flat, crystalline silicon wafers. In spite of several decades of intense research into the properties and potential applications of silicon, the surface chemistry of this material has only recently begun to be investigated in a systematic fashion.[1] As electronic devices on silicon become progressively smaller, the fraction of atoms residing on or near the surface becomes significant.[2] The chemical nature of these interface atoms thus plays a crucial role in the proper functioning and characteristics of the device. While native oxide on silicon has proven extremely useful in electronically passivating bulk silicon, much attention is being directed towards the synthesis of organic monolayers which can be modified upon demand for specific requirements. By tapping into the vast resources of organic and organometallic chemistry, a wide variety of functionalities can be synthesized and incorporated which will allow for fine tailoring of surface characteristics for a broad range of applications, some of which are outlined in this review. Because the surface chemistry of non-oxidized silicon is still in its infancy, several different approaches have been taken to first understand its reactivity, and then to subsequently exploit the reactivity to prepare stable, sophisticated interfaces. This review will focus exclusively on the chemistry involving formation of organic monolayers on both flat and porous silicon surfaces bound directly to the underlying bulk material through silicon–carbon bonds, some examples of which are shown in Fig. 1. Wet bench-top reactions are emphasized although recent advances utilizing ultra-high vacuum (UHV) conditions will be outlined. Capping of silica and glass surfaces with alkyl-, alkoxy- and chloro-silanes has been reviewed elsewhere.[3]

Professor Jillian Buriak was born in Toronto, Canada in 1967. She received her A. B. Degree from Harvard University in 1990 and pursued undergraduate research with Professor Andrew R. Barron. After teaching high school sciences in the Fiji Islands on a Catherine Innes Ireland Fellowship from Radcliffe College, she commenced her doctoral studies in 1991 with Professor John A. Osborn at the Université Louis Pasteur in Strasbourg, France. Upon completion of her PhD in 1995, she carried out two years of post-doctoral research with Professor M. Reza Ghadiri at The Scripps Research Institute in La Jolla, California. In 1997 she joined the faculty at Purdue University as an Assistant Professor of Inorganic Chemistry.

Flat, single crystal silicon

Single crystal silicon wafers of high purity are commercially available and relatively inexpensive due to their wide use in microelectronic applications. The most common surface orientations are Si(111) and Si(100) (*vide infra*) although other Si(*hkl*) orientations are known.[1] Upon exposure to air, single crystal silicon becomes rapidly coated with a thin, native oxide that can be removed chemically with fluoride ion or thermally under UHV conditions. Depending upon the desired electronic properties, silicon wafers are doped in a controlled fashion with electron donating (P, As, Sb: *n*-type) or withdrawing (B: *p*-type) impurities to render the intrinsic material more highly conducting.

Porous silicon

While much of the effort towards preparation of organic monolayers on silicon has been directed towards flat, single crystal surfaces, a substantial body of research has been dedicated to porous silicon functionalization.[2] Porous silicon is a potentially revolutionary variant of crystalline silicon[4] because of its tunable electro-, photo- and chemo-luminescent properties.[5] While bulk silicon is an extremely poor light emitter, porous silicon can achieve quantum efficiencies in excess of 10%, rendering it technologically important for optoelectronic applications, that is, incorporation of both optical and electronic elements into integrated circuits.[6] Because it is easily prepared through simple galvanostatic,[7] chemical (stain),[8] or photochemical[9] etches from silicon wafers ('bucket' chemistry),[5] porous silicon could be readily integrated with existing silicon-based integrated circuit (IC) manufacturing processes. Other non-silicon-based light emitting materials such as GaAs or organic light emitting compounds will require

extensive modification of the IC processes for their incorporation into silicon-based chips.

Porous silicon has a highly complex nanoscale architecture made up of one-dimensional crystalline nanowires and zero-dimensional nanocrystallites as demonstrated in Fig. 2. This material has elicited publication of over 4000 papers[10] since the discovery of its photoluminescence in 1990 which is testament not only to its technological potential, but to the fundamental interest in understanding the luminescence phenomena of nanocrystalline particles.[11] The major barrier preventing commercial applications of porous silicon is the instability of its native interface, a metastable Si–H termination (*vide infra*), and thus surface chemistry has proven to be a crucial element for the technological success of this material. The photoluminescence of porous silicon depends strongly upon the surface passivation, with certain functionalities (*i.e.* halogens)[12] resulting in complete quenching of light emission. While highly debated in the literature, it is generally accepted that quantum confinement effects, arising from recombination of entrapped electron-hole pairs (excitons) within the boundaries of nanocrystallites/nanowires with diameters of *ca.* 2 nm, are responsible.[2,5] Surface states associated with various interface species can have dramatic quenching effects if they provide sites for non-radiative recombination of the excitons.[13] The precision of organic chemistry promises to allow for fine tuning of these important interfacial effects, leading ultimately towards an understanding of the role of surface states on semiconducting nanoparticles in general. The nature of the surface bond, sterics, conjugation, and electronics of organic substituents can all be modulated at will and should provide: (i) stable porous silicon surfaces, (ii) modifiable surface characteristics, and (iii) potential to interface with organic conductor/semiconductors/LEDs and biologically relevant molecules for an array of applications.

Wet chemical functionalization strategies

For the preparation of functionalized, non-oxidized silicon interfaces, silicon–hydride terminated surfaces generally serve as an ideal starting point (Fig. 3). Si–H passivation is only metastable with respect to oxidation under ambient conditions, thus precluding long-term use in most cases. These surfaces can, however, be handled in air for tens of minutes with little degradation which renders them accessible to chemists and materials scientists wishing to use standard Schlenk and glove box techniques.[14] Silicon–hydride termination of commercial, native oxide capped flat crystal silicon wafers is carried out quickly and efficiently in under 10 min using commercially available fluoride sources. Dilute (1–2%) aqueous HF treatment of a Si(100) wafer yields the (100) dihydride $=SiH_2$ capped surface, and 40% aqueous NH_4F of a Si(111) wafer provides the atomically flat (111) monohydride ≡SiH terminated surface.[15] Porous silicon, when etched through standard procedures involving HF, is also hydride terminated but is coated with $–SiH_3$, $=SiH_2$, ≡SiH groups in a variety of different local orientations and environments owing to the porous nature of the material.[16] All the freshly etched silicon hydride terminated surfaces are chemically homogeneous (> 99% H termination) which is essential for clean reactions.

The hydride terminated surfaces are extremely useful surface precursors because the Si–H and Si–Si bonds can serve as chemical handles through which functionalization can be mediated. The body of literature involving functionalization of soluble, molecular silicon–hydride and silicon–silicon containing compounds is vast.[17] Several of these reactions for molecular compounds have been adapted and applied to surfaces, as described here. Other reactions, on the other hand, have no molecular equivalents since they utilize the underlying bulk electronic properties of the semiconducting silicon.

The chemistries of hydride terminated porous and flat, single crystal silicon surfaces are closely related and, with few exceptions, a novel reaction found to operate on one surface usually has some degree of success on the other.[18] Porous silicon is especially attractive due to its high surface area which renders analysis relatively straightforward through conventional transmission Fourier transform IR (FTIR) or diffuse reflectance IR (DRIFT) spectroscopy. As a result, routine characterization of this material is practical and facile for most chemists. Flat surfaces offer, on the other hand, a much more structurally homogeneous surface that is extremely useful for controlled reactivity studies. The general mechanistic trends for flat and porous silicon interfaces are very closely related and thus are discussed here interchangeably.

Hydrosilylation involving a radical initiator

Hydrosilylation involves insertion of an unsaturated bond into a silicon–hydride group as shown in Fig. 4. Alkyne and alkene hydrosilylation on Si–H terminated surfaces yields alkenyl and alkyl termination, respectively. The first example of hydrosilylation of non-oxidized Si–H passivated silicon was carried out by Chidsey and coworkers in 1993 on flat crystal Si(111)

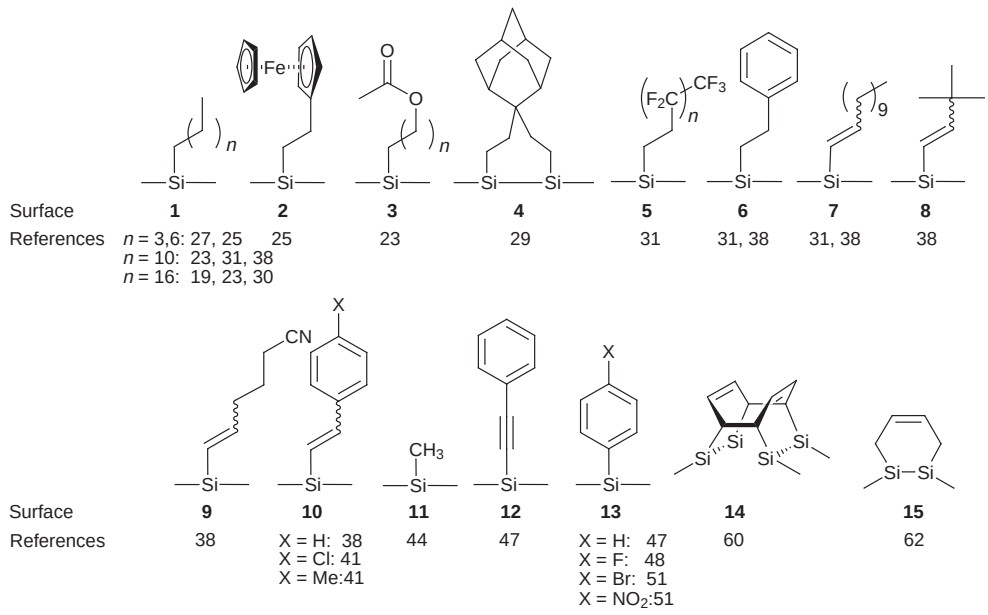

Fig. 1 Examples of organic monolayers formed on various silicon surfaces, bound through Si–C bonds.

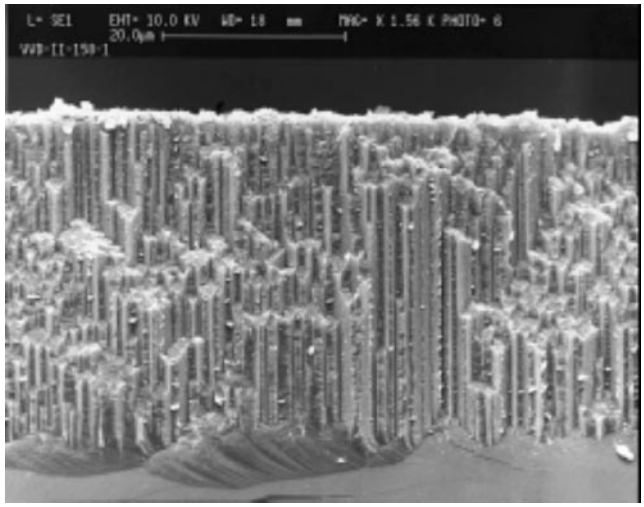

Fig. 2 Cross-sectional scanning electron micrograph (SEM) of a 30 μm thick porous silicon layer electrochemically etched on a (100) single-crystal wafer. The pores here are on the order of μm but through variation of the etching conditions, a wide range of pore sizes (from 2 nm to μm) is easily accessed. Professor M. J. Sailor is thanked for his kind permission to use this figure from ref. 2. Reproduced with permission from Wiley-VCH.

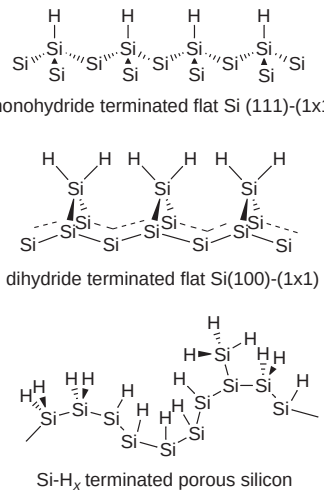

Fig. 3 The Si(111), (100) and porous silicon hydride terminated surfaces discussed here. The flat Si(111) (1 × 1) surface is capped with only one hydride to satisfy the tetravalency of the silicon atoms. The dihydride flat Si(100) (1 × 1) is shown but monohydride Si(100) (2 × 1) and mixed mono- and di-hydride Si(100) (3 × 1) surfaces are also possible.[1]

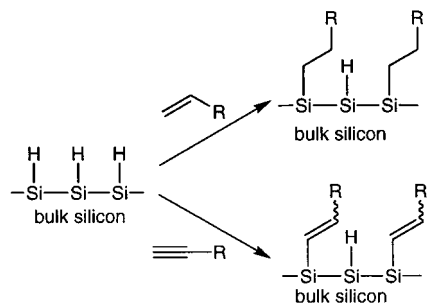

Fig. 4 Hydrosilylation of alkenes or alkynes involves insertion of the carbon–carbon unsaturated bond into the silicon–hydride bond, yielding alkyl and alkenyl terminated surfaces, respectively.

surfaces.[19] Insertion of alkenes into surface bound Si–H groups, in the presence of a diacyl peroxide radical initiator, provided high quality alkyl monolayers at 100 °C. Monolayers prepared from octadecene, yielding octadecyl groups on the surface (surface **1**, Fig. 1), are densely packed and tilted approximately 30° from the surface normal. As a result of the good coverage provided by the film, the silicon surfaces demonstrate excellent stability and withstand extended boiling in aerated chloroform, water, acid (2.5 M H_2SO_4 in 90% dioxane, v/v) and base (10% aqueous 1 M NH_4OH), and are resistant to fluoride (immersion in 48% aqueous HF). Under ambient conditions in air, little oxidation of the silicon surface is observed, indicating the usefulness of this approach for technological applications.

The authors propose a radical mechanism for monolayer formation under these conditions. The initiator, the diacyl peroxide, undergoes homolytic cleavage to form two acyloxy radicals which decompose to carbon dioxide and an alkyl radical.

$$[RC(O)O]_2 \rightarrow 2RC(O)O\cdot$$
$$RC(O)O\cdot \rightarrow R\cdot + CO_2$$

The alkyl radical can then abstract H· from a surface Si–H group to produce a silicon radical.

$$R\cdot + HSi\equiv \rightarrow RH + \cdot Si\equiv$$

Because silyl radicals are known to react extremely rapidly with olefins, formation of a silicon carbon bond is the next probable step.[20]

$$R'CH{=}CH_2 + \cdot Si\equiv \rightarrow R'(CH\cdot)CH_2Si\equiv$$

The carbon-based radical can then abstract a hydrogen atom either from a neighboring Si–H group or from the allylic position of an unreacted olefin.

The majority of studies carried out by this group involved perhydroalkenes but the ω-Cl terminated olefin, 11-chloroundec-1-ene, produced good quality monolayers with chloride termination. As suggested by the authors, further functionalization of the surface through the chloride is possible. Hydrosilylation of the alkyne, hexadecyne, produced a good quality monolayer and as noted in a footnote,[21] may be bound to the silicon surface through a vinyl group as would be expected. The use of the bromide terminated olefin, 11-bromoundec-1-ene, however, produced a poorly organized monolayer, perhaps due to the incompatibility of the Br with the radical nature of the reaction.

Thermally induced hydrosilylation

Control experiments carried out by Chidsey and co-workers during their investigations of diacylperoxide initiated olefin hydrosilylation on Si(111) surfaces indicated that the reaction could occur in the absence of diacylperoxide initiator at higher temperatures (≥150 °C), almost certainly through homolytic Si–H cleavage.[22]

$$HSi\equiv \rightarrow \cdot H + \cdot Si\equiv$$

The silyl radical will then proceed to react with the olefin to form the silicon–carbon bond. This result was pursued by Sudhölter and coworkers on hydride terminated Si(100).[23] Working at 200 °C, a number of different olefins were examined for their propensity to form stable monolayers. 2 h contact time produced closely packed monolayers when long-chain aliphatic alkenes (12–18 C, surface **1**, Fig. 1) were used as judged by X-ray reflectivity, ATR IR spectroscopy and contact angle measurements. With ω-ester substituted alkenes, ester terminated alkyl surfaces were prepared (surface **3**, Fig. 1) and then subsequently cleaved with $LiAlH_4$ (Scheme 1) to yield the hydrophilic, hydroxy-terminated silicon surface.

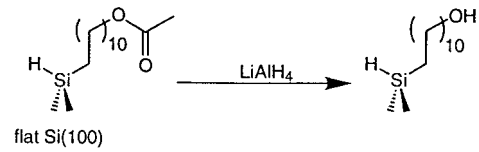

Scheme 1

This reaction clearly demonstrated that alkyl monolayers on silicon are robust enough to tolerate further chemical reactions,

and can be built upon directly to produce more sophisticated surfaces. Alcohol-terminated alkenes could not be utilized directly through this method because they react with the surface through the hydroxy group, yielding ill defined monolayers. Thus traditional protecting group strategies may be viable options when preparing functional films on silicon. Recent work has demonstrated that aliphatic monolayers produced on hydride terminated Si(111) and Si(100) through this reaction are also stable up to 615 K under vacuum which indicates that organic monolayers on silicon can be thermally resistant.[24]

Thermally induced hydrosilylation of alkynes and alkenes has been applied to Si–H terminated porous silicon surfaces. Horrocks and Houlton reported that refluxing porous silicon for 18–20 h at 110–180 °C in an aliphatic alkyne or alkene yields alkyl monolayers (surface **1**, Fig. 1).[25] Alkyne hydrosilylation does not produce surface bound vinyl groups as one would expect, presumably because it undergoes two hydrosilylations. Hydrosilylation of vinyl ferrocene (surface **2**, Fig. 1) was particularly interesting since it allows for electrochemical investigations of the ethylferrocene terminated surface. While these surfaces demonstrate good stability to boiling base (75% KOH–25% EtOH, pH 12), significant photoluminescence quenching due to the thermal hydrosilylation is observed (Fig. 7, *vide infra*). Porous silicon is inherently fragile and appears to degrade under extended reflux conditions.

Photochemical hydrosilylation (UV)

It is known in the organic and organometallic literature that UV irradiation can promote hydrosilylation of unsaturated compounds[26] due to homolytic cleavage of Si–H bonds, as is the case with thermal induction. UV photoinduction, however, takes place at room temperature and thus provides a way to avoid thermal input which could be harmful to delicate or small features on a silicon chip. Minimal input of thermal energy would be preferable in any IC manufacturing process (thermal budget). Chidsey and coworkers showed in 1997 that irradiation of a hydride terminated Si(111) surface with UV light (185 and 253.7 nm) in the presence of an aliphatic alkene like pent-1-ene or octadec-1-ene (surface **1**, Fig. 1) brought about hydrosilylation in 2 h at room temperature.[27] Interestingly, these surfaces were further functionalized through a biphasic (gas/solid) photoinduced (351 nm) free radical chlorosulfonylation of the terminal methyl groups and then reacted with ethylenediamine (Scheme 2).[28] The authors propose binding of biomolecules to the amino terminus for investigation by scanning probe microscopy (SPM), sensing, and surface related assays. UV irradiation derived from a Xe UV lamp (24 h) has also been used to hydrosilylate divinyladamantane on Si(111) surfaces for use as a solid substrate for chemical vapor deposition (CVD) of diamond films (surface **4**, Fig. 1).[29]

These results were followed up by Effenberger *et al.* who found that irradiation with substantially longer wavelengths, up to 385 nm, for 20–24 h were also effective in promoting alkene hydrosilylation on Si(111) surfaces (surface **1**, Fig. 1).[30] Using masking techniques, they photopatterned the surface to produce areas of differing wettabilities as visualized under a microscope.

Photochemical hydrosilylation (white light)

Recently, Stewart and Buriak demonstrated that a simple white light source could induce hydrosilylation of alkenes and unconjugated alkynes on Si–H terminated photoluminescent porous silicon surfaces at room temperature in minutes.[31] Illumination of an unfiltered tungsten ELH bulb (GE slide projector bulb) of moderate intensity (22–44 mW cm^{-2}) on a photoluminescent porous silicon sample wetted with an alkene or alkyne (surfaces **1**, **5**–**7**, Fig. 1) induces surface hydrosilylation as demonstrated schematically in Fig. 5. Because the reaction is photoinduced, photopatterning can be easily carried out with simple optical apparatus to prepare spatially defined areas of differing chemical functionalities. For instance, use of a f/75 reducing lens and a mask produced with a high quality laser printer can achieve features as small as 30 μm. Examples of larger scale photopatterning on porous silicon produced from n-type silicon crystal wafers are shown in Fig. 6. As demonstrated in Fig. 6(b)–(d) long aliphatic substituents on the surface, here dodecyl groups, can sufficiently protect the surface from boiling alkali. The remaining, unpatterned areas of Si–H termination dissolve rapidly under these conditions in what can be viewed as a lithographic process. Dodecyl terminated samples will tolerate boiling for 30 min in aerated aqueous KOH (pH 10) solution, conditions under which freshly etched (Si–H terminated) porous silicon will dissolve in seconds. These surfaces are not, however, as stable as those produced through Lewis acid mediated hydrosilylation (*vide infra*, Hydrosilylation mediated by metal complexes) which will resist several hours of contact with alkali at 100 °C. The unpatterned areas of surface Si–H groups can, instead of undergoing dissolution, hydrosilylate (white light induced) a second alkene or alkyne to produce domains of differing terminations. This provides an extremely useful method of hydrosilylating porous silicon surfaces at room temperature with simple white light illumination.

The mechanism of this reaction still remains to be determined. Monochromatic experiments indicated that the degree of incorporation increased with shorter wavelengths (450 > 550 > 650 nm) as measured by transmission FTIR. Because wavelengths as long as 400 nm will promote alkene hydrosilylation on hydride terminated Si(100) surfaces, the blue end of the white light illumination may induce homolytic Si–H cleavage to produce silicon radicals.[26] Alternatively, photogenerated holes on the photoluminescent porous silicon surface are produced upon light soaking which are subsequently attacked by alkyne or alkene nucleophiles.[32] Electron deficient alkynes (phenylacetylene, 4-methylphenylacetylene and 4-chlorophenylacetylene) require long reaction times (12 h) and are generally poorly incorporated, supporting a mechanism involving nucleophilic attack.[33] We are presently vigorously investigating this reaction through electron paramagnetic resonance (EPR) spectroscopy and chemical means in order to distinguish between surface radical reactions and potential involvement of the underlying electronic properties of the silicon nanocrystallites and nanowires which make up the porous silicon matrix.

The light mediated reaction appears very gentle and, depending upon the chemical groups incorporated, preserves most of the intrinsic photoluminescence of the porous silicon

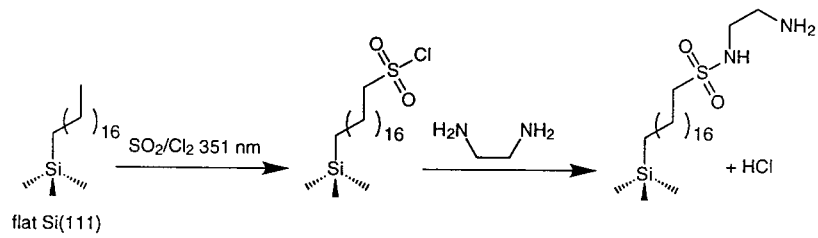

Scheme 2

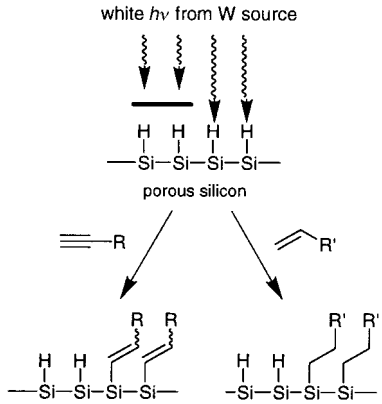

Fig. 5 Illumination of photoluminescent porous silicon samples with white light in the presence of an alkene or alkyene induces hydrosilylation, yielding alkyl and alkenyl termination, respectively. The reaction takes place at room temperature in 30–60 min, with white light of moderate intensity (22–44 mW cm^{-2}).[31] Masking techniques allow for preparation of spatially defined areas of chemical functionalities.

(Fig. 7). Dodecyl groups (surface **1**, Fig. 1), having no unsaturation, maintain 97% of the photoluminescence whereas dodecenyl termination (surface **7**, Fig. 1), bound to the surface through a vinyl group, preserves 61%. A small red shift of the photoluminescence of *ca.* 10 nm is observed. This functionalization strategy could, therefore, be important for preparation of optoelectronic porous silicon devices and sensors.

Hydrosilylation mediated by metal complexes

Because Pt(0) complexes and colloids are extremely effective catalysts for the hydrosilylation of alkenes with soluble, molecular silanes,[34] Zazzera *et al.* examined their potential on hydrogen terminated flat Si(100) surfaces.[35] Using 3,4-dichlorobutene as the olefin and platinum(0)–divinyltetramethyldisiloxane as the catalyst precursor, they observed chloride incorporation (from the Cl-containing olefin) on the surface as determined by XPS and surface mass spectrometry (TOF-SIMS) after 45 min at room temperature. *In situ* ATR IR spectroscopy indicated consumption of surface SiH_2 groups, supporting a hydrosilylation mechanism. They found, however, that the platinum complex also catalyzed oxidation of the silicon surface although this competing reaction could be reduced by minimizing trace water and utilizing a large excess of olefin.

Other workers have found that late transition metal complexes, in general, are problematic with respect to Si–H terminated porous silicon.[36] Exposure of freshly etched porous silicon to Wilkinson's catalyst, $RhCl(PPh_3)_3$, and the palladium complexes $PdCl_2(PEt_3)_2$ or $Pd(OAc)_2$/1,1,3,3-tetramethylbutyl isocyanide in the presence of alkynes,[37] resulted in blackening of the surfaces due to apparent metal deposition which thoroughly quenched the photoluminescence. Substantial oxidation was also noted even if considerable precautions were taken.

In order to avoid late transition metals and their accompanying problems of oxidation and metal deposition on porous silicon, Buriak and Allen utilized a Lewis acid to mediate hydrosilylation of alkynes and alkenes.[38] Lewis acid catalyzed or mediated hydrosilylation reactions seemed ideal for functionalization of porous silicon because of the mild reaction conditions involved and high selectivity and specificity of the corresponding solution phase reaction.[39] $AlCl_3$ is an effective catalyst for alkenes as well which suggested that Lewis acid mediated surface chemistry would not be limited to alkynes.[39b,c] Since $EtAlCl_2$ is soluble in non-polar solvents whereas $AlCl_3$ is not, it was chosen as the Lewis acid to avoid multiphasic reactions on the surface of porous silicon.[40] A wide range of alkynes and alkenes were smoothly hydrosilylated on Si–H passivated porous silicon at room temperature (surfaces **6**–**10**, Fig. 1), yielding vinyl and alkyl terminated surfaces, re-

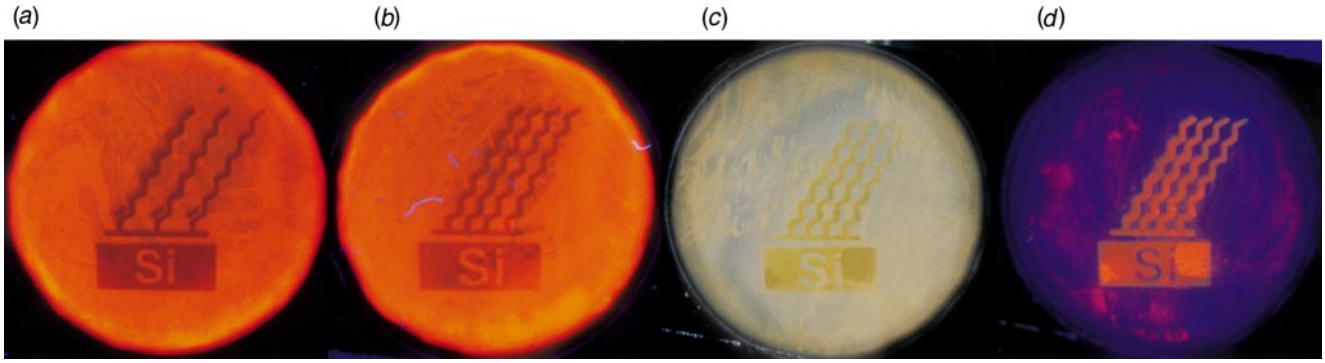

Fig. 6 Photographs of 12 mm diameter photoluminescent porous silicon samples prepared through white light promoted hydrosilylation of dodec-1-yne (surface **7**) and dodec-1-ene (surface **1**) through masking procedures.[31] (a) Surface **7** appears as the darkened, red-shifted patterned area when illuminated with a 365 nm hand-held UV lamp. The other areas of the wafer are unfunctionalized (native Si–H termination). (b) Surface **1** (ref-shifted patterned area) upon illumination with 365 nm light. (c) Sample from (b) after boiling in aerated, aqueous KOH (pH 12) solution for 15 s. The unfunctionalized porous silicon (grey area) has dissolved while the hydrosilylated surface (surface **1**, golden area) remains intact. (d) Illumination of the surface from (c) with a 365 nm hand held UV lamp. The PL of the hydrosilylated area (surface **1**) remains intact while most of the unfunctionalized PL is destroyed. This figure has been reproduced from ref. 31 with permission from Wiley-VCH.

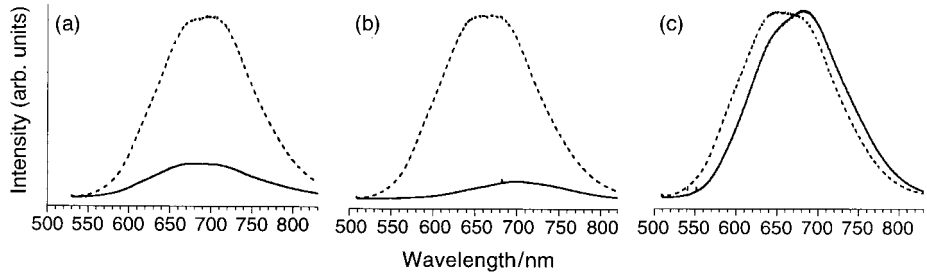

Fig. 7 Photoluminescence spectra of 1-dodecene hydrosilylation (surface **1**) on n-type porous silicon (440 nm excitation). The dotted spectrum is that of freshly etched porous silicon, and the solid that of the resulting dodecyl terminated surface. (a) Lewis acid mediated,[38] (b) thermally induced (2 h reflux in neat dodec-1-ene),[36] (c) white light promoted (60 min reaction at 22 mW cm^{-2} white light).[31]

spectively. By using an excess of $EtAlCl_2$, alkynes with coordinating functional groups (ester, hydroxy and cyano groups) could also be incorporated onto the surface. One equivalent of the Lewis acid complexes the coordinating group and the remainder mediates the hydrosilylation reaction. We have found, thus far, the reaction to be independent of silicon doping and morphology.

The effects of the reaction on photoluminescence have been studied in some detail. In all cases, at least 75% of the intrinsic photoluminescence is lost, as shown for dodec-1-ene in Fig. 7, although it can be partially restored through boiling in alkali or soaking in HF solutions.[41] Conjugated functionalities, such as styrenyl termination (surface **10**, Fig. 1), result in complete loss of photoluminescence with no possibility for recovery. Neither electron donating nor withdrawing substituents (chloro or methyl) on the conjugated styrenyl group have any effect on the photoluminescence. Sailor and Song observed similar effects for phenylacetylide termination (*vide infra*, Reactions of alkyl/aryl carbanions) in which a phenyl ring is conjugated through an alkyne linker (surface **12**, Fig. 1). These results suggest that surface states associated with the conjugated group result in efficient non-radiative recombination of the excitons produced upon irradiation with blue or UV light.

That the reaction is indeed hydrosilylation is strongly supported by the following experimental results. Consumption of Si–H groups can be clearly seen through difference FTIR spectra taken before and after the reaction with an alkyne or alkene.[36] The procedure with dodec-1-yne produces a surface bound vinyl group whose ν(C=C) of this olefin can be clearly distinguished in the transmission FTIR at 1595 cm^{-1} as shown in Fig. 8. It was proven through chemical means that this

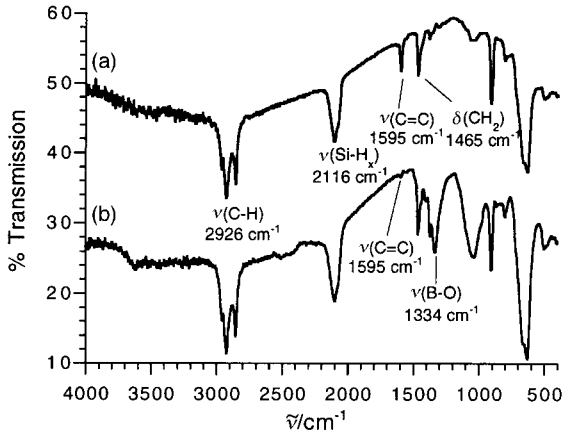

Fig. 8 FTIR (transmission mode) of monolayers prepared through: (a) hydrosilyation of dodec-1-yne mediated by $EtAlCl_2$ on porous silicon resulting in covalent attachment of a dodecenyl group (surface **7**) and (b) hydroboration of the surface-bound olefin of the dodecenyl group with 0.8 M BH_3·THF. The ν(C=C) vanishes upon hydroboration, as would be expected for an olefinic substituent. Reprinted with permission from *J. Am. Chem. Soc.* (ref. 38), Copyright 1998, American Chemical Society.

functionality is indeed a double bond. The dodecenyl terminated surface was hydroborated with excess 0.8 M BH_3·THF in THF under nitrogen followed by quenching of the surface in air and rinsing with excess THF.[42] Almost quantitative disappearance of the stretch at 1595 cm^{-1} was observed by transmission FTIR in Fig. 8(b), with concomitant appearance of a new stretch at 1334 cm^{-1} which corresponds to the B–O stretching frequency.[43] The stereochemistry of the borane addition has not been determined although it is expected that the boron atom will add preferentially to the least hindered carbon, that being the carbon β to the surface silyl group.

The hydrophobic, alkyl and alkenyl terminated surfaces are very stable under highly demanding chemical conditions. The dodecenyl functionalized surface (surface **7**, Fig. 1) will resist at least 4 h of boiling in aerated solutions of 25% EtOH–75% aqueous KOH (pH 10) with little change in the FTIR spectrum; Si–H terminated porous silicon dissolves in seconds. The surprising increase in photoluminescence of dodecyl and dodecenyl terminated porous silicon under these conditions may be due to a secondary basic etch at defect sites although this observation remains to be clarified.[41] Long term stability studies under ambient conditions are underway but preliminary results indicate that dodecenyl terminated porous silicon derived from p-type wafers is at least an order of magnitude more resistant to oxidation, as judged by FTIR spectroscopy. This route appears to be a promising, low temperature means of stabilizing porous silicon, and incorporating a broad range of chemical functionalities for preparation of 'smart', sophisticated silicon devices.

Reactions of alkyl/aryl carbanions

The use of alkyl Grignard and alkyl lithium nucleophiles on silicon surfaces was first investigated by Chazalviel, Ozanam and coworkers.[44] Silicon–methyl terminated porous silicon derived from p-type single crystal silicon (surface **11**, Fig. 1) was demonstrated to be electrochemically accessible through treatment of the native Si–H passivated surface with a methyl Grignard or methyl lithium organometallic under anodic conditions. As proposed by the authors, silicon hydride groups are consumed through a transmetallation reaction, forming silicon-methyl groups and either MgHX or LiH as by-products of the reaction. The stability of the surfaces increases an order of magnitude with respect to accelerated air oxidation at 100 °C as determined by FTIR spectroscopy. This electrochemical reaction is especially interesting since it has no obvious chemical equivalent for soluble, molecular silanes;[45] the semiconducting properties of the underlying silicon are harnessed to effect the chemistry.[46]

Song and Sailor[47] and Kim and Laibinis[48] subsequently investigated the effects of Grignard and alkyl and aryl lithium reagents without an electronic bias. The range of carbanion nucleophiles that could be bound to the surface of porous silicon through Si–C bonds was extended and detailed mechanistic studies were carried out. The mechanism proposed for silicon–carbon bond formation, shown in Scheme 3, involves attack of the weak Si–Si bond (Si–Si = 215–250 kJ mol^{-1}, Si–H = 323 kJ mol^{-1})[49] by the carbonanion nucleophile (MR). Soluble molecular disilanes react in a similar manner.

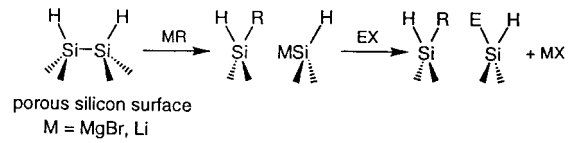

Scheme 3

The resulting silyl anion on the porous silicon surface can be further reacted with an electrophile (EX), offering the possibility to form mixed surfaces.

The effects of carbanion functionalization on the photoluminescence of porous silicon have also been investigated in some detail. Methyl termination, as examined by Chazalviel and coworkers,[44] has little effect on the photoluminescence intensity of p-type porous silicon. Sailor and Song observed that a conjugated alkyne (surface **12**, Fig. 1) results in irreversible quenching of the intrinsic photoluminescence that could not be recovered by rinsing with HF solutions. It was found, however, that simple phenyl[47] or 4-fluorophenyl[48] termination (surface **13**, Fig. 1) resulted in only minor quenching which points to the interesting possibility of using the surface functionalities to tune the photoluminescence and underlying optoelectronics of the material.

Alkylation of flat silicon surfaces with alkyl Grignards or lithium reagents through a two-step route has also been demonstrated by Lewis and Weinberg.[50] Chlorination of a hydride terminated flat Si(111) crystal with PCl_5 for 20–60 min

at 80–100 °C produced a chloride terminated silicon surface. Transmetallation with an organolithium or Grignard at 80 °C for 30 min to 8 days produced LiCl or MgXCl, and an alkyl group bound to the silicon surface through an Si–C linkage. Surfaces with long alkyl termination are more resistant to oxidation under ambient conditions and to boiling in aerated chloroform and water. Thermal desorption and XPS experiments indicate that ≡Si–OR linkages are not formed which provides support for the expected Si–C bond formation event.

Electrochemical diazonium reduction

Electrochemistry has also been used to produce close-packed phenyl monolayers (surface **13**, Fig. 1) on hydride terminated flat n-type Si(111) surfaces (Scheme 4).[51]

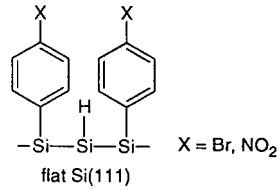

Scheme 4

Application of a negative potential of *ca.* 1 V to a dilute HF solution containing a 4-nitro- or bromo-benzene diazonium salt results in production of aryl radical and dinitrogen.

$$^{+}N{\equiv}N–Ar–X + e^{-} \rightarrow \cdot\ Ar–X + N_2\ (X = Br \text{ or } NO_2)$$

The aryl radical can then abstract a surface hydride to form silicon radicals which can react with another aryl radical to form the silicon–carbon bond.

$$\cdot\ Ar–X + {\equiv}Si–H \rightarrow {\equiv}Si\cdot + H–Ar–X$$
$${\equiv}Si\cdot + \cdot\ Ar–X \rightarrow {\equiv}Si–Ar–X$$

The covalent nature of the phenyl bonding to the surface is demonstrated by their stability to aqueous 40% HF solutions, and XPS and Rutherford backscattering (RBS) measurements. Because this reaction utilizes the electrode nature of the semiconducting silicon, no clear reaction parallels can be found for soluble, molecular silanes. One important advantage of this approach is that the process is cathodic, thus making the surface electron rich during the reaction which renders it less susceptible to nucleophilic attack by water, supressing oxidation.

Ultra high vacuum (UHV) functionalization strategies

The reactivity of clean silicon surfaces, in absence of a hydrogen monolayer, has been studied intensively by a number of groups under ultra high vacuum (UHV) conditions.[1] The activity of these surfaces is very different from that of the metastable Si–H terminated materials which provides further insight into the structures and properties of flat silicon. The thermally reconstructed Si(100) (2 × 1) surface (Fig. 9), with no

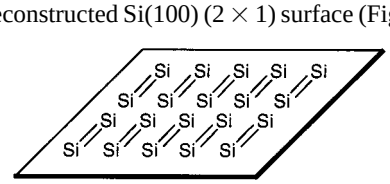

Fig. 9 Schematic diagram of the Si=Si dimers oriented on a Si(100) surface under UHV conditions.

hydrogen capping, has recently been shown to be capable of a number of remarkable cycloaddition reactions that have parallels to organic reactions. The surface silicon atoms pair into dimers connected by a σ and a π bond, thus having essentially double bond character. Use of 4° miscut off-axis Si(100) single crystal wafers allows for highly rotationally oriented samples in which all the Si=Si dimers are pointed in the same direction, yielding anisotropic surfaces on a centimeter length scale. The silicon–silicon double bonds are highly reactive, and have been exploited to produce ordered monolayers through the chemistry described here.

[2 + 2] Reactions of alkynes and alkenes with reconstructed Si(100)

Early work on 'relatively simple' unsaturated hydrocarbons such as ethylene, propylene, acetylene and benzene have been shown to chemisorb on Si(100) (2 × 1) surfaces and are able to resist temperatures of up to 550–600 K.[52] It was suggested that alkenes add to clean Si(100) (2 × 1) surfaces to form a disilicon substituted aliphatic $–CH_2CH_2–$ bridge through a formal [2 + 2] cycloaddition (Scheme 5).

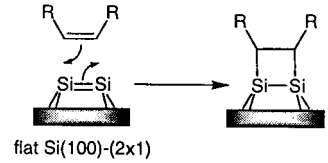

Scheme 5

Two new Si–C σ bonds form due to cleavage of the π bonds in the alkene and disilylene. Electron energy loss spectroscopy (EELS) suggests rehybridization of the two sp^2 carbons to sp^3 although the fate of the remaining Si–Si σ bond is still unclear.[53] Acetylene reacts in a similar [2 + 2] fashion yielding a disilicon-substituted alkene and involves a change in hybridization at the carbon from sp to sp^2 in this case.[54] Concerted [2 + 2] cycloadditions are symmetry-forbidden which suggests a low-symmetry pathway.[55]

Hamers *et al.* have recently described an elegant extension of this series of reactions involving the π bonds of organic species containing C=C bonds.[56] A wide range of complex cyclic olefins react in this manner at moderate temperatures (50–100 °C), including cyclopentene,[57] 3-pyrroline,[53] pyrrolidone,[58] norbornadiene,[53] cycloocta-1,5-diene,[59] and cyclooctatetraene.[60] The [2 + 2] addition of cyclooctatetraene (surface **15**, Fig. 1) is especially interesting since it appears to add to the surface through a double cycloaddition, leaving two alkene groups per molecule exposed through which further chemistry could be carried out.[60] Scanning tunneling microscopy (STM) images of the cyclooctatetraene functionalized surface are shown in Fig. 10, revealing the long range order of the samples and formation of only one major surface species.

Diels–Alder ([4 + 2]) reactions of dienes with reconstructed Si(100)

Konecny and Doren predicted,[61] and Bent and coworkers demonstrated experimentally,[62,63] that the double bond character of the reconstructed Si(100) (2 × 1) surface could act as a dienophile in a Diels–Alder [4 + 2] type reaction (Scheme 6).

Chemisorption of buta-1,3-diene (surface **15**, Fig. 1) or 2,3-dimethylbuta-1,3-diene onto the Si(100) (2 × 1) surface at room temperature results in an efficient Diels–Alder reaction, forming two Si–C σ bonds and one unconjugated, internal olefin. FTIR spectroscopy, thermal desorption, near edge X-ray absorption fine structure and deuterium labeling studies assisted in the determination of surface composition. A reinvestigation of the 2,3-dimethylbuta-1,3-diene reaction on Si(100) (2 × 1) by Hamers and coworkers supports the observation of a Diels–Alder [4 + 2] cycloaddition for 80% of the molecules although they note a minor (20%) [2 + 2] cycloaddition product as well.[64]

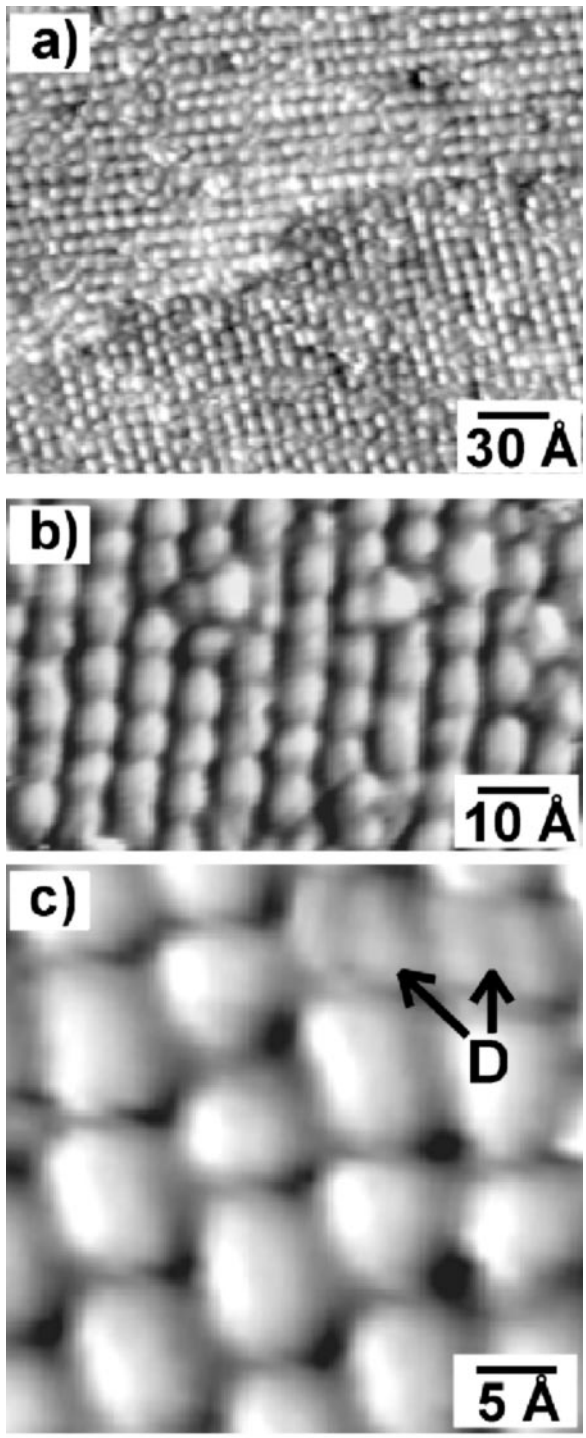

Fig. 10 Scanning tunneling microscopy (STM) images of the Si=Si dimer terminated Si(100) surface after exposure to cyclooctatetraene to form surface **15** (Fig. 1); (a) demonstrates the long range anisotropy and ordering of the surface while (b) and (c) reveal the absorption pattern of the molecules. 'D' refers to a minority species comprising < 5% of the surface features. Professor Robert J. Hamers is gratefully acknowledged for permission to reproduce this figure from ref. 60(*a*). Reprinted with permission from *J. Phys. Chem.* (ref. 60(*a*)), Copyright 1998, American Chemical Society.

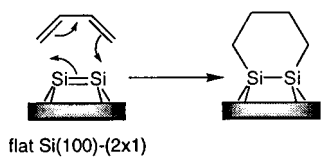

Scheme 6

In the case of cyclohexa-1,3-diene, 55% of the surface products arise from the [4 + 2] addition, 35% the [2 + 2] and 10% and unknown product. The [4 + 2] products are predicted to be thermodynamically more stable but because surface temperature has little affect on product distributions, it is suggested that the reaction is under kinetic control.

Directions for functionalized silicon surfaces: present and future

Tunable, stabilized silicon surfaces will have a broad array of technologically important applications. Flat, non-oxidized silicon surfaces functionalized with ordered organic monolayers have obvious potential in microelectronics. Gate oxides in metal oxide semiconductor transistors (MOSFETs) may be replaced with an organic monolayer since the resistivity could be modulated through organometallic/organic synthesis.[56] Aliphatic substituents will provide obvious insulating properties but conjugated, unsaturated organic moieties could allow for fine tuning of the surface conductivity. Interfacing of silicon microelectronic circuits with neuronal networks and other biologically relevant systems is a fascinating direction that has received much attention in recent years.[65] Surface properties are crucial and thus the power of organometallic/organic chemistry on silicon could play an important role.

Functionalized, stable porous silicon surfaces have an immense variety of potential uses which partially explains the explosion of interest in this material since 1990.[2,5] Applications include use as chemical sensors,[66] microelectronics,[67] photonics,[68] optoelectronic devices[13] such as electroluminescent displays,[69] photodetectors,[13] and as a matrix for photopumped tunable lasers.[70] The biocompatability of porous silicon has been examined *in vivo* and *in vitro* within a simulated body fluid (SBF) environment.[71] Hydroxyapatite, a major constituent of bone, forms on the porous silicon surface and thus is a bioactive material with interesting applications as a biological implant.[72]

Porous silicon as a sensor is a particularly exciting application because of its high surface area which can render it more sensitive than a flat silicon chip, and the two (at least), unrelated signal transduction modes (read-out mechanisms) that are accessible. Early observations by Sailor and coworkers indicated that physisorbed molecular adsorbates such as methanol, benzene, dichloromethane (from the vapor or as a liquid)[73] or NO[74] on the native Si–H terminated porous silicon surface reversibly quench the photoluminescence. Thus quenching of the photoluminescence could serve as a visible wavelength read-out for sensing of chemical vapors or gaseous molecules in general. The second signal transduction mode for a porous silicon-based sensor involves an optical interferometric event, unrelated to the previously described photoluminescence quenching scheme.[75] Thin porous silicon films exhibit Fabry–Perot fringe patterns created by multiple reflections of white light on the air–porous silicon and porous silicon–bulk silicon interfaces. A change of the index of refraction of the porous silicon matrix, induced by absorbance of a material with a different index of refraction within the pores, will cause a shift in the fringe pattern. Oxidized porous silicon has been functionalized with a number of biologically relevant molecules such as biotin and has been shown to sense and quantify streptavidin binding.[75] Clearly, for exquisitely selective and sensitive binding, surface chemistry is of extreme importance since binding groups must be incorporated. The organometallic chemistry described here on non-oxidized silicon surfaces is highly relevant to the preparation of sensors because of the high sophistication of these surfaces and excellent stability required.

Recent work by Whitesides and coworkers has outlined a fascinating approach towards generation of small structures through soft lithography.[76] An elastomer stamp or mold is used to repeatedly and accurately pattern self-assembled monolayers

(SAMs) on surfaces, producing spatially defined arrays of chemical functionalities and interface characteristics. Recent work has demonstrated the compatability of soft lithographic techniques with standard SiO_2/Si fabrication processes.[77] At this writing, however, no results concerning utilization of soft lithography to form monolayers on non-oxidized silicon have been revealed in the literature, but with the strong technological interest in preparing small features of tunable electronic and chemical characteristics on oxide-free silicon, it is almost certainly only a matter of time.[78] Several room-temperature processes involving monolayer preparation through Si–C bonds, as described here, are under development and could be applicable to soft lithography.

Conclusions

The development of novel, organometallic reactions on non-oxidized silicon is clearly an exciting, rapidly growing field still in exploratory stages. A number of unrelated approaches have been pursued through wet chemical, electrochemical, and UHV techniques, generating preliminary trends and contributing to a better understanding of the technologically important silicon surface. The goal of exercising perfect control over the surface characteristics of silicon is a tempting one which promises both academic and commercial rewards.

Acknowledgements

The Camille and Henry Dreyfus Foundation is thanked for a New Faculty Award (1997–2002), and Purdue University for financial assistance. I would like to thank my collaborators, Matthew J. Allen, Michael P. Stewart, and Janet M. Holland for their contributions to the work referenced here. Professor Michael J. Sailor of UCSD and Professor Robert J. Hamers of the University of Wisconsin, Madison are gratefully acknowledged for permission to reprint Fig. 2 and 10 from references 2 and 60(*a*), respectively.

References

1 H. N. Waltenburg and J. T. Yates, *Chem. Rev.*, 1995, **95**, 1589.
2 M. J. Sailor and E. J. Lee, *Adv. Mater.*, 1997, **9**, 783.
3 A. Ulman, *Introduction to Thin Organic Films: From Langmuir Blodgett to Self-Assembly*, Academic Press, Boston, MA, 1991.
4 L. T. Canham, *Appl. Phys. Lett.*, 1990, **57**, 1046.
5 A. G. Cullis, L. T. Canham and P. D. J. Calcott, *J. Appl. Phys.*, 1997, **82**, 909.
6 B. Hamilton, *Semicond. Sci. Technol.*, 1995, **10**, 1187.
7 A. Halimaoui, in *Properties of Porous Silicon*, ed. L. T. Canham, INSPEC, London, 1997, p.12.
8 M. T. Kelly, J. K. M. Chun and A. B. Bocarsly, *Appl. Phys. Lett.*, 1994, **64**, 1693.
9 N. Noguchi and I. Suemune, *Appl. Phys. Lett.*, 1994, **62**, 1429; O. K. Anderson, T. Frello and E. Veje, *J. Appl. Phys.*, 1995, **78**, 6189.
10 SciFinder (CAS/STN database) found on 22/03/99 3980 papers using the term 'porous silicon', excluding 'oxide' and 'silica'.
11 L. T. Canham, in *Properties of Porous Silicon*, ed. L. T. Canham, INSPEC, London, 1997, p. 249.
12 J. M. Lauerhaas and M. J. Sailor, *Science*, 1993, **261**, 1567.
13 M. J. Sailor, J. L. Heinrich and J. M. Lauerhaas, *Semiconductor Nanoclusters*, P. V. Kamat and D. Meisel, Elsevier, Amsterdam, 1996, vol. 103, p. 209.
14 B. J. Tufts, A. Kumar, A. Bansal and N. S. Lewis, *J. Phys. Chem.*, 1992, **96**, 4581.
15 G. S. Higashi, Y. J. Chabal, G. W. Trucks and K. Raghavachari, *Appl. Phys. Lett.*, 1990, **56**, 656; G. S. Higashi, R. S. Becker, Y. J. Chabal and A. J. Becker, *Appl. Phys. Lett.*, 1991, **58**, 1656.
16 R. C. Anderson, R. S. Muller and C. W. Tobias, *J. Electrochem. Soc.*, 1993, **140**, 1393; A. Grosman and C. Ortega, in *Properties of Porous Silicon*, ed. L. T. Canham, INSPEC, London, 1997, p. 145.
17 *The Chemistry of Organic Silicon Compounds*, ed. S. Patai and Z. Rappoport, John Wiley and Sons, New York, 1989.
18 For example of reactions that are successful on both hydride terminated flat and porous silicon: (*a*) thermally induced hydrosilylation, refs. 19, 23 and 25; (*b*) photoelectrochemical esterification; ref. 46; (*c*) reaction of alkyl and aryl carbanions, P. E. Laibinis and N. Y. Kim, *Fall Meeting of the Materials Research Society*, Boston, MA, 1998, abstract F3.5; (*d*) alkoxylation with ROH (where R = H, alkyl), ref. 1 and N. Y. Kim and P. E. Laibinis, *J. Am. Chem. Soc.*, 1997, **119**, 2297.
19 (*a*) M. R. Linford and C. E. D. Chidsey, *J. Am. Chem. Soc.*, 1993, **115**, 12631; (*b*) M. R. Linford, P. Fenter, P. M. Eisenberger and C. E. D. Chidsey, *J. Am. Chem. Soc.*, 1995, **117**, 3145.
20 C. Chatgilialoglu, *Acc. Chem. Res.*, 1992, **25**, 188.
21 In footnote 33 of ref. 19(*b*), the authors note that surface hydrosilylation of hexadecyne produces a small peak at 1600.8 cm^{-1} which they state suggests a surface bound vinyl group. Indeed, Lewis acid and white light mediated hydrosilylation of dodecyne on porous silicon yields a strong ν(C=C) vibration at 1595 cm^{-1} which corroborates their assumption: see refs. 31, 36 and 38.
22 J. A. Labinger, in *Comprehensive Organic Synthesis*, ed. B. M. Trost and I. Fleming, Pergamon, New York, 1991, vol. 8, p. 699.
23 A. B. Sieval, A. L. Demirel, J. W. M. Nissink, M. R. Linford, J. H. van der Maas, W. H. de Jeu, H. Zuilhof and E. J. R. Sudhölter, *Langmuir*, 1998, **14**, 1759.
24 M. M. Sung, J. Kluth, O. W. Yauw and R. Maboudian, *Langmuir*, 1997, **13**, 6164.
25 J. E. Bateman, R. D. Eagling, D. R. Worrall, B. R. Horrocks and A. Houlton, *Angew. Chem., Int. Ed.*, 1998, **37**, 2683.
26 I. Fleming, in *Comprehensive Organic Chemistry*, ed. N. Jones, Pergamon, New York, 1979, vol. 3, p. 568.
27 J. Terry, M. R. Linford, C. Wigren, R. Cao, P. Pianetta and C. E. D. Chidsey, *Appl. Phys. Lett.*, 1997, **71**, 1056; J. Terry, R. Mo, C. Wigren, R. Cao, G. Mount, P. Pianetta, M. R. Linford and C. E. D. Chidsey, *Nucl. Instrum. Methods. Phys. Res., Sect. B*, 1997, **133**, 94.
28 P. Wagner, S. Nock, J. Spudich, W. D. Volkmuth, S. Chu, R. L. Cicero, C. P. Wade, M. R. Linford and C. E. D. Chidsey, *J. Struct. Biol.*, 1997, **119**, 189.
29 E. Leroy, O. M. Küttel, L. Schlapbach, L. Giraud and T. Jenny, *Appl. Phys. Lett.*, 1998, **73**, 1050.
30 F. Effenberger, G. Götz, B. Bidlingmaier and M. Wezstein, *Angew. Chem., Int. Ed.*, 1998, **37**, 2462.
31 M. P. Stewart and J. M. Buriak, *Angew. Chem., Int. Ed.*, 1998, **23**, 3257. Recent work in our group indicates that the reaction proceeds much more efficiently with photoluminescent samples, regardless of initial doping: M. P. Stewart and J. M. Buriak, unpublished results.
32 J. L. Heinrich, A. Lee and M. J. Sailor, *Mater. Res. Soc. Symp. Proc.*, 1995, **358**, 605.
33 J. March, *Advanced Organic Chemistry*, Wiley-Interscience, New York, 4th edn., 1992, p. 748.
34 L. N. Lewis, *J. Am. Chem. Soc.*, 1990, **112**, 5998.
35 L. A. Zazzera, J. F. Evans, M. Deruelle, M. Tirrell, C. R. Kessel and P. McKeown, *J. Electrochem. Soc.*, 1997, **144**, 2184.
36 J. M. Holland, M. P. Stewart, M. J. Allen and J. M. Buriak, *J. Solid State Chem.*, in press.
37 Hydrosilylation with Wilkinson's catalyst: B. Marciniec and J. Gulinski, *J. Organomet. Chem.*, 1993, **446**, 15; Bis-silylation with palladium complexes: Y. Ito, M. Suginome and M. Murakami, *J. Org. Chem.*, 1991, **56**, 1948.
38 J. M. Buriak and M. J. Allen, *J. Am. Chem. Soc.*, 1998, **120**, 1339.
39 (*a*) N. Asao, T. Sudo and Y. Yamamoto, *J. Org. Chem.*, 1996, **61**, 7654; (*b*) K. Oertle and H. Wetter, *Tetrahedron Lett.*, 1985, **26**, 5511; (*c*) K. Yamamoto and M. Takemae, *Synlett*, 1990, 259.
40 Asao *et al.* showed that $EtAlCl_2$ and $AlCl_3$ work equally well as catalysts for hydrosilylation of alkynes (see ref. 39*a*).
41 J. M. Buriak and M. J. Allen, *J. Lumin.*, 1998, **80**, 29.
42 A. Pelter, K. Smith and H. C. Brown, *Borane Reagents*, Academic Press, San Diego, 1988, pp. 166–167.
43 L. J. Bellamy, *The Infra-Red Spectra of Complex Molecules*, Methuen and Company Ltd, New York, 1960, p. 348.
44 C. Viellard, M. Warntjes, F. Oxanam and J.-N. Chazalviel, *Proc. Electrochem. Soc.*, 1996, **95**, 250.
45 There are scattered examples of electrochemical hydrosilylation of alkenes with soluble, molecular silanes. See, for example: O. Y. Okhlobystin and N. T. Berberova, *Dokl. Akad. Nauk. SSSR*, 1993, **332**, 599.
46 Sailor and coworkers have previously demonstrated a photoelectrochemical reaction on n-type derived porous silicon which results in silyl ester formation on the surface. There is no molecular equivalent because hole migration to the surface silicon atoms drives the process: E. J. Lee, T. W. Bitner, J. S. Ha, M. J. Shane and M. J. Sailor, *J. Am. Chem. Soc.*, 1996, **118**, 5375.
47 J. H. Song and M. J. Sailor, *J. Am. Chem. Soc.*, 1998, **120**, 2376.
48 N. Y. Kim and P. E. Laibinis, *J. Am. Chem. Soc.*, 1998, **120**, 4516.
49 F. A. Cotton and G. Wilkinson, *Advanced Inorganic Chemistry*, John Wiley and Sons, New York, 5th edn., 1988, p. 266.

50 A. Bansal, X. Li, I. Lauermann, N. S. Lewis, S. I. Yi and W. H. Weinberg, *J. Am. Chem. Soc.*, 1996, **118**, 7225.
51 C. Henry de Villeneuve, J. Pinson, M. C. Bernard and P. Allongue, *J. Phys. Chem. B*, 1997, **101**, 2415.
52 M. J. Bozack, W. J. Choyke, L. Muehlhoff and J. T. Yates, *Surf. Sci.*, 1986, **176**, 547; M. J. Bozack, P. A. Taylor, W. J. Choyke and J. T. Yates, *Surf. Sci. Lett.*, 1986, **177**, L933; M. J. Bozack, W. J. Choyke, L. Muelhoff and J. T. Yates, *J. Appl. Phys.*, 1986, **60**, 3750; J. Yoshinobu, H. Tsuda, M. Onchi and M. Nishijima, *J. Chem. Phys.*, 1987, **87**, 7332; S. Gokhale, P. Trischberger, D. Menzel, W. Widdra, H. Dröge, H.-P. Steinrück, U. Birkenbeuer, U. Gutdeutsch and N. Rösch, *J. Chem. Phys.*, 1998, **108**, 5554; B. Borovsky, M. Krueger and E. Ganz, *Phys. Rev. B*, 1998, **57**, R4269.
53 J. Hovis, S. Lee, H. Liu and R. J. Hamers, *J. Vac. Sci. Technol. B*, 1997, **15**, 1153.
54 P. A. Taylor, R. M. Wallace, C. C. Cheng, W. H. Weinberg, M. J. Dresser, W. J. Choyke and J. T. Yates, *J. Am. Chem. Soc.*, 1992, **114**, 6754.
55 H. Liu and R. J. Hamers, *J. Am. Chem. Soc.*, 1997, **119**, 7593.
56 J. T. Yates, *Science*, 1998, **279**, 335.
57 R. J. Hamers, J. S. Hovis, S. Lee, H. Liu and J. Shan, *J. Phys. Chem. B*, 1997, **101**, 1489.
58 H. B. Liu and R. J.Hamers, *Surf. Sci.*, 1998, **416**, 354.
59 J. S. Hovis and R. J. Hamers, *J. Phys. Chem. B*, 1997, **101**, 9581.
60 (*a*) J. S. Hovis and R. J. Hamers, *J. Phys. Chem. B*, 1998, **102**, 687; (*b*) D. F. Padowitz and R. J. Hamers, *J. Phys. Chem. B*, 1998, **102**, 8541.
61 R. Konecny and D. Doren, *J. Am. Chem. Soc.*, 1997, **119**, 11 098.
62 A. V. Teplyakov, M. J. Kong and S. F. Bent, *J. Am. Chem. Soc.*, 1997, **119**, 11100.
63 A. V. Teplyakov, M. J. Kong and S. F. Bent, *J. Chem. Phys.*, 1998, **108**, 4599.
64 J. S. Hovis, H. B. Liu and R. J. Hamers, *J. Phys. Chem. B*, 1998, **102**, 6873.
65 M. S. Ravenscroft, K. E. Bateman, K. M. Shaffer, H. M. Schessler, D. R. Jung, T. W. Schneider, C. B. Montgomery, T. L. Custer, A. E. Schaffner, Q. Y. Liu, Y. X. Li, J. L. Barker and J. J. Hickman, *J. Am. Chem. Soc.*, 1998, **120**, 12 169 and references therein.
66 M. J. Sailor, in *Properties of Porous Silicon*, ed. L. T. Canham, INSPEC, London, 1997, p. 364.
67 V. P. Bondarenko and V. A. Yakovtseva, in *Properties of Porous Silicon*, ed. L. T. Canham, INSPEC, London, 1997, p. 343.
68 M. Thönissen, M. Krüger, G. Lerondel and R. Romestain, Properties of Porous Silicon, ed. L. T. Canham, INSPEC, London, 1997, p. 349; M. Van Belle, *Photonics Spectra*, 1998, **32**, (**10**), 57.
69 V. V. Doan and M. J. Sailor, *Science*, 1992, **256**, 1791.
70 L. T. Canham, *Appl. Phys. Lett.*, 1993, **63**, 337.
71 L. T. Canham, *Adv. Mater.*, 1995, **7**, 1033; L. T. Canham, in *Properties of Porous Silicon*, ed. L. T. Canham, INSPEC, London, 1997, p. 371.
72 X. Li, J. L. Coffer, Y. Chen, R. F. Pinizzotto, J. Newey and L. T. Canham, *J. Am. Chem. Soc.*, 1998, **120**, 11 706.
73 J. M. Lauerhaas, G. M. Credo, J. L. Heinrich and M. J. Sailor, *J. Am. Chem. Soc.*, 1992, **114**, 1911.
74 J. Harper and M. J. Sailor, *Anal. Chem.*, 1996, **68**, 3713.
75 A. Janshoff, K. P. S. Dancil, C. Steinem, D. P. Greiner, V. S.-Y. Lin, C. Gurtner, K. Motesharei, M. J. Sailor and M. R. Ghadiri, *J. Am. Chem. Soc.*, 1998, **120**, 12 108.
76 Y. Xia and G. M. Whitesides, *Angew. Chem. Int. Ed.*, 1998, **37**, 551.
77 N. L. Jeon, J. Hu, G. M. Whitesides, M. K. Erhardt and R. G. Nuzzo, *Adv. Mater.*, 1998, **10**, 1466.
78 In Table 4 of ref. 76, Xia and Whitesides summarize the solid substrates and molecular precursors that form self-assembled monolayers (SAMs). The work of the groups of Chidsey (ref. 19) and Lewis (ref. 50) is mentioned.

Paper 9/00108E

Synthesis and structures of heterometallic trinuclear clusters $[CpFe(CO)_2]_2(\mu_3\text{-}S_2)W(CO)_5$ and $Cp_2Fe_2(CO)_3(\mu\text{-}CO)(\mu_3\text{-}S)W(CO)_5$ and kinetic study of migration of the $W(CO)_5$ moiety in the disulfido complex

Katsuaki Kuge, Hiromi Tobita and Hiroshi Ogino*

Department of Chemistry, Graduate School of Science, Tohoku University, Sendai 980-8578, Japan.
E-mail: ogino@agnus.chem.tohoku.ac.jp

Received (in Cambridge, UK) 2nd March 1999, Accepted 4th May 1999

The reaction of $CpFe(CO)_2Br$, NaSH and $W(CO)_5(THF)$ gave two Fe_2W clusters, one with a μ_3-S_2 and the other with a μ_3-S; in the former cluster $W(CO)_5$ moiety migration on the disulfido ligand was observed by variable-temperature ^1H NMR spectroscopy.

Heterometallic cluster synthesis is widely studied aiming to find new methods of building up clusters systematically. Complexes containing sulfur ligands are often applied as building blocks for polynuclear clusters owing to the remaining coordination ability of sulfur ligands to metal moieties through their lone pairs. In addition, clusters containing a wide variety of coordination modes of sulfur ligands are fascinating from the structural point of view.[1] Simple addition of an $M(CO)_5$ moiety (M = group 6 metal) to sulfido ligands is frequently used for the synthesis of heterometallic sulfur clusters with various bridging sulfido ligands.[2] By contrast, addition of an $M(CO)_5$ moiety to disulfido ligands is rare.[3] Here, we report the synthesis of two new clusters with an Fe_2W core *via* addition of $W(CO)_5$. One of the clusters contains a new type of Fe_2W core, and migration of the $W(CO)_5$ moiety on the disulfido ligand bridging the two $CpFe(CO)_2$ moieties was observed by variable-temperature ^1H NMR spectroscopy.

Reaction of $CpFe(CO)_2Br$ with an excess of NaSH in THF at room temperature resulted in the formation of a brown solution. After 2 h, TLC indicated the disappearance of $CpFe(CO)_2Br$, but isolation and identification of the reaction product was unsuccessful. Addition of $W(CO)_5(THF)$ in THF to the reaction mixture at room temperature gave two heterometallic trinuclear clusters $[CpFe(CO)_2]_2(\mu_3\text{-}S_2)W(CO)_5$ **1** and $Cp_2Fe_2(CO)_2(\mu\text{-}CO)(\mu_3\text{-}S)W(CO)_5$ **2** in 30 and 11% yields, respectively (Scheme 1).

A crystal structure analysis of **1** (Fig. 1)† shows that two $CpFe(CO)_2$ moieties are bridged by a $\eta^1:\eta^1$-S_2 ligand, and one of the sulfur atoms in the S_2 ligand is coordinated to a $W(CO)_5$ moiety in an η^1 mode. The W atom surrounded by one S and five CO ligands adopts an octahedral geometry, and both of Fe(1) and Fe(2) atoms adopt a three-legged piano stool geometry. There are no bonds between the three metal centres. The W–S(2) bond [2.582(2) Å] is slightly longer than normal W–S dative bonds (2.522–2.57 Å)[2] encountered in clusters having a $W(CO)_5$ moiety coordinated to a bridging sulfido ligand. The Fe(1)–S(1) and Fe(2)–S(2) distances [2.292(2) and 2.307(2) Å] are similar to those of trisulfido complex $[CpFe(CO)_2]_2(\mu\text{-}S_3)$ (2.283 and 2.280 Å) and tetrasulfido complex $[CpFe(CO)_2]_2(\mu\text{-}S_4)$ (2.276 Å).[4] The S(1)–S(2) bond [2.076(2) Å] is longer than the S–S distances found in $[CpRu(PMe_3)_2]_2(\mu\text{-}S_2)^{2+}$ (1.962 Å)[5] and $[(NH_3)_5Ru]_2(\mu\text{-}S_2)^{4+}$ (2.014 Å).[6] The Fe(2)–S(2)–S(1) bond angle [116.86(7)°] is larger than that of Fe(1)–S(1)–S(2) [107.49(9)°] because of the coordination of a $W(CO)_5$ moiety to the S(2) atom. Trinuclear clusters bridged by only one disulfido ligand are rare.[4] Complex **1** is the first example of a trinuclear

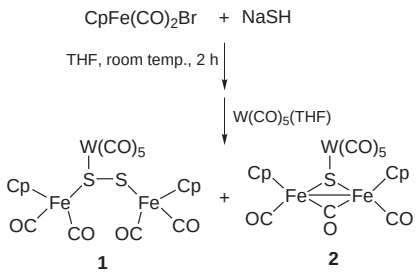

Scheme 1

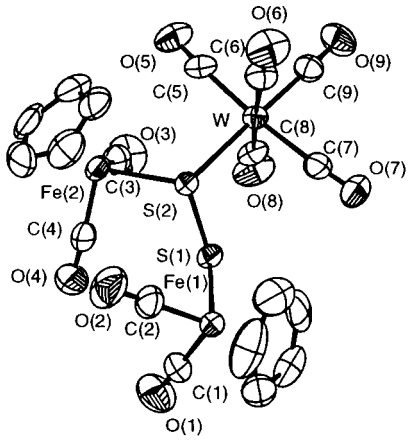

Fig. 1 ORTEP view of **1** with 50% thermal ellipsoids. Selected bond lengths (Å) and angles (°): Fe(1)–S(1) 2.292(2), Fe(2)–S(2) 2.307(2), W–S(2) 2.582(2), S(1)–S(2) 2.076(2), Fe(1)–C(1) 1.756(8), Fe(2)–C(3) 1.76(1), Fe(1)–C(2) 1.763(7), Fe(2)–C(4) 1.776(9), W–C(5) 2.026(8), W–C(6) 2.042(8), W–C(7) 2.047(8), W–C(8) 2.047(8), W–C(9) 1.974(8), Fe(1)–S(1)–S(2) 107.49(9), Fe(2)-S(2)–S(1) 109.20(9).

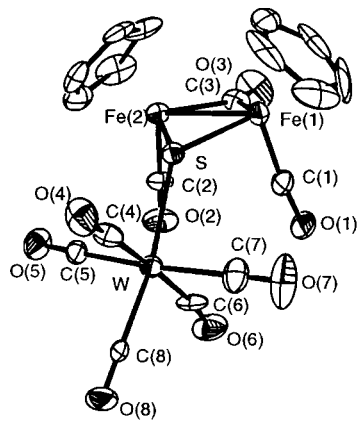

Fig. 2 ORTEP view of **2** with 30% thermal ellipsoids. Selected bond lengths (Å) and angles (°): Fe(1)–S 2.239(6), Fe(2)–S 2.228(6), W–S 2.547(6), Fe(1)–Fe(2) 2.592(4), Fe(1)–C(1) 1.75(2), Fe(2)–C(2) 1.81(2), Fe(1)–C(3) 1.94(2), Fe(2)–C(3) 1.95(3), W–C(4) 2.02(2), W–C(5) 2.02(2), W–C(6) 2.09(3), W–C(7) 2.07(2), W–C(8) 1.99(2), Fe(1)–S–Fe(2) 70.9(2).

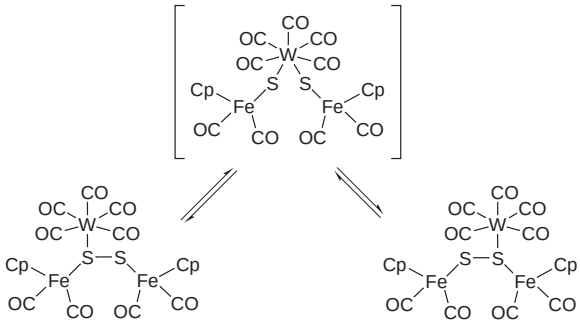

Scheme 2

cluster connected by only one disulfido ligand in an $\eta^1:\eta^1:\eta^1$ fashion.

The X-ray structure analysis of **2** (Fig. 2)† shows that two iron atoms are directly bonded to each other [Fe–Fe 2.592(4) Å] with the bond bridged by a CO ligand and a μ_3-S ligand to form an Fe(1)–S–Fe(2)–C(3) four-membered ring, and a $W(CO)_5$ moiety is coordinated to the μ_3-S ligand. Two Cp ligands are mutually *cis* and the $W(CO)_5$ moiety is at the *anti* position with respect to the two Cp ligands. The W atom has an octahedral geometry. The W–S bond [2.547(6) Å] is close in length to that of **1** suggesting a dative bond character. The Fe(1)–S and Fe(2)–S distances [2.239(6) and 2.228(6) Å] lie within the typical range for Fe–S bonds [2.18–2.26 Å].[7]

It is noteworthy that in the ^{1}H NMR spectrum of **1** at 296 K, only one broad peak for the ring protons of the Cp ligands was observed at δ 4.22. Taking account of the crystal structure of **1** in Fig. 1 in which the $W(CO)_5$ moiety is bound to only one of the two sulfur atoms, the spectrum clearly shows that the $W(CO)_5$ moiety is migrating between two sulfur atoms faster than the NMR time scale to make the two Cp ligands equivalent. At lower temperature (250 K), the signal for the Cp ligands decoalesced to two singlets at δ 3.96 and 4.17.

Abel *et al.* previously observed a 1,2-shift of a $W(CO)_5$ moiety between two sulfur atoms in $W(CO)_5(Me_3SiCH_2SSCH_2SiMe_3)$.[8] Based on the activation parameters for this reaction ($\Delta H^{\ddagger}$ = 71.6 ± 1.8 kJ mol^{-1}, $\Delta S^{\ddagger}$ = −8.7 ± 5.4 J mol^{-1} K^{-1} and $\Delta G^{\ddagger}_{298}$ = 74.2 ± 0.2 kJ mol^{-1}), they proposed an intermediate in which the lone pairs of both sulfur atoms were coordinated to the $W(CO)_5$ moiety. The activation parameters for **1** determined by complete lineshape analysis are $\Delta H^{\ddagger}$ = 75.9 ± 3.1 kJ mol^{-1}, $\Delta S^{\ddagger}$ = 55.4 ± 10.6 J mol^{-1} K^{-1} and $\Delta G^{\ddagger}_{298}$ = 59.4 ± 6.2 kJ mol^{-1}. These values are consistent with the intramolecular mechanism. However, the somewhat larger $\Delta S^{\ddagger}$ value for our system may be reasonably explained by an alternative mechanism shown in Scheme 2 involving oxidative addition of the S–S bond, where the transition state is expected to be looser than that in Abel's mechanism. Intramolecular oxidative addition of a coordinated disulfide to a W^0 center to give a seven-coordinate bis(thiolato)tungsten(II) intermediate has been proposed in $W(CO)_3(phen)(RSSR)$ complexes.[9]

Notes and references

† *Crystal data*: for **1**: $C_{19}H_{10}O_9Fe_2S_2W$, M = 741.95, monoclinic, space group $P2_1/c$ (no. 14), a = 17.174(6), b = 7.096(4), c = 19.452(4) Å, β = 92.26(2)°, V = 2368(1) Å^3, T = 293 K, Z = 4, μ(Mo-Kα) = 62.80 cm^{-1}, $R(R_w)$ = 0.030 (0.044) for 5445 unique data with $I > 3\sigma(I)$. For **2**: $C_{18}H_{10}O_8Fe_2SW$, M = 681.88, orthorhombic, space group $Pca2_1$ (no.29), a = 16.896(9), b = 9.848(5), c = 12.815(10) Å, V = 2132(3) Å^3, T = 293 K, Z = 4, μ(Mo-Kα) = 68.68 cm^{-1}, $R(R_w)$ = 0.039 (0.051) for 2790 unique data with $I > 3\sigma(I)$. CCDC 182/1242. See http://www.rsc.org/suppdata/cc/1999/1061/ for crystallographic files in .cif format.

1 A. Müller, W. Jagermann and J. H. Enemark, *Coord. Chem. Rev.*, 1982, **46**, 245; A. Müller and E. Diemann, *Adv. Inorg. Chem.*, 1987, **31**, 89; J. Wachter, *Angew. Chem., Int. Ed. Engl.*, 1989, **28**, 1613.

2 A. A. Pasynskii, I. L. Eremenko, Y. V. Rakitin, B. Orazsakhatov, V. M. Novotortsev, O. G. Ellert, V. T. Kalinnikov, G. G. Aleksandrov and Y. T. Struchkov, *J. Organomet. Chem.*, 1981, **210**, 377; A. Winter, I, Jibril and G. Huttner, *J. Organomet. Chem.*, 1983, **247**, 259; R. D. Adams, J. E. Babin, J.-G. Wang and W. Wu, *Inorg. Chem.*, 1989, **28**, 703; R. D. Adams, J. E. Babin, P. Mathur, K. Natarajan and J.-G. Wang, *Inorg. Chem.*, 1989, **28**, 1440; R. D. Adams, J. E. Babin and J.-G. Wang, *Polyhedron*, 1989, **8**, 2351.

3 H. Brunner, G. Gehart, J. C. Leblanc, C. Moise, B. Nuber, B. Stubenhofer, F. Volpato and J. Wachter, *J. Organomet. Chem.*, 1996, **517**, 47.

4 M. A. El-Hinnawi, A. A. Aruffo, B. D. Santarsiero, D. R. McAlister and V. Schomaker, *Inorg. Chem.*, 1983, **22**, 1585.

5 J. Amarasekera, T. B. Rauchfuss and S. R. Wilson, *Inorg. Chem.*, 1987, **26**, 3328.

6 R. C. Elder and M. Trkula, *Inorg. Chem.*, 1977, **16**, 1048.

7 P. J. Vergamini and G. J. Kubas, *Prog. Inorg. Chem.*, 1976, **21**, 261.

8 E. W. Abel, S. K. Bhargava, P. K. Mittal, K. G. Orrell and V. Sik, *J. Chem. Soc., Dalton Trans.*, 1985, 1561.

9 R. F. Lang, T. D. Ju, G. Kiss, C. D. Hoff, J. C. Bryan and G. J. Kubas, *Inorg. Chem.*, 1994, **33**, 3899.

Communication 9/01660K

ChemComm

Convergent synthesis of the ABCDE ring framework of ciguatoxin

Kenji Maeda, Tohru Oishi, Hiroki Oguri and Masahiro Hirama*

Department of Chemistry, Graduate School of Science, Tohoku University, and CREST, Japan Science and Technology Corporation (JST), Sendai 980-8578, Japan. E-mail: hirama@ykbsc.chem.tohoku.ac.jp

Received (in Cambridge, UK) 19th April 1999, Accepted 4th May 1999

An alkylation–metathesis sequence is shown to be a powerful method to synthesize the ABCDE ring framework of ciguatoxin 1.

Ciguatoxin (CTX1B, **1**) is the principal toxin that causes ciguatera poisoning.[1] Its gigantic structure and unique agonist activity against the sodium channel have attracted considerable attention among synthetic organic chemists.[2] During the course of our synthetic studies directed toward **1**, we developed an efficient method of constructing *trans*-fused 6,*n*,6,6-tetracyclic ether systems (*n* = 7–10) by combining intermolecular alkylation and ring-closing metathesis (RCM) reactions.[3] We describe herein a convergent synthesis of the ABCDE ring framework **2** of **1** starting from the AB ring **4** and E-ring fragments **5**, using the described alkylation–metathesis strategy (Scheme 1).

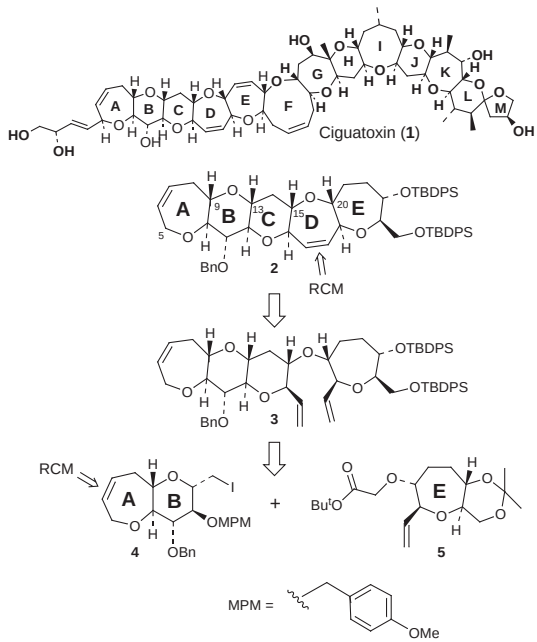

Scheme 1

The synthesis of the iodide **4** is shown in Scheme 2. Tri-*O*-acetyl-D-glucal was converted to **6** *via* methanolysis of the acetate and successive protection of the resulting triol as the tetraisopropyldisiloxanediyl (TIPDS) and benzyl ether. Epoxidation of **6** using Spilling's method[4] followed by addition of CH_2=$CHCH_2MgBr$ resulted in the formation of **7** in 53% overall yield. Allylation of the secondary alcohol of **7** gave **8**, which was subjected to RCM reaction using Grubbs' catalyst, $(PCy_3)_2Cl_2Ru$=CHPh **9**[5] to afford the 7,6-bicyclic system **10** in 94% yield.[6] The TIPDS group of **10** was removed using TBAF and the 1,3-diol was converted to the *p*-methoxybenzylidene acetal **11**. Reductive cleavage of the benzylidene acetal with DIBAL-H followed by conversion of the resulting primary alcohol to an iodide gave **4** regioselectively.[7]

Alkylation of the *tert*-butyl ester **5**, which was readily prepared from D-glucose[8] with **4** using LDA in the presence of 1,3-dimethyl-3,4,5,6-tetrahydro-2(1*H*)-pyrimidone (DMPU) gave a separable mixture of the desired diastereomer **12** and the epimer **13** in a 3 : 2 ratio in 58% combined yield (Scheme 3). When HMPA was used instead of DMPU in this alkylation

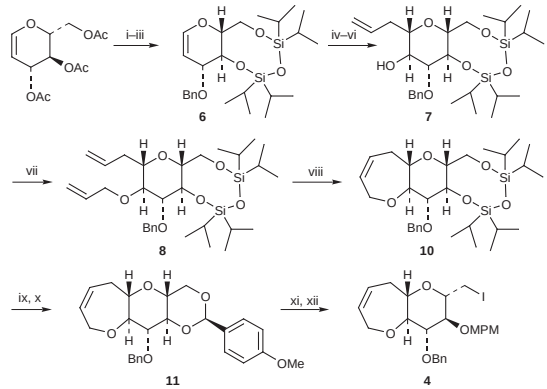

Scheme 2 *Reagents and conditions*: i, K_2CO_3 (cat.), MeOH; ii, $(TIPDS)Cl_2$, pyridine; iii, BnBr, NaH, DMF, THF, 0 °C to room temp., 63% (3 steps); iv, NBS, THF–H_2O (9 : 1); v, KHMDS, 18-crown-6, toluene, −75 to 0 °C, 4 h; vi, H_2C=$CHCH_2MgBr$, 0 °C to room temp., 53% (3 steps); vii, H_2C=$CHCH_2Br$, NaH, 0 °C to room temp., 93%; viii, **9** (cat.), CH_2Cl_2, 94%; ix, TBAF, THF; x, PPTS (cat.), *p*-$MeOC_6H_4CH(OMe)_2$, $(CH_2Cl)_2$; xi, DIBAL-H, CH_2Cl_2, −78 to −20 °C, 75% (3 steps); xii, I_2, PPh_3, imidazole, toluene, 82%.

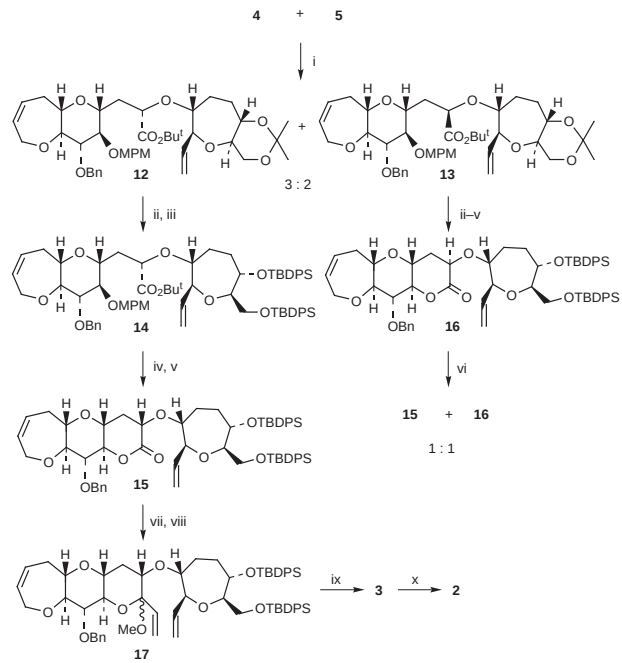

Scheme 3 *Reagents and conditions*: i, LDA, DMPU, THF, −78 to 0 °C, 58% (based on recovery of **4**; 23%); ii, PPTS (cat.), MeOH; iii, TBDPSCl, imidazole, DMF, 71% (2 steps); iv, DDQ, $(CH_2Cl)_2$–H_2O (20 : 1), 91%; v, CSA (cat.), toluene, 80 °C, 80%; vi, imidazole, toluene, reflux, 80% (**15** : **16** = 1 : 1); vii, H_2C=$CHMgBr$, Et_2O, −78 to −60 °C, 91%; viii, CSA (cat.), $HC(OMe)_3$, CH_2Cl_2, 75%; ix, $BF_3{\cdot}OEt_2$, Et_3SiH, CH_2Cl_2, −45 °C, 96%; x, **9**, CH_2Cl_2, 40 °C, 93%.

reaction, the ratio became 1 : 1. Although further attempts to improve the diastereoselectivity and to epimerize **13** were unsuccessful at this stage, we found that the epimerization could be obtained at a later stage (*vide infra*). Acidic methanolysis of the acetonide **12** followed by protection of the resulting 1,3-diol as TBDPS ethers gave **14**. Removal of the *p*-methoxybenzyl group using DDQ followed by treatment with CSA in toluene at 80 °C gave the δ-lactone **15**. The epimeric lactone **16** was also synthesized from **13** in an analogous manner. This lactone was found to undergo epimerization by treatment with imidazole in toluene under reflux to give a separable 1 : 1 mixture of **15** and **16** in 80% yield, while stronger bases such as Bu^{t}OK and DBU caused only decomposition. Thus, the undesired epimer **13** was successfully converted into **15**. Treatment of the lactone **15** with CH_2=CHMgBr followed by conversion of the resultant hemiacetal to the corresponding methyl acetal afforded **17** as a 1 : 1 mixture of anomers. Reduction of the anomeric mixture **17**[9] with Et_3SiH in the presence of $BF_3{\cdot}OEt_2$[10] gave **3** as a single isomer in 96% yield. Finally RCM reaction of **3** with Grubbs' catalyst **9** at 40 °C in CH_2Cl_2 gave the ABCDE ring **2** in 93% yield.[11]

In conclusion, we have demonstrated that the alkylation–metathesis strategy is versatile for the convergent synthesis of the pentacyclic segment **2** of **1**. Further studies directed toward the total synthesis of **1** are currently in progress in our laboratory.

Notes and references

1 M. Murata, A. M. Legrand, Y. Ishibashi, M. Fukui and T. Yasumoto, *J. Am. Chem. Soc.*, 1990, **112**, 4380; M. Satake, A. Morohashi, H. Oguri, T. Oishi, M. Hirama, N. Harada and T. Yasumoto, *J. Am. Chem. Soc.*, 1997, **119**, 11325.

2 For recent synthetic studies, see: T. Oishi, M. Shoji, K. Maeda, N. Kumahara and M. Hirama, *Synlett*, 1996, 1165; T. Oishi, K. Maeda and M. Hirama, *Chem. Commun*., 1997, 1289; T. Oishi, M. Shoji, N. Kumahara and M. Hirama, *Chem. Lett*., 1997, 845; T. Oishi, Y. Nagumo and M. Hirama, *Synlett*, 1997, 307; S. Hosokawa and M. Isobe, *Synlett*, 1996, 351; T. Oka, K. Fujiwara and A. Murai, *Tetrahedron*, 1996, **37**, 1179; E. Alvarez, M. Delgado, M. T. Díaz, L. Hanxing, R. Pérez and J. D. Martín, *Tetrahedron Lett.*, 1996, **37**, 2865; J. L. Ravelo, A. Regueiro, E. Rodríguez, J. A. Vera and J. D. Martín, *Tetrahedron Lett.*, 1996, **37**, 2869; S. Hosokawa, K. Kira and M. Isobe, *Chem. Lett.*, 1996, 473; M. Inoue, M. Sasaki and K. Tachibana, *Tetrahedron Lett.*, 1997, **38**, 1611; T. Oka, K. Fujiwara and A. Murai, *Tetrahedron Lett.*, 1997, **38**, 8053; M. Inoue, M. Sasaki and K. Tachibana, *Angew. Chem., Int. Ed.*, 1998, **37**, 965; M. Sasaki, T. Noguchi and K. Tachibana, *Tetrahedron Lett*., 1999, **40**, 1337.

3 T. Oishi, Y. Nagumo and M. Hirama, *Chem. Commun*., 1998, 1041.

4 C. H. Marzabadi and C. D. Spilling, *J. Org. Chem*., 1993, **58**, 3761.

5 P. Schwab. R. H. Grubbs and J. W. Ziller, *J. Am. Chem. Soc.*, 1996, **118**, 100.

6 M. Delgago and J. D. Martín, *Tetrahedron Lett.*, 1997, **38**, 6299.

7 R. Johansson and B. Samuelsson, *J. Chem. Soc., Chem. Commun*., 1984, 201.

8 I. Kadota, A. Ohno, Y. Matsukawa and Y. Yamamoto, *Tetrahedron Lett.*, 1998, **39**, 6373.

9 We found that reduction of the ketal rather than the corresponding hemiacetal using Et_3SiH and $BF_3{\cdot}OEt_2$ gave a remarkably higher yield of the reduction product; 0–70% yield in the case of hemiacetal under the same reduction conditions. Also see ref. 3.

10 D. L. Lewis, J. K. Cha and Y. Kishi, *J. Am. Chem. Soc.*, 1982, **104**, 4976.

11 The stereochemistry of **2** was unambiguously determined by ^{1}H NMR analysis. *Selected data* for **2**: δ_H (500 MHz, $CDCl_3$) 0.98 (9H, s, TBDPS), 0.99 (9H, s, TBDPS), 1.55 (1H, q, *J* 11.4, H14$_{ax}$), 1.53–1.60 (1H, m, H22), 1.62–1.69 (1H, m, H22′), 1.71–1.78 (1H, m, H21), 2.05–2.14 (1H, m, H21′), 2.29 (1H, dt, *J* 11.4, 4.1, H14$_{eq}$), 2.31-2.38 (1H, m, H8), 2.64 (1H, ddd, *J* 16.0, 7.7, 3.5, H8′), 3.08–3.15 (2H, m, H12, H13), 3.28(0) (1H, ddd, *J* 8.4, 7.7, 3.8, H9), 3.28(5) (1H, ddd, *J* 11.4, 8.9, 4.1, H15), 3.31–3.40 (2H, m, H20, H24), 3.35 (1H, dd, *J* 9.0, 8.4, H10), 3.48 (1H, t, *J* 9.0, H11), 3.62–3.70 (3H, m, H23, H25, H25′), 3.88 (1H, dq, *J* 8.9, 2.3, H16), 4.01 (1H, dq, *J* 16.0, 2.8, H5), 4.12 (1H, dq, *J* 9.0, 2.3, H19), 4.29 (1H, dd, *J* 16.0, 5.7, H5′), 4.83 (1H, d, *J* 11.5, C*H*$_2$Ph), 4.89 (1H, d, *J* 11.5, C*H*$_2$Ph), 5.64 (1H, dt, *J* 13.0, 2.3, H18), 5.77 (1H, dddd, *J* 11.8, 5.1, 3.5, 2.8, H7), 5.83 (1H, dt, *J* 13.0, 2.3, H17), 5.87 (1H, ddt, *J* 11.8, 5.7, 2.8, H6), 7.23–7.43 (17H, m, Ph), 7.52–7.56 (4H, m, Ph), 7.59–7.66 (4H, m, Ph).

Communication 9/03063H

ChemComm

Reductive deamination of α-amino carbonyl compounds by means of samarium iodide

Toshio Honda* and Fumihiro Ishikawa

Faculty of Pharmaceutical Sciences, Hoshi University, Ebara 2-4-41, Shinagawa-ku, Tokyo 142-8051, Japan. E-mail: honda@hoshi.ac.jp

Received (in Cambridge, UK) 19th April 1999, Accepted 4th May 1999

Reaction of α-amino carbonyl compounds with SmI_2 in THF–HMPA in the presence of a proton source afforded the deamination products, where the fragmentation occurred between the nitrogen and the carbon α to the carbonyl group.

SmI_2 was firstly, introduced as a useful synthetic tool in organic synthesis by Kagan and co-workers,[1] and thereafter, this reagent rapidly became an established reagent for developing a variety of useful and unique transformations.[2] Although much effort has been devoted to studying the reductive deoxygenation of α-hydroxy or α-alkoxy carbonyl compounds employing SmI_2 as a powerful one-electron reducing reagent, its application to the deamination of α-amino carbonyl compounds has received relatively little attention. Attractive examples of the reductive deamination reaction were reported by Molander and Stengel using 2-acylaziridines and 4-acylazetidin-2-one as starting materials [eqn. (1)],[3] where the leaving amino groups were

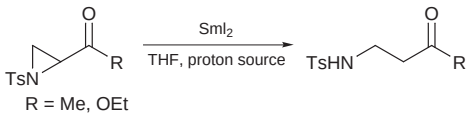

R = Me, OEt (1)

involved in highly strained three- or four-membered rings. Similar SmI_2-promoted carbon–nitrogen bond cleavage reactions were also employed in the reductive removal of an *N*-substituted benzotriazolyl group,[4] and in the isonitrile–nitrile rearrangement.[5]

In continuation of our work on the synthesis of biologically active natural products using SmI_2,[6] we were interested in researching a general deamination reaction of α-amino carbonyl compounds [eqn. (2)], and here report our successful results

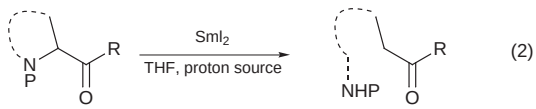

P = alkyl, acyl
R = alkyl, OR′ (2)

concerning systematic investigation of SmI_2-promoted reductive deamination.

Initially, we applied the SmI_2-promoted deamination reaction to phenylalanine derivatives,[7] and the results obtained are summarised in Table 1. Based on the results, it was concluded that reductive deamination with SmI_2 is applicable to the wide variety of amino functions including primary, secondary and tertiary amines, and also amide groups. The deamination usually took place within 30 min in the presence of a proton source, such as MeOH or pivalic acid, to give methyl dihydrocinnamate in high yields, although a relatively prolonged reaction time was required in the case of benzyl-substituted amines as leaving groups. The reductive deamination was typically carried out as follows: a solution of SmI_2 (2.5 mmol) and HMPA (2.5 mmol) in THF (12 cm^3) and a solution of proton source (MeOH or pivalic acid, 1.25 mmol) in THF (5 cm^2) were successively added dropwise to a stirred solution of an α-amino ester (0.5 mmol) in THF (10 cm^3) at 0 °C, and the resulting solution was allowed to warm to room temperature. A stream of air was bubbled through the solution, and an excess of Celite in Et_2O and saturated aqueous $NaHCO_3$ (2 cm^3) were added. The solution was filtered and the filtrate was washed with brine. The organic layer was separated, dried and evaported to give a residue, which was subjected to column chromatography on silica gel.

Table 1 Reductive deamination of phenylalanine derivatives[a]

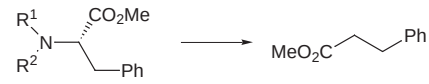

R^1	R^2	Proton source	Reaction time	Yield (%)
H	H	MeOH	30 min	73
H	H	Pivalic acid	15 min	80
H	Me	MeOH	30 min	71
H	Bn	MeOH	2.5 h	85
Me	Me	MeOH	< 5 min	90
Bn	Bn	MeOH	4 h	93
H	Ac	MeOH	15 min	99

[a] Reaction conditions: starting material (0.5 mmol); SmI_2 (5 equiv.); HMPA (5 equiv.); proton soruce (2.5 equiv.); solvent (THF); 0 °C to room temperature.

The reactions of proline derivatives[8] (Table 2) and ethyl pipecolinate derivatives[9] (Table 3), where the leaving amino groups were involved in the cyclic systems, under the same reaction conditions as above gave the corresponding deamination products in good yields. The deamination could be applied not only to α-amino esters but also to α-amino ketones. Thus, treatment of α-acetylpiperidine derivatives[10] with SmI_2 also

Table 2 Reductive deamination of proline derivatives[a]

Starting material	Product	Proton source	Reaction time	Yield (%)
		MeOH Pivalic acid	30 min 10 min	62 73
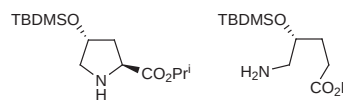		MeOH	1.5 h	88
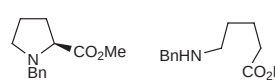		MeOH	9 h	82
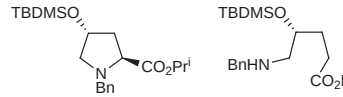		MeOH	7.5 h	99

[a] Reaction conditions: starting material (0.5 mmol); SmI_2 (5 equiv.); HMPA (5 equiv.); proton source (2.5 equiv.); solvent (THF); 0 °C to room temperature.

Table 3 Reductive deamination of 2-acetylpiperidine and ethyl pipecolinate derivatives, and a phthalimide derivative[a]

Starting material	Product	R	Reaction time	Yield (%)
	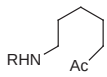	Me	1 min	87
		Bn	1 min	96
		Ac	<5 min	94
		Boc	<5 min	96
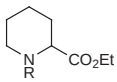	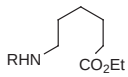	Me	<5 min	86
		Bn	<5 min	89
		Ac	45 min	78
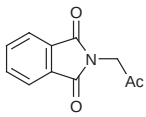	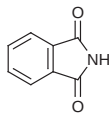	—	1 min	72

[a] Reaction conditions: starting material (0.5 mmol); SmI_2 (5 equiv.); HMPA (5 equiv.); MeOH (2.5 equiv.) was used as a proton source; solvent (THF); 0 °C to room temperature.

provided the desired compounds, in high yields, in which both alkyl and acyl derivatives of amines could be used as leaving groups (Table 3). Interestingly, the reaction of *N*-(2-oxopropyl)phthalimide with SmI_2 in THF–HMPA in the presence of MeOH yielded phthalimide in 72% yield (Table 3). The products obtained were well-characterised by spectroscopic data including microanalysis, or by direct comparison with the authentic samples.

We next investigated the effect of proton sources, and found that *N*,*N*-dimethylaminoethanol (DMAE) was also effective for this reaction as well as MeOH and pivalic acid (Table 4). It should be noted that this reaction can be carried out under neutral reaction conditions in the presence of other functional groups, such as alkyl ester, alkyl ether, imide and amide groups. Moreover, this reaction proceeded in the presence or absence of HMPA, however, the presence of HMPA proved desirable in terms of yields and reaction times (Tables 2, 3 and 4). These results were in agreement with those observed in the reductive deoxygenation reactions, since HMPA was recognised to increase the rate of the reaction of SmI_2.[11]

As can be seen in Table 2, the fragmentation product bearing a primary amino function sometimes afforded the cyclisation compound. This type of conversion will provide a useful route for the synthesis of naturally occurring or biologically interesting piperidine derivatives in optically active forms. Indeed,

Table 4 Investigation of the proton sources and the effect of HMPA in reductive deamination[a]

Starting material	Product	Proton source	Reaction time	Additive	Yield (%)
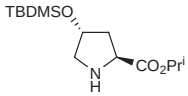	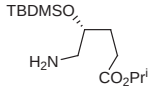	MeOH	5 h	none	65
		Pivalic acid	40 min	HMPA	82
		DMAE	45 min	HMPA	90
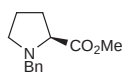	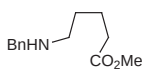	MeOH	18 h	none	85
		Pivalic acid	1 h	HMPA	92
		DMAE	2 h	HMPA	78
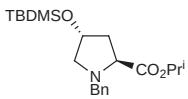	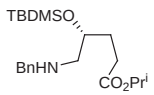	MeOH	36 h	none	76
		Pivalic acid	45 min	HMPA	88
		DMAE	1.5 h	HMPA	93
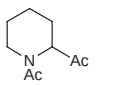	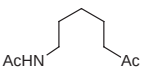	MeOH	12 h	none	50
		Pivalic acid	<5 min	HMPA	86
		DMAE	10 min	HMPA	71

[a] Reaction conditions: starting material (0.5 mmol); SmI_2 (5 equiv.); proton source (2.5 equiv.); additive (5 equiv.); solvent (THF); 0 °C to room temperature.

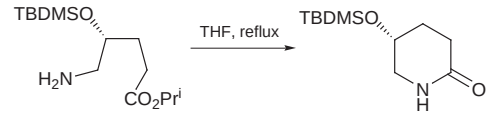

Scheme 1

heating of isopropyl δ-amino-γ-*tert*-butyldimethylsiloxyvalerate in THF for 2 days gave 5-*tert*-butyldimethylsiloxy-2-piperidone in 75% yield (Scheme 1).

In summary, we have described a general reductive deamination reaction employing SmI_2 in THF–HMPA. This reaction proceeds in relatively high yield under mild reaction conditions and seems to be applicable to the wide variety of α-amino carbonyl compounds. Utilisation of this reaction in the synthesis of natural products is under investigation. This work was supported by the Ministry of Education, Science, Sports and Culture of Japan.

Notes and references

1 P. Girard, J. L. Namy and H. B. Kagan, *J. Am. Chem. Soc.*, 1980, **102**, 2693.

2 Reviews: J. Inanaga, *J. Org. Synth. Chem.*, 1989, **47**, 200, J. A. Soderquist, *Aldrichim. Acta*, 1991, **24**, 15; D. P. Curran, T. L. Fevig, C. P. Jasperse and M. J. Totleben, *Synlett*, 1992, 943; G. A. Molander, *Chem. Rev.*, 1992, **92**, 29: G. A. Molander and C. R. Harris, *Chem. Rev.*, 1996, **96**, 307; G. A. Molander and C. R. Harris, *Tetrahedron*, 1998, **54**, 3321 and references cited therein.

3 G. A. Molander and P. J. Stengel, *J. Org. Chem.*, 1995, **60**, 6660; G. A. Molander and P. J. Sangel, *Tetrahedron*, 1997, **53**, 8887; N. H. Kawahara and M. Goodman, *Tetrahedron Lett.*, 1999, **40**, 2271.

4 J. M. Aurrecoechea and A. Fernandez-Acebes, *Tetrahedron Lett.*, 1993, **34**, 549; J. M. Aurrecoechea and A. Fernandez-Acebes, *Synlett*, 1996, 39; A. R. Katritzky, M. Qi, D. Feng and D. A. Nichols, *J. Org. Chem.*, 1997, **62**, 4121.

5 H.-Y. Kang, A. N. Pae, Y. S. Cho, H. Y. Koh and B. Y. Chung, *Chem. Commun.*, 1997, 821.

6 T. Honda, S. Yamane, K. Naito, K. and Y. Suzuki, *Heterocycles*, 1994, **37**, 515; T. Honda, F. Ishikawa and S. Yamane, *J. Chem. Soc., Chem. Commun.*, 1994, 499; T. Honda, S. Yamane, K. Naito and Y. Suzuki, *Heterocycles*, 1995, **40**, 301; T. Honda, F. Ishikawa and S. Yamane, *J. Chem. Soc., Perkin Trans. 1*, 1996, 1125; T. Honda, S. Yamane, F. Ishikawa and M. Katoh, *Tetrahedron*, 1996, **37**, 12177; T. Honda, M. Katoh and S. Yamane, *J. Chem. Soc., Perkin Trans. 1*, 1996, 2219; T. Honda and M. Katoh, *Chem. Commun.*, 1997, 369.

7 The starting phenylalanine derivatives were prepared from the methyl ester by the known procedures; *N*-methyl derivative: M. C. Allen, W. Fuhrer, B. Tuck, R. Wade and J. M. Wood, *J. Med. Chem.*, 1989, **32**, 1652; *N*,*N*-dimethyl derivative: T. Hayashi, M. Konishi, M. Fukushima, K. Kanehira, T. Hioki and M. Kumada, *J. Org. Chem.*, 1983, **48**, 2195; *N*-benzyl derivative: F. Effenberger, U. Burkard and J. Willfahrt, *Liebigs Ann. Chem.*, 1986, 314; *N*,*N*-dibenzyl derivative: B. D. Gray and P. W. Jeffs, *J. Chem. Soc., Chem. Commun.*, 1987, 1329; *N*-acetyl derivative: M. J. Burk, J. E. Feaster, E. H. Harlow and L. Richard, *Tetrahedron: Asymmetry*, 1991, **2**, 569; *N*-Boc derivative: M. Sakaitani and Y. Ohfune, *J. Org. Chem.*, 1990, **55**, 870.

8 *N*-Benzylproline methyl ester was prepared from methyl prolinate: V. Ferey, P. Vedrenne, L. Toupet, T. L. Gall and C. Mioskowski, *J. Org. Chem.*, 1996, **61**, 7244; isopropyl 4-*tert*-butyldimethylsiloxyprolinate was prepared by silylation of the corresponding ester, which on *N*-benzylation with BnBr and NaH gave the *N*-benzyl derivative.

9 *N*-Substituted pipecolinates were prepared from ethyl pipecolinate by alkylation with the suitable alkyl halide and Pr^i_2NEt or by acetylation with Ac_2O.

10 2-Acetyl-*N*-alkylpiperidine derivatives were prepared from ethyl pipecolinate *via* four steps involving *N*-alkylation with alkyl halide, hydrolysis of the ester, conversion of the acid to the Weinreb's amide (S. Nahm and S. M. Weinreb, *Tetrahedron Lett.*, 1981, **22**, 3815), and treatment of the amide with MeMgBr; the *N*-acetyl compound was derived from the *N*-benzyl derivative by reductive debenzylation over Pd/C in the presence of Ac_2O; the *N*-Boc derivative was prepared according to the known procedure: S. Aoyagi, T.-C. Wang and C. Kibayashi, *J. Am. Chem. Soc.*, 1993, **115**, 11393.

11 J. Inanaga, M. Ishikawa and M. Yamaguchi, *Chem. Lett.*, 1987, 1485.

Communication 9/03073E

Highly active supported palladium catalyst for the regioselective synthesis of 2-arylpropionic acids by carbonylation

S. Jayasree, A. Seayad and R. V. Chaudhari*

Homogeneous Catalysis Division, National Chemical Laboratory, Pune- 411 008, India. E-mail: rvc@ems.ncl.res.in

Received (in Cambridge, UK) 30th March 1999, Accepted 5th May 1999

A catalyst system consisting of supported palladium in the presence of phosphine ligands, TsOH and LiCl catalyses the carbonylation of 1-arylethanols to 2-arylpropionic acids with significantly improved activity and regioselectivity; the catalyst can be recycled with no loss in activity and selecivity.

Carbonylation of 1-arylethanols is of great interest since it provides an environmentally benign route[1] for the synthesis of anti-inflammatory drugs such as Ibuprofen, Naproxen *etc*. The importance of this route can be clearly demonstrated from the commercialisation of an Ibuprofen process at Texas in 1992 by Hoechst Celanese Corporation based on the carbonylation of 1-(4-isobutylphenyl)ethanol using a palladium complex catalyst.[2] The desired high selectivity (> 98%) for Ibuprofen was achieved only at very high pressures[3] (16–34 MPa). This homogeneous palladium catalyst system gave lower TOF† (50–100 h^{-1}) and selectivity (< 68%) at lower pressures (~ 6.8 MPa).[4] Additives such as $CuCl_2$ were reported to improve the selectivity under similar conditions.[5] In another study, a biphasic catalyst with a water soluble palladium complex[6] has been reported but in this case also, very low reaction rates (TOF = 2.3 h^{-1}) and lower Ibuprofen selectivity (70%) were observed.

Here we report, for the first time, highly active and selective supported palladium and platinum catalyst systems for the synthesis of 2-arylpropionic acids from the corresponding 1-arylethanols. Supported palladium combined with PPh_3, LiCl and TsOH provides very high TOF (3375 h^{-1}) and more importantly high selectivity (99.5%) for 2-arylpropionic acids at lower pressures (5.4 MPa). The activity as well as the selectivity was substantially higher compared to previous reports under identical conditions. The catalyst was recycled four times with no loss in activity and selectivity, attaining a total TON of 55,000. These results indicate that this new catalyst system (Pd-C/PPh_3/TsOH/LiCl) is highly efficient and provides significant improvement over the current state of the art for the synthesis of 2-arylpropionic acids.

In a typical experiment, the supported catalyst,‡ the substrate, the phosphine ligand, LiCl, TsOH, H_2O and the solvent (methyl ethyl ketone) were charged into a stirred pressure reactor and the reaction was carried out at 5.4 MPa of CO partial pressure at 115 °C under 1100 rpm for a specified time. The reaction mixture was analysed by gas chromatography§ and the products were further characterized by GC-MS and NMR.

Typical results for the carbonylation of 1-(4-isobutylphenyl)-ethanol (*p*-IBPE) using different catalysts, supports, promoters and ligands are presented in Table 1. Pt/C provided comparatively lower activity than Pd/C. Other supports such as γ-alumina and H-ZSM-5 were also useful. Different acid and halide sources were checked and were found to not significantly effect the catalytic activity. The nature of the phosphine ligand has a strong influence on the catalytic activity, as evidenced from Table 1. No reaction was observed with diphos ligands such as dppb, unlike the catalyst system reported by Ali *et al.* for the carbonylation of olefins.[7]

It was important to understand whether the reaction occurs heterogeneously or homogeneously (by soluble complexes of Pd formed *in situ*). For this purpose, liquid phase reaction samples were withdrawn during reaction and also after the end of the reaction (on cooling of the contents). The analysis of the liquid phase, after the reaction, for Pd content by atomic absorption spectroscopy showed < 0.1 ppm of Pd in solution, but the sample withdrawn under the reaction conditions showed significant leaching of Pd (1.5 ppm Pd). This indicates that the reaction is more likely to be homogeneously catalysed and the enhanced activity and selectivity is due to the combination of Pd with PPh_3 and promoters like TsOH, and LiCl. At the same time, readsorption of Pd onto the support after the reaction facilitates repeated recycling. Thus, the proposed catalyst system offers significant advantages, not only with respect to activity and selectivity, but also to catalyst recycling.

Intermediate sampling for the carbonylation of *p*-IBPE showed that the reaction proceeds through the formation of 4-isobutylstyrene and 1-(4-isobutylphenyl)ethyl chloride as the intermediates. Here the question was, which intermediate is undergoing carbonylation? To make this point clear, the carbonylation of 4-isobutylstyrene was performed in the absence of LiCl. The reaction was found to be very slow (TOF = 300 h^{-1}) with very poor Ibuprofen selectivity (65%). But in

Table 1 Carbonylation of 1-(4-isobutylphenyl)ethanol (*p*-IBPE) to give Ibuprofen using supported palladium and platinum catalysts[a]

Catalyst	Ligand	*t*/h	Conversion (%)	Selectivity (%)	TOF/h^{-1}
1% Pd/C	PPh_3	4.2	96	99.2	3375
1% Pd/γ-alumina	PPh_3	5.5	92	99.5	2475
1% Pd/H-ZSM-5	PPh_3	5.8	90	99.0	2285
1% Pt/C	PPh_3	24	90	99.2	550
Pd metal[b]	PPh_3	8	97	99.3	90
1% Pd/C	P(*p*-Tol)$_3$	4.5	94	98.5	3062
1% Pd/C	P(*p*-FPh)$_3$	5.9	95	99.5	2384
1% Pd/C	P(Cy)$_3$	24	50	99.5	308
1% Pd/C[c]	PPh_3	8	91	99.0	1676
1% Pd/C[d]	PPh_3	6	93	98.5	2272

[a] *Conditions:* *p*-IBPE (14.04 mmol), catalyst (10 mg), phosphine (0.1908 mmol), TsOH (5.6052 mmol), LiCl (5.6052 mmol), H_2O (67 mmol), methyl ethyl ketone (21 ml), P_{CO} = 5.4 MPa, T = 115 °C. [b] Pd metal (2 mg). [c] HCl (5.6052 mmol) instead of TsOH and LiCl. [d] Bu_4NCl instead of LiCl.

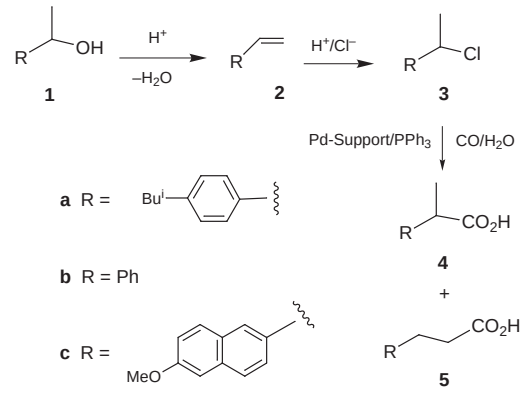

Scheme 1

Table 2 Synthesis of 2-arylpropionic acids by carbonylation[a]

Substrate	*t*/h	Conversion (%)	Selectivity (%)	TOF/h^{-1}
1a	4.2	96	99.2	3375
2a	4	92	99.1	3400
3a	4	90	99.3	3300
1b	13	90	98	1010
2b	4.6	92	98	2900
1c	24	90	99	552

[a] *Conditions:* Substrate (14.04 mmol), catalyst (10 mg), phosphine (0.1908 mmol), TsOH (5.6052 mmol), LiCl (5.6052 mmol), H_2O (67 mmol), methyl ethyl ketone (21 ml), P_{CO} = 5.4 MPa, T = 115 °C.

the presence of LiCl the catalytic activity and Ibuprofen selectivity were the same as that of *p*-IBPE carbonylation. Under similar conditions, 1-(4-isobutylphenyl)ethyl chloride also showed the same catalytic activity and selectivity behaviour. This indicates that in the presence of LiCl, the major reaction pathway is the carbonylation of the chloro derivative, as shown in Scheme 1.

The catalyst system was also applicable for the carbonylation of various 1-arylethanols and their corresponding olefin and chloro analogues, as demonstrated in Table 2. In all cases, high TOF and 2-arylpropionic acid selectivity were achieved.

In summary, in the presence of phosphines, TsOH and LiCl, with supported palladium and platinum as the catalyst systems, the carbonylation of 1-arylethanols to 2-arylpropionic acids occurs with high activity and regioselectivity with efficient recycling of the catalyst.

S. J. and A. S. thank the Council of Scientific and Industrial Research, India, for a research fellowship.

Notes and references

† TOF = Turn over frequency = number of moles of Ibuprofen produced per mole of metal per hour.

‡ The catalysts were prepared by wet impregnation of the chloride salts of the metals followed by reduction using formaldehyde (for carbon) or sodium formate (for alumina and H-ZSM-5).

§ Analysis of the components was by GC (FFAP capillary column 25 m × 0.2 mm, FID)

1 R. A. Sheldon, *Chem. Ind.*, 1992, 903; C. B. Dartt and M. E. Davis, *Ind. Eng. Chem. Res*., 1994, **33**, 2887.
2 J. N. Armor, *Appl. Catal*., 1991, **78**,141.
3 V. Elango, D. G. Kenneth, M. M. Alan, M. N. Graham, Z. G. Edward and S. B. Lee, EP 400 892, 1990.
4 A. Seayad, A. A. Kelkar and R. V. Chaudhari, *Stud. Surf. Sci. Catal*., 1998, **113**, 883.
5 E. J. Jang, K. H. Lee, J. S. Lee and Y. G. Kim, *J. Mol. Catal. A: Chem.*, 1999, **138**, 25.
6 G. Papadogianakis, L. Maat and R. A. Sheldon, *J. Chem. Technol. Biotechnol*., 1997, **70**, 83; G. Papadogianakis, G. Verspui, L. Maat and R. A. Sheldon, *Catal. Lett.*, 1997, **47**, 43.
7 B. E. Ali, G. Vasapollo and H. Alper, *J. Org. Chem.*, 1993, **58**, 4739.

Communication 9/02541C

Cu_2O: a catalyst for the photochemical decomposition of water?

Petra E. de Jongh,* Daniel Vanmaekelbergh and John J. Kelly

Debye Institute, Utrecht University, PO Box 80 000, 3508 TA Utrecht, The Netherlands. E-mail: pjongh@phys.uu.nl

Received (in Basel, Switzerland) 15th February 1999, Accepted 24th April 1999

The photoelectrochemical properties of polycrystalline Cu_2O electrodes are discussed with regard to the application of the oxide as a photocatalytic material for water splitting.

Recently, illuminated Cu_2O was reported to act as a stable catalyst for water splitting. Hydrogen and oxygen were evolved in a vigorously stirred suspension of Cu_2O particles, without a noticeable decrease in activity over a period of 1900 h.[1] This was very surprising since single crystalline Cu_2O is known to be photocathodically unstable.[2] The mechanism of water splitting and the precise role of the Cu_2O are still unclear.[1,3] Photocatalysis at a p-type semiconductor such as Cu_2O implies that the majority charge carriers (holes) oxidize water to oxygen, while the photogenerated minority charge carriers (electrons) reduce water to hydrogen. These reactions can be studied electrochemically; at positive potentials an anodic dark current due to oxygen evolution is expected, and at negative potentials a cathodic photocurrent accompanied by hydrogen evolution. We were already involved in research on electrodeposited polycrystalline Cu_2O layers,[4] and decided to study the photoelectrochemistry of these layers with respect to the decomposition of water.

We prepared well defined Cu_2O consisting of 0.1–1 μm crystals on a transparent, fluorine-doped tin oxide substrate by reduction of Cu^{2+} from a saturated copper(II) lactate aqueous solution. This technique has been described elsewhere.[4–8] Films were grown galvanostatically at 55 °C and pH 11 at a current density of 0.2 mA cm^{-2}. In the X-ray diffraction spectra only peaks due to Cu_2O were found. A bandgap of 1.9 eV was estimated from the optical absorption, in good agreement with literature values. Absorption at wavelengths >600 nm due to CuO was not seen. Scanning electron microscopy showed only well defined crystals. No changes in appearance or photoelectrochemical properties were found on keeping the Cu_2O layers in air for months.

The photoelectrochemical properties were investigated using a three electrode set-up with 0.5 M Na_2SO_4 as electrolyte solution. This method has the advantage that the cathodic and anodic reactions on the Cu_2O working electrode can be studied separately; they are accompanied by the reduction or oxidation of water at the platinum counter electrode. In the dark an anodic current, corresponding to the oxidation of the Cu_2O [eqn. (1)], was observed at potentials above 0.0 V *vs.* SCE (all redox potentials[9] are *vs.* SCE and at pH 7):

$$Cu_2O + 2\ OH^- + 2h^+ \rightarrow 2\ CuO + H_2O \quad E = -0.05\ V \quad (1)$$

The CuO slowly dissolves. In the presence of oxygen, a small steady state dark current was observed at negative potentials. When the solution was thoroughly purged with argon this dark current could be reduced to <1 μA cm^{-2}.

Under illumination, a large cathodic photocurrent was observed with an air-saturated solution under strong convection. This photocurrent started at a potential between 0.0 and 0.1 V, and the photocurrent spectrum was in good agreement with the Cu_2O absorption spectrum. Fig. 1(a) shows the current at −0.4 V *vs.* SCE under chopped 350 nm illumination. At low light intensities the photocurrent increased linearly with increasing photon flux; quantum efficiencies of 50% were measured for a photon flux below 5×10^{14} s^{-1} cm^{-2}. At higher light intensities

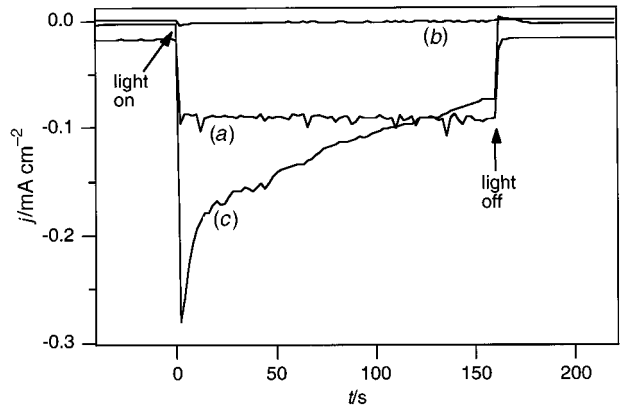

Fig. 1 Current density at −0.4 V measured on a 0.5 μm thick Cu_2O electrode illuminated with 350 nm (5×10^{15} s^{-1} cm^{-2}) in 0.5 M Na_2SO_4 solution: (a) bubbled with air, (b) bubbled with Ar and (c) bubbled with Ar and with 40 mM MV^{2+} added to the solution.

the photocurrent levels off. When the solution was carefully purged with argon, the cathodic photocurrent was very low (≈ 1 μA cm^{-2}) as is shown in Fig. 1(b). It is clear that the current observed in air-saturated solution is due to oxygen reduction, for instance *via* eqn. (2).

$$O_2 + 2\ H_2O + 2e^- \rightarrow H_2O_2 + 2\ OH^- \quad E = +0.03\ V \quad (2)$$

The hydrogen peroxide is further reduced to water. The high intensity photocurrent limit was close to the limiting current density for oxygen reduction at a platinized indium tin oxide electrode under the same hydrodynamic conditions. Obviously, the photocathodic reduction of oxygen on Cu_2O is extremely efficient. On the other hand, the reduction of water to hydrogen seems negligible. If appropriate deposition conditions were used, the Cu_2O layers, in contrast to single crystalline electrodes,[2] proved to be surprisingly stable under photocathodic conditions. The photocurrent due to oxygen reduction was constant over long periods, even when the photon flux exceeded the oxygen flux to the electrode surface. No evidence was found for the formation of copper due to the reduction of Cu_2O ($E = -0.19$ V). The small photocurrent observed in argon-purged solutions is very likely due to the reduction of traces of oxygen left in the solution.

The methylviologen (1,1-dimethyl-4,4-bipyridinium) system, $MV^{2+}/MV^{\cdot+}$ has a redox potential of −0.60 V *vs.* SCE,[10] which is close that of hydrogen. Fig. 1(c) shows a photocurrent transient for an Ar purged 0.5 M Na_2SO_4 solution containing 40 mM $[MV]Cl_2$. In the absence of oxygen, the photocurrent quantum efficiency was initially very high. However, the photocurrent decreased rapidly with time. This is likely due to the formation of a MV^0 layer on the electrode surface. The $MV^{\cdot+}$ radical cation, which is formed upon reduction of MV^{2+}, can be further reduced to MV^0; redox potentials of −1.1 to −1.3 V are reported for this reaction.[10–12] MV^0 is not soluble in aqueous solutions and is known to form blocking films on the electrode surface.[13] This is in good agreement with the observation that the photocurrent is restored as soon as air is admitted to the cell. Oxygen is known to oxidize MV^0 to MV^{2+} very effectively. Obviously the kinetics for the reduction of MV^{2+} are much more efficient than those for the reduction of water.

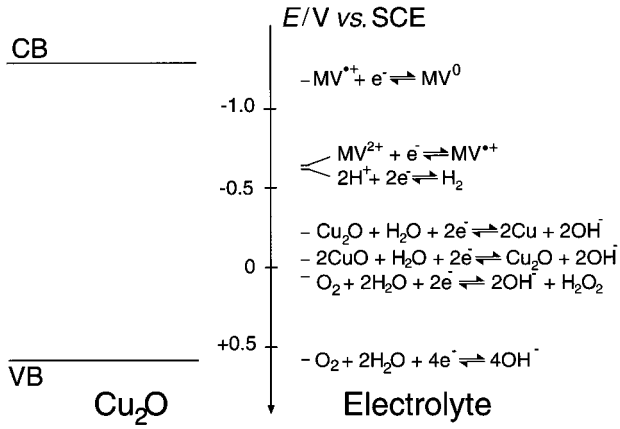

Fig. 2 Overview of the redox potentials of the relevant reactions with respect to the estimated position of the Cu_2O band edges.

It is interesting, in the light of our results, to examine the requirements that have to be met if Cu_2O is to function as a photocatalyst for water splitting. It is crucial that both the reduction and oxidation reactions of water are thermodynamically possible, and that these reactions are kinetically favourable. Fig. 2 shows the redox potentials of the relevant reactions with respect to the positions of the Cu_2O band edges.[2] To reduce water, the electron Fermi level and hence also the conduction band edge must be at an energy higher than that corresponding to the reduction potential for water, which at pH 7 is −0.65 V. The estimated position of the edge of the Cu_2O conduction band is −1.4 V.[2] This means that a large overpotential is available for the reaction. However, our measurements show that in the absence of other redox species no significant cathodic photocurrent is found in aqueous electrolyte. In the presence of oxygen or the methylviologen cation very efficient photocathodic reactions were found. The reduction of water must be kinetically highly unfavourable at our illuminated Cu_2O. To enable the oxidation of water, the Cu_2O valence band edge must be at an energy below that corresponding to the oxidation potential of water, which at pH 7 is *ca.* +0.57 V. The edge of the valence band was estimated to be at +0.6 V.[2] It is unlikely that the valence band edge lies at a much lower energy. This can be deduced from the bandgap of 2 eV and the fact that the position of the conduction band edge must be significantly more negative than −1.2 V *vs.* SCE if the photocathodic reduction of $MV^{\cdot+}$ (E = −1.2 V *vs.* SCE) is to be possible. As a consequence (almost) no overpotential is available for the oxidation of water. Furthermore, the oxidation of Cu_2O, with a redox potential of −0.05 V, is thermodynamically considerably more favourable. Our results show that the anodic current in the dark corresponds at least partly to oxidation of the oxide. Therefore, although the Cu_2O is stable under photocathodic conditions, stability under open circuit illumination is unlikely.

On the basis of these results it seems questionable if water can be split at Cu_2O *via* a normal photocatalytic reaction. However, our polycrystalline layers show long term stability under photocathodic conditions, and a surprisingly high quantum efficiency for the photocathodic reduction of both oxygen and the methylviologen cation. Therefore Cu_2O could be a promising material, not for direct photoelectrochemical water splitting, but in conjunction with a suitable redox system as a p-type photoelectrode in an electrochemical photovoltaic cell.

Notes and references

1 M. Hara, T. Kondo, M. Komoda, S. Ikeda, K. Shinohara, A. Tanaka, J. Kondo and K. Domen, *Chem. Commun.*, 1998, 357.
2 H. R. Schöppel and H. Gerischer, *Ber. Bunsenges. Phys. Chem.*, 1971, **75**, 1237.
3 S. Ikeda, T. Takata, T. Kondo, G. Hitoki, M. Hara, J. N. Kondo, K. Domen, H. Hosono, H. Kawazoe and A. Tanaka, *Chem. Commun.*, 1998, 2158.
4 P. E. de Jongh, D. Vanmaekelbergh and J. J. Kelly, *Z. Phys. Chem.*, in press.
5 T. D. Golden, M. G. Shumsky, Y. Zhou, R. A. Vanderwerf, R. A. van Leeuwen and J. A. Switzer, *Chem. Mater.*, 1996, **8**, 2499.
6 D. Tench and L. F. Warren, *J. Electrochem. Soc.*, 1983, **130**, 869.
7 A. E. Rakhshani and J. Varghese, *Sol. Energy Mater.*, 1987, **15**, 237.
8 A. P. Chatterjee, A. K. Mukhopadhyay, A. K. Chakraborty, R. N. Sasmal and S. K. Lahiri, *Mater. Lett.*, 1991, **11**, 358.
9 *Standard Potentials in Aqueous Solutions*, ed. A. J. Bard, R. Parsons and J. Jordan, IUPAC, New York, 1985.
10 C. L. Bird and A. T. Kuhn, *Chem. Soc. Rev.*, 1981, **10**, 49.
11 M. Heyrovsky, *J. Chem. Soc., Chem. Commun.*, 1987, 1856.
12 D. W. Bahnemann, C. H. Fischer, E. Janate and A. Henglein, *J. Chem. Soc., Faraday Trans. 1*, 1987, **83**, 2559.
13 G. H. Schoenmakers, R. Wagenaar and J. J. Kelly, *Ber. Bunsenges. Phys. Chem.*, 1996, **100**, 1169.

Communication 9/01232J

ChemComm

$[Ru\{MeC(CH_2EMe)_3\}_2](CF_3SO_3)_2$: the first homoleptic hexaseleno- and hexatelluro-ether complexes

William Levason, Simon D. Orchard and Gillian Reid*

Department of Chemistry, University of Southampton, Highfield, Southampton, UK SO17 1BJ.
E-mail: gr@soton.ac.uk

Received (in Basel, Switzerland) 9th March 1999, Accepted 29th April 1999

The preparations of the first examples of homoleptic hexaseleno- and hexatelluro-ether complexes, $[Ru\{MeC(CH_2EMe)_3\}_2](CF_3SO_3)_2$ (E = Se or Te) are described; the crystal structure of the former shows both ligands binding facially to the Ru^{II} centre, with the Se-based lone pairs in the *syn* arrangement.

Recently we embarked on a comparative study of the binding characteristics of thio-, seleno- and telluro-ether ligands to transition metal centres and we have shown that to low-valent group 6 and group 7 metal centres E→M donation increases in the order S < Se << Te.[1] Despite this, multidentate telluroether ligands are very rare, and the only reported tritelluroether complex is *fac*-$[Mn(CO)_3\{MeC(CH_2TeMe)_3\}]CF_3SO_3$.[2] We have already reported the synthesis, structures and properties of a range of multidentate and macrocyclic selenoether ligand complexes, and, in light of the prediction that telluroethers will show enhanced donating abilities, we have begun to investigate the synthesis and properties of multidentate telluroethers and their complexes with the platinum group metals. There are no examples with homoleptic hexaseleno- or hexatelluro-ether coordination to octahedral metal complexes. Typically two or more of the six coordination sites are occupied by halogen co-ligands which greatly influence the metal ion properties.[3] We report here the preparation, spectroscopic and structural characterisation of the first homoleptic hexaseleno- and hexatelluro-ether complexes, $[Ru\{MeC(CH_2EMe)_3\}_2](CF_3SO_3)_2$ (E = Se or Te).

$[Ru(dmf)_6](CF_3SO_3)_3$[4] reacts with 2 mol. equiv. of $MeC(CH_2EMe)_3$ (E = Se or Te) in refluxing MeOH solution to give yellow coloured solutions containing the hexa-substituted ruthenium(II) species $[Ru\{MeC(CH_2EMe)_3\}_2](CF_3SO_3)_2$.† These species can be isolated by addition of Et_2O to the concentrated solutions and filtration. The electrospray mass spectra (MeCN) show peaks with isotope distributions consistent with the doubly charged species $[Ru\{MeC(CH_2EMe)_3\}_2]^{2+}$ (E = Se, *m/z* centred at 402; E = Te, *m/z* centred at 548). IR spectroscopy shows peaks associated with coordinated triselenoether or telluroether, as well as absorptions characteristic of the $CF_3SO_3^-$ anion. The $^{77}Se\{^1H\}$ and $^{125}Te\{^1H\}$ NMR spectra of the complexes show single resonances at δ 120 and 204, respectively. Given that pyramidal inversion at an $Ru–SeR_2$ or $Ru–TeR_2$ unit is expected to be slow,[5,6] the observation of only one resonance in each case indicates that each coordinated ligand adopts a *syn* configuration.

Repeated attempts were made to obtain single crystals of one of these compounds suitable for an X-ray crystal structure analysis. Crystals of the selenoether complex were eventually obtained by diffusion of Et_2O into a solution of the complex in $MeNO_2$. A data set collected at 150 K gave rather broad peaks and did not refine satisfactorily. Data collection was therefore repeated at a slower scan-speed on a second sample at room temperature, yielding better quality data. The crystal structure‡ shows an ordered centrosymmetric $[Ru\{MeC(CH_2SeMe)_3\}_2]^{2+}$ cation with the Ru atom occupying a crystallographic inversion centre, giving a half-cation and one $CF_3SO_3^-$ anion in the asymmetric unit. Within the cation the Ru^{II} centre is coordinated to two tridentate, facially bound selenoether ligands, to give a slightly distorted octahedral arrangement with Ru–Se 2.4808(7), 2.4701(7), 2.4781(6) Å (Fig. 1). The Se–Ru–Se angles involved in the six-membered chelate rings are very close to 90°, and the Me substituents are oriented in the propeller-like arrangement associated with the configuration. This is consistent with the *syn* configuration deduced from $^{77}Se\{^1H\}$ NMR spectroscopy. The Ru–Se distances compare with 2.396(1)–2.465(1) Å in *cis*-$\{RuCl_2([16]aneSe_4)\}$ ([16]$aneSe_4$ = 1,5,9,13-tetraselenacyclohexadecane) and 2.465(3)–2.479(3) Å in *trans*-$[RuCl(PPh_3)([16]aneSe_4)]^+$.[6]

The electronic spectrum of $[Ru\{MeC(CH_2SeMe_3\}_2](CF_3SO_3)_2$ shows two d–d transitions, $^1A_{1g} \rightarrow {}^1T_{1g}$ and $^1A_{1g} \rightarrow {}^1T_{2g}$ at 25975 and 29940 cm^{-1} respectively, as well as intense charge transfer transitions at higher energy. Analysis of the spectrum[7] leads to approximate values of 10 *Dq* and *B* of 25000 and 250 cm^{-1}, respectively. These values can be compared with $\{Ru(H_2O)_6\}^{2+}$ (17700 and 425), $[Ru(en)_3]^{2+}$ (25450 and 390)[7] and $[Ru([9]aneS_3)_2]^{2+}$ ([9]$aneS_3$ = 1,4,7-trithiacyclononane) (28400 and 290 cm^{-1}).[8] These data indicate that the selenoether tripod, like [9]$aneS_3$, is a strong field ligand with a high degree of covalent character in the Ru–Se bonds. The electronic spectrum of $[Ru\{MeC(CH_2Te-$

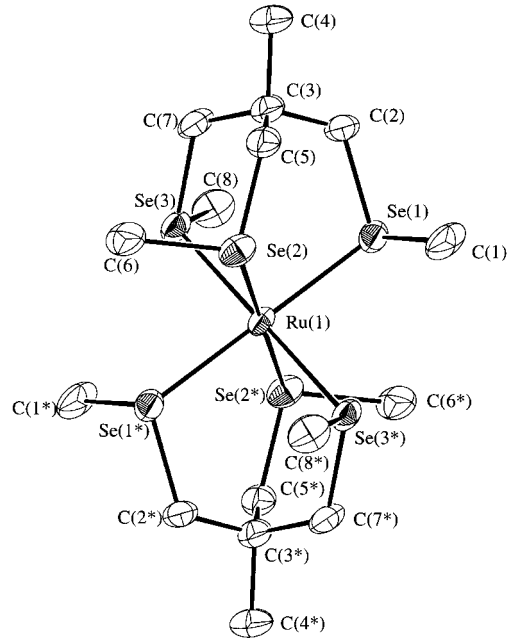

Fig. 1 View of the structure of $[Ru\{MeC(CH_2SeMe)_3\}_2]^{2+}$ with the numbering scheme adopted. H atoms are omitted for clarity, atoms marked * are related by a crystallographic inversion centre and ellipsoids are drawn at the 40% probability level. Selected bond lengths (Å) and angles (°): Ru–Se(1) 2.4808(7), Ru–Se(2) 2.4701(7), Ru–Se(3) 2.4781(6); Se(1)–Ru–Se(2) 90.18(2), Se(1)–Ru–Se(3) 89.02(2), Se(2)–Ru–Se(3) 87.56(2)°.

$Me)_3\}_2](CF_3SO_3)_2$ is less informative since the charge transfer transitions tail into the visible region and completely obscure the metal-centred transitions.

Cyclic voltammetry on $[Ru\{MeC(CH_2SeMe)_3\}_2](CF_3SO_3)_2$ (MeCN solution, 0.1 mol dm^{-3} $NBu^n_4BF_4$ supporting electrolyte) shows an irreversible reduction at −2.0 V *vs.* Fc/Fc^+ and a quasi-reversible oxidation at 1.18 V *vs.* Fc/Fc^+ which is assigned to the $Ru^{II/III}$ redox couple. This oxidation potential is considerably higher than for *trans*-$[RuCl_2([16]aneSe_4)]$ ($E_{1/2}$ = 0.32 V *vs.* Fc/Fc^+),[6] reflecting the presence of six soft Se donor atoms around the Ru^{II} centre in the former. $[Ru\{MeC(CH_2TeMe)_3\}_2](CF_3SO_3)_2$ shows no oxidative activity, only an irreversible reduction at −1.52 V *vs.* Fc/Fc^+. The relatively high potentials for these processes probably reflect the high stability of the low-spin d^6 Ru^{II} species within the strong field Se_6 or Te_6 coordination sphere, and strongly suggest that these ligands will be capable of supporting other $[ML_6]^{x+}$ species (L = Se or Te) for a wide variety of metals, thus promoting very different electronic environments at the metal centres.

We thank the University of Southampton and the EPSRC for support and Johnson Matthey plc for generous loans of $RuCl_3$.

Notes and references

† Satisfactory analytical and spectroscopic data were obtained.

‡ *Crystal data*: $C_{18}H_{36}F_6O_6RuS_2Se_6$, M = 1101.42, triclinic, space group $P\bar{1}$, a = 8.8436(5), b = 11.6692(15), c = 8.7056(8) Å, α = 107.369(9), β = 91.648(7), γ = 106.530(7), V = 815.62(14) Å^3, Z = 1, D_c = 2.242 g cm^{-3}, μ(Mo-Kα) = 73.68 cm^{-1}. Rigaku AFC7S four-circle diffractometer. Data collection at 293 K using Mo-Kα X-radiation (λ = 0.71073 Å), gave 2875 unique reflections (R_{int} = 0.0162) which were used in all calculations. The structure was solved using direct methods[9] and developed by iterative cycles of least-squares refinement[10] and difference Fourier synthesis. While the centrosymmetric cation is ordered, the $CF_3SO_3^-$ anion, which occupies a general position, shows rather high thermal parameters, particularly those associated with the F and O atoms. However, attempts to model this disorder by refining partial site occupancies were not successful, hence the atoms were refined with unit occupancies and high thermal parameters. While low temperature data collection would normally be expected to reduce the thermal motion and improve the structure quality, a data set from a different crystal collected previously at 150 K gave broad peaks and a significantly poorer fit to the data. Anisotropic thermal parameters were refined for all non-H atoms and H atoms were included in fixed, calculated positions. The weighting scheme $w^{-1} = \sigma^2(F_0) + (0.0634P)^2 + 2.2211P$, where $P = (F_0^2 + 2F_c^2)/3$, gave satisfactory agreement analyses. At final convergence, R_1 = 0.0539, wR_2 = 0.1106 (all data), R_1 = 0.0373, wR_2 = 0.1011 [$I \geqslant 2\sigma(I)$], S = 1.032 for 178 parameters. CCDC 182/1245. See http://www.rsc.org/suppdata/cc/1999/1071/ for crystallographic files in .cif format.

1 W. Levason, S. D. Orchard and G. Reid, *Organometallics*, 1999, **18**, 1275; A. J. Barton, W. Levason and G. Reid, *J. Organomet. Chem.*, 1999, in press.
2 W. Levason, S. D. Orchard and G. Reid, *J. Chem. Soc., Dalton Trans.*, 1999, 823.
3 E. G. Hope and W. Levason, *Coord. Chem. Rev.*, 1993, **122**, 109.
4 R. J. Judd, R. Cao, M. Biner, T. Armbruster, H.-B. Burgi, A. E. Merbach and A. Ludi, *Inorg. Chem.*, 1995, **34**, 5080.
5 W. Levason, S. D. Orchard, G. Reid and V.-A. Tolhurst, *J. Chem. Soc., Dalton Trans.*, 1999, in press.
6 W. Levason, J. J. Quirk, G. Reid and S. M. Smith, *J. Chem. Soc., Dalton Trans.*, 1997, 3719.
7 A. P. B. Lever, *Inorganic Electronic Spectoscopy*, Elsevier, Amsterdam, 2nd edn., 1984.
8 S. C. Rawle, T. J. Sewell and S. R. Cooper, *Inorg. Chem.*, 1987, **26**, 3769.
9 SHELXS-86, G. M. Sheldrick, *Acta Crystallogr., Sect. A*, 1990, **46**, 467.
10 SHELXL-97, G. M. Sheldrick, Univesity of Göttingen, 1997.

Communication 9/01930H

Metal-capped α-cyclodextrins: the crowning of the oligosaccharide torus with precious metals

Dominique Armspach and Dominique Matt

UMR 7513 CNRS, Université Louis Pasteur, Groupe de Chimie Inorganique Moléculaire, 1 rue Blaise Pascal, F-67008 Strasbourg Cedex, France. E-mail: dmatt@chimie.u-strasb.fr and armyou@chimie.u.strasb.fr

Received (in Cambridge, UK) 12th April 1999, Accepted 29th April 1999

The synthesis of diphosphino α-cyclodextrins (α-CDs) and their capping by transition metals are described; one of the complexes has been tested in biphasic catalytic hydroformylation.

Multidentate ligands preorganised around a macrocyclic platform have attracted much interest in recent years in view of their ability to shape the coordination sphere of metals in a specific manner as well as to provide well defined cavities or clefts.[1] The combination of both features could lead to the development of new metal catalysts with enhanced selectivities and activities. In addition, it may be anticipated that the presence of a bulky cavity will provide protection against undesired side reactions if properly positioned with respect to the metal centre. These issues have, in some respect, been addressed by use of monosubstituted cyclodextrins (CDs) bearing a pendant catalytic site.[2–4] However, until now, no synthetic methodology has been developed for *capping* a CD with a catalytically active transition metal unit. Exact positioning of the metal at the cavity mouth appears to be essential for fully exploiting the intrinsic properties of CDs in terms of water-solubility, chirality and steric crowding. In this preliminary communication, we report on the synthesis of the first C_2-symmetrical diphosphines based on α-CD and describe how these ligands undergo efficient capping of the oligosaccharide torus with catalytically important transition metals.†

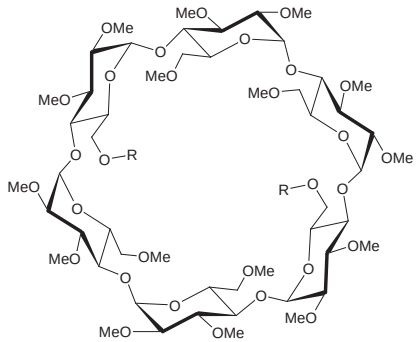

1 R = $C(C_6H_4Bu^t)_3$
2 R = H
3 R = Ms
4a R = 3-C_6H_4I
4b R = 4-C_6H_4I
5a R = 3-$C_6H_4PPh_2$
5b R = 4-$C_6H_4PPh_2$

All ligands mentioned here were derived from diol **2** which was obtained in gram-scale quantities and good yield (87%) by acidic cleavage[5] of 6A,6D-di-*O*-tris(*p*-*tert*-butylphenyl)methyl-per-*O*-methyl-α-CD **1**[6] with HBF_4 (34%) in Me_3CN. Diol **2** was converted into dimesylate **3** in 90% yield. Treatment of the latter with 3-iodophenol or 4-iodophenol and K_2CO_3 in DMF afforded respectively di-iodo CDs **4a** and **4b** which on Stelzer's palladium-catalysed cross coupling[7] with diphenylphosphine gave phosphine-based ligands **5a** and **5b** in 69 and 70% overall yields, respectively.

^1H as well as ^{13}C and ^{31}P NMR spectra of diphosphines **5a**† and **5b**† clearly show the presence of the expected twofold molecular symmetry which indicates free rotational motion of the triarylphosphine fragments. For example, the ^{31}P NMR spectrum of either **5a** or **5b** consists of a single singlet respectively at δ −4.5 and −6.8.

According to CPK‡ models, ligand **5a** possesses the right geometrical features to promote the formation of *trans-P,P*-chelates upon metal complexation. Evidence for the latter was given by studying the coordination of **5a** with metals prone to form linear arrangements. Thus, treatment of **5a** with $AgBF_4$ led to the C_2-symmetric complex P–Ag–P **6**. Likewise, its gold analogue **7** was cleanly obtained by reacting in CH_2Cl_2 the *in situ* prepared complex [Au(thf)(SC_4H_8)]BF_4 (SC_4H_8 = tetrahydrothiophene) with **5a** in high yield. The complex is air stable

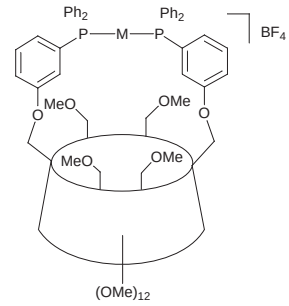

6 M = Ag
7 M = Au

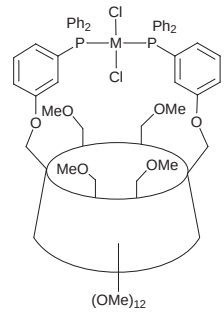

8a M = Pt
9a M = Pd

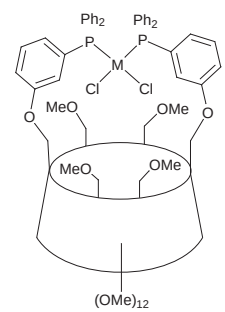

8b M = Pt
9b M = Pd

and can be subjected to chromatography on silica gel without noticeable decomposition, an unusual feature for complexes of that type. Similarly, treatment of **5a** with [$PtCl_2(PhCN)_2$] (mixture of *cis* and *trans* isomers) led to the exclusive formation of *trans-P,P*-chelate complex **8a**. However, exposure of a refluxing ethanolic solution of **8a** to sunlight produced after a week a 65:35 equilibrium mixture of **8a** and *cis* chelate **8b**. These compounds could easily be separated by column chromatography without detection of any interconversion during the separation. Molecular-weight determination using vapour phase osmometry (CH_2Cl_2) gave masses of 1890 and 1950 for **8a** and **8b**, respectively [M(calc.) = 1984]. This

Table 1 Selected MS and spectroscopic data for complexes **6**–**11**

Compound	FAB-MS [*m*/*z* (%)]	$^{31}P\{^{1}H\}$ NMR[a] δ_P (*J*(PM)/Hz)	^{1}H NMR[b] δ_H of MeO-$6^{B,E}$ and MeO-$6^{C,F}$
6	1825 (100), $[M - BF_4]^+$ 1841 (45), $[M - BF_4 + O]^+$	14.2 (495)	2.88, 3.17
7	1913 (100), $[M - BF_4]^+$ 1930 (13), $[M - BF_4 + O]^+$	15.4	3.17, 3.26
8a	1982[d] (20), M^+	21.4 (2642)	3.03, 3.05
8b	1912 (100), $[M - 2Cl]^+$ 1947[d] (75), $[M - Cl]^+$	15.3 (3669)	3.20, 3.29
9a	1859 (50), $[M - Cl]^+$	24.5	3.03, 3.04
9b	1894 (30), M^+	33.5[c]	3.21, 3.26
10a	1947 (75), $[M - Cl]^+$	19.1 (2633)	3.00, 3.16
10b	1982[d] (13), M^+	13.4 (3681)	3.01, 3.10
11	1819 (100), $[M - Cl - CO]^+$ 1847 (15), $[M - Cl]^+$ 1854 (95), $[M - CO]^+$	29.7	3.00, 3.10

[a] In $CDCl_3$ (ext. ref.: H_3PO_4). [b] In $CDCl_3$. [c] The stereochemistry about the palladium centres was assigned empirically according to ref. 8. [d] The monomeric nature of this complex was confirmed by vapour phase osmometry.

clearly demonstrates the monomeric nature of both compounds.§ Moreover, the reaction between ligand **5a** and $[PdCl_2(PhCN)_2]$ (*cis* and *trans* isomers) afforded a rapidly interconverting 80 : 20 equilibrium mixture of *trans*-chelate **9a** and *cis*-chelate **9b** as evidenced by ^{31}P NMR spectroscopy[8] (Table 1). In addition, unlike **5a**, ligand **5b** gave with $[PtCl_2(PhCN)_2]$ both *trans* chelate **10a** and the corresponding *cis* chelate **10b** (not drawn) as a 40 : 60 mixture.¶ Their

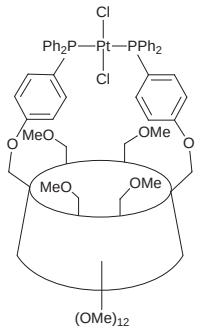

10a

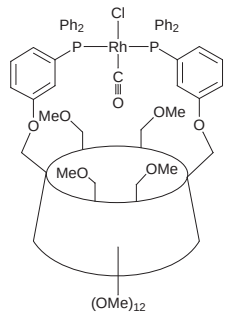

11

separation could not be achieved since they interconvert rapidly in solution. Clearly, the phosphine fragments in **5a**, less so in **5b**, are arranged on the cyclodextrin platform so as to favour *trans* chelation. Full evidence for the latter was given by the reaction of $[\{Rh(CO)_2Cl\}_2]$ in dichloromethane with **5a** which quantitatively yielded complex **11**.† The $^{31}P\{^{1}H\}$ NMR spectrum of **11** displays a single doublet [*J*(Rh–P) 127.1 Hz] in agreement with the expected *trans*-P,P stereochemistry.

Complex **11** possesses the essential features known to be important for a hydroformylation catalyst. Indeed, **11** catalyses the conversion of oct-1-ene into the corresponding aldehydes in H_2O–MeOH (conversion and chemoselectivity > 99% after 18 h).‖ Selectivity of linear to branched aldehydes (n : i) is of the order of 70 : 30, which is unexceptional for rhodium(I) bis-(phosphine) complexes. Similarly, the turn-over frequency** (70 h^{-1}) compares well with standard nonionic hydroformylation catalysts. Unfortunately, low water-solubility prevents **11** acting as a supramolecular catalyst as evidenced by the outcome of the catalytic tests which are typical of classical systems both in terms of activity and selectivity. Although **11** is only present in the methanol–water phase in the first place, transfer of the catalyst to the oct-1-ene–aldehydes phase was found to take place during the reaction.

A synthetic methodology has been designed for the preparation of highly preorganised diphosphines based on α-CD. Such ligands promote the formation of chelate complexes in which the P_2 unit rigidly holds a metal centre at the mouth of the cavity. Water-soluble analogues of the aforementioned species are expected to form inclusion complexes in water with substrates that can react catalytically *via* the metal centre. It is hoped that these combined features will improve existing hydroformylation and hydrogenation catalysts both in terms of activity and selectivity.

Notes and references

† Satisfactory elemental analyses have been obtained for all compounds. *Selected data*: for **5a**: ^{1}H NMR ($CDCl_3$): δ 3.21 (s, 6H, C*H*$_3$O-6), 3.22 (s, 6H, C*H*$_3$O-6), 3.47 (s, 6H, C*H*$_3$O), 3.48 (s, 6H, C*H*$_3$O), 3.50 (s, 6H, C*H*$_3$O), 3.64 (s, 6H, C*H*$_3$O), 3.65 (s, 6H, C*H*$_3$O) , 3.66 (s, 6H, C*H*$_3$O), 3.09–4.02 (m, 32H, H-2, H-3, H-4, H-5, H-$6^{B,C,E,F}$), 4.30–4.36 (m, 4H, H-$6^{A,D}$), 4.97 (d, 2H, ^{3}J 3.2 Hz, H-1), 5.01 (d, 2H, ^{3}J 3.2 Hz, H-1), 5.06 (d, 2H, ^{3}J 3.2 Hz, H-1), 6.82 (t, 2H,^{3}J 7.2 Hz, aromatic H), 6.88–7.00 (m, 4H, aromatic H), 7.22–7.33 (m, 22H, aromatic H). $^{13}C\{^{1}H\}$ NMR ($CDCl_3$): δ 57.87 (×3) (*C*H$_3$O-2), 58.79, 58.93 (*C*H$_3$O-6), 61.72 (×3) (*C*H$_3$O-3), 67.69 (C-$6^{A,D}$), 70.79 and 71.18 (×2) (C-5), 71.25 (×2) (C-$6^{B,C,E,F}$), 81.27 (×3), 82.05 (×3), 82.28, 82.40 and 82.93 (C-2, C-3, C-4), 100.02 (×3) (C-1), 114.65 (s, C_{para}), 120.28 [d, ^{2}J(C,P) 24.8 Hz, C_{ortho}], 126.08 [d, ^{2}J(C,P) 15.3 Hz, C_{ortho}], 128.53 [d, ^{3}J(C,P) 6.7 Hz, C_{meta}], 128.70 (s, C_{para}), 129.45 (d, ^{3}J(C,P) 6.5 Hz, C_{meta}), 133.87 [d, ^{2}J(C,P) 19.6 Hz, C_{ortho}], 137.08 (d, ^{1}J(C,P) 8.5 Hz, aromatic C_{quat}], 138.91 [d, ^{1}J(C,P) 12.0 Hz, aromatic C_{quat}], 158.85 [d, ^{3}J(C,P) 9.9 Hz, C_{meta}]. $^{31}P\{^{1}H\}$ NMR ($CDCl_3$): δ = − 4.5 (s). FAB MS, *m*/*z* (%): 1717 (100) $[M + H]^+$.

For **5b**: $^{31}P\{^{1}H\}$ NMR ($CDCl_3$): δ = − 6.8 (s). FAB MS, *m*/*z* (%): 1739 (100) $[M + Na]^+$.

For **11**: IR (KBr) *ν*/cm^{-1}: 1977m (C≡O). ^{1}H NMR ($CDCl_3$): δ 3.00 (s, 6H, C*H*$_3$O-6), 3.10 (s, 6H, C*H*$_3$O-6), 3.46 (s, 6H, C*H*$_3$O), 3.50 (s, 6H, C*H*$_3$O), 3.51 (s, 6H, C*H*$_3$O), 3.64 (s, 6H, C*H*$_3$O), 3.66 (s, 12H, C*H*$_3$O), 3.08–3.84 (m, 30H, H-2, H-3, H-4, H-$5^{B,C,E,F}$, H-$6^{B,C,E,F}$), 4.19–4.26 (m, 4H, H-6b^{A,D}, H-$5^{A,D}$), 4.65–4.71 (m, 2H, H-6a^{A,D}), 4.99 (d, 2H, ^{3}J 3.2 Hz, H-1), 5.03 (d, 2H, ^{3}J 3.2 Hz, H-1), 5.05 (d, 2H, ^{3}J 3.2 Hz, H-1), 6.98–7.67 (m, 28H, aromatic H). $^{13}C\{^{1}H\}$ NMR ($CDCl_3$): δ 57.72, 57.79 and 58.08 (CH_3O-2), 58.87 (×2) (CH_3O-6), 61.79 (×3) (CH_3O-3), 68.12 (C-$6^{A,D}$), 69.95 (C-$5^{A,D}$), 70.28 and 70.61 (C-$6^{B,C,E,F}$), 71.30 (×2) (C-$5^{B,C,E,F}$), 81.26, 81.36 (×2), 82.02 (×2), 82.11, 82.18, 82.34 and 83.62 (C-2, C-3, C-4), 99.68 and 99.98 (C-$1^{B,C,E,F}$), 100.77 (C-$1^{A,D}$), 116.04, 122.96, 127.92, 128.12, 132.02, 133.92 and 134.34 (aromatic CH), 129.86, 133.45 and 158.34 (aromatic C_{quat}). $^{31}P\{^{1}H\}$ NMR ($CDCl_3$): δ 29.7 [d, *J*(P,Rh) 127.1 Hz].

‡ CPK stands for Corey-Pauling-Koltun.

§ Mass spectrometry cannot be reliably employed for mass determination for these neutral MCl_2 complexes as peaks due to ion–molecule reactions were detected in the spectra (intensity *ca*. 4% for **8b**).

¶ Vapour phase osmometry measurements (CH_2Cl_2) gave a mass of 1820 for the mixture **10a**/**10b**, thus confirming the monomeric nature of both compounds.

‖ *Conditions*: 40 bar CO–H_2 (1 : 1), 60 °C, H_2O–MeOH (6 : 4), [**11**] = 1.2 × 10^{-3} M, [oct-1-ene] = 0.47 M.

** Turn-over frequency in mol aldehydes formed per mole Rh per hour, averaged over 3.5 h at 60% conversion.

1 C. Wieser, C. B. Dieleman and D. Matt, *Coord. Chem. Rev.*, 1997, **165**, 93.
2 M. Reetz and J. Rudolph, *Tetrahedron: Asymmetry*, 1993, **4**, 2405.
3 M. Sawamura, K. Kitayama and Y. Ito, *Tetrahedron: Asymmetry*, 1993, **4**, 1829.
4 M. T. Reetz and S. R. Waldvogel, *Angew. Chem. ,Int. Ed. Engl.*, 1997, **36**, 865.
5 A. W. Coleman, C.-C. Lin and M. Miocque, *Angew. Chem.*, 1992, **104**, 1402.
6 D. Armspach and D. Matt, *Carbohydr. Res.*, 1998, **310**, 129.
7 O. Herd, A. Hessler, M. Hingst, M. Tepper and O. Stelzer, *J. Organomet. Chem.*, 1996, **522**, 69.
8 S. O. Grim and R. L. Keiter, *Inorg. Chim. Acta*, 1970, **4**, 56.

Communication 9/02879J

ChemComm

Imine allylation by allylic trimethylsilanes *via in situ* formation of *N*-tosyliminium species from carbonyl compounds and toluene-*p*-sulfonamide with $SnCl_2$ and *N*-chlorosuccinimide: regioselection and diastereoselection

Yoshiro Masuyama,* Jiro Tosa and Yasuhiko Kurusu

Department of Chemistry, Sophia University, 7-1 Kioicho, Chiyoda-ku, Tokyo 102-8554, Japan.
E-mail: y-masuya@hoffman.cc.sophia.ac.jp

Received (in Cambridge, UK) 8th April 1999, Accepted 5th May 1999

***N*-Tosyliminium species, prepared *in situ* from carbonyl compounds and $TsNH_2$ with $SnCl_2$ and *N*-chlorosuccinimide, undergo nucleophilic addition of allylic silanes (imine allylation) to produce the corresponding homoallylic amines; the imine allylation by but-2-enyltrimethylsilane with aldehydes and $TsNH_2$ leads to regio- and diastereoselection to produce *anti* 1-substituted 2-methylbut-3-enylamines.**

Lewis acid-catalysed allylations of imines or iminium species with allylic silane or tin reagents are one of the most effective methods for the introduction of an amino group into carbon skeletons.[1, 2] However, some imines and iminium species are unstable to water or heat, and their purification is difficult *via* recrystallization, distillation and chromatography. The allylation of imines or iminium species, prepared *in situ* from carbonyl compounds and amines, would therefore be a synthetically useful strategy.[3–7] We have reported that *N*-chlorosuccinimide (NCS) and $SnCl_2$ can be utilized for the aldol-type reaction of isopropenyl acetate with oxycarbenium ions derived from either aldehydes with alcohols or lactols.[8] A key step in the aldol-type reaction is probably the formation of alkoxytrichlorotins, which react with aldehydes to form oxycarbenium ions. We hoped that, using NCS–$SnCl_2$, aldehydes could be transformed into *N*-tosyliminium species with $TsNH_2$, in analogy to alcohols giving oxycarbenium ions, and that the *N*-tosyliminium species could undergo nucleophilic addition with allylic silanes (imine allylation).[9]

As a consequence of the investigation of imine allylation by allyltrimethylsilane **1** with benzaldehyde and some amines under various conditions, it was proved that starting with a solution of $SnCl_2$ (1.1 mmol), $TsNH_2$ (1 mmol) and benzaldehyde (**2**; R^1 = Ph, R^2 = H, 1 mmol) in CH_2Cl_2 (3 ml) in an ice-bath, the addition of NCS (1.1 mmol) in CH_2Cl_2 (5 ml) followed by allyltrimethylsilane (**1**, 1.5 mmol) after 2 h afforded *N*-tosyl-1-phenylbut-3-enylamine (**3**; R^1 = Ph, R^2 = H) in a 96% yield (Scheme 1). Benzylamine, benzamide, and *tert*-butyl carbamate were ineffective in the reaction under the same conditions as those used with $TsNH_2$. This allylation probably needs amines or amides bearing an acidic proton on nitrogen for the formation of the trichlorotin amide; as shown in Scheme 2, $TsNH_2$ reacts with **A**, derived from NCS and $SnCl_2$, to form **B**, which undergoes nucleophilic addition to benzaldehyde (R = Ph) to form **C** followed by **D**. The imine allylation by **1** with various carbonyl compounds and $TsNH_2$ was carried out under the same conditions as those for benzaldehyde described above. Representative results are summarized in Table 1. Any aldehyde, including aromatic aldehydes bearing either an electron-withdrawing group (entries 2 and 3) or an electron-donating group (entries 4–6), aliphatic aldehydes (entries 8–10) and an α,β-unsaturated aldehyde (entry 11) can be used in the imine allylation. In the cases of aldehydes bearing a coordinate group,

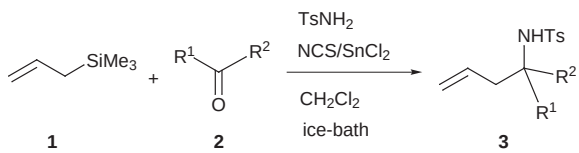

Scheme 1

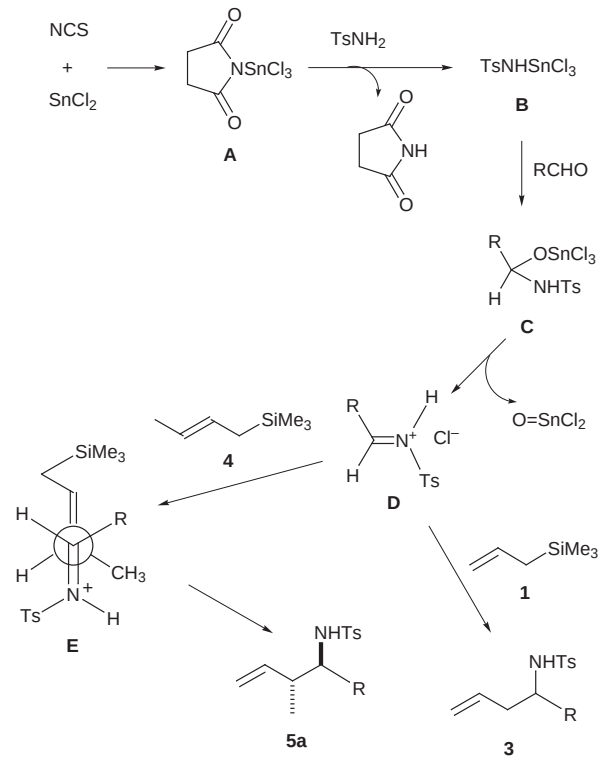

Scheme 2

Table 1 Imine allylation by **1** with **2**, $TsNH_2$, NCS and $SnCl_2$ to give **3**

Entry	R^1	R^2	*t*/h	Yield[a] (%)
1	Ph	H	6	96
2	4-ClC_6H_4	H	6	90
3	4-NCC_6H_4	H	6	92
4	4-MeC_6H_4	H	8	81
5	4-$MeOC_6H_4$	H	10	75
6	3,4-$(CH_2O_2)C_6H_3$	H	15	47
7	2-Furyl	H	15	28
8	C_6H_{13}	H	15	64
9	*c*-C_6H_{11}	H	15	70
10	$PhCH_2CH_2$	H	10	86
11	PhCH = CH	H	15	52
12	$(CH_2)_4$		20	26
13	$(CH_2)_5$		20	38
14	Ph	Me	20	17

[a] Isolated yields.

Table 2 Diastereoselective imine allylation by but-2-enyltrimethylsilane **4** to give **5**[a]

Entry	R	*t*/h	Yield[b] (%)	**5s** : **5a**[c]
1	Ph	6	91	11 : 89
2	4-ClC_6H_4	15	87	11 : 89
3	4-MeC_6H_4	15	73	10 : 90
4	C_6H_{13}	15	48	8 : 92
5	*c*-C_6H_{11}	15	62	9 : 91

[a] The imine allylation by **4** (1.5 mmol) was carried out with aldehydes (1 mmol), $TsNH_2$ (1 mmol), $SnCl_2$ (1.1 mmol) and NCS (1.1 mmol) in CH_2Cl_2 (3 ml) by the same method as that for the allylation by **1**. [b] Isolated yields. [c] The ratio was determined by ^1H NMR (JEOL GX-270).

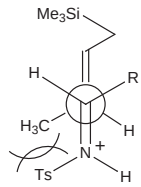

Fig. 1 Antiperiplanar transition state of **4**

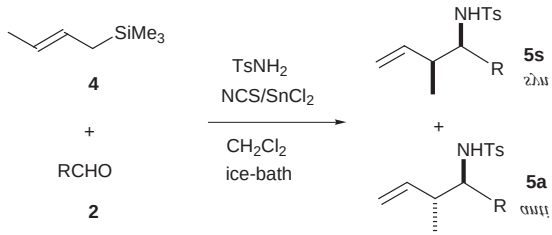

Scheme 3

3,4-methylenedioxybenzaldehyde and furan-2-carbaldehyde exhibited low yields (entries 6 and 7), and pyridine-2-carbaldehyde did not react under the given conditions. Ketones can also undergo the imine allylation to be converted into the corresponding homoallylic amines in unsatisfactory yields (entries 12–14).

The imine allylation of but-2-enyltrimethylsilane (**4**)† with some aldehydes and $TsNH_2$ under the same conditions as those of **1** caused γ-*anti*-addition to afford *anti* 1-substituted 2-methylbut-3-enylamines **5a** in good yields, as summarized in Table 2 (Scheme 3).‡ The γ-*anti*-addition probably occurs *via* an acyclic antiperiplanar transition state (**E**) between **4** and **D** (Scheme 2), due to steric hindrance between the tosyl group and the methyl group (Fig. 1).[4,9]

Notes and references

† But-2-enyltrimethylsilane (**4**; *E* : *Z* = 86 : 14) was prepared by the reaction of but-2-enyltrichlorosilane, derived from 1-chlorobut-2-ene and trichlorosilane with CuCl and Et_3N, with MeMgI (ref. 10).

‡ The stereochemistry was determined by comparison of ^1H NMR data of primary homoallylic amines (R = Ph, C_6H_{13}), which were produced by removal of the tosyl group (ref. 9), with those in the literature (ref. 11).

1 For a review, see: Y. Yamamoto and N. Asao, *Chem. Rev.*, 1993, **93**, 2207.
2 For recent papers, see: D.-K. Wang, L.-X. Dai and X.-L. Hou, *Tetrahedron Lett.*, 1995, **36**, 8649; C. Bellucci, P. G. Cozzi and A. Umani-Ronchi, *Tetrahedron Lett.*, 1995, **36**, 7289; T. Basile, A. Bocoum, D. Savoia and A. Umani-Ronchi, *J. Org. Chem.*, 1994, **59**, 7766.
3 For the reaction of allylic silane and tin reagents with formaldehyde and amines, see: S. D. Larsen, P. A. Grieco and W. F. Fobare, *J. Am. Chem. Soc.*, 1986, **108**, 3512; P. A. Grieco and A. Bahsas, *J. Org. Chem.*, 1987, **52**, 1378.
4 For the reaction of allylic silanes with aldehydes and carbamates, see: S. J. Veenstra and P. Schmid, *Tetrahedron Lett.*, 1997, **38**, 997; J. S. Panek and N. F. Jain, *J. Org. Chem.*, 1994, **59**, 2674.
5 For the reaction of allyltributyltin with aldehydes and arylamines, see: S. Kobayashi, S. Iwamoto and S. Nagayama, *Synlett*, 1997, 1099.
6 For the allylation of iminiums prepared in situ from α-alkoxymethylcarbamate, see: Y. Yamamoto and M. Schmid, *J. Chem. Soc., Chem. Commun.*, 1989, 1310; N. Kise, H. Yamazaki, T. Mabuchi and T. Shono, *Tetrahedron Lett.*, 1994, **35**, 1561.
7 For the allylation of iminium species prepared *in situ* from *N*-alkyl-*N*-trifluoromethanesulfonyloxyamide, see: R. V. Hoffman, N. K. Nayar, J. M. Shankweiler and B. W. Klinekole III, *Tetrahedron Lett.*, 1994, **35**, 3231.
8 Y. Masuyama, Y. Kobayashi, R. Yanagi and Y. Kurusu, *Chem. Lett.*, 1992, 2039; Y. Masuyama, Y. Kobayashi and Y. Kurusu, *J. Chem. Soc., Chem. Commun.*, 1994, 1123.
9 For the allylation of only aromatic sulfonimines, prepared beforehand, with allylic bromides and indium, see: T. H. Chan and W. Lu, *Tetrahedron Lett.*, 1998, **39**, 8605.
10 N. Furuya and T. Sukawa, *J. Organomet. Chem.*, 1975, **96**, C1.
11 R. W. Hoffmann and A. Endersfelder, *Liebigs Ann. Chem.*, 1987, 215.

Communication 9/02789K

Highly donor-doped (110) layered perovskite materials as novel photocatalysts for overall water splitting

Hyun G. Kim, Dong W. Hwang, Jindo Kim, Young G. Kim and Jae S. Lee*

Department of Chemical Engineering and School of Environmental Engineering, Pohang University of Science and Technology, San 31 Hyoja-dong, Pohang, 790-784, Korea. E-mail: jlee@postech.ac.kr

Received (in Cambridge, UK) 12th April 1999, Accepted 6th May 1999

Highly donor-doped (110) layered perovskite materials with a generic composition of $A_mB_mO_{3m+2}$ (m = 4, 5; A = Ca, Sr, La; B = Nb, Ti) loaded with nickel have been found to be efficient photocatalysts for overall water splitting with quantum yields as high as 23% under UV irradiation.

Among various methods of solar energy conversion, photocatalytic splitting of water into H_2 and O_2 has received most attention because of its potential to obtain directly clean and high-energy containing H_2 from abundant H_2O. Since its discovery in 1972,[1] water splitting with semiconductor photocatalysts under ultraviolet (UV) irradiation has become the subject of extensive studies.[2–4] However, quantum yields (% of absorbed photons that have been actually used to generate a photoreaction product) for well known photocatalysts such as TiO_2 and $SrTiO_3$ are very low (*ca.* <1%). Recently, (100) layered perovskite materials such as $K_4Nb_6O_{17}$ and $A_4Ta_xNb_{6-x}O_{17}$ (A = K, Rb) were found by Domen and coworkers to be much more efficient, showing quantum yields of *ca.* 5%.[5,6] This greatly improved quantum yield has been attributed to the use of their interlayer spaces as reaction sites. Inoue *et al.*[7] have reported an efficient water splitting over RuO_2–$BaTi_4O_9$ with a tunnel structure. However, it is desirable to find photocatalytic materials with even higher quantum yields in order for the water splitting to become a viable method to solve both energy and environmental problems in the future.

Here, we report a group of novel photocatalysts for overall water splitting with photon yields as high as 23% under UV irradiation. The materials are a series of homologous structures based on perovskite-type slabs with a generic composition of $A_mB_mO_{3m+2}$ (m = 4, 5; A = Ca, Sr, La; B = Nb, Ti) loaded with nickel. Unlike the (100) layered perovkite-type materials reported by the Domen group, our materials have the perovskite slabs parallel to (110) relative to the perovskite structre and are highly donor-doped. These structural and electronic characteristics are believed to be responsible for the much improved quantum yields.

For the preparation of the photocatalysts, *ca.* 10 g of commercial powders of metal carbonates and oxides were mixed in a desired composition and pressed in the form of a pellet. Pellets were calcined at 1123–1173 K for 6 h in an electric furnace and sintered at 1273–1623 K for 5 h. The presence of the (110) perovskite phase in the sintered ceramics was confirmed by X-ray diffraction (XRD) analysis using Cu-Kα radiation. Particle sizes of 0.5–8 μm were obtained by pulverizing the sintered pellets in a mortar. In order to obtain photocatalysts exhibiting high activities for water splitting, it was essential to load a transition metal on our perovskite materials and nickel was found to be the most effective. Thus, perovskite powders were impregnated with an aqueous $Ni(NO_3)_2$ solution to give a Ni loading of 1 wt% which was determined to be the optimum loading that gave the highest rate of water splitting. Ni-loaded $A_mB_mO_{3m+2}$ (m = 4, 5) catalysts were reduced with dihydrogen at 973 K, and then oxidized with oxygen at 473 K. This reduction–oxidation procedure was found to be an effective method to obtain active photocatalysts based on (100) layered perovskite materials.[5,6]

The photocatalytic decomposition of water was carried out at room temperature in a closed gas circulation system using a high pressure Hg lamp (450 W) placed in an inner irradiation-type quartz reaction cell. The catalyst (1.0 g) was suspended in distilled water (350 mL) by magnetic stirring. The rates of H_2 and O_2 evolution were determined by a gas chromatograph.

Fig. 1 shows a typical time course of H_2 and O_2 gas evolution for the photocatalytic decomposition of water over Ni/$Sr_2Nb_2O_7$. Note that $Sr_2Nb_2O_7$ is the reduced formula of $Sr_4Nb_4O_{14}$, the first member of the series $A_mB_mO_{3m+2}$ with m = 4. The catalyst produces H_2 (402 μmol h^{-1}) and O_2 (198 μmol h^{-1}) in a stoichiometric ratio (H_2 : O_2 = 2 : 1). In early studies of water splitting, the simultaneous evolution of O_2 and H_2 (*overall* water splitting) had been a challenge due to the difficulty of O_2 formation and the rapid reverse reaction between the two products. Furthermore, the reaction proceeds at steady rates with no indication of catalyst deactivation for 20 h during which the mol of H_2 produced are greater than the mol of the catalyst by factors of *ca.* 50 for Ni and *ca.* 2 for Nb contained in the whole catalyst. Since two electrons are needed to produce a molecule of H_2 from water, the latter corresponds to the turnover number of 4 if all Nb atoms have participated in the water splitting. This demonstrates that *overall* water splitting on this material proceeds *catalytically*.

Table 1 summarizes results of water decomposition and catalyst characterization for a number of photocatalysts. Our (110) layered perovskite catalysts ($Ca_2Nb_2O_7$, $Sr_2Nb_2O_7$, $La_2Ti_2O_7$ and $La_4CaTi_5O_{17}$) are compared with previously known (100) layered perovskite catalysts ($K_4Nb_6O_{17}$ and $K_4Ba_2Ta_3O_{10}$) and bulk-type TiO_2 catalyst (Degussa P-25), all under the same reaction conditions. $La_4CaTi_5O_{17}$ is the second member of $A_mB_mO_{3m+2}$ with m = 5. All perovskite-type catalysts were loaded with Ni, while Pt was loaded onto TiO_2 because Pt is known to be the best modifier for TiO_2. The BET surface areas of all perovskite-type photocatalysts fabricated by sintering at 1250 °C for 5 h are 4–5 m^2 g^{-1}. The band gap energies estimated from UV–VIS diffuse reflectance spectra of all catalysts are in the UV energy region of 3.1–4.3 eV. A

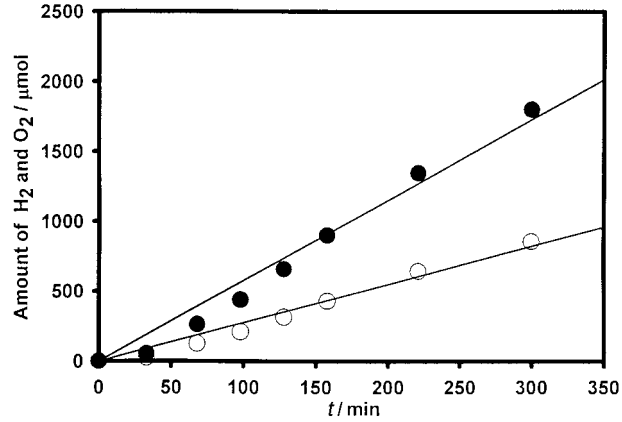

Fig. 1 Time courses of H_2 (●) and O_2 (○) evolution from distilled water over Ni (1.0 wt%)/$Sr_2Nb_2O_7$.

Table 1 Physical properties, H_2 evolution rates and quantum yields for various photocatalysts

Catalyst[a]	BET surface area/m^2 g^{-1}	Band gap/eV	Second harmonic generation	Rate of H_2 evolution/μmol h^{-1}	Quantum yield (%)
$Ca_2Nb_2O_7$	4.2	4.3	Yes	101	7 (< 288 nm)
$Sr_2Nb_2O_7$	5.1	4.1	Yes	402	23 (< 300 nm)
$La_2Ti_2O_7$	5.2	3.2	No	441	12 (< 360 nm)
$La_4CaTi_5O_{17}$	4.9	3.8	No	499	20 (< 320 nm)
TiO_2	50.0	3.1	—	0.3	< 1 (< 360 nm)
$K_4Nb_6O_{17}$	4.5	3.3	No	210	5 (< 360 nm)
$KBa_2Ta_3O_{10}$	4.2	3.5	No	150	8 (< 350 nm)

[a] All perovskite-type catalysts were loaded with Ni [1.0 wt% for (110) layered materials and 0.1 wt% for (100) layered materials] while 1.0 wt% Pt was loaded onto TiO_2.

second harmonic generation (SHG) in $Ca_2Nb_2O_7$, $La_2Ti_2O_7$ and $K_4Nb_6O_{17}$ ceramics was checked by using a fundamental wave of a pulsed Nd^{3+}:YAG laser at wavelength of 1064 nm as the incident light since $Sr_2Nb_2O_7$ is a known non-linear optical material showing SHG.[8] Although a SHG was clearly observed in $Ca_2Nb_2O_7$, $La_2Ti_2O_7$ and $K_4Nb_6O_{17}$ ceramics exhibited no SHG.

It is clear that (110) layered perovskite catalysts are, as a group, much more active than previously known (100) layered perovskite or bulk-type TiO_2 for the photocatalytic decomposition of water into H_2 and O_2 under UV irradiation. The rate of H_2 evolution over Pt/TiO_2 was a mere 0.3 μmol h^{-1}. Dramatic improvement is observed for Ni-doped (100) layered perovskites and still further for (110) layered perovskites. The quantum yield of H_2 evolution over photocatalysts was estimated by using the chemical actinometer ferrioxalate[9] [$Fe(C_2O_4)_3^{3-}$] based on known photon absorbance during the reduction of Fe^{3+} to Fe^{2+}. The quantum yield is the more meaningful parameter than the rate of H_2 evolution itself to gauge the performance of a photocatalyst because the rate is normalized against the absorbed photons. The photon flux from the UV lamp varies depending on the wavelength and, hence, the quantum yield is not necessarily proportional to the rate of H_2 production when semiconductors of different band gaps are used as catalysts. Yet, it is again clear that (110) layered perovskite materials are superior to previously known photocatalysts also in terms of the quantum yield. In fact, to the best of our knowledge, the quantum yield of 23% is the highest among reported semiconductor photocatalysts for overall water splitting. The quantum yield of 5% for $K_4Nb_6O_{17}$ is in agreement with the previous reports for the same material.[5,6]

Examination of quantum yields listed in Table 1 reveals that the superior performance of $A_mB_mO_{3m+2}$ (m = 4,5) is general and not limited to one specific composition. Probably, their structure is important for photocatalytic activity. Compounds with structures that are composed of slabs with distorted perovskite-type atomic configurations are classifed into two groups according to the geometrical relations of the slabs to the perovskite structure.[10] The slabs in (100) layered perovskites[11,12] are obtained by cutting the perovskite structure parallel to (100) and those in (110) layered perovskites[13] are parallel to (110).

As mentioned, (100) layered perovskites[5,6] or tunnel structures[7] have received attention recently since they are much more active than the generally used TiO_2 or $SrTiO_3$ for photocatalytic water splitting. The high activity of these materials has been attributed to effective utilization of interlayer space as reaction sites. We have discovered that the (110) layered perovskites of $A_mB_mO_{3m+2}$ (m = 3, 4; A = Ca, Sr, La; B = Nb, Ti) are still more active with unprecedentedly high quantum yields. These novel photocatalysts are of a layered structure and hence the contribution of interlayer space as reaction sites is expected as in (100) layered perovskite materials. Yet, we have to consider other factors to account for the further increased quantum yields.

If the TiO_2 component of $CaTiO_3$ or $SrTiO_3$ with the ideal perovskite structure is completely replaced by Nb_2O_5, the product is $Ca_2Nb_2O_7$ or $Sr_2Nb_2O_7$. The replacement of Ti^{4+} by Nb^{5+} results in excess electrons and slabs of a distorted perovskite structure of m unit cells thick in order to accommodate excess oxygen.[13] This also occurs when Ca^{2+} or Sr^{2+} is replaced by La^{3+} as in $La_2Ti_2O_7$. This structural substitution gives highly donor-doped (110) layered perovskite materials $A_4B_4O_{14}$, commonly denoted as $A_2B_2O_7$. When a part of the oxygen is lost, the next structure $A_5B_5O_{17}$ in the series is obtained as in $La_4CaTi_5O_{17}$. In the photocatalytic water splitting over a semiconductor, excited electron–hole pairs are generated when the catalyst is illuminated with light having energy equal to or greater than the band gap. The principal challenge is how to suppress the energy-wasteful recombination of the formed electron–hole pairs. Recombination is usually much more facile than the subsequent steps needed for water cleavage. In a semiconductor–liquid interface, the electron–hole pairs are separated by the electric field present in the depletion layer. It is expected that the highly donor-doped (110) perovskite would create a narrower depletion layer than undoped perovskite as is observed for metal-ion doped TiO_2.[14] Band bending would then take place on a depletion layer with a narrower width or become more drastic.[15] Finally, the increased band bending would allow more efficient charge separation and enhance the overall quantum yield of water splitting.

This work has been supported by LG Corporate Institute of Technology.

Notes and references

1 A. Fujishima and K. Honda, *Nature*, 1972, **238**, 37.
2 D. Duonghong, E. Borgarello and M. Gratzel, *J. Am. Chem. Soc.*, 1981, **103**, 4685.
3 T. C. Liu, G. L. Griffin and S. S. Chan, *J. Catal.*, 1985, **94**, 108.
4 S. J. Sato and J. M. White, *J. Phys. Chem.*, 1981, **85**, 336.
5 K. Domen, A. Kudo and A. Shinozaki, *J. Chem. Soc., Chem. Commun.*, 1986, 356.
6 K. Sayama, H. Arakawa and K. Domen, *Catal. Taday*, 1990, **28**, 175.
7 Y. Inoue, T. Niiyama and Y. Asai, *J. Chem. Soc., Chem. Commun.*, 1992, 579.
8 A. W. Sleight, F. C. Zumsteg and J. R. Barkley, *Mater. Res. Bull.*, 1978, **13**, 1247.
9 J. Granifo and G. Ferraudi, *J. Phys. Chem.*, 1985, **10**, 1206.
10 N. Ishizawa, F. Marumo and T. Kawamura, *Acta Crystallogr., Sect. B*, 1975, **31**, 1912.
11 S. N. Ruddlesden and P. Popper, *Acta Crystallogr.*, 1958, **10**, 54.
12 M. Dion, M. Gann and M. Tournoux, *Mater. Res. Bull.*, 1981, **16**, 142.
13 D. M. Smyth, D. Liu and X. Yao, *Mater. Res. Bull.*, 1992, **27**, 387.
14 J. Kiwi, in *Homogeneous and Heterogeneous Photocatalysis*, ed. E. Pelizzetti and N. Serpone, D. Reidel, Dordrecht, 1986, p. 275.
15 M. Schiavello and A. Sclafani, in *Photocatalysis; Fundamentals and Applications*, ed. N. Serpone and E. Pelizzetti, John Wiley & Sons, New York, 1989, p. 159.

Communication 9/02892G

Nitration of cyclic vinylsilanes with acetyl nitrate: effect of silyl moiety and ring size

Govindagouda S. Patil and Gopalpur Nagendrappa*

Department of Chemistry, Bangalore University, Bangalore 560001, India. E-mail: nagendrappa@mailcity.com

Received (in Cambridge, UK) 25th March 1999, Accepted 4th May 1999

Reaction of $AcONO_2$ with common ring vinylsilanes gives the corresponding α,β-unsaturated 1-nitrocycloalkenes, and with medium and large ring vinylsilanes it produces novel 1,1-dinitro 2-nitrates.

The reaction of $AcONO_2$ with olefins leads to a plethora of products, which include isomeric nitro acetates, nitro nitrates and nitroalkenes.[1,2] However, the desired α,β-unsaturated nitroalkenes are obtained at best as only very minor products or not at all.[3] The results have been rationalized by proposing an oxazetidine intermediate, a [2 + 2] cycloadduct of a nitryl cation with an olefin.[1] Because of the well-known propensity of vinylsilanes to undergo regiospecific electrophilic substitution,[4] we considered that they could be nitrated[5] to the synthetically versatile α,β-unsaturated nitroalkenes.[6] This has now been realized in the case of common ring vinylsilanes. However, the medium and large ring vinylsilanes give different but interesting and novel products.

The nitration procedure is very simple. The cyclic vinylsilane (2.5 mmol) in CH_2Cl_2 (2 ml) at −15 °C was treated dropwise with $AcONO_2$[7] (5 mmol). After stirring the mixture for about half an hour (the disappearance of the vinylsilanes was monitored by GC), water was added and the mixture worked up in the usual manner. The products were purified by silica gel chromatography [2% EtOAc–light petroleum (bp 60–65 °C)].

For the present study, a series of 1-trimethylsilylcycloalkenes consisting of three common rings (**1**–**3**), one medium ring (**4**) and one large ring (**5**, a 1 : 1 mixture of *cis* and *trans* isomers) was employed.[8] The three common ring vinylsilanes **1**–**3** gave, in moderate to good isolated yields, the corresponding 1-nitrocycloalkenes **6**–**8** (Scheme 1), which were identical to authentic compounds.[3,5] No other products were detected in any of these cases.

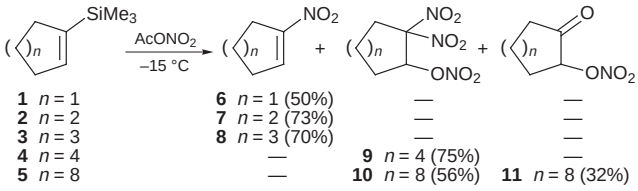

1 *n* = 1 — **6** *n* = 1 (50%) — —
2 *n* = 2 — **7** *n* = 2 (73%) — —
3 *n* = 3 — **8** *n* = 3 (70%) — —
4 *n* = 4 — — **9** *n* = 4 (75%) —
5 *n* = 8 — — **10** *n* = 8 (56%) **11** *n* = 8 (32%)

Scheme 1

1-Trimethylsilylcyclooctene **4** produced a single solid product, which was identified as 2,2-dinitrocyclooctyl nitrate **9**. 1-Trimethylsilylcyclododecene **5** (a 1 : 1 mixture of *cis* and *trans* isomers) gave a 2 : 1 mixture of the dinitro nitrate **10** and the keto nitrate **11** (Scheme 1), which were separated by repeated fractional crystallization from light petroleum (bp 60–65 °C). Compounds **9**–**11** were characterized by their spectral and elemental analysis data.[9] The expected 1-nitrocycloalkenes were not detected in either of these cases. This is in stark contrast to the results of nitration of cyclooctene, which was found to behave like the common ring cycloalkenes.[1]

The smooth conversion of the cyclic vinylsilanes **1**–**3** to the corresponding 1-nitrocycloalkenes **6**–**8** as the sole products is strikingly dissimilar to the complex results obtained in the nitration of their unsilylated analogues.[1] This clearly underlines the powerful influence of silicon in directing this transformation. The apparently different results from the medium and large ring vinylsilanes **4** and **5** can also be attributed to control by the silicon moiety.

All the results of $AcONO_2$ reaction with the cyclic vinylsilanes **1**–**5** can be rationalized by a mechanistic scheme involving the initial formation of a [2 + 2] cycloaddition intermediate **12**–**16** (Scheme 2), following the proposal of Borisenko *et al.* who based it on theoretical calculation and experimental results of $AcONO_2$ reaction with cycloalkenes.[1]

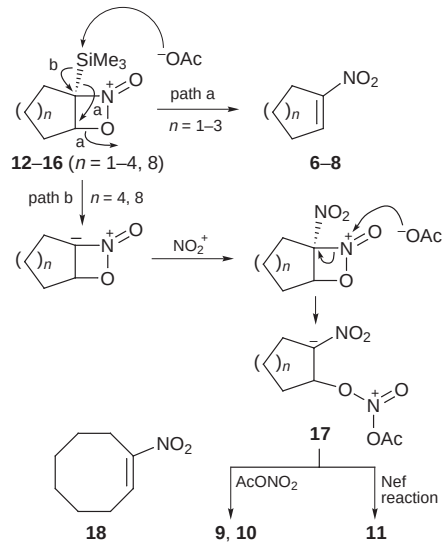

Scheme 2

In the present case, the regiospecificity is presumed to arise from the well-known β-silicon effect[4] which directs the electrophile NO_2^+ to attack the α position. Since the loss of silicon is more rapid than that of a β-proton in the β-elimination reactions of β-silicon-containing substrates, the further transformation of **12**–**16** is guided by this process. The β-elimination in **12**–**16** to the nitroolefinic products **6**–**8** occurs if silicon and the β-leaving group (C–O bond) attain the antiperiplanar geometry,[10] which is achieved when the carbocycles in **12**–**16** have the required conformation (*e.g.* cyclohexane in the chair form with α-C–$SiMe_3$ and β-C–O bonds being axial-axial *trans*). All the intermediates **12**–**16** from the vinylsilanes **1**–**5** can accommodate this conformational demand, but only those (**12**–**14**, *n* = 1–3) from the common ring vinylsilanes eventually lead to the 1-nitrocycloalkenes **6**–**8** (Scheme 2, path a). In the case of medium and large rings, the more rapid changes in their conformations and transannular interactions[10] probably diminish the life-time of the crucial conformation in which silicon and the leaving group are antiparallel to such an extent that the intermediate takes a different route to give the observed products (Scheme 2, path b).

We verified and confirmed that **9** is not formed from **4** *via* 1-nitrocyclooctene **18**. When **18**, prepared by a literature procedure,[11] was treated with $AcONO_2$ under conditions identical to those used for the nitration of **4**, the starting

nitrocycloalkene **18** was recovered intact. We presume that the formation of **10** from **5** follows a similar route.

Additional evidence for this mechanistic scheme is the fact that no 1,2-nitro acetate, 1,2-nitro nitrate or transannular products are produced from any of the cyclic vinylsilanes **1**–**5**, unlike the reported results of the nitration of cycloalkenes under similar conditions.[1]

The formation of the keto nitrate **11** is likely to be due to a Nef-type transformation[12] of a possible intermediate **17**, which can also give the dinitro nitrate.

Our work demonstrates that nitration of cyclic vinylsilanes can be accomplished, though the nature of the products is dependent on the ring size, in that the common rings give the 1-nitrocycloalkenes and rings larger than seven-membered rings will produce novel dinitro nitrates.

The authors thank the DST and the CSIR, New Delhi, for financial support of this work and a fellowship to GSP. Some of the equipment used in this work was donated by the Alexander von Humboldt Foundation, Germany.

Notes and references

1 A. A. Borisenko, A. V. Nikulin, S. Wolfe, N. S. Zefirov and N. V. Zyk, *J. Am. Chem. Soc.*, 1984, **106**, 1074 and references cited therein.

2 G. A. Olah, R. Malhotra and S. C. Narang, *Nitration : Methods and Mechanisms*, VCH, New York, 1989.

3 For some of the procedures for the preparation of 1-nitroalkenes, see J. R. Hwu, K.-L. Chen and S. Ananthan, *J. Chem. Soc., Chem. Commun.*, 1994, 1425; S. E. Denmark and L. R. Marcin, *J. Org. Chem.*, 1993, **58**, 3850; A. Kamimura, T. Kawai and A. Kaji, *J. Chem. Soc., Chem. Commun.*, 1987, 1550; E. J. Corey and H. Estreicher, *J. Am. Chem. Soc.*, 1978, **100**, 6294; R. Ballini and C. Palestini, *Tetrahedron Lett.*, 1994, **35**, 5731; R. S. Varma, R. Dahiya and S. Kumar, *Tetrahedron Lett.*, 1997, **38**, 5131.

4 B. Chiavarino, M. E. Crostoni and S. Fornarini, *J. Am. Chem. Soc.*, 1998, **120**, 1523; J. B. Lambert, *Tetrahedron*, 1990, **46**, 2677; S. G. Wierschke, J. Chandrasekhar and W. L. Jorgensen, *J. Am. Chem. Soc.*, 1985, **107**, 1496; J. S. Panek, *Comprehensive Organic Synthesis*, ed. B. M. Trost, Pergamon, London, 1991, vol. 1, part 1, p. 579; I. Fleming, A. Barbero and D. Walter, *Chem. Rev.*, 1997, **97**, 2063.

5 An unsuccessful attempt to nitrate cyclic vinylsilanes has been previously reported, but without revealing the details: E. J. Corey and H. Estreicher, *Tetrahedron Lett.*, 1980, **21**, 1113.

6 See for example, M. Ayerbe, A. Arrieta and F. P. Cossio, *J. Org. Chem.*, 1998, **63**, 1795; S. E. Denmark and J. A. Dixon, *J. Org. Chem.*,1997, **62**, 7086; E. Dumez, J. Rodriguez and J.-P. Dulcere, *Chem. Commun.*, 1997, 1831; S. E. Denmark and A. Thorarensen, *Chem. Rev.*,1996, **96**, 137.

7 $AcONO_2$ was prepared by adding 0.375 g of conc. HNO_3 (1.40 density, AR Grade, Merck) to Ac_2O (5 ml, distilled over P_2O_5); see ref. 1.

8 G. Nagendrappa, *Synthesis*, 1980, 704.

9 *Selected data* for **9**: mp 56–58 °C; ν_{max}/cm^{-1} 1652, 1595, 1564; $\delta_H(CDCl_3)$ 6.19 (dd, *J* 7.6 and 1.4, 1H), 2.94–2.63 (m, 2H), 2.45–2.30 (m, 1H), 2.12–1.99 (m, 1H), 1.89–1.77 (m, 4H), 1.59–1.44 (m, 4H); $\delta_C(CDCl_3)$ 121.5 (s), 78.7 (d), 32.3 (t), 30.6 (t), 25.9 (t), 25.8 (t), 24.8 (t), 21.8 (t); $\delta_O(CDCl_3)$ 596.3, 445.2, 352.9; *m/z* 264 (1%, $M^+ + 1$), 171 (3), 95 (37), 81 (34), 67 (37), 55 (72), 46 (100, NO_2^+), 41 (67) (Found: C, 36.73; H, 5.03; N, 16.01. $C_8H_{13}N_3O_7$ requires: C, 36.51; H, 4.98; N, 15.96%). For **10**: mp 80–82 °C; ν_{max}/cm^{-1} 1667, 1595, 1569; $\delta_H(CDCl_3)$ 6.08 (d, *J* 9.9, 1H), 2.58–2.39 (m, 2H), 2.03–1.83 (m, 1H), 1.60–1.28 (m, 17H); $\delta_C(CDCl_3)$ 120.4, 74.9, 32.5, 26.6, 25.6, 25.0, 22.3, 22.1, 22.0, 21.8, 21.6, 19.6 (Found: C, 45.11; H, 6.81; N, 12.83. $C_{12}H_{21}N_3O_7$ requires: C, 45.14; H, 6.63; N, 13.16%). For **11**: mp. 89–91 °C; ν_{max}/cm^{-1} 1729, 1652, 1636; $\delta_H(CDCl_3)$ 5.29 (q, *J* 3.3, 1H), 2.81–2.71 (m, 1H), 2.50–2.40 (m, 1H), 2.14–1.85 (m, 3H), 1.64–0.88 (m, 15H); $\delta_C(CDCl_3)$ 204.3, 85.5, 34.8, 26.2, 26.1, 25.9, 23.7, 22.6, 22.2, 21.8, 21.0, 19.2 (Found: C, 59.05; H, 8.85; N, 5.38.$C_{12}H_{21}NO_4$ requires: C, 59.24; H, 8.70; N, 5.76%).

10 E. L. Eliel and S. H. Wilen, *Stereochemistry of Organic Compounds*, Wiley, New York, 1994, ch. 11, pp. 762–771.

11 W. K. Seifert, *Org. Synth.*, 1988, **Coll. Vol. 6**, 837.

12 J. R. Hwu and B. A. Gilbert, *J. Am. Chem. Soc.*, 1991, **113**, 5917 and references cited therein.

Communication 9/02388G

ChemComm

Formation of the bidentate [$Ph_2SNC(Me)N(H)$] ligand by metal-assisted sulfimide addition to acetonitrile; X-ray crystal structure of [$Pt(Ph_2SNH)(Ph_2SNC(Me)NH)Cl]Cl{\cdot}MeCN$

Paul F. Kelly* and Alexandra M. Z. Slawin

Department of Chemistry, Loughborough University, Loughborough, Leicestershire, UK LE11 3TU. E-mail: P.F.Kelly@lboro.ac.uk

Received (in Basel, Switzerland) 4th March 1999, Accepted 1st May 1999

In contrast to similar reactions of Cu, Co and Pd species, the platinum(II) complex [$Pt(MeCN)_2Cl_2$] reacts with Ph_2SNH (ratio 1 : 2) in MeCN *via* a metal assisted addition of the sulfimide to the acetonitrile to give [$Pt(Ph_2SNH)(Ph_2SNC(Me)NH)Cl]Cl{\cdot}MeCN$, the first example of a complex of the bidentate [$Ph_2SNC(Me)N(H)$] ligand.

As part of our continuing interest in the coordination chemistry of sulfur–nitrogen species[1] we have recently reported on the reactivity of *S*,*S*′-diphenylsulfimide, Ph_2SNH **1**, towards a number of metal centres. For example, during investigations into its reactivity towards $CuCl_2$ we showed that the N-bound 2 : 1 complex, *trans*-[$CuCl_2(Ph_2SNH)_2$], forms readily *via* reaction in MeCN. Though such a product was not unexpected, it proved to be unusual in its ability to crystallise in either square-planar or pseudo-tetrahedral geometries.[2] Such isomerism appears to be unique for a neutral Cu(II) species, indicating that the ligand properties of **1** are not as simple as one might

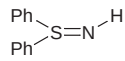

1

imagine. This conclusion is backed up by the observation that [$Co(Ph_2SNH_2)_6]Cl_2$ exhibits strong, concerted, directed hydrogen bonding between both sets of triple N–H units on either side of the coordination octahedron and the chloride counter ions.[3] These results, backed up by the obvious potential of the sulfimides in general as functionalised ligands, prompted us to investigate the coordination chemistry of **1** further by addressing its ability to coordinate to Pt and Pd centers.

Many aspects of the latter chemistry prove to be quite straightforward;[4] thus salts of $[Pd_2X_6]^{2-}$ (X = Cl or Br) form $[PdX_3(Ph_2SNH)]^-$ or [$Pd(Ph_2SNH)_4]X_2$ depending upon reaction stoichiometry while 4 equivalents of **1** react slowly with $[PPh_4]_2[PtCl_4]$ in CH_2Cl_2 to give [$Pt(Ph_2SNH)_4]Cl_2$. There is no evidence from either X-ray crystallographic or IR spectroscopic studies that such products contain **1** as anything other than simple N-bound ligands. During such work, however, we noted that the product of the reaction of **1** with [$Pt(MeCN)_2Cl_2$] (ratio 2 : 1) in acetonitrile† generated crystalline material the IR spectrum of which was unusual in that it exhibited a very strong, broad N–H peak at 3071 cm^{-1} (of the type we have more usually seen associated with cationic sulfimide complexes) and extra bands not normally associated with the Ph_2SNH ligand (at 1540, 1249 and 807 cm^{-1}). As such data were not consistent with the simple formulation [$Pt(Ph_2SNH)_2Cl_2$] we investigated the complex by X-ray crystallography.‡

The structure obtained for **2** (which includes an acetonitrile of solvation) is shown in Fig. 1. Although two of the four coordination sites on the platinum contain expected ligands (N-bound **1** and a chloride) the other two sites are taken up by the nitrogen and sulfur atoms of a chelating [$Ph_2SNC(Me)N(H)$] ligand. Close inspection of the latter and the overall metallocycle of which it is part reveals a number of important points about the reaction and its product. First of all it is clear that during the course of the reaction one of the sulfimide units has added to an acetonitrile and completed the metallocycle by binding to the platinum through a sulfur. Within this metallocycle the S–N distance appears to be virtually identical to that in the unreacted, coordinated sulfimide ligand (1.625 *cf.* 1.618 Å) indicating that this may be best represented as a double bond. Of the two C–N bonds one, N(14)–C(13), is significantly shorter than the other (1.302 *cf.* 1.358 Å) indicating a higher bond order. Thus we can approximate the bonding within the neutral ligand to N(H)=C(Me)N=SPh_2 though as with most sulfimide systems this obviously constitutes something of an over simplification. Bond distances and angles within the coordinated unreacted sulfimide unit are not significantly different to those noted in other complexes of **1**. A point of note about the structure comes with the fact that there are significant H-bonding interactions between the two N–H bonds and the free chloride (average of the two H···Cl distances being 2.26 Å). It is possible that this is a contributory factor in the significant deviation of the N(2)–Pt–S(1) angle from linear (167.6°). In the light of this structure the unexpected IR spectrum may be explained; the strong N–H band comes about thanks to the hydrogen bonding in the system, while the other bands may be assigned to C–N stretches and deformations. The structure is also backed up by the ^1H and ^{13}C NMR data (the latter, for example, showing the CH_3–C carbons at δ 19.0 and 183.6 respectively). One final important feature of the structure comes from the fact that it constitutes the first example of a sulfimide unit binding through the sulfur atom as opposed to the nitrogen.

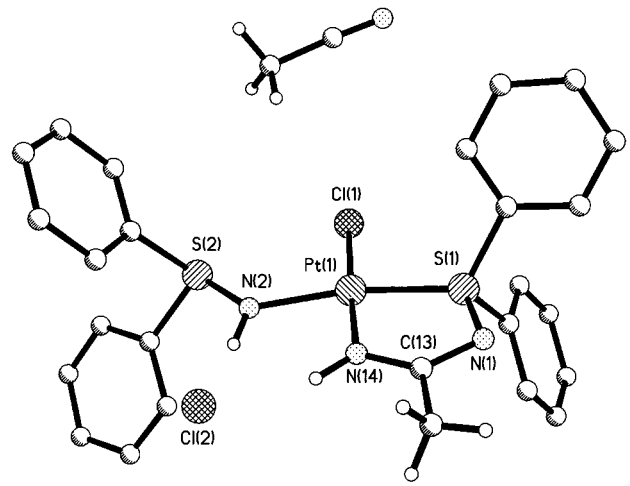

Fig. 1 X-Ray crystal structure of **2**·MeCN. Selected bond distances (Å) and angles (°): Pt–S(1) 2.1876(12), S(1)–N(1) 1.625(4), N(1)–C(13) 1.358(6), C(13)–N(14) 1.302(6), N(14)–Pt 1.989(4), Pt–Cl(1) 2.3191(14), Pt–N(2) 2.012(4), N(2)–S(2) 1.618(4); Pt–S(1)–N(1) 106.7(2), S(1)–N(1)–C(13) 110.8(3), C(13)–N(14)–Pt 119.1(3), N(2)–Pt–S(1) 167.56(14), N(2)–Pt–Cl(1) 94.36(14), Cl(1)–Pt–S(1) 97.84(5), N(2)–Pt–N(14) 87.8(2), Pt–N(2)–S(2) 127.5(3).

A number of aspects of this reaction are noteworthy. One important feature is that it can be repeated using $Pt(MeCN)_2Cl_2$ in CH_2Cl_2; in this case it is clear that coordinated MeCN ligands must be reacting as we no longer have the excess of the ligand in the form of the solvent. Additionally, it should be noted that **1** does not react with MeCN in the absence of the metal centre. Thus the solid retrieved after removal of the solvent from a solution of **1** in MeCN after stirring for 1 h at either ambient temperature, or indeed at reflux temperature, has an identical IR spectrum to the starting material. The choice of metal is also crucial; as we have already noted we have seen no evidence of this type of reaction occurring during reactions involving Co and Cu and attempts to observe analogous reactions using $Pd(MeCN)_2Cl_2$ or $[Pd(MeCN)_4][BF_4]_2$ also fail. Thus the reaction would appear to be specific to Pt, at least amongst the aforementioned metals. This brings us to the question of the reaction mechanism. It is possible that the first stage of the reaction involves coordination of one **1** ligand followed by reaction with the remaining coordinated MeCN. At present we regard this as a less likely option as it implies that coordination to the metal is activating the sulfimide towards attack by MeCN. If this were the case one might suspect that $[Pt(Ph_2SNH)_4]Cl_2$ (from **1** + $[PPh_4]_2[PtCl_4]$ in CH_2Cl_2) would be prone to reaction with this solvent; in fact it can be dissolved in boiling MeCN and, after precipitation by cooling, shows no change in its IR spectrum. In addition it should be remembered that **2** exhibits one unreacted sulfimide ligand. The other possible route involves nucleophilic addition of the sulfimide to the nitrilic carbon followed by proton transfer and coordination of the sulfur *via* loss of the remaining MeCN. This is conceptually a very simple route, the only drawback coming from the fact that it would require the sulfimide/acetonitrile addition to be faster or more efficient than simple substitution. Some justification for this comes with the observation that platinum appears to be less effective (or at least slower) at binding **1** than lighter metals. Thus while conversion of $[Pd_2X_6]^{2-}$ to $[Pd(Ph_2SNH)_4]X_2$ takes place in a matter of minutes, $[Pt(Ph_2SNH)_4]Cl_2$ only forms from $[PPh_4]_2[PtCl_4]$ over the course of many days. In addition, the $[Pt(PMe_2Ph)_2(Ph_2SNH)Cl]^+$ cation forms a solution equilibrium with $Pt(PMe_2Ph)_2Cl_2$ upon addition of Cl^-.[4] We thus favour the second of the two reaction mechanisms; this conclusion is backed up by the fact that nucleophilic addition to coordinated nitriles is well documented.[5] It should also be noted that preliminary work indicates that this reaction can be mirrored for other nitriles such as propionitrile and benzonitrile.

The metallocycle formed in this reaction is a very rare example of a transition metal based MNCNS cyclic system; indeed there would only appear to be one other example of such a unit characterised by X-ray crystallography, namely that found in $[Pt\{PhSNC(MeC_6H_4)NNC(MeC_6H_4)NSPh\}(PPh_3)]$,[6] though here it is a part of a tridentate ligand system (the X-ray structure of recently formed $[Pt\{N(H)C(Ph)N(H)S\}(dppe)]^+$ was not reported, though the species does indeed contain the cyclic PtNCNS unit[7]). In fact we can extend this further and say that with the exception of cases where X = S (the very well known and much studied dithiadiazolyls) the *only* other structure of the type *cyclo*-XNCNS to be found in a search of the Cambridge Structural Database[8] is one in which X = O.[9]

To conclude, we can say that the reaction of $Pt(MeCN)_2Cl_2$ with **1** provides an efficient, high yield route to a very rare structural system, *via* a metal-assisted activation unprecedented for a sulfimide. It is quite feasible that the neutral ligand thus formed will prove to be labile, providing an efficient route to new imine-substituted sulfimide systems; work towards this end is underway.

The authors acknowledge Johnson Matthey for loans of precious metals.

Notes and references

† A solution of $[PtCl_2(MeCN)_2]$ (61 mg, 0.18 mmol) in MeCN (20 ml) was treated with a solution of **1** (71 mg, 0.35 mmol) in the same solvent (5 ml) added over a period of 2 min with stirring. Upon continuous stirring the resulting yellow solution suddenly precipitated a pale yellow solid (time required for precipitation to start varied from experiment to experiment, ranging from < 1 to 10 min; in all cases, however, once started precipitation was very rapid). The mixture was stirred for a further 30 min then allowed to settle whereupon the solvent was decanted, the solid washed with cold MeCN (10 ml) and then Et_2O (10 ml) and dried *in vacuo* to give a pale yellow product. Yield 92 mg, 74%.

Recrystallisation from hot MeCN gave 60 mg (48% based upon original amount of Pd used) of well formed crystalline material, though the solution retained a significant yellow colour even after cooling indicating that some reaction/decomposition had occurred during the heating process, hence the lowering of yield. There was no significant difference in the IR spectra of the crude and recrystallised material. X-Ray crystallography confirmed the formulation as $[Pt(Ph_2SNH)(Ph_2SNC(Me)NH)Cl]Cl$ with no solvated MeCN present, though this X-ray data is not presented in full here. Found: C, 42.6; H, 3.3; N, 5.9%. Calc. for $C_{26}H_{25}Cl_2N_3PtS_2$: C, 44.0; H, 3.6; N, 5.9%. ^{1}H NMR ($CDCl_3$) δ 10.4 (1H, s, NH), 7.99 (8H, m, CH), 7.63 (2H, m, CH), 7.59 (4H, m, CH), 7.50 (6H, m, CH), 2.50 (3H, s, CH_3); ^{13}C NMR ($CDCl_3$) δ 183.6 (NCN), 138.2, 135.7, 134.0, 132.1, 130.0, 129.9, 128.0 (phenyl groups), 19.0 (CH_3).

A similar reaction occurred when $PtCl_2$ was dissolved in hot MeCN (effectively forming the same starting material *in situ*) and then **1** added. In this case recrystallisation gave product with one MeCN of crystallisation {*i.e.* $[Pt(Ph_2SNH)(Ph_2SNC(Me)NH)Cl]Cl\cdot MeCN$} as shown by X-ray crystallography and microanalysis (Found: C, 44.5; H, 3.9; N, 7.6%; Calc. for $C_{28}H_{28}Cl_2N_4PtS_2$: C, 44.8; H, 3.8; N, 7.5%). It is not clear why the two recrystallisations gave solvated and unsolvated materials.

IR spectroscopy confirmed that an identical product is formed if the $Pt(MeCN)_2Cl_2$ reaction is performed in CH_2Cl_2.

‡ *Crystal data* for **2**: all measurements were made on a Siemens SMART diffractometer with graphite monochromated Mo-Kα radiation. Data were collected using small slices: 12830 data collected. $C_{28}H_{28}Cl_2N_4PtS_2$, M = 750.65, monoclinic, space group $P2_1/n$, a = 13.223(1), b = 10.941(1), c = 20.912(1) Å, β = 100.302(1)°, U = 2976.5(1) Å^3, Z = 4, T = 293 K. μ(Mo-Kα) = 5.11 mm^{-1}, λ = 0.71073 Å, F(000) = 1472. R_1 = 0.0268, wR_2 = 0.0486 [$I > 2\sigma(I)$], 4267 independent reflections (4217 observed).

CCDC 182/1247. See http://www.rsc.org/suppdata/cc/1999/1081/ for crystallographic files in .cif format.

1 P. F. Kelly, A. M. Z. Slawin and A. Soriano-Rama, *J. Chem. Soc., Dalton Trans.*, 1996, 53 and references therein.
2 P. F. Kelly, A. M. Z. Slawin and K. W. Waring, *J. Chem. Soc., Dalton Trans.*, 1997, 2853.
3 P. F. Kelly, A. M. Z. Slawin and K. W. Waring, *Inorg. Chem. Commun*, 1998, **1**, 249.
4 P. F. Kelly, A. C. Macklin, A. M. Z. Slawin, K. W. Waring and R. Yates, in preparation.
5 B. N. Storhoff and H. C. Lewis, *Coord. Chem. Rev.*, 1977, **23**, 1; S. J. Bryan, P. G. Huggett, K. Wade, J. A. Daniels and J. R. Jennings, *Coord. Chem. Rev.*, 1982, **44**, 149.
6 T. Chivers, K. McGregor and M. Parvez, *J. Chem. Soc., Chem. Commun.*, 1993, 1021.
7 N. Feeder, R. J. Less, J. M. Rawson and J. N. B. Smith, *J. Chem. Soc., Dalton Trans.*, 1998, 4091.
8 3D Search and Research Using the Cambridge Structural Database, F. H. Allen and O. Kennard, *Chem.-Des. Automat. News*, 1993, **8**, 1; 31.
9 J. P. Chupp, D. J. Dahm and K. L. Leschinsky, *J. Heterocycl. Chem.*, 1975, **12**, 485.

Communication 9/01783F

A versatile synthetic strategy for construction of large oligomers: binding and photophysical properties of a nine-porphyrin array

Chi Ching Mak,[a] Didier Pomeranc,[a] Marco Montalti,[b] Luca Prodi[b] and Jeremy K. M. Sanders*[a]

[a] *Cambridge Centre for Molecular Recognition, University Chemical Laboratory, Lensfield Road, Cambridge, UK CB2 1EW. E-mail: jkms@cam.ac.uk*

[b] *Dipartimento di Chimica 'G. Ciamician', Università degli Studi di Bologna, I-40126 Bologna, Italy*

Received (in Cambridge, UK) 19th January 1999, Accepted 6th May 1999

Mitsunobu coupling of a free base porphyrin tetraacid with four equivalents of a monohydroxy metalloporphyrin dimer leads to a highly non-polar dendritic nine-porphyrin array that is readily separated from more polar products resulting from incomplete coupling; photophysical measurements reveal an energy transfer process from the peripheral metalloporphyrins to the central free-base porphyrin unit.

Covalently-linked dendritic arrays of porphyrins are of interest for their photophysical and electrochemical properties, but they present a substantial synthetic challenge.[1,2] In particular, the chromatographic separation of successive generations, or of incomplete generations, becomes increasingly difficult. One solution has centred on the control of the chromatographic properties of the products, by varying the peripheral groups of the porphyrins between generations.[2] We now present a more versatile strategy based on Mitsunobu coupling of alcohols and acids to give esters.[3,4] The key feature of this approach is the simultaneous Mitsunobu couplings of a multi-acid (or multi-alcohol) central core with several peripheral components, giving only one non-polar product; any incompletely coupled products will be significantly more polar and therefore easily separated. Here, we illustrate the strategy by describing the synthesis, binding and photophysical properties of the flexible nine-porphyrin array **1**. In the following communication[5] we apply the same strategy to a mixed-metal 'star-shaped' porphyrin pentamer.

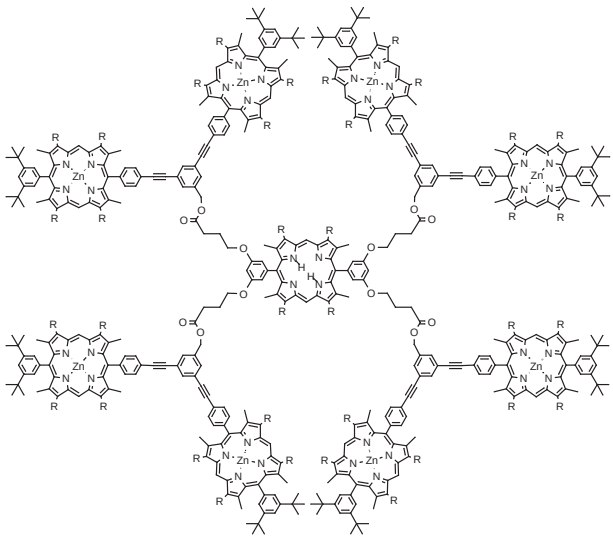

1 R = *n*-hexyl

The key to the synthesis of **1** is the availability of the appropriately-functionalised porphyrin tetra-acid **2** and porphyrin dimer **3**. In order to avoid solubility problems, all the porphyrin units in **1** have the same hydrophobic methyl and hexyl β-substitution pattern. Preparation of the porphyrin tetra-acid **2** involves condensation of aldehyde **4** with dipyrromethane **5** (generated *in situ*) followed by base hydrolysis. Recrystallisation from methanol gave pure **2**† in 21% overall yield. Unlike most other porphyrin acids, **2** is soluble in organic solvents such as THF or acetone. The synthesis of porphyrin dimer **3** has been reported previously.[2] Mitsunobu condensation of **2** with 4 equiv. of **3** in THF afforded **1**† in 69% yield as a purple solid which was easily separated from incompletely coupled side products and unreacted **2** and **3** by silica gel chromatography. Diagnostic resonances in the ^{1}H NMR spectrum of **1** are identified at $\delta -2.34$ for the inner NH protons, and at δ 5.00 for the eight benzylic protons of the peripheral units. Additional confirmation for the preparation of **1** was obtained by a peak at *m/z* = 10045 in the MALDI-TOF spectrum (M_r $C_{664}H_{846}N_{36}O_{12}Zn_8$ = 10047).

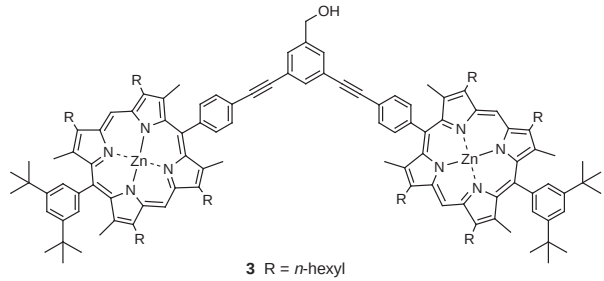

3 R = *n*-hexyl

As in the less flexible nine-porphyrin array that we reported earlier,[2] the rigid porphyrin dimer moieties in **1** can be brought together by cooperative binding to the bidentate ligand diazabicyclo[2.2.2]octane (DABCO). Titration of DABCO with **1** [Fig. 1(a)] gives a characteristic Soret maximum at 420 nm which is due to exciton coupling between the parallel porphyrin units.[6] This exciton-coupled maximum was attained with *ca.* 10 equiv. of DABCO, which is comparable to the less-flexible nine-porphyrin array we described earlier.[2] However, the present flexible system is effectively unfolded again by $< 10^4$ equiv. of DABCO, rather than the 10^6-fold excess required by the rigid system. This reflects the larger number of conformations available to the more flexible system. Exciton-

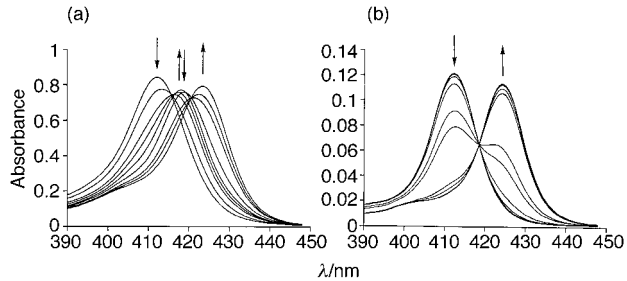

Fig. 1 UV–VIS titration (CH_2Cl_2) of DABCO (as a 2–4 × 10^{-4} M solution) *vs.* (a) **1** (number of equiv. added per nine-porphyrin array: 0, 1.1, 2.3, 4.0, 10.8, 22.7, 680, 1814, 7940) and (b) **3** (both as 2–5 × 10^{-7} M solutions).

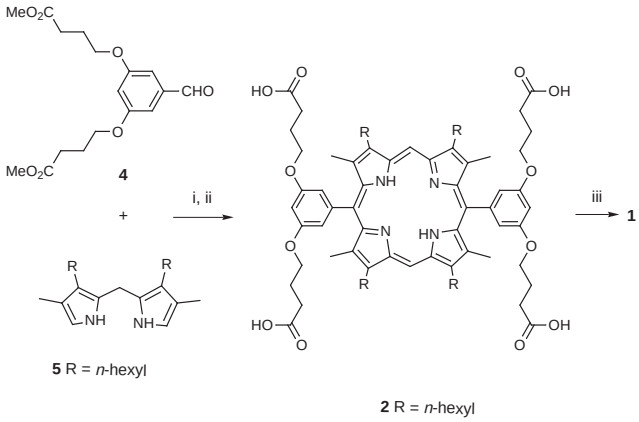

Scheme 1 *Reagents and conditions*: i, TFA (−20 °C to room temp.), DDQ; ii, Na_2CO_3 (water–THF–ethanol), reflux; iii, **3** (4 equiv.), DEAD, PPh_3.

coupled spectra are not observed when the rigid porphyrin dimer **3** is titrated with DABCO [Fig. 1(b)].

The absorption spectrum of **1** approximates a superposition of the spectra of the constituent monomeric porphyrins, suggesting a relatively weak electronic interaction between the porphyrins. The fluorescence quantum yield of **3** (Φ_f = 0.035, τ = 1.6 ns, 298K) is nearly identical to that of the monomeric porphyrin precursors, indicating the absence of quenching processes. The luminescence properties of **1** indicate that both the fluorescence quantum yield and lifetime of the singlet excited state of the Zn porphyrin units are reduced 2.5 fold at 298 K relative to a monomeric Zn porphyrin. Furthermore, excitation spectra demonstrate a parallel sensitization of the fluorescence of the free base porphyrin by the Zn porphyrin. These results show that energy is transferred[7] from the peripheral units to the core with *ca.* 60% efficiency ($k_{ET} = 9 \times 10^8\ s^{-1}$). The transferred energy is subsequently emitted by the core free base porphyrin (Φ_f = 0.10) with an efficiency nearly identical to that of a monomeric free base porphyrin. Calculations indicate that the most likely mechanism of energy transfer is the Förster type.[8] The Zn porphyrin phosphorescence of **1** is completely quenched at 77 K, probably because of an energy transfer process to the triplet excited state localised on the central free base porphyrin, the phosphorescence of which is rarely observed.

In summary, we have described a synthetic strategy in which the chromatographic properties of the desired product have been designed to differ from the strarting materials and side products. We have applied this approach to the preparation of a nine-porphyrin array (for which the photophysical properties have been presented), but clearly this methodology has the potential to be generalised for mixed metal systems[4] or to other types of dendritic structures.

We thank the EPSRC, Croucher Foundation and MURST for financial support.

Notes and references

† *Selected data* for **2**: anal. Found: C, 71.99; H, 7.98; N, 4.06. Calc. for $C_{76}H_{102}N_4O_{12}$: C, 72.23; H, 8.13; N, 4.43%. δ_H (250 MHz, DMSO-d_6) −2.62 (s, 2H, N*H*), 0.86 [t, *J* 7.2 Hz, 12H, $(CH_2)_5CH_3$], 1.25–1.55 [2 × m, 16H, $(CH_2)_3(CH_2)_2CH_3$], 1.70 [qnt, *J* 7.2 Hz, 8H, $(CH_2)_2CH_2(CH_2)_2CH_3$], 1.90–2.20 [2 × m, 16H, $CH_2CH_2(CH_2)_3CH_3$ and $CH_2CH_2CO_2H$), 2.41 (t, *J* 7.2 Hz, 8H, $CH_2CH_2CO_2H$), 2.62 (s, 12H, pyrrolic CH_3), 3.80–4.20 [m, 8H, $CH_2(CH_2)_4CH_3$], 4.15 (t, *J* 6.4 Hz, 8H, $ArOCH_2CH_2$), 7.00 (t, *J* 2.1 Hz, 2H, Ar*H*), 7.21 (d, *J* 2.1 Hz, 4H, Ar*H*), 10.18 (s, 2H, *meso-H*), 12.12 (s, 4H, CO_2H); δ_C (DMSO-d_6) 14.3, 22.6, 24.8, 26.4, 29.9, 30.6, 31.8, 33.4, 67.6, 96.8, 102.4, 112.8, 118.2, 136.5, 141.0, 143.3, 143.7, 144.7, 159.6, 174.5; UV–VIS (THF): positive FAB *m/z* 1265 [(M+H)$^+$]; λ_{max} (log ε) 408 (5.44), 504 (4.77), 580 (4.69), 538 (4.64), 610 (4.55). **1**: anal. Found: C, 78.46; H, 8.41; N, 4.84. Calc. for $C_{664}H_{846}N_{36}O_{12}Zn_8 \cdot 3H_2O$: C, 78.95; H, 8.50; N, 4.99%. δ_H (250 MHz, $CDCl_3$) −2.34 (s, 2H, N*H*), 0.85–1.00 [m, 108H, $(CH_2)_5CH_3$], 1.25–1.85 [3 × m, 216H, $(CH_2)_2(CH_2)_3CH_3$] 1.55 (s, 144H, *Bu*^{t}), 2.00–2.30 [2 × m, 80H, $CH_2CH_2(CH_2)_3CH_3$ and $CH_2CH_2CO_2$), 2.43 (s, 48H, pyrrolic CH_3), 2.49 (s, 48H, pyrrolic CH_3), 2.61 (t, *J* 7.7 Hz, 8H, $CH_2CH_2CO_2$), 2.78 (s, 12H, core pyrrolic CH_3), 3.60–4.30 [2 × m, 80H, $CH_2(CH_2)_4CH_3$ and $ArOCH_2CH_2$], 5.00 (s, 8H, CO_2CH_2Ar), 7.00–7.10 (m, 2H, core Ar*H*), 7.31–7.39 (m, 4H, core Ar*H*), 7.63–8.15 (overlapping m, 68H, Ar*H*), 10.05 (s, 16H, *meso–H*), 10.31 (s, 2H, *meso–H*); δ_C ($CDCl_3$) 14.2, 14.7, 15.0, 15.6, 22.9, 24.8, 26.7, 26.9, 27.0, 30.1, 30.9, 31.8, 32.1, 33.4, 35.3, 65.3, 67.4, 89.1, 91.1, 97.6, 102.4, 112.9, 117.7, 118.0, 121.0, 122.6, 124.4, 128.1, 130.8, 133.5, 134.5, 136.3, 136.9, 137.5, 138.6, 141.6, 142.6, 143.5, 144.2, 144.6, 145.0, 146.2, 146.5, 147.3, 148.1, 149.8, 159.5, 172.9; UV–VIS (CH_2Cl_2): λ_{max} (log ε) 412 (6.46), 538 (5.19), 576 (4.91).

1 For some covalent porphyrin arrays containing more than five porphyrin units, see: G. M. Dubowchik and A. D. Hamilton, *J. Chem. Soc., Chem. Commun.*, 1987, 293; S. Anderson, H. L. Anderson and J. K. M. Sanders, *J. Chem. Soc., Perkin Trans. 1*, 1995, 2255; D. L. Officer, A. K. Burrell and D. C. W. Reid, *Chem. Commun.*, 1996, 1657; O. Mongin, C. Papamicaël, N. Hoyler and A. Gossauer, *J. Org. Chem.*, 1998, **63**, 5568; H. A. M. Biemans, A. E. Rowan, A. Verhoeven, P. Vanoppen, L. Latterini, J. Foekema, A. P. H. J. Schenning, E. W. Meijer, F. C. de Schryver and R. J. M. Nolte, *J. Am. Chem. Soc.*, 1998, **120**, 11 054; A. Nakano, A. Osuka, I. Yamazaki, T. Yamazaki and Y. Nishimura, *Angew. Chem., Int. Ed.*, 1998, **37**, 3023.

2 C. C. Mak, N. Bampos and J. K. M. Sanders, *Angew. Chem., Int. Ed. Engl.*, 1998, **37**, 3020.

3 O. Mitsunobu, *Synthesis*, 1981, 1; D. L. Hughes, *Org. React.*, 1992, **42**, 335.

4 This strategy has been used effectively for dendrimer syntheses based on small conventional building blocks: see F. Zeng and S. C. Zimmerman, *J. Am. Chem. Soc.*, 1996, **118**, 5326.

5 C. C. Mak, N. Bampos and J. K. M. Sanders, *Chem. Commun.*, 1999, following communication.

6 C. A. Hunter, J. K. M. Sanders and A. J. Stone, *Chem. Phys.*, 1989, **133**, 395; C. A. Hunter, M. N. Meah and J. K. M. Sanders, *J. Am. Chem. Soc.*, 1990, **112**, 5773.

7 Efficient energy transfer from peripheral zinc porphyrins to a central free base porphyrin has been observed in some five-porphyrin arrays: J. Davila, A. Harriman and L. R. Milgrom, *Chem. Phys. Lett.*, 1987, **136**, 427; S. Prathapan, T. E. Johnson and J. S. Lindsey, *J. Am. Chem. Soc.*, 1993, **115**, 7519.

8 T. Förster, *Faraday Discuss. Chem. Soc.*, 1959, **27**, 7.

Communication 9/00513G

Ru(II)-centred porphyrin pentamers as coordination building blocks for large porphyrin arrays

Chi Ching Mak, Nick Bampos and Jeremy K. M. Sanders*

Cambridge Centre for Molecular Recognition, University Chemical Laboratory, Lensfield Road, Cambridge, UK CB2 1EW. E-mail: jkms@cam.ac.uk

Received (in Cambridge, UK) 19th January 1999, Accepted 6th May 1999

Ru(II)-centred porphyrin pentamers have been synthesised with Ni or Zn porphyrins at the peripheral sites; these elaborate systems have been used as building blocks for large porphyrin arrays through their coordination chemistry with bidentate and tetradentate ligands; coordination of a sterically unhindered pentamer to a free-base tetrapyridylporphyrin yields a 21 porphyrin array.

We report here the preparation of covalent Ru-centred porphyrin pentamers which can then be assembled into larger arrays by coordination to multidentate ligands.[1,2] This highly convergent and efficient approach is illustrated with the preparation of an array of 21 porphyrins that contains units in three different metallation states; it is complementary to the fully covalent[3] and photochemical[4] approaches we have reported elsewhere.

Mitsunobu condensation[5] of Ni–porphyrin **1**[6] with porphyrin tetra-acid **2** (0.25 equiv.) in THF afforded the core free-base porphyrin pentamer **3** in 58% yield as a purple solid.† This multiple Mitsunobu strategy ensures that the desired fully-coupled pentamer is the only non-polar product; it is therefore readily isolated and purified. The MALDI-TOF mass spectrum of **1** gave the anticipated MH^+ ion at *m/z* 5185. Metallation of **3** with $Ru_3(CO)_{12}$ in refluxing toluene[7] provided the Ru-centred pentamer **4** as a deep red solid in 66% yield. The lack of reactive functional groups in **3** avoids any significant Ru-mediated side reactions during metallation. The ^{1}H NMR properties and the presence of new peaks at *m/z* 5283 and 10566 in the MALDI mass spectrum corresponding to $[(M - CO)^+]$[8,9] and $[(2M - 2CO)^+]$,[9] confirmed the successful metallation. In an inverted Mitsunobu approach, the core Ru–porphyrin diol **5**[10] was esterified with 2 equiv. of the acid dimer **6**[11] to give the more rigid pentamer **7** in 21% yield. The MALDI-TOF spectrum revealed the expected peaks at *m/z* 5432 $[(M - CO)^+]$ and 10950 $[(2M - 2CO)^+]$.

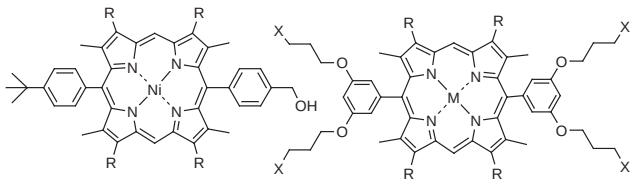

1 = NiPorCH$_2$OH

2 M = 2H; X = CO$_2$H
3 M = 2H; X = CO$_2$CH$_2$NiPor
4 M = Ru^{II}–CO; X = CO$_2$CH$_2$NiPor
9 M = Ru^{II}–CO; X = OH

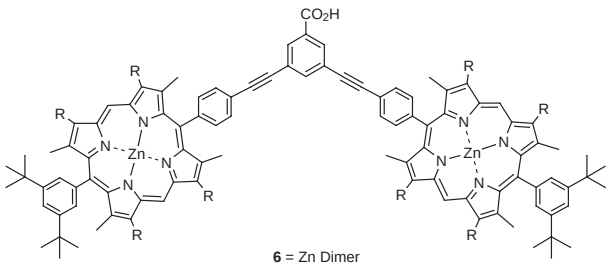

6 = Zn Dimer

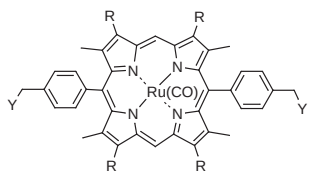

5 Y = OH
7 Y = Zn Dimer

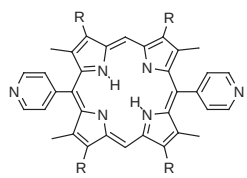

8

R = *n*-hexyl

The central Ru-ion dominates the coordination chemistry of pentamers **4** and **7**, with the strength of binding to N-ligands decreasing in the order Ru ≫ Zn ≫ Ni. Pyridyl ligands, such as those presented in this work, bind very tightly to ruthenium porphyrins, forming rigid well characterisable complexes.[4] However, the extremely high binding affinities make NMR and UV titrations impractical. With this in mind, addition of < 0.5 equiv. of diazabicyclo[2.2.2]octane (DABCO) to a 4–7 mM solution of **4** in $CDCl_3$ leads to exclusive Ru-coordination as shown in Fig. 1(a), where the sharp DABCO chemical shifts in the ^{1}H NMR spectrum are characteristic of the equilibrium between mono- and bi-nuclear porphyrin complexes, in slow exchange on the NMR chemical shift timescale. DABCO is a sufficiently small ligand that steric interaction between the peripheral porphyrins on the two porphyrin pentamers inhibits complete formation of a 10-porphyrin array. Titration of 0.5 equiv. of the larger bridging dipyridyl porphyrin ligand **8** with **4** results in exclusive formation of the 11-porphyrin array **4**·**8**·**4** as judged by the upfield shifts of the NH and pyridyl protons of **8** (as the 2,6-pyridyl protons of **8** shift upfield from δ 9.00 to 1.60, any 1 : 1 complex would be immediately apparent in the spectrum).

Adding a tetra-aryl ruthenium monomer to free-base tetrapyridyl porphyrin indicated that the 0.5 ppm highfield shift of the NH resonance is additive with each coordinated ruthenium monomer (free base $\delta_{NH} = -2.90$, mono-coordinated $\delta_{NH} = -3.35$, di-coordinated $\delta_{NH} = -3.87$, tri-coordinated $\delta_{NH} = -4.30$, tetra-coordinated $\delta_{NH} = -4.92$). The chemical shift of the porphyrin inner NH protons is therefore diagnostic of the number of porphyrins coordinating to the tetradentate porphyrin ligand, so that binding 4 equiv. of monomer **9** shifts the NH signal from $\delta -2.90$ to -4.91, by about 0.5 ppm per equivalent of **9** [Fig. 2(a)]. Reaction of 4 equiv. of rigid pentamer **7** with tetrapyridyl porphyrin gives rise to a high-field resonance at $\delta -4.75$ (Fig. 2(b)] suggesting the formation of a 21-porphyrin array [Fig. 1(b)]. The steric congestion associated with coordination of the more flexible pentamer **4** however, is so great that the product distribution is dominated by the coordination of only three such pentamers about the tetrapyridyl porphyrin, as is apparent by the shift of the NH protons [$\delta -4.25$, Fig. 2(c)]. Preliminary experiments with an extended analogue of tetrapyridyl porphyrin show that, four molecules of

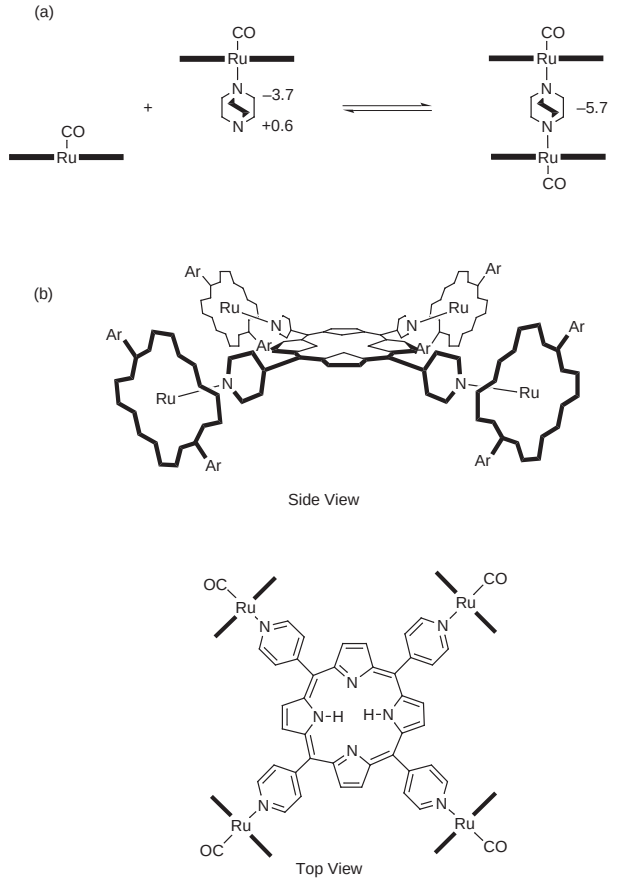

Fig. 1 (a) Equilibria and characteristic chemical shifts observed when Ru(II)–porphyrins bind DABCO; (b) cartoon representations of the assembly formed by coordination of four Ru–porphyrins to tetrapyridylporphyrin.

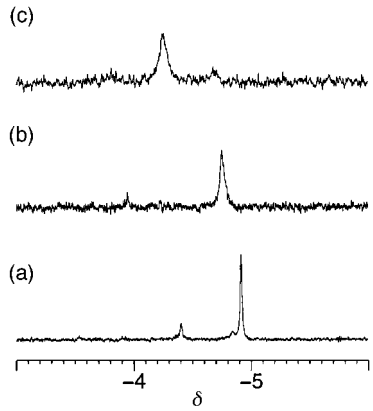

Fig. 2 Selected region of the ^{1}H NMR spectrum (500 MHz, $CDCl_3$, 300 K) showing the NH protons of tetrapyridylporphyrin in the presence of: (a) 4 equiv. of monomer **9**, (b) 4 equiv. of pentamer **7**, (c) 4 equiv. of pentamer **4**.

4 can now be accommodated if the steric constraints can be released, resulting in a NH resonance at δ *ca.* −4.90. The remote porphyrins of **4** and **7** appear to have little effect on the NH chemical shift of the coordinating pyridyl porphyrins.

In summary we have demonstrated that a combination of covalent and coordination chemistry provides a versatile approach for the assembly of very large porphyrin arrays. Elsewhere we show how photolytic removal of the Ru-bound CO ligand, followed by additional ligation can produce even more elaborate arrays.[4]

We thank the Croucher Foundation and the University of Cambridge for financial support and S. L. Darling for a sample of **8**.

Notes and references

† All new compounds gave satisfactory ^{1}H and ^{13}C NMR spectra, MALDI-TOF mass spectra and analytical values. In particular, the ^{1}H NMR spectra of pentamers gave the correct integrated intensities for the four peripheral *vs*. single core porphyrin.

1 For recent reviews of porphyrin arrays, see: C.-T. Chen, in *Comprehensive Supramolecular Chemistry: Coordination Polymers*, ed. J. L. Atwood, J. E. D. Davies, D. D. Macnicol and F. Vögtle, Pergamon Press, New York, 1996, vol. 5, no. 4, pp. 91; J. K. M. Sanders, in *Comprehensive Supramolecular Chemistry: Templated Chemistry of Porphyrin Oligomers*, ed. J. L. Atwood, J. E. D. Davies, D. D. Macnicol and F. Vögtle, Pergamon Press, New York, 1996, vol. 9, no. 4, pp. 131; M. D. Ward, *Chem. Soc. Rev.*, 1997, **26**, 365.

2 For Ru–porphyrin monomers used as a building block towards porphyrin arrays, see: H. L. Anderson, C. A. Hunter and J. K. M. Sanders, *J. Chem. Soc., Chem. Commun.*, 1989, 226; K. Funatsu, A. Kimura, T. Imamura and Y. Sasaki, *Chem. Lett.*, 1995, 765; E. Alessio, M. Macchi, S. Heath and L. G. Marzilli, *Chem. Commun.*, 1996, 1411; K. Funatsu, T. Imamura, A. Ichimura and Y. Sasaki, *Inorg. Chem.*, 1998, **37**, 1798; W. T. S. Huck, A. Rohrer, A. T. Anilkumar, R. H. Fokkens, N. M. M. Nibbering, F. C. J. M. van Veggel and D. N. Reiahoudt, *New. J. Chem.*, 1998, **22**, 165.

3 (*a*) C. C. Mak, N. Bampos and J. K. M. Sanders, *Angew. Chem., Int. Ed.*, 1998, **37**, 3020; (*b*) C. C. Mak, D. Pomeranc, M. Montalti, L. Prodi and J. K. M. Sanders, *Chem. Commun.*, 1999 (preceding communication).

4 S. L. Darling, C. C. Mak, N. Bampos, N. Feeder, S. J. Teat and J. K. M. Sanders, *New. J. Chem.*, 1999, **23**, 359.

5 O. Mitsunobu, *Synthesis*, 1981, 1; D. L. Hughes, *Org. React.*, 1992, **42**, 335.

6 **1** was prepared on a gram scale by mixed condensation of 4-*tert*-butyl- and 4-hydroxymethyl-benzaldehydes with the appropriate pyrromethane followed by metallation. For related syntheses see: A. Vidal-Ferran, N. Bampos and J. K. M. Sanders, *Inorg. Chem.*, 1997, **36**, 6117; Z. Clyde-Watson, A. Vidal-Ferran, L. J. Twyman, C. J. Walter, D. W. J. McCallien, S. Fanni, N. Bampos, R. S. Wylie and J. K. M. Sanders, *New. J. Chem.*, 1998, **22**, 493.

7 M. Barley, J. Y. Becker, G. Domazetis, D. Dolphin and B. R. James, *Can. J. Chem.*, 1983, **61**, 2389.

8 M. Frauenkron, A. Berkessel and J. H. Gross, *Eur. Mass. Spectrom.*, 1997, **3**, 427.

9 In MALDI TOF spectra, Ru(II) CO porphyrins generally give, in addition to an (M − CO) ion, peaks corresponding to the dimer [2M − 2CO]: C. C. Mak and J. K. M. Sanders, to be submitted.

10 **5** was prepared from 4-hydroxymethylbenzaldehyde in an analogous procedure to that reported previously: V. Marvaud, A. Vidal-Ferran, S. J. Webb and J. K. M. Sanders, *J. Chem. Soc., Dalton Trans.*, 1997, 985.

11 Bis-porphyrinic benzoic acid **6** was prepared from 3,5-diiodobenzoic acid in a similar fashion to a previously reported bis-porphyrinic benzyl alcohol.[3a]

Communication 9/00517J

ChemComm

Synthesis of volicitin: a novel three-component Wittig approach to chiral 17-hydroxylinolenic acid

Georg Pohnert,* Thomas Koch and Wilhelm Boland*

Max-Planck-Institut für Chemische Ökologie, Tatzendpromenade 1a, D-07745 Jena, Germany.
E-mail: pohnert@ice.mpg.de

Received (in Liverpool, UK) 10th March 1999, Accepted 22nd April 1999

A short stereoselective synthesis of both enantiomers of *N*-(17-hydroxylinolenoyl)-L-glutamine (volicitin) 12, an elicitor of plant volatile biosynthesis from beet armyworm salivary secretion, is described; the protected 17-hydroxylinolenic acid 4 moiety of volicitin 12 was prepared in a one pot bis-Wittig reaction.

Plants are able to respond to herbivore damage by *de novo* biosynthesis of a characteristic blend of volatiles that attracts the natural enemies of the attacking insect.[1] Feeding on the leaf is accompanied by introduction of salivary secretions that may contain high and/or low molecular weight compounds activating the plant's defense. Established elicitors are a β-glucosidase from the regurgitant of *Pieris brassicae* caterpillars[2] and the recently identified *N*-(17-hydroxylinolenoyl)-L-glutamine (volicitin) **12** from beet armyworm oral secretion.[3] Like the microbial metabolite coronatine, which strongly induces volatile biosynthesis in plants,[4] volicitin **12** is also an amphiphilic compound that consists of a nonpolar lipid moiety joined to an amino acid by an amide linkage. First experiments with synthetic volicitin revealed that biological activity is highly dependent on the stereochemistry of the amino acid.[3] A conjugate of (±)-17-hydroxylinolenic acid and L-glutamine proved to be highly active, while the corresponding conjugate with D-glutamine was virtually inactive. The configuration of the 17-hydroxy group of the fatty acid has not been addressed to date.

Here we report an efficient synthesis of both enantiomers of TBDMS protected 17-hydroxylinolenic acid methyl ester **4** based on a novel three component bis-Wittig approach. Subsequent deprotection and coupling with L-glutamine yielded both volicitin diastereomers (17*R*)- and (17*S*)-**12**, respectively.

According to Scheme 1, the fatty acid skeleton is readily assembled in a single operation *via* a bis-Wittig approach, based on the *Z*-hex-3-ene-1,6-diol-derived symmetric bifunctional Wittig salt **2**.[5] In order to suppress the formation of symmetric by-products **5** and **6**, resulting from statistical coupling of the three components **1**,[6] **2** and **3**, the reaction conditions were carefully optimised. While addition of a 1 : 1 mixture of the aldehydes **1** and **3** to the ylide **9** resulted in the expected statistical product ratio of **4**, **5** and **6**, successive addition of the aldehydes to **9**, in conjunction with optimised temperatures during the stepwise reaction, afforded high yields of the protected 17-hydroxylinolenic acid **4**. This result suggested

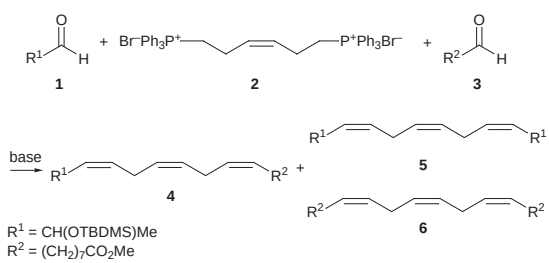

Scheme 1

different reactivity of the bis-functional ylide **9** and the monofunctional intermediates like **10**. Thus, if only 1 equiv. of aldehyde **1** was added to a cold solution (−100 °C) of the bis-ylide **9**, generated from the bis-phosphonium salt with 2.1 equiv. of KHMDS,[7] a preferential formation of the mono-ylide **10** was observed after slow warming to −20 °C. Recooling to −78 °C and addition of 1 equiv. of aldehyde **3** afforded the cross-coupled product **4** in high yield. According to GLC-MS analysis, the amount of the two symmetric products **5** and **6** was less than 20% of the product mixture. Furthermore, the amount of symmetric coupling products could be suppressed even more efficiently by using the aluminium alkoxide **8**, generated by reduction of TBDMS-protected D- or L-lactic acid methyl ester **7** with DIBAL-H at low temperature, as the first carbonyl equivalent (Scheme 2).[8]

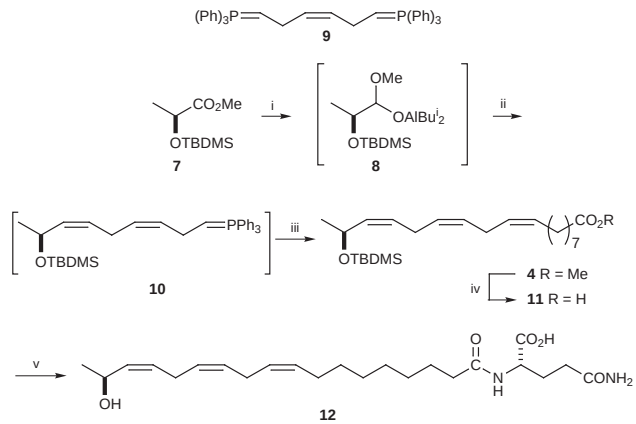

Scheme 2 *Reagents and conditions*: i, DIBAL-H, Et_2O, −78 °C; ii, **9** [prepared from **2** in THF using 2 equiv. $KN(SiMe_3)_2$, −78 to 0 °C], −78 °C, add **8**, warm to room temp.; iii, −78 °C, **3**, warm to room temp.; iv, LiOH, THF–H_2O; v, NEt_3, THF, $ClCO_2Et$, −10 °C, then Gln, NaOH, room temp.

During warming to room temperature, the silylated aldehyde **1** is presumably slowly released from the intermediate aluminium complex **8** and reacts instantaneously with the bis-ylide **9** to give the ylide **10**. After 30 min at room temperature, the solution was recooled (−78 °C), before 1.2 equiv. of the 9-oxo ester **3** were added. Following work-up, the silylated (17*R*)- or (17*S*)-hydroxylinolenic acid **4** could be isolated in 42% overall yield.† Less than 10% of the symmetrical coupling products **5** and **6** could be detected. Use of the configurationally stable aluminium complex **8** had the additional advantage that the sensitive chiral C_3 synthon **1** reacted without racemisation under the basic Wittig conditions. Both products, (17*S*)- and (17*R*)-**4**, proved to be of >97% ee by Mosher ester analysis of the end products (17*S*)- and (17*R*)-**12** (volicitin).‡ ^{13}C NMR analysis revealed the configuration of the 9- and 15-double bonds to be of >95% *Z*.

Saponification of **4** with aqueous LiOH in THF[7] afforded TBDMS protected 17-hydroxylinolenic acid **11** in 86% yield. Coupling of **11** with glutamine was achieved using the ethyl carbonate mixed anhydride method. Acidic workup of the crude

product resulted in simultaneous deprotection, and pure volicitin **4** could be separated from excess glutamine by RP-MPLC-chromatography.§ The significance of the chiral centre for the induction of plant volatile biosynthesis is currently being evaluated. Detailed results together with information on the mode of signaling of the compound will be presented elsewhere.

The three-component Wittig reaction described here opens a new and highly versatile route to the skipped triene substructures occurring in a large variety of natural products. The central building block **2** is readily available on a multi-gram scale,[5] and one-pot product formation with good stereoselectivities allows its universal use as a building block in the synthesis of highly unsaturated fatty acids and related compounds. Like the previously introduced di-n-butyl-1-stannacyclohexa-2,5-diene[9] as a bifunctional building block for the formation of skipped dienes, the bis-Wittig approach also has universal potential, allowing the direct assembly of at least three homoconjugated double bonds from simple precursors in a single operation.

Financial support by the *Deutsche Forschungsgemeinschaft* (SPP 716) Bonn, and the *Fonds der Chemischen Industrie*, Frankfurt, is gratefully acknowledged. We thank the *BASF*, Ludwigshafen, and the *Bayer AG*, Leverkusen, for generous supplies of chemicals and solvents and Dr N. J. Oldham for proof-reading of the manuscript.

Notes and references

† Experimental procedure: A cold (−78 °C) suspension of the Wittig salt **2** (700 mg, 0.91 mmol) in dry THF (15 ml) was treated with $KN(SiMe_3)_2$ in hexane (3.8 ml of a 0.5 M solution). The solution was allowed to warm to 0 °C, stirred for 10 min and recooled (−78 °C). An ethereal solution of the aluminate **8** (2.3 ml, 0.4 M, pre-cooled to −78 °C) was added (ref. 6,8). The mixture was allowed to warm to room temperature and stirring was continued for 1 h before recooling to −78 °C. Then, a solution of **3** (203 mg in 1 ml THF) was added and the mixture was allowed again to reach room temperature. Hydrolysis with sat. NH_4Cl, extraction with Et_2O and column chromatography on SiO_2 yielded the protected ester **4** as a colourless, viscous liquid. Yield: 161 mg (42%).

‡ Both enantiomers of **12** were esterified with excess (*R*)-(−)-α-methoxy-α-(trifluoromethyl)phenylacetyl chloride in the presence of DMAP and Et_3N (ref. 10). After the reaction was complete (no starting material could be detected *via* NMR analysis) the ee of **12** was determined by integration of the isolated 17-hydroxylinolenic acid C(18)-methyl doublet [δ 1.35 for (17*S*)-**12** and δ 1.42 for (17*R*)-**12**].

§ *Selected data* for **12**: $[\alpha]_{589}^{22}$ +3 (*c* 0.83, CH_2Cl_2) [(17*S*)-**12**]; $[\alpha]_{589}^{22}$ −4.0 (*c* 0.82, CH_2Cl_2) [(17*R*)-**12**]; δ_H (CD_3OD, 500 MHz) 5.3–5.17 (m, 6H), 4.50 (dq, 1H, *J* 6.8, 6.36), 4.25 (dd, 1H, *J* 4.8, 3.9), 2.75 (m, 2H), 2.69 (t, 2H, *J* 5.8), 2.21–2.16 (m, 2H), 2.12 (t, 2H, *J* 7.3), 2.07–1.95 (m, 1H), 1.95 (q, 2H, *J* 6.5), 1.87–1.77 (m, 1H), 1.49 (t, 2H), 1.29–1.18 (m, 10H), 1.07 (d, 3H, *J* 6.36); δ_C (CD_3OD, 125 MHz), 176.761, 175.404, 174.169, 134.418, 130.237, 128.657, 128.190, 127.690, 127.680, 63.396, 52.376, 35.867, 31.799, 29.704, 29.339, 29.269, 29.227, 27.623, 27.177, 25.868, 25.787, 25.519, 22.970. See ref. 3 for mass spectroscopic data.

1 M. K. Stowe, T. C. J. Turlings, J. H. Loughrin, W. J. Lewis and J. H. Tumlinson, *Proc. Natl. Acad. Sci. U.S.A.*, 1995, **92**, 23 and references cited therein.
2 M. L. Mattiacci, M. Dicke and M. A. Posthumus, *Proc. Natl. Acad. Sci. U.S.A.*, 1995, **92**, 2036.
3 H. T. Alborn, T. C. J. Turlings, T. H. Jones, G. Stenhagen, J. H. Loughrin and J. H. Tumlinson, *Science*, 1997, **276**, 945.
4 W. Boland, J. Hopke, J. Donath, J. Nüske and F. Bublitz, *Angew. Chem., Int. Ed. Engl.*, 1995, **34**, 1600.
5 P. Fiedler, Dissertation, Universität Karlsruhe (TH), 1980. Experimental details for the preparation of **2** will be reported elsewhere.
6 S. K. Massad, L. D. Hawkins and D. C. Baker, *J. Org. Chem.*, 1983, **48**, 5180.
7 K. C. Nicolaou, J. Y. Ramphal and Y. Abe, *Synthesis*, 1989, 898.
8 W. Boland, P. Ney and L. Jaenicke, *Synthesis*, 1980, 1015.
9 E. J. Corey, J. Kang, *Tetrahedron Lett.*, 1982, **23**, 1651.
10 J. A. Dale, D. L. Dull and H. S. Mosher, *J. Org. Chem.*, 1969, **34**, 2543.

Communication 9/02020I

Direct observation of 1,2-didehydronaphthalene in a low temperature argon matrix: consecutive photolysis of 1,2-naphthalenedicarboxylic anhydride

Tadatake Sato, Masaya Moriyama, Hiroyuki Niino and Akira Yabe*

National Institute of Materials and Chemical Research (NIMC), Higashi, Tsukuba, 305-8565, Japan. E-mail: yabe@nimc.go.jp

Received (in Cambridge, UK) 23rd March 1999, Accepted 27th April 1999

1,2-Didehydronaphthalene (1-naphthyne) was produced in a low temperature argon matrix by wavelength-selective photolysis of 1,2-naphthalenedicarboxylic anhydride, which was confirmed by comparison of its FTIR spectrum with the theoretical IR spectrum calculated by density functional theory.

Arynes, benzyne and its congeners, have attracted great interest because of their ability to participate in a wide variety of organic reactions and their peculiar structures containing a strained triple bond. Among them, only the simplest member, *o*-benzyne, has been thoroughly characterized by its direct observation using matrix isolation spectroscopy.[1] Recently, its peculiar structure has been discussed on the basis of both experimental and theoretical results. The length of the triple bond in *o*-benzyne estimated by ^{13}C dipolar NMR[2] has shown that theoretical calculations, particularly calculations at the density functional theory (DFT) level, have provided reasonably accurate geometries of such an unstable species.[3] On the other hand, larger arynes, dehydrogenated polycyclic aromatic hydrocarbon molecules (PAHs), have scarcely been characterized by direct observation, although dehydrogenated and/or ionized PAHs have been recognized as important components of the interstellar medium.[4] Whereas some experimental results of ionized species are available,[5] little data on dehydrogenated PAHs have been presented: there is only one brief experimental report on 2-naphthyne.[6] Herein we wish to report the first direct observation of 1-naphthyne in a low temperature argon matrix. The FTIR spectrum of this compound is discussed on the basis of DFT calculation (B3LYP/6-31G** level).[7]

1,2-Naphthalenedicarboxylic anhydride **1** was photolyzed in an argon matrix at 11 K. During the experiment, the pressure in a sample chamber was kept under 10^{-5} Torr. Crystallites of **1** were vaporized at 50 °C and co-deposited with argon (99.9999%) onto a CsI plate.[8] It has been reported that the efficiency of photo-decomposition of anhydrides decreases as the pressure of a buffer gas increases in the gas phase and approaches zero in a condensed medium.[9] Therefore, a high intensity light is necessary to photolyze the anhydride in a cryogenic matrix.[10] Moreover, the choice of an appropriate wavelength for photolysis is quite important in order to suppress the multiple reactions proceeding simultaneously. Since the lowest transition band of matrix-isolated **1** observed was at 356 nm in its UV-VIS absorption, we used the third harmonic pulse of Nd:YAG laser (355 nm, 10 Hz, 4 mJ cm^{-2} $pulse^{-1}$) to photolyze **1**. The photolysis was followed by FTIR spectroscopy. Irradiation at 355 nm led to the diminution of the intensities of all the IR bands of **1** and concomitant growth of new IR bands ascribable to the first intermediate **2**[11] and CO_2 (2343 and 666 cm^{-1}). No IR band due to CO appeared in this photolysis. Thus it was confirmed that selective decarboxylation of **1** resulted in the formation of a $C_{10}H_6$–CO species **2**. Naphtho[*a*]cyclopropanone (in parentheses in Scheme 1) is a possible structure for **2** by analogy with the photolysis of phthalic anhydride.[1a] Indeed, the observed FTIR bands, except the C=O stretching bands, were in good agreement with the calculated vibrational bands of naphtho[*a*]cyclopropanone.[11] Meanwhile, four bands ascribed to this mode were observed at

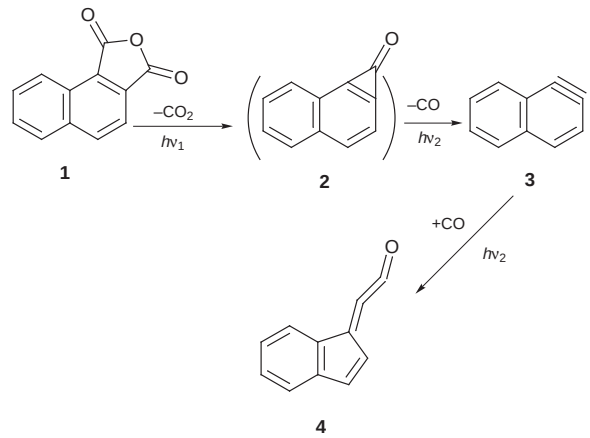

Scheme 1

1832, 1843, 1856 and 1873 cm^{-1}, although only one band was predicted theoretically for the C=O stretching mode. Such complex IR bands have often been observed for ketenes in cryogenic matrices.[12] Thus, we tentatively assigned **2** to naphtho[*a*]cyclopropanone. This compound was stable under prolonged irradiation at 355 nm.

To photolyze **2**, a high-pressure mercury lamp (500 W) was used through a 20 cm water filter and a UV-cut off glass filter (> 290 nm) since the UV absorption edge of **2** was observed at 320 nm in the matrix. In contrast to the photolysis of **1**, compound **2** was photolyzed in a rather short time upon irradiation. New bands due to the second intermediate **3** (Table 1) and CO (2142 cm^{-1}) appeared, while the IR bands of **2** disappeared upon irradiation. In particular, since the band of CO

Table 1 Observed FTIR data for **3** in an argon matrix and calculated data for 1-naphthyne

Observed for **3**		Calculated for 1-naphthyne	
$\tilde{\nu}$/cm^{-1}	Integrated intensity[a] (relative value)	$\tilde{\nu}^b$/cm^{-1}	IR intensity km mol^{-1}
452.2	43	390.4	70
558.4	22	538.4	14
—		701.6	5
749.3	37	736.3	26
799.4	42*	786.4	42
1072.3	11	1066.7	16
1077.2	8	1076.6	5
1494.7	11	1494.7	9
1537.2	6	1521.1	8
—		1600.1	11
		3065.6	10
3028.0, 3048.3, 3088.8	38	3078.3	22
		3088.1	16
		3092.3	21

[a] For comparison with calculated values, integrated intensities were normalized based on the value marked by an asterisk. [b] Scaled by 0.9614.[14]

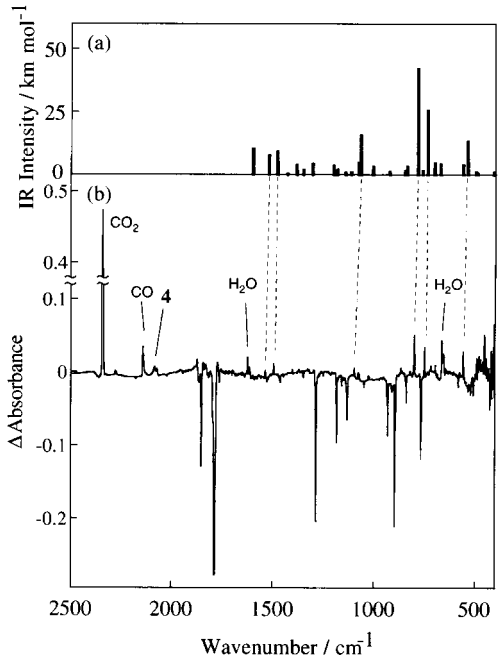

Fig. 1 (a) Theoretical IR spectrum of 1-naphthyne calculated at the B3LYP/6-31G** level. Frequencies have been scaled by a factor of 0.9614.[14] (b) Difference FTIR spectrum before and after irradiation of **1** with 95000 pulses of THG of Nd:YAG laser followed by 1.5 min with a high-pressure mercury lamp (> 290nm). Positive peaks correspond to **3** and negative peaks to **1**.

appeared with diminution of all the C=O stretching bands of **2**, it was revealed that a $C_{10}H_6$ species was formed by decarbonylation of **2**. The observed IR spectrum was compared with the theoretical IR spectrum of 1-naphthyne calculated at B3LYP/6-31G** level.[13] As shown in Fig. 1, all the predicted bands with intensities > 5 km mol^{-1} (listed in Table 1), except those at 701.6 and 1600 cm^{-1}, were observed in the experimental spectrum. The latter two bands could not be identified probably because of overlap with those of CO_2 and H_2O produced by the inevitable small leakage in the apparatus. Frequency deviations for all the bands except that observed at 452 cm^{-1} were within 20 cm^{-1}. These deviations are reasonably small at the computational level.[13] On the other hand, the relatively large deviation (62 cm^{-1} underestimated) for the band at 452 cm^{-1} can be explained as follows. The band is due to the ring deformation mode containing angular motions of the C–C≡C moiety. In the vibrational analysis of *o*-benzyne at the same computational level, the frequency of the corresponding mode was underestimated by 83 cm^{-1} from the observed frequency.[1a] Therefore, this deviation appears to be peculiar to the triple bond in arynes at the computational level. Moreover, no other IR bands ascribed to by-products formed by ring opening[15] or ring deformation[16] were observed. Thus, we conclude that the obtained $C_{10}H_6$ species can be assigned to 1-naphthyne.

Incidentally, in view of the keen debate concerning *o*-benzyne,[1] we should comment on the stretching mode of the C–C triple bond in **3**. For 1-naphthyne, the frequency and intensity of this mode were predicted as 1988 cm^{-1} and 0.0983 km mol^{-1}, respectively. Although we could observe all the bands with predicted intensity > 5 km mol^{-1}, the observation of the C≡C stretching band of 1-naphthyne was not possible under our experimental conditions.

By prolonged irradiation (> 290 nm) of **3**, new IR bands slowly appeared at 2084 and 2072 cm^{-1}. These bands could be ascribed to benzocyclopentadienylideneketene **4** according to the literature.[1a] This result shows that **3** reacts easily with CO to form **4** upon the irradiation. This reaction also occurred upon irradiation using the fourth harmonic pulse of the Nd:YAG laser (266 nm, 10 Hz, 3 mJ cm^{-2} pulse^{-1}). By contrast, 2-naphthyne[17] did not form the corresponding ketene upon irradiation at 266 nm. These results indicate differences in reactivity of the two naphthynes. The characteristics of the triple bond in arynes should be responsible for their reactivity. In the calculated geometries of these naphthynes, the lengths of triple bonds in these naphthynes were apparently different; 1.241 and 1.260 Å for 1- and 2-naphthynes, respectively.

In conclusion, we successfully produced 1-naphthyne by wavelength-selective photolysis of **1** in a low temperature argon matrix. Observed differences in reactivity of the two naphthynes is of interest from the viewpoint of their reactivity–structure profile. Further detailed study is in progress.

We are grateful to Prof. Curt Wentrup (University of Queensland, Australia) for helpful suggestions and discussions.

Notes and references

1 See, for example: (*a*) J. G. Radziszewsky, B. A. Hess Jr. and R. Zahradnik, *J. Am. Chem. Soc.*, 1992, **114**, 52; (*b*) J. G. G. Simon, N. Münzel and A. Schweig, *Chem. Phys. Lett.*, 1990, **170**, 187; (*c*) R. Warmuth, *Angew. Chem., Int. Ed. Engl.*, 1997, **36**, 1347 and references therein.
2 A. M. Orendt, J. C. Facelli, J. G. Radziszewski, W. J. Horton, D. M. Grant and J. Michl, *J. Am. Chem. Soc.*, 1996, **118**, 846.
3 H. J. Jiao, P. V. R. Schleyer, B. R. Beno, K. N. Houk and R. Warmuth, *Angew. Chem., Int. Ed.*, 1998, **36**, 2761.
4 See, for example: E. Pauzat, D. Talbi and Y. Ellinger, *Astron. Astrophys.*, 1995, **293**, 263; E. Pauzat, D. Talbi and Y. Ellinger, *Astron. Astrophys.*, 1997, **319**, 318; S. R. Langhoff, *J. Phys. Chem.*, 1996, **100**, 2819 and references therein.
5 See, for example, D. M. Hudgins and L. J. Allamandola, *J. Phys. Chem. A.*, 1997, **101**, 3472; S. P. Ekern, A. G. Marshall, J. Szczepanski and M. Vala, *J. Phys. Chem. A.*, 1998, **102**, 3498 and references therein.
6 H. A. Weimer, B. J. McFarland, S. Li and W. Weltner Jr., *J. Phys. Chem.*, 1995, **99**, 1824.
7 Gaussian 94, Revision E.2, M. J. Frisch, G. W. Trucks, H. B. Schlegel, P. M. W. Gill, B. G. Johnson, M. A. Robb, J. R. Cheeseman, T. Keith, G. A. Petersson, J. A. Montgomery, K. Raghavachari, M. A. Al-Laham, V. G. Zakrzewski, J. V. Ortiz, J. B. Foresman, J. Cioslowski, B. B. Stefanov, A. Nanayakkara, M. Challacombe, C. Y. Peng, P. Y. Ayala, W. Chen, M. W. Wong, J. L. Andres, E. S. Replogle, R. Gomperts, R. L. Martin, D. J. Fox, J. S. Binkley, D. J. Defrees, J. Baker, J. P. Stewart, M. Head-Gordon, C.Gonzalez, and J. A. Pople, Gaussian, Inc., Pittsburgh PA, 1995.
8 **1** (Ar matrix, 11K) UV-VIS (λ/nm): 356, 349, 339, 333, 324, 319, 311, 306, 250, 248, 243, 211. FTIR ($\tilde{\nu}$/cm^{-1}): 3098vw, 3068vw, 1852m, 1787s, 1461w, 1348w, 1286s, 1182m, 1158w, 1131m, 931m, 896s, 839m, 767m, 747w, 582w, 507w.
9 J. Lohmann, *J. Chem. Soc., Faraday Trans.*, 1971, 814.
10 The quantum yield of the photolysis of **1** isolated in the argon matrix was estimated as *ca.* 10^{-4}.
11 **2** (Ar matrix, 11 K) UV-VIS (λ/nm): 316, 309, 303, 296, 290, 278, 268, 238s, 231, 225. Observed FTIR bands ($\tilde{\nu}$/cm^{-1}) and theoretically-predicted frequencies (cm^{-1}) and intensity (km mol^{-1}) in parentheses : 3047vw, 2074vw, 3084vw (3069, 7; 3080, 16; 3089, 15; 3092, 12), 1832m, 1842m, 1856m, 1872m, (1875, 915; C = Ostr), — (1604, 22), 1579vw (1570, 37), 1568vw (1552, 14), 1510w (1495, 37), 1448vw (1428, 8), 1329vw (1326, 6), — (1316, 8), — (1092, 9), — (967, 6), 820w (809, 39), 774w (763, 8), 748w (737, 20), 645w (664, 25), — (594, 20), 493w (488, 10).
12 For example: R. F. C. Brown, N. R. Browne, K. J. Coulston, F. W. Eastwood, M. J. Irvine, A. D. E. Pullin and U. E. Wiersum, *Aust. J. Chem.*, 1989, **42**, 1321.
13 At the computational level, the vibrational frequencies of *o*-benzyne were predicted with reasonable accuracy. Although some vibrational modes containing the motion of the C≡C moiety showed relatively large deviation, the rms deviation between calculated (scaled by 0.9614[14]) and observed[1a] frequencies was 40.7 cm^{-1}.
14 Scaling factor for B3LYP/6-31G* level was used: A. P. Scott and L. Radom, *J. Phys. Chem.*, 1996, **100**, 16 502.
15 M. Moriyama, T. Ohana and A. Yabe, *J. Am. Chem. Soc.*, 1997, **119**, 10 229.
16 R. F. C. Brown, *Pure Appl. Chem.*, 1990, **62**, 1981.
17 2-Naphthyne was directly formed from 2,3-naphthalenedicarboxylic anhydride upon irradiation at 266 nm and showed a similar FTIR spectrum to that reported.[6]

Communication 9/02315A

Perfluorotributylamine as a probe molecule for distinguishing internal and external acidic sites in zeolites by high-resolution ^{1}H MAS NMR spectroscopy

Weiping Zhang, Ding Ma, Xianchun Liu, Xiumei Liu and Xinhe Bao*

State Key Laboratory of Catalysis, Dalian Institute of Chemical Physics, Chinese Academy of Sciences, Dalian 116023, P R China. E-mail: xhbao@ms.dicp.ac.cn

Received (in Cambridge, UK) 14th January 1999, Accepted 4th May 1999

^{1}H MAS NMR spectra of perfluorotributylamine adsorbed on HZSM-5 zeolites loaded with or without molybdenum show that it is a promising probe molecule for distinguishing the internal and external acidic sites in zeolites as well as for determining the position of silanols and some non-framework Al species.

Molybdenum-loaded HZSM-5 zeolites are promising catalysts for the conversion of methane to benzene under non-oxidative conditions.[1–7] The acidic sites in HZSM-5 zeolites are thought to play an important role in the aromatization of the primary product, ethylene, to benzene.[2,3] Until now, it has not been easy to distinguish the internal and external acidic sites in zeolites and to obtain quantitatively the concentration of acidic sites on the external surface of zeolites, though some methods such as IR spectroscopy[8,9] have been developed for the characterization of the external acidic sites of zeolites using base molecules with different sizes. High-resolution ^{1}H MAS NMR is a direct and senstitive tool able to characterize the local environment of protons in zeolites, and different acidic sites can be distinguished by chemical shifts induced by selective adsorption of certain probe molecules.[10] Here we use ^{1}H MAS NMR spectroscopy for quantitative determination of external acidity, as well as the position of non-acidic hydroxy groups (silanols) and some non-framework Al species of the zeolites, using perfluorotributylamine [$(n\text{-}C_4F_9)_3N$] as a probe molecule. Perfluorotributylamine is a weakly basic molecule with a diameter of 0.94 nm,[11] and is much larger than the pore size of microporous zeolites such as ZSM-5 (0.55 nm) and Y (0.74 nm).

NaZSM-5 zeolite samples with controlled particle sizes were prepared by varying the duration and temperature of crystallization as well as the amount of alkali metal salt such as NaCl.[12] Fully exchanged HZSM-5 with a Si/Al ratio of 28 (determined by ^{29}Si MAS NMR, and consistent with the value of 25 obtained by inductively coupled plasma analysis) was obtained by ion exchange of NaZSM-5 with a 0.4 M aqueous solution of NH_4NO_3. A Mo-HZSM-5 sample was prepared by impregnating the above-mentioned HZSM-5 zeolites (average particle sizes 70 nm by transmission electron microscopy) with an aqueous solution of $(NH_4)_6Mo_7O_{24}$, and calcined in air at 773 K.

In order to simulate catalytic reaction conditions in an environment suitable for NMR spectroscopy, we designed and fabricated a special device for on-line treatment of zeolite samples (Fig. 1).[13] With this system, the solid samples can be heated up to *ca.* 1000 K in a vacuum for dehydration, and can be exposed to several different gases together or separately. After treatment, the sample can be filled *in situ* into a NMR rotor by a tamper, sealed with a cap from the plug rack and transferred to the spectrometer without exposure to air. In the present experiment, the zeolites were dehydrated typically at 673 K and a pressure below 10^{-2} Pa for 10–20 h. Selective adsorption of perfluorotributylamine (from Acros Organics) was performed by exposing the dehydrated sample to saturated vapor at room temperature for 30 min. After equilibration, the samples were degassed at 298 K to remove the physical adsorbates on the surface.

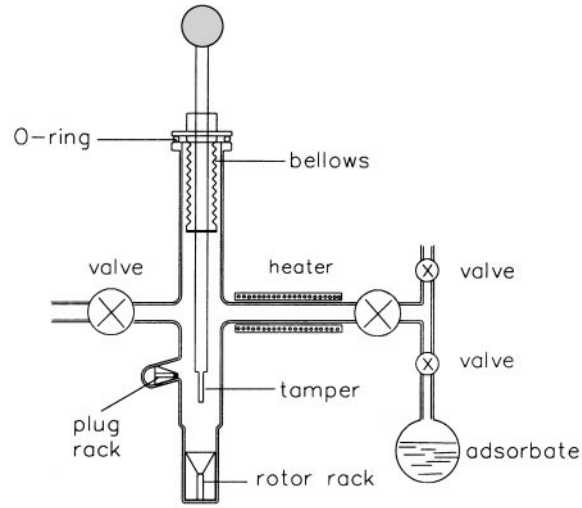

Fig. 1 Schematic diagram of the evacuating, loading and sealing apparatus of the solid samples for the solid-state MAS NMR study.

^{1}H MAS NMR spectra were recorded at 400.1 MHz on a Bruker DRX-400 spectrometer with a BBO MAS probe using 4 mm ZrO_2 rotors. The pulse width was 1 μs for a $\pi/10$ pulse, and 200 scans were accumulated with a 4 s recycle delay. Samples were spun at 8 kHz, and chemical shifts were referenced to a saturated aqueous solution of sodium 4,4-dimethyl-4-silapentanesulfonate. The Bruker software WINNMR was employed for deconvolution using fitting of Gaussian–Lorentzian lineshapes.

The upper curves in Fig. 2 show the ^{1}H MAS NMR spectra of HZSM-5 zeolite and a sample loaded with 6 wt% molybdenum before adsorption of perfluorotributylamine. At least five peaks can be clearly observed in the ^{1}H MAS NMR spectra (see the corresponding quantitatively deconvoluted spectra in Fig. 2). Besides the usually observed bridging hydroxy peak at about δ 3.9, the non-framework AlOH peak at δ 2.4 and the non-acidic silanol peak at about δ 1.7 can be identified. Moreover, a broad resonance at about δ 5.8 is also visible, which is ascribed to a second Brønsted site having an additional electrostatic interaction with the zeolite framework.[10] The narrow signal at about δ 4.9 can be assigned to an extremely small amount of water residing in the zeolite cages.[14] It is apparent from these spectra that the total ^{1}H signal intensity decreases upon loading molybdenum, and the resonances at δ 1.7 and 2.4 are preferentially reduced compared to those at δ 3.9 and 5.8. These results reveal that in the 6 wt% Mo–HZSM-5 sample prepared by impregnation, the molybdate ions preferentially react with the silanols and the non-framework AlOH groups on the surface of the zeolites. After adsorption of perfluorotributylamine, the intensity of the peak at δ 3.9 decreases, while that of the peak at about δ 5.8 ppm increases [see upper and lower curves in Fig. 2(*a*)]. This fact suggests that a portion of the bridging hydroxy groups located on the external surface of the zeolite interact with the perfluorotributylamine to form perfluorotributylaminium ions whose resonance signal

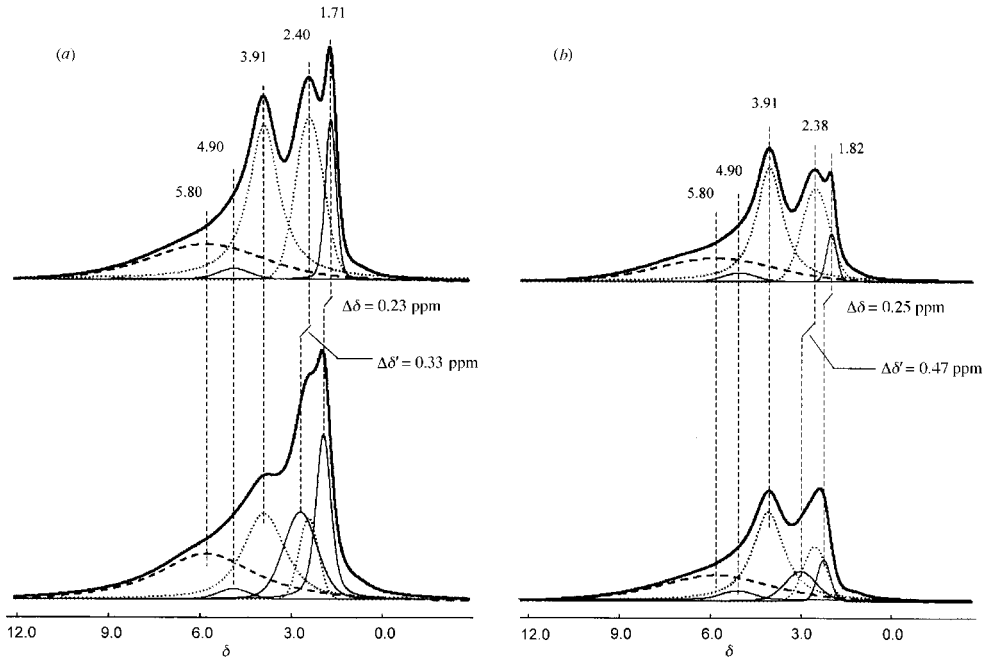

Fig. 2 ^{1}H MAS NMR spectra, with deconvolution, of (*a*) HZSM-5 zeolite and (*b*) 6 wt% Mo-HZSM-5, (top) before and (bottom) after adsorption of perfluorotributylamine, recorded at a resonance frequency of 400.1 MHz with a sample spinning rate of 8 kHz and 200 scans.

appears at about δ 6.0, while those at the internal surface are not accessible to perfluorotributylamine, so their chemical shift is unchanged. Based on these results, and after careful deconvolution of the obtained spectra, the concentration of Brønsted acid sites on the external surface of the zeolites can be calculated by (eqn. 1),

$$C_{\text{ext.surf.}} = (1 - A_1/A_2) \times 100\% \quad (1)$$

where A_1 and A_2 denote the integral area of the peak at δ 3.9 after and before adsorption of perfluorotributylamine, respectively (quantitatively deconvoluted spectra are also shown in Fig. 2). According to eqn. (1), the concentration of Brønsted acid sites on the external surface for HZSM-5 zeolites (70 nm) is 32%, while that for the 6 wt% Mo-HZSM-5 is 9%. This result, combined with the fact that the peak intensity at δ 3.9 decreases after Mo-loading clearly demonstrates that the Brønsted acidic sites on the external surface of the HZSM-5 zeolite can also react with the molybdate ions during sample preparation.

In addition, the resonance position of silanols of the samples shifts from about δ 1.7 to about δ 2.0 after adsorption of perfluorotributylamine. This low-field shift of over 0.2 ppm confirms that a weak hydrogen bond between the SiOH and the N of perfluorotributylamine is formed due to its relatively high deprotonation energy (ΔE_{DP} = 1427 kJ mol^{-1}). [15] Thus most of the silanols of the given samples are located on the external surface, and not at the lattice defects of the internal surface in the zeolites. By reasonable deconvolution, the > 0.3 ppm low-field shift of the non-framework Al resonance after adsorption of perfluorotributylamine demonstrates that some of the non-framework Al atoms exist on the external surface of the zeolites. Their concentration on the external surface can also be calculated *via* eqn. (1). Thus for HZSM-5 zeolites without Mo and with 6 wt% Mo, the concentrations are 65 and 51%, respectively. This also suggests that molybdate ions react with the non-framework AlOH groups on the external surface of the zeolites during sample preparation. From the above discussion, it is clearly demonstrated that there are at least three kinds of molybdenum species existing on the external surface of the HZSM-5 zeolite, *i.e.* Mo interacting with silanols, non-framework AlOH groups and Brønsted acidic sites on the external surface, respectively. These observations are consistent with the suggestion presented by Lunsford and co-workers[5,6] that impregnated Mo remains predominantly on the external surface of the zeolite, *via* studies comparing different preparation methods such as impregnation and solid state ion exchange. These Mo species are very likely associated with the activation of methane to form ethylene (and H_2) as the sole primary product, which aromatizes further on the Brønsted acidic sites to produce benzene and methylbenzene.[3]

In conclusion, this paper reports a feasible method for distinguishing the internal and external acidic sites in zeolites. After dehydration of the zeolites in a patented device capable of *in situ* sample pretreatments, and then adsorption of perfluorotributylamine as a probe, the Brønsted acidity distribution between the internal and external surfaces of the zeolites can be determined by ^{1}H MAS NMR spectroscopy. Meanwhile, the position of silanols and some non-framework Al species can also be identified.

We gratefully acknowledge the support of the National Natural Science Foundation of China and the Ministry of Science and Technology of China through the Climbing Project.

Notes and references

1 L. Wang, L. Tao, M. Xie, G. Xu, J. Huang and Y. Xu, *Catal. Lett.*, 1993, **21**, 35.
2 L. Chen, L. Lin, Z. Xu, Z. Li and T. Zhang, *J. Catal.*, 1995, **157**, 190.
3 Y. Xu, S. Liu, L. Wang, M. Xie and X. Guo, *Catal. Lett.*, 1995, **30**, 135.
4 S. Liu, Q. Dong, R. Ohnishi and M. Ichikawa, *Chem. Commun.*, 1997, 1455.
5 B. M. Weckhuysen, D. Wang, M. P. Rosynek and J. H. Lunsford, *J. Catal.*, 1998, **175**, 338.
6 B. M. Weckhuysen, D. Wang, M. P. Rosynek and J. H. Lunsford, *J. Catal.*, 1998, **175**, 347.
7 B. M. Weckhuysen, M. P. Rosynek and J. H. Lunsford, *Catal. Lett.*, 1998, **52**, 31.
8 A. Corma, V. Fornés and F. Rey, *Zeolites*, 1993, **13**, 56.
9 J. Take, T. Yamaguchi, K. Miyamoto, H. Oyawa and M. Misono, *Stud. Surf. Sci. Catal.*, 1986, **28**, 495.
10 M. Hunger, *Catal. Rev.- Sci. Eng.*, 1997, **39**, 345.
11 J. Take, H. Yoshioka and M. Misono, *Proceedings of the Ninth International Conference on Catalysis*, ed. M. J. Philips and M. Ternan, The Chemical Institute of Canada, Ottawa, 1988, p. 372.
12 V.P. Shiralkar, P. N. Joshi, M. J. Eapen and B. S. Rao, *Zeolites*, 1991, **11,** 511.
13 X. Liu, Q. Zhao and X. Bao, CN 98 2 38330.4, 1998.
14 M. Hunger, D. Freude and H. Pfeifer, *J. Chem. Soc., Faraday Trans.*, 1991, **87**, 657.
15 E. Brunner, *J. Mol. Struct.*, 1995, **355**, 61.

Communication 9/00396G

Solvothermal reaction route to nanocrystalline semiconductors $AgMS_2$ (M = Ga, In)

Junqing Hu,[a,b] Qingyi Lu,[a,b] Kaibin Tang,*[a,b] Yitai Qian,*[a,b] Guien Zhou[b] and Xianming Liu[b]

[a] *Structure Research Laboratory, University of Science and Technology of China, Hefei, 230026, P.R. China. E-mail: kbtang@.ustc.edu.cn*

[b] *Department of Chemistry, University of Science and Technology of China, Hefei, 230026, P.R. China*

Received (in Cambridge, UK) 9th March 1999, Accepted 7th May 1999

Nanocrystalline semiconductors $AgGaS_2$ and $AgInS_2$ with particle sizes ranging from 5 to 12 nm are prepared by a solvothermal reaction in the temperature range 180–230 °C.

The study of nanometre sized crystallites provides an opportunity to observe the evolution of material properties with size.[1] Studies of semiconductor nanostructures with size-dependent optical and electronic properties are motivated by potential applications which include quantum-dot lasers and high-speed non-linear optical switches.[2,3] Therefore, current attention has focussed on the development of new methods for the preparation of nanocrystalline semiconductors.

I–III–VI_2 chalcopyrite semiconducting compounds such as $AgGaS_2$ and $AgInS_2$ have been shown to be useful linear and non-linear optical materials.[4,5] The band gaps and optical properties of many of these ternary sulfur containing chalcopyrites have been reported.[6,7] Considerable progress has been made in the synthesis of I–III–VI_2 semiconductor crystallites.[8,9] However, the reported preparative routes were traditional solid-state reaction methods which require high processing temperatures (800–1000 °C), long reaction times, and special apparatus. Vacancies or interstitial defects in the chalcopyrite lattice cause these compounds to have poor crystal quality and poor optical transparency.[10] As we know, different preparative methods have important effects on the resulting microstructure and physical properties of materials. Recently, various solution chemical synthesis techniques have been utilized to prepare some fascinating materials. This chemical method allows the particle size and their distribution as well as their morphology to be controlled.[11]

Herein, we report a solvothermal synthetic route to the I–III–VI_2 nanocrystalline compounds $AgGaS_2$ and $AgInS_2$ in the temperature range 180–230 °C by using AgCl, Ga (or In) and S as the reactants. The synthetic reaction was carried out in an autoclave and can be represented by eqn. (1).

$$3AgCl + 4M + 6S \xrightarrow[180–230\ °C]{\text{solvent}} 3AgMS_2 + MCl_3\ (M = Ga, In) \quad (1)$$

In this process, the coordinating solvent plays an important role in the formation of $AgGaS_2$ and $AgInS_2$.

In a typical procedure, analytical grade AgCl (1.0 g), Ga (0.648 g) or In (1.068 g), and S (0.447 g) were put into an autoclave of 50 mL capacity and then the autoclave was filled with ethylenediamine up to 85% of the total volume. The autoclave was maintained at 180–230 °C for 10 h and then allowed to cool to room temperature. The precipitates were filtered off and washed sequentially with CS_2, absolute ethanol, dilute acid, aqueous ammonia solution and distilled water, to remove the residual impurities (*e.g.* elemental sulfur and chloride). After drying in a vacuum at 70 °C for 2 h, a final dark yellow product was obtained.

The obtained samples were characterized by X-ray powder diffraction (XRD), operating on a Japan Rigaku Dmax-γA X-ray diffractometer with graphite-monochromated Cu-Kα radiation (λ = 1.5418 Å). The morphology and particle size of the final products were determined by transmission electron microscopy (TEM) images taken with a Hitachi H-800 transmission electron microscope. X-Ray photoelectron spectra (XPS) were recorded on a VGESCALAB MKII X-ray photoelectron spectrometer, using non-monochromated Mg-Kα radiation as the excitation source.

Fig. 1(a) shows the XRD pattern of an $AgGaS_2$ sample prepared by the solvothermal synthetic process. All the peaks could be indexed to the tetragonal $AgGaS_2$ phase with cell constants a = 5.7538 and c = 10.3026 Å, in agreement with reported data in the literature.[12] No characteristic peaks of other impurities such as Ga or Ag_2S, were observed. Fig. 1(b) shows the XRD pattern of an $AgInS_2$ sample. All the reflections could be indexed to the pure chalcopyrite phase $AgInS_2$ with lattice parameters a = 5.8652 and c = 11.1992 Å, in good agreement with the literature values.[13] The broadened nature of these diffraction peaks indicate that the grain sizes of the samples are on the nanometre scale. The average sizes of the particles are 6 and 10 nm, for $AgGaS_2$ and $AgInS_2$, respectively, as estimated by the Scherrer equation.

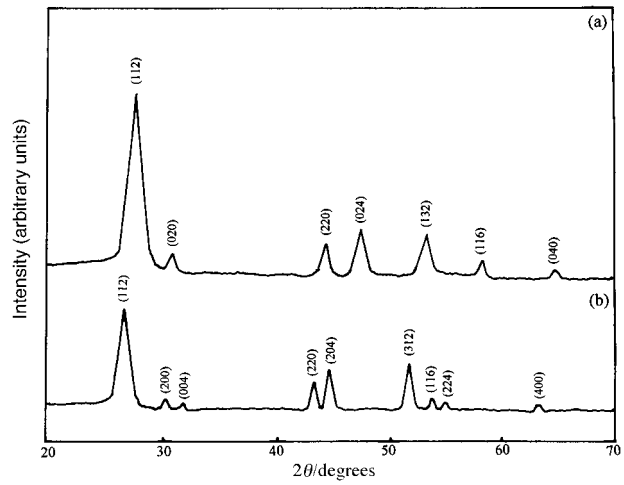

Fig. 1 XRD patterns of samples of (*a*) $AgGaS_2$ and (*b*) $AgInS_2$ prepared by solvothermal reaction.

The quality of the samples was also characterized by XPS. No obvious impurities, *e.g.* chloride ion or elemental sulfur, could be detected in the samples, indicating that the level of impurities is lower than the resolution limit of XPS (1 at%). Quantification of the XPS peaks gave Ag : Ga : S atomic ratios of 1 : 1.08 : 2.10.

Fig. 2 shows TEM images of as-prepared nanocrystalline $AgGaS_2$ and $AgInS_2$. It can be seen that the samples consist of uniform spherical particles. The diameters of the particles are in the range 5–7 and 9–12 nm, respectively, in accord with the XRD results.

It is well known that solvents can influence the reaction pathway. In our experiments, different solvents were tested and the results revealed that the coordinating ability of the solvent played an important role in the formation of nanocrystalline

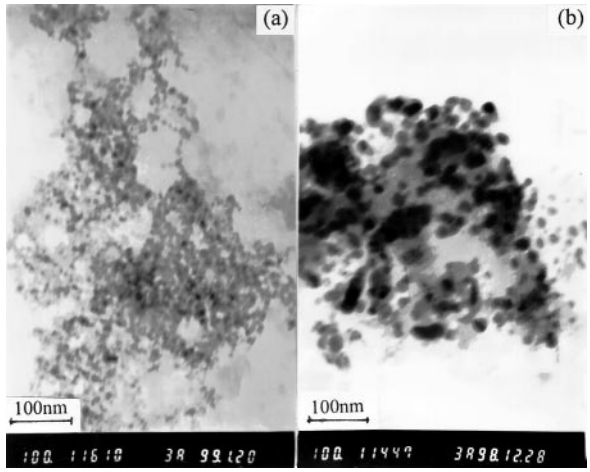

Fig. 2 TEM images of (*a*) $AgGaS_2$ and (*b*) $AgInS_2$ as in Fig. 1.

$AgGaS_2$. Ethylenediamine, a bidentate solvent, was selected due to its strong N-chelation ability and basicity. It can act as a bidentate ligand to form a relatively stable Ag^+ complex, which can incorporate dissolved sulfur as seen for other amine solvents.[14,15] As the temperature was increased, Ga melted and the formation of $AgGaS_2$ may be through a liquid-solution diffusion process. This route thus differs substantially from solid state reactions which require high temperature to overcome higher activation energy barriers. When pyridine, showing weaker binding and basicity, was used as solvent, keeping the other reaction conditions constant, the reaction was incomplete and the product purity was lower. A non-polar solvent, benzene, having no chelating ability or basicity, was also tried. According to XRD analysis, the reaction in benzene did not produce $AgGaS_2$, and the product was mostly unreacted AgCl and Ga. The influence of reaction temperature and time on the formation of $AgGaS_2$ were also studied. The optimum conditions for the formation of nanocrystalline $AgGaS_2$ is at a temperature of 180–230 °C for 10 h. If the temperature was lower than 150 °C, or the time was shorter than 5 h, the crystallinity of the $AgGaS_2$ was lower. If the temperature was higher than 250 °C or the time longer than 12 h, the particles were larger and the product was contaminated by carbonization of the solvent.

In summary, we have succeeded in the synthesis of nanocrystalline $AgGaS_2$ and $AgInS_2$ by solvothermal reaction. The structure and property of the solvent can strongly influence the reaction process. The method presented herein provides uniform particles with narrow size distribution which may be further enhanced by use of other solvents. This method can be readily employed to prepare other nanocrystalline I–III–VI_2 materials such as $AgMSe_2$, $CuMS_2$ (M = Ga, In). A detailed study on this synthesis method is in progress.

Financial support of this work by the National Natural Science Foundation of China is gratefully acknowledged.

Notes and references

1 C. B. Murray, D. J. Norris and M. G. Bawendi, *J. Am. Chem. Soc*., 1993, **115**, 8706.
2 L. Brus, *Appl. Phys. A*., 1991, **53**, 465.
3 M. Nirmal, B. O. Dabbousi, M. G. Bawendi, J. J. Macklin, J. K. Trautman, T. D. Harris and L. E. Brus, *Nature*, 1996, **383**, 802.
4 S. C. Abrahams and J. L. Bernstein, *J. Chem. Phys*., 1973, **59**, 1625.
5 I. Yonenaga, K. Sumino, E. Niwa and K. Masumoto, *J. Cryst. Growth*, 1996, **167**, 616.
6 B. Tell and H. M. Kasper, *Phys. Rev B; Condens. Matter*., 1971, **4**, 4455.
7 H. Matthes, R. Viehmann and N. Marschall, *Appl. Phys. Lett*., 1975, **26**, 237.
8 B. F. Levine, *Phys. Rev B; Condens. Matter*., 1973, **7**, 2600.
9 R. K. Route, R. S. Feigelson and R. J. Raymakers, *J. Cryst. Growth*, 1976, **33**, 239.
10 N. Yamamoto, K. Yokota and H. Horinaka, *J. Cryst. Growth*, 1990, **99**, 747.
11 J. Moon, T. Li, C. A. Randall, J. H. Adair, *J. Mater. Res*., 1997, **12**, 189.
12 JCPDS, 27-615.
13 JCPDS, 25-1330.
14 C. O. Kienitz, C. Thone and P. G. Jones, *Inorg. Chem.*, 1996, **35**, 3990.
15 Y. Cheng, T. J. Emge and J. G. Brennan, *Inorg. Chem.*, 1996, **35**, 342.

Communication 9/02218J

ChemComm

The first organoelement oxides containing three different metals; synthesis and structure of (Ph_2SiOR_2SnOMO) [R = $(CH_2)_3NMe_2$; M = Bu^t_2Sn, Bu^t_2Ge, PhB]† ‡

Jens Beckmann, Klaus Jurkschat,* Nicole Pieper and Markus Schürmann

Lehrstuhl für Anorganische Chemie II, Fachbereich Chemie der Universität Dortmund, D-44221 Dortmund, Germany. E-mail: kjur@platon.chemie.uni-dortmund.de

Received (in Cambridge, UK) 26th March 1999, Accepted 12th May 1999

***Umpolung* of ring strain by intramolecular Sn–N Lewis acid–Lewis base interaction is the key for the synthesis of the first organoelement oxides of the type (Ph_2SiOR_2SnOMO) [R = $(CH_2)_3NMe_2$; M = Bu^t_2Sn, Bu^t_2Ge, PhB] which hold potential as precursors to tertiary metal oxides.**

Recently, we reported the syntheses and structures of stannasiloxanes such as *cyclo*-$R_2Si(OSnBu^t_2)_2O$ (**1**, R = Bu^t; **2**, R = Ph),[1a,b] *cyclo*-$(Ph_2SiOR_2SnO)_2$ [**3**, R = Bu^t; **4**, R = $(CH_2)_3NMe_2$],[1b,c] *cyclo*-$R_2Sn(OSiPh_2)_2O$ [**5**, R = Bu^t; **6**, R = $(CH_2)_3NMe_2$],[1c,d] and of the germastannoxanes *cyclo*-$Bu^t_2Sn(OGePh_2)_2O$ **7**.[1c] Such compounds are of potential interest as molecular precursors for the synthesis by ring-opening polymerisation of inorganic polymers.[1d,2] The stannasiloxane $Bu^t_2Sn(OSiPh_2)_2O$ **5** contains a six-membered ring in solution but is the first well-defined polystannasiloxane in the solid state. The ring strain in **5** is the thermodynamic driving force for the polymerisation which however, is compensated in solution by entropy of a large number of monomers, *i.e.*, six-membered rings.[1d] In contrast, the related borasiloxane *cyclo*-PhB($OSiPh_2)_2O$ **8** is a six-membered ring both in solution and in the solid state.[2b] The reaction of the eight-membered stannasiloxane ring *cyclo*-$(Ph_2SiOBu^t_2SnO)_2$ (**3**) with 2/3 mol equivalents *cyclo*-$(Bu^t_2SnO)_3$ quantitatively provided *in situ* the six-membered stannasiloxane ring $Ph_2Si(OSnBu^t_2)_2O$ **2**. However, this reaction is also an equilibrium and removal of the solvent quantitatively yielded the starting compounds *cyclo*-$(Bu^t_2SnO)_3$ and **3**.[1b]

In contrast, the reaction of the eight-membered intramolecularly coordinated stannasiloxane ring *cyclo*-$(Ph_2SiOR_2SnO)_2$ [**4**, R = $(CH_2)_3NMe_2$] with *cyclo*-$(Bu^t_2SnO)_3$ afforded the first *cyclo*-stannasiloxane **9** containing two different substituted tin atoms (Scheme 1).§

Furthermore, the reaction of compound **4** with di-*tert*-butylgermanium dihydroxide $Bu^t_2Ge(OH)_2$ and phenylboronic acid $PhB(OH)_2$ gave the first organoelement oxides **10** and **11**, respectively, being composed of three different metals or metalloids in the same ring (Scheme 1).§

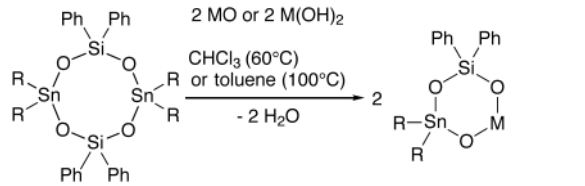

9, M = Bu^t_2Sn, R = $(CH_2)_3NMe_2$
10, M = Bu^t_2Ge, R = $(CH_2)_3NMe_2$
11, M = PhB, R = $(CH_2)_3NMe_2$

Scheme 1

† Dedicated to Professor Dietmar Seyferth on the occasion of his 70th birthday.

‡ This work contains part of the Ph.D. thesis of N. Pieper, Dortmund University 1998, and of the intended Ph.D. thesis of J. Beckmann.

It seems that the intramolecular Sn–N coordination increases the ring strain in the eight-membered *cyclo*-stannasiloxane **6** but decreases the ring strain in the six-membered rings **9**–**11**. This means, the formation of **9**–**11** is favoured by both enthalpy and entropy.

The molecular structures¶ of compounds **10** and **11** are shown in Fig. 1 and 2, respectively. Compound **9** is isostructural with **10**. The Sn(1) atoms in **9**–**11** exhibit distorted octahedral configurations with the carbon atoms in mutual *trans* and the oxygen and nitrogen atoms in *cis* positions. The deviation from the ideal octahedral geometry is documented by the C(1)–Sn(1)–C(11) angles of 149.3(2)–152.30(2)° and the N(1)–Sn–N(2) angles of 105.4(1)–109.58(9)°. The O(1)–Sn(1)–O(3) angles fall in the range 90.30(8)–95.45(9)°. The intramolecular Sn–N distances in **9**–**11** [2.620(3)–2.764(3) Å] are shorter as compared to the Sn–N contacts in the eight-membered *cyclo*-stannasiloxane **4** [2.721(4)/2.811(4) Å].[1c] The Sn–N distances are quite different within each of the compounds **9**–**11**. This corresponds with previous observations on the intramolecularly coordinated organotin sulfide $\{[Me_2N(CH_2)_3]_2SnS\}_2$.[3]

Compared to the ^{119}Sn NMR chemical shifts in solution the ^{119}Sn MAS NMR spectra of **9**–**11** exhibit shifts of 52.9, 30.3 and 9.5/17.8 ppm‖ to low frequency which hints, especially for **10** and **11**, at a stronger Sn–N coordination in the solid state.

The synthetic concept introduced within this paper should also apply for the synthesis of organoelement oxides containing

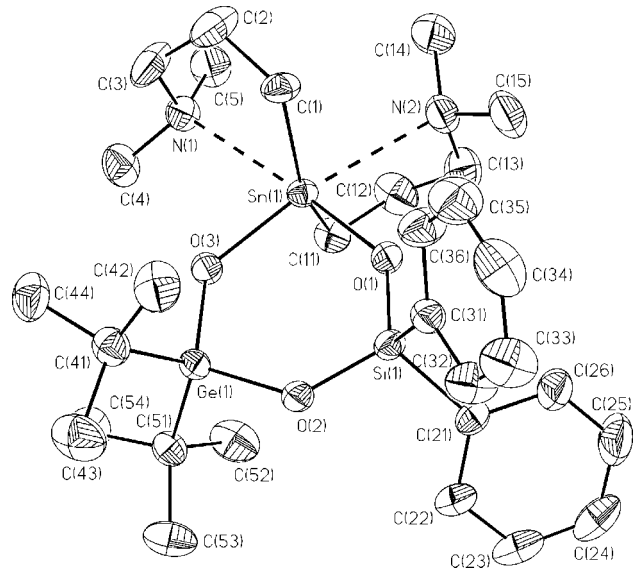

Fig. 1 General view of a molecule of **10** showing 30% probability displacement ellipsoids and the atom numbering. The hydrogen atoms were omitted for clarity. Selected bond lengths (Å) and angles (°): Sn(1)–O(1/3) 2.010(2)/2.022(2), Sn(1)–N(1/2) 2.648(3)/ 2.752(3); O(1)–Sn(1)–O(3) 93.89(8), O(1)–Si(1)–O(2) 113.5(1); O(2)–Ge(1)–O(3) 109.1(1). Compound **9** is isostructural; Ge(1) is replaced by Sn(2). Sn(1)–O(1/3) 1.998(2)/2.026(2), Sn(1)–N(1/2) 2.683(3)/2.764(3); O(1)–Sn(1)–O(3) 95.45(9), O(1)–Si(1)–O(2) 114.2(1), O(2)–Sn(2)–O(3) 106.69(9).

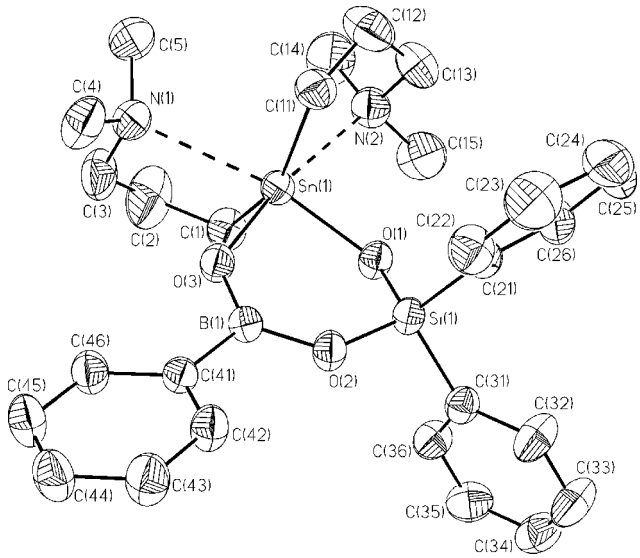

Fig. 2 General view of a molecule of **11** showing 30% probability displacement ellipsoids and the atom numbering. The hydrogen atoms were omitted for clarity. Selected bond lengths (Å) and angles (°): Sn(1)–O(1/3) 2.038(2)/2.054(2) (2.017(2)/2.050(2)), Sn(1)–N(1/2) 2.620(3)/2.681(3) (2.649(3)/2.65(2)); O(1)–Sn(1)–O(3) 90.30(8)(91.75(8)); O(1)–Si(1)–O(2) 110.4(1) (112.9(1)), O(2)–B(1)–O(3) 124.2(3) (123.5(3)). The values given in parentheses refer to the second, symmetrically independent molecule of **11** in the unit cell which is not shown.

both main group elements and transition metals. Such compounds are of increasing interest as single source precursors for mixed metal oxides[4] which find applications in heterogeneous catalysis[5a] or for solar cells.[5b]

We thank the Deutsche Forschungsgemeinschaft and the Fonds der Chemischen Industrie for financial support.

Notes and references

§ Literature procedures were used to prepare *cyclo*-$(R_2SnOSiPh_2O)_2$ (**3**, R = Bu^t;[1b] **4**, R = $(CH_2)_3NMe_2$[1c]], *cyclo*-$(Bu^t_2SnO)_3$[6a] and Bu^t_2-$Ge(OH)_2$.[6b]

Synthesis and selected spectroscopic data: 1,1-*di-tert-butyl*-3,3-*bis*(3-*dimethylaminopropyl*)-5,5-*diphenyl*-2,4,6-*trioxa*-5-*sila*-1,3-*distannacyclohexane* **9**: 1,1,5,5-tetrakis(3-dimethylaminopropyl)-3,3,7,7-tetraphenyl-2,4,6,8-tetraoxa-3,7-disila-1,5-distannacyclooctane **4** (500 mg, 0.495 mmol) and di-*tert*-butyltin oxide (246 mg, 0.330 mmol) were dissolved in chloroform (10 mL). The reaction mixture was kept at 60 °C for 12 h. The solvent was evaporated *in vacuo* and the residue recrystallised from *n*-hexane to give 271 mg (38 % yield) of **9** as colourless crystals, mp 135 °C. $^{29}Si\{^1H\}$ NMR δ −40.4 [$^2J(^{29}Si–O–^{119}Sn)$ 31 Hz]; $^{119}Sn\{^1H\}$ NMR δ −93.3 [$^2J(^{119}Sn–O–^{119/117}Sn)$ 371 Hz], −191.7 [$^2J(^{119}Sn–O–^{119/117}Sn)$ 377 Hz]; $^{119}Sn\{^1H\}$ MAS NMR: δ −92.7 [$^2J(^{119}Sn–O–^{119/117}Sn)$ 381 Hz], −244.6. MS: *m/z*: 697 ($C_{26}H_{41}N_2O_3SiSn_2^+$), 639 ($C_{22}H_{31}N_2O_3SiSn_2^+$), 583 ($C_{20}H_{28}O_3SiSn_2^+$), 206 ($C_5H_{12}Sn^+$). Elemental analysis (%): found: C, 47.81, H, 7.18, N, 3.65. Calc. for $C_{30}H_{52}N_2O_3Sn_2Si$: C 47.78, H 6.95, N 3.71%. Molecular weight ($CHCl_3$): found.: 543 g mol^{-1}; calc. for $C_{30}H_{52}N_2O_3Sn_2Si$: 754 g mol^{-1}.

1,1-*di-tert-butyl*-3,3-*bis*(3-*dimethylaminopropyl*)-5,5-*diphenyl*-3-*germa*-2,4,6-*trioxa*-5-*sila*-1-*stannacyclohexane* **10**: 1,1,5,5-tetrakis(3-dimethylaminopropyl)-3,3,7,7-tetraphenyl-2,4,6,8-tetraoxa-3, 7-disila-1, 5-distannacyclooctane **4** (500 mg, 0.495 mmol) and di-*tert.*-butylgermanium dihydroxide (240 mg, 1.087 mmol) were dissolved in toluene (15 mL). The reaction mixture was kept at 100 °C for 2 d. The solvent was distilled off and the residue was recrystallised from *n*-hexane to give 268 mg (36 % yield) of colourless crystals of **10**, mp. 148 °C. $^{29}Si\{^1H\}$ NMR δ −42.2 [$^2J(^{29}Si–O–^{119/117}Sn)$ 32 Hz]; $^{119}Sn\{^1H\}$ NMR δ −231.6; $^{119}Sn\{^1H\}$ MAS NMR: δ −261.9. MS: *m/z*: 707 ($C_{30}H_{51}N_2O_3GeSiSn^+$), 650 ($C_{26}H_{42}N_2O_3GeSiSn^+$), 621 ($C_{25}H_{39}NO_3GeSiSn^+$), 536 ($C_{20}H_{28}O_3GeSiSn^+$), 478 ($C_{16}H_{18}O_3GeSiSn^+$), 206 ($C_5H_{12}Sn^+$). Elemental analysis (%): found: C, 51.09; H, 7.57; N, 3.92; calc. for $C_{30}H_{52}N_2O_3GeSiSn$: C, 50.89; H, 7.40; N, 3.96. Molecular weight ($CHCl_3$): found: 657 g mol^{-1}; calc. for $C_{30}H_{52}N_2O_3GeSiSn$: 708 g mol^{-1}.

3,3-*bis*(3-*dimethylaminopropyl*)-3,5,5-*triphenyl*-3-*bora*-2,4,6-*trioxa*-5-*sila*-1-*stannacyclohexane* **11**: 1,1,5,5-tetrakis(3-dimethylaminopropyl)-3,3,7,7-tetraphenyl-2,4,6,8-tetraoxa-3,7-disila-1, 5-distannacyclooctane **4** (455 mg, 0.450 mmol) and phenylboronic acid (110 mg, 0.902 mmol) were dissolved in chloroform (10 mL). The reaction mixture was kept at 60 °C for 12 h. The solvent was removed *in vacuo* and the residue was recrystallised from *n*-hexane to give 335 mg (61% yield) of colourless crystals of **11**, mp 132 °C. $^{29}Si\{^1H\}$ NMR δ −38.7 [$^2J(^{19}Si–O–^{119/117}Sn)$ 19 Hz]; $^{119}Sn\{^1H\}$ NMR δ −259.1; $^{119}Sn\{^1H\}$ MAS NMR: δ −268.6, −276.9. MS: *m/z* 609 ($C_{28}H_{38}N_2O_3BSiSn^+$), 523 ($C_{23}H_{26}NO_3BSiSn^+$), 430 ($C_{17}H_{21}NO_2BSiSn^+$), 206 ($C_5H_{12}NSn^+$). Elemental analysis (%): found: C 55.25, H 6.85, N 4.50; calc. for $C_{28}H_{39}N_2O_3BSiSn$: C 55.20, H 6.45, N 4.60. Molecular weight ($CHCl_3$): found: 517 g mol^{-1}; calc. for $C_{28}H_{39}N_2O_3BSiSn$: 609 g mol^{-1}.

^1H and ^{13}C NMR data for compounds **9**–**11** can be viewed electronically, see: http://www.rsc.org/suppdata/1999/1095/.

¶ The structures of **9**–**11** were refined in the triclinic space group $P\bar{1}$.

9: $C_{30}H_{52}N_2O_3SiSn_2$, M_r = 754.21, crystal dimensions: 0.70 × 0.18 × 0.15 mm, a = 9.302(1), b = 10.824(1), c = 17.897(1) Å, α = 81.611(1), β = 88.994(1), γ = 85.935(1)°, V = 1778.1(3) Å^3, Z = 2, μ = 1.467 mm^{-1}, D_c = 1.409 Mg m^{-3}, D_m = 1.420(2) Mg m^{-3}, $2\theta_{max}$ = 29.61°, 21528 measured, 8738 (R_{int} = 0.032) independent and 5324 observed reflections with $I > 2\sigma(I)$, $R1$ = 0.036, $wR2$ = 0.0748 for 355 parameters, S = 0.907, Δ/ρ_{max} = 0.672 e Å^{-3}.

10: $C_{30}H_{52}GeN_2O_3SiSn$, M_r = 708.11, crystal dimensions: 0.40 × 0.20 × 0.20 mm, a = 9.190(1), b = 10.833(1), c = 17.730(1) Å, α = 80.144(1), β = 89.614(1), γ = 86.402(1)°, V = 1735.6(3) Å^3, Z = 2, μ = 1.649 mm^{-1}, D_c = 1.355 Mg m^{-3}, $2\theta_{max}$ = 25.66°, 23559 measured, 6102 (R_{int} = 0.035) independent and 4234 observed reflections with $I > 2\sigma(I)$, $R1$ = 0.031, $wR2$ = 0.0604 for 355 parameters, S = 0.950, Δ/ρ_{max} = 0.277 e Å^{-3}.

11: $C_{28}H_{39}BN_2O_3SiSn$, M_r = 609.20, crystal dimensions: 0.20 × 0.10 × 0.10 mm, a = 10.630(1), b = 17.201(1), c = 17.300(1) Å, α = 100.001(1), β = 90.737(1), γ = 104.343(1)°, V = 3012.9(4) Å^3, Z = 4, μ = 0.917 mm^{-1}, D_c = 1.343 Mg m^{-3}, D_m = 1.387(2) Mg m^{-3}, $2\theta_{max}$ = 25.68°, 41 109 measured, 10 578 ($R_{int.}$ = 0.024) independent and 7733 observed reflections with $I > 2\sigma(I)$, $R1$ = 0.031, $wR2$ = 0.0735 for 696 parameters, S = 0.999, Δ/ρ_{max} = 0.442 e Å^{-3}.

CCDC 182/1261. See: http://www.rsc.org/suppdata/cc/1999/1095/ for crystallographic files in .cif format.

‖ The unit cell of **11** consists of two independent conformers and consequently two signals are observed in the $^{119}Sn\{^1H\}$ MAS NMR spectrum.

1 (*a*) J. Beckmann, K. Jurkschat, B. Mahieu and M. Schürmann, *Main Group Met. Chem.*, 1998, **21**, 113; (*b*) J. Beckmann, B. Mahieu, W. Nigge, D. Schollmeyer, K. Jurkschat and M. Schürmann, *Organometallics*, 1998, **17**, 5697; (*c*) J. Beckmann, K. Jurkschat, U. Kaltenbrunner, N. Pieper and M. Schürmann, *Organometallics*, 1999, **18**, 1586; (*d*) J. Beckmann, K. Jurkschat, D. Schollmeyer and M. Schürmann, *J. Organomet. Chem.*, 1997, **543**, 229.

2 (*a*) I. Manners, *Angew. Chem.*, 1996, **108**, 1712; (*b*) D. A. Foucher, A. J. Lough and I. Manners, *Inorg. Chem.* 1992, **31**, 2034.

3 K. Jurkschat, S. Van Dreumel, G. Dyson, D. Dakternieks, T. J. Bastow, M. E. Smith and M. Dräger, *Polyhedron*, 1992, **11**, 2747.

4 (*a*) M. Veith, S. Mathur and V. Huch, *J. Am. Chem. Soc.*, 1996, **118**, 903; (*b*) M. Veith, S. Mathur and V. Huch, *Inorg. Chem.*, 1996, **35**, 7295.

5 (*a*) A. de Mallmann, O. Lot, N. Perrier, F. Lefebvre, C. Santini and J. M. Basset, *Organometallics*, 1998, **17**, 1031; (*b*) V. M. Jimenez, J. A. Mejias, J. P. Espinos and A. R. Gonzales-Elipe, *Surf. Sci.*, 1996, **366**, 545.

6 (*a*) H. Puff, W. Schuh, R. Sievers, W. Wald and R. Zimmer, *J. Organomet. Chem.*, 1984, **260**, 271; (*b*) H. Puff, S. Franken, W. Schuh and W. Schwab, *J. Organomet. Chem.* 1983, **254**, 33.

Communication 9/02428J

First crystallographic structure determination of an oligothiophene metal π-complex

Gerhard Grüner,[a] Tony Debaerdemaeker[b] and Peter Bäuerle*[a]

[a] *Abteilung Organische Chemie II, Universität Ulm, Albert-Einstein-Allee 11, 89081 Ulm, Germany. E-mail: peter.baeuerle@chemie.uni-ulm.de*

[b] *Sektion Röntgen- und Elektronenbeugung, Universität Ulm, Albert-Einstein-Allee 11, 89081 Ulm, Germany*

Received (in Cambridge, UK) 22nd March 1999, Accepted 4th May 1999

A novel oligothiophene metal π-complex containing the, as yet, longest α-conjugated oligothiophene as ligand is described; characterisation by X-ray and other physicochemical methods clearly reveals the influence of the metal units upon the electronic and the geometric structure.

Oligothiophenes represent ideal model compounds for the corresponding polydisperse conducting polymers[1] and novel materials used in organic transistors[2] or light emitting devices.[3] Therefore, the tailoring of the electronic properties by electronically active substituents,[4] the replacement of thiophene moieties by other heteroaromatic units,[5] and the coordination of transition metals to an oligothiophene core lead to pronounced alterations of the (electronic) properties.[6] The molecular arrangement of the oligothiophenes in the solid state may be crucial for the performance of the devices.[2] However, X-ray data for oligothiophenes have been sparse, since the growth of suited single crystals is very difficult, and the crystals often contain intrinsic disorder and defects.[5,7]

Herein we present the synthesis and characterisation of $[(CpRu)_2(\eta^6,\eta^6\text{-DB5T})](PF_6)_2$ **4**, a novel bis-ruthenium π-complex of 'benzo-capped' quinquethiophene **3**. In contrast to other examples,[6] the planar and stiff terminal benzo[*b*]thiophene units provide good stability and an optimal influence of the metal fragments onto the electronic properties.

According to Scheme 1, 4,7-di-*n*-butylbenzo[*b*]thiophene **1**[8] was reacted with Bu^nLi and bromine to yield the 2-bromo derivative **2** in 69% yield. Nickel-catalysed cross-coupling of the Grignard reagent of **2** and 5,5″-dibromoterthiophene yielded oligothiophene (DB5T) **3** (56%). The doubly ruthenated quinquethiophene $[(CpRu)_2(\eta^6,\eta^6\text{-DB5T})](PF_6)_2$ **4** was effectively formed by the reaction of **3** with two equiv. of $[CpRu(MeCN)_3]PF_6$ [9] (73% yield). The resulting metal complex **4** was purified by reprecipitation and is stable in air, is highly soluble in polar solvents such as dichloromethane, 1,2-dichloroethane, and in coordinating solvents such as acetone.†

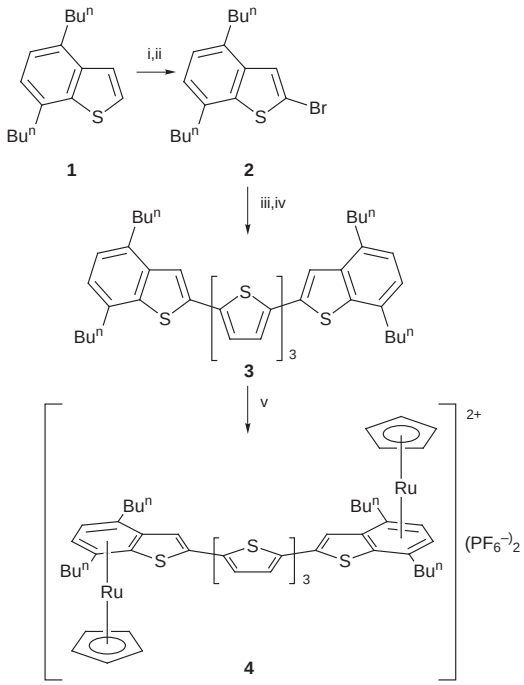

Scheme 1 *Reagents and conditions*: i, Bu^nLi, THF, −20 °C; ii, Br_2, −20 °C; iii, Mg; iv, $Ni(dppp)Cl_2$, Et_2O, Br–T_3–Br; v, $[CpRu(MeCN)_3]PF_6$, $C_2H_4Cl_2$, reflux.

Various 2D NMR spectroscopic experiments enabled the assignment of all ^1H and ^{13}C resonances in comparison to the non-complexed quinquethiophene **3**. The $CpRu^+$-fragments are exclusively η^6-bound to the anellated benzene rings. Owing to the influence of the metal, the proton resonances of the terminal benzo[b]thiophene units are strongly shifted upfield ($\Delta\delta$: $H^{3'''',3''''}$ = −0.20, $H^{5'''',5''''}$ = −1.02, $H^{6'''',6''''}$ = −1.00 ppm). In contrast, resonances of the central terthiophene moiety are shifted downfield ($\Delta\delta$: $H^{4,4''}$ = +0.18, $H^{3,3''}$ = +0.13, $H^{3',4'}$ = +0.14 ppm). The most pronounced changes in the ^{13}C NMR spectra are evident for the benzo carbons ($\Delta\delta$: $C^{3a''''}$, $C^{3a''''}$ = −32.3, $C^{4''''}$, $C^{4''''}$ = −34.5, $C^{5''''}$, $C^{5''''}$ = −39.8, $C^{6''''}C^{6''''}$ = −42.0, $C^{7''''}$, $C^{7''''}$ = −36.2, $C^{7b'''',7b''''}$ = −30.4 ppm).

To enable comparison with the non-complexed oligothiophene DB5T **3**, the electronic properties of metal complex **4** were determined by optical measurements and by cyclic voltammetry. In the absorption spectrum metallation of the oligothiophene causes a displacement of the unstructured π–π^* transition to lower energies and a decrease of the absorption coefficient [**3**: λ_{max} (lg ε) = 436 nm (4.76); **4**: λ_{max} (lg ε) = 454 nm (4.72)]. The emission spectrum of **3** exhibits a structured band at λ_{max} = 501 nm. Owing to a strong metal ligand interaction the fluorescence of **4** at λ_{max} = 533 nm is strongly quenched. The electrochemical characterisation of **3** reveals two fully reversible oxidation waves corresponding to two one electron transfer steps ($E°_1$ = 0.39 V, $E°_2$ = 0.75 V *vs*. Fc/Fc^+). As typical for electron-rich oligothiopenes, no reduction process can be observed in the negative potential regime ($E \geq -2$ V). Owing to the electron withdrawing character of the metal fragments, oxidation of **4** is shifted to positive potentials ($E°_1$ = 0.75 V, $E°_2$ = 1.06 V *vs*. Fc/Fc^+). Additionally, in the CV of **4** a reversible two electron reduction wave arises at $E°_3$ = −1.76 V *vs*. Fc/Fc^+ which corresponds well to the values obtained for other $[CpRu(arene)]^+PF_6^-$ salts.[10] Thus, the oxidation process is located on the oligothiophene core, whereas reduction occurs at the metal fragments.

Since no splitting of the reduction wave can be seen, electron transfer to the ruthenium centers occurs at the same energy indicating none, or at best weak, interaction *via* the conjugated π system (Fig. 1).

Small ruby red crystals of the oligothiophene metal complex **4** suitable for X-ray structure determination were grown by recrystallisation from CH_2Cl_2–Et_2O.‡ Views of the molecule in Fig. 2 verify the composition of the molecule. The oligothiophene core is nearly coplanar exhibiting small interplanar angles (ring 1,2: 5.0°; ring 2,3: 9.4°). Rather unique *syn*

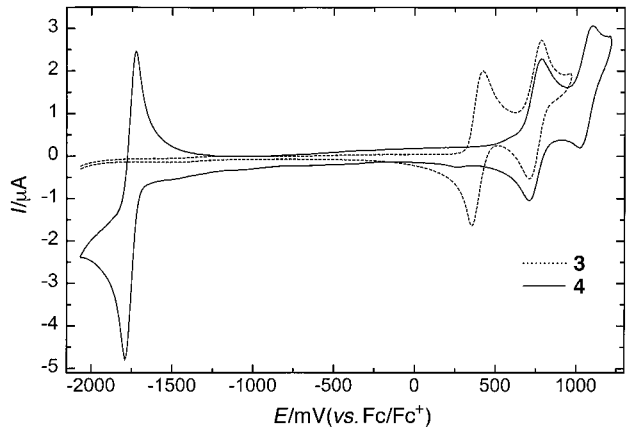

Fig. 1 Cyclic voltammograms (c = 10^{-3} mol l^{-1} substrate in CH_2Cl_2–TBAHFP (0.1 M), v = 100 mV s^{-1}; Pt disk working electrode, Pt wire counter electrode, Ag/AgCl reference electrode internally calibrated with the Fc/Fc^+-couple) of metallated oligothiophene [(CpRu)$_2$(η^6,η^6-DB5T)]$(PF_6)_2$ **4** (solid line) in comparison to the non-metallated ligand **3** (dashed line).

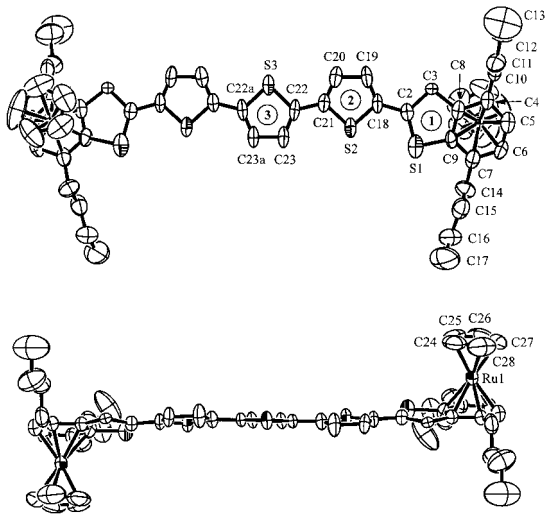

Fig. 2 ORTEP front view of oligothiophene metal complex **4** showing atomic labeling, 50% thermal ellipsoids (top). Side view of **4** (bottom). The PF_6^- counter ions have been omitted for clarity. Selected bond distances (Å): S(1)–C(2) 1.706(14), Ru(1)–C(4) 2.232(13), S(1)–C(9) 1.720(12), Ru(1)–C(5) 2.181(14), C(2)–C(3) 1.600(15), Ru(1)–C(6) 2.185(13), C(3)–C(8) 1.621(15), Ru(1)–C(7) 2.210(14), C(8)–C(9) 1.425(18), Ru(1)–C(8) 2.263(12), C(8)–C(4) 1.439(17), Ru(1)–C(9) 2.251(13), C(4)–C(5) 1.432(19), Ru(1)–C(24) 2.170(19), C(5)–C(6) 1.360(20), Ru(1)–C(25) 2.186(17), C(6)–C(7) 1.410(18), Ru(1)–C(26) 2.178(18), C(7)–C(9) 1.392(18), Ru(1)–C(27) 2.159(19), C(2)–C(18) 1.449(16), Ru(1)–C(28) 2.140 (20).

conformations of the terminal benzo[*b*]thiophene units are observed with respect to the central all *anti* terthiophene moiety which shows quite normal bond length and angles. The occurrence of *syn* conformers in coplanar arrangements has only been verified once previously in a mixed pentamer containing four thiophene and one 1,3,4-oxadiazole unit.[5] In accordance with the NMR assignments, the $CpRu^+$-fragments are η^6-coordinated to the terminal benzene rings and not η^5 to any thiophene ring. The two metal fragments are directed to opposite sides with respect to the oligothiophene plane representing one of two possible isomers.§ Simultaneously, the butyl side chains on each benzo[*b*]thiophene unit point in the opposite direction with respect to the coordinated metal. The distances Ru–C5/C6 are found to be shorter than Ru–C8/C9 indicating a transversal displacement of the metal atom by 0.07 Å from the center of the benzene ring to the ends of the molecule. This has been observed in the benzo[*b*]thiophene complex [(CpRu)(η^6-benzo[*b*]thiophene)]BF_4 and other transition-metal complexes containing fused arene ligands.[11] As a consequence, bonds C2–C3, C3–C8, and S1–C9 are longer than expected, while the corresponding bond angles are distorted.

Current efforts in our laboratory are now directed to the variation of the length of the oligothiophene ligand and variation of the transition metal.

We gratefully acknowledge a grant (Landesgraduiertenstipendium) for G. G. and Degussa AG for a generous gift of ruthenium trichloride.

Notes and references

† All new compounds had spectral (^{1}H NMR, ^{13}C NMR, UV–VIS) and microanalytical properties (C, H, S) consistent with the assigned structures.

‡ *Crystal data*: [(CpRu)$_2$(η^6,η^6-DB5T)]$(PF_6)_2$ **4**: $C_{54}H_{58}F_{12}P_2Ru_2S_5$, M = 1359.38, monoclinic, space group *I*2/*a*, a = 14.444(2), b = 16.998(3), c = 27.623(3) Å, β = 99.94(1)°, V = 6680.3(16) Å^3, Z = 2, D_c = 1.352 g cm^{-3}, crystal dimensions 0.15 × 0.27 × 0.77 mm, T = 220(2) K, μ = 0.721 cm^{-1} (analytical absorption correction). Intensity data were collected on a STOE-IPDS image-plate diffractometer [Mo-Kα radiation (λ = 0.71073 Å), graphite monochromator] in the φ rotation scan mode. 5186 unique reflections were measured and used in the refinement. The structure was solved by direct methods with the XMY93 program system.[12] The molecule is located on a crystallographic twofold axes passing through S3 and between C23 and C23a. Refinement (SHELXL93)[13] of positional and anisotropic thermal parameters for all non-hydrogen atoms converged to R = 0.0937 for 1873 reflections with $F_o \geq 4\sigma(F_o)$. The relatively poor R value is probably due to a disordered PF_6^- anion which was therefore only refined isotropically and to a high anisotropy of the terminal atoms. These effects could not be eliminated by low-temperature data collection.

CCDC 182/1243. See: http://www.rsc.org/suppdata/1999/1097/ for crystallographic files in .cif format.

§ Evidently, during the crystallization process only one possible isomer of compound **4** precipitated. The other isomer would comprise the same conformation of the oligothiophene core but with the two metal centers on the same side. Both isomers, presumably present in solution, can not be distinguished in NMR experiments.

1 P. Bäuerle, *Oligothiophenes* in *Electronic Materials: The Oligomeric Approach*, ed. G. Wegner and K. Müllen, Wiley-VCH, Weinheim, 1998, pp. 105–197.
2 G. Horowitz, *Adv. Mater*., 1998, **10**, 365.
3 F. Geiger, M. Stoldt, P. Bäuerle, H. Schweizer and E. Umbach, *Adv. Mater*., 1993, **5**, 922; G. Horowitz, P. Delannoy, H. Bouchriha, F. Deloffre, J.-L. Fave, F. Garnier, R. Hajlaoui, M. Heyman, F. Kouki, P. Valat, V. Wittgens and A. Yassar, *Adv. Mater*., 1994, **6**, 752; K. Uchiyama, H. Akimichi, S. Hotta, H. Noge and H. Sakaki, *Synth. Met*., 1994, **63**, 57.
4 J. Roncali, *Chem. Rev*., 1992, **92**, 711.
5 U. Mitschke, E. Mena-Osteritz, T. Debaerdemaeker, M. Sokolowski and P. Bäuerle, *Chem. Eur. J*., 1998, **4**, 2211.
6 D. D. Graf, N. C. Day and K. R. Mann, *Inorg. Chem*., 1995, **34**, 1562; D. D. Graf and K. R. Mann, *Inorg. Chem*., 1997, **36**, 141, 150; M.-G. Choi, D.-J. Jeong and M. Lee, *Mol. Cryst. Liq. Cryst*., 1997, **295**, 121; D. H. Kim, B. S. Kang, S. M. Lim, K.-M. Bark, B. G. Kim, M. Shiro, Y.-B. Shimand S. C. Shin, *J. Chem. Soc. Dalton Trans*., 1998, 1893.
7 D. Fichou and C. Ziegler, *Structure and Properties of Oligothiophenes in the Solid State: Single Crystals and Thin Films*, in *Handbook of Oligo- and Polythiophenes*, ed. D. Fichou, Wiley-VCH, Weinheim, 1999, pp. 183–282.
8 G. Grüner, M. Schlögl, T. Debaerdemaeker and P. Bäuerle, *Eur. J. Org. Chem*., in preparation.
9 T. P. Gill and K. R. Mann, *Organometallics*, 1982, **1**, 485.
10 O. V. Gusev, M. A. Ievlev, M. G. Peterleitner, S. M. Peregudova, L. I. Denisovich, P. V. Petrovskii and N. A. Ustynyuk, *J. Organomet. Chem*., 1997, **534**, 57 (*E vs.* SCE corresponds to *E vs.* Fc/Fc^+ −0.4 V).
11 S. C. Huckett, L. L. Miller, R. A. Jakobson and R. J. Angelici, *Organometallics*, 1988, **7**, 686.
12 T. Debaerdemaeker, *Z. Kristallogr*., 1993, **206**, 173.
13 G. M. Sheldrick, SHELXL93, University of Göttingen, 1993.

Communication 9/02249J

A homobimetallic vanadium d^2–d^2 complex $(Cp_2V)_2(3\eta:4\eta\text{-}Me_3SiC{\equiv}C{-}C{=}C{-}C{\equiv}CSiMe_3)$: structure and magnetism

Robert Choukroun,*[a] Christian Lorber,[a] Bruno Donnadieu,[a] Bernard Henner,[b] Richard Frantz[b] and Christian Guerin[b]

[a] *Equipe Précurseurs Moléculaires et Matériaux, Laboratoire de Chimie de Coordination du CNRS, 205 route de Narbonne, 31077, Toulouse Cedex, France. E-mail: choukrou@lcc.toulouse.fr*

[b] *Laboratoire 'Chimie Moléculaire et Organisation du Solide', UMR CNRS 5637, Université de Montpellier, 2 Place E. Bataillon, F-34095 Montpellier Cedex 5, France*

Received (in Cambridge, UK) 24th March 1999, Accepted 7th May 1999

The d^2–d^2 homobimetallic complex $(Cp_2V)_2(3\eta:4\eta\text{-}Me_3SiC{\equiv}C{-}C{=}C{-}C{\equiv}CSiMe_3)$ was synthesized from $Me_3SiC{\equiv}C{-}C{\equiv}C{-}C{\equiv}CSiMe_3$ and Cp_2V and characterized by an X-ray crystal structure; magnetic moment measurements from 300 to 2 K indicated a weak antiferromagnetic *J* exchange coupling of -3.7 cm^{-1}.

The chemistry of transition metal alkynyl and related complexes continues to be an attractive focus, and among its differing chemical and physical properties, their potential non-linear optical properties are of interest.[1] Furthermore, a rich acetylenic chemistry has recently been described with group 4 transition metals in which the synthon 'Cp_2Zr' played an important part.[2] Our research group has extended this concept to group 5 with the reactive isolable vanadocene Cp_2V complex.

The remarkable oxidative addition of vanadocene Cp_2V **1** to ethynyl –C≡C– bonds was demonstrated early and a vanadocyclopropene structure was established.[3] In previous papers, we established that Cp_2V reacts with $Cp'_2Zr(C{\equiv}CPh)_2$ to give $Cp_2V(\mu\text{-}\eta^2:\eta^4\text{-}C{\equiv}C{-}C{\equiv}CPh)ZrCp'_2$, with a vanadacyclopropane moiety containing two planar tetracoordinated carbons on the butadiyne ligand[4] or with the phosphane $ArP(C{\equiv}CPh)_2$ to give the adduct $Cp_2V(PhC{=}C)P(C{\equiv}CPh)Ar$.[5] Alternatively, two Cp_2V units can be added to a diethynyl ligand RC≡C–C≡CR (R = $SiMe_3$, Ph) to give a homobimetallic V^{IV}–V^{IV} system $(Cp_2V)_2(1{-}2\eta:3{-}4\eta\text{-}RC{=}C{-}C{=}CR)$ where the Cp_2V units are in *cis* or *trans* positions depending on the nature of R.[6] As such, particular attention is given to the reactivity of Cp_2V with a triyne $Me_3SiC{\equiv}C{-}C{\equiv}C{-}C{\equiv}CSiMe_3$[7] **2**, to establish a synthetic route to an ethynyl vanadium-bridged complex.

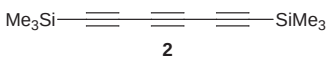

2

Addition of a pentane solution of **1** (2 or 3 equiv.) to **2** leads to a crystalline black solid $(Cp_2V)_2(3\eta:4\eta\text{-}Me_3SiC{\equiv}C{-}C{=}C{-}C{\equiv}CSiMe_3)$ **3**,† fully characterized by an X-ray structure

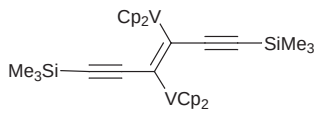

3

determination (Fig. 1).‡ Surprisingly, the vanadium atom has an oxidative state of +3, instead of the expected classical V^{IV} which to our knowledge has been observed in all other cases. The main feature of **3** is the bonding mode of the two vanadocene moieties which are attached to both the internal carbon atoms of the triyne *via* a single σ-type V–C(11a) bond of length 2.165 Å which raises the vanadium oxidation state from +2 to +3. The geometrical alteration of ligand **2** is reflected by the *trans* configuration of the triyne: the nearly linear –C–C≡CSiMe$_3$ moiety [C(11a)C(12)C(13) 165.5°, C(12)C(13)Si(1) 173.2°] forms a 113.4° angle with the C(11a)C(11a′) bond. The sum of the angles around C(11a) (nearly 360°) as well as the 1.381 Å bond length of C(11)–C(11a′) (in accord with a double bond) indicate an sp^2-ethylene structure. The SiC_6Si skeleton and the vanadium atoms are in the same plane and the dihedral angle between the plane of the Cp_2V unit (obtained from the centroids of the Cp rings and the vanadium atom) and the plane of the SiC_6Si ligand is 98.66°.

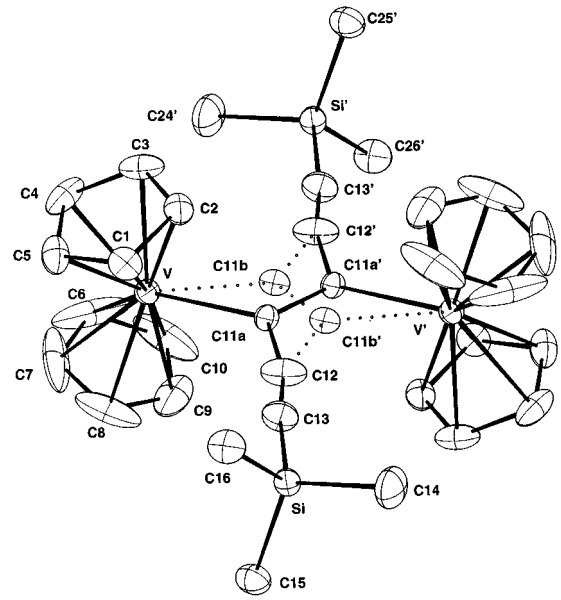

Fig. 1 Molecular structure of **3**. Selected distances (Å) and angles (°), hydrogen atoms omitted: V–C(11a) 2.165(4), C(11a)–C(11a′) 1.381(9), C(11)–C(12) 1.476(5), C(12)–C(13) 1.206(4), V···V′ 5.25, V–Cp 1.947(av.); Cp–V–Cp 147.8(av.) [Cp are the centroids of the C_5H_5 rings C(1)–C(5), C(6)–C(10)].

Variable-temperature magnetic susceptibility measurements have been carried out on the V^{III} homobimetallic d^2–d^2 species **3**.§ The effective moment μ_{eff} is 4.01 μ_B at 300 K, which is consistent with two vanadium(III) units ($\mu_{theor} = 2[\sqrt{\Sigma S(S+1)}] = 4$ for two non-interacting d^2 vanadium atoms). If the two magnetically equivalent d^2 centers are totally non-interacting, then μ_{eff} should remain constant over a large temperature range. The effective moment μ_{eff} decreases to 1.51 μ_B at 2 K. Fig. 2 shows a plot of the molar susceptibility per dimer χ_m, *vs.* *T*. The solid line represents a good fit and was considered to account for the observed dependence with an exchange interaction model, having a weak antiferromagnetism with $J = -3.7$ cm^{-1}.[8]

When 1 equiv. of **1** was treated with only 1 equiv. of **2** in pentane, tiny brown needles were obtained. Unfortunately, efforts to obtain suitable crystals for an X-ray diffraction analysis have to date failed. Elemental analysis and magnetic

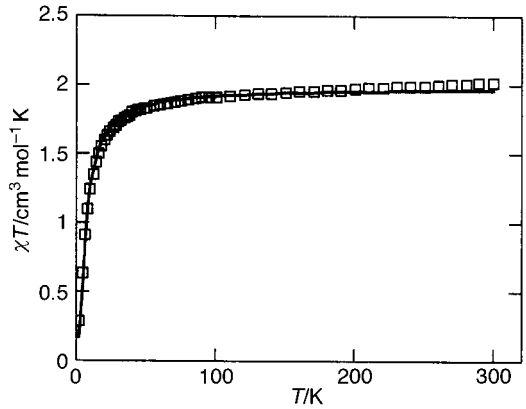

Fig. 2 Temperature dependance of molar magnetic susceptibilities per vanadium (□) of **3**; the solid line results from a least-squares theoritical fit.

studies (μ_{eff} = 1.9 μ_B) are in agreement with a vanadium(IV) atom bound to **2**,† and a vanadocene cyclopropene structure such as $Cp_2V(3–4\eta^2\text{-}Me_3SiC{\equiv}C–C{=}C–C{\equiv}CSiMe_3)$ **4** can be suggested. Treatment of **4** in C_6D_6 with another equiv. of **1** leads

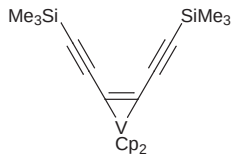

4

to **3**, as revealed by ^{1}H NMR spectroscopy (the ^{1}H NMR spectrum of paramagnetic **3** in C_6D_6 consists of an observable low field broad signal of Cp at δ 124 and a well resolved Me_3Si signal at δ 1.0. A comproportionation reaction between V^{IV} (**4**) and V^{II} (**1**) to give $2V^{III}$ (**3**) is probably operative but a mechanistic description must await further experimental evidence.

In summary, the reaction of **1** with a triyne ligand led to a homobimetallic d^2–d^2 complex. This unexpected reactivity seems to be due to the odd parity of the number of C≡C bonds in **2**.[7] It would be interesting experimentally to test other odd-yne ligands to understand the ligand/metal effects and efforts are currently being made in this direction.

Notes and references

† Satisfactory elemental analysis results were obtained for compounds **3** and **4**.

‡ *Crystallographic data* for **3**: $C_{32}H_{38}Si_2V_2$, M = 580.72, monoclinic, space group $P2_1/c$, a = 11.214(2), b = 113.778(2), c = 10.797(1) Å, β = 112.72(1)°, V = 1538.76 Å^3, Z = 4, D_c = 1.66 g cm^{-3}, μ = 6.82 cm^{-1}, $R(R_w)$ = 0.033(0.036) for 1719 unique data and 173 parameters, GOF = 1.08. Data collection was performed at *ca.* 180 K on a IPDS STOE diffractometer using graphite-monochromated Mo-Kα radiation. The structure was solved by direct methods and subsequent difference Fourier maps. A disordered distribution was observed for C(11) and the best model to fit the electronic density was to consider two positions C(11a) and C(11b) with a ratio of occupancy of 0.6/0.4. CCDC 182/1256. See http://www.rsc.org/suppdata/cc/1999/1099/ for crystallographic files in .cif format.

§ Magnetic susceptibilities were determined using a SQUID susceptometer within the temperature range 2–300 K. Using a Heisenberg Hamiltonian $H = -JS_AS_B$ with the local spin $S_A = S_B = 1$, the magnetic interaction was estimated with a model for dinuclear compounds [eqn. (1)].[9] The J and g parameters were determined by least-squares fitting. The agreement factor R [eqn. (2)] = 2.89 × 10^{-4}. The average value of the g-factor was 1.996.

$$\chi = \frac{2N\beta^2}{kT} g^2 \frac{e^x + 5e^{3x}}{1 + 3e^x + 5e^{3x}} \quad (x = J/kT) \tag{1}$$

$$R = \frac{\Sigma(\chi_m^{obs} - \chi_m^{calc})^2}{\Sigma(\chi_m^{obs})^2} \tag{2}$$

1 H. S. Nalwa and S. Miyata, *Nonlinear Optics of Organic Molecules and Polymers*, CRC Press, Boca Raton, FL, 1997; L. K. Myers, C. Langhoff and M. E. Thompson, *J. Am. Chem. Soc.*, 1992, **114**, 7560.

2 S. L. Buchwald and R. D. Broene, *Comprehensive Organometallic Chemistry II*, ed. E. W. Abel, F. G. Stone and G. Wilkinson, Pergamon Press, Fort Collins, vol. 12, ch. 7.4; J. A. Labinger, *Comprehensive Organic Chemistry*, ed. B. M. Trost and I. Fleming, Pergamon Press, New York, 1991, vol. 8, p. 667; see, for example: N. Suzuki, D. Y. Kondakov and T. Takahashi, *J. Am. Chem. Soc.*, 1994, **116**, 3431; B. P. Warner, M. Davis and S. L. Buchwald, *J. Am. Chem. Soc.*, 1994, **116**, 5471; M. R. Kesti and R. M. Waymouth, *Organometallics*, 1992, **11**, 1095; C. Lebefer, W. Baumann, A. Tillack, R. Kempe, H. Gorls and U. Rosenthal, *Organometallics*, 1996, **15**, 3486; H. Lang, W. Frosch, I. Y. Wu, S. Blau and B. Nuber, *Inorg. Chem.*, 1996, **35**, 6266; V. Varga, J. Hiller, M. Polasek, U. Thewalt and K. Mach, *J. Organomet. Chem.*, 1996, **515**, 57.

3 G. Fachinetti, C. Floriani, A. Chiesi-Villa and C. Guastini, *Inorg. Chem.*, 1979, **18**, 2282; J. L. Petersen and L. Griffith, *Inorg. Chem.*, 1980, **19**, 1852.

4 C. Danjoy, J. Zhao, B. Donnadieu, J.-P. Legros, L. Valade, R. Choukroun, A. Zwick and P. Cassoux, *Chem. Eur. J.*, 1998, **4**, 1100; R. Choukroun and P. Cassoux, *Acc. Chem. Res.*, 1999, in press.

5 R. Choukroun, Y. Miquel, B. Donnadieu, A. Igau, C. Blandy and J.-P. Majoral, *Organometallics*, 1999, **18**, 1795.

6 R. Choukroun, B. Donnadieu, I. Malfant, S. Haubrich, R. Frantz, C. Guerin and B. Henner, *Chem. Commun.*, 1997, 2315.

7 The central C≡C ethynyl bond of **2**, which is more electron-rich than the other C≡C ethynyl bonds may favor the reaction at the central core of the ligand; G. N. Patel, *J. Polym. Sci. Polym. Phys. Ed.*, 1979, **17**, 1591; Y. Rubin, S. S. Lin, C. B. Knobler, J. Anthony, A. M. Boldi and F. Diederich, *J. Am. Chem. Soc.*, 1991, **113**, 6943; F. Diederich, Y. Rubin, O. L. Chapman and N. S. Goroff, *Helv. Chim. Acta*, 1994, **77**, 1441; H. D. Kalinowski, S. Berger and S. Braun, *Carbon-13 NMR Spectroscopy*, J. Wiley, New York, 1988; C. Guerin and B. Henner, unpublished results.

8 The observed magnetic behaviour could equally well arise from a non-interacting distorted monomeric vanadium(II) centre; B. N. Figgis, J. Lewis and F. E. Mabbs, *J. Chem. Soc.*, 1960, 2480; B. N. Figgis, J. Lewis, F. E. Mabbs and G. A. Webb, *J. Chem. Soc. A*, 1966, 1411; D. J. Machin and F. E. Mabbs, *Magnetism and Transition Metal Chemistry*, Chapman and Hall, London, 1973, ch. 4 and 5.

9 O. Kahn, *Molecular Magnetism*, VCH, New York, 1993, p. 114.

Communication 9/02370D

Reversible methyl group migration between osmium and tin in reactions of osmium trimethylstannyl complexes

Clifton E. F. Rickard, Warren R. Roper,* Timothy J. Woodman and L. James Wright*

Department of Chemistry, The University of Auckland, Private Bag 92019, Auckland, New Zealand.
E-mail: w.roper@auckland.ac.nz

Received (in Cambridge, UK) 13th April 1999, Accepted 10th May 1999

Treatment of the coordinatively unsaturated osmium trimethylstannyl complex, $Os(SnMe_3)Cl(CO)(PPh_3)_2$ 1, with either pyridine (py) or sodium acetate results in methyl migration from tin to osmium, giving the structurally characterised complexes, $Os(Me)(SnClMe_2)(py)(CO)(PPh_3)_2$ 2 or $Os(Me)(SnMe_2OC[Me]O)(CO)(PPh_3)_2$ 3, respectively: the methyl migration is reversible and treatment of $Os(Me)(SnClMe_2)(py)(CO)(PPh_3)_2$ with CO gives the trimethylstannyl complex, $Os(SnMe_3)Cl(CO)_2(PPh_3)_2$.

α-Migration, as shown in eqn. (1), is an established feature of organometallic chemistry.[1] In the closely related metal silyl complex chemistry many transformations have been observed which imply the intermediacy of metal silylene complexes generated by 1,2-migration of an R group as in eqn. (2).[2] In one instance, when R = H, *reversible* 1,2-migration has been reported for a platinum silyl complex.[3] Since there is a substantial number of well characterised stannylene complexes[4] it can be envisaged that the type of interconversion represented in eqn. (3) might play a part in understanding the reactions

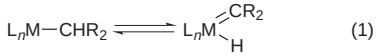

(1)

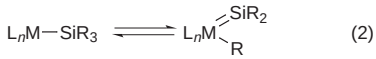

(2)

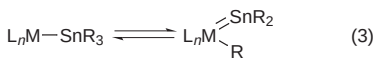

(3)

undergone by metal stannyl and metal stannylene complexes. Indeed, free, stable stannylenes have been inserted into metal–halogen bonds.[4] A further observation relevant to this idea is that $Ru[Sn(C_6H_4Me\text{-}p)_3]Cl(CO)(PPh_3)_2$ readily decomposes in solution to $Ru(C_6H_4Me\text{-}p)Cl(CO)PPh_3)_2$.[5] We describe herein new reactions undergone by the osmium trimethylstannyl complex, $Os(SnMe_3)Cl(CO)(PPh_3)_2$ **1**, in which (i) a methyl group migrates to osmium and this is accompanied by either a chloride transfer to tin forming a chlorodimethylstannyl ligand, or by formation of a bridging acetatodimethylstannyl ligand, (ii) an example of reverse migration of a methyl group from osmium to tin to reform the trimethylstannyl ligand, and (iii) the crystal structures of the two products of methyl migration to osmium, $Os(Me)(SnClMe_2)(py)(CO)(PPh_3)_2$ **2** (py = pyridine) and $Os(Me)(SnMe_2OC[Me]O)(CO)(PPh_3)_2$ **3**.

$Os(SnMe_3)Cl(CO)(PPh_3)_2$ **1**, when treated with CO, $CNC_6H_4Me\text{-}p$, or sodium dimethyldithiocarbamate, gives the expected six coordinate trimethylstannyl complexes, $Os(SnMe_3)Cl(CO)_2(PPh_3)_2$, $Os(SnMe_3)Cl(CO)(CNC_6H_4Me\text{-}p)(PPh_3)_2$, or $Os(SnMe_3)(\eta^2\text{-}S_2CNMe_2)(CO)(PPh_3)_2$.[6,7] We now report that reaction of **1** with pyridine (Scheme 1) leads not to the expected six-coordinate complex, '$Os(SnMe_3)Cl(py)(CO)(PPh_3)_2$', but rather to the colourless, methyl-migrated product, $Os(Me)(SnClMe_2)(py)(CO)(PPh_3)_2$ **2** in 64% isolated yield. That methyl group migration has occurred in the formation of **2** is revealed by the ^1H NMR spectrum which shows the osmium-bound methyl group as a triplet at δ 0.15 ($^3J_{HP}$ 6.62 Hz) (syntheses and other data for **2** and **3** are given in footnote †). This structural assignment was fully confirmed

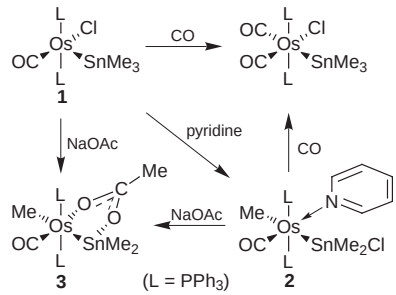

Scheme 1

by a crystal structure determination.‡ The structure of **2** is shown in Fig. 1, along with selected bond lengths and angles. The osmium–tin bond distance of 2.6741(4) Å does not differ substantially from the corresponding distances found in other osmium stannyl complexes. The osmium–bound methyl group is found to lie *trans* to the tin atom, with the angle C–Os–Sn at 175.30(12)°. The osmium–methyl bond length of 2.249(5) Å is similar to that observed in both $Os(Me)(H)(CO)_2(PPr^i_3)_2$ [2.198(17) Å][8] and $Os(Me)(I)(CO)_2(PMe_3)_2$ [2.174(15) Å].[9] The geometry around the tin centre is quite symmetrical with the angles Os–Sn–C(3), Os–Sn–C(4) and Os–Sn–Cl(1), all close to 120°.

Remarkably, when compound **2** is treated with CO, pyridine is displaced but the compound formed is not '$Os(Me)(SnMe_2Cl)(CO)_2(PPh_3)_2$'. Instead, the trimethylstannyl complex, $Os(SnMe_3)Cl(CO)_2(PPh_3)_2$, is obtained in 80% isolated yield, where the methyl group has migrated back to the tin atom and chloride has returned to osmium. It may be significant for this

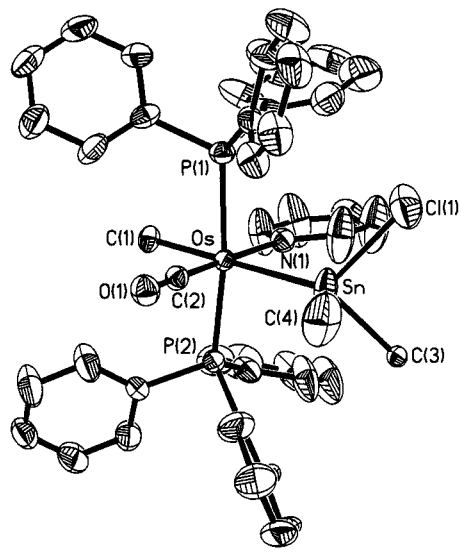

Fig. 1 Crystal structure of **2**. Selected bond lengths (Å) and angles (°): Os–Sn 2.6741(4), Os–C(1) 2.249(5), Os–N(1) 2.251(4), Sn–Cl(1) 2.422(2), Os–Sn–C(3) 123.47(11), Os–Sn–C(4) 120.9(2), Os–Sn–Cl(1) 119.17(6), C(3)–Sn–C(4) 99.5(3), C(1)–Os–Sn 175.30(12).

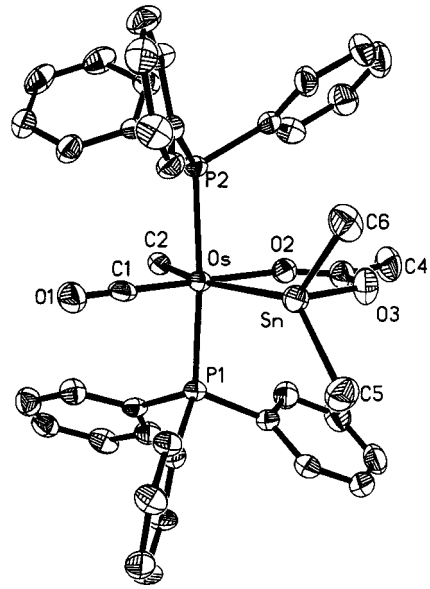

Fig. 2 Crystal structure of **3**. Selected bond lengths (Å) and angles (°): Os–Sn 2.6766(4), Os–C(2) 2.183(5), Os–O(2) 2.183(4), Sn–O(3) 2.143(4), Os–Sn–C(5) 131.22(19), Os–Sn–C(6) 129.70(18), C(5)–Sn–C(6) 98.2(3), C(2)–Os–Sn 158.77(15).

transformation that solutions of **2** are red suggesting that partial pyridine dissociation occurs to give a coordinatively unsaturated species in solution.

Treatment of **1** with sodium acetate also gives a methyl-migrated product, $\overline{Os(Me)(SnMe_2OC[Me]O)}(CO)(PPh_3)_2$ **3** (Scheme 1). The same compound is accessible from a reaction between **2** and sodium acetate. The ^{1}H NMR spectrum of **3** shows the osmium-bound methyl group as a triplet at δ 0.25 ($^3J_{HP}$ 7.12 Hz). The structure was confirmed by a crystal structure determination.‡ The molecular geometry of **3** is shown in Fig. 2, along with selected bond lengths and angles. The acetate bridges across the osmium–tin bond forming a five-membered chelate ring. The osmium–tin bond distance of 2.6766(4) Å does not differ substantially from the corresponding distances found in other osmium stannyl complexes. The osmium–methyl bond length is 2.183(5) Å, and the osmium-bound methyl group is found to lie *trans* to the tin atom, with the angle C–Os–Sn at 158.77(15)°. This considerable deviation from linearity is no doubt a consequence of the small O–Os–Sn angle required by the bridging acetate ligand. The osmium atom, the osmium-bound methyl, the carbonyl, the tin atom and the acetate ligand are all coplanar. The geometry around the tin centre is far from tetrahedral with C(5), C(6), Sn, and Os almost coplanar. The sum of the angles made by the two methyl groups and the osmium atom about tin is 359.1°, with the tin atom lying only 0.127(3) Å from the plane through C(5), C(6) and Os. The acetate oxygen, O(3), is bound to tin at a distance of 2.143(4) Å and the O(3)–Sn bond is perpendicular to the Os, Sn, C(5), C(6) plane. These structural parameters are compatible with some base-stabilised stannylene character in the bonding of the tin ligand. The tin resonance found in the ^{119}Sn NMR spectrum of **3** is a triplet signal at δ 392.94 ($^2J_{SnP}$ 119.4 Hz).

We have as yet no mechanistic information regarding these methyl group migrations. However, from the observations depicted in Scheme 1 and discussed herein, it is clear that methyl migration occurs only when a coordinatively unsaturated osmium stannyl species is accessible. It is possible that such a species is in an equilibrium of the type shown in eqn. (3).

T. J. W. is grateful to the Royal Society (London) for the award of a postdoctoral fellowship.

Notes and references

† *Synthesis of* $Os(Me)(SnClMe_2)(py)(CO)(PPh_3)_2$ **2**: $OsHCl(CO)(PPh_3)_3$ (1.00 g, 0.960 mmol) was added directly to a solution of trimethylvinyltin (1.00 g, 5.23 mmol) in a mixture of benzene (18 mL) and toluene (18 mL) and heated to reflux under nitrogen. The mixture was then photolysed with a 1000 W tungsten/halogen lamp held 10 cm from the flask, the heat of the lamp being sufficient to maintain reflux. After 7 min the photolysis was stopped. The resulting red solution of $Os(SnMe_3)Cl(CO)(PPh_3)_2$ **1** was cooled to 0 °C in an ice bath and pyridine (2 mL) was added. The red colour changed rapidly to pale yellow. The reaction was maintained at room temperature for 30 min and then the solvent was removed *in vacuo*. Recrystallisation from dichloromethane–ethanol gave **2** as a white microcrystalline solid in 63.8% yield. ν_{max}(Nujol mull)/cm^{-1}: 1878 (CO); δ_H($CDCl_3$, 400.133 MHz, 300 K) 0.15 [t, 3H, OsCH_3, ^3J(PH) 6.62 Hz], 0.24 [s, 6H, SnCH_3, ^2J(SnH) 21.0 Hz), 6.95–7.60 (m, 35H, PPh_3 and pyridine); δ_{Sn}($CDCl_3$, 149.144 MHz, 300 K) 186.63 [t, ^2J(SnP) 110.4 Hz]. Calc. for $C_{45}H_{44}NOClP_2OsSn$: C, 52.93; H, 4.34; N, 1.37. Found: C, 53.52; H, 4.32; N, 1.26%.

Synthesis of $\overline{Os(Me)(SnMe_2OC[Me]O)}(CO)(PPh_3)_2$ **3**: to the red solution of $Os(SnMe_3)Cl(CO)(PPh_3)_2$ **1** produced as described above but cooled only to 40 °C, was added NaO_2CMe (0.080 g, 0.975 mmol) dissolved in a mixture of ethanol (10 mL) and water (5 mL). The colour of the solution changed from deep red to pale yellow over 10 s. The reaction mixture was then stirred at room temp. for 30 min. Solvent removal *in vacuo* provided a pale yellow solid which was recrystallised from dichloromethane–ethanol to give colourless microcrystals of **3** in 76.4% yield, mp 167–171 °C. ν_{max}(Nujol mull)/cm^{-1}: 1881 (CO), 1535 (O_2CMe); δ_H($CDCl_3$, 400.133 MHz, 300 K) −0.19 [s, 6H, Sn·CH_3, ^2J(SnH) 21.4 Hz], 0.25 [t, 3H, OsCH_3, ^3J(PH) 7.12 Hz], 0.71 (s, 3H, O_2CCH_3), 7.25–7.70 (m, 30H, PPh_3); δ_{Sn}($CDCl_3$, 149.144 MHz, 300) 392.94 [t, ^2J(SnP) 119.4 Hz]. Calc. for $C_{42}H_{42}O_3P_2SnOs$: C, 52.24; H, 4.38%. Found: C, 53.53; H, 4.38%.

‡ *Crystal data*: **2**·CH_2Cl_2: crystals were grown from dichloromethane–ethanol. $C_{45}H_{44}ClNOP_2OsSn\cdot CH_2Cl_2$, M = 1106.02, triclinic, space group $P\bar{1}$, a = 9.6249(1), b = 12.5510(2), c = 19.6568(3) Å, α = 96.708(1), β = 97.968(1), γ = 107.02(1)°, U = 2217.36(5) Å^3, F(000) = 1088, D_c = 1.657 g cm^{-3}, Z = 2, μ(Mo-Kα, λ = 0.71073 Å) = 3.714 mm^{-1}. Intensity data were collected to a θ limit of 27.45° on a Siemens 'SMART' diffractometer[10] at 203(2) K and corrected for absorption.[11] The structure was solved using Patterson methods[12] and refined by full-matrix least squares analysis on F^2 employing SHELXL97.[13] All non-hydrogen atoms were allowed to assume anisotropic motion, except C(3) which was refined isotropically. Hydrogens were placed in calculated positions and refined using a riding model. Refinement converged to 0.0384 (R_w = 0.0944) for 9304 reflections for which $I > 2\sigma(I)$.

3·CH_2Cl_2: crystals were grown from dichloromethane–ethanol. $C_{42}H_{42}O_3OsP_2Sn\cdot CH_2Cl_2$, M = 1050.51, triclinic, space group $P\bar{1}$, a = 9.8487(1), b = 11.9753(2), c = 18.5656(3) Å, α = 95.559(1), β = 101.214(1), γ = 103.598(1)°, U = 2064.36(5) Å^3, F(000) = 1032, D_c = 1.690 g cm^{-3}, Z = 2, μ(Mo-Kα, λ = 0.71073 Å) = 3.924 mm^{-1}. Intensity data were collected to a θ limit of 27.40° on a Siemens 'SMART' diffractometer[10] at 203(2) K and corrected for absorption.[11] The structure was solved by direct methods[12] and refined by full-matrix least-squares analysis on F^2 employing SHELXL97.[13] All non-hydrogen atoms were allowed to assume anisotropic motion. Hydrogens were placed in calculated positions and refined using a riding model. Refinement converged to 0.0401 (R_w = 0.0721) for 7401 reflections for which $I > 2\sigma(I)$.

CCDC 182/1258. See http://www.rsc.org/suppdata/cc/1999/1101/ for crystallographic files in .cif format.

1 R. H. Crabtree, *The Organometallic Chemistry of the Transition Metals*, Wiley, New York, 2nd edn., 1994, p. 176.
2 K. H. Pannell and H. K. Sharma, *Chem. Rev.*, 1995, **95**, 1351; T. D. Tilley, *Comments Inorg. Chem.*, 1990, **10**, 37.
3 G. P. Mitchell and T. D. Tilley, *J. Am. Chem. Soc.*, 1998, **120**, 7635.
4 M. F. Lappert and R. S. Rowe, *Coord. Chem. Rev.*, 1990, **100**, 267.
5 G. R. Clark, K. R. Flower, W. R. Roper and L. J. Wright, *Organometallics*, 1993, **12**, 259.
6 P. D. Craig, K. R. Flower, W. R. Roper and L. J. Wright, *Inorg. Chim. Acta*, 1995, **240**, 385.
7 C. E. F. Rickard, W. R. Roper, T. J. Woodman and L. J. Wright, *Chem. Commun.*, 1999, 837.
8 M. A. Esteruelas, F. J. Lahez, J. A. Lopez, L. A. Oro, C. Schlünken, C. Valero and H. Werner, *Organometallics*, 1992, **11**, 2034.
9 G. Bellachioma, G. Cardaci, A. Macchioni and P. Zanazzi, *Inorg. Chem.*, 1993, **32**, 547.
10 SMART and SAINT, Siemens Analytical Instruments Inc., Madison, WI, 1994.
11 R. H. Blessing, *Acta Crystallogr., Sect. A*, 1995, **51**, 33.
12 SHELXTL, Siemens Analytical Instruments Inc., Madison, WI, USA, 1994.
13 G. M. Sheldrick, SHELXS-97, Program for the Solution of Crystal Structures, Universität Göttingen, Germany, 1997.

Communication 9/02938I

Oxidation catalysis over functionalized metalloporphyrins fixated within ultralarge-pore transition metal-doped silicate supports

Lei Zhang, Tao Sun and Jackie Y. Ying*

Department of Chemical Engineering, Massachusetts Institute of Technology, Cambridge, MA 02139, USA. E-mail: jyying@mit.edu

Received (in Bloomington, IN, USA) 22nd January 1999, Accepted 29th April 1999

Amine-functionalized metalloporphyrins stably fixated on well-defined ultralarge-pore Nb-doped silicates provided excellent catalytic oxidation activity for bulky substrates.

Numerous efforts have focused on fixating enzyme-mimic metalloporphyrin catalysts to prevent self-oxidation of the active centers and to achieve easy recovery of the catalysts.[1,2] Conventional supports for metalloporphyrins include polymer resins, amorphous porous silicas, layered clays and zeolites.[2] Leaching of the porphyrins from conventional supports and steric hindrance of the catalyst due to matrix pore geometry represent major impediments to the development of effective heterogenized metalloporphyrin catalysts. To prevent distortion of the porphyrin macrocycles and to facilitate the diffusion of reactants and products in catalytic reactions, it would be ideal to employ an inorganic support with a well-defined pore structure having pore openings > 2 nm. MCM-41 silicate[3] with its unique hexagonally-packed mesoporous structure represents an attractive host for supporting the large metalloporphyrin molecules.[4,5] A highly active oxidation catalyst has been prepared by anchoring of Ru-porphyrins *via* axial nitrogen ligands to the surface of MCM-41 modified with 3-aminopropyltriethoxysilane.[4]

Our laboratory has successfully synthesized novel transition metal oxide analogs of MCM-41 (*e.g.* Nb–TMS1 and Ta–TMS1) using a covalent linkage between the amine surfactant molecules and the transition metal precursors to ensure strong interaction between the templating agents and the inorganic species during the self-assembly process.[6] In this study, we have introduced transition metal dopants into the MCM-41 silicate framework to provide distinct sites for covalent bonding with the intentionally chosen NH_2 substituents on porphyrin macrocycles. This strategy effectively fixates the porphyrins without engaging their metal centers, leaving the latter accessible as active sites for oxidation catalysis. This technique is different from previous reports, which employed MCM-41 grafted with bulky compounds for ligand bonding with porphyrins,[4] or involved encapsulation of porphyrins through hydrothermal synthesis or ion-exchange *via* hindered diffusion in MCM-41 with relatively small mesopore size (22–24 Å).[5] By directly anchoring the porphyrin molecules onto the pore walls, steric effects associated with the support structure can be minimized. The importance of active site accessibility is further illustrated in this study, which presents a first investigation on the effects of pore size and porphyrin loading on the conversion of bulky substrates during oxidation catalysis.

Nb-doped mesoporous silicates NbSil-R (where R represents the precursor Si-to-Nb atomic ratio) were synthesized by mixing an aqueous cetyltrimethylammonium bromide (CTAB) surfactant solution with a 10 wt% aqueous tetramethylammonium silicate solution, followed by the addition of niobium ethoxide.[7] To increase the pore size of Nb-doped silicates, a mixture of cationic and neutral surfactants was used in the derivation of ultralarge-pore NbSi4-R.† Both NbSi4-R and NbSil-R gels were washed with ethanol and water, filtered and calcined at 540 °C in air for 6 h for surfactant removal. To examine the effect of support microstructure on catalytic activity, an amorphous Nb-doped silica gel was synthesized by sol–gel processing of tetraethoxysilane and niobium ethoxide under acidic conditions in the absence of surfactant templating agents. Iron porphyrins were introduced to the various calcined Nb-doped silicate supports by stirring in $CHCl_3$ for 24 h at room temp. The amine-functionalized iron porphyrins, Fe(III)T_{NH_2}PPBr, were prepared using a modified literature procedure.[8]

X-Ray diffraction (XRD) patterns illustrated the hexagonally-packed pore structure of our Nb-doped mesoporous silicate samples.[7] There was negligible hysteresis in the adsorption–desorption isotherms of NbSil-5.4 and NbSi4-20, and narrow BJH (Barrett–Joyner–Halenda) pore size distributions centered at 24 and 33 Å (Table 1) were noted for these two samples, respectively. NbSil-5.4 and NbSi4-20 possessed BET (Brunauer–Emmett–Teller) surface areas of 1140 and 864 $m^2\ g^{-1}$, respectively. By contrast, the amorphous Nb-doped SiO_2 sample had a type I isotherm characteristic of microporous materials (pore size < 20 Å) and a BET surface area of 557 $m^2\ g^{-1}$.

The diffuse-reflectance UV–VIS spectrum of the supported FeT_{NH_2}PPBr catalysts showed a broad Soret absorption band at 420 nm, indicating the presence of iron porphyrins in the mesoporous matrix. The appearance of the Q band implies no distortion of the conjugated porphyrin plane[9] in the large pore

Table 1 Oxidation over supported or unsupported FeT_{NH_2}PPBr catalysts under ambient conditions[a]

Support	Nb (wt%)	Fe[b]/ mg	Surface area/ $m^2\ g^{-1}$	Pore size/Å	Substrate	Conversion[c] (%)	Selectivity			TON/mol (mol Fe)$^{-1}$	Duration/h
							Oxide	1-ol	1-one		
—	—	0.69	—	—	Cyclohexene	100	79.4	13.3	7.3	40	2
NbSil-5.4	7.72	0.75	1140	24	Cyclohexene	86	58.2	25.1	17.7	32	2
NbSi4-20	6.00	0.14	864	33	Cyclohexene	85	78.9	12.1	9.0	170	2
—	—	0.14	—	—	Cyclooctene	85	100	—	—	170	5
NbSil-5.4	7.72	0.75	1140	24	Cyclooctene	57	100	—	—	21	5
NbSil-11.4	3.64	0.36	1477	23	Cyclooctene	42	100	—	—	33	5
NbSi4-20	6.00	0.14	864	33	Cyclooctene	98	100	—	—	196	5
Nb-doped silica gel	8.60	0.36	557	< 20	Cyclooctene	14	100	—	—	11	5

[a] Reaction conditions: 1 ml substrate, 4 ml CH_2Cl_2 and 0.5 mmol iodosobenzene. [b] Total Fe content from unsupported porphyrin catalysts, or from 100 mg of supported porphyrin catalysts. [c] Conversion was determined by GC and based on moles of iodobenzene formed during the reaction in air.

opening of our mesoporous support. The mesostructure of the Nb-doped mesoporous silicates was preserved upon $FeT_{NH_2}PPBr$ loading, as indicated by XRD. In addition, the absence of XRD peaks associated with iron porphyrin crystallites demonstrated that the iron porphyrins were highly dispersed in the mesoporous matrix. N_2 adsorption–desorption analyses confirmed that the iron porphyrins were loaded within the pore channels of the Nb-doped mesoporous silicates. For example, $FeT_{NH_2}PPBr$/NbSi4-20 has a lower BET surface area (666 $m^2\ g^{-1}$), pore volume (0.89 $cm^3\ g^{-1}$) and average pore size (32 Å), compared to the unloaded NbSi4-20 support (864 $m^2\ g^{-1}$, 1.14 $cm^3\ g^{-1}$, 33 Å).

The heterogeneous metalloporphyrin catalysts were tested at ambient conditions in a 25 ml batch micro-reactor (Table 1). Epoxidation of cyclohexene over $FeT_{NH_2}PPBr$/NbSil-5.4 gave a total conversion of 86% after only 2 h. In addition to cyclohexene oxide, cyclohex-2-en-1-ol and cyclohex-2-en-1-one were found as by-products possibly *via* allylic oxidation. Allylic oxidation might be initiated by O_2, resulting in cyclohexenyl peroxyl radicals.[10] Allylic oxidation has also been observed during cyclohexene epoxidation over polymer-supported iron porphyrin catalysts, which yielded cyclohex-2-en-1-one as the main product.[11] In comparison, significantly greater selectivity to cyclohexene oxide (58.2%) was achieved with our supported catalyst. This might be attributed to faster diffusion of the cyclohexene oxide products out of the mesoporous structure, thus alleviating further oxidation. The unsupported metalloporphyrin catalysts provided a faster reaction rate and produced an even better epoxide selectivity (79.4%) since there were no steric hindrance effects associated with substrate diffusion. We found that the use of a Nb-doped silicate support with larger pores greatly facilitated substrate diffusion. When loaded with $FeT_{NH_2}PPBr$, NbSi4-20 with 33 Å pores led to significantly higher epoxide selectivity (78.9%) than NbSil-5.4 (24 Å pores, 58.2% selectivity). Cyclohexene conversions over these two supported catalysts were similar after 2 h, even though a lower $FeT_{NH_2}PPBr$ loading was employed in NbSi4-20.

We also examined cyclooctene as a substrate that is less prone to O_2 oxidation than cyclohexene. Unlike cyclohexene, the selectivity to epoxide was 100% in the oxidation of cyclooctene. The conversion after 5 h of reaction was higher for $FeT_{NH_2}PPBr$/NbSil-5.4 than for $FeT_{NH_2}PPBr$/NbSil-11.4, as the higher Nb dopant concentration of the former allowed for a greater maximum metalloporphyrin loading level (Table 1). However, TON decreased with increased metalloporphyrin loading in the NbSil-R supports, suggesting that not all the metalloporphyrin sites were accessible to the bulky substrates for epoxidation catalysis, possibly due to the pore size constraint of the support matrix (23–24 Å).

The effect of support pore size on catalytic conversion of cyclooctene was examined systematically to investigate the role of diffusional restriction in the heterogenized catalysts. Among the various systems examined, $FeT_{NH_2}PPBr$ supported on sol–gel derived amorphous Nb-doped silica showed the lowest activity after 5 h (14% conversion, TON = 11). This could be attributed to steric constraints within this microporous support. With an identical Fe loading of 0.36 mg, mesoporous NbSil-11.4 provided 3 times greater activity (42% conversion, TON = 33) than microporous Nb-doped silica gel. Using mesoporous NbSi4-20, which has a larger pore size (33 Å) than NbSil-11.4 (23 Å), 98% epoxidation of cyclooctene was achieved in < 5 h despite the lower Fe loading (0.14 mg). An excellent TON of 196 was achieved over $FeT_{NH_2}PPBr$/NbSi4-20, which was even higher than that attained by the homogeneous $FeT_{NH_2}PPBr$ system (TON = 170). For both $FeT_{NH_2}PPBr$/NbSi4-20 and unsupported $FeT_{NH_2}PPBr$, a similar catalyst loading of 0.14 mg Fe was introduced to the reactant solution. The greater TON over $FeT_{NH_2}PPBr$/NbSi4-20 suggested that highly dispersed iron porphyrins fixated within supports of sufficiently large pore dimensions would have no diffusional constraints that inhibit substrate conversion, while preventing the detrimental self-oxidation of metalloporphyrins experienced in homogeneous systems. Our studies clearly showed that the support microstructure and iron porphyrin loading were important factors governing the catalyst performance.

During the course of the oxidation reactions, no catalyst leaching was detected in our systems, as indicated by the absence of the characteristic Soret band associated with free $Fe(III)T_{NH_2}PPBr$ in the UV–VIS spectra of the reaction solutions. This confirmed that $Fe(III)T_{NH_2}PPBr$ was stably immobilized within the porous Nb-doped silicate framework *via* the N–Nb ligand interaction. We further examined catalytic performance over multiple oxidation cycles, and found no degradation in conversion over our supported catalyst systems for at least three oxidation cycles. These studies demonstrated the effectiveness of heterogenizing catalysts through strong catalyst–support interactions, which could be established easily *via* appropriate doping of the porous support. The flexibility of pore size tailoring in Nb-doped mesoporous silicates further enabled us to optimize the activity of supported iron porphyrins by providing full accessibility to the catalytic sites. Such catalyst design considerations can be applied broadly to achieve heterogenized catalysts of bulky, stereospecific enzyme and organometallic complexes for effective and efficient synthesis of fine chemicals and pharmaceuticals.

This work was supported by the David and Lucile Packard Foundation and the Camille and Henry Dreyfus Foundation.

Notes and references

† Synthesis of NbSi4-R. 5 mmol of CTAB and 2.5 mmol of tetradecylamine (Acros) were first dissolved in 108 g of water. 11.4 g of tetraethoxysilane (United Chemical) were gradually added to the surfactant solution at room temp. and stirred for 30 min. A measured amount of niobium ethoxide was then introduced dropwise into the loosley-bonded silica gel. The resulting gel mixture was adjusted to pH 11 with the addition of tetraethylammonium hydroxide, and stirred for 3 h at ambient conditions before subjected to hydrothermal treatment at 120 °C for 4 days.

1 D. Ostovic, G. S. He and T. C. Bruice, in *Metalloporphyrins in Catalytic Oxidations*, ed. R. A. Sheldon, Marcel Dekker, New York, 1994, ch. 2.
2 B. Meunier, *Chem. Rev*., 1992, **92**, 1411.
3 C. T. Kresge, M. E. Leonowicz, W. J. Roth, J. C. Vartuli and J. S. Beck, *Nature*, 1992, **359**, 710; A. Monnier, F. Schüth, Q. Huo, D. Kumar, D. I. Margolese, R. S. Maxwell, G. D. Stucky, M. Krishnamurthy, P. Petroff, A. Firouzi, M. Janicke and B. F. Chmelka, *Science*, 1993, **261**, 1299; P. T. Tanev and T. J. Pinnavaia, *Science*, 1995, **267**, 865; H. Yang, A. Kuperman, N. Coombs, S. Mamiche-Afara and G. A. Ozin, *Science*, 1996, **379**, 703.
4 C.-J. Liu, S.-G. Li, W.-Q. Pang and C.-M. Che, *Chem. Commun*., 1997, 65; C.-J. Liu, W.-Y. Yu, S.-G. Li and C.-M. Che, *J. Org. Chem*., 1998, **63**, 7364.
5 B. T. Holland, C. Walkup and A. Stein, *J. Phys. Chem. B*, 1998, **102**, 4301.
6 D. M. Antonelli and J. Y. Ying, *Angew. Chem., Int. Ed. Engl*., 1996, **35**, 426; D. M. Antonelli, A. Nakahira and J. Y. Ying, *Inorg. Chem*., 1996, **35**, 3126; D. M. Antonelli and J. Y. Ying, *Chem. Mater*., 1996, **8**, 874; T. Sun and J. Y. Ying, *Nature*, 1997, **389**, 704.
7 L. Zhang and J. Y. Ying, *AIChE J*., 1997, **43**, 2793.
8 J. Collman, R. R. Gagne, C. A. Reed, T. R. Halbert, G. Lang and W. T. Robinson, *J. Am. Chem. Soc*., 1975, **97**, 1427.
9 P. Rothemund, *J. Am. Chem. Soc*., 1939, 2012.
10 J. T. Groves and D. V. Subramanian, *J. Am. Chem. Soc*., 1984, **106**, 2177.
11 D. R. Leanord and J. R. Lindsay Smith, *J. Chem. Soc., Perkin Trans. 2*, 1990, 1917.

Communication 9/00629J

Donor complexes of bis(1-indenyl)phenylborane dichlorozirconium as isospecific catalysts in propene polymerization

Manfred T. Reetz,* Marc Willuhn, Christian Psiorz and Richard Goddard

Max-Planck-Institut für Kohlenforschung, Kaiser-Wilhelm-Platz 1, D-45470 Mülheim/Ruhr, Germany.
E-mail: reetz@mpi-muelheim.mpg.de

Received (in Cambridge, UK) 30th March 1999, Accepted 7th May 1999

Chiral boron-bridged *ansa*-type zirconocenes can be prepared in a few simple steps; various donor molecules such as Et_2O, THF or PMe_3 undergo complexation at boron leading to catalysts having vastly different catalytic properties in Ziegler–Natta polymerization of propene; the PMe_3-containing catalyst is the most active and stereoselective (96% isotacticity).

The nature of substituents and the substitution pattern of titanocenes and zirconocenes are known to exert a pronounced influence on their activity and selectivity as catalysts in Ziegler–Natta polymerization.[1] Recently, several zirconocenes borylated at the Cp-moiety have been prepared and tested as catalysts.[2,3] None of them showed activity in the polymerization of propene, and some even failed to polymerize ethene,[3] possibly due to decomposition caused by the co-catalyst methylalumoxane (MAO) which is generally required as an activator. Here, we describe the synthesis of donor-coordinated *ansa*-type zirconocenes **1** and their use as catalysts in the

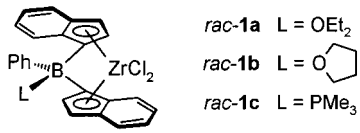

production of polypropene (PP). Significantly, it turns out that the nature of the donor ligand L determines the activity and stereoselectivity of the catalytic system, *i.e.* it can be used as a handle to control the polymerization.

The starting point for the synthesis of zirconocenes **1** was bis(1*H*-inden-1-yl)phenylborane **4**, readily accessible as a 1:1 mixture of *rac*- and *meso*-stereoisomers by the reaction of dichlorophenylborane **2** with indenyllithium **3** (Scheme 1). Although it was possible to convert **4** into the corresponding dianion by treatment with lithium bis(trimethylsilyl)amide (LiHMDS),[4] at least 20% of indenyllithium **3** was formed as an undesired side-product. This problem was solved by first isomerizing **4** into the thermodynamically more stable compound **5** in 95% yield by the action of catalytic amounts of PPr^i_3 and then effecting double deprotonation. Upon reacting $ZrCl_4$ with the intermediate dianion, a 1:1 mixture of *rac*-**1a** and *meso*-**1a** as well as non-identified side-products were formed.

Following removal of solid components, the solution was cooled to −20 °C, from which diastereomerically pure *rac*-**1a** crystallized as an orange–red solid in 12% yield. It was unambiguously characterized by ^{1}H, ^{11}B and ^{13}C NMR spectroscopy. Treatment of *rac*-**1a** with a solvent mixture of THF and CH_2Cl_2 led to the formation of *rac*-**1b** whereas the reaction with PMe_3 in toluene afforded adduct *rac*-**1c**. In both cases it was possible to obtain crystals suitable for an X-ray structural analysis (Fig. 1).† It should be mentioned that a different boron-bridged zirconocene has been described previously, but it was not possible to obtain crystals for an X-ray structural analysis, nor did it show activity towards ethene polymerization.[3] PMe_3 has been used to form adducts with other borylated metallocenes.[2c] The present C_1-symmetric compounds are structurally similar. In the case of *rac*-**1b** the angle between zirconium and the center of the two five-membered rings is 122.3(8)° (mean), which lies between that of the known Me_2C-bridged bis(indenyl)dichlorozirconium (118.2°)[5] and that of the Me_2Si-bridged analog (127.8°).[6] For *rac*-**1c** this angle was found to be 121.5(7)°, similar to that in *rac*-**1b**. Nevertheless, the Zr···B–O angle in*rac*-**1b** [120.4(6)°] is significantly smaller than the Zr···B–P angle in *rac*-**1c** [131.3(2)°].

In order to test the complexes in olefin polymerization, activation by treatment with MAO in toluene for 5 min was performed in all cases. Although compound *rac*-**1a** was found to be a fairly active catalyst (200–2600 kg PE mol[Zr]$^{-1}$ h^{-1})

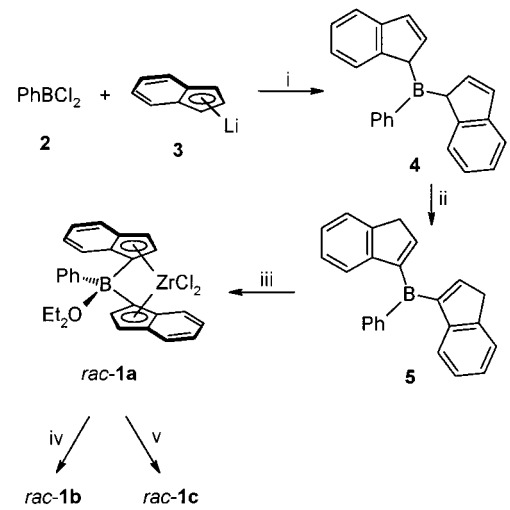

Scheme 1 *Reagents and conditions*: i, Et_2O, −70 to 20 °C, 12 h (75–85%); ii, PPr^i_3 (2 mol%), Et_2O, 20 °C, 16 h (85%); iii, (*a*) LiHMDS (2.05 equiv.), Et_2O, −70 to 20 °C, 10 h; (*b*) $ZrCl_4$ (1 equiv.), toluene–Et_2O, −70 to 20 °C, 12 h; iv, THF–CH_2Cl_2 (1:1); v, PMe_3 (7 equiv.), toluene, −70 to 20 °C (21%).

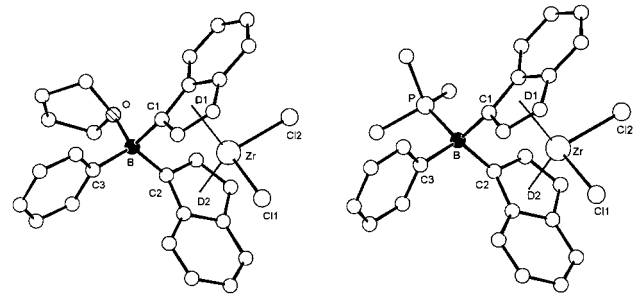

Fig. 1 Molecular structures of *rac*-**1b** (left) and *rac*-**1c** (right). Selected interatomic distances (Å) and angles (°): left (mean of two independent molecules): Zr···B 3.117(8), B–O 1.626(4), B–C3 1.603(5), Cl1–Zr–Cl2 99.5(3), D1–Zr–D2 122.3(8), Zr···B–O 120.4(6), Zr···B–C3 132.1(3), O–B–C3 107.5(2), C1–B–C2 101.5(2); right: Zr···B 3.173(3), B–P 2.006(3), B–C3 1.618(4), Cl1–Zr–Cl2 96.58(3), D1–Zr–D2 121.5(7), Zr···B–P 131.3(2), Zr···B–C3 126.7(4), P–B–C3 102.0(2), C1–B–C2 99.4(2).

Table 1 Polymerization of propene with *rac*-**1c** in toluene as solvent and MAO as activator[a]

T/°C	Al : Zr	Productivity/kg PP mol[Zr]$^{-1}$ h^{-1}	10^{-3} M_w/g mol^{-1}	Tacticity (% mmmm-pentades)
20	1000	326	315	96
40	220	783	161	93
40	1000	1052	129	90
40	5000	1232	97	93
60	1000	174	62	85

[a] *Polymerization conditions*: 2 bar propene, 1 h, *ca*. 30 μmol l^{-1} [Zr].

for ethene polymerization producing high molecular weight polymer ($M_w \approx 700000$ g mol^{-1} as determined by GPC), this complex turned out to be a rather poor catalyst for the polymerization of propene. For example, using a Al/Zr ratio of 1000, activities of only 10–75 kg PP mol[Zr]$^{-1}$ h^{-1} were observed at room temperature with the production of atactic oily PP ($M_w \approx 20000$ g mol^{-1}). In contrast, the phosphine adduct *rac*-**1c** displayed remarkably high activity and stereoselectivity (Table 1). ^{13}C NMR spectra of typical PP samples obtained at various polymerization temperatures demonstrate high degrees of isotacticity, *e.g.* 96% isotacticity at room temperature.

Thus, complex *rac*-**1c** is the first boron-bridged zirconocene which catalyzes the polymerization of propene. It competes well with other *ansa*-type zirconocenes, especially with respect to isotacticity and molecular weight.[5,6] Since the ether analog *rac*-**1a** is a poor catalyst, it is obvious that the nature of the donor ligand at boron is crucial. A possible explanation is that for *rac*-**1a** excess MAO induces decomplexation of the donor ligand, thereby initiating the decomposition of the *ansa*-metallocene, whereas for *rac*-**1c** the donor ligand PMe_3 remains bonded to boron throughout the polymerization. Whatever the exact explanation may be, it is clear that the use of PMe_3 provides a handle to control activity and tacticity. It remains to be seen whether other phosphines or different donor ligands induce similar effects.

Notes and references

† *Crystal data: rac*-**1b**: $C_{28}H_{25}BCl_2OZr$, M_r = 550.41, orange prism, crystal size 0.28 × 0.32 × 0.49 mm, a = 10.746(1), b = 15.510(3), c = 16.308(3) Å, α = 62.15(1), β = 82.92(1), γ = 83.25(1)°, U = 2379.2(7) Å^3, T = 293 K, triclinic, space group $P\bar{1}$ (no. 2), Z = 4, D_c = 1.54 g cm^{-3}, μ = 0.71 mm^{-1}. Enraf-Nonius CAD4 diffractometer, Mo-Kα X-radiation, λ = 0.71069 Å. 11215 measured reflections, no absorption correction, 10815 unique, 8006 observed [$I > 2.0\sigma(F_o^2)$]. The structure was solved by direct methods (SHELXS-97) and refined by full-matrix least-squares (SHELXL-97) on F^2 for all data with Chebyshev weights to R = 0.038 (obs.), wR = 0.105 (all data), 595 parameters, S = 1.02, H atoms riding, max. shift/error 0.001, residual ρ_{max} = 0.775 e Å^{-3}. CCDC 000/000.

rac-**1c**: $C_{27}H_{26}BCl_2PZr\cdot2.5CH_2Cl_2$, M_r = 766.69, orange prism, crystal size 0.18 × 0.32 × 0.32 mm, a = 33.5561(8), b = 10.9508(2), c = 20.6866(6) Å, β = 121.201(2)°, U = 6502.1(3) Å^3, T = 100 K, monoclinic, space group $C2/c$ (no. 15), Z = 8, D_c = 1.57 g cm^{-3}, μ = 0.98 mm^{-1}. Siemens SMART diffractometer, Mo-Kα X-radiation, λ = 0.71073 Å. 34678 measured reflections, no absorption correction, 11860 unique, 8996 observed [$I > 2.0\sigma(F_o^2)$]. The structure was solved by direct methods (SHELXS-97) and refined by full-matrix least-squares (SHELXL-97) on F^2 for all data with Chebyshev weights to R = 0.062 (obs.), wR = 0.137 (all data), 357 parameters, S = 1.13, H atoms riding, max. shift/error 0.001, residual ρ_{max} = 2.678 e Å^{-3} (0.789 Å from Cl6 in solute).

CCDC 182/1257. See http://www.rsc.org/suppdata/cc/1999/1105/ for crystallographic files in .cif format.

1 Reviews: *Ziegler Catalysts: Recent Scientific Innovations and Technological Improvements*, ed. G. Fink, R. Mülhaupt and H. H. Brintzinger, Springer, Berlin, 1995; M. Bochmann, *J. Chem. Soc., Dalton Trans.*, 1996, 255; H.-H. Brintzinger, D. Fischer, R. Mülhaupt, B. Rieger and R. Waymouth, *Angew. Chem.*, 1995, **107**, 1255; *Angew. Chem., Int. Ed. Engl.*, 1995, **34**, 1143; see also: L. Resconi, F. Piemontesi, I. Camurati, O. Sudmeijer, I. E. Nifant'ev, P. V. Ivchenko and L. G. Kuz'mina, *J. Am. Chem. Soc.*, 1998, **120**, 2308; I.-M. Lee, W. J. Gauthier, J. M. Ball, B. Iyengar and S. Collins, *Organometallics*, 1992, **11**, 2115.

2 (*a*) M. T. Reetz, H. Brümmer, M. Kessler and J. Kuhnigk, *Chimia*, 1995, **49**, 501; (*b*) M. Bochmann, S. J. Lancaster and O. B. Robinson, *J. Chem. Soc., Chem. Commun.*, 1995, 2081; (*c*) D. S. Stelck, P. J. Shapiro, N. Basickes and A. L. Rheingold, *Organometallics*, 1997, **16**, 4546: (*d*) R. Duchateau, S. J. Lancaster, M. Thornton-Pett and M. Bochmann, *Organometallics*, 1997, **16**, 4995; (*e*) S. J. Lancaster, M. Thornton-Pett, D. M. Dawson and M. Bochmann, *Organometallics*, 1998, **17**, 3829; (*f*) J. Ruwwe, G. Erker and R. Fröhlich, *Angew. Chem.*, 1996, **108**, 108; *Angew. Chem., Int. Ed. Engl.*, 1996, **35**, 80.

3 K. A. Rufanov, V. V. Kotov, N. B. Kazennova, D. A. Lemenovskii, E. V. Avtomonov and J. Lorberth, *J. Organomet. Chem.*, 1996, **525**, 287; K. Rufanov, E. Avtomonov, N. Kazennova, V. Kotov, A. Khvorost, D. Lemenovskii and J. Lorberth, *J. Organomet. Chem.*, 1997, **536**–**537**, 361; personal communication from K. A. Rufanov to M. Willuhn, 1997.

4 For the use of weakly nucleophilic bases for the deprotonation of cyclopentadienyl- and indenyl-boranes see also: G. E. Herberich and A. Fischer, *Organometallics*, 1996, **15**, 58; G. E. Herberich, E. Barday and A. Fischer, *J. Organomet. Chem.*, 1998, **567**, 127; E. Barday, B. Frange, B. Hanquet and G. E. Herberich, *J. Organomet. Chem.*, 1999, **572**, 225.

5 A. Z. Voskoboynikov, A. Y. Agarkov, E. A. Chernyshev, I. P. Beletskaya, A. V. Churakov and L. G. Kuz'mina, *J. Organomet. Chem.*, 1997, **530**, 75.

6 W. A. Herrmann, J. Rohrmann, E. Herdtweck, W. Spaleck and A. Winter, *Angew. Chem.*, 1989, **101**, 1536; *Angew. Chem., Int. Ed. Engl.*, 1989, **28**, 1511.

Communication 9/02543J

Control of copper(II) coordination geometry *via* supramolecular assembly of ligands in the solid state

David J. White,*[a] Leroy Cronin,[a] Simon Parsons,[a] Neil Robertson,[a] Peter A. Tasker*[a] and Adrian P. Bisson[b]

[a] *Department of Chemistry, The University of Edinburgh, Joseph Black Building, Kings Buildings, West Mains Rd., Edinburgh, UK EH9 3JJ. E-mail: P.A.Tasker@ed.ac.uk*

[b] *Zeneca Specialties plc, PO Box 42, Hexagon House, Blackley, Manchester, UK M9 8ZS*

Received (in Cambridge, UK) 19th March 1999, Accepted 6th May 1999

The high density and strength of intermolecular hydrogen bonding between amine and sulfonamide units in the complex [Cu(Tstn)$_2$] [TstnH = *N*-(3-aminopropyl)-4-methylbenzenesulfonamide] give rise to energetically unfavourable coordination geometries at the copper centres in the solid state, in a manner analogous to the entatic state forced on metal active sites in metalloenzymes through secondary and tertiary protein structures.

The blue copper sites, present in several protein environments, exhibit a number of characteristics, derived from unusual electronic structures, that distinguish them from small molecule, copper(II) complexes.[1,2] These characteristics arise from distorted coordination geometries at the metal centre. The mismatch between the coordination environment supplied by the protein (determined by its amino acid sequence and hydrogen bonded structure), and that preferred by the metal centre (determined by electronic and steric effects) leads to this metastable 'entatic' or 'rack' state.[3,4] Entatic states have been modelled in small molecules by using rigid, predisposed[5] or sterically hindered ligands.[6] Although hydrogen bonded systems have been widely studied due to their potential to control solid state geometries[7] their application in imposing 'entatic states' in simple metal complexes has not been described previously.

In the system presented here we have used an unhindered ligand to engineer a high density of hydrogen bond donors and acceptors into a copper(II) complex, which lead to a large number of intermolecular interactions in the solid state. The copper(II) complex [Cu(Tstn)$_2$] exists in two crystalline forms which differ only in the disposition of intermolecular hydrogen bonds, but which have distorted copper coordination geometries that differ markedly from each other and from that seen in solution.

Reaction of TstnH, **1**, with copper acetate in boiling methanol gives a deep blue solution which, on evaporation at ambient temperature, deposits a dark blue crystalline compound, **2,** identified as [Cu(Tstn)$_2$].† If evaporation is prevented and the solution is instead left to stand at ambient temperature in a sealed vessel, it deposits a bright green crystalline compound, **3**, with the same molecular formula, [Cu(Tstn)$_2$]. In solution (DMF) the electronic and electrospray mass spectra of **2** and **3** are identical, suggesting that a single species is present. The compounds can be interconverted by dissolution in hot methanol; evaporation produces **2**, whilst crystallization on cooling and standing produces **3**, regardless of the starting complex. The marked difference in colour and in the measured solid state visible spectra, in the FTIR spectra and in the melting behaviour of the two solids led us to determine X-ray crystal structures for both to define the origin of these differences.‡

The asymmetric unit of the blue compound, **2**, contains two almost isostructural but independent [Cu(Tstn)$_2$] molecules (weighted rms deviation 1.062 Å) in which the ligands chelate the metal through deprotonated sulfonamide and amine nitrogens (Fig. 1). The coordination geometry (Table 1) at copper is highly distorted square planar (dihedral angles between the chelate planes 36.4 and 34.5° in the two independent molecules). All the amine protons form intermolecular hydrogen bonds (Table 2) to sulfonamide oxygens resulting in zigzag

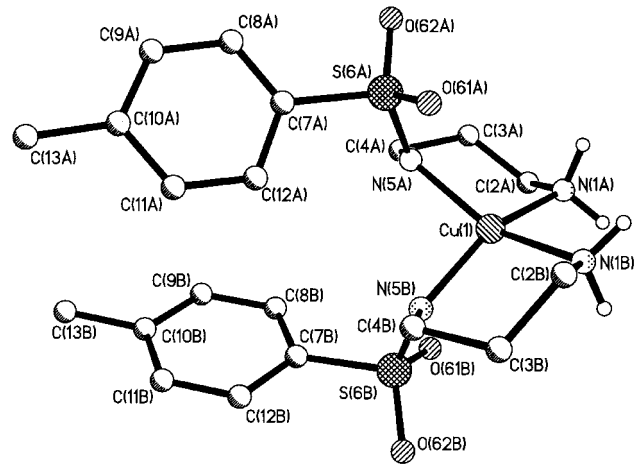

Fig. 1 Molecular structure of **2**. Only amine hydrogens are shown. Selected bond distances and angles for **2** are given in Table 1.

Table 1 Selected bond distances (Å) and angles (°) in **2** and **3**

	2	**3**		**2**	**3**
Cu1–N1A	2.023(7)	2.001(5)	N1A–Cu1–N1B	91.8(2)	95.01(16)
Cu1–N1B	2.013(7)	2.009(5)	N1A–Cu1–N5A	91.2(3)	93.3(2)
Cu1–N5A	1.970(8)	1.946(6)	N1A–Cu1–N5B	154.5(4)	138.3(2)
Cu1–N5B	1.954(8)	1.959(6)	N1B–Cu1–N5A	153.7(4)	137.1(2)
S6A-O61A	1.448(7)	1.445(4)	N1B-Cu1-N5B	90.5(3)	93.7(2)
S6A-O62A	1.449(7)	1.463(5)	N5A-Cu1-N5B	97.9(2)	107.33(18)

Table 2 Hydrogen bonded distances (Å) and angles (°) in **2** and **3**

	H···O	N–H···O	N···O
2			
N1A–H1A1···O61D	2.170	172.6(9)	3.075(12)
N1A–H1A2···O62B	2.068	170.5(9)	2.969(12)
N1B–H1B1···O61B	2.181	172.9(9)	3.086(11)
N1B–H1B2···O62D	2.072	173.1(8)	2.977(11)
N1C–H1C1···O62C	2.178	168.3(9)	3.075(11)
N1C–H1C2···O62A	2.052	163.2(9)	2.934(12)
N1D–H1D1···O61A	2.139	172.7(9)	3.044(12)
N1D–H1D2···O61C	1.996	170.4(9)	2.898(12)
3			
N1A–H1A1···O62A	2.086	153.1(6)	2.927(6)
N1A–H1A2···O62B	2.344	141.2(5)	3.106(6)
N1B–H1B1···O62B	2.058	151.9(5)	2.893(6)
N1B–H1B2···O62A	2.405	140.4(5)	3.160(6)

Note: the N-H distances were fixed at 0.91 Å. H-bonds were assigned using the Platon program[13] to interactions of the oxygen and nitrogen atoms that were < 3.12 Å.

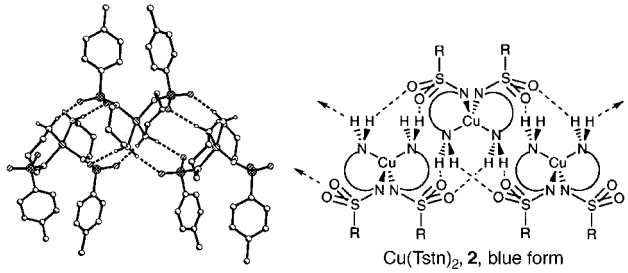

Fig. 2 Hydrogen bonded interactions in the solid state structure of **2** and a schematic representation of these interactions. Selected distances are given in Table 1.

chains of the complex extending through the structure (Fig. 2).

The asymmetric unit of the green compound, **3**, contains a single [Cu(Tstn)$_2$] molecule (Fig 3). The copper centre has a more nearly tetrahedral geometry; the dihedral angle between the two chelate planes is 58.4° and the N1–Cu–N5 chelate angles are larger, 93.3(2) and 93.7(3)°, than in **2** (average 90.9°). One of the oxygen atoms on each sulfonamide group forms two hydrogen bonds to amine protons. All of the amine protons are therefore involved in hydrogen bonds and each complex has eight S=O···H–N interactions, four as the donor and four as the acceptor. This results in the formation of a linear one dimensional hydrogen bonded polymer of [Cu(Tstn)$_2$] molecules (Fig. 4). Both **2** and **3** are very insoluble materials, dissolving only very slowly in polar solvents, reflecting the large number of intermolecular interactions. The number of hydrogen bonds that each molecule is involved in is the same in each structure. However, the mean of the O···N distances is shorter in **2** and the mean of the O···H–N angles is closer to 180°, suggesting that the hydrogen-bonded interactions are stronger than those in **3**. A survey of the CSD[8] reveals that the majority of copper(II) N_4 complexes with 1,3-diaminopropane based ligands are square planar[9] and deviation from this geometry is only observed with very bulky ligands.[6] The significant distortion toward the energetically unfavourable tetrahedral geometry observed in **2** and **3** appears to be a consequence of the system seeking the lowest free energy in the solid state *via* formation of very stable hydrogen bonding networks favoured by the ligands. This offers the intriguing possibility of controlling the electronic and magnetic properties of metal centres in the solid state using simple ligands designed to provide a matrix with unusual coordination sites for metals. Whilst such an approach is analogous to the entatic state[3] binding sites in proteins, unlike these, the unusual geometries are unlikely to be preserved in solution.

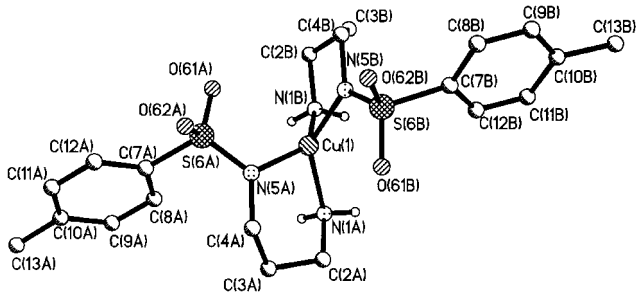

Fig. 3 Molecular structure of **3**. Only amine hydrogens are shown. Selected bond distances and angles are given in Table 1.

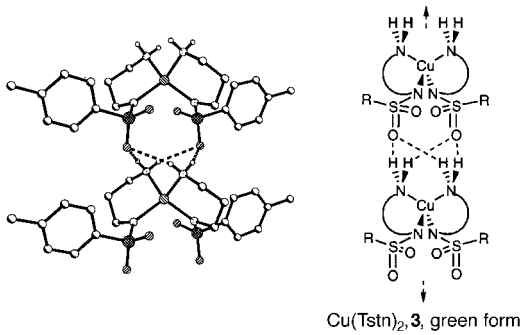

Fig. 4 Hydrogen bonded interactions in the solid state structure of **2** and a schematic representation of these interactions. Selected distances are given in Table 1.

We thank Mr J. Millar and Mr. W. Kerr for obtaining NMR spectra, Mr A. Taylor and Mr H. MacKenzie for mass spectra, Ms. L Eades for elemental analyses and Dr R. O. Gould and Mr. S. G. Harris for help in collecting X-ray data. Thanks to the Royal Society of Edinburgh (N. R.), the Leverhume Trust (L. C.) and Zeneca Specialties plc for funding.

Notes and references

† *Experimental procedures*: **1**: this was prepared by a modification of the method described by Kirsanov and Kirsanova.[10]

2: A solution of **1** (0.228 g, 1 mmol) in boiling methanol (10 mL) was added to a solution of copper acetate hydrate (0.1 g, 0.5 mmol) also in methanol (10 mL). Immediately a dark, ink blue solution was obtained. The solution was filtered hot then allowed to cool to room temperature. Evaporation of solvent at ambient temperature over 24 h gave dark blue crystals. These were collected by filtration, washed with methanol (3 × 5 mL), then diethyl ether (2 × 5 mL) and dried *in vacuo* (22 mg, 20% yield). Crystals suitable for X-ray diffraction were obtained by evaporation of a saturated methanol solution of the complex; mp 170 °C, decomp. 200 °C (Found: C, 46.39; H, 5.60; N, 10.60. Calc. for $C_{20}H_{30}N_4CuO_4S_2$: C, 46.36; H, 5.84; N, 10.81%); UV–VIS [λ_{max}/nm (ε dm^3 mol^{-1} cm^{-1})]: dmf, 620 (135); reflectance, 495; MS (FAB, nba) *m/z* [Cu(Tstn)$_2$]$^+$ 518.

3: This complex was prepared in an identical manner to **2**. However, instead of evaporating the dark blue solution it was left to stand in a sealed vessel at ambient temperature for 48 h giving bright green crystals. These were collected by filtration, washed with methanol (3 × 5 mL), then diethyl ether (2 × 5 mL) and dried *in vacuo* (24 mg, 22% yield). Crystals suitable for X-ray diffraction could be obtained using this method; mp (18 °C decomp.) 200 °C (Found: C, 46.36; H, 5.91; N, 10.79. Calc. for $C_{20}H_{30}N_4CuO_4S_2$: C, 46.36; H, 5.84; N, 10.81%). UV–VIS [λ_{max}/nm (ε dm^3 mol^{-1} cm^{-1})]: dmf, 620 (135); reflectance, 510. MS (FAB, nba) *m/z* [Cu(Tstn)$_2$]$^+$ 518.

‡ *Crystal data:* both structures were solved by Patterson methods (DIRDIF)[11] and refined against F^2 (SHEXL-97).[12] **2**: $C_{20}H_{30}N_4CuO_4S_2$, M = 518.14, monoclinic, space group $P2_1/c$, a = 15.019(6), b = 24.783(10), c = 12.873(8) Å, β = 101.43(4)°, U = 4696(4), Z = 8, D_c = 1.466 g cm^{-3}, T = 220(2) K, μ (Cu-K$_\alpha$) = 3.26 mm^{-1}, wR_2 = 0.1923 (8543 independent reflections), R = 0.0612 [$F > 4\sigma(F)$].

3: $C_{20}H_{30}N_4CuO_4S_2$, M = 518.14, monoclinic, space group C2/c, a = 32.427(7)), b = 6.1076(15), c = 23.254(5) ≈, β = 96.30(3)°, U = 4577.6(19), Z = 8, D_c = 1.504 gcm^{-3}, T = 220(2) K, μ (Mo-Kα) = 1.171 mm^{-1}, wR_2 = 0.1157 (4050 independent reflections), R = 0.0524 [$F > 4\sigma(F)$]. CCDC 182/1246. See http://www.rsc.org/suppdata/cc/1999/1107/ for crystallographic files in .cif format.

1 H. B. Gray and E. I. Solomon, in *Copper Proteins*, ed. T. G. Spiro, Wiley, New York, 1981, pp 1–39.
2 E. I. Solomon, in *Copper Coordination Chemistry*, ed. K. Karlin and J. Zubieta, Adenin Press, New York, 1982, pp 1–22.
3 R. J. P. Williams, *Eur. J. Biochem.*, 1995, **234**, 363.
4 B. G. Malström, *Eur. J. Biochem.*, 1994, **223**, 711.
5 T. C. Higgs and C. J. Carrano, *Inorg. Chem.*, 1997, **36**, 291.
6 J. McMaster, R. L. Beddoes, D. Collison, D. R. Eardley, M. Helliwell and C. D. Garner, *Chem. Eur. J.*, 1996, **2**, 685.
7 D. Braga and F. Grepioni, *J. Chem. Soc., Dalton Trans.*, 1999, 1.
8 D. A. Fletcher, R. F. McMeeking and D. J. Parkin, *J. Chem. Inf. Comput. Sci.*, 1996, **36**, 746.
9 See, for example B. Morosin and J. Howatson, *Acta Crystallogr., Sect. B*, 1970, **26**, 2062.
10 A. V. Kirsanov and N. A. Kirsanova, *J. Gen. Chem. USSR*, 1962, **32**, 877.
11 P. T. Beurskens, G. Beurskens, W. P. Bosman, R. d. Gelder, S. Garcìa-Granda, R. O. Gould, R. Israël and J. M. M. Smits, DIRDIF-96, University of Nijmegen, The Netherlands, 1996.
12 G. M. Sheldrick, SHELXL-97, University of Göttingen, Germany, 1997.
13 A. L. Spek. *Acta Crystallogr., Sect. A*, 1990, **46**, C34.

Communication 9/02196E

ChemComm

Stereoselective Yang cyclizations of α-amido ketones

Axel G. Griesbeck,* Heike Heckroth and Johann Lex

Institute of Organic Chemistry, University of Cologne, Greinstr. 4, D-50939 Köln, Germany.
E-mail: griesbeck@uni-koeln.de

Received (in Liverpool, UK) 4th March 1999, Accepted 29th April 1999

The photocyclization of methyl-substituted α-acetamido butyrophenone derivatives is highly stereoselective and leads to 2-aminocyclobutanols with complete control of three new stereogenic centers.

The term Yang cyclization describes the formation of cyclobutanols from 1-hydroxytetramethylene biradicals which are produced *via* photochemical γ-hydrogen abstraction.[1] In the course of this reaction up to eight diastereoisomers could be formed from one chiral substrate molecule. Three subsequent steps influence the chemo- and stereoselectivity of this reaction: (i) γ-H abstraction, (ii) biradical dynamics and (iii) biradical combination *vs.* cleavage reaction. Triplet excited carbonyls give rise to triplet 1,4-biradicals and, consequently, the lifetime of these intermediates (100–1000 ns)[2] rises due to slow spin inversion processes (ISC). The γ-H abstraction proceeds most likely through a six-membered chair-like transition state.[3] Detailed mechanistic investigations have been performed by Wagner and co-workers which also included stereochemical probing.[4] During our studies on photochemical transformations of enantiomerically pure α-amino acids (N-activation mode)[5] we became interested in using Yang cyclizations as a simple tool for the synthesis of 2-aminocyclobutanols (C-activation mode). As substrates α-acetamido butyrophenone derivatives **1a**–**f** were synthesized from the corresponding amino acids by a three-step reaction protocol.[6] The photochemical behaviour of these compounds was investigated by irradiation with light λ > 320 nm in benzene solutions (Scheme 1). The *tert*-leucine derivative **1a** gave the cyclobutanol **2a** (Φ_C = 0.11 ± 0.02) and the Norrish II fragmentation product **3** (Φ_F = 0.08 ± 0.02).[7] The Yang cyclization product was isolated in 45% yield as a single diastereoisomer. The *tert*-leucine **1a** and the leucine derivative **1b**, respectively, were transformed into cyclobutanols with only one additional stereogenic center and thus solely show the influence of a given stereogenic center on a proximate radical center. In both cases, the *cis*-diastereoisomers were formed with ds > 96%.

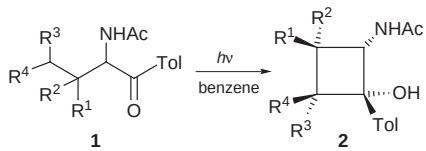

1 **2**

	R^1	R^2	R^3	R^4	C/F
a	Me	Me	H	H	50:50
b	H	H	Me	Me	49:51
c	Me	H	H	H	74:26
e	H	H	Me	H	33:67
f	H	H	Et	H	48:52

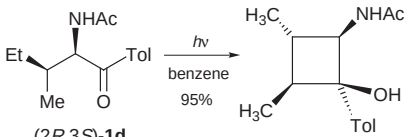

(2*R*,3*S*)-**1d** **2d**

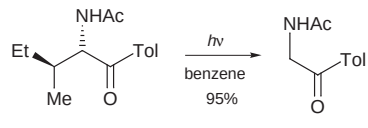

(2*S*,3*S*)-**1d** **3**

Scheme 1 C/F = cyclization/fragmentation ratio.

Characteristic NMR shifts were observed for H-2 (δ 4.2–4.8) and the methyl groups in **2b** which showed strong anisotropic effects ($\Delta\delta$ = 0.45 ppm).[8] Additional proof came from the X-ray structure analysis for **2b** (Fig. 1).† A reasonable explanation for the high 1,2-asymmetric induction might be an intramolecular hydrogen bond at the stage of the triplet 1,4-biradical which has already been described for Yang cyclizations of α-ester-substituted ketones.[9] The valine derivative **1c** cyclized more efficiently (Φ_C = 0.19 ± 0.02) and gave the cyclobutanol **2c** in 74% yield with ds > 96%. The relative configuration was established *via* X-ray structure analysis.† Two explanations for the high 1,3-asymmetric induction are possible: selective γ-H abstraction from one of the diastereotopic methyl groups or non-selective γ-H abstraction followed by selection at the biradical stage (radical combination *vs.* cleavage and/or hydrogen back transfer). Biradical dynamics most likely were responsible for the results obtained with the isoleucine and alloisoleucine derivatives (2*S*,3*S*)-**1d** and (2*R*,3*S*)-**1d**. Whereas the (2*S*,3*S*)-isomer gave exclusively the Norrish II cleavage product **3**, (2*R*,3*S*)-**1d** cyclized efficiently to give the cyclobutanol **2d**. The latter compound again was formed diastereoisomerically pure (*i.e.* ds > 96%) with complete control of the three newly formed stereogenic centers. X-Ray structure analysis completed the configuration analysis.†

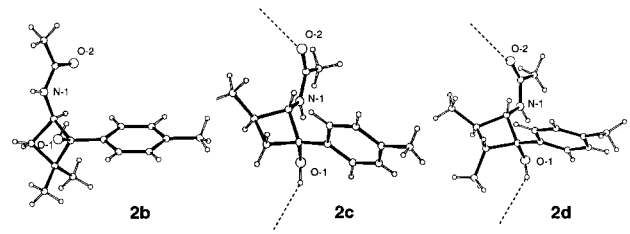

2b **2c** **2d**

Fig. 1 Crystal structures of the cyclobutanols **2b**, **2c** and **2d**.

Finally, the unbranched substrates **2e** and **2f** (from norvaline and norleucine, respectively) were investigated. Both substrates preferentially showed fragmentation and, as a minor reaction path, formation of the cyclobutanols **2e**,**f** with excellent diastereoselectivity. Thus, the radical coupling step also proceeds with high *inherent* stereoselectivity in addition to the 1,2-*induced* stereoselectivity.

In the mechanistic scenario (*vide supra*) for the Yang cyclization process *induced* and *inherent* diastereoselectivity are related to two different steps: biradical dynamics and spin inversion coupled with radical-radical combination. This relation is depicted in Scheme 2 for substrate (2*R*,3*S*)-**2d**. After hydrogen abstraction from the more reactive methylene group, equilibration of the triplet 1,4-biradical leads to three possible conformers, *anti*, *syn* and *syn*′. The energies of these species were calculated using the PM3 method. The cyclization path is not available from the *anti*-isomer, however, this structure is less favourable compared with the *syn*-isomer. Hydrogen

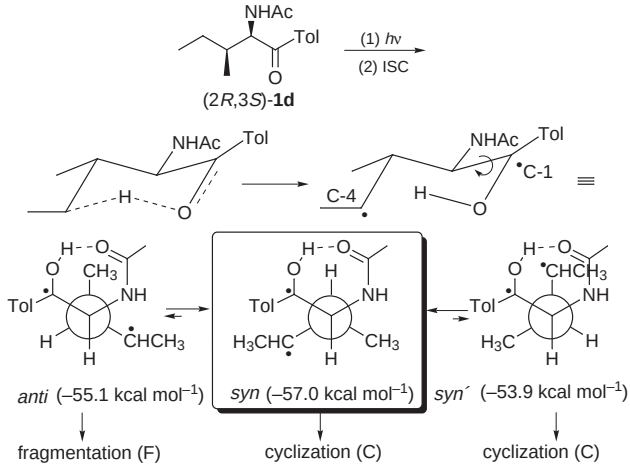

Scheme 2 Mechanistic scenario for the photocyclization of (2*R*,3*S*)-**1d**.

bonding stabilizes all three possible conformers and is the major contribution to the high 1,2-asymmetric induction.

The reverse is the case for (2*S*,3*S*)-**2d** and fragmentation dominates the reaction due to the more stable triplet *anti* 1,4-biradical. This theory however, does not take into account the fact that the calculated biradical minima structures are not necessarily identical with the actual ISC-reactive structures. Spin–orbit coupling, the major contribution to triplet/singlet ISC, is higher for *syn*-biradicals[10] and depends on the orientation of the p-orbitals localized at the spin-bearing carbon atoms.[11] An orthogonal orientation of these orbitals prior to C–C bond formation leads to a *trans* arrangement of the methyl at C-4 and the tolyl group at C-1 (inherent diastereoselectivity). Thus, the *induced* and *inherent* stereoselectivity of the Yang cyclization can be correlated with different selection stages of the reaction.

This work was supported by the Deutsche Forschungsgemeinschaft, the Fonds der Chemischen Industrie and the Universität zu Köln (postgraduate grant for H. H.)

Notes and references

† *Crystal data* for **2b**: $C_{15}H_{21}NO_2 \cdot 1/2H_2O$ (from MeOH), M = 256.3, monoclinic, a = 12.840(1), b = 18.077(1), c = 12.920(1) Å, β = 90.62(1)°, space group $C2/c$, Mo-Kα, 11448 reflections measured, 1748 reflections with $I > 2\sigma(I)$, R_1 = 0.058, wR_2 = 0.117. For **2c**: $C_{14}H_{19}NO_2$ (from MeOH), M = 233.3, monoclinic, a = 7.459(1), b = 11.63(2), c = 15.652(3) Å, β = 102.67(2)°, space group $P2_1/c$, Mo-Kα, 2478 reflections measured, 1202 reflections with $I > 2\sigma(I)$, R_1 = 0.064 , wR_2 = 0.119. For **2d**: $C_{15}H_{21}NO_2$ (from MeOH), M = 247.33, orthorhombic, a = 7.546(1), b = 11.848(1), c = 15.712(1) Å, space group $P2_12_12_1$, Mo-Kα, 3096 reflections measured, 1942 reflections with $I > 2\sigma(I)$, R_1 = 0.050, wR_2 = 0.099. CCDC 182/1248. See http://www.rsc.org/suppdata/cc/1999/1109/ for crystallographic files in .cif format.

1 N. C. Yang and D.-D. H. Yang, *J. Am. Chem. Soc.*, 1958, **80**, 2913.
2 J. C. Scaiano, *Acc. Chem. Res.*, 1982, **15**, 252; L. J. Johnston and J. C. Scaiano, *Chem. Rev.*, 1989, **89**, 521.
3 A. E. Dorigo, M. A. McCarrick, R. J. Loncharich and K. N. Houk, *J. Am. Chem. Soc.*, 1990, **112**, 7508; R. R. Sauers and L. A. Edberg, *J. Org. Chem.*, 1994, **59**, 7061.
4 P. J. Wagner and B.-S. Park, *Org. Photochem.*, 1991, **11**, 227; P. J. Wagner, in *Handbook of Photochemistry and Photobiology*, ed. W. M. Horspool and P.-S. Song, CRC Press, Boca Raton, 1995, p. 449.
5 A. G. Griesbeck, *Chimia*, 1998, **52**, 272; A. G. Griesbeck, *EPA Newsl.*, 1998, 3; A. G. Griesbeck, *Liebigs Ann. Chem.*, 1996, 1951.
6 O. Itoh, T. Honnami, A. Amano, K. Murata, Y. Koichi and T. Sugita, *J. Org. Chem.*, 1992, **57**, 7334.
7 Quantum yields by actinometry (GC product analyses) using valerophenone as standard with Φ_F = 0.33: P. J. Wagner and A. E. Kemppainen, *J. Am. Chem. Soc.*, 1972, **94**, 7495.
8 F. D. Lewis and T. A. Hilliard, *J. Am. Chem. Soc.*, 1972, **94**, 3852.
9 T. Hasegawa, Y. Arata, M. Endoh and M. Yoshioka, *Tetrahedron*, 1985, **41**, 1667; T. Hasegawa, Y. Arata and A. Kageyama, *Tetrahedron Lett.*, 1983, **24**, 1995.
10 M. Klessinger, *Pure Appl. Chem.*, 1997, **69**, 773.
11 A. G. Griesbeck, S. Stadtmüller and H. Mauder, *Acc. Chem. Res.*, 1994, **27**, 70.

Communication 9/01723B

ChemComm

Regulation of α/β-folding of a designed peptide by haem binding

Seiji Sakamoto, Ikuo Obataya, Akihiko Ueno and Hisakazu Mihara*†

Department of Bioengineering, Faculty of Bioscience and Biotechnology, Tokyo Institute of Technology, Nagatsuta, Yokohama 226-8501, Japan. E-mail: hmihara@bio.titech.ac.jp

Received (in Cambridge, UK) 26th April 1999, Accepted 12th May 1999

A designed peptide H2α17-I bound Fe^{III}–mesoporphyrin (haem); and the haem-binding prevented the peptide forming β-sheet aggregates by facilitating the formation of an α-helix tetramer, indicating that the folding state of artificially designed peptides could be regulated by cofactor binding.

Iron porphyrins occur widely in nature as cofactors of haemproteins and display diverse functions. In addition to the wide range of iron porphyrin reactions, iron porphyrins are important factors in defining the three-dimensional (3D) structure of haemproteins, because the removal of a porphyrin cofactor from natural haemproteins caused perturbation and/or destabilization of protein 3D structures.[1–4] So far, in the field of *de novo* protein design, considerable effort has been devoted to construction of polypeptide 3D structure conjugated with porphyrin molecules *via* chelation[5–7] or covalent linkage with peptides.[8–11] However, to establish an artificial haemprotein that meets the minimal requirements for its function, it will be necessary to understand the role of porphyrin cofactors as structural elements of haemproteins. In a previous paper, we described the design of a two-α-helix peptide H2α17-L, whose binding to Fe^{III}–mesoporphyrin (haem) stabilized an α-helical structure and induced a change in the molecular-assembly of the peptide from a monomeric to a tetrameric form.[7b] These results demonstrated that the haem had a significant effect on the 3D-structure and molecular association of an artificially designed polypeptide. Here we examine the effects of amino acid disposition around the axial ligand on the haem-binding property, using novel designed peptides H2α17-I and H2α17-V. Furthermore, we found that the haem binding affected the secondary structure and molecular-association state of the peptide H2α17-I.

The design of H2α17-I and H2α17-V was based on that of the template peptide H2α17-L,[7b] which took an α-helix structure in the buffer both with and without bound haem. The amino acid sequences of H2α17-I and H2α17-V were identical to that of H2α17-L except for their hydrophobic residues (Fig. 1). In the cases of H2α17-I and H2α17-V, hydrophobic Ile and Val residues, respectively, were introduced at the 5th, 6th, 12th and 13th positions instead of the Leu residues of H2α17-L. In the designed α-helix structure, four hydrophobic residues per helix could be arranged around the His[9] to make a hydrophobic haem binding site and a haem would be deployed between the two helices. In the cases of H2α17-I and H2α17-V, however, it was predicted that the folded state of the amphiphilic α-helical sequences would be significantly destabilized by the introduction of four Ile or Val residues, which prefer a β-strand rather than an α-helix structure.[12] Additionally, when the peptide sequences were drawn as a β-sheet model, the peptide could take a kind of amphiphilic β-sheet structure. However, the haem will bind to the folded-state of an α-helical structure with higher affinity than to that of a β-structure, because the hydrophobic residues, which form the hydrophobic haem-binding site, can be arranged around the His,[9] only when the peptides take an α-helix structure. The peptides were synthesized by solid-phase method using Fmoc chemistry and purified with semi-preparative HPLC. The peptides H2α17-I and H2α17-V gave molecular ion peaks at *m/z* 4011.9 [$(M + H)^+$] (calc. 4011.7) and 3898.8 [$(M + H)^+$] (calc. 3899.0), respectively, on matrix assisted laser desorption ionization of time-of-flight mass spectrometry.

Circular dichroism (CD) studies revealed that the peptides H2α17-I and H2α17-V showed typical α-helical patterns with double negative maxima at 207 and 222 nm in trifluoroethanol (TFE), which was known to be an α-helix stabilizing solvent.[13] Upon dilution in 2.0×10^{-2} mol dm^{-3} Tris HCl buffer (pH 7.4) from TFE stock solution of H2α17-I and H2α17-V (final TFE concentration was 1.0%), the peptides showed CD spectra typical of a β-structure with a single negative maximum at 218 nm and a positive maximum at 198 nm (Fig. 2). Additionally, Fourier transform infrared (FT-IR) spectra of the peptides in cast films exhibited narrow peaks for the amide I and II bands: H2α17-I, 1630 and 1555 cm^{-1}; H2α17-V, 1627 and 1553 cm^{-1}, respectively. These wavenumbers were characteristic of a β-structure rather than an α-helix or a random structure.[14] In the absence of haem, H2α17-I and H2α17-V gave no peak on the size exclusion column, suggesting that the peptides formed β-sheet aggregates in multiple states. The formation of β-sheet aggregates was also confirmed by the binding of Congo Red dye, which stains β-sheet proteins, such as amyloid and prion proteins.[15a] Because the template peptide H2α17-L took an α-helix structure and was in a monomeric form under the same conditions, the β-conformation of the peptides in the buffer is due to the high β-propensity of the Ile and Val residues.

On the contrary to the above results, when the TFE stock solution of H2α17-I was diluted with buffer containing haem (1.0 equiv.), the peptide showed a typical α-helical pattern with

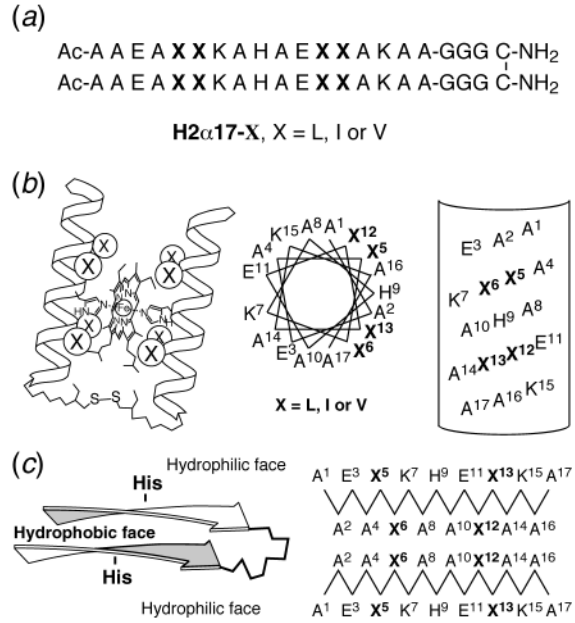

Fig. 1 Structure of the designed peptides. (*a*) Amino acid sequence of H2α17-I and H2α17-V. (*b*) Illustration of the two-α-helix peptide structure bound to the haem, and helix wheel and net drawings of the 17-peptide. (*c*) Schematic illustration of the β-structure of the 17-peptide.

† PRESTO, JST at Tokyo Institute of Technology.

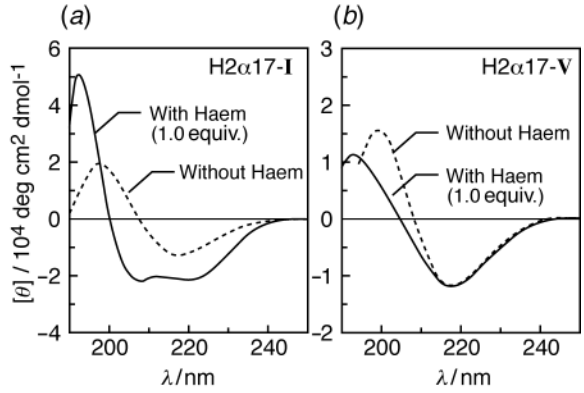

Fig. 2 CD spectra of (*a*) H2α17-I and (*b*) H2α17-V in the absence and presence of haem (1.0 equiv.) in the buffer (pH 7.4) containing 1% TFE at 25 °C. [peptide] = 1.0×10^{-5} mol dm^{-3}.

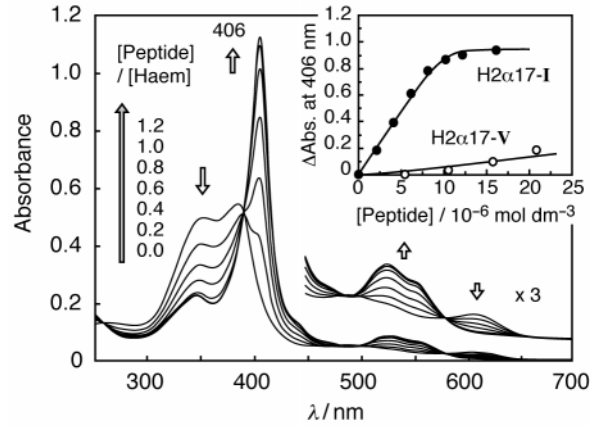

Fig. 3 UV-VIS spectra of haem with increasing H2α17-I concentration in the buffer, pH 7.4 at 25 °C. The TFE solution of the peptide was added to the buffer solution of haem (final TFE content; 1.5%). [haem] = 1.0×10^{-5} mol dm^{-3}. Inset: Plots of absorbance at the Soret band of haem as a function of concentration, peptide (●) H2α17-I and (○) H2α17-V.

double negative maxima at 208 and 222 nm in the buffer (containing 1.0% TFE) (Fig. 2). From the ellipticity at 222 nm ($[\theta]_{222}$ = −22 500 deg cm^2 dmol^{-1}), the α-helicity was estimated as 71%.[16] Size-exclusion chromatography and sedimentation equilibrium studies revealed that the peptide H2α17-I was in a tetrameric form (MW_{obs} = 18 000, 3.9-mer) after haem binding, as was observed in H2α17-L.[7b] That is, the haem binding induced a drastic alteration of the secondary structure and molecular association state from β-sheet aggregates to an α-helical tetrameric assembly. The peptide H2α17-I folded into a β-structure at acidic pH (4.0–6.0) in the presence and absence of haem. Because the pK_a of His is reported as *ca*. 6.4,[17] the pH effect is attributed to the protonation of the His side chains such that they cannot act as ligands. Therefore, we concluded that H2α17-I folded into an α-helix structure *via* haem binding through a ligation with His residues. In contrast, the peptide H2α17-V took a β-structure even in the presence of haem at pH 7.4, suggesting that H2α17-V could not bind the haem effectively. CD studies demonstrated that the secondary structure and molecular assembly of the designed peptide was regulated by the haem binding. Although the α-form (with haem) was completely denatured with 6.0 mol dm^{-3} urea (urea denaturation midpoint; $[\text{urea}]_{1/2}$ = 2.7 mol dm^{-3}, free energy of unfolding; ΔG_{H_2O} = −7.6 kJ mol^{-1}), the CD spectrum of the β-form (without haem) was not changed even with 7.0 mol dm^{-3} urea, indicating that the β-form is much more stable than the α-form. Thus, the alternation of peptide α/β folding appeared to be regulated by a kinetic mechanism rather than a thermodynamic one. Even in the absence of haem, immediately after dilution from the TFE solution, it is predicted that the peptide takes an α-helix structure,[15] although the α-helix structure is unstable and the rapid transition from the α- to the β-form follows. In the presence of haem, however, the haem binds the metastable α-form and prevents the peptide progressing to a β-form. Indeed, after formation of the β-sheet structure, the peptide could not bind the haem and the α-helix structure was not recovered by the addition of haem.

To further characterize the haem binding with the peptides, UV-VIS titration of the haem was carried out in buffer. With increasing concentration of H2α17-I an increase of the Soret band at 406 nm and a decrease of the band at 355 nm of haem were observed (Fig. 3). The UV-VIS spectrum of haem in the presence of peptide resembles those of natural cytochromes with low-spin six-coordinate iron.[7] The binding constant (K_a), determined from the absorbance change at the Soret band using a single site binding equation, was 1.0×10^7 dm^3 mol^{-1} (Fig. 3, inset), comparable to that of H2α17-L (K_a = 1.1×10^7 dm^3 mol^{-1}).[7b] On the other hand, addition of H2α17-V caused little increase of the Soret band, indicating that the peptide could not bind the haem effectively in this concentration range. The computer modeling study suggested that the side chain of the Val residue was too small to make effective van der Waals contact with the porphyrin plane, when the haem was positioned between the helices with energetically favorable side-chain torsional angles of the His ligands.[10,11] Additionally, the hydrophobicity of Val is lower than that of Ile and Leu,[18] These results revealed that the nature of amino acids at the haem binding site was important for the effective haem-binding by the two-α-helix peptides. There is enough hydrophobicity and van der Waals volume in Leu and Ile for effective haem binding in the two-α-helix form.

In conclusion, we successfully designed and synthesized the peptide H2α17-I with the unique property that the folding state was controlled by the haem-binding. The haem binding prevented the peptide from forming β-sheet aggregates by facilitating the formation of an α-helix tetramer. These findings indicate the importance of haem cofactor as a structural element of artificial haem-conjugated proteins and polypeptides. This kind of work will lead to studies to construct mini-haemproteins and elucidate their folding and application.

Notes and references

1 M. S. Hargrove and J. S. Olson, *Biochemistry*, 1996, **35**, 11 310.
2 W. R. Fisher, H. Taniuchi and C. J. Anfinsen, *J. Biol. Chem.*, 1973, **248**, 3188.
3 C. D. Moore, O. N. Al-Misky and J. T. Lecomte, *Biochemistry*, 1991, **30**, 8357.
4 Y. Feng and S. G. Sligar, *Biochemistry*, 1991, **30**, 10 150.
5 R. E. Sharp, C. C. Moser, F. Rabanal and P. L. Dutton, *Proc. Natl. Acad. Sci. U.S.A.*, 1998, **95**, 10 465.
6 H. K. Rau, N. DeJonge and W. Haehnel, *Proc. Natl. Acad. Sci. U.S.A.*, 1998, **95**, 11 526.
7 (*a*) S. Sakamoto, S. Sakurai, A. Ueno and H. Mihara, *Chem. Commun.*, 1997, 1221; (*b*) S. Sakamoto, A. Ueno and H. Mihara, *Chem. Commun.*, 1998, 1073; (*c*) S. Sakamoto, A. Ueno and H. Mihara, *J. Chem. Soc., Perkin Trans. 2*, 1998, 2395.
8 T. Sasaki and E. T. Kaiser, *J. Am. Chem. Soc.*, 1989, **111**, 380.
9 H. Mihara, Y. Haruta, S. Sakamoto, N. Nishino and H. Aoyagi, *Chem. Lett.*, 1996, 1; H. Mihara, K. Tomizaki, T. Fujimoto, S. Sakamoto, H. Aoyagi and N. Nishino, *Chem. Lett.*, 1996, 187.
10 F. Nastri, A. Lombardi, G. Morelli, O. Maglio, G. D'Auria, C. Pedone and V. Pavone, *Chem. Eur. J.*, **3**, 340.
11 D. A. Williamson and D. R. Benson, *Chem. Commun.*, 1998, 961.
12 P. Y. Chou and G. D. Fasman, *Biochemistry*, 1974, **13**, 222.
13 N. E. Zhou, B.-Y. Zhu, C. M. Kay and R. S. Hodges, *Biopolymers*, 1992, **32**, 419.
14 W. K. Surewicz, H. H. Mantsch and D. Chapman, *Biochemistry*, 1993, **32**, 389.
15 (*a*) Y. Takahashi, A. Ueno and H. Mihara, *Chem. Eur. J.*, 1998, **4**, 2475; (*b*) D. Hamada, S. Segawa and Y. Goto, *Nat. Struct. Biol.*, 1996, **3**, 868.
16 J. M. Scholtz, H. Qian, E. J. York, J. M. Stewart and R. L. Baldwin, *Biopolymers*, 1991, **31**, 1463.
17 C. Tanford, *Adv. Protein Chem.*, 1962, **17**, 69.
18 D. M. Engelman, T. A. Steitz and A. Goldman, *Annu. Rev. Biophys. Biophys. Chem.*, 1986, **15**, 321.

Communication 9/03320C

ChemComm

Decarboxylative elimination of enol triflates as a general synthesis of acetylenes

Ian Fleming* and Chandrashekar Ramarao

Department of Chemistry, Lensfield Road, Cambridge, UK CB2 1EW. E-mail: if10000@cam.ac.uk

Received (in Liverpool, UK) 9th March 1999, Accepted 28th April 1999

Decarboxylative elimination of a range of enol triflates 11 of β-keto esters gives acetylenes 12.

We established long ago in a series of papers[1,2] that enol arenesulfonates **1** derived from acylmalonates underwent concerted decarboxylative elimination to give acetylenic acids **2** (Scheme 1), provided that the group R was cation-stabilising. Thus the reaction worked if the group R was aryl, vinyl or cyclopropyl, but not if it was alkyl or ethynyl, a severe limitation which deterred us from investigating the synthetic potential of this reaction any further. In the meantime, better leaving groups than arenesulfonate have been developed,[3] and so we have returned to this remarkably mild reaction to see if it could be made into a more general synthesis of acetylenes.

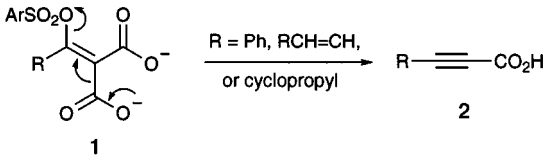

Scheme 1

Although we know of no relevant quantitative data for elimination reactions, it is known that 1-adamantyl trifluoromethanesulfonate (triflate) undergoes S_N1 solvolysis 10^5 to 10^6 times faster than the corresponding toluene-*p*-sulfonate (tosylate),[4] and that ethyl triflate undergoes S_N2 solvolysis in AcOH 10^4 faster than ethyl tosylate.[5] We also knew that the rate of the decarboxylative elimination **1** → **2** was sensitive to how good the leaving group was, although not quite to the same extent as an S_N1 reaction. Thus the decarboxylative elimination had a ρ value for *p*-substituted benzenesulfonates of 1.16,[2] whereas the S_N1 reaction of 1-adamantyl arenesulfonates has a ρ value of 1.76.[6] Putting these facts together implied that enol triflates ought to undergo decarboxylative elimination much faster than enol arenesulfonates, and quite probably fast enough to work for those cases that had failed before. We carried out the sequence in Scheme 2 to prepare the enol triflate dicarboxylic acids **5**, and dissolved them in aqueous $NaHCO_3$. They cleanly gave the acetylenic acids **2a**–**d**, having alkyl and ethynyl groups R, showing that the main limitation in our earlier work had been overcome.

With a more general reaction now at our disposal, we investigated whether the second carboxylic acid group was necessary. It had always been possible that the second carboxylate ion, present in all our earlier reactions, had accelerated the decarboxylative elimination by a Coulombic repulsion. We prepared the enol triflate **7** (Scheme 3). On treatment with base this gave the terminal acetylene **8**, showing that the second carboxy group was unnecessary. In this case, K_2CO_3 in refluxing acetone proved to be better than aqueous $NaHCO_3$.

We also prepared a small range of acetylenes **12** and **14** with alkyl groups on both sides (Scheme 4), again with greater success using K_2CO_3 in acetone as the base. We were not successful in our efforts to prepare an enol triflate with branched alkyl groups on both sides of the intended triple bond, neither of the β-keto esters **15** giving an enol triflate, although we were successful with examples having branched chains separately on each side, as in the synthesis of the acetylenes **12c** and **14**. We

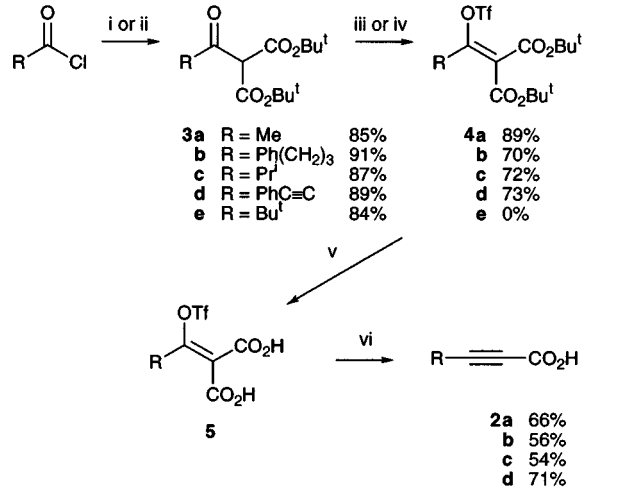

Scheme 2 *Reagents and conditions*: i, $CH_2(CO_2Bu^t)_2$, $Mg(OEt)_2$; ii, $CH_2(CO_2Bu^t)_2$, Et_3N; iii, Tf_2O, Et_3N, CH_2Cl_2, 0 °C → rt, 3 h; iv, NaH, Et_2O, 0 °C, 1 h, then Tf_2O, 0 °C, then rt, 1 h; v, TFA, rt, 30 min; vi, $NaHCO_3$, H_2O, rt, 12 h.

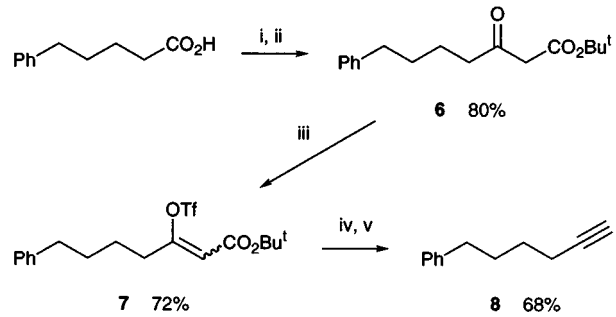

Scheme 3 *Reagents and conditions*: i, carbonyldiimidazole, THF, rt, 1 h; ii, $LiCH_2CO_2Bu^t$, −78 °C, 1 h; iii, NaH, Et_2O, 0 °C, 1 h, then Tf_2O, 0 °C → rt, 1 h; iv, TFA, rt, 30 min; v, K_2CO_3, Me_2CO, reflux, 4 h.

were also unable to prepare an enol triflate adjacent to a *tert*-butyl group when we treated di-*tert*-butyl pivaloylmalonate **3e** with a variety of bases and Tf_2O.

Except for these limitations, we now have a fairly general synthesis of acetylenes based on a β-keto ester system (Scheme 5), with a wide variety of methods for incorporating or attaching the groups R^1 and R^2 on each side of the ketone group,[7] some of which are illustrated by the standard but far from opitimised methods we used in Schemes 2–4. The overall transformation is similar to that achieved by Zard's intriguing reaction,[8] in which β-keto esters are treated successively with hydroxylamine and with $NaNO_2$ and iron(II) sulfate, but the pathway described here is mechanistically more straightforward, and probably less apt to give byproducts.

The following is a representative recipe for the preparation of the enol triflate and for the decarboxylative elimination. The keto-ester **13c** (7 g, 26.7 mmol) in dry Et_2O (50 cm^3) was added to a prewashed suspension of NaH (60% dispersion in mineral oil, 2.13 g, 53.4 mmol) at 0 °C and stirred for 1 h. Tf_2O (6.6 cm^3, 40.0 mmol) was added and the reaction mixture was stirred for 1 h at 0 °C and 1 h at room temperature. The mixture was cooled

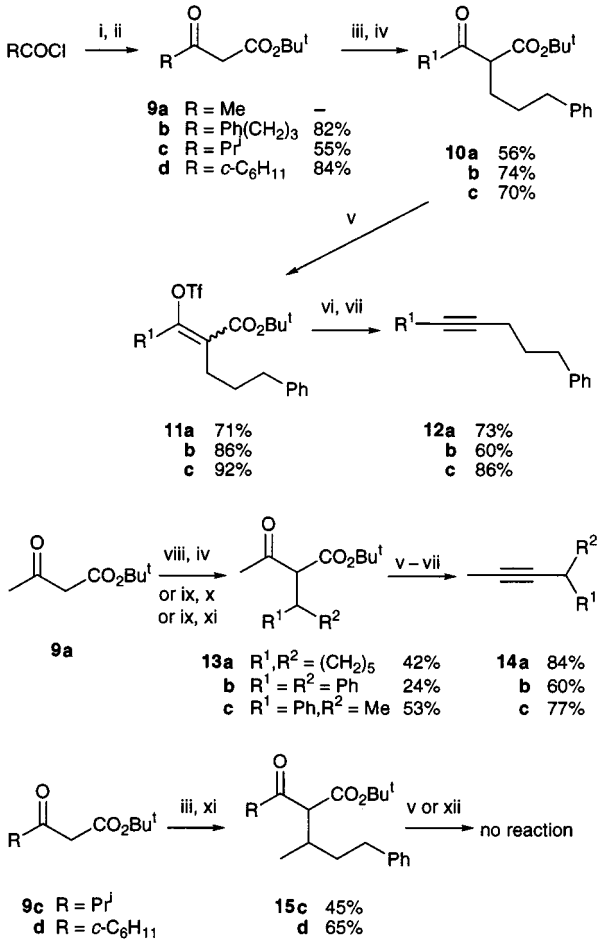

Scheme 4 *Reagents and conditions*: i, Meldrum's acid, Py, CH_2Cl_2, 0 °C → rt, 3 h; ii, Bu^{t}OH, toluene, reflux, 4 h; iii, $Ph(CH_2)_2CHO$, $TiCl_4$, Py, THF, rt, 16 h; iv, H_2, Pd/C, MeOH, rt, 12 h; v, NaH, Et_2O, 0 °C, 1 h, then Tf_2O, 0 °C → rt, 2 h; vi, TFA, rt, 30 min; vii, K_2CO_3, Me_2CO, reflux, 4–5 h; viii, cyclohexanone, $TiCl_4$, Py, CH_2Cl_2, rt, 16 h; ix, PhCHO, *c*-$C_5H_{10}NH$, EtOH, 5 °C, 14 h; x, Ph_2CuLi, THF, −78 °C, 1 h; xi, Me_2CuLi, THF, −78 °C, 1 h; xii, Tf_2O and several other bases: KH, 2,6-di-*tert*-butylpyridine, *etc.*

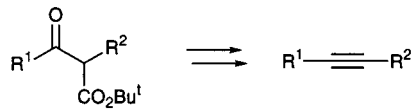

Scheme 5

and quenched carefully with water and extracted with Et_2O (2 × 60 cm^3). The extract was washed with saturated $NaHCO_3$ (60 cm^3) and brine (60 cm^3), dried ($MgSO_4$) and evaporated under reduced pressure to give 3-*tert*-butoxycarbonyl-4-phenylpent-2-en-2-yl trifluoromethanesulfonate (8.94 g, 85%); R_f [EtOAc–light petroleum (bp 40–60 °C), 20 : 80] 0.77; ν_{max} (film)/cm^{-1} 1721 (C=O) and 1602 (Ph); δ_H(250 MHz; $CDCl_3$) 7.3–7.2 (5H, m, Ph), 3.86 (1H, q, *J* 7.3, PhC*H*), 2.1 (3H, s, *Me*C=C), 1.57 (3H, d, *J* 7.2, *Me*CH) and 1.31 (9H, s, Bu^t). The triflate was unstable and had to be used in the next step without further characterisation. The triflate (8.94 g, 22.7 mmol) was stirred in TFA (10 cm^3) for 40 min at room temperature. The excess TFA was removed under reduced pressure to give a light yellow–brown solid, which was dissolved in acetone (50 cm^3). K_2CO_3 (7.3 g, 53.4 mmol) was added and the reaction mixture refluxed for 4 h, cooled, poured into water and extracted with Et_2O. The extract was washed with dilute HCl (50 cm^3), water (50 cm^3) and brine (50 cm^3), dried ($MgSO_4$), and evaporated under reduced pressure. The residue was chromatographed [SiO_2, light petroleum (bp 40–60 °C)] to give the 4-phenylpent-2-yne[9] **14c** (2.97 g, 77% from the keto ester); R_f [EtOAc–light petroleum (bp 40–60 °C), 10 : 90] 0.85; ν_{max}(film)/cm^{-1} 1450 (Ph); δ_H(250 MHz; $CDCl_3$) 7.4–7.2 (5H, m, Ph), 3.72 (1H, m, PhC*H*), 1.88 (3 H, d, *J* 2.5, *Me*C≡C) and 1.47 (3H, d, *J* 7.2, *Me*CH); δ_C(250 MHz; $CDCl_3$) 144−, 128.4+, 126.8+, 126.4+, 82, 77.5−, 31.9+, 24.6+ and 3.6+ (+ indicates methyl or methine and − indicates methylene or quaternary carbon).

We thank Avra Laboratories, Hyderabad, for a maintenance grant (C. R.).

Notes and references

1 I. Fleming and J. Harley-Mason, *J. Chem. Soc.*, 1963, 4771 and 4778; E. J. D. Brown and J. Harley-Mason, *J. Chem. Soc.*, 1966, 1390; I. Fleming and C. R. Owen, *J. Chem. Soc. (C)*, 1971, 2013.
2 I. Fleming and C. R. Owen, *J. Chem. Soc. (B)*, 1971, 1293.
3 T. W. Bentley, in *The Chemistry of Sulphonic Acids, Esters and their Derivatives*, ed. S. Patai and S. Rappoport, Wiley, Chichester, 1991, pp. 671–696.
4 K. Takeuchi, K. Ikai, T. Shibata and A. Tsugeno, *J. Org. Chem.*, 1988, **53**, 2852.
5 A. Streitwieser, Jr., C. L. Wilkins and E. Kiehlmann, *J. Am. Chem. Soc.*, 1968, **90**, 1598. See also: M. G. Ahmed, R. W. Alder, G. H. James, M. L. Sinnott and M. C. Whiting, *J. Chem. Soc., Chem. Commun.*, 1968; 1533; D. N. Kevill and G. M. Lin, *Tetrahedron Lett.*, 1978, 949; J. F. Garrity and J. W. Prodolliet, *Tetrahedron Let.*, 1982, **23**, 417.
6 D. N. Kevill, K. C. Kolwyck, D. M. Shold and C.-B. Kim, *J. Am. Chem. Soc.*, 1973, **95**, 1065.
7 S. Benetti, R. Romagnoli, C. De Risi, G. Spalluto and V. Zanirato, *Chem. Rev.*, 1995, **95**, 1065.
8 J. Boivin, L. ElKaim, P. G. Ferro and S. Z. Zard, *Tetrahedron Lett.*, 1991, **32**, 5321; J. Boivin, S. Huppé and S. Z. Zard, *Tetrahedron Lett.*, 1995, **36**, 5737; J. Boivin, S. Huppé and S. Z. Zard, *Tetrahedron Let.*, 1996, **37**, 8735.
9 J. C. Gilbert, D. H. Giamalva and U. Weerasooriya, *J. Org. Chem.*, 1983, **48**, 5251.

Communication 9/01921I

ChemComm

Sono-electrosynthesis: electrode depassivation and trapping of insoluble redox products

Richard P. Akkermans, Sarah L. Roberts and Richard G. Compton*

Physical and Theoretical Chemistry Laboratory, Oxford University, South Parks Road, Oxford, UK OX1 3QZ. E-mail: compton@ermine.ox.ac.uk

Received (in Cambridge, UK) 16th March 1999, Accepted 7th May 1999

The electrosynthesis of water-insoluble products such as *leuco*-Methylene Green from soluble precursors can be accomplished using an emulsion formed *via* insonation so that the organic phase constantly extracts the product and simultaneously prevents the electrode passivation which would occur in aqueous solution alone.

The introduction of power ultrasound into electrochemical systems has many benefits,[1,2] including first, extremely enhanced mass transport resulting from acoustic streaming[3] or microjetting,[4] and second, electrode activation arising from cavitational erosion.[5] In addition sonication has been used to permit the electrochemical study of essentially water-insoluble organic species in aqueous solution.[6,7]

Here we report a new and general use of ultrasonically generated emulsions in electrosynthesis. Many potentially viable electrode processes are inhibited if not entirely passivated by the adsorption, precipitation or polymerisation of reaction products or intermediates on the electrode surface. This note addresses two such reactions in aqueous solution, first the two-electron reduction of Methylene Green[8–10] (MG, **1**) to *leuco*-Methylene Green, and second the oxidation of iodide to solid iodine,[11–13] both at platinum electrodes.

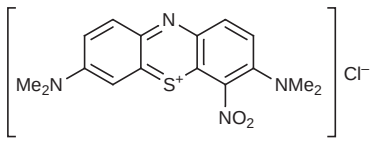

1

The presence of an organic phase which emulsifies under insonation is shown to lead to (i) 'clean' useful voltammetry, (ii) the extraction of reduction products and (iii) the preservation of electrode activity where in aqueous solution alone passivation would preclude useful electrosynthesis.

Experiments were conducted using a 250 ml sonovoltammetric cell at 20 °C, which incorporated a 13 mm diameter, 20 kHz titanium tipped ultrasonic horn probe (Sonics & Materials). Ultrasound power levels up to 50 W cm^{-2} were employed[14,15] and electrochemical measurements carried out using a commercial three-electrode potentiostat (Eco-Chemie, Utrecht) except that the horn probe was electrically isolated as previously reported.[16] Full descriptions of sonoelectrochemical and sonovoltammetric procedures have appeared elsewhere.[17]

Cyclic voltammograms for 0.2 and 2 mM aqueous solutions of Methylene Green in 0.1 M KCl, buffered at pH 6.5 ± 0.1 with 0.2 M KH_2PO_4, were recorded in quiescent solution. A typical 'silent' voltammogram is shown in Fig. 1. The two peaks can be attributed to the processes in eqn. (1) and (2), where *l*-MG is *leuco*-Methylene Green. The two-electron character of each wave was evidenced first by Tafel analysis and second by the observation that the reduction potentials shifted by *ca.* 30 mV per pH unit in the pH range 6 to 8 consistent with a two-electron, one proton reduction. Notice the large 'stripping' peak corresponding to the re-oxidation of the insoluble surface-bound *leuco*-Methylene Green.

$$MG_{(aq)} + H^+ + 2e^- \rightleftharpoons l\text{-}MG_{(s)} \quad E^{red}_{peak} = -0.09 \text{ V } vs. \text{ SCE} \quad (1)$$

$$MG_{(aq)} + H^+ + 2e^- \rightleftharpoons l\text{-}MG_{(aq)} \quad E^{red}_{peak} = -0.22 \text{ V } vs. \text{ SCE} \quad (2)$$

When 25 W cm^{-2} of power ultrasound is introduced into the cell the voltammetry changes markedly due to the significantly enhanced mass transport and is shown in Fig. 2. Notice first that a much larger stripping peak is seen corresponding to the greater deposition resulting from the enhanced currents flowing due to the increased mass transport. Second, whilst there is a mass-transport limited current analogous to a polarogram relating to the two-electron processes, reflecting the constant flux of material due to steady-state convection/diffusion, the wave at the more negative potential shows a progressive decrease of signal at potentials negative of *ca.* −0.23 V *vs.* SCE. This electrode passivation was also seen (i) under silent conditions and (ii) during hydrodynamic voltammetry (for example at a channel electrode) and effectively precludes the electro-

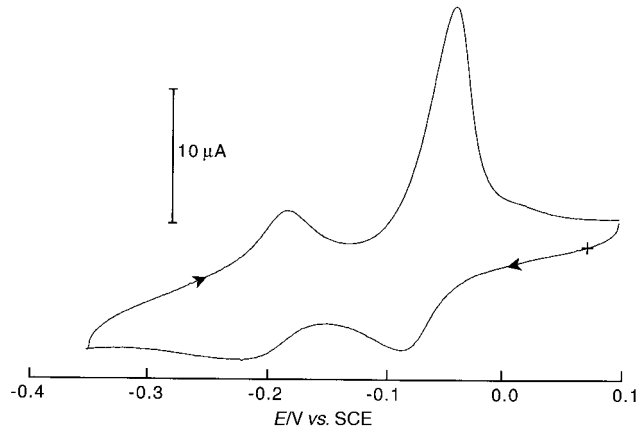

Fig. 1 'Silent' cyclic voltammogram of 0.2 mM MG in 0.1 M KCl/0.2 M $KH_2PO_{4(aq)}$ at pH 6.5. Scan rate was 10 mV s^{-1} and the working electrode was a 6 mm diameter Pt disc.

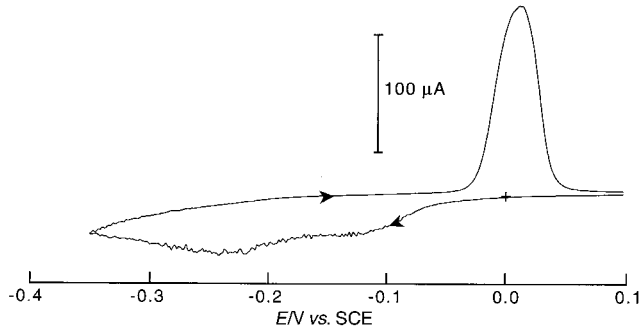

Fig. 2 Cyclic voltammogram of 0.2 mM MG in 0.1 M KCl/0.2 M $KH_2PO_{4(aq)}$ at pH 6.5. 25 W cm^{-2} ultrasound was employed at a horn-to-electrode distance of 22 mm. Scan rate was 10 mV s^{-1} and the working electrode was a 6 mm diameter Pt disc.

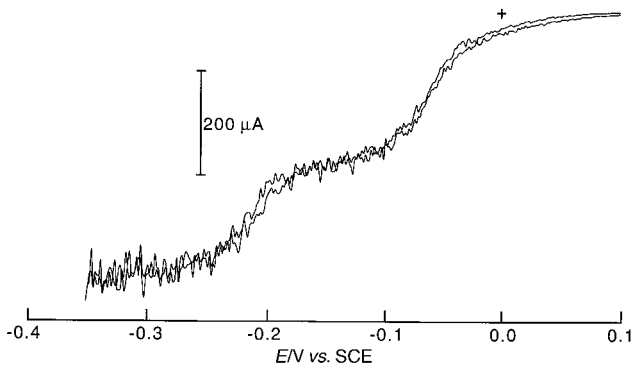

Fig. 3 Cyclic voltammogram of 2 mM MG in 0.1 M KCl/0.2 M $KH_2PO_{4(aq)}$ at pH 6.5 and 20% (v/v) toluene (emulsified). 18 W cm^{-2} ultrasound was employed at a horn-to-electrode distance of 19 mm. Scan rate was 10 mV s^{-1} and the working electrode was a 6 mm diameter Pt disc.

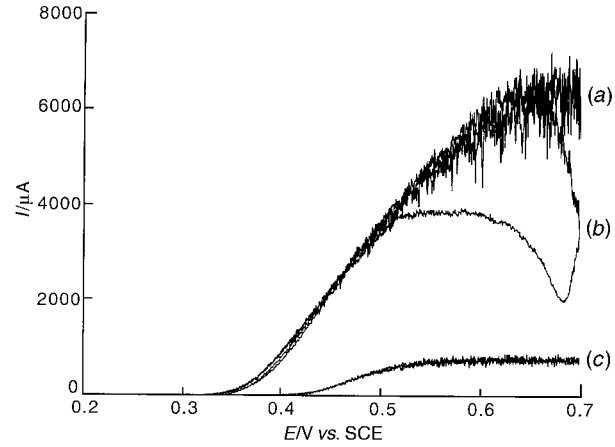

Fig. 4 Cyclic voltammograms on a 6 mm Pt disc electrode at 10 mV s^{-1} for (*a*) 1 mM and (*b*) 10 mM KI in 0.125 M H_2SO_4. 18 W cm^{-2} ultrasound was employed at a horn-to-electrode distance of 12 mm. Trace (*c*) is as for (*b*) except that 10% (v/v) of the aqueous solution was replaced with CH_2Cl_2 and emulsified.

synthetic generation of useful quantities of *leuco*-Methylene Green. However when voltammetry is conducted using a 20% (v/v) solution of toluene in water and 18 W cm^{-2} ultrasound is utilised to form an emulsion, the sonovoltammetry is very different, as shown in Fig. 3. Now, two steady-state sigmoidal reduction waves are observed with no evidence of a stripping peak on sweeps to positive potentials. Similar effects were seen using n-octane instead of toluene. We attribute this to the solubility of the reduction product in the emulsified organic phase that bathes the electrode surface. This was confirmed using a 30 min sono-electrolysis experiment during which the potential of the solution (200 ml of 2 mM MG in 0.1 M KCl/ 0.2 M KH_2PO_4 at pH 6.5 and 50 ml of toluene) was maintained at −0.35 V *vs.* SCE under ultrasound. The toluene reaction mixture was then isolated under argon, evaporated to dryness and the product dissolved in octane for UV-visible characterisation of the *leuco* base *via* the peak at 263 nm.[18]

Examination of Fig. 3 shows two roughly equal waves corresponding to the two electron reduction of Methylene Green giving respectively solid *l*-MG and aqueous phase *l*-MG. The former, of course, is rapidly removed by the emulsion. The relative sizes of the two waves reflect the amount of material that can nucleate and adsorb in the case of the first wave and the fact that the overall magnitude of the two waves taken together reflects the rate of mass transport of MG to the electrode surface. The scope for 'clean' voltammetric measurements in otherwise passivating systems in the presence of ultrasound is evident.

The oxidation of iodide at platinum electrodes is complicated by the formation of solid iodine at higher concentrations when the solubility of iodine is exceeded (1.1 mM in water at 25 °C).[19] Cyclic voltammetry of 1 and 10 mM aqueous solutions of KI in 0.125 M H_2SO_4 was performed under 19 W cm^{-2} ultrasound at a horn to electrode distance of 12 mm. This is shown in Fig. 4. At the higher concentration the voltammetry deviates from the expected steady-state behaviour and heavy electrode passivation leads to current fall-off. When 10% (25 ml) of the aqueous solution was replaced with CH_2Cl_2 and the mixture was emulsified, steady-state behaviour was achieved and is seen in Fig. 4(*c*). This was confirmed spectroscopically to be due to the dissolution of iodine from the platinum electrode.

Sonication is a convenient and effective alternative to the use of high-speed stirring and/or detergents for the promotion of emulsions for electrochemistry,[20] although the possibility of a small amount of parallel chemistry resulting from sono-decomposition of the solvents (water, toluene and dichloromethane) should be noted.

The use of the sono-emulsion technique to depassivate electrochemical systems promises much for synthetic, mechanistic and analytical studies and can be expected to considerably broaden the range of chemical systems amenable to electrochemical study.

We thank the EPSRC for a studentship for R. P. A. and for financial support (grant no. GR/L/36413) under the Analytical Sciences program.

Notes and references

1 D. J. Walton and S. S. Phull, *Adv. Sonochem.*, 1996, **4**, 205.
2 R. G. Compton, J. C. Eklund and F. Marken, *Electroanalysis*, 1997, **7**, 509.
3 F. Marken, R. P. Akkermans and R. G. Compton, *J. Electroanal. Chem.*, 1996, **415**, 55.
4 J. Klima, C. Bernard and C. Degrand, *J. Electroanal. Chem.*, 1995, **399**, 147.
5 R. G. Compton, J. C. Eklund, S. D. Page, G. H. W. Sanders and J. Booth, *J. Phys. Chem.*, 1994, **98**, 12410.
6 F. Marken, R. G. Compton, S. D. Bull and S. G. Davies, *Chem. Commun.*, 1997, 995.
7 F. Marken and R. G. Compton, *Electrochim. Acta*, 1998, **43**, 2157.
8 Q. Chi and S. Dong, *Anal. Chim. Acta*, 1994, **285**, 125.
9 Y. Zhu and S. Dong, *Electrochim. Acta*, 1990, **35**, 1139.
10 D.-M. Zhou, H.-Q. Fang, H.-Y. Chen, H.-X. Ju and Y. Wang, *Anal. Chim. Acta*, 1996, **329**, 41.
11 L. M. Dané, L. J. J. Janssen and J. G. Hoogland, *Electrochim. Acta*, 1968, **13**, 507.
12 Y. A. Yaraliyev, *Electrochim. Acta*, 1984, **29**, 1213.
13 Y. Chen, H. Zhang and B. Wu, *J. Electroanal. Chem.*, 1992, **335**, 321.
14 T. J. Mason, J. P. Lorimer and D. M. Bates, *Ultrasonics*, 1992, **30**, 140.
15 M. A. Margulis and A. N. Mal'tsev, *Russ. J. Phys. Chem.*, 1969, **43**, 592.
16 F. Marken and R. G. Compton, *Ultrason. Sonochem.*, 1996, **2**, S131.
17 R. G. Compton, J. C. Eklund and S. D. Page, *J. Phys. Chem.*, 1995, **99**, 4211.
18 A. T. Vartanyan, *Opt. Spektrosk.*, 1956, **1**, 478.
19 S. Swathirajan and S. Bruckenstein, *J. Electroanal. Chem.*, 1980, **112**, 25.
20 S. Schweizer, J. F. Rusling and Q. Huang, *Chemosphere*, 1994, **28**, 961.

Communication 9/02217A

Formation and structure of unusual [2 + 1] adducts of citronellal and oligo(hydroxy)benzenes

Bart Forier, Suzanne Toppet, Luc Van Meervelt and Wim Dehaen*

Department of Chemistry, Katholieke Universiteit Leuven, Celestijnenlaan 200F, 3001 Heverlee (Leuven), Belgium. E-mail: wim.dehaen@chem.kuleuven.ac.be

Received (in Liverpool, UK) 25th February 1999, Accepted 28th April 1999

Citronellal reacts with electron rich oligo(hydroxy)benzenes in an acid catalyzed condensation reaction to afford unusual [2 + 1] adducts which are characterized with mass and NMR spectroscopy, and X-ray crystallography.

Resorcinarenes are an important class of electron rich cyclophanes, which have been used extensively as hosts for ammonium ions, amino acids, polyols and saccharides.[1] They are also the starting materials for container molecules such as cavitands and carcerands.[2] Their success is to a major extent due to their convenient one step synthesis involving the [4 + 4] acid catalyzed condensation of aldehydes and resorcinol. Both aromatic and aliphatic aldehydes can be used, and in many cases the *rccc* stereoisomer is formed preferentially.

With the goal of introducing chirality to these resorcinarenes in a simple way, we tried the acid-catalyzed condensation of citronellal with resorcinol, following literature procedures.[1] To our joy, large amounts of a white crystalline material were formed. However, the spectral data did not correspond with the desired [4 + 4] adduct **1**. This was clear by the absence of signals corresponding to phenolic hydrogens both in the ^{1}H NMR (taken at 400 MHz) and IR spectra. Moreover, the double bond had disappeared, as was clear from the shift of the methyl groups from δ 2.1 in citronellal to δ 1.1 in the product, and the disappearance of the signal of the vinyl hydrogen in the ^{1}H NMR spectrum. Notably, the product formed was not optically active, and in fact racemic citronellal was used in all subsequent reactions. Very soon it became apparent that a [2 + 1] adduct between citronellal and resorcinol, corresponding to an interesting bis(spirocyclohexane)benzodifuran **2**, had formed. The yield was 66% based on citronellal, rising to 77% when a 2 : 1 ratio of starting materials was used (Scheme 1).[3] The structure of **2** agrees with the mass spectrum (*m/z* 382). The ^{1}H NMR spectrum shows doublet absorptions (6H) at δ 0.9, and a singlet (12H) at δ 1.1 for the hydrogens of the methyl groups. A number of multiplet signals between δ 1.3 and 1.9 (total 18H) correspond to the cyclohexyl protons. Two singlets (each 1H) at δ 6.18 and 6.61 can be assigned to the aromatic H-8 and H-4 of the benzodifuran. Furthermore, in the ^{13}C NMR spectrum the aliphatic quaternary carbons are diagnostic: they show up at δ 45.7 (C-3,6 of benzodifuran) and 91.8 (C-2,7 of benzodifuran). The aromatic signals at δ 93.4 (CH-8 of benzodifuran) and 115.5 (CH-4 of benzodifuran) are within the expected values.

Although citronellal and resorcinol both are very common chemicals, we have found no earlier reference to compound **2** in the literature. To test the generality of this cyclocondensation reaction, other phenols were combined with citronellal. Phenol itself did not give a defined condensation product, but the isomeric hydroquinone gave a [2 + 1] adduct (*m/z* 382) in good yield (72%). However, careful investigation of the ^{1}H and ^{13}C NMR spectra showed that the product is not the (by now) expected benzo[1,2-*b*:4,5-*b*′]difuran **3** but a doubly bridged benzo[1,2-*b*: 4,5-*b*′]dioxocane **4** (Scheme 2). The ^{1}H NMR spectrum shows the methyl groups now all appear as doublets at δ 0.96, 0.97 and 1.10 (each 6H). A multiplet at δ 1.16 (2H) is well separated from the bulk of the aliphatic protons (14 H between δ 1.53 and 1.91). The former signal clearly corresponds to the two hydrogens at C-3,10 which undergo the shielding influence of the aromatic anisotropy. Another well-separated aliphatic signal is the doublet at δ 2.60 corresponding to the benzylic H-6,13. In the aromatic region of the spectrum, the expected singlet (2H) at δ 6.41 is found. In the ^{13}C NMR spectrum the diagnostic signals are from one aliphatic quaternary carbon (C-2,9) at δ 78.2 and one aromatic CH at δ 113.2. The product **4** is not optically active due to its centre of symmetry.

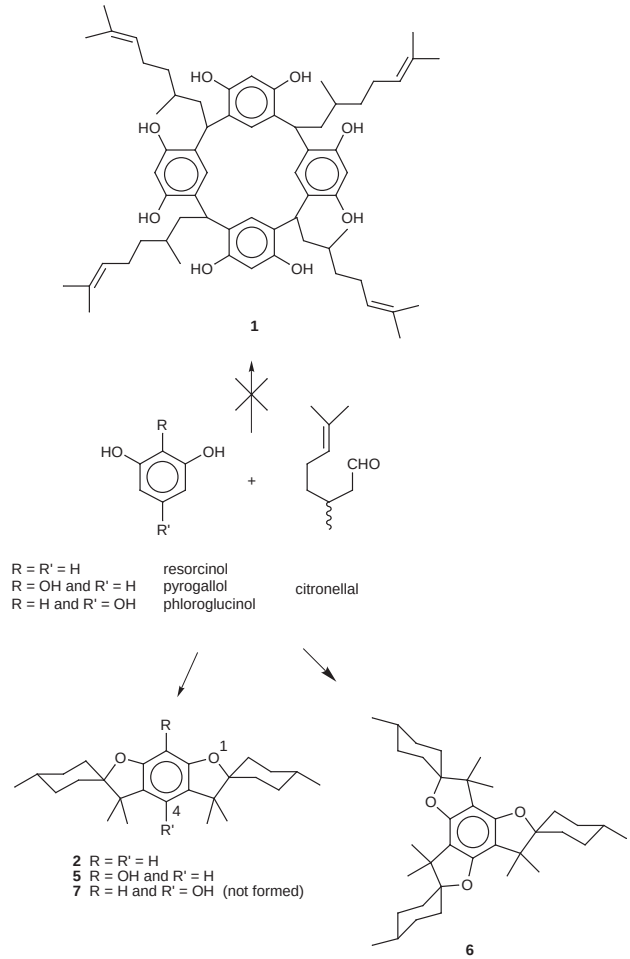

Scheme 1

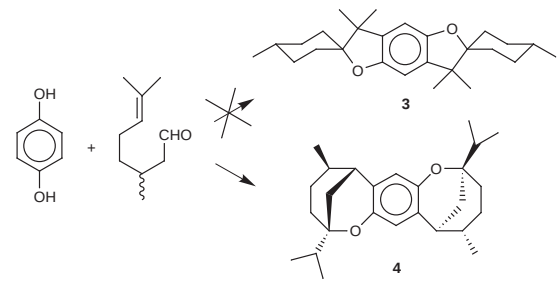

Scheme 2

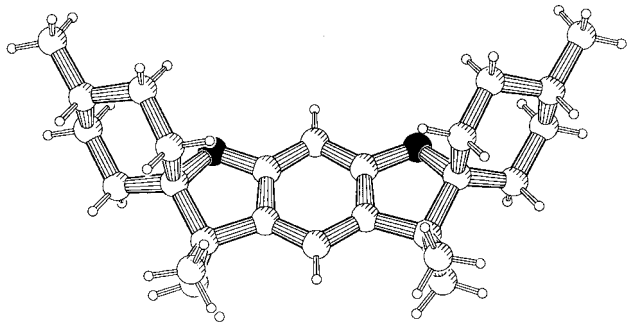

Fig. 1 X-Ray structure of **2**.

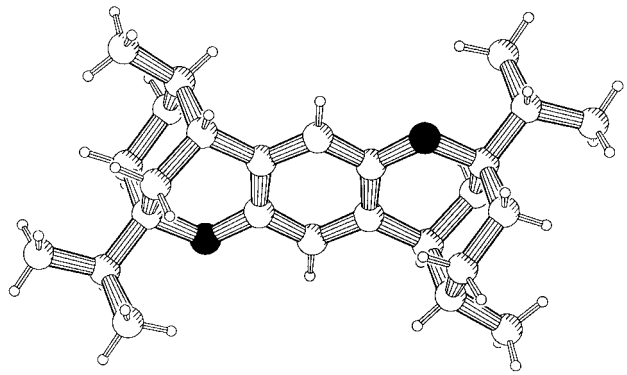

Fig. 2 X-Ray structure of **4**.

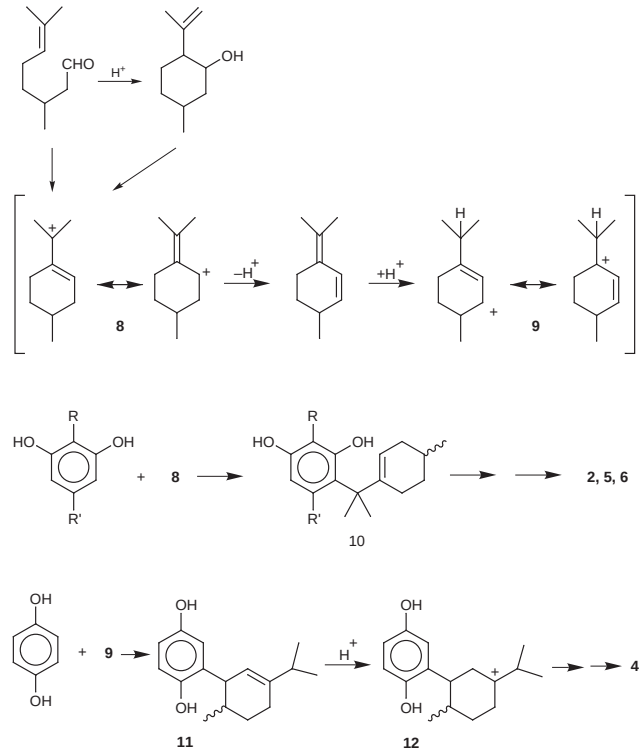

Scheme 3

Pyrogallol afforded product **5** with citronellal, having structure and yield (63%) comparable with compound **2**. The isomeric phloroglucinol gave a fair yield (33%) of an inseparable mixture of four diastereoisomers, corresponding to a [3 + 1] adduct **6** (*m/z* 534). The [2 + 1] adduct **7**, which should be theoretically possible, was not present (Scheme 1). The ^{1}H and ^{13}C NMR spectra of this mixture, which was not further investigated, showed similarity to that of the resorcinol adduct **2**.

Crystals of **2** and **4** were grown from an acetone–MeOH mixture and the molecular structures of **2** and **4** were confirmed by X-ray diffraction.[4] The molecular shape of compound **2** is determined to a large extent by the conformation of the different rings (Fig. 1). The central ring system is slightly bent: the angle between the best planes through both tetrahydrofuran rings is 14.5°. Both cyclohexane rings have a chair conformation with the methyl substituent in the equatorial position and the *gem*-dimethyl carbon in the equatorial position in order to reduce possible steric hindrance. Compound **4** possesses an internal centre of symmetry (Fig. 2). The tetrahydropyran ring has a clear envelope conformation with the isopropyl group attached in the equatorial position. The cyclohexane ring, oriented axially with respect to the previous ring, has a chair conformation with the methyl substituent in the axial position.

Citronellal is known to cyclize in acidic medium, in fact this is a way to prepare isopulegol.[5] When the condensations of resorcinol and hydroquinone were carried out with isopulegol, the adducts **2** and **4** were formed in comparable yields (75 and 76%, respectively) as for the reactions based on citronellal.

Via a number of intermediates, involving acid-catalyzed isomerizations, the stabilized cationic species **8** and **9** can form in the reaction mixture (Scheme 3). Obviously, **8** is more stable than **9** and will be preferentially formed. Resorcinol, pyrogallol and phloroglucinol are significantly more reactive than hydroquinone towards electrophilic substitution and, therefore, they can react with the stabilized cation **8** with the formation of the intermediate **10**, which after protonation will cyclize with the phenol function. It is interesting to note that even when the reactants are combined in a 1 : 1 ratio, only the [2 + 1] adduct **2** is obtained. Apparently, the intermediate [1 + 1] adduct is significantly more reactive than resorcinol itself.

Hydroquinone will only react with the less stabilized cation **9**, and the intermediate **11** will be protonated selectively with the formation of the tertiary carbenium ion **12**, and ultimately the bridged compound **4**. A similar singly bridged [2 + 1] condensation product resulting from the acid catalyzed condensation of resorcinol and 2-cyclohexenone was reported recently.[6]

We thank the Ministerie voor Wetenschapsbeleid, the F.W.O. Vlaanderen and the University for their continuing support. B. F. thanks the I.W.T for a predoctoral fellowship.

Notes and references

1 P. Timmerman, W. Verboom and D. N. Reinhoudt, *Tetrahedron*, 1996, **52**, 2663

2 D. J. Cram and J. M. Cram, *Container Molecules and their Guests*, *Monographs in Supramolecular Chemistry*, ed. J. F. Stoddart, Royal Society of Chemistry, Cambridge, 1994, vol. 4; R. G. Chapman and J. C. Sherman, *Tetrahedron*, 1997, **53**, 15911

3 All new compounds described were characterized by IR, mass, ^{1}H and ^{13}C NMR spectroscopy and gave correct C, H elemental analysis.

4 *Crystal data*: intensity data were collected at 16 °C on a Siemens P4 diffractometer using Mo-Kα radiation (λ = 0.71073 Å). Data were corrected for Lp effects, but not for absorption. For **2**: $C_{26}H_{38}O_2$, M = 382.56, triclinic, $P\bar{1}$, a = 6.604(1), b = 11.265(3), c = 15.797(4) Å, α = 106.96(2), β = 90.41(2), γ = 93.45(2)°, V = 1121.7(4) Å^3, Z = 2, D_c = 1.133 g cm^{-3}, μ(Mo-Kα) = 0.069 mm^{-1}, F(000) = 420, crystal size 0.5 × 0.1 × 0.1 mm, 2716 independent reflections. Final R = 0.0535 for 1912 reflections with $I > 2\sigma(I)$ and $\omega R2$ = 0.1490 for all data. For **4**: $C_{26}H_{38}O_2$, M = 382.56, monoclinic, $P2_1/n$, a = 8.555(2), b = 10.668(2), c = 12.247(2) Å, β = 108.14(1)°, V = 1076.1(4) Å^3, Z = 2, D_c = 1.181 g cm^{-3}, μ(Mo-Kα) = 0.069 mm^{-1}, F(000) = 420, crystal size 0.45 × 0.25 × 0.25 mm, 1893 independent reflections. Final R = 0.0393 for 1598 reflections with $I > 2\sigma(I)$ and $\omega R2$ = 0.1084 for all data. The structures were solved by direct methods (SHELXTL). Refinement on F^2 was carried out by full-matrix least-squares (SHELXTL) with anisotropic displacement parameters for non-H atoms and riding isotropic H atoms (C–H distance free to refine). CCDC 182/1255. See http://www.rsc.org/suppdata/cc/1999/1117/ for crystallographic data in .cif format.

5 K. Bauer, D. Garbe and H. Surburg, *Common Fragrance and Flavor Materials*, 3rd edn., Wiley-VCH, Weinheim, 1997.

6 P. Livant, T. R. Webb and W. Xu, *J. Org. Chem.*, 1997, **62**, 737.

Communication 9/01553A

Catalysis in the core of a carbosilane dendrimer

G. Eric Oosterom, Richard J. van Haaren, Joost N. H. Reek, Paul C. J. Kamer and Piet W. N. M. van Leeuwen*

Institute of Molecular Chemistry, University of Amsterdam, Nieuwe Achtergracht 166, 1018 WV Amsterdam, The Netherlands. E-mail: pwnm@anorg.chem.uva.nl

Received (in Cambridge, UK) 25th March 1999, Accepted 12th May 1999

The synthesis of a series of diphosphine ligands having phosphorus donor atoms in the core of a carbosilane dendrimer and their use in palladium catalysed allylic alkylation is described.

Dendrimers are fascinating molecules owing to their unique physical and chemical properties.[1] From the beginning catalysis has been recognised as one of their main potential applications, but so far only a few examples have appeared in the literature.[2–5] Two general strategies for the construction of dendritic catalysts can be applied: (1) multiple catalytic sites at the periphery of the dendrimer and (2) one (or more) catalytic site(s) in the core of the dendrimer.

Previously, we and others have reported examples of the periphery strategy.[2,3] This approach has the major advantage that the catalyst can be removed from the product mixture *via* nanofiltration and reused.[3,4]

Recently, a number of groups reported core-functionalised dendrimers as examples of the second strategy.[5] Some of these so-called 'dendrizymes' showed that the substrate selectivity of the catalytic reaction changed with increasing generations.[6]

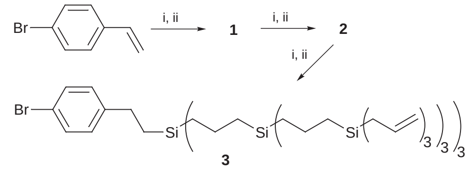

Scheme 1 *Reagents and conditions*: i, $HSiCl_3$, [Pt], rt, 2 h, 100%; ii, $BrMgCH_2CH{=}CH_2$, Et_2O, rt, 100%.

Here we describe the synthesis of carbosilane dendritic wedges using *p*-bromostyrene as starting compound. The bromide can be used to construct a new type of ligand embedded in the apolar dendrimer. The dendritic analogues of dppf [bis(diphenylphosphino)ferrocene] were synthesised as examples of such core-functionalised dendrimers. Initial experiments show that palladium complexes of these dendrimers are active catalysts in allylic alkylation reactions and a significant change in the product selectivity is observed for the largest dendrimer.

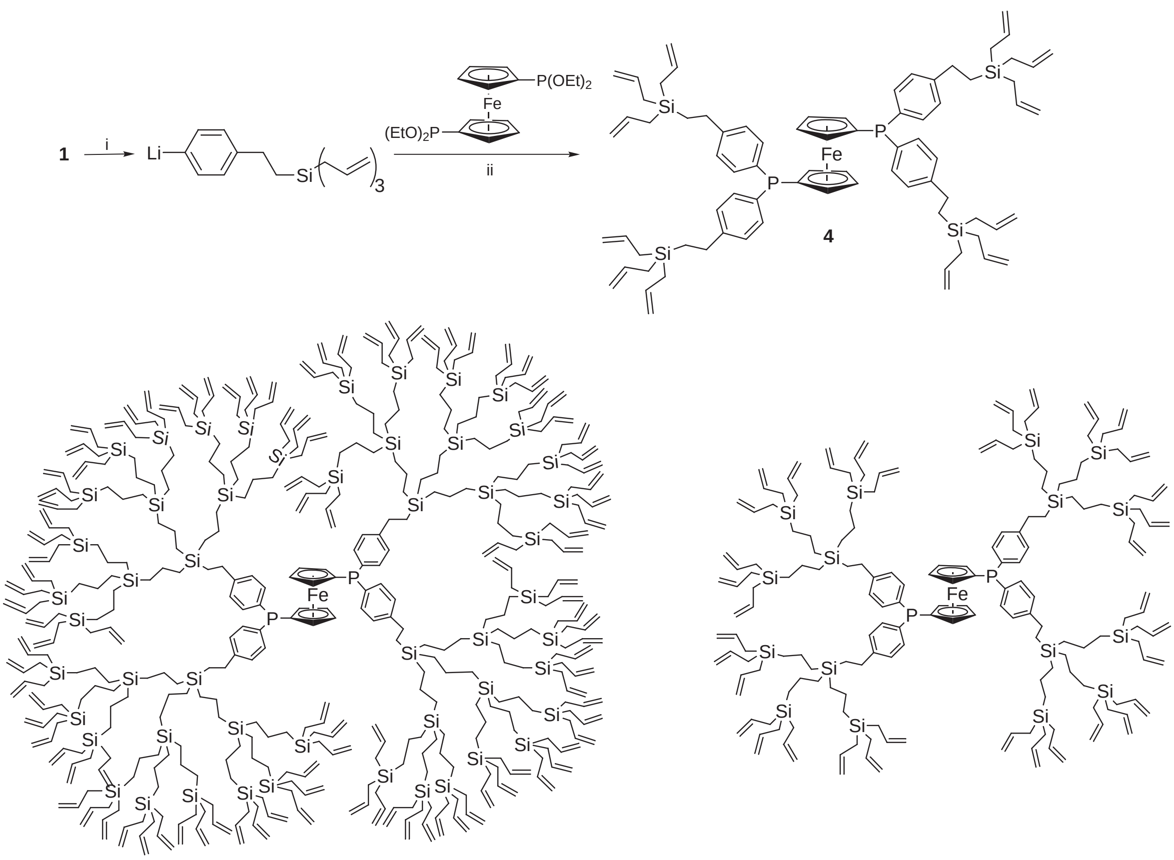

Scheme 2 *Reagents and conditions*: i, BuLi, THF, −78 °C; ii, THF, −78 °C.

Table 1 Activity and selectivity in the allylic alkylation of 3-phenylallyl acetate with diethyl 2-sodio-2-methylmalonate after 60 min[a]

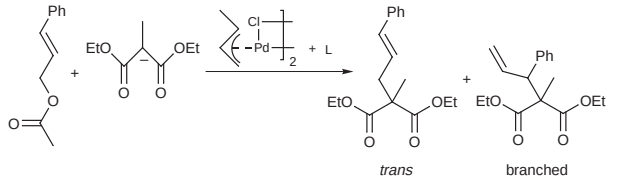

L	Conversion (%)[b]	*trans* product (%)[c]
—	8	96 (±1.0)
dppf	72	90 (±0.7)
4	76	88 (±1.2)
5	58	87 (±0.8)
6	17	79 (±0.4)

[a] Conditions: 0.25 μmol $[crotyl\text{-}PdCl]_2$, 0.5 μmol **L**, 6.0 ml THF, 0.5 mmol 3-phenylallyl acetate, 1.0 mmol malonate, 0.05 mmol decane, rt. [b] All catalytic reactions reached full conversion in 24 h. [c] The selectivity of the reaction was independent of the conversion.

The carbosilane wedges **1**–**3** (Scheme 1) were prepared in a divergent manner starting from *p*-bromostyrene, using a two-step methodology.[7] These steps involve a platinum-catalysed hydrosilylation with $SiHCl_3$ followed by reaction with an excess of allylmagnesium bromide yielding wedges **1** to **3**. Under optimised reaction conditions the wedges were obtained quantitatively, purified by flash chromatography and characterised by ^1H and ^{13}C NMR spectroscopy, elemental analysis, and FAB and MALDI-TOF mass spectrometry. The bromobenzene moiety can be used to synthesise a core-functionalised dendrimer in a convergent way. After lithiation using BuLi at −78 °C, these wedges were made to react with tetraethyl ferrocene-1,1′-diylbis(phosphonite)[8] yielding the bidentate ligands **4**–**6** with molecular weights up to 8567 (Scheme 2). These compounds were purified by column chromatography and analysed by ^1H and ^{31}P NMR spectroscopy, MALDI-TOF mass spectrometry and elemental analysis.†

Palladium dichloride complexes were prepared by stirring the ligand with $Pd(MeCN)_2Cl_2$ in CH_2Cl_2 for 60 min during which the solution turned red. ^{31}P NMR spectroscopy confirmed complete complexation of the ligand in a bidentate *cis* fashion. The signal of the free ligand around δ −18 was completely replaced by a singlet around δ +32.

After it was shown that these novel core-functionalised dendrimers formed similar Pd complexes as dppf, the catalytic activity of the compounds was tested in palladium catalysed allylic alkylation. In a typical experiment, crotylpalladium chloride dimer was added to a THF solution of the ligand and the mixture was incubated for 1 h at room temperature. 3-Phenylallyl acetate, decane (internal standard) and diethyl 2-sodio-2-methylmalonate were added.‡ The reactions were followed by GC analysis of samples taken from the reaction mixture. All the Pd complexes of the dendritic phosphines were catalytically active (see Table 1), producing mainly the linear *trans* product. The *cis* product was not observed. As indicated by the similar conversion for dppf and **4**, the allyl end groups do not interfere in the catalytic reaction. As expected, the rate of the reaction decreased using the higher generation catalysts. This effect, also found by others,[5,9] is due to more difficult mass transport with increasing steric bulk of the dendritic wedges, and is most pronounced when going from generation 2 to 3.

Remarkably, the size of the dendrimers determined also the selectivity of the allylic alkylation reaction; Pd–**6** yielded significantly more of the branched product. This change in selectivity might be due to the increasing steric bulk of the dendrimer hindering the attack of the nucleophile on the Pd–allyl. The apolar microenvironment created by the carbosilane wedges could also be the reason for this observed selectivity effect. Current research is aiming at a detailed insight in the nature of the dendritic effect and extending the synthetic approach to other core functionalities.

We thank the Netherlands Foundation for Chemical Research (CW) and the Netherlands Organisation for Scientific Research (NWO) for financial support and P. G. Emmerink for experimental assistance.

Notes and references

† *Selected data* for **4**: $\delta_H(CDCl_3)$ 0.94 (m, 8H, $SiCH_2CH_2Ph$), 1.62 (d, 24H, $SiCH_2CH$), 2.64 (m, 8H, $SiCH_2CH_2Ph$), 4.02 (d, 4H, H_{Fc}), 4.09 (d, 4H, H_{Fc}), 4.87 (d, 12H, $CHCH_2$), 4.92 (dd, 12H, $CHCH_2$), 5.79 (m, 12H, $CHCH_2$), 7.12 (d, 8H, H_{ar}), 7.22 (d, 8H, H_{ar}); $\delta_P(CDCl_3)$ −18.39. For **5**: $\delta_H(CDCl_3)$ 0.61 (t, 24H, $SiCH_2CH_2CH_2Si$), 0.67 (t, 24H, $SiCH_2CH_2Si$), 0.84 (m, 8H, $SiCH_2CH_2Ph$), 1.38 (m, 24H, $SiCH_2CH_2CH_2Si$), 1.59 (d, 72H, $SiCH_2CH$), 2.56 (m, 8H, $SiCH_2CH_2Ph$), 4.06 (d, 4H, H_{Fc}), 4.15 (d, 4H, H_{Fc}), 4.85 (d, 36H, $CHCH_2$), 4.90 (dd, 36H, $CHCH_2$), 5.78 (m, 36H, $CHCH_2$), 7.11 (d, 8H, H_{ar}), 7.26 (dd, 8H, H_{ar}); $\delta_P(CDCl_3)$ − 18.53. For **6**: $\delta_H(CDCl_3)$ 0.54 (t, 96H, $SiCH_2CH_2CH_2Si$), 0.66 (t, 96H, $SiCH_2CH_2CH_2Si$), 0.82 (m, 8H, $SiCH_2CH_2Ph_2$), 1.29 (m, 96H, $SiCH_2CH_2CH_2Si$), 1.56 (d, 216H, $SiCH_2CH$), 2.54 (m, 8H, $SiCH_2CH_2Ph$), 4.04 (br s, 4H, H_{Fc}), 4.14 (br s, 4H, H_{Fc}), 4.83 (d, 108H, $CHCH_2$), 4.88 (dd, 108H, $CHCH_2$), 5.75 (m, 108H, $CHCH_2$), 7.11 (d, 8H, H_{ar}), 7.23 (brs, 8H, H_{ar}); $\delta_P(CDCl_3)$ − 17.9; *m/z* (MALDI-TOF) 8679 [M + Ag].

‡ In catalysis isolated complexes gave similar results as *in situ* complexes.

1 G. R. Newkome, C. N. Moorefield and F. Vögtle, *Dendritic Molecules*, Verlag-Chemie, Weinheim, Germany, 1996.
2 J. W. J. Knapen, A. W. van der Made, J. C. de Wilde, P. W. N. M. van Leeuwen, P. Wijkens, D. M. Grove and G. van Koten, *Nature*, 1994, **372**, 659.
3 J.-J. Lee, W. T. Ford, J. A. Moore and Y. Li, *Macromolecules*, 1994, **27**, 4632; D. Seebach, R. E. Marti and T. Hintermann, *Helv. Chim. Acta*, 1996, **79**, 1710; M. T. Reetz, G. Lohmer and R. Schwickardi, *Angew. Chem., Int. Ed. Engl.*, 1997, **36**, 1526; T. Marquardt and U. Lüning, *Chem. Commun.*, 1997, 1681; C. Köllner, B. Pugin and A. Togni, *J. Am. Chem. Soc.*, 1998, **120**, 10274; R. A. Gossage, J. T. B. H. Jastrzebski, J. van Ameijde, S. J. E. Mulders, A. J. Brouwer, R. M. J. Liskamp and G. van Koten, *Tetrahedron Lett.*, 1999, **40**, 1413.
4 U. Kragl and C. Dreisbach, *Angew. Chem., Int. Ed. Engl.*, 1996, **35**, 642.
5 H. Brunner, *J. Organomet. Chem.*, 1995, **500**, 39; P. Bhyrappa, J. K. Young, J. S. Moore and K. S. Suslick, *J. Am. Chem. Soc.*, 1996, **118**, 5708; H.-F. Chow and C. C. Mak, *Macromolecules*, 1997, **30**, 1228; H.-F. Chow and C. C. Mak, *J. Org. Chem.*, 1997, **62**, 5116; S. Yamago, M. Furukawa, A. Azuma and J.-I. Yoshida, *Tetrahedron Lett.*, 1998, **39**, 3783.
6 For a review about dendrimers as biological mimics: D. K. Smith and F. Diederich, *Chem. Eur. J.*, 1998, **4**, 1353.
7 A. W. van der Made and P. W. N. M. van Leeuwen, *J. Chem. Soc., Chem. Commun.*, 1992, 1400; L.-L. Zhou and J. Roovers, *Macromolecules*, 1993, **26**, 963; D. Seyferth, T. Kugita, A. L. Rheingold and G. P. A. Yap, *Organometallics*, 1995, **14**, 5362.
8 M. J. Burk and M. F. Gross, *Tetrahedron Lett.*, 1994, **35**, 9363.
9 I. Morao and F. P. Cossío, *Tetrahedron Lett.*, 1997, **38**, 6461.

Communication 9/02392E

Regioselective one-step synthesis of *trans*-3,*trans*-3,*trans*-3 and *e,e,e* [60]fullerene tris-adducts directed by a C_3-symmetrical cyclotriveratrylene tether

Gwénaël Rapenne,[a] Jeanne Crassous,[b] André Collet,*[b] Luis Echegoyen*[c] and François Diederich*[a]

[a] *Laboratorium für Organische Chemie, ETH-Zentrum, Universitätstrasse 16, CH-8092 Zürich, Switzerland. E-mail: diederich@org.chem.ethz.ch*

[b] *Laboratoire de Stéréochimie et des Interactions Moléculaires, CNRS UMR 5532, Ecole Normale Supérieure de Lyon, 46 Allée d'Italie, 69364 Lyon Cedex 07, France*

[c] *Department of Chemistry, University of Miami, Coral Gables, FL 33124, USA*

Received (in Cambridge, UK) 22nd April 1999, Accepted 12th May 1999

The first covalent cyclotriveratrylene (CTV)–C_{60} adducts were prepared by the tether-directed Bingel reaction, which gave the two C_3-symmetrical *trans*-3,*trans*-3,*trans*-3 and *e,e,e* tris-adducts with a high degree of regioselectivity.

The preparation of higher covalent adducts of buckminsterfullerene (C_{60}) with interesting electrochemical[1] or chiroptical properties[2] is currently under intense investigation. The tether-directed remote functionalisation method developed in the Diederich group for this purpose has proved to be very powerful because of its high regio- and stereoselectivity.[3] This methodology has been used successfully to prepare enantiomerically pure *cis*-3 bis-adducts with inherently chiral functionalisation patterns[2] or cyclophane-type crown ether[4a] and porphyrin[4b,5] conjugates with interesting redox properties, in which the second chromophore is doubly connected to the *trans*-1 positions at the two poles of the carbon sphere. Many functionalisation reactions of C_{60} leading to a variety of mono- and bis-adducts have been reported.[6] In contrast, only a few examples of tris-adducts have been described.[2a,7,8] In theory, bis-adducts of C_{60} derived from Bingel cyclopropanation reactions[9] can exist as eight different regioisomers, seven of which have been detected and isolated.[7a] The number of possible regioisomers increases to 46 in the case of tris-adducts in which three of the thirty 6-6 bonds (bonds between two six-membered rings) have been cyclopropanated.[6b] In 1994, Hirsch and co-workers reported the stepwise preparation of such tris-adducts and eventually obtained the *trans*-3,*trans*-3,*trans*-3 and *e,e,e* regioisomers together with other isomers, after tedious separation and purification.[7a]

Here we report the tether-directed regioselective synthesis of two new C_3-symmetrical tris-adducts having *trans*-3,*trans*-3,*trans*-3 and *e,e,e* structures, respectively, in one step from C_{60}. Cyclotriveratrylene (CTV) is well-suited in size and shape to interact favorably with C_{60}.[10] The affinity between these two molecules, which is reinforced by the electron donor character of CTV and the electron acceptor properties of C_{60}, has been evidenced by the formation of a crystalline complex in which C_{60} adopts a nesting position at van der Waals contact distance above the concave surface of the CTV macrocycle.[10a] These features prompted us to utilize a C_3-symmetric tris-malonate derivative of CTV, such as (±)-**2**, as a template for preparing tris-aducts of C_{60} by the tether-directed Bingel reaction (Scheme 1). The required (±)-**2** was obtained in one step by reacting the C_3-symmetrical CTV derivative (±)-**1**[11] with 3.3 equiv. of ethyl malonyl chloride (room temperature, CH_2Cl_2–pyridine). After column chromatography (SiO_2, CH_2Cl_2 → CH_2Cl_2–1% MeOH), (±)-**2** was obtained in 77% yield as a colorless solid.

The Bingel reaction of (±)-***2*** with C_{60} was carried out in the presence of 9 equiv. of DBU and 3 equiv. of I_2. After 4 h, two products (±)-**3** and (±)-**4** had formed which were separated by column chromatography (SiO_2 H, CH_2Cl_2 → CH_2Cl_2–2% MeOH) and isolated in 11 and 9% yield, respectively. FAB-MS spectra† of (±)-**3** and (±)-**4** displayed the molecular ions expected for the tris-adducts shown in Scheme 1. This is the first example of tris-adduct formation by a one-step tether-directed Bingel addition.

The C_3-symmetry of the two adducts was established using NMR spectroscopy. The ^{1}H NMR spectra of (±)-**3** and (±)-**4** display the usual features for a C_3-CTV unit, *i.e.* two singlets for the aromatic H-atoms, one singlet for the OMe groups and the characteristic AB quartet for the CH_2 bridges. This means that the adducts must themselves possess a C_3 axis that is common to the CTV and the C_{60} subnits. The ^{13}C NMR spectra (Fig. 1), showing 20 resolved peaks for the fullerene C-atoms of (±)-**3** and 18 for those of (±)-**4**, support this conclusion. Since among all the possible regioisomers only the *trans*-3,*trans*-3,*trans*-3 and *e,e,e* trist-adducts exhibit such a symmetry (the *cis*-1,*cis*-1,*cis*-1 tris-adduct cannot form for steric reasons), the structures

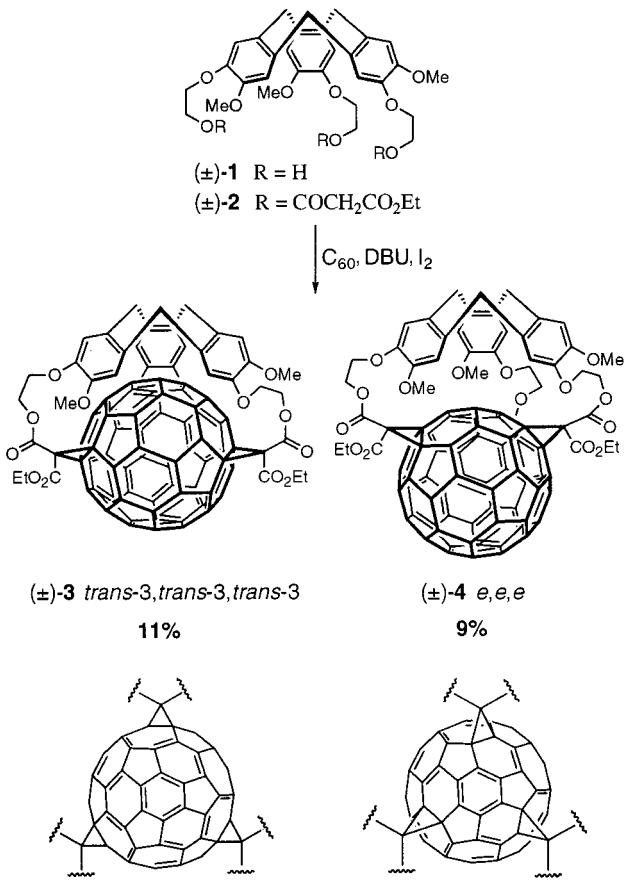

Scheme 1

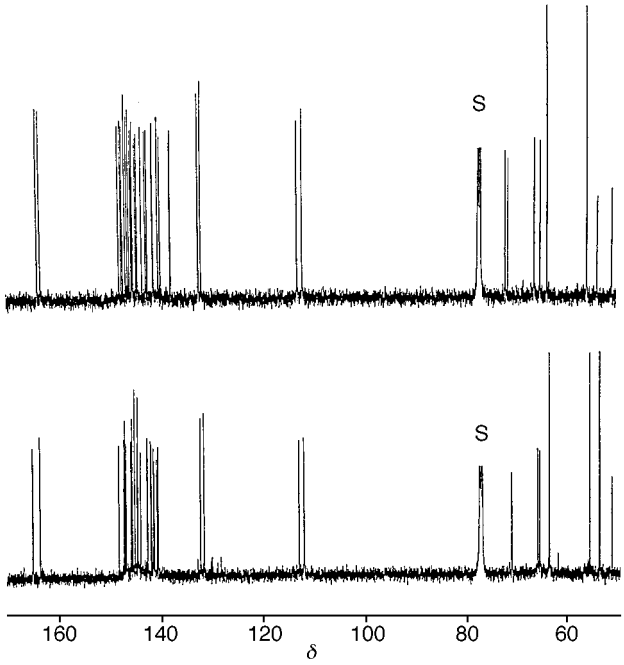

Fig. 1 ^{13}C NMR (125 MHz, $CDCl_3$) spectra of (*a*) tris-adduct (±)-**3** and (*b*) tris-adduct (±)-**4**; S stands for solvent.

of the two new tris-adducts were thus unambiguously established.

Since all attempts at transesterification to give the corresponding known tris(diethyl malonate) adducts[7a] failed, the structures of the two compounds were initially assigned with the help of UV-visible spectroscopy (CH_2Cl_2). Regioisomer (±)-**3** exhibits a cherry-red colour and (±)-**4** an orange–red colour, which are the same as those previously reported for the regioisomeric *trans*-3,*trans*-3,*trans*-3 and *e*,*e*,*e* tris(diethyl malonate) adducts, respectively.[7a] This difference is reflected in an additional absorption band at λ_{max} = 422 nm in the UV-visible spectrum of (±)-4.

The assignment of (±)-**3** and (±)-**4** as the *trans*-3,*trans*-3,*trans*-3 and *e*,*e*,*e* isomers, respectively, was further supported by a close comparison of their NMR spectra with those of analogous untethered tris-cyclopropanated C_{60} derivatives.[7a,b] The ^{13}C NMR chemical shifts of the bridgehead sp^3-C-atoms in the fullerene shell have been shown to appear at higher field in the *e*,*e*,*e* than in the *trans*-3,*trans*-3,*trans*-3 regiosomer, whereas the opposite behaviour has been observed for the methano bridge C-atom. The ^{13}C NMR resonances for the cyclopropane fragments were in fact observed at δ 71.63, 71.11 (bridgehead) and 50.61 (bridge) for (±)-**3** and at δ 70.73, 70.66 (bridgehead) and 51.07 (bridge) for (±)-**4**. The structural assignment was further corroborated by the position of the ^{1}H NMR resonance of the axial protons in the methylene bridges of the CTV fragment. For the tris-adduct (±)-**4** (δ 4.65), this signal is nearly unaffected with respect to that observed for the free CTV (±)-**2** (δ 4.74) whereas for (±)-**3**, it is significantly downfield shifted to δ 5.33. This indicates a much greater proximity of the CTV fragment to the fullerene core with its deshielding pentagon rings, which is expected for the *trans*-3,*trans*-3,*trans*-3 regioisomer, as shown in Scheme 1.

The total yield of tris-adducts is 20%, with a distribution of 55% of *trans*-3,*trans*-3,*trans*-3 and 45% of *e*,*e*,*e* regioisomer. Given the low statistical yield of 0.5% for (±)-**3** and 1% for (±)-**4** (among the 46 possible tris-adduct regioisomers), one can assume that the CTV template is largely responsible for this high degree of regioselectivity.

Since a splitting and doubling of the NMR signals is observed neither for (±)-**3** nor for (±)-**4**, one can expect the triply tethered reaction to be diastereoselective. We are currently investigating the use of optically pure C_3-CTV **2**[12] as starting material in order to confirm this diastereoselectivity, which opens new perspectives in the preparation of optically active derivatives of C_{60} and other fullerenes.

This work was supported by the Swiss National Science Foundation, the CNRS and the US National Science Foundation (CHE-9816503). G. R. is grateful for a Lavoisier postdoctoral fellowship of the French Ministry of Foreign Affairs.

Notes and references

† *Selected data* for (±)-**3**: cherry-red solid; $\lambda_{max}(CH_2Cl_2)$/nm (ε/dm^3 mol^{-1} cm^{-1}) 297 (33 100), 316 (25 500), 488 (2810), 570 (1250, sh); δ_H(500 MHz, $CDCl_3$) 6.61 (s, 3 H), 6.55 (s, 3 H), 5.33 [d, *J* 12.5, 3 H, CTV-CH_2(ax)], 4.63 (m, 6 H), 4.45 (m, 6 H), 4.13 (m, 3 H), 4.02 (m, 3 H), 3.63 (s, 9 H), 3.37 [d, *J* 12.5, 3 H, CTV-CH_2(eq)], 1.42 (t, *J* 7.1, 9 H); δ_C(125 MHz, $CDCl_3$) 164.13, 163.55, 148.36, 147.89, 147.59, 147.06, 146.69, 146.31, 145.97, 145.73, 145.68, 145.53, 144.97, 144.67, 143.74, 143.00, 142.66, 141.64, 141.49, 140.60, 140.14, 138.16, 132.67, 132.11, 113.17, 112.15, 71.63, 71.11, 65.80, 64.65, 63.32, 55.42, 53.41, 50.61, 14.10; *m*/*z* (HR-FAB$^+$-MS) 1596.2839 (M$^+$, calc. 1596.2841). For (±)-**4**: orange–red solid; $\lambda_{max}(CH_2Cl_2)$/nm (ε/dm^3 mol^{-1} cm^{-1}) 296 (43 600), 319 (30 000), 422 (2450), 486 (3270), 568 (1550); δ_H(500 MHz, $CDCl_3$) 6.56 (s, 3 H), 6.53 (s, 3 H), 4.93 (m, 3 H), 4.82 (m, 3 H), 4.65 [d, *J* 14.5, 3 H, CTV-CH_2(ax)], 4.47 (m, 6 H), 4.15 (m, 6 H), 3.58 (s, 9 H), 3.38 [d, *J* 14.5, 3 H, CTV-CH_2(eq)], 1.40 (t, 9 H); δ_C (125 MHz, $CDCl_3$) 164.96, 163.57, 148.32, 147.44, 147.34, 147.14, 146.95, 146.02, 145.73, 145.22, 144.78, 144.58, 144.10, 142.69, 142.06, 141.89, 141.55, 141.40, 140.87, 140.62, 132.32, 131.65, 112.93, 111.95, 70.73, 70.66, 65.53, 65.10, 63.30, 55.24, 53.40, 51.07,14.10 *m*/*z* (HR-FAB$^+$-MS) 1596.2835 (M$^+$, calc. 1596.2841).

1 L. Echegoyen and L. E. Echegoyen, *Acc. Chem. Res.*, 1998, **31**, 593.
2 (*a*) J.-F. Nierengarten, T. Habicher, R. Kessinger, F. Cardullo, F. Diederich, V. Gramlich, J. P. Gisselbrecht, C. Boudon and M. Gross, *Helv. Chim. Acta*, 1997, **80**, 2238; (*b*) M. Taki, Y. Nakamura, H. Uehara, M. Sato and J. Nishimura, *Enantiomer*, 1998, **3**, 231; (*c*) H. Isobe, H. Tokuyama, M. Sawamura and E. Nakamura, *J. Org. Chem.*, 1997, **62**, 5034.
3 F. Diederich and R. Kessinger, *Acc. Chem. Res.*, in the press.
4 (*a*) J.-P. Bourgeois, L. Echegoyen, M. Fibbioli, E. Pretsch and F. Diederich, *Angew. Chem., Int. Ed. Engl.*, 1998, **37**, 2118; (*b*) J.-P. Bourgeois, F. Diederich, L. Echegoyen and J.-F. Nierengarten, *Helv. Chim. Acta*, 1998, **81**, 1835.
5 E. Dietel, A. Hirsch, E. Eichhorn, A. Rieker, S. Hackbarth and B. Röder, *Chem. Commun.*, 1998, 1981.
6 (*a*) A. Hirsch, *Top. Curr. Chem.*, 1999, **199**, 1; (*b*) A. Hirsch, *The Chemistry of the Fullerenes*, Thieme, Stuttgart, 1994.
7 See for example: (*a*) A. Hirsch, I. Lamparth and H. R. Karfunkel, *Angew. Chem., Int. Ed. Engl.*, 1994, **33**, 437; (*b*) F. Djojo and A. Hirsch, *Chem. Eur. J.*, 1998, **4**, 344; (*c*) T. Hamano, K. Okuda, T. Mashino, M. Hirobe, K. Arakane, A. Ryu, S. Mashiko and T. Nagano, *Chem. Commun.*, 1997, 21.
8 For tether-directed preparations of tris-adducts, see: L. Isaacs, F. Diederich and R. F. Haldimann, *Helv. Chim. Acta*, 1997, **80**, 317; F. Cardullo, P. Seiler, L. Isaacs, J.-F. Nierengarten, R. F. Haldimann, F. Diederich, T. Mordasini-Denti, W. Thiel, C. Boudon, J.-P. Gisselbrecht and M. Gross, *Helv. Chim. Acta*, 1997, **80**, 343.
9 C. Bingel, *Chem. Ber.*, 1993, **126**, 1957.
10 (*a*) J. W. Steed, P. C. Junk, J. L. Atwood, M. J. Barnes, C. L. Raston and R. S. Burkhalter, *J. Am. Chem. Soc.*, 1994, **116**, 10 346; (*b*) J. L. Atwood, M. J. Barnes, M. G. Gardiner and C. L. Raston, *Chem. Commun.*, 1996, 1449; (*c*) H. Matsubara, A. Hasegawa, K. shiwaku, K. Asano, M. Uno, S. Takahashi and K. Yamamoto, *Chem. Lett.*, 1998, 923; (*d*) H. Matsubara, T. Shimura, A. Hasegawa, M. Semba, K. Asano and K. Yamamoto, *Chem. Lett.*, 1998, 1099.
11 J. Canceill, J. Gabard and A. Collet, *J. Chem. Soc., Chem. Commun.*, 1983, 122; J. Canceill, J. Gabard and A. Collet, *J. Am. Chem. Soc.*, 1984, **106**, 5997; G. Vériot, J. P. Dutasta, G. Matouzenko and A. Collet, *Tetrahedron*, 1995, **51**, 389.
12 A. Collet, in *Comprehensive Supramolecular Chemistry*, ed. F. Toda, Pergamon, 1996, vol. 6, ch. 9, pp. 281–303.

Communication 9/03226F

Rod-like ruthenium(II) coordination polymers: synthesis and properties in solution

Steffen Kelch and Matthias Rehahn*

Polymer Institute, University of Karlsruhe, Kaiserstrasse 12, D-76128 Karlsruhe, Germany.
E-mail: Matthias.Rehahn@t-online.de

Received (in Basel, Switzerland) 1st March 1999, Accepted 1st May 1999

Well defined coordination polymers obtained *via* the conversion of 4,4″-bis(2,2′:6′,2″-terpyridine)-2′,5′-dihexyl-*p*-terphenyl and activated ruthenium(III) show intrinsic viscosities of up to [*η*] ≈ 300 mL g^{-1} and a tremendous polyelectrolyte effect in salt-free DMA solution proving both their high molecular weights and considerable chain stiffness.

Soluble ruthenium(II) coordination polymers of well defined constitution are of actual interest because of their electronic, photooptical, magnetic and catalytic properties.[1–8] Moreover, they represent important reference systems for the profound analysis of polyelectrolyte behaviour in solution which is a field of research that urgently needs appropriate model polymers. Recently, we described the first high-molecular-weight ruthenium(II) coordination polyelectrolytes **1**.[9–11] These polymers have a rigid, randomly coiled backbone and display characteristic polyelectrolyte behaviour in salt-free solutions. To further deepen the understanding of the structure–property relationship of these rather unusual coordination polyelectrolytes it is worthwhile to also make available ruthenium(II) coordination polymers which have rod-like backbones. We therefore decided to prepare polymers **2** *via* the conversion of 4,4″-bis(2,2′:6′,2″-terpyridine)-2′,5′-dihexyl-*p*-terphenyl **5** and an activated ruthenium(III) species such as **6**,[12] and thus *via* a procedure which has only been used so far for the preparation of mono- and oligonuclear ruthenium complexes (Scheme 1).

Polyelectrolytes **2** were expected to be readily soluble because of their flexible *n*-hexyl side chains[13] and to have a rod-like shape because of (i) the constitution of the bis-tridentate ligand monomers and (ii) the octahedral coordination sphere around the transition-metal atoms. The required ligand monomer **5** was prepared in almost quantitative yields and high purity *via* the Pd-catalysed condensation of 4′-(*p*-bromophenyl)-2,2′:6′,2″-terpyridine **3**[14] and 2,5-dihexylbenzene-1,4-diboronic acid **4**[15] in a heterogeneous mixture of toluene and 1 M aqueous Na_2CO_3, and its constitution was verified using ^{1}H [Fig. 1(a)] and ^{13}C NMR spectroscopy.

Prior to the polymer synthesis itself, several model studies were performed to find out the optimum reaction conditions for the conversion **5** + **6** → **2** which guarantee selective and practically quantitative formation of the $[Ru(tpy)_2]^{2+}$ motif (tpy = 2,2′:6′,2″-terpytidine). These conditions should further prevent formation of defect structures within the chains of **2** which could destroy its rod-like shape. In the course of these experiments, DMA–butan-1-ol was found to be the solvent mixture of choice for our purpose. The conversion of $RuCl_3 \cdot 3H_2O$ with $AgBF_4$–acetone, on the other hand, provided us the appropriately reactive metal monomer **6**.[12] Finally, knowledge of the chemical shifts of all absorptions of both possible chain termini of **2** is imperative for NMR end-group analysis which is a convenient method for the estimation of the

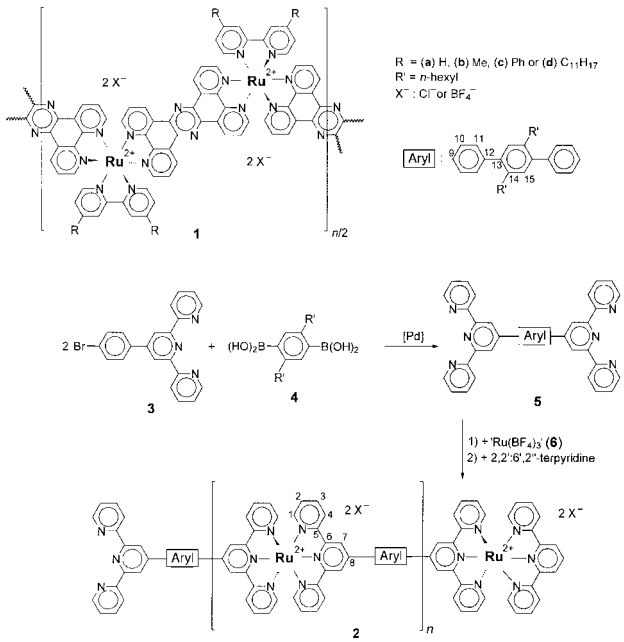

Scheme 1

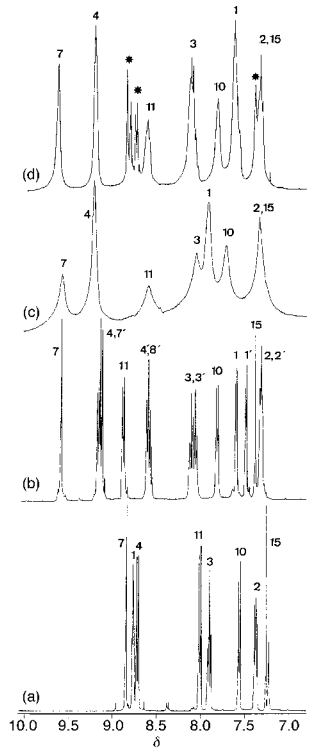

Fig. 1 400 MHz ^{1}H NMR spectra of (a) ligand monomer **5**, (b) the dinuclear model complex [(tpy)Ru(**5**)Ru(tpy)](BF$_4$)$_4$, (c) the high-molecular-weight polymer **2** and (d) a tpy-terminated low-molecular-weight polymer **2**, recorded in $CDCl_3$ (a), DMSO-d_6 (b, d) and DMA-d_9 (c), respectively, at room temperature. The signal assignment is according to the numbering specified in Scheme 1.

achieved degree of polymerisation (P_n). Therefore, the dinuclear complex [(tpy)Ru(**5**)Ru(tpy)](BF$_4$)$_4$ was prepared *via* the conversion of **5** with 2 equiv. of an activated ruthenium(III)–terpyridine complex which was obtained *via* the treatment of [Ru(tpy)Cl$_3$][16] with AgBF$_4$–acetone. The resulting dinuclear complex subsequently allowed the identification of all NMR absorptions that are caused by [Ru(tpy)$_2$]$^{2+}$ end-groups of **2** (right-hand side terminus of **2** in Scheme 1; [see Fig. 1(b) for its ^{1}H NMR spectrum]. For the tpy-termini of **2** (left-hand side terminus of **2** in Scheme 1), on the other hand, monomer **5** itself is the appropriate model compound [Fig. 1(a)]. Coordination polymers **2** were prepared under the optimised reaction conditions. For this purpose, an appropriate quantity of RuCl$_3$·3H$_2$O was first converted into the activated metal monomer **6** and subsequently heated with exactly 1 equiv. of ligand monomer **5** in butan-1-ol–DMA for 5 d. The product was precipitated in practically quantitative yields as a dark red, fibrous material which readily and completely redissolved in DMA or DMSO. Its constitution was analysed using ^{1}H and ^{13}C NMR spectroscopy. Fig. 1(c) displays a representative ^{1}H NMR spectrum of the product.

All intense absorptions clearly correspond to the inner-chain repeating units of **2**. No signals were found, on the other hand, of defect structures or of end-groups. In order to prove that such absorptions are not only covered by the broad signals of the repeating units, further polymerisations were carried out where a slight excess of either ligand monomer **5** or metal monomer **6** was used. In the latter case, 5% of tpy was added to the reaction mixture prior to work-up to produce well defined [Ru(tpy)$_2$]$^{2+}$ chain termini (Scheme 1). As expected, additional signals that correspond to the respective end-groups were observed in the NMR spectra of all these latter polymers. As an example, Fig. 1(d) displays the ^{1}H NMR spectrum of a polymer **2** prepared by using an excess of **5**.

We conclude that end-groups are reliably detectable by NMR despite the broad and intense absorptions of the polymer backbone but obviously have intensities below the limits of accuracy of the NMR method for polymers **2** prepared from an exact 1 : 1 equivalence of comonomers **5** and **6**. Moreover, formation of cyclic oligomers can be excluded because of the rod-like shape of **2**. It is evident, therefore, that very high-molecular-weight polymers were produced: considering the limits of the NMR method, we estimate average degrees of polymerisation of $P_{n(NMR)} \geqslant 30$ ($M_n \geqslant 36\,000$ g mol^{-1}) for the best products synthesized so far.

The hydrodynamic behaviour of **2** was analysed by viscosimetry to further support its high P_n and its rod-like shape. In DMA–0.02 M NH$_4$PF$_6$ solution—where intermolecular Coulomb interactions between the charged macromolecules are screened out—the high-molecular-weight samples of **2** show intrinsic viscosities of up to $[\eta] \approx 300$ mL g^{-1}. These values are *ca.* one order of magnitude higher than those reported for the randomly coiled reference polymers **1** ($[\eta] \leqslant 25$ mL g^{-1}). Moreover, a value of $[\eta] \approx 300$ mL g^{-1} is not only the highest intrinsic viscosity ever observed for a ruthenium(II) coordination polymer but also of the same order of magnitude as the intrinsic viscosities observed for purely covalent rod-like macromolecules such as poly(*p*-phenylenes)[16,17] or polyimides.[18] These results thus strongly support the high values of P_n and the rod-like shape of **2**.

In a second series of experiments, the hydrodynamic behaviour of a high- ($P_n \geqslant 30$) and a low-molecular-weight ($P_n \leqslant 10$) sample of **2** was studied in pure DMA where the intermolecular Coulomb interactions between the macromolecules are in operation. Under these conditions, the high-molecular-weight sample displays a very pronounced polyelectrolyte effect, *i.e.* a maximum in the Huggins plot of $(\eta_{sp}/c_p)_{max} \approx 2000$ mL g^{-1} at a polymer concentration of $c_P \approx 5 \times 10^{-6}$ g mL^{-1}. Nevertheless, the maximum is also clearly detectable for the low-molecular weight polymer **2** where a value of $(\eta_{sp}/c_P)max \approx 500$ mL g^{-1} is reached at a polymer concentration of $c_P \approx 5 \times 10^{-6}$ g mL^{-1}. Finally, the maximum is again less pronounced {$(\eta_{sp}/c_P)max \approx 100$ mL g^{-1}} for the high-molecular-weight but randomly coiled reference polymer **1a** and appear at a polymer concentration of $c_P \approx 7 \times 10^{-6}$ g mL^{-1}. These results highlight the tremendous influence of the chain length and in particular the shape of the macromolecules on their hydrodynamic behaviour also in solutions of low ionic strength. Comparably high-molecular-weight ($P_n \geqslant 30$) but randomly coiled reference polymers **1** reach maxima of $(\eta_{sp}/c_p)_{max} \approx 100$ mL g^{-1} at the best.

Finally, UV–VIS spectra were recorded in DMA solution of the mononuclear complex [Ru(tpy)$_2$](PF$_6$)$_2$, the dinuclear complex [(tpy)Ru(**5**)Ru(tpy)](BF$_4$)$_4$ and the high-molecular-weight polymer **2** to analyse the absorption behaviour of the [Ru(tpy)$_2$]$^{2+}$ motif as a function of the number of complexes present in one molecule. In all cases, intense absorptions are observed at wavelengths below $\lambda = 380$ nm (ligand-centered $\pi^* \leftarrow \pi$ transitions) and at wavelengths above $\lambda = 400$ nm (metal-to-ligand charge-transfer transitions). No evidence is found in these spectra that might be interpreted as the result of intramolecular electronic interaction between the metal centers in the dimeric and polymeric species. This conclusion is further supported by cyclic voltammetry performed in DMF–NBu$_4$BF$_4$ solution: half-wave potentials of $E_{1/2}^{ox} = 1.20$, 1.24 and 1.25 V are found for the metal-localized first oxidation in the case of the mononuclear complex [Ru(tpy)$_2$](PF$_6$)$_2$, the dinuclear complex [(tpy)Ru(**5**)Ru(tpy)](BF$_4$)$_4$, and the high-molecular-weight polymer **2**, respectively.

Therefore, in full agreement with previous studies on related oligomeric complexes,[19] polymer **2** can be considered as a sequence of electonically nearly independent ruthenium(II) complexes. Presently, we are analysing the spectroscopic and electrochemical behaviour of polymers **2** in more detail.

The authors are grateful to Professor M. Ballauff, Karlsruhe, for his support of this work. We would like to thank Dr W. M. Meyer and Mr C. Sieber, MPI for Polymer Research, Mainz, for skillful technical assistance (cyclic voltammetry) as well as the Deutsche Forschungsgemeinschaft for financial support of the present work.

Notes and references

1 M. Rehahn, *Acta Polym.*, 1998, **49**, 201.
2 F. Ciardelli, E. Tsuchida and D. Wöhrle, *Macromolecule-Metal-Complexes*, Springer, Berlin, 1996.
3 V. Balzani, A. Juris, M. Venturi, S. Campagna and S. Serroni, *Chem. Rev.*, 1996, **96**, 759.
4 A. Harriman and R. Ziessel, *Chem. Commun.*, 1996, 1707.
5 J.-M. Lehn, *Supramolecular Chemistry*, VCH, Weinheim, 1995.
6 E. C. Constable and A. M. W. Chargill Thompson, *J. Chem. Soc., Dalton Trans.*, 1995, 1615.
7 E. C. Constable, A. M. W. Cargill Thompson, P. Harveson, L. Macko and M. Zehnder, *Chem. Eur. J.*, 1995, **1**, 360.
8 J.-P. Sauvage, J.-P. Collin, J.-C. Chambron, S. Guillerez, C. Coudret, V. Balzani, F. Barigelletti, L. DeCola and L. Flamigni, *Chem. Rev.*, 1994, **94**, 993.
9 R. Knapp, A. Schott and M. Rehahn, *Macromolecules*, 1996, **29**, 478.
10 S. Kelch and M. Rehahn, *Macromolecules*, 1997, **30**, 6185.
11 S. Kelch and M. Rehahn, *Macromolecules*, 1998, **31**, 4102.
12 M. Beley, S. Chodorowski, J.-P. Collin, J.-P. Sauvage, L. Flamigni and F. Barigelletti, *Inorg. Chem.*, 1994, **33**, 2543.
13 M. Ballauff, *Angew. Chem., Int. Ed. Engl.*, 1989, **28**, 253.
14 W. Spahni and G. Calcaferri, *Helv. Chim. Acta*, 1984, **67**, 450.
15 M. Rehahn, A.-D. Schüter and G. Wegner, *Makromol. Chem.*, 1990, **191**, 1991.
16 B. P. Sullivan, J. M. Calvert and T. Meyer, *Inorg. Chem.*, 1980, **19**, 1404.
17 A.-D. Schüter and G. Wegner, *Acta Polym.*, 1993, **44**, 59.
18 L. Schmitz and M. Ballauff, *Polymer*, 1995, **36**, 879.
19 J.-P. Collin, P. Lainé, J.-P. Launay, J.-P. Sauvage and A. Sour, *J. Chem. Soc., Chem. Commun.*, 1993, 434.

Communication 9/01638D

ChemComm

Synthesis of a novel rigid tetrathiafulvalene-σ-*p*-benzoquinone diad (TTF-σ-Q) with inherent structural configuration suitable for intramolecular charge-transfer

Evgeny Tsiperman, Tal Regev, James Y. Becker,* Joel Bernstein, Arkady Ellern, Vladimir Khodorkovsky,* Alex Shames and Lev Shapiro

Department of Chemistry, Ben-Gurion University of the Negev, 84105, Beer-Sheva, Israel.
E-mail: becker@bgumail.bgu.ac.il

Received (in Cambridge, UK) 22nd March 1999, Accepted 6th May 1999

The synthesis of a novel D–A diad, involving a TTF moiety covalently linked to *p*-benzoquinone *via* a rigid spacer, shows a bent structure in the solid state which provides intrinsic through-space intramolecular charge-transfer interaction.

Since the discovery[1] of the first organic metal in 1973, much attention has been devoted to the investigation of TTF, its derivatives and analogs, as electron donor components of many charge transfer (CT) complexes and ion radical salts.[2] In order to control the stoichiometry of the D (donor) and A (acceptor) components and the degree of charge-transfer in CT complexes, which are crucial parameters in the design of 'organic metals', the concept of D–A–D and A–D–A triads was developed,[3] in which the D and A fragments are integral parts of a single molecule. Several D–TCNQ–D,[3] D–TCNAQ–D[4] and A–TTF–A[5] systems have been studied. In this context, TTF-σ-TCNQ systems have obvious appeal,[6] but have proved to be an elusive goal.[7,8] However, systems involving TTF-π-TCNQ are known.[9]

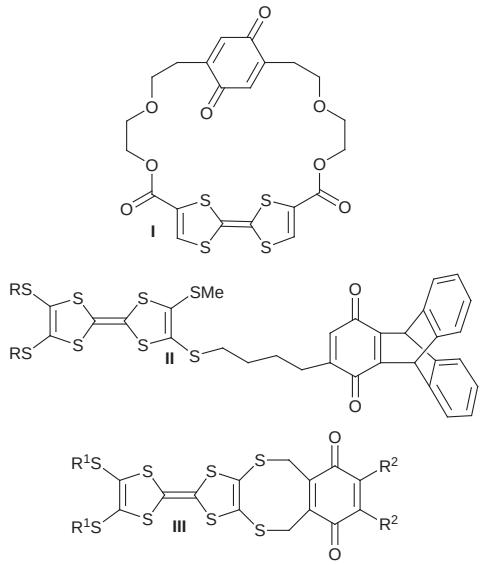

'TTF-σ-quinone' systems are known both in cyclic (**I**)[10] and non-cyclic (**II**) derivatives.[11] Recently, rigid TTF-σ-quinone derivatives (**III**) (containing two linking σ bonds) were synthesized.[12] In none of these systems, was an intramolecular CT band discernible in the UV–VIS spectrum, for different reasons.[8] Evidently, there is a need to design a molecule in which both the distance and orientation between the TTF and the quinone moieties are fixed, in order to achieve a CT interaction.

We now present the synthesis (Scheme 1), electrochemistry, X-ray structure and intramolecular charge-transfer properties of new rigid TTF-σ-Q (**6a**,**b**) molecules, involving TTF moieties chemically linked to *p*-benzoquinone by nonconjugated rigid cyclic rings, *via* two σ linkers. This type of molecule could be a potential precursor for TTF-σ-TCNQ systems. The unique bent structure of **6a** in the solid state (Fig. 1), in which the plane of the D moiety lies above the plane of the A moiety, with essentially eclipsed overlap, affords the first example of a non-cyclic system with built-in through-space σ-type interaction between the π-systems of the D and A components.[13] The synthesis of **6** involves two cycloaddition reactions[14] to afford **3** as the sole *R*,*S*,*R*,*S* stereoisomer in which the 1,3-dithiole-2-thione moiety is located opposite to the aryl ring, probably due to steric hindrance in the *S*,*R*,*R*,*S* isomer. The hydrogens on the carbons adjacent to the sulfur atoms are orientated in the same spatial direction with respect to the bent planes of the molecule. This configuration was confirmed by X-ray structure determination for the 'oxo' derivative **4**, which was generated from **3** (2 mmol). The latter reaction and the following ones

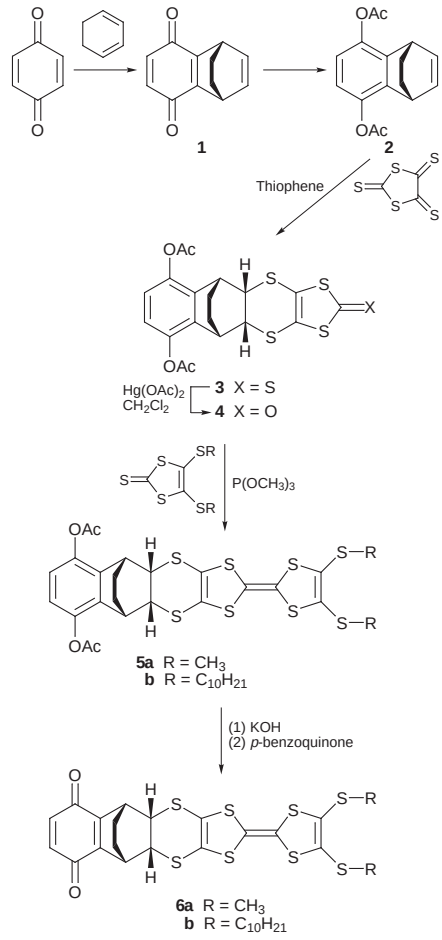

Scheme 1

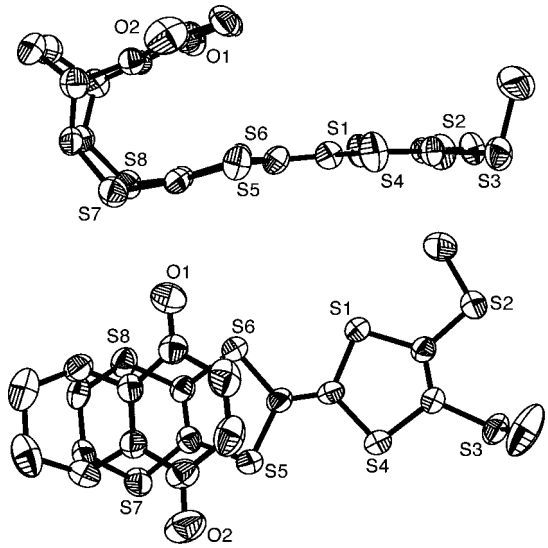

Fig. 1 ORTEP drawing of **6a** at the 50% probability level. Hydrogen atoms and the numbering of the carbon atoms have been omitted for clarity. Side-view of the molecule (above) and view in the plane of the TTF moiety (below).

which are described in Scheme 1 were performed according to known procedures.[15] Products **6a** and **6b** were separated from their reaction mixtures by silica gel column chromatography (CH_2Cl_2); both had a deep green color.

The UV–VIS spectrum of **6a** shows a broad absorption band in the 550–950 nm region, centered at *ca.* 685 nm ($\varepsilon \sim 310$), which points to a weak charge transfer interaction. The spectra were recorded at various concentrations of **6a**, and the extinction coefficient of this low energy band varied in accordance with Beer–Lambert law. Therefore, this band is assigned to an intramolecular charge-transfer interaction.

The cyclic voltammogram[16] of **6a** shows two one-electron reversible oxidation waves at $E^1_{1/2} = 0.55$ and $E^2_{1/2} = 0.825$ V, characteristic for tetraalkylthio-TTF derivatives,[2a] and two reversible reduction waves, one at −0.525 V (one-electron) and a smaller one at −1.20 V, for the reduction of the disubstituted *p*-benzoquinone moiety. (At slower scan rates a trace of an ill-defined 'third' reversible couple is observed in between the above two reduction waves, which is related to a product derived from the decomposition of the dianion.) Product **6b** affords a similar cyclic voltammogram pattern, with similar redox potentials. It is generally expected that a weak CT interaction will not affect the redox potentials pattern given by the relatively insensitive cyclic voltammetry technique.

Deep green needles of **6a**[17] were crystallized from CH_2Cl_2 by slow evaporation of the solvent. The X-ray structure (Fig. 1) verifies the bent configuration of the molecule and shows that the acceptor *p*-benzoquinone moiety is spatially located above the donor dimethylthio-TTF unit. Indeed, the intramolecular distance between the face-to-face planes of the donor and acceptor moieties is 3.29 Å, which may be compared to the plane-to-plane distances between donor and acceptor molecules in crystal packings of mixed-stacks intermolecular charge transfer of HMTSF–TCNQ[18] and ET–TCNQ[19] complexes. The apparently low degree of CT in the ground state of **6** was also confirmed by EPR measurements, which after sunlight irradiation gave rise to a photoinduced intramolecular electron transfer process, resulting in the appearance of broad signals (yet to be analyzed), with two '*g*' factors ($g_1 = 2.0050$; $g_2 = 2.0064$).

Compounds **6a** and **6b** are among the first examples of systems with inherent intramolecular through space charge transfer properties. Their synthesis opens up a way to obtain new compounds with controllable overlap between the donor and acceptor units, as well as controllable degree of charge transfer, *e.g.* by changing the strength of the acceptor moiety. Also, it is noteworthy that **6b** and its derivatives could be potential candidates for constructing Langmuir–Blodgett films and investigating their physical properties.

Notes and references

1 J. P. Ferraris, D. O. Cowan, V. Walatka and J. H. Perlstein, *J. Am. Chem. Soc*., 1973, **95**, 948; L. B. Coleman, M. J. Cohen, D. J. Sandman, F. G. Yamagishi, A. F. Garito and A. Heeger, *Solid State Commun*., 1973, **12**, 1125.

2 (*a*) V. Y. Khodorkovsky and J. Y. Becker, in *Organic Conductors: Fundamentals and Applications*, ed. J. P. Farges, Marcel Dekker, New York, 1994, ch. 3, p. 75; (*b*) J. R. Ferraro and J. M. Williams, *Introduction to Synthetic Electrical Conductors*, Academic Press, London, 1987; (*c*) K. Bechgaard, in *Structure and Properties of Molecular Crystals*, ed. M. Pierrot, Elsevier, Amsterdam, 1990, p. 235; (*d*) J. M. Williams, A. J. Schultz, U. Geiser, K. D. Carlson, A. M. Kini, H. H. Wang, W.-K. Kwok, M.-H. Whangbo and J. E. Shirber, *Science*, 1991, **252**, 1501; (*e*) A. E. Underhill, *J. Mater. Chem*., 1992, **2**, 1; *J. Mater. Chem*., 1995, **5**, 1469.

3 J. Y. Becker, J. Bernstein, S. Bittner, N. Levi and S. S. Shaik, *J. Am. Chem. Soc*., 1983, **105**, 4468; J. Y. Becker, J. Bernstein, S. Bittner, N. Levi, S. S. Shaik and N. Zer-Zion, *J. Org. Chem*., 1988, **53**, 1689.

4 P. de Miguel, M. R. Bryce, L. M. Goldenberg, A. Beeby, V. Khodorkovsky, L. Shapiro, A. Niemz, A. O. Cuello and V. Rotello, *J. Mater. Chem*., 1998, **8**, 71.

5 M. P. Le Paillard and A. Robert, *Bull. Soc. Chim. Fr*., 1992, **129**, 205; A. Robert and D. Lorcy, *Molecular Engineering for Advanced Materials*, ed. J. Becher and K. Schaumburg, NATO ASI Series C, vol. 456, Kluwer, Dordecht, 1994, p. 251.

6 A. Aviram and M. A. Ratner, *Chem. Phys. Lett*., 1974, **29**, 277.

7 C. A. Panetta, J. Bachdadchi and R. M. Metzger, *Mol. Cryst. Liq. Cryst*., 1984, **107**, 103.

8 M. R. Bryce, *Adv. Mater*., 1999, **11**, 11.

9 H. Nadizadeh, D. L. Mattern, J. Digleton, X-L. Wu and R. M. Metzger, *Chem. Mater*., 1994, **6**, 268; L. M. Goldenberg, J. Y. Becker, O. Paz-Tal Levi, V. Y. Khodorkovsky, L. M. Shapiro, M. R. Bryce, J. P. Cresswell and M. C. Petty, *J. Mater. Chem*., 1997, **7**, 901; N. A. Bell, R. A. Broughton, J. S. Brooks, T. A. Jones, S. C. Thorpe and G. J. Ashwell, *J. Chem. Soc., Chem. Commun*., 1990, 325.

10 R. M. Moriarty, A. Tao, R. Gilardi, Z. Song and S. M. Tuladhar, *Chem. Commun*., 1998, 157

11 S. Scheib, M. P. Cava, J. W. Baldwin and R. M. Metzger, *J. Org. Chem*., 1998, **63**, 1198.

12 J. L. Segura, N. Martin, C. Seoane and M. Hanack, *Tetrahedron Lett*., 1996, **37**, 2503; M. Gonzales, B. Illescas, N. Martin, J. L. Segura, C. Seoane and M. Hanack, *Tetrahedron*, 1998, **54**, 2853.

13 It is important to distinguish here between the interacting orbitals and the type of interaction. The interacting systems are π-orbitals orientated essentially in an end-to-end fashion (σ-type interaction) rather than a parallel orientation (π-type interaction).

14 O. Diels and K. Alder, *Chem. Ber*., 1929, **62B**, 2337; O. Neilands, Ya. Katsens and Y. Kreitsberga, SU 1428753 (*Chem. Abstr*., 1989, **110**, P95252); O. Neilands, Y. Katsens and Y. Kreitsberga, *Zh. Org. Khim*., 1989, **25**, 658 (*Chem. Abstr*., 1989, **111**, 194689k).

15 A. Krief, *Tetrahedron*, 1986, **42**, 1209 and references therein.

16 In MeCN–CH_2Cl_2(2 : 1)–0.1 M Bu_4NClO_4 on glassy carbon working electrode. Potentials are quoted *vs*. Ag/AgCl reference electrode at 50 mV s^{-1} scan rate.

17 *Crystal data* for **6a**: A shiny deep green needle (0.4 × 0.15 × 0.15 mm) of $C_{20}H_{16}O_2S_8$ was used for X-ray intensity data measurements on a standard Bruker SMART CCD 1000™ diffractometer [λ(Mo-Kα) = 0.711069 Å, graphite monochromator, a scan width of 0.3° in ω and exposure time of 10 s frame^{-1}, detector–crystal distance = 4.95 cm]. A total of 1080 frames were collected and integrated with the Bruker Saint software package using a wide-frame integration algorithm. The crystal is monoclinic, space group $P2_1$, at 298 K, $a = 8.486(1)$, $b = 8.770(1)$, $c = 15.430(3)$ Å, $\beta = 98.740(3)°$, $Z = 2$, $V = 1135.0(3)$ Å^3, $F(000) = 560$, 7221 reflections were collected ($2\theta < 56.82°$), of which 4931 reflections were independent ($R_{int} = 3.18\%$) and 2823 with $F_o > 4\sigma(F_o)$. Data were corrected for absorption using SADABS program. The structure was solved by direct methods and refined by least-squares in full-matrix approximation: 273 parameters, $R1 = 4.04\%$, $wR2 = 6.20\%$, GOF = 0.796. Bruker SHELX Software package was used for all calculations and drawings. CCDC 182/1252. See http://www.rsc.org./suppdata/cc/1999/1125 for crystallographic data in .cif format.

18 T. J. Kistemmacher, T. J. Emge, A. N. Bloch and D. O. Cowan, *Acta Crystallogr*., 1982, **B38**, 1193.

19 T. Mori and H. Inokuchi, *Bull. Chem. Soc. Jpn.*, 1987, **60**, 402.

Communication 9/02277E

Stereochemical course of the reduction step in the formation of 2-*C*-methylerythritol from the terpene precursor 1-deoxyxylulose in higher plants

Duilio Arigoni,*[a] José-Luis Giner,[b] Silvia Sagner,[c] Juraithip Wungsintaweekul,[c] Meinhart H. Zenk,[c] Klaus Kis,[d] Adelbert Bacher,[d] and Wolfgang Eisenreich[d]

[a] *Laboratorium für Organische Chemie, Eidgenössische Technische Hochschule, Universitätsstrasse 16, CH-8092 Zürich, Switzerland. E-mail: arigoni@org.chem.ethz.ch*
[b] *Department of Chemistry, State University of New York, ESF, Syracuse, NY 13210, USA*
[c] *Lehrstuhl für Pharmazeutische Biologie, Universität München, Karlstrasse 29, D-80333 Munich, Germany*
[d] *Lehrstuhl für Organische Chemie und Biochemie, Technische Universität München, Lichtenbergstrasse 4, D-85747 Garching, Germany*

Received (in Cambridge, UK) 19th March 1999, Accepted 4th May 1999

Feeding of 1-deoxy-D-[3-^{2}H]xylulose to leaves of the tree *Liriodendron tulipifera* affords 2-*C*-methyl-*D*-erythritol labelled specifically in the H_{Si} position of C-1.

Over the last few years evidence has been accumulated in different laboratories for the existence in eubacteria, algae and higher plants of an alternative mevalonate-independent metabolic pathway for the formation of isopentenyl pyrophosphate (IPP, **3**) and dimethylallyl pyrophosphate (DMAPP, **4**), the two universal building blocks of terpene biosynthesis (Scheme 1).[1] The first C_5 intermediate in this pathway, 1-deoxyxylulose 5-phosphate **1a**, is assembled from pyruvic acid and glyceraldehyde 3-phosphate in a decarboxylative reaction that requires the participation of thiamine pyrophosphate as a cofactor, and genes specifying for the corresponding synthase have been cloned from *Escherichia coli*[2] and from *Mentha piperita*.[3] The isolation of a NADPH-dependent reductoisomerase from *E. coli* capable of catalyzing the transformation of **1a** into 2-*C*-methylerythritol 4-phosphate **2a** has been described recently.[4] While the remaining steps of the sequence remain unknown, it has been shown that the (*E*)-methyl group of DMAPP **4** and the terminal methylene group of IPP **3** acquire label from 1-deoxy[3-^{2}H]xylulose **1b** (H• = D) in *E. coli*[5] as well as in cell cultures of *Catharanthus roseus*.[6] In addition, the specific localization of this label in the H_E position of the IPP generated in the plant system rules out DMAPP as the committed precursor of IPP along the deoxyxylulose pathway.[6] Supporting evidence for the same conclusion has been obtained in work with secretory cells from *M. piperita*.[7]

The well documented efficiency of leaves of the tree *Liriodendron tulipifera* in converting exogenous 1-deoxyxylulose **1b** into 2-*C*-methylerythritol **2b**[8] was exploited in the present study for investigating the stereochemical course of the reduction step of this transformation in a feeding experiment involving the easily accessible 1-deoxy[3-^{2}H]xylulose **1b** (H• = D).[9] For this purpose the leaf stems were immersed into a 18.5 mM solution of the precursor at room temperature and under natural daylight illumination. After two days the desired product was isolated from the biomass as described.[8] Following careful purification by HPLC on a column of Rezex Phenomenex (300 × 7.8 mm), using distilled water as eluent and a refractometer as the detecting system, the biosynthetic sample was converted into the known bis-acetonide **5**.[10]† Assignments of all the ^{1}H and ^{13}C NMR signals were obtained for an unlabeled reference specimen of **5** by two dimensional homonuclear (COSY, NOESY) and heteronuclear (HMQC) experiments. The data are summarized in Table 1 and Fig. 1. Specifically, the assignment of the ^{1}H NMR signals at δ 3.64

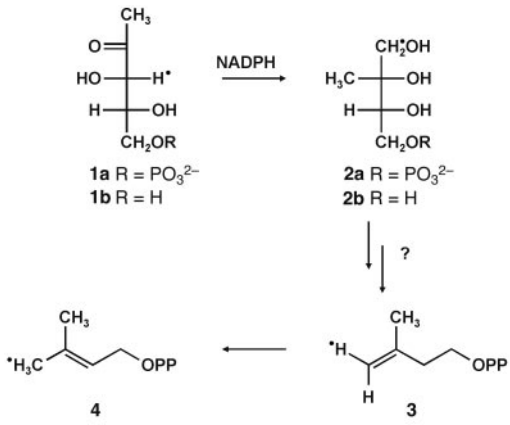

Scheme 1

Table 1 NMR data of 1,2:3,4-di-*O*-isopropylidene-2-*C*-methylerythritol **5** in $CDCl_3$. The transmitter frequency for ^{1}H was 500.13 MHz

Position	δ_H (mult, *J*/Hz)	δ_C
1 (*Re*)	3.64 (d, 8.7)	72.89
1 (*Si*)	3.95 (d, 8.7)	
2	—	80.96
2′	1.26 (s)	19.18
3	4.00 (t, 6.5)	78.37
4 (*Re*)	3.80 (dd, 8.7, 5.9)	65.35
4 (*Si*)	3.94 (dd, 8.6, 7.2)	
5-CH_3 (*Re*)	1.27 (s)	26.49
5-CH_3 (*Si*)	1.28 (s)	27.15
6-CH_3 (*Re*)	1.32 (s)	26.09
6-CH_3 (*Si*)	1.23 (s)	24.61
5	—	109.47[a]
6	—	109.51[a]

[a] Assignments may be interchanged.

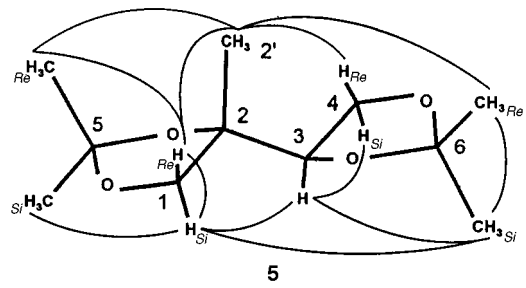

Fig. 1 Predominant conformation of **5** as reconstructed from two-dimensional NOESY experiments. Observed interactions are indicated by curved lines.

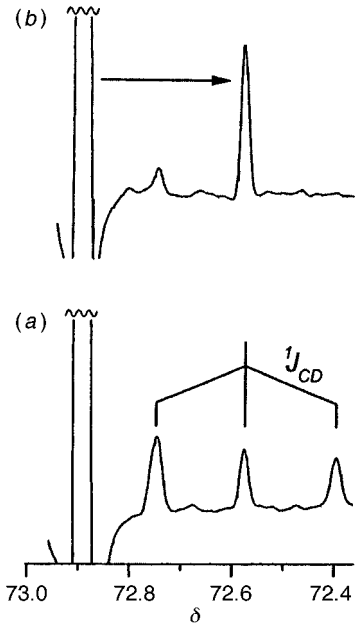

Fig. 2 ^{13}C NMR signals of C-1 in **5** derived from the feeding experiment: (*a*) ^{1}H-decoupled, (*b*) ^{1}H,^{2}H-decoupled.

and 3.95 to H_{Re} and H_{Si} of C-1, respectively, is well-supported by the network of NOE interactions detailed in Fig. 1. Monodeuteration at C-1 in the sample of **5** derived from the feeding experiment was evidenced by the appearance in the proton-decoupled ^{13}C NMR spectrum of a new triplet (J_{CD} = 22.5 Hz) with an upfield shift of −313 ppb from the normal signal at δ 72.89 (Fig. 2a). Under ^{2}H-decoupling conditions this triplet collapsed to a singlet (Fig. 2b) with an intensity of 4% relative to the overall intensity of the C-1 signal. In addition, the ^{2}H NMR spectrum of the compound displayed a single signal at δ 3.96, thus ensuring that the deuterium was specifically localized in the H_{Si} position of C-1.

On the basis of this evidence the stereochemical course of the conversion **1b** → **2b** can now be depicted as in Fig. 3a (R = H). The reaction is likely to occur through the intermediacy of the corresponding phosphoric acid monoesters (R = PO_3^{2-}).[4] Comparison with the mechanistically related steps involved in the biosynthesis of valine and isoleucine[11] (*cf.* Fig. 3b) reveals a close stereochemical matching, which suggests that in each of the reactions there is a steric necessity for the migrating group and the reducing cofactor to be located on opposite faces of the planes defined by the respective hydrogen-bridged α-hydroxycarbonyl substructures.

This work was supported by grants from the Deutsche Forschungsgemeinschaft (SFB 369) and the Fonds der Chemischen Industrie. Financial support by Novartis International AG, Basel (to D. A.) is gratefully acknowledged.

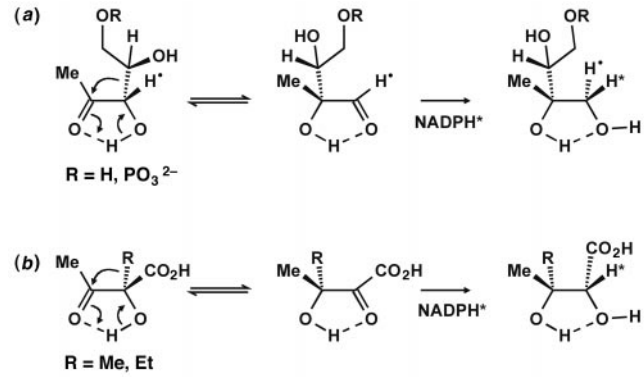

Fig. 3 (*a*) Stereochemical course of the 1-deoxyxylulose conversion into 2-*C*-methylerythritol. (*b*) stereochemical course of reductoisomerase reactions in the biosynthesis of valine (R = Me) and isoleucine (R = Et).

Notes and references

† In improvement of the original procedure a solution of 21 mg of **2b** in 8 ml of acetone was treated with 2 ml of 2.2 M $ZnCl_2 \cdot Et_2O$ in CH_2Cl_2 at room temperature for 24 h; after addition of 20 ml of $CHCl_3$ the organic phase was washed with $NaHCO_3$ (5%) and water, dried with $MgSO_2$ and concentrated to a crude oil, which was purified on a column of silica gel (0.5 × 10 cm) with hexane–EtOAc (3 : 1 v/v) as the solvent to yield pure **5** in a yield of 77%.

1 For reviews, see W. Eisenreich, M. Schwarz, A. Cartayrade, D. Arigoni, M. H. Zenk and A. Bacher, *Chem. Biol.*, 1998, **5**, R221; M. Rohmer, *Prog. Drug Res.*, 1998, **50**, 135.
2 G. A. Sprenger, U. Schörken, T. Wiegert, S. Grolle, A. A. de Graaf, S. V. Taylor, T. Begley, S. Bringer-Meyer and H. Sahm, *Proc. Natl. Acad. Sci. U.S.A.*, 1997, **84**, 12856; L. M. Lois, N. Campos, S. R. Putra, K. Danielsen, M. Rohmer and A. Boronat, *Proc. Natl. Acad. Sci. U.S.A.*, 1998, **95**, 2105.
3 B. M. Lange, M. R. Wildung, D. McCaskill and R. Croteau, *Proc. Natl. Acad. Sci. U.S.A.*, 1998, **95**, 2100.
4 S. Takahashi, T. Kuzuyama, H. Watanabe and H. Seto, *Proc. Natl. Acad. Sci. U.S.A.*, 1998, **95**, 9879.
5 J.-L. Giner, B. Jaun and D. Arigoni, *Chem. Commun.*, 1998, 1857.
6 D. Arigoni, W. Eisenreich, C. Latzel, S. Sagner, T. Radykewicz, M. H. Zenk and A. Bacher, *Proc. Natl. Acad. Sci. U.S.A.*, 1999, **96**, 1309.
7 D. McCaskill and R. Croteau, *Tetrahedron Lett.*, 1999, **40**, 653.
8 S. Sagner, W. Eisenreich, M. Fellermeier, C. Latzel, A. Bacher and M. H. Zenk, *Tetrahedron Lett.*, 1998, **39**, 2091.
9 J.-L. Giner, *Tetrahedron Lett.*, 1998, **39**, 2749.
10 T. Anthonsen, S. Hagen and M. A. E. Sallam, *Phytochemistry*, 1980, **19**, 2375.
11 R. K. Hill, S. Sawada and S. M. Arfin, *Bioorg. Chem.*, 1979, **8**, 175 and references cited therein.

Communication 9/02216C

First total synthesis of (+)-koninginin D

Gang Liu and Zhiqin Wang*

Shanghai Institute of Organic Chemistry, Chinese Academy of Sciences, 354 Feng Lin Lu, Shanghai 200032, China. E-mail: wangzq@pub.sioc.ac.cn

Received (in Cambridge, UK) 17th February 1999, Accepted 29th April 1999

A total synthesis of (+)-koninginin D (1) is described; the absolute configuration of the immediate antecedent of 1 is shown to have the configuration 7*R*,9*S*,10*S* by X-ray diffraction analysis.

(+)-Koninginin D, a biologically active natural product, was isolated from the culture of *Trichoderma koningii* Oudem by Ghisalberti *et al.* in 1989.[1] The structure and relative stereochemistry were determined as shown in structure **1.** Since

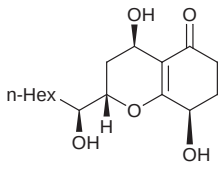

(+)-koninginin D **1**

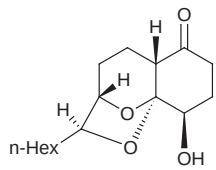

(–)-koninginin A

then four congeners of koninginin D have been isolated (koninginin A, B, C and E).[2] In 1995 Mori and Abe[3] and Xu and Zhu[4] published the total synthesis and absolute configuration of (−)-koninginin A independently. Here we report the total synthesis of (+)-koninginin D.

Mori constructed chiral centers C_9 and C_{10} of (−)-koninginin A *via* the Sharpless asymmetric dihydroxylation, while Xu used tartaric acid as the starting material to establish the two chiral vicinal hydroxy groups. Because koninginins A–E were isolated from a culture of the same species of microorganism, we suggested that (+)-koninginin D has the same absolute configuration at C_9 and C_{10} as that of (−)-koninginin A. Our retrosynthetic analysis of (+)-koninginin D is shown in Scheme 1.

The synthesis of **4** is shown in Scheme 2. According to the known procedure[5] (+)-tartaric acid was transformed to diol **7**, which when treated with TsCl and $C_5H_{11}MgBr$ afforded monoalkylated acetonide **8** in 48.5% yield. Compound **8** was transformed to the iodo compound with NaI, which when reacted with CH_2=CHMgBr in the presence of CuI gave **9**.[6] Ozonolysis of **9** afforded **4**. The overall yield of **4** from **7** is 30% (5 steps).

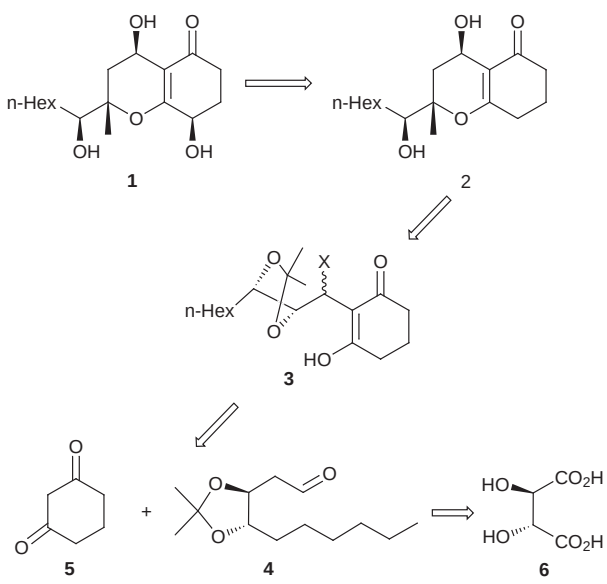

Scheme 1

The condensation of **4** and cyclohexane-1,3-dione **5** was performed by the method described by Paquette *et al.*,[7] giving **10** and a small amount of the Michael addition product **11** (Scheme 3)

Treatment of **10** with dilute HCl in acetone resulted in deprotection and cyclization furnishing **12**. Under the reaction of $Hg(OAc)_2$ in AcOH the PhS group of **12** was replaced by an AcO group, affording **13** and a small amount of **14**. X-Ray diffraction analysis revealed that the C_7 acetoxy group of **13** is *trans* to the β-alkyl group.† Since the chiral centers C_9 and C_{10}

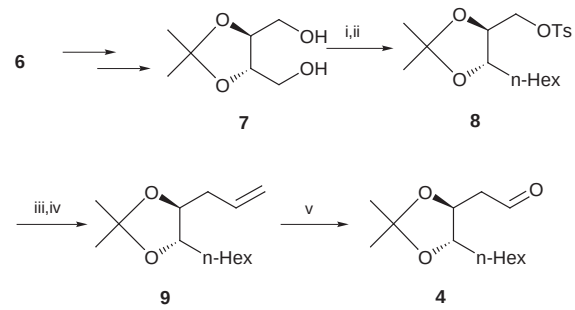

Scheme 2 *Reagents and conditions*: i, TsCl, CH_2Cl_2, Et_3N, rt, 6 h, 95%; ii, $C_5H_{11}MgBr$, THF, Li_2CuCl_4, −78 °C to rt, 5 h, 51%; iii, NaI, DMF, 80 °C, 2 h, 91%; iv, CH=CHMgBr, CuI, HMPA, THF, −30 to 10 °C, 20 h, 75%; v, O_3, CH_2Cl_2, MeOH, −78 °C, 91%.

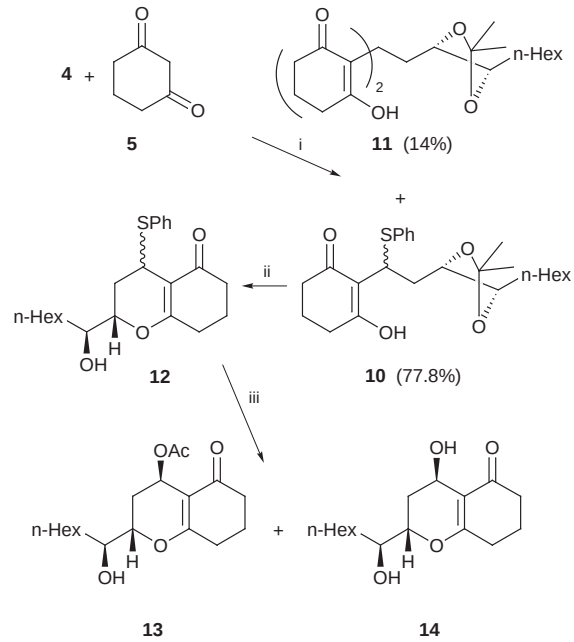

Scheme 3 *Reagents and conditions*: i, PhSH, SiO_2, CH_2Cl_2, 30–35 °C; ii, 2 M HCl, acetone, rt, 24 h, 87%; iii, AcOH, $Hg(OAc)_2$, rt, 5 h, 84%.

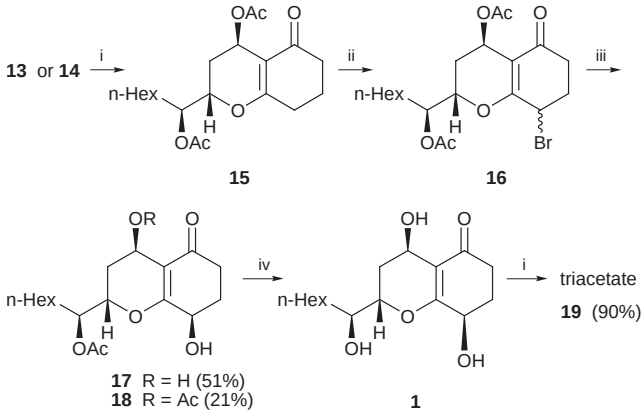

Scheme 4 *Reagents and conditions*: i, Ac_2O, Et_3N, DMAP, rt, 2 h, 95%; ii, NBS, AlBN, CCl_4, reflux, 2 h, 69%; iii, NaI, dioxane, $CaCO_3$, H_2O, reflux, 48 h, 72%; iv, MeOH, Na_2CO_3, H_2O, rt, 1 h, 91%.

of **13** came from (+)-tartaric acid the absolute configuration of **13** can be assigned as 7*R*,9*S*,10*S*. Both of **13** and **14** treated with Ac_2O gave **15**. Attempts to introduce a hydroxy group at C_4 *via* allylic oxidation of **15** with reagents like SeO_2, $SeO_2{\cdot}SiO_2$, $Hg(OAc)_2$, $Pb(OAc)_4$ and $AcOBu^t$ failed.

Allylic bromination of **15** with NBS gave **16** in fairly good yield. Nucleophilic substitution of **16** *via* the method described by Wu [8] produced a mixture of 4β-hydroxy compounds **17** and **18**, both of which upon hydrolysis gave (+)-koninginin D **1** as a white powder, mp 140–142 °C (hot plate); $[\alpha]_D^{20}$ 171 (*c* 0.125, $CHCl_3$) [ref. mp 122–123 °C, $[\alpha]_D$ +166.9 (*c* 0.3, $CHCl_3$)] (Scheme 4). The H^1 NMR, C^{13} NMR and mass spectra of **1** and its triacetate **19** were identical with those of natural (+)-koninginin D and its triacetate, respectively.‡ The overall yield of (+)-koninginin D from tartaric acid was 4.1% (15 steps).

Notes and references

† *Crystal data* for **13**: $C_{18}H_{28}O_5$, *M* = 324.42, orthorhombic, *a* = 13.690(4), *b* = 25.900(3), *c* = 5.179(3) Å, *V* = 1836(1) Å^3, *T* = 293 °C, *P*2,2,2 (#19), *Z* = 4, μ(Mo-Kα) = 0.84 cm^{-1}, 2487 reflections measured, 2487 unique (R_{int} = 0.000) which were used in all calculations. The final $wR(F^2)$ was 0.057 [for 1140 observed reflections with $I > 2.00\sigma(I)$]. CCDC 182/1244. See http://www.rsc.org/suppdata/cc/1999/1129/ for crystallographic files in .cif format.

‡ Selected data for **1**: δ_H(300 MHz, $CDCl_3$) 4.68 (dd, *J* 1, 2, 1H), 4.49 (q-like, *J* 4.8, 1H), 4.11 (ddd, *J* 2.2, 4.6, 12.1, 1H), 3.72 (q, *J* 6.4, 1H), 2.60 (ddd, *J* 4.74, 5.58, 17.00, 1H), 2.30 (m, 1H), 2.20 (m, 1H), 2.00 (m, 2H), 1.60 (m, 3H), 1.40–1.25 (m, 8H), 0.88 (t, *J* 6.80, 3H); δ_C(75 MHz, $CDCl_3$) 198.3, 171.4, 114.6, 77.0, 73.0, 66.7, 57.7, 34.0, 33.2, 31.8, 31.1, 29.3, 29.2, 25.4, 22.7, 14.1; *m/z* 298 (M^+, 1.3%), 281 (32.9), 262 (20.1), 242 (7.1), 209 (6.6), 191 (8.3), 166 (29.0), 165 (100), 155 (26.0), 139 (25.2), 109 (14.2) [$C_{16}H_{24}O_4$ (M − H_2O) requires 280.1675 found 280.1683]. For **19** $[\alpha]_D^{20}$ +127.4 (*c* 0.58, $CHCl_3$); δ_H(300 MHz, $CDCl_3$) 5.80 (m, 1H), 5.64 (t, *J* 4.90, 1H), 5.06 (td, *J* 3.82, 6.60, 1H), 4.14 (ddd, *J* 2.2, 3.7, 12.8, 1H), 2.63 (m, 1H), 2.39 (m, 1H), 2.20 (m, 1H), 2.13 (s, 3H), 2.07 (s, 3H), 2.04 (s, 3H), 1.99 (m, 1H), 1.75 (m, 1H), 1.65 (m, 2H), 1.25–1.30 (m, 9H), 0.87 (t, *J* 6.9, 3H); δ_C(75 MHz, $CDCl_3$) 194.8, 170.5, 169.8, 168.5(2), 112.2, 74.3, 73.0, 66.6, 59.7, 32.9, 31.7, 30.0, 29.3, 29.1, 26.5, 25.2, 22.6, 21.2, 20.9, 20.8, 14.1; *m/z* 380 (M^+ −44, 11.3%), 365 (17.7), 322 (14.7), 321 (25.0), 305 (67.4), 279 (7.9), 262 (14.4), 245 (44.4) 233 (14.0), 191 (15.8), 165 (15.3), 149 (17), 43 (100) ($C_{22}H_{32}O_8$: calc. C, 62.24; H, 7.60. Found: C, 61.93; H, 7.74%).

1 R. W. Dunlop, A. Simon, K. Sivasihamparam and E. L. Ghisalberti, *J. Nat. Prod.*, 1989, **52**, 67.
2 E. L. Ghisalberti, C. Y. Rowland, *J. Nat. Prod.*, 1993, **56**, 1799; S. R. Parker, H. G. Cutler and P. R. Schreiner, *Biosci. Biotechnol. Biochem.*, 1995, **59**, 1747.
3 K, Mori and K. Abe, *Polish J. Chem.*, 1994, **68**, 2255 ; K, Mori and K, Abe, *Liebigs Ann.*, 1995, 943.
4 X. X. Xu and Y. H. Zhu, *Tetahedron Lett.*, 1995, **36**, 9173.
5 E. Hungerbuhler and D. Seebuch *Helv. Chim. Acta*, 1981, **64**, 687.
6 S. H. Kang and S. B.Lee *Chem. Commu.*, 1998, 761.
7 K. Fuchs and L. A.Paquette, *J. Org. Chem.*, 1994, **59**, 528.
8 R. B. Zhao and Y. L. Wu, *Acta Chim. Sinica*, 1989, 87.

Communication 9/01320B

A zwitterionic carbene–plumbylene adduct

Frank Stabenow, Wolfgang Saak and Manfred Weidenbruch*

Fachbereich Chemie, Universität Oldenburg, D-26111 Oldenburg, Germany

Received (in Liverpool, UK) 13th April 1999, Accepted 28th April 1999

4,5-Dimethyl-1,3-diisopropylimidazol-2-ylidene reacts with bis(2,4,6-triisopropylphenyl)plumbylene to furnish the adduct 4 as yellow crystals; an X-ray structure analysis of 4 revealed a very long lead–carbon bond of 254.0(5) pm and a pyramidal lead centre with a bending angle of 70.5°.

Since the first isolation of thermally stable carbenes of the imidazol-2-ylidene type[1] the chemistry of this class of compounds has undergone vigorous developments, which were recently reviewed.[2] The nucleophilicity of these molecules is reflected, for example, in the formation of adducts with GeI_2,[3] $SnCl_2$,[4] and even a diarylstannylene.[5] Lead(II) derivatives of this carbene system were previously unknown. We now report on the formation and structure of the first adduct between a plumbylene and an imidazol-2-ylidene.

Compound **1** (Scheme 1) which we recently prepared[6] is the first diplumbene having a Pb=Pb double bond length and *trans*-bending angle of the sizes predicted by theoretical calculations.[7–9] Although **1** is indefinitely stable in the solid state under exclusion of light and air, it decomposes in solution to furnish predominately the plumbylene molecules **2** as a consequence of the low Pb=Pb bond dissociation energy, calculated to be merely 24 kJ mol^{-1} for the parent compound $H_2Pb{=}PbH_2$.[9] Addition of the carbene **3**[10] to a violet solution of **2** in toluene results in a spontaneous change in the colour of the solution to orange. Replacement of the toluene by *n*-hexane and cooling to −30 °C then affords compound **4** as yellow crystals in 43% yield. The adduct **4** is sensitive to light and air and the solid decomposes at room temperature. It is only stable in solution in the presence of an excess of **2**. All attempts to record NMR and electron spectra of pure **4** have failed because deposition with formation of 1,3,5-triisopropylbenzene occurs even at −70 °C in C_7D_8 solution.

Accordingly, our determination of the constitution of **4** is based solely on a low-temperature, X-ray crystallographic analysis (Fig. 1)† which, however, does reveal some interesting features. The Pb–C(carbene) bond length of 254.0(5) pm is unusually long and is probably one reason for the lability of the molecule. While the carbon atom C(1) exhibits an almost planar environment, the lead atom shows a pyramidal arrangement of its substituents as reflected by the bending angle of θ = 70.5° between the plane of the atoms C(12)–Pb–C(27) and the Pb–C(1) vector.

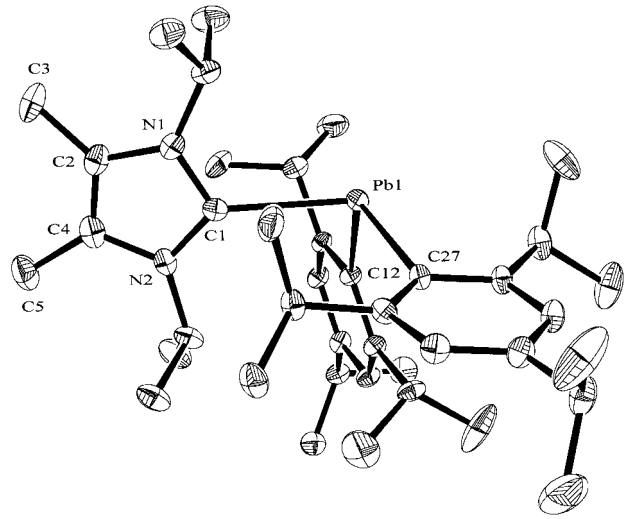

Fig. 1 Molecular structure of **4** (50% probability, hydrogen atoms omitted). Selected bond lengths (pm) and angles (°): C(1)–Pb 254.0(5), C(12)–Pb 237.6(4), C(27)–Pb 238.3(4), C(1)–N(1) 135.7(6), C(1)–N(2) 136.3(6), N(1)–C(2) 139.3(7), N(2)–C(4) 140.3(7), C(2)–C(4) 134.0(8), C(12)–Pb–C(27) 105.3(1), C(12)–Pb–C(1) 90.1(1), C(27)–Pb–C(1) 108.8(1), N(1)–C(1)–N(2) 104.6(4).

These results clearly indicate that, of the two possible electronic forms of the molecule **4** (Scheme 2) (the plumbene form **4a** and the zwitterionic form **4b**), the latter dominates. Further evidence in support of the existence of **4b** is provided by the Pb–C(*ipso*) bond lengths which are 8 pm longer than those in **1**.[6] Similarly, density functional theory calculations for the parent compound $H_2Pb{=}CH_2$, predicting a planar molecule with a Pb=C bond length of 204.5 pm,[8] are also suggestive of the loose adduct **4b** rather than a molecule with a Pb=C double bond of type **4a**. A bonding situation formally similar to that of **4b** may be present in the cyclopropylidene adduct of a diaminoplumbylene in which, however, the Pb=C bond length is 12 pm shorter such that the molecule is accordingly more stable.[11]

Although germenes and stannenes are now well-established,[12] molecules with Pb=C double bonds remain unknown. All attempts to achieve this goal by reaction of **2** and similarly constructed plumbylenes[13] with electrophilic carbenes of the cryptodiborylcarbene type[14] have been unsuccessful. This seems to indicate that diarylplumbylenes preferably participate in bond-forming reactions with nucleophilic rather than electro-

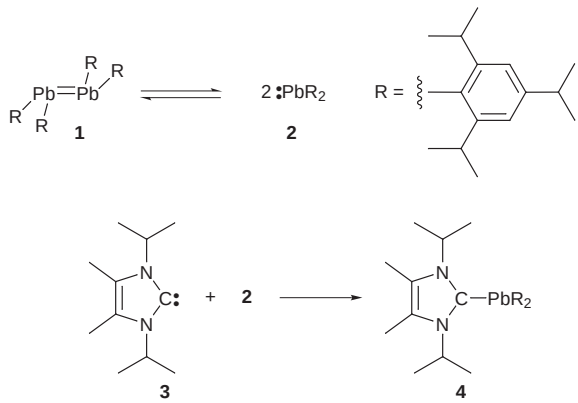

Scheme 1

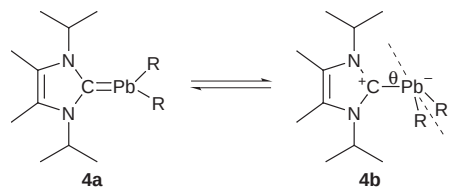

Scheme 2

philic carbenes, a consequence of the relativistic contraction of the 6s electron pair of lead.[15]

Financial support of our work by the Deutsche Forschungsgemeinschaft and the Fonds der Chemischen Industrie is gratefully acknowledged.

Notes and references

† *Crystal data* for **4**: $C_{41}H_{66}N_2Pb$, M = 794.15, crystal dimensions 0.71 × 0.63 × 0.30 mm^3, triclinic, space group $P\bar{1}$, a = 1056.88(7), b = 1108.20(6), c = 1791.80(8) pm, α = 72.784(6), β = 88.671(7), γ = 85.959(8)°, V = 1999.6(2) × 10^6 pm^3, Z = 2, D_c = 1.319 g cm^{-3}, λ(Mo-Kα) = 71.033 pm, T = 193(2) K, $2\theta_{max}$ = 52°, unique reflections 7260, observed [$I > 2\sigma(I)$] 6313, parameters 397. The structure was solved by direct methods (SHELXS-97) and refined by full-matrix least-squares techniques against F^2 (SHELXL-97). Hydrogen atoms were placed in the calculated positions, and all other atoms were refined anisotropically; R = 0.0311, $wR2$ (all data) = 0.0733. CCDC 182/1254. See http://www.rsc.org/suppdata/cc/1999/1131/ for crystallographic data in .cif format.

1 A. J. Arduengo III, R. L. Harlow and M. Kline, *J. Am. Chem. Soc.*, 1991, **113**, 361.
2 Review: W. A. Herrmann and C. Köcher, *Angew. Chem.*, 1997, **109**, 2256; *Angew. Chem., Int. Ed. Engl*., 1997, **36**, 2162.
3 A. J. Arduengo III, H. V. R. Dias, J. C. Calabrese and F. Davidson, *Inorg. Chem.*, 1993, **32**, 1541.
4 N. Kuhn, T. Kratz and R. Boese, *Chem. Ber.*, 1995, **128**, 245.
5 A. Schäfer, M. Weidenbruch, W. Saak and S. Pohl, *J. Chem. Soc., Chem. Commun.*, 1995, 1157.
6 M. Stürmann, W. Saak, H. Marsmann and M. Weidenbruch, *Angew. Chem.*, 1999, **111**, 145; *Angew. Chem., Int. Ed.*, 1999, **38**, 187.
7 G. Trinquier and J. P. Malrieu, *J. Am. Chem. Soc.*, 1987, **109**, 5303; G. Trinquier, *J. Am. Chem. Soc.*, 1990, **112**, 2130.
8 H. Jacobsen and T. Ziegler, *J. Am. Chem. Soc.*, 1994, **116**, 3667.
9 K. W. Klinkhammer, T. F. Fässler and H. Grützmacher, *Angew. Chem.*, 1998, **110**, 114; *Angew. Chem., Int. Ed.*, 1998, **37**, 124.
10 N. Kuhn and T. Kratz, *Synthesis*, 1993, 561.
11 H. Schumann, M. Glanz, F. Giergsdies, F. E. Hahn, M. Tamm and A. Grzegorzewski, *Angew. Chem.*, 1997, **109**, 2328; *Angew. Chem., Int. Ed. Engl.*, 1997, **36**, 2232.
12 Review: J. Escudié, C. Couret and H. Ranaivonjatovo, *Coord. Chem. Rev.*, 1998, **178**–**180**, 565.
13 M. Stürmann, M. Weidenbruch, K. W. Klinkhammer, F. Lissner and H. Marsmann, *Organometallics*, 1998, **17**, 4425.
14 H. Klusik and A. Berndt, *Angew. Chem.*, 1983, **95**, 895; *Angew. Chem., Int. Ed. Engl*., 1983, **22**, 877; Review: A. Berndt, *Angew. Chem.*, 1993, **105**, 1034; *Angew. Chem., Int. Ed. Engl.*, 1993, **32**, 985.
15 P. Pyykkö, *Chem. Rev.*, 1988, **88**, 563.

Communication 9/02919B

ChemComm

N–H activation *vs.* C–H activation: ruthenium-catalysed regioselective hydroamination of alkynes and hydroarylation of an alkene with *N*-methylaniline

Yuko Uchimaru

National Institute of Materials and Chemical Research, Tsukuba, Ibaraki 305, Japan.
E-mail: y_uchimaru@home.nimc.go.jp

Received (in Cambridge, UK) 22nd March 1999, Accepted 12th May 1999

Phenylacetylene and its derivatives undergo regioselective insertion into the N–H bond of *N*-methylaniline in the presence of $Ru_3(CO)_{12}$ catalyst to afford *N*-methyl-*N*-(α-styryl)anilines in high yields, whereas styrene reacts with the *ortho* C–H bond of *N*-methylaniline giving 2-(1-phenylethyl)-*N*-methylaniline.

Transition metal complex-catalysed hydroamination of carbon–carbon double or triple bonds with non-tertiary amines is an attractive method for carbon–nitrogen bond formation. Indeed, various *intramolecular* hydroamination reactions of aminoalkenes and aminoalkynes have been reported to date.[1,2a] Although several examples of *intermolecular* reactions[2–5] have been also reported, the substrates for these reactions are usually limited to highly reactive or strained carbon unsaturated compounds.[4] We have found that ordinary alkynes undergo hydroamination with aromatic amines in the presence of a catalytic amount of $Ru_3(CO)_{12}$. This is the first example of ruthenium-catalysed *intermolecular* hydroamination. In addition, the same ruthenium complex catalyses regioselective hydroarylation reaction of an alkene with an aromatic amine *via ortho* C–H bond activation. We report here these ruthenium complex-catalysed reactions.

A mixture of phenylacetylene (**1a**, 0.25 mmol), *N*-methylaniline (**2a**, 2.5 mmol), and $Ru_3(CO)_{12}$ (0.0125 mmol Ru) was heated at 70 °C in a sealed glass tube under nitrogen. After 18 h, **1a** was completely consumed and *N*-methyl-*N*-(α-styryl)aniline (**3a**) was regioselectively formed in 85% GLC yield (based on the amount of **1a** charged) (Table 1, run 1). GLC and GC-MS analyses indicated that isomers of **3a** were less than 2% yield.† A similar result was obtained under milder conditions (50 °C, 3 d). In a separate four-fold scale reaction, **3a** was isolated in 61% yield by Kugelrohr distillation and was fully characterised by ^1H and ^{13}C NMR, IR and GC-MS analyses.‡

The catalytic activity of several transition metal complexes was also examined for the present reaction (**1a** : **2a** : catalyst = 1 : 10 : 0.05 mol ratio, 70 °C, 18 h). A ruthenium complex $[RuCl_2(CO)_3]_2$ was found to promote the reaction. However, the catalyst $Ru_3(CO)_{12}$ was more effective; 85% yield of **3a** with $Ru_3(CO)_{12}$, 69% with $[RuCl_2(CO)_3]_2$. In addition, the amine **2a** was more selectively transformed to **3a** with $Ru_3(CO)_{12}$ (96% selectivity based on the amount of **2a** consumed) than with $[RuCl_2(CO)_3]_2$ (74%). Other transition metal complexes such as $[RuCl_2(p\text{-cymene})]_2$, $RuCl_2(PPh_3)_3$, $[RuCl_2(cod)]_n$ $[CpRu(CO)_2]_2$, $Fe(CO)_5$, $Co_2(CO)_8$, $Co_4(CO)_{12}$, $PdCl_2(PPh_3)_2$ and Cp_2ZrMe_2 were ineffective. Thus, $Ru_3(CO)_{12}$ was the most effective among the complexes examined.

Table 1 Hydroamination of alkynes catalysed by $Ru_3(CO)_{12}$[a]

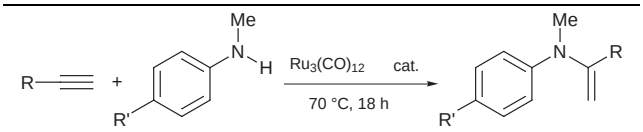

1 **2** **3**

Run	1	R	2	R′	3	Yield (%)[b]
1	**1a**	Ph	**2a**	H	**3a**	85
2	**1b**	*p*-MeC_6H_4	**2a**	H	**3b**	78
3	**1c**	*p*-FC_6H_4	**2a**	H	**3c**	88
4	**1a**	Ph	**2b**	Me	**3d**	76
5	**1d**	Cyclohex-1-enyl	**2a**	H	**3e**	77

[a] **1** 0.25 mmol; **2** 2.5 mmol; $Ru_3(CO)_{12}$ 0.0125 mmol/Ru; 70 °C for 18 h. [b] GLC yields based on the charged amount of alkyne **1**.‡

Table 1 summarises the results of the reactions of alkynes **1a**–**d** with *p*-substituted *N*-methylanilines **2a**,**b**. In all cases, the corresponding enamines **3a**–**e** were obtained in high yields. The results of *p*-substituted phenylacetylenes **1a**–**c** (runs 1–3) suggest that an electron-withdrawing substituent at the *para*-position increases the yield of **3**. The tendency was more clearly observed when the reactions were carried out under the retarded reaction conditions (**1** : **2a** = 1 : 1 mol/mol, in toluene, 70 °C, 18 h); the yields of products: **3c** (26%) > **3a** (13%) > **3b** (4%).§ A conjugated enyne, 1-ethynylcyclohexene (**1d**) also underwent hydroamination with **2a** to give enamine **3e** under similar conditions (run 5).

Surprisingly, when styrene (**4**) was used instead of alkynes, the reaction course was completely different. As shown in Scheme 1, the hydroarylation product, 2-(1-phenylethyl)-*N*-methylaniline (**5**), was selectively obtained in 83% yield after heating a mixture of **4** (0.25 mmol), **2a** (0.25 mmol), $Ru_3(CO)_{12}$ (0.0125 mmol Ru) and toluene (0.2 ml) at 150 °C for 19 h.‡ The hydroamination product was not detected at all. Treatment of the same mixture at 70–100 °C reaction temperature resulted in complete recovery of both starting materials **2a** and **4**. Previously a $[RhCl(PEt_3)_2]_2$–lithium amide system was reported to promote hydroarylation of norbornene with aniline.[4d] In this system, however, not only hydroarylation, but also hydroamination proceeded at the same time, and the combined yields for both reactions were not high. Therefore we believe that our present reaction is the first successful example of transition-metal complex-catalysed hydroarylation of an alkene with an aromatic amine.[6]

A plausible mechanism for hydroamination of alkyne is shown in Scheme 2, which involves (i) oxidative addition of the N–H bond of amine **2** to a coordinatively unsaturated ruthenium(0) centre giving the (amido)ruthenium hydride **6**,[7,8] (ii) coordination of alkyne **1** to the ruthenium centre to form complex **7**, followed by (iii) intramolecular nucleophilic attack of the nitrogen lone pair of **7** on the coordinated carbon–carbon triple bond,[4a,d] and (iv) reductive elimination of enamine **3** from the vinyl ruthenium species **8** to reproduce the coordinatively unsaturated ruthenium(0) centre.¶ The trend of the relative

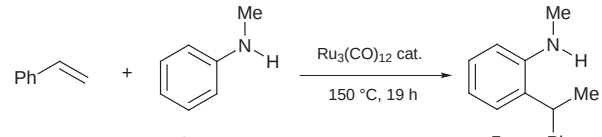

4 **2a** **5**

Scheme 1

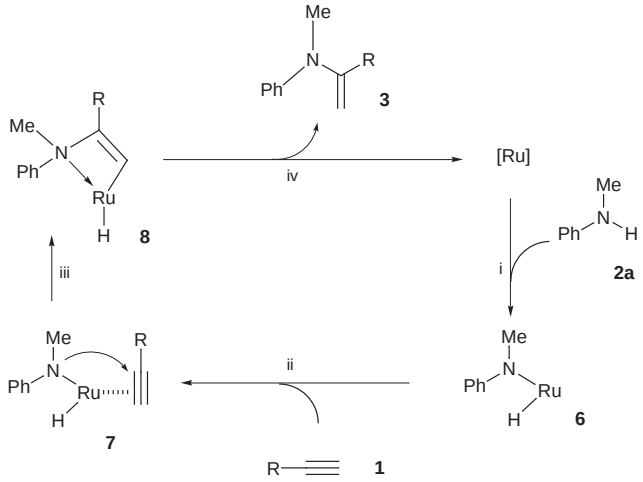

Scheme 2

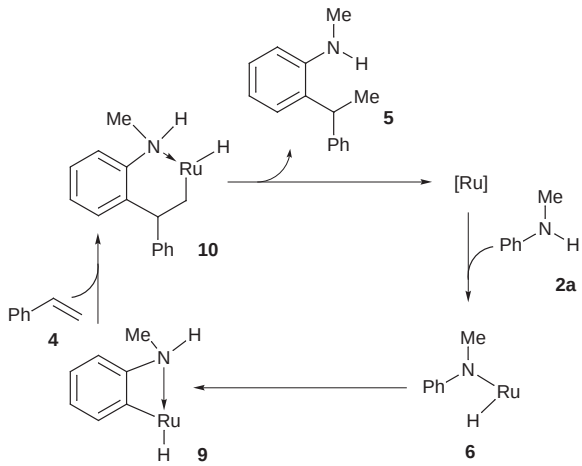

Scheme 3

reactivities of *para*-substituted phenylacetylenes **1a**–**c** toward **2a** (*vide supra*) is consistent with step (iii). On the other hand, the striking difference in the reaction course for styrene (hydroarylation) may be explained by a mechanism depicted in Scheme 3. Probably because of the lower coordination ability of the carbon–carbon double bond to the metal centre,[8] the styrene analogue of complex **7** might not be produced from the (amido)ruthenium hydride complex **6**. Instead, if *ortho* C–H bond activation[9] takes place to form complex **9**, hydroarylation product **5** could be formed *via* a ring expansion reaction of the strained four-membered ruthenacycle **9** with styrene followed by reductive elimination from the resulting six-membered ruthenacycle **10**.

To summarize, we have found the first examples of ruthenium-complex catalysed regioselective hydroamination and hydroarylation of carbon–carbon multiple bonds with *N*-methylaniline. The reaction course depends on the structure of the unsaturated substrate. Studies on other substrates and the mechanism are in progress.

Notes and references

† Trimers of **1a**, such as 1,2,4-triphenylbenzene and 1,3,5-triphenylbenzene, were detected in 5 and 2% yields, respectively.

‡ All the products in this study were known and were identified by ^{1}H and ^{13}C NMR, IR and GC-MS analyses or by comparison with authentic samples. For synthesis of authentic samples of the enamines, see J. Barluenga, F. Aznar, R. Liz and R. Rodes, *J. Chem. Soc., Perkin Trans. 1*, 1980, 2732. For an authentic sample of 2-(1-phenylethyl)-*N*-methylaniline, see M. M. Aly, M. Z. Badr, A. M. Fahmy and S. A. Mahgoub, *Acta Chim. Hung.*, 1985, **120**, 15.

§ Recoveries of the starting materials are as follows; for the reaction of **1c** (**1c** 69%, **2a** 72%), for the reaction of **1a** (**1a** 85%, **2a** 86%), for the reaction of **1b** (**1b** 94%, **2a** 96%).

¶ Since activation of an N–H bond of aniline by $Ru_3(CO)_{12}$ was reported to take place under reaction conditions similar to those in the present reaction [see ref. 7(*a*)], we propose a mechanism with the (amido)ruthenium hydride **6** involved as an intermediate [step (i)]. However, because of the relatively high coordination ability of the carbon–carbon triple bond with the metal centre, we cannot completely exclude the possibility of another mechanism which includes alkyne coordination to the Ru metal centre followed by nucleophilic attack of an amine nitrogen at the activated carbon–carbon triple bond.

1 See for a review of intramolecular hydroamination, L. S. Hegedus, *Angew. Chem., Int. Ed. Engl.*, 1988, **27**, 1113.

2 See for reviews of intermolecular hydroamination: (*a*) T. E. Müller and M. Beller, *Chem. Rev.*, 1998, **98**, 675; (*b*) J.-J. Brunet, *Gazz. Chim. Ital.*, 1997, **127**, 111; (*c*) J.-J. Brunet, D. Neibecker and F. Niedercorn, *J. Mol. Catal.*, 1989, **49**, 235.

3 A. M. Baranger, P. J. Walsh and R. G. Bergman, *J. Am. Chem. Soc.*, 1993, **115**, 2753; Y. Li and T. J. Marks, *Organometallics*, 1996, **15**, 3770; A. Haskel, T. Straub and M. S. Eisen, *Organometallics*, 1996, **15**, 3773; M. S. Eisen, T. Straub and A. Haskel, *J. Alloys Compd.*, 1998, **271**–**273**, 116.

4 (*a*) A. L. Casalnuovo, J. C. Calabrese and D. Milstein, *J. Am. Chem. Soc.*, 1988, **110**, 6738; (*b*) P. J. Walsh, A. M. Baranger and R. G. Bergman, *J. Am. Chem. Soc.*, 1992, **114**, 1708; (*c*) A. L. Seligson and W. C. Trogler, *Organometallics*, 1993, **12**, 744; (*d*) J.-J. Brunet, G. Commenges, D. Neibecker and K. Philippot, *J. Organomet. Chem.*, 1994, **469**, 221; (*e*) R. Dorta, P. Egli, F. Zürcher and A. Togni, *J. Am. Chem. Soc.*, 1997, **119**, 10857; (*f*) I. Nakamura, H. Itagaki and Y. Yamamoto, *J. Org. Chem.*, 1998, **63**, 6458 and references cited therein.

5 Rhodium-catalysed hydroamination of styrene and hex-1-ene has recently been reported as a side reaction of oxidative amination, see ref. 2(*b*).

6 Murai *et al.* reported several examples of ruthenium-catalysed hydroarylation of alkenes and alkynes with aromatic ketones, imines, and esters: S. Murai, N. Chatani and F. Kakiuchi, *Pure. Appl. Chem.*, 1997, **69**, 589 and references cited therein.

7 (*a*) E. Sappa and L. Milone, *J. Organomet. Chem.*, 1973, **61**, 383; (*b*) G. C. Hsu, W. P. Kosar and W. D. Jones, *Organometallics*, 1994, **13**, 385.

8 J. P. Collmann, L. S. Hegedus, J. R. Norton and R. G. Finke, *Principles and Applications of Organotransition Metal Chemistry*, University Science Books, Hill Valley, CA, 1987.

9 J. F. Hartwig, R. G. Bergman and R. A. Andersen, *J. Am. Chem. Soc.*, 1991, **113**, 3404.

Communication 9/02240F

Lanthanum(III) capture of 18-crown-6 in the cavity of *p*-sulfonatocalix[4]arene

Alexander Drljaca,[a] Michaele J. Hardie,[a] Julian A. Johnson,[b] Colin L. Raston[a] and Helen R. Webb[a]

[a] *Department of Chemistry, Monash University, Clayton, Melbourne, Victoria, 3168, Australia. E-mail: c.raston@sci.monash.edu.au*

[b] *CSIRO Minerals, Clayton, Melbourne, Victoria, 3168, Australia*

Received (in Columbia, MO, USA) 2nd March 1999, Accepted 13th April 1999

Aqueous solutions of sodium *p*-sulfonatocalix[4]arene, 18-crown-6 and lanthanum(III) trichloride at pH 2.5 afford the 'ferris wheel' type supercation: [{Ln^{3+}⊂(18-crown-6)$(OH_2)_3$}∩{(*p*-sulfonatocalix[4]arene^{4-} + 2H^+)}]$^+$ isolated as the chloride with numerous waters of crystallisation.

The coordination selectivity exhibited by calixarenes toward rare earth cations has been widely investigated because of its implications for separation science.[1] Of particular interest are the interactions with the highly charged and water-soluble sodium *p*-sulfonatocalixarenes.[2–5] These show remarkable inclusion properties for both ionic and neutral molecules (especially the smaller sized calix[4 and 5]arenes).[5–8] As crown ethers are good lanthanide complexants[9] it was anticipated that they would also be useful supramolecular synthons. Thus the species formed when combining a rare earth cation, crown ether, and sodium *p*-sulfonatocalixarene was explored. Whilst these systems may ultimately prove important for the separation of lanthanides, the assembly of such multicomponent arrays is of interest in itself.

Herein we report the results of the interaction between the cone-shaped sodium *p*-sulfonatocalix[4}arene, 18-crown-6, and lanthanum(III) chloride in aqueous media. The interplay between the two macrocycles has proved effective in stabilising, and in some cases selectively crystallising, a broad range of highly charged polynuclear aqua cations. Specifically, $[Cr_2(OH)_2(H_2O)_8]^{4+}$, $[Cr_3(OH)_4(H_2O)_{10}]^{5+}$ and $[Cr_4(OH)_6(H_2O)_{12}]^{6+}$, and $[Al_3O_4(OH)_{12}(OH)_{24}(H_2O)_{12}]^{7+}$ have been identified.[10] The main counterions are globular-like ionic capsules or superanions [{Na^+⊂(18-crown-6)$(OH_2)_2$}⊂{(*p*-sulfonatocalix[4]arene^{4-})$_2$}]$^{7-}$ (Θ^{7-}), which vary their crown ether conformation and degree of protonation with the polynuclear cation. A variety of cohesive forces are present in these solid-state ionic capsules, including hydrogen bonding, electrostatic, π-stacking, and van der Waals interactions. Additionally, the crown ether and the calixarene exhibit a complementarity of curvature, albeit after some geometric pre-organisational requirements. In the present study a new type of assembly results whereby the crown ether (containing a lanthanide and three water molecules) resides in one calixarene, as a perched structure, like a 'ferris wheel' with the rotation axis about a metal to O-centre of a sulfonate group. This supercation has a single positive charge and hence two of the sulfonate groups are protonated, as [{Ln^{3+}⊂(18-crown-6)$(OH_2)_3$} ∩ {(*p*-sulfonatocalix[4]arene^{4-} + 2H^+)}]$^+$ ([X]$^+$). It is noteworthy that the formation of an ionic capsule, Θ^{7-} or the partially protonated forms, is precluded in the present study by (i) the lanthanide ions effectively competing with sodium to form the central ionic core, demanding a different coordination environment, and/or (ii) the trivalent positive charge of the metal ion being insufficient to overcome the electrostatic repulsion between two calixarenes in the ionic capsule (at least for the pH of the solutions studied).

The complex [X]$^+$[Cl]$^-$.10H_2O crystallised from an aqueous solution of sodium *p*-sulfonatocalix[4]arene,[11,12] 18-crown-6, and lanthanum trichloride hexahydrate[12] at pH 2.5 (which was adjusted using perchloric acid) (Scheme 1).† Using small-scale reactions varying in 0.5 pH units, it was established that

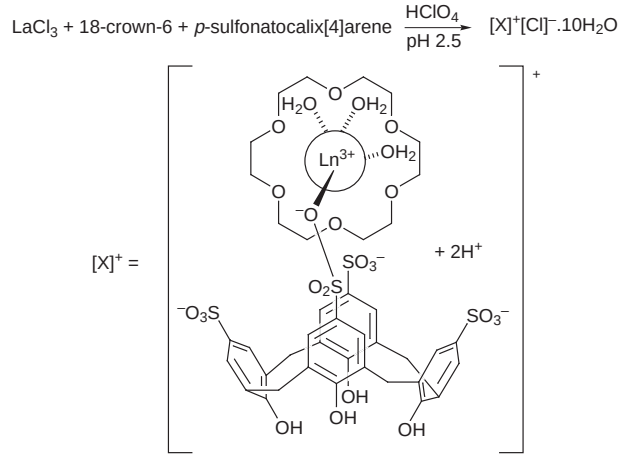

Scheme 1

crystallisation occurred over a narrow pH range (2.5–3). The proposed composition of this structure is reinforced by electron microprobe results which show that lanthanum and chloride are present, and in an equivalent stoichiometric ratio.

Crystals suitable for X-ray diffraction‡ deposited over several days. They crystallised in the space group $P3_1$ with the supercation [X]$^+$, the counter ion, and ten water molecules in the asymmetric unit. Results are reported in Fig. 1 and 2. As can be

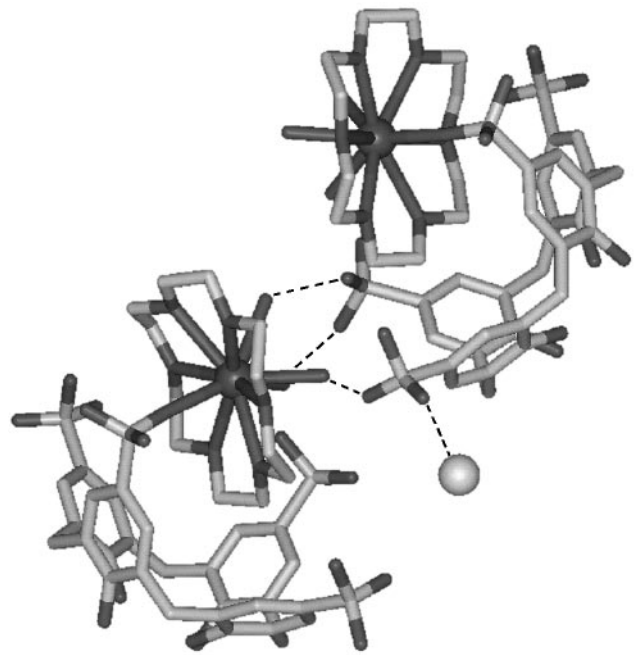

Fig. 1 Projection of two supercations [X]$^+$ in **1** showing associations between sulfonate groups and coordinated waters and sulfonate groups and chloride ions; hydrogen atoms have been removed for clarity and implied hydrogen-bonding interactions are represented by dashed lines.

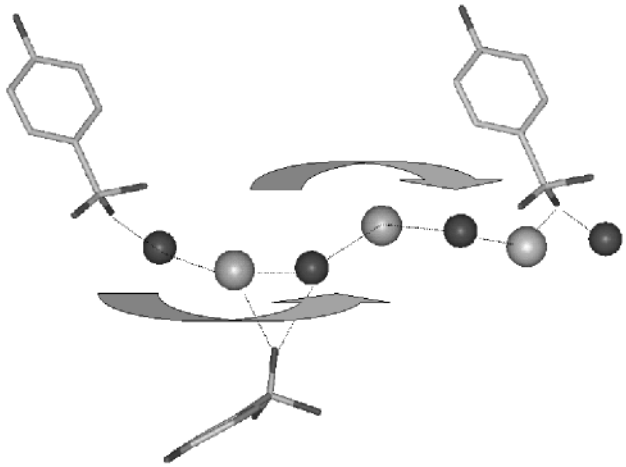

Fig. 2 Hydrogen bonded helical array of supercations, chlorides and waters of crystallisation. Only one phenyl group of each supercation is shown for clarity.

seen, the lanthanide is bound symmetrically by the six crown ether oxygen atoms [La–O = 2.654(5) to 2.733(5) Å] (Fig. 1). Assisted by the complementarity of curvature, this moiety resides in the cavity of the calixarene *via* a La–sulfonate linkage [La–O = 2.418(5) Å] and van der Waals interactions. The metal centre also has three water molecules attached at 2.557(5), 2.558(5) and 2.542(5) Å, on the opposite side to the sulfonate group relative to the plane of the crown ether, and these hydrogen bond to a single adjacent supercation (Fig. 1, O···O distances = 2.696, 2.799, 2.916 Å). The coordination environment around the lanthanide is unexceptional.[13]

Complementarity of curvature of the crown ether with that of the calixarene is achieved by the splaying of two opposite phenol groups (with torsion angles between the opposite phenol groups of 140.5 and 79.9°). In comparison the analogous angles in the ionic capsules Θ^{7-} range from 93–100°, and 46–59° respectively.[10] Due to the linkage between the metal and the calixarene, in the present structure the plane of the crown ether is rotated towards the cavity of the calixarene by 51.6° with respect to the vector of symmetrical approach. Within the crystal lattice an infinite helical array of the supercations, chloride counterions and water is formed through hydrogen bonding associations (Fig. 2).

In conclusion, using a combinatorial approach we have gained access to a novel supercation comprised of four components. By varying the pH in a systematic way, there is scope for constructing a wide range of structural types for such multicomponent systems.

Support of this research from the Australian Research Council is gratefully acknowledged.

Notes and references

† *Synthesis*: Using an excess of the metal salt, 13 mg of $LaCl_3.6H_2O$ (3.8×10^{-2} mmol), 15.5 mg of *p*-sulfonatocalix[4]arene (1.89×10^{-2} mmol) and 5 mg of 18-crown-6 (1.89×10^{-2} mmol) were dissolved in *ca.* 1 ml of water and the pH adjusted to 2.5 using a few drops of concentrated perchloric acid (65%). A yield of 13% was obtained (*ca.* 3 mg). Electron microprobe: lanthanum and chlorine are present in an equal ratio.

‡ *Crystal data* for **1**: $C_{40}H_{72}ClLaO_{35}S_4$, M_r = 1415.59; trigonal (hexagonal setting), $P3_1$, $a = b$ = 20.1097(3), c = 13.2080(3) Å, V = 4625.7 Å^3, Z = 3, μ = 0.963 mm^{-1} (no correction), 25935 data collected, 12878 unique (R_{int} = 0.044), number of parameters = 729, final GoF = 1.038, R_1 = 0.0591 [on 11332 observed data with $I > 2\sigma(I)$], wR_2 = 0.1720, (all data). Data were collected at 123(1) K on an Enraf-Nonius KappaCCD diffractometer using Mo-Kα radiation (λ = 0.71073 Å). The structure was solved by direct methods (SHELXS-97) and refined using full-matrix least-squares on F^2 (SHELXL-97). All nonhydrogen atoms were refined anisotropically except for two disordered water positions that were refined isotropically, and all C-H hydrogens were fixed at geometrically estimated positions. Interestingly, a crystal with a corresponding unit cell [trigonal (hexagonal setting), $P3_1$, $a = b$ = 20.0838(3), c = 13.1953(2) Å] was also isolated from a solution prepared in an analogous way using lanthanum *tris*(trifluoromethanesulfonate) nonahydrate. Perchloric acid was not required to acidify the solution to *ca.* pH 2.5. Electron microprobe results indicate that lanthanum and fluorine are present, but not chlorine. CCDC 182/1251. See http://www.rsc.org/suppdata/cc/1999/1135/ for crystallographic data in .cif format.

1 J.-C. G. Bunzli and J. A. Harrowfield, *Lanthanide Ions and Calixarenes*, in *Calixarenes: A Versatile Class of Macrocyclic Compounds*, ed. J. Vicens and V. Bohmer, Kluwer, Boston, 1991.

2 J. Atwood and S. Bott, *Water Soluble Calixarene Salts. A Class of Compounds with Solid-State Structures Resemblng Those of Clays*, in *Calixarenes: A Versatile Class of Macrocyclic Compounds*, ed. J. Vicens and V. Bohmer, Kluwer, Boston, 1991.

3 S. Shinkai, H. Koreishi, K. Ueda, T. Arimura and O. Manabe, *J. Am. Chem. Soc.*, 1987, **109**, 6371.

4 J. Atwood, G. Orr, N. Means, F. Hamada, H. Zang, S. Bott and K. Robinson, *Inorg. Chem.*, 1992, **31**, 603.

5 J. W. Steed, C. P. Johnson, C. L. Barnes, R. K. Juneja, J. L. Atwood, S. Reilly, R. L. Hollis, P. H. Smith and D. L. Clark, *J. Am. Chem. Soc.*, 1995, **117**, 11426.

6 A. W. Coleman, S. G. Bott, S. D. Morley, C. M. Means, K. D. Robinson, H. Zhang and J. L. Atwood, *Angew. Chem., Int. Ed. Engl.*, 1988, **27**, 1361.

7 J. L. Atwood, A. W. Coleman, H. Zhang and S. G. Bott, *J. Inclusion Phenom.*, 1989, **7**, 203.

8 J. L. Atwood, F. Hamada, K. D. Robinson, G. W. Orr and R. L. Vincent, *Nature*, 1991, **349**, 683.

9 R. Rogers and C. Bauer, *Structural Chemistry of Metal–Crown Ether and Polyethylene Glycol Complexes Excluding Groups 1 and 2*, in *Comprehensive Supramolecular Chemistry*, ed. J. Atwood, J. Davies, D. Macinol and F. Vogtle, Pergamon, New York, 1996, vol. 1, p. 315.

10 A. Drljaca, M. J. Hardie, C. L. Raston and L. Spiccia, *Chem. Eur. J.*, in the press; A. Drljaca, M. J. Hardie and C. L. Raston, to be published.

11 S. Shinkai, S. Mori, T. Tsubaki, T. Sone and O. Manabe, *Tetrahedron Lett.*, 1984, **25**, 5315.

12 J. Harrowfield, D. Kepert, J. Patrick and A. White, *Aust. J. Chem.*, 1983, **36**, 483.

13 F. Cotton and G. Wilkinson, *Advanced Inorganic Chemistry*, 5th edn., Wiley, 1998, p. 959.

Communication 9/02095K

Cyclam as a supramolecular synthon: infinite stacked arrays to encapsulation in superanions

Samantha Airey, Alexander Drljaca, Michaele J. Hardie and Colin L. Raston*

Department of Chemistry, Monash University, Clayton, Melbourne, Victoria 3168 Australia.
E-mail: c.raston@sci.monash.edu.au

Received (in Columbia, MO, USA) 2nd March 1999, Accepted 13th April 1999

Cyclam crystallised from $CHCl_3$–hexane gives infinite, hydrogen bonded assembled columns; in acidic aqueous media (pH 2) in the presence of sodium *p*-sulfonatocalix[4]arene and the dichromium(III) aqua ion, the superanion or ionic capsule $[[H_4(cyclam)]^{4+} \subset \{(p\text{-sulfonatocalix[4]arene}^{4-})_2\}]^{4-}$ crystallises as the salt of $[Cr_2(OH)_2(H_2O)_8]^{4+}$.

Cyclam (1,4,8,11-tetraazacyclotetradecane) is a traditional macrocyclic ligand in metal ion chemistry.[1] It can be di- or tetra-protonated at low pH to form cationic macrocycles. The tetra-protonated form $[H_4(cyclam)]^{4+}$ adopts an *exodentate* conformation[2] while the di-protonated $[H_2(cyclam)]^{2+}$ and neutral molecule adopt an *endodentate* conformation.[3,4] The neutral molecule has four nitrogen centres capable of hydrogen bonding, as donor and/or acceptor groups, and in this regard its potential in supramolecular chemistry, at least where one of the modes in intermolecular interplay involves hydrogen bonding, is yet to be realised. Both the di- and tetra-protonated forms, on the other hand, have been used as templates in crystal engineering studies, forming polymeric arrays with a variety of anions.[2,3] In exploring this chemistry we have discovered two remarkable, disparate, hydrogen bonding arrays. One of these is the crystallisation of solvent free, pure cyclam from $CHCl_3$–hexane solutions.

The other hydrogen bonding array is associated with the formation of a new ionic capsule where the $[H_4(cyclam)]^{4+}$ is shrouded by two *p*-sulfonatocalix[4]arenes, *viz* $[[H_4(cyclam)]^{4+} \subset \{(p\text{-sulfonatocalix[4]arene}^{4-})_2\}]^{4-}$ (Θ^{4-}), isolated as the salt of the dichromium(III) cation $[Cr_2(OH)_2(H_2O)_8]^{4+}$. The bowl-shaped, highly charged and water soluble *p*-sulfonatocalixarenes, usually used as their sodium salts, show remarkable inclusion properties for ionic guests and neutral molecules, for both calix[4 and 5]arenes.[5] As to the ionic capsule reported, we note that these classes of compounds have only recently been established, but with a metal crown ether complex in the centre of the capsule, $[\{Na^+ \subset (18\text{-crown-6})(OH_2)_2\} \subset \{(p\text{-sulfonatocalix[4]arene}^{4-})_2\}]^{7-}$, which is effective in crystallising, in some cases selectively, the polynuclear cations $[M_2(OH)_2(H_2O)_8]^{4+}$, $[M_3(OH)_4(H_2O)_{10}]^{5+}$ and $[M_4(OH)_6(H_2O)_{12}]^{6+}$ (M = Cr or Rh), and $[Al_{13}O_4(OH)_{12}(OH)_{24}(H_2O)_{12}]^{7+}$.[6] Ionic capsules relate to other contemporary studies on self-assembly of neutral molecular capsules,[7] as does the formation of a 1:1 crown ether to calixarene perched structure with lanthanum(III) in the crown ether, $[\{Ln^{3+} \subset (18\text{-crown-6})(OH_2)_3\} \cap \{(p\text{-sulfonatocalix[4]arene}^{4-} + 2H^+)\}]^+$.[8] The ionic capsule is without precedence, and its ability to crystallise as a dichromium(III) aqua cation suggests it has potential in forming complexes of a wide range of large cationic species, with ultimate applications in separation science. A key feature of the ionic capsules is the complementarity of curvature of the cyclam with the calixarene, albeit with some geometrical preorganisational requirements.

Complex $[Cr_2(OH)_2(H_2O)_8]^{4+}\Theta^{4-}$ crystallised from a solution of cyclam, sodium *p*-sulfonatocalix[4]arene, and the perchlorate salt of the dichromium(III) cation, with the pH adjusted to 2 using perchloric acid (Scheme 1).† This is the only example of an ionic capsule where the charge on the superanion matches that required by the polynuclear cation, without the need to invoke some degree of protonation of the superanion, unlike for complexes involving $[\{Na^+ \subset (18\text{-crown-6})(OH_2)_2\} \subset \{(p\text{-sulfonatocalix[4]arene}^{4-})_2\}]^{7-}$, which can adjust the degree of protonation depending on the polynuclear cation.

Crystals suitable for X-ray diffraction studies of cyclam and $[Cr_2(OH)_2(H_2O)_8]^{4+}\Theta^{4-}.6(H_2O)$‡ deposited over several days. Both crystallise in $P\bar{1}$ systems with the two independent cyclams residing over centres of symmetry (Fig. 1), or the ionic capsule and cation residing over inversion centres (Fig. 2). Cyclam has been reported to have an *endodentate* conformation[4] although a detailed structure is not available.[9] Cyclam (Fig. 1) has two opposite NH groups in the plane of and directed into the centre of the macrocycle, which form intramolecular hydrogen bonds across the 1,3-diamine groups at N–H···N distances of 2.243 and 2.273 Å (corresponding N···N 2.934 and 2.948 Å) and angles at the hydrogen of 135.7 and 133.1°. These are slightly longer interactions than the intramolecular hydrogen bonding observed for $[H_2(cyclam)]^{2+}$.[3] The remaining two N–H groups are directed away from the macrocycle and form

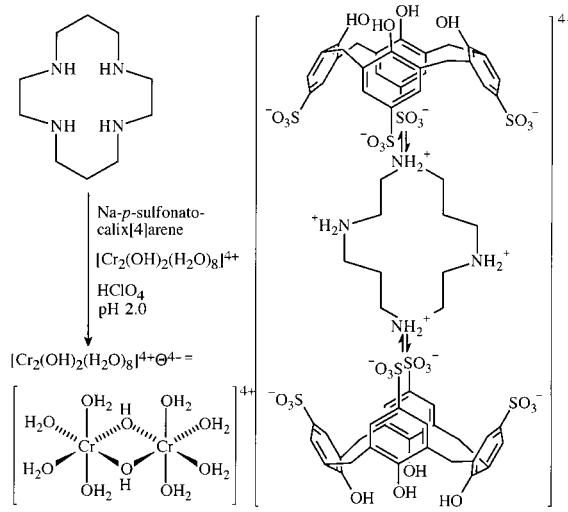

Scheme 1

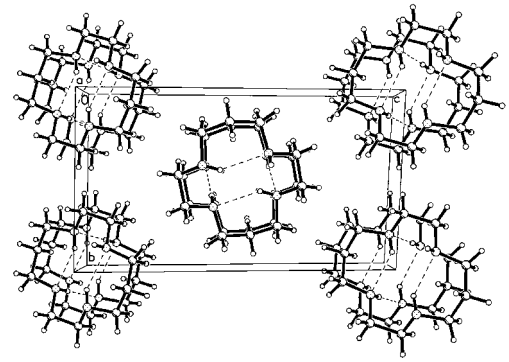

Fig. 1 Packing diagram for cyclam showing the intermolecular hydrogen bonded columnar arrays and intramolecular hydrogen bonding (hydrogen bonds indicated by dashed lines).

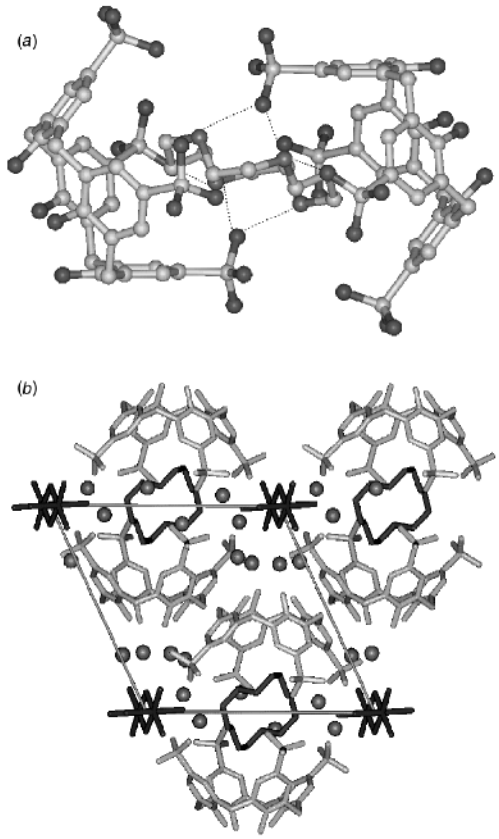

Fig. 2 Projection of (*a*) the superanion $[[H_4(cyclam)]^{4+} \subset \{(p\text{-sulfonatocalix[4]arene}^{4-})_2\}]^{4-}$ (Θ^{4-}), hydrogen atoms have been removed for clarity and implied hydrogen-bonding interactions are represented by dashed lines, and (*b*) unit cell and packing in $[Cr_2(OH)_2(H_2O)_8]^{4+}\Theta^{4-}.6(H_2O)$.

intermolecular N–H···N hydrogen bonds giving columns of cyclam held together by alternating pairs of intermolecular hydrogen bonds at N–H···N distances of 2.296 and 2.267 Å (corresponding N···N 3.155 and 3.143 Å). The intermolecular hydrogen bonds are considerably more direct than the intramolecular hydrogen bonds with N–H···N angles of 178.1 and 177.0°.

In the structure of $[Cr_2(OH)_2(H_2O)_8]^{4+}\Theta^{4-}.6(H_2O)$ the $[H_4(cyclam)]^{4+}$ is locked within the capsule by an intricate hydrogen bonded array [Fig. 2(*a*)]. Protons were not found crystallographically and the hydrogen bonding network is implied through numerous close N···O contacts ranging from 2.61 to 2.83 Å. There are close N···O contacts, in addition to those shown in Fig. 2(*a*), with a sulfonate group of another capsule and a water molecule, hence each N-centre is associated with at least two hydrogen bonds, which, along with its *exodentate* conformation,[2] is good evidence that the cyclam is the tetra-protonated species $[H_4(cyclam)]^{4+}$. The capsule itself is not as symmetrical as those containing crown ether,[6] with the two bowl cavities offset relative to each other, presumably to maximise hydrogen bonding and for geometrical complementarity between the interacting hydrophobic components of the cyclam and calixarene. The conformation of the calixarene, however, is more symmetrical than for the crown ether ionic capsules where two opposite phenol groups are splayed apart, with dihedral angles 93–100° relative to the other two, dihedral angle 46–59°.[6] In the present structure the corresponding dihedral angles are 81 and 52°. Packing of the capsules within the crystal lattice shows sulfonate to hydroxy hydrogen bonding between calixarenes of adjacent capsules (O···O separations of 2.87 and 2.90 Å) complemented by a slightly displaced π stacking of phenyl groups (centroid separation 3.62 Å, closest C···C = 3.43 Å, torsion angle between aromatic faces = 0°) [Fig. 2(*b*)]. The dichromium cations sit at the hydrophilic equator of the capsules [Fig. 2(*b*)], with close O···O contacts between the coordinated waters and sulfonate groups ranging from 2.62 to 2.77 Å. The geometry of the dichromium cation is unexceptional[6,10] and deviates from strict octahedral coordination.

Overall, we have established new supramolecular chemistry of cyclam, that of pure cyclam as a reference point in the area, and that of the capsule which gives further insight into construction of ionic capsules.

Support of this research from the Australian Research Council is gratefully acknowledged.

Notes and references

† Synthesis of $[Cr_2(OH)_2(H_2O)_8^{4+}\Theta^{4-}$: An aqueous solution of sodium *p*-sulfonatocalix[4]arene and cyclam in 2 : 1 proportions was added to an aqueous solution of $[Cr_2(OH)_2(H_2O)_8][ClO_4]_4$ and the pH of the mixture was adjusted to pH 2.0 with aqueous $HClO_4$. Pale green crystals of $[Cr_2(OH)_2(H_2O)_8]^{4+}\Theta^{4-}$ grew as a hexahydrate over several weeks. Crystals were sensitive to loss of solvent, becoming opaque on removal from mother liquor.

‡ Data were collected at 123(1) K on an Enraf-Nonius KappaCCD diffractometer with Mo-Kα radiation, λ = 0.71073 Å. Structures were solved by direct methods (SHELXS-97) and refined by full-matrix least-squares on F^2 (SHELXL-97). *Crystal data* for Cyclam: $C_{10}H_{24}N_4$, M_r = 200.33, crystal size = 0.23 × 0.18 × 0.13 mm, triclinic, $P\bar{1}$, a = 4.6353(3), b = 8.5958(6), c = 15.2418(10) Å, α = 90.704(3), β = 96.743(4), γ = 99.336(4)°, V = 594.80(6) Å^3, Z = 2, μ = 0.07 mm^{-1} (no correction), $2\theta_{max}$ = 60.14°, 4366 data collected, 2989 unique (R_{int} = 0.023), 223 parameters, final GoF = 1.040, R_1 = 0.0498 [on 2198 observed data with $I > 2\sigma(I)$], wR_2 = 0.1099 (all data). All nonhydrogen atoms were refined anisotropically and all hydrogen atoms were located in the difference map and fully refined isotropically. For $[Cr_2(OH)_2(H_2O)_8^{4+}\Theta^{4-}.6(H_2O)$: $C_{33}H_{77}CrN_2O_{27}S_4$, M_r = 1114.21, crystal size = 0.18 × 0.08 × 0.04 mm, triclinic, $P\bar{1}$, a = 10.9916(3), b = 14.8774(5), c = 15.3517(6) Å, α = 63.836(1), β = 86.583(2), γ = 80.499(2)°, V = 2222.03(13) Å^3, Z = 2, μ = 0.545 mm^{-1} (no correction), $2\theta_{max}$ = 54.44°, 37347 data collected, 9727 unique (R_{int} = 0.146), 613 parameters, final GoF = 2.277, R_1 = 0.1644 [on 9727 observed data with $I > 2\sigma(I)$], wR_2 = 0.2347 (all data). All nonhydrogen atoms were refined anisotropically and C–H hydrogens were fixed at geometrically calculated positions. High residuals are a consequence of the extremely small, needle-like crystals obtained and poor data quality indicated by the high R_{int}. CCDC 182/1249. See http://www.rsc.org/suppdata/cc/1999/1137/ for crystallographic files in .cif format.

1 L. Lindoy, *The Chemistry of Macrocyclic Ligand Complexes*, Cambridge University Press, Cambridge, 1989.
2 S. Subramanian and M. J. Zaworotko, *J. Chem. Soc., Chem. Commun.*, 1993, 952; S. Subramanian and M. J. Zaworotko, *Can. J. Chem.*, 1993, **71**, 433; S. Subramanian and M. J. Zaworotko, *Can. J. Chem.*, 1995, **73**, 415.
3 G. Ferguson, C. Glidewell, R. M. Gregson and P. R. Meehan, *Acta Crystallogr., Sect. B*, 1998, **54**, 139.
4 N. F. Curtis, *Coordination Chemistry of Macrocyclic Compounds*, ed. G. A. Melson, Plenum, New York, 1979, ch. 4, p. 237.
5 See for example: J. W. Steed, C. P. Johnson, C. L. Barnes, R. K. Juneja, J. L. Atwood, S. Reilly, R. L. Hollis, P. H. Smith and D. L. Clark, *J. Am. Chem. Soc.*, 1995, **117**, 11426; A. W. Coleman, S. G. Bott, S. D. Morley, C. M. Means, K. D. Robinson, H. Zhang and J. L. Atwood, *Angew. Chem., Int. Ed. Engl.*,1988, **27**, 1361; J. L. Atwood, A. W. Coleman, H. Zhang and S. G. Bott, *J. Inclusion Phenom.*, 1989, **7**, 203; J. L. Atwood, F. Hamada, K. D. Robinson, G. W. Orr and R. L. Vincent, *Nature*, 1991, **349**, 683; S. Shinkai, K. Araki, T. Matsuda, N. Nishiyama, H. Ikeda, I. Takasu and M. Iwamoto, *J. Am. Chem. Soc.*, 1990, **112**, 9053.
6 A. Drljaca, M. J. Hardie, C. L. Raston and L. Spiccia, *Chem. Eur. J.*, 1999, in the press; A. Drljaca, M. J. Hardie and C. L. Raston, unpublished work.
7 J. Kang and J. Rebek, *Nature*, 1997, **385**, 50; T. Heinz, D. M. Rudkevich and J. Rebek, *Nature*, 1998, **394**, 764; L. R. MacGillivray and J. L. Atwood, *Nature*, 1997, **389**, 469; M. M. Conn and J. Rebek Jr., *Chem. Rev.*, 1997, **97**, 1647 and references therein.
8 A. Drljaca, M. J. Hardie, J. A. Johnson, C. L. Raston and H. R. Webb, *Chem. Commun.*, 1999, 1135.
9 Cambridge Structural Database, F. H. Allen and O. Kennard, *Chem. Des. Automat. News*, 1993, **8**, 1 and 31.
10 L. Spiccia, H. Stoeckli-Evans, W. Marty and R. Giovanoli, *Inorg. Chem.*, 1987, **26**, 474; A. Drljaca, D. C. R. Hockless, B. Moubaraki, K. S. Murray and L. Spiccia, *Inorg. Chem.*, 1997, **36**, 1988.

Communication 9/02124H

Octaphenylcyclotetrasiloxane confinement of C_{60} into double columnar arrays

Ian E. Grey,[a] Michaele J. Hardie,[b] Timothy J. Ness[b] and Colin L. Raston*[b]

[a] *CSIRO Division of Minerals, Box 312 Clayton South, Melbourne, Victoria 3169 Australia*
[b] *Department of Chemistry, Monash University, Clayton, Melbourne, Victoria 3168 Australia. E-mail: c.raston@sci.monash.edu.au*

Received (in Columbia, MO, USA) 2nd March 1999, Accepted 13th April 1999

Excess octaphenylcyclotetrasiloxane [{$SiPh_2$(μ-O)}$_4$] and C_{60} in toluene affords the 1 : 1 supramolecular complex as a hemi-toluene solvate where the fullerenes are arranged in double columnar arrays shrouded by edge on, interlocking siloxanes.

Host–guest and supramolecular chemistry of the electron-deficient fullerenes has focused mainly on the use of more traditional host or receptor molecules including cyclodextrins,[1] and container molecules with hydrophobic pockets lined with aromatic rings, notably calixarenes,[2–6] resorcinarenes,[7] and cyclotriveratrylene and related molecules.[8,9] A recent development is the confinement of C_{60} and C_{70} (and other globular molecules) in complementary cavities of rigid nickel(II) macrocycles.[10] Here the interaction may be synergic with the likelihood of fullerene to metal electron density flow as well as the reverse for the unsaturated rings of the host in contact with the fullerene. However, in general, encouraging inherently weak host–guest interactions involving a fullerene is facilitated by the complementarity of curvature of the host with that of the fullerene, as is having a host with a rigid structure such that there is no pre-organisation energy requirement prior to complexation with the fullerene.[10]

In further exploring the use of rigid receptor molecules to 'recognise' fullerenes we have investigated the interplay of octaphenylcyclotetrasiloxane [{$SiPh_2$(μ-O)}$_4$] with C_{60} and find it forms a 1 : 1 complex in the solid state. In principle, the siloxane can act as a multi-divergent receptor molecule with six concave surfaces surrounding the central core. Molecular mechanics suggests that these surfaces have complementarity of curvature with that of C_{60} and that there is little pre-organisation for complexation which is associated with simple torsion along the Si–C bonds. Despite this, the isolated complex has the siloxane acting as a single receptor site with C_{60}, in one of the four cavities which is edge-on relative to the tetrasiloxane plane (**1**). This is unexpected given that the two faces above and below

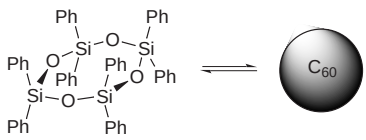

1

the siloxane plane have deeper cavities. Rather a phenyl ring of one siloxane molecule is directed into one of these cavities of another siloxane. This was also found in the structure of the siloxane itself but had been overlooked,[11] and surprisingly there is no inter-siloxane molecule π-stacking. The structure is also noteworthy in that the fullerenes are aligned in double columnar arrays; this structural motif is unusual, restricted to an organometallic inclusion complex[12] and a charge transfer complex with a thiafulvalene.[13] Moreover, this is the first report of a siloxane–C_{60} host–guest complex, and C_{70} fails to form a complex under similar conditions.

Dark red crystals of the 1 : 1 complex as a toluene hemi-solvate, [{$SiPh_2$(μ-O)}$_4$]C_{60}(toluene)$_{0.5}$, were obtained by slow diffusion of Pr^iOH vapour into a toluene solution of C_{60} and excess siloxane, ratio *ca.* 1 : 10.† Many other ratios and solvents, and solvent mixtures, were unsuccessful in forming the complex. The IR of the complex showed the superposition of peaks corresponding to the three components in the lattice, as expected for weakly associated species. In solution, UV–VIS studies show very little change in the range 400 to 800 nm, unlike in other systems,[5,8,13] and there was little change in the NMR spectroscopic data. Thus the interactions in solution are inherently weak.

In the structure derived from X-ray diffraction studies,‡ a molecule of each of the supramolecular synthons and half a toluene molecule residing over a centre of inversion comprise the asymmetric unit; results are presented in Fig. 1 and 2. The side-on interaction of the fullerene with the siloxane is unsymmetrical; two of the four phenyl rings attached to the same silicon centre have the closest contacts to the fullerene at 3.70 Å. The two phenyl rings on the other silicon associated with the same edge of the siloxane are positioned such that there

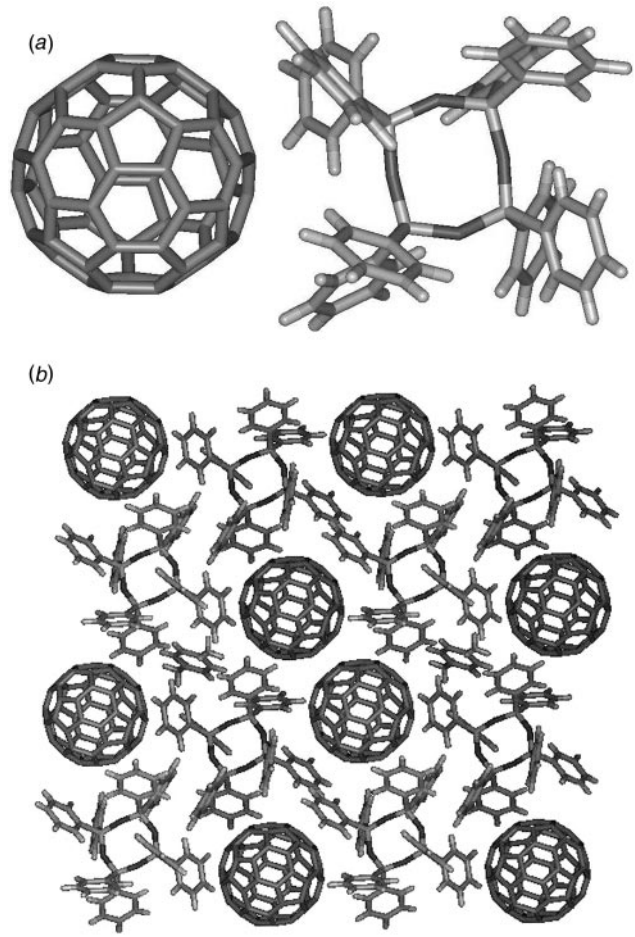

Fig. 1 The structure of [{$SiPh_2$(μ-O)}$_4$]C_{60}(toluene)$_{0.5}$ showing (*a*) the two interacting supramolecular synthons, and (*b*) the extended interplay projected down the axis, the direction of the double columnar arrays of fullerenes; the toluene molecules are disordered over centres of inversion.

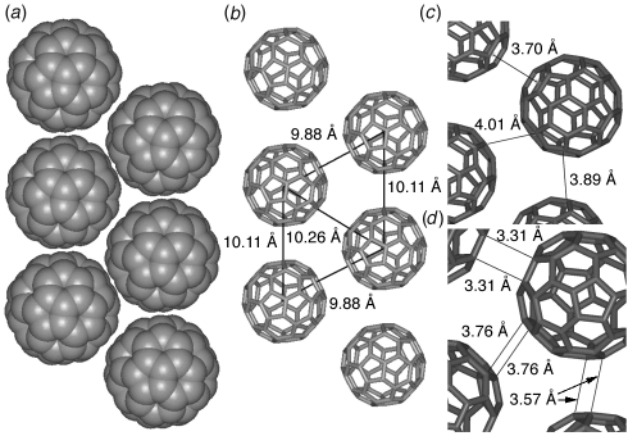

Fig. 2 The double columnar array of fullerenes in $[\{SiPh_2(\mu\text{-}O)\}_4]C_{60}(toluene)_{0.5}$ showing (*a*) space filling packing, (*b*) fullerene centroid–centroid separations, (*c*) inter-fullerene ring centroid separations, and (*d*) closest fullerene contacts.

is no π-stacking between the two components, and indeed, the protons on the phenyl rings are the atoms in immediate contact with the fullerene [Fig. 1(*a*)]. This type of C–H···C_{60} interaction has precedence in one other structure, notably that of $[C_{60} \subset (L)_2]$ (L = *p*-benzylhexahomooxacalix[3]arene).[3]

In the upper and lower cavity of the siloxane, there are either one or two phenyl rings orientated with the C–H groups towards the centre of the siloxane ring. These orientations preclude any interaction of the fullerene in the clefts. One 'upper' phenyl ring of one siloxane molecule is pointing into the 'lower cavity' of the same siloxane one unit cell away in the direction of the *a* axis [Fig. 1(*b*)]. This interlocking stacking motif is similar to that found in the crystal structures of the pure siloxane.[11] The predilection towards this type of stacking for the siloxane may be one of the factors influencing its interplay with the fullerene.

Fig. 2 shows the pairs of C_{60} columns. Analysis of the centroid-to-centroid distances of the C_{60} molecules shows that the packing is not as regular as close packing, with the positions of the C_{60} molecules in one column slightly offset, so they are closer to one of the nearest neighbours in the other column. The centroid-to-centroid distances are 10.11 Å within a column and either 9.88 or 10.26 Å between columns for the nearest neighbours. The shortest of these distances compare with the very short, dipole induced inter-fullerene distances in the single columnar arrays of C_{60} found in a calix[4]arene–C_{60} complex, *viz*. 9.8782(5) Å.[6] Within a single column of C_{60} molecules, the closest centroid to centroid approach for two C_6 rings is 3.89 Å, with the rings offset, so that the centroids are not directly opposite each other. The closest approach between C_6 ring centroids occurs between the columns at 3.70 Å. The closest C···C contact is 3.31 Å. The siloxane molecules appear to interact between columns, and with other C_{60} and toluene molecules [Fig. 1(*b*)]. With a few exceptions,[3,4,8] inter-fullerene interactions play a major role in the structures of supramolecular complexes of C_{60},[2,5–8,10,12,13] and this is further corroborated in the present structure. Establishing the ground rules for inter-fullerene interactions is important in understanding the competing interactions associated with the formation of discrete host–guest supermolecules.

This report clearly demonstrates the ability of a simple siloxane to self-assemble with C_{60}. From here there is the exciting prospect of stronger binding by incorporating extended aryl arms on the siloxane, and to extend the work to the analogous octa-aryloctasiloxanes $[\{Si(aryl)(\mu\text{-}O)\}_8]$.

The support of this work by the Australian Research Council is gratefully appreciated.

Notes and references

† *Synthesis* of $[\{SiPh_2(\mu\text{-}O)\}_4]C_{60}(toluene)_{0.5}$: Slow diffusion of Pr^iOH into a toluene solution of C_{60} (10 mg, 0.014 mmol) and the siloxane (100 mg, 0.130 mmol) in toluene (5 ml) over four weeks afforded colourless crystals (60 mg) of the siloxane which were separated manually from the deep red needles of the fullerene–siloxane complex, 4 mg, 19% yield. Found: C, 85.92; H, 2.60. $C_{111.5}H_{43.5}O_4Si_4$ requires, C, 85.85; H, 2.84%.

‡ *Crystal data* for $[\{SiPh_2(\mu\text{-}O)\}_4]C_{60}(toluene)_{0.5}$: Data were collected on an Enraf Nonius KappaCCD diffractometer with Mo-Kα radiation (λ = 0.71073 Å) and were corrected for Lorenzian and polarisation effects but not absorption. The structure was solved by direct methods (SHELXS-97) and refined anisotropically with full-matrix least-squares on F^2 (SHELXL-97). Hydrogen atoms were located in the difference map and refined isotropically. $C_{111.5}H_{43.5}O_4Si_4$, M = 1559.3, triclinic, space group $P\bar{1}$, a = 10.1145(4), b = 19.0653(8), c = 19.2258(7) Å, α = 82.250(5), β = 75.960(5), γ = 78.414(5)°, U = 3509.0(2) Å^3, Z = 2, D_c = 1.476 g cm^{-3}, T = 123(1) K, μ = 0.153 mm^{-1}, 22635 reflections collected, 12344 unique (R_{int} = 0.065), 7715 reflections observed, 1241 parameters, R_1 = 0.0513 (observed data), wR_2 = 0.1063 (all data). CCDC 182/1250. See http://www.rsc.org/suppdata/cc/1999/1139/ for crystallographic data in .cif format.

1 T. Anderson, G. Westman, G. Stenhagen, M. Sundahi and O. Wennerstrom, *Tetrahedron Lett.*, 1995, **36**, 597 and references therein; A. Harada and S. Takahashi, *J. Chem. Soc., Chem. Commun.*, 1988, 1352.

2 J. L. Atwood, G. A. Koutsantonis and C. L. Raston, *Nature*, 1994, **368**, 229; T. Suzuki, K. Nakashima and S. Shinkai, *Chem. Lett.*, 1994, 699; R. M. Williams, J. M. Zwier and J. W. Verhoeven, *J. Am. Chem. Soc.*, 1994, **116**, 6965; T. Suzuki, K. Nakashima and S. Shinkai, *Tetrahedron Lett.*, 1995, **36**, 249; K. Akao, K. Ikeda, T. Suzuki and S. Shinkai, *Tetrahedron Lett.*, 1996, **37**, 73; C. L. Raston, J. L. Atwood, P. J. Nichols and I. B. N. Sudria, *Chem. Commun.*, 1996, 2615; T. Haino, M. Yanase and Y. Fukazawa, *Tetrahedron Lett.*, 1997, **38**, 3739; A. Ikeda and S. Shinkai, *Chem. Rev.*, 1997, **97**, 1713; A. Ikeda, M. Yoshimura and S. Shinkai, *Tetrahedron Lett.*, 1997, **38**, 2107; N. S. Isaacs, P. J. Nichols, C. L. Raston, C. A. Sandoval and D. Young, *Chem. Commun.*, 1997, 1839; L. J. Barbour, G. W. Orr and J. L. Atwood, *Chem. Commun.*, 1997, 1439; J. L. Atwood, L. J. Barbour, C. L. Raston and I. B. N. Sudria, *Angew. Chem., Int. Ed. Engl.*, 1998, **37**, 981.

3 J. L. Atwood, L. J. Barbour, P. J. Nichols, C. L. Raston and C. A. Sandoval, *Chem. Eur. J.*, in the press.

4 T. Haino, M. Yanase and Y. Fukozawa, *Angew. Chem., Int. Ed.Engl.*, 1997, **36**, 3, 259; K. Tsubaki, K. Tanaka, T. Kinoshita and K. Fuji, *Chem. Commun.*, 1998, 895; T. Haino, M. Yanase and Y. Fukozawa, *Angew. Chem., Int. Ed. Engl.*, 1997, **37**, 7 and 997; T. Haino, M. Yanase and Y. Fukozawa, *Tetrahedron Lett.*, 1997, **38**, 3739.

5 A. Drijaca, C. Kepert, C. L. Raston, C. A. Sandoval, L. Spiccia and T. D. Smith, *Chem. Commun.*, 1997, 195.

6 L. J. Barbour, G. W. Orr and J. L. Atwood, *Chem. Commun.*, 1998, 1901.

7 K. N. Rose, L. J. Barbour, G. W. Orr and J. L. Atwood, *Chem. Commun.*, 1998, 407.

8 J. L. Atwood, M. J. Barnes, R. S. Burkhalter, P. C. Junk, J. W. Steed and C. L. Raston, *J. Am. Chem. Soc.*, 1994, **116**, 10 346; J. L. Atwood, M. J. Barnes, M. G. Gardiner and C. L. Raston, *Chem. Commun.*, 1996, 1449.

9 H. Matsuhara, A. Heasegawa, K. Shiwaku, K. Asano, M. Uno, S. S. Takahashi and K. Yamamoto, *Chem. Lett.*, 1998, 923.

10 P. C. Andrews, J. L. Atwood, L. J. Barbour, P. J. Nichols and C. L. Raston, *Chem. Eur. J.*, 1998, **4**, 1382; J. M. Marshall, P. D. Croucher, P. J. Nichols and C. L. Raston, *Chem. Commun.*, 1999, 193; P. D. Croucher, P. J. Nichols and C. L. Raston, *J. Chem. Soc., Dalton Trans.*, 1999, 279.

11 D. Braga and G. Zanotti, *Acta Crystallogr., Sect. B*, 1980, **36**, 950; Y. E. Ovchinnikov, V. E. Shklover, Y. T. Stuchkov, V. V. Dementev and T. M. Frunze, *Metalloorg. Khim.*, 1988, **1**, 1117.

12 J. D. Crane and P. B. Hitchcock, *J. Chem. Soc., Dalton Trans.*, 1993, 2537.

13 A. Izuoka, T. Tachikawa, T. Sugawara, Y. Saito and H. Shinohara, *Chem. Lett.*, 1992, 1049.

Communication 9/01719D

Formation of bamboo-like nanocarbon and evidence for the quasi-liquid state of nanosized metal particles at moderate temperatures

Yongdan Li,* Jiuling Chen, Yanmei Ma, Jinbao Zhao, Yongning Qin and Liu Chang

Department of Catalysis Science and Technology and State Key Lab on C1 Chemical Technology, School of Chemical Engineering, Tianjin University, Tianjin 300072, China. E-mail: ydli@tju.edu.cn

Received (in Cambridge, UK) 22nd March 1999, Accepted 12th May 1999

Carbon nano-filament formation in hydrocarbon and syngas based catalytic processes is fatal for supported metal catalysts as this leads to deactivation and crushing, and hence limitation of carbon deposition has been a major topic in catalysis.[1–5] Recently, the deliberate preparation of catalytically grown nanocarbons has been investigated because of their specific structure and potential for application in many fields.[6–8] Many nanocarbon conformations have been reported, such as tubular, coiled, helical, branched, octopus, *etc*. and have been found to be sensitive to the reaction conditions and catalyst properties.[9–14] Catalytic hydrocarbon decomposition[9–13] or arc-discharge evaporation of graphite[14–18] have been often used as preparation methods, though in the latter case, the presence of a metal is necessary as catalyst in the form of either vapor or droplets of melt. The selective preparation of a given formation is a challenge to catalysis researchers. Here, several nanocarbon conformations are shown to be formed with high morphological purity from methane on a copper–nickel–alumina catalyst, and some interesting phenomena related to the nanosized metal are reported.

A catalyst with a mol ratio Ni:Cu:Al of 75:15:10 was prepared by coprecipitation. The precipitate has a Feitknecht compound structure, which in ideal composition has formula $Ni_6Al_2CO_3(OH)_{16}\cdot 4H_2O$, However, here part of the Ni was replaced by Cu, the amount of Al was reduced, and the structure was distorted. After calcination, an NiO like phase is observed but with scattered XRD peaks. During reduction uniformly nanometer sized Ni-Cu alloy was obtained, as shown in Figs. 1 and 2. It is interesting that no structural information of other components except for NiO and Ni appeared in the XRD profiles of the oxidized and reduced state, respectively. Detailed catalyst preparation and reaction conditions have been published elsewhere.[9,10]

When this catalyst is exposed to methane–nitrogen (v/v = 1:2), at 773 K, and after the reaction rate reduced to zero, a large amount [93.5 mg C(mg Ni)$^{-1}$] of morphologically pure octopus carbon was formed. As shown in Fig. 3, the metal particles are polyhedral and are the origin of several nanocarbon fibers. When the temperature was 1023 K, and with the same feed, a large amount of hollow nanocarbon tubes are produced as shown in Fig. 4, with rare stick-shaped nanocarbon formed at the same time.

When this catalyst was exposed to methane–hydrogen (1:2, v/v) at temperatures of 1003 and 1043 K, a large amount of

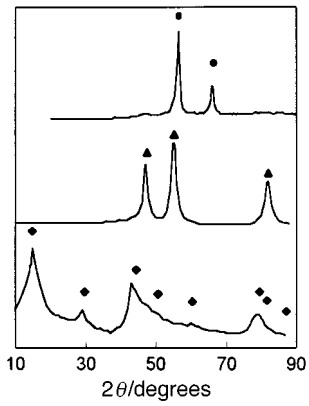

Fig. 1 XRD patterns of the catalyst and precursors: (◆) precipitate precursor, marked points are the position and height of the peaks of $Ni_6Al_2CO_3(OH)_{16}\cdot 4H_2O$; (▲) calcined material, marks are the peaks of NiO; (●) catalyst in reduced state, marks are the peaks of nickel.

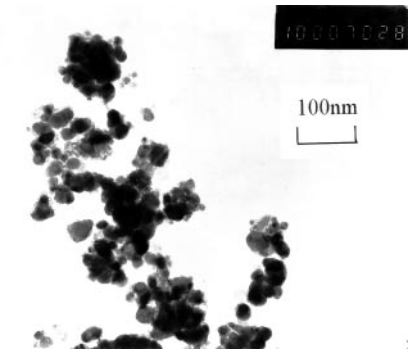

Fig. 2 TEM image of the catalyst in the reduced state.

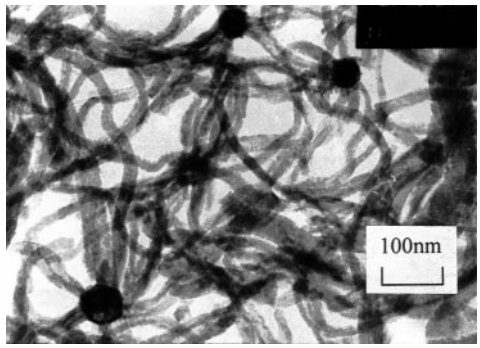

Fig. 3 Octopus carbon grown on the catalyst in methane–nitrogen at 773 K.

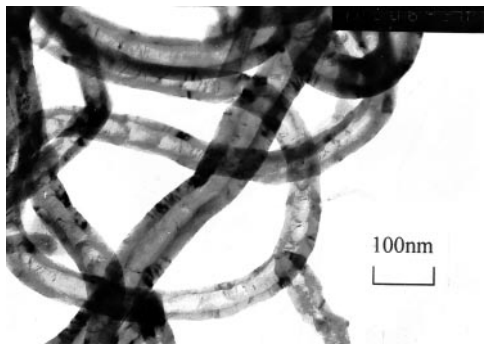

Fig. 4 Carbon nanotubes grown on the catalyst in methane–nitrogen at 1023 K.

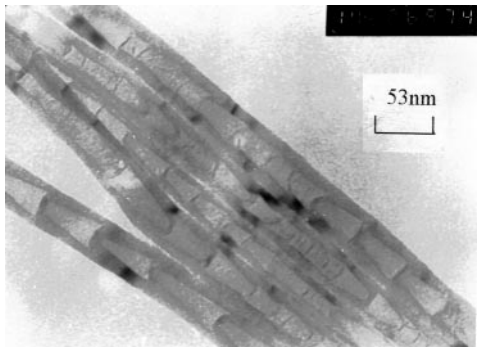

Fig. 5 Bamboo-shaped carbon grown on the catalyst in methane–hydrogen at 1043 K.

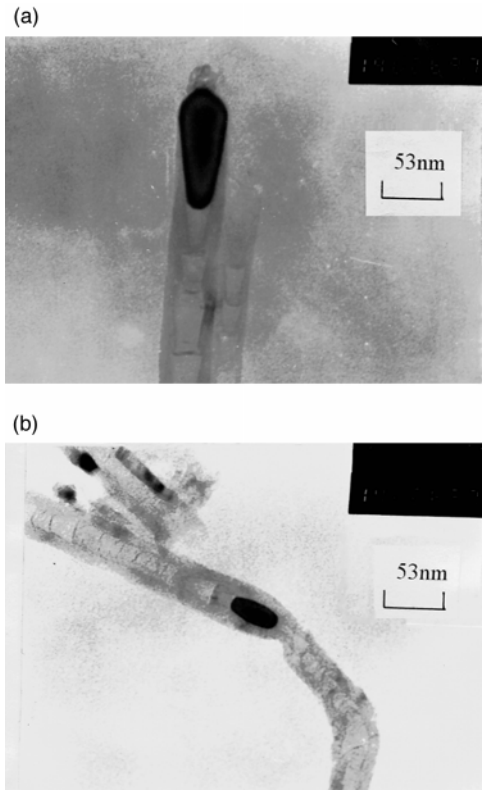

Fig. 6 Bamboo-shaped carbon grown on the catalyst in methane–hydrogen at 1003 K with encapsulated metal.

bamboo-shaped nanocarbon was obtained in a high morphology purity. The bamboo-shaped carbons formed under several conditions are shown in Figs. 5 and 6.

These conformations of carbon have been reported previously, though they were found together with other forms. Adveeva *et al.*[19] has reported octopus-shaped carbon, which was formed under nearly the same conditions as in this work. Saito[14] and Kovalevski and Safronov[20] reported separately bamboo-like carbons formed either from arc-discharge evaporation of graphite or from catalytic pyrolysis of hydrocarbons at 2223–2873 K. They attributed the formation of bamboo-like carbon to the catalytic effect of melted droplets of metal.[14,20]

Inspections of Figs. 2 and 3 show that the metal particles before reaction are irregularly shaped while after reaction at 773 K they are polyhedral, indicating recrystallization during induction of carbon formation. Micrographs in Fig. 6 show clearly that the metal, either at the tip of the carbon fiber or encapsulated inside, resembles a drop of mercury in a glass capillary, indicating that it is in a quasi-liquid state during reaction. Although no metal tip was found in Figs. 4 and 5, due to the crushing of the nanotubes before TEM observation, the carbon shows the same structure growth indicating the catalytic function of the liquid like metal. The shape of the carbon shows that it was formed by jumping of the metal tip at regular time intervals over similar distances. This can only be explained by supposing that the metal is in a quasi-liquid state with high surface energy and poor wetting ability towards graphite carbon. The highest temperature studied for these reactions was 1043 K, which is far below the melting point of the metals either in the pure or alloyed state. The melting point of nickel is 1728 K, while that of copper is 1357.5 K.[21] A Ni–Cu alloy with the same composition as the catalyst here has a melting point of 1423 K.[21] Some literature[22,23] has proposed metal carbide formation in this system, however, the temperature of Ni_3C formation is 1773–2373 K and the lowest melting temperature of a C–Ni alloy (atomic ratio 9 : 91) is 1573 K.[24] The existence of the metal in a quasi-liquid state at *ca*. 1000 K can only be attributed to the size effect of the metal at the nanometer level and the interfacial effect between nanocarbon and nanometal.

Results presented here suggest that (1) The conformation of a nanocarbon is sensitive to the reaction conditions and catalyst, and its morphological purity can be controlled. (2) The Ni–Cu/Al_2O_3 catalyst used here can catalyze nanocarbon formation both in the solid and molten state. (3) The Ni–Cu alloy undergoes recrystallization during induction of carbon formation producing pure octopus carbon in methane–nitrogen at 773 K, while a catalyst prepared under the same conditions but without doping of copper showed different behaviour.[10] (4) Ni–Cu alloy exists in the reaction system at as a quasi-liquid state at moderate temperatures owing to its nanosize and interfacial effects. (5) These phenomena may help to validate reaction mechanisms for nanocarbon formation on metals.

Notes and references

1 D. L. Trimm, *Catal. Rev.-Sci. Eng.*, 1977, **16**, 155.
2 C. H. Bartholomew, *Catal. Rev.-Sci. Eng.*, 1982, **24**, 67.
3 X. Y. Wu, J. Y. Zhang and L. Chang, *Stud. Surf. Sci. Catal.*, 1987, **34**, 208.
4 Q. Zhuang, Y. N. Qin and L. Chang, *Appl. Catal.*, 1991, **70**, 1.
5 R. T. K. Baker, *Stud. Surf. Sci. Catal.*, 1991, **68**, 1.
6 J. W. Mintmire and C. T. White, *Carbon*, 1995, **33**, 893.
7 R. S. Ruoff and D. C. Lorents, *Carbon*, 1995, **33**, 925.
8 R. T. K. Baker, *Carbon*, 1989, **27**, 315.
9 Y. D. Li, J. L. Chen, L. Chang and Y. N. Qin, *J. Catal.*, 1998, **178**, 76.
10 Y. D. Li, J. L. Chen and L. Chang, *Appl. Catal. A*, 1997, **163**, 45.
11 N. M. Rodriguez, *J. Mater. Res.*, 1993, **8**, 3233.
12 S. Motojima, S. Asakura, T. Kasemura, S. Takeuchi and H. Iwanaga, *Carbon*, 1996, **34**, 289.
13 G. G. Tibbetts, *J. Cryst. Growth*, 1984, **66**, 632.
14 Y. Saito, *Carbon*, 1995, **33**, 979.
15 C. H. Kiang, W. A. Goddard, R. Beyers and D. S. Bethune, *Carbon*, 1995, **33**, 903.
16 S. Amelinckx, X. B. Zhang, O. Bernaerts, X. F. Zhang, V. Ivanov and J. B. Nagy, *Science*, 1994, **265**, 635.
17 X. K. Wang, X. W. Lin, V. P. Dravid, J. B. Ketterson and R. P. H. Chang, *Appl. Phys. Lett.*, 1993, **62**, 1881.
18 W. Z. Li, S. S. Xie, L. X. Qian, B. H. Chang, B. S. Zou, W. Y. Zhou, R. A. Zhao and G. Wang, *Science*, 1996, **274**, 1701.
19 L. B. Adveeva, O. V. Goncharova, D. I. Kochubey, V. I. Zaikovskii, L. M. Plyasova, B. N. Novgorodov and Sh. K. Shaikhutdinov, *Appl. Catal. A*, 1996, **141**, 117.
20 V. V. Kovalevski and A. N. Safronov, *Carbon*, 1998, **36**, 963.
21 *Eryuan Hejin Zhuangtai Tuji (Phase Diagram of Binary Alloy Systems)*, ed. J. Q. Yu, W. Z. Yi, B. D. Chen and H. J. Chen, Shanghai Keji Publisher, Shanghai, China, 1987, p. 249 (in Chinese).
22 I. Alstrup and M. T. Taveres, *J. Catal.*, 1993, **139**, 513.
23 A. J. H. M. Kock, P. K. de Bokx, E. Boellaard, W. Klop and J. W. Geus, *J. Catal.*, 1985, **96**, 468.
24 *Tiehejin Cidian (Dictionary of Iron Alloys)*, ed. X. P. Zhang and C. J. Liu, Liaoning Keji Publisher, Shenyang, China, 1996, p. 317 (in Chinese).

Communication 9/02281C

Cyclodimerization and Diels–Alder reaction of a spiroepoxycyclohexadienone with an *o*-quinodimethane structure

Vincent Bonnarme,[a] Martine Mondon,[a] Alain Cousson[b] and Jean-Pierre Gesson*[a]

[a] *Laboratoire de Chimie XII, Université de Poitiers et CNRS, 40 avenue du Recteur Pineau, 86022 Poitiers, France. E-mail: jean-pierre.gesson@campus.univ-poitiers.fr*

[b] *Laboratoire Léon Brillouin, CE Saclay, 91191 Gif sur Yvette, France*

Received (in Liverpool, UK) 8th March 1999, Accepted 29th April 1999

Oxidation of 3-hydroxymethyl-2-naphthol with periodate affords a single *exo-syn* dimer arising from the intermediate *ortho* quinonoid spiroepoxycyclohexadienone; the latter can also be trapped by reactive dienophiles.

Spiroepoxycyclohexadienones are easily obtained from the corresponding 2-hydroxymethylphenols upon $NaIO_4$ oxidation.[1] Like related *ortho*-quinones, quinols and quinol acetates, these dienones easily dimerize *via* a concerted $4\pi+2\pi$ process.[2] Indeed, cycloaddition with various dienophiles (dienes, alkenes, styrenes, enol ethers and esters, enamides) readily occurs to give highly functional adducts.[3] The preparation of similar, albeit stable, dienones in the naphthalene series has been also reported from 2-hydroxymethyl-1-naphthol[4] and 1-hydroxymethyl-2-naphthol.[5]

In this respect, we became interested in the preparation of spirodienone **1** possessing a reactive *ortho*-quinomethane structure which could lead to benzo-fused bicyclo[2.2.2] adducts with dienophiles. This material was prepared from the known 3-hydroxymethyl-2-naphthol[6] **2**, easily obtained in two steps from 3-hydroxy-2-naphthoic acid (MeOH, H^+, 90%; $LiAlH_4$, 86%) (Scheme 1). Upon $NaIO_4$ oxidation (MeOH, H_2O, 20 °C), a single dimeric compound, **3**, mp 201–203 °C, was isolated in 67% yield. This material is characterized, apart from signals of aromatic and CH_2O protons, by two sharp singlets at δ 3.52 and 4.23. This is consistent with only one of the four possible symmetrical head-to-head dimers resulting from *endo* or *exo* and *syn* or *anti* (with respect to the epoxide oxygen) approaches (two of these structures have C_2 symmetry and two are *meso*). The exclusive formation of the *exo-syn* dimer was secured by an X-ray analysis of **4**† (Fig. 1) obtained after $NaBH_4$ reduction and acetylation (Scheme 1). Such orbital symmetry forbidden dimerizations (a formal $\pi^4s + \pi^4s$ process) have already been observed with *ortho*-quinonoid species, usually under irradiation.[7] For example, *in situ* generated 2-benzopyran-3-one has been reported by Bleasdale[8] to give mainly photodimer **5** in unspecified low yield,‡ and Schlosser[9] has described the spontaneous dimerization to **6** (74%) of an

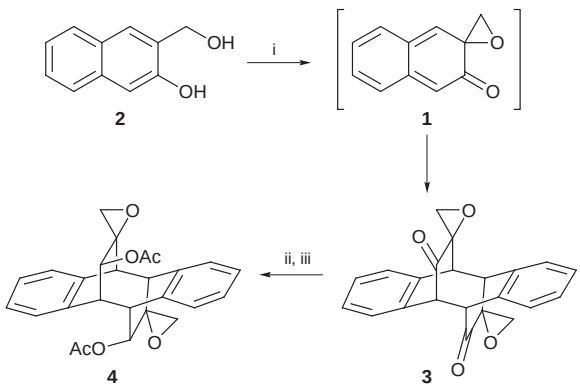

Scheme 1 *Reagents and conditions*: i, $NaIO_4$ (1.1 equiv.), MeOH, 90 min, rt; ii, $NaBH_4$ (1.1 equiv.), 0 °C, 10 min ; iii, Ac_2O, Py, 12 h, rt.

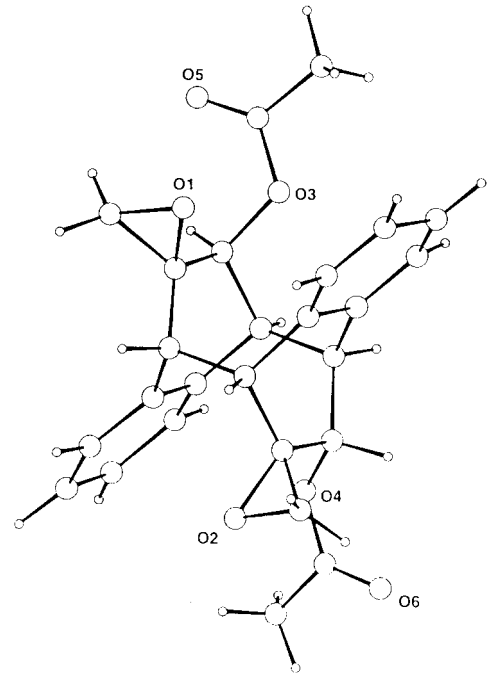

Fig. 1 Crystal structure of **4**.

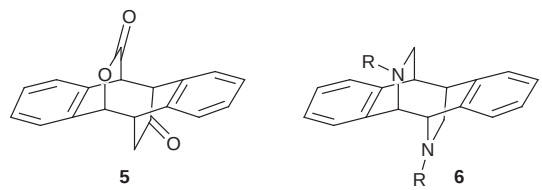

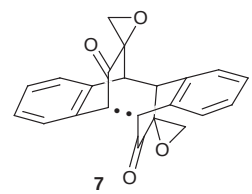

ortho-quinomethane derived from MeOH elimination of a tetrahydroquinoline. As suggested by Trahanovsky to explain the dimerization of 2,3-dimethylene-2,3-dihydrofuran,[10] **3** probably results from the intermediate diradical **7**, arising from the less hindered *exo-syn* approach of two monomers **1.**

The high facial selectivity observed in the reduction of **3** with $NaBH_4$ is also noteworthy since reduction of α,β-epoxy ketones with hydrides predominantly occurs *syn* to the oxygen epoxide.[11,12] On the other hand, Okada[13] has shown that $NaBH_4$ reduction of 2,3-benzo-fused norbornen-7-one proceeds *syn* to the phenyl ring, while *anti* reduction of 5,6-benzo-fused bicyclo[2.2.2]octan-2-one has been reported[12b] with $LiAlH_4$.

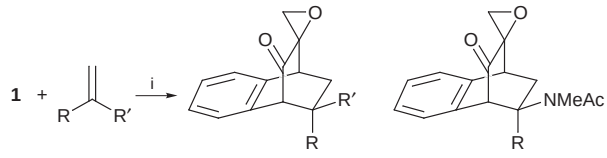

8 R = OEt, R′ = H
9a R = H, R′ NMeAc
9b R = NMeAc, R′ = H
10 R = *p*-MeOC$_6$H$_4$, R′ = H
11a R = OMe, R′ = Me
11b R = Me, R′ = OMe

9c

Scheme 2 *Reagents and conditions*: i, $NaIO_4$ (1.1 equiv.), dienophile (5 equiv.), MeOH–H_2O, 2–12 h, rt.

The π-facial selectivity of the reduction observed here is not controlled by the epoxide group, but this may be due to steric hindrance from the remote phenylene group rather than stereoelectronic control by the nearest phenyl ring.

Then, *in situ* cycloaddition of dienone **1** was attempted by carrying out the oxidation step in presence of 5 equiv. of dienophile (Scheme 2). Ethoxyethene and *N*-methyl-*N*-vinylacetamide add to **1** to give **8** (82%) and **9a–c** (70%) without notable dimer formation, unlike the less reactive 4-methoxystyrene, which gave **10** (42%) together with **3** (30%), and 2-methoxyprop-2-ene, which gave **11a** (25%), **11b** (4%) and **3** (44%). As expected, *syn-endo* cycloadition is observed in most cases, except for the enamide which exhibits low selectivity, giving *syn-exo* (**9a**), *syn-endo* (**9b**) and *anti-exo* (**9c**)§ adducts in a 2 : 1 : 1 ratio (a high *syn-exo* selectivity has been observed with enamides for a related spirocyclohexadienone[3d] and for a pyrone[14]).

In summary, oxidation of 3-hydroxymethyl-2-naphthol affords chiral dimer **3** possessing C_2 symmetry in a rigid framework, and trapping of the unstable dienone **1** is possible at room temperature with electron-rich dienophiles. Such adducts may serve as useful templates for the preparation of rigid phenethylamine derivatives[15] or of tetrahydronaphthalene derivatives after cleavage of the α,β-epoxy ketone moiety.[16]

Notes and references

† *Selected data* for **4**: mp 190 °C; δ_H(300 MHz, $CDCl_3$) 1.81 (s, 6 H, Ac), 2.50 (AB q, *J* 6, 4 H, CH_2O), 3.14 (s, 2 H, ArC*H*), 3.89 (d, *J* 2, 2 H, ArC*H*), 5.12 (d, *J* 2, 2 H, C*H*OAc), 7.30 (m, 8 H); δ_C 20.4, 46.0, 51.4, 55.0, 58.7, 70.4, 127.0, 127.4, 129.1, 130.1, 138.9, 139.1, 170.2.

Crystal data for **4**: $C_{28}H_{24}O_6$, M_r = 1729.89, monoclinic, *a* = 16.578(7), *b* = 25.37(1), *c* = 20.826(8) Å, *β* = 105.99(7)°, *V* = 8420(2) Å^3, space group $P2_1/n$, *Z* = 16, D_c = 1.36 g cm^{-3}, *F*(000) = 3659.166, colourless prismatic crystal stable in air, μ(Cu-Kα) = 0.754 mm^{-1}, 3030 independent reflections with $I \geq 3\sigma(I)$ were used in the structural analysis. The structure was solved using direct methods (ref. 17) and refined using least-squares calculations (ref. 18). Positional and anisotropic thermal parameters of all atoms except hydrogen were refined. Hydrogen atom positions were calculated, an equivalent isotropic thermal parameter was given for hydrogen atom groups. Finally *R* = 9.39%, R_w = 10.53% and *S* = 1.53 for 1250 refined parameters and 3030 reflections. A Chebychev polynomial with three coefficients was used in the weighting scheme. There are four independent molecules in the asymmetric unit and, although this is rather rare, no significant difference between these molecules was evidenced. CCDC 182/1253. See http://www.rsc.org/suppdata/cc/1999/1143/ for crystallographic data in .cif format.

‡ The analoguous isoquinolin-3-ol is reported to give a head-to-tail *exo* photodimer (ref. 19).

§ All new compounds were fully characterized by ^{1}H, ^{13}C NMR and HRMS except for adducts **9a** and **9b** which could not be separated by chromatography. *Selected data* for **9a**: δ_H 1.70 (ddd, *J* 14.2, 5.1 and 2.7, 1H), 2.03 (s, 3H), 2.18 (s, 3 H), 2.72 (ddd, *J* 14.2, 10.6 and 2.8), 5.58 (ddd, *J* 10.6, 5.1 and 2.5). For **9b**: δ_H 1.85 (ddd, *J* 14.2, 5.4 and 2.5), 2.14 (s, 3 H), 2.22 (s, 3 H), 2.76 (ddd, *J* 14.2, 10 and 2.5), 4.67 (ddd, *J* 10, 5.4 and 2.5). For **9c**: δ_H 2.13 (s, 3 H), 2.24 (m, 2 H), 2.90 (s, 3 H), 5.17 (ddd, *J* 9.6, 7.9 and 2.5).

1 E. Adler, S. Brasen and H. Miyake, *Acta Chem. Scand.*, 1971, **25**, 2055; H.-D. Becker, T. Bremholt and E. Adler, *Tetrahedron Lett.*, 1972, 4205.
2 E. Adler and K. Holmberg, *Acta Chem. Scand.*, 1974, **B28**, 465.
3 (*a*) V. Singh and B. Thomas, *J. Chem. Soc., Chem. Commun.*, 1992, 1211; (*b*) J.-P. Gesson, L. Hervaud and M. Mondon, *Tetrahedron Lett.*, 1993, **34**, 2941; (*c*) V. Singh and M. Porinchu, *Tetrahedron*, 1996, **52**, 7087; (*d*) C. Bachmann, V. Bonnarme, A. Cousson, M. Mondon and J.-P. Gesson, *Tetrahedron*, 1999, **55**, 433.
4 M. Tius and N. K. Reddy, *Synth. Commun.*, 1994, **24**, 859.
5 J.-P. Gesson, M. Mondon and N. Pokrovska, *Synlett*, 1997, 1395.
6 Y. Tanoue, A. Terada, I. Seto, Y. Umezu and O. Tsuga, *Bull. Soc. Chim. Jpn.*, 1988, **61**, 1221.
7 C. W. G. Fishwick and D. W. Jones, in *The Chemistry of the Quinonoid Compounds*, ed. S. Patai and Z. Rappoport, Wiley, 1988, vol. 2, part 1, pp. 403–453; J. L. Charlton and M. M. Alaudin, *Tetrahedron*, 1987, **43**, 2873.
8 D. A. Bleasdale, D. W. Jones, G. Maier and H. P. Reisenauer, *J. Chem. Soc., Chem. Commun.*, 1983, 1095.
9 G. Simig and M. Schlosser, *Tetrahedron Lett.*, 1994, **35**, 3081.
10 C. H. Chou and W. S. Trahanovsky, *J. Am. Chem. Soc.*, 1986, **108**, 4138.
11 P. Chautemps and J.-L. Pierre, *Tetrahedron*, 1976, **32**, 549; P. A. Bartlett, *Tetrahedron*, 1980, **36**, 2.
12 (*a*) T .W. Hart and B. Vacher, *Tetrahedron Lett.*, 1992, **33**, 3009; (*b*) M. J. Brienne, D. Varech and J. Jacques, *Tetrahedron Lett.*, 1974, 1233.
13 K. Okada, S. Tomita and O. Masaji, *Tetrahedron Lett.*, 1986, **27**, 2645.
14 K. Afarinkia, N. T. Daly, S. Gomez-Farnos and S. Joshi, *Tetrahedron Lett.*, 1997, **38**, 2369.
15 J. C. Barrish, S. H. Spergel, S. Moreland and S. A. Hedberg, *Bioorg. Med. Chem. Lett.*, 1992, **2**, 95.
16 K. Holmberg, H. Kirudd and G. Westin, *Acta Chem. Scand.*, 1974, **B28**, 913.
17 G. M. Sheldrick, SHELXS86, Program for the solution of crystal structures, 1986, University of Göttingen, Germany.
18 D. J. Watkin, J. R. Carruthers and P. W. Betteridge, CRYSTALS Software, 1985, Chemical Crystallography Laboratory, University of Oxford, England.
19 D. W. Jones, *J. Chem. Soc. (C)*, 1969, 1729.

Communication 9/01914F

Geometric control of cage architecture; observation of ligand-selective behaviour in the structures of $[\{As_2(NCy)_4\}_2M_4]$ (M = Na, Cu; Cy = C_6H_{11})

Alan Bashall,[a] Michael A. Beswick,[b] Eilis A. Harron,[b] Alexander D. Hopkins,[b] Sara J. Kidd,[b] Mary McPartlin,[a] Paul R. Raithby,[b] Alexander Steiner[c] and Dominic S. Wright*[b]

[a] *School of Chemistry, University of North London, London, UK N7 8DB*
[b] *Department of Chemistry, Lensfield Road, Cambridge, UK CB2 1EW. E-mail: dsw1000@cus.cam.ac.uk*
[c] *Department of Chemistry, Crown Street, Liverpool, UK L69 7ZD*

Received (in Cambridge, UK) 15th April 1999, Accepted 13th May 1999

The structure of $[\{As_2(NCy)_4\}_2Cu_4]$ reveals a dramatic change in the metal coordination mode compared to that found in the Sb analogue $[\{Sb_2(NCy)_4\}_2Cu_4]$, resulting in the distortion of the Cu_4 core from a square-planar to a butterfly shape and providing the first illustration of ligand-selective cage modification in such heterobimetallic species; in contrast the square-planar Na_4 arrangement found in $[\{Sb_2(NCy)_4\}_2M_4]$ (M = Na, Cu, Ag) is retained in $[\{As_2(NCy)_4\}_2Na_4]$.

In recent years the synthesis of nitrogen-containing anion ligands of Groups 15 and 16 [such as isoelectronic $S(NR)_3^{2-}$ [1] and $Sb(NR)_3^{3-}$ [2]] has provided new opportunities for the assembly of molecular cages containing a broad spectrum of mixed-element compositions.[3] However, most studies of the coordination chemistry of these and related systems have involved the alkali or alkaline earth metals[3,4] and no studies have so far indicated that changing the Group 15 or 16 elements within a particular family of ligands has any major effect on the coordination behaviour or on the nature of the cage formed for a particular metal. Studies of $[\{Sb_2(NCy)_4\}_2M_4]$ (M = Li,[5] Na,[6] Cu, Ag[4a,b]) have shown that the geometries of the supported M_4 cores arise from the compromise between the predominant rigidity of the $[Sb_2(NCy)_4]^{2-}$ ligand and the bonding demands of the coordinated metal ions. These influences are responsible for the switch from a tetrahedral Li_4 core for the Li complex to essentially square-planar M_4 cores in the Na, Cu(I) and Ag(I) complexes, and for the accompanying greater involvement of the μ_2- and exocyclic-N donor centres of the $[Sb_2(NCy)_4]^{2-}$ ligand in the latter. The recent synthesis of $[\{As_2(NCy)_4\}_2Li_4]$,[7,8] a source of the $[As_2(NCy)_4]^{2-}$ ligand, provides the opportunity for assessing the impact of differing geometric demands on cage architecture for a closely related ligand. We report here the first observation of ligand-selective modification for such a heterometallic cage.

In order to provide comparison with the related Sb systems, the Na complex $[\{As(NCy)_4\}_2Na_4]$ **1** and $[\{As_2(NCy)_4\}_2Cu_4]$ **2** were prepared. Complex **1** was obtained from the reaction of $As(NMe_2)_3$ with $CyNH_2$ followed by the addition of CyNHNa. Transmetallation of **1** with CuCl gave **2** (Scheme 1).†

The low-temperature X-ray study of **1**‡ (Fig. 1) shows that the complex has a cage structure consisting of two $[As(NCy)_4]^{2-}$ anions which coordinate four Na^+ cations using a combination of their μ-N and exocyclic-N donor sites. This overall structure and the rhombic arrangement of the Na^+ cations at the centre of the cage is identical to that occurring in the Sb analogue $[\{Sb_2(NCy)_4\}_2Na_4]$[6] and in the Cu and Ag complexes $[Sb_2(NCy)_4]_2M_4$ (M = Cu, Ag).[4a,b] However, although still essentially planar and possessing similar Na···Na distances (av. 3.17 Å) the Na_4 core in **1** is significantly more distorted than that in $[\{Sb_2(NCy)_4\}_2Na_4]$ (with alternating Na···Na···Na angles of av. 99.6 and av. 80.4° *cf.* av. 93.5 and 86.4° [6]).

In view of the similarity between **1** and the analogous Sb complex $[\{Sb_2(NCy)_4\}_2Na_4]$ it was anticipated that the Cu(I) complex $[\{As_2(NCy)_4\}_2Cu_4]$ **2** would exhibit the same overall structure as $[\{Sb_2(NCy)_4\}_2Cu_4]$[2] (in which essentially the same coordination mode as that found in **1** is preserved). However, the low-temperature X-ray study of 2‡ reveals that replacement of the Na^+ cations with Cu^I results in a dramatic change in the cage architecture. Rather than the μ-N and exocyclic-N centres of the two $[As_2(NCy)_4]^{2-}$ ligands bridging the alternate Cu···Cu edges of the Cu_4 core (as occurs in the Sb analogue[2]), the N atoms of each coordinate separate Cu ions in a manner not previously observed. This change in bonding mode results in essentially linear Cu(I) geometries [N–Cu–N 175.4(2)°]. The consequence of the asymmetrical coordination of the Cu centres of **2** [exocyclic-N–Cu 1.854(4), μ-N–Cu 1.949(4) Å] is that the Cu_4 core now has a butterfly-shape (rather than planar) arrangement. The switch from a symmetrical to an asymmetrical coordination mode corresponds to a 45° rotation of the Cu_4 core, a result of which is that the As_2N_2 and Cu_4 rings are now eclipsed.

The structural pattern found in **1** and in the Sb analogue, $[\{Sb_2(NCy)_4\}_2Na_4]$, stems from the presence of essentially ionic metal–ligand interactions which favour a ligand mode that maximises the coordination number of Na^+. In complexes containing Cu^I the preference for an essentially linear geometry can be satisfied by maintaining this same coordination mode (as

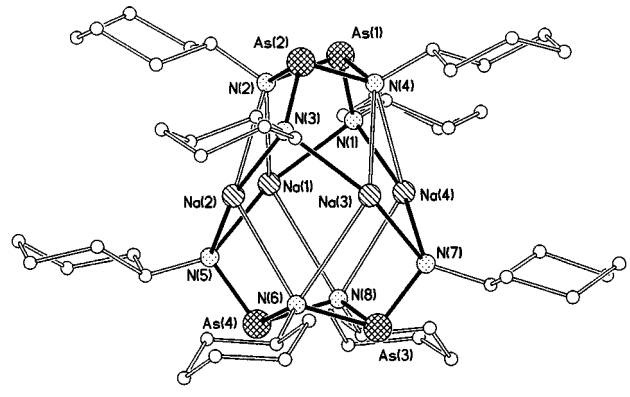

Fig. 1 Structure of cage molecules of **1** {a similar coordination mode and cage arrangement is also found in $[\{As_2(NCy)_4\}_2M_4]$ (M = Na, Cu, Ag)}. H-atoms have been omitted for clarity. Key bond lengths (Å) and angles (°); As(1)–N(1) 1.80(1), As(1)–N(2) 1.94(1), As(1)–N(4) 1.94(1), As(2)–N(3) 1.80(1), As(2)–N(4) 1.992(1), As(2)–N(2) 1.95(1), As(3)–N(7) 1.78(1), As(3)–N(6) 1.93(1), As(3)–N(8) 1.94(1), As(4)–N(5) 1.78(1), As(4)–N(8) 1.92(1), As(4)–N(6) 1.96(1), range exocyclic-N–Na 2.28(1)–2.37(1), range μ-N–Na 2.68(1)–2.99(1), Na···Na mean 3.17; As–(μ-N)–As means 93.0 (μ-N)–As–(μ-N) mean 78.8, (μ-N)–As–(*exo*-N) mean 103.8, (*exo*-N)–Na–(*exo*-N) mean 156.9, (μ-N)–Na–(μ-N) mean 122.9, Na···Na(2,4)···Na mean 99.6, Na···Na(1,3)···Na mean 80.4.

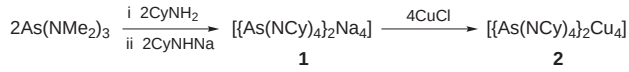

Scheme 1

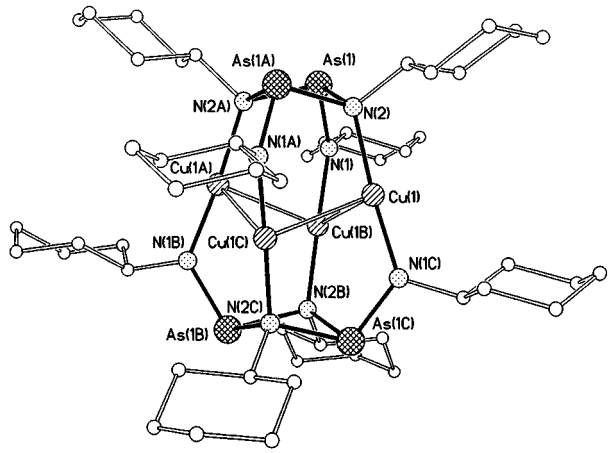

Fig. 2 The unique cage arrangement found in **2**. H-atoms have been omitted for clarity. Key bond lengths (Å) and angles (°); As(1)–N(2) 1.955(4), As(1)–N(2a) 1.949(4), As(10–N(1) 1.767(4), N(1)–Cu(1b) 1.854(4), N(2b)–Cu(1b) 1.927(4), Cu(1)···Cu(1b) 2.692(1); N(2)–As(1)–N(2a) 80.4(2), As(1)–N(2)–As(1a) 94.3(2), N(2)–As(1)–N(1) 104.3(4), N(2a)–As(1)–N(1) 104.0(2), N(1)–Cu(1b)–N(2b) 175.4(2), Cu(1b)···Cu(1)···Cu(1c) 83.4(2), dihedral angles between the As_2N planes in the As_2N_2 rings 143.2, and the Cu_3 planes of the Cu_4 core 126.0.

occurs in [{$Sb_2(NCy)_4$]$_2Cu_4$]^2). This symmetrical arrangement has the advantage that the Cu centres can increase their coordination numbers by additional weak interactions with the μ-N donor sites. However, with the more compact $[As_2(NCy)_4]^{2-}$ ligand adoption of the same mode would presumably destabilise the complex since the consequent compression of the Cu_4 core would lead to unfavourably short Cu···Cu contacts (*ca.* 2.46 Å; *cf.* 2.56 Å in Cu metal).[9] The alternative adopted in **2** gives a release from this effect since the asymmetrical ligand mode results in puckering of the Cu_4 core {with a resulting increase in Cu···Cu separation to 2.692(1);*cf.* 2.57 Å in [{$Sb_2(NCy)_4$}$_2Cu_4$]^2, but still maintains a linear Cu coordination geometry,

This study shows for the first time that geometric changes brought about by substitution of one Group 15 element for another within a particular family of poly-imido ligands can have large effects on the cage produced. This finding has important implications to the targeted design of cages with a particular structure and to the possibility of selective coordination involving ligands based on p block element frameworks.

We gratefully acknowledge the EPSRC (A. D. H., S. J. K., P. R. R., M. McP.), the Leverhulme Trust (M. A. B.) and Electron Industries (A. D. H.) for financial support.

Notes and references

† *Syntheses*: **1**; a mixture of [$PhCH_2Na$} (0.46 g, 4 mmol) and $CyNH_2$ (0.46 ml, 4 mmol) in a toluene (10 ml) was heated briefly to reflux, with the formation of a pale yellow precipitate. In a separate Schlenk tube, a mixture of $As(NMe_2)_3$ (2.5 ml, 4.0 mmol) and $CyNH_2$ (0.46 ml, 4 mmol) in toluene (10 ml) was briefly heated to reflux. This solution (cooled to room temperature) was added to the first, with the formation of a clear yellow solution which became orange after bringing to reflux (2 min). A small amount of solid was removed by filtration and careful reduction of the filtrate under vacuum resulted in precipitation of a small amount of white solid. Hexane (1 ml) was added and the precipitate was warmed into solution. Storage at room temp. (72 h) gave small, colourless needles of **1** (0.63 g, 54%). Final decomp. 192 °C. IR (Nujol, NaCl), ν_{max} = 1094m, 1067, 1019m, 798m, 750w. ^{1}H NMR (+25 °C, d_6-benzene, 250 MHz), δ 3.67 (m 2H, α-C–H Cy), 2.63 (m 2H, α-C–H Cy), 2.20–1.0 (m 40 H, –CH_2– Cy). Satisfactory elemental analysis (C, H, N) was obtained.

2; a mixture of **1** (1.22 g, 1.0 mmol) and CuCl (0.46 g, 4.6 mmol) in toluene (20 ml) was briefly heated to reflux then stirred (3 h). A cloudy grey–green suspension was formed which was filtered off to give a yellow filtrate. The solution was reduced under vacuum until precipitation commenced, this being warmed back into solution. Storage at room temp. (72 h) gave small, colourless needles of **2** (0.07 g, 5% first batch). Decomp. 188 °C. ^{1}H NMR (+25 °C, d_6-benzene, 250 MHz), δ 3.65 (2H, m α-C–H of Cy), 3.55 (2H, m α-C–H of Cy), 2.7–1.1 (40 H, overlapping m, –CH_2– of Cy). Satisfactory elemental analysis (C, H, N) was obtained.

‡ *Crystal data*: **1**; $C_{48}H_{88}As_4Na_4N_8$, M = 1168.90, orthorhombic, space group *Pbca*, Z = 8, a = 24.883(5), b = 37.424(8), c = 11.980(9) Å, V = 11156(9) Å^3, μ(Mo-Kα) = 2.446 mm^{-1}, T = 180(2) K. Data were collected on an Siemens-Stoe AED diffractometer and corrected for absorption using ψ-scans. Of a total of 9314 reflections collected, 6096 were independent (R_{int} = 0.068). The structure was solved by direct methods and refined by full-matrix least squares on F^2. Final $R1$ = 0.105 [$I > 2\sigma(I)$] and $wR2$ = 0.264 (all data).[10] The high R values for **1** are due to poor crystal quality. Maximum peaks in the Fourier synthesis can be assigned to a shadow image of the molecule in the crystal structure. Refinement of these peaks as As and Na positions give an occupation of 8% for the shadow image. However, in the final refinement the shadow image was omitted owing to rather high correlation factors and lack of convergence.

2; $C_{48}H_{88}As_4Cu_4N_8$, M = 1331.10, tetragonal, space group $I4_1/a$, Z = 4, a = 24.046(3), b = 24.046(3), c = 9.941(3) Å, V = 5748(2) Å^3, μ(Mo-Kα) = 3.783 mm^{-1}, T = 223(2) K. Data were collected on a Siemens P4 diffractometer and corrected for absorption using ψ-scans. Of a total of 2653 reflections collected, 2001 were independent (R_{int} = 0.044). The structure was solved by direct methods and refined by full-matrix least squares on F^2. Final $R1$ = 0.044 [$I > 2\sigma(I)$] and $wR2$ = 0.076 (all data).[10] CCDC 182/1259. See http://www.rsc.org/suppdata/cc/1999/1145/ for crystallographic files in .cif format for compound **1**.

1 R. Fleischer, S. Freitag, F. Pauer and D. Stalke, *Angew. Chem.*, 1996, **108**, 208; *Angew. Chem., Int. Ed. Engl.*, 1996, **35**, 204; T. Chivers, X. Gao, M. Parvez and G. Schatte, *Inorg. Chem.*, 1996, **35**, 4094.
2 M. A. Beswick, N. Choi, C. N. Harmer, A. D. Hopkins, M. A. Paver, M. McPartlin, P. R. Raithby, A. Steiner, M. Tombul and D. S. Wright, *Inorg. Chem.*, 1998, **37**, 2177.
3 M. A. Beswick and D. S. Wright, *Coord. Chem. Rev.*, 1998, **176**, 373; M. A. Beswick, M. E. G. Mosquera and D. S. Wright, *J. Chem. Soc., Dalton Trans.*, 1998, 2437 and references therein.
4 For examples involving other metals, see for example: (*a*) M. A. Beswick, C. A. Harmer, P. A. Paver, P. R. Raithby, A. Steiner and D. S. Wright, *Inorg. Chem.*, 1997, **36**, 1740; (*b*) D. Barr, A. J. Edwards, S. Pullen, M. A. Paver, M.-A. Rennie, P. R. Raithby and D. S. Wright, *Angew. Chem.*, 1994, **106**; 1960; *Angew. Chem., Int. Ed. Engl.*, 1994, **33**, 1875; (*c*) D. F. Moser, I. Schranz, M. C. Gerrety, L. Stahl and R. J. Staples, *J. Chem. Soc., Dalton Trans.*, 1999, 751.
5 R. A. Alton, D. Barr, A. J. Edwards, M. A. Paver, M.-A. Rennie, C. A. Russell, P. R. Raithby and D. S. Wright, *J. Chem. Soc, Chem. Commun.*, 1994, 1481.
6 A. Bashall, M. A. Beswick, C. N. Harmer, A. D. Hopkins, M. McPartlin, M. A. Paver, P. R. Raithby and D. S. Wright, *J. Chem. Soc., Dalton Trans.*, 1998, 1389.
7 M. A. Beswick, E. A. Harron, A. D. Hopkins, P. R. Raithby and D. S. Wright, *J. Chem. Soc., Dalton Trans.*, 1999, 107.
8 See also I. Schranz, L. Stahl and R. J. Staples, *Inorg. Chem.*, 1998, **37**, 1493, for the related $[P_2(NBu^t)_4]^{2-}$ ligand.
9 Assuming that the Cu atoms would be located at the mid-points of N(1)–N(1B), N(1)–N(1C), N(1A)–N(1C), N(1A)–N(1B).
10 SHELXTL PC version 5.03, Siemens Analytical Instruments, Madison, WI, 1994.

Communication 9/03010G

ChemComm

Novel reagents for targeted cleavage of RNA sequences: towards a new family of inorganic pharmaceuticals

Alavattam Sreedhara, Anjali Patwardhan and J. A. Cowan*

Evans Laboratory of Chemistry, The Ohio State University, 100 West 18th Avenue, Columbus, Ohio 43210 USA

Received (in Bloomington, IN, USA) 10th February 1999, Accepted 27th April 1999

Copper kanamycin degrades cognate RNA targets at concentrations as low as picomolar levels at physiological pH and temperature, but shows no chemistry with random RNA or DNA molecules, thereby demonstrating potential for development as a novel antiviral agent.

RNA-binding ligands that selectively disrupt RNA–protein interactions are of potential therapeutic value.[1] Both the absence of a cellular repair mechanism for RNA and the structural diversity of RNA motifs make these attractive drug targets.[1,2] Aminoglycoside antibiotics have been demonstrated to inhibit protein translation by recognition of 16S rRNA,[3,4] to inhibit the binding of the HIV Rev protein to its viral RNA recognition element, the Rev response element (RRE),[5] and also to inhibit the activity of hammerhead ribozymes,[6] group I intron ribozymes,[7] and the binding of HIV Tat peptide to TAR-RNA.[8] Solution structures have been determined for RNA complexed with a variety of aminoglycosides (paromomycin, ribostomycin, neamine, gentamicin).[9] Given the cognitive qualities of these molecules, we sought to develop metal derivatives that would not only inhibit protein binding to target RNA molecules, but better, would mediate destruction of the target. Hydrolysis of RNA by metal ion complexes has attracted considerable attention, since sequence-specific agents that catalyze the destruction of mRNA represent a new therapeutic approach.[10] Typically, high concentrations of complex, reaction times of several hours to days, and extremes of temperature and pH are used.[10b,11] Recently, RNA cleavage under milder conditions has been described.[12]

Herein, we report our finding that copper complexes of the aminoglycosides neomycin B and kanamycin A (Fig. 1) exhibit efficient RNA cleavage activity at physiological pH and temperature. Acetylation protection and ^{13}C NMR studies have been reported for the reaction of Cu^{2+} and kanamycin A that support the structure shown.[13] We have isolated the blue Cu^{2+}(kanamycin) complex **1** from the reaction of 1 : 1 kanamycin A and $CuSO_4$, and also Cu^{2+}(kanamycin)$_2$ **2** and Cu^{2+}-neomycin **3** complexes from reaction mixtures of 2 : 1 kanamycin A and $CuSO_4$, and 1 : 1 neomycin B and $CuSO_4$, respectively, as previously described.[14] Complex **1** was found to be stable in aqueous solution for more than one day, however, complexes **2** and **3** were less stable and formed precipitates within 4 h. For this reason, our attention focused on **1**.

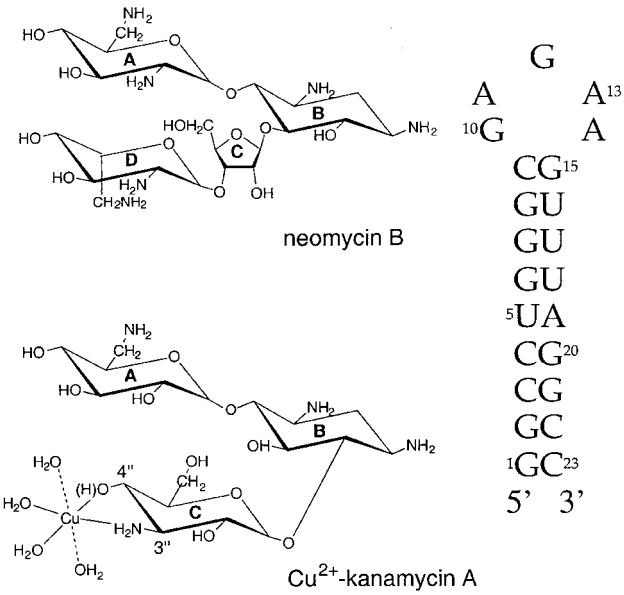

Fig. 1 Structures of the aminoglycosides used in this study (the copper complex of kanamycin A is shown), and a schematic illustration of the stem loop structure adopted by R23 (ref. 16).

A modified 23-mer RNA aptamer (hereafter termed R23) with a high binding affinity for neomycin B[15] (Fig. 1) was selected for a preliminary investigation of cleavage chemistry. The NMR solution structure of the neomycin B complex of R23 shows the aminoglycoside bound to the major groove through electrostatic and hydrogen bonding interactions with the amine and hydroxy groups of rings A and B, while the C and D sugar rings are pendant and can potentially chelate metal ions (Fig. 1).[16] Kanamycin A lacks the ribose ring C and two amine groups in ring D of neomycin B; however, neither ring contributes significantly to binding,[16] and so it is presumed that kanamycin A and neomycin B bind in a similar manner. In fact a comparison with published data indicates that rings A and B appear to form a conserved structural motif for recognition and binding to ribosomal RNA.[9]

Cleavage chemistry of **1** with either 5′-^{32}P end- or body-labeled R23 was examined in the absence and presence of the coreactants, H_2O_2 and ascorbate. R23 was incubated at 37 °C for 30 min to 1 h with various concentrations of **1**, and products were separated on a 19% denaturing polyacrylamide sequencing gel (Fig. 2). The cleavage sites were assigned by comparison with products generated by both alkaline hydrolysis and G-specific RNase T1 digestion. Data in Fig. 2(*a*) shows that cleavage of 5′-end-labeled R23 by **1** alone is not random, but rather specific cleavage sites were observed (lanes 2–4). Two sites of cleavage could be identified: one in the loop region at A^{14}/G^{15}, and the other in the stem region at C^4/U^5. This cleavage data is consistent with the NMR solution structure of R23 RNA bound to neomycin B, which shows binding of the aminoglycoside antibiotic in the loop region $A^{13}A^{14}G^{15}$, and in the stem region $U^5G^6G^7G^8$. The cleaved products co-migrate with products generated by partial alkaline hydrolysis [Fig. 2(*a*), lane 8]. Under these conditions, almost 70% cleavage of R23 is observed under hydrolytic conditions within 1 h.†

Although the hydrolysis of RNA by **1** is appreciable, addition of H_2O_2 or ascorbic acid increase the cleavage efficiency dramatically. Addition of 10 or 100 μM H_2O_2 to 30 μM R23 in the presence of as little as 50 pM **1** led to extensive cleavage—a truly catalytic multiturnover reaction with a ratio of catalyst to substrate of almost 1 : 10^6. Control experiments carried out in the absence of **1** and the presence of up to 100 μM H_2O_2 showed no background cleavage. Moreover, use of aqueous Cu^{2+} and H_2O_2 at concentrations where **1** demonstrated cleavage of R23 were ineffective for the former. Addition of 200 μM ascorbic acid to R23 treated with 20 nM **1** also showed extensive cleavage with almost 100% digestion of the parent RNA [Fig. 2(*b*], however, the relative concentrations of **1** required to effect cleavage of R23 in the presence of H_2O_2 and ascorbate indicates

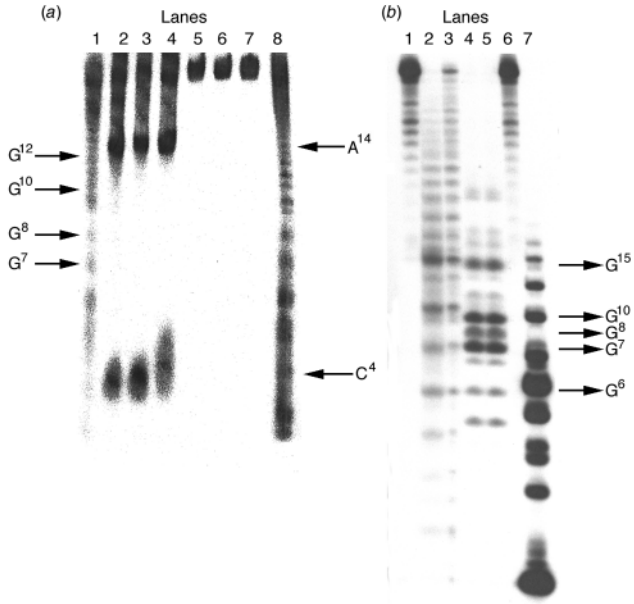

Fig. 2 (*a*) Autoradiograph of a 19% denaturing polyacrylamide electrophoretic gel for the cleavage of 5′-end-labeled R23 RNA by **1** at 37 °C for 2 h (ref. 18). Lane 1, R23 + 0.5 units RNase T 1; lane 2, R23 + 10 μM **1**; lane 3, R23 + 50 μM **1**; lane 4, R23 + 100 μM **1**; lane 5, R23; lane 6, R23 + 100 μM $CuSO_4$; lane 7, R23 + 100 μM kanamycin. Cleavage reactions were carried out in Tris-HCl (20 mM; pH 7.5) and contain *ca.* 1 μM RNA. Captions on the left indicate G-specific cleavage by RNase T1, while those on the right indicate sites giving rise to cleavage products of R23 following reaction with **1**. (*b*) Autoradiograph of a 19% denaturing polyacrylamide electrophoretic gel for the cleavage of uniformly-labeled R23 RNA by **1** at 37 °C for 1 h. Lane 1, R23; lane 2, R23 + 0.1 M NaOH; lane 3, R23 + Na_2CO_3/$NaHCO_3$ buffer; lane 4, R23 + 0.25 units RNase T 1; lane 5, R23 + 0.5 units RNase T1; lane 6, R23 + 1 μM $CuSO_4$/100 μM ascorbate; lane 7, R23 + 20 nM **1**/100 μM ascorbate. Cleavage reactions were carried out in Tris-HCl (20 mM; pH 7.5) and contain *ca.* 10 nM RNA. Captions on the right indicate G-specific cleavage by RNase T1 in lanes 4 and 5. Standard procedures for ^{32}P-labeling of R23 RNA, alkaline and RNase T1 digestion, and SDS-PAGE experiments were used (ref. 18).

that the former is more efficient in promoting oxidative damage. The products generated from ascorbate induced cleavage with **1** [Fig. 2(*b*), lane 7] were more numerous (most likely indicative of limited hydroxyl radical migration away from the copper ion), and offset relative to bands generated by backbone hydrolysis, consistent with a distinct oxidative cleavage pathway.‡ Again, control experiments show no background cleavage in the absence of **1** but in the presence of aqueous Cu^{2+} and ascorbate [Fig. 2(*b*), lane 6]. Recently we have demonstrated that **1** mediates oxidative cleavage of DNA through reactive copper-oxo or copper-hydroxo species.[14] Similarly, here we have used a spectrophotometric assay to identify formation of hydroxyl radical by use of rhodamine B.[14] The change in the λ_{552} absorbance from rhodamine was monitored in the presence of **1** (or reducing agents) alone, and with added ascorbate or H_2O_2. While **1** (or reducing agents) alone did not result in degradation of the dye, a combination of **1** with ascorbate or H_2O_2 led to a rapid decrease in λ_{552}, demonstrating that **1** is capable of producing reactive oxygen species only in the presence of reducing agents. These reactive oxygen species are capable of mediating oxidative damage to nucleic acids,[14] however, such hydroxyl radicals could not be trapped by rhodamine in the presence of a nucleic acid substrate. This indicates that the radicals formed are localized on or close to the copper ion, and are non-diffusible. Thus, the products from reaction of **1** with R23 RNA in the presence of H_2O_2 or ascorbic acid are indicative of an oxidative mechanism, mediated by a copper redox couple, with the concomitant release of hydroxyl radicals.

A primary reason for cleavage efficiency at low complex concentration arises from the high binding affinity for an R23 target site.[3,15,16] No cleavage products were observed after treating R23 with comparable concentrations of either aqueous Cu^{2+} or metal-free aminoglycoside alone (Fig. 2). To determine if cleavage by **1** was selective toward this particular structured RNA (R23), we examined the cleavage efficiency of linear oligo($A_{12\text{-}18}$) and poly(C), and double-strand poly(A).poly(U), each of which binds aminoglycosides weakly. No cleavage was detected by an FPLC assay, supporting the notion that tight binding of **1** to a target RNA is required for cleavage. Similar cleavage efficiencies for plasmid DNA were observed only at much higher complex concentrations (0.1 to 0.5 μM) as a result of the significantly lower binding affinity relative to a cognate structured RNA motif.[14] Artificial ribonucleases based on oligonucleotide-appended metal-based Lewis acidic functional groups represent an antisense approach for effective RNA cleavage.[12] Recognition of structured RNA targets[17] over linear RNA and DNA sequences by aminoglycoside antibiotics, coupled with the site-directed degradative capacity of their copper complexes, may render metalloaminoglycosides as novel and attractive therapeutic agents for the treatment of viral disease, and provide an alternative to the antisense approach. Experiments to test the antiviral activity of such complexes are in progress.

Supported in part by the National Science Foundation (CHE-9706904). J. A. C. is a Camille Dreyfus Teacher-Scholar (1994–1999). A. S. thanks OSU for the award of a University Postdoctoral Fellowship (1997–1998). We thank D. R. Schoenberg and K. Cunningham (Department of Pharmacology, OSU), and M. Foster (Department of Chemistry, OSU) for experimental advice and assistance with gel electrophoresis.

Notes and references

† Also consistent with efficient cleavage, under both oxidative and hydrolytic conditions, is the rapid increase in absorbance in UV–VIS spectra resulting from loss of hypochromism from interacting base pairs.
‡ Strand cleavage by a hydrolytic mechanism that is mediated through a 2′-OH leads to formation of 5′-OH and a terminal phosphate at the cleavage site. Cleavage by an oxidative path can lead to destruction of the ribose ring and base release, resulting in band positions that are offset from hydrolytic controls, as observed in Fig. 2(*b*) (lane 7).

1 T. Hermann, and E. Westhof, *Curr. Opin. Biotechnol.*, 1998, **9**, 66; K. Michael and Y. Tor, *Chem. Eur. J.*, 1998, **4**, 2091.
2 N. D. Pearson and C. D. Prescott, *Chem. Biol.*, 1997, **4**, 409.
3 P. Purohit and S. Stern, *Nature*, 1994, **370**, 659.
4 D. Moazed and H. F. Noller, *Nature*, 1987, **327**, 389.
5 M. L. Zapp, S. Stern and M. R. Green, *Cell*, 1993, **74**, 969.
6 T. K. Stage, K. J. Hertel and O. C. Uhlenbeck, *RNA*, 1995, **1**, 95.
7 U. Von Ahsen, J. Davies and R. Schroeder, *J. Mol. Biol.*, 1992, **226**, 935.
8 H.-Y Mei, A. A. Galan, N. S. Halim, D. P. Mack, D. W. Moreland, K. B. Sanders, H. N. Truong and A. W. Czarnik, *Bioorg. Med. Chem. Lett.*, 1995, **5**, 2755.
9 D. Fourmy, M. I. Recht, S. C. Blanchard and J. D. Puglisi, *Science*, 1996, **274**, 1367; M. I. Recht, D. Fourmy, S. C. Blanchard, K. D. Dahlquist and J. D. Puglisi, *J. Mol. Biol.*, 1996, **262**, 421.
10 (*a*) B. N. Trawick, A. T. Daniher and J. K. Bashkin, *Chem Rev.*, 1998, **98**, 939 and references cited therein; (*b*) J. K. Bashkin, E. I. Frovola and U. Sampath, *J. Am. Chem. Soc.*, 1994, **116**, 5981.
11 E. L. Hegg, K. A. Deal, L. L. Kiessling and J. N. Burstyn, *Inorg. Chem.*, 1997, **36**, 1715.
12 D. Magda, M. Wright, S. Crofts, A. Lin and J. Sessler, *J. Am. Chem. Soc.*, 1997, **119**, 6947; R. Haener, J. Hall, A. Pfuetzer and D. Huesken, *Pure Appl. Chem.*, 1998, **70**, 111; H. Inoue, T. Furukawa, M. Shimuzu, T. Tamura, M. Matsui and E. Ohtsuka, *Chem. Commun.*, 1999, 45.
13 S. Hanessian and G. Patil, *Tetrahedron Lett.*, 1978, 1031 and 1035.
14 A. Sreedhara and J. A. Cowan, *Chem. Commun.*, 1998, 1737.
15 M. G. Wallis, U. von Ahsen, R. Schroeder, and M. Famulok, *Chem. Biol.*, 1995, **2**, 543.
16 J. A. Cowan, D. Wang, K. Natarajan and T. Ohyama, manuscript submitted.
17 C. S. Chow and F. M. Bogdan, *Chem. Rev.*, 1997, **97**, 1489.
18 J. F. Milligan and O. C. Uhlenbeck, *Methods Enzymol.*, 1989, **180**, 51.

Communication 9/01140D

Long-lived charge separation in a donor–acceptor dyad adsorbed in mesoporous MCM-41

Vinoda Kuchi, Anna M. Oliver, Michael N. Paddon-Row* and Russell F. Howe*

School of Chemistry, University of New South Wales, Sydney, 2052, Australia. E-mail: r.howe@unsw.edu.au

Received (in Cambridge, UK) 19th March 1999, Accepted 14th May 1999

Irradiation of a rigid donor–{6-bond-bridge}–acceptor dyad [donor = dimethoxynaphthalene (DMN); acceptor = dicyanovinyl (DCV)] occluded within the pores of mesoporous MCM-41 containing aluminium leads to the formation of the DCV radical anion of the dyad with a lifetime of days.

Photoinduced charge separation in covalently linked dyads such as **1** occurs extremely rapidly, a result of strong electronic coupling mediated by a through-bond (TB) mechanism.[1] However the lifetimes of the resulting charge-separated (CS) states are short (nanosecond scale[2]), which is also a consequence of strong TB electronic coupling. We now report that photolysis of **1**,[1b] which has been occluded within the pores of mesoporous MCM-41, leads to a charge separation in which the host material participates, the final state of which has a lifetime measured in days.

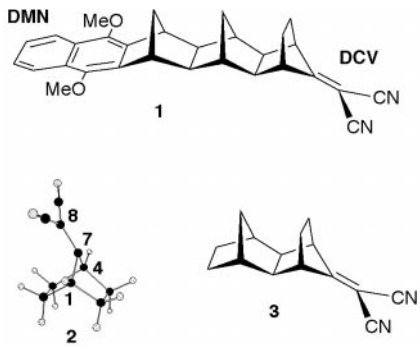

The ability of microporous zeolite hosts to stabilize organic radical cations and anions is well documented.[3] Mallouk *et al.* showed that the rates of charge recombination in a series of Ru^{II}–viologen dyads adsorbed at the external surface of several microporous zeolites were slowed by a factor of 10^5 relative to the same molecules in solution.[4] This dramatic stabilization of the charge-separated state in a molecule only partly occluded within a porous solid prompted us to begin a study of dyads totally occluded within the pores of the larger pore size (mesoporous) zeolite analog, MCM-41. The test dyad selected was **1**, which comprises a dimethoxynaphthalene (DMN) donor coupled to a dicyanovinyl (DCV) acceptor covalently linked to a rigid σ-bonded hydrocarbon bridge.

MCM-41 is a mesoporous silica containing a regular array of uniform linear one-dimensional pores with an approximately hexagonal cross section and a diameter determined by the particular surfactant molecule used in the synthesis.[5,6] Although the original preparations of MCM-41 were pure silica materials, it is also possible to incorporate aluminium into the synthesis to form mesoporous aluminosilicate zeolite analogs (hereafter designated AlMCM-41) with pores large enough to easily accommodate molecules such as **1**.[7] The pore volume of AlMCM-41 (0.22 $cm^3\ g^{-1}$) is sufficient to occlude up to 50 wt% of **1**. FTIR and ^{13}C NMR measurements on samples of AlMCM-41 (Si:Al = 15) loaded up to this level by impregnating the dehydrated AlMCM-41 with a CH_2Cl_2 solution of **1** under nitrogen showed that the molecule was adsorbed intact into the pores of the AlMCM-41.† Irradiation of loaded samples *in vacuo* at wavelengths where the DMN chromophore absorbs (below 310 nm) gave the EPR signal shown in Fig. 1(*a*). This signal grew in intensity with irradiation time for several hours, and was stable in the dark *in vacuo* for at least one day. The first derivative spectrum shows evidence of poorly resolved hyperfine splitting‡ which was enhanced by recording the second harmonic spectrum [Fig. 1(*b*)]; this shows clearly five hyperfine components. The second harmonic spectrum could be approximately simulated by assuming an isotropic hyperfine coupling with two equivalent ^{14}N nuclei and a coupling constant of 1.8 Gauss [Fig. 1(*c*)]. The actual hyperfine coupling in the observed spectra is clearly not completely isotropic; nevertheless the spectrum appears to be that expected for the DCV radical anion moiety in **1**. This identification was supported by B3LYP[8] DFT calculations of the isotropic hyperfine coupling constant for the model dicyanovinylnorbornane radical anion **2**.§ The calculated coupling constants are 1.76 and 1.34 Gauss using the 3-21G and 631G basis sets, respectively.

No EPR signal was observed when the corresponding experiment was carried out in MCM-41 containing no aluminium, *i.e.* the photoinduced formation of the radical anion of **1** appears to require the presence of aluminium on the MCM-41 framework. Conventional aluminosilicate zeolites are known to contain electron donor sites capable of transferring an electron to strong acceptors such as tetracyanoethylene.[9] Adsorption of TCNE from CH_2Cl_2 solution into dehyrated MCM-41 gave the

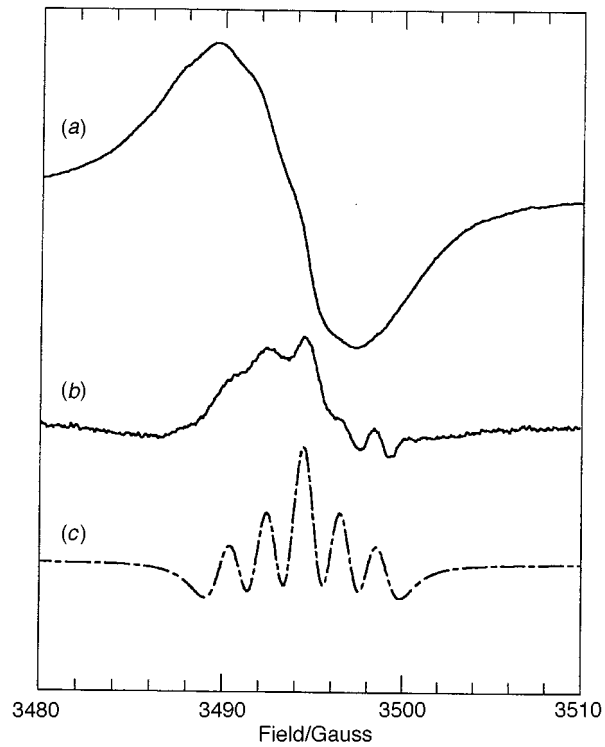

Fig. 1 (*a*) EPR spectrum of **1** in AlMCM-41 following irradiation *in vacuo* at room temperature; (*b*) second harmonic EPR spectrum; (*c*) computer simulation of (*b*) assuming isotropic hyperfine coupling to two equivalent ^{14}N nuclei of 1.8 Gauss.

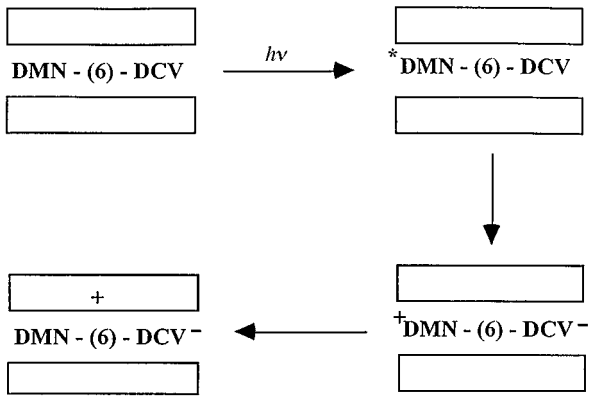

Fig. 2 Schematic of the proposed mechanism for the formation of the long-lived radical anion of **1**.

EPR spectrum of the radical anion only when the MCM-41 contained aluminium, and not with the all-silica form, confirming the role of aluminium in the framework in generating electron donor sites.

It is unlikely that the radical anion of **1** is formed in AlMCM-41 by direct electron transfer from the host, since the reduction potential of the DCV group is 1.5 V more negative than that of TCNE,[10] and the EPR signal was not observed without irradiation. This was confirmed by adsorbing the molecule **3** which contains no electron donor group into AlMCM-41; this gave no EPR signal in the dark or upon irradiation.

Our proposed explanation for the observed photoformation of the stable radical anion of **1** when it is adsorbed in AlMCM-41 (but not MCM-41 containing no aluminium) is shown schematically in Fig. 2: photoinduced intramolecular charge separation is followed immediately by hole transfer from the DMN cation radical to the MCM-41, leaving a stable DCV radical anion.

The ability of the host to stabilize the radical anion in this way clearly depends critically on the relative rates of charge recombination within the charge-separated state of the dyad and hole transfer to the host. We plan flash photolysis experiments to quantify these rates and to determine quantum yields, as has been done in solution[1] and for zeolite adsorbed species.[4] Better characterization of the electron donor (hole acceptor) sites in the AlMCM-41 host is also necessary. The many variations possible in this system (varying the Al content of the host, the pore size, the length of the hydrocarbon spacer and the redox properties of the dyad) provide intriguing opportunities to understand more fully and control electron transfer processes in heterogeneous systems.

An exciting aspect of our preliminary findings is that they offer the possibility of transducing photonic energy into truly long-lived energetic species possessing useful chemical potential. Furthermore, the generation of long-lived charge separation in mesoporous materials need not be restricted to rigid multichromophoric systems, but should occur with non-rigid systems as well. This is a very important conjecture, from the viewpoint of synthetic facility, and its validity will be tested.

We thank the Australian Research Council for support and Mr Paul Harvey for assistance and advice on the NMR studies.

Notes and references

† The adsorbed molecule gave FTIR and ^{13}C NMR spectra closely similar to those of the parent compound. Primary evidence for adsorption within the pores of MCM-41 came from observation of FTIR spectra: the ν(OH) band due to silanol groups within the pores of MCM-41 was broadened and shifted to lower frequency, indicating a weak hydrogen bonding interaction with **1**.

‡ No improvement in resolution was achieved by recording the spectrum at 77 K.

§ Geometry optimization of **2** was carried out under C_s symmetry constraint using the UB3LYP theoretical model and the 3-21G and 6-31G(d) basis sets. The UB3LYP/6-31G(d) and UB3LYP/3-21G optimized structures are nearly identical.

1 (*a*) M. N.Paddon–Row, *Acc. Chem. Res.*, 1994, **27**, 18; (*b*) H. Oevering, M. N. Paddon–Row, H. Heppener, A. M. Oliver, E. Cotsaris, J. W. Verhoeven and N. S. Hush. *J. Am. Chem. Soc.*, 1987, **109**, 3258.
2 M. N.Paddon–Row, A. M. Oliver, J. M.Warman, K. J. Smit, M. P. deHaas, H. Oevering and J. W.Verhoeven, *J. Phys. Chem.*, 1988, **92**, 6958.
3 K. B. Yoon, *Chem. Rev.*, 1993, **93**, 321; K. B.Yoon and J. K. Kochi, *J. Am. Chem. Soc.* 1996, **118**, 12 710; L. Brancaleon, D. Brousmiche, V. J. Rao, L. J. Johnston and V. J. Ramamurthy, *J. Am. Chem. Soc.*, 1998, **120**, 4926.
4 E. S. Brigham, P. T. Snowden, Y. I. Kim and T. E. Mallouk, *J. Phys. Chem.*, 1993, **97**, 8650; E. H. Yonemoto, Y. I. Kim, R. H. Schmehl, J. O. Wallin, B. A. Shoulders, B. R. Richardson, J. F. Haw and T. E. Mallouk, *J. Am. Chem. Soc.*, 1994, **116**, 10 557.
5 J. S. Beck, J. C.Vartuli, W. J. Roth, M. E. Leonwicz, C. T. Kresge, K. D. Schmitt, C. T. Chu, D. H. Olson, E. W.Sheppard, S. B. McCullen, J. B. Higgins and J. L. Schlenker, *J. Am. Chem. Soc.*, 1992, **114**, 10 834.
6 X. S. Zhao, G. Q. Lu and G. J. Millar, *Ind. Eng. Chem. Res.*, 1995, **35**, 2075.
7 J. M. Kim, J. H. Kwak, S. Jun and R. Ryoo, *J. Phys. Chem.*, 1995, **99**, 16 742.
8 A. D. Becke, *J. Chem. Phys.*, 1993, **98**, 5648; C. Lee, W. Yang and R. G. Parr, *Phys. Rev. B*, 1988, **37**, 785; Gaussian 94, Gaussian Inc, Pittsbugh, PA,1995.
9 B. D. Flockhart, L. McLoughlin and R. C. Pink, *J. Catal.*, 1972, **25**, 305.
10 S. L.Murov, I. Carmichael and G. L. Hug, *Handbook of Photochemistry*, 2nd edn., Marcel Dekker, NY, 1993.

Communication 9/02187F

Highly stereocontrolled access to a tetrahydroxy long chain base using *anti*-selective additions

Makoto Shimizu,* Manabu Kawamoto and Yasuki Niwa

Department of Chemistry for Materials, Mie University, Tsu, Mie 514-8507, Japan.
E-mail: mshimizu@chem.mie-u.ac.jp

Received (in Cambridge, UK) 25th March 1999, Accepted 12th May 1999

Complete diastereostereoselection was attained for the addition of acetylide and benzyloxymethyl anions to a chiral aldehyde and an imine derived from *meso*-tartaric acid, leading to a facile synthesis of (2*S*,3*S*,4*R*,5*R*,6*Z*)-2-amino-1,3,4,5-tetrahydroxyoctadecene as its pentaacetyl derivative in enantiomerically pure form.

Increasing interest in the field of cerebrosides prompted us to investigate an easy access to this class of compounds in a highly stereocontrolled fashion.[1] In conjunction with the amino polyols which recently have attracted the interest of chemists, several 2-amino-1,3,4,5-tetrahydroxyoctadecene derivatives have been found in bovine spinal cords and human brains as well as in green and red algae.[2] Among them, (2*S*,3*S*,4*R*,5*R*,6*Z*)-2-amino-1,3,4,5-tetrahydroxyoctadecene **1**, the long-chain base

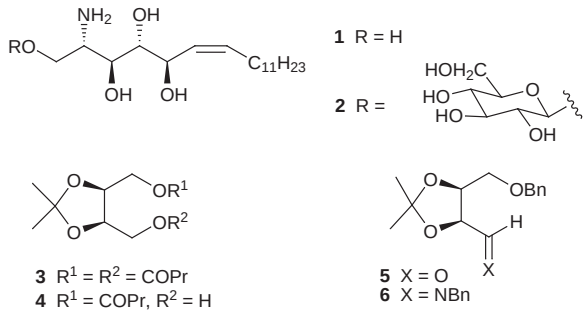

(LCB) part of a new cerebroside **2**, was isolated from the latex of *Eupohorbia characias L* and its structure has been elucidated.[3] The biological importance of such cerebrosides, especially the imparted bioactivities, makes this compound a useful target for synthesis. To the best of our knowledge, however, only two approaches to tetrahydroxy-LCB **1** have been reported; one starting from D-mannose[4a] and the other from D-glutamic acid.[4b] There still appear to be important problems of stereocontrol,[5] and we focused on the topic of stereocontrol in the addition of nucleophiles to chiral aldehydes and imines to find a solution to these problems. We have recently reported that complete *anti*-stereocontrol has been attained in an addition of nucleophiles to the chiral aldehyde derived from L-serine, leading to a short synthesis of (2*S*,3*S*,4*R*)-phytosphingosine,[6] while *syn*-selective addition of nucleophiles has also been successfully used for the synthesis of deoxybiotin.[7] In these studies, a non-chelation- or chelation-type transition state was thought to be crucial for such complete *anti*- or *syn*-stereoselection, respectively.[5–7] For the synthesis of tetrahydroxy-LCB **1**, the *anti*-stereocontrolled construction of the contiguous asymmetric carbons is likely to be difficult, as can be seen from its structure. Here we describe a new stereocontrolled approach to tetrahydroxy-LCB **1** using a tandem *anti*-selective addition of nucleophiles to the chiral aldehyde **5** and the imine **6** derived from *meso*-tartaric acid.

The chiral aldehyde **5**[8] was prepared in good overall yield in enantiomerically pure form starting from *meso*-tartaric acid using lipase-mediated desymmetrization as a crucial step. *meso*-Tartaric acid was converted into dibutyrate **3** *via* diethyl ester formation (cat. TsOH, EtOH) and acetonization (cat. TsOH, 2,2-dimethoxypropane, benzene, 94% yield for two steps) followed by reduction ($LiAlH_4$, THF, 84%) and bis-acylation (*n*-butyryl chloride, Et_3N, CH_2Cl_2, 75%). The dibutyrate **3** was treated with Lipase Amano PS in phosphate buffer–acetone at room temperature for 5 h to give the mono-ester **4** in 93% yield with > 99% ee.[9] The protection of the hydroxy functionality with an ethoxyethyl group (cat. PPTS, ethyl vinyl ether, CH_2Cl_2) was followed by hydrolysis of the ester moiety (K_2CO_3, MeOH). The benzyl etherification of the resulting ethoxyethyl ether (KHMDS, BnBr, THF) and hydrolysis of the ethoxyethyl group (cat. PPTS, PrOH) gave the alcohol, which was oxidized using the Swern oxidation to give the aldehyde **5** in enantiomerically pure form in 66% overall yield from the mono-ester **4**.†

As shown in Table 1, the *anti*-selective addition of acetylide to aldehyde **5** was conducted with triisopropoxytitanium acetylide **7** as described earlier[7,10] to give the desired adduct *anti*-**8** in 98% yield as single diastereomer (entry 1),‡ whereas modest *syn*-selectivity was observed with halomagnesium, lithium, or dichlorocerium acetylide (entries 2–5).

The *anti*-propargyl alcohol *anti*-**8** was then transformed into the imine **13** possessing the functionalities necessary for the synthesis of tetrahydroxy-LCB **1** *via* the following sequences: protection of the hydroxy group with TBDMS (TBDMSCl, imidazole, DMF, **9**: 95%); partial reduction of the triple bond

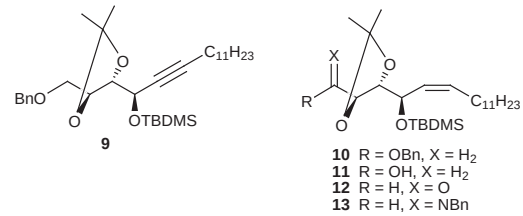

under the Lindlar conditions [H_2, Pd/$BaSO_4$, quinoline, MeOH, **10**: 99%, ($Z : E$ = > 99 : < 1)]; removal of the benzyl protecting group (Ca, liq. NH_3, **11**, 86%); Swern oxidation of the hydroxy group (oxalyl chloride, DMSO, Et_3N, CH_2Cl_2, **12**: 93%); benzylimination ($BnNH_2$, Et_2O, **13**: 100%).

Table 1 Addition of dodecylacetylide to aldehyde **5**

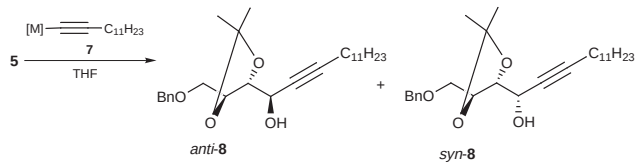

Entry	[M]	*T*/°C	Yield (%)[a]	*anti* : *syn*[b]
1	$Ti(OPr^i)_3$	−78–0	98	> 99 : < 1
2	MgBr	−78–0	43	40 : 60
3	MgCl	−50–0	66	24 : 76
4	Li	−78–0	43	27 : 73
5	$CeCl_2$	−78–rt	48	23 : 77

[a] Isolated yields. [b] Determined by ^1H and ^{13}C NMR analyses.

Table 2 Addition of nucleophiles to imine **6**

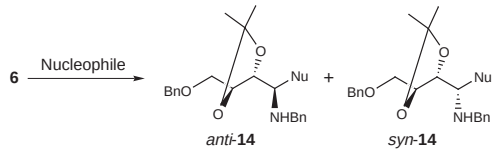

anti-**14** *syn*-**14**

Entry	Nucleophile	Solvent	*T*/°C	Additive (equiv)	Yield (%)[a]	*anti*:*syn*[b]
1	Li-dithianide	THF	−50–rt	none	33	< 1 : > 99
2	Li-dithianide	THF	−50–0	BF_3•Et_2O (4.0)	78	> 99 : < 1
3	LiC≡CTMS	THF	−78–rt	none	17	< 1 : > 99
4	LiC≡CTMS	THF	−78–0	BF_3•Et_2O (4.0)	55	> 99 : < 1
5	2-FurylLi	THF	−78–rt	none	16	< 1 : > 99
6	2-FurylLi	THF	−78–rt	BF_3•Et_2O (4.0)	34	> 99 : < 1
7	TMSCN	CH_2Cl_2	−78–rt	BF_3•Et_2O (4.0)	48	88 : 12
8	$LiCH_2OBn$[c]	THF	−78–0	BF_3•Et_2O (4.0)	78	> 99 : < 1

[a] Isolated yields. [b] Determined by HPLC analysis (Merck Hibar Column). [c] Preparation of this anion, see ref. 12.

For the introduction of a hydroxymethyl moiety into the imine **13**, three types of nucleophiles were investigated for the addition reaction in terms of diastereoselectivity, in which the imine **6** was used as a model substrate, and Table 2 summarizes the results.

As shown in Table 2, lithium dithianide in THF added to the imine **6** to give *syn*-**14** (Nu = 1,3-dithiane) as the sole product, whereas reversal of the diastereoselectivity was observed in the same reaction conducted in the presence of an excess BF_3•Et_2O, giving *anti*-**14** stereospecifically (entries 1 and 2).[7] Similar trends of reversal of the diastereoselectivity were observed in the cases with the lithium acetylide and 2-furyllithium (entries 3–6). TMSCN in the presence of BF_3•Et_2O[11] also effected the predominant formation of the *anti*-adduct *anti*-**14** (Nu = CN) (entry 7). For the preparation of tetrahydroxy-LCB, the use of a hydroxymethyl anion equivalent was more preferable in terms of functional group manipulation and, therefore, benzyloxymethyllithium[12] was used for the addition in the presence of BF_3•Et_2O to give *anti*-**14** (Nu = $BnOCH_2$) as the sole product in good yield (entry 8). This high selectivity is most probably explained in terms of non-chelation (for *anti*-adduct) and chelation transition states (for *syn*-adduct).

Thus, addition of benzyloxymethyllithium to the imine **13** was conducted as in the case with **6** in the presence of BF_3•Et_2O to give, as expected, the desired *anti*-adduct **15** exclusively in

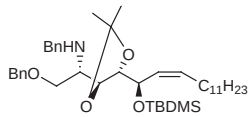

15

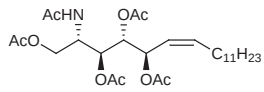

16

32% yield.§ Deprotection of the benzyl group was carried out with Na-NH_3, and subsequent hydrolysis with TFA followed by acetylation gave the pentaacetyl derivative **16** of tetrahydroxy-LCB **1** in 11% overall yield from **15**.¶

In conclusion, the present synthesis using a tandem *anti*-addition reaction to the chiral aldehyde and the imine realizes a rapid access to biologically important molecules in a highly stereocontrolled fashion. Since the level of the diastereoselectivity attained on the addition of nucleophiles to α-hydroxy aldehyde and imine was extremely high, this procedure may be applied to the syntheses of a variety of amino polyols of biological importance in a stereocontrolled manner.

Notes and references

† The enantiomeric purity was determined by HPLC using a chiral stationary column (Daicel OJ).

‡ To a solution of tridecyne (1.63 g, 647 mmol) in 70 ml of THF was added BuLi (1.68 M in n-hexane, 4.62 ml, 7.76 mmol) at −78 °C, and the mixture was stirred at −78 °C for 30 min. A solution of $ClTi(OPr^i)_3$ (1.0 M in n-hexane, 7.8 ml, 7.76 mmol) was added to the mixture at −78 °C and it was allowed to stand at −60 °C for 1 h. A solution of **5** (647 mg, 2.58 mmol) in THF (35 ml) was added to the resulting mixture at −78 °C, and the mixture was stirred at that temperature for 2 h. After usual work-up, the crude oil was purified by flash silica gel chromatography to give the propargyl alcohol *anti*-**8** (1.09 g, 98%) as a colorless oil.

§ To a solution of $SnCl_2$ (214 mg, 1.15 mmol) in THF (2 ml) was added a solution of LiBr (100 mg, 1.15 mmol) in THF (2 ml) and the mixture was stirred at room temperature for 30 min. A solution of $BnOCH_2Cl$ (180 mg, 1.15 mmol) in THF (2 ml) was added to the resulting mixture, to which was added BuLi (1.68 M in n-hexane, 2.74 ml, 4.61 mmol) at −78 °C, and stirred for 1 h at that temperature. BF_3•Et_2O (164 mg, 1.152 mmol) was added to the mixture and after 10 min a solution of **13** prepared *in situ* from **12** (131 mg, 0.288 mmol) and $BnNH_2$ (32.4 mg, 0.302 mmol) in THF (2 ml) was added at −78 °C, and the whole mixture was gradually warmed to 0 °C. After usual work-up, the crude oil was purified on preoperative TLC to give **15** (60.7 mg, 32%) as a colorless oil.

¶ The spectral properties are identical with the reported data (ref. 4).

1 Y. Hannun and R. M. Bell, *Science*, 1989, **243**; C. Djerassi and W. K. Lam, *Acc. Chem. Res*., 1991, **24**, 69; A. Olivera and S. Spiegel, *Nature*, 1993, **365**, 557.

2 H. S. Garg, M. Sharma, D. S. Bhakuni, B. N. Paramanik and A. K. Bose, *Tetrahedron Lett*., 1992, **33**, 1641; C. B. Rao and C. Satyanarayana, *Indian J. Chem., Sect. B*, 1994, **33B**, 97.

3 G. Falsone, F. Cateni, F. Katusian, H. Wagner, O. Seligmann, G. Pellizer and F. Asaro, *Z. Naturforsch, Teil B: Chem. Sci*., 1993, **48**, 1121; G. Falsone, F. Cateni, G. Visintin, V. Lucchini, H. Wagner and O. Seligmann, *Farmaco*, 1994, **49**, 167.

4 (*a*) Y.-L. Li and Y.-L. Wu, *Tetrahedron Lett*., 1995, **36**, 3875; (*b*) H. Yoda, T. Oguchi and K. Takabe, *Tetrahedron: Asymmetry*, 1996, **7**, 2113.

5 For reviews, see, J. Jurczak and A. Golebiowski, *Chem. Rev*., 1989, **89**, 149; *Comprehensive Organic Synthesis*, ed. B. M. Trost and I. Fleming, Pergamon, Oxford, 1991, vol. 1 and references cited therein; A. Dondoni and D. Perrone, *Aldrichim. Acta*, 1997, **30**, 35.

6 M. Shimizu, I. Wakioka and T. Fujisawa, *Tetrahedron Lett*., 1997, **38**, 6027.

7 T. Fujisawa, M. Nagai, Y. Koike and M. Shimizu, *J. Org. Chem*., 1994, **59**, 5865.

8 A. Dondoni and P. Merino, *Synthesis*, 1992, 196; P. Munier, A. Krusinski, D. Picq and D. Anker, *Tetrahedron*, 1995, **51**, 1229.

9 For lipase-mediated kinetic resolution of this kind of diol, see, M. Pottie, V. der Eycken and M. Vandewalle, *Tetrahedron: Asymmetry*, 1991, **2**, 329; H. J. Bestmann and L. Bauriegel, *Tetrahedron Lett*., 1995, **36**, 853.

10 F. Tabusa, T. Yamada, K. Suzuki and T. Mukaiyama, *Chem. Lett*., 1984, 405.

11 D. A. Evans, G. L. Carroll and L. K. Truesdale, *J. Org. Chem*., 1974, **39**, 914 and references cited therein.

12 E. J. Corey and T. M. Eckrich, *Tetrahedron Lett*., 1983, **24**, 3163; W. C. Still, *J. Am. Chem. Soc*., 1978, **100**, 1481.

Communication 9/02386K

Typeset and printed by Black Bear Press Limited, Cambridge, England

Confinement and recognition of icosahedral main group cage molecules: fullerene C_{60} and *o*-, *m*-, *p*-dicarbadodecaborane(12)

Michaele J. Hardie and Colin L. Raston*

Department of Chemistry, Monash University, Clayton, Melbourne, Victoria 3168, Australia.
E-mail: c.raston@sci.monash.edu.au

Received (in Cambridge, UK) 29th January 1999, Accepted 1st March 1999

Supramolecular chemistry of icosahedral main group cage molecules, fullerene C_{60} and the carboranes *o*-, *m*- , *p*-$B_2C_{10}H_{12}$, is of interest in the purification of these molecules and in building up novel materials. The non-polarised, spherical like nature of C_{60} requires specific shape and electronic complementarity between the interacting supramolecular synthons which leads to polarisation of the fullerene, whereas for the carboranes, hydrogen bonding involving the C–H groups, including the formation of bifurcated hydrogen bonds [C–H···(N,O)$_2$], and C–H···π interactions, along with shape complementarity, facilitate the self assembly process. Insight into future prospects in this field is presented.

Background

Highly symmetrical icosahedral molecules have captured the imagination of the chemical sciences community and beyond. This is particularly the case since 1985 with the discovery of a new allotropic form of carbon now known as the family of electron deficient fullerenes for which C_{60} is the most abundant and widely studied, having a truncated icosahedral structure.[1] A plethora of organic chemistry of C_{60} resulted in the 1990s which pertains to addition reactions across the 6,6′ position ring junction of two six membered rings, in accordance with the double bonds avoiding the five membered rings of the polyhedron.[2] Exohedral metal complexes of C_{60}, the metal to fullerene binding usually associated with the same 6,6′ positions of the fullerene, are also known,[3] as are endohedral species,[4] and the electrochemical behaviour of C_{60} is remarkable showing reversible reduction to C_{60}^{6-}.[5] Then there is the supramolecular chemistry of C_{60},[6] which is a focus of this article, with advances coming mainly from our research group, and those of Atwood, Fuji, Fukazawa, Matsubara, Shinkai, Verhoeven, and Wennerstrom.

Another focus of this article is the supramolecular chemistry of the related icosahedral main group cage molecules, the carboranes, 1,2-, 1,7-, 1,12-dicarbadodecaborane(12), *viz* *o*-, *m*-, *p*-$C_2B_{10}H_{12}$ (hereafter abbreviated *o*-, *m*-, and *p*-carborane). These carboranes have a rich organometallic chemistry (direct metal–carbon bonds),[7] and a rich organic chemistry associated with replacing one or more hydrogen atoms of the C–H groups as well as the boron atoms.[8] The supramolecular chemistry of the carboranes is even less developed than that of C_{60}. This is surprising given the nexus between these cages, and that unlike C_{60}, the carboranes have been known for several decades.[9] Fullerene C_{60} and the carboranes are all remarkably thermally stable, icosahedral cages with not too dissimilar diameters of 10.0 and ≈8 Å respectively.

In embracing the principles of supramolecular chemistry for C_{60} and the carboranes, the goal is to encourage the association of two or more components (a molecular cage and a second or more supramolecular synthon) in an organised array using weak intermolecular forces, namely van der Waals, hydrogen bonding, electrostatic and labile coordination interactions.[10] Such interactions are inherently weak and some can be comparable to crystal packing and other competing forces. Gaining control over these interactions is a major challenge and underpins much of the basic aims and ideals of supramolecular chemistry.[10] Complementarity of shape of the interacting synthons is important, as is taking advantage of the electron deficient nature of C_{60} and the acidic nature of the C–H groups of the carboranes[9] in optimising interactions between the two different synthons, in effectively negating competing solvent–cage, cage–cage, and host–host interactions.

The overall chemistry of the higher fullerenes is less developed than that of C_{60} with the supramolecular chemistry limited to a few reports, and for completeness, and that given one of the host–guest complexes of C_{70} is isomorphous with that of the C_{60} analogue,[11] the supramolecular chemistry of C_{70} is also included herein.

Fullerene C_{60} (and C_{70})

Fullerene C_{60} (and C_{70}) form supramolecular complexes with a variety of hydrophobic host systems including calixarenes, **1**,[5,11–28] oxacalix[3]arenes, **2**,[20,21,29] and related resorcina[4]-arenes, **3**,[30] and cyclotriveratrylene, **4,** R = Me (=

Professor C. L. Raston FRACI is an ARC Senior Research Fellow (1998) and recipient of an ARC Special Investigator Award (1998), Department of Chemistry, Monash University. He completed a Ph.D. under the guidance of Professor Allan White, and after postdoctoral studies with Professor Michael Lappert at the University of Sussex, he was appointed Lecturer at the University of Western Australia (1981) then to the Chair of Chemistry, Griffith University (1988) being awarded a D.Sc. there in 1993, and in 1995 moved to Monash University. Professor Raston received the RACI Burrows Award in 1994, and the H. G. Smith Award in 1996. Research interests cover aspects of main group, supramolecular and green chemistry, and he has published over 360 papers. In 1996 he chaired the 17th International Conference on Organometallic Chemistry, and in 1997 was President of the RACI.

Dr M. J. Hardie is a Postdoctoral Research Fellow at Department of Chemistry, Monash University. She completed a Ph.D. at the University of Melbourne (1996) under the guidance of Assoc. Prof. Richard Robson and Dr Bernard Hoskins, and joined Prof. Raston's research group after postdoctoral studies with Dr Alison Edwards at the University of Melbourne then Prof. A. Alan Pinkerton at the University of Toledo, Ohio (1996). Research interests include supramolecular chemistry and crystallography.

CTV),[5,28,31,32] and related molecules,[33] Ni(II) macrocycles, **5**,[34] as well as complexes with γ-cyclodextrin (included a silica supported system),[35] azacrown ethers,[36] and a porphyrazine.[37] There is also complexation of C_{60} or C_{70} by hydrogen bonded hydroquinones in a super-cube,[38] and with thiafulvalenes.[6,39] We have focused on hydrophobic systems, **1**–**4**, and related saddle shaped Ni(II) macrocycles, **5**,[34] and the work encompasses the incorporation of C_{60} into mesoporous silica.[28]

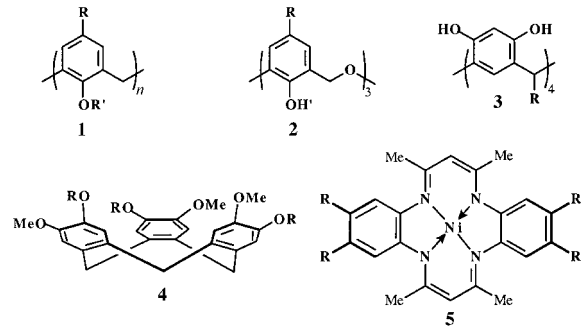

Calix[6,8]arenes

In 1994 we[12] and Shinkai and coworkers[13] reported the use of *p-tert*-calix[8]arene for the retrieval of high purity C_{60} from toluene solutions of fullerite derived from carbon soot, involving the recrystallisation of the precipitate from toluene followed by decomposition of the 1 : 1 complex when added to chlorinated hydrocarbons in which the fullerene is only sparingly soluble, Scheme 1. The resulting C_{60} is > 99.5% pure

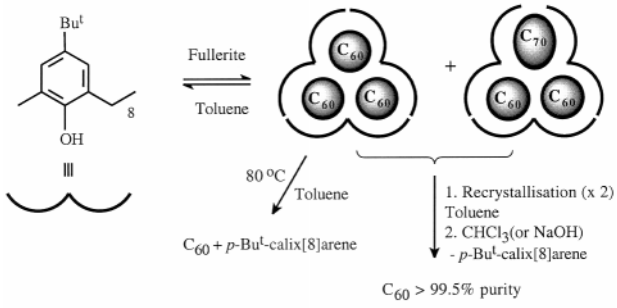

Scheme 1

whereas the initially formed precipitate contains up to 11% C_{70}. An independent study on the solid state ^{13}C NMR spectrum of the 1 : 1 complex between C_{60} and this calixarene has been reported.[18] Since the original foregoing reports, significant advances have been made in understanding the nature of the host–guest complex,[4,5,14] albeit with some conflicting reports, and in building up complex arrays based on other calixarenes, notably calix[5,6]arenes[11,21] and substituted calix[4,5,6,8]arenes,[15,16,19–28] and a resorcinarene.[30] This includes electrochemical studies, both solid state and solution, for C_{60} with calix[4,5,8]arenes and CTV.[5]

The 1 : 1 complex of C_{60} with *p-tert*-butylcalix[8]arene crystallises essentially quantitatively from toluene in the presence of *ca*. 10% excess of the calixarene. Decomposition of the complex by chloroform or dichloromethane possibly relates to the formation of a C–H···π interaction between the chlorinated solvent and aromatic rings of the calixarene taking precedence over the host–fullerene interactions. This type of interaction is found in dichloromethane inclusion complexes of calix[4]arenes.[40] Pure C_{70} does not form a complex with the same calixarene in toluene, but does so in benzene, crystallising as the 2 : 1 complex, $(C_{70})_2$(*p*-calix[8]arene).[15] Interestingly C_{70} also forms a 2 : 1 complex with *p-tert*-butylcalix[6]arene and its precipitation from toluene solutions can be used to retrieve 87% purity C_{70} from C_{60} depleted fullerite.[12]

The *p-tert*-butylcalix[8]arene–C_{60} complex has a resonant inter-fullerene molecular transition at 470 nm,[14] similar to that observed in thin films of C_{60}.[36] Formation of the complex possibly involves a monomeric 1 : 1 transient intermediate, Fig. 1, which distorts the electron cloud of the fullerene[14] resulting in micelle-like formation featuring fullerene–fullerene interactions in the interior core with the fullerenes encapsulated by the host calixarene molecules, Scheme 1. Additional ^{13}C CP MAS NMR data[41] suggest that no well ordered structure of the complex exists and a variety of modifications are possible in the solid state. Nevertheless there is a common underlying ratio of *ca*. 2 : 6[18] for two different types of *tert*-butylphenyl groups. A structure which is consistent with this ratio has each calixarene in the double cone conformation spanning two fullerenes. This double cone conformation of the calixarene would require minimal perturbation of the H-bonded phenol network relative to uncomplexed *p-tert*-butylcalix[8]arene. Determination of the number of fullerenes in the cluster comes from molecular mechanics[14] with the minimised structure for [$(C_{60})_3$(*p-tert*-butylcalix[8]arene)$_3$] shown in Fig. 1. C_{70} is complexed by *p-tert*-butylcalix[8]arene only in the presence of C_{60}, which is consistent with an aggregate of fullerenes with at least one of the C_{60} molecules replaced by C_{70}, the maximum molar incorporation of C_{70} in the complex being 15 ± 1.0%.[14] Comparison of the X-ray powder diffraction pattern of the C_{60} complex with that containing some C_{70}[41] is consistent with some isomorphous replacement of C_{60} by C_{70}. Incorporating more than one molecule of C_{70} per trimer of fullerenes, Scheme 1, may be too disruptive to the tight fullerene/calixarene meshing as suggested by molecular mechanics. Reports on the electrochemistry of the *p-tert*-butylcalix[8]arene complex have the complex breaking apart on reduction (at 400 mV more negative potential).[5] The vibrational spectrum of the complex has also been probed, using

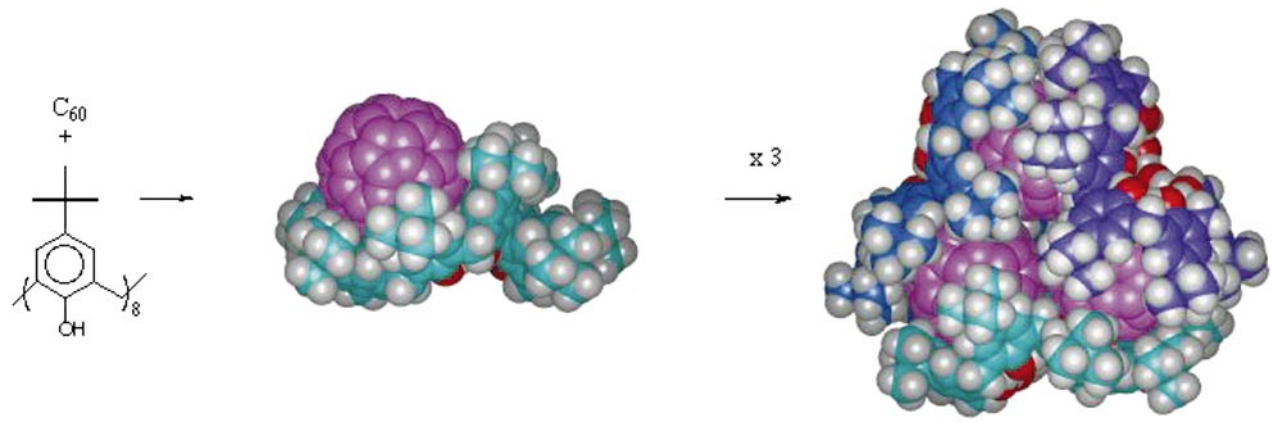

Fig. 1 Formation of the micelle like species [$(C_{60})_3$(*p-tert*-butylcalix[8]arene)$_3$] *via* a monomeric transient 1 : 1 intermediate (C_{60})(*p-tert*-butylcalix[8]-arene).[14]

Raman, IR and neutron scattering,[16] with the results consistent with the C_{60} molecules being almost isolated, suggesting any fullerene–fullerene interactions are weak. Other calix[8]arene complexes have been reported, **1** (n = 8, R = Pr^i or Et).[15]

The fullerene rich calix[6]arene complex, $(C_{60})_2$(calix[6]-arene), has been structurally authenticated[11] and as expected[6] the calixarene is in double cone conformation and associated with two fullerenes, one in each cavity as a perched structure. This arrangement resembles the jaws of a pincer acting on two adjacent spheres, and can be regarded as a building component for the three dimensional structure which has fullerene–fullerene contacts close to 10.0 Å, as well as fullerenes interacting with the aromatic rings *exo*- to the two shallow cavities, Fig. 2. Fullerene C_{70} forms the analogous 2 : 1 complex

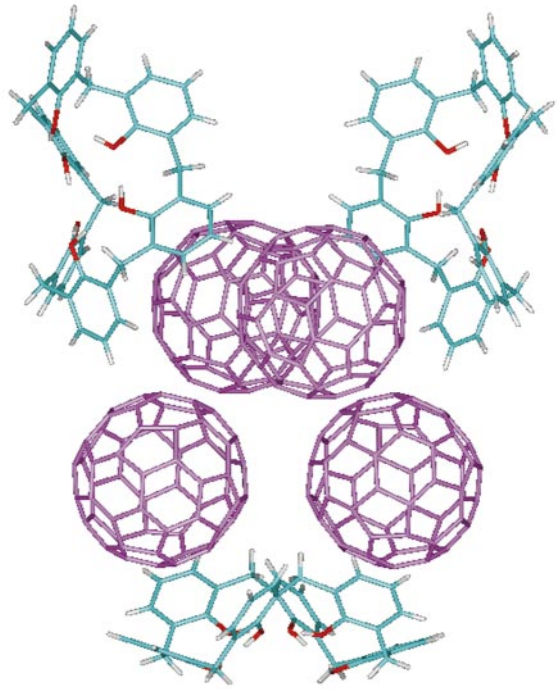

Fig. 2 Extended structure of $(C_{60})_2$(calix[6]arene) showing the double cone conformation of the calix[6]arene and interfullerene interactions.[11]

and is surprisingly isostructural with the C_{60} complex, both crystallising in space group $P4_12_12$. The principle axis of the fullerene is aligned such that the end of the fullerene close to this axis, where the curvature of the cage is similar to that of C_{60}, resides in the cavity. The double cone conformations provide further credence for the proposed structure of *p*-(C_{60})(*p*-*tert*-butylcalix[8]arene), and suggest the other 2 : 1 complexes, *p*-(C_{70})$_2$(*p*-*tert*-butylcalix[6,8]arene),[15] are also likely to have the calixarenes in the double cone conformation with a fullerene in each cavity. A calix[6]arene bearing *N*,*N*-dialkylaniline or *m*-phenylenediamine units forms complexes of C_{60} in toluene solution, with association constants of 7.9–1.1 × 10^2 dm^3 mol^{-1}.[19]

Calix[5]arenes and oxacalix[3]arenes

For the calix[6,8]arenes pre-organisation of the calixarenes *via* torsion along the C–CH_2–C moieties within the macrocycle is required for complexation with C_{60}. While both the calix-[4,5]arenes prefer the cone conformation, and are thus organised for host–guest formation, only the cavity of the calix[5]arene is large enough for binding C_{60} (but *exo*-cavity complexation is also possible—see below). The oxacalix[3]-arenes require minimal torsion for complementarity of curvature with C_{60}.[29]

Calix[5]arene itself forms a 1 : 1 complex with C_{60},[11,21] and other calix[5]arenes give either 1 : 1 or 2 : 1 complexes.[22] Molecular mechanics gives maximum overlap of the π-cloud of the calixarenes with the C_{60} where there is alignment of a C_5 axis of the fullerene with the C_5 axis of the calixarene.

p-Benzylcalix[5]arene and *p*-benzylhexahomooxacalix[3]ar-ene form 2 : 1 complexes with C_{60} from toluene solutions, as the octa-toluene solvate in the case of the calix[5]arene. In both structures the fullerene is shrouded by two staggered, *trans*-host molecules in cone conformations either with dangling benzyl groups, calix[5]arene, or edge on to the fullerene benzyl groups, oxacalix[3]arene, Fig. 3.[29] Either the benzyl groups are now

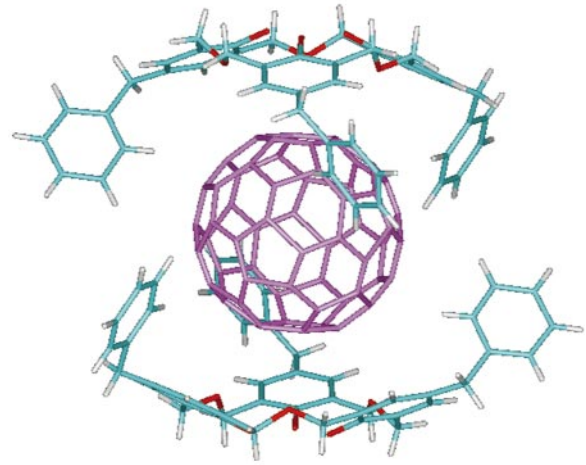

Fig. 3 The supermolecule [(C_{60})(*p*-benzylhexahomooxacalix[3]arene)$_2$].[29] The encapsulation of the fullerene by two oxacalix[3]arenes precludes the formation of extended supramolecular arrays *via* interfullerene interactions as were seen in Fig. 2.

directed away from the fullerene, θ = 180°, or are such that there are C–H···fullerene interactions, θ = 90°, Scheme 2. In

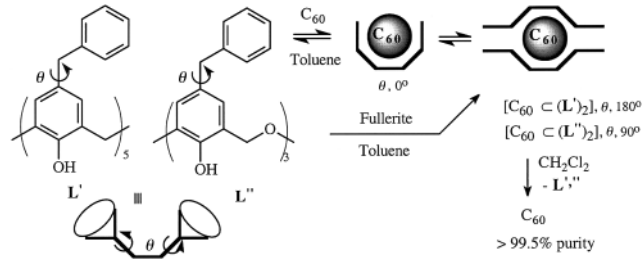

Scheme 2

both C_{60} structures, the alignment of the symmetry axis of the calixarene with the same symmetry element of C_{60}, C_5 and C_3, respectively, highlights the importance of symmetry matching in designing host molecules for fullerenes. This maximises the points of contact and efficiency of π–π interactions between the two interacting moieties. The only other authenticated structure with C_{60} encapsulated by two container molecules, hence precluding interfullerene contacts, is a calix[5]arene complex with three methyl and two iodo groups (1,3 disposition) in the *p*-positions of the upper rim.[22] The synthesis of covalently linked biscalix[5]arenes capable of encapsulating C_{60} or C_{70} has also been reported with binding constants indicating that C_{70} is bound preferentially.[23]

Even a 1 : 1 mixture of calixarenes, L′ or L″, with C_{60} in toluene, Scheme 2, still gives the 2 : 1 complexes in the solid, and in both cases it is also the exclusive complex formed when treating a fullerite mixture in toluene, from which C_{60} [> 99.5% purity (HPLC)] can be readily isolated on the addition of methylene chloride and represents an effective one step purification of C_{60}.

Solution studies on complexation of L′ with C_{60} in toluene give an association constant, K_1 = 2800 ± 200 dm^3 mol^{-1} at low concentrations of the calixarene, and K_2 = 230 ± 50 dm^3 mol^{-1} at higher concentrations. This is consistent with the initial formation of the 1 : 1 complex [C_{60} ⊂ (L′)], followed by

the formation of a 2 : 1 supermolecule, [$C_{60} \subset (L')_2$], and is in agreement with densitometry studies which support the displacement of two toluene molecules from L′ in toluene and formation of 1 : 1 complex in solution, $q = 0°$, Scheme 2.[24] The K_1 values for related 1 : 1 [$C_{60} \subset$ (substituted-calix[5]arene)] complexes studied by Fukazawa and coworkers are 2120 and 76 $\pm 5 \times 10^3$ dm^3 mol^{-1} in toluene.[22] In these studies there was no report of a second equilibrium. Similar UV–VIS studies involving L″ suggest the presence of more than one species in solution, the overall 2 : 1 association constant is estimated to be *ca.* 100 dm^3 mol^{-1}. In contrast, Fuji and coworkers[20] obtained a 1 : 1 association constant of 35.6 dm^3 mol^{-1} for a related oxacalixarene (R = Bu^t, **2**; or 64 ± 5 dm^3 mol^{-1} in an independent study[21]) and C_{60} in toluene, and obtained 1 : 1 complexes rather than a 2 : 1 complex in the solid state, showing interfullerene interactions.[20] Other solution studies on oxacalix-[3]arenes and calix[5]arenes have also been reported[21,25] including the electrochemical behaviour.[5]

Calix[4]arenes and resorcina[4]arene

Shinkai and coworkers screened a wide range of calixarenes for complexation of C_{60} in toluene and found little change in the electronic spectrum for the calix[4]arenes, and thus no evidence for complexation.[21] Nevertheless, some calix[4]arenes have been shown to form stable crystalline complexes with C_{60}, including (i) *p*-phenylcalix[4]arene which has a toluene molecule in the cavity, the overall structure dominated by fullerene–fullerene and *exo*-calixarene–fullerene interactions,[42] (ii) *p*-bromocalix[4]arene propyl ether, the structure showing very close interfullerene contacts in a columnar structure, which most likely results in opposing induced dipoles from the unidirectionally aligned calixarenes,[26] and (iii) *p*-iodocalix-[4]arene benzyl ether where the fullerenes are ordered without appreciable interfullerene interactions.[27] There is also a resorcin[4]arene, R = CH_2CH_2Ph, **2**, which has a molecular capsule derived from head to head hydrogen bonding of two resorcinarenes and propan-2-ol molecules, with the fullerene arranged in columns.[30] The fourfold symmetry of calixarenes and resorcinarenes relates to complexation of octaphenylcyclotetrasiloxane, [{$SiPh_2(\mu\text{-}O)$}$_4$], with C_{60} in toluene. The 1:1 supramolecular complex is a hemi-toluene solvate where the fullerenes are arranged in double columnar arrays shrouded by edge on siloxanes, the siloxanes interlocking by one of the phenyl groups of one molecule residing in the cavity of another.[43]

Cyclotriveratrylene

Complexation of C_{60} in toluene solutions of CTV results in polymeric structures in the solid, either a fullerene rich phase $(C_{60})_{1.5}$(CTV), or a 1 : 1 phase (C_{60})(CTV).[31,32] The structures are dominated by fullerene–fullerene interactions, and each CTV has a C_{60} associated within the cavity of the CTV as a 'ball and socket' nanostructure. For $(C_{60})_{1.5}$(CTV) the fullerenes collectively comprise a two dimensional close packed array with half of the fullerenes devoid of CTV, Fig. 4.[31] Solvated host–guest species, [(CTV)(C_{60})], are formed first in solution. This results in polarisation of the fullerene promoting aggregation which is evident by a resonant interfullerene transition band as 475 nm. The substituted analogue **4**, R = allyl, with C_{60} shows only solvated host–guest species.

The incorporation of aromatic pendant arms on CTV leads to strong binding of C_{60}, that of *N*-methylpyrrole showing the highest association constant, 48 × 103 dm^3 mol^{-1} in benzene. With six benzoyl arms a 1:1 complex forms in the solid state with two host molecules surrounding one fullerene, with a second 'bare' C_{60} in the lattice.[33] The host molecule, R = benzoyl, **4**, can be used to retrieve C_{60} from fullerite.[33] A planar analogue of CTV with a central six membered ring (without the bridging methylene units of CTV) forms a 1 : 2 complex in the solid state with isolated fullerenes surrounded by four planar molecules.[44]

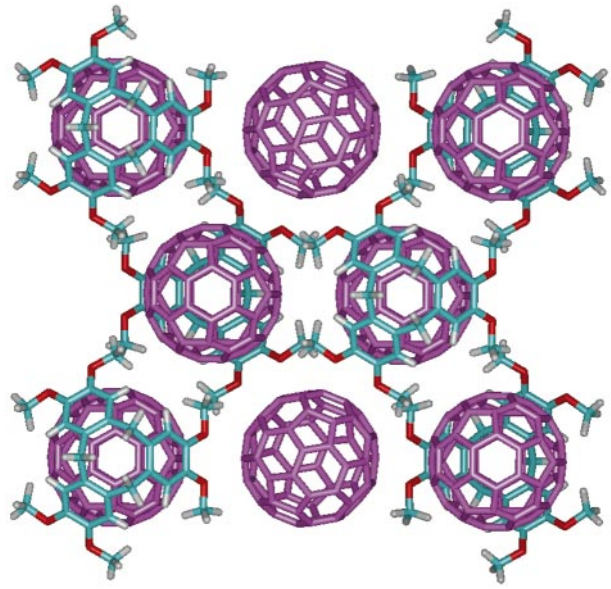

Fig. 4 Crystal packing of $(C_{60})_{1.5}(CTV)\cdot C_7H_6$.[31]

Nickel(II) macrocycles

Compound **5**, R = H, has two divergent concave surfaces in a saddle shape arrangement which arises from the otherwise unfavourable interactions between the methyl groups and the adjacent H-atoms on the aromatic rings.[34] It can act as a divergent heterotopic receptor towards C_{60}, or it can self-associate into dimeric species which in turn can act as a divergent homotopic receptor, for smaller clusters such as *o*-carborane (see below),[34] and also with the phosphorus chalcogenides P_4(S or Se)$_3$, Scheme 3.[34,45]

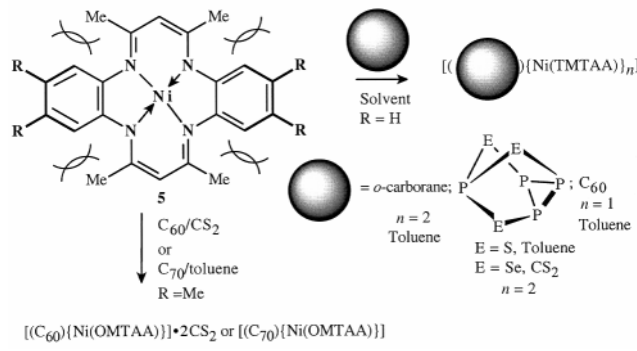

Scheme 3

In the structure of (C_{60})Ni(TMTAA) (TMTAA = tetramethyltetraazaannulene), Scheme 3, two host molecules shroud the fullerene such that a fullerene is in the saddle of one Ni(TMTAA) molecule with the methyl groups directed towards it and in the opposite saddle of another Ni(TMTAA) molecule, the overall host–guest contacts form a continuous zigzag array, Fig. 5, with the fullerenes forming a corrugated two dimensional sheet.[34] Cu(II) and Zn(II) TMTAA molecules similarly bind C_{60} and are isostructural with the Ni(II) analogue.[46] For R = Me, **5**, (= OMTAA) a 1 : 1 complex is formed with C_{60}, isolated as [Ni(OMTAA)C_{60}]$(CS_2)_2$. The extended supramolecular array is based on linear chains of close contact C_{60} molecules, and linear chains of π-stacked alternating molecules of C_{60} and Ni(OMTAA) with adjacent chains running in opposite directions and thus cancelling out dipole moments, Fig. 6. Surprisingly the same macrocycle forms a 1:1 complex with C_{70} which is isostructural with the C_{60} complex of Ni(TMTAA), *viz*. zigzag alternating C_{70}–Ni(OMTAA) chains with corrugated sheets of close contact C_{70} molecules.[47] In all of

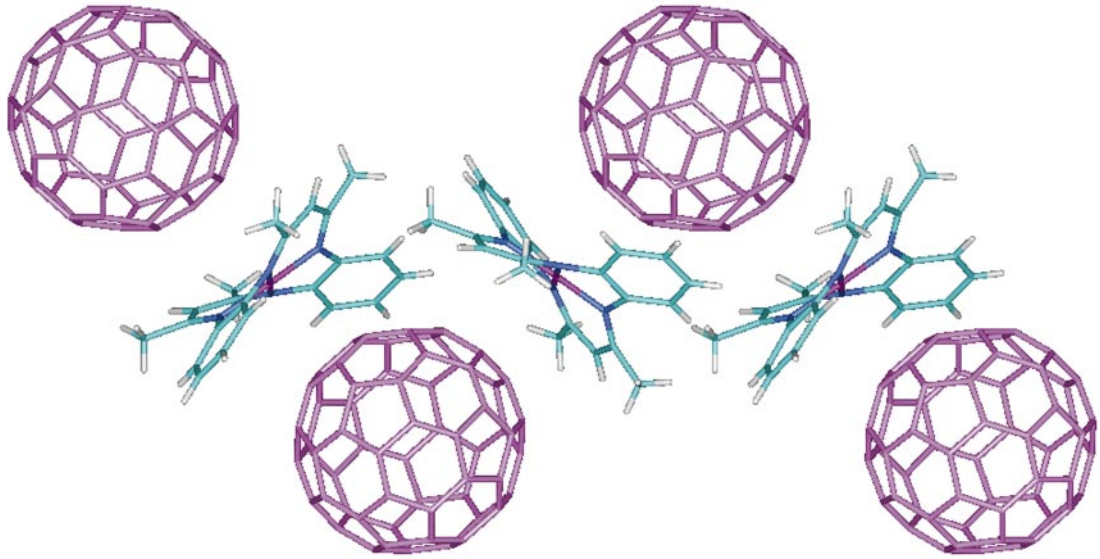

Fig. 5 The continuous zigzag array of [(C_{60}){Ni(TMTAA)}], highlighting the host–guest interactions between the C_{60} and both types of Ni(TMTAA) saddle.[34]

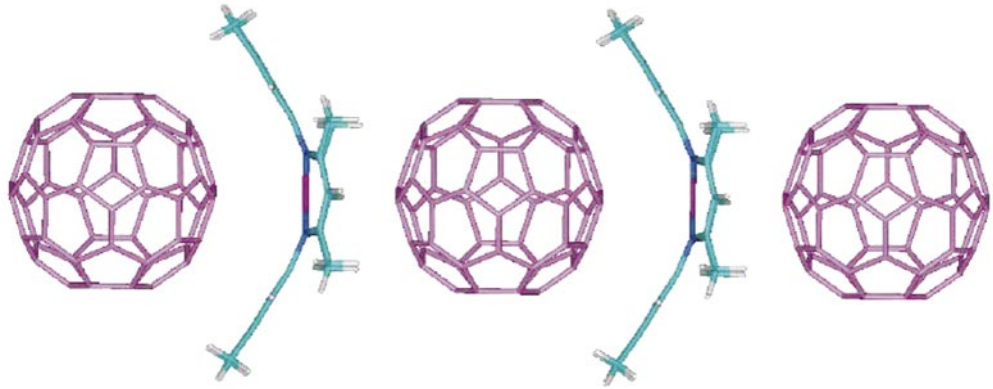

Fig. 6 The linear chains of π stacked C_{60} and Ni(OMTAA) molecules in [{Ni(OMTAA)}(C_{60})]·2CS_2.[47]

these Ni(II) macrocycle structure there are no significant contacts between the metal centres and the fullerenes. As in other systems there is evidence for the formation of 1 : 1 solvated supermolecules in solution which then go on to form micelle like species.[28,32,45] A planar Co(II) octaethylporphyrin also forms a 2 : 1 complex with C_{60} (and C_{70} and $C_{60}O$) in a 'bent metallocene' arrangement, with contacts of the metal to the fullerene in between van der Waals type interactions and a direct metal–fullerene interaction.[3] Here only one face of the macrocycle interacts with a fullerene, unlike in the C_{60} and C_{70} structures of Ni(TMTAA) and Ni(OMTAA). A silica supported zinc(II) tetraphenylporphyrin used in a HPLC column can separate metallofullerenes from C_{60} and higher fullerenes.[48]

Mesoporous silica studies

In addressing the difficulties in identifying and encouraging host–guest interactions of C_{60}, a new amorphous mesoporous silica (= $MPSiO_2$) with sufficient pore size to allow mobilisation of C_{60} was developed.[28] The material has a narrow range of pores, *ca*. 5.4 nm, which are large enough to accommodate small aggregates of fullerenes and associated host molecules, at least for small aggregates where conventional particle size analysis would be difficult. When this material is loaded with C_{60} it offers a qualitative test for supramolecular complexation of the fullerene, and the silica devoid of C_{60} is a material for uptake of preformed micelle like species ⩽5.4 nm in diameter.

Contact of magenta coloured toluene solutions of C_{60} with $MPSiO_2$ results in magenta colouration of the silica. Subsequent addition of toluene solutions of a variety of calixarenes and CTV yields brown–yellow material which shows a new broad resonant interfullerene transition band at *ca*. 450 nm. This is consistent with the formation of aggregates of C_{60}, most likely as part of micelle-like structures with the fullerene cores surrounded by host molecules in the pores of $MPSiO_2$, represented in Fig. 7. As an example, the addition of CTV

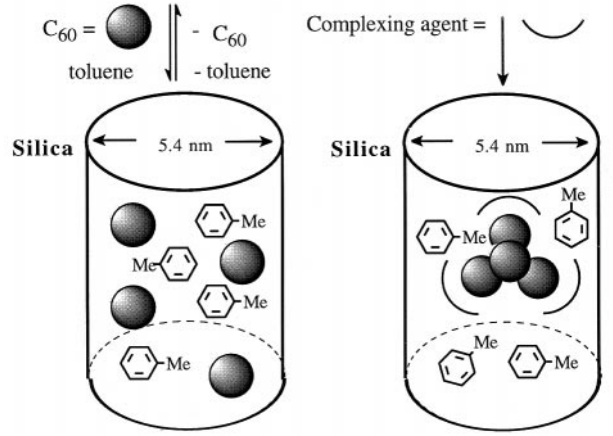

Fig. 7 Schematic representation of the formation of C_{60}–host aggregates inside the pores of mesoporous silica.

solutions to the mesoporous silica with premobilised C_{60} gives a spontaneous change in colour (magenta to brown) whereas addition of preformed solutions of C_{60} and CTV which are

brown show little mobilisation of fullerenes into the channels, and thus the micelle like species present in the solution have diameters ⩾ 5.4 nm.[28] Fullerene C_{60} has also been incorporated into molecular sieves (gas phase diffusion).[49]

Aggregation of fullerenes has been suggested in the incorporation of C_{60} into membranes,[50] and fullerene aggregates (mean diameter 10 nm) have been established in the solubilisation of C_{60} in aqueous media, with a band at 440 nm assigned to aggregate formation (*cf.* 450 nm for the above systems).[51] Aggregation of C_{60} is also prevalent in dissolution of the fullerene in a wide range of solvents, with significant reduction in its solubility.[52]

Carboranes

The C–H groups of carboranes are acidic[9] and intermolecular C–H···O,N hydrogen bonding is important in the supramolecular chemistry of carboranes, Fig. 8.[53–57] This includes

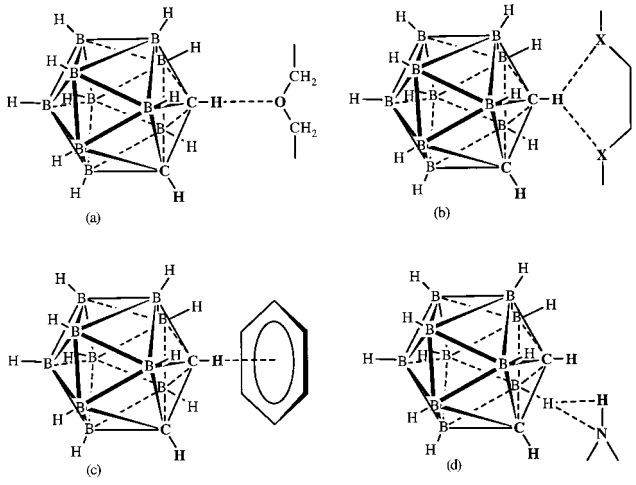

Fig. 8 Established types of interactions of carboranes (shown for the *o*-isomer): (a) classical C–H···O hydrogen bond, (b) bifurcated hydrogen bond, X = O (1,2-dimethoxylbenzene systems), N (in *o*-phenanthroline), (c) non-classical C–H···π hydrogen bond, and (d) B–H···H–N interplay.

bifurcated hydrogen bonding for 1,2-di(methoxy)benzenes and *o*-phenanthroline,[56,57] Fig. 8(b). Also important are the C–H···π-aromatic ring interactions, Fig. 8(c), where the $C–H_{carborane}$ is directed towards the centroid of an aromatic ring as a Coulombic interaction between a polarised C–H bond and the basic π-electrons of an aromatic ring, and can be regarded as a non-classical hydrogen bond.[53] This is calculated to be energetically favoured by 2.74 kcal mol^{-1},[53] at the 6-31G* level, for the model system of benzene interacting with *o*-carborane. The protons on carbon of the carborane have a residual charge of +0.299 *cf.* 0.068–0.091 for the hydrogen atoms on boron. Such non-classical hydrogen bonding has precedence in dichloromethane[40] inclusion complexes of calix[4]arenes. A less common type of interaction in complexes of carboranes involves B–H···H–N interplay with amines, Fig. 8(d).[58]

Theoretical calculations on a model system of *o*-carborane and 1,2-dimethoxybenzene give the $C–H_{carborane}···(O)_2$ interaction energetically favoured by 5.48 kcal mol^{-1}.[57] This is close to double the calculated energy of 2.74 kcal mol^{-1} for a single $C–H_{carborane}···\pi$ interaction.[53] This highlights a delicate balance between the carborane being involved in bifurcated hydrogen *versus* C–H···π bonding in the cavity of the CTV.

Host–guest chemistry

The first host–guest complexes of carboranes were the 1 : 1 complexes with α-, β- and γ-cyclodextrin, and a 2 : 1 complex for α-cyclodextrin.[59] Presumably in the 2 : 1 complex the carborane is shrouded by two host molecules, [(*o*-carborane)⊂(α-cyclodextrin)$_2$], which is related to C_{60} forming a 2:1 complex for the larger γ-cyclodextrin, noting the smaller cyclodextrins here do not form complexes with the fullerene.[35] The self-assembled ionic capsule, **6**, arising from interplay between (ethylenediamine)palladium(II)$^{2+}$ ions and four triply bridging pyridyl ligands, with the metal centres at the corners of an octahedron and the pyridyl ligands centred at the corners of a tetrahedron, has a large internal volume capable of binding four *o*-carborane molecules, presumably as a tetrahedral aggregate.[60] This encapsulation renders the carboranes water soluble, as do the cyclodextrin complexes.[59]

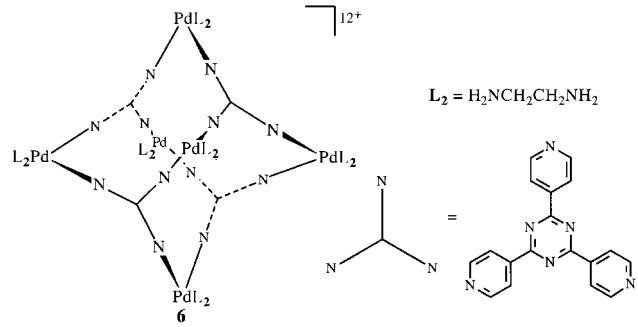

Other systems deal with hydrophobic host container molecules and the natures of the species formed are more substantiated with several X-ray structure determinations. These have shallow cavities and the resulting 1:1 supermolecules are at best described as perched structures. These involve calix[5]arene[56] and cyclotriveratrylene (= CTV).[53,57] Compounds prepared thus far and structurally authenticated are summarised in Scheme 4. A symmetrically tris-allyl substituted

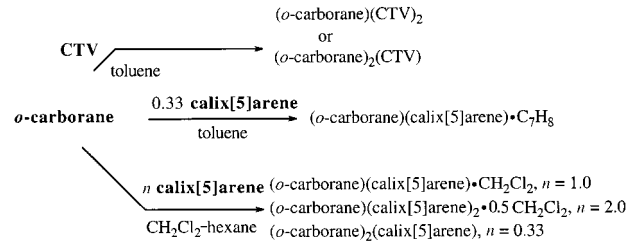

Scheme 4

analogue of CTV with a deeper cavity forms a 1 : 1 complex with *o*-carborane,[53] but has yet to be fully characterised. These complexes have IR shifts for $\nu_{C–H}$ of the carborane to lower energy, and a shift to higher energy for $\nu_{B–H}$,[53–57] consistent with the presence of non-classical hydrogen bonding for the C–H bonds with dispersal of the extra charge on the carbons resulting in strengthening of the B–H bonds.

The calix[5]arene–*o*-carborane complexes have a common structural motif in the solid state with a 1 : 1 ball and socket nanostructure comprised of the carborane in a cone shaped calixarene.[56] The carboranes interact with the calixarene most likely *via* the non-classical C–H···π hydrogen bonding, Fig. 8(c), and in all cases the C–H vectors of the carborane are directed towards aromatic rings of the host molecule. The interplay of the supermolecules with the other components, solvent, additional calixarene or carborane builds up the supramolecular arrays. In (*o*-carborane)(calix[5]arene)·CH_2Cl_2[56] the ball-and-socket units organise into larger dimeric supermolecules with calixarene hydroxy groups facing each other, forming a hydrophilic core shown in Fig. 9.

In (*o*-carborane)(calix[5]arene)·C_7H_8[56] the (*o*-carborane)∩(calix[5]arene) supermolecules stack along the same direction. The *endo*-cavity *o*-carborane of one supermolecule has contacts to the hydroxy groups of the next (*o*-carborane)∩(calix[5]arene). The calixarene rich complex (*o*-carborane)(calix[5]arene)$_2$·0.5CH_2Cl_2[56] has a remarkable structure with both calix-

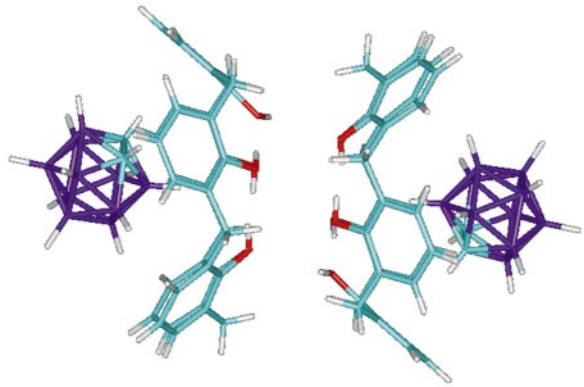

Fig. 9 The dimeric [(*o*-carborane)∩(calix[5]arene)]$_2$ nano-structure of [(calix[5]arene)(*o*-carborane)]·CH_2Cl_2. The dimer acts as a divergent receptor.[56]

[5]arene molecules acting as host molecules in quite distinct manners. One calixarene acts as a host molecule for the *o*-carborane, forming the ball-and-socket arrangement while the other acts as a secondary host for the (*o*-carborane)∩(calix-[5]arene) assembly *via* π···π interactions forming the [(*o*-carborane)∩(calix[5]arene)]∩(calix[5]arene) nano-structure illustrated in Fig. 10. The complexation of a host–guest species by a secondary host is relatively uncommon.

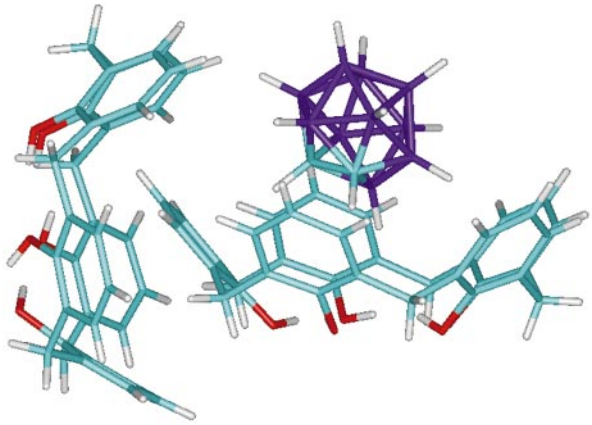

Fig. 10 The [(*o*-carborane)∩(calix[5]arene)]∩(calix[5]arene) nanostructure of [(calix[5]arene)$_2$(*o*-carborane)·0.5CH_2Cl_2].[56]

In the structure of (*o*-carborane)$_2$(calix[5]arene)[56] the carborane forms both *endo* and *exo* associations with the host calixarene, Fig. 11, with the second *o*-carborane forming a weak association with the hydroxy groups of the calixarene through one triangular face of the icosahedron. The *endo* and *exo* carboranes form pairs of cage molecules. The association of carboranes is also prevalent in the 1 : 1 complex of aza-18-crown-6 with *o*-carborane which forms an intercalation compound (see below),[55] and in the interplay between the four carboranes in the ionic capsule, **1**.[60]

In all the structures of the supermolecules [(*o*-carborane)∩(calix[5]arene)] the cage molecule is not a snug fit in the calixarene and thus while the formation of these complexes in solution is entropically driven there is some degree of torsional flexibility in the cone conformation of the calixarene to adapt to both the interactions with the cavity guest and the surroundings. Fullerene C_{60} in contrast has an excellent complementarity of curvature with calix[5]arenes in general (see above) and the calixarenes are in symmetrical conformations with little or no torsion mobility. In contrast, host–guest complexes of CTV and *o*-carborane clearly show a more snug fit of the cage species in the cavity of the host molecule, *i.e.* there is greater complementarity of curvature of the two supramolecular synthons. Surprisingly CTV also has complementarity with C_{60}[31,32] and the ability of CTV to accommodate spherical like molecules

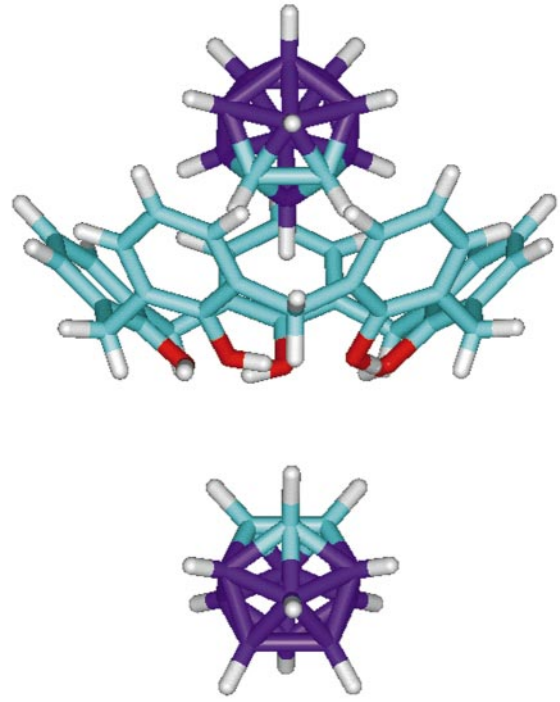

Fig. 11 The *exo* and *endo* associated *o*-carboranes of [(*o*-carborane)$_2$(calix[5]arene)].[56]

with different diameters (8 Å carborane *cf.* 10 Å C_{60}) relates to a shallower cavity of the rigid CTV relative to the diameter of the host molecule.

The structure of the 2 : 1 complex of CTV and *o*-carborane, Scheme 4, is comprised of 1 : 1 supermolecules of CTV and *o*-carborane, (*o*-carborane)∩(CTV),[53] the other CTV forming a zigzag π-stacked column with the inter-CTV contacts at the van der Waals limit. This type of association of CTV molecules is common even in inclusion complexes of CTV where the guest species are not in the cavities of the CTV molecules, the so called α-phase for CTV.[61] Thus the formation of complexes of *o*-carborane, and also C_{60}, with the guest species in the cavity of the CTV represents a major development in CTV chemistry. Non-bonded contact distances of the supermolecule (*o*-carborane)∩(CTV) show that three hydrogens of a triangular face of the icosahedron are directed towards the aromatic rings of the CTV albeit unsymmetrically, Fig. 12. This most likely arises from the energetically favoured $C–H_{carborane}\cdots\pi$ hydrogen bonds to two aromatic rings of the CTV *versus* repulsion between the B–H and the third aromatic ring of the CTV.

In (*o*-carborane)$_2$(CTV)[57] one of the carborane molecules forms three symmetry equivalent bifurcated hydrogen bonds to the methoxy groups of three equivalent CTV molecules, Fig. 8(b).[57] All three interactions originate from the same triangular face of the carborane icosahedron and, due to symmetry imposed disorder, each of the three carborane centres involved has 2/3 carbon and 1/3 boron character. A puckered hexagonal 2D hydrogen bonded network is formed, shown in Fig. 13. All CTV molecules within the grid, and indeed throughout the crystal lattice, have their bowl vertices pointing in the same direction. The second *o*-carborane molecule resides in the receptor sites forming a ball-and-socket (*o*-carborane)∩(CTV) nanostructure throughout the hydrogen bonded grid. The host–guest interplay within the supermolecule (*o*-carborane)∩(CTV) in the 2 : 1 complex is remarkably different to that found in (*o*-carborane)(CTV)$_2$. Here the alignment of the carborane within the CTV cavity is symmetrical with all carborane C–H vectors directed away from the CTV aromatic rings, Fig. 13.[57] However, the difference is consistent with the inherently weak interactions holding the supermolecule together.

^{1}H NMR spectra recorded in toluene for the 2 : 1 complex [(*o*-carborane)(CTV)$_2$] show rapid exchange processes occurring

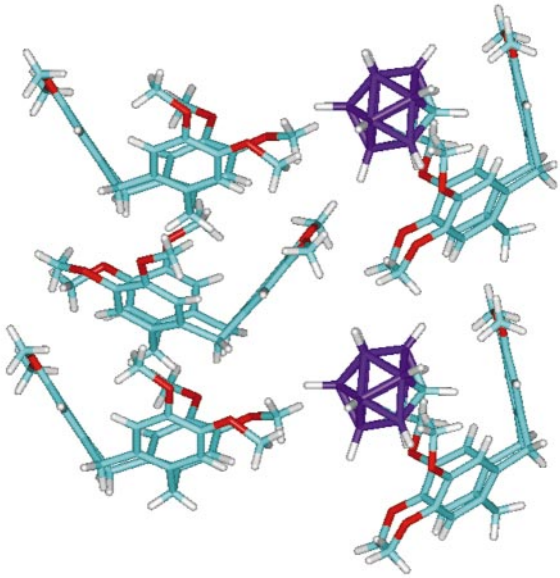

Fig. 12 Section of the crystal structure of [(*o*-carborane)(CTV)$_2$] showing the host–guest species and π stacked CTV molecules.[53]

between complexed and uncomplexed carborane. No significant changes to the ^{1}H NMR of CTV in the complexed and uncomplexed systems were evident. Variation in mole fraction of the carborane relative to CTV showed a non-linear relation with the chemical shift of the carborane C–H protons which implies that complexation is not a simple 1:1 supermolecule formation. The inability to fit the NMR data to this simple model indicates that *o*-carborane binds both *endo* and *exo* to the cavity of the CTV.

The nickel(II) macrocycle Ni(TMTAA), Scheme 3, can act as a divergent heterotopic receptor towards C_{60},[34] or it can self-associate into dimeric species which in turn can act as a divergent homotopic receptor, and this is found in the complex of *o*-carborane, and also for the phosphorus chalcogenides P_4(S or Se)$_3$.[34,46] In the solid state structure the *o*-carborane resides in the saddle of two Ni(TMTAA) molecules as bent sandwich like supermolecules with the two host molecules adjacent to each other, Fig. 14. The sandwich supermolecules form extended structures by locking together the pendant phenyl rings of one Ni(TMTAA) of one supermolecule with that of Ni(TMTAA) of another with the methyl groups all directed towards the cage. Alternatively the structures can be viewed as two associated Ni(TMTAA) molecules acting as a divergent receptor for two *o*-carboranes. The two Ni(TMTAA) moieties are at 90° to each other, and this is driven by the complementarity of curvature of the interlocking components, as well as by Ni···π-arene interactions.

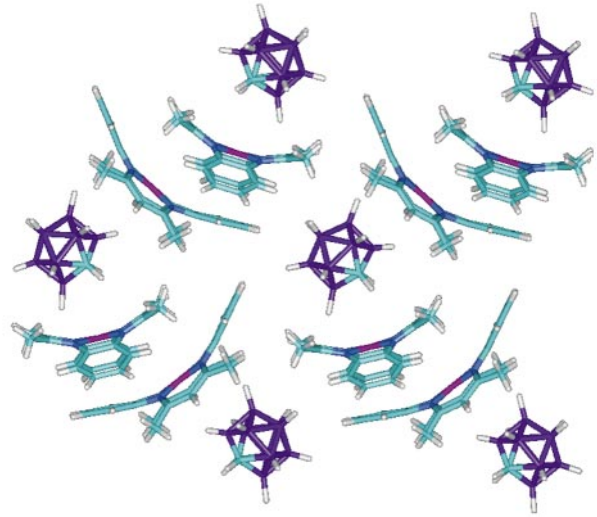

Fig. 14 Crystal stucture of [(*o*-carborane){Ni(TMTAA)}$_2$].[34]

Diaza-18-crown-6, [1,4,10,13-tetraoxa-7,16-diazacyclooctadecane] forms a 1:1 host–guest complex with *o*-carborane,[55] Scheme 5. While aza-18-crown-6, [1,4,10,13-tetraoxa-7-azacyclooctadecane] gives a 1:1 complex it is an intercalation compound with alternating layers of *o*-carboranes and crown ethers (see below). The striking difference in structure

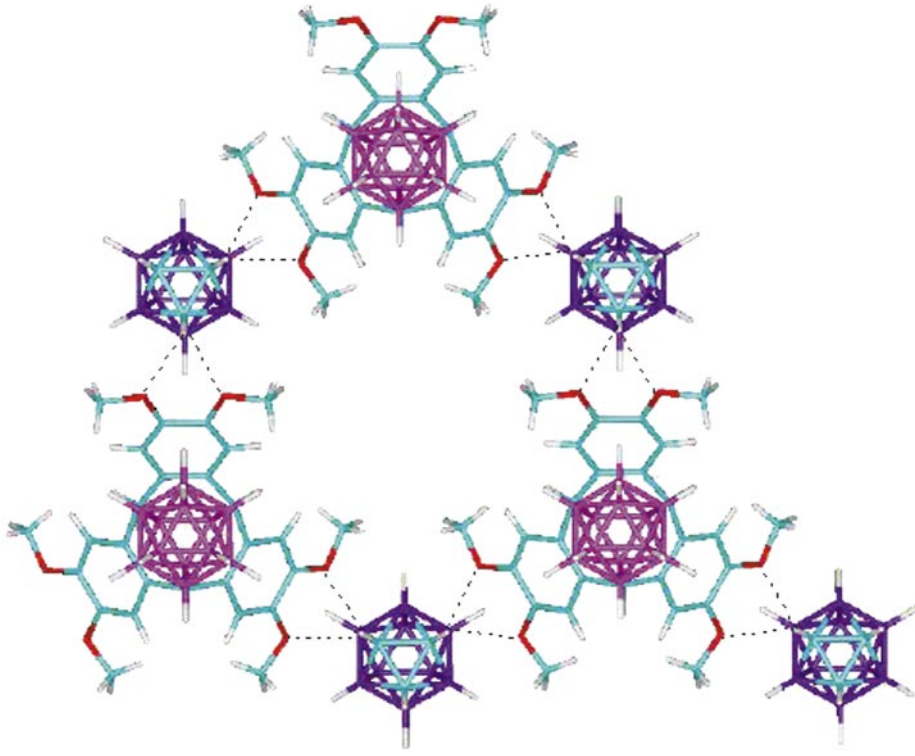

Fig. 13 Section of the crystal structure of [(*o*-carborane)$_2$(CTV)], showing the 2D hexagonal network formed through bifurcated B/C–H···O hydrogen bonds around the CTV, and guest carboranes (in pink).[57]

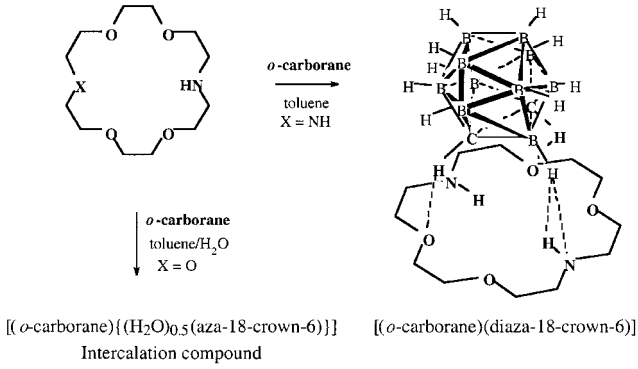

Scheme 5

between the two complexes reflects the delicate balance between weak intermolecular interactions, host–host, host–guest and guest–guest, which are within the realms of crystal packing forces.

In the supermolecules of [(*o*-carborane)∩(diaza-18-crown-6)], three H-atoms of a triangular face of the *o*-carborane polyhedron bearing the two carbon atoms reside above the diaza-18-crown-6. The two components are linked through $C–H_{carborane}\cdots O$ hydrogen bonding interactions, Fig. 8(a) coupled with B–H···H–N, Fig. 8(d), interplay. The H···H distance is close to the upper limit for unconventional dihydrogen bonds established for B–H···H–N contacts in aminoboranes.[58] The $O\cdots H_{carborane}$ distances are similar to those found in the *o*-, *m*-, and *p*-carborane adducts with HMPA.[54] A $\nu_{C–H}$ shift of the carborane of 33 cm^{-1} to lower energy and $\nu_{B–H}$ shift to higher energy of 25 cm^{-1} is observed.

Theoretical studies give the docking of the carborane with diaza-18-crown-6 to be favoured by 9.32 kcal mol^{-1}.[55] The optimised C–H···O distances at 2.471 Å compare well with experimental values at 2.49 Å, whereas optimised B–H···N and B–H···H–N at 2.924 and 2.721 Å, respectively are much longer than experimental values at 2.34 and 2.15 Å, and analogous distances in aminoboranes.[58] The reason for this is unclear. The high error in the position of the H-atom attached to nitrogen in [(*o*-carborane)∩(diaza-18-crown-6)] may be a problem, and the short B–H···H–N contacts for aminoboranes[58] arise from residual negative charge on the H-atoms attached to boron, *cf.* positive charge in [(*o*-carborane)∩(diaza-18-crown-6)].

^{1}H NMR in benzene at 25 °C for a range of concentrations of diaza-18-crown-6 (0.0–0.14 M) for a fixed *o*-carborane concentration (0.07 M) resulted in shifts in the *o*-carborane C–H resonance from δ 2.05–2.20 and the N–H resonance for diaza-18-crown-6 from δ 2.26–2.85. A near linear relationship indicate a low equilibrium constant (< 5 dm^3 mol^{-1}), eqn. (1).

$$o\text{-carborane} + \text{diaza-18-crown-6} \overset{\text{benzene}}{\rightleftharpoons} [(o\text{-carborane}) \cap (\text{diaza-18-crown-6})] \quad (1)$$

For *m*-carborane small differences in the chemical shift for C–H relative to a 1 : 1 mixture of the carborane and diaza-18-crown-6 indicate little or no complexation. Furthermore there is no complex formation in the solid state. Presumably the ability for *m*-carborane to form two C–H···O interactions within the same supermolecule while maintaining the crown conformation of the host is lost. The different binding prowess of *o*- and *m*-carborane suggests that separation of isomeric carboranes *via* selective binding is possible rather than using conventional chromatography.[9] Interestingly, ^{1}H NMR data show the corresponding *N*,*N*′-dibenzyldiaza-18-crown-6 forms a complex with *o*-carborane in benzene but attempts to isolate this complex were unsuccessful.[55]

Crystal structures of the 1 : 1 complexes of hexamethylphosphoramide (HMPA) with *o*-, *m*- and *p*-carboranes derived from toluene solutions have been reported.[54] The three complexes show extensive C–H···O hydrogen bonding and all adopt quite different supramolecular structures, commensurate with their differing arrangement of C–H sites. The *o*-isomer gives a dimeric structure, $C–H_{carborane}\cdots O$ 1.54(4)–1.60(4) Å, whereas the other isomers give polymeric structures with the HMPA O-centre bridging to two C–H groups from different carborane molecules (see below).

Tetrameric macrocycles mercuracarborand-4 and octaethylmercuracarborand-4 can also act as hosts for *closo*-$B_{12}H_{12}^{2-}$, as well as related globular borane anions *closo*-$B_{10}H_{10}^{2-}$ and *closo*-$B_{10}I_{10}^{2-}$.[7]

Extended arrays

The polymeric structures of [(*m*-, *p*-carborane)(HMPA)][54] have the O-centre of HMPA bridging to two C–H groups from different carborane molecules. Polymeric structures are also found in $(o\text{-carborane})_2$(CTV) and (C_{70})(*o*-carborane)(CTV)·1,2-dichlorobenzene.[57] Here hydrogen bonding is also prevalent, but involving bifurcated units, Fig. 8(b), rather than the classical hydrogen bond, Fig. 8(a). In the ternary system C_{70}–*o*-carborane–CTV–1,2-dichlorobenzene, each *o*-carborane interacts with two CTV molecules and in turn, each CTV is hydrogen bonded to two carboranes forming an infinite helical chain, Fig. 15. The CTV cavities are directed outwards from the helices, and each CTV complexes one C_{70} molecule. It is noteworthy that in the absence of carborane, C_{70} fails to form a complex with CTV, in contrast to C_{60} which forms two complexes, (C_{60})(CTV) and $(C_{60})_{1.5}$(CTV),[31,32] and that C_{60}

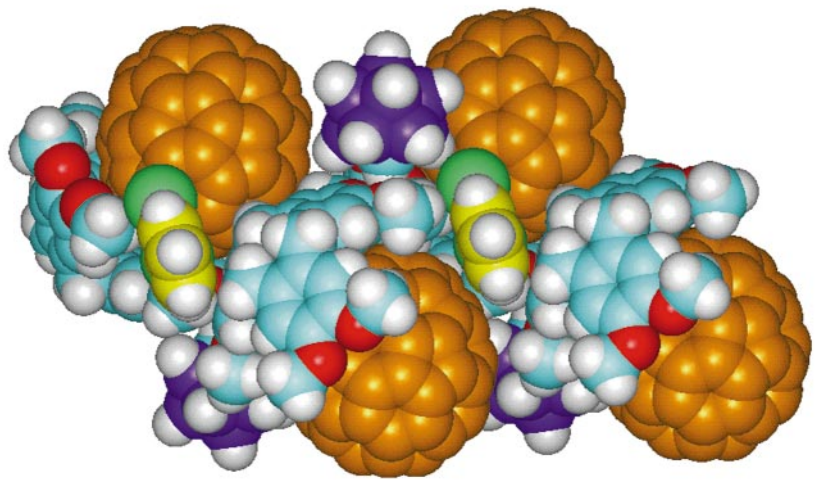

Fig. 15 Side view of a helix in [(C_{70})(*o*-carborane)(CTV)·1,2-dichlorobenzene] showing the binding of C_{70} molecules within the CTV bowls.[57]

and CTV in the presence of *o*-carborane also affords $(C_{60})_{1.5}$(CTV).

Inclusion/intercalation chemistry

Monoaza-18-crown-6 also gives a 1 : 1 complex, Scheme 5, with *o*-carborane but this is an intercalation complex, Fig. 16.[55]

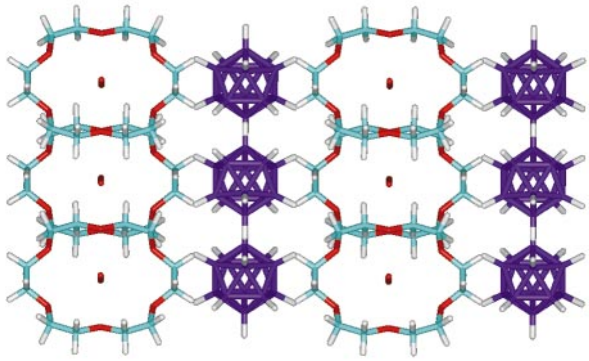

Fig. 16 Projection of [(*o*-carborane){$(H_2O)_{0.5}$⊂(aza-18-crown-6)}].[55]

Moreover, the crown ether requires a water molecule in its cavity for the complex to form, and the isolated material has a 50% occupancy of water in the cavity, [(*o*-carborane)-{$(H_2O)_{0.5}$⊂(aza-18-crown-6)}]. ^{1}H NMR of a mixture of the *o*-carborane and crown ether suggests intimate contact of the two components in solution, but in this case host–host and guest–guest interactions are predominant in the solid state. A similar effect was observed in the absence of moisture but in this case no host–guest or intercalation complex was isolated.

Although the structure of [(*o*-carborane){$(H_2O)_{0.5}$⊂(aza-18-crown-6)}] is highly disordered, it clearly shows the absence of any close intermolecular contacts like those observed in [(*o*-carborane)∩(diaza-18-crown-6)]. The polarised clusters form a two dimensional sheet, the nearest intercarborane contacts C/B–H···H–B/C at 2.41 Å.

Future prospects

Both icosahedral C_{60} and carboranes have recently gained prominence in supramolecular chemistry, the cohesion of the supermolecules and solid state structures coming from different interactions. Solvent molecules can also play a vital role in determining the crystal packing and overall topology of the systems. Interactions involving C_{60} or carboranes with themselves, including the formation of micelle like species for C_{60}, and with solvent and other molecules has potential in assembling complex structures. Complexation of other cage molecules is even less established and the ground rules for their confinement are beginning to emerge. Foremost is the use of rigid concave host molecules with complementarity of curvature with the cage molecule; any pre-organisational energy requirements of flexible host molecules may be at the expense of host–guest complexation. Moreover, combining carboranes with container molecules capable of the bifurcated hydrogen bonding with the carborane (such as CTV) offers scope for swaying the competing energies of interaction in favour of host–guest complexes (for cage molecules other than for carborane—demonstrated for C_{70}) where the host–guest components otherwise fail to assemble.

The ability to purify C_{60} by supramolecular complexation is noteworthy. The primary process in the binding of C_{60} is the formation of a host–guest species with polarisation of the fullerene resulting in aggregation of the fullerenes. The fate of this is complete encapsulation of a single fullerene, the formation of a stable micelle-like structure (in mesoporous silica as well as in bulk solution), or the breakdown of the latter resulting in crystallisation of pure C_{60}, Scheme 6. Complexation of higher fullerenes is a synthetic goal as is the complexation of

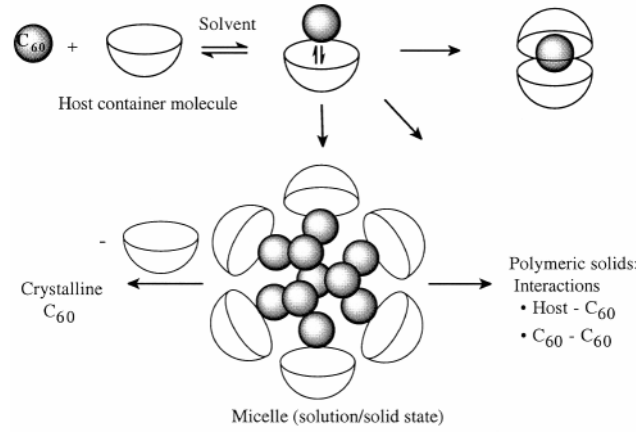

Scheme 6

reduced fullerenes, for which the associated complexes are likely to possess unusual properties. This may be possible using the receptor macrocycle M(TMTAA) where the metal centre is easily oxidised, M^{2+}(TMTAA) → $[M^{2+n}(TMTAA)]^{n+}$, *via* electron transfer to the cage molecule. The binding of carboranes is largely through C–H···O,N hydrogen bonds, and C–H···π-cloud interaction, with some evidence for the association of the carboranes.

A major advance in supramolecular chemistry is the ability to construct large encapsulating supermolecules assembled by hydrogen bonding[62] or metal coordination chemistry.[60] These systems have very large internal voids and in principle could accommodate, and incarcerate, several fullerenes, as has been achieved for four carboranes,[60] and even larger main group cages species. Finally the supramolecular chemistry has exciting possibilities in stabilising new species, in their separation from complex mixtures, and in generating novel structures and materials.

Acknowledgments

The authors wish to acknowledge the contribution from coworkers over several years at Monash University and Griffith University, and the collaboration with Professor J. L. Atwood, University of Missouri—Columbia, and Dr R. J. Blanch, ADFA, University of NSW. Financial support from the Australian Research Council and the Department of Industry, Science and Tourism is gratefully appreciated.

Notes and references

1 H. W. Kroto, J. R. Heath, S. C. O'Brien, R. F. Curl and R. E. Smalley, *Nature*, 1985, **318**, 162.
2 See, for example: M. Prato, *J. Mater. Chem.*, 1997, **7**, 1097; F. Diederich and C. Thilgen, *Science*, 1996, **271**, 317.
3 A. L. Balch and M. M. Olmstead, *Chem. Rev.*, 1998, **98**, 2123 and references therein.
4 See for example: F. D. Weiss, J. L. Elkind, S. C. O'Brien, R. F. Curl and R. E. Smalley, *J. Am. Chem. Soc.*, 1988, **110**, 4464.
5 See for example: S. A. Olsen, A. M. Bond, R. G. Compton, G. Lazarev, P. J. Mahon, F. Marken, C. L. Raston, V. Tedesco and R. Webster, *J. Phys. Chem.*, 1998, **102**, 2641 and references therein; Z. Chen, J. M. Fox, P. A. Gale, A. J. Pilgrim, P. D. Beer and M. J. Rosseinsky, *J. Electroanal. Chem.*, 1995, **392**, 101; D. E. Cliffel, A. J. Bard and S. Shinkai, *Anal. Chem.*, 1998, **70**, 4146.
6 C. L. Raston, *Comprehensive Supramolecular Chemistry*, ed. J. L. Atwood, J. E. D. Davies, D. D. Macnicol and F. Vögtle, Pergamon, Oxford, 1996, vol. 1 and references therein.
7 See for example: M. F. Hawthorne and Z. Zheng, *Acc. Chem. Res.*, 1997, **30**, 267 and references therein.
8 V. I. Bregadze, *Chem. Rev.*, 1992, **92**, 209 and references therein.
9 R. N. Grimes, *Carboranes*, Academic Press, New York, 1970.
10 J.-M. Lehn, *Supramolecular Chemistry, Concepts and Perspectives*, VCH, Weinheim, 1995.
11 J. L. Atwood, L. J. Barbour, C. L. Raston and I. B. N. Sudria, *Angew. Chem., Int. Ed.*, 1998, **37**, 981.

12 J. L. Atwood, G. A. Koutsantonis and C. L. Raston, *Nature*, 1994, **368**, 229.
13 T. Suzuki, K. Nakashima and S. Shinkai, *Chem. Lett.*, 1994, 699.
14 C. L. Raston, J. L. Atwood, P. J. Nichols and I. B. N. Sudria, *Chem. Commun*., 1996, 2615.
15 T. Suzuki, K. Nakashima and S. Shinkai, *Tetrahedron Lett.*, 1995, **36**, 249.
16 B. Paci, G. Amoretti, G. Arduini, G. Ruani, S. Shinkai, T. Suzuki, F. Ugozzoli and R. Caciuffo, *Phys. Rev. B*, 1997, **53**, 5566.
17 R. M. Williams and J. W, Verhoeven, *Recl. Trav. Chim. Pays-Bas Belg.*, 1992, **111**, 531.
18 R. M. Williams, J. M. Zwier and J. W. Verhoeven, *J. Am. Chem. Soc.*, 1994, **116**, 6965.
19 K. Araki, K. Akao, A. Ikeda, T. Suzuki and S. Shinkai, *Tetrahedron Lett.*, 1996, **37**, 73.
20 K. Tsubaki, K. Tanaka, T.Kinoshita and K. Fuji, *Chem. Commun.*, 1998, 895.
21 A. Ikeda and S. Shinkai, *Chem. Rev*., 1997, **97,** 1713; A. Ikeda, M. Yoshimura and S. Shinkai, *Tetrahedron Lett.*, 1997, **38,** 2107.
22 T. Haino, M. Yanase and Y. Fukazawa, *Tetrahedron Lett.*, 1997, **38**, 3739; T. Haino, M. Yanase and Y. Fukazawa, *Angew. Chem., Int. Ed. Engl.*, 1997, **36**, 259.
23 T. Haino, M. Yanase and Y. Fukazawa, *Angew. Chem., Int. Ed.*, 1998, **37**, 997.
24 P. J. Nichols, C. L. Raston, C.A. Sandoval and D. J. Young, *Chem. Commun.*, 1997, 1839.
25 A. Ikeda, Y. Suzuki, M. Yoshimura and S. Shinkai, *Tetrahedron*, 1998, **54**, 2497.
26 L. J. Barbour, G. W. Orr and J. L. Atwood, *Chem. Commun*., 1998, 1901.
27 L. J. Barbour, G. W. Orr and J. L. Atwood, *Chem. Commun*., 1997, 1439.
28 A. Drijaca, C. Kepert, L. Spiccia, C. L. Raston, C. A. Sandoval and T. D. Smith, *Chem. Commun*., 1997, 195.
29 J. L. Atwood, L. J. Barbour, P. J. Nichols, C. L. Raston, and C. A. Sandoval, *Chem. Eur. J*., 1999, **5**, 990.
30 K. N. Rose, L. J. Barbour, G. W. Orr and J. L. Atwood, *Chem. Commun*., 1998, 407.
31 J. L. Atwood, M. J. Barnes, R. S. Burkhalter, P. C. Junk, J. W. Steed and C. L. Raston, *J. Am. Chem. Soc*., 1994, **116**, 10346.
32 J. L. Atwood, M. Barnes, M. G. Gardiner and C. L. Raston, *Chem. Commun*., 1996, 1449.
33 H. Matsubara, A. Hasegawa, K. Shiwaku, K. Asano, M. Uno, S. S. Takahashi and K. Yamamoto, *Chem. Lett.*, 1998, 923.
34 P. C. Andrews, J. L. Atwood, L. J. Barbour, P. J. Nichols and C. L. Raston, *Chem. Eur. J*., 1998, **4**, 1384.
35 K. Cabrera, G. Wieland and M. Schafer, *J. Chromatogr.*, 1993, **644**, 396; T. Andersson, G. Westman, G. Stenhagen, M. Sundahl and O. Wennerström, *Tetrahedron Lett.*, 1995, **36**, 597 and references therein; Z. Yoshida, H. Takekuma, S. Takekuma and Y. Matsubara, *Angew. Chem., Int. Ed. Engl.*, 1994, **33**, 1597 and references therein.
36 F. Diedrich, J. Effing, U. Jonas, L. Jullien, T. Plesnivy, H. Ringsdorf, C. Thilgen and D. Weinstein, *Angew. Chem., Int. Ed. Engl.*, 1992, **31**, 1599.
37 D. M. Eichhorn, S. Yang, W. Jarrell, T. F. Baumann, L. S. Beall, A. J. P. White, D. J. Williams, A. G. M. Barrett and B. M. Hoffman, *J. Chem Soc., Chem. Commun.*, 1995, 1703.
38 O. Ermer, *Helv. Chim. Acta*, 1991, **74**, 1339; O. Ermer and C. Röbke, *J. Am. Chem. Soc.*, 1993, **115**, 10077.
39 A. Izuoka, T. Tachikawa, T. Sugawara, Y. Saito and H. Shinohara, *Chem. Lett.*, 1992, 1049; A. Izuoka, T. Tachikawa, T. Sugawara, Y. Suzuki, M. Konno, Y. Saito and H. Shinohara, *J. Chem. Soc., Chem. Commun.*, 1992, 1472.
40 J. L. Atwood, S. G. Bott, C. Jones and C. L. Raston, *J. Chem. Soc., Chem. Commun.*, 1992, 1349.
41 J. L. Atwood, C. L. Raston and J. A. Ripmeester, unpublished results.
42 J. L. Atwood, C. L. Raston and I. B. N. Sudria, unpublished results.
43 I. E. Grey, M. J. Hardie, T. J. Ness and C. L. Raston, *Chem. Commun.*, in press.
44 L. Y. Chiang, J. W. Swirczewski, K. Liang and J. Millar, *Chem. Lett.*, 1994, 981.
45 P. D. Croucher, P. J. Nichols and C. L. Raston, *J. Chem. Soc., Dalton Trans*., 1999, 279.
46 P. D. Croucher, P. J. Nichols, C. L. Raston and N. Smith, unpublished results.
47 J. M. Marshall, P. D. Croucher, P. J. Nichols and C. L. Raston, *Chem. Commun.*, 1999, 193.
48 I. Xiao, M. R. Savina, G. B. Martin, A. H. Francis and M. E. Meyerhoff, *J. Am. Chem. Soc*., 1994, **116**, 9341.
49 M. Anderson, J. Shi, D. A. Leigh, A. E. Moody, F. A. Wade, B. Hamilton and S. W. Carr, *J. Chem. Soc., Chem. Commun*., 1993, 533; A. Gügel, K. Müllen, H. Reichert, W. Schmidt, G. Schün, F. Schüth, J. Spickermann, J. Titman and K. Unger, *Angew. Chem., Int. Ed. Engl.*, 1993, **32**, 556.
50 H. Hüngerbuhler, D. M. Guldi and K.-D. Asmus, *J. Am. Chem. Soc*., 1995, **115**, 3386.
51 A. Beeby, J. Eastoe and R. H. Heenan, *J. Chem. Soc., Chem. Commun.*, 1994, 173.
52 R. S. Ruoff, D. S. Tse, R. Malhotra and D. C. Lorents, *J. Phys. Chem.*, 1993, **97**, 3379.
53 R. J. Blanch, M. Williams, G. D. Fallon, M. G. Gardiner, R. Kaddour and C. L. Raston, *Angew. Chem., Int. Ed. Engl*., 1997, **36**, 504.
54 M. G. Davidson, T. G. Hibbert, J. A. K. Howard, A. Mackinnon and K. Wade, *Chem. Commun.*, 1996, 2285.
55 P. D. Godfrey, W. J. Grigsby, P. J. Nichols and C. L. Raston, *J. Am. Chem. Soc*., 1997, **119**, 9283.
56 M. J. Hardie and C. L. Raston, *Eur. J. Inorg. Chem*., 1999, 195; and unpublished results.
57 M. J. Hardie, P. D. Godfrey and C. L. Raston, *Chem. Eur. J.*, 1999, in press.
58 T. B. Richardson, S. deGala, R. H. Crabtree and P. E. M. Seigbahan, *J. Am. Chem. Soc.*, 1995, **117**, 12875.
59 A. Harada and S. Takahashi, *J. Chem. Soc., Chem. Commun.*, 1988, 1352.
60 T. Kusukawa and M. Fujita, *Angew. Chem., Int. Ed. Engl.*, 1998, **37**, 3142.
61 J. Canceill, A. Collet and G. Gottarelli, *J. Am. Chem. Soc.*, 1984, **106**, 5997.
62 L. R. MacGillivray and J. L. Atwood, *Nature*, 1997, **389**, 469; T. Heinz, D. M. Rudkevich and J. Rebek, *Nature*, 1998, **394**, 764 and references therein.

Paper 9/00787C

Synthesis and photoelectrochemical properties of a self-assembled monolayer of a ferrocene–porphyrin–fullerene triad on a gold electrode

Hiroshi Imahori,*[a] Hiroko Yamada,[a] Shinichiro Ozawa,[a] Kiminori Ushida[b] and Yoshiteru Sakata*[a]

[a] *The Institute of Scientific and Industrial Research, Osaka University, 8-1 Mihoga-oka, Ibaraki, Osaka 567-0047, Japan. E-mail: imahori@sanken.osaka-u.ac.jp; sakata@sanken.osaka-u.ac.jp*

[b] *The Institute of Physical and Chemical Research (RIKEN), 2-1 Hirosawa, Wako, Saitama 351-0198, Japan*

Received (in Cambridge, UK) 22nd April 1999, Accepted 27th May 1999

A self-assembled monolayer of a ferrocene–porphyrin–C_{60} triad has been prepared to mimic efficient vectorial electron transport across a photosynthetic membrane.

In photosynthesis a key process for the conversion of light to chemical energy is initial electron transfer (ET) events in the reaction center complex. The ultrafast and unidirectional multistep ET takes place along well-arranged pigments embedded in the transmembrane proteins, leading to a generation of a charge-separated state across the membrane with a quantum efficiency (Φ) of nearly 100%. There have been numerous synthetic attempts to mimic this highly efficient process. Some of them, such as triads, tetrads, and pentads, produce a long-lived, charge-separated state with a high quantum yield.[1] However, efficient conversion (overall Φ = 1–10%) of light to photocurrents or chemical products *via* the charge-separated state has been hampered, because of the difficulty of assembling the donor–acceptor linked molecules unidirectionally in artificial membranes such as lipid bilayer and Langmuir–Blodgett membranes.[2–4] Self-assembled monolayers (SAMs)[5] are an alternative and promising approach to organize the donor–acceptor molecules on electrodes owing to their uniform and well-ordered structures.[6,7] Here we report the first preparation and photoelectrochemical properties of a SAM of a ferrocene (Fc)–porphyrin (P)–C_{60} triad **1** on a gold electrode.

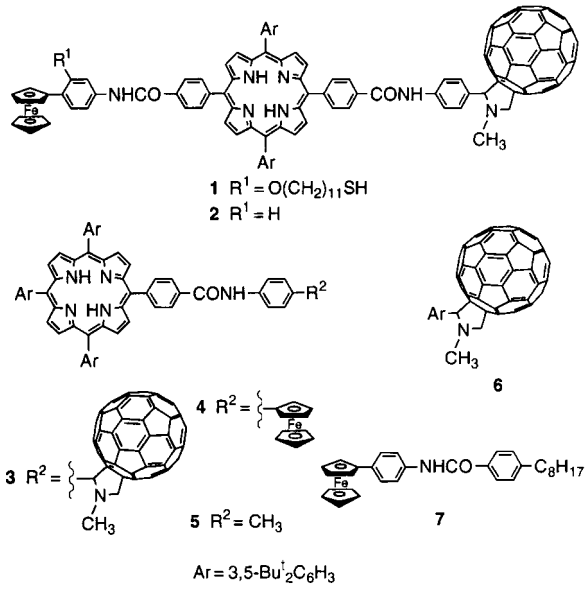

The synthetic route to **1** is shown in Scheme 1. Aminophenylferrocene **8** was prepared in three steps from ferrocene. Formyl-protected aniline **9** was synthesized in two steps from 4-nitrobenzaldehyde. Cross-condensation of porphyrin bis(acid chloride) **10** with **8** and **9** in benzene in the presence of pyridine, followed by acidic hydrolysis, afforded ferrocene–prophyrin **11** in 23% yield.[8] Bromide **11** was converted to thiol **12** *via* thioesterification with potassium thioacetate and subsequent base deprotection. The triad **1** was obtained by 1,3-dipolar cycloaddition using **12**, *N*-methylglycine, and C_{60} in toluene in 54% yield.[9] The reference compounds **2**–**7** were also prepared. Their structures were verified by spectroscopic analyses including ^{1}H NMR and MALDI-TOF mass spectra.†

The absorption spectrum of **2** in THF is essentially a linear combination of those of **5**, **6** and **7**, indicating no evidence for strong interaction among these chromophores. Absorption due to the porphyrin is much stronger relative to the C_{60} and the ferrocene, showing that the porphyrin is a major absorber of photons. Fluorescence spectra of **2** and **3** in THF are quenched strongly as compared with that of **5** when excited at the Soret band under the same concentration (relative intensities: 0.14 for **2**, 0.19 for **3**). In contrast, the relative fluorescence intensity of **4** *vs.* **5** (0.60) is much larger, suggesting that quenching of the excited singlet porphyrin (^{1}P*) by the attached C_{60} is a dominant deactivation pathway in **1**.

A cyclic voltammetric experiment using **1** on Au in CH_2Cl_2 containing 0.1 M Bu^nNPF_6 electrolyte with a sweep rate of 100 mV s^{-1} was performed to estimate the surface coverage. The adsorbed amount of **1** on Au was calculated from the charge of the anodic peak of the ferrocene to be 1.9×10^{-10} mol cm^{-2} (86 Å^2 molecule^{-1}), which is comparable to the porphyrin–polyalkanethiols ($0.8–2.0 \times 10^{-10}$ mol cm^{-2})[7,10] and C_{60}–polyalkanethiols ($1.3–2.0 \times 10^{-10}$ mol cm^{-2})[11,12] on gold electrodes. Assuming that the triad is packed perpendicularly to the gold surface, then the occupied area of one molecule is calculated to be *ca.* 87 Å^2 for hexagonal packing of the C_{60} moieties, which is consistent with the experimental value. Therefore, we can conclude that the triad molecules are well-packed with almost perpendicular orientation on the gold surface.

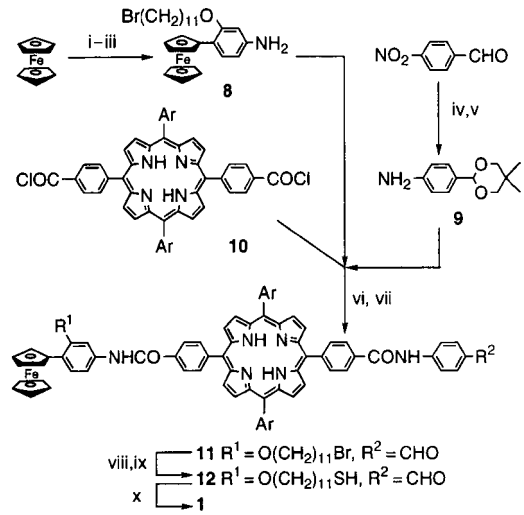

Scheme 1 *Reagents and conditions*: i, H_2SO_4, 2-amino-5-nitrophenol, 13%; ii, 1,11-dibromoundecane, K_2CO_3, 88%; iii, H_2, Pd/C, 84%; iv, neopentyl glycol, TsOH, 95%; v, H_2, Pd/C, 69%; vi, pyridine; vii, TFA, H_2SO_4, 23% (2 steps); viii, potassium thioacetate, 81%; ix, KOH, 50%; x, *N*-methylglycine, C_{60}, 54%.

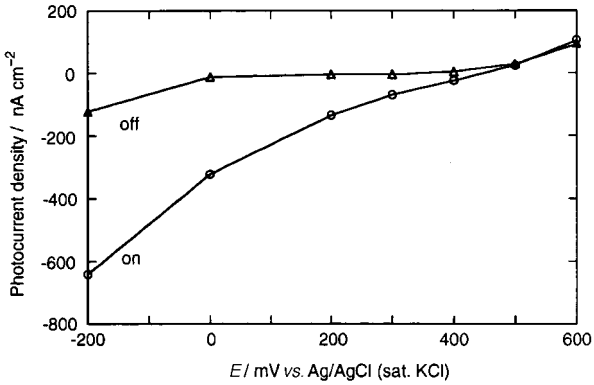

Fig. 1 Photocurrent *vs.* applied potential curves for the triad cell when the light is on (○) and off (△): λ = 438.5 nm (60 μW cm^{-2}), O_2-saturated 0.1 M Na_2SO_4 solution.

Photoelectrochemical measurements using **1** on Au in a three electrode system were carried out in an oxygen-saturated 0.1 M Na_2SO_4 solution. Fig. 1 shows current–potential curves under an illumination of 438.5 (±4.9) nm light (60 μW cm^{-2}). The SAM showed a photoelectrochemical response when the light was switched on and off. The photocurrent was reduced by argon bubbling of the solution and recovered to the initial state by successive oxygen bubbling. The results indicate that $C_{60}^{\cdot-}$ gives an electron to O_2 to produce $O_2^{\cdot-}$.[6] The intensity of the photocurrent in the present system is larger by two orders of magnitude than that of the porphyrin–polyalkanethiol systems,[10] implying that the C_{60} and ferrocene moieties are responsible for the higher efficiency. An increase in the cathodic photocurrent with an increase of the negative bias to the gold electrode demonstrates that the photocurrent flows from the gold electrode to the counter electrode through the electrolyte. The cathodic photocurrent dramatically increased as the potential applied dropped below +500 mV, which is in good agreement with the redox potential of ferrocene [+0.51 V (Fc/Fc$^{\cdot+}$)] (Fig. 1). This indicates that the photocurrent generation is controlled by the ET rate between the gold electrode and the ferrocene, similar to the porphyrin–ferrocene SAM system.[7] When methyl viologen (MV^{2+}) was employed as an electron carrier, the time profile of the photocurrent was dependent on the concentration of MV^{2+}. The initial and stable photocurrents increased with an increase of the MV^{2+} concentration under the argon- or oxygen-saturated conditions, implying that MV^{2+} also accepts an electron from $C_{60}^{\cdot-}$ to generate $MV^{\cdot+}$.

In the absorption spectra the Soret band of **1** on Au in air using the transmission mode is broad and red-shifted by 11 nm, compared with that of **2** in THF. This behavior is similar to that of the polymethylenethiol-linked porphyrin systems on gold electrodes.[7,10] This suggests increased π–π interaction among the porphyrin moieties within the SAM, which is quite consistent with the results obtained using cyclic voltammetry. The action spectrum of the cell roughly agrees with the absorption spectrum of **1** on Au, indicating that the porphyrin is the major photoactive species for photocurrent generation.

Quantum efficiency based on the number of photons absorbed by **1** on Au was calculated using the input power (60 μW cm^{-2} at 438.5 nm), the photocurrent density, and the estimated absorbance on Au (0.059). Under the optimal conditions using the oxygen-saturated solution with 30 mM MV^{2+}, we obtained a net photocurrent density of 660 nA cm^{-2} at −200 mV from the triad cell. Thus, the quantum yield is found to be 25%, which is more than two times larger than the highest value (11%) among the previous reports of photosynthetic multistep ET across artificial membranes and at monolayer-modified metal electrodes.[2–4,6,7,10,12]

The photocurrent generation may be explained as follows. On the basis of the fluorescence quenching experiments together with previously reported results,[6,13,14] photoinduced ET or charge-transfer occurs from $^1P^*$ [−0.82 V ($^1P^*/P^{\cdot+}$)] to C_{60} [−0.64 V($C_{60}/C_{60}^{\cdot-}$)] rather than from Fc to $^1P^*$. The resulting $C_{60}^{\cdot-}$ transfers an electron to diffusing electron carriers such as oxygen [−0.48 V ($O_2/O_2^{\cdot-}$)] and/or MV^{+2} [−0.62 V $MV^{+2}/MV^{\cdot+}$)], which eventually give an electron to the counter electrode. On the other hand, successive charge shift (CSH) occurs from Fc to $P^{\cdot+}$ [+1.08 V ($P/P^{\cdot+}$)], then from the gold electrode to $Fc^{\cdot+}$, resulting in the recovery of the initial state and a net vectorial electron flow from the gold electrode to the counter electrode through the monolayer and the electrolyte. There is a plausible explanation for the remarkable high efficiency in the system. We have shown that $^1P^*$ within the SAM on gold electrodes is strongly quenched by the gold electrodes.[10] This means that (i) initial photoinduced ET from $^1P^*$ to the first acceptor must compete with deactivation due to the gold electrode and (ii) the CSH to the second acceptor is much faster than charge recombination to the ground state. Utilization of C_{60} with its small reorganization energy may fully satisfy these requirements and improve the quantum yield greatly.[6,12,13,15]

In conclusion, a SAM of a ferrocene–porphyrin–C_{60} has been prepared for the first time. The high quantum yield implies that a combination of fullerenes and SAMs is promising for applications in materials science. Although our interpretation of the photocurrent generation mechanism is consistent with the results obtained by the electrochemical and photoelectrochemical measurements, further details must await photodynamical experiments in solutions and on a gold surface as well as structural studies on the monolayer.

This work was supported by Grant-in-Aids for COE Research and Scientific Research on the Priority Area of Electrochemistry of Ordered Interfaces and Creation of Delocalized Electronic Systems from the Ministry of Education, Science, Sports and Culture, Japan. Y. S. thanks the Mitsubishi Foundation for financial support.

Notes and references

† *Selected data* for **1**: δ_H(270 Mz; $CDCl_3$) 8.89 (d, *J* 5, 2H), 8.88 (d, *J* 5, 2H), 8.80 (d, *J* 5, 2H), 8.76 (d, *J* 5, 2H), 8.71 (br s, 1H), 8.36 (d, *J* 8, 2H), 8.29 (d, *J* 8, 4H), 8.20 (d, *J* 8, 2H), 8.19 (br s, 1H), 8.05 (s, 4H), 7.97 (d, *J* 8, 2H), 7.81 (s, 2H), 7.74 (s, 1H), 7.67 (br s, 2H), 7.58 (d, *J* 8, 1H), 7.10 (d, *J* 8, 1H), 4.85 (s, 2H), 4.63 (d, *J* 10, 1H), 4.43 (s, 1H), 4.30 (s, 2H), 4.18 (t, *J* 7, 2H), 4.09 (s, 5H), 3.82 (d, *J* 10, 1H), 2.69 (s, 3H), 2.53 (q, *J* 7, 2H, C*H*$_2$SH), 1.99 (quintet, *J*, 2H), 1.7–1.2 (m, 53H), −2.80 (br s, 2H).

1 M. R. Wasielewski, *Chem. Rev.*, 1992, **92**, 435.
2 P. Seta, E. Bienvenue, A. L. Moore, P. Mathis, R. V. Bensasson, P. A. Liddell, P. J. Pessiki, A. Joy, T. A. Moore and D. Gust, *Nature*, 1985, **316**, 653.
3 M. Fujihira, *Mol. Cryst. Liq. Cryst.*, 1990, **183**, 59.
4 G. Steinberg-Yfrach, J.-L. Rigaud, E. N. Durantini, A. L. Moore, D. Gust and T. A. Moore, *Nature*, 1998, **392**, 479.
5 A. Ulman, *Introduction to Ultrathin Organic Films*, Academic Press, San Diego, 1991.
6 H. Imahori, S. Ozawa, K. Ushida, M. Takahashi, T. Azuma, A. Ajavakom, T. Akiyama, M. Hasegawa, S. Taniguchi, T. Okada and Y. Sakata, *Bull. Chem. Soc. Jpn.*, 1999, **72**, 485.
7 K. Uosaki, T. Kondo, X.-Q. Zhang and M. Yanagida, *J. Am. Chem. Soc.*, 1997, **119**, 8367.
8 K. Tamaki, H. Imahori, Y. Nishimura, I. Yamazaki and Y. Sakata, *Chem. Commun.*, 1999, 625.
9 M. Maggini, G. Scorrano and M. Prato, *J. Am. Chem. Soc.*, 1993, **115**, 9798.
10 H. Imahori, H. Norieda, S. Ozawa, K. Ushida, T. Azuma, K. Tamaki and Y. Sakata, *Langmuir*, 1998, **14**, 5335.
11 C. A. Mirkin and W. B. Caldwell, *Tetrahedron*, 1996, **52**, 5113.
12 H. Imahori, T. Azuma, A. Ajavakom, S. Ozawa, H. Yamada, H. Norieda, K. Ushida and Y. Sakata, *Chem. Commun.*, 1999, 557.
13 H. Imahori and Y. Sakata, *Adv. Mater.*, 1997, **9**, 537.
14 N. Martín, L. Sánchez, B. Illescas and I. Pérez, *Chem. Rev.*, 1998, **98**, 2527.
15 D. M. Guldi and K.-D. Asmus, *J. Am. Chem. Soc.*, 1997, **119**, 5744.

Communication 9/03237A

Superior performance of a chiral catalyst confined within mesoporous silica

Brian F. G. Johnson,*[a] Stuart A. Raynor,[a] Douglas S. Shephard,[a] Thomas Mashmeyer,[ab] John Meurig Thomas,*[b] Gopinthar Sankar,[b] Stefen Bromley,[b] Richard Oldroyd,[b] Lynn Gladden[c] and Mike D. Mantle[c]

[a] *Department of Chemistry, The University of Cambridge, Lensfield Road, Cambridge, UK CB2 1EW. E-mail: bfgj1@cam.ac.uk*

[b] *Davy-Faraday Research Laboratories, The Royal Institution of Great Britain, 21 Albemarle Street, London, UK W1X 4BS*

[c] *Department of Chemical Engineering, The University of Cambridge, New Museum Site, Cambridge, UK CB2 3QZ*

Received (in Cambridge, UK) 26th March 1999, Accepted 12th May 1999

A chiral catalyst from the ligand 1,1′-bis(diphenylphosphino)ferrocene (dppf) anchored to the inner walls of the mesoporous support MCM-41 and co-ordinated to Pd^{II} has been shown to exhibit a degree of regioselectivity and enantiomeric excess, in the allylic amination of cinnamyl acetate, which is far superior to that of its homogeneous counterpart or that of a surface-bound analogue attached to a non-porous silica.

Stereo- and regio-selective catalysis lies at the heart of current developments in pharmaceutical, agrochemical and cognate industries.[1–3] The recognition that a small amount of a chiral catalyst may yield large quantites of a targeted chiral product has already led to the development of several ingenious methods for the design of such catalysts. These include modified metals,[4] metal oxides[5] and zeolites,[6,7] and the so-called 'ship-in-bottle' or 'tea-bag' systems.[8–10] In this work we have been able to demonstrate that a chiral ligand derived from 1,1′-bis(diphenylphosphino)ferrocene (dppf) bonded to an active metal centre (in this case Pd^{II})† and tethered, *via* a molecular link of appropriate length, to the inner walls of a mesoporous silica support (MCM-41, *ca*. 30 Å diameter) yields a degree of catalytic regioselectivity as well as an enantiomeric excess that is far superior to either the homogeneous counterpart or the cabosil-bound catalyst (Cabosil is a non-porous, high-area silica).

Our conceptual methodology was to take a homogeneous system of known catalytic behaviour and, by performing suitable modifications, to tether this catalyst within the mesopore.[11] Care is taken to ensure that all activity is confined to the internal surface of the MCM-41 channels. This is achieved by selectively deactivating the external surface of the support. We have shown previously by electron microscopy, on functionalised mesopores stained with Ru_6-based clusters, that this is a reliable and satisfactory method.[12]

Our approach to the preparation of the catalytic system is shown in Scheme 1. The mesoporous framework was first treated with Ph_2SiCl_2 under *non-diffusive conditions* to deactivate the exterior walls of the material. The interior walls of this same material were then derivatised with 3-bromopropyltrichlorosilane to give the activated MCM-41 **1**.

The ferrocenyl-based ligand, (*S*)-1-[(*R*)-1′,2-bis(diphenylphosphino)ferrocenyl]ethyl-*N*,*N*′-dimethylethylenediamine **2**, was prepared from ferrocene by literature methods.[13,14] On

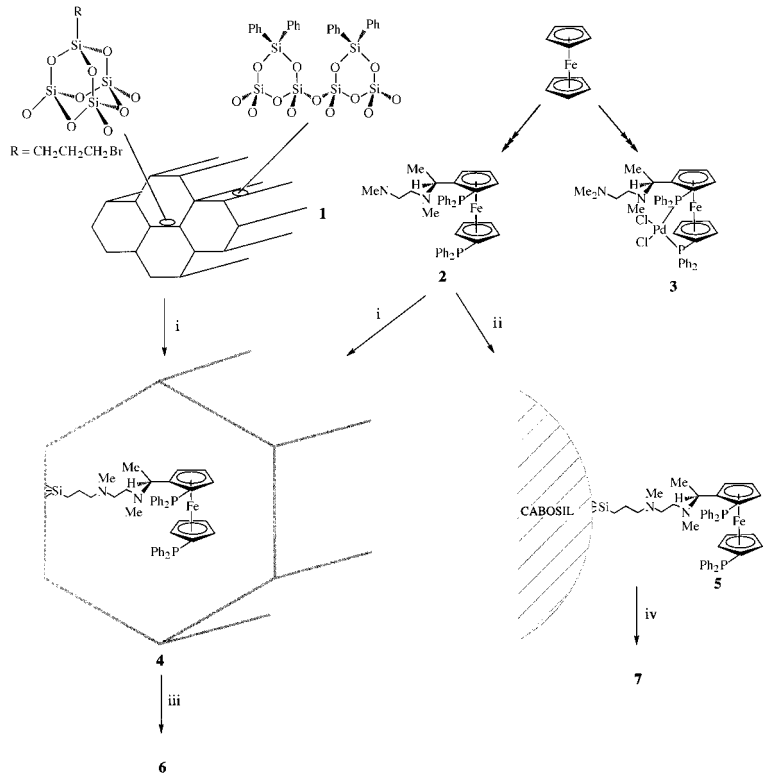

Scheme 1 The synthetic routes used in the preparation of the homogeneous catalyst **3**, the mesopore-supported **6** and the carbosil-bound **7**. *Reagents and conditions*: formation of **1**(a) Ph_2SiCl_2–THF, 25 °C, (b) $Cl_3SiCH_2CH_2CH_2Br$–THF, −78 °C; i, THF, 25 °C; ii, THF, 25 °C; iii $PdCl_2$–MeCN–THF, 25 °C; iv $PdCl_2$–MeCN–THF, 25 °C.

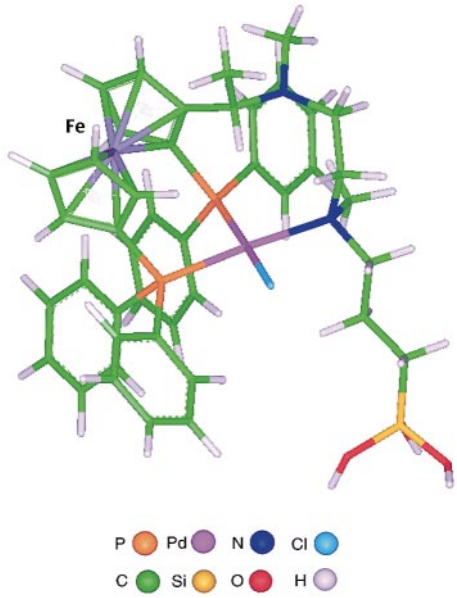

Fig. 1 Computer model of the catalytic centre inside MCM-41.

treatment of the activated MCM-41 **1** with an excess of **2** yields the chiral catalytic precursor **4** which, on reaction with $PdCl_2$–MeCN, gives the required catalyst **6**. In a separate experiment the closely related cabosil-supported catalyst **7** was prepared in a similar manner from surface-activated cabosil and **2** followed by addition of the required palladium(II) salt.

The catalyst **6** was fully characterised by a range of techniques. First, the structural integrity of the MCM-41 catalytic precursor **4** was established by MAS NMR and EXAFS spectroscopy. The presence of the tethered ferrocenyl catalysts was confirmed by comparison of the ^{13}C MAS NMR spectrum of **4** with that of the unattached precursor **2**. Apart from the additional signals arising from the propyl tethering unit the spectra were essentially the same. Examination of the ^{31}P MAS NMR of **2** and **4** showed identical chemical shift values. On incorporation of the Pd^{II} ion to yield the active catalyst **6**, significant changes in the aliphatic region of the ^{13}C MAS NMR and in the ^{31}P MAS NMR spectra were noted. Two ^{31}P resonances at δ 15.9 and 34.4 were recorded, clearly indicating two different phosphorous environments, these have been assigned as one being *trans* to a nitrogen and the other being *trans* to a chloride.[15] The change in the aliphatic region of the ^{13}C MAS NMR corresponds to changes in the methyl resonances of the amines, further corroborating the assignment of the ^{31}P spectrum. This entire arrangement was borne out by a detailed EXAFS analysis of **6**. The coordination environment of the cationic species within the mesopore is depicted in Fig. 1.

In testing our catalysts we decided to use an allylic amination reaction between cinnamyl acetate and benzylamine (Scheme 2). This reaction has two possible products: a straight chained product (which is favoured due to the retention of the delocalised π system) and a chiral branched product. The aim of the reaction is to produce the greatest possible yield of the branched product with the highest possible enantiomeric excess

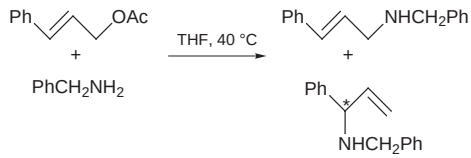

Scheme 2 The catalytic reaction between cinnamyl acetate and benzylamine.

Table 1 Catalytic results

Catalyst[a]	Conversion[b] (%)	Straight chain[c] (%)	Branched (%)	ee[d] (%)
3 (*S*)	76	99+	—	—
7 (*S*)	98	98	2	43
6 (*S*)	99+	49	51	99+
6 (*R*)	99+	50	50	93

[a] Symbols in parentheses denote chirality of the directing group. [b] % Conversion is stated relative to the use of benzylamine. [c] Regio- and enantio-selectivity determined by gas chromatography on a Chiraldex G-DA column (Alltech) with γ-cyclodextrin as the active phase (20 m). *Conditions*: He pressure 12.5 psi; temperature ramped 50–180 °C at 10 °C min^{-1} and then held for the duration of the run. [d] Major stereoisomer possesses the same chirality as the catalyst. Retention time *ca.* 38 min.

(ee). Three catalysts were examined: the homogeneous {(*S*)-1-[(*R*)-1′,2-bis(diphenylphosphino)ferrocenyl]ethyl-*N*,*N*′-dimethylethylenediamine} palladium dichloride **3**, the cabosil-supported one **7** and that attached within the mesoporous material **6**. Preliminary results of the studies are listed in Table 1. With the homogeneous catalyst **3** the reaction is directed solely towards the straight chain product whilst catalyst **7** shows some of the desired regioselectivity by producing 2% of the branched product. Unfortunately the enantioselectivity of the reaction is relatively low with an ee of 43%. The use of the mesopore-confined catalyst **6** promotes a dramatic change in the regioselectivity of the reaction, producing 51% of the branched product. The enantioselectivity of the catalysis is also greatly improved relative to the cabosil-bound catalyst with the ee approaching 100%.

These results indicate that the control exercised by the MCM-41 on the activity of the ferrocenyl catalyst is considerable. The profound changes in the regio- and enantio-selectivity are clearly apparent from the data listed in Table 1. Other, related systems are currently under investigation.

This work was supported by the EPSRC, ICI (Wilton) and the Newton Trust (S. A. R.), a Royal Society Fellowship and Peterhouse (D. S. S).

Notes and references

† Other metal ions, *e.g.* Rh(I) may also be employed.

1 R. Noyori, *Asymmetric Catalysis in Organic Synthesis*, Wiley, New York, 1994.
2 J. M. Brown and S. G. Davies, *Nature*, 1994, **370**, 418.
3 *Advances in Catalytic Processes: Asymmetric Chemical Transformations*, ed. M. Boyle, JAI, Greenwich, CT, vol. 1.
4 A. Pfalz and T. Heinz, *Top. Catal.*, 1997, 4, 229.
5 A. Baiker, *Curr. Opin. Solid State Mater. Sci., 1998*, **3**, 86.
6 *Top Catal*., ed. D. G. Blackmond and W. Leitner, 1997, **4**, Part 1.
7 A. Corma, M. Iglesias, C. del Pino and F. Sanchez, *J. Chem. Soc., Chem. Commun.*, 1991, 1253.
8 J. M. Thomas, *Philos. Trans. R. Soc. London, Ser. A*, 1990, **333**, 173.
9 C. L. Hill, *Activation and Functionalisation of Alkanes*, Wiley, New York, 1989.
10 M. J. Sabater, A. Corma, A. Domenech, V. Fornes and H. Garcia, *Chem. Commun.*, 1997, 1285.
11 J. M. Thomas, T. Maschmeyer, B. F. G. Johnson and D. S. Shephard, *J. Mol. Catal.*, 1999, **141**, 139.
12 D. S. Shephard, W. Z. Zhou, T. Mashmeyer, J. M. Matters, C. L. Roper, S. Parsons, B. F. G. Johnson and M. J. Duer, *Angew. Chem., Int. Ed.*, 1998, **37**, 2719.
13 G. W. Gokel and I. K. Ugi, *J. Chem. Educ.*, 1972, **49**, 294.
14 T. Hayashi, T. Mise, M. Fukushima, M. Kagotani, N. Nagashima, Y. Hamada, A. Matsumoto, S. Kawakami, M. Konishi, K. Yamamoto and M. Kumada, *Bull. Chem. Soc. Jpn.*, 1980, **53**, 1138.
15 T. Suzuki, M. Kita, K. Kashiwabara and F. Fujita, *Bull. Chem. Soc. Jpn.*, 1990, **63**, 3434; P. J. Stang, D. H. Cao, S. Siato and A. M. Arif, *J. Am. Chem. Soc.*, 1995, **117**, 6273.

Communication 9/02441G

Permanent blockade of *in situ*-generated acid Brønsted sites of vanadyl pyrophosphate catalysts by pyridine during the partial oxidation of toluene

Andreas Martin,* Ursula Bentrup, Bernhard Lücke and Angelika Brückner

Institut für Angewandte Chemie Berlin-Adlershof e.V., Rudower Chaussee 5 D-12484 Berlin, Germany. E-mail: a.martin@aca-berlin.de

Received (in Cambridge, UK) 6th April 1999, Accepted 20th May 1999

The permanent blockade of *in situ*-formed Brønsted-acid OH groups and an effective lowering of the catalyst acidity during the partial oxidation of toluene to benzaldehyde is demonstrated by an efficient method using a continuous dosing of pyridine to the feed that leads to drastically increased aldehyde selectivities.

Vanadium phosphates (VPO) are well known as catalysts for selective O- and N-insertion reactions of aliphatics and methylaromatics.[1,2] Recently, we have studied the ammoxidation of toluene on vanadyl pyrophosphate [$(VO)_2P_2O_7$] in detail and obtained knowledge on the formation of benzaldehyde, acting as a reaction intermediate.[3] Therefore, the idea arose to test these catalysts for the partial oxidation of toluene. However, the catalytic performance of these solids is rather poor: benzaldehyde selectivities >40% could only be reached at toluene conversions <5% and mainly carbon oxides were identified as by-products in the effluent. A number of further oxidised intermediates (cyclic anhydrides are of prime importance) that remain chemisorbed on the catalyst surface were detected by FTIR spectroscopy.[4] The reason for the rather low aldehyde selectivity can be seen in a very strong adsorption of toluene and/or intermediates on the rather acidic surface of the VPO catalyst as confirmed by *in situ*-EPR measurements carried out recently.[4] Furthermore, it is also supposed that the existence of M–OH sites could be involved in the oxidation of the aromatic nucleus, leading to total oxidation.[5]

Here, we present investigations on the partial oxidation of toluene to benzaldehyde with vanadyl pyrophosphate used as catalyst, especially on the effect of Brønsted-acid OH groups of the catalyst surface using *in situ*-FTIR spectroscopy. A procedure is proposed to block such *in situ*-generated acid OH groups by pyridine. Additionally, an effective increase of the basicity of the catalyst surface can be reached that might enhance the desorption rate of the desired aldehyde.

$(VO)_2P_2O_7$ (VPP) was generated by the usual dehydration of $VOHPO_4{\cdot}0.5H_2O$ used as precursor compound (723 K, 4 h, 10 l h^{-1} N_2). The catalytic properties were determined during the oxidation of toluene to benzaldehyde, using a fixed bed quartz-glass reactor. The catalyst (0.5 g) was applied as sieve fraction (1–1.25 mm) and mixed with an equal portion of quartz glass (1 mm) to avoid local overheating. The effluent was analysed by GC and the formation of CO/CO_2 was permanently followed by non-dispersive IR photometry. The *in situ*-FTIR investigations were carried out on a Bruker IFS 66 FTIR spectrometer using self-supporting discs with a diameter of 20 mm and a weight of 50 mg, mounted in an heated IR cell.

Fig. 1 depicts FTIR spectra of adsorbates of the partial oxidation of toluene (air– toluene = 100 : 1, 573 K) on VPP [*(a)* fresh VPP, *(b)* VPP pretreated with water vapour (4.2 mmol h^{-1} H_2O in air, 30 min) at 573 K prior to feed exposure). Beside the bands of the aromatic ring vibration (1605, 1500 cm^{-1}) and that of the adsorbed benzaldehyde (1678 cm^{-1}), the bands of cyclic anhydrides (1858, 1783 cm^{-1}) always appeared. These cyclic anhydrides can be considered as total oxidation precursors.[6] Additionally, Fig. 1 also shows FTIR spectra of air–benzaldehyde mixtures (air–benzaldehyde = 91 : 1) adsorbed at 573 K on the parent VPP sample *(c)* and on a VPP specimen pretreated with water vapour as mentioned above *(d)*. Normally, the benzaldehyde adsorption is characterised by the appearance of two vibration bands at *ca.* 1720 and 1705 cm^{-1} assigned as carbonyl stretching vibrations. In the spectrum of the water vapour pretreated sample a further carbonyl stretching band at 1685 cm^{-1} has been observed. The shift of the carbonyl band to lower wavenumbers points to a weakening of the C=O bond. This effect can be explained by a strengthening of the adsorption of the aldehyde[7] by interaction of neighbouring OH groups with the carbonyl groups probably *via* hydrogen bonding. This can also be seen in the case of the toluene–air adsorption under working conditions [Fig. 1, spectra *(a)* and *(b)*]: The carbonyl band is obviously shifted to lower wavenumbers, independent of the catalyst pretreatment, *i.e.* the water produced during the catalytic reaction causes the same effect as has been found for the water vapour pretreatment of the catalyst. This behaviour explains the findings of the recent *in situ*-EPR measurements[4] and provides a reason for the strong chemisorption of aldehyde intermediates and therefore, their subsequent oxidation in consecutive reactions.

Scheme 1 illustrates these ideas. The VPP catalyst surface consists of vanadyl dioctahedra units linked *via* V–O–P bridges with the phosphate tetrahedra of the pyrophosphate chains. A toluene molecule is chemisorbed on the Lewis sites *via* its π-electron system. An electrophilic attack on the methyl group leads to a methylene-like species, water is probably eliminated by the collaboration of bulk oxygen, which is in turn replaced by gas-phase oxygen. Thus, benzaldehyde is formed that is able to desorb, but simultaneously, the liberated water molecule can attack the neighbouring V–O–P bond, generating OH groups (V–OH and P–OH) which interact with benzaldehyde *via* hydrogen bonding and its fast desorption is markedly hindered.

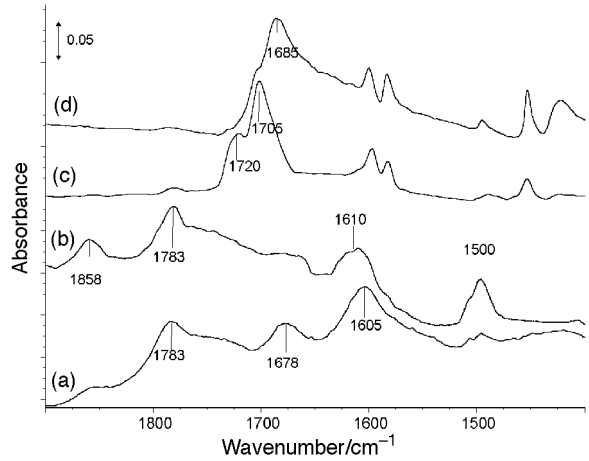

Fig. 1 FTIR spectra of adsorbates on a $(VO)_2P_2O_7$ catalyst at 673 K: (a) air–toluene flow (molar ratio = 100 : 1, 4.2 mmol toluene h^{-1}, 60 min), (b) the same air–toluene flow after water vapour pretreatment (4.2 mmol H_2O h^{-1} in air, 30 min), (c) air–benzaldehyde flow (molar ratio = 91 : 1, 2.3 mmol benzaldehyde h^{-1}, 60 min) and (d) the same air-benzaldehyde flow after water vapour pretreatment (4.2 mmol H_2O h^{-1} in air, 30 min).

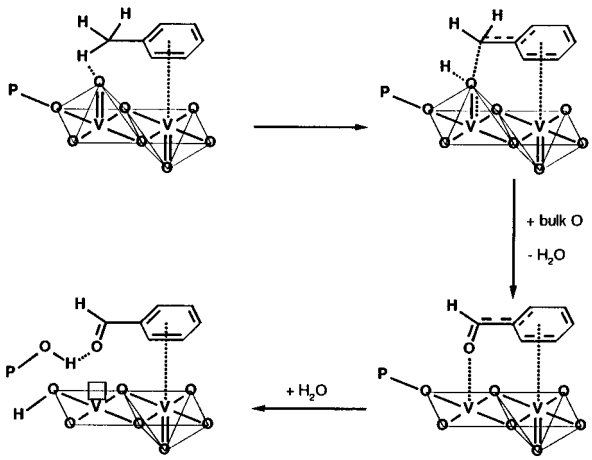

Scheme 1

The blockade or poisoning of OH groups by alkali metal cations[8] or tertiary amines[9] prior to use is already known but also *in situ*-poisoning experiments have been described. Nag *et al.*[10] observed a benzaldehyde selectivity increasing effect on MoO_x/TiO_2 catalysts at 633 K by introduction of pyridine pulses to a toluene-containing feed. This selectivity increase was accompanied by a sudden drop in the toluene conversion; acid sites (Brønsted as well as Lewis sites being necessary for toluene chemisorption) were immediately blocked. The authors concluded that the total oxidation is connected with relatively strong acid sites.

However, the idea arose to block the OH groups generated under VPP catalyst working conditions permanently. Thus, the task was to find a blocking agent that meets diverse requirements; (i) the blocking agent can be continuously dosed, (ii) it should not be involved in the catalytic reaction and (iii) sites of catalytic activity should not be covered.

Therefore, we attempted to use pyridine as an unoxidizable 'co-feed' and the FTIR spectra of Fig. 2 demonstrate the effect. Spectrum (a) shows the known spectrum if toluene and air are dosed. A continuous admixture of water vapour to such a feed causes no significant change of adsorbed species, additionally, a broad band of adsorbed water (1618 cm^{-1}) is observed as demonstrated in spectrum *(b)*. However, if a 4 wt% aqueous pyridine solution is used instead of pure water, spectrum *(c)* is obtained. This spectrum reveals the existence of pyridinium ions (Brønsted-acid sites) at 1540 cm^{-1} as well as coordinatively bound pyridine (Lewis-acid sites) at 1448 cm^{-1} but surprisingly, only low intensity bands of cyclic anhydrides and no band of adsorbed benzaldehyde are observed. One could suppose that no reaction occurred but the catalytic investigations prove the opposite. The beneficial effect of pyridine on the product desorption has also been demonstrated by *in situ*-EPR measurements. Changes of the EPR signal shape due to strong adsorption were found to be reversible by adding a 4 wt% aqueous pyridine solution to the feed, while no such effect was observed by adding water only. Fig. 3 depicts the selectivity data using a similar VPP catalyst during catalytic runs at 663 K; the toluene conversion amounts to *ca.* 12 mol%. It is clearly shown that the admixture of water vapour does not influence the selectivity but the addition of pyridine reveals a nearly threefold improvement of selectivity to benzaldehyde at constant conversion rates. Thus, pyridine is able to block the Brønsted-acid sites generated during the reaction and also to increase the surface basicity of the catalyst; otherwise, it seems unlikely that the chemisorption of toluene, occurring *via* the Lewis sites is markedly influenced.

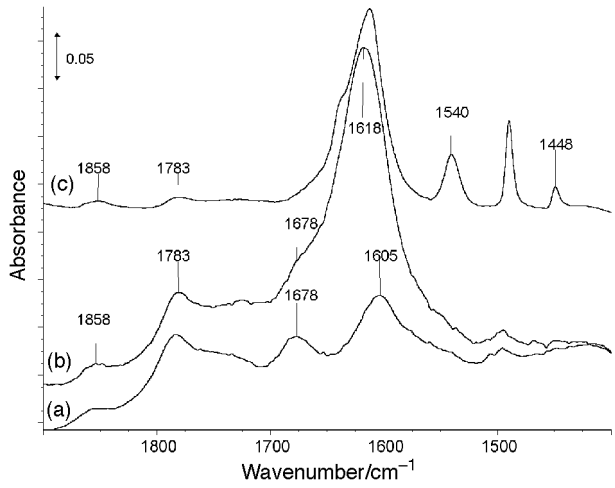

Fig. 2 FTIR spectra of intermediates of the partial oxidation of toluene on a $(VO)_2P_2O_7$ catalyst at 573 K: (a) air-toluene flow (molar ratio = 100 : 1, 4.2 mmol toluene h^{-1}, 60 min), (b) air–toluene–water vapour flow (molar ratio = 100 : 1 : 1, 4.2 mmol toluene h^{-1}, 60 min) and (c) air–toluene–water vapour (containing 4 wt% pyridine) flow (molar ratio = 100 : 1 : 1, 4.2 mmol toluene h^{-1}, 60 min).

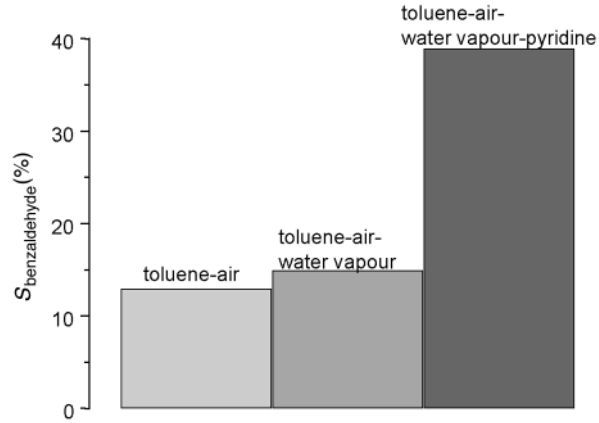

Fig. 3 Benzaldehyde selectivity of the partial oxidation of toluene over a $(VO)_2P_2O_7$ catalyst at 663 K and a *W*/*F* (total flow) = *ca.* 1 g h mol^{-1} using the following feed compositions: (a) air–toluene flow (molar ratio = 100 : 1), (b) air–toluene–water vapour flow (molar ratio = 100 : 1 : 1) and (c) air–toluene–water vapour (containing 4 wt% pyridine) flow (molar ratio = 100 : 1 : 1). Toluene conversion: 12 mmol in each case.

The demonstrated continuous tuning of the acid–base properties of the catalyst surface by a permanent blockade of *in situ*-generated OH groups, accompanied by the increase of the surface basicity of the surface results in drastically increased partial oxidation product selectivities.

The authors thank Mrs U. Wolf for experimental assistance and the Federal Ministry of Education and Research, Germany for financial support (project No. 03 C 0279 0).

Notes and references

1 *Vanadylpyrophosphate Catalysts*, ed. G. Centi, *Catal. Today*, 1993, **16**.
2 A. Martin and B. Lücke, *Catal. Today*, 1996, **32**, 279.
3 Y. Zhang, A. Martin, H. Berndt, B. Lücke and M. Meisel, *J. Mol. Catal. A: Chem.*, 1997, **118**, 205.
4 A. Martin, U. Bentrup, A. Brückner and B. Lücke, *Catal. Lett.*, 1999, **59**, 61.
5 A. Kaszonyi, M. Antol, M. Hronec, G. Delahay and D. Ballivet-Tkatchenko, *Collect. Czech. Chem. Commun.*, 1995, **60**, 505.
6 S. L. T. Andersson, *J. Catal.*, 1986, **98**, 138.
7 A. J. van Hengstum, J. Pranger, S. M. van Hengstum-Nijhuis, J. G. van Ommen and P. J. Gellings, *J. Catal.*, 1986, **101**, 323.
8 M. Ponzi, C. Duschatzky, A. Carrascull and E. Ponzi, *Appl. Catal. A: Gen.*, 1998, **169**, 373.
9 C. Brönnimann, T. Mallat and A. Baiker, *J. Chem. Soc., Chem. Commun.*, 1995, 1377.
10 N. K. Nag, T. Fransen and P. Mars, *J. Catal.*, 1981, **68**, 77.

Communication 9/02700I

ChemComm

New luminescent ruthenium complexes with extended π systems

G. Albano,[a] P. Belser,*[a] L. De Cola*[b] and M. T. Gandolfi[c]

[a] *Institute of Inorganic Chemistry, University of Fribourg, Pérolles, CH-1700 Fribourg, Switzerland. E-mail: peter.belser@unifr.ch*
[b] *IMC, University of Amsterdam, Nieuwe Achtergracht 166, 1018 WV Amsterdam, The Netherlands*
[c] *Department of Chemistry 'G. Ciamician', University of Bologna, I-40126 Bologna, Italy*

Received (in Basel, Switzerland) 3rd February 1999, Accepted 24th April 1999

New Ru(II) complexes are presented as potential luminescent sensors, fluorescent labels and DNA photoprobes.

Owing to their remarkable properties, Ru(II) polypyridyl complexes are used in several areas.[1,2,3] The chelating ligands play an important role in determining the properties of such systems.[4] In $[Ru(dppz)(bpy)_2]^{2+}$ the dppz (dipyrido[3,2-*a*:2,3-*c*]phenazine) ligand is suitable for the direct formation of a charge transfer excited state,[5] which is an important requirement for solar energy conversion. Furthermore dppz contains an extended aromatic system which can bind *via* π–π interaction to the DNA helix.[6] Along this line, two novel phenanthroline-type ligands, CN_2-np (naphtho[2,3-*f*][1,ω]phenanthroline-9,14-dicarbonitrile) and np (naphtho[2,3-*f*][1,ω]phenanthroline) have been prepared, which present some structural features similar to those of dppz. Fukui function calculations[7] indicate that, dppz, CN_2-np and, to a minor extent, np can be considered as comprising a bpy chelating subunit anchored to a remote accepting anthracene-type site (9,10-anthracenedicarbonitrile and anthracene respectively). One could therefore expect that the photophysical and electrochemical properties of $[Ru(CN_2\text{-np})(bpy)_2]^{2+}$ and $[Ru(np)(bpy)_2]^{2+}$ would be related to those of $[Ru(dppz)(bpy)_2]^{2+}$, however, we have found some new different interesting features. Since the system of $[Ru(dppz)(bpy)_2]^{2+}$ is still the subject of controversial discussion, the following results will help in the understanding of such complexes.

The CN_2-np ligand was synthesized by condensation of *o*-xylylene dicyanide and 1,10-phenanthroline-5,6-dione in basic conditions. Successive decarboxylation of CN_2-np in basic conditions gives the np ligand (Scheme 1). $[Ru(np)(bpy)_2](PF_6)_2$ was prepared by heating the np ligand with 1 equiv. of $Ru(bpy)_2Cl_2\cdot 2H_2O$ in methoxyethanol at 120 °C under argon for 15 h (yield after chromatographic plate purification: 19%). $[Ru(CN_2\text{-np})(bpy)_2](PF_6)_2$ was prepared by heating the CN_2-np ligand with 1 equiv. of $Ru(bpy)_2Cl_2\cdot 2H_2O$ in ethylene glycol for 6 min in a microwave oven (yield after chromatographic plate purification: 26%).[8]

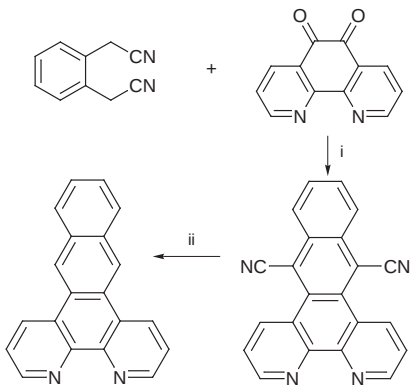

Scheme 1 *Reagents and conditions*: i, 10% solution of NaOEt in EtOH, room temp., 36 h, yield: 90%; ii, KOH, EtOH, argon, reflux, 12 h, yield: 57%.

Electrochemical data (Table 1) show that oxidation is a reversible metal centered Ru(III)/Ru(II) process for both $[Ru(CN_2\text{-np})(bpy)_2]^{2+}$ and $[Ru(np)(bpy)_2]^{2+}$ and the $E_{1/2}$ values obtained are very similar to those reported for $[Ru(bpy)_3]^{2+}$. This suggests that CN_2-np and np are similar to bpy with respect to their coordination ability to ruthenium: the σ donating properties of the two ligands are the same as those of bpy and the back donation from the Ru(II) ion is localized on bpy orbitals having π* character and does not involve the anthracene-type fragment of the two ligands. For $[Ru(CN_2\text{-np})(bpy)_2]^{2+}$, owing to the presence of withdrawing groups (CN), the added electron in the first reduction product and the lowest excited state are expected to be localized on CN_2-np. The first reduction wave of $[Ru(CN_2\text{-np})(bpy)_2]^{2+}$ occurs at a potential (−0.75 V in MeCN) very close to that of the free ligand (−0.79 V in DMSO, identical to that of 9,10-anthracenedicarbonitrile) and 0.27 V less negative than that of $[Ru(dppz)(bpy)_2]^{2+}$, in agreement with a stronger electron accepting character of 9,10-anthracenedicarbonitrile with respect to phenazine (Table 1). The further three monoelectronic reduction steps in $[Ru(CN_2\text{-np})(bpy)_2]^{2+}$ occur close to those of the three first reduction waves of $[Ru(bpy)_3]^{2+}$. This indicates that, after reduction of the anthracenedicarbonitrile fragment, reduction at the two chelating bpy ligands and at the bpy part of the CN_2-np ligand takes place. The last reduction step (−1.67 V) is localized on the bpy moiety of CN_2-np, since it occurs at a potential value less negative than the third reduction wave of $[Ru(bpy)_3]^{2+}$, as expected for bpy connected to an acceptor unit. The first two reduction potentials of $[Ru(np)(bpy)_2]^{2+}$ are very similar to those for $[Ru(bpy)_3]^{2+}$. The reduction potential of the free ligand np (−1.86 V) is similar to that of anthracene (−1.90 V).

Preliminary photophysical measurements show that $[Ru(CN_2\text{-np})(bpy)_2]^{2+}$ and $[Ru(np)(bpy)_2]^{2+}$ behave very differently from each other. The photophysical data are reported in Table 2 where values for $[Ru(bpy)_3]^{2+}$ and $[Ru(dppz)(bpy)_2]^{2+}$ are also listed. The photophysical properties of $[Ru(np)(bpy)_2]^{2+}$ resemble those of $[Ru(bpy)_3]^{2+}$ despite the presence of

Table 1 Electrochemical data[a]

	$E_{1/2}(Ru^{II/III})$/V	E_{red}/V			
			'bpy' centered		
$[Ru(CN_2\text{-np})(bpy)_2]^{2+}$	1.25	−0.75	−1.30	−1.50	−1.67
$[Ru(dppz)(bpy)_2]^{2+}$	1.24	−1.02	−1.44	−1.67	
$[Ru(np)(bpy)_2]^{2+}$	1.24		−1.38	−1.55	
$[Ru(bpy)_3]^{2+}$	1.29		−1.33	−1.52	−1.76
CN_2-np		−0.79[b]			
9,10-anthracenedicarbonitrile		−0.79[b]			
dppz		−1.11[b]			
Phenazine		−0.77[c]			
np		−1.86[b]			
Anthracene		−1.90[b]			

[a] Unless otherwise noted, redox potentials were measured in MeCN *vs.* SCE at room temp.; $NBu^t_4PF_6$ as supporting electrolyte. [b] In DMSO. [c] In DMF, ref. 5.

Table 2 Photophysical data[a]

	Absorption	Emission (298 K)		Emission (77 K)
	λ_{max}/nm (10^{-4} ε/dm^3 mol^{-1} cm^{-1})	λ_{max}/nm (τ/ns)	$10^{-3}\phi_{em}$	λ_{max}/nm (τ/μs)
$[Ru(CN_2\text{-np})(npy)_2]^{2+}$	439 (1.46), 398 (1.26), 380 (1.19), 309 (5.44), 290 (8.42), 256 (3.67), 228 (3.66)	700[b] (120) 610[b,c] (1700, 185)	0.5 2.0[c]	587 (7.1), 660 (464)
$[Ru(ddpz)(bpy)_2]^{2+}$	448 (1.57), 366 (1.55), 357 (1.56), 352 (sh) 315 (sh), 284 (9.36), 255 (4.18), 212 (5.00)	667 (229) 610[c] (260)	390	624 (2.6)
$[Ru(np)(bpy)_2]^{2+}$	452 (1.51), 292 (6.68), 256 (3.13)	610 (170) 610[c] (834)	16 82[c]	578 (6.6)
$[Ru(bpy)_3]^{2+}$	452 (1.45), 345 (sh), 323 (sh), 285 (8.71), 250 (2.51), 238 (2.95), 208 (sh), 185 (8.91)	611 (190) 611[c] (1000)	12 60[c]	600 (4.1)

[a] Unless otherwise noted, photophysical measurements were made in MeCN and emission spectra at 77 K were recorded in butyronitrile. [b] Maximum value of a multicomponent band. [c] De-aerated solution.

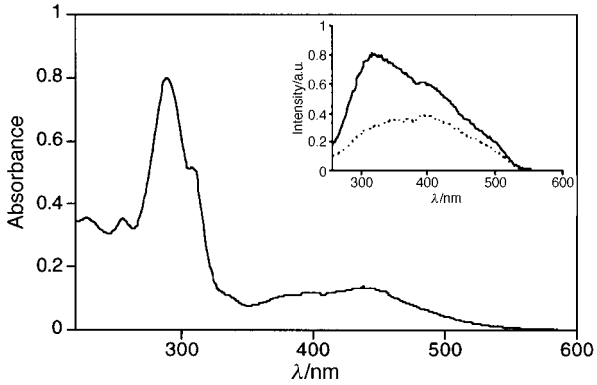

Fig. 1 Absorption spectrum of $[Ru(CN_2\text{-np})(bpy)_2]^{2+}$ in MeCN solution (1.5×10^5 M). Inset: luminescence spectra in aerated (----), and de-aerated (—), MeCN solution.

an extended π system condensed with the bpy ligand. For $[Ru(CN_2\text{-np})(bpy)_2]^{2+}$ the absorption spectrum, recorded in acetonitrile solution, shows the visible region broad bands due to absorption to different ^{1}MLCT excited states, involving both the bpy (higher energy) and the CN_2-np (lower energy) ligands (Fig. 1). It is interesting that CN_2-np shows rather low energy π–π* transitions (350–400 nm), that are also present in the complex, while the higher energy absorption bands are attributed to bpy π–π* transitions. In CH_2Cl_2 solution fluorescence of the free ligand occurs at 427 nm, while no phosphorescence emission was detected even at low temperature. We expect, however, a separation between the singlet and the triplet excited states very similar to that reported for the 9,10-anthracenedicarbonitrile,[9] and therefore a triplet state falling in the 700 nm region. The emission spectrum of $[Ru(CN_2\text{-np})(bpy)_2]^{2+}$ at room temperature in an aerated MeCN solution shows a very broad, multicomponent and weak band centered at 700 nm (Fig. 1). In deaerated solution however the maximum of this band shifts to higher energy and has two different excited state lifetimes (Table 2, and Fig. 1). Such photophysical investigation suggests the presence of two non-equilibrated charge transfer excited states; one state localized on the bpy moiety and the other lower energy state involving the anthracenedicarbonitrile unit. They appear to show different sensitivity to dioxygen, as reflected in their different lifetimes.

At low temperature the excited state lifetime (Table 2) for the lowest energy emitting state of $[Ru(CN_2\text{-np})(bpy)_2]^{2+}$ is far too long (464 μs) to be assigned to a pure ^{3}MLCT excited state. The long lived luminescence at low temperature could be attributed to a smaller degree of excited state distortion owing to the greater delocalization of the excited electron in the CN_2-np π* system as similarly reported by Meyer and coworkers[10] for a series of ruthenium complexes. However, for $[Ru(CN_2\text{-np})(bpy)_2]^{2+}$ the effect is really drastic, and in the absence of the CN groups, no effect due to delocalization is observed. Therefore the presence of a low lying triplet state centered on the CN_2-np ligand, close in energy to the lowest ^{3}MLCT excited state, should play an important role. When the solution is frozen, the ^{3}MLCT excited states move to higher energy and the intraligand (IL) state becomes the low lying excited state with a longer lifetime (Table 2). Such intraligand excited states have been previously observed in transition metal complexes.[11] The extremely long excited state lifetime is of course a very appealing property for the use of such a complex as a luminescent sensor or fluorescent label.

As mentioned above, $[Ru(np)(bpy)_2]^{2+}$ in MeCN shows emission properties similar to those of $[Ru(bpy)_3]^{2+}$. However in aqueous buffered solution an enhancement of the luminescence quantum yield in the presence of DNA, is observed as reported for $Ru(dppz)(phen)_2]^{2+}$.[12] With respect to $[Ru(dppz)(phen)_2]^{2+}$, $[Ru(np)(bpy)_2]^{2+}$ is already strongly luminescent in aqueous solution (in the absence of DNA), the quantum yield of luminescence is increased only by a factor of 2.5 ($\geqslant 10^6$ for $[Ru(dppz)(phen)_2]^{2+}$) and a simple monoexponential decay is observed in presence of increasing amounts of DNA. $[Ru(CN_2\text{-np})(bpy)_2]^{2+}$ shows, under the same conditions as above, a lowering of the absorption coefficient in the presence of DNA. In particular the bands at 350–400 nm corresponding to π–π* transitions of CN_2-np are diminished with increasing DNA concentration. This suggests binding of the anthracenedicarbonitrile unit of the ligand to the DNA helix.

This work was supported by MURST, CNR and the Swiss National Science Foundation. The authors would like to thank Professor V. Balzani for helpful discussion and Nunzio Salluce for help in some measurements.

Notes and references

1 K. Kalyanasundaran, *Coord. Chem. Rev.*, 1982, **46**, 159.
2 A. Juris, V. Balzani, F. Barigelletti, S. Campagna, P. Belser and A. von Zelewsky, *Coord. Chem. Rev.*, 1988, **84**, 85.
3 A. M. Pyle, J. P. Rehman, R. Meshoyrer, C. V. Kumar, N. J. Turro and J. K. Barton, *J. Am. Chem. Soc.*, 1989, **111**, 3051; J. M. Kelly, A. B. Tossi, D. J. MacDonnell and C. OhUigin, *Nucleic Acids Res.*, 1985, **13**, 6017.
4 F. Barigelletti, P. Belser, A. von Zelewsky, A. Juris and V. Balzani, *J. Phys. Chem.*, 1985, **89**, 3680.
5 E. Amouyal, A. Homsi, J.-C. Chambron and J.-P. Sauvage, *J. Chem. Soc., Dalton Trans.*, 1990, 1841.
6 A. E. Friedman, J.-C. Chambron, J.-P. Sauvage, N. J. Turro and J. K. Barton, *J. Am. Chem. Soc.*, 1990, **112**, 4960.
7 F. Gilardoni, J. Weber, H. Chermette and T. R. Ward, *J. Phys. Chem.*, 1998, **102**, 3607.
8 The compounds have been fully characterised and the data will be reported in a subsequent full paper.
9 S. L. Murov, I. Carmichael and G. L. Hug, *Handbook of Photochemistry*, Dekker, New York, 2nd edn., 1993 and references therein.
10 G. F. Strouse, J. R. Schoonover, R. Duesing, S. Boyde, W. E. Jones Jr. and T. J. Meyer, *Inorg. Chem.*, 1995, **34**, 473.
11 A. I. Baba, H. E. Ensley and R. H. Schmehl, *Inorg. Chem.*, 1995, **34**, 1198; A. I. Baba, J. R. Shaw, J. A. Simon, R. T. Thummel and R. H. Schmehl, *Coord. Chem. Rev.*, 1998, **171**, 43.
12 C. Hiort, P. Lincoln and B. Nordén, *J. Am. Chem. Soc.*, 1993, **115**, 3448.

Communication 9/00911F

ChemComm

A new method for the synthesis of chromium(IV) oxide at ambient pressure†

K. Ramesha and J. Gopalakrishnan*

Solid State and Structural Chemistry Unit, Indian Institute of Science, Bangalore 560 012, India.
E-mail: gopal@sscu.iisc.ernet.in

Received (in Cambridge, UK) 13th April 1999, Accepted 18th May 1999

The reaction $CrO_3 + 2NH_4X \rightarrow CrO_2 + 2\ NH_3 + H_2O + X_2$ (X = Br, I), which occurs quantitatively at 120–150 °C, provides a convenient method for the synthesis of CrO_2; unlike conventional methods, the method reported here does not require the use of high pressure for the synthesis of this technologically important material.

Chromium(IV) oxide, CrO_2, is unique among the rutile-type transition metal dioxides,[1] exhibiting ferromagnetic (T_c = 395 K) and metallic properties.[2] Because of these properties, the material finds application as a magnetic recording medium in the form of tapes. In recent years, there has been a renewed interest in this material in view of the realization[3] that it is a 'half-metallic' ferromagnet [*i.e.*, the majority (spin-up) electrons are delocalized, while the minority (spin-down) electrons are localized, having a semiconductor-like gap in the density-of-states] with a nearly 100% spin polarization[4] at the Fermi energy. An important consequence of the half-metallic nature is that films of CrO_2 exhibit a low-field tunneling-type magnetoresistance[5] that appears promising for application.

Since CrO_2 is a metastable phase[2] (decomposing at > 288 °C at 1 atm pressure of O_2), all the methods reported for its synthesis require high pressures.[2] Hydrothermal decomposition of aqueous solutions of CrO_3 at elevated temperatures and pressures (typically 480 °C and 2 kbar) is a common method for the synthesis of polycrystalline CrO_2 powders.[2] Growth of single crystals[6] however require much higher temperatures (900–1300 °C) and pressures (60–65 kbar).

Considering the technological and scientific importance of CrO_2, we developed a new method for its synthesis at ambient pressure. Our method is based on the low-temperature (120–150 °C) reduction of CrO_3 by NH_4I/NH_4Br followed by annealing the solid product at temperatures below the decomposition point of CrO_2. The method crucially depends on the solid state reaction given by eqn. (1)

$$CrO_3 + 2\ NH_4X \rightarrow CrO_2 + 2\ NH_3 + X_2 + H_2O \qquad (1)$$

which occurs quantitatively between 120 and 150 °C. Here, we describe the details of synthesis of crystalline CrO_2 by this method and its characterization.

Stoichiometric quantities of CrO_3 (20 mmol) and NH_4X (X = Br, I) (40 mmol) corresponding to eqn. (1) were thoroughly mixed under CCl_4. The mixture, taken in a Pyrex glass tube connected to a vacuum line, was heated slowly *in vacuo* (*ca.* 10^{-5} Torr) under continuous pumping conditions as described earlier.[7] Copious evolution of I_2/Br_2 occurred around 120 °C. The temperature was raised to 150 °C and held at this value until the evolution of I_2/Br_2 ceased (2–3 h). The liberated I_2/Br_2 condensed in a liquid nitrogen trap provided a quantitative measure of the extent of the reduction.[7] Significantly, reaction (1) does not occur with NH_4Cl. This is consistent with the redox characteristics of Cr^{VI} which oxidizes I^- and Br^- but not Cl^- in aqueous solutions.[8]

The black solid product of reaction (1) was stable in air; it was however non-magnetic and amorphous to X-rays [Fig. 1(a)]. Pellets of this product were annealed in evacuated sealed glass tubes at various temperatures and times. We found that annealing at 195 ± 5 °C for one week yielded crystalline CrO_2 with rutile structure. The lattice parameters, a = 4.419 (1), c = 2.915 (1) Å, derived from the X-ray powder diffraction pattern [Fig. 1(b)] are in excellent agreement with the values reported for CrO_2 in the literature.[9] Determination of oxygen content by iodometric titration revealed that the product is stoichiometric ($CrO_{1.99\pm0.02}$).

Measurement of electrical resistivity and magnetic susceptibility revealed that the CrO_2 prepared here is metallic and ferromagnetic as expected. The resistivity and susceptibility data of our samples (Fig. 2) are comparable to the corresponding data reported in the literature[5] for bulk polycrystalline samples

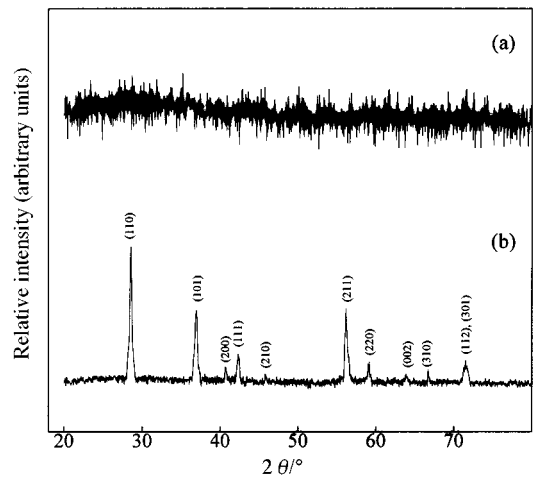

Fig. 1 Powder XRD patterns (Cu-Kα) of (a) solid product of reaction (1) with NH_4I and (b) product (a) annealed at 195 ± 5 °C for one week corresponding to crystalline CrO_2.

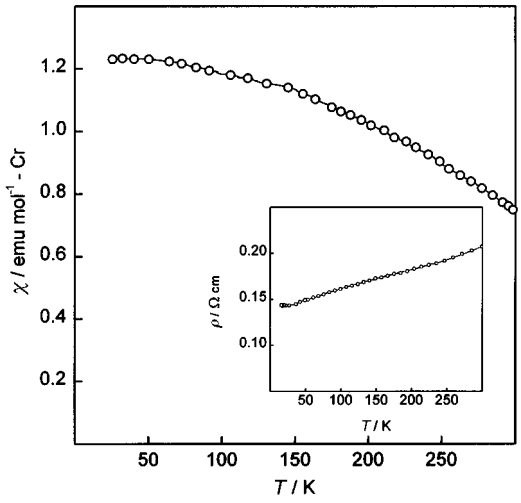

Fig. 2 Temperature dependence of magnetic susceptibility of CrO_2 measured at 0.5 T. Inset shows the temperature dependence of electrical resistivity of the same sample.

† Contribution No. 1412 from the Solid State and Structural Chemistry Unit.

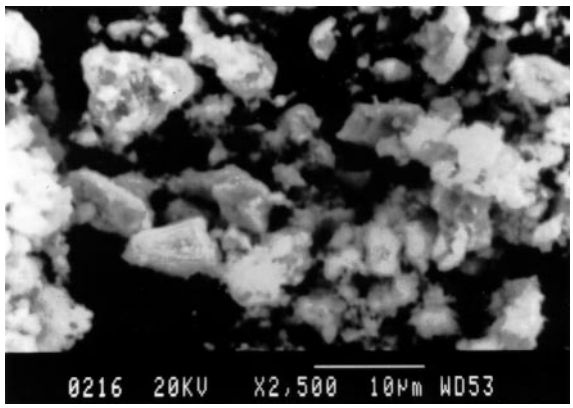

Fig. 3 SEM image of crystalline CrO_2.

as well as films of CrO_2. An SEM study showed that the samples are fairly crystalline, the particle sizes being in the range of a few μm (Fig. 3).

We believe that the key to the success of the method lies in the quantitative nature of reaction (1) which can be controlled to give an average oxidation state of Cr^{IV} in the solid state by using the required quantity of NH_4I/NH_4Br in the reaction mixture. This is in contrast to reactions between Cr^{VI} and I^-/Br^- in aqueous media, which proceed directly to give Cr^{III}; *i.e.* Cr^{VI} is not accessible as a stable species in aqueous media by redox reactions. An investigation of the X-ray morphous CrO_2 would throw light on the mechanism of reaction (1) which stabilizes Cr^{VI} in the solid state.

We can also prepare rutile-related (monoclinic) VO_2 as well as solid solutions of $Cr_{1-x}V_xO_2$ by the same method starting from V_2O_5 and V_2O_5–CrO_3 mixtures. Therefore, we believe that the method described here can be extended to the synthesis of other metastable oxides containing Cr^{IV} and/or V^{IV}, in general.

We thank the Department of Science and Technology, Government of India (Project No. SP/S1/H-17/97) for financial support. K. R. thanks the Council of Scientific and Industiral Research, New Delhi for the award of a fellowship.

Notes and references

1 D. B. Rogers, R. D. Shannon, A. W. Sleight and J. L. Gillson, *Inorg. Chem.*, 1969, **8**, 841.
2 B. L. Chamberland, *CRC Crit. Rev. Solid State Mater. Sci.*, 1977, **7**, 1.
3 K. P. Kämper, W. Schmitt, G. Güntherodt, R. J. Gambino and R. Ruf, *Phys. Rev. Lett.*, 1987, **59**, 2788.
4 R. J. Soulen Jr., J. M. Byers, M. S. Osofsky, B. Nadgorny, T. Ambrose, S. F. Cheng, P. R. Broussard, C. T. Tanaka, J. Nowak, J. S. Moodera, A. Barry and J. M. D. Coey, *Science*, 1998, **282**, 85.
5 H. Y. Hwang and S.-W. Cheong, *Science*, 1997, **278**, 1607.
6 B. L. Chamberland, *Mater. Res. Bull.*, 1967, **2**, 827.
7 V. Bhat and J. Gopalakrishnan, *J. Chem. Soc. Chem. Commun.*, 1986, 1644.
8 J. Bassett, R. C. Denney, G. H. Jeffery and J. Mendham, *Vogel's Textbook of Quantitative Inorganic Analysis*, Longman, London, 4th edn., 1978, p. 51.
9 JCPDS-International Centre for Diffraction Data Card No. 43–1040.

Communication 9/02927C

ChemComm

Nb_2Te_3, a niobium sesquitelluride with Te_2^{2-} groups

Holger Kleinke and Wolfgang Tremel*

Institut für Anorganische Chemie und Analytische Chemie, Universität Mainz, Duesbergweg 10-14, D-55099 Mainz, FRG. E-mail: tremel@indigotrem1.chemie.uni-mainz.de

Received (in Cambridge, UK) 8th March 1999, Accepted 18th May 1999

The new binary compound Nb_2Te_3 was synthesized by reduction of $NbTe_2$ with Ga metal; different from the formally analogous Ta_2Te_3 it crystallizes in the Mo_2As_3 structure type; based on the results of band structure calculations Nb_2Te_3 is metallic with quasi one-dimensional metal electronic properties.

In spite of the spectacular progress made in fields such as supramolecular[1] or nanochemistry,[2] new binary and seemingly simple compounds still continue to be found. Typical examples are early transition metals chalcogenides: about ten new binary phases such as TaS_3,[3] Ta_6Te_5,[4] Ta_3S_2,[5] Ta_2Se,[6], Hf_3Te_2,[7] and $Ti_{11}Se_4$[8] have been reported during the past decade; all of them display a unique structure type. At first sight it may seem surprising that binaries of such simple compositions have escaped detection until recently.

Even more surprising is that these compounds challenge our basic assumptions about the chemistry of the early transition elements and our chemical understanding in general. The chemistries of Zr and Hf are considered nearly identical,[9] and the situation is similar for their Group 5 congeners, Nb and Ta. Furthermore, the opportunity for metal segregation in mixed-metal systems allows the formation of pseudobinaries such as $Nb_{1.72}Ta_{3.28}S_2$[10] which have no counterpart in the binary systems.[11] The existence and structure of none of the above compounds could be predicted *a priori* and a rationalization of their structures *a posteriori* does not give conclusive hints why the binary chalcogenides of the early transition metals display as many differences as they do, even after accounting for differences in metal–metal bond strengths.[12]

In the quest for new metal-rich early transition metal cluster compounds with interstitial atoms we have investigated reactions in the system M/A/Q (M = Nb, Ta; A = B, Ga, C, Si; Q = S, Se, Te). Nb_2Te_3 was prepared by reducing $NbTe_2$ with Ga at 1000 °C.[13] According to the results of the X-ray structure determination† Nb_2Te_3 crystallizes in the Mo_2As_3 structure type.[14] The unit cell contains eight metal atoms (two crystallographically different metal atoms per asymmetric unit) in a distorted octahedral Te coordination. The basic motif of the structure are double chains of edge-sharing $NbTe_6$ octahedra, **1**.

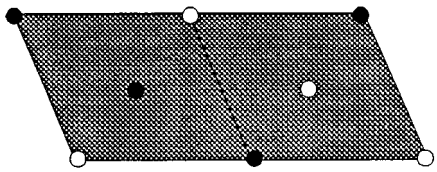

1

Motif **1** is a common fragment in structures derived from the NiAs or CdI_2 tye, but it is also encountered in the structures of metal oxide bronzes[15] and chalcogenides such as Nb_3Q_4[16] (Q = S, Se, Te) and Nb_2Se_3.[17] Most of these compounds have intriguing physical properties, because they represent borderline cases between metallic and non-metallic behavior.[15] Each octahedron of **1** shares one common face with the octahedron of an adjacent double chain. A view of the structure along the short axis *b* is provided in Fig. 1. A special feature of the structure is that four of the twelve octahedral voids in the unit cell remain empty; the empty holes are compressed in such a way as to give rise to the formation of Te_2 pairs with Te–Te distances of 2.915(3) Å, As a result, one third of the Te atoms are involved in Te–Te bonding. Moreover, the cations are shifted from the centers of the octahedra in such a way as to give rise to zigzag Nb–Nb chains along the *b* direction. The Nb(1) atoms are moved off their ideal positions by *ca.* 0.6 Å in the direction of one octahedral face. In this way, Nb(1)–Nb(1) chains are formed with metal–metal distances of 3.001(5) Å, which are only 5% longer than those in Nb metal. Nb(2) atoms also form chains along the *b* direction, but in these chains the Nb(2)–Nb(2) distances are, at 3.095(3) Å, considerably longer. Formally, Nb_2Te_3 may be viewed as $(Nb^{2.5+})_4(Te^{2-})_4(Te_2^{2-})$.

In contrast to the homologous Ta_2Te_3,[18] which crystallizes in a peculiar layer structure, Nb_2Te_3 adopts the Mo_2As_3 structure. The sesquiselenides Nb_2Se_3 and Ta_2Se_3 crystallize in another unique structure type,[17] whereas the corresponding sulfides are unknown. It is established that metal tellurides are distinctly different from the sulfides and selenides[19] because Te has a higher tendency to form chalcogen–chalcogen bonds;[20] still, it seemed to be a general rule that in metal chalcogenides with a metal/non-metal ratio > 2 no chalcogen–chalcogen bonds are formed. Thus, several questions need to be answered: (i) why does Nb_2Te_3 crystallize in the Mo_2As_3 structure type, *i.e.* what is the reason for the partial oxidation of Te in Nb_2Te_3? (ii) What are the electronic properties of Nb_2Te_3? (iii) Why are Nb_2Te_3 and Ta_2Te_3 structurally so different? We cannot answer the latter question; a general answer to (i) might be given in terms of 'redox competition'.[20] The lower electronegativity of Te compared to its lighter group homologues leads to a partial overlap of the metal d block and the Te centered valence band. As a result, there is an electron transfer from Te to the metal, *i.e.* Nb is reduced at the expense of Te. In order to probe the electronic structure of Nb_2Te_3 we have performed tight-binding band calculations.[21] Fig. 2 shows the t_{2g} subbands of Nb_2Te_3 along the symmetry lines corresponding to the *a*, *b* and *c* directions. The energy bands are flat along X–Γ, moderately

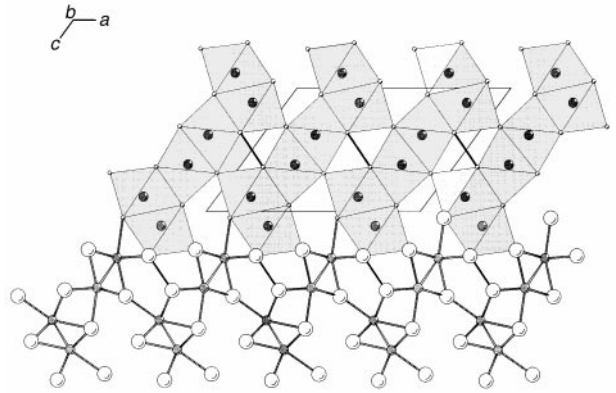

Fig. 1 View of the Nb_2Te_3 structure along *b*. Selected distances (Å): Nb(1)–Te(1) 2.883(3) (2×), Nb(1)–Te(2) 2.865(3), Nb(1)–Te(3) 2.738(3), Nb(1)–Te(3) 2.765(3) (2×) Nb(2)–Te(1) 2.904(3) (2×), Nb(2)–Te(2) 2.759(4) (2×), Nb(2)–Te(2) 2.776(3), Nb(2)–Te(3) 2.924(3), Te(1)–Te(1) 2.915(3), Nb(1)–Nb(1) 3.095(5) (2×), Nb(2)–Nb(2) 3.001(3) (2×).

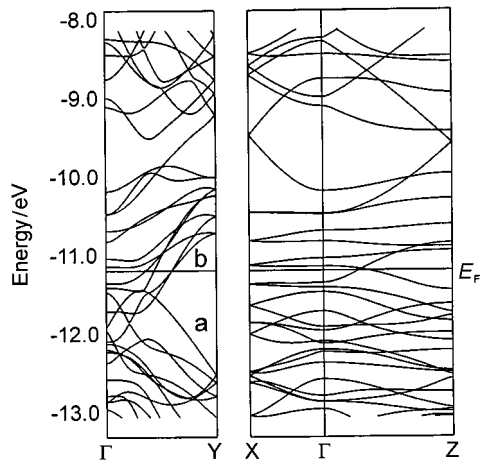

Fig. 2 Low-lying d-block bands of Nb_2Te_3: (a) along the chain direction Γ–Y; (b) along the main directions X–Γ–Z perpendicular to the chain direction. The Fermi level for Nb_2Te_3 is indicated by the horizontal bar.

disperse along Γ–Z, and highly disperse along Γ–Y. The Fermi level cuts through the middle of several steep bands; consequently, we expect metallic properties. The electronic structure may be understood in terms of the building blocks **1**, Nb_2Te_6 chains. Each of the chains **1** leads to six low-lying d block bands which originate from the t_{2g} levels of each metal. The lowest two of these bands have Nb–Nb bonding character, the two highest bands are Nb–Nb antibonding, and the remaining two bands are non-bonding with respect to the metal atoms. The unit cell of Nb_2Te_3 contains four of these chains, consequently, there must be eight bonding (labeled a in Figure 2), eight non-bonding (labeled b) and eight antibonding bands (not shown). For a $d^{2.5}$ electron count the lowest two bands of subset b are filled, and strongly anisotropic behavior is expected for Nb_2Te_3. If the bands are half-filled, a Peierls distortion may be expected. This situation is encountered for Tc_2As_3 (d^3),[22] which exhibits a superstructure of the Mo_2As_3 type and undergoes a displacive phase transition at high temperatures.

In summary, we have prepared niobium sesquitelluride, Nb_2Te_3, a new binary phase whose structure is distinctly different from those of the other known Group 5 sesquichalcogenides. It is the first early transition metal chalcogenide whose structure contains a dichalcogenide group. It is predicted to be a low-dimensional metal. For a half-filled t_{2g} subband (as observed for Tc_2As_3) a Peierls-distorted system is expected.

This work was supported by the Deutsche Forschungsgemeinschaft and the Fonds der Chemischen Industrie. We are indebted to Heraeus Quarzschmelze Hanau (Dr. Höfer) for a generous gift of silica tubes.

Notes and references

† *Crystal data* for Nb_2Te_3 at 25 °C: monoclinic, space group *C*2/*m* (no. 12), a = 15.073(2), b = 3.610(1), c = 10.775(2) Å, β = 126.59°, V = 470.76(10) Å, Z = 4, λ = 0.71073 Å, D_c = 8.022 g cm^{-3}, μ(Mo-Kα) = 22.77 mm^{-1}, crystal needle-like, dimensions 0.004 × 0.004 × 0.2 mm, θ_{max} = 54°, data collected at 25° on a Nicolet P2$_1$ four circle diffractometer, number of reflections, 1902, unique data with $F_o > 4\sigma(F_o)$, 767, number of variables, 32. Structure solved and refined using the SHELXTL program system. A numerical absorption correction was applied to the data (min., max. transmission, 0.86, 0.93). Final R, R_w = 0.070, 0.052. CCDC 182/1263.

1 J. M. Lehn, *Supramolecular Chemistry*, VCH Publishers, Weinheim, 1995. *Supramolecular Architecture*, ed. T. Bein, *ACS Symp Ser.*, 1992, vol. 499.
2 G. A. Ozin, *Adv. Mater.*, 1992, **4**, 612.
3 A. Meerschaut, L. Guemas and J. Rouxel, *J. Solid State Chem.*, 1981, **36**, 118.
4 M. Conrad and B. Harbrecht, *IVth European Conference on Solid State Chemistry*, Dresden, 1992.
5 H. Wada and M. Onoda, *Mater. Res. Bull.*, 1989, **24**, 1991; S.-J. Kim, K. S. Nanjundaswamy and T. Hughbanks, *Inorg. Chem.*, 1991, **30**, 159.
6 B. Harbrecht, *Angew. Chem.*, 1989, **101**, 1696; *Angew. Chem., Int. Ed. Engl.*, 1989, **28**, 1660.
7 R. L. Abdon and T. Hughbanks, *Angew. Chem.*, 1994, **106**, 2414; *Angew. Chem., Int. Ed. Engl.*, 1994, **33**, 2328.
8 T. E. Weirich, R. Ramlau, A. Simon, S. Hovmüller and X. Zhou, *Nature*, 1996, **382**, 144.
9 F. A. Cotton and G. Wilkinson, *Advanced Inorganic Chemistry*, Wiley, New York, 5th edn., 1988, p. 777.
10 X. Yao and H. F. Franzen, *J. Am. Chem. Soc.*, 1991, **113**, 1425.
11 X. Yao, G. Marking and H. F. Franzen, *Ber. Bunsen-Ges. Phys. Chem.*, 1992, **96**, 1552.
12 M. Köckerling and H. F. Franzen, *Croat. Chim. Acta*, 1995, **68**, 683.
13 In a typical reaction, 2 mmol (0.696 g) of $NbTe_2$ were reacted with 1 mmol Ga (0.070 g) at 1000 °C for 3 weeks in an evacuated quartz tube which had been dried *in vacuo* at 1000 °C before loading the starting components. The reaction products were Nb_2Te_3 and GaTe. Single crystals for the X-ray structure determination were obtained from the product mixture. Attempts to prepare single phase material from the elements or by reduction of $NbTe_2$ with Nb in the temperature range 500–1200 °C failed and lead to the formation of mixtures of $NbTe_2$ and Nb_3Te_4 instead. Similarly, attempts to grow single crystals of Nb_2Te_3 by vapor transport with halogens of TeX_4 (X = Cl, Br, I) only led to the formation of $NbTe_2/Nb_3Te_4$ mixtures.
14 P. Jensen, A. Kjekshus and T. Skansen, *Acta Chem. Scand.*, 1966, **20**, 1003; L. H. Dietrich and W. Jeitschko, *J. Solid State Chem.*, 1986, **63**, 377.
15 E. Canadell and M.-H. Whangbo, *Chem. Rev.*, 1991, **91**, 965; E. Canadell and M.-H. Whangbo, *Int. J. Mod. Phys. B*, 1993, **7**, 4005.
16 K. Selte and A. Kjekshus, *Acta Crystallogr.*, 1964, **17**, 1568. A. F. J. Ruysink, F. Kadijk, A. J. Wagner and F. Jellinke, *Acta Crystallogr., Sect. B*, 1968, **24**, 1614.
17 Nb_2Se_3; F. Kadijk, R. Huisman and F. Jellinek, *Acta Crystallogr., Sect. B*, 1968, **24**, 1102. Mo_2S_3; R. DeJonge, T. J. A. Popma, G. A. Wiegers and F. Jellinke, *J. Solid State Chem.*, 1970, **2**, 188.
18 M. Conrad and B. Harbrecht, *J. Less-Common Met.*, 1992, **187**, 181.
19 J. Rouxel, *Chem. Eur. J.*, 1996, **2**, 1053.
20 See, for example: W. Tremel, *Angew. Chem.*, 1991, **103**, 900; *Angew. Chem., Int. Ed. Engl.*, 1991, **30**, 840 and references therein.
21 M.-H. Whangbo and R. Hoffmann, *J. Am. Chem. Soc.*, 1978, **100**, 6093; M.-H. Whangbo, R. Hoffmann and R.-B. Woodward, *Proc. R. Soc. London, Ser. A*, 1979, **366**, 23. Nb parameters from ref. 12; Te parameters from ref. 20.
22 W. Jeitschko and L. H. Dietrich, *J. Solid State Chem.*, 1985, **57**, 59.

Communication 9/01822K

ChemComm

Ligand reorganization energies as a basis for the design of synergistic metal ion extraction systems

Mark L. Dietz,*[a] Andrew H. Bond,[a] Benjamin P. Hay,[b] Renato Chiarizia,[a] Vincent J. Huber[a] and Albert W. Herlinger[a]

[a] *Chemistry Division, Argonne National Laboratory, 9700 S. Cass Avenue, Argonne, IL 60439, USA. E-mail: mark_dietz@qmgate.anl.gov*

[b] *Environmental Molecular Sciences Laboratory, Pacific Northwest National Laboratory, PO Box 999, Richland, WA 99352, USA*

Received (in Cambridge, UK) 9th April 1999, Accepted 19th May 1999

In the extraction of alkaline earth cations by acidic organophosphorus extractants, a correlation has been demonstrated between the effectiveness of the stereoisomers of dicyclohexano-18-crown-6 as synergists and the strain energy associated with conversion of the unbound crown ether to its complexed form.

Metal ion separations comprise an important part of numerous industrial processes and constitute an essential first step in many chemical analyses. Among metal ion separation methods, liquid–liquid extraction (LLX) has found particularly wide use, a consequence of its selectivity, physical simplicity, and ease of scale-up. The extraction of a metal ion from an aqueous phase into an organic solvent requires, among other things, that electroneutrality be maintained. For neutral extractants, this is accomplished by coextraction of anions into the organic phase:

$$M^{n+}{}_{(aq)} + n\ X^{-}{}_{(aq)} + E_{(org)} \Leftrightarrow MX_n{\cdot}E_{(org)}$$

For common inorganic anions (*e.g.* Cl^-, NO_3^-), satisfactory metal extraction requires the use of organic solvents capable of either efficiently solvating a hydrophilic anion or of dissolving high concentrations of water,[1,2] a requirement that significantly reduces the number of practical LLX solvents. This limitation can be largely overcome, however, by employing organophilic anions, in particular, the anionic form of any of a number of alkylphosphoric, carboxylic or sulfonic acid extractants. Frequently, combinations of neutral and acidic extractants exhibit synergistic properties, yielding metal ion extraction greater than the sum of that observed for the individual extractants. Strong, size-selective synergism has been reported, for example, for alkaline earth cation extraction by certain combinations of crown ethers (CE) and organophosphorus acids (HA).[3,4] Despite numerous reports describing synergistic effects,[5–7] there have been few systematic investigations of the factors governing their magnitude. As a result, guidelines for the design of synergistic systems capable of the efficient and selective extraction of a desired cation are lacking. Recently, Hay *et al.*[8,9] have shown that ligand reorganization energies calculated using molecular mechanics methods can be employed to make quantitative predictions of the relative metal ion binding affinities of a variety of ligands containing a fixed number of donor atoms but differing in conformation. In the present work, we demonstrate that these methods provide the basis of a systematic approach to the design of synergistic metal ion extraction systems.

The crown ether dicyclohexano-18-crown-6 (DCH18C6) has five different stereoisomers,[10] each varying with respect to *cis*/*trans* isomerism at the point of ring fusion and *syn*/*anti* isomerism between cyclohexano substituents across the macrocyclic cavity. For the extraction studies, distribution ratios ($D_M = [M]_{org}/[M]_{aq}$) for Ca^{2+}, Sr^{2+} and Ba^{2+} were determined between aqueous buffers (pH ≈ 1.5–5) and toluene solutions of individual DCH18C6 stereoisomers and/or bis-*n*-octyl-, bis-2-ethylhexyl- or bis(diisobutylmethyl)-phosphoric acid [abbreviated HDOP, HDEHP and HD(DiBM)P, respectively] using standard radiometric methods. Continuous variation studies showed metal extraction to be negligible for the crown ether alone, permitting the synergistic constant to be defined simply as the ratio of the extraction constants in the presence and absence of DCH18C6 for each dialkylphosphoric acid. Acid dependency studies (Fig. 1), in which metal distribution ratios were determined as a function of pH at constant HA concentration either alone or in the presence of a stereoisomer of DCH18C6, indicated that while no significant synergistic effects are observed for Ca^{2+}, the extraction of both Sr^{2+} and Ba^{2+} is synergized by addition of DCH18C6. In nearly all cases, the magnitude of the synergistic effect was found to vary in the order:

cis-syn-cis (A) > *cis-anti-cis* (B) > *cis-trans* (E) > *trans-syn-trans* (C) ⩾ *trans-anti-trans* (D)

Slope analysis of these acid dependences, along with similar treatment of the extractant dependencies of the D_M values at constant pH and consideration of the continuous variation results, permits delineation of the equilibria describing alkaline earth cation extraction in these systems. In the absence of DCH18C6, the equilibrium expression can be written as follows:

$$K_{ex} = ([M(HA_2)_2{\cdot}nHA]_{org}[H^+]_{aq}{}^2)/([M^{2+}]_{aq}[(HA)_2]_{org}{}^{(2+n/2)})$$

where $n = 1$ for Ca^{2+} and 2 for Sr^{2+} and Ba^{2+}. For Sr^{2+} and Ba^{2+} in the presence of DCH18C6, this expression becomes:

$$K_{ex,s} = ([M(HA_2)_2{\cdot}DCH18C6]_{org}[H^+]_{aq}{}^2)/([M^{2+}]_{aq}[(HA)_2]_{org}{}^2\,[DCH18C6]_{org})$$

[The use of $(HA)_2$ to represent the alkylphosphoric acid in both sets of equilibria follows from the known dimeric state of these acids in toluene[5,11] and the absence of interaction between DCH18C6 and HA in the organic phase, confirmed by vapor pressure osmometry.] The synergistic constant, K_s, is defined as the ratio of $K_{ex,s}$ to K_{ex}, and corresponds to the organic phase reaction that leads to the formation of the final Sr^{2+} or Ba^{2+} complexes:

$$M(HA_2)_2{\cdot}2HA_{(org)} + DCH18C6_{(org)} \rightleftharpoons M(HA_2)_2{\cdot}DCH18C6_{(org)} + (HA)_{2\,(org)}$$

Fig. 2 depicts the relationship between the synergistic constants (*i.e.* the magnitude of the synergistic effect) for strontium and barium extraction and the ligand reorganization energy,[8,9] ΔU_{reorg}, for the complexation of Sr^{2+} and Ba^{2+} by the various stereoisomers of DCH18C6. The ligand reorganization energy represents the extent to which complex formation between the crown ether and a metal ion induces steric strain in the crown ether and, therefore, indicates the degree of binding site preorganization characteristic of each stereoisomer. Ligand reorganization energy is defined as the sum of two structural reorganization components: the energy required to convert the free ligand from its minimum energy conformer to one

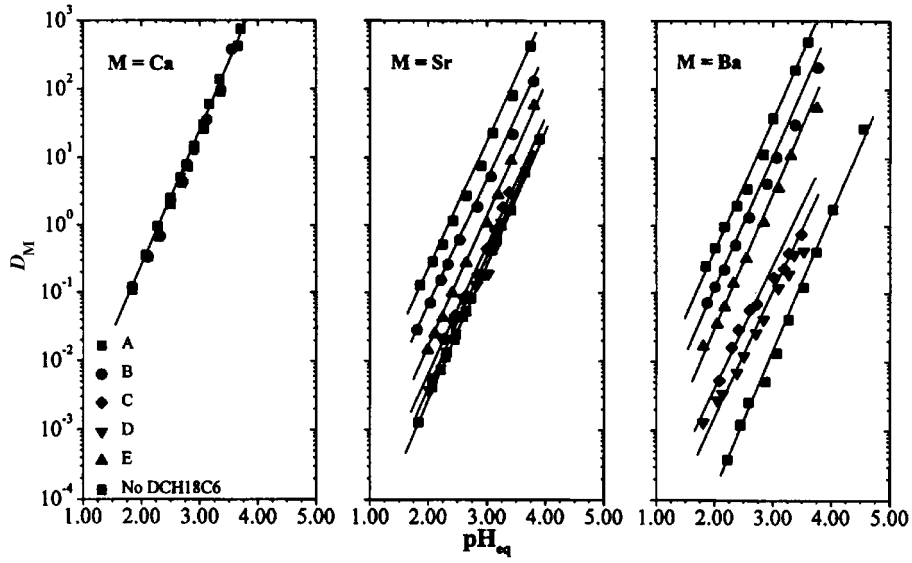

Fig 1. D_M *vs.* equilibrium pH for Ca^{2+}, Sr^{2+} and Ba^{2+} extraction by bis-*n*-octylphosphoric acid (HDOP) in toluene, both alone and in the presence of the stereoisomers of DCH18C6. Conditions: [HDOP] = 0.10 M; [DCH18C6] = 0.025 M in toluene; $[M(NO_3)_2]$ = 0.001 M; T = 23 ± 2 °C. (The least squares lines have a fixed slope of 2, consistent with the extraction equilibria.)

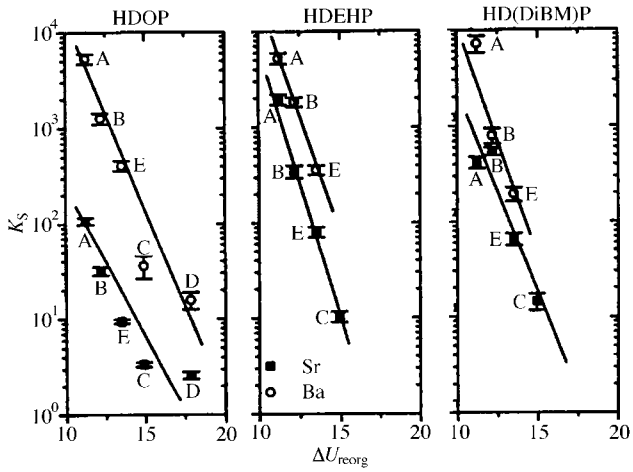

Fig 2. Relationship between the synergistic constants for Sr^{2+} and Ba^{2+} extraction and the ligand reorganization energy of the DCH18C6 stereoisomers.

predisposed for binding, ΔU_{conf}, and the energy difference between the binding conformer and the ligand conformation in the metal complex, ΔU_{comp}. Ligands highly preorganized for binding (*i.e.* 'sterically efficient' ligands) exhibit small ΔU_{reorg} values. As shown in Fig. 2, there exists an inverse linear relationship between log K_s and ΔU_{reorg}, providing strong evidence that the primary factor determining the magnitude of synergistic effects is the reorganization energy (and therefore, the metal ion binding affinity) of the neutral ligand, in this case, the various DCH18C6 stereoisomers. It appears that steric factors related to branching of the alkyl chains of the organophilic acid anion also play a role (Fig. 2), but the influence of these factors is clearly more limited.

To our knowledge, this work represents the first report of a correlation between the magnitude of a synergistic effect and ligand reorganization energies and thus, the first demonstration of the utility of molecular mechanics methods in guiding the design of synergistic metal ion separation systems. Given the widespread interest in crown ether-based separation processes and the enormous variety of both macrocyclic polyethers and organophilic acid anions available, these results are certain to have a significant impact on the development of improved systems for both analytical-scale and large-scale metal separations.

This work was performed under the auspices of the Office of Basic Energy Sciences, Division of Chemical Sciences, and the Environmental Management Sciences Program of the Offices of Science and Environmental Management, United States Department of Energy, under contract number W-31-109-ENG-38.

Notes and references

1 Y. Marcus and L. E. Asher, *J. Phys. Chem.*, 1978, **82**, 1246.
2 E. P. Horwitz, M. L. Dietz and D. E. Fisher, *Solvent Extr. Ion Exch.*, 1990, **8**, 199.
3 W. F. Kinard and W. J. McDowell, *J. Inorg. Nucl. Chem.*, 1981, **43**, 2947.
4 M. L. Dietz, R. Chiarizia, E. P. Horwitz, R. A. Bartsch and V. Talanov, *Anal. Chem.*, 1997, **69**, 3028.
5 T. Sekine and Y. Hasegawa, *Solvent Extraction Chemistry: Fundamentals and Applications*, Marcel Dekker, New York, 1977.
6 Z. B. Alfassi and C. M. Wai, *Preconcentration Techniques for Trace Elements*, CRC Press, Boca Raton, FL, 1992.
7 M. K. Beklemishev, S. G. Dmitrienko and N. V. Isakova, in *Macrocyclic Compounds in Analytical Chemistry*, ed. Y. A. Zolotov, John Wiley & Sons, New York, 1997.
8 B. P. Hay, J. R. Rustad and C. J. Hostetler, *J. Am. Chem. Soc.*, 1993, **115**, 11 158.
9 B. P. Hay, in *Metal-Ion Separation and Preconcentration: Progress and Opportunities*, ed. A. H. Bond, M. L. Dietz and R. D. Rogers, American Chemical Society, Washington, DC, 1999.
10 I. J. Burden, A. C. Coxen, J. F. Stoddart and C. M. Wheatley, *J. Chem. Soc., Perkin Trans. 1*, 1977, 220.
11 A. Sastre, N. Miralles and E. Bosch, *Anal. Chim. Acta*, 1997, **350**, 197.

Communication 9/02842K

ChemComm

Formation of an organometallic coordination polymer from the reaction of silver(I) with a non-complimentary lariat ether

Paul D. Prince,[a] Peter J. Cragg[b] and Jonathan W. Steed*[a]

[a] *Department of Chemistry, King's College London, Strand, London, UK WC2R 2LS. E-mail: jon.steed@kcl.ac.uk*
[b] *School of Pharmacy, University of Brighton, Cockcroft Building, Lewes Road, Brighton, E. Sussex, UK BN2 4GJ*

Received (in Columbia, MO, USA) 1st January 1999, Accepted 10th May 1999

The 'Ag^{I}(15-crown-5)' core moiety is a versatile supramolecular synthon, which is able to satisfy its coordination requirements using a variety of capping ligands; in the presence of the lariat ether *N*-allylaza-15-crown-5 an infinite organometallic coordination polymer is formed.

The design of supramolecular hosts for metal cations is based upon the proposition that the more complementary a host is to the guest the stronger the binding will be.[1–3] This is especially true in cases where the host is rigidly preorganised for guest complexation, as in the case of the spherands.[4] It follows from this well established fact that the majority of synthetic effort is geared towards the matching of host and guest electronic, steric and topological properties in order to maximise their mutual affinity. Clearly therefore, a successful host serves to confirm the rationality of its design. An interesting caveat of this line of reasoning is that potentially much information on host design may be gained by examination of cases in which the host is *not* complementary to the guest. In such cases the host–guest system is necessarily forced to distort in order to accommodate the conflicting requirements of each partner, with consequent diminution of affinity. The degree of distortion should furnish useful information about the tolerances on what may, and may not be termed 'complementary'.

Recently we have looked at a number of sterically and electronically non-complementary systems.[5–10] As part of these studies we reported the reaction of 'hard' oxygen donor ligands with the soft Ag^{I} cation to give complexes [Ag(L)][SbF_6] (L = 15-crown-5, **1a**; benzo-15-crown-5, **1b**).[7] In contrast to the usual linear or tetrahedral geometries of Ag^{I}[11] this results in the formation of two unusual seven-coordinate systems in which the 'Ag(15-crown-5)$^{+}$' core is capped by interactions with two oxygen atoms of the second macrocycle. The non-complementary nature of the hard base–soft acid interaction is exemplified in the long Ag–O bonding distances which ranged from 2.512(2) to 2.633(2) Å, compared with typical Ag–N_{amine} distances of *ca*. 2.2–2.4 Å.[12] Similar weak Ag–O_{ether} interactions have been noted recently in a range of β-diketonato glyme derivatives, which are of interest as CVD precursors.[13] This unsymmetrical sandwich geometry suggests that the Ag(15-crown-5)$^{+}$ core may be relatively stable and that the more loosely bound bidentate macrocycle could be readily replaced by other ligands, particularly those which are *more* complementary for the soft metal cation.

With this in mind we examined the reaction of Ag[SbF_6] with aza-15-crown-5 **2** since binding constant measurements demonstrate that Ag^{+} has a significantly greater affinity for *N*-donor ligands.[14] This reaction gave a virtually quantitative yield of a further 1:2 complex of formula [Ag(aza-15-crown-5)$_2$][SbF_6] **3**. The X-ray crystal structure of this material (Fig. 1)† proved to be approximately isomorphous with complex **1**. The key difference between the more complementary azacrown and its O-donor analogues is that in complex **3** the 'Ag(aza-15-crown-5)$^{+}$' core is capped by the nitrogen atom of a monodentate azacrown ligand, as opposed to two oxygen atoms in compounds **1**. It is likely that this is a direct result of the greater affinity of Ag^{I} for nitrogen, resulting in Ag–N distances of 2.304(2) and 2.2759(19) Å (core and cap respectively), compared to Ag–O distances in the range 2.6807(16)–2.7199(16) Å. Indeed the conformation of the capping crown ligand is entirely different because the driving force directing *two* donor atoms at the metal ion is no longer present. Interestingly this results in a significant offset to the crystal packing, which is dominated by C–H···O hydrogen bonding interactions to the non-coordinated oxygen atoms of the capping crown.[7] For compound **1a** this weak hydrogen bond results in an offset of the sandwich cation pairs giving a long crystallographic *a* axis (the direction of intermolecular chain propagation; 8.448 *vs*. 8.263 Å) and a larger monoclinic angle *β*. For compound **3** the weakly hydrogen bonded cation pairs are more directly on top of one another, reducing *β* from 101.4 to 98.8°. It is particularly noteworthy that it is the pairwise C–H···O interactions, of distances C···O 3.398(2) and 3.568(2) Å, H···O 2.58 and 2.62 Å (C–H normalised to 0.99 Å), which dominate the inter-cation packing, and not interactions to the more polar N–H moiety, which forms a long *intramolecular*

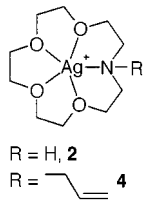

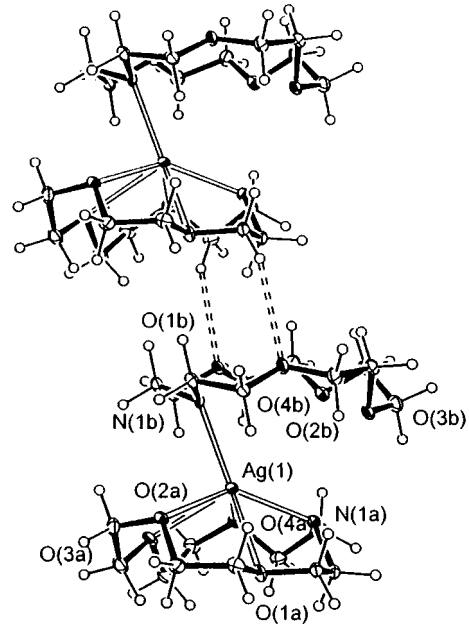

Fig. 1 Intermolecular interactions in [Ag(aza-15-crown-5$_2$][SbF_6] **3**. Selected bond distances (Å): Ag(I)–O(1A) 2.7193(15), Ag(1)–O(2A) 2.7449(16), Ag(1)–O(3A) 2.6807(16), Ag(1)–O(4A) 2.7199(16), Ag(1)–N(1A) 2.304(2), Ag(1)–N(1B) 2.2759(19).

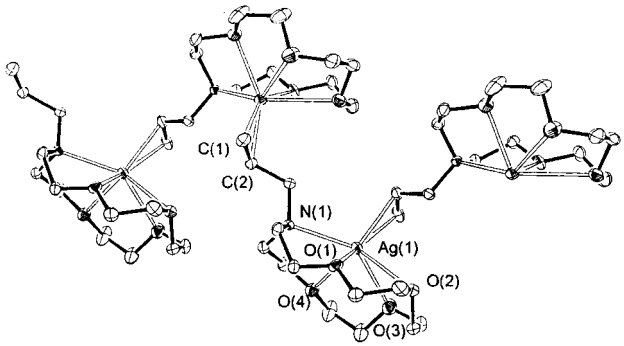

Fig. 2 The coordination polymer {[Ag(*N*-allylaza-15-crown-5)]}$_\infty$ **5**. Selected bond distances (Å): Ag(1)–C(1)′ 2.363(4), Ag(1)–C(2)′ 2.393(4), Ag(1)–O(1) 2.400(2), Ag(1)–O(2) 2.711(3), Ag(1)–O(3) 2.773(3), Ag(1)–O(4) 2.485(3), Ag(1)–N(1) 2.515(4) Å.

hydrogen bond to the distal oxygen atom of the capping azacrown, N(1A)···O(3B) 3.034(2) Å. The proton attached to N(1B) forms a bifurcated hydrogen bond to the oxygen atoms of the same crown ring, N···O 2.698(2) and 2.712(2) Å. Again, these do not affect the crystal packing because they are entirely intramolecular. The packing is however, further supported by C–H···F interactions[15–17] to the SbF_6^- anions, with shortest H···F distances 2.51–2.57 Å.

These results suggest that the interaction of derivatives of the Ag(15-crown-5)$^+$ core with further ligands with more affinity for Ag^I than etheric oxygen may prove of interest. In particular the affinity of Ag$^+$ for C-donor ligands has been well established, with the cation typically interacting with olefins and individual double bonds of arenes to form complexes such as [Ag([2.2.2]paracyclophane)]$^+$.[18] Furthermore Gokel and coworkers have noted a marked linearity between the electronic effect of the substituent on the aryl ring of the lariat and Ag$^+$ binding affinity in aryl lariat ethers[19] which is not reflected in the analogous interactions with Na$^+$ and K$^+$, which may arise from direct Ag–π interactions. Accordingly we examined the reaction of Ag[SbF_6] with the simple *N*-allyl lariat ether **4**.‡ This resulted in the formation of a polymeric complex {[Ag(allylaza-15-crown-5)][SbF_6]}$_\infty$ **5** again consisting of a substituted Ag(aza-15-crown-5)$^+$ core unit analogous to compounds **1** and **3** with a pendant allyl side arm. This side arm, while too short to wrap around and coordinate to the same Ag^I centre, is able to take the role of the second crown ether in complexes **1** and **3** resulting in an organometallic coordination polymer, with Ag–C distances of 2.363(4) and 2.393(4) Å (Fig. 2). This compares to distances of 2.49–2.68 for a range of recently reported Ag^I complexes of polyaromatic hydrocarbons[20] and typical distances of 2.40–2.60 Å[2] and confirms a full coordination interaction. Also remarkable is the Ag–N distance of 2.515(4) Å, which is *longer* than the distances from the metal cation to the two oxygen atoms nearest to the *N*-allyl moiety, Ag–O(1) 2.400(2) and Ag–O(4) 2.483(3) Å (*cf.* compounds **1** and **3**). The distal Ag–O distances are in the region of 2.74 Å. This striking difference may be rationalised by the delocalisation of the tertiary nitrogen atom lone pair onto the olefinic susbstituent,[21] and on steric grounds in which the relatively plastic coordination environment of the Ag^I ion is placing itself spatially where it may most effectively bond to the ext unit in the polymeric chain. Further evidence in support of this latter suggestion comes from the fact that the shortest Ag–O distances in **3** are to the oxygen atoms farthest away from the nitrogen atom. Again, the crystal packing is supported by C–H···F interactions to the SbF_6^- anion (shortest 2.48 Å).

We thank the EPSRC and King's College London for funding of the diffractometer system and Dr L. J. Barbour for the program X-Seed[23] used in the X-ray structure determinations. Grateful acknowledgement is also given to the EPSRC Chemical Database Service at Daresbury and to the Nuffield Foundation for the provision of computing equipment.

Notes and references

† *Crystal data*: **3**: $C_{20}H_{42}AgF_6N_2O_8Sb$, M = 782.18, monoclinic, space group $p2_1/n$, a = 8.2633(2), b = 13.7364(3), c = 25.8077(4) Å, β = 98.752(2)°, U = 2895.27(10) Å^3, Z = 4, μ = 16.92 cm^{-1}, T = 100 K, Refelections measured: 15 220, unique data: 6596 (R_{int} = 0.050), parameters: 352, R_1 [$F^2 > 2\sigma(F^2)$] = 0.0293, wR_2 (all data) = 0.0653.

5: $C_{13}H_{25}AgF_6NO_4Sb$, M = 602.96, orthorhombic, space group $Pn2_1a$, a = 9.3842(4), b = 9.4558(2), c = 21.5735(9) Å, U = 1914.33(12) Å^3, Z = 4, μ = 25.08 cm^{-1}, T = 100 K, Reflections measured: 13 305, unique data: 3460 (R_{int} = 0.027), parameters: 236, R_1 [$F^2 > 2\sigma(F^2)$] = 0.0231, wR_2 (all data) 0.0598.

CCDC 182/1264.

‡ *N*-Allylaza-15-crown-5 was prepared through direct combination of aza 15-crown-5 and 3-bromoprop-1-ene in dry diethyl ether in the presence of triethylamine and was identical in all respects to that prepared by an alternative procedure.[22]

1 *Comprehensive Supramolecular Chemistry*, ed. J. L. Atwood, J. E. D. Davies, D. D. MacNicol and F. Vögtle, Pergamon, Oxford, 1996, vol. 1.
2 F. Vögtle, *Supramolecular Chemistry*, Wiley, Chichester, 1991.
3 J.-M. Lehn, *Supramolecular Chemistry*, VCH, Weinheim, 1995.
4 D. J. Cram, *Angew. Chem., Int. Ed. Engl.*, 1986, **25**, 1039.
5 J. W. Steed, H. Hassaballa and P. C. Junk, *Chem. Commun.*, 1998, 577.
6 J. W. Steed and P. C. Junk, *J. Chem. Soc., Dalton Trans.*, 1999, in press.
7 P. D. Prince and J. W. Steed, *Supramol. Chem.*, 1998, **10**, 155.
8 J. W. Steed, P. C. Junk and B. J. McCool, *J. Chem. Soc., Dalton Trans.*, 1998, 3417.
9 J. W. Steed and K. Johnson, *J. Chem. Soc., Dalton Trans.*, 1998, 2601.
10 H. Hassaballa, J. W. Steed, P. C. Junk and M. R. J. Elsegood, *Inorg. Chem.*, 1998, **37**, 4666.
11 F. A. Cotton and G. Wilkinson, *Advanced Inorganic Chemistry*, Wiley-Interscience, New York, 5th edn., 1988.
12 G. Orpen, L. Brammer, F. H. Allen, O. Kennard, D. G. Watson and R. Taylor, *J. Chem. Soc., Dalton Trans.*, 1989, S1.
13 J. A. Darr, M. Poliakoff, A. J. Blake and W.-S. Li, *Inorg. Chem.*, 1998, **37**, 5491.
14 R. M. Izatt, K. Pawlak and J. S. Bradshaw, *Chem. Rev.*, 1991, **91**, 1721.
15 J. A. K. Howard, V. J. Hoy, D. O'Hagan and G. T. Smith, *Tetrahedron*, 1996, **52**, 12 613.
16 S. J. Borwick, J. A. K. Howard, C. W. Lehmann and D. O'Hagan, *Acta Crystallogr., Sect. C*, 1997, **53**, 124.
17 F. Grepioni, G. Cojazzi, S. M. Draper, N. Scully and D. Braga, *Organometallics*, 1998, **17**, 296.
18 H. C. Kang, A. W. Hanson, B. Eaton and V. Boekelheide, *J. Am. Chem. Soc.*, 1985, **107**, 1979.
19 D. A. Gustowski, V. J. Gatto, J. Mallen, L. Echegoyen and G. W. Gokel, *J. Am. Chem. Soc.*, 1987, **52**, 5172.
20 M. Munakata, L. P. Wu, T. Kuroda-Sowa, M. Mackawa, Y. Suenaga, G. L. Ning and T. Kojima, *J. Am. Chem. Soc.*, 1998, **120**, 8610.
21 A. W. Czarnik, *Acc. Chem. Res.*, 1994, **27**, 302.
22 R. A. Schultz, B. D. White, D. M. Dishong, K. A. Arnold and G. W. Gokel, *J. Am. Chem. Soc.*, 1985, **107**, 6659.
23 L. J. Barbour, *X-Seed*, A program for the graphical interpretation and elucidation of crystallographic data, University of Missouri, Columbia, 1999.

Communication 9/00252I

A cubic–cubic phase transition of 4′-*n*-hexacosyloxy-3′-nitrobiphenyl-4-carboxylic acid (ANBC-26)

Shoichi Kutsumizu,*[a] Tatsuya Ichikawa,[b] Shuichi Nojima[c] and Shinichi Yano[b]

[a] *Instrumental Analysis Center,Gifu University, 1-1 Yanagido, Gifu 501-1193, Japan. E-mail: kutsu@cc.gifu-u.ac.jp*
[b] *Department of Chemistry, Faculty of Engineering,Gifu University, 1-1 Yanagido, Gifu 501-1193, Japan*
[c] *School of Materials Science, Japan Advanced Institute of Science and Technology (JAIST), 1-1 Asahidai, Tatsunokuchi, Nomi, Ishikawa 923-1292, Japan*

Received (in Cambridge, UK) 14th April 1999, Accepted 14th May 1999

Lengthening of the alkoxyl group of 4′-*n*-alkoxy-3′-nitrobiphenyl-4-carboxylic acids to C_{26} produced two types of cubic mesophases with *Im*3*m* and *Ia*3*d* symmetries, where the *Im*3*m* cubic phase is transformed into the *Ia*3*d* cubic phase at 162 °C on heating.

Optically isotropic cubic mesophases are currently attracting much interest in the field of supramolecular chemistry because of their fundamental interest in the mysterious transformation with adjacent optically anisotropic mesophases (*e.g.* lamellar, hexagonal) and because of their biological significance.[1] They can occur in a wide range of chemical systems, such as liquid crystals, biological lipid-water, and block copolymers, and their formation depends on temperature and their molecular structure and composition. Our understanding in this field is, however, far from complete.

4′-*n*-alkoxy-3′-nitrobiphenyl-4-carboxylic acids have a relatively simple molecular structure which consists of a nitrobiphenylcarboxylic acid core and a long alkoxyl tail (see Fig. 2, top). These compounds, designated as ANBC-*n* (*n* is the number of carbons in the alkoxyl groups), were first synthesized by Gray *et al*.[2] and have been investigated by several researchers;[3–6] they show a cubic phase denoted cubic D (CubD) on both heating and cooling when $n \geqslant 16$, with the temperature region of this phase becoming wider with increasing *n* (up to $n = 22$).[3,4] For the $n = 16$ and 18 homologues, the structure type of the CubD phase has been already identified as space group *Ia*3*d*,[5,6] but the structure at the molecular level is still unclear. Here, we report a homologue having a very long chain of $n = 26$ which forms two types of cubic phases, one with *Im*3*m* symmetry and the other with *Ia*3*d* symmetry, with the *Im*3*m* cubic phase transforming into the *Ia*3*d* cubic phase at 162 °C on heating. This is the first example of a thermotropic cubic–cubic phase transition in one-component systems, although two examples have been reported in lyotropic binary or ternary mixtures on varying the water content.[7–9]

The $n = 26$ homologue, ANBC-26, was prepared by three steps: first, *n*-hexacosyl bromide was prepared by a Grignard-type reaction between *n*-hexadecyl bromide and 1,10-dibromodecane, and then, according to the established method of Gray *et al*.,[2] the obtained bromide was reacted with 4′-hydroxybiphenyl-4-carboxylic acid to give 4′-*n*-hexacosyloxybiphenyl-4-carboxylic acid (ABC-26), finally, nitration of ABC-26 gave ANBC-26. The final white powder product was purified by repeated recrystallization from ethanol, and the purity was checked by elemental analysis, thin layer chromatography, ^{1}H NMR, and differential scanning calorimetry (DSC).

The DSC trace of ANBC-26 shows the following phase sequence on the first heating curve (1H): crystal 1·86 °C·crystal 2·103 °C·smectic C (SmC)·123 °C·cubic I (Cub I)·162 °C cubic II (Cub II)·194 °C· structured liquid (I_1)·200 °C·isotropic liquid (I_2), with associated entropy changes of 86, 124, 6, 0.3, 9 and 15 J mol^{-1} K^{-1}, respectively. Identification of the phase type was by both texture observation using a polarizing optical microscope and small-angle X-ray scattering (SAXS). The structure of the I_1 phase has been discussed elsewhere.[3,4] The cooling process is more complicated and has not been fully characterized; the phase sequence determined so far is I_2·198 °C I_1·192 °C·hexagonal columnar phase·189 °C·Cub II·93 °C·SmC 76 °C·crystal. On second heating (2H), the sample showed crystallization of residual glassy domains at 79 °C, but was otherwise identical with the 1H scan.

Fig. 1 shows the SAXS patterns of ANBC-26 at (a) 130.4 °C and (b) 170.4 °C, on heating, where $q = (4\pi/\lambda)\sin\theta$, $\lambda = 0.154$ nm and 2θ = scattering angle (Mac Science M18XHF X-ray generator and Huxley–Holms optics). At 130.4 °C, 11 observed peaks are arranged almost symmetrically with respect to the beam stopper (not shown here), showing the following ratios of spacings: $\sqrt{3}$:$\sqrt{4}$:$\sqrt{5}$:$\sqrt{6}$:$\sqrt{7}$:$\sqrt{8}$:$\sqrt{9}$:$\sqrt{10}$:$\sqrt{12}$:$\sqrt{13}$:$\sqrt{15}$. Since the ratios $\sqrt{7}$ and $\sqrt{15}$ are not compatible with any cubic lattices, the sequence of numbers must be doubled. Therefore, the obtained ratios are $\sqrt{6}$:$\sqrt{8}$:$\sqrt{10}$:$\sqrt{12}$:$\sqrt{14}$:$\sqrt{16}$:$\sqrt{18}$:$\sqrt{20}$:$\sqrt{24}$:$\sqrt{26}$:$\sqrt{30}$, which is characteristic of a body-centered cubic symmetry *Im*3*m*, and thus the parameter of the unit cell is $a = 20.02 \pm 0.02$ nm. The pattern abruptly changed at *ca*. 155 °C on heating, and at 170.4 °C [Fig. 1 (b)], only two peaks with a ratio of $\sqrt{6}$:$\sqrt{8}$ are seen. The pattern was very often dissymmetric with respect to the beam stopper, as shown in the inset, reflecting orientation of the Cub II domains in the glass capillary tube. Since ANBC-26 is achiral, only the space group *Ia*3*d* matches the absence of diffractions with lower indices (100), (110), (111), (200) and (210). The cell parameter is estimated as $a = 12.30 \pm 0.04$ nm. The higher-temperature Cub II phase has the same symmetry as

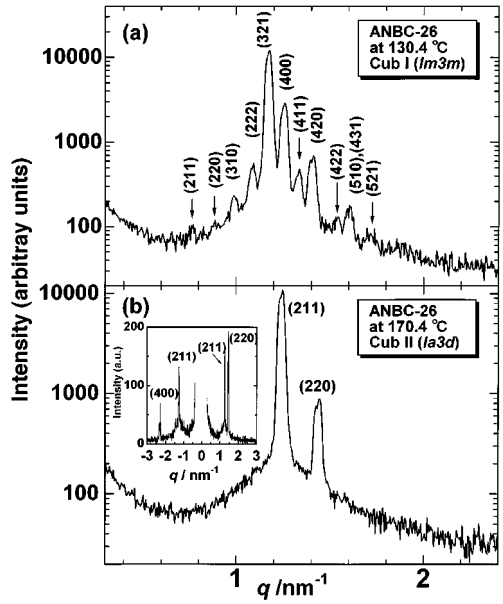

Fig. 1 SAXS patterns of ANBC-26 recorded (a) at 130.4 °C and (b) at 170.4 °C, on heating. Miller indices are also shown. In (b), the inset shows a second pattern for the same sample under the same thermal conditions.

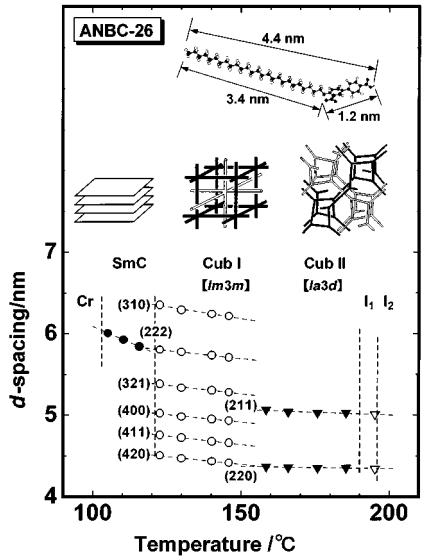

Fig. 2 Plots of *d*-spacing *vs*. temperature for ANBC-26 on heating. The molecular structure of ANBC-26 and model structures of the SmC, Cub I and Cub II phases are shown in the upper and middle part of this figure, respectively.

the CubD phase of ANBC-16[5] and −18.[6] On the other hand, the cubic phase of a 3′-cyano analogue with n = 18 (4′-*n*-octadecyloxy-3′-cyanobiphenyl-4-carboxylic acid) was identified in space group *Im*3*m*,[6] and this phase and the lower-temperature Cub I phase are of the same type.

ANBC-26 thus shows three liquid-crystalline phases, the SmC phase with a lamellar structure, and two types of cubic phases, one with *Im*3*m* symmetry and the other with *Ia*3*d* symmetry, on heating. Schematic models for these three structures are depicted in the middle part of Fig. 2. According to the models proposed for lyotropic systems by Luzzati and coworkers,[9] both cubic phases are visualized as two sets of networks of rods, which are interwoven but not connected. For the *Im*3*m* cubic phase, the rods are connected 6-by-6 at right angles so that they are directed parallel to one of three lattice axes, while in the *Ia*3*d* cubic phase, the rods are connected 3-by-3, forming two sets of helix-like networks, where each helix is linked with other four helices. In ANBC-26, the aromatic part and CO_2H group form these jointed rods, while the aliphatic chain fills out the free space between the rods.

In order to gain insight into the transformation process along the SmC–Cub I (*Im*3*m*)–Cub II (*Ia*3*d*) phase sequence, the *d*-spacings of diffraction peaks are plotted *vs*. temperature in the lower part of Fig. 2. Several interesting points are noted:

(1) The layer thickness of the SmC phase decreases as the temperature approaches the SmC–Cub I transition temperature. When the SmC layer is transformed into the SmA layer, the tilt angle of the molecular long axis against the layer normal usually reaches zero and thus the layer thickness increases. Therefore, the 'thinning' of the SmC layers may be characteristic of the SmC phase that exhibits any cubic phase at the higher temperature side.

(2) At the SmC to Cub I transition, the SmC layer thickness is equal to the (222) interplanar distance of the Cub I phase with *Im*3*m* symmetry. This suggests the existence of the so-called epitaxial relation[10] between the SmC layer planes and the (222) planes of the Cub I phase. In the *Im*3*m* cubic phase with a cell parameter a, one 6-by-6 connection point is located at (000) and the other at ($\frac{1}{2}a$,$\frac{1}{2}a$,$\frac{1}{2}a$), and the distance between them is ($\sqrt{3}$)a/2, while the (222) spacing is given by ($\sqrt{3}$)a/6. Hence, three layers should exist between the two connection points.

(3) In the Cub I phase, the diffraction of highest intensity is the (321) peak while the (211) diffraction peak is the highest in the Cub II phase; both spacings, however, show a discontinuity at the Cub I to Cub II phase transition.

(4) In the Cub I phase temperature range, the unit cell parameter a decreases with increasing temperature, showing a *negative* thermal volume expansion [$(1/a^3)(\mathrm{d}(a^3)/\mathrm{d}T) = -4 \times 10^{-2}$ K^{-1}]. This trend continues but is greatly reduced (-6×10^{-4} K^{-1}) for temperatures in the Cub II phase range. Bruce and coworkers reported a similar negative thermal volume expansion (-1.5×10^{-3} K^{-1}) for the *Ia*3*d* cubic phase of a silver(I) alkoxystilbazole complex.[11] It seems that negative thermal volume expansion is characteristic of cubic mesophases (fluid nature).

Finally, we comment on two issues. The first relates to the molecular structure characteristics of ANBC-26. A shorter alkoxyl homologue, *e.g.* ANBC-18, shows an *Ia*3*d* cubic phase, and the length of the aliphatic chain is estimated at 2.2 nm in the extended form, which is about twice the length of the aromatic core moiety (1.2 nm). For ANBC-26, the aliphatic chain length is 3.4 nm, about three times larger than the core length (see Fig. 2). The lengthening of the aliphatic chain unexpectedly produced two types of cubic phases on heating. Moreover, this lengthening also much improved the thermal stability among this series of compounds, as confirmed by thermal gravimetry.

Second, paying attention to the location of the methyl end groups in the two cubic lattices, they form curved interfaces so as to wrap the jointed rods. These interfaces are alternative sets of description for cubic phases and are denoted infinite periodic minimal surfaces (IPMS); three fundamental cubic IPMS have been reported, the Schwarz P and D and Schöen Gyroid G surfaces, which correspond to three bicontinuous cubic phases with symmetries *Im*3*m*, *Pn*3*m* and *Ia*3*d*, respectively.[12] Hyde *et al*. pointed out that three bicontinuous cubic IPMS are mathematically interrelated to each other by a Bonnet transformation *without change in curvature*.[12] This means that phase transitions between the three cubic phases should occur without heat exchange, provided that only the elastic energy of the system is taken into consideration. This may be a reason why only one type of cubic phase has been observed to date in a given thermotropic cubic system; also our observation of a very small entropy change (0.3 J mol^{-1} K^{-1}) for the Cub I–Cub II phase transition is consistent with this expectation.

In conclusion, ANBC-26 shows an interesting polymorphism, including two cubic mesophases with *Im*3*m* and *Ia*3*d* symmetries, and a structured liquid I_1 phase. We anticipate that our finding will lead to a more complete understanding of cubic molecular organization and its transformation to and from other types, especially in thermotropic liquid crystalline systems.

Notes and references

1 S. Diele and P. Göring, in *Handbook of Liquid Crystals*, ed. D. Demus, J. Goodby, G. W. Gray, H.-W. Spiess and V. Vill, Wiley–VCH, Weinheim, 1998, vol. 2B, pp. 887-900.
2 G. W. Gray, B. Jones and F. Marson, *J. Chem. Soc.*, 1957, 393.
3 D. Demus, G. Kunicke, J. Neelsen and H. Sackmann, *Z. Naturforsch., Teil A.*, 1968, **23**, 84; D. Demus, D. Marzotko, N. K. Sharma and A. Wiegeleben, *Kristall. Technol.*, 1980, **15**, 331.
4 S. Kutsumizu, M. Yamada and S. Yano, *Liq. Cryst.*, 1994, **16**, 1109; S. Kutsumizu, R. Kato, M. Yamada and S. Yano, *J. Phys. Chem., B*, 1997, **101**, 10 666.
5 A. Tardieu and J. Billard, *J. Phys. Coll.*, 1976, **37**, C3-79.
6 A. M. Levelut and Y. Fang, *Coll. Phys., Coll. 7*, 1991, **51**, C7-229; A. M. Levelut and M. Clerc, *Liq. Cryst.*, 1998, **24**, 105.
7 W. Longley and T. J. McIntosh, *Nature*, 1983, **303**, 612.
8 K. Larsson, *Nature*, 1983, **304**, 664.
9 P. Mariani, V. Luzzati and H. Delacroix, *J. Mol. Biol.*, 1988, **204**, 165.
10 Y. Rançon and J. Charvolin, *J. Phys. Chem.*, 1988, **92**, 2646.
11 B. Donnio, B. Heinrich, T. Gulik-Krzywicki, H. Delacroix, D. Guillon and D. W. Bruce, *Chem. Mater.*, 1997, **9**, 2951.
12 S. T. Hyde, S. Andersson, B. Ericsson and K. Larsson, *Z. Kristallogr.*, 1984, **168**, 213.

Communication 9/02975C

Synthesis of organometallic solids by protonation of $Cp^*M(CN)_3^{n-}$ (M = Rh, Ir, Ru)

Stephen M. Contakes, Michael Schmidt and Thomas B. Rauchfuss*

School of Chemical Sciences and the Frederick Seitz Materials Research Laboratory, University of Illinois at Urbana-Champaign, Urbana, IL 61801, USA. E-mail: rauchfuz@uiuc.edu

Received (in Bloomington, IN, USA) 16th March 1999, Accepted 18th May 1999

Protonation of aqueous acetone solutions of $[Cp^*Ir(CN)_3]^-$ produces the two-dimensional organometallic solid $(H_3O)[Cp^*Ir(CN)_3]\cdot Me_2CO$ wherein 14 Å diameter channels ($Ir_4C_8N_8O_4$) contain exchangeable solvent molecules; the analogous Ru and Rh tricyanide complexes are also susceptible to proton-induced polymerization.

The synthesis of solids based on organic[1] and metal organic subunits[2] from molecular precursors is a mature but still growing theme.[3] Organometallic solids are less well developed,[4] although the face-capping C_5R_5 ligands should be convenient for limiting the degrees of freedom in condensation processes. Molecular cages have been prepared by the reaction of *fac*-octahedral tritopic Lewis base $CpM(CN)_3^-$ with *fac*-octahedral tritopic Lewis acids Cp^*M^{2+} and $Mo(CO)_3$.[5–7] The complementary interaction of $Cp^*M(CN)_3^-$ with the pyramidal tritopic receptor[8] H_3O^+ is now shown to afford extended structures featuring two-dimensional net structures[9] (Scheme 1).

Aqueous solutions of $NEt_4[Cp^*Ir(CN)_3]$ **1** react upon mixing with protic acids (HOTf, HCl, HOTs) to produce the colorless solid $(H_3O)[Cp^*Ir(CN)_3]$ **2** in 82% isolated yield.† The yield is proportional to the stoichiometry of the acid, consistent with a cooperative process *vs.* formation of species of intermediate degrees of condensation (*e.g.* $H[Cp^*Ir(CN)_3]_2^-$). Base reverses the polymerization process, affording intact $Cp^*Ir(CN)_3^-$ [eqn. (1)].

$$\{(H_3O)[Cp^*Ir(CN)_3]\}_n \underset{H^+}{\overset{OH^-}{\rightleftharpoons}} [Cp^*Ir(CN)_3]^- \qquad (1)$$

IR measurements on **2** show two ν_{CN} bands (2156 and 2137 cm^{-1}) in the region for hydrogen bonded (or bridging) CN ligands. Compound **2** is completely insoluble in common solvents except methanol, wherein it dissociates to give free $[Cp^*Ir(CN)_3]^-$, as indicated by ^1H NMR measurements (δ 1.945, as for **1**). Conductivity measurements on 10^{-3} M MeOH solutions confirm that **2** is a 1:1 electrolyte (Λ_M of 96 Ω cm^2 mol^{-1}).

Crystals of **2** were obtained by layering an acetone solution of HOTf (10 mM) over an (10 mM) $CHCl_3$ solution of $NEt_4[Cp^*Ir(CN)_3]$ for 48 h.‡ The resulting crystals readily desolvate to give powders, even at 0 °C. The crystallographic analysis reveals a layered structure of formula $[Cp^*Ir(CN)_3]H_3O\cdot Me_2CO$. The corrugated sheets consist of $Cp^*Ir(CN)_3^-$ ions triply bridged *via* hydrogen bonds to H_3O^+ ions (Fig. 1). As in the previously described molecular boxes,[13,14] there is complementary connectivity of the Lewis base $[M(CN)_3]$ and Lewis (in this case Brønsted) acid (H_3O^+). The layers feature alternating 24- and 12-membered rings composed, respectively, of $Ir_4C_8N_8O_4$ and $Ir_2C_4N_4O_2$ atoms (ignoring H atoms). Owing to the linearity of the Ir–C–N···O linkages, the 24-membered rings are approximately octagonal and the 12 membered rings are approximately square. The 'cross window' distances in the 24-membered rings are *ca.* 14 (Ir···Ir) and *ca.* 13 Å (O···O). The 12- and 24-membered rings are eclipsed, leaving large channels that extend through the solid along the *a* axis (interlayer distance of 6.976 Å).

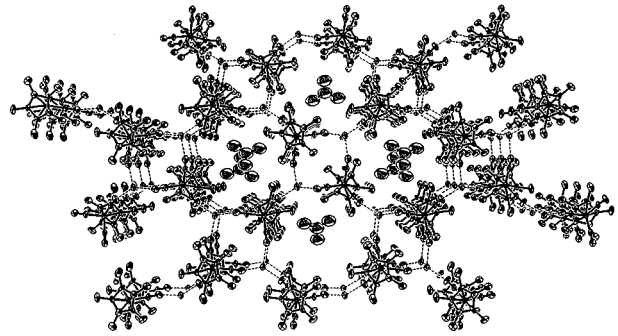

Fig. 1 Fragment of one layer of $(H_3O)[Cp^*Ir(CN)_3]\cdot Me_2CO$ viewed down the *a* axis. The acetone molecules occupy the octagonal channels (thermal ellipsoids set at the 50% probability level).

The octagonal channels in **2** are filled with acetone molecules that are subject to large thermal motion. It is thus understandable that this material easily desolvates. The lability of the solvent in **2** was examined by thermogravimetry, which confirms that acetone evolution reversibly occurs in the range 25–65 °C. Solvent *exchange* also occurs readily for *solid* **2**. To prove this point, samples of $\mathbf{2}\cdot Me_2CO$ were exposed to the *vapor* of fluoroacetone, which is virtually isosteric with acetone (Fig. 2). The TGA curves of the resultant material show an increase in the solvent weight loss from *ca.* 12% (*vs.* 12.0% theoretical) to *ca.* 15% (14.8% theoretical for $\mathbf{2}\cdot(CH_2F)MeCO$.

While the synthesis, spectroscopy, and solubility properties of $(H_3O)[Cp^*Rh(CN)_3]$ **3** are virtually identical to that of **2**, the rhodium species is significantly less stable. Thus **3** decomposes after several hours in refluxing $CHCl_3$ with evolution of HCN to produce, *inter alia*, $\{[Cp^*Rh]_7(CN)_{12}\}^{2+}$; the analogous decomposition of **2** requires 3 weeks.[6] This reaction illustrates the potential utility of the acid-catalysed condensation, somewhat analogous to the decarbonylation route used to prepare polynuclear metal carbonyls.

Hydrogen bonding interactions also play a significant role in the chemistry of $Cp^*Ru(CN)_3^{2-}$, which is of interest as a precursor to electroactive solids and cages. This species was readily prepared from the reaction of $Cp^*Ru(MeCN)_3^+$ with 3 equiv. of NaCN but it is difficult to separate the product from contaminating salts. Treatment of the crude product with HOTf (2 equiv) produced the polymer $H_2[Cp^*Ru(CN)_3]$ **4** as a white

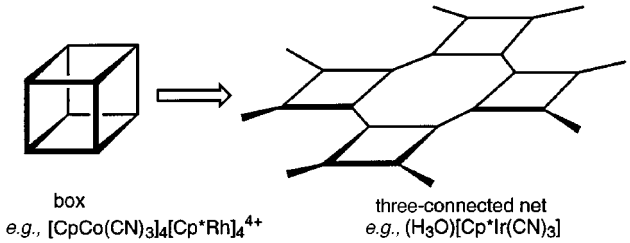

Scheme 1

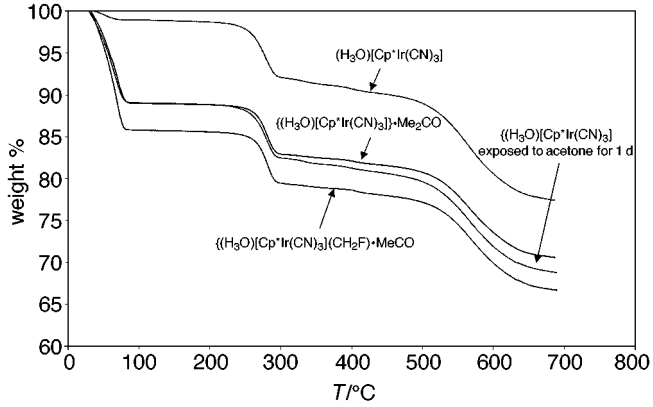

Fig. 2 TGA results for solvent exchange of $(H_3O)[Cp^*Ir(CN)_3]$-derived solids. From the top: $(H_3O)[Cp^*Ir(CN)_3]$, $(H_3O)[Cp^*Ir(CN)_3]\cdot Me_2CO$, vacuum-dried $(H_3O)[Cp^*Ir(CN)_3]$ after exposure to acetone vapor (24 h, 298 K), $(H_3O)[Cp^*Ir(CN)_3]\cdot\cdot Me_2CO$ that had been exposed to $(CH_2F)MeCO$ vapor (24 h, 298 K).

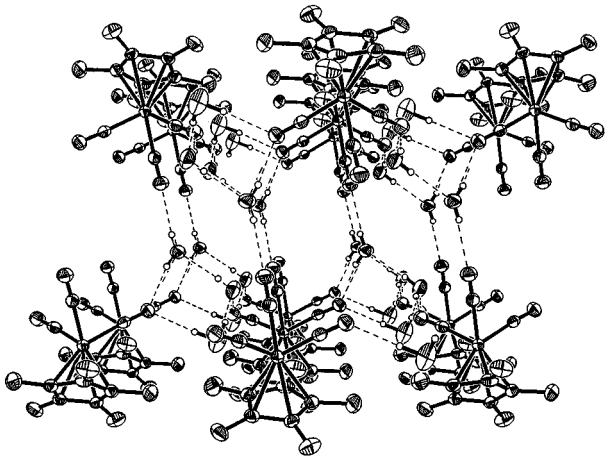

Fig. 3 Side view of one layer of hydrated anions in $[NEt_4]_2[Cp^*Ru(CN)_3]\cdot 3H_2O$ (thermal ellipsoids at the 50% probability level). Selected average bond lengths and angles: Ru–CN 1.995 Å, C–N 1.165 Å, Ru–C–N 176.8°, NC–Ru–CN 89.3°.

precipitate. Depolymerization was effected by treatment of aqueous suspensions of **4** with aqueous NEt_4OH to give analytically pure CH_2Cl_2-soluble $[NEt_4]_2[Cp^*Ru(CN)_3]$ **5** ($E_{1/2}$ = −729 mV *vs.* Fc/Fc^+). Crystallographic characterization‡ of the beige crystals of **5** revealed a hydrate with a layered structure wherein the hydrophobic and hydrophilic subunits are segregated (Fig. 3).

This research was supported by the Department of Energy. The following agencies provided fellowship support: NSF graduate fellowship (S. M. C.), Feodor Lynen postdoctoral fellowship (M. S.), and Alexander von Humboldt Senior Fellowship (T. B. R.).

Notes and references

† *Data for new compounds*: $\{(H_3O)[Cp^*Ir(CN)_3]\}$ **2**: 82% yield; ν_{CN} 2162, 2128 cm^{-1}; ^1H NMR (CD_3OD): δ_{Cp^*} 2.040. Anal. CHN. $\{(H_3O)[Cp^*Rh(CN)_3]\}$ **3**: 84% yield, ν_{CN} 2156, 2137 cm^{-1}. ^1H NMR (CD_3OD): δ_{Cp^*} = 1.945; Anal. CHN. $H_2[Cp^*Ru(CN)_3]$ **4**: 80% yield; Anal. CHN; ^1H NMR (CD_3OD): δ_{Cp^*} 1.90; ν_{CN} 2096, 2057, 2001 cm^{-1}. $[NEt_4]_2[Cp^*Ru(CN)_3]\cdot 3H_2O$ **5**: 63% yield. Anal. CHN; ^1H NMR: δ_{Cp^*} 1.90; ν_{CN} 2052, 2019 cm^{-1}. CV (MeCN): quasi-reversible oxidation at −729 mV *vs.* Fc/Fc^+.

‡ *Crystal data*: $(H_3O)[Cp^*Ir(CN)_3]\cdot C_3H_6O$ (M = 482.58), monoclinic, space group $P2_1/c$, 0.06 × 0.05 × 0.05 mm, a = 6.9764(2), b = 15.9021(5), c = 16.7178(6) Å, β = 90.8730(10)°, V = 1854.45(10) $Å^3$, Z = 4, D_c = 1.728 g cm^{-3}, T = 198(2) K; λ(Mo-Kα) = 0.71073 Å, 9590 reflections, 3268 independent (R_{int} = 0.1555), $R1$ = 0.0854, wR2 (on F^2) = 0.1397.

$[NEt_4]_2[Cp^*Ru(CN)_3]\cdot 3H_2O$ (M = 628.90), monoclinic, space group $P2_1/c$, 0.22 × 0.34 × 0.38 mm, a = 15.7795(7), b = 14.8677(7), c = 15.2447(7) Å, β = 109.4830(10)°, V = 3371.7(3) $Å^3$, Z = 4; D_c = 1.239 g cm^{-3}, T = 173(2) K; λ(Mo-Kα) = 0.71073 Å; 21890 reflections, 8054 independent (R_{int} = 0.0338), $R1$ = 0.0312, $wR2$ (on F_2) = 0.0763.

CCDC 182/1263.

1 D. J. Cram, *Nature*, 1992, **356**, 29; *Chemtech*, 1987, **17**, 120.
2 M. Fujita, M. Aoyagi, F. Ibukuro, K. Ogura and K. Yamaguchi, *J. Am. Chem. Soc.*, 1998, **120**, 611; M. Fujita and K. Ogura, *Coord. Chem. Rev.*, 1996, **148**, 249; O. M. Yaghi, H. L. Li, and T. L. Groy, *Inorg. Chem.*, 1997, **36**, 4292; O. M. Yaghi, G. M. Li and H. L. Li, *Nature*, 1995, **378**, 703.
3 J.-M. Lehn, *Supramolecular Chemistry*, VCH, Weinheim, 1995.
4 J. Lewis, P. R. Raithby and W. Y. Wong, *J. Organomet. Chem.*, 1998, **556**, 219; I. Manners, *Angew. Chem., Int. Ed. Engl.*, 1996, **35**, 1602; S. S. H. Mao, F. Q. Liu and T. D. Tilley, *J. Am. Chem. Soc.*, 1998, **120**, 1193; U. H. F. Bunz, *Pure Appl. Chem.*, 1996, **68**, 309; C. Gorman, *Adv. Mater.*, 1998, **10**, 295.
5 K. K. Klausmeyer, S. R. Wilson and T. B. Rauchfuss, *Angew. Chem., Int. Ed.*, 1998, **37**, 1808; K. K. Klausmeyer, S. R. Wilson and T. B. Rauchfuss, *J. Am. Chem. Soc.*, 1999, **121**, 2705.
6 S. M. Contakes, K. K. Klausmeyer, R. M. Milberg, S. R. Wilson and T. B. Rauchfuss, *Organometallics*, 1998, **19**, 3633.
7 Studies on related cages based on $[9]aneN_3$ in place of Cp ligands: J. L. Heinrich, P. A. Berseth and J. R. Long, *Chem. Commun.*, 1998, 1231.
8 D. Braga, F. Grepioni and G. R. Desiraju, *J. Organomet. Chem.*, 1997, **548**, 33.
9 A. F. Wells, *Structural Inorganic Chemistry*, Clarendon Press, Oxford, 1984.

Communication 9/02115I

Novel cyclic hexanuclear complexes containing quadruply bonded units joined by μ_6-carbonate ions

Maw-Cherng Suen,[a] Gwo-Wei Tseng,[a] Jhy-Der Chen,*[a] Tai-Chiun Keng[b] and Ju-Chun Wang[b]

[a] *Department of Chemistry, Chung-Yuan Christian University, Chung-Li, Taiwan, R.O.C.*
[b] *Department of Chemistry, Soochow University, Taipei, Taiwan, R.O.C.*

Received (in Cambridge, UK) 28th April 1999, Accepted 24th May 1999

Three complexes {[*trans*-$Mo_2(O_2CCF_3)_2$(μ-dppa)]$_3$(μ_6-CO_3)(μ_2-X)$_3$}F [X = Cl, Br or I; dppa = *N*,*N*-bis(diphenylphosphino)amine], are reported, which are the first cyclic, hexanuclear complexes containing quadruply bonded units joined by carbonate ions.

Complexes containing metal–metal multiple bonds have already been the subject of many studies of their structures and reactivities.[1] Quadruply bonded dinuclear complexes were found to be able to dimerize to form cyclic rectangular clusters. Pairs of dinuclear molecules undergo [2 + 2] cycloaddition by loss of the δ components of the quadruple bonds with the two single bonds formed joining the triply bonded dimers together.[2] Recently tetranuclear complexes of the type $[Mo_2(DArF)_3]_2(\mu\text{-}H)_2$ (DArF = *N*,*N*′-diarylformamidinate, Ar = *p*-tolyl or *p*-anisyl) containing quadruply bonded dimolybdenum units joined by μ-hydride ions have been prepared by reaction of $Mo_2(DArF)_3Cl_2$ and $NaHBEt_3$.[3] To investigate the bonding mode of the carbonate ion in the dimolybdenum complex, we studied the reaction of [*trans*-$Mo_2(O_2CCF_3)_2(MeCN)_6][BF_4]_2$ with K_2CO_3 and *N*,*N*′-bis(diphenylphosphino)amine (dppa) in CH_2Cl_2. The reaction afforded a novel cyclic, hexanuclear complex containing quadruply bonded units joined by carbonate ions and axially bridged by chloride atoms. The synthesis and structural characterization of this complex and its bromo and iodo analogue form the subject of this report.

The chloro complex, {[*trans*-$Mo_2(O_2CCF_3)_2$(μ-dppa)]$_3$(μ_6-CO_3)(μ-Cl)$_3$}F **1** was prepared by reaction of [*trans*-$Mo_2(O_2CCF_3)_2(MeCN)_6][BF_4]_2$ with K_2CO_3 and dppa in CH_2Cl_2.† The chloride atoms in **1** are presumably obtained from the CH_2Cl_2 solvent. The transfer of chloride atoms from the CH_2Cl_2 solvent to quadruply bonded complexes has been observed during the preparation of the complexes $Mo_2Cl_3(O_2C\text{-}Me)$(etp) {etp = bis[2-(diphenylphosphino)ethyl]phenylphosphine} and $Mo_2Cl_3(O_2CMe)$(tetraphos-2) {tetraphos-2 = tris[2-(diphenylphosphino)ethyl]phosphine}.[4] Reaction of [*trans*-$Mo_2(O_2CCF_3)_2(MeCN)_6][BF_4]_2$ with dppa and K_2CO_3 in MeCN, followed by addition of ZnX_2 (X = Br or I), afforded complexes of the type [*trans*-$Mo_2(O_2CCF_3)_2$(μ-dppa)]$_3$(μ_6-CO_3)(μ_2-X)$_3$}F (X = Br, **2**; X = I, **3**).† The appearance of the F ions in **1**–**3** can be ascribed to the dissociation of the BF_4^- ions to give F^- and BF_3, which has been observed during the preparation of a linear trichromium complex $[Cr_3(dpa)_4(F)(FBF_3)](BF_4)$ [dpa$^-$ = anion of bis(2-pyridyl)-amine].[5]

Crystals of **1**–**3** are isomorphous and conform to the space group *C*2/*c* with four molecules in each unit cell.‡ Fig. 1 shows a representative ORTEP diagram for the cations of **1**–**3**. The molecule resides on a C_2 axis passing through atoms X(1), O(8), C(1) and N(2) and bisecting the Mo(3)–Mo(3a) bond. The core structure is remarkable in that three sets of quadruply bonded $Mo_2(O_2CCF_3)_2$(μ-dppa) units are joined by a carbonate group (CO_3^{2-}) and axially bridged by three halide atoms. The metal atoms in each $Mo_2(O_2CCF_3)_2$(μ-dppa) unit are bridged by a dppa ligand and two $CF_3CO_2^-$ groups which are *trans* to each other. Table 1 lists selected bond distances and angles. The Mo–Mo distances for all three complexes are very similar and are normal for Mo–Mo quadruple bonds. The Mo–X distances are relatively long, indicating only weak Mo–X interactions. The Mo–X distances, which show a strong dependence on the nature of the halogen atoms, increase from X = Cl to I. Noticeably, while the angles of Mo–X–Mo decrease from X = Cl to I, the Mo–Mo–X angles become more linear. Each molecule of the three cations can be viewed as three sets of edge-sharing bioctahedra, shown as **I** (Scheme 1), linked by adjacent $CF_3CO_2^-$ groups and dppa ligands, and quadruply bonded by

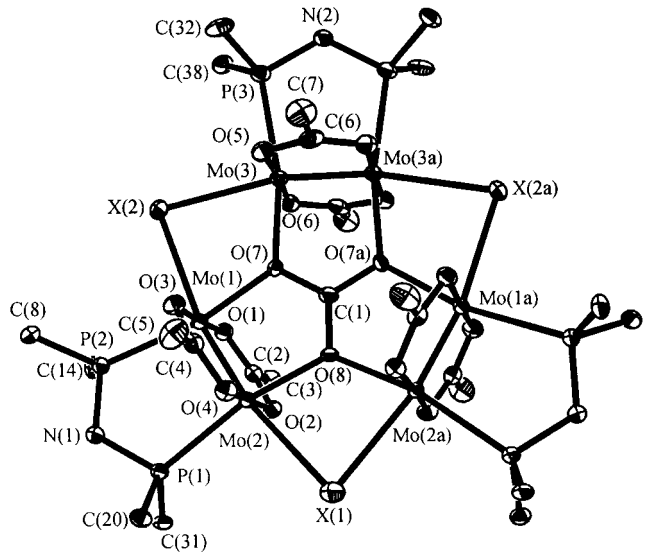

Fig. 1 A representative ORTEP drawing for complexes **1** (X = Cl), **2** (X = Br) and **3** (X = I). The F atoms of the CF_3 groups are removed and the phenyl carbon atoms are designated by their first atoms for clarity.

Table 1 Selected bond distances (Å) and angles (°) for **1** (X = Cl), **2** (X = Br) and **3** (X = I)

	X = Cl	X = Br	X = I
Mo(1)–Mo(2)	2.153(1)	2.152(1)	2.150(1)
Mo(3)–Mo(3a)	2.155(1)	2.148(1)	2.154(2)
Mo(1)–X(2)	2.828(2)	2.958(1)	3.202(1)
Mo(2)–X(1)	2.926(3)	3.029(1)	3.195(1)
Mo(3)–X(2)	2.862(2)	2.994(1)	3.202(1)
Mo(1)–X(2)–Mo(3)	82.9(1)	78.8(1)	72.7(1)
Mo(2)–X(1)–Mo(2a)	81.7(1)	77.8(1)	72.3(1)
Mo(1)–Mo(2)–X(1)	167.9(1)	170.0(1)	173.2(1)
Mo(2)–Mo(1)–X(2)	169.2(1)	171.6(1)	173.1(1)
Mo(3a)–Mo(3)–X(2)	168.2(1)	170.0(1)	173.9(1)

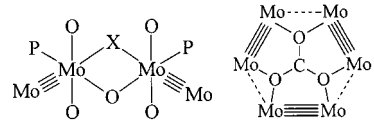

I **II**

Scheme 1

the adjacent molybdenum atoms. The average separations of the two metal centers in **I** are 3.799, 3.790 and 3.804 Å for **1**, **2** and **3**, respectively, indicating no metal–metal interaction.

The cations of **1**–**3** show the μ_6-CO_3^{2-} (3L, 6M)[6] anions bridging the six metal centers through the three oxygen atoms of the carbonate group. Such a coordination mode of μ_6-CO_3^{2-} has been seen in the complexes $[(VO)_6(\mu_6\text{-}CO_3)(\mu\text{-}CO_3)(OH)_9]^{5-}$,[7] in which simple μ_6-bridging was seen for the carbonate ion, and in $[Na_2Nd_4L_4(CO_3)L'_4]$ {H_3L = [(*o*-$HOC_6H_4CH{=}NCH_2)_2CH$]H, L′ = tetrahydrofuran or L'_2 = 1,2-dimethoxyethane},[8] where one carbonate oxygen bridges two sodium atoms and each of the others bridges one sodium and two neodymium atoms. The carbonate coordination in **1**–**3** appears unique in bridging three pairs of multiply bonded metal atoms.

Hexametallic complexes exhibit a fascinating variety of structural patterns.[9] Aggregates are known with the six metal centers as a planar edge-bridged square, a puckered hexagon, an edge-linked bitetrahedron, an edge-bridged tetrahedron, a face-capped tetrahedron and less regular arrays.[9] No complexes of these types containing multiply bonded metal centers have been reported. The cations of complexes **1**–**3** therefore represent a unique structural type for cyclic transition-metal M_6 complexes. The six metal atoms are shifted from their mean planes in pseudo-hexagonal, planar rearrangements, shown as **II** (Scheme 1), by only 0.059, 0.049 and 0.023 Å for **1**, **2** and **3**, respectively. Complexes **1**–**3** are in marked contrast to the cyclic complex $[Mo_6O_8(OEt)_6Cl_8]$[10] which exhibits a chair configuration of metal atoms incorporating three Mo–Mo single bonds. The only trimer of quadruply bonded dimers that has been reported is the linear complex $[Mo_6(O_2CCHF_2)_{12}(bpy)$ (bpy = 2,2′-bipyridine), which comprises a central, quadruply bonded $Mo_2(O_2CCHF_2)_4$ unit whose axial ligands are two $[Mo_2(O_2CCHF_2)_2(bpy)_2](O_2CCHF_2)_2$ units.[11]

We thank the National Science Council of the Republic of China for support.

Notes and references

† $[Mo_2(O_2CCF_3)_2(MeCN)_6](BF_4)_2$ (0.25 g, 0.30 mmol), K_2CO_3 (0.014 g, 0.10 mmol) and dppa (0.12 g, 0.30 mmol) were placed in a flask containing 10 mL CH_2Cl_2. The mixture was stirred at room temp. for 3 h to yield a red solution. The volume of the solvent was reduced and *n*-hexane added to induce precipitation. The red solid was then filtered off and washed with diethyl ether and then redissolved in CH_2Cl_2. Layering of the red solution with diethyl ether gave well formed red crystals. The crystals were collected and dried *in vacuo*. Yield: 0.11 g (43%). [Calc. for $C_{85}H_{63}Cl_3F_{19}Mo_6N_3O_{15}P_6$ (*M* = 2595.29): C, 39.34; H, 2.54; N, 1.62. Found: C, 38.94; H, 2.85; N, 1.50%. IR (KBr disk): 3427 br, 3053 br, 1577 m, 1434 m, 1191 m, 1165 m, 1097 m, 927 m, 799 s, 737 m, 694 m, 526 m. UV–VIS: λ = 513 nm (MeCN). $^{31}P\{^1H\}$ NMR ($CDCl_3$): δ 11.7. Complexes **2** and **3** were prepared by reactions of $[Mo_2(O_2CCF_3)_2(MeCN)_6](BF_4)_2$ (0.25 g, 0.30 mmol), K_2CO_3 (0.014 g, 0.10 mmol) and dppa (0.12 g, 0.30 mmol) with $ZnBr_2$ (0.067 g, 0.3 mmol) and ZnI_2 (0.096 g, 0.3 mmol), respectively, in MeCN. The other procedures were similar to those for **1**. Yield for **2**: 0.12 g (43 %) [Calc. for $C_{85}H_{63}Br_3F_{19}Mo_6N_3O_{15}P_6$ (*M* = 2728.61): C, 37.42; H, 2.33; N, 1.54. Found: C, 37.58; H, 2.43 ; N, 1.54%]. IR (KBr disk): 3452 br, 3058 br, 1590 m, 1435 m, 1275 m, 1203 m, 1152 m, 1100 m, 730 s, 691 m, 529 m. UV–VIS: λ = 508 nm (MeCN). $^{31}P\{^1H\}$ NMR ($CDCl_3$): δ 11.4. Yield for **3**: 0.081 g (30 %) [Calc. for $C_{85}H_{63}I_3F_{19}Mo_6N_3O_{15}P_6$ (*M* = 2869.61): C, 35.58; H, 2.21; N, 1.46. Found: C, 35.32; H, 2.11 ; N, 1.50%]. IR (KBr disk): 3566 br, 3057 br, 1618 m, 1436 m, 1190 m, 1165 m, 1099 m, 741 s, 696 m, 528 m. UV–VIS: λ = 503 nm (MeCN). $^{31}P\{^1H\}$ NMR ($CDCl_3$): δ 10.6 in $CDCl_3$.

‡ *Crystal data*: for **1**, $C_{97}H_{91}Cl_{11}F_{19}Mo_6N_3O_{17}P_6$, *M* = 3083.1, monoclinic, space group *C*2/*c*, *a* = 27.783(2), *b* = 17.091(1), *c* = 27.085(1) Å, β = 107.147(1)°, V = 12289(2) Å^3, *Z* = 4, D_c = 1.67 g cm^{-3}, μ = 0.999 mm^{-1}, 17303 reflections measured, no. of unique reflections = 8674 (R_{int} = 0.0401), no of parameters = 749, *R* = 0.0620 and R_w = 0.0722[$F > 4\sigma(F)$].

For **2**, $C_{97}H_{91}Br_3Cl_8F_{19}Mo_6N_3O_{17}P_6$, *M* = 3216.5, monoclinic, space group *C*2/*c*, *a* = 27.573(2), *b* = 17.203(1), *c* = 27.301(2) Å, β = 106.462(1)°, *V* = 12419(2) Å^3, *Z* = 4, D_c = 1.72 g cm^{-3}, μ = 1.889 mm^{-1}, 28959 reflections measured, no. of unique reflections = 8952 (R_{int} = 0.0459), no of parameters = 696, *R* = 0.0555 and R_w = 0.0754 [$F > 4\sigma(F)$].

For **3**: $C_{93}H_{75}I_3F_{19}Mo_6N_7O_{15}P_6$, *M* = 2985.7, monoclinic, space group *C*2/*c*, *a* = 29.983(2), *b* = 17.336(1), *c* = 23.514(1) Å, β = 114.462(1)°, *V* = 11125(1) Å^3, *Z* = 4, D_c = 1.78 g cm^{-3}, μ = 1.666 mm^{-1}, 15724 reflections measured , no. of unique reflections = 7418 (R_{int} = 0.0363), no of parameters = 661, *R* = 0.0561 and R_w = 0.0683 [$F > 4\sigma(F)$].

The diffraction data of **1**–**3** were collected on a Siemens CCD diffractometer, which was equipped with graphite-monochromated Mo-Kα (λ = 0.71073 Å) radiation. Structure solution was carried out using SHELXTL PLUS. During structural refinement, it was found that the three F atoms of one of the three trifluoroacetate groups of complex **1** and all the F atoms of the trifluoroacetate groups of complex **3** were disordered. The occupancies of the disordered F atoms were set to be 0.5 and refined as the other normal atoms.

CCDC 182/1267. See: http://www.rsc.org/suppdata/1999/1185/ for crystallographic files in .cif format.

1 F. A. Cotton and R. A. Walton, *Multiple Bonds between Metal Atoms*, Oxford University Press, London, 2nd edn., 1993; R. H. Cayton, M. H. Chisholm, J. C. Huffman and E. B. Lobkovsky, *J. Am Chem. Soc.*, 1991, **113**, 8709; K. Mashima, M. Tanaka and K. Tani, *J. Am Chem. Soc.*, 1997, **119**, 4307, and references cited therein.

2 T. R. Ryan and R. E. McCarley, *Inorg. Chem*., 1982, **21**, 2072; F. A. Cotton and G. L. Powell, *Inorg. Chem*., 1983, **22**, 871; F. A. Cotton and M. Shang, *J. Cluster Sci*., 1991, **2**, 121; R. T. Carlin and R. E. McCarley, *Inorg. Chem*., 1989, **28**, 3432; J.-D. Chen and F. A. Cotton, *J. Am. Chem. Soc.*, 1991, **113**, 5857; F. A. Cotton, B. Hong and M. Shang, *Inorg. Chem*., 1993, **32**, 4876.

3 F. A. Cotton, L. M. Daniels, G. T. Jordan IV, C. Lin and C. A. Murillo, *J. Am. Chem. Soc.*, 1998, **120**, 3398.

4 C.-T. Lee, S.-F.Chiang, C.-T. Chen, J.-D. Chen and C.-D. Hsiao, *Inorg. Chem.*, 1996, **35**, 2930.

5 F. A. Cotton, L. M. Daniels, C. A. Murillo and I. Pascual, *J. Am. Chem. Soc.*, 1997, **119**, 10 223

6 F. A. Cotton and G. Wilkinson, *Advanced Inorganic Chemistry*, John Wiley & Sons, New York, 5th edn., 1988, pp. 481–483.

7 T. C. W. Mak, P.-J. Li, C.-M. Zheng and K.-Y. Huang, *J. Chem. Soc., Chem. Commun.*, 1986, 1597.

8 G. B. Deacon, T. Feng, D. C. R. Hockless, P. C. Junk, B. W. Skelton, and A. H. White, *Chem. Commun.*, 1997, 342.

9 I. G. Dance, in *Comprehensive Coordination Chemistry*, ed. G. Wilkinson, R. D. Gillard and J. A. McCleverty, Pergamon, New York, 1987, vol. 1, pp. 135–177.

10 C. Limberg, S. Parsons and A. J. Downs, *J. Chem. Soc., Chem. Commun.*, 1994, 497.

11 E. F. Day, E. J. C. Huffman, K. Folting and G. Christou, *J. Chem. Soc., Dalton Trans.*, 1997, 2837.

Communication 9/03410B

Novel layered lithium nitridonickelates; effect of Li vacancy concentration on N co-ordination geometry and Ni oxidation state

Marten G. Barker,[a] Alexander J. Blake,[a] Peter P. Edwards,[b] Duncan H. Gregory,*[a] Thomas A. Hamor,[b] Daniel J. Siddons[a] and Susan E. Smith[a]

[a] *School of Chemistry, University of Nottingham, University Park, Nottingham, UK NG7 2RD*
[b] *School of Chemistry, University of Birmingham, Edgbaston, Birmingham, UK B15 2TT.*
E-mail: Duncan.Gregory@Nottingham.ac.uk

Received (in Oxford, UK) 14th April 1999, Accepted 21st May 1999

New compounds in which nickel is substituted for lithium in lithium nitride show evidence of high lithium vacancy concentrations and an ordering of these vacancies to form new structural variants.

The chemistry of transition metal ternary nitrides has recently been the subject of intense study.[1] However, the reactions of lithium nitride with the first row transition elements were first studied over fifty years ago.[2–4] A number of different compositions and structures are observed for the resulting lithium nitridometallates, some of the most common being based either on an antifluorite structure[2] or on a modification of the lithium nitride structure itself.[3] Late first row transition nitridometallates such as those formed with Co, Ni and Cu favour this latter structure type. The transition metal (M), in these compounds, partially substitutes for lithium between Li_2N planes to form $Li_{3-x}M_xN$ but the limit of substitution, *x*, is below unity. The parent binary nitride, Li_3N, is a lithium ion conductor.[5] Control of *x* has implications both structurally and in terms of the conductivity of materials. We report here the synthesis and structure of two new layered nitridonickelates.

New ternary lithium nitrides were synthesised by reaction of excess lithium nitride with nickel foil under a positive pressure of nitrogen gas. All manipulations were carried out in an argon or nitrogen-filled evacuable glove box. Lithium nitride (Li_3N) was prepared by reaction of gaseous nitrogen with cleaned lithium metal (5–6 g) dissolved in liquid sodium at 650 °C.[6] Ternary nitrides were prepared by reaction of Li_3N with a nickel foil (99.9% BDH) tube. The tube was placed inside a stainless-steel crucible, sealed in a stainless steel vessel under a positive pressure of nitrogen (*ca*. 2 atm) and heated to 750 °C for 24 h. The vessel was cooled and opened in a nitrogen filled glove box. The reaction yielded a gold coloured coating of crystalline product on the nickel foil. The air-sensitive crystals were isolated, loaded and sealed in capillaries.

Structure solution and refinement reveals two distinct products with compositions $Li_5Ni_3N_3$ and LiNiN.[7] Both compounds have structures closely related to Li_3N, with alternate layers of Li–N sheets and metal ions stacked perpendicular to the *c*-axis. The proposed structures of both compounds exhibit lithium vacancy ordering not seen in lithium nitride or the previously reported $Li_{3-x}M_xN$ compounds. Furthermore, Li ion vacancy concentrations in these lithium nitridometallates are well above the 1–2% level usually observed in Li_3N. This Li vacancy ordering enforces changes in space group with vacancy concentration and the approximate doubling of the $Li_5Ni_3N_3$ *a*-parameter relative to the Li_3N unit cell dimensions. It was almost impossible to discriminate between ordered and disordered models for the LiNiN structure by X-ray diffraction.[8]

It is useful to compare and contrast the structures of the nitridonickelates and the parent compound, Li_3N in terms of the nitrogen coordination environment. Lithium nitride, Li_3N is composed of layers of N-centred hexagonal bipyramids which stack along the *c*-axis. [Li_2N] planes (where each N is surrounded by a 'graphitic-like' hexagon of six Li atoms) are interconnected by Li atoms between layers (in the apical positions of the hexagonal bipyramids) [Fig. 1(a)].† In the nitridonickelates, Ni replaces Li in these 'apical' sites between layers additionally creating Li vacancies in the [Li_2N] planes. Hence there is an evolution of nitrogen co-ordination geometry with vacancy concentration. In $Li_5Ni_3N_3$ [Fig. (1b)] the nitrogen coordination is effectively reduced to '6 + 1' (distorted pentagonal bipyramidal). Within the Li–N planes, nitrogen is now surrounded by five lithium ions. In reality, the in-plane Li(1)–N(1) distance [2.42(4) Å] is much larger than the sum of

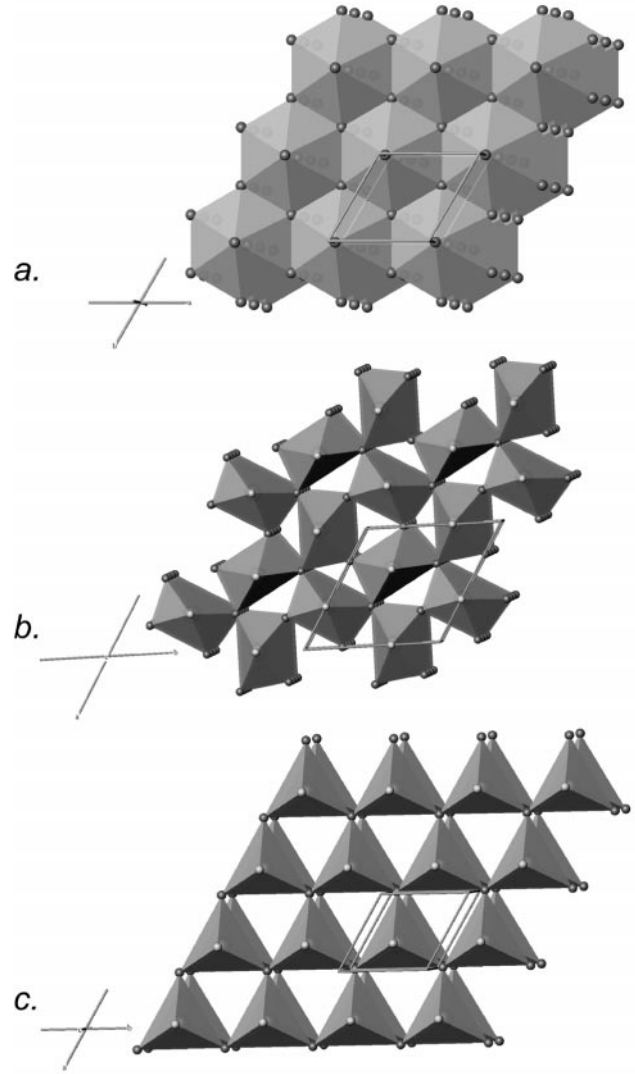

Fig. 1 Structure of (a) Li_3N, showing edge sharing of N(Li_8) polyhedra in the *ab* plane (b) $Li_5Ni_3N_3$, showing vertex sharing of N(Li_4Ni_2) polyhedra in the *ab* plane and creation of Li vacancies (c) LiNiN, showing vertex sharing of N(Li_3Ni_2) polyhedra in the *ab* plane and creation of Li vacancies.

the ionic radii[9] and the nitrogen coordination is closer to distorted octahedral than pentagonal bipyramidal. Li coordination within planes is both three- and two-fold. The N-centred polyhedra are linked by vertices both in the *ab* plane and along *c*. In the proposed structure of LiNiN [Fig. (1c)], the nitrogen coordination is reduced further to five (trigonal bipyramidal). The N coordination and the *intra*-layer linking in this compound are akin to that in the high-pressure form of Li_3N (β-Li_3N, with the Na_3As structure),[10] although the stacking of layers is altered. As in $Li_5Ni_3N_3$, the N-centred polyhedra are linked by vertices in three dimensions. The lithium coordination in the Li–N planes in LiNiN is exclusively trigonal planar as in the Li_3N parent structure. In both nitridonickelates, Li–N planes are linked *via* infinite, perpendicular N–Ni–N chains. In LiNiN, as in Li_3N, these chains are straight whereas in $Li_5Ni_3N_3$ they are slightly bent.

The Li-N bond lengths in both $Li_5Ni_3N_3$ [mean distance: 2.086(5) Å, excluding the interaction at 2.42(4) Å] and LiNiN [2.1697(6) Å] are of the same order as those observed in the parent binary nitride (2.130 Å).[11] The interplane Ni–N distances [1.777(1) Å in $Li_5Ni_3N_3$ and 1.7700(5) Å in LiNiN] are considerably shorter than the equivalent Li(2)–N distance in Li_3N (1.939 Å).[11] The Ni–N bond lengths are similar to those (Li,Ni)–N distances derived from *c*-parameters of $Li_{3-x}Ni_xN$ solid solution members[2] and are only marginally shorter than those observed in other nitridonickelate(I) species such as CaNiN (1.7904 Å)[12] and SrNiN [average: 1.81(4) Å].[13] These distances indicate the likely significant covalent (π) character of the Ni–N bond in nitridonickelates. Besides the $Li_{3-x}M_xN$ compounds, perhaps the most closely related structure to $Li_5Ni_3N_3$ and LiNiN is that of Li_4FeN_2, also a defect variant of Li_3N. In the nitridoferrate, however, metal vacancies occur *between* [Li_2N] planes (*i.e.* on iron positions) and the structure can be described by the formulation $Li_2(Fe_{0.5}\square_{0.5})N$ (where □ is a vacancy). The equivalent interplanar metal–nitrogen (Fe–N) distance in Li_4FeN_2 is 1.86(1) Å; longer than those observed in the nickel nitrides.

The nitridonickelates can be regarded as vacancy-ordered layer compounds, $Li_{3-x-y}Ni_x\square_yN$. In these examples, $x = 1$, $y = 0.333$ in $Li_5Ni_3N_3$ and $x = 1$, $y = 1$ in LiNiN. Besides affecting the nitrogen coordination environment, the other consequence of removing lithium is to increase the nickel valency and oxidation states above one become possible. $Li_5Ni_3N_3$ contains Ni^{I}/Ni^{II} ($Ni^{1.33+}$) whereas LiNiN contains exclusively divalent nickel. During the course of this study, the related nitridonickelate $Li_{5.69}Ni_{2.31}N_3$ was reported which also adopts the $P\bar{6}2m$ structure isotypic with $Li_5Ni_3N_3$.[14] In this case, $x = 0.77$, $y = 0.3333$ and Ni has an oxidation state of 1.43.

Bond valence calculations[15] performed for the nitridonickelates yielded the following values: (a) LiNiN: Li = 0.7, Ni = 1.9, N = −2.6; (b) $Li_5Ni_3N_3$: Li(1) = 0.7, Li(2) = 0.8, Ni = 1.9, N = −3.0. While the Li and N site valences compare well with Li_3N, perhaps more interesting is the magnitude of the Ni valences. These would suggest that Ni is present as predominantly Ni(II). Calculations performed on original $Li_{3-x}Ni_xN$ compositions, with (Li/Ni)–N bond lengths derived from *c*-parameters, produce similar values. In some cases, these absolute values may be artificially high since π-bonding contributions in transition metal nitrides lead to bonds shorter than anticipated from 'purely ionic' contributions. However, the inference is that regardless of the Li/Ni distribution on the interplanar site, creation of Li vacancies in the [Li_2N] plane is inevitable to maintain charge balance. There is a striking paucity of reliable structural data for the earlier reported $Li_{3-x}M_xN$ compounds. The increase in *a*-parameters with increasing *x* in these compounds suggests that substitution of transition metals for lithium *between* [Li_2N] planes also engenders structural change *within* those planes (albeit in a *disordered* manner). Neutron diffraction is a crucial tool in determining the site occupancy of light elements. Only '$Li_{2.5}Cu_{0.5}N$' has been examined by powder neutron diffraction (PND) and this compound was found to contain *ca.* 15% Li vacancies in the [Li_2N] plane (giving a refined composition $Li_{2.2}Cu_{0.5}N$).[16]

The ionic and electronic conductivity and the magnetic behaviour of $Li_{3-x}M_xN$ (M = Co, Ni) nitrides have been examined previously.[17] We are preparing $Li_{3-x-y}Ni_x\square_yN$ materials in bulk to investigate their electronic and magnetic properties. The effect of increased Li^+ ion vacancies and nickel oxidation states may have exciting implications for conductivity and magnetism in these lithium ternary nitrides.

The authors thank the EPSRC, British Telecom (S. E. S.) and the Royal Society (P. P. E.) for supporting this work and also the EPSRC for the award of an Advanced Fellowship to D. H. G.

Notes and references

† Colour versions of Fig. 1 along with an additional figure showing the structure of Li_3N, $Li_5Ni_3N_3$ and LiNiN connected by vertices along the *c*-axis can be accessed electronically (see http://www.rsc.org/suppdata/cc/1999/1187).

1 See, for example: D. H. Gregory, *J. Chem. Soc., Dalton Trans.*, 1999, 259; R. Niewa and F. J. DiSalvo, *Chem. Mater.*, 1998, **10**, 2733.

2 See, for example: R. Juza and F. Hund, *Z. Anorg. Allg. Chem.*, 1948, **257**, 1; R. Juza, H. H. Weber and E. Meyer-Simon, *Z. Anorg. Allg. Chem.*, 1953, **273**, 48.

3 W. Sachsze and R. Juza, *Z. Anorg. Allg. Chem.*, 1949, **259**, 278.

4 R. Juza, K. Langer and K. von Benda, *Angew. Chem.*, 1968, **80**, 373; *Angew. Chem., Int. Ed. Engl.*, 1968, **7**, 360.

5 U. V. Alpen, *J. Solid State Chem.*, 1979, **29**, 379.

6 Cleaned, pure lithium was added to an excess of molten sodium contained in a stainless-steel crucible at 250 °C. The cooled crucible was sealed inside a stainless-steel distillation vessel which was evacuated and filled with nitrogen gas (*ca.* 2 atm). The vessel was heated to 650 °C with the nitrogen pressure monitored using a pressure transducer. Excess Na was removed by vacuum distillation at 350 °C for 12 h.

7 *Crystal data*: $Li_5Ni_3N_3$, $M = 252.9$, hexagonal space group $P\bar{6}2m$ (no. 189), $a = 6.475(3)$, $c = 3.555(2)$ Å, $Z = 1$, $V = 129.1(3)$ Å^3, $D_c = 3.253$ g cm^{-3}, $\mu = 10.67$ mm^{-1}. 868 reflections measured at 293(2) K, 109 independent ($R_{int} = 0.0712$). Data collected on a Rigaku R-Axis II area detector diffractometer with graphite monochromated Mo-Kα radiation ($\lambda = 0.71073$ Å). The structure was solved by direct methods with SHELXS-86[a], and refined by least squares within SHELXL-93.[b] $w = 1/[\sigma^2(F_o^2) + (0.040P)^2 + 0.59P]$ where $P = (F_o^2 + 2F_c^2)/3$ $R1 = 0.0351$, $wR2 = 0.0884$.

LiNiN, $M = 79.66$, hexagonal space group $P\bar{6}m2$ (no.187) , $a = 3.758(1)$, $c = 3.540(1)$ Å, $Z = 1$, $V = 43.30(2)$ Å^3, $D_c = 3.055$ g cm^{-3}. $\mu = 10.606$ mm^{-1}, 1440 reflections measured at 297(2) K, 171 independent ($R_{int} = 0.024$). Data collected on a Stadi-4 diffractometer with Mo-Kα radiation ($\lambda = 0.71073$ Å). The structure was solved by direct methods with SHELXL-86[a] and refined by least squares within SHELXL-93.[b] $w = 1/[\sigma^2(F_o^2) + (0.0584\,P)^2]$ where $P = (F_o^2 + 2F_c^2)/3$. $R1 = 0.0374$, $wR2 = 0.0803$. (*a*) G. M. Sheldrick, *Acta Crystallogr., Sect. A*, 1990, **46**, 467; (*b*) G. M. Sheldrick, SHELXL-93, Program for Crystal Structure Refinement, University of Gottingen, Gottingen, Germany, 1993.

CCDC 182/1262. See http://www.rsc.org/suppdata/cc/1999/1187/ for crystallographic files in .cif.format.

8 The alternative disordered model was refined in space group *P*6/*mmm* with an *R*1 factor higher by 0.01 (0.046). The key differences compared to the $P\bar{6}m2$ model are the partial occupancy of the interplane site by Li (Li:Ni = 0.23:0.87) and disordered Li vacancies in the Li–N planes giving a Li(2) site partial occupancy (0.55).

9 W. H. Baur, *Crystallogr. Rev.*, 1987, **1**, 59

10 H. J. Beister, S. Haag, R. Kniep, K. Strössner and K. Syassen, *Angew. Chem.*, 1988, **100**, 1116; *Angew. Chem., Int. Ed. Engl.*, 1988, **27**, 1101.

11 A. Rabenau and H. Schultz, *J. Less-Common Met.*, 1976, **50**, 155.

12 M. Y. Chern and F. J. DiSalvo, *J. Solid State Chem.*, 1990, **88**, 459.

13 T. Yamamoto, S. Kikkawa and F. Kanamaru, *J. Solid State Chem.*, 1995, **115**, 353.

14 J. Klatyk, P. Hohn and R. Kniep, *Z. Kristallogr.*, 1998, **213**, 31.

15 N. E. Brese and M. O'Keeffe, *Acta Crystallogr., Sect. B*, 1991, **47**, 192.

16 M. T. Weller, S. E. Dann, P. F. Henry and D. B. Currie, *J. Mater. Chem.*, 1999, **9**, 283.

17 N. A. Martem'yanov, V. Kh. Tamm, V. P. Obrosov and Z. S. Martem'yanova, *Inorg. Mater.* 1995, **31**, 65.

Communication 9/02962A

'Adding' stable functional complementary, nucleophilic and electrophilic clusters: a synthetic route to $[\{(SiW_{11}O_{39})Mo_3S_4(H_2O)_3(\mu\text{-}OH)\}_2]^{10-}$ and $[\{(P_2W_{17}O_{61})Mo_3S_4(H_2O)_3(\mu\text{-}OH)\}_2]^{14-}$ as examples

Achim Müller,*[a] Vladimir P. Fedin,[a,b] Christoph Kuhlmann,[a] Heinz-Dieter Fenske,[c] Gerhard Baum,[c] Hartmut Bögge[a] and Björn Hauptfleisch[a]

[a] *Fakultät für Chemie der Universität, Lehrstuhl für Anorganische Chemie I, Postfach 100131, D-33501 Bielefeld, Germany. E-mail: a.mueller@uni-bielefeld.de*
[b] *Institute of Inorganic Chemistry, Russian Academy of Sciences, pr. Lavrentjeva 3, Novosibirsk 630090, Russia*
[c] *Institut für Anorganische Chemie, Kaiserstr. 12, D-76131 Karlsruhe, Germany*

Received (in Basel, Switzerland) 20th April 1999, Accepted 18th May 1999

Stable functional complementary clusters, *i.e.* of the electrophilic and nucleophilic type, can be 'added' resulting in the planned formation of the related reaction products: the high-yield synthesis of the crystalline compounds $[Me_2NH_2]_{10}[\{(SiW_{11}O_{39})Mo_3S_4(H_2O)_3(\mu\text{-}OH)\}_2]\cdot 20H_2O$ 1 and $[Me_2NH_2]_{14}[\{(P_2W_{17}O_{61})Mo_3S_4(H_2O)_3(\mu\text{-}OH)\}_2]\cdot 25H_2O$ 2 containing the related $\{Mo_3S_4\}^{4+}$ as well as $\{W_{11}O_{39}\}^{8-}$ and $\{W_{17}O_{61}\}^{10-}$ clusters as constituents, respectively, is a good example.

The deliberate synthesis of large clusters by 'adding' or 'linking' smaller ones, which are stable in solution under certain reaction conditions, is a challenge for the inorganic chemist. The aqua ion $[Mo_3S_4(H_2O)_9]^{4+}$ can for instance be regarded as an archetypical electrophilic building block in this respect since the H_2O ligands are labile and can be easily substituted by nucleophilic cluster anions with donor functions and therefore act formally as ligands. Here, we report the deliberate high-yield synthesis of the title species and provide two examples of the potentially large class of compounds having complementary functional polyoxometalate[1] and chalcogenide clusters as constituents.[2]

In an acidic medium two electrophilic $[Mo_3S_4(H_2O)_9]^{4+}$ [3] aqua cations react with two monovacant lacunary anions $\{[SiW_{11}O_{39}]^{8-}$ [4] or $[P_2W_{17}O_{61}]^{10-}$ [5]$\}$ to yield the cluster species $[\{(SiW_{11}O_{39})Mo_3S_4(H_2O)_3(\mu\text{-}OH)\}_2]^{10-}$ **1a** and $[\{(P_2W_{17}O_{61})Mo_3S_4(H_2O)_3(\mu\text{-}OH)\}_2]^{14-}$ **2a** respectively, which were isolated as the Me_2NH_2 salts **1** and **2** in high yield.†‡ It is important to note that the structure of the reaction products of the complementary educts can be predicted by considering (a) the preferred octahedral coordination of molybdenum, (b) the easily removable H_2O ligands of the $[Mo_3S_4(H_2O)_9]^{4+}$ aqua ion, and (c) the number of oxygen atoms in the lacunary-type anions $[SiW_{11}O_{39}]^{8-}/[P_2W_{17}O_{61}]^{10-}$ acting as strong donors. Under the same conditions, other products should (preferably) not be formed.

Single crystal X-ray structure determinations have revealed that the yellow–brown diamagnetic compounds $[Me_2NH_2]_{10}[\{(SiW_{11}O_{39})Mo_3S_4(H_2O)_3(\mu\text{-}OH)\}_2]\cdot 20H_2O$ **1** and $[Me_2NH_2]_{14}[\{(P_2W_{17}O_{61})Mo_3S_4(H_2O)_3(\mu\text{-}OH)\}_2]\cdot 25H_2O$ **2** contain the discrete cluster anions **1a** and **2a**, $[Me_2NH_2]^+$ cations, and crystal water molecules in their lattices.§ Fig. 1 and 2 show perspective views of the structures of **1a** and **2a** both having a central core built up by two $\{Mo_3S_4(H_2O)_3\}^{4+}$ fragments connected through two hydroxo bridging groups which are *cis* to the μ_3-S core atoms. [Note that in $[Mo_3S_4(H_2O)_9]^{4+}$, the H_2O ligands in *cis* position to the μ_3-S atom are more acidic than the c-H_2O ligands in *trans* position;[6] the protonation of the bridging oxygen atoms clearly follows from bond valence sum (BVS) calculations.[7]]

The two nucleophilic lacunary anions, of the Keggin type $\{[SiW_{11}O_{39}]^{8-}\}$ and of the Dawson type $\{[P_2W_{17}O_{61}]^{10-}\}$, can be considered as negatively charged ligands which replace coordinated H_2O ligands of the electrophilic educt (during the reaction). In this respect the monovacant lacunary anions with four oxygen donor atoms can be regarded as inorganic equivalents of a porphyrin ligand.[1c] In agreement with our

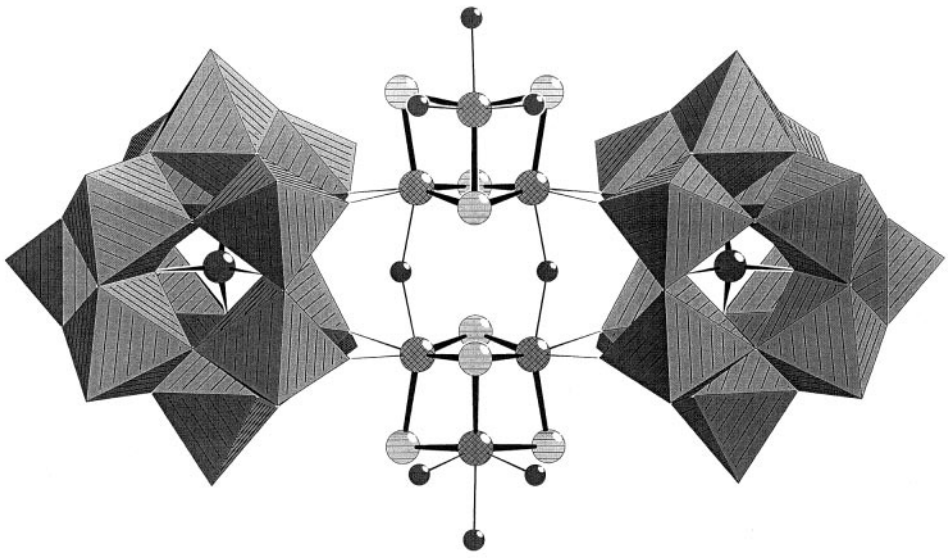

Fig. 1 Structure of the cluster anion **1a** distinguishing between the building units or constituents: $\{Mo_3S_4\}$ fragments in ball-and-stick and $\{W_9\}$ fragments in polyhedral representation.

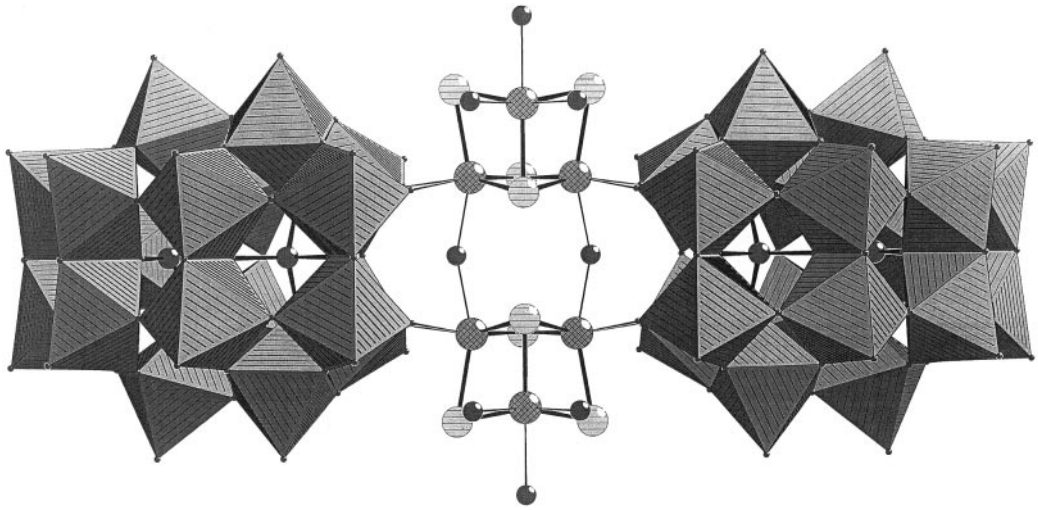

Fig. 2 Structure of the cluster anion **2a** showing the $\{Mo_3S_4\}$ and $\{W_{17}\}$ fragments as building units or constituents.

concept—the addition of stable clusters—the geometrical parameters of the constituents of the anions **1a** and **2a** are practically identical to those of the cluster educts.[8–10]

Compounds **1** and **2** are stable in air and in aqueous solutions (pH = 1–7). Heating **1** or **2** in concentrated hydrochloric acid leads to the reverse reaction, *i.e.* to the reformation of the $[Mo_3S_4(H_2O)_9]^{4+}$ cluster in quantitative yields.

The relative abundance of the different cluster constituents of **1a** and **2a** is also confirmed by the IR, Raman, UV–VIS and ^{31}P NMR spectra. The characteristic UV–VIS spectra indicate not only the presence of $\{Mo_3S_4\}^{4+}$ units possessing a d^6 electron configuration[2*a*] but also that these are almost electronically uncoupled. The characteristic vibrational spectra show bands due to the almost uncoupled vibrations of the constituents, while the ^{31}P NMR spectrum of **2a** [in a buffered aqueous solution (0.5 M $MeCO_2Na$–0.05 M $MeCO_2H$)] shows, consistent with the solid-state structure of **2**, signals in the intensity ratio 1 : 1.

We believe that the strategy of reacting appropriate stable nucleophilic and electrophilic, *i.e.* functional complementary, clusters may be of general importance for the synthesis of this type of compound.

We thank Dipl.-Chem. F. Peters and M. Schmidtmann for their collaboration and the Deutsche Forschungsgemeinschaft as well as the Fonds der Chemischen Industrie for financial support.

Notes and references

† *Synthesis* of $[Me_2NH_2]_{10}[\{(SiW_{11}O_{39})Mo_3S_4(H_2O)_3(\mu\text{-}OH)\}_2]\cdot 20H_2O$ **1**: to an aqueous acetate buffered (0.5 M $MeCO_2Na$–0.05 M $MeCO_2H$) solution (30 ml) of $K_8[\alpha\text{-}SiW_{11}O_{39}]\cdot 13H_2O$ (1.65 g; 0.51 mmol), 3.55 ml of a solution of 0.144 M $[Mo_3S_4(H_2O)_9]^{4+}$ (0.51 mmol) in 2 M HCl was added under vigorous stirring. The pH of the solution was adjusted to 1.8 by adding 6 M HCl dropwise. After stirring the yellow–brown solution for 15 min, Me_2NH_2Cl (2.0 g) was added and the reaction mixture was heated (80 °C) for 20 min. The solution was cooled to room temp. and allowed to stand for 3–5 days. The yellow–brown crystals which precipitated were filtered off, washed with water (5 °C) and dried over $CaCl_2$. Yield: 1.48 g of **1** (81%). Correct elemental analysis for C, H, N, S and H_2O. UV–VIS data [0.5 M $MeCO_2Na$–0.05 M $MeCO_2H$ buffer, absorption, λ/nm (ε/dm^3 mol^{-1} cm^{-1})]: 380 (16000), 450 (sh), 630 (800). IR (solid, KBr pellet, ν/cm^{-1}): 1612m [$\delta(H_2O)$], 1461m, 1411w, 1162w, 1016 (sh), 999m/950s/889s [ν(W=O)], 818m, 761s, 522m. FT-Raman (solid, λ = 1064nm, ν/cm^{-1}): 970s/913m/889m [ν(W=O)], 830m, 522w, 437s, {ν_s[Mo_3-(μ_3-S)]}, 360w, 335w, 282m, 236m, 198w.

‡ *Synthesis* of $[Me_2NH_2]_{14}[\{(P_2W_{17}O_{61})Mo_3S_4(H_2O)_3(\mu\text{-}OH)\}_2]\cdot 25H_2O$ **2**. The same method was applied for the preparation of **2** using $K_{10}[\alpha\text{-}P_2W_{17}O_{61}]\cdot 20H_2O$ (1.50 g; 0.305 mmol) and 2.13 ml of 0.144 M $[Mo_3S_4(H_2O)_9]^{4+}$ (0.305 mmol) in 2 M HCl. Yield: 1.34 g of **2** (86%). Correct elemental analysis for C, H, N and H_2O. UV–VIS data (0.5 M $MeCO_2Na$–0.05 M $MeCO_2H$ buffer, absorption, λ/nm): 365 (sh), 465 (sh), 620 (sh). IR (solid, KBr pellet, ν/cm^{-1}): 1612m [$\delta(H_2O)$], 1461m, 1412w, 1085s, 1053m, 1017m, 942s/913s [ν(W=O)], 768s, 522m. FT-Raman (solid, λ = 1064 nm, ν/cm^{-1}): 1015w, 974vs, 883s, 519w, 437s {ν_s[Mo_3-(μ_3-S)]}, 365m, 337w, 284w, 232m, 170w. ^{31}P NMR (0.5 M $MeCO_2Na$–0.05 M $MeCO_2H$ buffer solution, 85% H_3PO_4 as external reference): δ −6.58 (1P), −13.22 (1P).

§ *Crystal data*: $C_{20}H_{134}Mo_6N_{10}O_{106}S_8Si_2W_{22}$ **1**: M = 7144.37, monoclinic, space group $C2/m$, a = 24.820(5), b = 20.980(4), c = 26.870(5) Å, β = 97.24(3)°, U = 13880(5) Å^3, Z = 4, D_c = 3.419 g cm^{-3}, $2\theta_{max}$ = 54°, T = 200(2) K, μ = 18.91 mm^{-1}, R = 0.051 for 9300 reflections with $I > 2\sigma(I)$; STOE IPDS Image Plate diffractometer, Mo-Kα radiation, graphite monochromator. The structure was solved using direct methods and refined with the programs SHELXS-86 and SHELXL-97.

$C_{28}H_{176}Mo_6N_{14}O_{155}P_4S_8W_{34}$ **2**: M = 10396.73, orthorhombic, space group $Cmcm$, a = 22.419(5), b = 15.110(3), c = 56.036(11) Å, U = 18983(7) Å^3, Z = 4, D_c = 3.638 g cm^{-3}, $2\theta_{max}$ = 54°, T = 183(2) K, μ = 21.11 mm^{-1}, R = 0.123 for 8616 reflections with $I > 2\sigma(I)$; AXS SMART diffractometer, Mo-Kα radiation, graphite monochromator. The structure was solved using the program SHELXS-97 and refined using the program SHELXL-97 (all programs from G. M. Sheldrick, University of Göttingen). The structure was also refined in several lower symmetrical space groups, which lead to up to 2% lower R values. However, as no significant deviations from the higher symmetry were observed, *Cmcm* was chosen for the final refinements. In both compounds not all cations could be located due to Me_2NH_2/H_2O disorder problems.

The figures were prepared with the program DIAMOND (K. Brandenburg, *Diamond-Informationssystem für Kristallstrukturen*, Crystal Impact GbR, Germany).

CCDC 182/1262. See http://www.rsc.org/suppdata/cc/1999/1189/ for crystallographic files in .cif format.

1 (*a*) M. T. Pope, *Heteropoly and Isopoly Oxometalates*, Springer, Berlin, 1983; (*b*) *Polyoxometalates: From Platonic Solids to Anti-Retroviral Activity*, ed. M. T. Pope and A. Müller, Kluwer, Dordrecht, 1994; (*c*) M. T. Pope and A. Müller, *Angew. Chem., Int. Ed. Engl.*, 1991, **30**, 34; (*d*) A. Müller, F. Peters, M. T. Pope and D. Gatteschi, *Chem. Rev.*, 1998, **98**, 239.

2 (*a*) A. Müller, R. Jostes and F. A. Cotton, *Angew. Chem., Int. Ed. Engl.*, 1980, **19**, 875; (*b*) A. Müller. E. Diemann, R. Jostes and H. Bögge, *Angew. Chem., Int. Ed. Engl.*, 1981, **20**, 934; (*c*) M. Draganjac and T. B. Rauchfuss, *Angew. Chem., Int. Ed. Engl.*, 1985, **24**, 742; (*d*) A. Müller, *Polyhedron*, 1986, **5**, 323; (*e*) T. Shibahara, *Adv. Inorg. Chem.*, 1991, **37**, 143; (*f*) T. Shibahara, *Coord. Chem. Rev.*, 1993, **123**, 73; (*g*) I. Dance and K. Fisher, *Prog. Inorg. Chem.*, 1994, **41**, 637; (*h*) D. M. Saysell and A. G. Sykes, *J. Cluster Sci.*, 1995, **6**, 449; (*i*) T. Saito, in *Early Transition Metal Clusters with π-Donor Ligands*, ed. M. H. Chisholm, VCH, New York, 1995, p. 63; (*j*) T. Saito and H. Imoto, *Bull. Chem. Soc. Jpn.*, 1996, **69**, 2403.

3 T. Shibahara and H. Akashi, *Inorg. Synth.*, 1992, **29**, 260.

4 A. Teze and G. Herve, *Inorg. Synth.*, 1990, **27**, 85.

5 R. Contant, *Inorg. Synth.*, 1990, **27**, 104.

6 C. A. Routledge and A. G. Sykes, *J. Chem. Soc., Dalton Trans.*, 1992, 325.

7 Calculation of bond valence sums according to I. D. Brown, in *Structure and Bonding in Crystals*, ed. M. O'Keeffe and A. Navrotsky, Academic Press, New York, 1981, p. 1.

8 H. Akashi, T. Shibahara and H. Kuroya, *Polyhedron*, 1990, **9**, 1671.

9 T. J. R. Weakley, *Polyhedron*, 1987, **6**, 931.

10 K. Y. Matsumoto and Y. Sasaki, *Bull. Chem. Soc. Jpn.*, 1976, **49**, 156.

Communication 9/03170G

ChemComm

A fluorescent molecular thermometer based on the nickel(II) high-spin/low-spin interconversion

Marianne Engeser, Luigi Fabbrizzi,* Maurizio Licchelli and Donatella Sacchi

Dipartimento di Chimica Generale, Università di Pavia, via Taramelli 12, I-27100 Pavia, Italy. E-mail: fabbrizz@.unipv.it

Received (in Basel, Switzerland) 9th March 1999, Accepted 17th March 1999

The temperature of a fluid can be measured through a variation of the fluorescence emission intensity of a naphthalene fragment covalently linked to a Ni^{II} tetraaza-macrocyclic complex, which undergoes a temperature dependent spin interconversion equilibrium.

Luminescence is an easily detectable property which can be used to signal the occurrence of molecular events in real time and in real space. One of the first and most fascinating examples refers to the monitoring of the Ca^{2+} concentration inside the cell during muscle contraction by means of a specific chelating agent equipped with a fluorophore, using fluorescence microscopy as an investigating tool.[1] Since then, luminescent molecular receptors capable of sensing a variety of analytes (H^+,[2] s- and d-block metal ions,[3,4] anions,[5] amino acids)[6] have been developed. Most of them have been designed by following a two-component approach, *i.e.* by covalently linking a receptor subunit displaying selective affinity towards the envisaged substrate to a luminescent fragment.[7] Sensing is based on the occurrence of an intercomponent process (*e.g.* electron transfer) between the luminophore and the receptor, whose extent has to be distinctly different before and after recognition.

The success of the above outlined modular approach prompted us to the design of a two-component luminescent sensor of a physical rather than a chemical quantity: temperature. In the envisaged system, the luminescent fragment must be covalently linked to a bistable subunit, whose states A and B interact to a different extent with the nearby luminophore. Most importantly, the transition from A to B should be fast, reversible and controlled by temperature. We considered that the temperature dependent spin state interconversion of a transition metal centre could represent a convenient process to profit from, in order to build up a luminescent molecular thermometer. In particular, we looked at the high-spin/low-spin crossover of the Ni^{II} ion in a tetraaza coordinative environment like that offered by cyclam, **1**.[8]

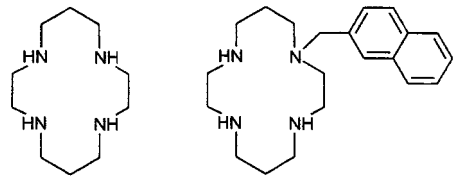

1 **2**

In this connection, we prepared a series of Ni^{II} complexes with the quadridentate macrocycle **2**, in which the naphthalene fluorescent fragment has been linked to the cyclam framework through a $–CH_2–$ spacer.† Complexes of formula $Ni^{II}(\mathbf{2})X_2$ were isolated as either yellow diamagnetic or blue–violet paramagnetic solids, depending upon the nature of the anion X^-. Poorly coordinating anions (ClO_4^-, $CF_3SO_3^-$) favour the formation of the yellow low-spin complexes, which have a square-planar stereochemistry. Anions of stronger coordinating tendencies (Cl^-, NCS^-, NO_3^-) stabilize the high-spin state, occupying the two apical positions of a slightly distorted octahedron. The stereochemical feature of high- and low-spin Ni^{II} complexes of cyclam and analogues have been ascertained through X-ray diffraction studies on a number of complexes.[9]

Spin-state and stereochemistry are maintained when the $Ni^{II}(\mathbf{2})X_2$ complexes are dissolved in non-coordinating solvents. When $X^- = ClO_4^-$, $CF_3SO_3^-$, a band at 470 nm (ε = 102 and 104 $dm^3\ mol^{-1}\ cm^{-1}$, respectively), typical for a low-spin square Ni^{II} tetramine complex is observed in $CHCl_3$ solution. Such a band is absent for $X^- = Cl^-$, NCS^-, NO_3^-, the less intense d–d bands of the high-spin form at 520 nm being observed. Very interestingly for sensing purposes, the two spin states exert a different influence on the emission properties of the proximate naphthalene subunit. In particular, the emission intensity in a $CHCl_3$ solution is remarkably higher for low-spin complexes (Quantum yield, Φ = 0.019 for ClO_4^-, 0.020 for $CF_3SO_3^-$) than for high-spin complexes (Φ = 0.009 for NO_3^-, 0.005 for NCS^-, 0.007 for Cl^-). Note that Φ values of the complexes are in any case substantially lower than that observed for plain naphthalene (Φ = 0.21 in ethanol). Transition metals typically quench the emission of a luminophore through two distinct mechanisms: electron transfer (eT) and energy transfer (*via* double electron exchange, ET). In particular, when the luminescent fragment is linked to a nitrogen atom of cyclam through a $–CH_2–$ spacer, the Ni^{II} centre tends to quench fluorescence through an ET mechanism.[10] This has been confirmed in the present work by the fact that when a solution of a $Ni^{II}(\mathbf{2})X_2$ complex in the glass forming butyronitrile solvent is brought to liquid nitrogen temperature, fluorescence is not revived at all, a behaviour suggestive of the occurrence of a double electron exchange.[11]

The ET based quenching mechanism involves the circular motion of electrons between the MO levels of the photo-excited fluorophore and the partially filled d orbitals of the Ni^{II} centre. The energy sequence of the latter orbitals changes with the metal spin-state and stereochemistry and this may affect the feasibility and rate of the double electron exchange process, thus determining a different quenching efficiency. The intimate details of the quenching mechanism have not been defined at this stage of the investigation. However, it is important to note that the considered two-component system contains a control subunit capable of existing in two states of comparable stability, which affect to a different extent the emission of the nearby covalently linked fluorescent fragment.

Ni^{II} complexes of cyclam and cyclam-like macrocycles in coordinating solvents like water and MeCN give an equilibrium mixture of the high- and low-spin forms.[8] In solution, the apical sites of the octahedral complex are occupied by two solvent molecules, S. The two species interconvert according to the following equilibrium:

$$[Ni^{II}(L)S_2]^{2+} \rightleftharpoons [Ni^{II}(L)]^{2+} + 2S \qquad (1)$$

blue, high-spin octahedral — yellow, low-spin square-planar

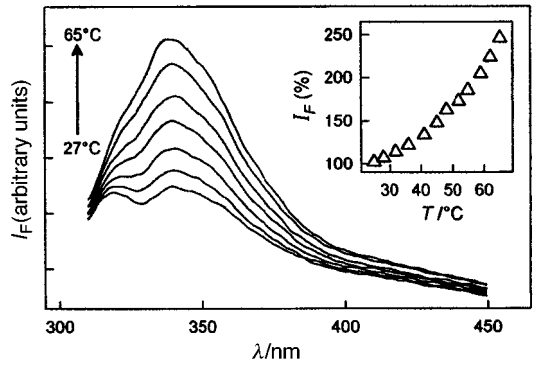

Fig. 1 Emission spectra of a 10^{-5} M MeCN solution of $[Ni^{II}(\mathbf{2})](ClO_4)_2$ recorded over the temperature range 27–65 °C (some spectra are omitted for clarity). I_F *vs.* temperature profile is shown in the inset.

The constant associated to the equilibrium (1) can be evaluated through the absorbance of the yellow form.[8] For a 10^{-3} M MeCN solution of $[Ni^{II}(\mathbf{2})](ClO_4)_2$, at 25 °C, $K = 4 \times 10^{-1}$: thus, the low-spin species is present at 30% and the high-spin species at 70%. The high-spin→low-spin conversion is typically endothermic, *i.e.* a temperature increase favours the formation of the yellow form. For a concentration $c \geqslant 10^{-3}$ M, this effect can be followed through an increase of the intensity of the d–d absorption band at 470 nm. In a very diluted concentration scale ($10^{-5} \leqslant c \leqslant 10^{-7}$ M), the temperature effect can be monitored through I_F, the intensity of the emission band of the naphthalene fragment: in particular, the temperature increase makes I_F increase appreciably.

Fig. 1 displays the emission spectra of an MeCN solution 10^{-5} M in $[Ni^{II}(\mathbf{2})](ClO_4)_2$ recorded over the temperature range 27–65 °C. The inset displays the corresponding I_F, *vs.* temperature profile. When decreasing temperature, I_F quickly decreases following the same profile. Thus, the $[NI^{II}(\mathbf{2})]^{2+}$ complex can be considered as a thermometric probe operating at the molecular level, and the I_F *vs. T* profile of the inset of Fig. 1 provides its calibration curve. Owing to the hydrophobic nature of the naphthyl substituent, $[Ni^{II}(\mathbf{2})](ClO_4)_2$ is not soluble in water even at a concenration as low as 10^{-7} M. It is soluble, however, in water–MeCN (20 : 80 v/v) and water–dioxane (50 : 50 v/v) mixtures, where it displays a similar temperature dependent emission behaviour over the temperature intervals 25–70 and 25–75 °C, respectively.

Other luminescent systems whose emission varies with temperature have been previously reported. In contrast to what is observed in the present study, in most cases a temperature increase depresses luminescence.[12] In these systems, there exists a non-emitting state, NR, slightly higher in energy than the S_1 emitting state. A temperature increase populates the NR state, which undergoes non-radiative decay, thus causing a decrease of the luminescence intensity. An increase of the emission intensity with increasing temperature was observed in the case of 'delayed fluorescence' displayed by some luminescent molecules (*e.g.* eosin).[13]

Light-emitting systems whose emission intensity varies with temperature can be used as probes for spatially and temporally resolved temperature measurement in any fluid including those of biological interest. Lipophilic fluorescent molecules displaying a decreasing emission with increasing temperature were proposed as optical thermometers of cell membranes.[14]

The two-component approach described here and the use of a metal containing a magnetically bistable subunit like $[Ni^{II}(cyclam)]^{2+}$ appears especially versatile for the construction of a fluorescent thermometer, used at a non-invasive concentration level. Thanks to the modular nature of the system, the fluorophore can be replaced at will, for instance to impart solubility in water or to provide emission in the desired wavelength interval, provided that an efficient energy transfer mechanism keeps operating.

This work has been supported by CNR (Progetto Finalizzato Biotecnologie). M. E. is grateful to the ERASMUS Bureau of the European Union for an ECTS grant.

Notes and references

† **2**: cyclam **1** (2 g, 0.01 mol) was dissolved in hot toluene (100 mL) and 2-bromomethylnaphthalene (0.442 g, 0.002 mol) dissolved in the minimum amount of toluene added. The resulting solution was refluxed for 6 h and then cooled to room temp. The ammonium salts and the excess cyclam were filtered off and the resulting clear solution washed with 5% aqueous NaOH (3×25 mL) and water (2×25 mL). After drying over $MgSO_4$, toluene was distilled off to give compound **2** as a pale yellow oil; yield 61%. MS (ESI): 341 [M + H^+]. The NMR spectrum was in accord with the proposed structure.

$[Ni(\mathbf{2})](CF_3SO_3)_2$: a solution of **2** (0.34 g, 1 mmol) in toluene (10 mL) was heated at reflux and a solution of $Ni(CF_3SO_3)_2$ (0.36 g, 1 mmol) in ethanol (10 mL) was added. After refluxing for 1 h, the solution was cooled to room temperature and concentrated at the rotary evaporator. The orange–yellow precipitate was filtered and washed with diethyl ether; yield 92%. MS (ESI): 547 [M − CF_3SO_3]. Correct elemental analysis (C, H, N). The other Ni^{II} complexes were obtained by a similar method.

1 R. Y. Tsien, *Biochemistry*, 1980, **19**, 2396.
2 R. A. Bissell, A. P. de Silva, H. Q. N. Gunaratne, P. L. M. Lynch, G. E. M. Maguire and K. R. A. S. Sandanayake, *Chem. Soc. Rev.*, 1992, 187.
3 A. P. de Silva, H. Q. N. Gunaratne, T. Gunnlaugsson, A. J. M. Huxley, C. P. McCoy, J. T. Rademacher and T. E. Rice, *Chem. Rev.*, 1997, **97**, 1515.
4 L. Fabbrizzi, M. Licchelli, P. Pallavicini, A. Perotti and D. Sacchi, *Angew. Chem., Int. Ed. Engl.*, 1994, **33**, 1975; *Angew. Chem.*, 1994, **106**, 2051.
5 L. Fabbrizzi, I. Faravelli, G. Francese, M. Licchelli, A. Perotti and A. Taglietti, *Chem. Commun.*, 1998, 971.
6 L. Fabbrizzi, G. Francese, M. Licchelli, A. Perotti and A. Taglietti, *Chem. Commun.*, 1997, 581.
7 R. A. Bissell, A. P. de Silva, H. Q. N. Gunaratne, P. L. M. Lynch, G. E. M. Maguire, C. P. McCoy and K. R. A. S. Sandanayake, *Top. Curr. Chem.*, 1993, **168**, 243.
8 L. Fabbrizzi and L. Sabatini, *Inorg. Chem.*, 1979, **18**, 438.
9 B. Bosnich, R. Mason, P. J. Pauling, G. B. Robertson and M. L. Tobe, *Chem. Commun.*, 1965, 97 {$[Ni^{II}(cyclam)Cl_2]$, high-spin]; L. Prasad, S. C. Nyburg and A. McAuley, *Acta Crystallogr., Sect. C*, 1987, **43**, 1038 {$[Ni^{II}(cyclam)](ClO_4)_2$, low-spin}.
10 V. Balzani and F. Scandola, *Supramolecular Photochemistry*, Ellis Horwood, Chichester, 1991.
11 L. Fabbrizzi, M. Licchelli, P. Pallavicini, A. Perotti, A. Taglietti and D. Sacchi, *Chem. Eur. J.*, 1996, **2**, 167.
12 A. P. de Silva, H. Q. N. Gunaratne, K. L. Jayasekera, S. O'Callaghan and K. R. A. S. Sandanayake, *Chem. Lett.*, 1995, 123; W. J. Dressick, J. Cline, J. N. Demas and B. A. DeGraff, *J. Am. Chem. Soc.*, 1986, **108**, 7567; N. Sabbatini, M. Guardigli, I. Manet, F. Bolletta and R. Ziessel, *Inorg. Chem.*, 1994, **33**, 955.
13 C. A. Parker, *Adv. Photochem.*, 1964, **2**, 305.
14 C. F. Chapman, Y. Liu, G. J. Sonek and B. J. Tromberg, *Photochem. Photobiol.*, 1995, **62**, 416.

Communication 9/01931F

ChemComm

Synthesis and characterization of iron(III) complexes of a new ligand containing a potentially bridging carboxylate; structural characterization of a helical tetranuclear iron complex

Vladimir M. Trukhan,[a] Cortlandt G. Pierpont,[b] Kenneth B. Jensen,[c] Ebbe Nordlander[d] and Albert A. Shteinman[a]

[a] *Institute of Chemical Physics, 142432 Chernogolovka, Russia*
[b] *Department of Chemistry and Biochemistry, University of Colorado, Boulder, CO 80309-0215, USA*
[c] *Department of Chemistry, Odense University, DK-5230 Odense M, Denmark*
[d] *Inorganic Chemistry 1, Chemical Center, Lund University, Box 124, S-221 00 Lund, Sweden. E-mail: Ebbe.Nordlander@inorg.lu.se*

Received (in Basel) 21st December 1998, Accepted 9th April 1999

Reaction of the new polydentate ligand 2,6-bis{3-[*N*,*N*-di(2-pyridylmethyl)amino]propoxy}benzoic acid (LH) with $Fe(ClO_4)_3$ followed by addition of chloroacetic acid leads to the formation of the tetranuclear complex $[\{Fe_2OL(ClCH_2CO_2)_2\}_2](ClO_4)_4$, the crystal structure of which reveals that it consists of two $Fe^{II}_2(\mu\text{-}O)(\mu\text{-}RCO_2)_2$ cores that are linked *via* the two L ligands in a helical structure, with the carboxylate moieties of the two ligands forming a hydrogen-bonded pair at the center of the helix.

A number of Fe_2O complexes have been synthesized to model the spectroscopic and structural properties of μ-oxo-μ-carboxylato diiron sites in proteins such as soluble methane monooxygenase (sMMO), ribonucleotide reductase (RNR) and hemerythrin.[1] In many cases, such biomimetic complexes have been found to be relatively unstable.[1,2] Efforts have therefore been made to prepare framework polydentate ligands that may stabilize complexes of this type,[3] examples include ligands in which multidentate nitrogen bases that bind to metals in a capping manner are linked to alkoxo or phenoxo groups capable of bridging two metals.[4] Binucleating polydentate ligands in which nitrogen donors are linked to a carboxylate moiety should be even more relevant for the modelling of μ-oxo-μ-carboxylate diiron sites because the carboxylate bridges in these enzymes are part of the protein.[5,6] Two successful[7,8] and two unsuccessful[9,10] attempts have been reported for the preparation of dinuclear iron complexes containing similar ligands; in these ligands, the carboxylate is one of the 'peripheral' donors at the terminus of a polydentate ligand. Here we report the synthesis of a new ligand containing a potentially bridging carboxylate moiety which is a part of the spacer that links two di(picolyl)amine groups. Reaction of this ligand with an iron(III) salt followed by addition of chloroacetic acid leads to the formation of a tetranuclear complex which consists of two linked $Fe^{III}_2(\mu\text{-}O)$ dimers.

The ligand 2,6-bis{3-[*N*,*N*-di(2-pyridylmethyl)amino]-propoxy}benzoic acid (LH) has been prepared in a three-step synthesis with a general overall yield of *ca*. 60% (Scheme 1). The products LMe and LH (Scheme 1) have been identified by ^{1}H NMR spectroscopy, microanalysis and, in the case of LMe, FAB mass spectrometry. The ^{1}H NMR spectra of LMe and LH are identical except for the methyl resonance at δ 3.61 that is present in the spectrum of LMe.†

Reaction of LH with 2 equiv. of $Fe(ClO_4)_3$ in methanol leads to the formation of a green–yellow product, which has tentatively been assigned the formula $[Fe_2OL(H_2O)_2](ClO_4)_3$ **1** on the basis of UV–VIS, IR, ^{1}H NMR spectroscopy and microanalysis.‡ Addition of 10 equiv. of chloroacetic acid to a solution of **1** in ethanol results in the formation of a brown complex **2**. The UV–VIS and ^{1}H NMR spectra§ of complex **2** indicate that it contains a μ-oxo-bis-μ-carboxylate diiron core. The assignments of the ^{1}H NMR spectra of **1** and **2** are based on their similarities to the spectra of oxo-bridged diiron complexes of related ligands, *viz*. $\{PyCH_2\}_2N(CH_2)_nCO_2^-$ (n = 1,2).[11] All features in the NMR spectra of **1** and **2** appear in the range δ 0–28, indicative of relatively strong antiferromagnetic coupling between the iron atoms. There are broad features above δ 20 (PyCH_2 and *o*-Py protons), sharper peaks at δ 15–18 (*m*-Py protons), and a very sharp peak at δ *ca*. 6 (*p*-Py protons). In addition, there are sharp peaks of the spacer polymethylene chain at δ 3–9. However, the mass spectrum of **2** (*vide infra*) and the analytical data suggest that it is a tetranuclear complex (a 'dimer of dimers') rather than a simple diiron complex.

It was possible to grow crystals of **2** from a MeOH–MeCN solution. In order to confirm the proposed tetranuclear structure and to assess whether the carboxylate moiety of **2** acts as a bridge between the metals, the crystal structure of **2** was determined.¶ The molecular structure of **2** is shown in Fig. 1. The Fe–O–Fe moieties are bridged by two chloroacetates while the non-bridging facial positions are filled by two di(picolyl)-amine moieties from two molecules of L so that the two L ligands link the two diiron–μ-oxo units. The average Fe–μ–oxo distance is 1.79 Å and the average Fe–O–Fe angle is 121.8°; the intra-dimer Fe-Fe distances are 3.102(4) Å [Fe(1)–Fe(2)] and 3.138(4) Å [Fe(3)–Fe(4)] while the interdimer Fe–Fe distances vary from *ca*. 10.5 Å to 10.8 Å . Complex **2** is structurally and, to some extent, chemically related to previously structurally characterized tetranuclear *bis*-Fe_2O species[12] but there are several features of the molecular structure of **2** that render it unique. The conformation of the linking ligands is such that the whole molecule acquires a helical shape; the dihedral angle between the Fe–O–Fe planes in **2** is 42.5°. The center of the helix is held together through the central carboxylates of the two

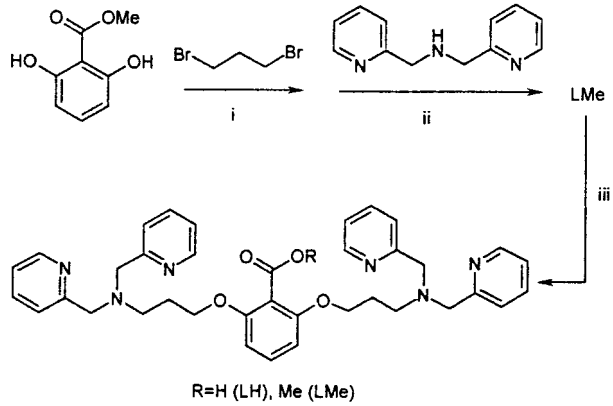

Scheme 1 Synthetic route to LMe and LH. *Reagents and conditions*: i, Me_2CO, K_2CO_3, 72 h, 94% yield; ii, Et_3N, 96 h, 77% yield; iii, KOH–EtOH–H_2O, 12 h, 84% yield.

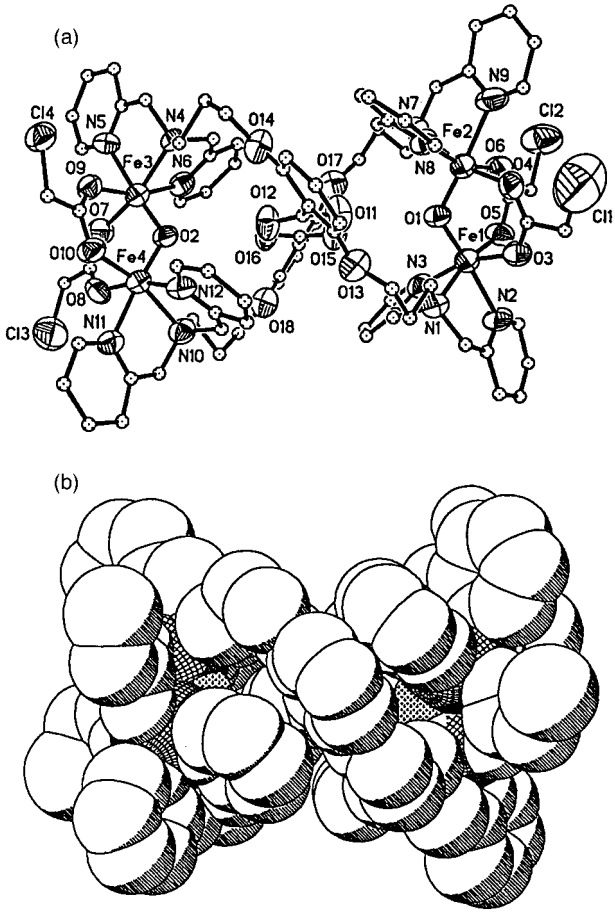

Fig. 1 (a) XP[13] and (b) space-filling drawings of the molecular structure of **2**, showing the atom labeling scheme. Thermal ellipsoids are drawn at the 20% level. Selected distances (Å) and angles (°): Fe(1)–O(1) 1.776(6), Fe(2)–O(1) 1.787(6), Fe(3)–O(2) 1.794(6), Fe(4)–O(2) 1.786(6), Fe(1)–N(1) 2.196(8), Fe(1)–N(2) 2.215(9), Fe(1)–N(3) 2.100(10), Fe(1)–O(3) 2.028(8), Fe(1)–O(5) 2.013(7), Fe(1)–O(1)-Fe(2) 121.1(4), Fe(3)–O(2)–Fe(4)122.5(4).

L ligands which form a hydrogen-bonded pair, the O(11)–O(15) and O(12)–O(16) distances are 2.61 and 2.60 Å, respectively. It is usually observed that the tertiary nitrogen atoms of di(picolyl)amines coordinate *trans* to the μ-oxo ligand in this type of diiron–oxo species but in **2**, the tertiary amines are coordinated *cis* to the oxo ligand and *trans* to one of the bridging carboxylates so that the apices by the bridging oxygens of the Fe_2O units point towards each other. It is likely that the 'girdle' that is formed by the hydrogen-bonded pair of central carboxylates prevents the two ligands from binding to the Fe_2O unit in the favoured coordination mode, instead they bind in the observed 'inverted' coordination mode.

Repeated attempts to detect the molecular ion of **2** by electrospray mass spectrometry (ESMS) have thus far proven unsuccessful. However, we do detect prominent peaks at *m/z* 952, 601 and 426; these peaks are consistent with the molecular formulation(s) $\{[Fe_4L_2(ClCH_2CO_2)_2](ClO_4)_{4-x}\}^{x+}$ (x = 2–4, respectively). Furthermore, we have prepared a number of other carboxylate derivatives of **1**. It appears that in solution, these iron–oxo carboxylate species are in equilibrium with other complexes of similar composition, the nature of which is currently under investigation. We are currently preparing a number of derivatives of LH containing other nitrogen donors and are attempting to use these ligands to synthesize structural and functional model complexes for the active sites of sMMO and RNR R2.

This research was supported by grants from the Russian Foundation for Basic Research (no. 97-03-32253), INTAS (no. 97-1289), the Swedish Natural Science Research Council (NFR) and the Royal Swedish Academy of Sciences. C. G. P. thanks the STINT foundation for financial support. We thank Professor Fred Menger and Prof. Jean-Pierre Tuchagues for useful synthetic information and Maria Johansson for assistance with the crystallographic data collection.

Notes and references

† LMe: ^{1}H NMR ($CDCl_3$, 25 °C): δ 8.50 (d, 4H, py-H$^\alpha$), 7.58 (t, 4H, py-H$^\beta$), 7.46 (d, 4H, py-H$^\delta$), 7.19 (t, 1H, Ar-H,*p*), 7.11 (t, 4H, py-H$^\eta$), 6.46 (d, 2H, Ar-H,*m*), 3.98 (t, 4H, OCH_2), 3.82 (s, 8H, pyCH_2N), 3.61 (s, 3H, OCH_3), 2.70 (t, 4H, NCH_2), 1.96 (t, 4H, CH_2). FAB-MS, *m/z* (rel. intensity, %): 647 (M, 100), 554 (M–CH_2py, 40), 448 (M − 2CH_2py, 45). Anal. $C_{38}H_{42}N_6O_4$. Calc.: C, 70.56; H, 6.55; N, 13.00. Found: C, 69.9; H, 6.85; N, 13.6%.

LH: ^{1}H NMR ($CDCl_3$, 25 °C): 8.50 (d, 4H, py-H$^\alpha$), 7.58 (t, 4H, py-H$^\beta$), 7.46 (d, 4H, py-H$^\delta$), 7.19 (t, 1H, Ar-H,*p*), 7.11 (t, 4H, py-H$^\eta$), 6.46 (d, 2H, Ar-H,*m*), 3.98 (t, 4H, OCH_2), 3.82 (s, 8H, pyCH_2N), 2.70 (t, 4H, NCH_2), 1.96 (t, 4H, CH_2). Anal. $C_{37}H_{40}N_6O_4$. Calc.: C, 70.23; H, 6.37; N, 13.28; Found: C, 70.57; H, 6.54; N, 12.99%.

‡ $[Fe_2OL(H_2O)_2](ClO_4)_3$ **1**: UV–VIS [MeCN; λ_{max}/nm (ε_M(Fe)dm^3 mol^{-1} cm^{-1})]: 220 (35000), 259 (20000), 330 (4000), 474 (659), 520sh (535), 724 (97). IR (KBr), ν/cm^{-1}:1608, 1541 (CO_2, as), 1463, 1419 (CO_2, s), 537 (Fe–O–Fe, s), 473. ^{1}H NMR (CD_3CN, 25 °C): δ 26 (*o*-py), 15.4, 14.0 (pyCH_2N), 11.6, 11.3 (*m*-py), 8.9, 8.6 (*m*-Ph), 8.0 (*p*-Ph), 7.3 (*p*-py), 6.7, 4.4, 3.9, 3.6 (CH_2). Anal. $C_{37}H_{43}Cl_3Fe_2N_6O_{19}$. Calc.: C, 40.63; H, 3.96; N, 7.68; Cl, 9.72; Found: C, 40.47, H, 4.10, N, 7.69; Cl, 10.20%.

§ $[\{Fe_2OL(ClCH_2CO_2)_2\}_2](ClO_4)_4$ **2**: UV–VIS [MeCN; λ_{max}/ nm (ε_M(Fe)/ dm^3 mol^{-1} cm^{-1}): 211 (23000), 245sh (15000), 344 (4200), 380sh (3100), 472 (840), 510 (730), 555sh (220), 721 (155). IR (KBr), ν/cm^{-1}: 1687 (CO_2H), 1607 (py), 1570 (CO_2, as), 1463, 1418 (CO_2, s), 536 (Fe–O–Fe). ^{1}H NMR (CD_3CN, 25 °C): δ 28 (*o*-py), 15.6 (pyCH_2N), 12.0 (*m*-py), 11.5 (O_2CCHCl), 8.5 (*m*-Ph), 7.8 (*p*-Ph), 7.4 (*p*-py), 6.7, 5.4, 4.1 (CH_2).

¶ *Crystal data*: $C_{84}H_{80}Cl_8Fe_4N_{12}O_{36.75}$, brown, crystal dimensions 0.23 × 0.21 × 0.18 mm, M = 2352.60, triclinic, space group $P\bar{1}$ (no. 2), a = 16.4575(3), b = 17.8346(2), c = 19.3790(3) Å, α = 77.521(1), β = 89.245(1), γ = 86.432(1)°, U = 5542.9(2) Å^3, Z = 2, D_c = 1.410 Mg m^{-3}, μ = 0.788 mm^{-1}, F(000) = 2404, 45710 reflections collected (1.1 < θ < 31.8°) at 293(2) K, 31848 independent reflections used in the structure refinement [$F_o > 2\sigma(F_o)$], R_1 (F) = 0.0973, wR_2 (F^2) = 0.2047, goodness-of-fit (F^2) = 0.854. Data were collected with a Siemens SMART CCD area detector, using graphite-monochromated Mo-*K*α radiation (λ = 0.71069 Å) from a Rigaku rotating anode X-ray generator. The intensity measurements were corrected for Lorentz, polarization and absorption effects. The positions of the metal atoms were found by direct methods,[13] and all the non-hydrogen atoms were located from difference Fourier syntheses. The hydrogen atoms were placed in calculated positions. A disorder in the orientations of the CH_2Cl groups of the chloroacetates containing Cl3A and Cl1A was detected and was successfully modelled; the conformations shown in Fig. 1 are favoured. The final refinement was carried out by full-matrix least-squares calculations[13] on F^2 and with anisotropic thermal parameters for all non-hydrogen atoms. CCDC 182/1215. See http://www.rsc.org/suppdata/cc/1999/1193/ for crystallographic files in .cif format.

1 D. M. Kurtz, Jr., *Chem. Rev.*, 1990, **90**, 585.
2 S. Ménage, E. C. Wilkinson, L. Que, Jr. and M. Fontecave, *Angew. Chem., Int. Ed. Engl.*, 1995, **34**, 203.
3 L. Berchet, M. N. Collomb-Dunand-Sauthier, P. Dubordeaux, W. Moneta, A. Deronzier and J.-M. Latour, *Inorg. Chim. Acta*, 1998, **282**, 243.
4 D. E. Fenton and H. Okawa, *Chem. Ber./Recl. Trav. Chim. Pays-Bas*, 1997, **130**, 433.
5 D. M. Kurtz, Jr., *JBIC*, 1997, **2**, 159.
6 A. A. Shteinman, *FEBS Lett.*, 1995, **362**, 5.
7 C. Hemmert, M. Verelst and J.-P. Tuchagues, *Chem. Commun.*, 1996, 617.
8 V. M. Trukhan and A. A. Shteinman, *Russ. Chem. Bull.*, 1997, **46**, 202.
9 A. Hazell, K. B. Jensen, K. J. McKenzie and H. Toftlund, *J. Chem. Soc., Dalton Trans.*, 1993, 3249.
10 V. M. Trukhan, I. L. Eremenko, N. S. Ovanesyan, A. A. Pasynskii, I. A. Petrunenko, V. V. Strelets and A. A. Shteinman, *Russ. Chem. Bull.*, 1996, **45**, 1981.
11 S. Ménage and L. Que, Jr., *New J. Chem.*, 1991, **15**, 431.
12 *Cf.* N. Arulsamy, J. Glerup and D. J. Hodgson, *Inorg. Chem.*, 1994, **33**, 3043 and references therein.
13 Structure determination, refinement and data presentation were carried out using programs contained in the SHELXTL Crystal Structure Determination Package, V; Siemens Industrial Automation, Inc.; Madison, WI, 1995.

Communication 8/09888C

ChemComm

Evidence for the presence of Mo(VI), W(VI) or Re(VII) species in silica-based materials. New approaches to highly dispersed oxo-species in mesoporous silicates

Jean-Yves Piquemal,[a] Emmanuel Briot,[a] Maxence Vennat,[a] Jean-Marie Brégeault,*[a] Geneviève Chottard[b] and Jean-Marie Manoli[c]

[a] *Systèmes Interfaciaux à l'Echelle Nanométrique, Université de Paris 6 and CNRS-ESA 7069, Case 196, 4 Place Jussieu, F-75252 Paris Cedex 05, France. E-mail: bregeaul@ccr.jussieu.fr*

[b] *Chimie des Métaux de Transition, Université de Paris 6 and CNRS-ESA 7071, Case 42, 4 Place Jussieu, F-75252 Paris Cedex 05, France*

[c] *Réactivité de Surface, Université de Paris 6 and CNRS-UMR 7609, Case 178, 4 Place Jussieu, F-75252 Paris Cedex 05, France*

Received (in Cambridge, UK) 30th March 1999, Accepted 18th May 1999

d^0 Transition metal-containing mesoporous molecular sieves are synthesized by the hydrolysis of tetraethyl orthosilicate in aqueous acid, in the presence of neutral or anionic low-condensed Mo(VI) or W(VI) oxo–peroxo or Re(VII) polyoxo species and a cationic surfactant; the materials have a nearly homogeneous distribution of the dopants and promising catalytic activities.

The recent discovery of mesoporous oxides offers novel possibilities for preparing transition metal-containing materials.[1] Most procedures in acidic (or basic) media require careful control of the rate of hydrolysis of the precursors, *e.g.* alkoxides. In acidic media, with $[MoO_4]^{2-}$, $[WO_4]^{2-}$, *etc.*, large iso-(or hetero-) polyoxometalates (POMs, M = Mo or W) are formed.[2–4] These POMs can be dispersed (or grafted) onto molecular sieves such as MCM-41,[5] but are not so easily inserted into pure mesoporous silica as they limit wall growth and/or lead to phase segregation. Previous work demonstrates that low-nuclearity neutral or anionic peroxo species can be prepared in 'MO_3/H_2O_2–H_2O–H_3O^+' precursor systems.[6,7]

In this work, we consider the electrostatic interaction of these peroxo species with silicate moieties (operating mode A), in the counter-ion-mediated $S^+X^-I^+$ pathway, as a means of incorporating molybdenum(VI), tungsten(VI) or rhenium(VII) into mesoporous silica. [S^+ = quaternary ammonium ion surfactant, *e.g.* cetyltrimethylammonium ($CTMA^+$); X^- = Cl^- and/or anionic oxo–peroxo species; I^+ = inorganic silicate precursor (tetraethyl orthosilicate, TEOS).[1] This procedure is compared with methods involving, or generating, polyoxometalates[8] or oxo species interacting with TEOS also in the $S^+X^-I^+$ pathway (operating mode B). The data (Table 1) show that mode A, with Mo or W oxo–peroxo species (run 1, sample A_{Mo}, wt% Mo ≈ 4.05; run 4, sample A_W, wt% W ≈ 7.55) leads to a higher M content than in the initial gel. On the other hand, with $[MeReO(O_2)_2(H_2O)]$ synthesized from '$[Me_3ReO_3]$ (denoted MTO)/H_2O_2–H_2O–H_3O^+' mixtures (run 6, sample A_{Re}, wt% Re ≈ 0.90) the rhenium content is low and a better incorporation can be obtained with aqueous $H^+[ReO_4]^-$ (run 7, sample B_{Re}, wt% Re ≈ 2.5). These results differ from those obtained with basic media (S^+I^- pathway),[1] which correspond to lower loadings of the M species (M = Mo, W or Re) incorporated into the framework of the silica matrix (see, for example, run 3, sample C_{Mo}).

The X-ray data for $(Si/M)_{initial}$ ≈ 50 are similar to those obtained for pure mesoporous silica. Samples A_{Mo}, A_W, A_{Re} and B_{Re} show higher order reflections such as (110), (200), *etc.*, which suggests that they have greater long-range order than samples B_{Mo} and B_W. Because of the relatively low metal content in these materials (Table 1), additional crystalline phases, if any, cannot be identified from the X-ray diffraction patterns, except for $(Si/Mo)_{initial} \leqslant 30$ for example, but some of them can be identified by laser Raman spectroscopy.

This method is very useful for characterizing detemplated materials with Mo or W prepared by the oxo–peroxo (mode A, Table 1) or the oxo-polyoxo route (mode B). Sensitivity to water vapour has been shown by identification of supported $H_4[SiMo_{12}O_{40}]$. (aq), while in an anhydrous atmosphere, there is no evidence for any crystalline phase or known product (*e.g.* MoO_3). Sample B_{Mo} gives a Raman spectrum corresponding to a mixture of high purity silica MCM-41 and the Keggin unit, '$SiMo_{12}$'. The Raman spectra of the W-MCM-41 prepared by the oxo–peroxo route (sample A_W) and by the polyoxo mode (sample B_W) are shown in Fig. 1. They include bands that originate from the SiO_2 matrix [*ca.* 1100, 800 (very weak) and 490 cm^{-1}] as well as from the tungsten oxo species. Bands attributed to the symmetric stretching mode of the terminal

Table 1 Metal (Mo, W or Re) content, interplanar spacing, average pore diameter, wall thickness and BET surface area (S_{BET})[a] in mesoporous silicates

Run	Operating Mode with M[b]	Si/M molar ratio: Gel	Si/M molar ratio: Calcined product	d_{100} spacing/Å	Unit cell parameter a_o/Å	Average pore diameter[c]/Å	Wall thickness[d]/Å	S_{BET}/ $m^2\ g^{-1}$
1	A_{Mo}	50	35	32	37	18	19	1072 ± 60
2	B_{Mo}	50	52	32	37	16	21	1176 ± 60
3	C_{Mo}	50	180	36	41.5	17	24.5	1037 ± 40
4	A_W	50	35	33.5	39	18	21	921 ± 60
5	B_W	50	45	33	38	16	22	897 ± 40
6	A_{Re}	50	300	31.1	36	15	21	1200 ± 60
7	B_{Re}	50	110	31.9	37	16	21	1015 ± 60

[a] These parameters refer to the calcined materials. [b]A corresponds to the oxo–peroxo route ($S^+X^-I^+$ pathway); B to the oxo or polyoxo mode ($S^+X^-I^+$ pathway); C is typical of synthesis in basic medium with $[MoO_2(acac)_2]$ as the molybdenum(VI) precursor (S^+I^- pathway). [c] Measured by BJH method (desorption). [d] Wall thickness given by the difference between a_o and the average pore diameter.

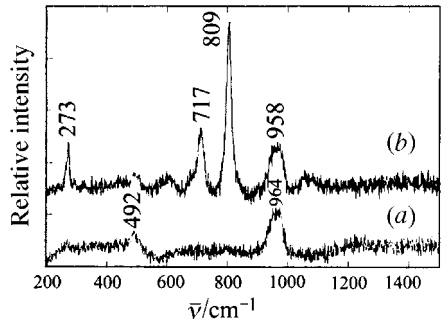

Fig. 1 Raman spectra of mesoporous tungstosilicate [W]-MCM-41; molecular sieves prepared by the oxo-peroxo route (a) and by the oxo–polyoxo mode (b).

W=O bonds are observed at 964 or 958 cm^{-1}. This assignment is still questionable:[9] terminal Si–O stretching of SiOH···OW 'defective sites' may also contribute. For sample A_W [Fig. 1(a)], no Raman bands due to crystalline WO_3 (*vide infra*) or to '$WO_3{\cdot}2H_2O$'[10] [960 (sharp), 685-662 (broad), 380 and 268 cm^{-1}] are observed. The minor Raman band at 215 cm^{-1}, associated with the W–O–W deformation mode,[11] is absent from these spectra but it must be kept in mind that W–O–W linkage can nevertheless exist, since the pore walls of M-MCM-41 resemble amorphous materials rather than crystalline molecular sieves. On the other hand, the Raman spectra of B_W materials, prepared by the aqueous method using ammonium metatungstate, $(NH_4)_6[H_2W_{12}O_{40}]$ or $Na_2[WO_4]$, at ambient temperature and calcined in air at 920 K [Fig. 1(b)], exhibit strong bands due to crystalline WO_3[10–12] at 809, 717 and 273 cm^{-1}, which are assigned to the stretching modes and to the deformation mode (δ) of the O–W–O moieties.[10] The observation of very strong Raman features due to crystalline WO_3 (sample B_W) indicates the formation of a very poorly dispersed SiO_2-supported tungsten oxide phase. Therefore, when the sample is heated, the polytungstate ions transform readily into bulk WO_3 surface species. The achievement of highly dispersed Mo, W and even Re oxo species for these silica-based materials obtained by the aqueous method is attributed to the low nuclearity of the species stabilized by H_2O_2, *e.g.* $\{MO(O_2)_2(H_2O)_2\}$, (M = Mo, W)[7] or $[MeRe(O_2)_2(H_2O)]$, or more simply by $[ReO_4]^-$.

Typical A_{Mo}, A_W, A_{Re} and B_{Re} samples exhibit a reversible, nearly hysteresis-free, type IV isotherm. Nitrogen BET surface areas (Table 1) are in the same range. Desorption hysteresis is not observed for A_{Mo}, A_W, A_{Re} and B_{Re}: a high degree of pore blocking does not occur in these samples but may do so in B_{Mo} and B_W. Mean pore sizes of *ca.* 18 Å (A_{Mo} and A_W) and 16 Å (B_{Mo} and B_W) are found by the BJH method, which is considered to underestimate the real pore size. These values are in fair agreement with TEM measurements, as is the wall thickness (19–22 Å).

X-Ray EDS experiments used to locate and quantify submicroscopic distributions of the Mo, W or Re species reveal that the Mo or W distribution in the typical $A_{Mo\ or\ W}$ solid is nearly homogeneous; the relative at %Mo[W] being 1.75[2.8] with a difference of 0.7[0.6] between maximum and minimum values.

However, B_{Mo} and B_W have a very inhomogeneous molybdenum or tungsten distribution; the average value is *ca.* 3.0 wt% (B_{Mo}) and values as high as 7.4% are also found, typical differences between maximum and minimum values being 7%. These results compare well with the other data; they indicate that there is a high dispersion or a 'quasi-homogeneous distribution' of the Mo or W sites in samples A, while in samples B there is a less ordered distribution between two (or more) phases as a consequence of phase segregation (*vide supra*).

Syntheses in acidic media would appear to be better than the basic S^+I^- pathway for the incorporation of M into mesoporous silica. The oxo–peroxo route, for Mo(VI) and W(VI), and the perrhenic acid route for Re(VII) in the $S^+X^-I^+$ mediated pathway are evidently better than synthesis with oxo–polyoxo species in acidic media for obtaining d^0 metal sites distributed throughout the bulk in spatially uniform states. Even if molybdenum(VI), tungsten(VI) and rhenium(VII) are not statistically and perfectly distributed in the hexagonal cell, high incorporation levels (Si/Mo $\simeq$ 35) never achieved before[1] can be obtained with high dispersion of the M species in the framework of the mesoporous materials. Samples A_{Mo} catalyze the oxidation of (*R*)-(+)-limonene with TBHP–decane mixtures (conversion 90%, selectivity to epoxides $\geqslant$98%). Different leaching behaviours are observed as a consequence of the different catalyst preparation methods; they are also related to the nucleophilicity of the reactants and to surface properties. Samples A_M and B_{Re} are also efficient catalysts for oct-1-ene methathesis, some of them without addition of Bu_4Sn or Ph_2SiH_2 cocatalysts. Work is in progress to control these systems better and to optimize epoxidation and metathesis results.

Notes and references

† *Preparation of samples:* A_{Mo} and A_W: MoO_3 (0.36 g, 2.5 mmol) [$WO_3{\cdot}H_2O$ (0.625 g, 2.5 mmol)] was first reacted with 15 wt% aqueous H_2O_2 (5 ml, 24.5 mmol). After 1 h stirring at 60 °C the solution, denoted A_1, was cooled to room temp. [followed by centrifugation (15 min at 2000 rpm)]. TEOS ($\approx$28 ml, 0.125 mol) was mixed with a solution of CTMACl (20 ml, 15 mmol) and 12.5 M HCl (92 ml, 1.15 mol) in H_2O ($\approx$220 ml, 17 mol); solution A_1 (Mo or W: 2.5 mmol) was then quickly added. The composition of the gel was: 1 TEOS:0.12 CTMACl:8.9 HCl:136 H_2O:0.19 H_2O_2:0.02 MoO_3. The reaction mixture was stirred (200 rpm) at ambient temperature for 1 h. The pale yellow [white] solid was isolated by filtration, washed with distilled water and dried over P_4O_{10} to give the initial sample. After efficient drying at room temperature, the powder was calcined in air (200 cm^3 min^{-1}, 1 K min^{-1}) from ambient temperature to 880–920 K (samples maintained at the final temperature for 4 h) to give sample A_{Mo} [A_W].

B_{Mo} and B_W: syntheses were adapted from methods previously described[13] for $(Si/Mo)_{initial} \approx 100$ mol/mol. To a solution of CTMACl (7.3 g, 0.02 mol) and 12.5 M HCl (8 ml, 0.1 mol) in H_2O (270 ml, 15 mol) were added precursor K_2MoO_4 (0.48 g, 2 mmol) [Na_2WO_4 (0.59 g, 2 mmol)] and TEOS (22.3 ml, 0.1 mol). The reaction mixture was stirred vigorously at ambient temperature for 24 h, then filtered, washed and treated as above for A_{Mo} and A_W.

A_{Re} and B_{Re}: MTO was prepared by a slightly modified version of the published method[14] starting from 10 g of Re_2O_7 in an overall yield of 85% after silica gel chromatography and recrystallization. $HReO_4$ was prepared from H_2O_2 (30% m/v) and metallic rhenium. A_{Re} and B_{Re} were prepared by a modification of the A_{Mo}, A_W and B_{Mo}, B_w pathways.

1 J. Y. Ying, C. P. Mehnert and M. S. Wong, *Angew. Chem., Int. Ed.*, 1999, **38**, 56.
2 M. T. Pope, *Heteropoly and Isopoly Oxometalates*, Springer, Berlin, 1983.
3 L. Karakonstantis, C. Kordulis and A. Lycourghiotis, *Langmuir*, 1992, **8**, 1318.
4 J.-P. Jolivet, *De la Solution à l'Oxyde*, InterEditions/CNRS Editions, Paris, 1994.
5 I. V. Kozhevnikov, A. Sinnema, R. J. J. Jansen, K. Pamin and H. van Bekkum, *Catal. Lett.*, 1995, **30**, 241.
6 J.-Y. Piquemal, C. Bois and J.-M. Brégeault, *Chem. Commun.*, 1997, 473.
7 J.-Y. Piquemal, S. Halut and J.-M. Brégeault, *Angew. Chem., Int. Ed. Engl.*, 1998, **37**, 1146.
8 I. V. Kozhevnikov, *Chem. Rev.*, 1998, **98**, 171.
9 E. Duprey, P. Beaunier, M.-A. Springuel-Huet, F. Bozon-Verduraz, J. Fraissard, J.-M. Manoli and J.-M. Brégeault, *J. Catal.*, 1997, **165**, 22.
10 M. F. Daniel, B. Desbat, J. C. Lassegues, B. Gerand and M. Figlarz, *J. Solid State Chem.*, 1987, **67**, 235.
11 D. S. Kim, M. Ostromecki, I. E. Wachs, S. D. Kohler and J. G. Ekerdt, *Catal. Lett.*, 1995, **33**, 209.
12 S. Colque, E. Payen and P. Grange, *J. Mater. Chem.*, 1994, **4**, 1343.
13 W. Zhang, J. Wang, P. T. Tanev and T. J. Pinnavaïa, *Chem. Commun.*, 1996, 979.
14 H. Rudler, J. Ribeiro Gregorio, B. Denise, J.-M. Brégeault and A. Deloffre, *J. Mol. Catal. A : Chem.*, 1998, **133**, 255.

Communication 9/02537E

ChemComm

STM observation of 12-hydroxyoctadecanoic acid and its 4,4′-bipyridinium salt self-assembled on a graphite surface†

Pu Qian,*‡ Hiroshi Nanjo, Toshiro Yokoyama and Toshishige M. Suzuki*

Tohoku National Industrial Research Institute, 4-2-1 Nigatak, Miyagino-ku, Sendai, 983-8551 Japan.
E-mail: B.Sen@tniri.go.jp (P.Qian) and suzuki@tniri.go.jp (T.M.Suzuki)

Received (in Cambridge, UK) 15th February 1999, Accepted 17th May 1999

Self-assembled monolayers of the gelling agent, 12-hydroxyoctadecanoic acid and its 4,4′-bipyridinium salt have been observed on the solution graphite interface using scanning tunnelling microscopy (STM) and the molecular patterns are discussed wth respect to the intermolecular hydrogen bond network.

Some types of amphiphiles act as gelling agents for organic solvents.[1] Among them, 12-hydroxyoctadecanoic acid (12-HOA) has attracted extensive attention from fundamental as well as practical points of view.[2–4] A wide range of solvents can be gelled by 12-HOA and hence this reagent has been applied to the recovery of spilled oil or disposal of used kitchen oil.[1] It has been pointed out that non-covalent weak interactions are responsible in controlling the self-assembling mode and the stabilization of aggregates.[1,4,5] The presence of the hydroxyl group in 12-HOA seems particularly important to the gelling ability of 12-HOA since stearic acid does not show this property. A structural model of a 12-HOA aggregate has been proposed by Terech *et al.* on the basis of neutron and X-ray scattering investigations.[6] An infinite network of hydrogen bonds between hydroxy groups has been suggested to stabilize the plate-like building unit, which is interconnected leading to construction of a three-dimensional fibrous polymer.[6]

Scanning tunnelling microscopy (STM) has provided molecular images of self-assembled molecules at atomic resolution.[7,8] Monolayers of self-assembled amphiphiles including fatty acids have been directly observed at solution–solid interfaces by STM and the morphologies of the two dimensional crystals discussed and interpreted in terms of intra- and inter-molecular hydrogen bonds.[9–12] We have attempted to observe directly the molecular patterns of the monolayers formed with 12-HOA and stearic acid as well as their 4,4′-bipyridinium salts, to clarify the molecular interaction, especially the role of the hydrogen bond network on the molecular assembly and gel formation ability.

A warm solution (*ca.* 0.5 wt%) of racemic 12-HOA (Aldrich Co.) in octylbenzene was applied on the surface of freshly cleaved highly oriented pyrolytic graphite (HOPG). Upon cooling to room temperature (23–26 °C), the solution became a gel. We have successfully observed the STM image of a self-assembled monolayer of 12-HOA on the HOPG surface under an organic gel layer.[13] Fig. 1(a) and 2(a) show the STM images of 12-HOA and stearic acid over a scan area of 10 × 10 nm along with their possible geometries [Fig. 1(b) and 2(b)]. Edges

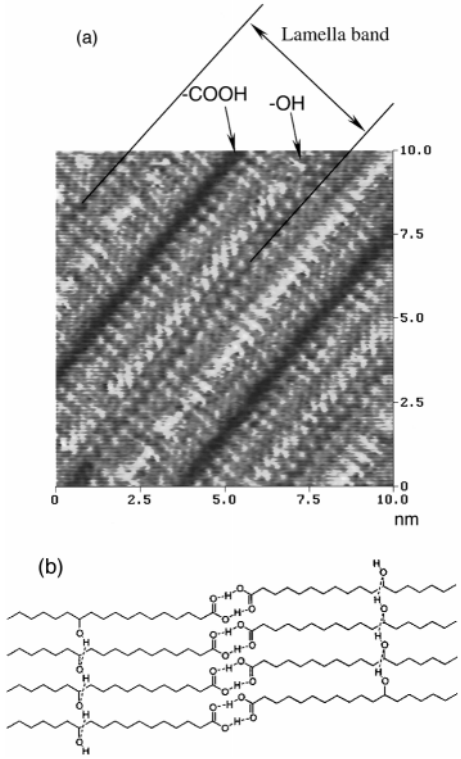

Fig. 1 (a) The STM image (10 × 10 nm) of a 12-HOA monolayer self-assembled on an HOPG surface. The image was obtained in constant current mode with a tungsten tip. Bias voltage and tunneling current were −1.47 V (tip negative) and 266 pA, respectively. (b) A possible geometry of the molecular alignment.

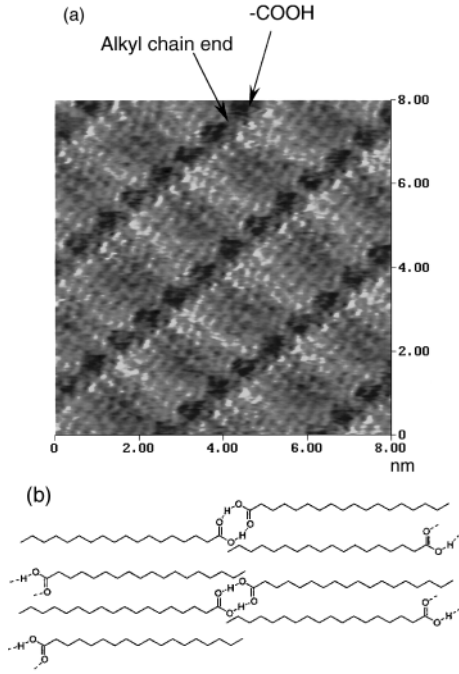

Fig. 2 (a) The STM images (8 × 8 nm) of a stearic acid monolayer self-assembled on an HOPG surface. The image was obtained in constant current mode with a tungsten tip. Bias voltage and tunneling current were −1.58 V (tip negative) and 682 pA, respectively. (b) A possible geometry of the molecular alignment.

† Colour versions of the STM images in Fig. 1–3 can be electronically accessed (http://www.rsc.org/suppdata/cc/1999/1197).
‡ Post doctoral fellow for Intelligent Cosmos Research Institute, Japan.

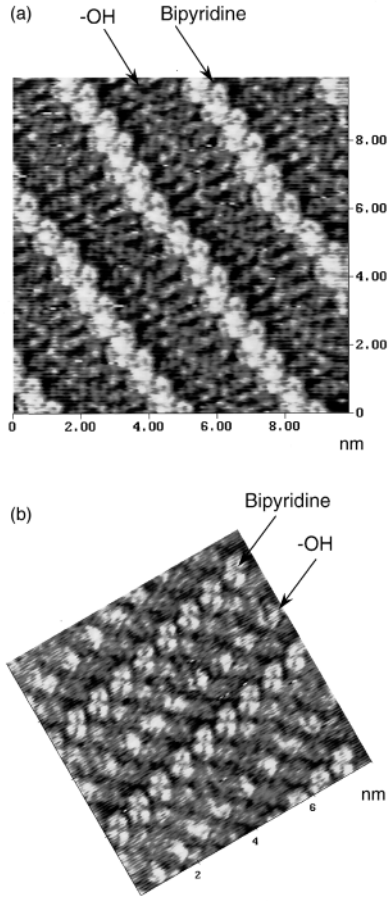

Fig. 3 The STM images of a self-assembled monolayer of 12-HOA-bpy. These two molecular orientations are mirror images. The images were obtained in constant current mode with a tungsten tip. (a) The scan area is 10 × 10 nm; bias voltage and tunneling current were 1.18 V (tip positive) and 216 pA, respectively. (b) The scan area is 8 × 8 nm; bias voltage and tunneling current were 1.41 V (tip positive) and 459 pA, respectively.

of multi-layers were not observed in any STM images indicating that the observed images are those of monolayers. Like stearic acid, 12-HOA molecules orient parallel to each other and thick dark areas are observed. The molecular axis orients perpendicularly to the dark stripes forming a centrosymmetric molecular pattern. An interdigitated geometry, in which the head groups alternately point in opposite directions has been suggested for the molecular alignment of stearic acid[9] and other saturated fatty acids[9] (Fig. 2). Thus the dark moiety has been assigned to carboxyl head groups.[9] The distance between the dark regions for stearic acid corresponds to its molecular length (*ca.* 2.5 nm) whereas that for 12-HOA is roughly double the molecular length of 12-HOA assuming that the alkyl chain is fully expanded. Therefore, the 12-HOA molecules are likely to associate in a head to head manner at carboxylic acid groups located in adjacent rows. Two brighter bands observed between thick black stripes can be attributed to the hydroxy groups on the C12 positions. The zigzag shaped dark area at the center of the image corresponds to the lamella boundary between the alkyl chain terminii. The possible molecular alignment is depicted in Fig. 1(b) where intermolecular hydrogen bonds effectively link 12-HOA molecules to form a macromolecular sheet. This molecular pattern, involving an infinite hydrogen bond network, coincides with the plate-like structure in the internal building block of 12-HOA aggregates proposed by Terech *et al.*[6]

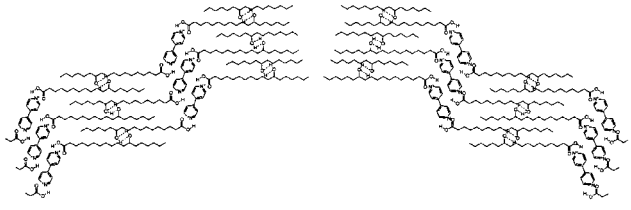

Fig. 4 Schematic representation of a possible molecular alignment for a 12-HOA–bpy monolayer.

In order to confirm our interpretation to the observed images, we have attempted to insert 4,4′-bipyridine (bpy) as a marker between carboxyl groups. A conjugated π-electron system such as bpy might be prominent in a molecular image since areas of higher electronic conductance tend to give brighter images. A mixture of 12-HOA and bpy (2:1) in octylbenzene solution formed a monolayer on HOPG, the molecular image of which is shown in Fig. 3. Remarkably bright regions corresponding to bpy moieties are now observed while the thick dark stripes disappeared. A similar phenomenon is observed in the monolayer image of bpy and stearic acid. Therefore the thick dark band in Fig. 1(a) can consistently be assigned to the region where hydrogen bonded carboxyl head groups are located. Bipyridine molecules sandwiched with 12-HOA appear to be inclined with respect to the alkyl chain at an angle of *ca.* 30°. The distance between the bpy centers is *ca.* 3.6–3.7 nm, which is much longer than that estimated from the molecular lengths of 12-HOA (2.5 nm) and bpy. When the alkyl chains in adjacent rows are associated at the hydroxyl groups as shown in Fig. 4, the observed bpy separations can be rationalized. Interestingly, enantiomeric molecular patterns are found in this system [Fig. 3(a) and 3(b)]. One plausible interpretation is that the racemate 12-HOA–bpy monolayer spontaneously segregates into different domains due to homochiral association at hydroxy groups.[12,14] Fig. 4 shows the proposed molecular arrangement of a 12-HOA–bpy monolayer in which hydroxy groups in vicinal rows are associated to form a polymeric hydrogen bond network. The infinite network of hydrogen bonds might play an important role for building up of the supramolecular assembly of aggregates. It is of note that the bpy salt of 12-HOA also shows gelling ability towards various solvents.

This research was performed as a part of Regional Consortium R&D program conducted by The New Energy and Industrial Technology Development Organization.

Notes and references

1 P. Terech and R. G. Weiss, *Chem. Rev.*, 1997, **97**, 3133.
2 A. T. Polishuk, *J. Am. Soc. Lubr. Eng.*, 1977, **33**, 133.
3 Y. Uzu, *J. Jpn. Oil Chem. Soc.*, 1975, **24**, 261.
4 T. Tachibana, T. Mori and K. Hori, *Bull. Chem. Soc. Jpn.*, 1981, **54**, 73; *Nature*, 1979, **278**, 578.
5 K. Hanabusa, M. Matsumoto, T. Miki, T. Koyama and H. Shirai, *J. Chem. Soc., Chem. Commun.*, 1994, 1401; K. Hanabusa, Y. Yamada, M. Kimura and H. Shirai, *Angew. Chem., Int. Ed. Engl.*, 1996, **35**, 1949.
6 P. Terech, *Prog. Colloid Polym. Sci.*, 1996, **102**, 64; P. Terech, V. Rodriguez, J. D. Barnes and G. B. McKenna, *Langmuir*, 1994, **10**, 3406.
7 D. P. E. Smith, J. K. H. Hörber, G. Binnig and H. Nejoh, *Nature*, 1990, **344**, 641.
8 J. P. Rabe and S. Buchholz, *Science*, 1991, **253**, 442.
9 M. Hibino, A. Sumi and I. Hatta, *Jpn. J. Appl. Phys.*, 1995, **34**, 610; 3354.
10 P. C. M. Grim, S. De Feyter, A. Gesquière, P. Vanoppen, M. Rücker, S. Valiyaveettil, G. Moessner, K. Müllen and F. C. De Schryver, *Angew. Chem., Int. Ed. Engl.*, 1997, **36**, 2601.
11 D. M. Cyr, B. Venkataraman, G. W. Flynn, A. Black and M. Whitesides, *J. Phys. Chem.*, 1996, **100**, 13 747.
12 P. Qian, H. Nanjo, T. Yokoyama and T. M. Suzuki, *Chem. Lett.*, 1998, 1133.
13 The STM images were obtained with a NanoScope IIIa (Digital Instruments.)
14 D. M. Walba and F. Stevens, *Acc. Chem. Res.*, 1996, **29**, 591.

Communication 9/01218D

ChemComm

Efficient, general synthesis of silylketenes *via* an unusual rhodium mediated Wolff rearrangement

Stephen P. Marsden* and Wai-Kit Pang

Department of Chemistry, Imperial College of Science, Technology and Medicine, London, UK SW7 2AY. E-mail: s.marsden@ic.ac.uk

Received (in Liverpool, UK) 30th March 1999, Accepted 12th May1999

Silylketenes bearing a range of substituents (alkyl, alkenyl, aryl, heteroaryl) are prepared by an unusual rhodium mediated Wolff rearrangement of the corresponding silyl diazo ketones.

Silylketenes are potentially extremely versatile intermediates in organic synthesis.[1] These readily isolable ketenes exhibit extraordinary stability in comparison with their non-silylated counterparts; furthermore, whilst their reactivity shares some common modes with the parent compounds, silylketenes also display a unique and useful chemistry unavailable to their non-silylated counterparts. The development of these compounds as routine synthetic intermediates has been hampered to some extent by the paucity of methods for their preparation in terms of yield and functional group tolerance.[2] We report herein a convenient new high-yielding and general preparation of silylketenes based upon a remarkable rhodium(II) octanoate mediated Wolff rearrangement of silylated diazo ketones.

We have previously disclosed results of our investigations into the chemistry of silylated diazo esters. In particular, we have shown that these compounds undergo intramolecular C–H insertion reactions upon treatment with rhodium(II) carboxylate catalysts in refluxing benzene, giving rise to α-silyl γ-lactones[3] (by insertion into the ester group) or oxasilacyclopentanes[4] (by insertion into ethers attached to the silicon). We were therefore interested in examining the behaviour of silylated diazo ketones under similar conditions. However, upon treatment of 1-diazo-1-(triethylsilyl)nonan-2-one[5] **1a** with rhodium(II) octanoate in benzene at room temperature, a rapid and quantitative (by ^{1}H and ^{13}C NMR) conversion to heptyl(triethylsilyl)ketene **2a** occurred (Scheme 1, Table 1). The ketene could be separated from the rhodium catalyst by chromatography, but the 79% isolated yield of the ketene indicates that some decomposition occurs during purification, possibly through hydration. In order to verify the structure of the ketene, we treated the crude reaction mixture with 1.2 equiv. of $BnNH_2$ in CH_2Cl_2 at room temperature to produce the corresponding α-silyl benzylamide **3a**, which was isolated in 91% yield.

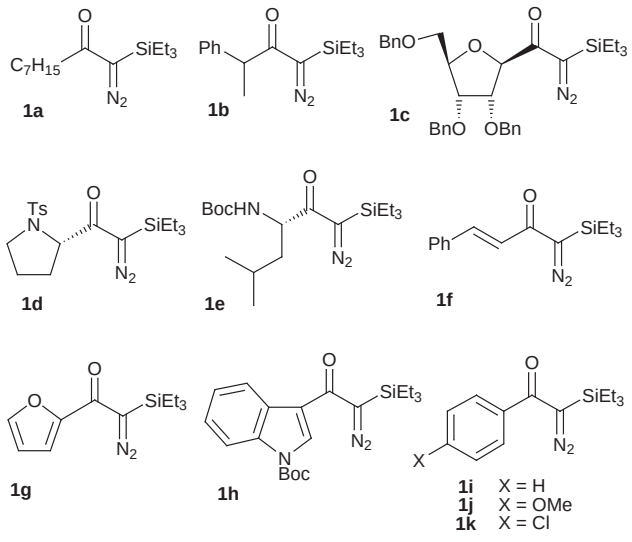

We next began to examine the functional group tolerance of this new method. As shown in Table 1, the synthesis appears to be general for a range of diazo ketones. The crude reaction mixtures were examined by ^{1}H and ^{13}C NMR to assess the purity of the ketenes prior to isolation by chromatography and/or derivitisation to the stable α-silyl benzylamides. Conversion to the silylketenes was found to be very clean in all cases, with the exception of ketenes **2e**, **2f** and **2i** which contained some minor contaminants. The isolated yields in Table 1 are lower than the observed spectroscopic purities, suggesting that some decomposition (possibly through hydration of the ketene) occurs on chromatography.

Aliphatic substituents are well tolerated (diazo ketones **1a**–**e**), including those derived from sugars (**1c**) and amino acids (**1d**,**e**). Higher temperatures were required for the decomposition of diazo ketones **1b**–**e**, possibly reflecting the increased hindrance to attack of the catalyst at the diazo carbon from the branched side-chains. The crude ketene **2e** contained unidentified contaminants which could potentially arise from interception of the intermediate carbenoid by the carbamate protecting group, or by intermolecular N–H insertion.

Alkenyl substituted diazo ketone **1f** furnished ketene **2f** after treatment with the catalyst at 80 °C. This ketene was contaminated with some minor components and was isolated pure in only 33% yield; however the 75% isolated yield of the benzylamine adduct attests to the dominance of the ketene pathway. Heteroaromatic substituents were also tolerated, with

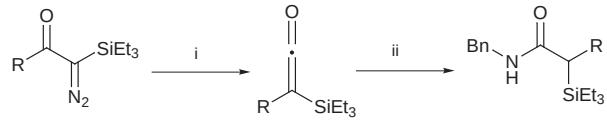

Scheme 1 *Reagents and conditions:* i, 1 mol% $Rh_2(O_2CC_7H_{15})_4$, PhH, room temp. to 80 °C; ii, 1.2 equiv. $BnNH_2$, CH_2Cl_2, room temp.

Table 1 Formation of silylketenes by Rh catalysed Wolff rearrangement

Diazo ketone	*T*/°C (*t*/min)	Ketene	Yield (%)[a]	Amide	Yield (%)[b]
1a	20 (10)	**2a**	79	**3a**	91
1b	50 (5)	**2b**	80	**3b**	—[c]
1c	50 (15)	**2c**	41	**3c**	63
1d	80 (30)	**2d**	45	**3d**	0
1e	80 (20)	**2e**	12	**3e**	27
1f	80 (10)	**2f**	33	**3f**	75
1g	60 (30)	**2g**	46	**3g**	87
1h	40 (10)	**2h**	57	**3h**	82
1j	50 (15)	**2i**	54	**3i**	47
1j	20 (5)	**2j**	54	**3j**	60
1k	60 (10)	**2k**	49	**3k**	56

[a] Figures quoted are isolated yields of pure ketene. [b] Yields of amide obtained over two steps from the diazo ketone, without isolation of the ketene. [c] No amide isolated from the reaction with $BnNH_2$.

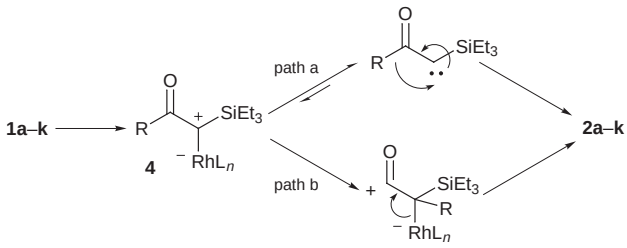

Scheme 2

2-furyl and indol-3-yl substituted diazo ketones **1g**,**h** rearranging smoothly to the corresponding ketenes **2g**,**h**.

The electronic influence of the diazo ketone substituent upon reactivity is illustrated by the rearrangement of aryl diazo ketones **1i**–**k**. Decomposition of the phenyl-substituted diazo ketone **1i** occurred at 50 °C to give ketene **2i**. Introducing an electron-releasing *p*-methoxy group to the aromatic ring in diazo ketone **1j** allowed the rearrangement to occur at ambient temperature, while the presence of an electron-withdrawing *p*-chloro group in **1k** required the reaction to be carried out at 60 °C. This order of reactivity could be due to the differing electron density available at the diazo carbon for coordination to the rhodium catalyst, or may reflect the development of a partial positive charge on the migrating group during the rearrangement (*vide infra*). The formation of ketene **2i** was accompanied by some minor by-products which were apparent in the ^{13}C NMR spectrum. The ^{1}H NMR spectrum was not sufficiently resolved to allow an estimation of purity of the crude material, but the 54% isolated yield of the pure ketene reflects a lower limit of the efficiency of the reaction.

Alkyl,[6] aryl[6] and alkenyl[7] substituted silylketenes have previously been prepared from silylated diazo ketones by photolysis, or in a few cases by treatment with copper(I) triflate.[6b] However, the formation of silylketenes from the reaction of silylated diazo ketones with rhodium(II) octanoate is somewhat surprising, since it is a generally held view that the use of rhodium catalysts for diazo ketone decomposition suppresses Wolff rearrangement[8] with only isolated exceptions.[9] That the rhodium(II) octanoate is intimately involved in the rearrangement is supported by the fact that no ketene formation was observed in reactions carried out in the absence of catalyst. We suggest two possible explanations for this anomalous behaviour of silyl diazo ketones. The first is that the silyl group destabilises the putative carbenoid intermediate **4** by the tendency of silicon to destabilise α-positive charges,[10] and also potentially by virtue of its bulk. This leads to decomplexation of the metal (path a, Scheme 2) and subsequent Wolff rearrangement from the free carbene. However, in our studies on silyl diazoacetate decomposition we have seen significant catalyst effects upon the stereochemical outcome of insertion reactions,[3] which argues against a decomplexation of the metal catalyst in this closely related system. We therefore suggest a second mechanism for the rearrangement, based upon the ability of silicon to stabilise β-positive charge.[10] Migration of the diazo ketone substituent in the rhodium carbenoid **4** generates an acyl cation which is stabilised by the β-silyl group (path b, Scheme 2). Loss of the σ-bound rhodium species furnishes the ketene and regenerates the catalyst.

In summary a mild, efficient and functional group tolerant synthesis of silylketenes is presented, proceeding *via* an unusual rhodium mediated Wolff rearrangement. Further investigations of this process, as well as synthetic applications of the silylketenes, are now in hand.

We thank the EPSRC for a Quota studentship, the Nuffield Foundation, Pfizer Central Research and the Zeneca Strategic Research Fund for financial support, and Johnson Matthey plc for the generous loan of rhodium salts. We also thank one of the referees for bringing ref. 9 to our attention.

Notes and references

1 A. Pommier, P. J. Kocienski and J. M. Pons, *J. Chem. Soc., Perkin Trans. 1*, 1998, 2105.
2 T. T. Tidwell, *Ketenes*, Wiley-Interscience, New York, 1995, pp. 348–354.
3 S. P. Marsden and W.-K. Pang, *Tetrahedron Lett.*, 1998, **39**, 6077.
4 S. N. Kablean, S. P. Marsden and A. M. Craig, *Tetrahedron Lett.*, 1998, **39**, 5109.
5 All of the silyl diazo ketones were prepared by C-silylation of the corresponding diazo ketones with triethylsilyl triflate, according to: T. Allspach, H. Gümbel and M. Regitz, *J. Organomet. Chem.*, 1985, **290**, 33.
6 (*a*) G. Maas and R. Brückmann, *J. Org. Chem.*, 1985, **50**, 2801; (*b*) R. Brückmann, K. Schneider and G. Maas, *Tetrahedron*, 1989, **45**, 5517.
7 J. L. Loebach, D. M. Bennett and R. L. Danheiser, *J. Am. Chem. Soc.*, 1998, **120**, 9690; J. L. Loebach, D. M. Bennett and R. L. Danheiser, *J. Org. Chem.*, 1998, **63**, 8380.
8 S. Bien and Y. Segal, *J. Org. Chem.*, 1977, **42**, 1685; G. B. Gill, in *Comprehensive Organic Synthesis*, ed. B. M. Trost and I. Fleming, Pergamon, Oxford, 1991, vol. 3, p. 88.
9 The rhodium catalysed decomposition of ethyl (*E*)-5-aryl-2-diazo-3-oxopent-4-enoates results in products assumed to arise *via* Wolff rearrangement and ketene decomposition. See: E. C. Taylor and H. M. L. Taylor, *Tetrahedron Lett.*, 1983, **24**, 5453.
10 E. Colvin, *Silicon in Organic Synthesis*, Butterworths, London, 1981.

Communication 9/02549I

Multiple site dioxygenase-catalysed *cis*-dihydroxylation of polycyclic azaarenes to yield a new class of bis-*cis*-diol metabolites

Derek R. Boyd,*[a] Narain D. Sharma,[a] Jonathan G. Carroll,[a] Christopher C. R. Allen,[b] David A. Clarke[b] and David T. Gibson[c]

[a] *School of Chemistry, The Queen's University of Belfast, Belfast, UK BT9 5AG. E-mail: dr.boyd@qub.ac.uk*
[b] *QUESTOR Centre, The Queen's University of Belfast, Belfast, UK BT9 5AG*
[c] *Department of Microbiology and the Center for Biocatalysis and Bioprocessing, The University of Iowa Iowa City, Iowa, 52242, USA*

Received (in Cambridge, UK) 26th March 1999, Accepted 17th May 1999

The enhanced stability of new mono-*cis*-dihydrodiol bacterial metabolites of tricyclic azaarenes has facilitated the dioxygenase-catalysed formation and isolation of the corresponding bis-*cis*-dihydrodiols (*cis*-tetraols) and a three step chemoenzymatic route to the derived arene oxide mammalian metabolites.

Dioxygenase-catalysed oxidation of mono- and poly-cyclic arenes by bacteria occurs widely in the environment.[1–3] Dioxygenase enzymes catalyse monohydroxylation (at benzylic and allylic centres), dihydroxylation (at alkene and arene bonds), and a combination of both yielding triol bioproducts (trihydroxylation of alkyl arenes).[1–3] *cis*-Dihydrodiol bioproducts are however very poor substrates for arene dioxygenase enzymes and prior to this communication no report of remote site bis-*cis*-dihydroxylation (tetrahydroxylation) has appeared.

The biodegradation of polycyclic aromatic hydrocarbons (PAHs) in eucaryotic systems, *e.g.* plants, animals and fungi, has frequently been found to proceed *via* monooxygenase-catalysed epoxidation followed by isomerisation to phenols or epoxide hydrolase-catalysed hydrolysis to *trans*-dihydrodiols.[4,5] In a typical example the oxidation of acridine **1A** using rat liver enzymes yielded 2-hydroxyacridine and *trans*-dihydrodiol **6** *via* the arene oxide intermediate **5A** (Scheme 1).[6–8]

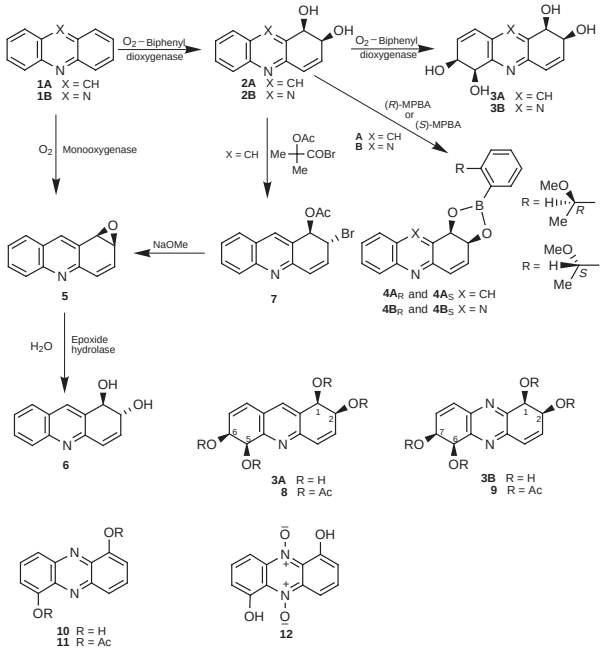

Scheme 1

Other studies have shown that remote site oxidation of PAHs can occur with animal liver enzymes to yield combinations of phenol, epoxide and *trans*-diol derivatives in different benzene rings.[9–12] The small quantities of metabolites, *e.g.* bis-*trans*-dihydrodiols, available from such monooxygenase-catalysed (cytochrome-P450) oxidations[9] are generally insufficient to allow rigorous structural or stereochemical analysis.

cis-Dihydrodiol metabolites resulting from oxidation at the 5,6-bond of the bicyclic azaarenes quinoline,[13] 2-chloroquinoline [14] and 2-methoxyquinoline[14] were isolated using a mutant strain (UV4) of the bacterium *Pseudomonas putida* (a source of toluene dioxygenase). These bioproducts were found to be remarkably stable in comparison with their carbocyclic analogues, *e.g.* the 1,2-*cis*-dihydrodiol of naphthalene. On this premise it was anticipated that the corresponding *cis*-dihydrodiol metabolites **2A** and **2B**, if formed from the tricyclic azaarenes acridine **1A** and phenazine **1B**, would be much more stable and consequently could prove to be valuable synthetic intermediates.

Acridine **1A** was biotransformed using a mutant strain of the bacterium *Sphingomonas yanoikuyae* B8/36 (a source of biphenyl dioxygenase, BPDO) following the reported procedure.[15] After removal of the bacterial cells the bioproducts were then extracted with EtOAc to yield a relatively polar compound (R_f 0.2, 5% MeOH in $CHCl_3$) which was identified by spectral methods (NMR, MS) and elemental microanalysis as dihydrodiol **2A**. ^{1}H NMR spectroscopy established that *cis*-dihydroxylation had occurred exclusively at the 1,2-position ($J_{1,2}$ 4.7 Hz). Reaction of *cis*-diol **2A** ($[\alpha]_D$ +72, MeOH) with (*R*)-(+)- and (*S*)-(−)-2-(1-methoxyethyl)phenylboronic acid (MPBA) yielded the boronate derivatives $\mathbf{4A}_R$ and $\mathbf{4A}_S$ respectively. ^{1}H NMR analyses of the boronates confirmed that *cis*-diol **2A** was enantiopure (> 98% ee); the absolute configuration was determined as (*1R,2S*) by application of the empirical ^{1}H NMR rule earlier established for a series of MPBA derivatives from other *cis*-dihydrodiol metabolites of PAHs [15, 16] (Table 1). The (*1R,2S*) configuration for *cis*-diol **2A**

Table 1 Yields, optical rotations and absolute configurations for metabolites **2A**, **2B**, **3A** and **3B** obtained using *S. yaniokuyae* B8/36, and derivatives **8**, **9** and **5**

Compound	Isolated yield (%)	$[\alpha]_D/10^{-1}$ deg cm^2 g^{-1} (solvent)	Absolute configuration
2A	50–55	+72 (MeOH)	1*R*,2*S*
2B	40	+102 (MeOH)	1*R*,2*S*
3A	12	+266 (Pyridine)	1*R*,2*S*,5*R*,6*S*
3B	15	+180 (MeOH)	1*R*,2*S*,6*R*,7*S*
8	95	+63 ($CHCl_3$)	1*R*,2*S*,5*R*,6*S*
9	95	+83 ($CHCl_3$)	1*R*,2*S*,6*R*,7*S*
5	55	+30 ($CHCl_3$)	1*R*,2*S*

was independently confirmed by a stereochemical correlation process involving oxidative degradation of the derived 1,2-diacetoxy-1,2,3,4-tetrahydroacridine to give (2*S*,3*S*)-(−)-dimethyl (2,3-diacetoxy)adipate of known configuration.[17]

In later biotransformation studies of acridine **1A**, total removal of water from the centrifuged culture medium at 35–40 °C under reduced pressure, followed by extraction of the semi-solid residue with EtOAc–MeOH (9:1) yielded a mixture of *cis*-diol **2A** and a more polar metabolite (R_f 0.15, 12% MeOH in $CHCl_3$) which was identified as the bis-*cis* diol **3A** (Table 1) on the basis of ^{1}H NMR (COSY, NOE) and MS data and formation of tetraacetate **8**. The chirality of the bis-*cis*-diol **3A** suggested that it was formed by initial *cis*-dihydroxylation of acridine **1A** at the 1,2-bond on the *Si*:*Si* face of the molecule followed by further *cis*-dihydroxylation at the 5,6-bond again on the *Si*:*Si* face to yield the (*1R,2S,5R,6S*) enantiomer exclusively. Confirmation that the bis-*cis*-diol **3A** had been derived from the mono-*cis*-diol **2A** was obtained by its addition as substrate to *S. yaniokuyae* B8/36. The samples of bis-*cis*-diol **3A**, isolated from metabolism of either acridine **1A** or the mono-*cis*-diol **2A**, were found to be indistinguishable.

Biotransformation of phenazine **1B** with *S. yaniokuyae* B8/36 or *Pseudomonas putida* 9816/11 (a source of naphthalene dioxygenase, NDO), and the normal extraction procedure yielded, in both cases, a mono-*cis*-dihydrodiol (R_f 0.45, 10% MeOH in $CHCl_3$, 5% yield from NDO and 40% yield from BPDO) which was identified as *cis*-1,2-dihydroxy-1,2-dihydrophenazine **2B** from ^{1}H NMR ($J_{1,2}$ 4.3 Hz) and MS analyses. Formation of MPBA derivatives $\mathbf{4B}_R$ and $\mathbf{4B}_S$ of the mono-*cis*-diol **2B** and their ^{1}H NMR analyses established that it was enantiopure (> 98% ee) and of (*1R,2S*) configuration from both bacterial mutant strains. Application of the improved extraction procedure (EtOAc–MeOH after removal of water from the centrifuged bioextracts) led to the isolation of a mixture of (*1R,2S*)-mono-*cis*-diol **2B** with a second metabolite (R_f 0.12, 15% MeOH in $CHCl_3$) from the *S. yaniokuyae* B8/36 biotransformation. This very polar bioproduct was identified as the phenazine bis-*cis*-dihydrodiol **3B** from NMR, MS and CD spectral data and formation of tetraacetate **9**; the structure was confirmed by aromatisation (thermal dehydration) and acetylation of the resulting bis-phenol **10** to yield 1,6-diacetoxyphenazine **11**.[18]

When (*1R,2S*)-mono-*cis*-diol **2B** was added as substrate to *S. yaniokuyae* the bis-*cis*-diol **3B** was isolated as the sole metabolite. The CD spectra of the bis-*cis*-diols **3A** and **3B** were found to be very similar, as anticipated. Thus the absolute configurations **(***1R,2S,5R,6S***)** and **(***1R,2S,6R,7S***)** were assigned for metabolites **3A** and **3B**, respectively**.** 1,6-Dihydroxyphenazine **10**, obtained by dehydration of the metabolite bis-*cis*-dihydrodiol **3B**, and the derived 1,6-dihydroxyphenazine 5,6-dioxide (iodinin) **12** have also been isolated from among a range of phenazine antibiotics produced as secondary metabolites in other bacterial systems.[19]

A further manifestation of the stability of the mono-*cis*-dihydrodiol **2A** became apparent from the reaction with 2-acetoxyisobutyryl bromide. It was anticipated that the resulting product, 1-acetoxy-2-bromo-1,2-dihydroacridine **7**, would aromatise spontaneously. However, compound **7** proved to be sufficiently stable to be isolated and identified by ^{1}H NMR analysis (crude yield *ca.* 80%) prior to treatment with NaOMe to yield (*1R,2S*)-(+)-1,2-epoxy-1,2-dihydroacridine (acridine 1,2-oxide, **5**). Thus the eucaryotic metabolite **5**, derived from acridine **1A**, was obtained as a single enantiomer in two steps with an overall yield of *ca.* 55% from the procaryotic metabolite **2A**. This procedure compares favourably with our earlier method for the synthesis of enantiopure acridine 1,2-oxide **5**, an eight step synthesis with an overall yield of 18%.[4,8] It also represents a significant improvement over an earlier five step method for the synthesis of enantiopure arene oxides of PAHs from the corresponding *cis*-dihydrodiols.[20]

Preliminary studies have indicated that the two-step synthetic procedure (**2A**→**7**→ **5**) used for the arene oxide synthesis is also applicable to other relatively stable *cis*-dihydrodiol metabolites of bi- and tri-cyclic azaarenes, *e.g.* the *cis*-dihydrodiols of 2-chloroquinoline (5,6- and 7,8-).[14] All arene oxide derivatives of azaarenes (*e.g.* acridine 1,2-oxide **5**) were found to hydrolyse, under aqueous conditions, to the corresponding *trans*-dihydrodiols (*e.g.* **6**) by exclusive nucleophilic attack at the allylic position.[7,8] The *cis*-dihydrodiol **2A** was also a minor hydrolysis product of arene oxide **5**.[8]

Recent studies of the bacterial metabolism of tetracyclic arene substrates, each containing two bay regions (chrysene and benzo[*b*]naphtho[2,1-*d*]thiophene), using *S. yanoikuyae* B8/36, have shown the formation of relatively unstable bis-*cis*-dihydrodiols as minor metabolites (0.3 and 3% yield, respectively).[21] Thus the new family of enantiopure arene tetraol metabolites arising from sequential *cis*-dihydroxylation on the arene *Si*:*Si* face is not confined to the linear azaarene series and more examples are anticipated.

We thank the U.S. Public Health Service grant GM29909 from the National Institute of General Medical Sciences (D. T. G.), the BBSRC (N. D. S) and the QUESTOR Centre (C. C. R. A and D. T. C.), for financial support. We also wish to acknowledge the valuable experimental assistance provided by Eric Becker and Heiko Nieke (Fachhochschule Mannheim under the EU Socrates Programme).

Notes and references

1 D. T. Gibson and V. Subramanian, in *Microbial Degradation of Organic Compounds*, ed. D. T. Gibson, Marcel Dekker, New York, 1984, p. 181.
2 S. M. Resnick, K. Lee and D. T. Gibson, *J. Ind. Microbiol*., 1996, **17**, 438.
3 D. R. Boyd and G. N. Sheldrake, *Nat. Prod. Rep*., 1998, 309.
4 D. R. Boyd and N. D. Sharma, *Chem. Soc. Rev*., 1996, 289.
5 S. C. Barr, N. Bowers, D. R. Boyd, N. D. Sharma, L. Hamilton, R. A. S. McMordie and H. Dalton, *J. Chem. Soc., Perkin Trans. 1*, 1998, 3443.
6 K. D. McMurtrey and C. Welch, *J. Liq. Chromatogr*., 1986, **9**, 2949.
7 D. R. Boyd, M. R. J. Dorrity, L. Hamilton, J. F. Malone and A. Smith, *J. Chem. Soc., Perkin Trans. 1*, 1994, 2711.
8 D. R. Boyd, R. J. H. Davies, L. Hamilton, J. J. McCullough, J. F. Malone, H. P. Porter, A. Smith, J. M. Carl, J. M. Sayer and D. M. Jerina, *J. Org. Chem.*, 1994, **59**, 984.
9 K. L. Platt and I. Reischmann, *Mol. Pharmacol*., 1987, **32**, 710.
10 D. R. Thakker, H. J. Yagi, M. Sayer, U. Kapur, W. Levin, R. L. Chang, A. W. Wood, A. H. Conney and D. M. Jerina, *J. Biol. Chem*., 1984, **260**, 11 249.
11 M. Boroujerdi, H. C. Kung, A. G. E. Wilson and M. W. Anderson, *Cancer Res*., 1981, **41**, 951.
12 H. Glatt, A. Seidel, O. Ribeiro, C. Kirkby, P. Hirom and F. Oesch, *Carcinogenesis*, 1987, **8**, 1621.
13 D. R. Boyd, N. D. Sharma, M. R. J. Dorrity, M. V. Hand, R. A. S. McMordie, J. F. Malone, H. P. Porter, J. Chima, H. Dalton and G. N. Sheldrake, *J. Chem. Soc., Perkin Trans. 1*, 1993, 1065.
14 D. R. Boyd, N. D. Sharma, J. G. Carroll, J. F. Malone and C. C. R. Allen, *Chem. Commun.*, 1998, 683.
15 D. R. Boyd, N. D. Sharma, R. Agarwal, S. M. Resnick, M. J. Schocken, D. T. Gibson, J. M. Sayer, H. Yagi and D. M. Jerina, *J. Chem. Soc., Perkin Trans. 1*, 1997, 1715.
16 S. M. Resnick, D. S. Torok and D. T. Gibson, *J. Org. Chem*., 1995, **60**, 3546.
17 D. R. Boyd, N. D. Sharma, R. Boyle, J. F. Malone, J. Chima, and H. Dalton, *Tetrahedron: Asymmetry*, 1993, **4**, 1307.
18 A. Albini, G. F. Bettinetti, E. Fasani and G. Minoli, *J. Chem. Soc., Perkin Trans. 1*, 1978, 299.
19 T. Hiroshi, S. Takashi, I. Masaur, Y.Hisashi and I. Yoshihiko, *Agric. Biol. Chem*., 1988, **52**, 301.
20 D. R. Boyd, N. D. Sharma, R. Agarwal, N. A. Kerley, R. A. S. McMordie, A. Smith, H. Dalton, A. J. Blacker and G. N. Sheldrake, *J. Chem. Soc., Chem. Commun.*, 1994, 1693.
21 D. R. Boyd, N. D. Sharma, F. Hempenstall, M. A. Kennedy, J. F. Malone, C. C. R. Allen, S. Resnick and D. T. Gibson, *J. Org. Chem.*, 1999, in the press.

Communication 9/02427A

ChemComm

Synthesis of pseudo-oligosaccharides by a sequence of yne-ene cross metathesis and Diels–Alder reaction

Stephan C. Schürer and Siegfried Blechert*

Institut für Organische Chemie, Sekr. C3, Technische Universität Berlin, Straße des 17. Juni 135, D-10623 Berlin, Germany. E-mail: sibl@wap0105.chem.tu-berlin.de

Received (in Liverpool, UK) 21st April 1999, Accepted 17th May 1999

Various pseudo oligosaccharides were prepared by a combination of selective yne-ene cross metathesis and Diels–Alder reaction from readily available monosaccharide building blocks.

Oligosaccharides have been implicated as key participants in a number of biological processes including signal transduction and a wide range of recognition events.[1] Because of this tremendous biological importance, carbohydrates have aroused much interest in synthetic and medicinal chemistry.[2]

During recent years the number of applications of olefin metathesis as a very mild and competitive synthetic method[3] has been considerably increased, due to the availability of well-defined catalysts, in particular Grubbs' well-established ruthenium initiator $Cl_2(PCy_3)_2Ru{=}CHPh$ (**Ru**, Cy = cyclohexyl).[4] However, olefin metathesis has rarely been used in carbohydrate chemistry. Most applications are ring closing metatheses (RCM) for the synthesis of monosaccharide derivatives[5] and few examples exist for ring opening metathesis polymerisation (ROMP) involving carbohydrates.[6] A very recent publication describes the homodimerisation of a number of olefinated pyranosides.[7] Selective cross metatheses employing monosaccharide building blocks have not been studied, apart from some isolated examples.[8,9] Nonetheless, the selective cross coupling of monosaccharide building blocks is very intriguing since the diversity of accessible carbohydrate derivatives is much higher compared to simple homodimerisation.

A selective cross metathesis between a terminal alkyne and a terminal alkene yielding 1,3-disubstituted butadienes has been found recently in our laboratory.[9] These 1,3-dienes, formed by yne-ene cross metathesis, represent attractive starting materials for subsequent Diels–Alder reactions (Scheme 1).

However, little is known about Diels–Alder transformations of nonactivated acyclic 1,3-dienes,[10] which are regarded as poor substrates for Diels–Alder reactions. As there were no examples of Diels–Alder reactions incorporating carbohydrate-substituted 1,3-butadienes, we started investigations on yne-ene cross metatheses of monosaccharide building blocks and subsequent Diels–Alder transformations, providing an easy and very flexible access towards pseudo-oligosaccharides.

Introducing acetylated 1-*O*-allyl- and 1-*O*-propargyl-glycopyranoside as the alkene and alkyne components to yne-ene cross metathesis followed by $MeAlCl_2$-catalysed Diels–Alder reaction with methyl vinyl ketone yielded compounds **1** and **2**, respectively (Fig. 1).†

A number of allyl- and propargyl-substituted carbohydrate building blocks was then prepared and introduced to yne-ene cross metathesis followed by Diels–Alder transformation according to Scheme 2. The combination of acetylated 1-*O*-allyl- and 1-*O*-propargyl-glyco- and -galacto-pyranosides afforded pseudo-oligosaccharides **3** and **4** in high yields.‡

A problem of all cross metathesis reactions that has not been solved as yet is the formation of *E*/*Z* mixtures,[3] usually resulting in stereoisomeric mixtures after subsequent transformations. Although the described Diels–Alder reaction proceeds with excellent regioselectivity, diastereomeric mixtures are obtained, due to the incorporation of *E*/*Z* mixtures of the carbohydrate-substituted 1,3-dienes. The diastereomers refer to the relative configuration of the cyclohexene substituents. However, this disadvantage can be overcome by equilibration into the thermodynamically more stable *trans*-configuration using NaOMe in MeOH–THF with simultaneous cleavage of any acetate protective groups (Scheme 2).

This equilibration–deprotection strategy has been successfully applied to the preparation of compounds **8**–**10**, where acetyl- and benzyl-protected β-D-glyco- and β-D-galacto-pyranosides with glycosidic and nonglycosidic linkage of the respective carbohydrate residue have been employed.

In addition to the described Lewis acid catalysed Diels–Alder reactions of 1,3-dienes we focused on aza-Diels–Alder transformations, since these would provide access to biologically interesting pipecolic acid derivatives substituted by two variable carbohydrates (Scheme 3).

As dienophiles we employed *N*-trichloroethylidene toluene-*p*-sulfonamide and ethyl (4-tolylsulfonylimino)acetate. Similar

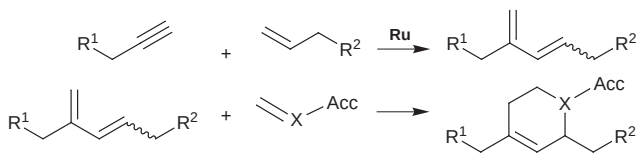

Scheme 1

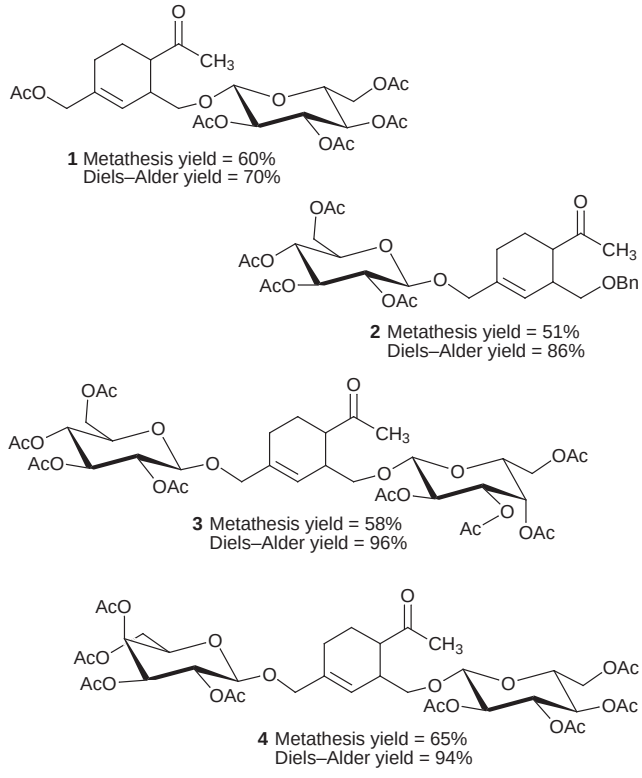

Fig. 1 Yields of **1**–**4**.

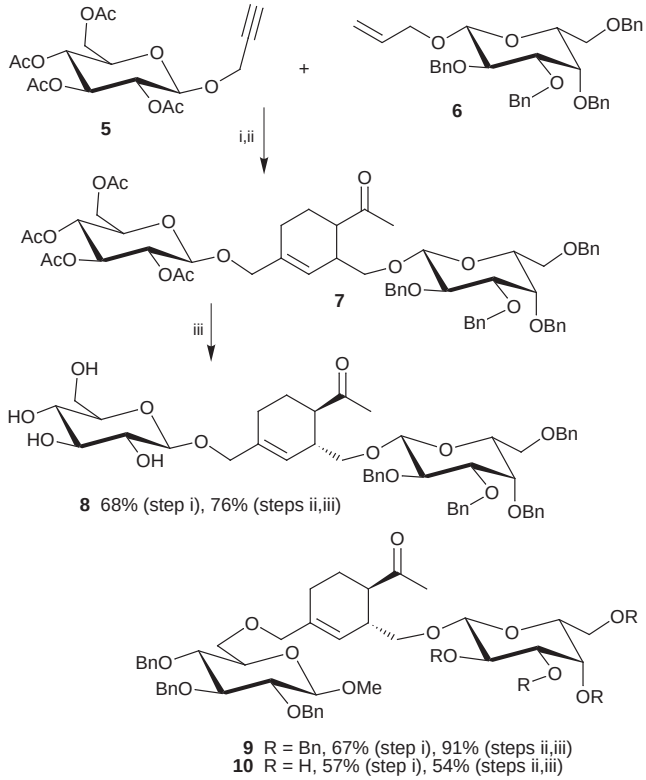

Scheme 2 *Reagents and conditions*: i, **Ru** (10%), CH_2Cl_2; ii, methyl vinyl ketone, $MeAlCl_2$, CH_2Cl_2–PhMe, −35 °C; iii, NaOMe, MeOH–THF.

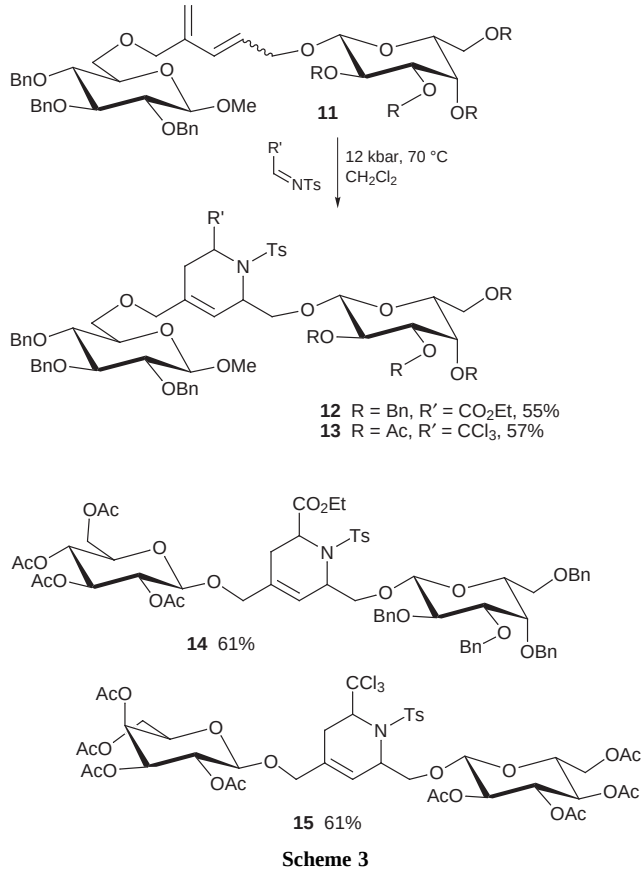

Scheme 3

to the Diels–Alder reactions described above, acetyl- and benzyl-protected β-D-glyco- and β-D-galacto-pyranosides with glycosidic and nonglycosidic linkages have been introduced to aza-Diels–Alder transformations, which were found to proceed with moderate to reasonable yield and excellent regioselectivity under 12 kbar pressure at 70 °C in CH_2Cl_2 to yield pseudo-oligosaccharides **12**–**15**.

In conclusion, we have developed a general sequence of selective yne-ene cross metathesis, Diels–Alder transformation and equilibration–deprotection for the synthesis of various biologically interesting carbohydrate derivatives. The combination of different monosaccharide building blocks and dienophiles has been demonstrated and should potentially give rise to a large number of pseudo-oligosaccharides of the types presented. Further investigations to explore the scope of the described reactions are now in progress.

We are thankful to the Fonds der Chemischen Industrie for financial support and to Priv. Doz. Dr J. Jakupovic for NMR characterisation of some of the presented compounds.

Notes and references

† *Yne-ene cross metathesis*: 5 mol% of **Ru** was added to a solution of 0.5 mmol of alkyne and 1.5–2.0 equiv. of alkene in CH_2Cl_2 (0.2 M concentration). After 12 h stirring another 5 mol% of **Ru** was added. After an additional 18 h the product was purified by column chromatography.

$MeAlCl_2$-catalysed Diels–Alder reaction: To a solution of 100 μmol of 1,3-diene and 20 equiv. of methyl vinyl ketone in 3 ml of CH_2Cl_2 and 1 ml of toluene, $MeAlCl_2$ (3 equiv.) was added at −78 °C. The reaction was stirred for 24 h at −35 °C and then quenched at −78 °C by addition of 10 equiv. of Et_3N and 1 ml of MeOH, followed by filtration through silica gel, concentration, and purification by column chromatography.

Equilibration and deprotection: The cycloadducts were stirred with 0.02 M NaOMe in MeOH–THF (1 : 1, v/v) at 0.01 M concentration for 12 h and then neutralised by addition of weakly acidic ion exchange resin, followed by filtration and purification by column chromatography.

High pressure aza-Diels–Alder reaction: A solution of 100 μmol of 1,3-diene and 1.5–2.0 equiv. of dienophile (0.2 M concentration) in CH_2Cl_2 was heated in a Teflon tube to 70–75 °C under 12 kbar pressure for 40 h. The product was purified by column chromatography.

‡ All prepared pseudo-oligosaccharides have been characterised by ^1H NMR, ^{13}C NMR, FAB-MS and IR spectroscopy. Additional 2D NMR spectra (COSY, HMQC, TOCSY, HMBC) have been obtained.

1 For references see: R. A. Dwek, *Chem. Rev.* 1996, **96**, 683; R. Roy, in *Carbohydrate Chemistry*, ed. G. J. Boons, Chapman and Hall, UK, 1998, p. 243; *Glycosciences, Status and Perspectives*; ed. H.-J. Gabius and S. Gabius, Chapman and Hall, Weinheim, 1997, p. 291; S. Hakamori and Y. Zhang, *Chem. Biol.*, 1997, **4**, 97; R. Roy, *Curr. Opin. Struct. Biol.*, 1996, **6**, 692; L. L. Kiessling and N. L. Pohl, *Chem. Biol.*, 1996, **3**, 71; N. J. Bovin and H.-J. Gabius, *Chem. Soc. Rev.*, 1995, **24**, 413.

2 For recent references see: K. J. Yarema and C. R. Bertozzi, *Curr. Opin. Chem. Biol.*, 1998, **2**, 49; *Carbohydrates in Drug Design*, ed. Z. J. Witczak and K. A. Nieforth, Marcel Decker, New York, 1997.

3 General reviews on olefin metathesis: R. H. Grubbs and S. Chang, *Tetrahedron*, 1998, **54**, 4413; S. K. Armstrong, *J. Chem. Soc., Perkin Trans. 1*, 1998, 371; M. Schuster and S. Blechert, *Angew. Chem.*, 1997, **109**, 2124; *Angew. Chem., Int. Ed. Engl.*, 1997, **36**, 2036.

4 P. Schwab, M. B. France, J. W. Ziller and R. H. Grubbs, *Angew. Chem.*, 1995, **107**, 2179; *Angew. Chem., Int. Ed. Engl.*, 1995, **34**, 2039.

5 For recent examples see: O. Sellier, P. Van de Weghe, D. Le Nouen, C. Strehler and J. Eustache, *Tetrahedron Lett.*, 1999, **40**, 853; D. J. Holt, W. D. Barker, P. R. Jenkins, D. L. Davies, S. Garrat, J. Fawcett, D. R. Russel and S. Ghosh, *Angew. Chem.*, 1998, **110**, 3486; *Angew. Chem. Int. Ed.*, 1998, **37**, 3298; H. S. Overkleeft, P. Bruggeman, U. K. Pandit, *Tetrahedron Lett.*, 1998, **39**, 3869; H. Ovaa, M. A. Leeuwenburgh, H. S. Overkleeft, G. A. van der Marel and J. H. van Boom, *Tetrahedron Lett.*, 1998, **39**, 3025; A. Fürstner and T. Müller, *J. Org. Chem.*, 1998, **63**, 424; F. E. Ziegler and Y. Wang, *J. Org. Chem.*, 1998, **63**, 426.

6 K. Nomura and R. R. Schrock, *Macromolecules*, 1996, **29**, 540; C. Fraser and R. H. Grubbs, *Macromolecules*, 1995, **28**, 7248; K. H. Mortell, M. Gingras and L. L. Kiessling, *J. Am. Chem. Soc.*, 1994, **116**, 12053.

7 R. Dominique, S. K. Das and R. Roy, *Chem. Commun.*, 1998, 2437.

8 J. Feng, M. Schuster and S. Blechert, *Synlett*, 1997, 129; M. Schuster, N. Lucas and S. Blechert, *Chem. Commun.*, 1997, 823; M. Schuster and S. Blechert, *Tetrahedron Lett.*, 1998, **39**, 2295.

9 R. Stragies, M. Schuster and S. Blechert, *Angew. Chem.*, 1997, **109**, 2628; *Angew. Chem., Int. Ed. Engl.*, 1997, **36**, 2518.

10 W. R. Roush and D. A. Barda, *J. Am. Chem. Soc.*, 1997, **119**, 7402.

Communication 9/03208H

Taming the coil: stabilizing a model hemoprotein fold *via* macrocyclization and peptide helix capping

Dahui Liu, Kyung-Hoon Lee and David R. Benson*

Department of Chemistry, University of Kansas, Lawrence, KS 66045-0046, USA.
E-mail: dbenson@caco3.chem.ukans.edu

Received (in Columbia, MO, USA) 16th February 1999, Accepted 17th May 1999

An N-terminal helix capping motif combined with a C-terminal disulfide bridge stabilizes the fold of a designed hemoprotein model.

Structural stability of many proteins is enhanced by disulfide bonds[1] or by coordination of metal ions to groups of amino acid side chain ligands.[2] Induction of helicity in short peptides has also been accomplished using these and other side chain-side chain interactions.[3] Employing a related approach, we achieved moderate helix induction upon histidine (His) to iron coordination in covalent peptide–porphyrin adducts known as peptide-sandwiched mesohemes (PSMs).[4] Similar helix induction was obtained in a disulfide-dimerized peptide upon complexation of a cobalt(III) porphyrin.[5] To aid our goal of creating small hemoprotein mimics having protein-like stability, we have been exploring ways to further reduce peptide conformatioal flexibility in our designs. The successful use of aromatic side chain–porphyrin interactions in the PSMs has recently been reported.[6]

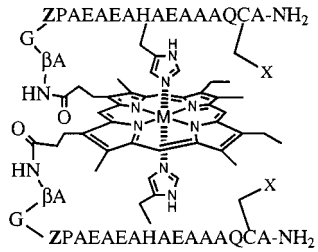

A = Ala; C = Cys; E = Glu; G = Gly; H = His; Q = Gln; P = Pro

1 X,X = S–S; Z = Asn; M = Fe^{III}
2 X = SAcm; Z = Asn; M = Fe^{III}
3 X = SAcm; Z = Gln; M = Fe^{III}
4a,b X,X = S–S; Z = Asn; M = Co^{III}

Herein we report preliminary results with **1**, in which extraordinarily high helix content is achieved through a combination of Fe–His coordination, an N-terminal helix capping motif, and macrocyclization *via* disulfide bond formation.

Lack of hydrogen bonding partners for the first and last few amino acids in a peptide helix results in fraying at each terminus.[7] Protein helices often terminate with a capping motif, which reduces the number of unsatisfied hydrogen bonding sites.[8] In the capping box motif, an amino acid with a hydrogen-bond acceptor on its side chain is situated prior to the first N-terminal helical residue. The side chain of this Ncap hydrogen bonds to the backbone amide NH of the third residue in the helix (N3), which otherwise would not have a hydrogen bonding partner other than water. The side chain of N3 (commonly glutamic acid; Glu) reciprocates by hydrogen-bonding to the backbone amide of the Ncap. The importance of side chain entropy in this end-cap motif is highlighted by the fact that asparagine (Asn) is one of the best Ncap residues in peptides while glutamine (Gln) is one of the worst.[9]

One of the most common amino acids at the first position (N1) of protein helices is proline (Pro).[10] Pro is especially useful at N1 as its backbone ϕ angle (which is ideal for residing in a helix) is fixed by its cyclic structure. Lack of a backbone amide hydrogen further works in favor of Pro at N1, as it needs no hydrogen bonding partner.

Based on the above considerations, Asn, Pro and Glu were selected as the Ncap, N1 and N3 residues in the design of **1**. The backbone torsional angles of Asn were set at the average values observed for Ncap residues in natural proteins (ϕ = −94°; ψ = 167°),[8] while the side chain torsional angles of the His residue coordinated to iron mesoporphyrin IX (MP-IX) were set at the favorable combination χ_1/χ_2 = 180°/−90°.[4,11] When His adopts this combination the peptide helix axis lies at an angle of *ca.* 30° relative to the porphyrin plane and the sulfhydryl group of a cysteine (Cys) residue located i + 7 from His is level with the porphyrin edge and just beyond it.[5] Separating Pro and His by five helical amino acids directed the α-amine of Asn toward the propionate groups of MP-IX, while the sequence β-alanine-glycine (β-Ala-Gly) nicely bridged the gap between the two. When a second peptide was incorporated on the other side of MP-IX, the two Cys residues were situated within bonding distance of one another. Fig. 1 shows a predicted energy minimized structure of **1**.[12]

The bis acetamidomethyl (Acm) protected precursor of **1** (**2**) serves to show how the disulfide linkage in **1** influences its structure and stability. We also prepared an analogue of **2** in which the Ncap Asn has been replaced by Gln (**3**) in order to determine whether Asn functions as intended in our design. Syntheses of **2** and **3** were accomplished using methods previously reported for the PSMs.[4] Brief treatment of **2** with iodine in aqueous 2,2,2-trifluoroethanol (TFE) cleanly yielded **1**.

Circular dichroism (CD) spectra of **1**–**3** are shown in Fig. 2. Using the mean residue ellipticity at 220 nm (θ_{220}) we calculate[13] that the peptides in **2** are 64% helical in aqueous solution at 8 °C (Table 1; only amino acids 4–18 are included in the calculation, as only these residues are predicted to be within the helix). In contrast, helix content in **3** is only 45% in water. The high helicity of acyclic **2** supports the choice of His placement in the peptide sequence, while the results with **3** confirm a helix-stabilizing role for the Ncap Asn. The helix stabilizing solvent TFE increases helix contents of **2** and **3** to 88 and 83%, respectively (Table 1). Finally, comparing spectra of **1** and **2** in H_2O (Fig. 2; Table 1) reveals that macrocyclization strongly increases peptide helix content as predicted. TFE

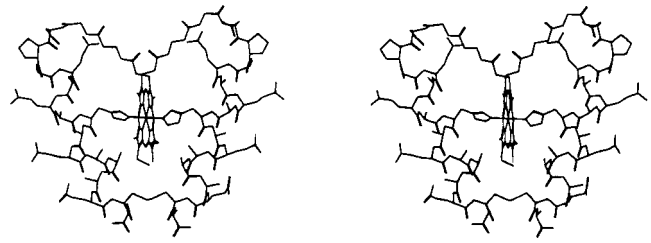

Fig. 1 Structure of one diasteromer of **1** predicted from molecular modeling studies.

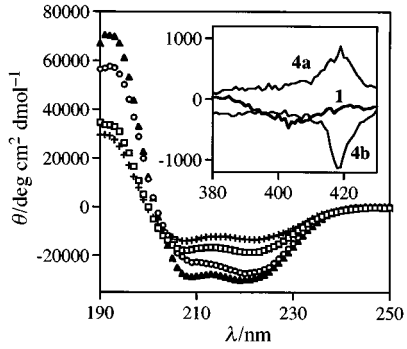

Fig. 2 Far-UV CD spectra of **1** in H_2O (○) and 3:1 (v/v) H_2O–TFE (▲) and of **2** (□) and **3** (+) in H_2O. Inset: Soret region spectra of **1**, **4a** and **4b** in H_2O. All samples were buffered at pH 7.0 with 2 mM potassium phosphate and all spectra were recorded at 8 °C.

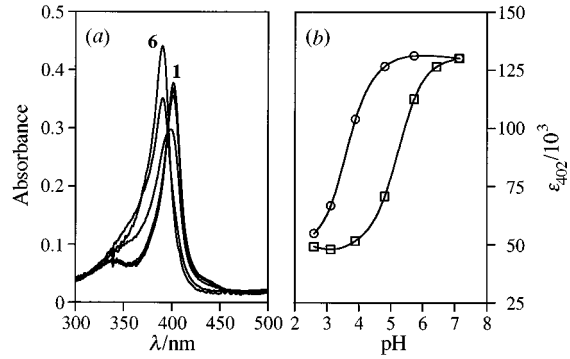

Fig. 3 (*a*) UV/vis spectra of **1** recorded as a function of pH. Spectrum 1: pH 7.1; Spectrum 6: pH 2.6. (*b*) Plots of extinction coefficient (ε) at Soret λ_{max} *vs.* pH for **1** (○) and **2** (□). All data were recorded at 22 °C.

Table 1 CD data for **1**–**4** in H_2O and in 3:1 (v/v) H_2O–TFE

	θ_{220}/deg cm² dmol^{-1} [a] (% Helix)[b]	
Compound	H_2O	3:1 (v/v) H_2O–TFE
1	−27 400 (94)	−30 000 (102)
2	−18 700 (64)	−25 800 (88)
3	−13 300 (45)	−24 000 (83)
4a	−25 500 (87)	−27 800 (95)
4b	−27 800 (95)	−30 100 (102)

[a] θ_{max} = −29 300 deg cm² dmol^{-1}. [b] Percent helix values are shown in parentheses.

further increases helix content in **1** from 94% to the theoretical maximum, although the relative intensities of the 208 and 220 nm bands in the two solvents suggest that TFE may cause additional changes to the structure of **1**.

The heme chromophore can contribute ellipticity in the far-UV region of CD spectra of hemoproteins and hemoprotein models.[14] Calculated helix contents reported in Table 1 must therefore be considered estimates only. Nonetheless, because the chromophore and the mode of attachment of peptide to porphyrin are the same in **1**–**3**, it is reasonable to assume that an increase in the absolute value of θ_{220} represents a proportional increase in peptide helix content.

PSMs built from MP-IX exist in two interconvertible diastereomeric forms.[4] Pavone and co-workers have reported that the two diastereomers of bis-His coordinated hemoprotein models constructed from Co^{III} deuteroporphyrin IX can be separated because His–Co^{III} bonds are exchange-inert.[15] We thus prepared and isolated the two diastereomers of the Co^{III} analogue of **1** (**4a** and **4b**). Helix contents of **4a** and **4b** are different, although both are very high. The CD Soret bands of **4a** and **4b** are of opposite sign but nearly equal intensity, whereas the Soret band of **1** is negative (Fig. 2, inset). That the helix contents of **1** and **4b** are nearly identical (and greater than **4a**) and each exhibits a negative Soret suggests that the diastereomer of **1** which corresponds to **4b** predominates at equilibrium. The diastereomer of **1** shown in Fig. 1 is the one predicted to be favored based on molecular modeling studies.

The intramolecular His ligands in **1**–**3** result in Fe–His coordination being strongly favored at neutral pH. However, because Fe–His bonds are exchange labile, at pH values near or below the pK_a of His, protonation of His competes with Fe–His coordination.[4] Protonation of His requires initial scission of the Fe–His bond, which results in conversion of heme from the low spin (S = 1/2; Soret λ_{max} = 402 nm) to the high spin (S = 5/2; Soret λ_{max} = 390 nm) form. One of our predictions with **1** was that the disulfide bridge would stabilize the folded (bis-His coordinated) form of the molecule relative to **2** by reducing the conformational freedom of its peptides in the unfolded form. We thus recorded UV/vis spectra of **1** and **2** in water as a function of pH (Fig. 3). For **2**, spectral changes are observed at pH values as high as 6. No changes were observed in UV/vis spectra of **1**, however, until pH < 5, illustrating the predicted stability enhancement of bis-His coordinated **1**.

In conclusion, we have shown that a combination of motifs commonly encountered in protein structures can provide considerable structural stabilization to hemoprotein models built from short peptides. The results illustrate the power of computer-aided *de novo* design in creating protein mimics having desired structural characteristics. Future work will be aimed at systematically investigating the influence of the Ncap, N1 and N3 residues in **1** and **2** on the stability of the folded form of each molecule. We also plan a detailed study of the three-dimensional structures of **4a** and **4b** using ^{1}H NMR, which will include an examination of how TFE influences peptide architecture.

This work was supported by NIH grant R29-GM52431.

Notes and references

1 T. E. Creighton, *BioEssays*, 1988, **8**, 57.
2 J. P. Glusker, *Adv. Protein Chem.*, 1991, **42**, 1.
3 J. C. Phelan, N. J. Skelton, A. C. Braisted and R. S. McDowell, *J. Am. Chem. Soc.*, 1997, **119**, 455 and references therein.
4 P. A. Arnold, D. R. Benson, D. J. Brink, M. P. Hendrich, G. S. Jas, M. L. Kennedy, D. T. Petasis and M. Wang, *Inorg. Chem.*, 1997, **36**, 5306.
5 P. A. Arnold, W. R. Shelton and D. R. Benson, *J. Am. Chem. Soc.*, 1997, **119**, 3181.
6 D. A. Williamson and D. R. Benson, *Chem. Commun.*, 1998, 961.
7 A. Chakrabartty and R. L. Baldwin, *Adv. Protein Chem.*, 1995, **46**, 141.
8 E. T. Harper and G. D. Rose, *Biochemistry*, 1993, **32**, 7605; A. J. Doig, M. W. MacArthur, B. J. Stapley and J. M. Thornton, *Protein Sci.*, 1997, **6**, 147.
9 A. J. Doig, A. Chakrabartty, T. M. Klinger and R. L. Baldwin, *Biochemistry*, 1994, **33**, 3396.
10 J. S. Richardson and D. C. Richardson, *Science*, 1988, **240**, 1648.
11 P. Chakrabarti, *Protein Eng.*, 1990, **4**, 57.
12 SYBYL molecular modeling software ver. 6.01, Tripos Associates, St. Louis, MO.
13 P. C. Lyu, J. C. Sherman and N. R. Kallenbach, *Proc. Natl. Acad. Sci. U.S.A.*, 1991, **88**, 5317.
14 D. R. Benson, B. R. Hart, X. Zhu and M. B. Doughty, *J. Am. Chem. Soc.*, 1995, **117**, 8502 and references therein.
15 G. D'Auria, O. Maglio, F. Nastri, A. Lombardi, M. Mazzeo, G. Morelli, L. Paolillo, C. Pedone and V. Pavone, *Chem. Eur. J.*, 1997, **3**, 350.

Communication 9/01312A

ChemComm

Aerobic catalytic oxidative coupling of 2-naphthols and phenols by $VO(acac)_2$

Der-Ren Hwang, Cheu-Pyeng Chen and Biing-Jiun Uang*

Department of Chemistry, National Tsing Hua University, Hsinchu, Taiwan 300, Republic of China.
E-mail: bjuang@chem.nthu.edu.tw

Received (in Cambridge, UK) 10th March 1999, Accepted 17th May 1999

In the presence of a catalytic amount of $VO(acac)_2$, oxidative coupling of 2-naphthol or phenol derivatives with molecular oxygen occurred at room temperature and selectively gave the corresponding *ortho–ortho* coupling products in moderate to high yields.

Optically active 1,1′-bi-2-naphthol and its derivatives have been widely used in enantioselective synthesis as a source of chirality.[1] There are some known methods for the oxidative coupling of 2-naphthols to give 1,1′-bi-2-naphthols using stoichiomeric amounts of oxidant,[2–4] and some methods employing catalytic oxidative coupling. These methods either use an expensive oxidant (such as AgCl) with low yield,[4c] require the preparation of a complex catalyst [such as CuCl(OH)·TMEDA, $CuSO_4(Al_2O_3)$] before the coupling reaction,[5,6] or perform the reaction at higher temperature [$CuSO_4(Al_2O_3)$, $FeCl_3$].[2a] Oxovanadium complexes were found to have specific catalytic activity towards organic syntheses especially in oxidation reactions.[7] A vast number of synthetic reactions which utilize oxovanadium(v), *i.e.* $VOCl_3$ and VOF_3, as oxidants have been documented, as exemplified by the oxidative coupling of phenols in natural product synthesis.[8] Due to the fact that $VOCl_3$ and VOF_3 are moisture sensitive, hazardous materials,[9] they are not easy to use in practice. Thus it is important to find a more convenient method for the oxidative coupling of phenols. Here we report a convenient oxidative coupling method for 2-naphthols and phenols with molecular oxygen as the oxidant in the presence of a catalytic amount (10 mol%) of $VO(acac)_2$, an inexpensive and stable catalyst (Scheme 1).[10]

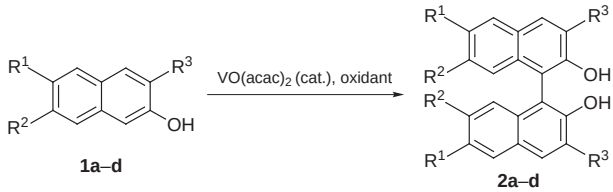

1a–d **2a–d**

Scheme 1

To achieve a catalytic cycle in the vanadium mediated coupling of phenols, one has to find an oxidant which will oxidize V^{IV} to V^{V} and will not interfere with the coupling reaction during the catalytic cycle. At the outset, a system consisting of 2-naphthol **1a**, 10 mol% $VO(acac)_2$ and oxidants such as H_2O_2, Bu^tOOH and Oxone was studied. Although 2-naphthol was consumed completely in these cases, only trace amounts of the coupling product **2a** were detected. The remaining materials were intractable. Then, $NaIO_4$ and NH_4IO_4 were used as oxidants. After reaction for 24 h under similar reaction conditions, most of the starting material was recovered and there was no coupling product. Finally, when molecular oxygen was used as oxidant and the reaction was conducted in CH_2Cl_2 at room temperature for 24 h, **1a** was consumed and **2a** was obtained in 92% yield after chromatographic purification.† The coupling product was present only in trace amounts when the reaction was conducted in MeOH.

In the case of 6-bromo-2-naphthol **1b**, the coupling reaction was completed in 24 h to give **2b** in 90% yield. The reactivity of electron-donating and electron-withdrawing group substituted 2-naphthols was apparently different. Coupling of **1c** was finished within 9 h, but gave a lower yield due to the formation of some intractable materials. The coupling reaction of 3-(methoxycarbonyl)-2-naphthol **1d** was very sluggish. It gave a 35% yield of **2d** after 120 h, and 62% of **1d** was recovered (Table 1).

Table 1 Oxidative coupling of 2-naphthol and derivatives catalyzed by $VO(acac)_2$[a]

Napthol	R^1	R^2	R^3	*t*/h	Product[b]	Yield (%)
1a	H	H	H	24	**2a**	92
1b	Br	H	H	24	**2b**	90
1c	H	OMe	H	9	**2c**	76
1d	H	H	CO_2Me	120	**2d**	35

[a] The reactions were run with 10 mol% $VO(acac)_2$ in CH_2Cl_2 at room temperature under 1 atm O_2. [b] Compounds **2a–d** were identified according to data reported in ref. 6.

Coupling of phenol under similar reaction conditions was unsuccessful; there was no detectable amount of 1,1′-biphenol present. When 2,4-dimethylphenol **3a** and 2,3,5-trimethylphenol **3b** were subjected to the coupling reaction, the corresponding *ortho–ortho* coupling products **4a** and **4b** were obtained in moderate yields (Table 2). These two reactions are similar in terms of reaction rate. Prolonged reaction time did not give a better yield of coupling product. In the latter case, 28% of **3b**

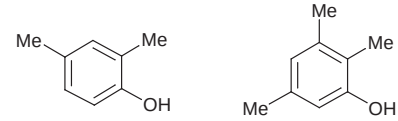

3a **3b**

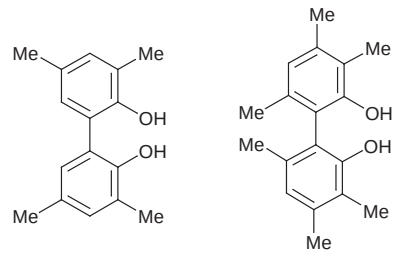

4a **4b**

Table 2 Oxidative coupling of alkyl substituted phenols catalyzed by $VO(acac)_2$[a]

Phenol	*t*/h	Product[b]	Yield (%)
3a	120	**4a**	66
3b	48	**4b**	62

[a] Reaction conditions were similar to those for **1a–d**. [b] **4a**,**b** were characterized according to data reported in ref. 11.

was recovered. Reaction of **3a** for 120 h gave a similar yield of **4a** but no **3a** was recovered. Instead, some intractable material was formed.

In conclusion, a facile oxidative coupling method that selectively coupled 2-naphthol or phenol derivatives to the corresponding *ortho–ortho* coupling products, 1,1′-bi-2-naphthols or 1,1′-bi-2-phenols, with molecular oxygen in the presence of a catalytic amount of $VO(acac)_2$ in moderate to high yields has been demonstrated.

We are grateful to the National Science Council, Republic of China, for support of this work.

Note and references

† *Typical procedure*: A stirred mixture of 2-naphthol (144 mg, 1 mmol), and $VO(acac)_2$ (26.5 mg, 0.1 mmol) in CH_2Cl_2 (10 ml) was exposed under an atmospheric pressure of molecular oxygen at room temperature for 24 h. The mixture was then filtered through a short column of silica gel and the silica gel was washed with EtOAc (40 ml). The filtrate was concentrated and purified by column chromatography (SiO_2, hexane–EtOAc = 5:1) to afford the coupling product **2a** (131 mg, 92%, mp 215–217 °C ; lit., [4a] 216–218 °C). On a 100 mmol scale, 75–78% of the coupling product was obtained.

1 For recent reviews see: C. Rosini, L. Franzini, A. Raffaelli and P. Salvadori, *Synthesis*, 1991, 503; H. B. Kagan and O. Riant, *Chem. Rev*., 1992, **92**, 1007; K. Mikami and M. Shimizu, *Chem. Rev*., 1992, **92**, 1021; (d) L. Pu, *Chem. Rev*., 1998, **98**, 2405.

2 (*a*) F. Toda, K. Tanaka and S. Iwata, *J. Org. Chem*. 1989, **54**, 3007; (*b*) R. Pummerer, E. Prell and A. Rieche, *Ber*., 1926, **59**, 2159; (*c*) B. Feringa and H. Wynberg, *J. Org. Chem*., 1981, **46**, 2547.

3 M. J. S. Dewar and T. Nakaya, *J. Am. Chem. Soc*., 1968, **90**, 7134; K. Yamamoto, H. Fukushima, Y. Okamoto, K. Hatada and M. Nakazaki, *J. Chem. Soc., Chem. Commun.*, 1984, 1111.

4 (*a*) B. Feringa and H. Wynberg, *Tetrahedron Lett.*, 1977, **18,** 4447; (*b*) J. Brussee, J. L. G. Groenendijk, J. M. te Koppele and A. C. A. Jansen, *Tetrahedron*, 1985, **41**, 3313; (*c*) M. Smrcina, J. Polakova, S. Vyskocil and P. Kocovsky, *J. Org. Chem*., 1993, **58**, 4534.

5 M. Noji, M. Nakajima and K. Koga, *Tetrahedron Lett.*, 1994, **35,** 7983.

6 T. Sakamoto, H. Yonehara and C. Pac, *J. Org. Chem*.,1994, **59**, 6859.

7 For a recent review see: T. Hirao, *Chem. Rev*., 1997, *97*, 2707.

8 M. A. Schwartz, R. A. Holton and S. W. Scott, *J. Am. Chem. Soc.*, 1969, **91**, 2800; J. D. White, R. J. Butlin, H.-G. Hahn and T. Johnson, *J. Am. Chem. Soc.*, 1990, **112**, 8595; D. A. Evans, C. J. Dinsmore, D. A. Evrard and K. M. DeVries, *J. Am. Chem. Soc.*, 1993, **115**, 6426; D. L. Comins and L. A. Morgan, *Tetrahedron Lett.*, 1991, **32,** 5919; W. L. Carrick, G. L. Karapinka and G. T. Kwiatkowski, *J. Org. Chem*., 1969, **34**, 2388.

9 M. K. O'Brien and B. Vanasse, in *Encyclopedia of Reagents for Organic Synthesis*, ed. L. A. Paquette, Wiley, New York, 1995, vol. 8, pp. 5482–5485.

10 B. E. Rossiter, in *Encyclopedia of Reagents for Organic Synthesis*, ed. L. A. Paquette, Wiley, New York, 1995, vol. 8, pp. 5479–5482.

11 For **4a** see: G. Sartori, R. Maggi, F. Bigi, A. Arienti, G. Casnati, G. Bocelli and G. Mori, *Tetrahedron*, 1992, **48,** 9483; for **4b** see: D. R. Armstrong, C. Cameron, D. C. Nonhebel and P. G. Perkins, *J. Chem. Soc., Perkin Trans. 2* 1983, 581.

Communication 9/01934K

The Ru(=CHPh)$Cl_2(PCy_3)_2$-initiated ring-opening metathesis polymerization of 7-*tert*-butoxybicyclo[2.2.1]hepta-2,5-diene: regeneration of initiator and the implied formation of macrocycles

Kenneth J. Ivin,*[a] Alan M. Kenwright[b] and Ezat Khosravi[b]

[a] *12, St. Michael's Gardens, South Petherton, Somerset, UK TA13 5BD. E-mail: kjivin@compuserve.com*
[b] *IRC in Polymer Science and Technology, University of Durham, UK DH1 3LE*

Received (in Cambridge, UK) 16th March 1999, Accepted 10th May 1999

The ring-opening metathesis polymerization (ROMP) of 7-*tert*-butoxybicyclo[2.2.1]hepta-2,5-diene initiated by Ru(=CHPh)$Cl_2(PCy_3)_2$ proceeds rapidly in organic solvents with almost complete consumption of initiator to form propagating ruthenium carbene species that are then converted slowly but not completely back to initiator, implying a secondary ring-closing metathesis reaction at the chain ends to form macrocycles.

The ROMP of the title monomer (7-TBONBD) initiated by $MoCl_5/Me_4Sn/Et_2O$ and $OsCl_3$ is known to give polymers containing both *anti* and *syn* units, depending on which double bond is opened in the propagation step (Scheme 1). The double bonds formed between the rings are mainly *trans* in the first case, and *cis* in the second.[1]

The ROMP of this monomer (M) has now been studied in various solvents at 20 °C, initiated by the well-defined ruthenium carbene complex[2] Ru(=CHPh)$Cl_2(PCy_3)_2$, (I), using ^{1}H, ^{13}C and ^{31}P NMR to follow the reaction. In $CDCl_3$, with $[I]_o$ = 0.0176 mol l^{-1}, $[M]_o$ = 1.016 mol l^{-1}, $[M]_o/[I]_o$ = 57.7, $t_{½}$ for the polymerization of M was about 3 min and most of the initiator was also rapidly consumed. The polymer consisted largely of *anti* units, with 34% *cis* double bonds between the rings. The consumption of M was slower in both CD_2Cl_2 ($t_{½}$ ~12 min) and C_6D_6 ($t_{½}$ ~17 min) under comparable conditions, but the *cis* content was similar. Experiments at $[M]_o/[I]_o$ = 5–10 allowed the determination of the ratio of propagation to initiation rate constants, k_p/k_i, from $[M]_o/[I]_o$ and the value of $[I]/[I]_o$ immediately after the completion of polymerization.[3] These gave k_p/k_i ~ 15, independent of solvent.

Fig. 1 is a stack plot of the carbene proton region taken at intervals over a period of 12 h for the reaction in $CDCl_3$, after the monomer had been consumed. This shows several remarkable and unexpected features, in particular (i) fine structure for the propagating species (P_n) which is not due to spin coupling, (ii) the regeneration of I at the expense of P_n, and (iii) the formation of another carbene species (X).

The positions of the three P_n lines (δ 19.38, 19.36, 19.33) were the same in a 400 MHz spectrum as in the 500 MHz spectrum. The fine structure is therefore not due to PH_α ^3J coupling nor to $H_\alpha H_\beta$ ^3J coupling. The absence of PH_α coupling is normal in ruthenium carbene complexes containing two PCy_3 ligands as in the initiator,[2] but the absence of $H_\alpha H_\beta$ coupling is very abnormal. Thus in complexes of the type [Ru]=CHR containing two PCy_3 ligands, $^3J_{\alpha\beta}$ ranges from 5.0 (R = Et) to 10.5 Hz (R = CH=CPh_2).[2,4–6] In the present case it would appear therefore that (i) rotation about the C_α–C_β bond in the propagating species is severely restricted by the interaction between the PCy_3 ligands and the enchained cyclopentene ring, (ii) the favoured conformation (**1**) has a HC–CH dihedral angle close to 90°; and (iii) the observed fine structure is due to sensitivity of the chemical shift to the *c/t* isomerism of the adjacent double bond and to the *m/r* isomerism of the adjacent dyad. The intensity pattern of the three P_n lines (31 : 39 : 30) can be interpreted in terms of similar *c/t* and *m/r* splittings (giving rise to three lines rather than four), a *cis* content of 34%, and somewhat different tacticities (*m/r* ratio) with respect to the adjacent *cis*- and *trans*-centred dyads.

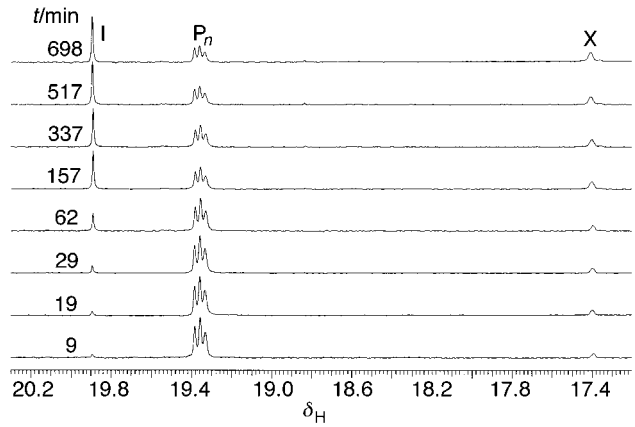

Fig. 1 Carbene proton region as a function of reaction time (t) in the 500 MHz ^{1}H NMR spectrum. Solvent $CDCl_3$: $[I]_o$ = 0.0176 mol l^{-1}, $[M]_o$ = 1.016 mol l^{-1}. P_n is the propagating species; X, see text. The intensities were referenced to the total integral of the δ 4.0–2.7 region (H-1,4 + H-7 signals). There was an overall loss of carbene proton signal of 24% during the first 700 min.

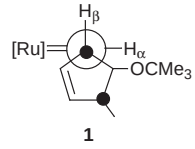

1

The regeneration of I (δ 19.89) at the expense of P_n can only occur by a ring-closing metathesis reaction in which the entire chain forms a macrocycle and the PhCH= end group re-attaches itself to the ruthenium centre (Scheme 2). When a second batch of monomer was added, [I] again fell to a very low level and slowly recovered, while [P_n] immediately rose and then again declined. However X (δ 17.40) did not fall but continued to

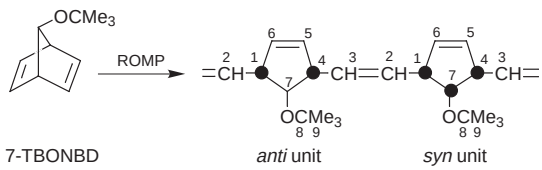

Scheme 1

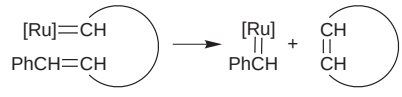

Scheme 2

grow. The relative intensities of the three P_n lines (Fig. 1) remained unchanged during the reversion of P_n to I, indicating that the probability of ring closure is independent of the stereochemistry close to the Ru=C bond.

When a small amount of ethyl vinyl ether was added to a portion of the reaction mixture in $CDCl_3$ some time after the first addition of monomer, the peaks due to species I, P_n and X all disappeared and new carbene proton peaks appeared at δ 18.91 (2%), in the position expected for [Ru]=CH_2,[5] and δ 14.54 (98%), attributed to [Ru]=CHOEt. The P_n chains had thus been terminated to give mainly vinyl end groups. GPC measurements on polymers that had been terminated just before and some time after the second addition of monomer showed the expected increase in molecular weight after the second addition, but in both cases the distributions were broad and unimodal for the main fraction. The DP was of the same order of magnitude as $[M]_o/[I]_o$ so that back-biting at other points in the chain to yield smaller cyclic oligomers cannot be a serious competitor, probably because of the difficulty of access of the Ru=C bond to double bonds situated between two substituted rings.

GPC traces of polymers that had been made in CD_2Cl_2 and terminated (i) immediately after consumption of monomer, and (ii) later after the initiator had been regenerated, showed differences in the low molecular weight region (300–700) consistent with the presence of different proportions of linear and cyclic oligomers, but further work is needed to characterise the species associated with the observed peaks.

Regeneration of initiator was also observed for the reaction in CD_2Cl_2 and C_6D_6 except that the whole process was somewhat slower than in $CDCl_3$ and the P_n signal consisted of two lines instead of three, in the ratio 28:72 in CD_2Cl_2 (δ 19.44, 19.40 relative to initiator δ 20.02) and 24:76 in C_6D_6 (δ 19.66, 19.60 relative to initiator δ 20.31). This is consistent with the presence of four underlying structures (*c/m*, *c/r*, *t/m*, *t/r*) of which three have the same chemical shift.

When the reaction was carried out in CD_2Cl_2 in the presence of added PCy_3 ($[PCy_3]/[I]_o$ = 1.88) it was greatly retarded (factor of ~50) but followed the same general course with eventual complete consumption of M, regeneration of I, and the formation of X. This strongly suggests a mechanism in which a PCy_3 ligand must first be released from the initiator before monomer can be coordinated to the Ru centre and react by metathesis. The magnitude of the effect was consistent with a constant for the dissociation of the PCy_3 ligand from the initiator of the order of 10^{-5} mol l^{-1}.

The reaction in CD_2Cl_2 was also followed by ^{31}P NMR. The initiator gave a singlet (δ 37.24), while P_n gave four signals (δ 36.80, 36.45, 36.36, 36.10) of approximately equal intensity. After the consumption of monomer, these rose and fell respectively as for the ^{1}H NMR signals. A small peak also emerged at δ 11.52 (PCy_3), and grew in parallel with the X peak in the ^{1}H NMR spectrum. By analogy with the recent work of Grubbs [7] one may speculate that X is a monophosphine complex formed by displacement of one of the PCy_3 ligands in P_n by chelation of an oxygen atom (in the polymer chain) to the Ru centre. A number of other small peaks appeared in the ^{31}P NMR spectrum between δ 55 and 25, comparable in intensity with that at δ 11.52, one of which may be due to the PCy_3 ligand in X. The slow rate of formation of X may arise from the necessity for the C_α–C_β bond in **1** to rotate against a substantial barrier to a position where the adjacent oxygen atom comes into juxtaposition with the ruthenium centre. Conversion of P_n to X does not go to completion and is probably a slow equilibrium process [eqn. (1)].

$$P_n \rightleftharpoons X + PCy_3 \quad (1)$$

It appears that the regeneration of initiator is peculiar to the ROMP of 7-TBONBD initiated by $Ru(=CHPh)Cl_2(PCy_3)_2$. To date we have been unable to observe this phenomenon using this initiator with other monomers, *e.g.* norbornene, or this monomer with other initiators, *e.g.* $Mo(=CHCMe_3)(=NAr)(OCMe_3)_2$.

We thank Dr J. G. Hamilton for providing a sample of monomer, and Mrs C. F. Heffernan for technical assistance.

Notes and references

1 J. G. Hamilton and J. J. Rooney, *J. Chem. Soc., Chem. Commun.*, 1992, 370.
2 P. Schwab, M. B. France, J. W. Ziller and R. H. Grubbs, *Angew. Chem., Int. Ed. Engl.*, 1995, **34**, 2039.
3 K. J. Ivin and J. C. Mol, *Olefin Metathesis and Metathesis Polymerization*, Academic Press, London 1997, p. 232.
4 S. T. Nguyen, L. K. Johnson, R. H. Grubbs and J. W. Ziller, *J. Am. Chem. Soc.*, 1992, **114**, 3974.
5 S. T. Nguyen, R. H. Grubbs and J. W. Ziller, *J. Am. Chem. Soc.*, 1993, **115**, 9858.
6 Z. Wu, A. D. Benedicto and R. H. Grubbs, *Macromolecules*, 1993, **26**, 4975.
7 B. R. Maughon and R. H. Grubbs, *Macromolecules*, 1997, **30**, 3459.

Communication 9/02073J

ChemComm

Size and shape evolution of core–shell nanocrystals

C. J. Zhong,* W. X. Zhang, F. L. Leibowitz and H. H. Eichelberger

Department of Chemistry, State University of New York at Binghamton, Binghamton, New York 13902, USA. E-mail: cjzhong@binghamton.edu

Received (in Columbia, MO, USA) 20th April 1999, Accepted 19th May 1999

The findings of an investigation of temperature-manipulated size and shape evolution for pre-formed decanethiolate–encapsulated gold nanocrystals are described.

Monolayer-encapsulated metal nanoparticles are of considerable technological interest because of the potential electronic, optical, magnetic, catalytic and sensing applications emerging from the core–shell combinations.[1,2] Part of our motivation stems from the opportunities of manipulating such structural properties as interfacial building blocks towards fine-tunable electrode nanomaterials.[3] One important advance emerging from various synthetic strategies[4–16] is the two-phase method, which was first reported by Schiffrin and coworkers[4,5] and has been extensively utilized.[1,4–8] This relatively simple method, which involves transferring an aqueous tetrachloroaurate ($AuCl_4^-$) precursor into an organic phase followed by reduction in the presence of thiols (RSH), has been proven very effective for synthesizing core sizes ranging from 1.5 to 5 nm by controlling the RSH/Au ratio and reaction temperature.[4–8] Narrow-size preparation and shape control are the ultimate synthetic challenges. Relatively little is, however, known about shape control for such composite nanomaterials,[12–16] though examples have recently been demonstrated for platinum nanoparticles by manipulating precursor ratios,[14] or introducing 'shape-inducing reagent'.[15] In view of the molecular and crystal natures of such core–shell systems, size and shape are inherently a dynamic process and an evolution may occur as a result of changes in chemical potentials of the particles. Such a process is the basis of crystallography involving nucleation, dissolution and growth,[18,19] but to our knowledge has not been studied for the core–shell type systems. Here, we describe the preliminary results of an investigation of such a process of pre-formed thiolate-encapsulated gold nanoparticles by manipulating temperatures.

Thiolate-encapsulated gold nanoparticles were prepared first by the two-phase method.[4,6] Briefly for decanethiolate-encapsulated nanoparticles, after transferring an aqueous $AuCl_4^-$ by tetraoctylammonium bromide (98%) into a toluene phase, decanethiol (DT, 96%) was added at a 2:1 ratio of DT/Au, and followed by adding an excess (12 ×) of an aqueous reducing agent ($NaBH_4$, 99%). The reaction produced a dark-brown solution of the DT-encapsulated nanoparticles, which was then subjected to two types of sample handling procedures. In the first procedure, the solvent was removed by rotary evaporator (at *ca.* 50 °C) yielding a black and waxy product, DT/Au(**1**). In the second procedure, the solution was brought to *ca.* 110 °C under reduced pressure for *ca.* 30 min. Upon this treatment, the solution showed a color change from brownish to pinkish. We note here two observations for the heating treatment. First, simply heating the solution at temperatures between 50 and 110 °C did not lead to any color change. Secondly, a color change occurred under conditions of the concentration rising to *ca.* 10-fold and the temperature to 100–115 °C. A systematic study of the related factors is in progress. This treatment was performed after the formation of the encapsulated nanoparticles, a procedure different from temperature control during the synthesis.[8] After removing solvent, the gray and powdery product, DT/Au(**2**), was collected. Both **1** and **2** were subjected to subsequent cycles of suspension in ethanol and acetone and centrifugation for at least four times to ensure a complete removal of non-nanoparticle materials.

These two samples, DT/Au(**1**) and DT/Au(**2**), were first examined by transmission electron microscopy (TEM). Fig. 1 presents two representative TEM images from the two samples. For the DT/Au(**1**) sample [Fig. 1(*a*)], the result displays an average core size of *ca.* 2.0 nm with *ca.* 80% populations within the range 1.5–2.5 nm. The crystal shapes, though not clearly identifiable with the TEM resolution, appear non-uniform. These microscopic features are in good agreement with those reported previously for samples prepared under similar conditions.[8] A previous study has determined that the most likely shape for such a core size is a truncated octahedron.[12] In contrast to the results shown for the DT/Au(**1**) sample, two striking features are evident for the DT/Au(**2**) sample [Fig. 1(*b*)]. First, it displays an increased core size with a narrow distribution in which more than 90% populations are within the range 4.7–5.7 nm (average 5.2 nm). Second, a close examination of the particle shapes indicates a 'hexagon' outline for an observable percentage of the particles. Clearly, an evolution in both size and shape of the particles has occurred from DT/Au(**1**) to DT/Au(**2**) samples. While not reported for thiolate-encapsulated nanocrystals, temperature-induced changes in size and morphology, including quasimelting, coalescence and sintering of fine particles, have indeed been reported for metal or metal oxide crystals or nanocrystals.[18,19] The size and shape evolution of our encapsulated nanoparticles in the solution may involve a

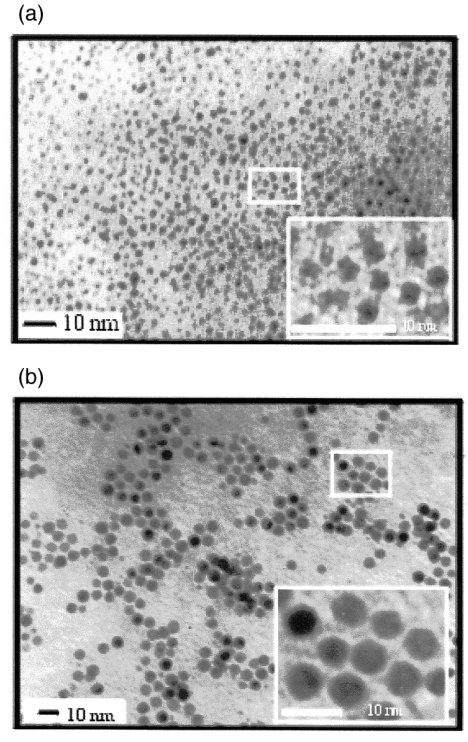

Fig. 1 TEM micrographs of two DT-encapsulated Au nanocrystal samples: (a) DT/Au(**1**) and (b) DT/Au(**2**) on carbon-coated TEM grids. The insert represents an enlarged view of the indicated area.

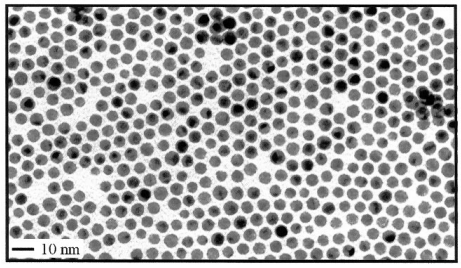

Fig. 2 TEM micrograph of the ordered domain features for DT/Au(**2**) on a carbon-coated TEM grid.

balance of the chemical potentials *via* desorption and re-adsorption of the shell components and coalescence of the cores as the driving force for the eventual size and shape.

Another remarkable feature for the evolved nanocrystals was the formation of long range order upon casting a solution of the DT/Au(**2**) sample onto a TEM grid and evaporating the solvent. As shown in Fig. 2, large domains of long range self-organizations are evident. Two-dimensional ordered arrays with a hexagon-type arrangement can also be identified. Similar long range orders have recently been reported for alkanethiolate-encapsulated gold nanoparticles that were prepared without temperature treatment, for examples, by fractionalized dodecanethiolate-encapsulated gold particles,[12] by gas-phase synthesis followed by solution-phase encapsulation,[10] and most recently by two-phase synthesized gold particles coated with quaternary ammonium ion pairs.[5] Our observation serves as an intriguing example for the long range ordering for the encapsulated nanocrystals prepared by the temperature treatment. In an excellent agreement with the notion that the encapsulating chains are likely interdigitated between opposing alkyl shells,[1,5,10,12] the determined average core–core (edge-to-edge) distance of *ca.* 1.5 nm is indeed close to the expected chain length of DT (1.4–1.5 nm).

Two sets of spectroscopic data further confirmed the observed evolution and the associated structural properties. First, the optical properties for the samples before and after the size and shape evolution were determined by measurement of adsorption in the visible region. Optically, fine particles display surface plasmon resonance bands with intensity and energy strongly dependent on size. The UV-VIS spectrum for DT/Au(**1**) in hexane displays an identifiable surface plasmon band envelope around 510 nm. The shape and position of this band is in agreement with those previously reported for similar particle sizes.[8] In contrast, the spectrum for the DT/Au(**2**) sample exhibits an increased intensity for the 520 nm band. This result, without an apparent shift in energy, is consistent with an increase in core size, a well documented phenomenon.[6,8,12]

Secondly, the structural properties of the encapsulating monolayer shells were characterized using IR spectroscopy. Two pieces of evidence emerge from the spectral similarities and differences (Fig. 3) between these two samples. First, the overall similarity in both high and low energy regions suggests the absence of major structural changes such as decomposition and transformation. Second, a close examination of the C–H stretching region provides diagnostic information about ordering properties of the alkyl chains in the shell. While bands corresponding to methyl stretching (2955 and 2872 cm^{-1}) show little change, a shift to lower wavenumbers is identified for the asymmetric and symmetric methylene stretching bands from DT/Au(**1**) (2920 and 2950 cm^{-1}) to DT/Au(**2**) (2917 and 2948 cm^{-1}). As extensively studied for both monolayers on planar[17] and on nanocrystal gold,[6,8] such a shift is diagnostic of the more crystalline nature[25] of the monolayer on larger particles. These results, combined with the optical data, confirm the evolution of the smaller-sized to larger-sized nanocrystals with the integrity of the final encapsulating shell structures maintained.

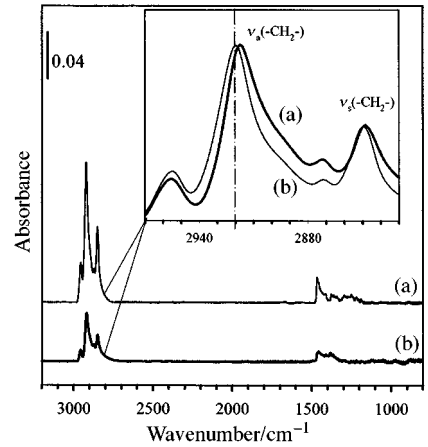

Fig. 3 FTIR spectra for (a) DT/Au(**2**) and (b) DT/Au(**1**) samples in KBr pallets. The insert represents a normalized view in the C–H stretching region.

Finally, we note that similar microscopic and spectroscopic characteristics have also been observed for samples with alkanethiolate shell components of different chain lengths.

A further systematic investigation to unravel the mechanistic aspects is in progress.

Notes and references

1 M. J. Hostetler and R. J. Murray, *Curr. Opin. Colloid Interface Sci.*, 1997, **2**, 42 and references therein.
2 G. Schon and U. Simon, *Colloid Polym. Sci.*, 1995, **273**, 101; 1995, **273**, 202.
3 C. J. Zhong, W. X. Zheng and F. L. Leibowitz, *Electrochem. Commun.*, 1999, **1**, 72.
4 M. Brust, M. Walker, D. Bethell, D. J. Schiffrin and R. Whyman, *J. Chem. Soc., Chem. Commun.*, 1994, 801.
5 J. Fink, C. J. Kiely, D. Bethell and D. J. Schiffrin, *Chem. Mater.*, 1998, **10**, 922.
6 M. J. Hostetler, J. J. Stokes and R. W. Murray, *Langmuir*, 1996, **12**, 3604.
7 M. J. Hostetler, C. J. Zhong, B. K. H. Yen, J. Anderegg, S. M. Gross, N. D. Evans, M. D. Porter and R. W. Murray, *J. Am. Chem. Soc.*, 1998, **120**, 9396.
8 M. J. Hostetler, J. E. Wingate, C. J. Zhong, J. E. Harris, R. W. Vachet, M. R. Clark, J. D. Londono, S. J. Green, J. J. Stokes, G. D. Wignall, G. L. Glish, M. D. Porter, N. D. Evans and R. W. Murray, *Langmuir*, 1998, **14**, 17.
9 R. G. Freeman, K. C. Garbar, K. J. Allison, R. M. Bright, J. A. Davis, A. P. Guthrie, M. B. Hommer, M. A. Jackson, P. C. Smith, D. G. Walter and M. J. Natan, *Science*, 1995, **267**, 17.
10 R. P. Andres, J. D. Bielefeld, J. I. Henderson, D. B. Janes, V. R. Kolagunta, C. P. Kubiak, W. J. Mahoney and R. G. Osifchin, *Science*, 1996, **273**, 1690.
11 R. Elghanian, J. J. Storhoff, R. C. Mucic, R. L. Letsinger and C. A. Mirkin, *Science*, 1997, **277**, 1078.
12 R. L. Whetten, J. T. Khoury, M. M. Alvarez, S. Murthy, I. Vezmar, Z. L. Wang, P. W. Stephens, C. L. Cleveland, W. D. Luedtke and U. Landman, *Adv. Mater.*, 1996, **8**, 428.
13 Z. L. Wang, J. M. Petroski, T. C. Green and M. A. El-Sayed, *J. Phys. Chem. B*, 1998, **102**, 6145.
14 T. S. Ahmadi, Z. L. T. C. Wang, T. C. Green, A. Henglein and M. A. El-Sayed, *Science*, 1996, **272**, 1924.
15 Y.-Y. Yu, S.-S. Chang, C.-L. Lee and C. R. C. Wang, *J. Phys. Chem. B*, 1997, **101**, 6661.
16 M. Giersig and P. Mulvaney, *Langmuir*, 1993, **9**, 3408.
17 M. D. Porter, T. B. Bright, D. L. Allara and C. E. Chidsey, *J. Am. Chem. Soc.*, 1987, **109**, 3559.
18 M. Miki-Yoshida, S. Tehuacanero and M. Jose-Yacaman, *Surf. Sci.*, 1992, **274**, 569.
19 S. Lijima and P. M. Ajayan, *J. Appl. Phys.*, 1991, **70**, 5138.

Communication 9/03165K

The first neutral homoleptic lanthanoid pyrazolates, including the mixed oxidation state species $[Yb_2(Bu^t_2pz)_5]$ (Bu^t_2pz = 3,5-di-*tert*-butylpyrazolate), from a simple new synthesis of pyrazolate complexes

Glen B. Deacon,*[a] Alex Gitlits,[a] Brian W. Skelton[b] and Allan H. White[b]

[a] *Chemistry Department, Monash University, Clayton, Victoria 3168, Australia. E-mail: Glen.Deacon@sci.monash.edu.au*

[b] *Department of Chemistry, University of Western Australia, Nedlands, WA 6907, Australia*

Received (in Columbia, MO, USA) 6th April 1999, Accepted 19th May 1999

Reaction of 3,5-di-*tert*-butylpyrazole (Bu^t_2pzH) with lanthanoid metals and mercury at 220 °C in the absence of an added solvent yields $[Ln(Bu^t_2pz)_3]$ (Ln = Nd, Sm), $[Eu(Bu^t_2pz)_2]$ and $[Yb_2(Bu^t_2pz)_5]$, which is a mixed oxidation state complex with the structural arrangement $[(\eta^2\text{-}Bu^t_2pz)Yb^{II}(\mu\text{-}\eta^2:\eta^2\text{-}Bu^t_2pz)_2Yb^{III}(\eta^2\text{-}Bu^t_2pz)_2]$.

Pyrazolate coordination chemistry[1] has recently been stimulated by expansion of recognised binding modes from the long standing (i) $\mu\text{-}\eta^1:\eta^1$, (ii) η^2 and (iii) η^1 (N-bonded)[1] to (iv) $\mu_3\text{-}\eta^1:\eta^2:\eta^1$, (v) $\mu\text{-}\eta^2:\eta^2$, (vi) $\pi\text{-}\eta^1$ (C-bonded), (vii) η^3 and (viii) η^5.[2–6] In addition, a 14-year restriction of η^2 coordination to f-block elements has been removed by recent examples of η^2-bonding to d-block[7] and main group elements.[8] Although there are now a wide variety of synthetic routes to rare earth pyrazolates,[3,5,9,10] no structurally characterised neutral homoleptic pyrazolatolanthanoid(II or III) complexes, $[Ln(R_mpz)_n]$ (n = 2 or 3; R possible substituents, m = 0–3), have been prepared,[11] presumably because the large size of Ln^{n+} leads to attachment of coligands, often derived from the synthesis solvent, giving $[Ln(R_mpz)_3(L)_x]$ (*e.g.* L = dme, thf, Ph_3PO, x = 1–3)[9] or $[Ln(R_mpz)_2(L)_x]$ (*e.g.* L = dme, x = 2).[3,10] Neutral homoleptic complexes would be of major structural interest, because of the need to attain coordination saturation in the absence of coligands. We now report that both di- and tri-valent neutral homoleptic pyrazolatolanthanoid complexes $[Ln(Bu^t_2pz)_n]$ (Bu^t_2pz = 3,5-di-*tert*-butylpyrazolate, n = 2 or 3), and the novel mixed oxidation state complex $[Yb_2(Bu^t_2pz)_5]$, can be prepared by a new synthesis of pyrazolate complexes. The method has potential general applicability to pyrazolates of electropositive metals.

Reaction of 3,5-di-*tert*-butylpyrazole with an excess of lanthanoid metal and mercury under vacuum at 220 °C without added solvent, followed by extraction with toluene and crystallisation yielded $[Yb_2(Bu^t_2pz)_5]$ **1**, $[Eu(Bu^t_2pz)_2]$ **2**, $[Sm(Bu^t_2pz)_3]$ **3** and $[Nd_2(Bu^t_2pz)_6]$ **4** in satisfactory yield.† The oxidation state diversity suggests the method has considerable versatility.

$$Ln + nBu^t_2pzH \xrightarrow{Hg} [Ln(Bu^t_2pz)_n] + n/2\ H_2\ (n = 2, 2.5 \text{ or } 3)$$

The dried complexes (single crystals of **1** and **4** were toluene solvates) gave satisfactory C, H, N, Ln analyses for the above compositions. For **1**, **3** and **4**, visible/near IR absorptions characteristic[12] of the appropriate Ln^{3+} ions were observed. X-Ray structures of **1**·PhMe‡ and **4**·2PhMe‡[13] revealed a bimetallic mixed oxidation state complex and a dimeric structure $[\{Nd(\eta^2\text{-}Bu^t_2pz)_2(\mu\text{-}\eta^2:\eta^2\text{-}Bu^t_2pz)\}_2]$[13] respectively (below). Neither **2** or **3** have yet been obtained as single crystals, but divalent **2** requires a $\mu\text{-}\eta^2:\eta^2$ pyrazolate bridged dimeric or associated structure to have reasonable coordination number whilst **3** is expected to have a dimeric structure similar to **4**. However, a monomer parent ion for **3**, in contrast to the absence of metal-containing ions for **4**, does leave open the possibility of a monomeric six-coordinate structure. The ^1H NMR spectrum of **1** in d_8-THF is indicative of dissociation into separate $Yb(Bu^t_2pz)_2$ and $Yb(Bu^t_2pz)_3$ complexes owing to solvent coordination.

The molecular structure of **1** (Fig. 1),‡ determined for the toluene solvate, shows a six-coordinate Yb^{2+} ion with one terminal $\eta^2\text{-}Bu^t_2pz$ ligand linked through two $\mu\text{-}\eta^2:\eta^2\text{-}Bu^t_2pz$ groups to an eight-coordinate Yb^{3+} which has two terminal $\eta^2\text{-}Bu^t_2pz$ ligands. It is only the second complex with $\mu\text{-}\eta^2:\eta^2$-pyrazolate coordination. The oxidation states of Yb(1) and Yb(2) (Fig. 1) are clearly evident from the bond distances. Thus, terminal (ter) Yb(1)–N(12) [2.334(7) Å] is comparable with $Yb\text{–}N_{ter}$ [2.404(6) and 2.378(5) Å] of $[\{Yb(\eta^2\text{-}Bu^t_2Pz)(\mu\text{-}\eta^2:\eta^2\text{-}Bu^t_2pz)(thf)\}_2]$[3] when the difference in ionic radii (0.06 Å)[14] between six- and seven-coordinate Yb^{2+} is considered. In addition $Yb(2)\text{–}N_{ter}$ distances [2.287(7) and 2.270(7) Å] are comparable with Er–N of eight-coordinate $[Er(Bu^t_2pz)_3(thf)_2]$ [2.274(7)–2.386(8) Å, av. 2.34 Å][9c] (ionic radius Er^{3+} > Yb^{3+}

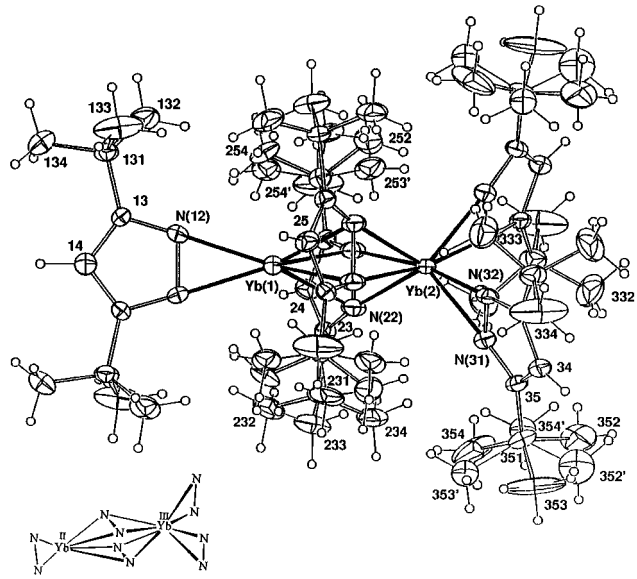

Fig. 1 Molecular projection of **1**; 20% probability ellipsoids are shown for the non-hydrogen atoms, hydrogens having arbitrary radii of 0.1 Å. Key carbon atoms are denoted by number only. [Insert: Yb(1) and Yb(2) coordination spheres]. Selected bond distances (Å) and angles (°): Yb(1)–N(12,21,22) 2.334(7), 2.534(8), 2.587(8); Yb(2)–N(21,22,31,32) 2.402(8), 2.425(8), 2.287(7), 2.270(7), N(12)–N(12*) 1.43(1), N(21)–N(22) 1.37(1), N(31)–N(32) 1.38(1); Yb(1)···C(23,24,25) 3.167(9), 3.468(10), 3.109(10); N(12)–Yb(1)–N(21,22,12*,21*,22*) 131.6(3), 145.0(3), 35.6(3), 138.7(3), 125.7(3); N(21)–Yb(1)–N(22,21*,22*) 31.1(2), 84.0(3), 76.1(3); N(22)–Yb(1)–N(22*) 85.1(3); N(21)–Yb(2)–N(22,31,32,21*,22*,31*,32*) 33.1(3), 138.5(3), 169.3(3), 89.8(3), 81.7(3), 94.0(3), 82.9(3); N(22)–Yb(2)–N(31,32,22*,31*,32*) 106.8(3), 137.2(3), 92.3(3), 120.7(3), 96.0(3), N(31)–Yb(2)–N(32,31*,32*) 35.3(3), 109.4(3), 96.7(3); N(32)–Yb(2)–N(32*) 105.4(3), Yb(1)–N(21,22)–Yb(2) 93.1(3), 91.3(3). The molecule has mirror symmetry, the mirror lying horizontal and almost normal to the page. Symmetry generated atoms are denoted by asterisks.

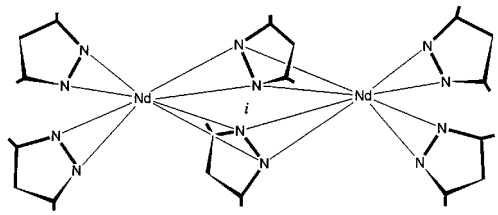

Fig. 2 Simplified representation of the structure of **4**, displaying the Nd/Bu^t_2pz connectivity.[13]

by *ca.* 0.02 Å for the same CN)[14] and with < Yb–N > (2.30$_5$ Å) of eight-coordinate [Yb(η^2-Ph_2pz)$_3$(dme)][13] (Ph_2pz = 3,5-diphenylpyrazolate). Furthermore, it can be calculated from existing lanthanoid pyrazolate structural data (*e.g.* refs. 3, 5, 9, 10) and lanthanoid ionic radii[14] that if Yb(1) were in oxidation state (III) a much shorter Yb–N_{ter} of 2.17 Å would be expected and if Yb(2) were Yb(II), a much longer < Yb–N_{ter} > of 2.44 Å would be expected. Both bridging pyrazolate groups of **1** are tilted towards divalent Yb(1) with the pyrazolate ring planes angled at 59.0(3)° to the Yb(1)···Yb(2) axis, *cf.* 90° for symmetrical bridging. Consequently, C(23) and C(25), but not the more distant (by ≥0.3 Å) C(24), of each μ-η^2:η^2-Bu^t_2pz ligand, may interact marginally with Yb(1). Subtraction of the ionic radius[14] for six-coordinate Yb^{2+} from Yb···C(23) and Yb···C(25) (Fig. 1 legend) gives 2.14 and 2.09 Å, respectively, which are near the upper limit (2.16 Å) of similarly derived values for complexes with inter- and intra-molecular π-arene···Ln coordination![15] Such interactions would enhance the coordination number of Yb(1) from the low value of six.

The connectivity of **4**[13] is shown in Fig. 2. There is no interaction of the Ln metals with toluene of crystallization in either **1** or **4**, since Ln···C(PhMe) and Ln···H(PhMe) separations lie outside the generous limits of 3.6 and 3.3 Å, respectively, for **1** and 3.7 and 3.4 Å for **4**.

1 is a rare example of a molecular compound combining lanthanoids in both II and III oxidation states and the first with pyrazolate ligands. Other examples of molecular lanthanoid(II, III) complexes include [{$Yb^{III}(C_5Me_5)_2$}$_2Yb^{II}$(μ-CCPh)$_4$],[16a] [$Yb^{III}(C_5Me_5)_2$(μ-F)$_2Yb^{II}(C_5Me_5)$]$_2$,[16b] [$Yb^{III}(C_5Me_5)_2$(μ-F)-$Yb^{II}(C_5Me_5)_2$],[16c] [$Yb^{III}Ph_2$(thf)(μ-Ph)$_3Yb^{II}$(thf)$_3$],[16d] [{$(C_5Me_4{}^iPr)_2Sm$}$_2$(μ-Cl)],[16e] and [$Sm^{III}(C_5Me_5)_2$(μ-C_5H_5)$Sm^{II}(C_5Me_5)_2$].[16f]

Structures of **1**·PhMe and **4**·2PhMe, suggest that the lanthanoid elements may prefer the newly recognised[3] μ-η^2:η^2 pyrazolate coordination mode as a means of attaining coordination saturation in [Ln($R_m$pz)$_n$] (n = 2 or 3) complexes. The range of different oxidation state products obtained from reaction (1) to this stage indicates that the method should be generally applicable for the homoleptic lanthanoid pyrazolates, and may also extend to pyrazolates of other electropositive metals, with the alkaline earths, uranium and aluminium being of particular interest. Indeed there is a near precedent for barium, where reaction of 3,5-dimethylpyrazole with Ba metal in *refluxing thf* yields the structurally uncharacterized Ba-(Me_2pz)$_2$.[17]

We are grateful to the Australian Research Council for support and for an Australian Postgraduate Award to A. G.

Notes and references

† All operations were carried out under an atmosphere of purified N_2 or Ar or under vacuum because of the extreme sensitivity of the compounds to air and moisture.

Representative syntheses: **1**: a mixture of Yb powder (2.00 g, 11.6 mmol), Bu^t_2pzH (0.52 g, 2.9 mmol) and mercury metal (two drops) was heated in a sealed tube under vacuum at 220 °C for 5 h. The dark red product was extracted with hot toluene (50 ml) yielding a dark red solution which was concentrated to 3 ml. The solution was then cooled at −20 °C for two days giving dark-red crystals of **1**·PhMe. The crystalline product was then dried at 80 °C under vacuum affording **1** (0.48 g, 67%) (Found: C, 53.00; H, 7.60; N, 11.35; Yb, 27.53. $C_{55}H_{95}N_{10}Yb_2$ requires C, 53.16; H, 7.71; N, 11.28; Yb, 27.85). IR (Nujol): ν/cm^{-1} 1560w, 1504s, 1314m, 1251s, 1227s, 1206s, 1019s, 993s, 794s. ^{1}H NMR (d_8-THF): δ 5.84 [s, 2H, H4 pz (Yb^{II})], 1.27 [s, 36H, Bu^t (Yb^{II})], −15.76 [vbr s, Bu^t (Yb^{III}) (satisfactory integration could not be obtained because of broadening)], −41.94 [s, 3H, H4, pz (Yb^{III})]. EIMS (70 eV) m/z 532 ([$Yb(Bu^t_2pz)_2$]$^+$, 9%), 180 ($Bu^t_2pzH^+$, 21). λ_{max} (PhMe)/nm (ε/dm^3 mol^{-1} cm^{-1}): 402 (351), 484sh (186), 925 (8), 945 (7), 976 (18), 981 (15).

4: a mixture of Nd powder (1.15 g, 8.0 mmol), Bu^t_2pzH (0.72 g, 4.0 mmol) and mercury metal (two drops) was heated in a sealed tube at 220 °C for 24 h. The reaction product was extracted with hot toluene (50 ml) giving a pale blue solution which was reduced in volume. Pale blue crystals of **4**·2PhMe appeared in a few hours. The product was dried at 80 °C under vacuum affording **4** (0.44 g, 48%) (Found: C, 58.07; H, 8.61; N, 12.57; Nd, 21.29. $C_{66}H_{114}N_{12}Nd_2$ requires C, 58.11; H, 8.42; N, 12.32; Nd, 21.15%). IR (Nujol): ν/cm^{-1} 1558w, 1523m, 1505s, 1414s, 1362s, 1303m, 1278w, 1253s, 1224s, 1206m, 1018s, 1006m, 980s, 808m, 796s, ^{1}H NMR (d_8-THF): δ 4.93 (s, 108H, Bu^t), 21.53 (s, 6H, H4 pz). λ_{max} (PhMe)/nm (ε/dm^3 mol^{-1} cm^{-1}): 532 (2), 578 (30), 591 (57), 744 (5). Analogous preparations gave **2** (95%) and **3** (57%).

‡ *Crystallographic data*: **1**·PhMe, [$Yb_2(Bu^t_2pz)_5$]·PhMe≡$C_{62}H_{103}N_{10}Yb_2$, M = 1334.7 orthorhombic, *Pnna* (no. 52), a = 20.92(1), b = 20.371(5), c = 15.990(9) Å, V = 6814 Å^3. D_c (Z = 4) = 1.30$_1$ g cm^{-3}. 12698 absorption corrected four circle diffractometer data (2θ–θ scan mode, $2\theta_{max}$ = 50°; monochromatic Mo-Kα radiation, λ = 0.7107$_3$ Å; T = 295 K) merged to 5998 unique (R_{int} = 0.030), 3248 [$I > 2\sigma(I)$] refining to R = 0.053, R_w (statistical weights) = 0.064, anisotropic thermal parameter forms for Yb, N, C, (x, y, z, U_{iso})$_H$ constrained at estimates. Two Bu^t groups are modelled as rotationally disordered, site occupancies 0.56(1), 0.72(1) and complements, the toluene also being disordered and modelled with constrained geometry. **4**·2PhMe.[13] Unit cell data (153 K), triclinic, $P\bar{1}$, a = 12.4301(9), b = 13.807(1)°, c = 14.015(1) Å, α = 119.480(1), β = 96.436(1), γ = 95.262(1)°, V = 2050 Å^3. CCDC 182/1268.

1 S. Trofimenko, *Chem. Rev.*, 1972, **72**, 497; S. Trofimenko, *Prog. Inorg. Chem.*, 1986, **34**, 115; G. La Monica and G. A. Ardizzoia, *Prog. Inorg. Chem.*, 1997, **46**, 151; A. P. Sadimenko and S. S. Basson, *Coord. Chem. Rev.*, 1996, **147**, 247; J. E. Cosgriff and G. B. Deacon, *Angew. Chem., Int. Ed.*, 1998, **37**, 286.

2 C. Yélamos, M. J. Heeg and C. H. Winter, *Inorg. Chem.*, 1998, **37**, 3892.

3 G. B. Deacon, E. E. Delbridge, B. W. Skelton and A. H. White, *Angew. Chem., Int. Ed.*, 1998, **37**, 2251.

4 L. R. Falvello, J. Forniés, A. Martin, R. Navarro, V. Sicilia and P. Villarroya, *Chem. Commun.*, 1998, 2429.

5 G. B. Deacon, E. E. Delbridge and C. M. Forsyth, *Angew. Chem., Int. Ed.*, 1999, **38**, 1766.

6 J. R. Perera, M. J. Heeg, H. B. Schlegel and C. H. Winter, *J. Am. Chem. Soc.*, 1999, **121**, 4536.

7 D. Röttger, G. Erker, M. Grehl and R. Fröhlich, *Organometallics*, 1994, **13**, 3897; I. A. Guzei, G. P. A. Yap, A. L. Rheingold, H. B. Schlegel and C. H. Winter, *J. Am. Chem. Soc.*, 1997, **119**, 3387; I. A. Guzei and C. H. Winter, *Inorg. Chem.*, 1997, **36**, 4415; I. A. Guzei, G. P. A. Yap and C. H. Winter, *Inorg. Chem.*, 1997, **36**, 1738.

8 D. Pfieffer, M. J. Heeg and C. H. Winter, *Angew. Chem., Int. Ed.*, 1998, **37**, 2517.

9 Ln(III): *e.g.* (*a*) T. D. Culp, J. G. Cederberg, B. Bieg, T. F. Kuech, K. L. Bray, D. Pfeiffer and C. H. Winter, *J. Appl. Phys.*, 1998, **83**, 4918; (*b*) J. E. Cosgriff, G. B. Deacon, G. D. Fallon, B. M. Gatehouse, H. Schumann and R. Weimann, *Chem. Ber.*, 1996, **129**, 953 and references therein; (*c*) J. E. Cosgriff, G. B. Deacon, B. M. Gatehouse, H. Hemling and H. Schumann, *Aust. J. Chem.*, 1994, **47**, 1223.

10 Ln(II): G. B. Deacon, E. E. Delbridge, B. W. Skelton and A. H. White, *Eur. J. Inorg. Chem.*, 1998, 543; 1999, 751.

11 For the sole complex with such a composition, *viz* Yb(pz)$_3$, see G. Bielang: Doctoral Dissertation, Univ. Hamburg, 1979.

12 W. T. Carnall, in *The Absorption and Fluorescence Spectra of Rare Earth Ions in Solution, in Handbook on the Physics and Chemistry of Rare Earths*, ed. K. A. Gschneider and L. Eyring, North-Holland, Amsterdam, 1979, vol. 3, ch. 24.

13 G. B. Deacon, E. E. Delbridge, A. Gitlits, B. W. Skelton and A. H. White, to be published.

14 R. D. Shannon, *Acta Crystallogr., Sect. A.*, 1976, **32**, 751.

15 G. B. Deacon and Q. Shen, *J. Organomet. Chem.*, 1996, **511**, 1.

16 (*a*) J. M. Boncella, T. D. Tilley and R. A. Andersen, *J. Chem. Soc., Chem. Commun.*, 1984, 710; (*b*) C. J. Burns, D. J. Berg and R. A. Andersen, *J. Chem. Soc., Chem. Commun.*, 1987, 272; (*c*) C. J. Burns and R. A. Andersen, *J. Chem. Soc., Chem. Commun.*, 1989, 136; (*d*) M. N. Bochkarev, V. V. Khramenkov, Y. F. Rad'kov and L. N. Zakharov, *J. Organomet. Chem.*, 1992, **429**, 27; (*e*) W. J. Evans, K. J. Forrestal and J. W. Ziller, *Polyhedron*, 1998, **17**, 4015; (*f*) W. J. Evans and T. A. Ulibarri, *J. Am. Chem. Soc.*, 1987, **109**, 4292.

17 A. Steiner and D. Stalke, *Inorg. Chem.*, 1995, **34**, 4846.

Communication 9/02675D

ChemComm

Chiral recognition and the determination of optical purity of some amino acid ester salts using monosaccharides as chiral selectors under liquid secondary ion mass spectral conditions†

P. Krishna,[a] S. Prabhakar,[a] M. Manoharan,[b] E. D. Jemmis[b] and M. Vairamani*[a]

[a] *Mass Spectrometry Centre, Indian Institute of Chemical Technology, Hyderabad-500 007, India. E-mail: vairamani@iict.ap.nic.in*

[b] *School of Chemistry, University of Hyderabad, Hyderabad-500 046, India*

Received (in Cambridge, UK) 24th March 1999, Accepted 19th May 1999

Naturally occuring monosaccharides D-mannose, D-galactose and D-glucose have been used for the first time as co-matrices for chiral recognition and for the determination of optical purity of the enantiomers of α-amino acid methyl ester hydrochlorides.

Mass spectrometry does not ordinarily distinguish optically active isomers. Recently, Sawada *et al.* reported the Fast Atom Bombardment (FAB) mass spectrometric estimation of the enantiomeric excess of amines and amino acid methyl esters *via* host–guest complexation using deuterated chiral crown ethers as chiral hosts.[1,2] This is an excellent method to estimate enantiomeric excess using a few micrograms of the amine, and is useful in combinatorial approaches towards the synthesis of chiral compounds. Polar chiral matrices have not so far been used as part of the mass spectral techniques for the study of chiral recognition.[3] It would be ideal if naturally occurring and readily available substrates could be used as chiral hosts for such a process. We have tested some hexoses as chiral co-matrices for gas phase chiral discrimination by Liquid Secondary Ion Mass Spectrometry (LSIMS) and found them suitable for such analyses.

Herein, we report the first observations concerning the enantioselectivity of naturally-occurring underivatized sugars D-mannose **1**, D-galactose **2** and D-glucose **3** as polar hosts towards alanine **4**, leucine **5** and phenylglycine **6** methyl esters (*R* and *S* isomers of **4**, **5** and **6**). We have also shown that this method could be used for the determination of the optical purity of **4** using the corresponding enantiomeric methyl-d_3 ester as an internal reference, employing the LSIMS technique following the enantiomer-labelled guest method of Sawada *et al.*[4–10] In the present study, we report a high degree of enantioselectivity of D-sugars towards amino acid methyl ester hydrochlorides, presumably through the host–guest complexation.

A typical LSIMS sample solution was prepared by mixing the following solutions: (i) 20 μl of a 0.5 M aqueous solution of D-mannose, (ii) 10 μl of a 0.5 M methanolic solution of D-methyl-d_3 alaninate hydrochloride, and (iii) 10 μl of a 0.5 M methanolic solution of L-methyl alaninate hydrochloride in 50 mg of glycerol (for the ee experiments, solutions of different ee were prepared by mixing appropriate quantities of 0.5 M methanolic solutions of both D- and L-methyl alaninate hydrochlorides). The above individual solution (2 μl) was loaded on to the stainless steel target of the LSIMS probe and the mass spectra were recorded.[11]

The amino acid methyl ester hydrochlorides **4**–**6** form fairly abundant adduct ions with the three monosaccharides, namely D-mannose, D-galactose and D-glucose, in the presence of glycerol as the matrix. In order to quantify the chiral discrimination parameter of the sugar we followed the enantiomer-labelled guest method recommended by Sawada *et al.*,[6] and used labelled D-amino acid methyl ester hydrochloride as the internal standard. The LSI mass spectrum of an equimolar mixture of L-methyl alaninate hydrochloride (L-**4**) and the reference D-methyl-d_3 alaninate hydrochloride (d_3-D-**4**) taken using D-mannose as a chiral co-matrix in presence of glycerol shows that the sugar forms a favourable adduct with the L-isomer [Fig. 1(*a*)]. The near absence of an isotope effect in the formation of the host–guest adduct is seen in the LSI mass spectrum of an equimolar mixture of D-methyl alaninate hydrochloride and the D-methyl-d_3 alaninate hydrochloride under identical experimental conditions [Fig. 1(*b*)]. The relative abundances of labelled D-enantiomer (*m/z* 287) and unlabelled D-enantiomer (*m/z* 284) adducts are almost identical. The existence of a chirality effect in the gas phase under LSIMS conditions is further supported by cross-chiral examination of an equimolar mixture of D-methyl alaninate hydrochloride and L-methyl-d_3 alaninate hydrochloride [Fig. 1(*c*)] wherein the

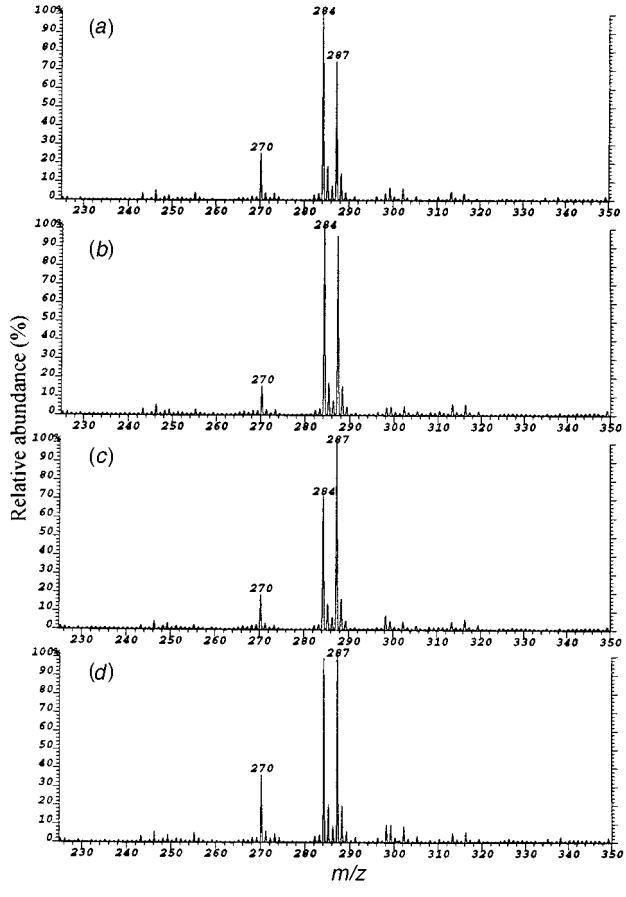

Fig. 1 LSI mass spectrum of 1:1 mixtures of methyl alaninate hydrochlorides in the presence of D-mannose as co-matrix in glycerol: (*a*) D-methyl-d_3 and L-methyl, (*b*) D-methyl-d_3 and D-methyl, (*c*) L-methyl-d_3 and D-methyl, and (*d*) L-methyl-d_3 and L-methyl.

† IICT communication number 4256.

Table 1 IRIS values for α-amino acid methyl ester hydrochlorides

Substrate	IRIS value[a]		
	D-mannose	D-galactose	D-glucose
(*S*)-Ala-OMe	0.71 ± 0.03	0.71 ± 0.02	0.70 ± 0.02
(*R*)-Ala-OMe[b]	1.40 ± 0.01	—	—
(*S*)-Leu-OMe	0.75 ± 0.01	0.75 ± 0.01	0.76 ± 0.01
(*S*)-Ph-Gly-OMe	0.68 ± 0.01	0.67 ± 0.01	0.66 ± 0.01

[a] The IRIS value shown is an average of two sets of IRIS values; each is an average of 10 consecutive experiments. [b] (*S*)-Methyl-d_3 alaninate hydrochloride was used as an internal reference.

labelled L-enantiomer (L-**4**) is used as the reference. The preference of D-mannose towards the L-enantiomer is now seen as an increased abundance of the adducts corresponding to the labelled enantiomer (*m/z* 287), to the same extent as observed in Fig. 1(*a*). Again an equimolar mixture of labelled and unlabelled L-methyl alaninate hydrochloride gives adducts of almost equal abundance [Fig. 1(*d*)] showing the absence of an isotope effect.

LSI mass spectral analysis of L-methyl leucinate hydrochloride **5** and L-methyl phenylglycinate hydrochloride **6** using the corresponding d_3-labelled D-enantiomer as reference also gave similar results in the presence of all three sugars. It should be pointed out that all three monosaccharides studied have shown a preference for the L-amino acid ester hydrochloride prepared from the L-amino acids that are naturally occurring. The relative peak intensity of the diastereomeric host–guest complex ion I_R and I_S, for the *R*-enantiomer (D-amino acid) and *S*-enantiomer (L-amino acid), respectively, can be taken as a measure of the selectivity of the host sugar towards the amino acid methyl ester hydrochloride guest [eqn. (1)] as proposed by Sawada *et al.*[6]

$$I_R/I_S = \text{IRIS (abbreviation)} \quad (1)$$

The IRIS values for the amino acid esters using sugars as comatrices are given in Table 1. The utility of this approach in determining the enantiomeric excess of amino acid methyl ester hydrochlorides was tested using methyl alaninate hydrochloride as an example. Thus mixtures containing different enantiomeric excesses (ees) of methyl alaninate hydrochloride were prepared and the LSI mass spectra taken using the D-methyl-d_3 alaninate hydrochloride as the internal standard. The plot of I_{R-d_3}/I_S as a function of ee is found to give a linear plot with a correlation coefficient of 0.99 (Fig. 2), validating the idea that mass spectral techniques can be used for the determination of the optical purity of chiral compounds.

Semiempirical AM1 calculations are also supportive of the observed higher stability of protonated sugar–amino acid ester complexes of the L-amino acids studied as compared to the corresponding D-isomers. This study was performed making hydrogen bonds *via* the chiral ammonium ion hydrogens with the ring oxygen, the anomeric oxygen of the sugar, and the C_6 oxygen of the sugar. A detailed investigation of the theoretical results is in progress.

Thus the present study has shown that monosaccharides show chiral discrimination towards amino acid ester salts and that this can be observed under LSIMS conditions. In the case of the amino acid esters studied, the L-isomers form more abundant adducts with sugars than the D-isomers. By using the methyl-d_3 ester of one enantiomer as an internal standard, it is possible to determine the enantiomeric excess of the respective compound

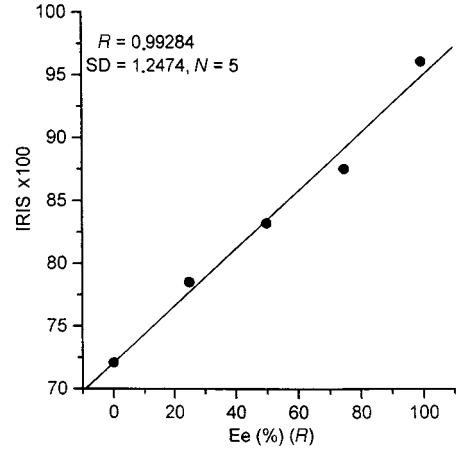

Fig. 2 A plot of IRIS values *vs.* ee for methyl alaninate hydrochlorides. Each point represents the average IRIS value optained for 10 consecutive experiments; standard deviation: < 1.0%.

by LSI mass spectrometry in the presence of a monosaccharide and glycerol. Further extension of this work to the study of other chiral compounds is in progress.

We thank the Director, IICT, for facilities and constant encouragement. A Fellowship from UGC, New Delhi, (to P. K.) is gratefully acknowledged. This work was supported in part by DST, New Delhi, India.

Notes and references

1 M. Sawada, H. Yamaoka, Y. Takai, Y. Kawai, H. Yamada, T. Azuma, T. Fujioka and T. Tanaka, *Chem. Commun.*, 1998, 1569.
2 Y.-N. Wu, Y.-P. Tu, Y.-J. Pan, Y.-Z. Chen, M. Cui, F.-R. Song and S.-Y. Liu, *Anal. Lett.*, 1997, **30**, 1399.
3 M. Sawada, *Chiral mass spectrometry*, in *Biological Mass Spectrometry: Present and Future*, ed. T. Matsu, R. M. Caprioli, M. L. Gross and Y. Sayama, Wiley, New York, 1994, p. 639.
4 M. Sawada, Y. Takai, H. Yamada, J. Nishida, T. Kaneda, R. Arakawa, M. Okamoto, K. Hirose, T. Tanaka and K. Naemura, *J. Chem. Soc., Perkins Trans. 2*, 1998, 701.
5 M. Sawada, *Mass Spectrom. Rev.*, 1997, **16**, 73.
6 M. Sawada, Y. Takai, H. Yamada, S. Hirayama, T. Kaneda, T. Tanaka, K. Kamada, T. Mizooku, S. Takeuchi, K. Ueno, K. Hirose, Y. Tobe and K. Naemura, *J. Am. Chem. Soc.*, 1995, **117**, 7726.
7 M. Sawada, Y. Takai, H. Yamada, T. Kaneda, K. Kamada, T. Mizooku, K. Hirose, Y. Tobe and K. Naemura, *J. Chem. Soc., Chem. Commun.*, 1994, 2497.
8 M. Sawada, Y. Okumura, M. Shizuma, Y. Takai, Y. Hidaka, H. Yamada, T. Tanaka, T. Kaneda, K. Hirose, S. Misumi and S. Takahashi, *J. Am. Chem. Soc.*, 1993, **115**, 7381.
9 M. Sawada, Y. Okumura, H. Yamada, Y. Takai, S. Takahashi, T. Kaneda, K. Hirose and S. Misumi, *Org. Mass Spectrom.*, 1993, **28**, 1525.
10 M. Sawada, M. Shizuma, Y. Takai, H. Yamada, T. Kaneda and T. Hanafusa, *J. Am. Chem. Soc.*, 1992, **114**, 4405.
11 All the LSI mass spectra were recorded on an AutoSpec (Micromass, Manchester, UK) mass spectrometer using an OPUS V3.IX data system. The samples were ionized using a primary ion beam of caesium ions of 25 kV at the source temperature of 46 °C. The desorbed ions were accelerated to 8 kV. The spectra were obtained with a magnet scan rate of 3 s per decade over a mass range of *m/z* 1–400 under continuum mode. The IRIS values presented here are an average of 10 successive experiments and an averaged spectrum from each experiment is obtained *via* the accumulation of 15 consecutive scans.

Communication 9/02366F

ChemComm

Synthesis and domino reactions of 1,1-bis(hydroxymethyl)allenes

Peter Langer*

Institut für Organische Chemie der Georg-August-Universität Göttingen, Tammannstraße 2, 37077 Göttingen, Germany. E-mail: planger@uni-goettingen.de

Received (in Cambridge, UK) 15th February 1999, Accepted 12th April 1999

The reaction of dilithiated 1,1-diphenylallene with aryl ketones provides a convenient access to novel 1,1-bis(hydroxymethyl)allenes, which undergo Friedel–Crafts-type domino reactions upon treatment with TsOH.

Domino reactions of alkynes have been used for the efficient synthesis of carbocycles and polycyclic aromatic hydrocarbons (PAHs).[1] Hydroxymethylalkynes have been converted into the more labile allenes and cumulenes which have then been used *in situ* for the preparation of [4]radialenes, macrocycles and 1,2-dihydrocyclobutaarenes.[2] However, only a few domino reactions using allenes as starting materials have been reported so far.[3] Herein, we report a convenient synthesis of 1,1-bis(hydroxymethyl)allenes.[4] These new difunctionalized substrates are used as starting materials in a unimolecular cationic domino reaction. In this context the first, to the best of our knowledge, Nazarov–Friedel–Crafts tandem reaction of an allene is reported which we believe represents a new type of domino process.

1,1-Diphenyl-3,3-dilithioallene **2** was generated in one pot by treatment of the TBDMS enol ether **1** with an excess of LDA in THF, a reaction recently developed by us.[5] The reaction of **2** with 2 equiv. of aryl ketones **3a**–**e** regioselectively provided the colourless bis(hydroxymethyl)allenes **4a**–**e** (Scheme 1, Table 1).† Due to the steric hindrance of the allenic phenyl groups, the sterically crowded allenes **4a**–**e** were regioselectively formed and isolated in high yields.

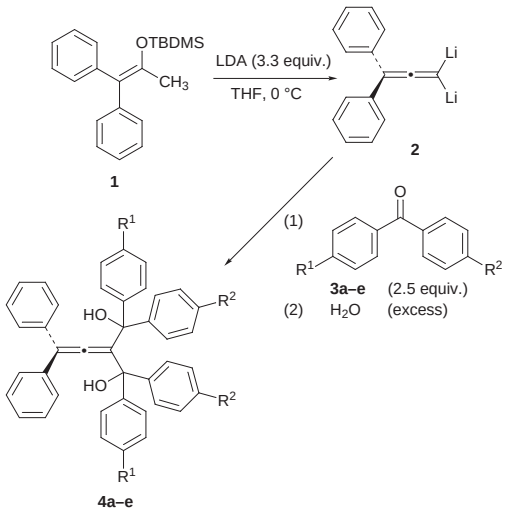

Scheme 1

Table 1 Synthesis of **4** and **5**

			Isolated yield (%)	
4/**5**	R^1	R^2	**4**	**5**
a	H	H	80	85
b	MeO	H	62	73
c	MeO	MeO	75	76
d	Me	Me	76	83
e	Cl	Cl	71	86

Treatment of allenes **4a**–**e** with TsOH in toluene resulted in elimination of 2 equiv. of water and selective formation of the orange coloured 5,10,10,11-tetraaryl-10*H*-benzo[*b*]fluorenes **5a**–**e** in very good yields (Scheme 2, Table 1).‡ In the case of allene **4b** containing two asymmetric carbon atoms, the cyclization proceeded regioselectively *via* the *p*-methoxyphenyl rather than the phenyl group to give **5b** in good yield. Pentafulvenes related to **5** have been used as intermediates in the synthesis of fullerene fragments.[6] Due to their curved structure, 10*H*-benzo[*b*]fluorenes **5a**–**e** are chiral as demonstrated by separation of the two atropic enantiomers of **5a** by HPLC using a chiral stationary phase.§

The formation of 10*H*-benzo[*b*]fluorenes **5** can be explained by a Nazarov–Friedel–Crafts domino reaction. Carbocation **I** is initially generated by dehydration (Scheme 2). The central allene carbon atom is attacked by the *ortho* carbon atom of one

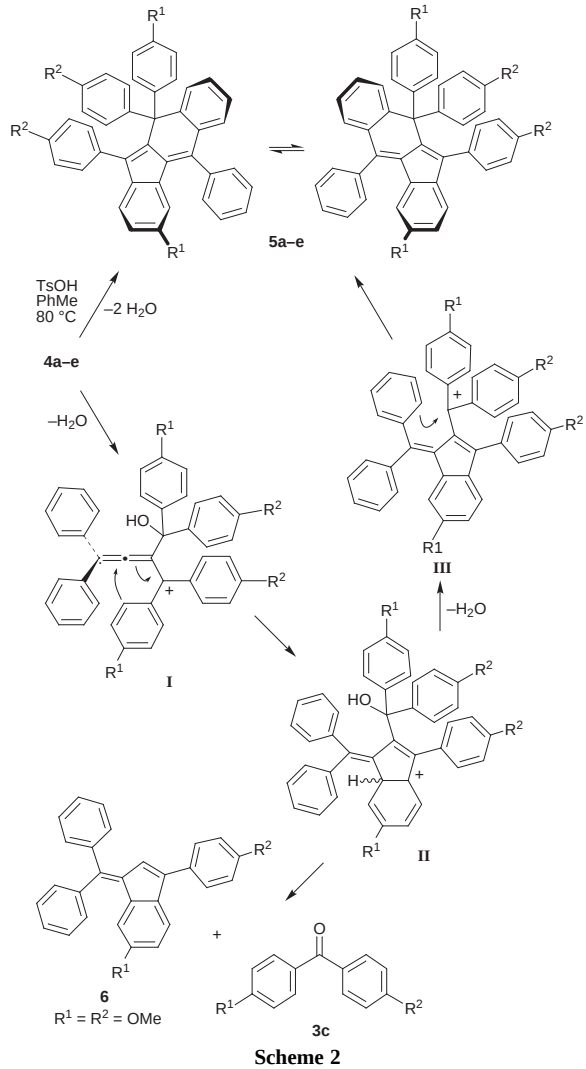

Scheme 2

of the aryl groups with formation of a five-membered ring to give intermediate **II**. Aromatization and dehydration subsequently lead to formation of the cationic intermediate **III**. The *ortho* carbon of the allene-derived phenyl group is attacked by the carbocation neighboring the ketone derived aryl groups. Aromatization finally leads to the products **5a**–**e**. The mechanism suggested is supported by the following observation: starting with the *p*-methoxyphenyl-substituted allene **4c**, the benzofulvene **6** is obtained as a minor product in 10% yield. Formation of **6** can be explained by formation of the benzofulvene moiety and subsequent elimination of bis(*p*-methoxyphenyl) ketone or, alternatively, by initial elimination of the ketone, formation of a cumulene (*vide infra*) and subsequent isomerization of the latter.

It is noteworthy that in the domino reaction leading to **5a**–**e** the allenic phenyl group became *sterically* accessible for the cationic π-cyclization only after the previous cyclization involving the rigid allene moiety had occurred. The reaction cascade thus represents a combination of cyclizations as observed for mono(hydroxymethyl)allenes[7a] and for aryl-substituted bis(hydroxymethyl)alkenes $Ar_2C{=}C[C(OH)Ar_2]_2$. The latter have been used as precursors for the generation of (hexaaryltrimethylene)methane dications.[7b]

The reaction of dilithioallene **2** with 2 equiv. of fluorenone and xanthone gave the colourless allenes **4f** and **4g** in 72 and 68% yields, respectively. As minor products, the yellow coloured cumulenes **7a** and **7b** were isolated in 10 and 14%

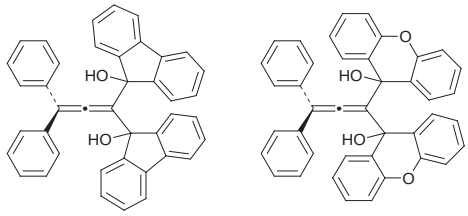

4f

4g

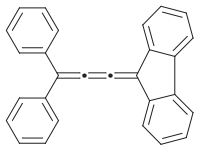
7a

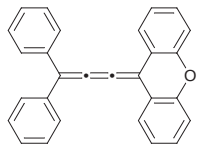

7b

yields. Treatment of the allenes **4f** and **4g** with TsOH resulted in elimination of fluorenone or xanthone and formation of the cumulenes **7a** and **7b** in 85 and 70% yields, respectively, rather than in cyclization. Previously, formation of cumulenes has only been observed for α-unsubstituted (hydroxymethyl)-allenes.[8] In the case of **4f**, the striking difference between the course of the dehydration reactions of the allenes **4a**–**e** and **4f**–**g** can be explained by the fact that cyclization would lead to a strained unsaturated 5,5,6-ring system.[9] In addition, the anti-aromatic character of the fluoren-9-yl cation in the ground state and the rigid character of the ketone-derived subunits of **4f** and **4g** presumably direct the course of the reaction.[10]

P. L. thanks Professor A. de Meijere and Professor D. Seyferth for their support and Professor A. Mannschreck for his help with the separation of the enantiomers of **5a**. Financial support from the Fonds der Chemischen Industrie (Liebig-scholarship and funds for P. L.) is gratefully acknowledged.

Notes and references

† *Preparation* of **4a**. A THF solution (10 ml) of **1** (950 mg, 2.95 mmol) was added to a THF solution of LDA which was prepared by addition of BuLi (1.6 M solution in hexane) to a THF solution (30 ml) of Pr^i_2NH (3.3 equiv.) at 0 °C. The solution was stirred at 20 °C for 6 h during which time the colour of the solution became deep red. A THF solution (10 ml) of benzophenone (1.34 g, 7.38 mmol) was added at −78 °C by syringe. The temperature was allowed to rise to 20 °C within 12 h to give a deep blue solution. The mixture was poured into water (50 ml) and was extracted with Et_2O. The combined yellow coloured organic layers were dried ($MgSO_4$), filtered and the solvent removed *in vacuo*. Purification by column chromatography (Et_2O–light petroleum 1 : 5 → 1 : 1) afforded the allene **4a** (1.31 g, 80%) as a colourless solid, mp 110 °C (decomp.); δ_H($CDCl_3$, 200 MHz): 3.82 (s, 2 H, OH), 6.32 (m, 4 H, Ph), 7.10–7.40 (m, 26 H, Ph); δ_C($CDCl_3$, 50 MHz): 82.90 (C, *C*OH), 114.85, 116.11 (C, *C*=C=*C*), 126.79, 127.91, 128.04 (CH, Ph), 127.18, 127.29, 127.83 (CH, Ph), 136.56, 146.56 (C, Ph), 205.26 (C, C=*C*=C); ν_{max}(KBr)/cm^{-1} 3385 (w), 3057 (w), 1949 (m, C=C=C), 1598 (w), 1493 (m), 1447 (m), 1348 (w), 1177 (w), 1031 (m), 698 (s). *m/z* (CI, H_2O): 539 (M^{+}+1 − H_2O), 521 (M^{+}+1 − $2H_2O$), 357 (100%, $Ph_2C{=}C{=}CPh_2$ + 1). (Calc. for $C_{41}H_{32}O_2$: C, 88.46; H, 5.79. Found: C, 88.23; H, 5.75%.) All new compounds gave correct spectroscopical data and elemental analyses and/or high resolution mass data.

‡ *Preparation* of **5a**: Allene **4a** (200 mg, 0.36 mmol) and TsOH (60 mg) were heated in toluene (30 ml) at 80 °C for 2 h. The colour of the solution changed from light yellow to deep orange. The crude mixture was purified by column chromatography (Et_2O–light petroleum = 1 : 5 → 1 : 1) to give **5a** (159 mg, 85%) as orange coloured crystals, mp 176 °C (decomp.); δ_H($CDCl_3$, 200 MHz) 6.20 (d, *J* 7, 1 H, Ar), 6.56 (m, 2 H, Ar), 6.71 (d, *J* 7, 1 H, Ar), 6.11 (dd, *J* 7, *J* 1.5, 1 H, Ar), 6.41 (m, 2 H, Ar), 6.58 (m, 3 H, Ar), 6.85–7.25 (m, 18 H, Ar); δ_C($CDCl_3$, 50 MHz): 57.42 (C, *C*Ph_2), 119.89, 123.25, 124.70, 126.05, 126.23, 127.33, 127.34, 127.81, 127.99, 128.08, 128.20, 128.77, 128.99, 129.28, 130.14, 130.15, 130.37 (CH, Ar), 133.57, 133.81, 134.32, 135.51, 137.78, 139.80, 140.13, 142.24, 145.54, 145.82, 147.23 (C, Ar); ν_{max}(KBr)/cm^{-1} 3056 (m), 3024 (m), 2924 (m), 1600 (m), 1492 (m), 1448 (m), 1368 (w), 1076 (w), 1032 (w), 760 (s), 744 (s), 724 (s), 700 (s); *m/z* (FAB) 521 (100%, M^{+} + 1). (Calc. for $C_{41}H_{28}$: C, 94.58; H, 5.42. Found: C, 94.27; H, 5.50%.)

§ Conditions (a) stationary phase: tris(phenylcarbamoyl)cellulose/SiO_2; eluent: EtOH; UV detection: λ = 320 nm; polarimetric detection: λ = 436 nm; *c* = 1 mg ml^{-1} (injection of 50 μl); *P* = 63 bar; *T* = 25 °C; flow: 0.5 ml min^{-1}; t_1 = 9 min; k_1' = 0.44. The results were independently confirmed by the use of different conditions: (b) stationary phase: triacetylcellulose/SiO_2; eluent: MeOH; UV detection: λ = 278 nm; polarimetric detection: λ = 405 nm; *c* = 1 mg ml^{-1} (injection of 150 μl); *P* = 68 bar; *T* = 25 °C; flow: 1.0 ml min^{-1}; t_1 = 12.6 min; k_1' = 0.60.

1 For reviews of domino reactions, see: L. F. Tietze and U. Beifuss, *Angew. Chem., Int. Ed. Engl.*, 1993, **32**, 131; A. de Meijere and F. E. Meyer, *Angew. Chem., Int. Ed. Engl.*, 1994, **33**, 2379.
2 H. Hopf and G. Maas, *Angew. Chem., Int. Ed. Engl.*, 1992, **31**, 931; F. Toda, K. Tanaka, I. Sano and T. Isozaki, *Angew. Chem., Int. Ed. Engl.*, 1994, **33**, 1757; H. Hopf, P. G. Jones, P. Bubenitschek and C. Werner, *Angew. Chem., Int. Ed. Engl.*, 1995, **34**, 2367.
3 S. Blechert, R. Knier, H. Schroers and T. Wirth, *Synthesis* 1995, 592; R. Grigg, V. Loganathan, V. Sridharan, P. Stevenson, S. Sukirthalingam and T. Worakun, *Tetrahedron*, 1996, **52**, 11 479; M. Schmittel, M. Strittmatter and S. Kiau, *Angew. Chem., Int. Ed. Engl.*, 1996, **35**, 1843; T. Doi, A. Yanagisawa, S. Nakanishi, K. Yamamoto and T. Takahashi, *J. Org. Chem.*, 1996, **61**, 2602; H. Nemoto, M. Yoshida and K. Fukumoto, *J. Org. Chem.*, 1997, **62**, 6450.
4 A 1,1-bis(hydroxymethyl)allene has been previously prepared by a different route in 17% yield: H. Mori, K. Ikoma and S. Katsumura, *Chem. Commun.*, 1997, 2243.
5 P. Langer, M. Döring and D. Seyferth, *Chem. Commun.*, 1998, 1927.
6 S. Hagen, M. S. Bratcher, M. S. Erickson, G. Zimmermann and L. T. Scott, *Angew. Chem., Int. Ed. Engl.*, 1997, **36**, 406.
7 (*a*) F. Toda, N. Ooi and K. Akagi, *Bull. Chem. Soc. Jpn.*, 1971, **44**, 1050; (*b*) N. J. Head, G. A. Olah and G. K. S. Prakash, *J. Am. Chem. Soc.*, 1995, **117**, 11 205.
8 F. W. Nader and C.-D. Wacker, *Angew. Chem., Int. Ed. Engl.*, 1985, **24**, 851.
9 For comparison, see: G. Dyker, F. Nerenz, P. Siemsen, P. Bubenitschek and P. G. Jones, *Chem. Ber.*, 1996, **129**, 1265.
10 M. Hoang, T. Gadosy, H. Ghazi, D.-F. Hou, A. C. Hopkinson, L. J. Johnston and E. Lee-Ruff, *J. Org. Chem.*, 1998, **63**, 7168.

Communication 9/01208G

Sequence dependent energy transfer from DNA to an anthryl probe: discrimination between GC and IC sequences

Challa V. Kumar* and Emma H. Asuncion

Department of Chemistry, 55 N. Eagleville Road, U-60, University of Connecticut, Storrs, CT 06269-3060, USA. E-mail: cvkumar@nucleus.chem.uconn.edu

Received (in Columbia, MO, USA) 19th January 1999, Accepted 5th May 1999

Singlet–singlet energy transfer from ionosine-cytosine sequences of DNA to an anthryl probe has been observed, but no energy transfer occurs from guanine-cytosine sequences.

Understanding the interaction of small molecules with the DNA double helix and establishing how these interactions vary with the DNA sequence is crucial for deciphering how small molecules may influence DNA structure and function.[1] Metal ions, heterocyclic cations, and natural antibiotics bind to DNA and the DNA binding studies with these ligands have been useful in cancer research.[2] Sequence dependent energy transfer from the DNA bases to *N*-ethyl-9-anthrylmethylamine hydrochloride (*N*-Et-AMAC, Fig. 1) is reported here. Upon excitation of the DNA bases, energy transfer to the anthryl chromophore (Fig. 2) has been observed from ionosine-cytosine sequences but not from guanine-cytosine sequences.

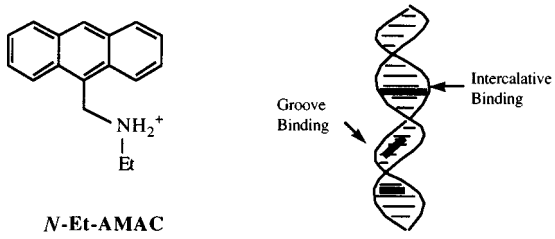

Fig. 1 Structure of the anthryl probe used for energy transfer studies with DNA, and graphical presentation of the intercalative and groove binding of organic ligands to the DNA helix.

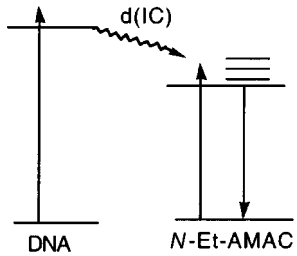

Fig. 2 Energy transfer scheme illustrating the sensitized emission from the anthryl chromophore bound to the DNA double helix.

Addition of calf thymus DNA (CT DNA) to a solution of *N*-Et-AMAC results in dramatic decreases in probe absorbance (Fig. 3). The concentration of the probe was kept constant (5 μM) while varying the DNA concentration from 0 to 400 μM. The large hypochromism (62%) accompanying the binding implies strong electronic interactions between the probe and the DNA bases.[3] No such hypochromism was observed when anthryl probes were allowed to bind to polyelectrolytes, sodium dodecylsulfate micelles, or proteins.[4] The above absorption data were used to construct Scatchard plots and a binding constant of 1.2×10^4 mol^{-1} has been estimated for *N*-Et-AMAC with CT DNA. Marginally higher binding constants have been observed with poly(dI-dC) and poly(dG-dC) (2.4×10^4 and 2.7×10^4 mol^{-1}, respectively) when compared to that with CT DNA. Additional evidence for the binding of *N*-Et-AMAC to the DNA helix was obtained from circular dichroism and from viscometric studies. Strong induced circular dichroism spectra were observed in the anthryl chromophore absorption region, when DNA was added to *N*-Et-AMAC.

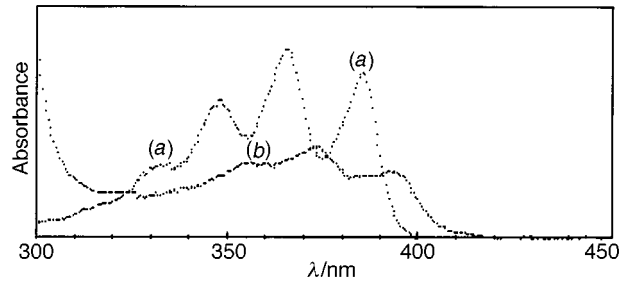

Fig. 3 Absorption spectra of *N*-Et-AMAC (9.7 μM) (*a*) in the absence and (*b*) in the presence of calf thymus DNA (400 μM). Absorbance full scale is 0.1.

The high affinity binding of *N*-Et-AMAC to the DNA helix was exploited in energy transfer studies. Singlet–singlet energy transfer from the DNA bases to 9-anthrylmethylamine hydrochloride was reported from this laboratory, previously.[3] The energy transfer from AT sequences was facile while no energy transfer was observed with GC sequences. In the case of *N*-Et-AMAC, however, energy transfer was observed from ionosine-cytosine (IC) sequences but not from guanine-cytosine (GC) sequences, providing a simple fluorescence method for discrimination between different DNA bases.

Evidence for sequence dependent singlet–singlet energy transfer was obtained from the fluorescence excitation spectra. Emission from *N*-Et-AMAC is monitored at 425 nm while varying the excitation wavelength from 260 to 410 nm (Fig. 4). Excitation in the DNA absorption region (260–300 nm) resulted in strong emission from the anthryl chromophore. Different DNA sequences were used to evaluate the dependence of

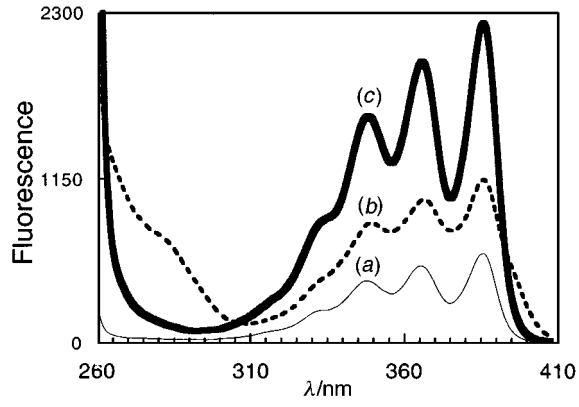

Fig. 4 Fluorescence excitation spectra of *N*-Et-AMAC (2.5 μM) in the presence of (*a*) poly(dI-dC) (99 μM) and (*b*) poly(dG-dC) (97 μM), and (*c*) in the absence of DNA.

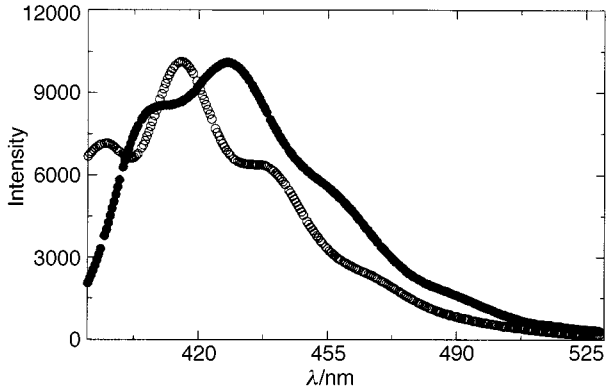

Fig. 5 Fluorescence spectra of *N*-Et-AMAC (5 μM) bound to CT DNA (54 μM) while exciting at (○) 350 and (●) 270 nm. The spectra are normalized to the same height, and no such red shifted emission was observed from *N*-Et-AMAC bound to poly(dG-dC).

energy transfer efficiencies on the DNA sequence and the curves obtained with GC and IC sequences are shown. Light absorption by the probe in the 260–320 nm region is weak, with a broad valley appearing in this window (thick line, Fig. 4). Light absorption by the DNA and subsequent energy transfer to the anthryl excited state is expected to result in sensitized anthryl emission. Accordingly, strong excitation bands in the 260–300 nm region were observed for *N*-Et-AMAC in the presence of IC sequences (dashed line). No such excitation bands appear in the spectrum of *N*-Et-AMAC when bound to poly(dG-dC) (thin line). The fluorescence spectral maxima of *N*-Et-AMAC, under these conditions, correspond to that of the probe bound to DNA (shown below), and the sensitized emission observed with poly(dI-dC) is indeed from the anthryl chromophore.

The *N*-Et-AMAC emission spectra when bound to DNA has distinct peaks at 395, 415 and 440 nm (Fig. 5, direct excitation at 360 nm), similar to those of the free chromophore, and these spectra are independent of the DNA sequence. However, when the excitation was shifted to 270 nm (into the DNA absorption region), new red-shifted emission at 405, 428, and 455 nm was observed (Fig. 5). This new emission was assigned to the chromophores bound to the DNA that are sensitized by the DNA excited states. Such red shifted emission was not observed when *N*-Et-AMAC was bound to poly(dG-dC) (270 nm excitation). These data, clearly suggest sequence dependent sensitization of anthryl fluorescence by the DNA base pairs. If the energy transfer does occur from DNA to the anthryl chromophore, then the excitation bands corresponding to the sensitizer absorption bands should appear in the excitation spectra. These are shown in Fig. 4. *N*-Et-AMAC does not have any absorption bands in the 260–320 nm region and thus, lends itself to the testing of the energy transfer hypothesis. The excitation spectra clearly indicate strong absorption in the 260–300 nm region and this absorption band is absent in the anthryl absorption spectra (bound to DNA or free). This interpretation is strengthened by the fact that the corresponding new excitation bands are absent in the presence of poly(dG-dC) and therefore, the results indicate the sequence dependence of the energy transfer process.

Exothermic energy transfer from all the DNA bases to the anthryl probe may be expected, considering the large singlet excited state energies of DNA bases (34000–35000 cm^{-1}).[5] The strong overlap of the DNA fluorescence spectra (300–400 nm) with the absorption of spectrum of *N*-Et-AMAC, and the fairly large excitation coefficients for the *N*-Et-AMAC absorption transitions suggest facile energy transfer from the DNA singlet excited states to the anthryl chromophore. Hence, the sequence dependence for energy transfer observed here is unexpected. Back energy transfer from the anthryl excited state to the DNA excited states is expected to be highly endothermic and slow. The clear dependence of the energy transfer on the DNA base sequence is suggestive of the ability of the anthryl excited state to differentiate between different DNA base pairs.

Light energy is nearly equally absorbed by all DNA base pairs in the 265–280 nm window. The excitation is known to migrate over a few base pairs along the DNA chain.[5] AT base pairs are four times less likely to trap excitation than GC pairs, and excitation localized at the GC sites is quenched efficiently at the singlet level *via* non-radiative paths, resulting in low fluorescence quantum yields.[5,6] The DNA fluorescence intensity, therefore, decreases with increased GC content of the DNA.[5] Rapid singlet–singlet energy transfer, therefore, is more likely to occur from the AT sites than from the GC sites. Energy transfer from DNA to *N*-Et-AMAC is expected to be sequence dependent and to be least efficient at GC sites. Such sequence dependence, however, was not observed with ethidium bromide (a known intercalator) and one could argue that the energy migration along the helix is slower than energy transfer to ethidium bromide, resulting in no sequence dependence. An alternative explanation for the sequence dependent energy transfer from DNA to *N*-Et-AMAC may have to do with the redox potentials of the bases. The oxidation potentials of different nucleotides are known to vary as GGG < GG < G < A < C < T.[7] One possibility is that the singlet excited states of GC base pairs are quenched by *N*-Et-AMAC by electron transfer rather than by energy trasnfer, due to the low oxidation potential of G compared to other bases.

The sequence dependence of energy transfer may arise from a combination of the excited state properties of the anthryl chromophore as well as those of the DNA bases. All DNA sequences quench the fluorescence from *N*-Et-AMAC with similar efficiencies [quenching constants for CT DNA, poly d(GC) and poly d(IC) sequences are 1.23×10^4, 1.43×10^4 and 1.24×10^4 M^{-1}, respectively). The quenching constants are nearly the same within experimental error and these data cannot account for the new excitation and emission bands presented here. Therefore, the overall sequence dependence may arise from a combination of facile energy transfer from the excited states of IC sequences and rapid electron transfer from the excited GC base pairs. While the exact mechanism of the sequence dependence for energy transfer is beyond the scope of this report, the current observations are being exploited in sequence dependent DNA cleavage studies.[8]

We thank the University of Connecticut Research Foundation for financial support of this work, and Willy B. Tan for experimental assistance.

Notes and references

1 Special issue on RNA/DNA Cleavage, *Chem. Rev.*, 1998, **98**; H. Suenaga and K. Nakashima, *J. Chem. Soc., Perkin Trans. 1*, 1998, 1263; H. H. Thorp, C. C. Cheng and J. G. Goll, *J. Am. Chem. Soc.*, 1995, **117**, 2970; T. D. Tullius, in *Bioorganic Chemistry: Nucleic Acids*, ed. S. M. Hecht, OUP, New York, 1996.

2 H. Tamura and H. Fujita, *Chem. Lett.*, 1997, **8**, 711; M. J. Absalon, W. Wu and J. Stubbe, *Biochemistry*, 1995, **34**, 2076; E. Farinas, J. D. Tan, N. Baidya and P. K. Mascharak, *J. Am. Chem. Soc.*, 1993, **115**, 2996; T. Saito, M. Kitamura and T. Shimidzu, *Nucleosides Nucleotides*, 1994, **13**, 1607.

3 C. V. Kumar and E. Asuncion, *J. Am. Chem. Soc.*, 1993, **115**, 8547; C. V. Kumar and E. Asuncion, *J. Chem. Soc., Chem. Commun.*, 1992, 470.

4 E. H. Asuncion, PhD Thesis, University of Connecticut, 1994.

5 J. Eisinger, *J. Photochem. Photobiol.*, 1968, **7**, 597; S. M. Bishop, M. Malone and D. Phillips, *J. Chem. Soc., Chem. Commun.*, 1994, 871.

6 *Photochemistry and Photobiology of Nucleic Acids*, ed. S. Y. Wang, Academic Press, New York, vol. 1, p. 23.

7 I. Saito, M. Takayama, H. Sugiyama and K. Nakatani, *J. Am. Chem. Soc.*, 1995, **117**, 6406; H. Sugiyama and L. Saito, *J. Am. Chem. Soc.*, 1996, **118**, 7063.

8 C. V. Kumar, W. B. Tan and P. W. Betts, *J. Inorg. Biochem.*, 1997, **66**, 177.

Communication 9/00542K

ChemComm

Evidence for unusually strong intramolecular hydrogen bonding in highly nonplanar porphyrins

Maria S. Somma, Craig J. Medforth,* Nora Y. Nelson, Marilyn M. Olmstead, Richard G. Khoury and Kevin M. Smith

Department of Chemistry, University of California, Davis, CA 95616, USA. E-mail: medforth@indigo.ucdavis.edu

Received (in Corvallis, OR, USA) 23rd March 1999, Accepted 27th April 1999

The ^{1}H NMR spectra of the 5,10,15,20-tetraalkylporphyrins 2–4 reveal a large downfield shift of the signal for the NH protons and a reduction in the activation energy for NH tautomerism as the alkyl substituents become larger; these unusual changes can be rationalized in terms of greatly enhanced intramolecular hydrogen bonding of the NH protons as the bulkier substituents distort the macrocycle from planarity and contract the porphyrin core.

A novel and highly diagnostic feature of the ^{1}H NMR spectra of porphyrins **1** is the presence of a signal at very high field (typically δ −2 to −4) arising from the NH protons.[1,2] Herein, we describe ^{1}H NMR studies of the tetraalkylporphyrins **2**–**4** which provide the first example of a porphyrin with an NH signal far downfield of this 'fingerprint' region. We then propose a mechanism to explain this novel behavior, as well as the unusually facile tautomerism of the NH protons also observed in this porphyrin, and show that this mechanism is consistent with structural parameters determined using X-ray crystallography.

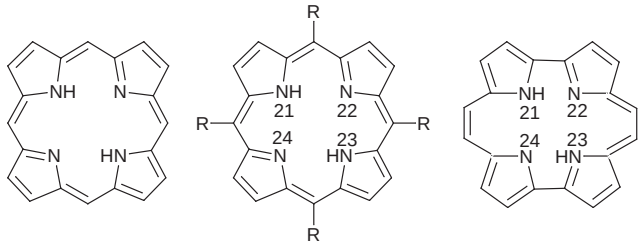

1 **2** R = C_5H_{11}; **3** R = Pr^i; **4** R = Bu^t **5**

The investigated 5,10,15,20-tetraalkylporphyrins **2**–**4** were prepared using published procedures[3] and their ^{1}H NMR spectra were recorded at a frequency of 300 MHz using $CDCl_3$ as the solvent. The ^{1}H NMR spectrum of the pentyl substituted porphyrin **2** showed a signal for the NH protons at δ −2.64, which is within the chemical shift range expected for the NH protons in porphyrins.[1,2] However, the spectrum of porphyrin **3** with more bulky isopropyl substituents showed a significant downfield shift of the NH signal to δ −1.80. In the case of porphyrin **4**, which has the even more bulky *tert*-butyl substituents, a very large downfield shift was seen for the NH signal (δ +1.58) and it was far downfield of the range expected for porphyrins.[1,2]

Large chemical shift changes in the ^{1}H NMR spectra of porphyrins are usually attributed to differences in the contribution from the porphyrin ring current effect.[1,2,4] Given the greater nonplanar distortions observed for metal complexes of tetraalkylporphyrins with larger alkyl substituents[5,6] it is plausible that the downfield shift of the NH signals is the result of a decrease in the porphyrin ring current. However, this approach is unsatisfactory because the ring current decrease determined for some cobalt(III) complexes of **4** is quite small (only about 5%).[7] Moreover, a change in the ring current would not account for the changes in the activation energies for NH tautomerism also observed in these porphyrins. For example, the activation energy for NH tautomerism in **2** measured using NMR spectroscopy ($\Delta G^{\ddagger}_{238}$ = 50 kJ mol^{-1}) was found to be similar to that measured for other nominally planar porphyrins ($\Delta G^{\ddagger}_{298}$ = 50±3 kJ mol^{-1}).[4] In addition, as with other porphyrins, the activation energy for tautomerism in **2** increased upon replacement of the inner hydrogens with deuteriums ($\Delta G^{\ddagger}_{283}$ = 60 kJ mol^{-1} in **2** *vs.* $\Delta G^{\ddagger}_{298}$ = 57±2 kJ mol^{-1} in regular porphyrins).[4] However, the activation energy for tautomerism in **3** was significantly reduced in both the dihydro ($\Delta G^{\ddagger}_{183}$ = 38 kJ mol^{-1}) and dideutero ($\Delta G^{\ddagger}_{233}$ = 50 kJ mol^{-1}) forms, and in porphyrin **4** there was no evidence of a dynamic process in either the dihydro or dideutero forms even at the lowest temperatures studied (182 K) indicating an extremely low activation energy.

In order to explain these changes in the NH chemical shifts and activation energies for NH tautomerism, we propose an alternative model in which there is also a substantial increase in intramolecular hydrogen bonding as the substituents become larger. This hydrogen bonding will produce an additional downfield shift for the NH protons, and should also lower the activation energies for tautomerism because intramolecular hydrogen bonding is analogous to the transition state for tautomerism where the hydrogens are co-shared by adjacent nitrogen atoms.[4,8] Such strong intramolecular hydrogen bonding has not previously been postulated in porphyrins, although this phenomenon has been invoked by Vogel and co-workers[9] to explain similar NMR behavior in the porphyrin isomer porphycene **5**. In porphycene, the unusual 'oblong' geometry of the macrocycle appears to provide both short N–N distances (N21–N22 2.83 Å, N21–N24 2.63 Å) and a nearly linear arrangement of a hydrogen bond between N21 and N24. In the case of porphyrins **2**–**4** it seemed likely that the increased intramolecular hydrogen bonding suggested by the NMR studies might be the result of the bulkier alkyl substituents forcing the porphyrin rings to adopt increasingly ruffled conformations, as seen for metal complexes of related tetraalkylporphyrins.[5,6] This ruffling distortion would contract the porphyrin core and shorten the distance between adjacent nitrogen atoms, thereby enhancing intramolecular hydrogen bonding.

The crystal structures of porphyrins **2**–**4** were determined† to see if they were consistent with this model. As can be seen in Fig. 1, the porphyrins with larger substituents do show increased ruffling of the macrocycle. This ruffling will maximize core contraction compared to other nonplanar distortion modes[10] and will also keep the nitrogen and hydrogen atoms in the porphyrin plane. Hence, the crystal structures show precisely the kind of nonplanar deformation expected to enhance intramolecular hydrogen bonding and produce the effects observed in the ^{1}H NMR spectra. Furthermore, the much larger effects seen in the NMR spectra of porphyrin **4** can be related to the significantly greater core contraction seen for this porphyrin (the average distance between the adjacent nitrogen atoms in **4** is only 2.71 Å *vs.* 2.89 Å in **3** and 2.91 Å in **2**). Note

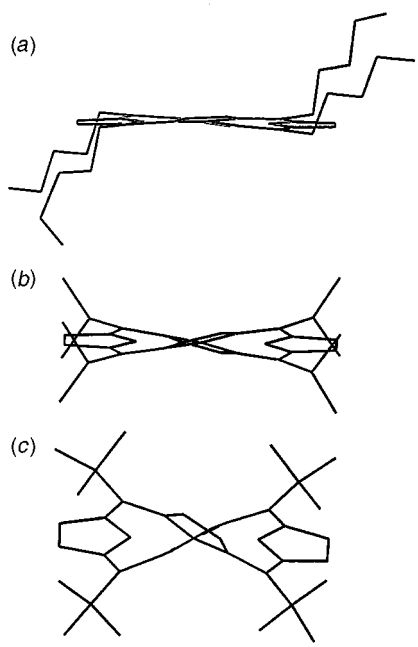

Fig. 1 Side-on views of the crystal structures of porphyrins (*a*) **2**, (*b*) **3** and (*c*) **4**. Hydrogen atoms have been omitted for clarity.

that a more detailed analysis of the pattern of hydrogen bonding within the porphyrin cores was also attempted but did not yield any definitive results. For example, the hydrogens in **4** were localized on an opposing pair of pyrrole rings and tilted towards adjacent nitrogen atoms (NH 21 towards N24 and NH 23 towards N22) possibly suggesting some additional deformation as a result of the severe core contraction. However, a review of other tetraalkylporphyrin crystal structures revealed similar NH tilting even in nominally planar systems.[3]

The studies reported here show that intramolecular hydrogen bonding in porphyrins can be strongly enhanced by a specific type of nonplanar distortion (ruffling), and also provide another example of the sometimes unexpected ways in which nonplanarity can affect the properties of porphyrins.[11] The fact that enhanced intramolecular hydrogen bonding has not previously been noted in other extremely nonplanar porphyrins is probably related to the predominantly saddle conformations[12] adopted by these molecules, where tilting of the pyrrole rings out of the porphyrin plane will disfavor intramolecular hydrogen bonding. Indeed, recent studies of such porphyrins have shown downfield shifts of the NH protons in some solvents due to increased *intermolecular* hydrogen bonding.[13] Finally, it is should be noted that this new information about hydrogen bonding in porphyrins, together with recent studies showing that even large nonplanar distortions result in only modest decreases in the porphyrin ring current effect,[7] suggests that the practice of using the chemical shift of the NH protons as an indicator of structurally induced changes in the porphyrin ring current may need to be approached with more caution.

This work was supported by grants from the National Institutes of Health (HL 22252) and the National Science Foundation (CHE-96-23117). C. J. M. gratefully acknowledges financial support from Professor J. A. Shelnutt (Sandia National Laboratories) through U.S. Department of Energy Contract DE-AC04-94AL85000.

Notes and references

† *Crystal data* for **2**: $C_{40}H_{54}N_4$, crystals were grown *via* slow diffusion of MeOH into a solution of **2** in THF, dimensions 0.20 × 0.38 × 0.55 mm, orthorhombic, space group $P2_12_12_1$, a = 13.416(2), b = 15.734(3), c = 16.473(2) Å, V = 3477.2(9) Å^3, Z = 4 (M = 590.87). Diffraction data were collected on a Syntex $P2_1$ diffractometer with a graphite monochromated sealed tube X-ray source [λ(Cu-Kα) = 1.54178 Å] at 130(2) K in $\theta/2\theta$ scan mode to $2\theta_{max}$ = 133.9°. Of 3466 reflections measured (+h,+k,+l), all were independent and 3229 had $I > 2\sigma$ (T_{max} = 0.77, T_{max} = 0.91, ρ_{calc} = 1.129 g cm^{-3}, μ = 0.497 mm-1). The structure was solved by direct methods and refined (based on $F2$ using all independent data) by full-matrix least-squares methods with 398 parameters (Siemens SHELXTL ver. 5.03). All non-hydrogen atoms were refined with anisotropic thermal parameters. Hydrogen atom positions were generated by their idealized geometry and refined using a riding model, except for the hydrogen atoms bonded to the pyrrole nitrogen atoms. In this case, electron density corresponding to a hydrogen atom was present at each pyrrole ring in difference Fourier maps, so each of the nitrogens was assigned a hydrogen at 0.5 occupancy. No absorption correction was applied. The final difference map had a largest peak of 1.45 e Å^{-3} and a largest hole of −0.40 e Å^{-3}. Final R factors were $R1$ = 0.0615 (observed data) and $wR2$ = 0.166 (all data).

For **3**: $C_{32}H_{38}N_4$, crystal grown *via* slow diffusion of cyclohexane into a solution of **3** in CH_2Cl_2, dimensions 0.24 × 0.24 × 0.14 mm, orthorhombic, space group $Fdd2$, a = 20.257(4), b = 20.999(4), c = 12.373(3) Å, V = 5263(2) Å3, Z = 8 (M = 478.66). Diffraction data were collected on a Syntex $P2_1$ diffractometer with a graphite monochromated sealed tube X-ray source [λ(Cu-Kα) = 1.54178 Å] at 130(2) K in $\theta/2\theta$ scan mode to $2\theta_{max}$ = 113.0°. Of 996 reflections measured (+h,+k,+l), 920 were independent (R_{int} = 0.038), and 817 had $I > 2\sigma$ (T_{min} = 0.88, T_{max} = 0.93, ρ_{calc} = 1.203 g cm^{-3}, μ = 0.546 mm^{-1}). The structure was solved by direct methods and refined (based on F^2 using all independent data) by full matrix least-squares methods with 168 parameters (SHELXS-86, SHELXL-93). All non-hydrogen atoms were refined with anisotropic thermal parameters. Hydrogen atom positions (except for the core pyrrolic NHs) were generated by their idealized geometry and refined using a riding model. Core hydrogen atoms, located in a difference Fourier map, were found to be localized on one opposing pair of pyrrole nitrogen atoms and were refined freely. An empirical absorption correction was applied using XABS2 (ref. 14). The final difference map had a largest peak of 0.19 e Å^{-3} and a largest hole of −0.22 e Å^{-3}. Final R factors were $R1$ = 0.0475 (observed data) and $wR2$ = 0.1272 (all data). CCDC 182/1265.

Full details of the crystal structure of **4** and related metal complexes of this porphyrin will be presented shortly (ref. 15).

1 H. Scheer and J. J. Katz, in *Porphyrins and Metalloporphyrins*, ed. K. M. Smith, Elsevier, Amsterdam, 1975, 399.
2 T. R. Janson and J. J. Katz, in *The Porphyrins*, ed. D. Dolphin, Academic Press, New York, 1979, vol. 4, p. 1.
3 M. O. Senge, I. Bischoff, N. Y. Nelson and K. M. Smith, *J. Porphyrins Phthalocyanines*, 1999, **3**, 99.
4 C. J. Medforth, in *The Porphyrin Handbook*, ed. K. M. Kadish, K. M. Smith and R. Guilard, Academic Press, Burlington, MA, 1999, in the press.
5 W. Jentzen, M. C. Simpson, J. D. Hobbs, X. Song, T. Ema, N. Y. Nelson, C. J. Medforth, K. M. Smith, M. Veyrat, M. Mazzanti, R. Ramasseul, J.-C. Marchon, T. Takeuchi, W. A. Goddard III and J. A. Shelnutt, *J. Am. Chem. Soc.*, 1995, **117**, 11 085.
6 M. O. Senge, T. Ema and K. M. Smith, *J. Chem. Soc., Chem. Commun.*, 1995, 733.
7 C. J. Medforth, C. M. Muzzi, K. M. Shea, K. M. Smith, R. J. Abraham, S. Jia and J. A. Shelnutt, *J. Chem. Soc., Perkin Trans. 2*, 1997, 839.
8 Z. Smedarchina, M. Z. Zgierski, W. Siebrand and P. W. Kozlowski, *J. Chem. Phys.*, 1988, **109**, 1014.
9 E. Vogel, M. Kocher, H. Schmickler and J. Les, *Angew. Chem., Int. Ed. Engl.*, 1986, **25**, 257.
10 X.-Z. Song, L. Jaquinod, W. Jentzen, D. J. Nurco, S. Jia, R. Khoury, J. Ma, C. J. Medforth, K. M. Smith and J. A. Shelnutt, *Inorg. Chem.*, 1998, **37**, 2009.
11 J. A. Shelnutt, X.-Z. Song, W. Jentzen, J.-G. Ma, S.-L. Jia, W. Jentzen and C. J. Medforth, *Chem. Soc. Rev.*, 1998, **27**, 31.
12 D. J. Nurco, C. J. Medforth, T. P. Forsyth, M. M. Olmstead and K. M. Smith, *J. Am. Chem. Soc.*, 1996, **118**, 10 918.
13 J. Takeda and M. Sato, *Chem. Lett.*, 1995, 971.
14 S. Parkin, B. Moezzi and H. Hope, *J. Appl. Crystallogr.*, 1995, **28**, 53.
15 K. M. Barkigia, M. W. Renner, N. Y. Nelson, R. Khoury, K. M. Smith, D. Holten, M. C. Piqueras, C. M. Rohlfing, S. Jia, J. A. Shelnutt and J. Fajer, unpublished work.

Communication 9/02339I

ChemComm

NMR detection of thermal and photochemical dihydrogen addition products of mono- and tri-nuclear ruthenium complexes containing carbonyl and triphenylphosphine ligands through *para*-hydrogen induced polarisation

Christopher J. Sleigh, Simon B. Duckett,* Roger J. Mawby and John P. Lowe

Department of Chemistry, University of York, York, UK YO10 5DD. E-mail: sbd3@york.ac.uk

Received (in Cambridge, UK) 26th April 1999, Accepted 25th May 1999

Enhancement of NMR signals by *para*-hydrogen induced polarisation is shown to facilitate the detection of isomers of $Ru(CO)_2(H)_2(PPh_3)_2$ and $Ru(CO)_3(H)_2(PPh_3)$ which contain inequivalent hydride ligands, and to demonstrate that $Ru_3(CO)_9(PPh_3)_3$ adds H_2 to form $Ru_3(CO)_8(H)(\mu\text{-}H)(PPh_3)_3$, as well as undergoing fragmentation to form $Ru(CO)_3(H)_2(PPh_3)$.

We have shown that the enhanced absorption and emission signals observed in NMR spectra of complexes incorporating hydrogen nuclei derived from *para*-enriched hydrogen[1] (p-H_2) can be used to detect and characterise materials present at concentrations too low for detection by normal NMR methods.[2] In particular, using this approach we have been able to identify minor all-*cis* isomers of $Ru(CO)_2(H)_2L_2$ (L = PMe_2Ph or PMe_3) that were previously unknown.[3] Here we extend this approach by demonstrating how both $Ru(CO)_3(H)_2(PPh_3)$ **1** and $Ru(CO)_2(H)_2(PPh_3)_2$ **2** behave with p-H_2. We show that two isomers of both **1** and **2** are detectable, and demonstrate that $Ru_3(CO)_9(PPh_3)_3$ reacts with hydrogen to yield new clusters containing bridging and terminal hydride ligands and also fragments to $Ru(CO)_3(H)_2(PPh_3)$. The precursors required for these studies, $Ru(CO)_3(PPh_3)_2$, $Ru_3(CO)_9(PPh_3)_3$ and *trans*-*cis*–*cis*-$Ru(CO)_2(H)_2(PPh_3)_2$ **2a**, were prepared by standard methods.[4] These complexes were selected for study because, despite the fact that ruthenium/carbonyl/triphenylphosphine species have been implicated in catalytic cycles involving H_2, their reactivity towards H_2 is only poorly understood.[5–7]

When a benzene-d_6 solution of $Ru(CO)_3(PPh_3)_2$ under 3 atm of p-H_2 was warmed to 353 K, no change in the ^{1}H NMR spectrum of the solution was detected. However, when a similar solution, also under p-H_2 was photolysed for 2 min, an NMR spectrum recorded at 308 K contained enhanced resonances at δ −6.67 (H_a, dd, J_{PH} 15.9, J_{HH} −5.4 Hz) and δ −7.34 (H_b, dd, J_{PH} 61.6, J_{HH} −5.4 Hz) [Fig 1(a)]. The values for J_{PH} suggested that the species responsible for these resonances, **1a**, contained a single PPh_3 ligand lying *cis* to H_a and *trans* to H_b. The p-H_2 enhanced complex **1a** was further characterised by 2D NMR,[8] allowing the ^{31}P resonance to be located at δ 20.3. In order to obtain ^{13}C data, ^{13}CO-labelled $Ru(CO)_3(PPh_3)_2$ was photolysed with p-H_2. In the resulting ^{1}H NMR spectrum of ^{13}CO-labelled **1a**, the H_a resonance showed an additional doublet splitting (J_{CH} 27.8 Hz) indicative of a *trans* H–Ru–CO arrangement. Two ^{13}CO resonances were detected at δ 197.6 and 199.5 by a ^{1}H–^{13}C HMQC experiment. The data indicated that **1a** was the *mer* isomer of $Ru(CO)_3(H)_2(PPh_3)$. This complex has not previously been observed by NMR, although high pressure IR studies have indicated its existence.[6] Surprisingly, in the corresponding ^{1}H–^{31}P correlation, additional resonances corresponding to the *fac* isomer of $Ru(CO)_3(H)_2(PPh_3)$ **1b** were detected which were missed in the original ^{1}H NMR spectrum owing to coincidental overlap with the resonance due to H_a of **1a**.

A very weak hydride resonance could also be seen in the ^{1}H NMR spectra of the photolysed solutions at δ −6.35 (t, J_{PH} 23.2 Hz). This was shown to be due to the *trans*–*cis*–*cis* isomer of $Ru(CO)_2(H)_2(PPh_3)_2$ **2a** by comparison with the spectrum of an authentic sample (see above). Under normal H_2, and after prolonged photolysis, **2a** was the only detectable product.

When the solution containing $Ru(CO)_3(PPh_3)_2$ and **1a** enhanced with p-H_2 was warmed to 328 K, the hydride resonances for **1a** broadened substantially, and a second pair of polarised hydride resonances appeared at δ −6.27 (ddd, J_{PH} 26.4, 19.1, J_{HH} = −7.1 Hz) and −7.52 (ddd, J_{PH} 75.1, 33.0, J_{HH} −7.1 Hz). Resonances for two inequivalent ^{31}P nuclei, both doublets with J_{PP} 32.0 Hz, were located in the ^{1}H–^{31}P spectrum at δ 50.2 and 41.6. It was concluded that the species responsible for the new resonances was the previously undetected all-*cis* isomer of $Ru(CO)_2(H)_2(PPh_3)_2$ **2b**.

A ^{1}H–^{1}H PHIP–EXSY experiment, recorded at 308 K, contained exchange peaks that indicated that the hydride ligands of *mer*-$Ru(CO)_3(H)_2(PPh_3)$ **1a** were interchanging positions with a rate constant of 40 s^{-1}. Even at higher temperatures, however, no peaks connected the resonances of **1a** to those of **2b**, suggesting that the interchange may be intramolecular,

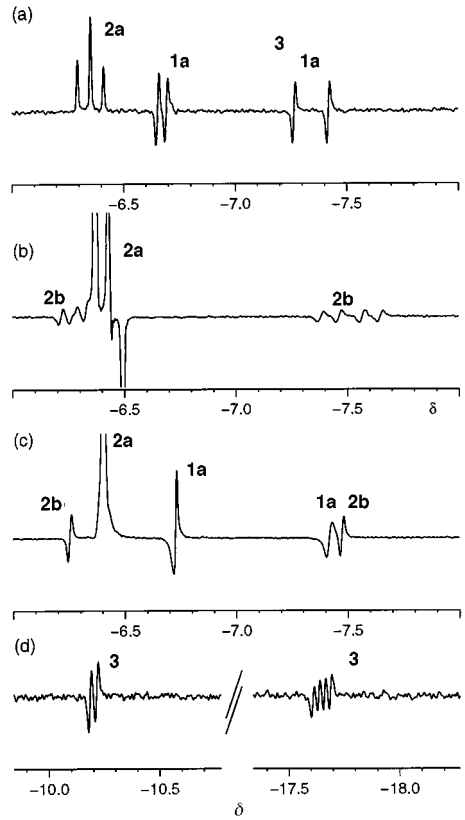

Fig 1 NMR spectra of reaction products obtained with p-H_2 in C_6D_6 showing the hydride region only. The antiphase components arise in transitions involving protons that originate from p-H_2. (a) ^{1}H spectrum of **1a** generated after UV irradiation of a sample of $Ru(CO)_3(PPh_3)_2$ at 308 K; (b) ^{1}H spectrum of **2b** at 328 K; (c) ^{1}H spectrum of a sample of **2a** warmed with p-H_2 in the presence of CO at 318 K; (d) ^{1}H spectrum of **3** generated from a sample of $Ru_3(CO)_9(PPh_3)_3$ at 308 K.

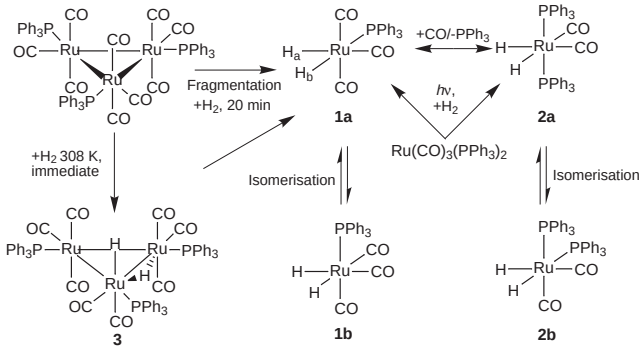

Scheme 1

perhaps a trigonal twist process similar to that reported for $Ru(CO)(H)_2(PPh_3)_3$.[9]

The interconversions between **2a**, **2b** and **1a** were further investigated using an authentic sample of **2a**. When a benzene-d_6 solution of **2a** was heated under 3 atm of *p*-H_2 to 328 K, no signals for **1a** were visible in the ^{1}H NMR spectrum, but the hydride resonances for **2b** were again observed [Fig. (1b)]. An NMR tube containing a fresh solution of **2a** was then placed under 1 atm of CO, frozen and then filled with 3 atm of *p*-H_2. When the solution was warmed to 318 K, the enhanced hydride resonances of **1a** and **2b** were observed [Fig. 1(c)]. Evidently **2a** readily undergoes replacement of PPh_3 by CO. We have recently adapted an NMR probe to allow a sample to be irradiated by UV light from a HgXe arc while NMR spectra are recorded.[10] ^{1}H NMR spectra recorded during photolysis of a benzene-d_6 solution $Ru(CO)_3(PPh_3)_2$ under 3 atm of *p*-H_2 at 292 K showed large enhanced hydride signals due to **1a** and a small non-enhanced signal due to **2a**. The signals for **1a** were not observed in the absence of UV radiation, confirming that, in this case, hydrogen exchange between **1a** and free H_2 is photochemical rather than thermal.

Many phosphine-substituted derivatives of $Ru_3(CO)_{12}$ have been characterised and studied, but the reactions of these complexes with hydrogen are less well understood.[11] We have therefore used *p*-H_2 to monitor the reaction of $Ru_3(CO)_9(PPh_3)_3$ with hydrogen. Nevinger *et al*. used a complex synthetic procedure to obtain a species believed to be $Ru_3(CO)_{11}H(\mu\text{-}H)$, whose ^{1}H NMR spectrum contained hydride resonances at δ −11.79 and 18.55.[12] We recorded the ^{1}H NMR spectrum of a benzene-d_6 solution of $Ru_3(CO)_9(PPh_3)_3$ under *p*-H_2 at 308 K, and detected enhanced resonances at δ −10.20 (dd, J_{PH} 11.2, J_{HH} −6.0 Hz) and −17.64 (ddd, J_{PH} 21.2,10.4, J_{HH} −6.0 Hz) for two mutually coupled hydrides in a species **3** [Fig. 1(d)]. The chemical shifts and couplings to phosphorus suggested that the former resonance represented a terminal hydride *cis* to a phosphine and the latter a hydride bridging two ruthenium atoms and *cis* to a phosphine ligand on each ruthenium. A 2D experiment located the resonances for the corresponding ^{31}P nuclei at δ 44.4 (coupled to both hydrides) and −17.6 (coupled only to the terminal hydride). From this evidence it appeared that **3** was the 48-electron cluster $Ru_3(CO)_8H(\mu\text{-}H)(PPh_3)_3$, with the structure shown in Scheme 1. The third ^{31}P nucleus was not detected by the 2D experiment because it is not coupled to either hydride. Complex **3**, which is comparable to both $Ru_3(CO)_{11}H(\mu\text{-}H)$ and $Os_3(CO)_{10}H(\mu\text{-}H)L$ (L = PPh_3 or CD_3CN),[13] is presumably formed by a simple substitution of CO by H_2.

After 20 min at 308 K, resonances for isomer **1a** of $Ru(CO)_3H_2(PPh_3)$ had appeared in the ^{1}H NMR spectrum of the solution. Consequently, either unreacted $Ru_3(CO)_9(PPh_3)_3$ or $Ru_3(CO)_8H(\mu\text{-}H)(PPh_3)_3$ fragment under hydrogen to yield mononuclear ruthenium complexes under relatively mild conditions. This observation is interesting, given that mixtures of $Ru_3(CO)_{12}$ and PPh_3 have been used in hydroformylation catalysis and $Ru(CO)_3(H)_2(PPh_3)$ has been implicated as an intermediate in hydroformylation.[5,7] No *para*-hydrogen enhanced products, either tri- or mono-nuclear, were detected on treating $Ru_3(CO)_{12}$ with *p*-H_2 either in the presence or the absence of UV irradiation.

Here, we have established some features of the ruthenium carbonyl/triphenylphosphine/hydrogen system, which shows some important differences from those with PMe_2Ph and PMe_3. Furthermore, we have established the feasibility of using *p*-H_2 to probe photochemical reactions, H_2 addition to clusters, and cluster fragmentations.

We are grateful to the EPSRC (C. J. S. and spectrometer), the University of York (J. P. L.), Bruker UK (spectrometer) and the Royal Society for financial support. We appreciated helpful discussions with Professor R. N. Perutz, Dr M. K. Whittlesey and Dr J. M. Lynam. A generous loan of ruthenium trichloride from Johnson Matthey is also gratefully acknowledged.

Notes and references

† *Selected spectroscopic data* for **1a**, **1b**, **2a**, **2b** and **3**: NMR spectra in C_6D_6 at 400.13 MHz (^{1}H) and 202.45 MHz (^{31}P) recorded on 5 mm samples in a 5 mm inverse geometry probe. **1a**: ^{1}H δ_H(328 K) −6.67 [H_a, *J*(PH) 15.9, *J*(COH) 27.8, *J*(HH) −5.4 Hz], −7.34 [H_b, *J*(PH) 61.6, *J*(HH) −5.4 Hz]. δ_P(328 K) 20.3 (s). δ_C(328 K); 199.5 d [*J*(PC) 8.4 Hz], 197.6 [d *J*(PC) 4.6 Hz]. **1b**: δ_H(308 K) −6.68 [*J*(PH) 23 Hz], δ_P(328 K) 55.1 (s). **2a**: δ_H(295 K) −6.35 [H, *J*(PH) 23.2 Hz]. δ_P(295 K) 57.7 (s). δ_C(295 K) 202.0 [t, *J*(PC) 8.3 Hz]. **2b**: δ_H(328 K) −6.27 [H_c, *J*(PH) 26.4, 19.1, *J*(HH) −7.1 Hz], −7.52 [H, *J*(PH) 75.1, 33.0, *J*(HH) −7.1 Hz]. δ_P(328 K) 50.2 d [*J*(PP) 32 Hz], 41.6 [d, *J*(PP) 32 Hz]. **3**: δ_H(300 K) −10.20 [H, *J*(PH) 11.2, *J*(HH −6.0 Hz], −17.64 [H, *J*(PH) 21.2, 10.4, *J*(HH) −6.0 Hz]. δ_P (308 K) 44.4 (s) and 31.2 (s).

1 C. R. Bowers and D. P. Weitekamp, *J. Am. Chem. Soc.*, 1987, **109**, 5541; R. Eisenberg, *Acc. Chem. Res.*, 1991, **24**, 110; J. Natterer and J. Bargon, *Prog. Nucl. Magn. Reson. Spectrosc.*, 1997, **31**, 293.
2 B. Duckett and R. Eisenberg. *J. Am. Chem. Soc*., 1993, **115**, 5292; P. D. Morran, S. A. Colebrooke, S. B. Duckett, J. A. B. Lohmann and R. Eisenberg. *J. Chem. Soc., Dalton Trans*., 1998, 3363.
3 S. B. Duckett, R. J. Mawby and M. G. Partridge, *Chem. Commun*., 1996, 383.
4 N. Ahmad, J. J. Levison, S. D. Robinson and M. F. Uttley. *Inorg. Synth.*, 1974, **15**, 50; M. I. Bruce, G. Shaw and F. G. A. Stone. *J. Chem. Soc., Dalton Trans*., 1972, 2094.
5 P. Kalck, Y. Peres and J. Jenck. *Adv. Organomet. Chem*. 1991, **32**, 121.
6 R. Whyman, *J. Organomet. Chem.*, 1973, **56**, 339.
7 E. M. Gordon and R. Eisenberg, *J. Organomet. Chem.*, 1986, **306**, C53.
8 S. B. Duckett, G. K. Barlow, M. G. Partridge and B. A. Messerle, *J. Chem. Soc., Dalton Trans*. 1995, **20**, 1427; S. Hasnip, S. B. Duckett, D. R. Taylor and M. J. Taylor. *Chem. Commun.*, 1998, 923.
9 G. E. Ball, and B. E. Mann, *J. Chem. Soc., Chem. Commun*., 1992, 561. We note that although we have no direct evidence that **1a** and **1b** interconvert, this is the case for the PMe_3, $AsMe_2Ph$ and PMe_2Ph analogues of **2**.
10 This will be reported fully elsewhere, however, we note that two UV transmitting liquid light guides were employed in conjunction with a modified narrow-bore probe that was used in a wide-bore magnet.
11 M. I. Bruce, M. J. Liddell, O. bin Shawkataly, C. A. Hughes, B. W. Skelton and A. H. White, *J. Organomet. Chem.*, 1988, **347**, 207.
12 L. R. Nevinger, J. B. Keister and J. Maher, *Organometallics*, 1990, **9**, 1900.
13 S. Aime, R. Gobetto and D. Canet, *J. Am. Chem. Soc.*, 1998, **120**, 6770; A. J. Deeming, *Adv. Orgnaomet. Chem.*, 1986, **26**, 1.

Communication 9/03321A

ChemComm

Evidence for a common Ru(P)$(NO)_2$ intermediate in photochemical and synthesis pathways involving Ru(TmTP)(NO)(ONO) and excess nitric oxide

Ivan M. Lorkovic and Peter C. Ford*

Department of Chemistry, University of California, Santa Barbara, CA 93106, USA. E-mail: ford@chem.ucsb.edu

Received (in Bloomington, IN, USA) 4th March 1999, Accepted 19th May 1999

Optical and IR spectra of the intermediate formed from the reaction of Ru(CO)(TmTP) with NO are compared with transient UV–VIS and FTIR spectra of photochemical intermediates formed from the photolysis and recovery of Ru(TmTP)(NO)(ONO) in the presence of NO; comparison reveals that the two pathways share a common intermediate, which IR spectral properties suggest to be *trans*-Ru(TmTP)$(NO)_2$.

The reaction chemistry of nitric oxide has drawn renewed attention owing to the established biological roles of NO and its interactions with metal centers in mammalian cardiovascular systems, in immunology and in various human disease states.[1–4] In this context we have been studying reactions of NO with metal porphyrin complexes,[5–7] and we and others have shown that the reaction of Ru^{II}(CO)(P) (P^{2-} = a porphyrinato dianion) with excess NO in hydrocarbon solvents forms the nitrito nitrosyl complex Ru(P)(NO)(ONO).[5,8] The other product is 1 equiv. of N_2O [eqn. (1)].[8] Other metal centers have long been known to facilitate the NO disproportionation in the presence of excess nitric oxide.[9,10]

$$Ru(P)(CO) + 4\,NO \longrightarrow Ru(P)(NO)(ONO) + N_2O \qquad (1)$$

Stopped flow kinetics studies in this laboratory with P = TmTP (tetra-*m*-tolylporphyrinate) or OEP (octaethylporphyrinate) have shown that the reaction in eqn. (1) proceeds by several steps.[6] There is a discernable intermediate **X** with a composition consistent with that of Ru(P)$(NO)_2$, and this reacts further by a pathway second order in [NO] to give Ru(P)(NO)(ONO).

$$Ru(P)(CO) + 2\,NO \rightleftharpoons \mathbf{X} + CO \qquad (2)$$

$$\mathbf{X} + 2\,NO \longrightarrow Ru(P)(NO)(ONO) + N_2O \qquad (3)$$

Parallel work in this laboratory has been concerned with the photochemistry of various Ru(P)(NO)(ONO).[11] Flash photolysis in benzene was shown to give two primary photoproducts, which were proposed to be Ru^{III}(P)(ONO) (resulting from photolabilization of NO) and Ru^{II}(P)(NO) (resulting from photolabilization of NO_2) both of which react with the excess NO to reform Ru(P)(NO)(ONO). Reformation of Ru(TmTP)(NO)(ONO) **1** from Ru^{III}(TmTP)(ONO) was shown to proceed by second order recombination with NO ($k_A = 5.5 \times 10^8$ dm^3 mol^{-1} s^{-1}). The regeneration of **1** from Ru(TmTP)(NO) **2** proved to be more circuitous; first there is a second order reaction of **2** with NO ($k_B = 4.5 \times 10^7$ dm^3 mol^{-1} s^{-1}) to form yet another transient species **Y**, then a much slower reaction of **Y** with excess NO to give **1**.[11]

On the basis of similarities in their optical spectra and reactivities, **X** and **Y** were suggested to be the same species, namely Ru(TmTP)$(NO)_2$. The OEP complex behaves similarly.[11] We present here a comparison of the UV–VIS and IR spectra of the photochemically prepared intermediate **Y** to those of **X** which was prepared by rapid mixing techniques in the thermal reaction of Ru(TmTP)(CO) plus NO. These data provide compelling evidence that the thermal and photochemical routes do indeed share a common intermediate. Also, IR analysis of the transient species of the thermal reaction confirms that N_2O production occurs during the second step of the thermal reaction, and that the isomerization of a predicted transient nitrosyl nitro species to **1** (Scheme 1) occurs too quickly to be observed by stopped flow techniques.

The optical spectral changes observed upon rapid mixing of cyclohexane solutions of NO and Ru(TmTP)(CO) are virtually identical in profile and time dependence to the changes observed using toluene as solvent.[6] In short, the carbonyl complex (Q band λ_{max} at 528 nm; $\varepsilon = 2.5 \times 10^3$ dm^3 mol^{-1} cm^{-1}) gives way, within 5 ms after mixing, to an intermediate (546 and 580 nm; 16×10^4 and 5×10^4 dm^3 mol^{-1} cm^{-1}), which reacts slowly ($k_{obs} = 0.3$ s^{-1}), in a second step, to give **1** (561 nm; 10.2×10^3 M^{-1} cm^{-1}). Furthermore the difference optical spectrum observed, after flash photolysis of a solution of **1** in cyclohexane in the presence of NO (5 mM) is indistinguishable from the difference spectrum between **X** and **1**.

Fig. 1(a) shows the IR spectral changes associated with the generation of **Y** within 1 μs after flash photolysis of **1** in cyclohexane solutions containing 5 mM NO (previously reported[11] but included here for purposes of comparison). Fig. 1(b) shows IR spectral data generated using a custom built, hand driven stopped-flow reactor to mix Ru(TmTP)(CO) with NO in a 1 mm pathlength IR cell. This difference spectrum was generated by subtracting the product spectrum generated by mixing identical concentrations of NO and Ru(TmTP)(CO) and waiting about 20 s from the initial spectrum seen immediately after mixing. The positive peaks represent the initial species formed, *i.e.* **X**, while the negative peaks can be largely attributed to the ruthenium containing product **1**, although the small peak at 2215 cm^{-1} is attributed to the formation of N_2O. Successive difference spectra show the positive and negative peaks returning to baseline as the intermediate **X** undergoes reaction with NO to form **1** and the transient spectra converge on the product spectrum. The intensities of the negative peaks in Fig. 1(a) represent *ca.* 95% of the maximum ΔA possible as determined by subtracting the product solution spectrum from

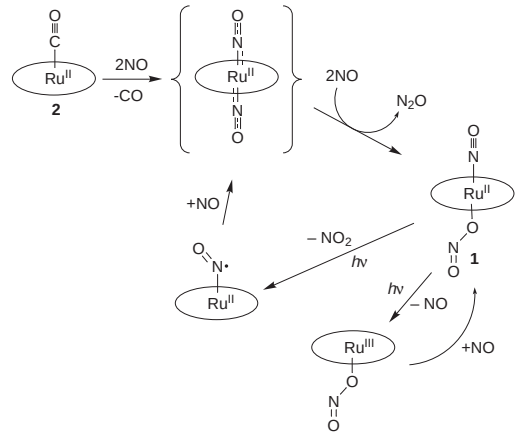

Scheme 1

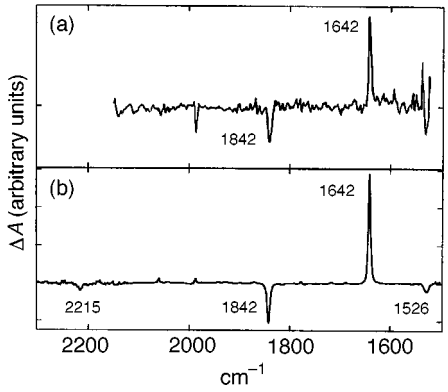

Fig. 1 (a) Long term (8–20 μs) FTIR difference spectrum observed using a step scan instrument after flash photolysis of a solution of **1** (200 μM) in cyclohexane in the presence of NO (5 mM).[11] (b) FTIR difference spectrum obtained by subtraction of the product spectrum recorded 15 s after mixing from the transient spectrum in cyclohexane recorded *ca*. 0.2 s after mixing of Ru(CO)(TmTP) (150 μM after mixing) with NO (3.9 mM) in a flow experiment. For both top and bottom spectra, the small peaks observed between 1900 and 2100 are solvent subtraction errors and correspond exactly to cyclohexane peaks.

that of pure cyclohexane. Thus, the subsequent reaction of **X** with NO has proceeded by only *ca*. 5%, and one can use the previously determined rate constant for this process to estimate the elapsed time after mixing at *ca*. 0.2 s. In this time frame, the starting material Ru(TmTP)(CO) would have reacted to completion ($k_{obs} = k_1[NO] = 3.8 \times 10^3$ s^{-1}).

It is clear from a comparison of Fig. 1(a) with 1(b) that the photolysis of **1** in the presence of NO and the reaction of Ru(CO)(TmTP) with NO generate the same intermediate, *i.e.* that **X** and **Y** are both Ru(TmTP)$(NO)_2$. There are several additional implications of these data. First, the negative peaks at 1527 and 1842 cm^{-1} show the same absorbance ratio (*ca*. 1/5) as observed for independently purified **1** in cyclohexane. This indicates that the negative peak at 1842 cm^{-1} does not overlap with a positive absorbance arising from **X**. (The small peaks visible at 1790, 1990 and 2060 cm^{-1} are due to imperfect solvent subtraction and correspond exactly to peaks in the cyclohexane spectrum). The peak at 1642 cm^{-1} is the sole characteristic absorbance of **X** with appreciable intensity between 2300 and 1500 cm^{-1}. Therefore the absorption coefficient at 1642 cm^{-1} may be estimated as 9000 dm^3 mol^{-1} cm^{-1} by intensity comparison to the negative ν_{NO} peak at 1842 cm^{-1} (3300 dm^3 mol^{-1} cm^{-1}) for **1**. The integrated intensity of the former is *ca*. 2.3 as strong as the latter.

There still remains some ambiguity with respect to the likely structure of **X**. Two possibilities would be the six coordinate dinitrosyl species implied above by the formula Ru(TmTP)$(NO)_2$ in either the *cis* or *trans* configurations. The *cis* dinitrosyl appears quite unlikely since it should show two IR active ν_{NO} bands, but only one was detected. In contrast, a linear array of two *trans* NO ligands bound to the metal in a centrosymmetric *ca*. D_{4h} point group should show a single IR band, the antisymmetric A_{2u} stretching mode of the two diatomic ligands with roughly twice the transition dipole strength of a single nitrosyl stretch. The symmetric A_{1g} stretch should not be IR active. Although ν_{NO} frequencies as low as 1600 cm^{-1} have been reported for linear or near linear metal nitrosyls,[12] the 1642 cm^{-1} remains unexpectedly low for a linear M–NO, since such bonding is commonly viewed as the result of NO^+coordination. A possible explanation would be that the two additional electrons necessary for the dinitrosyl formulation of **X** are in π* molecular orbital(s) delocalized over the five atom ONRuNO structure, thus giving a lower effective NO bond order, hence a lower ν_{NO}. The IR data are also consistent with a *trans*-Ru$(NO)_2$ structure with Ru–N–O angles less than 180° if the two NO groups are positioned in a manner to maintain a center of inversion (C_{2h} symmetry). Observation of but a single, sharp ν_{NO} band would appear to require a strong thermodynamic preference for this centrosymmetric configuration under the reaction conditions, unless there is very poor coupling between two such oscillators positioned on opposite sides of the Ru(P) plane.[13]

The difference spectrum Fig. 1(b) also shows a negative peak at 2215 cm^{-1} which decays back to baseline on the same time scale as the other negative peaks. This indicates that N_2O is formed concomitantly with **1** during the second stage in the reaction sequence in approximately the stoichiometry indicated by eqn. (3).[14] Although the final step in the mechanism described by Scheme 1 would be isomerization of an initially formed N-coordinated nitro complex to the O-bound nitrito analogue, the stopped-flow IR experiment gave no indication of intermediates between **X** and **1**. Thus, either this linkage isomerization is much faster than the trimolecular reaction of **X** with NO or this process leads to direct formation of the nitrito product.

This work was supported by the National Science Foundation (CHE-9726889) and by a Collaborative UC/Los Alamos Research (CULAR) Initiative grant from Los Alamos National Laboratory. The stopped flow spectrophotometer was purchased with an Instrumentation grant from the National Science Foundation (CHE 9522259). We thank Dr Brian Lee for intellectual contributions to this research.

Notes and references

1 L. J. Ignarro, G. M. Buga, K. S. Wood, R. E. Byrns and G. Chaudhuri, *Proc. Natl. Acad. Sci. USA*, 1987, **84**, 9265.
2 S. Moncada, R. M. J. Palmer and E. A. Higgs, *Pharmacol. Rev.*, 1991, **43**, 109.
3 D. A. Wink, I. Hanbauer, M. B. Grisham, F. Laval, R. W. Nims, J. Laval, J. Cook, R. Pacelli, J. Liebmann, M. Krishna, P. C. Ford and J. B. Mitchell, *Curr. Top. Cellular Regulation*, 1996, **34**, 159.
4 *Methods in Nitric Oxide Research*, ed. M. Feelish and J. S. Stamler, John Wiley and Sons, Chichester, England, 1996 and references therein.
5 K. M. Miranda, X. Bu, I. Lorkovic and P. C. Ford, *Inorg. Chem.*, 1997, **36**, 4838.
6 I. M. Lorkovic and P. C. Ford, *Inorg. Chem.*, 1999, **38**, 1467.
7 L. E. Laverman, M. Hoshino and P. C. Ford, *J. Am. Chem. Soc.*, 1997, **119**, 12663.
8 K. M. Kadish, V. A. Adamian, E. V. Caemelbecke, Z. Tan, P. Tagliatesta, P. Bianco, T. Boschi, G.-B. Yi, M. A. Khan and G. B. Richter-Addo, *Inorg. Chem.*, 1996, **35**, 1343.
9 D. Gwost and K. G. Caulton, *Inorg. Chem.*, 1974, **13**, 414.
10 R. D. Feltham, *Inorg. Chem.*, 1964, **3**, 119; R. D. Feltham and J. T. Carriel, *Inorg. Chem.*, 1964, **3**, 121.
11 I. M. Lorkovic, K. M. Miranda, B. Lee, S. Bernhard, J. R. Schoonover and P. C. Ford, *J. Am. Chem. Soc.*, 1998, **120**, 11674.
12 G. B. Richter-Addo and P. Legzdins, *Metal Nitrosyls*, Oxford University Press, New York, 1992, ch. 2 and references therein.
13 A referee has suggested another structure for **X**, namely Ru(P)-(N(O)NO), formed by reaction of NO with the coordinated NO of Ru(P)(NO). However, this formulation for **X** would be predicted to give products for the isotopic exchange experiments where Ru(TmTP)-(NO)(ONO) was photolyzed in the presence of $^{15}N^{18}O$ different from those observed (ref. 11). Those products can indeed be explained on the basis of formation of a dinitrosyl Ru(P)$(NO)_2$ intermediate. Another argument against this formulation would be that –N(O)NO ligand would also be expected to give two strong ν_{NO} bands yet only one new band was detected in the 1500–2300 cm^{-1} region. No new bands were seen in the 1000–1500 cm^{-1} region either; however, in that region there are several windows possibly obscured by solvent interference.
14 Based on the estimated absorption coefficients for N_2O, the yield of nitrous oxide in the second stage of the reaction was *ca*. 65% that of **1**, but the small intensity of the signal at 2215 cm^{-1} as well as possible pathways for N_2O loss add to the uncertainty of this value.

Communication 9/01779H

Solid oxide fuel cell using Co doped La(Sr)Ga(Mg)O_3 perovskite oxide with notably high power density at intermediate temperature

Tatsumi Ishihara, Takaaki Shibayama, Miho Honda, Hiroyasu Nishiguchi and Yusaku Takita

Department of Applied Chemistry, Faculty of Engineering, Oita University, Dannoharu 700, Oita 870-1192, Japan. E-mail: isihara@cc.oita.u.ac.jp

Received (in Cambridge, UK) 12th April 1999, Accepted 19th May 1999

Power generation characteristics of fuel cells was greatly improved by using $La_{0.8}Sr_{0.2}Ga_{0.8}Mg_{0.115}Co_{0.085}O_3$ as electrolyte. In particular, the maximum power density attained a value of 1.53 and 0.50 W cm^{-2} at 1073 and 873 K, respectively, in an H_2–O_2 cell when the thickness of electrolyte was 0.18 mm.

Solid oxide fuel cells (SOFCs) represent a new and clean electric power generation system. At present, Y_2O_3 stabilized -ZrO_2 (YSZ) is commonly used as the electrolyte of solid oxide fuel cells. Since the oxide ion conductivity of YSZ is fairly low, a thin electrolyte film without gas leakage and an excessively high operating temperature (1273 K) are essential to achieve high power density. On the other hand, advantages for SOFCs such as high efficiency and increased variety of usable fuels can be obtained at decreased temperatures such as 1073 K. Furthermore, choice of the materials for cell stacking becomes wider; in particular, cheap refractory metals such as stainless steel are usable upon decreasing the operating temperature down to 900 K. Consequently, a decrease in operating temperature is of importance for the development of cheap but reliable cells.[1] It is, therefore, of great importance to develop new electrolyte materials which exhibit high oxide ion conduction over a wide oxygen partial pressure. In our previous study, oxide ion conductivity in perovskite oxides were investigated and it was found that the $LaGaO_3$-based perovskite type oxide exhibits high oxide ion conductivity,[7,8] comparable with that of CeO_2-based oxide. In particular, $LaGaO_3$ doped with Sr for La and Mg for Ga sites (LSGM) exhibits high oxide ion conductivity over a wide oxygen partial pressure.[9–12] Furthermore, it was found that doping a small amount of Co into Ga sites of $LaGaO_3$ was effective in improving the oxide ion conductivity, albeit with the appearance of a small amount of hole conductivity.[13] Although the electrical conductivity monotonously increased, the transport number of oxide ion decreased with increasing Co content. Considering the transport number and oxide ion conductivity, the optimized composition of Co doped $LaGaO_3$ was $La_{0.8}Sr_{0.2}Ga_{0.8}Mg_{0.115}Co_{0.085}O_3$ (denoted LSGMC). Power generation characteristics of SOFCs with LSGMC as electrolyte was thus studied.

All specimens used in this study were prepared by conventional solid state reaction techniques employing powders of La_2O_3, Ga_2O_3, MgO, $SrCo_3$ and CoO (99.5%, Kishida). Details of the preparation procedure can be found elsewhere.[4,13] Sintering was performed at 1773 K for 6 h in air. Platinum paste was applied on both faces of sintered sample disks followed by calcination at 1223 K for 30 min.

In our previous study, for the application of LSGM as electrolyte to SOFCs, it was found that $Sm_{0.5}Sr_{0.5}CoO_3$ and Ni were appropriate for the cathode and the anode, respectively.[12] Using the same cathode and anode in this study, LSGMC was chosen as the electrolyte to develop SOFCs operable at intermediate temperatures. The initial SOFC fabricated in this study consisted of a single planar type cell of 20 mm diameter and the anode and cathode were both of 5 mm diameter. Pure O_2 or dry air and H_2 mixed with H_2O (3 vol%) were fed to the cathode and the anode, respectively, at 100 ml min^{-1}. The power generation characteristics were measured by a four probe method and a galvanostat was used to provide the electrical load.

The temperature dependence of the maximum power density together with the open circuit potential are shown in Fig. 1. The power generation characteristics of the cells using air and pure oxygen are also compared at 1073 K (Fig. 1). Open circuit potentials were slightly smaller than the theoretical values owing to hole conduction at high oxygen partial pressure, however, they remain > 1.0 V at all temperatures for both H_2–O_2 and H_2–air cells. On the other hand, notably large power densities are exhibited at all temperatures. When O_2 is used as oxidant, maximum power densities at 1273 and 1073 K are 1.40 and 0.77 W cm^{-2}, respectively. Furthermore, even at 873 K, the maximum power density is as high as 0.19 W cm^{-2}. At present, YSZ is the most common electrolyte for SOFCs. However, the maximum power density of an H_2–O_2 cell using YSZ as the electrolyte under the same conditions is only 0.38 and 0.06 W cm^{-2} at 1293 and 1073 K, respectively. Since the ionic conductivity of YSZ at 1273 K is almost the same as that of LSGMC at 923 K, it is expected that equivalent performances would potentially be achieved at considerably lower temperatures for LSGMC. The power density of the cell was slightly decreased by changing the oxidant from O_2 to air as shown in Fig. 1, however, the maximum power density was still higher than 700 mW cm^{-2} at 1073 K. It is generally observed that the power density is greatly decreased by changing the oxidant from O_2 to air. However, in this case the decrease in the power density was not large. This may result from hole conduction in LSGMC at high oxygen partial pressure. Since an extremely large power density was exhibited for both H_2–O_2 and H_2–air cells, LSGMC is highly attractive as the electrolyte of intermediate temperature SOFCs.

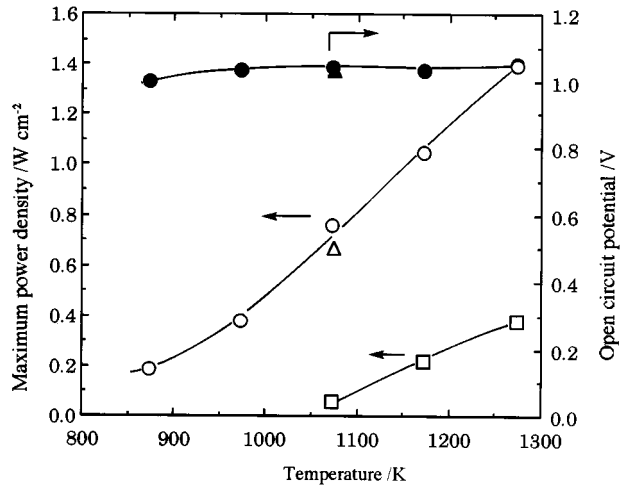

Fig. 1 Temperature dependence of electrical power generation characteristics of SOFCs containing $La_{0.8}Sr_{0.2}Ga_{0.8}Mg_{0.115}Co_{0.085}O_3$ as electrolyte. Thickness of electrolyte = 0.5 mm, $Sm_{0.5}Sr_{0.5}CoO_3$ cathode and Ni anode. (●) Open circuit potential and (○) maximum power density for an H_2–O_2 cell with LSGMC electrolyte. (△) Open circuit potential and (▲) maximum power density for an H_2–air cell with LSGMC electrolyte. (□) Maximum power density for an H_2–O_2 cell with $Zr_{0.84}Y_{0.16}O_4$ electrolyte.

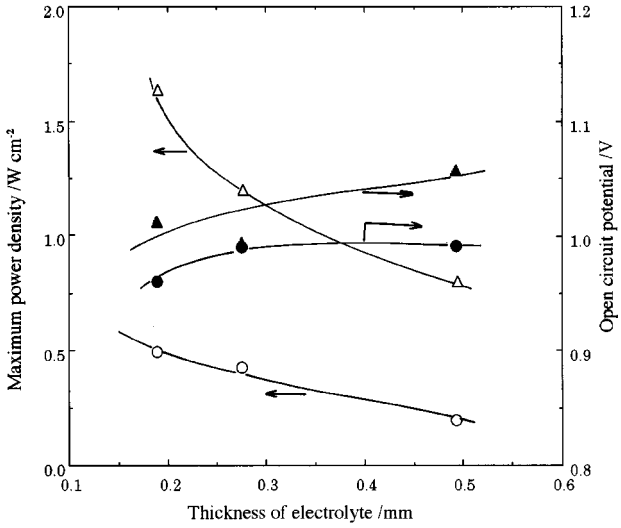

Fig. 2 Terminal voltage and power density of H_2–O_2 cells as a function of thickness of electrolyte. Ni and $Sm_{0.5}Sr_{0.5}CoO_3$ were used as anode and cathode, respectively. 873 K: (○) maximum power density and (●) open circuit potential. 1073 K: (△) maximum power density and (▲) open circuit potential.

A large part of the internal resistance of the present cell is ohmic resistance which is almost comparable to that of ionic conductivity in LSGMC. Therefore, it is reasonable to expect higher power density from a thinner LSGMC electrolyte and thus the effect of electrolyte thickness was studied. Fig. 2 shows the open circuit potential and power density of H_2–O_2 cells as a function of thickness of electrolyte. The power density of the cell monotonously increases with decreasing thickness of the electrolyte. In particular, the maximum power density reached a value of 1.53 and 0.50 W cm^{-2} at 1073 and 873 K, respectively, when the thickness of electrolyte was 0.18 mm (Fig. 2). On the other hand, the open circuit potential was decreased with decreasing thickness of the electrolyte because the contribution of hole conduction was more significant upon increasing the gradient in oxygen partial pressure. However, the open circuit potential was always > 1.0 V at 1073 K for an SOFC utilizing an LSGMC thin plate. At 0.18 mm electrolyte thickness, however, the open circuit potential was decreased to 0.94 V at 873 K, since the transport number of oxide ion was decreased. Fig. 3 shows the power generation characteristics of an LSGMC cell with 0.18 mm thick electrolyte. It is obvious that extremely large power density was attained for this cell even at 873 K. The current density at short circuited conditions at this temperature was 2.5 A cm^{-2} and furthermore, the power density at 0.7 V was as high as 352 mW cm^{-2}. This power density was comparable to that of a molten carbonate fuel cell operating at 923 K.

In light of the notably high oxide ion conductivity of LSGMC, we believe that today's SOFCs can be improved to yield higher power outputs at lower operating temperatures. The consequences of operation at low temperatures, are increased reliability of the cell with use of a reasonably priced metallic element, *e.g.* stainless steel, the removal of a requirement of an excessively thin electrolyte film and availability of more compact geometries which leads to easy maintenance and

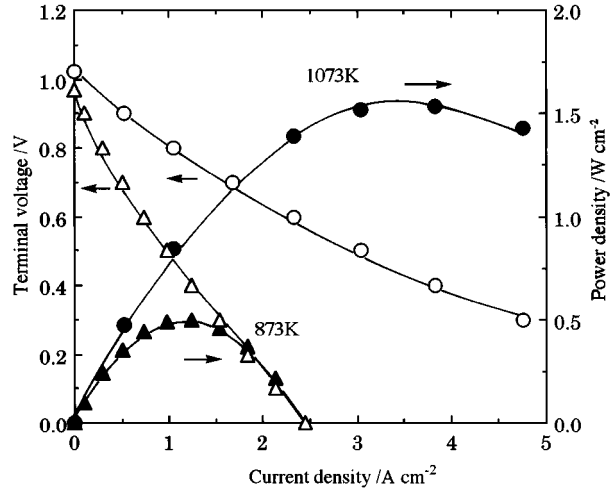

Fig. 3 Current–potential and current–power density curves of an SOFC utilizing 0.189 mm thick LSGMC at 873 and 1073 K with H_2 and O_2. (○) *I–V* curves and (●) *I–P* curves at 1073 K. (△) *I–V* curves and (▲) *I–P* curves at 873 K.

durability. These factors are major advantages arising from the use of the proposed electrolyte (LSGMC) for the next generation of power generators.

The authors would like to acknowledge the financial support from the 2nd Toyota High-technology Research Grant Program and Nissan Research Foundation. Part of this study was also supported by the Proposal-Based New Industry Creative Type Technology R&D Promotion Program from the New Energy and Industrial Technology Development Organization (NEDO) of Japan.

Notes and references

1 C. B. Choudary, H. S. Maiti and E. C. Subbarao, *Solid Electrolytes and Their Applications*, ed. E. C. Subbarao, Plenum Press, New York 1980, p. 40.
2 N. Q. Minh and T. Takahashi, *Science and Technology of Ceramic Fuel Cells*, Elsevier, Amsterdam, 1995.
3 S. De Souza, S. V. Visco and L. C. D. Jonghe, *J. Electrochem. Soc.*, 1997, **144**, L35.
4 T. Ishihara, H. Matsuda and Y. Takita, *J. Am. Chem. Soc.*, 1994, **116**, 3801.
5 M. Feng and J. B. Goodenough, *Eur. J. Solid State Inorg. Chem.*, 1994, **31**, 663.
6 K. Huang, M. Feng and J. B. Goodenough, *J. Am. Ceram., Soc.*, 1996, **79**, 1100.l
7 P. Huang and A. Petric, *J. Electrochem. Soc.*, 1996, **143**, 1644.
8 K. Nomura and S. Tanabe, *Solid State Ionics*, 1997, **98**, 229.
9 J. Drennan, V. Zelizko, D. Hay, F. T. Ciacchi, S. Rajendran and S. P. S. Badwal, *J. Mater. Chem.*, 1997, **7**, 79.
10 R. T. Baker, B. Gharbage and F. M. B. Marques, *J. Electrochem. Soc.*, 1997, **144**, 3130.
11 J. W. Stevenson, T. R. Armstrong, D. E. McCready, L. R. Pederson and W. J. Weber, *J. Electrochem. Soc.*, 1997, **144**, 3613.
12 T. Ishihara, H. Minami, H. Matsuda, H. Nishiguchi and Y. Takita, *Chem. Commun.*, 1996, 929.
13 T. Ishihara, H. Furutani, T. Yamada and Y. Takita, *Ionics*, 1997, **3**, 209.

Communication 9/02899D

A novel *in situ* simultaneous polymerization–hydrolysis technique for fabrication of polyacrylamide–semiconductor MS(M = Cd, Zn, Pb) nanocomposites

Yong Zhou,[a] Shuhong Yu,[a] Cuiying Wang,[a] Xiaoguang Li,[b] Yurui Zhu[a] and Zuyao Chen*[a]

[a] *Department of Chemistry, University of Science and Technology of China, Hefei, Anhui 230026, P. R. China. E-mail: zhz@mail.ustc.edu.cn*

[b] *Department of Materials Science and Engineering, University of Science and Technology of China, Hefei, Anhui 230026, P. R. China*

Received (in Cambridge, UK) 12th April 1999, Accepted 17th May 1999

Polyacrylamide(PAM)–semiconductor MS (M = Cd, Zn, Pb) nanocomposites with homogeneously well dispersed semiconductor nanoparticles in the polymer matrices were prepared by a novel *in situ* simultaneous polymerization–hydrolysis technique (SPH).

The synthesis and characterization of inorganic-organic polymer nanocomposites has received much intense research interest,[1] owing to their optical, electrical, catalytic and mechanical properties,[2,3] and potential applications in microelectronics.[4]

Many methods have been exploited to prepare semiconductor–polymer nanocomposites. Organization of semiconductor nanoparticles in an orderly fashion in a matrix may provide potential applications of their special properties, whereas polymers are expected to provide good mechanical and optical properties, conferring high kinetic stability on nanometer-sized semiconductor particles.

Meissner *et al.*[5] first reported a system involving dispersed semiconductor/polymer arrangements by physically embedding monograin CdS particles of *ca.* 40 μm diameter in a thin, nonconducting polyurethane membrane and various photoprocesses were examined. Later, a new method of incorporation of dispersed semiconductor CdS throughout an ionically conductive Nafion polymer membrane was developed.[6] Recently, CdS/polystyrene,[7] CdS/PS–P2VP[polystyrenes–block–poly(vinylpyridine)s],[8] PbS/S–MA(styrene–methylacrylic copolymer)[9] and PbS/E–MAA(ethylene–15% methacrylic acid copolymer) composites have been prepared in different polymer matrices using a variety of methods.[10] The multisemiconductor nanocomposite Cu_2S/CdS/ZnS was also successfully prepared in polystyrene by ion exchange.[11] Wang and Herron reported, for the first time, the synthesis of CdS/PVK(*N*-polyvinylcarbazole) polymer composite by using $Cd_{10}S_4Ph_{12}$ as precursor.[12] Currently, the use of amphiphilic block copolymer (ABC) micelles opens a doorway to utilize these materials as 'nanoreactors' for the formation of inorganic nanocrystals.[1,13] Other block copolymer system/metal sulfide nanoparticles have been prepared by addition of H_2S.[14]

Here, we report a novel *in situ* simultaneous polymerization–hydrolysis technique (SPH) for preparing polyacrylamide–semiconductor MS (M = Cd, Zn, Pb) nanocomposites in aqueous systems. The so-called SPH technique is based on the mechanism of the simultaneous polymerization of organic monomer and formation of semiconductor nanoparticles. It was found that the semiconductor nanoparticles (CdS, ZnS, PbS) were homogeneously well dispersed in the polyacrylamide matrices. The present SPH technique may provide a new route to prepare other metal sulfide–polymer hybrid nanocomposites.

In a typical procedure, the CdS–polyacrylamide (CdS–PAM) nanocomposite was prepared in an aqueous system. 0.01 mol $CdCl_2$ and 0.01 mol NH_2CSNH_2 were added to a 100 ml of 5.0 mol l^{-1} acrylamide(AM) monomer aqueous solution. Then, 0.01 g AIBN (2,2′-azobisisobutyronitrile) as radical initiator was added to the above solution. The mixture solution was put into a stainless-steel tank with a Teflon inner and heated in an oven at 140 °C for 12 h. The product obtained was washed with distilled water and absolute ethanol, dried at room temperature and ground into a powder for characterization.

The X-ray powder diffraction (XRD) pattern for the product was determined at a scanning rate of 0.02° s^{-1} in the 2θ range from 5–65°, using Japanese Rigaku Dmax γ_A-ray diffractometer with high-intensity Cu-Kα radiation (λ = 0.151478 nm) and a graphite monochromater was set at the diffracted radiation. The UV–VIS absorption spectrum was recorded with a Shimadzu UV-200 spectrophotometer. TEM images were taken with a Hitachi model H-800 transmission electron microscope, using an accelerating voltage of 200 kV.

Fig.1 shows the XRD pattern of a CdS–PAM nanocomposite obtained by the present SPH technique at 140° for 12 h. The broad peak at *ca.* 23° corresponds to the PAM phase. Cubic phase CdS nanoparticles were obtained. Not all diffraction peaks of the CdS nanoparticles can be observed in the XRD pattern of the CdS–PAM nanocomposite because of interference from the broad diffraction peaks for the PAM phase. However, the diffraction peaks for cubic CdS for $2\theta > 40°$ can clearly be seen.

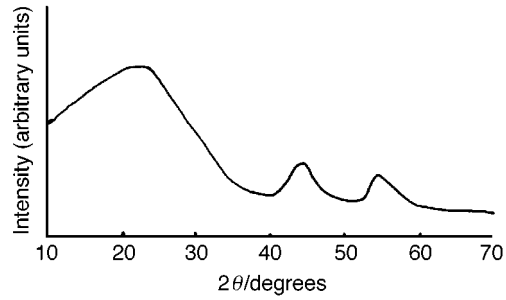

Fig. 1 The XRD pattern of a CdS–PAM nanocomposite prepared by the *in situ* simultaneous polymerization–hydrolysis technique (SPH) at 140 °C for 12 h.

The UV–VIS absorption spectrum of the CdS–PAM nanocomposite, dispersed in ethanol, was measured using pure PAM dispersed in ethanol as a reference solution.

The resulting spectrum shows λ_{max} for the CdS nanoparticles in the CdS/PAM nanocomposite at *ca.* 476 nm, *i.e.* blue-shifted relative to bulk CdS (515 nm).[15]

Fig. 2 shows a TEM image of the CdS–PAM nanocomposite powder. The image shows that the CdS nanoparticles prepared by the present SPH technique were homogeneously well dispersed in the PAM matrix. A histogram of the CdS nanoparticles (Fig. 3) shows a distribution of particle sizes in the range 2–10 nm.

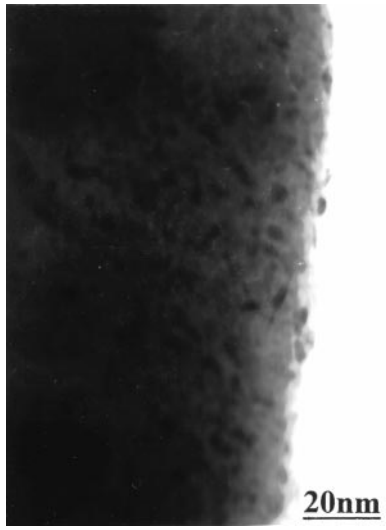

Fig. 2 TEM image of a CdS–PAM nanocomposite prepared by the *in situ* simultaneous polymerization–hydrolysis technique (SPH) at 140 °C for 12 h.

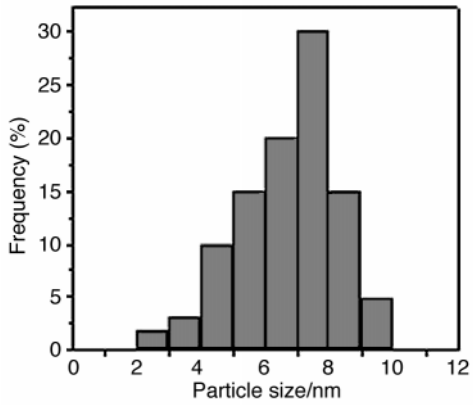

Fig. 3 Higtogram of CdS nanoparticle size in a CdS–PAM nanocomposite prepared by the present *in situ* SPH technique.

It is well known that the radical initiator AIBN decomposes at 45–65 °C, according to eqn. (1).

$$Me_2C(CN)-N=N-C(CN)Me_2 \xrightarrow{45\text{–}65\ ^\circ C} 2\ Me_2C^{\bullet}(CN) + N_2 \qquad (1)$$

The resulting radicals initiate the polymerization of the acrylamide (AM) monomer. Accompanying polymerization, CdS nanoparticles are also simultaneously formed by hydrolysis of NH_2CSNH_2 as described in eqns. (2) and (3).

$$NH_2CSNH_2 + 2H_2O \xrightarrow{Hydrolysis} 2NH_3 + CO_2 + H_2S \qquad (2)$$

$$Cd^{2+} + H_2S \longrightarrow CdS + 2H^+ \qquad (3)$$

Therefore, the obtained CdS nanoparticles can be homogeneously well dispersed in the PAM matrix. Further studies demonstrate that the average size of CdS nanoparticles in the absence of AM monomer obtained under the same preparation conditions as for the CdS–PAM nanocomposite, is *ca.* 20 nm which is larger than that of the CdS nanoparticles in the CdS–PAM nanocomposite. The reason may be that the reaction medium becomes more and more viscous as polymerization of the AM monomer proceeds, which is favorable for preventing the aggregation of initially formed CdS nanoparticles.

Fig. 4 TEM image of a ZnS–PAM nanocomposite prepared by the *in situ* simultaneous polymerization–hydrolysis technique (SPH) at 140 °C for 12 h.

We have also prepared ZnS–PAM and PbS–PAM nanocomposites *via* the present SPH technique by using $Zn(NO_3)_2$ and $Pb(NO_3)_2$ instead of $CdCl_2$. Fig. 4 shows the TEM image for the ZnS–PAM nanocomposite. It was found that the ZnS nanoparticles were also homogeneously well dispersed in the PAM matrix with a size of *ca.* 5–15 nm. The TEM image for the PbS–PAM nanocomposite indicates that the size of the PbS nanoparticles is *ca.* 10–20 nm.

In summary, CdS–PAM, ZnS–PAM and PbS–PAM nanocomposites with homogeneous dispersion of the metal sulfide nanoparticles in the polymer matrices were prepared by a novel *in situ* simultaneous polymerization–hydrolysis technique (SPH). The polymerization reaction of the AM monomer is favorable for preventing the aggregation of initially formed semiconductor nanoparticles. The present *in situ* SPH technique may provide a new route to prepare other metal sulfide semiconductor–polymer hybrid nanocomposites.

This work was supported by the National Nature Science Foundation of China (No. 59572031 and 19772049).

Notes and references

1 M. Antonietti and C. Göltner, *Angew. Chem., Int. Ed. Engl.*, 1997, **36**, 910.
2 D. M. Bigg, *Polym. Compos.*, 1996, **7**, 125.
3 L. T. Chang and C. C. Yen, *J. Appl. Polym. Sci.*, 1995, **55**, 371.
4 G. Schmid, *Chem. Rev.*, 1992, **92**, 1709.
5 D. Meissner, R. Memming and B. Kastening, *Chem. Phys. Lett.*, 1983, **96**, 34.
6 M. Krishnan, J. R. White, M. A. Fox and A. Bard, *J. Am. Chem. Soc.*, 1983, **105**, 7002.
7 J. M. Huang, Y. Yang, B. Yang, S. Y. Liu and J. C. Shen, *Polym. Bull.*, 1996, **36**, 337.
8 M. Möller, *Synth. Met.*, 1991, **41**, 1159.
9 M. Y. Gao, Y. Yi, B. Yang, F. L. Beng and J. C. Shen, *J. Chem. Soc., Chem. Commun.*, 1994, 2777.
10 Y. Wang, A. Suna, W. Mahler and R. Kesowski, *J. Chem. Phys.*, 1987, **87**, 7315; W. Mahler, *Inorg. Chem.*, 1988, **27**, 435.
11 Jinman Huang, Yi Yang, Bai Yang, Shiyong Liu and J. C. Shen, *Polym. Bull.*, 1996, **37**, 679.
12 Y. Wang and N. Herron, *Chem. Phys. Lett.*, 1992, **200**, 71.
13 A. Roescher and Möller, *Adv. Mater.*, 1995, **7**, 151.
14 M. Moffitt and A. Eisenberg, *Chem. Mater.*, 1995, **7**, 1178.
15 Y. M. Gao, P. Wu, J. Baglio, K. M. Dwight and A. Wold, *Mater. Res. Bull.*, 1989, **24**, 1215.

Communication 9/02891I

Syntheses of neutral iron, ruthenium and manganese half-sandwich vinylidene complexes. Crystal structure of $Fe(SnPh_3)(CO)(=C=CHPh)(\eta\text{-}C_5H_5)$

Harry Adams, Simon G. Broughton, Stephen J. Walters and Mark J. Winter*

Department of Chemistry, The University, Sheffield, UK S3 7HF. E-mail: Mark.Winter@Sheffield.ac.uk

Received (in Basel, Switzerland) 5th January 1999, Accepted 7th April 1999

Treatment of various anionic acyls $[M(SnPh_3)(CO)(COCH_2R)(\eta\text{-}C_5H_5)]^-$ (M = Fe, Ru) and acyls $[Mn(CO)_2(COCH_2R)(\eta\text{-}C_5H_4Me)]^-$ with MeCOCl affords acyl(oxy) carbenes $M(SnPh_3)(CO)\{=C(OCOMe)CH_2R\}(\eta\text{-}C_5H_5)$ and $[Mn(CO)_2\{=C(OCOMe)CH_2R)\eta\text{-}C_5H_4Me)]$ which formally eliminate $MeCO_2H$ to form neutral half-sandwich vinylidene complexes $M(SnPh_3)(CO)(=C=CHR)(\eta\text{-}C_5H_5)$ and complexes $Mn(CO)_2(=C=CHR)(\eta\text{-}C_5H_4Me)$.

Vinylidene complexes $L_nM(=C=CR^1R^2)$ have attracted a great deal of interest[1] over the last 15 years, partly due to the proposed intermediacy of vinylidene species in the Fischer–Tropsch process,[2] and also due to their ability to act as catalysts for alkyne polymerisation[3] and condensation[4] reactions. These complexes are prepared generally through either the rearrangement of alk-1-ynes at a metal centre, or through alkylation or protonation of the β-carbon of acetylide ligands. In the case of the Group 8 transition metals, the vast majority of these complexes are *cationic*. A very small number of neutral Group 7 and 8 half-sandwich vinylidene complexes are known.[5–7] We outline here a new method for the preparation of a class of *neutral* iron, ruthenium and manganese vinylidene complexes, the neutrality of which is expected to have important consequences for subsequent chemistry.

Recently, we reported the isolation of a number of unusually stable acyl(oxy) carbene species $M(SnPh_3)(CO)\{=C(OCOR)Ph\}(\eta\text{-}C_5H_5)$ (M = Fe, Ru; R = Me, Ph, Bu^t).[8] These are formed through the reaction of acid chlorides RCOCl with the anionic acyls $[M(SnPh_3)(CO)(COPh)(\eta\text{-}C_5H_5)]^-$. We now find that the corresponding anions $[M(SnPh_3)(CO)(COCH_2R)(\eta\text{-}C_5H_5)]^-$ **3**, **4** (Scheme 1) are available from the reactions of $LiCH_2R$ with $M(SnPh_3)(CO)_2(\eta\text{-}C_5H_5)$ **1**, **2**. These also react with MeCOCl, but while the expected acyl(oxy) carbenes $M(SnPh_3)(CO)\{=C(OCOMe)CH_2R\}(\eta\text{-}C_5H_5)$ **5** and **6** do indeed form, and are detectable by IR spectroscopy at low temperatures, the products isolated at ambient temperature are, unexpectedly, the *neutral* vinylidenes $M(SnPh_3)(CO)(=C=CHR)(\eta\text{-}C_5H_5)$ (R = H, Pr, Me, Ph) **7** and **8**.† These products correspond to the formal loss of $MeCO_2H$ from the intermediate acyl(oxy) carbenes $M(SnPh_3)(CO)\{=C(OCOMe)CH_2R\}(\eta\text{-}C_5H_5)$. The presence of protons on the carbon α to the carbene is *essential* for vinylidene formation, as is the presence of the labile acyl(oxy) substituent. We note here a previous report in which the *cationic* iron vinylidene complexes $[Fe(PPh_3)(CO)(=C=CR_2)(\eta\text{-}C_5H_5)]^+$ (R = H, Me) are prepared through loss of CF_3SO_3H from intermediate triflate-substituted carbenes of the form $[Fe(PPh_3)(CO)\{=C(OSO_2CF_3)CHR_2\}(\eta\text{-}C_5H_5)]^+$.[9]

The method for vinylidene preparation presented here is versatile in that it allows the direct preparation of rare examples of unsubstituted vinylidene complexes, as well as examples bearing methyl and phenyl substituents, in a single step from readily available starting materials. Yields are good. The method also works for different metals. For instance, the corresponding reactions of the manganese compound $Mn(CO)_3(\eta\text{-}C_5H_4Me)$ **9** (Scheme 2) afford the neutral vinylidenes $M(CO)_2(=C=CHR)(\eta\text{-}C_5H_4Me)$ (R = Pr, Ph) **10** as red oils.‡

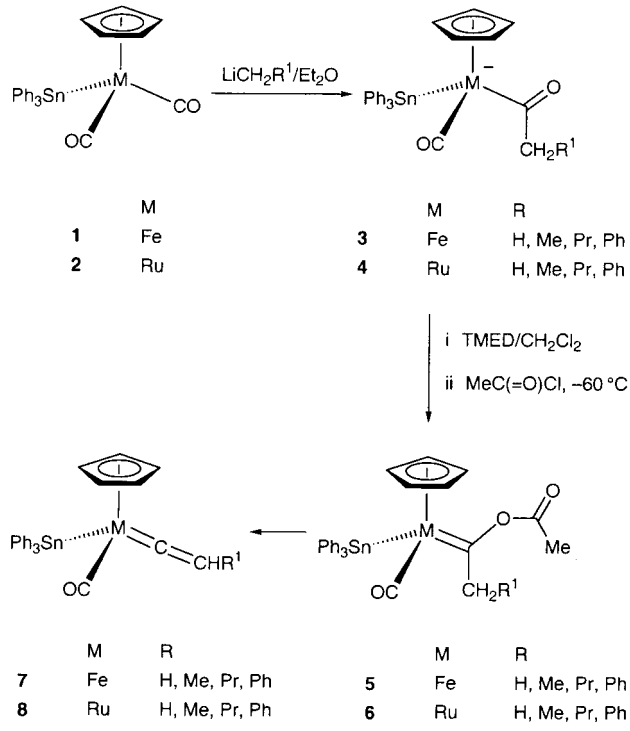

	M
1	Fe
2	Ru

	M	R
3	Fe	H, Me, Pr, Ph
4	Ru	H, Me, Pr, Ph

	M	R
7	Fe	H, Me, Pr, Ph
8	Ru	H, Me, Pr, Ph

	M	R
5	Fe	H, Me, Pr, Ph
6	Ru	H, Me, Pr, Ph

Scheme 1

The new complexes exhibit spectroscopic data typical for vinylidene complexes. For example, the parent complex **7** (R = H)§ shows a medium strength absorption [$\nu_{CO}(CH_2Cl_2)$ 1637 cm^{-1}] in its IR spectrum. This is attributed to the C=C stretch and signals at $\delta_C(CDCl_3)$ 346.2 and 105.3 in its ^{13}C NMR spectrum due to the vinylidene α- and β-carbons respectively. The presence of a singlet for the vinylidene protons in the ^1H NMR of the complex indicates that vinylidene rotation is facile at ambient temperature.

The nature of one compound **7** (R = Ph)¶ is further illustrated by a crystallographic study (Fig. 1), carried out in order to understand the vinylidene parameters. The Fe=C bond length of 1.744(4) Å is very short, reflecting the excellent π-acceptor properties[10] of the vinylidene fragment. The C=C bond length of 1.312(5) Å is in accord for a vinylidene complex, and reflects a bond order of *ca.* two. The vinylidene fragment itself is linear [Fe–C(7)–C(8) 179.7(3)°], and shows an orientation that corresponds both with theoretical studies[10] and with previously

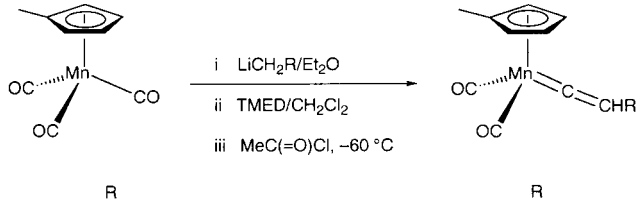

	R
9	Pr, Ph

	R
10	Pr, Ph

Scheme 2

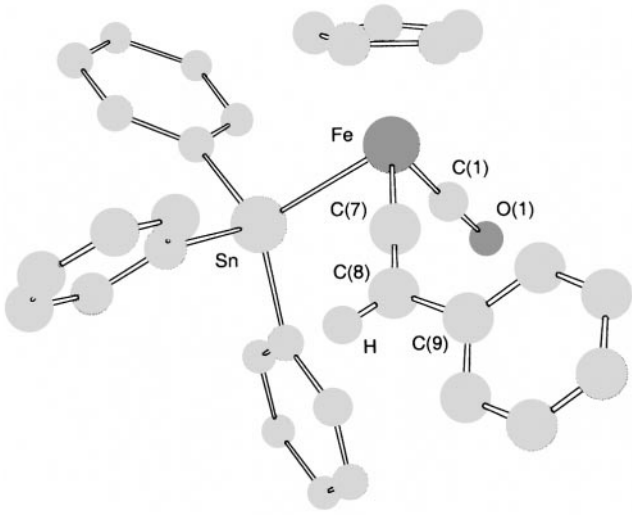

Fig. 1 Molecular structure of Fe($SnPh_3$)(CO)(=C=CHPh)(η-C_5H_5) **7** (R = Ph). Selected bond lengths (Å): Fe–C(7) 1.744(4), C(7)–C(8) 1.312(5), C(8)–C(9) 1.471(6).

reported structures of cationic iron and ruthenium vinylidene complexes.[11,12] As expected on steric grounds, the phenyl substituent occupies a position *anti* to the triphenyltin group. The vinylidene fragment does not adopt a truly horizontal conformation: the angle between the vinylidene plane and the plane defined by the centroid of the cyclopentadienyl ring, iron atom and C(7) is 73° rather than 90°. The twist is anticlockwise as viewed along C(8)–C(7)–Fe, and presumably minimizes steric interactions between the vinylidene hydrogen substituent and the triphenyltin group.

Notes and references

† Ru($SnPh_3$)(CO)(=C=CH_2)(η-C_5H_5) **8** (R = H): yellow, mp 112–113 °C. Found: C, 54.66; H, 3.81%; $[M]^+$ 570; $C_{32}H_{26}FeOSn$ requires C, 54.75; H, 3.89%; $[M]^+$ 570. IR (CH_2Cl_2, cm^{-1}) ν_{CO} 1972s, $\nu_{C=C}$ 1637m; δ(toluene-d_8) 7.75–7.63 (m, 6H, *o*-SnPh), 7.30–7.10 (m, 9H, *m*-, *p*-SnPh), 4.78 (s, 5H, η-C_5H_5), 3.85 (s, 2H, J_{SnH} 35, Ru=C=CH_2); δ_C($CDCl_3$) 336.3 (Ru=C), 200.3 (CO), 143.5 (*ipso*-SnPh), 136.7 (J_{SnC} 40, *o*-SnPh), 128.0 (J_{SnC} 47, *m*-, *p*-SnPh), 97.7 (Ru=C=*C*H_2), 88.4 (η-C_5H_5).

‡ $Mn(CO)_2$(=C=CHPh)(η-C_5H_4Me) **10** (R = Ph): red oil. Found C, 65.26; H, 4.29%; $[M - 2CO]^+$ 236; $C_{32}H_{26}FeOSn$ requires C, 65.74; H, 4.42%; $[M - 2CO]^+$ 236. IR (light petroleum, cm^{-1}) ν_{CO} 2006s, 1952, $\nu_{C=C}$ 1647m, 1630m, 1621m, 1598m, 1575m; δ_H($CDCl_3$) 7.35–7.25 (m, 2H, *o*-Ph), 7.20–7.05 (m, 3H, *m*-, *p*-Ph), 6.70 (s, 1H, =C=CH), 5.00 (m, 2H, η-C_5H_4Me), 4.95 (m, 2H, η-C_5H_4Me), 2.05 (s, 3H, Me), δ_C($CDCl_3$) 380 (Mn=C), 226.5 (CO), 133.3 (*ipso*-Ph), 128.6 (*o*-, *m*-Ph), 125.2 (*p*-Ph), 124.2 (*o*-, *m*-Ph), 122.4 (=C=*C*HPh), 88.1 (η-C_5H_4Me); 86.4, (η-C_5H_4Me), 13.7 (Me).

§ Fe($SnPh_3$)(CO)(=C=CH_2)(η-C_5H_5) **7** (R = H): yellow, mp 101–103 °C (decomp.). Found: C, 69.67; H, 4.01%; $[M]^+$ 526; $C_{26}H_{22}FeOSn$ requires C, 59.48; H, 4.22%, $[M]^+$; 526. IR (CH_2Cl_2, cm^{-1}) ν_{CO} 1962s, $\nu_{C=C}$ 1633m; δ_H($CDCl_3$) 7.65–7.54 (m, 6H, *o*-SnPh), 7.42–7.26 (m, 9H, *m*-, *p*-SnPh), 4.89 (s, 5H, η-C_5H_5), 4.57 (s, 2H, J_{SnH} 34, Fe=C=CH_2); δ_C($CDCl_3$) 346.2 (Fe=C), 214.4 (CO), 143.7 (*ipso*-SnPh), 136.7 (J_{SnC} 37, *o*-SnPh), 128.2 (*m*-, *p*-SnPh), 105.3 (Fe=C=*C*H_2), 85.4 (η-C_5H_5).

¶ Fe($SnPh_3$)(CO)(=C=CHPh)(η-C_5H_5) **7** (R = Ph): red–orange, mp 134–136 °C (decomp.). Found: C, 63.53; H, 4.17%; $[M]^+$ 602; $C_{32}H_{26}FeOSn$ requires C, 63.94; H, 4.36%; $[M]^+$ 602. IR (CH_2Cl_2, cm^{-1}) ν_{CO} 1966s, $\nu_{C=C}$ 1650m, 1640m, 1626m, 1593m, 1574w; δ_H($CDCl_3$) 7.63–7.53 (m, 6H, *o*-SnPh), 7.40–7.06 (m, 14H, *m*-, *p*-SnPh with Fe=C=CH*Ph*), 6.03 (s, 1H, J_{SnH} 19, Fe=C=C*H*Ph), 4.99 (s, 5H, η-C_5H_5); δ_C($CDCl_3$) 354.5 (Fe=C), 213.7 (CO), 143.4 (J_{SnC} 379, *ipso*-SnPh), 136.6 (J_{SnC} 38, *o*-SnPh), 132.1 (*ipso*-Fe=C=CH*Ph*), 128.7 (*o*- or *m*-Fe=C=CH*Ph*), 128.2 (*m*-, *p*-SnPh), 126.8 (Fe=C=*C*HPh), 125.9 (*p*-Fe=C=CH*Ph*), 124.9 (*o*- or *m*-Fe=C=CH*Ph*), 85.6 (η-C_5H_5).

Crystal data for **7** (R = Ph): monoclinic, a = 14.334(5), b = 10.318(4), c = 19.761(10) Å, β = 111.09(4)°, U = 2727(2) $Å^3$, Z = 4, D_c = 1.464 g cm^{-3}, space group $P2_1/n$ (a non standard setting of $P2_1/c$, no. 14), Mo-Kα radiation ($\bar{\lambda}$ = 0.71073 Å), μ(Mo-Kα) = 1.469 mm^{-1}, F(000) = 1208. Data were collected in the range $3.5 < 2\theta < 50°$ (ω-scan), 4801 independent reflections (R_{int} = 0.0340), final R = 0.0355, with allowance for the thermal anisotropy of all non-hydrogen atoms. CCDC 182/1225.

1 M. I. Bruce, *Chem. Rev.*, 1991, **91**, 197.
2 L. E. McCandlish, *J. Catal.*, 1983, **83**, 362.
3 S. J. Landon, P. M. Shulman and G. L. Geoffroy, *J. Am. Chem. Soc.*, 1985, **107**, 6739.
4 B. M. Trost and R. J. Kulawiec, *J. Am. Chem. Soc.*, 1992, **114**, 5579.
5 T. Braun, P. Steinert and H. Werner, *J. Organomet. Chem.*, 1995, **488**, 169.
6 L.-J. Baker, C. E. F. Rickard, W. R. Roper, S. D. Woodgate and L. J. Wright, *J. Organomet. Chem.*, 1998, **565**, 153.
7 A. B. Antonova, N. E. Kolobova, P. V. Petrovsky, B. V. Lokshin and N. S. Obezyuk, *J. Organomet. Chem.*, 1977, **137**, 55.
8 H. Adams, C. A. Maloney, J. E. Muir, S. J. Walters and M. J. Winter, *J. Chem. Soc., Chem. Commun.*, 1995, 1511.
9 B. E. Boland-Lussier, M. R. Churchill, R. P. Hughes and A. L. Rheingold, *Organometallics*, 1982, **1**, 628.
10 N. M. Kostic and R. F. Fenske, *Organometallics*, 1982, **1**, 974.
11 R. L. Beddoes, C. Bitcon, R. W. Grime, A. Ricalton and M. W. Whiteley, *J. Chem. Soc., Dalton Trans.*, 1995, 2873.
12 M. P. Gamasa, J. Gimeno, E. Lastra, B. M. Martin, A. Anillo and A. Tiripicchio, *Organometallics*, 1992, **11**, 1373.

Communication 9/00004F

ChemComm

A novel stationary phase for chiral chromatography: poly-L-leucine supported on porous graphitic carbon and its application to the separation of the enantiomers of chiral epoxides

Elizabeth J. Kelly,[a] David M. Haddleton,[a] David H. G. Crout,*[a] Paul Ross[b] and James Dutton[b]

[a] *Department of Chemistry, University of Warwick, Coventry, UK CV4 7AL. E-mail: d.h.g.crout@warwick.ac.uk*
[b] *Hypersil, Chadwick Road, Astmoor, Runcorn, Cheshire, UK WA7 7PR*

Received (in Liverpool, UK) 17th February 1999, Accepted 19th May 1999

A novel chiral stationary phase consisting of poly-L-leucine supported on porous graphitic carbon has been shown to be effective in the separation of the enantiomers of epoxides 1-5 by chiral high performance liquid chromatography.

The separation of enantiomers using chiral stationary phases in high performance liquid chromatography is an important technique for both the analysis and preparation of chiral compounds.[1] The use of polysaccharide derivatives, first described by Okamoto *et al*.,[2] has been primarily responsible for the increase in accessibility of this technique. Polysaccharides, cellulose and amylose, in particular, are derivatised through the formation of carbamate residues which results in highly crystalline polymers. The recognition of chirality in analytes is attributable not only to the inherent chirality of the carbohydrate components of the polymer, but also on the substantial helical nature of the tertiary structure.[3]

Polymers are finding wide-spread use as chiral catalysts in asymmetric synthesis. For example, Julia[4] and Roberts[5] have shown that poly-L-leucine functions as an asymmetric catalyst for the epoxidation of certain α,β-unsaturated ketones. The use of polymeric α-amino acids in synthesis has been reviewed.[6] However, the basis of enantiorecognition in this system has not been conclusively determined.[7] The factors involved are no doubt similar to those responsible for the enantioselectivity of chiral stationary phases in adsorption chromatography. An understanding of the mechanism of enantiorecognition in both systems would undoubtedly enhance the development of these techniques.[8] Colonna *et al*. have suggested that enantiorecognition is attributable to hydrogen bonding between the ketone functionality and the amide NH groups of the polymer backbone.[8] More recently Roberts and co-workers discussed the chiral architecture of poly-L-leucine and suggested that the enantiorecognition was induced mainly by the amino terminus of the peptide.[9]

The remarkable selectivity generated by poly-L-leucine in the Julia–Colonna system led us to explore the use of poly-L-leucine supported on porous graphitic carbon (PLL-PGC) as a chiral stationary phase for HPLC. Poly-L-leucine with derivatised end groups has been previously described in the enantioseparation of D- and L-leucine dipeptides.[10] The separation of a racemic mixture using PLL-PGC provides evidence for the level of interaction between poly-L-leucine and the analyte.

Poly-L-leucine was synthesised by ring opening polymerisation of L-leucine *N*-carboxyanhydride, using either 1,2-diaminoethane as initiator, resulting in polymer with amino functionality at both termini of the polymer chain, or water as initiator. Molecular mass information is difficult to obtain owing to the low solubility of this crystalline polymer. However, using highly acidic solutions (1% TFA and 1% formic acid respectively) both MALDI-TOF-MS and ESI-MS spectra of poly-L-leucine produced with 1,2-diaminoethane as initiator were obtained. In MALDI-TOF-MS the observed ions range from *m/z* 647.1 to 2116.1 (DP 5 to 18). The highest mass singly charged ion observed in electrospray ionisation had *m/z* 1759.3 (DP 15).

Poly-L-leucine was adsorbed onto the surface of porous graphitic carbon through the slow evaporation of a solution in 5% TFA in EtOH. The stationary phase was subsequently slurry packed under high pressure into high performance liquid chromatography columns. Columns giving the best performance were obtained using poly-L-leucine that had been continuously extracted (Soxhlet) with DMF–EtOH (5:1) for 48 h. The epoxides **1**-**5**, all but one of which correspond to the

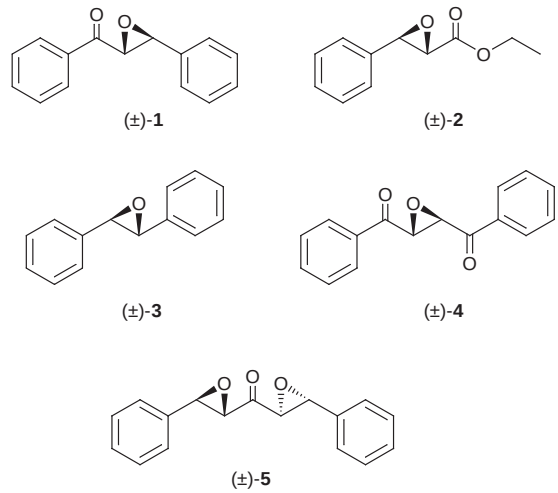

epoxide of an α,β-unsaturated ketone or ester, were analysed by reversed-phase HPLC. The results are given in Table 1. In all cases complete resolution of the two enantiomers was achieved. Fig. 1 shows the chromatogram recorded for the separation of the enantiomers of chalcone α,β-epoxide **1**. When racemic mixtures of **1**–**5** were eluted on an uncoated porous graphitic column, no separation of enantiomers was observed. The retention times of epoxides **1**-**5** were much greater than those observed with PLL-PGC. For example, the elution of chalcone α,β-epoxide from the uncoated column did not begin until 15 min after injection. Elution was complete after 25 min.

Table 1 HPLC data for the resolution of the enantiomers of epoxides **1**-**5** by poly-L-leucine supported on porous graphitic carbon[a]

Compound	k_1	k_2	α
1	4.35	10.68	2.56
2	4.33	5.82	1.34
3	2.05	2.42	1.18
4	5.58	12.45	2.13
5	6.47	12.30	1.90

[a] Solvent system: MeCN–H_2O (90 : 10 v/v), 0.5 cm^3 min^{-1}; column: 250 × 4.8 mm, $k = (t_R - t_0)/t_0$; k_1 = capacity factor for the first eluted peak; k_2 = capacity factor for the second eluted peak; α is the separation factor and is defined as $\alpha = k_2/k_1 = (t_{R2} - t_0)/(t_{R1} - t_0)$.

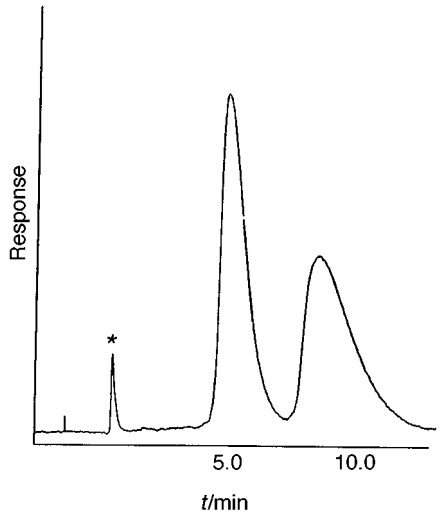

Fig. 1 Enantioseparation of epoxide **1** using PGC-PLL. Mobile phase: MeCN–H_2O (90 : 10 v/v), flow rate = 1.0 cm^3 min^{-1}; t_0 is marked with acetone (*).

The use of poly-L-leucine as an asymmetric catalyst for epoxidation has been largely confined to α,β-unsaturated ketones. The separation of *trans*-stilbene oxide **3** suggests that the mechanism of enantiorecognition is dominated by the chirality of the epoxide and its interaction with the polymer, and not by the presence of the carbonyl group. Compounds **6**-**9** were

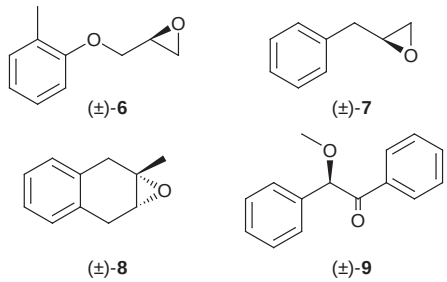

not separated on the PLL-PGC column. Comparison between this group and compounds **1**-**5** suggests the presence of an epoxide group with an attached phenyl or benzoyl substituent is necessary for successful separation of enantiomers. Although the number of examples is limited, these results do suggest that there is a parallel between the ability of poly-L-leucine to catalyse asymmetric epoxidation of α,β-unsaturated ketones and its ability to resolve the corresponding epoxides on PLL-PGC columns.

In summary we have demonstrated the use of a poly(amino acid)-coated porous graphitic carbon as an effective stationary phase in chiral HPLC. Poly-L-leucine has been shown to be an excellent alternative to cellulose as a stationary phase for the separation of the enantiomers of chiral epoxides. The parallel between the effectiveness of poly-L-leucine in catalysing the epoxidation of α,β-unsaturated ketones with high stereodiscrimination, and its effectiveness in resolving racemic mixtures of the same epoxides in the chiral HPLC system described above, suggests that the same factors are responsible for the stereoselectivity exhibited by both systems. It also suggests that the degree of separation of enantiomers of a given epoxide in the PLL-PGC system might be used to predict the effectiveness of poly-L-leucine as a catalyst for the epoxidation of the corresponding α,β-unsaturated ketones.

We thank Hypersil for financial support (to E. J. K.) and Professor K. R. Jennings and Dr A. Millar for electrospray ionisation mass spectrometry.

Notes and references

1 *A Practical Approach to Chiral Separations by Liquid Chromatography*, ed. G. Subramanian, VCH, New York, 1994.
2 Y. Okamoto, M. Kawashima and K. Hatada, *J. Am. Chem. Soc.*, 1984, **106**, 5357.
3 T. D. Booth, W. J. Lough, M. Saeed, T. A. G. Nocter and I. W. Wainer, *Chirality*, 1997, **9**, 173.
4 S. Banfi, S. Colonna, H. Molinari, S. Julia and J. Guixer, *Tetrahedron*, 1984, **40**, 5207.
5 W. Kroutil, M. E. Lasterra-Sanhez, S. J. Maddrell, P. Mayon, P. Morgan, S. M. Roberts, S. R. Thornton, C. J. Todd and M. Tuter, *J. Chem. Soc., Perkin Trans. 1*, 1996, 2837.
6 S. Ebrahim and M. Wills, *Tetrahedron: Asymmetry*, 1997, **8**, 3163.
7 L. Pu, *Tetrahedron: Asymmetry*, 1998, **9**, 1457.
8 S. Colonna, H. Molinari, S. Banfi, S. Julia, J. Masana and A. Alvarez, *Tetrahedron*, 1983, **39**, 1635.
9 P. A. Bentley, W. Kroutil, J. A. Littlechild and S. M. Roberts, *Chirality*, 1997, **9**, 198.
10 C. Hirayama, H. Ihara and K. Tanaka, *J. Chromatogr.*, 1988, **450**, 271.

Communication 9/01367I

ChemComm

An efficient carbonylation of aryl halides catalysed by palladium complexes with phosphite ligands in supercritical carbon dioxide

Yoshihito Kayaki,[a] Yushi Noguchi,[a] Seiji Iwasa,[a] Takao Ikariya*[a] and Ryoji Noyori[b]

[a] *Department of Chemical Technology, Tokyo Institute of Technology and CREST, Japan Science and Technology Corporation, O-okayama, Meguro-ku, Tokyo 152-8552, Japan. E-mail: tikariya@o.cc.titech.ac.jp*

[b] *Department of Chemistry and Research Center for Materials Science, Nagoya University, Chikusa, Nagoya 464-8602, Japan*

Received (in Cambridge, UK) 13th April 1999, Accepted 24th May 1999

The carbonylation of aryl halides catalysed by CO_2 soluble Pd complexes with trialkyl or triaryl phosphite ligands proceeds rapidly in $scCO_2$, in which the rate of the reaction is higher than those attained in solution phase reactions.

Supercritical fluids (SCFs) are attractive alternatives to organic solvents as reaction media for chemical reactions for a number of reasons. These reasons include their pressure tunable physical properties and solvent powers as well as the high miscibility of the reactant gases, efficient mass transfer, local clustering, and possible weakening of the solvation of the reactants.[1] In particular, homogeneous transition metal-catalysed reactions involving gaseous reactants in SCFs have been intensively investigated, *e.g.* hydrogenation of olefins,[1a,2] hydroformylation,[3] hydrogenation of carbon dioxide,[4] and oxidation by O_2.[2e,5] However, no discernible benefit in terms of rate was obtained by performing the reactions under supercritical conditions except for a rapid hydrogenation of supercritical carbon dioxide ($scCO_2$) with Ru complexes[4] and an olefin hydroformylation catalysed by Rh complexes.[3b,c] This report describes the first carbonylation reactions of aryl halides catalysed by CO_2 soluble Pd complexes which proceed rapidly in $scCO_2$. The rate of the reaction is higher than those attained in solution phase reactions.

We first examined the intramolecular carbonylation of 2-iodobenzyl alcohol **1**[6] catalysed by palladium complex $[PdCl_2(MeCN)_2]$ **3a** in a supercritical mixture of CO_2 and CO (P_{CO_2} = 200 atm and P_{CO_2} = 10 atm)† at 130 °C (Table 1). The reaction proceeds smoothly in the presence of 2.2 equiv. of Et_3N (**1**:Pd:Et_3N = 5000:1:11000) to give phthalide, **2** in a moderate yield, with the TON (turnover number, mol product per mol catalyst) = 2190 after 2 h. A visual inspection of the reaction mixture in the window-equipped reactor vessel confirms that all the reactants as well as the product **2** are soluble in $scCO_2$, although the catalyst **3a** is only partly soluble. The reaction was started by introducing CO_2 and then CO into the reactor containing the reactants and the catalyst at the reaction temperature (Method A). In this procedure, the reaction proceeded rapidly in the liquid phase which formed before reaching the supercritical homogeneous state. Therefore, the outcome of the reaction is at least partly due to the reaction in the liquid phase. In fact, the reaction performed in a liquid phase consisting of **1** and Et_3N without CO_2 under otherwise identical conditions (neat condition) (substrate:catalyst = 5000:1, P_{CO} = 10 atm, 130 °C, 2 h) produced **2** with a TON of 3570. Such reactions in the liquid phase can be prevented by separating the catalyst from the reactants using a small glass container (Method B, standard procedure).‡ Reactions using this standard procedure gave a TON of 120 after 2 h and 1880 after 18 h as shown in Table 1, which clearly indicates that the carbonylation proceeds in the homogeneous $scCO_2$ phase.

Encouraged by the marked catalytic activity of the less soluble catalyst precursor **3a** in $scCO_2$, we then tried to employ Pd complexes with trialkyl phosphite ligands, which are highly soluble even in nonpolar hydrocarbons.[7] The solubility test clearly demonstrated that 1×10^{-2} mmol (5.1 mg) of $[PdCl_2\{P(OEt)_3\}_2]$ **3b** were dissolved in $scCO_2$ (300 atm) at 130 °C in a 50 mL reactor vessel. The success of this strategy is shown by the greater TON attained in the reaction catalysed by **3b** under the standard conditions mentioned above compared to that with **3a**. The reaction of **1** with **3b** proceeded efficiently at 130 °C in a homogeneous single phase containing all the reactants and the catalyst to provide quantitatively the product **2** (Table 1).

The phosphite compounds are the best choice of ligand for an increase in the solubility of the Pd complex. The compound's structure and electronic properties strongly affect the outcome of the reactions, as listed in Table 1. The $scCO_2$ soluble Pd complexes with trialkyl or triphenyl phosphite ligands (**3b** and **3c**) are highly efficient catalyst precursors. The complex **3g** with PMe_3 ligands was less reactive because the strongly coordinated ligand retards slightly the reaction in $scCO_2$ as observed in conventional liquid solvents.[8] Replacement of the phenyl groups in PPh_3 with methoxy groups (**3d** and **3e**) facilitates the carbonylation due to an increase in the solubility of the Pd catalyst precursor. On the other hand, the reaction with the CO_2 insoluble PPh_3 complex **3f** proceeded rapidly almost to completion accompanied with metal deposition. One possible explanation is that the phosphorous ligand-free, CO_2 soluble Pd carbonyl species[9,10] generated might be extracted into the

Table 1 Pd complex catalysed carbonylation of 2-iodobenzyl alcohol **1** in $scCO_2$[a]

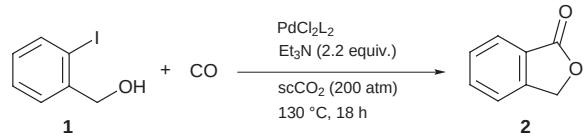

1 **2**

Run	L (Pd complex)	Medium (atm)	CO/atm	*t*/h	TON
1[b]	MeCN **3a**	CO_2 (200)	10	2	2190
2[c]	MeCN **3a**	—	10	2	3570
3	MeCN **3a**	CO_2 (200)	10	2	120
4	MeCN **3a**	CO_2 (200)	10	18	1880
5	$P(OEt)_3$ **3b**	CO_2 (200)	10	18	5000
6	$P(OPh)_3$ **3c**	CO_2 (200)	10	18	4510
7	$PPh(OMe)_2$ **3d**	CO_2 (200)	10	18	4470
8	$PPh_2(OMe)$ **3e**	CO_2 (200)	10	18	3880
9	PPh_3 **3f**	CO_2 (200)	10	18	4800
10	PMe_3 **3g**	CO_2 (200)	10	18	3180
11	$P(OEt)_3$ **3b**	CO_2 (200)	1	18	4650
12	$P(OEt)_3$ **3b**	CO_2 (200)	5	18	5000
13	$P(OEt)_3$ **3b**	toluene[d]	1	18	3100
14	$P(OEt)_3$ **3b**	toluene[d]	5	18	3800

[a] Reaction was conducted at 130 °C in a 50 mL reaction vessel containing 0.1 μmol of Pd catalyst (10 μl DMF solution), substrate and Et_3N (Method B). Substrate:Pd catalyst:Et_3N = 5000:1:11000. TON = product mol/catalyst mol. [b] The catalyst was not separated from the substrate (Method A). [c] Neat. [d] 50 ml.

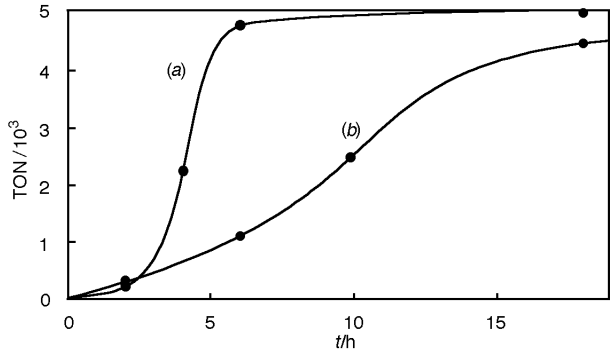

Fig. 1 Time *vs*. TON plots for the carbonylation of **1** catalysed by $[PdCl_2\{P(OEt)_3\}_2]$ **3b**, in (*a*) $scCO_2$ (standard procedure) or (*b*) toluene (substrate : catalyst = 5000 : 1, catalyst = 0.1 μmol).

$scCO_2$ phase, where the carbonyl complex effects the reaction highly efficiently and is deactivated during the later stages of the reaction because of the lack of a stabilizing ligand in the $scCO_2$ phase. In order to increase the solubility of the transition metal complexes in $scCO_2$, ligand modifications such as replacement of ligands containing aryl substituents to ligands bearing alkyl or perfluoroalkyl groups or introduction of CO_2-philic ponytails as substituents on the aryl groups have been developed previously.[4b,c,11] The use of phosphonate ligands has proved to be a practical alternative ligand modification for increasing the solubility of transition metal complexes in supercritical fluids.

The advantage of performing the carbonylation in supercritical fluids is that there is no marked effect of the CO pressure on the TON values obtained in $scCO_2$. Because of the higher diffusivity of $scCO_2$ compared to organic solvents as well as the high solubility of CO in this medium, the carbonylation even at 1 atm of CO pressure (CO : substrate = *ca*. 1.5 : 1) proceeded to near completion (TON = 4650). The yield of the product **2** (TON ~ 5000) is independent of the CO pressure over a range of 1–5 atm in $scCO_2$ (200 atm), whereas the reaction in toluene under otherwise identical conditions provided lower TON values (3100–3800) over a range of 1–5 atm of CO. The time conversion curve obtained by batch-wise experiments, illustrated in Fig. 1, as well as direct monitoring of the reaction by on-line FTIR revealed that the reaction proceeds rapidly to completion within 3–4 h after a *ca*. 2 h induction period.

The phosphonate–Pd catalyst can be applied to the intermolecular carbonylation of iodobenzene **4** and methanol (substrate : catalyst = 500 : 1) under the standard conditions in $scCO_2$ to yield methyl benzoate (TON = 260). Further optimization of the reaction is now in progress.

In conclusion, the carbonylation of aryl halides catalysed by Pd complexes with phosphonate ligands proceeds rapidly in $scCO_2$. The rate of the reaction is higher than that in the liquid phase.

Notes and references

† **SAFETY WARNING:** Operators of high-pressure equipment should take proper precautions to minimize the risk of personal injury [ref. 4(*b*)].

‡ *Standard procedure* for the carbonylation: The reactor equipped with a small vial was charged with argon gas in a desiccator. Then, a DMF (10 ml) solution of Pd catalyst (0.1 mmol) was charged in this vial, and the reactor was placed in an oven. After reaching the desired temperature of 130 °C (for *ca*. 1.5 h), a mixture of the substrate (0.5 mmol) and Et_3N (1.1 mmol) was added into the reactor (outside the vial) with a syringe through an opening against a flow of CO_2. Subsequently, CO (1–10 atm) was introduced, and then CO_2 (200 atm) was added with an HPLC pump. After stirring for 18 h, the reactor was cooled in a bath of MeOH and dry ice. The mixture of CO and CO_2 was vented, and the reactor was slowly warmed to room temperature. The yield of **2** was determined by ^{1}H NMR and GC analyses of $CDCl_3$ solutions of the products. On-line analysis was conducted by using a reactor vessel connected to the FT-IR equipment (JASCO FT/IR-610). The reaction was monitored by collecting spectra at intervals over the period of the reaction.

1 Recent reviews; (*a*) P. G. Jessop, T. Ikariya and R. Noyori, *Science*, 1995, **269**, 1065; (*b*) P. G. Jessop, T. Ikariya and R. Noyori, *Chem. Rev.*, 1999, **99**, 475.

2 (*a*) P. G. Jessop, T. Ikariya and R. Noyori, *Organometallics*, 1995, **14**, 1510; (*b*) M. J. Burk, S. Feng, M. F. Gross and W. Tumas, *J. Am. Chem. Soc.*, 1995, **117**, 8277; (*c*) J.-L. Xiao, S. C. A. Nefkens, P. G. Jessop, T. Ikariya and R. Noyori, *Tetrahedron Lett.*, 1996, **37**, 2813; (*d*) S. Kainz, D. Koch and W. Leitner, *Selective Reactions of Metal-Activated Molecules*, ed. H. Werner and W. Schreier, Vieweg, Wiesbaden, 1998, pp. 151–156; (*e*) S. Buelow, P. Dell'Orco, D. K. Morita, D. Pesiri, E. Birnbaum, S. Borkowsky, S. Feng, L. Luan, D. Morgenstern and W. Tumas, *Green Chemistry*, ed. O. T. Anastas and T. C. Williamson, OUP, New York, 1998, pp. 265–285.

3 (*a*) J. W. Rathke, R. J. Klingler and T. R. Krause, *Organometallics*, 1991, **10**, 1350; (*b*) S. Kainz, D. Koch, W. Baumann and W. Leitner, *Angew. Chem.*, 1997, **109**, 1699; *Angew. Chem., Int. Ed. Engl.*, 1997, **36**, 1628; (*c*) D. Koch and W. Leitner, *J. Am. Chem. Soc.*, 1998, **120**, 13 398; (*d*) D. R. Palo and C. Erkey, *Ind. Eng. Chem. Res.*, 1998, **37**, 4203; (*e*) I. Bach and D. J. Cole-Hamilton, *Chem. Commun.*, 1998, 1463.

4 (*a*) P. G. Jessop, T. Ikariya and R. Noyori, *Nature*, 1994, **368**, 231; (*b*) P. G. Jessop, Y. Hsiao, T. Ikariya and R. Noyori, *J. Am. Chem. Soc.*, 1996, **118**, 344.

5 K. M. Dooley and F. C. Knopf, *Ind. Eng. Chem. Res.*, 1987, **26**, 1910; G. J. Suppes, R. N. Occhiogrosso and M. A. McHugh, *Ind. Eng. Chem. Res.*, 1989, **28**, 1152; P. Srinivas and M. Mukhopadhyay, *Ind. Eng. Chem. Res.*, 1994, **33**, 3118; X.-W. Wu, Y. Oshima and S. Koda, *Chem. Lett.*, 1997, 1045; P. G. Jessop, *Top. Catal.*, 1998, **5**, 95; U. Kreher, S. Schebesta and D. Walther, *Z. Anorg. Allg. Chem.*, 1998, **624**, 602.

6 A. Cowell and J. K. Stille, *J. Am. Chem. Soc.*, 1980, **102**, 4193.

7 Y. Kayaki, I. Shimizu and A. Yamamoto, *Bull. Chem. Soc. Jpn.*, 1997, **70**, 1141.

8 The TON values obtained from 18 h reactions in toluene under otherwise identical conditions decrease in the order: $P(OEt)_3$ > PMe_3.

9 $[PdCl_2\{PPh_3\}_2]$ complex is known to react with CO in in Et_3N containing alcohols to give several kinds of Pd carbonyls and PPh_3. M. Hidai, M. Kokura and Y. Uchida, *J. Organomet. Chem.*, 1973, **52**, 431.

10 $[Pd(CO)_4]$ is known to be thermally unstable; J. H. Darling and J. S. Ogden, *J. Chem. Soc., Dalton Trans.*, 1973, 1079.

11 A. F. Lagante, B. N. Hansen, T. J. Bruno and R. E. Sievers, *Inorg. Chem.*, 1995, **34**, 5781; Y. H. Lin, N. G. Smart and C. M. Wai, *Trends Anal. Chem.*, 1995, **14**, 123; A. V. Yazdi and E. J. Beckmann, *Ind. Eng. Chem. Res.*, 1997, **36**, 2368; R. P. Hughes and H. A. Trujillo, *Organometallics*, 1996, **15**, 286; M. A. Carroll and A. B. Holmes, *Chem. Commun.*, 1998, 1395; D. K. Morita, D. R. Pesiri, S. A. David, W. H. Glaze and W. Tumas, *Chem. Commun.*, 1998, 1397.

Communication 9/02942G

ChemComm

Control of the free radical reaction by dynamic coordination: unique reactivity of pyridylethyl-substituted tin hydrides

Seiji Suga, Takao Manabe and Jun-ichi Yoshida*

Department of Synthetic Chemistry and Biological Chemistry, Graduate School of Engineering, Kyoto University, Kyoto 606-8501, Japan. E-mail: yoshida@sbchem.kyoto-u.ac.jp

Received (in Cambridge, UK) 11th May 1999, Accepted 26th May 1999

Tin hydrides having one or two pyridyl groups show unique reactivity in the reduction of alkyl halides under radical conditions, indicating the potential of intramolecular coordination for the control of radical reactions.

The importance of polar effects in radical reactions has attracted significant interest for many years,[1] and solvent effects[2] and anchimeric assistance[3] have been reported for various reactions involving free radicals. We report here unique reactivity of tin hydrides having pyridyl groups, suggesting the potential of intramolecular coordination for the control of radical reactions. This opens a new aspect of free radical chemistry. We also report the remarkable intermolecular effect of pyridyl groups in tin hydride reduction.

In recent work we have found the stabilization of cation radical intermediates by dynamic coordination to tin, which in turn favors the electron transfer from tetraalkylstannanes.[4] In connection with our interest in controlling chemical reactions by dynamic intramolecular coordination,[5,6] we envisioned that similar coordination might also be effective for the tin radical **1**. Thus, we synthesized tin hydrides having one or two pyridyl groups for coordination such as **2** and **3** and examined their reaction with organic halides under radical conditions (Scheme 1).[7]

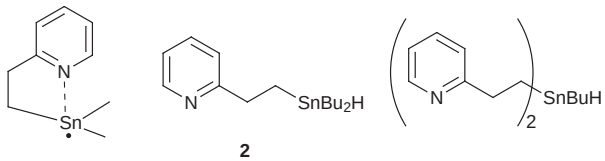

1 **2** **3**

Tin hydrides **2** and **3** were synthesized by the $LiAlH_4$ reduction of the corresponding tin halides.[4,8] The fact that the chemical shift from the ^{119}Sn NMR spectrum (in C_6D_6) of **2** (δ −88.270) is similar to that of Bu_3SnH (δ −87.210) indicated the absence of coordination of the pyridyl group to tin. This sharply contrasts to the ^{119}Sn NMR spectrum of the corresponding tin halide, which indicates the presence of a definite coordination of the pyridyl group to tin.[4]

The reduction of organic halides with **2**, however, exhibited unique features in contrast to that with Bu_3SnH (Table 1). Although primary alkyl bromides were reduced smoothly with **2**, the corresponding chlorides were unchanged under the same conditions.[9] *sec*-Alkyl chlorides and aromatic chlorides were also completely inactive towards **2** under these conditions. In the case of Bu_3SnH, however, such organic chlorides were reduced, albeit slowly. The unique reactivity of **2** seems to be ascribed to the lower reactivity of tin radical **1** towards organic halides (Scheme 2).

The reduction of alkyl bromides with **2** was completely retarded by the addition of a catalytic amount of hydroquinone

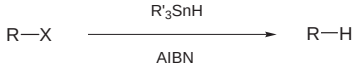

Scheme 1

Table 1 Reduction of organic halides with tin hydrides under radical conditions[a]

	Yield of RH (%)[b]		
Organic halide	Bu_3SnH	**2**	**3**
$C_{12}H_{25}Cl$	75	0	0
$C_{12}H_{25}Br$	97	97	39
$C_{12}H_{25}I$	96	98	97
$Ph(CH_2)_3Cl$	52	0	0
$Ph(CH_2)_3Br$	100	99	56
$Ph(CH_2)_3I$	100	99	94
1-Naphthyl-Cl	12	0	0
1-Naphthyl-Br	93	90	20
1-Naphthyl-I	97	97	96
$C_8H_{17}CClHCH_3$	75	0	0

[a] Reactions were normally carried out with 0.10 mmol of organic halide, 0.12 mmol of tin hydride, and 0.01 mmol of AIBN in 0.4 ml of benzene at 60 °C for 2 h under an atmosphere of argon. [b] Determined with GC using an internal standard.

(0.1 equiv.), indicating that the reaction proceeded by a radical chain mechanism. The facile 5-*exo* cyclization[10] shown in Scheme 3 also supported a radical mechanism. The ratio of 5-*exo*/6-*endo* was similar to that observed for Bu_3SnH. The high yields of the cyclized products also demonstrates the utility of **2** for radical carbon–carbon bond formation.[11]

In order to get deeper insight into the unique reactivity of **2**, we examined the effect of the pyridyl group on the stability of the tin radical with molecular orbital calculations.[12] The geometry optimization of a model compound, 2-$PyCH_2CH_2SnMe_2$ radical, gave three structures (Fig. 1). The coordinated structures **A** and **B** are more stable than non-coordinated structure **C**, indicating that the coordination does

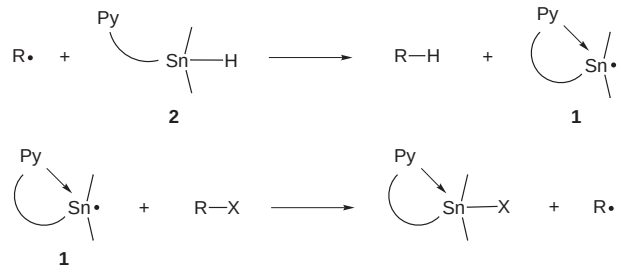

Scheme 2

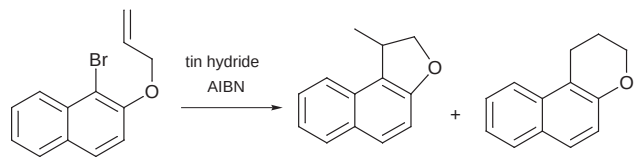

2	93%	9 : 1
Bu_3SnH	80%	9 : 1

Scheme 3

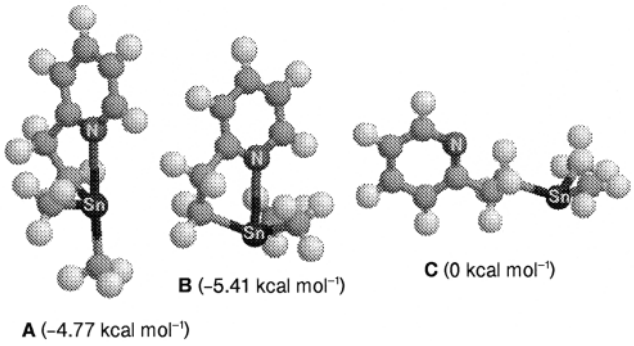

Fig. 1 Optimized structures of the 2-Py$CH_2CH_2SnMe_2$ radicals and their relative energies obtained by molecular orbital calculations (MP2/LANL2DZ).

take place at the radical. Such stabilization might decrease the reactivity of tin radicals towards organic halides,[13] although a detailed discussion should be reserved until kinetic data are available.

The reactivity of the tin hydride having two pyridyl groups, compound **3**, was also studied (Table 1). Although organic iodides were reduced smoothly with **3**, the reactions of organic bromides were much slower. Organic chlorides were almost inactive towards **3**. These data naturally imply that the second pyridyl group further decreases the reactivity of the tin radical.

It is notable that the introduction of the second pyridyl group gives us a bonus, *i.e.* easy separation and recovery of the tin halide after the reaction.[14] The tin halide derived from **3** can be completely separated by acid extraction and recovered by a follow-up base extraction, although the tin halide derived from **2** cannot be separated in a similar fashion. The easy protonation of the second pyridyl group seems to be responsible for this phenomena because the first pyridyl group should be used for coordination to the tin halide (*vide supra*).

In order to examine the effect of intermolecular coordination on the reactivity of the tin radical, we carried out the radical reduction of organic halides with Bu_3SnH in the presence of an additive such as pyridine and 2,2'-bipyridyl (Fig. 2). For the reduction of the alkyl bromide, the reaction took place smoothly even in the presence of such additives. The reduction of the alkyl chloride, however, was retarded significantly with an increase in the amount of additive. It is especially remarkable that the reaction was almost completely suppressed in the presence of 0.25 equiv. of bipyridyl. These results clearly indicate that the reactivity of tin radicals can be controlled even by intermolecular coordination.

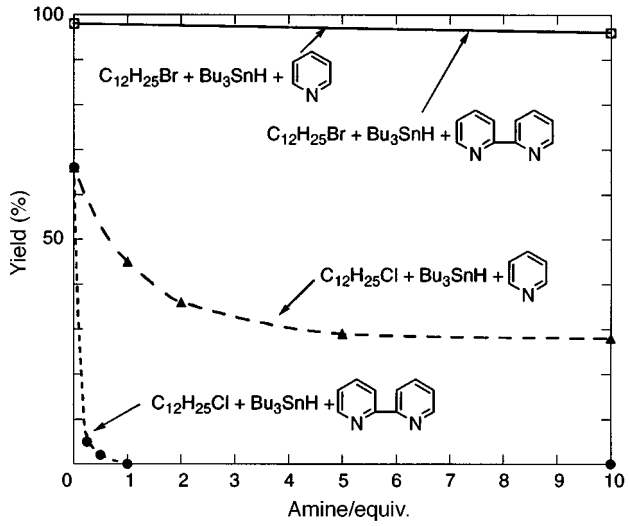

Fig. 2 Effect of pyridine and 2,2′-bipyridyl as additives on the reduction of alkyl halides by Bu_3SnH.

In summary, the results described above demonstrate the potential of dynamic coordination for the control of radical reactions. Future studies will hopefully delineate the detailed mechanistic role of the coordination.

We thank Professor Ilhyong Ryu, Osaka University, for valuable suggestions and discussions. This work was supported by a Grant-in-Aid for Scientific Research from Monbusho.

Notes and References

1 M. W. Wong, A. Pross and L. Radom, *J. Am. Chem. Soc.*, 1994, **116**, 11 938; M. W. Wong, A. Pross and L. Radom, *J. Am. Chem. Soc.*, 1993, **115**, 11 050 and references therein.

2 S. Hadida, M. S. Super, E. J. Beckman and D. P. Curran, *J. Am. Chem. Soc.*, 1997, **119**, 7406; L. Valgimigli, K. U. Ingold and J. Lusztyk, *J. Org. Chem.*, 1996, **61**, 7947; M. S. Workentin, N. P. Schepp, L. J. Johnston and D. D. M. Wayner, *J. Am. Chem. Soc.*, 1994, **116**, 1141; S. S. Kim, S. Y. Kim, S. S. Ryou, C. S. Lee and K. H. Yoo, *J. Org. Chem.*, 1993, **58**, 192, and references therein.

3 C. J. Easton and M. C. Merrett, *J. Am. Chem. Soc.*, 1996, **118**, 3035; R. A. Jackson, K. U. Ingold, D. Griller and A. S. Nazran, *J. Am. Chem. Soc.*, 1985, **107**, 208; K. J. Shea, D. C. Lewis and P. S. Skell, *J. Am. Chem. Soc.*, 1973, **95**, 7768; P. S. Skell, D. L. Tuleen and P. D. Readio, *J. Am. Chem. Soc.*, 1963, **85**, 2849; W. Thaler, *J. Am. Chem. Soc.*, 1963, **85**, 2607.

4 J. Yoshida and M. Izawa, *J. Am. Chem. Soc.*, 1997, **119**, 9361. See also J. Yoshida, S. Suga, K. Fuke and M. Watanabe, *Chem. Lett.*, 1999, 251.

5 Our results contrast with the pioneering work of Vedejs, which indicated that the intramolecular coordination of the amino group enhanced the reducing ability towards carbonyl groups: E. Vedejs, S. M. Duncan and A. R. Haight, *J. Org. Chem.*, 1993, **58**, 3046.

6 Tin hydride reductions: I. Shibata, T. Yoshida, A. Baba and H. Matsuda, *Chem. Lett.*, 1991, 307; I. Shibata, T. Yoshida, A. Baba and H. Matsuda, *Chem. Lett.*, 1989, 619. Stille Coupling: E. Vedejs, A. R. Haight and W. O. Moss, *J. Am. Chem. Soc.*, 1992, **114**, 6556. Electrophilic reactions: B. Jousseaume and P. Villeneuve, *J. Chem. Soc., Chem. Commun.*, 1987, 513; J. C. Podesta, A. B. Chopa and L. C. Koll, *J. Chem. Res.* (S), 1986, 308; H. G. Kuivila, J. E. Dixon, P. L. Maxfield, N. M. Scarpa, T. M. Topka, K.-H. Tsai and K. R. Wursthorn, *J. Organomet. Chem.*, 1975, **86**, 89.

7 Reduction with 2-(4-pyridyl)ethyldibutyltin hydride has been reported: D. L. J. Clive and W. Yang, *J. Org. Chem.*, 1995, **60**, 2607.

8 M. F. Mahon, K. C. Molloy and P. C. Waterfield, *Organometallics*, 1993, **12**, 769.

9 The reactivity of alkyl bromides is 10^3–10^6 times greater than that of alkyl chlorides, see D. P. Curran, C. P. Jasperse and M. J. Totleben, *J. Org. Chem.*, 1991, **56**, 7169 and references therein.

10 A. N. Abeywickrema, A. L. J. Beckwith and S. Gerba, *J. Org. Chem.*, 1987, **52**, 4072; the 6-*endo* cyclization product might arise *via* a tandem rearrangement from the 5-*exo* product.

11 B. Giese, *Radicals in Organic Synthesis: Formation of Carbon-Carbon Bonds*, Pergamon, Oxford, 1986; D. P. Curran, *Synthesis*, 1988, 417.

12 The molecular orbital calculations were carried out using Gaussian 94W. Revision B.2, M. J. Frisch, G. W. Trucks, H. B. Schlegel, P. M. W. Gill, B. G. Johnson, M. A. Robb, J. R. Cheeseman, T. Keith, G. A. Petersson, J. A. Montgomery, K. Raghavachari, M. A. Al-Latham, V. G. Zakrzewski, J. V. Ortiz, J. B. Foresman, C. Y. Peng, P. Y. Ayala, W. Chen, M. W. Wong, J. L. Andres, E. S. Replogle, R. Gomperts, R. L. Martin, D. J. Fox, J. S. Binkley, D. J. Defrees, J. Baker, J. P. Stewart, M. Head-Gordon, C. Gonzalez and J. A. Pople, Gaussian, Inc., Pittsburgh PA, 1995. Geometries were optimized and vibrational frequencies were determined.

13 K. Fukui, *Acc. Chem. Res.*, 1971, **4**, 57; I. Fleming, *Frontier Orbitals and Organic Chemical Reactions*, Wiley, London, 1976.

14 Several approaches to easy work-up and separation of tin halides have been developed. For example, D. Crich and S. Sun, *J. Org. Chem.*, 1996, **61**, 7200; D. P. Curran and S. Hadida, *J. Am. Chem. Soc.*, 1996, **118**, 2531; E. Fouquet, M. Pereyre and A. L. Rodriguez, *J. Org. Chem.*, 1997, **62**, 5242. See also ref. 7.

Communication 9/03795K

Simple synthesis of enantiomers of 6-hydroxyalkan-4-olides by stereoselective hydrogenation of methyl 4,6-dioxoalkanoates

Stefan Schulz

Institut für Organische Chemie, TU Braunschweig, Hagenring 30 D-38106 Braunschweig, Germany. E-mail: stefan.schulz@tu-bs.de

Received (in Liverpool, UK) 10th March 1999, Accepted 14th May 1999

A simple method for the synthesis of (*S*,*S*)- or (*R*,*R*)-6-hydroxyalkan-4-olides, components of the pheromonal secretion of the butterfly *Idea leuconoe*, in high ee by enantioselective hydrogenation of 4,6-diketo esters with a commercial available Ru–BINAP catalyst is described.

During our studies on the pheromone system of males of the large danaine butterfly *Idea leuconoe*[1,2] we identified the previously unknown 6-hydroxyalkan-4-olides with chain-lengths between 10 and 13 carbon atoms. They seem to act synergistically with the other pheromone components and are probably involved in male–male interactions.[2] Therefore a synthesis of the pure enantiomers was needed to elucidate their absolute configuration and further investigate their ecological role.

High ee and dr of diols have been observed in Ru–BINAP catalyzed stereoselective hydrogenations of β-diketones.[3,4] We reasoned that 4,6-diketo esters might also be good substrates for such hydrogenations. Experiments with 3,5-diketo esters showed poor selectivity using the employed catalyst $[NH_2Et_2]^+$-$[\{RuCl(BINAP)\}_2(\mu\text{-}Cl)_3]^-$ between the diketo and the β-keto ester functionalities,[5] coupled with moderate enantioselectivity. In addition, the results could be interpreted as a preferred ligation of the ester group over the keto group.[5,6] On the other hand, small structural differences of the end groups are recognized by the catalyst, so that products with high dr and ee can be obtained, as has been shown by the hydrogenation of hexane-2,4-dione.[4] Therefore, the preferred reduction of the 4,6-diketo system in the presence of an ester group seemed to be possible. To the best of our knowledge, the only stable and commercially available chiral Ru–BINAP catalysts are [RuCl((*R*)-BINAP)(*p*-cymene)]Cl [(*R*)-**6**] and its (*S*)-enantiomer (Fluka). These catalysts have been regarded as ineffective below 60 °C in catalytic hydrogenations of dicarbonyl compounds.[6,7] Nevertheless, their application in the hydrogenation of allylic alcohols[8] and experience from our laboratories[9] showed that they can be effective catalysts in the reduction of β-keto esters at 80 °C and 40 bar hydrogen pressure, the upper limits of the equipment available to us. For example, hydrogenation of methyl 3-oxononanoate in the presence of (*S*)-**6** yielded methyl (*S*)-**3**-hydroxynonanoate in quantitative yield and 97.4% ee.

The major lactone in the secretion of *Idea leuconoe* is 6-hydroxyundecan-4-olide **8**. The 4,6-diketo ester required for its synthesis can be easily prepared starting from hexanal **1**. Reaction with ethyl diazoacetate yielded ethyl 3-oxooctanoate **2**,[10] which was acylated with 3-methoxycarbonylpropionyl chloride **3** (Scheme 1). Krapcho de-ethoxycarbonylation[11] of the product **4** then lead to the required precursor, methyl 4,6-dioxoundecanoate **5**. Hydrogenation at 40 bar H_2 and 80 °C in the presence of (*S*)-**6** for two days yielded a mixture of (*S*,*S*)-**8** and methyl (*S*,*S*)-4,6-dihydroxyundecanote **7**,† verified by chemical correlation as described below. The ester **7** could be smoothly transformed into (*S*,*S*)-**8** by column chromatography over silica, and subsequent treatment of the product with old $CHCl_3$ or TsOH. The dr and ee were determined by GC on a chiral phase (Lipodex E), which allowed separation of all enantiomers. The dr varied in different experiments between 95 and 99%, while the ee of the major enantiomer varied between 93 and 95%. The ee of the minor diastereomer could only be estimated to be between 0 and 20% because of the small amount isolated. Several lactones with chain lengths between C_{10} and C_{13} have been prepared with similar results by this method.

Finally, a chemical correlation was needed to see whether the stereochemical outcome of the reaction was as expected. Therefore, our synthesis of *rac*-6-hydroxydodecan-4-olide[1] was modified to obtain compounds with defined stereochemistry. Allylation of methyl 4-oxobutanoate with allyl(diisopinocampheyl)borane derived from (−)-α-pinene furnished (*S*)-hept-6-en-4-olide.[12] After ozonolysis, the labile and slowly epimerising aldehyde (*S*)-6-oxohexan-4-olide was alkylated with hexylmagnesium bromide, yielding a diastereomeric mixture of the hydroxy lactones, enriched in the (4*S*)-enantiomers. In a second experiment, *rac*-6-oxohexan-4-olide was alkylated using dihexylzinc in the presence of (1*R*,2*R*)-1,2-bis(trifluoromethylsulfonylamino)cyclohexane to yield a mixture enriched in the (6*S*)-enantiomers.[13] Gas chromatographic analysis of these mixtures and the racemate allowed unambiguous assignment of the (4*S*,6*S*)-configuration in the hydro-

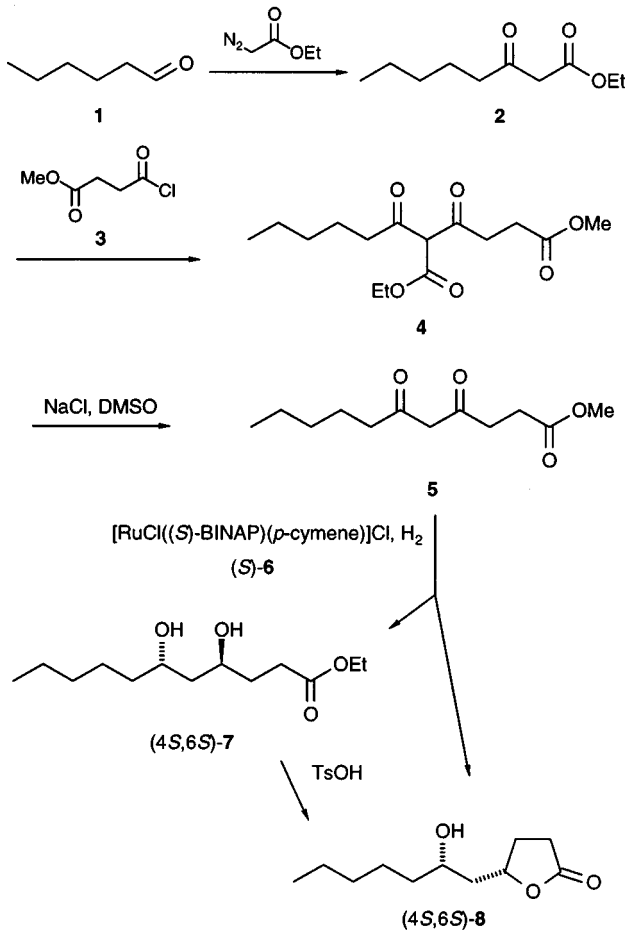

Scheme 1

genation products obtained with (*S*)-**6**. The result is in accord with the enantioselective hydrogenations of β-diketones with Ru-BINAP catalysts described in the literature.[3,4] Obviously the alkyl and ester groups are clearly differentiated by the catalyst.

Work is in progress to expand the described methodology to other compounds and optimize it by using other catalysts. This method bears considerable potential for the synthesis of building blocks, because of the two stereocenters and three differentiated carbon atoms in an alkyl chain.

I thank W. Luttmer for technical assistance. Financial support from the Deutsche Forschungsgemeinschaft is gratefully acknowledged.

Notes and references

† *Synthesis* of (4*S*,6*S*)-6-hydroxyundecan-4-olide: A stainless steel autoclave lined with Teflon and equipped with a stirring bar was charged with 200 mg of methyl 4,6-dioxoundecanoate and 5 ml of absolute MeOH. The solution was freed from air by repeatedly applying and releasing nitrogen pressure.

Approximately 10 mg of the catalyst (*S*)-**6** was added maintaining a steady flow of nitrogen to minimize contact with air. Then the autoclave was closed, a pressure of 40 atm applied, and finally heated to 80 °C for two days. When all educt was consumed (TLC control), the autoclave was cooled, the solvent removed, the product taken up in Et_2O and finally filtered over Celite. TLC control showed two spots, corresponding to **8** and **7**, which could be separated at this point by chromatography, if desired. Treatment of the crude mixture with a small amount of TsOH in CH_2Cl_2 transformed **7** into **8**. The product was then purified by chromatography over silica after removal of TsOH with saturated $NaHCO_3$ solution. Yield: 160 mg (91%); $[\alpha]_D^{22}$ +64.4 (*c* 1.30, Et_2O); δ_H(500 MHz, $CDCl_3$) 0.89 (t, 3H, H-11, *J* 6.9), 1.25–1.52 (m, 8H, H-7–H-10), 1.68 (ddd, 1H, H5, $J_{4,5}$ 3.3, $J_{5,6}$ 9.8, $J_{5,5'}$ 14.5), 1.80 (ddd, 1H, H-5′, $J_{5',6}$ 2.6 $J_{4,5'}$ 9.5), 1.90 (ddt, 1H, H-3, $J_{3,4}$ 8.5, $J_{2,3}$ 9.5, $J_{3,3'}$ 12.5), 2.38 (m, 1H, H-3′, $J_{3',4}$ 6.5), 2.55 (m, 2H, H-2), 3.89 (m, 1H, H-6), 4.80 (dddd, 1H, H-4); δ_C(100 MHz, $CDCl_3$) 13.98 (C-11), 22.58 (C-9), 25.14 (C-8), 28.52 (C-3), 28.86 (C-2), 31.70 (C-10), 38.02 (C-7), 43.16 (C-5), 68.54 (C-6), 78.10 (C-4), 177.09 (C-1).

1 S. Schulz and R. Nishida, *Bioorg. Med. Chem.*, 1996, **4**, 341.
2 R. Nishida, S. Schulz, C. H. Kim, H. Fukami, Y. Kuwahara, K. Honda and N. Hayashi, *J. Chem. Ecol.*, 1996, **22**, 949.
3 M. Kitamura, T. Ohkuma, S. Inoue, N. Sayo, H. Komobayashi, S. Akutagawa, T. Ohta, H. Takaya and R. Noyori, *J. Am. Chem. Soc.*, 1988, **110**, 629.
4 H. Kawano, Y. Ishii, M. Saburi and Y. Uchida, *J. Chem. Soc., Chem. Commun.*, 1988, **35**, 87.
5 L. Shao, H. Kawano, M. Saburi and Y. Uchida, *Tetrahedron*, 1993, **49**, 1997.
6 D. J. Ager and S. A. Laneman, *Tetrahedron: Asymmetry*, 1997, **8**, 3327.
7 K. Mashima, K. Kusano, M. Sato, Y. Matsumura, K. Nozaki, H. Komobayashi, N. Sayo, Y. Hori, T. Ishizaki, S. Akutagawa, H. O. T. Takaya and R. Noyori, *J. Org. Chem.*, 1994, **59**, 3064.
8 T. Eguchi, K. Arakawa, T. Terachi and K. Kakinuma, *J. Org. Chem.*, 1997, **62**, 1924.
9 A. Hefetz, T. Taghizadeh and W. Francke, *Z. Naturforsch.*, 1996, **51c**, 409.
10 C. R. Holmquist and E. J. Roskamp, *J. Org. Chem.*, 1989, **54**, 3258.
11 A. P. Krapcho, *Synthesis*, 1982, 893.
12 U. S. Racherla and H. C. Brown, *J. Org. Chem.*, 1991, **56**, 401.
13 M. J. Rozema, A. Sidduri and P. Knochel, *J. Org. Chem.*, 1992, **57**, 1956.

Communication 9/02022E

Synthesis of carbocycles by insertion of 1,1-dihalo-1-lithio species into zirconacycles

Nicolas Vicart† and Richard J. Whitby*

Department of Chemistry, Southampton University, Southampton, UK SO17 1BJ. E-mail: rjw1@soton.ac.uk

Received (in Liverpool, UK) 4th March 1999, Accepted 14th May 1999

1,1-Dihalo-1-lithio species (halogenocarbenoids) undergo double insertion into the carbon–zirconium bonds of a zirconacyclopent-ane or -ene to produce, after hydrolysis, bicyclo[3.3.0]oct-anes and -enes.

The intramolecular coupling of 1,*n*-dienes and -enynes induced by the zirconocene ('Cp_2Zr') equivalent zirconocene(but-1-ene) (generated *in situ* from dibutylzirconocene[1]) is a powerful method for ring construction.[2] It is important for efficient use of the transition metal to develop elaboration methods for the zirconacycles formed as intermediates. Of particular interest is their transformation into carbocycles by replacement of zirconium with carbon. Carbonylation to form cyclopent-anones and –enones by the mechanism shown in Scheme 1 is one method.[3] We extended this to the addition of isocyanides, where the zirconocene η^2-imine complex analogous to **2** could be trapped by insertion of a variety of alkenes, alkynes, and carbonyl compounds.[4] The direct formation of five-membered carbocyclic rings from zirconacycles has also been observed in a tandem allenyl carbenoid/aldehyde addition.[5] Takahashi has formed cyclopentadiene products from zirconacyclopentadienes by 1,1-addition to propynoates and copper catalysed addition to 3-iodopropenoates, and from zirconacyclopentenes by copper catalysed addition to acyl chlorides.[6]

We have developed a range of ring expansions of five-membered zirconacycles to six-membered homologues through the insertion of carbenoids (1-lithio-1-halo species), analogous to the formation of **1** (Scheme 1).[7] Here we describe how the insertion of 1,1-dihalo-1-lithio species allows the formation of five-membered carbocycles in a fashion analogous to the formation of **2** (Scheme 1).

Our first experiments were performed using the simplest halocarbenoid, lithiodichloromethane (**6a**).[8] Negishi has reported the formation of diphenylmethane from diphenylzirconocene and $LiCHCl_2$.[9] A solution of the zirconacyclopentane **4** in THF was formed from the diene **3** by the usual method.[1] Addition of CH_2Cl_2 followed by the slow addition of LDA at −78 °C and then hydrolysis gave a mixture of the protonolysis product of **4** and the anticipated product **10a** (Scheme 2 and Table 1, entry 1). Increasing the excess of $LiCHCl_2$ gave complete reaction of the zirconacycle **4**, but afforded **10a** mixed with products in which more than one molecule of the carbenoid had been incorporated. By using the bulkier carbenoid, $LiBr_2CPr$ (**6b**), generated *in situ* by deprotonation of 1,1-dibromobutane,[8] the multiple insertion pathway was eliminated and compound **10b** was isolated as the single product in good yield (Table 1, entry 2).‡ The likely mechanism is shown in Scheme 2. Deprotonation of **5b** by LDA gave the halogenocarbenoid **6b** which adds to **4** to produce the ate-complex **7b**. A 1,2-metallate rearrangement[9,10] to afford **8b** is followed by a diotropic rearrangement[11] to give **9b**. The formation of **9b** was confirmed by quenching the reaction at −78 °C with D_2O to afford the deuterated product **11** in 71% yield (Scheme 3). It is notable that both the formation of **8b** and its rearrangement to **9b** are fast at −78 °C. For the clean synthesis of **10b** it was important to maintain the reaction temperature below −50 °C until quenching, otherwise the by-product **12** was formed. We were pleased to find that allowing the reaction mixture to warm to room temperature before quenching gave **12** (86%) as the only product. Quenching with D_2O confirmed that the metal had

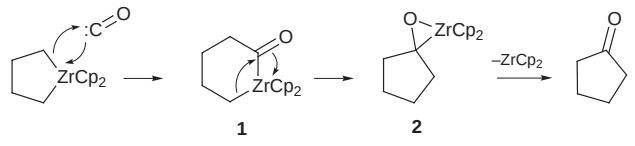

Scheme 1

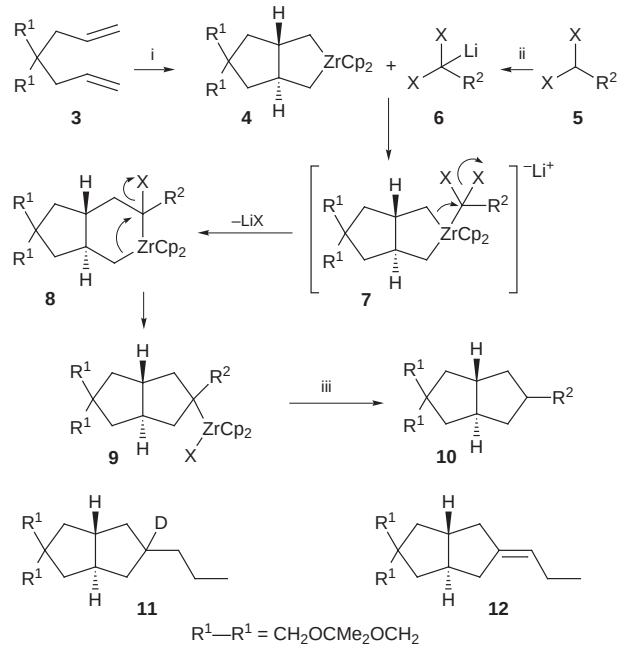

Scheme 2 *Reagents and conditions:* i, Cp_2ZrCl_2, BuLi (2 equiv.), −78 °C to room temp., THF; ii, R^2X_2CH (**5**) (1.5 equiv.), LDA (1.7 equiv.), −78 °C (−95 °C for **5e**) to −55 °C over 2 h; iii, MeOH, $NaHCO_3$ −78 °C to room temp., then room temp., 16 h.

Table 1 Reaction of dihalogenocarbenoids with zirconacyclopentane **4**

	Dihalide				
Entry	**5**	R^2	X	Product	Yield (%)[a]
1	**5a**	H	Cl	**10a**	< 15[b]
2	**5b**	Pr	Br	**10b**	66
3	**5c**	OMe	Cl	**10c**	68
4	**5d**	$SiMe_2Ph$	Cl	**10d**	71
5	**5e**	CN	Cl	**10e**	48

[a] Yields of isolated product after chromatography based on **3**. [b] Not separated from the hydrolysis product of **4**.

† Present address: Laboratoire des fonctions azotées et oxygénés complexes, Université de Rouen, IRCOF, UPRES A 6014, F76821 Mt. St. Aignan Cedex, France.

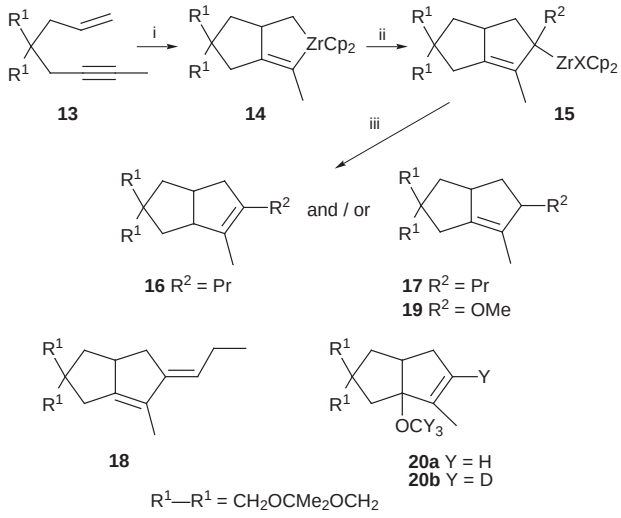

Scheme 3 *Reagents and conditions:* i, Cp_2ZrCl_2, BuLi (2 equiv.), −78 °C to room temp., THF; ii, R^2X_2CH (**5b** or **5c**) (1.5 equiv.), LDA (1.7 equiv.), −78 to −55 °C over 2 h, iii, hydrolysis as in Table 2.

Table 2 Reaction of dihalogenocarbenoids **5b** and **c** with **14**

Entry	5	Hydrolysis conditions	Products (ratios)[a]	Yield (%)[b]
1	**5b**	AcOH, −78 °C	**16** + **17** (36:64)	75
2	**5b**	MeOH–aq. $NaHCO_3$, 20 °C	**16** + **17** + **18** (29:44:27)	81
3	**5c**	AcOH, −78 °C	**19a**[c]	77
4	**5c**	MeOH–aq. $NaHCO_3$, −78 °C	**19a** + **20a** (47:53)	64
5	**5c**	CD_3OD–D_2O, −78 °C	**19b** + **20b** (45:55)	55

[a] Product ratios by NMR. [b] Isolated yields after chromatography based on **13**. [c] 72:28 ratio of diastereoisomers.

been lost by this stage, and a reasonable mechanism is a β-hydride elimination process (dehydrozirconation).

Metallation of dichloromethyl methyl ether **5c** with LDA in the presence of **4** gave the methoxy-substituted cyclopentane **10c** in good yield after protonolysis (Table 1, entry 3). Attempts to insert the carbenoid derived by lithiation of dichloromethyl(trimethyl)silane failed due to self condensation[12] and only the hydrolysis product of **4** was recovered. We found that the lithium derivative **6d** of the bulkier dichloromethyl(dimethyl)phenylsilane inserted into **4** efficiently to give silane **10d** (Table 1, entry 4) on protonolysis.

To avoid self condensation of the carbenoid precursor dichloroacetonitrile **5e** we added it to a mixture of LDA and the zirconacycle **4** in THF at −95 °C.[13] The cyanide **10e** was then isolated in moderate yield on hydrolysis (Table 1, entry 5).

When zirconacyclopentene **14** was treated with 1.5 equiv. of the *in situ* generated lithium carbenoid **6b** an inseparable mixture of **16** and **17** was formed (Scheme 3, Table 2, entry 1). Both **16** and **17** were formed as single diastereoisomers (estimated >93:7 detection limits). The formation of the mixture of **16** and **17** is easily rationalised by rapid allylic rearrangement of the initially formed organozirconium species **15**, indeed an η^3-allylzirconocene representation is probably most accurate. There is little to differentiate the two ends of the allylic system so a mixture of hydrolysis products is to be expected. Hydrolysis at 20 °C gave the diene **18** as a side product (Table 2, entry 2) presumably formed by a similar mechanism to the formation of **12**. The small amount of **18** produced compared with the formation of **12** is a reflection of the greater stability towards β-hydride elimination of the η^3-allyl *cf.* η^1-tertiary alkyl bonded zirconium.

Using dichloromethyl methyl ether **5c** as the carbenoid precursor, acidic quench of the reaction gave the single regioisomeric product **19** as a separable 72:28 mixture of diastereoisomers in good yield (Table 2, entry 3). When MeOH was used during the quench, we isolated a mixture of one diastereoisomer of **19** (the major one of the preceding experiment) and one diastereoisomer of **20a** (Table 2, entry 4). Quenching with CD_3OD gave a mixture of deuterated **19** and **20b** (Table 2, entry 5). Moreover, treatment of a sample of the minor diastereoisomer of **19** in THF with MeOH in the presence of Cl_2ZrCp_2 induced its fast transformation into **20a**. Formation of **20** is then due to an acid catalyzed $S_{N'}$ substitution of the methoxy group of **19** by the alcohol, probably *via* a carbocation. We have previously observed the 1,3-transposition of an amino group and the $S_{N'}$ replacement of an amino group by a hydroxy group in similar systems.[4a]

In conclusion, we have shown that selected halogenocarbenoids insert into a zirconacyclopentane to produce the related five-membered carbocyclic rings *via* sequential 1,2-metallate, and diotropic rearrangements. The yields are good for a tandem reaction sequence in which three carbon–carbon bonds are formed. Extension of the methodology to a zirconacyclopentene was complicated by poor regio- and/or diastereo-selectivity.

We gratefully acknowledge the European Community for financial support (TMR program, contract ERB-FMIBCT 97-2839). R. J. W. thanks Pfizer Central Research for generous uncommitted financial support.

Notes and references

‡ All compounds gave satisfactory ^1H and ^{13}C NMR (300 MHz), FTIR and LRMS spectra together with correct HRMS or microanalysis. All compounds were obtained pure except **10a** (mixture with hydrolysis product of **4**) and the regioisomers **16**/**17** which were characterised as the mixture.

1 C. Rousset, D. Swanson, F. Lamaty and E.-I. Negishi, *Tetrahedron Lett.*, 1989, **30**, 5105.
2 E.-I. Negishi, in *Comprehensive Organic Synthesis*, ed. B. M. Trost and I. Fleming, Pergamon, Oxford, 1991, vol. 5, p. 1163; R. D. Broene, in *Comprehensive Organometallic Chemistry II*, ed. E. W. Abel, F. G. A. Stone and G. Wilkinson, Pergamon, Oxford, 1995, vol. 12, p. 323; N. Uesaka, M. Mori, K. Okamura and T. Date, *J. Org. Chem.*, 1994, **59**, 4542; M. I. Kemp, R. J. Whitby and S. J. Coote, *Synthesis*, 1998, 557; E.-I. Negishi, S. M. Ma, T. Sugihara and Y. Noda, *J. Org. Chem.*, 1997, **62**, 1922.
3 C. J. Rousset, D. R. Swanson, F. Lamaty and E.-I. Negishi, *Tetrahedron Lett.*, 1989, **30**, 5105; E.-I. Negishi, S. J. Holmes, J. M. Tour, J. A. Miller, F. E. Cedrebaum, D. R. Swanson and T. Takahashi, *J. Am. Chem. Soc.*, 1989, **111**, 3336.
4 (*a*) J. M. Davis, R. J. Whitby and A. Jaxa-Chamiec, *Synlett*,1994, 110; (*b*) G. D. Probert, R. J. Whitby and S. J. Coote, *Tetrahedron Lett.*, 1995, **36**, 4113 and references cited therein.
5 G. J. Gordon and R. J. Whitby, *Chem. Commun.*, 1997, 1321.
6 T. Takahashi, Z. Xi, M. Kotora, C. Xi and K. Nakajima, *Tetrahedron Lett.*, 1996, **37**, 7521; T. Takahashi, W. Sun, C. Xi and M. Kotora, *Chem. Commun.*, 1997, 2069; M. Kotora, C. Xi and T. Takahashi, *Tetrahedron Lett.*, 1998, **39**, 4321.
7 S. F. Fillery, G. J. Gordon, T. Luker and R. J. Whitby, *Pure Appl. Chem.*, 1997, **69**, 633 and references cited therein.
8 J. Villieras and M. Rambaud, *Synthesis*, 1980, 644.
9 E.-I. Negishi, K. Akiyoshi, B. O'Conner, K. Takagi and G. Wu, *J. Am. Chem. Soc.*, 1989, **111**, 3089.
10 P. Kocienski and C. Barber, *Pure Appl. Chem.*, 1990, **62**, 1933.
11 G. Erker, R. Petrenz, C. Kruger, F. Lutz, A. Weiss and S. Werner, *Organometallics*, 1992, **11**, 1646; T. Takahashi, Z. Xi, R. Fischer, S. Huo, C. Xi and K. Nakajima, *J. Am. Chem. Soc.*, 1997, **119**, 4561; K. Kasai, Y. H. Liu, R. Hara and T. Takahashi, *Chem. Commun.*, 1998, 1989.
12 G. L. Larson and O. Rosario, *J. Organomet. Chem.*, 1979, **168**, 13.
13 P. Coutrot, *Bull. Soc. Chim. Fr.*, 1974, 1965.

Communication 9/01722D

Self assembly of a diphenanthrolinylpyrene-bridged Cu^{I} trimer

Céline Bonnefous, Nathalie Bellec† and Randolph P. Thummel*

Department of Chemistry, University of Houston, Houston, Texas 77204-5641, USA. E-mail: thummel@uh.edu

Received (in Columbia, MO, USA) 26th February 1999, Accepted 27th April 1999

The ligand 1,8-di(1,10-phenanthrolin-2-yl)pyrene has been prepared and complexed with Cu^{I} such that three ligands bridge a triangular arrangement of three metals resulting in a symmetrical helical assembly with each pyrene layered between two phenanthrolines at optimum π-stacking distance.

The use of metals and appropriate bridging ligands has become a dominant theme in the construction of some interesting three dimensional arrays.[1] Cu^{I} is particularly useful in this regard since many of its diimine complexes are labile, allowing ligand interchange to occur until the most thermodynamically stable assembly has been attained.[2] This report will focus on a Cu^{I} trimer of a diphenanthrolinylpyrene ligand **3**.

The Friedel–Crafts diacetylation of pyrene affords a mixture of the 1,3-, 1,6- and 1,8-diacetyl derivatives from which the pure 1,8-isomer **1** can be isolated.[3] When this material is treated with 2 equiv. of 8-aminoquinoline-7-carbaldehyde,[4] a 93% yield of 1,8-di(1,10-phenanthrolin-2-yl)pyrene **3** was obtained (Scheme 1). Treatment of this ligand in MeCN–CH_2Cl_2 (3:4) with 1 equiv. of $[Cu(MeCN)_4]ClO_4$ afforded a crude material which upon extraction with MeCN provided a 36% yield of the complex $[(Cu\mathbf{3})_3](ClO_4)_3$.

Constable and co-workers[5] have reported a system where two 6-substituted 2,2′-bipyridines joined by a 1,3-phenylene spacer bridged two metals while Sauvage and co-workers[6] have prepared a related di-1,10-phenanthrolinyl analogue. We expected a similar 2:2 combination of metal and ligand, which would afford a complex where the bridging pyrene moieties would be held co-facial to one another. This premise appeared to be supported by the high symmetry of the ^{1}H NMR spectrum (Fig. 1).

At 300 MHz the free ligand shows eleven well resolved signals between δ 7.75 and 9.05: three AB quartets for $H_{2,3}$, $H_{3',4'}$ and $H_{5',6'}$; singlets at δ 8.59 (H_9) and 8.40 (H_4); and a typical three proton pattern for H_7, $H_{8'}$ and $H_{9'}$. The complex also shows eleven well resolved signals with some shifted substantially upfield. The electrospray mass spectrum showed two major peaks at high mass. The peak at *m/z* 622, corresponding to $[(Cu\mathbf{3})_n]^{n+}$, established the 1:1 relationship of ligand and metal while the peak at *m/z* 983, corresponding to $[(Cu\mathbf{3})_3(ClO_4)]^{2+}$, indicated the trinuclear nature of the system.

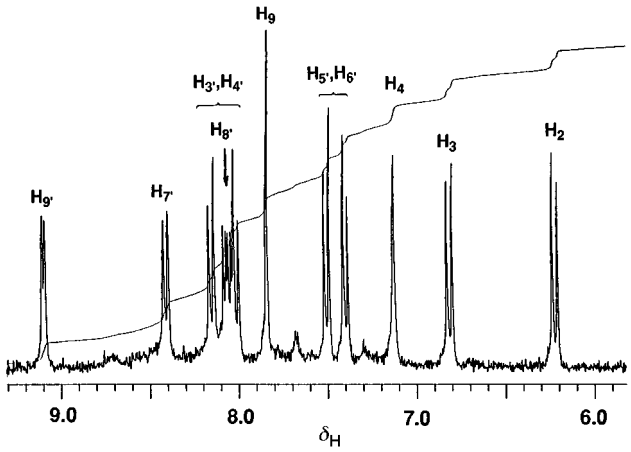

Fig. 1 300 MHz ^{1}H NMR spectrum of $[(Cu\mathbf{3})_3](ClO_4)_3$ at 25 °C in DMSO-d_6.

The structure of the complex was revealed by an X-ray analysis of a crystal grown from DMSO solution. Unfortunately the crystal quality was poor so that only a preliminary structure of the cation could be obtained. An ORTEP drawing of the cation is shown in Fig. 2 and Table 1 provides a summary of selected structural features. The geometry around copper is quite distorted. Each 1,10-phenanthroline unit binds to the metal through a short bond (1.96–1.99 Å) using the distal nitrogen N_{10}. The internal nitrogen N_1 forms a much longer bond to the metal (2.10–2.16 Å). We have seen similar bond distortions in the Cu^{I} complex of a highly twisted 2,2′-biquinoline derivative.[7] The tetrahedral geometry is also distorted. The N1–Cu–N10 chelation angles are relatively normal (80.9–81.5°) but the

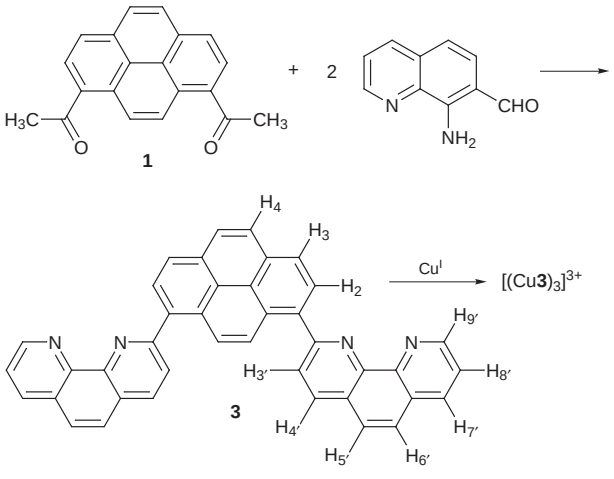

Scheme 1

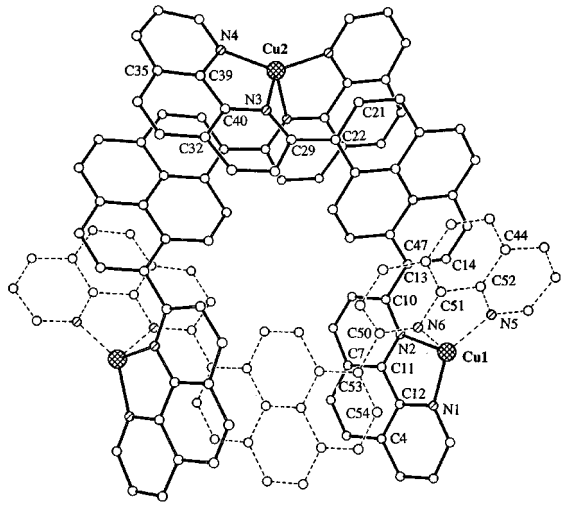

Fig. 2 ORTEP diagram of the cation of $[(Cu\mathbf{3})_3](ClO_4)_3$ with atomic numbering for key atoms.

† Visiting scholar from the University of Rennes, France.

Table 1 Selected geometric parameters for $[(Cu\mathbf{3})_3]^{3+}$ according to the numbering scheme in Fig. 2

Bond lengths (Å)		Bond angles (°)	
Cu1–N1	1.96 (0.0139)	N1–Cu1–N2	81.47 (0.59)
Cu1–N2	2.16 (0.0130)	N5–Cu1–N6	81.37 (0.54)
Cu1–N5	1.98 (0.0141)	N3–Cu2–N4	80.89 (0.47)
Cu1–N6	2.10 (0.0118)	N1–Cu1–N5	146.05 (0.63)
Cu–N3	2.14 (0.0113)	N1–Cu1–N6	121.94 (0.52)
Cu2–N4	1.99 (0.0108)	N2–Cu1–N5	123.12 (0.52)
		N2–Cu1–N6	96.52 (0.44)

Dihedral angles (°)			
N4–C39–C40–N3	1.65 (1.79)	Cu1–N1–C12–C4	170.65 (1.14)
N6–C51–C52–N5	2.67 (2.11)	Cu1–N2–C11–C7	168.04 (1.14)
N2–C11–C12–N1	4.59 (2.08)	Cu1–N5–C52–C44	167.98 (1.16)
N2–C10–C13–C14	59.73 (1.90)	Cu1–N6–C51–C4	168.13 (1.22)
N6–C50–C53–C54	57.75 (2.95)	Cu2–N3–C40–C32	168.63 (1.11)
N3–C29–C22–C21	58.34 (1.80)	Cu2–N4–C39–C35	170.75 (1.09)

N–Cu–N angles involving two different ligands are less regular with N1–Cu–N6 and N2–Cu–N5 being 122 and 123°, respectively, while N1–Cu–N5 is about 24° larger and N2–Cu–N6 is about 26° smaller. The planes of the two phenanthrolines are not orthogonal to one another. The extent to which the Cu lies out of the plane of the phenanthroline ring can be assessed by examining the C_a–C_b–N–Cu dihedral angle where C_a and C_b denote the two carbons common to pyridine and the central benzo-ring of phenanthroline. These angles range from 168–171°, where the ideal angle would be 180°, again indicating some distortion of tetrahedral geometry,

This cation has D_3 symmetry so that all three ligands are identical having the same helical twist about the phen–pyrene–phen bonds (57.8–59.7°). The phenanthroline rings are fairly planar with N_1–C–C–N_{10} dihedral angles of 1.7–4.6°. What is truly remarkable about the cation structure is the manner in which the aromatic rings π-stack, a pyrene being layered between two phenanthrolines to form three triple decked stacks which define a donut-shaped assembly (see Fig. 3 for stereoview). The stacking of the three rings is well organized and the average distance of any atom in a phenanthroline ring to the mean plane of the layered pyrene ring is 3.6 Å, which is approximately the optimal π-stacking distance. The increased surface area of pyrene as well as its ability to form well organized π-stacked arrays apparantly dictates the nuclearity of the complex. A similar effect for an Ag^+ trimer has recently been reported by Williams and co-workers.[8]

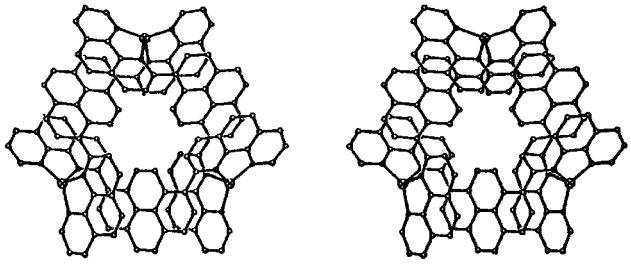

Fig. 3 Stereoview of the cation of $[(Cu\mathbf{3})_3](ClO_4)_3$.

From the stereodrawing, we notice that the hydrophobic cavity of the molecule consists of eighteen methine units. At the interior of the cavity are the C_9 and C_{10} hydrogens of the three pyrene units. On one face of the cavity are the C_3 and C_4 hydrogens of one set of three phens and on the other face are the C_3 and C_4 hydrogens of the other set of phens. The approximate diameter of the cavity is estimated to be about 3 Å by measuring the distance between opposing sets of atoms. If the van der Waals radii of the atoms are taken into account, the cavity size shrinks to about 1.8 Å. To verify that this cavity is indeed too small to accommodate a hydrophobic guest, we added Bu_2O to an NMR sample of $[(Cu\mathbf{3})_3](ClO_4)_3$ in DMSO-d_6 but no change was observed from the chemical shift values of the uncomplexed species.

Knowing the three dimensional structure, we can now more confidently assign the proton resonances in Fig. 1. The singlet for H_9 on the interior of the donut is downfield from the singlet for H_4 on the exterior. Similarly $H_{3'}$ and $H_{4'}$ are assigned as the downfield AB quartet. Due to the twist about the pyrene–phen bond, H_2 is held over the shielding region of the neighboring phen and found at higher field (δ 6.22).

To evaluate other features of the trimer, it became useful to prepare a monomeric analogue and hence the ligand 2-(pyren-1-yl)-1,10-phenanthroline **4**[9] was complexed in a 2:1 fashion with Cu^I. An NMR spectrum of the crude reaction product showed two sets of peaks in a 2:1 ratio which were attributed to conformational differences about the 2,1′-bond of ligand **4** in the complex.

The electronic absorption spectra (MeCN) of the ligands show long wavelength absorptions at 374 (log ε 4.53) for **3** and 342 nm (log ε 4.44) for **4**. The lower energy absorption of **3** is attributed to the presence of two phen substituents. The complexes show absorptions at 379 (log ε 4.76) and 473 nm (log ε 4.00) for $[(Cu\mathbf{3})_3]^{3+}$ and 346 (log ε 4.61) and 453 nm (log ε 3.50) for $[Cu(\mathbf{4})_2]^+$. The more intense, shorter wavelength band relates to the corresponding ligand absorption. The weak longer wavelength band is assigned to a characteristic metal to ligand charge transfer (MLCT) which gives the complexes their red color. The absorbance of the trimer appears at lower energy and is approximately 50% more intense than the monomer due to the 3:2 ratio of pyrene found in these two complexes.

Upon excitation into their lowest energy bands, the ligands exhibit strong pyrene-based emissions at 434 (**4**) and 450 nm (**3**). For the corresponding complexes these bands are greatly reduced in intensity possibly due to quenching by the copper center. Excitation into the MLCT bands of the complexes revealed only very weak luminescence.

The half-wave oxidation potentials for the two Cu^I complexes were determined by cyclic voltammetry and found to be virtually identical at +0.31 V (*vs.* SCE). This value compares with +0.67 V for $[Cu(dmp)_2]+$ (dmp = 2,9-dimethylphen).[10] It is noteworthy that the monomeric system is considerably more reversible than the trimer. The question of whether one or more electrons was being transferred in the oxidation of $[(Cu\mathbf{3})_3]^{3+}$ was addressed by controlled potential coulometry at 0.8 V, which indicated that only one copper in the trimer is being oxidized to Cu^{II}.

We would like to thank the Robert A. Welch Foundation and the National Science Foundation (CHE-9714998) for financial support of this work, Dr Eric van Caemelbecke for assistance with the electrochemical measurements, and Dr Jim Korp for assistance with the X-ray determination.

Notes and references

1 C. J. Jones, *Chem. Soc. Rev.*, 1998, **27**, 289.
2 P. N. W. Baxter, J.-M. Lehn, B. O. Kneisel and D. Fenske, *Chem. Commun.*, 1997, 2231 and references cited therein.
3 L. T. Scott and A. Necula, *J. Org. Chem.*, 1996, **61**, 386; R. G. Harvey, J. Pataki and H. Lee, *Org. Prep. Proceed Int.*, 1984, **16**, 144.
4 C.-Y. Hung, T.-L. Wang, Z. Shi and R. P. Thummel, *Tetrahedron*, 1994, **50**, 10 685; E. C. Riesgo, X. Jin and R. P. Thummel, *J. Org. Chem.*, 1996, **61**, 3017.
5 E. C. Constable, M. J. Hannon and D. A. Torcher, *Angew. Chem., Int. Ed. Engl.*, 1992, **31**, 230; E. C. Constable, M. J. Hannon and D. A. Tocher, *J. Chem. Soc., Dalton Trans.*, 1993, 1883.
6 C. O. Dietrich-Buchecker, J.-P. Sauvage, A. De Cian and J. Fischer, *J. Chem. Soc., Chem. Commun.*, 1994, 2231,
7 Y. Jahng, D. Kimble, E. C. Riesgo and R. P. Thummel, *Inorg. Chem.*, 1997, **36**, 5390.
8 C. Provent, S. Hewage, G. Brand, G. Bernardinelli, L. J. Charbonnière and A. F. Williams, *Angew. Chem., Int. Ed. Engl.*, 1997, **36**, 1287; A. Williams, *Chem. Eur. J.*, 1997, **3**, 15.
9 J. A. Simon, S. L. Curry, R. H. Schmehl, T. R. Schatz, P. Piotrowiak, X. Jin and R. Thummel, *J. Am. Chem. Soc.*, 1997, **119**, 11 012.
10 M.-T. Youinou, R. Ziessel and J.-M. Lehn, *Inorg. Chem.*, 1991, **30**, 2144.

Communication 9/01677E

Synthesis and anti-HIV activity of 1,3-dithiolane nucleosides

Nghe Nguyen-Ba, William L. Brown, Laval Chan, Nola Lee, Livio Brasili, Dominique Lafleur and Boulos Zacharie*

BioChem Pharma Inc., 275 Armand-Frappier Blvd., Laval, Québec, Canada H7V 4A7

Received (in Corvallis, OR, USA) 3rd March 1999, Accepted 20th May 1999

The potent activity displayed by 3′-azido-3′-deoxythymidine (AZT)[1] against human immunodeficiency virus (HIV) provides impetus for the development of novel nucleoside analogues.[2] Unfortunately, those compounds with the natural stereochemistry possess undesirable pharmacological properties[3] and are susceptible to the development of resistant stains of HIV.[3,4] In an attempt to overcome some of these detrimental side effects, the carbohydrate moiety of 2′,3′-dideoxynucleoside analogs has been replaced by other five membered rings.[3d,4] It has been demonstrated that hetero-substitution of these rings has a profound effect on the biological activity of the resulting nucleoside analogue[5] as displayed by (−)-2′-deoxy-3′-thiacytidine (3TC, Epivir) **1**.[5c,6]

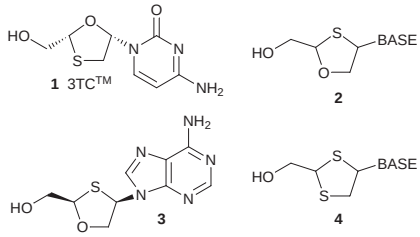

As part of an ongoing search for new anti-AIDS leads, we further explored this class of thioribonucleosides. These compounds possess improved metabolic stability to phosphorylases which cleave the glycosidic bond in nucleosides.[7] Recently, we reported the anti-HIV activity of 2,4-disubstituted 1,3-oxathiolane nucleosides **2** by transposing the sulfur and oxygen atoms of **1**.[4a] In this series, the (−)-adenine derivative **3** with the natural configuration was found to be twice as active as ddI in MT-4 cells. We further modified the oxathiolane ring by replacement of the oxygen atom of **2** with sulfur. This is exemplified by the general structure **4**. Here we report the synthesis and anti-HIV activity of this class of compounds.

The synthetic route to (±)-1,3-dithiolane compounds is based upon coupling a persilylated heterocyclic base with a dithiolane moiety **5** bearing a suitable leaving group Y at the 4-position under Vorbruggen's conditions.[8] Two approaches were considered for the preparation of the ring **5**. The first route is the introduction of a leaving group at position 4 using peroxide derivatives. For example, dithiolane **6** was prepared by treating **5a** with benzoyl peroxide in refluxing benzene (Scheme 1).[9]

The second approach offers a more general route for the synthesis of the key intermediate 1,3-dithiolane **11**† with a variety of displaceable leaving groups at C-4. Our synthetic strategy was based on the preparation of 1,3-dithiolan-4-one **9**, followed by reduction and acylation to give 4-acyloxy-1,3-dithiolane **11** (Scheme 2). Thus, reaction of freshly distilled $ClCH_2COCl$ with excess NaSH (3 equiv.) in absolute ethanol at −10 °C gave **7**[10] in quantitative yield. The crude product was

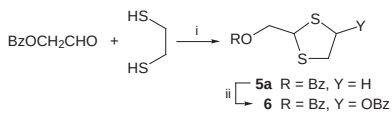

Scheme 1 *Reagents and conditions*: i, C_6H_6, TSA; ii, BzOOH, C_6H_6, heat.

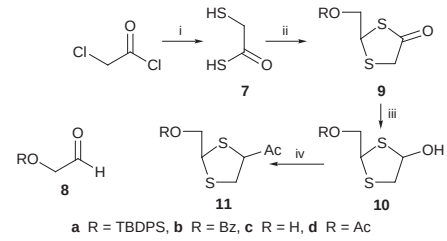

Scheme 2 *Reagents and conditions*: i, NaSH, absolute EtOH, −10 °C; ii, **8**, ZnI_2, CH_2Cl_2; iii, DIBAL-H, PhMe or BH_3·THF, $B(MeO)_3$; iv, AcOCl, Py.

immediately treated with aldehyde **8** in the presence of ZnI_2 as catalyst in CH_2Cl_2[11] to give the desired (±)-1,3-dithiolan-4-one **9** in moderate yield (50–60%). The initial synthetic procedure was based upon using the TBDPS protecting group for the hydroxy function of **9**. Reduction of **9a** with DIBAL-H (1.1 equiv.) in toluene gave thiolactol **10a** which was subsequently acylated to give the key intermediate **11a** in high yield. The silyl protecting group was later replaced by a benzoate group in order to facilitate the separation of the *cis* and *trans* nucleoside isomers. Applying the same conditions to reduce the benzoate **9b** did not result in any reduction product. However, using excess of DIBAL-H (3 equiv.) was successful and both the thiolactone and the benzoate function were reduced to give diol **10c** in 40% yield. Compound **10c** was then bis-acylated giving intermediate **11d** in high yield. Efforts were then directed to scale-up this procedure. Unfortunately, the DIBAL-H reduction proved particularly intractable. We therefore investigated other reducing agents that are selective and require little work-up. Only BH_3·THF (1.2 equiv.) catalyzed by $B(OMe)_3$ (1 equiv.) gave satisfactory results. The reduction was completed in 16 h and the product **10b** was obtained in 95% yield. This compound was then acylated to give the expected product **11b**. Following the same procedure, a number of different leaving groups (Bz, *m*-$ClC_6H_4CH_2$ and *p*-$O_2NC_6H_4CH_2$) were successfully introduced at C_4 of the sugar moiety **11**.

Compound **11b** is suitable for coupling with silylated cytosine or 5-fluorocytosine under refluxing conditions in CH_2Cl_2 and in the presence of $SnCl_4$ (Scheme 3). This gave the desired nucleoside analogue **12** or **13** as a 1 : 2 mixture of *cis* and *trans* isomers in moderate yields. Replacement of $SnCl_4$ with TMSI altered the ratio of the isomers. For example, compound **6** reacted with silylated N-acetylcytosine to give a mixture of the *cis* and *trans* nucleosides **12** in 62% yield with a slight predominance of the *cis* isomer.[9] Similar results were obtained using other leaving groups at C_4. This did not improve the yield

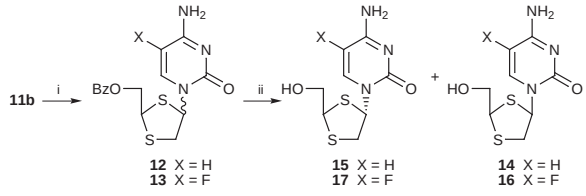

Scheme 3 *Reagents and conditions*: i, 2,4-Bis(trimethylsilyloxy)pyrimidine, $ClCH_2CH_2Cl$, $SnCl_4$, reflux, 16 h; ii, NH_3, MeOH.

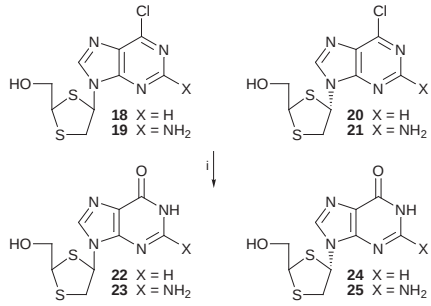

Scheme 4 *Reagents and conditions*: i, 25% aq. Me_3N–H_2O, 55–65%.

or the *cis*:*trans* ratio. The next step was the separation of the isomers **12** or **13**. This was achieved by flash chromatography on silica gel by prior acetylation of the amino group (cytosine) or by reverse chromatography HPLC after deprotection (5-fluorocytosine). The protecting groups were then removed by treatment with methanolic ammonia to give the desired nucleosides **14**–**17** in high yields. The relative stereochemistry of these products was assigned by difference NOE spectra.

Similarly, uracil, thymine, adenine and guanine derivatives were produced from **11b** using the same conditions. However, in the case of hypoxanthine and guanine analogs **22**–**25**, synthesis was undertaken by treating the corresponding 6-chloropurine or 2-amino-6-chloropurine derivatives **18**–**21** with 20 equiv. of an aqueous Me_3N solution in water (Scheme 4).

The anti-HIV activity of (±)-1,3-dithiolane nucleoside analogues was evaluated in MT-4 (human T helper) cells at concentrations up to 100 μg ml^{-1} and compared with 3TC™ (Epivir)[12] and the 5-fluoro derivative (FTC).[13] In this assay, only *cis* cytosine and 5-fluorocytosine derivatives **14** and **16** displayed inhibitory activity at ID_{50} of 9.3 and 4.8 μg ml^{-1} and were not cytotoxic at 100 μg ml^{-1}, whereas 3TC™ and FTC showed anti-HIV activity at 0.3 and 0.14 μg ml^{-1}, respectively. All the other nucleosides did not exhibit antiviral activity with no cytotoxicity up to 100 μg ml^{-1}. In contrast, *cis* and *trans* 6-chloropurine derivatives **18** and **20** showed cytotoxicity at CD_{50} of 10 μg ml^{-1}.

Described herein is a novel class of anti-HIV (±)-1,3-dithiolane nucleoside analogues. The biological results demonstrate that replacement of an oxygen atom of the oxathiolane with sulfur causes reduction in antiviral activity. It should be noted that compounds **14** and **16** are racemic. Resolution of the enantiomers may improve the activity. Therefore, enantiomeric separations of the racemic *cis* **14** was undertaken by chiral HPLC.[14] This gave the two enantiomers **26** and **27** in a

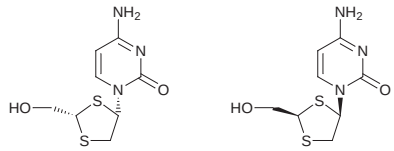

26 $[\alpha]_D^{25}$ +75 (*c* 0.10, H_2O) **27** $[\alpha]_D^{25}$ –70 (*c* 0.10, H_2O)

reasonable yield. It was found that isomer **27** possesses the natural configuration as evidenced by enzymatic resolution of the racemic mixture. Thus treatment of the mixture of the two enantiomers with cytidine deaminase converted only **27** to its corresponding uracil derivative. However, the unnatural enantiomer **26** was recovered and characterized by comparison of HPLC retention time and optical rotation with the previously isolated isomer. Both enantiomers were submitted for anti-HIV evaluation. Neither of the two compounds displayed improved antiviral activity.

We thank Drs T. Bowlin and R. Storer for reading the manuscript, Drs P. Hopewell and N. Cammack of Glaxo Group Research for testing the compounds, Ms L. Bernier and J. Dugas for technical assistance with HPLC separation of enantiomers, and Ms L. Marcil for secretarial and technical assistance.

Notes and references

† *Selected data* for **10b**: colorless oil; δ_H($CDCl_3$): 8.03 (m, 2H), 7.57 (dt, 1H, *J* 7, 1), 7.44 (t, 2H, *J* 7), 5.85 (m, 1H), 4.84 and 4.76 (t's, 1H, *J* 7), 4.68 and 4.39 (m's, 1H), 4.48 and 4.27 (m's, 1H), 3.30 (m, 2H), 2.85 (m, 1H). For **16**: δ_H(DMSO-d_6) 8.34 (d, 1H, *J* 7.5), 7.83 (br s, 1H), 7.59 (br s, 1H), 6.39 (m, 1H), 5.57 (t, 1H, *J* 5.5), 4.62 (t, 1H, *J* 6), 3.75 (t, 2H, *J* 6), 3.59 (m, 2H). For **17**; δ_H(DMSO-d_6) 8.10 (d, 1H, *J* 7 Hz), 7.78 (br s, H), 7.54 (br s, 1H), 6.41 (t, 1H, *J* 2), 5.36 (t, 1H, *J* 5.5), 4.81 (t, 1H, *J* 7 Hz), 3.45 (m, 4H). For **19**: δ_H(DMSO-d_6) 8.45 (s, 1H), 7.03 (br s, 2H), 6.40 (t, 1H, *J* 4), 5.53 (t, 1H, *J* 6), 4.73 (t, 1H, *J* 7), 3.80 (dd, 1H, *J* 13, 4.5), 3.74 (t, 2H, *J* 6), 3.63 (dd, 1H, *J* 13, 5); δ_C(DMSO-d_6) 159.80, 153.49, 150.01, 141.95, 123.61, 65.57, 64.52, 56.23, 42.93; HRMS (FAB): M^+ calc. for $C_9H_{11}ClN_5OS_2$ 304.00937, found 304.00880. For **21**: δ_H(DMSO-d_6) 8.34 (s, 1H), 7.02 (br s, 2H), 6.44 (t, 1H, *J* 3), 5.41 (t, 1H, *J* 6), 4.86 (t, 1H, *J* 7), 3.58 (m, 3H), 3.49 (m, 1H); HRMS (FAB): M^+ calc. for $C_9H_{11}ClN_5OS_2$ 304.00937, found 304.00840. For **26**: mp 108–110 °C; δ_H(DMSO-d_6) 8.06 (d, 1H, H-6′, *J* 7.63), 7.20 (br d, 2H, NH_2), 6.47 (t, 1H, *J* 4.4), 5.74 (d, 1H, *J* 7.42) 5.50 (t, 1H), 4.61 (t, 1H, *J* 6.5 Hz), 3.74 (t, 2H, *J* 6.00 Hz), 3.46 (dd, 1H, *J* 4.30, 12.9), and 3.36 (dd, 1H, *J* 4.1, 10.4); HRMS (FAB): M^+ calc. for $C_8H_{12}N_3O_2S_2$ 246.03709, found 246.03610. For **27**: mp 200–202 °C (decomp.); δ_H(DMSO-d_6) 7.90 (d, 1H, *J* 7.35), 7.17 (br d, 2H), 6.48 (d, 1H, *J* 3.72), 5.69 (d, 1H, *J* 7.47), 5.38 (t, 1H), 4.74 (t, 1H, *J* 6.83), 3.43 (m, 4H); HRMS (FAB): M^+ calc. for $C_8H_{12}N_3O_2S_2$ 246.03709, found 246.034640.

1 H. Mitsuya, J. K. Weinhold, P. A. Furman, M. H. St-Clair, S. Nusinoff-Lehrman, R. C. Gallo, D. Bolognesi, D. W. Barry, S. Broder, *Proc. Natl. Acad. Sci. U.S.A.*, 1985, **82**, 7096.

2 H. Mitsuya and S. Broder, *Proc. Natl. Acad. Sci. U.S.A.*, 1986, **83**, 1911; R. Yarchoan, H. Mitsuya, R. V. Thomas, J. M. Pluda, N. R. Hartman, C.-F. Perno, K. S. Marczyk, J.-P. Allain, D. G. Johns and S. Broder, *Science*, 1989, **245**, 412; T.-S. Lin, R. F. Schinazi and W. H. Prusoff, *Biochem. Pharmacol.*, 1987, **36**, 2713.

3 (*a*) R. W. Klecker, J. M. Collins, R. Yarchoan, R. Thomas, J. F. Jenkins, S. Broder, C. E. Myers Cli, *Pharmacol. Ther.*, 1987, **47**, 407; (*b*) M. S. Hirsch and J. C. Kaplan, *Antimicrob. Agents Chemother.*, 1987, **31**, 939; (*c*) R. Yarchoan, *Lancet*, 1988, **i**, 76; (*d*) M. L. Peterson and R. Vince, *J. Med. Chem.*, 1991, **34**, 2787 and references cited therein.

4 (*a*) B. Belleau, L. Brasili, L. Chan, M. D. DiMarco, B. Zacharie, N. Nguyen-Ba, H. J. Jenkinson, J. A. V. Coates, J. M. Cameron, *Bioorg. Med. Chem. Lett.*, 1993, **3**, 1723; (*b*) M. J. Bamford,D. C. Humber, R. Storer, *Tetrahedron Lett.*, 1991, **32**, 271 and references cited therein; (*c*) J. Branalt and I. Kvarnstrom, *J. Org. Chem.*, 1996, **61**, 3604 and references cited therein.

5 (*a*) T. S. Mansour, C. A. Evans, M. A. Siddiqui, M. Charron, B. Zacharie, N. Nguyen-Ba, N. Lee and B. Korba, *Nucleosides Nucleotides*, 1997, **16**, 993; (*b*) H. Soudeyns, X. J. Yao, Q. Gao, B. Belleau, J.-L. Kraus, N. Nguyen-Ba, B. Spira and M. A. Wainberg, *Antimicrob. Agents Chemother.*, 1991, **35**, 1386; (*c*) J. A. V. Coates, N. Cammack, H. J. Jenkinson, I. M. Mutton, B. A. Pearson, R. Storer, J. M. Cameron and C. R. Penn, *Antimicrob. Agents Chemother.*, 1992, **36**, 202; (*d*) M. W. Chun, D. H. Shin, H. R. Moon, J. Lee, H. Park and L. S. Jeong, *Bioorg. Med. Chem. Lett.*, 1997, **7**, 1475.

6 *U.S. Pat.* 05047407, BioChem Pharma Inc.; M. A. Nowak, S. Bon hoeffer, A. M. Hill, R. Bochme, H. C. Thomas and H. McDade, *Proc. Natl. Acad. Sci. U.S.A.*, 1996, **93**, 4398.

7 J. A. Secrist III, K. N. Tiwari, A. T. Shortnacy-Fowler, L. Messini, J. M. Riordan and J. A. Montgomery, *J. Med. Chem.*, 1998, **41**, 3865; M. R. Dyson, P. L. Coe and R. T. Walker, *J. Med. Chem.*, 1991, **34**, 2782.

8 H. Vorbruggen, K. Krolikiewicz and B. Bennua, *Chem. Ber.*, 1981, **114**, 1234.

9 N. Nguyen-Ba, W. Brown, N. Lee and B. Zacharie, *Synthesis*, 1998, 759.

10 M. Therien, J. Y. Gauthier and R. N. Young, *Tetrahedron Lett.*, 1988, **29**, 6733.

11 J. Y. Gauthier, T. Henien, L. Lo, M. Therien and R. N. Young, *Tetrahedron Lett.*, 1988, **29**, 6729.

12 J. M. Cameron, P. Collis, M. Daniel, R. Storer and P. Wilcox, *Drugs Future*, 1993, **18**, 319 and references cited therein.

13 L. W. Frick, L. St-John, L. C. Taylor, G. R. Painter, P. A. Furman, D. C. Liotta, E. S. Furfine and D. J. Nelson, *Antimicrob. Agents Chemother.*, 1993, **37**, 2285.

14 Chiral Column: Cyclobond I 2000 Beta-RSP 4.6 mm ID × 250 mm; mobile phase 10% MeCN–0.05% (AcOH–Et_3N, pH 6.74); pressure 965 psi and flow rate 0.50 ml min^{-1}. For **26**: t_R = 19.880 min; for **27**: t_R = 22.201 min.

Communication 9/01927H

ChemComm

Palladium catalysed allylation reactions in ionic liquids

Weiping Chen, Lijin Xu, Craig Chatterton and Jianliang Xiao*

Leverhulme Centre for Innovative Catalysis, Department of Chemistry, University of Liverpool, Liverpool, UK L69 7ZD. E-mail: j.xiao@liv.ac.uk

Received (in Cambridge, UK) 26th April 1999, Accepted 24th May 1999

Palladium catalysed allylic alkylation and amination reactions have been demonstrated to proceed readily in the room temperature ionic liquid 1-butyl-3-methylimidazolium tetrafluoroborate ([bmim][BF_4]) with easy catalyst/solvent recycling and no need to generate separately the carbanion nucleophiles.

Room temperature ionic liquids consisting of 1,3-dialkylimidazolium cations and their counter ions have attracted growing interest in the last few years.[1–8] These ionic liquids offer an attractive alternative to conventional organic liquids for clean synthesis, as they are easy to recycle and possess no effective vapor pressure. As with water and perfluoro solvents, they also offer the potential for easy catalyst/product separation, owing to their limited miscibility with many common organic liquids. A few types of catalytic reactions have been carried out in these and related ionic liquids; recent examples include Friedel–Crafts reactions,[1,4] Diels–Alder reactions,[2] alkylations,[3] olefin dimerisation and oligomerisation,[5–7,9] hydrogenation,[8] Heck reaction[10] and hydroformylation.[11] We report herein the first examples of palladium catalysed allylic alkylation and amination reactions in the ionic liquid [bmim][BF_4]. [bmim][BF_4] has a liquid range down to −81 °C. It is miscible with polar compounds such as lower alcohols but immiscible with less polar compounds such as toluene and Et_2O. Many organometallic compounds have been found to display good solubility in this liquid.

Palladium(0) catalysed allylic alkylations of soft carbon nucleophiles represent a very useful tool for organic synthesis.[12] As summarised by Hegedus, the alkylation reactions are usually conducted by mixing stabilised carbanions with a substrate-catalyst mixture in THF and then heating the resultant mixture at reflux.[13] The carbanions are generated separately using bases such as NaH in dipolar solvents like THF. Catalyst and solvent recycling, which will undoubtedly be difficult with conventional solvents, has rarely been addressed for these reactions.[14] Prompted by Seddon's recent report on *in situ* generation of anions in the alkylaton of indole and 2-naphthol in [bmim][PF_6],[3] we examind the room temperature, one-pot alkylation of the active methylene compounds **A**–**F** by 1,3-diphenylallyl acetate in [bmim][BF_4] (Scheme 1). The results are presented below.

The alkylation of dimethyl malonate **A** by 3-acetoxy-1,3-diphenylprop-1-ene was investigated first. The catalyst or catalyst precursor was formed by heating $Pd(OAc)_2$ (2 mol%, based on the acetate) with PPh_3 (8 mol%) in [bmim][BF_4] at 80 °C for 20 min. The ionic liquid was then cooled to ambient temperature, and the reaction started by adding the substrates and K_2CO_3. ^{1}H NMR monitoring showed that the alkylation was complete after 5 h reaction time at ambient temperature. The initial rate was slightly lower, due perhaps to the dissolution of the substrates and base or to the formation of active Pd^0 species at the beginning of the reaction. A few variables have been identified to be important for the success of the alkylation in [bmim][BF_4] (Table 1). (i) As with allylic alkylations in molecular solvents,[13] no reaction takes place in the ionic liquid without PPh_3. (ii) The reaction rate decreases markedly when the molar ratio of PPh_3:$Pd(OAc)_2$ is less than 4:1. Thus, with 3 equiv. (relative to palladium acetate) of PPh_3, the conversion of the acetate was only 50% after 15 h reaction time and, with 1 equiv. of PPh_3, a much lower conversion of 13% was observed. (iii) The reaction is slower without initial heating of $Pd(OAc)_2$ and PPh_3 in [bmim][BF_4]. Thus, heating of $Pd(OAc)_2$ and PPh_3 with the substrates in the absence of [bmim][BF_4] followed by reaction in the ionic liquid at ambient temperature for 15 h afforded only a 68% conversion. As a base, K_2CO_3 and DBU are equally effective but, in the case of the latter, the reaction mixture is homogeneous. K_2CO_3 only partly dissolves in [bmim][BF_4] under the reaction conditions. The quantity of palladium used can be lowered to 0.2 mol% without affecting the 100% conversion for reactions carried out overnight.

Using the procedures developed for dimethyl malonate, the alkylation was extended to the active methylene compounds **B**–**F**. The results are summarised in Table 2. All the reactions were completed with 100% conversion within the time indicated when using DBU as the base. The lower yield obtained with the acetylacetone **C** was partly due to double alkylation. Alkylation of the amido malonate **F** was sluggish at room temperature, but the reaction proceeded smoothly at 50 °C to give the product with 86% isolated yield. For the reactions involving methyl acetoacetate **B** and methyl cyanoacetate **D**, the product was a 1:1 mixture of two diastereomers. Replacing DBU with K_2CO_3 resulted in lower conversions for the substrates **B**–**F** under identical conditions; the reason is not immediately clear.

Using similar procedures, we also tested the amination of 1,3-diphenylallyl acetate. The amination by pyrrolidine pro-

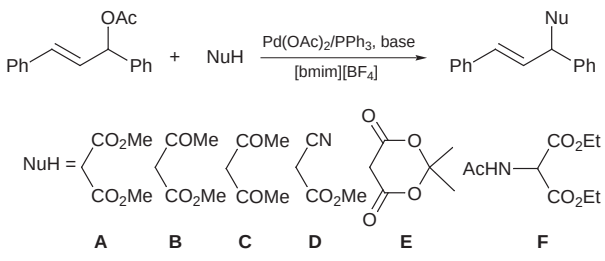

Scheme 1

Table 1 Palladium catalysed allylic alkylations in [bmim][BF_4] under various conditions[a]

PPh_3/$Pd(OAc)_2$	*t*/h	Conversion (%)
0	48	0
1	15	13
2	15	36
3	15	50
4	5	100
4	15	68[b]
4	15	100[c]

[a] General reaction conditions: 1.0 mmol of 3-acetoxy-1,3-diphenylprop-1-ene, 2 mol% $Pd(OAc)_2$, 1.5 mmol of dimethyl malonate and 2.0 mmol of K_2CO_3 in 1 ml of [bmim][BF_4] at ambient temperature. Before starting the reaction, $Pd(OAc)_2$ and PPh_3 were heated at 80 °C for 20 min in the ionic liquid. [b] $Pd(OAc)_2$, PPh_3 and the substrates were heated at 80 °C before introducing the base and ionic liquid at ambient temperature. [c] 0.2 mol% $Pd(OAc)_2$.

Table 2 Palladium catalysed allylations in [bmim][BF_4] with various nucleophiles[a]

NuH	Base	*t*/h	Yield (%)[b]
A	K_2CO_3	5	91
B	DBU	15	87[c]
C	DBU	15	54
D	DBU	14	88[c]
E	DBU	15	79
F	DBU	12	86[d]

[a] The reaction conditions were the same as the general reaction conditions given in Table 1, unless otherwise indicated. All the reactions completed with 100% conversion. [b] Isolated yield. [c] The product was a 1:1 mixture of two diastereomers. [d] Reaction was carried out at 50 °C.

ceeded readily to give the corresponding 1,3-diphenylallylamine with 100% conversion. Unlike the alkylations, no additional base is required in this transformation.

Catalyst separation/recycling appears to be difficult under the conditions established above, because the organic compounds and the ionic liquids form a homogeneous mixture and so catalyst separation *via* phase separation is not feasible. Further, extraction of the products with solvents of various polarity resulted in significant leaching of palladium species out of the ionic liquid. However, replacing PPh_3 with the hydrophilic phosphine P(*m*-$C_6H_4SO_3Na)_3$ led to effective recycling of the catalyst-containing ionic liquid phase; the catalyst along with the ionic liquid was reused three times without losing activity in the alkylation of dimethyl malonate. The product was extracted with toluene after each cycle of the reaction.

In summary, we have demonstrated that allylic alkylation and amination can effectively be performed in the room temperature ionic liquid [bmim][BF_4] with the additional benefit of easy catalyst/solvent recycling. Ionic liquids like this provide an ideal environment where ionic intermediates may be generated *in situ* and stabilised therein. Reactions in such media offer an attractive 'greener' alternative to the conventional processes where volatile organic solvents are frequently employed and catalyst reuse is difficult to implement.

We are indebted to the EPSRC and the University of Liverpool Graduates Association (Hong Kong) for postdoctoral research fellowships (W. C. and L. X.), and to the Leverhulme Centre for Innovative Catalysis for a LCIC studentship (C. C.).

Notes and references

1 A. Stark, B. L. MacLean and R. D. Singer, *J. Chem. Soc., Dalton Trans*., 1999, 63.
2 T. Fischer, A. Sethi, T. Welton and J. Woolf, *Tetrahedron Lett*., 1999, **40**, 793.
3 M. J. Earle, P. B. McCormac and K. R. Seddon, *Chem. Commun*., 1998, 2245.
4 C. J. Adams, M. J. Earle, G. Roberts and K. R. Seddon, *Chem. Commun*., 1998,2097.
5 L. C. Simon, J. Dupont and R. F. de Souza, *Appl. Catal. A: Gen.*, 1998, **175**, 215.
6 J. E. L. Dullius, P. A. Z. Suarez, S. Einloft, R. F. de Souza, J. Dupont, J. Fischer and A. DeCian, *Organometallics*, 1998, **17**, 815.
7 Y. Chauvin, H. Olivier, C. N. Wyrvalski, L. C. Simon and R. F. de Souza, *J. Catal*., 1997, **165**, 275.
8 A. L. Monteiro, F. K. Zinn, R. F. de Souza and J. Dupont, *Tetrahedron: Asymmetry*, 1997, **8**, 177.
9 B. Ellis, W. Keim and P. Wasserscheid, *Chem. Commun*., 1999, 337.
10 W. A. Herrmann and V. P. W. Bohm, *J. Organomet. Chem*., 1999, **572**, 141.
11 N. Karodia, S. Guise, C. Newlands and J.-A. Andersen, *Chem. Commun*., 1998, 2341.
12 G. Giambastiani and G. Poli, *J. Org. Chem*., 1998, **63**, 9608 and references therein.
13 L. S. Hegedus, in *Organometallics in Synthesis*, ed. M. Schlosser, Wiley, Chichester, 1994.
14 R. Kling, D. Sinou, G. Pozzi, A. Choplin, F. Quignard, S. Busch, S. Kainz, D. Koch and W. Leitner, *Tetrahedron Lett*., 1998, **39**, 9439.

Communication 9/03323H

Singlet–triplet bistability in a 1,3-phenylene-based bis(aminoxyl) diradical

Andrzej Rajca,* Kan Lu, Suchada Rajca and Charles R. Ross, II†

Department of Chemistry, University of Nebraska, Lincoln, NE 68588-0304, USA. E-mail: arajca@unlinfo.unl.edu

Received (in Columbia, MO, USA) 8th March 1999, Accepted 26th April 1999

Rapid quenching of the title bis(aminoxyl) 1 in 2-methyltetrahydrofuran from ambient temperature to cryogenic temperatures (5 K or below) produces 1 in its singlet state, which slowly converts at low temperatures, with an S-shaped time-dependence, to the triplet ground state.

1,3-Phenylene-based diradicals are ubiquitous building blocks for both high-spin polyradicals and molecular magnets.[1,2] Although 1,3-phenylene is the most reliable mediator of ferromagnetic coupling in organics, it is well established that severe bond torsions in 1,3-phenylene-based diradicals may result in singlet ground states.[3–5] Therefore, different bond torsions associated with selected conformers may allow for the same diradical to be obtained in either a singlet or triplet ground state. Such a phenomenon was recently reported for a different class of organic diradicals, which have been obtained in either a singlet or triplet state, depending on the photon energy in the photochemical generation or the solvent.[6–8] However, the rate of such conformationally mediated conversion between the different spin states in diradicals was not observed.[8] Now we report the singlet and triplet ground state in a 1,3-phenylene-based diradical, 4,6-bis(trifluoromethyl)-*N*,*N*′-di-*tert*-butyl-1,3-phenylenebis(aminoxyl) **1**, with an observable rate of conversion between the low- and high-spin states.

Synthesis of **1** is outlined in Scheme 1. X-Ray crystallography, EPR, ^{1}H NMR, MS, IR and elemental analysis data confirm the structure and suggest a purity of > 95%.

X-Ray crystallography indicates that the aminoxyl moieties are twisted out of the plane of the 1,3-phenylene with torsional angles of −70 (C5–C6–N2–O2) and 49° (C3–C2–N1–O1); both oxygens point toward the trifluoromethyl groups.[9] The geometry and conformation of the trifluoromethyl groups suggests negligible radical–fluorine hyperconjugation (Fig. 1).[10]

The $\Delta m_s = 1$ region of the X-band EPR spectrum of **1** in frozen 2-MeTHF has six broad peaks consistent with a triplet state. The two inner most resonances show resolved hyperfine coupling with the two nitrogens; the center resonance, which would correspond to a monoradical impurity, is negligible. The spectral width of 0.0321 Tesla is constant in the 10–65 K range and it is of similar magnitude to that found for other 1,3-phenylene-connected bis(aminoxyl)s.[3,4,11] The $\Delta m_s = 2$ signal is also observed (Fig. 2). In the ^{1}H NMR spectrum of a 0.05 mol dm^{-3} solution of **1** in $CDCl_3$, two prominent peaks at −16 (broad) and 1.1 ppm (narrow) have a relative intensity of 36 : 1, they are assigned to the *tert*-butyl groups associated with the aminoxyl moiety and the diamagnetic impurity (presumably a hydroxyamine moiety), respectively.[12] Molecular ions in the EI MS for **1** and the dihydroxyamine **2** (Scheme 1) show a *m/z* difference corresponding to two hydrogen atoms.

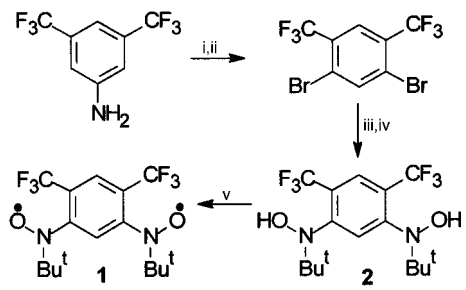

Scheme 1 *Reagents and conditions*: i, Br_2, Fe, CH_2Cl_2; ii, $NaNO_2$, H_2SO_4, EtOH (45% for 2 steps); iii, Bu^{t}Li, Et_2O; iv, (Bu^{t}NO)$_2$; v, Ag_2O, $CHCl_3$ (20% for 3 steps).

† Current address: Department of Structural Biology, St. Jude Children's Hospital, 332 N. Lauderdale St., Memphis, TN 38105, USA.

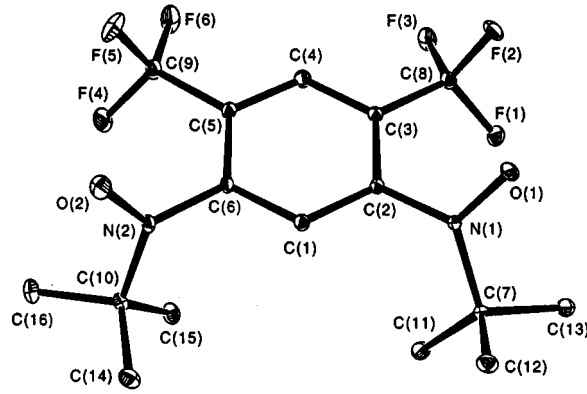

Fig. 1 Molecular structure of **1** in the solid state at 50 K; thermal ellipsoids at the 50% probability. The hydrogens are not shown.

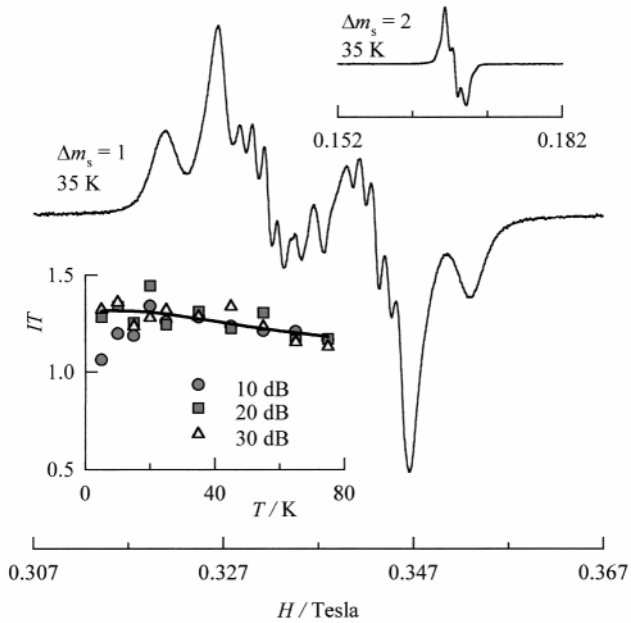

Fig. 2 The EPR spectrum of 0.001 mol dm^{-3} **1** in 2-MeTHF. Zero field splitting parameters for an $S = 1$ state are: $|D/hc| \approx 0.015$ cm^{-1} and $|E/hc| \approx 0.001$ cm^{-1}. Lower insert: plot of the product (IT) of the intensity (I) for the $\Delta m_s = 2$ resonance and the temperature (T) *vs.* T at three settings of microwave power (10, 20 and 30 dB); the 20 and 30 dB data are amplified by the consecutive factors of 3.2 ≈ $(10)^{1/2}$. The values of I are obtained by numerical double integration of the $\Delta m_s = 2$ region. The solid line corresponds to a numerical fit with the singlet–triplet energy gap corresponding to $2J/k = 80$ K (ref. 14) (J is a coupling constant from the Heisenberg Hamiltonian, $H = -2J\boldsymbol{S}_1\cdot\boldsymbol{S}_2$ with $|\boldsymbol{S}_1| = |\boldsymbol{S}_2| = 1/2$).

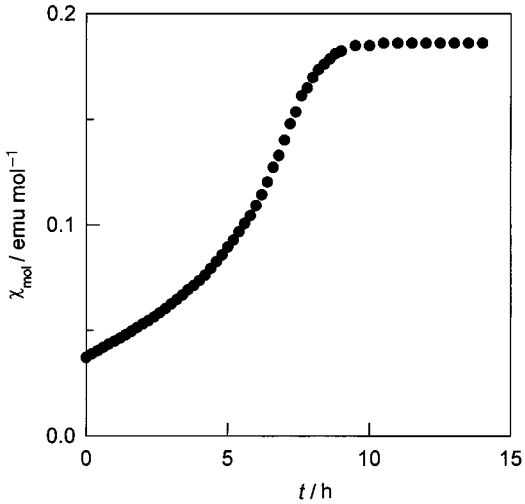

Fig. 3 Plot of molar magnetic susceptibility (χ_{mol}) *vs.* time, following rapid cooling of **1** (0.62 ± 0.07 mg) in 2-MeTHF (*ca.* 0.05 ml) from ambient temperature to 5 K. The applied magnetic field is 0.5 Tesla.

A sample of **1** in 2-MeTHF (10^{-2} mol dm^{-3}) was inserted, at a moderately rapid rate (5–10 min), into a SQUID magnetometer/susceptometer sample chamber kept at approximately 5 K. After establishing a stable temperature in the sample chamber (*ca.* 5 min), and an additional brief equilibration (2–5 min), the molar magnetic susceptibility (χ_{mol}) was measured at a constant applied magnetic field (H = 0.05–0.5 Tesla) as a function of time.[13] S-shaped plots were obtained, in which χ_{mol} increases about five times (Fig. 3).[13] The onset of a sharp rise in χ_{mol} is random and varies from several minutes to several hours. Gradual cooling of **1** in 2-MeTHF, *e.g.* temperature sweep from 290 to 5 K at 3, 5 or 10 K min^{-1}, gives the equilibrium value of χ_{mol} at 5 K. Analogous S-shaped plots are obtained at 1.8 and 2 K. The observed phenomena are solvent dependent; the time-dependence of χ_{mol} was not found for **1** in tetrahydrofuran (THF) or toluene (constant χ_{mol} *vs.* time).

Diradical **1** in 2-MeTHF was kept at 1.8 or 5 K until χ_{mol} (*vs.* time) reached a constant value, and then magnetization (M) was measured at T = 1.8 and 5 K as a function of H = 0–5 Tesla. The fit of the M *vs.* H/T data to the Brillouin functions gives S = 1, indicating a triplet ground state. Furthermore, the plateau value of χ_{mol} = 0.19 at 5 K (Fig. 3) is in good agreement with χ_{mol} = 0.20, as expected for a predominantly triplet ground state at 5 K. The plot of IT *vs.* T, where I is the intensity of the EPR signal in the Δm_S = 2 region, slightly decreases at the higher end of the 10–75 K range (Fig. 2). Therefore, the triplet ground state is slightly depopulated at higher temperatures, suggesting a small energy gap between the triplet and the excited singlet state within the same conformer (weak ferromagnetic coupling) or conversion to another conformer with different ordering of states.

One of the most straightforward rationalizations for these results is by invoking two conformers (conformational isomers) for **1** with different torsions about the C(1,3-phenylene)–N bonds.[3] The low temperature conformer has a triplet ground state, probably with a rather small (Heisenberg $2J/k$ < 100 K) singlet–triplet energy gap.[14] The high temperature conformer has a singlet ground state (at least, at low temperatures), with a non-negligible singlet–triplet energy gap. Upon rapid quenching from ambient temperature to 5 or 1.8 K, the high temperature conformer (or a large fraction of) is frozen in 2-MeTHF glass. Because the singlet–triplet thermal equilibration within the same conformer will remain very fast, the singlet ground state is predominantly populated in the 1.8–5 K range for the high temperature conformer. The observed S-shaped increase of χ_{mol} *vs.* time in the 1.8–5 K range would involve a conformational change from the high temperature to the low temperature conformer. The resultant dramatic change between the population of the singlet *vs.* triplet states is responsible for a typically five-fold increase in χ_{mol}. The S-shape and random time span for the completion of the conformational change are associated with various glassy matrix effects, *e.g.* random distribution of non-equivalent sites in the matrix.[15] A somewhat vexing problem is the preference for the singlet ground state in the high temperature conformer. This would require overcoming the entropic advantage of the triplet state (m_s degeneracy) by other sources of entropy or enthalpy, *e.g.* relatively low energy vibrational modes in the singlets or different solvation in the liquid *vs.* glassy 2-MeTHF. Unfortunately, there are no structural data for the singlet state (or states) of **1**.

Although conformational isomers were invoked in studies of some organic di- and poly-radicals, the time-dependence of the magnetic susceptibility of **1** in 2-MeTHF is unprecedented and calls for prudent interpretation of magnetic data for organic molecules, especially in glassy matrices.[6] Ultimately, a rational design of spin-bistable diradicals (or polyradicals) may provide organic analogues of metal ion based spin crossover compounds.[16]

This research was supported by the National Science Foundation (CHE-9510096 and CHE-9806954).

Notes and references

1 A. Rajca, J. Wongsriratanakul, S. Rajca and R. Cerny, *Angew. Chem., Int. Ed.*, 1998, **37**, 1229; K. K. Anderson and D. A. Dougherty, *Adv. Mater.*, 1998, **10**, 688; K. Sato, M. Yano, M. Furuichi, D. Shiomi, T. Takui, K. Abe, K. Itoh, A. Higuchi, K. Katsuma and Y. Shirota, *J. Am. Chem. Soc.*, 1997, **119**, 6607; A. Rajca, S. Rajca and S. R. Desai, *J. Chem. Soc., Chem. Commun.*, 1995, 1957; A. Rajca, *Chem. Rev.*, 1994, **94**, 871.

2 H. Iwamura, K. Inoue and N. Kaga, *New J. Chem.*, 1998, 201.

3 M. Dvolaitzky, R. Chiarelli and A. Rassat, *Angew. Chem., Int. Ed. Engl.*, 1992, **31**, 180.

4 F. Kanno, K. Innoue, N. Koga and H. Iwamura, *J. Am. Chem. Soc.*, 1993, **115**, 847; J. Fujita, M. Tanaka, H. Suemune, N. Koga, K. Matsuda and H. Iwamura, *J. Am. Chem. Soc.*, 1996, **118**, 9347.

5 S. Fang and M.-S. Lee, *J. Am. Chem. Soc.*, 1995, **117**, 6727; K. Okada, T. Imakura, M. Oda, H. Murai and M. Baumgarten, *J. Am. Chem. Soc.*, 1996, **118**, 3047; A. Rajca and S. Rajca, *J. Chem. Soc., Perkin Trans. 2*, 1998, 1077.

6 L. C. Bush, R. B. Heath and J. A. Berson, *J. Am. Chem. Soc.*, 1993, **115**, 9830; L. C. Bush, L. Maksimovic, X. W. Feng, H. S. M. Lu and J. A. Berson, *J. Am. Chem. Soc.*, 1997, **119**, 1416.

7 D. A. Schultz, A. K. Boal and G. T. Farmer, *J. Am. Chem. Soc.*, 1997, **119**, 3846.

8 J. A. Berson, *Acc. Chem. Res.*, 1997, **30**, 238.

9 *Crystal data* for **1**: $C_{16}H_{20}F_6N_2O_2$, M = 386.34, monoclinic, a = 5.849(2), b = 31.360(200), c = 9.436(6) Å, β = 93.8600(5)°, V = 1726.9(111) Å^3, T = 50(2) K, space group $P2_1/n$ (14), Z = 4, μ(AgKα) = 0.08 mm^{-1}. Structure solved by direct methods and refined by full-matrix least-squares on F^2. 5018 reflections observed [$F_o > 4\sigma(F_o)$]. Final refinement statistics: $wR(F2)$ = 0.1168, $R(F)$ = 0.0502, GooF = 1.079. CCDC 182/1278. See http://www.rsc.org/suppdata/cc/1999/1249/ for crystallographic files in .cif format.

10 On the side of the relatively less twisted aminoxyl moiety in **1**, C8 (CF_3 group) and N1 (aminoxyl) are 0.16 and 0.15 Å, respectively, from the plane defined by the six carbons of the benzene ring (RMS 0.014 Å). All C–F bond lengths are 1.34 Å.

11 A. Calder, A. R. Forrester, P. G. James and G. R. Luckhurst, *J. Am. Chem. Soc.*, 1969, **91**, 3724.

12 The chemical shift of −17 ppm is found for protons of the Bu^t group in 2-methyl-*N*-*tert*-butylphenylaminoxyl: A. Calder, A. R. Forrester, J. W. Emsley, G. R. Luckurst and R. A. Storey, *Mol. Phys.*, 1970, **18**, 481. Treatment of **1** in $CDCl_3$ in an NMR tube with phenylhydrazine gives quantitatively dihydroxyamine **2**, as expected.

13 A Quantum Design MPMS5S SQUID instrument was used with either standard or continuous temperature control. An approximate correction for diamagnetism (χ_{dia}) for each sample was obtained from extrapolation of χ *vs.* $1/T$ (χ = total magnetic susceptibility) plots using the data in the T = 160–280 K range in the cooling mode of the MPMS5S. Typical values $\chi_{dia} \approx 4 \times 10^{-8}$ emu are an order of magnitude less than the total χ in the 5–1.8 K range.

14 The estimate of the Heisenberg coupling constant, J/k = 40 K (Fig. 2), can only be very approximate, as conformational effects may interfere with a simple two-state model.

15 W. Siebrand and T. A. Wildman, *Acc. Chem. Res.*, 1986, **19**, 238.

16 O. Kahn and C. J. Martinez, *Science*, 1998, **279**, 44.

Communication 9/01906E

Rotaxane construction with a binaphthol-derived crown ether

Stuart J. Cantrill,[a] Matthew C. T. Fyfe,[a] Aaron M. Heiss,[a] J. Fraser Stoddart,*[a] Andrew J. P. White[b] and David J. Williams[b]

[a] *Department of Chemistry and Biochemistry, University of California, Los Angeles, CA 90095, USA. E-mail: stoddart@chem.ucla.edu*

[b] *Department of Chemistry, Imperial College, South Kensington, London, UK SW7 2AY*

Received (in Columbia, MO, USA) 16th March 1999, Accepted 20th May 1999

Secondary dialkylammonium ions thread through the cavity of (*RS*)-benzo-2,2′-binaphtho[26]crown-8 to create [2]pseudorotaxanes, one of which was stoppered to produce a [2]rotaxane—incorporating the chiral binaphthyl unit—that was characterised by NMR spectroscopy, mass spectrometry and X-ray crystallography.

There is currently a resurgence of interest in the employment of binaphthyl-containing macrocyclic hosts in supramolecular chemistry,[1] principally because of the potential for the chiral binaphthyl unit to associate diastereoselectively with racemic guest mixtures. However, the pioneering studies in this area took place more than a quarter of a century ago when, in 1973, Cram and his associates[2] described the synthesis of chiral binaphthyl-incorporating crown ethers, *e.g.* (*R*)-2,2′-binaphtho[20]crown-6 [(*R*)-BN20C6, Fig. 1], that exhibit enantiomeric recognition[3] of racemic *primary alkylammonium* ($R^1R^2CHNH_3^+$) ions, *e.g.* (*RS*)-α-methoxycarbonylbenzylammonium [(*RS*)-**1**$^+$], during the formation of face-to-face complexes. More recently, we discovered that crown ethers with suitably sized cavities, *e.g.* dibenzo[24]crown-8 (DB24C8), are pierced by *secondary dialkylammonium* ($R^1CH_2NH_2^+CH_2R^2$) ions, *e.g.* dibenzylammonium (**2**$^+$), producing[4] [2]pseudorotaxanes—and, ultimately, rotaxanes[5]—by means of, *inter alia*, hydrogen bonds. Here, we demonstrate that the expanded racemic binaphthol-derived crown ether (*RS*)-benzo-2,2′-binaphtho[26]crown-8 [(*RS*)-BBN26C8†] can be penetrated by $R^1CH_2NH_2^+CH_2R^2$ ions to produce (Fig. 1) [2]pseudorotaxanes.[6] This observation has resulted in the synthesis of a racemic binaphthyl-containing [2]rotaxane that has been characterised by NMR spectroscopy, mass spectrometry and X-ray crystallography.

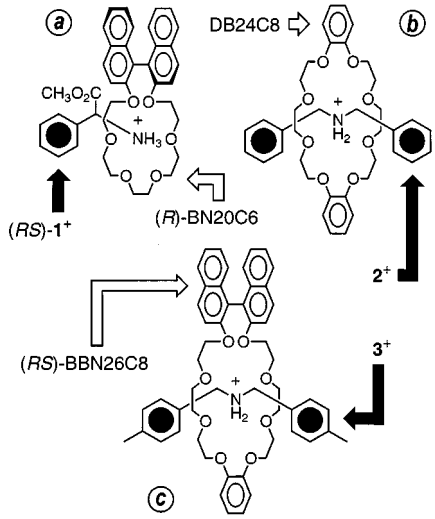

Fig. 1 Several complexes produced by the intermolecular association of crown ethers with ammonium ions. (*a*) Face-to-face complex [(*R*)-BN20C6·(*RS*)-**1**]$^+$. (*b*) [2]Pseudorotaxane [DB24C8·**2**]$^+$. (*c*) [2]Pseudorotaxane [(*RS*)-BBN26C8·**3**]$^+$.

The first indication that (*RS*)-BBN26C8 forms pseudorotaxane complexes with $R^1CH_2NH_2^+CH_2R^2$ ions was provided by FAB mass spectrometry. The FAB mass spectrum of a 1:1 CH_2Cl_2 solution of (*RS*)-BBN26C8 and bis(*p*-methylbenzyl)ammonium hexafluorophosphate[4a] (**3**·PF_6) reveals a strong supramolecular ion at *m/z* 851, corresponding to [(*RS*)-BBN26C8·**3**]$^+$. Complex formation was also indicated in solution by ^{1}H NMR spectroscopy. The ^{1}H NMR spectrum [400 MHz, $CDCl_3$–CD_3CN (3:1), 300 K] of an equimolar solution of (*RS*)-BBN26C8 and **3**·PF_6 shows that, like[4] [DB24C8·**2**]$^+$, the complex [(*RS*)-BBN26C8·**3**]$^+$ exchanges slowly with its uncomplexed constituents on the NMR timescale, signals being observed for (1) [(*RS*)-BBN26C8·**3**]$^+$ itself, (2) free (*RS*)-BBN26C8 and (3) uncomplexed **3**$^+$. In other words, even though the 26-membered macroring of (*RS*)-BBN26C8 is two atoms larger than that of DB24C8, the cavity is still small enough for the relatively bulky aryl rings of the cation to have some difficulty threading. The fact that so many different species are equilibrating slowly with one another on the NMR timescale, coupled with the crown ether's C_2 symmetry, means that the signals associated with the polyether/benzylic CH_2 and aromatic CH portions of the spectrum, located at δ 2.84–4.15 and 6.53–7.80, respectively, are extremely complicated. However, the signals for the CH_3 protons in both the free and complexed states of **3**$^+$ are well separated from one another, resonating at δ 2.23 and 2.13, respectively. From an analysis of the relative intensities of these signals, an association constant (K_a) of 960 ± 100 M^{-1} was calculated for [(*RS*)-BBN26C8·**3**][PF_6] by using the single-point method.[4] Noticeably, this K_a is much lower than that obtained for the [DB24C8·**3**][PF_6] complex (1900 ± 200 M^{-1}) under identical conditions, indicating that replacing one of DB24C8's catechol units with the less preorganised binaphthol residue lowers the complex stability.‡

Next, we investigated the application of the (*RS*)-BBN26C8–$R^1CH_2NH_2^+CH_2R^2$ recognition motif to rotaxane synthesis. Gratifyingly, the [2]rotaxane (*RS*)-**4**·O_2CCF_3 was isolated§ in 42% yield when (*RS*)-BBN26C8 was reacted (Scheme 1) with

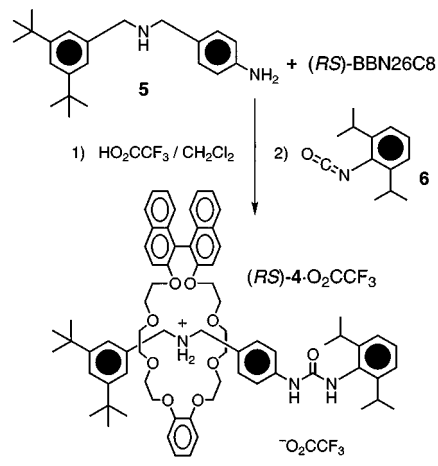

Scheme 1

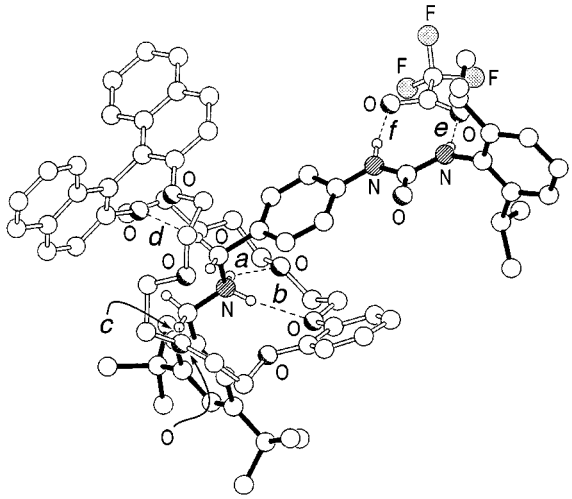

Fig. 2 X-Ray crystal structure of the (*R*)-enantiomer of [2]rotaxane (*RS*)-**4**·O_2CCF_3. Hydrogen bonding distances and angles {[X···O], [H···O] distances (Å), [X–H···O] angles (°)}: (*a*) 2.86, 2.12, 139; (*b*) 2.95, 2.08, 160; (*c*) 3.28, 2.39, 153; (*d*) 3.21, 2.29, 160; (*e*) 2.86, 2.00, 161; (*f*) 2.89, 2.00, 168.

p-aminobenzyl-*m*,*m*′-di-*tert*-butylbenzylamine (**5**), HO_2CCF_3 and *o*,*o*′-diisopropylphenyl isocyanate (**6**).[5] This interlocked compound is completely stable to column chromatography, indicating that the *m*,*m*′-di-*tert*-butylphenyl and *o*,*o*′-diisopropylphenyl termini of the rotaxane's 'dumbbell' component are sufficiently bulky to ensure that dissociation does not occur. Further evidence for the stability of the [2]rotaxane architecture is provided by the FAB mass spectrum of (*RS*)-**4**·O_2CCF_3, where the base peak, observed at *m/z* 1153, corresponds to the ion [(*RS*)-**4**]$^+$. Although the ^{1}H NMR spectrum (400 MHz, CD_3CN, 300 K) of (*RS*)-**4**·O_2CCF_3 displays numerous sets of complicated multiplets, a comparison of the integrals associated with resonances for both (*RS*)-BBN26C8 and the dumbbell component reveals that both species are present in a 1 : 1 ratio in the rotaxane. Interestingly, the peaks associated with the benzylic C$H_2NH_2^+$ protons do not lie in the 'expected' δ 4.45–4.75 range,[5] presumably as a direct consequence of the binaphthyl unit's shielding effect. In this instance, a ^{1}H–^{13}C HMQC experiment revealed that two sets of signals, ranging from δ 3.78–3.94 and 4.01–4.24, occur for these protons. The ^{13}C NMR spectrum (100 MHz, CD_3CN, 300 K) of (*RS*)-**4**·O_2CCF_3 is also intriguing and demonstrates that the crown ether is desymmetrised, *i.e.* the C_2 axis is negated, upon its incorporation into the [2]rotaxane architecture. The presence of the unsymmetrical dumbbell makes BBN26C8's two halves heterotopic and, hence, *all* of its 38 carbon atoms anisochronous. A total of 55 of the 60 ^{13}C NMR signals anticipated¶ for (*RS*)-**4**·O_2CCF_3 were observed in the spectrum (several of the heterotopic carbon atoms resonate at the same frequency).

The X-ray analysis‖ of the rotaxane (*RS*)-**4**·O_2CCF_3 reveals (Fig. 2) that the binaphthol-derived crown ether BBN26C8 encircles the dumbbell's NH_2^+ centre. Stabilisation of the [2]rotaxane architecture occurs principally *via* a combination of [N$^+$–H···O] and [C–H···O] hydrogen bonding involving the NH_2^+ centre, its adjacent CH_2 groups and the crown ether's oxygen atoms. There is also a near-parallel (5°), partial overlap between one of the BBN26C8 naphthalene rings and the *p*-toluidinyl ring of the dumbbell (mean interplanar separation 3.6 Å), indicative of a supplementary weak π–π stacking interaction. The $^-O_2CCF_3$ anion hydrogen bonds to the two urea NH groups.[5] There are no inter-[2]rotaxane interactions of note.

To summarise, we have established that $R^1CH_2NH_2^+CH_2R^2$ ions penetrate the cavity of binaphthol-derived crown ether (*RS*)-BBN26C8, generating [2]pseudorotaxanes that may be capped to form [2]rotaxanes. The preparation of these pseudorotaxanes and rotaxanes, which incorporate the chiral binaphthyl unit, augurs well for future studies on (1) the concepts of supramolecular chirality,[7] (2) the preferential recognition[3] of a chiral $R^1CH_2NH_2^+CH_2R^2$ ion over its enantiomer by either (*R*)- or (*S*)-BBN26C8 in the production of diastereoisomeric pseudorotaxanes[8] and (3) the synthesis of optically active rotaxanes.[9]

Notes and references

† (*RS*)-BBN26C8 was acquired in 42% yield by reaction of (*RS*)-1,1′-bi-2-naphthol with *o*-bis(2-{2-[2-(*p*-tolylsulfonyloxy)ethoxy]ethoxy}ethoxy)benzene (which was prepared using a method similar to that employed to obtain the corresponding *p*-derivative: M. J. Gunter, D. C. R. Hockless, M. R. Johnston, B. W. Skelton and A. H. White, *J. Am. Chem. Soc.*, 1994, **116**, 4810) in MeCN in the presence of Cs_2CO_3 and CsOTs.

‡ By the same token, Cram's group discovered (D. S. Lingenfelter, R. C. Helgeson and D. J. Cram, *J. Org. Chem.*, 1981, **46**, 393) that the binaphthol-derived crown ether BN20C6 binds RNH_3^+ ions less well than its 2,3-dihydroxynaphthalene-derived congener.

§ It should be noted that **4**·O_2CCF_3 was obtained as a racemic mixture, the rotaxane's chirality arising only by virtue of the C_2-symmetric binaphthyl unit. Here, cycloenantiomerism (C. Yamamoto, Y. Okamoto, T. Schmidt, R. Jäger and F. Vögtle, *J. Am. Chem. Soc.*, 1997, **119**, 10 547), a phenomenon that would lead to the formation of two diastereoisomeric pairs of enantiomers, does not occur, because (*RS*)-BBN26C8 has two homotopic faces by virtue of its C_2 axis of rotation.

¶ Free (*RS*)-BBN26C8, dumbbell and anion give rise to 19, 20 and two signals, respectively, in their ^{13}C NMR spectra. Thus, the ^{13}C NMR spectrum of rotaxane (*RS*)-**4**·O_2CCF_3 would be expected to exhibit a total of 41 signals if no desymmetrisation were to occur.

‖ X-Ray quality single crystals were obtained by vapour diffusion of *n*-C_5H_{12} into a CH_2Cl_2 solution of (*RS*)-**4**·O_2CCF_3. *Crystal data*: $[C_{73}H_{90}N_3O_9][O_2CCF_3]\cdot 2CH_2Cl_2$, M = 1436.4, monoclinic, $P2_1/n$ (no. 14), a = 13.281(3), b = 30.528(2), c = 21.593(2) Å, β = 96.80(1)°, V = 8694(2) Å^3, Z = 4, D_c = 1.097 g cm^{-3}, μ(Cu-Kα) = 17.2 cm^{-1}, F(000) = 3040, T = 173 K; Siemens P4 rotating anode diffractometer, ω-scans, 12673 independent reflections; structure solved by direct methods, all major occupancy non-hydrogen atoms of cations and anions refined anisotropically (non-hydrogen atoms of solvent molecules isotropically) using full-matrix least-squares, based on F^2, to give R_1 = 0.138, wR_2 = 0.342 for 5299 independent observed reflections [$|F_o| > 4\sigma(|F_o|)$, $2\theta \leqslant 120°$] and 950 parameters. CCDC 182/1269.

1 L. Pu, *Chem. Rev.*, 1998, **98**, 2405.
2 E. P. Kyba, M. G. Siegel, L. R. Sousa, G. D. Y. Sogah and D. J. Cram, *J. Am. Chem. Soc.*, 1973, **95**, 2691.
3 X. X. Zhang, J. S. Bradshaw and R. M. Izatt, *Chem. Rev.*, 1997, **97**, 3313.
4 (*a*) P. R. Ashton, M. C. T. Fyfe, S. K. Hickingbottom, J. F. Stoddart, A. J. P. White and D. J. Williams, *J. Chem. Soc., Perkin Trans. 2*, 1998, 2117; (*b*) M. C. T. Fyfe and J. F. Stoddart, *Adv. Supramol. Chem.*, 1999, **5**, 1.
5 S. J. Cantrill, D. A. Fulton, M. C. T. Fyfe, J. F. Stoddart, A. J. P. White and D. J. Williams, *Tetrahedron Lett.*, 1999, **40**, 3669.
6 E. Ishow, A. Credi, V. Balzani, F. Spadola and L. Mandolini, *Chem. Eur. J.*, 1999, **5**, 984.
7 M. Suárez, N. Branda, J.-M. Lehn, A. Decian and J. Fischer, *Helv. Chim. Acta*, 1998, **81**, 1.
8 M. Asakawa, P. R. Ashton, W. Hayes, H. M. Janssen, E. W. Meijer, S. Menzer, D. Pasini, J. F. Stoddart, A. J. P. White and D. J. Williams, *J. Am. Chem. Soc.*, 1998, **120**, 920.
9 T. Schmidt, R. Schmieder, W. M. Müller, B. Kiupel and F. Vögtle, *Eur. J. Org. Chem.*, 1998, 2003.

Communication 9/02096I

ChemComm

Cooperative halide, perrhenate anion–sodium cation binding and pertechnetate extraction and transport by a novel tripodal tris(amido benzo-15-crown-5) ligand

Paul D. Beer,*[a] Peter K. Hopkins[a] and James D. McKinney[b]

[a] *Department of Chemistry, Inorganic Chemistry Laboratory, University of Oxford, South Parks Road, Oxford, UK OX1 3QR*

[b] *BNFL, Springfields, Preston, Lancashire, UK PR4 0XJ*

Received (in Cambridge, UK) 29th April 1999, Accepted 25th May 1999

A new tripodal tris(amido benzo-15-crown-5) ligand L[1] cooperatively binds chloride, iodide and perrhenate anions *via* co-bound crown ether complexed sodium cations and efficiently extracts and transports the pertechnetate anion from simulated aqueous nuclear waste solutions *via* cooperative ion-pair binding effects.

Ion pair recognition, the simultaneous complexation of cationic and anionic guest species by multisite receptors, is a new, emerging and topical field of coordination chemistry.[1–6] These heteroditopic ligands can be designed to exhibit novel cooperative and allosteric behaviour whereby the binding of one charged guest can influence, through electrostatic and conformational effects, the subsequent coordination of the pairing ion. Such systems have potential as new selective extraction and transportation reagents for ion pair species of environmental importance. As a consequence of discharges from nuclear fuel reprocessing plants the radioactive pertechnetate anion TcO_4^- is alleged to have a detrimental effect on the environment.[7] Approaches to the removal of pertechnetate anion from waste include liquid–liquid coextraction with metal complexed crown ethers,[8] lipophilic arsonium[9] and ferrocenium[10] salts and π-transition metal–cyclotriveratrylene derivatives.[11] In order to demonstrate, to the best of our knowledge for the first time, the practical usage of ion-pair cooperativity for extraction of such a toxic anionic guest species, we report here the synthesis of a new tripodal tris(amido benzo-15-crown-5) ligand L[1] that cooperatively binds halide and perrhenate anions *via* crown ether complexation of sodium cations, and also efficiently extracts and transports the pertechnetate anion from simulated aqueous nuclear waste *via* cooperative ion-pair binding effects. The target ligand L[1] containing a tripodal tetrahedral amide hydrogen bond donor anion recognition site in combination with crown ether cation binding moieties was synthesised in 55% yield by condensation of tris(2-aminoethyl)amine (tren) **1** with 3 equiv. of 4-chlorocarbonylbenzo-15-crown-5[12] **2** in the presence of Et_3N in CH_2Cl_2 (Scheme 1). Analogous synthetic procedures using appropriate acid chlorides were used to prepare the tripodal model ligands L[2] and L[3] in 30 and 29% yield respectively.

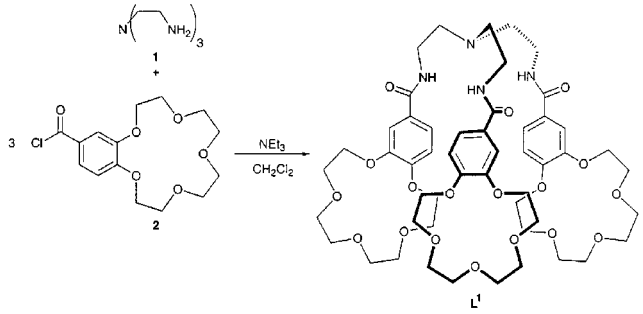

Scheme 1

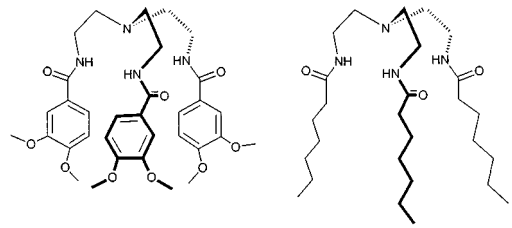

The anion binding properties of L[1]–L[3] were initially investigated by ^{1}H NMR titration studies with Cl^-, I^- and ReO_4^- in $CDCl_3$ solution. The latter two anions were chosen as I^- has approximately the same size and charge density as TcO_4^-, and ReO_4^- is an isostructural analogue. The addition of all three anions (as their Bu_4N^+ salts) to $CDCl_3$ solutions of L[1]–L[3] caused significant downfield perturbations of the respective ligand's amide protons by up to $\Delta\delta$ = 1.41 ppm, indicating anion binding is taking place in the tripodal amide vicinity of the ligand. Analysis of the resulting titration curves with the computer program EQNMR[13] suggested 1:1 complex stoichiometry in all cases and the determined stability constant values are presented in Table 1. The magnitudes of the stability constants shown in Table 1 are relatively modest, reflecting the neutrality of the ligands; all three ligands exhibit the largest stability constant with chloride. Because nuclear waste discharges typically contain high concentrations of sodium cations it was of interest to investigate the mode of binding of this particular cationic guest to L[1]. Unfortunately solubility problems prevented use of ^{13}C NMR titration techniques.† By monitoring the picrate chromophore, UV-visible spectroscopic titration experiments with sodium picrate and L[1] in 1:1 THF–CH_2Cl_2 indicated that at high concentrations of sodium cation (*i.e.* ⩾ 3 equiv.) unsurprisingly, one sodium cation is bound in each benzo-15-crown-5 moiety. However at lower concentrations, the observation of a well documented bathochromic shift of the picrate chromophore to 377 nm[14] indicated the additional presence of a 1:1 charge separated sandwich complex. Interestingly, alkali metal picrate extraction experiments with L[1] (Table 2) revealed an extraction preference for $Na^+ > K^+ > Cs^+$. In order to elucidate cooperative ion-pair binding effects

Table 1 Anion stability constant data

	K^a/M^{-1}		
Ligand	Cl^-	I^-	ReO_4^-
L[1]	60	30	40
L[2]	75	40	40
L[3]	40	20	30

[a] Determined in $CDCl_3$ at 298 K, errors estimated to be ⩽10%. [L] = 1 × 10^{-2} M.

Table 2 Extraction of metal picrates by L^1

Picrate	Extraction[a] (%)
Na	80
K	40
Cs	15

[a] Aqueous phase: 1×10^{-4} M metal picrate; $CDCl_3$ phase: 1×10^{-3} M L^1 at 298 K.

^{1}H NMR anion titration experiments with L^1 were repeated in the presence of 1 equiv. of sodium picrate and EQNMR determined stability constant values are present in Table 3. Clearly there is a significant increase in the strength of binding for all anions in the presence of 1 equiv. of sodium cation; in the case of ReO_4^- the increase is greater than twenty-fold. This positive cooperativity may be attributed to the increased electrostatic attraction between the positively charged $L^1 \cdot Na^+$ complex and the guest anion. The complexed metal cation may also affect the spatial arrangement of the ligand and enhance the relative acidity of the ligand's amide protons, leading to stronger hydrogen bonding of the anionic guest. It is noteworthy that the anion selectivity trend displayed by L^1 is altered in the presence of sodium. With no metal cation present, L^1 binds Cl^- in preference to ReO_4^-, however on addition of sodium cation, ReO_4^- is more strongly bound (Table 3), which suggests the binding of the metal cation preorganises L^1 for tetrahedral anionic guest recognition.

Table 3 Stability constants for L^1 anion binding in the presence and absence of sodium picrate in $CDCl_3$

Anion	K/M^{-1}
Cl^-	60[a]
Cl^- ($+Na^+$)[b]	520[c]
I^-	30[a]
I^- ($+Na^+$)[b]	390[c]
ReO_4^-	40[a]
ReO_4^- ($+Na^+$)[b]	840[c]

[a] At 298 K, errors estimated to be ⩽10%. [b] Titration carried out in the presence of 1 equiv. of sodium picrate. [c] At 298 K, errors estimated to be ⩽15%.

Encouraged by these cooperative ion pair binding results, pertechnetate extraction experiments were carried out using conditions that simulated nuclear waste streams. The aqueous phase contained ammonium pertechnetate (100 ppm) and sodium nitrate (2.35 M) and the pH was adjusted to basic conditions (pH = 11) using NaOH. The organic phase consisted of CH_2Cl_2 solutions of L^1–L^3 and benzo-15-crown-5 at concentrations of 1.5×10^{-2} M for the tripodal ligands and 4.5×10^{-2} M for the crown ether. Equal volumes (2 ml) of each solution were mixed, and rapidly shaken. Inductively coupled plasma mass spectrometry (ICP-MS) and ^{99}Tc NMR were used to determine the concentrations of pertechnetate in the respective phases. L^1 extracted *ca.* 70% TcO_4^- whereas benzo-15-crown-5 achieved *ca.* 20% extraction after 5 min.‡ No increase in percentage extraction occurred after this time. Interestingly the tripodal ligands L^2 and L^3 containing no crown moieties displayed respectively less than 10 and 0% extraction of TcO_4^- even after 24 h. The distribution coefficients for TcO_4^- extraction by all the ligands are shown in Fig. 1. The distribution coefficient D for L^1 of 2.3 represents a greater than twenty-fold and ten-fold enhancement in extraction efficiency when compared to L^2 and benzo-15-crown-5, respectively. This important result suggests that a crown ether cation binding site covalently linked to a tripodal amide anion coordinating cavity creates a new efficient extraction reagent for TcO_4^- which operates *via* similar cooperative ion-pair binding effects as

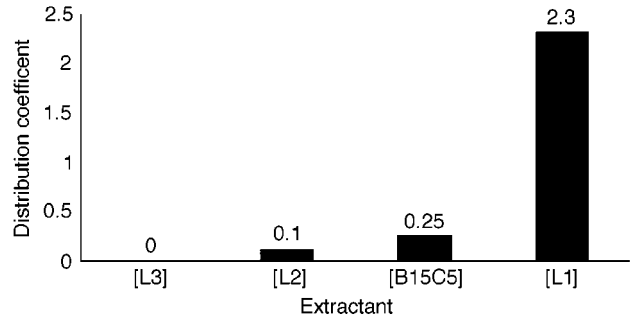

Fig. 1 Distribution coefficients for pertechnetate extraction by L^1–L^3 and benzo-15-crown-5. Organic phase: CH_2Cl_2, concentration of L^1–L^3 = 1.5×10^{-2} M, benzo-15-crown-5 = 4.5×10^{-2} M; aqueous phase: 100 ppm NH_4TcO_4, 2.35 M $NaNO_3$, pH 11, T = 298 K.

noted in the NMR titration experiments. Preliminary U-tube membrane transport investigations using the same aqueous conditions as described previously for the extraction experiments as the source of the aqueous phase revealed a six-fold increase in the rate of transport of TcO_4^- by L^1 (flux = 6.3×10^{-8} mol h^{-1}) over transport mediated by benzo-15-crown-5 (flux = 1.0×10^{-8} mol h^{-1}).

In summary, the new tripodal heteroditopic ligand L^1, by virtue of having both anion and cation recognition sites, has been demonstrated to cooperatively bind chloride, iodide and perrhentate anions *via* co-bound crown ether complexed sodium cations, and is a more efficient extraction and carrier transporting reagent for the pertechnetate anion when compared to monotopic ligands L^2, L^3 and benzo-15-crown-5.

We thank BNFL for a studentship (P. K. H.) and the EPSRC for use of the mass spectrometry service at University College, Swansea.

Notes and references

† ^{1}H NMR titration studies with L^1 and Na^+ unfortunately proved too complicated to monitor, to enable binding stoichiometries to be determined.

‡ In analogous extraction experiments at neutral pH, L^1 extracted 65% TcO_4^-.

1 M. T. Reetz, C. M. Niemeyer and K. Harris, *Angew. Chem., Int. Ed. Engl.*, 1991, **30**, 1472.
2 D. M. Rudkevich, Z. Brzozka, M. Palys, H. C. Visser, W. Verboom and D. N. Reinhoudt, *Angew. Chem., Int. Ed. Engl.*, 1994, **33**, 467.
3 K. I. Kinnear, D. P. Mousley, E. Arafar and J. C. Lockhart, *J. Chem. Soc., Dalton Trans.*, 1994, 3637.
4 P. D. Beer, M. G. B. Drew, R. J. Knubley and M. I. Ogden, *J. Chem. Soc., Dalton Trans.*, 1995, 3117.
5 J. Scheerder, J. P. M. van Duynhoven, J. F. J. Engbersen and D. N. Reinhoudt, *Angew. Chem., Int. Ed. Engl.*, 1996, **35**, 1090.
6 J. E. Redman, P. D. Beer, S. W. Dent and M. G. B. Drew, *Chem. Commun.*, 1998, 231; P. D. Beer and S. W. Dent, *Chem. Commun.*, 1998, 825.
7 T. M. Beasley and H. V. Lorz, *Technetium in the Environment*, ed. G. Desmet and C. Myttenacrc, Elsevier, London, 1986.
8 M. G. Jalhoom, *J. Radioanal. Nucl. Chem.*, 1986, **104**, 131.
9 T. Omori, Y. Muraoka and H. Suganuma, *J. Radioanal. Nucl. Chem.*, 1994, **178**, 237.
10 J. F. Clark, D. L. Clark, G. D. Whitener, N. C. Schroeder and S. H. Strauss, *Environ. Sci. Technol.*, 1996, **30**, 3124.
11 J. L. Atwood, K. T. Holman and J. W. Steed, *Chem. Commun.*, 1996, 1401.
12 R. Ungaro, B. El Hay and J. Smid, *J. Am. Chem. Soc.*, 1976, **98**, 5198.
13 M. J. Hynes, *J. Chem. Soc., Dalton Trans.*, 1993, 311.
14 K. H. Wong, M. Bourgoin and J. Smid, *J. Chem. Soc., Chem. Commun.*, 1974, 715.

Communication 9/03440D

ChemComm

Synthesis of primary amides by lipase-catalyzed amidation of carboxylic acids with ammonium salts in an organic solvent

Mike J. J. Litjens, Adrie J. J. Straathof,* Jaap A. Jongejan and Joseph J. Heijnen

Delft University of Technology, Kluyver Laboratory for Biotechnology, Julianalaan 67, 2628 BC Delft, The Netherlands. E-mail: straathof@stm.tudelft.nl

Received (in Liverpool, UK) 30th March 1999, Accepted 12th May 1999

The synthesis of butyramide and oleamide, by *Candida antarctica* lipase B-catalyzed amidation of the carboxylic acids, in an organic solvent with ammonium bicarbonate or ammonium carbamate as a source of ammonia results in good yields, making prior activation of the acids unnecessary.

Primary amides are important derivatives of several types of carboxylic acids, such as fatty acids and amino acids. In addition, enantioselective amidation of chiral acids may be used as an alternative to esterification in kinetic resolution processes. However, direct reaction of carboxylic acids with ammonia requires extreme conditions (200 °C, 7 bar anhydrous ammonia).[1] This may lead to the formation of byproducts in the production of heat sensitive amides such as oleamide. A selective reaction under mild conditions is therefore desirable.

For amidation of aliphatic acids with ammonia, lipases have been considered as the catalyst, but they have been rejected because the formation of a carboxylate anion would lead to precipitation of the ammonium carboxylate rather than formation of the acyl–enzyme complex and subsequent reaction with ammonia.[2,3] For this reason amides are usually synthesized from a neutral and activated form of the acid, such as the acid chloride (which takes away the need for a catalyst) or an ester. For example, De Zoete *et al.*[2] developed a one-pot procedure for the esterification and subsequent ammoniolysis using *Candida antarctica* lipase B (CALB) to catalyze both steps. In many cases it would be attractive if such an activation step could be avoided.

A recent thermodynamic study on the hydrolysis and ammoniolysis of the ester butyl butyrate indicates that the unactivated butyric acid should react efficiently with ammonia under mild conditions in anhydrous methyl isobutyl ketone (MIBK).[4] We decided to verify these thermodynamic predictions experimentally.

Here we demonstrate that primary amides can indeed be formed in good yields under mild reaction conditions, by direct amidation of the carboxylic acids (Scheme 1). The amidation of butyric acid to form butyramide and water serves as a model reaction, using CALB as the biocatalyst. The reaction is performed in MIBK at 25 °C, and ammonium salts that partly dissolve during the course of the reaction are used as a convenient source of ammonia. The experiments were carried out in 33 ml closed glass vessels containing 25 ml dry MIBK with various butyric acid concentrations (concentrations are mentioned in Fig. 1). Immobilized CALB (15 mg) (Novozym 435, a kind gift of NOVO Nordisk, with a catalytic activity of approximately 11000 PLU g^{-1} preparation) and solid ammonium bicarbonate or ammonium carbamate (*ca.* 2.5 mmol) were added, and the suspension was stirred. Samples were taken through a septum to prevent the escape of gas during sampling, and were immediately centrifuged and analyzed for butyric acid and butyramide by GC.

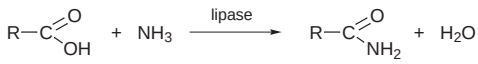

Scheme 1

The experimental results are very encouraging, yields at equilibrium for the amide (after 17 days) were found to be 80–90% when using ammonium bicarbonate and 90–100% when using ammonium carbamate as the source of ammonia (Fig. 1). In addition the model predictions agree reasonably well with the experimental results. No butyramide was formed in the absence of the enzyme, thus the amidation is enzyme-catalyzed. Fig. 1 shows that the amidation proceeds better with ammonium carbamate than with ammonium bicarbonate as the source of ammonia. Model calculations show that this results from the combined effect of a higher ammonia concentration and a lower water concentration. Ammonium bicarbonate dissolves as one equivalent of ammonia, water, and carbon dioxide, whereas ammonium carbamate dissolves as two equivalents of ammonia and one equivalent of carbon dioxide. It is obvious that an increased concentration of ammonia improves the yield at equilibrium, and that an increased concentration of water, which is a coproduct of the amidation, decreases the yield at equilibrium.

With ammonium carbamate as the source of ammonia, the yields obtained in the present experiments approach the optimized yields of the two-step process by De Zoete *et al.*[2] for the synthesis of octanamide and oleamide from the carboxylic acids *via* the esters. The yield of our direct enzymatic amidation may be improved by increasing the ammonia concentration. According to the model calculations[4] the ammonia concentration is below 30 mmol l^{-1} under the experimental conditions employed. Up to 230 mmol l^{-1} of ammonia may be used by saturating the reaction medium with gaseous ammonia.[4] The removal of reaction water, for example by molecular sieves, may further improve the yield.

To estimate the productivity of CALB in our one-step procedure as compared to the two-step procedure by De Zoete *et al.*,[2] an experiment was performed with oleic acid as the substrate. The experimental conditions were similar to those mentioned for butyric acid, except that the temperature was

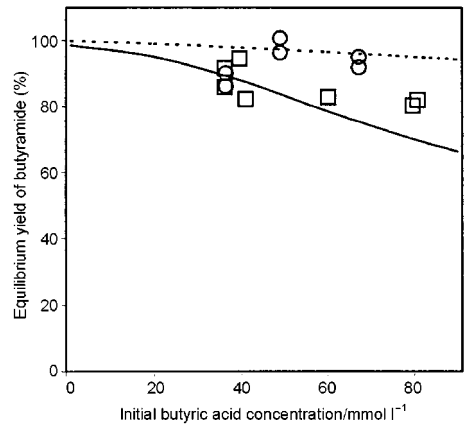

Fig. 1 Yields of butyramide at equilibrium for various initial butyric acid concentrations with solid ammonium bicarbonate (□, —) or solid ammonium carbamate (○, ···) as the source of ammonia. Markers are measured data, lines are predictions using the model presented in ref. 4.

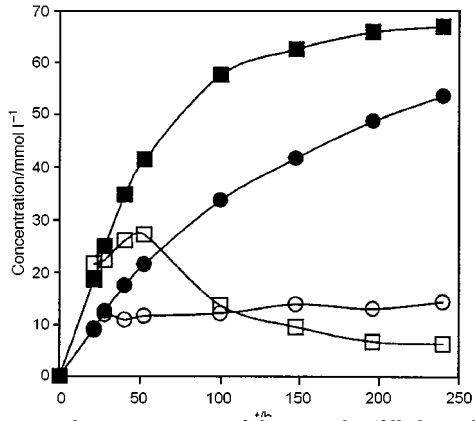

Fig. 2 Measured concentrations of butyramide (filled symbols) and dissolved butyric acid (empty symbols) for a CALB-catalyzed amidation of 70 mmol l^{-1} butyric acid in MIBK. In experiment A (□), 115 mmol l^{-1} ammonia is released gradually by dissolving ammonium carbamate. In experiment B (○), the same amount of ammonia is added in one portion.

35 °C and the enzyme concentration was 1 g l^{-1}. With 1.3 mmol ammonium carbamate as the source of ammonia, 48 mmol l^{-1} oleic acid was converted into oleamide in 95% yield in 4 days. This corresponds to a productivity of 11 mmol oleamide per gram of immobilized enzyme per day, which is more than twice the productivity calculated from the experiment by De Zoete *et al.*,[2] which was performed at 60 °C. Immobilized CALB is highly stable even at 60–80 °C.[5]

Thus, the direct amidation of aliphatic carboxylic acids with ammonia proceeds well, despite the commonly held belief that such a reaction might not be feasible. For this reason we expect that the acid is present mainly in its undissociated form, and not as the unreactive carboxylate. The ammonia concentrations that result from the dissolution of the ammonium salts are apparently sufficient for amidation of the acid, but are not so high that they cause precipitation of the acid as its ammonium salt. Model calculations[4] for butyric acid concentrations of 70 mmol l^{-1} in MIBK predict that ammonia concentrations of 115 mmol l^{-1} cause an equilibrium situation where most of the butyric acid is precipitated, and therefore not available to the enzyme. However, if the ammonia concentration is kept below 30 mmol l^{-1}, then the dissolved butyric acid concentration is much higher. For this reason it is important to add the necessary amount of ammonia gradually, for instance by adding it as slowly dissolving ammonium carbamate. The influence of a gradual addition of ammonia on the reaction rate is demonstrated by the experiments shown in Fig. 2. In a similar experimental setup as described above, 140 mmol l^{-1} butyric acid was dissolved in dry MIBK at 25 °C. In experiment A, 10 ml of this solution was diluted with 10 ml dry MIBK, and 115 mmol l^{-1} ammonia was added as 1.15 mmol solid ammonium carbamate. In experiment B 10 ml of the butyric acid solution was diluted with 10 ml MIBK that previously had been saturated with ammonia, thereby adding the same total amount of ammonia as in experiment A. Immobilized CALB (24 mg) was added to both experiments. Fig. 2 shows that the gradual addition of ammonia through dissolving ammonium carbamate (experiment A) results in higher dissolved butyric acid concentrations and therefore higher amidation rates than the instantaneous addition of the same amount of ammonia (experiment B). In this example the rate of amidation is increased by a decreased ammonia concentration.

In a recent publication Cerovsky and Kula[6] report that low yields (between 0.5 and 38%) of dipeptide amides have been obtained in the protease-catalyzed amidation of the C-terminal carboxylic group of dipeptides. The reactions were performed in MeCN with dissolved ammonium bicarbonate as the source of ammonia. This shows that the reaction described by us is also applicable to other compounds. However, the low solubility of the dipeptides in the organic medium was thought to limit the yield. For substrates of CALB such as aliphatic acids we do not expect any such limitations.

In conclusion we have demonstrated that the direct enzymatic amidation of butyric acid and oleic acid with ammonia is a feasible reaction. Using a widely applicable, commercially available and robust lipase preparation, high yields are achieved under mild reaction conditions. We intend to optimize this amidation reaction and apply it to other carboxylic acids.

We thank Dr Ulf Hanefeld for helpful discussions and for carefully reading the manuscript. This work was financially supported by the Ministry of Economic Affairs, the Ministry of Education, Culture and Science, and the Ministry of Agriculture, Nature Management and Fishery in the framework of an industrially relevant research program of the Netherlands Association of Biotechnology Centers in the Netherlands (ABON).

Notes and references

1 R. Opsahl, in *Kirk-Othmer Encyclopedia of Chemical Technology*, 4th edn., ed. J. I. Koschwitz and M. Howe-Grant, Wiley, New York, 1992, vol. 2, pp. 346–356.
2 M. C. De Zoete, A. C. Kock-van Dalen, F. van Rantwijk and R. A. Sheldon. *J. Mol. Catal. B: Enzym.*, 1996, **2**, 19.
3 N. Öhrner, C. Orrenius, A. Mattson, T. Norin and K. Hult, *Enzyme Microb. Technol.*, 1996, **19**, 328.
4 M. J. J. Litjens, M. Sha, A. J. J. Straathof, J. A. Jongejan and J. J. Heijnen, *Biotechnol. Bioeng.*, in the press.
5 E. M. Anderson, K. M. Larsson and O. Kirk, *Biocatal. Biotransform.*, 1998, **16**, 181.
6 V. Cerovsky and M. R. Kula, *Angew. Chem., Int. Ed.*, 1998, **37**, 1885.

Communication 9/04060I

ChemComm

A new technique for anchoring homogeneous catalysts

Robert Augustine,* Setrak Tanielyan, Stephen Anderson and Hong Yang

Center for Applied Catalysis, Chemistry Department, Seton Hall University, South Orange, NJ 07079, USA. E-mail: augustro@shu.edu

Received (in Corvallis, OR, USA) 21st April 1999, Accepted 4th May 1999

Heteropoly acids have been found to serve as anchoring agents between a support material and the metal atom of a homogeneous catalytic complex.

Interest in the ability to attach active homogeneous catalysts to an insoluble support material has been on-going for over twentyfive years.[1–5] To date, virtually every example of such supported homogeneous catalysts has involved some method for placing a ligand in or on a solid material and then using this 'heterogenized' ligand to prepare a catalytic complex. With this form of attachment, the metal atom could be removed by a ligand exchange reaction possibly with some of the product, substrate molecules or other species present in the reaction mixture. In most cases the activity and selectivity of these heterogenized complexes were lower than those observed with the corresponding homogeneous species and on attempted re-use the activity and selectivity of these heterogenized complexes were frequently lost. This approach, which requires the incorporation of the ligand onto a solid material, is particularly difficult to apply with most of the chiral ligands used in the highly efficient enantioselective homogeneous catalysts in use today.

We describe here a procedure by which a preformed homogeneous complex can be anchored to a variety of support materials, with the resulting catalyst being at least as active as the homogeneous species and capable of being re-used many times with no loss of activity or selectivity and no evidence of catalyst leaching.[6]

These heterogenized catalysts have been prepared by using a heteropoly acid such as phosphotungstic acid (PTA) as the anchoring agent to attach a complex to a support material. This is accomplished by adding a solution of the heteropoly acid (20 μmol in 2.5 ml of alcohol) with vigorous stirring to a suspension of the support material (300 mg in 10 ml of alcohol), with stirring continued for about 3 h followed by the removal of the liquid and thorough washing of the solid. This solid is then suspended in another 10 ml of degassed alcohol and a solution of the homogeneous catalyst (20 μmol in 1 ml of alcohol) is added under an inert atmosphere, with stirring, over a 30 min period. Stirring is continued for 8 to 12 h under an inert atmosphere, the liquid removed and the solid washed thoroughly until no color is observed in the wash liquid. This material can be used directly or dried for future use.

In some of our initial work with alumina supports, a slight color was sometimes imparted to the reaction mixture which, at first, was thought to indicate some leaching of the complex. However, analysis of these reaction mixtures showed that they contained not only rhodium but also tungsten and aluminum, which indicated that this loss occurred by attrition of the alumina and not by any leaching of the complex. Using EtOH in the preparation and reaction procedures successfully removed this problem.

It has been reported that Rh and Ir complexes react with a heteropoly acid to give a material in which the metal atom is attached to the heteropoly acid through the oxygen atoms on its surface.[7] Attachment of the heteropoly acid to a support such as alumina takes place by interaction of the hydroxy groups of the acid with the support.[8] The result is the attachment of the complex to the support using a heteropoly acid with bonding to the metal atom. The ^{31}P MAS NMR chemical shifts for the phosphorous atom in PTA, PTA on alumina and the Rh(DiPamp) supported on PTA–Al_2O_3 both before and after use in a hydrogenation were all identical, showing that the PTA remained intact throughout the entire preparation and reaction sequence.[9]

The data presented in Table 1 show the reaction rate and product ee for successive hydrogenations of methyl 2-acetamidoacrylate (**1**) run over a Rh(DiPamp) complex supported on PTA treated Montmorillonite K as well as the corresponding data obtained using the homogeneous catalyst. The first use of the heterogeneous catalyst was slower than that observed with the homogeneous catalyst and the product ee was also lower. However, when the first product mixture was removed from the reactor and a fresh solution of the starting material added to the heterogeneous, anchored catalyst, subsequent re-use proceeded significantly faster than the homogeneously catalyzed reaction with higher product ees observed as well. This catalyst was re-used fifteen times with no loss of activity or selectivity. Analysis of the product mixtures showed that if any rhodium was present it was there in an amount below the detection limit, which corresponded to less than 1 ppm. While we are not certain of the reason for the increase in activity after the first use of the heterogeneous catalyst, the fact that in some reactions the catalyst changed from yellow to a light gray–violet on use and back to yellow on exposure to air suggests that this activation may be the result of some partial reduction of the tungsten in the PTA.

One of the advantages of this approach to anchoring homogeneous catalysts is its apparent generality, in that this procedure can be used to anchor a variety of pre-formed active homogeneous catalysts onto a number of different supports. In Table 2 are listed the reaction rate and product ee data observed for the hydrogenation of **1** over several Rh complexes anchored to alumina along with the corresponding homogeneous catalyst data, while in Table 3 are given the data for the hydrogenation of **1** using Rh(DiPamp) anchored on different supports. We have also used these anchored homogeneous catalysts for the hydrogenation of a number of other prochiral substrates such as methyl 2-acetamidocinnamate, 2-actamidocinnamic acid, dimethyl itaconate and 2-methylhex-2-enoic acid. A Ru(BINAP)

Table 1 Reaction rate and product ee data from the multiple hydrogenations of **1** over a Rh(DiPamp)–PTA–Montmorillonite catalyst[a]

Use number	Rate[b]	Product ee (%)
Homogeneous	0.25	76
1	0.18	67
2	1.20	92
3	1.26	94
6	1.49	96
9	1.29	97
15	[c]	97

[a] Hydrogenation run at 25 °C under 1 atm H_2 using 20 μmol of supported Rh(DiPamp) to saturate 0.8 mmol of **1** for each run. [b] In mol of H_2 per mol Rh per min. [c] Rate data for this run were lost due to a computer malfunction.

Table 2 Reaction rate and product ee data from the multiple hydrogenations of **1** over Rh(Ligand)–PTA–alumina catalysts along with the data from the homogeneously catalyzed hydrogenations[a]

Ligand	Use number	Anchored		Homogeneous	
		Rate[b]	Ee (%)	Rate[b]	Ee (%)
DiPamp	1	0.32	90	0.25	76
	3	1.67	93		
Prophos	1	2.0	68	0.26	66
	3	2.6	63		
Me-Duphos	1	1.8	83	3.3	96
	3	4.4	95		
BPPM	1	3.75	21	7.4	84
	3	8.15	87		

[a] Hydrogenation run at 25 °C under 1 atm H_2 using 20 μmol of supported Rh(ligand) to saturate 0.8 mmol of **1** for each run. [b] In mol of H_2 per mol Rh per min.

Table 3 Reaction rate and product ee data from the multiple hydrogenations of **1** over a Rh(DiPamp) catalyst on different PTA modified supports[a]

Support	Use number	Rate[b]	Ee (%)
Montmorillonite K	1	0.18	67
	3	1.26	94
Carbon	1	0.07	83
	3	0.41	90
Alumina	1	0.32	90
	3	1.67	93
Lanthana	1	0.38	91
	3	0.44	92

[a] Hydrogenation run at 25 °C under 1 atm H_2 using 20 μmol of supported Rh(ligand) to saturate 0.8 mmol of **1** for each run. [b] In mol of H_2 per mol Rh per min.

complex anchored to PTA treated alumina was used for successive hydrogenations of **1** and dimethyl itaconate with the reaction rate and product ee increasing after the first use in both cases. Analysis of the product mixtures from these reactions found no detectable ruthenium present.

In every instance, the reaction rates and product ee were at least equal to and frequently better than the results obtained using the corresponding homogeneous catalyst, especially when the catalysts were re-used. In some instances, even the first use of the catalyst gave superior results. Heteropoly acids other than PTA were also successful anchoring agents.

This anchoring procedure has also been applied to achiral complexes with similar results. For instance, hydrogenation of hex-1-ene over a Wilkinson's catalyst anchored to PTA treated alumina proceeded 2–3 times faster than the corresponding homogeneously catalyzed reaction, even on the first use of the heterogenized material. A Rh(dppb) complex anchored to a PTA modified alumina was used for several successive hydrogenations of hex-1-ene with a combined substrate : catalyst ratio of about 8000 : 1. An analysis of the product mixtures from these reactions found no detectable rhodium present.

This research was supported by grants CTS-9312533 and CTS-9708227 from the United States National Science Foundation and financial support from The Engelhard Corporation.

Notes and references

1 J. P. Collman, L. S. Hegedus, M. P. Cooke, J. R. Norton, G. Dolcetti and D. N. Marquardt, *J. Am. Chem. Soc.*, 1972, **94**, 1789.
2 W. Dumont, J.-C. Poulin, T. P. Daud and H. B. Kagan, *J. Am. Chem. Soc.*, 1973, **95**, 8295.
3 L. L. Murrell, *Advanced Materials in Catalysis*, Academic Press, New York, 1977, ch. 8.
4 V. Isaeva, A. Derouault and J. Barrault, *Bull. Soc. Chim. Fr.*, 1996, **133**, 351.
5 U. Nagel and J. Leipold, *Chem. Ber.*, 1996, **129**, 815.
6 S. K. Tanielyan and R. L. Augustine, *U.S. Pat. Appl.*, 08/994,025; *PCT Int. Appl.*, WO-9828074; *Chem. Abstr.*, 1998, **129**, 109217.
7 M. Pohl, D. K. Lyon, N. Mizuno, K. Nomiya and R. G. Finke, *Inorg. Chem.*, 1995, **34**, 1413.
8 Y. Izumi, R. Hasere and K. Urabi, *J. Catal.*, 1983, **84**, 402.
9 The MAS NMR spectra were obtained by Xiaolin Yang, Engelhard Corp., Iselin, NJ, USA.

Communication 9/03205C

ChemComm

An extremely mild and stereocontrolled construction of 1,2-*cis*-α-glycosidic linkages *via* benzyl-protected glycopyranosyl diethyl phosphites

Hiroko Tanaka, Hiroki Sakamoto, Ai Sano, Seiichi Nakamura, Makoto Nakajima and Shunichi Hashimoto*

Graduate School of Pharmaceutical Sciences, Hokkaido University, Sapporo 060-0812, Japan.
E-mail: hsmt@pharm.hokudai.ac.jp

Received (in Cambridge, UK) 9th April 1999, Accepted 14th May 1999

A highly stereocontrolled 1,2-*cis*-α-glycosidation reaction under conditions mild enough for acid-labile alcohols has been developed using benzyl-protected glycopyranosyl diethyl phosphites as glycosyl donors in the presence of 2,6-di-*tert*-butylpyridinium iodide and tetrabutylammonium iodide.

Due to the rapidly recognised biological significance of the saccharide residues of carbohydrate-containing biomolecules, the rational design and development of stereocontrolled glycosidation reactions[1] are of growing importance not only in carbohydrate chemistry but also in medicinal chemistry.[2] One of the current topics in this area is the emergence of glycosyl phosphites as a new family of glycosyl donors,[3–6] the effectiveness of which has been demonstrated well by high-yield and α-selective sialylation[3a,4a,b] using sialyl phosphite as a donor and TMSOTf as a promoter. As yet another advantage of glycosyl phosphites, we recently reported that glycosidations of benzyl-protected glycopyranosyl diethyl phosphites with a variety of acceptor alcohols could be effected with the aid of $BF_3{\cdot}OEt_2$ as a promoter at −78 °C to exhibit the highest 1,2-*trans*-β-selectivity known to date for glycosidations without neighboring group participation.[7] During the course of mechanistic investigations of the reaction, we found that the glucopyranosyl phosphite **1**† could not be directly activated by $BF_3{\cdot}OEt_2$ at −78 °C. This result, together with the finding that the trimethylsilyl ether **10** derived from *O*-6-unprotected glycoside **9** did not serve as a glycosyl donor (Scheme 1),

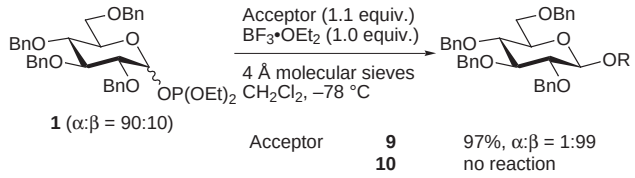

Scheme 1

suggested that glycosidation should be effected with the aid of the BF_3–acceptor alcohol complex[8] which functioned as a proton donor to activate the phosphite group to give oxocarbenium ion and diethyl phosphite. Although TfOH is known to activate the phosphite **1** to give mainly 1,2-*trans*-β-glucosides,[4c] there has been no reported attempt to use promoters with much lower Brønsted acidity. At this stage, we envisaged that if the phosphite group could be activated using promoters such as pyridinium iodides, the glycosidation process *via* glycopyranosyl iodide coupled with Lemieux's *in situ* anomerisation method[9] might lead to the construction of 1,2-*cis*-α-glycosidic linkages under extremely mild reaction conditions.[10–12] Herein, we report a new aspect of glycosidations with benzyl-protected glycopyranosyl diethyl phosphites, wherein the combined use of 2,6-di-*tert*-butylpyridinium iodide (DTBPI)[13] as a promoter and tetrabutylammonium iodide as an additive proves to be the superior choice for allowing exceptionally high levels of 1,2-*cis*-α-selectivity, as well as glycosylations of even highly sensitive aglycones.

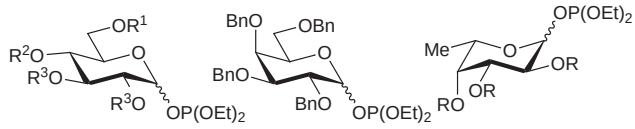

1 $R^1 = R^2 = R^3$ = Bn
2 $R^1 = R^2 = R^3$ = *p*-$ClC_6H_4CH_2$
3 R^1 = Tr, $R^2 = R^3$ = Bn
4 R^1 = TBDPS, $R^2 = R^3$ = Bn
5 R^1, R^2 = PhCH, R^3 = Bn

6

7 R = Bn
8 R = *p*-$ClC_6H_4CH_2$

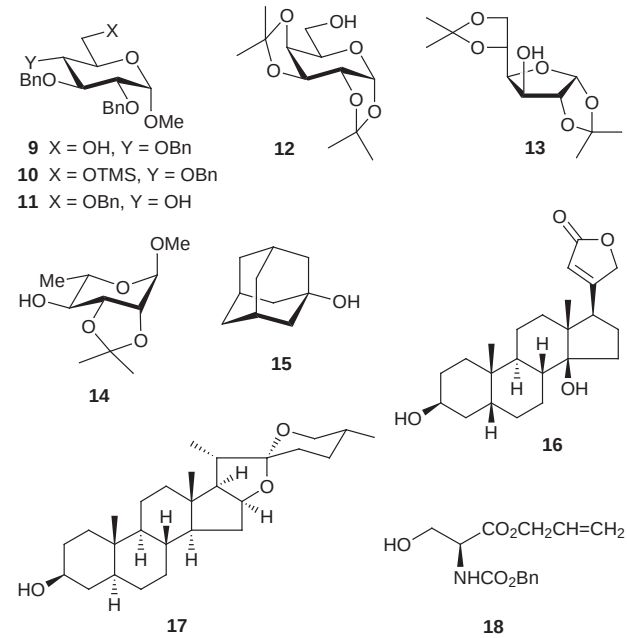

9 X = OH, Y = OBn
10 X = OTMS, Y = OBn
11 X = OBn, Y = OH

12

13

14

15

16

17

18

Since it is well-documented that glycosylations of less nucleophilic alcohols favor 1,2-*cis*-α-glycosides, we first examined glycosidation of **1** with **9** with a high reactivity in order to make an assessment as accurately as possible. After considerable experimentation, it was found that coupling of **1** (α:β = 90:10 or 75:25, 1.1 equiv.) with **9** (1.0 equiv.) in CH_2Cl_2 in the presence of DTBPI (1.2 equiv.) and pulverised 4 Å molecular sieves proceeded at room temperature for 48 h to afford the corresponding 1,2-*cis*-disaccharide in 85% yield with an α:β ratio of 92:8 (Table 1, entry 1). Since TLC and ^1H NMR analyses showed that *in situ* conversion of **1** into the α-glucopyranosyl iodide[14] proceeded to completion within 30 min irrespective of the anomeric composition of the donor, the glycosidation of the iodide *via in situ* anomerisation was presumed to be the rate-determining step. As expected, the addition of Bu_4NI (1.2 equiv.) to the above mixture facilitated the anomerisation process and shortened the reaction time to 24 h, providing the disaccharide in 84% yield with the same α-selectivity as above (entry 2).‡§

In order to clarify the scope and limitations of the present method, we then explored the glycosidation of glycosyl phosphites **1**–**8**† with a range of acceptor alcohols. The

Table 1 1,2-*cis*-Glycosidation reaction with glycopyranosyl diethyl phosphites[a]

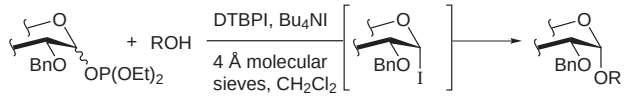

Entry	Donor[b]	Acceptor	*t*/h	Yield[c] (%)	α : β[d]
1[e]	**1**	**9**	48	85	92 : 8
2	**1**	**9**	24	84	92 : 8
3	**1**	**11**	48	59	95 : 5
4	**1**	**12**	24	91	94 : 6
5	**1**	**13**	48	81	92 : 8
6	**1**	**15**	48	88	91 : 9[f]
7	**1**	**16**	48	89	90 : 10
8	**1**	**17**	36	92	92 : 8
9	**2**	**9**	24	88	95 : 5[g]
10	**3**	**9**	48	88	96 : 4[g]
11	**4**	**9**	48	91	96 : 4[g]
12	**5**	**9**	48	80	90 : 10[g]
13	**6**	**9**	48	85	95 : 5[g]
14	**6**	**14**	24	94	93 : 7[g]
15	**6**	**18**	48	87	93 : 7
16	**7**	**9**	3	82	88:12
17	**7**	**12**	4	95	89 : 11[g]
18	**8**	**9**	4	87	95 : 5
19	**8**	**12**	4	95	93 : 7[g]

[a] Donor : acceptor : DTBPI : Bu_4NI molar ratio = 1.1 : 1.0 : 1.2 : 1.2. [b] The anomeric ratio of the phosphites: **1**, 90 : 10; **2**, 61 : 39; **3**, 50 : 50; **4**, 83 : 17; **5**, 66:34; **6**, 52 : 48; **7**, 49 : 51; **8**, 57 : 43. [c] Isolated total yield based on the acceptor alcohol used. [d] Determined by HPLC (column, Zorbax® Sil, 4.6 × 250 mm; eluent, 9–30% EtOAc in hexane or 14–22% THF in hexane; flow rate, 1.5 ml min^{-1}). [e] In the absence of Bu_4NI. [f] Determined by 125 MHz ^{13}C NMR. [g] Determined by 500 MHz ^1H NMR.

examples highlighted in Table 1 deserve some comment. In all cases except for the exceedingly sterically hindered, unreactive *O*-4-unprotected glycoside **11** (entry 3), the present glycosidations were found to offer a high-yielding entry to 1,2-*cis*-linked glycosides and disaccharides, utilising conditions under which highly acid-sensitive alcohols such as digitoxigenin **16** and tigogenin **17** were safely glycosylated (entries 7 and 8). While glycosidations of the D-gluco- and D-galactopyranosyl donors **1** and **6** displayed high levels of α-selectivity with various alcohols of different reactivities (entries 1–8 and 13–15), that of L-fucopyranosyl donor **7** was found to exhibit less satisfactory selectivity (entries 16 and 17). However, the α-selectivity was greatly improved by switching the protective group from a benzyl group to a *p*-chlorobenzyl group (entries 18 and 19),[15] although only a small enhancement was observed with the D-glucopyranosyl donor (entry 9). According to a general trend,[10,16] protection of the *O*-6 hydroxy group as a bulky triphenylmethyl or *tert*-butyldiphenylsilyl ether gave further enhanced α-selectivities of up to 96 : 4 (entries 10 and 11). In this regard, it is also of interest that the present protocol could be advantageously extended to glycosidation with 4,6-*O*-benzylidene-protected glucopyranosyl donor **5** (entry 12).[11]

In conclusion, the present method constitutes an exceptionally mild and general procedure for the highly stereocontrolled construction of 1,2-*cis*-α-glycosidic linkages. Thus, we have now developed a stereoselective entry to either 1,2-*cis*-α-glycosides or 1,2-*trans*-β-glycosides using glycosyl phosphites as common glycosyl donors by proper choice of the reaction conditions.

This research was supported in part by a Grant-in-Aid (No.08557119) from the Ministry of Education, Science, Sports and Culture of Japan.

Notes and references

† Glycopyranosyl diethyl phosphites **1**–**8** were readily prepared from the corresponding glycopyranoses according to the reported procedure (ref. 7), the anomeric ratios of which were determined by 109 MHz ^{31}P NMR using 85% H_3PO_4 as an external standard.

‡ Typical experimental procedure: A solution of **1** (72.6 mg, 0.11 mmol) in CH_2Cl_2 (1 ml) was added to a mixture of **9** (46.4 mg, 0.1 mmol), DTBPI (38.3 mg, 0.12 mmol), Bu_4NI (44.3 mg, 0.12 mmol) and pulverised 4 Å molecular sieves (50 mg). The whole mixture was stirred at room temperature for 24 h. Standard workup followed by column chromatography (silica gel, 6 : 1 hexane–AcOEt) furnished the corresponding disaccharide (82.9 mg, 84%) as a 92:8 mixture of α- and β-anomers.

§ The combined use of 2,6-di-*tert*-butylpyridinium bromide and Bu_4NBr under otherwise identical conditions (reaction time; 48 h) provided the disaccharide with the α : β ratio of 87 : 13 in 80% yield.

1 For recent reviews see: K. Toshima and K. Tatsuta, *Chem. Rev*., 1993, **93**, 1503; G.-J. Boons, *Tetrahedron*, 1996, **52**, 1095; *Modern Methods in Carbohydrate Synthesis*, ed. S. H. Khan and R. A. O'Neil, Harwood, Amsterdam, 1996.

2 *Synthetic Oligosaccharides*, *ACS Symp. Ser.* No. 560, ed. P. Kovác, ACS, Washington, D.C., 1993; *Carbohydrates in Drug Design*, ed. Z. J. Witczak and K. A. Nieforth, Marcel Dekker, New York, 1997.

3 (*a*) T. J. Martin and R. R. Schmidt, *Tetrahedron Lett.*, 1992, **33**, 6123; (*b*) T. Müller, R. Schneider and R. R. Schmidt, *Tetrahedron Lett.*, 1994, **35**, 4763.

4 (*a*) H. Kondo, Y. Ichikawa and C.-H. Wong, *J. Am. Chem. Soc.*, 1992, **114**, 8748; (*b*) M. M. Sim, H. Kondo and C.-H. Wong, *J. Am. Chem. Soc.*, 1993, **115**, 2260; (*c*) H. Kondo, S. Aoki, Y. Ichikawa, R. L. Halcomb, H. Ritzen and C.-H. Wong, *J. Org. Chem*., 1994, **59**, 864.

5 Y. Watanabe, C. Nakamoto, T. Yamamoto and S. Ozaki, *Tetrahedron*, 1994, **50**, 6523.

6 H. Schene and H. Waldmann, *Eur. J. Org. Chem*., 1998, 1227.

7 S. Hashimoto, K. Umeo, A. Sano, N. Watanabe, M. Nakajima and S. Ikegami, *Tetrahedron Lett.*, 1995, **36**, 2251.

8 The pK_a values of BF_3–alcohol complexes are estimated to be +1.0 to +7.3: K. S. Minsker, V. A. Babkin and G. E. Zaikov, *Int. J. Polym. Mater*., 1995, **28**, 77.

9 R. U. Lemieux, K. B. Hendriks, R. V. Stick and K. James, *J. Am. Chem. Soc*., 1975, **97**, 4056.

10 We previously developed 1,2-*cis*-α-glycosidation with benzyl-protected glycopyranosyl phosphorodiamidimidothioates in the presence of 2,6-lutidinium toluene-*p*-sulfonate and Bu_4NI, however, this method suffered from lengthy preparation of the glycosyl donors: S. Hashimoto, T. Honda and S. Ikegami, *Tetrahedron Lett.*, 1990, **31**, 4769.

11 It has recently been reported by Waldmann's group that LiI-mediated glycosidation reactions with glycopyranosyl phosphates in a 1 M solution of $LiClO_4$ in CH_2Cl_2 gave 1,2-*cis*-glycosides *via in situ* generated glycopyranosyl iodides in moderate yields and with appreciable α-selectivity: U. Schmid and H. Waldmann, *Liebigs Ann./Recl*., 1997, 2573.

12 T. Uchiyama and O. Hindsgaul, *Synlett*, 1996, 499; J. Gervay and M. J. Hadd, *J. Org. Chem*., 1997, **62**, 6961.

13 Y. Okamoto and Y. Shimakawa, *J. Org. Chem*., 1970, **35**, 3752.

14 B. Ernst and T. Winkler, *Tetrahedron Lett*., 1989, **30**, 3081.

15 S. Koto, S. Inada, N. Morishima and S. Zen, *Carbohydr. Res*., 1980, **87**, 294; N. L. Pohl and L. L. Kiessling, *Tetrahedron Lett*., 1997, **38**, 6985.

16 S. Houdier and P. J. A. Vottero, *Carbohydr. Res*., 1992, **232**, 349; G.-J. Boons, S. Bowers and D. M. Coe, *Tetrahedron Lett*., 1997, **38**, 3773; K. Fukase, Y. Nakai, T. Kanoh and S. Kusumoto, *Synlett*, 1998, 84.

Communication 9/02845E

ChemComm

syn-Diastereoselective carbonyl allylation by 1- or 3-substituted prop-2-en-1-ols with tin(II) iodide and tetrabutylammonium iodide

Yoshiro Masuyama,* Takanori Ito, Kentaro Tachi, Akihiro Ito and Yasuhiko Kurusu

Department of Chemistry, Sophia University, 7-1 Kioicho, Chiyoda-ku, Tokyo 102-8554, Japan.
E-mail: y-masuya@hoffman.cc.sophia.ac.jp

Received (in Cambridge, UK) 22nd March 1999, Accepted 17th May 1999

1-Substituted or 3-substituted prop-2-en-1-ols cause *syn*-diastereoselective carbonyl allylation with tin(II) iodide and tetrabutylammonium iodide *via* the formation of 3-substituted prop-2-enylpolyiodotins to produce *syn*-1,2-disubstituted but-3-en-1-ols.

Barbier-type carbonyl allylation is one of the most convenient methods for the introduction of allylic functions.[1] Allylic metal reagents in the allylation reaction are generated *in situ* from allylic halides, which are usually prepared from allylic alcohols in advance. Thus, it should be an important aim to generate allylic metal reagents from available and storable allylic alcohols directly. We have already reported carbonyl allylations by allylic alcohols with tin(II) chloride, which need a catalytic amount of palladium complexes such as $PdCl_2(PhCN)_2$, $Pd(PPh_3)_4$ and so on.[2] We here report that allylic alcohols serve as carbonyl allylating agents without the palladium complexes *via* the use of tin(II) iodide and tetrabutylammonium iodide (TBAI),[3] and that the carbonyl allylation by 1- or 3-substituted prop-2-en-1-ols with tin(II) iodide and TBAI exhibits *syn*-diastereoselectivity,[4] in contrast to the palladium-catalysed *anti*-diastereoselective carbonyl allylation by 3-substituted (*E*)-prop-2-en-1-ols with tin(II) chloride in 1,3-dimethylimidazolidin-2-one (DMI).[5]

Prop-2-en-1-ol (**1**) slowly caused allylation of benzaldehyde without palladium catalysts in the presence of tin(II) iodide, TBAI and NaI under the same conditions (namely at room temperature in DMI containing a small amount of H_2O) which gave the best results for the carbonyl allylation by allylic halides with tin(II) halides and tetrabutylammonium halides;[4] 15–20 °C, 166 h, 17% yield. When the temperature was raised to 60 °C, prop-2-en-1-ol (**1**) was amenable to the allylation of various aldehydes, as summarized in Table 1. Use of less than 2 equiv. of tin(II) iodide with respect to benzaldehyde lowered the yield (SnI_2 (2 mmol), 60 °C, 66 h, 61%). Tin(II) bromide slowed down the allylation of benzaldehyde (72 h, 38%), and no reaction occurred with tin(II) chloride, under the same conditions as those of the allylation with tin(II) iodide.

Table 1 Carbonyl allylation by **1** with SnI_2, TBAI and NaI[a]

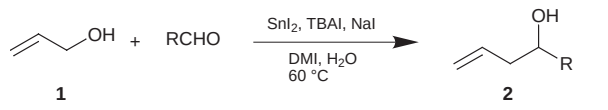

R	*t*/h	Yield[b] of **2** (%)
Ph	41	77
4-MeC_6H_4	54	55
4-ClC_6H_4	45	79
$PhCH_2CH_2$	72	64
c-C_6H_{11}	62	36
C_6H_{13}	35	52
CH_2=$CH(CH_2)_8$	46	54

[a] The allylation of aldehydes (1 mmol) by prop-2-en-1-ol (2 mmol) was carried out with SnI_2 (3 mmol), TBAI (0.25 mmol) and NaI (2.5 mmol) in DMI (3 ml) and H_2O (0.1 ml) at 60 °C. [b] Isolated yields.

Diastereoselective allylation of benzaldehyde (1 mmol) by (*E*)-but-2-en-1-ol (**3**; R = Me, R′ = H, 2 mmol) was investigated with tin(II) iodide (3 mmol) and TBAI (1 mmol) at 60 °C in various solvents containing a small amount of H_2O; DMI (19 h, 74%, *syn*:*anti* = 83:17) is superior to other solvents (THF, 26 h, 74%, *syn*:*anti* = 83:17; DMF, 72 h, 18%, *syn*:*anti* = 67:33; H_2O, 72 h, 31%, *syn*:*anti* = 89:11; DMI without H_2O, 72 h, 25%, *syn*:*anti* = 71:29) for both reactivity and diastereoselectivity. The results in the diastereoselective carbonyl allylation by some 1- or 3-substituted prop-2-en-1-ols† with SnI_2, TBAI and NaI in DMI–H_2O are summarized in Table 2. Allylic alcohols bearing an aliphatic group at the α- or γ-position can be applied to the *syn*-diastereoselective carbonyl allylation. In contrast, (*E*)-cinnamyl alcohol bearing an aromatic group at the γ-position exhibits *anti*-selectivity, similar to the palladium-catalysed carbonyl allylation with tin(II) chloride.

The *syn*-diastereoselective carbonyl allylation by 1- or 3-substituted prop-2-en-1-ols, except (*E*)-cinnamyl alcohol, with tin(II) iodide and TBAI probably proceeds *via* (i) the transformation of the prop-2-en-1-ol into 1-substituted 3-iodoprop-1-ene **A**, which is then converted into 3-substituted prop-2-enylpolyiodotin **B**, and (ii) the formation of an acyclic antiperiplanar transition state **C** between 3-substituted prop-2-enylpolyiodotin **B**, in which the tin has no Lewis acidity, and an aldehyde, as shown in Scheme 1.[4]‡ The tin in (*E*)-cinnamylpolyiodotin, derived from (*E*)-cinnamyl alcohol with tin(II) iodide and TBAI, may have Lewis acidity owing to (σ–

Table 2 Diastereoselective carbonyl allylation with SnI_2, TBAI and NaI[a]

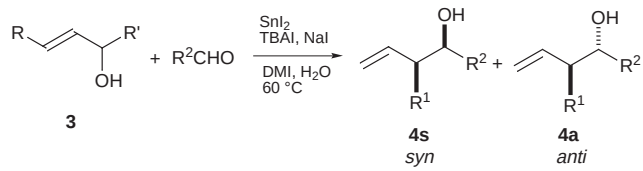

Allylic alcohol			Product			
R	R′	*t*/h	R^1	R^2	Yield[b] of **4** (%)	Ratio[c] **4s**:**4a**
Me	H	47	Me	Ph	76	82:18
Me	H	65	Me	4-MeC_6H_4	50	81:19
Me	H	47	Me	4-ClC_6H_4	79	82:18
Me	H	71	Me	$PhCH_2CH_2$	58	67:33
Me	H	72	Me	*c*-C_6H_{11}	37	67:33
Me	H	46	Me	C_6H_{13}	61	75:25
Me	H	78	Me	CH_2=$CH(CH_2)_8$	56	78:22
H	Me	91	Me	Ph	51	82:18
H	Me	87	Me	C_6H_{13}	45	77:23
Ph	H	24	Ph	Ph	49	1:99[d]
Pr	H	48	Pr	Ph	80	70:30

[a] The allylation of aldehydes (1 mmol) by allylic alcohols (2 mmol) was carried out with SnI_2 (3 mmol), TBAI (0.25 mmol) and NaI (2.5 mmol) in DMI (3 ml) and H_2O (0.1 ml) at 60 °C. [b] Isolated yields. [c] The ratio was determined by ^{1}H NMR spectroscopy (JEOL GX-270 or Λ-500) and/or GC (Capillary column PEG 20M 0.25 mm × 30 m). [d] See ref. 5.

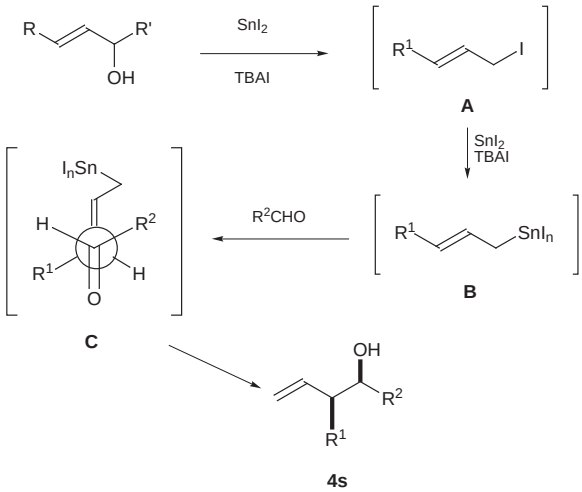

Scheme 1

p)π conjugation between the tin–allylic carbon σ-bond and an electron-deficient olefinic β-carbon in the (*E*)-cinnamyl group.[6] Thus, (*E*)-cinnamylpolyiodotin probably causes *anti*-addition to aldehydes *via* the formation (coordination) of chair-like six-membered cyclic transition states.[2,5]

Notes and references

† Starting allylic alcohols [prop-2-en-1-ol, (*E*)-but-2-en-1-ol, but-1-en-3-ol (*E*)-cinnamyl alcohol and (*E*)-hex-2-en-1-ol] were purchased from Tokyo Chemical Industry Co., Ltd.

‡ Allylic alcohol are known to cause α-regioselective carbonyl allylation with Me_3SiCl, NaI and H_2O–Sn (or SnI_2). (ref. 3). The tin intermediates in this reaction were assumed to be allylic (μ-iodo)ditin compounds. Since our reaction system contains an excess of iodides, triiodostannate is probably formed, preventing the formation of Sn–I–Sn bonds, and thus allylic (μ-iodo)ditin species. Thus, the thermodynamically stable γ-substituted allylic tin intermediate **B** probably causes the expected γ-addition to aldehyde to produce 1,2-disubstituted but-3-en-1-ol **4**.

1 For a review, see: Y. Yamamoto and N. Asao, *Chem. Rev.*, 1993, **93**, 2207.

2 For reviews of palladium-catalysed carbonyl allylation by allylic alcohols with tin(II) chloride, see: Y. Masuyama, *J. Synth. Org. Chem. Jpn.*, 1992, **50**, 202; Y. Masuyama, in *Advances in Metal-Organic Chemistry*, ed. L. S. Liebeskind, JAI Press, Greenwich, 1994, vol. 3, p. 255.

3 For an α-regioselective carbonyl allylation by allylic alcohols, see: Y. Kanagawa, Y. Nishiyama and Y. Ishii, *J. Org. Chem.*, 1992, **57**, 6988.

4 For a *syn*-diastereoselective carbonyl allylation by allylic halides with SnI_2 and TBAI, see: Y. Masuyama, M. Kishida and Y. Kurusu, *Tetrahedron Lett.*, 1996, **37**, 7103; Y. Masuyama, A. Ito and Y. Kurusu, *Chem. Commun.*, 1998, 315.

5 J. P. Takahara, Y. Masuyama and Y. Kurusu, *J. Am. Chem. Soc.*, 1992, **114**, 2577.

6 For *anti*-diastereoselective carbonyl allylation by (*E*)-cinnamyltributyltin or (*E*)-cinnamyltriphenyltin with $BF_3{\cdot}Et_2O$ in CH_2Cl_2, see: M. Koreeda and Y. Tanaka, *Chem. Lett.*, 1982, 1299.

Communication 9/02233C

Typeset and printed by Black Bear Press Limited, Cambridge, England

ChemComm
FEATURE ARTICLE

The asymmetric Birch reduction and reduction–alkylation strategies for synthesis of natural products

Arthur G. Schultz

Department of Chemistry, Rensselaer Polytechnic Institute, Troy, NY 12180-3590, USA. E-mail: schula@rpi.edu

Received (in Cambridge, UK) 4th March 1999, Accepted 25th March 1999

Synthetic applications of the asymmetric Birch reduction and reduction–alkylation are reported. Synthetically useful chiral intermediates have been obtained from chiral 2-alkoxy-, 2-alkyl-, 2-aryl- and 2-trialkylsilyl-benzamides I and the pyrrolobenzodiazepine-5,11-diones II. The availability of a wide range of substituents on the precursor benzoic acid derivative, the uniformly high degree of diastereoselection in the chiral enolate alkylation step, and the opportunity for further development of stereogenic centers by way of olefin addition reactions make this method unusually versatile for the asymmetric synthesis of natural products and related materials.

Introduction

The Birch reduction has been used by several generations of synthetic organic chemists for the conversion of readily available aromatic compounds to alicyclic synthetic intermediates.[1] Birch reductions are carried out with an alkali metal in liquid NH_3 solution usually with a co-solvent such as THF and always with an alcohol or related acid to protonate intermediate radical anions or related species. One of the most important applications of the Birch reduction is the conversion of aryl alkyl ethers to 1-alkoxycyclohexa-1,4-dienes. These extremely valuable dienol ethers provide cyclohex-3-en-1-ones by mild acid hydrolysis or cyclohex-2-en-1-ones when stronger acids are used (Scheme 1).

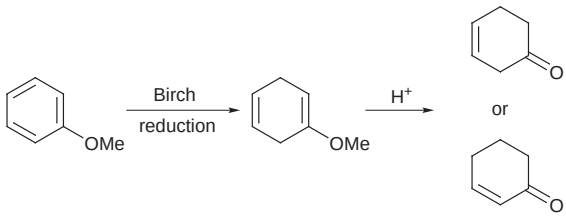

Scheme 1

The Birch reduction of derivatives of 2-methoxybenzoic acid followed by alkylation of the intermediate enolate is of even greater strategic value. The resulting chiral cyclohexa-1,4-dienes are converted to 2,2-disubstituted cyclohex-3-en-1-ones by hydrolysis of the enol ether. If the carboxylic acid is used in the reduction step, then treatment of the intermediate cyclohexa-1,4-diene with acid results in hydrolysis–decarboxylation to give 2-substituted cyclohex-2-en-1-ones (Scheme 2).

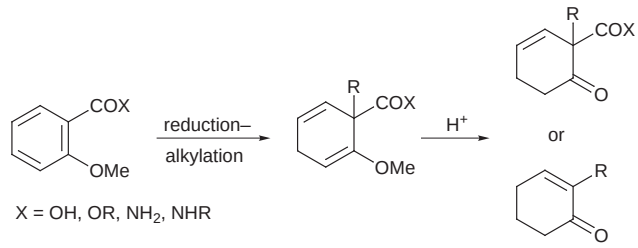

Scheme 2

Against this backdrop of prior investigation, we initiated a program directed at the development of an asymmetric version of the Birch reduction and reduction–alkylation of derivatives of benzoic acid.[2] We opted to make use of a chiral auxiliary covalently bound to the carboxylic acid group and after a brief screening of possible candidates were delighted to find that the inexpensive amino acid (*S*)-proline and its product of reduction by $LiAlH_4$, (*S*)-pyrrolidine-2-methanol, served beyond all reasonable expectation. It has been demonstrated that 2-alkoxy-, 2-alkyl-, 2-aryl- and 2-trialkylsilyl-benzamides of general structure **I** can be effectively utilized in asymmetric organic synthesis of a wide range of synthetic targets. It was necessary to develop a different protocol for the anthranilic acids; the pyrrolobenzodiazepine-5,11-diones **II**, obtained by condensation of 1 equiv. of (*S*)-proline with the corresponding isatoic anhydride, provided a remarkably flexible solution to the incorporation of nitrogen substitution on the derived cyclohexane ring.

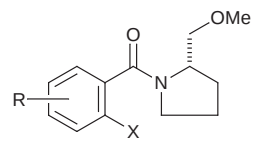

I X = OMe, alkyl, aryl, SiR_3
R = H, OMe, alkyl, aryl

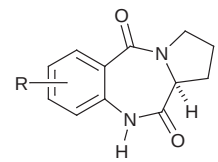

II R = H, alkyl

Much of the characterization of reactivity of **I** (X = OMe) and some of the early applications of **I** and **II** to asymmetric organic synthesis were reviewed in 1990.[3] The focus of this feature article is on recent developments with greatly expanded sets of substrates corresponding to the generalized structures **I** and **II**. Particular attention is devoted to the utilization of these substrates for the asymmetric synthesis of natural products and related materials.

Arthur Schultz is the William Weightman Walker Professor of Chemistry at Rensselaer Polytechnic Institute. He received his BS degree from the Illinois Institute of Technology and his PhD in organic chemistry from the University of Rochester under the supervision of Richard Schlessinger. From 1970 to 1972 he was a postdoctoral fellow at Columbia University with Gilbert Stork. He began his academic career at Cornell University and moved to RPI in 1978. His research interests include asymmetric organic synthesis, the development of new synthetic methods, the synthesis of natural products, and synthetic and mechanistic organic photochemistry. He is the recipient of an NIH MERIT Award 1992–2002.

Tools for asymmetric synthesis

At the outset of our studies of the reactivity of **I** and **II**, it was necessary to investigate claims that tertiary benzamides were inappropriate substrates for the Birch reduction. It had been reported that reduction of *N*,*N*-dimethylbenzamide with sodium in NH_3 in the presence of *tert*-butyl alcohol gave benzaldehyde and a benzaldehyde–ammonia adduct. We found that the competition between reduction of the amide group and the aromatic ring was strongly dependent on reaction variables, such as the alkali metal (type and quantity), the availability of a proton source more acidic than NH_3, and reaction temperature. Reduction with potassium in NH_3–THF solution at −78 °C in the presence of 1 equiv. of *tert*-butyl alcohol gave the cyclohexa-1,4-diene **2** in 92% isolated yield (Scheme 3). At the other extreme, reduction with lithium in NH_3–THF at −33 °C in the absence of *tert*-butyl alcohol gave benzaldehyde and benzyl alcohol as major reaction products.[4]

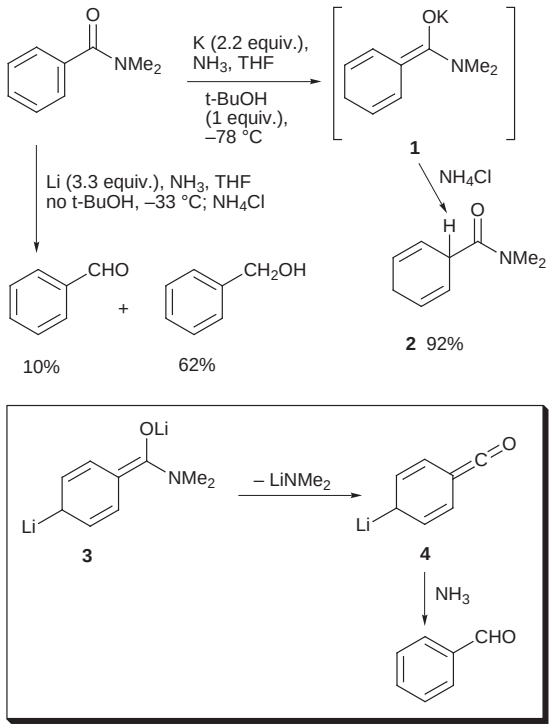

Scheme 3

Reduction of the aromatic nucleus in *N*,*N*-dimethylbenzamide occurs by an initial single electron transfer to give a radical anion. Protonation of the radical anion generates a radical and a second electron transfer gives the amide enolate **1**. Protonation of the cross-conjugated trienolate moiety in **1** occurs α to the incipient carbonyl group to give the cyclohexa-1,4-diene **2**.[1]

Amide group reduction probably occurs by the mechanism shown in Scheme 3. Two-electron transfer without protonation would give dianion **3**. Elimination of $LiNMe_2$ from **3** would give **4** (an acyl anion equivalent) and protonation of **4** at the carbonyl group would give benzaldehyde.

Because dianion formation appears to be more important when lithium rather than potassium is used, many of the Birch reductions and reduction–alkylations of **I** and **II** that have been developed utilize potassium as the reducing metal. Piperylene is added prior to the alkylation reagent to consume any remaining metal and thereby prevent reduction of the alkylation reagent. In the event that the alkylation reagent is unstable to strong bases (*e.g.* homoallylic and arylethyl halides) LiBr is added to reduce the basicity of the reaction medium.

Birch reduction of the chiral benzamide **5** generates the amide enolate **6** (Scheme 4). This enolate has been characterized by NMR spectroscopy and by an extensive examination of the effects of changes in alkali metal, solvent, reaction temperature and substituents near the reaction center on the diastereoselectivity of enolate alkylation.[5] These data have been reviewed before[3] and will not be discussed here. For this presentation it is sufficient to note that the alkylation reagent reacts with enolate **6** preferentially from the least hindered face away from the methoxymethyl group on the chiral auxiliary.

Diastereoselectivities for alkylation of enolate **6** are outstanding. Alkylation with MeI gives **7** (R = Me) as the major product diastereomer in a ratio of 260 : 1 with respect to the minor diastereomer **8**. A wide range of alkylation reagents have been examined including allylic, benzylic, homoallylic, alkoxymethyl, cyanomethyl, and arylethyl halides.

It is important to perform both the Birch reduction of **5** and the alkylation of enolate **6** at −78 °C. Enolate **6** obtained directly from **5** at low temperatures is considered to be a 'kinetic enolate'. A 'thermodynamic enolate' obtained from **6** by equilibration techniques has been shown to give an opposite sense of stereoselection on alkylation.[5] Although a comprehensive study of this modification has not been carried out, diastereoselectivities for formation of **8** were found to be greater than 99 : 1 for alkylations with MeI, EtI, and $PhCH_2Br$. Thus, it should be possible to obtain both enantiomers of a target structure by utilization of a single chiral benzamide.[6,7]

It has been demonstrated that excellent diastereoselectivities for enolate alkylation also are obtained when alkyl substituents are positioned at C(4), C(5) or C(6) of benzamide **5**.[5] Aryl[8] and methoxy[9] substituents at C(5) also are compatible, but a methyl group at C(3) leads to an inversion of the diastereoselectivity of enolate alkylation. The inverted sense of stereoselection is thought to be a result of a disruption of the internal chelation shown in enolate **6** by steric effects of the neighboring methyl substituent.[5]

A more traveled route to the absolute configuration represented by cyclohexa-1,4-diene **8** involves Birch reduction–alkylation of benzoxazepinone **9**.[2,5] This heterocycle is best prepared by the base-induced cyclization of the amide obtained from 2-fluorobenzoyl chloride and (*S*)-pyrrolidine-2-methanol.[10] The molecular shape of enolate **10** is such that the hydrogen at the stereogenic center provides some shielding of the α-face of the enolate double bond. Thus, alkylation occurs primarily at the β-face of **10** to give **11** as the major diastereomer. The diastereoselectivity for alkylation with methyl iodide is only 85:15, but with more sterically demanding alkyl halides such as ethyl iodide, allyl bromide, 4-bromobut-1-ene *etc.*, diastereoselectivities are greater than 98 : 2.

Birch reduction–alkylation of 2-alkyl- and 2-trimethylsilylbenzamides corresponding to structure **12** has provided a very general route to cyclohexa-1,4-dienes of type **14**. Enolate **13** has been used to explain the alkylation diastereoselectivities for over twenty cases in which the substituent X is varied from a group as small as methyl to groups as large as CH_2CH_2Ph or $SiMe_3$.[11,12] As with enolate **5**, the alkylation reagent reacts preferentially from the less hindered face of enolate **13** to give **14**.

Companion reactions that serve to expand the scope of the asymmetric Birch reduction–alkylation strategy

The development of facial selective addition reactions of cyclohexa-1,4-dienes **7** and **14** has greatly extended the value of the asymmetric Birch reduction–alkylation. For example, amide directed hydrogenation[13] of **15** with the Crabtree catalyst system occurs with outstanding facial selectivity *syn* to the amide carbonyl group to give **16** (Scheme 5).[11]

The reluctance of tertiary amides to undergo hydrolysis, especially those produced in the Birch reduction–alkylation with a quaternary center next to the carbonyl group, has inspired the development of a variety of intramolecular transacylation reactions as illustrated by the cleavage of the SEM ether in **16**

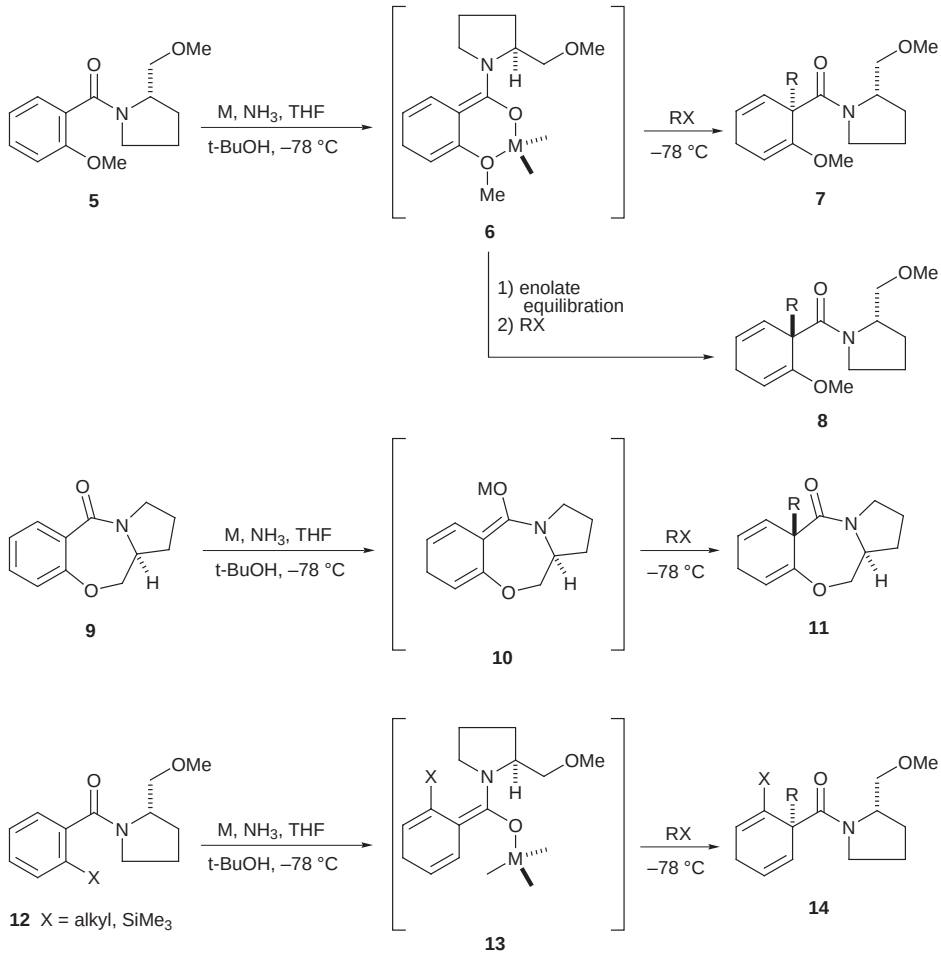

Scheme 4

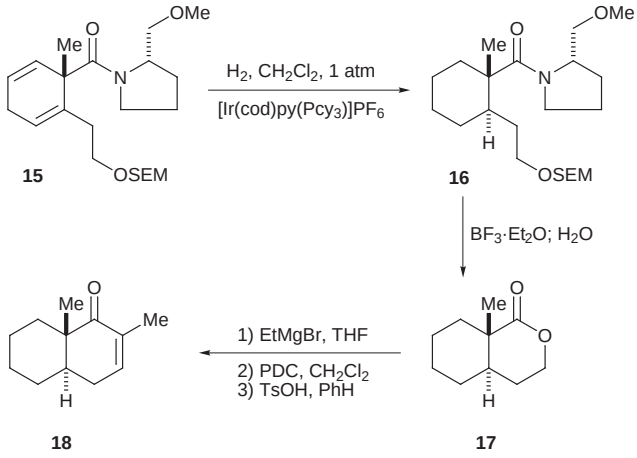

Scheme 5

and subsequent cyclization of the resulting alcohol to give lactone **17**. It is noteworthy that the chiral auxiliary can be removed at this stage by a simple partitioning of the reaction mixture between an organic solvent and aqueous acid.

Lactone **17** was converted to the *trans* fused octalone **18** by a classical Grignard-type carboannulation. Variations of the organometallic reagent used in the conversion of **17** to **18** and modifications of the substrate and alkylation reagent utilized to produce **15** afford unusually flexible options for the preparation of annulated cyclohexanes.

An application to the asymmetric synthesis of enantiomerically pure *trans*-hexahydroanthracen-9-ones is shown in Scheme 6. It should be possible to carry out a second stereoselective reductive alkylation of the benzoyl group in **22** as was demonstrated in the related hydrofluoren-9-one and hydrophenanthren-9-one series.[14] The key to the development of synthetic strategies involving consecutive Birch reduction–alkylations will depend on sequential activations of aromatic rings toward alkali metal in ammonia reduction; carbonyl activation is illustrated by the conversion of **21** to **22** in Scheme 6.

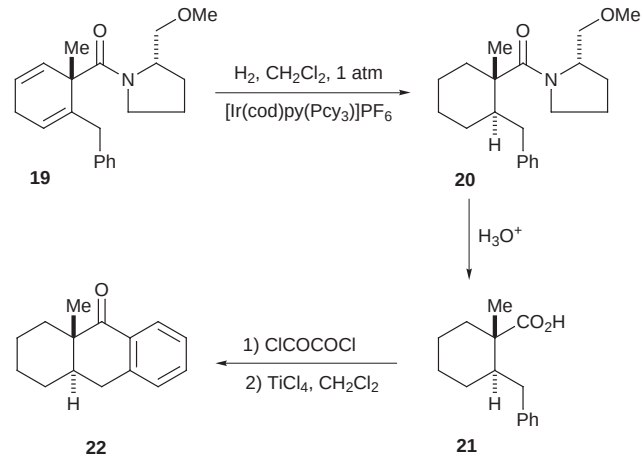

Scheme 6

Bis-allylic oxidation of **23** and related cyclohexa-1,4-dienes provides a convenient and general preparation of cyclohexa-2,5-dien-1-ones (Scheme 7).[15] These cross-conjugated dienones are substrates for a variety of photochemical rearrangement and intramolecular cycloaddition reactions.[16] Amide-directed hydrogenations of dienones **24a** and **24b** with the homogeneous iridium catalyst afford cyclohexanones **25a** and **25b**, containing three stereogenic centers on the six-

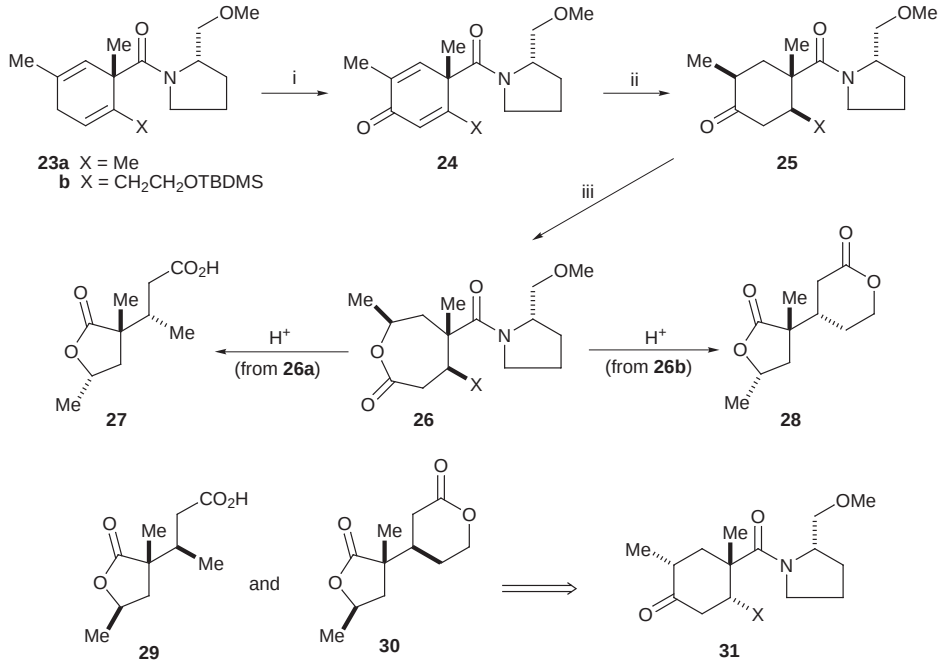

Scheme 7 *Reagents*: i, PDC, t-BuOOH, Celite, PhH; ii, H_2, [Ir(cod)py(Pcy$_3$)]PF_6, CH_2Cl_2, 1 atm; iii, MCPBA.

membered ring. Opposite stereoselectivity is obtained with heterogeneous catalysts such as rhodium on alumina or palladium on carbon to give cyclohexanones **31a** and **31b**.[17] X-Ray structural studies[18] demonstrate the importance of the bulky amide group in directing heterogeneous catalytic hydrogenation to the distal face of the cyclohexa-2,4-dienone ring.

We were interested in applications of the high level of stereocontrol associated with the asymmetric Birch reduction–alkylation to problems in acyclic and heterocyclic synthesis. The pivotal disconnection of the six-membered ring is accomplished by utilization of the Baeyer–Villiger oxidation (Scheme 7). Treatment of cyclohexanones **25a** and **25b** with MCPBA gave caprolactone amides **26a** and **26b** with complete regiocontrol. Acid-catalyzed transacylation gave the butyrolactone carboxylic acid **27** from **26a** and the bis-lactone **28** from **26b**; cyclohexanones **31a** and **31b** afforded the diastereomeric lactones **29** and **30**.[17]

Chiral butyrolactones of type **27** and **28** have substantial value in asymmetric synthesis because they contain readily differentiable difunctional group relationships (*e.g.* 1,5-dicarboxylic acid, 1,4-hydroxycarboxylic acid, 1,6-hydroxycarboxylic acid, 1,6-diol *etc.*) that would be difficult to assemble by existing asymmetric condensation and pericyclic processes. Applications of these chiral derivatives of glutaric acid to syntheses of indole, indoline and quinolinone alkaloids are illustrated in Schemes 16–18.

A structural requirement for the asymmetric Birch reduction–alkylation is that a substituent must be present at C(2) of the benzoyl moiety to desymmetrize the developing cyclohexa-1,4-diene ring (Scheme 4). However, for certain synthetic applications, it would be desirable to utilize benzoic acid itself. The chemistry of chiral benzamide **12** (X = $SiMe_3$) was investigated to provide access to non-racemic 4,4-disubstituted cyclohex-2-en-1-ones **33** (Scheme 8).[19] Alkylation of the enolate obtained from the Birch reduction of **12** (X = $SiMe_3$) gave cyclohexa-1,4-dienes **32a–d** with diastereoselectivities greater than 100 : 1.[20] These dienes were efficiently converted in three steps to the chiral cyclohexenones **33a–d**.

A very effective method for removal of the chiral auxiliary from cyclohexenones **34** involves treatment with I_2 in THF–H_2O to give the iodolactones **35** (Scheme 9). These highly functionalized chiral cyclohexanones have figured prominently in the asymmetric synthesis of natural products; *e.g.* Scheme 15. Furthermore, selective cleavage of the cyclohexanone ring in **35**

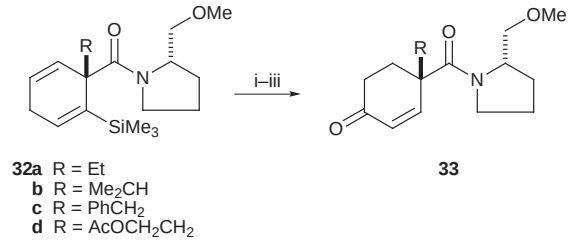

Scheme 8 *Reagents*: i, PDC, t-BuOOH; ii, H_2, Pd/C; iii, $CuCl_2$, DMF.

with LiOH under aqueous conditions affords the butenolide carboxylic acids **36**.[21] A competing fragmentation process initiated by addition of hydroxide ion to the lactone carbonyl group gives the 4-hydroxycyclohexenones **37**. Yields for formation of the butenolide **36** are in the range of 80 to 90% when relatively large groups are present at C(2). On the other hand, the 4-hydroxycyclohexenone **37** is obtained in 72% yield when R^1 = H and R^2 = Me.

A different mode of fragmentation of the lactone ring in **35** occurred to give butyrolactone **38** when anhydrous lithium alkoxides were used in place of metal hydroxides under aqueous conditions (Scheme 10). It is noteworthy that **36**, **37** and **38** (R^1 = H) are all formed without racemization. Although we are only in the early stages of development of the chemistry of iodolactones **35**, it is already clear that there is considerable potential for utilization of the butenolides derived from **35** as scaffolds for construction of carbocyclic and heterocyclic ring

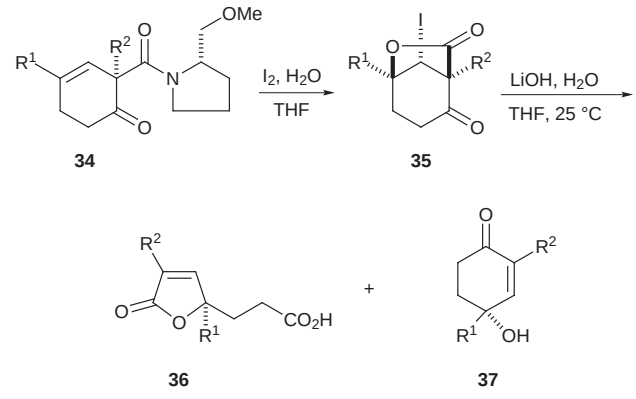

Scheme 9

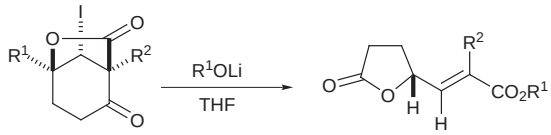

35 38

Scheme 10

systems by way of intramolecular radical and dipolar addition reactions.[21]

Cyclohexenones **34** also undergo a highly diastereoselective dihydroxylation to give *cis*-diols **39** (Scheme 11).[22] These diol amides are converted to hydroxylactones **40** by an acid-catalyzed process involving retro aldol–realdolization prior to transacylation. The enantiomers of hydroxylactones **40** are obtained from iodolactones **35** by iodide exchange with 2,2,6,6-tetramethylpiperidin-1-yloxy free radical (TEMPO) followed by reductive cleavage of the TEMPO derivative with Zn in HOAc. The enantiomeric purity of the hydroxylactones prepared by either route is 95–98% ee.

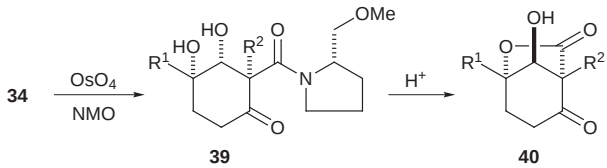

39 40

Scheme 11

Reaction of enolate **5** with excess NH_4Cl at −78 °C gave the α-protonated amide **41** as a 4 : 1 mixture of diastereomers.[5] This degree of stereoselectivity was considered to be unacceptable for applications in asymmetric organic synthesis. However, the chiral 2-substituted cyclohex-2-en-1-one **42**, obtained from **41** by enol ether hydrolysis along with double bond migration, undergoes conjugate addition reactions with Grignard reagents and related organometallic derivatives with moderate to good regio- and stereo-control.[23] Considerably more selective addition reactions of **42** occur with allyl silanes (the Sakurai reaction) and enol silyl ethers (the Mukaiyama–Michael addition).[24] Treatment of the conjugate adduct with *N*-methylhydroxylamine releases the chiral auxiliary to give a 1-methyltetrahydrobenzisoxazolin-3-one; *e.g.* **43**, 96% ee. Heterocycle **43** provides 2,3-disubstituted cyclohexanones **44** by a reduction–alkylation sequence (Scheme 12).[24]

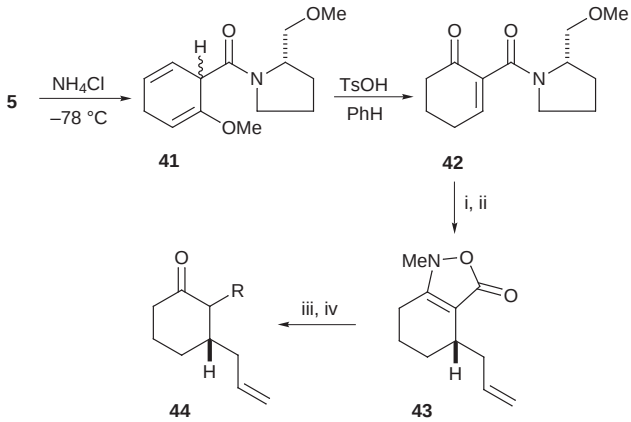

41 42 43 44

Scheme 12 *Reagents*: i, $H_2C{=}CHCH_2SiMe_3$, $TiCl_4$; ii, MeNHOH, H^+; iii, Li, NH_3–THF; RX.

Applications to the asymmetric synthesis of natural products and related materials

What truly distinguishes the asymmetric Birch reduction–alkylation protocol from other methods for preparation of non-racemic cyclohexane derivatives is (i) the accessibility of aromatic carboxylic acids with substituents ranging from heteroatoms to alkyl and aryl groups to tethered functionality available for subsequent strategic applications, (ii) the uniformly high degree of diastereoselection in the chiral enolate alkylation step, and (iii) the opportunity for further development of stereogenic centers on the resulting chiral cyclohexa-1,4-diene ring system by facial-selective addition reactions.

The tricyclic sesquiterpene longifolene has served as a vehicle for the illustration of new strategies for organic synthesis.[25] Both enantiomers have been obtained from natural sources; (+)-longifolene occurs in several *Pinus* species and is commercially available while the rare (−)-longifolene has been found in certain liver mosses.[26] We elected to prepare (−)-longifolene **49** from the cyclohexa-1,4-diene **45**, obtained from the Birch reduction–alkylation of benzoxazepinone **9** in 96% yield with a diastereomeric excess of greater than 98% (Scheme 13).[27]

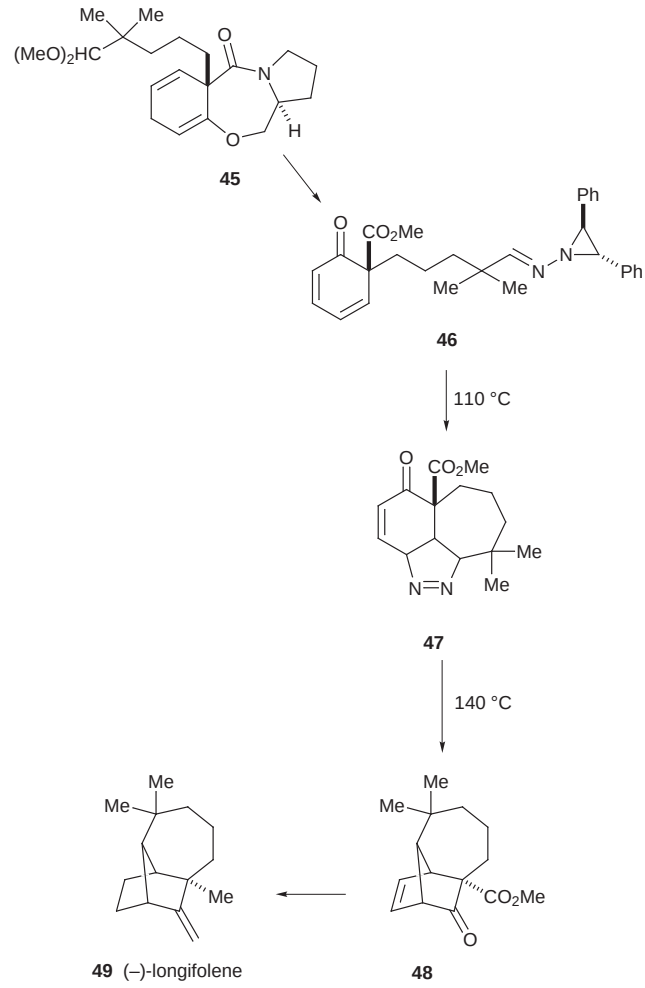

45 46 47 48

Scheme 13

Cyclohexadiene **45** was converted to **46** by what has proven to be a general method for preparation of the cyclohexa-2,4-dien-1-one ring system.[28] Fragmentation of the aziridinyl imine in **46** at 110 °C gave an intermediate diazoalkane which underwent an intramolecular 1,3-dipolar cycloaddition to give the pyrazoline **47**. At 140 °C, pyrazoline **47** expelled N_2 and rearranged to the tricyclic ketone **48**. The development of this and related bicyclizations[29] illustrated a practical synthetic equivalence of an intramolecular diene–carbene 4 + 1 cycloaddition in the cyclohexa-2,4-dien-1-one series.

The 2-azaspiro[5.5]undecane group of alkaloids occur in certain plants of the genus *Nitraria*. There has been some interest in the biological activity of these alkaloids because their structures are similar to the histrionicotoxins, a group of

1-azaspiro[5.5]undecane alkaloids found only in dendrobatid frogs.[30] The first asymmetric syntheses of (+)-sibirine **50**, (+)-nitramine **51** and (−)-isonitramine **52** from the chiral benzamide **5** and benzoxazepinone **9** established the absolute configuration of these alkaloids (Scheme 14).[31]

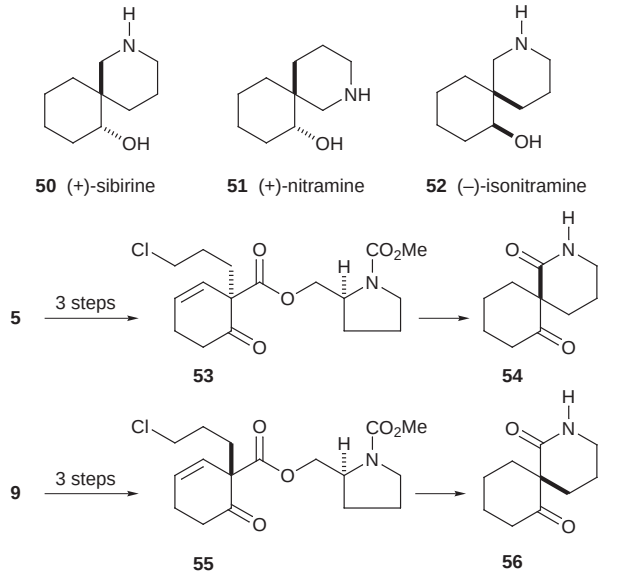

Scheme 14

The diastereomerically related keto esters **53** and **55**, activated for removal of the chiral auxiliary, were obtained from **5** and **9**. The requisite nitrogen atom was introduced by an azide displacement of chloride and at an opportune stage of the synthesis an intramolecular aminolysis of the carboxylic ester provided the enantiomerically related keto lactams **54** and **56**. Although shorter routes to these popular synthetic targets have been reported in recent years, the conversion of **9** to (−)-isonitramine (ten steps, 50% overall yield) clearly illustrates the efficiency of the asymmetric Birch reduction–alkylation strategy for construction of the azaspiroundecane ring system.

Lycorine is the most abundant alkaloid in plants of the *Amaryllidaceae*. Several syntheses of racemic lycorine had been reported prior to our initiation of studies directed at an asymmetric synthesis of the unnatural enantiomer **64**.[32] A common theme in all of the syntheses of (±)-lycorine has been the utilization of either an intermolecular or intramolecular Diels–Alder construction of the key C-ring of the alkaloid. This six-membered ring presents a rather formidable synthetic challenge because of the four contiguous stereogenic centers, the *trans* 1,2-diol moiety, and the juxtaposition of the aromatic substituent and the carbon–carbon double bond.

The first asymmetric total synthesis of (+)-lycorine is outlined in Scheme 15. While our earlier applications of the Birch reduction–alkylation of chiral benzamide **5** were focused on target structures with a quaternary stereocenter derived from C(1) of the starting benzoic acid derivative, the synthesis of **64** demonstrates that the method also is applicable to the construction of chiral six-membered rings containing only tertiary and trigonal carbon atoms.[33]

Birch reduction–alkylation of **5** with 2-bromoethyl acetate was carried out with complete facial selectivity to give **57**. This tetrafunctional intermediate was converted to the bicyclic iodolactone **58** (> 99% ee) from which the radical cyclization substrate **59** was prepared. The key radical cyclization occurred with complete regio- and facial-selectivity and subsequent stereoselective reduction of the resulting tertiary radical gave **60** with the required *trans* BC ring fusion.[34] The allylic alcohol unit of (+)-lycorine was obtained by a photochemical radical decarboxylation, **62** → **63**.

The eburnamine–vincamine alkaloids found in plants of the dogbane family provided a useful testing ground for application

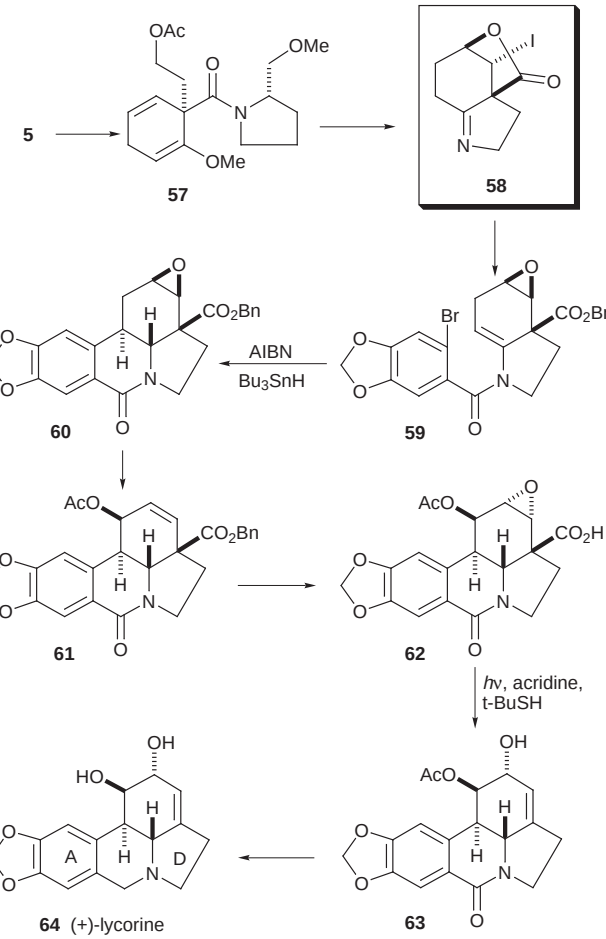

Scheme 15

of the butyrolactone synthesis outlined in Scheme 7 to the construction of nitrogen heterocycles (Scheme 16). An asymmetric total synthesis of (+)-apovincamine **71** began with the Birch reduction–ethylation of the chiral 2-methoxy-5-methylbenzamide **65** to give **66** (diastereomer ratio > 100 : 1).[35] Tryptamine was coupled to the butyrolactone carboxylic acid **67**, and the resulting amide was converted to the keto aldehyde **69**. An acid-catalyzed cyclization of **69** followed by a base-induced elimination of MeOH provided the key *cis*-fused diene lactam **70**, which was converted to (+)-apovincamine **71** by a sequence of steps involving reduction of the ene lactam with $LiAlH_4$ and oxidation of the methyl substituent by an electrophilic dibromination.

The butyrolactone route to alkaloids was demonstrated again with a synthesis of **77**, the core structure of the *Melodinus* alkaloid (+)-meloscine **72** (Scheme 17).[36] The synthetic strategy features an early incorporation of the aromatic ring in **72** as the 5-benzyl substituent in **73**. The Mannich bicyclization of **75** provides the key *cis*-pyridin-6-one **76**, from which the remaining ring in **77** is assembled by an oxidative cleavage of the *N*-allyl group and acid-catalyzed cyclization of the resulting keto aldehyde. It is expected that (+)-meloscine **72** will be prepared from a derivative of **73** containing a modified 5-benzyl substituent. The asymmetric Birch reduction–alkylation will provide a latent vinyl group to accommodate the substitution at C(20) of **72**.[37]

The versatile cyclohexa-1,4-diene **32a** has served as an intermediate for synthesis of (−)-eburnamonine **81** and the *Aspidosperma* alkaloid (−)-aspidospermidine **84** (Scheme 18).[38] Butyrolactone carboxylic acids **78** and **82** were prepared from **32** by modification of the methodology outlined in Scheme 7. The key Pictet–Spengler-type cyclization of **79** under conditions of kinetic control gave an 18 : 1 mixture of **80** and its C(3) β-epimer in 93% yield. Subsequent hydroboration

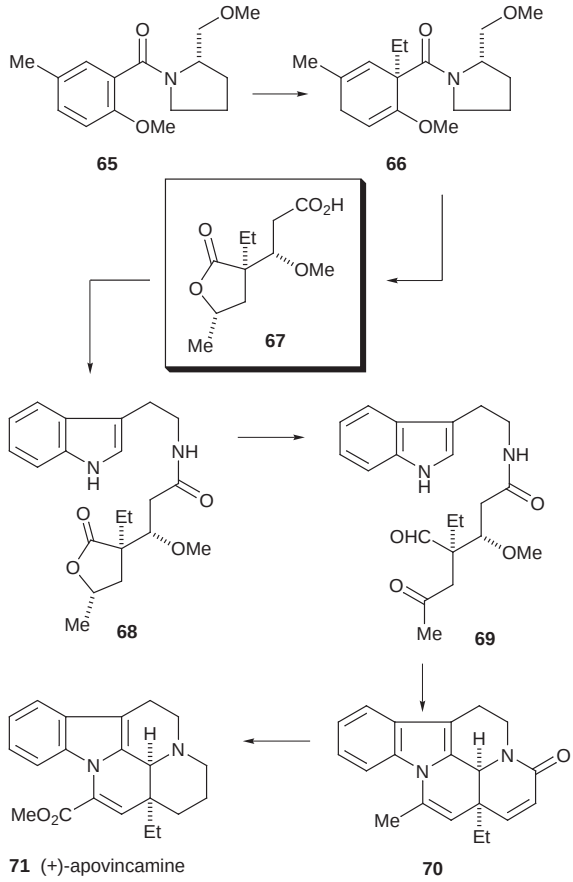

Scheme 16

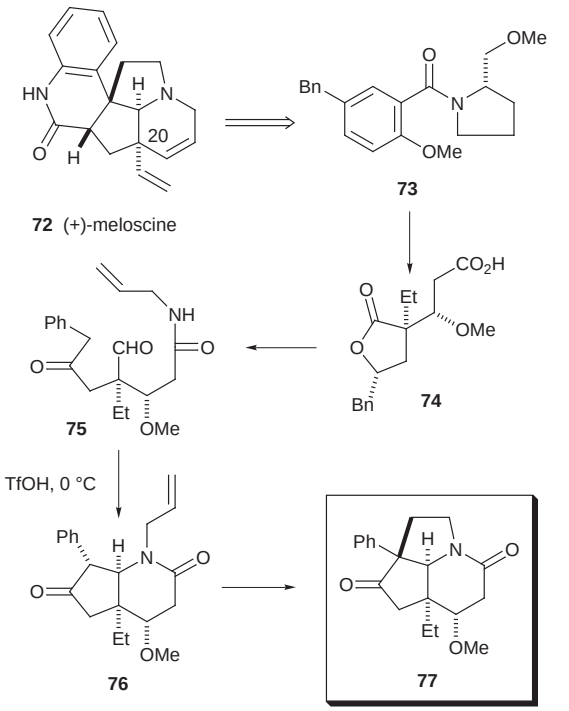

Scheme 17

of **80** and oxidation of the intermediate primary alcohol gave (−)-eburnamonine **81** in a total of 12 steps from the chiral benzamide **12** (X = $SiMe_3$) and 17% overall yield.

The classical Harley–Mason cyclization was utilized *en route* to (−)-aspidospermidine **84**.[39] The synthesis of **84** required 12 steps from the chiral benzamide **12** (X = $SiMe_3$) and was carried out with an overall yield of 19%.

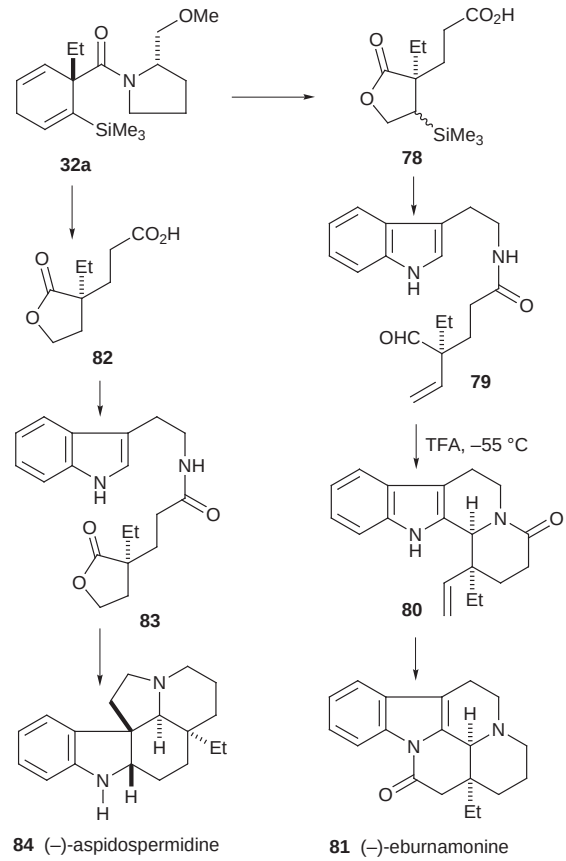

Scheme 18

Birch reduction–methylation of the 2,3-dialkyl substituted benzamide **85** (Scheme 19) provided the cyclohexa-1,4-diene **86** with diastereoselectivity comparable to that observed with the 2-alkylbenzamides illustrated in Scheme 4. Cyclohexadiene **86** was converted to iodolactone **87** and reduction of **87** with Bu_3SnH occurred with exclusive equatorial delivery of hydrogen to give the axial methoxyethyl derivative **88**. Lactone **88** was converted to the Caribbean fruit fly pheromone (+)-epianastrephin **90** (> 98% ee) in 9.5% overall yield from the chiral benzamide **85**.[40]

The hasubanan alkaloids are of pharmacological interest because of their structural resemblance to the morphine alkaloids.[41] The first asymmetric synthesis of a hasubanan alkaloid, (+)-cepharamine **99**, is shown in Scheme 20.[42] The synthesis is highly convergent as a result of the Birch reduction of **91** and alkylation with **92** to give the cyclohexa-1,4-diene **93** in 95% yield. Conversion of **93** to **94** and radical cyclization of **94** gave the hydrophenanthrene **95a**. An exchange of protecting

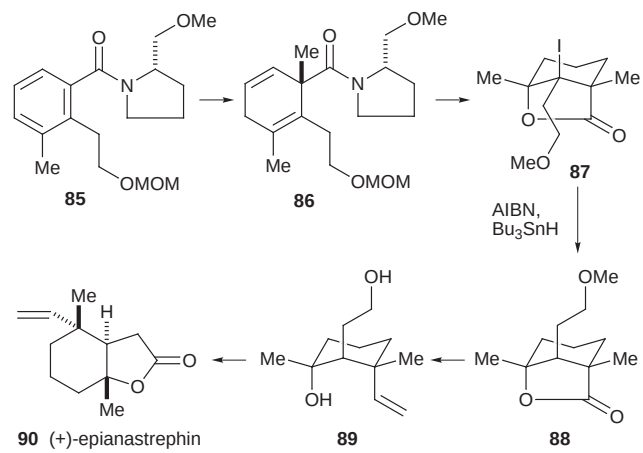

Scheme 19

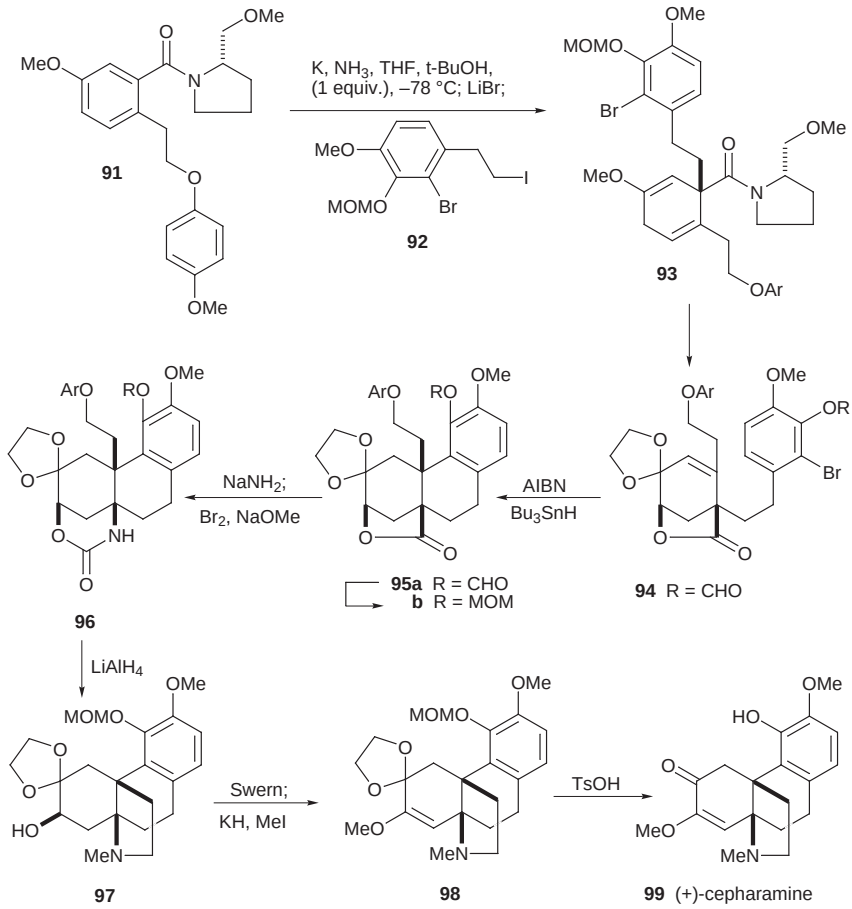

Scheme 20

group was followed by a very efficient Hofmann-type rearrangement of **95b** with internal capture of the resulting isocyanate by the neighboring OH group to give the cyclic carbamate **96**. Formation of the *cis*-fused *N*-methylpyrrolidine ring was then carried out in one experimental operation by treatment of **96** with $LiAlH_4$ in refluxing THF. Swern oxidation of **97** to the corresponding ketone followed by *O*-alkylation of the ketone enolate afforded enol ether **98**. Acid-catalyzed ketal and MOM ether hydrolysis proceeded without disruption of the enol ether to give (+)-cepharamine **99**. The synthesis of **99** required 16 steps from the chiral benzamide **91** and was carried out with an overall yield of 12%.

Applications of pyrrolobenzodiazepine-5,11-diones

The pyrrolobenzodiazepine-5,11-diones **II** have been utilized in asymmetric syntheses of both the *cis*- and *trans*-decahydroquinoline alkaloids (Schemes 21 and 22). For example, reduction of **100** with 4.4 equiv. of potassium in the presence of 2 equiv. of t-BuOH, followed by protonation of the resulting enolate with NH_4Cl at −78 °C gave the *cis*-fused tetrahydrobenzene derivative **101**.[43] Amide-directed hydrogenation of **101** gave the hexahydrobenzene derivative with diastereoselectivity greater than 99 : 1. Removal of the chiral auxiliary and adjustment of the oxidation state provided aldehyde **103** which was efficiently converted to the poison frog alkaloid (+)-pumiliotoxin C.

Reduction of all three of the double bonds in the pyrrolobenzodiazepine-5,11-dione **105** with excess potassium provides the corresponding *trans* fused hexahydrobenzene derivative **106** in high yield with complete stereochemical control. The preparation of (+)-perhydro-219A **108** from **106** has been reported[13] and a general method of preparation of derivatives of *trans*-2-aminocyclohexanecarboxylic acid (*e.g.* **107**) has recently appeared.[44]

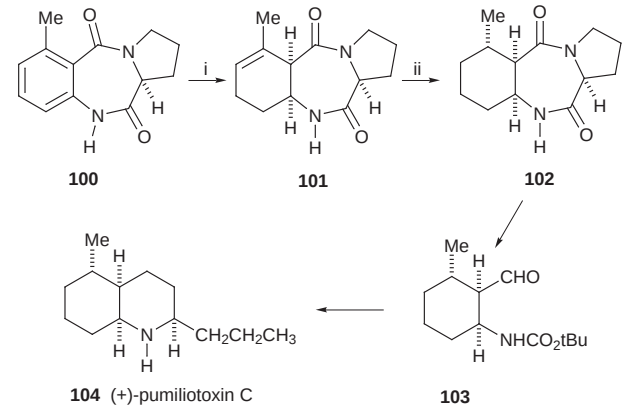

Scheme 21 *Reagents*: i, K (4.4 equiv.), NH_3, THF, t-BuOH (2 equiv.); NH_4Cl; ii, H_2 $[Ir(cod)py(Pcy_3)]PF_6$

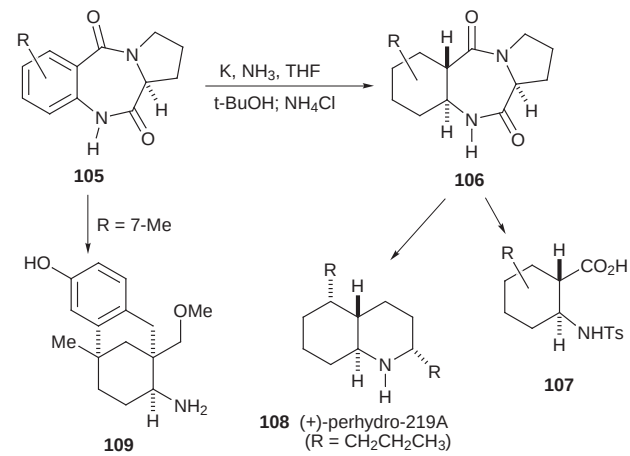

Scheme 22

The enolates obtained by reduction of two of the double bonds in **105** undergo completely stereoselective alkylation to give *cis*-fused tetrahydrobenzene derivatives in excellent yield. Structural analogues of the morphine alkaloids have been prepared by way of reduction–alkylation of **105** with *p*-alkoxybenzyl halides; *e.g.* **109**. One of these analogues has displayed high affinity for the κ-opioid receptor and anti-nociceptive studies have demonstrated that this analogue is a full κ-agonist.[45]

Conclusions and future considerations

Chiral benzamides **I** and the pyrrolobenzodiazepine-5,11-diones **II** have proven to be effective substrates for asymmetric organic synthesis. Although the scale of reaction in our studies has rarely exceeded the 50 to 60 g range, there is no reason to believe that considerably larger-scale synthesis will be impractical. Applications of the method to more complex aromatic substrates and to the potentially important domain of polymer supported synthesis are currently under study. We also are developing complementary processes that do not depend on a removable chiral auxiliary but rather utilize stereogenic centers from the chiral pool as integral stereodirectors within the substrate for Birch reduction–alkylation.[46]

Acknowledgements

I thank my talented and enthusiastic co-workers for their many significant contributions and the National Institutes of Health (GM 26568 and GM 33061) for generous financial support.

Notes and references

1 For recent reviews of the Birch reduction, see: J. M. Hook and L. N. Mander, *Nat. Prod. Rep.*, 1986, **3**, 35; P. W. Rabideau and Z. Marcinow, *Org. React.*, 1992, **42**, 1.

2 For the first report of an asymmetric Birch reduction–alkylation, see: A. G. Schultz and P. Sundararaman, *Tetrahedron Lett.*, 1984, **25**, 4591.

3 A. G. Schultz, *Acc. Chem. Res.*, 1990, **23**, 207.

4 A. G. Schultz and M. Macielag, *J. Org. Chem.*, 1986, **51**, 4983.

5 A. G. Schultz, P. Sundararaman, M. Macielag, F. P. Lavieri and M. Welch, *Tetrahedron Lett.*, 1985, **26**, 4575; A. G. Schultz, M. Macielag, P. Sundararaman, A. G. Taveras and M. Welch, *J. Am. Chem. Soc.*, 1988, **110**, 7828.

6 Chiral benzamide **5** is available from Aldrich Chemical Co.

7 For an application of the 'thermodynamic enolate' obtained from **5**, see: P. Magnus, F. Tavares and N. Westwood, *Tetrahedron Lett.*, 1997, **38**, 1341.

8 A. G. Schultz, M. Dai, S.-K. Khim, L. Pettus and K. Thakkar, *Tetrahedron Lett.*, 1998, **39**, 4203.

9 Unpublished results of S. Kirincich, RPI laboratories.

10 A. G. Schultz, D. J. P. Pinto, M. Welch and R. K. Kullnig, *J. Org. Chem.*, 1988, **53**, 1372.

11 A. G. Schultz and N. J. Green, *J. Am. Chem. Soc.*, 1991, **113**, 4931.

12 A. G. Schultz and L. Pettus, *Tetrahedron Lett.*, 1997, *38*, 5433.

13 P. J. McCloskey and A. G. Schultz, *J. Org. Chem.*, 1988, **53**, 1380.

14 For the first report of Birch reductions and reduction–alkylations of chiral 2-phenylbenzamides, see: A. G. Schultz, M. Macielag, D. E. Podhorez and J. Suhadolnik, *J. Org. Chem.*, 1988, **53**, 2456.

15 A. G. Schultz, A. G. Taveras and R. E. Harrington, *Tetrahedron Lett.*, 1988, **29**, 3907.

16 A. G. Schultz, *CRC Handbook of Organic Photochemistry and Photobiology*, ed. W. H. Horspool, CRC Press, London, p. 685, 716.

17 A. G. Schultz, D. K. Hoglen and M. A. Holoboski, *Tetrahedron Lett.*, 1992, **33**, 6611.

18 A. G. Schultz, A. G. Taveras, R. E. Taylor, F. S. Tham and R. K. Kullnig, *J. Am. Chem. Soc.*, 1992, **114**, 8725.

19 A. G. Schultz and L. Pettus, *Tetrahedron Lett.*, 1997, **38**, 5433.

20 Alkylation of the enolate with MeI gave the product corresponding to **32** with a diastereoselectivity of only 3.2 : 1. However, the diastereoselectivity for methylation of the enolate generated from **12** (X = $SiEt_3$) gave an improved diastereoselectivity of 10:1; unpublished results of Dr L. Pettus, RPI laboratories.

21 A. G. Schultz, M. Dai, S.-K. Khim, L. Pettus and K. Thakkar, *Tetrahedron Lett.*, 1998, **39**, 4203.

22 A. G. Schultz, M. Dai, F. S. Tham and X. Zhang, *Tetrahedron Lett.*, 1998, **39**, 6663.

23 A. G. Schultz and R. E. Harrington, *J. Am. Chem. Soc.*, 1991, **113**, 4926.

24 A. G. Schultz and H. Lee, *Tetrahedron Lett.*, 1992, **33**, 4397.

25 For the first total synthesis of (±)-longifolene, see: E. J. Corey, M. Ohno, R. B. Mitra and P. A. Vatakencherry, *J. Am. Chem. Soc.*, 1964, **86**, 478.

26 S. Huneck and S. Klein, *Phytochemistry*, 1967, **6**, 383.

27 A. G. Schultz and S. Puig, *J. Org. Chem.*, 1985, **50**, 916.

28 A. G. Schultz and J. P. Dittami, *Tetrahedron Lett.*, 1983, **24**, 1369; A. G. Schultz, J. P. Dittami, F. P. Lavieri, C. Salowey, P. Sundararaman and M. B. Szymula, *J. Org. Chem.*, 1984, **49**, 4429; A. G. Schultz, F. P. Lavieri and T. E. Snead, *J. Org. Chem.*, 1985, **50**, 3086; A. G. Schultz, R. R. Staib and K. K. Eng, *J. Org. Chem.*, 1987, **52**, 2968; A. G. Schultz, R. E. Harrington and F. S. Tham, *Tetrahedron Lett.*, 1992, **33**, 6097.

29 A. G. Schultz, J. P. Dittami and K. K. Eng, *Tetrahedron Lett.*, 1984, **25**, 1255; A. G. Schultz, K. K. Eng and R. K. Kullnig, *Tetrahedron Lett.*, 1986, **27**, 2331.

30 J. W. Daly, H. M. Garraffo and T. S. Spande, in *The Alkaloids*, ed. G. A. Cordell, Academic Press, New York, 1993, vol. 43, pp. 185–288.

31 P. J. McCloskey and A. G. Schultz, *Heterocycles*, 1987, **25**, 437.

32 A. G. Schultz, M. A. Holoboski and M. S. Smyth, *J. Am. Chem. Soc.*, 1996, **118**, 6210.

33 For the earlier asymmetric total synthesis of (+)-1-deoxylycorine, see: A. G. Schultz, M. A. Holoboski and M. S. Smyth, *J. Am. Chem. Soc.*, 1993, **115**, 7904.

34 For a study of facial selectivity and regio- and stereo-control in radical cyclizations of related chiral enamides, see: A. G. Schultz, P. R. Guzzo and D. M. Nowak, *J. Org. Chem.*, 1995, **60**, 8044.

35 A. G. Schultz, W. P. Malachowski and Y. Pan, *J. Org. Chem.*, 1997, **62**, 1223.

36 A. G. Schultz and M. Dai, *Tetrahedron Lett.*, 1999, **40**, 645.

37 A. G. Schultz and N. J. Green, *J. Am. Chem. Soc.*, 1992, **114**, 1824.

38 A. G. Schultz and L. Pettus, *J. Org. Chem.*, 1997, **62**, 6855.

39 J. Harley-Mason and M. Kaplan, *J. Chem. Soc., Chem. Commun.*, 1967, 915.

40 A. G. Schultz and S. J. Kirincich, *J. Org. Chem.*, 1996, **61**, 5626.

41 M. Matsui, in *The Alkaloids*, ed. A. Brossi, Academic Press, New York, 1988, vol. 33, pp. 307–347.

42 A. G. Schultz and A. Wang, *J. Am. Chem. Soc.*, 1998, **120**, 8259.

43 A. G. Schultz, P. J. McCloskey and J. J. Court, *J. Am. Chem. Soc.*, 1987, **109**, 6493.

44 A. G. Schultz and C. W. Alva, *Org. Synth.*, 1996, **73**, 174.

45 A. G. Schultz, A. Wang, C. Alva, A. Sebastian, S. D. Glick, D. C. Deecher and J. M. Bidlack, *J. Med. Chem.*, 1996, **39**, 1956.

46 A. G. Schultz and Y.-J. Li, *Tetrahedron Lett.*, 1996, **37**, 6511; A. G. Schultz and S. J. Kirincich, *J. Org. Chem.*, 1996, **61**, 5631; A. G. Schultz and Y.-J. Li, *Tetrahedron Lett.*, 1997, **38**, 2071; A. G. Schultz, T. J. Guzi, E. Larsson, R. Rahm, K. Thakkar and J. M. Bidlack, *J. Org. Chem.*, 1998, **63**, 7795.

Paper 9/01759C

2,5-Di-(*tert*-butyl)phospholyl sandwich complexes containing group 14 elements (Ge, Sn, Pb). Synthesis, molecular structure, and ring transfer chemistry of $[M(PC_4H_2Bu^t_2)_2]$ (M = Sn, Pb)

Kareen Forissier, Louis Ricard, Duncan Carmichael* and François Mathey*

Laboratoire 'Hétéroéléments et Coordination', CNRS UMR 7653, DCPH Ecole Polytechnique, 91128 Palaiseau Cedex, France. E-mail: Duncanc@mars.polytechnique.fr

Received (in Basel, Switzerland) 12th April 1999, Accepted 26th May 1999

Structurally characterised tin and lead sandwich compounds are shown to contain aromatic phospholyl ligands which can be transferred to rhodium and iridium centres under mild conditions.

The coordination chemistry of phospholyl ligands towards transition metals is an area reaching maturity[1] and a number of recent studies have also highlighted the chemistry of alkali metal phospholides.[2] However, simple π complexes involving monophospholyl ligands and elements of the p block have yet to appear.[3] Lying somewhere between the classical ionic chemistry of the phospholide anions and covalent transition metal phospholyls, these complexes may answer some interesting questions concerning the nature of the metal–phospholyl bond and the potential for η^5–η^1 equilibria. Furthermore, it seems reasonable to assume that they will be useful reagents.[4]

We present here the synthesis of three group 14 sandwich complexes **1**–**3** containing the 2,5-di(*tert*-butyl)phospholyl ligand and the molecular structures of $[Pb(PC_4H_2Bu^t_2)_2]$ **1** and

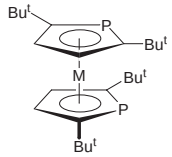

M = Pb, **1**; Sn, **2**; Ge, **3**

$[Sn(PC_4H_2Bu^t_2)_2]$ **2**. Using the 2,5-di-(*tert*-butyl)phospholyl ligand[5] diminishes the potential for electron-transfer chemistry† at the relatively redox-sensitive tin and lead centres and allows comparisons to be made with the published complexes $[M(NC_4H_2Bu^t_2)_2]$ (M = Sn **4**,[6a] Pb **5**[6b]) and $[M(C_5H_3Bu^t_2)_2]$ (M = Ge **6**, Sn **7**, Pb **8**[7a]).

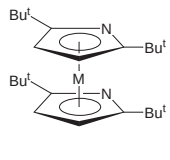

M = Sn, **4**; Pb, **5**

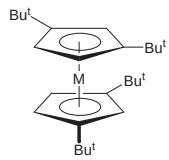

M = Ge, **6**; Sn, **7**; Pb, **8**

Stirring THF solutions containing $[Li(PC_4H_2Bu^t_2)(THF)_2]$ **10**[5] with MCl_2 (M = Sn, Pb) for 30 min at room temp. followed by evaporation to dryness *in vacuo*, extraction of $[M(PC_4H_2Bu^t_2)_2]$ into pentane and crystallisation at −78 °C produced air and moisture-sensitive deep (Pb, **1**) and pale (Sn, **2**) yellow cubes in *ca.* 80% yield. A similar procedure using GeI_2 gave $[Ge(PC_4H_2Bu^t_2)_2]$ **3** (50%) as a pale yellow powder.‡

X-Ray diffraction studies upon single crystals of the isostructural lead and tin compounds (Fig. 1 and 2, respectively) show two discrete molecular η^5 complexes within each unit cell.§ In each case, the Bu^t groups almost perfectly eclipse the phosphorus and CH functionalities, thus relieving nonbonding

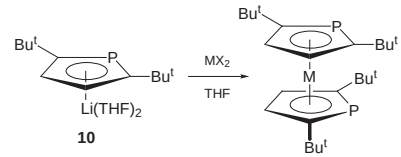

10

M = Pb, **1**; Sn, **2**; Ge, **3**

interactions between the rings. The angles at the intersection of the planes defined by the flat phospholyl ligands (Pb: 17.3; Sn: 19.2°) predictably[1] resemble the cyclopentadienyl-derived stannocenes and plumbocenes more than the aza-analogues **4** and **5**. The tilt of 5.7° for the phospholyl ring in the related phospharuthenocene[5] suggests that these angles may simply reflect the preferred geometry of the 2,5-di-(*tert*-butyl)phospholyl ligand rather than any significant electronic drive for a bent metallocene structure. Thus, the small $^1J_{PSn}$ coupling in **2**¶ probably reflects high *s*-electron character in both the P *and* the Sn lone pair orbitals.[7b,8] The equalisation of bond lengths within the phospholyl component indicates extensive delocalisation (Table 1)[9] which is confirmed by the large intracyclic $^1J_{PC}$ coupling constants ([Pb = 51.4, Sn = 48.5 and Ge = 47.0 Hz; *cf.* $(Me_3Sn)PC_4H_2Bu^t_2$ **9**, (27.5 Hz) and the delocalised $[Li(PC_4H_2Bu^t_2)(THF)_2]$ **10** (47.0 Hz), $[Ru(C_5Me_5)(PC_4H_2Bu^t_2)]$ **11** (62.7 Hz), **12** (65.3 Hz)]. These data suggest strongly that the rings are highly aromatic.

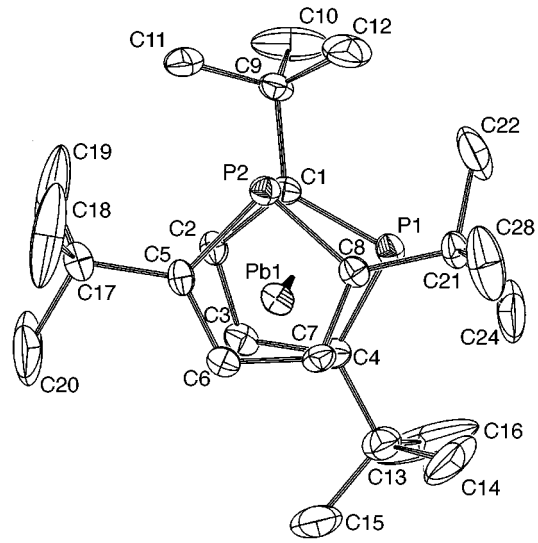

Fig. 1 Molecular structure of one of the essentially identical molecules of $[Pb(PC_4H_2Bu^t_2)_2]$ **1**, found in the unit cell. Selected bond lengths (Å): Pb(1)–P(1) 2.8732(8), Pb(1)–P(2) 2.9012(7), Pb(1)–C(1) 2.763(3), Pb(1)–C(2) 2.796(3), Pb(1)–C(3) 2.863(3), Pb(1)–C(4) 2.872(3), Pb(1)–C(8) 2.820(3), Pb(1)–C(7) 2.860(3), Pb(1)–C(6) 2.905(3), Pb(1)–C(5) 2.895(3), P(1)–C(1) 1.789(3), P(1)–C(4) 1.787(3), P(2)–C(5) 1.787(3), P(2)–C(8) 1.785(3), C(1)–C(2) 1.385(4), C(2)–C(3) 1.530(4), C(3)–C(4) 1.381(4), C(5)–C(6) 1.391(4), C(6)–C(7) 1.415(4), C(7)–C(8) 1.390(4).

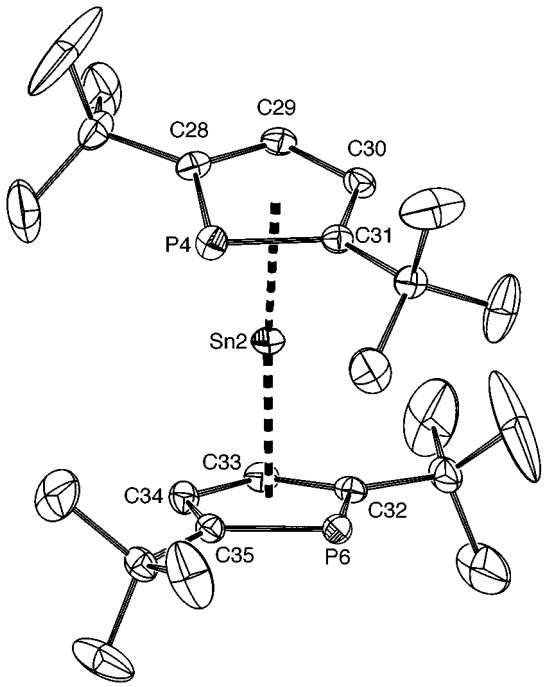

Fig. 2 Molecular structure of one of the essentially identical molecules of $[Sn(PC_4H_2Bu^t_2)_2]$ **2**, found in the unit cell. Selected bond lengths (Å): Sn(2)–P(4) 2.8018(7), Sn(2)–P(6) 2.8348(7), Sn(2)–C(28), 2.822(3), Sn(2)–C(29) 2.825(3), Sn(2)–C(30) 2.741(3), Sn(2)–C(31) 2.688(3), Sn(2)–C(32) 2.854(3), Sn(2)–C(33) 2.871(3), Sn(2)–C(34) 2.813(3), Sn(2)–C(35) 2.770(3), P(4)–C(31) 1.788(3), P(4)–C(28) 1.794(3), P(6)–C(32) 1.785(3), P(6)–C(35) 1.790(3), C(28)–C(29) 1.372(4), C(29)–C(30) 1.425(4), C(30)–C(31) 1.385(4), C(32)–C(33) 1.393(4), C(33)–C(34) 1.419(4), C(34)–C(35) 1.384(4).

Table 1 Bond length equalisation in selected phospholyl motifs

Complex	*r*(C=C)/Å	*r*(C–C)/Å	Ref.
$[Mo_2(PC_4H_2Bu^t_2)_2(CO)_4]$	1.407	1.425	*a*
$[PC_4Me_4][Li(tmeda)]$	1.396	1.424	*b*
$[Pb(PC_4H_2Bu^t_2)_2]$	1.387	1.417	*c*
$[Sn(PC_4H_2Bu^t_2)_2]$	1.384	1.422	*c*
$PhCH2PC_4H_4$	1.343	1.438	*d*

References: (*a*) D. Carmichael, L, Ricard and F. Mathey, *J. Chem. Soc., Chem. Commun.*, 1994, 2489; (*b*) T. A. Douglas, K. H. Theopold, B. S. Haggerty and A. L. Rheingold, *Polyhedron*, 1990, **9**, 209; (*c*) this work; (*d*) P. Coggan and A. T. McPhail, *J. Chem. Soc., Dalton Trans.*, 1973, 1888.

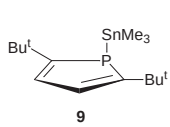

9

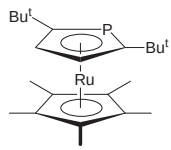

11

Complexes **1**–**3** are hydrocarbon-soluble and may also be recovered unchanged after several days at room temperature in dichloromethane. Such solution properties suggest a significant covalent contribution to the metal–ring interaction and imply some potential as 'mild' sources of phospholyl ligands. This has been confirmed in studies of the reactivity of $[M(cod)Cl]_2$ towards warm dichoromethane solutions of **1**, which permitted clean and quantitative isolation of the new compounds $[M(cod)(PC_4H_2Bu^t_2)]$ (M = Rh, **12**, yellow; M = Ir, **13**, orange) after filtration from $PbCl_2$.

Thus, in addition to their theoretical interest, these main group complexes may be useful precursors for the synthesis of further metal phospholyl compounds.

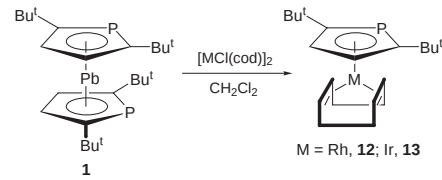

1

We thank Ecole polytechnique for a studentship (to K. F.) and CNRS for support.

Notes and references

† To date, attempts to prepare bis(3,4 dimethylphospholyl)plumbocene by an analogous route have failed.

‡ *Selected spectroscopic data:* (NMR: C_6D_6, Bruker AC200; MS: HP5989B). **1** δ_P 75. δ_C 168.3 ($^1J_{PC}$ 51.4, $^1J_{PbC}$ 50.9), 123.7 ($^2J_{PC}$ 3.4, $^1J_{PbC}$ 73.0). δ_H 6.90 ($^3J_{PH}$ 4.2). **2** δ_P 62 ($^1J_{SnP}$ 74.7). δ_C 166.2 ($^1J_{PC}$ 48.5, $^1J_{SnC}$ 10.6), 125.5 ($^1J_{PC}$ 4.6, $^1J_{SnC}$ 53.4). δ_H 6.90 ($^3J_{PH}$ 4.2, $^3J_{SnH}$ 10.6). **3** δ_P 67. δ_C 161.2 ($^1J_{PC}$ 47.5). MS −ve CI(NH_3) *m/z* (%): 464 (2) [M^+], 195 (100) [$PCl_{12}H_{20}$]. δ_P −3.8 ($^1J_{RhP}$ 15.2). δ_C 138.0 ($^1J_{PC}$ 62.7, $^1J_{RhC}$ 13.5), 95.7 ($^2J_{PC}$ 13.7), 65.3 ($^1J_{RhC}$ 13.7), 33.8 ($^2J_{RhC}$ 6.1), δ_H 5.46 ($^3J_{PH}$ 4.4). EI-MS *m/z* (%): 406 (81) [M^+], 347 (100) [$M^+ - C_4H_9$]. **13** δ_P −28.1. δ_C 128.1 ($^1J_{PC}$ 65.6), 93.2 ($^2J_{PC}$ 4.6), 49.3, 34.4 δ_H 5.46 ($^3J_{PH}$ 4.4). EI-MS *m/z* (%): 496 (31) [M^+], 437 (38) [$M^+ - C_4H_9$].

§ *Crystal structure determinations*: for **1**: $C_{24}H_{40}P_2Pb$, M = 597.69, yellow plate (0.22 × 0.16 × 0.14 mm) from pentane. Data collected at 150.0(1) K on an Enraf Nonius Kappa CCD diffractometer using Mo-Kα (λ = 0.71073 Å) radiation and graphite monochromator; solved with the maXus package and refined using SHELXL97; monoclinic, space group $P2_1/n$, a = 16.0550(2), b = 20.3550(4), c = 16.4910(3) Å, β = 101.323(1)°, V = 5284.35(16) Å^3, Z = 8, D_c = 1.503 g cm^{-3}, μ = 6.513 cm^{-1}, F(000) = 2368, reflections collected = 10807, maximum θ = 26.37°, used = 9859 [$F^2 > 2\sigma(F^2)$]. Final agreement factors: wR_2 = 0.0635, R_1 = 0.0237, GOF = 1.010, $\Delta\rho$ max./min. = 1.616(0.093)/−0.831(0.093) e Å^{-3}.

For **2**: $C_{24}H_{40}P_2Sn$, M = 509.19, pale yellow plate (0.20 × 0.20 × 0.15 mm) from pentane, monoclinic, space group $P2_1/n$, a = 16.0460(2), b = 20.3280(2), c = 16.3740(2) Å, β = 101.089(6)°, V = 5241.20(11) Å^3, Z = 8, D_c = 1.291 g cm^{-3}, μ = 1.104 cm^{-1}, F(000) = 2112, reflections collected = 10683, maximum θ = 26.35°, used = 9926 [$F^2 > 2\sigma(F^2)$]. Data collected and processed as above. Final agreement factors wR_2 = 0.0754, R_1 = 0.0278, GOF = 1.034, $\Delta\rho$ max./min. = 1.354(0.069)/−0.921(0.069) e Å^{-3}.

CCDC 182/1270. See http://www.rsc.org/suppdata/cc/1999/1273/ for crystallographic files in .cif format.

¶ No PbP coupling could be observed at room temp. for **1** (C_6D_6, ^{31}P = 81 MHz).

1 K. B. Dillon, F. Mathey and J. F. Nixon, *Phosphorus; the Carbon Copy*, Wiley, Chichester, 1998.
2 T. A. Douglas and K. H. Theopold, *Angew. Chem., Int. Ed. Engl.*, 1989, **28**, 1367; F. Paul, D. Carmichael, L. Ricard and F. Mathey, *Angew. Chem., Int. Ed. Engl.*, 1996, **35**, 1125.
3 A bis(η^1phospholyl)indium 'ate' complex is known: T. A. Douglas, K. H. Theopold, B. S. Haggerty and A. L. Rheingold, *Polyhedron*, 1990, **9**, 209. Nixon and coworkers have also briefly communicated π complexes of a more elaborate 1,2,4-triphospholyl ring: (η^5-triphospholyl)indium: C. Callaghan, G. B. Clentsmith, F. G. N. Cloke, P. B. Hitchcock, J. F. Nixon and D. M. Vickers, *Organometallics*, 1999, **18**, 793; (η^5-triphospholyl)(η^5-pentamethylcyclopentadienyl)plumbocene: see ref. 1, p. 330.
4 See, for example, F. Nief and F. Mathey, *J. Chem. Soc., Chem. Commun.*, 1988, 770.
5 D. Carmichael, L. Ricard and F. Mathey, *J. Chem. Soc., Chem. Commun.*, 1994, 1167.
6 (*a*) N. Kuhn, G. Henkel and S. Stubenrauch, *Angew. Chem., Int. Ed. Engl.*, 1992, **31**, 778. (*b*) N. Kuhn, G. Henkel and S. Stubenrauch, *J. Chem. Soc., Chem. Commun.*, 1992, 760.
7 (*a*) P. Jutzi and R. Dickbreder, *J. Organomet. Chem.*, 1989, **373**, 301; for reviews, see: (*b*) P Jutzi, *J. Organomet. Chem.*, 1990, **400**, 1; (*c*) P Jutzi, *Adv. Organomet. Chem.*, 1986, **26**, 217; (*d*) P. Jutzi and N. Burford, *Chem. Rev.*, 1999, **99**, 969.
8 C. J. Jameson and H. S. Gutowski, *J. Chem. Phys.*, 1969, **51**, 2790.
9 See, for example, P. v. R. Schleyer, P. K. Freeman, H. Jiao and B. Goldfuss, *Angew. Chem., Int. Ed. Engl.*, 1995, **34**, 337.

Communication 9/02909E

ChemComm

Chemical insight from crystallographic disorder: structural studies of a supramolecular β-cyclodextrin/coumarin photochemical system

Tom J. Brett,[ab] Jennifer M. Alexander,[a] Joanna L. Clark,[ab] Charles R. Ross II[ab]† Gerard S. Harbison,[a] and John J. Stezowski*[ab]

[a] *Department of Chemistry, University of Nebraska-Lincoln, Lincoln, Nebraska 68588-0304, USA. E-mail: jstezowski@unl.edu*

[b] *Center for Materials Research and Analysis, University of Nebraska-Lincoln, Lincoln, Nebraska 68588-0113, USA*

Received (in Columbia, MO, USA) 16th March 1999, Accepted 26th April 1999

From a combination of X-ray crystallography, solid-state NMR, and theoretical calculations, a model of a β-cyclodextrin (β-CD)–coumarin inclusion complex has been developed which characterizes the complex as a 2:3 β-CD–coumarin system with the coumarin molecules located in β-CD dimer 'reaction nano-tubes'; the model explains the reported yield for the coumarin photodimerization reaction carried out in powdered solids.

Several important contributions have been made to determine the mechanistic and controlling factors that produce given reaction outcomes in solid-state photochemical reactions.[1] Most such studies have focused on reactions carried out in neat crystals; however, co-crystallizing or 'host' media have been used to produce reaction outcomes not observed in neat crystals,[2] thus expanding the arsenal of the solid-state photochemist to produce a desired result. Detailed studies of such important systems at the molecular level are much less common.

β-Cyclodextrin (β-CD), a cyclic oligomer made of seven D-glucose units, is an example of one such host system in which the outcome of photochemical reactions can be modified.[3] An example system is the photodimerization of coumarin and coumarin derivatives. Upon photolysis, coumarin and its derivatives can give four structural isomers, the product ratio of which in solution is strongly influenced by the solvent polarity and the multiplicity of the excited state involved.[4] Product distributions in neat crystals and co-crystals have been found to correspond to the pre-irradiation disposition of the molecules in the crystal.[5,6] A study of the photodimerization of coumarin and coumarin derivatives in crystalline powder β-CD complexes has been reported.[7] However, these complexes were not subjected to detailed structural studies. The β-CD–coumarin complex presents an especially interesting model system for the study of intermolecular solid-state photochemical reactions in supramolecular systems. Scheme 1 illustrates the photochemical reaction in the supramolecular complex.

Not unexpectedly, room temperature X-ray crystallographic studies of the β-CD–coumarin complex[8] present a feature common to crystallographic studies of β-CD complexes: disorder. Although there is disorder of the guests at room temperature, difference Fourier maps ($F_o - F_c$) clearly reveal three general sites for coumarin molecules per cyclodextrin dimer (Fig. 1). Solid-state ^{13}C magic angle spinning NMR experiments with decoupling verified the 2:3 host:guest (H:G) ratio.[9] This finding corrects the previous characterization of this system as a 2:2 H:G system, and, as will be described below, helps to explain the previously reported 64% yield in the photodimerization reaction.[7] The disorder present was such that the coumarin orientations could not be determined unambiguously from conventional difference electron density maps. The shape of the difference electron density plots corresponding to the guest coumarins is flat and elliptical (like naphthalene), hence the general layout of the coumarins is definable.

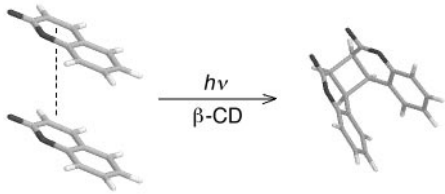

Scheme 1

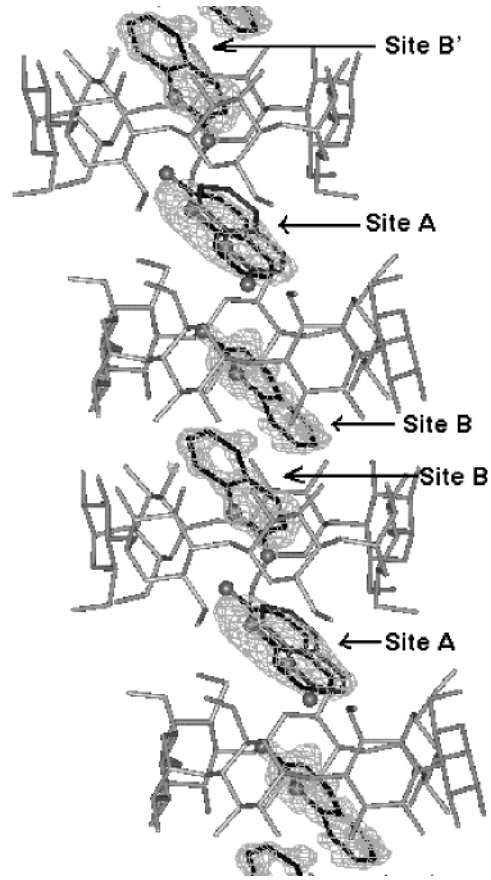

Fig. 1 Structure of the β-CD–coumarin 'reaction nano-tube' with the difference electron density ($F_o - F_c$) in the CD overlaid. CDs are in grey while coumarin molecules are shaded as follows: carbon = black; oxgen = light grey balls. Coumarin molecules at crystallographically disordered site A are shaded with black carbons for one orientation and grey carbons for the other ortientation. Waters of crystallization are omitted for clarity. The β-CD dimer stacks are roughly parallel to the crystallographic *c*-axis. See text for details. See: http://www.rsc.org/suppdata/cc/1999/1275/ for a colour version of this figure.

† Current address: Department of Structural Biology, St. Jude Children's Research Hospital, Memphis, TN 38105-2794, USA.

However, the direction of orientation (defined by which direction the carbonyl points) is not obvious. Consequently, lattice energy calculations[10] were employed to probe the most energetically favorable arrangement of coumarin orientations. The calculations indicate that an antiparallel pair of coumarin molecules in the center of the β-CD dimer (sites B and B′) is favored, while the orientation at site A must be aligned parallel with one of these two molecules. Because of space group symmetry, the orientation at site A is necessarily disordered; this coumarin sits on a crystallographic two-fold axis, but does not itself posses two-fold symmetry. The consequence is that site A's orientation is such that it could react with either site B or site B′. Either case requires some migration of the guest coumarins to bring the molecular orbitals involved closer to each other, which should be allowed in the CD's non-constraining environment.[11]

Analysis of these experiments produces an intriguing model that provides insight into the photochemical behavior of the system. The β-CD dimers pack in the crystal in a 'channel packing' motif,[12] in which the dimers stack one on top of another producing channels parallel to the *c* axis throughout the crystal allowing for interaction between guests in adjacent CD dimer cavities. The coumarin molecule at site A actually resides at the dimer-stacking interface. Even though the pair of molecules at site B is only separated by about 3.65 Å, they are antiparallel and cannot react without reorientation to give the observed *syn*-HH dimer.[13] Thus, the photodimerization likely happens between a coumarin molecule at site A and one either at site B or site B′ (depending on their respective orientations). On average, this leaves one of the three coumarin molecules per β-CD dimer unreacted, making the maximum theoretical yield 67%.

We conclude that the β-CD environment described here behaves not as a 'reaction nano-vessel', an environment where the interactions of import occur only within a single β-CD dimer, but rather as a 'reaction nano-tube', an environment where there is a considerable amount of interaction between molecules in adjacent β-CD dimers. This 'reaction nano-tube' allows for a 2:3 H:G ratio and limits the theoretical yield to 67%. In addition, the study nicely illustrates that important chemical information can be determined for complex, disordered systems by structural studies using complementary methods.

Funding for this work was provided by the NSF (CHE-9812146). We thank Dr X. C. Zeng for assistance with the theoretical calculations and for helpful discussions, and Cerestar USA, Inc. (Hammond, IN) for samples of β-CD.

Notes and references

1 For example see: V. Ramamurthy and K. Venkatesan, *Chem. Rev.*, 1987, **87**, 433 and references therein.
2 V. Ramamurthy, in *Photoprocesses of Host–Guest Complexes in the Solid State*, ed. V. Ramamurthy, VCH, New York, 1991, p. 303.
3 V. Ramamurthy, *Tetrahedron*, 1986, **42**, 5753.
4 D. O. Cowan and R. L. Drisko, *Elements of Organic Photochemistry*, Plenum, New York, 1976.
5 K. Gnanaguru, N. Ramasubbu, K. Venkatesan and V. Ramamurthy, *J. Org. Chem.*, 1985, **50**, 2337.
6 J. N. Moorthy and K. Venkatesan, *J. Org. Chem.*, 1991, **56**, 6957.
7 J. N. Moorthy, K. Venkatesan and R. G. Weiss, *J. Org. Chem.*, 1992, **57**, 3292.
8 *Crystal data* for $(C_{42}H_{70}O_{35})\bullet(C_9H_6O_2)_{1.5}\bullet 12H_2O$: M_r = 1570.38, monoclinic, space group *C2* (no. 5), a = 19.322(2), b = 24.641(3), c = 16.050(2) Å, β = 108.759(8)°, Z = 4, D_c = 1.442 g cm^{-3}, crystal size 0.5 × 0.4 × 0.1 mm, λ = Mo-Kα, T = 293(2) K. Data were collected on an automated Siemens P4 diffractometer with a sealed tube source. 6778 unique reflections (R_{int} = 0.0403) were collected to $2\theta_{max}$ = 50°. The structure was solved by molecular replacement of the β-CD coordinates from an isomorphous structure. Coumarin sites were located in difference electron density maps ($F_o - F_c$). Coumarin molecules in orientations determined from the lattice energy calculations were refined as rigid bodies. Least-squares refinement on F^2 of 835 parameters was carried out using SHELXL97 (G. M. Sheldrick, *SHELXL97, Program for the Refinement of Crystal Structures.* University of Göttingen, Germany, 1997) and converged to a final R_1 = 0.0893, wR_2 = 0.2037 and GOF = 1.239 for 3369 reflections with $F_o > 4\sigma(F_o)$. All non-hydrogen atoms were treated anisotropically except those of the coumarin molecules and low occupancy waters. Hydrogens on carbon atoms were generated geometrically and were fixed in a riding model. A final difference electron density map showed no distinct features with ρ_{max} = 0.46 and ρ_{min} = −0.33 e Å^{-3}. CCDC 182/1260. See http://www.rsc.org/suppdata/cc/1999/1275/ for crystallographic data in .cif format.
9 ^{13}C MAS spectra were obtained at 7.1 T with a standard Bloch decay pulse sequence on a sample of about 200 mg of hydrated crystalline complex. The dynamics of the guest made cross-polarization ineffective. 2048 transients were averaged, with an 80 s delay between acquisitions to allow spin relaxation. The spinning speed used was 4 kHz; at this speed, no rotational sidebands were observed. Assignments for coumarin resonances were deduced by comparison with a reference solution NMR spectrum (Aldrich). Assignments for β-CD resonances were deduced by comparison with previously published results (M. J. Gidley and S. M. Bociek, *J. Chem. Soc., Chem. Commun.*, 1986, 1223). Overlapping peaks were deconvolved to obtain integrated spectral intensities. Spectral shifts were referenced to the high frequency resonance of adamantane, and converted to a TMS scale by adding 38.56 ppm. The shifts obtained (relative to TMS), along with intensities, are as follows: δ_C 160 (3C), 154 (3C), 143 (3C), 131 (3C), 128 (3C), 124 (3C), 119 (3C), 117 (3C), 116 (3C), 104 (14C), 81 (14C), 73 (42C), 60 (14C).
10 Lattice energy calculations were performed using the CrystalPacker module in Cerius^2 (Molecular Simulations). Calculations performed were single point energy calculations with coumarin molecules located at positions from the crystallographic model. For the calculations, the orientations at site B and B′ were fixed as: an antiparallel pair, a parallel pair pointing in the +*c* direction, and a parallel pair pointing in the −*c* direction. With each of the fixed arrangements at site B, the orientation at site A was varied to each of the four orientations possible, and each time the energy was calculated. The low energy arrangements displayed an antiparallel pair at site B and B′ with site A aligned parallel to either of the molecules at site B or B′.
11 T. J. Brett, S. Liu, P. Coppens and J. J. Stezowski, *Chem. Commun.*, 1999, 551.
12 D. Mentzafos, I. M. Mavridis, G. LeBas and G. Tsoucaris, *Acta Crystallogr.*, 1991, **B47**, 746.
13 The *syn*-HH dimer was the reported product of the study in ref. 7. We verified formation of this product in our crystals as follows: the reaction product was extracted with CH_2Cl_2 and the crystal structure of the isolated photoproduct verified that it was the *syn*-HH dimer. The coordinates of this structure have also been deposited.

Communication 9/02092F

ChemComm

Multiphase catalysis using water-soluble metal complexes in supercritical carbon dioxide

Bhalchandra M. Bhanage,[a] Yutaka Ikushima,[b] Masayuki Shirai[a] and Masahiko Arai*[a]

[a] *Institute for Chemical Reaction Science, Tohoku University, Katahira, Aoba-ku, Sendai 980-8577, Japan. E-mail: marai@icrs.tohoku.ac.jp*

[b] *Tohoku National Industrial Research Institute, Nigatake, Miyagino-ku, Sendai 983-8551, Japan*

Received (in Cambridge, UK) 4th May 1999, Accepted 28th May 1999

Hydrogenation of cinnamaldehyde was performed in a supercritical carbon dioxide–water biphasic catalyst system, which eliminates gas–liquid–liquid mass transfer and gives better activity and selectivity.

Supercritical carbon dioxide ($scCO_2$) is considered as an ecologically benign and economically feasible reaction medium for metal catalyzed reaction.[1] It has several advantages such as nonflammability, lack of toxicity, absence of a gas–liquid phase boundary and possible simplifications in work up. This makes $scCO_2$ an alternative to conventional solvents. The physicochemical properties of $scCO_2$ can be tuned within a certain range by adjusting the pressure and temperature. Use of organometallic catalysts in $scCO_2$ is interesting, as demonstrated in some previous works.[2] Water-soluble organometallic catalysis has widened the scope of homogeneous catalysis in practice as it gives easy separation of catalyst and reactants/products, which is an important step towards the development of environmentally friendly processes.[3] Hoechst AG is operating a 300,000 tonnes per annum plant for hydroformylation of propylene using Rh and a water-soluble phosphine complex in a biphasic mode of operation. Several new concepts such as use of co-solvents[4] and surface active ligands,[5] interfacial catalysis using catalyst binding ligands,[6] supported aqueous phase catalysis,[7] and supported ethylene glycol phase catalysis[8] have emerged to improve poor reaction rates, which are due to limitations in liquid–liquid mass transfer and/or solubility of reactants. Considering the advantages of $scCO_2$ as a reaction medium and water-soluble metal complexes, there is a need to combine these two approaches to develop a truly environmentally friendly process (see Table 1). This eliminates the use of organic solvents and also gives easy catalyst/product separation and catalyst recycling. Here we demonstrate integration of biphasic catalysis and supercritical carbon dioxide using hydrogenation of an α,β-unsaturated aldehyde, cinnamaldehyde. This gives significant enhancement in the reaction rate and selectivity to cinnamyl alcohol and easy separation of the catalyst and reactants/products.

Hydrogenation of α, β-unsaturated aldehydes to give unsaturated alcohols with high selectivity is a challenging task due to several possible side reactions using heterogeneous metal supported catalysts.[9,10] However, good selectivity and activity were reported with $Ru–PPh_3$ based catalysts using homogenous and biphasic catalyst systems.[11] Table 2 summarizes the present results for hydrogenation of cinnamaldehyde using several catalyst systems.† Under the conditions used, unsaturated alcohol (UOL) and saturated aldehyde (SAL) were the main products with other very minor products. All the catalysts were reduced with H_2 for 1 h at 40 °C in order to form the active catalytic species. The catalytic chemistry for hydrogenation of α,β-unsaturated aldehydes using Ru–TPPTS [TPPTS = $P(C_6H_4SO_3Na)_3$] has already been explored well by earlier investigators.[11] In homogeneous reaction systems gas–liquid mass transfer is a key rate determining parameter. In the case of toluene solvent, 29% conversion was obtained with 92% selectivity to UOL. Homogeneous catalysis in general suffers from the major drawback of catalyst and product separation and, hence, the concept of biphasic catalysis has emerged. When this system is converted to a biphasic mode of operation keeping all parameters constant, the conversion of cinnamaldehyde drops from 29% to 11%, retaining the selectivity performance (Table 2, run 3). The important parameters such as gas–liquid–liquid mass transfer and liquid–liquid mass transfer (*i.e.* solubility of substrate in catalyst phase) are key factors in controlling the rate of reaction. In this case the substrate, cinnamaldehyde, has finite solubility in the catalyst phase, and therefore that is not a major limitation unlike hydroformylation of higher olefins in a biphasic mode of operation.[3–6] When this reaction is subjected to $scCO_2$ as medium instead of an organic solvent like toluene, the $RuCl_3–PPh_3$ catalyst system performs very poorly (run 2). It is mainly due to the very poor solubility of the phosphine ligand in $scCO_2$. Visual observation through a sapphire window confirms that solid catalyst particles are suspended in $scCO_2$. Since there is no interaction of catalyst and reactants, a poor reaction rate is observed. Presently, many researchers are working on enhancing the solubility of phosphine ligands in

Table 1 Catalysis using metal complexes

System	Type	Advantages	Disadvantages
Homogeneous	Gas–liquid	High activity and selectivity	Catalyst/product separation; gas–liquid mass transfer; organic solvent needed
Biphasic (organic–water)	Gas–liquid–liquid	High selectivity; high activity possible with water soluble substrates; easy catalyst separation and recycling	Low reaction rates for water insoluble substrates; gas–liquid–liquid mass transfer limits rate of reaction; organic solvent needed
SAPC	Gas–liquid–liquid (on solid support)	High activity and selectivity; product separation by phase separation; easy catalyst recycling	Organic solvent needed; stability of catalyst film on solid support
Biphasic (supercritical solvent–water)	Supercritical fluid–liquid	High selectivity; high activity possible with water soluble substrates; easy catalyst separation and recycling; organic solvent not needed	Poor solvating ability of many supercritical fluids
SAPC in supercritical solvent	Supercritical fluid–liquid (on solid support)	High activity and selectivity; product separation by phase separation; easy catalyst recycling; use of organic solvent is avoided	Poor solvating ability of many supercritical fluids

Table 2 Hydrogenation of cinnamaldehyde using various catalyst systems[a]

Run	Reaction type	Catalyst precursor	Ligand	Solvent system	Pressure/MPa		Conversion (%)	Selectivity (%)	
					$scCO_2$	H_2		UOL	SAL
1	Homogeneous	$RuCl_3$	PPh_3	toluene	—	40	29	92	8
2	Homogeneous	$RuCl_3$	PPh_3	$scCO_2$	140	40	1.5	89	11
3	Biphasic	$RuCl_3$	TPPTS	toluene–water	—	40	11	92	8
4	Biphasic	$RuCl_3$	TPPTS	$scCO_2$–water	140	40	38	99	0.5
5	Biphasic	$RhCl_3$	TPPTS	$scCO_2$–water	140	40	35	—	100
6	Biphasic	$Pd(OAc)_2$	TPPTS	$scCO_2$–water	140	40	22	—	100
7	SAPC	$RuCl_3$	TPPTS	toluene–water	—	40	13	93	7
8	SAPC	$RuCl_3$	TPPTS	$scCO_2$–water	140	40	44	96	4

[a] Reaction conditions: Catalyst precursor: 0.012 mmol; ligand/Ru: 8; T = 40 °C; cinnamaldehyde: 7.8 mmol; toluene (for 1,3,7): 25 cm^3; time: 2 h; water: 0.5 cm^3; silica (for 7,8): 1.5 g.

$scCO_2$ by using flourous substituents.[12] Biphasic catalytic systems such as $scCO_2$–water (runs 4–6) give much better conversion than conventional biphasic reactions (11 to 38%) and normal homogenous modes of operation (29 to 38%). This catalyst system differs from conventional gas–liquid and gas–liquid–liquid catalytic hydrogenation, since gas–liquid and gas–liquid–liquid mass transfer are completely eliminated in the case of $scCO_2$ as solvent. The concentration of hydrogen in a supercritical mixture of H_2 (85 bar) and CO_2 (120 bar) at 50 °C is 3.2 M, while the concentration of H_2 in THF under the same pressure is only 0.4 M.[13] This property of $scCO_2$ allows a reduction in viscosity and an increase in diffusion rate as compared with the liquid phase, so that transport to and from the catalyst phase is no longer a limiting factor. This causes significant rate enhancement as observed in Table 2 and might be advantageous in improving selectivity performance. $RuCl_3$ as metal precursor gives 99% selectivity towards UOL (run 4), while $RhCl_3$ and $Pd(OAc)_2$ give 100% selectivity towards SAL. Earlier investigators have already examined this feature. Supported aqueous phase catalysis (SAPC) in which the metal complex is supported on a solid surface like silica has been successfully used for biphasic reactions which have substrate solubility limitations. SAPC can also be used in $scCO_2$ as solvent and better activity and selectivity were observed when compared with toluene as solvent (12.4 to 44%). Although the application of SAPC is not particularly attractive in the case of hydrogenation of cinnamaldehyde (since it has finite solubility in the catalyst phase), it may be more attractive in the case of water insoluble substrates.

In conclusion, $scCO_2$–water was shown to be a good alternative solvent system for conventional biphasic catalytic systems. This eliminates gas–liquid–liquid mass transfer limitations due to the very high solubility of reactant gases in $scCO_2$.

We thank the Japan Society for Promotion of Science (JSPS) for financial support.

Notes and references

† Typical experimental procedure for an experiment involving the $scCO_2$–water biphasic catalytic system is as follows: $RuCl_3$ (0.012 mmol) and TPPTS (0.096 mmol) dissolved in water (0.5 cm^3) were charged to a 50 cm^3 reactor maintained at 40 °C. Hydrogen (10 bar) was introduced into the reactor and left for 1 h. Cinnamaldehyde (7.8 mmol) was introduced into the reactor after depressurizing the hydrogen. Hydrogen (40 bar) and liquid carbon dioxide were subsequently introduced into the reactor using a JASCO Model 880-PU syringe pump and compressed to the desired pressure (180 bar). The pump delivered the CO_2 at a flow rate of 3.5 ml min^{-1}. Pressure control was achieved using a JASCO Model 880-81 back pressure regulator. The reaction was started by stirring the mixture with a magnetic stirrer and continued for 2 h. After reaction, the pressure was released and the reaction mixture was analyzed *via* GC (Shimadzu GC-8A, Ucon Oil 8HB 2000 Uniport B, 6 m). Details of the experimental apparatus and procedures are described elsewhere (ref. 14).

1 *Chem. Rev.*, 1999, **99**; G. Kaupp, *Angew. Chem.*, 1994, **106**, 1519; *Angew Chem., Int. Ed. Engl.*, 1994, **33**, 1452; M. Poliakoff, S. M. Howdle and S. G. Kazarian, *Angew. Chem.*, 1995, **107**, 1409; *Angew. Chem., Int. Ed. Engl*., 1995, **34**, 1275; P. G. Jessop, T. Ikaria and R. Noyori, *Science*, 1995, **269**, 1065.

2 P. G. Jessop, T. Ikariya and R. Noyori, *Nature*, 1994, **368**, 231; A. Furstner, D. Koch, K. Langemann, W. Leitner and C. Six, *Angew Chem., Int. Ed. Engl.*, 1997, **36**, 2466; J. W. Rathke, R. J. Klingler and T. R. Krause, *Organometallics*, 1991, **10**, 1350.

3 *Applied Homogeneous Catalysis by Organometallic Complexes*, ed. B. Cornils and W. A. Herrmann, VCH, Weinheim, 1996; B. Cornils, W. A. Herrmann and R. W. Eckl, *J. Mol. Catal. A*, 1997, **116** 27; W. A. Herrmann and B. Cornils, *Angew. Chem., Int. Ed. Engl*., 1997, **36**, 1048.

4 R. M. Deshpande, Purwanto, H. Delmas and R. V. Chaudhari, *Ind. Chem. Eng. Res*., 1996, **35**, 3927; Purwanto and H. Delmas, *Catal. Today*, 1995, **24**, 135.

5 H. Ding and B. E. Hanson, *J. Chem. Soc., Chem. Commun*., 1994, 2747; H. Ding, B. E. Hanson and J. Bakos, *Angew. Chem., Int. Ed. Engl*., 1995, **34**, 1645.

6 R. V. Chaudhari, B. M. Bhanage, R. M. Deshpande and H. Delmas, *Nature*, 1995, **373**, 501; *US Pat.* 5498801 (1996); 5650546 (1997).

7 J. P. Arhancet, M. E. Davis, J. S. Merola and B. E. Hanson, *Nature*, 1989 **339**, 454; J. P. Arhancet, M. E. Davis, J. S. Merola and B. E. Hanson, *J. Catal.*, 1990, **121**, 327.

8 K. T. Wan and M. E. Davis, *Nature*, 1994, **370**, 449.

9 P. Gallezot and D. Richard, *Catal. Rev.-Sci. Eng.*, 1998, **40**, 81 and references cited therein; V. Ponec, *Appl. Catal. A*., 1997, **149**, 27.

10 M. Arai, H. Takahashi, M. Shirai, Y. Nishiyama and T. Ebina, *Appl. Catal. A*., 1999, **176**, 229; M. Arai, A. Obata, K. Usui, M. Shirai and Y. Nishiyama, *Appl. Catal. A.*, 1996, **146**, 381; M. Arai, K. Usui, M. Shrai and Y. Nishiyama, *Stud. Surf. Sci. Catal.*, 1995, **91**, 923; M. Arai, K. Usui and Y. Nishiyama, *J. Chem. Soc., Chem. Commun.*, 1993, 1853.

11 J. M. Grosselin, C. Mercier, G. Allmang and F. Grass, *Organometallics*, 1991, **10**, 2126; M. Hernandez and P. Kalck, *J. Mol. Catal. A*, 1997, **116**, 117 and 130; A. J. Carrasquel, J. Marino, F. A. Lopez, D. E. Paez, I. Rojas and N. Valecia, *J. Mol. Catal. A*, 1997, **116**, 157; F. Joo, J. Kovacs, A. C. Benyei and A. Katho, *Catal. Today*, 1998, **42**, 441.

12 D. Koch and W. Leitner, *J. Am. Chem. Soc.*, 1998, **120**, 13 398; D. R. Palo and C. Erkey, *Ind. Eng. Chem. Res.*, 1998, **37**, 4203.

13 *Hydrogen and Deuterium*, ed. C. L. Young, Solubility Data Series, Pergamon, Oxford, 1981, vol. 5/6.

14 Y. Ikushima, N. Saito, K. Hatakeda, S. Ito, M. Arai and K. Arai, *Ind. Eng. Chem. Res.*, 1992, **31** 569; Y. Ikushima, N. Saito and M. Arai, *J. Phys. Chem.*, 1992, **96**, 2293.

Communication 9/03528A

ChemComm

High yields of diazabicycloalkanes and oxazabicycloalkanes containing medium and large rings from rhodium-catalysed hydroformylation reactions without the need for high dilution conditions

David J. Bergmann, Eva M. Campi, W. Roy Jackson* and Antonio F. Patti

Department of Chemistry, Monash University, Clayton, Victoria, 3168 Australia.
E-mail: w.r.jackson@sci.monash.edu.au

Received (in Cambridge, UK) 6th May 1999, Accepted 1st June 1999

Rhodium-catalysed reactions of *N*-alkenyl-1,3-diaminopropanes and *N*-alkenylaminoethanols give diazabicycloalkanes and oxazabicycloalkanes containing medium or large rings in excellent yields.

We have previously reported the preparation of 1,5-diazabicyclo[4.3.0]nonane and 1,5-diazabicyclo[4.4.0]decane in high yield by rhodium-catalysed reactions of appropriate *N*-alkenyl-1,3-diaminopropanes **1** (n = 1 or 2) with H_2/CO.[1] The reactions presumably involve cyclisation of an initially formed diaminoaldehyde **2** to form an aminopropyl substituted cyclic iminium salt **3** or enamine which subsequently cyclises to give the bicyclic product **4** (Scheme 1). It has been well established that the amino function of an aminoalkene rapidly coordinates to the rhodium atom[2] and as only very low ratios of rhodium to substrate are used (typically 1:100 or greater) it seemed probable that the newly formed aldehyde function should be in close proximity to the rhodium-coordinated amino function and thus cyclisation rather than polymerisation be preferred even for medium and large ring systems. There is indirect evidence that iminium species contained in medium or large rings are susceptible to polymerisation reactions.[3] Thus the possibility that a pendant amino or hydroxy function could be used to trap any such reactive cyclic iminium species was investigated as a general route to the synthesis of bicyclic heterocycles containing medium or large rings.

A series of *N*-alkenyl-1,3-diaminopropanes **1** and *N*-alkenylaminoethanols **5** were thus reacted with H_2/CO under a range of conditions and the results are summarised in Table 1.

Excellent yields of compounds **4a** and **6a** containing a thirteen-membered ring fused to six- or five-membered heterocycles were obtained when BIPHEPHOS[4] was used as a ligand in reactions of the primary amine **1a** and the alcohol **5a** (entries 1 and 2). Use of this ligand in hydroformylation reactions has been shown to lead to almost complete regioselectivity for the terminal aldehyde.[1,4,5] The products **4a** and **6a** from these reactions showed no evidence for any compounds containing a methyl-substituted twelve-membered ring which would arise from the products of internal rather than terminal hydroformylation. Reaction of the primary amine **1b** under these conditions led to polymerisation and only a poor yield (28%) of the bicyclic compound containing a ten-membered ring was obtained when the reaction temperature was decreased to 40 °C (entry 3). A reaction of the related secondary amine **1c** however gave an excellent yield of the bicyclic product **4c** using PPh_3 as a ligand at 80 °C (entry 4). The product contained *ca.* 10% of compound arising from branched-chain aldehyde. A reaction using BIPHEPHOS with a 1:1 ratio of H_2/CO gave a complex mixture whose ^{1}H NMR spectrum suggested that some hydrogenation of the intermediate iminium species **3** and possibly the substrate **1c** had occurred. Accordingly a reaction was carried out using a 1:5 H_2/CO gas ratio as this has been shown to minimise the problems associated with substrate hydrogenation.[6] The bicycle **4c** containing a ten-membered ring was now obtained in excellent yield and with >95% regioselectivity (entry 5). The related aminoethanol **5b** behaved in an identical fashion with excellent yields (*ca.* 93%) of bicyclic compound **6b** containing a ten-membered ring being obtained (entries 6 and 7). Again the reaction involving BIPHEPHOS appeared to be virtually regiospecific.

A reaction of the primary amine **1d** using BIPHEPHOS as ligand at 80 °C gave only polymeric material but a good yield (74%) of the (6,8) bicycle **4d** was obtained when the reaction

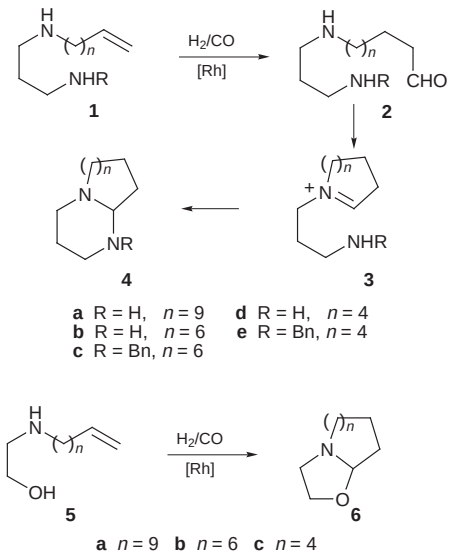

Scheme 1

Table 1 Rhodium-catalysed reactions of *N*-alkenyl-1,3-diaminopropanes **1** and *N*-alkenylaminoethanols **5** with H_2/CO[a]

Entry	Reactant	n	R	T/°C	Ligand	Ratio H_2/CO	Product (ring sizes)	Yield[b] (%)
1	**1a**	9	H	80	BIPHEPHOS	1:1	**4a** (6,13)	80
2	**5a**	9	—	80	BIPHEPHOS	1:1	**6a** (5,13)	80
3	**1b**	6	H	40	BIPHEPHOS	1:1	**4b** (6,10)	28
4	**1c**	6	Bn	80	PPh_3	1:1	**4c** (6,10)	95[c]
5	**1c**	6	Bn	80	BIPHEPHOS	1:5	**4c** (6,10)	95
6	**5b**	6	—	80	PPh_3	1:1	**6b** (5,10)	93[c]
7	**5b**	6	—	80	BIPHEPHOS	1:5	**6b** (5,10)	93
8	**1d**	4	H	50	BIPHEPHOS	1:1	**4d** (6,8)	74
9	**1e**	4	Bn	80	BIPHEPHOS	1:5	**4e** (6,8)	95
10	**1e**	4	Bn	80	PPh_3	1:1	**4e** (6,8)	14[d]
11	**5c**	4	—	80	PPh_3	1:1	**6c** (5,8)	92[c]

[a] Reaction conditions: Substrate (0.5–1 mmol) with substrate: $[Rh(OAc)_2]_2$:ligand = 200:1:4 in benzene (5–10 ml) for 20 h with an initial gas pressure (H_2 + CO) of 2.76 MPa (400 psi). [b] Isolated yields; products from reactions using BIPHEPHOS as ligand contained >95% of linear derived material. [c] Containing *ca.* 10% branch-chain derived product. [d] The (6,7) bicyclo compound arising from initial internal hydroformylation was the major product (38%).

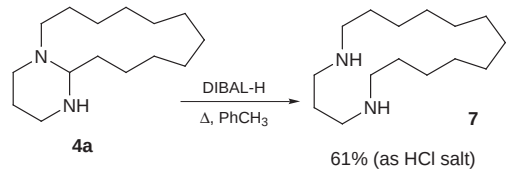

Scheme 2

temperature was reduced to 50 °C (entry 8). An excellent yield (95%) of almost regiopure material was obtained from a reaction of **1e** using BIPHEPHOS with a 1:5 H_2/CO ratio (entry 9). In contrast a reaction using PPh_3 as ligand surprisingly gave the (6,7) bicyclo product arising from initial internal hydroformylation as the major product with only a small amount (14%) of the (6,8) compound **4e** (entry 10). However a reaction of the related aminoalcohol **5c** under these conditions gave an excellent yield (92%) of bicyclic products consisting mainly of **6c** together with *ca*. 10% of the methyl-substituted (5,7) compound.

The potential of the bicyclic diamines as precursors of monocyclic diamino compounds was illustrated by ring opening of the (6,13) bicyclic amine **4a** and the related (6,6) compound which was available from previous work.[1] Reactions of these compounds with DIBAL-H in toluene led to formation of 1,5-diazacycloheptadecane **7** and 1,5-diazacyclodecane respectively in good yield (*ca*. 60%) (Scheme 2).[7]

We thank the Australian Research Council for support and provision of a postgraduate award (to D. J. B.) and Johnson Matthey Pty Ltd for a loan of rhodium.

Notes and references

1 D. J. Bergmann, E. M. Campi, W. R. Jackson, Q. J. McCubbin and A. F. Patti, *Tetrahedron*, 1997, **53**, 17 449.
2 M. E. Krafft, L. J. Wilson and K. D. Onan, *Organometallics*, 1988, **7**, 2528; E. M. Campi, W. R. Jackson, Q. J. McCubbin and A. E. Trnacek, *J. Organomet. Chem*., 1997, **539**, 147.
3 E. M. Campi, W. R. Jackson, Q. J. McCubbin and A. E. Trnacek, *Aust. J. Chem*., 1996, **49**, 219.
4 G. D. Cuny and S. L. Buchwald, *J. Am. Chem. Soc*., 1993, **115**, 2066.
5 G. D. Cuny and S. L. Buchwald, *Synlett*, 1995, 519; I. Ojima, M. Tzamarioudaki and M. Eguchi, *J. Org. Chem*., 1995, **60**, 7078; I. Ojima, D. M. Iula and M. Tzamarioudaki, *Tetrahedron Lett*., 1998, **39**, 4599.
6 T. Rische and P. Eilbracht, *Synthesis*, 1997, 1331.
7 H. Yamamoto and K. Maruoka, *J. Am. Chem. Soc*., 1981, **103**, 4186; R. Alder, E. Heilbronner, E. Honegger, A. B. McEwen, R. E. Moss, E.Olefirowicz, P. A. Petillo, R. B. Sessions, G. R. Weisman, J. M. White and Z.Yang, *J. Am. Chem. Soc*., 1993, **115**, 6580.

Communication 9/03638E

ChemComm

Synthesis, resolution and racemization study of helically twisted *o*-terphenyls

Jian Ping Gao, Xian Sheng Meng, Timothy P. Bender, Sean MacKinnon, Valerie Grand and Zhi Yuan Wang*

Department of Chemistry, Carleton University, 1125 Colonel By Drive, Ottawa, Ontario, Canada K1S 5B6. E-mail: wangw@ccs.carleton.ca

Received (in Corvallis, OR, USA) 19th February 1999, Accepted 26th May 1999

The synthesis, resolution and racemization studies of helical *o*-terphenyls, useful chiral building blocks are reported.

Understanding of the structure–chiroptics relationships of helical molecules is of theoretical and synthetic importance. Systematic distortion of helical aromatic systems by disturbance of the conjugated π-electron array,[1] from conformationally rigid helicences[2] (*e.g.* **1a**) to less rigid helically twisted

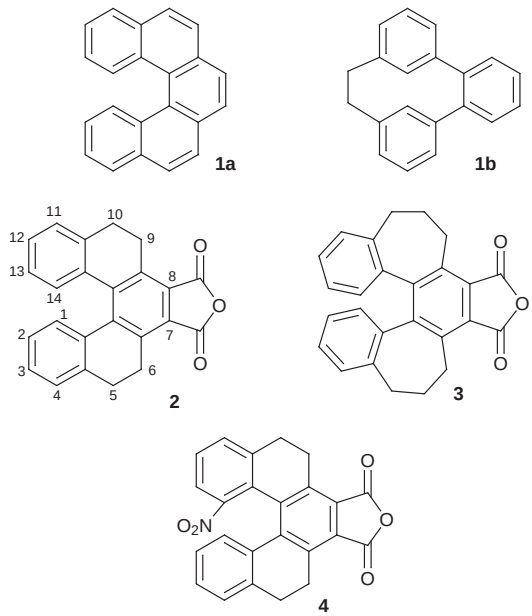

o-terphenyl (*e.g.* **1b**),[3] provides a useful way to gain knowledge about chiroptics of organic molecules. In order to gain further insight into the chiroptical properties of the helical *o*-terphenyl system, *o*-terphenyls **2**, **3** and **4**, which are structurally related to *o*-terphenyl **1b,** were chosen for study. Compounds **2**[4] and **3**[5] contain the same *o*-terphenyl moiety as **1b** but it is bridged by two ethylene or propylene units, respectively. Little is known about the resolution and chiroptical properties of bridged helical *o*-terphenyls such as **2** and **3**. Considering the similarity in π-conjugation, it occurred to us that, if resolvable and stable, optically pure bridged *o*-terphenyl derivatives would have a high optical activity as [5]helicene does. Moreover, these *o*-terphenyl derivatives are advantageously more soluble than fully aromatized helicenes and can be made on a large scale from readily available starting materials through a non-photocyclization route.[4] We recently introduced the nitro, amino and isocyanato groups into *o*-terphenyl **2** at the C-1 (*e.g.* **4**[7a]) and C-3 positions[6,7] and obtained several polymers using functionalized **2**.[7a,d,e] Therefore, resolved *o*-terphenyls **2**–**4** would be valuable building blocks for making optically active compounds and polymers. To resolve these *o*-terphenyl derivatives, chemical and chromatographic resolutions and recrystallization were attempted. Chemical resolution of **4** was achieved using brucine.[8] Since dextrorotatory [5]helicene has *P* helicity,[9] this resolved laevorotatory helical *o*-terphenyl **4** should have *M* helicity. Attempted on chemical resolution of **2** using the same route was unsuccessful, as the corresponding acid ethyl ester had no optical activity. Chromatographic separation using a chiral column was attempted for compounds **2**, **3** and **4**.[10] Racemic **4** could be readily resolved by this means. However, anhydride **2** came out as a single peak under the same chromatographic conditions using different solvent systems. Surprisingly, compound **3** gave two well-resolved peaks and the *M* enantiomer was obtained in high optical purity.

The resolved (*M*)-**4** showed very large specific optical rotations (*e.g.* −1518 at 589 nm and −7100 at 436 nm), comparable to that of (*M*)-[5]helicene (−1670 at 589 nm and −4950 at 436 nm, Table 1). Its CD spectrum [Fig. 1(*a*)] shows a strong negative band near 370 nm and a positive peak around 290 nm. In comparison with (*M*)-**4**, the resolved **3** displayed a rather low optical rotation (−55 at 589 nm). The striking difference in optical rotation between **3** and **4** is believed to be mainly due to variation in the degree of π-electron delocalization within the terphenyl moiety. Calculations have shown that optical rotations of helically twisted aromatic systems depend largely on the extended π-electron conjugation.[11] There is only a slight change in the geometry of the terphenyl moiety going from ethylene linkages in **4** to propylene linkages in **3**, as indicated by the X-ray structure analyses. The terphenyl unit in **4** is quite planar, the nitrobiphenyl unit being twisted by 37.4° and the other biphenyl being twisted by 29.1° (Fig. 2).[12] However, the biphenyl moiety in **3** has a large twist of 58°, indicating that the π-electrons of the terphenyl unit in **3** are less delocalized than those in **4**. Similarly, resolved **1b** was reported to have an optical rotation of 3210 at 365 nm and a smaller twist angle of about 47.8°. The UV-VIS spectra [Fig. 1(*b*)] of **2** and **4** display two strong peaks near 365 and 285 nm, whereas **3** had two bands centered at 330 and 270 nm. These absorption data further confirm a decrease in π-electron conjugation from **4** to **3**. Thus, the π-electron conjugation in the helically twisted *o*-terphenyl system directly relates to the strength of the optical rotation at a given wavelength. The greater the conjugation, or the smaller the twist angle is, the higher the optical rotation.

Thermal racemization studies were carried out at 49.8 °C (±0.1 °C) for (*M*)-**4**, and at 22.0 °C (±0.1 °C) for resolved **3**. The results are listed in Table 1, together with those of **1a** and **1b** for comparison. The half-life ($t_{1/2}$) of racemization at 49.8 °C was determined to be 2340 min for (*M*)-**4**, longer than that (62.7 min at 57 °C) of (*M*)-[5]helicene (**1a**).[2] Accordingly, the racemization barrier for compound (*M*)-**4** (27.7 kcal mol^{-1}) is higher than that (23.5 kcal mol^{-1}) of [5]helicene. As the lower helicenes racemize faster than higher ones,[2d,13,14] helical *o*-terphenyls having a substituent larger than hydrogen at the inner C_1-position are expected to have an increased barrier for

Table 1 Specific optical rotations and racemization half-life times ($t_{1/2}$) of resolved helical *o*-terphenyls and [5]helicene

Compound	Helicity	$[\alpha]_{589}$	$[\alpha]_{546}$	$[\alpha]_{436}$	$t_{1/2}$/min
3	*M*	−55	−94	−349	1100 (22.0 °C)
4	*M*	−1518	−1998	−7100	2340 (49.8 °C)
1a	*M*	−1670	−2025	−4950	62.7 (57.0 °C)
1b	*M*	−3210[a]			243.4 (100 °C)

[a] At 365 nm, 20 °C.

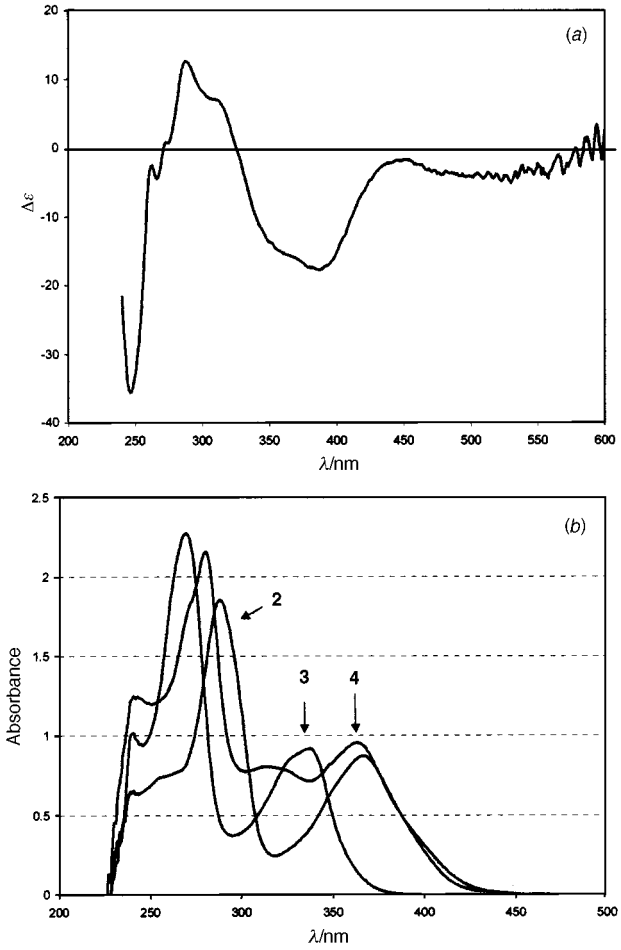

Fig. 1 (*a*) CD spectrum of (*M*)-**4** and (*b*) UV-VIS spectra of **2**–**4**.

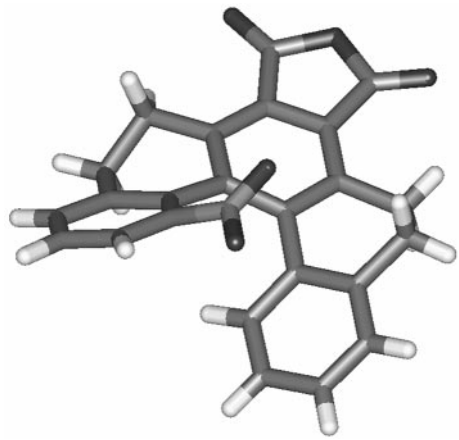

Fig. 2 Molecular geometry of **4** determined by X-ray analysis (ref. 12).

thermal racemization, which allows for effective resolution.[14] The X-ray structure of **4** shows a substantial overlapping between the nitro group and the opposite benzene ring. For compound **2**, although the terphenyl unit adopts a helical conformation and has a higher degree of π-conjugation (smaller twist angle of 32.4°) than compound **3**, the degree of overlapping between the two terminal benzene rings is probably too small to allow for resolution at ambient temperatures. Comparing compounds **2** and **3**, the former is conformationally unstable and racemizes rapidly at ambient temperatures. Owing to two extra CH_2 units, **3** has the two terminal rings overlapped to a great enough extent to allow for resolution but still easily racemizes with a half-life time of 1100 min at 22 °C. In comparison, **1b** was successfully resolved and had a racemization activation energy of about 30 kcal mol^{-1}, which is close to that (27.7 kcal mol^{-1}) of **4** and higher than that (23.5 kcal mol^{-1}) of **1a**.

In conclusion, chemical resolution of the bridged C_1-substituted helical *o*-terphenyls can be achieved. The racemization barrier depends on the degree of overlapping of the two terminal rings and optical activity relates to the degree of π-conjugation of the *o*-terphenyl moiety.

The Natural Sciences and Engineering Research Council of Canada financially supported this work. The authors would like to acknowledge Dr Gary Enright (NRC Canada) for the X-ray analysis of **4**.

Notes and references

1 S. Grimme, J. Harren, A. Sobanski and F. Vögtle, *Eur. J. Org. Chem.*, 1998, 1491.
2 (*a*) K.P. Meurer and F. Vögtle, *Top. Curr. Chem.*, 1985, **127**, 1; (*b*) W. H. Laarhoven and W. J. C. Prinsen, *Top. Curr. Chem.*, 1984, **125**, 63; (*c*) R. H. Martin, *Angew. Chem., Int. Ed. Engl.*, 1974, **13**, 649; (*d*) C. Goedicke and H. Stegemeyer, *Tetrahedron Lett.*, **1970**, 937.
3 M. Wittek, F. Vögtle, G. Stühler, A. Mannschreck, B. M. Lang and H. Irngartinger, *Chem. Ber.*, 1983, **116**, 207.
4 H. A. Weidlich, *Ber.*, 1938, **71**, 1203; F. Bergmann, H.E. Eschinazi and M. Neeman, *J. Org. Chem.*, 1943, **8**, 179.
5 Y. Altman and D. Ginsburg, *J. Chem. Soc.*, 1961, 1498. Single crystals of racemic **3** suitable for X-ray analysis were obtained by slow evaporation of an acetone solution. *Crystal data* for **3:** $C_{26}H_{20}O_3$, M = 380.42, orthorhombic, space group *Pccn*, μ = 0.085 mm^{-1}, a = 35.753(2), b = 14.2245(7), c = 7.5267(4) Å, V = 3827.8(3) $Å^3$, T = 296 K, Z = 8, measured reflections 21719, unique reflections = 4579, R(int) = 0.0431.
6 J. P. Chen, J. P. Gao and Z. Y. Wang, *Polym. Int.*, 1997, **44**, 83.
7 (*a*) Z. Y. Wang, Y. Qi, T. P. Bender and J. P. Gao, *Macromolecules*, 1997, **30**, 764; (*b*) Y. Qi, J. P. Gao, T. P. Bender and Z. Y. Wang, *Polym. Prepr.*, 1996, **37**, 276; (*c*) Z. Y. Wang, J. P. Gao, T. P. Bender, Y. Qi, S. MacKinnon, L. Kuang, J. P. Chen and X. S. Meng, *Polym. Prepr.*, 1997, **38**, 153; (*d*) T. P. Bender, Y. Qi, J. P. Gao and Z. Y. Wang, *Macromolecules*, 1997, **30**, 6001; (*e*) T. P. Bender and Z. Y. Wang, *J. Polym. Sci. Part A: Polym. Chem.*, 1998, **36**, 1349.
8 The mixture of racemic **4** (2.96 g, 7.46 mmol) and brucine (3.30 g, 8.38 mmol) in 380 ml of absolute ethanol was heated to reflux until TLC showed no more anhydride. The reaction solution was then cooled to room temperature. On standing overnight, a crop of yellow crystals separated, which was filtered off, washed with ethanol and dried under vacuum to give 2.20 g of **4**·brucine salt: $[\alpha]_D^{22}$ = +640. Recrystallization twice of the first crop from CH_2Cl_2–EtOH raised the optical rotation to +665, which on decomposition with HCl afforded the corresponding acid esters: 1.08 g, $[\alpha]_D^{22}$ +1406 (c = 0.098, $CHCl_3$); ν_{max}(KBr)/cm^{-1} 1728, 1697(C=O); δ_H(400 MHz, $CDCl_3$) 1.43 (t, 3H), 2.66 (m, 1H), 2.81 (m, 5H), 3.01 (m, 1H), 3.19 (m, 1H), 4.44 (q, 2H), 6.69 (d, 1H), 6.90 (t, 1H), 7.21 (t, 1H), 7.30 (d, 1H), 7.33 (t, 1H), 7.47 (d, 1H), 7.59 (d, 1H); δ_C(50 MHz, $CDCl_3$) 169.4 and 169.2 (C=O, ester), 174.7 and 174.4 (C=O, acid). The mother liquor of the first crop was left open to air at room temperature for several days and the second crop precipitated out. The yellow solid was then filtered off, washed with ethanol and dried under vacuum to give 1.18 g of **4**·brucine salt ($[\alpha]_D^{22}$ −739), which upon treatment with HCl produced the acid ester: $[\alpha]_D^{22}$ −1243 (c 0.093, $CHCl_3$); ν_{max}(KBr)/cm^{-1} 1727, 1698 (C=O). Heating the acid ester ($[\alpha]_D^{22}$ −1243, *e.g.*, 150 mg) at 50 °C under vacuum (5 mmHg) for 6 h, followed by recrystallization once from hexane–CH_2Cl_2 afforded optically pure (*M*)-**4:** $[\alpha]_D^{22}$ −1518 (c 0.050, $CHCl_3$).
9 I. G. Stará, I. Stary, M. Tichý, J. Závada and V. Hanuš, *J. Am. Chem. Soc.*, 1994, **116**, 5084; H. J. Bestmann and W. Both, *Angew. Chem., Int. Ed. Engl.*, 1972, **11**, 296; J. Tribout, R.H. Martin, M. Doyle and H. Wynberg, *Tetrahedron Lett.*, 1972, 2839.
10 Column (S,S)-Whelk-01 from Regis Technologies Inc. USA; using 2–10% Pr^iOH in hexane at 25 °C at a flow rate of 1 ml min^{-1}.
11 V. Buss and K. Kolster, *Chem. Phys.*, 1996, **203**, 309.
12 Single crystals of racemic **4** suitable for X-ray analysis were obtained on slow evaporation of a CH_2Cl_2 solution. *Crystal data* for **4**: $C_{24}H_{15}NO_5$, M = 397.38, triclinic, space group $P\bar{1}$, μ = 0.10 mm^{-1}. a = 8.1376(6), b = 11.0822(8), c = 11.2149(8) Å, α = 103.642(8), β = 98.747(7), γ = 108.001(8)°, V = 906.64(11) $Å^3$, T = −100 °C, Z = 2, measured reflections = 5254, unique reflections = 4159, R(int) = 0.016. CCDC 182/1271.
13 R. H. Martin and M. J. Marchant, *Tetrahedron*, 1974, **30**, 347.
14 R. H. Janke, G. Haufe, E.-U. Würthwein and J. H. Borkent, *J. Am. Chem. Soc.*, 1996, **118**, 6031.

Communication 9/01474H

1,3-Thiaphosphole and 1,3-thiarsole are aromatic

Arthur J. Ashe III* and Xinggao Fang

Department of Chemistry, The University of Michigan, Ann Arbor, MI 48109-1055, USA. E-mail: ajashe@umich.edu

Received (in Corvallis, OR, USA) 14th May 1999, Accepted 24th May 1999

Treatment of 3,3-dibutyl-2,3-dihydro-1,3-thiastannole with either PBr_3 or $AsCl_3$ followed by DBU affords 1,3-thiaphosphole or 1,3-thiarsole, respectively.

Studies on the series pyridine (**1**), phosphabenzene (**2**) and arsabenzene (**3**) have contributed handsomely to our understanding of the concepts of aromaticity and multiple bonding between carbon and the heavier main group atoms.[1–4] 1,3-Thiazole (**4**),[5] 1,3-thiaphosphole (**5**) and 1,3-thiarsole (**6**) form a similar series of aromatic heterocycles. Heavily substituted derivatives of **5**, *e.g.* **8**[6] and **9**,[7] have been prepared although thiarsole remains unknown. A preparation of the unsubstituted heterocycles is desirable and would allow study of the intrinsic properties of the parent rings. We now report on a one step synthesis of **5** and **6** and on some properties of the compounds.

Our synthesis is analogous to the original preparation of **2** and **3**.[3] Heating 3,3-dibutyl-2,3-dihydro-1,3-thiastannole (**10**)[8] in tetraglyme with 1 equiv. of PBr_3 followed by treatment with DBU allows distillation of **5** in 10% yield (Scheme 1). Similar treatment of **10** with $AsBr_3$ followed by DBU allows distillation of **6** in 22% yield. Compounds **5** and **6** are air sensitive liquids which are most conveniently handled in dilute solutions.

The ^{1}H NMR spectra of **4**, **5** and **6** (Table 1) show very low field signals, downfield from those of thiophene (**7**). The most characteristic feature of the spectra is the particularly low field signals due to protons which are adjacent to the group 15 heteroatoms. This shift, which is also shown by the series **1**–**3**, is apparently caused by the large magnetic anisotropies of the π-bound group 15 heteratoms.[9] However the low field signals for the more remote protons H(5) of **5** and **6** are probably due to the effects of an aromatic ring current.[10] The ^{13}C NMR chemical shifts for C(2) and C(4) also occur at low field as is typical of carbon atoms which are π-bound to heavier group 15 elements.[9,11] Lastly, the ^{31}P shift of **5** (δ 211.3) is virtually identical to those of **8** and **9** which indicates **5** has a π-bound phosphorus(III).[12]

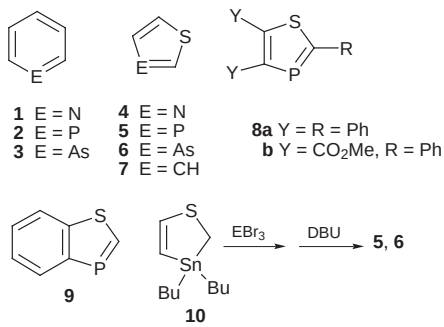

Scheme 1

The mass spectra of **4**, **5** and **6** show intense molecular ions which are the base peaks. Like **2** and **3**[3] the major daughter peaks for thiaphosphole and thiarsole are due to loss of acetylene. The loss of HCE (E = N, P, As) is rather less important for **5** and **6** than for **4**.[13]

The UV spectrum of 1,3-thiazole shows intense peaks at 208 (2550) and 233 nm (3750),[14] which have been assigned to π→π* excitations. The spectrum of **5** in hexane shows peaks at 215 (12,000), 249 (3000) and 274 nm (5000), while that of **6** shows peaks at 225 (14,000), 267 (6200) and 290 nm (9800). The progressive red shift of the corresponding bands with increasing atomic number of the heteroatoms corresponds to a smaller gap between the bonding and antibonding orbitals for the heavier heterocycles. This trend is confirmed by performing Hartree–Fock level *ab initio* molecular orbital calculations for **5**[15] and **6** with the RHF/6-31+G* basis set.[16] The optimized structural parameters of **5** listed in Table 2 do not differ significantly from those reported for the X-ray structures of the substituted derivative **8**. The calculated structures are consistent with those of planar aromatic heterocycles.

Since acid catalyzed proton isotopic exchange is the simplest aromatic substitution reaction,[17] it was of interest to examine the behavior of **5** and **6** in deuteroacids. Compound **5** is rapidly destroyed by CF_3CO_2D, but shows no H/D exchange on extended heating in CH_3CO_2D. Heating **6** with excess CH_3CO_2D–$CDCl_3$ (1:2) to 100 °C for 22 h leads to the incorporation of two deuterium atoms.[18] The rate of exchange at C(2) is 1.5 times faster than at C(4) with no detectable exchange at C(5). Under identical conditions thiophene does not show exchange[19] but the more reactive indole shows H/D exchange at C(3) at a similar rate.[20] Thus like arsabenzene,[21] 1,3-thiaarsole shows the reactivity of a highly activated aromatic ring.

We are grateful to the NSF for financial support of this work.

Table 1 Comparison of the ^{1}H and ^{13}C NMR parameters of thiophene (**7**), 1,3-thiazole (**4**), 1,3-thiaphosphole (**5**) and 1,3-thiarsole (**6**)[a,b]

	Compound			
Parameter	**7**	**4**	**5**[c]	**6**
$\delta_{H(2)}$	7.35	8.88	8.87 (J_{PH} 35.7 Hz)	9.93
$\delta_{H(4)}$	7.13	7.98	8.16 (J_{PH} 43.4 Hz)	8.94
$\delta_{H(5)}$	7.35	7.41	8.37 J_{PH} 9.1 Hz)	8.48
$J_{H(2)\,H(4)}$/Hz	0.9	0	2.2	2.2
$J_{H(2)\,H(5)}$/Hz	3.0	2.0	1.4	1.4
$J_{H(4)\,H(5)}$/Hz	5.0	3.2	6.9	7.0
$\delta_{C(2)}$	124.2	152.7	153.8 (J_{CP} 60.4 Hz)	167.9
$\delta_{C(4)}$	126.2	143.4	144.6 (J_{CP} 51.3 Hz)	155.7
$\delta_{C(5)}$	124.2	118.6	138.8 (J_{CP} 15.4 Hz)	139.5

[a] Solvent $CDCl_3$. [b] ^{1}H NMR (400 MHz) and ^{13}C NMR (126 MHz). [c] ^{31}P NMR (162 MHz), δ 211.3.

Table 2 Selected bond lengths for **8b** compared with the calculated bond lengths for **5** and **6**.

	Bond length/Å		
Bond	**8b** (E = P)[a]	**5** (E = P)	**6** (E = As)
S(1)–C(2)	1.70	1.71	1.70
C(2)–E(3)	1.72	1.69	1.79
E(3)–C(4)	1.76	1.78	1.88
C(4)–C(5)	1.36	1.35	1.34
C(5)–S(1)	1.71	1.72	1.72

[a] Ref 7(*c*).

Notes and references

† *Experimental procedure* for **6**: A solution of $AsBr_3$ (0.96 g, 3.65 mmol) in 2 ml of tetraglyme was added to a solution of **10** (0.98 g, 3.21 mmol) in 4 ml of tetraglyme at −30 °C. The mixture was heated to 85 °C for 15 h and then cooled to 60 °C. DBU (1.00 ml, 6.69 mmol) was added and the mixture was stirred for 3 h at this temperature. Pot-to-pot distillation (0.01 torr, 25 °C) gave the desired product as a yellow liquid (100 mg, 22%). Compound **6** is extremely air sensitive and brief exposure leads to a white intractable precipitate; *m/z* 146 (100%), 120 (51), 75 (13), 45 (19). Compound **5** was prepared in the same manner; *m/z* 102 (100%), 76 (47), 57 (24), 45 (29).

1 G. Märkl, *Angew. Chem.*, 1966, **78**, 907; *Angew. Chem., Int. Ed. Engl.*, 1966, **5**, 846.
2 P. Jutzi and K. Deuchert, *Angew. Chem.*, 1969, **81**, 1051; *Angew. Chem., Int. Ed. Engl.*, 1969, **8**, 991; H. Vermeer and F. Bickelhaupt, *Angew. Chem.*, 1969, **81**, 1052; *Angew. Chem., Int. Ed. Engl.*, 1969, **8**, 992.
3 A. J. Ashe III, *J. Am. Chem. Soc.* 1971, **93**, 3293.
4 G. Märkl, *Chem. unserer Zeit*, 1982, **16**, 139; A. J. Ashe III, *Top. Curr. Chem.*, 1982, **105**, 1; A. J. Ashe III, in *Comprehensive Heterocyclic Chemistry II*, vol. ed. A. McKillop, Pergamon, Oxford, 1996, vol. 5, p. 669.
5 A. Dondoni and P. Merino, in *Comprehensive Heterocyclic Chemistry II*, vol. ed. I. Shinkai, Pergamon, Oxford, 1996, vol. 3, p. 373.
6 K. Issleib and R. Vollmer, *Tetrahedron Lett.*, 1980, **21**, 3483.
7 (*a*) G. Märkl, E. Eckl, U. Jakobs, M. L. Ziegler and B. Nuber, *Tetrahedron Lett.*, 1987, **28**, 2119; (*b*) W. Rösch, H. Richter and M. Regitz, *Chem. Ber.*, 1987, **120**, 1809; (*c*) G. Märkl, W. Hölzl, A. Kallmünzer, M. L. Ziegler and B. Nuber, *Tetrahedron Lett.*, 1992, **33**, 4421.
8 A. J. Ashe, III, X. Fang and J. W. Kampf, *Organometallics*, 1999, **18**, 1821.
9 A. J. Ashe III, R. R. Sharp and J. W. Tolan, *J. Am. Chem. Soc.*, 1976, **98**, 5451.
10 J. D. Memory and N. K. Wilson, *NMR of Aromatic Compounds*, Wiley, New York, 1982; P. J. Garratt, *Aromaticity*, Wiley, New York, 1986.
11 T. C. Klebach, H. vanDongen and F. Bickelhaupt, *Angew. Chem.*, 1979, **91**, 423; *Angew. Chem., Int. Ed. Engl.*, 1979, **18**, 395.
12 K. Karaghiosoff and A. Schmidpeter, *Phosphorus Sulfur*, 1988, **36**, 217.
13 K. H. Pannell, C. C.-Y. Lee, C. Párkányi and R. Redfearn, *Inorg. Chim. Acta*, 1975, **12**, 127; G. M. Clarke, R. Grigg and D. H. Williams, *J. Chem. Soc. (B)*, 1966, 339.
14 H. G. Heller, D. Auld and K. Salisbury, *J. Chem. Soc. (C)*, 1967, 682.
15 For prior calculation on **4**, see: L. Nyulászi, P. Várnai, S. Krill and M. Regitz, *J. Chem. Soc., Perkin Trans. 2*, 1995, 315.
16 Gaussian 94, Rev. B.3, M. J. Frisch, G. W. Trucks, H. B. Schlegel, P. M. W. Gill, B. G. Johnson, M. A. Robb, J. R. Cheeseman, T. Keith, G. A. Petersson, J. A. Montgomery, K. Raghavachari, M. A. Al-Laham, V. G. Zakrzewski, J. V. Ortiz, J. B. Foresman, C. Y. Peng, P. Y. Ayala, W. Chen, M. W. Wong, J. L. Andres, E. S. Replogle, R. Gomperts, R. L. Martin, D. J. Fox, J. S. Brinkley, D. J. Defrees, J. Baker, J. P. Stewart, M. Head-Gordon, C. Gonzalez and J. A. Pople, Gaussian, Inc., Pittsburgh, PA, 1995.
17 A. R. Katritzky and R. Taylor, *Adv. Heterocycl. Chem.*, 1990, **47**, 7, 87; 142.
18 The D incorporation was followed using GC/MS and ^{1}H NMR spectroscopy.
19 W. J. Archer, *J. Chem. Soc., Perkin Trans. 2*, 1982, 295.
20 D. M. Muir and M. C. Whiting, *J. Chem. Soc., Perkin Trans. 2*, 1976, 388.
21 A. J. Ashe, III, W.-T. Chan, T. W. Smith and K. M. Taba, *J. Org. Chem.*, 1981, **46**, 881.

Communication 9/04044G

First example of the atom transfer radical polymerisation of an acidic monomer: direct synthesis of methacrylic acid copolymers in aqueous media

E. J. Ashford, V. Naldi, R. O'Dell,† N. C. Billingham* and S. P. Armes*

School of Chemistry, Physics and Environmental Science, University of Sussex, Falmer, Brighton, UK BN1 9QJ. E-mail: s.p.armes@sussex.ac.uk

Received (in Oxford, UK) 11th May 1999, Accepted 1st June 1999

Sodium methacrylate is polymerised directly *via* atom transfer radical polymerisation (ATRP) in aqueous media using a poly(ethylene oxide)-based macro-initiator; the resulting poly(ethylene oxide-*block*-sodium methacrylate) copolymers were obtained in good yield and have narrow molecular weight distributions as evidenced by aqueous GPC.

Recently there has been considerable interest[1–3] in atom transfer radical polymerisation (ATRP), which allows the facile synthesis of styrenic[1,2] and (meth)acrylate[3] homopolymers and copolymers with predetermined degrees of polymerisation and narrow polydispersities. ATRP is usually performed either in bulk or in non-aqueous media and is remarkably tolerant of functional groups. For example, Matyjaszewski and co-workers demonstrated that ATRP can be carried out in the presence of ethylene carbonate, MeOH, MeCN, pyridine or PPh_3 with little or no deleterious effects.[4] More recently, Coca *et al.* have reported successful ATRP of a hydrophilic monomer, 2-hydroxyethyl acrylate, in 50% aqueous solution at 90 °C.[5]

Near-monodisperse acidic copolymers can be readily prepared *via* anionic (group transfer) polymerisation using either *tert*-butyl or benzyl methacrylate as a protected monomer for methacrylic acid.[6,7] In principle ATRP can also be used for such protected monomer syntheses, but in practice Haddleton and co-workers have reported very slow polymerisation for sterically hindered monomers such as *tert*-butyl methacrylate.[8] Moreover, in a recent review article, Patten and Matyjaszewski state that 'acrylic and methacrylic acid cannot be polymerised with currently available ATRP catalysts, because these monomers react rapidly with the metal complexes to form metal carboxylates that are inefficient deactivators and cannot be reduced to active ATRP catalysts'.[9] We report herein the successful ATRP of sodium methacrylate directly in water. Given the problems discussed above, this approach promises to be a useful and versatile route to model acidic copolymers.

Our ATRP formulation (see Scheme 1) is based on that described by Matyjaszewski's group and comprises a monofunctional poly(ethylene oxide) macro-initiator, a $Cu^{I}Br$ catalyst and 2,2′-bipyridine (bipy). This ligand was selected because it is commercially available, readily forms a water-soluble complex with Cu^{I} and, unlike the *N*-alkyl-2-pyridylmethanimine ligands reported by Haddleton and co-workers,[8,10] is not prone to hydrolytic instability. The macro-initiator was synthesised by reacting a monomethoxy-capped poly(ethylene oxide) with 2-bromoisobutyryl bromide according to Jankova *et al.*[11] An ^{1}H NMR spectrum of the purified macro-initiator is shown in Fig. 1(*a*). After several freeze-thaw and de-gassing cycles, the ATRP of sodium methacrylate was carried out at 90 °C under dry nitrogen in doubly-distilled, de-ionised water (*ca.* pH 9). The initial monomer concentration was 33 vol% based on solvent, the initiator concentration was 0.07–0.11 mol dm^{-3} (depending on the molecular weight of the target polymer) and the molar ratio of macro-initiator:$Cu^{I}Br$:bipy was 2:2:5. Polymerisations were terminated by pouring the

† Present address: Cambridge Display Technology, 181a Huntingdon Road, Cambridge, UK CB3 0DJ.

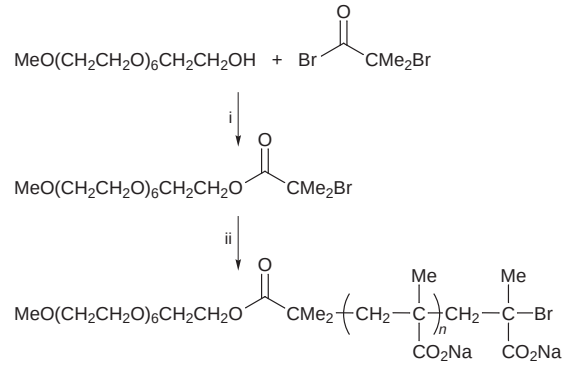

Scheme 1 *Reagents and conditions*: i, Et_3N, toluene, 0 °C, 12 h; ii, sodium methacrylate, $Cu^{I}Br$, bipy, H_2O, 90 °C, 21 h.

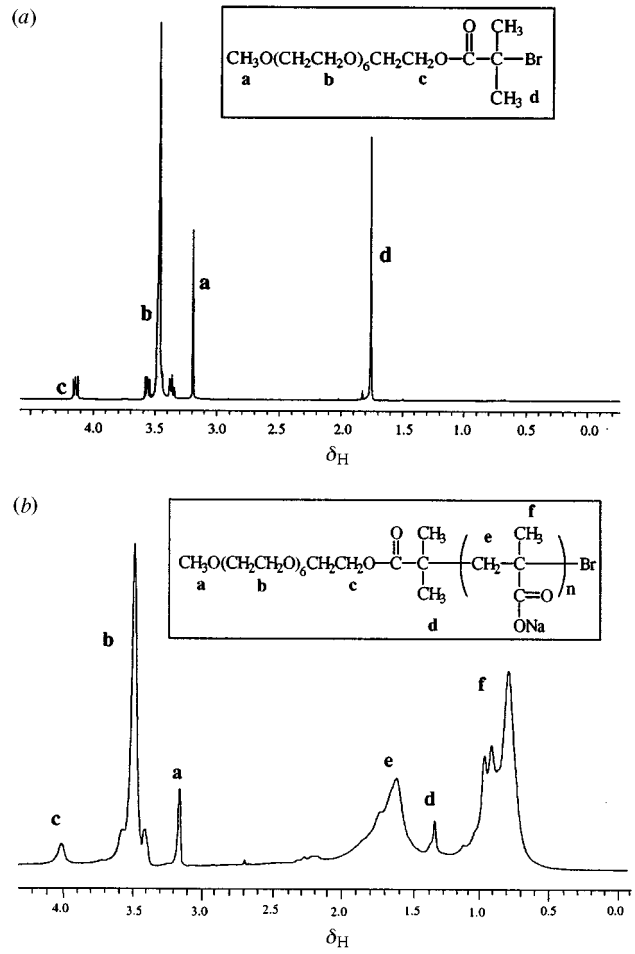

Fig. 1 ^{1}H NMR spectra for (*a*) the methoxy-capped poly(ethylene oxide) macro-initiator and (*b*) the poly(ethylene oxide-*block*-sodium methacrylate) synthesised using this macro-initiator (entry 3 in Table 1).

Table 1 A summary of the molecular weights, polydispersities and copolymer compositions of the poly(ethylene oxide-*block*-sodium methacrylate)s synthesised using aqueous ATRP

	Initiator	[Initiator]/ mmol	[Monomer]/ mmol	*t*/h	M_n Theory[b]	M_n NMR	M_n GPC[c]	M_w/M_n (GPC)[c]	Conversion (%)[d]
1	**1**	1.67	46.0	4.3	1645	2000	1500	1.30	47
2	**1**	1.67	46.0	6.2	2660	2500	2100	1.30	76
3	**1**	1.67	46.0	21.0	2800	3100	2900	1.27	80
4	**1**	1.0	92.5	17.0	7560	7400	7300	1.20	72
5[e]	—	0.0	46.0	21.0	—	—[i]	20200	2.18	82
6[f]	—	0.0	46.0	21.0	—	—[i]	4600	2.32	44
7	[g]	1.67	46.0	21.0	416	—[i]	3250	2.55	13
8	[h]	1.67	46.0	21.0	384	—[i]	2000	2.29	12
9	**2**	1.06	29.6	21.0	1540	1600	1300	1.23	44

[a] All reactions carried out with [CuBr]:[initiator]:[bipyridine] = 2:2:5, under nitrogen at 90 °C in degassed aqueous solution. [b] Calculated using the following formula: M_n (Theory) = 108.07(Δ[Monomer]/[Initiator]*p*), where *p* = fractional conversion. [c] Aqueous GPC details: Pharmacia Biotech Superdex® 200 HR 10/30 FPLC® column; eluent: 20% MeCN (HPLC grade) + 80% (0.01 M Na_2HPO_4 + 0.05 M $NaNO_3$); flow rate = 0.5 ml min^{-1}; pH 7–8; poly(sodium styrene-4-sulfonate) standards. [d] Reaction mixture was precipitated into EtOH and dried to constant weight. [e] Control reaction: performed with 5 g monomer and 15 ml water only. [f] Control reaction: catalyst and ligand present, but no initiator. [g] Initiator is sodium bromoisobutyrate. [h] Sodium bromoisobutyrate was used as the initiator, in the presence of monomethoxy-capped poly(ethylene oxide) (1.67 mmol). [i] M_n cannot be calculated from ^{1}H NMR spectra since the end groups are not known.

reaction solution into excess EtOH in order to isolate the precipitated copolymer [the Cu^I catalyst, bipy ligand and sodium methacrylate monomer are all soluble in EtOH]. Copolymer molecular weights, polydispersities and yields are summarised in Table 1. Moderate to good yields, good control over molecular weight and narrow polydispersities (M_w/M_n < 1.30) were achieved under ATRP conditions (see entries 1–4).

A proton NMR spectrum (D_2O) of a poly(ethylene oxide-*block*-sodium methacrylate) [entry 3, Table 1] clearly shows signals arising from the macro-initiator at δ 3.15 and 3.35–3.65. In order to demonstrate genuine block copolymer formation, the isolated polymers were subjected to Soxhlet extraction with refluxing THF for 3 h (the macro-initiator is THF-soluble). The NMR spectra obtained before and after THF extraction were identical, confirming that the macro-initiator is covalently attached to the poly(sodium methacrylate) chains. The peak integrals assigned to the ethylene oxide residues can also be used to determine the block copolymer M_n by end-group analysis. These values are included in Table 1 and are in reasonably good agreement with the aqueous GPC data.

Virtually all vinyl monomers are susceptible to radical initiation if heated for prolonged periods, even in the absence of initiator. Thus it was no surprise that non-living thermally-initiated polymerisation occurred on heating an aqueous solution of sodium methacrylate to 90 °C for 21 h in the absence of any macro-initiator or catalyst; the resulting polymer had a broad molecular weight distribution and a relatively high molecular weight (see entry 5, Table 1). Similarly, heating an aqueous solution of sodium methacrylate in the presence of the Cu^IBr and bipy ligand, but in the absence of initiator (entry 6), yielded polymer of high polydispersity (M_w/M_n = 2.32) but much lower molecular weight. Here the Cu^I [or traces of Cu^{II} formed by oxidation] probably acts as a polymerisation retarder.[12] Both control experiments support the hypothesis that the macro-initiator initiates ATRP of sodium methacrylate.

Subsequent experiments confirmed that the choice of pH is critical for successful ATRP. Below pH 6, sodium methacrylate does not undergo ATRP; the bipy ligand becomes protonated and no longer solubilises the Cu^IBr catalyst. Above pH 6, controlled polymerisation is evident and the optimum pH lies between 8 and 9. It is well known that the rate of radical polymerisation of methacrylic acid in water is very sensitive to pH.[13] However, this reaction usually favours low pH, because at high pH the rate of propagation is reduced due to the build-up of anionic charge density on the polymer backbone. In the present case it appears that there is a balance between reduced propagation at high pH and competing protonation of the ligand at low pH. Furthermore, synthesis of high molecular weight poly(sodium methacrylate) by aqueous ATRP has so far proved problematic: relatively broad molecular weight distributions are obtained if target molecular weights are greater than 10000.

Choice of initiator is also important. Polymerisation of sodium methacrylate using sodium 2-bromoisobutyrate as initiator (entry 7) gave only low conversion and polydisperse polymer, with an M_n much higher than expected. To determine whether the ethylene oxide residues of the macro-initiator might be contributing to the polymerisation, we performed the same reaction in the presence of the monomethoxy-capped poly(ethylene oxide) starting material, with no improvement (entry 8). In contrast, the monomeric analogue of the macro-initiator, 2-hydroxyethyl 2-methyl-2-bromopropionate **2**, successfully initiated the polymerisation of sodium methacrylate (entry 9) to produce near-monodisperse homopolymer, but with somewhat lower monomer conversion (44%).

In summary, we have demonstrated that ATRP of sodium methacrylate works well in aqueous media. Well-defined low molecular weight poly(sodium methacrylate)-based blocks can be prepared directly, without requiring protection chemistry for the carboxylic acid residues.

We thank FMC for financial support and for permission to publish this work.

Notes and references

1 S. G. Gaynor, J. S. Wang and K. Matyjaszewski, *Macromolecules*, 1995, **28**, 8051.
2 T. E. Patten, J. Xia, T. Abernathy and K. Matyjaszewski, *Science*, 1996, **272**, 866.
3 M. Sawamoto and M. Kamigaito, *Trends Polym. Sci.*, 1996, **4**(**11**), 371.
4 K. Matyjaszewski, Y. Nakagawa and C. B. Jasieczek, *Macromolecules*, 1998, **31**, 1535.
5 S. Coca, C. B. Jasieczek, K. L. Beers and K. Matyjaszewski, *J. Polym. Sci., Part A: Polym. Chem.*, 1998, **36**, 1417.
6 J. Mykytiuk, S. P. Armes and N. C. Billingham, *Polym. Bull.*, 1992, **29**, 139.
7 S. P. Rannard, N. C. Billingham, S. P. Armes and J. Mykytiuk, *Eur. Polym. J.*, 1993, **29**, 407.
8 D. M. Haddleton, M. C. Crossman, B. H. Dana, D. J. Duncalf, A. M. Heming, D. Kukulj and A. J. Shooter, *Macromolecules*, 1999, **32**, 2110.
9 T. E. Patten and K. Matyjaszewski, *Adv. Mater.*, 1998, **10**, 901.
10 D. M. Haddleton, C. Waterson, P. J. Derrick, C. B. Jasieczek and A. J. Shooter, *Chem. Commun.*, 1997, 683.
11 K. Jankova, X. Y. Chen, J. Kops and W. Batsberg, *Macromolecules*, 1998, **31**, 538.
12 E. Collinson, F. S. Dainton, D. R. Smith, G. J. Trudel and S. Tazuke, *Faraday Discuss. Chem. Soc.*, 1960, **29**, 188.
13 G. Blauer, *J. Polym. Sci.*, 1953, **11**, 189.

Communication 9/03773J

$[Ga_2Cl_4(dioxane)_2]_x$: molecular structure and reactivity of a polymeric gallium(II) halide containing two five-coordinate gallium atoms about a Ga–Ga bond

Pingrong Wei, Xiao-Wang Li and Gregory H. Robinson*

Department of Chemistry, The University of Georgia, Athens, GA 30602-2556, USA.
E-mail: robinson@SUNCHEM.uga.edu

Received (in Columbia, MO, USA) 20th April 1999, Accepted 21st May 1999

A polymeric 1,4-dioxane adduct of gallium(II) chloride, $[Ga_2Cl_4(dioxane)_2]_x$, containing two five-coordinate gallium atoms about a Ga–Ga bond [Ga–Ga 2.3825(9) Å], reacts with 1,4-dilithiotetraphenylbutadiene affording an unusual Ga(II)–tetraphenylbutadiene complex.

The first organometallic compound unambiguously shown to contain a Ga–Ga bond, $[(Me_3Si)_2HC]_2Ga–Ga[CH(SiMe_3)_2]_2$ [Ga–Ga 2.541(1) Å], isolated from reaction of $LiCH(SiMe_3)_2$ with gallium(II) bromide bis(dioxane), $Ga_2Br_4(dioxane)_2$, was reported only a decade ago.[1] In the solid state, $Ga_2Br_4(dioxane)_2$ resides in a *trans* geometry about a Ga–Ga bond of 2.395(6) Å.[2] The solid state structure of the corresponding bis(dioxane) adduct of gallium(II) chloride, $Ga_2Cl_4(dioxane)_2$, assumes a similar *trans* geometry about a comparable Ga–Ga bond of 2.406(1) Å.[3] In both $Ga_2Br_4(dioxane)_2$ and $Ga_2Cl_4(dioxane)_2$, the gallium atoms are four-coordinate tetrahedral—each bonding to two halide atoms, one dioxane adduct, and the remaining gallium atom. Herein, we report a polymeric 1,4-dioxane adduct of gallium(II) chloride, $[Ga_2Cl_4(dioxane)_2]_x$ **I**,[4] wherein both gallium atoms reside in five-coordinate trigonal bipyramidal environments about a Ga–Ga bond. The polymeric structure of **I** is interesting as it is notably different from previously reported Ga(II) halides. Moreover, **I** is shown to react with 1,4-dilithiotetraphenylbutadiene affording $[(PhC{=}CPhPhC{=}CPh)]Ga[(Cl)Li(OEt_2)_2]_2$[5] **II** (Scheme 1).

Compound **I** is significant as it represents a rare example of two five-coordinate gallium atoms about a Ga–Ga bond. Compound **II** involves cleavage of the Ga–Ga bond affording a Ga(II)–tetraphenylbutadiene complex.

From the discovery of cyclogallenes,[6–8] metalloaromatic Ga_3^{2-} ring systems, to reports of a gallyne,[9,10] a Ga_2^{2-} organometallic analog of acetylene, this laboratory has been interested in the dynamics of the Ga–Ga bond. These discoveries notwithstanding, this laboratory remained intrigued by the chemistry of the simple bis(dioxane) adducts of gallium halides, $Ga_2X_4(dioxane)_2$ (X = Cl, Br) and their well documented ability to stabilize both the Ga(II) oxidation state and the Ga–Ga bond. To this end, we sought to isolate triclinic crystals of $Ga_2Cl_4(dioxane)_2$ and explore its reactivity. To our great surprise, we obtained orthorhombic crystals of $[Ga_2Cl_4(dioxane)_2]_x$ **I** (Fig. 1).[11] It is possibly noteworthy that **I** was crystallized in our laboratory at room temperature while crystallization in the original preparation by Small and Worrall[2] took place at 0 °C. While **I** has a number of similarities with $Ga_2Cl_4(dioxane)_2$ and $Ga_2Br_4(dioxane)_2$ (*i.e.* the dioxane adducts are in the chair form), the differences are quite remarkable. Most striking about **I** is the five-coordinate, almost idealized trigonal bipyramidal coordination about both gallium atoms [O–Ga–O 179.10(10)°] while maintaining a Ga–Ga bond. It is particularly noteworthy that **I** is a rare example of a dimeric gallane consisting of two five-coordinate gallium atoms about a Ga–Ga bond. The trigonal bipyramidal coordination notwithstanding, it is also surprising that the Ga–Ga bond distance of 2.3825(9) Å in **I** is shorter than the values reported for both $Ga_2Br_4(dioxane)_2$ [2.395(6) Å] and $Ga_2Cl_4(dioxane)_2$ [2.406(1) Å]. Indeed, the Ga–Ga bond in **I** is considerably shorter than the cyclogallene Ga–Ga bond distances of 2.441(1) and 2.4187(5) Å reported for $Na_2[(Mes_2C_6H_3)Ga]_3$ and $K_2[(Mes_2C_6H_3)Ga]_3$, respectively, involving trigonal planar coordinated gallium atoms. The independent Ga–O bond distance of 2.4087(19) Å in **I** is considerably longer than the mean values of 2.03(2) and 2.027(2) Å reported for $Ga_2Br_4(dioxane)_2$ and $Ga_2Cl_4(dioxane)_2$, respectively. However, the Ga–O bond length of **I** compares well with the Ga–O(axial)

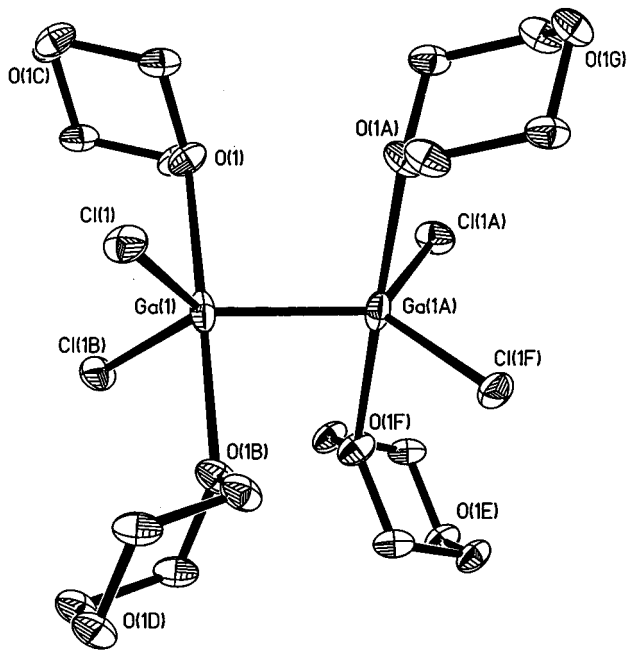

Fig. 1 Molecular structure of $[Ga_2Cl_4(dioxane)_2]_x$ **I**. Bond distances (Å) and angles (°): Ga(1)–Ga(1a) 2.3825(9), Ga(1)–Cl(1) 2.1721(7), Ga(1)–O(1) 2.4087(19), O(1)–C(2) 1.439(3), Cl(1b)–Ga(1)–Cl(1) 112.75(5), Cl(1b)–Ga(1)–Ga(1a) 123.62(2), Cl(1)–Ga(1)–Ga(1a) 123.62(2), Cl(1b)–Ga(1)–O(1) 89.46(5), Cl(1)–Ga(1)–O(1) 90.05(5), Ga(1a)–Ga(1)–O(1) 90.45(5), Cl(1b)–Ga(1)–O(1b) 90.05(5), Cl(1)–Ga(1)–O(1b) 89.46(5), Ga(1a)–Ga(1)–O(1b) 90.45(5), O(1)–Ga(1)–O(1b) 179.10(10). (Symmetry codes: a: $-x+1/2, -y+1/2, z$; b: $x, -y+1/2, -z+1/2$; c: $-x, -y+1, -z+1$; d: $-x, y-1.2, z-1/2$; e: $x+1/2, -y+1, z-1/2$; g: $x+1/2, y-1/2, -z+1$).

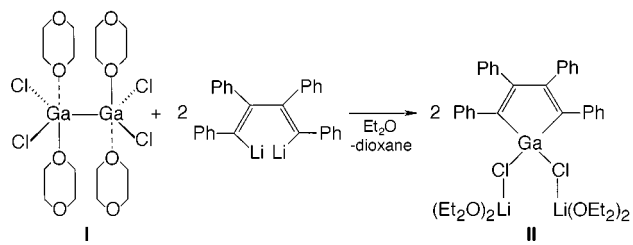

Scheme 1

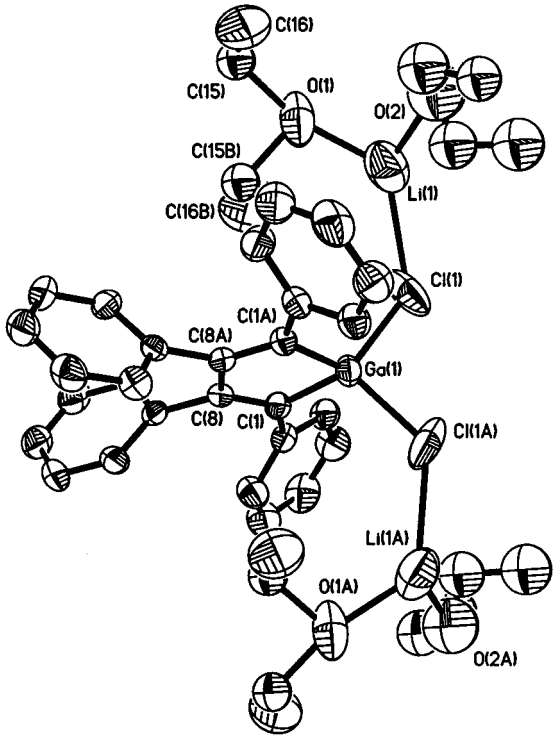

Fig. 2 Molecular structure of $[(PhC{=}CPhPhC{=}CPh)]Ga[(Cl)Li(OEt_2)_2]_2$ **II**. Bond distances (Å) and angles (°): Ga(1)–C(1a) 1.966(4), Ga(1)–C(1) 1.966(4), Ga(1)–Cl(1a) 2.2306(18), Ga(1)–Cl(1) 2.2305(18), Cl(1)–Li(1) 2.625(18), Li(1)–O(1) 2.07(2), Li(1)–O(2) 2.31(2); C(1a)–Ga(1)–C(1) 91.4(3), (1a)–Ga(1)–Cl(1a) 115.56(15), C(1)–Ga(1)–Cl(1a) 116.17(13), C(1a)–Ga(1)–Cl(1) 116.17(13), C(1)–Ga(1)–Cl(1) 115.57(15), Cl(1a)–Ga(1)–Cl(1) 102.68(14), (1)–Cl(1)–Li(1) 125.8(4). (Symmetry codes: a, $y + 1/3$, $x - 1/3$, $-z + 1.6$; b: $y + 1/3$, $x - 1/3$, $-z + 7/6$).

distances of 2.450(5) and 2.278(5) Å reported for the trigonal bipyramidal coordinated gallium atom in the azacrown ether complexation of the dimethylgallium fragment of $[(Me_2Ga)$-(diaza-18-crown-6)$[GaMe_3]_2$.[12] Also noteworthy, a view of the unit cell of **I** reveals an extended array stabilized by Cl···H(dioxane) interactions at contacts of 2.836 Å. Effectively, these interactions allow the dioxane moieties to loosely associate $Ga_2Cl_4(dioxane)_2$ units in infinite chains within the unit cell.

The tetraphenylbutadiene ligand is potentially useful in organogallium chemistry. Indeed, this ligand was utilized in the stabilization of the recently reported spirogallane anion, $[(PhC{=}CPhPhC{=}CPh)_2Ga]^-$.[13] Reaction of **I** with 1,4-dilithiotetraphenylbutadiene yields the interesting gallium(II) product **II** (Fig. 2).[11] **II** resides about a two fold mirror plane passing through the Ga(1) atom and bisecting the C(8)–C(8a) bond. The coordination about the gallium atom is distorted tetrahedral. The Ga–C bonds in **II** are a little shorter than those reported for the spirogallane. Although the mechanism which affords **II** remains unclear, Ga–Ga bond cleavage was clearly involved. Moreover, it is interesting that instead of the system eliminating LiCl, the lithium atoms, stabilized by diethyl ether, remained in the coordination sphere *via* bridging chlorine atoms [Li(1)–Cl(1)–Ga(1) bond angle is 125.8(4)°]. The Ga–Cl bond distance of 1.966(4) Å in **II** is considerably shorter than the values of 2.177(5) and 2.201(5) Å for $(Mes_2C_6H_3)_2GaCl$[14] and $[(Pr^i{}_3C_6H_2)_2C_6H_3GaCl_2]_2$,[15] respectively.

We are grateful to the National Science Foundation (G. H. R.: CHE-95-9520162) and to the donors of the Petroleum Research Fund, administered by the American Chemical Society, for support of this work.

Notes and references

1 W. Uhl, M. Layh and T. Hildenbrand, *J. Organomet. Chem.*, 1989, **364**, 289.
2 R. W. H. Small and I. J. Worrall, *Acta Crystallogr., Sect. B*, 1982, **38**, 250.
3 J. C. Beamish, R. W. H. Small and I. J. Worrall, *Inorg. Chem.*, 1979, **18**, 220.
4 Inside the drybox (M. Braun Labmaster 130) Ga_2Cl_4 (Aldrich Chemical Co.) (17.8 mmol, 5 g) was dissolved in 1,4-dioxane (25 mL). The resulting mixture was filtered and the solution was allowed to stand at room temperature for several days resulting in colorless cubic crystals (4 g, 62% yield). Mp 158–159 °C. Anal. (E + R Microanalytical Laboratories, Parispanny, NY) Calc. (found) $Ga_2Cl_4(dioxane)_2$: C, 21.00 (21.17); H, 3.50 (2.90%). The less than ideal hydrogen analysis may be due to the loosely associated solvent molecules. ^{1}H NMR (300 MHz, 298 K, THF-d_8): δ 3.52 (m, 2H, $-OCH_2$); ^{13}C NMR (300 MHz, 298 K, THF-d_8): δ 72.7 ($-OCH_2$).
5 A suspension of 1,4-dilithiotetraphenylbutadiene in diethyl ether (50 mL), obtained from reaction of diphenylacetylene (Aldrich Chemical Co.) (10 mmol, 1.78 g) and lithium (10 mmol, 0.071 g), was added to a diethyl ether solution of **I** (2.5 mmol, 1.14 g) at −78 °C. After stirring for 3 h at −78 °C, the system was allowed to slowly warm to room temperature, stirring continued overnight. The resulting solution was separated from the precipitate by filtration, and concentrated to about a half of its volume, and then kept at −20 °C for several days. Yellow crystals were obtained (1.0 g, 31%). Mp 92 °C. Anal. Calc. (found) $Ph_4C_4GaCl_2Li_2(Et_2O)_3$: C, 65.50 (65.07); H, 6.82 (6.54%). ^{1}H NMR (300 MHz, 298 K, THF-d_8): δ 1.07 (m, 18H, $-OCH_2CH_3$), 3.35 (m, 12H, $-OCH_2CH_3$), 6.68–7.15 (br, m, 20H, Ph H); ^{13}C NMR (300 MHz, 298 K, THF-d_8): δ 15.7 ($-OCH_2CH_3$), 66.3 ($-OCH_2CH_3$), 123.7, 125.1, 127.4, 127.5, 130.2, 131.5, 141.6, 143.6, 148.8, 149.6.
6 X.-W. Li, W. T. Pennington and G. H. Robinson, *J. Am. Chem. Soc.*, 1995, **117**, 7578.
7 X.-W. Li, Y. Xie, P. R. Schreiner, K. D. Gripper, R. C. Crittendon, C. F. Campana, H. F. Schaefer, III and G. H. Robinson, *Organometallics*, 1996, **15**, 3798.
8 Y. Xie, P. R. Schreiner, H. F. Schaefer, III, X.-W. Li and G. H. Robinson, *J. Am. Chem. Soc.*, 1996, **118**, 10 635.
9 J. Su, X.-W. Li, R. C. Crittendon and G. H. Robinson, *J. Am. Chem. Soc.*, 1997, **119**, 5471.
10 Y. Xie, R. S. Grev, J. Gu, H. F. Schaefer, III, P. v. R. Schleyer, J. Su, X.-W. Li and G. H. Robinson, *J. Am. Chem. Soc.*, 1998, **120**, 3773.
11 X-Ray intensity data were measured at room temperature on a Bruker SMART TM CCD-based X-ray diffractometer system with graphite-monochromated Mo-Kα radiation (λ = 0.710 73 Å). *Crystallographic data*: For **I**: orthorhombic, space group *Pnnn* (no. 48) with unit cell parameters a = 8.2481(1), b = 8.277(1), c = 11.385(1) Å, V = 777.4(2) Å^3, Z = 8. Refinement converged at $R1$ = 0.024 and wR_2 = 0.059.
For **II**: trigonal, space group $R\bar{3}c$ (no. 167) with unit cell parameters a = 45.008(4), c = 10.413(1) Å, V = 18.268(3) Å^3, Z = 36. Refinement converged at $R1$ = 0.052 and wR_2 = 0.131.
CCDC 182/1272.
12 B. Lee, W. T. Pennington and G. H. Robinson, *Organometallics*, 1990, **9**, 1709.
13 J. Su, S. D. Goodwin, X.-W. Li and G. H. Robinson, *J. Am. Chem. Soc.*, 1998, **120**, 12 994.
14 X.-W. Li, W. T. Pennington and G. H. Robinson, *Organometallics*, 1995, **14**, 2109.
15 J. Su, X.-W. Li and G. H. Robinson, *Chem. Commun.*, 1998, 2015.

Communication 9/03166I

Methods for effecting monofunctionalization of $(CH_2{=}CH)_8Si_8O_{12}$

Frank J. Feher,*[a] Kevin D. Wyndham,[a] Richard K. Baldwin,[a] Daravong Soulivong,[a] Joseph D. Lichtenhan[bc] and Joseph W. Ziller[a]

[a] *Department of Chemistry, University of California, Irvine, CA 92697-2025, USA. E-mail: fjfeher@uci.edu*
[b] *Air Force Research Laboratory, Edwards Air Force Base, CA 93524-7680, USA*
[c] *Hybrid Plastics, Inc., 18237 Mt. Baldy Circle, Fountain Valley, CA 92708, USA*

Received (in Bloomington, IN, USA) 16th February 1999, Accepted 21st May 1999

A new method is described for effecting selective monofunctionalization of $CH_2{=}CH)_8Si_8O_{12}$ 2: reaction of 2 with triflic acid (TfOH) produces $(TfOCH_2CH_2)(CH_2{=}CH)_7Si_8O_{12}$ 3, which reacts with nucleophiles (*e.g.* H_2O or 2-mercaptopyridine) to produce $(XCH_2CH_2)(CH_2{=}CH)_7Si_8O_{12}$ (4 X = OH, 5 X = SC_5H_4N); acylation of 4 with *p*-$O_2NC_6H_4COCl$ affords (*p*-$O_2NC_6H_4CO_2CH_2CH_2)(CH_2{=}CH)_7Si_8O_{12}$ 6; catalytic hydrogenation of 4 affords $(HOCH_2CH_2)Et_7Si_8O_{12}$ 7.

Polyhedral oligosilsesquioxanes (POSS) have recently attracted interest as building blocks for hybrid inorganic/organic materials.[1–5] Many families of POSS monomers are now known, but some of the most promising monomers are cube-octameric frameworks with a single polymerizable pendant group (*e.g.* **1**).[6,7] As part of a general effort to identify cost-effective ways

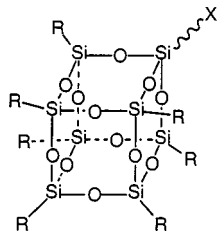

1 X = polymerizable pendant group

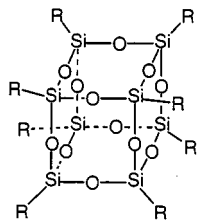

2 R = vinyl

for manufacturing POSS monomers on a large scale, we have been exploring potential methods for preparing POSS monomers from inexpensive $R_8Si_8O_{12}$ frameworks.[8–10] Here, we outline a new strategy for preparing POSS monomers from $(CH_2{=}CH)Si_8O_{12}$ **2**. This strategy, which involves addition of triflic acid (TfOH) to a C=C bond of the vinylsilsesquioxane, produces an attractive precursor for the preparation of cube-octameric POSS monomers containing seven vinyl or ethyl groups and one unique pendant group.

Vinylsilsesquioxane **2**, which is readily available from the hydrolytic condensation of $(CH_2{=}CH)SiCl_3$,[11,12] undergoes a wide variety of useful transformations, including free-radical addition reactions,[13] catalytic hydrogenation,[14] Diels–Alder reactions,[15] epoxidation[4] and olefin metathesis.[8] With eight potentially reactive vinyl groups, reactions of **2** often produce complicated product mixtures. Under the right conditions, however, reactions of **2** can be quite selective for the functionalization of a single vinyl group.

The reaction of **2** with TfOH† (1 equiv., CH_2Cl_2, 25 °C) occurs quickly upon mixing to afford a new silsesquioxane product in good yield (*ca.* 40–45%) (Scheme 1).‡ Based on the known reactivity of $R_8Si_8O_{12}$ frameworks toward TfOH[9,10] and the tendency of some vinylsilanes to undergo protodesilylation or rearrangement,[16] we expected to observe cleavage of Si–O–Si linkages and/or Si–C bonds. Instead, both the ^{13}C and ^{29}Si NMR spectra were consistent with a compound possessing a C_3-symmetric Si_8O_{12} framework, and the ^1H NMR spectrum exhibited an AA′BB′ coupling pattern characteristic of $R_7Si_8O_{12}(CH_2CH_2X)$ frameworks.[17] Based on the reaction stoichiometry and the ^1H chemical shift for the CH_2X group (δ 4.75, t, J 12 Hz), this compound was assigned as **3**; this assignment was confirmed by multinuclear NMR data (^{13}C, ^{29}Si, ^{19}F) and a high resolution mass spectrum. To the best of our knowledge, this is the first example of triflic acid addition to a vinylsilane.

Triflate **3** could not be isolated in pure form because it readily co-crystallizes with **2**. However, crude product mixtures containing **3** react with a variety of nucleophiles to afford substitution products that can be easily isolated as pure compounds. For example, hydrolysis of **3** (acetone or dioxane–aqueous Na_2CO_3) produces **4**, which was identified on the basis of compelling multinuclear NMR data, a high resolution mass spectrum, and a preliminary single crystal X-ray diffraction study.§ Reaction of **3** with 2-mercaptopyridine affords **5**.¶ In both cases, separation of the product from unreacted **2**, as well as small amounts of products derived from functionalization of more than one vinyl group (*vide infra*), can be accomplished by flash chromatography on SiO_2.

In contrast to most compounds containing $SiCH_2CH_2OH$ groups, **4** does not undergo facile base-catalyzed elimination of ethylene to produce SiOH groups. It is also resistant to acid-catalyzed dehydration. This unexpected stability, which is probably due to a strong preference for *trans*-diaxial orientation of the Si_8O_{12} framework and OH group, allows **4** to be used as a precursor to a wide range of potentially useful compounds. For example, both acylation of **4** to **6** (*p*-$O_2NC_6H_4COCl$, CH_2Cl_2–pyridine, 50 °C, 8 h) and the catalytic hydrogenation of **4** to **7** (10% Pd/C, 100 psig H_2, Et_2O, 25 °C, 20 h) occur in quantitative NMR yield.¶

Unlike TfOH-induced Si–O–Si cleavage reactions of $R_8Si_8O_{12}$, which can afford high yields of a single product at complete conversion, functionalization of POSS pendant groups is normally selective for monofunctionalization[18] only at low conversion (< 10% based on $R_8Si_8O_{12}$). At higher conversion the monofunctionalization reaction no longer enjoys a large statistical advantage and the formation of many polyfunctional products is usually observed. For the reaction of **2** with TfOH described above, the selectivity for monofunctionalization is *ca.* 85–90% as judged by multinuclear NMR spectra and EI mass spectra obtained on crude product mixtures. Under these conditions, difunctionalized products are

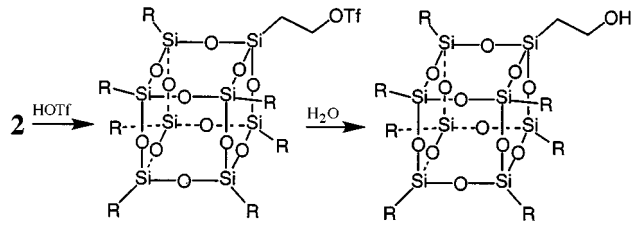

3 R = vinyl **4** R = vinyl

Scheme 1

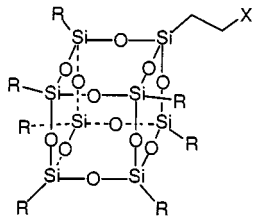

5 R = vinyl; X = 

6 vinyl $O_2CC_6H_4NO_2$

7 ethyl OH

also produced in yields of *ca.* 10–15% (based on the amount of **2** consumed). Higher selectively for monofunctionalization can be achieved by performing the reaction to lower conversion, but larger amounts of unreacted **2** must be recovered and the absolute mass yield of **3** is correspondingly lower. We have not been able to separate or isolate any of the triflates derived from addition of TfOH to vinyl groups on **2**. However, hydrolysis of the crude product mixture cleanly transforms all CH_2CH_2OTf groups into CH_2CH_2OH groups and produces a mixture of alcohols that can be efficiently separated by chromatography. A full account of our efforts to control the extent of functionalization and isolate synthetically useful quantities of polyfunctional products will be reported separately.

In summary, the addition of triflic acid to vinyl groups of **2** provides the basis for a fundamentally new method for preparing functionalized silsesquioxanes. Frameworks containing seven vinyl or ethyl groups and one unique pendant group are particularly easy to prepare, but both the rich reaction chemistry of vinylsilsesquioxanes and the ease with which multiply functionalized derivatives can be isolated in synthetically useful quantities provide access to a wide range of potentially useful compounds.

These studies were supported by the Air Force Research Laboratory (Edwards AFB). We are grateful to Dr John Greaves (UCI) for obtaining high-resolution mass spectra of **3**–**7**.

Notes and references

† TfOH = CF_3SO_3H

‡ Triflic acid (TfOH, 1 equiv.) was added to a solution of **2** (188 mg, 0.297 mmol) in CH_2Cl_2. After 3 h at 25 °C, the reaction mixture was diluted with CH_2Cl_2, washed with saturated aqueous Na_2CO_3, dried over $MgSO_4$, and evaporated to afford 180 mg of a white solid. Analysis by NMR spectroscopy (^{1}H, ^{13}C, ^{29}Si) and mass spectrometry indicated that the crude product contains mainly **3** (40–45%), unreacted **2** (50%) and small amounts of products resulting from addition of TfOH to more than one vinyl group. For **3**: ^{1}H NMR (500 MHz, $CDCl_3$, 25 °C): δ 6.25–5.75 (m, 21H), 4.73 (t, *J* 12 Hz, 2H, CH_2OTf), 1.50 (t, *J* 12 Hz, 2H, $SiCH_2$). ^{13}C{^{1}H} NMR (125 MHz, $CDCl_3$, 25 °C): δ 137.40, 137.24, 137.03 (rel. int. 3:3:1 for CH_2), 128.39, 128.29, 128.09 (rel. int. 1:3:3 for CH), 118.5 (q, *J* 320 Hz, CF_3), 75.15 (CH_2OTf), 14.89 ($SiCH_2$). ^{29}Si{^{1}H} NMR (99 MHz, $CDCl_3$, 25 °C): δ −71.61, −80.08, −80.14 (rel. int: 1:3:4). ^{19}F{^{1}H} NMR (470.13 MHz, $CDCl_3$, 21 °C): δ −139.45. EI (70 eV, 200 °C) exact mass for M^+ (found): *m/z* 781.9020 (781.9041).

§ The hydrolysis of crude **3** was performed in wet acetone–CH_2Cl_2. Analysis (^{1}H, ^{13}C, ^{29}Si NMR) of the crude product obtained after evaporation of the solvent indicated complete conversion of $SiCH_2CH_2OTf$ to $SiCH_2CH_2OH$. Flash chromatography on silica with CH_2Cl_2 afforded **4** as a white solid, which was recrystallized from CH_2Cl_2 at −35 °C. For **4**: ^{1}H NMR (500 MHz, $CDCl_3$, 25 °C): δ 6.15–5.90 (m, 21H), 3.85 (t, *J* 7.2 Hz, 2H, CH_2OH), 1.18 (t, *J* 7.2 Hz, 2H, $SiCH_2$). ^{13}C{^{1}H} NMR (125 MHz, $CDCl_3$, 25 °C): δ 137.07, 137.05, 136.95 (rel. int. 3:3:1 for CH_2), 128.58, 128.56 (rel. int. 4:3 for CH), 58.48 (CH_2OH), 17.28 ($SiCH_2$). ^{29}Si{^{1}H} NMR (99 MHz, $CDCl_3$, 25 °C): δ −68.00, −80.16, −80.36 (rel. int. 1:3:4). EI (70 eV, 200 °C) exact mass for M^+ (found): *m/z* 649.9528 (649.9520).

Crystal data for **4**: $C_{16}H_{26}O_{13}Si_8$, *M* = 651.09, rhombohedral, space group $R\bar{3}$, *a* = *b* = 13.4510(8), *c* = 13.9408(12) Å, γ = 120°, *V* = 2184.4(3) Å^3, *T* = 158 K, *Z* = 3, μ = 0.426 mm^{-1}, 4488 reflections collected, 1152 independent reflections with $I > 2\sigma(I)$, R_1 = 0.0811, wR_2 = 0.2285. The CH_2CH_2OH group exhibits $\bar{3}$ disorder because the crystallographic center of inversion is located at the center of the Si_8O_{12} framework.

CCDC 182/1295. See http://www.rsc.org/suppdata/cc/1999/1289/ for crystallographic files in .cif format.

¶ For **5**: ^{1}H NMR (500.2 MHz, $CDCl_3$, 25 °C): δ 8.38 (m, CH, 1H), 7.63 (m, CH, 1H), 7.24 (s, CH, 1H), 7.10 (m, CH, 1H), 6.1–5.9 (m, $CH{=}CH_2$, 21H), 3.31 (t, CH_2S, 2H), 1.22 (t, CH_2Si, 2H). ^{13}C{^{1}H} NMR (125.8 MHz, $CDCl_3$, 25 °C): δ 159.4 (s, CH), 148.0 (s, CH), 138.0 (s, CH) 137.308, 137.256, 137.22 (s, $CH{=}CH_2$, rel. int. 3:3:1), 128.785, 128.765, (s, $CH{=}CH_2$, rel. int. 3:4), 122.9 (s, CH), 119.9 (s, CH), 25.44 (s, CH_2S), 12.84 (s, $SiCH_2$). ^{29}Si{^{1}H} NMR (99.4 MHz, $CDCl_3$, 25 °C): δ −68.8 (s, $SiCH_2CH_2S$), −79.95, −80.00 (s, rel. int. 4:3). Mass spectrum (EIMS) *m/z* calc. for $C_{21}H_{29}O_{12}NSSi_8$: $[M]^+$ 742.9565, found 742.9564.

For **6**: ^{1}H NMR (500.2 MHz, $CDCl_3$, 25 °C) δ: 8.26–8.19 (m, $C_6H_4NO_2$, 4H), 6.16–5.84 (m, $SiCH{=}CH_2$, 21H), 4.52 (t, CH_2O, 2H), 1.37 (t, $SiCH_2$, 2H). ^{13}C{^{1}H} NMR (125.8 MHz, $CDCl_3$, 25 °C): δ 164.55 (s, CO), 150.45 (s, C-quat), 137.398, 137.13 (br, $SiCH{=}CH_2$, rel. int. 3:4), 135.72 (s, C-quat), 130.710 (s, CH), 128.45 (s, $SiCH{=}CH_2$), 123.50 (s, CH), 62.269 (s, CH_2O), 12.92 (s, $SiCH_2$). ^{29}Si{^{1}H} NMR (99.4 MHz, $CDCl_3$, 25 °C): δ −69.0 (s, $SiCH_2CH_2O$), −80.1, −80.3 (s, rel. int. 4:3). Mass spectrum (ESMS) *m/z* calc. for $C_{23}H_{29}O_{16}NSi_8$: $[M]^+$ 798.9640, found 798.9640.

For **7**: ^{1}H NMR (500.2 MHz, $CDCl_3$, 25 °C): δ 3.81 (t, *J* 8.0 Hz, CH_2OH, 2H), 1.60 (br, OH, 1H), 1.09 (t, *J* 7.6 Hz, CH_2CH_2OH, 2H), 0.993 (t, $SiCH_2CH_3$, 21H), 0.60 (q, $SiCH_2CH_3$, 14H). ^{13}C{^{1}H} NMR (125.8 MHz, $CDCl_3$, 25 °C): δ 58.83 (s, CH_2CH_2O), 17.58 (s, CH_2CH_2O), 6.47 (s, $SiCH_2CH_3$), 4.00 (s, $SiCH_2CH_3$). ^{29}Si{^{1}H} NMR (99.4 MHz, $CDCl_3$, 25 °C): δ −65.6, −65.7, −68.8 (s, rel. int. 3:4:1). Mass spectrum (EIMS) *m/z* calc. for $C_{16}H_{40}Si_8O_{13}$: $[M - H]^+$ 663.0545, found 663.0487.

1 J. J. Schwab and J. D. Lichtenhan, *Appl. Organomet. Chem.*, 1998, **12**, 707.
2 J. D. Lichtenhan, *Comments Inorg. Chem.*, 1995, **17**, 115.
3 A. Lee and J. D. Lichtenhan, *Macromolecules*, 1998, **31**, 4970.
4 C. Zhang and R. M. Laine, *J. Organomet. Chem.*, 1996, **521**, 199.
5 R. M. Laine, C. X. Zhang, A. Sellinger and L. Viculis, *Appl. Organomet. Chem.*, 1998, **12**, 715.
6 A. Tsuchida, C. Bolln, F. G. Sernetz, H. Frey and R. Mulhaupt, *Macromolecules*, 1997, **30**, 2818.
7 T. S. Haddad and J. D. Lichtenhan, *Macromolecules*, 1996, **29**, 7302.
8 F. J. Feher, D. Soulivong, A. G. Eklund and K. D. Wyndham, *Chem. Commun.*, 1997, 1185.
9 F. J. Feher, D. Soulivong and A. E. Eklund, *Chem. Commun.*, 1998, 399.
10 F. J. Feher, D. Soulivong and F. Nguyen, *Chem. Commun.*, 1998, 1279.
11 P. G. Harrison, C. Hall and R. Kannengiesser, *Main Group Met. Chem.*, 1997, **20**, 515.
12 M. G. Voronkov, T. N. Martynova, R. G. Mirskov and V. I. Belyi, *Zh. Obshch. Khim.*, 1979, **49**, 1522.
13 R. Weidner, N. Zeller, B. Deubzer and V. Frey, in *Organooligosilsesquioxanes*, *US Pat.* 5047492, 10th September 1991 (Wacker-Chemie GmbH).
14 V. M. Kovrigin, V. I. Lavrent'ev and N. V. Sinegubova, *J. Gen. Chem. USSR*, 1987, **57**, 995.
15 V. M. Kovrigin, V. I. Lavrent'ev and V. M. Moralev, *J. Gen. Chem. USSR*, 1986, **56**, 2049.
16 I. Fleming, J. Dunoques and R. Smithers, *Org. React.*, 1989, **37**, 57.
17 F. J. Feher, J. J. Schwab, D. M. Tellers and A. Burstein, *Main Group Chem.*, 1998, **2**, 169.
18 G. Calzaferri, D. Herren and R. Imhof, *Helv. Chim. Acta*, 1991, **74**, 1278.

Communication 9/01308C

ChemComm

Tetraorganodistannoxanes: formation of a novel *cis*-ladder†

Marcus Schulte,[a] Markus Schürmann,[a] Dainis Dakternieks[b] and Klaus Jurkschat*[a]

[a] *Lehrstuhl für Anorganische Chemie II der Universität Dortmund, D-44221 Dortmund, Germany. E-mail: kjur@platon.chemie.uni-dortmund.de*

[b] *School of Biological and Chemical Sciences, Deakin University, Geelong,Vic. 3217, Australia*

Received (in Basel, Switzerland) 25th February 1999, Accepted 21st May 1999

Reaction of the acetylenic-bridged ditin precursor $[Me_3SiCH_2(Cl_2)SnCH_2(Me_2)Si]_2C_2$ 1 with the oxygen source $(Bu^t_2SnO)_3$ results exclusively in formation of the dimeric tetraorganodistannoxane $\{[Me_3SiCH_2(Cl)SnCH_2(Me_2)SiC{\equiv}CSi(Me_2)CH_2Sn(Cl)CH_2SiMe_3]O\}_2$ 2 which has the hitherto unknown *cis*-configuration; this is retained during the quantitative conversion of 2 into the hydroxy-substituted analogue $\{[Me_3SiCH_2(OH)SnCH_2(Me_2)SiC{\equiv}CSi(Me_2)CH_2Sn(Cl)CH_2SiMe_3]O\}_2$ 3.

Dimeric tetraorganodistannoxanes $[R_2(X)SnOSn(X)R_2]_2$ (X = halogen, OH, R′CO_2, NCS; R, R′ = alkyl, aryl)[1–5] have been reported to be efficient homogeneous catalysts in various organic reactions such as transesterification under virtually neutral conditions,[6] highly selective acylation of alcohols,[7] urethane formation[8] and alkyl carbonate synthesis.[9]

We recently reported the syntheses and structures of tetraorganodistannoxanes $\{[R(X)SnCH_2ZCH_2Sn(X)R]O\}_n$ which contain tri- or tetra-methylene bridges between the two tin atoms. These compounds exhibit either a double ladder or a dimeric structure (n = 4; R = CH_2SiMe_3; X = Cl, OH; Z = CH_2),[10] [n = 2, 4; R = CH_2SiMe_3, CH_2CMe_3, CH_2CHMe_2; X = Cl, OAc; Z = CH_2, $(CH_2)_2$, $SiMe_2$],[11] [n = 2; R = $CH(SiMe_3)_2$; X = F; Z = CH_2].[12] Also recently reported was the first triple ladder $\{[R(Cl)Sn(CH_2)_3Sn(Cl)(CH_2)_3Sn(Cl)R]O_{1.5}\}_4$ (R = CH_2SiMe_3),[13] in this case three tin atoms are connected by trimethylene bridges.

In the double ladders $\{[R(Cl)SnCH_2ZCH_2Sn(Cl)R]O\}_4$ [R = CH_2SiMe_3; Z = CH_2, $(CH_2)_2$] the distance between the two $Sn_4Cl_4O_2$ layers is 6.04 and 7.07 Å, respectively, which is too small to contemplate any host–guest chemistry. With the goal to increase the $Sn_4Cl_4O_2$ interlayer separation, we synthesised the precursor of a double ladder containing a rigid acetylene spacer, $[Me_3SiCH_2(Cl_2)SnCH_2(Me_2)Si]_2C_2$, **1**.‡

However, reaction of **1** with $(Bu^t_2SnO)_3$ resulted in quantitative formation of the dimeric tetraorganodistannoxane **2**§ rather than the anticipated tetrameric double ladder compound (Scheme 1).

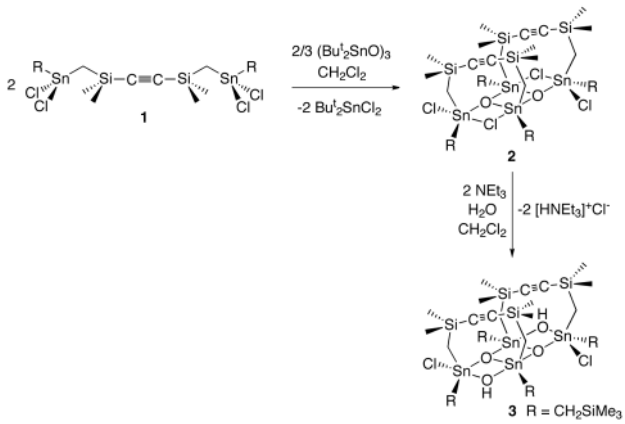

Scheme 1 Synthesis of the tetraorganodistannoxanes **2** and **3**.

† This work contains part of the intended PhD thesis of M. Schulte.

Somewhat surprisingly, the crystal structure (Fig. 1) of **2**¶ shows that both acetylenic spacer groups are on the same side of the tetraorganodistannoxane ladder core, *i.e.* **2** adopts the lower symmetry *cis*-configuration as compared to the usual *trans*-configuration.[12] The origin of this geometric disposition is not clear. Each tin atom has a distorted trigonal bipyramidal geometry. For the exocyclic tin atoms, two carbons and one oxygen occupy the equatorial positions and two chlorines occupy the axial positions, while for the endocyclic tin atoms the equatorial positions are occupied by two carbons and one oxygen and the axial positions by one oxygen and one chlorine. The shortest Sn–O bond lengths are found for the exocyclic tins [Sn(1)–O(1) 2.024(3) Å, Sn(4)–O(2) 2.018(2) Å] and the longest Sn–O bonds exist in the Sn_2O_2 ring [Sn(2)–O(2) 2.132(3) Å, Sn(3)–O(1) 2.159(3) Å]. It is worth noting that the Sn(2)–O(2) bond corresponds to the longer Sn(2)–Cl(2) bond [2.641(1) Å] whereas the Sn(3)–O(1) bond corresponds to the shorter Sn(3)–Cl(4) bond [2.512(2) Å]. The chlorine atoms Cl(1) and Cl(3) are non-bridging [Sn(2)–Cl(3) 3.490(1) Å, Sn(3)-Cl(1) 3.497(1) Å]. The torsion angles involving the bridging chlorine atoms [Sn(1)–O(1)–Sn(2)–Cl(2) 7.93(7)°,

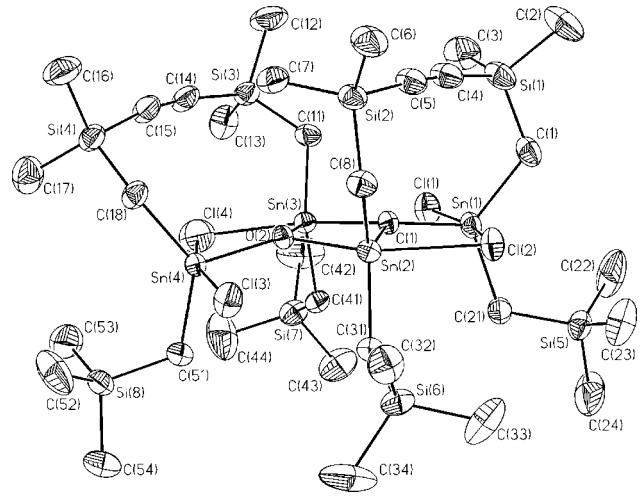

Fig. 1 Crystal structure of *cis*-$\{[Me_3SiCH_2(Cl)SnCH_2(Me_2)SiC{\equiv}CSi(Me_2)CH_2Sn(Cl)CH_2SiMe_3]O\}_2$ **2**, showing 30% probability ellipsoids. Hydrogen atoms are omitted for clarity. Selected bond lengths (Å) and angles (°): Sn(1)–O(1) 2.024(3), Sn(1)–Cl(1) 2.453(1), Sn(1)–Cl(2) 2.740(1), Sn(2)–O(1) 2.058(3), Sn(2)–O(2) 2.132(3), Sn(2)–Cl(2) 2.641(1), Sn(2)–Cl(3) 3.490(1), Sn(3)–O(1) 2.159(3), Sn(3)–O(2) 2.049(3), Sn(3)–Cl(1) 3.497(1), Sn(3)–Cl(4) 2.512(2), Sn(4)–O(2) 2.018(2), Sn(4)–Cl(3) 2.507(1), Sn(4)–Cl(4) 2.503(2), O(1)–Sn(1)–Cl(1) 88.29(8), O(1)–Sn(1)–Cl(2) 76.28(8), O(1)–Sn(1)–C(1) 122.7(2), O(1)–Sn(1)–C(21) 112.5(2), Cl(1)–Sn(1)–Cl(2) 164.57(4), O(1)–Sn(2)–O(2) 74.4(1), O(1)–Sn(2)–Cl(2) 78.11(8), O(1)–Sn(2)–C(8) 121.0(1), O(1)–Sn(2)–C(31) 106.6(1), O(2)–Sn(2)–Cl(2) 152.36(7), O(1)–Sn(3)–O(2) 74.0(1), O(2)–Sn(3)–Cl(4) 77.72(8), O(2)–Sn(3)–C(11) 114.0(2), O(2)–Sn(3)–C(41) 108.4(1), O(1)–Sn(3)–Cl(4) 151.59(8), O(2)–Sn(4)–Cl(3) 86.29(8), O(2)–Sn(4)–Cl(4) 78.46(9), O(2)–Sn(4)–C(18) 113.7(2), O(2)–Sn(4)–C(51) 113.7(2), Cl(3)–Sn(4)–Cl(4) 163.50(6), Si(1)–C(4)–C(5) 173.7(5), Si(2)–C(5)–C(4) 176.0(5), Si(3)–C(14)–C(15) 171.8(4), Si(4)–C(15)–C(14) 169.9(4), Sn(1)–O(1)–Sn(2)–Cl(2) 7.93(7), Sn(3)–O(2)–Sn(4)–Cl(4) 6.74(8), Sn(2)–O(1)–Sn(3)–O(2) 8.0(1).

Sn(3)–O(2)–Sn(4)–Cl(4) 6.74(8)°] and the Sn_2O_2 ring [Sn(2)–O(1)–Sn(3)–O(2) 8.0(1)°] reveal a distortion from planarity which originates from ring strain in the two nine-membered Sn–O–Sn–C–Si–C≡C–Si–C rings. This ring strain is also manifested in the deviation of the Si–C≡C angles from the ideal value of 180° [Si(1)–C(4)–C(5) 173.7(5)°, Si(2)–C(5)–C(4) 176.0(5)°, Si(3)–C(14)–C(15) 171.8(4)°, Si(4)–C(15)–C(14) 169.9(4)°]. All four Sn–C–Si frameworks are bent into the same direction which results in an intramolecular stacking of the two nine-membered rings. There is no intramolecular or intermolecular interaction between two spacers [shortest intramolecular distance C(7)···C(18) 3.827(7) Å].

The dimeric nature of the material is retained in solution as was verified by molecular weight determination (calc. for **2**: M = 1334 g mol^{-1}, found in CH_2Cl_2: M = 1383 g mol^{-1}). The ^{119}Sn NMR spectrum in $CDCl_3$ contains two signals of equal integral ratio at δ −132.4 (C_2SnO_2Cl) and at δ −75.8 (C_2SnOCl_2) indicating the presence of a single isomer in solution. However, these data do not provide unambiguous information about which of the two possible isomers is present in solution.

The tetrachloro-substituted distannoxane **2** reacts almost quantitatively with triethylamine–water to give the dihydroxy-substituted distannoxane **3**.‖ Again, the *cis*-isomer of **3** is formed exclusively in the solid state‡ (Scheme 1).

In aqueous solution compound **3** does not undergo further hydrolysis. Also for **3** the dimeric structure is retained in solution as was verified by molecular weight determination (calc. for **3**: M = 1297 g mol^{-1}, found in CH_2Cl_2: M = 1349 g mol^{-1}). The ^{119}Sn NMR spectrum in $CDCl_3$ shows two signals of equal integral ratio at δ −153.1 and −152.2 revealing the presence of a single isomer only, but as stated for compound **2** it is not evident which of the two isomers is actually present.

These preliminary results reveal that the silicon containing acetylenic spacer $CH_2(Me_2)SiC{\equiv}CSi(Me_2)CH_2$ plays an essential role in controlling the structure of the distannoxane dimers **2** and **3**. Further studies on this class of compounds will focus on the catalytic activity of spacer bridged distannoxanes such as **2** and **3**.

We thank the Deutsche Forschungsgemeinschaft and the Fonds der Chemischen Industrie for financial support.

Notes and references

‡ The detailed synthesis of **1** and the crystal structure of **3** will be presented in a forthcoming full paper.

§ *Synthesis and selected spectroscopic data* for **2**: to a solution of **1** (500 mg, 0.69 mmol) in dry CH_2Cl_2 (10 ml) was added dropwise a solution of (Bu^t_2SnO)$_3$ (172 mg, 0.23 mmol) in dry CH_2Cl_2 (10 ml). The mixture was stirred for 3 h at room temp. The solvent and the resulting $Bu^t_2SnCl_2$ were removed *in vacuo* to afford **2** as an amorphous colourless solid with mp 158–160 °C in quantitative yield (461 mg, 0.35 mmol). Single crystals were grown from hexane at 4 °C. Anal. Calc. for $C_{32}H_{76}O_2Cl_4Sn_4Si_8$: C, 28.80, H, 5.74. Found: C, 29.10, H, 5.60% ^{1}H NMR ($CDCl_3$, 400.13 MHz, 25 °C) δ 0.13 (s, 18H, $SiMe_3$), 0.18 (s, 18H, $SiMe_3$), 0.26 (s, 6H, $SiMe_2$), 0.31 (s, 6H, $SiMe_2$), 0.32 (s, 6H, $SiMe_2$), 0.34 (s, 6H, $SiMe_2$), 0.63 [d, 2H, ^2J(^{1}H–^{1}H) 12 Hz, CH_2], 0.81 [d, 2H, ^2J(^{1}H–^{1}H) 12 Hz, CH_2], 0.92 [d, 2H, ^2J(^{1}H–^{1}H) 12 Hz, CH_2], 0.93 [d, 2H, ^2J(^{1}H–^{1}H) 13 Hz, CH_2], 0.94 [d, 2H, ^2J(^{1}H–^{1}H) 12 Hz, CH_2], 1.02 [d, 2H, ^2J(^{1}H–^{1}H) 12 Hz, CH_2], 1.05 [d, 2H, ^2J(^{1}H–^{1}H) 13 Hz, CH_2], 1.19 [d, 2H, ^2J(^{1}H–^{1}H) 13 Hz, CH_2]. ^{13}C{^{1}H} NMR ($CDCl_3$, 100.63 MHz, 25 °C) δ 0.00 ($SiMe_2$), 0.95 ($SiMe_2$), 1.22 ($SiMe_3$), 1.61 ($SiMe_2$), 1.82 ($SiMe_3$), 2.18 ($SiMe_2$), 17.32 (CH_2), 19.45 (CH_2), 20.23 (CH_2), 20.58 (CH_2), 114.54 (C≡C), 117.81 (C≡C). ^{29}Si{^{1}H} NMR ($CDCl_3$, 79.49 MHz, 25 °C) δ −19.4 [2Si, ^2J($^{117/119}$Sn–^{29}Si) 67 Hz, $SiMe_2$], −19.2 [2Si, ^2J($^{117/119}$Sn–^{29}Si) 72 Hz, $SiMe_2$], 1.1 [2Si, ^2J($^{117/119}$Sn–^{29}Si) 19 Hz, $SiMe_3$], 1.2 [2Si, ^2J($^{117/119}$Sn–^{29}Si) 24 Hz, $SiMe_3$]. ^{119}Sn{^{1}H} NMR ($CDCl_3$, 149.21 MHz, 25 °C) δ −132.4 [2Sn, ^2J($^{117/119}$Sn–^{119}Sn) 63, 109/114 Hz, C_2SnO_2Cl], −75.8 [2Sn, ^2J($^{117/119}$Sn–^{119}Sn) 63, 111/116 Hz, C_2SnOCl_2].

¶ *Crystal data* for **2**: $C_{32}H_{76}Cl_4O_2Si_8Sn_4$, M_r = 1334.21, triclinic space group $P\bar{1}$, a = 13.240(1), b = 15.536(1), c = 16.387(1)Å, α = 78.643(1), β = 75.868(1), γ = 68.096(1)°, V = 3011.7(4) Å^3, Z = 2, D_c = 1.471 Mg m^{-3}, F(000) = 1328, λ(Mo-Kα) = 0.71069 Å, μ = 2.000 mm^{-1}, T = 291(1)K, final R = 0.032 for 7455 unique observed [$F > 4.0\sigma(F)$] diffractometer data. CCDC 182/1274. See http://www.rsc.org/suppdata/cc/1999/1291/ for crystallographic files in .cif format.

‖ *Synthesis and selected spectroscopic data for* **3**: to a solution of **2** (400 mg, 0.30 mmol) in CH_2Cl_2 (10 ml) was added water (10 ml) and Et_3N (61 mg, 0.60 mmol). The mixture was stirred for 3 h at room temperature. After addition of CH_2Cl_2 (20 ml) and water (20 ml) the phases were separated. The organic phase was washed with saturated NH_4Cl (20 ml) and water (20 ml), dried over Na_2SO_4, filtered and evaporated *in vacuo* to give **3** as an amorphous colourless solid with mp 207–208 °C in 97% yield (378 mg, 0.29 mmol). **3** can be recrystallized from CH_2Cl_2–hexane (1 : 1) to afford a crystalline colourless solid. Anal. Calc. for $C_{32}H_{78}O_4Cl_2Sn_4Si_8$: C, 29.62, H, 6.06. Found: C, 29.60; H, 6.10%. ^{1}H NMR ($CDCl_3$, 400.13 MHz, 25 °C) δ 0.11 (s, 18H, $SiMe_3$), 0.12 (s, 18H, $SiMe_3$), 0.21 (s, 6H, $SiMe_2$), 0.24 (s, 6H, $SiMe_2$), 0.33 (s, 6H, $SiMe_2$), 0.39 (s, 6H, $SiMe_2$), 0.40 [d, 2H, ^2J(^{1}H–^{1}H) 12 Hz, CH_2], 0.44 [d, 2H, ^2J(^{1}H–^{1}H] 12 Hz, CH_2), 0.50 [d, 2H, ^2J(^{1}H–^{1}H) 12 Hz, CH_2], 0.58 [d, 2H, ^2J(^{1}H–^{1}H) 13 Hz, CH_2], 0.59 [d, 2H, ^2J(^{1}H–^{1}H) 13 Hz, CH_2], 0.66 [d, 2H, ^2J(^{1}H–^{1}H) 13 Hz, CH_2], 0.77 [d, 2H, ^2J(^{1}H–^{1}H) 12 Hz, CH_2], 1.02 [d, 2H, ^2J(^{1}H–^{1}H) 13 Hz, CH_2], 2.96 [s, 2H, ^2J($^{117/119}$Sn–^{1}H) 8 Hz, OH]. ^{13}C{^{1}H} NMR ($CDCl_3$, 100.63 MHz, 25 °C) δ 0.32 ($SiMe_2$), 1.28 ($SiMe_2$), 1.33 ($SiMe_2$), 1.40 ($SiMe_3$), 1.61 ($SiMe_2$), 1.85 ($SiMe_3$), 11.44 (CH_2), 13.17 (CH_2), 15.29 (CH_2), 15.57 (CH_2), 117.65 (C≡C), 117.74 (C≡C). ^{29}Si{^{1}H} NMR ($CDCl_3$, 79.49 MHz, 25 °C) δ −19.1 [2Si, ^2J($^{117/119}$Sn–^{29}Si) 55 Hz, $SiMe_2$], −18.7 [2Si, ^2J($^{117/119}$Sn–^{29}Si) 49 Hz, $SiMe_2$], 1.2 [2Si, ^2J($^{117/119}$Sn–^{29}Si) 52 Hz, $SiMe_3$], 1.4 [2Si, ^2J($^{117/119}$Sn–^{29}Si) 52 Hz, $SiMe_3$]. ^{119}Sn{^{1}H} NMR ($CDCl_3$, 149.21 MHz, 25 °C) δ −153.1 [2Sn, ^2J($^{117/119}$Sn–^{119}Sn) 50, 88/92 Hz], −152.2 [2Sn, ^2J($^{117/119}$Sn–^{119}Sn) 50, 90/94 Hz].

1 R. Okawara and M. Wada, *J. Organomet. Chem.*, 1963, **1**, 81.
2 D. C. Gross, *Inorg. Chem.*, 1989, **28**, 2355 and references therein.
3 A. G. Davies, *Organotin Chemistry*, VCH, Weinheim, 1997, pp. 138–154.
4 F. Ribot, C. Sanchez, A. Meddour, M. Gielen, E. R. T. Tiekink, M. Biesemans and R. Willem, *J. Organomet. Chem.*, 1998, **552**, 177 and references therein.
5 O. Primel, M.-F. Llauro, R. Pétiaud and A. Michel, *J. Organomet. Chem.*, 1998, **558**, 19 and references therein.
6 J. Otera, N. Dan-Oh and H. Nozaki, *J. Org. Chem.*, 1991, **56**, 5307 and references therein.
7 A. Orita, A. Mitsutome and J. Otera, *J. Org. Chem.*, 1998, **63**, 2420 and references therein.
8 R. P. Houghton and A. W. Mulvaney, *J. Organomet. Chem.*, 1996, **517**, 107.
9 E. N. Suciu, B. Kuhlmann, G. A. Knudsen and R. C. Michaelson, *J. Organomet. Chem.*, 1998, **556**, 41.
10 D. Dakternieks, K. Jurkschat, D. Schollmeyer and H. Wu, *Organometallics*, 1994, **13**, 4121.
11 M. Mehring, M. Schürmann, I. Paulus, D. Horn, K. Jurkschat, A. Orita, J. Otera, D. Dakternieks and A. Duthie, *J. Organomet. Chem.*, 1999, **574**, 176.
12 B. Zobel, M. Schürmann, K. Jurkschat, D. Dakternieks and A. Duthie, *Organometallics*, 1998, **17**, 4096.
13 M. Mehring, M. Schürmann, H. Reuter, D. Dakternieks and K. Jurkschat, *Angew. Chem. Int. Ed. Engl.*, 1997, **36**, 1112.

Communication 9/01557D

A cluster growth route to quantum-confined CdS nanowires

Ping Yan, Yi Xie,* Yitai Qian and Xianming Liu

Structure Research Laboratory, and Department of Chemistry, University of Science and Technology of China, Hefei, Anhui, 230026, P.R. China. E-mail: yxie@ustc.edu.cn

Received (in Cambridge, UK) 8th March 1999, Accepted 29th April 1999

Quantum-confined CdS nanowires with diameters around 4 nm and lengths ranging from 150 to 250 nm were grown for the first time from cadmium bis(diethyldithiocarbamate) $[Cd(DDTC)_2]_2$ by removal of the four thione groups with ethylenediamine (en) at 117 °C for 2 min.

Semiconductor crystallites that are small in comparison to the bulk exciton diameter show quantum confinement effects, which have been intensely studied, and a number of good reviews have mirrored this development.[1,2] Various methods for the production of II–VI and III–V nanocrystals with narrow size distributions in the desired size range of between 1 and 15 nm in diameter have been developed.[3]

Special attention has been paid to one-dimensional structures, such as nanotubes and nanowires owing to their interesting properties.[4] However the challenge of fabricating such 1D structures is substantial because technologically useful quantum wires require lateral dimensions of < *ca*. 10 nm. Such a precision level is a formidable technological challenge.[5]

Recently very long CdTe nanowires[6] were fabricated by the molecular-beam epitaxy (MBE) growth technique, however, their diameters are much larger than 10 nm. Considering the small exciton diameter of CdS (6 nm), the preparation of quantum confined CdS nanowires (of diameter < 6 nm) is even more difficult. A promising route is deposition of semiconductors into anodic aluminium oxide membrane filters or nuclear track-etched polycarbonate membranes with small pores; the smallest semiconductor nanowire obtained by this method to date is 9 nm.[7]

Here, quantum confined CdS nanowires were successfully obtained for the first time from a cluster precursor $Cd_2(S_2CNEt_2)_4$, which can be regarded as an inorganic core $[Cd_2S_2]$ with four capping groups.[8] Nucleophilic attack by ethylenediamine at the thione carbon can lead to removal of the capping groups. This process is shown in Scheme 1 and the resulting organic product has been characterized.[9]

The inorganic Cd_2S_2 cores can then combine with each other and under appropriate chemical and physical environment, $[Cd_2S_2]$ may preferentially grow along a unique direction and result in a one-dimensional structure.

In a typical process, 1 g of $[Cd(S_2CNEt_2)]_2$, prepared by precipitation from a stoichiometric mixture of $NaS_2CN(C_2H_5)_2$ and $CdCl_2$ in water, was dissolved in 30 ml ethylenediamine in a flask, and then heated to reflux (117 °C), and maintained at this temperature for 2 min. The yellowish precipitate obtained was filtered off and washed with ethanol.

The X-ray diffraction (XRD)† pattern of the nanowires is shown in Fig. 1. All the reflections, to within experimental

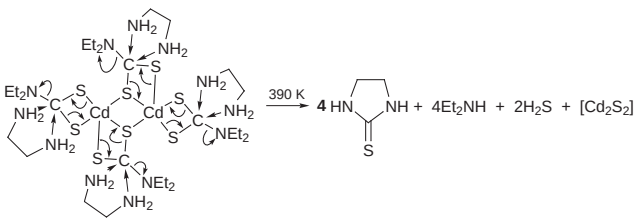

Scheme 1

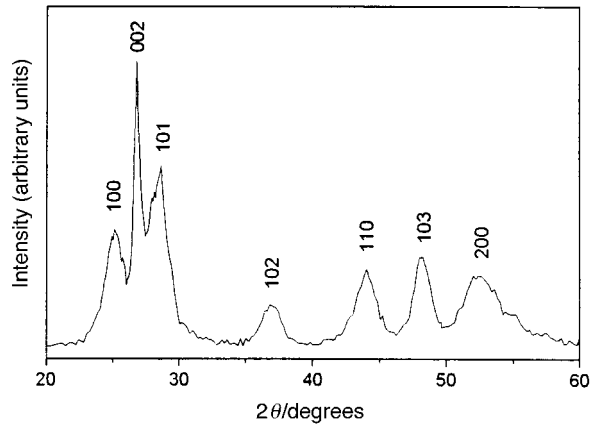

Fig. 1 XRD pattern for CdS nanowires.

error, fit that of bulk hexagonal CdS.[10] The (002) diffraction peak, the second strongest peak in bulk hexagonal CdS, is unusually narrow and strong, indicating a preferential growth along the *c* axis in the product. Using the Scherrer formula[11] on the (*hk*0) peaks (100) (110) and (200), the average diameter of the nanowires is estimated as 4.0 nm. This is confirmed by transmission electron microscopy (TEM)‡ images (Fig. 2), which reveal straight-line shapes and uniform diameters of *ca*. 4 nm and lengths ranging from 150 to 250 nm. IR spectroscopy was carried out to examine the purity of the product, and indicated the absence of both DDTC and ethylenediamine, suggesting a high degree of purity.

Fig. 3(a) shows the absorption spectrum of a sample dispersed in distilled water. The clear maximum at 455 nm is assigned to the optical transition of the first excitonic state.[2] The average particle diameter, as calculated from the maximum of the absorption curve (λ_m = 455 nm) is 3.8 nm[2] in good agreement with the TEM and XRD results. Since the onset of the absorption spectrum generally represents the larger end of

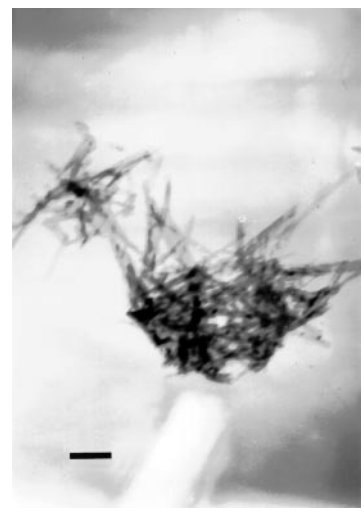

Fig. 2 TEM images of the nanowires (scale bar, 50 nm).

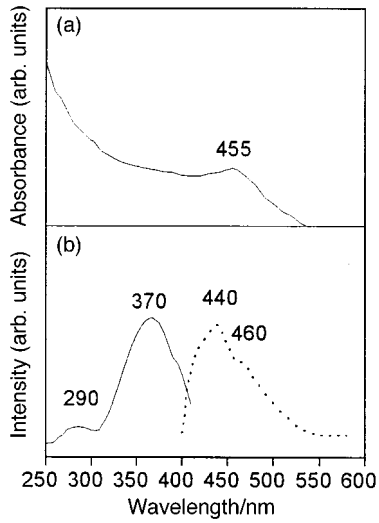

Fig. 3 (a) Absorption spectrum of a CdS sample dispersed in H_2O. (b) Excitation (solid line) and photoluminescence (dashed line) spectra of CdS nanowires. The spectra were taken in reflection geometry. The excitation wavelength for the emission spectrum was 370 nm, and the monitoring wavelength for the excitation spectrum was 440 nm.

the size distribution,[12] the position of the absorption edge (λ_e = 515 nm) shows that the lengths of the nanowires (150–250 nm) are much larger than the exciton diameter of CdS (6 nm). The large difference between sizes calculated from λ_e and λ_m, which can be related to the width of the particle size distribution, is characteristic for nanowires. The clear appearance of a blue-shift of the absorption peak relative to bulk CdS indicates that the CdS nanowires are quantum-confined. The excitation spectrum (monitoring wavelength at 440 nm) shows absorption bands at 290 and 370 nm [Fig. 3(b)]. Under photoluminescent excitation at 370 nm, the nanowires emit blue light at 440 and 460 nm [Fig. 3(b)] with a 55 nm blue shift relative to bulk CdS. These features are close to the optical absorption edge of CdS, suggesting a near band-edge emission.

When $[Cd(DDTC)_2]_2$ is thermolyzed at 250 °C for 30 min in trioctylphosphine oxide (TOPO), the morphology for most of the CdS nanocrystallites was reported to be thin plates.[13] In our experiments, other nucleophiles such as pyridine and diethylamine were also tested to remove the capping groups, however, no wire-like products were obtained. These results show that ethylenediamine plays a critical role in the formation of wire structures and probably serves as a director for the growth of the intermediate inorganic $[Cd_2S_2]$ core. Ethylenediamine has been extensively used as a template in solvothermal processes. For example, Li *et al*.[14] reported that elemental reaction of Cd and S in ethylenediamine resulted in CdS nanorods with diameters of 25–40 nm[14] although no detailed mechanism was proposed.

In summary, quantum-confined CdS nanowires with diameters of *ca*. 4 nm and lengths ranging from 150 to 250 nm have been grown for the first time from $[Cd(DDTC)_2]_2$, by removal of the four thione groups with ethylenediamine (en) at 117 °C for 2 min. Further studies may extend the method for the preparation of other quantum-confined nanowires.

Financial support from the Chinese National Foundation of Natural Science Research through the Outstanding Youth Science Fund and Huo Yingdong Foundation for Young Teachers is gratefully acknowledged. This work is also supported by the Climbing Plan from the State Science and Technology Commission of China.

Notes and references

† XRD patterns were obtained on a Japan Rigaku D/Max γA rotation anode X-ray diffractometer with Ni-filtered Cu-Kα radiation (λ = 1.54178 Å).
‡ TEM measurements were made on a Hitachi H-800 transmission electron microscope with an accelerating voltage of 200 kV.

1 A. P. Alivisatos, *Science*, 1996, **271**, 933.
2 H. Weller, *Angew. Chem., Int. Ed. Engl*., 1993, **32**, 41.
3 X. Peng, J. Wickham and A. P. Alivisatos, *J. Am. Chem. Soc*., 1998, **120**, 5343.
4 A. M. Morales and C. M. Lieber, *Science*, 1998, **279**, 208.
5 M. Sundaram, S. A. Chalmers, P. F. Hopkins and A. C. Gossard, *Science*, 1991, **254**, 1326.
6 B. P. Zhang, W. X. Wang, T. Yasuda, Y. Segawa, H. Yaguchi, K. Onabe, K. Edamatsu and T. Itoh, *Mater. Sci. Eng. B*, 1998, **51**, 224.
7 D. Routkevitch, T. Bigioni, M. Moskovits and J. M. Xu, *J. Phys. Chem*., 1996, **100**, 14037.
8 A. Domenicano, L. Torelli, A. Vaciago and L. Zambonelli, *J. Chem. Soc. A*, 1968, 1351.
9 K. Ramadas and N. Janarthanan, *J. Chem. Res. S*, 1998, 228.
10 Joint Committee on Powder Diffraction Standards (JCPDS), File No. 41-1049, CdS.
11 H. P. Klug and L. E. Alexander, in *X-Ray Diffraction Procedures for Polycrystalline and Amorphous Materials*, Wiley, New York, 1962, p. 491.
12 M. Moffitt, L. McMahon, V. Pessel and A. Eisenberg, *Chem. Mater*., 1995, **7**, 1185.
13 T. Trindade, P. O'Brien and X. Zhang, *Chem. Mater*., 1997, **9**, 523.
14 Y. D. Li, H. W. Liao, Y. Ding, Y. T. Qian, L. Yang and G. Zhou, *Chem. Mater*., 1998, **10**, 2301.

Communication 9/01821B

Catalytic enantioselective aryl transfer: asymmetric addition of diphenylzinc to aldehydes

Carsten Bolm* and Kilian Muñiz

Institut für Organische Chemie der RWTH Aachen, Professor-Pirlet-Str. 1, D-52074 Aachen, Germany. E-mail: carsten.bolm@oc.rwth-aachen.de

Received (in Liverpool, UK) 17th May 1999, Accepted 26th May 1999

The asymmetric addition of diphenylzinc to aldehydes in the presence of catalytic amounts of a planar chiral ferrocene-based hydroxy oxazoline affords products with enantiomeric excesses of up to 96%.

The asymmetric addition of organozinc reagents (ZnR_2) to aldehydes is a well understood process in which the transferred moiety R is generally an alkyl group such as methyl, ethyl or isopropyl. A variety of chiral compounds catalyse this process yielding the corresponding secondary alcohols with excellent enantiomeric excesses.[1] In contrast, asymmetric transition metal catalysed C–C bond formations between aldehydes and suitable *aryl* transfer reagents are still rare.[2] In this context, Fu described the addition of diphenylzinc to 4-chlorobenzaldehyde which, in the presence of 3 mol% of a planar chiral azaferrocene, gave the product with 57% ee.[3] So far, this has been the only report on this type of arylation.[4,5] In a complementary approach, Miyaura recently described the rhodium catalysed addition of phenylboronic acid to naphthaldehyde. In the presence of an axially chiral monophosphine as ligand, an enantiomeric excess of 41% ee was obtained for the product.[6]

We have recently investigated the influence of planar chirality on asymmetric alkylation reactions catalysed by a series of ferrocenyl hydroxy oxazolines.[7–9] Within this project, the syntheses and catalytic applications of compounds **1a** and **1b** have been described.[7b] We have now employed these

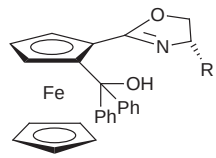

1a R = Bu^t
b R = Ph

ferrocenes in asymmetric arylations by catalysed addition of diphenylzinc to aldehydes.[10] First, the reaction conditions were optimised using 4-chlorobenzaldehyde (**2**) as substrate (Table 1).

Even with as little as 3 mol% of ferrocene **1a** quantitative formation of **3** was observed, indicating the efficiency of this catalysis (Table 1, entry 1). HPLC using a chiral stationary phase revealed an enantiomeric excess of 64% for the resulting secondary alcohol. By incresing the catalyst loading to 5 and 10 mol%, the ee of **3** was raised to 82 and 88% ee, respectively (entries 2, 3). Ferrocene **1b** proved to be equally efficient and gave identical results (entry 5). Finally, the reaction temperature was lowered to −20 °C. Still, high conversion was achieved, but the increase in ee was only minor (entry 4). It is of note that the absolute configuration of the product is *R*, indicating that the face selectivity of the catalysis is unchanged with regard to the related alkylation reactions described before.[7] Such unchanged selectivity had also been reported by Fu,[3] but contrasts the findings by Soai observed in reactions with *in situ* formed diphenylzinc.[1d,5a]

Table 1 Asymmetric addition of diphenylzinc to 4-chlorobenzaldehyde (**2**) in the presence of catalytic amounts of ferrocene **1a** or **1b**

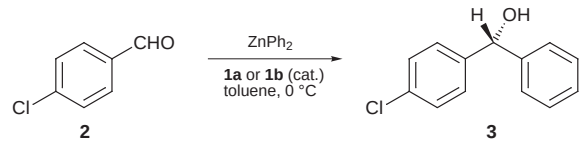

2 **3**

Entry	Ferrocene (mol %)	*t*/h	Yield[a] (%)	Ee of **3**[b] (%)	Configuration[c]
1	**1a** (3)	12	99	64	*R*
2	**1a** (5)	15	99	82	*R*
3	**1a** (10)	14	99	88	*R*
4[d]	**1a** (10)	11	92	90	*R*
5	**1b** (10)	13	99	88	*R*

[a] Isolated yield after column chromatography. [b] Determined by HPLC using a chiral stationary phase (Chiralcel OB, *n*-hexane–Pr^{i}OH = 4:1, 1.0 ml min^{-1}). [c] Determined by comparison of the optical rotation with literature values. [d] Reaction was carried out at −20 °C.

In order to guarantee a reasonable catalytic process, the catalysts loading was limited to 5 mol% and the reaction temperature was maintained at 0 °C in further studies. Under these conditions, several other aldehydes were submitted to the asymmetric arylation using ferrocene **1a** as catalyst precursor (Table 2).

Several conclusions can be drawn from these results: unsubstituted or *para*-substituted aromatic aldehydes give the highest enantioselectivities (entries 1, 2). *ortho*-Substituents at the aryl group lower the product ee of aromatic substrates (entries 3, 4). Aliphatic aldehydes give enantioselectivities up to a 75% ee as obtained for acetaldehyde (entries 5, 6). A sterically

Table 2 Asymmetric addition of diphenylzinc to various aldehydes in the presence of 5 mol% of ferrocene **1a**

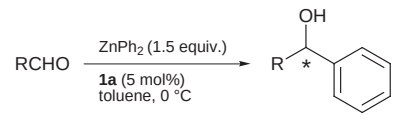

Entry	R	*t*/h	Yield[a] (%)	Ee[b] (%)	Configuration[d]
1	4-ClC_6H_4	15	99	82	*R*
2	Ferrocenyl	11	89	⩾96[c]	*R*
3	2-BrC_6H_5	14	98	31	*R*
4	1-Naphthyl	14	99	28	*R*
5	Me	15	94	75	*S*
6	Ph$(CH_2)_2$	10	91	50	*S*
7	Bu^t	16	99	56	*S*
8	2-Pyridyl	12	98	3	*R*

[a] Isolated yield after column chromatography. [b] Determined by chiral HPLC on stationary phase. [c] Determined by ^{1}H NMR in the presence of Eu(tfc)$_3$. [d] Determined by comparison of the optical rotation with literature values.

demanding *tert*-butyl group does not allow a high ee (entry 7).

The low enantioselectivity in the arylation of 2-formylpyridine (entry 8) is due to a competitive uncatalysed nonselective reaction of diphenylzinc with the substrate itself.[11] Unlike all other arylations where a dark orange to red solution was obtained, in this case the reaction mixture turns light yellow immediately after the addition of the aldehyde. A control experiment in the absence of **1a** showed a solution of identical colour. From this reaction mixture the product alcohol was isolated in 97% yield. Thus, we assume that the arylation of this substrate is initiated by the pyridine itself leading to a product which then is able to catalyse its own formation in an non-stereoselective manner giving racemic pyridyl alcohol.[1*d*,12,13]

In order to reveal details of the nature of the active catalytic species, a catalysis with scalemic **1b** was performed: arylation of 4-chlorobenzaldehyde (**2**) in the presence of 10 mol% of **1b**, which had an enantiomeric excess of 57%, led to the formation of (*R*)-4-chlorophenyl(phenyl)methanol [(*R*)-**3**] with 48% ee. From this correlation between the enantiomeric excesses of the ferrocene and the product[13] we conclude that heterodimeric species are not involved in the catalytic conversion of the substrate. This is in accordance with our previous results for related alkylation reactions with non-enantiopure ferrocenyl oxazolines.[7–9,14]

In summary, we have described a novel catalytic system for asymmetric arylations of various differently substituted aldehydes employing diphenylzinc as organometallic aryl source.

We are grateful to the Fonds der Chemischen Industrie and to the Deutsche Forschungsgemeinschaft (DFG) within the Collaboraive Research Center (SFB) 380 ‘Asymmetric Synthesis by Chemical and Biological Methods’ for financial support.

Notes and references

1 (*a*) R. Noyori, *Asymmetric Catalysis in Organic Synthesis*, Wiley, New York, 1994, ch. 5, p. 255; (*b*) R. Noyori and M. Kitamura, *Angew. Chem., Int. Ed. Engl.*, 1991, **30**, 49; (*c*) K. Soai and S. Niwa, *Chem. Rev.*, 1992, **92**, 833; (*d*) K. Soai and T. Shibata, *J. Synth. Org. Chem. Jpn.*, 1997, **55**, 994; (*e*) D. Seebach, D. A. Plattner, A. K. Beck, Y. M. Wang, D. Hunziker and W. Petter, *Helv. Chim. Acta*, 1992, **75**, 2171.

2 (*a*) For a pioneering report on an asymmetric phenylation in the presence of stoichiometric amounts of a chiral titanium–BINOL complex, see: D. Seebach, A. K. Beck, S. Roggo and A. Wonnacott, *Chem. Ber.*, 1985, **118**, 3673; (*b*) For a later catalytic version employing Ti–TADDOLates, see: B. Weber and D. Seebach, *Tetrahedron*, 1994, **50**, 7473.

3 P. I. Dosa, J. C. Ruble and G. C. Fu, *J. Org. Chem.*, 1997, **62**, 444.

4 For the addition of $ZnPh_2$ to prochiral ketones, see: P. I. Dosa and G. C. Fu, *J. Am. Chem. Soc.*, 1998, **120**, 445.

5 Other reports on $ZnPh_2$ additions to aldehydes: (*a*) K. Soai, Y. Kawase and A. Oshio, *J. Chem. Soc., Perkin Trans. 1*, 1991, 1613; (*b*) J. Hübscher and R. Berner, *Helv. Chim. Acta*, 1990, **73**, 1068. However, these reactions employ *in situ* generated $ZnPh_2$ from $ZnCl_2$ and a Grignard precursor and seem not to involve a defined $ZnPh_2$ species as had already been discussed in ref. 1(*c*), 3.

6 M. Sakai, M. Ueda and N. Miyaura, *Angew. Chem. Int. Ed.*, 1998, **37**, 3475.

7 (*a*) C. Bolm, K. Muñiz Fernández, A. Seger and G. Raabe, *Synlett*, 1997, 1051; (*b*) C. Bolm, K. Muñiz Fernández, A. Seger, G. Raabe and K. Günther, *J. Org. Chem.*, 1998, **63**, 7860.

8 K. Muñiz Fernández, PhD thesis, RWTH Aachen, 1999.

9 C. Bolm, K. Muñiz and J. P. Hilderbrand, *Org. Lett.*, in press.

10 Diphenylzinc was perchased from Strem (ref. 3) and stored as a 2.0 M solution in toluene. Under these conditions $ZnPh_2$ proved to be stable over a long period of time.

11 Recent examples of *asymmetric* autocatalyses: T. Shibata, S. Yonekubo and K. Soai, *Angew. Chem., Int. Ed.*, 1999, **38**, 659; T. Shibata, J. Yamamoto, N. Matsumoto, S. Yonekubo, S. Osanai and K. Soai, *J. Am. Chem. Soc.*, 1998, **120**, 12 157; C. Bolm, A. Seger and F. Bienewald, *Organic Synthesis Highlights III*, ed. J. Mulzer and H. Waldmann, Wiley-VCH, Weinheim, 1998, p. 79.

12 For a structurally related pyridyl alcohol in asymmetric $ZnEt_2$ additions, see: C. Bolm, M. Zehnder and D. Bur, *Angew. Chem., Int. Ed. Engl.*, 1990, **29**, 205; C. Bolm, G. Schlingloff and K. Harms, *Chem. Ber.*, 1992, **125**, 1191.

13 C. Girard and H. B. Kagan, *Angew. Chem., Int. Ed.*, 1998, **37**, 2922; C. Bolm, *Advanced Asymmetric Synthesis*, ed. R. Stephenson, Capman and Hall, London, 1996, p. 9. M. Avalos, R. Babiano, P. Ciutas, J. L. Jiménez and J. C. Palacios, *Tetrahedron: Asymmetry*, 1997, **8**, 2997.

14 To date, there is only one report on a non-linear effect (NLE) for a ferrocene ligand in an asymmetric diethylzinc addition: G. Nicolosi, A. Patti, R. Morrone and M. Piattelli, *Tetrahedron: Asymmetry*, 1994, **5**, 1639.

Communication 9/03884A

Synthesis and α-substitution reactions of methoxime derivatives of alkene-carbon monoxide alternating copolymers

Paveena Khansawai, R. Michael Paton* and David Reed

Department of Chemistry, The University of Edinburgh, West Mains Road, Edinburgh, UK EH9 3JJ. E-mail: r.m.paton@ed.ac.uk

Received (in Cambridge, UK) 28th April 1999, Accepted 1st June 1999

Poly(1-methoxyiminotrimethylene) 5 and poly[(1-methoxyiminotrimethylene)-*co*-(1-methoxyimino-3-methyltrimethylene)] 6, prepared by reaction of ethene/propene–carbon monoxide alternating copolymers with methoxylamine, undergo α-substitution on treatment with BuLi followed by addition of electrophiles such as MeI.

Alternating copolymers of alkenes and carbon monoxide are proving to be useful starting materials for the preparation novel functionalised polymers.[1–5] Reaction can take place at individual ketone groups or at 1,4-dione units; for example, the ketones can be converted to their 1,3-dioxolane derivatives by acid-catalysed reaction with 1,2-diols,[4] whereas with primary amines Paal–Knorr condensation of 1,4-diones affords poly(ethylenepyrroles).[2] We have previously described[5] the conversion of ethene-carbon monoxide copolymer **1** (E-CO) and

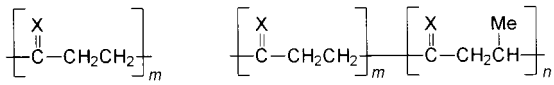

1 X = O (E-CO)
3 X = NOH
5 X = NOMe

2 X = O (EP-CO)
4 X = NOH
6 X = NOMe

ethene/propene–carbon monoxide copolymer **2** (EP-CO) to polyketoximes **3** and **4** on treatment with hydroxylamine. We now report that reaction with methoxylamine affords the corresponding methoxime polymers **5** and **6**, and that these readily undergo base-induced reactions with electrophiles at the α-methylene group.

Reaction of E-CO or EP-CO with methoxylamine in pyridine at room temperature resulted in slow dissolution of the polymer and complete conversion of the ketone groups to their methoxime derivatives. In a typical experiment a suspension of E-CO (M_n = 1500, 100 mg) was stirred with a four-fold excess of methoxylamine hydrochloride (595 mg) in pyridine (10 ml) at room temperature for two days. The resulting homogeneous solution was poured into water (50 ml) and the product extracted into $CHCl_3$. Washing with aq. Na_2CO_3 and water, drying, and removal of the solvent afforded poly(1-methoxyiminotrimethylene) **5** as a pale yellow gum (71%), which was purified by precipitation from $CHCl_3$ by addition of MeOH. EP-CO (m = 0.99, n = 0.01)† and EP-CO (m = 0.85, n = 0.15)‡ reacted similarly, yielding poly[(1-methoxyiminotrimethylene)-*co*-(1-methoxyimino-3-methyltrimethylene)] **6**. The products were identified from their spectroscopic properties§ by comparison with the corresponding polyketoximes **3** and **4**, and with 2,5-bis(methoxyimino)hexane **7**¶ and 3,6,9-tris(methoxyimino)undecane **8**¶ which were prepared as model compounds by methoximation of hexane-2,5-dione and undecane-3,6,9-trione respectively. For polymethoxime **5** the conversion of ketone units in the polymer to methoximes is evident from the infrared spectrum in which the carbonyl absorption at 1690 cm^{-1} is replaced by a C=N peak at 1630 cm^{-1}. Furthermore in the ^{13}C NMR spectrum the carbonyl absorptions of the starting material at 208–210 ppm are absent and there are new characteristic peaks for the imino carbons at 158.57 and 158.48 ppm, similar to those found at 161–157 ppm for the *E,E-*, *E,Z-* and *Z,Z*-isomers of model dimethoxime **7** and at 161–158 ppm for trimethoxime **8**. There are also signals for the methylene carbons at 30.63, 30.50, 30.03, 29.88, 25.35, 25.07, 24.43 and 24.13 ppm, similar to those reported[5] for polyketoxime **3**. The multiplicity of peaks in this region is attributed to the presence of *syn-anti*, *syn-syn*, *anti-anti* and *anti-syn* combinations of neighbouring oximes; those at higher frequency (29–31 ppm) are assigned to the α-*anti*-carbons by comparison with literature data for methoxyimino compounds.[6] The presence of methoxy groups is shown by signals at 3.78 (^1H) and 61.10 (^{13}C) ppm. Unlike the precursor alkene–carbon monoxide copolymers (**1**, **2**) and the polyoximes (**3**, **4**) all the new polymethoximes show good solubility in a range of organic solvents, thus giving increased scope for modification reactions.

All previous modifications have involved manipulation of the carbonyl groups, either singly or as 1,4-dione or 1,4,7-trione units. Functionalisation of the backbone methylene groups has not been achieved so far, largely due to the very low solubility of these polymers in common organic solvents. The availability of the new polymethoxime derivatives described above provided the opportunity to examine the feasibility of base-induced α-substitution reactions with electrophiles, as illustrated in Scheme 1.

Preliminary experiments were carried out using the model methoximes **7** and **8** in order to establish suitable reaction conditions and also to facilitate spectroscopic identification of the polymer products. Treatment of dimethoxime **7** (1.16 mmol) in THF at −78 °C with BuLi (3.52 mmol), followed by addition of MeI (3.55 mmol) afforded, on work-up, a mixture of compounds **9** and **10** (96% combined yield). Trimethoxime **8** reacted similarly yielding a mixture of α-methylated products (62%), of which compounds **11** and **12** are representative examples. The corresponding reactions of methoximes **7** and **8** with BnBr afforded α-benzylated products **13**/**14** (24%) and *e.g.* **15**/**16** (58%) respectively. The *syn* selectivity of the lithiation process[6,7] was established by reacting dimethoxime **7** with BuLi in THF at −78 °C and quenching the resulting solution with [*O*-^2H]methanol. The isolated product was shown by NMR spectroscopy to be predominantly a mixture of mono- and dideuterio compounds **17** and **18**, together with some unreacted

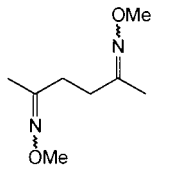

7

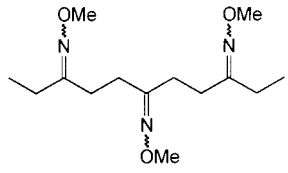

8

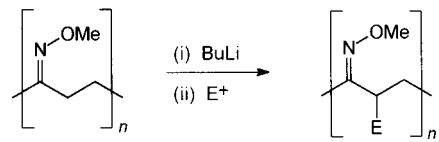

Scheme 1

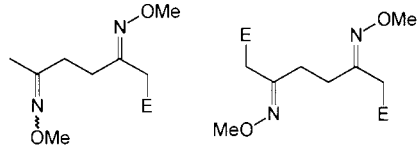

9 E = Me
13 E = Bn
17 E = D

10 E = Me
14 E = Bn
18 E = D

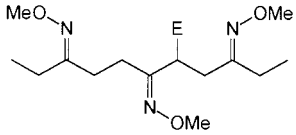

11 E = Me
15 E = Bn
19 E = D

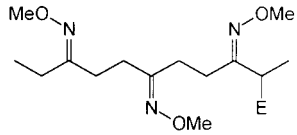

12 E = Me
16 E = Bn
20 E = D

starting material. α-Deuteration at the *syn* methyl is confirmed by the presence of a peak at 1.79 ppm in the ^{2}H NMR spectrum; there is also a corresponding reduction of *ca*. 30% in the intensity of the signal for the protons of this group in the ^{1}H spectrum, with part of the singlet at 1.79 ppm in the starting material being replaced by a 1:1:1 triplet at 1.75 ppm. The analogous reaction of trimethoxime **8** resulted in 8% deuterium incorporation, representing an average of one hydrogen atom being replaced per molecule. Deuterium NMR peaks at 2.16, 2.27 and 2.44 ppm indicate isotopic substitution at several of the syn α-methylene positions, *e.g*. **19**/**20**.

Having established that directed α-substitutions could be accomplished on the model compounds the reactions of the polymethoximes were studied under similar conditions. To test the extent of anion formation a sample of EP-CO-derived polymethoxime **6** (m = 0.99, n = 0.01) was treated with BuLi (5 equiv.), excess [*O*-^{2}H]methanol added to the resulting solution, and the recovered polymer examined by NMR spectroscopy. α-Substitution in the product **21** is confirmed by

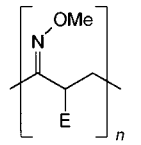

22 E = Me or H
23 E = Bn or H

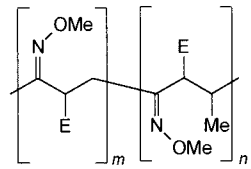

21 E = D or H
24 E = Me or H
25 E = Bn or H

the presence of a peak at 2.45 ppm in the ^{2}H NMR spectrum very similar to that observed for the model compounds **19**/**20**; there is also a *ca*. 15% reduction in the intensity of the signal for the methylene protons in the ^{1}H spectrum, indicating that on average there are ~0.6 deuterium atoms per methoxime unit.

These results suggested that multiple electrophilic substitutions on the polymer backbone should be possible, and to test the feasibility of introducing alkyl substituents by this means the polymethoxime polyanions were reacted with MeI and BnBr. E-CO-derived polymethoxime **5** (100 mg) in dry THF was treated with BuLi (1.0 equiv.) at −78 °C and MeI (1.0 equiv) added to the resulting solution. After stirring for 2 h at −78 °C and warming to 0 °C the mixture was quenched with water and the product extracted into Et_2O. Drying, removal of the solvent *in vacuo* and precipitation from $CHCl_3$ solution by addition of MeOH afforded a pale yellow gum (60 mg). The NMR spectra of the product **22** were broadly similar to those observed for the polymethoxime **6** (m = 0.85, n = 0.15) previously prepared by methoximation of the alternating copolymer of carbon monoxide and 85% ethene/15% propene. The introduction of the methyl substituents was confirmed by the appearance of a new proton doublet signal at 1.00 ppm with a 6.7 Hz coupling to the adjacent backbone CH; by comparison with the oximino methyl signal the extent of reaction was estimated as 29%. In the ^{13}C NMR spectrum there are additional peaks for the ethylidene group at 16.28, 16.67 (CH_3) and 29.27, 36.00 ppm (CH). The reaction of E-CO polymethoxime **5** with BnBr proceeded similarly, yielding a yellow gum (**23**) which was purified by precipitation from $CHCl_3$ by addition of MeOH. The NMR spectra of the product showed characteristic peaks for the benzylidene group [7.1–7.3 ppm (Ph*H*); 37.52 (*C*HPh), 126.13, 128.18, 128.69 (Ph*C*H), 139.34 ppm (Ph*C*)] similar to those observed for model compounds **13**–**16**. From the proton spectrum it was estimated that there were on ~0.3 benzyl groups per methoxime unit. The corresponding reactions of BuLi / MeI and BuLi / BnBr with EP-CO-derived polymethoximes **6** (m = 0.99, n = 0.01) and **6** (m = 0.85, n = 0.15) proceeded in a similar manner to afford modified polymers **24** and **25**. On the basis of the deuterium exchange experiments it is presumed that for all the alkylated polymers the substituents are introduced *syn* to the methoximino group.

In conclusion, the conversion of the ketone groups in alkene–carbon monoxide copolymers to methoximes allows directed α-substitution reactions to be carried out on the polymer backbone. Previous modification reactions have all involved functionalisation at the carbonyl groups; the results described above therefore represent the first examples involving reaction at the alkene units. It is anticipated that a range of novel polymers will be accessible by reaction with appropriate electrophiles.

We thank BP Chemicals for the supply of the ethene/propene–carbon monoxide alternating copolymers, and the Royal Thai Government for a Scholarship (P. K.).

Notes and references

† Alternating copolymer of CO and 99% ethene/1% propene.
‡ Alternating copolymer of CO and 85% ethene/15% propene.
§ NMR spectra were acquired on either a Bruker WH360 (^{1}H, ^{2}H, ^{13}C) or Bruker AC250 (^{13}C) spectrometer.
¶ Compounds **7** and **8** were mixtures of *E*- and *Z*-isomers.

1 A. Sen, *Adv. Polym. Sci.*, 1986, **73/74**, 125.
2 *E.g.* J.-T. Chen, Y.-S. Yeh and A. Sen, *J. Chem. Soc., Chem. Commun.*, 1989, 965; A. Sen, Z. Jiang and J.-T. Chen, *Macromolecules*, 1989, **22**, 2014; Z. Jiang and A. Sen, *Macromolecules*, 1992, **25**, 880.
3 Z. Jiang, S. Sanganeria and A. Sen, *J. Polym. Sci., Polym. Chem. Ed.*, 1994, **32**, 841.
4 M. J. Green, A. R. Lucy, S.-Y. Lu and R. M. Paton, *J. Chem. Soc., Chem. Commun.*, 1994, 2063.
5 S.-Y. Lu, R. M. Paton, M. J. Green and A. R. Lucy, *Eur. Polym. J.*, 1996, **32**, 1285.
6 S. Shatzmiller and R. Lidor, *Synthesis*, 1983, 590.
7 T. A. Spencer and C. W. Leong, *Tetrahedron Lett.*, 1975, 3889; R. R. Fraser and K. L. Dhawan, *J. Chem. Soc., Chem. Commun.*, 1976, 674; H. Ensley and R. Lohr, *Tetrahedron Lett.*, 1978, 1418.

Communication 9/03411K

Exchange reaction of a decanethiol self-assembled monolayer with porphyrin disulfides observed by surface plasmon enhanced fluorescence spectroscopy

Akito Ishida* and Tetsuro Majima

The Institute of Scientific and Industrial Research, Osaka University, Mihogaoka 8-1, Ibaraki, Osaka 567-0047, Japan. E-mail: ishida@sanken.osaka-u.ac.jp

Received (in Cambridge, UK) 27th April 1999, Accepted 8th June 1999

The treatment of a decanethiol SAM with a solution of a porphyrin disulfide gives a SAM inlaid with the porphyrin chromophores adopting J-aggregate-like partially stacked and well oriented structures by site-selective exchange reaction in the SAM.

Molecular exchange in a self-assembly monolayer (SAM) is a fundamental subject of surface science, and experimental[1–4] and theoretical[5] approaches to the reaction process have been developed. Here, we report the exchange reactions of decanethiol SAMs with porphyrin disulfides having trimethylene (**1a**) or decamethylene (**1b**) chains using surface plasmon (SP)

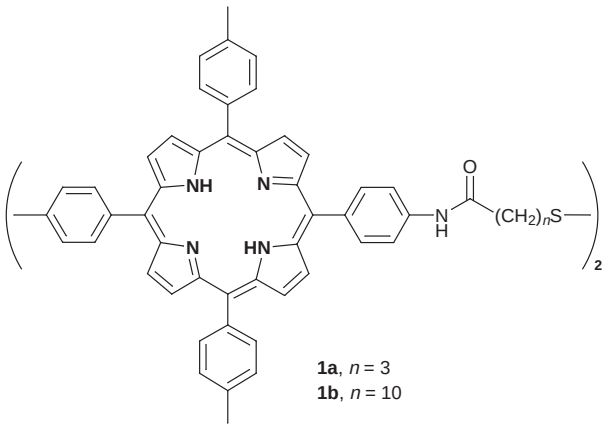

1a, $n = 3$
1b, $n = 10$

enhanced fluorescence spectroscopy.† SP is an effective excitation method for photo-functional molecules on a gold or silver film to give enhanced fluorescence,[6–8] and we employed p-polarization to observe the anisotropy‡ as well as other fluorescence properties.

Decanethiol SAMs were prepared by immersion of bare gold films on BK-7 right-angle prisms in a 1 mmol dm^{-3} 1,2-dichloroethane (DCE) solution of decanethiol for 5 h. The resulting decanethiol SAMs were then very carefully immersed into 50 μmol dm^{-3} DCE solutions of **1a** or **1b**, for a suitable time. After carefully washing the surface with DCE, the fluorescence properties were measured by SP excitation in air.[6] Fig. 1 shows changes in the fluorescence properties for the exchange reaction of decanethiol SAMs by **1a** and **1b**, as a function of the immersion time. The remarkable differences demonstrate that the exchange efficiency as well as the motion of the *transplanted* porphyrin chromophores in the SAM depended strongly upon the methylene chain length of **1**.

Very weak fluorescence of the porphyrin with rather large anisotropy was observed independently of the immersion time for **1a** even after a few minutes. This indicates that no exchange reaction with **1a** occurred except for fast exchange in a few minutes. It is well known that decanethiol gives a very tight and densely packed SAM on a flat gold surface. The trimethylene chains of **1a** are too short to penetrate the decanethiol SAM for interaction between the disulfide group and the surface and thus **1a** did not induce an exchange reaction.§

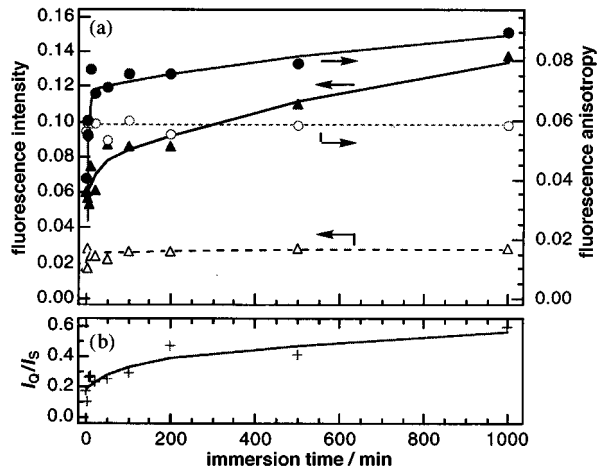

Fig. 1 Changes in the fluorescence properties for the exchange reaction; (a) anisotropy: (○) **1a**, (●) **1b** and intensity (△) **1a**, (▲) **1b**; (b) intensity ratio between the Soret and Q-bands (I_Q/I_S) of the excitation spectrum for **1b**. An almost constant I_Q/I_S value of 1.5 was observed for **1a**.

The very weak fluorescence observed for **1a** is probably attributed to the very small numbers of porphyrin-linked trimethylenethiol groups attached on the gold surface at defects in the decanethiol SAM. Because the porphyrin-linked trimethylene thiols have capped the defects, no further exchange reaction can occur.

In sharp contrast to **1a**, significant increases of fluorescence intensity and anisotropy were observed for **1b** at an initial immersion time of 50 min. These changes demonstrate effective exchange by **1b**, and the resulting porphyrin-linked decanethiols in the SAM are gradually ordered and lose their freedom of motion as the exchange reaction proceeds. The increase of the anisotropy can be rationalized by the increase of π–π stacking of the porphyrin chromophores which causes a characteristic change in the absorption spectrum. This is reflected in the SP enhanced fluorescence excitation spectra shown in Fig. 2.

The Q-bands increased strikingly with increased the immersion time.¶ It is well known that the π–π stacking of porphyrins

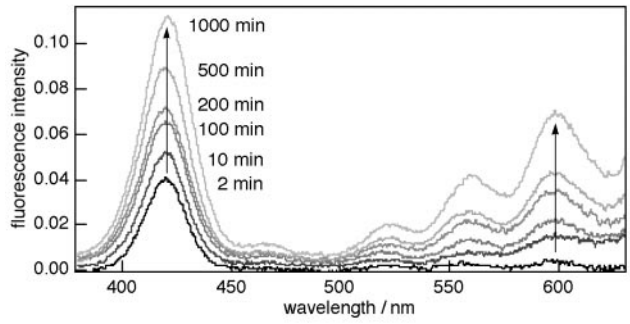

Fig. 2 Changes in the SP enhanced fluorescence excitation spectra for the exchange reaction of a decanethiol SAM with a 50 μmol dm^{-3} DCE solution of **1b** (λ_{em} = 725 nm; λ_{ex} = 425 nm).

reduces the intensity of the Soret band and that the relative ratio between the Soret and Q-bands (I_Q/I_S) increases.[9] Therefore, the changes in the excitation spectra demonstrate that the initially formed monomeric porphyrin-linked decanethiols in the SAM gradually change to a stacked structure as the exchange reaction proceeds. Because the excitation spectrum after 1000 min immersion shows maxima of the Soret bands at 420 and 470 nm, the porphyrin chromophores seem to adopt partially stacked structures similar to J-aggregates.[9] The increase of the fluorescence anisotropy is attributable to the increase of well oriented stacked structures which are more inflexible than the monomeric porphyrin chromophores.

Two possible mechanisms are presumed for the gradual stacking; (i) lateral migration of the porphyrin-linked decanethiol units exchanged at random in the SAM,‖ or (ii) site-selective exchange reaction nearby initially exchanged porphyrin-linked decanethiols. We have carried out the successive exchange reaction using a zinc complex of **1b** (**1b**–Zn) followed by **1b**. A decanethiol SAM was immersed into a 50 μmol dm^{-3} DCE solution of **1b**–Zn for 3 min and the resulting SAM showed characteristic fluorescence of the Zn–porphyrin (Fig. 3). This SAM was then immersed into a 50 μmol dm^{-3} DCE solution of **1b** for 30 s. After this treatment, the fluorescence of the Zn–porphyrin completely disappeared and was replaced by fluorescence of the free-base porphyrin (Fig. 3). This demonstrates fluorescence resonance energy transfer (FRET) from the Zn–porphyrin chromophores to the neighboring free-base porphyrin chromophores which have a lower singlet excitation energy than that of the Zn–porphyrin.** Because the efficiency of FRET is highly dependent upon the distance between the donor and acceptor, the free-base porphyrin chromophores must be exchanged nearby the Zn–porphyrin chromophores. The small numbers of initially exchanged porphyrin chromophores are likely to disturb the surrounding decanethiol SAM so leading to active sites, or act to increase the local concentration of **1b** by π–π interactions.

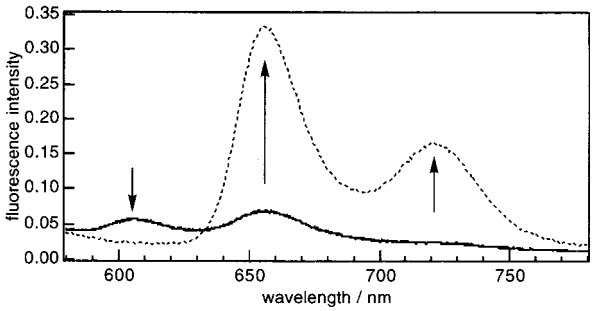

Fig. 3 The fluorescence spectra of the decanethiol SAM exchanged by a 50 μmol dm^{-3} DCE solution of **1b**–Zn for 3 min before (——) and after (- - - -) successive treatment with a 50 μmol dm^{-3} DCE solution of **1b** for 30 s (λ_{ex} = 420 nm).

We have demonstrated that the treatment of a decanethiol SAM with **1b** gives a SAM inlaid with the porphyrin chromophores adopting J-aggregate-like partially stacked and well oriented structures by site-selective exchange reaction.

This work was supported by a Grant-in Aid for Scientific Research from the Ministry of Education, Science, Sports and Culture of Japan (A. I. and T. M.), and Research Area of 'Fields and Reactions' in PRESTO Project of JST Corporation (A. I.), NEDO (A. I.), and the Kansai Research Foundation (A. I.).

Notes and references

† The porphyrin disulfides were synthesized and purified by reported procedures (T. Akiyama, H. Imahori and Y. Sakata, *Chem. Lett.*, 1994, 1147). A 50 nm gold film was directly evaporated on the hypotenuse face of a 15 × 15 × 15 mm BK-7 right-angle prism at a pressure of $< 6 \times 10^{-4}$ Pa, rinsed with 1,2-dichloroethane (DCE) and dried in class-100 air.

‡ The degree of polarization (r) of the β bands are calculated by the fluorescence intensities at parallel ($I_{\|}$) and perpendicular ($I_{\perp}$) polarizer configurations as $r = (I_{\|} - I_{\perp}) / (I_{\|} + 2I_{\perp})$.

§ The inefficient exchange reaction of **1a** may also be a consequence of **1a** having an odd number of methylene units. This may result in steric or kinetic barriers such as unfavorable orientation of the porphyrin chromophores of **1a** initially adsorbed in the decanethiol SAM.

¶ The fluorescence excitation spectrum of a porphyrin SAM by SP excitation shows enormous magnification of the Q-bands compared with the absorption and excitation spectra by direct photoirradiation on the surface due to the field enhancement effect which is much more considerable for the wavelength region of the Q-bands than that of the Soret-band.[6]

‖ The treatment of a bare gold surface with a mixture of **1b** and **1b**–Zn gave a SAM containing both of the chromophores in the same ratio as in the original mixture which suggests similar exchange rates for **1b** and **1b**–Zn. Consequently, we can rule out the possibility that the initially exchanged Zn–porphyrin-linked decanethiol units may be selectively forced out by added **1b** resulting in disappearance of the fluorescence.

** The changes in the fluorescence properties of the decanethiol SAM after 5 min immersion in a solution of **1b** were observed in air. After 15 h, small increases in the anisotropy and enhancement of the Q-bands were barely observed. This suggests that the lateral migrations of the porphyrin-linked decanethiols in the decanethiol SAM proceed slowly in air.

1 C. Cotton, A. Glidle, G. Beamson and J. M. Cooper, *Langmuir*, 1998, **14**, 5139.
2 K. Kajikawa, M. Hara, H. Sasabe and W. Knoll, *Jpn. J. Appl. Phys., Part 2*, 1997, **36**, 1116.
3 P. E. Laibinis, M. A. Fox, J. P. Folkers and G. M. Whitesides, *Langmuir*, 1991, **7**, 3167.
4 J. B. Schlenoff, M. Li and H. Ly, *J. Am. Chem. Soc.*, 1995, **117**, 12 528.
5 W. Mizutani, T. Ishida and H. Tokumoto, *Appl. Surf. Sci.*, 1998, **130**–**132**, 792.
6 A. Ishida, Y. Sakata and T. Majima, *Chem. Commun.*, 1998, 57.
7 H. Yokota, K. Saito and T. Yanagida, *Phys. Rev. Lett.*, 1998, **80**, 4606.
8 R. E. Benner, R. Dornhaus and R. K. Chang, *Opt. Commun.*, 1979, **30**, 145.
9 R. F. Khairutdinov and N. Serpone, *J. Phys. Chem. B*, 1999, **103**, 761.

Communication 9/03334C

ChemComm

The restoration of pyrene fluorescence of a Cu^{II}–β-cyclodextrin–pyrene complex

Swadeshmukul Santra, Peng Zhang and Weihong Tan*

Department of Chemistry and UF Brain Institute, The University of Florida, Gainesville, FL 32611-7200, USA. E-mail: tan@chem.ufl.edu

Received (in Corvallis, OR, USA) 23rd April 1999, Accepted 3rd June 1999

A new photochemical mechanism has been developed to restore the fluorescence of an interesting complex of copper ion–pyrene–cyclodextrins upon interaction with glutamate.

We describe a new photochemical mechanism to restore the fluorescence of an interesting complex of copper(II) ion–cyclodextrin–pyrene upon interaction with glutamate. This process will enable us to understand cyclodextrin (CD) based chemistry and to develop novel techniques for amino acid analysis. Cyclodextrins have been widely used in many areas including chemistry, material science and biotechnology.[1,2] They are sugar molecules having the structure of a hollow truncated cone with a hydrophobic cavity. Cyclodextrins (host) are capable of encapsulating appropriately sized fluorophores (guest) in their hydrophobic cavity by forming inclusion complexes.[1,2] These complexes can be formed based on four possible intermolecular interactions.[2] The inclusion of pyrene molecules inside the cavity of cyclodextrins has been well-studied.[3,4] Upon inclusion of a fluorophore, CDs offer a more protective microenvironment and generally enhance the luminescence of the guest molecule by shielding the excited species from quenching and non-radiative decay processes that occur in bulk solution. In general, the guest molecule loses its solvation sphere upon entering the cyclodextrin cavity, and solvent molecules are simultaneously expelled out from the cavity. On the other hand, copper(II) (Cu^{2+}) ions can (i) quench the fluorescence *via* a photo-induced electron transfer process which involves a transfer of electron from the fluorophore in the excited state to the metal ion;[5] (ii) form complexes with CDs in alkaline solutions;[6] and (iii) bind with L-glutamate,[7] a tridentate ligand. Cu^{2+}–CD complexes are capable of binding organic molecules in the cavity,[8] and Cu^{2+} can bind strongly with EDTA in alkaline media leaving free CDs in solution.[9]

Here we report a new mechanism for fluorescence enhancement based on the above-described chemical reactions taking place in aqueous media. A new Cu^{2+}–β-CD–pyrene ternary complex is prepared in which the pyrene fluorescence is quenched by the Cu^{2+} ion, as shown in Scheme 1. Cu^{2+} is weakly bound to the deprotonated secondary hydroxy groups of β-CD.[6] It is expected that strong chelating agents, such as amino acids, will bind to the Cu^{II} complex, leaving free β-CD–pyrene and resulting in fluorescence restoration. We have chosen glutamate, a major excitatory neurotransmitter in the central nervous system,[10] as an example to demonstrate the principle that the ternary complex has strong capability of binding amino acids. The restoration of the pyrene fluorescence in this study is accomplished upon the addition of glutamate.

To demonstrate the principle, we have used a fluorescence spectroscopic method to characterize the complexes synthesized at different stages of the chemical reactions shown in Scheme 1. All the experiments were done at room temperature using a Perkin-Elmer Luminescence Spectrometer [Model LS 50B, UK]. Fluorescence spectra of the solutions prepared at different stages of the process were recorded with the same pyrene concentration of 2×10^{-8} M. First, a stock solution of pyrene was prepared in cyclohexane. A calculated amount of the pyrene stock solution was added to a cuvette, and the cyclohexane was evaporated by dry nitrogen. A trace amount of pyrene was thus obtained for the preparation of experimental solutions for spectroscopic analysis. The solutions were stirred for 24 h and 12 h before and after, respectively, the addition of the required amount of solid β-CD to make its concentration in the solution 0.01 M. It was assumed that pyrene molecules were completely dissolved in all solutions. Fig. 1(*a*) and (*b*) show an almost two-fold fluorescence enhancement of the pyrene emission in β-CD [Fig. 1(*b*)] when compared to the free pyrene emission in 1 M NaOH solution [Fig. 1(*a*)]. Second, we added 0.01 M Cu^{2+} solution [$CuSO_4 \cdot 5H_2O$] to the above complex solution followed by stirring for 2 h. No precipitate of $Cu(OH)_2$ was observed and the resulting complex formed in the solution (deep blue in color) was non-fluorescent, as shown by Fig. 1(*c*). The enhanced fluorescence of pyrene complexed with β-CD was quenched by Cu^{2+} due to electron transfer. In the third step, glutamate was added to the same solution. The fluorescence spectrum of the resulting new solution is shown in Fig. 1(*d*). It is clear that the addition of glutamate to the complex solution resulted in complete restoration of pyrene fluorescence. This restoration is due to the removal of Cu^{2+} from the ternary complex. The pyrene fluorescence band is slightly distorted in Fig. 1(*d*), showing a larger full width at half maximum (FWHM). Although the vibrational structure of the pyrene fluorescence bands remained intact, their relative intensity ratios varied when compared to those of free pyrene, and pyrene encapsulated inside the β-CD cavity. The strongest vibrational peak of the pyrene fluorescence band at 374 nm became a shoulder after the complex interacted with glutamate. We also obtained excitation spectra for all the solutions at different stages of the process, as shown in the left side of Fig. 1. Overall,

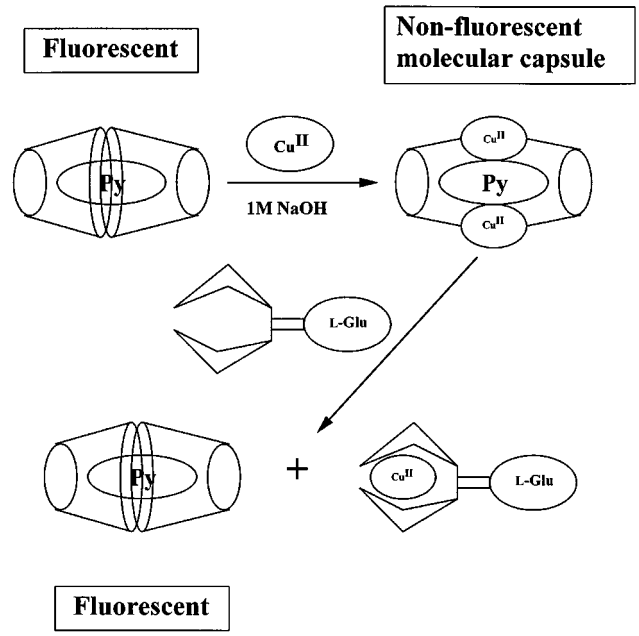

Scheme 1 Proposed mechanism for the formation of a ternary Cu^{2+}–β-CD–pyrene molecular capsule and the restoration of pyrene fluorescence upon interaction with glutamate.

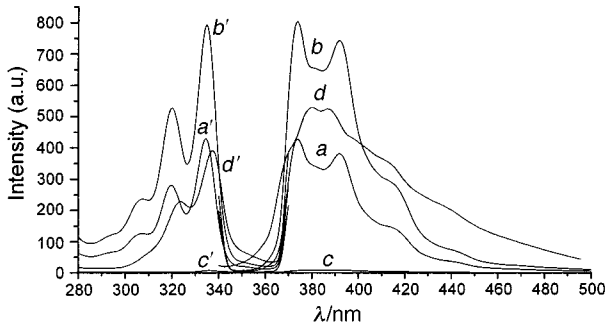

Fig. 1 Fluorescence emission spectra [λ_{exc} = 335 nm] (right) and fluorescence excitation spectra [λ_{em} = 374 nm] (left); (*a*) and (*a*′): free pyrene [*A* = 16018 au]; (*b*) and (*b*′): pyrene encapsulated in β-CD (0.01 M) cavity [*A* = 31346 au]; (*c*) and (*c*′): in the presence of 0.01 M Cu^{II} [*A* = 412 au]; (*d*) and (*d*′): after addition of 1.87 M glutamate [*A* = 30566]; [pyrene] = [2×10^{-8} M] and *A* = 392 au for the background. *A* is the uncorrected total area under the pyrene fluorescence band.

similar results to those from the fluorescence spectra were obtained. This further supports the proposed mechanisms of this series of chemical reactions. The total area under the fluorescence band for the restored emission and the emission before Cu^{2+} addition were the same. Based on the total area under each emission band as shown in Fig. 1, there is a more than 1500 times {(30566 − 392)/(412 − 392) = 1510} enhancement of fluorescence yield. This result clearly shows that there is no loss of fluorescence yield even in the solution phase, where there is a huge amount of other ionic substances. It is thus expected that an amino acid sensor, such as a glutamate sensor, developed in this manner will be highly sensitive.

One of the most important steps in this series of chemical reactions is the quenching of fluorescence by Cu^{2+}. One key question that has to be answered is how much Cu^{2+} has to be added to the complex solution in order to totally quench the pyrene fluorescence. We thus studied the effect of [Cu^{2+}] on the quenching of pyrene fluorescence. Fluorescence spectra of the complex solutions with various amounts of Cu^{2+} were taken, and the fluorescence intensity at 374 nm was used to monitor the effect of Cu^{2+} on pyrene fluorescence quenching. As shown in Fig. 2, pyrene emission decreased exponentially as the [Cu^{2+}] increased to about 0.01 M. There was no change essentially in fluorescence intensity as more Cu^{2+} was added to the solution. 0.01 M happened to be the concentration of β-CD in the complex solution. This suggests the stoichiometry of the formation of the Cu^{2+}–β-CD complex be of 1:1. Further increase of [Cu^{2+}] led to its precipitation as $Cu(OH)_2$. Based on the crystal structure of β-CD–pyrene–alcohol complex,[11] we thus propose a 2:2:1 Cu^{2+}–β-CD–pyrene molecular capsule, as shown in Scheme 1. The reaction between glutamate and the ternary complex in solution could take place in a single step (glutamate binds directly with the ternary complex) or in two steps (glutamate binds with the free Cu^{2+} ion which is in equilibrium with the ternary complex). Detailed kinetic measurements are being carried out to understand both the quenching and the restoration mechanisms.

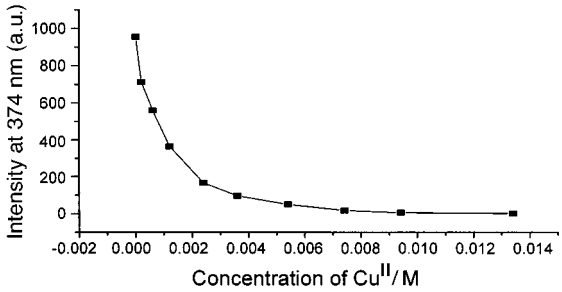

Fig. 2 Effect of copper ion concentration on the fluorescence intensity of pyrene emission in the β-CD–pyrene inclusion complex.

When different amounts of glutamate were used to restore the pyrene fluorescence, we observed a dramatic increase in fluorescence of pyrene in the complex solution. This provides an essential basis for designing a Cu^{2+}–β-CD–pyrene based bioanalysis assay for amino acids. Presently a few strategies are being pursued to take advantage of the dramatic rise of the restored fluorescence to achieve excellent detection capability. The selectivity for individual amino acid analysis could appear as a major disadvantage of this mechanism. But some of our preliminary studies have revealed that different amino acids have different binding capabilities with the copper(II) ion. We have also found that the same ternary copper(II) complex displays different sensitivity ranges for different amino acids. It is thus possible that ultrasensitive assays could be developed for glutamate and other interesting neurotransmitters. Another possible application of this photochemical mechanism could be amino acid analysis by capillary electrophoresis or HPLC using the ternary complex by either on-column or post-column reactions. We will also explore optical fiber technology to covalently bind the ternary complex for biosensor development.[12]

In conclusion, we report here for the first time the restoration of pyrene fluorescence in a Cu^{2+}–β-CD–pyrene ternary complex upon interaction with glutamate. The restoration is complete and fast. Based on Cu^{2+} concentration experiments, we have proposed a feasible molecular interaction mechanism of the complexes formed *via* a few interesting chemical reactions. The Cu^{2+}–β-CD–pyrene complex has a molecular ratio of 2:2:1. The formation of the ternary complex and the restoration of pyrene fluorescence by glutamate demonstrate the feasibility of a bioanalysis technique for the detection of glutamate and other similar ligands. The principle operates similarly to a molecular beacon (non-fluorescent probe) used for the detection of DNA sequences in the target through a hybridization process followed by the restoration of quenched fluorescence.[13] The chemistry involved in the present technique is relatively simple. Synthesis of the complex capsule can be carried out in the solution phase which should facilitate the usage of this capsule as a biosensor for *in vivo* glutamate monitoring. This inclusion system may also become a new model for multifactorial biological systems for molecular recognition and for mimicking active transport or concentration of substances.

This work was supported by US NSF Career Award CHE-9733650, by the Whitaker Foundation Biomedical Engineering Award and by US Department of Defense Office of Naval Research Young Investigator Award N00014-98-1-0621.

Notes and references

1 J. Szejtli, *Cyclodextrins and their Inclusion Complexes*, Academiai Kiado, Budapest, 1982.
2 D. B. Amabilino and J. F. Stoddart, *Chem. Rev*., 1995, **95**, 2725; A. Harada, L. Li and M. Kamachi, *Nature*, 1993, **364**, 516.
3 T. Yorozu, M. Hoshino and M. Imamura, *J. Phys. Chem.*, 1982, **86**, 4426.
4 H. Yang and C. Bohne, *J. Phys. Chem.*, 1996, **100**, 14 533.
5 T. Nakamura, A. Kira and M. Imamura, *Bull. Chem. Soc. Jpn.*, 1984, **57**, 2033.
6 Y. Matsui and D. Suemitsu, *Bull. Chem. Soc. Jpn.*, 1985, **58**, 1658.
7 C. M. Gramaccoili and R. E. Marsh, *Acta Crystallogr*., 1966, **21**, 594.
8 O. Egyed and V. Weiszfeiler, *Vib. Spectrosc*., 1994, **7**, 73.
9 Y. Matsui and K. Kinugawa, *Bull. Chem. Soc. Jpn.*, 1985, **58**, 2981.
10 J. A. Zivin and D. W. Choi, *Sci. Am*., July 1991, **265**, 56; J. Cordek, X. Wang and W. Tan, *Anal. Chem*., 1999, **71**, 1529.
11 K. A. Udachin and J. A. Ripmeester, *J. Am. Chem. Soc*., 1998, **120**, 1080.
12 W. Tan, *Trends Anal. Chem.*, 1998, **17**, 501; J. P. Alarie and T. Vo-Dinh, *Talanta*, 1991, **38**, 529.
13 X. Fang, X. Liu, S. Schuster and W. Tan, *J. Am. Chem. Soc*., 1999, **121**, 2921.

Communication 9/03244D

ChemComm

Transmission electron microscopic and small angle X-ray diffraction investigations of $Au_{55}(PPh_3)_{12}Cl_6$ microcrystals†

Günter Schmid,*[a] Raphael Pugin,[a] Thomas Sawitowski,[a] Ulrich Simon[a] and Bernd Marler*[b]

[a] *Institut für Anorganische Chemie der Universität Essen, Universitätsstrasse 5-7, D-45117 Essen, Germany. E-mail: guenter.schmid@uni-essen.de*

[b] *Institut für Mineralogie der Ruhr-Universität Bochum, Universitätsstrasse 150, D-44780 Bochum, Germany. E-mail: bernd.marler@ruhr-uni-bochum.de*

Received (in Basel, Switzerland) 7th April 1999, Accepted 31st May 1999

Micrometer sized crystals of close packed $Au_{55}(PPh_3)_{12}Cl_6$ clusters are formed from dichloromethane solution and are investigated by transmission electron microscopy and small angle X-ray diffraction.

After a period of almost 20 years of investigation of the cluster compound $Au_{55}(PPh_3)_{12}Cl_6$ since its first synthesis we have now succeeded in making microcrystals in preparative amount. Transmission electron microscopic studies and small angle X-ray diffraction indicate a simple close packed arrangement of the spherical clusters correlating with an effective cluster distance of 2.3 nm in very good agreement with the actual cluster size of 2.1–2.2 nm.

The cluster compound $Au_{55}(PPh_3)_{12}Cl_6$ was first described in 1981.[1] In the meantime a large number of papers followed, describing its chemical and physical properties.[2–8] The compound became of extraordinary significance owing to its quantum size behavior. With respect to this property Au_{55} clusters are the most promising particles for applications in future nanoelectronics.[9]

The development of the physical and chemical characteristics of the easily available $Au_{55}(PPh_3)_{12}Cl_6$ cluster[10] was accompanied by the disadvantage of its non-crystalline nature. Thus, solid state investigations had to be performed with pellets or thin layers. Investigations of solutions suffered from their ready decomposition so that much effort has been required to reach our present knowledge of this cluster.

We have now succeeded in obtaining microcrystals of $Au_{55}(PPh_3)_{12}Cl_6$ in preparative quantities. The reason for having failed to obtain such crystalline particles previously is simply because they are too small to be distinguished directly and because long-standing electron microscopic investigations were exclusively focused on the imaging of single clusters from very dilute solutions. However, fast evaporation of the solvent from concentrated dichloromethane solutions of $Au_{55}(PPh_3)_{12}Cl_6$ results in the formation of well shaped crystals in the size range of hundreds of nanometers up to a few micrometers. Transmission electron microscopy (TEM) and small angle X-ray diffraction (SAXRD) of such microcrystals were used to establish their structure. Samples for the TEM investigations were simply prepared from a drop of a saturated solution of $Au_{55}(PPh_3)_{12}Cl_6$ in CH_2Cl_2 added onto the grid. After evaporation of the solvent the TEM images showed well shaped, mainly hexagonal, crystals (Fig. 1).

In contrast to the case of dilute solutions, only a few single clusters could be observed. Magnification of such crystals established their monocrystalline character. The high magnification of a crystal edge in Fig. 2, thin enough for TEM, allowed the determination of more structural details.

The distance between parallel columns is 2.0–2.1 nm. Supposing a fcc arrangement of the clusters, this distance corresponds to an effective cluster distance of 2.3–2.4 nm, in good agreement with the calculated cluster diameter if van der Waals distances between the PPh_3 ligands of neighboring clusters are considered. Cluster distances of 2.3 nm could also directly be determined from the TEM image in Fig. 2. Fig. 3

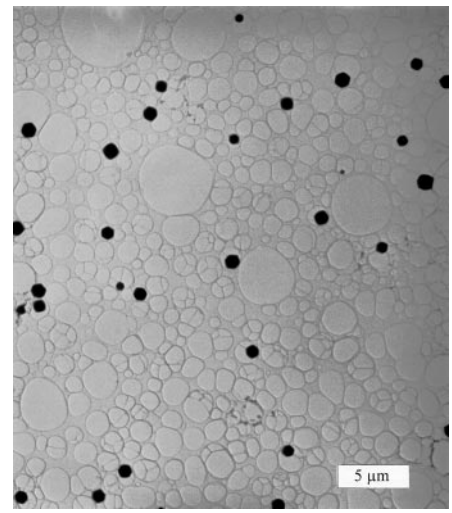

Fig. 1 Transmission electron microscopic (TEM) image of well shaped microcrystals of $Au_{55}(PPh_3)_{12}Cl_6$. Most of the crystals are *ca.* 1 μm in diameter.

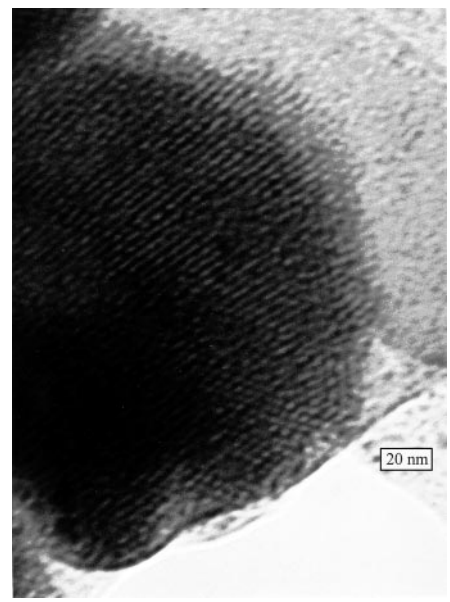

Fig. 2 High resolution TEM image of a $Au_{55}(PPh_3)_{12}Cl_6$ microcrystal. The monocrystalline particle shows cluster rows with a separation of 2.0–2.1 nm in accord with a hexagonal close-packed arrangement of the spherical clusters. The cluster distance can be determined as 2.3 nm.

† Dedicated to Professor Helmut Werner on the occasion of his 65th birthday.

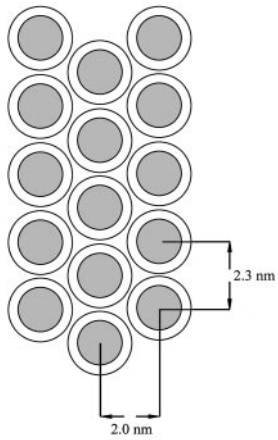

Fig. 3 Schematic view of the cluster arrangement in the microcrystals.

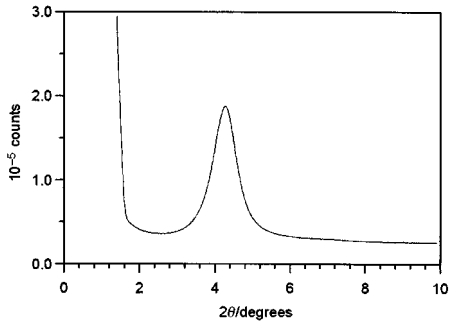

Fig. 4 Result of small angle X-ray diffraction (SAXRD) measurements on $Au_{55}(PPh_3)_{12}Cl_6$ microcrystals. The 2θ angle of 4.3° corresponds to a *d* value of 2.05 nm, in accord with the TEM results.

schematically represents the situation observed in the high resolution TEM images.

Samples for SAXRD experiments have also been prepared by fast evaporation of the solvent of concentrated dichloromethane solutions of $Au_{55}(PPh_3)_{12}Cl_6$. The black powder consisted almost exclusively of microcrystals as shown in Fig. 1. The result of the SAXRD experiments is shown in Fig. 4.

Only one strong reflection of 2θ = 4.3° is registered, corresponding to a *d*-value of 2.05 nm in accord with the average distance from TEM of 2.05 nm. This might correspond to a hexagonal close packing, if observed along the [111] direction.

Based on our knowledge of the quantum size behavior of individual clusters, the availability of nanocrystalline microcrystals now opens new routes for their use in three-dimensional single electron tunneling (SET) devices. A crystal of the size of $1 \times 1 \times 1$ μm contains *ca.* 10^8 clusters. The combination of such microcrystals by appropriate linkers is in principle possible and so could be a vehicle to a future nanotechnology.

Notes and references

‡ *Sample preparation*: the synthesis of $Au_{55}(PPh_3)_{12}Cl_6$ was carried out following ref. 10. For TEM investigations, a drop of a concentrated solution of $Au_{55}(PPh_3)_{12}Cl_6$ in dichloromethane, was added onto a carbon covered grid and dried. SAXRD measurements were performed with the powdery cluster material as synthesized.

TEM images were accomplished with a Philips FEG CM 200 microscope while for SAXRD measurements a Siemens D 5000 was used.

1 G. Schmid, R. Boese, R. Pfeil, F. Bandermann, S. Meyer, G. H. M. Calis and J. W. A. van der Velden, *Chem. Ber.*, 1981, **114**, 3634.
2 Summarizing the literature up to 1994; G. Schmid, in *Clusters and Colloids-From Theory to Applications*, ed. G. Schmid, VCH, Weinheim, 1994.
3 B. A. Smith, J. Z. Zhang, U. Giebel and G. Schmid, *Chem. Phys. Lett.*, 1997, **270**, 139.
4 Y. Volokitin, J. Sinzig, L. J. de Jongh, G. Schmid and I. I. Moiseev, *Nature*, 1996, **384**, 621.
5 L. F. Chi, M. Hartig, T. Drechsler, Th. Schwaak, C. Seidel, H. Fuchs and G. Schmid, *Appl. Phys. A*, 1998, **66**, 187.
6 L. F. Chi, S. Rakers, M. Hartig, H. Fuchs and G. Schmid, *Thin Solid Films*, 1998, **327**–**329**, 520.
7 G. Schmid and L. F. Chi, *Adv. Mater.*, 1998, **10**, 515.
8 G. Schmid, R. Pugin, J.-O. Malm and J.-O. Bovin, *Eur. J. Inorg. Chem.*, 1998, 813.
9 U. Simon, *Adv. Mater.*, 1998, **10**, 1487.
10 G. Schmid, *Inorg. Synth.*, 1990, **7**, 214.

Communication 9/02741F

ChemComm

An open-framework iron phosphate with large voids, exhibiting spin-crossover

Amitava Choudhury,[ab] Srinivasan Natarajan[a] and C. N. R. Rao*[ab]

[a] *Chemistry and Physics of Materials Unit, Jawaharlal Nehru Centre for Advanced Scientific Research, Jakkur P.O., Bangalore 560 064, India. E-mail: cnrrao@jncasr.ac.in*

[b] *Solid State and Structural Chemistry Unit, Indian Institute of Science, Bangalore 560 012, India*

Received (in Cambridge, UK) 7th May 1999, Accepted 8th June 1999

A novel iron phosphate, $[(C_4N_3H_{16})(C_4N_3H_{15})]^{5+}$-$[Fe_5F_4(H_2PO_4)(HPO_4)_3(PO_4)_3]^{5-}\cdot H_2O$, consisting of a Fe–O/F–Fe network crosslinked by PO_4 groups is shown to possess unusually large elliptical voids of 24 T atoms (T = Fe, P) and to exhibit a gradual low- to high-spin transformation.

Amongst the variety of open-framework metal phosphates investigated in recent years, those of transition metals are of particular interest not only because of the novelty in their structures, but also because of their properties of potential value. One of the important objectives in synthesizing open-framework transition metal phosphates is the possibility of obtaining new solids with novel magnetic properties. Several open-framework iron phosphates have been synthesized and characterized in recent years,[1–3] but most of them order antiferromagnetically with the exception of one, which shows ferrimagnetic behavior at low temperatures.[4] Open-framework cobalt phosphates also order antiferromagnetically.[5] We have synthesized a new iron phosphate, exhibiting spin-crossover, which is rather unusual in an oxidic material. The material also has several noteworthy structural features which include the presence of infinite Fe–O/F–Fe chains, large voids formed by 24 T atoms (T = Fe, P), crosslinking by PO_4 tetrahedra.

The new iron phosphate $[(C_4N_3H_{16})(C_4N_3H_{15})]^{5+}[Fe_5F_4(H_2PO_4)(HPO_4)_3(PO_4)_3]^{5-}\cdot H_2O$ **I**, was prepared by employing hydrothermal methods in the presence of diethylenetriamine (DETA).† The light green colored crystals of **I** belonged to the monoclinic space group $P2_1/n$ and since the asymmetric unit of **I** contains 59 non-hydrogen atoms and it is convenient to describe the structure in terms of small building blocks. The three-dimensional structure of **I** can be considered as made from layers along the [001] direction, consisting of a network of FeO_6, FeO_5F and FeO_4F_2 octahedra and PO_4 tetrahedra (Fig. 1). The framework has the formula $[Fe_5F_4(H_2PO_4)(HPO_4)_3(PO_4)_3]^{5-}$. Charge neutrality is achieved by the presence of the organic structure-directing amine (DETA) in its protonated form. There are two molecules of DETA in the unit cell, one triply protonated and the other doubly protonated. The layers are connected to each other *via* phosphate groups, completing the three-dimensional architecture (Fig. 2). This connectivity creates large elliptical voids bound by 24 T atoms (T = Fe, P) forming one-dimensional channels along the [010] direction, within which the DETA and water molecules reside. The width of the channels is 15.3 × 4.5 Å (longest and shortest atom—atom contact distances, not including van der Waals radii). To our knowledge, this is the first open-framework iron phosphate material with such large voids. The layers themselves contain pores bound by 8 T atoms (T = Fe, P) and the H_2PO_4 groups protrude into this opening rendering the pores inaccessible. Along the [100] direction, the structure has another narrow channel bound by 16 T atoms and the protruding H_2PO_4 and HPO_4 moieties occupy this channel.

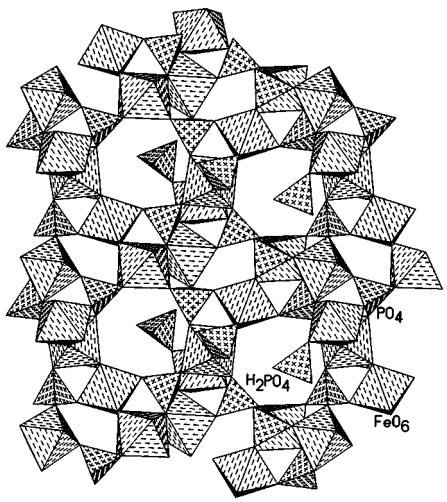

Fig. 1 Layer type arrangement in **I** along the [001] direction. Note that the H_2PO_4 moieties project into the eight-membered pores within the layers.

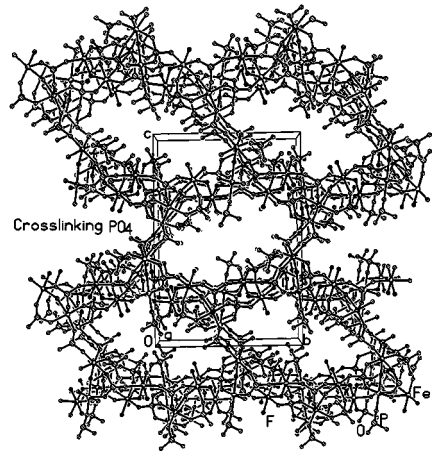

Fig. 2 Structures of **I**, showing large elliptical tunnels along the [010] direction. Note that the walls of the tunnels are composed of PO_4 tetrahedra. Amine and water molecules are not shown for clarity.

The most striking aspect of the structure of **I** is the cationic sub-network of Fe atoms. The connectivity between the various iron–oxygen(fluorine) octahedra is such that infinite Fe–O/F–Fe polymeric chains are formed as shown in Fig. 3(a). This network results from the presence of three-coordinate oxygen atoms and fluorine bridges in the structure. The Fe–O/F–Fe polymeric chains and the phosphate tetrahedra are so connected as to give rise to channels which appear as though they are decorated by PO_4 tetrahedra. This material may, thus, be considered to be an infinite iron–oxy fluoride network, $Fe_2O_{3-x}F_x$($x \leqslant 0.4$), crosslinked by the phosphate groups. Pillaring of layers in framework solids is not common, the only such material being an indium phosphate,[6] where the pillaring is by InO_6 octahedra. The crosslinking by PO_4 tetrahedra found in **I** is analogous to the pillaring in the indium phosphate.[6]

Besides its novel structural features, the iron phosphate **I** also exhibits unusual magnetic properties. Magnetic susceptibility measurements show that the magnetic moment increases gradually from 2.0 μ_B around 20 K to *ca*. 6.0 μ_B around 250 K [Fig. 3(b)]. The low-temperature moment corresponds to that of low-spin Fe^{III} ($^2T_{2g}$) and the high-temperature moment to that of

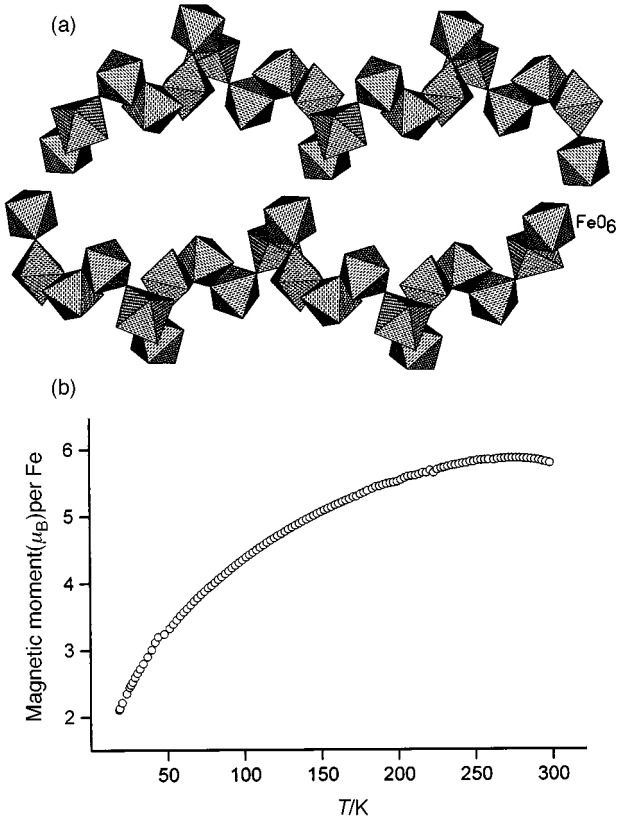

Fig. 3 Network of Fe–O/F octahedra along the [100] direction. The network shows strong anisotropy and is crosslinked by PO_4 tetrahedra (not shown). (b) Temperature variation of the magnetic moment.

high-spin Fe^{III} ($^6A_{1g}$). The variation of the magnetic moment [Fig. 3(b)] is characteristic of a gradual spin-crossover similar to that found in some iron(III) complexes.[7] Mössbauer spectra recorded at 298 and 50 K show the presence of the high- and low-spin Fe^{III} ions, respectively, with characteristic differences in the isomer shift and the quadruple splitting (δ = 0.32, 0.1 and ΔE_Q = 0.34, 1.03 mm s^{-1}). The occurrence of spin-crossover in Fe^{III} ions in an oxide material is rather unusual and suggests that the possibility of internal pressure being exerted on the Fe–O polyhedra.

In summary, the synthesis of a novel open-framework iron phosphate with interesting structure and magnetic properties has been accomplished. The presence of Fe–O/F–Fe chains and large one-dimensional channels decorated by phosphate groups are two of the novel features of the material. The occurrence of a smooth magnetic spin-crossover as a function of temperature is noteworthy in that iron(III) oxides generally have Fe^{III} in the high-spin state.

A. C. thanks the Council of Scientific and Industrial Research (CSIR), Government of India for the award of a research fellowship.

Notes and references

† The title compound was synthesized from an iron phosphate gel containing DETA as a structure-directing agent. iron(III) chloride, phosphoric acid (85 wt%), DETA, HF and water in a ratio 1:6:3:1:200 were mixed and stirred until homogeneous. The mixture was sealed in a 23 ml Teflon-lined, stainless steel autoclave (Parr, USA) and heated at 180 °C for 72 h. The resulting product, containing predominantly light green crystals, was filtered off and washed thoroughly with deionized water. A suitable single crystal (0.06 × 0.06 × 0.08) was carefully selected under a polarizing microscope. The crystal structure determination was performed on a Siemens SMART CCD diffractometer equipped with a normal focus, 2.4 kW sealed-tube X-ray source (Mo-Kα radiation, λ = 0.71073 Å) operating at 50 kV and 40 mA. A hemisphere of intensity data were collected in 1321 frames with ω scans (width of 0.30° and exposure time of 30 s per frame).

Crystal data for $[(C_4N_3H_{16})(C_4N_3H_{15})]^{5+}[Fe_5F_4(H_2PO_4)(HPO_4)_3(PO_4)_3]^{5-}\cdot H_2O$, **I**: monoclinic, space group $P2_1/n$ (no. 14), a = 9.670(1), b = 15.618(1), c = 22.563(1), β = 90.82(1)°, V = 3407.1(1) Å^3, Z = 4, M = 1254.1, μ = 1.915 mm^{-1} and D_c = 1.836(1) g cm^{-3}. A total of 13848 reflections were collected at 298 K in the θ range 1.59–23.19° and merged to give 4844 unique data (R_{int} = 0.065) of which 3635 with $I > 2\sigma(I)$ were considered to be observed. The structure was solved by direct methods with SHELXS-86[8] and difference Fourier synthesis. Final R = 0.06, R_w = 0.13 and S = 1.13 were obtained for 541 parameters. Part of the hydrogen atoms were located initially in the difference Fourier maps and for the final refinements, hydrogen atoms for both the framework as well as the amine molecules were placed geometrically and held in the riding mode. Final Fourier map minimum and maximum: −1.009 and 0.908. Full-matrix least-squares structure refinement against $|F^2|$ were carried out with SHELXTL-PLUS program package.[9]

CCDC 182/1280. See: http://www.rsc.org/suppdata/cc/1999/1305/ for crystallographic files in .cif format.

1 K.-H. Lii, Y.-F. Huang, V. Zima, C.-Y. Huang, H.-M. Lin, Y.-C. Jiang, F.-L. Liao and S.-L. Wang, *Chem. Mater.*, 1998, **10**, 2599 and references therein; Z. A. D. Lethbridge, P. Lightfoot, R. E. Morris, D. S. Wragg, P. A. Wright, Å. Kvick and G. Vaughan, *J. Solid State Chem.*, 1999, **142**, 455.
2 J. R. D. DeBord, W. M. Reiff, R. C. Haushalter and J. Zubieta, *J. Solid State Chem.*, 1996, **125**, 186; J. R. D. DeBord, W. M. Reiff, C. J. Warran, R. C. Haushalter and J. Zubieta, *Chem. Mater.*, 1997, **9**, 1994.
3 M. Cavellec, D. Riou and G. Ferey, *J. Solid State Chem.*, 1994, **112**, 441; M. Cavellec, D. Riou, J.-M. Greneche and G. Ferey, *Zeolites*, 1996, **17**, 252; M. Cavellec, C. Egger, J. Linares, M. Nogues, F. Varret and G. Ferey, *J. Solid State Chem.*, 1997, **134**, 349.
4 M. R. Cavellec, J.-M. Greneche, D. Riou and G. Ferey, *Chem. Mater.*, 1998, **10**, 2434.
5 P. Feng, X. Bu and G. D. Stucky, *Nature*, 1997, **388**, 735; X. Bu, P. Feng and G. D. Stucky, *Science*, 1997, **278**, 2080.
6 A. M. Chippindale, S. J. Brech, A. R. Cowley and W. M. Simpson, *Chem. Mater.*, 1996, **8**, 2259.
7 M. S. Haddad, M. W. Lunch, W. D. Ferderer and D. N. Hendrickson, *Inorg. Chem.*, 1981, **20**, 123.
8 G. M. Sheldrick, SHELXS-86 Program for Crystal Structure Determination, Universität Göttingen, 1986, *Acta Crystallogr., Sect. A*, 1990, **46**, 467.
9 G. M. Sheldrick, SHELXTL-PLUS Program for Crystal Structure Refinement, Universität Göttingen, 1993.

Communication 9/03683K

ChemComm

5,10,15-Triphenylcorrole: a product from a modified Rothemund reaction

Roberto Paolesse,*[a] Laurent Jaquinod,[b] Daniel J. Nurco,[b] Sonia Mini,[a] Francesco Sagone,[a] Tristano Boschi[a] and Kevin M. Smith[b]

[a] *Dipartimento di Scienze e Tecnologie Chimiche, Università di Roma Tor Vergata, 00133 Roma, Italy. E-mail: roberto.paolesse@uniroma2.it*

[b] *Department of Chemistry, University of California, Davis, CA 95616, USA. E-mail: kmsmith@ucdavis.edu*

Received (in Corvallis, OR, USA) 23rd April 1999, Accepted 1st June 1999

One-pot synthesis of 5,10,15-triphenylcorrole has been achieved by reaction of benzaldehyde with an excess of pyrrole; the triphenylphosphinocobalt complex of 5,10,15-triphenylcorrole has been structurally characterized using X-ray crystallography.

5,10,15,20-Tetraphenylporphyrin **1** is probably the most ubiquitous synthetic porphyrin and it has often been utilized to study biomimetic and/or catalytic systems.[1,2] Its success in these roles is probably due to the relatively easy synthetic approach to **1**, which is obtained by condensation of pyrrole and benzaldehyde.[3] Since the first synthetic approach reported by Rothemund,[4] a huge number of studies related to the synthetic aspects of **1** have been reported in the literature.[3] Different reaction conditions have been utilized and the reaction mechanism has been minutely discussed, but until recently[5–9] the possibility that other macrocycles might be generated from this reaction had been ignored. This aspect has now been investigated and different macrocycles have been isolated and characterized from the Rothemund reaction; these include the 'N-confused'-porphyrin **2** (NC-TPP)[5,6] and 5,10,15,20-tetraphenylsapphyrin **3** (TPS)[7] from the standard pyrrole/benzaldehyde condensation, and a *meso*-hexa(pentafluorophenyl)hexaphyrin, in low yield, from a related reaction.[8] While a study by Lindsey and Geier established the scope of the formation of NC-TPP and TPS, additional pigments were observed but in very low yield and therefore were not characterized.[9]

During our studies on the chemistry of corrole, we reported the formation of a *meso*-phenyl-β-substituted corrole from the cobalt catalyzed cyclization of a hydroxybenzylpyrrole,[10] the first intermediate in the condensation of pyrrole and benzaldehyde. This result, and knowledge that the ring-expanded sapphyrin system was also isolated,[7] caused us to suspect that 5,10,15-triphenylcorrole **4** might also be another, albeit diminutive, product of the Rothemund reaction. Two examples of *meso*-substituted corroles have since been reported in the literature;[11,12] these corroles were obtained as by-products of the expected porphyrins in the reaction of pyrrole and aldehydes. These examples further supported our hypothesis that corroles might be obtained from the condensation of pyrrole and aldehydes, but because of the low yields and the particular aldehydes used, these results cannot be generalized. Here we report that, under certain defined conditions, triphenylcorrole **4** is formed in reasonable yield from the Rothemund reaction;† cobalt was easily inserted into **4** and the corresponding triphenylphosphino complex **5** was structurally characterized.

Pyrrole and benzaldehyde (3:1 molar ratio) were reacted in refluxing AcOH for 4 h with spectrophotometric monitoring. Following work-up and chromatographic separation on alumina, triphenylcorrole **4** was obtained in 6% yield (unoptimized) as red–green crystals. The expected tetraphenylporphyrin **1** was also obtained from this reaction in yields comparable with those of **4**, indicating that under these modified conditions the ring closure to corrole is competitive with the formation of the larger porphyrin macrocycle; trace amounts of NC-TPP were also observed. [5,6] When the reaction was carried out in propionic acid[14] (for 2 h) the yields of corrole were slightly lower. The choice of reaction conditions is critical for the formation of useful amounts of **4**.

The ^{1}H NMR spectrum of **4** shows broad AB patterns for the β-pyrrolic protons because of the reduced symmetry of the corrole ring. Spectrophotometry of **4** provided the optical spectrum shown in Fig 1. The Soret band appears at 416 nm (ε 101 000), without significant shift with respect to that of **1**; three

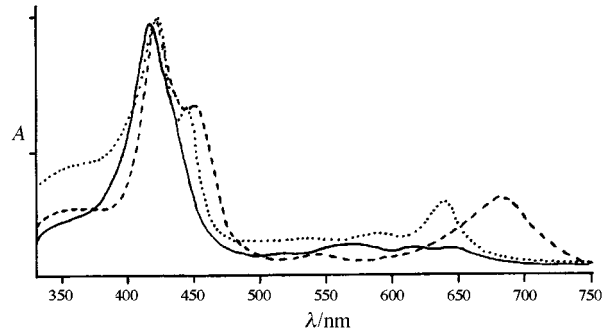

Fig. 1 Optical spectra of **4** in CH_2Cl_2 (solid line), in DMF (dotted line) and in AcOH (dashed line). Absorbances are normalized to their maxima.

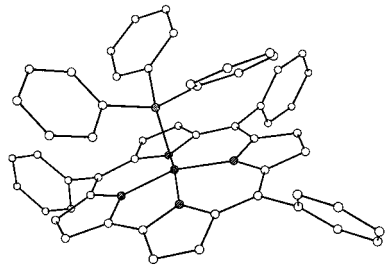

Fig. 2 Molecular structure of **5**; hydrogen atoms have been omitted for clarity.

broad Q bands are present in the 570–650 nm region. It is interesting to note that **4** is more acidic than the corresponding β-octaalkyl analogues[15] because DMF is sufficiently basic to give the corresponding monoanion derivative without addition of bases, as evidenced by the visible spectrum (Fig. 1) recorded in DMF. The same spectrum is obtained by addition of a few drops of base (NaOH 10% in water) to a methanolic solution of **4**. The monocation of **4** was formed in AcOH, as is also shown in Fig. 1. Addition of increasing amounts of H_2SO_4 to the AcOH solution of **4** led to further changes in the visible absorption spectrum; these indicated additional protonation processes which have not yet been characterized, but which do not involve disruption of the conjugated pathway (*i.e.* no removal of the Soret band). In the case of β-octaalkylcorroles[16,17] protonation at the 5-position in H_2SO_4 has been proposed on account of the disappearance of the Soret band in the electronic absorption spectrum.

The insertion of the cobalt(III) ion into **4** was performed by reaction of corrole and $Co(OAc)_2$ in refluxing MeOH in the presence of PPh_3 to give the corresponding complex **5** in 88% yield. The ^{1}H NMR spectrum of **5** is similar to that of **4**, but with more resolved resonances. The axial phosphine ligand shows three sets of resonances for the *ortho*, *meta* and *para* protons, in accord with observations in the corresponding β-octaalkylcorrole complexes,[10,18] indicating that the PPh_3 ligand does not suffer from steric interactions with the *meso*-phenyl groups.

The electronic spectrum of **5** shows a Soret band at 385 nm (ε 51 000) and a Q band centered at 561 nm (ε 11 500). Its EI mass spectrum shows an $[M - PPh_3]^+$ ion, while use of the FAB technique allowed observation of the molecular ion without loss of the axial ligand.

The structure of **5** was determined by X-ray crystallography.‡ Compound **5** was slightly non-planar with a 0.069 Å mean deviation of the macrocyclic atoms from the corrole mean plane. The conformation observed resembles the porphyrin-type dome conformation.[20] The central Co^{III} ion featured M–N bond lengths of 1.863(2), 1.891(2), 1.886(2) and 1.867(2) Å; the two shortest of these bonds involved the nitrogens adjacent to the C_α–C_α linkage. This is typical of metallocorroles and has been observed in the crystal structures of other corroles.[10,21] In **5**, the Co^{III} ion is displaced from the corrole mean plane by 0.389 Å and the Co–P bond length is 2.201(1) Å.

In conclusion, we have shown that the synthesis of **4**, even at only 6% yield, permits the corrole field to utilize and exploit a direct analogue of tetraphenylporphyrin; this should provide a starting point for further development of the comparative chemistry of this contracted macrocyclic system.

This work was supported by grants from CNR-Italy (MADESS II project no. 97.01380.PF48) and the US National Science Foundation (CHE-96-23117) and National Institutes of Health (HL-22252).

Notes and references

† After the present paper had been submitted and reviewed, a report of the synthesis of 5,10,15-tris(pentafluorophenyl)corrole from pyrrole and pentafluorobenzaldehyde appeared (ref. 13). These authors showed that using their conditions with pyrrole and benzaldehyde does not afford 5,10,15-triphenylcorrole (**4**). We thank a reviewer for informing us of the imminent publication of this article.

‡ *Crystal data* for **5**: Crystals were grown by slow diffusion of MeOH into a CH_2Cl_2 solution of **5** ($C_{55}H_{38}N_4PCo$). The selected crystal (0.28 × 0.52 × 0.54 mm) had a triclinic unit cell, space group $P\bar{1}$ and cell dimensions a = 8.5269(8), b = 13.1028(13), c = 18.161(2) Å, α = 94.284(8), β = 92.308(8), γ = 97.677(8)°, V = 2002.6(3) Å^3 and Z = 2 (FW = 844.8). Data were collected on a Siemens R3 m/V diffractometer with a sealed tube source [λ(Mo-Kα) = 0.71073 Å] at 130(2) K in ω scan mode to $2\theta_{max}$ = 55.0°. Of 9795 reflections measured (+h, ±k, ±l) all were independent and 7351 had $I > 2\sigma$ (T_{min} = 0.78, T_{max} = 0.89, ρ_{calc} = 1.40 g cm^{-3}, μ = 0.515 μ^{-1}). The structure was solved by direct methods and refined (based on F^2 using all data except for three suppressed reflections) by full-matrix least-squares methods with 550 parameters (Siemens SHELXTL ver. 5.03). Hydrogen atom positions were generated by their idealized geometry and refined using a riding model. An empirical absorption correction was applied (ref. 19). Final R factors were $R1$ = 0.041 (observed data) and $wR2$ = 0.112 (all data). CCDC 182/1277.

1 R. A. Sheldon, in *Metalloporphyrins in Catalytic Oxidations*, ed. R. A. Sheldon, Marcel Dekker, New York, 1994, p. 1.
2 B. Morgan and D. Dolphin, *Struct. Bonding (Berlin)*, 1987, **64**, 115.
3 J. S. Lindsey, in *The Porphyrin Handbook*, ed. K. Kadish, K. M. Smith and R. Guilard, Academic Press, San Diego, 1999, Book 1, ch. 2.
4 P. Rothemund, *J. Am. Chem. Soc*., 1939, **61**, 2912.
5 P. J. Chmielewski, L. Latos-Grazynski, K. Rachlewicz and T. Glowiak, *Angew. Chem., Int. Ed. Engl.*, 1994, **33**, 779.
6 H. Furuta, T. Asano and T. Ogawa, *J. Am. Chem. Soc.*, 1994, **116**, 767.
7 P. J. Chmielewski, L. Latos-Grazynski and K. Rachlewicz, *Chem. Eur. J.*, 1995, **1**, 68.
8 M. G. P. M. S. Neves, R. M. Martins, A. C. Tome, A. J. D. Silvestre, A. M. S. Silva, V. Felix, M. G. B. Drew and J. A. S. Cavaleiro, *Chem. Commun*., 1999, 385.
9 G. R. Geier III and J. S. Lindsey, *J. Org. Chem*., 1999, **64**, 1596.
10 R. Paolesse, S. Licoccia, G. Bandoli, A. Dolmella and T. Boschi, *Inorg. Chem.*, 1994, **33**, 1171.
11 E. Rose, A. Kossanyi, M. Quelquejeu, M. Soleilhavoup, F. Duwavran, N. Bernard and A. Lecas, *J. Am. Chem. Soc.*, 1996, **118**, 1567.
12 N. M. Loim, E. V. Grishko, N. I. Pyshnograeva, E. V. Vorontsov and V. I. Sokolov, *Izv. Akad. Nauk. Ser. Khim.*, 1994, **5**, 925; *Chem. Abstr*., 1995, **122,** 187 733.
13 Z. Gross, N. Galili and I. Saltsman, *Angew. Chem., Int. Ed.*, 1999, **38**, 1427.
14 A. D. Adler, F. R. Longo, J. D. Finarelli, J. Goldmacher, J. Assour and L. J. Korsakoff, *J. Org. Chem*., 1967, **32**, 476.
15 A. W. Johnson and I. T. Kay, *J. Chem. Soc.*, 1965, 1620.
16 M. J. Broadhurst, R. Grigg, G. Shelton and A. W. Johnson, *J. Chem. Soc., Perkin Trans. 1*, 1972, 143.
17 R. Grigg., R. J. Hamilton, M. L. Jozefowicz, C. H. Rochester, R. J. Terrel and H. Wickwar, *J. Chem. Soc., Perkin Trans. 2*, 1973, 407.
18 M. Conlon, A. W. Johnson, W. R. Overend, D. Rajapaksa and C. M. Elson, *J. Chem. Soc., Perkin Trans. 1*, 1973, 2281.
19 S. R. Parkin, B. Moezzi and H. Hope, *J. Appl. Crystallogr.*, 1995, **28**, 53.
20 W. Jentzen, X.-Z. Song and J. A. Shelnutt, *J. Phys. Chem. B*, 1997, **101**, 1684.
21 S. Will, J. Lex, E. Vogel, H. Schmickler, J.-P. Gisselbrecht, C. Haubtmann, M. Bernard and M. Gros, *Angew. Chem., Int. Ed. Engl.*, 1997, **36**, 357; E. Vogel, S. Will, A. S. Tilling, L. Neumann, J. Lex, E. Bill, A. X. Trautwein and K. Wieghardt, *Angew. Chem., Int. Ed. Engl.*, 1994, **33**, 731.

Communication 9/03247I

High separation selectivity with imperfect zeolite membranes

Elena Piera, Joaquin Coronas, Miguel Menéndez and Jesús Santamaría*

Department of Chemical and Environmental Engineering, University of Zaragoza, 50009, Zaragoza, Spain. E-mail: iqcatal@posta.unizar.es

Received (in Cambridge, UK) 16th April 1999, Accepted 8th June 1999

In spite of the presence of inter-crystalline defects, high selectivities can be obtained in the separation of gas phase mixtures with zeolite membranes.

The development and application of zeolite membranes constitutes a swiftly expanding area where the data published over a period of a few months often suffice to change the prevailing view on the status of development (population of defects, crystal orientation, *etc.*) of a specific family of zeolite membranes, or on the transport mechanism for a given separation. A well known example of the rapidly changing concepts in the field refers to the misnaming of zeolite membranes as molecular-sieving membranes. Nowadays there are numerous examples (see refs. *e.g.* 1–3) of 'reverse selectivity' membranes, *i.e.* membranes where the largest molecule is selectively separated because of preferential adsorption that leads to pore blockage.

Another widely used presumption in this area establishes that, if a high separation selectivity (a two to three-digit figure is often considered as sufficiently high) is observed, then one can claim that a 'defect-free' or 'almost defect-free' membrane has been obtained. This article deals with this perception by demonstrating that defective membranes are nevertheless capable of high separation selectivities, if tested under a suitable set of operating conditions.

The work was carried out using silicalite membranes, which are probably the most widely studied zeolite membranes. They were prepared by *in situ* hydrothermal synthesis onto stainless steel supports having 1 μm diameter pores. In order to confine the permeation area, the ends of the stainless steel porous supports (11 mm i.d., 16 mm o.d.) were soldered to non-permeable tubes of the same material and diameter.

The membranes were prepared by hydrothermal synthesis according to the directions in ref. 1, except that Aerosil 300 was used instead of Aerosil 130. The molar composition of the gel was: 21 SiO_2: 788 H_2O: 3, NaOH: 1 TPABr, (TPABr = tetrapropylammonium bromide). The gel was cloudy and thin, with a pH of 11.0. The support tube was wet with water, and then one end of the wet tube was wrapped with Teflon tape, plugged with a Teflon cap and filled with the synthesis gel. The other end was also wrapped with tape and plugged with another Teflon cap. The tube was placed vertically in a Teflon-lined autoclave, and the autoclave in a convection stove at 443 K for 8–15 h. XRD measurements (not shown) carried out on membranes synthesized using this procedure indicated that pure silicate was formed on the stainless steel support.

The separation measurements were performed with the membrane placed in a stainless steel separation module where it was sealed with silicone o-rings. The gaseous feed stream containing the desired partial pressure of TIPB (1,2,4,5-tetra-isopropylbenzene) or water and He was obtained by mixing in variable proportions two mass-flow controlled streams of He, one of which [82 cm^3(STP) min^{-1}] had been bubbled through TIPB or water saturators. The gas mixture was fed into the tube (retentate) side of the membrane, and allowed to permeate through the membrane wall. The permeate side was swept with 83 cm^3(STP) min^{-1} of carrier gas (N_2). Retentate and permeate sides were usually at atmospheric pressure.

Before running an experiment the membranes were heated to 753 K at a rate of 1 K min^{-1}, and then calcined at this temperature for 8 h, in order to remove any adsorbed species. The separation selectivities given below were calculated as the ratios of permeances, using the log (mean partial pressure) difference in the calculations. The composition of the feed stream was accurately determined by feeding it directly into the sampling loop of the on-line gas chromatography. Similarly, when steady state was reached, which often meant keeping the membrane under continuous flow for *ca.* 2 h, samples at the exit of both the permeate and retentate sides were analyzed by on-line gas chromatography.

A first series of experiments was carried out to verify the presence of inter-crystalline defects on the membrane, and to evaluate their contribution to the total permeation flux. To this end, a He steam was saturated with TIPB at a temperature of 373 K (in order to have a sufficiently high vapour pressure of TIPB), and then fed to the retentate side of the membrane. The permeation of TIPB was measured as a function of temperature and then compared to that of He when the same experiment was carried out without TIPB. Since TIPB has a kinetic diameter of 0.87 nm, higher than the average channel diameter of silicalite (0.55 nm), the TIPB flux observed can be ascribed to permeation through inter-crystalline defects.

The results of TIPB permeation experiments are shown in Fig. 1. It is interesting that at the lowest temperature tested for permeation of TIPB/He mixtures, the permeation of He is almost completley blocked by TIPB (giving a TIPB/He selectivity over 800). This is probably due to capillary condensation of TIPB in the intercrystalline voids, blocking the access of He to the zeolite membrane. For increasingly higher temperatures the access to zeolite pores was progressively freed, and the He permeance increased. It must be noted, however, that the TIPB permeance was little affected, which again agrees with the assumption that TIPB does not use the zeolite pore network, but the inter-crystalline defects. Since a relatively high permeance of TIPB [$(1.5–3.2) \times 10^{-8}$ mol m^{-2} s^{-1} Pa^{-1}] was observed throughout the temperature interval tested, it can be concluded that the silicalite membrane has a very significant concentration of inter-crystalline defects.

A more meaningful comparison can be established between water (kinetic diameter 0.265 nm) and He (kinetic diameter 0.26 nm) both of which are able to transit easily through the zeolite

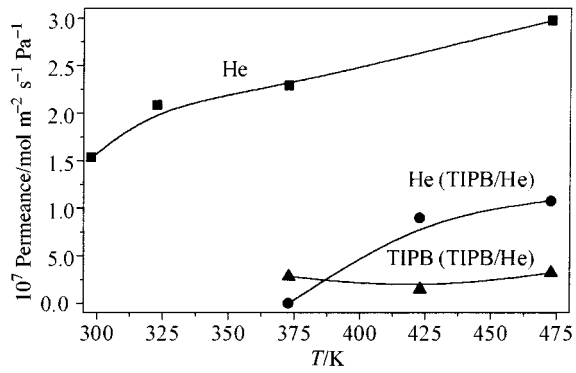

Fig. 1 He single gas permeance and He and TIPB permeances in the TIPB/He mixture as a function of temperature; partial pressure of TIPB in the feed = 1.1 kPa.

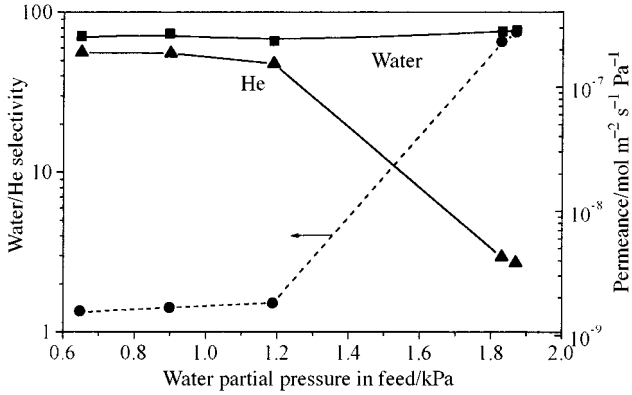

Fig. 2 He and water permeances and water/He separation selectivity in the water/He mixture as a function of the water partial pressure in the feed; temperature = 297 K.

pore network. Besides, since silicalite is an organophilic zeolite a significant interaction with water (preferential adsorption) is not expected. The experiments carried out with water–He mixtures are in general agreement with these assumptions (Fig. 2). A nearly constant value (1.3–1.5) to the water/He selectivity is obtained at water partial pressures in the feed of 1.1 kPa and lower. In spite of this low value of selectivity, it can be said that the membrane shows some water/He selectivity (about four times the Knudsen value of 0.47). This could be the result of blocking of the zeolite pores by water, which is the only condensable component present in the feed.

However, as the water partial pressure in the feed was increased to 1.9 kPa, a dramatic change takes place: the He flux is reduced by two orders of magnitude and the water/He selectivity increases markedly. This is due to blocking of most of the non-zeolite pores (*i.e.* inter-crystalline defects) by capillary condensation of water. The size of these defects can be approximately estimated by the Kelvin equation as 2.5–3 nm, much larger than the zeolite pores. In spite of these defects, a water/He selectivity of 74 is obtained at a water partial pressure in the feed of 1.9 kPa (Fig. 2).

Financial support from DGICYT (QUI97-1085), DGA (P94/97) and Fundación Repsol is gratefully acknowledged.

Notes and references

1 M. D. Jia, B. Chen, R. D. Noble and J. L. Falconer, *J. Membr. Sci.*, 1994, **90**, 1.
2 A. Giroir-Fendler, J. Peureux, H. Mozzanega and J. A. Dalmon, *Stud. Surf. Sci. Catal.*, 1996, **111**, 127.
3 E. Piera, A. Giroir-Fendler, H. Moueddeb, J. A. Dalmon, J. Coronas, M. Menéndez and J. Santamaria, *J. Membr. Sci.*, 1998, **142**, 97.

Communication 9/03036K

Self-assembly of a [2 × 2] hydrogen bonded grid

Piotr Lipkowski,[a] Anna Bielejewska,[a] Huub Kooijman,[b] Anthony L. Spek,[b]† Peter Timmerman*[a] and David N. Reinhoudt*[a]

[a] *Laboratory of Supramolecular Chemistry and Technology, MESA+ Research Institute, University of Twente, PO Box 217, NL-7500 AE Enschede, The Netherlands. E-mail: d.n.reinhoudt@ct.utwente.nl.*

[b] *Bijvoet Center for Biomolecular Research, Crystal and Structural Chemistry, Utrecht University, Padualaan 8, NL-3584 CH Utrecht, The Netherlands*

Received (in Liverpool, UK) 28th April 1999, Accepted 3rd June 1999

Formation of 24 cooperative hydrogen bonds drives the spontaneous assembly of a rigid bifunctional trimelamine and bis(barbituric acid) to give selectively the [2 × 2] hydrogen-bonded grid, in preference to the corresponding [1 × 1] or polymeric assemblies.

In 1992 Youinou and co-workers reported the formation of a $[Cu_4(dppn)_4](CF_3SO_3)_4$ complex in which the dppn [3,6-bis(2′-pyridyl)pyridazine] ligands are perpendicularly oriented pairwise around four Cu^+ centers thus forming a sandwich-type complex.[1] Very similar structures generally referred to as [*n* × *n*] 'metallosupramolecular grids' have been reported by Lehn and co-workers.[2–4] Information storage both on the *covalent* and on the *supramolecular* level determines the overall size [*n* × *n*] and shape (grid *vs.* helix) of the assembly.[5] We are currently investigating the self-assembly of [*n* × *m*] hydrogen-bonded grids using the melamine–barbituric acid (M•BA) binding motif.[6] The formation of six cooperative hydrogen bonds between dimelamine **1** and 5,5-diethylbarbituric acid (DEB) (K_{ass} = 7.6 × 10^4 M^{-1} in $CDCl_3$) restricts the rotations around the $C_{triazine}$–NH, the NH–CH_2, and the CH_2–C_{phenyl} bonds in **1**, giving the semi-rigid flat assembly **1**•DEB.[7] Here we describe the formation of [2 × 2] grid $\mathbf{2b}_2$•$\mathbf{3}_2$, the simplest example of this type of hydrogen-bonded assemblies.[8] The grid has been fully characterized by 2D NMR spectroscopy, MALDI-TOF mass spectrometry, and vapor pressure osmometry (VPO).

The synthesis of trimelamine **2b** starts from cyanuric chloride *via* successive reactions with Bn_2NH (1.0 equiv.) and $BuNH_2$ (1.0 equiv.), followed by refluxing in neat *m*-xylylenediamine to give **4** in 92% yield (Scheme 1). Reaction of **4** with cyanuric chloride (0.5 equiv.) and subsequent aminolysis of the corresponding chloride **2a** with excess of NH_3 gives **2b** in 85% yield.[9] Bis(barbituric acid) derivative **3** was synthesized starting with the alkylation of diethyl 2-ethylmalonate with 1,3-diiodopropane in 35% yield,[10] followed by reaction with urea (NaOEt/EtOH) in 25% yield.[11]

Assembly of **2b** and **3** can in principle lead to three different hydrogen-bonded structures (see Scheme 1), *i.e.* the [1 × 1] assembly **2b•3**, the [2 × 2] (grid) assembly $\mathbf{2b}_2$•$\mathbf{3}_2$, and the polymeric assembly $[\mathbf{2b•3}]_n$. Bis(barbituric acid) **3** was designed such that the formation of the [1 × 1] assembly, which would be preferred on entropic grounds,† is impossible. The short *n*-propyl spacer does not allow two barbituric acid moieties of one molecule of **3** to bind simultaneously to both binding sites of one molecule of **2b**. The X-ray crystal structure of free **3**‡ [see Fig. 1(*a*)] clearly confirms this picture and shows that the conformation adopted in the solid state is fully consistent with formation of the [2 × 2] grid $\mathbf{2b}_2$•$\mathbf{3}_2$ [see Fig. 1(*b*)]. Furthermore, the high extent of preorganization in the monomeric units **2b** and **3** reduces the likelihood of hydrogen-bonded polymerization ($[\mathbf{2b•3}]_n$).

Addition of 1.0 equiv. of **2b** to a suspension of **3** in $CDCl_3$ results in rapid dissolution of both components. Conclusive evidence for the formation of assembly $\mathbf{2b}_2$•$\mathbf{3}_2$ comes from VPO measurements which give an average MW of 2500, very close to the calculated MW of 2800.§ Furthermore, MALDI-TOF mass spectrometry after Ag^+ labeling[12] shows a small but distinct signal for the Ag^+ complex of $\mathbf{2b}_2$•$\mathbf{3}_2$ (*m/z* 2924; calc. for $C_{152}H_{180}N_{44}O_{12}$•$^{109}Ag^+$ = 2924) together with that for the (open) **2b•3** (not shown) (*m/z* 1517; calc. for $C_{76}H_{90}N_{22}O_6$•$^{109}Ag^+$ = 1517). The presence of the latter is due to destruction of assembly $\mathbf{2b}_2$•$\mathbf{3}_2$ upon addition of AgO_2CCF_3, most likely due to strong coordination of Ag^+ to the hydrogen-bonded triazine nitrogen.¶

The ^{1}H NMR spectrum of the 1:1 mixture of **2b** and **3** in $CDCl_3$ confirms the exclusive formation of the [2 × 2] grid $\mathbf{2b}_2$•$\mathbf{3}_2$. The spectrum of $\mathbf{2b}_2$•$\mathbf{3}_2$ at 60 °C [see Fig. 2(*a*)] shows a broad signal at δ14.0 (NH_{barb}), a singlet at δ 7.65 ppm (ArH) and two signals at δ 7.1 (NH_{xylyl} + ArH) and 6.76 (NH_{xylyl}). Both the NH_{butyl} and the NH_2 protons coincide with the aromatic proton signals for the four benzyl groups (δ 7.4–7.2). Furthermore, three singlets at δ 4.84, 4.62 and 4.51 (CH_2Ar) and a doublet at δ 3.33 [$NHCH_2(CH_2)_2CH_3$] are observed. At lower temperatures (< 30 °C), two signals are observed at δ 14.6 and 14.0, one broad and one sharp,‖ and a complex pattern of signals

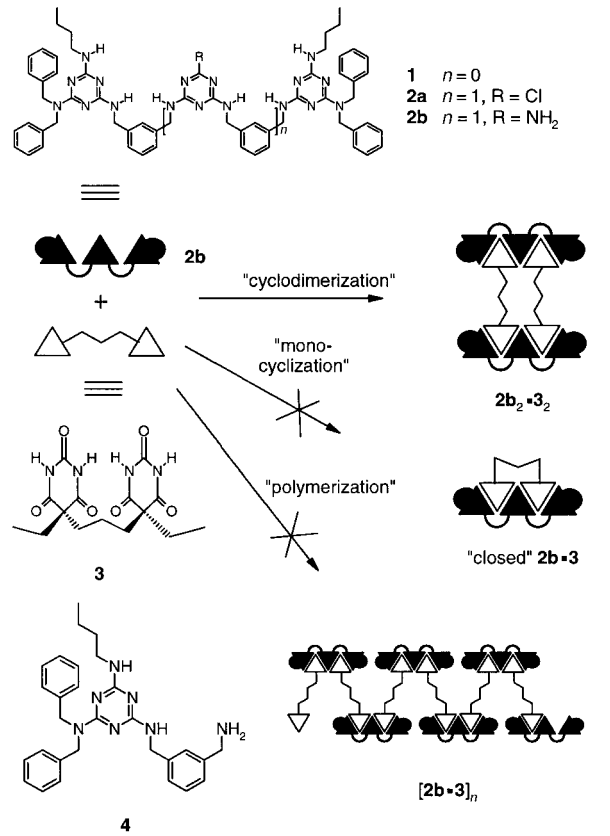

Scheme 1 Representation of the different types of hydrogen-bonded assemblies (*i.e.* [1 × 1], [2 × 2] and [*n* × *n*]) that can be formed *via* hydrogen bond formation between trimelamine **2b** and bis(barbituric acid) **3**. Only the [2 × 2] assembly is experimentally observed.

† Address correspondence concerning crystallography to this author.

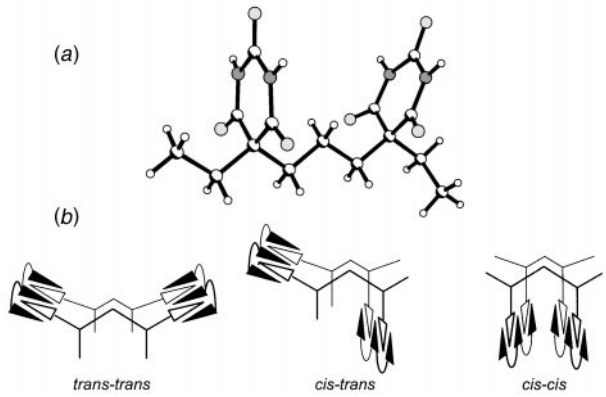

Fig. 1 (*a*) X-Ray crystal structure of **3**; white (small and large) atoms represent hydrogen and carbon atoms, grey (light and dark) atoms represent oxygen and nitrogen atoms. The barbiturate moiety [containing atom O(5)] is slightly distorted from planarity towards an envelope conformation (maximum deviation from the least-squares plane is 0.131(1) Å [for C(7)]). This distortion is most likely caused by the acceptance of intermolecular hydrogen bond formation [involving O(5) and O(6)]. (*b*) Three isomeric conformations of the [2 × 2] assembly $\mathbf{2b}_2$•$\mathbf{3}_2$.

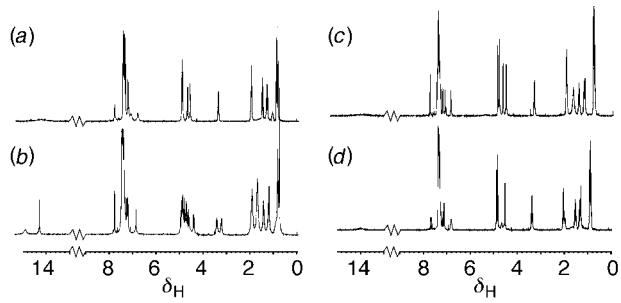

Fig. 2 ^{1}H NMR spectra (400 MHz) of (*a*) [2 × 2] assembly $\mathbf{2b}_2$•$\mathbf{3}_2$ at 60 °C; (*b*) [2 × 2] assembly $\mathbf{2b}_2$•$\mathbf{3}_2$ at −40 °C; (*c*) [1 × 1] assembly **2b**•DEB_2 at −40 °C; (*d*) 1:1 mixture of [2 × 2] assembly $\mathbf{2b}_2$•$\mathbf{3}_2$ and [1 × 1] assembly **1**•DEB at 20 °C.

for the CH_2Ar protons and for the $NHCH_2(CH_2)_2CH_3$ protons is observed [see Fig. 2(*b*)]. The absence of any other signals in the δ 15–13 region clearly rules out the presence of alternative assemblies (*i.e.* [1 × 1] or polymeric) or the existence of more than one isomeric form [*trans-trans*, *cis-trans* and *cis-cis*, see Fig. 1(*b*)]. The less symmetrical *cis-trans* isomer can be ruled out based on symmetry arguments, but which of the two other isomers is the most stable one is at present unknown.

The decoalescence of the proton signals for the two heterotopic NH_{barb} protons around 30 °C clearly illustrates the much higher kinetic stability of grid $\mathbf{2b}_2$•$\mathbf{3}_2$ compared to assembly **2b**•DEB_2, which shows an averaged (broad) signal around δ 14.0 for these two protons even at −50 °C [see Fig. 2(*c*)]. The reason is that exchange of these protons in $\mathbf{2b}_2$•$\mathbf{3}_2$ involves the simultaneous cleavage of 12 hydrogen bonds, while exchange in **2b**•DEB_2 only requires six hydrogen bonds to be broken. Interestingly, the exchange between the two NH_{barb} protons in $\mathbf{2b}_2$•$\mathbf{3}_2$ is significantly faster in the presence of an equivalent amount of the two-component assembly **1**•DEB [averaged signal around δ 14.0 is observed, see Fig. 2(*d*)]. This is due to the fact that components **1** and DEB temporarily occupy the non-hydrogen bonded sites in **2b**•DEB_2 during the exchange process, thus decreasing the activition barrier for this process.[13]

Finally we studied the thermodynamic stability of $\mathbf{2b}_2$•$\mathbf{3}_2$ as compared to that of **2b**•DEB_2 and $\mathbf{1}_2$•**3**. The melting point index for hydrogen-bonded assemblies I_{T_m} = HB/(N − 1) predicts that an equimolar mixture of [1 × 2] assembly **2b**•DEB_2 (I_{T_m} = 6) and [2 × 1] assembly $\mathbf{1}_2$•**3** (I_{T_m} = 6) is thermodynamically unstable, and would rearrange to give preferentially the [2 × 2] assembly $\mathbf{2b}_2$•$\mathbf{3}_2$ (I_{T_m} = 8) and [1 × 1] assembly **1**•DEB (I_{T_m} = 6).[14] Analysis of the ^{1}H NMR spectrum of a 1:1 mixture of **2b**•DEB_2 and $\mathbf{1}_2$•**3** clearly shows that neither one of the two assemblies is present. Diagnostic is the absence of the characteristic resonances at δ 7.0 and 4.7. This experiment confirms the assumption that the thermodynamic stability of grid $\mathbf{2b}_2$•$\mathbf{3}_2$ is significantly higher than that of **2b**•DEB_2 and $\mathbf{1}_2$•**3**. Further studies on how structural parameters influence the stability of [2 × 2] grids are currently in progress.

This work was supported in part (A. L. S.) by the Netherlands Foundation of Chemical Research (SON) with financial aid from the Netherlands Organisation for Scientific Research (NWO).

Notes and references

† Based on the melting point index for hydrogen-bonded assemblies I_{T_m} = HB/(N − 1) (where HB = number of H-bonds in the assembly and N = number of monomeric units in the assembly) (ref. 14), the stability of [1 × 1] assembly **2b•3** is higher (I_{T_m} = 12) than [2 × 2] assembly $\mathbf{2b}_2$•$\mathbf{3}_2$ (I_{T_m} = 8) and the polymeric assembly [**2b•3**]$_n$ (I_{T_m} = 6).

‡ *Crystal data* for **3**: $C_{15}H_{20}N_4O_6$, M_r = 352.35, colourless, block-shaped crystal (0.2 × 0.2 × 0.3 mm), triclinic, space group $P\bar{1}$ (no. 2) with a = 6.5364(6), b = 10.8100(12), c = 11.7511(12) Å, α = 79.960(5), β = 85.799(6), γ = 88.868(6)°, V = 815.38(14) Å^3, Z = 2, D_c = 1.435 g cm^{-3}, F(000) 372, μ(Mo-Kα) = 0.1 mm^{-1}, 23889 reflections measured, 3717 independent, R_{int} = 0.0582, (1.6 < θ < 27.4°, T = 150 K, Mo-Kα radiation, graphite monochromator, λ = 0.71073 Å) on an Enraf-Nonius Kappa-CCD area detector on rotating anode. Data were collected for Lp effects but not for absorption. The structure was solved by automated direct methods (SHELXS96). Refinement on F^2 was carried out by full-matrix least-squares techniques (SHELXL-96) for 286 parameters. Hydrogen atoms were located on a difference Fourier map and their coordinates were included as parameters in the refinement. Refinement converged at a final w$R2$ value of 0.0898, $R1$ = 0.0317 [for 3522 reflections with $F_o > 4\sigma(F_o)$], S = 1.023. A final difference Fourier showed no residual density outside –0.24 and 0.32 e Å^{-3}. CCDC 182/1276. See http://www.rsc.org/suppdata/cc/1999/1311/ for crystallographic data in .cif format.

§ The experimentally determined average MW is slightly lower than the calculated MW, because assembly $\mathbf{2b}_2$•$\mathbf{3}_2$ is in equilibrium with the free components **2b** and **3** (concentration dependant on association constant of the complex). Moreover, the presence of a small excess of one of the components [~5% deviation from exact 1:1 stoichiometry (w/w)] will further decrease the average MW.

¶ Destruction of assembly $\mathbf{2b}_2$•$\mathbf{3}_2$ by Ag^+ ions was confirmed independantly by ^{1}H NMR spectroscopic measurements, which show the gradual disappearance (over several hours) of the proton signals after the addition of AgO_2CCF_3.

‖ The broadness of these signals is related to the proton exchange rate with residual water present. The NH_{barb} proton bound to the *outer* melamine unit (δ 14.6) is much broader than the NH_{barb} proton bound to the *inner* melamine unit (δ 14.0), because this proton is more exposed to the solvent (breakage of 3 *vs*. 6 hydrogen bonds).

1 M.-T. Youinou, N. Rahmouni, J. Fischer and J. A. Osborn, *Angew. Chem., Int. Ed. Engl.*, 1992, **31**, 733.
2 P. N. W. Baxter, J.-M. Lehn, J. Fischer and M.-T. Youinou, *Angew. Chem., Int. Ed. Engl.*, 1994, **33**, 2284.
3 P. N. W. Baxter, J.-M. Lehn, B. Kneisel and D. Fenske, *Chem. Commun.*, 1997, 2231.
4 G. S. Hanan, D. Volkmer, U. S. Schubert, J.-M. Lehn, G. Baum and D. Fenske, *Angew. Chem., Int. Ed. Engl.*, 1997, **36**, 1842.
5 J.-M. Lehn, *Supramolecular Chemistry, Concepts and Perspectives*, VCH, Weinheim, 1995.
6 S.-K. Chang and A. D. Hamilton, *J. Am. Chem. Soc.*, 1988, **110**, 1318; J.-M. Lehn, M. Mascal, A. DeCian and J. Fischer, *J. Chem. Soc., Chem. Commun.*, 1990, 479; J. P. Mathias, E. E. Simanek, J. A. Zerkowski, C. T. Seto and G. M. Whitesides, *J. Am. Chem. Soc.*, 1994, **116**, 4316.
7 C. M. Marjo, unpublished results.
8 J. Yang, E. Fan, S. J. Geib and A. D. Hamilton, *J. Am. Chem. Soc.*, 1993, **115**, 5314.
9 J. P. Mathias, E. E. Simanek and G. M. Whitesides, *J. Am. Chem. Soc.*, 1994, **116**, 4326.
10 A. C. Cope, H. L. Holmes and H. O. House, *Org. React.*, 1957, **9**, 107.
11 E. Fischer and A. Dilthey, *Ann.* 1904, **335**, 334.
12 K. A. Jolliffe, M. Crego Calama, R. Fokkens, N. M. M. Nibbering, P. Timmerman and D. N. Reinhoudt, *Angew. Chem., Int. Ed.*, 1998, **37**, 1294.
13 J. Rao, J. Lahiri, L. Isaacs, R. M. Weis and G. M. Whitesides, *Science*, 1998, **280**, 708.
14 M. Mammen, E. E. Simanek and G. M. Whitesides, *J. Am. Chem. Soc.*, 1996, **118**, 12614.

Communication 9/03446C

ChemComm

Deprotonation of low-spin mononuclear iron(III)–hydroperoxide complexes give transient blue species assigned to high-spin iron(III)–peroxide complexes

Kenneth B. Jensen, Christine J. McKenzie,* Lars Preuss Nielsen, Jens Zacho Pedersen and Henrik Molina Svendsen

Department of Chemistry, University of Southern Denmark, Odense Campus, 5230 Odense M, Denmark. E-mail: chk@chem.ou.dk

Received (in Cambridge, UK) 14th April 1999, Accepted 24th May 1999

Purple iron(III)–hydroperoxide complex ions [Fe(Rtpen)(η^1-OOH)]$^{2+}$ can be reversibly deprotonated to give transient blue species showing spectroscopic properties transient with iron(III)–peroxide complexes; a novel ferryl species is produced in MS/MS experiments with the iron(III) hydroperoxide ion.

Dioxygen activation chemistry by a single iron atom occurs in some non-heme iron enzymes[1] and the antitumor drug bleomycin (BLM).[2] The characterisation of model mononuclear non-heme Fe(III)–peroxide species is expected to aid the structural elucidation of similar species in the catalytic cycles of these non-heme iron biomolecules. In recent years several biologically relevant transient mononuclear non-heme iron(III)–hydroperoxide model systems have been identified in solution.[3–5] These species are proposed to contain end-on (η^1) hydroperoxide ligands. The only mononuclear non-heme complex proposed to contain a side-on (η^2) peroxide ligand is [Fe(edta)O_2].[6,7]

A mononuclear iron(II) complex of the pentadentate ligand *N*-methyl-*N*,*N*′,*N*′-tris(2-pyridylmethyl)ethane-1,2-diamine (metpen) [Fe(metpen)Cl](PF_6) when treated with an excess of H_2O_2 in hydroxylic solvents generates purple solutions.[3] The UV-VIS and EPR spectra of this solution show features comparable to other reported Fe(III)–η^1-OOH systems[5] and bleomycin,[2] supporting formulation of the transient purple species as the low-spin Fe(III)–hydroperoxo compound [Fe(metpen)(η^1-OOH)]$^{2+}$. By carrying out simple ligand modifications of the parent metpen ligand we have continued this work towards the ultimate aim of solid state characterisation, and we communicate here the spectroscopic identification of new unique mononuclear Fe(III)–peroxide species obtained by deprotonation of the hydroperoxide species [Fe(Rtpen)(η^1-OOH)]$^{2+}$, where Rtpen is the generic abbreviation for the ligand series; *N*-ethyl-*N*,*N*′,*N*′-tris(2-pyridylmethyl)ethane-1,2-diamine (ettpen) and *N*-benzyl-*N*,*N*′,*N*′-tris(2-pyridylmethyl)-ethane-1,2-diamine (bztpen).

The yellow crystalline iron(II) and iron(III) complexes [Fe(Rtpen)Cl]A and [Fe(Rtpen)Cl]$(A)_2$ (A = ClO_4 or PF_6), are prepared by the reaction of each ligand with either iron(II) or iron(III) chloride in dry methanol followed by addition of a salt of the counter anion. Crystal structures of the iron(II) compounds have been obtained. The iron(III) species are not stable in solution: their reduced counterparts and orange iron(III) compounds, formulated as [(Rtpen)ClFe(μ-O)FeCl(Rtpen)]$(A)_2$, can be isolated from aged solutions of [Fe(Rtpen)Cl]$(A)_2$. The reactions of the iron(II) and iron(III) compounds with an excess of hydrogen peroxide in hydroxylic solvents generate purple solutions which are stable for hours. There is a time lag of a few seconds before the appearance of the purple colour when the iron(II) starting materials are used. This time lag supports the notion of a rate-determining formation of an intermediate low-spin iron(III) compound (detected by EPR) before a ligand exchange reaction with deprotonated hydroperoxide. A possible reaction scheme is presented in Scheme 1. By using the iron(III) starting materials [Fe(bztpen)Cl]$(A)_2$ (A = ClO_4 or PF_6), formation of the hydroperoxide species is expedited since formation of the purple colour is, in these cases, instantaneous. The purple chromophores are proposed to be the low-spin Fe(III)–hydroperoxide complexes containing end-on bound hydroperoxide ligands, [Fe(Rtpen)(OOH)]$^{2+}$ with spectroscopic characteristics similar to those we reported[3] for [Fe(metpen)(OOH)]$^{2+}$. The addition of ammonia, triethylamine or pyridine to the purple solutions produces a transient blue colour. If the base is first added to methanolic solutions of [Fe(Rtpen)Cl]$^+$ followed by hydrogen peroxide the blue solution is generated directly. Subsequent addition of hydrochloric acid to the blue solutions regenerates the purple solution. This cycle can be repeated several times with the same solution indicating a reversible acid/base equilibrium. We assign the blue species to a novel iron(III)–peroxide compound derived from the deprotonation of the purple [Fe(Rtpen)(OOH)]$^{2+}$. The spectroscopic data obtained so far is consistent with a mononuclear high-spin iron(III) complex with either side-on (η^2) or end-on (η^1) peroxide coordination (Scheme 1).

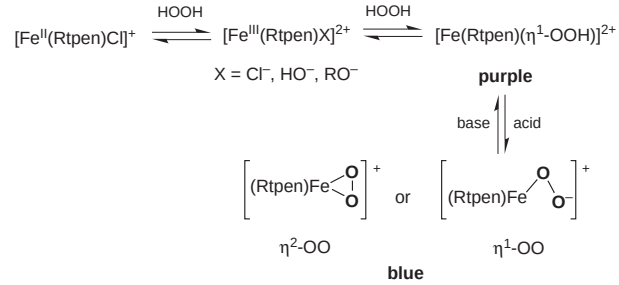

Scheme 1

UV-VIS spectra for [Fe(ettpen)Cl]PF_6 and its proposed purple Fe(III)–hydroperoxide and blue iron(III)–peroxide derivatives are shown in Fig. 1. Similar data were obtained for the other members of the series.[8] The difference in the maxima assigned to the peroxide to iron(III) charge-transfer band in the purple and blue species is consistent with expected increased donor strength of the O_2^{2-} *vs.* O_2H^- ligand. However this simple argument is complicated by a concomitant spin change of the iron atom (see EPR results below).

Peaks assigned to both the complexes, [Fe(bztpen)(OOH)]$^+$ and [Fe(bztpen)(OO)]$^{2+}$ are observed in the ESI mass spectra of the purple solutions (Fig. 2). Consistent with the proposed acid/base equilibrium the ratio between *m/z* 511.2 and 256.1 ions increases in spectra of the blue solutions (*m/z* 511.2 is weak in Fig. 2). A prominent peak (often the most intense) at *m/z* 247.6 can be assigned to the ferryl species, [Fe(bztpen)O]$^{2+}$. Collision induced dissociation (CID) of the ion at *m/z* 256.1 produces ions at *m/z* 247.6, 239.6 and 194.6. The first two of these ions are assigned to the ferryl species [Fe(bztpen)O]$^{2+}$ and a ferrous species [Fe(bztpen)]$^{2+}$, and explained by loss of a hydroxyl and hydrosuperoxide radical, respectively, from [Fe(bztpen)(OOH)]$^{2+}$. The third peak is assigned to [Fe(bztpen − C_7H_6)]$^{2+}$. In order to determine whether or not the peaks at *m/z* 239.6 and 194.6 could be the result of the decomposition of the *m/z* 247.6

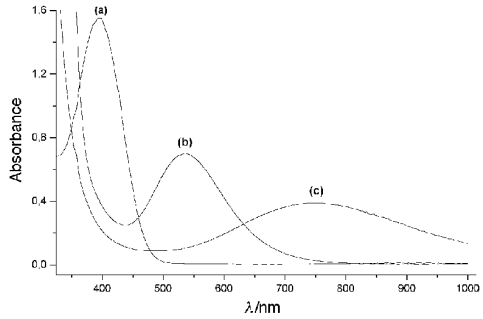

Fig. 1 UV-VIS spectra of (a) 7.5×10^{-4} M [Fe(ettpen)Cl]PF_6 in MeOH, (b) after addition of 300 equiv. of H_2O_2 and followed by (c) addition of 35 equiv. of Et_3N.

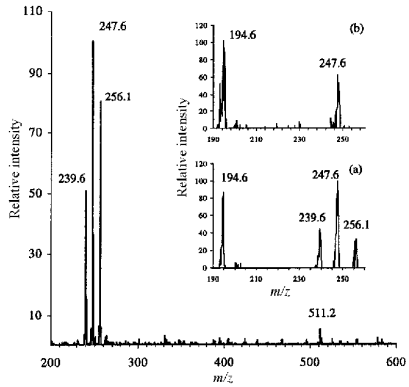

Fig. 2 The ESI mass spectrum of the purple solution generated by the reaction of [Fe(bztpen)Cl]$(ClO_4)_2$ with 100 equiv. of H_2O_2 in ethanol. Inserts show the CID spectra of the (a) *m/z* 256.1 and (b) *m/z* 247.6 ions. Assignments: *m/z* 256.1, [Fe(bztpen)(OOH)]$^{2+}$; 511.2, [Fe(bztpen)(OO)]$^{+}$; 247.6, [Fe(bztpen)O]$^{2+}$; 239.6, [Fe(bztpen)]$^{2+}$; 194.6, [Fe(bztpen − C_7H_6)]$^{2+}$.

ion {[Fe(bztpen)O]$^{2+}$} as well as, or rather than the hydroperoxide ion, [Fe(bztpen)(OOH)]$^{2+}$ a second MS/MS experiment on the *m/z* 247.6 ion was performed. This resulted only in the generation of the *m/z* 194.6 ion. Loss of 106 mass units from [Fe(bztpen)O]$^{2+}$ can be ascribed to loss of the mass equivalent to benzaldehyde, and intramolecular oxo transfer from the ferryl to the dangling benzyl group seems to be a plausible explanation. The iron(II) species which is expected to remain after benzaldehyde loss, [Fe^{II}(bztpen − C_7H_6)]$^{2+}$ (= {[Fe^{IV}(bztpen)O] − C_7H_6O}$^{2+}$) fits with observation of the *m/z* 194.6 ion. In contrast, the CID spectrum obtained under similar conditions of the *m/z* 511.2 ion {[Fe(bztpen)O_2]$^{+}$} does not show any of the peaks assignable to [Fe^{IV}(bztpen)O]$^{2+}$; instead only the ligand decomposition reaction is observed. In summary reaction proceeds *via* Scheme 2.

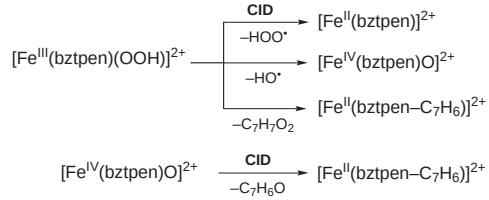

Scheme 2

The comparative ease of O–O (and Fe–O) bond cleavage in [Fe(metpen)(OOH)]$^{2+}$ compared with [Fe(metpen)(OO)]$^{+}$ observed in the MS/MS experiments is in agreement with the expectation that hydroperoxide species are more reactive (in solution) towards the O–O bond cleavage to give highly reactive ferryl oxidants, compared to their peroxide counterparts. It is for this reason, for example, iron(III) hydroperoxide species are proposed in the DNA degradation process catalysed by bleomycin.[2]

EPR spectra of the purple solutions generated from the reaction of [Fe(bztpen)Cl]PF_6 or [Fe(bztpen)Cl]$(PF_6)_2$ with hydrogen peroxide show overlapping rhombic signals indicative of two low-spin Fe(III) species, their relative intensities depending on the amount of hydrogen peroxide added and the time lag. These results are consistent the formation of [Fe(bztpen)(η^1-OOH)]$^{2+}$ (g = 2.20, 2.16, 1.96) and its precursor, [Fe^{III}(bztpen)X]$^{2+}$, X = Cl^-, OH^- or OR^-, (g = 2.32, 2.14, 1.93) as depicted in Scheme 1. The EPR spectra of blue solutions produced by the addition of base develop new signals at g = 7.60 and 5.74 due to formation of a high-spin iron(III) species. A direct relationship between the concentration of the high-spin species in the EPR spectra and the absorbance of the 748 nm band was verified by recording EPR spectra on a series of frozen solutions in which the blue chromophore showed different concentrations. A calibration of the EPR signals was made.[9]

It is tempting to make a structural assignment of seven coordination for the high-spin blue Fe(III)–peroxide species, *i.e.* [Fe(bztpen)(η^2-OO)]$^{+}$, however other structural alternatives cannot be excluded, *e.g.* [Fe(bztpen)(η^1-OO)]$^{+}$ or six-co-ordinated iron(III) with side-on peroxide and a non-co-ordinated ligand picolyl pendant arm. The possibility that the blue species is a dinuclear μ:η^2,η^2-O_2 species analogous to the dicopper hemocyanin model of Kitajima *et al.*[10] appears to be eliminated since the expected strong antiferromagnetic coupling would cause EPR silence.

In summary, the partial spectroscopic characterisation of three biologically relevant non-heme Fe(III)(O_2H), Fe(III)(O_2) and Fe(IV)O (mass spectrometry only) motifs has been achieved. To our knowledge this is the first observation of the acid–base chemistry of non-heme Fe(III)–peroxo species.

This work was supported by a grant to C. J. M. from the Danish Natural Science research council. We are grateful to a referee for suggesting the EPR calibration and UV-VIS–EPR spectroscopy correlation experiments.

Notes and references

1 L. Que and R. Y. N. Ho, *Chem. Rev.*, 1996, **96**, 2607.
2 J. W. Sam, X.-J. Tang and J. Peisach, *J. Am. Chem. Soc.*, 1994, **116**, 5250; R. J. Guajardo, J. D. Tan and P. K. Mascharak, *Inorg. Chem.*, 1994, **33**, 2838.
3 I. Bernal, I. M. Jensen, K. B. Jensen, C. J. McKenzie, H. Toftlund and J. P. Tuchagues, *J. Chem. Soc., Dalton Trans.*, 1995, 3667.
4 K. B. Jensen, Ph.D. Thesis, Odense University, Denmark, 1997.
5 C. Kim, K. Chen, J. Kim and L. Que, Jr, *J. Am. Chem. Soc.*, 1997, **119**, 5964; M. Lubben, A. Meetsma, E. C. Wilkinson, B. Feringa and L. Que, Jr., *Angew. Chem., Int. Ed. Engl.*, 1995, **34**, 2048; Y. Zang, T. E. Elgren, Y. Dong and L. Que, Jr, *J. Am. Chem. Soc.*, 1993, **115**, 811.
6 S. Ahmad, J. D. McCallum, A. K. Shiemke, E. H. Appelman, T. M. Loehr and J. Sanders-Loehr, *Inorg. Chem.*, 1988, **27**, 2230.
7 F. Neese and E. I. Solomon, *J. Am. Chem. Soc.*, 1998, **120**, 12 829.
8 Purple species, λ_{max}/nm: [Fe(metpen)(OOH)]$^{2+}$, 536; [Fe(ettpen)-(OOH)]$^{2+}$, 536: blue species, λ_{max}/nm: [Fe(metpen)(OO)]$^{2+}$, 748; [Fe(ettpen)(OO)]$^{2+}$, 747.
9 The related compounds [Fe(tpen)]$(ClO_4)_3$ [tpen = *N*,*N*,*N*′,*N*′-tetrakis(2-pyridylmethyl)ethane-1,2-diamine and Na[Fe(edta)] (edta^{4-} = ethylendiaminetetraacetate) were used to calibrate the low-spin iron(III) and high-spin iron(III) signals, respectively. Possible differences in the rates of relaxation for the various iron compounds were eliminated by calibrating at several probe temperatures. Thus an estimation of the percentage conversion in the reactions with hydrogen peroxide was made. 100% of the iron(II) species [Fe(bztpen)Cl]$^{+}$ can be converted to the low-spin iron(III) species [Fe(bztpen)X]$^{2+}$ and [Fe(bztpen)OOH]$^{2+}$ (relative amounts depending on the H_2O_2 excess); 25% of the low-spin [Fe(bztpen)OOH]$^{2+}$ can be converted to the high-spin signal assigned to [Fe(bztpen)OO]$^{+}$. There are two factors which might be responsible for the apparent incomplete conversion: (i) All the reactions are in equilibrium (as depicted in Scheme 1) and the iron(II) species are favoured. (ii) Decomposition of all or some of the iron(III) species depicted in Scheme 1 and formation of EPR silent oxo-bridged dimers. In support of the second explanation peaks assignable to [(bztpen)Cl-Fe(μ-O)FeCl(bztpen)]$^{2+}$ (*m/z* 522) are indeed observed in ESI mass spectra of the purple and blue solutions.
10 N. Kitajima, K. Fujisawa, C. Fujimoto, Y. Moro-oka, S. Hashimoto, T. Kitagawa, K. Toriumi, K. Tatsumi and A. Nakamara, *J. Am. Chem. Soc.*, 1992, **114**, 1277.

Communication 9/02985K

X-Ray structure and theoretical studies of $RuH_2(\eta^2\text{-}H_2)(\eta^2\text{-}H\text{-}SiPh_3)(PCy_3)_2$, a complex with two different η^2-coordinated σ bonds

Khansaa Hussein,[a]† Colin J. Marsden,[a] Jean-Claude Barthelat,[a] Venancio Rodriguez,[b] Salvador Conejero,[b] Sylviane Sabo-Etienne,*[b] Bruno Donnadieu[b] and Bruno Chaudret[b]

[a] *Laboratoire de Physique Quantique, IRSAMC (UMR 5626), Université Paul Sabatier, 118 route de Narbonne, 31062 Toulouse Cedex 4, France*

[b] *Laboratoire de Chimie de Coordination du CNRS, 205 route de Narbonne, 31077 Toulouse Cedex 04, France. E-mail: sabo@lcc-toulouse.fr*

Received (in Basel, Switzerland) 25th February 1999, Accepted 11th June 1999

Weak interactions between the silicon and the hydrides are responsible for the stabilization of the title complex bearing two different coordinated σ-bonds, (η^2-H_2) and (η^2-H–$SiPh_3$).

Nowadays the existence of η^2-dihydrogen or η^2-silane coordination to a metal centre is well established.[1–3] These η^2-H–X species (X = H, Si) are often considered as a representation of the arrested oxidative addition of dihydrogen or silanes to a metal center. They are thus often invoked in many catalytic reactions such as hydrogenation or hydrosilylation.[1–4] When considering the small number of complexes accommodating two σ-HX bonds, one important question is to determine the factors that promote the formation of such species. Indeed, there are only two thermally stable bis(dihydrogen) complexes[3] $[RuH_2(H_2)_2(PCy_3)_2]$ **1** and $[Tp^*RuH(H_2)_2]$, and we have recently described a new family of bis(silane) complexes $[RuH_2\{(\eta^2\text{-H–}SiR_2)_2X\}(PR'_3)_2]$ in which the disilane ligand acts as a chelate and is coordinated to the ruthenium *via* two σ-H–Si bonds.[5]

Here, we present the first structural characterization of a mixed σ-(H–H) and σ-(H–Si) complex $RuH_2(\eta^2\text{-}H_2)(\eta^2\text{-H–}SiPh_3)(PCy_3)_2$ **2** as well as theoretical studies highlighting the importance of weak formally non-bonding interactions between the silicon and the classical hydrides.

In 1994, we reported our first results concerning the reactivity of **1** toward weakly coordinating ligands such as N_2 and $HEPh_3$ (E = Si, Ge).[6] Substitution of two or one dihydrogen ligands was observed leading to $RuH_2(N_2)_2(PCy_3)_2$ and $RuH_2(\eta^2\text{-}H_2)(\eta^2\text{-H–}EPh_3)(PCy_3)_2$ respectively. The silane complex **2** was obtained by addition of 1 equiv. of $HSiPh_3$ to a pentane suspension of **1**. On the basis of NMR data and T_1 measurements, we proposed a formulation for **2** in which the two phosphine ligands were in a *trans* position, in agreement with the presence of such bulky phosphines. However, we have now succeeded in growing crystals and have obtained new information from the X-ray diffraction study. The molecular structure is shown in Fig. 1 and the principal distances and angles are listed in Table 1.‡ Two molecules are found in the asymmetric unit; however, as no significant differences are observed, we present here only the data concerning one molecule. Surprisingly, the phosphines are in a *cis* configuration with a P1–Ru–P2 angle of 109.71(5)°. The classical hydride H4 is *trans* to one phosphine with a P1–Ru–H4 angle of 166.5(14)° whereas the hydrogen H5 involved in the σ-H–Si bond is *trans* to the other phosphine with a P2–Ru–H5 angle of 170.7(11)°. The second classical hydride H3 is *trans* to the dihydrogen ligand H1–H2 with H3–Ru–H1 and H3–Ru–H2 angles of 163(2) and 168(2)°, respectively.

The (η^2-Si–H) coordination is confirmed by a significant lengthening of the Si–H5 bond: 1.72(3) Å (*ca.* 1.49 Å in free silanes). The Ru–H bond lengths vary from 1.47(4) to 1.66(2) Å with the two Ru–H distances involving the dihydrogen ligand markedly higher. The dihydrogen ligand is characterized by a H1–H2 distance of 0.82(2) Å, a value in agreement with an unstretched dihydrogen complex as highlighted by its high reactivity [addition of H_2 or N_2 results in immediate elimination of the silane and formation of the corresponding bis(dihydrogen) or bis(dinitrogen) complex]. The Si···H4 distance of 1.83(3) Å is below the limit of 2 Å normally admitted for σ-Si–H bonds. Thus the silicon is almost symmetrically bonded to H5 and H4, as can be seen from the H–Ru–Si angles of 45.9(11) and 50.2(10)°. In addition the Si···H3

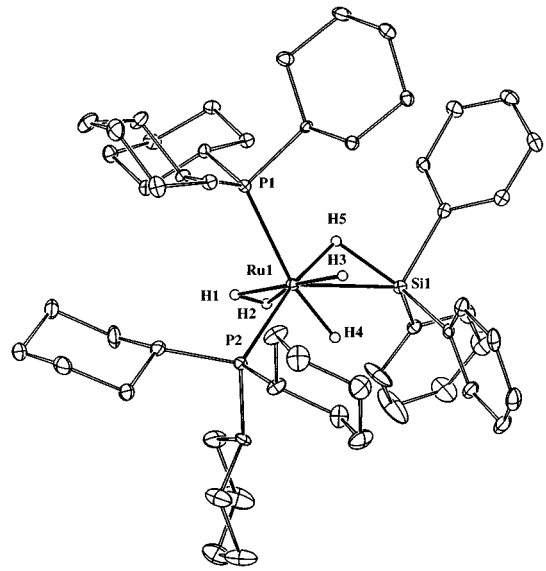

Fig. 1 ORTEP[12] drawing of compound **2**.

Table 1 Calculated geometrical parameters for the $RuH_2(\eta^2\text{-}H_2)(\eta^2\text{-H–}SiH_3)(PH_3)_2$ ground-state isomer and X-ray data for **2**[a]

	B3LYP	X-ray		B3LYP	X-ray
Ru–H1	1.807	1.66(2)	Ru–H2	1.785	1.64(2)
Ru–H3	1.626	1.49(4)	Ru–H4	1.641	1.47(4)
Ru–H5	1.643	1.54(4)	Si–H5	1.946	1.72(3)
Si···H3	2.116	2.40(4)	Si···H4	2.071	1.83(3)
H1–H2	0.849	0.82(2)	Ru–Si	2.394	2.3846(18)
Ru–P1	2.370	2.4058(17)	Ru–P2	2.367	2.3921(16)
H3···H4	2.301	2.22(2)			
P1–Ru–P2	98.9	109.71(5)	P1–Ru–H4	171.8	166.5(14)
P2–Ru–H5	177.6	170.7(11)	Si–Ru–H5	53.8	45.9(11)
Si–Ru–H3	60.0	72.6(14)	Si–Ru–H4	58.3	50.2(10)
H1–Ru–H2	27.4	28.9(8)	H2–Ru–H3	162.9	168(2)
P1–Ru–Si	114.4	118.49(6)	P2–Ru–Si	124.9	124.85(6)

[a] See Fig. 1 for labelling of the atoms. Distances are in Å and angles in °.

† Permanent address: Department of Chemistry, Faculty of Sciences, University Al Baath, Homs, Syria.

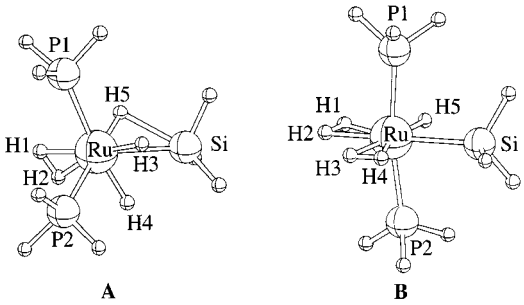

Fig. 2 The B3LYP-optimized structures of isomers **A** and **B**.

distance is 2.40(3) Å, allowing further Si···H interactions as also found by theoretical calculations. Similar interactions are also responsible for the *cis* geometry for the two PCy_3 ligands in the ruthenium complexes $RuH_2\{(\eta^2\text{-H–}SiR_2)_2X\}(PR'_3)_2$ accommodating two σ-Si–H bonds.[5b]

DFT/B3LYP calculations using a relativistic small-core pseudopotential and a [5s,5p,3d] contracted Gaussian basis for ruthenium[7] were performed on the model complex $RuH_2(\eta^2\text{-}H_2)(\eta^2\text{-H–}SiH_3)(PH_3)_2$.§ Geometry optimizations followed by vibrational frequency analyses allow identification of five singlet local minima. The structure of the most stable isomer **A** in Fig. 2 (C_1 symmetry) closely resembles that found by X-ray diffraction for **2**; we note that location of H atoms by X-ray diffraction is subject to considerable uncertainties, and that the computed P1–Ru–P2 bond angle would increase by about 7° if the PH_3 ligands were replaced by a more realistic model, such as PMe_3.[5b] Optimized geometrical parameters are listed in Table 1 for comparison. The origin of the unusual *cis* geometry for the two phosphines can be found in the presence of two attractive non-bonded interactions between the silicon atom and the two classical hydrides H3 and H4;[10] the attractive nature of these interactions is shown by the Mulliken population analysis.¶ Indeed, the calculated Si···H3 and Si···H4 distances, 2.116 and 2.071 Å, respectively, are much shorter than the sum of the van der Waals radii of silicon and hydrogen (3.3 Å). Such interactions are precluded geometrically in the four other isomers (all having *trans* phosphines). The lowest-energy of these is better described as a hydrido(silyl) complex $RuH(SiH_3)(\eta^2\text{-}H_2)_2(PH_3)_2$ (**B** in Fig. 2); it is only 8 kJ mol^{-1} above **A** [17 kJ mol^{-1} by single-point CCSD(T) calculations]. Relative B3LYP energies of the other isomers vary from 16 to 41 kJ mol^{-1}. Binding energies of the SiH_4 and H_2 ligands have been calculated from the $RuH_2(\eta^2\text{-}H_2)(PH_3)_2$ and $RuH_2(\eta^2\text{-H–}SiH_3)(PH_3)_2$ fragments.‖

As pointed out very recently by Corey and Braddock-Wilking in their impressive review on the reactions of hydrosilanes with transition-metal complexes, 'Several variations of interactions seem to occur between silanes and metals, from full oxidative addition to that of arrested addition with an interaction between a metal orbital and a Si–H sigma bond'.[2b] We have shown here how important additional Si···H interactions are; they control the coordination geometry at the metal centre. This type of bonding deserves special attention for future studies, given that it involves energies comparable to those in the 'dihydrogen bonds'** recently described by several groups,[11] and that it might well be of primary importance in catalytic silicon transformations.

This work is supported by the CNRS. We thank the Centre National Universitaire Sud de Calcul, Montpellier, France (project irs 1013) for a generous allocation of computer time.

Notes and references

‡ *Crystal data* for **2**: $C_{58}H_{91}OP_2SiRu$, M = 995.59, triclinic, space group $P\bar{1}$, T = 160(2) K, a = 12.7694(16), b = 20.991(3), c = 21.691(2) Å, α = 94.763(14), β = 103.677(14), γ = 98.202(15)°, V = 5550.0(12) Å^3, Z = 4, μ = 0.342 mm^{-1}, reflections collected/unique = 44792/16676, $R1$ = 0.0381, $wR2$ = 0.0626. The H1–H5 atoms were located on difference Fourier syntheses; their coordinates were refined with isotropic thermal parameters. CCDC 182/1287. See http://www.rsc.org/suppdata/cc/1999/1315/ for crystallographic files in .cif format.

§ All calculations were performed with the Gaussian 94 program.[8] The Si and P atoms were described by standard pseudo-potentials developed in Toulouse[9] with a double-zeta plus polarization basis set. A double-zeta plus polarization basis was used for the hydrogen atoms, except for those of the phosphine ligands (DZ only).

¶ We obtain non-negligible positive overlap populations between Si and H3 or H4 of 0.05 and between Si and H5 of 0.09 (0.40 in free SiH_4).

‖ The energy differences between the products and the reactants are −92.7 kJ mol^{-1} for SiH_4 and −73.8 kJ mol^{-1} for H_2. Further details on related complexes will be published elsewhere.

** Intramolecular hydrogen bonding between a hydride and a hydrogen bond donor.

1 For reviews on dihydrogen complexes chemistry: G. J. Kubas, *Acc. Chem. Res.*, 1988, **21**, 120; R. H. Crabtree, *Acc. Chem. Res.*, 1990, **23**, 95; P. G. Jessop and R. H. Morris, *Coord. Chem., Rev.*, 1992, **121**, 155; D. M. Heinekey and W. J. Oldham Jr., *Chem. Rev.*, 1993, **93**, 913; R. H. Crabtree, *Angew. Chem., Int. Ed. Engl.*, 1993, **32**, 789; M. A. Esteruelas and L. A. Oro, *Chem. Rev.*, 1998, **98**, 577.

2 For reviews on silane complexes: (*a*) U. Schubert, *Adv. Organomet. Chem.*, 1990, **30**, 151; (*b*) J. Y. Corey and J. Braddock-Wilking, *Chem. Rev.*, 1999, **99**, 175.

3 S. Sabo-Etienne and B. Chaudret, *Coord. Chem. Rev.*, 1998, **178**–**180**, 381.

4 M. L. Christ, S. Sabo-Etienne and B. Chaudret, *Organometallics*, 1995, **14**, 1082; F. Delpech, S. Sabo-Etienne, B. Donnadieu and B. Chaudret, *Organometallics*, 1998, **17**, 4926.

5 (*a*) F. Delpech, S. Sabo-Etienne, B. Chaudret and J. C. Daran, *J. Am. Chem. Soc.*, 1997, **119**, 3167; (*b*) F. Delpech, S. Sabo-Etienne, B. Chaudret, J. C. Daran, K. Hussein, C. J. Marsden and J.-C. Barthelat *J. Am. Chem. Soc.*, 1999, in press.

6 S. Sabo-Etienne, M. Hernandez, G. Chung, B. Chaudret and A. Castel, *New J. Chem.*, 1994, **18**, 175.

7 V. Rodriguez, S. Sabo-Etienne, B. Chaudret, J. Thoburn, S. Ulrich, H.-H. Limbach, J. Eckert, J.-C. Barthelat, K. Hussein and C. J. Marsden, *Inorg. Chem.*, 1998, **37**, 3475.

8 Gaussian 94, M. J. Frisch, G. W. Trucks, H. B. Schlegel, P. M. W. Gill, B. G. Johnson, M. A. Robb, J. R. Cheeseman, T. A. Keith, G. A. Petersson, J. A. Montgomery, K. Raghavachari, M. A. Al-Laham, V. G. Zakrewski, J. V. Ortiz, J. B. Foresman, J. Cioslowski, B. B. Stefanov, A. Nanayakkara, M. Challacombe, C. Y. Peng, P. Y. Ayala, W. Chen, M. W. Wong, J. L. Andres, E. S. Replogle, R. Gomperts, R. L. Martin, D. J. Fox, J. S. Binkley, D. J. Defrees, J. Baker, J. P. Stewart, M. Head-Gordon, C. Gonzalez and J. A. Pople, Gaussian, Inc., Pittsburgh PA, 1995.

9 Y. Bouteiller, C. Mijoule, M. Nizam, J.-C. Barthelat, J.-P. Daudey, M. Pélissier and B. Silvi. *Mol. Phys.*, 1988, **65**, 2664.

10 G. I. Nikonov, L. G. Kuzmina, D. A. Lemenovskii and V. V. Kotov, *J. Am. Chem. Soc.*, 1995, **117**, 10 133; M.-F. Fan and Z. Lin, *Organometallics*, 1998, **17**, 1092.

11 See, for example, R. H. Crabtree, P. E. M. Siegbahn, O. Eisenstein, A. L. Rheingold and T. F. Koetzle, *Acc. Chem. Res.*, 1996, **29**, 348; S. Park, A. J. Lough and R. H. Morris, *Inorg. Chem.*, 1996, **35**, 3001; J. A. Ayllon, S. Sabo-Etienne, B. Chaudret, S. Ulrich and H.-H. Limbach, *Inorg. Chim. Acta*, 1997, **259**, 1; A. Castellanos, J. A. Ayllon, S. Sabo-Etienne, B. Donnadieu, B. Chaudret, W. Yao, K. Kavallieratos and R. H. Crabtree, *C. R. Acad. Sci.* 1999, in press.

12 C. K. Johnson, ORTEP, Report ORNL-5138, Oak Ridge National Laboratory, Oak Ridge, TN, 1976.

Communication 9/01558B

ChemComm

Nickel nanowires of 4 nm diameter in the cavity of carbon nanotubes

Bhabendra K. Pradhan, Takashi Kyotani* and Akira Tomita

Institute for Chemical Reaction Science, Tohoku University, 2-1-1 Katahira, Aoba-Ku, Sendai 980-8577, Japan. E-mail: kyotani@icrs.tohoku.ac.jp

Received (in Cambridge, UK) 24th May 1999, Accepted 14th June 1999

Nickel nanowires of 4 nm diameter were formed in the cavity of carbon nanotubes with an inner diameter of 20 nm.

There has been an increasing interest in the fabrication of ferromagnetic metal nanowires in terms of their fundamental importance as well as potential application in magnetic recording technology. Recently, such nanowires have been often prepared by a template technique[1] that involves electrochemical deposition of metal into nanometer-wide channels of anodic aluminium oxide films,[2,3] polycarbonate track etched membranes[4,5] or nanochannel array glass.[6] The obtainable lowest diameter by such methods is restricted by the lowest attainable inner diameter of the nanochannels in the template materials. None of the nanochannels in the above host materials can easily reach an inner diameter of < 10 nm. Therefore, the template method does not allow the construction of ferromagnetic metal nanowires with a diameter of < 10 nm. Here we report a unique nickel nanowire formation by metal–organic chemical vapor deposition (MOCVD) in the cavity of carbon-coated nanochannels of anodic aluminium oxide film. The diameter of the nickel nanowires prepared by this method is uniformly 4 nm, which is much smaller than the inner diameter (*ca.* 20 nm) of the carbon-coated nanochannels.

Previously, we demonstrated that monodisperse carbon nanotubes with uniform size (length, diameter and thickness) can be prepared by the following template carbonization technique;[7,8] pyrolytic carbon deposition in the uniform and straight channels of anodic aluminium oxide film and then liberation of the carbon from the film by dissolving the template. With a similar method, but using a catalyst, Martin and coworkers prepared more highly crystallized carbon nanotubes.[9] Furthermore, by applying this template technique, we and then Martin *et al.* prepared platinum or iron-filled uniform carbon nanotubes in which the metal or metal oxide was present as nanorods or nanoparticles.[10–12] In this study, we attempted to insert nickel into carbon nanotubes. The previously described anodic oxidation[7,8] of an electropolished aluminium plate was used to prepare a porous anodic aluminium oxide film with a channel diameter of *ca.* 30 nm and the film diameter and thickness were 20 mm and *ca.* 75 μm, respectively. The film was subjected to carbon deposition by thermal decomposition of propene (1.2% in N_2) at 800 °C, which resulted in uniform coating of carbon on the channel walls. The resultant carbon-coated film was then subjected to metal–organic chemical vapor deposition (MOCVD) of nickelocene [$Ni(C_5H_5)_2$] in the following manner. Nickelocene was vaporized at 105 °C (corresponding to a vapor pressure of 0.6 kPa) and the film was exposed to the vapor with H_2 gas (50% in N_2) at a total flow rate of 100 cm^3(STP) min^{-1} at 275 °C for 0.25 or 1 h. After the MOCVD, the film was treated with 10 M NaOH solution at 150 °C in an autoclave for 6 h to dissolve the anodic aluminium oxide. Nickel/carbon nanotube composites were obtained as an insoluble fraction. The composites were observed with a transmission electron microscope (TEM; JEOL, JEM-2010) equipped with an energy dispersive X-ray spectrometer (Noran, 644G3SES).

Fig. 1(a) shows a bright field TEM image of the nickel/carbon nanotube composites prepared by MOCVD for 1 h. The image exhibits a carbon nanotube with a diameter of *ca.* 30 nm, containing a single nanowire of 500 nm in length and 4 nm in diameter. Fig. 1(b) shows the electron diffraction pattern taken from the nickel/carbon nanotube composite [Fig. 1(a)]. The pattern presents a pair of arcs from the carbon (002) reflection. In addition to the reflection from the carbon tube, two pairs of sharp diffraction spots were observed, which can be indexed as (111) and (222) reflections from fcc nickel metal. Apart from the sharp spots, there are several spots from nickel metal (220) and (331) reflections. An energy dispersive X-ray spectrum taken from this nanowire confirms the presence of nickel with no signal corresponding to oxygen. Both the diffraction pattern and elemental analyses suggest that the nanowire is pure nickel metal rather than a nickel compound. The appearance of the nickel (111) and (222) reflections not as a ring, but as a pair of symmetrical spots, indicates high orientation of the (111) planes in the nickel nanowire [Fig. 1(a)]. Judging from the positions of (111) and (222) spots, we can conclude that the (111) planes run parallel to the axis of the nickel wire. This was further confirmed by the lattice fringe image discussed below.

Fig. 2 shows a high resolution TEM image of a nanowire-containing carbon nanotube prepared under the same conditions as in Fig. 1(a). In this image, the lattice fringes of the nanowire which are located near the inner wall of the carbon nanotube are clearly observed and the lattice planes are parallel to the wire axis. The regular spacing of the observed lattice planes was 0.20 nm, which corresponds to the separation of (111) planes of fcc nickel metal. For all the nanowires we observed in this study, such preferable orientation of (111) planes was found without any clear grain boundaries. This accords with the result of the electron diffraction [Fig. 1(b)]. From these findings, we concluded that each of these nickel nanowires is a slender single crystal.

In order to examine the formation of nickel nanowire at an early stage, we carried out the MOCVD for a shorter time, *i.e.* 15 min. We observed many nickel nanowires in the cavity of carbon nanotubes as shown in Fig. 3. In some cases, short nanowires are present at an angle to the tube axis. The length of

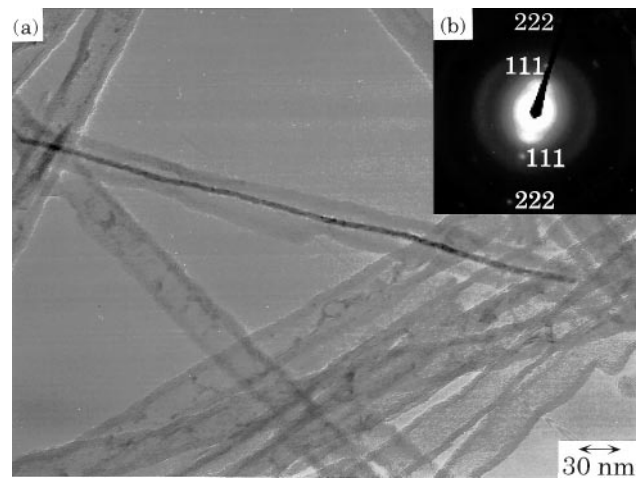

Fig. 1 (a) Low-magnification TEM image of a nickel/carbon nanotube composite prepared by MOCVD for 1 h at 275 °C. (b) Electron diffraction pattern taken from the nanowire-containing carbon nanotube (a).

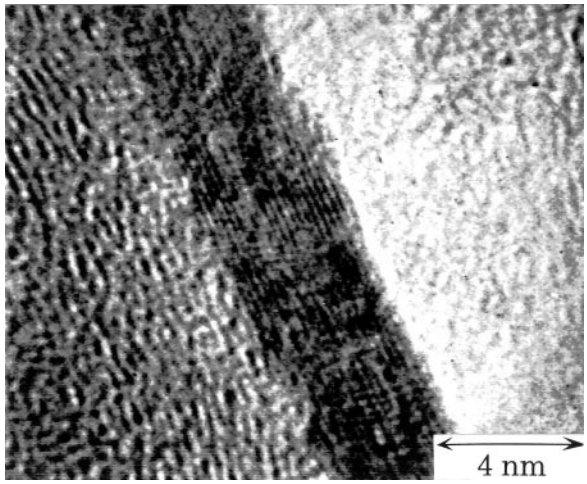

Fig. 2 High-resolution TEM image of a nickel wire near the inner wall of carbon nanotubes. The carbon nanotube/nickel nanowire composites was prepared by MOCVD for 1 h at 275 °C.

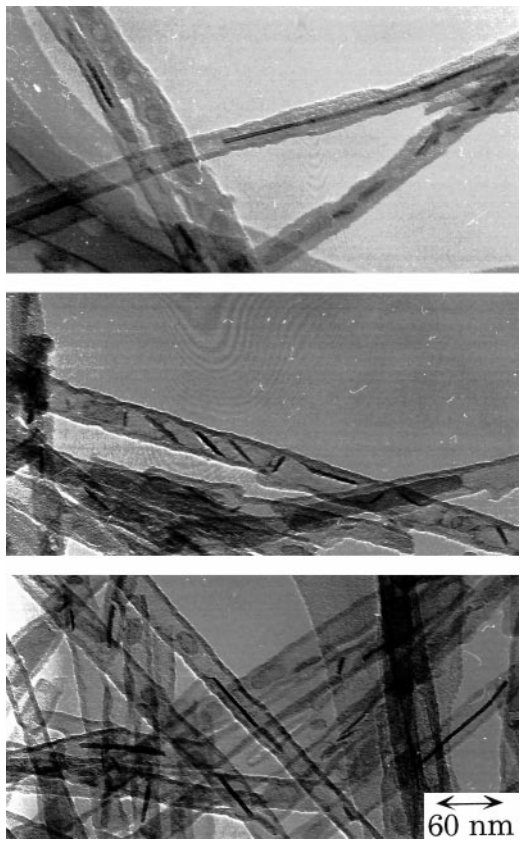

Fig. 3 Bright field TEM images at different areas for carbon tubes/nickel nanowire composites prepared by MOCVD for 15 min at 275 °C.

the nanowires varies from ten to a few hundred nm and the average length is less than that in Fig. 1(a). It was found that the nanowire diameter is rather uniform at *ca.* 4 nm irrespective of the MOCVD time period. This finding suggests preferred nanowire growth toward the direction parallel to (111) plane.

Among all the tubes we have examined with TEM, more than 50% of the tubes contained nickel nanowires with a uniform diameter of 4 nm. However, we did not observe any nanowires in the cavity of carbon nanotubes near their open ends. This implies that the growth of nickel nanowires occurred inside the carbon-coated nanochannels. Even though the nickel metal was formed in the nanochannels, the diameter of the resultant nanowires was less than the inner diameter of the nanochannels. At the present moment, we do not have a reasonable explanation for the formation of such thin nanowires, but we presume that the coated carbon plays some role in producing them.

The template method is considered to be a promising approach for the fabrication of metal nanowires of very small size.[2–6,13] In this method, the obtainable diameter of nanowires is, however, regulated by the inner diameter of the nanochannels in the template materials. To the best of our knowledge, the formation of metal nanowires with diameters smaller than that of the template has not been previously reported. Another important feature in our method is that nickel nanowires are always evident as encapsulated nanowires in the hollow interiors of uniform carbon nanotubes. Since metal-filled carbon nanotubes could have a variety of industrial applications,[14] there have been many attempts towards the production of carbon nanotubes filled with metal or metal compounds as nanowires.[15–20] However, as stated above, the diameter of the nanowires is always the same as the inner diameter of carbon nanotubes. Thus, the nanowire formation we have discovered here is a quite unique phenomenon and can provide a novel methodology for future nanofabrication technology.

This study was partly supported by the Ministry of Education, Science, Sports and Culture, Grant-in-Aid for Scientific Research on Priority Areas, No. 288 ‘Carbon Alloys’.

Notes and references

1 C. R. Martin, *Science*, 1994, **266**, 1961.
2 D. Davydov, J. Haruyama, D. Routkevitch, B. W. Statt, D. Ellis, M. Moskovits and J. M. Xu, *Phys. Rev. B: Condens. Matter*, 1998, **57**, 13 550.
3 F. Schlottig, M. Textor, N. D. Spencer, K. Sekinger, U. Shnaut and J.-F. Paulet, *Fresenius J. Anal. Chem.*, 1998, **361**, 684.
4 T. M. Whitney, J. S. Jiang, P. C. Searson and C. L. Chien, *Science*, 1993, **261**, 1316.
5 C. Schönenberger, B. M. I. van der Zande, L. G. J. Fokkink, M. Henny, C. Schmid, M. Krüger, A. Bachtold, R. Huber, H. Birk and U. Staufer, *J. Phys. Chem. B*, 1997, **101**, 5497.
6 P. P. Nguyen, D. H. Pearson, R. J. Tonucci and K. Babcock, *J. Electrochem. Soc.*, 1998, **145**, 247.
7 T. Kyotani, L. Tsai and A. Tomita, *Chem. Mater.*, 1995, **7**, 1427.
8 T. Kyotani, L. Tsai and A. Tomita, *Chem. Mater.*, 1996, **8**, 2109.
9 G. Che, B. B. Lakshmi, C. R. Martin, E. R. Fisher and R. S. Ruoff, *Chem. Mater.*, 1998, **10**, 260.
10 T. Kyotani, L. Tsai and A. Tomita, *Chem. Commun.*, 1997, 701.
11 B. Lakshmi, E. R. Fisher and C. R. Martin, *Nature*, 1998, **393**, 346.
12 B. K. Pradhan, T. Toba, T. Kyotani and A. Tomita, *Chem. Mater.*, 1998, **10**, 2510.
13 M. Sasaki, M. Osada, N. Sugimoto, S. Inagaki, Y. Fukushima, A. Fukuoka and M. Ichikawa, *Microporous Mesoporous Mater.*, 1998, **21**, 597.
14 M. Freemantle, *Chem. Eng. News*, 1996, **74**, 62.
15 P. M. Ajayan, T. W. Ebbesen, T. Ichihashi, S. Iijima, K. Tanigaki and H. Hiura, *Nature*, 1993, **362**, 522.
16 C. Guerret-Piecourt, Y. Le Bouar, A. Loiseau and H. Pascard, *Nature*, 1994, **372**, 761.
17 Y. K. Chen, M. L. H. Green and S. C. Tsang, *Chem. Commun.*, 1996, 2489.
18 A. A. Setlur, J. M. Lauerhaas, J. Y. Dai and R. P. H. Chang, *Appl. Phys. Lett.*, 1996, **69**, 345.
19 A. Loiseau and H. Pascard, *Chem. Phys. Lett.*, 1996, **256**, 246.
20 J. Y. Dai, J. M. Lauerhaas, A. A. Setlur and R. P. H. Chang, *Chem. Phys. Lett.*, 1996, **258**, 547.

Communication 9/04157E

Development of a selective TOCSY experiment and its use in analysis of a mixture of related compounds

Gary J. Sharman*

AstraZeneca Pharmaceuticals, Silk Road Business Park, Macclesfield, Cheshire, UK SK10 2NA.
E-mail: gary.sharman@alderley.zeneca.com

Received (in Cambridge, UK) 26th March 1999, Accepted 9th June 1999

A selective TOCSY experiment based on the recently described DPFGSE selective excitation sequence has been developed: it employs gradient purging pulses which result in excellent lineshapes free of antiphase dispersive components, and has proven useful in the identification of a number of impurities in a pharmaceutical intermediate.

Recently, Stott *et al.* have described a new method of selective excitation called 'double pulsed field gradient spin echo' (DPFGSE).[1,2] The method gives exceptionally clean selective excitation. They have used this selective excitation scheme to develop a one dimensional NOE experiment, the DPFGSE-NOE, which gives excellent quality NOE spectra devoid of the subtraction artefacts normally associated with the steady state NOE difference experiment.

Using this excitation scheme, we have developed a selective TOCSY experiment.[3–5] DANTE pulses have been used instead of shaped pulses within the DPFGSE sequence [Fig 1(*a*)], due to spectrometer hardware limitations, but the quality of the selective excitation remains high. This approach has the advantage of allowing the bandwidth of the selective excitation to be easily tailored by adjusting the DANTE delay. The TOCSY transfer can be achieved by a period of spin locking following on from the selective excitation. The DIPSI[6,7] sequence was chosen in this case. However, such a sequence can result in severely distorted lineshapes.[8,5] These distortions arise because any magnetisation which is not purely single component, prior to and after the period of spin locking, results in zero quantum coherence which gives an antiphase dispersive contribution to the lineshape. Thus poorer quality spectra are obtained and interpretation is less straightforward in that direct comparison with a proton spectrum or with expected multiplet patterns is not possible. This is clearly illustrated in Fig. 2(*a*), which shows a selective TOCSY spectrum of sucrose following excitation of the anomeric proton. The triplet due to H4 and the double doublet due to H2 are both severely distorted. A z-filter, employing a variable delay list,[9,10] is one way of reducing these undesired effects, but this necessitates long acquisition times as the phase cycle must be completed for each value of the z-filter delay, of which there are typically many. In addition, even with all parameters set up optimally, this method can never remove all of the phase anomalies.[8]

A superior method for removing these zero quantum effects is provided by dephasing in an inhomogenous B_0 field, as described by Davis *et al.*[8] The method is based around a period of spin locking which is executed concurrently with a gradient pulse, before and after the mixing sequence. This method gives exceptionally clean two dimensional TOCSY spectra,[8] and a similar scheme has been used by Dalvit in a 1D TOCSY.[4] The essence of the method is that zero quantum coherence precesses during the gradient pulse. Its offset becomes spatially dependent and it is therefore dephased. The pulse sequence incorporating these purging pulses and the DIPSI mixing sequence is shown in Fig. 1(*b*). Fig. 2(*b*) shows a selective TOCSY spectrum of a sucrose test sample—the lineshape and multiplet structure is greatly improved, and compares well to the normal proton spectrum.

The excellent selectivity of the DPFGSE sequence suggested to us that this TOCSY sequence might prove useful in the analysis of low level impurities in a mixture. This type of analysis could be tackled by LC-NMR,[11] but this technique is not without its problems. Replicating chromatography at the high loading levels required for LC-NMR is not always straightforward, and lower loading levels can lead to inadequate sensitivity. Also, instrument time is a factor, with probe changes

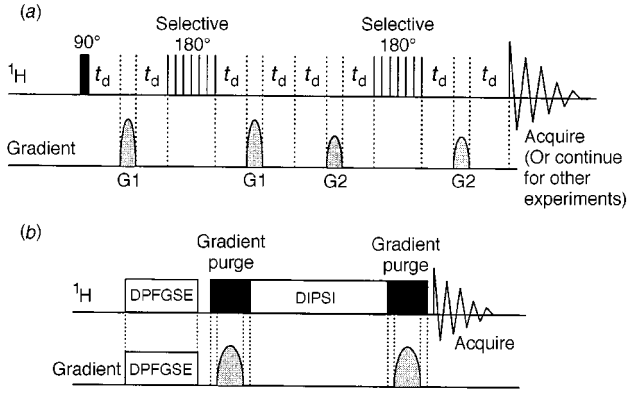

Fig. 1 (*a*) Pulse sequence for the DPFGSE selective excitation. The DANTE pulse consists of 200 π/200 pulses separated by a delay of 125 μs. (*b*) Additional pulses for the selective 1D-TOCSY experiment.

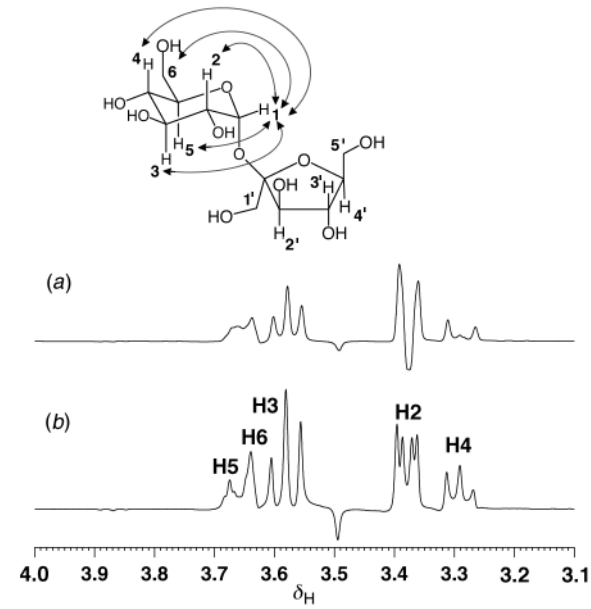

Fig. 2 (*a*) Selective TOCSY spectrum of sucrose obtained using only a period of DIPSI mixing after selective excitation. Phase distortions are apparent. (*b*) Selective TOCSY spectrum obtained using the sequence in Fig. 1(*b*), showing almost complete removal of distortions. The TOCSY mixing time was 100 ms, the purge spin lock 10 ms and the gradient pulse 9.8 ms at approximately 15 G cm^{-1} (a 100 μs delay precedes and follows the gradient).

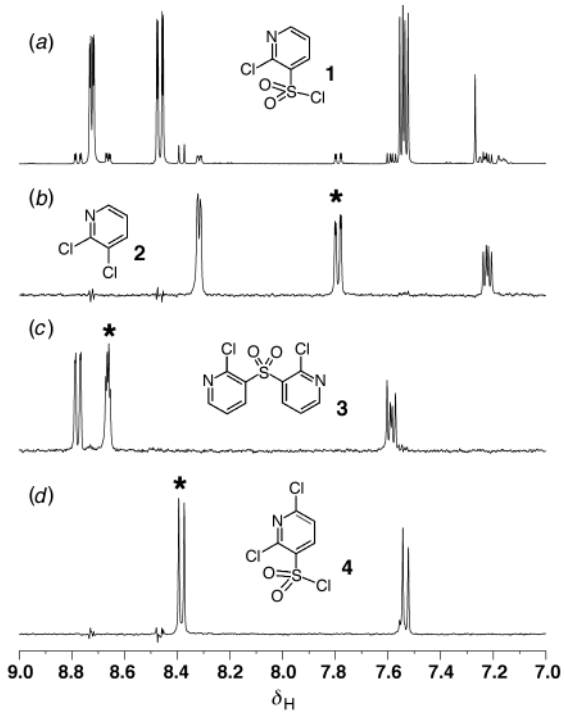

Fig. 3 (*a*) 400 MHz ^{1}H NMR spectrum of **1** in DMSO-d_6. A number of low level impurities are also apparent. (*b*)–(*d*) Selective 1D-TOCSY spectra obtained after selective excitation of the marked peaks. Each spectrum is consistent with the impurities **2**–**4**. Spectra in (*b*)–(*d*) acquired with 64 transients.

significantly increasing the time taken for analysis of a sample. Diffusion ordered spectroscopy[12,13] is perhaps a promising alternative, but this technique requires a significant difference in the diffusion coefficients of the species involved; this may well not be the case for typical impurities of related structure. The selective TOCSY experiment described above might provide another fast approach. The method would require that one impurity peak be resolved from other components. In these circumstances, a partial spectrum of the impurity could be acquired, and in the case of simple compounds consisting of one spin system, an essentially normal proton spectrum could be obtained.

This approach was tested on a sample which contained a number of impurities requiring identification. The major component in the mixture was the sulfonyl chloride **1**, but a number of other peaks were apparent in the spectrum [Fig. 3(*a*)]. Using the selective TOCSY experiment described above, the resonance at 7.8 ppm was excited, resulting in the spectrum shown in Fig. 3(*b*). This spectrum clearly shows the excellent suppression of the main component, together with a lineshape which compares favourably to that of the normal proton spectrum. The spectrum clearly represents a component in which the three aromatic protons are still present, but the relatively large chemical shift changes suggest different substituents to the main component. The spectrum is therefore consistent with that of the suspected impurity **2**. Similarly, selective excitation of the resonance at 8.65 ppm resulted in the spectrum shown in Fig. 3(*c*). As for the first impurity, the spectrum indicates a disubstituted pyridine system, but the similarity of chemical shifts to the main component suggests that these resonances are due to the dimeric sulfone **3**, another suspected impurity. Note that in this spectrum too, lineshape is good and the main component is well suppressed, despite the fact that the selectively excited proton is only 0.1 ppm from a resonance of the main component.

Finally, the resonance at 8.4 ppm was selectively excited. This gave rise to the 1D-TOCSY spectrum shown in Fig. 3(*d*). Clearly, this component exhibits only two proton resonances, indicating a tri-substituted product. It was therefore assigned to the dichloro sulfonyl chloride **4**, which was another suspected contaminant. Note that one of the two resonances in this component was completely overlapped with the main component in the normal proton spectrum. The excellent suppression of the main component, however, means that this peak can clearly be observed with its normal lineshape and doublet structure.

Overall, the three experiments took a total of 15 min to acquire. Subsequently, the sample was analysed by LC-NMR. This took several hours, including time for probe changes and setting up the chromatography. The conclusions reached were the same. Mass spectrometry also confirmed the identity of the three impurities.

The impurities in this sample were present at a level of approximately 4% w/w each. The level of suppression afforded by the selective TOCSY experiment is such that the residual peaks arising from the main component are approximately 2% of the level of each impurity. This figure suggests that the level at which impurities could be detected while retaining a useful degree of suppression of the main peak is rather lower than the 4% in this sample. It is estimated that 0.5% could be regarded as the limit of detection.

Of course, this selective TOCSY experiment will not give a complete, 'normal' spectrum of every component in every mixture; it may be that peaks are not resolved from the main component, or more complicated structures with many spin systems will not allow transfer to all parts of the molecule. However, in the case of many pharmaceutical compounds, we are looking for closely related impurities, and so a complete spectrum may not be necessary to obtain a structure. The elucidation of a different substitution pattern, or a 'missing' proton in a particular spin system, may be enough to define a structure, particularly when combined with mass spectrometry data. Also, the use of the related DPFGSE NOE experiment could allow parts of the molecule not in the same spin system to be accessed. Overall, it seems that this method, while not being a panacea for the analysis of all impurities, is nevertheless a useful technique which in this case has provided a fast answer to a real problem.

Notes and references

1 K. Stott, J. Keeler, Q. N. Van and A. J. Shaka, *J. Magn. Reson.*, 1997, **125**, 302.
2 K. Stott, J. Stonehouse, J. Keeler, T. L. Hwang and A. J. Shaka, *J. Am. Chem. Soc.*, 1995, **117**, 4199.
3 L. Braunschweiller and R. R. Ernst, *J. Magn. Reson.*, 1983, **53**, 521.
4 C. Dalvit and G. Bovermann, *Magn. Reson. Chem.*, 1995, **33**, 156.
5 T. Parella, *Magn. Reson. Chem.*, 1996, **34**, 329.
6 A. J. Shaka, C. J. Lee and A. Pines, *J. Magn. Reson.*, 1988, **77**, 274.
7 S. P. Rucker and A. J. Shaka, *Mol. Phys.*, 1989, **68**, 509.
8 A. Davis, G. Estcourt, J. Keeler, E. Laue and J. Titman, *J. Magn. Reson. Ser. A*, 1993, **105**, 167.
9 M. Rance, *J. Magn. Reson.*, 1987, **74**, 557.
10 R. Bazzo and I. D. Campbell, *J. Magn. Reson.*, 1988, **76**, 358.
11 See for example, L. Griffiths, *Anal. Chem.*, 1995, **67**, 22, 4091.
12 H. Barjat, G. A. Morris, S. Smart, A. G. Swanson and S. C. R. Williams, *J. Magn. Reson. Ser. B*, 1995, **108**, 2, 170.
13 D. H. Wu, A. D. Chen and C. S. Johnson, *J. Magn. Reson. Ser. A*, 1996, **121**, 88.

Communication 9/02459J

Dankasterone, a new class of cytotoxic steroid produced by a *Gymnascella* species from a marine sponge

Taro Amagata, Mitsunobu Doi, Makiko Tohgo, Katsuhiko Minoura and Atsushi Numata*

Osaka University of Pharmaceutical Sciences, 4-20-1 Nasahara, Takatsuki, Osaka 569-1094, Japan. E-mail: numata@oysun01.oups.ac.jp

Received (in Cambridge, UK) 13th May 1999, Accepted 9th June 1999

Dankasterone, produced by a strain of *Gymnascella dankaliensis* from the marine sponge *Halichondria japonica*, is a novel class of steroid with significant cytotoxicity against tumour cells in culture.

In our programme devoted to the search for new antitumour metabolites from microorganisms inhabiting the marine environment, we have found a number of antitumour and cytotoxic compounds and elucidated their structures.[1,2] As part of this study, we have previously isolated the cytotoxic gymnastatins[2,3] and gymnasterones[4] from a strain of *Gymnascella dankaliensis* (Castellani) Currah OUPS-N134 originally separated from the sponge *Halichondria japonica*. Further investigation for metabolites of this fungal strain has now led to the isolation of a structurally unique and cytotoxic steroid **1**, designated dankasterone.

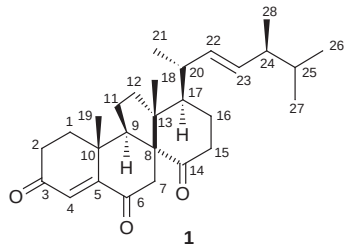

1

In this experiment, the fungal strain was cultivated in a medium which was prepared by replacement of glucose used for the previous experiment[2–4] by starch. The MeOH extract of the mycelium was purified by bioassay-directed fractionation employing a combination of Sephadex LH-20 and silica gel column chromatography and HPLC to afford dankasterone **1** as prisms.

Dankasterone **1** was assigned the molecular formula of $C_{28}H_{49}O_5$ as deduced from HREIMS. A close inspection of the ^{1}H and ^{13}C NMR spectral data† for **1** from DEPT and ^{1}H–^{13}C COSY experiments revealed the presence of six methyls including four secondary and two tertiary methyls, seven methylenes, five sp^3- hybridised methines, three quaternary sp^3-carbons, one disubstituted and one trisubstituted double bond, and one unconjugated and two conjugated ketones. The ^{1}H–^{1}H COSY analysis for the functional groups led to partial structures A (C-1 and C-2), B (C-9, C-11 and C-12) and C (C-15–C-17 and C-20–C-28), which were supported by HMBC correlations. The geometry of the disubstituted double bond was deduced from the coupling constants ($J_{23,24}$ 15.1 Hz) of the olefinic protons. The connection of the partial structures (A to C) and the remaining functional groups was determined on the basis of HMBC correlations. The typical correlations are as follows; H-1 and H-2 to C-3, H-4 to C-2, C-6 and C-10, H-19 to C-1, C-5, C-9 and C-10, H-7 to C-6, C-8 and C-13, H-9 to C-7, C-8, C-10 and C-14, H-15 to C-14, and H-18 to C-8, C-12, C-13 and C-17. Based on this evidence, the planar structure of **1** was elucidated.

The relative stereochemistry for **1** was established by NOESY experiments, which showed NOEs from 1-H$^\alpha$ to 9-H and 11-H$^\alpha$, 19-H to 1-H$^\beta$ and 11-H$^\beta$, 17-H to 9-H and 12-H$^\alpha$, and 18-H to 7-H$^\alpha$, 7-H$^\beta$ and 12-H$^\beta$. The relative stereostructure of **1** thus expected was cofirmed by X-ray structure analysis‡ on a single crystal of **1** (Fig. 1), which clarified the stereochemistry of the side chain. This compound is an unprecedented steroid with a 13(14→8)*abeo*-8-ergostane skeleton which is considered to have been reconstructed from ergostane through the 1,2-migration of C-13–C-14 bond to the C-8 position.

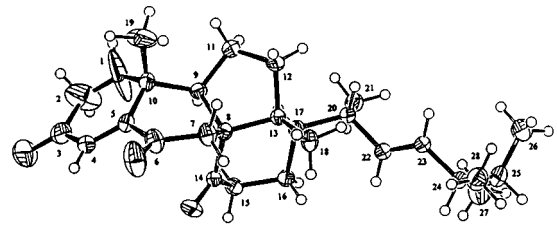

Fig. 1 X-Ray crystal structure for dankasterone **1**.

Dankasterone **1** exhibited significant cytotoxicity (ED_{50} 2.2 μg ml^{-1}) in the P-388 lymphocytic leukemia test system in cell culture. First isolation of this steroid with a unique carbon skeleton consisting of five-membered (C) and six-membered (D) rings has evoked great interest in what sort of biological activity it exhibits, compared with those of usual steroids.

Notes and references

† *Spectral data* for **1**: Prisms, mp 133–134 °C (MeOH), $[\alpha]_D^{26}$ +57.8 (*c* 0.7 in $CHCl_3$); HREIMS *m/z* 424.2988 (M^+), Δ − 1.3 mmu; λ_{max}(EtOH)/nm (log ε) 254 (4.02); ν_{max}(KBr)/cm^{-1} 1695, 1682, 1607; δ_H(500 MHz, $CDCl_3$) 0.81 (3H, d, *J* 6.8, 27-H), 0.84 (3H, d, *J* 6.8, 26-H), 0.91 (3H, d, *J* 6.8, 28-H), 0.98 (3H, s, 18-H), 1.09 (3H, d, *J* 6.8, 21-H), 1.26 (3H, s, 19-H), 1.47 (1H, octet, *J* 6.8, 25-H), 1.48 (1H, dd, *J* 13.2 and 4.2 , 17-H), 1.69 (1H, m, 16-H$^\beta$), 1.71 (1H, m, 12-H$^\alpha$), 1.77 (1H, dt, *J* 13.0 and 7.2, 12-H$^\beta$), 1.85 (1H, m, 11-H$^\beta$), 1.88 (1H, m, 24-H), 1.90 (1H, m, 16-H$^\alpha$), 2.02 (1H, m, 11-H$^\alpha$), 2.04 (1H, m, 1-H$^\beta$), 2.08 (1H, dd, *J* 13.4 and 5.1, 1-H$^\alpha$), 2.42 (1H, m, 20-H), 2.46 (1H, m, 2-H$^\alpha$), 2.48 (2H, m, 15-H), 2.50 (1H, d, *J* 16.8, 7-H$^\beta$), 2.53 (1H, dt, *J* 17.6 and 6.2, 2-H$^\beta$), 2.66 (1H, dd, *J* 16.8 and 1.3, 7-H$^\alpha$), 2.81 (1H, td, *J* 9.0 and 1.3, 9-H), 5.25 (1H, dd, *J* 15.1 and 5.0, 22-H), 5.29 (1H, dd, *J* 15.1 and 3.5, 23-H), 6.36 (1H, s, 4-H); δ_C(125.7 MHz, $CDCl_3$) 17.05 (C-18), 17.58 (C-28), 19.66 (C-27), 20.03 (C-26), 23.16 (C-16), 23.59 (C-21), 23.99 (C-19), 25.10 (C-11), 33.04 (C-25), 34.34 (C-2), 35.99 (C-10), 37.20 (C-20), 37.93 (C-15), 38.30 (C-12), 38.88 (C-1), 40.82 (C-7), 43.21 (C-24), 49.32 (C-17), 49.35 (C-9), 53.97 (C-12), 62.18 (C-8), 126.48 (C-4), 132.31 (C-22), 135.10 (C-23), 156.05 (C-5), 199.10 (C-3), 200.00 (C-6), 214.78 (C-14).

‡ *Crystal data* for **1**: $C_{28}H_{40}O_3$, *M* = 424.60, orthorhombic, $P2_12_12_1$, *a* = 12.667(3), *b* = 23.829(5), *c* = 8.134(4) Å, *V* = 2455.4(14) Å^3, *Z* = 4, d_x = 1.149 g cm^{-3}, *F*(000) = 928, μ(Cu-Kα) = 0.563 mm^{-1}. Data collection was performed on a Rigaku AFC5R using graphite-monochromated radiation (λ = 1.5418 Å); 5117 reflections were collected until θ_{max} = 70.14°, in which 3467 reflections were observed [$I > 2\sigma(I)$]. The crystal structure was solved by direct methods using SHELXS-86 (ref. 5). The structure was refined by full-matrix least-squares methods on F^2 using SHELXL-93 (ref. 6). In the structure refinements, non-hydrogen atoms were refined with anisotropic temperature factors. Hydrogen atoms were calculated on the geometrically ideal positions by the 'ride on' method, and were included in the calculation of structure factors with isotropic temperature factors. In the final stage, *R* = 0.0625, *Rw* = 0.1504 and *S* = 1.036 were obtained. CCDC 182/1288.

1 C. Iwamoto, K. Minoura, S. Hagishita, K. Nomoto and A. Numata, *J. Chem. Soc., Perkin Trans. 1*, 1998, 449 and references cited therein.
2 T. Amagata, M. Doi, T. Ohta, K. Minoura and A. Numata, *J. Chem. Soc., Perkin Trans. 1*, 1998, 3585 and references cited therein.
3 A. Numata, T. Amagata, K. Minoura and T. Ito, *Tetrahedron Lett*., 1997, **38**, 5675.
4 T. Amagata, K. Minoura and A. Numata, *Tetrahedron Lett*., 1998, **39**, 3773.
5 G. M. Sheldrick, SHELXS-86, Program for the Solution of Crystal Structures, University of Göttingen, Göttingen, 1986.
6 G. M. Sheldrick, SHELXS-93, Program for the Refinement of Crystal Structures from Diffraction Data, University of Göttingen, Göttingen, 1993.

Communication 9/03840J

ChemComm

Mg^0-promoted selective C–F bond cleavage of trifluoromethyl ketones: a convenient method for the synthesis of 2,2-difluoro enol silanes

Hideki Amii, Takeshi Kobayashi, Yasushi Hatamoto and Kenji Uneyama*

Department of Applied Chemistry, Faculty of Engineering, Okayama University, Tsushimanaka 3-1-1, Okayama 700-8530, Japan. E-mail: uneyamak@cc.okayama-u.ac.jp

Received (in Cambridge, UK) 7th May 1999, Accepted 8th June 1999

2,2-Difluoro enol silyl ethers were readily prepared by Mg^0 promoted selective defluorination of trifluoromethyl ketones in the presence of TMSCl, which involves C–F bond cleavage.

Difluoro enol silyl ethers are synthetic equivalents of enolates of α,α-difluoro ketones and useful synthons for difluoro compounds, which provide a wide repertoire of bioactive fluorinated compounds.[1] One of the well-established methods for preparing difluoro enol silyl ethers is dehalogenation from halodifluoromethyl groups.[2] Selective defluorination of the trifluoromethyl group is a promising method for preparing difluoro compounds due to the broad and easy availability of trifluoromethylated compounds. However, there are very few successful cases of the selective demonofluorination from a trifluoromethyl group.[3–7] Recently, we have reported electroreductive methods for difluoro enol silyl ethers[8] and difluoro enamines[9] using trifluoromethyl ketones and imines as starting materials. A key feature of these methodologies is the selectivity of defluorination which derives from the higher reduction potentials of the product enols and enamines than those of the parent keto systems.[8] Here, we report the first successful Mg^0-promoted selective defluorination of trifluoromethyl ketones **1** in the presence of TMSCl by means of a process involving C–F bond cleavage [eqn. (1)],[10] which provides a highly efficient access to a variety of 2,2-difluoro enol silyl ethers.

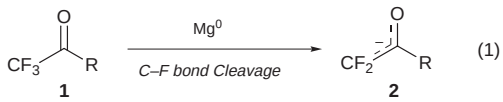

The reaction procedure is very simple. The mixture of **1a** (6.0 mmol), TMSCl and Mg[11] (12 mmol) in 2.4 ml of anhydrous THF was stirred at 0 °C for 20 min [eqn. (2)].† After filtration, the difluoro enol silyl ether **3a** was obtained in 91% NMR yield.

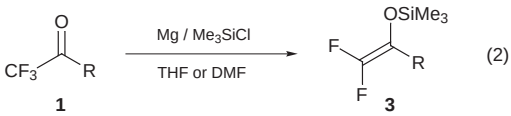

Compared to previously available methods, this methodology has several advantages: (i) the starting trifluoromethylated materials are readily available directly from trifluoroacetates; (ii) Mg as a reducing agent is cheap and easy to handle; and (iii) selective formation of 2,2-difluoro enol silyl ethers is achieved in a short reaction time.

As shown in Table 1, the same procedure for the selective formation of **3** works well for a diverse group of aromatic, heteroaromatic and aliphatic ketones, and the over-reduction products were not detected.

In the cases of aromatic and heteroaromatic ketones **1a–f**, the reactions were completed within 25 min at 0 °C in THF (entries 1–6), as compared with the case of aliphatic ketones (**1g** and **1h**) which required DMF as a solvent (entries 7 and 8).[12] Also,

Table 1 Mg^0-promoted defluorinative silylation of trifluoromethyl ketones **1**[a]

Entry	**1**	R	*T*/°C	*t*/min	Product **3**	Yield[b] (%)
1	**1a**	Ph	0	20	**3a**	91
2	**1b**	4-$MeOC_6H_4$	0	20	**3b**	89
3	**1c**	4-$CF_3C_6H_4$	0	20	**3c**	87
4	**1d**	4-ClC_6H_4	0	20	**3d**	98
5	**1e**	2-furyl	0	25	**3e**	97
6	**1f**	2-thienyl	0	25	**3f**	97
7[c]	**1g**	C_6H_{13}	0	30	**3g**	56
8[c]	**1h**	Cy	0	30	**3h**	62

[a] Unless otherwise stated, the reactions were performed on a 0.6 mmol scale in THF. [b] NMR yield, which was calculated by ^{19}F NMR integration of product **3** relative to 1,3-bis(trifluoromethyl)benzene internal standard. [c] DMF was used as solvent, and 8 equiv. of Mg was used.

aromatic and heteroaromatic ketones **1a–f** generally gave good yields, and the presence of electron-withdrawing and -donating groups had little effect on the yields. Notably, CF_3-arene and Cl-arene functionalities were compatible with the present reaction conditions; the reductive cleavage of the benzylic C–F bond[13] or aromatic C–Cl bond[14] did not occur (entries 3 and 4).

The formation of **3** can be explained by assuming the pathway pictured in Scheme 1. Initially, the intermediate ketyl species **4** is generated in the reaction of Mg^0 with a ketone **1**, which is further reduced to anion species **5** by Mg. The resultant β-fluorinated organomagnesium species **5** readily undergoes β-elimination to form **2**. In general, the cleavage of a C–F bond is not easy due to the large bond energy (*ca.* 552 kJ mol^{-1}). However, the bond breaking does occur rather easily when the CF_3 group is attached to a π-system because electron acceptance into the carbonyl group and subsequent extrusion of the fluoride ion may make large contributions to the driving force of the reaction. The reduction potential of aromatic ketones (**1a–f**) is more negative than that of aliphatic ones (**1g** and **1h**). Therefore, the difference in reactivity between aromatic ketones and aliphatic ones may derive from the tendency to form ketyl anion species **3**.

In particular, utilization of 2,2-difluoro enol silanes **3** is made in aldol reactions.[7] After simple filtration of the metal waste, the crude products **3** were used directly in the next reaction without

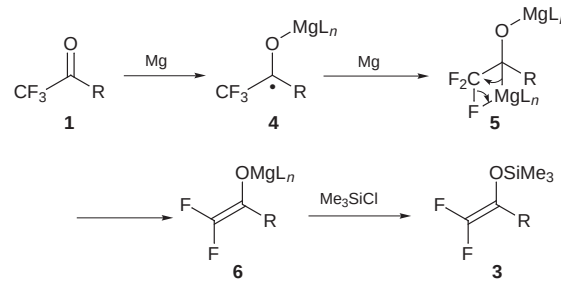

Scheme 1

purification due to the instability of **3**. When benzaldehyde was added to a solution of **3a** and $TiCl_4$ at −78 °C, the aldol adduct **7a** was formed [eqn. (3)] in 71% isolated yield (from **1a**).

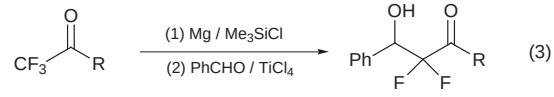

(3)

1a R = Ph — **7a** (71%)
d R = 4-ClC$_6$H$_4$ — **d** (78%)
g R = C$_6$H$_{13}$ — **g** (38%)
h R = Cy — **h** (42%)

In conclusion, Mg^0-promoted selective defluorination of a series of trifluoromethyl ketones provides a promising route to difluoro enol silanes.

We thank the SC-NMR laboratory of Okayama University for ^{19}F NMR analysis and the Ministry of Education, Science, Sports and Culture of Japan for financial support (Grant-in-Aid for Scientific Research, No. 09305058).

Notes and references

† *Typical procedure* for **3a**: To TMSCl (2.6 g, 24 mmol) in freshly distilled THF (24 ml) and Mg (290 mg, 12 mmol) cooled down to 0 °C under an argon atmosphere, trifluoroacetophenone (1.04 g, 6.0 mmol) was added dropwise and then stirred for an additional 20 min. After evaporation of most of the THF, hexane (20 ml) was added to the residue, and the resulting salt was filtered and the filtrate concentrated to give 1.21 g (*ca*. 0.53 mmol) of crude product (the crude product **3a** had purity > 95%).

To a solution of crude **3a** and benzaldehyde (1.27 g, 12 mmol) in CH_2Cl_2 (10 ml) cooled down to −78 °C, was added dropwise a solution of $TiCl_4$ (6 mmol) in CH_2Cl_2 (10 ml). Then the reaction mixture was quenched with aq. NH_4Cl, and the organic layer was washed with brine and dried over Mg_2SO_4. Purification of the products by chromatography on silica gel (hexane–EtOAc 5 : 1) provided **7a** (1.18 g, 71% from **1a**) as a colorless oil. *Selected data* for **7d**: 3512 cm^{-1} (ν_{OH}), 1696 cm^{-1} (ν_{CO}); δ_H($CDCl_3$, 200 MHz) 3.05 (d, *J* 3.6, 1 H), 5.35 (ddd, J_{HF} 18.6, 7.6, 3.6, 1 H), 7.2–7.5 (m, 7 H), 7.9–8.0 (m, 2 H); δ_F($CDCl_3$, 188 MHz, C_6F_6 as an internal standard) 45.2 (dd, J_{FF} 290.7, J_{HF} 18.6, 1 F), 56.9 (dd, J_{FF} 290.7, J_{HF} 7.6, 1 F).

1 J. P. Whitten, C. L. Barney, E. W. Huber, P. Bey and J. R. McCarthy, *Tetrahedron Lett.*, 1989, **30**, 3649; Z.-M. Qiu and D. J. Burton, *J. Org. Chem.*, 1995, **60**, 5570; K. Iseki, Y. Kuroki, D. Asada and Y. Kobayashi, *Tetrahedron Lett.*, 1997, **38**, 1447.
2 M. Kuroboshi, and T. Ishihara, *Bull. Chem. Soc. Jpn.*, 1990, **63**, 426.
3 Base-catalysed dehydrofluorination of 2,2,2-trifluoroethyl groups: J. A. Haward, W. H. Owton, J. M. Percy and M. K. Rock, *Tetrahedon*, 1995, **51**, 10 289; J. Ichikawa, T. Sonoda and H. Kobayashi, *Tetrahedon Lett.*, 1989, **30**, 1641.
4 Defluorination *via* Brook rearrangement for acylsilanes: F. Jin, Y. Xu and W. Huang, *J. Chem. Soc., Perkin Trans. 1*, 1993, 795; T. Brigaud, P. Doussot and C. Portella, *J. Chem. Soc., Chem. Commun.*, 1994, 2117.
5 Reductive dechlorofluorination of α-chloro-α-alkoxy-β,β-trifluoropropionates: G.-Q. Shi and W.-L. Cai, *J. Org. Chem.*, 1995, **60**, 6289.
6 S_N2' type reaction to trifluoromethyl groups: J.-P. Bégué, D. Bonnet-Delpon and M. H. Rock, *Synlett*, 1995, 659.
7 Reactions of the silyllithium and silylmagnesium reagents with trifluoromethyl ketones: I. Fleming, R. S. Roberts and S. C. Smith, *J. Chem. Soc., Perkin Trans. 1*, 1998, 1215.
8 K. Uneyama, K Maeda, T. Kato and T. Katagiri, *Tetrahedron Lett.*, 1998, **39**, 3741.
9 K. Uneyama and T. Kato, *Tetrahedron Lett.*, 1998, **39**, 587.
10 For a recent review on metal-mediated C–F bond activation, see: J. Burdeniuc, B. Jedlicka and R. H. Crabtree, *Chem. Ber./Recl.*, 1997, **130**, 145.
11 A flask containing Mg turnings was flame-dried under under vacuum, cooled, and then flushed with argon. Commercially available Mg turnings (Nacalai tesque, Inc.) were used without further activation of the magnesium surface, such as iodine, dibromoethane or ultrasound treatment.
12 Y. Ishino, Y. Kita, H. Maekawa, T. Ohno, Y. Yamasaki, T. Miyata and I. Nishiguchi, *Tetrahedron Lett.*, 1999, **40**, 1349.
13 Electroreductive defluorination of fluoromethylarenes: C. Saboureau, M. Troupel, S. Sibille and J. Périchon, *J. Chem. Soc., Chem. Commun.*, 1989, 1138; C. P. Andrieux, C. Combellas, F. Kanoufi, J.-M. Savéant and A. Thiébault, *J. Am. Chem. Soc.*, 1997, **119**, 9527.
14 For a recent review, see: V. V. Grushin and H. Alper, *Chem. Rev.*, 1994, **94**, 1047.

Communication 9/03681D

ChemComm

Bis(amido)magnesium mediated aldol additions: first structural characterisation of an amidomagnesium aldolate intermediate

John F. Allan, Kenneth W. Henderson* and Alan R. Kennedy

Department of Pure and Applied Chemistry, University of Strathclyde, 295 Cathedral Street, Glasgow, UK G1 1XL. E-mail: k.w.henderson@strath.ac.uk

Received (in Basel, Switzerland) 11th May 1999, Accepted 2nd June 1999

Bis(hexamethyldisilazido)magnesium has successfully been used to mediate aldol additions of selected ketones and aldehydes in hydrocarbon media, and the structure of an intermediate amido(aldolate), [{$(Me_3Si)_2$NMg[μ-OC(Me)-$Bu^tCH_2C(Bu^t)=O$]}$_2$] 17, produced by the self-coupled reaction of pinacolone has been characterised by X-ray crystallography.

Addition of the α carbon of an aldehyde or ketone to a second carbonyl unit is known as the aldol addition and has become one of the cornerstone reactions of modern synthetic chemistry.[1] Several methods have been developed to mediate this transformation, one of the most useful being the formation of a metal enolate by abstraction of a proton α to the carbonyl using a strong base. This is most commonly achieved through the use of lithium reagents and more specifically bulky lithium amides such as lithium diisopropylamide (LDA) and lithium hexamethyldisilazide (LHMDS).[2] We are interested in exploring the utility of amidomagnesium compounds as reagents to perform similar transformations since they are less reactive, more thermally stable and, in some instances, more selective than their lithium counterparts.[3] Magnesium has previously been used to mediate aldol additions *via* transmetallation of preformed lithium enolates with magnesium halides.[2] Reactions of this type have proved problematic due to 'salt-effects'.[4] In this respect, we have recently reported the presence of Schlenk-type equilibria for Hauser bases (R_2NMgX) and halomagnesium enolates, which complicates their use.[5] In comparison, bis(amido)magnesium compounds [$(R_2N)_2Mg$] have scarcely been studied as reagents.[6] In part this is due to complications with their synthesis, leading to troublesome side reactions of *in situ* prepared complexes.[7] These experimental problems have recently been overcome and we now report the use of bis(amido)magnesium compounds as reagents.[8] Herein we exploit an ether-free preparation of the bis(amide) [Mg{$N(SiMe_3)_2$}$_2$] **1**, and examine its utility in the aldol addition reaction.

A mixture of commercially available Bu_2Mg and 2 equivalents of hexamethyldisilazane was heated to reflux in heptane solution for several hours, and slow cooling to room temperature resulted in the crystallisation of **1** in high yield.[9] Crystalline **1** was then isolated and used as a stock reagent. In turn, reactions with pinacolone **2**, acetophenone **3**, hexan-2-one **4**, 3-methylbutan-2-one **5** and cyclohexanone **6** were performed (Scheme 1), and Table 1 lists the results of the aldol addition reactions mediated by **1**.†

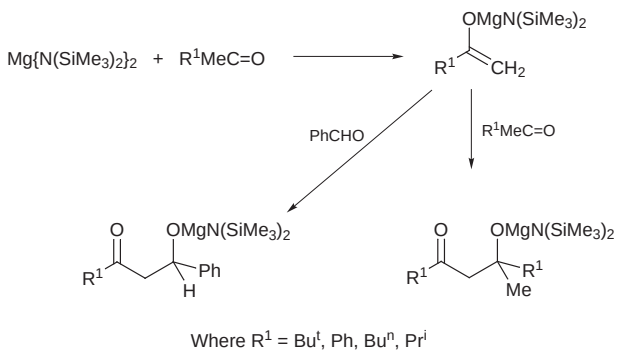

Scheme 1

Isolated yields from the ketone/aldehyde reactions compare favourably with lithium-mediated additions (reactions 1–5).[2] In most instances the reaction of the ketone enolates with

Table 1 Aldol addition reactions mediated by **1**

Entry	Ketone	Carbonyl added (mol. equiv.)	Major product	Yield (%)
1		PhCHO (1.5)	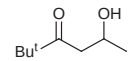 **7**	86
2		PhCHO (2)	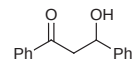 **8**	86
3	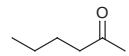	PhCHO (2)	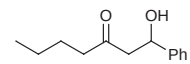 **9**	94
4		PhCHO (2)	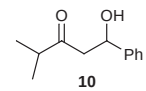 **10**	82
5		PhCHO (2)	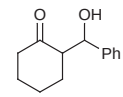 **11**	90
6	**2**	**2** (1)	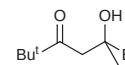 **12**	56
7	**3**	**3** (1)	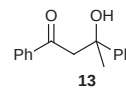 **13**	38
8	**4**	**4** (1)	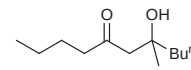 **14**	80
9	**5**	**5** (1)	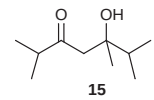 **15**	63
10	**6**	**6** (1)	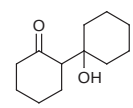 **16**	62

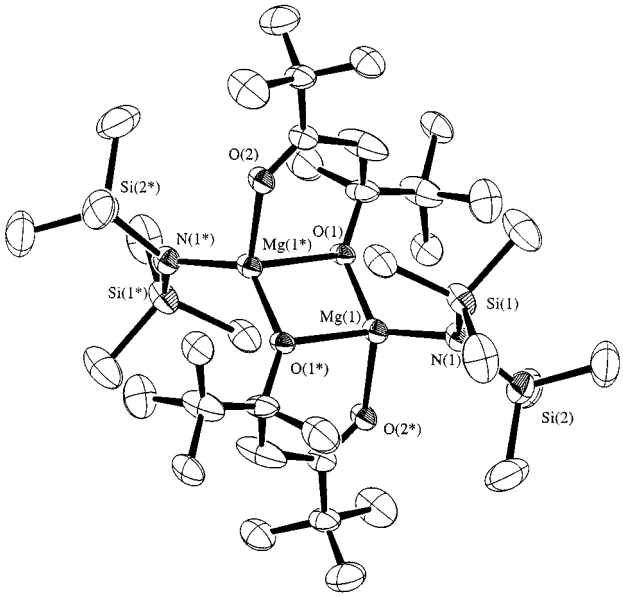

Fig. 1 Molecular structure of the major isomer of **17** with hydrogen atoms omitted for clarity. Key bond lengths (Å) and angles (°): Mg(1)–O(1) 1.9540(15), Mg(1)–O(1*) 1.9881(15), Mg(1)–N(1) 1.9920(19), Mg(1)–O(2*) 2.0619(15), O(1)–Mg(1)–O(1*) 85.90(6), O(1)–Mg(1)–N(1) 126.96(7), O(1*)–Mg(1)–N(1) 129.57(7), O(1)–Mg(1)–O(2*) 111.60(7), O(1*)–Mg(1)–O(2*) 87.18(6), N(1)–Mg(1)–O(2*) 108.51(7), C(7)–O(1)–Mg(1) 144.29(16), C(7)–O(1)–Mg(1*) 116.06(13), Mg(1)-O(1)–Mg(1*) 94.10(6), C(14)–O(2)-Mg(1*) 130.27(12).

benzaldehyde resulted in a small quantity (4–16%) of self-addition products. Significantly, this problem was overcome by adding 2 equivalents of the aldehyde to a solution of **1** before addition of the ketone. Also, no aldimine formation was detected.[10] Analogies with Corey's internal quench method for formation of silyl enol ethers are clear.[11]

It is known that ketone–ketone aldol coupling is usually less favourable than ketone–aldehyde additions. Using high temperature conditions (25–70 °C) the self-aldol reactions were found to proceed in reasonable yields (reactions 6–10).[12] The ability to perform these reactions at higher temperatures contrasts appreciably with the lithium analogues, where the aldolates commonly undergo retro-aldol reactions above −30 °C or eliminate LiOH to give enones.[2] With the systems reported here, the enone only becomes the major product after extended reflux. Furthermore, reactivity of both amide functions bonded to magnesium is suggested by reaction of 4 equivalents of **2** with **1** which yielded 55% of aldol product **12** (calculated with respect to ketone).

It should be noted that when polar donor solvents such as THF or HMPA were present, the yield of aldolate was significantly reduced (< 10% for entry 6). This is consistent with the observation that, in lithium-mediated reactions, increasing the solvent polarity increases yields of enolisation but disfavours addition. However, this effect appears to be more dramatic for magnesium, since the lithium reactions are commonly performed in THF solution. This may be a consequence of the magnesium centres being more sterically crowded than those of lithium, resulting in blocking of the incoming carbonyl.

The intermediate from the pinacolone self-coupled reaction, $[\{(Me_3Si)_2NMg[\mu\text{-}OC(Me)Bu^tCH_2C(Bu^t)=O]\}_2]$ **17**, was characterised by X-ray crystallography (Fig. 1).‡ The centrosymmetric structure is based on a *trans*-6,4,6-fused ring system in which each aldolate acts as both bridge and chelate.

Two superimposed isomers are present within the crystal lattice of **17**. The isomers differ in the conformation of the six-membered aldolate chelate rings where half-chair and twist-boat conformation are found in a ratio of 80.5(3):19.5(3). Chelate isomers are also found in aldolate derivatives of lithium,[13] zinc,[14] titanium[15] and aluminium.[16] These isomers adopt half-boat, chair, half-chair and twist boat structures, illustrating the shallow energy surface separating these conformations.

We would like to thank The Royal Society for a University Research Fellowship (K. W. H.), and Professor Robert E. Mulvey and Dr William J. Kerr for helpful discussions during the preparation of this manuscript.

Notes and references

† Base **1** (2 mmol) was suspended in 10 ml of hexane and cooled to −78 °C. Aldehyde (4 mmol) or alternatively ketone (2 mmol) was then added, followed by dropwise addition of the ketone (2 mmol). The aldehyde reactions were stirred at −78 °C for 30 min then quenched with 1 M HCl. The self-coupled reactions were warmed to room temperature and stirred for 48–72 h before quenching in 1 M HCl. Improved yields of **12** and **13** were obtained on heating the mixtures to reflux for several hours. Further improvements in yields are expected on optimising the reaction conditions.

‡ *Crystal data* for **17**: $C_{36}H_{82}Mg_2N_2O_4Si_4$, M = 768.02, T = 123(2) K, triclinic space group, $P\bar{1}$, a = 9.610(3), b = 11.381(2), c = 12.024(4) Å, α = 98.90(2), β = 104.00(2), γ = 105.996(19)°, U = 1191.5(5) Å^3, Z = 1, μ(Mo-Kα) = 0.185 mm^{-1}, D_c = 1.070 Mg m^{-3}, $2\theta_{max}$ = 56°, 6084 reflections collected, 5746 unique, (R_{int} = 0.0173) all were used in the calculations. The minor disorder component was treated isotropically with no hydrogen atoms attached. All other non-hydrogen atoms were treated anisotropically and all other hydrogens included in a riding model. The final $wR(F^2)$ was 0.1417 and conventional R was 0.0488. Programs were standard diffractometer control software and members of the SHELX family (G. M. Sheldrick, University of Göttingen, Germany). The structure was solved using direct methods and refined by full-matrix least-squares refinement on F^2. A single crystal of **17** was mounted in inert oil and transferred to the cold N_2 gas stream of the diffractometer.

CCDC 18/1286. See http://www.rsc.org/suppdata/cc/1999/1325/ for crystallographic files in .cif format.

1 C. H. Heathcock, in *Asymmetric Synthesis*, ed. J. D. Morrison, Academic Press, New York, 1983, vol. 3, pp. 111–212.; D. A. Evans, *ibid*., pp. 2–110; C. H. Heathcock, *Aldrichim. Acta*, 1990, **23**, 99.
2 H. O. House, D. S. Crumrine, A. Y. Teranishi and H. D. Olmstead, *J. Am. Chem. Soc*., 1973, **95**, 3310; F. Gaudemar-Bardone and M. Gaudemar, *J. Organomet. Chem*., 1976, **104**, 281.
3 P. E. Eaton, C. H. Lee and Y. Xiong, *J. Am. Chem. Soc*., 1989, **111**, 8016.
4 A. Loupy and B. Tchoubar, *Salt Effects in Organic and Organometallic Chemistry*, VCH, New York, 1991.
5 J. F. Allan, W. Clegg, K. W. Henderson, L. Horsburgh and A. R. Kennedy, *J. Organomet. Chem*., 1998, **559**, 173.
6 D. Bonafoux, M. Bordeau, C. Biran, P. Cazeau and J. Dunogues, *J. Org. Chem*., 1996, **61**, 5532; D. Bonafoux, M. Bordeau, C. Biran, and J. Dunoguès, *J. Organomet. Chem*., 1995, **493**, 27.
7 K. W. Henderson, J. F. Allan and A. R. Kennedy, *Chem. Commun*., 1997, 1149.
8 M. Westerhausen, *Trends Organomet. Chem*., 1997, **2**, 89.
9 This is a variation of the method from L. M. Engelhardt, B. S. Jolly, P. C. Junk, C. L. Raston, B. W. Skelton and A. H. White, *Aust. J. Chem*., 1986, **39**, 1337.
10 D. J. Hart, K. Kanai, D. G. Thomas and T. K. Yang, *J. Org. Chem*., 1983, **48**, 289.
11 E. J. Corey and A. W. Gross, *Tetrahedron Lett*., 1984, **25**, 495.
12 Magnesium anions have been used for the thermodynamic equilibration of aldolates: K. A. Swiss, W. B. Choi, D. C. Liotta, A. F. Abdel-Magid and C. A. Maryanoff, *J. Org. Chem*., 1991, **56**, 5978.
13 P. G. Williard and J. M. Salvino, *Tetrahedron Lett*., 1985, **26**, 3931.
14 S. C. Goel, M. Y. Chiang and W. E. Buhro, *J. Am. Chem. Soc*., 1991, **113**, 7069.
15 P. G. Cozzi, C. Floriani, A. Chiesivilla and C. Rizzoli, *Organometallics*, 1994, **13**, 2131.
16 M. B. Power, A. W. Apblett, S. G. Bott, J. L. Atwood and A. R. Barron, *Organometallics*, 1990, **9**, 2529.

Communication 9/03784E

ChemComm

Covalent and noncovalent interpenetrating planar networks in the crystal structure of {[Ni(4,4′-bipyridine)$_2$(NO$_3$)$_2$·2pyrene}$_n$

Kumar Biradha, Konstantin V. Domasevitch, Brian Moulton, Corey Seward and Michael J. Zaworotko*

Department of Chemistry, The University of Winnipeg, Winnipeg, Manitoba, R3B 2E9, Canada.
E-mail: mike.zaworotko@uwinnipeg.ca

Received (in Columbia, MO, USA) 16th February 1999, Accepted 9th June 1999

The crystal structure of {[Ni(4,4′-bipyridine)$_2$(NO$_3$)$_2$]·2pyrene}$_n$ reveals the first example of complementary, interpenetrating covalent and noncovalent 2D networks.

Crystal engineering of coordination polymer networks based upon multitopic ligands represents a growing area of coordination and supramolecular chemistry.[1,2] In this context, 2D square grid networks exemplify a particularly simple example of a predictable network. The primary reason for interest in such compounds has been their ability to afford controllable cavities that are suitable for enclathration of organic guest molecules (Scheme 1). A number of simple bifunctional spacer ligands have been examined, especially 4,4′-bipyridine (4,4′-bipy).[3–7] However, a phenomenon that mitigates against or even precludes enclathration is the filling of cavities by self-inclusion or interpenetration.[8] Interpenetrated structures have limited potential in the context of host–guest chemistry but have significant potential in terms of other bulk properties.[9] In this contribution, we report a compound that combines the above features: {[Ni(4,4′-bipy)$_2$(NO$_3$)$_2$]·2pyrene}$_n$ **1** which represents, to our knowledge, the first compound in which two very different types of 2D net interpenetrate: a square grid coordination polymer and a non-covalent planar net of pyrene molecules. A recent literature review[8] revealed that the only other example of a compound with different interpenetrating nets contains two nets of similar structure and composition.[10]

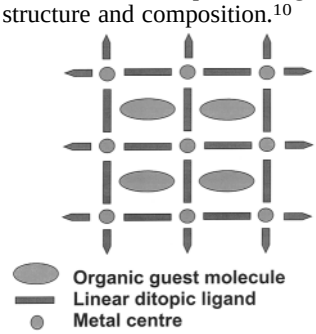

Scheme 1

A realistic motif for self-assembly of aromatic molecules is a 2D net that is sustained by edge-to-face stacking interactions. A distorted form of such a net coexists with [Ni(4,4′-bipy)$_2$(NO$_3$)$_2$] square grids in **1**. Blue crystals of **1** were grown by carefully layering a MeOH solution of Ni(NO$_3$)$_2$·6H$_2$O onto a MeOH solution of 4,4′-bipy and pyrene under ambient conditions.† The coordination networks [Fig. 1(a)] possess inner cavities of *ca*. 8 × 8 Å and stack parallel to one another with an interlayer separation of *ca*. 7.9 Å (corresponding to half the *c*-axis) and bear a close resemblance to the coordination array in [Cd(4,4′-bipy)$_2$(NO$_3$)$_2$]·2C$_6$H$_4$Br$_2$.[3] An additional factor that appears to influence the packing of the grids is weak CH···O hydrogen bonding between the 4,4′-bipy ligands and nitrate anions of the adjacent grids. C···O separations are in the range of 2.877–3.149 Å. The pyridyl rings of the 4,4′-bipy ligands are not coplanar and are twisted by 32.5–48.9°.

The pyrene nets [Fig. 1(b)] are sustained by edge-to-face interactions and contain cavities of dimensions *ca*. 6.5 × 3.5 Å. The shortest intermolecular C–C separations (3.518 Å) are similar to those reported for related compounds such as pyrene itself[11] and 1-propynylpyrene.[12] The planes of the neighboring molecules intersect at an angle of *ca*. 60° and there are no face-to-face stacking interactions between the molecules. The pyrene nets can be regarded as distorted (4,4) nets if the node is the point in space at which the vectors of the four pyrene planes intersect. An alternate interpretation is that nodes exist at the point of the edge-to-face interactions. The pyrene net could then be regarded as a distorted brick wall form of a (6,3) net.[8] It is important to note that either a (4,4) or a (6,3) planar net is complementary from a topological sense with the (4,4) coordination polymer net and ensures that the coordination

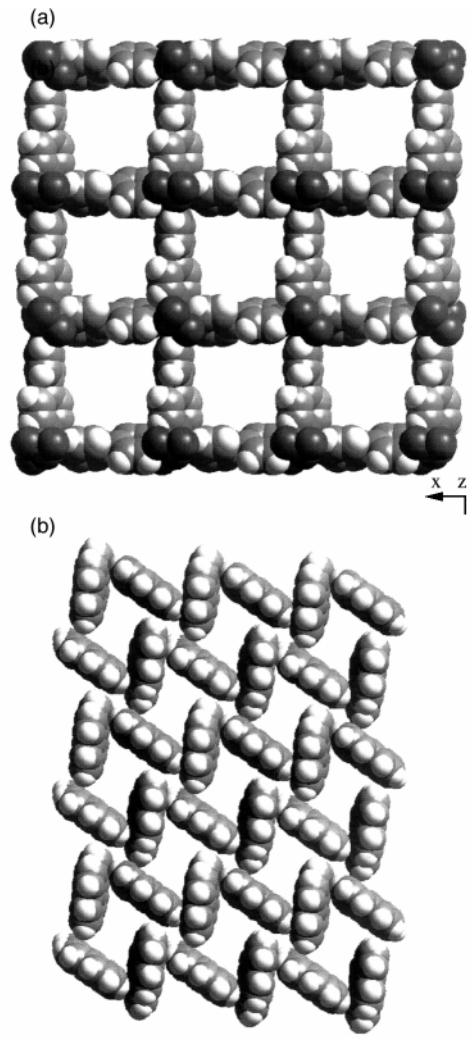

Fig. 1 (a) The square grid networks formed by [Ni(4,4′-bipy)$_2$(NO$_3$)$_2$] in **1**. Cavities have effective dimensions of *ca*. 8 × 8 Å. (b) An illustration of the pyrene (4,4) nets that exist in **1**. Cavities possess effective dimensions of *ca*. 6.5 × 3.5 Å.

polymer nets must pack in a staggered manner. Given that cavity size within the pyrene nets is complementary with the width and height of a single aromatic ring, it should be unsurprising that the pyrene nets thread orthogonally with the 4,4′-bipy ligands of the coordination polymer *via* face-to-face and edge-to-face interactions. The shortest carbon–carbon separation between the atoms of 4,4′-bipy ligands and pyrene molecules is *ca*. 3.40 Å and corresponds to face-to-face stacking (interplanar angle = 7.3°). The shortest C···O separations involving pyrene 3.20 Å may be attributed to $CH\cdots ONO_3$ hydrogen bonds. The calculated[13] volumes of the two nets are similar: 1548.5 and 1502.0 Å^3 for the covalent and noncovalent networks, respectively. This is to be expected based upon the observation that 4,4′-bipy square grids are self-complementary as they can interpenetrate in a two-fold fashion.[5] A view of the crystal packing is presented in Fig. 2.

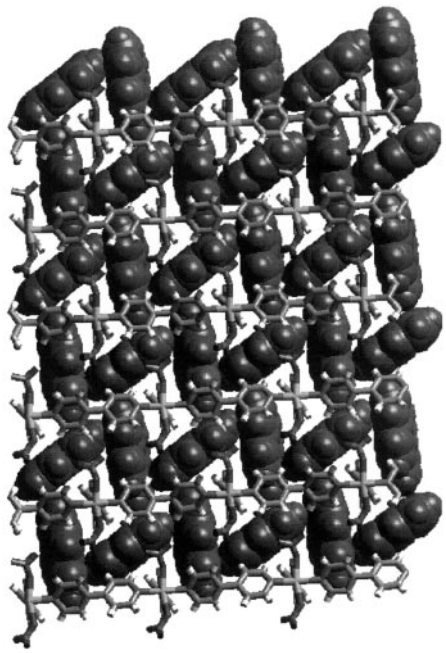

Fig. 2 A view of the crystal structure of **1** viewed down the *b*-axis. Note the stacking interactions between the pyrene molecules (space-filling mode) and square grid networks.

Interestingly, although both nets appear to be inherently centrosymmetric at first glance, the title compound crystallizes in the non-centrosymmetric space group *Pn* and is therefore polar. Pyrene molecules that lie opposite each other across the grid cavities in the *ac*-plane are clearly not related by inversion and are therefore crystallographically nonequivalent (Fig. 3). Indeed, they are not coplanar. Each set of four pyrene molecules in the *ac*-plane that surround the grid cavities adopts a bowl-like conformation and the bowls 'stack' in a parallel fashion along the *b*-axis. Additionally, the orientation of alternating pyrene molecules along the *b*-axis is slightly different, which leads to a doubling of the *b*-axis and the observed superstructure. An alternative possibility was also considered during structure refinement: random disposition of pyrene molecules in the crystal and crystallographic disorder. This artificial increase of the lattice symmetry did not afford a satisfactory refinement. Thus, the bulk polarity in **1** is a consequence of the symmetry of the supramolecular assembly of pyrene molecules.

In summary, the interpretation of the structure of **1** as interpenetrating covalent and noncovalent nets is to our knowledge unique and important in the context of understanding the structure and stoichiometry of compounds that are based upon interpenetrated covalent and noncovalent nets. **1** also illustrates how polarity in crystals can be generated from subtle packing of achiral components, as illustrated by the chiral nets of pyrenes. We are presently seeking other examples of compounds that contain complementary but chemically different nets.

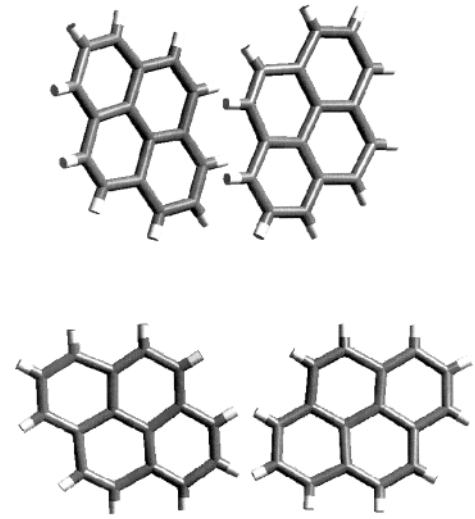

Fig. 3 An illustration of how the relative orientations of the pyrene molecules preclude a centre of inversion in **1**.

We acknowledge the generous financial support of the NSERC (Canada) in the form of a research grant (M. J. Z.).

Notes and references

† *Crystal data* for **1**: $C_{52}H_{36}N_6NiO_6$, monoclinic, space group *Pn*, a = 11.3602(6), b = 22.771(1), c = 15.8580(9) Å, β = 93.956(1)°, V = 4092.4(4) Å^3, Z = 4, D_c = 1.460 g cm^{-3}, λ = 0.7107 Å, $F(000)$ = 1864. 14 277 reflections out of 15 136 unique reflections measured at 200 K on a Siemens SMART/CCD diffractometer using the θ scan mode ($4 < 2\theta < 56°$) afforded on convergence final *R*-factors of $R1$ = 0.041 and $wR2$ = 0.103 (1172 parameters refined, the highest electron density peak and hole were 0.75−0.66 e Å^{-3}). H atoms were placed in calculated positions. All other atoms were anisotropically refined. The absolute structure could not be determined unambiguously as refinement of the absolute structure Flack parameter afforded a value of 0.48(2), although refinement in the other enantiomorph afforded $R1$ = 0.043. The crystallographic calculations were conducted using the SHELXS-86 and SHELXL-93 programs.[14,15]

CCDC 182/1281. See: http://www.rsc.org/suppdata/cc/1999/1327/ for crystallographic files in .cif format.

1 S. Kitagawa and M. Kondo, *Bull. Chem. Soc. Jpn.*, 1998, **71**, 1739.
2 B. F. Hoskins and R. Robson, *J. Am. Chem. Soc.*, 1990, **112**, 1546.
3 M. Fujita, Y. J. Kwon, S. Washizu and K. Ogura, *J. Am. Chem. Soc.*, 1994, **116**, 1151.
4 L. R. MacGillivray, R. H. Groeneman and J. L. Atwood, *J. Am. Chem. Soc.*, 1998, **120**, 2676.
5 R. W. Gable, B. F. Hoskins and R. Robson, *J. Chem. Soc., Chem. Commun.*, 1990, 1677.
6 S. Subramanian and M. J. Zaworotko, *Angew. Chem., Int. Ed. Engl.*, 1995, **35**, 2127.
7 J. Lu, T. Paliwala, S. C. Lim, C. Yu, T. Niu and A. J. Jacobsen, *Inorg. Chem.*, 1997, **36**, 923.
8 S. R. Batten and R. Robson, *Angew. Chem., Int. Ed.*, 1998, **37**, 1461.
9 V. R. Thalladi, S. Brasselet, H.-C. Weiss, D. Blaser, A. K. Katz, H. L. Carrell, R. Boese, J. Zyss, A. Nangia and G. R. Desiraju, *J. Am. Chem. Soc.*, 1998, **120**, 2563; W. Lin, Z. Wang and R.-G. Xiong, Materials Research Society, Fall 1998 Meeting, Boston, Abstract U1.1.
10 T. Soma and T. Iwamoto, *Acta Crystallogr., Sect. C*, 1996, **52**, 1200.
11 R. Allman, *Z. Kristallogr.*, 1970, **132**, 129.
12 J. T. Mague, M. Foroozesh, N. E. Hopkins, L. L.-S. Gan and W. L. Alworth, *J. Chem. Crystallogr.*, 1997, **27**, 183.
13 Cerius^2, v. 3.8, Molecular Simulations Inc., San Diego, 1998.
14 G. M. Sheldrick, SHELXS-86, *Acta Crystallogr., Sect. A*, 1990, **46**, 467.
15 G. M. Sheldrick, SHELXL-93, A system of computer programs for X-ray structure determination, University of Göttingen, 1993.

Communication 9/01311C

Convergent synthesis and 'surface' functionalization of a dendritic analog of poly(ethylene glycol)

Scott M. Grayson, Manikandan Jayaraman and Jean M. J. Fréchet*

Department of Chemistry, University of California, Berkeley, CA 94720-1460, USA.
E-mail: frechet@cchem.berkeley.edu

Received (in Corvallis, OR, USA) 23rd March 1999, Accepted 21st May 1999

Aliphatic polyether dendrons exhibit easily modified surface functionality.

Because of its water solubility and non-ionic character, linear poly(ethylene glycol) has been utilized widely for applications ranging from surfactants to biocompatible drug solubilizers.[1] Although a variety of dendrimers have been reported to date,[2] few possess the structural features that would endow them with analogous solubility properties. An early, imaginative, divergent approach towards aliphatic polyether dendrimers reported by Hall *et al*. over a decade ago[3] has not been widely used due to synthetic complications. We have recently reported an efficient convergent route to dendrons containing an aliphatic polyether backbone and peripheral benzyl ether protecting groups.[4] Now, we report a very versatile convergent synthesis of hydroxy-terminated aliphatic polyether dendrons that may be considered dendritic analogs of poly(ethylene glycol) because of the 2 : 1 carbon : oxygen ratio in the branched repeat unit. These dendrons may prove valuable in polymer therapeutics as a result of their compact shape, high polarity, and multiple chain end functionalities.[5]

The hallmark of a successful convergent synthesis is an aptly chosen monomer that enables simple, high-yielding activation and growth steps. Our monomer, 3-chloro-2-chloromethylprop-1-ene, is well suited for high-yield Williamson coupling with two dendritic alcohols, since its symmetrical and activated allylic functionalities afford the same product regardless of displacement mechanism (S_N1, S_N2, or S_N2'). The resulting olefinic dendron can then be converted to the primary dendritic alcohol in high yield and with excellent regioselectivity *via* standard hydroboration reaction conditions. Further growth results from a repetitive cycle of coupling and activation reactions to afford larger dendrons.

Ketals were chosen as the surface protecting groups primarily because they are unaffected by the basic conditions required throughout the synthesis. While several acetals and ketals were tested, the lipophilic nature of the dibutyl ketal protecting group confers upon these dendrons excellent solubility in hexanes, thus facilitating their purification by chromatography. In addition, these protecting groups allow a facile deprotection under mildly acidic conditions, exposing terminal hydroxy functionalities that can be further modified if desired.

The synthesis of the first generation terminal moiety, [G-1]-ol, was achieved by protecting two of the hydroxy functionalities of 1,1,1-tris(hydroxymethyl)ethane with nonan-5-one in the presence of $BF_3{\cdot}OEt_2$.[6] Reaction of the [G-1]-ol, **1**, NaH, and 3-chloro-2-chloromethylprop-1-ene, in the presence of catalytic amounts of KI and 18-crown-6 afforded the second generation alkene, **2**, in 84% yield. This alkene was converted effectively to the activated primary [G-2]-ol, **3**, through hydroboration with 9-BBN,[7] followed by oxidation in alkaline H_2O_2 (92%). Repetition of the coupling and activation steps led to the preparation of higher generation dendrons up to [G-4]-ene, **6** (Scheme 1). All of the materials were purified by flash column chromatography on silica gel using EtOAc–hexane as eluent and were obtained as transparent, viscous oils.

Identification of the focal functionality by NMR and FT-IR facilitated the characterization of these dendritic compounds. In

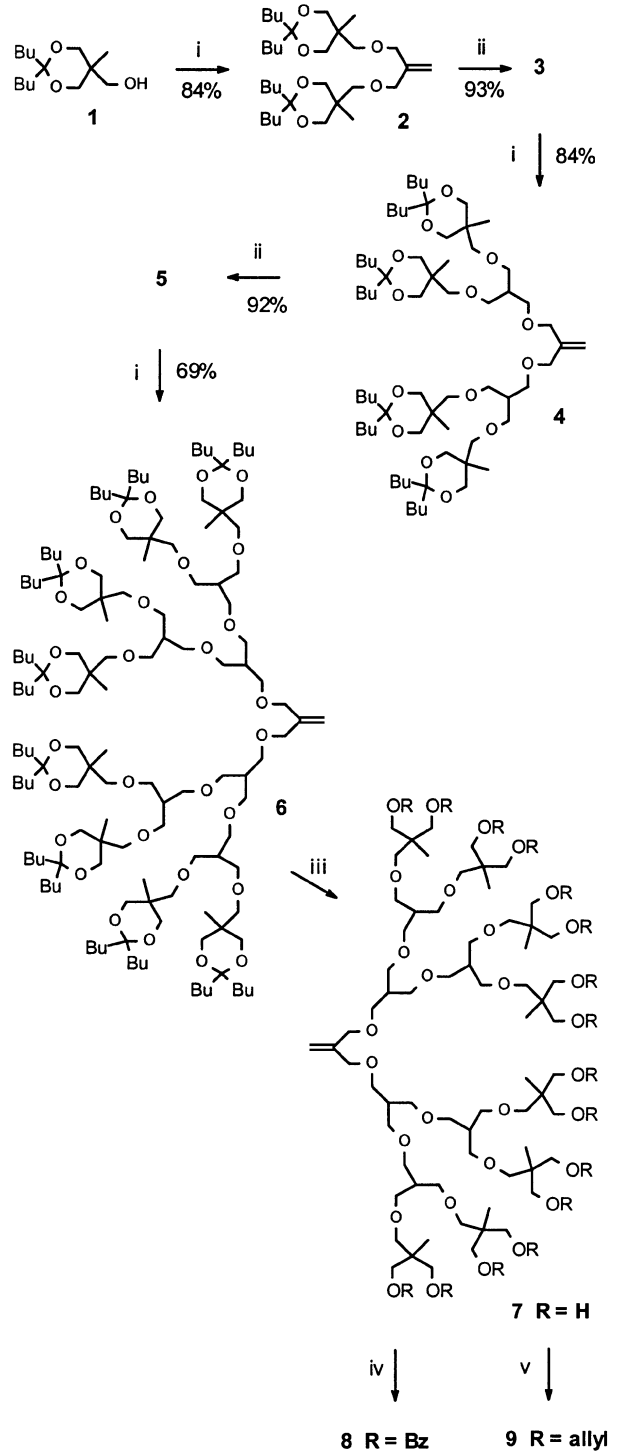

Scheme 1 *Reagents and conditions*: i, NaH, THF, KI, 18-crown-6, $(ClCH_2)_2C{=}CH_2$; ii, 9-BBN, THF, then H_2O_2–NaOH; iii, H^+ Resin, MeOH; iv, BzCl, pyridine; v, allyl bromide, NaH, DMA–THF.

Table 1 MS and SEC data for second, third, and fourth generation dendrons

Compound	Calculated MW	FAB/MALDI MW	SEC[a] M_n	PDI
[G-2]-ene	540.8	540.7	600	1.01
[G-2]-ol	558.8	558.7	720	1.00
[G-3]-ene	1169.8	1170	1400	1.00
[G-3]-ol	1187.8	1189	1420	1.00
[G-4]-ene	2427.6	2429	2450	1.01
[G-4]-ol	2445.6	2446	2470	1.01

[a] SEC analysis was performed using THF as the eluent and was calibrated against polystyrene standards.

$CDCl_3$ the dendritic alkenes showed a singlet at δ 5.15 in the ^{1}H NMR spectrum, peaks at δ 143 and 113 in the ^{13}C NMR spectrum, and an absorbance at 1650–1660 cm^{-1} in the FT-IR spectrum, corresponding to the focal carbon–carbon double bond. The dendrons with focal hydroxy functionalities exhibited a broad absorbance at 3300–3500 cm^{-1} in the FT-IR spectrum, as well as a triplet at δ 2.7 in the ^{1}H NMR spectrum and a peak at δ 63 in the ^{13}C NMR spectrum corresponding to the adjacent methylene. The integration ratio between the peripheral acetals and the focal functionality verified both the generation of the dendron, and the retention of all protection groups.

Molecular weights of the dendritic molecules were monitored by mass spectrometry (MS) using fast atom bombardment (FAB) MS for those below 1000 Daltons, and matrix assisted laser desorption ionization time of flight (MALDI-TOF) MS for those above 1000 Daltons. In addition, the narrow signal obtained by size exclusion chromatography (SEC) further confirmed the monodisperse nature of the compounds, as expected in a convergent dendrimer synthesis (Table 1).

Deprotection of the chain-ends of the dendrons was achieved using an acid cation exchange resin. Because of the highly polar character of the resultant hydroxy-terminated dendron, and the insolubility of the polymeric catalyst, the product, **7**, could be isolated in near quantitative yield by a simple filtration of its methanol solution. At the fourth generation, these hydroxy-terminated compounds exhibited the desired water solubility regardless of the focal functionality. This was expected as previous studies of dendrimers' physical properties verified that the solubility of dendritic polymers is dominated at higher generation by the peripheral functionalities.[8]

The high reactivity of the 'surface' hydroxy functionalities was confirmed through simple modification reactions (Scheme 1). For example, reaction of the sixteen free hydroxy groups of $(OH)_{16}$[G-4]ene, **7**, with a two-fold excess of BzCl in pyridine afforded the fully esterified product, **8**. Similarly, a nucleophilic substitution reaction was performed with **7**, NaH, and a two-fold excess of allyl bromide to produce the fully allylated dendron, **9**. Both reactions appeared to be quantitative, as no partially functionalized dendrons were isolated by chromatography or observed in the MALDI-TOF MS of the crude reaction mixture.

Characterization of the surface modified dendrons was also achieved by monitoring changes in functionality. The end-deprotected dendrons exhibited a broad absorbance at 3300–3500 cm^{-1} in the FT-IR spectrum corresponding to the multiple hydroxy functionalities. Conversion of the surface groups to benzoate esters resulted in the appearance of a characteristic narrow carbonyl absorbance at 1724 cm^{-1} in the FT-IR spectrum, as well as aromatic resonances in the ^{1}H NMR,

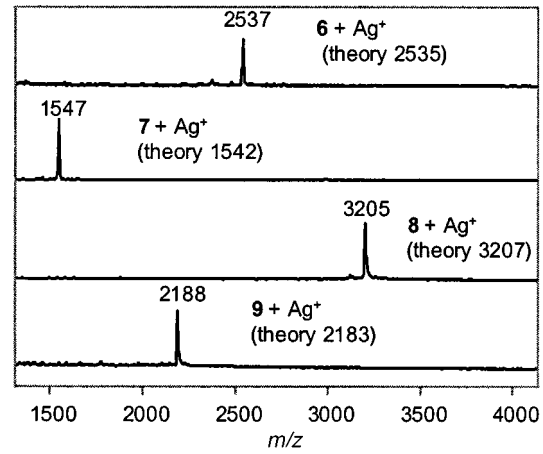

Fig. 1 MALDI-TOF MS data for the deprotection and derivatization of [G-4]-ene.

while the allyl ethers exhibited an alkene absorbance at 1646 cm^{-1} in the FT-IR spectrum as well as additional resonances for the vinyl protons (δ 5.2, 5.3, and 5.9) in the ^{1}H NMR. MALDI-TOF MS data of both functionalized dendrons exhibited a single peak with molecular weights corresponding closely to the expected values (Fig. 1.)

We believe that the unique and high yielding chemistry used in the preparation of these dendrons, as well as the flexibility of their functionalization at the focal point and at the chain ends, makes them suitable for broad use as building blocks in a variety of dendritic structures where they will complement the widely used aromatic polyethers we developed earlier.[9]

Financial support of this research by the U.S. Army Research Office (MURI program, DAAG55-97-0126) and the National Science Foundation (NSF-DMR #9816166) is gratefully acknowledged.

Notes and references

1 P. D. Senter, H. P. Svensson, G. J. Schreiber, J. L. Rodriguez and V. M. Vrudhula, *Bioconjugate Chem.*, 1995, **6**, 389; R. B. Greenwald, A. Pendri and D. Bolikal, *J. Org. Chem.*, 1995, **60**, 331.
2 J. M. J. Fréchet, *Science*, 1994, **263**, 1710; G. R. Newkome, C. N. Moorefield and F. Vögtle, *Dendritic Molecules*, VCH, New York, 1996.
3 A. B. Padias, H. K. Hall, Jr., R. McConnell and D. A. Tomalia, *J. Org. Chem.*, 1987, **52**, 5305.
4 M. Jayaraman and J. M. J. Fréchet, *J. Am. Chem. Soc.*, 1998, **120**, 12 996.
5 R. Duncan, P. Kopecekova, J. Strohalm, I. C. Hume, J. B. Lloyd and J. Kopecek, *Br. J. Cancer*, 1988, **57**, 147; L. W. Seymour, K. Ulbrich, P. S. Steyger, M. Brereton, V. Subr, J. Strohalm and R. Duncan, *Br. J. Cancer*, 1994, **70**, 636; P. Ferruti, S. Knobloch, E. Ranucci, R. Duncan and E. Gianasi, *Macromol. Chem. Phys.*, 1998, **199**, 2565; S. Wroblewski, P. Kopeckova, B. Rihova and J. Kopecek, *Macromol. Chem. Phys.*, 1998, **199**, 2601.
6 D. W. White, R. D. Bertrand, G. K. McEwen and J. G. Verkade, *J. Am. Chem. Soc.*, 1970, **92**, 7125.
7 E. F. Knight and H. C. Brown, *J. Am. Chem. Soc.*, 1968, **90**, 5280.
8 K. L. Wooley, J. M. J. Fréchet and C. J. Hawker, *Polymer*, 1994, **35**, 4489.
9 C. J. Hawker and J. M. J. Fréchet, *J. Chem. Soc., Chem. Commun.*, 1990, 1010; C. J. Hawker and J. M. J. Fréchet, *J. Am. Chem. Soc.*, 1990, **112**, 7638.

Communication 9/02340B

ChemComm

Exploring a chemical encoding strategy for combinatorial synthesis using Friedel–Crafts alkylation

Robin H. Scott, Colin Barnes, Ulrich Gerhard and Shankar Balasubramanian*

University Chemical Laboratory, University of Cambridge, Lensfield Road, Cambridge, UK CB2 1EW. E-mail: sb10031@cam.ac.uk

Received (in Liverpool, UK) 29th March 1999, Accepted 14th June 1999

The use of scandium(III) triflate and ytterbium(III) triflate-catalysed Friedel–Crafts alkylation to insert a set of hydroxymethyl pyrrole amide tags (1b–i) on to polystyrene resins under mild conditions and the encoding of a split and mix peptide library is demonstrated.

Combinatorial approaches to molecular problem solving are the subject of great conceptual and experimental exploration. The approach is dependent on the ability to rapidly generate and screen large and diverse libraries.[1,2] The split and mix synthesis method,[3] which generates 'one-bead-one-compound' libraries, is a powerful approach, although the identification of active compounds remains a technical issue. A variety of deconvolution protocols exist,[1,4] of which the chemical tag-based encoding strategy is an inexpensive and general method that can be employed without the need for specialised equipment.[5,6] Key issues associated with chemical tagging include: the need for convenient, orthogonal chemistry for the attachment of tags to resin beads without disruption of the library molecules; the design of tags that are sufficiently robust to withstand a wide range of chemistry; and a simple cleavage and sensitive analysis strategy for decoding.

We have explored the use of Lewis acid-catalysed Friedel–Crafts alkylation to insert tags directly into the aromatic rings of polystyrene or other electron rich aromatic rings incorporated into the polymer. Friedel–Crafts chemistry has previously been used to functionalise polystyrene resins.[7,8] Having studied a variety of hydroxymethyl aromatics, the pyrrole derivative **1a** (R^1 = H, R^2 = OMe) was found to have promising reactivity with toluene (used as a resin mimic), reacting in 80% yield after 12 h at room temperature using a scandium catalyst (Scheme 1).[9] Scandium(III) triflate has particular advantages as the choice of Lewis acid since it is relatively insensitive to water, catalyses alkylations with alcohols[10] and its use has been demonstrated for solid phase chemistry.[11]

A mixture of polar and non-polar solvents was essential to retain both resin swelling and solubility of the scandium triflate. Since only small amounts of each tag need be incorporated into a bead (typically 1% of the resin capacity equating to about 0.05% of the available aromatic rings), the model solution phase reaction used 100 equiv. of toluene. Therefore in these reactions, the tags were present at relatively low concentrations. For acceptable reaction rates (completion in < 1 day), the concentration of Lewis acid required was at millimolar levels (which often equates to several equivalents compared to the tags).

Owing to the high reactivity of the pyrollic tag molecule with toluene, more stable amide derivatives were also prepared starting from the fully substituted methyl 4-formyl-1,2,5-trimethylpyrrole-3-carboxylate **2** (Scheme 2). Pyrrole ester **2** was hydrolysed to the free acid, then coupled to a variety of secondary amines. Reduction of the formyl group with $NaBH_4$ on alumina gave the corresponding alcohols **1b–i** in overall yields of 54–90% and these were found to be stable at −20 °C for at least six months. Once attached to the resin loss of the encoding tag is unlikely as the amide linkage is chemically robust, although in principle a linkage of any choice could be utilised in this methodology.

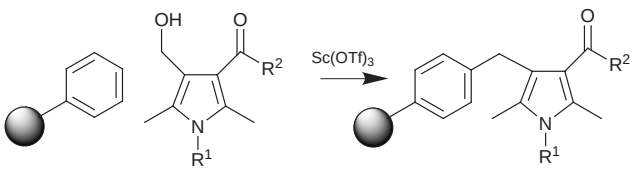

1

Scheme 1

Scandium-catalysed reaction of alcohol **1c** with toluene at room temperature was essentially complete in 2 days to give 74% of the desired product **3** and 23% of side product **4** (Table 1). Reaction of **1c** with the more reactive 1,3-dimethoxybenzene (DMB, 100 equiv.) resulted in a substantially improved reaction giving **5** in almost quantitative yield in only a few minutes. In the absence of an aromatic substrate, **1c** was shown to react slowly with itself in the presence of $ScOTf_3$ to form a dimer **4**, most likely by self-condensation and subsequent deformylation. These solution phase studies suggested that a resin containing a nucleophile more reactive than toluene would be less prone to side reactions.

The kinetics of pyrrole amide **1c** reacting with various polystyrene resins was followed by observing the loss of **1c** from the reaction mixture as compared to a control with no resin present. The observed reaction rate of amide **1c** with chloromethylpolystyrene **6** (Aldrich, 200–400 mesh) was comparable to the model studies with toluene (Table 1) under similar conditions. Reaction of **1c** with the more reactive, acetylated Wang resin **7** (Novabiochem, 200–400 mesh) gave the expected rate improvement leading to a half-life of 1.5 h as compared to 10.5 h for **6**. These reactivity studies are consistent with the observations made for the model reactions of **1c** with toluene and DMB and suggests that the resin environment does not impede the desired chemistry.

Chloromethylpolystyrene (Polymer Labs, 50–60 mesh, 1.8 mmol g^{-1}) was reacted with 3-methoxyphenol and subsequently 4-hydroxymethylphenol, to give the modified Wang resin **8**, which could be used for a library synthesis. However, some degree of cleavage of the Wang linker was observed when resin **8**, loaded with Fmoc-alanine, was treated with 10 mM

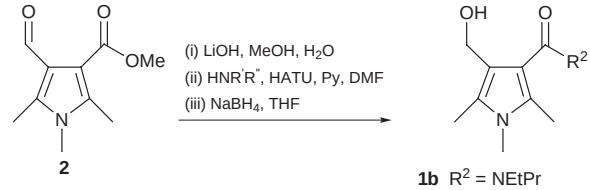

2

1b R^2 = NEtPr
c R^2 = NBu_2
d R^2 = $N(C_5H_{11})_2$
e R^2 = $N(C_6H_{13})_2$
f R^2 = $NMeC_{12}H_{25}$
g R^2 = $N(C_8H_{17})_2$
h R^2 = $N(C_{10}H_{21})_2$
i R^2 = $N(C_{12}H_{25})_2$

Scheme 2

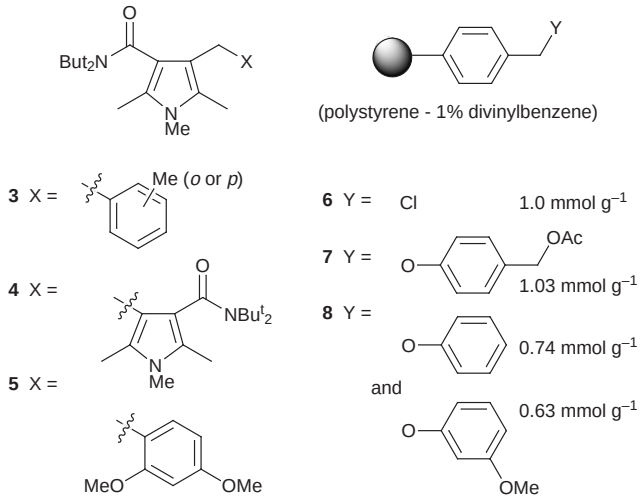

scandium triflate (6.2% cleavage in 3 h). It was found that ytterbium triflate, which has similar properties to scandium triflate, [12] was more compatible with Wang resin, giving only 0.9% cleavage of the linker in 3 h.

To demonstrate that this technology can be applied to the encoding of a combinatorial library, a split and mix[3] tripeptide library (*step 1*, ala, gly, leu; *step 2*, val, met, phe; *step 3*, trp, ser, ser-lys) was synthesised on resin **8** and encoded with alcohols **1d**–**1i**. Three batches of resin **8** were coupled to an amino acid using benzotriazol-1-yloxytris(pyrrolidino)phosphonium hexafluorophosphate (PyBOP) chemistry, the resin was capped with Ac_2O after each step and subsequently reacted with the appropriate encoding pyrroles **1d**–**i**, at 30 μmol g^{-1} of resin (approx. 300 pmol per bead, 3% compared to library loading) in 15 mM ytterbium triflate in 2 : 1 $ClCH_2CH_2Cl$–$MeNO_2$ for 16 h. The beads were then mixed and split and the Fmoc group removed ready for the next round of synthesis. The peptides, from single beads, were cleaved in TFA (95%), then the beads were subjected to hydrolysis with 5.6 M HCl to cleave the secondary amines from the encoding tags. The hydrolysate was dried *in vacuo* then reacted with dansyl chloride in the presence of Na_2CO_3 and analysed by fluorescence HPLC.

The only limitation revealed in this experiment was that no incorporation of the pyrroles was seen to beads that had incorporated methionine, presumably due to *S*-alkylation of the pyrrole tags. However, no other amino acid in the library appeared to interfere with the Friedel–Crafts encoding chemistry (notably phenylalanine and tryptophan). A number of beads were decoded and Fig. 1 shows a typical analysis of a single bead. The HPLC trace unambiguously identified the peptide from the encoding tags and the identity of the peptide was confirmed by electrospray mass spectrometry. The overall efficiency for incorporation, cleavage and detection for tags **1d**–**i** was 20 ± 10% based on a dansylated standard solution of the amines analysed under the same conditions.

Table 1 Friedel-Crafts reactions of **1c**[a]

Substrate (equiv.)	$ScOTf_3$/ mM	Reaction time/h	Unreacted **1c**[b] (%)	$t_{1/2}$/h for **1c**[c]	Yield (%)
None	10	24	63	> 48	**4** 37
None	20	48	31	17	**4** 69[d]
Toluene (100)	20	48	3	8	**3** 74[d] **4** 23[d]
DMB(40)	10	24	1	< 0.2	**5** 99[d]
Resin **6** (5)[e]	10	24	34	10.5	—
Resin **7** (4)[e]	10	24	2	1.5	—

[a] Reactions were carried out at room temperature in 2:1 $ClCH_2CH_2Cl$–$MeNO_2$ with 1 equiv. of **1c**. [b] Based on HPLC-ELSD analysis of the reaction mixture. [c] Half-lives measured in a more comprehensive study of the kinetics. [d] Products isolated and characterised by ^1H, ^{13}C NMR and FT-IR spectroscopy and high resolution mass spectrometry. [e] Compared to the loading.

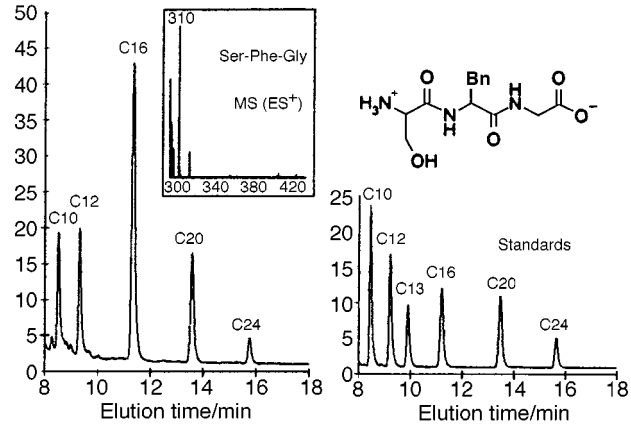

Fig. 1 Analysis of a bead: (*a*) mass spectrum of the cleaved peptide and (*b*) the HPLC trace of the cleaved tags (reverse phase, H_2O–MeCN, Novapak phenyl 1.5 × 150 mm column, excitation/emission at 340/500 nm).

These studies show that Friedel–Crafts insertion of such tags may be employed in a chemical encoding strategy. In this first instance, the methodology has been exemplified using secondary amine tags which were based on published work by the Affymax group,[5] however the pyrrole/Friedel–Crafts chemistry should also be suitable as a carrier for attachement of other tag moieties (*e.g.* MS tags) to a resin bead. In comparison with existing chemical encoding methods,[5,6] orthogonal protecting groups are not required and the tags are not randomly inserted but are directed into the resin backbone. Furthermore, it has been demonstrated that the insertion kinetics is tunable by doping the resin with electron-rich aromatics. The further application of this chemistry to the encoding of compound libraries is currently being carried out to evaluate its broader compatibility with other resins and chemistries.

We acknowledge the help of Michael Prodigalidad for the single bead analysis of peptides by mass spectrometry. We thank Zeneca Pharmaceuticals for a studentship to R. S. and the BBSRC (Grant # MOL04534). We acknowledge Chris Abell, David Hollinshead and Richard Shute for proofreading the manuscript and helpful discussions. S. B. is a Royal Society University Research Fellow.

Notes and references

1 M. A. Gallop, R. W. Barrett, W. J. Dower, S. P. A. Fodor and E. M. Gordon, *J. Med. Chem.*, 1994, **37**, 1233.
2 A. Nefzi, J. M. Ostresh and R. A. Houghten, *Chem. Rev.*, 1997, **97**, 449.
3 A. Furka, F. Sebestyen, M. Asgedom and G. Dibo, *Int. J. Pept. Protein. Res.*, 1991, **37**, 487.
4 A. W. Czarnik, *Proc. Natl. Acad. Sci. U.S.A.*, 1997, **94**, 12 738.
5 Z. J. Ni, D. Maclean, C. P. Holmes, M. M. Murphy, B. Ruhland, J. W. Jacobs, E. M. Gordon and M. A. Gallop, *J. Med. Chem.*, 1996, **39**, 1601.
6 H. P. Nestler, P. A. Bartlett and W. C. Still, *J. Org. Chem.*, 1994, **59**, 4723.
7 J. M. J. Frechet and M. J. Farrall, in *Chemistry and Properties of Crosslinked Polymers*, ed. S. S. Labana Academic Press, New York, 1977, pp. 59–83.
8 A. Warshawsky, R. Kalir and A. Patchornik, *J. Org. Chem.*, 1978, **43**, 3151.
9 Substituted benzyl alcohols were generally found to be much less reactive than hydroxymethylpyrroles under comparable conditions, as one would expect.
10 T. Tsuchimoto, K. Tobita, T. Hiyama and S. Fukuzawa, *Synlett*, 1996, 557.
11 S. Kobayashi, I. Hachiya and M. Yasuda, *Tetrahedron Lett.*, 1996, **37**, 5569.
12 S. Koboyashi, *Synlett*, 1994, 689.

Communication 9/02489A

ChemComm

Highly active ethylene polymerisation catalysts based on iron: an *ab initio* study

Edward A. H. Griffiths, George J. P. Britovsek, Vernon C. Gibson* and Ian R. Gould*

Department of Chemistry, Imperial College of Science, Technology and Medicine, South Kensington, London, UK SW7 2AY. E-mail: v.gibson@ic.ac.uk;i.gould@ic.ac.uk

Received (in Cambridge, UK) 22nd March 1999, Accepted 4th June 1999

Full *ab initio* calculations are described on an iron-based ethylene polymerisation catalyst bearing a 2,6-bis(imino)-pyridyl ligand.

The development of non-metallocene olefin polymerisation catalysts constitutes a highly active area of academic and industrial research.[1] In particular, late transition metal polymerisation catalysts have become of interest since the discovery by Brookhart and co-workers that Ni^{II} and Pd^{II} complexes containing bulky α-diimine ligands are capable of polymerising ethylene and higher α-olefins to high molar mass polymers.[2] These systems have been the subject of several theoretical investigations.[3–5] In parallel studies, we and Brookhart and co-workers have recently reported highly active ethylene polymerisation catalysts based on iron and cobalt bearing 2,6-bis(imino)pyridyl ligands.[6,7] Here, we present the first theoretical studies on this catalyst system, having assumed the generally accepted Cossee–Arlman polymerisation mechanism.[8] The key features of the reaction pathway are shown in Scheme 1.

Optimisations† were initially performed on the bis(2,6-diisopropylphenylimino)pyridyliron dichloride complex **A** shown in Scheme 1. From the table presented in Scheme 1 it can be seen that the level of agreement between the gas-phase calculated bond parameters and the experimental data[6] is generally good. The results are also in accord with the experimental magnetic moment,[6] since quintet multiplicity (S = 2) was found to correspond to a minimum energy structure within the C_s point group. The optimised structures **1**–**4**, obtained for the first insertion step, are shown in Fig. 1; a potential energy profile is shown in Fig. 2.

For the methyl cation **1** (Fig. 1), the iron atom lies in the plane defined by the bis(imino)pyridine nitrogens (3N-plane) to within 0.04 Å. The four-coordinate geometry around the iron centre is thus best described as distorted square planar. The

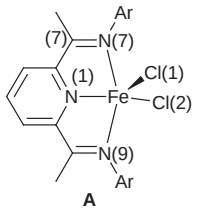

A

	Experimental	Calculated
Fe–Cl(1)	2.311(2) Å	2.36 Å
Fe–Cl(2)	2.266(2) Å	2.27 Å
Fe–N(1)	2.088(4) Å	2.11 Å
Fe–N(7)	2.250(4) Å	2.23 Å
C(7)–N(7)	1.285(6) Å	1.29 Å
N(1)–Fe–N(7)	73.2(1)°	73.4°
N(7)–Fe–Cl(2)	98.6(1)°	99.3°
N(1)–Fe–Cl(2)	147.9(1)°	149.1°
N(7)–Fe–N(9)	140.1(1)°	141.9°
N(1)–Fe–Cl(1)	94.62(12)°	85.4°

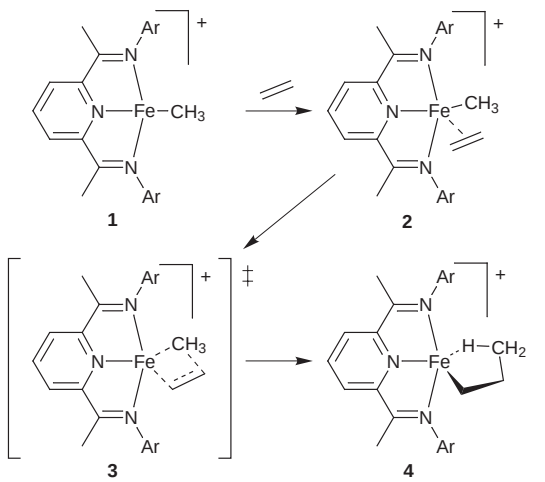

Scheme 1

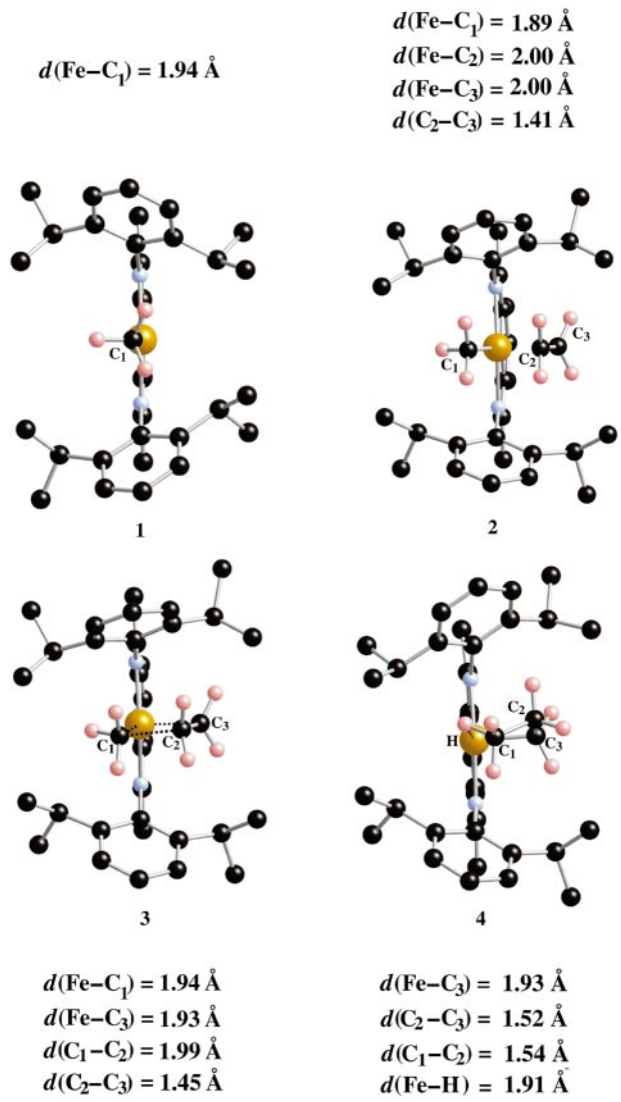

Fig. 1 The optimised structures of the reactant **1**, the ethylene π-complex **2**, the transition state **3**, and the γ-agostic product **4**. Selected atoms have been labelled. The pyridyl nitrogen is obscured by the iron atom.

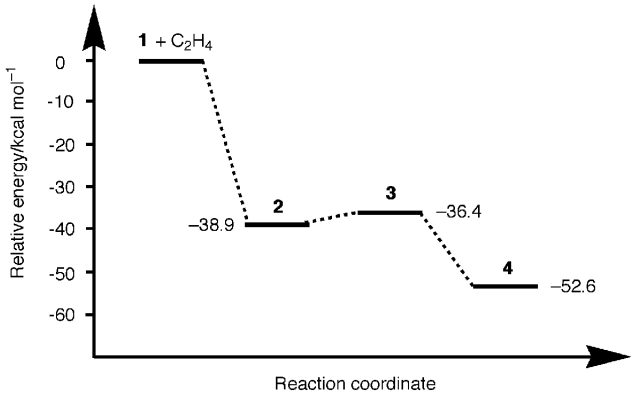

Fig. 2 Potential energy profile of ethylene insertion into the Fe–CH_3 bond of **1**.

distortion arises largely within the square plane due to the constrained nature of the ligand system, the N(imino)–Fe–N(imino) bond angle being 160.8°. Additionally, the methyl group (C_1) is bent out of the square plane by 6.4°. Compared to the dichloride (**A**), the Fe–N(imino) and Fe–N(pyridyl) distances have shortened considerably, presumably a consequence of the lower coordination number and the positively charged iron centre. The former now average 2.00 Å while the latter is 1.93 Å, the Fe–N(imino) distances vary by less than 0.01 Å in structures **1**–**4**; the Fe–C_1 distance is 1.94 Å. The 2,6-diisopropylphenyl rings have tilted relative to those in the dichloride by 9.1° and are now inclined at 70.3° to the 3N-plane.

In the structure of the ethylene π-complex **2** (Fig. 1), the methyl group has tilted further away from the 3N-plane to an inclination of 24.1° to accommodate the incoming ethylene. The geometry around the iron centre is now distorted trigonal bipyramidal with the N(pyridyl) atom, the methyl group and the complexed ethylene in the equatorial positions. The angle C_1–Fe-(midpoint of C_2–C_3) is 96.9°. The Fe–C_1 bond distance of 1.89 Å in the complex is shorter than in **1**; no rotation of the methyl group is observed. The iron atom lies at a distance of 2.00 Å to both olefinic carbons which are 1.41 Å apart. Additionally, the hydrogens of the ethylene are orientated away from the metal, consistent with partial re-hybridization of the carbon centres. The Fe–N(pyridyl) bond length shrinks slightly to 1.90 Å. In order to assist the approach of the olefin the 2,6-diisopropylphenyl rings have tilted through 18.6° away from the approach path of the incoming olefin. This tilting may protect the sterically less-hindered side of the metal centre from further coordination whilst insertion occurs. The binding energy of the ethylene is 38.9 kcal mol^{-1}.

In the transition state **3** (Fig. 1) the four centres involved, C_1–Fe–C_3–C_2, are nearly coplanar, the olefinic carbon C_2 lying only 0.08 Å above the C_1–Fe–C_3 plane. The methyl group is pulled back and is now inclined at 18.9° to the 3N-plane. Simultaneously the C_3 atom has moved from an equatorial to an apical site thus returning the geometry around the metal centre towards distorted square pyramidal with the basal site becoming vacant as the C_1–Fe bond is broken. The Fe–C_3 bond length shortens to 1.93 Å whilst the Fe–C_1 bond has elongated to 1.94 Å and the C_2–C_3 bond length has increased to 1.45 Å. The activation energy is 2.5 kcal mol^{-1}. This is a very low barrier indicating a facile insertion process.

For the insertion product **4** (Fig. 1), the carbon of the methyl group C_1 and the olefinic carbon C_2 have twisted below and above the plane containing the pyridyl nitrogen and the Fe–C_3 bond, respectively. This puckering of the propyl chain leads to a further tilting of the 2,6-diisopropylphenyl rings by 8.4° away from the propyl chain. A weak γ-agostic interaction has been formed in which the C_1–H bond length is stretched to 1.12 Å. The Fe–H distance is 1.91 Å and the Fe–N(pyridyl) distance is further shrunk to 1.82 Å. The structure is now distorted square pyramidal with the fourth basal site occupied by the agostic hydrogen of the propyl chain and C_3 occupying the apical site. The product **4** is lower in energy than **2** by 13.7 kcal mol^{-1}. Preliminary investigations have shown that the insertion of the second ethylene molecule is accompanied by a rearrangement of the propyl chain from the apical position to the in-plane site (*cf.* structure **1**).

In summary, full *ab initio* calculations have been performed on the bis(imino)pyridyliron ethylene polymerisation catalyst system, and key structures operating for the first monomer insertion within a cationic alkyl mechanism have been identified. The energetics associated with complexation and insertion are comparable with values calculated for the Ni^{II} α-diimine catalyst system, the barrier to insertion however is significantly lower.[3–5] Further studies are in progress on the propagation and termination steps for this new system.

We thank the EPSRC for a studentship (E. A. H. G.) and BP Amoco Chemicals for financial support.

Notes and references

† All *ab initio* calculations were carried out using the GAUSSIAN98 package (ref. 9). Geometry optimisations on the parent dichloride (**A**) were performed using the B3LYP, BP86 and B3P86 functionals. The B3P86 (ref. 10, 11) functional was found to give the best agreement with experiment (Scheme 1) and was thus employed to calculate the structures of the catalytic cycle. For the carbon and hydrogen atoms of the alkyl chain and the chlorine and nitrogen atoms, the 6-31G** (ref. 12) basis set was employed. For the iron atom the Ahlrichs (ref. 13) pVDZ basis set was used. The STO-3G (ref. 14) basis set was placed on all other atoms. The dichloride was calculated with C_s symmetry and quintet multiplicity (S = 2). The mirror plane contains the iron atom, the pyridyl nitrogen atom and both chlorine atoms. All structures **1**–**4** of the catalytic cycle were calculated without symmetry constraints; attempts to impose C_s symmetry led to higher energy structures. For the purpose of this study, the cationic Fe^{II} species have been assigned singlet (S = 0) multiplicities. Electronic wavefunction stability calculations reveal that **2**, **3** and **4** are all singlets. Frequency calculations were performed on all optimised structures to confirm the existence of true minimum energy structures for **1**, **2** and **4**. The first order saddle point of **3** was confirmed by the presence of a single imaginary frequency in the Hessian.

1 G. J. P. Britovsek, V. C. Gibson and D. F. Wass, *Angew. Chem., Int. Ed.*, 1999, **38**, 428.
2 C. M. Killian, D. J. Tempel, L. K. Johnson and M. Brookhart, *J. Am. Chem. Soc.*, 1996, **118**, 11664; L. K. Johnson, C. M. Killian and M. Brookhart, *J. Am. Chem. Soc.*, 1995, **117**, 6414.
3 L. Deng, T. K. Woo, L. Cavallo, P. M. Margl and T. Ziegler, *J. Am. Chem. Soc.*, 1997, **119**, 6177; L. Deng, P. M. Margl and T. Ziegler, *J. Am. Chem. Soc.*, 1997, **119**, 1094.
4 D. G. Musaev, M. Svensson, K. Morokuma, S. Strömberg, K. Zetterberg and P. E. M. Siegbahn, *Organometallics*, 1997, **16**, 1933; D. G. Musaev, R. D. J. Froese, M. Svensson and K. Morokuma, *J. Am. Chem. Soc.*, 1997, **119**, 367; D. G. Musaev, R. D. J. Froese and K. Morokuma, *New. J. Chem.*, 1997, **21**, 1269; D. G. Musaev, R. D. J. Froese and K. Morokuma, *Organometallics*, 1998, **17**, 1850.
5 P. E. M. Siegbahn, S. Strömberg and K. Zetterberg, *Organometallics*, 1996, **15**, 5542.
6 G. J. P. Britovsek, V. C. Gibson, B. S. Kimberley, P. J. Maddox, S. J. McTavish, G. A. Solan, A. J. P. White and D. J. Williams, *Chem. Commun.*, 1998, 849.
7 B. L. Small, M. Brookhart and A. M. A. Bennett, *J. Am. Chem. Soc.*, 1998, **120**, 4049.
8 P. Cossee, *J. Catal.*, 1964, **3**, 80.
9 GAUSSIAN98, Revision A.1, Gaussian Inc., Pittsburgh, PA, 1998.
10 J. P. Perdew, *Phys. Rev. B*, 1986, **33**, 8822.
11 A. D. Becke, *J. Chem. Phys.*, 1993, **98**, 5648.
12 W. J. Hehre, R. Ditchfield and J. A. Pople, *J. Chem. Phys.*, 1972, **56**, 2257.
13 A. Schaefer, H. Horn and R. Ahlrichs, *J. Chem. Phys.*, 1992, **97**, 2571.
14 W. J. Hehre, R. F. Stewart and J. A. Pople, *J. Chem. Phys.*, 1969, **51**, 2657.

Communication 9/02276G

ChemComm

A synthetic receptor for the Cbz-L-Ala-L-Ala-OH dipeptide sequence

Peter D. Henley and Jeremy D. Kilburn*

Department of Chemistry, University of Southampton, Southampton, UK SO17 1BJ. E-mail: jdk1@soton.ac.uk

Received (in Liverpool, UK) 28th April 1999, Accepted 26th May 1999

A novel bowl-shaped macrobicyclic receptor has been prepared and is a particularly strong and selective receptor for Cbz-L-Ala-L-Ala-OH ($-\Delta G_{ass}$ = 25 kJ mol^{-1} at 293 K in $CDCl_3$).

The development of synthetic receptors for biologically relevant substrates such as peptides[1] continues to be a fertile area of research. The bacterial cell wall precursor peptide L-Lys-D-Ala-D-Ala-OH represents a particularly interesting target because a selective receptor[2] for this peptide sequence might lead to mimics for the vancomycin family of antibiotics.[3] We have described several systems designed to act as receptors for peptides specifically with a free carboxylic acid terminus[1a,1e,4] and in particular we have prepared a series of receptors **1** which

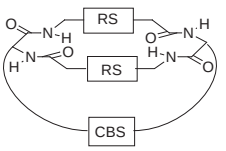

CBS = carboxylate binding site
RS = rigid spacer

1

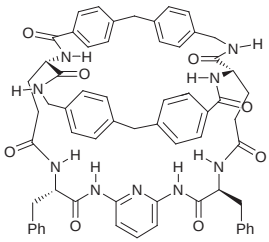

2

feature a specific binding site for the carboxylic acid terminus of peptide guests at the base of a bowl-shaped cavity.[4] Thus we have described macrobicycle **2**, which incorporates a diamidopyridine unit to serve as a carboxylic acid binding site and is an effective receptor for certain dipeptides, in particular for Cbz-β-Ala-D-Ala-OH, in chloroform solution.[4b] Despite the encouraging binding selectivities found for **2**, NMR and molecular modelling studies revealed it to be a highly flexible molecule, particularly in the portion derived from glutamic acid and phenylalanine, which links the diamidopyridine unit and the rim of the cavity. Thus **2** is far from preorganised for optimal binding of peptide guests. Here we describe a new bowl-shaped macrobicyclic receptor **13**, with increased rigidity in comparison to **2**, which has proved to be a particularly strong and selective receptor for Cbz-L-Ala-L-Ala-OH.

In order to produce a more rigid variant of our bowl-shaped receptors, we chose to link the bisarylmethane-derived rim used previously with a tyrosine derived aromatic unit, and a glutamic acid residue so that ultimately the side-chain methyl ester could be functionalised to give a water-soluble receptor.

The synthesis of macrobicycle **13** follows the strategy for the synthesis of **2** and related macrobicycles, with a double intramolecular cyclisation of a suitably activated acyclic precursor **12** as the key step (Scheme 1). Assembly of the cyclisation precursor then requires coupling together of the various amino acid building blocks around the carboxylic acid binding site, in this case diaminopyridine. Thus Cbz-L-glutamic acid γ-methyl ester was converted to the corresponding acid fluoride, using cyanuric fluoride and pyridine,[5] and coupled to diaminopyridine, which had been pretreated with *N*,*O*-bis-(trimethylsilyl)acetamide[6] to give **3** in 81% yield. Removal of the Cbz-protecting groups to yield the corresponding diamine **4** was readily achieved with Pd/C/H_2. Acid **5** was prepared by a

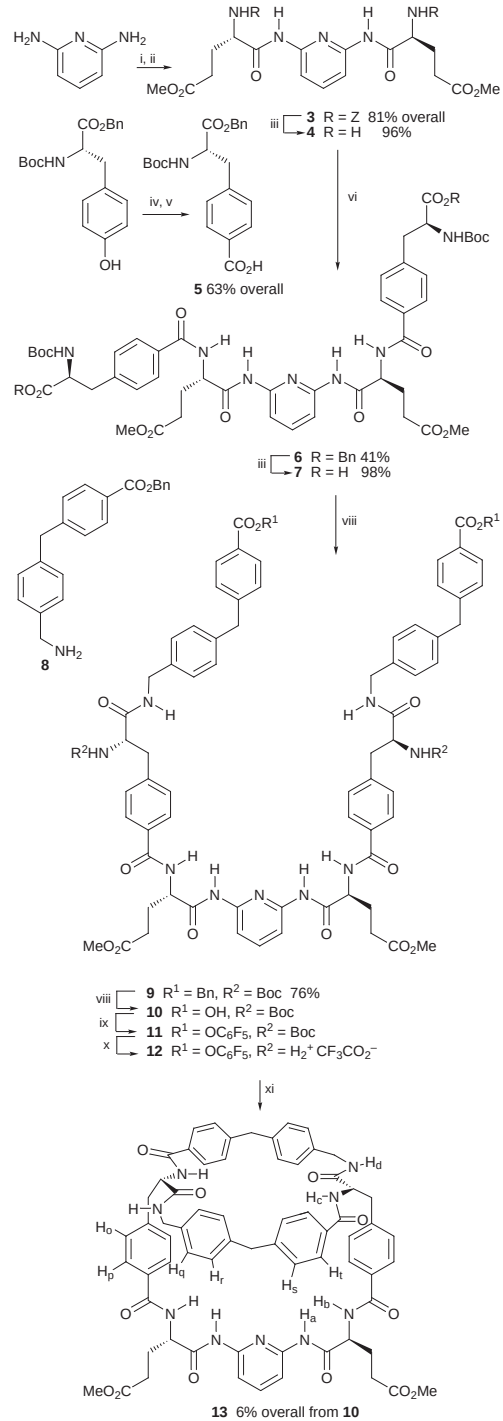

Scheme 1 *Reagents and conditions*: i, *N*,*O*-bis(trimethylsilyl)acetamide; ii, Cbz-L-Glu(OMe)-F, TBAF; iii, Pd, C, H_2, MeOH; iv, Tf_2O, pyridine, CH_2Cl_2; v, $Pd(OAc)_2$, $Ph_2P(CH_2)_3PPh_2$, KOAc, CO, DMSO, 65 °C, then 1 M HCl; vi, **5**, EDC, HOBT, DMAP, DMF; vii, **8**, EDC, HOBT, DMAP, DMF; viii, Pd, C, H_2, DMF; ix, F_5C_6OH, EDC, DMAP, DMF–THF (1:3 v/v); x, 10% TFA, CH_2Cl_2; xi, slow addition to a refluxing solution of Pr^i_2NEt in MeCN.

Table 1 Binding constants (K_{ass}) and free energies of complexation ($-\Delta G_{ass}$) for the 1:1 complexes formed between macrobicycle **13** and various substrates, in $CDCl_3$ at 20 °C

Entry	Substrate	K_{ass}[a]/M^{-1}	$-\Delta G_{ass}$/kJ mol^{-1}
1	Phenylacetic acid	2100 ± 100	18.6 ± 0.1
2	Cbz-L-Ala-OH	5300 ± 500	20.9 ± 0.3
3	Cbz-D-Ala-OH	800 ± 70	16.3 ± 0.3
4	Cbz-β-Ala-L-Ala-OH	2500 ± 130	19.0 ± 0.1
5	Cbz-L-Ala-L-Ala-OH	33000 ± 3200	25.3 ± 0.3
6	Cbz-D-Ala-D-Ala-OH	4500 ± 300	20.5 ± 0.2
7	Cbz-Gly-L-Ala-OH	1800 ± 150	18.3 ± 0.2
8	Cbz-Gly-D-Ala-OH	3100 ± 370	19.6 ± 0.3

[a] Errors were estimated from the quality of the fit of the experimental data to the calculated, by carrying out several titration experiments and by monitoring the shift of several protons (H_a, H_o, H_r) to obtain several estimates of K_{ass} and averaging the values obtained.

palladium catalysed carbonylation of the triflate derived from Boc-L-tyrosine benzyl ester.[7] In the presence of potassium acetate[8] and the bidentate dppp ligand,[9] the carbonylation worked well to give the desired acid **5** in 66% yield after aqueous acid work-up. Acid **5** was then coupled to diamine **4** using 1-(3-dimethylaminopropyl)-3-ethylcarbodiimide hydrochloride (EDC) and 1-hydroxybenzotriazole hydrate (HOBT), and the resulting diester **6** was debenzylated to give the diacid **7**, which in turn was coupled with the previously described amine **8**[4b] to give the protected cyclisation precursor **9**. Debenzylation of **9** and formation of the bispentafluorophenyl ester was followed by removal of the Boc protecting groups to give the bisamine salt **12**. Slow addition of **12** to a refluxing solution of Pr^i_2NEt in MeCN gave the desired macrobicycle **13**, but in only 6% yield overall from diacid **10**, after purification by column chromatography. The yield of the final cyclised product was disappointing and in previous syntheses of related compounds[4] the analogous sequence typically yielded ~30% of macrobicycle, but in the present case the low yield is probably attributable to the greater rigidity of the precursor and of the resulting macrobicycle.

Macrocycle **13** gave a well-resolved ^1H NMR spectrum in $CDCl_3$ which could be fully assigned with the help of 2D NMR experiments. Binding studies on macrobicycle **13** were therefore carried out with a number of Cbz-protected alanine derived amino acids and dipeptides in $CDCl_3$, using a standard ^1H NMR titration experiment, monitoring the shift of various signals, and analysing the resultant binding curves (Table 1).[10] In each binding experiment a 1:1 binding stoichiometry has been assumed which was generally supported by the good fit of the measured data to the theoretical model, on analysis. In each titration experiment significant downfield shifts of the signal for NH_a were observed ($\Delta\delta$ = 0.3–0.8 ppm), consistent with a strong association between the carboxylic acid and the amidopyridine moiety. Addition of corresponding methyl esters to a solution of **13** led to no significant changes in the ^1H NMR spectrum for **13**, further confirming the importance of the carboxylic acid–amidopyridine interaction in the observed binding. The addition of all carboxylic acid substrates, with the exception of phenylacetic acid (Table 1, entries 2–8), also led to large downfield shifts of the signals for NH_c ($\Delta\delta$ = 0.4–0.9 ppm) and addition of the dipeptide substrates (entries 5–8) led to large downfield shifts of NH_d ($\Delta\delta$ = 0.1–0.5 ppm) implicating these NHs in hydrogen bonding with the respective substrates. (The signal for NH_b was obscured by the aromatic region and could not be accurately monitored.) Significant shifts in the signals for the aromatic protons were also observed. In particular, addition of substrates incorporating an L-Ala-OH moiety (entries 2, 4, 5 and 7) led to an upfield shift of ArH_p ($\Delta\delta$ = 0.1–0.2 ppm) and a downfield shift of ArH_t ($\Delta\delta$ = 0.1– 0.3 ppm), whereas addition of substrates incorporating D-Ala-OH (entries 3, 6 and 8) gave much smaller shifts of ArH_p and ArH_t, but significant upfield shifts of both ArH_q and ArH_r ($\Delta\delta$ = 0.1–0.2 ppm).

The association constants for the various guests studied indicate that the receptor, while able to bind a range of substrates, is a particularly strong receptor for Cbz-L-Ala-L-Ala-OH ($-\Delta G_{ass}$ = 25.3 kJ mol^{-1}). The receptor is very selective for this substrate as evidenced by the fact that Cbz-L-Ala-L-Ala-OH is bound > 4 kJ mol^{-1} more strongly than Cbz-D-Ala-D-Ala-OH and ~7 kJ mol^{-1} more strongly than Cbz-Gly-L-Ala-OH. The latter result is particularly notable since the difference in binding energies (~7 kJ mol^{-1}) is the consequence of replacing a single proton with a methyl group at the second residue of the dipeptide (Gly → L-Ala), and is probably a consequence of the methyl group establishing a stabilising interaction with the bisarylmethane unit in the rim of the macrobicycle—which is evidenced by the large upfield shift of the signal for the methyl group ($-\Delta\delta \approx 0.7$ ppm) on complexation with macrobicycle **13**.[11]

Thus the increased rigidity, and hence preorganisation, introduced into the structure of macrobicycle **13** has provided a stronger and considerably more selective receptor than the previously described macrobicycle **2** and, whereas the latter was a better receptor for β-alanyl-D-α-amino acid substrates, macrobicycle **13** is selective for dipeptides derived from two α-amino acids, and in particularly for the significant L-Ala-L-Ala-OH sequence.

We thank the EPSRC for a studentship for P. H. and Dr Tobias Braxmeier and Dr Herbert Röttele (Karlsruhe University) for carrying out additional NMR experiments.

Notes and references

1 For recent examples of peptide receptors see (*a*) J. Dowden, P. D. Edwards, S. S. Flack and J. D. Kilburn, *Chem. Eur J.*, 1999, **5**, 79; (*b*) Md. A. Hossain and H.-J. Schneider, *J. Am. Chem. Soc.*, 1998, **120**, 11 208; (*c*) R. Breslow, Z. Yang, R. Ching, G. Trojandt and F. Odobel, *J. Am. Chem. Soc.*, 1998, **120**, 3536; (*d*) D. W. P. M. Löwik, M. D. Weingarten, M. Broekema, A. J. Brouwer, W. C. Still and R. M. J. Liskamp, *Angew. Chem.*, 1998, **37**, 1846; (*e*) M. Davies, M. Bonnat, F. Guillier, J. D. Kilburn and M. Bradley, *J. Org. Chem.*, 1998, **63**, 8696.

2 The *in vitro* antimicrobial activity, against selected Gram-positive bacteria, of a calixarene derived receptor for the dipeptide sequence D-Ala-D-Ala-OH has been described: A. Casnati, M. Fabbi, N. Pelizzi, A, Pochini, F. Sansone, R. Ungaro, E. Di Modugno and G. Tarzia, *Bioorg. Med. Chem. Lett.*, 1996, **6**, 2699.

3 H. R. Perkins, *Biochem. J.*, 1969, **111**, 195; D. H. Williams, *Nat. Prod. Rep.*, 1996, **13**, 469; D. H. Williams, M. S. Searle, M. S. Westwell, J. P. Mackay, P. Groves and D. A. Beauregard, *Chemtracts: Org. Chem.*, 1994, **7**, 133.

4 (*a*) G. J. Pernia, J. D. Kilburn, J. W. Essex, R. J. Mortishire-Smith and M. Rowley, *J. Am. Chem. Soc.*, 1996, **118**, 10 220; (*b*) C. P. Waymark, J. D. Kilburn and I. Gillies, *Tetrahedron Lett.*, 1995, **36**, 3051.

5 L. A. Carpino, D. Sadat-Aalaee, H. G. Chao and R. H. DeSelms, *J. Am. Chem. Soc.*, 1990, **112**, 9651.

6 S. Rajeswari, R. J. Jones and M. P. Cava, *Tetrahedron Lett.*, 1987, **28**, 5099.

7 J. W. Tilley, R. Sarabu, R. Wagner and K. Mulkerins, *J. Org. Chem.*, 1990, **55**, 906; X. Creary, B. Benage and K. Hilton, *J. Org. Chem.*, 1983, **48**, 2887.

8 S. Cacchi and A. Lupi, *Tetrahedron Lett.*, 1992, **33**, 3939.

9 R. E. Dolle, S. J. Schmidt and L. I. Kruse, *J. Chem. Soc., Chem. Commun.*, 1987, 904.

10 The binding constants were calculated by fitting the data to a 1:1 binding isotherm using NMRTit HG software, kindly provided by Professor C. A. Hunter, University of Sheffield. See: A. P. Bisson, C. A. Hunter, J. C. Morales and K. Young, *Chem. Eur. J.*, 1998, **4**, 845.

11 In view of the selectivity of macrobicycle **13** for Cbz-L-Ala-L-Ala-OH over Cbz-D-Ala-D-Ala-OH (Table 1, entries 5 and 6), and for Cbz-L-Ala-OH over Cbz-D-Ala-OH (entries 2 and 3), the preference for Cbz-Gly-D-Ala-OH over Cbz-Gly-L-Ala-OH (entries 7 and 8) is somewhat surprising. The origin of this selectivity is unclear at this stage and will need to be examined in further studies.

Communication 9/03449H

ChemComm

Manganese dioxide can oxidise unactivated alcohols under *in situ* oxidation–Wittig conditions

Leonie Blackburn, Xudong Wei and Richard J. K. Taylor*

Department of Chemistry, University of York, Heslington, York, UK YO10 5DD. E-mail: rjkt1@york.ac.uk

Received (in Liverpool, UK) 18th May 1999, Accepted 3rd June 1999

The *in situ* alcohol oxidation–Wittig reaction using manganese dioxide as the oxidant has been applied to semi-activated and, for the first time, unactivated alcohols to furnish the corresponding α,β-unsaturated esters.

Manganese dioxide is an extremely useful oxidant in organic chemistry.[1] Oxidations using manganese dioxide are particularly easy to perform as the oxidant is heterogeneous and the reaction work-up usually involves simple filtration and evaporation of the solvent. An important use of manganese dioxide is to convert primary alcohols into the corresponding aldehydes, although the process is limited to activated systems of the allylic/benzylic type. Recently, we described the development of an *in situ* manganese dioxide oxidation–Wittig process in which activated alcohols were treated with manganese dioxide in the presence of a stabilised Wittig reagent: the resulting aldehyde was trapped as it was formed to produce the homologated α,β-unsaturated ester [eqn. (1)].[2] This procedure is particularly useful in cases where the intermediate aldehyde is difficult to isolate (*e.g.* for reasons of volatility, toxicity, liability to oligomerisation).

$$RCH_2OH \xrightarrow[Ph_3P{=}CHE]{MnO_2,\ CH_2Cl_2,\ \text{room temp.}} RCH{=}CHE \qquad (1)$$

R = vinyl, alkynyl, phenyl; E = CO_2Et, *etc.*

Coincidentally, at around the same time, Barrett *et al.* reported the combined use of the Dess–Martin periodinane and stabilised phosphoranes,[3] and Matsuda's group employed barium permanganate in a similar process.[4]†

The simplicity of the manganese dioxide procedure referred to above, coupled with the toxicity of barium permanganate and the sensitivity, and hazardous preparation, of the Dess–Martin oxidant, prompted us to attempt to extend the scope of the process (Tables 1 and 2). Initial studies concentrated on alcohols which might be classified as 'semi-activated' (Table 1).‡ Thus, as expected, cyclopropylmethanol **1** underwent smooth *in situ* oxidation–Wittig reaction giving enoates **2** and **3**, as did the corresponding diol **4** producing dienoate **5**.

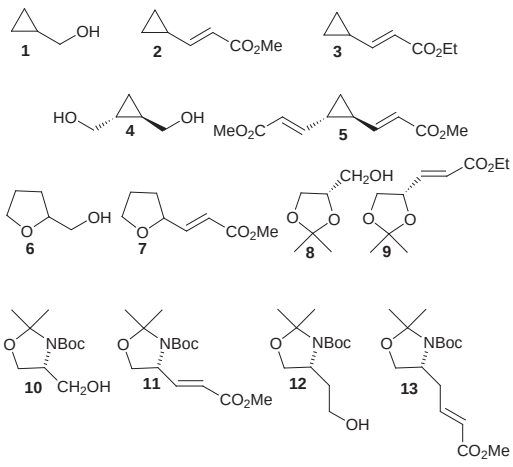

Such reactions should prove useful in the synthesis of cyclopropyl-based natural products.[3a]

Table 1 *In situ* oxidation–Wittig reactions on 'semi-activated' alcohols[a]

Substrate	Product	Solvent	*t*/h	Yield (%)	Configuration
1	**2**	toluene	4	80	>99% *E*
1	**3**	toluene	4	86	>99% *E*
4	**5**	$CHCl_3$	18	81	>99% *E*
6	**7**	$CHCl_3$	24	66	6:1 *E*:*Z*
8	**9**	toluene	20	74	3:1 *E*:*Z*[b]
10	**11**	toluene	18	58	>95% *E*[c]
12	**13**	$CHCl_3$	20	70	>95% *E*[d]

[a] Activated MnO_2 (Aldrich, *ca.* 10 equiv.) was added in three equal portions to a mixture of the alcohol and the stabilised Wittig reagent, Ph_3PCHCO_2R (1.2 equiv.), in the specified solvent which was heated under reflux for the specified time. [b] $[\alpha]_D^{20}$ +40.5 (*c* 1, $CHCl_3$); lit.,[6] +38.3 (*c* 2, $CHCl_3$). [c] $[\alpha]_D^{20}$ −65.5 (*c* 1, $CHCl_3$); lit.,[7] −65 (*c* 4.2, CH_2Cl_2). [d] $[\alpha]_D^{20}$ −27.9 (*c* 1.15, $CHCl_3$).

In this same study (Table 1), we also investigated the oxidation of alcohols containing a proximal heteroatom which might activate the alcohol to oxidation inductively and/or by providing a coordination site for the oxidant. Encouragingly, tetrahydrofurfuryl alcohol **6** furnished the desired α,β-unsaturated ester **7** in good yield. In contrast, oxidation of this alcohol to the corresponding aldehyde is reported to be problematic and at best yields of *ca.* 50% are obtained using tetrapropylammonium perruthenate (TPAP) and 4-methylmorpholine *N*-oxide (NMO).[5] The *in situ* reaction was also successfully applied to several related enantiomerically pure primary alcohols **8**, **10** and **12**. No racemisation was observed according to polarimeteric measurements[6,7] and good yields were obtained. During the course of this study McKervey *et al.* utilised our *in situ* oxidation–Wittig methodology to convert non-racemic protected γ-amino alcohols into the corresponding α,β-unsaturated esters and ketones without loss of stereochemical integrity.[8]

In order to establish the limitations of this process we treated a completely unactivated alcohol, decanol **14**, under the *in situ* manganese dioxide–Wittig conditions.

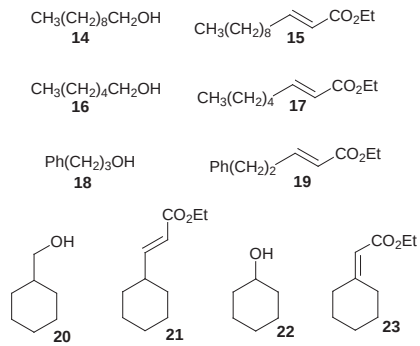

To our amazement (Table 2), enoate **15**[9] was obtained in 80% yield after 24 h reflux in toluene.§ This result was extremely surprising given the generally accepted view that manganese dioxide is not an effective oxidant for unactivated primary alcohols.[1] We therefore studied other unactivated primary

Table 2 *In situ* oxidation–Wittig reaction on unactivated alcohols[a]

Substrate	Product	Solvent	*t*/h	Yield(%)	Configuration
14	**15**	toluene	24	80	> 95% *E*
16	**17**	toluene	24	70	> 95% *E*
18	**19**	toluene	6	86	> 95% *E*
20	**21**	$CHCl_3$	20	51	> 99% *E*
22	**23**	toluene	24	< 1	

[a] Activated MnO_2 (Aldrich, *ca*. 10 equiv.) was added in three equal portions to a mixture of the alcohol and the stabilised Wittig reagent, Ph_3PCHCO_2R (1.2 equiv.), in the specified solvent which was heated under reflux for the specified time.

alcohols. Both hexanol **16** and 1-phenylpropan-3-ol **18** furnished the desired products **17** and **19**, respectively, in excellent yield. With cyclohexylmethanol **20**, the expected product **21** was obtained in reduced yield (51%); it seems likely that alkyl substitution at the β-position relative to the alcohol is responsible for the reduction in efficiency. A limitation to the process was realised when secondary alcohols were studied. As shown in Table 2, treatment of cyclohexanol **22** under the *in situ* oxidation–Wittig conditions gave only trace amounts of the desired enoate **23**. Similar results were also observed with pentan-3-ol and dihydrocholesterol, which both failed to yield the corresponding enoates. These results were not unexpected as both the oxidation of secondary alcohols and the Wittig reactions of stabilised phosphoranes with ketones are known to be difficult compared with the corresponding sequence commencing with primary alcohols.

We have carried out preliminary studies to try to rationalise these results. The most important point is that on treatment with manganese dioxide in the absence of a Wittig reagent, but under otherwise identical conditions, the primary alcohols gave only low yields of the corresponding aldehydes: for example, after reflux in toluene with manganese dioxide for 24 h, decanol gave decanal in only 12% yield, unreacted alcohol accounting for the balance of material. One possible explanation for the high conversions observed in the presence of the stabilised phosphoranes is that the primary alcohols are being converted into the corresponding aldehydes in small equilibrium quantities with the *in situ* Wittig reagent immediately trapping out the aldehyde. Alternatively it is possible that the phosphorane may be activating the oxidant or the alcohol (or the intermediate complex) to oxidation. Further mechanistic studies are in progress.¶

In summary, we have shown for the first time that unactivated primary alcohols can be efficiently oxidised using manganese dioxide under *in situ* Wittig conditions. Similar results are reported with 'semi-activated' alcohols producing a range of synthetically useful α,β-unsaturated esters.

We thank the EPSRC for a research fellowship (X. W.) and research studentship (L. B.). We are also grateful to Pfizer for additional financial support and to A. D. Campbell for carrying out the conversion of **12** into **13**.

Notes and references

† In preliminary studies, we have shown that chromium dioxide (Magtrieve™) can also be used for *in situ* oxidation–Wittig reactions.

‡ All new compounds were fully characterised spectroscopically and by HRMS.

§ Representative procedure: Activated manganese dioxide (0.3 g) was added to a stirred solution of decanol (158 mg, 1 mmol) and ethoxycarbonylmethylenetriphenylphosphorane (418 mg, 1.2 mmol) in toluene (25 ml) and the mixture was heated to reflux. Two further portions of manganese dioxide (*ca*. 0.3 g each) were added to the reaction over the first hour and then it was stirred and heated until TLC indicated that reaction was complete (*ca*. 24 h). The manganese dioxide was removed by filtration through Celite, the Celite was washed well with toluene, and the combined organic portions were concentrated *in vacuo* to *ca*. 1–2 ml. Column chromatography (light petroleum–Et_2O 5:1) gave ethyl *trans*-dodec-2-enoate (181 mg, 80%) as a colourless oil with spectroscopic data consistent with those published (ref. 9).

¶ Addition of Ph_3PO or pyridine to the manganese dioxide oxidation of decanol under toluene reflux (24 h) increases the yield from 12 to *ca*. 40%.

1 A. J. Fatiadi, *Synthesis*, 1976, 65 and 133; *Encyclopedia of Reagents for Organic Synthesis*, ed. L. A. Paquette, Wiley, Chichester, 1995, vol. 5, p. 3229.
2 X. Wei and R. J. K. Taylor, *Tetrahedron Lett.*, 1998, **39**, 3815.
3 (*a*) A. G. M. Barrett, D. Hamprecht and M. Ohkubo, *J. Org. Chem*., 1997, **62,** 9376; (*b*) C. C. Huang, *J. Labelled Compd. Radiopharm.*, 1987, **24**, 675; (*c*) D. Crich and X. Mo, *Synlett*, 1999, 67.
4 S. Shuto, S. Niizuma and A. Matsuda, *J. Org. Chem*., 1998, **63**, 4489.
5 F. Cominetti, A. Deagostino, C. Prandi and P. Venturello, *Tetrahedron*, 1998, **54**, 14603.
6 T. Morikawa, Y. Washio, S. Harada, R. Hanai, T. Kayashita, H. Nemoto, M. Shiro and T. Taguchi, *J. Chem. Soc., Perkin Trans. 1*, 1995, 271.
7 H. Priepke, R. Bruckner and K. Harms, *Chem. Ber*., 1990, **123**, 555.
8 S. B. Davies and M. A. McKervey, *Tetrahedron Lett*., 1999, **40**, 1229.
9 J. A. Elix, D. A. Venables and A. W. Archer, *Aust. J. Chem.*, 1994, **47**, 1345.

Communication 9/03980E

Catalysis of chlorosilane on the ring-expansion of cyclic acetals bearing a carbene precursor. Lewis acid–base effect on the oxonium ylide intermediate

Takashi Mori and Akira Oku*

Department of Chemistry and Materials Technology, Kyoto Institute of Technology, Matsugasaki, Sakyo-ku, Kyoto 606-8585, Japan. E-mail: oku@ipc.kit.ac.jp

Received (in Cambridge, UK) 17th May 1999, Accepted 8th June 1999

Rhodium catalyzed (1–0.1 mol%) decomposition of 2-(3-diazo-2-oxopropyl)-2-methyldioxolane 1a or 2-(3-diazo-1-methyl-2-oxopropyl)-2-methyldioxolane 1b in the presence of a catalytic amount of TMSCl (10 mol%), yielded 4,7-dioxocane 3a (91%) or 3b (49%), whereas similar reaction in the absence of TMSCl caused 1,2-rearrangement to give bicyclobutanones 2a or 2b, respectively; Lewis acid-base catalysis by TMSCl of the ring-expansion of a bicyclooxonium ylide intermediate is revealed.

It is well known that metal carbene complexes (or carbenoids) react with oxygen, nitrogen or sulfur compounds to form onium ylides and some are utilized for synthetic purposes.[1] Among them, ethereal oxonium ylides, the most short-lived species,[2] have been investigated recently. Nevertheless, they are so short-lived that their application to synthesis is limited to a few examples, *e.g.* [1,2]- and [2,3]-sigmatropic rearrangement.[3,4]

Johnson reported that a metal carbene complex generated from diazo ketone **1a** and $Rh_2(OAc)_4$ yielded [1,2]-rearrangement product **2a** as the major product (68%) and ring-expansion product **3a** in a minor amount (16%) (Scheme 1).[5] Recently, we reported that a protic nucleophile (*e.g.* MeOH, AcOH) protonates the ylide intermediate to form a bicyclic oxonium ion, suppressing the 1,2-rearrangement and facilitating three-carbon ring-expansion reactions.[6,7] In analogy to the ylide trapping method, we anticipated that a silyl cation may trap the ylide to form a silyl-substituted oxonium ion, ending up with a similar ring-expansion reaction. We report here the first evidence for Lewis acid–base catalysis by chlorosilanes of the oxonium ylides that is exerted in the three-carbon ring-expansion reaction.

In advance of the use of transition metal catalysts, we examined the stability of diazo ketone **1a** in the presence of various silyl reagents, because **1a** was suspected of decomposing in the presence of these species in the absence of the metal catalyst.[8] It was found that diazoketone **1a** decomposed only in the presence of TMSOTf.

The reaction of **1a** in the presence of $Rh_2(OAc)_4$ and various silyl reagents was performed as follows: the diazo ketone was slowly added to a solution of $Rh_2(OAc)_4$ (1 mol%) and the silyl reagent (1.0 equiv., initial concentration 0.1 mol dm^{-3}) at ambient temperature. After complete consumption of **1a**, the reaction was quenched with Et_3N and products were isolated by silica gel flash chromatography.

Choice of the silyl reagent was important. With TMSCN, the reaction did not take place, presumably because it poisoned the Rh catalyst. With TMSCl or TESCl, the expected ring-expansion product **3a** was obtained as the major product (80 or 44%, respectively). In both cases, minor products were [1,2]-rearrangement product **2a** and non-rearrangement product 2-(3-chloro-2-oxopropyl)-2-methyldioxolane.[9] In contrast, TBDMSCl (entry 4) did not give **3a**, probably because the chlorosilane was not reactive enough to capture the oxonium ylide. Again, TMSOAc gave **3a** although in low yield. Consequently, TMSCl was chosen as the most appropriate reagent, with which we examined the choice of solvent. Among those examined, benzene was the best for the production of **3** (CH_2Cl_2, 80%; benzene, 91%; THF, 68%).

Ring-expansion product **3a** seems likely to be formed by the elimination–hydrolysis of silyl ether **7** in the work-up procedure.[10] However, searching for this intermediate **7** by ^1H NMR in the reaction mixture (benzene-d_6,) was unsuccessful. Therefore, we assumed that the chlorosilane is acting as a catalyst[11]

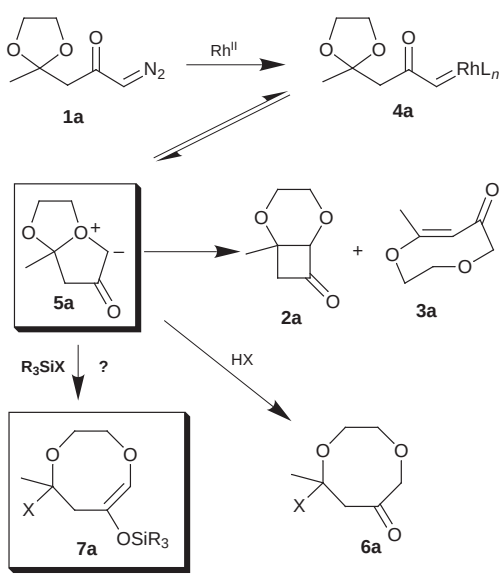

Scheme 1

Table 1 Effect of stoichiometry and concentration of TMSCl in the ring-expansion reaction

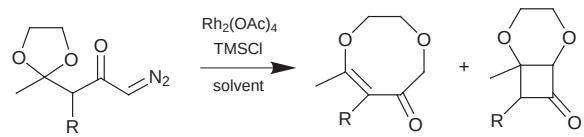

		TMSCl			
Entry[a]	Substrate	Equiv.	Init. conc./ mol dm^{-3}	Addition time/min	Products (%)
1	**1a**	—	—	—	**3a** (16), **2a** (68)[b]
2	**1a**	1.0	0.10	10	**3a** (91)
3	**1a**	0.5	0.05	10	**3a** (40), **2a** (20)
4	**1a**	0.1	0.01	10	**3a** (33), **2a** (37)
5	**1a**	0.1	0.10	10	**3a** (38), **2a** (12)
6	**1a**	0.1	0.10	120	**3a** (77)
7	**1b**	—	—	120	**2b** (58)[b]
8	**1b**	0.1	0.10	120	**3b** (27), **2b** (41)
9	**1b**	0.5	0.50	120	**3b** (42), **2b** (21)
10	**1b**	1.0	1.00	120	**3b** (49), **2b** (10)

[a] The amount of catalyst $Rh_2(OAc)_4$ was 1 mol% relative to **1** for entries 1–5, 0.1 mol% for entries 6–10. [b] Ref. 5.

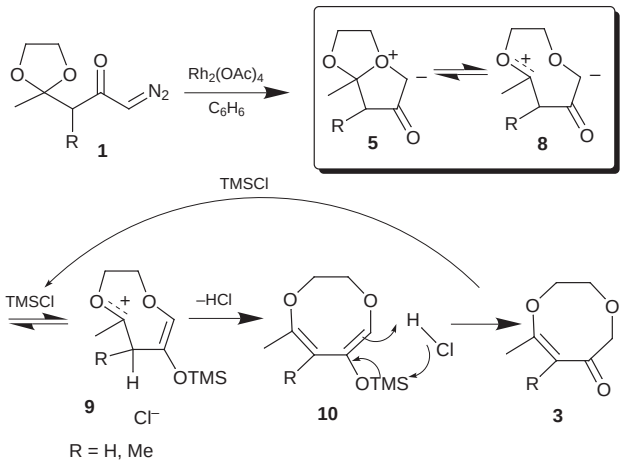

Scheme 2

and investigated the stoichiometric effect of TMSCl (Table 1, entries 2–6). It is clear that, as the molar amount of TMSCl *vs.* **1a** decreases, the yield of [1,2]-rearrangement product **2a** increases (entries 2–4). However, even with a decreased amount of chlorosilane (0.1 equiv.), the catalytic role of TMSCl can be exerted effectively under the following conditions: (1) the initial concentration of TMSCl is kept at a relatively high level, *e.g.* 0.1 mol dm^{-3} (entries 2, 5, 6); (2) the amount of $Rh_2(OAc)_4$ is as low as 0.1 mol% (entry 6); (3) the diazo ketone is added as slowly as possible (entry 6). Under such conditions, the oxonium ylide is formed in very low concentration and, although very short-lived, it can react effectively with the large excess of TMSCl.

Some of these optimized conditions were also applied to methyl-substituted diazo ketone **1b** (Table 1, entries 7–10). In the absence of chlorosilane (entry 7), **2b** was formed as the sole product,[5] whereas the addition of TMSCl to the reaction mixture increased the formation of ring-expansion product **3b**. Increasing both the molar amount and initial concentration of TMSCl also improved the yield of **3b** (entries 8–10).

On the basis of the above-mentioned findings, we propose the mechanism depicted in Scheme 2. First, the treatment of diazo ketone **1** with the transition metal catalyst generates oxonium ylide **5** *via* its carbenoid **4**, both being in equilibrium[12] (see Scheme 1). Ylide **5** is in equilibrium with zwitterion **8**, which is trapped by the chlorosilane to form oxocarbenium ion **9** in preference to the [1,2]-rearrangement. Ion **9** undergoes deprotonation with counter ion Cl^- to produce diene **10**, which results in the formation of final product **3**. Relatively low yields of **3b** in comparison with **3a** may be attributable to the steric effect encountered in the deprotonation of **9** where two methyl groups must adopt a (*Z*) disposition. The double bond structure of **3** has been described as *trans*.[5] If it is *trans*, the mechanism for the double bond formation from the ylide should be a concerted one, being inconsistent with a sequential profile of the present mechanism. Therefore, we measured the X-ray crystallographic structure of **3a** (mp 67 °C) to obtain a clear insight into the mechanism.† As shown in Fig. 1, the geometry of the enone is *cis*.

To summarize, $Rh_2(OAc)_4$ catalyzed decomposition of diazo ketones **1a** and **1b** in the presence of a catalytic amount of TMSCl yielded three-carbon ring-expansion products **3a** and **3b** in better yields than in the absence of the chlorosilane, while the catalyst role of TMSCL in this sequential reaction was verified.

This hitherto unknown catalysis by chlorosilanes in the control of ethereal oxonium ylides seems promising for its utilization with other onium ylides.

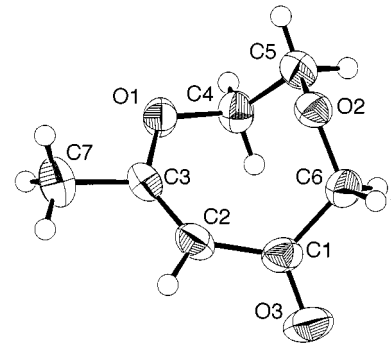

Fig. 1 Molecular structure of **3**. Selected torsion angles (°): O(1)–C(3)–C(2)–C(1) 7.9(4), C(1)–C(2)–C(3)–C(7) −175.7(2).

The authors are indebted to the skilled technical assistance of Dr Motoo Shiro, Rigaku X-Ray Research Laboratory (Tokyo), for the X-ray analysis of **3a**.

Notes and references

† *Crystal data* for $C_7H_{10}O_3$ **3**: M = 142.15, monoclinic, a = 13.686(1), b = 4.231(1), c = 14.018(2) Å, β = 117.924(3)° U = 721.9(2) $Å^3$, T = 296 K, space group $P2_1/a$ (no.14), Z = 4, μ(Mo-K) = 1.02 cm^{-1}, D_c = 1.308 g cm^{-3}, 1431 unique reflections measured. The structure was solved using direct methods and refined by full-matrix least-squares to R = 0.034 and wR = 0.046 for 948 reflections with $I > 3\sigma(I)$. $\Sigma w(|F_o| - |F_c|)^2$ was minimized. Single crystals of $C_7H_{10}O_3$ **3a** were obtained by recrystallization from hexane–Et_2O after purification by silica gel flash chromatography. CCDC 182/1283. See http://www.rsc.org/suppdata/cc/1999/1339/ for crystallographic data in .cif format.

1 For carbonyl ylides, see reviews: A. Padwa and S. F. Hornbuckle, *Chem. Rev*., 1991, **91**, 263; T. Ye and M. A. Mckervey, *Chem. Rev*. 1994, **94**, 1091; A. Padwa and M. D. Weingarten, *Chem. Rev*., 1996, **96**, 223.
2 (*a*) I. Naito, A. Oku, N. Ohtani, Y. Fujiwara and Y. Tanimoto, *J. Chem. Soc., Perkin Trans. 2*, 1996, 725; (*b*) H. Tomioka, N. Kobayashi, S. Murata and T. Ohtawa, *J. Am. Chem. Soc*., 1991, **113**, 8771.
3 F. G. West, B. N. Naidu and R. W. Tester, *J. Org. Chem.*, 1994, **59**, 6892; J. B. Brogan, C. B. Bauer, R. D. Rogers and C. K. Zerher, *Tetrahedron Lett*., 1996, **37**, 5053; M. P. Doyle, D. G. Ene, D. C. Forbes and J. S. Tedrow, *Tetrahedron Lett*., 1997, **38**, 4367.
4 J. S. Clark, A. G. Dosetter and W. G. Whittingham, *Tetrahedron Lett*., 1996, **37**, 5605; M. P. Doyle, V. Bagheri and E. Claxton, *J. Chem. Soc., Chem. Commun*., 1990, 46.
5 E. J. Roskamp and C. R. Johnson, *J. Am. Chem. Soc*., 1986, **108**, 6062.
6 For the ring-expansion of bicyclic oxonium ylides, see: A. Oku, S. Ohki, T. Yoshida and K. Kimura, *Chem. Commun*., 1996, 1077; A. Oku, N. Murai and J. Baird, *J. Org. Chem.* 1997, **62**, 2123; T. Mori, M. Taniguchi, F. Suzuki, H. Doi and A. Oku, *J. Chem. Soc., Perkin Trans. 1*, 1998, 3623.
7 For the ring-expansion of bicyclic oxonium ions, see: T. Kamada, G. Quing, M. Abe and A. Oku, *J. Chem. Soc., Perkin Trans. 1*, 1996, 413; T. Nakata, S. Nomura and H. Matukura, *Tetrahedron Lett*., 1996, **37**, 213, 217 and 6365.
8 A. B. Smith and R. K. Dieter, *Tetrahedron*, 1981, **37**, 2407.
9 When impure TMSCl was used, the yield of this by-product increased, probably because contaminant HCl reacted with diazo ketone **1a** to give it.
10 Work-up without Et_3N, decreased the yield of **3a**.
11 The Lewis acid character of the silyl cation is described in different reaction systems: S. Murata, M. Suzuki and R. Noyori, *J. Am. Chem. Soc.*, 1980, **102**, 3248; H. Sakurai, K. Sasaki and A. Hosomi, *Bull. Chem. Soc. Jpn.*, 1983, **56**, 3195; T. Sato, Y. Wakahara and H. Nozaki, *Tetrahedron Lett*., 1990, **31**, 1581; K. T. Hollis and B. Bosnich, *J. Am. Chem. Soc*., 1995, **117**, 4570.
12 The equilibrium was first reported in ref. 2(*a*), and then by T. Sueda, T. Nagaoka, S. Goto and M. Ochiai, *J. Am. Chem. Soc*., 1996, **118**, 10141.

Paper 9/03928G

ChemComm

A novel solid-phase reductive alkylation route to acridine and dansyl polyamine conjugates

Simon Carrington,[a] Jacques Renault,[b] Sophie Tomasi,[b] Jean-Charles Corbel,[b] Philippe Uriac[b] and Ian S. Blagbrough*[a]

[a] *Department of Pharmacy and Pharmacology, University of Bath, Bath, UK BA2 7AY. E-mail: prsisb@bath.ac.uk*
[b] *Pharmacochimie des Molécules de Synthèse et des Produits Naturels, Faculté de Pharmacie, Université de Rennes 1, 2 Avenue du Professeur Léon Bernard, 35043 Rennes Cedex, France*

Received (in Cambridge, UK) 19th May 1999, Accepted 11th June 1999

Solid-phase organic synthesis (SPOS) routes to target unsymmetrical polyamines and their acridinyl and dansyl conjugates have been developed based upon borane–pyridine complex (BAP) mediated reductive alkylation, azide reduction with triphenylphosphine, and the use of pent-4-enoyl (Pnt) as an orthogonal amine protecting group.

Polyamines and especially their unsymmetrical conjugates display a wide range of important biological activities making them useful as lead compounds for a wide range of potential therapies.[1] These medicinal chemical applications include potential anti-parasitic drugs as potent inhibitors of the enzyme trypanothione reductase[2] and cytotoxic compounds such as acridine–spermine conjugates that display significant sequence selectivity on binding to an oligonucleotide.[3] It has recently been shown that dansylated polyamines are novel glutamate (NMDA) receptor antagonists.[4] (−)-15-Deoxyspergualin, a potent immunosupressor, is a spermidine–guanidine conjugate for the treatment of corticoresistant acute renal graft rejection.[5] The regiocontrolled synthesis of unsymmetrical polyamine conjugates continues to attract the attention of bioorganic and synthetic chemists,[5–8] but these approaches often, of necessity, include a number of steps for orthogonal protecting group introduction and removal that makes the overall multistep syntheses certainly time consuming and sometimes low yielding. Furthermore, such solution-phase syntheses are simply not amenable to the rapid preparation of a wide range of conjugates for biological evaluation, and therefore attention has been turned recently to the use of solid-phase organic synthesis (SPOS) for the preparation of polyamine conjugates with the potential for compound-library design.[9–13] At the forefront of these studies are Bradley and co-workers who have addressed the synthesis of trypanothione (spermidine containing) libraries in their elegant studies of SPOS for polyamine amides and lactams.[9] Independently, Houghten and co-workers have recently used SPOS reductive alkylation to prepare diazepine derivatives and parallel SPOS borane reduction of triamides afforded large numbers of unsymmetrically substituted diethylenetriamines.[10]

We have designed a series of unsymmetrical polyamine conjugates **1**–**5** as targets to illustrate our proof of concept that reductive alkylation is a practical approach to such substituted compounds using SPOS methodologies. The potential of this reductive alkylation route is in the ability to prepare a range of linear unsymmetrical polyamines. By design, the amine distribution along the polymethylene chain can be varied, in a controlled manner, using the sequence elaborated below. Acridin-9-ylcarbonyl thermine **1** and thermospermine **2** require reductive alkylation of an aldehyde with an amine bound to the resin. The corresponding conjugate **3**, with a regiospecific methyl substituent, requires alkylation of this resin using a methyl ketone. Azide dansyl conjugate **4** and didansylated **5** will be prepared from the same resin-bound intermediate.[13] Azide aldehyde **9** was prepared from 4-bromobutyl acetate **6**, by azide nucleophilic displacement of the halide affording **7**

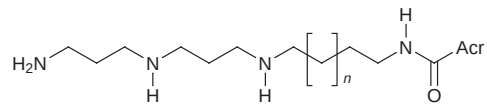

1 $n = 0$
2 $n = 1$

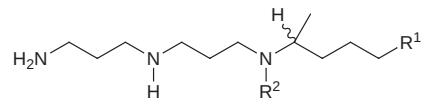

3 R^1 = NHCO-9-Acr, R^2 = H
4 $R^1 = N_3$, R^2 = Dan
5 R^1 = NHDan, R^2 = Dan

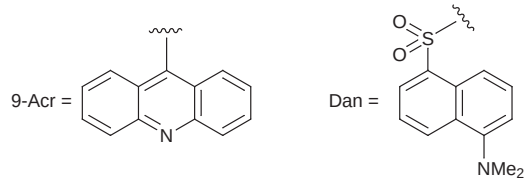

(NaN$_3$, DMSO, 25 °C, 16 h, 95%), ester saponification to azide primary alcohol **8** (2 M aq. NaOH, MeOH, 25 °C, 3 h, 85%), and then Swern oxidation of this alcohol to the desired aldehyde **9** (50%) (Scheme 1). Azide ketone **10** was prepared from the readily available 5-chloropentan-2-one (NaN$_3$, cat. NaI, DMSO, 50 °C, 18 h, 90%).[14] 3-Pent-4-enoylaminopropanal **12** was prepared from the corresponding 3-aminopropan-1-ol by *N*-acylation with the symmetrical anhydride Pnt$_2$O [15] affording amide primary alcohol **11** (CH_2Cl_2, 0 °C, 1 h, 72%) which was oxidised to the desired amide aldehyde **12** (PDC, CH_2Cl_2, 25 °C, 3 h, 76%).

Wang resin was activated under rigorously anhydrous conditions with 4-nitrophenyl chloroformate (*N*-methylmorpholine, CH_2Cl_2, 25 °C, 19 h) and then reacted with N^1-*tert*-butoxycarbonyl-N^1-(3-aminopropyl)-1,3-diaminopropane[2,6] (CH_2Cl_2, 16 h)[16] affording resin **13**. That this reaction went to completion was verified by the use of gel-phase ^{13}C NMR spectroscopy.[17] Reductive alkylation of portions of resin **13** with aldehyde **9**, ketone **10** and aldehyde **12** afforded resins **14**–**16** respectively (BAP, 3:1 DMF–EtOH, 48 h) (Scheme 2).[18] Washed and dried samples of resins **14** and **15** displayed characteristically strong IR bands (by diffuse reflectance) for the resin-bound azide functional group at 2090 cm^{-1}. Portions of these resins **14**–**16** were Boc protected (excess of Boc$_2$O, CH_2Cl_2, 2 × 12 h) on the newly formed secondary amines affording resins **17**–**19** respectively. A further portion of resin **15** was *N*-dansylated (2 equiv. dansyl chloride, 2 equiv. *N*-methylmorpholine, CH_2Cl_2, 2 × 18 h) and half of this product was cleaved from the resin (1:1 TFA–CH_2Cl_2, 25 °C, 2 h) to afford azide dansyl polyamine **4** as a white solid. The remaining half was reacted with PPh$_3$ and water (1 equiv. H$_2$O, THF, 2 ×

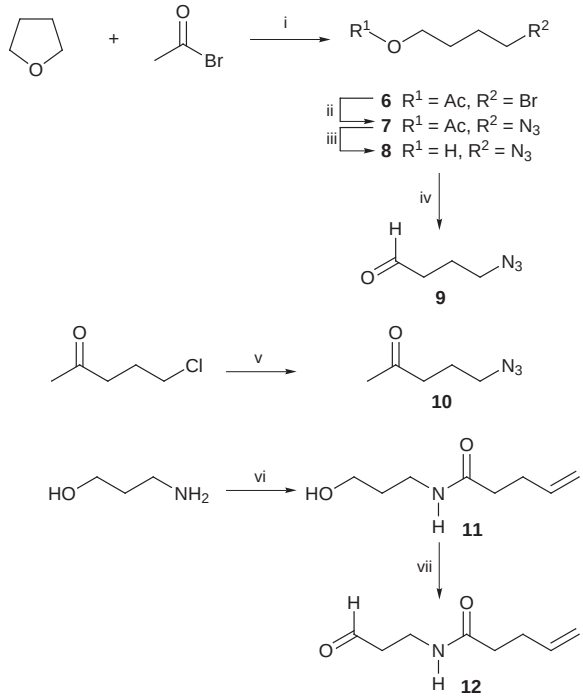

Scheme 1 *Reagents and conditions*: i, ZnBr, reflux; ii, NaN_3, DMSO; iii, 2 M aq. NaOH, MeOH; iv, $(COCl)_2$, DMSO, Et_3N, CH_2Cl_2 (Swern); v, NaN_3, cat. NaI, DMSO, 50 °C; vi, Pnt_2O, CH_2Cl_2; vii, PDC, CH_2Cl_2.

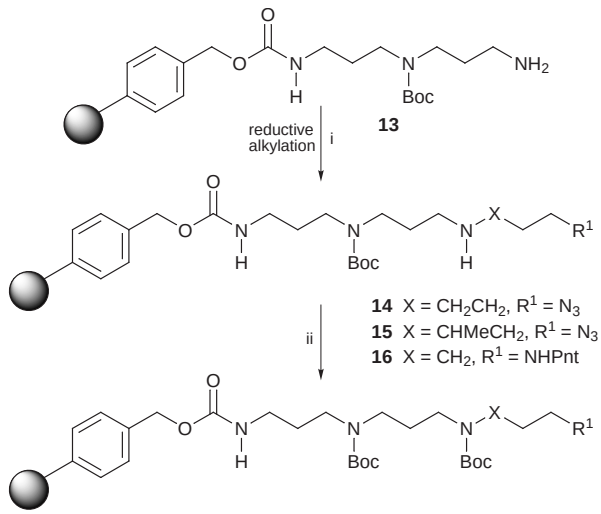

Scheme 2 *Reagents and conditions*: i, aldehyde or ketone, BAP, 3:1 DMF-EtOH; ii, Boc_2O, CH_2Cl_2; iii, PPh_3, H_2O, THF; iv, I_2, 1:1 H_2O–THF.

18 h) to convert the azide into a primary amine, which has previously been reported only for solution-phase synthesis,[5,19] and this newly formed amine was then *N*-dansylated. Cleavage from the resin yielded didansylated polyamine **5** as a white solid in 35% yield over the six steps (resin loading, reductive alkylation, dansylation, azide reduction, dansylation and resin cleavage). Resins **17** and **18** were similarly reacted with PPh_3 to afford resin-bound primary amines **20** and **21** respectively.

The Pnt group has been used to protect a variety of substituted amines including amino sugars[15] in solution phase, and nucleotides in SPOS.[20] The primary amine protected by a Pnt group in resin **19** was unmasked by treatment with I_2 and water (1:1 H_2O–THF, 25 ºC, 18 h) affording resin **22**.[15,20] Resin-bound amines **20**–**22** were acylated using acridine-9-carboxylic acid activated with N^1-hydroxybenzotriazole (DMF, 2 × 15 h). The resulting acylated resins were cleaved affording targets **1**–**3** as their free bases after final purification by flash column chromatography over silica gel (eluant 8:5:1 CH_2Cl_2–MeOH-conc. aq. NH_3)† in order to remove traces of triamine starting material which had been crosslinked.

Here we report a novel reductive alkylation SPOS route to unsymmetrical polyamines and their conjugates. The feasibility of preparing unsymmetrical polyamines anchored on Wang resin as a solid support, and then selective unmasking of amines to reveal sites for conjugation, will find ready applications. Furthermore, our SPOS uses of Pnt as an amine protecting group orthogonal to Boc, and of azide reduction with PPh_3 should have wide applicability in combinatorial chemistry where libraries of amines are constructed.

We thank the Atlantic Arc for Medicinal Chemistry (GP2A), the ARC (Association pour la Recherche sur le Cancer) and the Ligue Nationale contre le Cancer for financial support of this project. We acknowledge S. Sinbandhit and M. Le Roch (Université de Rennes 1) and A. J. Geall (University of Bath) for useful discussions and their input into these studies.

Notes and references

†Each acridine conjugate **1**–**3** was homogeneous by TLC (silica gel, eluant CH_2Cl_2–MeOH–conc. aq. NH_3 (8:5:1) and reverse-phase HPLC using a 5 μm Supelcosil ABZ + plus column eluting with 70:30 0.1% aq. TFA–MeCN, UV detection at 256 nm. Unoptimised yields were typically 5% over 6 steps.

1 I. S. Blagbrough, S. Carrington and A. J. Geall, *Pharm. Sci.*, 1997, **3**, 223 and references cited therein.
2 S. Carrington, A. H. Fairlamb and I. S. Blagbrough, *Chem. Commun.*, 1998, 2335 and references cited therein.
3 I. S. Blagbrough, S. Taylor, M. L. Carpenter, V. Novoselskiy, T. Shamma and I. S. Haworth, *Chem. Commun.*, 1998, 929 and references cited therein.
4 J. Chao, N. Seiler, J. Renault, K. Kashiwagi, T. Masuko, K. Igarashi and K. Williams, *Mol. Pharmacol*., 1997, **51**, 861.
5 P. Durand, P. Richard and P. Renaut, *J. Org. Chem.*, 1998, **63**, 9723 and references cited therein.
6 M. C. O'Sullivan, Q. Zhou, Z. Li, T. B. Durham, D. Rattendi, S. Lane and C. J. Bacchi, *Bioorg. Med. Chem.*, 1997, **5**, 2145.
7 S. K. Choi, K. Nakanishi and P. N. R. Usherwood, *Tetrahedron*, 1993, **49**, 5777; D. W. Huang, H. Jiang, K. Nakanishi and P. N. R. Usherwood, *Tetrahedron*, 1997, **53**, 12391.
8 B. T. Golding, A. Mitchinson, W. Clegg, M. R. J. Elsegood and R. J. Griffin, *J. Chem. Soc., Perkin Trans. 1*, 1999, 349.
9 I. R. Marsh, H. Smith and M. Bradley, *Chem. Commun.*, 1996, 941; I. R. Marsh, H. K. Smith, C. LeBlanc and M. Bradley, *Mol. Diversity*, 1997, **2**, 165; I. R. Marsh and M. Bradley, *Tetrahedron*, 1997, **53**, 17317; P. Page, S. Burrage, L. Baldock and M. Bradley, *Bioorg. Med. Chem. Lett.*, 1998, **8**, 1751.
10 A. Nefzi, C. Dooley, J. M. Ostresh and R. A. Houghten, *Bioorg. Med. Chem. Lett.*, 1998, **8**, 2273; A. Nefzi, J. M. Ostresh and R. A. Houghten, *Tetrahedron*, 1999, **55**, 335.
11 B. W. Bycroft, W. C. Chan, N. D. Hone, S. Millington and I. A. Nash, *J. Am. Chem. Soc.*, 1994, **116**, 7415; I. A. Nash, B. W. Bycroft and W. C. Chan, *Tetrahedron Lett.*, 1996, **37**, 2625.
12 G. Byk, M. Frederic and D. Scherman, *Tetrahedron Lett.*, 1997, **38**, 3219; G. Byk, C. Dubertret, V. Escriou, M. Frederic, G. Jaslin, R. Rangara, B. Pitard, J. Crouzet, P. Wils, B. Schwartz and D. Scherman, *J. Med. Chem.*, 1998, **41**, 224.
13 S. Tomasi, M. Le Roch, J. Renault, J.-C. Corbel, P. Uriac, B. Carboni, D. Moncoq, B. Martin and J.-G. Delcros, *Bioorg. Med. Chem. Lett.*, 1998, **8**, 635.
14 B. Carboni, M. Vaultier and R. Carrie, *Tetrahedron*, 1987, **43**, 1799.
15 R. Madsen, C. Roberts and B. Fraser-Reid, *J. Org. Chem.*, 1995, **60**, 7920.
16 D. M. Dixit and C. C. Leznoff, *J. Chem. Soc., Chem. Commun.*, 1977, 798.
17 G. C. Look, C. P. Holmes, J. P. Chinn and M. A. Gallop, *J. Org. Chem.*, 1994, **59**, 7588.
18 N. M. Kahn, V. Arumugam and S. Balasubramanian, *Tetrahedron Lett.*, 1996, **37**, 4819; E. E. Swayze, *Tetrahedron Lett.*, 1997, **38**, 8465 and 8643.
19 B. Carboni, A. Benalil and M. Vaultier, *J. Org. Chem.*, 1993, **58**, 3736.
20 R. P. Iyer, D. Yu, N. H. Ho, T. Devlin and S. Agrawal, *J. Org. Chem.*, 1995, **60**, 8132; I. Habus, J. Xie, R. P. Iyer, W.-Q. Zhou, L. X. Shen and S. Agrawal, *Bioconjugate Chem.*, 1998, **9**, 283.

Communication 9/04023D

Synthesis of single-wall carbon nanotubes by catalytic decomposition of hydrocarbons

J.-F. Colomer,*[a] G. Bister,[a] I. Willems,[a] Z. Kónya,[a] A. Fonseca,[a] G. Van Tendeloo[b] and J. B. Nagy[a]

[a] *Laboratoire de Résonance Magnétique Nucléaire, FUNDP, 61 rue de Bruxelles, B-5000 Namur, Belgium. E-mail: jean-francois.colomer@fundp.ac.be*

[b] *EMAT, University of Antwerp (RUCA), Groenenborgerlaan 171, B-2020 Antwerp, Belgium*

Received (in Cambridge, UK) 20th April 1999, Accepted 10th June 1999

Individual single-wall carbon nanotubes (SWNTs) and bundles can be obtained over different types of supported metal catalysts by decomposition of ethylene, similar to the synthesis of multi-wall carbon nanotubes.

Until now, laser evaporation[1] and electric arc discharge techniques[2] have been used to synthesise SWNTs in high yield, but many previous reports[3–5] have shown that the catalytic decomposition of hydrocarbons could be a possible way to produce SWNTs. In the present work, we describe the synthesis of SWNTs from ethylene decomposition on supported metal catalysts, prepared by impregnation of different supports. The 3d transition metals are known for their efficient production of single- and multi-wall nanotubes.[1,2,6] For this reason, Co, Ni, Fe and mixtures of these metals are used in our catalysts, to produce individual or bundles of SWNTs. Various supported metal catalysts are prepared on different supports (alumina and silica)† and with different metals (Co, Ni, Fe) and metal mixtures (Co-Fe, Ni-Co, Co-Fe, Co-Ni-Fe) by a method already described.[7] The role of the supports involves the dispersion of the metal particles. Catalysts are prepared by impregnating the support with an EtOH solution containing the appropriate concentration (2.5 wt% of each metal) of metal salts or mixture of metals salts. After sonication (1 h) and evaporation of EtOH, the material is dried at 150 °C (12–15 h) and ground into a fine powder. The synthesis of single-wall nanotubes was carried out in a fixed-bed reactor at 1080 °C (60 min). For each synthesis, a quartz boat containing about 200 mg of catalyst was placed in the center of the reactor. The gas flows of the ethylene–nitrogen mixture used were 30 and 80 ml min^{-1}, respectively. The abundance of SWNTs is estimated from TEM observations using JEOL 200CX and Phillips CM 20 instruments for low and high resolution measurements, respectively. The TEM images show unambiguously either the presence of individual SWNTs (with some small bundles) or principally the presence of abundant bundles of SWNTs. These bundles seem to be similar to those produced by arc discharge or laser evaporation techniques with the one difference, however, that they are longer (up to several μm). All the catalysts prepared are active in the formation of SWNTs, with varying efficiency. In fact, in all cases, SWNTs have been observed, but their abundance seems to be dependent on the nature of the metal and the type of support. The synthesis of SWNTs is more efficient for the metal catalysts supported on alumina than on fumed silica. Moreover, in the case of fumed silica using the same reaction parameters, the SWNTs are coated with a thick layer of amorphous carbon. Concerning the influence of the nature of the metal, it is very difficult to discrimate among the catalysts containing a single metal. For all the metals, individual SWNTs are observed, but Co and Fe seem to be more active than Ni. In addition, some SWNT bundles are also found in these samples. For the catalysts prepared from a mixture of metals, the best activity is found for Fe-Co and Fe-Co-Ni mixtures supported on alumina. On these two catalysts, a significant amount of SWNT bundles is observed (Fig. 1). The catalysts prepared from a mixture of metals are more efficient for SWNT production than those prepared with a single metal. The bundles of SWNTs are larger and longer than those synthesised by arc discharge and the laser evaporation. Details of these SWNT bundles are shown on Fig. 2, where a large bundle of about 20–35 nm of diameter can be observed [Fig. 2(*a*)]. Moreover, the SWNT diameter can be estimated by transmission electron microscopy: Fig. 2(*a*) shows that the SWNTs in the bundles have a uniform diameter and they form crystallite-like entities organized in a two-dimensional triangular lattice, with a lattice constant *a*, about 1.0 nm, corresponding to nanotubes of 0.7 nm in diameter separated by the van der Waals intertube distances of 3.4 Å. The diameter estimated for the SWNTs is around 0.7 nm. For comparison, a lattice constant of 1.7 nm has been given for the SWNT bundles produced by laser evaporation[1] and the smallest SWNTs organised in ropes found in the synthesis by arc discharge have 1.2–0.9 nm diameter when argon is used instead of helium.[8] The estimated diameter of SWNTs in the bundle is confirmed by Fig. 2(*b*) showing the cross section of the bundles which gives the same small diameter. In fact, on the top of this picture, some graphitic layers also appear and the distance between them is equal to 3.4 Å. These data confirm the accuracy of the value of the tube diameter. The tube diameters found for the SWNT bundles are the smallest produced until now. In the case of individual SWNTs, a distribution of diameter is also observed and individual SWNT diameters range from 1.6 to 5 nm. The tubes which have the largest diameter are often double-wall nanotubes. Most of the individual SWNTs have diameters

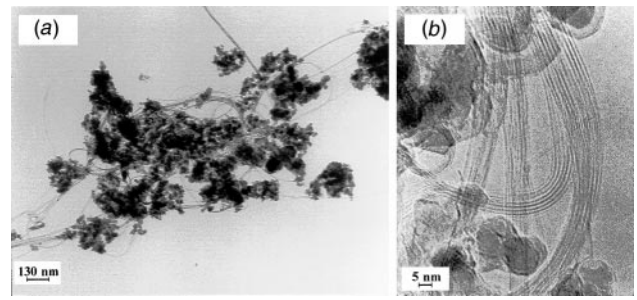

Fig. 1 (*a*) Low and (*b*) high resolution TEM images of SWNT bundles produced on Co-Ni-Fe/alumina catalyst by decomposition of ethylene at 1080 °C.

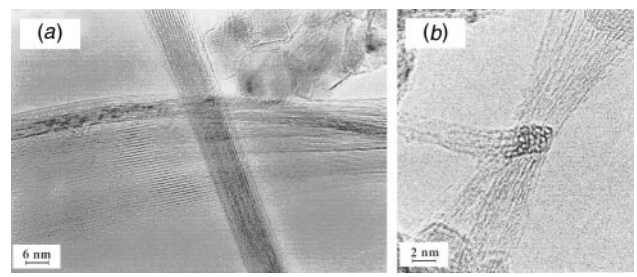

Fig. 2 TEM images of (*a*) large SWNT bundle and (*b*) higher magnification of SWNT bundle cross section.

around 1.8–2 nm. In comparison, isolated SWNTs have larger diameters than those produced by the other two techniques (around 1.4 nm). Recently, very small diameters (0.6–0.8 nm) were found for isolated SWNTs synthesised by the electric arc discharge method in the presence of argon.[8]

In the case of multi-wall carbon nanotubes (MWNT) synthesis, the influence of support on the growth mechanism is rather well-documented.[6] The mechanism depends on the interactions between the metal particles and the support. In the case of SWNTs produced by the catalytic process, Dai *et al.*[3] have proposed a growth mechanism close to that of MWNTs, because metal particles have been found trapped in the tip of SWNTs, and the diameter of the SWNTs is related to the size of the catalytic metal particle attached to their end. This fact could explain the large diameter distribution of isolated SWNTs (average diameter about 2 nm) synthesised by the catalytic decomposition of hydrocarbons compared to the ones obtained by the other techniques. In our different samples, no catalytic particles were found trapped at the end of the individual SWNTs, but the closed ends of the SWNTs are not incompatible with this proposed mechanism, where the individual SWNT could grow from a supported particle at one end and be closed at the other. This growth mechanism is strengthened by the fact that the synthesis of SWNTs can also be carried out at low temperature (750–850 °C)[5] similarly to the synthesis of multi-wall nanotubes.

In the formation of the SWNT bundles, the support does not seem to play an important role on the growth mechanism, contrary to what has previously been proposed.[4] Bundles of SWNTs were observed in all cases (on both alumina and silica) where the catalysts are composed of mixtures of metals. Possibly, the support plays a role in the dispersion of the metal on the surface, and influences the pyrolytic cracking of the hydrocarbon in certain cases, but the presence or the absence of SWNT bundles is not governed by the support. The formation of SWNT bundles increases when mixtures of metals are present. Possibly, the preparation of catalysts with mixtures of metals induces a better dispersion of the metals on the catalyst surface. Moreover, the formation of each SWNT in the bundle may not depend on a small metal particle, and the growth mechanism of SWNT bundles could be different for individual SWNTs. One of the hypotheses involves SWNT bundles grown from single bigger metal particles so that bundle formation would be linked to the nature of the metal surface. This hypothesis could also explain the presence of SWNT bundles in the samples synthesised on single metal supported catalysts. Reinforcing this hypothesis is the very small size of the SWNT diameters in the bundles compared to the diameter of isolated SWNTs (linked to the size of catalytic metal particle).

In conclusion, isolated SWNTs and SWNT bundles can be produced by catalytic decomposition of hydrocarbons. Supported catalysts containing either a single metal or a mixture of metals seem to induce the growth of isolated SWNTs or SWNT bundles, respectively. Bundles of SWNTs have been synthesised with very small and uniform diameter (around 0.7 nm), and isolated SWNTs with larger diameter (around 2 nm). In the near future, the synthesis conditions could be optimised to obtain SWNTs in large quantities, as is already the case for MWNTs obtained *via* catalytic decomposition of hydrocarbons.

The authors thank the European Commission, TMR contract NAMITECH, ERBFMRX-CT96-0067 (DG12-MIHT) and the Belgian Programme on Inter University Poles of Attraction initiated by the Belgian State, Prime Minister's Office of Science Policy Programming (4/10).

Notes and references

† Supports used are Alumina Al_2O_3 δ crystalline form from Degussa with surface area 100 $m^2\ g^{-1}$ and Silica SiO_2 type fumed with surface area 380 $m^2\ g^{-1}$.

1 A. Thess, R. Lee, P. Nikolaev, H. J. Dai, P. Petit, J. Robert, C. H. Xu, Y. H. Lee, S. G. Kim, A. G. Rinzler, D. T. Colbert, G. E. Scuseria, D. Tomanek, J. E. Fisher and R. E. Smalley, *Science*, 1996, **273**, 483.
2 C. Journet, W. K. Maser, P. Bernier, A. Loiseau, M. L. De La Chapelle, S. Lefrant, P. Deniart, R. Lee and J. E. Fisher, *Nature*, 1997, **388**, 756.
3 H. Dai, A. G. Rinzler, P. Nikolaev, A. Thess, D. T. Colbert and R. E. Smalley, *Chem. Phys. Lett.*, 1996, **260**, 471.
4 J. Kong, A. M. Cassell and H. Dai, *Chem. Phys. Lett.*, 1998, **292**, 567.
5 J. H. Hafner, M. J. Bronikowski, B. R. Azamian, P. Nikolaev, A. G. Rinzler, D.T. Colbert, A. Smith and R. E. Smalley, *Chem. Phys. Lett.*, 1998, **296**, 195.
6 S. Amelinckx, X. B. Zhang, D. Bernaerts, X. F. Zhang, V. Ivanov and J. B. Nagy, *Science*, 1994, **265**, 635.
7 C. E. Snyder, W. H. Mandevile, H. G. Tennent, L. K. Truesdale and J. J. Barber, *Int. Pat.* WO 9/07163, 1989.
8 C. Journet, PhD Thesis, Montpellier, 1998.

Communication 9/03142A

ChemComm
FEATURE ARTICLE

A variety of combinatorially linkable units as disposition:† from a giant icosahedral Keplerate to multi-functional metal–oxide based network structures

Achim Müller,* Paul Kögerler and Christoph Kuhlmann

Faculty of Chemistry, University of Bielefeld, Postfach 100131, D-33501 Bielefeld, Germany. E-mail: a.mueller@uni-bielefeld.de

Received (in Cambridge, UK) 22nd February 1999, Accepted 20th April 1999

In polyoxometalate chemistry a large variety of compounds, clusters and solid-state structures can be formed by linking together metal–oxygen building blocks. Interestingly, reactions based on libraries of virtual building blocks can be planned under appropriate conditions, resulting for instance in the high-yield synthesis of inorganic superfullerenes and giant ring-shaped, electron-rich, mixed-valence polyoxomolybdates with nanosized cavities. The latter species can continue to grow and also can be covalently linked together to form chains as well as layered mesoporous compounds with properties relevant for materials science. The largest polyoxometalate cluster obtained on the basis of such a growth process consists of 248 Mo atoms. Remarkably, such giant ring species can also act as hosts for other clusters forming new types of supramolecular compounds.

Introduction

In nature, complex molecular systems like proteins have evolved (*natura naturans*) which are perfectly suited to their functions. These are formed, at least formally, in a sequence of steps principally under dissipative conditions, that is far from thermodynamic equilibrium. The challenge for the chemist is to synthesize correspondingly complex multi-functional molecules also under non-dissipative conditions using one-pot reactions, without the need to separate and purify each single intermediate product. Relevant model reactions have been explored in solutions of simple oxoanions of the early transition metals. Novel types of molecular growth processes including a type of induced cascade and those with feedback effects have been discovered leading to a huge variety of unusual compounds regarding structures and properties.[1] The basis is constituted by a system with a variety of combinatorially linkable polyoxometalate building units either as existing or virtual species (as disposition) which are available on demand in a kind of 'library' depending on the boundary conditions.

† A disposition can be interpreted as the inherent tendency of an object or system (in this case molecules or ions or fragments of these) to act or react under certain characteristic conditions.

Achim Müller, born in Detmold, Germany, studied Chemistry and Physics and obtained his PhD (1965) and his Habilitation (1967) at the University of Göttingen under the supervision of O. Glemser. He is now Professor of Inorganic Chemistry at the University of Bielefeld. His research interests range from problems of molecular physics, vibrational spectroscopy, bioinorganic chemistry, molecular metal chalcogenide complexes and clusters, and supramolecular chemistry to aspects of philosophy of science.

Paul Kögerler, born in Vienna, Austria, studied chemistry at the University of Bielefeld. He received his Diploma in 1996. Currently he is completing his PhD on the magnetism, electronic properties and chemistry of polyoxometalate clusters under the supervision of Professor A. Müller.

Christoph Kuhlmann, born in Gronau, Germany, studied chemistry at the University of Bielefeld. He obtained his Diploma in 1997 and is currently engaged in his PhD work on the synthesis, structure and chemistry of polyoxometalate clusters under the supervision of Professor A. Müller.

In search of an archetypical system with linkable units as disposition: the generation of a superfullerene (giant ball) with more than 500 atoms and icosahedral symmetry as a relevant example

While molecular systems, even relatively large ones, can in principle be generated by successive steps of synthesis and isolation,[2] the formation of extremely large molecular systems, in particular those with unusual structures, properties, together with very high symmetry, *e.g.* those comparable to simple spherical viruses, requires a different method of approach.

If we intend to construct for instance a giant species similar in size and shape to spherical viruses with icosahedral (C_5 C_3 C_2) symmetry, we have to find a reaction system in which pentagonal units can first be generated, then get linked and be placed at the 12 corners of an icosahedron. In the case of polyoxomolybdates these pentagonal units ({(Mo)Mo_5} groups) consist of a central bipyramidal MoO_7 unit sharing edges with five MoO_6 octahedra. The {(Mo)Mo_5} unit is a constituent of the {Mo_8}-type unit abundant in many giant polyoxometalates (see below) in which, apart from the related densely packed {(Mo)Mo_5} unit, two more loosely bound MoO_6 octahedra occur. When linkers in the form of *doubly bridging units* are present in solution, for instance those of the classical $\{Mo^{V}_2O_4\}^{2+}$ type[3] (typically formed in reduced molybdate solutions in the presence of bidentate ligands) that can link these pentagonal units, an icosahedral molecular system with 12 of the mentioned pentagons and 30 of the mentioned linkers is formed. When for example acetate anions act as bridging ligands for the $\{Mo^{V}_2O_4\}^{2+}$ groups, the spherical cluster with the stoichiometry $[Mo^{VI}_{72}Mo^{V}_{60}O_{372}(MeCO_2)_{30}(H_2O)_{72}]^{42-}$ ({Mo_{132}}) results,[4] where the central Mo positions of the {(Mo)Mo_5} pentagons define the 12 corners, and the $\{Mo^{V}_2O_4\}^{2+}$ groups the 30 edges of an icosahedron (in agreement with Euler's well known formula). This corresponds to the formulation $[\{(Mo)Mo_5O_{21}(H_2O)_6\}_{12}\{Mo^{V}_2O_4(MeCO_2)\}_{30}]^{42-}$. Interestingly, the ball-like structure (Fig. 1) is also documented in the crystal structure (space group $Fm\bar{3}$) with cubic closest packed spheres of the salt $(NH_4)_{42}[Mo^{VI}_{72}Mo^{V}_{60}O_{372}(MeCO_2)_{30}$-

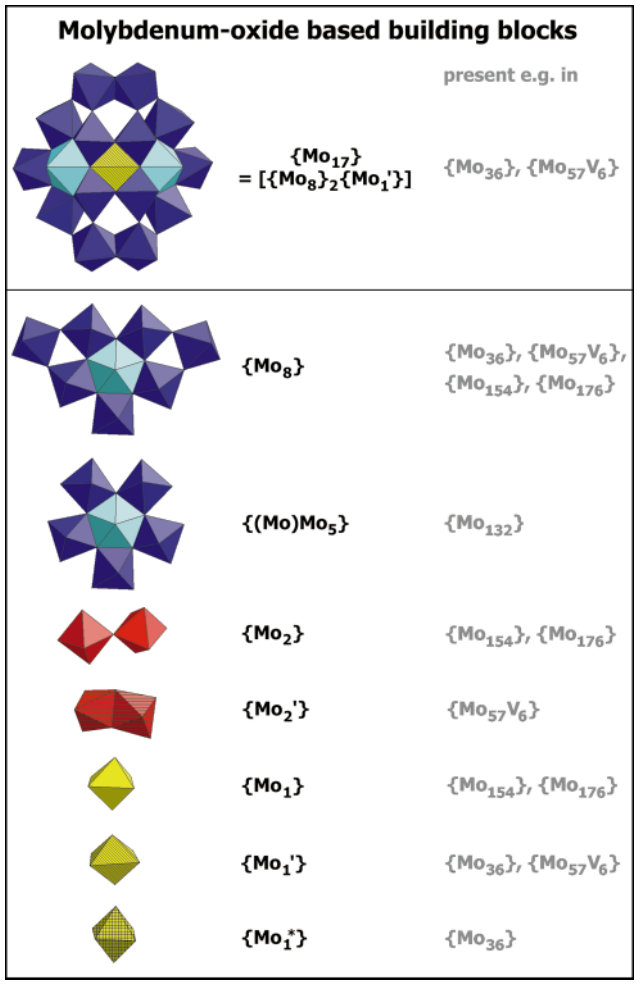

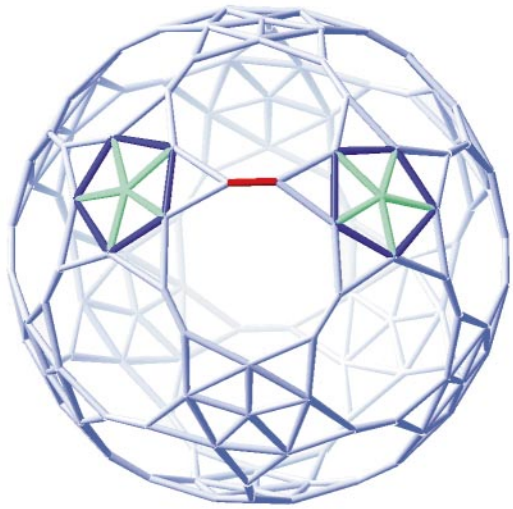

Fig. 1 Schematic representation of the 132 molybdenum atom framework of the Keplerate cluster highlighting its spherical nature. Two pentagonal {(Mo)Mo_5} groups (blue) linked by an {Mo^V–Mo^V} bridge (red) are emphasized.

$(H_2O)_{72}]\cdot xH_2O\cdot yMeCO_2NH_4$ ($x \approx 300$, $y \approx 10$). Remarkably, we are speaking about a molecular system having icosahedral symmetry although it is built up from more than 500 atoms. Despite the large number of normal vibrations the Raman spectrum shows just a few lines because only the A_g and the fivefold degenerate H_g modes are Raman active (Fig. 2).

This molecular system with 60 MoO_6 subunits or 12 related {(Mo)Mo_5} pentagons represents a topological model for

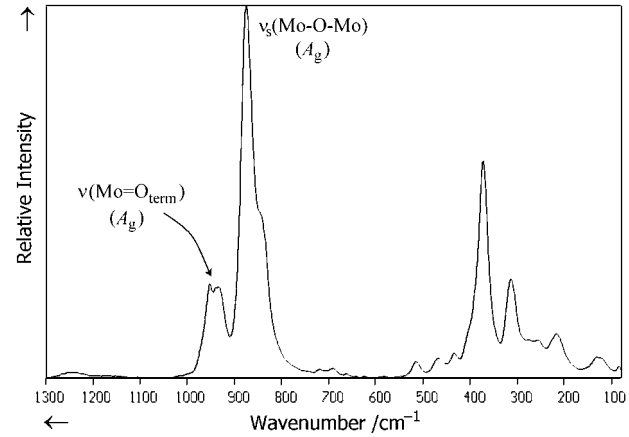

Fig. 2 Raman spectrum of $(NH_4)_{42}[Mo^{VI}_{72}Mo^{V}_{60}O_{372}(MeCO_2)_{30}(H_2O)_{72}]\cdot xH_2O\cdot yMeCO_2NH_4$ ($x \approx 300$, $y \approx 10$) (powder, λ_e = 1064 nm; ν_s stands for breathing).

spherical viruses, *e.g.* the most simple satellite tobacco necrosis virus (STNV) with 60 identical protein subunits (coded only by one gene) or 12 pentagonal capsomers (morphology units), each capsomer consisting of five protomers (for details see ref. 5 and Fig. 3). The wire-frame representation of the {Mo_{132}} cluster species additionally even suggests the structural/topological similarity to the more complex icosahedral virus capsids with a triangulation number of $T = 3$ (Fig. 4) (for details of virus structures and topologies see ref. 5 and 6).

More interestingly, on substituting the bridging acetate ligands by formate groups this smaller ligand allows a special type of organization of the *ca.* 60 encapsulated H_2O molecules: a related hydrogen-bonded cluster as guest system with an 'onion-type' structure which is induced by the peripheral spherical cluster shell (Fig. 5).[7]

It has been proposed to call the {Mo_{132}}-type cluster a Keplerate corresponding to Kepler's model of the cosmos and his concept of planetary motion, as described in his early opus *Mysterium Cosmographicum*.[8] In accordance with this speculative model, Kepler believed that the distances between the orbits of the planets could be explained if the ratios between the successive orbits were designed to be equivalent to the spheres successively circumscribed around and inscribed within the five Platonic solids. In analogy, the cluster correspondingly shows a spherical shell of terminal oxygen atoms in which an icosahedron spanned by the centers of the 12 {(Mo)Mo_5} pentagons, the Mo atoms of the central MoO_7 bipyramids, is inscribed (see Fig. 1).

We are convinced that this {Mo_{132}}-type cluster will be the starting point for the development of a Keplerate-type chemistry, also due to the fact that these types of species are stable in aqueous solution and allow the encapsulation of different types of guests into the cavity. Furthermore, a collection of the spherically shaped huge clusters is a useful model system for special dynamical aspects of solid-state chemistry, since it enables for instance the investigation of nucleation processes (which are still not understood) but probably also of the first principles of structure-forming processes.

With respect to this fascinating discovery of the giant icosahedral cluster it seems worthwhile to concentrate on general aspects of self-aggregation processes, especially those based on the relevant polyoxometalate library systems (for aspects of combinatorial chemistry see ref. 9). In these systems we can expect reaction pathways which will lead to an extreme variety of unusual molecular systems based on differently linkable virtual units as disposition in solution.

The route to nanoscaled structures

If such unusual species as the mentioned Keplerate can be formed by linking different well defined units as disposition, it

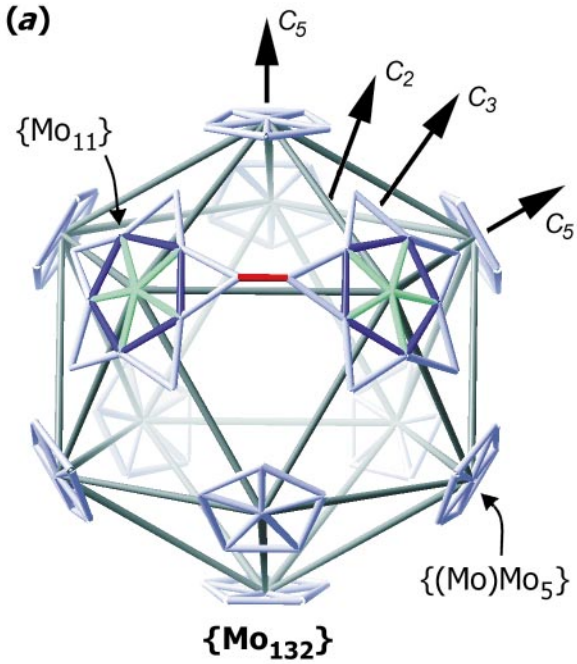

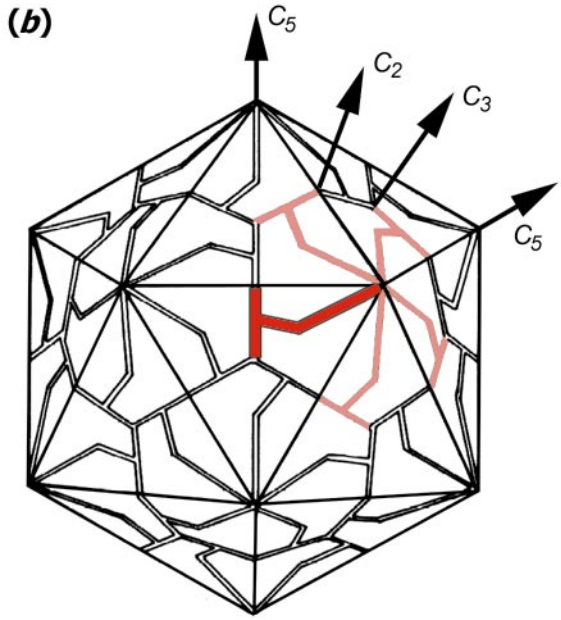

Fig. 3 Schematic representation of the icosahedron spanned by the centers of the {(Mo)Mo_5} subfragments of the {Mo_{132}}-type cluster (*a*) and of the satellite tobacco necrosis virus with triangulation number $T = 1$ (ref. 5) highlighting five of the protomers (red) (*b*). Two {Mo_{11}} units each formed by the {(Mo)Mo_5} groups and the five related Mo centers of the five neighbouring {$Mo^{V}_{2}O_4$}$^{2+}$ bridges are emphasized.

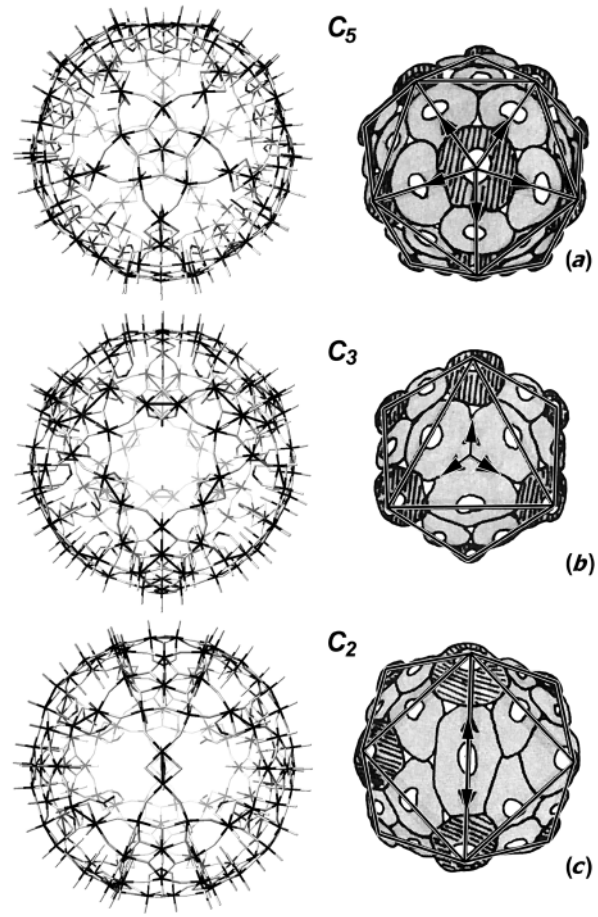

Fig. 4 Illustration of the structure of the {Mo_{132}}-type cluster (left) with perspective views along a fivefold (*a*), a threefold (*b*), and a twofold (*c*) symmetry axis in wire-frame presentations (used due to the structural complexity). For the purpose of comparison, corresponding schematic representations of an icosahedral virus capsid ($T = 3$) with 20 hexagonal and 12 pentagonal capsomers (morphology units) are presented [see ref. 6(*c*)]. In both systems, the C_5 axes cross the centers of the pentagonal units (hatched) (*a*), the C_3 axes cross the midpoint between three units (*b*), and the C_2 axes cross the center of the units (*c*). Whereas (*a*) refers to the centers of both the pentagonal {(Mo)Mo_5} units and the pentagonal capsomers which are located at the 12 corners of an icosahedron (see Fig. 3), (*b*) and (*c*) refer to the {Mo^{V}_{2}} units of the {Mo_{132}}-type cluster and the hexagonal capsomers, respectively.

is worthwhile to have a look at conditions which favour the corresponding emergence of molecular complexity including synthetic routes involving several successive reaction steps.

Optimal conditions for linking of fragments are:

- abundance of a huge variety of linkable units, *i.e.* building blocks and
- the possibility of generation of units (intermediates) with high free enthalpy to drive polymerization or growth processes, *e.g.* by formation of H_2O, of an easy structural change in the building units and blocks, of including hetero elements in the fragments, to form larger units which can be linked in different ways, to control the structure-forming processes by templates, to generate structural defects in reaction intermediates (*e.g.* leading to lacunary structures) in order to remove building units from large intermediates by the presence of appropriate reactants, to localize and delocalize electrons in different ways in order to gain versatility, to control and vary the charge of building parts (*e.g.* by protonation, electron transfer reactions, or substitution) and to limit growth by the abundance of appropriate terminal ligands, of generating fragments with energetically low-lying unoccupied molecular orbitals.

According to our present knowledge these conditions can only be optimally fulfilled in polyoxometalate systems which possess the relevant variety of molecular and electronic configurations, and not *e.g.* in silicate-based systems.

In generating large complex molecular species we have to realize that corresponding natural processes are effected by the (directed as well as non-directed) linking of (a huge variety of) basic and well defined preorganized (or stepwise organized) fragments. An impressive example of this, discussed in almost all textbooks on biochemistry, is the self-aggregation (reconstitution) process of the tobacco mosaic virus (TMV), which is based on preorganized units.[10] *This process more or less meets our strategy in controlling the linking of fragments to form larger units and linking the latter again.* The linking of building blocks containing 17 metal atoms ({Mo_{17}} units) to form cluster anions consisting of two or three of these units provides an archetypical example. The resulting two- or three-fragment

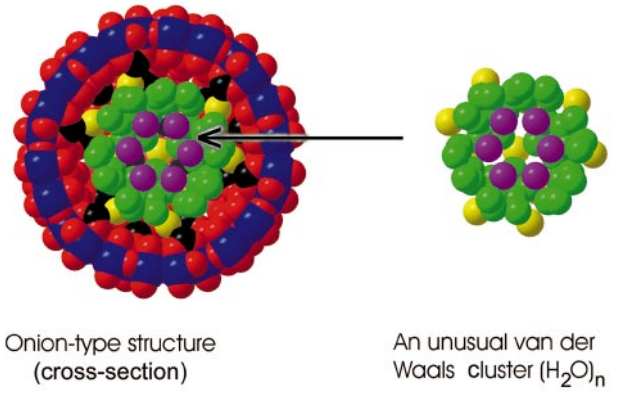

Fig. 5 Cross section through the equator of $[(H_2O)_n \subset Mo^{VI}_{72}Mo^{V}_{60}O_{372}(HCO_2)_{30}(H_2O)_{72}]^{42-}$ allowing a view into the cavity of the cluster shell and highlighting the hydrogen-bonded cluster formed by the encapsulated H_2O molecules (oxygen atoms) (*left*). The different shells spanned by encapsulated H_2O molecules are represented by spheres with different colours [violet shell (radius *ca*. 3.5 Å), green shell (6.2–6.9 Å) and yellow shell (8.2–8.7 Å) (*right*)]. Interestingly, the onion-like structure of the whole anion is completed by the three following outer shells consisting of (1) that of the 72 H_2O and 30 formate ligands coordinated to molybdenum atoms and pointing into the cavity (*ca* 10.5 Å), (2) that of the 132 molybdenum atoms (*ca* 13.1 Å) and (3) that of the terminal 132 oxygen atoms (*ca* 14.7 Å) (Mo centers: blue, O atoms: red, C atoms: black).

clusters are of the $\{Mo_{36}\}$ ($[\{MoO_2\}_2\{H_{12}Mo_{17}(NO)_2O_{58}(H_2O)_2\}_2]^{12-}$ = $[\{Mo_1{}^*\}_2(\{Mo_8\}_2\{Mo_1{}'\})_2]$) or of the $\{Mo_{57}M_6\}$ type (*e.g.* $[\{VO(H_2O)\}_6\{Mo_2(\mu\text{-}H_2O)_2(\mu\text{-}OH)\}_3\{Mo_{17}(NO)_2O_{58}(H_2O)_2\}_3]^{21-}$ = $[\{VO(H_2O)\}_6\{Mo_2{}'\}_3(\{Mo_8\}_2\{Mo_1{}'\})_3]$) (Fig. 6).[11,12]

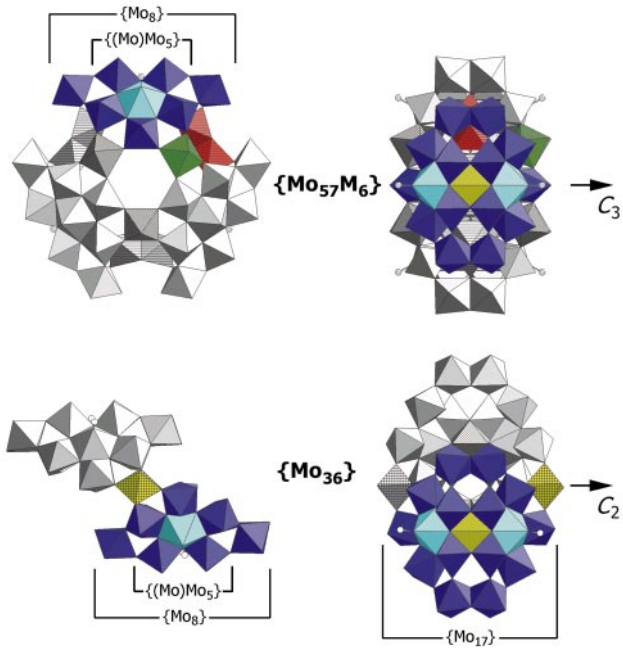

Fig. 6 Polyhedral representation of the $\{Mo_{57}M_6\}$ cluster with its basic building blocks and their constituents along the C_3 (*upper left*) and along one of the three C_2 axes (*upper right*): On the upper right, one $\{Mo_{17}\}$ building block consisting of one $\{Mo_1{}'\}$ and two $\{Mo_8\}$ groups, and on the upper left, one $\{Mo_8\}$ unit is shown in colour. Also shown in colour are one $\{Mo_2{}'\}$ group (built up from two face-sharing octahedra) and one MO_6 unit (green, cross-hatched). For comparison, the polyhedral representations of the $\{Mo_{36}\}$ cluster structure, consisting of two $\{Mo_{17}\}$ building blocks linked by two $\{Mo_1{}^*\}$ units (only one in colour), are shown in the related views, also highlighting one $\{Mo_8\}$ (*bottom left*) and one $\{Mo_{17}\}$ building block (*bottom right*). Of importance is the relation between $\{Mo_8\}$ and the pentagonal $\{(Mo)Mo_5\}$ groups (see text) ($\{Mo_8\}$: blue (central MoO_7 pentagonal bipyramid: cyan), $\{Mo_2{}'\}$: red hatched, $\{Mo_1{}'\}$: yellow hatched, $\{Mo_1{}^*\}$: yellow, cross-hatched).

The structure of the $\{Mo_{17}\}$ unit can furthermore be reduced to two $\{Mo_8\}$-type groups which are symmetrically linked by an $\{Mo_1{}'\}$-type unit. The $\{Mo_8\}$ building block, found in many other large polyoxometalate structures, is itself (as mentioned above) built up by a densely packed pentagonal $\{(Mo)Mo_5\}$ unit, containing a central MoO_7 or $MoO_6(NO)$ bipyramid sharing edges with five MoO_6 octahedra, and two more weakly bonded (sharing only corners) MoO_6 octahedra which can be more easily 'removed'. The pentagonal unit with a high formation tendency is for instance responsible for the formation of structures with icosahedral symmetry like the $\{Mo_{132}\}$-type cluster (for details, see Fig. 1).

With the $\{Mo_8\}$-type building block even very large and unusual clusters can be built up: subsequent to our publication[13] of a 3.5 nm-diameter wheel-shaped metal–oxide based cluster anion containing 154 molybdenum atoms *i.e.* $[Mo_{154}(NO)_{14}O_{448}H_{14}(H_2O)_{70}]^{28-}$ ($\{Mo_{154}\}$) and built up from 14 of the mentioned $\{Mo_8\}$ groups linked by 14 $\{Mo_2\}$- and 14 $\{Mo_1\}$-type units, respectively (Fig. 7,8), it was metaphorically stated in *New Scientist*

"Big wheel rolls back the molecular frontier".[14]

This signifies the enormous interest of modern chemistry to 'leave' the molecular world, characterized by rather small molecules or ions, and to 'proceed' to the meso- or nano-world with a view to discovering and investigating the new inherent phenomena and system qualities.

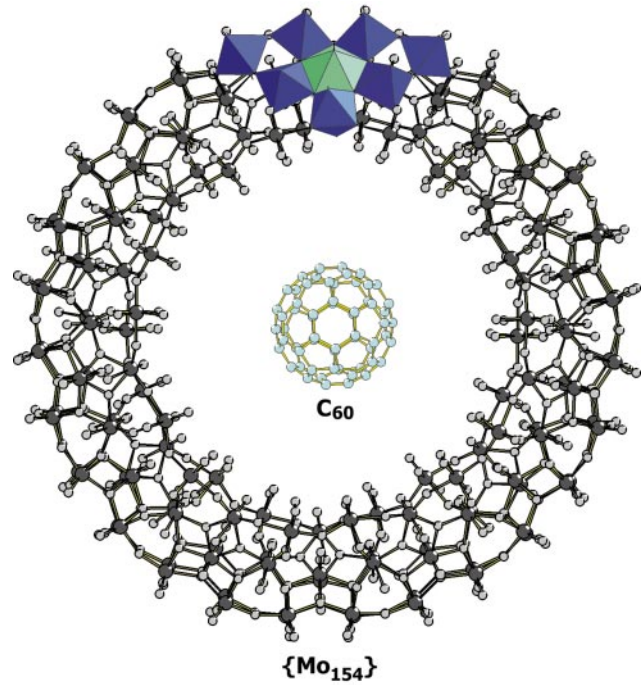

Fig. 7 Ball-and-stick representation of the $\{Mo_{154}\}$-type cluster $[Mo^{VI}_{126}Mo^{V}_{28}O_{462}H_{14}(H_2O)_{70}]^{14-}$ showing one $\{Mo_8\}$ unit (blue) with its central MoO_7 pentagonal bipyramid (cyan) in polyhedral representation. For the purpose of size-comparison, a C_{60} fullerene molecule is shown.

Remarkable is that *using the same reaction type*, i.e. *the acidification of aqueous solutions of the most simple tetrahedral oxoanions of the early transition elements of the type* $MO_4{}^{n-}$, *the resulting products span the three important areas of matter*, from the micro-, through the meso- (or nano-) to the macrostructures, the latter being characterized by crystallinity or translational invariance. In the present case the nano-structures are of particular interest owing to the huge structural variety of the related polyoxometalates. Additional external chemical interventions, *e.g.* those corresponding to the list given above, lead to an even greater structural diversity, for example in the presence of reducing agents (especially those with the possibility of multi-electron transfer), appropriate templates or hetero elements.

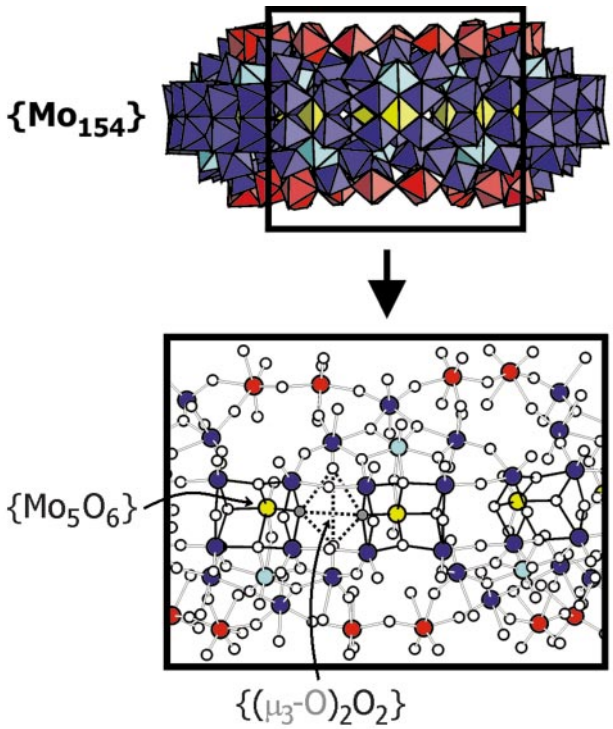

Fig. 8 Polyhedral representation of the tetradecameric $\{Mo_{154}\}$-type cluster with view perpendicular to that depicted in Fig. 7 (*top*) and structural details of cluster compartments in ball-and-stick representation (*bottom*). This representation highlights (1) three of the 14 (incomplete) double-cubane-type compartments each of which is spanned by five Mo centers (Mo–Mo = 3.4–4.0 Å) belonging to $\{Mo_8\}$- as well as $\{Mo_1\}$-type groups and six O atoms (the lowered bond valence sum (BVS) values of the corresponding Mo atoms with an average value of 5.6 prove, besides other experimental data, that two 4d electrons are trapped in each compartment), and (2) one of the 14 $\{(\mu_3\text{-O})_2O_2\}$-type compartments indicated by dotted lines which are located between two double-cubane-type compartments (the two characteristic μ_3-O atoms (dark grey, O–O = 3.07 Å) have an average BVS value of 1.2 indicating a degree of protonation; for details see ref. 34). ($\{Mo_8\}$: blue (central MoO_7 pentagonal bipyramid: cyan), $\{Mo_1\}$: yellow, $\{Mo_2\}$: red).

The use of the above-mentioned fundamental *linkable building units*, *e.g.* in the form of Platonic solids, enables the generation of molecular systems of higher structural variability and versatility compared to arrangements of aggregated metal atoms with spherical symmetry, which lead to pure metal clusters or ligand-stabilized clusters with metal cores. In the present case, the final macroscopic product is the crystalline metal oxide, in the latter, the crystalline metal. Important research in this area has been done by Schmid.[15]

The basic principles of the *one-pot reactions*, mainly those with feedback effects, non-linearity relations and induced cascades (see below), are of relevance for fundamental problems of prebiotic chemistry and conservative self-organization in general. *This is especially valid in the present case with reference to the combinatorially linkable (virtual) units as disposition*. The prebiotic situation is very well reflected by a citation from *Scientific American* that deals with the work of a well-known member of the Santa Fe institute:

> "[Stuart A.] Kauffman's simulations have led him to several conclusions. One is that when a system of simple chemicals reaches a certain level of complexity [...], it undergoes a dramatic transition, or phase change. The molecules begin spontaneously combining to create larger molecules of increasing complexity and catalytic capability. Kauffman has argued that this process of 'autocatalysis'—rather than the fortuitous formation of a molecule with the ability to replicate and evolve–led to life." [16]

On the other hand, one-pot reactions are, in principle, of industrial interest according to Dömling and Ugi's MCR (multi-component reaction)-type studies.[17]

Aspects of self-aggregation, related reaction types and synthesis

Preventing degradation as well as uncontrolled aggregation

The most suitable strategy to guarantee limited growth as well as synthetic aspects in the present case of polyoxometalate chemistry is based on the generation of sufficiently negatively charged fragments (intermediates formed during the aggregation process) enabling growth by avoiding both a possible degradation due to hydrolysis and an uncontrolled aggregation to network-type structures, leading for instance to the formation of the related oxides. This can be attained not only by substituting some metal centers of lower for ones of higher oxidation state or by substituting less positively charged for higher positively charged groups (*e.g.* by exchanging $[Mo(NO)]^{3+}$ for $[MoO]^{4+}$), but also by the (permanent) presence of an appropriate reducing agent or even different types of these. It is of utmost importance to keep the growing molecular system in solution, which can be achieved by avoiding a too high nucleophilicity of the peripheral oxygen atoms, thus preventing aggregation. This is accomplished for instance by the presence of a large number of H_2O ligands which cause the high solubility in protic media and/or terminal doubly bonded oxygen atoms of the O=Mo groups.

In the reaction system MoO_4^{2-}–H_2O–NH_2OH–$(X^VO_4^{3-})$ highly negatively charged species are abundant, for instance the highly soluble ion $[Mo^{VI}_8V^{IV}_4O_{36}(X^VO_4)]^{11-}$ (X = V; As; without protonation); the latter species can be trapped with electrophiles such as the As^{III} centers, resulting in the less soluble stable cluster species $[As^{III}_2Mo^{VI}_8V^{IV}_4O_{36}(As^VO_4)]^{5-}$ with lowered negative charge.[11c,e] Other negatively charged linkable (virtual) fragments as disposition, such as the $\{Mo_{17}\}$ unit which can be 'linked' in different ways by certain electrophilic metal centers (or linkers) such as Fe^{III} or $V^{IV}O^{2+}$, form larger systems, *e.g.* the three-fragment cluster of the $\{Mo_{57}M_6\}$ type with three $\{Mo_{17}\}$ units. A higher nucleophilicity of the fragments and a higher coordination number of the linkers can lead to giant species with a larger number of linked fragments (for the remarkable giant tungstate-based cluster of Pope and coworkers see below).

Spectroscopic detection of stability regions and conditions for further aggregation

The possibility of spectroscopic detection of the mentioned clusters in solution (*e.g.* by means of resonance-Raman spectroscopy) constitutes a good *base when studying conditions for the generation of ever larger species. Stability regions of the clusters can be determined and further possible aggregation processes under different conditions can be recognized upon changing the pH values and redox potentials*. Starting for instance with the above mentioned two-fragment $\{Mo_{36}\}$-type cluster with two $\{Mo_{17}\}$ groups, the three-fragment $\{Mo_{57}M_6\}$-type cluster with three $\{Mo_{17}\}$ groups is formed after adding for instance the strong electrophilic linker $V^{IV}O^{2+}$ under reducing conditions. In solutions containing this cluster, the (more reduced) wheel-shaped cluster $[Mo_{154}(NO)_{14}O_{448}H_{14}(H_2O)_{70}]^{28-}$ ($\{Mo_{154}\}$) forms upon further acidification and reduction ($\{Mo_{154}\}$-type clusters like the pure isopolyoxometalate analogue containing 14 $[MoO]^{4+}$ instead of 14 $[MoNO]^{3+}$ groups turned out to comprise the prototype of the molybdenum-blue species).[18] These clusters can be regarded as tetradecamers that meet D_{7d} symmetry if the hydrogen atoms are excluded and can be formally generated by linking 140 MoO_6 octahedra and 14 $MoO_6(NO)$ or MoO_7 pentagonal bipyramids, forming the building blocks of the $\{Mo_8\}$, $\{Mo_2\}$, and $\{Mo_1\}$ type which are each present in the tetradecameric cluster type 14 times.

Template-driven aggregation: an example

An important strategy often used is that of template-controlled linking especially of relatively small building units (for a review see ref. 19 but also ref. 20). It is for instance possible to link square pyramids built up by five oxygen atoms and a central vanadium atom to form cage systems. The resulting cage, *i.e.* the cluster shell, is formed complementary to the size and shape of the template which is finally encapsulated as guest in the reaction product. The relevant condensation process is initiated by adding negatively charged template ions to an aqueous solution containing vanadate ions in presence of a reducing agent which leads to the formation of polyoxovanadates (IV) or mixed-valent polyoxovanadates (IV,V). A spherically shaped halogenide anion (*e.g.* Cl^-) as template induces the formation of a spherically shaped cage, whereas the presence of the elongated azide anion results in an elongated (stretched) cluster cage (Fig. 9).[19,20] This procedure can also be regarded formally

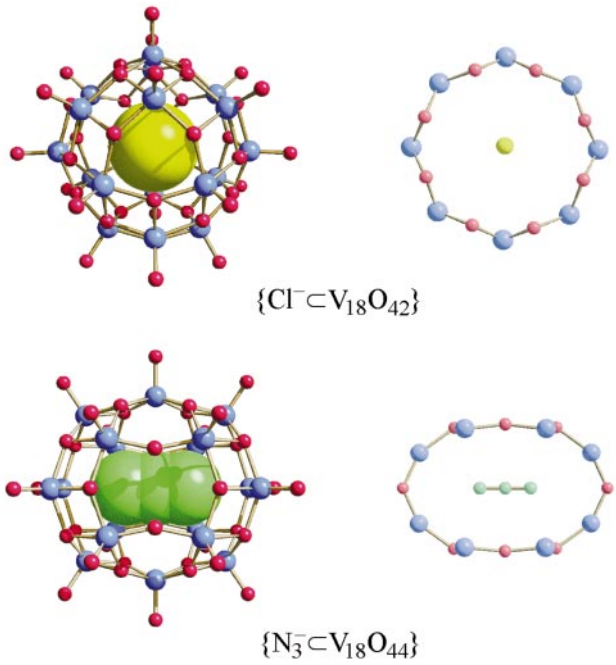

Fig. 9 Representation of the complementarity of the polyoxovanadate shell (host) formed by linking OVO_4 square pyramids (archetypical for the formation of relevant parts of concave host structures) and the encapsulated convex anion (guest) directing the linking as a template.

as a 'slaving' process according to Haken's concept of synergetics:[21] the template 'forces' or 'slaves' the square-pyramidal units to get aggregated in a uniform way. The analogy of the relevant host–guest system, in which the metal–oxygen cluster cage can be regarded as host and the enclosed anion as guest, to the endohedral fullerenes is evident (where in fact metal cations are present as guests). It should be noted that the interaction of the cluster shell with the anion is very weak (but cation stabilized) and consequently the cluster shells may be used as matrices for quasi-isolated anions.[22]

It is furthermore remarkable that all known resulting cluster shells can be regarded as sections of layers of vanadium pentoxide (V_2O_5).[19a,23] (The curvature of the cluster shell is due to the negative partial charges at the peripheral oxygen atoms.) This means that one can describe the cluster cages as being formally cut out from the layers of a crystalline compound.

Of particular interest is the case of *a template, generated in solution in an initial step, directing or determining the subsequent linking processes*: a cubane-type $\{V_4O_4(O_{term})_4\}$ fragment with the stoichiometry of amphoteric $V^{IV}O_2$, obviously primarily formed in solution, induces the formation of a cluster the structure of which has similarity with a segment of the (cubic) NaCl defect structure (Fig. 10).[24]

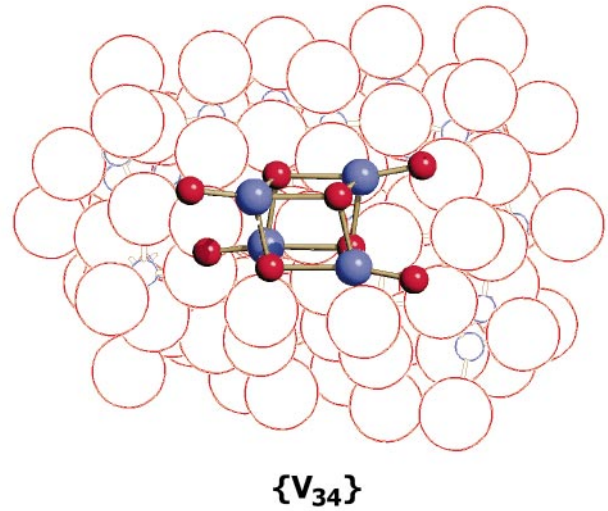

Fig. 10 Structure of the cluster anion $[V_{34}O_{82}]^{10-}$ with the highlighted $\{V_4O_4(O_{term})_4\}$ cubane-type central unit (formed initially in the reaction solution) acting formally as template, as in the case of the clusters of Fig. 9. The $\{V_{34}\}$-type cluster has similarity with a segment of the (cubic) NaCl defect structure (the 'shell' framework in space-filling, the central unit in ball-and-stick representation).

Molecular growth to complexity *via* an induced cascade

During natural evolution the emergence of more complex molecular structures from simpler ones occurred. In this context, basic principles of induced cascade reactions of the type given in Scheme 1 are of special relevance:

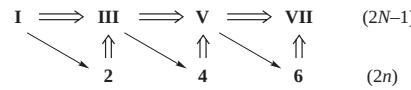

Scheme 1

The odd Roman numerals $2N - 1$ signify maturation steps of a molecular system in growth or development and the Arabic numerals $2n$ represent 'reagents' that react only with the special preliminary intermediate $2N - 1$. The 'species' $2n$ can themselves be products of self-assembly processes, but can remarkably be generated template-driven by the corresponding intermediate $2N - 1$. *In the latter case each intermediate* $2N - 1$ *carries information inducing the formation of the subsequent intermediate* $2n$ *(induced cascade-type reaction)* with which it then reacts thus demonstrating an interesting feedback effect.

One example for a growth process according to this model scheme has been investigated in detail: a cluster anion containing 37 molybdenum atoms ($[H_{14}Mo_{37}O_{112}]^{14-}$) is formed *via* intermediates,[25] one of which, the cluster of the type $\{Mo^{V}_{12}Mo^{VI}_{4}\}$ (containing an ε-Keggin-type nucleus capped by four electrophilic $\{Mo^{VI}O_3\}$ groups), can be isolated from the reaction medium[26a] (this $\{Mo_{16}\}$ fragment also resembles the core of other larger clusters with higher symmetry, such as $[XH_nMo_{42}O_{109}\{(OCH_2)_3CR\}_7]^{m-}$ with X = $Na(H_2O)_3^+$: n = 13, m = 9; n = 15, m = 7 or X = MoO_3: n = 14, m = 9; n = 13, m = 10).[26b] After the relevant reduction of the four surface constituents of the type $\{Mo^{VI}O_3\} \rightarrow \{Mo^{V}O_3\}$, the intermediate cluster acts both as nucleophile *and* template in directing the formation of two further electrophilic molybdenum-oxide based intermediates ($\{Mo_{10}\}$ and $\{Mo_{11}\}$). These subsequently react with their template (in a type of symmetry-breaking step) leading finally to the reaction product, the $\{Mo_{37}\}$-type cluster which remarkably has no (higher) symmetry element (Fig. 11). The most interesting aspect is that the former electrophilic $\{Mo^{VI}O_3\}$ groups are transformed into nucleophilic $\{Mo^{V}O_3\}$ ones after they have been attached to the cluster surface. The reduction of units on the cluster surface seems to be (1) the basis of the growth processes investigated here (as the growing system always has a nucleophilic surface)

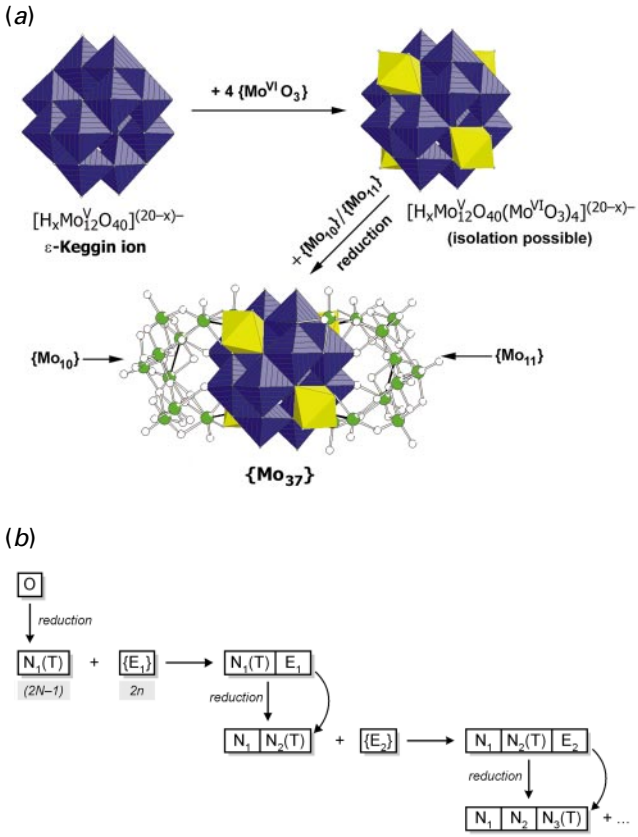

Fig. 11 (*a*) Schematic representation of a molecular growth process based on an induced cascade and molecular symmetry-breaking steps according to the reaction Scheme 1 (see text); the resulting $\{Mo_{37}\}$ cluster remarkably does not show any (higher) symmetry elements. (*b*) Reaction scheme corresponding to the growth process shown in (*a*), demonstrating principally the step-by-step procedure in which nucleophiles (such as the reduced ε-Keggin ion) attract electrophiles (such as $\{Mo^{VI}O_3\}$). Remarkably these can become nucleophiles ($\{Mo^{V}O_3\}$ units) on the surface of the cluster upon reduction. O denotes species at the beginning of a growth process (formally the non-reduced ε-Keggin ion). $N_i(T)$ denotes a nucleophilic intermediate/fragment produced under reducing conditions (of the type $2N-1$ according to Scheme 1, *e.g.* the reduced ε-Keggin ion) with a potential template function for the generation of the electrophilic intermediate E_i (of the type $2n$ according to Scheme 1, *e.g.* the $\{Mo^{VI}O_3\}$ groups).

and (2) the entering point into the world of open systems, since the reduction of the $\{Mo^{VI}O_3\}$ groups at the surface of the cluster can in principle be performed 'externally' by adding an appropriate reducing agent at the right time. It is important to note that these types of integrated constituents (here situated on the surface of a cluster) are more easily reduced than the discrete ones.

Large clusters and the correlated size(form)/complexity(functionality) pair

An increase in the size of a molecular system can *in principle* lead to multi-functionality whereby with increasing size of the system the correlated concept pair, form–function, can correspondingly become more and more important. This should be elucidated by the following examples:

(1) In the case of the mentioned $\{Mo_{57}M_6\}$-type cluster, it is possible to *place* (*or exchange*) *step-wise different* (*para*)-*magnetic centers* M *like* $Fe^{II/III}$ *and* $V^{IV}O^{2+}$ *in the respective linker positions*, thus allowing some control over the cluster's magnetic properties or even the tuning of these.[27] On the other hand the cluster in question exhibits cavities on its periphery. This is of special interest since these *cavities can be filled with positively charged units such as* $[MoO]^{4+}$ *under reducing conditions* (*i.e.* by increasing the nucleophilicity) *and can be emptied again upon oxidation* (Fig. 12). As mentioned earlier,

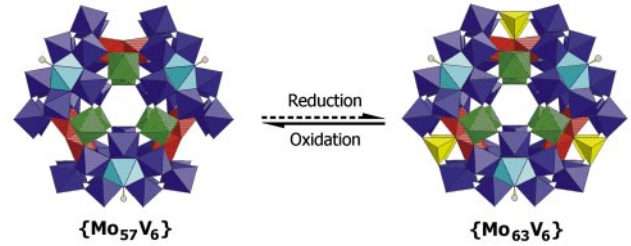

Fig. 12 Quasi-reversible molecular growth $\{Mo_{57}M_6\} \rightarrow \{Mo_{63}M_6\}$ based on a type of switchable sites: six electrophilic $[MoO]^{4+}$ groups (yellow tetrahedra) can (formally) be taken up step-wise under reducing conditions (by the nucleophilic cluster) to form finally the $\{Mo_{63}M_6\}$ cluster, but can be expelled when the latter cluster is oxidized (see text).

this seems to be the basic principle of the growth processes under consideration: aggregation or growth is due to interaction of nucleophilic growing species with electrophilic groups. The reaction, based on a kind of switchable sites, represents a type of model for uptake and release of metal centers in metal storage proteins under redox-active conditions.[25]

(2) A further nice example is presented by the cluster anion $\{Mo_{75}V_{20}\}$.[28] Interestingly, virtual $\{(Mo)Mo_5\}$ pentagons (as disposition) in solutions can be used as basic building blocks in presence of other building blocks to construct spherical species, *e.g.* derivatives of the $\{Mo_{132}\}$-type cluster with its 12 pentagonal $\{(Mo)Mo_5\}$ units. This leads for instance to the mentioned cluster anion which can be described with reference to one of the Archimedean solids, namely the icosidodecahedron with 30 corners and 32 faces. This Archimedean solid is formed by 12 pentagonal and 20 triangular faces built up by 20 V^{IV} and 10 Mo^{VI} centers while ten pentagonal faces of the icosidodecahedron are capped by the $\{(Mo)Mo_5\}$ pentagons (Fig. 13, 14). Besides the remarkable fact that the ten triangles,

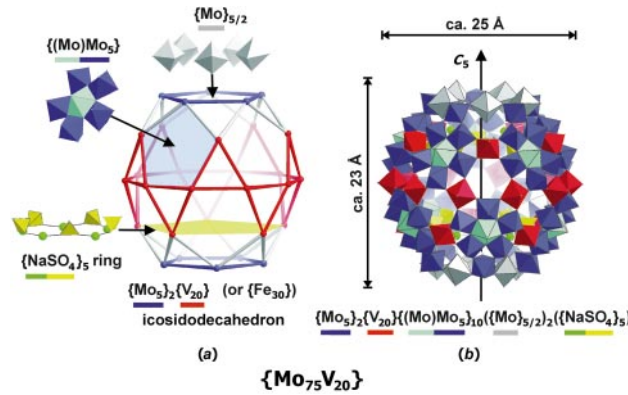

Fig. 13 (*a*) $\{V_{20}Mo_{10}\}$ framework structure of the $\{Mo_{75}V_{20}\}$-type cluster with 30 corners and 32 faces (20 triangles and 12 pentagons) spanned by 20 V^{IV} (red) and 10 Mo^{VI} (blue) centers (the Fe atoms of the related $\{Fe_{30}\}\{(Mo)Mo_5\}_{12}$-type cluster form a less distorted icosidodecahedron). Additional details: (1) one of the $\{(Mo)Mo_5\}$ units capping 10 pentagonal faces (Mo pentagonal bipyramid: light blue, Mo octahedra: dark blue), (2) pentagonal (under-occupied) array built up by the five MoO_6 octahedra capping the other two pentagonal faces (grey), (3) a 'magnetic' ring-shaped band formed by 10 $V^{IV}{}_3$ triangles having common corners (red) and (4) one of the two encapsulated $\{NaSO_4\}_5$-type rings (Na atoms: green, SO_4 tetrahedra: yellow). (*b*) Polyhedral representation of the (approximately) spherical structure of the complete $\{Mo_{75}V_{20}\}$-type cluster.

built up by the 20 V^{IV} centers, form an equatorial paramagnetic ring-shaped band with very strong antiferromagnetic exchange interactions, the cluster opens the doorway for new aspects of supramolecular chemistry because of the abundance of two $\{(NaSO_4)_5\}$-type rings inside the cavity. On the other hand it seems to be clear that the $V^{IV}O^{2+}$ groups should in principle be replaceable by Fe^{III} centers (as in the case of the $\{Mo_{57}M_6\}$-type cluster), which could enable a tuning of magnetic properties. In particular it could result in an isolation of clusters

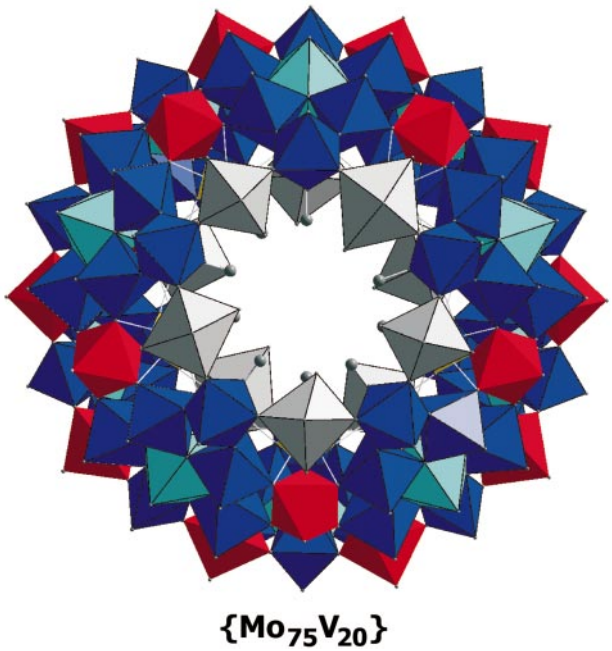

Fig. 14 Polyhedral representation of the $\{Mo_{75}V_{20}\}$-type cluster with a view along the C_5 axis, *i.e.* perpendicular to that depicted in Fig. 13(*b*) (colour code as in Fig. 13).

with an icosidodecahedral base spanned by 30 Fe centers. This for instance would correspond to a derivative of the $\{Mo_{132}\}$ cluster having also 12 $\{(Mo)Mo_5\}$ pentagons but the 30 $\{Mo^{V}{}_2O_4\}^{2+}$ groups replaced by 30 Fe^{III} centers.

(3) The *size/multi-functionality* concept pair can be elucidated very well by means of the giant wheel-type cluster, *e.g.* the tetradecameric $\{Mo_{154}\}$-type cluster and its properties:

1 It exhibits a nanometer-sized cavity, presenting new perspectives for a novel host–guest chemistry.
2 It has an extended hydrophilic inner and outer surface owing to the presence of 70 H_2O ligands.
3 It has a huge surface area which explains in part the high affinity towards adsorbents, such as charcoal or silk.
4 It renders a molecular model for catalytically active metal oxides.
5 The aqueous solution shows further aggregation tendencies: the formation of colloids of 40 nm hydrodynamic radius could be detected by means of dynamic light scattering and scanning electron microscopy.[29]
6 The periphery of the cluster ring shows a rather high electron density.
7 There are 14 uncoupled $\{Mo_5O_6\}$ (incomplete double-cubane) compartments, each of which carries two delocalized 4d electrons (comparable to a so-called electronic necklace, *i.e.* corresponding to an electron-storage system where the uncoupled storage elements are threaded like pearls on a string).[34]
8 It is possible to generate deliberately discrete structural defects on the inner surface of the cluster ring by abstracting positively charged $\{Mo_2\}$ groups using special ligands which have a high affinity to these groups (see below).
9 The ring-shaped units can be linked according to a type of crystal engineering: assembly owing to synergetically induced functional complementarity of distinct surface sites (see below).
10 It is possible to place molecules or replace ligands at different sites of the surface (thereby subsequently changing the properties) and to study direct reactions between the molecules placed inside the cavity.

Relevant compounds containing the ring-shaped units are presented in Table 1.

Table 1 Compounds with nanosized rings: building units (Fig. 8) and bond valence sum values relating to the structures[a]

Compound (with approximate crystal water content)[a]	Building units[b]	Structure	BVS[c] (Mo)	BVS[d] (μ_3-O)	Ref.
$(NH_4)_{28}[Mo_{154}(NO)_{14}O_{448}H_{14}(H_2O)_{70}]\cdot xH_2O$ ($x \approx 350$)	$\{Mo_2\}_{14}\{Mo_8\}_{14}\{Mo_1\}_{14}$	Discrete rings	5.7	1.2	13
$Na_{14}[Mo_{154}O_{462}H_{14}(MeOH)_8(H_2O)_{62}]\cdot xH_2O\cdot yMeOH$[e] ($x \approx 400$, $y \approx 10$)	$\{Mo_2\}_{14}\{Mo_8\}_{14}\{Mo_1\}_{14}$	Discrete rings	5.5	1.2	30
$Na_{15}\{0.5[Mo_{154}O_{462}H_{14}(H_2O)_{70}]\cdot 0.5[Mo_{152}O_{457}H_{14}(H_2O)_{68}]\}\cdot xH_2O$ ($x \approx 400$)	$\{Mo_2\}_{14}\{Mo_8\}_{14}\{Mo_1\}_{14}$ + $\{Mo_2\}_{13}\{Mo_8\}_{14}\{Mo_1\}_{14}$	Two different discrete rings, one of which possesses a defect	5.6 5.6	1.2 1.2	31
$Li_{16}[Mo_{176}O_{528}H_{16}(H_2O)_{80}]\cdot xH_2O (x \approx 400)$	$\{Mo_2\}_{16}\{Mo_8\}_{16}\{Mo_1\}_{16}$	Discrete rings	5.6	1.3	32
$Na_{16}[Mo_{176}O_{528}H_{16}(MeOH)_{17}(H_2O)_{63}]\cdot xH_2O\cdot yMeOH$ ($x \approx 600$, $y \approx 30$)	$\{Mo_2\}_{16}\{Mo_8\}_{16}\{Mo_1\}_{16}$	Discrete rings	5.7	1.3	33
$Na_{24}\{0.5[Mo_{144}O_{437}H_{14}(H_2O)_{56}]\cdot 0.5[Mo_{144}O_{437}H_{14}(H_2O)_{60}]\}\cdot xH_2O$ ($x \approx 350$)	$\{Mo_2\}_9\{Mo_8\}_{14}\{Mo_1\}_{14}$ + $\{Mo_2\}_9\{Mo_8\}_{14}\{Mo_1\}_{14}$	Discrete rings with defects and chains built up by rings with defects	—[f]	—[f]	34
$Na_{24}[Mo_{144}O_{437}H_{14}(H_2O)_{56}]\cdot xH_2O (x \approx 250)$	$\{Mo_2\}_9\{Mo_8\}_{14}\{Mo_1\}_{14}$	Chains built up by rings with defects	5.8	1.2	35
$Na_{22}[Mo_{146}O_{442}H_{14}(H_2O)_{58}]\cdot xH_2O (x \approx 250)$	$\{Mo_2\}_{10}\{Mo_8\}_{14}\{Mo_1\}_{14}$	Chains built up by rings with defects	5.6	1.2	31
$Na_{16}[Mo_{152}O_{457}H_{14}(H_2O)_{66.5}]\cdot xH_2O (x \approx 300)$	$\{Mo_2\}_{13}\{Mo_8\}_{14}\{Mo_1\}_{14}$	Layers built up by rings with defects	5.6	1.2	34
$Na_{21}[Mo_{154}O_{462}H_{14}(H_2O)_{54}(H_2PO_2)_7]\cdot xH_2O (x \approx 300)$	$\{Mo_2\}_{14}\{Mo_8\}_{14}\{Mo_1\}_{14}$	Layers with attached $H_2PO_2^-$ groups	5.6	1.2	36

[a] Formulae of some earlier reported compounds corrected according to the now accepted type of protonation for compounds with $b = 14$ building units (tetradecameric case) or $b = 16$ (hexadecameric case). [b] The general formula for the discrete pure molybdenum–oxide based unit is $[\{Mo^{VI}{}_2O_5(H_2O)_2\}^{2+}{}_{b-x}\{(Mo^{VI/V}{}_8O_{26}(\mu_3\text{-}O)_2H_m(H_2O)_3Mo^{VI/V})^{(4-m)-}\}_b]^{(2b-bm+2x)-} \equiv [\{Mo_2\}_{b-x}\{Mo_8\}_b\{Mo_1\}_b]^{(2b-bm+2x)-}$ [b = number of building units per set = number of compartments referring to Fig. 8 = number of protonations at the equatorial μ_3-O atoms or in the $\{(\mu_3\text{-}O)_2O_2\}$ compartment (for $m = 1$) = half of the (formal) number of Mo^{V} centers; x = number of defects or missing $\{Mo_2\}^{2+}$ units]. [c] Average BVS value for the Mo centers which span the b incomplete $\{Mo_5O_6\}$-type double cubanes, built up by (parts of) the $\{Mo_8\}$ and $\{Mo_1\}$ units (Fig. 8). The (formal) number of Mo^{V} centers per ring is for all compounds $2b$ (or two per compartment) according to the related constant BVS (Mo) values and other experimental data (see text). [d] Average BVS value for the μ_3-O atoms of the $b = 14$ or 16 $\{(\mu_3\text{-}O)_2O_2\}$-type compartments (Fig. 8), which indicates protonation at the equatorial μ_3-O atoms or within the $\{(\mu_3\text{-}O)_2O_2\}$compartments. The finally accepted value for the number of protons m per compartment is 1 mainly according to the results of the numerous cation analyses. This value corresponds to a disorder of the kind that only one of the two μ_3-O atoms of a compartment is protonated. This situation ($m = 1$) is also more plausible as the other possibility ($m = 2$) leads to a rather small H–H distance in the compartment (compare W. H. Baur, *Acta Crystallogr., Sect. B*, 1992, **48**, 745). [e] Because of the rather high resolution of the crystal structure, Na^+ positions could be determined for the first time, proving their importance for the structure formation. [f] The structure is not sufficiently resolved to calculate reasonable BVS values.

On route to larger and more complex systems: supramolecular and solid-state structures

An aspect of particular interest is the fact that the large ring-shaped synthons can assemble to form chains or layers (Table 1).[34–36] The assembly is based on the replacement of H_2O ligands at $\{Mo_2\}$ units (on rings) by oxygen atoms of terminal Mo=O groups (on other rings), the nucleophilicity of which is increased for instance by introducing electron donating (and the linking-introducing) ligands like $H_2PO_2^-$ at relevant neighbouring sites (Fig. 15). In this case a *layer compound* can be obtained.[36] In addition, as the process is based on reactions at the same type of amphiphilic $\{Mo_2\}$-type O=MoL (L = H_2O, $H_2PO_2^-$) units in different rings, the term synergetically

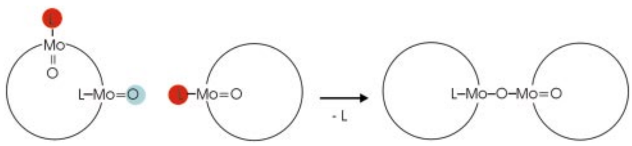

Fig. 15 Schematic representation of the basic assembly principles of ring-shaped cluster units forming the layers with $[Mo^{VI}_{126}Mo^{V}_{28}O_{462}H_{14}(H_2O)_{54}(H_2PO_2)_7]^{21-}$ units. The formation is based on the synergetically induced functional complementarity of the $\{Mo_2\}$-type O=Mo(L) (L = H_2O, $H_2PO_2^-$) sites of their surfaces: each precursor ring contains the corresponding virtual functional complementary O=Mo(H_2O) groups (becoming 'donors' due to the electron-donating $H_2PO_2^-$ replacing H_2O ligands and 'acceptors' without $H_2PO_2^-$ ligands).

induced functional complementarity seems to be justified. The hypophosphoric acid in this case acts both as reducing agent and H_2O-replacing ligand. Linking is in principle also possible by abstracting some $\{Mo_2\}$-type fragments using bidentate ligands, such as the formate anion, from the inner surroundings of the $\{Mo_{154}\}$-type cluster which also causes a higher nucleophilicity at the O=Mo(H_2O) sites of $\{Mo_2\}$ units in the neighbourhood. *Compounds with chains* having interesting electronic properties can be formed in this way (see Fig. 16 and Table 1).[31,34]

An even larger ring-shaped cluster than the tetradecameric $\{Mo_{154}\}$ type with 176 molybdenum atoms ($\{Mo_{176}\}$), *i.e.* with a hexadecameric structure, can be obtained containing correspondingly 16 instead of 14 sets of each of the three mentioned building blocks of the type $\{Mo_8\}$, $\{Mo_2\}$ and $\{Mo_1\}$ (Fig. 17, Table 1).[32,33] Under special reducing conditions the cluster system even starts growing again while two molybdenum–oxide fragments of the type $\{Mo_{36}O_{96}(H_2O)_{24}\}$ cover the cavity of the wheel-shaped cluster like hub-caps, resulting in an $\{Mo_{248}\}$-type cluster (Fig. 18).[37] This is in terms of the number of metal atoms the largest known cluster anion that has been structurally characterized so far. Remarkably the structure of the $\{Mo_{36}O_{96}(H_2O)_{24}\}$-type fragment is nearly identical to a segment of the solid-state structure of the compound Mo_5O_{14} (Fig.19).[38] This offers the possibility to model crystal growth under boundary conditions, especially the related initial nucleation process which is not understood at all. On the other hand,

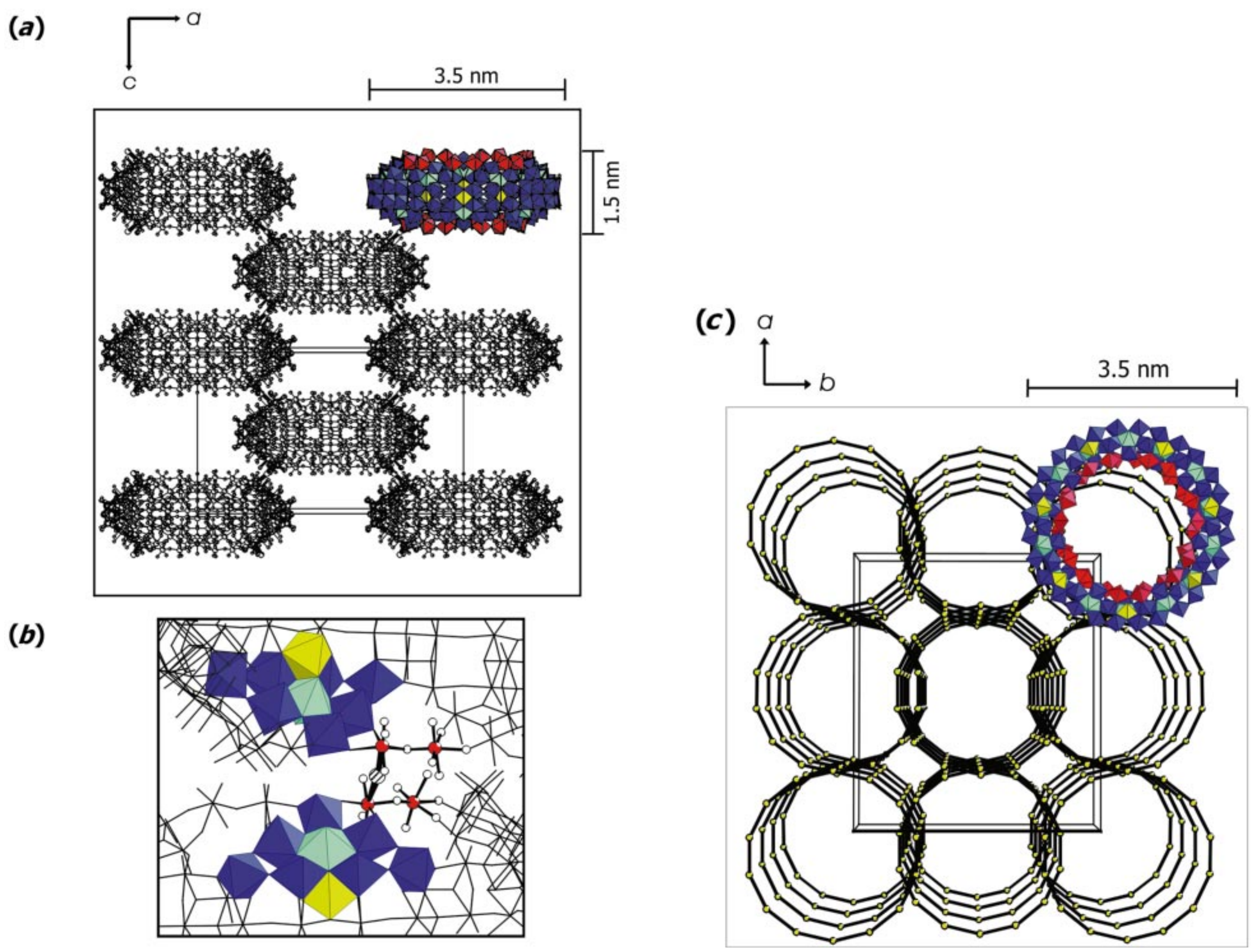

Fig. 16 (*a*) Ball-and-stick representation of the 'packing' of the covalently (in direction of the *b* axis) linked rings in crystals of $Na_{16}[Mo^{VI}_{124}Mo^{V}_{28}O_{429}(\mu_3\text{-}O)_{28}H_{14}(H_2O)_{66.5}]\cdot xH_2O$ ($x \approx 300$) ($\{Mo_{152}\}$) viewed along the crystallographic *b* axis. Each ring is connected to surrounding rings *via* Mo–O–Mo bridges of the O=Mo–O–Mo–OH_2 units, thus forming layer networks parallel to the *ac* plane. One ring is shown as basic unit in polyhedral representation ($\{Mo_2\}$ units: red, $\{Mo_8\}$: blue (central MoO_7 pentagonal bipyramid: cyan), $\{Mo_1\}$: yellow). (*b*) Detailed view of the bridging region between two cluster rings. One $\{Mo_8\}$ unit of each ring together with one $\{Mo_1\}$ unit is shown in polyhedral representation and one $\{Mo_2\}^{2+}$ (= $\{Mo^{VI}_2O_5(H_2O)_2\}^{2+}$) unit per ring in ball-and-stick representation (Mo centers: red). The bridging (disordered) oxygen centers are depicted as large, hatched circles (for clarity, the disorder in the bridging positions is not shown here). (*c*) Perspective view along the crystallographic *c* axis showing the framework with nanotubes which are filled with H_2O molecules and Na^+ cations. For clarity, only one ring is shown completely in polyhedral representation. For the other rings only the centers of the $\{Mo_1\}$ units (yellow) are given and connected. The diameter of the central cavity inside a ring in the crystal is at least 1.9 nm.

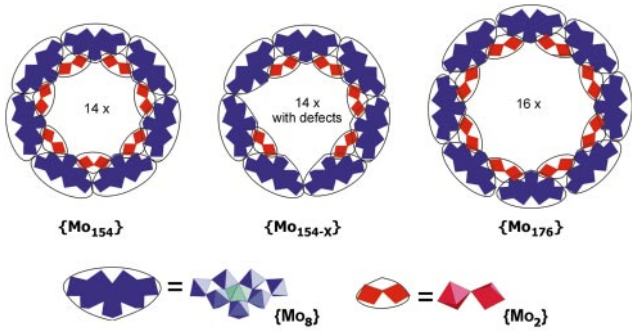

Fig. 17 Schematic comparison of the tetradecameric $\{Mo_{154}\}$- (with and without defects referring to missing $\{Mo_2\}$ groups) and hexadecameric $\{Mo_{176}\}$-type cluster showing the basic $\{Mo_8\}$ and $\{Mo_2\}$ units (the equatorial $\{Mo_1\}$ units are not visible in this representation).

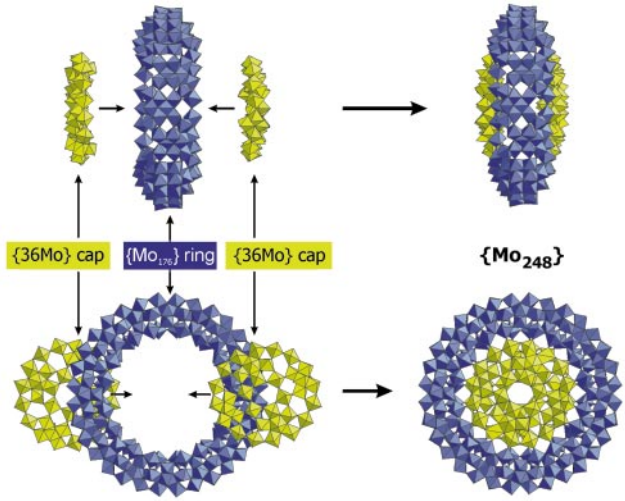

Fig. 18 Schematic representation of the growth process $\{Mo_{176}\} \rightarrow \{Mo_{248}\}$. The structure of one $\{Mo_{248}\}$ cluster can formally be decomposed into one $\{Mo_{176}\}$-type ring (blue) and two $\{Mo_{36}O_{96}(H_2O)_{24}\}$-type hub-caps (yellow).

this type of aggregation has relevance for metal-center assembly in biological systems, in particular in the case of special types of biomineralization in compartments.

In this context important work on large inorganic cluster systems based on copper selenide (*e.g.* $[Cu_{146}Se_{73}(PPh_3)_{30}]$),[39a] silver selenide (*e.g.* $[Ag_{172}Se_{40}(SeBu^n)_{92}(dppp)_4]$),[39b] metal cores (*e.g.* $[Al_{77}\{N(SiMe_3)_2\}_{20}]^{2-}$)[40] and polyoxotungstate systems (*e.g.* $[As_{12}Ce_{16}(H_2O)_{36}W_{148}O_{524}]^{76-}$)[41] should be mentioned, too.

The ring-shaped $\{Mo_{154}\}$-type clusters linked to chains can also act as hosts for smaller polyoxometalate guests, such as the (non-reduced) two-fragment $\{Mo_{36}\}$-type cluster.[42] In this novel supramolecular system the interaction between host and guest, which fits exactly into the cavity of the host, is due to 16 hydrogen bonds as well as the Coulomb interaction mediated by four sodium cations located between the negatively charged host and negatively charged guest (Fig. 20).

Facile and high-yield synthesis of the considered compounds with giant cluster anions

The precipitation and isolation of some of the giant cluster anions, mainly those with high solubility, caused difficulties for generations of chemists in the past, but also during the initial phase of our related investigations. Generations of chemists have for instance tried, without success, to isolate pure compounds or even a few crystals (only amorphous material obtained) from molybdenum blue solutions. These contain *e.g.* highly soluble giant cluster anions of the $\{Mo_{154}\}$ type which can be formed by reducing agents from molybdate solutions

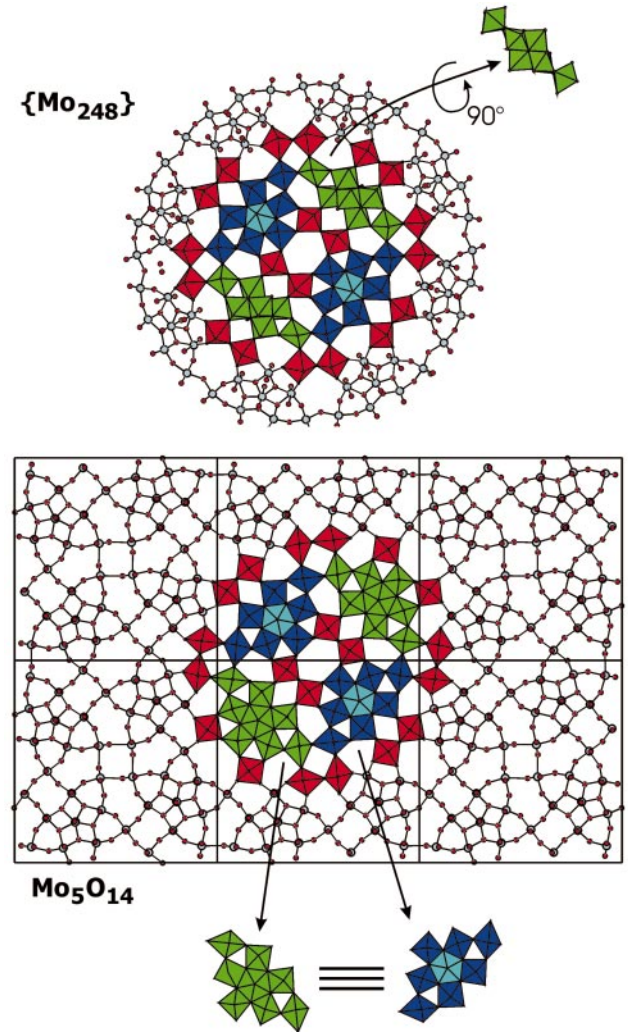

Fig. 19 Structural comparison of the hub-cap motif of the $\{Mo_{248}\}$ cluster and the related segment of the solid-state structure of Mo_5O_{14}. *Above*: schematic representation of one half of the $\{Mo_{248}\}$ cluster with a highlighted $\{Mo_{36}O_{96}(H_2O)_{24}\}$ hub-cap in polyhedral representation. *Below*: structure of Mo_5O_{14} viewed along the *c* axis [see ref. 38(*a*) for details]. Both the hub-caps and the Mo_5O_{14} layer sections each contain four $\{Mo_8\}$ entities surrounding two central $\{Mo_2\}$ units. A central ring of six MoO_6 octahedra is formed by these two $\{Mo_2\}$ units and two MoO_6 octahedra belonging to two opposite $\{Mo_8\}$ entities. Whereas in the case of the Mo_5O_{14} layer section the four $\{Mo_8\}$ entities (two blue; two green) are of the 'usual' type and occur in several of the discussed giant clusters with one central $\{(Mo)Mo_5\}$ pentagon which has two adjacent MoO_6 octahedra, only two of the four $\{Mo_8\}$ entities in the $\{Mo_{248}\}$ hub-caps have that structure. The other two $\{Mo_8\}$ units (in green) consist of a central fragment in which six Mo atoms span an $\{Mo_6\}$ octahedron which is linked to two *trans*-positioned edge-sharing MoO_6 octahedra ($\{Mo_8'\}$ entities). The layers of the solid-state structure of Mo_5O_{14} can be formed by formal superposition of the above-mentioned segment with 36 Mo centers $\{Mo_1\}$: yellow, $\{Mo_2\}$: red).

within minutes.[18,31] In the meantime, we have solved this problem: in the presence of a high electrolyte concentration (method of choice) the solubility is tremendously reduced so that the discrete $\{Mo_{154}\}$- and $\{Mo_{176}\}$-type clusters[30,31,33] and also related compounds with chain[31] and layer[36] structures could be obtained in a high-yield within a short time and in pure crystalline form. The same is valid for the $\{Mo_{132}\}$-Keplerate-type compound which can be obtained as very large crystals for which the precipitation is not problematical.

Where are we? Perspectives

Dynamic light scattering experiments on monodisperse solutions containing the $\{Mo_{154}\}$-type cluster show the presence of colloids with a hydrodynamic radius of *ca.* 40 nm which can

(*a*)

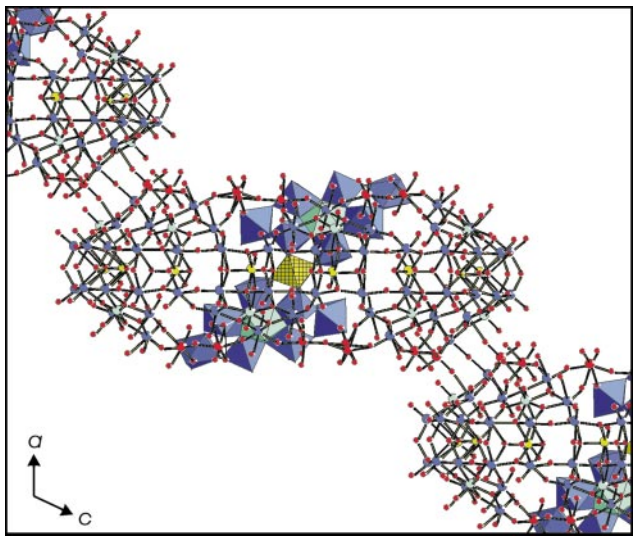

(*b*)

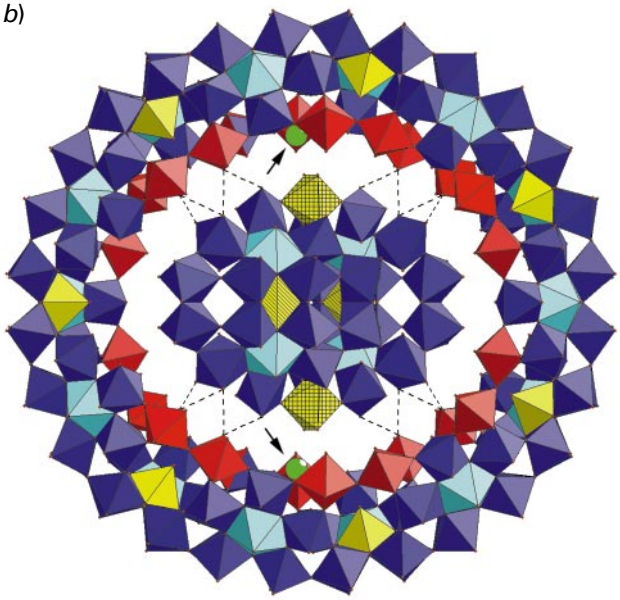

Fig. 20 Some structural details of the novel supramolecular system $\{Mo_{36} \subset Mo_{148}\}$ (occupation of the cavities: *ca.* 20%). (*a*) Part of the chain structure is shown, which is built up by linking ring-shaped cluster units $\{Mo_{148}\}$ (*i.e.* based on the $\{Mo_{154}\}$-type with three missing $\{Mo_2\}$ groups; only the front halves of the rings are shown for clarity). (*b*) View perpendicular to (*a*): the interaction between host and guest is due to 16 hydrogen bonds (dotted lines; O (host) ⋯ O (guest) = 2.744–2.965 Å) and (at least) four sodium cations (green, indicated by arrow, only two Na positions are visible in this perspective view) situated between host and guest. The sodium salt crystallizes in the space group *C*2/*m* (a = 29.425, b = 51.078, c = 30.665 Å, β = 114.85°).

also be isolated and visualized by scanning electron microscopy (Fig. 21).[29] *As the polyoxometalate chemistry covers therefore several orders of magnitude with respect to the number of atoms and the size of the clusters, its nomination as a "Powers of Ten"-type chemistry in accordance with the famous book title seems justified*. Referring to biological systems we are dealing with an order of magnitude comparable in principle to that of the above-mentioned spherical viruses.

Using combinatorially linkable (virtual) building units (as disposition) in solutions of polyoxometalates having library character, the linking of special groups, such as those of the pentagonal $\{(Mo)Mo_5\}$ type, by different types of linker groups or even paramagnetic (open shell) centers, opens new fascinating aspects and possibilities *e.g.* for structural chemistry, supramolecular chemistry, materials science and magneto-chemistry. 'Playing' with pentagons, besides from getting

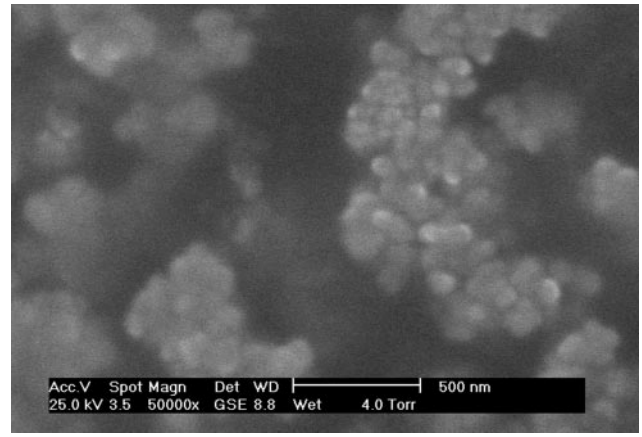

Fig. 21 Scanning electron microscope (Philips ESEM XL30, 25 kV, 3.0 Torr) image showing aggregates with a diameter of *ca.* 500 nm (based on smaller 80 nm particles) which are formed after evaporation of a methanolic solution of $Na_{22}[Mo_{146}O_{442}H_{14}(H_2O)_{58}]\cdot xH_2O$ ($x \approx 250$) (concentration: 0.1 mg ml^{-1}). It is evident that the aggregates tend to form larger arrangements.

several icosahedral-type clusters, is also of interest because of their role in the history of culture and aspects of solid-state physics.[43] Another interesting option is the study of chemical reactions at the surface of giant clusters, *e.g.* to replace H_2O ligands of the wheel-shaped clusters by amphiphilic (head/tail-type) ligands and place paramagnetic centers at the tail inside the cavity while the head replaces H_2O ligands of the parent system. The most interesting challenge will be of course to fill the cavities of the 'opened' ball-type $\{Mo_{132}\}$ cluster (which exists also as lacunary-type system) or through its apertures with a variety of different guests and also to place molecules inside the cavity of the ring- and ball-shaped clusters, which show a different reactivity to the discrete (isolated) ones.

Acknowledgements

We are grateful to the Deutsche Forschungsgemeinschaft and the Fonds der Chemischen Industrie for financial support.

Notes and references

1 A. Müller, F. Peters, M. T. Pope and D. Gatteschi, *Chem. Rev.*, 1998, **98**, 239; M. T. Pope and A. Müller, *Angew. Chem., Int. Ed. Engl.*, 1991, **30**, 34; M. T. Pope, *Heteropoly and Isopoly Oxometalates*, Springer, New York, 1983; *Polyoxometalates: From Platonic Solids to Anti-Retroviral Activity*, ed. M. T. Pope and A. Müller, Kluwer, Dordrecht, 1994.
2 K. C. Nicolaou and E. J. Sorensen, *Classics in Total Synthesis: Targets, Strategies, Methods*, VCH, Weinheim, 1996.
3 H. K. Chae, W. G. Klemperer and T. A. Marquart, *Coord. Chem. Rev.*, 1993, **128**, 209.
4 A. Müller, E. Krickemeyer, H. Bögge, M. Schmidtmann and F. Peters, *Angew. Chem., Int. Ed.*, 1998, **37**, 3360.
5 L. Liljas and B. Strandberg, in *Biological Macromolecules and Assemblies, Vol. I, Virus Structures*, ed. F. A. Jurnak and A. McPherson, Wiley, New York, 1984, p. 97.
6 (*a*) D. Voet and J. G. Voet, *Biochemistry*, Wiley, New York, 2nd edn., 1995; (*b*) B. Alberts, D. Bray, J. Lewis, M. Raff, K. Roberts and J. D. Watson, *Molecular Biology of the Cell*, Garland, New York, 3rd edn., 1994; (*c*) B. D. Davis, R. Dulbecco, H. N. Eisen and H. S. Ginsberg, *Microbiology*, Harper & Row, Philadelphia, 3rd edn., 1980; (*d*) S. C. Harrison, *Trends Biochem. Sci.*, 1984, **9**, 345.
7 A. Müller, V. P. Fedin, C. Kuhlmann, H. Bögge and M. Schmidtmann, *Chem. Commun.*, 1999, 927.
8 J. Kepler, *Mysterium Cosmographicum*, 1596. See also: M. Kemp, *Nature*, 1998, **393**, 123.
9 *Combinatorial Chemistry: Synthesis and Application*, ed. S. R. Wilson and A. W. Czarnik, Wiley, New York, 1997; N. K. Terrett, *Combinatorial Chemistry*, Oxford University Press, Oxford, 1998.
10 D. Voet and J. G. Voet, *Biochemistry*, Wiley, New York, 2nd edn., 1995, p. 1076.
11 First reports about the $\{Mo_{57}V_6\}$ cluster appeared in 1993 [(*a*) S. Zhang, G. Huang, M. Shao and Y. Tang, *J. Chem. Soc., Chem. Commun.*, 1993,

37; (*b*) A. Müller, E. Krickemeyer, S. Dillinger, H. Bögge, A. Proust, W. Plass and R. Rohlfing, *Naturwissenschaften*, 1993, **80**, 560]. Different related clusters were published later and errors concerning the first formula of the complicated system were corrected: (*c*) A. Müller, E. Krickemeyer, S. Dillinger, H. Bögge, W. Plass, A. Proust, L. Dloczik, C. Menke, J. Meyer and R. Rohlfing, *Z. Anorg. Allg. Chem.*, 1994, **620**, 599; (*d*) A. Müller, W. Plass, E. Krickemeyer, S. Dillinger, H. Bögge, A. Armatage, C. Beugholt and U. Bergmann, *Monatsh. Chem.*, 1994, **125**, 525; (*e*) A. Müller, W. Plass, E. Krickemeyer, S. Dillinger, H. Bögge, A. Armatage, A. Proust, C. Beugholt and U. Bergmann, *Angew. Chem., Int. Ed. Engl.*, 1994, **33**, 849; (*f*) A. Müller, H. Bögge, E. Krickemeyer and S. Dillinger, *Bull. Pol. Acad. Sci. Chem.*, 1994, **42**, 291. For details on the relevant basic $\{Mo_8\}$ unit see also: A. Müller and C. Beugholt, *Nature*, 1996, **383**, 296.

12 For the two-fragment cluster type see also K.-H. Tytko, B. Schönfeld, B. Buss and O. Glemser, *Angew. Chem., Int. Ed. Engl.*, 1973, **12**, 330 with the corrected formula in B. Krebs, S. Stiller, K.-H. Tytko and J. Mehmke, *Eur. J. Solid Inorg. Chem.*, 1991, **28**, 883.

13 A. Müller, E. Krickemeyer, J. Meyer, H. Bögge, F. Peters, W. Plass, E. Diemann, S. Dillinger, F. Nonnenbruch, M. Randerath and C. Menke, *Angew. Chem., Int. Ed. Engl.*, 1995, **34**, 2122.

14 D. Bradley, *New Sci.*, November Issue, 1995, **148**, 18.

15 G. Schmid, in *From Simplicity to Complexity in Chemistry–and Beyond, Part I*, ed. A. Müller, A. Dress and F. Vögtle, Vieweg, Wiesbaden, 1996, p. 149; see also: *Clusters and Colloids: From Theory to Applications*, ed. G. Schmid, VCH, Weinheim, 1996; G. Schmid, *J. Chem. Soc., Dalton Trans.*, 1998, 1077; see also ref. 40.

16 J. Horgan, *Sci. Am.*, June Issue, 1995, 74.

17 A. Dömling and I. Ugi, *Angew. Chem., Int. Ed. Engl.*, 1993, **32**, 563(916); I. Ugi, *Proc. Estonian Acad. Sci. Chem.*, 1995, **44**, 237.

18 *Gmelins Handbuch der Anorganischen Chemie, Molybdän*, Verlag Chemie, Berlin, 1935, pp. 134–147; *Gmelin Handbook of Inorganic Chemistry, Molybdenum Suppl., Vol. B3a*, Springer, Berlin, 8th edn., 1987, pp. 61–68. See also: A. Müller, J. Meyer, E. Krickemeyer and E. Diemann, *Angew. Chem., Int. Ed. Engl.*, 1996, **35**, 1206.

19 (*a*) A. Müller, H. Reuter and S. Dillinger, *Angew. Chem., Int. Ed. Engl.*, 1995, **34**, 2311; (*b*) A. Müller, *Nature*, 1991, **352**, 115.

20 A. Müller, R. Sessoli, E. Krickemeyer, H. Bögge, J. Meyer, D. Gatteschi, L. Pardi, J. Westphal, K. Hovemeier, R. Rohlfing, J. Döring, F. Hellweg, C. Beugholt and M. Schmidtmann, *Inorg. Chem.*, 1997, **36**, 5239; A. Müller, E. Krickemeyer, M. Penk, R. Rohlfing, A. Armatage and H. Bögge, *Angew. Chem., Int. Ed. Engl.*, 1991, **30**, 1674.

21 H. Haken, *Synergetics: An Introduction*, Springer, Berlin, 2nd edn., 1978.

22 A. Müller, E. Diemann, E. Krickemeyer and S. Che, *Naturwissenschaften*, 1993, **80**, 77. Also see reference 19 as well as M.-M. Rohmer, M. Bénard, J. Maestre and J.-M. Poblet, *Coord. Chem. Rev.*, 1998, **178–180**, 1019.

23 W. G. Klemperer, T. A. Marquart and O. M. Yaghi, *Angew. Chem., Int. Ed. Engl.*, 1992, **31**, 49; A. Müller, R. Rohlfing, E. Krickemeyer and H. Bögge, *Angew. Chem., Int. Ed. Engl.*, 1993, **32**, 909.

24 A. Müller, R. Rohlfing, J. Döring and M. Penk, *Angew. Chem., Int. Ed. Engl.*, 1991, **30**, 588.

25 A. Müller, J. Meyer, E. Krickemeyer, C. Beugholt, H. Bögge, F. Peters, M. Schmidtmann, P. Kögerler and M. J. Koop, *Chem. Eur. J.*, 1998, **4**, 1000.

26 (*a*) M. I. Khan, A. Müller, S. Dillinger, H. Bögge, Q. Chen and J. Zubieta, *Angew. Chem., Int. Ed. Engl.*, 1993, **32**, 1780; A. Müller, S. Dillinger, E. Krickemeyer, H. Bögge, W. Plass, A. Stammler and R. C. Haushalter, *Z. Naturforsch., Teil B*, 1997, **52**, 1301; (*b*) M. I. Khan and J. Zubieta, *J. Am. Chem. Soc.*, 1992, **114**, 10 058; M. I. Khan, Q. Chen, J. Salta, C. J. O'Connor and J. Zubieta, *Inorg. Chem.*, 1996, **35**, 1880.

27 A. Müller, W. Plass, E. Krickemeyer, R. Sessoli, D. Gatteschi, J. Meyer, H. Bögge, M. Kröckel and A. X. Trautwein, *Inorg. Chim. Acta*, 1998, **271**, 9; D. Gatteschi, R. Sessoli, W. Plass, A. Müller, E. Krickemeyer, J. Meyer, D. Sölter and P. Adler, *Inorg. Chem.*, 1996, **35**, 1926. For other related aspects, see: D. Gatteschi, A. Caneschi, L. Pardi and R. Sessoli, *Science*, 1994, **265**, 1054.

28 A. Müller, M. Koop, H. Bögge, M. Schmidtmann, F. Peters and P. Kögerler, *Chem. Commun.*, to be submitted.

29 A. Müller, W. Eimer, E. Diemann and C. Serain, in press.

30 A. Müller, E. Krickemeyer, S. Q. N. Shah, H. Bögge, M. Schmidtmann and B. Hauptfleisch, *Inorg. Chem.*, to be published.

31 A. Müller, S. K. Das, V. P. Fedin, E. Krickemeyer, C. Beugholt, H. Bögge, M. Schmidtmann and B. Hauptfleisch, *Z. Anorg. Allg. Chem.*, 1999, **625**, 1187.

32 A. Müller, E. Krickemeyer, H. Bögge, M. Schmidtmann, C. Beugholt, P. Kögerler and C. Lu, *Angew. Chem., Int. Ed.*, 1998, **37**, 1220; see also: C. Jiang, Y. Wei, Q. Liu, S. Zhang, M. Shao and Y. Tang, *Chem. Commun.*, 1998, 1937.

33 A. Müller, M. Koop, H. Bögge, M. Schmidtmann and C. Beugholt, *Chem. Commun.*, 1998, 1501.

34 A. Müller, E. Krickemeyer, H. Bögge, M. Schmidtmann, C. Beugholt, S. K. Das and F. Peters, *Chem. Eur. J.*, 1999, **5**, 1496.

35 A. Müller, E. Krickemeyer, H. Bögge, M. Schmidtmann, F. Peters, C. Menke and J. Meyer, *Angew. Chem., Int. Ed. Engl.*, 1997, **36**, 484.

36 A. Müller, S. K. Das, H. Bögge, C. Beugholt and M. Schmidtmann, *Chem. Commun.*, 1999, 1035.

37 A. Müller, S. Q. N. Shah, H. Bögge and M. Schmidtmann, *Nature*, 1999, **397**, 48; P. Ball, *Nature*, 1998, **395**, 745.

38 (*a*) A. Müller and B. Hauptfleisch, in preparation; (*b*) L. Kihlborg, *Ark. Kemi*, 1963, **21**, 427.

39 (*a*) H. Krautscheid, D. Fenske, G. Baum and M. Semmelmann, *Angew. Chem., Int. Ed. Engl.*, 1993, **32**, 1303; (*b*) D. Fenske, N. Zhu and T. Langetepe, *Angew. Chem., Int. Ed.*, 1998, **37**, 2640.

40 A. Ecker, E. Weckert and H. Schnöckel, *Nature*, 1997, **387**, 379.

41 K. Wassermann, M. H. Dickman and M. T. Pope, *Angew. Chem., Int. Ed. Engl.*, 1997, **36**, 1445.

42 A. Müller *et al.*, in preparation.

43 A. L. Mackay, in *Quasicrystals, Networks, and Molecules of Fivefold Symmetry*, ed. I. Hargittai, VCH, Weinheim, 1990.

Paper 9/01436E

ChemComm

Gold(III)-induced oxidation of glycine†

Juan Zou, Zijian Guo, John A. Parkinson, Yu Chen and Peter J. Sadler*

Department of Chemistry, University of Edinburgh, King's Buildings, West Mains Road, Edinburgh, UK EH9 3JJ. E-mail: P.J.Sadler@ed.ac.uk

Received (in Cambridge, UK) 1st April 1999, Accepted 11th June 1999

NMR investigations of isotopically-labelled glycine show that Au^{III} induces deamination and subsequent decarboxylation of the amino acid with formation of glyoxylic acid, NH_4^+, formic acid, CO_2 and metallic gold.

Several injectable 1:1 Au(I)–thiolate complexes and an orally-active Au(I)–phosphine complex are used clinically for the treatment of difficult cases of rheumatoid arthritis.[1] Their clinical application is limited, however, owing to severe host toxicity such as kidney damage and blood disorders. The molecular basis for these toxic side-effects of chrysotherapy is poorly understood[2] but recently Gleichmann *et al.*[3] have demonstrated that the oxidation of Au(I) to Au(III) *in vivo* may be responsible for some of the observed toxicity. In inflammatory situations, strong oxidants such as hypochlorite (ClO^-) and hydrogen peroxide (H_2O_2) are potentially available *in vivo* and can oxidise Au(I)–thiolates and Au(I)–phosphines to Au(III).[4] In view of this, and the antitumour activity of some Au(III) complexes,[5] it is important to understand the chemistry of Au(III)–biomolecule interactions. Surprisingly, there are only a few reports of reactions of Au(III) with amino acids, and these have focused on the sulfur-containing amino acids, namely cyst(e)ine and methionine.[6,7,8] Au(III) can cleave the disulfide bond of cystine to give the sulfonic acid[6,7] and can oxidise the sulfur of methionine stereospecifically to the sulfoxide.[8] We report here the first elucidation of the pathway of Au(III)-induced oxidation of the amino acid glycine. The identification of reaction intermediates and final products was made possible by the use of ^{13}C and ^{15}N isotopic labelling and multinuclear NMR spectroscopy.‡ The proposed stepwise oxidation mechanism provides a basis for obtaining further insights into the mechanism of gold drug toxicity.

Reactions of $[Au^{III}Cl_4]^-$ **1** with [^{15}N]glycine [^{15}N] **2** (1:2, starting pH 2.44)§ were monitored by 1D ^1H NMR (data acquired at intervals over a 12 h period) and by 2D [^1H, ^{15}N] HSQC-TOCSY NMR spectroscopy (acquired after 8 h of reaction).[9] On the basis of these results, a mechanism for the reaction of Au(III) with glycine can be proposed (Scheme 1). Initial coordination of Gly to Au(III) *via* the amino group gives $[AuCl_3(Gly\text{-}N)]$ **3** [δ(^1H): CH_2 3.85; δ($^1H/^{15}N$): $^{15}NH_2$ 6.88/2.6], which can undergo chelation to form $[AuCl_2(Gly\text{-}N,O)]$ **4** [δ(^1H): CH_2 3.75; δ($^1H/^{15}N$): $^{15}NH_2$ 6.75/−9.2]. The identification of the O,N-chelate **4** is based on chemical shift arguments compared with analogous Pt(II)–am(m)ine systems.[10] For example, δ(^{15}N) of S,N-chelated Met in [Pt(Hdien-*N*,*N*)(^{15}N-Met-*S*,*N*)] is *ca.* 10 ppm to lower frequency compared to monodentate Met in [Pt(dien)(^{15}N-Met-*N*)].[11] In our case, δ(^{15}N) for $^{15}NH_2$ of coordinated Gly differs by 12 ppm between the monodentate and O,N-chelate Au complexes.

Once formed, the chelate **4** appears to be unreactive. A two-electron transfer from Gly to Au(III) in **3** gives rise to a Au(I)–imine intermediate. Imines with a proton on N are seldom stable and are known to undergo fast hydrolysis to the corresponding aldehyde and NH_4^+.[12] An imine ligand on Au(I) would also be readily displaced by Cl^- and would hydrolyse to give glyoxylic acid **6** [^1H: δ 5.31(s)] with concomitant formation of NH_4^+ **5** [δ 7.09 (d, $^1J_{HN}$ 73 Hz)] and Au(0). The identity of **6** was revealed by further experiments. This species was stable over the pH range 1.45–12.3 and a pH titration gave an associated pK_a of 3.42. ^{13}C–{^1H} DEPT NMR data (CH group, ^{13}C: δ 89.4) suggested assignment to the aldehyde group of glyoxylic acid (lit.,[13] pK_a 3.46 at 298 K, I = 0). NMR spectra of glyoxylic acid recorded at the same pH (^1H: δ 5.36; ^{13}C: δ 173.6 and 89.7) further supported this assignment.

Both the Au(III)– and Au(I)–imine intermediates are too unstable to be observed by NMR during the reactions. The NH_4^+ produced reacts with $[AuCl_4]^-$ to give Au(III)-ammine adducts such as $[AuCl_3(NH_3)]$ **7**. This species was identified by reaction of **1** with $^{15}NH_4Cl$ (1:2, pH 2.98). It gave rise to a major HSQC cross-peak ($^1H/^{15}N$: δ 5.93/−12.9), which exhibited $^1H/^2H$ isotope shift effects[14–16] and chemical shifts very similar to those of **7**. Further substitution of Cl^- ligands by NH_3 is known to be difficult to achieve, and formation of $[Au(NH_3)_4]^{3+}$ requires the use of a large excess (super-saturated solutions) of NH_4^+ together with NH_3 gas.[17] Oxidative decarboxylation of glyoxylic acid *via* further reaction with Au(III) gives rise to formic acid **8**, carbon dioxide **9** and Au(0). This was confirmed by two separate reactions of **1** with glyoxylic acid to give formic acid **8** (^1H: δ 8.20, pH 1.52) and with 2-[^{13}C]Gly **2** to give [^{13}C]**8** (^1H: δ 8.20, $^1J_{CH}$ 218 Hz, ^{13}C: δ 166.4). Therefore formic acid is formed from the aldehyde

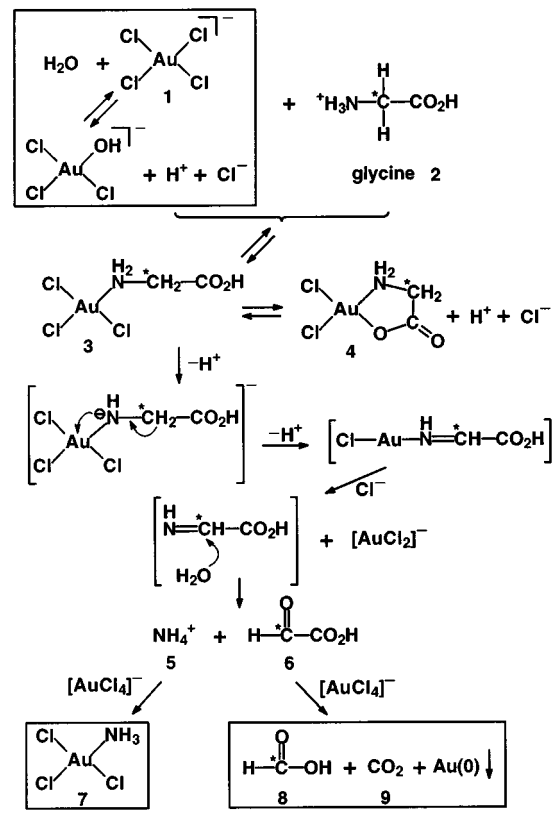

Scheme 1

† Reactions of $[Au^{III}Cl_4]^-$ **1** with [^{15}N]glycine as monitored by 1D ^1H NMR and 2D [^1H, ^{15}N] HSQC-TOCSY NMR can be viewed in electronic form, see: http://www.rsc.org/suppdata/cc/1999/1359/.

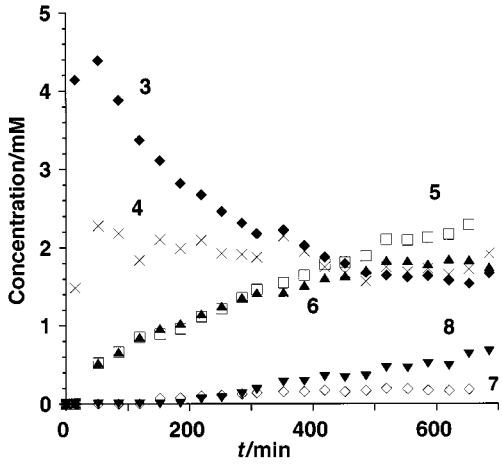

Fig. 1 Concentration *vs.* time profiles for species observed during the reaction of $[AuCl_4]^-$ **1** (15 mM) with [^{15}N]glycine ([^{15}N]**2**) (30 mM) at pH 2.87, 298 K. Concentrations were obtained from peak integrals using TSP as a standard. The profile for free Gly (*ca*. 70% unreacted after 10 h) is not shown.

group of glyoxylic acid. Formic acid can be further oxidised by Au(III) to give Au(0) and carbon dioxide,[18] but this step was not observed in the current study using 2-[^{13}C]Gly, probably due to the slow rate of the reaction at low pH.[18] The variations in concentration of the species observed by NMR during the reaction of **1** with [^{15}N]**2** with time are shown in Fig 1.

Reactions of **1** with [^{15}N]**2** at higher molar ratios gave rise to similar NMR spectra but higher product yields. For example, in the presence of a 10-fold excess of **1**, all [^{15}N]**2** reacted within 14 h. The ^{1}H NMR spectrum of a solution containing **1** and [^{15}N]**2** in a 1 : 2 molar ratio, pH 7.14, recorded after 14 h showed peaks for the CH_2 signal of [^{15}N]**2** at δ 3.56, together with singlets at δ 5.07 (assigned to the CH of glyoxylate) and at δ 8.46 (assigned to formate). The course of the reaction between **1** and **2** at physiological pH§ therefore appears to be similar to that at low pH. However, rapid proton exchange at pH 7[19] made it impossible to carry out a detailed ^{1}H,^{15}N NMR study.

The mechanism in Scheme 1 predicts that the products from the reaction§ of DL-alanine with $[AuCl_4]^-$ should be NH_4^+, pyruvic acid and acetylaldehyde. This was verified by ^{1}H and ^{13}C NMR spectroscopy, although the reaction was slower than that of Gly.

A parallel mechanism has recently been proposed for Fe(III)-assisted oxidative cleavage of a C–N bond.[20] Fe(III)-bound bis(2-pyridylmethyl)aminoacetate (BPG) is transformed into Fe(III)–bis(2-pyridylmethyl)amine *via* an Fe(III)–imine intermediate which undergoes hydrolysis with release of glyoxylic acid. Photodecomposition of complexes such as $[Co^{III}(Gly_3)]$ and $[Co^{III}(Ala_3)]$ have been reported to give rise to dipeptide amides, together with CO_2 and aldehydes.[21] Photoredox transformation of an Fe(III) complex with *N*-(phosphonomethyl)glycine has also been reported, and when irradiated with UV light the Gly derivative decomposes to give formaldehyde, ammonia and a new species containing phosphorus.[22] The reactions with Au(III) studied here were not activated by light.¶

Gold(III)-induced oxidation of Gly and related amino acids may be important in relation to the severe toxicity of gold drugs. It is possible that Au(III) can also deaminate the amino terminus of peptides and proteins. For example, during the reactions of Au(III) with tripeptides GGH and GGG, the formation of colloidal gold is observed together with other unidentified species.[23] Au(III) modification of peptides is likely to influence MHC peptide presentation and T cell recognition systems, allowing gold to have a major influence on the immune system.

We thank the Wellcome Trust (Wellcome Travelling Research Fellowship to J. Z), the Biotechnology and Biological Sciences Research Council, and the Engineering and Physical Science Research Council for their support for this work, the CVCP for an ORS Award to Y. C., Professor A. M. Sargeson (Australian National University) and Dr R. M. Hartshorn (University of Canterbury, New Zealand) for helpful discussion, and Johnson Matthey plc for loan of gold salts.

Notes and references

‡ NMR spectra were recorded at 298 K on a Brüker DMX 500 NMR spectrometer (^{1}H 500.13 MHz, ^{15}N 50.7 MHz), using the procedures described previously.[24] The 1D ^{13}C-{^{1}H} and 2D [^{1}H, ^{13}C] HETCOR NMR spectra were acquired using standard procedures.

§ NMR samples were prepared in 90% H_2O–10% D_2O (600 μl). Fresh solutions of $Na[AuCl_4]\cdot 2H_2O$ (30 mM) and Gly (60 mM) were prepared separately and then mixed in the following molar ratios (Au : Gly) at 298 K: 1 : 1, 2 : 1, 3 : 1, 5 : 1, 8 : 1, 10 : 1, 1 : 2 and 1 : 4. Fresh solutions of DL-Ala and $[AuCl_4]^-$ were mixed in a 2 : 1 molar ratio at 298 K. The concentration of $[AuCl_4]^-$ was 15 mM for all reactions. For reactions at neutral pH, the pH values of the solutions of $[AuCl_4]^-$ and Gly were adjusted separately prior to mixing, and remeasured immediately after mixing.

¶ The same products were observed for the reactions conducted under N_2 and in the absence of light.

1 C. F. Shaw III, *Perspect. Biol. Med*., 1979, **2**, 287; P. J. Sadler, *Struct. Bonding (Berlin)*, 1976, **29**, 171; K. C. Dash and H. Schmidbaur, *Met. Ions Biol. Syst*., 1983, **14**, 180; P. J. Sadler and R. E. Sue, *Metal-Based Drugs*, 1994, **1**, 107.
2 C. F. Shaw III, *Comments Inorg. Chem*., 1989, **8**, 233; S. L. Best and P. J. Sadler, *Gold Bull*., 1996, **29**, 87.
3 E. Gleichmann, D. Schuhmann and M. Kubickamuranyi, *Eur. J. Pharmacol*., 1990, **183**, 78.
4 C. F. Shaw III, S. Schraa, E. Gleichmann, Y. P. Grover, L. Dunemann and A. Jagarlamudi, *Metal-Based Drugs*, 1994, **1**, 351; K. Takahashi, P. Griem, C. Goebel, J. Gonzalez and E. Gleichmann, *Metal-Based Drugs*, 1994, **1**, 483.
5 R. V. Parish, B. P. Howe, J. P. Wright, J. Mack, R. G. Pritchard, R. G. Buckley, A. M. Elsome and S. P. Fricker, *Inorg. Chem*., 1996, **35**, 1659; P. Calamai, S. Carotti, A. Guerri, T. Mazzei, L. Messori, E. Mini, P. Orioli and G. P. Speroni, *Anti-Cancer Drug Des.*, 1998, **13**, 67.
6 C. F. Shaw III, M. P. Cancro, P. L. Witkiewicz and J. E. Eldridge, *Inorg. Chem.*, 1980, **19**, 3198; P. L. Witkiewicz and C. F. Shaw III, *J. Chem. Soc., Chem. Commun*., 1981, 1111.
7 D. H. Brown and W. E. Smith, *Am. Chem. Soc. Symp. Ser*., 1983, **209**, 401; W. E. Smith and J. Reglinski, *Perspect. Bioinorg. Chem.*, 1991, **1**, 183.
8 E. Bordignon, L. Cattalini, G. Natile and A. Scatturi, *J. Chem. Soc., Chem. Commun*., 1973, 878; G. Natile, E. Bordignon and L. Cattalini, *Inorg. Chem.*, 1976, **15**, 246; A. A. Isab and P. J. Sadler, *Biochim. Biophys. Acta*, 1979, **492**, 322.
9 To view supplementary data in electronic form see: http://www.rsc.org/suppdata/cc/1999/1359.
10 S. J. Berners-Price and P. J. Sadler, *Coord. Chem. Rev*., 1996, **151**, 1, and references therein.
11 Y. Chen, Z. Guo, P. del S. Murdoch, E. Zang and P. J. Sadler, *J. Chem. Soc., Dalton Trans*., 1998, 1503.
12 *Advanced Organic Chemistry: Reactions, Mechanisms, and Structure*, ed. J. March, John Wiley & Sons, New York, 1985, p. 784.
13 *Critical Stability Constants*, ed. A. E. Martell and R. M. Smith, Plenum Press, New York, 1977, p. 65.
14 T. C. Stringfellow, G. Wu and R. E. Wasylishen, *J. Phys. Chem. B*, 1997, **101**, 9651.
15 R. B. Calvert and J. R. Shapley, *J. Am. Chem. Soc*., 1978, **100**, 7726.
16 F. A. L. Anet and A. H. Dekmezian, *J. Am. Chem. Soc*., 1979, **101**, 5449.
17 L. H. Skibsted and J. Bjerrum, *Acta Chem. Scand., Ser. A*, 1974, **28**, 740.
18 B. S. Maritz and R. van Eldik, *J. Inorg. Nucl. Chem*., 1976, **38**, 1749.
19 *NMR of Proteins and Nucleic Acids*, ed. K. Wüthrich, John Wiley & Sons, New York, 1986, p. 24.
20 M.-C. Rodriguez, F. Lambert, I. Morgenstern-Badarau, M. Cesario, J. Guilhem, B. Keita and L. Nadjo, *Inorg. Chem*., 1997, **36**, 3525.
21 V. Balzani, V. Carassiti, V. Moggi and N. Sabbatini, *Inorg. Chem.*, 1965, **4**, 1247.
22 M. J. Sima, *Chem. Pap.—Chem. Zvesti*., 1997, **51**, 258.
23 S. L. Best, Ph. D. thesis, University of London, 1996.
24 N. Kratochwil, Z. Guo, P. del S. Murdoch, J. A. Parkinson, P. J. Bednarski and P. J. Sadler, *J. Am. Chem. Soc*., 1998, **120**, 8253; Y. Chen, Z. Guo, J. A. Parkinson and P. J. Sadler, *J. Chem. Soc., Dalton Trans*., 1998, 3577.

Communication 9/02646K

Multi-valent polymer of vancomycin: enhanced antibacterial activity against VRE

Hirokazu Arimoto,*[a] Kazuya Nishimura,[a] Tomoya Kinumi,[b] Ichiro Hayakawa[a] and Daisuke Uemura[c]

[a] *Department of Chemistry, Faculty of Science, Shizuoka University, Ohya, Shizuoka 422-8529, Japan. E-mail: scharim@ipc.shizuoka.ac.jp*
[b] *Department of Biochemistry and Cell Biology, National Institute of Infectious Diseases, Tokyo 162-8640, Japan*
[c] *Department of Chemistry, Graduate School of Science, Nagoya University, Chikusa, Nagoya 464-8602, Japan*

Received (in Cambridge, UK) 4th May 1999, Accepted 14th June 1999

A multivalent polymer of vancomycin, synthesized *via* ring-opening metathesis polymerization (ROMP), exhibited significant enhancement of antibacterial activity against vancomycin-resistant enterococci (VRE).

The history of the fight against infectious bacteria centers around the recurring problem of drug resistance. For example, the evolution of MRSA (methicilin-resistant *Staphylococcus aureus*), which resists almost all established antibiotics, is now a serious worldwide problem. Currently the only viable treatment for MRSA is vancomycin. However, VRE (vancomycin resistant enterococci) has emerged, and the possibility of this resistance being transferred to *S. aureus* is a cause of major concern.[1] Although much effort has been put forth to locate new antibiotics, no alternatives to vancomycin-class glycopeptides have been found. Thus, novel strategies to modify the glycopeptides to enhance their potency against VRE are in great demand.

We have been interested in the rapidly growing molecular design principle of multivalent or cluster effects for the enhancement of weak non-bonding interactions.[2,3] Although successful applications of this concept with sugar ligands have been reported, it has not been further generalized to the recognition of complex natural products or peptides.[4] Vancomycin binds to the D-Ala-D-Ala residue of the pentapeptide terminal of a bacterial biosynthetic intermediate through five hydrogen bonds.[5] Since this binding interferes with bacterial peptidoglycan biosynthesis, it is widely believed that strengthening the association could enhance antibacterial activity. We describe herein our preliminary attempts to enhance the potency of vancomycin-class antibiotics against VRE by the formation of vancomycin-based polymers (Fig. 1).

Vancomycin contains a variety of functional groups sensitive to basic, acidic and oxidative conditions,[6,7] which necessitates careful consideration of strategies for both the modification and polymerizations steps. We chose to pursue a ring-opening metathesis polymerization (ROMP) approach. Among the known ROMP catalysts, Grubb's ruthenium catalyst[8] appeared to be well suited, as it is tolerant to polar functional groups, and applications to sugars and protected oligopeptides have appeared. However, deactivation of the catalyst by free amino groups has been demonstrated, and the functional group tolerance of the catalyst to primary amide, carboxylic acids, and phenols has not been fully established.[9]

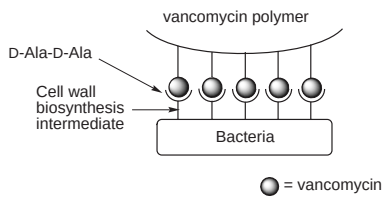

Fig. 1 Schematic presentation of the interaction of a vancomycin polymer with a bacterial cell wall biosynthesis intermediate.

Transformation of vancomycin to a ROMP monomer was accomplished as shown in Scheme 1. An aromatic aldehyde, which was linked to the metathesis-active norbornene unit, was appended onto vancomycin by regioselective reductive amination.[10] ^{1}H NMR and MALDI-TOF mass spectroscopy (*m/z* 1757, M + 1) data[11] were consistent with the structure of monomer unit **1**. The regioselectivity for the amino-sugar portion over the N-terminal secondary amine was further established through a fragmentation analysis of a PSD experiment on the MALDI-TOF mass spectra (*m/z* 617, average mass, see Scheme 1).

The ring-opening metathesis polymerization was investigated under two different sets of conditions. When the polymerization was conducted in aqueous emulsion condi-

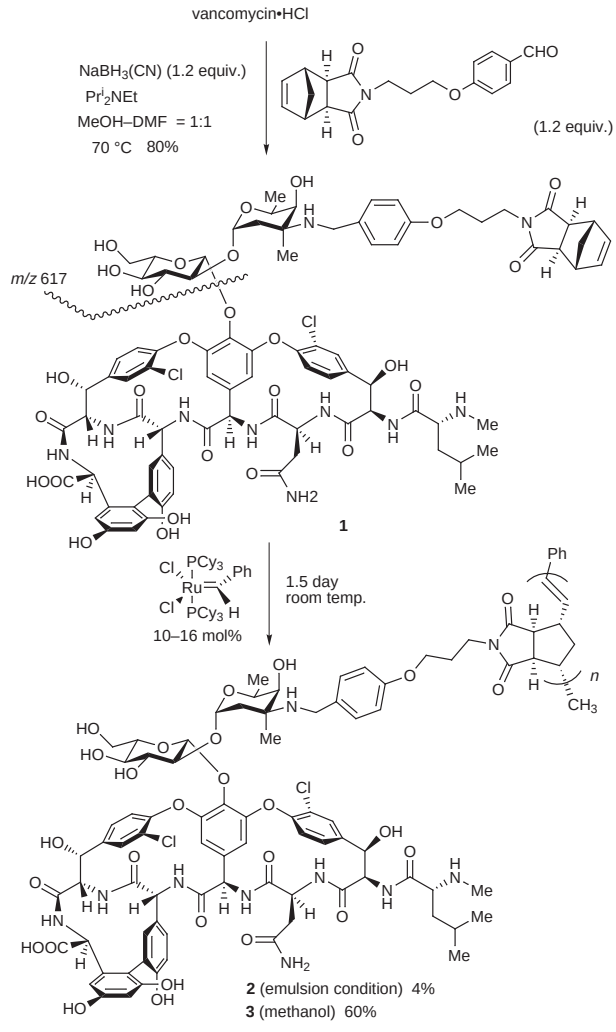

Scheme 1

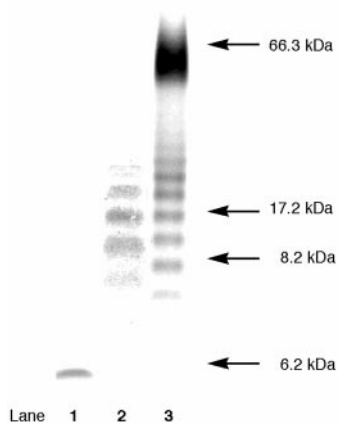

Fig. 2 Electrophoresis of compounds **1**–**3** [16% Tris–Tricine SDS–polyacrylamide gel (silver stained)]: lane 1 = monomer **1**; lane 2 = polymer **3**; lane 3 = polymer **2**.

tions,[12] the reaction was slow and the yield of polymer was only 4%. A significant improvement was observed with MeOH as the solvent in the standard homogeneous system. After 1.5 days reaction time, removal of unreacted monomer and catalyst by reversed phase column chromatography (Cosmosil 75C_{18}-OPN, MeCN–H_2O = 1:2, 1% TFA) afforded 60% yield of polymeric material **3**.[13] Polymerization was evidenced by broadened signals in the ^{1}H NMR spectra, as well as the disappearance of the norbornene olefinic proton signals. Polymer formation was also monitored by SDS-PAGE electrophoresis, which indicated the difference in molecular weight distribution of the two reactions (Fig. 2).

Antibacterial activities of monomer **1** and polymers **2** and **3** were thus evaluated (Table 1). The antibacterial properties of vancomycin were not affected by introduction of the norbornene unit present in **1**. In contrast, polymerization of **1** to **3** resulted in a significant (8 to 60 fold) enhancement of potency agaisnt VREs, with retention of practical MIC values against *S. aureus* and *Enterococci*. The reason for the marked differences in potency between **2** and **3** is not clear at this stage, but may be due either to the polymer weight distributions or to the substructural difference of each polymer. These results suggest that polyvalent polymers may be promising tools in the fight against multi-resistant bacteria.

Table 1 Antibacterial activities of compounds **1**–**3**

	MIC/μg ml^{-1}			
Compound	*S. aureus*[a]	*Entero-coccus*[b]	VRE (Van A)[c]	VRE (Van B)[d]
VCM	0.2	< 0.5	> 250	125
1	0.2	< 0.5	> 250	125
2	—	31	> 250	31
3	2.3	2	31	2

[a] Mean of six strains of *S. aureus*, which include clinically isolated MRSA. [b] *Enterococcus faecalis*. [c] NCB40. [d] RV1.

In conclusion, we have prepared multivalent polymers of vancomycin that displayed significant antibacterial activity enhancement against VRE. Further efforts towards the understanding of this enhancement will be reported in due course.

The authors thank Dr Yoshichika Arakawa, National Institute of Infectious Diseases, and Dr Kiyoshi Nakayama, Daiichi Pharmaceutical Co. Ltd., for antibacterial tests, Dr Masahiro Uritani, Shizuoka University, for SDS-PAGE analysis, and Professor William Moser of IUPUI for helpful discussions and for critiquing the manuscript. This research was partly supported by a Grant-in-Aid for Scientific Research from the Ministry of Education, Science, Sports and Culture, Japan and a Sasakawa Scientific Research Grant from the Japan Science Society.

Notes and references

1 For recent reviews on this field, see D. Niccolai, L. Tarsi and R. J. Thomas, *Chem. Commun.*, 1997, 2333. See also D. H. Williams and B. Bardsley, *Angew. Chem., Int. Ed.*, 1999, **38**, 1173.
2 M. Mammen, S. K. Choi and G. M. Whitesides, *Angew. Chem., Int. Ed.*, 1998, **37**, 2754.
3 L. L. Kiessling and N. L. Pohl, *Chem. Biol.*, 1996, **3**, 71.
4 For some examples of multivalent polymers with non-sugar ligands: V. C. Gibson, E. L. Marshall, M. North, D. A. Robson and P. J. Williams, *Chem. Commun.*, 1997, 1095; S. C. G. Biagini, V. C. Gibson, M. R. Giles, E. L. Marshall and M. North, *Chem. Commun.*, 1997, 1097.
5 D. H. Williams, *Nat. Prod. Rep.*, 1996, **13**, 469. In VanA and VanB resistance, pentapeptide terminals are changed from -D-Ala-D-Ala to -D-Ala-D-Lac, which makes the binding of vancomycin considerably weaker.
6 C. M. Harris, H. Kopecka and T. M. Harris, *J. Am. Chem. Soc.*, 1983, **105**, 6915.
7 Vancomycin is also sensitive to acidic and oxidative conditions, see R. Nagarajan and A. A. Schabel, *Chem. Commun.*, 1988, 1306; M. Adamczyk, J. Grote and S. Rege, *Bioorg. Med. Chem. Lett.*, 1998, **8**, 885 and references therein.
8 P. Schwab, M. B. France, J. W. Ziller and R. H. Grubbs, *Angew. Chem., Int. Ed. Engl.*, 1995, **34**, 2039.
9 For compatibility of metathesis catalysts with various functional groups, see review: S. K. Armstrong, *J. Chem. Soc., Perkin Trans. 1*, 1998, 371. See also R. H. Grubbs and S. Chang, *Tetrahedron*, 1998, **54**, 4413; M. L. Randall and M. L. Snapper, *J. Mol. Catal. A: Chem.*, 1998, **133**, 29.
10 R. D. G. Cooper, N. J. Snyder, M. J. Zweifel, M. A. Staszak, S. C. Wilkie, T. I. Nicas, D. L. Mullen, T. F. Butler, M. J. Rodriguez, B. E. Huff and R. C. Thomspon, *J. Antibiot.*, 1996, **49**, 575; M. J. Rodriguez, N. J. Snyder, M. J. Zweifel, S. C. Wilkie, D. R. Starck, R. D. Cooper, T. I. Nicas, D. L. Mullen, T. F. Butler and R. C. Thompson, *J. Antibiot.*, 1998, **51**, 560.
11 Monoisotopic mass.
12 D. M. Lynn, S. Kanaoka and R. H. Grubbs, *J. Am. Chem. Soc.*, 1996, **118**, 784.
13 We believe that monomer **1** was used as a trifuoroacetic acid salt, since the chromatographic purification of **1** was done by a TFA-containing solvent system. Thus, the key to the success in the metathesis polymerization may be the ammonium salt formation of two *sec*-amines in **1**, which prevented the deactivation of catalyst.

Communication 9/03529J

Formamides undergo in-plane bimolecular nucleophilic vinylic substitutions (S_N2) by the reaction with (*E*)-alkenyl(phenyl)iodonium tetrafluoroborates: stereoselective synthesis of (*Z*)-vinyl formates

Masahito Ochiai,* Shinji Yamamoto and Koichi Sato

Faculty of Pharmaceutical Sciences, University of Tokushima, 1-78 Shomachi, Tokushima 770-8505, Japan. E-mail: mochiai@ph2.tokushima-u.ac.jp

Received (in Cambridge, UK) 25th May 1999, Accepted 9th June 1999

Reported for the first time is the stereoselective synthesis of (*Z*)-vinyl formates, which involves in-plane bimolecular nucleophilic vinylic substitutions of (*E*)-β-alkylvinyl-(phenyl)iodonium tetrafluoroborates with formamides.

The chemistry of vinyl formates is relatively unexplored, mostly due to the lack of an efficient method for their syntheses. Baeyer–Villiger rearrangement of conjugated enals with H_2O_2 activated with selenium catalysts, *i.e.* SeO_2 and bis(2-nitrophenyl)diselenide, affords vinyl formates.[1] Ring opening of α,β-epoxysilanes with anhydrous formic acid, followed by *anti* β-elimination of silanol, was utilized to create the vinyl formate functionality of *Latia* luciferin.[2] A method for stereoselective synthesis of (*Z*)-vinyl formates is not available. We report herein, for the first time, stereoselective synthesis of (*Z*)-vinyl formates, which involves in-plane biomolecular nucleophilic vinylic substitutions of (*E*)-β-alkylvinyl(phenyl)iodonium tetrafluoroborates **1a**–**c** with formamides (Scheme 1).[3]

The vinyl S_N2 reaction has been considered to be a high-energy pathway and neglected for a long time.[4,5] However, we reported recently that use of aryliodonio groups as a leaving group with very high leaving ability makes possible the vinylic S_N2 pathway; thus, (*E*)-(β-alkylvinyl)iodonium salts **1a**–**c** on exposure to Bu_4NX (X = Cl, Br and I) at room temperature afford the corresponding (*Z*)-vinyl halides stereoselectively with exclusive inversion of configuration in high yields.[6,7] All of the kinetic results, secondary isotope effects, substituent effects of the leaving groups, the solvent effects, the pressure effects as well as stereochemistry of the substitutions firmly establish the in-plane S_N2 mechanism. Interestingly, we found reaction of (*E*)-(β-alkylvinyl)iodonium salts **1a**–**c** with *N*,*N*-disubstituted formamides gives (*Z*)-vinyl formates **2** stereoselectively with inversion of configuration: thus, heating of a solution of (*E*)-dec-1-enyl(phenyl)iodonium tetarfluoroborate **1a** in DMF at 50 °C for 6 h under nitrogen afforded the (*Z*)-vinyl formate **2a**† in a high yield (83%) (Table 1, entry 1). The

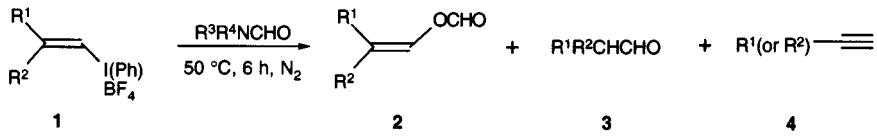

1 **2** **3** **4**

a $R^1 = C_8H_{17}$, R^2 = H, **b** $R^1 = Me_2CH(CH_2)_2$, R^2 = H, **c** $R^1 = Ph(CH_2)_3$, R^2 = H,
d $R^1 = Bu^t$, R^2 = H, **e** R^1 = Ph, R^2 = H, **f** R^1 = H, $R^2 = C_8H_{17}$, **g** $R^1 = Ph(CH_2)_3$, R^2 = Me

Scheme 1

Table 1 Nucleophilic vinylic substitution of alkenyl(phenyl)iodonium tetrafluoroborates **1** with formamides[a]

		Formamide		Product [yield (%)][b]				
Entry	**1**	R^3	R^4	**2**	**3**	Ratio[c]	**4**	Ratio[d]
1	**1a**	Me	Me	**2a** (83)	**3a** (12)	88:12	**4a** (5)	95:5
2	**1a**	Et	Et	**2a** (62)	**3a** (27)	69:31	**4a** (4)	95:5
3	**1a**	$(CH_2)_4$		**2a** (48)	**3a** (24)	67:33	**4a** (4)	94:6
4	**1a**	$(CH_2)_5$		**2a** (72)	**3a** (24)	75:25	**4a** (5)	95:5
5	**1a**	$(CH_2)_2O(CH_2)_2$		**2a** (77)	**3a** (23)	77:23	**4a** (6)	95:5
6	**1a**	Pr^i	Pr^i	**2a** (32)	**3a** (16)	67:33	**4a** (52)	48:52
7	**1a**	*c*-C_6H_{11}	*c*-C_6H_{11}[e]	**2a** (0)	**3a** (0)	—	**4a** (62)	0:100
8	**1a**	Ph	Me	**2a** (80)	**3a** (1)	99:1	**4a** (3)	97:3
9	**1a**	*p*-$MeOC_6H_4$	Me	**2a** (42)	**3a** (0)	100:0	**4a** (5)	89:11
10	**1a**	*p*-ClC_6H_4	Me	**2a** (59)	**3a** (0)	100:0	**4a** (2)	96:4
11	**1b**	Me	Me	**2b** (76)	**3b** (17)	81:19	**4b** (4)	96:4
12	**1b**	Pr^i	Pr^i	**2b** (42)	**3b** (26)	62:38	**4b** (18)	79:21
13	**1b**	Ph	Me	**2b** (47)	**3b** (1)	97:3	**4b** (0)	100:0
14	**1c**	Me	Me	**2c** (72)	**3c** (19)	79:21	**4c** (3)	97:3
15	**1c**	Pr^i	Pr^i	**2c** (0)	**3c** (0)	—	**4c** (52)	0:100
16	**1c**	Ph	Me	**2c** (31)	**3c** (1)	96:4	**4c** (1)	98:2
17	**1d**	Me	Me	**2d** (0)	**3d** (0)	—	**4d** (—)[f]	—
18	**1e**	Me	Me	**2e** (0)	**3e** (0)	—	**4e** (2)	—
19	**1f**[g]	Me	Me	**2f** (0)	**3f** (0)	—	**4a** (80)	0:100

[a] Reactions were carried out at 50 °C under N_2 for 6 h. [b] Yields were determined by GC. [c] Ratios of **2**:**3**. [d] Ratios of (**2** + **3**):**4**. [e] Reaction was carried out in a solution of $(c\text{-}C_6H_{11})_2NCHO$–DMF (3:1) at 82 °C. [f] Not determined. [g] **1f**: (*Z*)-dec-1-enyl(phenyl)iodonium perchlorate.

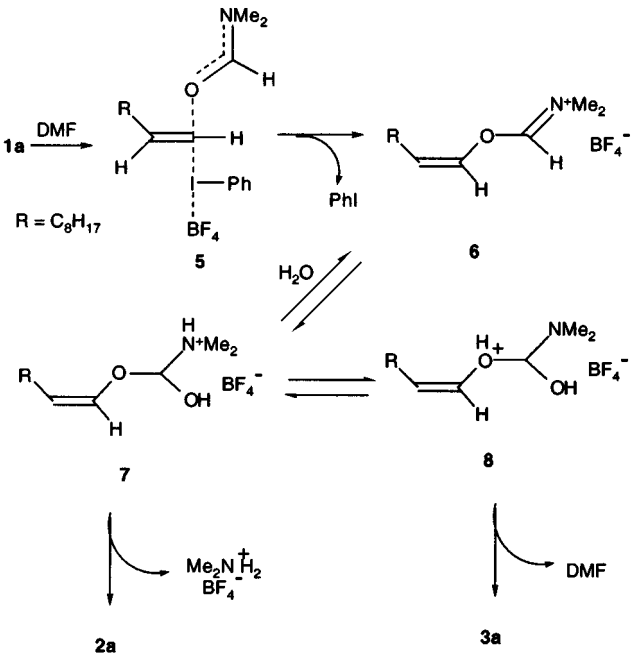

Scheme 2

reaction is highly stereoselective and no formation of the (*E*)-vinyl formate **2f** was detected by GC and 400 MHz ^{1}H NMR. The saturated aldehyde **3a** and the terminal alkyne **4a** were obtained as minor products in 12 and 5% yields.

N,*N*-Diethylformamide and *N*-formyl cyclic amines, *i.e. N*-formyl-pyrrolidine, -piperidine and -morpholine, similarly gave the (*Z*)-vinyl formate **2a** as a major product but with an increased amount of the aldehyde **3a** (entries 2–5). It is noted that the use of aromatic formamides such as *N*-formyl-*N*-methylanilines resulted in reactions almost free of the byproduct **3a** (entries 8–10). In contrast, the reaction course was dramatically changed when sterically demanding *N*,*N*-diisopropylformamide was used and a large amount of dec-1-yne **4a** (52%) was produced *via* elimination. With *N*,*N*-dicylohexylformamide, this elimination is the sole detectable pathway. Acetamides also act as good nucleophiles in this reaction; for instance, treatment of **1a** with *N*,*N*-dimethylacetamide at 50 °C for 6 h afforded stereoselectively (*Z*)-dec-1-enyl acetate in 62% yield, along with formation of **3a** (26%) and **4a** (7%).

The concerted vinylic S_N2 pathways are highly sensitive to the nature of β-substituents of the vinyliodonium salts and are inhibited or retarded when (*E*)-β-*tert*-butylvinyl- **1d** and (*E*)-β-phenylvinyliodonium salt **1e** were used in the reaction with halides.[6,8] This tendency was also kept in the reaction of iodonium salts **1d** and **1e** with DMF at 50 °C, which afforded no S_N2 products **2d** and **2e** (entries 17 and 18). Reaction of the (*Z*)-isomer with DMF resulted in extensive *anti* β-elimination to give **4a** in 80% yield, as reported previously.[6]

Scheme 2 illustrates a possible mechanism for formation of the (*Z*)-vinyl formate **2a** and the aldehyde **3a** from (*E*)-vinyliodonium salt **1a** by the reaction with DMF. Formamide on treatment with alkyl tosylates undergoes exclusive *O*-alkylation with no *N*-alkylation;[9] therefore, it seems reasonable to assume that the oxygen atom of DMF selectively attacks the (*E*)-vinyliodonium salt **1a** to produce the inverted (*Z*)-*O*-vinylimidonium salt **6** (Vilsmeier–Haack salt) *via* the vinylic S_N2 transition state **5**, which was stabilized by delocalization of the nitrogen lone-pair electrons. The hyper-leaving group ability of the phenyliodonio group would be responsible for the vinylic S_N2 reaction.[7] Subsequent attack of water will produce *N*-protonated tetrahedral species **7**, which collapses to **2a** with the ammonio group being released, or *O*-protonated tetrahedral species **8**, which collapses to **3a** with DMF being released.

The formate **2a** and the aldehyde **3a** seem to be kinetic products, since neither isomerization of the double bond of **2a** yielding **2f** nor hydrolysis of **2a** to the saturated aldehyde **3a** was observed under the conditions used. We believe that the ratios of the (*Z*)-vinyl formate **2a** to the saturated aldehyde **3a** might depend on the leaving ability of the ammonio groups, which will increase in the order $HN^+Pr^i_2$ < HN^+Et_2 < HN^+Me_2 < HN^+(Me)Ar. These hypotheses are in a good agreement with the observed ratios shown in Table 1.

Base-induced α-eliminations generating free alkylidene carbenes are a feasible process for β-alkylvinyliodonium salts.[10,11] The α-elimination pathway to yield the alkyne **4a**, which was established by analysis of the deuterium content (88%) of [1-^{2}H]dec-1-yne obtained by the reaction of β-deuterated **1a** with *N*,*N*-diisopropylformamide at 50 °C, would compete with the vinylic S_N2 reaction leading to the formation of **2** and **3**. The ratios of the vinylic S_N2 reaction *versus* the α-elimination shown in Table 1 clearly indicate that sterically demanding *N*,*N*-diisopropylformamide and *N*,*N*-dicyclohexylformamide will lead to steric retardation of the S_N2 pathway, which, in turn, results in formation of a large amounts of the alkyne **4**.

In general, bimolecular nucleophilic substitutions are favoured when a good nucleophile is present; however, formamides with rather low nucleophilicity undergo the vinylic S_N2 reaction under mild conditions. The origin of this unusual reaction is attributable to the hyper-leaving group ability of the phenyliodonio group.

Notes and references

† *Selected data* for **2a**: δ_H(400 MHz, $CDCl_3$) 0.88 (t, *J* 6.3, 3H), 1.2–1.44 (m, 12H), 2.16 (q, *J* 6.9, 2H), 4.99 (dt, *J* 7.5 and 6.9, 1H), 7.07 (d, *J* 7.5, 1H), 8.08 (s, 1H); δ_C(100 MHz, $CDCl_3$) 14.1, 22.7, 24.5, 29.1, 29.2, 29.3, 29.4, 31.9, 116.1, 132.7, 158.0; ν_{max}($CHCl_3$)/cm^{-1} 2920, 2850, 1725, 1665, 1460, 1380, 1170, 910; *m/z* (EI) 184 (M^+, 1%), 138 (4), 110 (8), 96 (19), 82 (38), 68 (32), 57 (100); HRMS calc. for $C_{11}H_{20}O_2$ (M^+), 184.1463, found 184.1470.

1 F. Nakatsubo, Y. Kishi and T. Goto, *Tetrahedron Lett.*, 1970, 381; L. Syper, *Tetrahedron*, 1987, **43**, 2853.
2 P. Magnus and G. Roy, *J. Chem. Soc., Chem. Commun.*, 1978, 297.
3 For reviews of organoiodanes, see: G. F. Koser, in *The Chemistry of Functional Groups, Supplement D*, Wiley, New York, 1983, ch. 18; M. Ochiai and Y. Nagao, *J. Synth. Org. Chem. Jpn.*, 1986, **44**, 660; R. Moriarty and O. Prakash, *Acc. Chem. Res.*, 1986, **19**, 244; M. Ochiai, *Rev. Heteroatom Chem.*, 1989, **2**, 92; Y. Kita, H. Tohma and T. Yakura, *Trends Org. Chem.*, 1992, **3**, 113; A. Varvoglis, *The Chemistry of Polycoordinated Iodine*, VHC, New York, 1992; G. F. Koser, in *The Chemistry of Functional Groups, Supplement D2*, Wiley, New York, 1995, ch. 21; T. Kitamura, *J. Synth. Org. Chem. Jpn.*, 1995, **53**, 893; P. J. Stang and V. V. Zhdankin, *Chem. Rev.*, 1996, **96**, 1123.
4 For reviews of nucleophilic vinylic substitutions, see: Z. Rappoport, *Acc. Chem. Res.*, 1981, **14**, 7; Z. Rappoport, *Recl. Trav. Chim. Pays-Bas*, 1985, **104**, 309.
5 For theoretical studies, see: D. R. Kelsey and R. G. Bergman, *J. Am. Chem. Soc.*, 1971, **93**, 1953; M. N. Glukhovtsev, A. Pross and L. Radom, *J. Am. Chem. Soc.*, 1994, **116**, 5961; V. Lucchini, G. Modena and L. Pasquato, *J. Am. Chem. Soc.*, 1995, **117**, 2297.
6 M. Ochiai, K. Oshima and Y. Masaki, *J. Am. Chem. Soc.*, 1991, **113**, 7059; T. Okuyama, T. Takino, K. Sato and M. Ochiai, *J. Am. Chem. Soc.*, 1998, **120**, 2275; T. Okuyama T. Takino, K. Sato, K. Oshima, S. Imamura, H. Yamataka, T. Asano and M. Ochiai, *Bull. Chem. Soc. Jpn.*, 1998, **71**, 243.
7 For leaving group ability of the aryliodonio groups, see: M. Ochiai, in *Chemistry of Hypervalent Compounds*, ed. K. Akiba, Wiley-VCH, New York, 1999, ch. 12; T. Okuyama, T. Takino, T. Sueda and M. Ochiai, *J. Am. Chem. Soc.*, 1995, **117**, 3360.
8 T. Okuyama and M. Ochiai, *J. Am. Chem. Soc.*, 1997, **119**, 4785; T. Okuyama, H. Oka and M. Ochiai, *Bull. Chem. Soc. Jpn.*, 1998, **71**, 1915.
9 B. C. Challis and J. A. Challis, *The Chemistry of Amides*, ed. J. Zabicky, Interscience, New York, 1970, ch. 13.
10 Formation of dec-1-yne **4a** from the vinyliodonium salt **1a** by the reaction with Et_3N has been firmly established to involve α-elimination–rearrangement pathways (ref. 11).
11 M. Ochiai, Y. Takaoka and Y. Nagao, *J. Am. Chem. Soc.*, 1988, **110**, 6565; M. Ochiai, M. Kunishima, S. Tani and Y. Nagao, *J. Am. Chem. Soc.*, 1991, **113**, 3135; M. Ochiai, K. Uemura and Y. Masaki, *J. Am. Chem. Soc.*, 1993, **115**, 2528; M. Ochiai, T. Sueda, K. Uemura and Y. Masaki, *J. Org. Chem.*, 1995, **60** 2624.

Communication 9/04220B

Deprotonated ethylenethiourea as a ligand in an unusual tetrameric gold(I) complex†

Peter G. Jones* and Steffi Friedrichs

Institut für Anorganische und Analytische Chemie, Technical University of Braunschweig, Postfach 3329, 38023 Braunschweig, Germany. E-mail: p.jones@tu-bs.de

Received (in Basel, Switzerland) 24th May 1999, Accepted 13th June 1999

The product of the reaction between $[(etu)_2Au]^+Cl^-$ (etu = imidazolidine-2-thione) and aqueous sodium hydroxide, previously described as $\{(etu)Au\}_2O$, is shown by X-ray analysis to be a tetramer with four gold(I) centres and four deprotonated etu ligands acting as *N*,*S*-donors.

Ethylenethiourea [imidazolidine-2-thione (etu)] is a well known ligand in the chemistry of gold(I); complexes such as $[(etu)_2Au]Cl\cdot H_2O$ were described as long ago as 1928.[1] Also reported[1] was $\{(etu)Au\}_2O$, apparently the product of the reaction between $[(etu)_2Au]Cl$ and aqueous sodium hydroxide. In the light of current knowledge, this complex would be unexpected because of the extremely low affinity of gold(I) centres for oxide ligands; as far as we are aware, there is no established example of such a complex. We have recently begun a study of hydrogen bonding in etu complexes of gold(I),[2] in the course of which we decided to re-examine the previous report.

The reaction between $[(etu)_2Au]Cl$ and aqueous alkalis is not difficult to reproduce; it leads immediately to a white precipitate, which is however practically insoluble in all common solvents. In such cases the slow diffusion of reacting solutions may lead to crystalline material; the careful layering of the three phases aqueous potassium hydroxide (bottom), ethyl acetate (centre) and ethanolic $[(etu)_2Au]Cl$ (top) indeed led to single crystals, albeit extremely small. An X-ray structure determination did however prove possible, exploiting the greater sensitivity of area detector technology.‡

The structure is shown in Fig. 1. It is a tetramer $[Au(etu - H)]_4$, where (etu − H) indicates an ethylenethiourea deprotonated at one nitrogen atom.§ The ligands coordinate through S and the deprotonated N atom, and there are two differently coordinated types of gold centre. Gold atoms Au2 and Au3 lie on twofold axes ½,½, *z* and are linearly coordinated by two nitrogen atoms [Au2–N12 2.04(1), Au3–N22 1.97(1) Å], whereas Au1 lies on a general position and is coordinated by two sulfur atoms [Au1–S1 2.284(4), Au1–S2 2.304(4) Å] in a distorted linear geometry [S–Au–S 169.8(2)°]. As far as we are aware, only one other complex of (etu − H) is known: $[Mo_2(py)_2(O_2CBu^t)_3(etu - H)]$.[3]

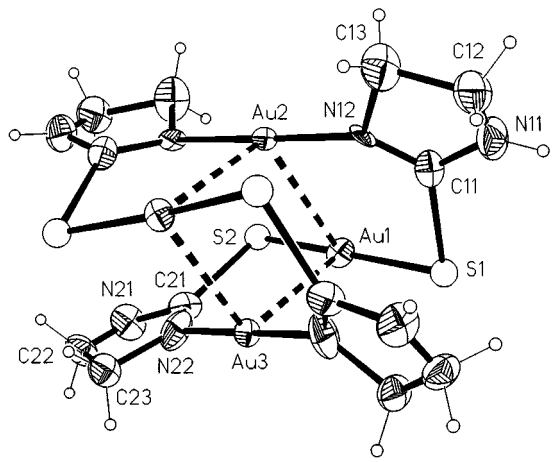

Fig. 1 Structure of the tetramer $[Au(etu - H)]_4$ in the crystal. Only the asymmetric unit is numbered. Ellipsoids represent 50% probability levels; H and S atom radii are arbitrary (see text).

† Dedicated to Professor Reinhard Schmutzler on the occasion of his 65th birthday.

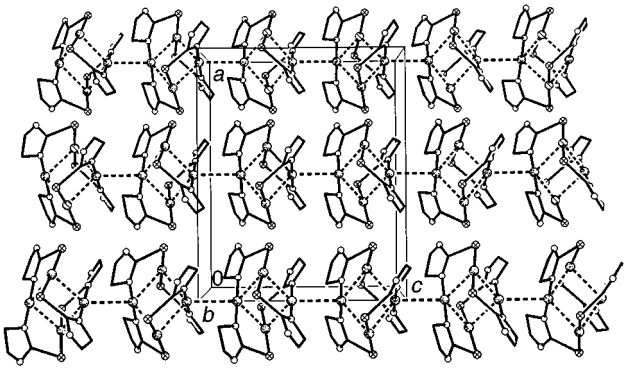

Fig. 2 Packing diagram of $[Au(etu - H)]_4$, showing the formation of chains of tetramers parallel to the *z* axis. Au···Au contacts are indicated by dashed lines. H atoms are omitted.

The tetramer contains a 16-membered ring comprising the gold atoms, all N and S donor atoms, and one C atom of each (etu − H) ligand. Within this ring, the gold atoms are connected *via* short Au···Au contacts Au1···Au2 2.972(1) and Au1···Au3 2.974(1) Å to form a rhombus with angles of 71.28(2)° at Au1 and 108.79(7)° at Au2. A similar arrangement was observed in the gold(I) thioacetate tetramer $[Au(MeCS_2)]_4$.[4] In the current structure, the tetramers are further linked into chains parallel to the *z* axis by contacts Au2···Au3′ 3.176(1) Å (Fig. 2). The non-bonded S···N distances are S2···N12′ 3.23 and S1···N22′ 3.24 Å.

The existence of oxide complexes of Au(I) thus still remains to be demonstrated, whereas the (etu − H) ligand has been found at gold for the first time. Investigations of the reactivity of the (etu − H) tetramer are in progress.

We thank the Fonds der Chemischen Industrie (Frankfurt) for financial support.

Notes and references

‡ X-Ray structure determination: A colourless needle (*ca.* 0.1 × 0.02 × 0.01 mm) was mounted in inert oil on a glass fibre. Data were measured using Mo-Kα radiation on a Bruker SMART 1000 CCD diffractometer. Absorption corrections were based on multiple scans (program SADABS). Structure solution and refinement proved difficult because of pseudo-symmetry; the gold atoms simulate an additional pseudo-mirror plane. The sulfur atoms were refined isotropically because the two components of the double image thus generated are closely adjacent. Otherwise, the structure was refined [as a racemic twin with components 0.54(2): 0.46(2)] anisotropically on F^2 using all reflections (program SHELXL-97[5]). Hydrogen atoms were placed in calculated positions (assuming planarity at nitrogen) and refined using a riding model. An extensive set of restraints

were employed to improve stability of refinement. In view of the severe pseudo-symmetry, bond lengths should be interpreted with caution.

Crystal data: $C_{12}H_{20}Au_4N_8S_4$, M = 794.98, orthorhombic, space group *Iba*2, a = 16.1973(9), b = 10.3143(6), c = 13.2818(7) Å, V = 2218.9(2) Å^3, Z = 4, μ = 26.7 mm^{-1}, T = −130 °C, Bruker SMART 1000 CCD diffractometer, 11373 reflections to $2\theta_{max}$ 56°, 2759 unique, 119 parameters, 154 restraints, $wR2$ = 0.081, $R1$ = 0.032, S = 1.03, max. $\Delta\rho$ 2.26 e Å^{-3}.

CCDC 182/1293. See http://www.rsc.org/suppdata/cc/1999/1365/ for crystallographic files in .cif format.

§ The chemical analysis was satisfactory: found. (calc.) for $C_{12}H_{20}Au_4N_8S_4$; C, 11.91 (12.09); H, 1.49 (1.69); N, 9.26 (9.40); S, 10.79 (10.75)%. It is instructive to compare these values with those quoted in 1928 for $C_6H_{12}Au_2ON_4S_2$:[1] C, 11.45 (11.7); H, 2.1 (2.0); N, 9.3 (9.1); S, 10.5 (10.4); Au, 64.8 (64.2)%.

1 G. T. Morgan and F. H. Burstall, *J. Chem. Soc.*, 1928, 143.
2 P. G. Jones and S. Friedrichs, manuscript in preparation.
3 R. H. Cayton, M. H. Chisholm, E. F. Putilina and K. Folting, *Polyhedron*, 1993, **12**, 2627.
4 O. Piovescana and P. F. Zanazzi, *Angew. Chem. Int. Ed. Engl.*, 1980, **7**, 579.
5 G. M. Sheldrick, SHELXL-97, a program for refining crystal structures, University of Göttingen, Germany, 1997.

Communication 9/04137K

1,2-Bis(chloromethylalumino)tetrafluorobenzene, an aluminium-based bifunctional Lewis acid with a perfluorinated backbone

Martin Tschinkl,[a] Robert E. Bachman[b] and François P. Gabbaï*[a]

[a] *Department of Chemistry, Texas A&M University, College Station, Texas 77843-3255, USA. E-mail: Gabbai@mail.chem.tamu.edu*

[b] *Department of Chemistry, Georgetown University, Washington, DC 20057, USA*

Received (in Columbia, Mo, USA) 17th March 1999, Accepted 20th May 1999

1,2-Bis(trimethylstannyl)tetrafluorobenzene reacts with chlorodimethylaluminium(III) to afford dimeric 1,2-bis-(chloromethylalumino)tetrafluorobenzene the structure of which has been determined by X-ray analysis.

Bidentate aluminium Lewis acids have recently emerged as promising tools for organic reaction catalysis[1] as well as for anion[2] and molecular recognition.[3] Experience gained in boron chemistry indicates that this class of compounds could also prove useful as activators for olefin polymerization with d^0-transition metal catalysts.[4,5] In this latter case, the use of strongly electron withdrawing substituents[6,7] appears to be required in order to yield very stable weakly coordinating anions.[8] As part of our continuing effort[9] in this direction, we now report the synthesis and characterization of dimeric 1,2-bis(chloromethylalumino)tetrafluorobenzene, a bidentate Lewis acid bearing a perfluorinated backbone.

1,2-Bis(trimethylstannyl)benzene has been shown to react with aluminium chlorides to yield 1,2-bis(alumino)benzene complexes.[10] In order to determine if a similar synthetic strategy could be applied to the preparation of perfluorinated systems, bis(trimethylstannyl)tetrafluorobenzene **1**[11] was allowed to react with chlorodimethylaluminium(III) in hexane (Scheme 1).† After 96 h, complete removal of the volatile components afforded a quantitative yield of **2**, which could be crystallized by slow evaporation of the solvent from a hexane solution. The identity of **2** was first inferred from the following salient NMR spectroscopic features.‡ ^{27}Al NMR indicated the presence of a tetra-coordinated aluminium center (δ 150, $\omega_{1/2}$ = 2700 Hz). The ^{19}F NMR spectrum allowed the possibility of fluoride activation[8] to be eliminated since two signals with multiplicity consistent with a AA′BB′ higher order spin system were observed. A high field singlet in both the ^{1}H and ^{13}C NMR spectrum could be assigned to the methylaluminium groups. While EI mass spectrometry allowed the detection of a peak corresponding to 1,2-bis(methylchloroalumino)tetrafluorobenzene, definitive identification of **2** was provided by a single crystal structure analysis (*vide infra*), which revealed its dimeric nature. In this respect, **2** differs from its perprotio analog 1,2-bis(methylchloroalumino)benzene which has been formulated as a monomer.[10] By analogy with the reaction of 1,2-bis(trimethylstannyl)benzene with chlorodimethylaluminium(III),[10] the formation of 1,2-bis(dimethylalumino)tetrafluorobenzene through trimethylstannyl chloride elimination could have been expected. In the present case however, the isolation of **2** is accompanied by formation of tetramethylstannane which was found among the volatile components of the reaction.

Table 1 Important bond lengths (Å) and angles (°) in the structure of **2**

Al(1)–C(11)	1.954(4)	Al(2)–Cl(24)	2.2778(14)	Al(3)–Cl(13)	2.2894(14)
Al(1)–Cl(12)	2.2808(15)	Al(2)–Cl(12)	2.2784(14)	Al(4)–C(22)	1.966(3)
Al(1)–Cl(13)	2.2812(16)	Al(3)–C(21)	1.959(4)	Al(4)–Cl(34)	2.720(14)
Al(2)–C(12)	1.955(4)	Al(3)–Cl(34)	2.2884(14)	Al(4)–Cl(24)	2.3003(15)

C(11)–Al(1)–Cl(12)	98.90(12)	Al(2)–Cl(12)–Al(1)	98.25(5)
Cl(12)–Al(1)–Cl(13)	101.73(6)	Al(1)–Cl(13)–Al(3)	120.12(6)
C(12)–Al(2)–Cl(12)	99.17(12)	Al(2)–Cl(24)–Al(4)	118.79(5)
Cl(24)–Al(2)–Cl(12)	99.63(6)	Al(4)–Cl(34)–Al(3)	99.11(5)
C(21)–Al(3)–Cl(34)	98.33(11)	C(12)–C(11)–Al(1)	121.8(3)
Cl(34)–Al(3)–Cl(13)	100.23(5)	C(11)–C(12)–Al(2)	120.2(3)
C(22)–Al(4) Cl(34)	99.20(11)	C(22)–C(21)–Al(3)	122.0(2)
Cl(34)–Al(4)–Cl(24)	100.75(5)	C(21)–C(22)–Al(4)	120.7(3)

Compound **2** crystallizes in the monoclinic space group $P2_1/c$ with four molecules in the unit cell.§ Important bond length and angles are listed in Table 1. As shown in Fig. 1, the complex approachs C_{2v} symmetry and adopts a conformation reminiscent of a wings-up butterfly. Each aluminium center is tetrahedrally coordinated and lies close to the plane containing its corresponding phenylene ligand [Al(1) 0.129 Å, Al(2) −0.144 Å,Al(3) 0.179 Å, Al(4) 0.018 Å]. There are two types of bridging chlorine atoms in the coordination sphere of each aluminium center. The chlorine atoms Cl(12) and Cl(34) bridge neighboring aluminium centers within the 1,2-bis(alumino)tetrafluorobenzene sub-units. They are thus responsible for the formation of [C_2AlClAl] five-membered rings which approach planarity [Σ(endocyclic angles) 538.32 and 539.33°]. The chloride coordination angles Al(1)–Cl(12)–Al(2) and Al(3)–Cl(34)–Al(4) of 98.25(5) and 99.11(5)° can be compared to the value of 94.83(4)° observed in the structure of the related tin-based bidentate complex 1,2-bis(dimethylchlorostannyl)benzene·HMPA.[12] The Al–Cl bond distances of **2** fall within the narrow range of 2.272(1)–2.300(1) Å with an average value of 2.28 Å. The chlorine atoms Cl(13) and Cl(24) connect the two 1,2-bis(alumino)tetrafluorobenzene sub-units into a symmetrical dimer and form an eight-membered $(AlCl)_4$ ring which adopts a crown conformation. The cofacial tetrafluorophenylene rings are essentially parallel (dihedral angle 6.4°). The distance between their respective centroids is relatively short (3.56 Å) and indicates the presence of an interaction.

In view of the low stability and sometimes explosive behavior of perfluoroaryl aluminium derivatives,[6] the isolation

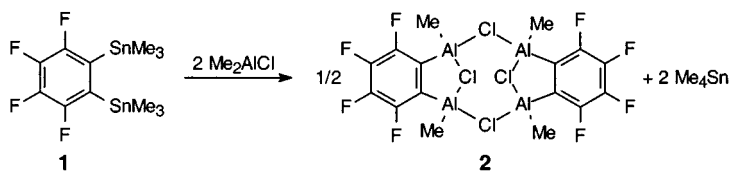

1 **2**

Scheme 1

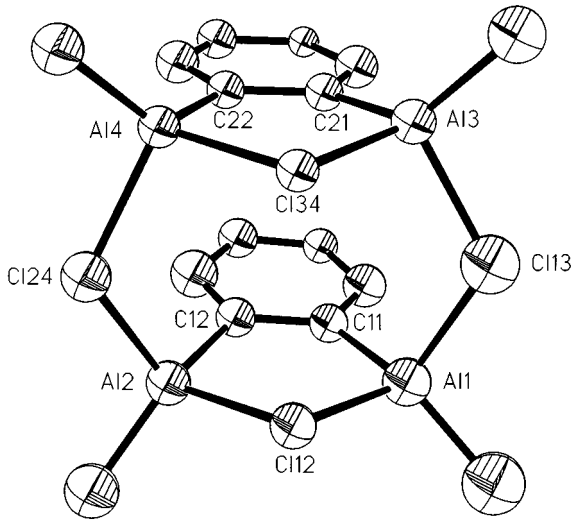

Fig. 1 ORTEP drawing of **2** with 50% probability ellipsoids; H and F atoms omitted for clarity.

of **2** is especially noteworthy. Analogous boron complexes such as 1,2-bis[bis(pentafluorophenyl)boryl]tetrafluorobenzene have been only very recently isolated.[13] Current studies are focussed on the use of 1,2-bis(alumino)tetrafluorobenzene complexes to abstract halides from a variety of substrates.

We thank the Department of Chemistry at Texas A&M University for making this work possible and Dr R. Shröck (Wacker) for the donation of precious chemicals. Financial support from the State of Bavaria/Technische Universität München and the DAAD (Promotionsstipendium, grant to M. T.) is gratefully acknowledged. The purchase of the X-ray diffractometer was made possible by a grant from the National Science Foundation (CHE-9115394); additional support for its purchase was provided by Georgetown University.

Notes and references

† *Synthesis of* **2**: *great caution should be exercised as aluminium complexes with perfluorinated aryl substituents have been reported to spontaneously explode.*[6] Chlorodimethylaluminium (374 mg, 4.04 mmol) was added to a solution of **1** (961 mg, 2.02 mmol) in hexane (5 mL) at room temp. The resulting solution was stirred for four days and filtered to remove traces of insoluble material. Evaporation of the solvent left a white residue that was exposed to a dynamic vacuum for 6 h at 50 °C. This procedure afforded a 95% yield (580 mg) of **2** (mp 79–80 °C). Elemental analysis. Calc. for $C_{16}H_{12}Al_4Cl_4F_8$: C, 31.69; H, 1.98. Found C, 31.05; H, 2.15%.

‡ *NMR data for* **1**, ^{1}H NMR (300 MHz, [$^2H_6$]benzene): δ −0.25 (s, 12 H, CH_3). ^{13}C NMR (75.4 MHz, [$^2H_6$]benzene: δ −8.4 (s, CAl) 126.8 (s, C-1/2) 140.7 (d, $^1J_{CF}$ 241.7 Hz, C-3/6) 152.1 (d, $^1J_{CF}$ 236.6 Hz, C-4/5). ^{19}F NMR (282.2 MHz, [$^2H_6$]benzene, $CFCl_3$ ext.); δ −121.22 (pseudo d, J_{FF} 19.5 Hz, 4 F, F-3/6) −151.88 (pseudo, d, J_{FF} 19.5 Hz, 4 F, F-4/5). ^{27}Al NMR (104.2 MHz, [$^2H_6$]benzene, $AlCl_3 \cdot 6H_2O$ ext.) δ 150 ($\omega_{1/2}$ 2700 Hz).

§ *Crystal and structure determination data for* **2**: X-ray data for **2** were collected at −100 °C on a Siemens SMART-CCD diffractometer using graphite monochromated Mo-Kα radiation (λ = 0.71073 Å). An irregularly shaped colorless plate of **2** *ca.* 0.1 × 0.3 × 0.4 mm in size was selected and mounted on a glass fiber with epoxy. The data were collected using 0.3°-wide ω-scans with a crystal to detector distance of 5.0 cm to yield a sphere (98% complete) of data to a resolution of 0.75 Å (2θ = 56.6°). The data was then truncated, on the basis of intensity statistics, at a resolution of 0.90 Å to yield a sphere (99.8% complete) of data ($2.08 \leqslant 2\theta \leqslant 23.23°$) composed of 19775 reflections (3549 unique, R_{int} = 0.0522). Other key crystallographic parameters are as follows: $C_{16}H_{12}Al_4Cl_4F_{12}$, M = 605.98, monoclinic, space group $P2_1/c$, a = 9.832(2), b = 9.855(2), c = 25.692(6) Å, V = 2484.9(9) Å^3, Z = 4, μ = 0.681 mm^{-1}. The structure was solved by direct methods and refined by full-matrix least squares against F^2 using the SHELXTL/PC (ver. 5.10) package. The refinement converged with residuals of $R1$ ($wR2$) = 0.0359 (0.0779) for 293 refined parameters and 3549 unique reflections [2505 with $I > 2\sigma(I)$].

CCDC 182/1273. See http://www.rsc.org/suppdata/cc/1999/1367/ for crystallographic files in .cif format.

1 T. Ooi, M. Tomoya and K. Maruoka, *Angew. Chem., Int. Ed.*, 1998, **37**, 2347.
2 W. Uhl, F. Hannemann, W. Saak and R. Wartchow, *Eur. J. Inorg. Chem.*, 1998, 921.
3 O. Saied. M. Simard and J. D. Wuest, *Organometallics*, 1998, **17**, 1128.
4 L. Jia, X. Yang, C. Stern and T. J. Marks, *Organometallics*, 1994, **13**, 3755.
5 K. Köhler, W. E. Piers, A. P. Jarvis, S. Xin, Y. Feng, A. M. Bravakis, S. Collins, W. Clegg, G. P. A. Yap and B. Marder, *Organometallics*, 1998, **17**, 3557.
6 T. Belgardt, J. Storre, H. W. Roesky, M. Noltemeyer and H.-G. Schmidt, *Inorg. Chem.*, 1995, **34**, 3821.
7 A. H. Cowley, G. S. Hair, B. G. McBurnett and R. A. Jones, *Chem. Commun.*, 1999, 437.
8 Y.-X. Chen, M. V. Metz, L. Li, C. L. Stern and T. J. Marks, *J. Am. Chem. Soc.*, 1998, **120**, 6287.
9 M. Tschinkl, A. Schier, J. Riede and F. P. Gabbaï, *Inorg. Chem.*, 1998, **37**, 5097.
10 J. J. Eisch, K. Mackenzie, H. Windisch and C. Krüger, *Eur. J. Inorg. Chem.*, 1998, 153.
11 T. Chivers, *J. Organomet. Chem.*, 1969, **19**, 75.
12 R. Altmann, K. Jurkschat and M. Schürmann, *Organometallics*, 1998, **17**, 5858.
13 V. C. Williams, W. E. Piers, W. Clegg, M. R. J. Elsegood, S. Collins and T. B. Marder, *J. Am. Chem. Soc.*, 1999, **121**, 3244.

Communication 9/02127B

ChemComm

MIB: an advantageous alternative to DAIB for the addition of organozinc reagents to aldehydes

William A. Nugent

DuPont Company, Central Research and Development, PO Box 80328, Wilmington, DE 19880-0328, USA. E-mail: william.a.nugent@usa.dupont.com

Received (in Corvallis, OR, USA) 14th May 1999, Accepted 10th June 1999

3-*exo*-Morpholinoisoborneol (MIB) catalyzes the addition of organozinc reagents to aldehydes in high enantiomeric excess and provides several advantages over the venerable amino alcohol ligand DAIB.

The addition of organozinc reagents to aldehydes catalyzed by enantiopure β-amino alcohols[1] represents the enantioselective counterpart of the Grignard addition reaction.[2] The extensive research on this transformation has been summarized in review articles.[3] The first ligand to provide high enantioselectivities in such reactions was 3-exo-dimethylaminoisoborneol (DAIB, **1b**) which was developed by Noyori and co-workers.[4] Despite the many alternative β-amino alcohol ligands[5] now available, interest in DAIB has remained remarkably high. Recent studies[6] provide detailed insight into the mechanism of DAIB-promoted additions and new applications of this venerable ligand continue to appear.[7]

While DAIB has enjoyed great success, three factors somewhat limit further extensions of this technology. (i) The most efficient synthesis, that developed by White and co-workers,[8] requires three steps for the conversion of parent amino alcohol **1a** to DAIB. (ii) DAIB is somewhat air-sensitive and slowly decomposes upon storage.[4] (iii) While DAIB-promoted addition of organozinc reagents to aromatic aldehydes proceeds in excellent enantiomeric excess, it has not yet proven possible to obtain similar ees in the case of α-branched aliphatic aldehydes.[4] Here we report that a simple structural modification circumvents these problems whilst retaining the desirable features of DAIB.

(2*R*)-(+)-3-*exo*-Aminoisoborneol (+)-**1a** was prepared by $LiAlH_4$ reduction of *anti*-(1*S*)-(−)-camphorquinone 3-oxime following the literature procedure.[8,9] Treatment of (+)-**1a** with commercial bis(2-bromoethyl) ether in the presence of excess Et_3N resulted in dialkylation of the amine nitrogen (Scheme 1).† Extractive work-up followed by crystallization from hexanes afforded (2*R*)-(+)-3-*exo*-morpholinoisoborneol **2** [(+)-MIB] as transparent crystals, mp 65–67 °C. The enantiomer (−)-MIB was prepared similarly from (−)-**1a**.

Like DAIB, MIB promotes the enantioselective addition of organozinc reagents to aldehydes (Scheme 2). The addition of Et_2Zn to a series of aldehydes under standard conditions (two-fold excess Et_2Zn in 2:1 hexane–toluene)‡ is summarized in Table 1. The reactions in Table 1 were quenched by addition of Ac_2O which quantitatively converts the intermediate zinc alkoxides to the corresponding acetate esters and allows direct analysis of the product mixture by chiral capillary column gas chromatography.[10] As exemplified by entries 1–4, addition of Et_2Zn to aromatic and heteroaromatic aldehydes proceeded cleanly with enantiomeric excesses similar to those reported using DAIB. Moreover, we were delighted to find that addition of Et_2Zn to several α-branched aliphatic aldehydes (entries 6–10) also proceeded in 97–99% enantiomeric excess. Only in the case of the straight-chain aliphatic aldehyde hexanal did the ee begin to erode. In all cases in Table 1 the major enantiomer of the product had the *R* absolute configuration, thus the sense of chirality obtained from (+)-MIB is the same as that obtained from (+)-DAIB.

Table 1 Enantioselective addition of Et_2Zn to aldehydes catalyzed by (+)-MIB[a]

Entry	Aldehyde	MIB/ mol%	*T*/°C	*t*/h	Yield (%)[b]	Ee (%)[b]
1	Benzaldehyde	2	0	3	98	98
2	*m*-Tolualdehyde	2	0	3	97	98
3	*p*-Fluorobenzaldehyde	5	0	3	98	98
4	3-Furaldehyde	5	0	6	91	97
5	Hexanal	5	0	3	96	91
6	Isobutyraldehyde	5	0	3	94	99
7	Cyclohexanecarboxaldehyde	5	0	3	94	99
8	2-Ethylbutyraldehyde	5	25	18	92	99
9	Cyclopropanecarboxaldehyde	5	0	3	91	98
10	Trimethylacetaldehyde	5	25	24	62	97

[a] All reactions contained aldehyde (3.0 mmol) and Et_2Zn (6.0 mmol) in 2:1 hexane–toluene (9 ml); for details see note ‡. [b] Determined by chiral capillary column gas chromatography on Cyclodex B stationary phase (J&W Scientific); in all cases (*R*)-enantiomer formed preferentially.

The reduced yield observed for addition of Et_2Zn to the tertiary aliphatic aldehyde trimethylacetaldehyde requires some comment. The limited yield can be traced to competing reduction of the the aldehyde to the zinc alkoxide of neopentyl alcohol which is subsequently acetylated under our reaction conditions (Scheme 3). The formation of minor amounts of BnOH as a side-product of DAIB-catalyzed addition of Et_2Zn to benzaldehyde has been noted by Noyori and co-workers.[11] In our experience, detectable amounts of primary alcohol are invariably formed during addition of organozinc reagents to aldehydes in the presence of β-amino alcohols. This side-reaction is most severe in the case of sterically bulky aldehydes bearing tertiary alkyl substituents. In contrast, for the other aldehydes in Table 1, this reductive pathway occurs to the extent of 2% or less for aromatic and primary aliphatic aldehydes (entries 1–5) and 5% or less for secondary aliphatic aldehydes (entries 6–9).

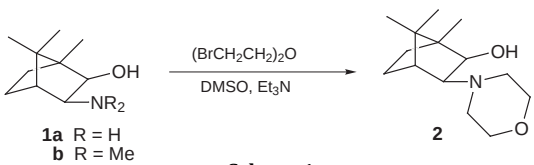

1a R = H
b R = Me

2

Scheme 1

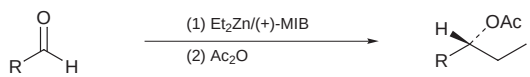

Scheme 2

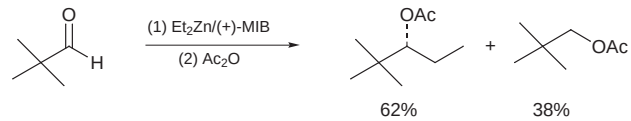

Scheme 3

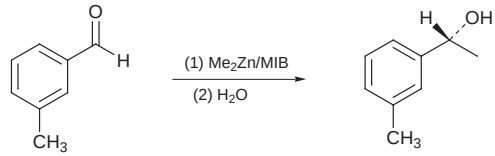

Scheme 4

MIB can also be used to effect the addition of Me_2Zn to aldehydes although longer reaction times are required to compensate for the lower reactivity of this organozinc reagent. Addition of Me_2Zn to *m*-tolualdehyde [18 h, room temperature, 5% (+)-MIB] afforded (*R*)-(+)-1-(*m*-tolyl)ethanol§ in 95% ee and 88% isolated yield after flash chromatography (Scheme 4).

It is also noteworthy that the crystalline nature of MIB imparts greater air-stability as compared with DAIB. A sample of MIB stored under air at ambient conditions for three months showed no degradation of spectroscopic properties nor catalytic performance when compared with freshly prepared material. Given the several advantages of MIB, we suggest that it should be considered as an alternative ligand for reactions where DAIB has previously been utilized.

Notes and references

† *Preparation* of (+)-**2**: Amino alcohol (+)-**1a** (4.53 g, 26.8 mmol) was dissolved in DMSO (25 ml) and Et_3N (10 ml). A solution of di(2-bromoethyl) ether (8.07 g, 90% pure, 31.3 mmol) in DMSO (20 ml) was added dropwise. After 72 h the mixture was added to 250 ml water and 60 ml 1 M NaOH and was extracted into Et_2O (3 × 100 ml). After removal of solvent at reduced pressure the product was taken up in Et_2O, extracted into 1 M HCl (50 ml), released with NaOH, and again extracted into Et_2O. After removal of volatiles, the residue was dissolved in hexanes (4 ml per g of crude product), filtered and cooled to −30 °C to produce **2** (2.95 g, 46%) as a white crystalline solid, mp 65–67 °C. ($C_{14}H_{25}NO_2$: Calc: C, 70.25; H, 10.53; N, 5.85; found: C, 70.18; H, 10.83, N, 5.94%). $\delta_H(C_6D_6)$ 0.69 (s, 3 H), 0.73 (m, 1 H), 0.88 (m, 1 H), 1.04 (s, 3 H), 1.15 (s, 3 H), 1.31 (td, 1 H), 1.52 (m, 1 H), 1.67 (d, 1 H), 1.99 (d, 1 H), 2.13 (br, 2 H), 2.31 (br, 2 H), 3.32–3.42 (m, 5 H total), 3.92 (br d, 1 H); $\delta_c(C_6D_6)$ 11.88, 21.10, 22.19, 27.99, 32.56, 45.35, 46.64, 49.52, 66.82, 73.37, 79.03 (as in the case of **1b**, one ^{13}C resonance is too broad to observe at room temperature); $[\alpha]_D^{25}$ +4.4, (*c* = 2.03, MeOH).

‡ *Typical procedure*: A solution of freshly distilled aldehyde (3.00 mmol), toluene (3.0 ml), internal standard (chlorobenzene or *tert*-butybenzene) and (+)-**2** (14.4 mg, 0.060 mmol) was cooled to 0 °C. After dropwise addition of 1.0 M Et_2Zn in hexane solution (6.0 ml, 6.0 mmol), the mixture was maintained at 0 °C for 3 h. Ac_2O (1.2 ml, 13 mmol) was added and the mixture was allowed to stand overnight prior to capillary column GC analysis on a Cyclodex B stationary phase (J&W Scientific).

§ *Optical rotation* data: $[\alpha]_D^{25}$ +40.5 (*c* = 1.48, EtOH), lit.[12] for (*R*)-enantiomer, $[\alpha]_D^{21}$ +40.4 (*c* 0.530, EtOH), lit.[12] for (*S*)-enantiomer, $[\alpha]_D^{21}$ −41.9 (*c* = 0.500, EtOH).

1 N. Oguni and T. Omi, *Tetrahedron Lett.*, 1984, **25**, 2823.
2 V. Grignard, *C. R. Hebd. Sceances Acad. Sci.* , 1900, **130**, 1322.
3 K. Soai and S. Niwa, *Chem. Rev.*, 1992, *92*, 833; R. Noyori, *Asymmetric Catalysis in Organic Synthesis*, Wiley, New York, 1994, ch. 5.
4 M. Kitamura, S. Suga, K. Kawai and R. Noyori, *J. Am. Chem. Soc.*, 1986, **108**, 6071.
5 See for example: L. Sola, K. S. Reddy, A. Vidal-Ferran, A. Moyano, M. A. Pericas, A. Riera, A. Alvarez-Larena and J.-F. Piniella, *J. Org. Chem.*, 1998, **63**, 7078; J. Beliczey, G. Giffels, U. Kragl and C. Wandrey, *Tetrahedron: Asymmetry*, 1997, **8**, 1529; A. Vidal-Ferran, A. Moyano, M. A. Pericas and A. Riera, *J. Org. Chem.*, 1997, **62**, 4970; K. Soai, S. Yokoyama and T. Hayasaka, *J. Org. Chem.*, 1991, **56**, 4264.
6 M. Kitamura, S. Suga, H. Oka and R. Noyori, *J. Am. Chem. Soc.*, 1998, **20**, 9800; M. Yamakawa and R. Noyori, *Organometallics*, 1999, **18**, 128.
7 P. I. Dosa and G. F. Fu, *J. Am. Chem. Soc.* 1998, **120**, 445; A. H. M. De Vries, J. F. G. A. Jansen and B. L. Feringa, *Tetrahedron*, 1994, **50**, 4479; W. Oppolzer and R. N. Radinov, *J. Am. Chem. Soc.*, 1993, **115**, 1593; W. Oppolzer, R. N. Radinov and J. De Brabander, *Tetrahedron Lett.*, 1995, **36**, 2607.
8 J. D. White, D. J. Wardup and K. F. Sundermann, *Org. Synth*., submitted for publication (procedure no. 2822); J. D. White, personal communication, March, 1999.
9 R. A. Chittenden and G. H. Cooper, *J. Chem. Soc. C*, 1970, 49.
10 W. A. Nugent, G. Licini, M. Bonchio, O. Bortolini, M. G. Finn and B. W. McCleland, *Pure Appl. Chem.*, 1998, **70**, 1071.
11 M. Kitamura, S. Okada, S. Suga and R. Noyori, *J. Am. Chem. Soc.*, 1989, **111**, 4028.
12 K. Nakamura, M. Kawasaki and A. Ohno, *Bull. Chem. Soc. Jpn.*, 1996, **69**, 1079.

Communication 9/04042K

ChemComm

Asymmetric synthesis of the core cyclopentane of viridenomycin

Mark P. Arrington and A. I. Meyers*

Department of Chemistry, Colorado State University, Fort Collins, Colorado 80523-1872, USA.
E-mail: aimeyers@lamar.colostate.edu

Received (in Corvallis, OR, USA) 20th April 1999, Accepted 28th May 1999

The fully substituted cyclopentene ring with three stereogenic centers has been efficiently constructed for the first time using chiral bicyclic lactams, the insertion of the quaternary center being the key step; ring opening of chiral sulfates to the correct 1,2-dihydroxy substituents also played a major role in reaching 1 in suitable form (18) for further study.

Recently, a natural product was isolated from the culture broth of an actinomycete identified as *Streptomyces gannmycicus*, and upon structure determination, it was found that this compound was identical to viridenomycin, a natural product that had been known for some time, but which had not been structurally characterized.[1] Viridenomycin has been shown to

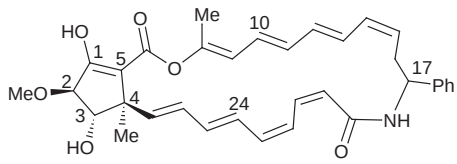

Viridenomycin

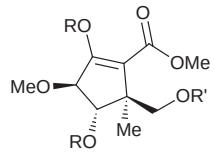

1

act as an antifungal antibiotic, and additionally has prolonged the survival of mice infected with B16 melanoma. It is structurally very similar to the natural product hitachimycin,[2,3] although viridenomycin has not yet been the subject of any reported synthetic efforts. It has, as its core, a highly functionalized cyclopentene ring **1** with three contiguous stereogenic centers, one of which is quaternary. Additionally, the absolute stereochemistry of viridenomycin is still unknown with the stereochemistry at C-17 still in question.

With our interest in chiral, bicyclic lactams as templates for a variety of enantiomerically pure compounds containing quaternary stereocenters, the C-4 position of viridenomycin suggested the possibility of an asymmetric synthesis.

The requisite chiral bicyclic lactam **2** (Scheme 1) was readily prepared by condensation of levulinic acid and enantiomerically pure natural valinol.[4] Treatment of **2** with LDA followed by MeI quench gave a mixture of products, containing primarily the desired α-methyl bicyclic lactam **3a**, in addition to some of the α,α-dimethylated compound **3b**.[5] The latter was only partially separable from the desired compound, so the crude product was simply carried on and directly treated again with LDA. The resulting enolate was quenched with $ClCO_2Me$, giving **3c** with high (> 98%) diastereoselectivity (NMR). Again, the α,α-dimethylated derivative **3b** was difficult to remove, and the mixture of **3b** and **3c** was carried forward. It had been previously observed[6] that acylating agents such as acid chlorides approached the lactam enolate in an *exo* fashion, so an *exo* approach to **3c** was hypothesized for the present transformation. The stereochemistry would be confirmed at a later time.

Reduction of the quaternary lactam ester **3c** with $NaBH_4$ in EtOH furnished the corresponding alcohol **4**, in high overall yield (65%) for the first three steps (**2**–**4**). The alcohol **4** was now easily separable from the accompanying α,α-dimethyl material **3b**. An X-ray crystal structure of alcohol **4** was obtained and confirmed that the hydroxymethyl group in **4** was indeed on the β-face of the molecule. This is the first published example of the lactam enolate of **2** acylating preferentially from the *exo* face. The hydroxymethyl side chain of **4** was transformed to its benzyl ether **5** in 96% yield, and the chiral auxiliary removed by reduction–hydrolysis to yield the cyclopentenone **6** with high efficiency (76%) for the three step process (**5** → **6**).

Studies were undertaken to access the allylic alcohol **7a**, *via* various reducing agents in anticipation of subsequent olefin dihydroxylation, to **9**. Since the benzyl protected hydroxymethyl side chain may be considered larger than the methyl group in **6**, it was expected that reducing agents should approach preferentially from the bottom face of the cyclopentenone **6**, to yield the β-OH group. It was found (Scheme 2) that the highest stereoselectivity could be realized (3.5 : 1) utilizing DIBAL-H[7] to afford **7a**. This modest selectivity was considered acceptable because the major isomer **7a** could be isolated in good (78%) yield, and the undesired α-OH isomer **7b** was also recyclable by oxidizing to the enone **6** with CrO_3 in high (86%) yield.

Repetitive reductions with DIBAL-H produced additional quantities of **7a**. The latter was converted to its *p*-methoxybenzyl (PMB) ether **8**, (KH, PMBCl) in 95% yield. Osmylation proceeded smoothly (90%) to give an inseparable mixture of diastereomeric diols **9** with relatively high (10 : 1) selectivity. The protons at C-2, C-3 (viridenomycin numbering) in **9** were sufficiently discernible in the NMR to determine the level of selectivity. Cyclic sulfate formation was accomplished using the Sharpless technique,[8,9] producing a single isomer (**10**) in

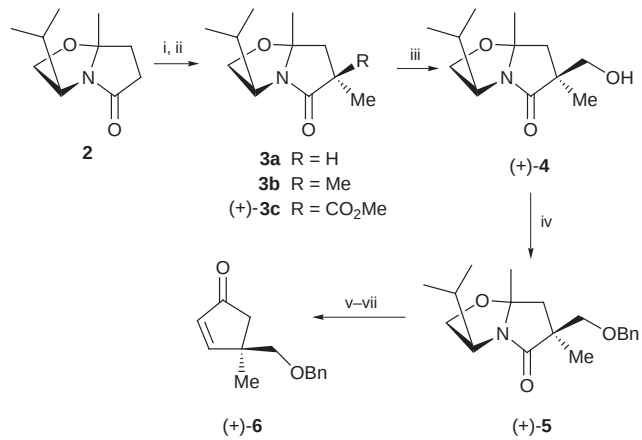

2

3a R = H
3b R = Me
(+)-**3c** R = CO_2Me

(+)-**4**

(+)-**6**

(+)-**5**

Scheme 1 *Reagents and conditions*: i, LDA, MeI, THF, −78 °C → rt; ii, LDA, $ClCO_2Me$, THF, −78 °C → rt (50 : 1 dr); iii, $NaBH_4$ (7 equiv.), EtOH, 0 °C → rt (65%, 3 steps); iv, NaH, BnCl, DMF, 0 °C → rt (95%); v, Red-Al (6.6 equiv.), THF, −25 °C, 2 d; vi, $NBu_4NH_2PO_4$ (50 equiv.), EtOH–H_2O (1 : 1); vii, KOH (0.1 equiv.), THF (76%, 3 steps).

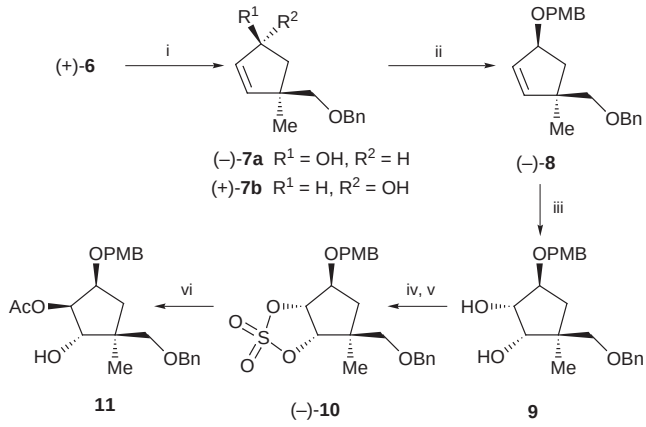

Scheme 2 *Reagents and conditions*: i, DIBAL-H (1.5 equiv.), THF. −78 °C (99%, 3.5:1 dr); ii, KH, (2.2 equiv.) PMBCl, DMF, 0 °C (95%); iii, $K_2OsO_2{\cdot}H_2O$, NMO, acetone–H_2O (3:1) (90%, 10:1 dr); iv, $SOCl_2$, Et_3N, CH_2Cl_2, 0 °C; v, $RuCl_3{\cdot}H_2O$, $NaIO_4$, CCl_4–H_2O–MeCN (1:1.4:1) (85%, 2 steps); vi, CsOAc (5 equiv.), DMF, 40 °C, then H_2SO_4, THF (99%, 9:1 dr).

satisfactory (77%) yield for the two steps. Caesium acetate opening of the sulfate **10** occurred with high regioselectivity (10:1) and yield (99%) to furnish the acetoxy alcohol **11** as the major regioisomer. In this case, the regioisomeric products were not separable and thus the mixture was carried forward.

Protection of the alcohol **11** (Scheme 3) was accomplished in excellent yield (96%) with TBDMSCl and imidazole affording the acetate **12** which was removed by K_2CO_3 in MeOH to give a quantitative crude yield of **13**. Methyl ether formation was accomplished on crude **13** in the usual manner to furnish methoxy derivative **14**. At this stage the regioisomeric impurity in **11** obtained by opening the cyclic sulfate was found to be separable and the slightly lower yield of this step (86%) reflects the removal of the undesired isomer.

It was now necessary to remove the PMB ether in **14**. Oxidative cleavage with CAN resulted in several products, thus

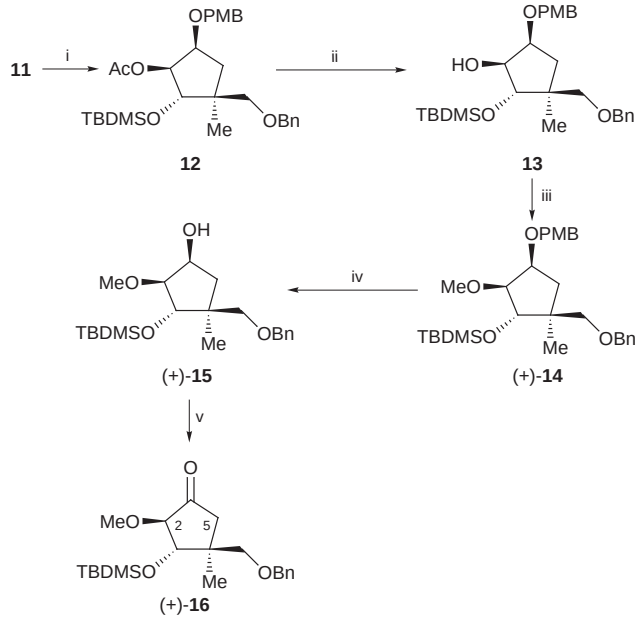

Scheme 3 *Reagents and conditions*: i, TBDMSCl, imidazole, DMAP (91%); ii, K_2CO_3, MeOH (100%); iii, NaH (2.5 equiv.), MeI, 0 °C (86%); iv, DDQ (1.3 equiv.), CH_2Cl_2–H_2O (5:1) (93%); v, $(COCl)_2$, DMSO, Et_3N, −78 °C (91%).

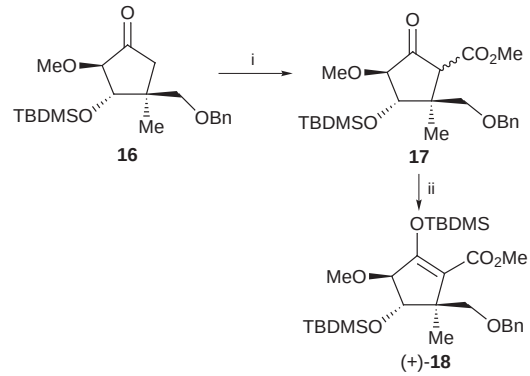

Scheme 4 *Reagents and conditions*: i, LDA, HMPA (25 equiv.), $NCCO_2Me$, −78 → −20 °C; ii, TBDNCl, imidazole, DMAP (40%, 2 steps).

the cleavage was performed with DDQ, which quickly removed the PMB group in good yield (93%) and gave the free C-1 alcohol **15**. Mild oxidation under Swern conditions produced the desired ketone **16** (91%).

The enolate of **16** was generated in the presence of HMPA[10] as cosolvent and warmed to −40°C before quenching with NCO_2Me. Enolate formation generated small amounts of the epimerized **16** and elimination products. However, the desired product **17** was the major constituent of the mixture, along with still significant quantities of undesired products. It appears from all of these experiments that the source of epimerization was not initial generation of the incorrect enolate, but was due to facile proton transfer processes after the addition of the electrophile.

Having obtained a quantity of the carboxylated derivative, **17**, attention was turned to isolation of the enol ester **18**, the intended target of this study (Scheme 4). Attempts to silylate **17** gave an enol ether, which was poorly characterized. By combining the two steps from **16** to **18** (no attempt was made to purify the β-keto ester **17**), the crude material was directly silylated and gave an overall yield of **18** of 40%. With the acquisition of **18**, all of the correct regio- and stereo-chemical features have been installed and the substituents at the 4- and 5-positions are in a position to further extend the synthesis to viridenomycin itself.

Further studies are in progress to introduce into **18** the 24-membered polyene ring of viridenomycin.

We are grateful to the NIH for financial support of this work.

Notes and references

1 M. Nakagawa, K. Furihata, Y. Hayakawa and H. Seto, *Tetrahedron Lett.*, 1991, **32**, 659.
2 T. Hasegawa, T. Kamiya, T. Henmi, H. Iwasaka and S. Yamatodani, *J. Antibiot.*, 1975, **28**, 167.
3 S. Omura, A. Nakagawa, K. Shibata and H. Sano, *Tetrahedron Lett.*, 1982 , **23**, 4713; I. Umezawa, H. Takeshima, K. Komiyama, Y. Koh, H. Yamamoto and M. Kawaguchi, *J. Antibiot.*, 1981, **34**, 259.
4 A. B. Smith, III, T. A. Rano, N. Chida, G. A. Sulikowski and J. L. Wood, *J. Am. Chem. Soc.*, 1992, **114**, 8008.
5 A. I. Meyers and D. Romo, *Tetrahedron*, 1991, **47**, 9503. A. I. Meyers and G. P. Brengel, *Chem. Commun.*, 1997, 1.
6 D. A. Sandham and A. I. Meyers, unpublished results.
7 A. Saito, A. Tanaka and T. Oritani, *Tetrahedron: Asymmetry*, 1996, **7**, 2923.
8 Y. Gao and K. B. Sharpless, *J. Am Chem. Soc.*, 1988, **110**, 7538.
9 B. Lohray, *Synthesis*, 1992, 1035.
10 C. Liotta and T. C. Caruso, *Tetrahedron Lett.*, 1985, **26**, 1599.

Communication 9/03160J

Copper zinc oxide catalysts for ambient temperature carbon monoxide oxidation

S. H. Taylor,[a] G. J. Hutchings[a] and A. A. Mirzaei[b]

[a] *Cardiff University, Department of Chemistry, PO Box 912, Cardiff, UK CF10 3TB. E-mail: taylorsh@cf.ac.uk*
[b] *Leverhulme Centre for Innovative Catalysis, University of Liverpool, Department of Chemistry, Liverpool, UK L69 3BX*

Received (in Cambridge, UK) 29th April 1999, Accepted 16th June 1999

Copper zinc oxide catalysts are effective for the ambient temperature carbon monoxide oxidation and display higher specific activity than the current commercial hopcalite catalyst.

The catalytic oxidation of carbon monoxide to carbon dioxide at ambient temperature and pressure is an important process for respiratory protection. In particular, the process is widely adopted by mining industries and has also found applications in deep sea diving and space exploration. Furthermore, new applications for the process such as reducing the deactivation of carbon dioxide lasers and applications for new sensors have been explored. In the last 10 years low temperature carbon monoxide oxidation has received renewed attention since Haruta *et al.* demonstrated that gold, highly dispersed on various oxides, forms catalysts active at sub-ambient temperatures.[1] However, the most widely used catalyst is the mixed copper manganese oxide hopcalite catalyst, $CuMn_2O_4$, first examined in 1921.[2,3] Both the gold based and the copper manganese oxide catalysts are important in terms of their high activity at ambient temperatures. It is the observation of high activity at low temperature which has stimulated significant recent interest in these types of catalysts.[4,5] It is interesting to consider whether other catalysts are capable of sustaining carbon monoxide oxidation at ambient temperature. Here, we present the first results showing that copper zinc oxide catalysts, prepared by co-precipitation, can display much higher activity for reaction than the current commercial hopcalite catalysts.

Catalysts were prepared using a co-precipitation technique under different atmospheres, including air, nitrogen, hydrogen and carbon dioxide. Aqueous solutions of $Cu(NO_3)_2{\cdot}3H_2O$ (0.25 mol l^{-1} Aldrich 99.999%) and $Zn(NO_3)_2{\cdot}6H_2O$ (0.25 mol l^{-1} Aldrich 99.999%) were pre-mixed in a 2:1 ratio. The resulting solution was stirred and heated to 80 °C in a round bottomed flask fitted with a condenser and equilibrated under a gas flow of 20 ml min^{-1} for 5 min. An aqueous solution of Na_2CO_3 (0.25 mol l^{-1} Aldrich 99.999%) was added to the continuously stirred flask until a pH in the range 6.8–7.0 was attained. At this stage the gas flow was passed through the solution and the precipitate allowed to age between 60 and 300 min. After ageing the precipitate was recovered by filtration, washed several times with hot distilled water and dried in air (120 °C for 16 h) and subsequently calcined in static air (550 °C for 6 h) to produce the catalyst. The hopcalite catalyst was also prepared in a similar manner using co-precipitation. The catalysts were characterised by powder X-ray diffraction. and nitrogen adsorption to determine the BET surface area.

The catalysts were tested for CO oxidation using a fixed bed laboratory microreactor. Typically CO (5% CO in He, 5 ml min^{-1}) and O_2 (50 ml min^{-1}) were fed to the reactor at controlled rates using mass flow controllers and passed over the catalyst (100 mg) at 20 °C. The products were analysed using on-line gas chromatography with a 3 m packed Carbosieve column. These conditions are equivalent to a total gas hourly space velocity of 33 000 h^{-1} and CO concentration of 0.45 vol%. Under these conditions the adiabatic temperature rise is < 7 °C and consequently the reactor temperature could readily be maintained isothermally at 20 °C.

All the copper zinc oxide catalysts, irrespective of the preparation atmosphere, showed appreciable activity for the oxidation of carbon monoxide at 20 °C. Blank reactions under the same conditions demonstrated no conversion. All the copper zinc oxide catalysts showed an initial decrease in activity over the first 30 min on line, but after this initial period steady state activity was maintained over the 500 min test period. Representative data for the catalysts prepared in an air atmosphere are shown in Fig. 1. The steady state activity of the aged copper zinc oxide catalysts derived from different atmospheres, and comparison with a copper manganese oxide catalyst are shown in Table 1.

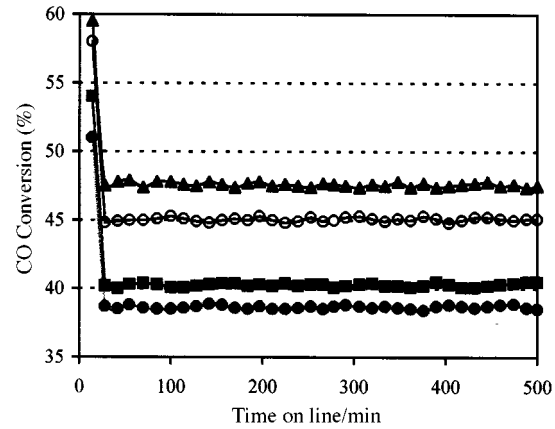

Fig. 1 Carbon monoxide conversion at 20 °C for aged catalysts prepared using air *vs.* time on line (GHSV = 33 000 h^{-1}, 100 mg catalyst, 0.45 vol% CO: Ageing time: (●) 60, (■) 120, (▲) 180 (○) 300 min.

The atmosphere used during co-precipitation has a marked influence on the activity of the copper zinc oxide catalysts. Regardless of ageing time, the general trend in terms of carbon monoxide conversion is air > hydrogen ≈ nitrogen > carbon dioxide. Increasing the catalyst ageing time up to 180 min increased the carbon monoxide conversion over all the copper zinc oxide catalysts. Increasing the ageing time to 300 min resulted in a slight decrease in conversion for the catalyst prepared in an air atmosphere, however, the catalysts prepared under the other atmospheres continued to show an increase in conversion. The catalyst surface areas were of similar magnitude regardless of the preparation atmosphere, however, there is a general increase in surface area as a result of increased ageing time. Although the overall conversion increases with ageing time the specific activity shows a gradual decrease.

Under our reaction conditions comparison of the copper zinc oxide catalyst has been made with the highly active copper manganese oxide catalyst.[6] The copper zinc oxide catalysts aged for < 180 min are all considerably more active than the copper manganese oxide catalysts. For example, the specific activity of copper zinc oxide aged for 60 min is greater than the

Table 1 Steady state activity for ambient temperature carbon monoxide oxidation (GHSV = 33 000 h^{-1}, 100 mg catalyst, 0.45 vol% CO)

Catalyst	Ageing time/min	Preparation atmosphere	Surface area/ $m^2\ g^{-1}$	CO conversion 10^{-16} (%)	Rate/molecules m^{-2}
CuO/ZnO	60	Air	29	38.8	1.50
CuO/ZnO	60	CO_2	26	20.5	0.88
CuO/ZnO	60	H_2	25	29.8	1.33
CuO/ZnO	60	N_2	27	30.4	1.26
Cu/Mn_xO_y	60	Air	28	9.9	0.39
CuO/ZnO	120	Air	36	40.2	1.35
CuO/ZnO	120	CO_2	28	21.5	0.86
CuO/ZnO	120	H_2	34	34.8	1.14
CuO/ZnO	120	N_2	32	33.2	1.16
$CuMn_xO_y$	120	Air	26	11.8	0.51
CuO/ZnO	180	Air	46	47.5	1.16
CuO/ZnO	180	CO_2	38	25.6	0.76
CuO/ZnO	180	H_2	41	40.2	1.10
CuO/ZnO	180	N_2	40	38.6	1.08
$CuMn_x/O_y$	180	Air	27	20.4	0.84
CuO/ZnO	300	Air	42	45.0	1.20
CuO/ZnO	300	CO_2	40	28.8	0.81
CuO/ZnO	300	H_2	45	42.4	1.06
CuO/ZnO	300	N_2	43	41.4	1.08
$CuMn_xO_y$	300	Air	30	49.5	1.85

corresponding copper manganese oxide catalyst by a factor >3.8. It is only once the copper manganese oxide catalyst has been aged for 300 min that it demonstrates higher activity. The optimum ageing time for the copper manganese oxide catalyst is 720 min showing a specific oxidation rate greater than the best copper zinc oxide by a factor of *ca.* 2.2.

Characterisation of the catalysts by powder X-ray diffraction showed that the preparation atmosphere and ageing process strongly influence the structure of the catalyst precursor. Hydrozincite $[Zn_5(CO_3)_2(OH)_6]$, gerhardite $[Cu_2(OH)_3NO_3]$, malachite $[Cu_2CO_3(OH)_2]$, aurichalcite $[(Cu,Zn)_5(CO_3)_2(OH)_6]$ and rosasite $](Cu,Zn)_2CO_3(OH)_2]$, were all determined and the relationship between preparation conditions and structure is considered to be complex. However, after calcination all the catalysts consisted of CuO and ZnO. The particle sizes of the oxides determined by X-ray line broadening decreased with increased ageing time, this effect was most marked with the catalyst prepared under air and carbon dioxide atmospheres, whilst under nitrogen and hydrogen atmospheres the effect was relatively minor. Temperature programmed reduction using hydrogen indicates that there may be some mixed oxide formation in the calcined catalyst. The catalysts were all similar by transmission electron microscopy, but subtle differences indicate that copper/zinc oxide solid solutions were formed and this is consistent with the evidence from temperature programmed reduction. The origin of the low temperature oxidation activity is unclear, but it appears that the highly dispersed CuO and ZnO, and the presence of solid solution phases formed during the controlled precipitation and ageing process are important.

At this stage no attempt has been made to optimise the activity of the copper zinc oxide catalysts, but it is clear that these catalysts show promising performance for the oxidation of carbon monoxide under ambient conditions. To the best of our knowledge this is the first reported study of copper zinc oxide catalyst prepared by co-precipitation under different atmospheres for the oxidation of carbon monoxide at low temperatures and these systems are now worthy of further investigation.

We thank Chris Kiely and Dave Whittle (University of Liverpool) for electron microscopy and Richard Joyner (Nottingham Trent) for useful discussion.

Notes and references

1 Haruta, N. Yamada, T. Kobayashi and S. Iijima, *J. Catal*., 1989, **115**, 301.
2 T. H. Rogers, C. S. Piggot, W. H. Bahlke and J. M. Jennings, *J. Am. Chem. Soc*., 1921, **43**, 1973.
3 H. A. Jones and H. S. Taylor, *J. Phys. Chem*., 1923, **27**, 623.
4 G. J. Hutchings, A. A. Mirzaei, R. W. Joyner, M. R. H. Siddiqui and S. H. Taylor, *Catal. Lett*., 1996, **42**, 21.
5 G. Fierro, S. Morpurgo, M. LoJacono and M. Inversi, *Appl. Catal. A*, 1988, **166**, 407.
6 E. J. Trimble, *Toxicology*, 1996, **115**, 41.

Communication 9/03426I

ChemComm

Evidence for the participation of a high-valent iron–oxo species in stereospecific alkane hydroxylation by a non-heme iron catalyst

Kui Chen and Lawrence Que, Jr.*

Department of Chemistry and Center for Metals in Biocatalysis, University of Minnesota, Minneapolis, Minnesota 55455, USA. E-mail: que@chem.umn.edu

Received (in Bloomington, IN, USA) 1st March 1999, Accepted 10th June 1999

The incorporation of ^{18}O from $H_2{}^{18}O$ into the product of stereospecific alkane hydroxylation by $[Fe^{II}(bpmen)(CH_3CN)_2](ClO_4)_2$–$H_2O_2$ provides the first strong evidence for the participation of a high-valent iron–oxo species in the mechanism of a non-heme iron catalyst.

The mechanisms for stereospecific hydrocarbon oxidation catalysed by iron-containing metalloenzymes have attracted significant interest in the chemical and biochemical communities.[1–3] Discrete high-valent iron-oxo species, formally Fe^V=O, have been proposed as oxidants in these reactions, *i.e.* a $[(Por\cdot)Fe^{IV}=O]^+$ species in alkane and alkene oxidation by cytochrome P450[1] and an $Fe^{IV}{}_2(\mu\text{-}O)_2$ intermediate in methane hydroxylation by methane monooxygenase.[4] In synthetic efforts to mimic these biological catalysts, both heme[5] and non-heme iron complexes[6,7] have been shown to be capable of catalysing alkane hydroxylation. Strong evidence has been obtained for the involvement of high-valent metal–oxo species on reactions involving some heme complexes and H_2O_2 from $H_2{}^{18}O$ exchange experiments,[8–11] but not for corresponding non-heme iron catalysts.[12,13] We have previously reported the first and thus far only example of stereospecific alkane hydroxylation by a non-heme iron catalyst, $[Fe^{II}(tpa)(CH_3CN)_2](ClO_4)_2$ **1** [tpa = tris(2-pyridylmethyl)amine, Fig. 1], in combination with H_2O_2.[7] Reported here are further studies on alkane hydroxylation by H_2O_2 catalysed by a related iron complex, $[Fe^{II}(bpmen)(CH_3CN)_2](ClO_4)_2$ **2** [bpmen = *N*,*N*′-dimethyl-*N*,*N*′-bis(2-pyridylmethyl)ethylene-1,2-diamine, Fig. 1], which exhibits higher catalytic activity. The incorporation of $H_2{}^{18}O$ into the oxidation product provides the first evidence that a non-heme iron catalyst can hydroxylate alkanes stereospecifically *via* a high-valent iron–oxo species.

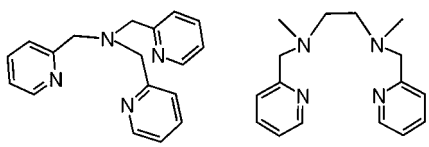

Fig. 1 Tetradentate ligands for non-heme Fe^{II} complexes **1** and **2**.

Complex **2** can be prepared from the reaction of equimolar amounts of $Fe^{II}(ClO_4)_2{\cdot}6H_2O$ and the ligand bpmen[14] in CH_3CN under Ar. Addition of diethyl ether into the CH_3CN solution gives a red solid, which can be recrystallised from CH_3CN–diethyl ether at 4 °C to afford red crystals suitable for crystallographic analysis (Fig. 2).† The crystal structure of **2** shows an iron(II) coordination sphere like that of **1**[15] with two solvent molecules in a *cis* geometry.

The alkane hydroxylation ability of **2** is superior to that of **1**. Under syringe pump conditions in CH_3CN solution in air,[7] 0.7 mM **2** catalyses the oxidation of cyclohexane with 10 equiv. H_2O_2 to afford 5.6(5) turnover (TN) of cyclohexanol and 0.7(2) TN of cyclohexanone within 30 min. The products account for 70% of the oxidant H_2O_2, which is much higher than the 40% conversion exhibited by **1**.[7] The high alcohol/ketone ratio obtained for **2** in air contrasts the much smaller ratios diagnostic of radical chain autoxidation found for other nonheme iron catalysts[6] and suggests the participation of a metal-based oxidant, as proposed in **1**–H_2O_2.[7]

Further mechanistic insight comes from ^{18}O-labeling experiments in the hydroxylation of cyclohexane.‡ With 10 equiv. H_2O_2 in the presence of 1000 equiv. $H_2{}^{18}O$, 18(3)% of the oxygen atom in the cyclohexanol product is ^{18}O-labeled. The complementary experiments with 10 equiv. $H_2{}^{18}O_2$ in the presence of 1000 equiv. H_2O show 84(4)% ^{18}O-labeled alcohol. These results demonstrate that O_2 is not involved in the reaction of **2**–H_2O_2. Furthermore, ^{18}O-incorporation can be significantly affected by the amount of $H_2{}^{18}O$ in the reaction solution. For example, with 200 equiv. $H_2{}^{18}O$, only 13(1)% of the cyclohexanol product is ^{18}O-labeled; and this value decreases further to 5.8(1)% in the presence of 50 equiv. $H_2{}^{18}O$. These observations show that the mechanism of alkane hydroxylation by **2**–H_2O_2 involves an oxidant capable of oxygen atom exchange with H_2O in competition with C–O bond formation.

The **2**–H_2O_2 combination is also capable of stereospecific alkane hydroxylation. The reaction of *cis*-1,2-dimethylcyclohexane with **2**–H_2O_2 affords 4.6(1) TN of *cis*-1,2-dimethylcyclohexanol and no isomeric *trans*-alcohol product. More interestingly, 26(1)% of the *cis*-alcohol product is ^{18}O-labeled when the reaction is carried out in the presence of 10 equiv. H_2O_2 and 1000 equiv. $H_2{}^{18}O$. Therefore, the oxidant responsible for stereospecific alkane hydroxylation can undergo oxygen-atom exchange with H_2O. Since the rate of epimerization of tertiary carbon radicals is quite fast (10^9 s^{-1}),[16] ^{18}O-exchange very likely happens prior to the interaction of the iron-based oxidant and the alkane C–H bond.

A mechanism for alkane hydroxylation by **2**–H_2O_2 combination is proposed based on the recent characterisation of Fe^{III}–OOH intermediates for several non-heme iron complexes

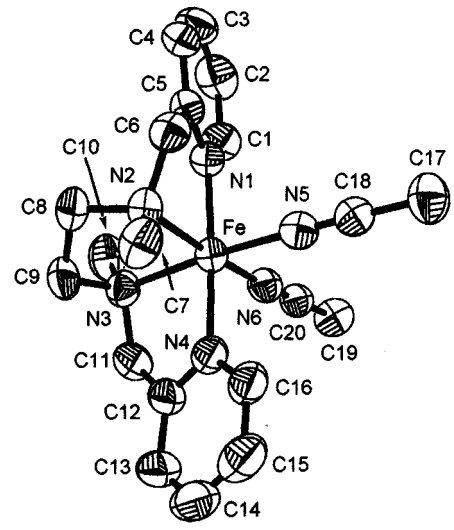

Fig. 2 Thermal ellipsoid plot of complex **2**. Ellipsoids are drawn at the 50% probability level. Hydrogen atoms are omitted for clarity.

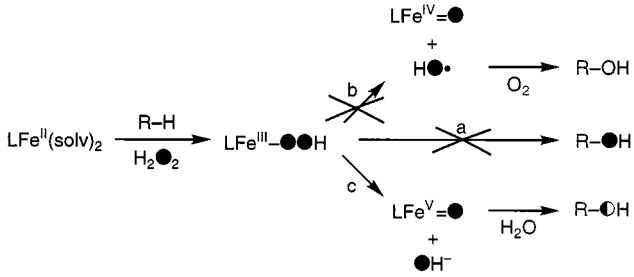

Scheme 1

(Scheme 1).[6j,7,17] Such an intermediate could attack the substrate directly [Scheme 1(a)] or undergo prior O–O bond scission. For the latter cases, homolysis of the O–O bond would afford Fe^{IV}=O and HO· [Scheme 1(b)], while heterolysis would give rise to Fe^{V}=O and HO^- [Scheme 1(c)]. The stereospecificity of *cis*-1,2-dimethylcyclohexane hydroxylation and lack of O_2 involvement in the reaction exclude the participation of hydroxyl radicals.[18] The observation of solvent exchange eliminates the possibility of direct attack of the Fe^{III}–OOH intermediate on the alkane substrate, since solvent exchange could not occur with such a species. The remaining mechanistic option is the heterolysis of the O–O bond to form a formally Fe^{V}=O species analogous to the $[(Por\cdot)Fe^{IV}=O]^+$ species observed for heme peroxidases and proposed for cytochrome P450.[1] Such a species would be capable of solvent exchange, provided its lifetime is long enough.[8–11, 19] Since solvent exchange is indeed observed for the stereospecific oxidation of *cis*-1,2-dimethylcyclohexane, a formally Fe^{V}=O intermediate must be involved in the **2**–H_2O_2 reaction. Complex **2** thus represents the first non-heme iron alkane hydroxylation catalyst for which evidence for a high-valent iron–oxo species has been obtained. Further studies into the nature of this species are in progress.

This work was supported by the National Institutes of Health (GM-33162).

Notes and references

† *Selected analytical data for* **2**. Elemental analysis. Calc. for $C_{20}H_{28}Cl_8FeN_6O_8$: C, 39.56; H, 4.65; N, 13.84; Cl, 11.68. Found: C, 39.41; H, 4.57; N, 13.76; Cl, 11.61%. X-Ray crystal data for $C_{20}H_{28}Cl_2FeN_6O_8$: M = 607.23, orthorhombic, space group $P2_12_12_1$, a = 9.984(2), b = 15.039(4), c = 17.653(2) Å, V = 2650.6(9) Å^3, T = 293(2) K, D_c = 1.522 g cm^{-1}, Z = 4, μ = 0.826 mm^{-1}, R [$I > 2\sigma(I)$] = 0.052 for 4642 independent reflections of the 5268 collected, R (all data) = 0.085. CCDC 182/1292. See http://www.rsc.org/suppdata/cc/1999/1375/ for crystallographic files in .cif format.

‡ $H_2{}^{18}O_2$ (ICON, 90%) or $H_2{}^{18}O$ (Isotec, 88.8% or ICON, 85 or 95%) was added to the reaction solutions in parallel experiments. Each product solution was treated with 0.1 mL 1-methylimidazole and 1 mL acetic anhydride to esterify the alcohol product (L. E. Elvebak, II, T. Schmitt and G. R. Gray, *Carbohydr. Res.*, 1993, **246**, 1). ^{18}O-incorporation was analysed by GC–CIMS (HP 5898, DB-5, and Finnigan MAT 95) with NH_3 as ionisation gas. Control experiments showed that cyclohexanol does not exchange its oxygen atom with H_2O under the experimental conditions.

1 M. Sono, M. P. Roach, E. D. Coulter and J. H. Dawson, *Chem. Rev.*, 1996, **96**, 2842.
2 L. Que, Jr. and R. Y. N. Ho, *Chem. Rev.*, 1996, **96**, 2607.
3 B. J. Wallar and J. D. Lipscomb, *Chem. Rev.*, 1996, **96**, 2625.
4 J. D. Lipscomb and L. Que, Jr., *J. Biol. Inorg. Chem.*, 1998, **3**, 331.
5 B. Meunier, *Chem. Rev.*, 1992, **92**, 1411.
6 (*a*) N. Kitajima, H. Fukui and Y. Moro-oka, *J. Chem. Soc., Chem. Commun.*, 1988, 485; (*b*) J. B. Vincent, J. C. Huffman, G. Christou, Q. Li, M. A. Nanny, D. N. Hendrickson, R. H. Fong and R. H. Fish, *J. Am. Chem. Soc.*, 1988, **110**, 6898; (*c*) W. Nam and J. S. Valentine, *New J. Chem.*, 1989, **13**, 677; (*d*) R. A. Leising, R. E. Norman and L. Que, Jr., *Inorg. Chem.*, 1990, **29**, 2553; (*e*) R. H. Fish, M. S. Konings, K. J. Oberhausen, R. H. Fong, W. M. Yu, G. Christou, J. B. Vincent, D. K. Coggin and R. M. Buchanan, *Inorg. Chem.*, 1991, **30**, 3002; (*f*) H.-C. Tung, C. Kang and D. T. Sawyer, *J. Am. Chem. Soc.*, 1992, **114**, 3445; (*g*) D. H. R. Barton and D. Doller, *Acc. Chem. Res.*, 1992, **25**, 504; (*h*) R. A. Leising, J. Kim, M. A. Pérez and L. Que, Jr., *J. Am. Chem. Soc.*, 1993, **115**, 9524; (*i*) R. M. Buchanan, S. Chen, J. F. Richardson, M. Bressan, L. Forti, A. Morvillo and R. H. Fish, *Inorg. Chem.*, 1994, **33**, 3208; (*j*) M. Lubben, A. Meetsma, E. C. Wilkinson, B. Feringa and L. Que, Jr., *Angew. Chem., Int. Ed. Engl.*, 1995, **34**, 1512; (*k*) I. W. C. E. Arends, K. U. Ingold and D. D. M. Wayner, *J. Am. Chem. Soc.*, 1995, **117**, 4710; (*l*) S. Ito, M. Suzuki, T. Kobayashi, H. Itoh, A. Harada, S. Ohba and Y. Nishida, *J. Chem. Soc., Dalton Trans.*, 1996, 2579; (*m*) B. Singh, J. R. Long, G. C. Papaefthymiou and P. Stavropoulos, *J. Am. Chem. Soc.*, 1996, **118**, 5824; (*n*) S. Ménage, J.-M. Vincent, C. Lambeaux and M. Fontecave, *J. Mol. Cat. A: Chem.*, 1996, **113**, 61; (*o*) C. Nguyen, R. J. Guajardo and P. K. Mascharak, *Inorg. Chem.*, 1996, **35**, 6273; (*p*) M. Kodera, H. Shimakoshi and K. Kano, *Chem. Commun.*, 1996, 1737; (*q*) S. Mukerjee, A. Stassinopoulos and J. P. Caradonna, *J. Am. Chem. Soc.*, 1997, **119**, 8097; (*r*) P. A. MacFaul, K. U. Ingold, D. D. M. Wayner and L. Que, Jr., *J. Am. Chem. Soc.*, 1997, **119**, 10594.
7 C. Kim, K. Chen, J. Kim and L. Que, Jr., *J. Am. Chem. Soc.*, 1997, **119**, 5964.
8 W. Nam and J. S. Valentine, *J. Am. Chem. Soc.*, 1993, **115**, 1772.
9 K. A. Lee and W. Nam, *J. Am. Chem. Soc.*, 1997, **119**, 1916.
10 S. J. Yang and W. Nam, *Inorg. Chem.*, 1998, **37**, 606.
11 J. Bernadou and B. Meunier, *Chem. Commun.*, 1998, 2167.
12 D. C. Heimbrook, S. A. Carr, M. A. Mentzer, E. C. Long and S. M. Hecht, *Inorg. Chem.*, 1987, **26**, 3835.
13 S. Ménage, J.-B. Galey, J. Dumats, G. Hussler, M. Seité, I. G. Luneau, G. Chottard and M. Fontecave, *J. Am. Chem. Soc.*, 1998, **120**, 13370.
14 H. Toftlund, E. Pedersen and S. Yde-Adersen, *Acta Chem. Scand., Ser. A*, 1984, **38**, 693.
15 Y. Zang, J. Kim, Y. Dong, E. C. Wilkinson, E. H. Appelman and L. Que, Jr., *J. Am. Chem. Soc.*, 1997, **119**, 4197.
16 A. M. Khenkin and A. E. Shilov, *New J. Chem.*, 1989, **13**, 659; P. J. Krusic, P. Meakin and J. P. Jesson, *J. Phys. Chem.*, 1971, **75**, 3438.
17 I. Bernal, I. M. Jensen, K. B. Jensen, C. J. McKenzie, H. Toftlund and J.-P. Tuchagues, *J. Chem. Soc., Dalton Trans.*, 1995, 3667; M. E. de Vries, R. M. La Crois, G. Roelfes, H. Kooijman, A. L. Spek, R. Hage and B. L. Feringa, *Chem. Commun.*, 1997, 1549; R. Y. N. Ho, G. Roelfes, B. L. Feringa and L. Que, Jr., *J. Am. Chem. Soc.*, 1999, **121**, 264; P. Mialane, A. Nivorojkine, G. Pratviel, L. Azéma, M. Slany, F. Godde, A. Simaan, F. Banse, T. Kargar-Grisel, G. Bouchoux, J. Sainton, O. Horner, J. Guilhem, L. Tchertanova, B. Meunier and J.-J. Girerd, *Inorg. Chem.*, 1999, **38**, 1085; G. Roelfes, M. Lubben, K. Chen, R. Y. N. Ho, A. Meetsma, S. Genseberger, R. M. Hermant, R. Hage, S. K. Mandal, V. G. Young, Jr., Y. Zang, H. Kooijman, A. Spek, L. Que, Jr. and B. L. Feringa, *Inorg. Chem.*, 1999, **38**, 1929.
18 C. Walling, *Acc. Chem. Res.*, 1975, **8**, 125.
19 R. J. Balahura, A. Sorokin, J. Bernadou and B. Meunier, *Inorg. Chem.*, 1997, **36**, 3488.

Communication 9/01678C

ChemComm

First η^1-ligated 2,4,6-tri-*tert*-butyl-1,3,5-triphosphabenzene complexes and the remarkable trihydration reaction of *trans*-$[PtCl_2(PMe_3)(P_3C_3Bu^t_3)]$ to *cis*-$[PtCl(PMe_3)(P_3O_3C_3H_5Bu^t_3)]$, containing the novel $CH(Bu^t)PH(O)C(Bu^t)PH(O)CH(Bu^t)P(O)$ ring system

Scott B. Clendenning, Peter B. Hitchcock and John F. Nixon*

School of Chemistry, Physics and Environmental Science, University of Sussex, Brighton, Sussex, UK BN1 9QJ

Received (in Cambridge, UK) 10th May 1999, Accepted 9th June 1999

The first examples of η^1-complexes of 2,4,6-tri-*tert*-butyl-1,3,5-triphosphabenzene are described, namely *trans*-$[PtCl_2(PR_3)(P_3C_3Bu^t_3)]$ (PR_3 = PMe_3, PEt_3, PMe_2Ph or $PMePh_2$) and their structures established by ^{31}P and ^{195}Pt NMR spectroscopy. The unusual molecular structure of *cis*-$[PtCl(PMe_3)(P_3O_3C_3H_5Bu^t_3)]$, containing the novel $CH(Bu^t)PH(O)C(Bu^t)PH(O)CH(Bu^t)P(O)$ ring system, which is formed by the trihydration of *trans*-$[PtCl_2(PMe_3)(P_3C_3Bu^t_3)]$ is also reported.

There is considerable current interest in the synthesis and ligating properties of compounds containing P–C multiple bonds.[1–4] Very recently[5,6] synthetic routes have been developed to 2,4,6-tri-*tert*-butyl-1,3,5-triphosphabenzene **1** and its structure and PE spectrum have just been reported.[7]

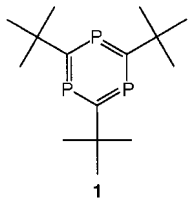

1

Although η^6-arene transition metal complexes occupy a key position in the development of contemporary organometallic chemistry, heteroarenes of the type EC_5R_5 (E = N, P, As, Sb or Bi) can also form η^1-ligated metal complexes unless bulky substituents such as *tert*-butyl groups in the 2,6-positions disfavour such interactions.[8] To date, no examples of η^1-bonded 2,4,6-tri-*tert*-butyl-1,3,5-triphosphabenzene complexes have been reported and only a handful of η^6-complexes of **1** are known such as the triple decker Sc(I) complex $[Sc_2(\eta^5\text{-}P_3C_2Bu^t_2)_2$ $(\eta^6\text{-}P_3C_3Bu^t_3)]$ the structure of which has been established by X-ray crystallography[9] and $[ML_n(\eta^6\text{-}P_3C_3Bu^t_3)]$, [$ML_n$ = $Mo(CO)_3$, $W(CO)_3$, $Mn(\eta^5\text{-}C_5H_5)$ or Ru(cod)],[10] whose stuctures have been proposed on the basis of NMR spectroscopic studies.

We now describe the first examples of η^1-bonded 2,4,6-tri-*tert*-butyl-1,3,5-triphosphabenzene platinum(II) complexes of the type *trans*-$[PtCl_2(PR_3)(S_3C_3Bu^t_3)]$ (PR_3 = PMe_3 **2**, PEt_3 **3**, PMe_2Ph **4** or $PMePh_2$ **5**) which are formed by treatment of **1**

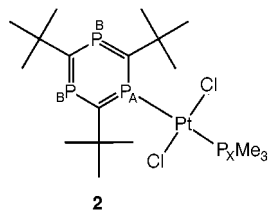

2

with the appropriate $[PtCl_2(PR_3)]_2$ complex in CH_2Cl_2 or $CHCl_3$ at room temperature. Attempts to make complexes of **1** by direct reaction with a variety of other metal halides such as MCl_4, (M = Ti or Zr), MCl_5 (M = Nb or Ta), CuX (X = Cl or I) were all unsuccessful as were ligand displacement reactions involving $[MCl_2(NCPh)_2]$ (M = Pd or Pt) and $[RhClL_n]$ (L = cyclooctene, n = 2; L = PPh_3, n = 3).

The $^{31}P\{^1H\}$ NMR spectrum of *trans*-$[PtCl_2(PMe_3)(P_3C_3Bu^t_3)]$ **2**, which is typical for all the complexes **2**–**5**, is shown in Fig. 1, and exhibits the characteristic coupling constant data expected for the *trans*-isomer. The ^{195}Pt NMR spectrum exhibits the expected doublet of doublets pattern.† Solution NMR data for the platinum complexes **3**–**5** containing the bulkier phosphines showed that, unlike complex **2**, there was always a significant concentration of the starting $[PtCl_2(PR_3)]_2$ complex present as well as unreacted **1** and several attempts to obtain crystalline complexes invariably led to further disproportionation. Not surprisingly it proved impossible to attach more than one $[PtCl_2(PR_3)]$ fragment to **1**.

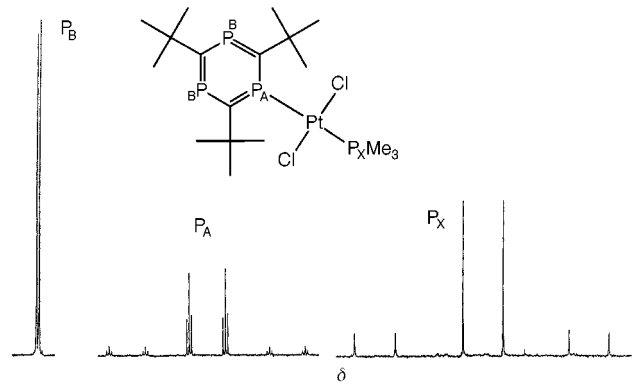

Fig. 1 $^{31}P\{^1H\}$ NMR spectrum of **2**.

It is interesting to compare the magnitude of the ^1J(PtP) coupling constant to the triphosphabenzene ring in **2** (2418 Hz) with that of the *trans* ligated PMe_3 (2901 Hz) indicating the smaller s-character of the P-lone pair in the triphosphabenzene. In the analogous 2,4,6-tri-*tert*-butyl-1-phosphabenzene[11] complex *trans*-$[PtCl_2(PMe_3)(PC_5H_2Bu^t_3)]$, synthesised in a similar manner, ^1J(PtP) is 2548 Hz, indicating that the presence of additional phosphorus atoms in the aromatic ring reduces the s-character of the P-lone pair electrons.

It has been previously shown that η^1-ligation of phosphaarenes can enhance their reactivity and we observe a remarkable reaction when **2** was recrystallised from CH_2Cl_2 in the air at room temperature. Addition of three water molecules to the coordinated triphosphabenzene ring occurs, together with HCl elimination, to afford the unusual complex $[PtCl(PM_3)\text{-}(P_3O_3C_3H_5Bu^t_3)]$ **6**. The molecular structure of **6**, which was established by a single crystal X-ray diffraction study‡ and is shown in Fig. 2, clearly results from addition of H_2O across each of the unsaturated P–C bonds in **2** in which the H adds to carbon and the OH to phosphorus in accord with the expected

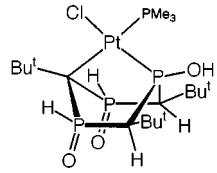

6

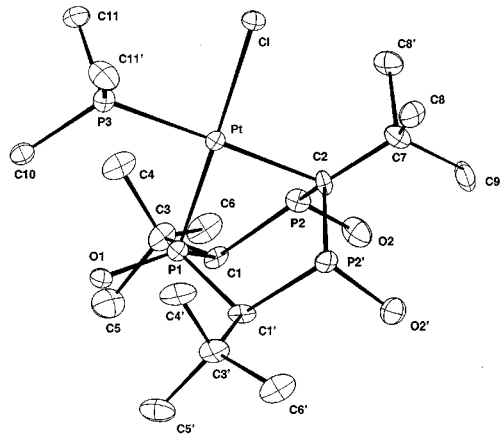

Fig. 2 Molecular structure of **6**. Selected distances (Å) and angles (°): Pt–P(1) 2.224(6), Pt–Cl 2.416(5), Pt–P(3) 2.273(6), Pt–C(2) 2.24(2), P(1)–O(1) 1.479(15), P(2)–O(2) 1.528(12), P(1)–C(1) 1.843(16), P(2)–C(2) 1.777(12), P(2)–C(1) 1.818(15); P(1)–Pt–C(2) 82.6(6), P(1)–Pt–P(3) 96.6(2), C(2)–Pt–P(3) 179.2(6), P(1)–Pt–Cl 178.84(19), C(2)–Pt–Cl 98.6(6), P(3)–Pt–Cl(1) 82.3(2), C(1)–P(1)–C(1′ 97.3(9), C(2)–P(2)–C(1) 109.3(8), P(2)–C(2)–P(2′ 114.6(12) P(2)–C(1)–P(1) 105.6(7)

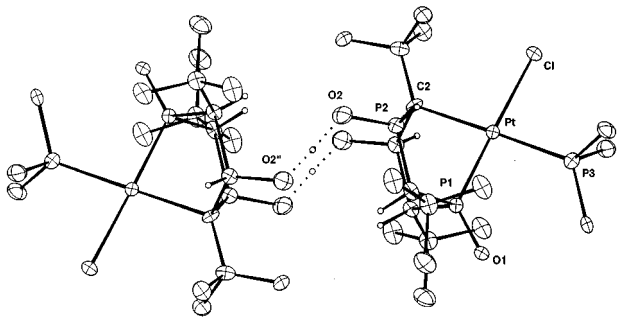

Fig. 3 Dimeric structure of **6**.

polarity of the bond. The resulting intermediate presumably then undergoes Arbusov-type rearrangement at *two* of the newly formed –P(OH)CHBu^t–centres to produce –PH(O)CHBu^t–ring fragments with the rearrangement at the third phosphorus centre unable to proceed because of ligation of the P atom to Pt. The accompanying loss of HCl and formation of a Pt–C bond leads to the observed product **6**. Mathey, Venanzi and their coworkers,[12–14] have previously noted selective addition of water and methanol to 2-pyridylphosphinines **7** and 2,2′-biphosphinines **8** coordinated to electrophilic metal centres as a result of the partial dearomatisation of the ligand.

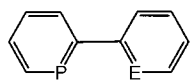

E = N **7** or P **8**

Complex **6** shows the following interesting features, (i) the structure consists of a H-bonded dimer; (ii) this H atom lies on a crystallographic twofold axis and was refined to a distance of 2.39 Å between O(2) and O(2)″; (iii) each individual molecule is bisected by a mirror plane through Pt and the ring C and P atoms to which it is bonded; (iv) the ring P–C bond lengths (ranging between 1.78 and 1.84 Å) are elongated compared with those in **1** and are typical for P–C single bonds; (v) the two P(2)=O double bond distances [1.528(12) Å] are similar to that of the formally single P(1)–O bond [1.479(15) Å] for the phosphorus attached to platinum. The structure suggests that the acidic H responsible for the dimeric structure of **6** may be capable of replacement by other cations, or substituted by organic groups, leading to significant structural changes (Fig. 3) and this is currently under study along with other aspects of the ligating behaviour of **1**.

We thank NSERC for a scholarship (for S. B. C.) and EPSRC for their continuing support (to J. F. N.) for phospha-organometallic chemistry.

Notes and references

† ^{31}P {^{1}H} NMR data: **2**: δP_A 203.0, δP_B 264.8, δP_X −18.3; $^1J(PtP_A)$ 2418, $^1J(PtP_X)$ 2886, $^2J(P_AP_B)$ 36.3, $^2J(P_AP_X)$ 543.3 Hz. **3**: δP_A 207.1, δP_B, 264.5, δP_X 12.1; $^1J(PtP_A)$ 2378, $^1J(PtP_X)$ 2884, $^2J(P_AP_B)$ 36.4, $^2J(P_AP_X)$ 508.5 Hz: **4**: δP_A, 202.5, δP_B, 265.4, δP_X −11.4; $^1J(PtP_A)$ 2487, $^1J(PtP_X)$ 2920, $^2J(P_AP_B)$ 36.6, $^2J(P_AP_X)$ 543.6 Hz. **5**: δP_A 200.4, δP_B 267.0, δP_X 1.3; $^1J(PtP_A)$ 2569, $^1J(PtP_X)$ 2961, $^2J(P_AP_B)$ 37.0, $^2J(P_AP_X)$ 545.5 Hz. **6**: $\delta P_{P(O)H}$ 31.4 [d, ^1J(PH) 552 Hz], $\delta P_{P(OH)}$ −0.6 [br, ^1J(PtP) 3155 Hz] $\delta P_{(PMe_3)}$, 10.1 [br, ^1J(PtP) 3181 Hz].

^{195}Pt NMR data (rel. K_2PtCl_6): **2**: δPt −3705; **3**: δPt −3738; **4**: δPt −3710; MS data (EI): **6**: *m*/*z* 660 (M^+).

‡ *Crystal data*: **6**, $C_{18}H_{41}ClO_3P_4Pt{\cdot}2.5CH_2Cl_2$, M = 872.2, orthorhombic, space group *Cmca* (no. 64), a = 14.508(9), b = 15.924(9), c = 29.018(12) Å, U = 6704(6) Å^3, Z = 8, D_c = 1.73 Mg m^{-3}, crystal dimensions 0.3 × 0.2 × 0.05 mm, F(000) = 3464, T = 173(2) K, Mo-Kα radiation (λ = 0.71073 Å). Data were collected on an Enraf-Nonius CAD4 diffractometer and of the total 2428 independent reflections measured, 1951 having $I > 2\sigma(I)$, were used in the calculations. The final indices [$I > 2\sigma(I)$] were $R1$ = 0.075, $wR2$ = 0.196. The complex lies on a crystallographic mirror plane and forms H-bonded dimers across a twofold rotation axis. All non-H atoms were anisotropic. H atoms were included in riding mode with U_{iso}(H) equal to 1.2eq(C) or 1.5eq(C) for methyl groups. The H-bonded H atom lies on a crystallographic twofold axis and was refined.

CCDC 182/1284. See http://www.rsc.org/suppdata/cc/1999/1377/ for crystallographic files in .cif format.

1 K. B. Dillon, F. Mathey and J. F. Nixon, *Phosphorus: The Carbon Copy*, John Wiley, Chichester, 1998, p. 366 and references therein.
2 J. F. Nixon, *Coord. Chem. Rev.*, 1995, **145**, 201.
3 J. F. Nixon, *Chem. Rev.*, 1988, **88**, 1327.
4 *Multiple bonds and low coordination in phosphorus chemistry*, ed. M. Regitz and O. J. Scherer, Georg Thieme Verlag, 1990, p. 496 and references therein.
5 P. Binger, S. Leininger, J. Stannek, B. Gabor, R. Mynott, J. Bruckmann and C. Kruger, *Angew. Chem., Int. Edn. Engl.*, 1995, **34**, 2227.
6 F. Tabellion, A. Nachbauer, S. Leininger, C. Peters, M. Regitz and F. Preuss, *Angew. Chem., Int. Edn.*, 1998, **37**, 1233.
7 R. Gleiter, H. Lange, P. Binger, J. Stannek, C. Krüger, J. Bruckmann, U. Zenneck and S. Kummer, *Eur. J. Inorg. Chem.*, 1998, 1619.
8 A. J. Ashe and J. C. Colburn, *J. Am. Chem. Soc.*, 1977, **99**, 8099. A. J. Ashe, W. Butler, J. C. Colburn and S. Abu-Orabi, *J. Organomet. Chem.*, 1985, **282**, 233.
9 P. L. Arnold, F. G. N. Cloke, P. B. Hitchcock and J. F. Nixon, *J. Am. Chem. Soc.*, 1996, **118**, 7630.
10 P. Binger, S. Stutzmann, J. Stannek, B. Gabor and R. Mynott, *Eur. J. Inorg. Chem.*, 1999, 83.
11 K. Dimroth and W. Mach, *Angew. Chem., Int. Edn. Engl.*, 1968, **7**, 460.
12 B. Schmid, L. M. Venanzi, A. Albinati and F. Mathey, *Inorg. Chem.*, 1991, **30**, 4693.
13 D. Carmichael, P. Le Floch and F. Mathey, *Phosphorus, Sulphur*, 1993, **77**, 255.
14 P. Le Floch, S. Mansuy, L. Ricard, F. Mathey, A. Jutand and C. Amatore, *Organometallics*, 1996, **15**, 3267.

Communication 9/03745D

High activity cobalt based catalysts for the carbonylation of methanol

Andrew C. Marr,[a] Evert J. Ditzel,[b] Attila C. Benyei,[a]† P. Lightfoot[a] and David J. Cole-Hamilton*[a]

[a] *School of Chemistry, University of St. Andrews, St. Andrews, Fife, Scotland, UK KY16 9ST. E-mail: djc@st-and.ac.uk*

[b] *BP Chemicals, Salt End, Hull, UK HU12 8DS*

Received (in Basel, Switzerland) 20th April 1999, Accepted 31st May 1999

[Cp*Co(CO)$_2$] in the presence of PEt$_3$ and MeI catalyses the carbonylation of methanol with initial rates up to 44 mol dm^{-3} h^{-1} before decaying to a second catalytic phase with rates of 3 mol dm^{-3} h^{-1}; [CoI(CO)$_2$(PEt$_3$)$_2$], which is trigonal bipyramidal with axial PEt$_3$ ligands, has been isolated from the final reaction solution.

Ethanoic acid is a bulk chemical of major importance in the polymer, paints and other industries. It is currently mainly manufactured by the carbonylation of methanol in the presence of iodomethane.[1] The first process of this kind used [Co$_2$(CO)$_8$] as the catalyst precursor, but the low activity and selectivity of this system meant that high temperatures and pressures (200 °C, 600 bar) were required and the selectivity to methanol was low.[2]

The discovery that rhodium[3] or iridium[4] based catalysts operate more selectively under much milder conditions (180 °C, 30 bar) led to these processes becoming favoured commercially. However, because of the much lower cost of cobalt than of its two platinum group metal congeners, there would be considerable interest if cobalt based systems that operated with high activity and selectivity under mild conditions could be discovered. In this paper, we report evidence that cobalt based systems can display very high activity and high selectivity.

Fig. 1 shows plots of gas (CO) uptake from a ballast vessel attached to an autoclave at constant pressure by solutions of [Cp*Co(CO)$_2$] under various conditions. [Cp*Co(CO)$_2$] in methanol containing methyl iodide shows relatively low activity but if 10 equivalents of PEt$_3$ are added, a dramatic increase in catalytic activity is observed. The reaction profile shows a very fast initial phase followed by a period with no activity and a further period where the activity is restored but to a level lower than that of the initial phase. This behaviour is reproducible. Addition of water to the system leads to a similar reaction profile, although the overall rates are higher than in the absence of water. The catalyst present during the second phase of the reaction carried out in the presence of water does not appear to be deactivated and the conversion to carbonylation product at the end of the reaction shown in Fig. 2 is *ca.* 41%. Since the major product under these conditions is methyl ethanoate, this represents *ca.* 80% of the methanol being consumed.

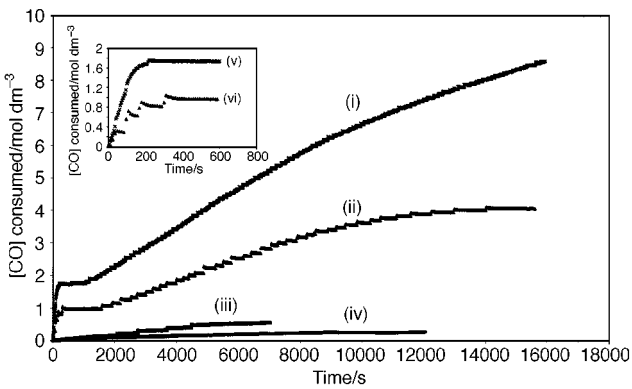

Fig. 1 CO uptake plots for methanol carbonylation reactions catalysed by: (i) [Cp*Co(CO)$_2$–PEt$_3$–H$_2$O; (ii) as (i) but no H$_2$O; (iii) as (ii), but no PEt$_3$; (iv) [Co$_2$(CO)$_8$]; inset: (v) and (vi) early stages of (i) and (ii), respectively.

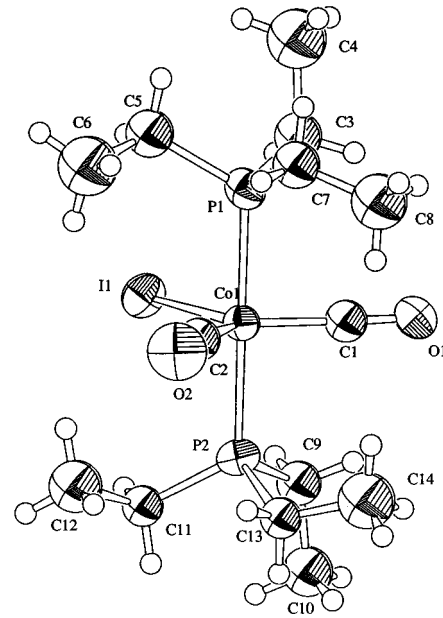

Fig. 2 X-Ray structure and numbering scheme for [CoI(CO)$_2$(PEt$_3$)$_2$]. Important bond lengths (Å) and angles (°): Co(1)–C(1) 1.75(2), Co(1)–C(2) 1.71(2), Co(1)–P(1) 2.208(6), Co(1)–P(2) 2.229(6), Co(1)–I(1) 2.649(3), C(1)–O(1) 1.14(2), C(2)–O(2) 1.17(2); I(1)–Co(1)–C(1) 114.4(7), I(1)–Co(1)–C(2) 118.6(7), I(1)–Co(1)–P(1) 89.5(2), I(1)–Co(1)–P(2) 89.9(2), C(1)–Co(1)–C(2) 127(1), C(1)–Co(1)–P(1) 89.7(7), C(1)–Co(1)–P(2) 89.8(7), C(2)–Co(1)–P(1) 90.5(7), C(2)–Co(1)–P(2) 90.5(7), P(1)–Co(1)–P(2) 179.0(3), Co(1)–C(1)–O(1) 175(1), Co(1)–C(2)–O(2) 173(2). There are two crystallographically distinct molecules in the asymmetric unit cell. The data for only one is reported here. The other is similar, except that only one ethyl group on one phosphine is *anti* to a Co–P bond.

Rates for the two phases of the reaction are presented in Table 1 and it should be noted that the conditions under which these reactions have been carried out are milder than those used for the industrial processes catalysed by rhodium or iridium systems. At 120 °C, the temperature of these studies, rates obtained with [RhCl(CO)$_2$]$_2$ as the catalyst precursor are of the order of 1 mol dm^{-3} h^{-1},[5] 44 times slower than the initial fast phase of the [Cp*Co(CO)$_2$]–PEt$_3$–H$_2$O system. The concentration of cobalt is 30 times that used for the rhodium catalyst so the actual activity of the cobalt system is 1.5 times the rate using rhodium. The high solubility and low cost of the cobalt system mean that it is possible to obtain industrially significant rates using the cobalt based system, even under the mild conditions used in this study.

GLC analysis of the liquid phase at the end of the reactions shows that the major product is methyl acetate, although acetic

† Current address: Chemistry Department, Kossuth Lajos University, Debrecen, Hungary.

Table 1 Rates of carbonylation of methanol under various conditions[a]

Catalyst	[Catalyst]/ mol dm^{-3}	[PEt_3]/ mol dm^{-3}	[MeOH]/ mol dm^{-3}	[MeI]/ mol dm^{-3}	[H_2O]/ mol dm^{-3}	Solution volume/cm^3	Initial rate/ mol dm^{-3} h^{-1}	TOF[b]/h^{-1}
[$Co_2(CO)_8$]	0.15	0	20.5	2.8	0	44.1	0.64	4.3
[Cp*Co(CO)$_2$]	0.09	0	24.5	0.15	0	51.6	0.32	3.6
[Cp*Co(CO)$_2$]	0.15	1.5	22.3	1.9	0	87.8	18.3, 1.1[c]	123, 7.1[c]
[Cp*Co(CO)$_2$]	0.15	1.5	22.2	1.8	4.5	4.3	43.9, 2.5[c]	314, 18[c]
[CoI(CO)$_2$(PMe_2Ph)$_2$][d]	2.7×10^{-3}	0	19.8	3.2	0	5.0	0.004	1.45
[RhCl(CO)$_2$]$_2$[e]	4.8×10^{-3}	0	—[f]	2.5	11.3	161	0.9[g]	188
[RhCl(CO)$_2$]$_2$[e]	4.8×10^{-3}	0	—[h]	2.4	2.3	164	0.6	125

[a] p_{CO} = 100 bar, T = 120 °C. Kinetic profiles were obtained using two different Hastelloy C autoclaves with different volumes. Reproducibility between the two reactors was checked by carrying out two identical reactions using identical concentrations. The reproducibility was ±15%. Reproducibility for the same autoclave was ±10%. [b] TOF is defined as the number of mol of CO consumed per mol of catalyst per hour. [c] Initial rate for the second active phase of the reaction. [d] Obtained from a 24 h batch reaction and analysis of the liquid phase products. [e] p_{CO} = 27 bar, but this reaction is zero order in p_{CO}. [f] Substrate added as methyl ethanoate (38.75 cm^3, 3.03 mol dm^{-3}), in ethanoic acid (64.9 cm^{-3}, 6.83 mol dm^{-3}); the reaction is zero order in [MeOH]. [g] Rises to 1.2 mol dm^{-3} as the reaction proceeds and [$RhI_2(CO)_2$]$^-$ forms.[6] [h] Substrate added as methyl ethanoate (23.82 cm^3, 1.83 mol dm^{-3}), in ethanoic acid (109.8 cm^{-3}, 11.4 mol dm^{-3}); the reaction is zero order in [MeOH].

acid is also formed, especially in the system containing added water. Traces of 1,1-dimethoxymethane (the acetal of ethanal) are also observed, but very much less than in the presence of [$Co_2(CO)_8$] based catalysts.

[Cp*Co(CO)$_2$] reacts with *e.g.* PMe_3 to give [Cp*Co(CO)(PMe_3)], which in turn reacts with iodomethane to give [Cp*Co(COMe)I(PMe_3)].[7] Since there is no induction period for the initial phase of the reaction, this suggests that the initial fast step of the carbonylation reaction is catalysed by [Cp*Co(CO)(PEt_3)]/[Cp*Co(COMe)I(PEt_3)]. We have carried out IR studies on a final solution from a reaction carried out in the presence of water [ν_{CO} 1989, 1973 (sh), 1905 cm^{-1}] to try to identify the cobalt species present during the second, slower but more prolonged catalytically active phase, and in addition have isolated a complex from the final reaction solution in the absence of water.

The isolated complex has been characterised by X-ray crystallography‡ as [CoI(CO)$_2$(PEt_3)$_2$], a trigonal bipyramidal complex with axial PEt_3 ligands (Fig. 2). [CoI(CO)$_2$(PEt_3)$_2$] gives rise to the strong peak at 1905 cm^{-1}, together with a weaker peak at 1973 cm^{-1}. The origin of the absorption at 1989 cm^{-1} is unclear, but evidence from other reactions suggests that the species giving rise to it is catalytically active and may be [Cp*Co(CO)I]$^-$. We have not isolated sufficient of [CoI(CO)$_2$(PEt_3)$_2$] to test its catalytic activity but the related [CoI(CO)$_2$(PMe_2Ph)$_2$] is active for methanol carbonylation (Table 1).

The isolation of [CoI(CO)$_2$(PEt_3)$_2$] from a solution containing excess MeI which would be expected efficiently to quaternise PEt_3 to [$PMeEt_3$]I, is surprising. However, we have shown by GCMS that free PEt_3 is present in the catalytic solutions and that the related [CoI(CO)$_2$(PMe_2Ph)$_2$] is formed if [CpCo(PMe_2Ph)CO] is used as a potential catalyst precursor, indicating either that phosphines can migrate between Co atoms without escaping the solvent cage, or that the solution can act as a source of free phosphine.

We conclude that careful design of cobalt based catalysts can give activities and selectivities that are comparable with those of their rhodium based analogues and because of the high solubility and low cost of the catalyst precursor, rates at low temperature can be higher than those currently observed under conditions used for the commercial rhodium or iridium based processes.

We thank BP Chemicals and the EPSRC for a CASE studentship (A. C. M.) and the European Community for support under a TEMPUS programme (A. C. B.). We also thank CATS, the Catalyst Evaluation and Optimisation Service funded by SHEFC for some of the kinetic measurements carried out by G. Schwarz and D. Foster.

Notes and references

‡ *Crystal data*: [$C_{14}H_{30}O_2CoIP_2$], M_r = 478.18, orthorhombic, space group $P2_12_12_1$, a = 15.95(1), b = 19.482(9), c = 13.312(10) Å, U = 4136(4) Å^3, Z = 8, D_c = 1.563 g cm^{-3}, F(000) = 1920.00, μ(Mo-Kα) = 24.58 cm^{-1}, λ = 0.71069 Å, T = 230 K. Crystal size, 0.3 × 0.25 × 0.2 mm. Of the 1917 reflections that were collected, $3 < 2\theta < 40.0°$ on a Rigaku AFC7S diffractometer, 1622 were observed. Structure solved by direct methods and expanded using Fourier techniques. The Co, I, P and O atoms were refined anisotropically, the C atoms isotropically. The maximum and minimum residual electron densities are 0.62 and −0.42 e A^{-3}. R = 0.040, R_w = 0.037. CCDC 182/1282.

1 M. J. Howard, M. D. Jones, M. S. Roberts and S. A. Taylor, *Catal. Today*, 1993, **18**, 325.
2 T. W. Dekleva and D. Forster, *Adv. Catal.*, 1986, **34**, 100.
3 F. E. Paulik and J. F. Roth, *Chem. Commun.*, 1968, 1578.
4 C. S. Garland, M. F. Giles and J. G. Sunley, *Eur. Pat.*, 643 034, 1995; *Chem. Abstr.*, 1995, **123**, 86573g.
5 J. Rankin, A. D. Poole, A. C. Benyei and D. J. Cole-Hamilton, *Chem. Commun.*, 1997, 1835.
6 J. Rankin, PhD Thesis, University of St. Andrews, 1997.
7 H. Werner, B. Heiser, B. Klingert and R. Dölfel, *J. Organomt. Chem.*, 1982, **240**, 179.

Communication 9/03169C

Palladium-catalysed formation of maleic anhydrides from CO, CO_2 and alk-1-ynes

Bartolo Gabriele,*[a] Giuseppe Salerno,*[a] Mirco Costa[b] and Gian Paolo Chiusoli[b]

[a] *Dipartimento di Chimica, Università della Calabria, 87030 Arcavacata di Rende, Cosenza, Italy. E-mail: b.gabriele@unical.it; g.salerno@unical.it*

[b] *Dipartimento di Chimica Organica e Industriale, Università di Parma, Viale delle Scienze, 43100 Parma, Italy*

Received (in Liverpool, UK) 8th April 1999, Accepted 20th May 1999

Carbon dioxide causes palladium-catalysed synthesis of unsaturated γ-lactones from alk-1-ynes and CO to shift towards maleic anhydrides.

We recently showed that working in dioxane–water at 80 °C under a 10 atm pressure of CO in the presence of PdI_2 and 10 equiv. of KI leads to catalytic reductive carbonylation of alk-1-ynes with formation of furan-2(5*H*)-ones (Scheme 1).[1] Oxidation of CO to CO_2 accounts for the stoichiometry of the process.

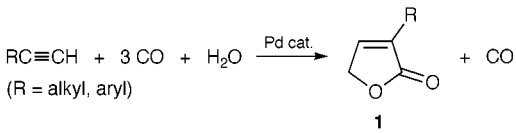

Scheme 1

We now find that in the presence of added CO_2 another catalytic reaction takes place, consisting of the formation of maleic anhydrides according to Scheme 2.

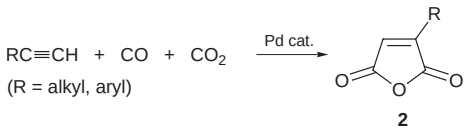

Scheme 2

Table 1 reports the results obtained with and without additional CO_2 pressure. By working under the same reaction conditions which selectively lead to furanones but under an additional 40 atm pressure of CO_2, the product distribution was clearly altered in favour of maleic anhydrides, although the overall reaction rate was decreased.

Both the presence of small amounts of water and the nature of Pd^{II} counterion were essential to the process, only traces of products being obtained under anhydrous conditions or using $PdCl_2$ and 10 equiv. of KCl as catalyst. Decomposition to Pd metal occurred only to a limited extent. In any case, Pd metal was not a catalytically active species for the present reaction, as shown by control experiments.

Table 1 Reactions of alk-1-ynes (100 equiv.) with CO (10 atm), CO_2 and H_2O (200 equiv.) in dry dioxane in the presence of PdI_2 (1 equiv.) and KI (10 equiv.), substrate conc.: 0.5 mmol ml^{-1} dioxane, T = 80 °C

Substrate	$P(CO_2)$/ atm	t/h	Yield (%)[a] 1	2
BuC≡CH	—	15	77[b]	7
BuC≡CH	40	64	32[c]	47
PhC≡CH	—	15	67	traces
PhC≡CH	40	24	30	34

[a] Based on starting alk-1-yne, by GLC. [b] 4-Butyl-2(5*H*)-furan-2-one (8%) was also detected in the reaction mixture. [c] 4-Butyl-2(4*H*)-furan-2-one (10%) was also present in the reaction mixture.

The effect of CO_2 can be rationalised in the following way (Scheme 3; anionic iodide ligands are omitted for simplicity). An I-Pd-CO_2H species,[2] stabilised by iodide ligands, is first generated from PdI_2, CO and H_2O and then inserts the alkyne and CO to give intermediate **I**. At this point two pathways are possible. Formation of furanones requries the intervention of a palladium hydride species,[3] which must derive from decarboxylation[4] of I-Pd-CO_2H, as shown in Scheme 3. Hydride exchange on complex **I** by H-Pd-I[5] followed by reductive cyclization of intermediate **II** leads to allylpalladium complex **III**, whose protonolysis affords **1** with regeneration of the catalytically active species [path (*a*)]. On the other hand, anhydrides can be formed *via* tautomerization of acylpalladium intermediate **I**[6] followed by elimination of Pd^0 and HI or I-Pd-H [path (*b*)]. This reaction is stoichiometric and reoxidation is needed to start a new cycle.[6,7] However, in the presence of an excess of CO_2 I-Pd-H can be reconverted into a catalytically active form. In fact, CO_2 may insert into the palladium hydride bond[8] with formation of either a I-Pd-CO_2H species (which can directly start a new cycle) or a Pd-O(CO)H species, whose protonolysis by HI would afford PdI_2. In both cases no reoxidation is needed and the anhydride cycle can go on. Moreover, in the presence of added CO_2, the decarboxylation equilibrium is shifted to the left and the anhydride cycle becomes competitive with the reduction pathway leading to furanones.

In summary, we have shown that under our conditions CO_2 strongly influences the distribution of products. In the presence of an excess of added CO_2 the resulting concentration of palladium hydride species is reduced in favour of Pd-CO_2H and/or Pd-O(CO)H species, thus minimising furanone formation and allowing the anhydride cycle to run.

The reaction reported here is the first example in which CO and CO_2 are used together for the catalytic formation of unsaturated cyclic anhydrides. The stoichiometric formation of an anhydride from a metallacyclic complex, CO and CO_2 in two steps was described some years ago.[9] In the recently reported

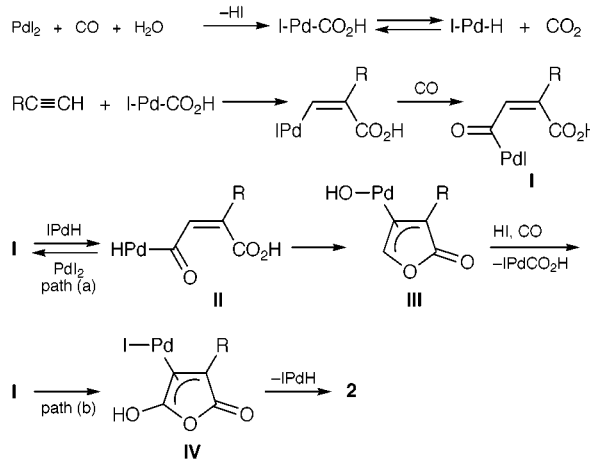

Scheme 3

oxidative cyclization–alkoxycarbonylation of propynylamines carried out in the presence of CO_2, the role of CO_2 in the catalytic cycle was very different (*in situ* generation of a propynyl carbamate, which then underwent cyclization and alkoxycarbonylation).[10]

The authors gratefully acknowledge the Ministero dell'Università e della Ricerca Scientifica e Tecnologica (MURST) for financial support (Progetto d'Interesse Nazionale PIN 9803026360).

Notes and references

1 B. Gabriele, G. Salerno, M. Costa and G. P. Chiusoli, *Tetrahedron Lett.*, 1999, **40**, 989.
2 This I-Pd-CO_2H species should form analogously to alkoxycarbonylpalladium halides but could not be isolated. Similar hydroxycarbonyl complexes are known with other metals, however; for representative examples, see Y.-X. He and D. Sutton, *J. Organomet. Chem.*, 1997, **538**, 49 and references cited therein.
3 B. Gabriele, G. Salerno, M. Costa and G. P. Chiusoli, *J. Organomet. Chem.*, 1995, **503**, 21.
4 R. Bertani, G. Cavinato, L. Toniolo and G. Vasapollo, *J. Mol. Catal.*, 1993, **84**, 165; B. Gabriele, G. Salerno, M. Costa and G. P. Chiusoli, *J. Mol. Catal. (A)*, 1996, **111**, 43.
5 For a recent review on methods of preparation and reactivity of hydrido complexes of palladium, see V. V. Grushin, *Chem. Rev.*, 1996, **96**, 2011.
6 B. Gabriele, M. Costa, G. Salerno and G. P. Chiusoli, *J. Chem. Soc., Perkin Trans. 1*, 1994, 83.
7 D. Zargarian and H. Alper, *Organometallics*, 1991, **10**, 2914.
8 For reviews on CO_2 insertion into the M–H bond, see M. E. Volpin and I. S. Kolomnikov, *Organomet. React.*, 1975, **5**, 590; X. Yin and J. R. Moss, *Coord. Chem. Rev.*, 1999, **181**, 27.
9 E. Carmona, E. Gutiérrez-Pueblo, J. M. Martin, A. Morge, M. Paneque, M. L. Poveda and C. Rui, *J. Am. Chem. Soc.*, 1989, **111**, 2883.
10 A. Bacchi, G. P. Chiusoli, M. Costa, B. Gabriele, C. Righi and G. Salerno, *Chem. Commun.*, 1997, 1209.

Communication 9/02814E

Thiazolium-dependent catalytic antibodies produced using a covalent modification strategy†

Fujie Tanaka, Richard A. Lerner* and Carlos F. Barbas III*

The Skaggs Institute for Chemical Biology and the Department of Molecular Biology, The Scripps Research Institute, 10550 North Torrey Pines Road, La Jolla, CA 92037, USA. E-mail: carlos@scripps.edu

Received (in Corvallis, OR, USA) 23rd March 1999, Accepted 1st June 1999

A thiazolium cofactor was introduced at a unique active site residue within antibodies that were generated by reactive immunization; the modified antibodies catalyzed a new cofactor-dependent reaction.

Enzymes effectively extend their catalytic scope by employing cofactors.[1] Consequently, in efforts to create novel cofactor-dependent protein catalysts several strategies have been developed.[2] Herein we report a novel approach which combines the unique features of catalytic antibodies derived from reactive immunization with a strategy for covalent modification that allows for the stable incorporation of a variety of cofactors. We further demonstrate the applicability of this strategy by preparing the first thiazolium-dependent catalytic antibodies.

Antibodies 38C2 and 33F12 were previously generated by reactive immunization with 1,3-diketone **1**.[3] These antibodies possess two key features which make them attractive as model systems for the development of cofactor-dependent catalysts: (i) they have unusually promiscuous active sites capable of binding a large variety of molecules and further transforming them chemically, and (ii) they contain a single highly reactive low pK_a lysine residue in their active site that is essential to their catalytic mechanism. The pK_as of the ε-amino groups of the LysH93 of 38C2 and 33F12 were determined to be 6.0 and 5.5, respectively.[3] Since this reactive lysine is the active nucleophile in Schiff base formation during the aldol reaction, we sought to take advantage of this reactivity and use it as a unique chemical handle for modification of these antibody catalysts. In earlier studies we have demonstrated that many β-dicarbonyl compounds are covalently yet reversibly bound as enaminones by these antibodies.[3] While β-dicarbonyl modified cofactors might be used to decorate the active sites of these antibodies with novel functionalities, we sought to develop a labeling strategy that would be irreversible and compatible with a wide range of cofactor chemistries. We reasoned that β-lactams[4] would form of a stable amide linkage to LysH93 (Scheme 1).

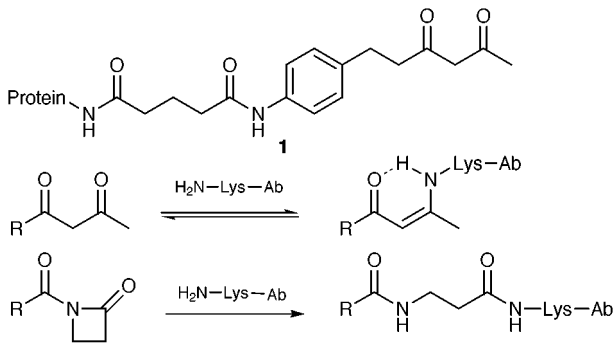

Scheme 1

To test this concept we synthesized a variety of β-lactam derivatives and studied their reactivity towards 38C2. The antibody 38C2 (20–30 μM active site) was first incubated with β-lactams (263 μM) in 5% MeCN– or DMSO–PBS (pH 7.4) at 25 °C. After 15–30 min and 14.5–40 h, the antibody active site was titrated by the addition of pentane-2,4-dione, followed by measurement of the characteristic enaminone absorption at 318 nm.[3] This assay effectively allows us to quantitate modification of the active site. Experiments with compounds **2**, **3** and **4**

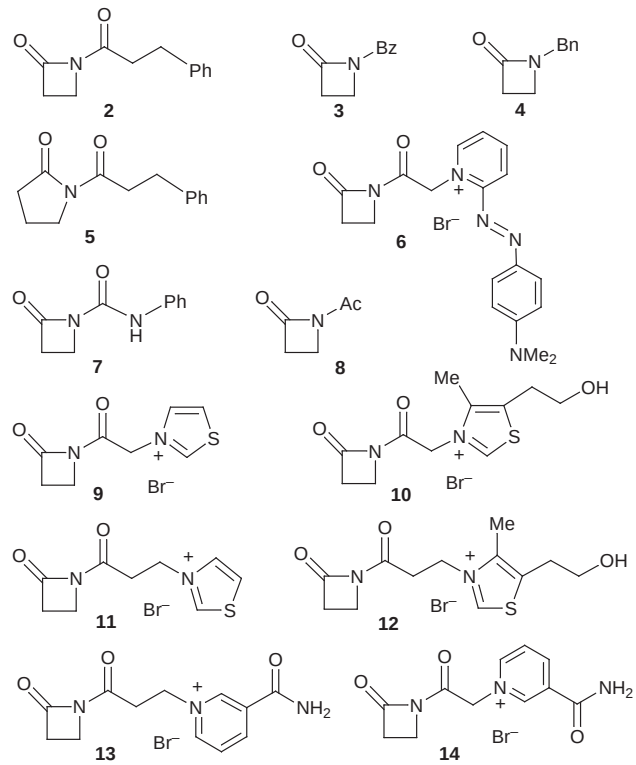

suggest that the enhanced reactivity of the β-lactam ring provided by the 1-acyl group present on **2** and **3** is required for reaction with the antibody. The 1-acyl group might also facilitate the reaction by positioning the molecule in the active site of the antibody. The β-lactam ring is in fact required for reactivity since γ-lactam **5**, which contains a stable amide linkage, does not react with the antibody. Although formation of an enaminone upon reaction of the antibody with pentane-2,4-dione is typically complete within 5 min, modification by the β-lactam compounds proceeds in a slow, time dependent fashion.[5] In the case of β-lactam **2**, 95% of the active sites remain unmodified after a 15 min incubation period. After 14.5 h of incubation, only 45% of the active sites remain unmodified. Reaction with these β-lactams was quantitatively inhibited by prior addition of pentane-2,4-dione to the antibody.

In order to determine the stoichiometry of the β-lactam modification, we first used mass spectrometry. The Fab

† Experimental details for the preparation and characterization of **2**–**14**, antibody labeling, characterization, and kinetics are provided as electronic supplementary information, see http//www.rsc.org/suppdata/cc/1999/1383/.

fragment of 38C2 (22 μM) was treated with compounds **2** and **4** (500 μM) for 65 h and the proteins were subsequently purified by gel filtration chromatography. MALDI-TOF mass spectra of the unmodified Fab 38C2, Fab 38C2 treated with **2**, and Fab 38C2 treated with **4** show centroid masses of *m*/*z* 48331, 48534 and 48326, respectively. Given the molecular weight of **2** (*m*/*z* 203), these data indicate that one molecule of **2** is incorporated per molecule of Fab 38C2. The Fab 38C2 was not modified with **4**, as expected based on our active site titration data.

To further support our conclusions, a spectrophotometric assay was also investigated. Violet colored compound **6** was reacted with 38C2 as described above. Absorbance measurements at 566 nm suggest that 65–80%[6] of the antibody was modified with **6.** Titration of this modified antibody by the addition of pentane-2,4-dione verifies that 69% of the active sites were modified. Further, an equivalent loss of aldolase activity from 38C2 was observed. To examine the chemistry by which compound **6** reacts with the active site, **6**-modified antibody 38C2 was treated with 500 mM hydroxylamine at room temperature for 27 h and subsequently purified. Spectrophotometric measurements of the resulting antibody at 566 nm revealed no loss of the chromophore, consistent with the formation of a stable amide linkage. While other active site residues such as tyrosine L41[3*d*] might be candidates for modification, hydroxylamine treatment would be expected to readily deacylate such an ester modification, thereby liberating the chromophore.[5] Additional studies indicated that antibody 38C2 was also covalently modified by compounds **7**–**14**.[7]

We also extended these studies to antibody 33F12, which differs from 38C2 by 18 amino acids. Examination of the rate of modification of 33F12 with 1-acylazetidin-2-ones **2**, **3** and **9** under the conditions described above revealed that antibody 33F12 reacted with these compounds at a rate 70–80% of that observed for 38C2. The studies described above are all consistent with a model wherein 1-acylazetidin-2-ones react with a single amine functionality within the active site of antibodies 38C2 and 33F12. Because of its unique chemical reactivity and structural accessibility, the ε-amino group of LysH93, common to both of these antibodies, is the most likely site for modification.

Given the diverse array of chemistries accessible to the B_1-dependent enzymes,[1,8,9] we chose to study the catalytic activity of antibodies modified with compounds **9** and **10**. We chose α-decarboxylation as a model reaction for the well studied thiamin-dependent enzyme pyruvate decarboxylase.[9] Antibody 38C2 (166 μM) was treated with **9** and **10** (10 mM) in 5% MeCN–PBS at room temperature for 51 and 66 h, respectively, followed by purification by gel filtration chromatography. More than 95% of the active sites were modified as determined by the enaminone assay previously described. Thiazolium-mediated decarboxylation of $PhCOCO_2H$ **15** was studied by HPLC using 40 μM of **9**-modified antibody 38C2 and 500 μM of **15** in 10% DMSO–aqueous buffer [(PBS, pH 7.4)/(200 mM bicine, pH 8.5) = 1:1]. Antibody 38C2 modified with **9** catalyzed the formation of BzOH[10] **16**, whereas unmodified antibody 38C2 and the antibody treated with **10** did not catalyze the reaction. The bulky substituents (Me and $HOCH_2CH_2$ groups) of **10** may present steric barriers to binding of the substrate **15**. When treated with **9,** antibody 33F12 also catalyzed this decarboxylation reaction. The modified antibodies 38C2 and 33F12 displayed typical Michaelis–Menten saturation kinetics; kinetic parameters were as follows: **9**-modified antibody 38C2, k_{cat} 2.1 × 10^{-3} min^{-1} and K_m 5.8 × 10^2 μM; **9**-modified antibody 33F12, k_{cat} 7.8 × 10^{-4} min^{-1} and K_m 2.7 × 10^2 μM. The rates of the antibody catalyzed reactions were compared with the rate of the thiazolium-catalyzed reaction, k_{thz} 1.0 × 10^{-8} μM^{-1} min^{-1}. Antibodies 38C2 and 33F12 modified with **9** therefore yield rate enhancements over thiazolium catalysis alone [$(k_{cat}/K_m)/k_{thz}$] of 370 and 290, respectively. The effective molarity of the cofactor (k_{cat}/k_{thz}) is therefore 0.21 M for 38C2 and 0.078 M for 33F12. These studies suggest that catalysis arises from sequestration of the substrate in proximity to the thiazolium cofactor. The relative hydrophobicity of the active site may also contribute to solvent mediated catalysis of the reaction.[11]

In summary, we have demonstrated that aldolase antibodies 38C2 and 33F12, prepared using reactive immunization, are specifically and covalently modified with a diverse range of 1-acylazetidin-2-ones. We have found that this methodology can be used for the production of novel thiazolium-dependent catalytic antibodies. The attachment system described above should also be useful for the diverse post-translational modification of biological libraries, such as phage displayed antibody libraries[12] which retain LysH93. This would allow for the *in vitro* evolution of cofactor-dependent catalysis. Because reactive immunization selects for catalysts that operate through covalent mechanisms, it presents us with a simple strategy for the generation of diverse antibody combining sites that retain a reactive chemical group in their active site.[3] As we have demonstrated here with aldolase antibodies, the active site remains amenable to labeling with cofactors, thereby providing a handle for extending the scope of catalytic antibodies. Since the chemist is not constrained to select cofactors from nature's pallet, unnatural yet catalytically interesting cofactors can be studied.

This study was supported in part by the NIH [CA27489].

Notes and references

1 C. Walsh, *Enzymatic Reaction Mechanisms*, ed. A. C. Bartlett and L. W. McCombs, W. H. Freeman and Company, New York, 1979.

2 For the introduction of cofactors into antibodies using cleavable affinity labels, see S. J. Pollack, G. R. Nakayama and P. G. Schultz, *Science*, 1988, **242**, 1038. For cofactor dependent catalytic antibodies, see P. G. Schultz and R. A. Lerner, *Science*, 1995, **269**, 1835; F. Tanaka, M. Oda and I. Fujii, *Tetrahedron Lett.*, 1998, **39**, 5057; S. I. Gramatikova and P. Christen, *Biol. Chem.*, 1996, **271**, 30583.

3 (*a*) J. Wagner, R. A. Lerner and C. F. Barbas III, *Science*, 1995, **270**, 1797; (*b*) C. F. Barbas III, A. Heine, G. Zhong, T. Hoffmann, S. Gramatikova, R. Bjornestedt, B. List, J. Anderson, E. A. Stura, I. A. Wilson and R. A. Lerner, *Science*, 1997, **278**, 2085; (*c*) G. Zhong, T. Hoffmann, R. A. Lerner, S. Danishefsky and C. F. Barbas III, *J. Am. Chem. Soc*., 1997, **119**, 8131; (*d*) T. Hoffmann, G. Zhong, B. List, D. Shabat, J. Anderson, S. Gramatikova, R. A. Lerner and C. F. Barbas III, *J. Am. Chem. Soc.*,1998, **120**, 2768; (*e*) G. Zhong, D. Shabat, B. List, J. Anderson, S. C. Sinha, R. A. Lerner and C. F. Barbas III, *Angew. Chem., Int. Ed.*, 1998, **110**, 2609.

4 Reactions of amines with benzylpenicillin have been reported: J. J. Morris and M. I. Page, *J. Chem. Soc., Perkin Trans. 2*, 1980, 212.

5 Covalent bond formation has been reported in the time-dependent inactivation of a catalytic antibody: B. Gigant, J.-B. Charbonnier, B. Golinelli-Pimpaneau, R. R. Zemel, Z. Eshhar, B. S. Green and M. Knossow, *Eur. J. Biochem.*, 1997, **246**, 471.

6 The range of extinction coefficients of the known dyes possessing the dimethylaminophenylazopyridinium group was used: M. Takeuchi, M. Taguchi, H. Shinmori and S. Shinkai, *Bull. Chem. Soc. Jpn.*, 1996, **69**, 2613; P. Schindler and G. Huber, *Enzyme Inhibitors, Proc. Meet.*; (Brodbeck, Urs,eds), Weinheim, Fed. Rep. Ger., *Verlag Chem.*, 1980, 169.

7 The observed order of the reactivity was: **3** > **11**–**13** > **2**, **9**, **10**, **14** > **8** > **7**. In studies of **3**, 90% of the active site was modified after 3 h whereas with **8**, 29% of the active site was modified after 40 h.

8 R. Kluger, *Chem. Rev.*, 1987, **87**, 863.

9 J. Hong, S. Sun, T. Derrick, C. Larive, K. B. Schowen and R. L. Schowen, *Biochim. Biophys. Acta*, 1998, **1385**, 187; S. Sun, G. S. Smith, M. H. O'Leary and R. L. Schowen, *J. Am. Chem. Soc.*, 1997, **119**, 1507 and references cited therein.

10 Aldehyde generation from the reaction intermediate in the decarboxylation has been reported to be a difficult process in the model reaction: see ref. 8 and Y. Chen, G. L. Barletta, K. Haghjoo, J. T. Cheng and F. Jodan, *J. Org. Chem.*, **1994**, *59*, 7714. However, atmospheric oxygen reacts with the intermediate and the hydrolysis gives the acid as the relatively easier process: A. I. Vovk and I. V. Murav'eva, *Russ. J. Gen. Chem.*, 1995, **65**, 119; A. I. Vovk and I.V. Murav'eva, *Russ. J. Gen. Chem.*, 1989, **59**, 1048; L. J. Dirmaier, G. A. Garcia, J. W. Kozarich and G. L. Kenyon, *J. Am. Chem. Soc.*, 1986, **108**, 3149.

11 J. Crosby and G. E. Lienhard, *J. Am. Chem. Soc.*, 1970, **92**, 5707.

12 D. R. Burton and C. F. Barbas III, *Adv. Immunol.*, 1994, **57**, 191.

Communication 9/02337B

N-Nitrosopiperidines with chirality solely due to hindered rotation about the N–N bond: enantioselective inclusion complexation with optically active hosts

Teresa Olszewska,[a] Maria J. Milewska,[a] Maria Gdaniec[b] and Tadeusz Połoński*[a]

[a] *Department of Chemistry, Technical University, 80-952 Gdańsk, Poland. E-mail: tadpol@chem.pg.gda.pl*
[b] *Faculty of Chemistry, A. Mickiewicz University, 60-780 Poznań, Poland*

Received (in Liverpool, UK) 3rd March 1999, Accepted 3rd June 1999

An efficient optical resolution of 4-substituted *N*-nitrosopiperidines achieved by enclathration with chiral diols was evidenced by X-ray crystallography and circular dichroism spectra in solution.

Hindered rotation about the partial double bond between the two adjacent nitrogen atoms in *N*-nitrosamines results in many unusual stereochemical and spectroscopic consequences.[1] In the absence of any improper symmetry axis the molecules of *N*-nitrosopiperidines, derived from symmetric amines, are chiral and may exist in two enantiomeric forms. Interconversion between the enantiomers occurs by rotation about the N–N bond (Scheme 1). The corresponding energy barrier is large enough (23–25 kcal mol^{-1})[2] to permit potential isolation of stereoisomers at ambient temperature.

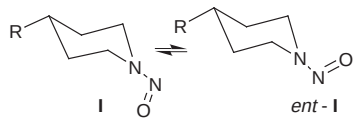

Scheme 1

The compounds **1**–**4**, owing their chirality solely to restricted rotation of the NO group, would be useful and extremely simple models for studying the chiroptical spectra of the nitrosamino

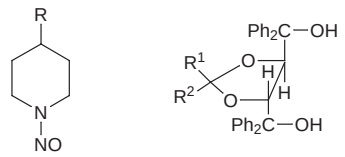

1 R = H
2 R = Me
3 R = Ph
4 R = CH_2Ph

5a $R^1 = R^2$ = Me
5b R^1–R^2 = $(CH_2)_4$

chromophore. The optical activity of nitrosamines has been the subject of numerous investigations and much speculation in recent years.[3] However, the resolution of racemic compounds devoid of additional functional groups usually poses a serious problem.[4] A method, which has received increasing attention in the last two decades, is the inclusion crystallization of racemates with optically active hosts.[5] This seems to be a promising approach also for our purpose. Recently, we have found that cholic acid crystal matrices show strong chiral recognition ability with the nitrosamines **1** and **2**, making it possible to detect their CD spectra in the solid state.[6] Unfortunately, this technique is restricted to rather small molecules and cholic acid did not form inclusion complexes with **3** and **4**.

Here we present a simple and general procedure for optical resolution of nitrosamines that also makes possible their isolation from the host matrices. We were particularly interested in obtaining easily crystallizing compounds, which stored in the solid state could retain their optical activity for very long periods. The nitrosamines **3** and **4** were among candidates that should satisfy these conditions. With use of (*R*,*R*)-(−)-**5a** and (*R*,*R*)-(−)-**5b** (TADDOLs), easily accessible from (+)-tartaric acid,[7] as the chiral hosts we were able to prepare optically active **3** and **4** in the crystal form and record their CD spectra in solution. The 1:1 complexes of **3** and **4** with **5a** were obtained by cocrystallization of equimolar amounts of the corresponding nitrosamine and the host diol from toluene–hexane. In the case of the diol **5b** and nitrosamine **4**, after choosing the proper component proportion, two types of inclusion compound can be prepared, with mp 109 and 131 °C (guest–host ratio of 1:1 and 1:2, respectively).

Usually separation of the optically active guest from the chiral diol can be accomplished chromatographically or by fractional distillation.[5,8] Obviously neither of these techniques can be used for unstable or rapidly racemising compounds. Taking advantage of the reported strong affinity of **5a**,**b** with secondary amines,[9] we succeeded in liberating of the enclathrated nitrosamines by a competitive complexation of the host diols with piperazine. This was possible because this amine forms a very stable and almost insoluble (in nonpolar solvents) 2:1 complex with **5b**. Therefore after addition of piperazine to a suspension of **4**·2(**5b**) in Et_2O at *ca*. 0 °C, followed by filtration of the precipitated piperazine complex and evaporation of the solvent, the optically active nitrosamine (−)-**4** was isolated; mp 62–63 °C, $[\alpha]_D^{21}$ −67.2 (*c* 1.25, C_6H_6). Compound

Table1 Circular dichroism (CD) data

Compound	Solvent[a]	λ/nm ([Θ])[b]
(−)-**3**	CD	376 (−510)
3·**5a**	T	373 (−2170)
3·**5b**	T	373 (−2080)
(−)-**4**	CD	373 (−1200)
4·5a	T	372 (1230)
4·**5b**	T	372 (−1880)
4·2(**5b**)	T	371 (−1550)

[a] CD = cyclohexane–dioxane (9:1), T = toluene. [b] Molecular ellipticity in deg cm^2 dmol^{-1}, measured immediately after dissolution of the sample.

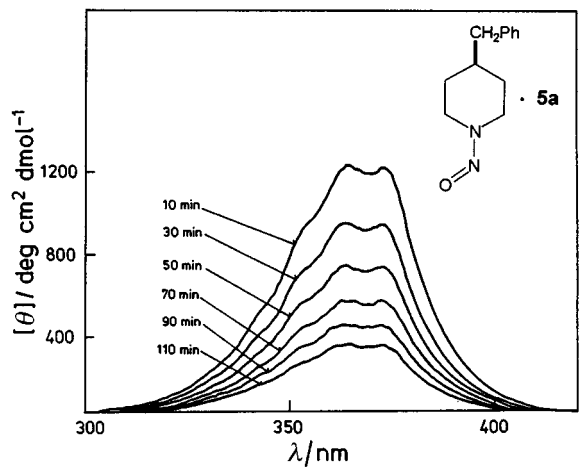

Fig. 1 Decay of the CD signal of **4**·**5a** in toluene at 22 °C.

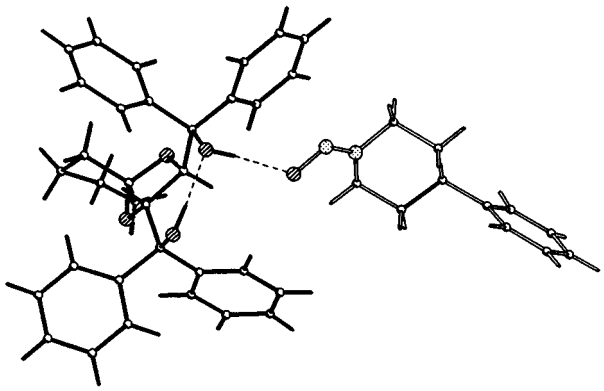

Fig. 2 Molecular structure of the complex **3**·**5b**. Broken lines represent the hydrogen bonds.

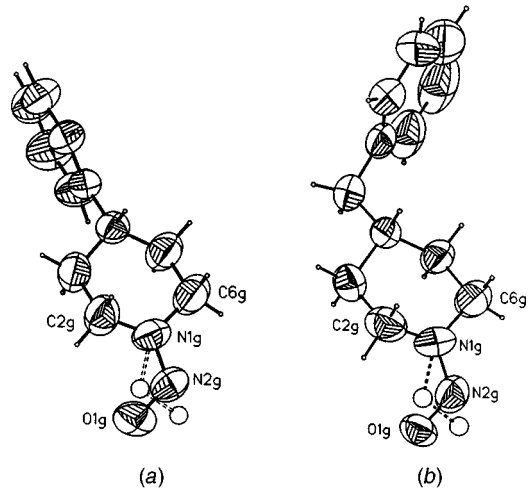

Fig. 3 ORTEP drawings of the guest nitrosamines (*a*) **3** and (*b*) **4** showing their absolute configurations.

(−)-**3** was prepared similarly; mp 66–67 °C, $[\alpha]_D^{21}$ −50.2 (*c* 1, C_6H_6).

The optical activity of the isolated nitrosamines is manifested by their chiroptical spectra in solution. Since the nitrosamine n–π* band does not interfere with the absorption of the phenyl chromophore in **5a**,**b**, the shape of the CD spectra of the complexed and free nitrosamines are essentially the same (Table 1). The CD curves observed in toluene solution show moderately strong Cotton effects corresponding to the nitrosamine n–π* electronic transition near 370 nm, which gradually decrease at room temperature (Fig. 1) due to a rapid racemization of (−)-**3** and (−)-**4**. A comparison of the CD sign of **4**·**5b** with that of **4**·2(**5b**) revealed the same configuration of the guest molecules included in both clathrates. In contrast, the opposite sign and slightly lower CD magnitude of **4**·**5a** to those shown by **4**·**5b** and **4**·2(**5b**) indicates a preferential complexation of the (+)-**4** enantiomer by the host **5a**.

The first order kinetics of the racemization process can be monitored by simple polarimetric measurements and we observed the racemisation half-life $t_{1/2}$ at 22 °C for **3** and **4** of 50 and 45 min, respectively. The calculated activation energy $\Delta G^{\ddagger}$ values of 22.0 and 21.9 kcal mol^{-1} for **3** and **4**, respectively, are comparable to the N–N rotation barrier heights obtained for *N*-nitrosopiperidines *via* NMR measurements.[2]

The X-ray crystallographic analysis of the clathrates **3**·**5b** (Fig. 2) and **4**·2(**5b**) revealed that one enantiomer of the guest nitrosamine was preferentially included in the crystals.† The absolute configurations of the guest molecules can be easily elucidated from the crystal structures of the clathrates and we found that in the case of the complexes **3**·**5b** and **4**·2(**5b**) the *S* configuration is preferred by (−)-**3** and (−)-**4** nitrosamine molecules (Fig. 3). However, a small degree of contamination of the inclusion crystals with the second nitrosamine enantiomer results in disorder of the N–NO group over two positions. A significant excess of the *S* enantiomer was determined from the refinement of the occupancy factors of two NO group positions although the exact enantiomeric ratio could not be determined due to a high correlation between the occupancy factors and dispalacement parameters of the N–NO group *via* the least-squares method. The X-ray structures of the clathrates showed that the piperidine ring in **3** and **4** assumes a chair conformation with the substituent at C-4 occupying the equatorial position. The nitroso oxygen is hydrogen bonded to one of the hydroxy groups of the host diol.

Notes and references

† Diffraction data were obtained on a Kuma KM-4 diffractometer with graphite monochromated Cu-Kα radiation (λ = 1.54178 Å). The structures were solved by direct methods with the program SHELXS-86 (ref. 10). Full-matrix least-squares refinement was carried out with SHELXL-93 (ref. 11). The *N*-nitroso groups in the guest molecules are disordered over two positions. Restraints were imposed on 1-2 and 1-3 distances and the planarity of the *N*-nitrosamino group during structure refinement. The minor components were refined with isotropic displacement parameters. *Crystal data* for **4**·2(**5b**): $2C_{33}H_{27}O_4{\cdot}C_{12}H_{16}N_2O$, M = 1189.44, monoclinic, space group $C2$, a = 35.720(7), b = 8.605(2), c = 23.661(5) Å, β = 117.94(3)°, V = 6425(2) Å^3, Z = 4, D_c = 1.230 g cm^{-3}, μ = 0.632 mm^{-1}, T = 293 K, crystal size 0.4 × 0.4 × 0.05 mm, θ_{max} = 60°, 4792 reflections measured, 4710 unique (R_{int} = 0.029) R_1 = 0.042, wR_2 = 0.107 for 3929 reflections with $I > 2\sigma(I)$ (R_1 = 0.062, wR_2 = 0.114 for all 4710 independent reflections). For **3**·**5b**: $C_{33}H_{27}O_4{\cdot}C_{11}H_{14}N_2O$, M = 682.83, monoclinic, space group $P2_1$, a = 11.292(2), b = 9.536(2), c = 17.654(4) Å, β = 97.04(2)°, V = 1886.7(7) Å^3, Z = 2, D_c = 1.202 g cm^{-3}, μ = 0.620 mm^1, T = 293 K, crystal size 0.5 × 0.15 × 0.03 mm, θ_{max} = 66°, 3511 reflections measured, 3418 unique (R_{int} = 0.024), R_1 = 0.0418, wR_2 = 0.1108 for 2633 reflections with $I > 2\sigma(I)$ (R_1 = 0.0696, wR_2 = 0.1271 for all 3418 independent reflections). CCDC 182/1275. See: http://www.rsc.org/suppdata/cc/1999/1385/ for crystallographic data in .cif format.

1 M. J. Milewska and T. Połoński, *Magn. Reson. Chem*., 1994, **32**, 631 and references cited therein; M. Gdaniec, M. J. Milewska and T. Połoński, *J. Org. Chem*., 1995, **60**, 7411; T. Połoński, M. Pham, M. J. Milewska and M. Gdaniec, *J. Org. Chem*., 1996, **61**, 3766; G. V. Shustov and A. Rauk, *J. Am. Chem. Soc*., 1995, **117**, 928.

2 J. D. Cooney, S. K. Brownstein and J. W. ApSimon, *Can. J. Chem*., 1974, **52**, 3028; R. K. Harris, T. Pryce-Jones and F. J. Swinbourne, *J. Chem. Soc., Perkin Trans. 2*, 1980, 476.

3 T. Połoński, M. J. Milewska and A. Katrusiak, *J. Am. Chem. Soc*., 1993, **115**, 11 410 and references cited therein.

4 H. Völter and G. Helmchen, *Tetrahedron Lett*., 1978, 1251.

5 F. Toda, *Top. Curr. Chem*., 1987, **140**, 43; F. Toda, in *Comprehensive Supramolecular Chemistry*, ed. D. D. MacNicol, F. Toda and R. Bishop, Pergamon, Oxford, 1996, vol. 6, pp. 465–516.

6 M. Gdaniec, M. J. Milewska and T. Połoński, *Angew. Chem., Int. Ed*., 1999, **38**, 392.

7 D. Seebach, A. K. Beck, R. Imwinkelried, S. Roggo and A. Wonnacott, *Helv. Chim. Acta*, 1987, **70**, 954; F. Toda and K. Tanaka, *Tetrahedron Lett*., 1988, **29**, 551.

8 F. Toda, *Supramol. Chem*., 1995, **6**, 159 and references cited therein; G. Kaupp, *Angew. Chem., Int. Ed. Engl*., 1994, **33**, 728.

9 E. Weber, N. Dörpinghaus and I. Goldberg, *J. Chem. Soc., Chem. Commun*., 1988, 1566; I. Goldberg, Z. Stein, E. Weber, N. Dörpinghaus and S. Franken, *J. Chem. Soc., Perkin Trans. 2*, 1988, 953.

10 G. M. Sheldrick, *Acta Crystallogr., Sect. A*, 1990, **46**, 467.

11 G. M. Sheldrick, SHELXL-93, Program for the Refinement of Crystal Structures, University of Göttingen, 1993.

Communication 9/01718F

Aerobic oxidation of α-hydroxycarbonyls catalysed by trichlorooxyvanadium: efficient synthesis of α-dicarbonyl compounds

Masayuki Kirihara,* Yuta Ochiai, Shinobu Takizawa, Hiroki Takahata and Hideo Nemoto*

Faculty of Pharmaceutical Sciences, Toyama Medical and Pharmaceutical University, Sugitani 2630, Toyama 930-0194, Japan. E-mail: kirihara@ms.toyama-mpu.ac.jp

Received (in Cambridge, UK) 6th May 1999, Accepted 8th June 1999

α-Hydroxycarbonyls were efficiently oxidized into α-dicarbonyls using a catalytic amount of trichlorooxyvanadium under an oxygen atmosphere.

α-Dicarbonyl compounds are important materials in synthetic organic chemistry.[1] They have been used as substrates for benzylic acid rearrangement[2] and starting materials for syntheses of heterocyclic compounds.[3] α-Dicarbonyl compounds are frequently obtained by the oxidation of α-hydroxycarbonyl precursors. Due to the sensitivity of the α-dicarbonyl compounds, special reagents and reaction conditions are required to prevent side reactions during the oxidation of the α-hydroxycarbonyls.[1] Although a number of methods have been developed to achieve this transformation, most of them suffer from drawbacks such as the use of stoichiometric amounts of corrosive acids or toxic metallic compounds that generate undesirable waste materials.†

We now describe the chemoselective aerobic oxidation of α-hydroxycarbonyls to α-dicarbonyls catalysed by high valent vanadium.‡

During the course of our study of the oxyvanadium-catalysed cleavage of α-hydroxy ketones, we found that the reaction of 2-hydroxycyclooctanone with a catalytic amount of dichloroethoxyoxyvanadium [$VO(OEt)Cl_2$] in MeCN under an oxygen atmosphere efficiently afforded cyclooctane-1,2-dione.[4]

We further examined the reaction, and found that α-dicarbonyl compounds could be efficiently obtained when trichlorooxyvanadium ($VOCl_3$) was used as the catalyst (Scheme 1).

First, we chose benzoin as the substrate and examined the reaction with several high valent vanadium catalysts in MeCN under an oxygen atmosphere (Table 1). Benzil was obtained in all cases, and the best result was obtained when $VOCl_3$ was used as the catalyst (run 2).

We then examined the reaction of benzoin with a catalytic amount of trichlorooxyvanadium in several solvents (Table 2). As noted in runs 1 and 2, MeCN and acetone are good solvents for this reaction.

The reaction of several α-hydroxy ketones with a catalytic amount of $VOCl_3$ in MeCN under an oxygen atmosphere provided the α-diketones in excellent yields.§ In all cases, the α-diketone was the sole product and no by-products were observed. These results are summarized in Table 3. The reaction

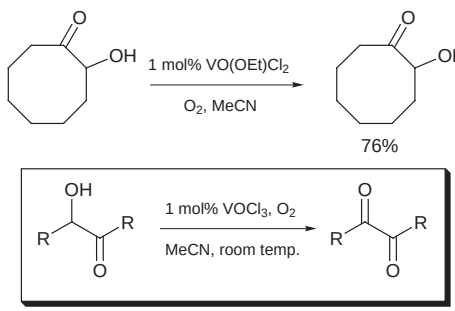

Scheme 1

Table 1 Reaction with different catalysts

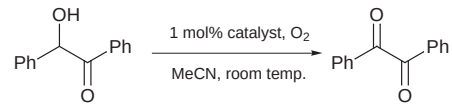

Run	Catalyst	*t*/h	Yield (%)
1	$VO(OEt)Cl_2$	1.5	94
2	$VOCl_3$	1.5	95
3	$VO(OEt)_3$	103	76
4	$VO(acac)_2$	127.5	76

Table 2 Reaction with different solvents

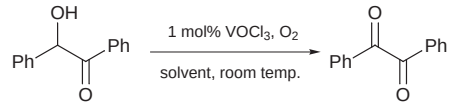

Run	Solvent	*t*/h	Yield (%)
1	MeCN	1.5	95
2	Acetone	2.5	94
3	CH_2Cl_2	21.5	84
4	AcOH	4.5	68
5	MeCN–H_2O (4:1)	307	57
6	Benzene	210.5	55

Table 3 Reaction with different α-hydroxy ketones

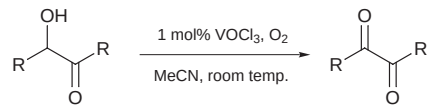

Entry	α-Hydroxy ketone	*t*/h	Yield (%)
1	R = Ph	1.5	95
2[a]	R = Ph	11	89
3	R = 4-ClC_6H_4	1.5	quant.
4	R = 4-$MeOC_6H_4$	1.5	quant.
5	R = C_9H_{19}	12	quant.
6	R = CH_2=$CH(CH_2)_7$	5.5	quant.
7[b]	R = $C_{15}H_{31}$	13.5	quant.
8	R = cyclohexyl	20	95
9	R–R = $(CH_2)_{10}$	8.5	quant.
10	R–R = $(CH_2)_{13}$	22.5	95
11	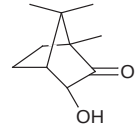	114	quant.

[a] The reaction was carried out in air. [b] The reaction was carried out under reflux.

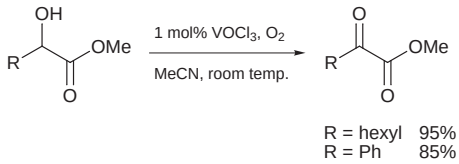

Scheme 2

of benzoin with a catalytic amount of $VOCl_3$ in MeCN in air also gave benzil in good yield (entry 2). It took longer to complete the reaction in the cases of the α-diketones having aliphatic substituents (entries 5–11). Interestingly, alcohols without a carbonyl moiety at their α-position did not react under the same conditions. α-Hydroxy esters were also efficiently oxidized to α-keto esters (Scheme 2).

As mentioned in a previous paper,[4] this reaction is not a simple radical oxidation, because this reaction was not influenced by a radical inhibitor.¶ A stoichiometric amount of $VOCl_3$ reacted with benzoin to afford benzil in the absence of oxygen (Scheme 3). This result means that molecular oxygen acts as a co-oxidant and reoxidizes the low valent vanadium that is formed.

We observed that the color of the reaction mixture was dark yellow at first, and then turned green in most cases. The 'green' of the reaction mixture strongly suggests the presence of V^{IV}

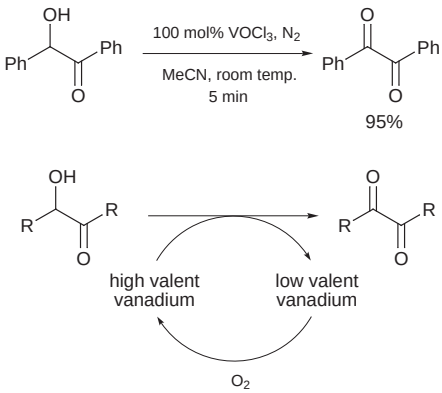

Scheme 3

species. Further study concerning aspects of the mechanism is currently underway.

We would like to express our appreciation to Professor Kan Kanamori, Toyama University, and Dr Yasushi Oda, Kyowa Hakko Kogyo Co., for their useful suggestions.

Notes and references

† We retrieved all the transformations of α-hydroxycarbonyl into α-dicarbonyl using REACCS (MDL Co., Ltd.), and found over 100 methods. Representative reports are cited in ref. 5.

‡ Two other aerobic oxidations of α-hydroxycarbonyls to α-dicarbonyls have been reported (ref. 6).

§ A typical experimental procedure is as follows: a mixture containing the α-hydroxycarbonyls (5.0 mmol), $VOCl_3$ (4.7 μl, 0.05 mmol) and MeCN (50 ml) was stirred at room temperature (or refluxed) under an oxygen atmosphere for 1.5–22.5 h. The mixture was quenched with saturated aq. $NaHCO_3$ and extracted with 20 ml × 3 of EtOAc. The combined organic extracts were washed with saturated aq. NH_4Cl and brine, dried over $MgSO_4$ and evaporated to afford the α-dicarbonyls.

¶ 2,6-di(*tert*-butyl)-*p*-cresol did not interfere with the reaction of $VOCl_3$ with benzoin in MeCN.

1 K. P. C. Vollhardt and N. E. Schore, *Organic Chemistry*, 2nd edn., Freeman, New York, 1994, pp. 924–929.
2 G. B. Gill, in *Comprehensive Organic Synthesis*, ed. G. Pattenden, Pergamon, New York, 1991, vol. 3, pp. 821–838.
3 I. Flament and M. Stoll, *Helv. Chim. Acta*, 1967, **50**, 1754; H. W. Rothkopf, D. Wöhrle, R. Müller and G. Kossmehl, *Chem. Ber*., 1975, **108**, 875; H. Wynberg and H. J. Kooreman, *J. Am. Chem. Soc*., 1965, **87**, 1739; W. W. Paudler and J. M. Barton, *J. Org. Chem*., 1966, **31**, 1720.
4 M. Kirihara, S. Takizawa and T. Momose, *J. Chem. Soc., Perkin Trans. 1*, 1998, 7.
5 J. S. Buck and S. S. Jenkins, *J. Am. Chem. Soc*., 1929, **51**, 2163; A. McKillop, B. P. Swann, M. E. Ford and E. C. Taylor, *Tetrahedron Lett*., 1970, 5281; A. McKillop, B. P. Swann, M. E. Ford and E. C. Taylor, *J. Am. Chem. Soc*., 1973, **95**, 3641; P. Girara and H. B. Kagan, *Tetrahedron Lett*., 1975, 4513; M. Besemann, A. Cornelis and P. Laszlo, *C. R. Acad. Sci. Ser. C*, 1984, **299**, 427; G.-S. Zhang, Q.-Z. Shi, M.-F. Chen and K. Cai, *Synth. Commun*., 1997, **27**, 9534; R. S. Varma, D. Kumar and R. Dahiya, *J. Chem. Res.* (*S*), 1998, 324.
6 M. P. L. Caton, G. Darbrough and T. Parker, *Tetrahedron Lett*., 1980, **21**, 1685; M. Singh and R. A. Misra, *Synthesis*, 1989, 403.

Communication 9/03622I

ChemComm

Extending the $n = 2$ Ruddlesden–Popper solid solution $La_{2-2x}Sr_{1+2x}Mn_2O_7$ beyond $x = 0.5$: synthesis of Mn^{4+}–rich compounds

Julie E. Millburn, John F. Mitchell* and Dimitri N. Argyriou

Materials Science Division, Argonne National Laboratory, Argonne, Illinois 60439, USA. E-mail: mitchell@anl.gov

Received (in Bloomington, IN, USA) 13th April 1999, Accepted 15th June 1999

Reported herein are the synthesis and room temperature crystal structures of the heretofore unknown, metastable manganites $La_{2-2x}Sr_{1+2x}Mn_2O_{7+\delta}$ ($0.5 \leqslant x \leqslant 0.9$) *via* high temperature ($T = 1650$ °C) quenching followed by low temperature ($T = 400$ °C) annealing to fill oxygen vacancies; this approach enables access to the electronic, magnetic, and structural properties of previously unexplored compositions in this important CMR system.

Mixed-valent manganite perovskites have received considerable attention in recent years, primarily because of the observation of colossal magnetoresistance (CMR) and more generally due to the unusually strong coupling among their lattice, spin, and charge degrees of freedom.[1–3] Although the focus of interest has primarily rested with the pseudocubic $Ln_{1-x}A_xMnO_3$ perovskites (A = Ca, Sr, Ba, Pb, Bi), naturally layered CMR materials have also attracted attention owing to their potential as model systems for low-dimensional physics[4–6] and because they exhibit substantially better low-field magnetoresistance than their three-dimensional perovskite counterparts.[7] Single phase synthesis has only been successfully achieved in the $n = 2$ Ruddlesden–Popper (RP) $La_{2-2x}Sr_{1+2x}Mn_2O_{7+\delta}$ manganite series for doping concentrations in the range $0.3 \leqslant x \leqslant 0.5$. Nonetheless, the structural, electronic, and magnetic phase diagram across this relatively narrow doping region is remarkably rich, displaying ferromagnetism, antiferromagnetism, canted states, spin rotations, and charge ordering.[7–11] Unfortunately, extension of the solid solution towards higher Mn^{4+} concentrations has heretofore proved unsuccessful,[12] with the notable exception of the synthesis of the $x = 1.0$ end member compound, $Sr_3Mn_2O_{7+\delta}$.[13, 14]

Here, we report on the synthesis and room temperature structural data of highly oxidized $La_{2-2x}Sr_{1+2x}Mn_2O_{7+\delta}$ phases with $0.5 \leqslant x \leqslant 0.9$. The importance of these materials for the continuing investigation and understanding of the physics of layered manganites is three-fold. First, they provide prototypes for appraisal of the interplay between aliovalent substitution and vacancy formation. Secondly, they provide models for further assessing the impact of Jahn–Teller distortions in these materials. Finally, they provide experimental data necessary to test theoretical predictions concerning the evolution of the magnetic ground state with dopant concentration.

Polycrystalline samples of $La_{2-2x}Sr_{1+2x}Mn_2O_{7+\delta}$, $0.5 \leqslant x \leqslant 0.9$, were prepared by high temperature, solid state reaction of La_2O_3 (Johnson-Matthey REacton 99.999%, pre-fired at 1000 °C in air for 12 h), $SrCO_3$ (Johnson-Matthey Puratronic 99.994%, dried at 150 °C in air for 12 h) and MnO_2 (Johnson-Matthey Puratronic 99.999%, pre-fired at 425 °C in flowing oxygen for 6 h, then slow cooled at 1 °C min^{-1} to room temperature). Stoichiometric quantities of the starting materials were mixed and fired in air as powders, at 900 °C for 24 h and then 1050 °C for a further 24 h. Samples were then pressed into 13 mm diameter pellets at 6000 lbs and ramped at 5 °C min^{-1} to 1650 °C. After 18 h each compound was quenched directly from the synthesis temperature into dry ice. As is the case for $Sr_3Mn_2O_{7+\delta}$,[2,14] the materials are metastable below 1650 °C and must be rapidly cooled to below 1000 °C to prevent decomposition. The black products were subsequently annealed for 12 h at 400 °C in flowing oxygen. Materials were reground between each firing. The Mn^{4+} content of the as-made and annealed materials was determined by iodometric titration against a standardized potassium thiosulfate solution. For each composition titrations were repeated several times to ensure accurate and consistent results (typically < 2% spread). Approximately 50 mg portions of as-made material were rapidly heated on a thermogravimetric analysis (TGA) balance to 400 °C in flowing oxygen, held at this temperature until no further weight change was observed, then quickly cooled to room temperature. Room temperature time-of-flight (TOF) powder neutron diffraction data were collected for the oxygen annealed samples on the Special Environment Powder Diffractometer (SEPD) at Argonne National Laboratory's Intense Pulsed Neutron Source (IPNS). All crystal structure analysis was performed by the Rietveld method using the GSAS program suite.[15]

The results of the titrations and the room temperature c/a ratio for the annealed samples as a function of x are plotted in Fig. 1. The individual lattice parameters for selected compositions are listed in Table 1. Data included for the $x = 1.0$ composition, $Sr_3Mn_2O_{7+\delta}$, are taken from ref. [13] Within the resolution of the SEPD instrument [$\pm 145° 2\theta$, $\Delta d/d$ (FWHM) = 0.0034] we find no evidence in our samples of the subtle phase separation previously reported for the $x = 0.5$ composition.[4]

Table 1 Room temperature lattice parameters from powder neutron diffraction data for $La_{2-2x}Sr_{1+2x}Mn_2O_7$ ($0.5 \leqslant x \leqslant 0.9$)

x	a/Å	c/Å
0.50	3.87470(3)[a]	20.0031(3)
0.55	3.87035(4)	19.9862(3)
0.60	3.86490(3)	19.9784(3)
0.75	3.84317(5)	19.9968(3)
0.80	3.83533(5)	20.0070(4)
0.90	3.81834(5)	20.0325(5)
1.00	3.79972(5)	20.0959(4)

[a] Numbers in parentheses are esds.

As shown in Table 1, the a lattice parameter monotonically decreases by 1.94% between $0.5 \leqslant x \leqslant 1.0$. In contrast, the c –axis shows a minimum at $x \approx 0.65$. This results in a smooth rise in the c/a ratio with increasing x (Fig. 1), a complete reversal of what is observed with increasing Mn^{4+} concentration in the $0.3 \leqslant x \leqslant 0.5$ region. This transformation in lattice behavior may reflect changes as a function of manganese oxidation state in the nature of d orbital occupation from in-plane to axial. It may also reflect a modification of the A–type magnetic ordering seen in this system at $x \sim 0.5$.[11] Theoretical predictions of the magnetic ground state by Maezono *et al.*,[16] for instance, depend upon a decreasing c/a ratio. In light of the present results, such calculations may require revision.

The as-made materials are found by titration to display an average Mn oxidation state of approximately +3.5 irrespective

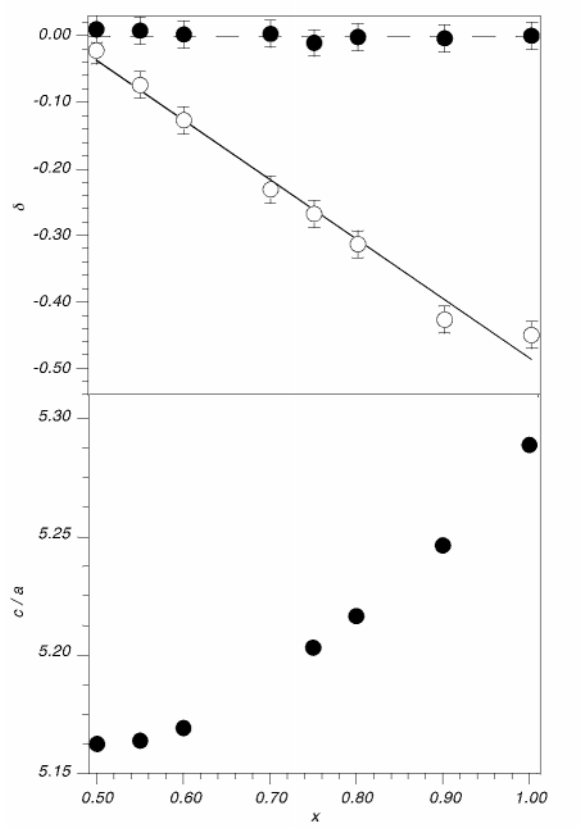

Fig. 1 Oxygen non-stoichiometry, δ, and c/a *vs.* x in $La_{2-2x}Sr_{1+2x}Mn_2O_{7+\delta}$ ($0.5 \leqslant x \leqslant 0.9$). Open circles represent data for the as-made, 1650 °C quenched samples, closed filled that for the low temperature oxygen annealed materials.

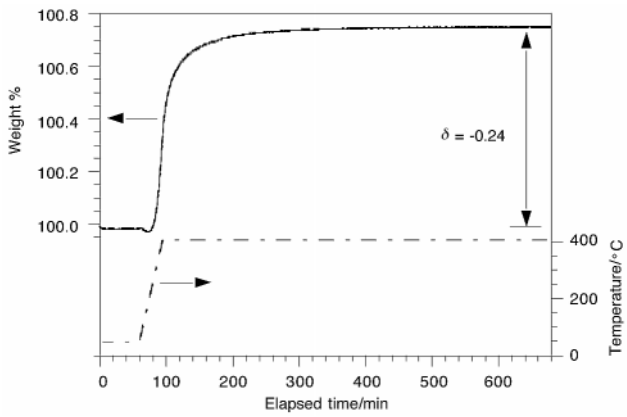

Fig. 2 Thermogravimetric analysis of as-made $La_{0.5}Sr_{2.5}Mn_2O_{7+\delta}$ under a flowing oxygen atmosphere.

of composition. Analogy with $Sr_3Mn_2O_{7+\delta}$[13] suggests this to be a consequence of the formation of oxygen vacancies in the materials during synthesis. Thermogravimetric analysis corroborates this hypothesis; illustrative results for the $x = 0.75$ composition are shown in Fig. 2. The observed weight gain indicates that a substantial quantity of oxygen is incorporated by the sample upon heating. Assuming the end-point corresponds to the stoichiometric material, $La_{0.5}Sr_{2.5}Mn_2O_{7.0}$, then the as-made compound may be formulated as $La_{0.5}Sr_{2.5}Mn_2O_{6.76}$, *i.e.* $\delta = -0.24(2)$. Since, the average manganese oxidation is given by $3 + x + \delta$, this value of δ corresponds to an oxidation state of +3.51(2) in good agreement with the titrimetric result of +3.48(2). Fig. 1 shows the monotonic decrease in δ (or increase in number of oxygen vacancies formed during synthesis) with x that gives rise to the constant, dopant independent Mn oxidation state. Once annealed at 400 °C in oxygen, all the materials are found to be stoichiometric, $\delta = 0.00(2)$. This is corroborated by refinement of the oxygen content in the powder neutron diffraction data: all oxygen site occupancies are unity within error. These findings suggest that the initial synthesis conditions impose an upper limit on the transition-metal oxidation state. In fact, in our experience, $Mn^{+3.5}$ is the maximum mean oxidation state attainable in a layered $n = 2$ manganite system by any high temperature route. Prior attempts to extend the solid solution beyond $x = 0.5$ in this and other $Ln_{2-2x}Sr_{1+2x}Mn_2O_7$ series by conventional high temperature solid state techniques results in the formation of mixed-phase materials.[12]

The use of a two-step procedure such as reported here, in which formation of vacancies within the structure is followed by low temperature oxygen annealing to yield the stoichiometric material, thus seems essential in providing access to compositions containing higher concentrations of Mn^{4+}. Access to these compositions will permit a more complete investigation of the interplay among structure, magnetism, and transport in layered manganites. Full characterization of the temperature-dependent crystallographic and magnetic structure of the compositions prepared here will be reported in a subsequent paper.

The authors thank Simine Short for assistance with the TOF powder neutron diffraction measurements. This work was supported by the U. S. Department of Energy, Basic Energy Sciences–Materials Sciences under contract W-31-109-ENG-38 (JEM, JFM) and W-7405-ENG-36 (DNA).

Notes and references

1 B. Raveau, A. Maignan and V. Caignaert, *J. Solid State Chem.*, 1995, **117**, 424.
2 A. Urushibara, Y. Moritomo, T. Arima, A. Asamitsu, G. Kido and Y. Tokura, *Phys. Rev. B*, 1995, **51**, 14 103.
3 P. G. Radaelli, M. Marezio, H. Y. Hwang, S. Cheong and B. Batlogg, *Phys. Rev. B*, 1996, **54**, 8992.
4 P. D. Battle, D. E. Cox, M. A. Green, J. E. Millburn, L. E. Spring, P. G. Radaelli, M. J. Rosseinsky and J. F. Vente, *Chem. Mater.*, 1997, **9**, 1042.
5 Y. Moritomo, Y. Tomioka, A. Asamitsu, Y. Tokura and Y. Matsui, *Phys. Rev. B.*, 1995, **51**, 3297.
6 J. F. Mitchell, D. N. Argyriou, J. D. Jorgensen, D. G. Hinks, C. D. Potter and S. D. Bader, *Phys. Rev. B*, 1996, **55**, 63.
7 Y. Moritomo, A. Asamitsu, H. Kuwahara and Y. Tokura, *Nature*, 1996, **380**, 141.
8 T. Kimura, Y. Tomioka, A. Asamitsu and Y. Tokura, *Phys. Rev. Lett.*, 1998, **81**, 5920.
9 D. N. Argyriou, J. F. Mitchell, J. B. Goodenough, O. Chmaissem, S. Short and J. D. Jorgensen, *Phys. Rev. Lett.*, 1997, **78**, 1568.
10 T. G. Perring, G. Aeppli, Y. Moritomo and Y. Tokura, *Phys. Rev. Lett.*, 1997, **78**, 3197.
11 K. Hirota, Y. Moritomo, H. Fujioka, M. Kubota, H. Yoshizawa and Y. Endoh, *J. Phys. Soc. Jpn.*, 1998, **67**, 3380.
12 R. Seshadri, C. Martin, M. Hervieu, B. Raveau and C. N. R. Rao, *Chem. Mater.*, 1997, **9**, 270.
13 J. F. Mitchell, J. E. Millburn, M. Medarde, S. Short and J. D. Jorgensen, *J. Solid State Chem.*, 1998, **141**, 599.
14 N. Mizutani, A. Kitazawa, O. Nobuyuki and M. Kato, *J. Chem. Soc. Jpn.*, 1970, **73**, 1097.
15 A. C. Larson and R. B. Von Dreele, General Structural Analysis System, Los Alamos Internal Report No. 86–748, 1990.
16 R. Maezono, *Personal Communication*, 1999.

Communication 9/02947H

A novel method for tailoring the pore-opening size of MCM-41 materials

X. Song Zhao,[a] G. Q. (Max) Lu*[a] and X. Hu[b]

[a] *Department of Chemical Engineering, The University of Queensland, St Lucia, Brisbane, Qld 4072, Australia. E-mail: maxlu@cheque.uq.edu.au*

[b] *Department of Chemical Engineering, Hong Kong University of Science and Technology, Clear Water Bay, Kowloon, Hong Kong*

Received (in Cambridge, UK) 26th April 1999, Accepted 21st June 1999

A novel pore tailoring method is proposed by which the pore-opening sizes of MCM-41 materials can be finely tuned without significant loss in pore volume and surface area.

The disclosure of the mesoporous molecular sieve MCM-41[1] has inspired a great deal of interest in catalysis, adsorption/separation and other fields,[2,3] in particular in processing bulk molecules.[4] Most excitingly, a recent study[5] shows that MCM-41 has a comparable cracking activity for long-chain hydrocarbons and even an increased activity for bulky hydrocarbons. This finding further shows the application potentials of MCM-41 in hydrocarbon processing such as in FCC (Fluid Catalytic Cracking) and Friedel–Crafts alkylation. However, for those catalytic reactions over MCM-41 materials studied so far, shape selectivity, which is of paramount importance, has not been observed. Normally, MCM-41 catalysts can lead to the thermodynamic equilibrium of the products owing to the existence of large mesopores.

Although the pore sizes of MCM-41 materials can be varied during synthesis by choosing various surfactants with different carbon chain lengths, the smallest pore size that can be obtained appears to be around 2 nm. It is obviously hard to observe any shape or size selectivity over these materials because the kinetic sizes of most of the products of catalytic reactions are smaller than this. Therefore, fine-tuning the pore diameter of MCM-41 by post modification is desirable and imperative to achieve shape-selective catalytic properties. In this study, we present a preliminary study on a novel pore modification method as schematically shown in Fig. 1. Through selectively removing the surfactant molecules occupied at both ends of the cylindrical pore (step A), we are able to tailor the pore-opening sizes of MCM-41 materials by deposing some modifying reagents such as tetraethylorthosilicate (TEOS) (step B). The main pore body can be protected against modification by the remaining surfactant molecules. In this way, the surface area and pore volume can be largely retained while the pore-opening sizes can be fine-tuned by the number of cycles of step B. Once the template is totally removed (step C), an ink-bottle-like pore-structured MCM-41 material results.

The parent mesoporous silica was prepared from the starting gel composition of 4.5 Na_2O:30 SiO_2:5.6 CTMACl:20 EtOH:2500 H_2O, (CTMACl = cetyltrimethylammonium chloride), at 100 °C for 3 days. The mixture was filtered off and extensively washed with deionized water and acetone to remove any residual ions and surfactants. A typical pore modification run is described as follows. (1) 100 g of the as-synthesized sample were dried at 120 °C overnight before adding to 500 ml of toluene under stirring for 2 h; 1.5 g of acetic acid was then added to the above mixture under stirring for another 2 h. The mixture was filtered off, washed with toluene and dried at 120 ^{0}C. (2) Part of the sample (*ca.* 2 g) was loaded into a chemical vapor deposition (CVD) system[6] and heated to 200 °C. At this temperature, tetraethylorthosilicate (TEOS) was fed from a saturator by high purity helium gas with a flow rate of 50 ml min^{-1} for 18 h. Chemical reaction occurred between surface silanol groups and TEOS *via* SiOH + $Si(OEt)_4 \rightarrow SiOSi(OEt)_3$ + EtOH. (3) The helium carrier gas was then switched to a water saturator to allow the attached $-Si(OEt)_3$ species to hydrolyze to generate new silanol groups for the subsequent modification runs. (4) The modified sample was calcined at 540 °C to remove the remaining surfactant molecules. Samples before and after modification were characterized by physical adsorption of nitrogen, benzene and water vapor, thermogravimetric analysis (TGA), and X-ray diffraction (XRD).

Some preliminary characterization results for a sample whose pore openings had been modified three times using TEOS are given below. Fig. 2 compares the nitrogen adsorption/desorption isotherms of the MCM-41 samples before and after modification, along with their physical adsorption data. The inset to Fig. 2 shows the Haorvath–Kawazoe pore size distribution (PSD) curves. It is seen that the pore-modified MCM-41 sample exhibits a type I isotherm with a small hystersis loop, different from the parent MCM-41 which shows

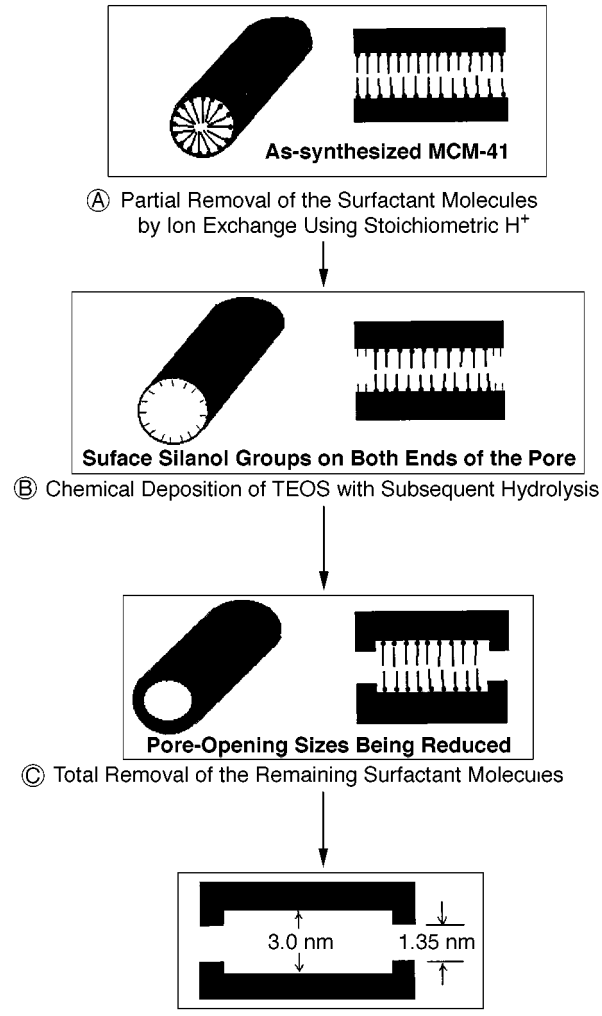

Fig. 1 Schematic model for tailoring the pore-opening size of MCM-41.

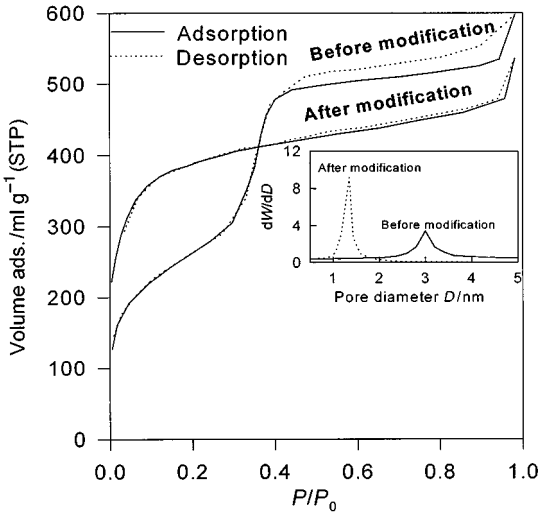

Fig. 2 Nitrogen adsorption/desorption isotherms and other physical adsorption data of the MCM-41 samples before and after pore modification.

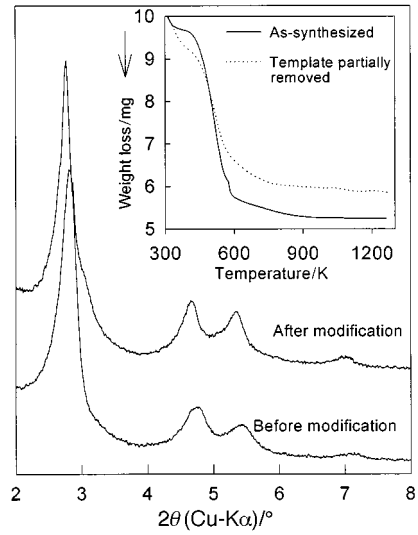

Fig. 3 XRD patterns of MCM-41 samples before and after modification and TGA curves of the parent and the template partially removed MCM-41 sample.

a type IV isotherm. The enhanced adsorption volume in the low relative pressure region indicates that the narrowed pore entrances (to the micropore size) enhanced the adsorption potential near the pore mouth region. The effective pore size, BET surface area, pore volume, benzene and water adsorption capacity had been reduced from 3.0 to 1.35 nm, 1120 to 886 m^2 g^{-1}, 0.86 to 0.69 ml g^{-1}, 8.3 to 6.5 mmol g^{-1} and 39 to 34 mmol g^{-1}, respectively, after three modification runs. These adsorption parameters support our hypothesis shown in Fig. 1 because of the fairly small reduction in porosity after modification (If the whole of the pores were modified, the pore volume would be decreased by about 80%, assuming the thickness of one silica layer to be 0.3 nm). However, the characteristic hysteresis loop for ink-bottle pore structures as documented[7] was not significant on the modified sample, presumably due to the short equilibrium time (60 s) used in our experiments. Further pore structure characterization work, along with shape-selective catalytic properties, are now being undertaken and a full paper will be published soon.

The XRD and TGA data shown in Fig. 3 further confirm our pore modification model. The XRD patterns of the MCM-41 samples before and after modification are essentially identical, demonstrating that the hexagonal pore structure was maintained after modification. The degree of template removal calculated from the TGA curves is *ca.* 15% based on anhydrous silica, indicating that most of the surfactant molecules remained inside the channels after being extracted by acetic acid solution in toluene. The 15% of the removed template is believed to be that occupying both ends of the pore.

To conclude, an effective, novel pore modification method has been proposed and the preliminary characterization data confirm our suggested modification model. This method allows for the tailoring of pore opening sizes of surfactant-templated mesophases without significant loss in pore volume and surface area.

Notes and references

1 J. S. Beck, C. Vartuli, W. J. Roth, M. E. Leonowicz, C. T. Kresge, K. D. Schmitt, C. T-W. Chu, D. H. Olson, E. W. Sheppard, S. B. McCullen, J. B. Higgins and J. L Schlenker, *J. Am. Chem. Soc.*, 1992, **114**, 10 834.
2 A. Sayari, *Chem. Mater.*, 1996, **8**, 1840.
3 X. S. Zhao, G. Q. Lu and G. J. Millar, *Ind. Eng. Chem. Res.*, 1996, **35**, 2075.
4 P. B. Venuto, *Stud. Surf. Sci. Catal.*, 1997, **105**, 811.
5 H. Koch and W. Reschetilowski, *Microporous Mesoporous Mater.*, 1998, **25**, 127.
6 H. P. Chu, L. Lei, X. Hu and P. L Yue, *Energy Fuels*, 1998, **12**, 1108.
7 J. H. de Bore, in *The Structure and properties of Porous Materials* ed., D. H. Everett and F. S. Stone, Butterworths, London 1958, p. 68.

Communication 9/03302E

A novel paramagnetic dithiadiazolyl radical: Crystal structure and magnetic properties of *p*-$BrC_6F_4CNSSN^{\bullet}$

Guillermo Antorrena,[a] John E. Davies,[b] Matthew Hartley,[b] Fernando Palacio,[a] Jeremy M. Rawson,*[b] J. Nicholas B. Smith[b] and Alexander Steiner[c]

[a] *Instituto de Ciencia de Materiales de Aragon, CSIC-Universidad de Zaragoza, Zaragoza, Spain E-50009*
[b] *Department of Chemistry, The University of Cambridge, Lensfield Road, Cambridge, UK CB2 1EW. E-mail: jmr31@cam.ac.uk*
[c] *Department of Chemistry, The University of Liverpool, Crown Street, Liverpool, UK L69 7ZD*

Received (in Cambridge, UK) 11th May 1999, Accepted 8th June 1999

The dithiadiazolyl radical *p*-$BrC_6F_4CNSSN^{\bullet}$ 2 retains its monomeric nature in the solid state; variable temperature magnetic studies on 2 indicate Curie–Weiss behaviour (θ = −27 K) above 60 K with an effective magnetic moment of 1.45 μ_B at room temperature; the absence of long-range magnetic order down to 1.8 K is attributed to the low dimensionality of the magnetic exchange pathway predicted on the basis of the inter-molecular S···N interactions.

The magnetic properties of the dithiadiazolyl radical *p*-NCC_6F_4CNSSN **1** are exceptional.[1,2] The β-phase of this compound is one of a small number of organic magnets and it exhibits a magnetic ordering temperature (36 K) unprecedented for an organic radical.[2] The singly-occupied molecular orbital (SOMO) of **1**, as with other dithiadiazolyl derivatives,[3] is a π-based orbital of a_2 symmetry (nodal at C) and is localised on the heterocyclic ring. Thus, to a first approximation, we may assume that variation of the substituent at C will have only minor effects on the electronic properties of the radical centre. Indeed, because of these negligible electronic effects, one of the most difficult tasks associated with this particular area of chemistry is to overcome the considerable dimerisation energy (*ca.* 35 kJ mol^{-1})[3] associated with these radicals. In **1**, a fortuitous combination of the fluorinated aromatic ring, coupled with strong CN···S interactions effectively compete with the natural tendency for spin-paired dimerisation.[1,2]

Recently, we have concentrated our efforts on a series of fluorinated derivatives, closely related to **1**. Herein, we report the synthesis and structure of *p*-BrC_6F_4CNSSN **2**, which represents only the second example of a dithiadiazolyl radical to retain its paramagnetic nature in the solid state.

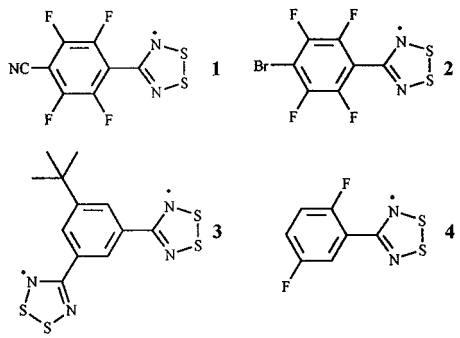

Radical **2** was prepared from BrC_6F_4CN using standard synthetic procedures[4] and was purified by vacuum sublimation (10^{-2} Torr, 80 °C), with recovered yields typically 14%, based on *p*-BrC_6F_4CN. Red crystals suitable for X-ray diffraction† were obtained by successive sublimations along a glass tube under dynamic vacuum.

The asymmetric unit (Fig. 1) comprises one molecule of **2** of unexceptional geometry, and with a large twist angle between C_6 and CN_2S_2 rings of 51.8° (*c.f.* α-**1** and β-**1** at 32° and 58°, respectively).[1,2] The majority of dithiadiazolyl radicals are associated *via* a close out-of-plane interaction between the two heterocyclic rings with S···S separations of 2.9–3.1 Å,[5] which facilitates at π*–π* interaction between the singly occupied molecular orbitals (SOMOs) based on each heterocyclic ring, thereby rendering them diamagnetic. In **2** the radicals pack in columns along the crystallographic *a*-axis (Fig. 2), although these out-of-plane contacts are much longer than normal out-of-plane contacts and fall in the range 3.675–3.999 Å, larger than those observed for the bis(dithiadazolyl) radical **3** [3.48(2)–3.61(2) Å][8] and the fluorinated dithiadiazolyl radical **4** [3.544(3) Å].[9] Whilst the molecular structures of **1** and **2** are similar, their solid state structures are different; radical **1** forms a chain-like motif through electrostatic CN···S interactions.[1,2] In the case of **2** the difference in electronegativity between Br and S (0.04) is much less than that observed between S and an sp-hybridised N (2.49) in **1**. Instead electrostatic interactions between S and the heterocyclic sp^2 N (electronegativity

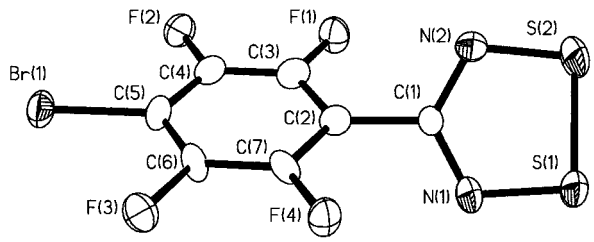

Fig. 1 Selected intramolecular bond lengths (Å) and angles (°) for **2**: S(1)–S(2) 2.070(4), S(1)–N(1) 1.640(8), S(2)–N(2) 1.624(9), C(1)–N(1) 1.317(14), C(1)–N(2) 1.327(12), N(1)–S(1)–S(2) 93.7(4), N(2)–S(2)–S(1) 95.5(3), C(1)–N(1)–S(1) 113.9(7), C(1)–N(2)–S(2) 112.8(7), N(1)–C(1)–N(2) 124.0(9).

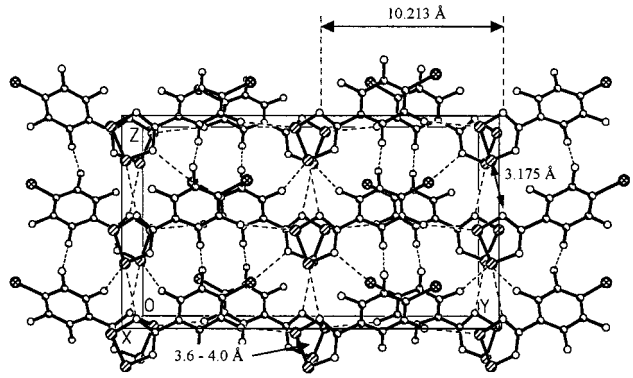

Fig. 2 Molecular packing diagram of **2** viewed perpendicular to the crystallographic *a*-axis, with selected intermolecular contacts labelled (see text for discussion).

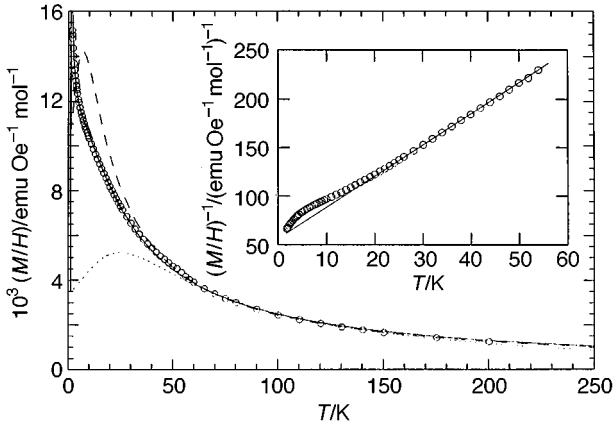

Fig. 3 Variation of M/H as a function of T (○) for **2** and several fits to modified Bonner–Fisher models: Bonner–Fisher with an additional diamagnetic term (·····); Bonner–Fisher considering that only 70% of the molecules contribute to the magnetism (-----) $J = -5.4(1)$ K; and Bonner–Fisher including a linear dependence $J(T)$ term and a paramagnetic term (——).

difference = 1.55) determine the crystal packing. This is manifested in a short intermolecular interaction [S(1)···N(2) 3.175(9) Å] close to the heterocyclic ring plane which links neighbouring molecules into chains along the *c*-axis. Whereas out-of-plane contacts around 3.0 Å lead to essentially diamagnetic solids, this close in-plane approach in **2** leads to retention of paramagnetism (see below).

Variable temperature magnetic susceptibility studies (ac and dc) under different applied magnetic fields were carried out on a microcrystalline sample of **2**. Diamagnetic corrections, were made for the sample holder and sample (Pascal's constants). The effective magnetic moment at high temperature [μ_{eff} = 1.45 μ_B at room temperature] is less than that expected for an $S = ½$ paramagnet and decreases slowly to 1.35 μ_B at 50 K before undergoing a more rapid decrease down to 0.5 μ_B at 1.8 K.

Above 60 K, the magnetic susceptibility follows the Curie–Weiss law with $\theta = -27 \pm 1$ K (Fig. 3, inset), although an extra and unjustified diamagnetic term ($\chi_d \approx -5 \times 10^{-4}$ emu mol^{-1}) must be added in order to explain the low values of μ_{eff}. Using a mean-field approximation, this value of θ would indicate a paramagnetic–antiferromagnetic phase transition at 27 K. However no evidence of long range magnetic order is observed and the linear field dependence of the susceptibility is corroborated at 5 K by a magnetisation *vs.* field plot.

On the other hand, for systems exhibiting low dimensional character (which is strongly suggested by the structure of **2**), a fit of the experimental data to the Bonner–Fisher model for an $S = ½$ Heisenberg chain gives $J = -19 \pm 5$ K and approximately the same χ_d term. This model predicts a broad maximum in χ at $T_{max} = 1.282 \times |J|$ K (24 ± 6 K), as a consequence of short range (low-dimensional) interactions (Fig. 3). However there is no broad maximum in χ observed down to 1.8 K and there is a marked deviation from the Bonner–Fisher model below 60 K. It has not been possible to fit the experimental data satisfactorily by simply including paramagnetic impurities or correction factors due to hypothetical sample degradation (Fig. 3).

These observations indicate a peculiar evolution of the susceptibility as a function of temperature, exhibiting paramagnetic behaviour with antiferromagnetic interactions ($J > 19$ K) in the high temperature range and weaker interactions at low temperatures. However, a surprisingly good fit is obtained throughout the temperature range by incorporating a simple linear dependence of the exchange parameter, J_2 [$J = -(0.31T + 8.2)$] in the Bonner–Fisher model (Fig. 3). In this case, there is no need to use an extra diamagnetic correction, although an additional paramagnetic term (corresponding to 3% of $S = ½$ paramagnetic impurity) is included to explain the large slope of the susceptibility below 10 K.

The absence of a transition to a magnetically ordered state must arise as a consequence of the crystal structure which necessarily precludes propagation of the magnetic exchange interaction throughout the solid above 1.8 K (the limiting low temperature of these measurements). The structure of **2** provides two potential pathways for propagation of the magnetic exchange interaction; either *via* the close in-plane interactions along the crystallographic *c*-axis; and/or *via* the out-of-plane interactions along the crystallographic *a*-axis (Fig. 2). Whilst the intermolecular S···N interactions in β-**1** lead to a diamond-like three-dimensional magnetic exchange pathway,[10] the dimensionality of **2** could, at best, be described as a two-dimensional net with layers separated by half the length (10.213 Å) of the crystallographic *b* axis. Thus the peculiar behaviour of *J* can be ascribed to either structural changes as the temperature decreases,[11] or to the presence of competing ferromagnetic and antiferromagnetic exchange interactions. In the first case, the temperature dependence of *J* will be a direct consequence of the modification of the exchange pathways, whereas in the second case it would just be a mathematical artefact to account for the rising of the magnetisation due to the ferromagnetic interactions. In order to provide a more solid basis to resolve this problem, low temperature structure determinations are in progress.

We would like to thank Ciba-Geigy and the MEC for studentships (J. N. B. S. and G. A., respectively), the Royal Society for an equipment grant (J. M. R.), the CICYT (Grant No. MAT94-043 and MAT97-0951), the British Council and the MEC for their support of international cooperation (J. M. R./F. P.).

Notes and references

† *Crystal data* for **2**: $C_7BrF_4N_2S_2$, $M = 332.12$, orthorhombic, space group *Aba*2, $a = 8.263(2)$, $b = 20.426(4)$, $c = 11.556(2)$ Å, $U = 1950.4(7)$ Å^3, $Z = 8$, $D_c = 2.262$ g cm^{-3}, $\lambda = 0.71073$ Å, $T = 150(2)$ K, μ(Mo-Kα) = 4.672 mm^{-1}, $F(000) = 1272$. Data were collected on a Rigaku AFC-7 four-circle diffractometer using an oil-coated rapidly cooled crystal of dimensions 0.35 × 0.25 × 0.20 mm using the ω–2θ method ($3.17 \leqslant \theta \leqslant 27.51°$). Of a total of 2292 collected reflections, 2175 were independent (R_{int} = 0.0449). The structure was solved by direct methods[5] and refined using full-matrix least squares[6] on F^2 to final values of R_1 [$F > 4\sigma(F)$] = 0.0643 and wR_2 = 0.1428 (all data), goodness of fit = 1.026; largest peak and hole in the final difference map were within +0.91, −0.59 e Å^{-3}; the refined Flack parameter [−0.02(2)] indicates the correct absolute structure.[7] CCDC 182/1279. See http://www.rsc.org/suppdata/cc/1999/1393/ for crystallographic files in .cif format.

1 A. J. Banister, N. Bricklebank, W. Clegg, M. R. J. Elsegood, C. I. Gregory, I. Lavender, J. M. Rawson and B. K. Tanner, *J. Chem. Soc., Chem. Commun.*, 1995, 679.
2 A. J. Banister, N. Bricklebank, I. Lavender, J. M. Rawson, C. I. Gregory, B. K. Tanner, W. Clegg, M. R. J. Elsegood and F. Palacio, *Angew. Chem., Int. Ed. Engl.*, 1996, **35**, 2533.
3 J. M. Rawson, A. J. Banister and I. Lavender, *Adv. Heterocycl. Chem.*, 1995, **62**, 137.
4 C. M. Aherne, A. J. Banister, I. B. Gorrell, M. I. Hansford, Z. V. Hauptman, A. W. Luke and J. M. Rawson, *J. Chem. Soc., Dalton Trans.*, 1993, 967.
5 SHELXS, G. M. Sheldrick, *Acta. Crystallogr., Sect. A.*, 1990, **46**, 467.
6 SHELXL 93, G. M. Sheldrick, University of Göttingen, 1993.
7 H. D. Flack, *Acta. Crystallogr., Sect. A.*, 1983, **39**, 876.
8 R. A. Beekman, R. T. Boeré, K. H. Moock and M. Parvez, *Can. J. Chem.*, 1998, **76**, 85.
9 A. J. Banister, A. S. Batsanov, O. G. Dawe, P. L. Herbertson, J. A. K. Howard, S. Lynn, I. May, J. N. B. Smith, J. M. Rawson, T. E. Rogers, B. K. Tanner, G. Antorrena and F. Palacio, *J. Chem. Soc., Dalton Trans.*, 1997, 2539.
10 P. J. Langley, J. M. Rawson, J. N. B. Smith, M. Schuler, A. Schweiger, F. Palacio, G. Antorrena, C. Hoffmann, G. Gescheidt, A. Quintel, P. Rechsteiner, R. Bachmann and J. Hulliger, *J. Mater. Chem.*, 1999, 1431.
11 A recent example of the effects of a second-order structural phase transition in a molecular magnetic compound can be found (L. R. Falvello, M. A. Hitchman, F. Palacio, I. Pascual, A. J. Schultz, H. Stratemeier, M. Toms, E. P. Urriolabeitia and D. M. Young, *J. Am. Chem. Soc.*, 1999, **121**, 2808.

Communication 9/03771C

ChemComm

LNA stereoisomers: *xylo*-LNA (β-D-*xylo* configured locked nucleic acid) and α-L-LNA (α-L-ribo configured locked nucleic acid)

Vivek K. Rajwanshi, Anders E. Håkansson, Britta M. Dahl and Jesper Wengel*

Center for Synthetic Bioorganic Chemistry, Department of Chemistry, University of Copenhagen, Universitetsparken 5, DK-2100 Copenhagen, Denmark. E-mail:wengel@kiku.dk

Received (in Cambridge, UK) 21st April 1999, Accepted 3rd June 1999

Synthesis of xylo-LNA containing one 2′-*O*,4′-*C*-methylene-β-D-xylofuranosyl thymine nucleotide monomer and α-L-LNAs containing one or four 2′-*O*,4′-*C*-methylene-α-L-ribofuranosyl thymine nucleotide monomer(s) has been accomplished using phosphoramidite chemistry with pyridine hydrochloride as activator; oligothymidylate α-L-LNA displays strongly enhanced affinity towards complementary RNA.

In a series of papers, Seela *et al.* have synthesized and studied xylo-DNA containing one or more 2′-deoxy-β-D-xylofuranosyl nucleotide(s).[1–4] Compared with the corresponding natural 2′-deoxy-β-D-ribofuranosyl oligonucleotide reference (**T**, thymine

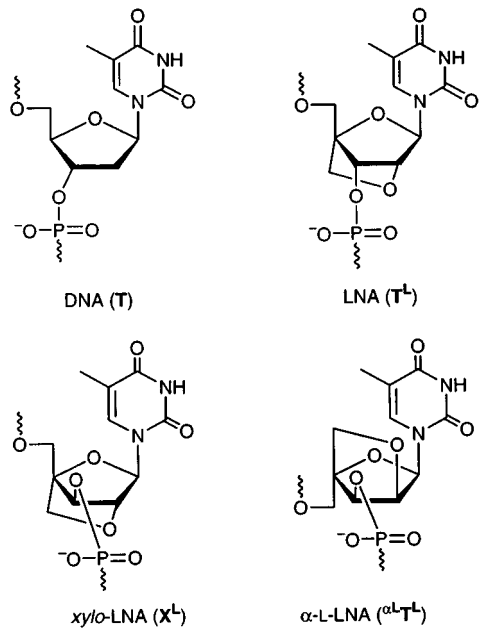

derivatives are shown for all the four different monomers), *xylo*-DNA generally displays decreased thermal affinity towards complementary single stranded DNA.[1–4] We[5–9] and others[10] have recently reported unprecedented thermal stabilities of duplexes involving LNA (Locked Nucleic Acid, $\mathbf{T^L}$)† and complementary single stranded DNA or RNA. Here the first stereoisomers of LNA are introduced, namely *xylo*-LNA ($\mathbf{X^L}$) containing one or more 2′-*O*,4′-*C*-methylene-β-D-xylofuranosyl nucleotide monomer(s), and α-L-LNA containing one or more 2'-*O*,4'-*C*-methylene-α-L-ribofuranosyl nucleotide monomer(s) ($^{\alpha L}T^L$).

Conversion of the thymine *xylo*-LNA nucleoside **1**[11] and the α-L-LNA nucleoside **4**,[12] which both were obtained from D-glucose, into the phosphoramidite building blocks **3** and **6**, respectively, was performed as depicted in Scheme 1. Nucleoside **1** was reacted first with 1.5 equiv. of 4,4′-dimethoxytrityl chloride (DMTCl) in anhydrous pyridine (25 h, room temperature) and then with an additional 1.0 equiv. (21 h, room temperature) to afford the 5′-*O*-DMT-protected *xylo*-LNA nucleoside **2**‡ in 50% yield after column chromatographic separation from the 3′-*O*-DMT isomer (isolated in 29% yield). Interactions (sterical interference and/or hydrogen bonding) between the three substituents at the α-face of the furanose ring are possible explanations for the unusually low reactivity, and low selectivity, towards dimethoxytritylation of the primary hydroxy group of nucleoside **1**. Subsequent phosphitylation of the 3′-hydroxy group afforded in 51% yield the phosphoramidite derivative **3**.§ The 5′-*O*-DMT-protected derivative **5**[12]¶ was obtained in 80% yield by debenzylation of nucleoside **4** and subsequently converted into the phosphoramidite **6** in low yield.‖

The oligomers were synthesized on an automated DNA synthesizer by use of the phosphoramidite approach.[13] Seela *et al.* have reported that the use of 3′-*O*-phosphoramidites in their syntheses of *xylo*-DNA required a ten-fold extension of the standard coupling time. Therefore they applied phosphonate chemistry for oligomerization of 5′-*O*-DMT protected 2′-deoxy-β-D-xylofuranosyl monomers.[3] Analogously, the coupling yield of amidite **3** was only 15% after 10 min coupling time using standard concentrations and 1*H*-tetrazole as activator (sequence 5′-$\mathbf{X^L}T_6$; coupling yields determined spectrophotometrically by the release of the 4,4′-dimethoxytrityl group after each coupling step). This inefficient coupling of **3**, which strongly contrasts with the nearly quantitative coupling of the parent diastereoisomeric LNA amidite,[5–7] is probably caused by steric hindrance during the reaction between the 5′-hydroxy group of 5′-OH-T_6 and the amidite **3**, the latter having three sterically demanding groups oriented towards the α-face of the furanose ring. In an attempt to improve the coupling yield of amidite **3**, syntheses of 5′-$\mathbf{X^L}T_6$ using different activators[14–16] and coupling times were performed (Table 1). These experiments showed that the use of pyridine hydrochloride as activator may indeed allow efficient coupling of sterically very hindered phosphoramidite building blocks. This is an important result as research in this area moves towards bicyclic,[9] tricyclic,[17] functionalized[9] and branched[18] oligonucleotides.

We then turned to the synthesis of the *xylo*-LNA and α-L-LNA sequences **8**–**10** shown in Table 2 using the optimized conditions (pyridine hydrochloride; 10 min coupling time)

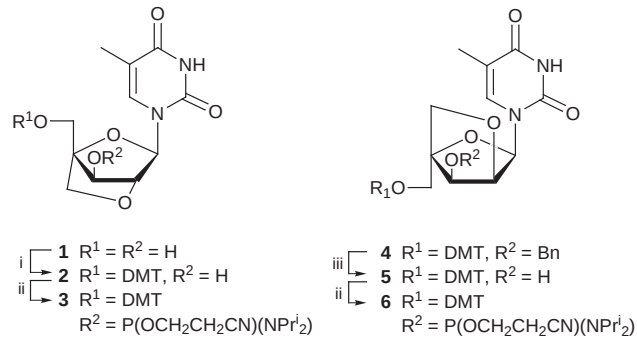

Scheme 1 *Reagents and conditions*: i, DMTCl, anhydrous pyridine (50%); ii, Pr^i_2NEt, 2-cyanoethyl *N*,*N*-diisopropylphosphoramidochloridite, anhydrous CH_2Cl_2 (**3**: 51%; **6**: 7%‖); iii, ammonium formate, Pd/C, MeOH (80%).

Table 1 Model syntheses of 5′-$\mathbf{X^L}T_6$

Activator	*t*/min	Yield[a,b] (%)
1*H*-Tetrazole	10 min	15
1*H*-Tetrazole	30 min	31
4,5-Dicyanoimidazole[c]	30 min	71
Pyridine hydrochloride[d]	10 min	> 99

[a] Refers to the coupling yield for amidite **3**. [b] The coupling yield of the unmodified ß-cyanoethyl T-amidite was > 99%. [c] Ref. 14. [d] Ref. 15,16.

Table 2 *Xylo*-LNA (**8**) and α-L-LNAs (**9** and **10**) synthesized; T_m values measured[a]

Sequence	dA_{14} Complement T_m/°C (ΔT_m/°C)	rA_{14} Complement T_m/°C (ΔT_m/°C)	Mass found $[M - H]^-$	Mass calc. $[M - H]^-$
7 5′-T_{14}	32	28		
8 5′-$T_7\mathbf{X^L}T_6$	19 (−13)	24 (−4)	4221.2	4223.8
9 5′-$T_7(^{\alpha L}\mathbf{T^L})T_6$	32 (±0)	33 (+5)	4225.4	4223.8
10 5′-$T_5(^{\alpha L}\mathbf{T^L})_4T_5$	36 (+1)	46 (+4.5)	4309.0	4307.8

[a] Melting temperatures (T_m values) obtained from the maxima of the first derivatives of the melting curves (A_{260} *vs.* temperature) recorded in medium salt buffer (10 mM sodium phosphate, 100 mM sodium chloride, 0.1 mM EDTA, pH 7.0) using 1.5 mM concentrations of the two complementary strands (assuming identical extinction coefficients for all modified and unmodified thymine nucleotides). Also shown are changes in T_m value *per modification* (ΔT_m) compared with the reference values obtained for **7**.

affording coupling yields of ~99% for amidite **3** and 97–99% for amidite **6**.** Contrary to amidite **6**, consecutive incorporation of amidite **3** resulted in reduced coupling yields (85–97%; sequences not shown). The oligomers **8**–**10** were synthesized in the DMT-off mode and directly ethanol-precipitated after cleavage from the solid support yielding products with > 90% purity as judged from capillary gel electrophoresis.

The results from preliminary binding studies in medium salt buffer are shown in Table 2. The thermal stability of complexes formed between *xylo*-LNA **8**, containing a single $\mathbf{X^L}$ monomer, and complementary single stranded DNA (dA_{14}) and RNA (rA_{14}) was significantly reduced (ΔT_m/mod = −13 and −4 °C, respectively) when compared with the unmodified T_{14} reference **7**. Contrary to this, the binding affinity of α-L-LNAs **9** and **10** was unchanged or slightly improved towards complementary DNA, and strongly increased towards complementary RNA (ΔT_m/mod = +4.5 and +5 °C). The latter results compare closely with our results obtained earlier for the corresponding LNA oligothymidylate sequences.[5] Modeling studies on monomers $\mathbf{X^L}$ and $^{\alpha L}\mathbf{T^L}$ clearly show their furanose conformations to be very different. Thus, whereas $\mathbf{X^L}$ is locked in a 3′-*endo* (N-type) conformation, $^{\alpha L}\mathbf{T^L}$ is locked in a 3′-*exo* (S-type) conformation. The preliminary binding data indicate that the inverted configuration at C-3′ (compared with *e.g.* LNA and DNA) in *xylo*-LNA monomer $\mathbf{X^L}$ causes an unfavorable local disruption of the regular duplex structures. However, the 2′-*exo* conformation of monomer $^{\alpha L}\mathbf{T^L}$ allows the formation of very stable hetero duplexes despite the configuration being inverted at both C-3′ and C-4′. In fact, superimposition of models of the LNA monomer $\mathbf{T^L}$ and the α-L-LNA monomer $^{\alpha L}\mathbf{T^L}$ reveals the possibility of a very close three-dimensional positioning of the thymine moieties and of the C-5′- and C-3′-oxygen atoms for the two monomers existing in locked 3′-*endo* and 3′-*exo* conformations, respectively.

The first LNA stereoisomers, *xylo*-LNA and α-L-LNA, have been synthesized using phosphoramidite chemistry on an automated DNA synthesizer applying extended coupling times and pyridine hydrochloride as activator. This synthetic method should be generally applicable for coupling of sterically hindered phosphoramidite building blocks. α-L-LNA containing one and four α-L-LNA monomers recognized complementary RNA with remarkably increased affinity. Currently, the binding properties of a variety of *xylo*-LNA and α-L-LNA oligomers are being studied in full detail.

The Danish Natural Science Research Council, The Danish Technical Research Council and Exiqon A/S are thanked for financial support. Dr Carl Erik Olsen and Dr Thomas Kofoed are thanked for recording MALDI-MS spectra.

Notes and references

† We have defined LNA as an oligonucleotide containing one or more 2′-*O*,4′-*C*-methylene-ß-D-ribofuranosyl nucleotide monomer(s).

‡ *Selected data* for **2**: $\delta_H(C_5D_5N)$ 13.12 (1H, br s, NH), 8.07 (1H, d, *J* 1.2, H-6), 7.84–7.00 (13H, m, DMT), 6.26 (1H, s, H-1′), 4.93 (1H, d, *J* 2.2, H-2′), 4.61 (1H, m, H-3′), 4.38 (1H, d, *J* 8.0, H-5″a), 4.30 (1H, d, *J* 8.0, H-5″b), 4.20 (1H, d, *J* 10.0, H-5′a), 3.87 (1H, d, *J* 10.0, H-5′b), 3.72 (3H, s, OCH_3), 3.71 (3H, s, OCH_3), 1.97 (3H, s, CH_3); *m/z* (FAB) 573 $[M + H]^+$ (found: C, 66.6; H, 5.7; N, 4.7; $C_{32}H_{32}N_2O_8.0.25H_2O$ requires C, 66.6; H, 5.7; N, 4.9%). This compound was acetylated on an analytical scale (Ac_2O, anhydrous pyridine) yielding a mono-acetate for which the signal for the H-3′ proton was found (^1H–^1H COSY NMR analysis) at δ 5.47 (compared with δ 4.61 for **2**) proving compound **2** as being the 5′-*O*-DMT derivative.

§ *Selected data* for **3**: $\delta_P(Me_3CN)$ 154.0, 151.8.

¶ *Selected data* for **5**: $\delta_H[(CD_3)_2SO]$ 11.39 (1H, br s, NH), 7.62 (1H, d, *J* 1.0, H-6), 7.44–6.89 (13H, m, DMT), 5.97 (1H, s, H-1′), 5.94 (1H, d, *J* 4.3, HO-3′), 4.44 (1H, d, *J* 4.3, H-3′), 4.23 (1H, s, H-2′), 4.13 (1H, d, *J* 8.4, H-5″a), 3.92 (1H, d, *J* 8.4, H-5″b), 3.74 (6H, s, OCH_3), 3.31 (2H, m, H-5′), 1.86 (3H, s, CH_3); *m/z* (FAB) 573 $[M + H]^+$.

‖ *Selected data* for **6**: δ_P(MeCN) 149.9, 149.3; *m/z* (FAB) 773 $[M + H]^+$. This phosphitylation has not yet been optimized and the yield was only 7% because of the need for repeated column chromatographic purification.

** All oligomers were prepared on a Biosearch 8750 DNA Synthesizer on CPG solid supports using the standard conditions of the synthesizer. However, the couplings of amidites **3** and **6** were performed with the changes described in the text and after premixing the amidite with the activator (1*H*-tetrazole 0.45 M; 4,5-dicyanoimidazole and pyridine hydrochloride 0.50 M) in anhydrous MeCN in a syringe followed by direct injection of this mixture into the column reactor during the coupling time applied. The 5′-*O*-DMT group was removed on the synthesizer immediately after completion of the sequences. Subsequent treatment with concentrated ammonia [32% (w/w), 12 h, 55 °C] and ethanol-precipitation afforded the product oligomers.

1 H. Rosemeyer and F. Seela, *Helv. Chim. Acta*, 1991, **74**, 748.
2 H. Rosemeyer, M. Krecmerova and F. Seela, *Helv. Chim. Acta*, 1991, **74**, 2054.
3 F. Seela, K. Wörner and H. Rosemeyer, *Helv. Chim. Acta*, 1994, **77**, 883.
4 F. Seela, M. Heckel and H. Rosemeyer, *Helv. Chim. Acta*, 1996, **79**, 1451.
5 S. K. Singh, P. Nielsen, A. A. Koshkin and J. Wengel, *Chem. Commun.*, 1998, 455.
6 A. A. Koshkin, S. K. Singh, P. Nielsen, V. K. Rajwanshi, R. Kumar, M. Meldgaard, C. E. Olsen and J. Wengel, *Tetrahedron*, 1998, **54**, 3607.
7 S. K. Singh and J. Wengel, *Chem. Commun.*, 1998, 1247.
8 A. A. Koshkin, P. Nielsen, M. Meldgaard, V. K. Rajwanshi, S. K. Singh and J. Wengel, *J. Am. Chem. Soc.*, 1998, **120**, 13 252.
9 J. Wengel, *Acc. Chem. Res.*, 1999, **32**, 301.
10 S. Obika, D. Nanbu, Y. Hari, J. Andoh, K. Morio, T. Doi and T. Imanishi, *Tetrahedron Lett.*, 1998, **39**, 5401.
11 V. K. Rajwanshi, R. Kumar, M. K. Hansen and J. Wengel, *J. Chem. Soc., Perkin Trans 1*, in the press.
12 A. E. Håkansson and J. Wengel, in preparation.
13 M. H. Caruthers, *Acc. Chem. Res.*, 1991, **24**, 278.
14 C. Vargeese, J. Carter, J. Yegge, S. Krivjansky, A. Settle, E. Kropp, K. Peterson and W. Pieken, *Nucleic Acids Res.*, 1998, **26**, 1046.
15 S. M. Gryaznov and R. L. Letsinger, *Nucleic Acids Res.*, 1992, **20**, 1879.
16 B. Greiner and W. Pfleiderer, *Helv. Chim. Acta*, 1998, **81**, 1528.
17 R. Steffens and C. J. Leumann, *J. Am. Chem. Soc.*, 1997, **119**, 11 548.
18 Y. Ueno, M. Takeba, M. Mikawa and A. Matsuda, *J. Org. Chem.*, 1999, **64**, 1211.

Communication 9/03189H

ChemComm

Bis(benzene)chromium: a pre-catalyst for the hydrosilation of ketones and aldehydes, and for the dehydrocoupling of triphenylsilane with primary alcohols†

Franck Le Bideau,[a] Josette Henique,[a] Edmond Samuel*[a] and Ch. Elschenbroich[b]

[a] *Ecole Nationale Supérieure de Chimie de Paris (UMR 7576 CNRS), 11 rue Pierre et Marie Curie, 75231 Paris Cedex 05, France. E-mail: samuel@ext.jussieu.fr*

[b] *Department of Chemistry, Philipps University, Marburg, Germany*

Received (in Basel, Switzerland) 15th February 1999, Accepted 10th June 1999

Bis(benzene)chromium is a valuable pre-catalyst for the hydrosilation of α-aryl carbonyl compounds as well as for the dehydrocoupling between primary alcohols and triphenylsilane.

For a number of years, the catalytic hydrosilation of ketones and aldehydes has been a widely used reaction in organic synthesis, known to be catalysed by a large number of transition metal compounds.[1–6] However, to our knowledge, bis(benzene)chromium (BBC) has never been used for this purpose, and moreover its known catalytic properties have been mentioned only in a very few instances.[7–10]

In this work, we show that under certain conditions, BBC is an active homogeneous catalyst for the hydrosilation of ketones and aldehydes as well as for the dehydrocoupling of primary alcohols with triphenylsilane.

The catalytic reaction was examined using different substrates **1** and a number of silanes **2** (**2**/**1** = 1.2 equiv.) in the presence of neutral BBC (6% mol) in benzene (or benzene-d_6) and under aerobic conditions (Scheme 1). With diphenylsilane and methylphenylsilane, compounds **3** were not stable on silica gel and were converted spontaneously to the corresponding alcohols **5** (MeOH, silica gel or acetone, HCl). The results are summarized in Table 1. It is of note that the hydrosilation reactions were generally clean as judged by the ^{1}H NMR spectra of the crude reaction mixtures. Thus silylenol ether, the main by-product resulting from dehydrogenative silylation, occasionally encountered with other catalysts,[1] was not detected in this case. The formation of polymers was accompanied by an increase in the aromatic signal intensity and the appearance of singlets (corresponding to SiH) in the range δ 5.5–6.0 was observed to a small extent.

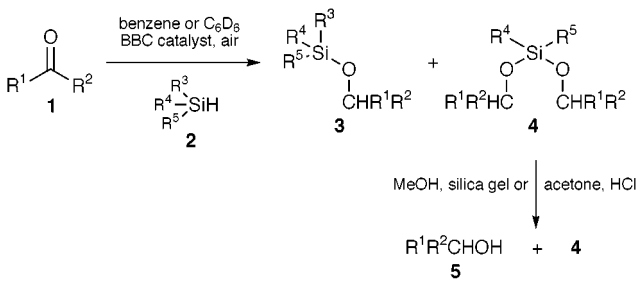

Scheme 1

Saturated ketones are not reactive under these conditions. For instance, acetone gave only traces of compound **3** after 24 h at 40 °C in benzene (Table 1, entry 2). On the other hand, and as judged from the ^{1}H NMR spectra of the crude reaction mixtures, with excess acetone (both as solvent and reactant), reaction occurs with total conversion of the silane. We have also attempted the reduction of carbon–carbon multiple bonds but without success, with hydrosilation of 2-cyclopenten-1-one occurring exclusively on the carbonyl function (Table 1, entry 4).

Different silanes were used in the hydrosilation of *para*-anisaldehyde (Table 1, entries 5–8). Ph_3SiH, Me_2PhSiH and Et_3SiH are not effective in this reaction, probably owing to steric hindrance. This can also explain the poor yields for compound **4** obtained with Ph_2SiH_2 (Table 1, entries 1–5). With a less hindered silane (Table 1, entry 6 *vs.* 5), **4** is obtained in 21% yield. Two ethoxysilanes were also examined (Table 1, entries 7 and 8) with success. The formation of **4** is attributed to a redistribution reaction of the silane prior to hydrosilation.[11,12]

In order to gain information about the nature of the species responsible for the catalytic process, *para*-anisaldehyde was reacted with dimethylethoxysilane under argon in the presence of freshly sublimed BBC, by saturating the solution of the aldehyde and the silane in benzene with argon prior to the addition of the arene complex (Scheme 2). No reaction occured after 18 h at room temperature. It follows that although BBC is

† Metal π complexes of benzene derivatives, part 54. Part 53: *Z. Anorg. Allg. Chem*., 1999, **625**, 875.

Table 1 Hydrosilation of ketones and aldehydes by BBC‡

		2			Yield (%)			
Entry	**1**	R^3	R^4	R^5	**3**	**4**	**5**	Conditions
1	Acetophenone	H	Ph	Ph	—	< 5	90	*a–c*
2	Acetone	H	Ph	Ph	tr.[d]	—	—	*b, e–g*
3	Piperonal	H	Ph	Ph		< 5	65	*a–c*
4	2-Cyclopenten-1-one	H	Ph	Ph	47	—	—	*a, e, g, h*
5	*p*-Anisaldehyde	H	Ph	Ph	—	< 5	95	*a–c*
6	*p*-Anisaldehyde	H	Me	Ph	—	21	72	*a*
7	*p*-Anisaldehyde	OEt	Me	Me	50	24	—	*a, f, i*
8	*p*-Anisaldehyde	OEt	OEt	Me	39	18	—	*a, f, h, i*

[a] Isolated yields after flash chromatography. [b] **4** and **5** were characterized by ^{1}H NMR. [c] 70 °C, 3 h. [d] tr = trace. [e] Yields are calculated by ^{1}H NMR with ferrocene as reference. [f] 40 °C, 24 h. [g] **4** was not detected [h] 25% starting material left. [i] Products **3** and **4** have been fully characterized.

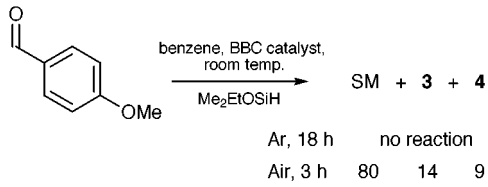

Scheme 2 (SM = starting material)

the catalytic precursor, hydrosilation is thought to proceed by the transient formation of a species generated by the reaction of O_2 with BBC in the presence of trace amounts of water.[13] The mechanism seems therefore to be completely different from the well established Chalk and Harrod oxidative addition process in the case of late transition metal catalyst complexes. Instead it may involve primary electron transfer to yield the radical pair BBC^+ $O_2^{-\cdot}$ and subsequent hydrogen atom abstraction from the silane by the hydroperoxide anion, thereby triggering a radical path for the hydrosilation. This option is currently being tested by means of EPR spectroscopy.

Under the same experimental conditions, primary alcohols led to fast dehydrocoupling in the presence of Ph_3SiH (Scheme 3) with vigorous gas evolution. Yields are of the same order as those reported in the literature for numerous other known catalysts.[14] Propargyl alcohol was thus converted to the corresponding silyl compound with the triple bond remaining intact. This reaction is an alternative, in the case of primary alcohols, to the protection method using bromotriphenylsilane in pyridine.[15]

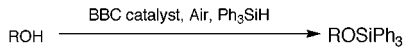

Scheme 3

It has been demonstrated that BBC can behave as an efficient spin trap[16] and reactions described above provide further support to the hitherto unsuspected usefulness of this well known sandwich compound in organic synthesis.

Notes and references

‡ *Typical procedure* (Table 1, entry 7): Dimethylethoxysilane (1.2 mmol) was added, at room temperature, to a solution of *p*-anisaldehyde (1 mmol) and BBC (0.06 mmol) in benzene (1 mL). After 3 h at 40 °C in the presence of air, the reaction mixture was concentrated. The residue was flash chromatographed affording **3** [light petroleum–diethyl ether (90 : 10)] and then **4** (dichloromethane).

3 : ^{1}H NMR (200 MHz, $CDCl_3$) δ 7.27 (2H, d, *J* 8.0 Hz), 6.88 (2H, d, *J* 8.0 Hz), 4.72 (2H, s), 3.81 (3H, s), 3.75 (2H, q, *J* 7.2 Hz), 1.21 (3H, t, *J* 7.2 Hz), 0.16 (6H, s); ^{13}C NMR (50 MHz, $CDCl_3$) δ 158.8, 132.5, 128.2, 113.6, 64.2, 58.1, 55.1, 18.1, −7.0; IR (neat) : 2966, 2930, 2860, 2840, 1613, 1514, 1465, 1256, 1077, 1037, 867, 841 cm^{-1}, MS (*m/z*) 240, 225, 195, 179, 121, 77; Anal. Calc. for $C_{12}H_{20}O_3Si$: C, 60.00; H, 8.32. Found : C, 59.11; H, 8.25%.

4 : ^{1}H NMR (200 MHz, $CDCl_3$) δ 7.25 (4H, d, *J* 8.7 Hz), 6.87 (4H, d, *J* 8.7 Hz), 4.69 (4H, s), 3.81 (6H, s), 0.18 (6H, s); ^{13}C NMR (50 MHz, $CDCl_3$) δ 158.8, 132.6, 128.1, 113.6, 64.1, 55.1, −2.9; IR (neat) : 2960, 2930, 2860, 2840, 1613, 1513, 1464, 1260, 1065, 1036, 860, 800 cm^{-1}; MS (*m/z*) 332, 211, 121, 91; Anal. Calc. for $C_{18}H_{24}O_4Si$: C, 65.02; H, 4.27. Found : C, 63.85; H, 7.40%.

1 I. Ojima, in *The Chemistry of Organic Silicon Compounds, Part 2*, ed. Z. Rappoport, Wiley, New York, 1983, p. 1479.
2 W. P. Weber, in *Silicon Reagents for Organic Synthesis*, Springer-Verlag, Berlin–Heidelberg–New York, 1983, p. 288.
3 I. Itsuno *Org. React.*, 1998, **52**, 440.
4 H. Brunner, H. Nishiyama and K. Itoh, in *Catalytic Asymmetric Synthesis*, ed. I. Ojima, VCH, New York, 1993, p. 303.
5 B. Marciniec and J. Gulinski *J. Organomet. Chem*, 1993, **446**, 15.
6 B. Marciniec, J. Gulinski, W. Urbaniak and Z. W. Kornetka, in *Comprehensive Handbook on Hydrosilylation*, ed. B. Marciniec, Pergamon, Oxford, 1992.
7 B. G. Gribov, D. D. Mozzhukhin, B. I. Kozyrkin and A. S. Strizhkova, *J. Gen. Chem. USSR*, 1972, **42**, 2521
8 Y. Tazima and S. Yuguchi, *Bull. Chem. Soc. Jpn.*, 1966, **39**, 2534.
9 Y.-Z. Huang and J. Q. Zhou *J. Organomet. Chem*, 1988, **348**, 235.
10 G. Fochi, *Organometallics*, 1988, **7**, 2255.
11 M. D. Curtis and P. S. Epstein, *Adv. in Organomet. Chem.*, 1981, **19**, 213.
12 S. Xin, C. Aitken, J. F. Harrod, Y. Mu and E. Samuel, *Can. J. Chem.*, 1990, **68**, 471.
13 The oxidation potential of the couple BBC–BBC^+ is −0.68 V *vs.* SCE. For oxidation of BBC, see ref. 7.
14 C. Lorentz and U. Schubert, *Chem. Ber.*, 1995, **128**, 1267.
15 T. W. Greene and P. G. M. Wutz, in *Protective Groups in Organic Synthesis*, Wiley, 2nd edn, New York, 1991, p. 50.
16 E. Samuel, D. Caurant, D. Gourier, Ch. Elschenbroich and K. Agbaria *J. Am. Chem. Soc.*, 1988, **120**, 8088.

Communication 9/01234F

Dispersion and reactivity of vanadium oxide catalysts supported on niobia

Komandur V. R. Chary,* Gurram Kishan and Thallada Bhaskar

Catalysis Section, Indian Institute of Chemical Technology, Hyderabad 500 007, India.
E-mail: kvrchary@iict.ap.nic.in

Received (in Cambridge, UK) 20th April 1999, Accepted 15th June 1999

Vanadium oxide catalysts supported on niobia are found to be highly active for ammoxidation of 3-picoline and it is found that the catalytic properties are directly related to the dispersion of vanadia.

Recently, there has been growing interest in the study of niobium-based materials as catalysts in various catalytic transformations.[1–7] Niobium(v) oxide can be used as a support, as a promoter and also as a unique solid acid. There are several advantages of using niobium(v) oxide as a catalyst support for vanadium oxide catalysts. These include the fact that (i) niobium is in the same group of the Periodic table as vanadium and is expected to have similar properties. (ii) Niobium(v) oxide is much more difficult to reduce than vanadium (easy reduction often causes low selectivity in oxidation reaction). (iii) Addition of niobium(v) oxide to a mixture of molybdenum and vanadium oxide improves the activity and selectivity during oxidation, ammoxidation and oxidative dehydrogenation reactions.[6,7]

Nicotinamide is an important chemical compound for the metabolism of human beings and animals, and is used as a food additive. It is usually synthesized by the ammoxidation of 3-picoline to nicotinonitrile and further hydrolysis of the nitrile formed.[8–11] Vanadium oxide catalysts, either unsupported or supported, are generally used for this ammoxidation process. We report here, for the first time, the use of V_2O_5 catalysts supported on niobium(v) oxide for ammoxidation of 3-picoline to nicotinonitrile. The purpose of this work is to determine the degree of dispersion of vanadium oxide supported on niobium(v) oxide and to understand the relation between activity of the catalysts and oxygen chemisorption sites.

Niobium(v) oxide was prepared by calcination of niobium pentoxide hydrate (Niobia HY-340 AD/1227, CBMM, Brazil) in air at 773 K for 4 h. A series of V_2O_5 catalysts with V_2O_5 loadings in the range 2–12 wt% supported on Nb_2O_5 (surface area 55 $m^2\ g^{-1}$) were prepared by impregnation with an aqueous solution containing ammonium metavanadate (Fluka). The catalysts were subsequently dried at 383 K for 16 h and calcined in air at 773 K for 5 h. Oxygen chemisorption was measured by a static method using a Pyrex glass system capable of supporting a vacuum of 10^{-6} Torr. Details of experimental set up have been given elsewhere.[14] Prior to chemisorption measurements, *ca.* 0.250 g of the sample was pre-reduced in a flow of hydrogen (40 ml min^{-1}) at 640 K for 2 h and the catalyst cell was evacuated at the same temperature for 1 h. Oxygen chemisorption uptakes were determined as the difference of two successive adsorption isotherms measured at 640 K.

A down-flow fixed bed reactor operating at atmospheric pressure and made of Pyrex glass was used for testing the catalysts during ammoxidation of 3-picoline to nicotinonitrile. About 2 g of catalyst diluted with an equal amount of quartz grains was charged into the reactor and was supported on a glass wool bed. Prior to introducing the reactant 3-picoline with a syringe pump, the catalyst was reduced at 673 K for 2 h in purified hydrogen flow (40 ml min^{-1}). After prereduction the reactor was fed with 3-picoline, ammonia and air, keeping mole ratio of 3-picoline : H_2O : NH_3 : air at 1 : 13 : 22 : 44 and contact time at 0.6 s. The reaction was carried out at various temperatures ranging from 573 to 683 K. The liquid products obtained (mainly nicotinonitrile) were analysed by gas chromatograph using an OV-17 column. Traces of carbon oxides were also formed during the reaction.

The oxygen chemisorption capacities of various V_2O_5/Nb_2O_5 catalysts are presented along with other information in Table 1. Pure Nb_2O_5 was also reduced under identical conditions and its oxygen uptake was taken into account for the supported catalysts. The results show that oxygen chemisorption capacities are found to increase with increase of vanadia content on niobia (Table 1). However, the dispersion of vanadia (O/V) is found to decrease steadily with increase of vanadia content (Table 1). Dispersion of vanadium oxide is defined as the fraction of total O atoms (determined from oxygen chemisorption) to total V atoms in the sample. The results of oxygen chemisorption results are further supported by powder X-ray diffraction results shown in Fig. 1, wherein a mixed vanadium–niobium oxide such as β-(Nb, V)$_2O_5$ (JCPDS card No: 16-132) was formed at moderately high vanadia content and increases with further increase of vanadia content. This β-(Nb, V)$_2O_5$ phase can be observed with d = 3.77, 3.56 and 3.40 Å for samples containing 10 and 12% V_2O_5 supported on Nb_2O_5 [Fig. 1(d) and (e)]. A decrease in dispersion of vanadia at higher loadings might be due to formation of β-(Nb, V)$_2O_5$.

According to Smits *et al.*,[6] the activity for oxidative dehydrogenation of propane was much reduced for samples containing the β-(Nb, V)$_2O_5$ phase. Wadsley and Andersson[13] also suggested that, in this phase the vanadium is replaced by the niobium present in isolated tetrahedral sites at the junction of blocks of NbO_6 octahedra. Thus the number of surface vanadium species are found to decrease when β-(Nb, V)$_2O_5$ is present in the catalyst.

The conversion and selectivity during ammoxidation of 3-picoline are reported in Table 1. The results show that conversion of 3-picoline increases up to 6% of V_2O_5 and did not

Table 1 Results of oxygen uptake, dispersion, oxygen atom site density, surface area and ammoxidation of 3-picoline for various V_2O_5/Nb_2O_5 catalysts

Sample	Wt% of V_2O_5 on Nb_2O_5	Surface area/ $m^2\ g^{-1}$	Oxygen uptake[a]/ μmol g^{-1}	Surface area[b] $m^2\ g^{-1}$	Oxygen atom site density/10^{18} m^{-2}	Dispersion[c] (O/Mo)	Ammoxidation of 3-picoline[d]	
							% Conversion	% Selectivity
1	2	50.2	83.1	57.0	1.76	0.76	73.80	97.60
2	4	48.7	161.2	49.0	3.96	0.73	80.20	95.70
3	6	46.7	217.9	49.1	5.35	0.66	90.30	98.05
4	8	44.1	249.6	45.7	6.58	0.57	88.60	96.60
5	10	43.6	300.9	45.2	8.03	0.54	85.70	97.20
6	12	44.2	340.6	46.2	8.88	0.51	82.85	95.30

[a] $T_{Reduction} = T_{Adsorption} = 640$ K. [b] BET surface area determined after oxygen chemisorption. [c] Dispersion = fraction of vanadium atoms at the surface assuming $O_{ads}/V_{surf} = 1$. [d] Reaction temperature = 683 K.

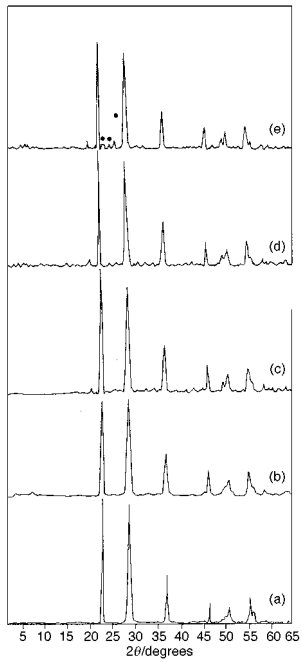

Fig. 1 X-Ray diffraction of V_2O_5/Nb_2O_5 catalysts: (a) 2%, (b) 4%, (c) 6%, (d) 10%, (e) 12% V_2O_5/Nb_2O_5. (●) Indicates XRD peaks arising from β-(Nb, V)$_2O_5$.

change appreciably at higher loadings. However, the selectivity of nicotinonitrile was found to be independent of vanadia loading in the catalyst. Watling *et al.*[7] also observed a similar trend in the activity for oxidative dehydrogenation (ODH) of propane over V_2O_5/Nb_2O_5 catalysts. They noticed that the rate of propane ODH first increases linearly with vanadia loading up to 6% and then remains constant at higher vanadia loadings. It is worth noting here that this vanadia loading corresponds closely to a theoretical monolayer capacity of V_2O_5 supported on a niobia having a specific surface area of 55 m^2 g^{-1}. This indicates that indeed a monolayer of vanadium oxide is formed at this concentration of V_2O_5 on niobium oxide.

The results of catalytic performance during ammoxidation can be explained by assuming that the active sites are due to vanadium ions at the surface, and the activity and selectivity of this site depends on the number of neighbouring vanadium and niobium ions. According to Smits *et al.*[14] the neighboring vanadium ions provide additional activity, while neighboring niobium ions improve the selectivity. The optimal activity and selectivity is shown a site having both vanadium and niobium as neighbors (V–O–V*–O–Nb).[14] At low vanadium loadings, the possibility of vanadium sites having a vanadium ion as a neighbour are low and thus the catalyst will be selective (Fig. 1) but not very active. The high activity for 6% V_2O_5/Nb_2O_5 catalyst might be due to presence of both vanadium and niobium as neighbors (monolayer loading). At higher loadings of V_2O_5 the activity remains constant due to formation of the new phase *i.e.* β-(Nb, V)$_2O_5$. This can be explained based on the assumption that not all the vanadium present in these catalysts contributes to the formation of mixed oxide phase.

To find the relation between the ammoxidation activity of 3-picoline and the dispersion of vanadia, a plot of 1/*X versus* the number of surface V_2O_5 moles is shown in Fig. 2, where *X* is the rate of picoline molecules converted per second per surface V_2O_5. A linear relationship passing through the origin was obtained, which clearly demonstrates that 3-picoline conversion is directly related to oxygen chemisorption measured at 640 K. As reported elsewhere, in connection with vanadium oxide catalysts supported on alumina[12] and on silica,[15] oxygen is chemisorbed at low temperatures selectively on coordinatively unsaturated sites (CUS), generated upon reduction, having a particular coordination environment. These sites are located on a highly dispersed vanadia phase, which is formed only at low

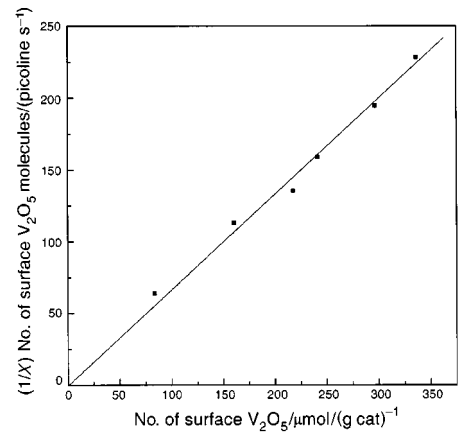

Fig. 2 Relationship between concentration of surface V_2O_5 and the rate of 3-picoline conversion.

vanadia loadings and remains as a 'patchy monolayer' on the support surface. At higher vanadia loadings, a second phase forms, in addition to the existing monolayer, and this post monolayer phase does not appreciably chemisorb oxygen. In light of the above, the correlation observed here, indicates that the catalytic functionality of the dispersed vanadium oxide phase supported on niobium(v) oxide is responsible for the ammoxidation of 3-picoline to nicotinonitrile is located on a patchy monolayer phase and that this functionality can be titrated by the oxygen chemisorption method described in this work.

Thus at low vanadia loadings the active vanadia phase is present in a highly dispersed state. However, at higher vanadia loadings, a mixed oxide containing β-(Nb, V)$_2O_5$ is formed. V_2O_5/Nb_2O_5 catalysts were highly active and selective for the conversion of 3-picoline to nicotinonitrile. The oxygen uptake is found to be directly related to the activity of the catalysts during 3-picoline ammoxidation to nicotinonitrile.

One of us (G. K.) thanks CSIR, New Delhi and T. B. thanks UGC, New Delhi for the award of a Senior Research Fellowships. The authors are also grateful to CBMM, Brasil for providing a hydrated niobia sample.

Notes and references

1 K. Tanabe, *Catal. Today*, 1990, **8**, 1.
2 K. Tanabe and S. Okazaki, *Appl. Catal. A*, 1995, **133**, 191.
3 J. R. H. Ross, R. H. H. Smits and K. Seshan, *Catal. Today*, 1993, **16**, 503.
4 J. Huuhtanen and S. L. T. Andersson, *Appl. Catal. A*, 1993, **98**, 159.
5 R. H. H. Smits, K. Seshan, J. R. H. Ross and A. P. M. Kentgens, *J. Phys. Chem.*, 1995, **99**, 9169.
6 R. H. H. Smits, K. Seshan, J. R. H. Ross, L. C. A. Van den Oetelaar, J. H. J. M. Helwegen, M. R. Anantharaman and H. H. Brongersma, *J. Catal.*, 1995, **157**, 584.
7 T. C. Watling, G. Deo, K. Seshan, I. E. Wachs and J. A. Lercher, *Catal. Today*, 1996, **28**, 139.
8 A. Andersson and S. T. Lundin, *J. Catal.*, 1979, **58**, 383.
9 A. Andersson, Jan-Olov Bovin and P. Walter, *J. Catal.*, 1986, **98**, 204.
10 B. V. Suvorov, A. D. Kagarlitskii, D. Kh. Semvaev, I. S. Kolodina and A. I. Loiko, Br. Pat. 1 317 064, 1973.
11 K. V. R. Chary, G. Kishan, T. Bhaskar and Ch. Sivraj, *J. Phys. Chem.*, 1998, **102**, 6792.
12 N. K. Nag, K. V. R. Chary, B. M. Reddy, B. Rama Rao and V. S. Subrahmanyam, *Appl. Catal.*, 1984, **9**, 225.
13 A. D. Wadsley and S. Andersson, in *Perspectives in Structural Chemistry*, ed. J. D. Dunitz and J. A. Ibers, Wiley, New York, 1970, vol. 3, p. 19.
14 R. H. H. Smits, K. Seshan, H. Leemreize and J. R. H. Ross, *Catal. Today*, 1993, **16**, 513.
15 N. K. Nag, K. V. R. Chary, B. R. Rao and V. S. Subrahmanyam, *Appl. Catal.*, 1989, **9**, 225.

Communication 9/03138C

Lithiated organophosphorus enamines: a new synthetic approach and the first crystal structures

William Clegg,[a] Robert P. Davies,[b] Lorraine Dunbar,[b] Neil Feeder,[b] Stephen T. Liddle,[a] Robert E. Mulvey,[c] Ronald Snaith*[b] and Andrew E. H. Wheatley[b]

[a] *Department of Chemistry, University of Newcastle, Newcastle upon Tyne, UK NE1 7RU*
[b] *Department of Chemistry, University of Cambridge, Cambridge, UK CB2 1EW. E-mail: rs10003@cam.ac.uk*
[c] *Department of Pure and Applied Chemistry, University of Strathclyde, Glasgow, UK G1 1XL*

Received (in Cambridge, UK) 21st April 1999, Accepted 16th June 1999

Made by a nitrile insertion/hydrogen migration process *via* $Ph_2P(O)CH_2Li$ and Bu^tCN, the enamide $Ph_2P(O)CH{=}C(Bu^t)N(H)Li$ and its TMEDA hemisolvate exist as tetrameric and dinuclear arrangements respectively: the novel structure of the starting lithiated phosphane oxide, also in its TMEDA hemisolvated form, is shown to contain Li–C contacts of two distinct types.

Previously we have described the nitrile insertion reaction and subsequent Lewis base-promoted ketimide to azaallyl rearrangement depicted in eqn. (1) (R = H or Pr^n).[1] Here we show

$$RCH_2Li + Bu^tC{\equiv}N \longrightarrow RCH_2(Bu^t)C{=}NLi \xrightarrow{HMPA} RC(H){=}C(Bu^t)N(H)Li{\cdot}HMPA \quad (1)$$

that this dual process can be extended to a functionalised group, R = $Ph_2P(O)$ in the lithiated phosphane oxide $Ph_2P(O)CH_2Li$, and that it can thereby occur without the aid of an external Lewis base. Such lithiated phosphane oxides are widely used as Horner–Wittig reagents[2] for the stereoselective synthesis of alkenes. As such, their metal–ligand bonding is of particular interest since in rare cases intimate C–Li contacts can contribute to the stability of these generally exclusively Li–O bonded molecules. For this reason we determined first the crystal structure of the starting lithiated phosphane oxide in its partially TMEDA-solvated form, $\{[Ph_2P(O)CH_2Li]_2{\cdot}TMEDA\}_2$ **1**, thereby revealing a unique tetranuclear arrangement which has in fact two distinct types of C–Li contact. The products of the nitrile insertion reactions of $Ph_2P(O)CH_2Li$, $\{Ph_2P(O)CH{=}C(Bu^t)N(H)Li\}_4$ **2** and $\{Ph_2P(O)CH{=}C(Bu^t)N(H)Li\}_2{\cdot}TMEDA$ **3**, have also been crystallographically characterised, so giving the first crystal structures of lithiated organophosphorus enamines. We also report some preliminary reactions of **2** which show that it can behave as either a C-based or a N-based nucleophile.

Although earlier attempts to produce crystals of the solvent-free parent compound $Ph_2P(O)CH_2Li$ failed,[3] we have now successfully crystallised its TMEDA hemisolvate **1**.† Despite a high *R* value, the key features of the solid-state structure of **1**‡ are clear-cut. Thus, although formally tetrameric, the centrosymmetric molecular structure of **1** (Fig. 1) is best regarded as a pseudo-dimer, constructed by the dimerisation of two dinuclear units. 'Dimerisation' operates through a strictly planar $(OLi)_2$ ring, a feature common to purely dinuclear lithiophosphane oxide dimers.[4] Each dinuclear unit accommodates two distinct Li atoms within a puckered (POLiOLiC) ring. With respect to individual monomeric (CPOLi) units, the short C26–Li1 contact [2.171(13) Å] within this six-membered ring is intermolecular. A bidentate TMEDA ligand completes the four-fold coordination of Li1. Fused onto the (POLiOLiC) ring is an (OPCLi) chelate ring, made possible by the C13–Li2 contact [2.340(13) Å]. Here, the carbanionic CH_2^- centre functions as

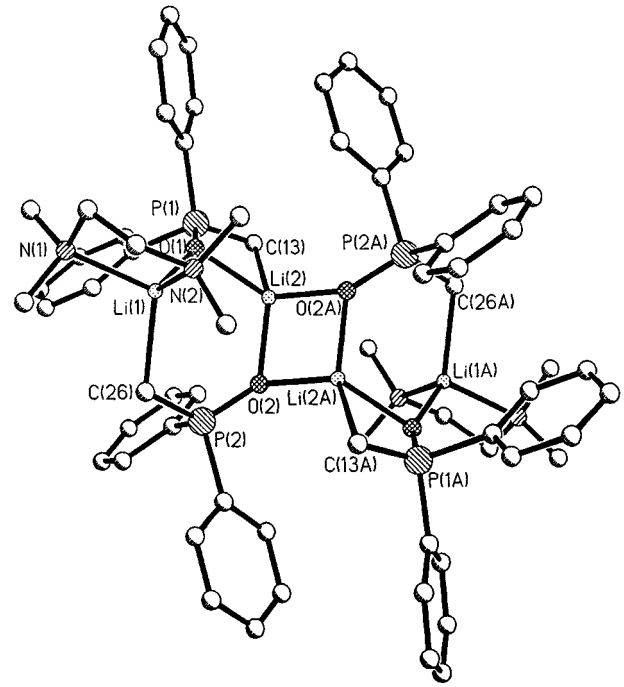

Fig. 1 Molecular structure of **1**. Hydrogen atoms are omitted for clarity.

an internal coordinating centre, to the exclusion of TMEDA (note that in the synthesis of **1** a 3:2 TMEDA:Li ratio was used). Crystallographic confirmation of Li–C contacts in lithiated phosphane oxides has so far been limited to those within (POCLi) chelates in non-solvated $\{Ph_2P(O)CHLiC(H)MeEt\}_4$[3] and to intermolecular ones in the dimer of fully TMEDA-solvated lithio *P*-isopropyl-1,3,2-dioxaphosphorinane 2-oxide[5] (their mean lengths of 2.230 and 2.228 Å, respectively, lie between those found in **1**). Both types of contact are uniquely combined within the structure of **1**, a fact directly attributable to its *partially* solvated nature (*i.e.* with non-solvated and solvated Li sites).

Having an in-built Lewis base function, $Ph_2P(O)CH_2Li$ does not require the participation of a donor solvent to convert to the enamide **2** on addition of nitrile [eqn. (2)]. Accordingly, a

$$Ph_2P(O)CH_2Li + Bu^tC{\equiv}N \longrightarrow \underset{\mathbf{2}}{Ph_2P(O)CH{=}C(Bu^t)N(H)Li} \xrightarrow{TMEDA} \underset{\mathbf{3}}{\tfrac{1}{2}[\{Ph_2P(O)CH{=}C(Bu^t)N(H)Li\}_2{\cdot}TMEDA]} \quad (2)$$

hexane–toluene solvent system was used.† No ketimide intermediate, as detected in the simple alkyl systems [eqn. (1)], is observable here, nitrile insertion and hydrogen transfer (from

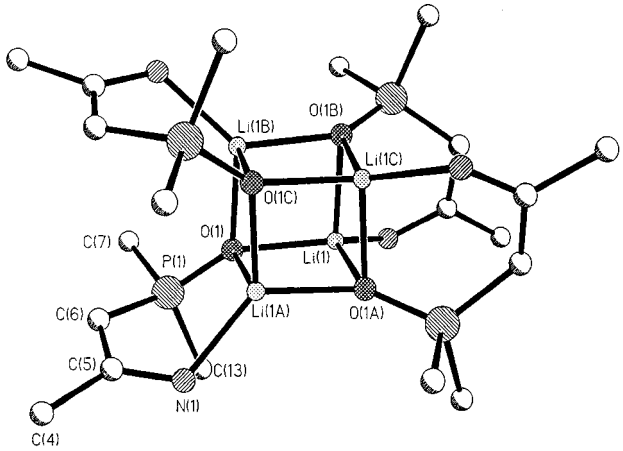

Fig. 2 Molecular structure of **2**. Only the *ipso*-C of Ph and the quaternary C of Bu^t groups are shown. Hydrogen atoms are omitted for clarity.

the CH_2 unit to the N atom) both having occurred. To make the hemisolvated derivative **3**, the same reaction is followed, but TMEDA is added subsequently [eqn. (2)].†

Based on a $(LiO)_4$ pseudocubane core, the molecular structure of **2** (Fig. 2)‡ has N atoms internally donating to the Li ones within (OPCCNLi) chelate rings. The most revealing feature is that relatively long PC⋯C [1.399(5) Å] and short C⋯N [1.310(4) Å] bond lengths within these rings indicate a delocalised arrangement with a high degree of imidoalkyl [RC(H)–C(Bu^t)=NH]$^-$ character, moreso than in the simple lithium azaallyl {Pr^{n}C(H)=C(Bu^t)N(H)Li·HMPA}$_2$ [1] [corresponding lengths: 1.345(3) and 1.390(3) Å]. Accordingly, the Li–N bond in **2** is short [1.958(6) Å; *cf* 2.012 Å (mean) in the latter], reflecting also the relatively strain-free conformation [CNLi angle, 119.2(3)°] of the six-membered chelate ring. No C–Li contacts are therefore necessary, so the *C*(H)*C*(Bu^t) atoms display sp^2 rather than sp^3 hybridisation. The second enamide structure **3** (Fig. 3)‡ is constructed around an asymmetrical, essentially planar $(LiO)_2$ rhomboidal ring. Chelation of Li1 by TMEDA forces the chelating (OPCCN) arms into a *cis* conformation with both N atoms internally donating to Li2: in this way both Li atoms attain (distorted tetrahedral) four coordination. The Li–O bond lengths within the OPCCNLi chelated units are significantly longer [2.075(6) Å] than those involving the TMEDA-solvated Li [1.913(6) Å]. These are counterbalanced by short Li–N(anion) bonds and long Li–N(TMEDA) bonds [1.990(5) and 2.094(7) Å, respectively]. Similarly, the wider bite size of the OPCCN ligand [99.5(1)°; *cf* 88.0(4)° for TMEDA] is offset by narrower O–Li2–O bond angles [94.8(4)° *cf*. 105.9(4)° for OLi1O]. As in **2**, the PC⋯C and C⋯N bond lengths in **3** [1.408(5) and 1.321(5) Å, respectively] suggest that the imidoalkyl canonical form again makes a substantial contribution to the enamide structure, and show therefore that the resonance delocalisation within the OPCCN anion is largely unaffected by the change in aggregation or the introduction of solvation.

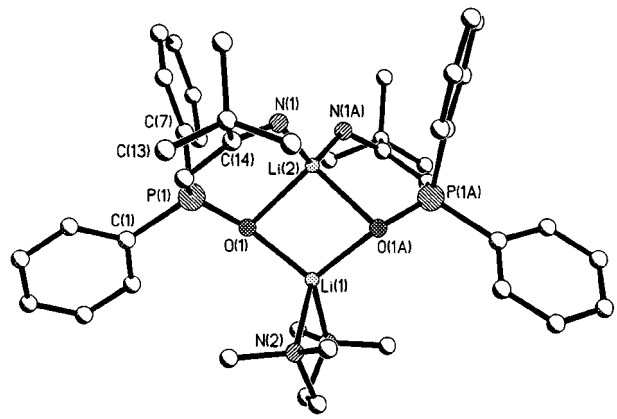

Fig. 3 Molecular structure of **3**. Hydrogen atoms are omitted for clarity.

Finally, quenching the lithium complexes **2** or **3** with suitable electrophiles can give access to new organophosphorus enamines. Related compounds of the type $Ph_2P(O)CH{=}C(R)N(H)R'$, made by nucleophilic addition of amines to 1-alkynylphosphine oxides,[6] are useful precursors to α,β-unsaturated ketimines and ketones. Interestingly, preliminary studies on **2** indicate that methanolysis affords $Ph_2P(O)CH{=}C(Bu^t)NH_2$ but that treatment with methyl iodide affords chiral $Ph_2P(O)CH(Me)$-C(Bu^t)=NH.† This ambi-(N- or C-) nucleophilic behaviour, and the potential uses of the products as unusual new ligands, are being explored further.

We thank the EPSRC (W. C., L. D., N. F.) for financial support, and St. Catharine's (R. P. D.) and Gonville & Caius (A. E. H. W.) Colleges for Research Fellowships.

Notes and references

† Standard inert-atmosphere Schlenk techniques were used for all syntheses. **1**: Bu^{n}Li (6 mmol in hexane) was added to a suspension of $Ph_2P(O)CH_3$ (6 mmol) in toluene (5 ml) containing TMEDA (3 mmol) at −78 °C. Warming to room temperature gave a yellow precipitate. Hexane was removed *in vacuo* and replaced by toluene (2 ml). Dissolution was achieved by heating the mixture following the addition of more TMEDA (6 mmol). Allowing the solution to cool gradually in a water bath afforded yellow rhomboidal crystals of **1** (yield, 36%; mp decomp. from 90 °C). **2**: $Ph_2P(O)CH_3$ (5 mmol) was suspended in toluene and chilled to −78 °C prior to the addition of Bu^{n}Li (5 mmol in hexane). Warmed to room temperature and treated with Bu^{t}CN (5 mmol) the solution changed from pale to dark yellow. It was then stirred for 30 min before being transferred to a 65 °C water bath and allowed to cool slowly. The solution deposited pale yellow cubic crystals of **2** (yield, 52%; mp decomp. from 175 °C). **3** : the synthesis of **2** was followed to the dark yellow solution stage. TMEDA (5 mmol) was subsequently added. Storing this solution at −30 °C for 4 days produced bright yellow crystals of **3** (yield, 48%; mp decomp. from 167 °C). **1**, **2** and **3** were also characterised by elemental analysis and NMR (^{1}H and ^{13}C) spectral data (to be published in a full paper). The quenched products were also characterised by their ^{1}H NMR spectra.

‡ *Crystal data for*: **1**: $C_{32}H_{40}Li_2N_2O_2P_2$, M = 560.48, monoclinic, space group $P2_1/n$, a = 12.683(2), b = 10.290(1), c = 24.527(3) Å, β = 98.782(3)°, U = 3163.5(7) Å^3, Z = 4, D_c = 1.177 g cm^{-3}, μ = 0.167 mm^{-1} (Mo-Kα, λ = 0.71069 Å), T = 160(2) K; R_w = 0.3095 on F^2 values of all 5560 unique data, conventional R = 0.1039 on F values of 3437 reflections with $F_o^2 > 2\sigma(F_o^2)$, 365 parameters; final difference map within ±0.68 e Å^{-3}. **2**: $C_{18.88}H_{22.25}LiNOP$, M = 317.04, tetragonal, space group $P4/n$, a = 16.472(2), c = 13.664(3) Å, U = 3707.4(10) Å^3, Z = 8, D_c = 1.136 g cm^{-3}, μ = 0.150 mm^{-1} (Mo-Kα, λ = 0.71069 Å), T = 180(2) K; R_w = 0.2018 on F^2values of all 3268 unique data, conventional R = 0.0618 on F values of 2390 reflections with $F_o^2 > 2\sigma(F_o^2)$, 206 parameters; final difference map within ±0.63 e Å^{-3}. **3**: $C_{21}H_{29}LiN_2OP$, M = 363.37, monoclinic, space group $C2/c$, a = 27.740(6), b = 9.803(2), c = 20.206(4) Å, β = 130.69(3)°, U = 4166.61(14) Å^3, Z = 8, D_c = 1.159 g cm^{-3}, μ = 0.143 mm^{-1} (Mo-Kα, λ = 0.71069 Å), T = 180(2) K; R_w = 0.1464 on F^2 values of all 3669 unique data, conventional R = 0.0634 on F values of 1998 reflections with $F_o^2 > 2\sigma(F_o^2)$, 245 parameters; final difference map within ±0.26 e Å^{-3}.

CCDC 182/1291. See http://www.rsc.org/suppdata/cc/1999/1401/ for crystallographic files in .cif format.

1 D. R. Armstrong, W. Clegg, L. Dunbar, S. T. Liddle, M. MacGregor, R. E. Mulvey, D. Reed and S. A. Quinn, *J. Chem. Soc., Dalton Trans.*, 1998, 3431.
2 L. Horner, H. Hoffmann, H. G. Wippel and G. Klahre, *Chem. Ber.*, 1959, **92**, 2499; J. Clayden and S. Warren, *Angew. Chem., Int. Ed. Engl.*, 1996, **35**, 241.
3 J. E. Davies, R. P. Davies, L. Dunbar, P. R. Raithby, M. G. Russell, R. Snaith, S. Warren and A. E. H. Wheatley, *Angew. Chem., Int. Ed. Engl.*, 1997, **36**, 2334.
4 *E.g.* see S. E. Denmark, K. A. Swiss and S. R. Wilson, *Angew. Chem., Int. Ed. Engl.*, 1996, **35**, 2515.
5 S. E. Denmark, K. A. Swiss, P. C. Miller and S. R. Wilson, *Heteroat. Chem.*, 1998, **9**, 209.
6 A. Portnoy, C. J. Morrow, M. S. Chattha, J. C. Williams and A. M. Aguiar, *Tetrahedron Lett.*, 1971, 1397.

Communication 9/03175H

Water-soluble [60]fullerene–cationic homooxacalix[3]arene complex which is applicable to the photocleavage of DNA

Atsushi Ikeda,[a] Tsukasa Hatano,[a] Masaru Kawaguchi,[a] Hikaru Suenaga[b] and Seiji Shinkai*[a]

[a] *Department of Chemistry and Biochemistry, Graduate School of Engineering, Kyushu University, Fukuoka 812-8581, Japan. E-mail: seijitcm@mbox.nc.kyushu-u.ac.jp*

[b] *Fukuoka Industrial Technology Center, 1465-5 Aikawa, Kurume Fukuoka 839-0861, Japan. E-mail: suenaga@bfri01.fitc.pref.fukuoka.jp*

Received (in Cambridge, UK) 14th May 1999, Accepted 14th June 1999

A new water-soluble, cationic homooxacalix[3]arene 1 was synthesized: this homooxacalix[3]arene solubilized [60]fullerene into water and the [60]fullerene–homooxacalix[3]arene complex acted as an efficient DNA photocleavage reagent.

The ready availability of [60]fullerene and its homologues has increasingly invited exploration of their outstanding new physical and chemical properties. Among them, one of the most important applications is medicial use: for example, they act as a singlet oxygen ($^1O_2$) photosensitizer[1,2] to cleave DNA[3–8] and as an inhibitor to suppress HIV protease activity.[9,10] In spite of their high potentials, however, applications have been very limited because of their poor water solubility. Several lines of effort have so far been devoted toward compensation for this drawback, for example, by introduction of water-soluble substituents,[3–6] mixing with water-soluble polymers,[7,11] and solubilization in γ-cyclodextrin (γ-CD)[12] and water-soluble calix[8]arenes.[13] We considered that among these methods, the host–guest method should be superior to others because (i) one can directly use 'unmodified [60]fullerene' which can generate $^1O_2$ more efficiently than other [60]fullerene derivatives,[14] (ii) one can suppress undesired photo-dimerization of [60]fullerene and (iii) dioxygen or substrates can collide with [60]fullerene more efficiently. Recently, we found that homooxacalix[3]arene and its derivatives can include [60]fullerene in their cavities.[15–18] This finding suggests that if a cationic homooxacalix[3]arene can solubilize [60]fullerene into water *via* host–guest interactions, the resultant [60]fullerene–homooxa[3]arene complex should be readily bound to DNA and might act as a DNA photocleavage reagent therein. With these objects in mind, we designed a new water-soluble cationic homooxacalix-[3]arene **1** with a cone conformation.

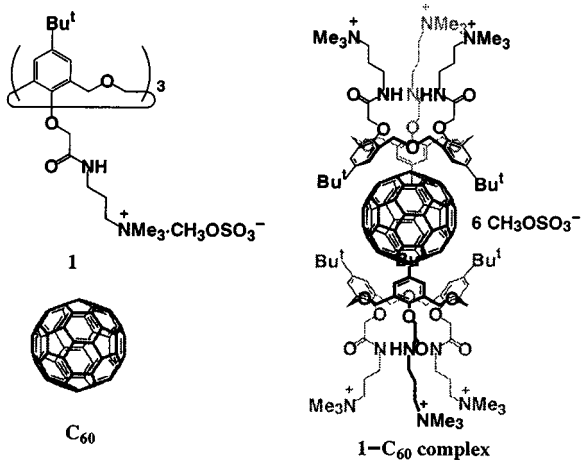

Water-soluble calixarene **1** was synthesized according to Scheme 1 and identified by ^{1}H NMR, FT-IR and ESI-TOF MS

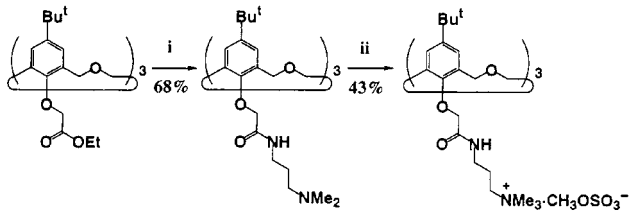

Scheme 1 *Reagents and conditions*: i, *N*,*N*-dimethylpropane-1,3-diamine, DMAP, NaH, THF–EtOH; ii, Me_2SO_4, THF.

spectroscopic evidence and elemental analysis.† The ^{1}H NMR data are consistent with a cone conformation.

Firstly, the critical aggregate concentration (CAC) of **1** was estimated by surface tension (Wilhelmy method). As shown in Fig. 1, the surface tension of **1** in pure water abruptly decreased at *ca*. 3 mmol dm^{-3}. One can consider, therefore, that compound **1** forms aggregates above this concentration. In the subsequent experiments, we set the concentration of **1** to 0.50 mmol dm^{-3}, where **1** exists discretely in aqueous solution.

[60]Fullerene (solid) was extracted into water containing **1** by sonication (10 min) followed by stirring (3 days).‡ After centrifugation (10 000 rpm, 15 min, 20 °C), the solution was characterized by UV–VIS absorption and ^{13}C NMR spectroscopic methods. The UV–VIS absorption spectrum of the **1**–[60]fullerene complex shows absorption maxima at 264, 341 and 438 nm assignable to solubilized [60]fullerene (Fig. 2). The

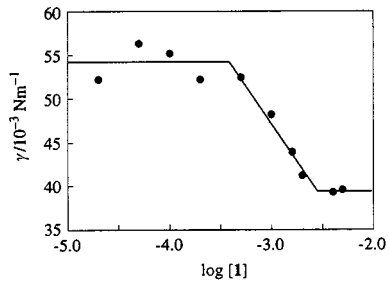

Fig. 1 Plot of surface tension *vs.* concentration of **1** at 25 °C.

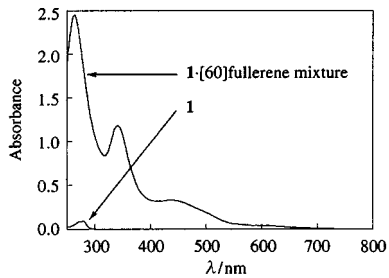

Fig. 2 Absorption spectra of **1** and **1**–[60]fullerene complex in water at 25 °C: [**1**] = 0.50 mmol dm^{-3}.

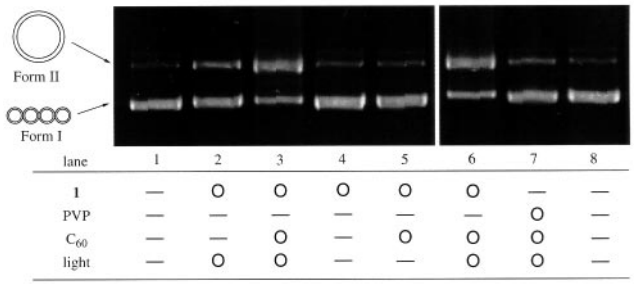

Fig. 3 Agarose gel electrophoretic patterns of DNA nicked by **1**–[60]fullerene complex. The reaction samples contained 93 μmol dm^{-3} of ColE1 supercoiled plasmid. Lanes 1 and 8: no chemicals in distilled water. Lane 2 and 4: 25 μmol dm^{-3} of **1**. Lanes 3, 5 and 6: 25 μmol dm^{-3} of **1** and 12 μmol dm^{-3} of [60]fullerene. Lane 7: 0.9 wt% PVP and 12 μmol dm^{-3} of [60]fullerene. Lanes 1–3 and 6–8: incubated under visible light irradiation at a distance of 10 cm by a 140 W Xe lamp (Sumita LS-140UV) at 25 °C for 6 h. Lanes 4 and 5: incubated in the dark for 6 h. After the addition of 10 mm^3 of 10% SDS solution and loading buffer (Wako) in this order, electrophoresis was performed using 0.9% agarose gel. The gel was stained with 0.3 μg dm^{-3} ethidium bromide and visualized on a UV transilluminator.

^{13}C NMR spectrum of the **1**–[60]fullerene complex shows a new peak (145.90 ppm) due to sp^2 carbon atoms of [60]fullerene. These results consistently support the view that [60]fullerene is solubilized into water by inclusion in **1**. We determined the concentration of solubilized [60]fullerene by elemental analysis of the dried sample obtained by evaporation of this solution. The analytical result shows that the concentration of [60]fullerene in the original aqueous solution was 0.24 mmol dm^{-3}. This indicates the ratio between **1** and [60]fullerene to be 2:1.§ From a dynamic light-scattering measurement (DLS: Otsuka Electronic DLS-7000), the particle size of the **1**–[60]fullerene complex was estimated to be 1.4 nm, which was comparable with the size of the **1**–[60]fullerene 1:2 complex (as simulated by a computational method). These results strongly support the view that the complex does not form large aggregates under the present experimental conditions.

The **1**–[60]fullerene complex was applied to the photocleavage of ColE1 supercoil plasmid. Under dark conditions, DNA was not cleaved even in the presence of these reagents (Fig. 3, lanes 4 and 5). Under visible light irradiation, the **1**–[60]fullerene complex clearly showed DNA-cleaving activity (lane 3). In lane 3, about 65% of supercoiled DNA (form I) was converted to nicked DNA (form II). On the other hand, compound **1** showed a weak DNA-cleaving activity by itself. We consider that 'cationic' **1** is bound to 'anionic' DNA to induce a conformational change in DNA, which facilitates the DNA photocleavage. For comparison, we carried out a control experiment using the poly(vinylpyrrolidone) (PVP)–[60]fullerene system.[7] The DNA-cleaving activity of the PVP–[60]fullerene system (lane 7) was obviously much lower than that of the **1**–[60]fullerene complex (lane 6) under visible light irradiation. Consequently, one can conclude that [60]fullerene included in 'cationic' **1** is transported onto 'anionic' DNA with the aid of electrostatic interactions and cleaves it with the aid of photoirradiation.

How was DNA cleaved by transported [60]fullerene? Foote *et al.*[19] proposed that two mechanisms have to be taken into consideration: type I is the photoinduced electron transfer from the guanine unit to [60]fullerene and type II is the reaction with $^1O_2$ photochemically generated by [60]fullerene. These two mechanisms can be distinguished by comparison of the results of the aerobic conditions with those of the anaerobic ones. We found that there is no significant difference between these two conditions: the yields of form II were 63% under the aerobic conditions, 63% under the anaerobic (N_2) conditions and 66% under the dioxygen-saturated conditions. The results suggest that the mechanism mainly operative in the present DNA photocleavage system is type I, which is basically in line with Foote's results.[19]

In conclusion, the present paper demonstrated that 'cationic' **1** can solubilize [60]fullerene into water and transport it to DNA. Hence, photocleavage can be readily accomplished therein using 'unmodified' [60]fullerene. To the best of our knowledge, this is one of a few successful examples in which 'unmodified' [60]fullerene is directly supplied to DNA. These findings imply, therefore, that the concepts cultivated in host–guest chemistry of [60]fullerene and its homologues are more fruitfully applied to medicinal chemistry.

Notes and references

† *Selected data* for **1**: δ_H(250 MHz, [$^2H_6$]DMSO) 8.11 (s, 3H, NH), 6.91 (s, 6H, ArH), 4.69 and 4.48 (each d, each 6H, $ArCH_2O$), 4.21 (s, 6H, OCH_2CO), 3.37 (s, 9H, CH_3OSO_3), 3.20–3.37 (m, 6H, NCH_2), 2.98–3.15 (m, 33H, NCH_3 and NCH_2), 1.93 (m, 6H, $CH_2CH_2CH_2$), 1.05 (s, 27H, Bu^t); *m/z* (ESI-TOF MS) 1270 ([M − $CH_3OSO_3^-$]$^+$).

‡ By a similar method, [70]fullerene can be also solubilized into water by inclusion in **1**.

§ We determined the stoichiometry between **1** and [60]fullerene by the C/N ratio of the elemental analysis and then calculated the ε of the **1**–[60]fullerene mixture to be 4.87×10^4 dm^3 mol^{-1} cm^{-1} (341 nm) *via* the UV–VIS absorption spectrum (Calc. for $C_{63}H_{108}N_6O_{21}S_3 \cdot 0.245C_{60} \cdot 3.5H_2O$: C, 57.6; H, 7.1; N, 5.2. Found C, 57.5; H, 6.6; N. 5.2%).

1 J. L. Arbogast, A. O. Darmanyan, C. S. Foote, Y. Rubin, F. N. Diederich, M. M. Alvarez, S. J. Anz and R. L. Whetten, *J. Phys. Chem.*, 1991, **95**, 11.
2 N. Martín, L. Sánchez, B. Illescas and I. Pérez, *Chem. Rev.*, 1998, **98**, 2527.
3 T. D. Ros and M. Prato, *Chem. Commun.*, 1999, 663.
4 Y.-Z. An, C.-H. B. Chen, J. L. Anderson, D. S. Sigman, C. S. Foote and Y. Rubin, *Tetrahedron*, 1996, **52**, 5179.
5 A. S. Boutorin, H. Tokuyama, M. Takasugi, H. Isobe, E. Nakamura and C. Hélène, *Angew. Chem., Int. Ed. Engl.*, 1994, **33**, 2462.
6 E. Nakamura, H. Tokuyama, S. Yamago, T. Shiraki and Y. Sugiura, *Bull. Chem. Soc. Jpn.*, 1996, **69**, 2143; H. Tokuyama, S. Yamago, E. Nakamura, T. Shiraki and Y. Sugiura, *J. Am. Chem. Soc.*, 1993, **115**, 7918.
7 Y. N. Yamakoshi, T. Yagami, S. Sueyoshi and N. Miyata, *J. Org. Chem.*, 1996, **61**, 7236.
8 N. Higashi, T. Inoue and M. Niwa, *Chem. Commun.*, 1997, 1507.
9 S. H. Friedman, D. L. DeCamp, R. P. Sijibesma, G. Srdanov, F. Wudl and G. L. Kenyon, *J. Am. Chem. Soc.*, 1993, **115**, 6506.
10 S. H. Friedman, P. S. Ganapathi, Y. Rubin and G. L. Kenyon, *J. Med. Chem.*, 1998, **41**, 2424.
11 Y. N. Yamakoshi, T. Yagami, K. Fukuhara, S. Sueyoshi and N. Miyata, *J. Chem. Soc., Chem. Commun.*, 1994, 517.
12 T. Anderson, K. Nilsson, M. Sundahl, G. Westman and O. Wennerström, *J. Chem. Soc., Chem. Commun.*, 1992, 604.
13 R. M. Williams and J. W. Verhoeven, *Recl. Trav. Chim. Pays-Bas*, 1992, **111**, 531.
14 T. Hamano, K. Okuda, T. Mashino, M. Hirobe, K. Arakane, A. Ryu, S. Mashiko and T. Nagano, *Chem. Commun.*, 1997, 21.
15 A. Ikeda, M. Yoshimura and S. Shinkai, *Tetrahedron Lett.*, 1997, **38**, 2107.
16 A. Ikeda, Y. Suzuki, M. Yoshimura and S. Shinkai, *Tetrahedron.*, 1998, **54**, 2497.
17 K. Tsubaki, K. Tanaka, T. Kinoshita and K. Fuji, *Chem. Commun.*, 1998, 895.
18 A. Ikeda, M. Yoshimura, H. Udzu, C. Fukuhara and S. Shinkai, *J. Am. Chem. Soc.*, 1999, **17**, 4291.
19 R. Bernstein, F. Prat and C. S. Foote, *J. Am. Chem. Soc.*, 1999, **121**, 464.

Communication 9/03872H

Enantiospecific synthesis of a planar chiral bidentate indenyl–alkoxide complex of zirconium using an axially chiral indene ligand

Robert W. Baker* and Brian J. Wallace

School of Chemistry, The University of Sydney, NSW 2006, Australia. E-mail: r.baker@chem.usyd.edu.au

Received (in Cambridge, UK) 10th May 1999, Accepted 22nd June 1999

The reaction of axially chiral (*M*)-1-(2′-methyl-3′-indenyl)-naphthalene-2-methanol 3 with $Zr(NEt_2)_4$ enantiospecifically provides the planar chiral complex (*P*)-bis(diethylamido)-[1-(2′-methyl-1′-indenyl)naphthalene-2-methoxo]-zirconium 7.

Planar chiral cyclopentadienylmetal complexes feature amongst the more successful stereoselective catalysts. They are usually obtained in enantiomerically pure form through resolution procedures, there being few methodologies allowing asymmetric synthesis. The most common approach[1] designed to avoid resolution utilises cyclopentadienyl ligands containing other stereogenic elements, rendering the faces of the ligand diastereotopic; however, stereoselectivity for the planar chiral element generated during metallation reactions is not guaranteed and separation of diastereoisomers may still be required. An approach extensively employed for 1,2-disubstituted ferrocenes involves the diastereoselective lithiation of complexes containing a chiral *ortho*-directing group.[2] An alternative to this is the enantioselective metallation of ferrocenes with achiral *ortho*-directing groups using a palladium(II) salt with an *N*-protected amino acid,[3] or a chiral lithium amide or an alkyllithium/chiral ligand complex.[2] Two other recently reported methods for the asymmetric synthesis of planar chiral cyclopentadienylmetal complexes are the displacement of chiral auxiliary ligands (L^{ch}) from half-sandwich complexes $Cp^*RuL_2{}^{ch}$ by planar prochiral cyclopentadienylmetals,[4] and the cyclisation of ferrocenyl diazoketones catalysed by chiral rhodium complexes.[5] We have proposed a ligand design whereby a second metal coordination site is constrained to one face of an asymmetrically substituted cyclopentadienyl ring through hindered rotation about the bond between the cyclopentadienyl ring and a naphthalene moiety; formation of chelating complexes using these ligands was anticipated to lead to the enantiospecific generation of a planar chiral cyclopentadienylmetal complex. Towards this objective, we have described approaches to the asymmetric synthesis of precursors to axially chiral chelating fluorene[6,7] and indene[8,9] ligands, employing ligand coupling reactions of sulfoxides. Here we demonstrate the potential of our ligand design with the enantiospecific synthesis of a planar chiral bidentate indenyl–alkoxide complex of zirconium using an axially chiral indene ligand.

We have described previously[9] that the reaction of (1*R*)-menthyl (*R*)-1-(*p*-tolylsulfinyl)naphthalene-2-carboxylate[7] with 2-methylindenyllithium during 30 min at 0 °C provides exclusively the −*ac*-rotamer of (1*R*)-menthyl (*S*)-1-(2′-methyl-1′-indenyl)naphthalene-2-carboxylate **1** in 50% yield and 70% de. The C1–C1′ bond of **1** was shown to be a stable stereogenic element that was conserved during subsequent prototropic shifts to 1-(2′-methyl-3′-indenyl)naphthalenes; thus, treatment of **1** with triethylamine provided **2** in 97% yield and 65% de, while LAH reduction gave **3** in quantitative yield and 70% ee. In order to obtain ligand **3** in enantiomerically pure form, a convenient procedure amenable to operation on a large scale has been developed (Scheme 1). Esterification of 1-bromo-2-naphthoic acid **4** (readily prepared from 2-methylnaphthalene)[10] with (1*R*)-menthol followed by displacement of the bromide with sodium thiophenoxide, furnished the phenylsulfide **5** in 94% overall yield. Oxidation of **5** with dimethyldioxirane, generated *in situ* using OXONE®, provided the sulfoxide **6** as a 58:42 mixture of epimers at sulfur (^{1}H NMR analysis) in 51% yield, accompanied by 46% of recovered **5**.† Reaction of **6** with 2-methylindenyllithium during 40 min at 0 °C furnished **1** and the +*ac*(*R*) isomer of **1**, in a ratio of 44:56, respectively (^{1}H NMR analysis), in 92% combined yield. This mixture was then quantitatively isomerised to a mixture of **2** and the *P*-epimer of **2**, in a ratio of 46:54, respectively,‡ on treatment with triethylamine. Fractional crystallisation, then recrystallisation from hexane solution furnished **2** in > 99% de‡ and 32% yield (maximum theoretical yield 46%). A single-crystal X-ray structure determination on **2**§ establishes the *M* absolute configuration at the chiral axis, which had been previously proposed on the basis of comparisons of CD spectra.[9] The rate of epimerisation of **2** to the *P*-epimer (ultimately affording a 1:1 mixture) has been determined by HPLC analysis in xylenes solution at reflux,‡ providing a barrier to rotation $\Delta G^{\ddagger}_{413}$ = 150.6 kJ mol^{-1}. Reduction of **2** of > 99% de‡ with LAH affords **3** quantitatively with > 99% ee.¶ While the barrier to rotation in **3** has not been determined, it can be anticipated to be higher again than that of **2**.[8]

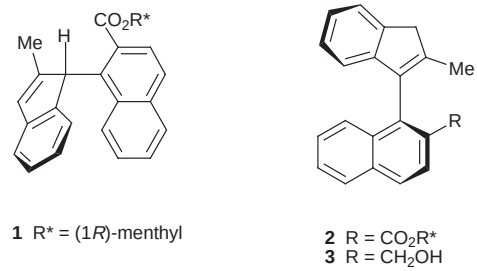

1 R* = (1*R*)-menthyl

2 R = CO_2R^*
3 R = CH_2OH

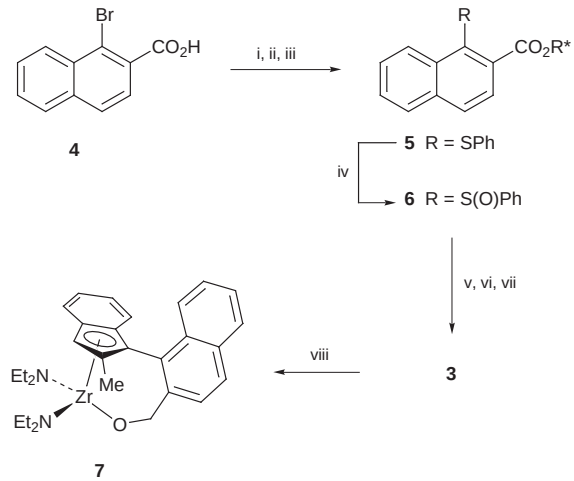

Scheme 1 *Reagents and conditions*: i, $SOCl_2$ (15 equiv.), 25 °C, 20 h; ii, (1*R*)-menthol (2 equiv.), pyridine (2 equiv.), CH_2Cl_2, 25 °C, 30 min; iii, PhSNa (1.2 equiv.), DMF, 60 °C, 20 h; iv, OXONE® (3 equiv.), $NaHCO_3$ (5 equiv.), acetone–MeCN–water (20:10:1), 5 °C, 20 h; v, 2-methylindenyllithium (1.3 equiv.), THF, 0 °C, 40 min; vi, NEt_3–toluene (1:1), reflux, 24 h; vii, LAH (5 equiv.), diethyl ether, 25 °C, 1 h; viii, $Zr(NEt_2)_4$ (1 equiv.), toluene, reflux, 16 h.

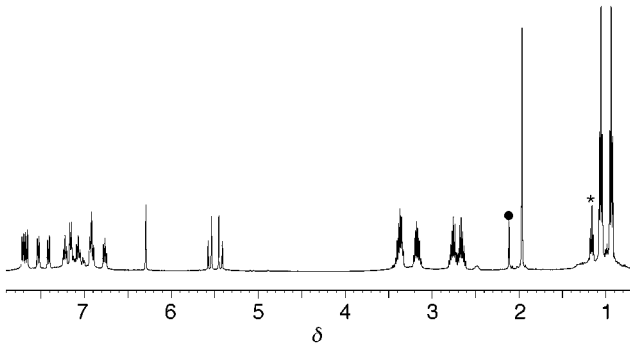

Fig. 1 ^{1}H NMR (400 MHz, C_6D_6) spectrum of complex **7**; unobscured signals of residual toluene and $Zr(NEt_2)_4$ are indicated by • and *, respectively.

With multigram quantities of enantiomerically pure **3** available, we next sought to prepare a bidentate indenyl–alkoxide metal complex[11] in order to demonstrate that the axial chirality of the ligand would indeed translate into planar chirality in the complex without loss of enantiomeric purity.‖ Initial attempts at metallation of **3** through formation of the dilithio species with BuLi, followed by reaction with $ZrCl_4$ in a variety of solvents, failed to produce any of the desired complex. Metallation was readily achieved, however, employing the amine elimination method.[13] Reaction of **3** with 1 equiv. of $Zr(NEt_2)_4$ in toluene solution under reflux for 16 h, followed by removal of the solvent, led to essentially quantitative conversion to the complex **7**,** as evident from inspection of the ^{1}H NMR spectrum of the crude product (Fig. 1).†† In particular, the methylene signal of the indene moiety of **3** (AB pattern centred at δ_H 3.65) is replaced by a singlet at δ_H 6.29 in **7**; the methylene signal of the naphthalenemethanol moiety of **3** (AB pattern centred at δ_H 4.63) is significantly deshielded on formation of **7** (AB pattern centred at δ_H 5.50); and the diastereotopic NEt_2 ligands of **7** appear as two distinct ABX_3 patterns. Consistent with the mononuclear structure proposed for **7**, the high field ^{1}H NMR spectrum of the crude product obtained in the reaction of *rac*-**3** with $Zr(NEt_2)_4$ was identical to that obtained with enantiomerically pure **3**, with additional signals being completely absent. Hydrolysis of complex **7** with dilute HCl solution quantitatively returned ligand **3** with > 99% ee.¶ It follows that complex **7** is also enantiomerically pure and can be assigned *P* absolute configuration (a single descriptor for configuration is used as the atropisomerism of the precursor ligand **3** is considered to be latent in the complex). We are currently examining the expansion of this approach to a wide range of ligands and metal complexes.

Notes and references

† A reaction sequence analogous to that from **4** to **6** was first developed in this laboratory by M. A. Foulkes using the isopropyl esters.

‡ Diastereoisomeric purity was determined by HPLC: a 4.6 × 250 mm column (Zorbax 5 μ silica, Jones) was used with 0.4% ethyl acetate–hexane as eluent at a flow rate of 1.5 ml min^{-1}, detection 254 nm, t_R: 17.4 min for **2** and 20.0 min for the *P*-epimer of **2**.

§ Details of the single-crystal X-ray structure determination of **2** will appear in the full account.

¶ Enantiomeric purity was determined by HPLC: a 4.6 × 250 mm column (Pirkle Type 1A, Regis) was used with 5% propan-2-ol/hexane as eluent at a flow rate of 1.5 ml min^{-1}, detection 254 nm, t_r: 9.5 min for **3** and 10.2 min for *ent*-**3**.

‖ Somewhat related to this work, Pregosin and coworkers[12] have reported that reaction of $Ru(OAc)_2$[(*M*)-6,6′-dimethoxybiphenyl-2,2′-diyl-bis{di(3,5-di-*tert*-butylphenyl)phosphine}] with MeLi affords a planar chiral $RuMe_2$ complex where Ru is coordinated to one phosphine together with an η^6-C_6H_3 moiety from one of the biaryl rings; however, the enantiomeric purity of this complex is not discussed.

** Complex **7** was isolated as an orange viscous oil which, to date, has resisted crystallisation. Consequently, the purity of **7** is dependant on the precision of the stoichiometry of the reaction between **3** and $Zr(NEt_2)_4$, *e.g.* the reaction product shown in Fig. 1 contains *ca.* 5 mol% unreacted $Zr(NEt_2)_4$.

†† *NMR data* for **7**: δ_H (400 MHz, C_6D_6, primed numbers refer to the indenyl moiety) 0.94, 2.65 and 2.74 (10H, ABX_3, *J* 14.0, 6.8, NEt_2), 1.05, 3.17 and 3.38 (10H, ABX_3, *J* 14.0, 6.8, NEt_2), 1.96 (3H, s, 2′-Me), 5.43 and 5.56 (2H, AB, *J* 15.6, CH_2O), 6.29 (1H, s, H-3′), 6.76 (1H, dd, *J* 7.6, 7.6, 6′-H), 6.89–6.94 (2H, m, 5′- and 7′-H), 7.07 (1H, dd, *J* 8.4, 6.8, 7-H), 7.15 (1H, d, *J* 8.4, 3-H), 7.22 (1H, dd, *J* 8.0, 6.8, 6-H), 7.41 (1H, d, *J* 8.4, 8-H), 7.53 (1H, d, *J* 8.4, 4′-H), 7.66 (1H, d, *J* 8.4, 4-H) and 7.71 (1H, d, *J* 8.0, 5-H); δ_C (100 MHz, C_6D_6) 140.3, 134.8, 133.5, 130.9, 128.5 (each C), 128.4, 128.1 (each CH), 127.6 (C), 126.8, 126.6 (each CH), 125.9 (C), 125.6, 125.0, 123.7, 123.5, 123.0, 121.7 (each CH), 110.4 (C), 97.2 (CH), 74.0 (CH_2), 45.02, 44.99 (each 2 × CH_2), 16.2, 15.7 (each 2 × CH_3) and 14.0 (CH_3).

1 R. L. Halterman, *Chem. Rev.*, 1992, **92**, 965 and references cited therein; R. L. Halterman, *Synthesis of Chiral Titanocene and Zirconocene Dichlorides*, in *Metallocenes*, ed. A. Togni and R. L. Halterman, Wiley-VCH, Weinheim, 1998, ch. 8, and references therein.

2 C. J. Richards and A. J. Locke, *Tetrahedron: Asymmetry*, 1998, **9**, 2377 and references therein.

3 V. I. Sokolov, L. L. Troitskaya and O. A. Reutov, *J. Organomet. Chem.*, 1979, **182**, 537.

4 U. Koelle, K. Bücken and U. Englert, *Organometallics*, 1996, **15**, 1376.

5 S. Siegel and H.-G. Schmalz, *Angew. Chem., Int. Ed. Engl.*, 1997, **36**, 2456.

6 R. W. Baker, T. W. Hambley and P. Turner, *J. Chem. Soc., Chem. Commun.*, 1995, 2509.

7 R. W. Baker, M. A. Foulkes and J. A. Taylor, *J. Chem. Soc., Perkin Trans. 1*, 1998, 1047.

8 R. W. Baker, T. W. Hambley, P. Turner and B. J. Wallace, *Chem. Commun.*, 1996, 2571, (Corrigendum, 1997, 506).

9 R. W. Baker, J. N. H. Reek and B. J. Wallace, *Tetrahedron Lett.*, 1998, **39**, 6573.

10 S. L. Colletti and R. L. Halterman, *Organometallics*, 1991, **10**, 3438.

11 For other examples of bidentate cyclopentadienyl–alkoxide complexes of Group IV metals see: B. Reiger, *J. Organomet. Chem.*, 1991, **420**, C17; Y.-X. Chen, P.-F. Fu, C. L. Stern and T. J. Marks, *Organometallics*, 1997, **16**, 5958; E. E. C. G. Gielens, J. Y. Tiesnitsch, B. Hessen and J. H. Teuben, *Organometallics*, 1998, **17**, 1652; S. D. R. Christie, K. W. Man, R. J. Whitby and A. M. Z. Slawin, *Organometallics*, 1999, **18**, 348.

12 N. Feiken, P. S. Pregosin and G. Trabesinger, *Organometallics*, 1997, **16**, 3735.

13 G. M. Diamond, R. F. Jordan and J. L. Petersen, *J. Am. Chem. Soc.*, 1996, **118**, 8024 and references therein.

Communication 9/03740C

ChemComm

Poly[(dibenzylidene)tetrathiapentalene]—the first linearly extended TTF polymer

Harald Müller,*[a] Fouad Salhi,[a] Bernadette Divisia-Blohorn,[b] Françoise Genoud,[b] Theyencheri Narayanan,[a] Maren Lorenzen[a] and Claudio Ferrero[a]

[a] *European Synchrotron Radiation Facility, B.P. 220, 38043 Grenoble, France. E-mail: mueller@esrf.fr*
[b] *UMR 5819 CEA-CNRS-UJF, Départment de Recherche Fondamentale sur la Matiére Condensée CEA-Grenoble, 38054 Grenoble Cedex 9, France*

Received (in Bristol, UK) 10th November 1998, Revised manuscript 10th June 1999, Accepted 10th June 1999

The preparation of the first π-conjugated TTF polymer composed entirely of vinylogous, linearly fused TTF moieties has been achieved by oxidative polymerization of 2,5-di(benzylidene)-1,3,4,6-tetrathiapentalene.

Numerous attempts to incorporate TTF into polymeric backbones have been spurred by the exciting solid state properties of TTF molecular conductors and aimed at a combination of the electrical conductivity exhibited by these radical cation salts with the enhanced processability of a polymer matrix.[1] The TTF polymers reported to date consist of essentially independent TTF entities attached to a conjugated polymer backbone or of linear chains composed of segregated TTF units linked through spacer groups *via* σ or π bonds.[1] In spite of the well-known tendency of TTF to form ordered stacks,[2] the interactions between individual TTF units in polymeric matrices are difficult to control in the solid state. Insufficient through-bond and through-space interactions as a consequence of lacking conjugation and structural disorder in TTF polymers may result in low conductivities in the oxidized state.[1]

Macromolecular structures composed of fully π-conjugated TTF units could possibly offer an interesting alternative to overcome these inherent drawbacks.[1f,g,3] Linearly annelated TTF entities appear to be particularly promising in that respect, since the radical cation salts of many dimeric, linearly fused TTF derivatives exhibit metallic conductivity.[4] Despite the exceptional solid state properties of molecular conductors based on dimeric TTF donor molecules, the preparation of polymeric analogues has not yet been reported.

Recently, we have disclosed a novel synthetic approach to vinylogous, extended TTF derivatives starting from tetrathiapentalenes as precursors.[5] Here we report the application of this method to the preparation of poly[(dibenzylidene)tetrathiapentalene] (**3**; PDB-TTP), the first conducting polymeric TTF derivative composed entirely of π-conjugated, linearly annelated TTF units.

The synthetic concept is based on the transformation of the tetrathiapentalene (TTP) precursor **1** into the corresponding bifunctional TTF derivative **2**.[5] Owing to its hybrid TTP/TTF character, compound **2** can undergo oligo- and polymerization reactions *via* radical intermediates, a behaviour which contrasts sharply with that commonly known for TTF vinylogues.[6] Suitable substituents, such as the phenyl rings of **1**, enhance the solubility of the monomer and prevent the growing TTF chain from precipitation and thus from an early termination of the polymerization reaction.

The key step of the oxidative polymerization involves the formation of the highly reactive radical $\mathbf{1}^{+\cdot}$ from 2,5-di(benzylidene)-1,3,4,6-tetrathiapentalene (**1**; DB-TTP), which dimerizes with subsequent dehydrogenation to the TTF derivative **2**.[5] The isolation of the stable intermediate **2** confirms that radica–radical coupling of $\mathbf{1}^{+\cdot}$ occurs *via* the benzylic carbon atoms and thus resembles closely the well-known oxidative dimerization of 1,4-dithiafulvenes to vinylogous TTF derivatives.[7] Contrary to ordinary TTF derivatives, however, **2** can be oxidized to the radical trication $\mathbf{2}^{3+\cdot}$ which through subsequent radical dehydrodimerization and oxidation steps, eventually yields a polymer of general formula **3**. The proposed polymerization mechanism is depicted in Scheme 1 and was established by detailed electrochemical investigations performed on **1** and independently synthesized **2**.[8]

Thin films of **3** were prepared on Pt disk electrodes in anhydrous dichloromethane by repeated potential cycling between 0 and + 1.6 V (**1**: 4 10^{-4} M; $Bu^n_4NPF_6$ 0.1M; CH_2Cl_2;

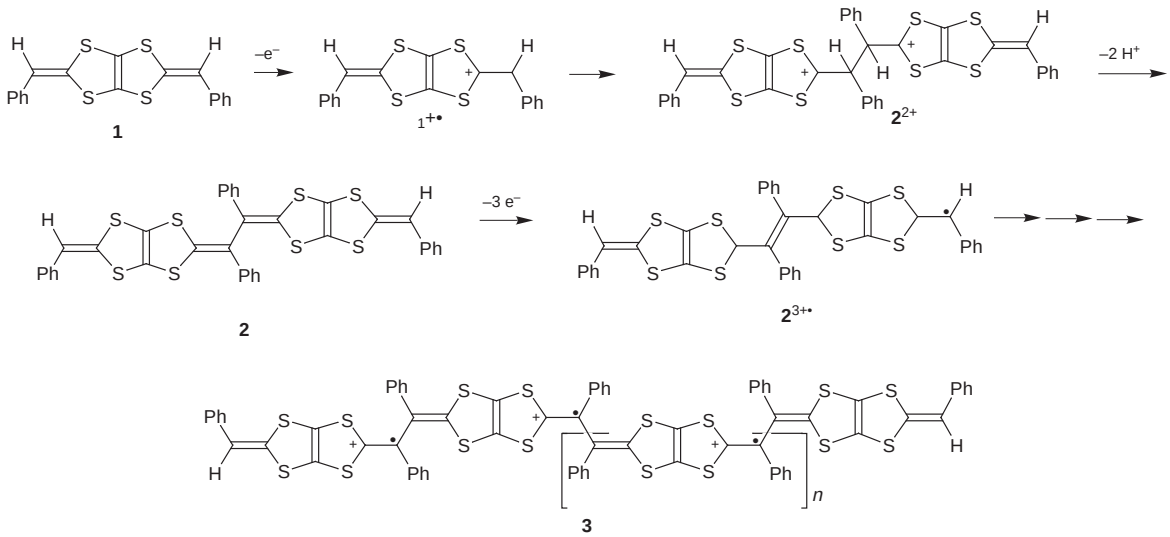

Scheme 1 Redox polymerization of monomer **1**. The counterions have been omitted for clarity, the polymer **3** is shown in a partially oxidized state. For an estimate of *n* see text.

Pt disc electrode ∅ 3 mm; v = 100 mV s^{-1}; 500 cycles) or by potentiostatic electrolysis at + 1.6 V [all potential values *versus* a saturated calomel electrode (SCE)].† The cyclic voltammogram of **1**, recorded during film synthesis, exhibited two irreversible waves (anodic peak potentials *ca.* + 0.8 and + 1.4 V) for the first sweep. Further scans showed the evolution of a new symmetrical redox wave at a less anodic potential (*ca.* + 0.6 V) indicating the formation of a new electroactive species. The peak currents of the latter increased continuously with each subsequent scan thus evidencing progressive deposit growth on the electrode surface.

The electrochemical response of a PDB-TTP film in monomer-free solution. The CV involves a sharp redox wave at a peak potential of *ca.* + 600 mV as well as several coalescing signals between + 900 and + 1500 mV, respectively. For simplicity, the latter will be considered as a single redox wave only. The amounts of charge transferred between 0 to + 700 mV and between + 700 to + 1500 mV are equal, as follows from an integration of the respective peak areas. The symmetrical signal shapes are characteristic of a surface-immobilized reversible redox system and hence in line with the postulated structure **3**.[9]

Results obtained by *in situ* EPR spectro-electrochemistry indicate that each peak potential coincides with a local maximum of the potential-dependent spin density. The relative ratio of the spin populations corresponding to the peak potentials of the first and second redox couple, respectively, is *ca.* 2 : 1. This value, together with the coulometric analysis of the peak areas makes plausible an assignment of the first redox couple to a partial oxidation state **3**, where a linearly extended chain bears one positive charge per vinylogous TTF unit. The removal of further electrons requires the unfavourable localization of positive charges on adjacent dithiole units and occurs in several steps between + 900 and + 1500 mV, where complete oxidation is reached. The resulting increase of the coulombic repulsion shifts the corresponding oxidation potentials towards higher values, simultaneously the number of charge carriers decreases as a consequence of spin recombination.

Continued potential cycling (500 cycles) of films in monomer-free solution between 0 and + 750 mV did not cause any loss in electroactivity, thus demonstrating high stability and pronounced electrochemical reversibility. A switching potential of + 1700 mV reduced the electroactivity by about 50% after 50 scans, presumably as a consequence of overoxidation.

Treatment of **1** with $NOPF_6$ (molar ratio 1 : 1.5) furnished the black, insoluble solid **3** in a yield of 80%, the analytical data of which are in good agreement with the partially oxidized structure **3** containing one counterion per repetitive unit.‡

MALDI-TOF and FAB MS of solid **3** gave intense peaks corresponding to the general formula $m/z = n(354)$ with $z = 1$. Fragments with m/z = 2412 (n = 6), 1416 (n = 4) and 1062 (n = 3) can unambiguously be assigned to structural elements comprising six, four and three monomer units, respectively. These results provide strong evidence for the presence of a linearly extended structure **3**, since the polymerization of **1** (m/z = 356) implies the formal abstraction of two hydrogen atoms per monomer unit within a chain, whereas the two terminal units loose only one hydrogen atom. The lower limit for the average molecular weight of **3** (without counterions) can thus be estimated to amount to at least eight monomer units, corresponding to a molecular weight of 2836 g mol^{-1}. TTF polymers comprising eight monomer units have been described in previous work.[10]

IR spectra of solid **3** exhibit a weak electronic absorption stretching from 3700 to *ca.* 1750 cm^{-1}, a behaviour typical of a semiconductor. Assuming a simple transition between the valence and the conduction band, the corresponding band gap amounts to a value of 217 meV. Intense bands at 1357 and 1248 cm^{-1} closely resemble features characteristic of TTF radical cation salts,[11] and thus corroborate the charged TTF structure **3**. Absorptions at 838 and 557 cm^{-1} confirm the presence of the hexafluorophosphate counterion. EPR spectra of compound **3** display a single, symmetrical line with a width of 6–8 G. The averaged g-factor is 2.0077, the spin density is *ca.* 2×10^{23} spins mol^{-1}. The electrical conductivity, as determined by four-probe measurements on compact samples of **3**, gave values of about 10^{-6} S cm^{-1}. For electrochemically deposited films the conductivities range from 5×10^{-3} to 5×10^{-4} S cm^{-1}. The latter values are among the highest reported to date for polymeric TTF derivatives.[1]

A typical small angle X-ray scattering (SAXS) pattern of compound **3** shows a diffuse scattering background with a sharp superimposed peak at $\boldsymbol{s}$ = 0.44 nm^{-1} and a large bump stretching from 0.6 $nm^{-1} \leqslant \boldsymbol{s} \leqslant$ 1.4 nm^{-1} where s is the modulus of the scattering vector. The observed feature is typical of a partially crystalline polymer comprising an ordered, crystalline phase randomly distributed in an amorphous matrix.[12] The single Bragg peak at $\boldsymbol{s}$ = 0.44 nm^{-1} indicates the presence of a crystalline phase with a d-spacing of 22.6 Å. The large bump of the intensity curve originates from the scattering contribution of both amorphous and crystalline phases. Wide-angle X-ray scattering (WAXS) data show essentially a considerable amorphous background with a few superimposed diffraction peaks in the range $2° \leqslant 2\Theta \leqslant 25°$ and hence support the macromolecular character of **3**.

In conclusion we have presented the synthesis of the first TTF main-chain polymer composed entirely of linearly fused TTF units starting from a tetrathiapentalene precursor. The synthetic approach is unique in its simplicity and contrasts the multistep procedures described in previous work.[1] Attempts to extend the scope of the synthetic approach and to tailor important polymer properties, such as solubility and conductivity by varying the substituents of the monomeric precursors are currently being investigated and will be presented in due course.

Notes and references

† The redox-potential of the ferrocene/ferrocenium couple under the conditions used is to +0.46 V *vs.* SCE.

‡ Compound **3**, black solid (from CH_3CN), mp (decomp.) > 200 °C. Anal: found C, 43.47, H, 2.30. $C_{18}H_{10}S_4PF_6$ requires C, 43.28, H, 2.02%.

1 (*a*) Y. Ueno, Y. Masuyama and M. Okawara, *Chem. Lett.*, 1975, 603; (*b*) C. U. Pittman, M. Narita and Y. F. Liang, *Macromolecules*, 1976, **9**, 360; (*c*) C. U. Pittman, Y. F. Liang and M. Ueda, *Macromolecules*, 1979, **12**, 541; (*d*) F. B. Kaufman, A. H. Schroeder, E. M. Engler, S. R. Kramer and J. Q. Chambers, *J. Am. Chem. Soc.*, 1979, **102**, 483; (*e*) G. Kossmehl and M. Rohde, *Macromolecules*, 1982, **9**, 541; (*f*) V. Q. Trinh, L. van Hinh, G. Schukat and E. Fanghänel, *J. Prakt. Chem.*, 1989, **331**, 826; (*g*) S. Frenzel, S. Arndt, R. M. Gregorius and K. Müllen, *J. Mater. Chem.*, 1995, **5**, 1529; (*h*) T. Yamamoto and T. Shimizu, *J. Mater. Chem.*, 1997, **7**, 1967.

2 J. R. Ferraro and J. M. Williams, *Introduction to Synthetic Organic Conductors*, Academic Press, 1987.

3 M. Adam and K. Müllen, *Adv. Mater.*, 1994, **6**, 439.

4 Y. Misaki, T. Ohta, N. Higuchi, H. Fujiwara, T. Yamabe, T. Mori, H. Mori and S. Tanaka, *J. Mater. Chem.*, 1995, **5**, 1571.

5 H. Müller, F. Salhi and B. Divisia-Blohorn, *Tetrahedron Lett.*, 1997, **38**, 3215.

6 Z. Yoshida, T. Kawase, H. Awaji, I. Sugimoto, T. Sugimoto, and S. Yoneda, *Tetrahedron Lett.*, 1983, **24**, 3469; Y. Yamashita, M. Tomura, M. B. Zaman and K. Imeda, *Chem. Commun.*, 1998, 1657.

7 P. Hapiot, D. Lorcy, A. Tallec and R. Carlier, *J. Phys. Chem.*, 1996, **100**, 14 823.

8 P. Hapiot, F. Salhi, B. Divisia-Blohorn and H. Müller, *J. Phys. Chem.*, submitted for publication; F. Salhi, PhD. Thesis, Université Joseph Fourier, Grenoble, 1999.

9 E. Laviron, *J. Electroanal. Chem.*, 1972, **39**, 1; H. Fujihara, H. Nakai, M. Yoshihara and T. Maeshima, *Chem. Commun.*, 1999, 737.

10 L. V. Hinh, G. Schukat and E. Fanghänel, *J. Prakt. Chem.*, 1979, **321**, 299.

11 R. Bozio, I. Zanon, A. Girlando and C. Pecile, *J. Chem. Phys.*, 1979, **71**, 2282.

12 L. A. Feigin and D. I. Svergun, *Structure Analysis by Small-Angle X-Ray and Neutron Scattering*, Plenum Press, 1987.

Communication 9/04761A

ChemComm

Novel synthesis of a vanadium–titanium aluminophosphate molecular sieve of MFI structure (VTAPO-5) and catalytic activity for the partial oxidation of methanol

M. P. Kapoor*[a] and Anuj Raj[b]

[a] *Osaka National Research Institute, 1-8-31 Midorigaoka, Ikeda, Osaka-563, Japan. E-mail: kapoor@onri.go.jp*
[b] *National Institute of Materials and Chemical Research, 1-1 Higashi, Tsukuba, Ibaraki-305, Japan*

Received (in Cambridge, UK) 14th May 1999, Accepted 15th June 1999

A new vanadium–titanium substituted aluminophosphate molecular sieve of MFI structure (VTAPO-5) was synthesized hydrothermally and found to be active and selective in partial oxidation of methanol; catalytic activity depends on the vanadium sites; however, the presence of titanium influences the reactivity of vanadium species during reaction.

Aluminophosphate (AlPO) molecular sieves classified as a new class of microporous crystalline inorganic solids are contemporary to the zeolites. A variety of AlPOs have been reported with a rich diversity of structures.[1,2] They are framework oxides with Al and P in tetrahedral coordination with oxygen. In spite of different structural properties from zeolites, AlPOs also apparently obey Loewenstein's rule with an avoidance of Al–O–Al bonds and thus include framework topologies analogous to zeolites. Although titanium and vanadium substitution is well documented in various topologies,[3–7] very little information on isomorphously substituted Ti and V AlPOs have been reported. Excluding the original patent on synthesis of some titanium containing AlPOs, only the synthesis and characterization of TAPSO-5,[8] and more recently TAPO-5, −11, −31 and –36 have been published.[9–11] Many important issues encountered in the synthesis and application of substituted AlPOs are still unaddressed. Very few reports are available in the literature regarding the catalytic behavior of substituted AlPOs such as TAPOs and VAPOs.

Ulagappan and Krishnasamy[8] found that TAPO-5 and -11 were active in phenol hydroxylation. Also some activity was reported for VAPO-5 and Ti-VPI-5 in the catalytic oxidation of cyclohexane to cyclohexanol using *tert*-butyl hydroperoxide (TBHP). Recently, it has shown that TAPOs of structure types AFI, AEL, ATO and ATS (TAPO-5, -11, -31 and -36 respectively) have comparable activities to titanium silicates (TS-1) in a series of oxidation reactions using dilute H_2O_2 (30 wt%) as the oxidant.[10,11] Vanadium–titanium catalysts, (either supported or impregnated) are widely used in industry for the partial oxidation of hydrocarbons and for the selective catalytic reduction of NO with NH_3. In the literature there are some interesting reports[12] concerning the structural characteristics of coprecipitated VTiO systems and their activity in *n*-butene oxidation for the selective production of acetaldehyde and acetic acid. In a very recent report[13] the nature of vanadium sites in a V/α-Ti phosphate catalyst for the oxidative dehydrogenation of ethane were investigated. Here, we report for the first time, the novel synthesis of vanadium–titanium aluminophosphate-5 (VTAPO-5), which is found to be an active and selective catalyst for the partial oxidation of methanol.

VTAPO-5 was synthesized using a gel composition 0.30 NPr_3 : 0.70 TPAOH : 0.02 TiO_2 : 0.047 V_2O5 : P_2O_5 : 42 H_2O. In a typical synthesis, the calculated amounts of phosphoric acid (85 wt%) and pseudoboehmite, as P and Al sources respectively, were mixed and dissolved in distilled water. Then vanadium and titanium as hydrated oxovanadium(IV) sulfate and titanium isopropoxide, respectively, were introduced dropwise to the homogenous gel under vigorous stirring. A mixture of tripropylamine (NPr_3) and TPAOH (an organic template as structure directing agent), was used to direct the MFI structure type in the VTAPO-5 molecular sieve and was slowly introduced into the gel. Finally the entire gel was further stirred for at least 1 h and transferred into a Teflon-coated stainless-steel autoclave for hydrothermal crystallization. Based on a series of systematic syntheses, pure and highly crystalline VTAPO-5 was synthesized aging the gel directly at 458 K for 200 h. After heating, the autoclave was cooled and solid product was separated by centrifugation and repeatedly washed with distilled water followed by drying at 358 K for 6 h followed by calcination in air at 813 K for 8 h. It was interesting that the systems involving only NPr_3 or TPAOH gave no VTAPO molecular sieve while pure VTAPO was obtained from the gel with a mixture of NPr_3 and TPAOH. Substituted TAPO-5 and VAPO-5 were also synthesized by essentially following a reported procedure,[10,14] using the gel composition TPAOH : 0.04 TiO_2 : P_2O_5 : 40 H_2O : NPr_3 : 0.047 V_2O_5 : P_2O_5 : 40 H_2O respectively.

The samples were characterized by X-ray diffraction (XRD), diffuse reflectance UV-VIS spectroscopy (DRS), Raman spectroscopy and ^{27}Al and ^{31}P MAS NMR. Pore volumes were measured by *n*-butane adsorption and N_2 adsorption methods (BET). Bulk chemical analysis was carried out using inductively coupled plasma atomic emission spectroscopy (ICP). Chemical and physical properties of all samples are given in Table 1.

The XRD patterns of TAPO-5 and VAPO-5 were similar to those reported earlier and confirm the purity of the crystallized product with the XRD pattern of VTAPO-5 being closer to that of pure TAPO-5. Intercalation of vanadium moieties in the framework can be discounted since no change in the basal spacing is observed. Pore plugging as well as evidence for an extraneous phase were checked by *n*-butane and nitrogen adsorption. The measured BET surface area for VTAPO-5 was 304 $m^2\ g^{-1}$ and the void volume was 0.121 ml g^{-1}. The amount

Table 1 Physico-chemical properties of substituted AlPOs.

	Chemical analysis				N_2 adsorption		*n*-Butane adsorption
Material	Ti	V	Al	P	S_{BET}/$m^2\ g^{-1}$	V_p/ml g^{-1}	V_p/ml g^{-1}
VTAPO-5	0.015	0.022	0.484	0.491	304	0.121	0.114
TAPO-5	0.028	—	0.489	0.481	311	0.117	0.110
VAPO-5	—	0.024	0.492	0.483	298	0.123	0.118

Table 2 Partial oxidation of methanol over substituted AlPOs

Material	Methanol Conversion (%)	Product selectivity (mol%)						
		HCHO	CO	$(CH_3)_2O$	CO_2	CH_3CHO	MF	FA
TAPO-5	0.01[a]	nd	nd	nd	nd	nd	nd	nd
VAPO-5	5.73[a]	79.2	12.6	5.8	3.4	nd	nd	nd
	7.28[b]	74.8	14.4	7.2	3.6	nd	nd	nd
	10.16[c]	69.2	16.3	9.4	5.1	nd	nd	nd
VTAPO-5	5.91[a]	31.4	20.7	6.0	3.1	8.1	29.5	1.2
	7.87[b]	22.9	22.2	7.3	3.3	9.3	33.4	1.6
	11.09[c]	13.8	24.4	9.6	4.5	10.7	35.3	1.7

Reaction conditions: Feed = 20% methanol in Ar; 10% O_2 in Ar, reaction temp. = 200 °C; F/W (contact time) = [a] 21400 (0.29 s), [b] 15600 (0.40 s), [c] 9800 (0.64 s); catalyst = 0.2 g; MF = methyl formate; FA = formic acid; nd = not detected.

of *n*-butane adsorbed at STP was 0.114 ml g^{-1}. The DRS UV–VIS spectrum of VTAPO-5 shows a single peak with λ_{max} 232–238 nm and no evident shoulder around 300 nm. This suggested that VTAPO-5 is free from anatase or extraframework species such as titanium or vanadium oxide, in line with the BET and *n*-butane adsorption results. Moreover, in all samples studied, no oxide species were detected by Raman spectroscopy. ^{31}P and ^{27}Al MAS NMR spectra of calcined TAPO-5, VAPO-5 and VTAPO-5 indicate that in all samples the aluminium was present in a tetrahedral environment and octahedral Al was absent as found in pseudoboehmite.[15] The ^{27}Al MAS NMR spectra of TAPO-5 and VAPO-5 show a main peak at δ 32.4 while VTAPO-5 showed a slight shift to δ 34.1. Similar results were obtained from ^{31}P MAS NMR spectra; a single ^{31}P band assigned to framework tetrahedral phosphorus was observed at δ −29.8 for VAPO-5 and TAPO-5 samples whereas VTAPO-5 showed a shift to δ −27.2. The overall characterization results indicates that the novel VTAPO and its analogs TAPO-5 and VAPO-5 are pure and well crystallized.

Previous work indicates that the incorporated metal environment is essentially the same for all substituted AlPO analogs and is quite different from that in metal silicates. However, VTAPO-5 is found to be an active catalyst for the partial oxidation of methanol. The catalytic measurements were carried out in a conventional continuous flow differential reactor system. The typical reaction products were methyl formate, formaldehyde, acetaldehyde dimethyl ether, formic acid, CO and CO_2. Measurement of formic acid was performed by acid–base volumetric analysis while other products were analyzed by gas chromatography. The methanol oxidation reaction results (at steady state) and reaction conditions are summarized in Table 2. The catalytic tests were conducted at 200 °C and measured at different contact times (space velocities) of the feed under differential conditions. TAPO-5 was found to be totally inactive for methanol oxidation at the reaction condition studied except for very low activity observed at higher temperature (> 280 °C). VAPO-5 showed a significant activity. The major products obtained were formaldehyde and CO along with small amount of CO_2 and dimethyl ether. On VTAPO a considerable quantity of methyl formate and acetaldehyde were obtained as major products in addition to CO, formaldehyde, CO_2 and dimethyl ether. For methanol oxidation the product formation is proposed to be accompanied by several known complex equlibrium reactions (1)–(7) (Scheme 1).

With regard to the influence of contact time of the feed on the activity and selectivity, the system clearly showed that increased contact time improves methanol conversion and selectivities to methyl formate, acetaldehyde and CO with a decrease in the selectivity to formaldehyde. Thus, it can be proposed that formaldehyde is the initial product of methanol partial oxidation and is an intermediate species in the production of methyl formate, acetaldehyde and CO while the formation of dimethyl ether and CO_2 are independent of the production of the major products. According to these results, the methanol chemisorbs on vanadium species as a surface methoxy (CH_3O), and depending on the nature of Ti sites present on the surfaces of the catalyst, can react *via* various pathways to form

$$2CH_3OH \rightleftharpoons (CH_3)_2O + H_2O \quad (1)$$

$$CH_3OH + \{O_2\} \rightleftharpoons HCHO + 2H^+ + 2e^- \quad (2)$$

$$CH_3OH + \{O_2\} \rightleftharpoons CO + 4H^+ + 4e^- \quad (3)$$

$$HCHO \rightleftharpoons CO + 2H^+ + 2e^- \quad (4)$$

$$CH_3OH + H_2O \rightleftharpoons CO_2 + 6H^+ + 6e^- \quad (5)$$

$$CH_3OH + H_2O \rightleftharpoons HCO_2H + 4H^+ + 4e^- \quad (6)$$

$$HCHO + CH_3OH \rightleftharpoons [CH_3OCH_2OH] \rightleftharpoons HCO_2CH_3 \quad (7)$$

Scheme 1

acetaldehyde, methyl formate, formaldehyde, dimethyl ether and carbon oxides. While titanium itself is not an active site for the partial oxidation of methanol, VTAPO-5 selectively generates methyl formate and acetaldehyde which are more complex than products generated from pure VAPO-5. Thus titanium plays an important role in catalysis possibly due to strong V–Ti interactions. Verification of the precise reaction mechanism is linked to the measurement of the quantity and nature of the active sites. The fact that titanium modifies the active reaction sites would explain why VAPO-5 does not produce acetaldehyde or methyl formate. Further investigation of the catalytic behavior of VTAPO-5 and analogous VAPO-5 catalysts in various hydrocarbon conversion reactions such as oxidative dehydrogenation and epoxidation are in progress.

Notes and references

1 W. M. Meier, D. H. Olson and Ch. Baerlocher, *Atlas of Zeolite structure Types*, Elsevier, Amsterdam–New York, 1996.
2 S. T. Wilson, B. M. Lok, C. A. Messina, T. R. Cannan and E. M. Flanigen, *J. Am. Chem. Soc*, 1982, **104**, 1146.
3 N. Taramasoo, G. Perego and B. Notari, *US Pat.* 4410501, 1983.
4 J. S. Reddy, R. Kumar and P. Ratnasamy, *Appl. Catal.*, 1990, **58**, L1.
5 M. A. Camblor, A. Corma, A. Martinez and J. Perez-Pariente, *J. Chem. Soc., Chem. Commun.*, 1992, 589.
6 J. Kornatovski, M. Sychev, S. Kuzenkov, K. Strnadova, W. Pilz, D. Kassner, G. Pierper and W. H. Baur, *J. Chem. Soc., Faraday Trans.*, 1995, **91**, 2217.
7 H. E. B. Lampers and R. A. Sheldon, *Stud. Surf. Sci. Catal.* 1997, **105**, 1061.
8 N. Ulagappan and V. Krishnasamy, *J. Chem. Soc., Chem. Commun.*, 1995, 589.
9 M. H. Z. Niaki, P. N. Joshi and S. Kaliaguine, *Chem. Commun.*, 1996, 47.
10 M. H. Z. Niaki, M. P. Kapoor and S. Kaliaguine, *J. Catal.*, 1998, 177, 231.
11 M. H. Z. Niaki, M. P. Kapoor and S. Kaliaguine, *Proc. 12th IZC*, Baltimore, USA, 1998, p. 1221.
12 W. E. Slinkard and P. B. DeGroot, *J. Catal*, 1981, **68**, 423.
13 J. S. Gonzalez, M. Martinez-Lara, M. A. Bañares, M. V. M. Huerta, E. R. Castellón, J. L. G. Fierro and A. J. Lopez, *J. Catal*, 1999, **181**, 280.
14 M. J. Haannepen and J. H. C. van Hooff, *Appl. Catal.*, 1997, **152**, 183; 203.
15 C. S. Blackwell and R. I. Patten, *J. Phys. Chem.*, 1988, **92**, 3965.

Communication 9/03876K

ChemComm

Transformations of *fac*-Re(dmbpy)(CO)$_3$(CO$_2$H) in the presence of carbon dioxide (dmbpy = 4,4′-dimethyl-2,2′-bipyridine)

Dorothy H. Gibson* and Xiaolong Yin

Department of Chemistry and Center for Chemical Catalysis, University of Louisville, Louisville, KY 40292, USA. E-mail: dhgibs01@athena.louisville.edu

Received (in Bloomington, IN, USA) 26th March 1999, Accepted 10th June 1999

Reactions of *fac*-Re(dmbpy)(CO)$_3$(CO$_2$H) 1 or *fac, fac*-Re(dmbpy)(CO)$_3$(CO$_2$)Re(dmbpy)(CO)$_3$ 2 with CO$_2$, in DMSO or DMF containing small amounts of water, lead to the bicarbonato complex, *fac*-Re(dmbpy)(CO)$_3$[OC(O)OH] 4; the formato complex, *fac*-Re(dmbpy)(CO)$_3$(OCHO) 5, is not a major product in any of these reactions.

The proposed intermediacy of metallocarboxylic acids in reductions of CO_2 catalyzed by ruthenium and rhenium polypyridyl complexes[1] has prompted our interest in the synthesis and chemistry of compounds of this type. Previously, the production of formate in the catalytic reactions has been attributed to CO_2 insertion into metal hydrides generated from decarboxylations of metallocarboxylic acids.[1] We recently described the first synthesis of a rhenium acid of this type, *fac*-Re(dmbpy)(CO)$_3$(CO$_2$H) **1**[2] which had been proposed to be an intermediate in electrocatalytic reductions of CO_2 by *fac*-Re(dmbpy)(CO)$_3$Cl.[1] Thermolysis of **1** in dimethyl formamide (DMF) gave the new CO_2-bridged compound, *fac, fac*-Re(dmbpy)(CO)$_3$(CO$_2$)Re(dmbpy)(CO)$_3$ **2**; the reactions could be photoassisted. We suggested that **2** was formed *via* β-hydride elimination from **1**, followed by CO_2 loss, to give *fac*-Re(dmbpy)(CO)$_3$H **3** as an intermediate.[2] Subsequent reaction of **3** with additional **1** was proposed to yield **2** (and hydrogen) as shown in Scheme 1. Since formate was absent from the thermolysis products of **1**, additional reactions of **1** and **2**, with and without CO_2, have been explored because of their relevance to proposed steps in the catalytic processes.[1]

Although the ^{1}H NMR spectrum of **1** can be obtained in DMF-d$_7$ at 0 °C, **1** is labile in this solvent at room temperature and readily converts to **2**.[2] We attempted to follow this transformation by ^{1}H NMR in order to probe for the intermediacy of hydride **3**. A solution of **1** in DMF-d$_7$ was prepared and the spectrum quickly recorded. The spectrum showed none of **3**, but did not correspond exactly to that of **2**[2] either; resonances appeared at the same chemical shift positions as those observed for **2**, but some were broadened (suggesting dynamic behavior) while others were sharp. After 1 h, all resonances had sharpened to those of **2** together with a small amount of a second compound, identified as the bicarbonato complex *fac*-Re(dmbpy)(CO)$_3$[OC(O)OH] **4**.† Importantly, the major features of the spectrum obtained from a sample of **1** after a few minutes in DMF-d$_7$ were reproduced by mixing equimolar quantities of hydride **3** and **1** in this solvent and quickly obtaining the spectrum. The hydride resonance at δ 1.8 had already disappeared by the time the spectrum could be observed, although the spectrum of **3**, alone, can easily be obtained under these conditions. Eventually, the mixture of **3** and **1** afforded **2**, a small amount of formate, *fac*-Re(dmbpy)(CO)$_3$(OCHO) **5**,[2,3] and a small amount of **4**.

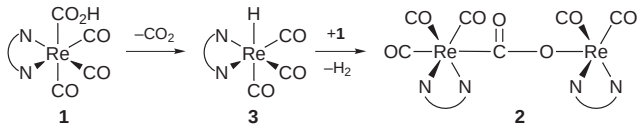

Scheme 1 N–N = 4,4′-dimethyl-2,2′-bipyridine

Compound **1** is more stable in DMSO-d$_6$ and its ^{1}H NMR spectrum can be obtained easily at room temperature. After about 40 min, however, all low field resonances of **1** (dmbpy ring and carboxyl H atoms) became broadened and new resonances that are analogous to those of **2** in this solvent appeared; no resonances for hydride **3** were observed. Compound **2** shows doublets at δ 8.44, 8.34, 7.31 and 7.15 and singlets at δ8.28 and 8.10 in DMSO-d$_6$; the new species showed resonances at all of these positions, but those at δ8.28 and 7.31 were broadened while the others were sharp. After about 2.5 h, all resonances of **1** had disappeared, but the two broadened resonances of the new species were still broadened. Such spectra have been reproduced several times with different samples of **1**; any disturbance (shaking, purging with N$_2$, *etc*.) of samples which have been allowed to stand for 2 h results in immediate transformation of this species to products, primarily **2**. In a separate experiment, a 73% yield of **2** together with 10% of **4** was obtained from a solution of **1** after 2 h standing in DMSO-d$_6$ under laboratory fluorescent lights followed by purging the solution with N$_2$; formate **5** was absent. However, a sample of **1**, dissolved in DMSO-d$_6$ and allowed to stand under laboratory fluorescent lights after purging with CO_2, generated bicarbonato complex **4** in 97% yield after 3 h.

The thermolysis, at ambient temperature, of an equimolar mixture of acid **1** and hydride **3** was followed by ^{1}H NMR spectroscopy in DMSO-d$_6$ in the same manner as for **1** alone. The spectrum was recorded 10 min after dissolving both compounds in the solvent; all resonances of the two substrates were broadened. After 40 min, the carboxyl proton of **1** and the hydride resonance of **3** had disappeared and broadened resonances characteristic of the species formed from **1** alone had appeared. Conversion to **2** occurred slowly, as before; again, formate **5** was not observed.

Other changes in thermolysis samples of **1** in DMSO-d$_6$ accompany changes in the ^{1}H NMR spectra; the initially yellow solutions darken and gas evolution becomes evident after 1.5 h (CO_2 is soluble at these concentrations). As the spectra change to more closely resemble **2**, the solutions become dark orange; with prolonged standing, the solutions become pale yellow and a precipitate of the sparingly soluble bicarbonato complex **4** appears. Thus, it is clear that CO_2 was liberated and available for the eventual production of **4.** Formate **5** was not observed as a product in the reactions conducted in DMSO, although it can be readily formed from hydride **3** and CO_2 in this solvent.[3]

Reactions of **2** were then conducted in DMF-d$_7$ or DMSO-d$_6$ together with 'bone-dry' CO_2[4] in order to provide further clarification. A solution of **2** in DMF-d$_7$ was purged with the CO_2 for a few minutes; during this time, the initially red solution became yellow and a yellow precipitate formed. Further analysis of the solution, and the precipitate, showed that **2** had converted completely to bicarbonate **4**. A similar experiment conducted with **2** in DMSO-d$_6$ showed approximately equal quantities of acid **1** together with **4** after 10 min; formate **5** was formed in only trace quantities in the experiment. Independently, we showed that the hydroxo complex, *fac*-Re(dmbpy)(CO)$_3$(OH)·H$_2$O **6**,[2] was rapidly converted to **4** in quantitative yield upon exposure to CO_2. These results suggest

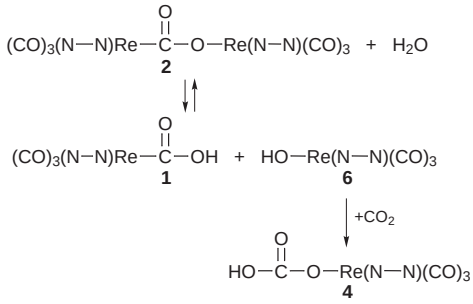

Scheme 2 N–N = 4,4′-dimethyl-2,2′-bipyridine

that the CO_2-bridged compound **2** exists in these solutions in equilibrium with a small amount of its hydrolysis products, acid **1** and hydroxo complex **6** (generated by adventitious water), and that subsequent conversion of **6** to **4** occurs quickly, and irreversibly, in the presence of CO_2. In DMF-d_7, the conversion of **2** proceeds to **4** rapidly; in DMSO-d_6, a mixture containing **4** and **1** can be observed because **1** is more stable in this solvent. These reactions are shown in Scheme 2. Although not typical of CO_2-bridged complexes of this type,[5] similar hydrolysis of one has been suggested previously;[6] the reverse reaction is facile and well known.[5]

In recent years, both intra- and inter-moleclar interactions between basic transition metal hydrides and H-donor reagents containing N–H or O–H groups have been well documented.[7] These have been described in terms of initial hydrogen bonding between the two species followed by formation of a dihydrogen ligand. A linear H···HO hydrogen bond has been suggested previously;[7d] thus, we suggest the pathway outlined in Scheme 3 for the transformation of **1** to **2**. The precise nature of the intermediate species leading to **2** is not known at present. However, the suggested partial conversion of **1** to **3**, followed by the reaction of **3** with additional **1** and loss of H_2 leading to **2**, is directly analogous to the reactions of other rhenium hydrides with weakly acidic, and protic, substrates. The poor solubility of **1** ensures that free H_2 cannot be spectroscopically observed in our reactions, although gas evolution is evident after the intermediate species develops. Also, the limited solubilities of **1** and **2** prevent low temperature NMR experiments or probes of H-bonding *via* IR spectra of the solutions for further information about the nature of the intermediate species; the existence of the intermediate is clear, however.

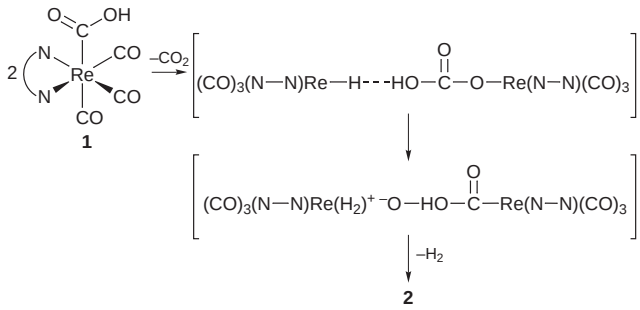

Scheme 3 N–N = 4,4′-dimethyl-2,2′-bipyridine

Previous spectral studies of the interactions of hydrides with hydroxylic species have been done in non-polar solvents to avoid competition for the hydroxyl hydrogen.[7] However, the very polar solvents (DMF and DMSO) used with **1** (or **1** and **3**) do not appear to disrupt the association of **1** with **3**. We conclude that it is this strong association with **1** that prevents hydride **3** from being accessible for reaction with CO_2 to form formate **5**.

The behavior of **1** in the presence of CO_2, in solvents and under the not rigorously dry conditions that are typically used in electrocatalytic reactions involving CO_2,[1] casts doubt on the intermediacy of **1** as a precursor to formate in the reactions. We have suggested[2,8] that metal formyl complexes, through the hydrides formed by their degradation, are more likely precursors to formates generated in the reactions. Rapidly in DMF solution, and more slowly in DMSO, acid **1** is transformed to products not identified in the catalytic reactions. Catalytic reactions conducted in acidic media, however, could yield CO as the result of carboxyl cleavage of either **1** or **2**.[1] Efforts are in progress to define the chemical behavior of these reactive compounds further.

This work has been supported by the United States Department of Energy (Division of Chemical Sciences, Office of Science).

Notes and references

† An authentic sample of **4** was obtained as follows: a flask containing a red solution of *fac*-Re(dmbpy)$(CO)_3OH{\bullet}H_2O$ **6**[2] (0.031 g, 6.6×10^{-2} mmol) in 10 mL of acetone was flushed with dry CO_2. The solution immediately changed to yellow and a yellow solid precipitated. The solid was collected by filtration and washed with acetone (2×5 mL). After drying under high vacuum, 0.025 g (75% yield) of **4** was obtained, mp 199–201 °C. Anal. Calc. for $C_{16}H_{13}N_2O_6Re{\bullet}H_2O$: C, 36.02; H, 2.83. Found: C, 36.13; H, 2.65%. IR ν_{CO} (KCl, DRIFTS): 2026s, 1906s, 1872s; ν_{OCOO} 1630m, 1422m, 1350m cm^{-1}. ^1H NMR (DMF-d_7): δ 9.21 (1H, br), 8.97 (2H, d, *J* 6 Hz), 8.68 (2H, s), 7.65 (2H, d, *J* 6 Hz) and 2.59 (6H, s). ^{13}C NMR (DMSO-d_6): δ 198.33, 194.62, 158.64, 154.96, 152.67, 152.49, 128.10, 124.72 and 20.96.

1 J. Hawecker, J. M. Lehn, and R. Ziessel, *J. Chem. Soc., Chem. Commun.*, 1983, 536; *Helv. Chim. Acta*, 1986, **69,** 1990; R. Ziessel, in *Catalysis by Metal Complexes: Photosensitization and Photocatalysis Using Inorganic and Organometallic Compounds*; ed. K. Kalyanasundaram and M. Grätzel, Kluwer Academic, Dordrecht, The Netherlands, 1993, p.217; P. Christensen, A. Hamnett, A. V. G. Mair and J. A. Timney, *J. Chem. Soc., Dalton Trans.*, 1992, 1455; F. P. A. Johnson, M. W. George, F. Hartl and J. J. Turner, *Organometallics*, 1996, **15**, 3374; N. Sutin, C. Creutz and E. Fujita, *Comments Inorg. Chem.*, 1997, **19**, 67.

2 D. H. Gibson and X. Yin, *J. Am. Chem. Soc.*, 1998, 1**20**, 11 200.

3 B. P. Sullivan and T. J. Meyer, *Organometallics*, 1986, **5**, 1500.

4 Matheson Gas Products, Inc., Morrisville, PA, USA.

5 D. H. Gibson, *Chem. Rev.*, 1996, **96**, 2063; S. M. Tetrick, C. Xu, J. R. Pinkes and A. R. Cutler, *Organometallics*, 1998, **17**, 1861.

6 M. A. Bennett, G. B. Robertson, A. Rokicki and W. A. Wickramasinghe, *J. Am. Chem. Soc.*, 1988, **110**, 7098.

7 See, for example: J. C. Lee, Jr., E. Peris, A. L. Rheingold and R. H. Crabtree, *J. Am. Chem. Soc.*, 1994, **116**, 11 014; W. Yao and R. H. Crabtree, *Inorg. Chem.*, 1996, **35**, 3007; A. J. Lough, S. Park, R. Ramachandran and R. H. Morris, *J. Am. Chem. Soc.*, 1994, **116,** 8356; S. Park, A. J. Lough and R. H. Morris, *Inorg. Chem.*, 1996, **35**, 3001; E. S. Shubina, N. V. Belkova, A. N. Krylov, E. V. Vorontsov, L. M. Epstein, D. G. Gusev, M. Niedermann and H. Berke, *J. Am. Chem. Soc.*, 1996, **118**, 1105; J. A. Ayllón, C. Gervaux, S. Sabo-Etienneand and B. Chaudret, *Organometallics*, 1997, **16**, 2000; N. V. Belkova, E. S. Shubina, A. V. Ionidis, L. M. Epstein, H. Jacobsen, A. Messmer and H. Berke, *Inorg. Chem.*, 1997, **36**, 1522; E. S. Shubina, N. V. Belkova, E. V. Bakhmutova, E. V. Vorontsov, V. I. Bakhmutov, A. V. Ionidis, C. Bianchini, L. Marvelli, M. Peruzzini and L. Epstein, *Inorg. Chim. Acta*, 1998, **280**, 302.

8 D. H. Gibson, B. A. Sleadd, M. S. Mashuta and J. F. Richardson, *Organometallics*, 1997, **16**, 4421.

Communication 9/02453K

ChemComm

Synthesis of highly ordered MCM-41 by micelle-packing control with mixed surfactants

Ryong Ryoo,* Chang Hyun Ko and In-Soo Park

Materials Chemistry Laboratory, Department of Chemistry and Centre for Molecular Science, KAIST, Taejon, 305-701, Korea. E-mail: rryoo@sorak.kaist.ac.kr

Received (in Cambridge, UK) 1st June 1999, Accepted 22nd June 1999

The mesoporous silica molecular sieve MCM-41 can be obtained in a highly ordered form with various pore diameters if micelle packing is suitably controlled with a mixture of *n*-alkyltrimethylammonium bromide and *n*-alkyltriethylammonium bromide according to the length of the C_{12}–C_{22} alkyl groups.

The periodic assemblage between surfactant micelles and inorganic layers is a versatile route to the synthesis of molecular sieves with uniform pore diameters in the mesopore range.[1–6] Previous work on the synthesis of such mesoporous silica molecular sieves referred to as MCM-41 and SBA-15 has revealed that the mesopore diameters can be controlled by using surfactants with different tail lengths and expanding the micelles with suitable organic additives.[2,6–8] Here, we point out that the structural order of the resultant mesoporous materials decreases with changing pore diameter, due to mismatches in the surfactant's head-to-tail packing ratio. We demonstrate that the structural order can be improved remarkably if mixed surfactants of *n*-alkyltriethylammonium bromides [$C_nH_{2n+1}NEt_3Br$ (n = 12, 14, 16, 20 and 22), ATEABr for brevity] and *n*-alkyltrimethylammonium bromides ($C_nH_{2n+1}NMe_3Br$, ATMABr) are used for the synthesis of MCM-41. The optimum mixing ratio can be tuned according to the length of the alkyl groups.

The ATEABr and ATMABr surfactants used for the synthesis of MCM-41 were received from Aldrich or synthesised in our laboratory. The synthesis of ATEABr was carried out by the reaction of 1-bromoalkane with triethylamine in acetonitrile solution under reflux.[9] ATMABr surfactants were synthesised similarly using 1-bromoalkane and trimethylamine, but the reaction was performed in a pressure vessel in order to prevent loss of trimethylamine. Synthesised surfactants were purified twice *via* dissolution in chloroform and subsequent recrystallisation by the addition of ethyl acetate.

The synthesis of the MCM-41 silica was performed in a manner similar to that reported in our previous work,[10,11] except for the use of ATEABr–ATMABr mixtures. An aqueous solution of sodium silicate with Na/Si = 0.5 (2.4 mass% Na_2O, 9.2 mass% SiO_2, 88.4 mass% H_2O) was used as the silica source. The silica source was added dropwise to an aqueous solution of an ATEABr–ATMABr mixture at a given temperature while the solution was stirred vigorously. After continuously stirring for 1 h, the resultant gel mixture was heated for 24 h at 373 K. The mixture after heating was cooled to the same temperature as before the initial mixing, and the pH of the mixture was adjusted to 10 with acetic acid. The mixture after the pH adjustment was heated again for 48 h at 373 K. pH adjustment and subsequent heating was repeated once more before the precipitated MCM-41 product was finally filtered off. The product was washed with EtOH–HCl–H_2O (84.1 : 1.0 : 14.9 mol/mol) and calcined in air at 823 K. The structural order of the product was estimated by its XRD pattern obtained on a Rigaku Miniflex (0.5 kW) instrument using Cu-Kα radiation with 0.01° 2θ step size and 1 s step time.

Fig. 1 shows highly resolved XRD patterns for the C_nMCM-41 samples obtained after optimisation of the starting compositions and mixing temperatures as listed in Table 1. C_n indicates

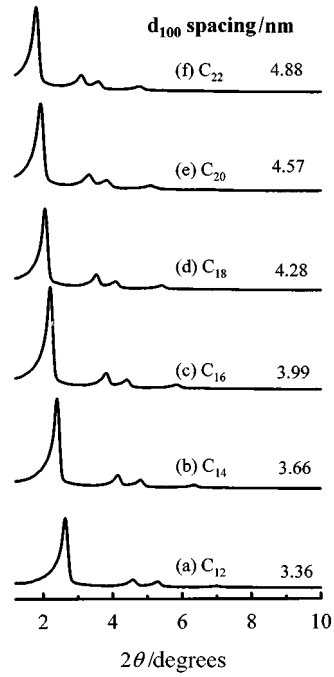

Fig. 1 XRD patterns for high-quality C_nMCM-41 samples obtained by the optimum synthesis conditions given in Table 1: (a) C_{12}, (b) C_{14}, (c) C_{16}, (d) C_{18}, (e) C_{20} and (f) C_{22}MCM-41. Samples were calcined in air at 823 K.

the number of carbon atoms in the alkyl chain of the surfactants. These results show that the optimum ATEABr/ATMABr ratio increased with increasing alkyl chain length in the surfactant. For the synthesis of C_{12} and C_{14}MCM-41, the addition of ATEABr was not beneficial and led to XRD line broadening and loss of intensity. The synthesis of C_{16}–C_{20}MCM-41 by the addition of ATEABr showed a significant improvement of the structural order up to an optimum ATEABr/ATMABr ratio, after which the structural order was progressively lost. The optimum ratio for ATEABr/ATMABr increased from C_{16} to C_{22}MCM-41 so that ATEABr was used as the single surfactant for C_{22}MCM-41. As reported in Table 1, the surfactant concentration and the mixing temperature were also optimised

Table. 1 Optimum conditions for synthesis of MCM-41

	ATMABr	ATEABr	H_2O	
Sample[a]	*x*	*y*	*z*	Mixing temp/K
C_{12}MCM-41	1.0	0.0	400	293
C_{14}MCM-41	1.0	0.0	400	293
C_{16}MCM-41	0.80	0.20	400	303
C_{18}MCM-41	0.66	0.34	400	328
C_{20}MCM-41	0.10	0.90	500	333
C_{22}MCM-41	0.0	1.0	500	338

[a] C_nMCM-41 denotes MCM-41 samples synthesised using a mixture of $C_nH_{2n+1}NMe_3Br$ and $C_nH_{2n+1}NEt_3Br$. The composition of the starting mixture was 4 SiO_2 : x C_nATMABr : y C_nATEABr : 1 Na_2O : z H_2O.

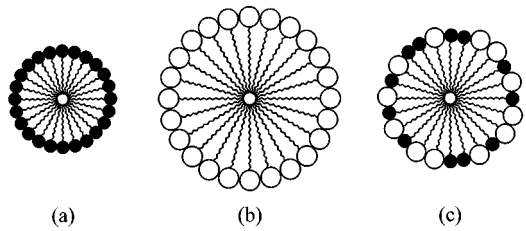

Fig. 2 Schematic models for the cross section of surfactant micelles. (a) The small NMe_3 head group is suitable for short alkyl tails, for the formation of the hexagonal C_{12}MCM-41 mesophase. (b) The large NEt_3 head group for C_{22}MCM-41. (c) The micelle packing in an intermediate case can be controlled with mixed surfactants.

according to the decrease in the solubility of the surfactants as the alkyl group size increases.

An explanation for the change in the optimal ATEABr/ATMABr ratio is depicted in Fig. 2. As Fig. 2(a) shows, small head groups are necessary to form a cylindrical micelle with short alkyl tails in the case of the C_{12} and C_{14}MCM-41 synthesis. If the tail length increases with the same head group, the resultant micelle structures are likely to be those with smaller surface curvatures such as for the cubic *Ia3d* and eventually the lamellar phase. Hence lamellar mesophases are most easily obtained when C_{22}ATMABr is used as a single surfactant for the synthesis of silica–surfactant mesostructures. The head group size should be increased by the substitution with C_{22}ATEABr in order to synthesise the hexagonal mesostructure [Fig. 2(b)]. The highly ordered XRD patterns for C_{16}–C_{20} MCM-41 in Fig. 1 indicate that the use of the ATMABr–ATEABr mixtures is an effective way for controlling the surface curvature of micelles for the hexagonal mesophase [Fig. 2(c)] and probably for the synthesis of other mesophases.

Highly ordered C_{22}MCM-41 can also be obtained using ATMABr as the single surfactant and sodium silicate as the silica source if the pH of the starting mixture is carefully adjusted to 8 before heating, as reported by Namba *et al.*[12] A lamellar or disordered mesophase is obtained if the pH is not adjusted at all, or adjusted after heating. The effect of the pH adjustment is evidence for the mesophase-formation mechanism that takes place co-operatively by the silica source and surfactants.[13] In this mechanism, the silicate anion participates as a part of the head-group moiety of the micelle. The size of the silicate species increases with decreasing pH, and consequently at low pH, the combination of the large silicate species with the small head of the ATMABr surfactant leads to the formation of a large head group that is suitable for the hexagonal mesophase. Thus, the optimum ATEABr/ATMABr ratio for MCM-41 synthesis depends not only on the length of the surfactant tails but also on the pH of the reaction mixture (Fig. 3). The reversibility of the formation of the silica–surfactant mesostructure is an another important factor that affects MCM-41 synthesis. The formation of the hexagonal mesophase at pH 8 is not easily reversed and consequently the synthesis becomes very sensitive to the timing and temperature for the pH adjustment during the silicate polymerisation. On the other hand, the synthesis using C_{22}ATEABr can be performed more easily at sufficiently high pH where the formation of the hexagonal mesostructure is reversible.

The surface curvature of micelles can also be controlled using other mixed surfactant systems such as cationic–neutral[14] and cationic–anionic.[15] For example, it has been reported that the use of ATMABr and poly(oxyethylene) alkyl ethers produced the cubic mesoporous silica molecular sieve MCM-48 in high yield [4.2 SiO_2/surfactant (mol/mol)] by hydrothermal synthesis at atmospheric pressure.[14] Mixed surfactants may be considered for finding mesoporous silica molecular sieves with

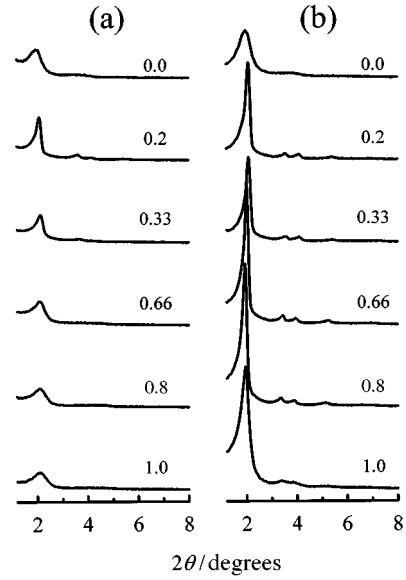

Fig. 3 XRD patterns for MCM-41 synthesised with 4 SiO_2:x C_{18}ATMABr:(1−x) C_{18}ATEABr:1 Na_2O:400 H_2O (mol/mol). Numbers denote the mole number x for C_{18}ATMABr. (a) Product, filtered and dried, after the starting mixture was heated for 24 h at 373 K. (b) Product, filtered and dried, after the pH of the heated mixture in (a) was adjusted to 10 and heated again for 48 h at 373 K.

new structures, as well as improving synthesis procedures for known materials. In addition, the same idea may be used to adjust the surfactant's head group size proportionally to the increase in the diameter of the micelle, when organic additives are used to increase the pore diameter.

This work was supported by the Korea Science and Engineering Foundation.

Notes and references

1 C. T. Kresge, M. E. Leonowicz, W. J. Roth, J. C. Vartuli and J. S. Beck, *Nature*, 1992, **359**, 710.
2 J. S. Beck, J. C. Vartuli, W. J. Roth, M. E. Leonowicz, C. T. Kresge, K. D. Schmitt, C. T-W. Chu, D. H. Olson, E. W. Sheppard, S. B. McCullen, J. B. Higgins and J. L. Schlenker, *J. Am. Chem. Soc.*, 1992, **114**, 10 834.
3 Q. Huo, D. I. Margolese, U. Ciesla, P. Feng, T. E. Gier, P. Sieger, R. Leon, P. M. Petroff, F. Schuth and G. D. Stucky, *Nature*, 1994, **368**, 317.
4 S. A. Bagshaw, E. Prouzet and T. J. Pinnavaia, *Science*, 1995, **269**, 1242.
5 R. Ryoo, J. M. Kim, C. H. Ko and C. H. Shin, *J. Phys. Chem.*, 1996, **100**, 17 718.
6 D. Zhao, J. Feng, Q. Huo, N. Melosh, G. H. Fredrickson, B. F. Chmelka and G. D. Stucky, *Science*, 1998, **279**, 548.
7 J. S. Beck, J. C. Vartuli, W. G. J. Kennedy, C. T. Kresge, W. J. Roth and S. E. Schramm, *Chem. Mater.*, 1994, **6**, 1816.
8 A. Corma, Q. Kan, M. T. Navarro, J. Perez-Pariente and F. Rey, *Chem. Mater.*, 1997, **9**, 2123.
9 M. J. Kim and R. Ryoo, *Chem. Mater.*, 1999, **11**, 487.
10 R. Ryoo and J. M. Kim, *J. Chem. Soc., Chem. Commun.*, 1995, 711.
11 J. M. Kim, J. H. Kwak, S. Jun and R. Ryoo, *J. Phys. Chem.*, 1995, **99**, 16 742.
12 S. Namba, A. Mochizuki and M. Kito, *Stud. Surf. Sci. Catal.*, 1998, **117**, 257.
13 A. Monnier, F. Schuth, Q. Huo, D. Kumar, D. Margolese, R. S. Maxwell, G. D. Stucky, M. Krishnamurty, P. Petroff, A. Firouzi, M. Janicke and B. F. Chmelka, *Science*, 1993, **261**, 1299.
14 R. Ryoo, S. H. Joo and J. M. Kim, *J. Phys. Chem*, in press.
15 F. Chen, L. Huang and Q. Li, *Chem. Mater.*, 1997, **9**, 2685.

Communication 9/04355A

An unusual reaction of ethyl 4-bromomethylbenzoate with the carbanion of substituted ethyl acetate

Ramesh C. Anand* and Archana Milhotra

Department of Chemistry, Indian Institute of Technology, Hauz Khas, New Delhi-110016, India.
E-mail: rcanand@chemistry.iitd.ernet.in

Received (in Cambridge, UK) 18th May 1999, Accepted 11th June 1999

Reaction of ethyl 4-bromomethylbenzoate with the carbanion of substituted ethyl acetate affords nucleophilic aromatic substitution of the bromomethyl group instead of the expected alkylation of the benzylic bromide.

In connection with a project on the synthesis of a natural product, we needed 2-(4-carboxyphenyl)propanoic acid **1** as

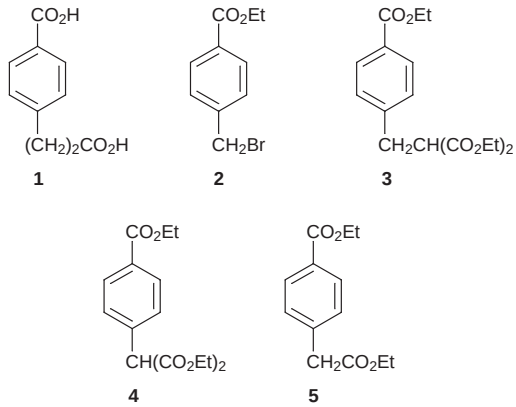

one of the intermediates. A straightforward procedure was employed to prepare this compound by alkylation of ethyl 4-bromomethylbenzoate **2** with the carbanion of diethyl malonate (generated by NaH in C_6H_6) followed by decarboxylation[1] of the resulting alkylated diethyl malonate **3** in aqueous DMSO containing NaCl. The crude product on purification by column chromatography afforded a white crystalline compound as the only product. The ^{1}H NMR and ^{13}C NMR spectra† did not support the expected structure of the diethyl ester of **1**, suggesting the structure to be **5**. In order to further corroborate the structure **5** of the product, it was synthesized by the literature[2] method and was found to be identical with the isolated product **5** of the present reaction (IR, ^{1}H NMR, ^{13}C NMR, mp and TLC). It is likely that an S_NAr mechanism[3] in this case is being preferred over the usual S_N reaction in spite of using a benzylic bromide. Such an S_NAr reaction with *ipso* attack on an aromatic ring having only one ethoxycarbonyl group resulting in the elimination of the bromomethyl group is quite unprecedented under the reaction conditions. Probably the nucleophile is attacking the aromatic carbon carrying the bromomethyl substituent to provide an intermediate **6** (Scheme 1), which in turn may eliminate either $CH_2(CO_2Et)_2$ to give starting compound **2**, or MeBr which may escape as a gas shifting the equilibrium to furnish the product **4**.

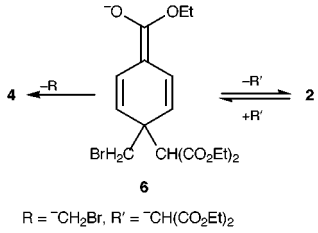

Scheme 1

Table 1 Results of reactions with various substituted acetates

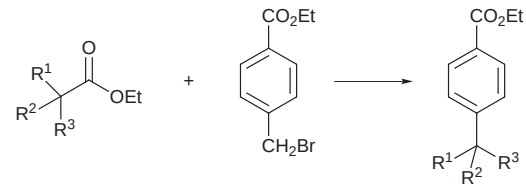

Reactant			Product				
R^1	R^2	R^3	No.	R^1	R^2	R^3	Yield[a] (%)
CO_2Et	H	H	**5**[b]	CO_2Et	H	H	63
H	CN	H	**7**[b]	H	CN	H	68
CO_2Et	Me	H	**8**	CO_2Et	Me	CO_2Et	75
Me	CN	H	**9**	Me	CN	CO_2Et	73

[a] The yield of the product is an average of the yields obtained in repeated experiments. The other product obtained from the chromatographic column was the unreacted starting compounds. [b] Isolated product after decarboxylation with NaCl in aq. DMSO (ref. 1).

This type of reaction has also been exhibited by the substituted ethyl acetate carbanions shown in Table 1 (studied so far). A detailed investigation of this reaction is in progress.

Financial assistance from C.S.I.R., New Delhi, in the form of Project No. 01 (1551)/98/EMR-II to R. C. A. and an R.A. to A. M. is gratefully acknowledged.

Notes and references

† *Selected data* for **5**: δ_H 1.17 (3H, t, *J* 7.2), 1.38 (3H, t, *J* 7.2), 3.27 (2H, s), 4.12 (2H, q, *J* 7.2), 4.37 (2H, q, *J* 7.2), 7.22 (2H, d, *J* 8.4), 7.92 (2H, d, *J* 8.4); δ_C 13.88, 14.34, 38.22, 60.59, 60.93, 127.43, 128.93, 129.50, 141.51, 166.42, 170.46. For **7**: δ_H 1.40 (3H, t, *J* 7.2), 3.12 (2H, s), 4.38 (2H, q, *J* 7.2), 7.31 (2H, d, *J* 8.1), 8.03 (2H, d, *J* 8.1); δ_C 14.22, 35.06, 37.76, 60.91, 120.41, 128.96, 129.71, 129.99, 141.41, 166.11. For **8**: δ_H 1.25 (6H, t, *J* 7.2), 1.36 (6H, m), 4.19 (4H, q, *J* 7.2), 4.36 (2H, q, *J* 7.2), 7.21 (2H, d, *J* 8.1), 7.94 (2H, d, *J* 8.1); δ_C 13.90, 14.21, 19.69, 54.63, 60.74, 61.32, 129.29, 129.88, 130.14, 141.55, 166.32, 171.51. For **9**: δ_H 1.28 (3H, t, *J* 7.2) 1.41 (6H, m), 4.21 (2H, q, *J* 7.2), 4.38 (2H, q, *J* 7.2), 7.24 (2H, d, *J* 8.1), 7.96 (2H, d, *J* 8.1); δ_C 14.11, 14.26, 19.71, 54.73, 60.74, 61.31, 129.62, 129.91, 130.21, 131.33, 141.62, 166.38, 171.54.

1 A. P. Krapcho, J. F. Weimaster, J. M. Eldridge, E. G. E. Jahngen, A. J. Lovey and W. P. Stephens, *J. Org. Chem.*, 1978, **43**, 138.
2 J. F. Codington and E. J. Mosettig, *J. Org. Chem.*, 1952, **17**, 1035.
3 J. March, *Advanced Organic Chemistry*, 4th edn., Wiley, New York, 1992, p. 641.

Communication 9/03959G

Thiacrown ether tetrathiafulvalene derivatives as redox responsive ligands

Franck Le Derf,[a] Miloud Mazari,[a] Nicolas Mercier,[a] Eric Levillain,[a] Pascal Richomme,[b] Jan Becher,[c] Javier Garín,[d] Jesus Orduna,[d] Alain Gorgues[a] and Marc Sallé*[a]

[a] *Laboratoire d'Ingénierie Moléculaire et Matériaux Organiques, UMR CNRS 6501, Université d'Angers, 2 Bd Lavoisier, F-49045 Angers, France. E-mail: salle@univ-angers.fr*
[b] *SC RMN, Université d'Angers, 2 Bd Lavoisier, F-49045 Angers, France*
[c] *Department of Chemistry, Odense University, Campusvej 55, DK-5230 Odense M, Denmark*
[d] *Instituto de Ciencia de Materiales de Aragon, Unidad de Nuevos Materiales Orgánicos, Facultad de Ciencias, CSIC-Universidad de Zaragoza E-50009 Zaragoza, Spain*

Received (in Liverpool, UK) 29th March 1999, Accepted 17th June 1999

Thiacrown ether TTF derivatives have been synthesized; one of them, whose X-ray molecular structure has been determined, is shown to combine Ag^+ recognition and reversible binding properties as a function of the electrochemical potential applied.

The design of redox-responsive ligands able to recognise cationic guests constitutes an area of active research.[1] In this context, a substantial amount of work has been devoted to the covalent association of a polyether subunit to the tetrathiafulvalene (TTF) moiety.[2,3]

Surprisingly, very few examples of *soft* ligands designed to bind transition metal cations, such as azacrown [4] or thiacrown [5] TTF analogues, have been described. Furthermore, all polythioether-TTFs described so far are poorly soluble, which has precluded any proper characterisation of their metal binding ability.[5]

We now report the synthesis of new sulfur ligands involving various polythioether chains connected to the 2,7-positions of the TTF core, as well as the selective Ag^+ complexing properties of one of them. Receptors **1**–**3**† were prepared (60%, 49% and 52% respectively) under high dilution conditions in DMF, from the [1 + 1] cyclocondensation of compound **4** [4] with suitable ω-dithiole polythioethers,[6] in the presence of caesium carbonate (Scheme 1). Compounds **1**–**3** whose structures were established by 2D NMR (DQF COSY, ROESY, HMQC, HMBC), were obtained as (*Z*/*E*) isomeric mixtures in relative amounts of 60:40 (**1**), 65:35 (**2**), 60:40 (**3**) as determined by ^{1}H-NMR.

X-Ray structural determination of (*Z*)-**1** shows that the increased chain length relative to the previously described thiacrown TTF derivative[5b] considerably decreases the degree of bending of the TTF skeleton (Θ = 16.4°) (Fig. 1). This constitutes a structural prerequisite in order to reach reversible redox processes.

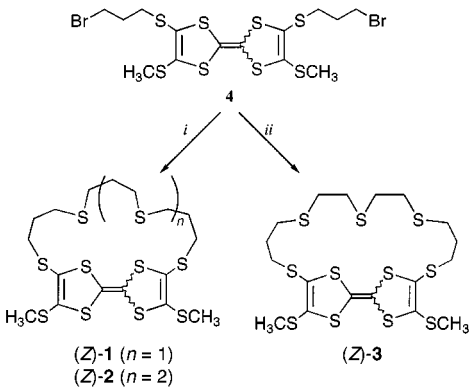

Scheme 1 *Reagents and conditions*: (i) propane-1,3-dithiol (synthesis of **1**), 4-thiaheptane-1,7-dithiol (synthesis of **2**), Cs_2CO_3, DMF; (ii) 3-thiapentane-1,5-dithiol, Cs_2CO_3, DMF.

Binding properties of compounds **1**–**3** were evaluated using different techniques (LSIMS, ^{1}H-NMR and cyclic voltammetry (CV)). LSIMS experiments show that the progressive addition of a silver triflate solution leads to the appearance of a peak corresponding to the formation of the 1:1 complex [**L**-Ag]$^+$. Notably, addition of an excess of Ag^+ results in formation of the additional [**L**-2Ag]$^+$ and [**L**-3Ag]$^+$ complexes in the case of ligands **1** and **2**.

For ligands **1** and **2**, this result may be attributed to the competing Ag^+ binding process between the thiacrown part and both terminal SC=CSCH$_3$ fragments, as observed for the parent tetramethylsulfanyl-TTF.[7]

This observation was confirmed by ^{1}H-NMR titration studies ($CDCl_3$–CD_3CN [1:1]), the signal corresponding to the methylsulfanyl fragments of **1** and **2** being the only one significantly affected by addition of $AgCF_3SO_3$.[8] For macrocycle **3**, the signals which are shifted to lower fields upon titration correspond to the polythioether methylene protons of the (*Z*) isomer only, confirming that in this case complexation preferentially involves the thiacrown cavity. This good Ag^+ binding ability of the polythioether chain in **3** may be attributed to a better orientation of the coordinating S atoms, contrary to compounds **1** and **2** for which insertion of propylene fragments cannot ensure a correct structural environment, as shown by X-ray data (Fig. 1).‡

Interestingly, the Ag^+ titration curves obtained from ^{1}H-NMR shifts for the crown ether methylene protons of **3** exhibit a plateau for 0.6 equiv. of added cation (Fig. 2). This result is in good agreement with the 60/40 ratio of (*Z*)-**3**/(*E*)-**3** isomers, confirming that Ag^+ binding occurs through the (Z)-isomer only. Analysis of these data with the program EQNMR [9] shows that the crown thioether recognition site of (*Z*)-**3** forms a 1:1 complex with Ag^+, with an average stability constant $K°$ = $10^{3.26}$ ($CDCl_3$–CD_3CN [1:1]).

As expected from the quasi-planar character of the TTF skeleton discussed above in the case of **1**, compounds **1**–**3** exhibit two reversible one-electron redox processes, with

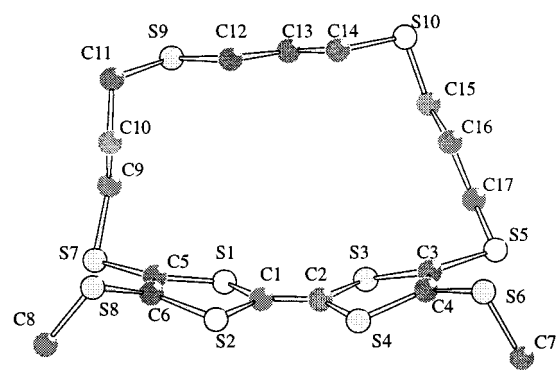

Fig. 1 X-Ray molecular structure of (*Z*)-**1**.

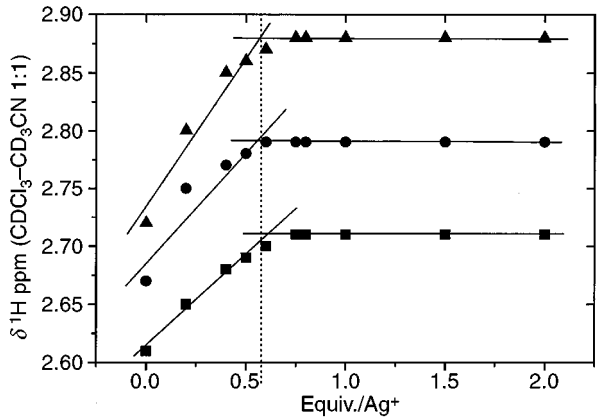

Fig. 2 Proton NMR titration curve of the perturbation of the CH_2S protons of the polythiaether bridge in **3,** upon addition of silver cation.

oxidation potentials similar to those observed for the parent tetramethylsulfanyl-TTF (*e.g.* compound **1**: E_1^{ox} = 0.59 V and E_2^{ox} = 0.89 V *vs*. Ag/AgCl). Whereas no change is observed in CV of compounds **1** and **2** upon addition of Ag^+ and in agreement with the solution NMR study, the progressive addition of controlled amounts of silver triflate to **3** results in a positive shift of E_1^{ox}. This phenomenon is attributed to the electrostatic inductive effect of the crown ether bound metal

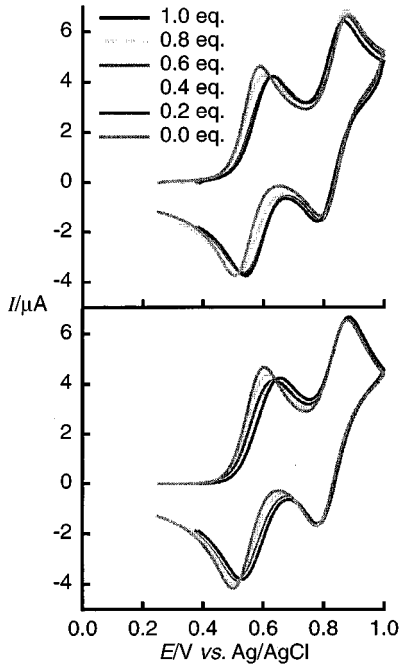

Fig. 3 Experimental (top) and simulated (bottom) cyclic voltammograms of **3** in the presence of increasing amounts of Ag^+. The simulated data were fitted to experimental results for **3** (10^{-3} mol L^{-1} in CH_2Cl_2–CH_3CN [1:1], Bu_4NPF_6 (0.1 mol L^{-1})) at 293 K and 100 mV s^{-1}. All simulations were carried out with the same set of parameters, only the Ag^+ equivalent concentration being changed according to the experimental voltammograms. Charge transfer parameters: $k_s = 3.5 \times 10^{-3}$ cm s^{-1}, $\alpha = 0.5$. Chemical reaction parameters: $K° = 3.35 \times 10^3$ L mol^{-1}, $k_f° = 1.3 \times 10^6$ L mol^{-1} s^{-1} and $K^{\cdot+} = 90$ L mol^{-1}, $k_f^{\cdot+} = 3 \times 10^7$ L mol^{-1} s^{-1}. Diffusion coefficient: $D = 3.6 \times 10^{-6}$ cm^2 s^{-1}.

cation which causes an increase of E_1^{ox} (Fig. 3). The fact that the E_2^{ox} remains unchanged is attributable to the expulsion of the metal ion from the cavity, due to the doubly charged TTF moiety. Values of the binding constant of the Ag^+ complex as a function the redox state of the TTF core in ligand **3** were evaluated using the DIGISIM 2.1® simulation program (BAS Inc.). A strong Ag^+ affinity is found for the neutral ligand (TTF: $K° = 10^{3.53}$) in good agreement with the value determined by ^{1}H-NMR. Oxidation of TTF into $TTF^{\cdot+}$ leads to a decrease of the complexation ability ($K^{\cdot+} = 10^{1.95}$) and to the expulsion of the metal for the dicationic TTF^{2+} state, as shown by the constant E_2^{ox} value ($K^{2+} \approx 0$).

It is noteworthy that no shift of E_1^{ox} has been observed upon addition of a wide variety of groups 1 or 2 or transition metal ions (Na^I, K^I, Cs^I, Mg^{II}, Ba^{II}, Cr^{III}, Ni^{II}, Zn^{II}, Cd^{II}),[10] which illustrates the good selectivity of ligand **3** for Ag^+.

In conclusion, the efficiency in modulation of the trapping properties of ligand **3** has been demonstrated thanks to an unprecedented metal cation binding ability among crown thioether TTF derivatives (neutral TTF state) associated the controllable releasing of the metal cation upon electrochemical oxidation to the dicationic TTF state.

Financial support DGES (PB 97-1186 and Action Intégrée HF 1997-0042) is gratefully acknowledged.

Notes and references

† All new compounds gave analytical and spectroscopic data consistent with their structures.

‡ *Crystal data* for (*Z*)-**1**: orange crystals, $C_{17}H_{24}S_{10}$, M = 547.91, triclinic, $P\bar{1}$, Z = 2, a = 9.482(3), b = 11.870(7), c = 12.393(5) Å, α = 80.90(4), β = 69.89(3), γ = 70.75(4)°, V = 1235(1) Å^3, Z = 2, D_c = 1.48 g cm^{-3}, T = 293 K, μ(MoKα) = 0.862 mm^{-1}, 7523 reflections measured, 3706 independent reflections (R = 0.016) with $I/\sigma(I) > 3$ available for calculations. The structure was solved by direct methods (SIR program of MoLEN), R = 0.054, R_W = 0.069 (use of F magnitude, 340 parameters, static disorder appears for several atoms (2 S and 2 C): each of them was located on two positions with half occupancy rate). CCDC 182/1319. See http://www.rsc.org/suppdata/cc/1999/1417/ for crystallographic data in .cif format.

1 For a recent review, see : P. L. Boulas, M. Gómez-Kaifer and L. Echegoyen *Angew. Chem. Int. Ed.*, 1998, **37,** 216.
2 (*a*) For a recent review, see : M. Brøndsted and J. Becher, *Liebigs Ann.*, 1997, 2177; (*b*) R. Dieing, V. Morisson, A. J. Moore, L. Goldenberg, M. R. Bryce, J. M. Raoul, M. C. Petty, J. Garin, M. Saviron, I. K. Lednev, R. E. Hester and J. N. Moore, *J. Chem. Soc., Perkin Trans. 2*, 1996, 1587.
3 F. Le Derf, M. Mazari, M. Sallé, N. Mercier, E. Levillain, P. Richomme, J. Becher, J. Garin, J. Orduna and A. Gorgues, submitted.
4 F. Le Derf, M. Sallé, N. Mercier, J. Becher; P. Richomme, A. Gorgues, J. Orduna and J. Garin, *Eur. J. Org. Chem.*, 1998, 1861.
5 (*a*) M. Wagner, S. Zeltner and R. M. Olk, *Liebigs Ann.*, 1996, 551; (*b*) T. Jorgensen, B. Girmay, T. K. Hansen, J. Becher, A. E. Underhill, M. B. Hursthouse, M. E. Harman and J. D. Kilburn, *J. Chem. Soc., Perkin Trans. 1*, 1992, 2907; (*c*) S. Zeltner, R. M. Olk, M. Wagner and B. Olk, *Synthesis*, 1994, 1445.
6 H. T. Stock and R. M. Kellog, *J. Org. Chem.*, 1996, **61**, 3093.
7 M. Munakata, L. P. Wu, X. Gan, T. K. Sowa and Y. Suenaga, *Mol. Cryst. Liq. Cryst.*, 1996, **284**, 319.
8 $AgCF_3SO_3$ 99+%, purchased from Aldrich.
9 M. J. Hynes, *J. Chem. Soc., Dalton Trans.*, 1993, 311.
10 Addition of $Cu(CF_3SO_3)_2$ or $Hg(CF_3CO_2)_2$ to **3** in CH_2Cl_2–CH_3CN led to oxidation of the ligand.

Communication 9/02497B

ChemComm

Total synthesis of (+)-rottnestol†

Ivona R. Czuba and Mark A. Rizzacasa*

School of Chemistry, The University of Melbourne, Parkville, Victoria 3052, Australia.
E-mail: m.rizzacasa@chemistry.unimelb.edu.au

Received (in Cambridge, UK) 2nd June 1999, Accepted 18th June 1999

The first total synthesis of the marine metabolite (+)-rottnestol is described.

Marine sponges provide a large range of novel and bioactive metabolites that generally fall into defined chemotaxonomic groups. Recently, some tetrahydropyran containing secondary metabolites have been isolated from sponges that are chemically quite different to compounds that were previously isolated from the same sources. Chemical investigation of the sponge genus *Haliclona* sp., collected around Rottnest Island off the coast of Western Australia, yielded the hemiketal rottnestol (**1**).[1] The structure of **1** was determined using NMR techniques and by comparison to the related compounds, the raspailols A (**2**) and

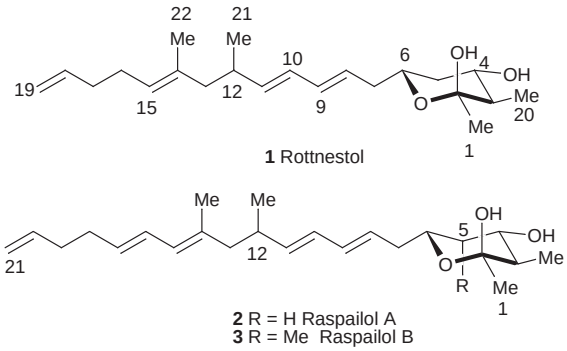

B (**3**), which were isolated from the sponge *Raspailia* sp. and possess antibiotic activity.[2] However, only small amounts of **1**–**3** were isolated which precluded oxidative degradation to determine the absolute configuration at C12.[1,2] We now report the first total synthesis of each of the possible C12 epimers of **1** which allowed for the assignment of the absolute configuration of this compound.

In designing a synthetic approach to both C12 epimers of **1**, we noted that a pivotal retrosynthetic bond cleavage would be between C9–C10. To generate this linkage, we elected to utilise a Stille cross-coupling protocol because of its remarkable success in constructing diene systems.[3,4] Therefore, coupling between an optically pure C10–C19 fragment **4** and a suitable vinylstannane such as **5** could provide each of the C12 epimers of **1** in a highly convergent manner.

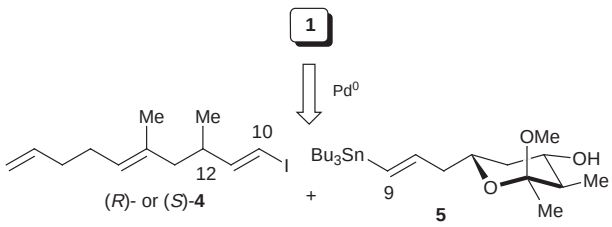

Our approach to the C12 isomers of **1** began with the synthesis of pyran fragment **5** as outlined in Scheme 1. Brown crotylmetallation[5] of the (*S*)-malic acid derived aldehyde **6**[6] followed by silylation provided alkene **7** in good yield. Wacker oxidation[7] using catalytic palladium chloride gave the ketone **8** which upon treatment with camphorsulfonic acid in MeOH afforded the pyran **9** as one anomer. Conversion of the alcohol **9** into an unstable triflate followed by lithium acetylide displacement and silyl group removal provided acetylene **10**. Radical hydrostannylation[8] of **10** in boiling benzene then afforded stannane **5** ready for Stille coupling.

The synthesis of both enantiomers of the sidechain vinyl iodide **4** is outlined in Scheme 2. Addition of but-3-enylmagnesium bromide to methacrolein gave the known allylic alcohol[9]

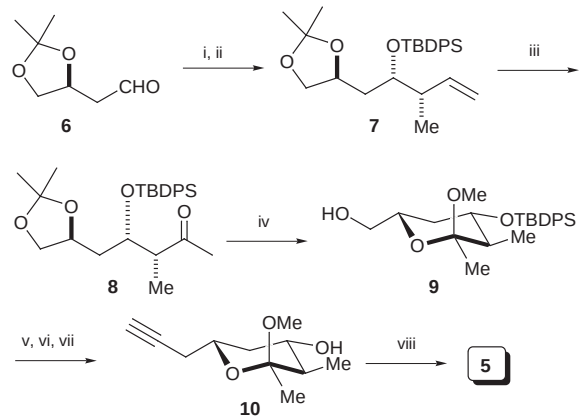

Scheme 1 *Reagents and conditions*: (i) (+)-Ipc_2B-(*Z*)-crotyl then NaOH, H_2O_2 (76%) (ii) TBDPSCl, imidazole, DMF (85%); (iii) 20 mol% $PdCl_2$, 1.1 equiv. CuCl, O_2, aq. DMF, 50 °C (85%); (iv) 20 mol% CSA, MeOH, RT, 3 h (72%); (v) Tf_2O, 2,6-lutidine, CH_2Cl_2, −78 °C; (vi) LiC≡CTMS, THF–HMPA, −78 to 0 °C; (vii) TBAF·$3H_2O$, THF, RT (71% for 3 steps); (viii) 1.1 equiv. Bu_3SnH, 10 mol% AlBN, benzene, reflux, 2 h (54%). Ipc = Isopinocampheyl.

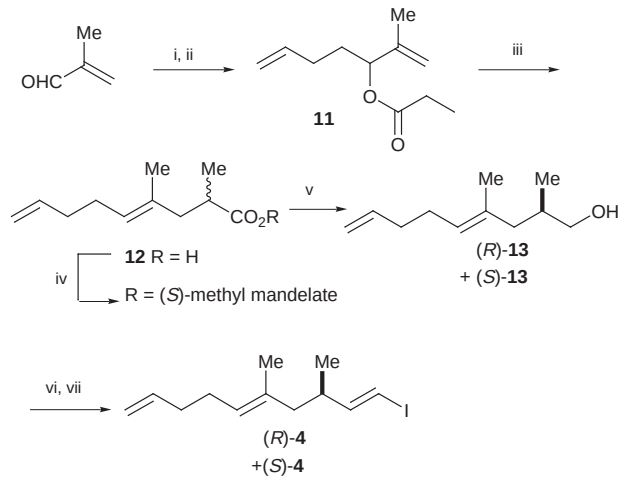

Scheme 2 *Reagents and conditions*: (i) CH_2=$CHCH_2CH_2MgBr$, Et_2O (65%); (ii) propionyl chloride, pyridine, CH_2Cl_2 (91%); (iii), LDA, THF–HMPA, TBSCl, −78 °C to rt, then aq. HCl (84%); (iv) (*S*)-methyl mandelate, DCC, 10 mol% DMAP, normal phase HPLC separation (86%); (v) $LiAlH_4$, Et_2O (86%); (vi) Dess–Martin reagent, CH_2Cl_2 (100%) (vii) 7.5 equiv. $CrCl_2$, 1.9 equiv. CHI_3, 6:1 dioxane–THF, rt (71%).

† Dedicated to Professor Robert E. Ireland on the occasion of his 70th birthday.

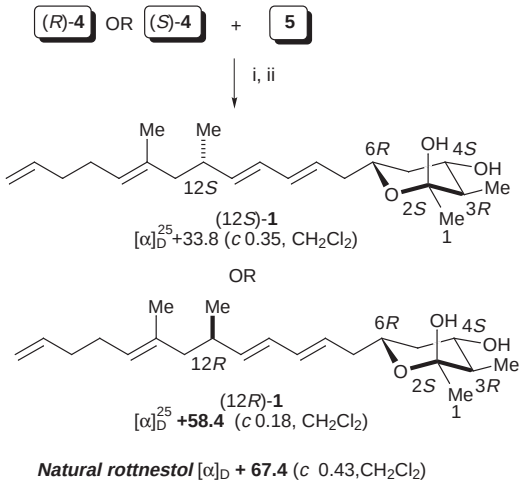

Natural rottnestol $[\alpha]_D$ **+ 67.4** (*c* 0.43,CH_2Cl_2)

Scheme 3 *Reagents and conditions*: (i) 10 mol% $Pd(MeCN)_2Cl_2$, i-Pr_2NEt, DMF, rt (54–62%); (ii) 5% aq. HCl, THF, 0 °C (55–66%).

which was propionylated to provide ester **11**. Ireland–Claisen rearrangement[10,11] of **11** gave the racemic acid **12** in high yield upon acidic work-up. Resolution of the α-methyl chiral acid **12** was achieved by conversion to the corresponding (*S*)-mandelate esters followed by HPLC separation of the diastereoisomeric (*R*,*S*)- and (*S*,*S*)-mandelates.[11] Reduction of each mandelate ester then gave the optically pure alcohols (*R*)-**13** {$[\alpha]_D^{25}$ +6.5 (*c* 1.0, $CHCl_3$)} and (*S*)-**13** {$[\alpha]_D^{25}$ −6.6 (*c* 1.0, $CHCl_3$)} and the absolute configurations of each were determined by the ^{1}H NMR analysis of the derived (*S*)-MTPA esters.[12,13]‡ Dess–Martin oxidation[14] of (*R*)- and (*S*)-**13** followed by vinyliodination[15] then provided iodides (*R*)- and (*S*)-**4**.

Palladium-mediated coupling of (*R*)- or (*S*)-**4** with stannane **5** proceeded smoothly§ and subsequent acid hydrolysis afforded (12*R*)- and (12*S*)-**1** respectively (Scheme 3). Not surprisingly, (12*R*)- and (12*S*)-**1** could not be differentiated by either ^{1}H or ^{13}C NMR spectroscopy and both were identical to rottnestol in all respects apart from the optical rotation of (12*S*)-**1**.¶ As shown in Scheme 3, (12*R*)-**1** possesses a rotation with the same sign and similar value to that of natural rottnestol[1] while (12S)-**1** had a much lower value. We therefore propose the absolute configuration of rottnestol (**1**) to be 2*S*,3*R*,4*S*,6*R*,12*R*. Application of this approach to the synthesis of the raspailols is now underway.

We thank Dr M. Boyd and Dr J. Beutler of the NCI Maryland, USA for the generous gift of natural rottnestol (**1**) for TLC comparison and copies of the ^{1}H and ^{13}C NMR spectra. This work was financially supported by the Australian Research Council.

Notes and references

‡ For the (*R*,*S*)-MTPA ester (derived from (*R*)-**13** and (*S*)-MTPA) the C1 methylene protons appear as a doublet at δ 4.14 (J = 5.2 Hz) while for the (*S*,*S*)-MTPA ester the same protons appear as well separated doublets of doublets at δ 4.03 (J = 10.8, 6.4 Hz) and 4.24 (J = 10.8, 4.8 Hz): see refs. 12 and 13.

§ Interestingly, the C4-TBDPS ether of **5** and (±)-**4** failed to undergo cross coupling under a variety of conditions.

¶ *Selected data* for (12*R*)- and (12*S*)-**1**: δ_H(400 MHz, C_6D_6) 0.97 (d, *J* 6.8, 3H, CH_3), 1.13 (d, *J* 6.4, 3H, CH_3), 1.14 (q, *J* 12.4, 1H, $H5_{ax}$), 1.18 (s, 3H, CH_3), 1.25 (m, 1H, H3), 1.50 (s, 3H, CH_3), 1.71 (ddd, *J* 12.4, 4.8, 2.4, 1H, $H5_{eq}$), 1.92 (dd, *J* 13.2, 7.6, 1H, $H13_a$), 2.05 (m, 5H, $H13_b$, H16, H17), 2.18 (ddd, *J* 14.0, 7.2, 6.8, 1H, $H7_a$), 2.34 (ddd, 14.0, 7.2, 6.8, 1H, $H7_b$), 3.58 (dt, *J* 10.4, 4.4, 1H, H4), 3.84 (m, 1H, H6), 5.00 (d, *J* 10.4, 1H, H19), 5.05 (dd, *J* 17.2, 1.6, 1H, H19), 5.17 (br t, *J* 6.4, 1H, H15), 5.54 (dd, *J* 14.4, 7.6, 1H, H11), 5.70 (dt, 14. 7.2, 1H, H8), 5.79 (m, 1H, H18), 6.10 (m, 1H, H10), 6.13 (m, 1H, H9); δ_C (100 MHz, C_6D_6) 12.3 (C20), 16.1 (C22), 20.1 (C21), 27.8 (C16), 28.2 (C1), 34.4 (C17), 34.9 (C12), 39.7 (C7), 41.3 (C5), 47.2 (C3), 47.9 (C13), 68.3 (C6), 69.7 (C4), 98.9 (C2), 114.8 (C19), 126.2 (C15), 128.4 (C8), 128.8 (C10), 133.2 (C9), 133.8 (C14), 138.75 (C11), 138.81 (C18).

1 K. L. Erickson, J. A. Beutler, J. H. Cardellina II and M. R. Boyd, *Tetrahedron*, 1995, **51**, 11953.
2 C. M. Cerda-García-Rojas and D. J. Faulkner, *Tetrahedron*, 1995, **51**, 1087.
3 J. K. Stille, *Angew. Chem., Int. Ed. Engl.*, 1986, **25**, 508.
4 V. Farina, V. Krishnamurthy and W. J. Scott, in *Organic Reactions*, ed. L. A. Paquette, Wiley, New York, 1997, pp. 1–652.
5 H. C. Brown and K. S. Bhat, *J. Am. Chem. Soc.*, 1986, **108**, 293.
6 J. W. Burton, J. S. Clark, S. Derrer, T. C. Stork, J. G. Bendall and A. B. Holmes, *J. Am. Chem. Soc.*, 1997, **119**, 7483.
7 J. Tsuji, *Synthesis*, 1984, 369.
8 A. J. Leusink and H. A. Budding, *J. Organomet. Chem.*, 1968, **11**, 533.
9 M. Nishizawa and R. Noyori, *Bull. Chem. Soc. Jpn.*, 1981, **54**, 2233.
10 R. E. Ireland and R. H. Meuller, *J. Am. Chem. Soc.*, 1972, **94**, 5897.
11 E. J. Corey and A. Tramontano, *J. Am. Chem. Soc.*, 1984, **106**, 462.
12 F. Yasuhara, S. Yamaguchi, R. Kasai and O. Tanaka, *Tetrahedron Lett.*, 1986, **27**, 4033.
13 F. D. Riccardis, L. Minale, R. Riccio, B. Giovannitti, M. Iorizzi and C. Debitus, *Gazz. Chim. Ital.*, 1993, **123**, 79.
14 D. B. Dess and J. C. Martin, *J. Am. Chem. Soc.*, 1991, **113**, 7277.
15 K. Takai, K. Nitta and K. Utimoto, *J. Am. Chem. Soc.*, 1986, **108**, 7408.

Communication 9/04379I

Catalytic radical acetylation of adamantanes with biacetyl by a cobalt salt under atmospheric dioxygen

Arata Kishi, Susumu Kato, Satoshi Sakaguchi and Yasutaka Ishii*

Department of Applied Chemistry, Faculty of Engineering and High Technology, Research Center, Kansai University, Suita, Osaka 564-8680, Japan. E-mail: ishii@ipcku.kansai-u.ac.jp

Received (in Cambridge, UK) 24th March 1999, Accepted 11th June 1999

Exposure of a mixture of adamantane and biacetyl under O_2 in the presence of $Co(OAc)_2$ (0.1 mol%) in AcOH led to 1-acetyladamantane (47%) and 1,3-diacetyladamantane (20%) as major products along with small amounts of adamantan-1-ol (4%) and adamantan-2-one (3%).

The introduction of an acyl group to alkanes is one of the most difficult transformations in organic synthesis. Until recently, there have been a few reports on the acetylation of cycloalkanes under irradiation of light or by using a radical initiator such as benzoyl peroxide.[1–4] Although the catalytic acetylation of alkanes is of interest and would be more useful in organic synthesis, such a method has not yet been developed. Here, we report the first successful catalytic radical acetylation of adamantanes using biacetyl as an acetylating agent by a cobalt salt under O_2 atmosphere [eqn. (1)].

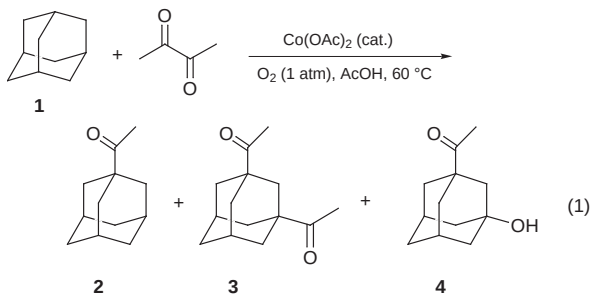

Table 1 shows the results for the acetylation of adamantane **1** with biacetyl under various conditions.† The acetylation of **1** with biacetyl in the presence of $Co(OAc)_2$ (0.1 mol%) and O_2 (1 atm) in AcOH at 60 °C for 2 h gave 1-acetyladamantane **2** (47%), 1,3-diacetyladamantane **3** (20%) and 3-acetyladamantan-1-ol **4** (6%) along with several oxygenated products such as adamantan-1-ol **5** (4%) and adamantan-2-one **6** (3%) (run 1). Photoacetylation of **1** with biacetyl is reported to form **2** in 13.8% under N_2 and 40% under O_2, but no diacetyl compound **3** is formed.[1] Therefore, our reaction provides an efficient catalytic method for the synthesis of acetyl derivatives of **1** which are technically interest compounds. When the acetylation was carried out for 4 h, **3** was obtained in preference to **2** (run 2). Among the solvents examined, AcOH was found to be the best solvent (runs 3 to 5). From the mechanistic point of view, it is important to note that no reaction takes place when a Co^{III} ion was employed in place of the Co^{II} ion (run 6). The reaction proceeded smoothly even in the presence of a very small amount (0.01 mol%) of $Co(OAc)_2$ or $Co(acac)_2$ at 80 °C to give **2** and **3** in satisfactory yields (runs 7 to 9). When the amount of biacetyl was reduced to half (3 equiv.) so that the concentration of biacetyl was halved with respect to O_2, the selectivity to **2** decreased and the amount of partly oxygenated **4** increased (run 10). In the absence of biacetyl, however, no reaction took place and the starting **1** was recovered unchanged (run 11). This fact shows that the aerobic oxidation of **1** is also induced by the presence of biacetyl. The reaction did not take place either in the presence of hydroquinone (0.1 mol%) or in the absence of O_2 (runs 12 and 13). These observations strongly suggest that a radical chain process is involved in the present acetylation, and that molecular oxygen is an essential component to promote the acetylation. Indeed, adamantyl radical, generated *in situ* from 1-bromoadamantane (3 mmol) by the action of Bu_3SnH (3.6 mmol) and AIBN (0.3 mmol) in AcOH (3 ml) reacted with biacetyl (18 mmol) and O_2 (1 atm) at 80 °C for 4 h to form **2** and **5** in 5 and 4% yields, respectively, although it abstracted more easily the hydrogen atom from the Bu_3SnH to give **1** (39%) as the major product. The reaction using benzil in place of biacetyl resulted in the recovery of the starting materials (run 14).‡

Table 1 Acetylation of **1** with biacetyl catalyzed by metal salts[a]

					Yield (%)				
Run	Metal salt (mol%)	Solvent	*t*/h	Conversion (%)	**2**	**3**	**4**	**5**	**6**
1	$Co(OAc)_2$ (0.1)	AcOH	2	94	47	20	6	4	3
2[b]	$Co(OAc)_2$ (0.1)	AcOH	4	99	22	37	10	2	4
3	$Co(OAc)_2$ (0.5)	AcOH	2	>99	10	30	11	1	4
4	$Co(OAc)_2$ (0.5)	$ClCH_2CH_2Cl$	2	65	51	4	trace	2	3
5	$Co(OAc)_2$ (0.5)	MeCN	2	2	trace	—	—	1	trace
6	$Co(acac)_3$ (0.1)	AcOH	2	no reaction					
7[c]	$Co(OAc)_2$ (0.01)	AcOH	4	98	21	35	9	2	5
8[c]	$Co(acac)_2$ (0.01)	AcOH	4	92	49	28	4	2	5
9[c]	$Co(OAc)_2$ (0.0025)	AcOH	4	77	51	14	1	2	3
10[d]	$Co(OAc)_2$ (0.5)	AcOH	4	98	20	25	16	4	4
11[e]	$Co(OAc)_2$ (0.5)	AcOH	2	no reaction					
12[f]	$Co(OAc)_2$ (0.5)	AcOH	2	no reaction					
13[g]	$Co(OAc)_2$ (0.5)	AcOH	2	no reaction					
14[h]	$Co(OAc)_2$ (0.5)	AcOH	4	no reaction					

[a] **1** (3 mmol) was allowed to react with biacetyl (6 equiv., 18 mmol) in the presence of a metal salt under O_2 (1 atm) in AcOH (3 ml) at 60 °C. [b] Polyfunctionalyzed products and adamantane-1,3-diol were also formed. [c] 80 °C [d] Biacetyl (3 equiv., 9 mmol) was used. [e] In the absence of biacetyl. [f] Hydroquinone (0.1 mol%) was added. [g] Under argon. [h] Benzil was used in place of biacetyl.

In order to gain insight into the role of cobalt salts in the present reaction, acetylations of **1** with biacetyl by Co^{II} and Co^{III} ions under O_2 (1 atm) at 75 and 80 °C were monitored by GC at appropriate time intervals (Fig. 1). The acetylation of **1** was efficiently catalyzed by Co^{II} at 75 °C, while the reaction with Co^{III} did not take place at all at this temperature. However, when the reaction temperature was raised to 80 °C, the acetylation of **1** by Co^{III} was prompted after an induction period of about 1 h. It is well-known that Co^{III} ions are reduced to Co^{II} ions by organic substrates such as toluene and cyclohexane *via* a one-electron transfer process.§ Therefore, the induction period of about 1 h observed at 80 °C would correspond to the time needed for the formation of Co^{II} by the one-electron transfer to Co^{III} from biacetyl and/or **1**. At 75 °C, however, owing to the difficulty of the electron transfer to Co^{III} from these substrates, no acetylation is induced. Therefore, if the reduction of Co^{III} to Co^{II} is performed by adding an additive like aldehyde, **1** was acetylated by Co^{III} even at 75 °C [eqn. (2)]. These findings indicate that the Co^{II} ion, which reacts easily with O_2 to generate labile dioxygen complexes such as a superoxocobalt(III) or μ-peroxocobalt(III) complex, plays an important role in the present acetylation [eqns. (3) and (4)].[7,8]

$$PhCHO + Co^{III} \longrightarrow PhCO\bullet + Co^{II} + H^{+} \quad (2)$$

$$L_nCo^{II} + O_2 \rightleftharpoons L_nCo^{III}\text{-}O\text{-}O\bullet \quad (3)$$
superoxocobalt(III)

$$L_nCo^{III}\text{-}O\text{-}O\bullet + L_nCo^{III} \rightleftharpoons L_nCo^{III}\text{-}O\text{-}O\text{-}Co^{III}L_n \quad (4)$$
μ-peroxocobalt(III)

Although the mechanistic details are still obscure, the fact that the acetylation did not take place with Co^{II} in the absence of O_2 or with Co^{III} even in the presence of O_2 suggests that a cobalt(III)–oxygen complex is the key species in the present acetylation of **1** with biacetyl. The resulting cobalt(III)-oxygen complex reacts with biacetyl to generate an acetyl radical which is readily trapped by O_2 under the present conditions to form an acetyl peroxyl radical [eqns. (5) and (6)]. The formed acetyl peroxyl radical undergoes hydrogen abstraction from **1** to form an adamantyl radical **7** and peracetic acid [eqn. (7)]. The formed radical **7** would react with biacetyl to give **2** and an acetyl radical which serves as a chain carrier in the reaction [eqn. (8)]. In addition, **7** reacts with O_2 to produce oxygenated products **5** and **6** [eqn. (9)]. Under the present reaction conditions in which O_2 exists in the reaction system, the direct abstraction of the hydrogen from **1** by the acetyl radical may be disregarded, since the rate of hydrogen abstraction from an alkane by acetyl radical is much slower than that of the addition of O_2 to acetyl radical.¶ The acetyl peroxyl radical can also abstract the hydrogen from **1** to form **7** and peracetic acid. It is probable that peracetic acid formed in the reaction is easily subjected to redox decomposition by Co ions to generate a radical species which acts as a radical carrier. In fact, the reaction of **1** (3 mmol) with biacetyl (18 mmol) under the influence of MCPBA (3.6 mmol) and Co^{III} (0.015 mmol) in acetic acid (3 ml) in an inert atmosphere at 60 °C for 1 h afforded **2** with 60% selectivity, although the conversion of **1** was low (5%) probably because of the rapid decomposition of MCPBA by Co ion.

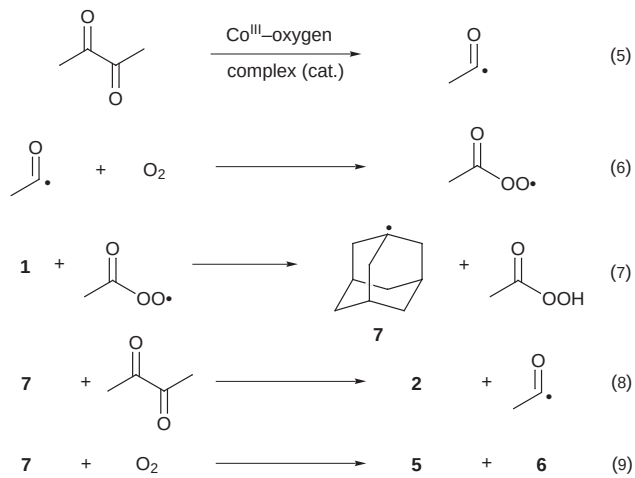

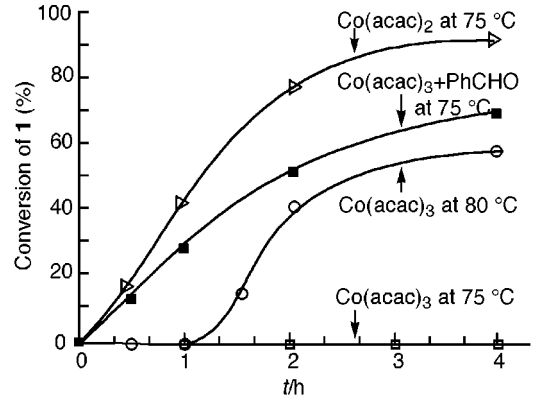

Fig. 1 Time-dependence curves for the conversion of **1** with biacetyl catalyzed by $Co(acac)_2$, $Co(acac)_3$ and $Co(acac)_3$ combined with benzaldehyde in AcOH at 75 or 80 °C. Conditions: **1** (3 mmol), biacetyl (18 mmol), AcOH (3 ml), cobalt salt (3.0×10^{-4} mmol), benzaldehyde (1.5×10^{-2} mmol).

In order to extend the present acetylation to substituted adamantanes, 1,3-dimethyladamantane **8** and **5** were allowed to react with biacetyl under the same reaction conditions as employed for **1** in Table 1, run 3. As expected, **8** was satisfactorily acetylated to the corresponding mono- and diacetyladamantanes in 54 and 21% yields, respectively. Similarly, **5** afforded **4** in 54% yield along with 3,5-diacetyladamantan-1-ol (7%). It is interesting to note that the reaction of **5** with biacetyl did not take place on the hydroxy function, which is different from the usual acetylation procedure using Ac_2O or AcCl, in which the hydroxy group is preferentially acetylated.

This work was partly supported by a Grant-in-Aid for Scientific Research (No.10450337) from Monbusho.

Notes and references

† *Typical reaction*: To a solution of adamantane **1** (3 mmol) and $Co(OAc)_2$ (0.1 mol%) in AcOH (3 ml) was added biacetyl (18 mmol), and the mixture was stirred under O_2 (1 atm) at 60 °C for 2 h. Products were isolated by column chromatography on silica gel with hexane–EtOAc.

‡ Treatment of biacetyl with O_2 in the presence of Co^{II} under these conditions afforded AcOH in 192% (based on Co^{II}), however, benzil was recovered unchanged by the same treatment.

§ The reaction of a Co^{III} ion with cyclohexane (ref. 5) or alkylbenzenes (ref. 6) is known to involve one-electron transfer from the substrate to Co^{III}, yielding a Co^{II} ion and radical cation which readily liberates H^+ to give an alkyl radical.

¶ The reaction of acetyl radical with O_2 is reported to occur very fast [$k = (1.8 \pm 0.5) \times 10^9$ M^{-1} s^{-1}] compared with the hydrogen abstraction from *n*-hexane by acetyl radical ($k \leqslant 5 \times 10^3$ M^{-1} s^{-1}) (ref. 9).

1 I. Tabushi, S. Kojo and Z. Yoshida, *Tetrahedron Lett.*, 1973, **26**, 2329.
2 I. Tabushi, S. Kojo and K. Fukunishi, *J. Org. Chem.*, 1978, **43**, 2370.
3 K. Fukunishi, A. Kohno and S. Kojo, *J. Org. Chem.*, 1988, **53**, 4369.
4 W. G. Bentrude and K. R. Darnall, *J. Am. Chem. Soc.*, 1968, **90**, 3588.
5 E. I. Heiba, R. M. Dessau and W. J. Koehl Jr., *J. Am. Chem. Soc.*, 1969, **91**, 6830.
6 A. Onopchenko and J. G. D. Shultz, *J. Org. Chem.*, 1973, **38**, 3729.
7 C. L. Wong, J. A. Switer, K. P. Balakrishnan and J. F. Endicott, *J. Am. Chem. Soc.*, 1980, **102**, 5511.
8 J. J. Bozell, B. R. Hames and D. R. Dimmel, *J. Org. Chem.*, 1995, **60**, 2398.
9 E. B. Carl, G. N. Anthony, M. R. David, U. I. Keith and L. Janusz, *Aust. J. Chem.*, 1995, **48**, 363.

Communication 9/02384D

ChemComm

Unexpected [2 + 2] cycloaddition between the P=O group of *P*-(2,4,6-triisopropylphenyl) P-heterocycles and dimethyl acetylenedicarboxylate

György Keglevich,*[a] Henrietta Forintos,[a] Áron Szöllõsy[b] and László Tõke[c]

[a] *Department of Organic Chemical Technology, Technical University of Budapest, 1521 Budapest, Hungary. E-mail: keglevich@oct.bme.hu*
[b] *Department of General and Analytical Chemistry, Technical University of Budapest, 1521 Budapest, Hungary.*
[c] *Research Group of the Hungarian Academy of Sciences at the Department of Organic Chemical Technology, Technical University of Budapest, 1521 Budapest, Hungary.*

Received (in Cambridge, UK) 1st June 1999, Accepted 22nd June 1999

The reaction of 1-(2,4,6-triisopropylphenyl)-1,2-dihydrophosphinine 1-oxide 1d with dimethyl acetylenedicarboxylate (DMAD) affords, surprisingly, oxaphosphetene 3 instead of the expected Diels–Alder cycloadduct; the unusual reactivity of the trialkylphenylphosphine oxides towards DMAD seems to be of general value.

The 1,2-dihydrophosphinine 1-oxides (**1**) with phenyl, alkyl or alkoxy substituents on the phosphorus atom proved to be valuable starting materials in the synthesis of phosphabicyclo-[2.2.2]octadienes **2** that are precursors of low-coordinated fragments, methylenephosphine oxides ($YP(O)CH_2$) useful in the phosphorylation of nucleophiles.[1–4] The cycloadducts (**2**) are obtained by the Diels–Alder reaction of dihydrophosphinine oxides **1** and DMAD (Scheme 1).[1,4] Other dienophiles, such as maleic acid derivatives were also utilised in the synthesis of bridged phosphorus heterocycles.[5,6]

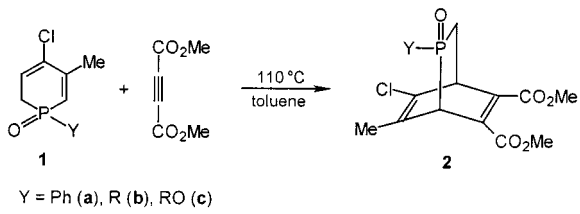

Scheme 1[1–4]

Recently, we have described the preparation of 1-(triisopropylphenyl)dihydrophosphinine oxide **1d** revealing unique properties due to the presence of the sterically demanding P-substituent.[7] We wished to utilise compound **1d** in the synthesis of *P*-(trialkylphenyl)phosphabicyclooctadiene **2d** (**2**, Y = 2,4,6-$Pr^i_3C_6H_2$) that seemed to be promising in the generation of a sterically hindered and hence a relatively stable methylenephosphine oxide (2,4,6-$Pr^i_3C_6H_2P(O)CH_2$).

The reaction of **1d** and DMAD in 1,2-xylene at 165 °C (in a bomb) did not lead, however, to cycloadduct **2d**, instead oxaphosphete **3** isomeric with **2d** could be isolated in 76% yield after column chromatography (Scheme 2). Cycloadduct **2** could not be detected, not even in traces. Spiro derivative **3** exhibited a δ_P value of 24.0 ($CDCl_3$). Similar 1,2-oxaphosphetes have never been reported in the literature. The 1,2-oxaphosphetes are, however, well-known intermediates in the Wittig reaction.[8] The structure of product **3** was confirmed by ^{13}C and ^1H NMR,[9] as well as two-dimensional correlation diagrams, such as HMQC and HMPC spectra. Elemental composition of **3** was supported by HRMS.

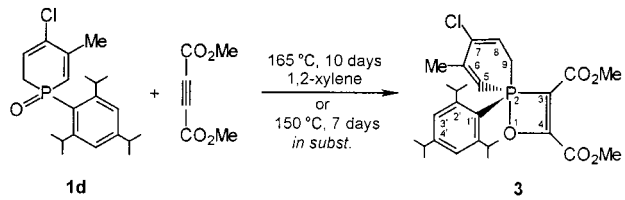

Scheme 2

This is the first case in which the P=O group of a phosphine oxide reacted with DMAD to furnish the 1,2-oxaphosphete ring. Moreover, the [2+2] cycloaddition was fully selective and the dihydrophosphinine ring of starting material **1d** remained intact.

We wished to evaluate if the above [2+2] cycloaddition is of general value for P-heterocycles with a *P*-triisopropylphenyl substituent. Hexahydrophosphinine oxide **4** obtained from **1d** by catalytic hydrogenation was reacted with DMAD at 150 °C in the absence of any solvent, to give oxaphosphete **5** in 58% yield after chromatography (Scheme 3). Starting from the 63–37% diastereoisomeric mixture of **4**, product **5** was also formed as a mixture of two isomers.[10]

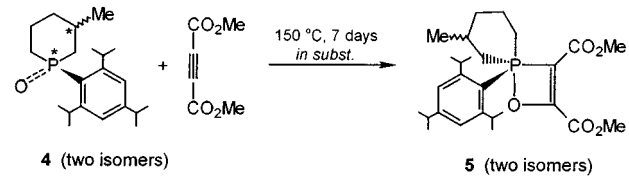

Scheme 3

Finally, it was examined if a P-heterocycle with a five-membered ring can be involved in the above type [2 + 2] cycloaddition. The interaction of 1-(triisopropylphenyl)dihydrophosphole oxide **6** and DMAD at 150 °C led again to the corresponding oxaphosphete (**7**). In this case the double-bond of the 2,5-dihydrophosphole moiety was, however, isomerised to afford the 2,3-dihydro hetero ring (Scheme 4). 2,5-Dihydrophospholes are known to undergo double-bond rearrangement on thermal treatment.[11] Product **7** was isolated in 83% yield in a clean reaction. The structure of spiro derivatives **5** and **7**[12] was confirmed by NMR and MS.

It is worth mentioning that the *P*-phenyl analogues of hexahydrophosphinine **4** and dihydrophosphole **6** did not enter into reaction with DMAD at 150–165 °C. This means that the electron-releasing ability of the triisopropylphenyl ring may be responsible for the new type of reactivity of the P=O group.

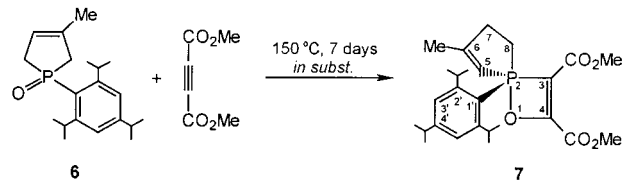

Scheme 4

To summarise our findings, it can be concluded that the reaction of DMAD with 5- and 6-membered P-heterocycles bearing a triisopropylphenyl substituent on the phosphorus atom affords the corresponding spiro derivative of 1,2-oxaphosphete. This type of [2+2] cycloaddition between the P=O group of tertiary phosphine oxides and the acetylene moiety of DMAD has not been observed previously and is, obviously, the consequence of the presence of the triisopropylphenyl substituent at the phosphorus atom. The reaction under discussion may be of general value and hence the cycloaddition of acyclic trialkylphenylphosphine oxides with DMAD may represent a new entry into the synthesis of *P*-aryl oxaphosphetes.

Future work will be directed towards the possible extension and the theoretical evaluation of the P=O + -C≡C- [2 + 2] cycloaddition reaction.

Thanks are due to FKFP (Grant No.: 363/1999) and OTKA (Grant No.: T029039) financial support.

Notes and references

1 L. D. Quin, J.-S. Tang and Gy. Keglevich, *Heteroatom. Chem*., 1991, **2**, 283.
2 L. D. Quin, J.-S. Tang, Gy. S. Quin and Gy. Keglevich, *Heteroatom. Chem*., 1993, **4**, 189.
3 Gy. Keglevich, K. Újszászy, L. D. Quin and Gy. S. Quin, *Heteroatom. Chem*., 1993, **4**, 559.
4 Gy. Keglevich, L. Tõke, Zs. Böcskei, D. Menyhárd and L. D. Quin, *Heteroatom. Chem*., 1995, **6**, 593.
5 Gy. Keglevich, K. Steinhauser, K. Ludányi and L. Tõke, *J. Organomet. Chem*., 1998, **570**, 49.
6 Gy. Keglevich, L. D. Quin, Zs. Böcskei, Gy. M. Keserû, R. Kalgutkar and P. M. Lahti, *J. Organomet. Chem*., 1997, **532**, 109.
7 Gy. Keglevich, Gy. M. Keserû, H. Forintos, Á. Szöllõsy, K. Ludányi and L. Tõke, *J. Chem. Soc., Perkin Trans. 1*, 1999, 1801.
8 E. Vedejs and C. F. Marth, *^{31}P NMR Detection and Analysis of Wittig Intermediates*, in *Phosphorus-31 NMR Spectral Properties in Compound Characterization and Structural Analysis*, ed. L. D. Quin and J. G. Verkade, VCH, New York, 1994, p. 297.
9 *Selected data* for **3**: $\delta_C(CDCl_3)$ 16.2 (J_{PC} 17.5, C^6–Me), 23.5 (J_{PC} 8.7, *o*-CH(*C*H$_3$)$_2$), 25.3 (*p*-CH(*C*H$_3$)$_2$), 30.0 (J_{PC} 62.8, C^9), 31.8 (J_{PC} 6.7, *o*-*C*HMe$_2$), 34.0 (*p*-*C*HMe$_2$), 50.6 (CH$_3$O), 51.5 (CH$_3$O), 74.4 (J_{PC} 107.4, C^3), 119.3 (J_{PC} 13.7, C^8), 121.6 (J_{PC} 94.3, C$^{1'}$), 122.5 (J_{PC} 85.0, C^5), 123.2 (J_{PC} 11.9, C$^{3'}$), 140.0 (J_{PC} 14.1, C^7), 152.7 (J_{PC} 11.3, C$^{2'}$), 153.0 (C$^{4'}$), 155.4 (J_{PC} 14.8, C^6), 166.4 (J_{PC} 14.8, C=O), 167.5 (J_{PC} 15.6, C=O), 182.4 (J_{PC} 6.1, C^4)
10 *Selected data* for **5**-**1**: $\delta_P(CDCl_3)$ 23.9 (69%), **5**-**2**: $\delta_P(CDCl_3)$ 29.1 (31%).
11 K. Hunger, U. Hasserodt and F. Korte, *Tetrahedron*, 1964, **20**, 1593; L. D. Quin, J. P. Gratz and T. P. Barket, *J. Org. Chem*., 1968, **33**, 1034.
12 *Selected data* for **7**: $\delta_P(CDCl_3)$ 39.5; $\delta_C(CDCl_3)$ 20.7 (J_{PC} 18.0, C^6-Me), 23.8 (J_{PC} 5.9, *o*-CH(*C*H$_3$)$_2$), 25.5 (*p*-CH(*C*H$_3$)$_2$), 26.0 (J_{PC} 59.2, C^8), 32.0 (J_{PC} 6.3, *o*-*C*HMe$_2$), 34.3 (*p*-*C*HMe$_2$), 35.7 (J_{PC} 6.8, C^7), 50.7 (CH$_3$O), 51.8 (CH$_3$O), 76.1 (J_{PC} 103.0, C^3), 116.3 (J_{PC} 88.6, C^5), 122.8 (J_{PC} 93.7, C$^{1'}$), 123.2 (J_{PC} 11.3, C$^{3'}$), 152.7 (C$^{2'}$), 152.8 (C$^{4'}$), 164.0 (J_{PC} 23.0, C^6), 167.0 (J_{PC} 14.3, C=O), 168.1 (J_{PC} 15.4, C=O), 182.5 (J_{PC} 6.2, C^4).

Communication 9/04422A

The gas-phase fragmentation of trineopentylstannyl cation: a rare example of β-methyl migration within a main group organometallic compound

Dainis Dakternieks,* Allan E. K. Lim and Kieran F. Lim

Centre for Chiral and Molecular Technologies, Deakin University, Geelong, 3217 Australia.
E-mail: dainis@deakin.edu.au

Received (in Cambridge, UK) 19th April 1999, Accepted 21st June 1999

The lowest-energy fragmentation pathway of trineopentylstannyl cation is the first example of β-methyl migration to an organotin compound in the gas-phase; the origin of the migrating methyl groups is confirmed by an isotopic labelling experiment.

The migratory insertion of an unsaturated compound into a transition metal–hydrogen (or carbon) bond is a well established reaction.[1] The β-hydrogen [eqn. (1)] and β-methyl [eqn. (2)]

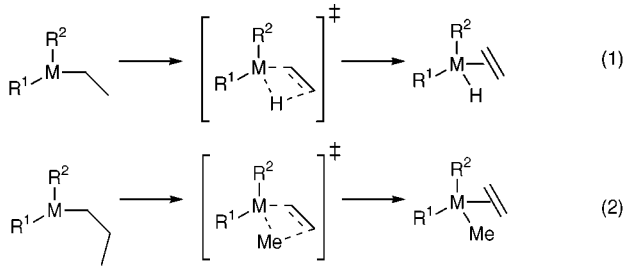

elimination processes, being microscopic reversals of the insertion process, are of fundamental importance in the many catalytic processes involving transition metals,[2–4] including Ziegler–Natta polymerization.[2]

Although these processes are primarily associated with transition-metal organometallic compounds, they are also known to occur within organoaluminium compounds.[5] In particular, trineopentylaluminium dissociates reversibly into $AlMe_3$ and isobutene at 200 °C [eqn. (3)].[6] Whilst the

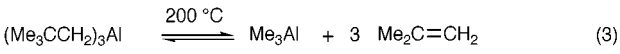

observations in these early works are now attributed to the β-Me elimination process,[5] to the best of our knowledge, there are no other examples of β-Me elimination in main group organometallic chemistry.

As part of a comprehensive study into the gas-phase fragmentation of organostannyl cations, we investigated the fragmentation of trineopentylstannyl cation $[(Me_3CCH_2)_3Sn]^+$ (**1**), derived from trineopentylstannyl trifluoromethanesulfonate (**2**),† using ESMS. Initially designed as a very mild method of analyzing large biomolecules,[7] ESMS has since been widely used as an investigative tool in organometallic solution chemistry.[8]

While there is still significant debate over the exact nature of the electrospray ionization process,[9] it basically entails spraying the analyte solution into the mass spectrometer source followed by evaporation of the solvent molecules. In-source CID of the analyte ions can be made to occur by increasing the potential difference (cone voltage) across the skimmer cones.[10] This allows analyses to start under *extremely* mild conditions and the energy of the ions analyzed can be gradually increased. Organotin compounds, the halides in particular, have been investigated within several ESMS studies.[11]

Analysis of a solution of **2** in acetonitrile is first performed under mild conditions,‡ at a cone voltage of 20 V. The

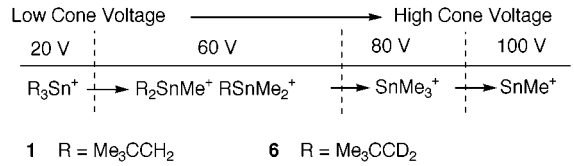

Scheme 1 Observed fragmentation patterns of **1** and **6**.

predominant species observed is the acetonitrile (solvent) adduct, [**1** + CH_3CN], along with a smaller peak corresponding to **1**.§ Increasing the cone voltage to 40 V causes dissociation of the acetonitrile adduct and **1** becomes the main species detected.

The cation **1** itself remains intact until the cone voltage is raised even further (~60 V), where the onset of fragmentation occurs. The fragmentation pattern observed is summarized in Scheme 1. For each neopentyl group lost, a methyl group remains on tin. No evidence for simple Sn–C bond cleavage was found. The presence of methyl residues on tin in the fragment ions can be rationalized through the two different pathways depicted in Scheme 2. The top pathway is analogous to the β-Me migration process known in transition metal complexes, whereas the bottom pathway resembles a well established[12] hydrocarbon pyrolysis process. Both reaction channels lead to the same products.

To resolve this issue, the deuterated trineopentylstannyl chloride (**4**) was synthesized *via* Scheme 3. The corresponding trifluoromethanesulfonate (**5**) was obtained *via* metathesis of **4** with silver trifluoromethanesulfonate. Subsequently the deuterated trineopentylstannyl cation (**6**) is derived from **5**.¶ In this case, the two different types of hydrogen atom in **6** are distinguished, allowing the discrimination between the two reaction channels.

Analysis of an acetonitrile solution of **5** as before, afforded the fragment ions of **6**. The results obtained are depicted in Scheme 1, this time with R being the deuterated neopentyl group. The *m/z* values of the isotope distributions of the fragment ions clearly show that the methyl residues on tin are not deuterium labeled, thus unambiguously identifying the source of the methyl residue as being from the β-position (Scheme 4).

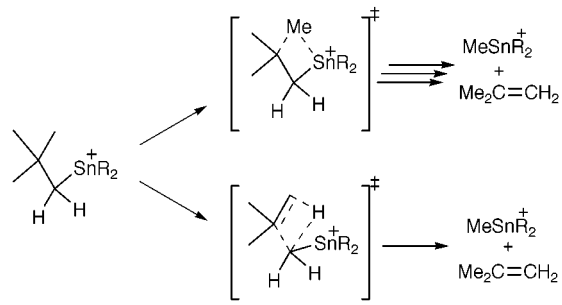

Scheme 2 Possible reaction channels for the fragmentation of **1**.

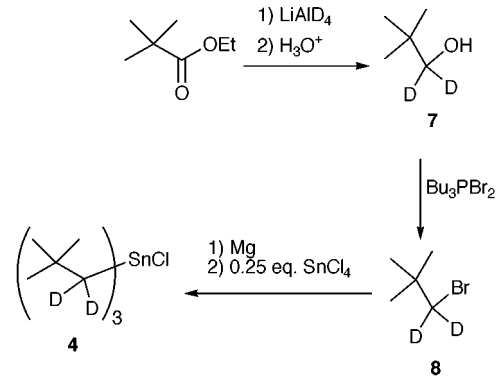

Scheme 3 Synthesis of deuterated trineopentylstannyl chloride analog **4**.

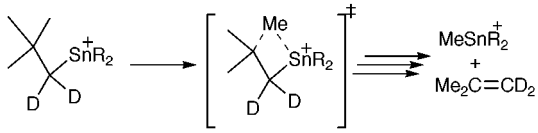

Scheme 4 Confirmed fragmentation pathway of **6**.

Repeating the ESMS in-source CID analyses on both **2** and **5** using deuterated acetonitrile as solvent and carrier afford the same daughter ions as when normal acetonitrile is used, thus eliminating the possibility that the acetonitrile solvent is the source of the CH_3 groups.

The observed β-Me elimination process is also reproducible under solvent-free (MS/MS) conditions.‖ Selecting and trapping the relevant cations **1** and **6** followed by CID using helium as a collision gas again afforded fragmentation as depicted in Scheme 1.

In conclusion, we believe this is the first report of an unusual β-Me elimination process occurring within an organotin compound. Whilst the observation of complex processes in the gas-phase is not uncommon using conventional (*e.g.* EI or CI) mass spectrometric techniques, it is extremely important to note that the β-Me elimination we observe using ESMS is the first occurring dissociation process to be observed upon gradually raising the cone voltage. This demonstrates that the β-Me elimination observed is the lowest-energy dissociation pathway for this cation, as opposed to being an exotic high-energy process. We suggest that this process occurs *via* β-Me migration to afford a thermodynamically stabilised β-stannyl cation, which then loses isobutene to give the daughter ion. These results would be consistent with known work[13] concerning the importance of the Group 14 β-effect in the reactivities of Group 14 organometallic species.

We thank the Australian Research Council for financial support and Deakin University and the Department of Education, Training, and Youth Affairs (DETYA), Australia, for the provision of an Overseas Postgraduate Research Scholarship to A. E. K. L.

Notes and references

† **2** was obtained from trineopentylstannyl chloride (**3**) *via* metathesis with silver trifluoromethanesulfonate. **3** was synthesized using literature methods (H. Zimmer, I. Hechenbleikner, O. A. Homberg and M. Danzik, *J. Org. Chem.*, 1964, **29,** 2632.) **3**: $^{119}Sn\{^1H\}$ NMR (111.87 MHz, $CHCl_3$) δ = 126.2; δ_H (299.98 MHz, $CDCl_3$): 1.09 (s, 27H, Me_3C), 1.54 [s, 6H, CH_2Sn, $^2J(^1H,^{119}Sn)$ = 47 Hz]; $^{13}C\{^1H\}$ NMR (75.44 MHz, $CDCl_3$) δ 32.36 (quaternary), 33.27 [CH_3, $^3J(^{13}C,^{119}Sn)$ = 40 Hz], 40.49 [CH_2Sn, $^1J(^{13}C,^{119}Sn)$ = 328 Hz]. ν(KBr)/ cm^{-1}) 2954, 2900, 2860, 1464, 1384, 1364, 1239, 1143, 1113, 1011, 736, 604; mp 110–111 °C [lit. 112.5–113.5 °C].

‡ The following general analysis procedure was used: approximately 100 mg of trineopentylstannyl chloride was combined with one equivalent of silver trifluoromethanesulfonate and stirred in 10 mL of dry CH_2Cl_2 for 15 to 30 min with protection from light. The resultant trineopentylstannyl trifluoromethanesulfonate solution was decanted from the AgCl precipitate and diluted with dry acetonitrile to a concentration of approximately 1 mM for ESMS analysis. ES mass spectra were obtained with a Micromass Platform II single quadrupole mass spectrometer using an acetonitrile mobile phase. Spectra were collected at cone voltages of 20, 40, 60, 80, and 100 V each. All peak assignments were unambiguously confirmed *via* comparison with calculated isotope distributions.

§ In all spectra low intensity peaks corresponding to the $[(R_3Sn)_2Tf]^+$ and (if the solvents used were not absolutely dry) $[(R_3Sn)_2OH]^+$ clusters were observed. MS/MS experiments confirm that the presence of these clusters do not have any bearing on the β-Me migration results observed.

¶ The deuterated trineopentylstannyl cation (**6**) was derived from tris(1,1-dideutero-2,2-dimethylpropyl)stannyl trifluoromethanesulfonate (**5**), which was obtained from tris(1,1-dideutero-2,2-dimethylpropyl)stannyl chloride (**4**) *via* metathesis with silver trifluoromethanesulfonate. The synthesis of **7** was achieved by modifying literature methods (I. Dostrovsky and F. S. Klein, *J. Chem. Soc.*, 1955, 4401; S. Sarel and M. S. Newman, *J. Am. Chem. Soc.*, 1956, **78**, 5416): ethyl trimethylacetate was reacted with $LiAlD_4$ to afford **7** in 61% yield; δ_H (299.98 MHz, $CDCl_3$) 0.87 (s, 9H, Me_3C), 2.03 (s, 1H, OH); $^{13}C\{^1H\}$ NMR (75.44 MHz, $CDCl_3$) δ = 25.91 (CH_3), 32.35 (quaternary), 72.50 (1:2:3:2:1 quintet, CD_2OH, $^1J(^{13}C,^2H)$ = 42 Hz). Using the literature (G. A. Wiley, R. L. Hershkowitz, B. M. Rein and B. C. Chung, *J. Am. Chem. Soc.*, 1964, **86,** 964) method of converting neopentyl alcohol into neopentyl bromide, **7** was converted to **8** in 50% yield; δ_H (299.98 MHz, $CDCl_3$) 1.04 (s, 9H, Me_3C); $^{13}C\{^1H\}$ NMR (75.44 MHz, $CDCl_3$) δ 27.69 (CH_3), 32.00 (quaternary), 47.57 (1:32.00 (quaternary), 47.57 (2:3:2:1 quintet, CD_2Br, $^1J(^{13}C,^2H)$ = 46 Hz); MS (70 eV): *m/z* (%): 57 (100) [$(CH_3)_3C^+$], 137 (11) [$^{79}BrCD_2(CH_3)_2C^+$], 139 (11) [$^{81}BrCD_2(CH_3)_2C^+$], 152 (1) [M^+ containing ^{79}Br], 154 (1) [M^+ containing ^{81}Br]. The Grignard reagent of **8** was formed by reaction of **8** with magnesium turnings in THF. Using this Grignard reagent, the literature procedure (H. Zimmer, I. Hechenbleikner, O. A. Homberg and M. Danzik, *J. Org. Chem.*, 1964, **29,** 2632) for the synthesis of **3** afforded **4** in 18% yield; $^{119}Sn\{^1H\}$ NMR (111.87 MHz, $CHCl_3$) δ 126.8; δ_H (299.98 MHz, $CDCl_3$) 1.09 (s, 27H, Me_3C); $^{13}C\{^1H\}$ NMR (75.44 MHz, $CDCl_3$) δ 31.95 (quaternary), 32.92 [CH_3, $^3J(^{13}C,^{119}Sn)$ = 40 Hz], 39.55 [1:2:3:2:1 quintet, CD_2Sn, $^1J(^{13}C,^2H)$ = 39Hz]. IR (KBr)/cm^{-1} ν 2954, 2900, 2860, 2194 (CD_2), 2133 (CD_2) 1461, 1391, 1364, 1238, 1049, 622; mp 113–114 °C

‖ MS/MS experiments were performed using standard isolation and excitation procedures on mass selected ions generated *via* electrospray ionization using a Finnigan model LCQ (San Jose, CA, USA) quadrupole ion trap mass spectrometer.

1 See, for example: Ch. Elschenbroich and A. Salzer, *Organometallics*, 2nd edn., VCH, New York, 1992.
2 (*a*) R. H. Crabtree, *The Organometallic Chemistry of Transition Metals*, Wiley, New York, 1988; (*b*) J. P Collman, L. S. Hegedus, J. R. Norton and R. G. Finke, *Principles and Applications of Organotransition Metal Chemistry*, University Science Books, Mill Valley, California, 1987; (*c*) A. Yamamoto, *Organotransition Metal Chemistry*, Wiley, New York, 1986.
3 See, for example: (*a*) G. Sini, S. A. Macgregor, O. Eisenstein and J. H. Teuben, *Organometallics*, 1994, **13,** 1049;. (*b*) A. D. Horton, *Organometallics*, 1996, **15,** 2675 and references therein.
4 (*a*) M. Etienne, R. Mathieu and B. Donnadieu, *J. Am. Chem. Soc.*, 1997, **119,** 3218; (*b*) B. C. Ankianiec, V. Christou, D. T. Hardy, S. K. Thomson and G. B. Young, *J. Am. Chem. Soc.*, 1994, **116**, 9963.
5 J. J. Eisch, in *Comprehensive Organometallic Chemistry*, ed. G. Wilkinson, F. G. A. Stone and E. W. Abel, Pergamon, Oxford, 1982, vol. 1, p. 610.
6 (*a*) K. Ziegler, *Angew. Chem.*, 1956, **68,** 721; (*b*) W. Pfohl, *Liebigs Ann. Chem.*, 1960, **629,** 207.
7 J. B. Fenn, M. Mann, C. K. Meng, S. F. Wong and C. M. Whitehouse, *Science*, 1989, **246,** 64.
8 (*a*) R. Colton, A. D'Agostino and J. C. Traeger, *Mass. Spectrom. Rev.*, 1995, **14,** 79 and (*b*) W. Henderson, B. K. Nicholson and L. J. McCaffrey, *Polyhedron*, 1998, **17**, 4291.
9 J. B. Fenn, *J. Am. Soc. Mass Spectrom.*, 1993, **4**, 524.
10 (*a*) S. Lacorte, C. Molina and D. Barceló, *J. Chromatogr. A*, 1998, **795**, 13 and (*b*) W. M. A. Niessen, *J. Chromatogr. A*, 1998, **794**, 407 and references therein.
11 (*a*) W. Henderson and M. J. Taylor, *Polyhedron*, 1996, **15**, 1957; (*b*) T. L. Jones and L. D. Betowski, *Rapid Commun. Mass Spectrom.*, 1993, **7**, 1003.
12 (*a*) K. F. Lim, R. G. Gilbert, T. C. Brown and K. D. King, *Int. J. Chem. Kinet.*, 1987, **19,** 373; (b) T. C. Brown, K. D. King and R. G. Gilbert, *Int. J. Chem. Kinet.*, 1988, **20,** 549.
13 J. B. Lambert, Y. Zhao, R. W. Emblidge, L. A. Salvador, X. Y. Liu, J. H. So and E. C. Chelius, *Acc. Chem. Res.*, 1999, **32**, 183.

Communication 9/03098K

ChemComm

First paddlewheel complex with a doubly-bonded Ir_2^{6+} core

F. Albert Cotton,*[a] Carlos A. Murillo*[ab] and Daren J. Timmons[a]

[a] *Laboratory for Molecular Structure and Bonding and Department of Chemistry, PO Box 30012 Texas A&M University, College Station, TX 77842-3012. E-mail: cotton@tamu.edu*

[b] *Department of Chemistry, University of Costa Rica, Ciudad Universitaria, Costa Rica. E-mail: murillo@tamu.edu*

Received (in Cambridge, UK) 14th June 1999, Accepted 29th June 1999

Reaction of $IrCl_3$ with Hhpp in refluxing ethanol (Hhpp = 1,3,4,6,7,8-hexahydro-2*H*-pyramido[1,2-*a*]pyrimidine) yields $Ir_2(hpp)_4Cl_2$, the first paddlewheel complex of Ir^{III}, with a short Ir–Ir distance of 2.495(1) Å, an average Ir–Cl distance of 2.643[6] Å, an Ir_2^{6+} core bridged by four hpp ligands with two axial chlorine atoms, and a double bond between the Ir atoms.

A great deal of understanding has come in the area of multiple bonds between transition metal atoms through the study of dinuclear paddlewheel-type complexes; however, there is very little depth to our knowledge for iridium. Indeed, there is only one paddlewheel complex containing an Ir_2^{4+} core and four bridging anionic ligands, namely $Ir_2(DTolF)_4$ (DTolF = *N*,*N*′-di-*p*-tolylformamidinate) **I**,[1] and the three-step synthesis of this was quite cumbersome. It appears that there are only seven other complexes containing a single bond between divalent iridium atoms that fall within the family of compounds broadly defined by **II**.[1,2]

Dinuclear complexes of iridium(III) are typically edge-sharing or face-sharing bioctahedra and have no metal–metal bonds because of the closed t_{2g}^6 configuration. There are a few complexes in which the short Ir–Ir bond distance is indicative of direct metal–metal bonding, *e.g.* $[Ir_2(\mu\text{-}H)_3H_2(PPh_3)_4]PF_6$,[3] 2.518 Å; $[(Cp^*Ir)_2(\mu\text{-}H)_3]ClO_4$,[4] 2.465 Å, but the close approach may be due to the $(\mu\text{-}H)_3$ bridging. No complex of the paddlewheel type has been reported for trivalent iridium.

It has been shown recently that bridging hpp, the monoanion of 1,3,4,6,7,8-hexahydro-2*H*-pyrimido[1,2-*a*]pyrimidine, stabilizes complexes of the type $M_2(hpp)_4$ (M = V,[5] Nb,[6] Cr,[5] Mo,[5] Ni,[7] and Pd[8]). Additionally, complexes containing an M_2^{6+} core have been made for M = Ru,[9] Re,[10] Mo,[11] and Pd.[8] The complex $[Mo_2(hpp)_4][BF_4]_2$ [11] is the sole example of an Mo_2^{6+} core supported by soft, binitrogen-donor ligands as the bridges and $Pd_2(hpp)_4Cl_2$ [8] is the only example of a single bond between trivalent palladium atoms. As a result, our interest has turned more towards the +3 oxidation state of the transition metals.

For many transition metals (*e.g.* Cr, Co, Ni, Pd, Ru, Rh), simple halide salts are often used as starting materials for the synthesis of a wide variety of paddlewheel complexes, but there is no general pathway for the analogous iridium complexes. Rhenium and osmium paddlewheel complexes are typically synthesized by ligand exchange using $Re_2Cl_8^{2-}$ and $Os_2(O_2CCH_3)_4Cl_2$, respectively, but no similar diiridium starting materials are available. However, one osmium complex, Os_2(hydroxypyridinato)$_4Cl_2$, was synthesized from $OsCl_3$ and the neutral ligand in refluxing ethanol.[12] This same method was tried with $IrCl_3$ and Hhpp and resulted in only the second example of an iridium paddlewheel complex and the first one containing Ir^{III}.

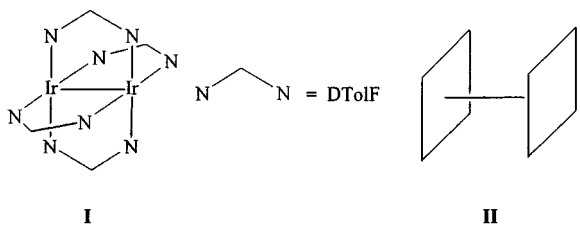

I **II**

Scheme 1

When $IrCl_3$ and Hhpp were stirred in ethanol at room temperature for several hours, no reaction occurred, but heating to reflux overnight resulted in a brown solution containing a small amount of solid.† Removal of the ethanol under reduced pressure left a brown residue, which was dissolved in a minimum amount of CH_2Cl_2. From this solution a dark purple band containing $Ir_2(hpp)_4Cl_2$ **1** (10% yield) was eluted first on a silica gel column with a 10 : 1 CH_2Cl_2–MeOH eluent. Crystals can be readily grown in air by evaporation or diffusion of hexanes into a dichloromethane solution. The solid is air stable and is not decomposed by water, in which it is sparingly soluble.

When an analogous reaction was conducted in toluene, the hot toluene became purple and a dark solid precipitated. Complex **1** was isolated from the toluene filtrate by evaporation. After washing with acetonitrile the yield was reproducibly *ca.* 10%. The dark solid is as yet uncharacterized.

Substitutions in low spin d^6 systems are known to be difficult,[13] and $IrCl_3$ is no exception; this may account for the low yields of $Ir_2(hpp)_4Cl_2$. Additionally it appears that $IrCl_3$ does not react at all with Li(hpp) in refluxing THF or CH_2Cl_2. It is possible that the conditions necessary to activate these reactions also lead to several side products. Clearly a more reactive starting material is desirable, but we have not found one yet as the number of suitable Ir^{III} complexes is rather small.

The structure‡ of **1**, a diiridium unit bridged by four hpp ligands with chlorine atoms bound in the axial positions, is shown in Fig. 1. The Ir–Ir *double* bond distance is 2.495(1) Å and the average Ir–Cl bond distance is 2.643[6] Å. There is no analog with which to make a comparison. The 'nearest kin' is $Ir_2(DTolF)_4$ which contain an Ir_2^{4+} core and a formal Ir–Ir *single* bond of length 2.524(3) Å,[1] a relatively small change of 0.029 Å from the metal–metal distance in **1**.

Compound **1** is paramagnetic with a room-temperature magnetic susceptibility that corresponds to two unpaired electrons. This observation could be accommodated on the basis of the classic molecular orbital ordering, $\sigma^2\pi^4\delta^2\delta^{*2}\pi^{*2}$. However, this is not necessarily the case. We recently reported[8] that $Pd_2(hpp)_4Cl$, which has two more electrons, has the configuration $\pi^4\delta^2\delta^{*2}\pi^{*4}\sigma^2$; the high energy of the σ orbital is traced to the very strong and short Pd–Cl bonds [2.474(4) Å]. In **1**, the Ir–Cl bond lengths are much longer [2.617(4) Å] and therefore the σ orbital will likely be lower in energy, although not necessarily at the bottom. However, as long as the σ orbital is below the π* orbitals, its actual position is not critical and the electronic configuraion of **1** will correspond to a net bond order of 2.

This work suggests several interesting ideas, such as reduction of the Ir_2^{6+} core to Ir_2^{4+} and the question of whether $Rh_2(hpp)_4Cl_2$ as well as $Rh_2(hpp)_4$ can be made. We are pursuing these matters.

We thank Dr Xiaoping Wang for the magnetic measurements and the National Science Foundation for financial support.

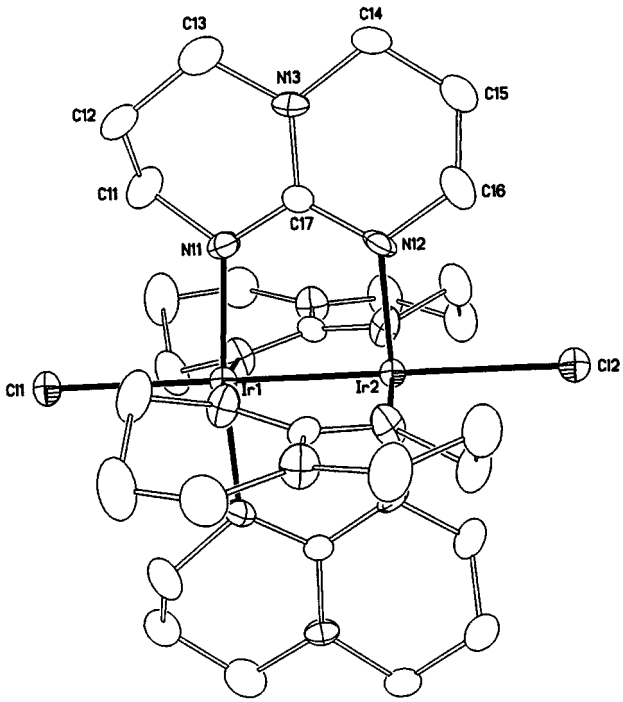

Fig. 1 The molecular structure of $Ir_2(hpp)_4Cl_2$; atoms are drawn at the 50% probability level. Selected bond distances (Å): Ir(1)–Ir(2) 2.495(1), Ir–Cl (av) 2.643[6], Ir–N (av) 2.01[1] Å; N–Ir–Ir–N torsion angle = 11.2(4)°.

Notes and references

† A flask was charged with $IrCl_3$ (0.2 g, 0.66 mmol), Hhpp (0.46 g, 3.3 mmol) and a stirring bar. Ethanol (40 ml) was added and the mixture was refluxed overnight resulting in a brown solution with a small amount of dark solid. All solvent was removed under vacuum and the brown residue dissolved in 10 ml CH_2Cl_2. A purple band was eluted on a silica gel column using a 10 : 1 CH_2Cl_2–MeOH eluent. After the solvent was evaporated, a purple solid, namely $Ir_2(hpp)_4Cl_2$, was isolated in 10% yield (0.034 g, 0.034 mmol). Purple crystals of **1** were grown by the slow diffusion of hexanes into a dichloromethane solution of **1**. IR (KBr, cm^{-1}): 2930w, 2848m, 1700w, 1653w, 1601vw, 1560w, 1526vs, 1465.3s, 1440vs, 1386m, 1309s, 1276m, 1212vs, 1140w, 1071vw, 1031vw, 759m, 407vw. UV–VIS (CH_2Cl_2) [λ/nm(ε/dm^3 mol^{-1} cm^{-1})]: 365 (3900), 396 (3900), 515 (4500), 550 (5700), 701 (6100). ^1H NMR ($CDCl_3$): δ 1.81 (br qnt, CH_2), 3.06 (t, CH_2), 5.40 (br, CH_2). $\chi_g = 3.9 \times 10^{-3}$ cm^3 mol^{-1}; $\mu_{obs} = 3.05$ μ_B. Elemental analysis: found (calc.): C, 33.23 (33.40); H, 4.79 (4.80); N, 15.91 (16.67)%.

‡ *Crystal data* for $Ir_2(hpp)_4Cl_2$: $C_{28}H_{48}N_{12}Ir_2Cl_2$, M = 1008.08, tetragonal, space group $P4/n$, a = 9.966(3), c = 15.907(6) Å, V = 1579.8(9) $Å^3$, Z = 2, μ(Mo-Kα) = 8.627 mm^{-1}. Data were collected at 213(2) K. The structure, refined on F^2, converged for 1036 unique reflections and 103 parameters to give $R1(F)$ = 0.038 and $wR2(F^2)$ = 0.080 with a goodness-of-fit of 1.150. CCDC 182/1318. See http://www.rsc.org/suppdata/cc/1999/1427/ for crystallographic data in .cif format.

1 F. A. Cotton and R. Poli, *Polyhedron*, 1987, **6**, 1625.
2 K. M. Dunbar, S. O. Majors and J. Sun, *Inorg. Chim. Acta*, 1995, **229**, 373 and references therein.
3 R. H. Crabtree, H. Felkin, G. E. Morris, T. J. King and J. A. Richards, *J. Organomet. Chem.*, 1976, **113**, C7.
4 R. O. Stevens, M. R. McLean, T. Wen, J. D. Carpenter, R. Bau and T. F. Koetzle, *Inorg. Chim. Acta*, 1989, **161**, 223.
5 F. A. Cotton and D. J. Timmons, *Polyhedron*, 1998, **17**, 179.
6 F. A. Cotton, J. H. Matonic and C. A. Murillo, *J. Am. Chem. Soc.*, 1997, **119**, 7889.
7 F. A. Cotton, C. A. Murillo and D. J. Timmons, unpublished work.
8 F. A. Cotton, J. Gu, C. A. Murillo and D. J. Timmons, *J. Am. Chem. Soc.*, 1998, **120**, 13 280.
9 J. L. Bear, Y. Li, B. Han and K. Kadish, *Inorg. Chem.*, 1996, **35**, 1395.
10 F. A. Cotton, J. Gu, C. A. Murillo and D. J. Timmons, *J. Chem. Soc., Dalton Trans.*, submitted.
11 F. A. Cotton, L. M. Daniels, C. A. Murillo and D. J. Timmons, *Chem. Commun.*, 1997, 1449.
12 F. A. Cotton and J. L. Thompson, *J. Am. Chem. Soc.*, 1980, **102**, 6437.
13 F. A. Cotton, G. Wilkinson, C. A. Murillo and M. Bochmann, *Advanced Inorganic Chemistry*, Wiley-Interscience, New York, 6th edn., 1999.

Communication 9/04698D

Self-assembled single-chain oligo(*p*-phenylene) amphiphiles: reversed micelles, vesicles and gels

Vladimir Sidorov,[a]† Trevor Douglas,[b] Sergey M. Dzekunov,[a] David Abdallah,[a] Bereket Ghebremariam,[a] Paul D. Roepe[a] and Stefan Matile*[a]‡

[a] *Department of Chemistry, Georgetown University, Washington, DC 20057-1227, USA. E-mail: matiles@gusun.georgetown.edu*

[b] *Department of Chemistry, Temple University, Philadelphia, 19122-2585, USA*

Received (in Cambridge, UK) 16th April 1999, Accepted 18th June 1999

The diverse supramolecular chemistry of a rigid, T-shaped single-chain amphiphile, including giant vesicles, spherical and tubular reversed micelles, and gels, is described in comparison to that of rigid-rod amphiphiles of different length.

Classical surfactants are single-chain amphiphiles that consist of a flexible lipophilic chain attached to a hydrophilic head group.[1–5] To better organize their dynamic micellar or vesicular suprastructures, design and synthesis of single-chain amphiphiles with either very short (< 11 Å)[2,4] or very long (rod-coil polymers)[6] rigid-rod subunits have been the subject of recent pioneering reports. Despite the potential importance for modern-day nanotechnology and biophysics, comparable studies with oligomeric rigid-rod single-chain amphiphiles are rare, presumably because of the formidable synthetic challenges involved.[7–9] We have recently considered self-assembly of oligo(*p*-phenylene) amphiphiles (*e.g.* **1**–**4**, Fig. 1) as a possible explanation for the poor binding of rigid-rod guests with either asymmetric (*e.g.* **1**) or hydrophobically mismatched (*e.g.* **3**, **4**) scaffolds to lipid bilayer hosts.[8–11] Here we report self-assembly of 'rigid-T' single-chain amphiphile **1** into giant vesicles ($\mathbf{1_v}$), reversed micelles ($\mathbf{1_m}$), and aqueous gels ($\mathbf{1_g}$) in comparison to amphiphilic oligo(*p*-phenylene) rods of different length (**2**–**4**) that yield vesicles only.

'Rigid-rod' vesicles $\mathbf{1_v}$–$\mathbf{3_v}$ were prepared with entrapped HPTS (8-hydroxypyrene-1,3,6-trisulfonic acid, a water soluble fluorescence probe). To obtain vesicles, fully hydrated mixed micellar solutions containing **1**–**4** (2 mM), octyl D-glucopyranoside (70 mM), HPTS (100 μM), and buffer (5–10 mM $Na_nH_{3-n}PO_4$, 0–100 mM NaCl, pH 6.4) were dialysed at 60–70 °C to remove detergent and external HPTS.[9–11] On the other hand, reversed micelles $\mathbf{1_m}$ were made from a solution of 'rigid-T' amphiphile **1** in biphasic systems composed of a nonpolar solvent (*e.g.* $CHCl_3$, CH_2Cl_2, xylene) and either acidic (pH 1, $\mathbf{1_{m(a)}}$) or basic (pH 13, $\mathbf{1_{m(b)}}$) water with HPTS. After brief sonication, rhythmical shaking (1 h, 1300 rpm), and centrifugation (10 min, < 3000*g*), most of the aqueous layer was a milky, foamlike emulsion. This emulsion was stable for more than two weeks but transformed into a gel ($\mathbf{1_g}$, gel point: 1.0 mg ml^{-1})[12] within 3–5 h after removal of the organic phase containing micellar $\mathbf{1_m}$.

The spectroscopic changes of rigid-rod chromophores **1**–**4** upon self-assembly, namely hypo-/hypsochromism of the ^1L transitions and bathochromic shifts for emission maxima, are listed in Table 1. The effects reached from minor changes for 'rigid T's' ($\mathbf{1_v}$/$\mathbf{1_m}$) to unambiguous H-aggregation[13] for rigid rods $\mathbf{2_v}$ and $\mathbf{3_v}$. This implied herringbone-type packing for self-assembled rods of 30 to 40 Å length with multiple constructive π–π-interactions at least for the latter case. An increased tendency toward herringbones for longer rods may further account for crystallization ($\mathbf{4_c}$) instead of vesiculation of deci(*p*-phenylene) **4** under identical conditions.

Consistent with the spectroscopic trends, differential scanning calorimetry (DSC) gave phase transitions for $\mathbf{1_v}$ but not for $\mathbf{2_v}$, $\mathbf{3_v}$ and $\mathbf{4_c}$. No distinct transitions for $\mathbf{1_g}$ indicated that vesicular $\mathbf{1_v}$ and the (according to cross-polarizing optical microscopy) amorphous crystalline gel strands in $\mathbf{1_g}$ were of different nature. Studies of the presumably involved bilayers with (Fig. 1a) or without (Fig. 1b) interdigitating 'T's' are ongoing to delineate the usefulness of rigid-T vesicles $\mathbf{1_v}$ with

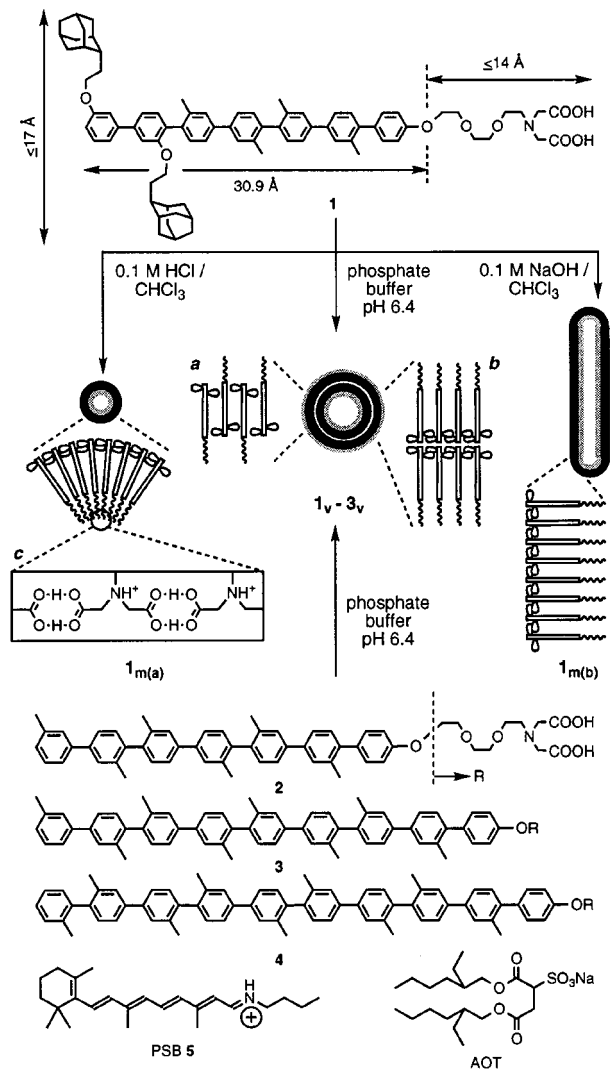

Fig. 1 Structure of oligo(*p*-phenylene)s **1**–**4**, PSB **5**, and AOT; schematic suprastructures for vesicular ($\mathbf{1_v}$–$\mathbf{3_v}$) and micellar ($\mathbf{1_m}$) self-assemblies.

† Present address: Department of Chemistry, University of Maryland, College Park, MD, USA.

‡ Present address: Department of Organic Chemistry, University of Geneva, Geneva, Switzerland.

Table 1 Spectroscopic data for self-assembled amphiphilic oligo(*p*-phenylene)s

	1[a]/Å	Micrographs[b]	λ^{e}_{max}/nm ($\Delta\lambda^{e}_{max}$/nm)[c]	λ^{a}_{max}/nm ($\Delta\lambda^{a}_{max}$/nm)[d]	Hypo.[e]
$\mathbf{1_{m(a)}}$	30.9	Micelles	372 (+2)	288 (−2)	0.70
$\mathbf{1_v}$	30.9	Vesicles	375 (+5)	288 (−2)	0.71
$\mathbf{2_v}$	30.9	Vesicles	386 (+19)	274 (−12)	0.43
$\mathbf{3_v}$	39.4	Vesicles	374 (+9)	276 (−10)	0.53
$\mathbf{4_c}$	43.6	Microcrystals	369 (+2)	258 (−28)	0.20

[a] Calculated length of rigid-rod subunit. [b] SEM, phase-contrast and/or fluorescence microscopy. [c] λ^{3}_{max}: emission maxima, $\Delta\lambda^{e}_{max}$: λ^{e}_{max} of self-assembly − λ^{e}_{max} of monomer in THF. [d] λ^{a}_{max}: absorption maxima, $\Delta\lambda^{a}_{max}$: λ^{a}_{max} of self-assembly − λ^{a}_{max} of monomer in THF. [e] Hypochromism (ε^{a}_{max} of self-assembly/ε^{a}_{max} of monomer in THF).

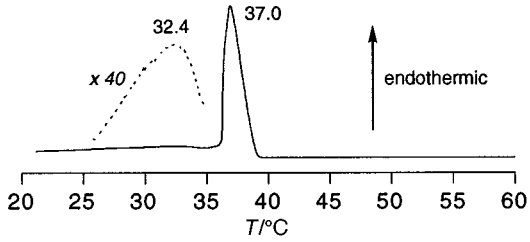

Fig. 2 DSC heating curve of $\mathbf{1_v}$ (scanning rate 1 °C min^{-1}).

T_c = 37.0 °C for applications such as temperature-controlled drug release (Fig. 2).

Optical fluorescence and phase-contrast micrographs contained mainly spherical microparticles for $\mathbf{1_v}$–$\mathbf{3_v}$ and $\mathbf{1_{m(a)}}$ with average diameters that increased with scaffold length and asymmetry ($\mathbf{2_v}$ < $\mathbf{3_v}$ < $\mathbf{1_{m(a)}}$ < $\mathbf{1_v}$, Fig. 3a). Microcrystals were observed for $\mathbf{4_c}$. Perhaps due to better resolution or, more likely, shrinking *in vacuo*, scanning electron microscopy (SEM) revealed nanoparticles for both 'rigid-T' vesicles ($\mathbf{1_v}$, Fig. 3b) and reversed micelles ($\mathbf{1_{m(a)}}$, Fig. 3c). Interestingly, vesicles ($\mathbf{1_v}$) appeared as cavities within precipitated $Na_nH_{3-n}PO_4$ buffer. The additional presence of '8-shaped' besides spherical vesicles implied facile fusion and fission (Fig. 3a/b).

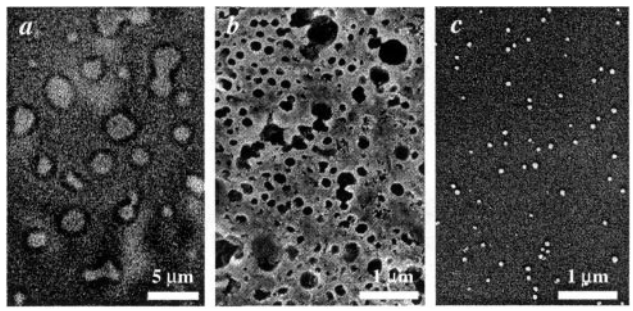

Fig. 3 Representative scanning electron and phase-contrast/fluorescence micrographs for self-assembled **1**–**3**. (a) Fluorescence micrograph for $\mathbf{3_v}$ (diameters: 1.7–3.3 μm). (b) Scanning electron micrograph for $\mathbf{1_v}$ (diameters: 80–260 nm). (c) Scanning electron micrograph for $\mathbf{1_{m(a)}}$ (diameters: 33–73 nm).

Compatibility with the harsh SEM-conditions indicated both stability and high water permeability. The latter was supported for $\mathbf{1_{m(a)}}$ in $CDCl_3$ by a water exchange rate of k = 1.7 ms^{-1} calculated from coalescence of the resonances for intramicellar bulk water (4.78 ppm, ω ([H_2O]/[**1**]) ≈ 100) and extramicellar acidic water (2.18 ppm) at 37.5 °C in the 300 MHz ^{1}H NMR spectra. Extraordinary stability of reversed micelles $\mathbf{1_{m(a)}}$ was further implied by the constant emission intensity of encapsulated HPTS upon dilution of $\mathbf{1_{m(a)}}$. Apparently, the critical micelle concentrations (cmc) of $\mathbf{1_{m(a)}}$ for formation (2 mM) and destruction (< 5 μM) differ significantly. Since rod-shaped **2**–**4** did not self-assemble under identical conditions, the T-shaped structure of **1** seems essential for micellization.[3] However, rapid destruction of $\mathbf{1_{m(a)}}$ by addition of $CuCl_2$, as well as a wormlike morphology for 'basic reversed micelles' $\mathbf{1_{m(b)}}$ (not shown) suggested additional importance of hydrogen bonding in between the hydrophilic iminodiacetate (IDA) termini of **1** for suprastructural organization and stabilization of $\mathbf{1_{m(a)}}$ (Fig. 1c).

Preliminary studies on reversed micelles $\mathbf{1_{m(a)}}$ as biomimetic receptor models revealed that protonated *N*-retinylidene-*n*-butylamine Schiff base (PSB) **5** bound to $\mathbf{1_{m(a)}}$ is not hydrolyzed by intramicellar bulk water.[5] The absorption maximum of PSB **5** surrounded by rigid-rod arene-arrays of the supramolecular host $\mathbf{1_{m(a)}}$ at 456 nm is 16 nm red-shifted compared to that of **5** within conventional AOT reversed micelles.[14] This observation reinforces the potential of $\mathbf{1_{m(a)}}$ as valuable biomimetic receptors. It is in support of the hypothesis that fine-tuning of the absorption of retinylidene Schiff base in bacteriorhodopsins may be governed by aromatic residues in the PSB binding pocket and/or by ring-chain coplanarization of PSB in addition to external point charges.[15]§

In summary, our results imply that single-chain 'rigid-T' amphiphiles are unique surfactants with suprastructural diversity beyond the limitations of comparable rigid-rod amphiphiles. Preliminary results with remarkably stable, water permeable, reversed micelles as biomimetic receptors and catalysts implied potential usefulness of 'rigid-T' amphiphiles in biological, organic and materials chemistry.

This research was supported by NIH (GM56147 (SM) and GM54516 (PDR)), an award from Research Corporation (SM), the donors of the Petroleum Research Fund, administered by the American Chemical Society (SM), Suntory Institute for Bioorganic Research (SUNBOR Grant (SM)), and Georgetown University. The authors thank Drs Naomi Sakai and Richard G. Weiss for discussion, and Dr Robert E. Bachman for access to DSC.

Notes and references

§ The effect of $\mathbf{1_{m(a)}}$ (160 μM in CH_2Cl_2) on the stereoselectivity of cyclopentadiene dimerization (*i.e.* an increasing relative yield of the *exo*-product from 14% to 27%) did not exceed the ordinary influence of reversed micelles.

1 J.-H. Fuhrhop and J. Köning, *Membranes and Molecular Assemblies: The Cytokinetic Approach*, The Royal Society of Chemistry, Cambridge, UK, 1994.
2 T. Kunitake, *Angew. Chem., Int. Ed. Engl.*, 1992, **31**, 709.
3 J. Israelachvili, *Intramolecular & Surface Forces*, 2nd edn., Academic Press, London, UK, 1991.
4 F. M. Menger and J. Ding, *Angew. Chem., Int. Ed. Engl.*, 1996, **35**, 2137.
5 A. Singh, C. Sandorfy and J. Fendler, *J. Chem. Soc., Chem. Commun.*, 1990, 233.
6 S. A. Jenekhe and X. L. Chen, *Science*, 1998, **279**, 1903.
7 J. M. Tour, *Chem. Rev.*, 1996, **96**, 537.
8 B. Ghebremariam, V. Sidorov and S. Matile, *Tetrahedron Lett.*, 1999, **40**, 1445.
9 B. Ghebremariam and S. Matile, *Tetrahedron Lett.*, 1998, **39**, 5335.
10 M. M. Tedesco, B. Ghebremariam, N. Sakai and S. Matile, *Angew. Chem., Int. Ed.*, 1999, **38**, 540.
11 C. Ni and S. Matile, *Chem. Commun.*, 1998, 755.
12 P. Terech and R. G. Weiss, *Chem. Rev.*, 1997, **97**, 3133.
13 B. Ghebremariam and S. Matile, *Enantiomer*, 1999, **4**, 127 and 139.
14 Y. Gat and M. Sheves, *J. Am. Chem. Soc.*, 1993, **115**, 3772.
15 H. Houjou, Y. Inoue and M. Sakurai, *J. Am. Chem. Soc.*, 1998, **120**, 4459.

Communication 9/03041G

Ionic liquids: a convenient solvent for environmentally friendly allylation reactions with tetraallylstannane

Charles M Gordon*[a] and Adam McCluskey*[b]

[a] *Department of Pure and Applied Chemistry, the University of Strathclyde, Thomas Graham Building, 295 Cathedral Street, Glasgow, UK G1 1XL. E-mail: c.m.gordon@strath.ac.uk*

[b] *Department of Chemistry, the University of Newcastle, University Drive, Callaghan, NSW 2308, Australia. E-mail: amcclusk@mail.newcastle.edu.au*

Received (in Liverpool, UK) 6th May 1999, Accepted 15th June 1999

Ionic liquids based on the 1-butyl-3-methylimidazolium cation have been used as solvents for the preparation in good yield of homoallylic alcohols from tetraallylstannane and a range of aldehydes.

In recent years chemists have striven to develop new synthetic methodologies and techniques which are more environmentally benign, work generally referred to under the title of 'clean technology'. Organostannanes are extremely useful reagents in organic synthesis, but are also notoriously environmentally unfriendly due to the presence of toxic tin residues. There have been a number of attempts to develop cleaner organostannane reagents and reaction conditions. Examples include the development of polymer supported organostannanes,[1] the use of water as solvent,[2] and water-soluble reagents.[3]

Room temperature ionic liquids are attracting increasing interest as environmentally benign reaction media for organic and organometallic synthetic chemistry, for example Friedel–Crafts[4] and hydrogenation reactions.[5] These solvents possess a number of interesting properties, notably their lack of vapour pressure, ease of reuse, lack of flammability, and large accessible temperature range. Furthermore, by alteration of the cation and anion it is possible to adjust the solubility properties of an ionic liquid, for example making it immiscible with water or certain organic solvents. Recent studies on Diels–Alder reactions in ionic liquids based on the 1-alkyl-3-methylimidazolium cation in conjunction with a variety of anions (*e.g.* PF_6^- and BF_4^-) have suggested reactivity patterns similar to those observed in alcoholic solvents.[6,7] Herein we report for the first time the combination of organostannane chemistry and ionic liquid methodology.

The allylation of aldehydes to produce homoallylic alcohols is a useful organic transformation, which has attracted considerable attention in recent years.[8] The most common method is the use of metal–allyl complexes, and one of us (AM) has recently reported the use of tetraallylstannane (**1**) for allylation under very mild conditions (Table 1).[9]

The reaction was found to be most efficient when carried out in MeOH solution. **1** has a number of advantages as a reagent compared with the allyltrialkylstannanes traditionally used for such reactions. In particular, all of the allyl ligands are transferred, leaving the tin by-product in the form of inorganic salt which is much more easily separated from the reaction mixture than organostannane residues resulting from allyltrialkylstannane reactions. Most importantly from a clean chemistry standpoint, as each molecule of **1** will react with four separate aldehyde molecules the reaction is extremely 'atom efficient', since the only reagent atom not incorporated into the product is tin.

The reaction of a range of aromatic and aliphatic aldehydes with **1** was investigated. In a typical experiment, the chosen aldehyde was stirred at room temperature for 16 h with 0.25 equiv. of **1** dissolved in 2 ml of the chosen ionic liquid. The ionic liquids employed were 1-butyl-3-methylimidazolium tetrafluoroborate ([bmim][BF_4]) and hexafluorophosphate ([bmim][PF_6]), which were prepared by literature methods.[10] On completion of the allylation reaction the ionic liquid was observed to be cloudy. Work-up was achieved simply by extraction of the reaction mixture with Et_2O followed by removal of the solvent.† This approach generally allowed isolation of products of excellent purity, unreacted starting material being the only contaminant in some cases, as discussed below. The cloudy residue was assumed to be the tin by-product, and this did not transfer into the Et_2O extracts. The yields obtained are listed in Table 1. Product characterisation was carried out using ^1H and ^{13}C NMR spectroscopy.

As can be seen in Table 1, excluding entry 5 the yields varied from 66–93% depending on the nature of the aldehyde employed. Such values are in good agreement with those previously reported for the equivalent reaction in MeOH solution.[9] Reactions were judged to have gone to completion if the ^1H and ^{13}C NMR spectra showed no signals for the aldehyde group. It should be noted that the small scale on which the reactions were carried out meant that mechanical losses were proportionately quite large, so larger scale preparations would be expected to give higher yields. The allylation of benzaldehyde in [bmim][PF_6] was investigated on a larger scale to confirm this. When 2.50 g of **1** (8.87 mmol) was reacted with 3.765 g of benzaldehyde (35.46 mmol) in 10 ml of ionic liquid, an isolated yield of 5.17 g (96%) of the homoallylic alcohol was obtained.

The reaction was observed to proceed to completion with simple aromatic aldehydes like benzaldehyde (entry 1). Similar behaviour was observed when electron-withdrawing substituents were present (*e.g. p*-Cl, entry 2), and the presence of weakly electron-donating substituents did not appear to hinder the reaction significantly. Thus good yields were obtained in the reactions of tolualdehyde (entry 3) and anisaldehyde (entry 4).

Table 1 Yields of homoallylic alcohol using [bmim][BF_4] and [bmim][PF_6] ionic liquids

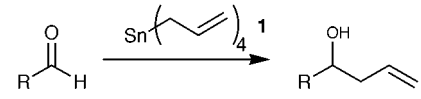

Entry	R	Yield (%) [bmim][BF_4]	[bmim][PF_6]
1	Ph	79[a]	82[a]
2	*p*-ClC_6H_4	93[a]	82[a]
3	*p*-MeC_6H_4	80[b]	72[b]
4	*p*-$MeOC_6H_4$	84[a]	76[b]
5	*p*-$Me_2NC_6H_4$	0	0
6	Pr	70[b]	70[b]
7	C_5H_{12}	72[b]	74[b]
8	*trans*-PhC=CMe	69[b]	66[b]
9	(*S*)-$Me_2C{=}CH(CH_2)_2CHMeCH_2$	73[b]	78[b]

[a] Isolated yield. [b] NMR yields.

Table 2 Results obtained using recycled ionic liquids

Entry	R	Cycle	Yield (%) [bmim][BF_4]	Yield (%) [bmim][PF_6]
1	Ph	1	79[a]	82[a]
2	Ph	2	82[a]	81[a]
3	Ph	3	78[a]	83[a]

[a] Isolated yield.

When a strongly electron-donating substituent such as Me_2N was present, however, only starting materials were obtained on work-up (entry 5). The greatly reduced reaction rate with electron-donating substituents was also observed in the reactions carried out in MeOH solution.[9]

The presence of significant amounts of unreacted **1** in the organic extracts from the reactions involving simple aliphatic aldehydes suggested that these did not go to completion (entries 6 and 7). No traces of unreacted aldehyde were observed in these cases, but these are probably sufficiently volatile to be lost during work-up. Traces of **1** were also found in the reaction products of *trans*-2-methylcinnamaldehyde (entry 8), suggesting that here too the reaction was incomplete. Yields obtained in all three cases were reasonable despite this.

The product of the (*S*)-(−)-citronellal reaction (entry 9) can contain both *threo*- and *erythro*-isomers. The NMR spectra suggested that any selectivity was modest at best, with peaks corresponding to each isomer being of almost identical intensity. This is perhaps not surprising given the combination of the small size of the methyl group and its distance from the reactive site. Similarly small degrees of selectivity have been reported in the crotylstannationation of citronellal carried out in aqueous solution using (*E/Z*)-Bu_2(MeCH=$CHCH_2$)SnCl.[11]

In general it was found that there was no contamination of the products with tin by-products when the reaction proceeded to completion. This was confirmed by recording ^{119}Sn NMR spectra of the organic products, which indicated that no tin was present in any form. In cases where partial conversion was observed, however, some **1** was found in the organic extracts. No contamination of the products with ionic liquid was observed, however. The reaction between **1** and benzaldehyde was monitored using ^{119}Sn NMR spectroscopy to attempt to determine the fate of the tin residues. A signal corresponding to **1** was observed at −45.8 ppm before addition of the benzaldehyde. This disappeared rapidly when the reagents were mixed, but no further ^{119}Sn signals were observed in either the ionic liquid or the organic product. The reaction was accompanied by the formation of an insoluble white residue, more noticeable than in the preparative experiments due to the lower volume of ionic liquid employed. Attempts were made to identify this species, but it proved to be relatively insoluble in all solvents investigated, and no signals were seen in the ^{119}Sn spectrum. It should be noted that these results contrast strongly with ^{119}Sn investigations carried out on the reaction in MeOH solution, where no insoluble product was observed, and signals were seen in the region −600 to −640 ppm which were assigned to polymeric tin(IV) methoxide species.[9c]

Little difference was found in the yields obtained using the two different solvents. Recycling of the ionic liquid was carried out for the reaction of benzaldehyde following an extremely straightforward protocol.‡ The results gained are shown in Table 2. It can be seen that no decrease in yield was observed in runs carried out using 'old' ionic liquid, and furthermore the products obtained were of the same purity as in the first run. In the case of the recycled $[PF_6]^-$ salt the purification removed all of the cloudy residue, while some cloudiness was observed in the recycled $[BF_4]^-$ salt, but this did not seem to impair the performance of the liquid.

At present the mechanism of the reaction is not clear. Previous studies on the reaction in MeOH have suggested the presence of an eight-membered ring transition state involving both reactants and the solvent.[9] The results presented here do not give any direct clue as to the role of the ionic liquid in this reaction. Further mechanistic investigations are currently in progress.

In conclusion, ionic liquids appear to be excellent solvents in which to carry out allylation reactions using tetraallylstannane. The reaction proceeds most readily with aromatic aldehydes, provided that no strongly electron donating substituent is present. The reaction is less rapid in aliphatic aldehydes, but it should be stressed that all of the investigations reported here were carried out at 15 °C. Allylation of an aldehyde containing a chiral centre gave little evidence for stereoselectivity in the reaction, although the example chosen was relatively unfavourable. Separation of the products from the ionic liquid is very straightforward, as is recycling of the liquid. The latter will be an important concern if ionic liquids are truly to be considered environmentally friendly solvents. Future work will address the reaction of a wider range of substrates, and a mechanistic investigation will be attempted, part of which will be an attempt to identify the insoluble tin by-product of the reaction.

We would like to thank the Royal Society of Edinburgh for the award of a BP Research Fellowship (C. M. G.), the University of Newcastle (A. M.) for financial support, and Dr Phil Dennison for assistance with the ^{119}Sn NMR spectroscopy.

Notes and references

† *Typical procedure for the allylation of alkanals by tetraallylstannane in ionic liquids.* Benzaldehyde (106 mg, 1 mmol) was placed in a 5 ml reaction vial with a spin vane. To this was added 2 ml of [bmim][BF_4] followed by tetraallylstannane (70.7 mg, 0.25 mmol), the septum cap was replaced, and the mixture stirred vigorously at room temperature (typically 15 °C) for 16 h. After this time the mixture was extracted with Et_2O (3 × 10 ml), the organic extracts were combined and dried over anhydrous $MgSO_4$. The Et_2O was removed *in vacuo* to yield a pale oil, 117 mg (79%).

‡ *Recycling of ionic liquids.* After complete reaction and work-up as described above, the ionic liquid could be used with no further treatment. Since this would result in the build-up of tin residues over a period of time, however, the procedure generally employed was to dissolve the ionic liquid in EtOAc (10 ml), and wash with water (2 × 5 ml) and brine (5 ml). Addition of Et_2O (20 ml) caused two layers to form, the lower being essentially pure ionic liquid.

1 W. P. Neumann and J. Junggebauer, *Tetrahedron*, 1997, **53**, 1361.
2 A. McCluskey, *Green Chem.*, 1999, **1**, 167.
3 R. Breslow and J. Light, *Tetrahedron Lett.*, 1990, **31**, 2957.
4 C. J. Adams, M. J. Earle, G. Roberts and K. R. Seddon, *Chem. Commun.*, 1998, 2097.
5 P. J. Dyson, D. J. Ellis, D. G. Parker and T. Welton, *Chem. Commun.*, 1999, 25.
6 (*a*) M. J. Earle, P. B. McCormac and K. R. Seddon, *Green Chem.*, 1999, **1**, 23; (*b*) T. Fischer, A. Sethi, T. Welton and J. Woolf, *Tetrahedron Lett.*, 1999, **40**, 793.
7 J. A. Berson, Z. Hamlet and W. A. Mueller, *J. Am. Chem. Soc.*, 1962, **84**, 297.
8 For reviews see: Y. Yamamoto and N. Asao, *Chem. Rev.*, 1993, **93**, 2207; J. A. Marshall, *Chem. Rev.*, 1996, **96**, 31
9 (*a*) A. Yanagisawa, H. Inoue, M. Morodome and H. Yamamoto, *J. Am. Chem. Soc.*, 1993, **115**, 10 356; (*b*) T. M. Cokley, R. L. Marshall, A. McCluskey and D. J. Young, *Tetrahedron Lett.*, 1996, **37**, 1905; (*c*) T. M. Cokley, P. J. Harvey, R. L. Marshall, A. McCluskey and D. J. Young, *J. Org. Chem.*, 1997, **62**, 1961; (*d*) A. McCluskey, I. Wayan Muderawan, Muntari and D. J. Young, *Synlett*, 1998, **8**, 909.
10 J. S. Wilkes and M. J. Zaworotko, *J. Chem. Soc., Chem. Commun.*, 1992, 965.
11 D. Furlani, D. Marton, G. Tagliavini and M. Zordan, *J. Organomet. Chem.*, 1988, **341**, 345.

Communication 9/03661J

ChemComm

Monomeric magnesium 1-azaallyl and β-diketiminato complexes derived from the bis(trimethylsilyl)methyl ligand: The X-ray structure of the four-coordinate planar magnesium complex [Mg{N(R)C(Bu^t)C(H)R}$_2$] and of [Mg({N(R)C(Ph)}$_2$CH)$_2$]†

Catherine F. Caro, Peter B. Hitchcock and Michael F. Lappert*

The Chemistry Laboratory, University of Sussex, Brighton,UK BN1 9QJ. E-mail: m.f.lappert@sussex.ac.uk

Received (in Basel, Switzerland) 25th May 1999, Accepted 17th June 1999

Reaction of [K{N(R)C(Bu^t)C(H)R}]$_n$ {[K(LL′)]$_n$} or [Li({N(R)C(Ph)}$_2$CH)]$_2$ {≡ [Li(LL)]$_2$} with magnesium bromide yielded the monomeric, crystalline magnesium complexes [Mg(LL′)$_2$] 1 or [Mg(LL)$_2$] 2, which have been structurally characterised; 1 has the magnesium atom in an unusual planar environment.

Monomeric magnesium complexes containing monoanionic bidentate ligands are rare. Four-coordinate examples have been based upon an alkyl-functionalised pyridyl or a 1,4-diazabutadiene ligand, [Mg{CR$_2$(C$_5$H$_4$N-2)}$_2$][1] or [Mg{N(Bu^t)(CH)$_2$N-(Bu^t)}$_2$][2] (R = SiMe$_3$), while the benzamidinate ligand [N(R)C(Ph)NR]$^-$ has generated a range of solvated monomeric Mg complexes [Mg{N(R)C(Ph)NR}$_2$L$_n$] (L = absent; L = PhCN, n = 1; or L = thf and n = 2).[3] Recent examples of main group metal β-diketiminates include [Al{N(*p*-Tol)C-(Me)C(H)C(Me)N(*p*-Tol)}Cl$_2$][4] (*p*-Tol = *p*-C$_6$H$_4$Me) and [Ba$_3$\{N(R′)C(Me)C(H)C(Me)NR′\}$_3$(NR$_2$)] (R = SiMe$_3$, R′ = C$_6$H$_{11}$).[5] The synthesis and reactions of some alkali metal α,ω-bis(trimethylsilyl)-1-azaallyl and α,β-diketiminates, including their role in preparing unusual transition metal and main group element complexes has been reviewed.[6] We now report the syntheses and structures of the magnesium bis(1-azaallyl) [Mg(LL′)$_2$] **1** (Scheme 1, step i) and bis(β-diketiminate) [Mg(LL)$_2$] **2** (Scheme 1, step ii) and the subsequent reaction of **1** with PhCN to yield the asymmetric β-diketiminato complex [Mg(LL″)$_2$] **3** (Scheme 1, step iii) [LL′ = N(R)C(Bu^t)C(H)R, LL = N(R)C(Ph)C(H)C(Ph)NR, LL″ = N(R)C(Bu^t)C(H)-C(Ph)NR, R = SiMe$_3$].

The new, pale yellow, air-sensitive, readily hydrocarbon-soluble, crystalline solids **1**–**3** gave satisfactory elemental analyses, NMR spectroscopic‡ and X-ray (**1** and **2**)§ data.

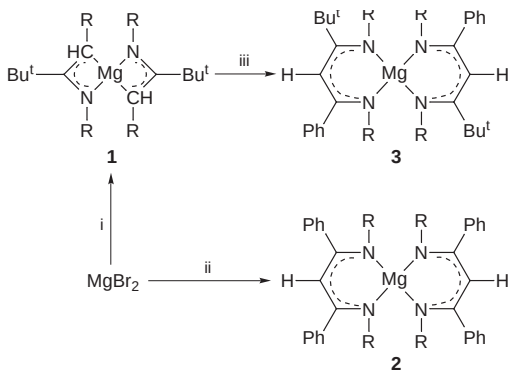

Scheme 1 Synthesis of the magnesium bis(1-azaallyl) and β-diketiminates **1**–**3**. *Reagents and conditions*: i, 2 K(LL′), pentane, 16 h, *ca*. 25 °C; ii, [Li(LL)]$_2$, pentane, 16 h, *ca*. 25 °C; iii, 2 PhCN, Et$_2$O, 2 h, −78 °C [LL′ = N(R)C(Bu^t)C(H)R, LL = {N(R)C(Ph)}$_2$CH].

† No reprints available.

The X-ray molecular structures of crystalline **1** and **2** are shown in Figs. 1 and 2.§ Especially noteworthy is that the centrosymmetric **1** exhibits a very unusual planar coordination geometry around the magnesium centre (*cf.*[1] the distorted tetrahedral geometry in [Mg{CR$_2$(C$_5$H$_4$N-2)$_2$}]). The ligands in **1** are bonded in a *trans*-chelate fashion forming with the magnesium atom a chair skeletal conformation. The angle

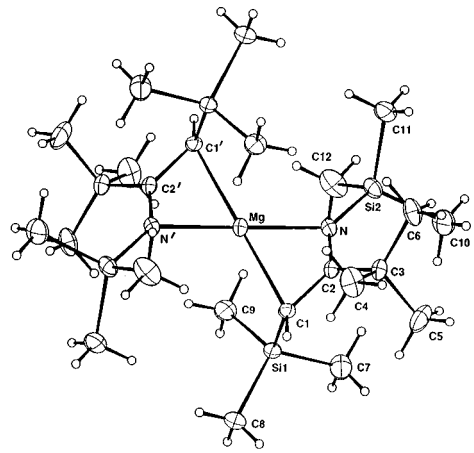

Fig. 1 Molecular structure of **1** with selected bond distances (Å) and angles (°): Mg–N 2.084(3), Mg–C(1) 2.284(4), Mg–C(2) 2.408(4), N–C(2) 1.347(5), C(1)–C(2) 1.405(6), C(2)–C(3) 1.546(6); N–Mg–N′ 180.0, C(1)–Mg–C(1)′ 180.0, N–Mg–C(1) 64.27(14), C(2)–N–Mg 86.3(2), N–Mg–C(1)′ 115.73(14), N–C(2)–C(1) 115.7(4), C(2)–N–Si(2) 140.7(3).

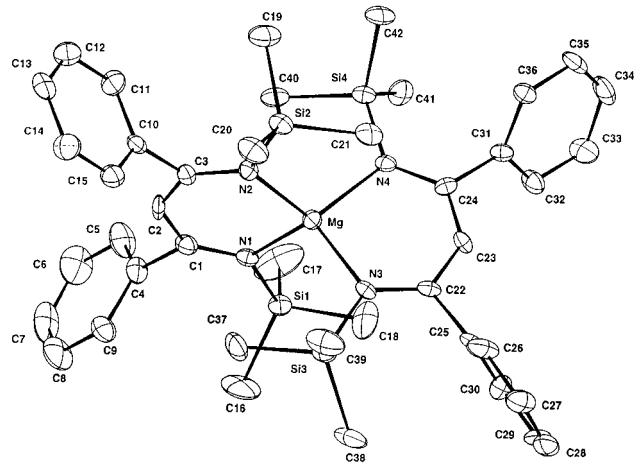

Fig. 2 Molecular structure of **2** with selected bond distances (Å) and angles (°): Mg–N(1) 2.096(8), Mg–N(2) 2.068(8), N(1)–C(1) 1.299(11), C(1)–C(2) 1.432(13), C(2)–C(3) 1.403(13), C(3)–N(2) 1.318(11), C(1)–C(4) 1.499(14); N(1)–Mg–N(2) 99.7(3), N(1)–Mg–N(3) 114.3(3), N(1)–Mg–N(4) 113.6(3), Mg–N(2)–C(3) 117.0(6), Mg–N(1)–C(1) 116.6(7), C(1)–C(2)–C(3) 131.5(9).

between the planes NC(2)C(1) and MgNC(1)N′C(1)′ is *ca.* 46°; the Mg–C(2) distance of 2.408(4) Å is too long for a single bond but lies within the sum of the van der Waals radii. The Mg–N bond of 2.084(3) Å is longer than the terminal Mg–N bonds [1.975(7) Å] in the three-coordinate magnesium amide [Mg(μ-NR_2)(NR_2)]$_2$,[7] but shorter than in the related magnesium complex [Mg{CR_2(C_5H_4N)-2}$_2$] (2.13(1) Å).[1] The N–C and C–C bond lengths lie in between values for single and double bonds; therefore, a degree of π-delocalisation is assumed. 'Ideal' planar magnesium geometry exists in the (tetraphenylporphyrinato)magnesium bis(methyl benzoate) clathrate.[8] Porphyrins are so rigid, that they often form a nearly planar geometry about a metal;[8–10] however, the 1-azaallyl ligand is not rigid and therefore it is very surprising that **1** is planar. This unusual geometry has also been observed for the Group 2 metal compound, [*trans*-Sr(NR_2)$_2$(μ-1,4-dioxane)], where the unexpected stereochemistry about the strontium atom was attributed to agostic intramolecular CH···Sr interactions [Sr···C 3.16(1) Å] with resultant widening of the Si–N–Si angles to 126.4°; the environment about the strontium atom was then best described as quasi-octahedral.[11] The polymeric dialkylmagnesium compound [Mg(CHR_2)$_2$]$_\infty$ is stabilised by intermolecular interactions of 2.535(4) Å between each magnesium atom and a γ-methyl group of a neighbouring Mg(CHR_2)$_2$.[12] In **1**, the closest possible intramolecular contacts (from a methyl group to the magnesium atom) are Mg···H 2.626(3) Å and Mg···C(9) 2.897(3) Å (within the limits of van der Waals forces); however, no significant lengthening of the C(9)–Si(1) bond or distortion of the geometry about the methyl group was observed. The large C(2)–N–Si(2) bond angle of 140.7(3)° in **1** may be due to steric repulsion between the $SiMe_3$ and Bu^t groups as no distortion of the geometry about the Si atoms was observed.

Preliminary first principle AIMPRO (a local density functional, pseudo-potential code[13]) calculations on the whole, isolated molecule, support the planar structure, being 9 kJ mol^{-1} lower in energy than the tetrahedral structure.¶ Such a small energy difference is possibly beyond the accuracy of the code, but indicates the viability of the planar Mg structure. Further calculations will be reported in the full paper. Using the CAChe™ mechanics program, using an enhanced MM2 parametrised force field,[14] we found that the tetrahedral structure is disfavoured by virtue of interligand repulsion between an $SiMe_3$ at the γ-C of one ligand and $SiMe_3$ at N of the other.

Crystalline **2** is the first structurally authenticated example of a simple magnesium β-diketiminate [a macrocyclic bis(ketiminate) is known[15]]. In **2** the magnesium atom is in a distorted tetrahedral environment. The ligands bind η^2 to the magnesium atom through the nitrogen atoms with no observed interactions from the C(1), C(2) or C(3) atoms to the magnesium, as in the related Li complex.[5] Each MgNCCCN skeleton is planar, as also is the case in the isoleptic transition metal Co^{II}, Ni^{II}, Cu^{II} or Pd^{II} compounds,[6,16] and in Sn(LL)Cl. This differs from the situation found in the complexes [Li(LL)]$_2$,[6] [Sn(LL)Me_3][6] or [Al(LL)Me_2][17] in which MLL is boat-shaped, [LL]$^-$ having some η^5- character. It may be that the latter group of complexes favour the boat conformation not only because of their having strong Lewis acid metal sites, but also because the metal is coordinatively unsaturated. Calculations will be reported in the full paper.

The two ligands in **2** are almost orthogonal to one another. The N–C and C–C bond lengths lie in between those for single and double N–C and C–C bonds. This, combined with the coplanarity of each ring, shows that there is a degree of π-delocalisation. The four Mg–N bond lengths in **2** are identical within estimated standard deviations and are similar to values reported for [Mg{N(Bu^t)$(CH)_2$N(Bu^t}$_2$].[2] The monomeric nature of **2** is presumably due to the $SiMe_3$ ligands preventing further attack at the metal centre, demonstrated by the relatively air-stable nature of **2**, as well as its surprising inertness to reaction with small donor molecules (*e.g.* PhCN), metal halides or even protic species.

We are grateful to Dr M. Heggie for the AIMPRO calculations, Professor F. G. N. Cloke for the CAChe™ data and thank EPSRC and FMC Corporation (Bromsgrove and Dr F. Reed) for a CASE award for C. F. C.

Notes and references

‡ Selected spectroscopic data [^{1}H at 300 MHz and ^{13}C{^{1}H} at 62.9 MHz in C_6D_6 (**1**–**3**)]. **1**: ^{1}H δ 0.29 ($SiMe_3$, s), 0.33 ($SiMe_3$, s), 1.19 (Bu^t, s) and 3.40 (CH, s); ^{13}C{^{1}H} δ 74.8 (CH) and 207.5 (C(2)). **2**: ^{1}H δ 0.32 ($SiMe_3$, s) and 5.23 (CH, s); ^{13}C{^{1}H} δ 3.8 ($SiMe_3$) and 107.7 (CH). **3**: ^{1}H δ 0.31 ($SiMe_3$, s), 0.73 ($SiMe_3$, s), 0.97 (Bu^t, s) and 5.52 (CH, s); ^{13}C{^{1}H} δ 104.6 (CH).

§ *Crystal data* for **1** and **2**: data for each of **1** and **2** were collected at 173(2) K on an Enraf-Nonius CAD4 diffractometer in the ω-2θ mode in the range $2 < \theta < 25°$ (**1**) or 23° (**2**). The structures were refined by full-matrix least squares on all F^2 (SHELXL 93).

1: $C_{24}H_{56}MgN_2Si_4$, M = 509.4, orthorhombic space group *Pbca*, a = 10.929(2), b = 17.815(4), c = 16.857(6) Å, U = 3282(2) Å^3, Z = 4, D_c = 1.03 g cm^{-3}, μ(Mo-Kα) = 0.21 mm^{-1}. Final residuals were R_1 = 0.064, for the 1729 with $I > 2\sigma(I)$ and wR_2 = 0.183 for all 2875 reflections.

2: $C_{42}H_{58}MgN_4Si_4{\cdot}C_5H_{12}$, M = 827.74, monoclinic space group $P2_1/c$ (no.14), a = 12.078(4), b = 35.114(8), c = 12.123(3) Å, β = 104.25(2)°, U = 4983(2) Å^3, Z = 4, D_c = 1.10 g cm^{-3} μ(Mo-Kα) = 0.17 mm^{-1}. Final residuals were R_1 = 0.094, for the 2971 with $I > 2\sigma(I)$, and wR_2 = 0.290 for all 6923 reflections. CCDC 182/1320.

¶ AIMPRO is a density functional code using non-conserving pseudopotentials, a wave function basis of atom-centred s,p Gaussians and a charge density fitted to s Gaussians. Three independent Gaussian exponents were used for H (for which the bare Coulomb potential was used), four for C and five each for N, Si and Mg. Geometry optimisation was by conjugate gradient and the local density approximation was employed.

1 M. J. Henderson, R. I. Papasergio, C. L. Raston, A. H. White and M. F. Lappert, *J. Chem. Soc., Chem. Commun.*, 1986, 672.
2 M. G. Gardiner, G. R. Hanson, M. J. Henderson, F. C. Lee and C. L. Raston, *Inorg. Chem.*, 1994, **33**, 2456.
3 (*a*) M. Westerhausen and H.-D. Hausen, *Z. Anorg. Allg. Chem.*, 1992, **615**, 27; (*b*) P. G. H. Uiterweerd, *DRS Thesis*, University of Groningen, 1997.
4 B. Qian, D. L. Ward and M. R. Smith, *Organometallics*, 1998, **17**, 3070.
5 W. Clegg, S. J. Coles, E. K. Cope and F. S. Mair, *Angew. Chem., Int. Ed.*, 1998, **37**, 796.
6 M. F. Lappert and D.-S. Liu, *J. Organomet. Chem*., 1995, **500**, 203.
7 M. Westerhausen and W. Schwarz, *Z. Anorg. Allg. Chem*., 1992, **609**, 39.
8 M. P. Byrn, C. J. Curtis, I. Goldberg, Y. Hsiou, S. I. Khan, P.A. Sawin, S. K. Tendick and C. E. Strouse, *J. Am. Chem. Soc*., 1991, **113**, 6549.
9 M. P. Byrn, C. J. Curtis, Y. Hsiou, S. I. Khan, P. A. Sawin, S. K. Tendik, A. Terzis and C. E. Strouse, *J. Am. Chem. Soc*., 1993, **115**, 9480.
10 N. S. Mani, L. S. Beall, T. Miller, O. P. Anderson, H. Hope, S. R. Parkin, D. J. Williams, A. G. M. Barrett and B. M. Hoffman, *J. Chem. Soc., Chem. Commun*., 1994, 2095.
11 F. G. N. Cloke, P. B. Hitchcock, M. F. Lappert, G. A. Lawless and B. Royo, *J. Chem. Soc., Chem. Commun.*, 1991, 724.
12 P. B. Hitchcock, J. A. K. Howard, M. F. Lappert, W.-P. Leung and S. A. Mason, *J. Chem. Soc., Chem. Commun.*, 1990, 847.
13 R. Jones and P. R. Briddon, *Identification of Defects in Semiconductors*, in *Semiconductors and Semimetals*, ed. M. Stavola, Academic Press, New York, 1997.
14 N. L. Allinger, *J. Am. Chem. Soc.*, 1977, **99**, 8127.
15 F. Corazza, C. Floriani, A. Chiesi-Villa, C. Guastini and S. Ciurli, *J. Chem. Soc., Dalton Trans.*, 1988, 2341.
16 J. R. Severn, *D.Phil. Thesis*, University of Sussex, 1998; R. Sablong, unpublished work, University of Sussex.
17 F. Coslédan, P. B. Hitchcock and M. F. Lappert, *Chem. Commun.*, 1999, 705.

Communication 9/04196F

Specific crosslinking of cell adhesive molecules by heterobifunctional glycopeptide synthesised on the basis of chemoenzymatic strategy

Shin-Ichiro Nishimura,*[a] Masao Matsuda,[a] Hidemitsu Kitamura[b] and Takashi Nishimura[b]

[a] *Laboratory for Bio-Macromolecular Chemistry, Division of Biological Sciences, Graduate School of Science, Hokkaido University, Sapporo 060-0810, Japan. E-mail: shin@glyco.sci.hokudai.ac.jp*

[b] *Division of Host Defense Mechanisms, Department of Immunology, Tokai University School of Medicine, Isehara 259-1193, Japan*

Received (in Cambridge, UK) 1st June 1999, Accepted 22nd June 1999

Heterobifunctional glycopeptide 1 composed of Neu5Acα-(2→3)Galβ(1→4)[Fucα(1→3)]GlcNAc (sialyl Lewis^x) and Lys-Gly-Arg-Gly-Asp-Ser (KGRGDS) having specific activity to bind concurrently with two different types of cell adhesive molecules such as selectins and integrins was synthesised on the basis of a combined chemical and enzymatic strategy.

It has been well documented that many kinds of cell adhesive molecules (CAMs) participate in a variety of biological phenomena such as cell–cell interactions and cell–extracellular matrix (ECM) interactions.[1–6] It should also be noted that collaboration of multiple and complex bindings between different types of cell surface receptors and their ligands greatly contribute to the construction of stable and specific cellular society.

In the present study, we designed a heterobifunctional glycopeptide **1** as a novel and potential glycoligand, because this artificial glycopeptide composed of Neu5Acα(2→3)Galβ≙(1→4)[Fucα(1→3)]GlcNAc (sialyl Lewis^x) and Lys-Gly-Arg-Gly-Asp-Ser (KGRGDS) was supposed to interact with two different types of families of cell adhesive proteins such as selectins and integrins concurrently. This type of synthetic heterobifunctional glycopeptide is strongly expected to become a novel class of antiflammatory and anticancer 'glycodrugs'.[7–9] Kunz *et al*. have reported a significant '*cis*' type interaction of the synthetic RGDS-sialyl Lewis^x with P-selectin as an IC_{50} value of 26 μM. In addition to this type of enhanced affinity of glycoligand with protein, we found an interesting '*trans*' type interaction of a novel glycoligand **1** involving a flexible peptide linker with two different protein receptors. Fig. 1 summarises some plausible mechanisms of '*cis*' and '*trans*' type interactions of glycoligand **1** with cell adhesive proteins.

Scheme 1 indicates a retrosynthetic route for compound **1**. Firstly, a key intermediate **2** was prepared by chemical synthesis from a simple *n*-pentenyl glycoside of *N*-acetyllactosamine **5**[10] and tetrapeptide derivative **4** as starting materials (Scheme 2). The terminal double bond of compound **5** was converted into a carboxy group by treating with potassium permanganate in 87% yield and the active ester of **6** was employed for the coupling reaction with the ε-amino group of Z-lysine to afford **7** in 71% yield. To achieve satisfactory flexibility in the spacer-arm between sialyl Lewis^x and RGDS and versatility in further chemical manipulation, H-Gly-OBn was combined with **7** to give *N*-acetyllactosamine-dipeptide derivative **8** in 83% yield. Consequently, deprotection of the benzyl ester and *O*-acetyl groups of **8** under alkaline conditions was allowed to proceed smoothly and gave compound **3** in 87% yield without racemization. Coupling reaction of the glycopeptide **3** with an unprotected disaccharide moiety with an amino-terminus generated from RGDS derivative **4** was carried out by employing diphenylphosphoryl azide[11] as a selective promoter of the carboxy group of the glycopeptide. A hexapeptide derivative **9** was obtained in 77% yield with no side reaction at the free hydroxy groups of the carbohydrate moiety. Removal of all

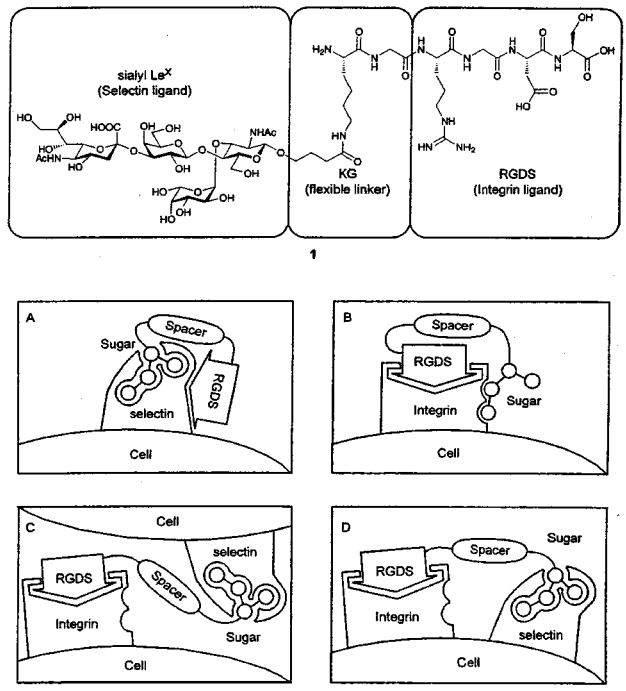

Fig. 1 Chemical structure of **1** and plausible mechanisms of binding of **1** with receptor molecules. (A) and (B) represent cooperative-type '*cis*' interactions, and (C) and (D) represent crosslinking-type '*trans*' interactions (crosslinking by glycopeptide), respectively.

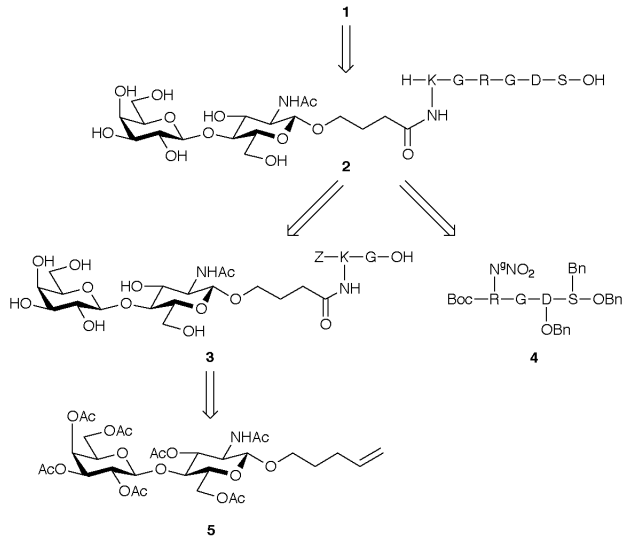

Scheme 1 Retrosynthetic route to cell adhesive glycopeptide **1** (CAGP **1**).

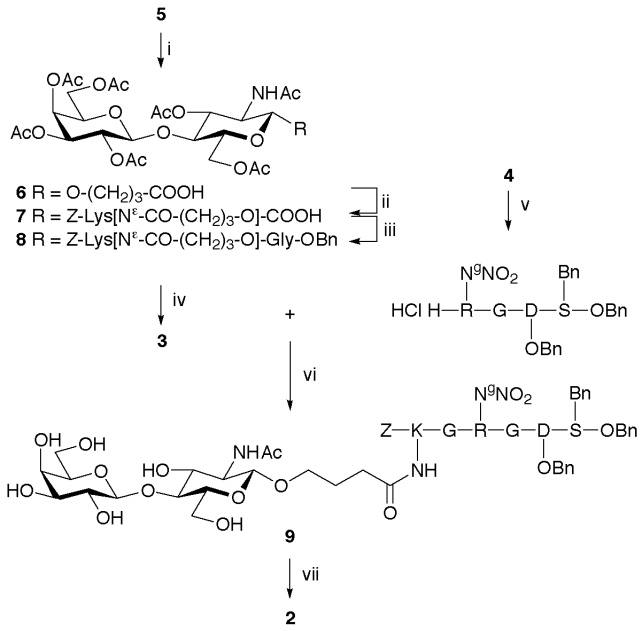

Scheme 2 *Reagents and conditions*: i, $KMnO_4$, AcOH aq., rt, 87%; ii, HONSu, DCC, DMF, 0 °C→rt, then Z-Lys, TEA, DMF–H_2O (9:1), rt, 71%; iii, DPPA, Gly-OBn, TEA, DMF, 0 °C→rt, 83%; iv, NaOMe, dry MeOH, rt, then 1 M NaOH aq., rt, ion exchange resin (Dowex 50W-X8), 87%; v, 2 M HCl–dioxane, 0 °C→rt; vi, DPPA, TEA, DMF, 0 °C→rt, 77% (over all yield from **4**); vii, Pd/C, H_2 gas, MeOH–H_2O, (1:1) rt, 99%.

protecting groups of the peptide moiety of **9** such as benzyl, nitro, and benzyloxycarbonyl groups was performed by standard hydrogenation in the presence of palladium on charcoal to give the intermediate **2** in 92% yield.

Subsequently, the glycopeptide **2** was employed as a substrate for the corresponding glycosyltransferases. It is of interest to examine the substrate specificity of the enzymatic glycosyltransfer reactions against non-natural glycopeptide **2**, since acceptability of synthetic glycoconjugates to the glycosyltransferases depends strongly on the nature of aglycons or supporting backbones.[12] In fact, a synthetic hexapeptide bearing an *N*-acetyllactosamine side chain through an appropriate hydrophobic linker (**2**) was proved to be an excellent substrate both for α(2"→3)sialyltransferase and for α(1→3)fucosyltransferase. The sialylation and fucosylation of compound **2** proceeded smoothly and glycopeptide **1** was isolated by preparative HPLC in 45% overall yield from **2** (Scheme 3).

The effect of hybridisation of the functional carbohydrate and peptide on the '*cis*' type interaction between glycoligand **1** and each protein was investigated by surface plasmon resonance (SPR). As anticipated, compound **1** binds P- and E-selectins more strongly than native sialyl Lewis^x, and association constants of **1** with P- and E-selectins were assumed to be 6.6×10^7 M^{-1} and 4.5×10^5 M^{-1}, respectively. It was also found that **1** inhibited interaction of human integrin β_1 with its monoclonal antibody more effectively than RGDS (IC_{50} = 0.55 mM).

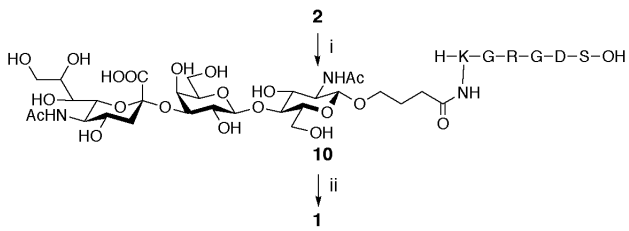

Scheme 3 *Reagents and conditions*: i, **2** (20 mg), CMP-Neu5Ac (25 mg), α-2,3-sialyltransferase (0.3 unit), calf intestine alkaline phosphatase (20 unit), BSA (10 mg), $MnCl_2 \cdot 4H_2O$, Triton CF-54, 50 mM sodium cacodylate buffer (2.0 mL, pH 7.4), 37 °C, 3 d, 80%; ii, **10** (15 mg), GDP-Fuc (10.3 mg), α-1,3-fucosyltranseferase V (10 munit), calf intestine alkaline phosphatase (1 unit), NaN_3, $MnCl_2 \cdot 4H_2O$, 100 mM HEPES buffer (1.0 mL, pH 7.5), 37 °C, 3 d, 56%.

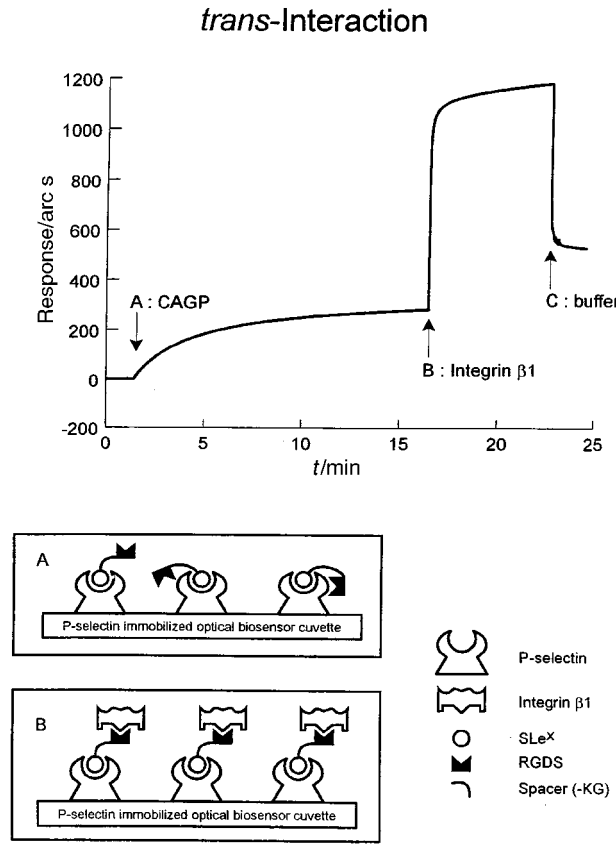

Fig. 2 Crosslinking of selectin and integrin by cell adhesive glycopeptide (CAGP) monitored by SPR method. The first arrow 'A' indicates the time point of the beginning of the injection of cell adhesive glycopeptide (20 μL, 1.3 mg mL^{-1}) to the P-selectin immobilised cuvette. The second arrow 'B' indicates the time point of the injection of integrin β1 (20 μL, 9.1 μg mL^{-1}) to this cuvette. The third arrow 'C' indicates the beginning of the buffer washout (200 μL of phosphate buffer solution). Integrin β1 was found to bind to CAGP-P-selectin complex as indicated by a significant increase in the response unit.

These successful results of cooperative '*cis*' interactions prompted us to examine the artificial crosslinking of selectin and integrin by the synthetic glycoligand. As indicated in Fig. 2, glycopeptide **1** exhibited the specific capacity to bind P-selectin and human integrin β_1 concurrently. We also have evidence that **1** could block the integrin-mediated adhesion of activated T cells to a collagen-coated plate at the same level as inhibition by a monoclonal antibody to integrin. Therefore, it is strongly suggested that synthetic glycopeptide **1** will become an effective practical tool, 'cell adhesive glycopeptide (CAGP)', to modulate immune responses through its inhibitory effect on lymphocyte-endothelial cell interaction.

Notes and references

1 T. A. Springer, *Nature*, 1990, **346**, 425.
2 R. O. Hynes and A. D. Lander, *Cell*, 1992, **68**, 303.
3 L. A. Lasky, *Science*, 1992, **258**, 964.
4 E. A. Clark and J. A. Ledbetter, *Nature*, 1994, **367**, 425.
5 L. Steinman, *Cell*, 1995, **80**, 7.
6 E. C. Butcher and L. J. Picker, *Science*, 1996, **272**, 60.
7 M. Matsuda and S.-I. Nishimura, *Peptide Chem.*, 1996, **1995**, 381.
8 U. Sprengard, G. Kretzschmar, E. Bartnik, C. Huls and H. Kunz, *Angew. Chem., Int. Ed. Engl.*, 1995, **34**, 990.
9 M. D. Pierschbacher, E. G. Hayman and E. Ruoslahti, *Proc. Natl. Acad. Sci. U.S.A.*, 1983, **80**, 1224.
10 S.-I. Nishimura, K. Matsuoka, T. Furuike, S. Ishii, K. Kurita and K. M. Nishimura, *Macromolecules*, 1991, **24**, 4236
11 T. Tsuda and S.-I. Nishimura, *Chem. Commun.*, 1996, 2779.
12 S.-I. Nishimura and K. Yamada, *J. Am. Chem. Soc.*, 1997, **119**, 10 555.

Communication 9/04362D

Ruthenium-catalysed multiple component transformations: one-step stereoselective synthesis of functional dienes from alkynes and carboxylic acids

Jacques Le Paih, Sylvie Dérien and Pierre H. Dixneuf*

UMR 6509 CNRS-Université de Rennes, Organométalliques et Catalyse: Chimie et Electrochimie Moléculaires, Campus de Beaulieu, 35042 Rennes, France. E-mail: pierre.dixneuf@univ-rennes1.fr

Received (in Liverpool, UK) 7th May 1999, Accepted 22nd June 1999

The precatalyst RuCl(cod)C_5Me_5 allows the head-to-head oxidative dimerization of terminal alkynes and the concommittent 1,4-addition of carboxylic acid to afford (1*E*,3*E*)-1-acyloxy-1,3-dienes in one step under mild conditions.

The development of catalysis towards the selective combination of several simple substrates to afford in one step a unique functional molecule in high yield constitutes an important contribution to the discovery of new synthetic methods for environmental impact. These reactions require toxic reagents to be banished, high selectivity and atom economy to avoid costly separations. Multiple component reactions selectively combining several molecules into only one[1,2] *via* the formation of more than two bonds constitute an important challenge for chemists. Recently, ruthenium catalysts, in particular, have been shown to promote the one-step addition of three simple substrates. Representative examples deal with the selective formation of polycyclic compounds,[3] bicyclic phenols,[4] tricyclic hydroquinones[5] or cyclopentenones *via* the catalytic trifunctional Pauson–Khand reaction.[6] The combination of functional arene derivatives with alkene and carbon monoxide *via* the activation of the inert (sp^2)C–H bond has led to aryl ketones.[7] 1,5-Diketones and (*E*)-vinyl chlorides can also be obtained in one step by three component addition of alkyne, unsaturated ketone and water,[8] or NH_4Cl,[9] respectively. The combination of two molecules of acetylene and acrylonitrile has just been achieved by a ruthenium catalyst and affords the heptatrienenitrile.[10]

We have shown recently that the catalyst precursor RuCl(cod)C_5Me_5 promotes the oxidative coupling of C≡C and C=C bonds of alkynes and allyl alcohol to generate either γ,δ-aldehydes[11] or performs the three-component synthesis of methylenetetrahydropyran acetal derivatives.[12] We now report a novel regio- and stereo-selective, three-component catalytic synthesis of functional 1,3-dienes, by one-step combination of two molecules of terminal alkynes and one of carboxylic acid to easily afford (1*E*,3*E*)-1,4-disubstituted-1-acyloxybuta-1,3-dienes [eqn. 1)].

The reaction of 2.5 mmol phenylacetylene with 1.25 mmol acetic acid in the presence of 5 mol% of RuCl(cod)C_5Me_5 (**A**) in 1 mL dioxane affords, after 20 h at room temperature 90% of only the (1*E*,3*E*)-1,4-diphenyl-1-acyloxybuta-1,3-diene **3a** stereoisomer [eqn. (2)]. This reaction corresponds to the highly regioselective head-to-head coupling of terminal alkynes with stereoselective 1,4-addition of the proton and the carboxylate. The stereochemistry of **3a** was established by NMR and NOE experiments.† The addition of $MeCO_2D$ to 2 equiv. of phenylacetylene, catalysed by 5% of **A**, afforded the corresponding PhCD=CH–CH=C(OAc)Ph derivative **3b** and showed the selective 1,4-addition of acetic acid to the conjugated diene skeleton.

The efficiency of the reaction drastically depends on the nature of the solvent. After 15 h the previous reaction leading to **3a**, performed at room temperature led to 37, 41, 49, 75 and 77% phenylacetylene conversion in toluene, CH_2Cl_2, MeCN, THF and dioxane, respectively. The corresponding addition of acetic acid to *p*-methoxyphenylacetylene and *p*-cyanophenylacetylene led to 85% of **4** and 81% of **5**, but after 42 and 0.5 h,

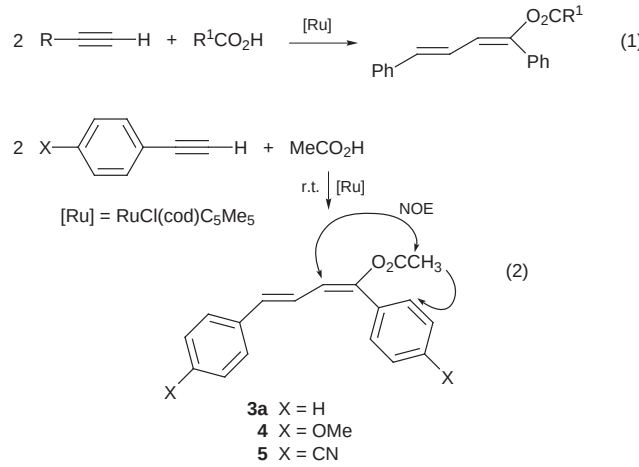

respectively, at room temperature [eqn. (2)], showing that an electron-withdrawing group on the phenyl ring drastically favours the reaction. The reaction also proceeds with alkylacetylenes but with a lower efficiency as hex-1-yne and oct-1-yne are transformed, under the **3a** formation conditions, into (1*E*,3*E*)-RCH=CH–CH=C(OAc)R **1** (R = Bu^n, 20%) and **2** (R = C_6H_{13}, 40%).

A variety of carboxylic acids have been added to phenylacetylene in the presence of catalyst **A** at room temperature and the corresponding dienes **6** were obtained (Scheme 1). It thus appears that strong carboxylic acids give a low yield of diene (**6a**: 30%), and the weaker acids ($pK_a > 4$) afford quantitative yields after 16–18 h of catalytic reaction at room temperature (**6d**–**6f**).

It has been shown recently that RuCl(cod)C_5R_5 precursors react with terminal alkynes to give, after cod ligand displacement, a complex resulting from the head-to-head, oxidative coupling of two molecules of alkyne at the ruthenium site[10,13,14] to give either a bis-carbene derivative[13,14] or, when a phosphine ligand is coordinated, a ruthenacyclopentadiene.[10] Moreover, we have shown that the addition of two equivalents of phenylacetylene to precursor **A** led to the formation and isolation of the metallacycle **B**, with a bis-carbene structure

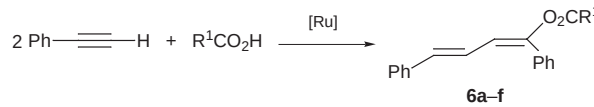

	R^1	*t*/h	Yield (%)
a	$CHCl_2$	15	30
b	CH_2CN	18	85
c	H	20	62
d	CH_2OMe	18	95
e	Ph	16	98
f	Bu^t	16	91

Scheme 1 *Reaction conditions*: alkyne (2.5 mmol), catalyst **A** (0.125 mmol), acid (1.25 mmol), dioxane (1 ml), stirred at room temperature for various reaction times (15–20 h).

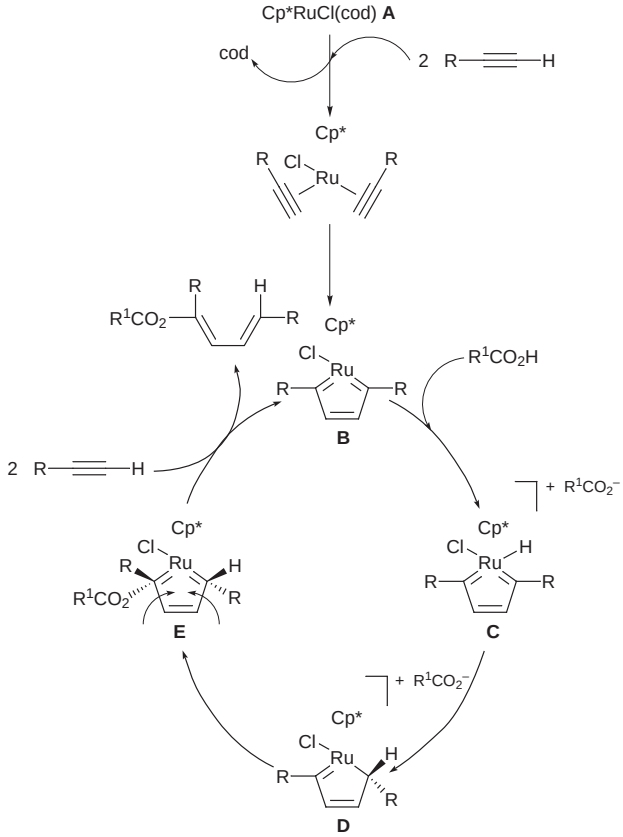

Scheme 2

(Scheme 2) which was previously obtained *via* a different route.[14] Consequently, Scheme 2 provides a possible mechanism leading to the formation of dienes **3**–**6**. Protonation of bis-carbene intermediate **B** can lead to the species **D**, *via* known carbene ligand insertion into a M–H bond.[15] The direct protonation of the carbene atom of **B** to afford **D** in one step cannot be ruled out. The species **E** arising from carboxylate addition to **D** is expected to generate (1*E*,3*E*)-dienes **3**–**6**. In support of this mechanism we have shown that the isolated complex **B** catalyses the formation of **3a** under conditions reported in Scheme 1 and that the substitution of acetic acid by NaO_2CMe in THF does not lead to any transformation of either phenylacetylene or complex **B**.

The above catalytic reaction represents a new example of multiple component addition of type 2A + B → C, performed under mild conditions with atom economy. It offers potential for the stereoselective preparation of functional dienes by 1,4-addition to the ruthenacycle intermediate resulting from oxidative coupling of two alkyne molecules at the ruthenium centre.

The authors are grateful to Dr Christian Bruneau for helpful discussions and MENRT for the award of a thesis grant to J. L. P.

Notes and references

† *Selected data* for **3a** Ph–C^4H=C^3H–C^2H=$C^1(O_2CCH_3)$Ph: δ_H ($CDCl_3$, 300 MHz) 2.23 (s, 3H, O_2CCH_3), 6.30 (d, 1H, *J* 11.2, H^2), 6.68 (d, 1H, *J* 15.6, H^4), 6.98 (dd, 1H, J_1 11.2, J_2 15.6, H^3), 7.3–7.5 (m, 10H, Ph). δ_H(C_6D_6, 300 MHz) 1.71 (s, 3H, O_2CCH_3), 6.31 (d, 1H, *J* 11.1, H^2), 6.49 (d, 1H, *J* 15.1, H^4), 7.00–7.16 (m, 9H, Ph + H^3), 7.46–7.54 (m, 2H, Ph). NOE experiments show the relative *cis* position of H2 and the O_2CCH_3 group. In $CDCl_3$, the irradiation at δ 2.23 leads to an increase in 2% of the signal at δ 6.30 (H2). In C_6D_6, irradiation at δ 1.71 leads to an increase in 1.5% of the signal of the two *ortho* protons of the phenyl group between δ 7.46 and 7.54 and an increase in 2% of the signal at δ 6.31 (H2). But the irradiation at δ 6.31 (H3) has no influence on the signals at δ 7.46 and 7.54 or δ 1.71.

1 I. Ugi, *Angew. Chem.*, 1962, **74**, 9; A. Dömling and I. Ugi, *Angew. Chem., Int. Ed. Engl.*, 1993, **32**, 563.
2 L. F. Tietze and U. Beifuss, *Angew. Chem.*, 1993, **105**, 137; L. F. Tietze and U. Beifuss, *Angew. Chem., Int. Ed. Engl.*, 1993, **32**, 131; G. H. Posner, *Chem. Rev.*, 1986, **86**, 831 ; B. M. Trost, *Angew. Chem., Int. Ed. Engl.*, 1995, **34**, 259.
3 Y. Yamamoto, H. Kitahara, R. Hattori and K. Itoh, *Organometallics*, 1998, **17**, 1910.
4 N. Chatani, Y. Fukumoto, T. Ida and S. Murai, *J. Am. Chem. Soc.*, 1993, **115**, 11 614.
5 T. Morimoto, N. Chatani, Y. Fukumoto and S. Murai, *J. Org. Chem.*, 1997, **62**, 3762; T. Kondo, N. Suzuki, T. Okada and T. Mitsudo, *J. Am. Chem. Soc.*, 1997, **119**, 6187.
6 N. Suzuki, T. Kondo and T. Mitsudo, *Organometallics*, 1998, **17**, 766.
7 N. Chatani, Y. Ie, F. Kakiuchi and S. Murai, *J. Org. Chem.*, 1997, **62**, 2604; E. J. Moore, W. R. Pretzer, T. J. O'Connell, J. Harris, L. LaBounty, L. Chou and S. S. Grimmer, *J. Am. Chem. Soc.*, 1992, **114**, 5888.
8 B. M. Trost, M. Portnoy and H. Kurihara, *J. Am. Chem. Soc.*, 1997, **119**, 836.
9 B. M. Trost and A. B. Pinkerton, *J. Am. Chem. Soc.*, 1999, **121**, 1988.
10 C. S. Yi, J. R. Torres-Luhian, N. Liu, A. L. Rheingold and I. A. Guzei, *Organometallics*, 1998, **17**, 1257.
11 S. Dérien, D. Jan and P. H. Dixneuf, *Tetrahedron*, 1996, **52**, 5511.
12 S. Dérien, L. Ropartz, J. Le Paih and P. H. Dixneuf, *J. Org. Chem.*, 1999, **64**, 3524; S. Dérien, B. Gomez-Vicente and P. H. Dixneuf, *Chem. Commun.*, 1997, 1405.
13 M. O. Albers, D. J. A. de Waal, D. C. Liles, D. J. Robinson, E. Singleton and M. B. Wiege, *J. Chem. Soc., Chem. Commun.*, 1986, 1680.
14 C. Gemel, A. La Pensée, K. Mauthner, K. Mereiter, R. Schmid and K. Kirchner, *Monatsh. Chem.*, 1997, **128**, 1189.
15 H. Le Bozec, J.-L. Fillaut and P. H. Dixneuf, *J. Chem. Soc., Chem. Commun.*, 1986, 1182; V. A. Osborn, A. Craig and M. J. Winter, *J. Chem. Soc., Chem. Commun.*, 1986, 1185.

Communication 9/03805A

ChemComm

Reaction of *N*-methyldihydropyridines with alkoxycarbene complexes of chromium and tungsten: sequential use of three carbonyl ligands of $Cr(CO)_6$ for the formation of polyoxygenated compounds

Henri Rudler,*[a] Andrée Parlier,[a] Blanca Martin-Vaca,[a] Eva Garrier[a] and Jacqueline Vaissermann[b]

[a] *Laboratoire de Synthèse Organique et Organométallique, UMR 7611, Université Pierre et Marie Curie T44-45, 4 place Jussieu 75252, Paris Cedex 5, France. E-mail: rudler@ccr.jussieu.fr*

[b] *Laboratoire de Chimie des Métaux de Transition, URA 419, Université Pierre et Marie Curie T44-45, 4 place Jussieu 75252, Paris Cedex 5, France.*

Received (in Liverpool, UK) 30th April 1999, Accepted 18th June 1999

***N*-methylpyridinium ylide complexes obtained from alkoxycarbene complexes of chromium and *N*-methyldihydropyridines easily insert successively a CO ligand to give α-alkoxy chromium acyl complexes, then a tethered triple bond and two additional CO groups to yield bicyclic butenolides.**

The use of stoichiometric amounts of transition metal complexes for the synthesis of organic compounds can only be acceptable if elaborate molecules are obtained and if, ideally, most of the ligands around the metal center can be incorporated in the final products. As examples of such reactions we can cite those involving Fischer carbene complexes for the cyclopropanation of olefins,[1] and for the synthesis of phenols[2] and pyrrolinones[3] from alkynes. As far as the balance of the metal ligands in these reactions is concerned, whereas only one CO ligand is used in the first case to form the carbene group which is then transferred to the double bond, two CO ligands of $M(CO)_6$ are incorporated in the two latter examples, one for the formation of the starting carbene complexes, the other one for the formation of respectively a phenol and a lactam.

The purpose of this communication is to describe for the first time a straightforward, room temperature triple insertion of CO groups from $Cr(CO)_6$ *via* carbene complexes, providing finally polycyclic polyoxygenated compounds *without* the need of external CO.[4]

The starting carbene complexes, containing either a tethered triple or double bond, were prepared from $Cr(CO)_6$ and $W(CO)_6$ *via* known routes.[5,6] Interaction of **1a** (M = Cr, R^1 = CH_2Ph) (2.02 g, 4.2 mmol) in CH_2Cl_2 (110 ml) at −10 °C, with an excess (3 equiv., 0.84 ml) of a mixture of 1,2 and 1,4 *N*-methyldihydropyridines in CH_2Cl_2 (10 ml) gave after 12 h at room temperature, the tetrahydrobenzofuranones **2a** (0.95 g, 65%) as a 77:23 mixture of two diastereoisomers which could be separated by fractional crystallization into an oil for the major isomer and white crystals (mp 153 °C) for the minor one. The microanalysis confirmed the insertion of two CO groups in the organic ligand of complex **1a**.† Both the IR spectrum (νCO, 1751 cm^{-1}, νC=C, 1662 cm^{-1}) and the ^{13}C NMR spectrum (δ CO, 172.9 and δ C≡C, 161.2 and 124.9) were in agreement with the presence of a butenolide. The fitting of the various carbon atoms was established by extensive NMR spectroscopy. The structure of the minor stereoisomer could finally be assessed by an X-ray analysis (Fig 1).‡ It confirmed the reduction of the starting carbene complex, the insertion of the triple bond and of two CO ligands and also established the stereochemistry of the various substituents with respect to H-7a, the hydrogen at the ring junction. The stereochemistry of the major product could be assessed by ^1H–^1H COSY and NOE experiments: in both compounds, the benzyl group is equatorial and *trans* with respect to H-7a.

Complex **1b** (M = Cr, R^1 = H) behaved similarly and led to a 10:1 mixture of diastereoisomers **2b**, the less abundant being obtained as white crystals, mp 90 °C. Its structure and thus the relative stereochemistry was again established both by NMR and by X-ray crystallography.§

When the same reaction was carried out on complex **1a** (M = W, R^1 = CH_2Ph), then the course of the reaction was different: product **3a** was isolated in 62% yield as a 2:1 mixture of isomers which were separated by silica gel chromatography. The NMR data of the minor isomer (yellowish crystals, mp 78 °C) confirmed the presence of a low field singlet at δ 7.70, of two diasteretopic hydrogens of an ethoxy group and of a carbonyl group, δ CO 200.7, belonging to a cyclohexenone.¶ Confirmation of structure **3** arose again from an X-ray analysis (Fig. 2).‡ As far as the mechanism of these transformations is concerned, we had already established that alkoxycarbene

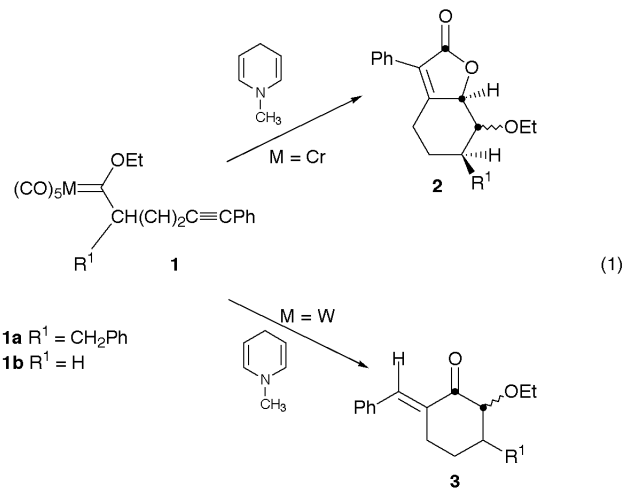

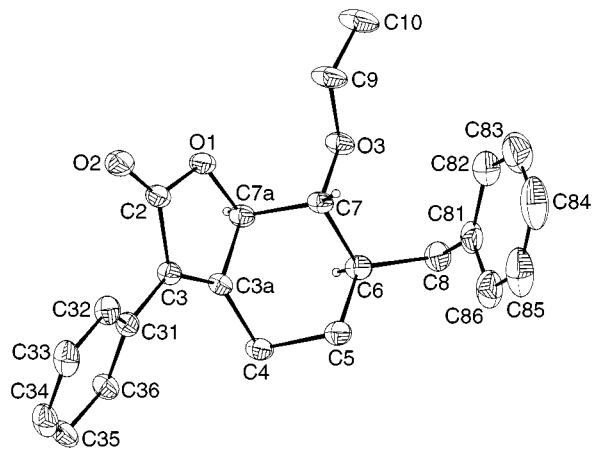

Fig. 1

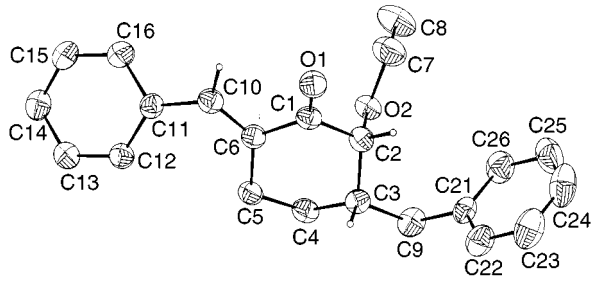

Fig. 2

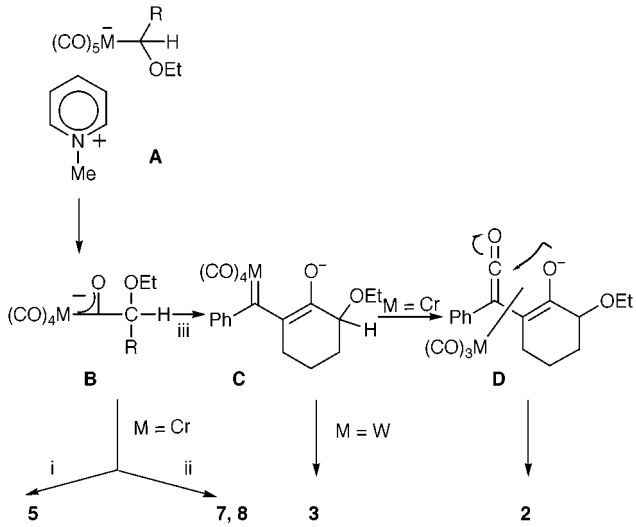

Scheme 1 i, R = Ph; ii, R = $(CH_2)_2CH{=}CH_2$; iii, R = $(CH_2)_3C{\equiv}CPh$.

complexes of chromium and tungsten were reduced by *N*-methyldihydropyridines into pyridinium metallates **A** (Scheme 1).[7]

Two sets of reactions allowed the assessement of the origin of **2** and **3** starting from the intermediate **A**: first, the reaction of **4** with *N*-methyldihydropyridines in the presence of cyclopent-2-en-1-one led to the 1,4 dicarbonyl compound **5** in 53% yield. This confirmed the formation of an ethoxy acyl metallate **B** from **A** and its addition to the conjugated ketone.[8–10]

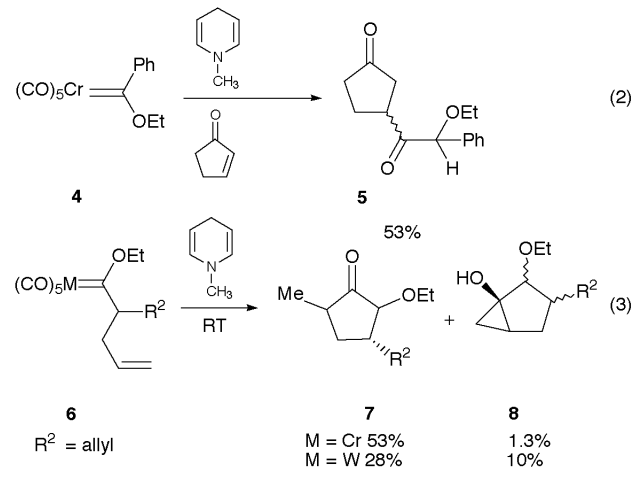

Second, reaction of complex **6** containing a tethered double bond led to a mixture of two possible products, **7** as the result of its intramolecular cyclopropanation by the oxycarbene function of **B**, and **8**, as the result of its insertion in the metal acyl bond of **B**.

If instead the R group in **A** and **B** contains a triple bond, then its insertion into the metal–carbon double bond of the oxycarbene complex **B** leads to a new carbene complex **C**: in the case of tungsten, no further reaction but protonation takes place giving **3**.

In the case of chromium, an additional CO insertion occurs leading to a ketene complex **D**. A nucleophilic intramolecular interaction between the oxygen atom and the central carbon of the ketene function, a reaction which has been well established in the case of aminocarbene complexes, will then give the lactone **2**.[3,10]

Thus, starting from $M(CO)_6$, and depending on the nature of the metal, either two (M = W) or three CO groups (M = Cr) were inserted leading to elaborate, functionalized molecules.This result confirms again the higher propensity of chromium to induce the insertion of carbonyl ligands and demonstrates for the first time that up to three carbonyl ligands of $Cr(CO)_6$ can be used as successive building blocks.

Notes and references

† *Selected data* for **2a**: δ_H 7.46–7.18 (m, 1H, ArH), 4.84 (d, *J* 4, 1H, H-7a), 4.20 (m, 1H, O*CH*), 3.70 (m, 1H, O*CH*), 3.35 (dd, *J* 13.5 and 8, 1H, Ph*CH*), 3.00 (dd, *J* 10.2 and 8.2, 1H, H-7), 2.98 (m, 1H, H-4), 2.35 (dd, *J* 13.5 and 9.6, 1H, Ph*CH*), 2.21 (dt, *J* 13.7 and 5, 1H, H-4), 1.96 (m, 2H, H-6, H-5), 1.33 (t, *J* 7.1, 3H, CH_3), 1.07 (m, 1H, H-5); δ_C 172.9, 162.2, 140.1, 129.9–124.9, 86.5, 86.4, 68.3, 43.2, 37.9, 29.4, 25.9, 16.0. Found: C, 79.24; H, 7.00. Calc. for $C_{23}H_{24}O_3$: C, 79.31; H, 6.89%.

‡ *Crystal data* for $C_{23}H_{24}O_3$ **2a**; *M* = 348.4, monoclinic, space group *Pc*, *a* = 11.198(5), *b* = 6.867(1), *c* = 12.192(18) Å, β = 90.26(7)°, *Z* = 2, D_c = 1.23 g cm^{-3} , μ = 0.75 cm^{-1}. 3075 data collected at room temperature on a Nonius CAD4 diffractometer. No absorption correction was applied. Anomalous dispersion terms and correction of secondary extinction were applied. The structure was solved by direct methods (SHELXS)[11] and refined by least-squares analysis using anisotropic thermal parameters for all non-hydrogen atoms. H atoms were located on a difference Fourier map, and only one overall isotropic parameter was refined. 1806 reflections, with $I < 3\sigma(I)$ were used to solve and refine the structure to R = 0.0511 and R_w = 0.0643 (Chebychev weighting scheme), 237 least-squares parameters. The programs used were CRYSTALS and CAMERON. For $C_{22}H_{24}O_2$ **3a**; *M* = 320.4, monoclinic, space group: $P2_1/n$, *a* = 9.028(4), *b* = 8.436(8), *c* = 24.178(8) Å, β = 99.33(3)°, *Z* = 4, D_c = 1.17 g cm^{-3}. 3663 data collected and structure solved as above with 1319 reflections to R = 0.0544 and R_w = 0.0645. CCDC 182/1297. See http://www.rsc.org/suppdata/cc/1999/1439/ for crystallographic data in .cif format.

§ The crystals of **2b** were not satisfactory for a precise X-ray structure determination.

¶ *Selected data* for **3a**: δ_H 7.70 (s, 1H, =*CH*Ph), 7.30–7.12 (m, 10H, ArH), 4.35–4.27 (dq, *J* 8.9 and 7.0, 1H, O*CHH*), 3.59–3.51 (dq, *J* 8.9 and 7.0, 1H, O*CHH*), 3.45 (d, *J* 10, 1H, O*CH*), 3.23–3.18 (dd, *J* 13.3 and 4.1, 1H, *CHH*Ph), 2.66–2.59 (dtd, *J* 16.2, 4.6, and 1.3, 1H, =C*CH*), 2.41–2.35 (dd, *J* 13.3 and 9.2, 1H, *CHH*Ph), 2.24–2.19 (m, 1H, *CH*CH_2), 2.09–2.05 (m, 1H, =C*CH*), 1.67–1.61 (m, 1H, *CHH*CH_2), 1.37 (dd, *J* 7 and 7, 3H, CH_3), 1.05–0.99 (m, 1H, *CHH*CH_2); δ_C 202.2 (CO), 139.5, 137.5, 135.1 (CH=), 130.2, 129.5, 128.6, 128.4, 126.2, 86.0, 67.3, 43.1, 38.7, 27.2, 26.6, 15.5. Found: C, 82.26; H, 7.54. Calc. for $C_{22}H_{24}O_2$: C, 82.46; H, 7.55%.

1 K. H. Dötz and E. O. Fischer, *Chem. Ber.*, 1972, **105**, 1356.
2 K. H Dötz, *Angew. Chem., Int. Ed. Engl.*, 1975, **14**, 644.
3 E. Chelain, R. Goumont, L. Hamon, M. Rudler, A. Parlier, H. Rudler, J. C. Daran and J. Vaissermann, *J. Am. Chem. Soc.*, 1992, **114**, 8088.
4 For an example of a multiple insertion of CO *under an external CO pressure* see M. F. Semmelhack, R. Tamura, W. Schnatter and J. Springer, *J. Am. Chem. Soc.*, 1984, **106**, 6363.
5 C. Alvarez, A. Pacreau, A. Parlier, H. Rudler and J. C. Daran, *Organometallics*, 1987, **6**, 1057.
6 E. Chelain, A. Parlier, M. Audouin, H. Rudler, J. C. Daran and J. Vaissermann, *J. Am. Chem. Soc.* , 1993, **115**, 10 568.
7 H. Rudler, M. Audouin, A. Parlier, B. Martin-Vaca, R. Goumont, T. Durand-Réville and J. Vaissermann, *J. Am. Chem. Soc.*, 1996, **118**, 12045.
8 E. J. Corey and L. S. Hegedus, *J. Am. Chem. Soc.*, 1969, **91**, 4926.
9 J. Y. Merour, J. L. Roustan, C. Charrier and J. Benaim, *J. Organomet. Chem.*, 1973, **51**, C24.
10 B. J. Söderberg, D. C. York, T. R. Hoye, G. M. Rehberg and J. A. Soriano, *Organometallics*, 1994, **13**, 4501.
11 G. M. Sheldrick, Program for the Refinement of Crystal Structures, University of Göttingen, Germany, 1986.

Communication 9/03474I

Diels–Alder and Michael addition reactions of indoles with masked *o*-benzoquinones: synthesis of highly functionalized hydrocarbazoles and 3-arylindoles

Ming-Fang Hsieh, Polisetti Dharma Rao and Chun-Chen Liao*

Department of Chemistry, National Tsing Hua University, Hsinchu, Taiwan 300. E-mail: ccliao@faculty.nthu.edu.tw

Received (in Cambridge, UK) 1st June 1999, Accepted 16th June 1999

Highly functionalized hydrocarbazoles and 3-arylindoles are prepared from commercially available 2-methoxyphenols and indoles.

The chemistry of indole[1] has been extensively investigated because of the wide-spread occurrence of its skeleton as a basic structural unit of various types of natural products with interesting and useful physiological properties.[2] It is well-known that indole behaves as an enamine towards electrophiles and undergoes Michael addition to electron-deficient alkenes.[1] In contrast, its dienophilic behavior has been reported only on a few occasions.[3–8] Indoles have been found to react as dienophiles in formal [4 + 2] cycloaddition reactions with 3,6-disubstituted 1,2,4,5-tetrazines,[3] tetrachlorothiophene 1,1-dioxide,[4] isoprene,[5] buta-1,3-diene,[5] cyclohexa-1,3-dienes[6] and quinodimethanes.[7] Indole magnesium salts were found to undergo facile cycloaddition reactions with 2-phenylsulfonyl-1,3-dienes.[8] However, indole participates in other types of cycloadditions as an electron-rich alkene.[1]

Masked *o*-benzoquinones (MOBs) are one of the most readily accessible types of cyclohexa-2,4-dienones with immense synthetic potential.[9,10] MOBs have been shown to be efficient dienes and they have been extensively used in this capacity in our laboratory.[9] Following our studies on Diels–Alder reactions of furans with MOBs,[11] we turned our attention to indoles. It was envisioned that if indoles could react with MOBs by cycloaddition, easy access to a variety of potentially useful hydrocarbazoles could be achieved. On the other hand, if indoles add to MOBs by a Michael addition a facile synthesis of highly substituted 3-arylindoles could be achieved. Accordingly, the reactions of selected MOBs **1a**–**c**, generated from phenols **2a**–**c** with a variety of indoles, were examined. We herein report that indoles **3a**–**e** undergo Diels–Alder or Michael addition to MOBs **1a**–**c** depending on the reaction temperature and substitution pattern, to furnish Diels–Alder adducts **4**–**8** or aromatized Michael adducts **9**–**11** in good yields.

In order to avoid their dimerization, MOBs were usually generated *in situ* from the corresponding 2-methoxyphenols in the presence of a reactive dienophile at a suitable temperature using (diacetoxyiodo)benzene (DAIB) in MeOH. Since indoles are known to react with DAIB,[12] an alternative procedure needed to be developed. Consequently, **1a**–**c** were generated from **2a**–**c** in MeOH by adding DAIB (1.0 equiv.) at 0 °C in MeOH and then an indole derivative was added. After the addition of an indole derivative, the temperature was elevated either to room temperature or to reflux (Schemes 1 and 2, Table 1).[13]

3-Methylindole (**3c**) reacted efficiently only at reflux to furnish the Diels–Alder adducts **6a**–**c** and products which could result *via* Michael addition were not descernible. The reactions of **3d** with **1a**–**c** were found to be sluggish and only Diels–Alder adducts **7a**–**c** were obtained in poor yields. At both room temperature and reflux, 2-methylindole (**3e**) underwent Michael addition to MOBs **1b** and **1c** followed by aromatization of the adducts to provide compounds **11b** and **11c** exclusively in excellent yields. Intriguingly, indole (**3a**) underwent cycloaddition at room temperature to furnish Diels–Alder adducts **4a**–**c** and Michael addition at reflux temperature to afford aromatized Michael adducts **9a**–**c** in good yields. 6-Bromoindole exhibited the same behavior as indole albeit with low efficiency.

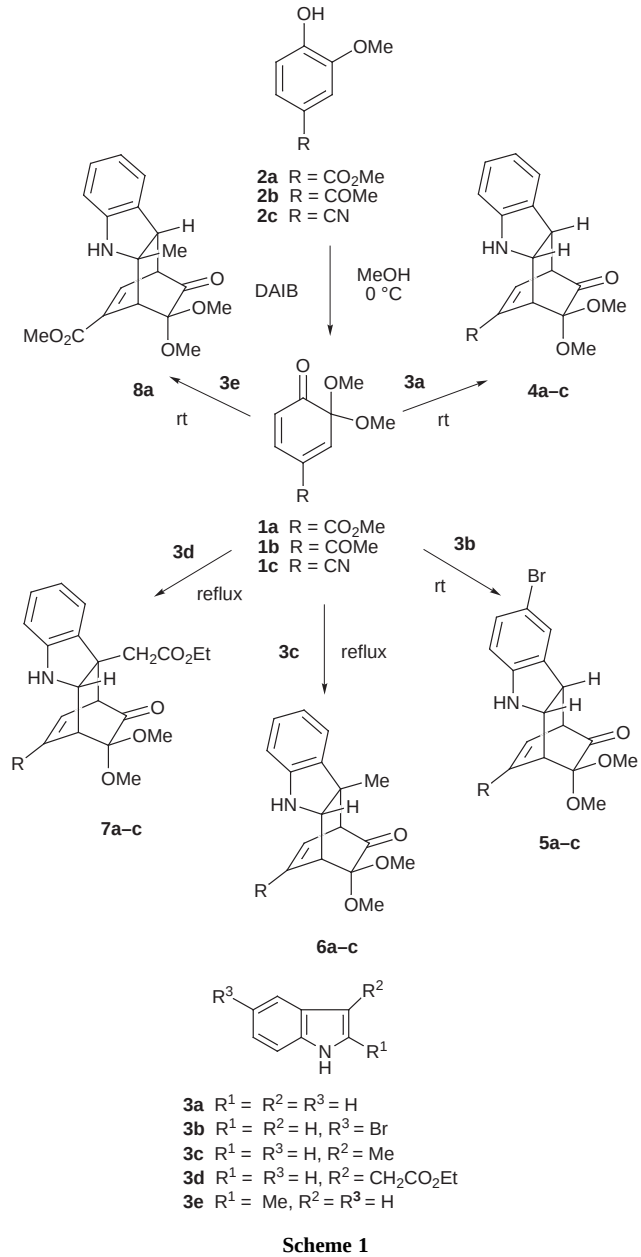

Scheme 1

The gross structures of all the products were determined by their IR, ^{1}H and ^{13}C NMR, DEPT, low- and high-resolution mass spectral analysis. The majority of these products provided satisfactory elemental analyses. The regioselectvity of the Diels–Alder reactions was determined by ^{1}H–^{1}H decoupling

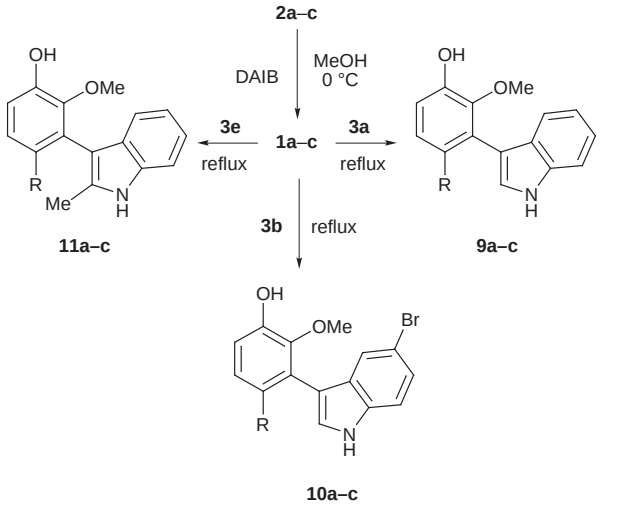

Scheme 2

Table 1 Diels–Alder and Michael addition reactions of indoles **3a–c** with MOBs **1a–c**

Entry	Indole derivative	MOB	Diels–Alder adduct	Yield (%)	Michael[b] adduct	Yield (%)
1	**3a**	**1a**	**4a**[a]	65	**9a**	96
2	**3b**	**1a**	**5a**[a]	50	**10a**	92
3	**3c**	**1a**	**6a**[b]	71	—	—
4	**3d**	**1a**	**7a**[b]	15	—	—
5	**3e**	**1a**	**8a**[a]	24	**11a**	86
6	**3a**	**1b**	**4b**[a]	70	**9b**	91
7	**3b**	**1b**	**5b**[a]	[c]	**10b**	90
8	**3c**	**1b**	**6b**[b]	54	—	—
9	**3d**	**1b**	**7b**[b]	37	—	—
10	**3e**	**1b**	—	—	**11b**	96
11	**3a**	**1c**	**4c**[a]	45	**9c**	53
12	**3b**	**1c**	**5c**[a]	23	**10c**	67
13	**3c**	**1c**	**6c**[b]	39	—	—
14	**3d**	**1c**	**7c**[b]	8	—	—
15	**3e**	**1c**	—	—	**11c**	75

[a] Add indole **3** to a solution of **1** in MeOH at 0 °C, then stir for **1** h at rt. [b] Add indole **3** to a solution of **1** in MeOH at 0 °C, then reflux for 1 h. [c] Not isolable.

experiments in all cases. Their stereoselectivity was predicted to be as shown based on our earlier results with furans[11] and is confirmed in the case of the adduct **7b** by its single crystal X-ray diffraction analysis.[14] Since in all cases the reactions furnished adducts resulting from *endo*-addition, these cycloaddition reactions appear to have followed all the ground rules of Diels–Alder reactions. On the other hand, the Michael addition appears to be highly regioselective. In all cases, only 1,6-addition took place. This result was confirmed by the NMR spectra of the aromatic Michael adducts **9**–**11** and by single crystal X-ray analysis in the case of **10a**.[14]

The exclusive cycloaddition of 3-substituted indoles **3c**,**d** and exclusive Michael addition of 2-methylindole to MOBs at both temperatures is probably due to steric factors. The dual reactivity of indoles lacking substituents needs to be understood. It was reasoned that the initially formed Diels–Alder adducts rearrange to the observed products **9**–**11** at high temperature. In order to test this hypothesis, the Diels–Alder adduct **4a** was refluxed in MeOH in the presence of indole and AcOH but only a complex mixture of products which contained no trace of **9a** was obtained. Hence an alternative mechanism, with **9**–**11** being produced *via* a Michael addition–aromatization sequence, is proposed. This concept has also gained support from the substitution pattern required for the success of these reactions. The presence of electron-withdrawing groups on C-4 of MOBs is essential for the success of these reactions. On the other hand, the presence of electron-withdrawing substituents on the 2- or 3-position of indole prevents both cycloaddition and Michael addition.

In conclusion these reactions are mechanistically interesting and help unravel a new class of dienes that can force indoles to act as dienophiles. These reactions provided easy access to a variety of multifunctional tetracyclic compounds and 3-aryl-indoles whose synthesis is otherwise difficult. The Diels–Alder adducts of indoles could potentially be useful starting materials in the total synthesis of indole monoterpenoid alkaloids and ellipticine-type compounds with antitumor activity.

We thank the National Science Council (NSC) of Taiwan, R.O.C for financial support. One of us, (P. D. R.) thanks NSC for a postdoctoral fellowship.

References and notes

1 R. J. Sundberg, *The Chemistry of Indoles*, Academic Press, New York, 1971; D. J. Chadwick, in *Comprehensive Heterocyclic Chemistry*, ed. A. R. Katritzky and C. W. Rees, Pergamon, Oxford, 1984, vol. 4, p. 155; R. A. Jones, in *Comprehensive Heterocyclic Chemistry*, ed. A. R. Katritzky and C. W. Rees, Pergamon, Oxford, 1984, vol. 4, p. 201; R. J. Sundberg, in *Comprehensive Heterocyclic Chemistry*, ed. A. R. Katritzky and C. W. Rees, Pergamon, Oxford, 1984, vol. 4, p. 313.

2 J. E. Saxton, *The Monoterpenoid Indole Alkaloids*, Wiley-Interscience, Chichester, 1994; J. E. Saxton, *Nat. Prod. Rep.*, 1997, **14**, 559 and references cited therein.

3 S. C. Benson, C. A. Polabrica and J. K. Snyder, *J. Org. Chem.*, 1987, **52**, 4610; M. Takahashi, H. Ishida and M. Kohmoto, *Bull. Chem. Soc. Jpn.*, 1976, **49**, 1725.

4 M. S. Raasch, *J. Org. Chem.*, 1980, **45**, 856.

5 E. Wenkert, P. D. R. Moeller and S. R. Piettre, *J. Am. Chem. Soc.*, 1988, **110**, 7188.

6 A. Gieseler, E. Steckhan, O. Wiest and F. Knoch, *J. Org. Chem.*, 1991, **56**, 1405.

7 J. H. Markgraff and D. E. Patterson, *J. Heterocycl. Chem.*, 1996, **33**, 109.

8 J.-E. Backvall and N. A. Plobeck, *J. Org. Chem.*, 1990, **55**, 4528.

9 D.-S. Hsu, P. D. Rao and C.-C. Liao, *Chem. Commun.*, 1998, 1795; P. D. Rao, C.-H. Chen and C.-C. Liao, *Chem. Commun.*, 1998, 155; P.-Y. Hsu, Y.-C. Lee and C.-C. Liao, *Tetrahedron Lett.*, 1998, **39**, 659; W.-C. Liu and C.-C. Liao, *Synlett*, 1998, 912; P.-Y. Hsiu and C.-C. Liao, *Chem. Commun.*, 1997, 1085; C.-S. Chu, P. D. Rao and C.-C. Liao, *Chem. Commun.*, 1996, 1537 and references cited therein.

10 R. Carlini, K. Higgs, C. Older and S. Randhawa, *J. Org. Chem.*, 1997, **62**, 2330; R. S. Coleman and E. B. Grant, *J. Am. Chem. Soc.*, 1995, **117**, 10 889; K. S. Feldman and S. M. Ensel, *J. Am. Chem. Soc.*, 1994, **116**, 3357; A. S. Mitchell and R. A. Russell, *Tetrahedron Lett.*, 1993, **34**, 545; M. G. Banwell and M. P. Collis, *J. Chem. Soc., Chem. Commun.* 1991, 1343 and references cited therein.

11 C.-H Chen, P. D. Rao and C.-C. Liao, *J. Am. Chem. Soc.*, 1998, **120**, 13 254; P. D. Rao, C.-H. Chen and C.-C. Liao, *Chem. Commun.*, 1999, 713.

12 R. M. Moriarty, C. J. Chany II and J. W. Kosmeder II, in *Encyclopedia of Reagents for Organic Synthesis*, ed. L. A. Paquette, Wiley, Chichester, 1995, vol. 2, p. 1479.

13 Procedure for Diels–Alder or Michael addition reactions of indoles **3** with **1a**–**c**. To a solution of **2** (1.0 mmol) in MeOH (10 ml) at 0 °C was added DAIB (1.0 mmol). After 10 min of stirring, an indole derivative **3** (5–20 mmol) was added at that temperature and the flask was rapidly warmed up to room temperature or to that of reflux by either removing the ice bath or transferring the reaction vessel to a preheated (100 °C) oil bath. The reaction mixture was stirred at either temperature for 1 h. Then MeOH was removed and the residue obtained was purified by flash chromatography on silica gel using 20% of ethyl acetate in hexanes as eluent to obtain Diels–Alder adducts or aromatized Michael adducts.

14 *Crystal data* for **7b**: $C_{22}H_{25}NO_6$, M = 399.43, monoclinic, a = 10.6487(1), b = 22.172(3), c = 8.588(2) Å, β = 95.726(1)°, V = 2017.5(5) Å^3, T = 293(2) K, space group $P2_1/c$, Z = 4, μ(Mo-Kα) = 0.096 mm^{-1}, 3545 reflections measured, 3545 unique (R_{int} = 0.0000). Final R indices [$I > 2\sigma(I)$] $R1$ = 0.0430, $wR2$ = 0.1261. For **10a**: $C_{17}H_{14}BrNO_4$, M = 376.20, triclinic, a = 9.0176(2), b = 9.4144(2), c = 10.3637(1) Å, α = 90.7060(1), β = 96.9180(1), γ = 117.1930(1)°, V = 774.62(2) Å^3, T = 293(2) K, space group $P\bar{1}$, Z = 2, μ(Mo-Kα) = 2.673 mm^{-1}, 7349 reflections measured, 3317 unique (R_{int} = 0.0347). Final R indices [$I > 2\sigma(I)$] $R1$ = 0.0349, $wR2$ = 0.0893. CCDC 182/1310. See http://www.rsc.org/suppdata/cc/1999/1441/ for crystallographic data in .cif format.

Communication 9/04366G

Typeset and printed by Black Bear Press Limited, Cambridge, England

ChemComm
FEATURE ARTICLE

Hydrolysis of DNA and RNA by lanthanide ions: mechanistic studies leading to new applications

Makoto Komiyama,*[a] Naoya Takeda[a] and Hidemi Shigekawa[b]

[a] *Department of Chemistry and Biotechnology, Graduate School of Engineering, The University of Tokyo, Hongo, Tokyo 113-8656 Japan. E-mail: mkomi@chembio.t.u-tokyo.ac.jp*

[b] *Institute of Applied Physics and Center for Tsukuba Advanced Research Alliance (TARA), University of Tsukuba, Tsukuba, Ibaraki 305-8573, Japan*

Received (in Cambridge, UK) 1st March 1999, Accepted 20th April 1999

A few years ago, the remarkable catalytic activity of lanthanide ions for the hydrolysis of nucleic acids was discovered. With Ce^{IV}, DNA was hydrolysed under physiological conditions. For RNA hydrolysis, the last three lanthanide ions (Tm^{III}, Yb^{III}, and Lu^{III}) are superb. Furthermore, artificial restriction enzymes for site-selective scission of DNA and RNA, essential tools for the future biotechnology, have been prepared by using the lanthanide complexes. The present article emphasizes the mechanistic aspects of the catalyses of these metal ions. Both DNA hydrolysis and RNA hydrolysis involve the cooperation of acid catalysis (by metal ion and/or metal-bound water) and base catalysis (by metal-bound hydroxide). The magnitudes of contributions of these catalyses, as well as the positions where they work, are primarily governed by the relative height of the energy-barrier for the formation of the pentacoordinated intermediate and that for its breakdown. The following conclusions have been obtained on the basis of various kinetic and spectroscopic evidence: (1) for the hydrolysis of both DNA and RNA, the catalytically active species are dinuclear hydroxo-clusters, (2) Ce^{IV} enormously activates DNA and promotes the formation of the pentacoordinated intermediate, and (3) the catalysis for RNA hydrolysis is mainly ascribed to the promotion of breakdown of the pentacoordinated intermediate.

Introduction

Non-enzymatic hydrolysis of DNA and RNA has attracted much interest, mainly because it is essential for further developments in biotechnology, molecular biology, therapy, and related fields.[1] In current biotechnology, the DNA of bacteria and viruses is manipulated using naturally-occurring enzymes. In the near future, however, we must deal with the DNA of higher animals and plants in order to widen the scope of applications. Is the currently employed technology directly applicable there? The answer is 'No'. First, the genomes of higher species are so large that the sequence-specificity of the restriction enzymes found in nature is too low to cut them solely at the desired site (most of them recognize a specific sequence composed of 4 or 6 DNA-bases).[2] Second, there are no natural enzymes showing sufficient sequence-specificity in RNA scission. Thus, artificial enzymes, which selectively hydrolyse DNA and RNA at the target position with a desired specificity, are crucially important. They may also be valuable tools for therapy, regulation of cell-growth, and other applications.

In order to prepare these artificial enzymes, catalysts for the scission of DNA and RNA are necessary. However, the phosphodiester linkages in DNA are enormously stable, and (until recently) could not be hydrolysed without using natural enzymes.[3,4] Non-enzymatic hydrolysis of RNA was also difficult. Several years ago, however, the remarkable catalytic activity of the lanthanide ions was discovered, and both DNA and RNA were for the first time hydrolysed at reasonable rates under physiological conditions.[5–7] The Ce^{IV} ion is the most active for DNA hydrolysis,[8,9] whereas Tm^{III}, Yb^{III} and Lu^{III} (the last three lanthanide ions) are quite effective for RNA hydrolysis.[10] The acceleration by these metal ions is as large as 10^8–10^{12} fold. Interestingly, these enormous activities are restricted to the lanthanide ions. Furthermore, artificial enzymes

Professor Makoto Komiyama was born in 1947 in Utsunomiya, Japan. After graduated from the University of Tokyo, he entered the Graduate School of this University, where he got his Ph.D. in 1975. After working in the USA as a postdoctoral fellow for Professor Myron L. Bender at Northwestern University, he got the position of Assistant Professor at the University of Tokyo in 1979. In 1987, he became an Associate Professor at the University of Tsukuba, and, since 1992, has been a full Professor of the University of Tokyo. His research areas involves bioorganic and bioinorganic chemistry (especially DNA and RNA hydrolysis), host–guest chemistry (cyclodextrins), functional polymers, and others. He received Awards for Young Scientists from the Chemical Society of Japan, the Japan IBM Science Award, an Award from the Rare Earth Society of Japan, and the Inoue Prize for Science.

Dr Naoya Takeda was born in 1968 in Chiba, Japan. Following his undergraduate education at the University of Tokyo, he obtained his Ph.D. from the University in 1998 under the supervision of Professor M. Komiyama. After working as an assistant staff member at the National Institute for Advanced Interdisciplinary Research, he is currently doing his postdoctoral work as a JSPS Research Fellow at the University of Tokyo. His research interests include bioorganic and bioinorganic chemistry.

Professor Hidemi Shigekawa was born in 1955 in Hiroshima, Japan. After graduated from the University of Tokyo, he entered the Graduate School of the University, and got a position of Assistant Professor there in 1980. After getting his Ph.D. in 1986, he worked at the Brook Haven National Laboratory (1987–1988) using the synchrotron radiation source, as a Postdoctoral Fellow for Dr J. Rowe of Bell Labs. In 1989, he became a lecturer at the University of Tsukuba, and has been an Associate Professor there since 1993. His main research is in the field of surface science using scanning tunneling microscopy and related techniques. He was awarded the Paper Award from the Surface Science Society of Japan in 1991 and 1998.

for site-selective scission of DNA and RNA were prepared by conjugating the lanthanide complexes to DNA oligomers (the sequence-recognizing moieties) (Fig. 1).[11,12] The DNA and

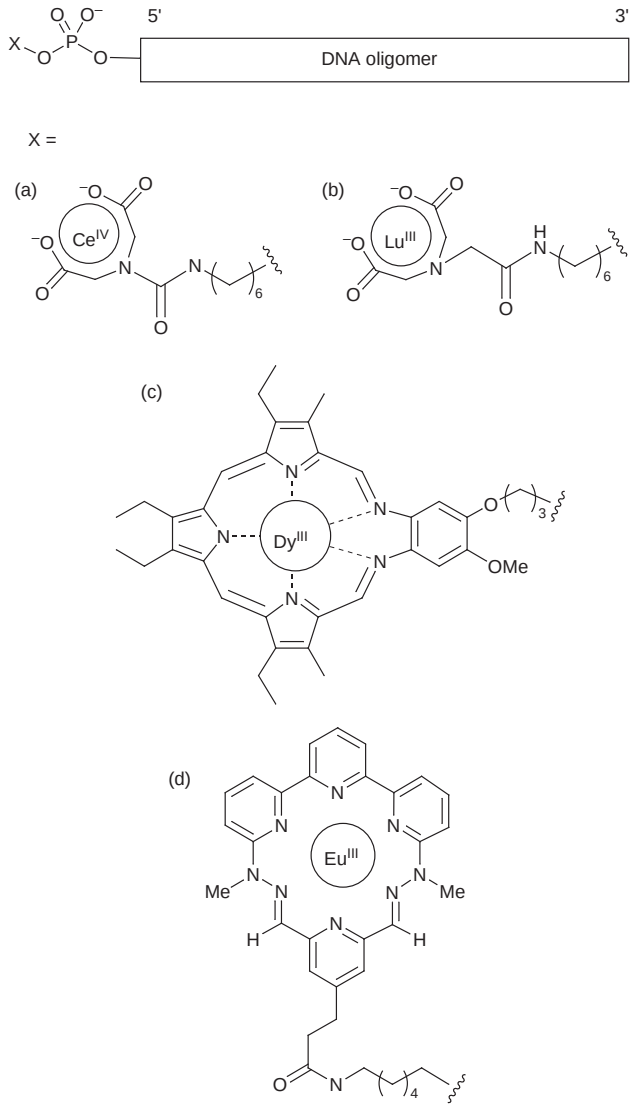

Fig. 1 Typical artificial enzymes for sequence-selective scission of (*a*) DNA and (b)–(d) RNA.

RNA fragments, obtained *via* scission, can be transformed into substrates for enzymatic manipulation. The synergy between lanthanide catalysis and biotechnology is straightforward.[13] A new era is imminent.

This paper focuses on the mechanistic aspects of the lanthanide catalysis for the hydrolysis of DNA and RNA. The following points are clarified on the basis of various kinetic and spectroscopic evidence: (a) what are the catalytically active species?, (b) where do the catalyses work in the course of the reactions?, and (c) why are the lanthanide ions highly active? The mechanisms of the catalyses for DNA and RNA are compared with each other, and also with those for the RNA hydrolysis by dinuclear complexes of non-lanthanide ions. The conclusions obtained here should pave the way to the rational design of still more active catalysts and also to versatile applications of these novel catalyses.

1 DNA hydrolysis by Ce^{IV}

1.1 Survey of the previous studies

The following features of Ce^{IV}-induced DNA hydrolysis have been already documented.[9]

(1) The DNA scission proceeds totally *via* the hydrolysis of phosphodiester linkages, without concurrent oxidative cleavage of the deoxyribose residues.

(2) At pH 7 and 50 °C, the half-life of the phosphodiester linkage in DNA is reduced to a few hours. The acceleration by Ce^{IV} is more than 10^{11} fold.

(3) The catalytically active species is formed from tetravalent Ce ion(s).

(4) Molecular oxygen is not necessary for the catalysis. Only when Ce^{III} salts (*e.g.* $CeCl_3$) are used as the catalysts, is molecular oxygen required to oxidize Ce^{III} to the catalytically active Ce^{IV}.

(5) The rate of DNA hydrolysis is almost constant from pH 2 to pH 8.5.

(6) The nucleic acid bases do not directly participate in the catalysis (the rate of DNA hydrolysis is almost independent of them).

(7) The reaction is accompanied by a notable D_2O solvent isotope effect (k_{H_2O}/k_{D_2O} = 2.2–2.4), showing a rate-limiting proton-transfer.

1.2 The rate-limiting step for DNA hydrolysis

The hydrolysis of DNA proceeds as a two-step reaction (Fig. 2). In the first step, a nucleophile (*e.g.* hydroxide ion) attacks the phosphorus atom, forming a pentacoordinated intermediate. In the second step, the 5′-OH of 2′-deoxyribonucleotide is removed from the phosphorus atom through the scission of the P–O bond [in non-enzymatic hydrolysis, the P–O(3′) scission can also take place]. In order to accelerate the whole reaction, the catalysts must promote the rate-limiting step. Unfortunately, however, it was not known which step is rate-limiting. Thus, the DNA analogues in Fig. 3, which possess better leaving groups

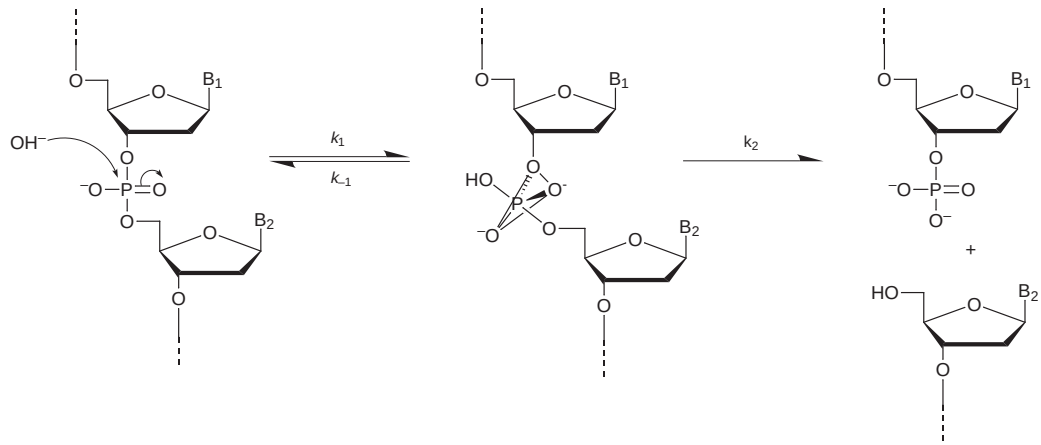

Fig. 2 The reaction pathway of DNA hydrolysis.

than DNA, were prepared as probes, and their hydrolysis rates were compared with the value for the native DNA.[14]

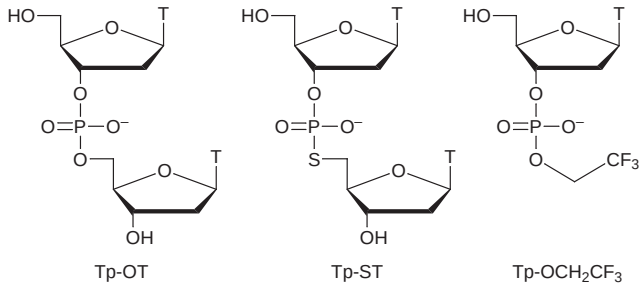

Fig. 3 DNA analogues possessing better leaving groups, as the probes of the rate-limiting step.

(1) Ce^{IV}-induced DNA hydrolysis. When the 5′-O atom of the thymidine in thymidylyl(3′–5′)thymidine (Tp-OT) is replaced with an S atom (the leaving group is changed from T-O^- to T-S^-), the dinucleotide analog (Tp-ST) is hydrolysed by Ce^{IV} around 1000 fold faster than is Tp-OT. The rate constants are 1.7×10^1 and 2.0×10^{-2} h^{-1}, respectively, when $[Ce^{IV}]_0$ = 10 mM at pH 7 and 30 °C. Similarly, the hydrolysis of Tp-OCH_2CF_3 is 75 fold faster than that of Tp-OT. The rate of hydrolysis monotonically increases with decreasing pK_a of the leaving group (the pK_as of T-SH, CF_3CH_2OH, and T-OH are around 11, 13, and 15, respectively). Apparently, the second-step (the scission of the P–O bond) is rate-limiting [the energy diagram is presented by the solid line in Fig. 4(*a*)]. If the first step were to be rate-limiting, the analogues should be hydrolysed at the same (or comparable) rate as Tp-OT.[15]

By using this result, the rate constant k_{obs} for the overall reaction in Fig. 2 is expressed by eqn. (1). The reaction involves the pre-equilibrium formation of the pentacoordinated intermediate.

$$k_{obs} = k_1k_2/k_{-1} \quad (1)$$

Accordingly, the hydrolysis of DNA is accelerated by (a) the increase in k_2 (promotion of the second-step) and/or (b) the increase in k_1/k_{-1} (stabilization of the pentacoordinated intermediate, with respect to the initial state). The activation free energy for the whole reaction ($\Delta G^{\ddagger}$) is the sum of ΔG_1 (the difference between the initial state and the pentacoordinated intermediate) and $\Delta G_2^{\ddagger}$ (the difference between the intermediate and the second-energy barrier).

The trivalent lanthanide ions also hydrolyse DNA, although the activities are far smaller (> 10^3 fold) than that of Ce^{IV}. Here, the second step is also rate-limiting. In contrast, non-lanthanide ions such as Mg^{II}, Zn^{II}, Co^{II}, Al^{III}, and Fe^{III} show no measurable catalysis under the same conditions.

(2) Alkaline hydrolysis. DNA is so stable that it is not hydrolysed at measurable rates even in highly alkaline solutions (*e.g.* in 1 M NaOH at 50 °C). Thus, the direct evaluation of the shape of the energy diagram using the probes in Fig. 3 has been unsuccessful.

However, the following argument shows that the energy diagram is almost symmetric, with respect to the position of the pentacoordinated intermediate: see the dotted line in Fig. 4(*a*). In the forward reaction of DNA hydrolysis, hydroxide ion is the nucleophile and the alkoxide ion of 5′-OH is the leaving group. In the backward reaction, the hydroxide ion and the alkoxide ion exchange positions. Since the pK_as of the conjugate acids of the hydroxide ion and the alkoxide ion are almost the same, their potentials as nucleophiles and the leaving groups are comparable.

1.3 Which step is promoted by the Ce^{IV} ion?

The Ce^{IV} ion accelerates DNA hydrolysis by 10^{11} fold or more, and thus the second step of the reaction must be promoted by this magnitude [see the energy diagrams in Fig. 4(*a*)]. Nevertheless, this step still remains rate-limiting in the whole reaction. Apparently, the first step is also accelerated by the Ce^{IV} ion to a similar (or greater) degree (otherwise, this step should become rate-limiting). The difference in the activation free energies between these two steps is not large. The pentacoordinated intermediate should also be stabilized by the metal ion.

As described later, the catalysis by Ce^{IV} is mainly ascribed to the decrease in ΔG_1, which is associated with the activation of the DNA. Note that the decrease in ΔG_1 necessarily lowers the height of the second barrier (with respect to the initial state), since $\Delta G^{\ddagger} = \Delta G_1 + \Delta G_2^{\ddagger}$.

1.4 Catalytically active species for the DNA hydrolysis

The Ce^{IV} ions form complex metal hydroxide gels when the pH is greater than 4. These heterogeneous systems are inappropriate for detailed kinetic analysis. However, it has been found that homogeneous mixtures can be obtained under highly acidic conditions (pH < 2.5).[16] Significantly, these mixtures have almost the same catalytic activity as the metal hydroxide gel (the hydrolysis of single-stranded DNA at pH 2 is only a few

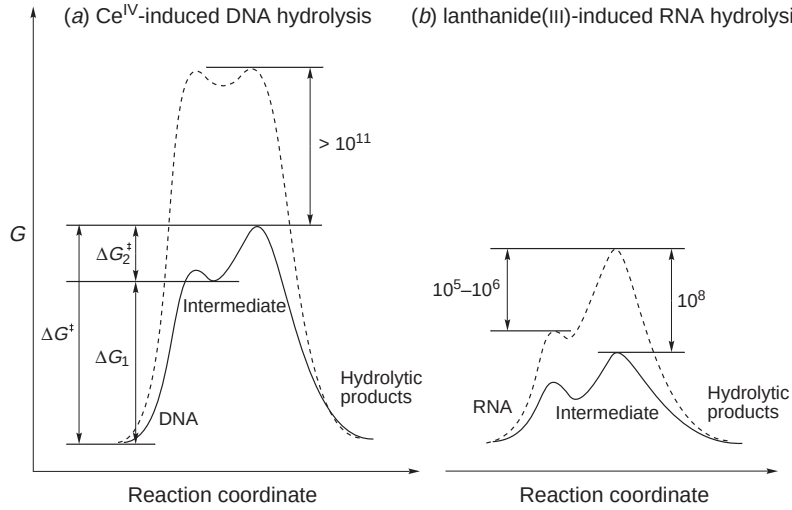

Fig. 4 Energy diagrams for (*a*) Ce^{IV}-induced DNA hydrolysis and (*b*) lanthanide(III)-induced RNA hydrolysis. The dotted lines show the diagrams for the corresponding alkaline hydrolysis.

fold slower than that at pH 7). Moreover, the concentrations of all the Ce^{IV}-derived species therein can be calculated using the equilibrium constants in the literature.[17] Thus, the catalytically active species for DNA hydrolysis in these homogeneous solutions have been investigated.[18,19]

(1) Hydrolysis of cyclic adenosine 3′,5′-monophosphate (cAMP). The hydrolysis of cAMP has many common features with DNA hydrolysis. First, both reactions are enormously (10^{11}–10^{12} fold) promoted by Ce^{IV}.[20] Second, the catalytic activity of Ce^{IV} is far greater than that of any other catalyst. Thirdly, both of the reactions proceed *via* the attack by OH^- (or H_2O) as external nucleophile. The six-membered cyclic phosphodiester in cAMP is activated by strain and is much more readily hydrolysed than the non-cyclic linkage in DNA. A variety of fundamental information on Ce^{IV}-induced DNA hydrolysis can be obtained from cAMP hydrolysis.[18]

In the reaction mixtures, six equilibria [eqn. (2)–(7)] hold.[17]

$$Ce^{IV} + H_2O \overset{K_{1,1}}{\rightleftharpoons} [Ce^{IV}(OH)]^{3+} + H^+, \quad pK_{1,1} = 1.1 \quad (2)$$

$$Ce^{IV} + 2H_2O \overset{K_{1,2}}{\rightleftharpoons} [Ce^{IV}(OH)_2]^{2+} + 2H^+, \quad pK_{1,2} = 0.3 \quad (3)$$

$$2\,Ce^{IV} + 2H_2O \overset{K_{2,2}}{\rightleftharpoons} [Ce^{IV}_2(OH)_2]^{6+} + 2H^+, \quad pK_{2,2} = 3.6 \quad (4)$$

$$2\,Ce^{IV} + 3H_2O \overset{K_{2,3}}{\rightleftharpoons} [Ce^{IV}_2(OH)_3]^{5+} + 3H^+, \quad pK_{2,3} = 4.1 \quad (5)$$

$$2\,Ce^{IV} + 4H_2O \overset{K_{2,4}}{\rightleftharpoons} [Ce^{IV}_2(OH)_4]^{4+} + 4H^+, \quad pK_{2,4} = 3.5 \quad (6)$$

$$6\,Ce^{IV} + 12H_2O \overset{K_{6,12}}{\rightleftharpoons} [Ce^{IV}_6(OH)_{12}]^{12+} + 12H^+, \quad pK_{6,12} = 15.4 \quad (7)$$

Thus, the equilibrium concentrations of all the Ce^{IV}-derived species (Ce^{4+}, $[Ce^{IV}(OH)]^{3+}$, $[Ce^{IV}(OH)_2]^{2+}$, $[Ce^{IV}_2(OH)_2]^{6+}$, $[Ce^{IV}_2(OH)_3]^{5+}$, $[Ce^{IV}_2(OH)_4]^{4+}$, and $[Ce^{IV}_6(OH)_{12}]^{12+}$) are evaluated by using the $K_{1,1}$, $K_{1,2}$, $K_{2,2}$, $K_{2,3}$, $K_{2,4}$, and $K_{6,12}$ values. As depicted in Fig. 5, the pH–rate constant profile (the

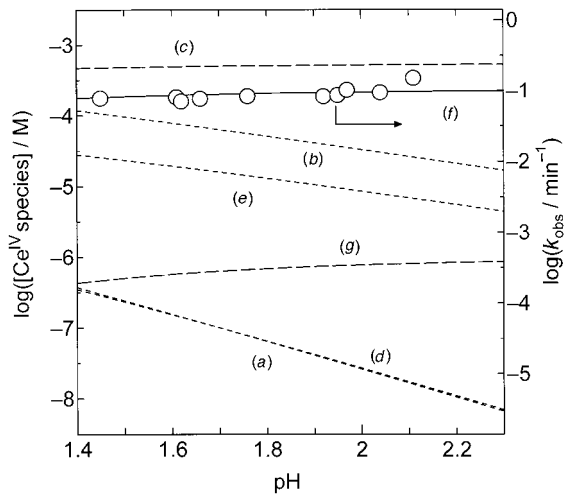

Fig. 5 The pH–rate constant profile for the cAMP hydrolysis by $Ce(NH_4)_2(NO_3)_6$ (10 mM) at 30 °C. The open circles are the experimental points. The equilibrium concentrations of the Ce^{IV}-derived species, calculated by using the *K* values in eqn. (2)–(7), are presented by the curved lines: (*a*) Ce^{4+}, (*b*) $[Ce^{IV}(OH)]^{3+}$, (*c*) $[Ce^{IV}(OH)_2]^{2+}$, (*d*) $[Ce^{IV}_2(OH)_2]^{6+}$, (*e*) $[Ce^{IV}_2(OH)_3]^{5+}$, (*f*) $[Ce^{IV}_2(OH)_4]^{4+}$, (*g*) $[Ce^{IV}_6(OH)_{12}]^{12+}$.

open circles) fits reasonably well the theoretical lines for the concentrations of $[Ce^{IV}(OH)_2]^{2+}$ [line (*c*)], $[Ce^{IV}_2(OH)_4]^{4+}$ [line (*f*)], and $[Ce^{IV}_6(OH)_{12}]^{12+}$ [line (*g*)]. These three species are the candidates for the catalytically active species. Note that the shapes of these lines are unanimously determined by the *K* values, whereas their positions (with respect to the right-hand side ordinate) can be moved vertically by changing the catalytic rate constants of the corresponding species.

In Fig. 6, the hydrolysis rate is plotted *vs.* $[Ce^{IV}(NH_4)_2(NO_3)_6]_0$

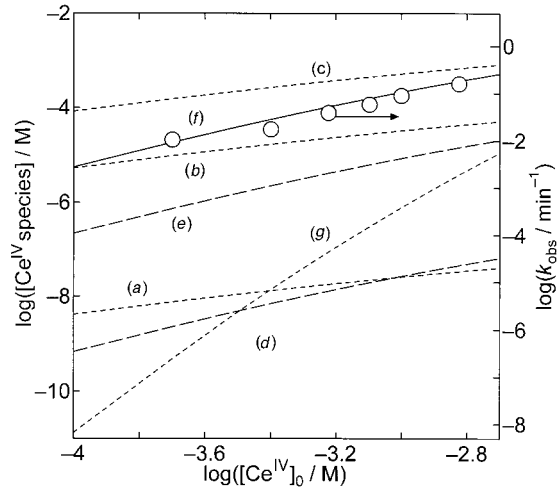

Fig. 6 The plots of the rate of cAMP hydrolysis *vs.* $[Ce(NH_4)_2(NO_3)_6]_0$ at pH 2.0 and 30 °C. The open circles are the experimental points, whereas the curved lines show the equilibrium concentrations of the corresponding species (see Fig. 5).

$(NO_3)_6]_0$. The experimental points agree well with the theoretical lines for $[Ce^{IV}_2(OH)_2]^{6+}$ [line (*d*)], $[Ce^{IV}_2(OH)_3]^{5+}$ [line (*e*)], and $[Ce^{IV}_2(OH)_4]^{4+}$ [line (*f*)]. Thus, only $[Ce^{IV}_2(OH)_4]^{4+}$ satisfies the results in both Figs. 5 and 6. This tetracationic bimetallic hydroxo cluster is the active species for the remarkable hydrolysis of cAMP.

(2) DNA hydrolysis. The Ce^{IV}-induced DNA hydrolysis has been analyzed in acidic solutions (pH 1.5–2.5) at 50 °C, exactly as described above for the cAMP hydrolysis.[19] It has been concluded that $[Ce^{IV}_2(OH)_4]^{4+}$ is also the active species. Of all the Ce^{IV} ions in the mixtures, only a small portion (20–30%) forms this bimetallic hydroxo-cluster (most of the rest exists as $[Ce^{IV}(OH)_2]^{2+}$), yet this species governs the whole reaction. Its catalytic activity is overwhelmingly greater than those of the other species. The cooperation of the two Ce^{IV} ions in the cluster is strongly indicated (*vide infra*).

From the viewpoints of biological and other practical applications, DNA hydrolysis at around pH 7 is the most important. In these mixtures, $[Ce^{IV}_2(OH)_4]^{4+}$ further aggregates, forming complicated gels. The bimetallic hydroxo clusters in the gels are the active species for DNA hydrolysis.

1.5. Activation of DNA by the Ce^{IV} ion

Why is Ce^{IV} ion highly effective for DNA hydrolysis? Why are the phosphodiester residues significantly activated by this metal ion? Do its f-orbitals play a significant role in the catalysis? In order to answer these questions, core-level photoelectron spectroscopy,[21] as well as EXAFS (extended X-ray absorption fine structure) and XANES (X-ray absorption near edge structure) measurements[22] were carried out. To simplify the analysis, diphenyl phosphate (DPP) was used as the specimen, in place of DNA.[23]

(1) Enormous electron-withdrawal from the phosphate by Ce^{IV}. Fig. 7 presents the core-level spectra for the 2*p* orbitals of the phosphorus atom of DPP in various lanthanide complexes. The electron-withdrawal by the metal ions from the phosphodiester linkage (and thus from the phosphorus atom), if any, is observed as the increase in the binding energy. It has been found that the binding energy of the orbitals in the Ce^{IV} complex is considerably greater than those for the complexes with La^{III}, Eu^{III}, Lu^{III}, and other non-lanthanide ions. Appar-

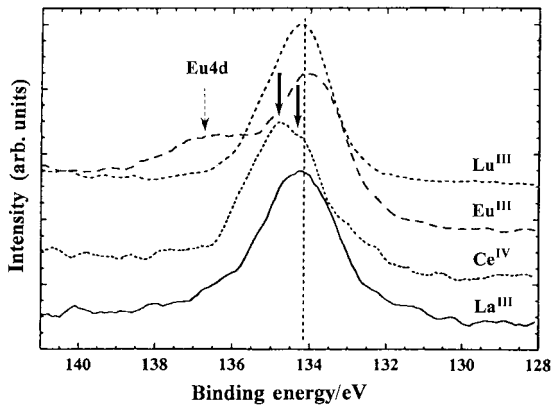

Fig. 7 Core-level spectra for the P2p orbital of DPP in the La^{III}, Ce^{IV}, Eu^{III}, and Lu^{III} complexes. $[Lanthanide\ ion]_0 / [DPP]_0 = 10$. The two bold arrows correspond to the P_H and P_L in Fig. 9.

ently, the Ce^{IV} ion exceeds the other metal ions in electron-withdrawing activity, and exceptionally promotes the electrophilicity of the phosphodiester linkage. The superiority of Ce^{IV} for the activation of DNA has been for the first time spectroscopically studied.

According to the L_3-XANES spectroscopy, 0.67 electrons exist in the 4f-orbitals of the Ce ion in the Ce^{IV}–DPP complex (these orbitals should be empty, if the Ce were to be really tetravalent). Upon complex formation, the electrons flow into the 4f-orbitals from the surroundings. In the DPP complexes of Ce^{III} and other lanthanide(III) ions, however, the corresponding electron-transfer to the metal(III) ions is not observed. The enormous activity of Ce^{IV} for DNA hydrolysis is primarily ascribed to the dominant electron-accepting activity, which is derived from the stability of its trivalent state. The lanthanide(III) ions cannot efficiently accept the electrons from DNA, since their divalent states are too unstable.

(2) Mixing of the orbitals of the phosphodiester linkage with those of Ce^{IV}. The electron-transfer from the phosphate to the Ce^{IV} ion occurs, at least partially, through the hybrid orbitals, which are formed from the 4f-orbitals of Ce^{IV} and the orbitals of the phosphorus atom (and/or of the oxygen atom) in the phosphate residue.[24] Consistently, a new energy state, related to this hybrid 4f-orbitals, appears near the Fermi level, when the Ce^{IV}–DPP complex is formed (Fig. 8). Neither free

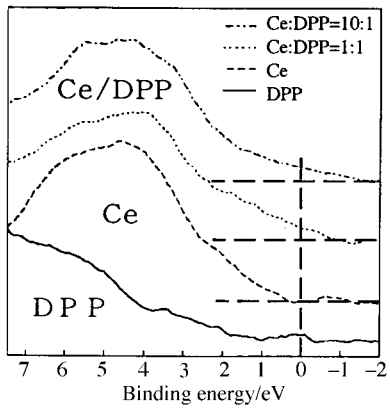

Fig. 8 X-Ray photoelectron spectra near the Fermi level.

DPP nor the Ce^{IV} hydroxo cluster (without DPP) has any energy-state density at this level. Since the 4f-orbitals of Ce^{IV} are lower in energy than those of the lanthanide(III) ions, and, at the same time, are widely spreading in space, they can efficiently interact with the orbitals of the phosphate. This mixing of the orbitals (as well as the resultant electron-transfer) would be still more efficient in the transition state, and decrease the activation free energy for the DNA hydrolysis.

(3) Structure of the Ce^{IV}–phosphate complex. According to detailed analysis of the core-level spectra, the phosphodiester is simultaneously coordinated to two Ce^{IV} ions, and enormously activated. As depicted in Fig. 9, the P2p signals of DPP in the

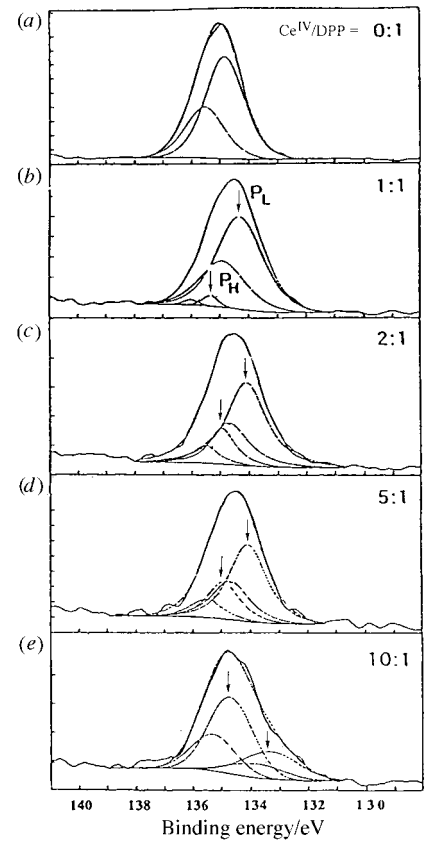

Fig. 9 Core-level spectra of the P2p orbital of DPP in the Ce^{IV}–DPP mixtures of different molar ratios. The peaks P_H and P_L correspond to the doublet signals of higher and lower binding energies.

Ce^{IV} complexes are composed of two components (P_H and P_L: each of the peaks is further split into a spin doublet). When the Ce^{IV} : DPP ratio is 1 : 1, the peak P_L of lower energy is predominant (b). Here, the phosphodiester linkage is bound to one Ce^{IV} ion and is only slightly activated (DNA hydrolysis hardly takes place). As the Ce^{IV} : DPP ratio increases [Fig. 9(*c*)–(*e*)], the intensity of P_H (of higher energy) gradually increases. This signal corresponds to DPP which is coordinated to two Ce^{IV} ions in the hydroxo cluster and is exceptionally activated by 'two-metal activation' (see Fig. 11). Consistently, the remarkable DNA hydrolysis occurs when Ce(IV) exists in excess to DNA.

These arguments are further substantiated by the EXAFS spectra in Fig. 10. In the absence of DPP [Fig. 10(*a*), (*b*)] the Ce^{IV} ions form metal hydroxo clusters (and the gel as their aggregates). Accordingly, the signal for the Ce–Ce distance is clearly observed at 3.6 Å (the position designated by the broken line). The signal at around 2.0 Å is for the Ce–O distance. Upon addition of DPP, the Ce–Ce signal rapidly weakens and is virtually nil at a Ce : DPP ratio of 1 : 1 [Fig. 10(*c*)]. Since the 1 : 1 Ce^{IV}–DPP complexes exist independently from each other (without mutual aggregation), the Ce–Ce signal is absent. When the Ce^{IV} : DPP ratio is > 1, however, the Ce–Ce signal appears again and gradually increases with increasing Ce : DPP ratio [Fig. 10(*d*), (*e*)]. Here, two Ce^{IV} ions are simultaneously interacting with one DPP molecule, and located in close

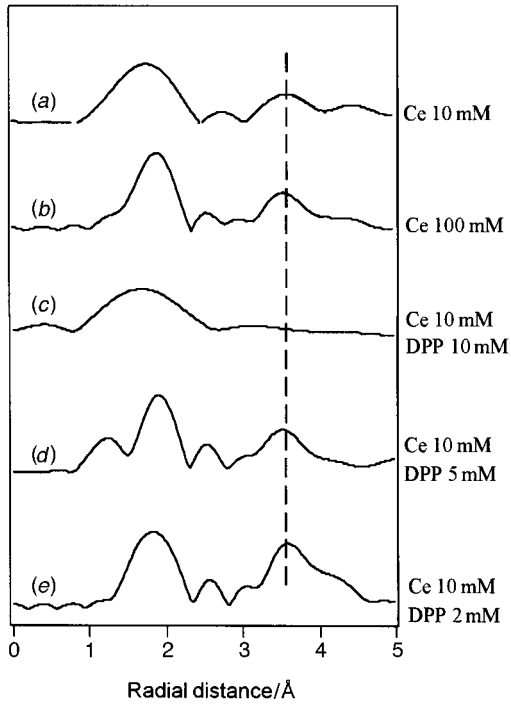

Fig. 10 EXAFS spectra for the Ce^{IV}–DPP systems.

proximity. Thus, these two Ce^{IV} ions are bound to each other, giving rise to the Ce–Ce signal.

1.6 Proposed mechanism for the DNA hydrolysis

The proposed mechanism is schematically depicted in Fig. 11. First, the phosphate residue is coordinated to the two Ce^{IV} ions in $[Ce^{IV}_2(OH)_4]^{4+}$ (the apparent association constant between Ce^{IV} and TpT is 10^3 M^{-1} at pH 2 and 50 °C).[9] As the result, the electrons of the phosphate are strongly withdrawn by the Ce^{IV} ions. Furthermore, the orbitals of the phosphate are mixed with the 4f-orbitals of Ce^{IV}, and form new hybrid orbital(s). These two factors greatly activate the phosphodiester linkage for the nucleophilic attack.

Then, the phosphate is attacked by the hydroxide ion coordinated to one of the two Ce^{IV} ions. According to the potentiometric titration, each of the Ce^{IV} ions releases three protons from its coordinated water to the aqueous phase, when the pH is increased from 0 to 4 (no proton is released above pH 4). Although this metal-bound hydroxide ion is a rather weak nucleophile, the phosphate is so activated (as described above) that the reaction can efficiently proceed. Furthermore, the hydroxide ion is located at quite a suitable position for the nucleophilic attack (the two Ce^{IV} ions in the bimetallic cluster have many coordinated water molecules, and at least one of them is placed appropriately for the purpose). Finally, the positive charges, accumulated in the Ce^{IV} hydroxo cluster (and also in the hydroxide gel as their aggregates), stabilize the negatively-charged transition state of DNA hydrolysis (the transition state is more negatively charged than the initial state, and is stabilized to a greater extent by the adjacent positive charges). Because of these factors, the pentacoordinated intermediate is efficiently formed.

In the breakdown of the intermediate, the water bound to Ce^{IV} functions as an acid catalyst. With this catalysis, the alkoxide ion of the 5′-OH of the 2′-deoxyribonucleotide (which is otherwise very unstable) can be promptly removed from the phosphorus atom. The large coordination number of the Ce^{IV} ions in the bimetallic cluster is favorable for the catalysis, exactly as described above for the first-step of DNA hydrolysis. The notable D_2O solvent isotope effect (see the Section 1.1) is associated with this proton transfer.

These arguments are supported by the fact that the activity of Ce^{IV} for DNA hydrolysis is substantially enhanced by cooperation with Pr^{III}.[25] When the Ce^{IV} : Pr^{III} ratio is 2, the activity is 10 fold greater than that of the Ce^{IV} ion (the Pr^{III} itself is virtually inactive under the reaction conditions employed). The catalysis occurs in the mixed hydroxo clusters, formed from these two metal ions in the reaction mixtures. Presumably, the Pr^{III} ion in this mixed cluster provides its metal-bound water as the acid catalyst, and promotes the second-step of DNA hydrolysis (the removal of the 5′-OH of 2′-deoxyribonucleotide). Under the reaction conditions (around pH 7), the Pr^{III}-bound water mostly remains undissociated ($pK_a \sim 9$),[26] and is superior as an acid catalyst to the Ce^{IV}-bound water. Although the $[Ce^{IV}(H_2O)_n]^{4+}$ ion is intrinsically a very strong acid (the pK_a for the first deprotonation is around 0),[26] it loses three protons at pH 0–4, and is only a weak acid at pH 7.[27]

On the $CeCl_3$-induced DNA hydrolysis under air, a mechanism, in which a hydrogen peroxide-like species (formed by the reduction of O_2 with the Ce^{III}) functions as the nucleophile, was proposed.[8b] However, this mechanism is unlikely, since Ce^{IV} salts satisfactorily hydrolyse DNA even in the complete absence of O_2.[8a,9] The role of O_2 is only to oxidize the Ce^{III} to the catalytically active Ce^{IV}, and not to provide the nucleophile. The nucleophile comes from the water.

2 Lanthanide(III) ion-induced hydrolysis of RNA

Since RNA has the 2′-OH of ribose as an intramolecular nucleophile towards the phosphorus atom, RNA is far more promptly (10^5–10^6 fold) hydrolysed than is DNA. Yet, non-enzymatic hydrolysis of RNA under physiological conditions is not easy (in order to hydrolyse RNA within an hour, for example, the catalyst must accelerate the reaction by 10^7-fold or more). Although a number of catalysts have been proposed,

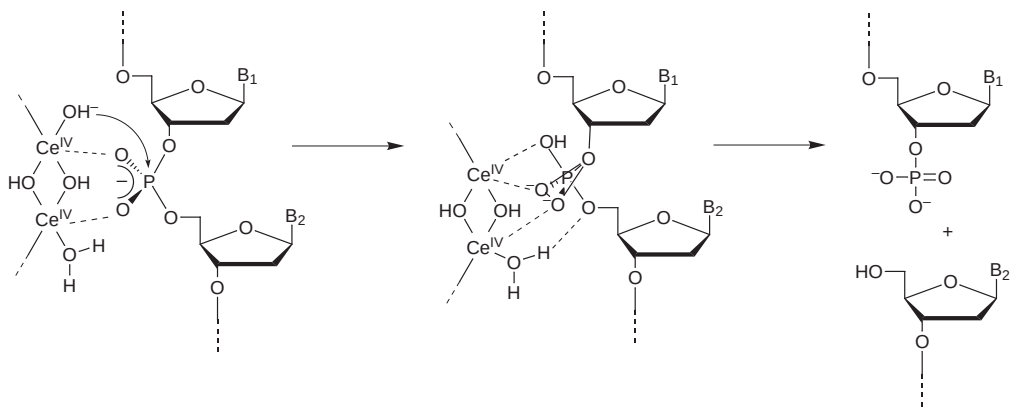

Fig. 11 Proposed mechanism of the Ce^{IV}-induced DNA hydrolysis [the P–O(5′) scission is presented here, although the P–O(3′) scission can also occur (see ref. 15)].

none of them exceeds (or is even comparable with) the lanthanide(III) ions in activity.

The catalytic activity of the lanthanide(III) ions at pH 7 monotonically increases with increasing atomic number.[10] With the last three (Tm^{III}, Yb^{III}, and Lu^{III}), RNA hydrolysis is completed within a few minutes at pH 7 and 30 °C. Interestingly, Ce^{IV}, which is the best for DNA hydrolysis, is not so active for RNA hydrolysis (its activity is comparable with that of Tb^{III}).

2.1 Catalytic species for RNA hydrolysis

The solvolysis chemistry of Nd^{III} is well known [eqn. (8) and (9)].[28] Thus, the Nd^{III}-induced hydrolysis of adenylyl(3′-5′)adenosine (ApA) has been kinetically analyzed in detail.[10] In

$$Nd^{III} + H_2O \overset{K_{1,1}}{\rightleftharpoons} [Nd^{III}(OH)]^{2+} + H^+ \quad pK_{1,1} = 9.4 \quad (8)$$

$$2Nd^{III} + 2H_2O \overset{K_{2,2}}{\rightleftharpoons} [Nd^{III}_2(OH)_2]^{4+} + 2H^+ \quad pK_{2,2} = 13.9 \quad (9)$$

the reaction mixtures, there exist three Nd^{III}-derived species: free Nd^{3+}, $[Nd^{III}(OH)]^{2+}$, and $[Nd^{III}_2(OH)_2]^{4+}$. The equilibrium concentration of each species can be calculated by using the $K_{1,1}$ and $K_{2,2}$ values.

As shown in Fig. 12, the logarithm of the rate of RNA hydrolysis steeply increases with increasing pH, up to pH 8, and

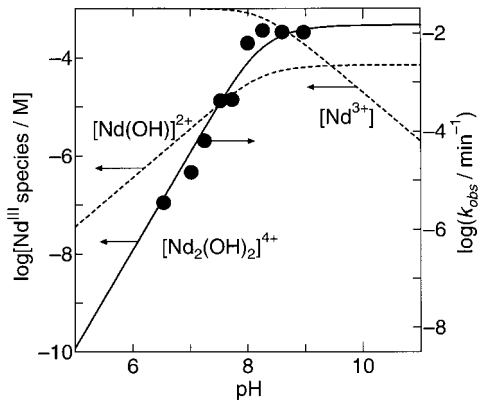

Fig. 12. The pH dependence of the rate of ApA hydrolysis by $NdCl_3$ (1 mM) at 30 °C. The closed circles are the experimental points, whereas the curved lines show the equilibrium concentration of the Nd^{III}-derived species.

then attains a plateau. The experimental points fit well the theoretical line showing the equilibrium concentration of $[Nd^{III}_2(OH)_2]^{4+}$ (the solid line). This bimetallic cluster is the active species for RNA hydrolysis (its formation is accompanied by the release of two protons, as shown by eqn. (9), and thus the pH–rate constant profile is so steep). This conclusion is further supported by the dependence of hydrolysis rate on the initial concentration of $Nd^{III}Cl_3$. In order to hydrolyse RNA efficiently, the bimetallic structure is essential. This finding is totally consistent with the fact that $[Ce^{IV}_2(OH)_4]^{4+}$ is the active species for Ce^{IV}-induced DNA hydrolysis.

2.2 Why does the activity of the lanthanide(III) ion at pH 7 increase with increasing atomic number?

The pH–rate constant profiles for all the lanthanide(III) ions have similar shapes, and are composed of (a) a steep straight line at lower pH and (b) a plateau at higher pH (see Fig. 13). The straight line corresponds to the formation of the active species $[Ln^{III}_2(OH)_2]^{4+}$ (Ln = lanthanide ion), whereas its formation is completed in the plateau.

As the atomic number increases, these profiles gradually shift towards the lower pH side. Accordingly, the concentration of the active species at pH 7 increases in this order. For example, Lu^{III} exists mostly as the bimetallic active species ($[Lu^{III}_2(OH)_2]^{4+}$) at pH 7. As the result, this metal ion is quite

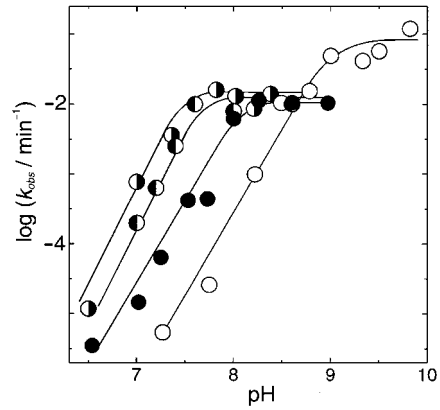

Fig. 13 The pH dependence of the rate of ApA hydrolysis by various lanthanide(III) chlorides (1 mM) at 30 °C: (○) La^{III}, (●) Nd^{III}, (◑) Tb^{III}, (◐) Lu^{III}. Only the typical results are presented here, since the shapes of the profiles for all the lanthanide(III) ions are similar and their positions monotonically shift towards lower pH side with increasing atomic number.

active for RNA hydrolysis in neutral solutions. For La^{III}, however, only a small fraction takes the active form at pH 7. Thus, Tm^{III}, Yb^{III}, and Lu^{III} are superior to the others, when the RNA hydrolysis is carried out under physiological conditions. In alkaline solutions, even the La^{III} ion mostly takes the active form and is sufficiently active.[29]

2.3 The rate-limiting step for RNA hydrolysis

When the 5′-O atom in RNA is replaced with a sulfur, the rate of alkaline hydrolysis of the corresponding phosphodiester linkage is increased by 10^5–10^6 fold.[30] Exactly as discussed in DNA hydrolysis (Section 1.2), the removal of the 5′-OH of the ribose from the phosphorus atom is rate limiting. Similarly, the lanthanide ion-induced RNA hydrolysis involves a rate-limiting removal of the 5′-OH.[10,31]

Based on these results, the energy diagrams are depicted in Fig. 4(*b*). The lanthanide(III) ions primarily accelerate the second step (the removal of the 5′-OH). At the same time, however, the first step (the intramolecular attack by the 2′-OH towards the phosphorus atom) is also promoted, to some extent ($> 10^{2-3}$ fold), so that the second-step remains rate-limiting (the RNA hydrolysis is accelerated by 10^8 fold). It is noteworthy that the first barrier in the alkaline hydrolysis of RNA is much lower than that in DNA hydrolysis [compare Fig. 4(*a*) with 4(*b*)]. The intramolecular attack by the 2′-OH is enormously efficient compared with the intermolecular reaction in the latter. Furthermore, the second barrier in the RNA hydrolysis (corresponding to $\Delta G_2^{\ddagger}$) is considerably higher than the first barrier (the rate difference is 10^5–10^6 fold). This is in contrast with the symmetric energy diagram in the DNA hydrolysis. The RNA hydrolysis involves the formation of a 2′,3′-cyclic monophosphate of the ribonucleotide as the first product, and a considerable strain is induced on the formation of this five-membered ring phosphate. The cyclic phosphate is much more reactive than RNA, and is rapidly hydrolysed to the 2′- or 3′-monophosphate as the final product.

2.4 Proposed mechanism of the RNA hydrolysis

First, the phosphodiester linkage in RNA is coordinated to the lanthanide(III) ion in the bimetallic cluster $[Ln^{III}_2(OH)_2]^{4+}$. In the following intramolecular nucleophilic attack by the 2′-OH towards the phosphorus atom, the hydroxide ion, bound to the metal ion(s), functions as the general base catalyst. Alternatively, the 2′-OH is directly coordinated to the metal ion, and its dissociation to alkoxide ion is facilitated.

In the breakdown of the resultant pentacoordinated intermediate, the metal-bound water (or the metal ion itself)

functions as the general acid catalyst. The water bound to the lanthanide(III) ions has a pK_a of around 8–9, which should be further decreased in the bimetallic clusters through the electron-withdrawal by the second metal(III) ion. This is quite appropriate for the present acid catalysis, since the RNA hydrolysis is carried out at around pH 7 (when the apparent activities of various acid catalysts are compared with each other at a predetermined pH, the activity increases as the pK_a gets closer to the pH).[31] The acid catalysis cooperates with the base catalysis in the hydroxo clusters, resulting in the prompt hydrolysis of RNA (Fig. 14).

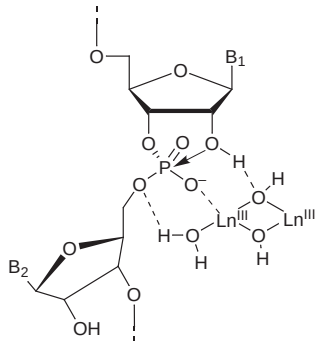

Fig. 14 Proposed mechanism of the lanthanide(III)-induced RNA hydrolysis.

3 DNA hydrolysis *vs.* RNA hydrolysis

What factor makes the Ce^{IV} ion the best for DNA hydrolysis? Why does RNA hydrolysis choose the lanthanide(III) ions? The energy diagrams in Fig. 4 give us some tips on these subjects. The energy diagram for the uncatalysed (alkaline) hydrolysis of DNA is virtually symmetric, and the heights of the first barrier and the second barrier are almost the same [the dotted line in Fig. 4(*a*)]. Under these conditions, the primary requirement for efficient catalysis is to *lower the energy barrier of the first step* (otherwise, the first barrier governs the rate of the whole reaction, no matter how much the second step is promoted). Second, the catalyst must stabilize the pentacoordinated intermediate with respect to the initial state [see eqn. (1)]. The Ce^{IV} ion satisfactorily fulfils these requirements, through the activation of the DNA by both (a) withdrawing the electrons from the phosphate in the 'two-metal activation' (Fig. 7 and 9) and (b) mixing its f-orbitals with those of the phosphate (Fig. 8). The second barrier is lowered with respect to the initial state, mainly because ΔG_1 is decreased. In contrast, the lanthanide(III) ions cannot activate DNA to such an extent that they are rather poor for DNA hydrolysis.

In uncatalysed hydrolysis of RNA [Fig. 4(*b*)], however, the second energy barrier is far higher than is the first energy barrier (10^5–10^6 fold difference in the reaction rate), as described in Section 2.3. Here, the promotion of the second step should directly accelerate the whole reaction (until it becomes lower than the first barrier). The promotion of the first step is not as essential as is the case in DNA hydrolysis. The lanthanide(III) ions are suitable for the acid catalysis in the second step, since they have many (8 or 9) coordinated water molecules and their pK_a values are close to the pH of the reaction mixtures (*vide ante*).[32]

4 From lanthanide ions to non-lanthanide ions

Soon after the remarkable catalysis by the lanthanide ions was discovered, many laboratories attempted to hydrolyse DNA and RNA by using non-lanthanide ions.[1] These catalysts, if available, should be useful for various practical applications (especially *in vivo*). It has been established that RNA can be hydrolysed by these metal ions, if two (or more) of them satisfactorily cooperate in dinuclear (or multi-nuclear) complexes (to date, there are no non-lanthanide complexes which can hydrolyse DNA of various sequences and structures).[33] In order to place the metal ions appropriately, various ligands have been designed. The control of acid/base properties of the metal ions (and of the water bound to them) is also important. For example, Zn^{II} ion itself is virtually inactive for RNA hydrolysis at pH 7. Mono-nuclear Zn^{II} complexes also exhibit poor activity. However, di- and tri-nuclear Zn^{II} complexes of pyridine-based ligands efficiently hydrolyse RNA (Fig. 15).[34,35] By attaching these zinc(II) complexes to DNA oligomers, sequence-selective artificial ribonucleases have been synthesized.[36]

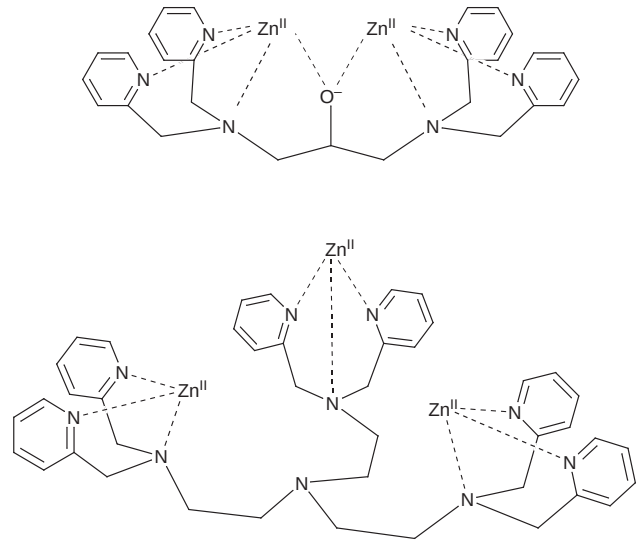

Fig. 15. Di- and tri-nuclear Zn^{II} complexes for RNA hydrolysis.

The lanthanide ions spontaneously form multi-nuclear clusters under physiological conditions, even in the absence of specific ligands. Two or more lanthanide ions are appropriately placed in these clusters, where bimetallic (or multi-metallic) synergism efficiently takes place. The 4f-orbitals activate the phosphates through orbital–orbital interactions. Furthermore, the acid/base properties of the coordinated water on the lanthanide ions are suitable for the catalysis at pH 7. Finally, the positively-charged reaction field, provided by the clusters, stabilizes the negatively-charged transition states for the hydrolysis of DNA and RNA. The combination of these factors gives rise to the remarkable activities of the lanthanide ions.

Conclusions

A few years ago, it was found that the lanthanide ions hydrolyse DNA and RNA under physiological conditions, and we have obtained useful tools to manipulate DNA and RNA without using naturally-occurring enzymes. However, the mechanistic details of these remarkable catalyses were not clear. In the present study, the following important conclusions have been obtained on the mechanisms of these catalyses.

(1) Tetracationic bimetallic hydroxo clusters are the active species ($[Ce^{IV}_2(OH)_4]^{4+}$ for DNA hydrolysis and $[Ln^{III}_2(OH)_2]^{4+}$ for RNA hydrolysis).

(2) The Ce^{IV} ion notably activates the phosphodiester linkages in DNA to nucleophilic attack, through (a) electron-withdrawal from the residues and (b) mixing its 4f-orbitals with their orbitals. As a result, the formation of the pentacoordinated intermediate is remarkably promoted.

(3) The catalysis for RNA hydrolysis is mainly ascribed to the acceleration of the breakdown of the pentacoordinated intermediate. The activity at pH 7 increases with increasing atomic number of the lanthanide(III) ion, since the concentration of the

active species (the bimetallic hydroxo cluster) increases in this order.

(4) In the lanthanide-induced hydrolysis of both DNA and RNA, the breakdown of the pentacoordinated intermediate is rate limiting.

These findings are valuable for the design of still more advanced catalysts for the hydrolysis of DNA and RNA, as well as artificial enzymes for site-selective scission of them. What should be clarified next is (1) what is the real nature of the orbital-mixing between the Ce^{IV} ion and the phosphate? and (2) how big a contribution is made to DNA activation by each of the electron-withdrawal and the orbital-mixing? In order to solve these problems, quantum-chemical analyses are under way. The application of lanthanide catalysis to biotechnology, molecular biology, and therapy are also currently being attempted.

Acknowledgements

The authors are indebted to all the co-workers and collaborators whose names are listed in the references. This study was partially supported by a Grant from the 'Research for the Future' Program of the Japan Society for the Promotion of Science (JSPS-RFTF97I00301) and Grants-in-Aid for Scientific Research from the Ministry of Education, Science, and Culture, Japan. A JSPS Research Fellowship for Young Scientists (for N. T.) is also acknowledged.

Notes and references

1 Recent reviews: M. Komiyama and J. Sumaoka, *Curr. Opin. Chem. Biol.*, 1998, **2**, 751; M. Oivanen, S. Kuusela and H. Lönnberg, *Chem. Rev.*, 1998, **98**, 961; B. N. Trawick, A. T. Daniher and J. K. Bashkin, *Chem. Rev.*, 1998, **98**, 939; G. Pratviel, J. Bernadou and B. Meunier, in *Advances in Inorganic Chemistry*, ed. A. G. Sykes, Academic Press, San Diego, 1998, vol. 45, p. 251; D. M. Perreault and E. V. Anslyn, *Angew. Chem., Int. Ed. Engl.*, 1997, **36**, 432; J. Chin, *Curr. Opin. Chem. Biol.*, 1997, **1**, 514; E. Kimura and T. Koike, in *Advances in Inorganic Chemistry*, ed. A. G. Sykes, Academic Press, San Diego, 1997, vol. 44, p. 229 and references cited therein.

2 The scission site of a restriction enzyme, which recognizes a sequence of 6 DNA bases, appears every 4^6 DNA bases (in average). If the DNA of the human beings, composed of more than 10^9 DNA bases, is treated with this restriction enzyme, the scission occurs at more than 10^5 sites.

3 The half-life of the phosphodiester linkage in DNA at pH 7 and 30 °C is estimated to be 200 million years. Although the linkage in RNA is much more reactive than that in DNA, its half-life is still 1000 years or so.

4 Supercoiled DNA, which is activated by strain and other factors, was reportedly cleaved *via* the hydrolytic pathway: L. A. Basile, A. L. Raphael and J. K. Barton, *J. Am. Chem. Soc.*, 1987, **109**, 7550; L. M. T. Schnaith, R. S. Hanson and L. Que, Jr., *Proc. Natl. Acad. Sci. U.S.A.*, 1994, **91**, 569; S. Hashimoto and Y. Nakamura, *J. Chem. Soc., Perkin Trans. 1*, 1996, 2623; R. Hettich and H.-J. Schneider, *J. Am. Chem. Soc.*, 1997, **119**, 5638.

5 DNA hydrolysis: Y. Matsumoto and M. Komiyama, *Nucleic Acids Symp. Ser.*, 1992, **27**, 33; M. Komiyama, K. Matsumura, K. Yonezawa and Y. Matsumoto, *Chem. Express*, 1993, **8**, 85; T. Shiiba, K. Yonezawa, N. Takeda, Y. Matsumoto, M. Yashiro and M. Komiyama, *J. Mol. Catal.*, 1993, **84**, L21.

6 RNA hydrolysis: K. Matsumura and M. Komiyama, *J. Chem. Soc., Chem. Commun.*, 1992, 640; J. R. Morrow, L. A. Buttrey, V. M. Shelton and K. A. Berback, *J. Am. Chem. Soc.*, 1992, **114**, 1903; J. R. Morrow and V. M. Shelton, *New J. Chem.*, 1994, **18**, 371; R. Breslow and D.-L. Huang, *Proc. Natl. Acad. Sci. U.S.A.*, 1991, **88**, 4080.

7 On the hydrolysis of various activated phosphoesters, see ref. 1.

8 (*a*) M. Komiyama, T. Shiiba, T. Kodama, N. Takeda, J. Sumaoka and M. Yashiro, *Chem. Lett.*, 1994, 1025; (*b*) B. K. Takasaki and J. Chin, *J. Am. Chem. Soc.*, 1994, **116**, 1121.

9 M. Komiyama, N. Takeda, Y. Takahashi, H. Uchida, T. Shiiba, T. Kodama and M. Yashiro, *J. Chem. Soc., Perkin Trans. 2*, 1995, 269.

10 K. Matsumura and M. Komiyama, *J. Biochem.*, 1997, **122**, 387.

11 Sequence-selective DNA scission: M. Komiyama, T. Shiiba, Y. Takahashi, N. Takeda, K. Matsumura and T. Kodama, *Supramol. Chem.*, 1994, **4**, 31; M. Komiyama, N. Takeda, T. Shiiba, Y. Takahashi, Y. Matsumoto and M. Yashiro, *Nucleosides Nucleotides*, 1994, **13**, 1297; M. Komiyama, *J. Biochem.*, 1995, **118**, 665.

12 Sequence-selective RNA scission: K. Matsumura, M. Endo and M. Komiyama, *J. Chem. Soc., Chem. Commun.*, 1994, 2019; J. Hall, D. Hüsken and R. Häner, *Nucleosides Nucleotides*, 1997, **16**, 1357; D. Magda, M. Wright, S. Crofts, A. Lin and J. L. Sessler, *J. Am. Chem. Soc.*, 1997, **119**, 6947.

13 J. Sumaoka, Y. Azuma and M. Komiyama, *Chem. Eur. J.*, 1998, **4**, 205.

14 N. Takeda, Y. Okada and M. Komiyama, unpublished results.

15 The electrophilicity of the phosphorus atom is not much altered by the O → S substitution, since the substitution of non-bridging oxygen in the phosphate to sulfur hardly affects the rate of hydrolysis. In Tp-OCH_2CF_3, the perturbation on the phosphorus atom is still smaller. In the Ce^{IV}-induced hydrolysis of Tp-OT, the P–O(3′) bond and the P–O(5′) bond are cleaved at almost the same rates (the resultant 5′- and 3′-monophosphates of thymidine are rapidly hydrolysed to thymidine as the final product, and thus are not much accumulated: see ref. 9). In the hydrolysis of Tp-ST and Tp-OCH_2CF_3, the P–S bond and P–O(5′) bond are exclusively cleaved.

16 Homogeneous hydrolysis of DNA at pH 7 by Ce^{IV}–saccharide complexes was reported: A. Kajimura, J. Sumaoka and M. Komiyama, *Carbohydr. Res.*, 1998, **309**, 345.

17 F. B. Charles Jr. and R. E. Mesmer, *The Hydrolysis of Cations*, Wiley, New York, 1976, p. 138.

18 J. Sumaoka, N. Takeda, Y. Okada, H. Takahashi, H. Shigekawa and M. Komiyama, *Nucleic Acids Symp. Ser.*, 1998, **39**, 137.

19 J. Sumaoka, K. Furuki and M. Komiyama, unpublished results.

20 J. Sumaoka, S. Miyama and M. Komiyama, *J. Chem. Soc., Chem. Commun.*, 1994, 1755.

21 H. Shigekawa, H. Ikawa, R. Yoshizaki, Y. Iijima, J. Sumaoka and M. Komiyama, *Appl. Phys. Lett.*, 1996, **68**, 1433.

22 H. Shigekawa, M. Ishida, K. Miyake, R. Shioda, Y. Iijima, T. Imai, H. Takahashi, J. Sumaoka and M. Komiyama, *Appl. Phys. Lett.*, 1999, **74**, 460.

23 The EXAFS and XANES measurements were carried out on samples frozen in liquid nitrogen.

24 Various characteristic properties of Ce compounds have been interpreted in terms of the formation of similar hybrid orbitals. For example, $CeRu_2$, $CeCo_2$, and $CeRh_3$ are non-magnetic, but show 4f-derived emission in their resonant photoemission spectra. Apparently, the 4f character is delocalized by the hybridization. The number of 4f electrons should be between 0 and 1 depending on the amount of the charge-transfer: A. Fujimori, *Phys. Rev. B*, 1983, **28**, 4489; A. Bianconi, H. Marcelli, R. Dexpert, A. Karnatak, T. J. Kotani and J. Petiau, *Phys. Rev. B*, 1987, **35**, 806 and references cited therein.

25 N. Takeda, T. Imai, M. Irisawa, J. Sumaoka, M. Yashiro, H. Shigekawa, and M. Komiyama, *Chem. Lett.*, 1996, 599. This Ce^{IV}/Pr^{III} combination is the most active catalyst for DNA hydrolysis ever reported.

26 J. Burgess, *Metal Ions in Solution*, Wiley, New York, 1978, p. 267.

27 Alternatively, Pr^{III} can provide its metal-bound hydroxide as the nucleophile. The hydroxide is a better nucleophile than the Ce^{IV}-bound hydroxide.

28 K. A. Burkov, L. S. Lilich, N. D. Ngo and A. Yu. Smirnov, *Russ. J. Inorg. Chem.*, 1973, **18**, 797.

29 P. Hurst, B. K. Takasaki and J. Chin, *J. Am. Chem. Soc.*, 1996, **118**, 9982.

30 X. Liu and C. B. Reese, *Tetrahedron Lett.*, 1995, **36**, 3413; J. B. Thomson, B. K. Patel, V. Jimenez, K. Eckart and F. Eckstein, *J. Org. Chem.*, 1996, **61**, 6273; R. G. Kuimelis and L. W. McLaughlin, *Nucleic Acids Res.*, 1995, **23**, 4753; D.-M. Zhou, N. Usman, F. E. Wincott, J. Matulic-Adamic, M. Orita, L.-H. Zhang, M. Komiyama, P. K. R. Kumar and K. Taira, *J. Am. Chem. Soc.*, 1996, **118**, 5862.

31 T. Shiiba and M. Komiyama, *Tetrahedron Lett.*, 1992, **33**, 5571.

32 The Brønsted relationship indicates that the intrinsic activity of acid catalysts increases with decreasing pK_a. However, the concentration of the active species (in the acidic form) at a predetermined pH decreases in this order. Thus, the net efficiency of the catalysis, determined by (the intrinsic activity of active species) × (the concentration of active species), takes the maximum when the pK_a is close to the reaction pH (see M. L. Bender, R. J. Bergeron and M. Komiyama, *The Bioorganic Chemistry of Enzymatic Catalysis*, Wiley, New York, 1984, ch. 6.

33 Some of the complexes in ref. 4 were proposed to be active for the hydrolysis of non-supercoiled DNA.

34 M. Yashiro, A. Ishikubo and M. Komiyama, *J. Chem. Soc., Chem. Commun.*, 1995, 1793.

35 M. Yashiro, A. Ishikubo and M. Komiyama, *J. Chem. Soc., Chem. Commun.*, 1997, 83.

36 S. Matsuda, A. Ishikubo, A. Kuzuya, M. Yashiro and M. Komiyama, *Angew. Chem., Int. Ed.*, 1998, **37**, 3284.

Paper 9/01621J

Metal-ion stabilization of photoinduced open colored isomer in crowned spirobenzothiapyran

Mutsuo Tanaka,[a] Kenji Kamada,[a] Hisanori Ando,[a] Takashi Kitagaki,[b] Yasuhiko Shibutani,[b] Setsuko Yajima,[c] Hidefumi Sakamoto[c] and Keiichi Kimura*[c]

[a] *Osaka National Research Institute, AIST, 1-8-13, Midorigaoka, Ikeda, Osaka 563-8577, Japan*
[b] *Department of Chemistry, Faculty of Engineering, Osaka Institute of Technology, 5-16-1, Ohmiya, Asahi-ku, Osaka 535-8585, Japan*
[c] *Department of Applied Chemistry, Faculty of Systems Engineering, Wakayama University, 930, Sakae-dani, Wakayama 640-8510, Japan. E-mail: kimura@sys.wakayama-u.ac.jp*

Received (in Cambridge, UK) 14th May 1999, Accepted 23rd June 1999

A spirobenzothiapyran derivative bearing a monoaza-12-crown-4 moiety affords significant thermal stability enhancement in the UV light induced colored merocyanine form of its photochromic moiety by metal-ion complexation of its crown ether moiety, although the complexation hardly induces the isomerization without photoirradiation.

Spirobenzopyrans[1] and spirobenzothiapyrans[2] are well-known photochromic compounds that isomerize to their corresponding merocyanine forms under UV light, and *vice versa* under visible light or heat. Such kinds of compounds have been studied extensively in view of photochromic devices.[3] However, the application of spirobenzothiapyrans to photochromic devices does not seem to be very easy due to the poor thermal stability of their open colored form. In our previous studies[4] on spirobenzopyrans bearing a monoazacrown ether moiety, we found that the spiropyran ring opening was facilitated by metal ion complexation of the crown ether moiety in the presence of metal ions. This resulted in the spiropyran ring opening even without UV light irradiation [Scheme 1(*a*)]. This finding prompted us to design spirobenzothiapyrans bearing a crown ether moiety, which we call crowned spirobenzothiapyrans, expecting facilitation of the thiapyran ring opening by metal ion complexation of the crown ether moiety. This in turn may allow the resulting spirobenzothiapyrans to be applicable for photochromic devices. Here we report preliminary results on significant stabilization of the photoinduced open colored isomer of a crowned spirobenzothiapyran in the presence of alkali metal ions, especially Li^+.

The synthesis of crowned spirobenzothiapyran **1** was carried out in accordance with Scheme 2. The conversion of the phenolic hydroxy group of crowned nitrosalicylaldehyde[4a] to the corresponding thiol group was attained by the reaction with $(CH_3)_2NCSCl$ at 0–25 °C in the presence of NEt_3, by refluxing in toluene, and by hydrolysis with KOH.[2d] The crowned thiosalicylaldehyde was then reacted with 2-methylene-1,3,3-trimethylindoline in refluxing EtOH to yield the spirobenzothiapyran bearing a monoaza-12-crown-4 moiety, **1**, which was purified by recrystallization from EtOH after preparative gel-permeation chromatography.† For comparison, we also synthesized a spirobenzothiapyran derivative bearing an oligooxyethylene moiety, **2**, in a similar way to **1**.

Absorption spectra of **1** and **2** were measured in MeCN in the presence and absence of an alkali metal perchlorate. The spectra of **1** and **2** were hardly changed by adding an equimolar amount of Li^+, Na^+, and K^+, unless irradiated by UV light. This means that isomerization to their merocyanine form by the thiapyran ring opening cannot proceed by metal ion complexation of their crown ether ring under dark conditions [Scheme 1(*b*)]. This isomerization behavior of **1** is very different from that of the spirobenzopyran bearing a monoaza-12-crown-4 moiety, the pyran ring of which can be opened readily by metal ion complexation even without UV light irradiation[4] [Scheme 1(*a*)], probably due to the polarity increase induced by the metal ion binding.

It should be noted that irradiation of 365 nm UV light‡ on the **1** solution containing Li^+ causes a drastic change in the absorption spectrum (Fig. 1). On the other hand, hardly any significant spectral change was observed in the **1** solution without any metal ion and with an equimolar amount of K^+. The Na^+ addition afforded only a slight spectral change (Fig. 1). Definitely, the metal ion complexing ability of the crown ether

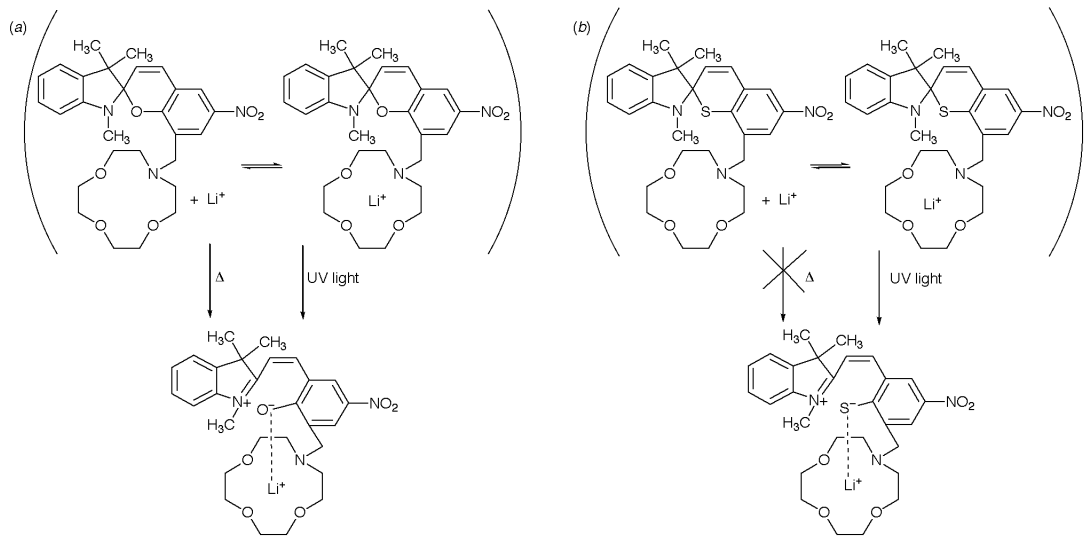

Scheme 1

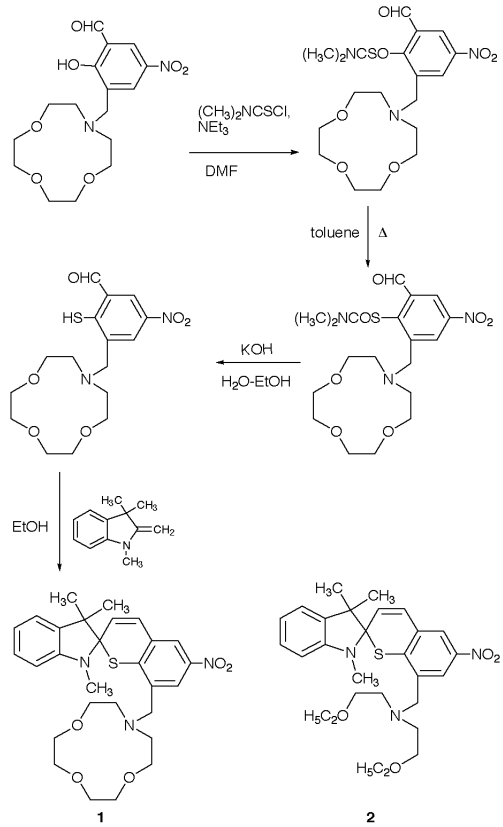

Scheme 2

moiety of **1** stabilizes the colored merocyanine isomer that is formed only on UV light irradiation, owing to the polarity enhancement. It is worth noting that the stabilization is highly selective for Li^+. In addition to the selective Li^+ binding with a monoaza-12-crown-4 moiety of **1**, some interaction between the thiolate anion and Li^+ complexed by the crown ether moiety probably contributes to the stabilization of the colored merocyanine isomer of **1,** as is the case with the Li^+ complex for merocyanine form of crowned spirobenzopyran (Scheme 1).[4c] This Li^+-specific stabilization of the photoinduced colored form of **1** is also supported by photochromism for a model compound carrying a linear oligooxyethylene moiety instead of a crown ether moiety, **2**. Since the linear oligooxyethylene moiety of **2** cannot bind a metal ion very powerfully, the presence of a metal

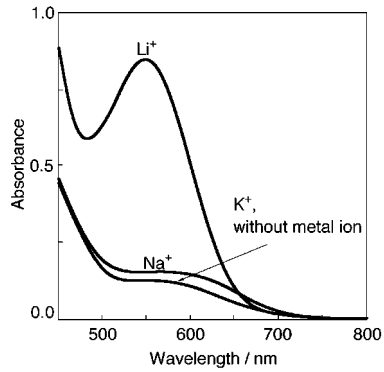

Fig. 1 Absorption spectra of crowned spirobenzothiapyran **1** under UV irradiation in the absence and presence of an alkali metal ion. **1** and alkali metal perchlorate: 2×10^{-4} mol dm^{-3} in acetonitrile.

ion, even Li^+, scarcely induced such UV light-induced isomerization to the open colored isomer as seen in the **1** system.

In order to elaborate the thermal stability of the open colored form of crowned spirobenzothiapyran **1** in MeCN, thermal decoloration of the **1** solution in the presence or absence of Li^+ was followed at room temperature by turning off UV the light.§ In the absence of Li^+, the thermal isomerization back to the spiropyran form was complete within 5 s. On the contrary, the thermal back-isomerization in the presence of Li^+ was very sluggish even by visible light irradiation, the half-life of the UV-induced merocyanine isomer being about 2 min. This again proves the Li^+ complexation-induced high stability of the colored merocyanine form in crowned spirobenzothiapyran **1**.

In conclusion, the crowned spirobenzothiapyran **1** exhibits characteristic photochromism as follows: i) the isomerization of **1** to its corresponding colored merocyanine form does not proceed even in the presence of any crown ether complexing metal ion, unless otherwise irradiated by UV light; ii) the Li^+-selective complexation of the crown ether moiety facilitates UV light induced isomerization (thiapyran ring opening) dramatically; and iii) the metal ion complexation stabilizes the colored merocyanine isomer thus formed to a great extent. Thus the photochromic crown ether seems to be promising for applications such as photochromic devices.

Notes and references

† *Selected data* for **1** : mp 146–148 °C; δ_H($CDCl_3$, 500 Hz) 1.23 (3H, s, CH_3), 1.37 (3H, s, CH_3), 2.68 (3H, s, NCH_3), 2.71 (4H, t, *J* 4, NCH_2), 3.53–3.77 (14H, m, OCH_2 and $PhCH_2N$), 5.98 (1H, d, *J* 6, CH=), 6.50 (1H, d, *J* 7.5, ArH), 6.85 (1H, t, *J* 7, ArH), 6.93 (1H, d, *J* 6, CH=), 7.06 (1H, d, *J* 6.5, ArH), 7.17 (1H, t, *J* 7.5, ArH), 7.93 (1H, s, ArH), 8.73 (1H, s, ArH). Calc. for $C_{28}H_{35}N_{30}O_5S$: H, 6.67, C, 64.00; N, 8.00; S, 6.10. Found: H, 6.63; C, 63.86; N, 7.86; S, 5.84%.

‡ The UV light, obtained by passing light of a 250 W Hg lamp through a light filter (wavelength 363.25 nm, $\Delta\mu/2$ 9.5 nm, transmittance 0.53), was introduced to the cell compartment of a spectrophotometer by using a glass fiber guide and was irradiated on the quartz cell containing a solution. The absorption spectra were therefore taken, while irradiating the measurement cell in the perpendicular direction to the measuring incident light.

§ The thermal coloration was followed by measuring the absorbance at 550 nm after UV light irradiation for 1.5 min.

1 (*a*) L. D. Taylor, J. Nicholson and R. B. Davis, *Tetrahedron Lett.*, 1967, 1585; (*b*) J. Sunamoto, K. Iwamoto, Y. Mohri and T. Kominato, *J. Am. Chem. Soc.*, 1982, **104**, 5502; (*c*) J. Anzai, A. Ueno and T. Osa, *J. Chem. Soc., Chem. Commun.*, 1984, 688; (*d*) M. Irie, T. Iwayanagi and Y. Taniguchi, *Macromolecules*, 1985, **18**, 2418; (*e*) H. Sasaki, A. Ueno, J. Anzai and T. Osa, *Bull. Chem. Soc. Jpn.*, 1986, **59**, 1953; (*f*) J. D. Winkler, K. Deshayes and B. Shao, *J. Am. Chem. Soc.*, 1989, **111**, 769; (*g*) F. Ciardelli, D. Fabbri, O. Pieroni and A. Fissi, *J. Am. Chem. Soc.*, 1989, **111**, 3470; (*h*) M. Inouye, M. Ueno, T. Kitao and K. Tsuchiya, *J. Am. Chem. Soc.*, 1990, **112**, 8977.

2 (*a*) R. S. Becker and J. Kolc, *J. Phys. Chem.*, 1968, **72**, 997; (*b*) S. Arakawa, H. Kondo and J. Seto, *Chem. Lett.*, 1985, 1805; (*c*) S. Tamura, N. Asai and J. Seto, *Bull. Chem. Soc. Jpn.*, 1989, **62**, 358; (*d*) M. Hirano, A. Miyashita and H. Nohira, *Chem. Lett.*, 1991, 209.

3 (*a*) R. C. Bertelson, *Photometric Process Involving Heterocyclic Cleavage in Photochromism*, ed. G. H. Brown, Wiley-Interscience, New York, 1971, ch. 3; (*b*) J. C. Crano and R. J. Guglielmetti, *Organic Photochromic and Thermochromic Compounds*, vol. 1, Main Photochromic Families, Plenum, New York, 1999.

4 (*a*) K. Kimura, T. Yamashita and M. Yokoyama, *J. Chem. Soc., Chem. Commun.*, 1991, 147; (*b*) K. Kimura, T. Yamashita and M. Yokoyama, *Chem. Lett.*, 1991, 965; (*c*) K. Kimura, T. Yamashita and M. Yokoyama, *J. Chem. Soc., Perkin Trans. 2*, 1992, 613; (*d*) K. Kimura, T. Yokoyama and M. Yokoyama, *J. Phys. Chem.*, 1992, **96**, 5614.

Communiication 9/03877I

ChemComm

Formal synthesis of roseophilin

Jeremy Robertson* and Richard J. D. Hatley

Dyson Perrins Laboratory, South Parks Road, Oxford, UK OX1 3QY.
E-mail: jeremy.robertson@chemistry.oxford.ac.uk

Received (in Cambridge, UK) 14th June 1999, Accepted 23rd June 1999

A thirteen step route to the tricyclic ketopyrrole core of roseophilin is presented in which the final step consists of a Paal–Knorr pyrrole synthesis that proceeds with *in situ* oxidation.

The intriguing structure of roseophilin, a cytotoxic antibiotic isolated from *Streptomyces griseoviridis* as disclosed by Seto in 1992,[1] has stimulated significant synthetic interest[2] culminating in Fürstner's elegant total synthesis of the racemate[3] and its analogues.[4] Our group has also been active in this area[5] and in this communication we outline a concise synthesis of the tricyclic ketopyrrole right hand half (±)-**10**. This route was

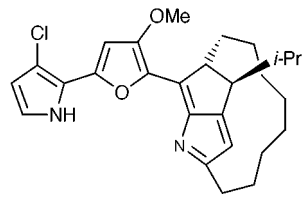

Roseophilin

designed to be easily tailored to provide access to either enantiomer of roseophilin as well as being sufficiently flexible that a range of roseophilin analogues could be prepared for biological evaluation.

At the outset of our investigations towards tricycles such as **10** we elected to form the pyrrole ring in the final step so that the energetic drive towards aromaticity would serve to override the adverse strain inherent in these molecules. In this respect our synthetic concept differs fundamentally from those of Fürstner,[2d,3,4] Fuchs,[2b,c] and Terashima.[2f] Our second guiding principle was to construct the thirteen membered ring by a free radical macrocyclisation[6] since our own studies[5a] had shown that bicyclo[10.2.1]pentadecenones could be obtained by this method.

Radical macrocyclisation precursor **6** was constructed in five steps from cyclopentenone derivative (±)-**1**[7] (Scheme 1) starting with conjugate addition[8] of *i*-PrMgCl which proceeded in essentially quantitative yield provided excess TMSCl (4.0 equiv.) was used to trap the enolate and Et_3N was added to the reaction mixture prior to aqueous work-up. Generation of the lithium enolate from the intermediate silyl enol ether, trapping with propargylic iodide (propargyl = prop-2-ynyl) **11**[9] and desilylation with fluorosilicic acid[10] afforded 1°-alcohol **2**. Yadav's procedure for converting 1°-propargyl alcohols into vinyl ketones[11] was unsuccessful when applied to this substrate as the hydrogen sulfide used in the work-up led to thiol adducts that could not be processed further. Eventually we found that treatment of alcohol **2** with $Hg(OAc)_2$ in acetic acid containing water (1.0 equiv.) then work-up after 30 min with dilute hydrochloric acid gave much improved results, a mixture being obtained consisting of the desired enone **3**, β-hydroxy ketone **4**, and the regioisomeric hydrolysis product **5** (4.5:1:1.5 respectively). These compounds were readily separable and the 1,4-adduct **4** could be dehydrated efficiently (MsCl, Et_3N, cat. DMAP; 93%) to give an acceptable overall yield of the radical precursor **6** after Finkelstein reaction.

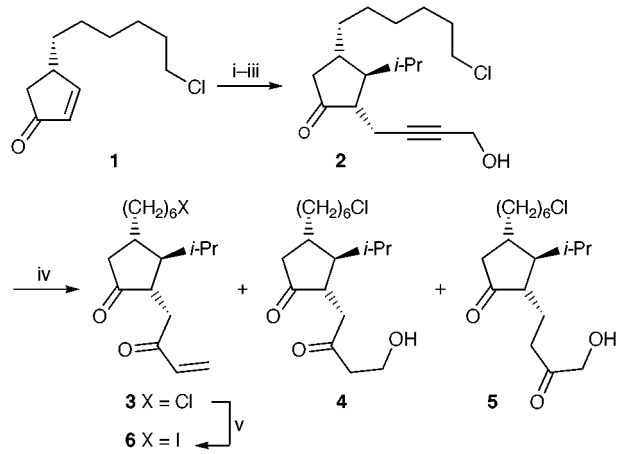

Scheme 1 *Reagents:* i. *i*-PrMgCl, CuI, LiCl, TMSCl, THF (96–99%); ii. MeLi then DMPU, **11**, THF (62%); iii. H_2SiF_6, aq. CH_3CN (96%); iv. $Hg(OAc)_2$, H_2O, AcOH then 5% aq. HCl (59% → **3**); v. NaI, butanone (88%).

The radical macrocyclisation required high dilution (2.5 mM) and slow addition (7 h) of the tin hydride in order to minimise direct reduction but enone hydrostannylation products could not be avoided. Work-up with thiophenol[12] facilitated isolation of the crystalline macrocyclic diketone **7** (Scheme 2) whose identity was confirmed by X-ray crystallography.[13] The *N*-benzyl pyrrole **9a** was formed straightforwardly but direct access to the *N*-unsubstituted analogue **9b** gave an indication of the strain in this system and forcing conditions were required (*cf.* ref. 14). Unfortunately we were unable to effect direct α-oxidation of either **9a** or the *N*-Boc analogue **9c** even though studies on compounds lacking the macrocyclic linking chain gave promising results.[15]

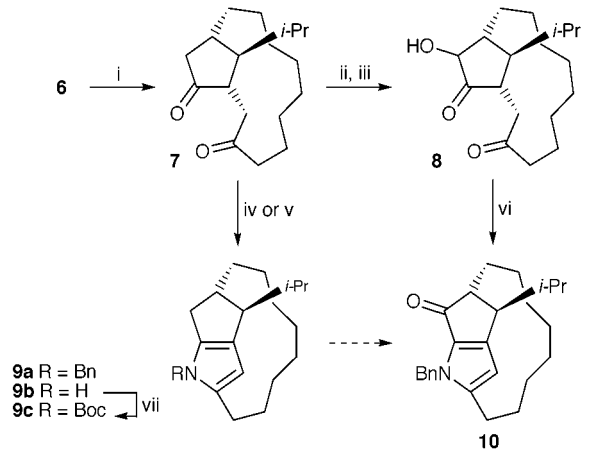

Scheme 2 *Reagents:* i. Bu_3SnH, AIBN, PhH (35–50%); ii. LDA, THF, −50 → 0 °C then TMSCl (55%, partial hydrolysis on SiO_2); iii. dimethyldioxirane (0.1 M in acetone), CH_2Cl_2 then aq. H_2SiF_6, CH_3CN (80%); iv. $BnNH_2$, AcOH, EtOH, 50 °C (60%); v. $(Me_3Si)_2NH$, Al_2O_3, 150 °C (sealed tube) (86%); vi. $BnNH_2$, AcOH, EtOH, 55 °C then 2 M aq. HCl, MeOH (25%); vii. KH, Boc_2O, THF (75%).

This problem proved insurmountable therefore we embarked on an attempt to effect oxidation prior to pyrrole formation which required a method for discriminating between the two carbonyl groups in diketone **7**. Treatment with LDA (1.1 equiv.) at −78 °C with an *in situ* TMSCl quench resulted in the sole formation of the doubly silylated compound **12** with a

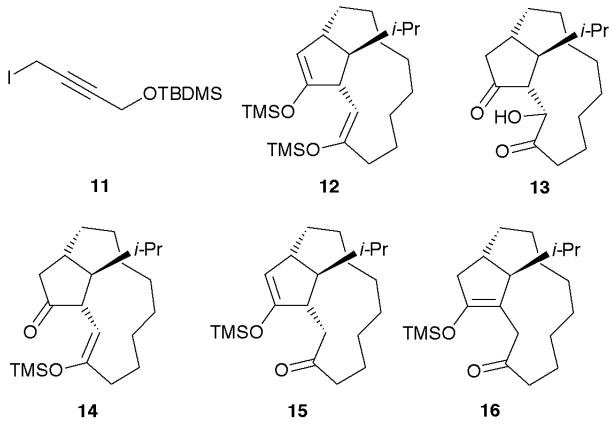

11 **12** **13**

14 **15** **16**

corresponding recovery of starting material. Furthermore, oxidation of bis-silyl enol ether **12** by MCPBA was selective for the macrocyclic position giving α-hydroxy ketone **13** in 70% isolated yield. An attempt to effect selective mono-desilylation[16] of **12** merely returned starting material.

Selective mono-silylation in the five-membered ring proved to be a challenging task as kinetic enolate formation with an *external* TMSCl quench led predominantly to silyl enol ether **14**. However a reasonable product ratio in favour of silyl enol ether **15** could be attained under equilibrating conditions although this compound could not be obtained free of the regioisomer **16** (3–4 : 1 ratio). This mixture was treated with dimethyldioxirane[17] to give, after desilylation, α-hydroxy ketone **8** (containing *ca*. 20% of the inseparable regioisomer). Overall yields for **7** → **8** were generally around 45% either with or without purification of the intermediate silyl enol ether mixture.

The final step, Paal–Knorr pyrrole synthesis from a 1,4-diketone bearing an unprotected α-hydroxy substituent, had no immediate precedent. Heating compound **8** with benzylamine in ethanolic acetic acid proved insufficient to drive the reaction to completion but, after consumption of the starting material, addition of 2.0 M hydrochloric acid in methanol was effective in delivering a pyrrole product. However this product did not contain a hydroxy group; in fact the ring closure was accompanied by an unexpected oxidation to afford a compound with spectroscopic data exactly matching those reported by Fürstner for the ketopyrrole **10**.

This route to ketopyrrole **10** not only stands as a formal total synthesis of (±)-roseophilin but opens the way to an enantiospecific synthesis because treatment of commercially available (4*R*)-(*tert*-butyldimethylsilyl)oxycyclopentenone[18] with 6-chlorohexylcuprate[5*a*] followed by elimination of the silyloxy group is expected to yield (*R*)-**1** from which a single enantiomer of roseophilin would follow. Currently we are optimising a new synthesis of the pyrrolylfuran left hand half and will report on this and our progress towards an enantiospecific total synthesis of roseophilin in due course.

We wish to thank the EPSRC for a studentship (RJDH), the EPSRC Mass Spectrometry Service Centre for exact mass measurements, Dr David J. Watkin for obtaining the X-ray structure of diketone **7**, and the Chemical Database Service at Daresbury.[19]

Notes and references

1 Y. Hayakawa, K. Kawakami, H. Seto and K. Furihata, *Tetrahedron Lett.*, 1992, **33**, 2701.
2 (*a*) S. Nakatani, M. Kirihara, K. Yamada and S. Terashima, *Tetrahedron Lett.*, 1995, **36**, 8461; (*b*) S. H. Kim and P. L. Fuchs, *Tetrahedron Lett.*, 1996, **37**, 2545; (*c*) S. H. Kim, I. Figueroa and P. L. Fuchs, *Tetrahedron Lett.*, 1997, **38**, 2601; (*d*) A. Fürstner and H. Weintritt, *J. Am. Chem. Soc.*, 1997, **119**, 2944; (*e*) T. Luker, W.-J. Koot, H. Hiemstra and W. N. Speckamp, *J. Org. Chem.*, 1998, **63**, 220; (*f*) T. Mochizuki, E. Itoh, N. Shibata, S. Nakatani, T. Katoh and S. Terashima, *Tetrahedron Lett.*, 1998, **39**, 6911.
3 A. Fürstner and H. Weintritt, *J. Am. Chem. Soc.*, 1998, **120**, 2817.
4 A. Fürstner, T. Gastner and H. Weintritt, *J. Org. Chem.*, 1999, **64**, 2361.
5 (*a*) J. Robertson, J. N. Burrows and P. A. Stupple, *Tetrahedron*, 1997, **53**, 14 807; (*b*) J. Robertson and J. N. Burrows, *Synthesis*,1998, 63; (*c*) N. Kuhnert, J. Peverley and J. Robertson, *Tetrahedron Lett.*, 1998, **39**, 3215.
6 (*a*) N. A. Porter, D. R. Magnin and B. T. Wright, *J. Am. Chem. Soc.* 1986, **108**, 2787; (*b*) S. Handa and G. Pattenden, *Contemp. Org. Synth.*, 1997, **4**, 196.
7 Prepared in 53% overall yield from 1-chlorooctan-8-ol: (i) Swern oxidation; (ii) *i*-Bu_2NH, K_2CO_3; (iii) $ClCH_2COCH_3$, NaI, 18C6, PhH; (iv) NaOH, aq. THF.
8 M. T. Reetz and A. Kindler, *J. Organomet. Chem.*, 1995, **502**, C5.
9 Prepared in 77% overall yield from butyne-1,4-diol: (i) TBDMSCl, imidazole, DMF; (ii) Ph_3P, I_2, imidazole, CH_2Cl_2.
10 A. S. Pilcher and P. DeShong, *J. Org. Chem.*, 1993, **58**, 5130.
11 J. S. Yadav, V. Prahlad and B. Muralidhar, *Synth. Commun.*, 1997, **27**, 3415.
12 J. Robertson, M. A. Peplow and J. Pillai, *Tetrahedron Lett.*, 1996, **37**, 5825.
13 Details of this structure will be provided in a full description of this work.
14 B. Rousseau, F. Nydegger, A. Gossauer, B. Bennua-Skalmowski and H. Vorbrüggen, *Synthesis*, 1996, 1336.
15 Details of these α-oxidations will be discussed in a separate report.
16 H. Urabe, Y. Takano and I. Kuwajima, *J. Am. Chem. Soc.*, 1983, **105**, 5703.
17 (*a*) W. Adam, L. Hadjiarapoglou and X. Wang, *Tetrahedron Lett.*, 1989, **30**, 6497; (*b*) W. Adam and F. Prechtl, *Chem. Ber.*, 1991, **124**, 2369; (*c*) W. Adam, J. Bialas and L. Hadjiarapoglou, *Chem. Ber.*, 1991, **124**, 2377.
18 We thank Sumitomo Chemical for a sample of this material.
19 D. A. Fletcher, R. F. McMeeking and D. Parkin, *J. Chem. Inf. Comput. Sci.*, 1996, **36**, 746.

Communication 9/04714J

ChemComm

One-pot synthesis of γ-lactams in a reaction cascade from α,β-unsaturated imines, CO and ethylene catalysed by $Ru_3(CO)_{12}$†

Daniel Berger and Wolfgang Imhof*

Institut für Anorganische und Analytische Chemie, August-Bebel-Str. 2, 07743 Jena, Germany. E-mail: cwi@rz.uni-jena.de

Received (in Cambridge, UK) 23rd April 1999, Accepted 22nd June 1999

The formation of 1,3-dihydropyrrol-2-one derivatives in moderate to excellent yields may be achieved by sequential insertion of CO and ethylene into C–H bonds of 1-azadienes catalysed by $Ru_3(CO)_{12}$; thus two new C–C bonds and a new center of asymmetry at C3 are produced *via* an intramolecular aldol condensation-like cyclization.

C–H activation reactions induced by transition metal compounds have aroused considerable interest as models for the initial steps of catalytic transformations of the ligands, *e.g.* in C–C coupling reactions. Thus in the past years inter- as well as intramolecular C–H activation reactions have been thoroughly reviewed.[1] In our recent work we investigated the reaction of aromatic imines towards $Fe_2(CO)_9$ which proceeds *via* C–H activation steps and subsequent intramolecular hydrogen migration reactions towards suitable acceptor sites in the ligand, producing di- or trinuclear iron carbonyl complexes.[2] On the other hand, it has been shown previously that aromatic imines may react with CO and/or a wide variety of olefins in the presence of catalytic amounts of $Ru_3(CO)_{12}$ to give the respective substitution products.[3] The C–C coupling reaction selectively takes place in the position *ortho* with respect to the imine substituent, and thus similar C–H activation steps to the ones which we observed in the stoichiometric reactions of the same ligands with $Fe_2(CO)_9$ may well be the initial steps of these catalytic reactions. The reaction of acyclic α,β-unsaturated imines with $Ru_3(CO)_{12}$ yields ruthenium carbonyl complexes, the formation of which also includes C–H activation steps, whereas treatment with $Fe_2(CO)_9$ produces (η^4-azadiene)$Fe(CO)_3$ complexes.[4,5]

Here we report the catalytic synthesis of γ-lactams, namely 1,3-dihydropyrrol-2-one derivatives, from α,β-unsaturated imines, CO and ethylene (Scheme 1).[6] From Scheme 1 it can be seen that variation of the organic substituent at nitrogen leads to different product distributions. Obviously CO and ethylene compete for the azadiene. In the case of the least electron donating organic moieties at the imine nitrogen, in addition to the pyrrol-2-one derivatives **1a** and **1b** two other compounds, **2a** and **2b** respectively, are formed in which one molecule of ethylene has inserted into the C–H bond at the β-carbon atom of the 1-azadiene. If R′ is *p*-$CF_3C_6H_4$ then **2a** is the main product

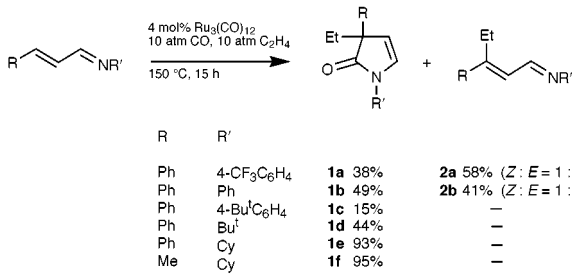

R	R′		
Ph	4-$CF_3C_6H_4$	**1a** 38%	**2a** 58% (*Z* : *E* = 1 : 2.5)
Ph	Ph	**1b** 49%	**2b** 41% (*Z* : *E* = 1 : 1)
Ph	4-$Bu^tC_6H_4$	**1c** 15%	–
Ph	Bu^t	**1d** 44%	–
Ph	Cy	**1e** 93%	–
Me	Cy	**1f** 95%	–

Scheme 1

† Experimental and spectral data for **1a–f** and **2a**,**b** are available from the RSC web site, see: http://www.rsc.org/suppdata/cc/1999/1457/

of the reaction. *Z* and *E* isomers are formed as can be demonstrated by IR and NMR spectroscopy. If the imine nitrogen and thus the whole π-system of the azadiene is nucleophilic enough the 1,3-dihydropyrrol-2-one derivatives **1c–f** are formed selectively. In these cases CO is obviously preferred for the first catalytic C–C coupling reaction. In the case of **1c** and **1d** the yields are quite low, presumably because of the higher steric demands of the *tert*-butyl groups. If the organic substituent at nitrogen is cyclohexyl the reaction produces **1e** and **1f** in nearly quantitative yield, so the steric as well as the electronic properties of the azadiene in those cases are ideal. Whether the starting material was cinnamaldehyde or croton aldehyde has no significant effect on the product distribution or the yield.

The formation of **1a–f** obviously proceeds *via* the catalytic incorporation of CO into the C–H bond at the β-carbon atom of the azadiene, followed by a nucleophilic attack of the imine nitrogen lone pair towards the aldehyde carbon closing the pyrrole ring. Compounds **1a–f** are then produced by a second catalytic C–C bond formation reaction by inserting one molecule of ethylene into the C–H bond *ortho* to the new carbonyl group in the 2-position of the pyrrole system (Scheme 2). By this reaction also a new chiral carbon atom at C3 is formed. This reaction sequence seems to us to be more reasonable than the other possibility, which would be for the intramolecular aldol condensation-like cyclization reaction to take place after the insertion of ethylene. If this were the reaction mechanism an ethyl group would have to be transferred from the carbonyl carbon atom to C3 of the pyrrolone system (Scheme 2). In addition, the reaction pathway we propose corresponds very well to the literature, in which C–C coupling

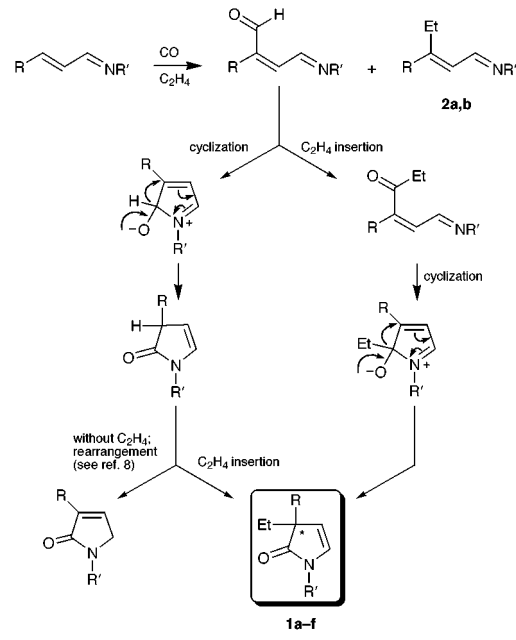

Scheme 2

reactions of olefins in the position *ortho* with respect to carbonyl groups have been reported using acetophenone derivatives as the starting material.[7] Parallel to our work Murai and coworkers very recently published a very similar reaction of azadienes with CO to yield the isomeric 1,5-dihydropyrrol-2-one derivatives.[8] They proposed a reaction mechanism in which as an intermediate a 1,3-dihydropyrrole-2-one derivative is formed which then isomerises to give the thermodynamically more stable 1,5-dihydropyrrol-2-one derivative (Scheme 2). Obviously in our reaction the second catalytic reaction of the pyrrol-2-one intermediate with ethylene to give **1a–f** is much faster than the rearrangement reaction, which we never observed. So this reaction offers the opportunity of selectively synthesising the thermodynamically less stable 1,3-dihydropyrrol-2-ones and in the same reaction building up a new center of chirality. Since γ-lactams are very interesting compounds with respect to pharmaceutical purposes,[9] the selective synthesis of 1,5-dihydropyrrol-2-one derivatives as reported by Murai as well as the synthesis of 1,3-dihydropyrrol-2-one derivatives we describe herein may both be useful synthetic strategies to achieve the selective synthesis of both isomers.

In the ^{1}H-NMR spectra of **1a–f** the most significant features are the two pyrrole hydrogen atoms at C4 and C5 which both give rise to doublets by coupling with each other in the range of δ 5.5 to 5.9 and δ 6.5 to 7.1, and the multiplet structures representing the CH_2 protons of the ethyl group attached to the new chiral center at C3 which clearly indicate that these two hydrogen atoms are diastereotopic. In the crystal structure determination of **1f** both enantiomers are observed to be statistically disordered in the lattice.[10] The bond lengths and angles show the values expected for a 1,3-dihydropyrrol-2-one. In addition, a quite strong intramolecular hydrogen bond is observed between the carbonyl oxygen atom and the methine hydrogen atom of the cyclohexyl substituent, which may be responsible for the downfield shift of the resonance of this hydrogen atom in the ^{1}H-NMR spectra of **1e** and **1f** at about δ 3.9 and the observation of five different CH_2 resonances for the cyclohexyl substituent in the ^{13}C-NMR spectrum of both compounds.

In conclusion we may say that the procedure described above allows the selective synthesis of 1,3-dihydropyrrol-2-one derivatives in a one-step synthesis. These compounds are produced *via* a reaction mechanism including two catalytic C–C bond formation reactions as well as the formation of a new center of chirality. Investigations on the reactivity of chiral azadienes in order to achieve diastereoselective reactions or reactions using catalysts derived from $Ru_3(CO)_{12}$ by substituting one or more CO groups by chiral ligands to achieve enantioselective reactions are under way and we will report these in due course.

The authors gratefully thank the Deutsche Forschungsgemeinschaft (SFB 436) for financial support.

Notes and references

1 (*a*) M. Brookhart and M. L. H. Green, *J. Organomet. Chem.*, 1983, **250**, 395; (*b*) E. C. Constable, *Polyhedron*, 1984, **3**, 1037; (*c*) J. Halpern, *Inorg. Chim. Acta*, 1985, **100**, 41; (*d*) R. H. Crabtree, *Chem. Rev.*, 1985, **85**, 245; (*e*) A. D. Ryabov, *Chem. Rev.*, 1990, **90**, 403; (*f*) *Selective Hydrocarbon Activation*, ed. J. A. Davies, VCH, Weinheim 1990; (*g*) B. A. Arndtsen, R. G. Bergman, T. A. Mobley and T. H. Petersen, *Acc. Chem. Res.*, 1995, **28**, 154; (*h*) R. H. Crabtree, *Chem. Rev.*, 1995, **95**, 987; (*i*) Y. Fujiwara, K. Takagi and Y. Taniguchi, *Synlett*, 1996, 591.

2 (*a*) W. Imhof, *J. Organomet. Chem.*, 1997, **533**, 31; (*b*) W. Imhof, *J. Organomet. Chem.*, 1997, **541**, 109; (*c*) W. Imhof, A. Göbel, D. Ohlmann, J. Flemming and H. Fritzsche, *J. Organomet. Chem.*, in the press; (*d*) W. Imhof, *Organometallics*, in the press.

3 (*a*) F. Kakiuchi, F. Yamauchi, N. Chatani and S. Murai, *Chem. Lett.*, 1996, 111; (*b*) T. Fukuyama, N. Chatani, F. Kakiuchi and S. Murai, *J. Org. Chem.*, 1997, **62**, 5647; (*c*) T. Fukuyama, N. Chatani, J. Tatsumi, F. Kakiuchi and S. Murai, *J. Am. Chem. Soc.*, 1998, **120**, 11 522.

4 (*a*) C. J. Elsevier, W. P. Mul and K. Vrieze, *Inorg. Chim. Acta*, 1992, **198–200**, 689 and literature cited therein; (*b*) W. P. Mul, C. J. Elsevier, L. H. Polm, K. Vrieze, M. C. Zoutberg, D. Heijdenrijk and C. H. Stam, *Organometallics*, 1991, **10**, 2247; (*c*) W. Imhof, *J. Chem. Soc., Dalton Trans.*, 1996, 1429.

5 W. Imhof, A. Göbel, D. Braga, P. De Leonardis and E. Tedesco, *Organometallics*, 1999, **18**, 736.

6 All compounds are characterised by GC, GC-MS, GC-IR and ^{1}H-NMR. In addition, **1e** and **1f** were characterised by ^{13}C-NMR, **1f** also by elemental analysis and X-ray structure determination. See note †.

7 M. Sonoda, F. Kakiuchi, N. Chatani and S. Murai, *Bull. Chem. Soc. Jpn.*, 1997, **70**, 3117.

8 T. Morimoto, N. Chatani and S. Murai, *J. Am. Chem. Soc.*, 1999, **121**, 1758.

9 (*a*) E. R. Gamzu, T. M. Hoover and S. I. Gracon, *Drug. Dev. Rev.*, 1989, **18**, 177; (*b*) S. Bertozzi and P. Salvadori, *Synth. Commun.*, 1996, **26**, 2659.

10 *Crystal data* for $C_{13}H_{21}NO$ **1f**: M = 207.31, orthorhombic, a = 20.476(1), b = 22.094(1), c = 11.4430(4) Å, V = 5176.8(5) Å^3, space group *Fdd*2. Z = 16, 1376 reflections measured, 1376 unique, 1253 observed reflections ($F_o^2 > 2\sigma(F_o^2)$), $R1$ = 0.0562, $wR2$ = 0.1395, GooF = 1.081, largest diff. peak 0.129 e Å^{-3}. CCDC 182/1302. See http://www.rsc.org/suppdata/cc/1999/1457/ for crystallographic data in .cif format.

Communication 9/03266E

ChemComm

Use of scandium tris(trifluoromethanesulfonate) as a Lewis acid catalyst in supercritical carbon dioxide: efficient Diels–Alder reactions and pressure dependent enhancement of *endo*:*exo* stereoselectivity

R. Scott Oakes, Toby J. Heppenstall, Najam Shezad, Anthony A. Clifford and Christopher M. Rayner*

School of Chemistry, University of Leeds, Leeds, UK LS2 9JT. E-mail: chrisr@chem.leeds.ac.uk

Received (in Liverpool, UK) 20th May 1999, Accepted 15th June 1999

The Diels–Alder reaction between various acrylates and cyclopentadiene in supercritical CO_2 are catalysed by scandium tris(trifluoromethanesulfonate); optimisation of CO_2 density leads to increased *endo*:*exo* selectivities compared to those obtained in conventional solvents.

The use of supercritical carbon dioxide ($scCO_2$) as an environmentally friendly non-toxic alternative to common organic solvents is an area of significant current interest.[1] Alongside the environmental aspects, $scCO_2$ also has additional benefits as a reaction medium, such as its ready availability, ease of removal and disposal and/or recycling. Other advantages which are particularly relevant for carrying out reactions in $scCO_2$ are: fine control of solvent properties by changes in temperature and pressure (*vide infra*); the ability to homogenise reaction substrates, electrically neutral metal complexes and gases like oxygen and hydrogen; enhanced diffusion rates; and potential for product processing.[2]

More recently, it has become apparent that there are more significant benefits to carrying out reactions in $scCO_2$. In our own laboratories we have recently reported that dramatic enhancements of diastereoselectivity are possible compared to those obtained in conventional solvents, simply by switching to $scCO_2$ and optimising the pressure and hence density of the reaction medium.[3] We have also recently shown that it is possible to fine tune the *endo*:*exo* selectivity of the Diels–Alder reaction between cyclopentadiene and methyl acrylate by controlling the density of the reaction medium by varying the temperature and pressure of the $scCO_2$.[4] It proved possible to change the *endo*:*exo* ratio from approximately 3:1 to 4:1. Whilst such a variation could be effected by changing solvent in a liquid phase reaction, it was of interest that similar variations could also be achieved in the same solvent, simply by altering its density. Such levels of selectivity and the slow rate of reaction were however of limited preparative value, and hence further investigations were warranted.

It is well known that Lewis acids catalyse Diels–Alder reactions and can improve their rate and stereoselectivity.[5] However, examples of conventional Lewis acid catalysis in $scCO_2$ are very limited.[6] It is known that fluorinated organometallic complexes have enhanced solubility in $scCO_2$, a factor we have recently exploited in the development of new C–C bond forming processes in $scCO_2$ using palladium sources such as $Pd(OCOCF_3)_2$.[7] We reasoned that related Lewis acidic complexes should also be capable of enhancing the rate and stereoselectivity of a Diels–Alder reaction such as that described above. Initial results of these studies are described below.

To follow on from our previous work, we decided to investigate catalysis of the Diels–Alder reaction between a variety of acrylates and cyclopentadiene (Scheme 1). Our initial studies concentrated on using *n*-butyl acrylate as dienophile as this was particularly convenient for product isolation and purification.

Scandium tris(trifluoromethanesulfonate) is widely used as a Lewis acid in a variety of reaction media.[8] Owing to its fluorinated nature, we believed it would also be suitable for use

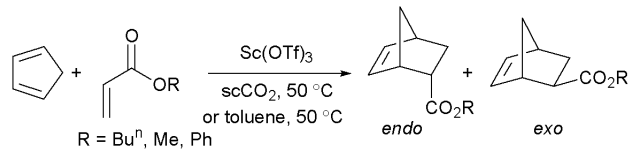

Scheme 1

in $scCO_2$. Initial results were encouraging. The reaction went to completion within 15 h at 50 °C, whereas the uncatalysed reaction was only 10% complete after 24 h under otherwise very similar conditions. In addition, a significant increase in *endo*:*exo* selectivity was observed as is common for Lewis acid catalysed Diels–Alder reactions.[5] We found that 6.5 mol% $Sc(OTf)_3$ catalyst gave good results, with no significant improvement at greater catalyst loading. In a conventional solvent such as toluene, an equivalent reaction gave a ratio of 10:1 *endo*:*exo* stereoselectivity. Changing to a significantly more polar solvent such as chloroform only had minimal effect on the selectivity (11:1 *endo*:*exo*). In $scCO_2$ at the same temperature (50 °C), variation of pressure (Fig. 1) allowed us to optimise the selectivity of this process,[9] with a maximum of 24:1 *endo*:*exo* being achieved, which is a considerable improvement, and further confirms our previous findings that significant enhancements of diastereoselectivity can be obtained by carrying reactions out in $scCO_2$ and optimising by varying the pressure and hence density of the reaction medium. Similar observations were observed with both phenyl and methyl acrylates, with *endo*:*exo* selectivities improving from 2:1 (toluene) to >8:1 ($scCO_2$, 1.09 g ml^{-1} density), and 4:1 (toluene) to >10:1 ($scCO_2$, 1.12 g ml^{-1} density) respectively.

It is of interest to note that, as was observed in our previous work, as pressure increases, the stereoselectivity rises to a maximum, and then begins to decrease. Note that this maximum

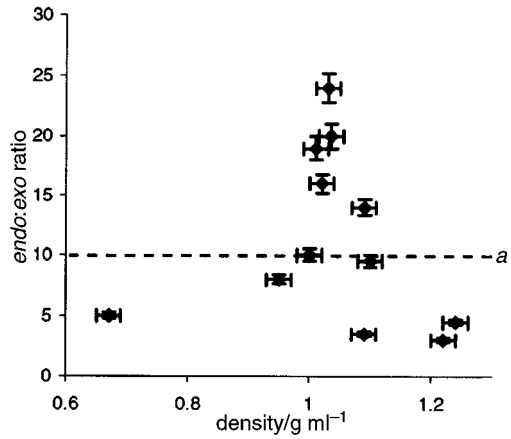

Fig. 1 Pressure dependent enhancement of *endo*:*exo* selectivity for Diels–Alder reaction between *n*-butyl acrylate and cyclopentadiene in $scCO_2$ catalysed by $Sc(OTf)_3$ at 50 °C. [a] 10:1 *endo*:*exo* selectivity observed in toluene at atmospheric pressure added for comparison.

occurs above the critical density of the medium and so is unlikely to be associated with clustering of molecules as is often proposed for effects observed around the critical point in near-supercritical fluids.[10] These new observations are consistent with the 'potential tuning' effect proposed in our previous paper[4] where the optimisation of the position and number of nearest neighbour solvent molecules with respect to a particular transition state was used to explain such a phenomenon. In such a case, an effect is observed which can be likened to a state of resonance between the solvent and reagents leading to an optimal selectivity for the reaction.

This work has now demonstrated the potential of Lewis acid catalysed reactions in $scCO_2$, and shown that enhanced rates and selectivities are possible. We are now further studying the origin and potential of this effect with respect to Diels–Alder reactions and other Lewis acid mediated reactions. The results of these studies will be reported in due course.

We are very grateful to the following members of the Leeds Cleaner Synthesis Group and their respective companies for funding and useful discussions: Dr Andrew Bridge, Rhône-Poulenc Rorer; Dr Mike Loft, Glaxo Research and Development; Julie MacRae, Pfizer Central Research; Dr William Sanderson, Solvay Interox; and Dr Ken Veal, SmithKline Beecham Pharmaceuticals.

Notes and references

1 A. A. Clifford, *Fundamentals of Supercritical Fluids*, Oxford University Press, 1998; A. A. Clifford, in *Supercritical Fluids*, ed. E. Kiran and J. M. H. Levelt Sengers, Kluwer, 1994, 449; see also ref. 3 and 4 and references cited therein.

2 See for example: L. E. McMahon, P. Timmins, A. C. Williams and P. York, *J. Pharm. Sci*., 1996, **85**, 1064; J. W. Tom, G. B. Lim, P. G. Debendetti and R. K. Prud'homme, in *Supercritical Fluid Engineering Science - Fundamentals and Applications*, ed. E. Kiran and J. F. Brennecke, ACS Symposium Series 514, 1993, ch. 11; P. G. Debendetti, *Supercritical Fluids*, ed. E. Kiran and J. M. H. Levelt Sengers, Kluwer, 1994, 719.

3 R. S. Oakes, A. A. Clifford, K. D. Bartle, M. Thornton-Pett and C. M. Rayner, *Chem. Commun*., 1999, 247.

4 A. A. Clifford, K. Pople, W. J. Gaskill, K. D. Bartle and C. M. Rayner, *J. Chem. Soc*., *Faraday Trans.*, 1998, **94**, 1451.

5 For a recent review see: C. P. Dell, *J. Chem. Soc., Perkin Trans. 1*, 1998, 3873.

6 See ref. 1 and references cited therein. Protic acid catalysed process have been reported including our own work on sulfur oxidation (ref. 3), see also: M. G. Hitzler, F. R. Smail, S. K. Ross and M. Poliakoff, *Chem. Commun.*, 1998, 359.

7 N. Shezad, R. S. Oakes, A. A. Clifford and C. M. Rayner, *Tetrahedron Lett.*, 1999, **40**, 2221.

8 For a recent review see: S. Kobayashi, *Eur. J. Chem*., 1999, 15.

9 Apparatus used is as previously described in ref. 3. *Typical procedure*: scandium tris(trifluoromethanesulfonate) (95 mg, 0.18 mmol, 6.5 mol%) was placed in a pressure vessel which was then sealed and charged to 50 bar pressure with CO_2. Agitation and heating was commenced, and a period of 20 min allowed for equilibration of conditions. *n*-Butyl acrylate (270 μl, 3.0 mmol) was injected into the system and the pressure increased to 80 bar. Cyclopentadiene (500 μl, 6.0 mmol, freshly cracked monomer) was injected and the pressure increased to the desired level. After 15 h, agitation and heating was stopped and the pressure released through a trap of diethyl ether (25 ml). The system was cleaned by further diethyl ether washes (2 × 1 ml). Filtration through Celite followed by solvent removal yielded the crude product mixture from which diastereomeric ratios were measured by ^{1}H NMR. Conversions were typically > 90%, and isolated yields > 80%. Density calibration was achieved by metering known amounts of carbon dioxide into the reaction vessel under standard reaction conditions (including reagents) using an ISCO 100D programmable syringe pump. Knowing the amount of carbon dioxide, the reactor volume and by observing the pressure, a calibration curve can be plotted for density versus pressure at constant temperature.

10 See for example: D. Andrew, B. T. Des Islet, A. Margaritis and A. C. Weedon, *J. Am. Chem. Soc.*, 1995, **117**, 6132; Y. Ikushima, N. Saito and M. Arai, *J. Phys. Chem.*, 1992, **96**, 2293.

Communication 9/04136B

ChemComm

Facile and general syntheses of 3- and/or 5-substituted 7*H*-pyrazolo[4,3-*e*]-1,2,4-triazolo[4,3-*c*]pyrimidines as a new class of potential xanthine oxidase inhibitors†

Tomohisa Nagamatsu* and Takayuki Fujita

Faculty of Pharmaceutical Sciences, Okayama University, Tsushima, Okayama 700-8530, Japan.
E-mail: nagamatsu@pheasant.pharm.okayama-u.ac.jp

Received (in Cambridge, UK) 7th May 1999, Accepted 24th June 1999

Convenient syntheses of 3- and/or 5-substituted 7*H*-pyrazolo[4,3-*e*]-1,2,4-triazolo[4,3-*c*]pyrimidines as a new class of potent xanthine oxidase inhibitors, involving the oxidative cyclisation of 4-alkylidenehydrazino- or 4-arylmethylidenehydrazino-1*H*-pyrazolo[3,4-*d*]pyrimidines with 70% nitric acid as the key step, are described.

As part of our studies on the synthesis[1] and biological evaluation[2] of novel fused pyrimidines, we initiated investigations aiming at designing new xanthine oxidase (XO) inhibitors. Among the fused purines prepared, the angular type purine analogues, 7*H*-1,2,4-triazolo[3,4-*i*]purines have been recently investigated for their potential XO inhibitory activities.[3] Allopurinol is known to inhibit XO[4] and is now widely employed in treatment of gout and hyperuricemia resulting from uric acid.[5–7] Although XO inhibitory activities have recently been discovered in some synthetic compounds,[8–10] no clinically effective XO inhibitors for the treatment of hyperuricemia have been developed since allopurinol was introduced for clinical use in 1963.[4] Herein, we report a facile strategy for general syntheses of the title compounds as a new class of potent XO inhibitors.

We have elucidated that 5-substituted 7*H*-1,2,4-triazolo[3,4-*i*]purines, especially the 5-oxo or 5-thioxo derivatives,[3] showed more potent bovine milk XO inhibitory activities than allopurinol. In contrast, few synthetic ways to prepare 7*H*-pyrazolo[4,3-*e*]-1,2,4-triazolo[4,3-*c*]pyrimidines, which are analogous to them, have been reported in the literature[11,12] or in patents[13] and several derivatives have been synthesized. However, none of the 5-substituted derivatives have been prepared up to now.

Our synthetic approach to the title compounds **4a**–**i** involved the preliminary synthesis of 6-chloro-4-hydrazino-1*H*-pyrazolo[3,4-*d*]pyrimidine (**2**) (79% yield) through the reaction of 2,4,6-trichloropyrimidine-5-carbaldehyde (**1**)[14] with anhydrous hydrazine (4 equiv.) in 2-methoxyethanol at 0 °C, followed by the reaction of **2** with an appropriate aldehyde (1.2–1.5 equiv.) in DMF at room temperature to yield the corresponding hydrazones **3c**–**i** in 60–93% yields as shown in Scheme 1.‡ In the light of this multiple step synthesis, a one-pot oxidative cyclisation starting from **3c**–**i** would be really attractive. Indeed, heating the hydrazones **3c**–**i** thus obtained with 70% nitric acid (*ca.* 5 equiv.) in DMF at 100 °C afforded the desired 3-substituted 7*H*-pyrazolo[4,3-*e*]-1,2,4-triazolo[4,3-*c*]-pyrimidin-5(6H)-ones (**4c**–**i**) accompanied with hydrolytic dechlorination in 60–85% yields (*Method A*).§ On the other hand, heating compound **2** with concentrated hydrochloric acid (50 parts) under reflux gave oxypurinol **5** (58% yield), which was confirmed by direct comparison with an authentic sample.[15] Then, treatment of the 4-thioxo derivative **6**, obtained by thiation of **5** according to the previously reported procedure,[15] with hydrazine monohydrate (17 equiv.) in ethanol under reflux afforded the 4-hydrazino derivative **7** in 71% yield. Compound **7** was subsequently cyclised to the corresponding **4a**,**b** (66–83% yields) by stirring with appropriate triethyl orthoesters (5 equiv.) in trifluoroacetic acid at room temperature (*Method B*).¶ Further, treatment of **7** with an appropriate aldehyde (1.5 equiv.) in DMF at room temperature gave the corresponding hydrazones **8b**–**i** in 74–95% yields. The intramolecular cyclisation of **8b**–**i** to the corresponding **4b**–**i** was also accomplished by

† Details of bovine milk xanthine oxidase inhibition by **4** and **10** are available from the RSC web site, see http://www.rsc.org/suppdata/cc/1999/1461/

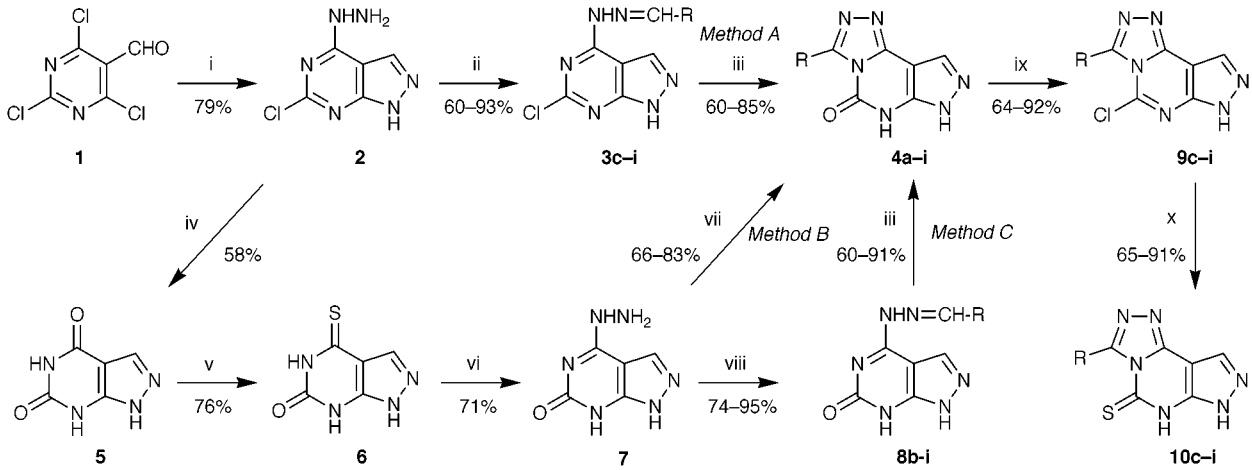

a R = H; **b** R = Me; **c** R = *n*-C_7H_{15}; **d** R = Ph; **e** R = 4-F-C_6H_4; **f** R = 4-Cl-C_6H_4; **g** R = 4-Me-C_6H_4; **h** R = 4-MeO-C_6H_4; **i** R = 4-O_2N-C_6H_4

Scheme 1 *Reagents and conditions*: i, anh. NH_2NH_2, $MeOCH_2CH_2OH$, 0 °C, 30 min; ii, RCHO, DMF, rt, 2–10 h; iii, 70% HNO_3, DMF, 100 °C, 1–5 h; iv, conc. HCl, reflux, 1 h; v, P_2S_5, pyridine, reflux, 2 h; vi, $NH_2NH_2{\cdot}H_2O$, EtOH, reflux, 10 min; vii, $RC(OEt)_3$, TFA, rt, 1 h; viii, RCHO, DMF, rt, 10 h; ix, $POCl_3$, reflux, 1–4 h; x, $(H_2N)_2C{=}S$, Bu^{s}OH, reflux, 0.5–2 h.

oxidation using 70% nitric acid (*ca.* 1.2 equiv.) in 60–91% yields in a similar manner as above (*Method C*).

In addition, we tried to prepare the 5-thioxo derivatives **10c**–**i**. Thus the key starting materials, 5-chloro derivatives **9c**–**i**, were readily prepared by refluxing the appropriate 5-oxo derivatives **4c**–**i** with phosphoryl chloride (100 parts) in 64–92% yields.‖ Then, thiation by reaction of **9c**–**i** with thiourea (1.2 equiv.) in butan-2-ol under reflux afforded the corresponding 5-thioxo derivatives **10c**–**i** in 65–91% yields.**

In conclusion, we accomplished the facile and general syntheses of not only oxypurinol **5** and 3- and/or 5-substituted 7*H*-pyrazolo[4,3-*e*]-1,2,4-triazolo[4,3-*c*]pyrimidines (**4** and **10**) as a new class of potential XO inhibitors but also 6-chloro-4-hydrazino-1*H*-pyrazolo[3,4-*d*]pyrimidine (**2**), which was an useful intermediate. The compounds (**4** and **10**) exhibited 100–760 fold more potent bovine milk XO inhibitory activities than that of allopurinol† and did not show any appreciable inhibition against the proliferation of T-cell acute lymphoblastic leukemia (CCRF-HSB-2). Further investigation of the present synthetic and XO inhibitory study is in progress and will be reported in detail shortly.

We are grateful to the SC-NMR Laboratory of Okayama University for 200 MHz ^{1}H NMR experiments. This work was partly supported by Grant-in-Aid for Scientific Research (C) (No. 09680570) from the Ministry of Education, Science, Sports and Culture, Japan.

Notes and references

‡ All new compounds **2**, **3c**–**i**, **7** and **8b**–**i** exhibited satisfactory elemental combustion analyses and mass and ^{1}H NMR spectral data consistent with structures indicated, and showed mps over 300 °C except for **3c** (mp 250 °C).

§ *Typical procedure*: A solution of **3c** (0.3 g, 1.02 mmol) with 70% nitric acid (0.5 ml, 5.55 mmol) in DMF (30 ml) was heated at 100 °C for 1 h. After the reaction was complete, the solution was concentrated to dryness *in vacuo* and treated with MeOH to afford the crystals **4c** (75%), which were collected by filtration and recrystallized from a mixture of DMF and EtOH. Other derivatives **4d** (85%), **4e** (72%), **4f** (71%), **4g** (67%), **4h** (61%) and **4i** (60%) were prepared in a similar manner to **4c** and recrystallized from a mixture of DMF and EtOH or water. The compounds **4c**–**i** showed mps above 300 °C, respectively. δ_H[60 or 200 MHz, $(CD_3)_2SO$] for **4c**: 0.86 (3H, t, *J* 6.54), 1.30 (8H, br s), 1.50–1.80 (2H, m), 2.50–2.95 (2H, m), 8.53 (1H, s), 12.41 (1H, br s), 13.50 (1H, br); for **4d**: 7.40–7.70 (3H, m), 7.90–8.35 (2H, m), 8.68 (1H, s), 12.60 (1H, br s), 13.60 (1H, br); for **4e**: 7.37 (2H, dd, *J* 8.82, 9.06), 8.22 (2H, dd, *J* 8.82, 5.88), 8.66 (1H, s), 12.59 (1H, br s), 13.65 (1H, br); for **4f**: 7.62 (2H, d, *J* 8.60), 8.17 (2H, d, *J* 8.60), 8.70 (1H, s), 12.62 (1H, br s), 13.66 (1H, br s); for **4g** (CF_3CO_2D): 2.54 (3H, s), 7.51 (2H, d, *J* 8.76), 8.03 (2H, d, *J* 8.76 Hz), 8.94 (1H, s); for **4h**: 3.85 (3H, s), 7.10 (2H, d, *J* 8.76), 8.12 (2H, d, *J* 8.76), 8.64 (1H, s), 12.60 (1H, br s), 13.50 (1H, br); for **4i**: 8.39 (4H, br s), 8.69 (1H, s), 12.70 (1H, br s), 13.60 (1H, br).

¶ *General procedure*: A solution of **7** (0.2 g, 1.2 mmol) with an appropriate triethyl orthoester (6 mmol) in trifluoroacetic acid (3 ml) was stirred at room temperature for 1 h. After the reaction was complete, the deposit was collected by filtration and recrystallized from DMF to yield the corresponding **4a** (mp > 300 °C, 66%) and **4b** (mp > 300 °C, 83%). δ_H[200 MHz, $(CD_3)_2SO$] for **4a**: 8.34 (1H, s), 8.62 (1H, s), 12.58 (1H, br s), 13.60 (1H, br s); for **4b**: 2.40 (3H, s), 8.54 (1H, s), 12.46 (1H, br s), 13.57 (1H, br s).

‖ All new compounds **9c**–**i** exhibited satisfactory elemental combustion analyses and mass and ^{1}H NMR spectral data consistent with structures indicated, and showed mps over 300 °C except for **9c** (mp 150 °C).

** *Typical procedure*: A solution of **9c** (0.3 g, 1.02 mmol) with thiourea (93 mg, 1.22 mmol) in Bu^{s}OH (15 ml) was heated under reflux for 1 h. After the reaction was complete, the solution was concentrated to dryness *in vacuo* and treated with EtOH to afford crystals of **10c** (mp 260–261 °C, 65%), which were collected by filtration and recrystallized from a mixture of DMF and water. Other derivatives **10d** (81%), **10e** (71%), **10f** (71%), **10g** (74%), **10h** (91%) and **10i** (77%) were prepared in a similar manner to **10c** and recrystallized from a mixture of DMF and EtOH or water. The compounds **10d**–**i** showed mps above 300 °C. It is noteworthy that the compounds **4**, **9** and **10** were reasonably stable in acid or alkali solution due to the substituents at the 5-position on the rings. δ_H[60 or 200 MHz, $(CD_3)_2SO$] for **10c**: 0.90 (3H, t, *J* 6.30), 1.31 (8H, br s), 1.55–2.10 (2H, m), 2.64–3.08 (2H, m), 8.63 (1H, s), 14.0 (1H, br), 14.38 (1H, br); for **10d**: 7.50–7.64 (3H, m), 8.10–8.30 (2H, m), 8.84 (1H, s), 14.0 (1H, br s), 14.35 (1H, br s); for **10e**: 7.40 (2H, dd, *J* 8.84, 8.90), 8.25 (2H, dd, *J* 8.84, 5.54), 8.75 (1H, s), 14.01 (1H, br), 14.37 (1H, br); for **10f**: 7.63 (2H, d, *J* 8.57), 8.20 (2H, d, *J* 8.57), 8.81 (1H, s), 14.01 (1H, br), 14.38 (1H, br); for **10g**: 2.40 (3H, s), 7.35 (2H, d, *J* 7.92), 8.10 (2H, d, *J* 7.92), 8.75 (1H, s), 13.90 (1H, br), 14.40 (1H, br); for **10h**: 3.85 (3H, s), 7.09 (2H, d, *J* 8.82), 8.14 (2H, d, *J* 8.82), 8.75 (1H, s), 14.0 (1H, br), 14.55 (1H, br); for **10i**: 8.41 (4H, br s), 8.77 (1H, s), 13.75 (1H, br), 14.25 (1H, br).

1 T. Nagamatsu and H. Yamasaki, *J. Chem. Soc., Chem. Commun*., 1995, 2041.
2 T. Nagamatsu, H. Yamasaki, T. Hirota, M. Yamato, Y. Kido, M. Shibata and F. Yoneda, *Chem. Pharm. Bull.*, 1993, **41**, 362.
3 T. Nagamatsu, Y. Watanabe, K. Endo and S. Imaizumi, PCT Int. Appl. WO 96 26 208, 1996 (*Chem. Abstr*., 1996, **125**, 247848j).
4 G. B. Elion, S. Callahan, H. Nathan, S. Bieber, R. W. Rundles and G. H. Hitchings, *Biochem. Pharmacol*., 1963, **12**, 85.
5 R. W. Rundles, J. B. Wyngaarden, G. H. Hitchings, G. B. Elion and H. R. Silberman, *Trans. Assoc. Am. Physicians*, 1963, **76**, 126.
6 T. F. Yü and A. B. Gutman, *Am. J. Med*., 1964, **37**, 885.
7 J. R. Klinenberg, S. E. Goldfinger, J. E. Seegmiller, *Ann. Intern. Med*., 1965, **62**, 639.
8 R. L. Wortmann, A. S. Ridolfo, R. W. Lightfoot, Jr and I. H. Fox, *J. Rheumatol.*, 1985, **12**, 540.
9 Y. Osada, M. Tsuchimoto, H. Fukushima, K. Takahashi, S. Kondo, M. Hasegawa and K. Komoriya, *Eur. J. Pharmcol*., 1993, **241**, 183.
10 G. Biagi, I. Giorgi, O. Livi, V. Scartoni, I. Tonetti and L. Costantino, *Farmaco*, 1995, **50**, 257.
11 G. A. Bhat and L. B. Townsend, *J. Chem. Soc., Perkin Trans. 1*, 1981, 2387.
12 F. Gatta, M. Luciani and G. Palazzo, *J. Heterocycl. Chem*., 1989, **26**, 613.
13 U. D. Treuner and H. Breuer, USP 4 053 474, 1977 (*Chem. Abstr*., 1977, **88**, 37826s), USP 4 124 764, 1978 (*Chem. Abstr*., 1978, **90**, 87508b); Ger. Offen. 2 838 029, 1979 (*Chem. Abstr*., 1979, **91**, 39492r).
14 F. Yoneda, Y. Sakuma, S. Mizumoto and R. Ito, *J. Chem. Soc., Perkin Trans. 1*, 1976, 1805.
15 R. K. Robins, *J. Am. Chem. Soc*., 1956, **78**, 784.

Communication 9/03676H

ChemComm

A new route to medium and large heterocyclic compounds

Tina Ventrice, Eva M. Campi, W. Roy Jackson* and Antonio F. Patti

Department of Chemistry, Monash University, Clayton, Victoria, Australia 3168.
E-mail: W.R. Jackson@sci.monash.edu.au

Received (in Cambridge, UK) 25th May 1999, Accepted 22nd June 1999

Hydrogenation of nitrobenzenes bearing aldehyde-containing substituents over heterogeneous platinum or palladium catalysts gives medium and/or large heterocyclic amines as a result of simple or dimeric cyclisation in moderate to good yields; a range of heteroatoms can be incorporated into the macrocycles, enhancing their potential as ligands.

The preparation of cyclic amines by hydrogenation of nitroaldehydes or nitroketones over platinum metal catalysts has been well established in the case of 5- and 6-membered heterocycles.[1] Recently the synthesis of a 17-membered cyclic amine has been reported in good yield (66%) by hydrogenolysis of a Cbz-protected aminoaldehyde with subsequent hydrogenation of the resulting cyclic iminium salt.[2] The reactions were carried out at relatively high dilution (4×10^{-3} M) in methanol using moderate amounts of a palladium hydroxide catalyst precursor (3.7×10^{-4} g atom of Pd) relative to substrate (2.3×10^{-1} mmol).

The above chemistry prompted us to explore a general synthesis of medium and large heterocycles based on the ready availability of nitrobenzenes bearing aldehyde-containing side chains **2** and **3** from hydroformylation[3] of the related nitroalkenes **1** (Scheme 1).[3,4] Good regio-control for the terminal aldehydes **2** can often be attained using the bulky bisphosphite ligand, BIPHEPHOS.[5] Use of triphenylphosphine or hydroformylation of allylic ethers[6] led to greater amounts of branched-chain aldehydes **3** but in all cases facile chromatographic separation of the branched and linear aldehydes was possible. The nitroaldehydes were reacted with hydrogen in methanol over 10% Pd/C and/or PtO_2 catalysts (Scheme 2). Standard conditions involved 1 atm H_2, ambient temperature, with Pd (5.6×10^{-5} g atom) for reaction on *ca.* 0.4 mmol scale with substrate concentration of 4.8×10^{-3} M. Larger amounts of Pt (3×10^{-4} g atom) were used, comparable with that described by the Japanese workers.[2] The results are summarised in Table1.

The monomeric compounds **5** and the dimeric compounds **6** were separated from any polymeric material and isolated in pure form by chromatography. Structures were assigned by ^{1}H and ^{13}C NMR spectroscopy and by electrospray (ESI) mass spectroscopy. Three representative products, the monomer **5n** as its *N*-benzoyl derivative and the dimers **6a** and **6g**, were fully characterised by single crystal X-ray structure determination.† Careful examination of the total product mixture by both adsorption chromotography and HPLC failed to show any evidence for the formation of trimers or other oligomers.

The yields of cyclic products obtained from *ortho*-substituted nitrobenzenes varied both with ring size and the pattern of heteroatom incorporation in the side chain. No clear trends emerged other than that in general compounds containing oxygen as the only heteroatom in the side chain gave lower yields of medium ring compounds, 9–11 membered (0–36%, entries 4–6, 8–10) than larger ring compounds, 13–22 membered (36–75%, entries 1, 4, 5, 9, 10, 13–15). Introduction of other heteroatoms had a marked influence. Reaction of compound **4b** containing sulfur in the side chain led only to an 8-ring monomer (entry 2) and two compounds **4f** and **4j** containing nitrogen in the side chain surprisingly gave only 9- and 11-membered ring compounds (entries 7 and 12). Introduction of ethyleneoxy units into the side chain in general led to improved yields over compounds containing carbon chains of similar lengths, *cf.* reactions of **4k** and **4l** (entries 13–15) with those of **4m** and **4n** (entries 16–18).

The *meta*- and *para*-substituted compounds **4o**–**4s** in all cases gave higher yields of dimeric compounds (entries 19–23).

An attempt was made to influence the yields of products by the addition of potential templating compounds to the reactions. Reactions of the compound **4i** were carried out with additives as summarised in Table 2.

Addition of the heavy metal salts Ag(OTf) and $La(OTf)_3$ dramatically influenced the ratio of products and resulted in exclusive formation of the eleven-membered heterocycle **5i** although the overall recovery of non-polymeric products was reduced. Energy minimisation calculations for interaction of one silver ion with the monomer **5i** and for two silver ions with the dimer **6i** were carried out.[7] The energy of the preferred conformation of the free monomer is similar to that of the preferred conformation when bonded to silver whereas serious distortion of the preferred conformation of the dimer is required in order to attain the conformation most suitable for bonding to two silver ions. Addition of glycine to the reaction had no effect on the yield or product distribution, perhaps not surprising as aqueous methanol was the reaction solvent.

The compounds have potential for use as novel ligands[8–10] and as constituents in molecular switching devices[11,12] and these applications are being evaluated.

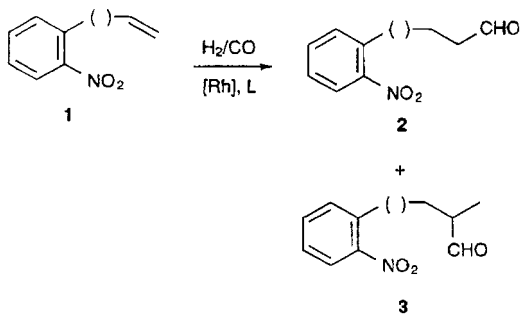

Scheme 1

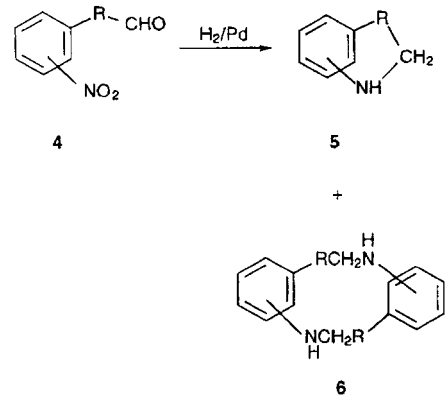

Scheme 2

Table 1 Isolated yields of heterocycles from hydrogenation of nitroaldehydes **4**[a]

Entry	Reactant	RCHO	Catalyst	Product yields[b] (%) Monomer **5**	Dimer **6**
1	**4a**	2-O$(CH_2)_2$CH(CH_3)CHO	Pd	14(8)	30(16)
2	**4b**	2-CH_2SCH_2CH(CH_3)CHO	Pt	20(8)	—(16)
3	**4c**	2-O$(CH_2)_3$CHO	Pd	33(8)	8(16)
4	**4d**	2-O$(CH_2)_4$CHO	Pd	—(9)	64(18)
5	**4d**	2-O$(CH_2)_4$CHO	Pt	—	75
6	**4e**	2-CH_2O$(CH_2)_3$CHO	Pd	—(9)	23(18)
7	**4f**	2-N(COPh)$(CH_2)_4$CHO	Pd	22(9)	–(18)
8	**4g**	2-O$(CH_2)_5$CHO	Pd	7(10)	20(20)
9	**4h**	2-O$(CH_2)_2$OCH_2CH(CH_3)CHO	Pd	—(10)	37(20)
10	**4i**	2-O$(CH_2)_2$O$(CH_2)_3$CHO	Pd	19(11)	36(22)
11	**4i**	2-O$(CH_2)_2$O$(CH_2)_3$CHO	Pt	22	18
12	**4j**	2-O$(CH_2)_2$N$(SO_2Me)(CH_2)_3$CHO	Pd	36(11)	—(22)
13	**4k**	2-O[$(CH_2)_2$O]$_2CH_2$CH(CH_3)CHO	Pd	56(13)	—(26)
14	**4l**	2-O[$(CH_2)_2$O]$_2(CH_2)_3$CHO	Pd	75(14)	6(18)
15	**4l**	2-O[$(CH_2)_2$O]$_2(CH_2)_3$CHO	58	—	
16	**4m**	2-O$(CH_2)_9$CH(CH_3)CHO	Pt	29(15)	18(30)
17	**4n**	2-O$(CH_2)_{11}$CHO	Pd	27(16)	19(32)
18	**4n**	2-O$(CH_2)_{11}$CHO	Pd	36	11
19	**4o**	3-O$(CH_2)_2$CH(CH_3)CHO	Pd	6(9)	39(18)
20	**4p**	3-O$(CH_2)_4$CHO	Pd	10(10)	17(20)
21	**4q**	4-O$(CH_2)_5$CHO	Pd	—(12)[c]	11(24)
22	**4r**	4-O$(CH_2)_2$O$(CH_2)_3$CHO	Pt	7(13)	22(26)
23	**4s**	4-O[$(CH_2)_2$O]$_2((CH_2)_3$CHO	Pt	—(16)	26(32)

[a] Reactions at ambient temperature with H_2 (1 atm, 0.1MPa) using a substrate concentration of 4.76×10^{-3} M in methanol with Pd (5.6×10^{-5} g atom) as 10% Pd on C and Pt (3×10^{-4} g atom) as PtO_2. [b] Ring size in parentheses. [c] Amino alcohol from reduction of CHO and NO_2 groups also formed (45%).

Table 2 Yields of monomer **5** and dimer **6** from hydrogenations of the nitroaldehyde **4i** with additives[a]

Additive	Yield (%)[b] **5i**	**6i**
—	19	36
Ag(OTf) 1 equiv.	30	—
Ag(OTf) 2 equiv.	33	—
La$(OTf)_3$ 1 equiv.	45	—
Glycine 1 equiv.[c]	21	33

[a] Reactions using Pd/C in methanol under conditions in footnote *a* in Table 1. [b] Isolated yield. [c] Glycine dissolved in a minimum amount of water (0.2 ml) and added to reaction in methanol (85 ml).

We thank the Australian Research Council for support and for provision of a postgraduate award (to TV) and Johnson Matthey Pty Ltd for loan of precious metals.

Notes and references

† *Crystal data* for **5n**: $C_{25}H_{33}NO_2$, M = 379.54, monoclinic space group $P2_1/n$, a = 9.3905(1), b = 23.1162 (5), c = 10.0908(2) Å, β = 99.648(1)°, U = 2159.46(6) Å^3, Z = 4, D_c = 1.167 g cm^{-3}, crystal dimensions 0.32 × 0.25 × 0.17 mm, T = 123(1) K, Mo-Kα, radiation λ = 0.71069 Å, μ = 0.73 cm^{-1}. Data were collected on a Nonius Kappa CCD diffractometer and of the total 15 217 reflections measured, 4843 unique (R_{int} = 0.021). Refinement on F, R_w = 0.039, $R1$ = 0.037 [for 3268 reflections with $I > 3\sigma(I)$]. For **6a**: $C_{22}H_{30}N_2O_2$, M = 354.49, orthorhombic space group *Pbca*, a = 7.045(5), b = 16.646(1), c = 16.866(1) Å, U = 1977.80(2) Å^3, Z = 4, D_c = 1.190 g cm^{-3}, crystal dimensions 0.20 × 0.18 × 0.08 mm, T = 173 (1) K, Mo-Kα, radiation λ = 0.71069 Å, μ = 0.76 cm^{-1}. Data were collected on a Nonius Kappa CCD diffractometer and of the total 13313 reflections measured, 2819 unique (R_{int} = 0.106). Refinement on F, R_w = 0.052, $R1$ = 0.064 [for 825 reflections with $I > 3\sigma(I)$]. For **6g**: $C_{24}H_{34}N_2O_2$, M = 382.54, monoclinic space group $P2_1$/c, a = 9.2424(5), b = 5.0502(1), c = 23.455(1) Å, β = 101.075(1)°, U = 1074.42(7) Å^3, Z = 2, D_c = 1.182 g cm^{-3}, crystal dimensions 0.35 × 0.15 × 0.11 mm, T = 173(1) K, Mo-Kα, radiation λ = 0.71069 Å, μ = 0.75 cm^{-1}. Data were collected on a Nonius Kappa CCD diffractometer and of the total 6885 reflections measured, 2820 unique (R_{int} = 0.041). Refinement on F, R_w = 0.052, $R1$ = 0.053 [for 1511 reflections with $I > 3\sigma(I)$]. CCDC 182/1323. See http://www.rsc.org.suppdata/cc/1999/1463/ for crystallographic data in .cif format.

1 P. N. Rylander, *Catalytic Hydrogenation in Organic Synthesis*, Academic Press, London, 1979, p. 132.
2 H. Ina, M. Ito and C. Kibayashi, *J. Org. Chem*., 1996, **61**, 1023.
3 E. M. Campi, W. R. Jackson and A. E. Trnacek, *Aust. J. Chem*., 1997, **50**, 807; D. Anastasiou, E. M. Campi, H. Chaouk and W. R. Jackson, *Tetrahedron*, 1992, **48**, 7467.
4 A. L. J. Beckwith and W. B. Gara, *J. Chem. Soc*., *Perkin Trans. 2*, 1975, 593; L. Garanti and G. Zecchi, *J. Heterocycl. Chem*., 1993, **30**, 559; G. Broggini, L. Garanti, G. Molteni and G. Zecchi, *Tetrahedron*, 1997, **53**, 3005.
5 G. D. Cuny and S. L. Buchwald, *J. Am. Chem. Soc.*, 1993, **115**, 2066; I. Ojima, D. M. Iula and M. Tzamarioudaki, *Tetrahedron Lett*., 1998, **39**, 4599.
6 C. Botteghi, R. Ganzerla, M. Lenarda and G. Moretti, *J. Mol. Catal*., 1987, **40**, 129; I. Amer and H. Alper, *J. Am. Chem. Soc*., 1990, **112**, 3674.
7 Insight II (v 4.0.0) (Discover) Molecular Modelling System; Molecular Simulations Inc., 9685 Scranton Road, San Diego, CA 92121-3752 (USA).
8 A. J. Leong, L. F. Lindoy, D. C. R. Hockless, G. F. Swiegers and S. B. Wild, *Inorg. Chim. Acta*, 1996, **246**, 371.
9 D. Parker and J. A. G. Williams, *J. Chem. Soc*., *Perkin Trans. 2*, 1995, 1305.
10 J. J. Christensen, D. J. Eatough and R. M. Izatt, *Chem. Rev*., 1974, **74**, 351; R. M. Izatt, J. S. Bradshaw, K. Pawlak, R. L. Bruening and B. J. Tarbet, *Chem. Rev*., 1992, **92**, 1261.
11 A. P. de Silva, H. Q. N. Gunaratne, T. Gunnlaugsson, A. J. M. Huxley, C. P. McCoy, J. T. Rademacher and T. E. Rice, *Chem. Rev*., 1997, **97**, 1515.
12 E. Ishow, A. Credi, V. Balzani, F. Spadola and L. Mandolini, *Chem. Eur. J.*, 1999, **5**, 984.

Communication 9/04168K

Coordination-structural change with pressure around atmospheric pressure in Zn(II) carboxylate salts of ethylene-methacrylic acid copolymer

Shinichi Yano,*[a] Muneatsu Nakamura[a] and Shoichi Kutsumizu[b]

[a] *Department of Chemistry, Faculty of Engineering, Gifu University, Yanagido 1-1, Gifu 501-1193, Japan. E-mail: yano@apchem.gifu-u.ac.jp*

[b] *Instrumental Analysis Center, Gifu University, Yanagido 1-1, Gifu 501-1193, Japan. E-mail: kutsu@cc.gifu-u.ac.jp*

Received (in Cambridge, UK) 6th May 1999, Accepted 22nd June 1999

Zn(II) carboxylate salts of ethylene-methacrylic acid copolymer undergo coordination-structural change by applying low pressure including atmospheric pressure at temperatures above 60 °C; the structure transforms from six-coordinate to four-coordinate, as the applied pressure increases from 0 to 3 MPa.

Ethylene-methacrylic acid copolymers neutralized with metal cation (E-MAA-*x*M, see Fig. 1) are representative ionic polymers (so-called ionomers which are defined as polymers functionalized with a small amount of pendant ionic groups).[1–3] The ionic groups are frequently phase-separated from the host hydrophobic polymer matrix to form ionic aggregates, resulting in physical properties superior to the host polymer. Therefore, E-MAA-*x*M, in general, consists of three phases of amorphous polyethylene, crystalline polyethylene, and ionic aggregation regions and hence undergoes a transitional change around 60 °C (T_i) (loss of order inside the ionic aggregations, according to our proposal[4]) and the melting of crystalline polyethylene region near 90 °C (T_m). E-MAA-60Zn is one of the most popular ionomers which have been marketed as wrapping sheets for foods, and plastics for golf balls and sport shoes by Du Pont since 1964.[5] In E-MAA-*x*Zn, it is known that the Zn(II) carboxylate salts can take either four-coordination or six-coordination structures, dependent on temperature or humidity,[6–9] but we have found that the coordination structure is changed with applied low pressure between 0 and 3 MPa above 60 °C. The present letter communicates this wonderful and unique transformation of the coordination structure in E-MAA-60Zn under low pressure including atmospheric pressure.

E-MAA-60Zn was supplied from Du Pont-Mitsui Polychemicals Co. Ltd. (Tokyo), where MAA content in E-MAA is 5.4 mol% and its degree of neutralization by Zn(II) cation is 60%; E-MAA is ACR-1560 of Du Pont-Mitsui Polychemicals Co. Ltd. and E-MAA-60Zn pellets were prepared by a melt reaction of E-MAA with a stoichiometric quantity of zinc oxide in an extruder.[10] The 10–30 μm thick films for IR measurements were prepared by compression-molding the pellets at 130 °C under 19.6 MPa.

The films obtained were annealed in a vacuum oven at 130 °C for 2 h under reduced pressure with a rotary pump (around 6.7×10^{-4} MPa because of a leak in the oven), and then cooled to room temperature at a rate of about 3 °C min^{-1}. After storing for more than 30 d at room temperature, this sheet was used as the starting sample in the following IR measurements. Differential scanning calorimetric measurements were made for the starting sample at a heating rate of 10 °C min^{-1} by use of a Seiko Denshi SSC-5000 calorimeter. The data showed an annealing peak near 52 °C, corresponding to the transition temperature of ionic aggregates (T_i) and the melting peak (T_m) of crystalline polyethylene regions near 88 °C, being well consistent with the previous data.[4]

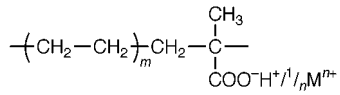

Fig. 1 Chemical structure of ethylene-methacrylic acid copolymer neutralized partially with metal cation (E-MAA-*x*M, MAA content = 5.4 mol%, M: metal cation, *x*: degree of neutralization in %).

IR spectra were measured with a Perkin-Elmer 1640 FT-IR spectrometer in the following two measuring procedures, where each trace was taken as the average of 16 scans at a resolution of 4 cm^{-1}.

(E-1) IR spectra under low pressures below 0.101 MPa: IR spectra were measured by use of a commercial gas cell (GL Sciences Co., Tokyo, Type GC-KBr) equipped with a hand-made heater. The starting film was placed in the gas cell two KBr windows and the pressure was controlled with N_2. Then, IR spectra were recorded at different temperatures.

(E-2) IR spectra under high pressures above 0.101 MPa: Under a pressure controlled by N_2 in an autoclave, the starting film was heated to 130 °C above T_m and annealed for 2 h, and then cooled to room temperature at a rate of about 3 °C min^{-1}. IR spectra were recorded at 30 °C.

Fig. 2(a) shows IR spectra of the starting E-MAA-60Zn in the wave number range from 500 to 2500 cm^{-1} at 30 °C. There are observed three characteristic peaks near 1624 and 1538 cm^{-1}, and near 1585 cm^{-1}, which have been assigned as antisymmetric stretching vibrations of COO$^-$, [ν_{as} (COO$^-$)], in six-(octahedral) coordination structure and that in four-(tetrahedral) coordination structure, respectively[6,7] (Coleman *et al.*[7] assumed that the 1536 and 1565 cm^{-1} bands are assigned to the six-coordination structure, and the 1537 and 1620 cm^{-1} bands to an acid salt structure, but here we assigned the bands at 1538 and 1624 cm^{-1}, and the weak band at 1565 cm^{-1} which is

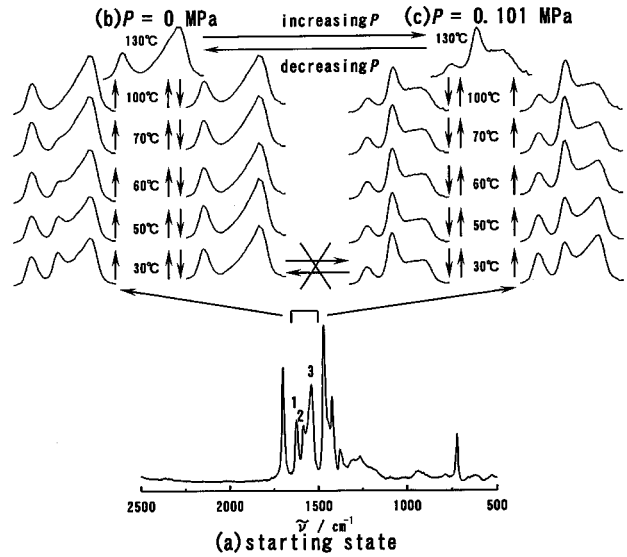

Fig. 2 IR spectrum in the wavenumber range from 500 to 2500 cm^{-1} (a), and variation of antisymmetric stretching vibration of COO$^-$ [ν_{as}(COO$^-$)] with temperature under P = 0 (b) and P = 0.101 MPa (atmospheric pressure) (c). 1 : 1624 cm^{-1}, 2 : 1585 cm^{-1} and 3 : 1538 cm^{-1} in (a).

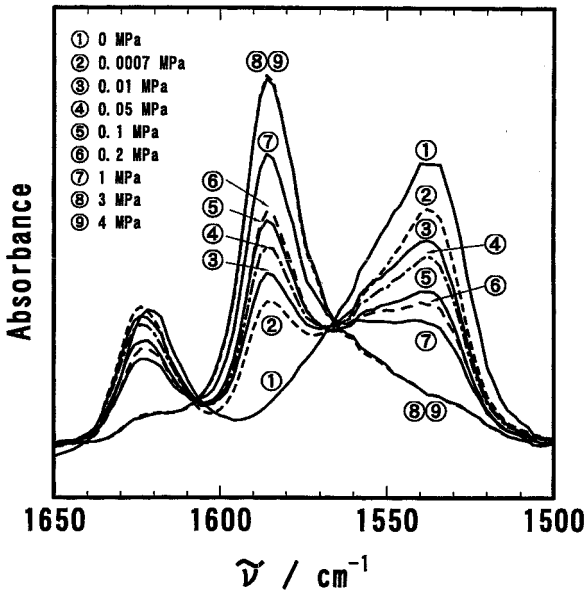

Fig. 3 Variation of antisymmetric stretching vibrations of COO^- [$\nu_{as}(COO^-)$] with pressure (P) at 30 °C. IR spectra were recorded at 30 °C for the samples cooled from the molten state of 130 °C under different constant pressures (P). The IR spectra (the coordination structure) are almost the same as those at 130 °C.

superimposed on the two bands, all to a six-coordination structure, because both structures are principally in six-coordination, and actually there would be a complicated distribution of the coordination structure over various structures from the six-coordination to the acid salt coordination). Fig. 2(b) and (c) show changes in the characteristic peaks of ν_{as} (COO^-) with varying temperature from 30 °C under two pressures [P = 0 (b) and P = 0.101 MPa (atmospheric pressure) (c) which is estimated about 0.137 MPa at 130 °C by the gaseous state function], where the measurements were done by use of the gas cell (E-1). When the starting sample is heated at P = 0, the ν_{as} (COO^-) band at 1585 cm^{-1} begins to be weakened from around 60 °C and disappears at 130 °C above T_m (88 °C), and as a result, only the bands at 1624 and 1538 cm^{-1} are seen at 130 °C. The IR spectra at 130 °C, exhibiting the two bands at 1624 and 1538 cm^{-1}, are unchanged during cooling to 30 °C. On the other hand, as temperature increases under P = 0.101 MPa, the 1585 cm^{-1} band becomes markedly intensified, accompanying the decrease of the 1624 and 1538 cm^{-1} bands, and becomes predominant at 130 °C. When P = 4 MPa, only the band at 1585 cm^{-1} was seen at 130 °C and the two bands at 1624 and 1538 cm^{-1} virtually disappeared, as described later. Consequently, these IR data indicate that the Zn(II) carboxylates in E-MAA-60Zn are in six-coordination at P = 0 and mostly in four-coordination when $P \geq 3$ MPa. At 130 °C, as P increases from 0, the coordination structure of the Zn(II) carboxylate undergoes a reversible transformation from a six-coordinate to a four-coordinate structure whose transformation rate was too fast to be detected on the present IR measurements. At 30 °C, the coordination structure, of course, is not changed with P, but when the temperature is elevated above 60 °C, it begins to be controlled by P again.

To examine the coordination structure under higher pressure above atmospheric pressure, we made IR spectral measurements at 30 °C for E-MAA-60Zn which was cooled to room temperature, after annealing at 130 °C for 2 h under different constant pressures of N_2 by use of an autoclave (E-2); the results are shown in Fig. 3, where the spectrum for P = 0 is that in Fig. 2 which was measured by use of the gas cell (E-1). Of course, the coordination structure at 30 °C copies that at 130 °C, as already described in Fig. 2. When P = 0 at 130 °C, the $\nu_{as}(COO^-)$ band appears near 1624 and 1538 cm^{-1}, corresponding to the six-coordinate structure, but as P increases, the two bands become weaker, and the 1585 cm^{-1} band is stronger, being predominant when $P \geq 3$ MPa. This pressure-dependent change was scarcely affected by the cooling rate from 130 °C. In Fig. 3, the pressure-dependent IR spectra for three $\nu_{as}(COO^-)$ bands show two isosbestic points near 1610 and 1570 cm^{-1}. The existence of two isosbestic points suggests that the structural transformation results from an equilibrium change between four- and six-coordination structures.

The pressure-dependent change in the coordination structure found in this work was also observed under Ar gas and the results were almost identical to those under N_2. Therefore, it was concluded that the coordination structure of Zn(II) carboxylate in E-MAA-60Zn is dependent on P at higher temperatures above around 60 °C. It has been reported that the coordination structure in some metal complexes is changed by adduct formation of gas molecules such as O_2 or under very high pressure,[10–13] but it is certainly surprising that the coordination structure changes with low pressure around atmospheric pressure. This novel finding, moreover, appears to have some significance in nature; for example it reminds us of relationships between physiological activity and coordination structure of some metal complexes in biological systems, and speaking boldly, physiological anomalies in deep sea, high mountains and cosmic space. Further studies are progressing for pressure-dependent coordination structures of metal complexes in various ionomers and also common metal complexes, for example pure metal alkyl carboxylates, in our laboratories and will be published elsewhere in the near future. In ethylene ionomers such as E-MAA-*x*M, the appearance and features of the pressure-dependent coordination structure seem to change sensitively depending on the host polymer, metal cation, its degree of neutralization and ion content.

The authors very much thank Professor Y. Sugi and Y. Kubota, Faculty of Engineering, Gifu University, for permitting us the use of an autoclave and their kind encouragement, and also Professor J. Uemura, Institute for Chemical Research, Kyoto University, for his valuable discussions and encouragement.

Notes and references

1 A. Eisenberg and M. King, *Ion-Containing Polymers*, Academic Press, New York, 1977.
2 M. Pineri and A. Eisenberg, *Structure and Properties of Ionomers, NATO ASI Series C, Vol. 198*, Reidel, Dordrecht, 1987.
3 S. Schlick, *Ionomers: Characterization, Theory, and Applications*, CRC Press, New York, 1996.
4 For example, K. Tadano, E. Hirasawa, Y. Yamamoto and S. Yano, *Macromolecules*, 1989, **22**, 226.
5 R. W. Rees and D. J. Vangham, *Polym. Prepr., Am. Chem. Soc., Div. Polym. Chem.*, 1965, **6**, 287.
6 B. A. Brozoski, M. M. Coleman and P. C. Painter, *Macromolecules*, 1984, **17**, 230.
7 M. M. Coleman, J. Y. Lee and P. C. Painter, *Macromolecules*, 1990, **23**, 2339.
8 K. Tsunashima, H. Nishioji, E. Hirasawa and S. Yano, *Polymer*, 1992, **33**, 1809.
9 T. Ishioka, *Polym. J.*, 1993, **25**, 1147.
10 E. Hirasawa, Y. Yamamoto, K. Tadano and S. Yano, *J. Appl. Polym. Sci.*, 1991, **42**, 351.
11 D. Voet and J. G.Voet, *Biochemistry*, Wiley, New York, 1990.
12 A. L. Crumbliss and F. Basolo, *J. Am. Chem. Soc*., 1970, **92**, 55.
13 R. van Eldik, *Inorganic High Pressure Chemistry: Kinetics and Mechanisms*, Elsevier, Amsterdam, 1986.

Communication 9/03629F

ChemComm

Hydrogen bonded antiparallel β-strand motifs promoted by 2,6-bis(carbamoylpeptide)pyridine

Qiang Yu,[a] Timothy E. Baroni,[a] Louise Liable-Sands,[b] Glenn P. A. Yap,[b] Arnold L. Rheingold[b] and A. S Borovik*[a]

[a] *Department of Chemistry, University of Kansas, Lawrence, KS 66045, USA. E-mail: aborovik@ukans.edu.*
[b] *Department of Chemistry, University of Delaware, Newark, DE 19716, USA*

Received (in Columbia, MO, USA) 5th January 1999, Accepted 3rd June 1999

A series of peptide dimers of 2,6-carbamoylpyridine have been isolated and their solid-state structures evaluated for the formation of strands motifs and lamellar architecture.

Many fibrous proteins found in nature (*e.g.* silks) have a significant amount of β-sheet structure which leads to lamellar architectures in the solid state.[1,2] The desirable physical properties associated with these proteins, such as high tensile strength, are proposed to result, in part, from their β-sheet structures.[1,2] Most attempts to duplicate these structural properties in synthetic systems have been hindered by difficulties in controlling secondary and tertiary peptide structures.[3] One useful approach to organize peptide structure is to incorporate a rigid template into the peptide backbone.[4,5] Our laboratory,[6] and that of Hamilton,[7] have been exploring the use of 2,6-bis[(2-carbamoylphenyl)carbamoyl]pyridine templates (**1**) to nucleate synthetic helices. Compounds with **1** have an inherent twist that results from the two appended phenyl rings being disposed on opposite faces of the planar 2,6-bis(carbamoyl)pyridine unit. We have found that replacing the phenyl groups with peptides would yield more planar compounds containing chiral clefts (**2**). In this design, direct intramolecular interactions between appended peptides are not possible; however intermolecular hydrogen bonding can occur to form supramolecular β-strands with antiparallel arrangements of peptides. We report herein our structural findings for a small family of peptide dimers.

Four dipeptides were synthesized that include all possible combinations of alanine and valine **2**(X,Y). Valine and alanine were chosen for their differing propensities to form β-sheets in proteins as shown by statistical[8] and thermodynamic studies.[9] Each pendant peptide arm was synthesized using standard DCC coupling protocol for Boc-protected amino acids.[10] Species **2**(X,Y) were obtained by treating THF solutions of the deprotected peptides with 2,6-bis(chlorocarbonyl)pyridine. All new compounds gave satisfactory FTIR, ^{1}H and ^{13}C NMR, FAB-MS, and elemental data.

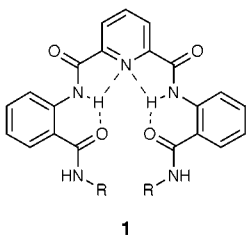

1

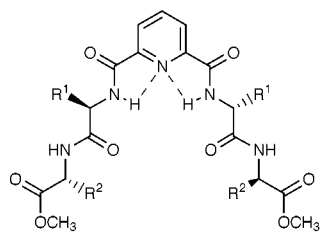

2(ala,ala): $R^1 = R^2 = CH_3$
2(val,val): $R^1 = R^2 = CH(CH_3)_2$
2(ala,val): $R^1 = CH_3$, $R^2 = CH(CH_3)_2$
2(val,ala): $R^1 = -CH(CH_3)_2$, $R^2 = CH_3$

NMR data in $CDCl_3$ obtained for the four peptide dimers suggest that the compounds are C_2 symmetric in solution. The chemical shift for the 2,6-carbamoylpyridine protons are observed at *ca.* 8.5 ppm which is indicative of intramolecular hydrogen bonding (*i.e.* $N–H_{amide}\cdots N_{py}$).[11] Moreover, the chemical shifts of these protons are sensitive to the presence of water. For **2**(val,ala), the resonance for these proton shifts downfield by 0.20 ppm with the addition of 1 equiv. of H_2O. Furthermore, the observed temperature dependence of the 2,6-carbamoyl protons of **2**(val,ala) in the presence of water ($\Delta\delta/\Delta T = -0.012$ ppm K^{-1}) is significantly greater than that under anhydrous conditions ($\Delta\delta/\Delta T = -0.0017$ ppm K^{-1}). Variable temperature ^{1}H NMR data also show that the chemical shift of the water present in **2**(val,ala) has a large temperature dependence of ($\Delta\delta/\Delta T = -0.0345$ ppm K^{-1}. Taken together these NMR data suggest the **2**(val,ala)·H_2O adduct forms *via* multiple hydrogen bonds.[12]

The solid state structures of **2**(val,ala)·H_2O and **2**(val,val)·H_2O were examined by single-crystal X-ray diffraction methods and agree with the structures suggested from solution studies. Both compounds crystallize in non-centrosymmetric space groups: **2**(val,ala)·H_2O in the tetragonal space group $P4_12_12_1$† and **2**(val,val)·H_2O in the orthorhombic space group $P2_12_12_1$.‡ The compounds have similar 'V'-shaped molecular structures with a guest water molecule residing in the chiral cleft formed by the two appended peptides [see Fig. 1 for **2**(val,val)·H_2O]. Species **2**(val,ala)·H_2O has exact C_2-symmetry where the axis bisects the pyridine ring and coincides with N(1) and O(9) of the water molecule. N(2)–H(2) of the carbamoyl moieties are involved in H-bonding between the pyridyl nitrogen [N(2)···N(1), 2.724(7) Å]. The guest water molecule also H-bonds to the internal valine carbonyl oxygens of each peptide as indicated by the heavy atom O(9)···O(2) distance of 3.097(7) Å. Compound **2**(val,val)·H_2O is not C_2-symmetric in the crystalline state; however, it also interacts with its guest water molecule through four H-bonding interactions: (i) O(9) H-bonds to carbamoyl N–H groups with N(2)···O(9) and N(4)···O(9) distances of 3.054(16) and 2.931(16) Å; and (ii) the water hydrogens H-bond to the appended peptides through the

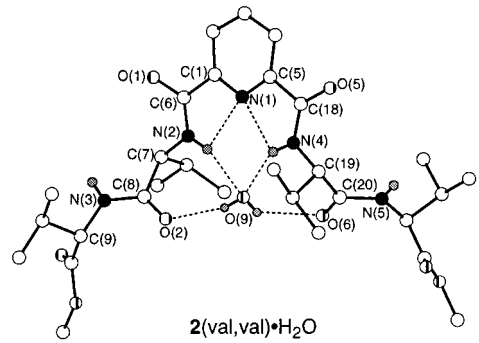

2(val,val)•H_2O

Fig. 1 Molecular structure of **2**(val,val)·H_2O. Selected distances (Å) and dihedral angles (°): N(2)–O(9) = 3.053(16); N(4)–O(9) = 2.928(15); C(30)–O(2) = 3.206(15); O(9)–O(2) = 2.830(16); O(9)–O(6) = 2.697(16); N(2)–C(7)–C(8)–N(3) = 136.3; N(4)–C(19)–C(20)–N(5) = 124.2; C(6)–N(2)–C(7)–C(8) = −130.9; C(18)–N(4)–C(19)–C(20) = −113.5.

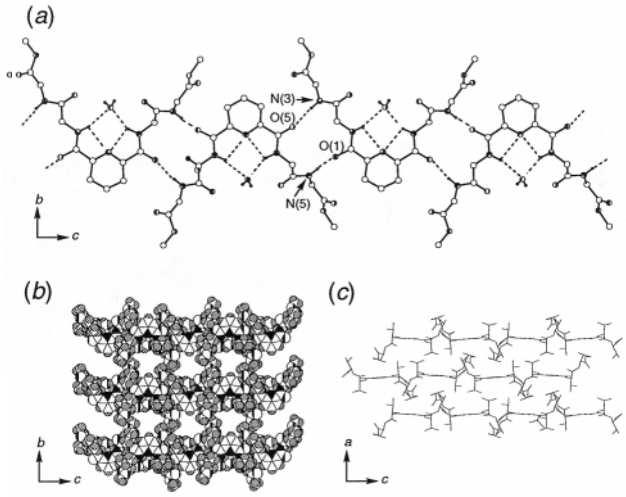

Fig. 2 Crystal lattice architecture in **2**(val,ala)·H_2O. (*a*) intermolecular hydrogen bonding network formed within antiparallel β-sheet (viewed along crystallographic *a*-axis, isopropyl groups removed for clarity), (*b*) lamella structure viewed in the *a*,*b* plane and (*c*) *a*,*c* plane. Chloroform solvent molecules removed for clarity.

internal valine carbonyl oxygens where heavy atom O(9)···O(2) and O(9)···O(6) distances are 2.830(15) and 2.698(15) Å.[13]

Although similar in molecular structure, **2**(val,val)·H_2O and **2**(val,ala)·H_2O have significantly different lattice architectures. Strand motifs are the dominant structural element found in the lattice of **2**(val,val)·H_2O. Individual strands are formed by an antiparallel arrangement of molecules connected by a network of intermolecular H-bonds which runs parallel to the crystallographic *c*-axis. Molecules within a strand have four intermolecular H-bonds, two bonds to each of its two nearest neighbors at distances of N(3)···O(5) = 2.860(16) and O(1)···N(5) = 2.970(18)Å [Fig. 2(*a*)]. The nearly coplanar positioning of the N(3)–H and C(6)–O(1) vectors (RMS planar deviation 0.064 Å) offers a favorable geometric arrangement for the formation of strands.

The strand motif in **2**(val,val)·H_2O resembles antiparallel β-strands (sheets) observed in proteins. The strands in this synthetic system have dihedral angles that are similar to the ψ (136°) and ϕ (−139°) angles found in protein antiparallel β-sheets.[14] The ψ angles for the internal valine in the molecular structure of **2**(val,val) are 136.2 and 124.2°, while those for ϕ are −130.9 and −113.5° (see legend to Fig. 1). These strand motifs assemble to produce sheets that lie in the crystallographic *b*,*c*-plane [Fig. 2(*b*)]. Note that each layer has an open framework which is formed by the interactions of peptides in neighboring strands. In **2**(val,val)·H_2O, the resultant open spaces within a layer are partially occupied by chloroform molecules. The arrangement of sheets within this crystal lattice is a lamellar structure [Fig. 2(*c*)].

In contrast to **2**(val,val)·H_2O, **2**(val,ala)·H_2O associates with neighboring molecules to form a three-dimensional network of hydrogen bonds which has neither strands nor a lamellar structure. Moreover, each molecule in the lattice of **2**(val,ala)·H_2O is involved in only two intermolecular H-bonds.[15] A possible explanation for the differences between the lattice architecture of **2**(val,ala)·H_2O and **2**(val,val)·H_2O is the magnitude of the molecular dihedral angles ψ and ϕ. In **2**(val,ala)·H_2O, the angles are ψ = −133.6° and ϕ = 118.6°, approximately 180° different than found for **2**(val,val)·H_2O (*vide supra*).

The β-strand formation observed in **2**(val,val)·H_2O and absent in **2**(val,ala)·H_2O is consistent with the results found in proteins, where valine and alanine confer different propensities for sheet formation. Moreover, β-sheets are often found in the interior of proteins where side chains engage in hydrophobic interactions with other units of secondary structure.[16] These interactions lead to alternating positioning of side chains that results in a 'tongue and groove' structure as observed in the lattice of **2**(val,val)·H_2O [Fig. 2(*c*)]. However, in **2**(val,ala)·H_2O the side chains do not permit the same long-range interactions, therefore an alternative lattice structure is adopted. The small size of **2**(val,val)·H_2O in comparison to proteins makes it particularly notable that antiparallel strand formation and lamellar structure is observed. Extension of this design to other peptide systems is currently under investigation.

We thank the NIH for financial support.

Notes and references

† *Crystal data* for **2**(val,ala)·H_2O: $C_{25}H_{37}N_5O_8·H_2$), crystal habit, blocks, space group $P4_12_12_1$, a = 12.535(3), c = 18.258(8) Å, V = 2868.9(19) Å^3, T = 231 K, Z = 4; μ = 0.98 cm^{-1}, 3535 reflections collected, 1649 independent reflections [$I > 2\sigma(I)$]. $R(F)$ = 0.0514, $R(wF^2)$ = 0.1024 with a GOF(F^2) = 0.94.

‡ *Crystal data* for **2**(val,val)·H_2O·$CHCl_3$: $C_{29}H_{45}N_5O_8·H_2O·1/2CHCl_3$, crystal habit, blocks, space group $P2_12_12_1$, a = 13,407(1), b = 14.817(2), c = 20.314(4) Å, V = 4035.5(8) Å^3, T = 298(2) K, Z = 4, μ = 1.76 cm^{-1}, 5123 reflections collected, 2303 independent reflections [$I > 2\sigma(I)$]. $R(F)$ = 0.0971, $R(wF^2)$ = 0.2597 with a GOF(F^2) = 1.175. CCDC 182/1285.

1 D. L. Kaplan, S. J. Lombardi, W. S. Muller and S. A. Fossey, in *Biomaterials*, ed. D. Byrom, Macmillin, UK, 1991, p. 1; *Silk Polymers*, ed. D. L. Kaplan, W. W. Adams, B. Farmer and C. Viney, *ACS Symp. Ser.* 544, ACS, Washington, DC, 1994; R. V. Lewis, *Acc. Chem. Res.*, 1992, **25**, 392.

2 A. H. Simmons, C. A. Michal and L. Jelinski, *Science*, 1996, **271**, 84; D. A. Tirrell, *Science*, 1996, **271**, 39.

3 Notable exceptions: M. T. Krechi, E. D. T. Adkins, A. J. Waddon, M. J. Fournier, T. L. Mason and D. A. Tirrell, *Science*, 1996, **265**, 1427; D. Choo, J. P. Schneider, N. R. Graciani and J. W. Kelly, *Macromolecules*, 1996, **29**, 355.

4 Recent reviews: J. P. Schneider and J. W. Kelly, *Chem. Rev.*, 1995, **95**, 2169; G. Tushsherer and M. Mutter, *Pure Appl. Chem.*, 1996, **68**, 2153; S. H. Gellman, *Acc. Chem. Res.*, 1998, **31**, 173.

5 Selected examples: D. S. Kemp and B. R. Bowen, *Tetrahedron Lett.*, 1988, **29**, 5077; A. B. Smith III, M. C. Guzman, P. A. Sprengeler, T. P. Keenan, R. C. Holcomb, J. L. Wood, P. J. Carroll and R. Hirschmann, *J. Am. Chem. Soc.*, 1994, **37**, 215; J. P. Schneider and J. W. Kelly, *J. Am. Chem. Soc.*, 1995, **117**, 2533; J. S. Nowick, S. Mahrus, E. M. Smith and J. W. Ziller, *J. Am. Chem. Soc.*, 1996, **118**, 1066.

6 T. Kawamoto, O. Prakash, A. L. Rheingold, B. A. Ostrander, A. L. Rheingold and A. S. Borovik, *Inorg. Chem.*, 1995, **34**, 4294; T. Kawamoto, B. S. Hammes, B. Haggerty, G. P. A. Yap, A. L. Rheingold and A. S. Borovik, *J. Am. Chem. Soc.*, 1996, **118**, 285; T. Kawamoto, B. S. Hammes, R. Ostrander, A. L. Rheingold and A. S. Borovik, *Inorg. Chem.*, 1998, **37**, 3424; Q. Yu, T. E. Baroni, L. Liable-Sands, A. L. Rheingold and A. S. Borovik, *Tetrahedron Lett.*, 1998, **39**, 6831.

7 Y. Hamuro, S. J. Geib and A. H. Hamilton, *Angew. Chem., Int., Ed. Engl.*, 1994, **33**, 446; Y. Hamuro, S. J. Geib and A. H. Hamilton, *J. Am. Chem. Soc.*, 1996, **118**, 7529; Y. Hamuro, S. J. Geib and A. H. Hamilton, *J. Am. Chem. Soc.*, 1997, **119**, 10 587.

8 P. Y. Chou and G. D. Fasman, *Biochemistry*, 1973, **12**, 211.

9 C. H. Kim and J. M. Berg, *Nature*, 1993, **362**, 267; D. L. Minor Jr. and P. S. Kim, *Nature*, 1994, **367**, 660; C. K. Smith, J. M. Withka and L. Regan, *Biochemistry*, 1994, **33**, 5510; D. L. Minor Jr. and P. S. Kim, *Nature*, 1994, **371**, 264.

10 M. Bodansky and A. Bodansky, *The Practice of Peptide Synthesis*, Springer-Verlag, New York, 1994.

11 The chemical shift of related protons in 2,6-carbamoylbenzene are at ~7.0 ppm.

12 See A. B. Kudryavtsev and W. Linert, *Physico-Chemical Applications of NMR*, World Scientific Publishing, Singapore, 1996, pp. 165–178.

13 An intermolecular C–H···O hydrogen bond is also observed between **2**(val,val) and the $CHCl_3$ solvate [C(30)···O(2) distance is 3.206(15) Å)]. Typical C–H···O hydrogen bond distances are ~3.4 Å: H.-B. Bürgi and J. D. Dunitz, *Structure Correlation*, VCH, New York, 1994.

14 T. E. Creighton, *Proteins-Structures and Molecular Principles*, Freeman, New York, 1984, pp. 221–225.

15 The intermolecular H-bonds between molecules in the lattice of **2**(val,ala)·H_2O are at distances of 2.954(7) and 3.307(6) Å for the N(3)–H···O(2) and C(3)–H···O(3) interactions.

16 For the influence of hydrophobic interactions in stabilizing sheet structures in proteins and synthetic systems see ref. 4 and B. Hazes and W. G. J. Hol, *Proteins: Struct. Funct. Genet.*, 1992, **12**, 278; Y. K. Tsang, H. Diaz, N. Graciani and J. W. Kelly, *J. Am. Chem. Soc.*, 1996, **116**, 3988; D. Neri, M. Billeter, G. Wider and K. Wüthrich, *Science*, 1992, **257**, 1559.

Communication 9/00541B

The complete and irreversible conversion of a *cis* carbon-substituted thiiranium ion into the *trans* isomer

Lucia Pasquato* and Giorgio Modena

Centro CNR Meccanismi di Reazioni Organiche (CMRO) and Dipartimento di Chimica Organica, Università di Padova, via Marzolo 1, 35131 Padova, Italy. E-mail: pasquato@chor.unipd.it

Received (in Liverpool, UK) 18th March 1999, Accepted 23rd June 1999

***t*-2-*tert*-Butyl-*t*-3-phenyl-*r*-1-methylthiiranium 1 isomerizes into the more stable (32.3 kJ mol^{-1}) *t*-2-*tert*-butyl-*c*-3-phenyl-*r*-1-methylthiiranium 2 in a complete and irreversible process (monitored by proton NMR at −30 °C) *via* an open benzylic carbenium ion.**

Thiiranium ions, the bridged intermediates in the addition of sulfenyl derivatives to alkenes,[1,2] are known to be among the most stable of the iranium ion family with respect to the isomeric open carbonium ions.[1,2] Isolation of these cyclic species[3] and their characterization in the solid state by X-ray structural determination[4–6] and in solution mainly by NMR spectroscopy[7,8] together with theoretical *ab initio* calculations[6,9] have provided detailed information on their structure.

Thiiranium ions are responsible for the complete *anti* stereospecificity of the additions of sulfenyl halides to alkenes. Few exceptions are known† and they concern, mainly, those alkenes having electron-donor substituents. For example, in the sulfenylation of vinyl ethers the thiiranium ion may be in equilibrium with the open carbonium ion stabilized *via* the mesomeric oxonium ion.[12]

Recently, we began to investigate the chemistry of stable and isolated thiiranium ions for mechanistic[8,13,14] as well as for synthetic reasons.[15] Bulky substituents at the ring carbons stabilize the ions, whereas phenyl substituents activate the α-carbon toward nucleophilic reactions. Here we report that we could observe, for the first time, the unexpected complete isomerization of the *t*-2-*tert*-butyl-*t*-3-phenyl-*r*-1-methylthiiranium **1** hexachloroantimonate into the *t*-2-*tert*-butyl-*c*-3-phenyl-*r*-1-methylthiiranium **2** hexachloroantimonate.

The *t*-2-*tert*-butyl-*c*-3-phenyl-*r*-1-methylthiiranium **2** hexachloroantimonate was prepared by reaction of (*E*)-3,3-dimethyl-1-phenylbut-1-ene with 1 equiv. of methylthio(bismethylthio)sulfonium hexachloroantimonate in CH_2Cl_2 at −20 °C.[14] Only the isomer having the phenyl ring *cis* to the *S*-methyl group is formed.[14] When we attempted the synthesis of the *t*-2-*tert*-butyl-*t*-3-phenyl-*r*-1-methylthiiranium **1** hexachloroantimonate by adding the same electrophile to the (*Z*)-3,3-dimethyl-1-phenylbut-1-ene at −20 °C, only the *trans* isomer **2** was obtained. The reaction repeated in CD_2Cl_2 and monitored by ^{1}H-NMR at −20 °C confirmed the exclusive formation of the *trans* thiiranium ion **2**.

However, the addition of CH_3SCl in CH_2Cl_2 at −78 °C to (*E*)- and (*Z*)-3,3-dimethyl-1-phenylbut-1-ene is completely stereoselective and hence the corresponding thiiranium ions must be the intermediates.

Indeed, when the reaction of the (*Z*)-alkene with $Me_3S_3SbCl_6$ was carried out at −50 °C in an NMR tube we could observe the slow formation of the *cis* thiiranium ion **1**.‡ The reaction is complete in about 30 min. Very diagnostic are the doublets relative to protons 2-H and 3-H which in the *trans* isomer are at 4.38 and 5.56 ppm respectively (*J* 12.0 Hz) whereas in the *cis* isomer 2-H and 3-H are doublets at 4.52 and 5.65 ppm (*J* 10.14 Hz). Also, the *S*-methyl group shows a singlet at 2.95 ppm in the *cis* isomer and at 2.16 ppm in the *trans* isomer.

Raising the temperature gradually up to −30 °C we observed the quantitative isomerization of the *cis* isomer **1** into the *trans* one ($t_{1/2}$ is about 2 h) without detecting any significant amount of (*Z*)-alkene suggesting that the isomerization occurs on the thiiranium ion itself, likely *via* a ring opening–ring closure process as depicted in Scheme 1.§

To confirm the hypothesis of Scheme 1, *i.e.* that the observed isomerization is due to an equilibrium between thiiranium ion and the corresponding carbonium ion, we prepared the *t*-2-*tert*-butyl-*t*-3-(3,5-dichlorophenyl)-*r*-1-methylthiiranium **3** hexachloroantimonate and the *t*-2-*tert*-butyl-*c*-3-(3,5-dichlorophenyl)-*r*-1-methylthiiranium **4** hexachloroantimonate, where the phenyl group is substituted by the more electronegative 3,5-dichlorophenyl residue, by addition of methylthio(bismethylthio)sulfonium hexachloroantimonate to (*Z*)- and (*E*)-1-(3,5-dichlorophenyl)-3,3-dimethylbut-1-enes¶ in CH_2Cl_2 at −60 °C.

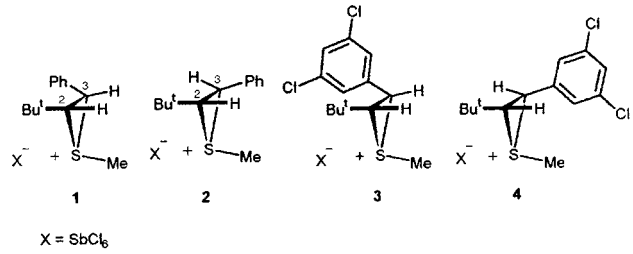

Scheme 1

As expected thiiranium ion **3** is much more stable than the homologous **1** in CD_2Cl_2. At 0 °C the compound is stable for more than 12 h.‖

Independent information on the relative stability of thiiranium ions **1** and **2** has been obtained by *ab initio* calculation.** Optimization at the RHF/3-21G*//RHF-3-21G* level gives an energy difference of 32.3 kJ mol^{-1} between the most stable *trans* and the *cis* isomer. The stronger steric interaction between the phenyl ring and the *cis tert*-butyl group in the ion **1** with respect to the steric interaction between the phenyl ring and the *S*-methyl group in the *trans* ion **2** may be responsible for the calculated energy difference.

In the optimized geometry relative to the *trans* thiiranium ion **2** the S–C(3) bond is 1.991 Å whereas the S–C(2) bond is 1.870 Å. The same bonds in the *cis* ion **1** are 1.855 and 1.884 Å respectively. The C(2)–C(3) bonds in the two isomers **1** and **2**

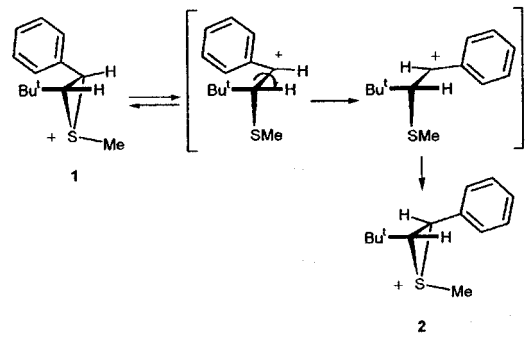

Scheme 2

are similar being 1.463 and 1.488 Å respectively. Very likely the *cis* interaction between the phenyl and the S–Me group in the ion **2** is minimized by stretching the S–C(3) bond. The much greater steric interaction between the *tert*-butyl and the *cis* phenyl moieties in the *cis* ion **1** is removed very efficiently by breaking the S–C(3) bond due to the presence of the phenyl ring which stabilizes the α positive charge in the open carbonium ion. Rotation around the C(2)–C(3) bond and closure to the *trans* ion **2** complete the rearrangement process (Scheme 1). The energy difference between the two ions ensures an irreversible reaction.

In conclusion, we have reported the isomerization of the *t*-2-*tert*-butyl-*t*-3-phenyl-*r*-1-methylthiiranium ion **1** to the more stable *trans* isomer **2** *via* an open benzylic carbonium ion. The different stability of these ions (32.3 kJ mol^{-1}) makes the process irreversible. Efforts are in progress in our laboratories to find suitable thiiranium ions to study the different reactivity modes of *cis* carbon-substituted thiiranium ions with respect to *trans* ones.

The authors thank Professor Vittorio Lucchini and Dr Alessandro Bagno for performing *ab initio* calculations.

Notes and references

† It has been reported that sulfenyl halides add stereospecifically to (*E*)- and (*Z*)-but-2-ene in the temperature range −34 to +146 °C (ref. 10). The corresponding thiiranium ions may be independently synthesized and they react with nucleophiles at −20 °C to give the non-isomerized adducts. However, a mixture of *erythro* and *threo* products, whose composition is independent of the starting thiiranium ion, is formed if the thiiranium ion salts are kept for some time at +20 °C (ref. 11).

‡ $\delta_H(CD_2Cl_2$, 200 MHz, −50 °C) 0.92 (9H, s, Bu^t); 2.95 (3H, s, Me), 4.52 (1H, d, *J* 10.14), 5.65 (1H, d, *J* 10.14), 7.45 (5H, m, Ph). $\delta_C(CD_2Cl_2$, 62.9 MHz, −50 °C) 23.46, 27.31, 33.88, 63.96, 75.02, 124.91, 127.42, 128.55, 129.14.

§ The stability of the (*Z*)-alkene was independently checked in CD_2Cl_2 in the range −30 to +25 °C by ^{1}H NMR.

¶ Both isomers were obtained from the corresponding alkyne prepared following the procedure reported in ref. 16. The (*Z*)-isomer was then obtained by hydroboration with catecholborane (ref. 17); the (*E*)-alkene was prepared by photochemical isomerization of the (*Z*)-isomer.

‖ The rather large difference in reactivity observed between *cis* thiiranium ions **1** and **3** is not unexpected since the reaction may be compared to a carbonium ion formation process from a neutral substrate. The difference in sigma values for phenyl and 3,5-dichlorophenyl is 2 × 0.37 which applied to a unimolecular process having rho values of −4 leads to an estimate value for the reactivity ratio of 10^{-3}.

** Spartan 5.0 program package, distributed by Wavefunction, Inc., Irvine, CA 92715.

1 G. Capozzi, G. Modena and L. Pasquato, *The Chemistry of Sulphenyl Halides and Sulphenamides*, ed. S. Patai, Wiley, Chichester, 1990, p. 403.
2 V. Lucchini, G. Modena and L. Pasquato, *Gazz. Chim. Ital.*, 1997, **127**, 177.
3 D. J. Pettit and G. K. Helmkamp, *J. Org. Chem.*, 1963, **28**, 2932.
4 G. I. Borodkin, Y. V. Gatilov, E. I. Chernyak and V. G. Shubin, *Izv. Akad. Nauk SSSR, Ser. Kim.*, 1985, 2826 (*Chem. Abstr.*, 1986, **105**, 208686); G. I. Borodkin, Y. V. Gatilov, E. I. Chernyak and V. G. Shubin, *Izv. Akad. Nauk SSSR, Ser. Kim.*, 1987, 2230 (*Chem. Abstr.*, 1987, **108**, 186453).
5 X. Huang, R. J. Batchelor, F. W. Einstein and A. J. Bennet, *J. Org. Chem.*, 1994, **59**, 7108.
6 L. Pasquato, R. Destro, V. Lucchini and G. Modena, *Phosphorus Sulfur Silicon Relat. Elem.*, in the press.
7 G. Capozzi, O. De Lucchi, V. Lucchini and G. Modena, *Tetrahedron Lett.*, 1975, 2603.
8 V. Lucchini, G. Modena and L. Pasquato, *J. Am. Chem. Soc.*, 1988, **110**, 6900; V. Lucchini, G. Modena and L. Pasquato, *J. Am. Chem. Soc.*, 1991, **113**, 6600.
9 Y. Kikuzono, T. Yamabe, S. Nagata, H. Kato and K. Fukui, *Tetrahedron*, 1974, **30**, 2197; J. W. Gordon, G. H. Schmid and I. G. Csizmadia, *J. Chem. Soc., Perkin Trans. 2*, 1975, 1722.
10 G. H. Schmid and V. M. Csizmadia, *Can. J. Chem.*, 1966, **44**, 1338.
11 W. A. Smit, M. Z. Krimer and E. A. Vorobieva, *Tetrahedron Lett.*, 1975, 2451; E. A. Vorobieva, M. Z. Krimer and W. A. Smit, *Izv. Akad. Nauk SSSR, Ser. Kim.*, 1976, 2743.
12 For example: K. C. Nicolaou, T. Ladduwahetty, J. L. Randall and A. Chucholowski, *J. Am. Chem. Soc.*, 1986, **108**, 2466; T. Sato, J. Otera and H. Nozaki, *J. Org. Chem.*, 1990, **55**, 6116; K. Kudo, Y. Hashimoto, M. Sukegawa, M. Hasegawa and K. Saigo, *J. Org. Chem.*, 1993, **58**, 579; D. K. Jones and D. C. Liotta, *Tetrahedron Lett.*, 1993, **34**, 7209; D. K. Jones and D. C. Liotta, *Adv. Mol. Model.*, 1995, **3**, 67.
13 V. Lucchini, G. Modena, M. Pasi and L. Pasquato, *J. Org. Chem.*, 1997, **62**, 7018.
14 M. Fachini, V. Lucchini, G. Modena, M. Pasi and L. Pasquato, *J. Am. Chem. Soc.*, 1999, **121**, 3944.
15 V. Lucchini, G. Modena and L. Pasquato, *J. Chem. Soc., Chem. Commun.*, 1994, 1565.
16 Z.-Y. Yang and D. J. Burton, *Tetrahedron Lett.*, 1990, **31**, 1369.
17 H. C. Brown and S. K. Gupta, *J. Am. Chem. Soc.*, 1972, **94**, 4370.

Communication 9/02221J

Coordination and oxidation of phosphine selenides with iodine: from cation pairs $[(R_3PSe)_2I^+]_2$ to (iodoseleno)phosphonium ions $[R_3PSeI]^+$ existing as guests in polyiodide matrices

Emma Seppälä, Frank Ruthe, Jörg Jeske, Wolf-W. du Mont* and Peter G. Jones

Institut für Anorganische und Analytische Chemie, Technische Universität Braunschweig, Postfach 3329, D-38023 Braunschweig, Germany. E-mail: w.du-mont@tu-bs.de

Received (in Basel, Switzerland) 23rd April 1999, Accepted 21st June 1999

An X-ray crystallographic study of adducts of trialkylphosphine selenides with > 1 equivalent of diiodine reveals that solid $Bu^t_3PSeI_3$ consists of cation pairs $[(Bu^t_3PSe)_2I^+]_2$ intercalated between I_5^- layers and that solid $R_2R'PSeI_7$ (R = Bu^t or Pr^i, R′ = Pr^i) contains $[R_2R'P–Se–I]^+$ cations with weak secondary I···I interactions to polyiodide networks.

Phosphine selenides $R_2R'P{=}Se$ are known act as donors towards dihalogen molecules, providing 1:1 adducts $R_2R'PSeX_2$.[1–7] *Molecular* structures have been determined for $R_2R'PSeI_2$ (type **A**, R, R′ = Ph, NMe_2, NEt_2,[3] and R = Bu^t, R′ = I[4]) and R_3PSeBr_2 (type **B**, R, R′ = NMe_2, C_6H_{11},[5] R = Bu^t, R′ = Pr^i or Bu^t[2,7]). Bromo- and iodo-selenophosphonium ions (type **D**) have been postulated as cations in ionic 1:1 adducts of phosphine selenide and dihalogen.[6] The first X-ray crystallographically characterised purely *ionic* solid 1:1 adduct was $(Pr^i_3PSe)_2I^+$ I_3^- **1a** (type **C**).[7] NMR spectra, however, suggest that in solutions of such 1:1 adducts equilibrium mixtures of several species are present.[2,6,7] Solutions prepared from $R_2R'P{=}Se$ (**2a**: R, R′ = Pr^i; **2b**: R = Bu^t, R′ = Pr^i; **2c**: R, R′ = Bu^t) and various amounts of I_2 always exhibit only one averaged ^{31}P NMR line accompanied by satellites arising from $^1J(^{77}Se,^{31}P)$, which decreases with increasing amounts of iodine. In CD_2Cl_2 solution, couplings $^1J(^{77}Se,^{31}P)$ are smaller than in C_6D_6 solution. Addition of < 5% of I_2 to $R_3P{=}Se$ leads to severe broadening and a slight downfield shift of the ^{77}Se NMR doublet. With larger amounts of I_2, as in the pure '1:1 adducts', the ^{77}Se resonances become too broad to be detected. This indicates kinetic lability of $R_3PSe–I_2$ systems and equilibration by exchange reactions that are fast on the ^{31}P and ^1H NMR time scales.

Such an equilibrium mixture is 'frozen' in solid $Bu^t_3PSeI_2$ **1c** [consisting of *molecular* $Bu^t_3PSe–I–I$ and *ionic* $(Bu^t_3PSe)_2I^+$ I_3^-].[2,7]

The transition from the molecular adduct $Bu^t_3PSeI_2$ to the cationic species $(Bu^t_3PSe)_2I^+$ is completed by adding slightly more iodine to solutions of **1c**. This leads to the solid compound $(Bu^t_3PSe)_2I^+$ I_5^- **3**. Cations with linear Se–I–Se arrangements that are well separated from each other and from the counter anions, are known from Se_6IAsF_6 and from related Se-coordinated $[L_2I]^+$ [L = *N*-methylbenzothiazole-2(3*H*)-selone].[8] Compound **3**, however, consists of *pairs* of cations $[(Bu^t_3PSe)_2I^+]_2$ [Fig. 1(a), (b)] intercalated into channels emerging from the corrugated structure of the polymeric I_5^- counter anion. The polymeric I_5^- ion creates channels between adjacent layers that offer suitable space for *pairs* of cations. Within these pairs, Se···Se contacts are shorter than the van der Waals radii; these cation pairs are well separated from the anionic network.

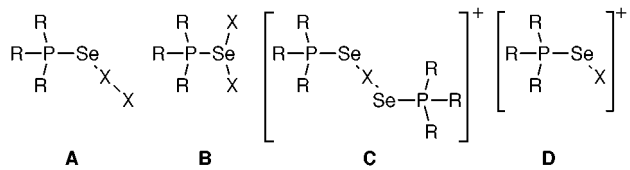

Scheme 1 Structural alternatives of phosphine selenide halogen adducts.

Use of an *excess* of iodine on $[I(py)_2]^+$ $[I_3]^-$ is known to provide solid $[I(py)_2]^+$ $[I_7]^-$.[9] Pr^i_3PSe **2a** and $Bu^t_2Pr^iPSe$ **2b** on reaction with excess iodine, however, do not form higher polyiodides of $(R_3PSe)_2I^+$ cations, but instead provide compounds of the composition $R_2R'PSeI_7$ **4a**, **4b** that represent the first examples of $[R_3PSeI]^+$ cations (type **D**). ^{31}P NMR spectra of these compounds exhibit, in comparison with **1a**, **1b**,[7] further decreased coupling constants $^1J(^{77}Se, ^{31}P)$, which are now similar to that of the type **B** molecular adduct $Pr^i_3PSeBr_2$, which contains a P–Se single bond.[7] The higher iodine content of $R_2R'PSeI_7$, compared with $(Me_2N)_3PSeI_4$ and $(Morph)_3PSeI_5$,[10] leads to improved separation of the $[R_2R'PSeI]^+$ cations of **4a** and **4b** from the surrounding weakly donating polyiodide networks.

Rather long cation–anion I···I distances in **4a** and **4b** (between 324.8 and 330 pm) correlate well with the shortest yet observed (P)–Se–I bonds (256.3–257.8 pm) in their $[R_2R'P–Se–I]^+$ cations.

The slight steric differences between the alkyl groups of the cations of **4a** and **4b** lead to quite different long-range order of their polyiodide anion structures. In solid **4b** (Fig. 2), one iodide anion [I(3)] bridges two of the $R_2R'PSeI^+$ cations and is in further contact with three I_2 molecules [*d*(I–I) 274–275 pm within the I_2 units], one of which [I(4)–I(5)] contacts the other I^- anion [I(6)]. I(6) is in contact with five I_2 molecules; of these, I(11)–I(12) is the only *terminal* I_2 molecule (Fig. 2). In solid **4a** (Fig. 3), one I^- [I(9)] is surrounded by two cations [$Pr^i_3P(1)$–Se(1)–I(1) and $Pr^i_3P(2)$–Se(2)–I(4)] and four I_2 molecules (when one I···I_2 distance of 368 pm is included), two (five-coordinated) I^- are in contact with one cation [I(7) with $Pr^i_3P(3)$–Se(3)–I(22), I(11) with $Pr^i_3P(4)$–Se(4)–I(5)] and four I_2 molecules, and the fourth I^- [I(20)] is surrounded by five I_2 molecules (Fig. 3).

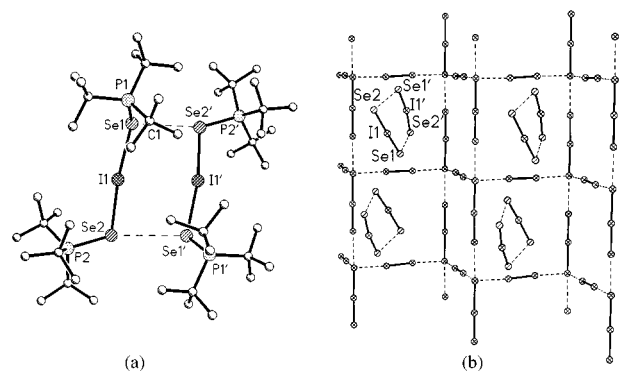

Fig. 1 (a) Cation pairs of **3**, selected bond lengths (pm) and angles (°): I1–Se2 273.7(1), I1–Se1 276.7(11), P1–Se1 218.6(2), P2–Se2 219.0(2), Se1···Se2′ 367.9(1), Se2–I1–Se1 170.3(3), P1–Se1–I1 112.6(7), P2–Se2–I1 111.5(7) (symmetry operator for generating equivalent atoms: −x, 1 + y, 0.5 − z); (b) Layer structure of **3**: Bu^t_3P groups omitted.

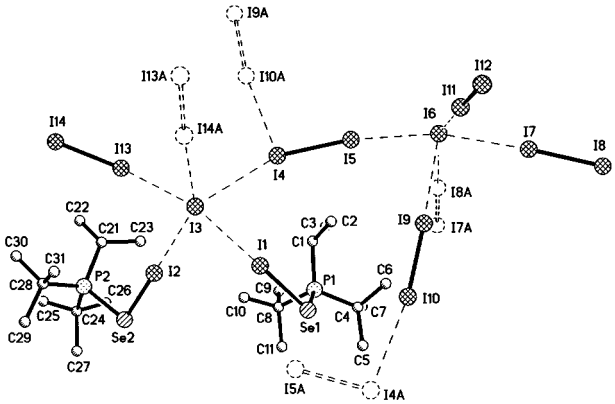

Fig. 2 Structure of **4b**, selected bond lengths (pm) and angles (°): I1–Se1 256.4(6), P1–Se1 223.5(1), I1···I3 330.2(4), I2–Se2 256.7(6), P2–Se2 223.7(1), I2···I3 324.8(5), P1–Se1–I1 102.1(3), P2–Se2–I2 101.6(4). Broken circles indicate atoms of other asymmetric units.

$[R_2R'P–Se–I]^+$ cations are also related to the rare class of alkane and arene selenenyl iodides R–Se–I[11–13] and with the (iodoseleno)imidazolium cation R^+–Se–I [*d*(Se–I) 259.1(5) pm] reported by Kuhn *et al.*[14] Compared with uncharged R–Se–I species,[11,13] all Se–I distances of the cations in **4a** and **4b** are slightly longer, which can be readily explained by the n → σ* nature of their anion-to-cation donor–acceptor interactions involving σ* orbitals of covalent Se–I bonds. We expect that the use of counter anions of low nucleophilicity will permit syntheses and studies of the electrophilicity of a larger number of stable (halogenoseleno)phosphonium ions of type **D**.

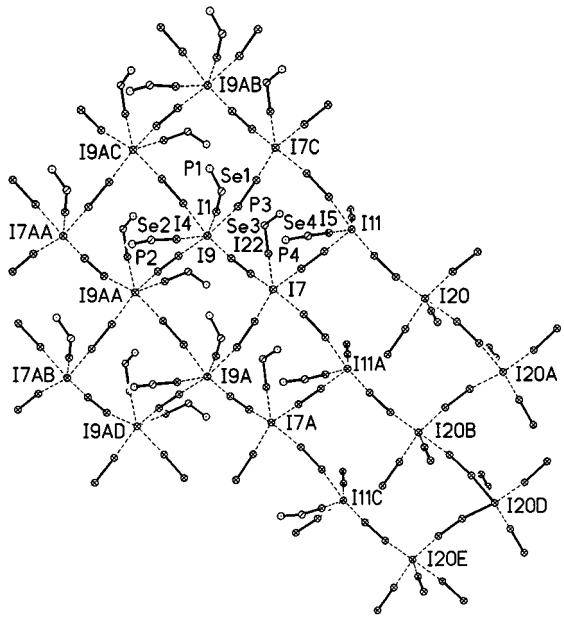

Fig. 3 Topology of I···I interactions within **4a**, selected bond lengths (pm) and angles (°): I1–Se1 256.3(2), P1–Se1 222.6(4), I1···I9 326.7(2), I4–Se2 256.4(2), P2–Se2 222.8(4), I4···I9 328.6(1), I22–Se3 257.1(2), P3–Se3 220.7(5), I22···I7 330.9(2), I5–Se4 257.8(2), P4–Se4 222.1(4), I5···I11 328.5(2), P1–Se1–I1 99.9(1), P2–Se2–I4 99.9(1), P3–Se3–I22 100.3(3), P4–Se4–I5 99.2(1); Pr^i groups omitted.

Notes and references

† *Crystal data*: **3**: $C_{27.5}H_{58}P_2Se_2I_6$; *M* = 1370.00, monoclinic, space group *C*2/*c*, *a* = 31.687(5), *b* = 13.955(2), *c* = 19.383(2) Å, *β* = 95.193(2)°, *U* = 8536.1(2) Å^3, *Z* = 8, D_c = 2.132 Mg m^{-3}, *μ* = 6.164 mm^{-1}, F(000) = 5112, 7530 independent reflections to 2*θ* max. 50°, *T* = 143 K, *S* = 1.155, *R*[*F*, > 4*σ*(*F*)] = 0.0519, *wR*(*F*^{2}) = 0.1541, 207 restraints and 358 parameters, highest peak 1.205 and deepest hole −2.128 e Å^{-3}.

4a: $C_{18}H_{42}P_2Se_2I_{14}$; *M* = 2254.98, orthorhombic, space group *Pna*2$_1$, *a* = 50.655(3), *b* = 15.5224(11), *c* = 12.5356(8) Å, *U* = 9856.7(1) Å^3, *Z* = 8, D_c = 3.039 Mg m^{-3}, *μ* = 10.348 mm^{-1}, *F*(000) = 7920, 23779 independent reflections to 2*θ* max. 56°, *T* = 143 K, *S* = 0.952, *R*(*F*, > 4*σ*(*F*)] = 0.0585, *wR*(*F*^{2}) = 0.1180, absolute structure factor *x* = 0.48(2), 397 restraints and 651 parameters, highest peak 3.177 and deepest hole −2.624 e Å^{-3}.

4b: $C_{11}H_{25}PSeI_7$; *M* = 1155.54, orthorhombic, space group $P2_12_12_1$, *a* = 12.6693(10), *b* = 16.4329(12), *c* = 25.2272(18) Å, *U* = 5252.1(7) Å^3, *Z* = 8, D_c = 2.923 Mg m^{-3}, *μ* = 9.714 mm^{-1}, *F*(000) = 4088, 15312 independent reflections to 2*θ* max. 60°, *T* = 143 K, *S* = 0.890, *R*[*F*, > 4*σ*(*F*)] = 0.0249, *wR*(*F*^{2}) = 0.0380, absolute structure factor *x* = 0.011(9), 126 restraints and 378 parameters, highest peak 1.743 and deepest hole −1.343 e Å^{-3}.

All X-ray datasets were collected with monochromated Mo-K*α* radiation (*λ* = 0.71073 Å) on a Stoe STADI-4 four-circle diffractometer (**3**) or a Bruker SMART 1000 CCD area detector (**4a**, **4b**). Absorption corrections were based on *ψ*-scans (**3**) or multiple scans (**4a**, **4b**). The structures were solved by direct methods and refined anisotropically by full-matrix least squares on *F*^{2}. H atoms were included using a riding model (except methyl groups in **4b**: refined as rigid groups). Structure **4a** was refined as a racemic twin; structure **3** contains half a molecule of toluene (disordered over an inversion centre) per formula unit. CCDC 182/1317. See: http://www.rsc.org/suppdata/cc/1999/1471/ for crystallographic files in .cif format.

‡ *^{31}P NMR data*: **1a** (300 K, CH_2Cl_2–C_6D_6): *δ* 65.3, $^1J(^{77}Se, ^{31}P)$ ±556 Hz; **1b** (300 K, C_6D_6): *δ* 76.2, $^1J(^{77}Se, ^{31}P)$ ±597 Hz, (300 K, CD_2Cl_2): *δ* 76.8, $^1J(^{77}Se, ^{31}P)$ ±547 Hz; **1c** (300 K, CH_2Cl_2–C_6D_6): *δ* 83.0, $^1J(^{77}Se, ^{31}P)$ ±593 Hz; **2b** (300 K, C_6D_6): *δ* 83.6, $^1J(^{77}Se, ^{31}P)$ ±704.8 Hz, (300 K, CD_2Cl_2): *δ* 83.8, $^1J(^{77}Se, ^{31}P)$ ±692.0 Hz; **3** (300 K, CD_2Cl_2): *δ* 83.0, $^1J(^{77}Se, ^{31}P)$ ±526 Hz; **4a** (300 K, CH_2Cl_2–C_6D_6): *δ* 66.5, $^1J(^{77}Se, ^{31}P)$ ±518 Hz; **4b** (300 K, CD_2Cl_2): *δ* 76.5, $^1J(^{77}Se, ^{31}P)$ ±528 Hz.

1 R. A. Zingaro and E. A. Meyers, *Inorg. Chem.*, 1962, **1**, 771; D. J. Williams and K. J. Wynne, *Inorg. Chem.*, 1976, **15**, 1449.
2 W.-W. du Mont, *Main Group Chem. News*, 1994, **2,** 18.
3 S. M. Godfrey, S. L. Jackson, C. A. McAuliffe and R. G. Pritchard, *J. Chem. Soc., Dalton Trans*., **1997**, 4499.
4 J. Jeske, W.-W. du Mont and P. G. Jones, *Chem. Eur. J.*, 1999, **5**, 385.
5 S. M. Godfrey, S. L. Jackson, C. A. McAuliffe and R. G. Pritchard, *J. Chem. Soc., Dalton Trans*., **1998**, 4201.
6 E. Krawczyk and A. Skowronska, *Phosphorus, Sulfur Silicon*, 1990, **51,** 329.
7 M. Bätcher, J. Jeske, F. Ruthe, E. Seppälä and W.-W. du Mont, unpublished work.
8 W. A. S. Nandana, J. Passmore and P. S. White, *J. Chem. Soc., Chem. Commun.*, **1983**, 526; F. Demartin, P. Deplano, F. A. Devillanova, F. Isaia, V. Lippolis and G. Verani, *Inorg. Chem.*, 1993, **32**, 3694.
9 E. E. Havinga and E. H. Wiebenga, *Acta Crystallogr.*, 1958, **11**, 733.
10 M. D. Rudd, S. V. Lindeman and S. Husebye, *Acta Chem. Scand.*, 1997, **51**, 689.
11 W.-W. du Mont, S. Kubiniok, K. Peters and H.-G. v. Schnering, *Angew. Chem.*, 1987, **99**, 820; *Angew. Chem., Int. Ed. Engl.*, 1987, **26**, 780.
12 W.-W. du Mont and I. Wagner, *Chem. Ber.*, 1988, **121**, 2109.
13 A. Martens-von Salzen, H.-U. Meyer and W.-W. du Mont, *Phosphorus, Sulfur Silicon*, 1992, **67**, 67; A. Martens-von Salzen, J. Jeske, W.-W. du Mont and P. G. Jones, *Phosphorus, Sulfur Silicon*, 1998, **136-138**, 545.
14 N. Kuhn, R. Fawzi, T. Kratz and G. Henkel, *Phosphorus, Sulfur Silicon*, 1996, **112**, 225.

Communication 9/03249E

ChemComm

Synthesis, crystal structure and ^{71}Ga MAS NMR spectroscopy of a novel gallium phosphatooxalate: $[Ga_5(OH)_2(C_{10}H_9N_2)(C_2O_4)(PO_4)_4]\cdot 2H_2O$

Ching-Yeh Chen,[a] Peter P. Chu[a] and Kwang-Hwa Lii*[ab]

[a] *Department of Chemistry, National Central University, Chungli, Taiwan 320, R.O.C. E-mail: liikh@cc.ncu.edu.tw*
[b] *Institute of Chemistry, Academia Sinica, Nankang, Taipei, Taiwan 115, R.O.C.*

Received (in Cambridge, UK) 22nd April 1999, Accepted 25th June 1999

The synthesis and characterization of a novel three-dimensional gallium phosphatooxalate is described; the structure consists of GaO_4 tetrahedra and GaO_6 octahedra linked by phosphate and oxalate groups to form two-dimensional sheets between which are GaO_4N square pyramids, generating tunnels in which the monoprotonated 4,4′-bipyridine molecules reside; ^{71}Ga MAS NMR confirms the presence of four-, five- and six-coordinate Ga atoms.

Open-framework materials have been the subject of intense research owing to their diverse structural chemistry and potential applications as ion-exchangers, catalysts and adsorbents.[1–3] Many of these materials are synthesized in the presence of an organic amine as structure-directing agent.[4–7] The organic moieties are usually accommodated in the structural voids, and in some cases can be removed by calcination or other treatments. In addition to the use of organic templates for preparing large-pore 3-D networks, the incorporation of organic multidentate ligands into the structure also creates a new route to open-framework materials. Advantages of using multidentate components can be realized by the enhancement in the thermal stability of the structure and the efficacy of rational design of crystalline solids through their coordinating propensities and geometries.[8] Recently, many research activities have focused on the synthesis of inorganic/organic hybrid materials; we have synthesized some interesting three-dimensional organically templated iron and indium phosphates.[9,10] There is equal interest in synthesizing 3-D GaPOs containing large apertures. Here, we report the synthesis and structural characterization of an inorganic/organic hybrid material, $[Ga_5(OH)_2(C_{10}H_9N_2)(C_2O_4)(PO_4)_4]\cdot 2H_2O$ **1**. Its unique framework structure is built up from three different types of gallium–oxygen polyhedra, oxalate and phosphate groups, forming channels in which the monoprotonated 4,4′-bipyridine molecules are located. ^{71}Ga solid state NMR has been applied to study the different coordination environments for gallium.

In a typical hydrothermal synthesis, a mixture of Ga_2O_3, 2-methylpiperazine, 4,4′-bipyridine, $C_2H_2O_4\cdot 4H_2O$, H_3PO_4 and H_2O in a molar ratio of 1 : 3 : 3 : 5 : 5 : 444 was sealed in a Teflon-lined acid digestion bomb and heated at 165 °C for 3 days under autogeneous pressure followed by slow cooling at 10 °C h^{-1} to room temperature. The resulting product consists of pale yellow plate-shaped crystals of **1** obtained in 69% yield based on Ga. A suitable pale yellow crystal was carefully selected for structure determination by single-crystal X-ray diffraction.† The product is monophasic as judged by the total consistency of its powder X-ray diffraction pattern with that simulated from the atomic coordinates derived from the single-crystal X-ray study. Elemental analysis confirmed its stoichiometry. (Anal. Found: C, 13.89; H, 1.44; N, 2.70. Calc.: C, 13.81; H, 1.45; N, 2.68%.) We have also carried out retro-syntheses and replaced 2-methylpiperazine with tetramethylammonium hydroxide; the resulting products are either monophasic with a very low yield or a mixture of **1** and a small amount of unidentified orange side product. Thermogravimetric analysis data in air for **1** showed a broad weight loss in several overlapping steps which begins gradually at 180 °C, has a maximum rate at *ca*. 450 °C and is incomplete by 975 °C. The final decomposition product is mainly $GaPO_4$ (JCPS: 31-0546). The weight loss in the initial step can be attributed to the loss of water molecules in the structural channels. The framework structure is stable up to 350 °C in air, as indicated from powder X-ray diffraction.

The three-dimensional framework of **1** consists of anionic sheets made of GaO_4 tetrahedra and GaO_6 octahedra connected *via* coordinating PO_4^{3-} and $C_2O_4^{2-}$ anions, and bridging GaO_4N square pyramids that interlink the sheets. The layer constructed from phosphates, oxalate and two types of Ga–O polyhedra in the *bc*-plane is shown in Fig. 1. Each GaO_4 tetrahedron is coordinated to four phosphate tetrahedra of which two connect one GaO_4 and two GaO_6 polyhedra in the same sheet while the other two connect one GaO_4, one GaO_6 and the bridging GaO_4N. Oxalate anions act as bis-bidentate ligands to two Ga(1) and form dimers of GaO_6 octahedra.

The coordination by the oxalate leads to a distorted octahedron for Ga(1), as indicated by the wide range of Ga–O bond lengths [1.887(3)–2.057(4) Å] and the O–Ga–O bond angle [81.5(1)°] subtended by the oxalate group. Connectivity between the dimers is *via* $P(1)O_4^{3-}$ and GaO_4N. Bond-valence calculations indicate that the bridging atom, O(11), between GaO_6 and GaO_4N is a hydroxo oxygen. The Ga(1)–O(11)–Ga(3) bond angle is 134.9(2)°. GaO_4N square pyramids, positioned in between the layers, join the GaO_6 and $P(2)O_4^{3-}$ from different layers, generating two types of tunnels parallel to the [001] direction (Fig. 2). Monoprotonated 4,4′-bipyridine cations are accommodated in the 12-membered void while the water molecules are located in the 8-membered channel. Ga(3) sits on a twofold axis and is bonded to four oxygens in the basal plane [Ga–O 1.869(4) Å (2×), 1.943(4) Å (2×)] and one nitrogen at the vertex [Ga–N 2.024(7) Å]. The two rings of 4,4′-bipy are twisted at an angle of 35.1°.

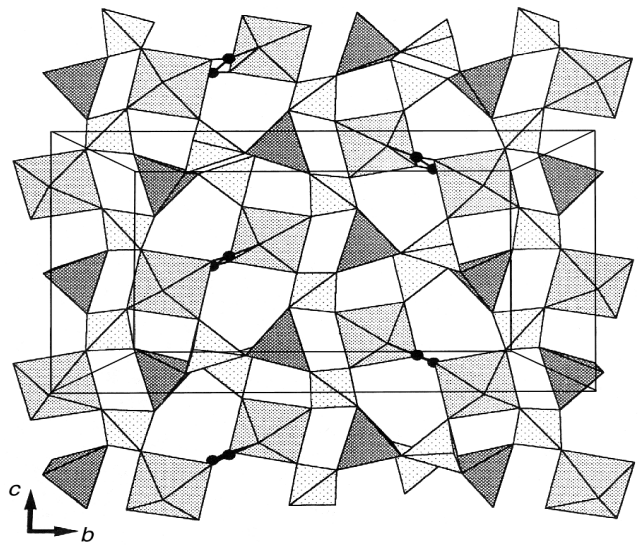

Fig. 1 Section of a sheet in **1** showing the connectivity among the Ga–O polyhedra, phosphate and oxalate anions. GaO_6 octahedra are medium grey, GaO_4 tetrahedra are dark grey and PO_4 tetrahedra are light grey. Solid circles are the carbon atoms of oxalate groups.

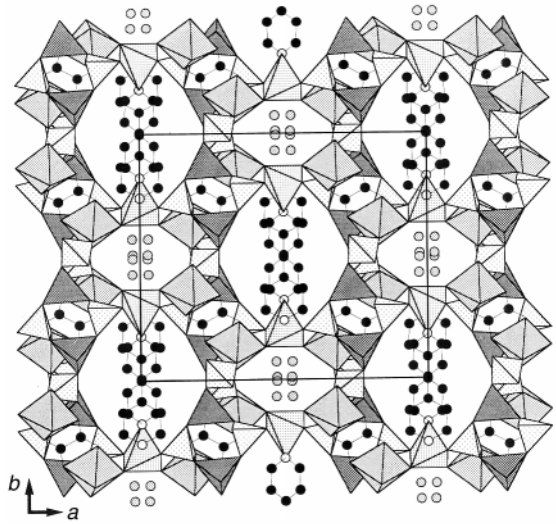

Fig. 2 Structure of **1** viewed along the [001] direction. Polyhedra with decreasing shading: GaO_4 tetrahedra, GaO_6 octahedra, GaO_4N square pyramids and PO_4 tetrahedra. Solid circles, C atoms; open circles, N atoms; stippled circles, water oxygen atoms.

The most interesting structural feature of **1** is the presence of GaO_6 octahedra, GaO_4N square pyramids and GaO_4 tetrahedra. In other microporous gallium phosphates, most frameworks are composed of some combinations of four-, five- or six-coordinate gallium atoms and PO_4 tetrahedra. $Rb_2[Ga_4(HPO_4)(PO_4)_4]\cdot 0.5H_2O$ and $GaPO_4$-14 are the other two examples in which gallium atoms have mixed four-, five- and six-coordination.[11,12] Because there is little known on solid state Ga NMR owing to intrinsic experimental difficulties,[13] it would be of great interest to investigate the correlation between the ^{71}Ga NMR of **1** and the structure. Fig. 3 shows the ^{71}Ga NMR spectrum (I = 3/2, ν = 121.84 MHz) with spinning rate of 12000 Hz and a single 45° pulse (a hard B_1 = 120 kHz is used). Chemical shifts were measured relative to the $[Ga(H_2O)_6]^{3+}$ ion in a gallium nitrate solution. Because there is a linear correlation between ^{27}Al and ^{71}Ga NMR chemical shifts in isostructural Al and Ga compounds,[14] the resonances at δ 116.4 and 94.0 correspond to tetrahedrally and octahedrally coordinated gallium, respectively. Interestingly, an additional resolved band at δ 66.8 is evident. We can compare the NMR spectrum of **1** with the ^{71}Ga MAS NMR of $[Ga_4(C_{10}H_9N_2)_2(PO_4)(H_{0.5}PO_4)_2(HPO_4)_2(H_2PO_4)_2(H_2O)_2]\cdot H_2O$ **2**,[15] where X-ray structure analysis shows only octahedral and tetrahedral gallium.Two bands at δ 94.0 and 116.4 were observed for **2**, while no band below δ 90 is evident. Therefore, we conclude that the resonance at δ 66.8 corresponds to the five-coordinate gallium (GaO_4N square pyramid). To our knowledge solid state NMR of five-coordinate gallium has not been documented previously. The splitting in the band at δ 116.4 reflects the residual line shape originated from the second order quadrupolar interaction associated with the large electric field gradient (efg) in the GaO_4 unit. By contrast, both GaO_6 and GaO_4N moieties show relatively smaller efg values. The large upfield shift for five-coordinate gallium is believed to be due to the strong shielding by directly bonded nitrogen.

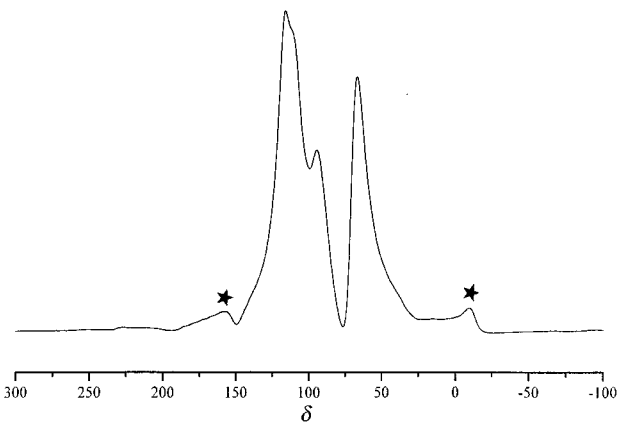

Fig. 3 ^{71}Ga MAS NMR spectrum for **1**. Asterisks denote spinning side bands.

In summary, this work illustrates that a novel gallium phosphatooxalate with a framework structure is synthesized hydrothermally and structurally characterized by single-crystal X-ray diffraction and ^{71}Ga MAS NMR spectroscopy. There is a good correspondence between the NMR spectrum and the structure.

We thank the Institute of Chemistry, Academia Sinica, National Science Council, and Chinese Petroleum Corp. for support, and Ms. F.-L. Liao and Prof. S.-L. Wang at the National Tsing Hua University for X-ray intensity data collection.

Notes and references

† X-Ray intensity data were collected on a Siemens SMART CCD diffractometer in 1271 frames with ω scans (width 0.30° and exposure time of 20 s per frame).

Crystal data for $[Ga_5(OH)_2(C_{10}H_9N_2)(C_2O_4)(PO_4)_4]\cdot 2H_2O$: monoclinic, space group $C2/c$, a = 18.3430(2), b = 15.9372(4), c = 9.1019(2) Å, β = 90.867(1)°, U = 2660.5(1) Å^3, Z = 4, M_r = 1043.74, D_c = 2.606 g cm^{-3}, μ(Mo-Kα) = 53.5 cm^{-1}, λ = 0.71073 Å, graphite monochromator, crystal dimensions 0.135 × 0.045 ×0.009 mm. Of the 2902 unique reflections collected ($2\theta_{max}$ = 56°, R_{int} = 0.0466), 2187 reflections were considered observed [$F_o > 4\sigma(F_o)$] after empirical absorption correction ($T_{min/max}$ = 0.826/0.942). Bond-valence calculations indicated that both Ga atoms are trivalent, O(11) had a valence sum of 1.24, and all other phosphate oxygens had values close to 2. The value for O(11) indicates that it is a hydroxo oxygen. The H atom was found in difference Fourier maps. Two lattice water sites, O(w1) and O(w2), were located in the structural tunnel. Both water oxygens initially showed very large thermal parameters. If the occupancy of O(w) is refined, the site occupancy factors obtained are 0.56(2) for O(w1) and 0.45(2) for O(w2), indicative of a half occupancy of the water of crystallization. The water hydrogens were not located. The 4,4′-bipyridine ligand acts as a monodentate ligand to Ga. To balance charge, the N atom which is not coordinated to Ga is protonated. The H atom which appears to be disordered over two positions, which are symmetry related by a twofold axis, is not included in the refinement. All other H atoms in 4,4′-bipyridine were located. Least-squares refinement (240 parameters) was performed with anisotropic thermal parameters for all non-hydrogen atoms and fixed isotropic thermal parameters (U = 0.05 Å^2) for all H atoms. $(\Delta\rho)_{max,min}$ = 0.79, −0.97 e Å^{-3}. The reliability factors converged to $R1$ = 0.0410, $wR2$ = 0.0921 and S = 1.072.

CCDC 182/1316. See http://www.rsc.org/suppdata/cc/1999/1473/ for crystallographic files in .cif format.

1 J. M. Thomas, *Angew. Chem., Int. Ed. Engl.*, 1994, **33**, 913.
2 A. K. Cheetham, H. Inokuchi and J. M. Thomas, *Curr. Opin. Solid State Mater. Sci.*, 1996, **1**, 55.
3 M. E. Davis, *Chem. Eur. J.*, 1997, **3**, 1745.
4 S. T. Wilson , B. M. Lock, C. A. Messina, T. R. Cannan and E. M. Flanigen, *J. Am. Chem. Soc.*, 1982, **104**, 1146.
5 R. C. Haushalter and L. A. Mundi, *Chem. Mater.*, 1992, **4**, 31.
6 G. Ferey, *C. R. Acad. Sci. Ser. C*, 1998, **1**, 1.
7 K.-H. Lii, Y.-F. Huang, V. Zima, C.-Y. Huang, H.-M. Lin, Y.-C. Jiang, F.-L. Liao and S.-L. Wang, *Chem. Mater.*, 1998, **10**, 2599.
8 O. M. Yaghi, G. Li and H. Li, *Nature*, 1995, **378**, 703.
9 H.-M. Lin, K.-H. Lii, Y.-C. Jiang and S.-L. Wang, *Chem. Mater.*, 1999, **11**, 519.
10 Y.-F. Huang and K.-H. Lii, *J. Chem. Soc., Dalton Trans.*, 1998, 4085.
11 K.-H. Lii, *Inorg. Chem.*, 1996, **35**, 7440.
12 J. B. Parise, *J. Chem. Soc., Chem. Commun.*, 1985, 606.
13 F. Fredoueil, D. Massiot, D. Poojary, M. Bujoli-Doeuff, A. Clearfield and B. Bujoli, *Chem. Commun.*, 1998, 175.
14 S. M. Bradley, R. D. Howe and R. A. Kydd, *Magn. Reson. Chem.*, 1993, **31**, 883.
15 C.-Y. Chen, P. P. Chu and K.-H. Lii, to be published.

Communication 9/03213D

Highly selective catalysts for conversion of ammonia to nitrogen in gasified biomass

Robert Burch* and Barry W. L. Southward

Catalysis Research Centre, Department of Chemistry, University of Reading, Whiteknights, Reading, UK RG6 6AD. E-mail: r.burch@reading.ac.uk

Received (in Cambridge, UK) 21st May 1999, Accepted 29th June 1999

Almost zero emissions of NO_x can be achieved in the catalytic combustion of simulated biomass mixtures containing substantial amounts of ammonia by use of a heteropolyacid catalyst.

Renewable energy sources, such as biomass, will be of increasing importance in the future as part of a strategy to lower the total emissions of CO_2. Recently, the combustion of biomass-derived gas (biogas) for combined heat and power generation has been studied.[1–3] However, conventional flame combustion processes create problems because biogas contains significant quantities of NH_3 (600–4000 ppm) in addition to fuel components (CO, H_2, CH_4) and on combustion the NH_3 is largely converted into NO_x. Catalytic combustion may overcome this problem but until now the selectivity for the conversion of NH_3 to N_2 is unsatisfactory, typically < 70%.[2,4] Here, we describe a newly discovered process for removing NH_3 from biogas with almost zero production of NO_x.

The novel solution to the selective oxidation of NH_3 in a biogas fuel which we have discovered is to differentiate the feed components on the basis of their chemical properties. The crucial discovery is that ammonia, being a basic molecule, can be differentiated from carbon monoxide and hydrogen by using a catalyst which contains acidic sites, to preferentially adsorb the ammonia. Combination with redox sites allows the selective oxidation of ammonia to nitrogen.

The catalyst selected was 12-tungstophosphoric acid, $H_3PW_{12}O_{40}$ (ex Acros, hereafter denoted HPW). It is a heteropoly acid material based upon the Keggin unit structure.[5] Such materials are well known for their strong and uniform acid sites arising from the charge balancing protons associated with the Keggin unit anion. In addition they also possess strong redox properties arising from surface and bulk electron transfer processes.[5]

Catalyst testing was performed in a standard quartz flow microreactor described previously[6] at a gas hourly space velocity (volume of reactants per volume of catalyst per hour) of 250 000 h^{-1}. The reaction mixture comprised 6.0% CO, 4.0% H_2, 0.5% O_2, 1050 ppm NH_3, and balance He. Product analysis was by mass spectrometry (Hiden DSMS) with NO_x emissions and residual NH_3 levels being confirmed using an external NH_3 oxidation reactor (with independent oxygen supply) coupled with a NO_x chemiluminescence detector (Signal series 4000). The partial salts of HPW were prepared by reflux of the parent acid with varying stoichiometries of KNO_3 (Analar ex Aldrich) to produce $K_{2.06}H_{0.94}PW_{12}O_{40}$ (hereafter KHPW) and $K_{2.66}H_{0.34}PW_{12}O_{40}$ (hereafter KPW) using a standard exchange process.[5] Temperature-programmed desorption of NH_3 was performed by saturation of the sample at 150 °C in 1% NH_3–He followed by purging in He. The sample was then ramped at 12 °C min^{-1} and the evolved species monitored by mass spectrometry.

Fig. 1 illustrates the NH_3 TPD profile of HPW. The strong and uniform acidity of the material is demonstrated by the single, sharp combination of desorption peaks at *ca.* 600 °C. These comprise H_2O, NH_3, N_2 and NO, the latter at two orders of magnitude lower concentration. This was a significant result since it demonstrated that NH_3 may be fixed on the Brønsted

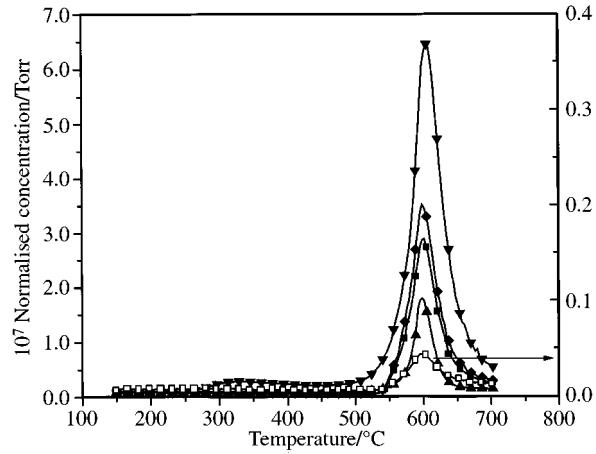

Fig. 1 NH_3 TPD results for HPW. Key: (□) NO (*m/z*) 30, (▲) N_2 (*m/z* 28), (▼) H_2O (*m/z* 18), (◆) NH_3 (*m/z* 17, corrected for H_2O contribution), (■) NH_3 (*m/z* 16).

acid sites of HPW and then converted into N_2 and H_2O by an internal reaction with labile oxygen from the Keggin anion. This reaction is presumed to proceed *via* the condensation of NO with NH_3, a proposal which is supported by temperature programmed reaction of a NO–CO–H_2 mix (1050 ppm 6.0%:4.0%) over NH_3 pretreated HPW. This yielded N_2 as the only product with peak N_2 production occurring at *ca.* 600 °C, the dissociation temperature of the NH_4–Keggin unit complex.[7] The amount of N_2 produced was consistent with a catalytic reaction between the NO and NH_3.

Fig. 2 shows the reaction of HPW pre-treated with NH_3 and then heated in the full reaction mixture. The results show that this material displays little or no catalytic function at temperatures below the NH_4^+ dissociation temperature. However, simultaneous with the onset of NH_4^+ dissociation there is a

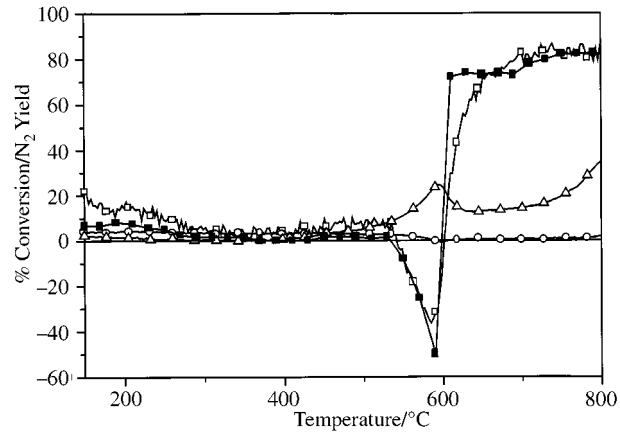

Fig. 2 Conversion profiles for simulated biomass stream over HPW. (6.0% CO, 4.0% H_2, 0.5% O_2, 1050 ppm NH_3 balance He). Key: (□) NH_3 conversion by MS (△) H_2 conversion by MS, (○) CO conversion by MS, (■) % N_2 yield by NO_x chemiluminescence.

sharp evolution of NO_x, as reflected in the negative N_2 production.

After this initial burst of NO_x, the catalyst then becomes active and highly selective for N_2 production, giving *ca.* 85% conversion of NH_3 and 100% selectivity to N_2. There is no measurable production of NO, NO_2, N_2O or HCN, and the nitrogen mass balance from both the mass spectrometry and NO_x analysis is 100% within experimental error. At the same time as we observe this very high conversion of ammonia, we see that the conversion of CO is $< 1\%$ and there is $< 20\%$ conversion of H_2 in the temperature range 600–750 °C.

These data for ammonia oxidation are consistent with an 'internal selective catalytic reduction' mechanism which can be summarised as follows. The Keggin unit oxidises the adsorbed NH_3 (trapped as NH_4^+) to NO_x using labile oxygen from the anion. The NO_x formed is retained briefly as part of the anion, and reacts with an NH_3 molecule to give N_2 and H_2O. The Keggin unit then re-oxidises by reaction with gas phase oxygen. This last step further accounts for the high chemical specificity of the process as it limits the concentration of active oxygen to react with CO and/or H_2. The rapid turnover between the proton and NH_4^+ states also prevents over reduction and collapse of the Keggin unit through dehydration,[8] with the result that the HPW is stable over the course of 6 h.

The requirement for protonic sites for the reaction was confirmed by the synthesis and testing of full and partial salts. The results in Fig. 3 show that, in comparison with the parent acid, KHPW displays a smaller NO_x formation (negative) peak and a lower activity, which increases gradually with temperature. KPW shows no negative NO_x peak and then an increasing level of N_2 production with temperature. For both the full and partial salts (KPW and KHPW) the activity for ammonia conversion to N_2 is much lower than for the HPA over most of the temperature range from 600–800 °C. The lower activity at *ca.* 600 °C is consistent with the requirement for acid sites to adsorb NH_3.

In conclusion, we have developed a strategy for the selective conversion of NH_3 from biomass-derived gases into N_2 by selective oxidation in competition with a large excess of CO and H_2. The key feature is the use of a catalyst which contains acid sites, to differentiate ammonia from CO and H_2, and redox properties, to oxidise the adsorbed species. Heteropoly acid catalysts have been used to demonstrate that the concept is viable and provides a novel way to overcome the NO_x formation associated with the direct combustion of biogas.

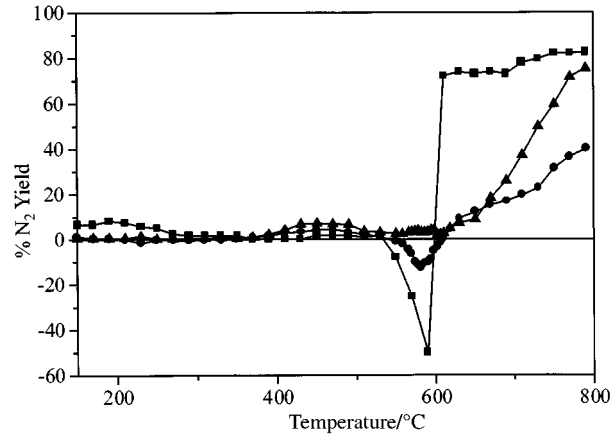

Fig. 3 N_2 production profiles for HPW and its salts. (6.0% CO, 4.0% H_2, 0.5% O_2, 1050 ppm NH_3 balance He). Key: (■) HPW ($H_3PW_{12}O_{40}$), (●) KHPW ($K_{2.06}H_{0.94}PW_{12}O_{40}$), (▲) KPW ($K_{2.66}H_{0.34}PW_{12}O_{40}$).

We are pleased to acknowledge the financial support of Alstom, DTI, and EPSRC through the FORESIGHT Challenge initiative. Helpful discussions with colleagues at Reading (Mr Matthieu Amblard), Cranfield University (Mr J. J. Witton, Professor B. Moss, Mr J. M. Przybylski, and Dr E. Noordally) and at Alstom (Mr M. Cannon) are gratefully acknowledged.

References

1 M. F. M. Zwinkels, G. M. Eloise Heginuz, B. H. Gregertsen, K. Sjöström and S. G. Järås, *Appl. Catal. A*, 1997, **148**, 325.
2 L. Lietti, C. Groppi, and C. Ramella, *Catal. Lett.*, 1998, **53**, 91.
3 *Development of Improved Stable Catalysts and Trace Element Capture for Hot Gas Cleaning*, DTI/ETSU/Clean Coal Power Generation Group, Project Profile 178, 1996.
4 E. M. Johansson, S. G. Jaras, *Catal. Today*, 1996, **47**, 359.
5 T. Okuhara, N. Mizuno and M. Misono, *Adv. Catal.*, 1996, **41**, 113.
6 M. Amblard, R. Burch and B. W. L. Southward, *Appl. Catal. B*, in press.
7 M. Amblard, R. Burch and B. W. L. Southward, *Clean Catalytic Combustion of Nitrogen-Bearing Biomass*, 4th International Workshop on Catalytic Combustion, San Diego, 1999.
8 B. W. L. Southward, J. Vaughan and C. T. O'Connor, *J. Catal.*, 1995, **153**, 293.

Communication 9/04088I

[$PdCl_2$($dppfO_2$-*O*,*O*′)]: a simple palladium(II) complex with a rare tetrahedral structure

Jeremy S. L. Yeo, Jagadese J. Vittal and T. S. Andy Hor*

Department of Chemistry, National University of Singapore, 3 Science Drive 3, Singapore 117543. E-mail: chmandyh@nus.edu.sg

Received (in Cambridge, UK) 19th May 1999, Accepted 1st June 1999

Single-crystal X-ray diffraction analysis of $PdCl_2$($dppfO_2$) [$dppfO_2$ = 1,1′-bis(oxodiphenylphosphoranyl)ferrocene] shows a rare tetrahedral geometry at a d^8 metal centre; physical and spectroscopic characterisations indicate a paramagnetic species.

The coordination and catalytic chemistry of 1,1′-bis(diphenylphosphino)ferrocene (dppf) has been reviewed.[1] There are ample examples in the recent literature that demonstrate the significance of this diphosphine ligand.[2] Like other phosphines, it can be readily oxidised to its mono- and di-oxide forms.[3] The structure of the latter, 1,1′-bis(oxodiphenylphosphoranyl)ferrocene ($dppfO_2$) is of interest to a number of groups, notably those of Hor,[3b] Pilloni,[3c] Postel[3d] and Hashmi.[3e] Phosphine oxides in general have attracted attention in view of their weak coordinating ability[4] and their function as co-catalysts,[5] crystallisation aids,[6] *etc*. The chemistry of Ph_3PO, the most familiar phosphine oxide, is well established.[4] The coordination ability of some diphosphine oxides[7] is also known, although less so for $dppfO_2$.[3] Our interest in Pd^{II}–dppf chemistry stems from the rich catalytic activities shown by many dppf complexes of Pd(II).[2b–h] Some of these complexes are susceptible to oxidation in solution and the decomposition product is generally assumed to be chiefly free $dppfO_2$.[3a] There is hitherto no report on the coordination chemistry of $dppfO_2$ with Pd(II) although such complexes with other diphosphine oxides are known.[7] Herein, we report the isolation of a simple Pd(II)–$dppfO_2$ complex with a rare mononuclear tetrahedral Pd(II) centre which, to our knowledge, has not been reported in the literature. It is well known that d^8 platinum metals overwhelmingly favour square planar structures and only Ni(II) forms a significant number of tetrahedral complexes.

Addition of $dppfO_2$ to [$PdCl_2(MeCN)_2$] in CH_2Cl_2 gives [$PdCl_2$($dppfO_2$-*O*,*O*′)] **1** in 81% yield.† This complex was originally obtained as a by-product in the reaction of [$Pd_2(dppf)_2(\mu\text{-}S)_2$] with COS. Its isolation contrasts with an earlier unsuccessful attempt to crystallise a palladium-containing triphenylphosphine oxide complex.[8] The IR spectrum of **1** (CH_2Cl_2) exhibits two strong ν(P–O) peaks at 1260 and 1269 cm^{-1}. The ^{31}P NMR spectrum in CD_2Cl_2[9] shows a broad peak at δ 34.0 and a minor resonance at δ 47.2, tentatively assigned to [$PdCl_2$(μ-$dppfO_2$)]$_2$. Upon standing for a week, this solution decomposes readily to give predominantly free $dppfO_2$ (δ 28.2). The electronic spectrum shows two bands at 20 264 [$^3T_1(F) \rightarrow {}^3A_2(F)$] and 26 900 cm^{-1} [$^3T_1(F) \rightarrow {}^3T_1(P)$], similar to that of a typical tetrahedral nickel(II) complex.[10] The magnetic moment[11] (2.48 μ_B) is lower than that of a typical Ni(II) tetrahedral complex (*ca.* 3.2 μ_B) but still consistent with paramagnetic Pd(II) with two unpaired electrons. The cyclic voltammogram shows a reversible one-electron couple with $E_{1/2}$ = 0.410 V (*vs.* [$FeCp_2$]$^+$–[$FeCp_2$]). Similar behaviour has been reported for $PdCl_2$(dppf) (0.430 V)[2a] and $dppfO_2$ (0.573 V).[3a] The remote possibility of an internal electron transfer that generates Pd(I) and Fe(III) is thereby eliminated. Similar observations were reported for some Cu(II)–$dppfO_2$ complexes[3f] and point to an oxygen-donating $dppfO_2$ ligand coordinated to a paramagnetic Pd(II) centre. The rarity of the postulated structure merited a crystallographic analysis.‡ This confirmed a mononuclear neutral complex with a chelating $dppfO_2$ and two terminal chlorides (Fig. 1). The near-ideal tetrahedral geometry at the Pd(II) centre is exemplified by the large intra- and inter-ligand angles [O1–Pd1–O2, Cl1–Pd1–Cl2 and O–Pd–Cl angles of 104.3(3), 120.4(2) and 107.8° (av.), respectively]. The dihedral angle between the {PdO_2} and {$PdCl_2$} planes (84.2°) also reflects a tetrahedral rather than a 'distorted square-planar' description. O-donation leads to lengthening of the P–O bonds (av. 1.512 Å) compared to those in $dppfO_2$ (1.495 Å[3]). This is also consistent with a stronger P–C (C_5 plane) bond (av. P–C 1.772 Å) compared to those in [$PdCl_2$(dppf)] (av. P–C 1.804 Å[2d]). There is little geometric distortion of the ferrocenyl C_5, moieties, the C_5 rings being planar with tilts of 3.6(7)° and torsional twist of < 2° (close to mirror symmetry). C1–P1 and C6–P2 deviate slightly from the mean plane by +0.12 and +0.008°, respectively.

The analogous $NiCl_2$($dppfO_2$) complex can be obtained only in poor yields from $NiCl_2 \cdot 6H_2O$ and $dppfO_2$ in propan-2-ol at room temperature or under reflux. Attempts to synthesise the platinum analogue have been unsuccessful. This is not surprising in view of the even stronger preference of Pt(II) for square planar coordination. The tetrahedral geometry of **1** is probably imposed by the large bite angle as a consequence of the sterically demanding chelating ring in $dppfO_2$. Its isolation demonstrates, for the first time, that tetrahedral Pd(II) is sustainable even in a mononuclear structure in which the metal centre is not constrained by neighbouring metal moieties.

[$PdCl_2$(dppf)] is probably the most well known dppf complex and finds extensive uses in catalysis (*e.g.* Grignard synthesis,[2b–d] hydrodehalogenation,[2f] *etc*.). Although this catalyst has demonstrated superior activity in many situations,[2d,e] in certain cases, its effectiveness is poor[2b,c] and reasons for this are

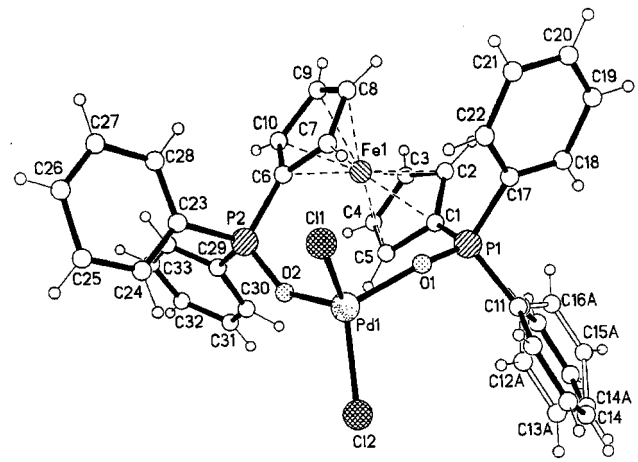

Fig. 1 Molecular structure of [$PdCl_2$($dppfO_2$-*O*,*O*′)]. Selected bond lengths (Å) and angles (°): Pd(1)–O(1) 1.974(8), Pd(1)–O(2) 1.968(7), Pd(1)–Cl(1) 2.222(4), Pd(1)–Cl(2) 2.204(3), P(1)–O(1) 1.495(9), P(2)–O(2) 1.529(6), P(1)–C(1) 1.780(9), P(1)–C(11) 1.781(10), P(1)–C(17) 1.781(9), P(2)–C(6) 1.764(11), P(2)–C(23) 1.785(13), P(2)–C(29) 1.791(10), O(1)–Pd(1)–O(2) 104.3(3), Cl(1)–Pd(1)–Cl(2) 120.4(2), O(1)–Pd(1)–Cl(1) 100.2(3), O(1)–Pd(1)–Cl(2) 112.7(3), O(2)–Pd(1)–Cl(1) 110.8(3), O(2)–Pd(1)–Cl(2) 107.3(2), P(1)–O(1)–Pd(1) 158.3(6), P92)–O(2)–Pd(1) 139.9(5).

presently not well understood. It is commonly accepted that $PdCl_2$(dppf) loses its catalytic efficiency after losing its phosphine ligand (in the form of $dppfO_2$) *via* $PdCl_2(dppfO_2)$. Isolation of **1** and its reasonable stability suggested that the current perception is not necessarily correct. The loss of activity rather may be linked to the geometric changes for Pd(II) upon oxidation of its dppf ligand. For example, we have recently demonstrated that C–C coupling and hydride transfer[2g,h] occur very efficiently on a planar Pd(II) core. Oxidative addition of tetrahedral Pd(0) gives a Pd(II) intermediate which must be geometrically rigid[12] for effective reductive elimination to occur. Loss of such rigidity could adversely affect the catalytic efficiency. Oxidation of the phosphine ligand also leads to a change in bite angle which would have an effect on catalytic activities.[13]

The authors acknowledge the National University of Singapore (NUS) for support (Grant RP 960664/A). We thank G. K. Tan for assistance in X-ray analysis, Y. P. Leong for assistance in the preparation of this manuscript and the technical staff of the department for professional support. Discussions with Y. K. Yan and Z. H. Loh are much appreciated. We thank the reviewers for some constructive feedback.

Notes and references

† *Synthesis* of [$PdCl_2$($dppfO_2$-*O*,*O*′)]: addition of $dppfO_2$ (0.074 g, 0.126 mmol) to a CH_2Cl_2 solution (40 cm^3) of [$PdCl_2(MeCN)_2$] (0.032 g, 0.125 mmol) resulted in a brown suspension that was stirred for 12 h. Filtration and concentration gave an orange solution. Layering of hexane on this solution gave red crystals of **1**, which were collected and washed with hexane and Et_2O (yield 81%). Found: C, 53.42; H, 4.02; Cl, 10.17. Calc. for $C_{34}H_{28}Cl_2O_2P_2FePd$: C, 53.47; H, 3.70; Cl, 9.28%.

‡ *Crystallographic data*: $C_{34}H_{28}Cl_2FeO_2P_2Pd$ **1**: M = 763.65, crystal dimensions: 0.33 × 0.18 × 0.13 mm, monoclinic, space group *Cc* (no. 9), a = 10.0444(2), b = 19.4070(3), c = 16.3157(1) Å, β = 91.340(2), V = 3179.58(8) $Å^3$, Z = 4, μ(Mo-Kα) = 1.321 mm^{-1}. 7985 reflections measured, 4010 unique (R_{int} = 0.0297), final $R1$ and $wR2$ values 0.0679 and 0.2104 for 3799 independent reflections [$I \geqslant 2\sigma(I)$] and 344 parameters. The data collection was performed at 295 K on a Bruker SMART CCD area-detector by the ω-scan method, within the limits $2.1 \leqslant \theta \leqslant 25.0°$. The data were corrected for absorption using an empirical method (SADABS[14a]) and the structure was solved by direct methods and refined by full-matrix least squares (SHELXTL[14b]). One of the phenyl rings (C11–C16) attached to P(1) was found to be disordered. Two disorder models (occupancies 0.7/0.3) were included in the least-squares refinements. Individual isotropic thermal parameters were refined for the major disorder component and common isotropic thermal parameter was refined for the other ring. Both the rings were treated as regular hexagons. Riding models were used to place all the hydrogen atoms in their idealized positions. CCDC 182/1307. See http://www.rsc.org.suppdata/cc/1999/1477/ for crystallographic data in .cif format.

1 K.-S. Gan and T. S. A. Hor, in *Ferrocenes—Homogeneous Catalysis, Organic Synthesis, Materials Science*, ed. A. Togni and T. Hayashi, 1995, ch. 1, p. 3; S.-W. A. Fong and T. S. A. Hor, *J. Cluster Sci*., 1998, **9**, 351.

2 (*a*) B. Corain, B. Longato, G. Favero, D. Ajò, G. Pilloni, U. Russo and F. R. Kreissl, *Inorg. Chim. Acta*, 1989, **157**, 259; (*b*) T. Kobayashi, T. Sakakura and M. Tanaka, *Tetrahedron Lett.*, 1985, **26**, 3463; (*c*) J. F. Hartwig, *Angew. Chem., Int. Ed.*, 1998, **37**, 2090; (*d*) T. Hayashi, M. Konishi, Y. Kobori, M. Kumada, T. Higuchi and K. Hirotsu, *J. Am. Chem. Soc.*, 1984, **106**, 158; (*e*) L. Schmitz, M. Rehahn and M. Ballauff, *Polymer*, 1993, **34**, 646; (*f*) B. Wei, S. H. Li, H. K. Lee and T. S. A. Hor, *J. Mol. Catal. A: Chem.*, 1997, **126**, L83; (*g*) Y. Xie, B.-M. Wu, F. Xue, S.-C. Ng, T. C. W. Mak and T. S. A. Hor, *Organometallics*, 1998, **17**, 3988; (*h*) Y. Xie, G. K. Tan, Y. K. Yan, J. J. Vittal, S.-C. Ng and T. S. A. Hor, *J. Chem. Soc., Dalton Trans.*, 1999, 773.

3 (*a*) G. Pilloni, B. Longato and B. Corain, *J. Organomet. Chem.*, 1991, **420**, 57; (*b*) Z.-G. Fang, T. S. A. Hor, Y.-S. Wen, L.-K. Liu and T. C. W. Mak, *Polyhedron*, 1997, **16**, 377; (*c*) G. Pilloni, B. Corain, M. Degano, B. Longato and G. Zanotti, *J. Chem. Soc., Dalton Trans*., 1993, 1777; (*d*) V. Munyejabo, M. Postel, J. L. Roustan and C. Bensimon, *Acta Crystallogr., Sect C.*, 1994, **50**, 224; (*e*) M. Bolte, F. Naumann and A. S. K. Hashmi, *Acta Crystallogr., Sect C.*, 1997, **53**, 178; (*f*) G. Pilloni, G. Valle, C. Corvaja, B. Longato and B. Corain, *Inorg. Chem.*, 1995, **34**, 5910.

4 (*a*) N. Burford, *Coord. Chem. Rev.*, 1992, **112**, 1 and references within; (*b*) C.-M. Che, T.-F. Lai, W.-C. Chung, W. P. Schaefer and H. B. Gray, *Inorg. Chem.*, 1987, **26**, 3907.

5 D. C. Billington, I. M. Helps, P. L. Pauson, W. Thomson and D. Willison, *J. Organomet. Chem.*, 1988, **354**, 233.

6 W. J. Evans, J. W. Grate and R. J. Doedens, *J. Am. Chem. Soc.*, 1985, **107**, 1671.

7 T. C. Blagborough, R. Davis and P. Ivison, *J. Organomet. Chem.*, 1994, **467**, 85; A. Bader and E. Lindner, *Coord. Chem. Rev.*, 1991, **108**, 27; R. J. Coyle, Y. L. Slovokhotov, M. Y. Antipin and V. V. Grushin, *Polyhedron*, 1998, **18**, 3059.

8 A. L. Spek, *Acta Crystallogr., Sect C.*, 1987, **43**, 1233.

9 Brüker AMX 500 spectrometer at 202.46 MHz; chemical shifts are externally referenced to 85% H_3PO_4.

10 N. N. Greenwood and A. Earnshaw, *Chemistry of the Elements*, Pergamon Press, New York, 1984, ch. 27, p. 1345.

11 Magnetic measurements were obtained on a Johnson Matthey MKII magnetic susceptibility balance. Observed magnetic susceptibility values were corrected for diamagnetism using Pascal's constants (B. N. Figgis and J. Lewis, *The Magnetochemistry of Complex Compounds*, in *Modern Coordination Chemistry*, ed. J. Lewis and R. G. Wilkins, Interscience, New York, 1960, ch. 6, p. 400) except for the diamagnetic contribution of $dppfO_2$ which is determined experimentally as -240×10^{-6} cm^3 mol^{-1}.

12 Geometric rigidity enables the *cis* ligands to be in close proximity and their labilisation under the influence of the *trans* ligands.

13 B. C. Hamann and J. F. Hartwig, *J. Am. Chem. Soc.*, 1998, **120**, 3694.

14 (*a*) SMART & SAINT Software Reference Manuals, version 4.0, Siemens Energy & Automation, Inc., Analytical Instrumentation, Madison, WI, 1996; (*b*) G. M. Sheldrick, *SADABS*, a software for empirical absorption correction, University of Göttingen, 1993.

Communication 9/04016A

$Mn^{II}(N_3)_2$(pyrazine). A 2-D layered structure consisting of ferromagnetically coupled 1-D $\{Mn(\mu\text{-}1,1\text{-}N_3)_2\}_n$ chains

Jamie L. Manson, Atta M. Arif and Joel S. Miller*

Department of Chemistry, University of Utah, 315 S. 1400 E., Salt Lake City, UT 84112-0850, USA. E-mail: jsmiller@chemistry.utah.edu

Received (in Bloomington, IN, USA) 20th April 1999, Accepted 21st June 1999

$Mn(N_3)_2$(pyz) (pyz = pyrazine) consists of ferromagnetically coupled linear chains of $\{Mn(N_3)_2\}_n$ comprised of μ-1,1-azido bridges together with μ-pyz ligands to afford 2-D planar layers.

In the last decade several families of molecule-based magnets have emerged,[1] including examples that exhibit ordering temperatures, T_c, in excess of 300 K.[2,3] For the latter high-T_c materials, both diamagnetic (cyanide) and paramagnetic ligands (tetracyanoethylene, TCNE) have been used to organize transition metal centers into 3-D networks. To better interpret magnetic properties of complex 3-D solids, reduced-dimensional structures, *i.e.* 1- and 2-D, are preferred to develop the necessary theoretical models. Recently, we have exploited the coordination chemistry of the dicyanamide ligand, $[N(CN)_2]^-$, which has produced a rich variety of polymeric architectures[4] with T_c values as high as 47 K.[5]

The azido ligand, N_3^-, unlike cyanide can bond two metal ions symmetrically either μ-1,1 through a terminal nitrogen which typically couple spins ferromagnetically, or μ-1,3 through both terminal nitrogens which couple spins antiferromagnetically.[6] Several monomeric,[7] dimeric[8] and polymeric[9] species typically with combinations of azido and pyridine-type ligands have been utilized to assemble a plethora of framework structures. $NMe_4[Mn(N_3)_3]$ is the only material where the metal coordination sphere contains only 1,3-N_3^- bridging ligands,[9a] while the others possess μ-1,3- or a mixture of μ-1,1- and μ-1,3-azido linkages, *i.e.* there are no characterized examples of polymeric solids that consist solely of μ-1,1-N_3^- bridging units. Hence, expecting ferromagnetic coupling, we sought to synthesize and structurally and magnetically characterize the first such example. Herein, we report the crystal structure and magnetic properties of $Mn^{II}(N_3)_2$(pyz), **1** (pyz = pyrazine).

The reaction of $MnCl_2$, NaN_3 and pyrazine in aqueous media leads to the formation of yellow plates of $Mn(N_3)_2$(pyz)† suitable for single crystal X-ray diffraction.‡ Each Mn^{II} ion is octahedrally coordinated to four different N_3^- ligands and two axial pyrazine ligands. In turn, each N_3^- ligand is μ-1,1-bound to two Mn^{II} metal centers. The MnN_6 octahedron is markedly distorted, with Mn–N_{azido} distances ranging from 2.198(12) to 2.270(14) Å (averaging 2.235 Å) and two equivalent Mn–N_{pyz} distances of 2.299(4) Å while *cis*-N–Mn–N angles range from 80.1(4) to 101.2(5)°. The Mn^{II}–N bond distances found for the MnN_4 equatorial plane are typical of azide coordination while the longer Mn–N_{pyz} distances are similar to those found in $Mn[N(CN)_2]_2$(pyz).[4b] The N–N distances of the azido ligand range from 1.091(18) to 1.248(17) Å (averaging 1.170 Å) and reflects typical double bond character, and as such, N(1)–N(2)–N(3) and N(4)–N(5)–N(6) bond angles are 178.5(14) and 179.4(13)°, respectively. Interestingly, the azide ligands do not reside within the Mn–N–Mn–N plane but form angles of 19.2(8) and 15.4(7)°. The solid consists of 1-D $\{Mn(N_3)_2\}_n$ linear chains linked *via* μ-pyz ligands to afford an extended 2-D layered network, Fig. 1, with intranetwork Mn···Mn separations of 3.412 (*via* azide) and 7.385 Å (*via* pyz) while the shortest internetwork Mn···Mn separation is 8.412 Å.

The magnetic susceptibility of **1** was measured between 2 and 300 K in a 1 kOe dc field upon warming. Above 10 K the data can be least-squares fit to the Curie-Weiss expression, $\chi \propto g/(T - \theta)$, with $g = 2.037(1)$ and $\theta = 5.51(3)$ K, Fig. 2, indicative of ferromagnetic coupling between the Mn^{II} metal sites joined *via* the μ-1,1-N_3^- ligands. The Lande-g value is in good agreement with the literature.[9c] χT has a value of 4.63 emu K mol^{-1} at 300 K, slightly larger than the expected value (4.38 emu K mol^{-1}) for isolated $S = 5/2$ Mn^{II} ions and due to ferromagnetic coupling increases gradually upon cooling to *ca.* 50 K. Below this temperature, χT increases to a maximum value of 9.7 emu K mol^{-1} at 5 K due to rapidly increasing ferromagnetic correlations between adjacent spin carriers. Upon cooling to 2 K, χT decreases quickly due to interchain antiferromagnetic interactions through the bridging pyrazine ligands. To determine the exchange parameters *via* each bridge type, χT was fit to the $S = 5/2$ Fisher chain model, $\chi_{1\text{-}D}$,[10] [eqn. (1)] in conjunction with an additional mean-field correction term, χ_{MF}, [eqn. (2)] assuming $z = 2$,[11] where N is Avogadro's number, μ_B is the Bohr magneton, k_B is the Boltzmann constant and z is the number of nearest neighbours. The best least squares fit parameters gave $g = 2.037(3)$, $J/k_B = 0.61(4)$ K, and J'/k_B

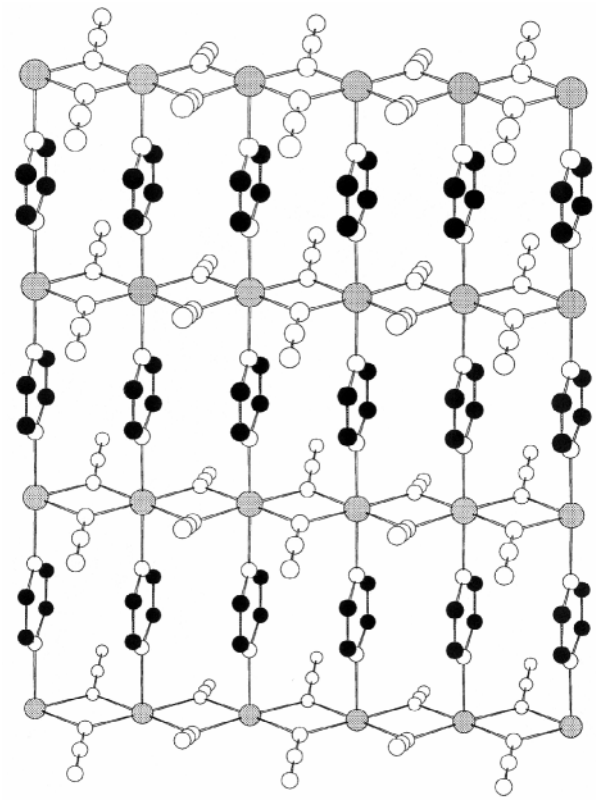

Fig. 1 Crystal structure of $Mn(N_3)_2$(pyz) showing a single 2-D layer. The shaded, open and filled spheres represent Mn, N and C, respectively. Hydrogen atoms have been omitted for clarity.

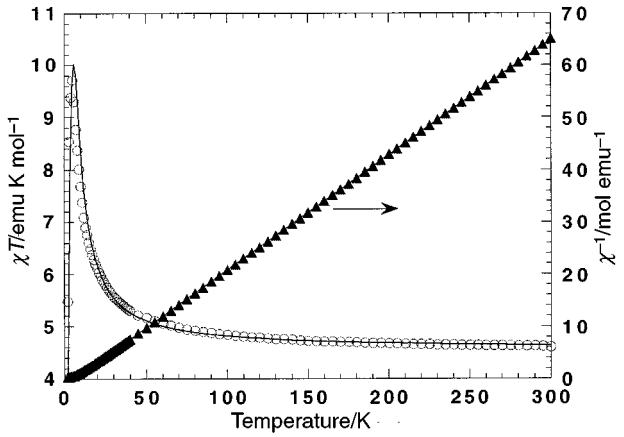

Fig. 2 Temperature-dependence of χT (○) and the reciprocal molar magnetic susceptibility, χ^{-1} (▲) for $Mn(N_3)_2(pyz)$. The heavy line denotes the theoretical fit of the data to eqn. (1) and (2).

$= -0.24(3)$ K for ferro- and antiferro-magnetic interactions *via* the azide and pyrazine ligands, respectively.

$$\chi_{1-D} = \frac{Ng^2\mu_B{}^2S(S+1)}{3k_BT} \bullet \frac{1+u(K)}{1-u(K)};$$

$$\text{where } u(K) = \coth K - 1/K \text{ and } K = \frac{2JS(S+1)}{k_BT} \qquad (1)$$

$$\chi_{MF} = \frac{\chi_{1-D}}{[1-\chi_{1-D}(2zJ'/Ng^2\mu_B{}^2)]} \qquad (2)$$

Weak ferromagnetic coupling is anticipated when the Mn–N–Mn bridge angles are appreciably less than 103–104°.[12] These angles are 97.9(5) and 101.2(5)° for **1** and hence suggest ferromagnetic coupling. Bridge angles approaching 105° give rise to strong ferromagnetic coupling due to accidental orthogonality of the magnetic d_{yz} orbital as shown by EHMO (extended Huckel molecular orbital) calculations.[13] By comparison, Mn–N–Mn angles of 104.6 and 101.0°, respectively, lead to J/k_B = 3.5 K for the dinuclear complex $(N_3)_2[Mn(terpy)_2]_2(X)_2$ (terpy = 2,2′:6′,2″-terpyridine; X = ClO_4^-, PF_6^-)[14] and 13.8 K for the alternating chain compound $[Mn(bipy)(N_3)_2]_n$.[13] A significantly reduced angle of 84.2° was reported for 2-D $[Ni(N_3)_2(tmeda)]_n$ (tmeda = *N*,*N*,*N*′,*N*′-tetramethylethylenediamine) which yielded antiferromagnetic exchange (−9.9 K) *via* the μ-1,1-N_3^- bridge.[15]

A broad maximum indicative of short-range antiferromagnetic ordering was observed at 2.7 K using low field $M(T)$ ($H_{dc} \leq 50$ Oe) and ac susceptibility measurements. For low dimensional solids, the actual ordering temperature lies below the maximum as elucidated by Fisher[10] from plots of $d\chi T/dT$, and for $Mn(N_3)_2(pyz)$, $T_N \approx 2$ K. Specific heat measurements are better suited to unambiguously identify T_N and are in progress. According to ac susceptibility, $\chi''(T)$ is frequency independent suggesting a non-glassy ground state. A shallow minimum at 3 K was observed in $\chi''(T)$, with the onset of spontaneous magnetization near 2 K and suggests the presence of a weak ferromagnetic ground state.

Isothermal magnetization experiments performed at 2 K show behavior typical of a soft ferromagnet as coercivity was not observed. Below *ca*. 6 kOe, the magnetization rises rapidly where a decrease in slope occurs, reaching a saturation magnetization, M_s, of 23530 emu Oe mol^{-1} at 50 kOe. This value is comparable, although slightly reduced, to the expected value of 27925 emu Oe mol^{-1} for isolated S = 5/2 ions.

The authors gratefully acknowledge the ACS-PRF (Grant #30722-AC5) and the U.S. Department of Energy (Grant #DE-FG03-93ER45504) for support of this work.

Notes and references

† A 3 mL aqueous solution of $MnCl_2{\cdot}4H_2O$ (1.6 mmol, 0.3169 g) was mixed with a H_2O solution (3 mL) containing NaN_3 (3.2 mmol, 0.2080 g) and pyrazine (1.6 mmol, 0.1281 g) affording small plate-like crystals suitable for X-ray diffraction. IR (Nujol, cm^{-1}): ν_s(azido) = 2098s, 2049m and ν_{as}(azido) = 1328m.

‡ *Crystal data* for $C_4H_4MnN_8$: M = 219.09, monoclinic *Cc*, a = 16.3458(17), b = 7.3848(5), c = 6.8236(7), β = 112.032 (4)°, U = 763.53(12) Å^3, Z = 4, D_c = 1.906 Mg m^{-3}, μ(Mo-Kα) = 1.690 mm^{-1}, T = 200.0 (1) K. The data were collected on an Enraf-Nonius KappaCCD diffractometer. Of 1230 data ($8 < 2\theta < 62°$), 928 were observed [$I > 2\sigma(I)$]. The structure was solved by direct methods using SIR97 and refined with SHELXL-97. All nonhydrogen atoms were refined anisotropically, while all hydrogen atoms were located but not refined, $R(F)$ = 0.0625, $R(wF)$ = 0.1659, and GOF = 1.038. CCDC reference number 182/1298. See http://www.rsc.org/suppdata/cc/1999/1479/ for crystallographic files in .cif format.

References

1 See, for example C. Mathonière, C. J. Nuttall, S. G. Carling and P. Day, *Inorg. Chem*., 1996, **35**, 1201; S. P. Sellers, B. J. Korte, J. P. Fitzgerald, W. M. Reiff and G. T. Yee, *J. Am. Chem. Soc*., 1998, **120**, 4662; K. Inoue, T. Hayamizu, H. Iwamura, D. Hashizume and Y. Ohashi, *J. Am. Chem. Soc*., 1996, **118**, 1803; H. Stumpf, L. Ouahab, Y. Pei, D. Grandjean and O. Kahn, *Science*, 1993, **261**, 447; F. Lloret, M. Julve, R. Ruiz, Y. Journaux, K. Nakatani, O. Kahn and J. Sletten, *Inorg. Chem*. 1993, **32**, 27.

2 S. Ferlay, T. Mallah, R. Ouahes, P. Veillet and M. Verdaguer, *Nature*, 1995, **378**, 701; Ø. Hatlevik, W. E. Buschmann, J. Zhang, J. L. Manson, M. Verdaguer and J. S. Miller, *Adv. Mater.*, 1999, **11**, in press.

3 J. M. Manriquez, G. T. Yee, R. S. McLean, A. J. Epstein and J. S. Miller, *Science*, 1991, **252**, 1415.

4 (*a*) J. L. Manson, C. Kmety, Q. Huang, J. Lynn, G. Bendele, S. Pagola, P. W. Stephens, A. J. Epstein and J. S. Miller, *Chem. Mater*., 1998, **10**, 2552; (*b*) J. L. Manson, C. D. Incarvito, A. L. Rheingold and J. S. Miller, *J. Chem. Soc., Dalton Trans*., 1998, 3705; (*c*) J. L. Manson, A. M. Arif and J. S. Miller, *J. Mater. Chem*., 1999, **9**, 979; (*d*) J. L. Manson, D. W. Lee, A. L. Rheingold and J. S. Miller, *Inorg. Chem*., 1998, **37**, 5966; (*e*) C. R. Kmety, J. L. Manson, Q. Huang, J. W. Lynn, R. W. Erwin, J. S. Miller and A. J. Epstein, *Phys. Rev. B: Condens*, in press; (*f*) J. L. Manson, A. M. Arif, C. D. Incarvito, L. M. Liable-Sands, A. L. Rheingold and J. S. Miller, *J. Solid State Chem*., in press.

5 J. L. Manson, C. R. Kmety, A. J. Epstein and J. S. Miller, *Inorg. Chem*., 1999, **38**, 2552.

6 J. Ribas, M. Monfort, X. Solans and M. Drillon, *Inorg. Chem*., 1994, **33**, 742.

7 M. Mikuriya, T. Fujii, T. Tokii and A. Kawamori, *Bull. Chem. Soc. Jpn*., 1993, **66**, 1675.

8 A. Escuer, R. Vicente, J. Ribas and X. Solans, *Inorg. Chem*., 1995, **34**, 1793.

9 See, for example: (*a*) F. A. Mautner, R. Cortés, L. Lezama and T. Rojo, *Angew. Chem., Int. Ed. Engl.*, 1996, **35**, 78; (*b*) A. K. Gregson and N. T. Moxon, *Inorg. Chem*., 1982, **21**, 586; (*c*) A. Escuer, R. Vicente, M. A. S. Goher and F. A. Mautner, *Inorg. Chem*., 1996, **35**, 6386; (*d*) A. Escuer, R. Vicente, M. A. S. Goher and F. A. Mautner, *Inorg. Chem*., 1998, **37**, 782; (*e*) L. K. Thompson, S. S. Tandon, F. Lloret, J. Cano and M. Julve, *Inorg. Chem*., 1997, **36**, 3301; (*f*) R. Cortés, L. Lezama, J. L. Pizarro, M. I. Arriortua and T. Rojo, *Angew. Chem., Int. Ed. Engl.*, 1996, **35**, 1810.

10 M. E. Fisher, *Am. J. Phys*., 1964, **32**, 343.

11 B. E. Myers, L. Berger and S. A. Friedberg, *J. Appl. Phys*., 1968, **40**, 1149.

12 J. Ribas, M. Monfort, B. K. Ghosh, X. Solans and M. Font-Bardia, *J. Chem. Soc., Chem. Commun*., 1995, 2375.

13 R. Cortés, M. Drillon, X. Solans, L. Lezama and T. Rojo, *Inorg. Chem*., 1997, **36**, 677.

14 R. Cortés, J. L. Pizarro, L. Lezama, M. I. Arriortua and T. Rojo, *Inorg. Chem*., 1994, **33**, 2697.

15 J. Ribas, M. Monfort, B. K. Ghosh and X. Solans, *Angew. Chem., Int. Ed. Engl*., 1994, **33**, 2087.

Communication 9/03406D

A facile reaction of Sb_2S_3 with $[CpCr(CO)_3]_2$: formation of a novel tetrachromium complex $[CpCr(CO)_3]_4(Sb_2S)$

Lai Yoong Goh,*[a] Wei Chen[b] and Richard C. S. Wong[b]

[a] *Department of Chemistry, National University of Singapore, Kent Ridge, Singapore 119260. E-mail: chmgohly@nus.edu.sg*

[b] *Department of Chemistry, University of Malaya, 50603 Kuala Lumpur, Malaysia*

Received (in Cambridge, UK) 6th May 1999, Accepted 1st July 1999

The reaction of $[CpCr(CO)_3]_2$ with Sb_2S_3 under mild reaction conditions led to the isolation of $[CrCp(CO)_2]_2S$ 4 and the new tetrachromium complex $[CpCr(CO)_3]_4(Sb_2S)$ 2, which has been characterized *via* a single crystal X-ray diffraction analysis.

Our earlier work has demonstrated the role of the 17-electron $CpCr(CO)_3$· species in the cleavage of the pnictogen tetrahedra P_4 and As_4,[1] and of mixed element P_4X_3 (X = S, Se) cages,[2] to generate complexes possessing a variety of geometries and structures. This communication reports the results from an extension of the investigation to Sb_2S_3.

In comparison to the organotransition metal complexes of the lighter elements of Group 15, those of antimony are scarce.[3] Most of the reported complexes derived from the reactions of the trihalo compounds SbX_3 or their alkyl derivatives, *e.g.* $RSbX_2$, R_2SbX, R_3Sb, $MeC(CH_2Sb)_3$ and $(Bu^tSb)_4$, with the anions of metal carbonyls, metal carbonyl clusters or cyclopentadienylmetal carbonyl fragments, as well as neutral transition metal fragments.[4] A few unique reactions generated antimony ligands from the reactions of elemental antimony with $[CpMo(CO)_3]_2$,[5] of the nortricyclic Zintl ion Sb_7^{3-} with $Ni(CO)_2(PPh_3)_2$[6] and of $S_8(Sb_2F_{11})$ with $Fe(CO)_5$.[7]

The reaction of $[CpCr(CO)_3]_2$ **1** with 6 mol equiv. of Sb_2S_3 in toluene under ultrasonication at ambient temperature for 48 h, led to the isolation of $[CpCr(CO)_3]_4(Sb_2S)$ **2** (19.3%), $[CpCr(CO)_2]_2(Cr{\equiv}Cr)$ **3** (5.8%) and $Cp_2Cr_2(CO)_4S$ **4** (46.6%) from the product mixture.† The tetrachromium complex **2** has been characterized spectroscopically‡ and by a single crystal X-ray diffraction analysis.§ Thermolysis of **2** at 80 °C, monitored by proton NMR spectral analysis, showed total degradation after 2 h to give **4** (28%), $Cp_4Cr_4S_4$ **5** (13%) and an insoluble as-yet-unidentified precipitate.

The reaction is represented in Scheme 1. In view of the facile dissociation of **1** into the 17-electron $CpCr(CO)_3$· monomeric species,[8] it is conceivable that the reaction proceeds *via* the attack of this reactive radical moiety on the ribbon-like polymeric structure of Sb_2S_3, cleaving the interlocking SbS_3 and SSb_3 tetrahedra in the structure,[9] producing the Cr_4Sb_2S complex **2** together with the Cr≡S≡Cr complex **4**, into which **2** also degrades under thermolytic conditions. Such reactions of Sb_2S_3 with an organometallic fragment under the mild conditions as utilised here is unprecedented, demonstrating the efficiency of the $CpCr(CO)_3$· species in the cleavage of the antimony–sulfur bonds of the polymeric structure of Sb_2S_3, as in the case of the cage molecules of the lighter elements of Groups 15/16.[1,2]

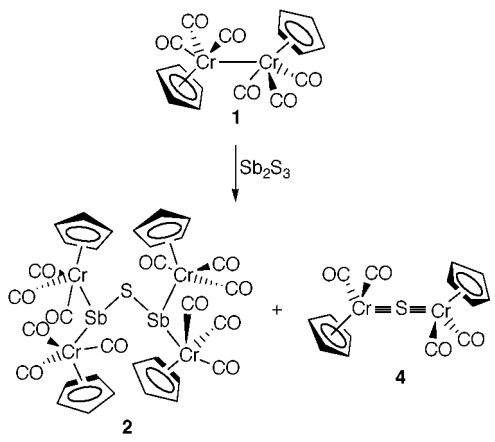

Scheme 1

An ORTEP plot of **2** is shown in Fig. 1. The molecule possesses an approximate C_2 symmetry with a butterfly configuration about the central sulfur atom. Each of the Sb atoms is coordinated to one S and two Cr atoms which form the base of a trigonal pyramid [angles ranging from 98.5(1) to 115.07(9)° at Sb1 and 98.8(1) to 114.83(9)° at Sb2]. Each Cr atom in turn is coordinated to one Cp ring and three CO ligands in a four-legged piano stool configuration. The Cr_2SbS fragments in the molecule belong to the electron precise pyramidal EM_2Y type[3c] [E = Sb, M = the 17-electron $CpCr(CO)_3$ fragment, Y = S]; the structure can be envisaged as the product of 'fusion' of two such units with the extrusion of a S atom, resulting in a bent Sb–S–Sb bridge [angle 93.9(3)°]. The Sb–Cr bond distances in **2** (2.837–2.849 Å) are longer than those found in $[\{Cr(CO)_5\}_3(\mu_3\text{-}Sb)]^-$ (2.624–2.636 Å)[10] and in $[Sb(Fe(CO)_4)_3\{Cr(CO)_5\}]^-$ (2.638 Å).[11] The Cr–Sb–Cr angles (115.07, 114.83°) are smaller than those in $[\{Cr(CO)_5\}_3(\mu_3\text{-}Sb)]^-$ (118.9, 122.2°).[10]

The new complex **2** is the first example of a transition metal complex containing a 'bare' antimony–sulfur bridging ligand with each antimony atom bonded to two metal atoms. The only other reported instance of such antimony–sulfur ligands, *viz.* the Sb_2S_6 ligand in the cationic cluster $[Fe_2(Sb_2S_6)(CO)_6]^{2+}$ is bonded to the Fe atoms only *via* its six S atoms.[7] The closest analogues to **2** are complexes containing an organoantimony–sulfur ligand, $\{(CO)_4Cr\}_n[(Ph_2Sb)_2S]$ and

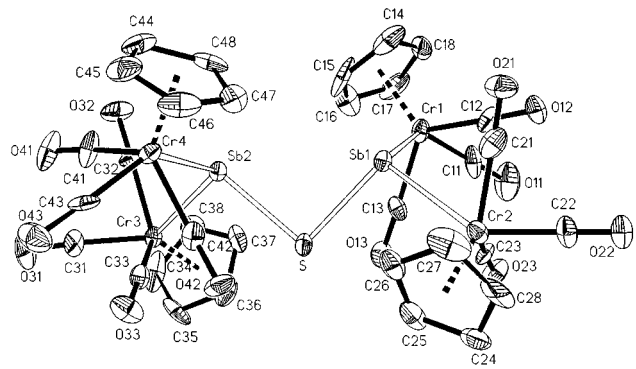

Fig. 1 Molecular structure of **2**. Selected bond lengths (Å) and angles (°): Sb1–S 2.466(5), Sb2–S 2.449(4), Sb1–Cr1 2.837(3), Sb1–Cr2 2.849(3), Sb2–Cr3 2.842(3), Sb2–Cr4 2.849(3), $Cp_{centroid}$–Cr 1.828–1.843; Sb1–S–Sb2 93.9(2), S–Sb1–Cr1 106.96(12), S–Sb1–Cr2 98.53(12), Cr1–Sb1–Cr2 115.07(9), S–Sb2–Cr3 98.82(12), Cr3–Sb2–Cr4 114.83(9), Cp–Cr–CO 112.4–125.0.

$\{(CO)_5Cr\}_n[(Ph_2Sb)_2S]$ (n = 1 or 2, depending on whether one or both Sb atoms are linked to Cr carbonyl fragments). Compared to **2**, the crystallographically characterized $\{(CO)_4Cr\}[(Ph_2Sb)_2S]$ complex possesses an Sb–S–Sb angle of 96.7(5)° and a Sb–Cr distance of 2.598(3) Å, much shorter than in **2**.[4l] Somewhat related parallels are the Mn⋍E⋍Mn 'inidene' complexes $[(MeCp)(CO)_2Mn]_2As_2E^-$ (E = S, Se)[12] and the ruthenium complex $(Cp^*Ru)_2(As_2S)_2$, the core structure of which consists of a Ru_2As_4 octahedron in which two edges are bridged by sulfur atoms.[13]

This work was supported by Grant RP3972673 of the National University of Singapore and Grant Nos. 09-02-03-0004 and 04-07-04-211 from the Malaysian Government.

Notes and references

† *Experimental procedure*: a deep green suspension of $[CpCr(CO)_3]_2$ **1** (100 mg, 0.25 mmol) and Sb_2S_3 powder (503 mg, 1.48 mmol) in toluene (20 ml) was ultrasonicated at ambient temperature for 48 h. The resultant orange–green reaction mixture was filtered through Celite (2 × 1 cm disc, *ca.* 1.5 g) and concentrated to *ca.* 20 ml. The filtrate was absorbed onto Celite (*ca.* 2 g) and concentrated to dryness before loading onto a silica gel column (2 × 10 cm) prepared in *n*-hexane–toluene (1:1). Elution gave four fractions: (i) a brownish green eluate in *n*-hexane–toluene (1:1, 25 ml), which on concentration gave deep green crystals of $Cp_2Cr_2(CO)_4S$ **4** (43 mg, 0.11 mmol, 46.6% yield). (ii) A deep green eluate in *n*-hexane–toluene (1:1, 10 ml), from which was obtained lustrous deep green crystals of the starting dimer **1** (23 mg, 0.057 mmol, 23.0% recovery). (iii) A dark green eluate in *n*-hexane–toluene (1:2, 20 ml) which yielded fine dark green crystalline $[CpCr(CO)_2]_2$ **3** (5 mg, 0.014 mmol, 5.8% yield). (iv) A dark brown eluate in THF (15 ml), which on concentration yielded fine black crystalline $Cp_4Cr_4(CO)_{12}Sb_2S$ **2** (26 mg, 0.024 mmol, 19.3% yield). Elemental analyses. Calc. C, 35.56; H, 1.85; Cr, 19.26; O, 13.33; Sb, 22.59; S, 2.96. Found: C, 35.0; H, 2.27; Cr, 19.03; Sb, 22.88; S, 2.95%.

‡ *Selected spectroscopic data*: ^{1}H NMR (100 MHz, C_6D_6): δ 4.52 (s, η^5-Cp). ^{13}C NMR (100 MHz, C_6D_6): δ 89.61 (η^5-Cp). IR (cm^{-1}, Nujol): ν(CO) 1986s, 1954m, 1901vs; other bands, 1066vw, 1025vw, 840w, 722w. MS (EI, 70 eV): *m/z* 622 $[Cp_2Cr_2(CO)_4Sb_2S]$, 468 $[Cp_2Cr_2(CO)_4Sb]$, 417 $[CpCr(CO)_2Sb_2]$, 346 $[Cp_2Cr_2(CO)_4]$, 295 $[CpCr(CO)_2Sb]$, 149 [CpCrS].

§ *Crystal data* for $C_{32}H_{20}O_{12}SCr_4Sb_2$ **2**: M_r = 1080.04, monoclinic, space group $P2_1/c$, a = 20.181(5), b = 12.400(4), c = 15.209(8) Å, β = 106.26(3)°, V = 3653.7(24)° Å^3, D_c = 1.963 g cm^{-3}, Z = 4, $2\theta_{max}$ = 24.99°, Mo-Kα = 0.71073 Å, ω-scan, T = 300 K. From 6413 reflections, 2446 were observed [$I > 2\sigma(I)$]. Lorentz-polarization and absorption corrections were applied (empirical), μ = 53.073 cm^{-1}, transmission$_{max./min.}$ = 99.93/61.12. The structure was solved by the direct method (SHELXS86) and refined on F^2 (SHELXL93). All non-hydrogen atoms (except C38 and C47) were refined anisotropically; C38 and C47 were refined isotropically as their temperature factors became non-positive. H atoms were generated geometrically and were allowed to ride on their respective carbon atoms. The final R and wR {w = $[\sigma^2(F_o^2) + (0.0139P)^2]^{-1}$ where $P = 1/3(F_o^2 + 2F_c^2)$} are 0.0836 and 0.1011, respectively, for 450 variables. The maximum residual peak is 0.945 e Å^{-3}. Diffraction-quality crystals of **2** were obtained as brownish black polyhedra from a saturated solution in THF after a week at −28 °C. A selected crystal was coated in epoxy glue, and X-ray diffraction measurements were made on a CAD4 diffractometer. CCDC 182/1303. See http://www.rsc.org/suppdata/cc/1999/1481/ for crystallographic files in .cif format.

1 L. Y. Goh, C. K. Chu, R. C. S. Wong and T. W. Hambley, *J. Chem.Soc., Dalton Trans.*, 1989, 1951; 1990, 977; L. Y. Goh, R. C. S Wong and E. Sinn, *J. Chem. Soc., Chem. Commun.*, 1990, 1484; *Organometallics*, 1993, **12**, 888; L. Y. Goh, R. C. S. Wong, W. H. Yip and T. C. W. Mak, *Organometallics*, 1991, **10**, 875.

2 L. Y. Goh, W. Chen and R. C. S. Wong, *Angew. Chem., Int. Ed. Engl.*, 1993, **32**, 1728; L. Y. Goh, W. Chen, R. C. S. Wong and K. Karaghiosoff, *Organometallics*, 1995, **14**, 3886; L. Y. Goh, W. Chen and R. C. S. Wong, *Phosphorus, Sulphur Silicon*, 1994, **93**–**94**, 209; L. Y. Goh, W. Chen, R. C. S. Wong, Z.-Y. Zhou and H. K. Fun, *Mendeleev Commun.*, 1995, 60; L. Y. Goh, W. Chen and R. C. S. Wong, *Organometallics*, 1999, **18**, 306.

3 For reviews, see: (*a*) O. J. Scherer, *Angew. Chem., Int. Ed. Engl.*, 1990, **29**, 1104; (*b*) J. Wachter, *Angew. Chem., Int. Ed.*, 1998, **37**, 750; (*c*) K. H. Whitmire, *Adv. Organomet.Chem.*, 1998, **42**, 1; (*d*) K. H. Whitmire, *J. Cluster Sci.*, 1991, **2**, 231.

4 Some references cited in ref. 3 above; also see for example: (*a*) M. Gorzellik, B. Nuber and M. L. Ziegler, *J. Organomet. Chem.*, 1992, **431**, 171; (*b*) N. C. Norman, N. L. Pickett, W. S. Storr, N. M. Boag and A. J. Goodby, *Polyhedron*, 1994, **13**, 2525; (*c*) W. Deck and H. Vahrenkamp, *Z. Anorg. Allg. Chem.*, 1991, **598**/**599**, 83; (*d*) W. Malisch and P. Panster, *J. Organomet. Chem.*, 1975, **99**, 421; (*e*) G. I. Nikonov, L. G. Kuzmina and J. A. K. Howard, *Organometallics*, 1997, **16**, 3723; (*f*) A.-M. Caminade, M. Veith, V. Huch and W. Malisch, *Organometallics*, 1990, **9**, 1798; (*g*) W. J. Evans, S. L. Gonzales and J. W. Ziller, *J. Chem. Soc., Chem. Commun.*, 1992, 1138; (*h*) J. Grobe, W. Golla, D. Le Van, B. Krebs and M. Läge, *Organometallics*, 1998, **17**, 5717; (*i*) J. Ellermann and A. Veit, *J. Organomet. Chem.*, 1985, **290**, 307; (*j*) H. J. Breunig and J. Pawlik, *Z. Anorg. Allg. Chem.*, 1995, **621**, 817; (*k*) H. J. Breunig, R. Rösler and E. Lork, *Angew. Chem., Int. Ed. Engl.*, 1997, **36**, 2819; (*l*) M. Wieber and N. Graf, *Z. Anorg. Allg. Chem.*, 1993, **619**, 1991, 2061.

5 J. R. Harper and A. L. Rheingold, *J. Organomet. Chem.*, 1990, **390**, C36.

6 S. Charles, B. W. Eichhorn and S. G. Bott, *J. Am. Chem. Soc.*, 1993, **115**, 5837.

7 G. W. Drake, G. L. Schimek and J. W. Kolis, *Inorg. Chem.*, 1996, **35**, 4534.

8 M. C. Baird, *Chem. Rev.*, 1988, **88**, 1217 and references cited therein; L. Y. Goh and Y. Y. Lim, *J. Organomet. Chem.*, 1991, **402**, 209 and references therein.

9 F. A. Cotton and G. Wilkinson, *Advanced Inorganic Chemistry*, Wiley-Interscience, New York, 5th edn., 1988, p. 404.

10 G. Huttner, U. Weber, B. Sigwarth, O. Scheidsteger, H. Lang and L. Zsolnai, *J. Organomet. Chem.*, 1985, **282**, 331.

11 K. H. Whitmire, M. Shieh and J. Cassidy, *Inorg. Chem.*, 1989, **28**, 3164.

12 Ch. Emmerich, G. Huttner and A. Asam, J. *Organomet. Chem.*, 1993, **447**, 71.

13 H. Brunner, B. Nuber, L. Poll, G. Roidl and J. Wachter, *Chem. Eur. J.*, 1997, **3**, 57.

Communication 9/03616D

ChemComm

Reversible metal-directed assembly of clusters of vesicles

Edwin C. Constable,*[a] Wolfgang Meier,[b] Corrinne Nardin[b] and Stefan Mundwiler[a]

[a] *Institut für Anorganische Chemie, Spitalstrasse 51, CH-4056 Basel, Switzerland. E-mail: constable@ubaclu.unibas.ch*

[b] *Institut für Physikalische Chemie, Klingelbergstrasse 80, CH-4056 Basel, Switzerland*

Received (in Cambridge, UK) 11th June 1999, Accepted 2nd July 1999

A terpy-functionalised phospholipid has been incorporated into lecithin vesicles and iron(II)-directed aggregation processes have been studied.

Self-assembly is a powerful methodology in supramolecular chemistry that allows the efficient formation of complex multidimensional structures from simple building blocks.[1] Much effort has been devoted to understanding the basic physical chemistry of self-assembled monolayers (SAMs), vesicles and micelles.[2] We have recently commenced a programme in which structural motifs with known self-assembly or molecular recognition paradigms are functionalised with metal-binding domains[3–5] and have described the formation and metal-initiated aggregation of SAMs bearing pendant 2,2′:6′,2″-terpyridine (terpy) motifs.[5] Here, we show that the introduction of a small amount of a terpy-functionalised phospholipid into 'normal' phospholipid vesicles leads to metal-initiated clustering and the formation of aggregates.

Hydrogenated L_α-lecithin **1** (a mixture of phospholipids with 31% R = $C_{16}H_{33}$, 59.75% R = $C_{18}H_{37}$, 5.71% R = $C_{20}H_{41}$ and 3.07% R = $C_{22}H_{45}$, average molecular mass 557 Da) was used as the host. A vesicle stock solution at a L_α-lecithin concentration of 10 mg cm^{-3} (1.8×10^{-2} M) was prepared;† the average vesicle mass was 3×10^7 g mol^{-1} corresponding to 54 000 molecules per vesicle and they have a mean hydrodynamic radius R_h of 54 nm and radius of gyration R_G of 51 nm as determined by dynamic and static light scattering.[6]‡ This gives $\rho = R_G/R_h = 0.944$ which is close to the theoretical value of $\rho = 1.0$ for hollow spheres.[7] The terpy-functionalised phospholipid **2** was prepared as previously described[5] and a 3 wt% amount added to the stock solution of the lecithin to give a total concentration of **2** of 3.29×10^{-4} M. The experimentally measured R_h and R_G were unchanged by the addition of the functionalised compound **2**, indicating no fundamental changes in the solution behaviour of **1** at this level of doping with **2**. The doping corresponds to an average of 970 molecules of **2** per vesicle. Freeze fracture replication transmission electron microscopy[8] revealed the presence of dispersed vesicles [Fig. 1(a)].

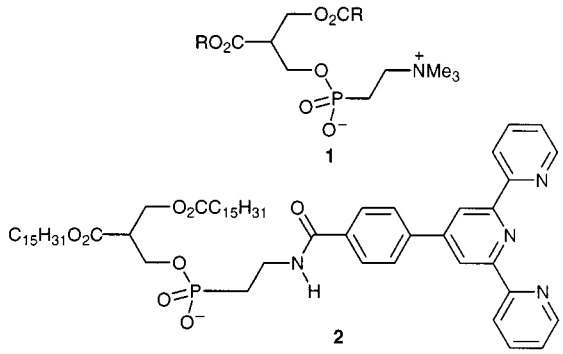

The free ligand **2** forms a typical purple iron(II) complex $[Fe(\mathbf{2})_2]^{2+}$ with a characteristic MLCT absorption maximum at 576 nm. Assuming that K_1 and K_2 for the formation of ML and ML_2 complexes are similar to those for terpy itself,[9] even with large excesses of iron, the 1:1 species is not of importance at *ca.* 0.1 mM ligand concentrations. The addition of aqueous $FeSO_4 \cdot 7H_2O$ to the modified vesicle solution resulted in a purple colour (λ_{max} 577–584 nm), indicating that the terpy is still available for coordination and that an $\{ML_2\}$ species is formed. Titration of aqueous Fe^{2+} into the stock solution reached a maximum absorbance at 582 nm at an M:**2** ratio of 0.7:1, compatible with the speciation calculations above and strongly suggesting that all of the terpy groups are on the *outer* surface of the vesicle.

The results of dynamic light scattering measurements as the iron(II) salt as titrated into the modified vesicle solution are presented in Fig. 2. The measured R_h increases smoothly past the 1:2 Fe^{2+}:**2** equivalence point until an Fe^{2+}:**2** ratio of *ca.* 4.5:1 is reached. After this point a rapid increase in the measured hydrodynamic radius occurs followed by precipitation of a violet solid when $[Fe^{2+}]$ reaches 1.76 mM. A control experiment with the stock solution in the absence of **2** showed

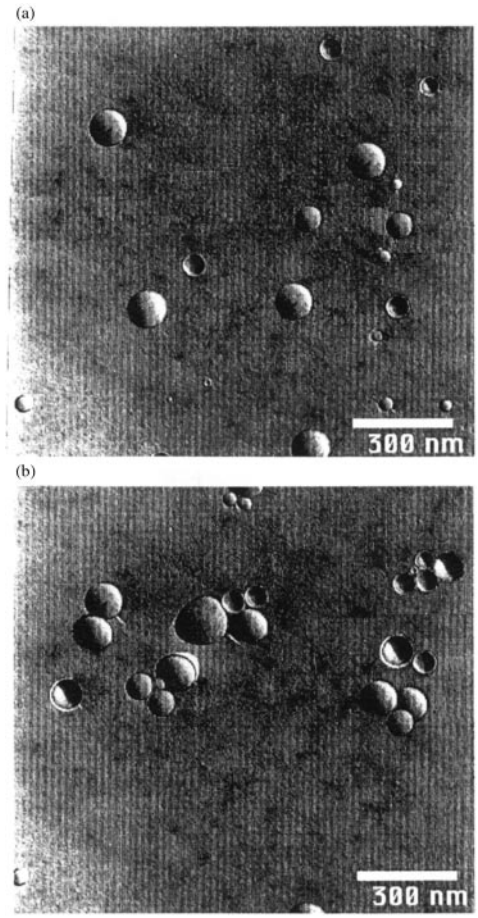

Fig. 1 (a) Freeze fracture electron micrograph of vesicles obtained with lecithin **1** (1.8×10^{-2} M) and **2** (3.29×10^{-4} M). No clustered vesicles are observed. (b) Freeze fracture electron micrograph of an identical vesicle solution after treatment with aqueous iron(II) sulfate to give an Fe^{2+}:**2** ratio of 4.5:1.

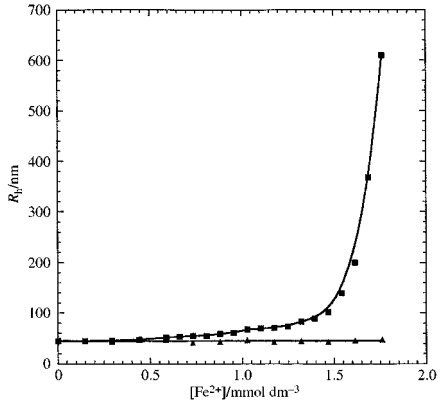

Fig. 2 Measured hydrodynamic radius of vesicles as a function of aqueous iron sulfate concentration. The data presented refer to the hybrid **1** + **2** vesicles (■) and to a control experiment with **1** alone (▲).

that the addition of the iron salt had no effect on the parent vesicles (Fig. 2). The aggregation process proved to be reversible, and the addition of a 100-fold molar excess of $Na_2(H_2edta)$ at 40 °C resulted in the discharge of the violet colour and restoration of the light scattering characteristics of the vesicle solution. At an Fe^{2+}:**2** ratio of 4.5:1, light scattering gave R_G = 108 nm and R_h = 106 nm consistent with an aggregation of the vesicles into clusters (see later). Metal-initiated transformation into giant vesicles can be rejected on the basis of the reversibility of the process upon addition of edta.

We propose that an aggregation process is occurring (Scheme 1) in which the surface terpy ligands are coordinating to the iron(II) centres. The low dilution of **2** within individual vesicles means that inter-vesicle coordination is favoured and each

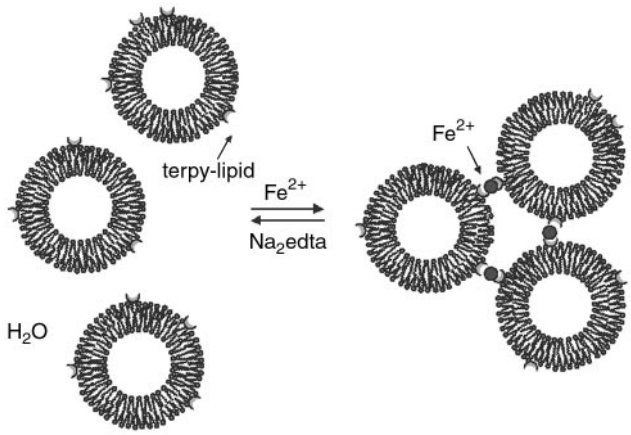

Scheme 1 Proposed iron(II) induced aggregation process of modified vesicles.

coordination event will clip two vesicles together. The high Fe^{2+}:**2** ratios needed before precipitation occurs represent the statistical factors involved in bringing two ligands together. The dimensions indicate an average aggregation state of 3.1 ± 1.1 vesicles in the clusters at a ratio of Fe^{2+}:**2** of 4.5:1 and an increase in size as the amount of iron is increased. It has previously been reported[10] that biotin-functionalised vesicles may be aggregated into clusters through interaction with streptavidin, but the approach we present here utilises a remarkably simple metal–ligand recognition process for the aggregation.

Direct evidence for the aggregation comes from cryomicroscopy. Fig. 1(b) shows a freeze fracture electron micrograph of the material at a ratio of Fe^{2+}:**2** of 4.5:1. At this concentration, microscopy reveals that only a very few single vesicles are present, the majority being aggregated into clusters.

In conclusion, we have shown that iron(II) salts may be used to assemble modified vesicles into clusters in a reversible process. We are currently investigating the extension of the chemistry to other metal ions with the aim of introducing specific redox, magnetic or photophysical properties into the aggregates.

We thank the University of Basel and the Schweizerischer Nationalfonds for financial support.

Notes and references

† **1** was deposited on the wall of a glass vessel by evaporation of a 1.8 M $CHCl_3$ solution and then hydrated in doubly distilled water to give a multilamellar liposome dispersion. This was repeatedly frozen in liquid nitrogen and thawed, followed by repeated extrusion through Nanopore filters of 100 nm pore size to form unilamellar vesicles.

‡ The results of the static and dynamic light scattering were obtained by extrapolation to zero concentration of vesicles by dilution of the stock solution with doubly distilled water. This indicates that the vesicles and the vesicle clusters are stable under these conditions of dilution.

1 See, *Comprehensive Supramolecular Chemistry*, ed. J. L. Atwood, J. E. D. Davies, D. D. MacNicol and F. Vögtle, Pergamon, Oxford, 1996, vol. 9 and references therein.
2 See, *Comprehensive Supramolecular Chemistry*, ed. J. L. Atwood, J. E. D. Davies, D. D. MacNicol and F. Vögtle, Pergamon, Oxford, 1996, vol. 7 and references therein.
3 E. C. Constable and S. Mundwiler, *Polyhedron*, in press.
4 E. C. Constable, C. E. Housecroft, R. Häner and A. Wirth, manuscript under revision.
5 E. C. Constable, S. Mundwiler and J. J. Ramsden, *J. Mater. Chem.*, (9/04388H) in press.
6 C. Schwarzwälder and W. Meier, *Macromolecules*, 1997, **30**, 4601.
7 W. Burchard in *Physical techniques for the study of food biopolymers*, ed. S. Ross-Murphy, Blackie Academic and Professional, Glasgow, 1994.
8 W. Meier, *Langmuir*, 1996, **12**, 6341.
9 W. W. Brandt and J. P. Wright, *J. Am. Chem. Soc.*, 1954, **76**, 3082.
10 S. Chiruvolu, S. Walker, J. Israelachvili, F.-J. Schmitt, D. Leckband and J. A. Zasadzinski, *Science*, 1994, **264**, 1753.

Communication 9/04665H

A layered silver sulfonate incorporating nine-coordinate Ag^{I} in a hexagonal grid

George K. H. Shimizu,*† Gary D. Enright, Chris I. Ratcliffe, Keith F. Preston, Jennifer L. Reid and John A. Ripmeester

Steacie Institute for Molecular Sciences, National Research Council of Canada, Ottawa, Ontario, K1A 0R6, Canada. E-mail: gshimizu@ucalgary.ca

Received (in Columbia, MO, USA) 3rd June 1999, Accepted 30th June 1999

Silver benzenesulfonate is an example of a layered 'inorgano–organic' solid where the inorganic component is comprised of sulfonate-bridged silver(I) centers and the organic moiety is a phenyl group; the resulting network of silver ions forms a planar hexagonal array incorporating a previously unobserved six-fold metal-bridging mode for the sulfonate ion.

Currently, there are numerous well studied examples of 'inorgano–organic' lamellar solids.[1] This term is used to describe layered solids containing a planar backbone, comprised solely of inorganic elements, which also incorporate organic moieties as covalently bound pendant groups. Organic derivatization of inorganic layers couples the skeletal rigidity of the inorganic lamellae with the structural diversity inherent to organic functionalization. The result can be a new compound with markedly different properties (solubility, intercalation, exfoliation) from the parent inorganic backbone. The principal sub-groups of complexes in this class include metal phosphonates,[2] and perovskite halides.[3] Whereas examples of lamellar networks with phosphonate groups abound,[2] lamellar 'inorgano–organic' systems employing sulfonates are virtually unknown.[4,5] Silver benzenesulfonate is a two-dimensional network from which the phenyl groups protrude from both sides. The resulting phenyl–silver(sulfonate)–phenyl trilayer then assembles by dispersive forces between the phenyl groups. The network of Ag–Ag bonds forms a nearly perfect hexagonal grid. Each Ag^{I} in the structure has nine atoms at less than van der Waals contact distances and each SO_3 group caps six different Ag^{I} centers. The observed η^6-coordination mode of the sulfonate group to metals is unprecedented.

Silver benzenesulfonate **1** may be generated by the addition of aqueous sodium benzenesulfonate to a solution of $AgNO_3$ in water. Concentration of this solution results in the precipitation of **1**, in very good yields, as a light gray solid.‡ Elemental analyses confirmed a 1 : 1 stoichiometry of Ag^{I} to benzenesulfonate. Diffusion of isopropyl ether into a MeOH solution of **1** resulted in the growth of extremely thin plate-like crystals suitable for an X-ray diffraction analysis.§

Silver benzenesulfonate forms a two-dimensional infinite array wherein the Ag^{I} centers are bridged by SO_3 groups to form layers and the phenyl moieties of the sulfonates protrude into the interlayer region (Fig. 1).[6] The asymmetric unit contains a single disordered silver benzenesulfonate unit. The interlayer distance, defined as the perpendicular distance between the layers of Ag^{I} ions, is 15.23(2) Å. The thickness of an individual lamella, defined as the region containing solely the Ag, S and O atoms, is 3.87(2) Å. The difference between these two values, 11.36(2) Å, constitutes the gallery height in the complex. Adjacent layers in the complex are slightly offset by 1.32(2) Å in a direction between the *a* and *b* axes. The benzenesulfonate has its major axis oriented *ca.* 14° off the normal to the plane containing the silver atoms. The interlayer phenyl group is disordered between two positions situated 81° apart about the major axis of the ring. NMR shows that at room temperature this disorder is dynamic.[7] The nearest distance between phenyl groups is 5.20(1) Å.[8] The structure is representative of the bulk phase as PXRD data was indexed to the same unit cell.[9]

The structure of **1** is extremely unusual both with respect to the coordination of the Ag^{I} ions and the mode of coordination of the sulfonate groups to the metals. Each Ag^{I} ion is nine-coordinate (Fig. 2) with a coordination sphere comprised of six sulfonate oxygen atoms [from six different sulfonate groups, Ag–O distances range from 2.42(1)–2.56(1) Å] and three bonds to other Ag ions [Ag–Ag 2.915(1) Å].[10] The geometry at each Ag^{I} may be considered as a distorted octahedron of oxygen donors, with three silver donors approaching in a trigonal plane bisecting the octahedron.[11] Congruently, the SO_3 groups must form bonds to six different Ag ions, each oxygen coordinating to two silver centres.[12] The six Ag–O distances span a smaller range than observed for the five Ag–O interactions in AgOTs [2.391(6)–2.700(3) Å].[4] Interestingly, the network of Ag–Ag

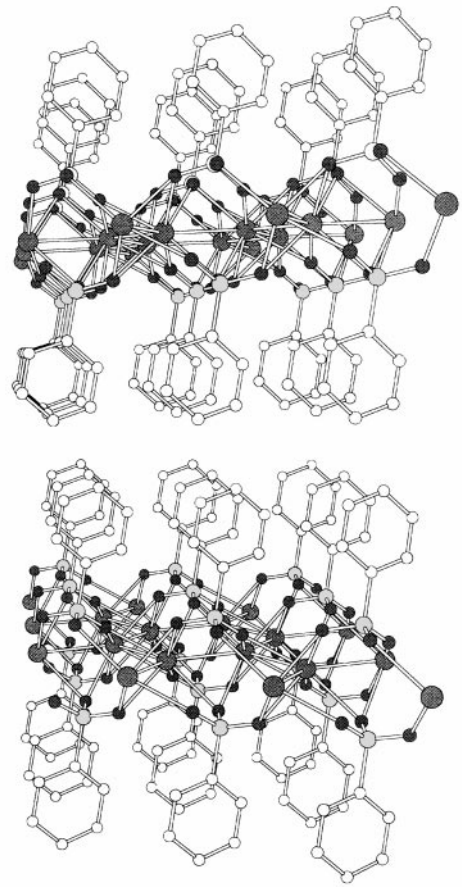

Fig. 1 Structure of **1** showing the overall lamellar network with phenyl groups protruding into the interlayer region. Disorder has been removed for clarity.

† Current address: Department of Chemistry, University of Calgary, 2500 University Drive N.W., Calgary, Alberta, T2N 1N4, Canada.

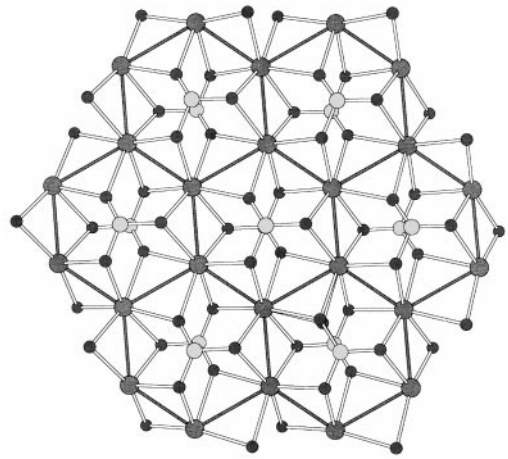

Fig. 2 View down onto a single lamella of the structure of **1** with phenyl rings and disordered oxygen atoms removed for clarity. Silver atoms: large circles, sulfur atoms: medium shaded circles, oxygen atoms: small circles. Note the hexagonal arrangement of the silver(I) centers and the nonavalent coordination mode, and the μ_6-sulfonate groups.

interactions forms a nearly perfect hexagonal grid reminiscent of graphite.[13,14] The hexagons are completely planar with the observed angles around the Ag periphery averaging to 120.0(1)° [the three different angles are 114.83(3), 116.12(3) and 128.79(3)°]. Each Ag hexagon is capped by an SO_3 group and the mean distance across a hexagon is 6.01(30) Å. The solely inorganic component of this structure, the $AgSO_3$ lamellae, possess almost hexagonal symmetry. The phenyl groups, however, cannot adopt this high symmetry necessitating a distortion in the overall structure to a triclinic, albeit pseudo-hexagonal, space group.[15] DSC–TGA analyses of a sample of silver benzenesulfonate revealed the sample to be completely stable to 139.7 °C at which point a reversible endothermic transition was observed in the DSC. A second non-reversible endothermic transition was observed at 198.2 °C followed by an exothermic transition with an onset temperature of 253.4 °C corresponding to loss of 43.9% of sample weight.

Silver(I) is a notoriously pliant ion with respect to its coordination sphere. Coordination numbers ranging from two to four are common[10] but examples of five- and six-coordinate Ag^I have also been observed.[16] Even in this light, the structure of **1** is remarkable. Silver benzenesulfonate possesses a fascinating structure both from the macroscopic viewpoint, the lamellar motif, and from the microscopic perspective, the highly unusual nine-coordinate Ag^I as well as a novel six-fold bridging mode for a coordinating sulfonate.The question of structure-directing effects (Ag–O *versus* Ag–Ag) in the silver sulfonate family will be resolved upon consideration of other derivatives.

Notes and references

‡ **1**: To a solution of $AgNO_3$ (1.44 g, 8.50 mmol) in H_2O (20 mL) was added a solution of sodium benzenesulfonate (1.53 g, 8.50 mmol) in H_2O (50 mL). A clear solution resulted which was concentrated to *ca.* 10 mL. A gray solid precipitated which was vacuum filtered, washed with cold water (2 mL) and dried. Yield: 1.78 g (6.72 mmol, 79%) CP MAS SS ^{13}C NMR (75 MHz) δ 144.1 (quat. arom), 127.5 (tert. arom). C, H analyses: calc. C, 27.19, H, 1.90: obs. C, 26.82, H, 1.84%. Diffusion of isopropyl ether into a MeOH solution of **1** gave plate-like crystals suitable for an X-ray analysis.

§ *Crystal data* for **1**: $C_{12}H_{10}Ag_2S_2O_6$, M = 530.06, colorless plates, triclinic, space group $P\bar{1}$, a = 5.1596(8), b = 5.1979(8), c = 15.296(2) Å, α = 86.75(2), β = 84.56(2), γ = 61.00(2)°, V = 357.2(1) Å^3, Z = 2, D_c 2.464 g cm^{-3}, R = 0.037, R_w = 0.043 and GOF = 1.27 for 161 parameters using 1540 [$F_o > 2.5\sigma(F_o)$] reflections. Mo-Kα radiation (λ = 0.71073 Å), μ(Mo-Kα) 3.05 mm^{-1}. Data collection temp. −100 °C. The data was collected on a Siemens SMART CCD diffractometer using the ω scan mode ($3 < 2\theta < 57.3°$) and solved using the NRCVAX suite of programs.[17] An initial refinement was attempted in $P\bar{1}$. The discovery from this of the $PhSO_3$ molecule disordered over two equally occupied positions then led us to consider the $P1$ space group. We were able to refine the structure (without disorder) in $P1$ to a residual $R_1(R_w)$ of 0.045 (0.063). However, under $P1$, strong correlations between parameters, non-positive definite thermal parameters, unacceptable C–C bond distances, higher residuals and an inconsistency with the NMR dynamics studies convinced us to accept the 50:50 disordered $P\bar{1}$ structure. The O and C atoms are all 50% occupied. The hydrogens were all placed in calculated positions. The partially occupied atoms in close contact (C1, C1a and C4, C4a) were refined isotropically. This structure was corroborated by CP MAS ^{13}C and ^2H SS NMR studies to be reported in detail elsewhere. CCDC 182/1311.

1 G. Alberti and U. Costantiono, in *Comprehensive Supramolecular Chemistry*, ed. J. L. Atwood, J. E. D. Davies, D. D. MacNicol and F. Vögtle, Elsevier Science, New York, 1996, vol. 7, ch. 1, pp. 1–24.

2 For α- and γ-Zr phosphonates, see: G. Alberti and U. Costantino, in *Inclusion Compounds*, ed. J. L. Atwood, J. E. Davies and D. D. MacNicol, Oxford University Press, New York, 1991, vol. 5, ch. 5, pp. 136–176; for a review to 1997, see, A. Clearfield, *Prog. Inorg. Chem.*, 1998, **47**, 371.

3 C. Bellito and P. Day, in *Comprehensive Supramolecular Chemistry*, ed. J. L. Atwood, J. E. D. Davies, D. D. MacNicol and F. Vögtle, Elsevier Science, New York, 1996, vol. 7, ch. 9, pp. 293–313.

4 G. K. H. Shimizu, G. D. Enright, C. I. Ratcliffe, G. S. Rego, J. L. Reid and J. A. Ripmeester, *Chem. Mater.*, 1998, **10**, 3282.

5 Sulfonates have been employed as H-bond acceptors in the generation of layered guanidinium sulfonates. Interestingly, in these complexes the sulfonate group forms six H-bonds much like the sulfonates herein form six-coordinate covalent bonds, see: V. A. Russell, C. C. Evans, W. Li and M. D. Ward, *Science*, 1997, **276**, 575; J. A. Swift, A. M. Pivovar, A. M. Reynolds and M. D. Ward, *J. Am. Chem. Soc.*, 1999, **121**, 5887; V. A. Russell, M. C. Etter and M. D. Ward, *J. Am. Chem. Soc.*, 1994, **116**, 1941.

6 Tetranuclear Ag^I clusters bridged by succinates have been previously observed, A. Michaelides, V. Kiritis, S. Skoulika and A. Aubry, *Angew. Chem., Int. Ed. Engl.*, 1993, **32**, 1495.

7 From CP MAS ^{13}C and ^2H solid state NMR, a model for the dynamics about the twofold axis of the phenyl ring consistent with the disorder was determined.

8 For a comparison with the structure of $Zr(O_3PPh)_2$, see: M. D. Poojary, H.-L. Hu, F. L. Campbell III and A. Clearfield, *Acta Crystallogr., Sect. B*, 1993, **49**, 996.

9 PXRD data of a bulk sample of silver benzenesulfonate was indexed to the following triclinic cell: a = 5.1564, b = 5.1956, c = 15.3099 Å, α = 86.785, β = 84.582, γ = 61.149°, V = 357.62 Å^3.

10 Moore and coworkers have recently performed a comprehensive search of the Cambridge Structural Database to quantify occurrences of metal ion geometries, see: D. Venkataraman, Y. Du, S. R. Wilson, P. Zhang, K. Hirsch and J. S. Moore, *J. Chem. Educ.*, 1997, **74**, 915. Their results, which are available at http://sulfur.scs.uiuc.edu, indicate Ag^I primarily occurs in linear, trigonal or tetrahedral coordination modes. No examples of nine-coordinate Ag^I are known. The Ag–Ag distances reported here are all significantly less than the van der Waals contact distance for Ag–Ag of 3.40 Å.

11 The most common geometry for nine-coordinate species, primarily observed for nonahydrated lanthanide complexes, is a tricapped trigonal prism, see F. A. Cotton and G. Wilkinson, *Advanced Inorganic Chemistry*, John Wiley, Toronto, 5th edn., 1988, p. 17. The present structure would fit this description if the two sulfonate groups bonded to each silver(I) were in an eclipsed orientation.

12 In a review of triflate binding, a listing of observed coordination modes of R–SO_3 to metals does not include the six-fold bridging mode observed here. See: G. A. Lawrance, *Chem. Rev.*, 1986, **86**, 17.

13 H. Zabel and S. A. Solin, *Graphite Intercalation Compounds I*, Springer Series in Material Science 14, Springer, Berlin, 1990.

14 Based upon the structural similarity to graphite, the prospect that the network may be a conductor was entertained. However, EPR spectra revealed a noiseless signal to 77 K, indicative that all the electrons were highly localized and the material is not a conductor.

15 For a hexagonal unit cell, the symmetry requirements are: $a = b$, $\alpha = \beta = 90$, $\gamma = 120°$. The observed unit cell parameters, with doubling of γ, are slight distortions from these conditions.

16 For examples of other penta- and hexa-coordinate Ag^I, see: K. A. Hirsch, S. R. Wilson and J. S. Moore, *Inorg. Chem.*, 1997, **36**, 2960; L. Carlucci, G. Ciani, D. M. Proserpio and A. Sironi, *Angew. Chem., Int. Ed. Engl.*, 1995, **34**, 1895; G. K. H. Shimizu, G. D. Enright, C. I. Ratcliffe, J. A. Ripmeester and D. D. M. Wayner, *Angew. Chem. Int. Ed.*, 1998, **37**, 1407.

17 E. J. Gabe, Y. LePage, J.-P. Charland, F. L. Lee and P. S. White, *J. Appl. Crystallogr.*, 1989, **32**, 384.

Communication 9/04445K

ChemComm

Towards multifold cycloswitching of biphotochromes: investigation on a bond-fused dihydroazulene/vinylheptafulvene and dithienylethene/dihydrothienobenzothiophene

Thomas Mrozek,[a] Helmut Görner[b] and Jörg Daub*[a]

[a] *Institut für Organische Chemie der Universität Regensburg, Universitätsstraße 31, D-93040 Regensburg, Germany. E-mail: joerg.daub@chemie.uni-regensburg.de*

[b] *Max-Planck-Institut für Strahlenchemie, D-45413 Mülheim an der Ruhr, Germany. E-mail: goerner@mpi-muelheim.mpg.de*

Received (in Liverpool, UK) 19th April 1999, Accepted 14th June 1999

The concept of molecular switching within a *cyclic* four-stage process is introduced on the basis of two structurally fused photochromic systems (A–D). The synthesis of 1,8a-dihydro-2,3-bis(2,5-dimethyl-3-thienyl)azulene-1,1-dicarbonitrile (open/closed A) is described; irradiation with UV light leads to an equilibrium of open/open B, open/closed A and closed/closed C, whereas B is thermally rearranged to A by ring closure of the vinylheptafulvene substructure.

The photochromes dihydroazulene (**DHA**)/vinylheptafulvene (**VHF**)[1] and dithienylethene (**DTE**)/dihydrothienobenzothiophene (**DHB**)[2] are based on all-carbon cyclizations, which differ in the number of participating bonds. **DHA/VHF** uses a five-bond and **DTE/DHB** a three-bond cyclization. The light-induced reversible isomerization reactions between open and closed forms have been intensively studied,[3] both systems were also optimized for multimode switching, *e.g.* redox-switch,[1e,2b] fluorescent switch.[1d,2d] From a mechanistic point of view both systems differ in that **DHA/VHF** has a photochemical forward and a thermal back-reaction, whereas in **DTE/DHB** both isomerizations occur photochemically.

There are no reports of biphotochromic systems containing both systems structurally condensed and therefore strongly coupled as shown in Scheme 1.[4] Photochrome **A**, for example, which contains **DTE** and **DHA** substructures fused by a common double bond, represents an energy minimum on a closed circuit established by the four photochromes **A**–**D**. A manifold of independent switching arises, which is likely to be controlled by substituents or functional units. Multimode switches, as shown in Scheme 1, are of interest for information handling at the molecular level.[2c,3,5] Here we report on the synthesis of the open/closed **A** ($R^1 = R^2 = CH_3$) and demonstrate the reversible interconversion of **A** into isomers **B** and **C**.

The synthesis[6] of **A** is shown in Scheme 2; the synthetic and analytical details will be published elsewhere.

(*Z*)-1,2-Bis(3-thienyl)ethenes[2a] are known to form stable atropisomers with perpendicular arrangement of ethene and thiophene substructures thus leading to three stereoisomers (a *meso* form with mirror symmetry and two enantiomeric forms with C_2 symmetry). Isomer **A** may give rise to eight stereoisomers consisting of four enantiomeric pairs of diastereomers due to the additional chiral center at C-8a.[1a,f] The ^{1}H-NMR at −50 °C (Fig. 1, top) reveals a 2 : 1 mixture of two atropisomers indicated by four pairs of singlets due to the thiophene's methyl groups: δ (stereoisomer 1) = 1.68, 1.80, 2.38, 2.46; δ (stereoisomer 2) = 1.77, 2.00, 2.34, 2.45. At room temperature the ^{1}H-NMR displays broadening of the methyl signals which is in agreement with fast equilibrating rotational isomers. We assume that the π–π repulsion of the neighbouring thiophenes favors the two stereoforms with pseudo-C_2 symmetry leading to two diastereomeric forms due to the chiral center at C-8a.

UV/Vis spectroscopy gives a detailed insight into the photochromic behaviour; the photochemically induced rearrangement was also monitored by IR (not shown) and ^{1}H-NMR. Irradiation of **A** in THF-d_8 at room temperature (quartz NMR tube, 254 nm[7a]) leads to a new compound, the structure of which is assigned to **C**. The methyl singlets at δ 1.90, 2.02, 2.20 and the doublet at δ 2.25 prove that only one isomer is formed (Fig. 1, bottom). Since the photochemical electrocyclization occurs in a conrotatory mode,[2] only one of the two pseudo-C_2 symmetric conformers will lead to the final product.

Irradiation of **C** with light $\lambda \geqslant 450$ nm[7b] restores the original spectrum of **A** completely. This clearly demonstrates the retroelectrocyclization of the 1,2-dihydrobenzene moiety of dihydrothienobenzothiophene **C**. Under the conditions of the ^{1}H-NMR experiment we could find no evidence for the formation of photochrome **B** under irradiation. This is due to the fast thermal back-reaction of the **VHF** substructure in **B** to the **DHA** form in **A**.

Irradiation with UV light, either steady-state (254, 313 or 366 nm) or pulsed (248, 308 or 354 nm),[1c] of **A** in non-polar solvents, *e.g.* cyclohexane (Fig. 2) and methylcyclohexane (MCH), leads to new strong absorption bands with maxima at

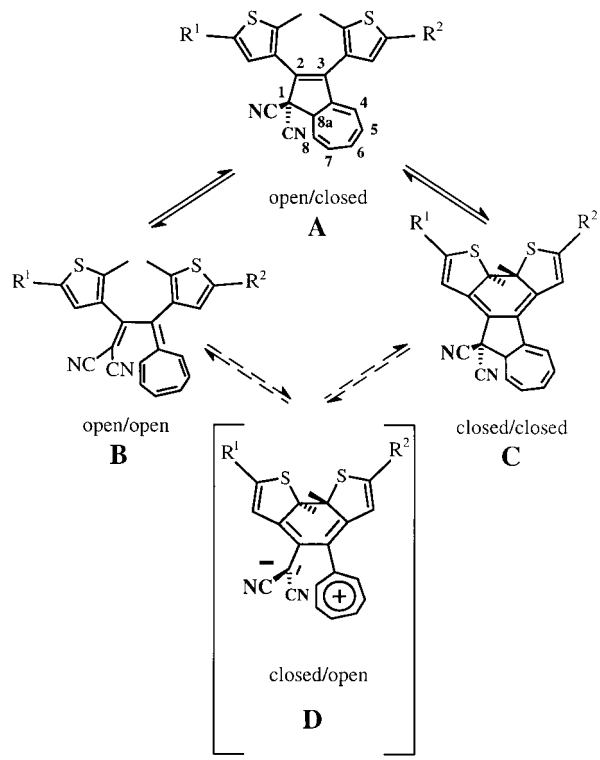

Scheme 1 Concept of a four-step cyclic process of biphotochromic compounds. The notation 'open/closed' for isomer **A** refers to the dithienyl moiety being in its 'open' state and the dihydroazulene moiety in a 'closed' one. This nomenclature is equally applied to forms **B**, **C** and **D**.

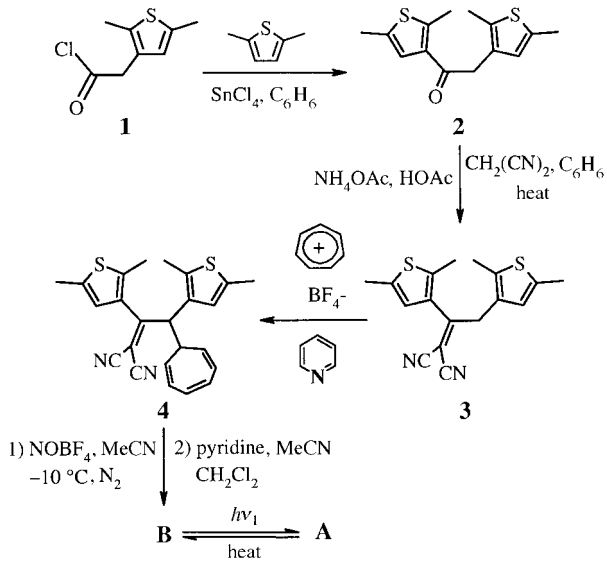

Scheme 2 Synthesis of open/closed **A**.

300, 360 and 480 nm within 10 ns. When the UV light is removed, the 300 nm peak slowly disappears and the visible band becomes less intense and is red-shifted to 510 nm. The latter findings are characteristic for **VHF** chromophores, which thermally revert back, reaction **B** → **A**.[1c] For comparison and reference, typical long wavelength absorption bands of chromophores **DHA**, **VHF**, **DTE** and **DHB** in various solvents are as follows: **DHA**:[1] 320–380 nm; **VHF**:[1] 410–470 nm; **DTE**:[2] 250–450 nm; **DHB**:[2] 420–820 nm.

Similar changes within 10 ns were observed for **A** in PhMe and polar solvents, *e.g.* DMF, MeCN, MeOH or EtOH, at room temperature, where after a few seconds or some minutes only the intense 360 nm band, in addition to the broader band centered at *ca.* 500 nm, were observed and no further spectral changes occur on heating. This is in agreement with the formation of **C** in the photochemical forward step. Note that the photochemical **A** → **B** forward and thermal **B** → **A** backward steps take place in all solvents. By irradiation with visible light ($\lambda \geqslant 450$ nm), **A** is completely restored.

Kinetic measurements quantify the solvent effects of the thermal ring closure. They follow a first order rate process. The corresponding pre-exponential factor (A), the activation energy (E_a) and the relaxation time ($\tau_{B\rightarrow A}$) at room temperature are given in Table 1. The activation parameters are similar, but they clearly demonstrate the trend that the more polar the solvent is, the faster the thermal rearrangement proceeds.

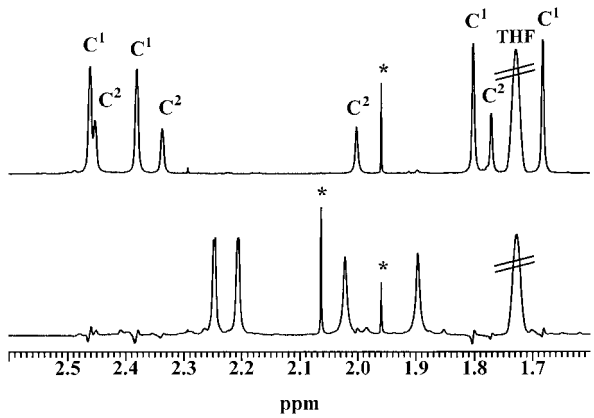

Fig. 1 Irradiation experiments of **A** in THF-d_8 (3.8×10^{-3} mol dm^{-3}) monitored by ^{1}H-NMR spectroscopy (−50 °C), representing the methyl signals. Top: precursor isomer **A** before irradiation; C^1,C^2 = methyl groups of the two conformers. Bottom: **A** after irradiation at room temperature (254 nm) for 5 h (photoconversion: *ca.* 50%) and subtraction of the upper spectrum (subtraction spectrum is shown). * = Unidentified signals.

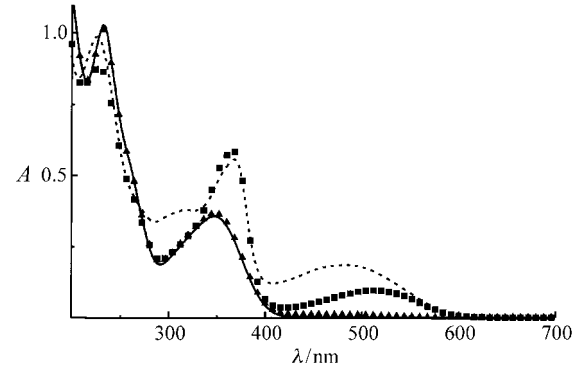

Fig. 2 Reversible irradiation of **A** in cyclohexane (4.4×10^{-5} mol dm^{-3}) at room temperature: **A** prior to (—) and after irradiation at 254 nm (----), after thermal relaxation (■) and after subsequent irradiation with visible light ($\geqslant 450$ nm), where **A** is restored (▲).

Table 1 Pre-exponential factor A, activation energy E_a and relaxation time $\tau_{B\rightarrow A}$ for the thermal ring-closure reaction[a]

Solvent	$A/10^{10}$ s^{-1}	E_a/kJ mol^{-1}	$\tau_{B\rightarrow A}$ s[b]	Temperature range/°C
MCH	20	82	1100	25–95
PhMe	1	70	130	25–110
DMF	100	78	30	25–130
MeCN	1	66	30	25–70
EtOH	0.5	64	25	0–70

[a] Obtained from Arrhenius plots, detection wavelength 475 nm and excitation wavelength λ_{exc} = 308 nm. [b] At 25 °C.

To summarize, both open/open **B** and closed/closed **C** are rapidly formed on irradiating open/closed **A**. **B** is thermally rearranged to **A,** and **C** can photochemically be reverted into **A**. Closed/open **D** has not yet been observed in the system with the substitution pattern $R^1 = R^2 = CH_3$. Appropriate donor and acceptor groups at the **DTE/DHB** moiety (R^1: acceptor subtituent; R^2: donor substituent) would make its formation likely.

Notes and references

1 (*a*) J. Daub, S. Gierisch, U. Klement, T. Knöchel, G. Maas and U. Seitz, *Chem. Ber*., 1986, **119**, 2631; (*b*) S. Gierisch and J. Daub, *Chem. Ber*., 1989, **122**, 69; (*c*) H. Görner, C. Fischer, S. Gierisch and J. Daub, *J. Phys. Chem*., 1993, **97**, 4110; (*d*) H. Spreitzer and J. Daub, *Liebigs Ann*., 1995, 1637; (*e*) H. Spreitzer and J. Daub, *Chem. Eur. J*., 1996, **2**, 1150; (*f*) M. Kaftory, M. Botoshansky, J. Daub, C. Fischer and A. Bross, *Acta. Crystallogr., Sect. C*, 1997, **53**, 1665.

2 (*a*) M. Irie and M. Mohri, *J. Org. Chem*., 1988, **53**, 803; (*b*) G. M. Tsivgoulis and J.-M. Lehn, *Chem. Eur. J*., 1996, **2**, 1399; (*c*) T. Tsujioka, M. Kume, Y. Horikawa, A. Ishikawa and M. Irie, *Jpn. J. Appl. Phys*., 1997, **36**, 526; (*d*) A. Fernandez-Acebes and J.-M. Lehn, *Adv. Mater*., 1998, **10**, 1519.

3 H. Dürr and H. Bouas-Laurent, *Photochromism Molecules and Systems*, Elsevier, Amsterdam, 1990; B. L. Feringa, W. F. Jaeger and B. de Lange, *Tetrahedron*, 1993, **49**, 8267; J. Daub, M. Beck, A. Knorr and H. Spreitzer, *Pure Appl. Chem*., 1996, **68**, 1399.

4 Examples of biphotochromic systems: J. Daub, K. M. Rapp. J. Salbeck and U. Schöberl, *Carbohydrates as Organic Raw Materials*, ed. F. W. Lichtenthaler, VCH, Weinheim, 1991, p. 323; L. Gobbi, P. Seiler and F. Diederich, *Angew. Chem., Int. Ed*., 1999, **38**, 674; H. Bleisinger, P. Scheidhauer, H. Dürr, V. Wintgens, P. Valat and J. Kossanyi, *J. Org. Chem*., 1998, **63**, 990; J. Daub, C. Fischer, S. Gierisch and J. Sixt, *Mol. Cryst. Liq. Cryst*., 1992, **217**, 177; H. Dürr in J. C. Crano and R. J. Guglielmetti, *Organic Photochromic and Thermochromic Compounds*, Plenum, New York, vol. 1, 1999, p. 223.

5 M. Irie, *Mol. Cryst. Liq. Cryst*., 1993, **227**, 263.

6 Analogous to ref. 1(*b*); T. Mrozek, *Diplomathesis*, University of Regensburg, 1997.

7 (*a*) UV-lamp (K. Benda, Laborgeräte und Ultraviolettstrahler); (*b*) High pressure Hg/Xe-cathode tip lamp with cut-off filter GG 455 (Schott).

Communication 9/03060C

Novel synthesis of isoprene from 3-methylbutan-2-one using phosphate catalysts

Graham J. Hutchings,*[a]† Ian D. Hudson,[a] Donald Bethell[a]‡ and Don G. Timms[b]

[a] *Leverhulme Centre for Innovative Catalysis, Department of Chemistry, University of Liverpool, Liverpool, UK L69 3BX. E-mail: hutch@cf.ac.uk*

[b] *Enichem Elastomers Ltd, Charleston Road, Hardley, Hythe, Southampton, UK SO4 6YY*

Received (in Cambridge, UK) 16th March 1999, Accepted 18th June 1999

$AlPO_4$ and BPO_4 catalyse the conversion of 3-methylbutan-2-one to isoprene in high yields *via* 2-methylbut-2-en-1-ol as an intermediate.

Isoprene is an important monomer for the stereoselective polymerisation to 1,4-*cis*-polyisoprene which is used in the manufacture of synthetic rubber. Isoprene is currently obtained from naphtha cracking but in recent years there has been continued interest in the identification of new synthetic routes. One interesting possibility is the dehydration of 2-methylbutanal which is available as a result of the commercialisation of the low pressure hydroformylation of butene.[1] BPO_4 has been shown to be an effective catalyst[2–4] for this reaction and can give 60–70% yield at high conversion, but deactivation can be rapid. Recently, we have shown[5] that BPO_4 can be readily reactivated using a simple high temperature treatment, thereby making these catalysts more suitable for industrial application. However, together with isoprene, 3-methylbutan-2-one is formed as a major by-product with both phosphate catalysts and this, at present, limits the commercial applicability of the process. Here we demonstrate that 3-methylbutan-2-one can be readily converted to isoprene using BPO_4 and $AlPO_4$ as catalysts. Furthermore, we demonstrate that isoprene and 3-methylbutan-2-one formation from 2-methylbutanal are linked by a common intermediate, 2-methylbut-2-en-1-ol. These results indicate that by recycling the 3-methylbutan-2-one by-product the overall yield of isoprene can be increased by $\geqslant$10% for both BPO_4 and $AlPO_4$ catalysts.

Boron phosphate (P:B = 1) was prepared by heating phosphoric acid (93 ml, 85%) with boric acid (100 g) at 60 °C for 1 h. Water (100 ml) was then added and the mixture was refluxed for 5 h and then dried (110 °C, 16 h) and calcined (350 °C, 4 h). The product was confirmed to be the cristabolite form of BPO_4 by X-ray diffraction. Aluminium phosphate (Al:P = 1) was prepared by the slow addition of aqueous ammonia (40 vol%, 5 °C), with continuous stirring, to an aqueous solution containing equimolar quantities of $AlCl_3$ and phosphoric acid (0.985 mol l^{-1}, 5 °C). Aqueous ammonia addition was continued until pH = 7.0 was attained. The white precipitate was aged (18 h, 20 °C) and collected by filtration, washed several times with propan-2-ol, dried (24 h, 120 °C) and calcined (3 h, 800 °C). Powder X-ray diffraction showed that the catalyst was a mixture of the cristabolite and tridymite phases of $AlPO_4$. Both these solids were screened (200–250 mesh), and pelleted and sieved (600–1000 μ) prior to use as catalysts. The phosphates were investigated as catalysts for the dehydration of 2-methylbutanal and isoprene was observed as the major product in agreement with our previous results.[5] For both BPO_4 and $AlPO_4$ the only by-product was 3-methylbutan-2-one which was formed at *ca.* 18–20% yield. In a separate set of reactions 3-methylbutan-2-one [0.67 ml (g catalyst)$^{-1}$ h^{-1}] was reacted over the phosphate catalysts (0.3 g) using a standard laboratory microreactor with nitrogen as a diluent (24 ml h^{-1}). Products were analysed using GC and satisfactory mass balances were obtained for all data presented. The results for BPO_4 at 325 °C and $AlPO_4$ at 400 °C are shown in Fig. 1. $AlPO_4$ required a higher reaction temperature than BPO_4 to observe a significant conversion level. Both catalysts convert 3-methylbutan-2-one to isoprene with high selectivity (80–95%) and at reasonable conversion levels. The catalyst performance was found to be very stable and, significantly, no appreciable deactivation was observed.

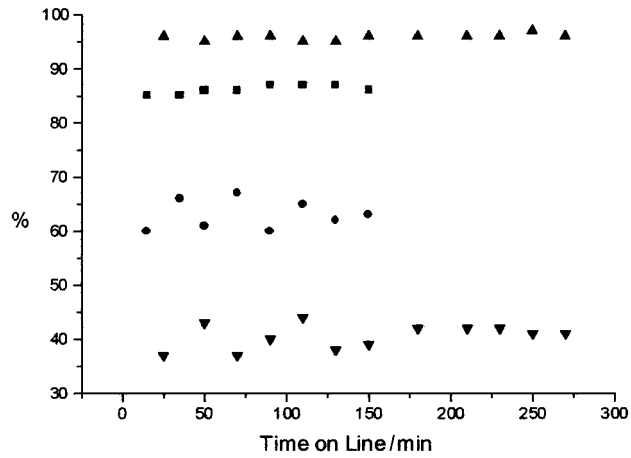

Fig. 1 Reaction of 3-methylbutan-2-one over (a) BPO_4 at 325 °C [(▼) conversion, (▲) isoprene selectivity] and (b) $AlPO_4$ at 400 °C [(■) conversion, (●) isoprene selectivity].

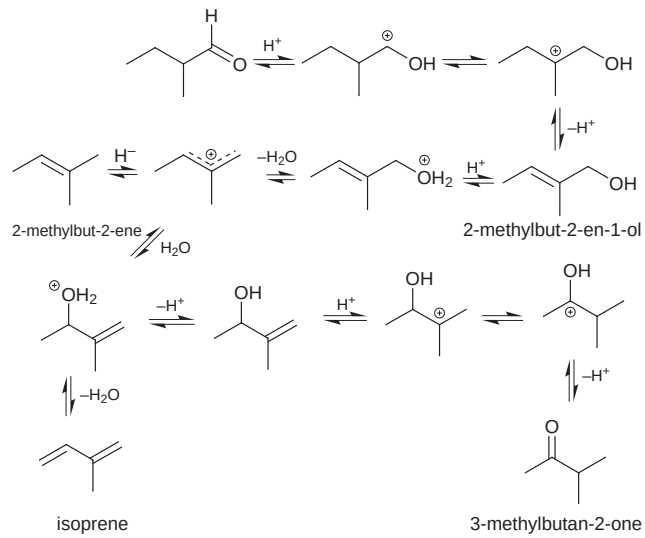

Scheme 1 Proposed mechanism for the conversion of 2-methylbutanal and 3-methylbutan-2-one to isoprene.

† Present address: Department of Chemistry, Cardiff University, PO Box 912, Cardiff, UK CF1 3TB.

‡ Present address: BNFL Ltd, Springfields Works, Salwick, Preston, UK PR4 0XJ.

The observation that both 2-methylbutanal and 3-methylbutan-2-one could be converted to isoprene with these catalysts prompted us to consider the reaction mechanism for these catalytic processes. We believe that 2-methylbut-2-en-1-ol is a central intermediate in the conversion of 2-methylbutanal into both isoprene and 3-methylbutan-2-one (Scheme 1). To test this proposal, 2-methylbut-2-en-1-ol was synthesised by reduction of 2-methylbut-2-enal with sodium borohydride in MeOH. 2-Methylbut-2-en-1-ol was then reacted [0.67 ml (g catalyst)$^{-1}$ h^{-1}] in a nitrogen diluent (24 ml min^{-1}) over BPO_4 (0.3 g) at 110 and 300 °C. At these temperatures, 2-methylbut-2-ene was a major product (*ca.* 10–40%) but in addition isoprene (37%), 2-methylbutanal (10%) and traces of 3-methylbutan-2-one were also observed and the conversion increased from 87% at 110 °C to 99% at 300 °C (Table 1). These results support the proposal that 2-methylbut-2-en-1-ol is a key intermediate in the conversion of 2-methylbutanal into both isoprene and 3-methylbutan-2-one.

This study indicates that the yield of isoprene from the dehydration of 2-methylbutanal, using $AlPO_4$ and BPO_4 catalysts, can be significantly enhanced if the major by-product, 3-methylbutan-2-one, is reacted over the same phosphate catalyst under the same reaction conditions. It is anticipated that this can be done *via* a recycle step and yield increases of *ca.* 10% for BPO_4 (from 72 to 82 at 325 °C) and 16% for $AlPO_4$ (from 56 to 72% at 400 °C) can be expected.

Table 1 Conversion of 2-methylbut-2-en-1-ol over BPO_4[a]

		Selectivity[b]		
T/°C	Conversion	2MBA	2MBE	I
110	87	12	49	39
300	99	25	47	10

[a] BPO_4 (0.3 g), 2-methylbut-2-en-1-ol [0.67 ml (g catalyst)$^{-1}$ h^{-1}], N_2 (24 ml min^{-1}. [b] 2MBA = 2-methylbutanal; 2MBE = 2-methylbut-2-ene; I = isoprene.

We thank EniChem Elastomers Ltd for financial support for this work.

Notes and references

1 P. J. Davidson, R. R. Hignett and D. T. Thompson, in *Catalysis*, A Specialist Periodical Report, ed. C. Kemball, Chemical Society, 1977, vol. 1, p. 369.
2 H. Fischer and G. Schunchel, *UK Pat.*, UK 1 385 348, 1975.
3 J. B. Moffat, *Rev. Chem. Intermed*., 1987, **8**, 1.
4 J. B. Moffat and A. Schmidtmeyer, *Appl. Catal.*, 1986, **28** , 161.
5 G. J. Hutchings, I. D. Hudson and D. G. Timms, *J. Chem. Soc., Chem. Commun.*, 1994, 2717.

Communication 9/02072A

ChemComm

Oxidative C(sp³)–C(sp³) bond cleavage reaction of an isopropyl group to give an acetyl group upon O_2-treatment of a labile cationic ruthenium species, $[Tp^{iPr}Ru(dppene)(OH_2)]^+$†

Yoshiaki Takahashi, Shiro Hikichi, Munetaka Akita* and Yoshihiko Moro-oka*

Research Laboratory of Resources Utilization, Tokyo Institute of Technology, 4259 Nagatsuta, Midori-ku, Yokohama 226-8503, Japan. E-mail: makita@res.titech.ac.jp

Received (in Cambridge, UK) 25th May 1999, Accepted 28th June 1999

Exposure of a cationic aquoruthenium(II) complex, $[Tp^{iPr}Ru(dppene)(OH_2)]^+$ [Tp^{iPr} = hydrotris(3,5-diisopropylpyrazolyl)borato; dppene = 1,2-bis(diphenylphosphino)ethene], to O_2 at ambient temperature results in oxidative cleavage of the C(sp³)–C(sp³) bond in an isopropyl group in the Tp^{iPr} ligand to give an acetyl functional group.

Oxygenation reactions mediated by a transition metal species are involved as key steps in organic synthesis and metabolic reactions, and selective aerobic oxygenation of hydrocarbyl functional groups has long been a challenging research target.[1] Transition metal–O_2 adducts have been studied extensively as pivotal intermediates of oxygenation reactions but the adducts may be too reactive to be isolated and they frequently oxidize external or internal functional groups including hydrocarbyl substrates. In contrast to a considerable number of C–H and C(sp²)=C(sp²) bond oxygenation reactions induced by O_2-treatment of a transition metal complex,[2] oxygenation of saturated C(sp³)–C(sp³) bond has few precedent examples.[3] During the course of our systematic synthetic study on dioxygen complexes coordinated by hydrotris(pyrazolyl)borato ligands (Tp^R),[4] we observed an oxidative cleavage reaction of a C(sp³)–C(sp³) bond in a ruthenium complex.

We attempted the synthesis of a ruthenium–dioxygen complex bearing the Tp^{iPr} ligand [Tp^{iPr} = hydrotris(3,5-diisopropylpyrazolyl)borato] by O_2-treatment of a coordinatively unsaturated cationic ruthenium(II) species, $[Tp^{iPr}Ru(diphosphine)]^+$ **1**$^+$ [diphosphine = Ph_2P–X–PPh_2: X = CH=CH (**a**: dppene), CH_2 (**b**: dppm), CH_2CH_2 (**c**: dppe)], which should be formed from labile cationic aquo complexes, $[Tp^{iPr}Ru(diphosphine)(OH_2)]^+$ **2**$^+$.[5,6] Exposure of the aquo complexes **2**$^+$ to O_2, however, did not afford the desired product but instead resulted in three different types of oxygenation reactions giving complexes **3**–**5** depending on the structure of the diphosphine ligand (Scheme 1).[7]

Stirring a methanol solution of the dppene complex **2a**OTf[5] (OTf = trifluoromethansulfonate) under an O_2 atmosphere (1 atm) at room temperature gave a mixture containing the red–brown diamagnetic complex **3**OTf (20 % isolated yield) as a major product. The three inequivalent 4-pz-H signals (^{1}H NMR)‡ indicated an unsymmetrical structure but **3**OTf could not be identified by the spectroscopic data alone. In addition, single crystals suitable for X-ray crystallography were not obtained. The coordinatively unsaturated species **1**$^+$ may be generated by an alternative method, *i.e.* dechlorination of the corresponding chloro complex **6** by the action of a Ag salt. Treatment of **6a** with $AgBF_4$ under O_2 atmosphere afforded **3**BF_4 showing spectroscopic properties† similar to those of the OTf salt and its molecular structure was determined by X-ray crystallography [Fig. 1(a)].‡ The most striking structural feature was formation of the acetyl group (C15–C14–O1) resulting from oxygenation of an isopropyl group in the Tp^{iPr} ligand proximal to the metal center, and coordination of the acetyl oxygen atom to the metal center leads to a distorted octahedral coordination geometry [N11–Ru1–N21 93.0(2)°, N11–Ru1–N21 77.8(2)°, N21–Ru1–Ru31 85.2(2)°, Ru1–P1 2.271(2) Å, Ru1–P2 2.297(2) Å, Ru1–O1 2.118(5) Å, Ru1–N11 2.051(5) Å, Ru1–N21 2.123(5) Å, Ru1–N31 2.180(7) Å]. In accord with the structure, a singlet signal at δ_H 1.66 (3H) assignable to the coordinated acetyl group was observed. The acetyl oxygen atom came from O_2 molecule as revealed by a labeling experiment using $^{18}O_2$. When the reaction was carried out in propan-2-ol, formation of methanol was detected by GLC analysis of the solution phase and, therefore, the removed methyl group should be converted to methanol. Thus interaction of the coordinatively unsaturated species **1a**$^+$ with O_2 resulted in unprecedented oxidative cleavage of the C(sp³)–C(sp³) bond in an isopropyl substituent under mild reaction conditions.

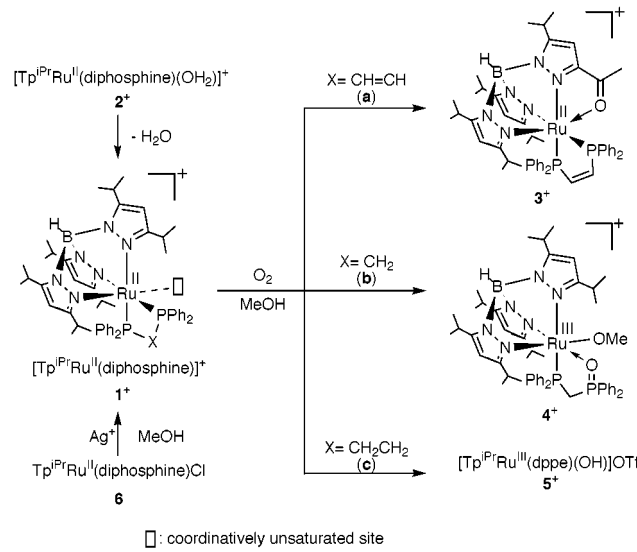

Scheme 1

In order to examine the generality of the oxygenation reaction, related diphosphine complexes **1b** and **1c**$^+$ were exposed to O_2. Although oxygenation of a hydrocarbyl group

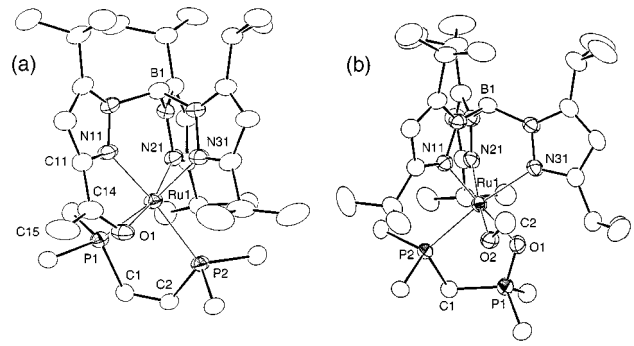

Fig. 1 Structures of the cationic parts of the oxygenated products, **3**BF_4 (a) and **4**PF_6 (b), drawn at the 30% probability level. For the phenyl groups only *ipso* carbons are shown for clarity and the acetyl part in **3**$^+$ is shaded.

did not occur, other types of oxygenation reactions were observed. Dechlorination of **6b** with $AgPF_6$ in MeOH under an O_2 atmosphere produced the red–brown paramagnetic complex **4**$^+$,† and its FD-MS data [*m/z* 998: Tp^{iPr}Ru(dppm)(OMe)(O)] suggested occurrence of oxygenation. X-Ray crystallography [Fig. 1(b)]‡ revealed that complex **4**$^+$ was a cationic ruthenium(III) complex with a 5-oxa-2,4-diphospharuthenacyclopentane structure resulting from oxygenation of one of the two phosphorus atoms in the dppm ligand, and the sixth coordination site was occupied by the methoxo ligand coming from the reaction solvent. In this case, an active oxidizing species bonded to the metal center should be trapped by the neighboring phosphorus atom to release strain of the four membered Ru–P–C–P ring in **2b**$^+$. Finally, treatment of the dppe complex **2c**PF_6 with O_2 resulted in one-electron oxidation of the ruthenium center coupled with deprotonation of the aquo ligand to give a hydroxo–Ru(III) complex **5**PF_6,† which was characterized by X-ray crystallography,‡ but no ligand oxygenation was observed. Complex cation **5**$^+$ is octahedral with a η^1-hydroxo ligand and it should be noted that the Ru–O distance [2.158(5) Å] is comparable to that in the cationic aquoruthenium(II) complex **2c** [2.148(8) Å] [5] but significantly longer than that in the Ru(II) analogue, Tp^{iPr}Ru(dppe)(OH) [2.067(4) Å].[8]

Thus O_2-treatment of the labile aquo–Ru(II) complexes **2**$^+$ resulted in oxidative C–C bond cleavage (dppene: **3**$^+$) or P-oxidation (dppm: **4**$^+$) or oxidation of the metal center (dppe: **5**$^+$) depending on the nature of the diphosphine ligands. The present oxygenation reactions should consist of complex multi-step reaction sequences, and several plausible mechanisms involving a combination of O–O homolysis, Ru–O homolysis, H-abstraction, ·OH-addition, epoxidation, *etc*. can be depicted. Although no other species could be isolated and further study is needed for clarification of the mechanisms, we propose a Ru(III)–η^1-superoxo species, [Tp^{iPr}Ru^{III}(dppe)(η^1-O_2^-)]$^+$, as a likely intermediate on the basis of the following consideration. In **1**$^+$, the chelating κ^3-Tp^{iPr} and κ^2-diphosphine ligands are tightly bound to the Ru center and the sixth coordination site originally occupied by the aquo ligand in **2**$^+$ is the only accessible coordination site. Coordination of an O_2 molecule, therefore, is feasible only in η^1-fashion (η^1-superoxo species). Because the oxygenation was observed only in alcohols, subsequent hydrogen abstraction from the solvent may lead to a hydroperoxo intermediate, which should induce oxidative C–C cleavage. In addition, the alcohol should also act as a reducing agent to regenerate a Ru(II) species like **3**$^+$. The Ru(II) system is in sharp contrast to the Rh(I) system, which undergoes oxidative addition of an O_2 molecule (two-electron oxidation process), and many (η^2-O_2)Rh(III) complexes were prepared by this method.[9] For elucidation of the mechanism of the O-atom transfer step, further experiments are now under way.

In summary, we reported oxidative C(sp^3)–C(sp^3) bond cleavage reaction induced by O_2-treatment of the coordinatively unsaturated Ru(II) species **1**$^+$. The present study revealed that such a highly active oxidizing species can be generated by simple exposure of a precursor **1**$^+$ to O_2 at ambient temperature. It is also notable that the reaction pathway is dependent on the electronic and structural features of the diphosphine ligand (*e.g.* strain of the diphosphametallacyclic structure and electron-donating ability of the diphosphine ligand).[10]

We are grateful to the Ministry of Education, Science, Sports, and Culture of the Japanese Government for financial support of this research (Grant-in-Aid for Scientific Research: No. 08102006).

Notes and references

† *Selected spectroscopic data*: for **3**BF_4: δ_H($CDCl_3$) 5.76, 5.65, 5.45 (1H × 3, s, 4-pz^{iPr} in Tp^{iPr}), 1.66 (3H, s, $COCH_3$). IR (KBr) ν_{BH} 2542 cm^{-1}. For **4**PF_6: ν_{BH} 2561 cm^{-1}. For **5**PF_6: ν_{OH} 3547 (sh), 3433, ν_{BH} 2552 cm^{-1}.

‡ X-Ray diffraction measurements were made on a Rigaku RAXIS IV imaging plate area detector with graphite-monochromated Mo-Kα radiation (λ = 0.71069 Å).

Crystal data: **3**BF_4·OEt_2: $C_{56}H_{74}B_2N_6O_2F_4P_2Ru$, M = 1123.84, T = −60 °C, triclinic, space group $P\bar{1}$, a = 14.960(4), b = 17.991(5), c = 12.659(3) Å, α = 104.15(2), β = 113.902(15), γ = 67.30(2)°, V = 2858.0(12) Å^3, Z = 2, D_c = 1.31 g cm^{-3}, μ = 3.9 cm^{-1}, $R1$ = 0.0878 for the 8133 unique data with $F > 4\sigma(F)$ ($wR2$ = 0.2484, for all 9085 data) and 671 parameters.

4PF_6: $C_{53}H_{71}BN_6O_2F_6P_3Ru$, M = 1142.95, T = −60 °C, monoclinic, space group $P2_1/n$, a = 13.076(2), b = 15.096(2), c = 29.955(5) Å, β = 101.324(3)°, V = 5798.3(14) Å^3, Z = 4, D_c = 1.31 g cm^{-3}, μ = 4.2 cm^{-1}, $R1$ = 0.0651 for the 8886 unique data with $F > 4\sigma(F)$ ($wR2$ = 0.1812 for all 10184 data) and 662 parameters.

5PF_6·THF: $C_{57}H_{79}BF_6N_6O_2P_3Ru$, M = 1199.05, T = −60 °C, triclinic, space group $P\bar{1}$, a = 13.452(5), b = 21.594(9), c = 11.612(3) Å, α = 102.06(2), β = 110.21(2), γ = 94.22(2)°, V = 3056.0(19) Å^3, Z = 2, D_c = 1.30 g cm^{-3}, μ = 4.0 cm^{-1}, $R1$ = 0.0890 for the 10023 unique data with $F > 4\sigma(F)$ ($wR2$ = 0.2426 for all 10667 data) and 755 parameters. CCDC 182/1300.

1 Leading references: R. A. Sheldon and J. K. Kochi, *Metal-Catalyzed Oxidations of Organic Compounds*, Academic Press, New York, 1981; *The Chemistry of Peroxides*, ed. S. Patai, John Wiley & Sons, Chichester, 1983; *Oxygen Complexes and Oxygen Activation by Transition Metals*, ed. A. E. Martel and D. T. Sawyer, Plenum Press, New York, 1988; *Organic Peroxides*, ed. W. Ando, John Wiley and Sons, Chichester, 1992; Thematic issue of *Chem. Rev.* (*Metal–Dioxygen Complexes*), *Chem . Rev.*, 1994, **94**, 567; G. Strukul, *Angew. Chem., Int. Ed. Engl.*, 1998, **37**, 1198; S. Murahashi, *Angew. Chem., Int. Ed. Engl.*, 1995, **34**, 2443.

2 See ref. 4(*b*) and references cited therein. For C=C cleavage reactions, see, for example, our paper dealing with model complexes of catechol dioxygenase. T. Ogihara, S. Hikichi, M. Akita and Y. Moro-oka, *Inorg. Chem.*, 1998, **37**, 2614.

3 Metalloenzymes which catalyze fragmentation of carbon skeleton *via* C–C cleavage (*e.g.* P-450) are known. V. Stajek, M. Miksch, P. Lueer, U. Matern and W. Boland, *Angew. Chem., Int. Ed* ., 1999, **38**, 400.

4 Pd–O_2: (*a*) M. Akita, T. Miyaji, S. Hikichi and Y. Moro-oka, *Chem. Commun.*, 1998, 1005; Co–OOR: (*b*) S. Hikichi, H. Komatsuzaki, M. Akita and Y. Moro-oka, *J. Am. Chem. Soc.*, 1998, **120**, 4699; Co, Ni–oxo; (*c*) S. Hikichi, M. Yoshizawa, Y. Sasakura, M. Akita and Y. Moro-oka, *J. Am. Chem. Soc.*, 1998, **120**, 10567; Mn–O_2: (*d*) H. Komatsuzaki, Y. Nagasu, K. Suzuki, T. Shibasaki, M. Satoh, F. Ebina, S. Hikichi, M. Akita and Y. Moro-oka, *J. Chem. Soc., Dalton Trans.*, 1998, 511; (*e*) H. Komatsuzaki, S. Ichikawa, S. Hikichi, M. Akita and Y. Moro-oka, *Inorg. Chem.*, 1998, **37**, 3652; V–O_2: (*f*) M. Kosugi, S. Hikichi, M. Akita and Y. Moro-oka, *J. Chem. Soc., Dalton Trans.*, 1999, 1369.

5 The dppene and dppm derivatives of **2**$^+$ and **6** were prepared according to the preparative method for the dppe complexes: see, Y. Takahashi, S. Hikichi, M. Akita and Y. Moro-oka, *Inorg. Chem.*, 1998, **37**, 3186.

6 The dehydrated, coordinatively unsaturated species **1c**$^+$ stabilized by an agostic interaction with a methyl C–H bond in the isopropyl group could be isolated. Y. Takahashi, S. Hikichi, M. Akita and Y. Moro-oka, *Organometallics*, 1999, **18**, 2571.

7 It was reported that (η^2-O_2)Ru(IV) complexes were obtained by O_2-treatment of the isoelectronic [(η^5-C_5R_5)Ru(diphosphine)]$^+$ species. K. Kirchner, K. Mauthner, K. Mereiter and R. Schmid, *J. Chem. Soc., Chem. Commun.*, 1993, 892; I de los Rios, M. J. Tenorio, J. Padilla, M. P. Puerta and P. Valerga, *J. Chem. Soc., Dalton Trans.*, 1996, 377; M. Sato and M. Asai, *J. Organomet. Chem.*, 1996, **508**, 121.

8 Y. Takahashi, S. Hikichi, M. Akita and Y. Moro-oka, unpublished work.

9 A η^2-peroxo complex with the Tp^{iPr} ligand, Tp^{iPr}Rh(O_2)(pz^{iPr}-H), was obtained by the oxidative addition method. Y. Takahashi, S. Hikichi, M. Akita and Y. Moro-oka, *Angew. Chem., Int. Ed.*, in press. For one-electron oxidation of Tp^{R}Rh complex, only one report appeared. N. G. Connelly, D. J. H. Emslie, B. Metz, A. G. Orpen and M. J. Quayle, *Chem. Commun.*, 1996, 2289.

10 Accoding to the E_L values defined and determined by Lever, the order of electron-donating ability is estimated as follows: dppene (0.49) > dppm (0.43) > dppe (0.28). A. B. P. Lever, *Inorg. Chem.*, 1990, **29**, 1271.

Communication 9/04218K

Remarkably stable self-assembled monolayers of new crown-ether annelated tetrathiafulvalene derivatives and their cation recognition properties†

Haiying Liu, Shenggao Liu and Luis Echegoyen*

Department of Chemistry, University of Miami, Coral Gables, FL 33124, USA. E-mail: echegoyen@miami.edu

Received (in Columbia MO) 26th May 1999, Accepted 23rd June 1999

Bis-thioctic ester derivatives of crown-ether annelated tetrathiafulvalenes (TTFs) form extremely stable self-assembled monolayers (SAMs) on gold electrodes and can recognize alkali metal ions by cyclic voltammetry.

The first TTF-functionalized SAMs, reported by Yip and Ward, were relatively unstable upon electrochemical probing and cycling.[1] Very recently a novel TTF compound containing four thiol groups was reported, which formed very robust SAMs on gold, and these were stable after repeated voltammetric cycling.[2] The use of such multiple anchoring sites provides very strong adherence of the compound to the metal surfaces, especially if the sulfur atoms are present within the same ring structure, in which case they exhibit a chelate effect.[3] For these reasons, the use of thioctic acid derivatives to anchor SAMs on metal surfaces has received considerable recent attention.[4] In addition, thioctic acid (1,2-dithiolane-3-valeric acid) is commercially available and easy to incorporate into a wide variety of structures *via* simple condensation reactions, as reported in the present work.

The incorporation of crown-ether groups into SAMs and their use as potential metal ion sensors were first reported almost simultaneously last year by Moore *et al.*[5] and by Flink *et al.*[6] In one case they prepared simple 12-crown-4 and 15-crown-5 derivatives with appended single chains terminated in a thiol group, and impedance spectroscopy was used to monitor ion binding events on the surface.[6] The other group reported crown-annelated TTF derivatives which also contained single alkyl chains terminated in thiol groups.[5] This work exploited the direct electrochemical response of the surface-confined crown-TTF groups to measure the effect of ion complexation, similar to previously reported work in homogeneous solution by Hansen *et al.*[7] However, these SAMs were apparently not very stable under various conditions and the electrochemical responses observed were very weak and poorly resolved.[5] Here we report the preparation of two bis-thioctic ester derivatives of crown-annelated TTFs, which form remarkably stable SAMs on gold and show very clear and reversible surface-confined electrochemistry and anodic shifts upon binding with alkali metal ions.

Compounds **1a**–**c** were directly synthesized in high yield by reacting the corresponding bis-alcohols with thioctic acid in CH_2Cl_2 in the presence of 1,3-dicyclohexylcarbodiimide (DCC) and 4-pyrrolidinopyridine or 4-(dimethylamino)pyridine (DMAP).[8] The corresponding crown-annelated TTF bis-alcohol precursors were prepared in reasonable yields following literature procedures.[9] The mono-alcohol precursor to prepare **1d** was obtained by reducing one of the ester groups of diester-EDT-TTF.[9b,10] It should be stressed that the synthetic method reported here to prepare crown-ether annelated tetrathiafulvalene derivatives with disulfide groups attached by reacting thioctic acid with derivatives of TTF incorporating hydroxy group(s) is general, straightforward and gives high yields.

Glass-sealed, ultra-clean spherical gold bead electrodes prepared from gold wire (99.9999%, diameter 250 μm) were

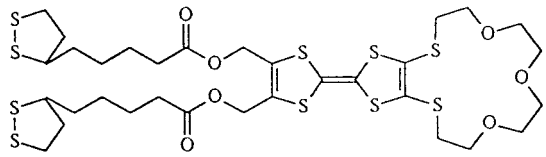

1a

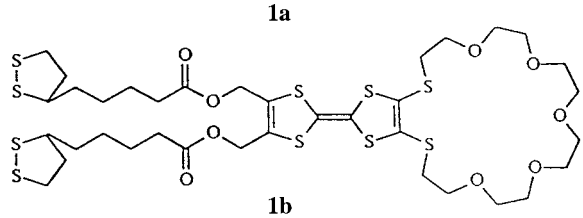

1b

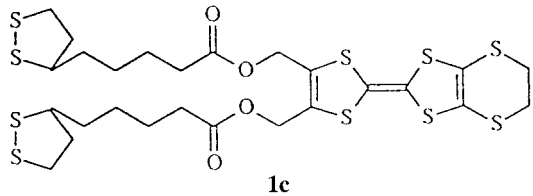

1c

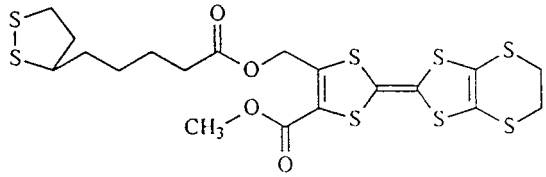

1d

dipped into 5 mM THF solutions of the corresponding bis-thioctic ester compounds **1a**–**d** for 24 h to form the corresponding SAMs.[11] After washing these with clean THF and allowing them to dry in air, these SAM modified electrodes were placed into 0.1 M Bu_4NPF_6–THF (or 0.1 M Bu_4NPF_6–CH_2Cl_2) and their cyclic voltammograms (CVs) recorded.[12] Fig. 1 shows the

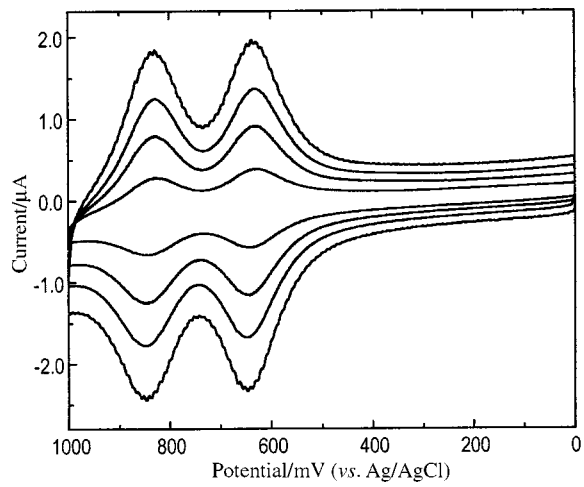

Fig. 1 Cyclic voltammetric analysis of the SAMs of **1a** in THF solution containing 0.1 M Bu_4NPF_6 at different scan rates: 100 (smallest current), 250, 400 and 600 mV s^{-1} (largest current).

† Data for compounds **1b**–**d** are available from the RSC web site, see http://www.rsc.org/suppdata/cc/1999/1493/

Table 1 Electrochemical data for the SAMs of the disulfides in THF solution containing 0.1 M Bu_4NPF_6 *vs.* an aqueous Ag/AgCl reference electrode

SAMs of compound	$E_{1/2}^1$/V (ΔE_p/mV)	$E_{1/2}^2$/V (ΔE_p/mV)	Coverage[a]
1a	0.64 (12)	0.85 (5)	1.15
1b	0.62 (20)	0.80 (15)	0.33
1c	0.65 (25)	0.90 (15)	1.58
1d	0.73 (58)	0.96 (70)	2.21

[a] In units of 10^{-10} mol cm^{-2}.

variable scan rate dependence of the CVs for SAMs of **1a** on gold in a THF-electrolyte solution. Both TTF-based oxidations are clearly observed and reversible, and their currents increase linearly with the scan rate, indicative of surface-confined behavior (Fig. 1).

This behavior is also evident from the Gaussian shapes of the peaks and the small potential difference between the anodic and cathodic peaks, 12 mV for the first oxidation at $E_{1/2}$ = +0.64 V (*vs.* an aqueous Ag/AgCl reference electrode and at v = 100 mV s^{-1}) and 5 mV for the second oxidation at $E_{1/2}$ = +0.85 V, see Table 1. Essentially identical behavior was observed for **1b**, **1c** and **1d**, but the SAMs of **1d** were much more unstable upon repeated potential cycling, with an 80% decrease in current after four cycles between 0 and +1.1 V. The potentials for the TTF-based oxidations are summarized in Table 1.

The SAMs derived from compounds **1a**, **1b** and **1c** were remarkably stable, exhibiting almost the same current response even after more than 100 potential scan cycles. Perhaps more impressively, these SAMs retained their stability over the course of several days, apparently indefinitely. In our hands, these are the most stable SAMs with which we have ever worked.

The effect of adding alkali metal ions to the THF solutions (typically 5 mM of MPF_6, with M = Li^+, Na^+ or K^+) varied for the different compound–M^+ combinations. The largest anodic shift was observed for **1b**–Na^+, and these cyclic voltammetric results are presented in Fig. 2.

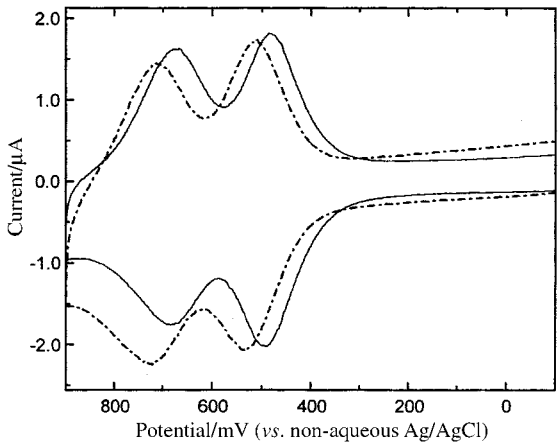

Fig. 2 Cyclic voltammetry of the SAMs of **1b** in THF solution containing 0.1 M Bu_4NPF_6 in the absence (solid line) and in the presence (dotted line) of 5.0 mM $NaPF_6$ at a scan rate of 400 mV s^{-1}. A non-aqueous Ag/AgCl containing 0.1 M Bu_4NPF_6 in THF was used as a reference electrode. Thus the potential axis is different from that in Fig. 1.

The first oxidation process was anodically shifted by 60 mV in this case, while the second oxidation was also shifted anodically, by 55 mV. This behavior is somewhat in contrast to that previously reported for crown-annelated TTF compounds in homogeneous solution, for which the first oxidation is shifted anodically, but the second remains unchanged, presumably due to electrostatically-induced decomplexation of M^+ following the first oxidation to form TTF^+–crown.[7] Either surface aggregation or cooperativity effects between neighboring crown rings on the SAMs could account for the different behavior observed here. The effects of the alkali metal ions tested on the CVs of **1a** and **1b** are summarized in Table 2.

Table 2 Shifts (mV) of redox potentials of the SAMs of **1a** and **1b** upon addition of alkali metal ion salts

Metal ion salt (5.0 mM)	SAMs of **1a**		SAMs of **1b**	
	$E_{1/2}^1$	$E_{1/2}^2$	$E_{1/2}^1$	$E_{1/2}^2$
$LiPF_6$	0	0	0	0
$NaPF_6$	+10	0	+60	+55
KPF_6	0	0	+20	+30

Note that Li^+ showed no effect on either of the crown compounds, while Na^+ showed the largest effect with both SAMs. K^+ induced a smaller anodic shift than Na^+, and only with **1b**. As expected, **1c** did not exhibit any cation-induced effects, since there is no crown ether ring present in the structure. All of these results indicate that the cation-induced shifts result from complexation between the crown rings and the metal ions.

In summary, electrochemically active SAMs have been prepared which are almost indefinitely stable and show promise as potential thin-film sensors for electrochemically inactive metal ions. Further work is underway to improve the selectivity properties of these SAMs.

This work was supported by the National Science Foundation, grants CHE-9816503 and DMR-9803088.

Notes and references

1 C. M. Yip and M. D. Ward, *Langmuir*, 1994, **10**, 549.
2 I. Fujihara, H. Nakai, M. Yoshihara and T. Maeshima, *Chem. Commun.*, 1999, 737.
3 Y.-S. Shon and T. R. Lee, *Langmuir*, 1999, **15**, 1136.
4 (*a*) Q. Cheng and A. Brajter-Toth, *Anal. Chem.*, 1992, **64**, 1998; (*b*) Y. Wang and A. E. Kaifer, *J. Phys. Chem. B*, 1998, 9922; (*c*) R. Blonder, I. Willner and A. F. Buckmann, *J. Am. Chem. Soc.*, 1998, **120**, 9335.
5 A. J. Moore, L. Goldenberg, M. R. Bryce, M. C. Petty, A. P. Monkman and S. N. Port, *Adv. Mater.*, 1998, **10**, 395.
6 S. Flink, B. A. Boukamp, A. v. d. Berg, F. C. J. M. van Veggel and D. N. Reinhoudt, *J. Am. Chem. Soc.*, 1998, **120**, 4652.
7 T. K. Hansen, T. Jorgensen, P. C. Stein and J. Becher, *J. Org. Chem.*, 1992, **57**, 6403.
8 All new compounds were fully characterized by spectroscopic techniques. *Selected data* for **1a**: isolated as a red–orange solid in 87% yield, ν (KBr)/cm^{-1} 2932 (s), 1710 (vs), 1630 (vs), 1542 (s), 1163 (s); δ_H($CDCl_3$/TMS) 4.91 (4H, s), 3.91 (4H, t, *J* 5.34), 3.74–3.67 (12H, m), 3.58 (4H, t, *J* 5.40), 3.19–3.14 (4H, m), 2.99 (2H, t, *J* 5.90), 2.45–2.37 (4H, m), 1.94–1.85 (2H, m), 1.79–1.63 (8H, m), 1.49–1.46 (4H, m); δ_C($CDCl_3$) 173.70, 173.17, 154.47, 142.04, 129.92, 128.82, 111.84, 108.38, 71.98, 71.51, 70.38, 60.38, 58.37, 56.36, 40.62, 38.95, 37.05, 36.19, 34.17, 26.72, 25.07; λ_{max}($CHCl_3$)/nm 327.5, 304.0; FAB$^+$-MS: *m/z* 862 (M^+, 60%), 864 (M^+ + 2, 100%); HRMS (FAB^+): *m/z* found 862.0453, calc. for $C_{32}H_{46}O_7S_{10}$: 862.0453. For data for **1b**–**d**, see footnote †.
9 (*a*) Detailed synthesis will be published elsehwere; (*b*) S. G. Liu, M. Cariou and A. Gorgues, *Tetrahedron Lett.*, 1998, **39**, 8663.
10 P. Blanchard, M. Sallé, G. Duguay, M. Jubault and A. Gorgues, *Tetrahedron Lett.*, 1992, **33**, 2685.
11 F. Arias, L. A. Godínez, A. E. Kaifer and L. Echegoyen, *J. Am. Chem. Soc.*, 1996, **118**, 6086.
12 All electrochemical experiments were performed using a BAS-100W system. Electrolyte solutions were prepared from recrystallized materials using spectroscopic grade solvents and purged with argon prior to use. A three-electrode configuration was used with a Ag/AgCl reference electrode and a platinum wire as the counter electrode. The geometric areas of the gold electrodes were calculated from the slopes of the linear plots of cathodic peak current *vs.* the square root of the scan rate obtained for the diffusion-controlled reduction of $Ru(NH_3)_6^{3+}$ [ref. 4(*b*)]. We employed a diffusion coefficient of 7.5×10^{-6} cm^2 s^{-1} (at 25 °C in 0.1 M NaCl). Typical values for the geometric area of the electrodes varied from 0.01 to 0.02 cm^2. Surface coverages of the SAMs of TTF derivatives were calculated by integration of the current during the first scan.

Communication 9/04249K

ChemComm

Opposite influence of calf thymus DNA on the rate of substitution of ethylenediamine, by thiourea, in the complex cations $[Pd(bpy)(en)]^{2+}$ and $[Pd(bromazepam)(en)]^{2+}$ (bromazepam = 7-bromo-1,3-dihydro-5-(2-pyridyl)-2*H*-1,4-benzodiazepin-2-one)

Matteo Cusumano,* Maria Letizia Di Pietro, Antonino Giannetto,* Maria Anna Messina and Francesco Romano

Dipartimento di Chimica Inorganica, Chimica Analitica e Chimica Fisica, University of Messina, Italy. E-mail: cusumano@chem.unime.it

Received (in Cambridge, UK) 4th June 1999, Accepted 29th June 1999

Calf thymus DNA inhibits the substitution of ethylenediamine, by thiourea, in $[Pd(bpy)(en)]^{2+}$ and catalyses the same reaction in $[Pd(bromazepam)(en)]^{2+}$ (bromazepam = 7-bromo-1,3-dihydro-5-(2-pyridyl)-2*H*-1,4-benzodiazepin-2-one); this kinetic effect can be related to the different binding modes of the two complexes to the biopolymer.

Inclusion in receptors such as cyclodextrins[1] as well as interactions with micelles[2] or polyelectrolytes[3] alter, often to a large extent, the physical properties and the reactivity of the interacting molecules. DNA can also, thanks to a variety of non-covalent interactions with small molecules,[4] produce these effects.[5] We report here an example in which calf thymus DNA exerts an opposite influence on the reactivity of the two similar palladium(II) complexes $[Pd(bpy)(en)](PF_6)_2$ and $[Pd(bromazepam)(en)](BF_4)_2$ (bromazepam = 7-bromo-1,3-dihydro-5-(2-pyridyl)-2*H*-1,4-benzodiazepin-2-one). For comparison, we report also the effect of DNA on the reactivity of $[Pd(en)_2]Cl_2$ and $[Pd(Me_4en)(py)_2](PF_6)_2$.

$[Pd(bromazepam)(en)](BF_4)_2$ was obtained by treating $[Pd(en)Cl_2]$[6] with $AgBF_4$ (ratio 1 : 2) in acetone, and then adding the corresponding amount of bromazepam. $[Pd(Me_4en)(py)_2](PF_6)_2$ was prepared by heating $[Pd(Me_4en)Cl_2]$, suspended in water, in the presence of an excess of pyridine. After dissolution of the complex, the product was obtained as a yellow precipitate by addition of NH_4PF_6. $[Pd(Me_4en)Cl_2]$,[7] $[Pd(bpy)(en)](PF_6)_2$[8] and $[Pd(en)_2]Cl_2$[6] were prepared by literature methods. Calf thymus DNA (Sigma) was purified as previously described.[9]

The complexes $[Pd(N–N)(en)]^{2+}$ (N–N = bpy or bromazepam) react with thiourea according to reaction (1). The nature of

$$[Pd(N–N)(en)]^{2+} + 2\ tu \longrightarrow [Pd(N–N)(tu)_2]^{2+} + en \quad (1)$$

the reaction products, isolated from water, was established by elemental analysis and ^1H NMR. The kinetics of ligand substitution, by thiourea, were followed spectrophotometrically, in the range 310–370 nm, at 25 °C. Under pseudo-first-order conditions with respect to the complex, the rate of reaction (1), which occurs in one observable step, is related to thiourea concentration by law (2). A good linear trend with zero

$$k_{obs} = k_2[tu]^2 \quad (2)$$

intercept, over the whole thiourea concentration range investigated, is obtained on plotting the k_{obs} values against the square of the thiourea concentration $[tu]^2$. If the reaction is monitored in the presence of calf thymus DNA ([DNA]/[Complex] = 6), the same rate law is observed; however DNA induces opposite changes in the rate of the reactions. Fig. 1 shows that, using the same experimental conditions ($I = 2.2 \times 10^{-2}$ mol dm^{-3} by addition of NaCl or $NaNO_3$; pH = 7 by using phosphate buffer; T = 25 °C), while the substitution of ethylenediamine in $[Pd(bpy)(en)]^{2+}$ is inhibited, the same reaction in $[Pd(bromazepam)(en)]^{2+}$ is accelerated. This kinetic effect can be related to the mode of interaction of the complexes with DNA. $[Pd(bpy)(en)]^{2+}$ intercalates to the double helix.[9,10] $[Pd(bromazepam)(en)]^{2+}$ binds externally, either docking in one of the grooves or simply electrostatically. No changes in the absorption spectrum of the latter complex nor any increase in the DNA viscosity are observed upon interaction. In addition, the increase in thermal denaturation temperature of the double helix, in the presence of $[Pd(bromazepam)(en)]^{2+}$ (1.4 ± 0.2 °C),† is much smaller than expected for a dicationic intercalator.[9] Intercalation protects the reaction centre from nucleophile attack making $[Pd(bpy)(en)]^{2+}$ unreactive; only the non-intercalated portion of this complex participates in the reaction and the

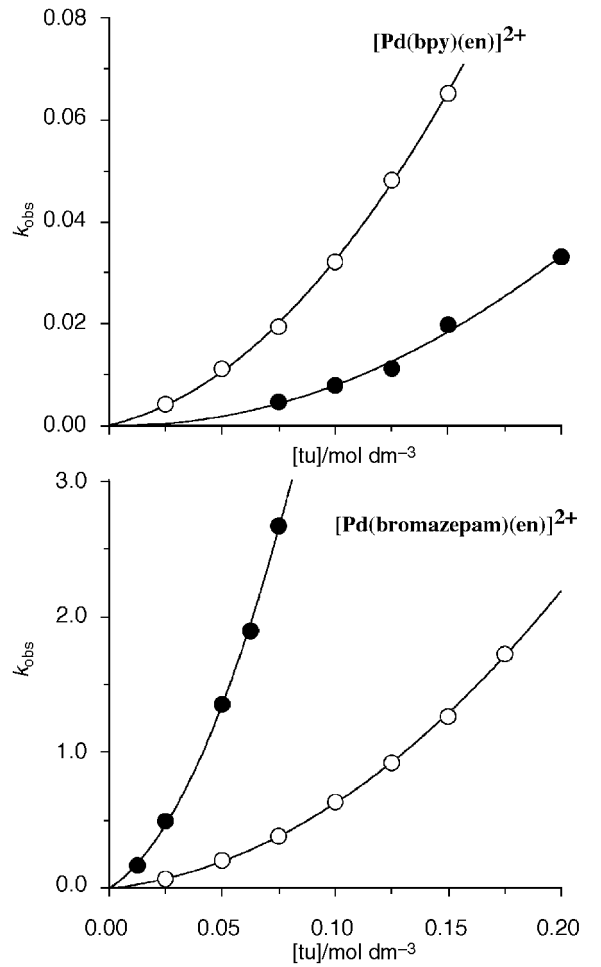

Fig. 1 Plot of k_{obs} against [tu] for reaction (1) (○) in the absence and (●) in the presence of DNA; 1.0×10^{-3} mol dm^{-3} phosphate buffer (pH 7) and 2.1×10^{-2} mol dm^{-3} NaCl or $NaNO_3$; T = 25 °C.

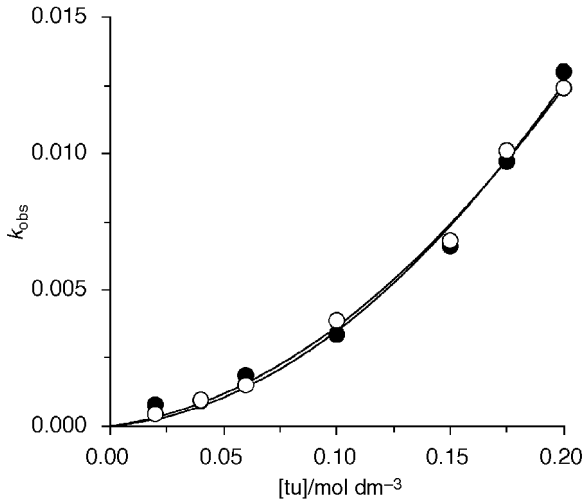

Fig. 2 Plot of k_{obs} against [tu] for reaction of $[Pd(Me_4en)(py)_2]^{2+}$ with thiourea (○) in the absence and (●) in the presence of DNA; 1.0×10^{-3} mol dm^{-3} phosphate buffer (pH 7) and 2.1×10^{-2} mol dm^{-3} NaCl or $NaNO_3$; T = 25 °C.

decreased concentration of one of the two reactants accounts for the decrease in the rate of substitution. In principle, an increase in the local concentration of the reagents can explain the catalytic effect of DNA; owing to its cationic nature [Pd(bromazepam)(en)]$^{2+}$ concentrates around DNA and if we assume that, for some reason, thiourea interacts with the biopolymer accumulating around it, enhanced concentration of the two reacting species would account for the observed acceleration in rate. More likely the observed catalytic effect is electronic in origin; the NH_2 hydrogen atoms of en are acidic[11] enough to interact with the DNA phosphate groups and so hydrogen bounding could stabilise the reaction intermediate with monodentate ethylenediamine. Kinetic data for the reaction of thiourea with $[Pd(en)_2]^{2+}$ and $[Pd(Me_4en)(py)_2]^{2+}$ corroborate this hypothesis. Both complexes bind externally to the double helix; however, while DNA catalyses the substitution of en, the rate of reaction for the latter complex, where no hydrogen atoms are available for interaction, is practically unaffected by the presence of the biopolymer (Fig. 2).

In conclusion, our data show that the observed kinetic effect of DNA on the reactivity of a small molecule can, in principle, be used as an indicator of its binding mode to the biopolymer.

Financial support from MURST and CNR is acknowledged.

Notes and references

† The thermal denaturation temperature of the complex–DNA mixture (1:10) was determined in 1.0×10^{-3} mol dm^{-3} phosphate buffer (pH 7) containing 7.8×10^{-6} mol dm^{-3} complex and 2.0×10^{-3} mol dm^{-3} NaCl.

1 A. Granados and R. H. de Rossi, *J. Am. Chem. Soc.*, 1995, **117**, 3690 and references therein.
2 C. A. Bunton and G. Savelli, *Adv. Phys. Org. Chem.*, 1986, **22**, 213.
3 H. Morawetz and B. Vogel, *J. Am. Chem. Soc.*, 1969, **91**, 563.
4 W. D. Wilson and R. L. Jones, *Intercalation Chemistry*, ed. M. S. Wittingham and A. J. Jacobson, Academic Press, New York, 1982, ch. 14.
5 R. F. Pasternack, E. J. Gibbs, R. Santucci, S. Shaertel, P. Ellinas and S. C. Sah, *J. Chem. Soc., Chem. Commun.*, 1987, 1771.
6 H. D. K. Drew, F. V. W. Pinkard, G. H. Preston and W. Wardlaw, *J. Chem. Soc.*, 1932, 1895.
7 M. Cusumano, A. Giannetto and A. Imbalzano, *Polyhedron*, 1998, **17**, 125.
8 L. E. Erikson, *J. Am. Chem. Soc.*, 1969, **91**, 6284.
9 M. Cusumano and A. Giannetto, *J. Inorg. Biochem.*, 1997, **65**, 137.
10 S. J. Lippard, *Acc. Chem. Res.*, 1978, **11**, 211.
11 W. G. Watt and D. G. Upchurch, *J. Am. Chem. Soc.*, 1968, **90**, 914.

Communication 9/04471J

The influence of A-cation disorder on the Curie temperature of ferroelectric $ATiO_3$ perovskites

Derek C. Sinclair[a] and J. Paul Attfield*[b]

[a] *Department of Engineering Materials, University of Sheffield, Mappin Street, Sheffield UK S1 3JD*
[b] *Department of Chemistry, University of Cambridge, Lensfield Road, Cambridge, UK CB2 1EW. E-mail: jpa14@chem.ac.uk*

Received (in Oxford, UK) 7th May 1999, Accepted 28th June 1999

The ferroelectric Curie temperature T_C in $ATiO_3$ perovskites is shown to increase linearly with the size variance of the A-site cation mixture [A = (Ba, Sr, Ca)] and this effect accounts for the unusual T_C variation in the $Ba_{1-x}Ca_xTiO_3$ system.

$BaTiO_3$ is a ferroelectric perovskite widely used in capacitors, thermistors and piezoelectric devices. The Curie temperature above which $BaTiO_3$ changes from being tetragonal and ferroelectric to cubic and paraelectric is T_C = 403 K.[1] The ferroelectricity arises from displacements of the Ti atoms towards one of the octahedrally coordinating oxygen atoms along the *c*-axis. A complete solubility exists between $BaTiO_3$ and $SrTiO_3$, and T_C decreases across the series to a value of 110 K for $SrTiO_3$.[2] This trend was ascribed to a cation size effect, in which the smaller Sr ion causes a reduction in the average radius of the A cation site and stabilises the cubic $ATiO_3$ structure to lower temperatures. By contrast, in the $Ba_{1-x}Ca_xTiO_3$ system, T_C rises from 403 K to a maximum value of 410 K at x = 0.08 before dropping to 391 K at the solid solution limit of x = 0.24.[3] This variation is not consistent with the above size effect.

It has recently been shown that the electronic and structural phase transition temperatures of several perovskite-type materials vary with the mean size and the size mismatch of the cations on the A-site.[4,5] Size is parameterised by the mean A-cation radius, $\langle r_A \rangle$, and A-site size mismatch is described by the statistical variance in the distribution of the radii, σ^2:

$$\sigma^2 = \langle r_A^2 \rangle - \langle r_A \rangle^2$$

σ^2 is defined for a mixture of many cations, but in a binary system such as A = $(Ba_{1-x}M_x)$, it reduces to:

$$\sigma^2 = x(1-x)(r_{Ba} - r_M)^2$$

and hence σ^2 varies quadratically with x. At a constant $\langle r_A \rangle$, the temperatures of the ferromagnetic metal to paramagnetic insulator transition in $AMnO_3$ perovskites (at which colossal magnetoresistances are observed),[6] and the superconducting critical transitions in A_2CuO_4 and ABa_2CuO_7 decrease linearly with increasing σ^2.[5,7] However, the orthorhombic–tetragonal structural transition in the A_2CuO_4 materials shows a strong linear increase with σ^2.[5] Here, we present the first systematic study of the influence of A site disorder on the properties of $BaTiO_3$-based ferroelectric perovskites.

Six (Ba, Sr, Ca)TiO_3 compositions (Table 1) were chosen to give a constant $\langle r_A \rangle$ = 1.454 Å but variable σ^2. $\langle r_A \rangle$ and σ^2 were calculated using standard values of nine-coordinate ionic radii.[8] 10 g samples were prepared by mixing appropriate quantities of $BaCO_3$, $SrCO_3$, $CaCO_3$ and TiO_2 (all 99.99+% pure) which were ground in an agate mortar and pestle with acetone for 15 min, fired in Pt foil boats at 1000 °C for 12 h, then reground for 15 min before refiring at 1200 and 1350 °C. Regrinding and refiring at 1350 °C for 12 h was repeated six times. The powders were milled in a planetary ball mill for 5 min rather than a mortar and pestle for the final three cycles. This lengthy preparative procedure was necessary as it is known to be difficult to homogenise low levels of alkaline earth dopants in $BaTiO_3$ powders.[9]

Table 1 Starting and EPMA analysed compositions for six $(Ba_{0.90+0.45x}Sr_{0.1-x}Ca_{0.55x})TiO_3$ samples and their A site cation size variances

Starting composition	Analysed formula[a]	σ^2/Å^2
$Ba_{0.900}Sr_{0.100}TiO_3$	$Ba_{0.91(3)}Sr_{0.09(3)}Ti_{1.0(4)}O_3$	0.0023
$Ba_{0.909}Sr_{0.080}Ca_{0.011}TiO_3$	$Ba_{0.90(2)}Sr_{0.09(2)}Ca_{0.01(2)}Ti_{1.02(2)}O_3$	0.0028
$Ba_{0.918}Sr_{0.060}Ca_{0.022}TiO_3$	$Ba_{0.92(1)}Sr_{0.06(1)}Ca_{0.02(1)}Ti_{1.02(2)}O_3$	0.0032
$Ba_{0.927}Sr_{0.040}Ca_{0.033}TiO_3$	$Ba_{0.93(1)}Sr_{0.04(1)}Ca_{0.03(1)}Ti_{1.02(2)}O_3$	0.0037
$Ba_{0.936}Sr_{0.020}Ca_{0.044}TiO_3$	$Ba_{0.94(1)}Sr_{0.02(1)}Ca_{0.04(1)}Ti_{1.02(2)}O_3$	0.0041
$Ba_{0.945}Ca_{0.055}TiO_3$	$Ba_{0.95(1)}Ca_{0.05(1)}Ti_{1.03(1)}O_3$	0.0047

[a] Formulae were calculated by normalising to Ba + Sr + Ca = 1.

The samples were characterised by electron probe microanalysis (EPMA), using a Cameca SX51 microprobe, and powder X-ray diffraction on a Stoe STADI/P diffractometer. The L_α line of Ba and the Kα line of Sr, Ti and Ca were used for the cation analysis, by employing calibration standards of $BaTiSi_3O_9$, $SrTiO_3$ and $CaSiO_3$ and the oxygen contents were calculated by difference. The EPMA showed the samples to be homogeneous with compositions consistent with the starting formulae (Table 1). The room temperature diffraction patterns were obtained with monochromated Cu-Kα_1 radiation and were all fully indexed in the tetragonal space group *P*4*mm*. A linear variation of lattice parameters with σ^2 is observed (Fig. 1), however, the cell volumes for all samples (64.10 ± 0.09 Å^3) were the same within error and showed no significant variation with σ^2.

The ferroelectric Curie temperatures, T_C, were found from permittivity and calorimetric measurements. Pellets for the permittivity experiments were cold pressed and fired overnight at 1350 °C in air. Impedance was measured between 25 and 180 °C over the frequency range 10–10^7 Hz with an applied voltage of 100 mV using a 4192 Hewlett Packard impedance analyser. Data obtained at fixed frequency of 1 kHz showed sharp permittivity *vs*. temperature profiles for all the samples, with no apparent broadening of the ferroelectric transition, T_C values were extracted from the permittivity maximum obtained

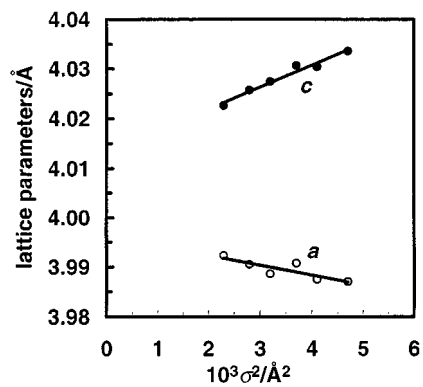

Fig. 1 Variation in the tetragonal lattice parameters of the $ATiO_3$ samples with σ^2 at 300 K.

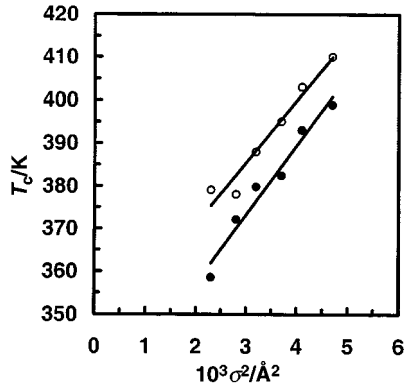

Fig. 2 Variation in T_C with σ^2. Open and filled circles correspond to data obtained from permittivity and DSC measurements, respectively.

on a heating cycle. Such values are dependent on the thermal history of the sample, as $BaTiO_3$-based materials show hysteresis on thermal cycling, so calorimetric measurements were used to confirm the T_C variation. Powdered samples were thermally cycled between 0 and 180 °C in a Polymers Lab differential scanning calorimeter at a heating rate of 10 °C min^{-1} and T_C values were extracted from the peak maximum associated with the endotherm in the cooling cycle. The two sets of T_C values are plotted *vs.* σ^2 in Fig. 2. A detailed analysis of the microstructure and electrical properties of the samples, which are sensitive to microstructural effects such as grain size and pellet density,[9] will be reported elsewhere.

The two sets of T_C values both show a strong linear increase with increasing A-cation size variance, σ^2, although the calorimetric values are systematically lower than those obtained from permittivity measurements. Linear fits to the permittivity and DSC results give slopes of $dT_C/d\sigma^2$ = 14500(400) and 16000(300) K Å^{-2}, and T_C^0 values (by extrapolation to σ^2 = 0) of 341(3) and 325(3) K, respectively, with fitting errors in parentheses. To estimate the contribution of cation size disorder to T_C in the $Ba_{1-x}Ca_xCa_xTiO_3$ series, the reported T_C values are shown together with disorder-corrected T_C^0 values in Fig. 3. These were calculated in the first approximation by extrapolating from T_C to σ^2 = 0 assuming a constant $dT_C/d\sigma^2$ = 15 000 K Å^{-2}, although a slight variation in $dT_C/d\sigma^2$ is expected across the series by comparison with other systems.[4] The resulting T_C^0 values show a near-linear fall with x comparable to the behaviour of T_C in the $Ba_{1-x}Sr_xTiO_3$ series.[2]

These results show that the ferroelectric transition temperature in doped $BaTiO_3$ materials is strongly influenced by

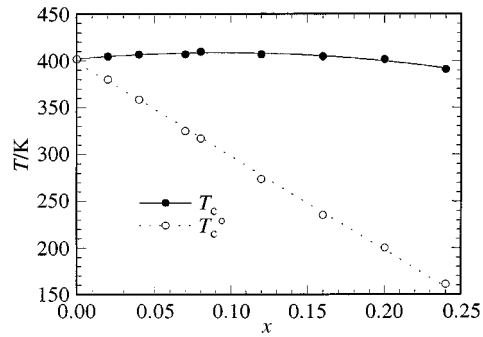

Fig. 3 The variation of T_C (from ref. 3) and the disorder corrected T_C^0 in the $(Ba_{1-x}Ca_x)TiO_3$ series.

both the average A cation size $< r_A >$ and the size variance σ^2. These effects initially oppose one another in substituted $(Ba_{1-x}M_x)TiO_3$ series where Ba is replaced by smaller M = Sr or Ca cations. As x increases, the decreasing $< r_A >$ *reduces* T_c but the increasing σ^2 *raises* T_C. The former reduction is essentially linear with $< r_A >$, as evidenced by the T_C^0 variation in Fig. 3, in apparent contrast to the size dependence of the previously studied electronic transitions, which decrease quadratically with $< r_A >$.[4,6] The linear increase of T_C with σ^2 is in keeping with the observed variation of the structural transition in A_2CuO_4 materials. Reducing $< r_A >$ in the $ATiO_3$ perovskites leads to tilts and rotations of the TiO_6 octahedra that destabilise the ferroelectrically ordered phase, whereas the local disorder associated with increasing σ^2 enables the ferroelectric distortions in the TiO_3 network to occur more easily and thereby stabilises the ferroelectric phase. This is supported by the data in Fig. 1, which show a divergence of the tetragonal a and c parameters as σ^2 increases.

The observed $dT_C/d\sigma^2 \approx$ 15 000 K Å^{-2} in our $ATiO_3$ series is smaller than the value of ≈50 000 K Å^{-2} found for the A_2CuO_4 structural transition,[5] which involves rotations but not distortions of the CuO_6 octahedra. However, $dT_C/d\sigma^2$ is comparable to the reported magnitudes of ≈20 000 K Å^{-2} for the metal–insulator transition in $AMnO_3$ perovskites.[4,6] This is accompanied by the formation of Jahn–Teller distortions of the MnO_6 octahedra *above* the transition,[10] whereas Ti displacements of comparable magnitude occur within the TiO_6 octahedra *below* the ferroelectric transition in $ATiO_3$ materials. Hence, the magnitude of $dT_C/d\sigma^2$ appears to be related to the degree of structural distortion occurring at the transition.

In conclusion, the ferroelectric–paraelectric transition temperature of $ATiO_3$ materials shows a strong linear increase with A-cation size variance. The σ^2 effect opposes the influence of the average A cation size and may be useful in stabilising ferroelectric phases to higher temperatures. In the $(Ba_{1-x}Sr_x)TiO_3$ series, the size effect dominates, so T_C falls with increasing x. However, Fig. 3 shows that the much greater σ^2 contribution in the $(Ba_{1-x}Ca_x)TiO_3$ series effectively cancels out the $< r_A >$ effect, leading to almost constant T_C values up to the observed maximum x = 0.24.

The authors thank James Marr and Susan Geddes for assistance with sample preparation, Dr Alison Coats for EPMA analysis and Dr Corrie Imrie and Brian Paterson for assistance with DSC measurements.

Notes and references

1 B. Jaffe, W. R. Cook and H. Jaffe, *Piezoelectric Ceramics*, Academic Press, London, 1971.
2 W. Jackson and W. Reddish, *Nature*, 1945, **56**, 717.
3 T. Mitsui and W. B. Westphal, *Phys. Rev.*, 1961, **124**, 1354.
4 J. P. Attfield, *Chem. Mater.*, 1998, **10**, 3239.
5 J. P. Attfield, A. L. Kharlanov, J. A. McAllister and L. M. Rodriguez-Martinez, *Mater. Res. Soc. Symp. Proc.*, MRS Fall Meeting, 1999, **547**, 15.
6 L. M. Rodriguez-Martinez and J. P. Attfield, *Phys. Rev. B: Condens. Matter*, 1996, **54**, R15622.
7 J. P. Attfield, A. L. Kharlanov and J. A. McAllister, *Nature*, 1998, **394**, 157.
8 R. D. Shannon, *Acta Crystallogr., Sect. A*, 1976, **32**, 751.
9 V. S. Tiwari, N. Singh and D. Pandey, *J. Am. Ceram. Soc.*, 1994, **77**, 1813.
10 L. M. Rodriguez-Martinez and J. P. Attfield, *Phys. Rev. B: Condens. Matter*, 1998, **58**, 246.

Communication 9/03680F

Transformations of alkynyl ligands at iron centres: alkenyl formation *via* addition of PPh_3 and enyne generation *via* head-to-head coupling and addition of benzene

Arthur J. Carty,*[a] Graeme Hogarth,*[ab] Gary D. Enright,[a] Jonathan W. Steed[c] and Dimitra Georganopoulou[c]

[a] *The Steacie Institute for Molecular Sciences, National Research Council of Canada, 100 Sussex Drive, Ottawa, Ontario, Canada K1A OR6. E-mail: Arthur.Carty@NRC.CA*

[b] *Department of Chemistry, University College London, 20 Gordon Street, London, UK WC1H 0AJ. E-mail: g.hogarth@ucl.ac.uk*

[c] *Department of Chemistry, King's College London, Strand, London, UK WC2R 2LS*

Received (in Basel, Switzerland) 7th May 1999, Accepted 13th June 1999

Thermolysis of $Fe_2(CO)_6(\mu\text{-}PPh_2)(\mu\text{-}C_2Bu^t)$ affords the binuclear alkenyl complex $Fe_2(CO)_5(\mu\text{-}PPh_2)(\mu\text{-}o\text{-}Ph_2PC_6H_4C{=}CHBu^t)$ and the trinuclear arene complex $Fe_3(CO)_4(\mu_3\text{-}o\text{-}PhPC_6H_4PPh)\{\mu_3\text{-}C(Bu^t)CCH{=}CBu^t\text{-}\eta^6\text{-}C_6H_5\}$ both resulting from a number of novel transformations including C–C bond formation and C–H and C–P bond cleavage and reformation.

Binuclear iron triad acetylide complexes such as $M_2(CO)_6(\mu\text{-}PPh_2)(\mu\text{-}C{\equiv}CR)$ have recently been exploited as novel precursors for the synthesis of multimetallic polycarbon materials *via* intermolecular coupling of alkynyl ligands.[1–4] For example, thermolysis of $Ru_2(CO)_6(\mu\text{-}PPh_2)(\mu\text{-}C{\equiv}CR)$ (R = Ph, Bu^t) affords several tetraruthenium clusters with C_4 chains formed by head-to-head or head-to-tail ynyl coupling, the nature of which depends on the acetylide substituent.[1,2] Similarly, in a remarkably specific, high yield reaction, the diiron complex $Fe_2(CO)_6(\mu\text{-}PPh_2)(\mu\text{-}C{\equiv}CPh)$ has been shown independently by ourselves[3] and Mays and coworkers[4] to undergo head-to-head carbon–carbon coupling generating the unusual tetrairon cluster $Fe_4(CO)_8(\mu\text{-}PPh_2)_2(\mu_4\text{-}C{\equiv}CPh)_2$ in which the face capping acetylides are linked through the tetrairon core by a short [1.596(4) Å] carbon–carbon contact. In an effort to extend this chemistry to other polycarbon systems we have studied the analogous thermolysis of $Fe_2(CO)_6(\mu\text{-}PPh_2)(\mu\text{-}C{\equiv}CBu^t)$ **1**. To our surprise, we have discovered that this leads to two new complexes formed *via* unprecedented transformations including carbon–carbon bond formation, and carbon–hydrogen and carbon–phosphorus bond cleavage and reformation. We describe herein the characterisation of these novel compounds $Fe_2(CO)_5(\mu\text{-}PPh_2)(\mu\text{-}o\text{-}Ph_2PC_6H_4C{=}CHBu^t)$ **2** and $Fe_3(CO)_4(\mu_3\text{-}o\text{-}PhPC_6H_4PPh)\{\mu_3\text{-}C(Bu^t)CCH{=}CBu^t\text{-}\eta^6\text{-}C_6H_5\}$ **3**.

Heating a toluene solution of **1** at 140 °C for 30 h resulted in a gradual darkening of the solution and disappearance of **1** as shown by IR spectroscopy, and led after chromatography to the isolation of orange $Fe_2(CO)_5(\mu\text{-}PPh_2)(\mu\text{-}o\text{-}Ph_2PC_6H_4C{=}CHBu^t)$ **2** (35%) and green $Fe_3(CO)_4(\mu_3\text{-}o\text{-}PhPC_6H_4PPh)\{\mu_3\text{-}C(Bu^t)CCH{=}CBu^t\text{-}\eta^6\text{-}C_6H_5\}$ **3** (10%) (Scheme 1). Spectroscopic data† and X-ray crystallography‡ established full details of the molecular structures and the nature of the coupled organic fragments.

Complex **2** (Fig. 1) is binuclear, the diiron centre being bridged by phosphido and alkenyl ligands. The latter carries the *tert*-butyl substituent at the β-carbon as expected, while the α-carbon is attached to the *ortho*-position of a 2-diphenylphosphino–C_6H_4 group and is *cis* to the Bu^t substituent. The diphenylphosphido functionality is coordinated to Fe(1) as a two-electron ligand. The two phosphorus ligands subtend an angle of 159.39(4)° at Fe(1) accounting for the relatively large phosphorus–phosphorus coupling constant of 75 Hz and the unique alkenyl proton lies *endo* to the phosphido bridge. While the structural features of the alkenyl group are similar to those of related diiron μ-alkenyl complexes the formation of a 2-diphenylphosphino–C_6H_4 substituent at C_α is quite unex-

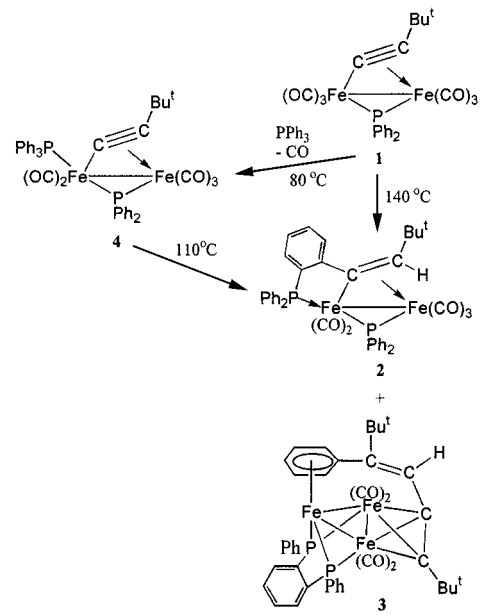

Scheme 1

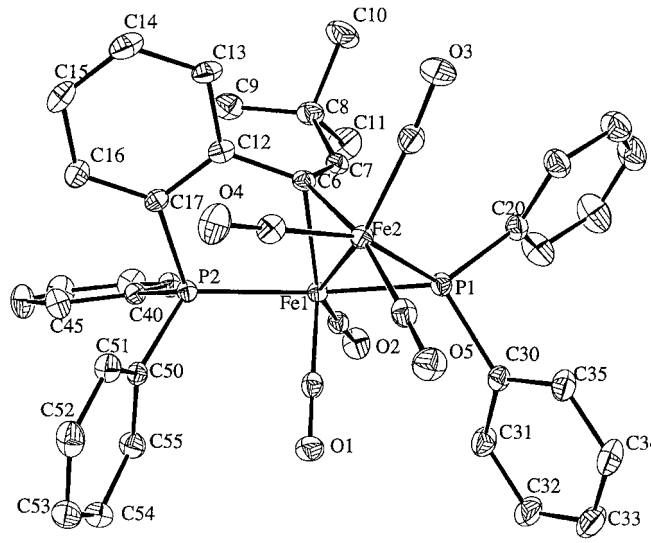

Fig. 1 Molecular structure of **2** with selected bond lengths (Å): Fe(1)–Fe(2) 2.5877(6), Fe(1)–P(1) 2.2220(10), Fe(1)–P(2) 2.2588(10), Fe(2)–P(1) 2.2269(10), Fe(1)–C(6) 2.080(3), Fe(1)–C(7) 2.307(3), Fe(2)–C(6) 2.020(3), C(6)–C(7) 1.383(5).

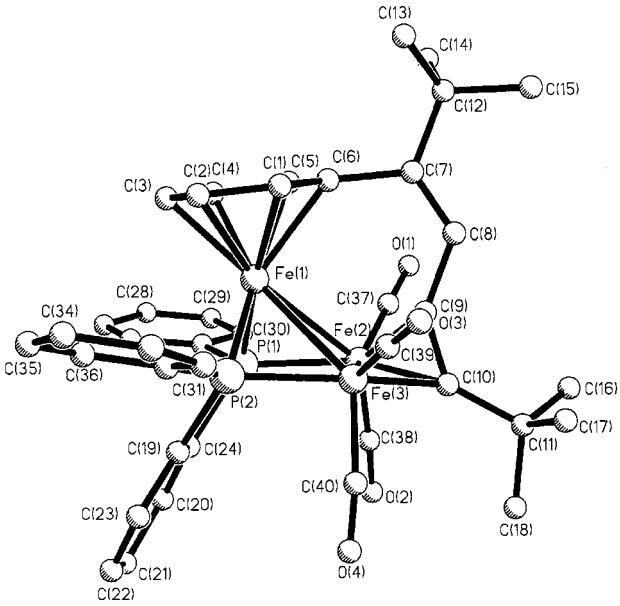

Fig. 2 Molecular structure of **3** with selected bond lengths (Å): Fe(1)–Fe(2) 2.696(2), Fe(1)–Fe(3) 2.689(3), Fe(2)–Fe(3) 2.438(2), Fe(1)–P(1) 2.184(4), Fe(1)–P(2) 2.191(4), Fe(2)–P(1) 2.165(4), Fe(3)–P(2) 2.155(4), Fe(1)–C(1) 2.119(14), Fe(1)–C(2) 2.097(13), Fe(1)–C(3) 2.104(12), Fe(1)–C(4) 2.089(11), Fe(1)–C(5) 2.142(12), Fe(1)–C(6) 2.156(12), Fe(2)–C(9) 2.020(11), Fe(3)–C(9) 1.982(12), Fe(2)–C(10) 2.041(11), Fe(3)–C(10) 2.034(11), C(1)–C(2) 1.412(18), C(2)–C(3) 1.374(18), C(3)–C(4) 1.411(18), C(4)–C(5) 1.398(17), C(5)–C(6) 1.461(17), C(1)–C(6) 1.433(17), C(6)–C(7) 1.490(17), C(7)–C(8) 1.294(16), C(8)–C(9) 1.469(16), C(9)–C(10) 1.335(16).

pected. Formally the new hydrocarbyl ligand can be derived from **1** by loss of CO and addition of PPh_3 across the alkynyl ligand. Indeed **2** is an isomer of $Fe_2(CO)_5(PPh_3)(\mu\text{-}PPh_2)(\mu\text{-}C{\equiv}CBu^t)$ **4**.[5] The latter is formed upon addition of PPh_3 to **1** under benzene reflux and we have now shown in a separate experiment that **4** cleanly converts to **2** in refluxing toluene. This may imply that upon thermolysis of **1**, PPh_3 is released which subsequently reacts with **1** to afford **2**.

The structure of trinuclear **3** (Fig. 2) is quite unprecedented and highly unusual for an Fe_3 cluster. It consists of a triiron core, one edge of which [Fe(2)–Fe(3) 2.438(2) Å] is significantly shorter than the other two [Fe(1)–Fe(2) 2.696(2), Fe(1)–Fe(3) 2.689(3) Å]. One face of the cluster is capped by an *ortho*-phenylenebis(phenylphosphido) bridge,[6] while the second is spanned by a new enyne ligand namely 2,2,7,7-tetramethyl-3-phenylocta-3-en-5-yne. The acetylinic triple bond acts as a four-electron donor, binding in perpendicular fashion to the short iron–iron vector, while the phenyl ring is coordinated as an η^6-ligand to Fe(1). The average iron–carbon (2.118 Å) and carbon–carbon (1.415 Å) bond lengths for the η^6-ligand fall within the ranges associated with mononuclear iron–arene complexes.[7] All bonds to the substituted aryl carbon C(6) are elongated with respect to the other carbons in the ring, an effect probably due to the strain imposed on the hydrocarbyl ligand to maximise metal–alkyne bonding. Two iron centres also bear two carbonyls giving the cluster the expected 48-electron count. Although there is no crystallographic plane of symmetry, the molecule has an approximate plane containing Fe(1)C(3)C(6)C(7)C(8)C(9)C(10) and bisecting Fe(2)–Fe(3) and P(1)–P(2) hence accounting for the relatively simple NMR data.

While the precise mechanism of formation of **2** and **3** from **1** is unknown, the nature of the new ligands and the nuclearity of **3** imply key bond breaking and bond making processes: (i) P–C(Ph) cleavage of a $\mu\text{-}PPh_2$ bridge and scavenging of released phenyl groups by phosphido and hydrocarbyl ligands; (ii) addition of a C–H bond of a phenylphosphine across a coordinated triple bond—we believe that this observation is unprecedented; (iii) head-to-head coupling of acetylide ligands and intermolecular condensation at binuclear metal centres; (iv) coupling of PPh_2 and PPh fragments *via* orthophosphination of a phenyl ring to afford a six-electron donor $PhPC_6H_4PPh$ ligand in **3**; (v) loss of carbonyl groups and η^6-coordination of an aryl substituent to afford a carbonyl free iron atom. Again, we are unaware of any comparable reacton.

We are currently examining the thermal and photochemical transformations of other binuclear phosphido bridged acetylides to gain further insights into the factors governing these novel processes.

We are grateful to the National Research Council of Canada and the Natural Sciences and Engineering Research Council for financial support of this work.

Notes and references

† *Spectroscopic data*: for **2**: IR (C_6H_{14}) ν(CO) 2030s, 1977vs, 1967m, 1954s, 1932m cm^{-1}; ^1H NMR ($CDCl_3$): δ 8.0–7.1 (m, Ph, 24H), 3.36 (dd, *J* 9.1, 2.5, 1H, H_β), 0.29 (s, 9H, Bu^t): ^{31}P NMR ($CDCl_3$): δ 179.8 (d, *J* 75, $\mu\text{-}PPh_2$), 73.4 (d, *J*, 75, PPh_2) (85% H_3PO_4): MS(FAB+) *m/z* 781 (M + 1); Anal. Calc. for $Fe_2C_{41}H_{34}O_5P_2{\cdot}0.25CH_2Cl_2$. C, 61.78, H, 4.31. Found: C, 62.21, H 4.24%. For **3**: IR (C_6H_{14}) ν(CO) 1981s, 1954s, 1915s, 1909m cm^{-1}; ^1H NMR ($CDCl_3$): δ 8.01 (s, 4H, Ph), 7.97 (s, 1H, C=CH), 7.53 (s, 6H, Ph), 6.87 (s, 4H, Ph), 6.30 (t, *J* 6.2, 1H, Ar), 4.43 (m, 2H, Ar), 4.30 (d, *J* 5.0, 2H, Ar), 1.89 (s, 9H, Bu^t), 1.04 (s, 9H, Bu^t): ^{31}P NMR ($CDCl_3$): δ 225.0 (s) (85% H_3PO_4): MS(FAB+) *m/z* 813 (M + 1); Anal. Calc. for $Fe_3C_{40}H_{38}O_4P_2$. C, 59.11; H, 4.68. Found: C, 59.48; H, 4.53%.

‡ *Crystal data*: for **2**: X-ray intensity data were collected on a Siemens CCD diffractometer using Mo-Kα radiation and the ω-scan mode; *T* = 173 K, $Fe_2C_{41}H_{34}O_5P_2$, M_r = 780.35, monoclinic, space group $P2_1/n$, *a* = 11.8359(10), *b* = 17.5456(11), *c* = 17.3929(11) Å, β = 92.545(5)°, *F*(000) = 1612, D_c = 1.436 g cm^{-3}, *Z* = 4, μ = 0.93 mm^{-1}, 2θ(max) = 57.5°, $R(R_w)$ = 0.0480 (0.0470) for 5812 reflections [$I > 2.5\sigma(I)$] and 587 parameters.

For **3**: X-ray intensity data were collected on a Nonius KappaCCD diffractometer using Mo-Kα radiation and the ϕ scan mode; *T* = 100 K, $Fe_3C_{40}H_{38}O_4P_2$, M_r = 812.19, monoclinic, space group *Ia*, *a* = 13.6479(14), *b* = 35.838(3), *c* = 15.1837(18) Å, β = 90.55(5)°, *F*(000) = 3344, D_c = 1.453 g cm^{-3}, *Z* = 8, μ = 1.28 mm^{-1}, 2θ(max) = 50°, $R(R_w)$ = 0.1089 (0.1737) for 11982 reflections [$I > 2\sigma(I)$] and 884 parameters. There are two independent molecules in the asymmetric unit but they do not differ significantly. CCDC 182/1294.

1 Y. Chi, A. J. Carty, P. Blenkiron, E. Delgado, G. D. Enright, W. Wang, S.-M. Peng and G. Lee, *Organometallics*, 1996, **15**, 5269.
2 E. Delgado, Y. Chi, W. Wang, G. Hogarth, P. J. Low, G. D. Enright, S.-M. Peng, G.-H. Lee and A. J. Carty, *Organometallics*, 1998, **17**, 2936.
3 A. J. Carty, G. Hogarth, G. Enright and G. Frapper, *Chem. Commun.*, 1997, 1883.
4 J. E. Davies, M. J. Mays, P. R. Raithby and K. Sarveswaran, *Angew. Chem., Int. Ed. Engl.*, 1997, **36**, 2688.
5 W. F. Smith, J. Yule, N. J. Taylor, H. N. Paik and A. J. Carty, *Inorg. Chem.*, 1977, **16**, 1593.
6 E. P. Kyba, M. C. Kerby, R. P. Kashyap, J. A. Mountzouris and R. E. Davis, *Organometallics*, 1989, **8**, 852; E. P. Kyba, M. C. Kerby, R. P. Kashyap, J. A. Mountzouris and R. E. Davis, *J. Am. Chem. Soc.*, 1990, **112**, 105; M. D. Soucek, H.-S. Chiou and E. P. Kyba, *J. Organomet. Chem.*, 1993, **456**, 255.
7 T. S. Cameron, A. Linden, K. C. Sturge and M. J. Zaworotko, *Helv. Chim. Acta*, 1992, **75**, 294.

Communication 9/03919H

Resolution of coupled electron transfer–ion transfer processes at liquid/liquid interfaces by visualisation of interfacial concentration profiles

Jie Zhang, Christopher J. Slevin and Patrick R. Unwin*

Department of Chemistry, University of Warwick, Coventry, UK CV4 7AL. E-mail: P.R.Unwin@warwick.ac.uk

Received (in Cambridge, UK) 10th June 1999, Accepted 23rd June 1999

A powerful approach for investigating heterogeneous electron transfer (ET) reactions at liquid/liquid (oil/water) interfaces is described and illustrated with studies of the reactions between $IrCl_6^{2-}$ or $Fe(CN)_6^{3-}$ in an aqueous phase and decamethylferrocene (DMFc) or ferrocene (Fc) in 1,2-dichloroethane (DCE).

ET reactions that occur at the interface between two immiscible electrolyte solutions (ITIES) are of considerable fundamental and industrial interest,[1] as well as representing a simple, useful analogue of redox processes that occur across cell menbranes.[2,3] Surprisingly, ET kinetics at ITIES are still poorly understood[4] and difficult to investigate unambiguously, because conventional electrochemical methods measure a total current flow which does not discriminate between ET and coupled ion transfer (IT).[5–7] To circumvent this problem, differential cyclic voltabsorptometry was recently combined with UV-VIS spectroscopy, to determine whether the products of an ET process crossed the interface.[8] A similar, earlier approach,[9,10] employed fluorescence as the spectroscopic probe. An *in-situ* EPR cell has also recently been developed to detect and monitor paramagnetic species produced as a result of ET at ITIES.[11]

While spectroscopic methods have provided improved insights into ET at liquid/liquid interfaces, they necessarily place demands on the types of reactants and products that can be studied.[12] Here, we describe a novel approach for investigating ET kinetics at ITIES, based on microelectrochemical measurement at expanding droplets (MEMED)[13,14] which, we show, allows all of the reactant and product distributions adjacent to the interface to be visualised. In this way, not only can the kinetics of the ET reaction be determined, but the extent to which the products are involved in coupled IT processes can readily be identified.

In the MEMED technique,[13,14] the ITIES is created by flowing a feeder liquid through a fine capillary tip (100–200 μm internal diameter), so that droplets form and grow periodically in a second receptor phase, immiscible with the first, analogous to the dropping mercury electrode[15] or electrolyte dropping electrode.[16,17] In contrast to these methods, however, MEMED determines the individual concentration profiles of products or reactants extending from the droplet surface into the receptor phase using a probe ultramicroelectrode (UME), positioned adjacent to the capillary. In the studies here, we used a 1 or 0.5 μm radius Pt disc working electrode held at a potential to detect a specific reactant or product by local diffusion-limited electrolysis. The current for the species of interest was recorded as a function of time, as droplets grew towards the tip, and converted to a concentration-distance profile.

We consider the redox reaction between Fc or DMFc (which we denote as Fc′) in DCE and either $IrCl_6^{2-}$ or $Fe(CN)_6^{3-}$ in the aqueous phase (denoted by Ox_{aq}):

$$Fc'_{DCE} + Ox_{aq} \xrightarrow{k} Fc'^{+} + Red_{aq} \quad (1)$$

where k is a first-order rate constant for the heterogeneous reaction. The objective was to determine k and identify whether the products (particularly Fc'^{+}) crossed the interface, by recording the concentration profiles for all four species in eqn. (1). This was achieved by expanding a DCE droplet containing Fc′ into an aqueous phase containing Ox and recording the Ox and Red profiles with the UME in the aqueous phase. Subsequently, an aqueous droplet, containing Ox, was expanded into the DCE phase and the profiles for Fc′ and Fc'^{+} recorded in DCE.

In all experiments, the potential across the interface was established by using the potential-determining ClO_4^- ion in each phase.[18] Fig. 1 and 2 show the concentration profiles for the reactants and products in the receptor phase for the reaction between $IrCl_6^{2-}$ and either Fc or DMFc. The concentrations have been normalised with respect to the bulk reactant concentrations, $[IrCl_6^{2-}]^*$ or $[Fc']^*$, and plotted against the separation, d, between the probe and droplet surface. The initial driving force for the reactions is governed by the difference in the formal potentials of the $IrCl_6^{2-}/IrCl_6^{3-}$ couple and the Fc′/Fc'^{+} couple, $\Delta E°$, and the relative potential drop, $\Delta\phi$, across the ITIES. This was determined by measuring the difference in the half-wave potentials, $\Delta E_{1/2}$, of the reversible couples in the two phases *versus* saturated calomel (SCE) reference electrode in the aqueous phase:

$$\Delta E_{1/2} = \Delta E° + \Delta\phi \quad (2)$$

For the $IrCl_6^{2-}$–Fc reaction $\Delta E_{1/2}$ was *ca.* 0.40 V, while for the $IrCl_6^{2-}$–DMFc reaction $\Delta E_{1/2}$ was *ca.* 0.70 V. These are

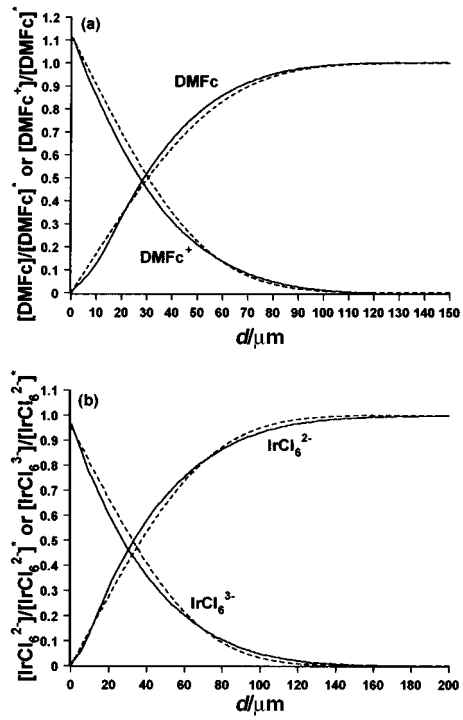

Fig. 1 Normalised concentration profiles (solid lines) of the reactants and products in the DCE (a) and aqueous (b) receptor phases for the reaction between DMFc (DCE) and $IrCl_6^{2-}$ (aqueous). Drop times and final sizes were (a) 5.54 s and 0.96 mm, and (b) 6.32 s and 1.00 mm. The theoretical profiles (dashed lines) are for a transport-controlled reaction, with no transfer of the product ions.

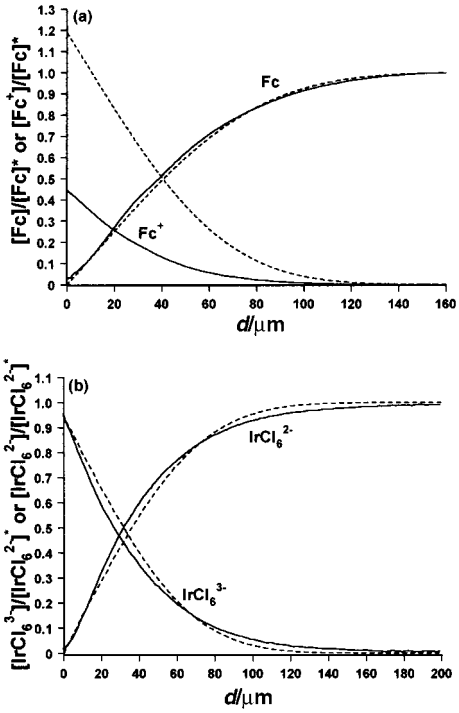

Fig. 2 Normalised concentration profiles (solid lines) of the reactants and products in the DCE (a) or aqueous (b) receptor phase for the reaction between Fc (DCE) and $IrCl_6^{2-}$ (aqueous). Drop times and final sizes were (a) 5.54 s and 0.96 mm, and (b) 6.32 s and 1.00 mm. The theoretical profiles (dashed lines) are for a transport-controlled reaction, with no transfer of the product ions.

relatively large driving forces and consequently the $IrCl_6^{2-}$ and $IrCl_6^{3-}$ profiles in both cases indicate that the reaction is transport-controlled ($k > 0.1$ cm s^{-1}), with the concentration of $IrCl_6^{2-}$ falling to zero at the surface of the droplet. There is generally good agreement between the experimental and theoretical profiles, calculated based on the following convective–diffusion equation, which applies close to the interface of the expanding droplet:[13,14]

$$\frac{\partial c_i}{\partial t} = D_i \frac{\partial^2 c_i}{\partial r^2} - \frac{q}{2\pi}\left(\frac{1}{r^2} - \frac{1}{r_o^2}\right)\frac{\partial c_i}{\partial r} \qquad (3)$$

D_i and c_i are the diffusion coefficient and concentration of the reactant, i = R, or product, i = P, in the receptor phase, respectively. The spherical coordinate, starting at the centre of the drop, is denoted by r; q is the volume flow rate, and r_o is the (time-dependent) drop radius.

The interfacial boundary condition is:

$$r = r_o: \quad -D_R \frac{\partial c_R}{\partial r} = D_P \frac{\partial c_P}{\partial r} = k c_R \qquad (4)$$

where R and P are, respectively, $IrCl_6^{2-}$ and $IrCl_6^{3-}$ for the aqueous receptor phase or Fc′ and Fc′$^+$ for the DCE receptor phase. Eqn. (4) assumes that neither the product nor the reactant in the receptor phase partition into the droplet. Semi-infinite no-flux boundary conditions apply at a long distance from the ITIES. Measured values of $D_{IrCl_6^{2-}} = 6.8 \times 10^{-6}$ cm^2 s^{-1} and $D_{IrCl_6^{3-}} = 7.5 \times 10^{-6}$ cm^2 s^{-1} were employed to calculate the concentration profiles.

The DMFc and DMFc$^+$ profiles (Fig. 1) for the DCE receptor phase also show a good fit to a transport-controlled process, with $k > 0.1$ cm s^{-1}, calculated using $D_{DMFc} = 7.5 \times 10^{-6}$ cm^2 s^{-1} and $D_{DMFc^+} = 6.0 \times 10^{-6}$ cm^2 s^{-1}. The excellent agreement between the DMFc$^+$ experimental and theoretical profiles indicates that DMFc$^+$ does not cross the ITIES under the defined experimental conditions, and that charge neutrality must be maintained by ClO_4^- transfer from the aqueous phase to the DCE phase. In contrast, while the Fc profile in Fig. 2 indicates that the $IrCl_6^{2-}$–Fc reaction is clearly transport-controlled, the Fc$^+$ profile indicates a substantial loss of Fc$^+$ which can be attributed to transfer across the interface from the DCE to the aqueous phase.[5]

The reaction between $Fe(CN)_6^{3-}$ and DMFc was also investigated. Although DMFc was proposed as an ideal electron donor for ET studies at ITIES,[6] earlier investigations concluded that no ET reaction could be observed between DMFc and $Fe(CN)_6^{3-}$ at the DCE/aqueous interface.[6] In this study, DMFc and DMFc$^+$ were measured in a DCE receptor phase, while forming an aqueous droplet containing $Fe(CN)_6^{3-}$. The results clearly showed that an ET reaction occur between $Fe(CN)_6^{3-}$ and DMFc, evidenced by a decrease in DMFc and formation of DMFc$^+$ close to the interface. The process was characterised by a first-order heterogeneous reaction rate constant of $(2.0 \pm 0.2) \times 10^{-3}$ cm s^{-1}. The smaller rate constant with $Fe(CN)_6^{3-}$ compared to $IrCl_6^{2-}$ as the electron acceptor can be attributed to a lower driving force, $\Delta E_{1/2} = 0.086$ V.

In summary, MEMED is a promising technique for studying ET reactions at ITIES. Determining all of the reactant and product distributions adjacent to the ITIES allows interfacial ET kinetics to be determined unambiguously, and the nature of any coupled IT processes is revealed.

We thank the EPSRC (GR/L15074) and Zeneca for support. J. Z. also gratefully acknowledges scholarships from the ORS scheme and the University of Warwick. Helpful discussions with Dr John Atherton and John Umbers (Zeneca Huddersfield Works) are much appreciated.

Notes and references

1 A. G. Volkov, D. W. Deamer, D. L. Tanelian and V. S. Markin, *Liquid Interfaces in Chemistry and Biology*, Wiley, New York, 1998; P. F. Barbara, T. J. Meyer and M. A. Ratner, *J. Phys. Chem.*, 1996, **100**, 13148.
2 R. B. Gennis, *Biomembranes: Molecular Structure and Function*, Springer-Verlag, New York, 1989.
3 J. Koryta, *Electrochim. Acta*, 1979, **24**, 293.
4 M. Tsionsky, A. J. Bard and M. V. Mirkin, *J. Am. Chem. Soc.*, 1997, **119**, 10785.
5 J. Hanzlik, Z. Samec and J. Hovorka, *J. Electroanal. Chem.*, 1987, **216**, 303.
6 V. J. Cunnane, G. Geblewicz and D. J. Schiffrin, *Electrochim. Acta*, 1995, **44**, 3005.
7 C. Wei, A. J. Bard and M. V. Mirkin, *J. Phys. Chem.*, 1995, **99**, 43.
8 Z. Ding, P.F. Brevet and H. H. Girault, *Chem. Commun.*, 1997, 2059.
9 T. Kakiuchi and Y. Takasu, *Anal. Chem.*, 1994, **66**, 1853.
10 T. Kakiuchi and Y. Takasu, *J. Electroanal. Chem.*, 1995, **381**, 5.
11 R. A. W. Dryfe, R. D. Webster, B. A.Coles and R. G. Compton, *Chem. Commun.*, 1997, 779.
12 Z. Ding, D. J. Fermin, P. F. Brevet and H. H. Girault, *J. Electroanal. Chem.*, 1998, **458**, 139.
13 C. J. Slevin and P. R. Unwin, *Langmuir*, 1997, **13**, 4799.
14 C. J. Slevin and P. R. Unwin, *Langmuir*, 1999, in press.
15 C. M. A. Brett and A. M. Oliveira Brett, *Electrochemistry*, Oxford University Press, 1993, p.158.
16 S. Kihara, M. Suzuki, K. Ogura, S. Umetani, M. Matsui and Z. Yoshida, *Anal. Chem.*, 1986, **58**, 2954.
17 R. M. Allen and D. E. Williams, *Faraday Discuss.*, 1996, **104**, 281.
18 The aqueous phase contained 0.25 mol dm^{-3} $NaClO_4$ and 0.1 mol dm^{-3} NaCl, while the DCE phase contained 0.1 mol dm^{-3} tetra-*n*-hexylammonium perchlorate (THAP). The DCE phase contained either 1×10^{-2} mol dm^{-3} Fc′ (droplet) or 1×10^{-3} mol dm^{-3} Fc′ (receptor), while the aqueous phase contained 1×10^{-2} mol dm^{-3} Ox (droplet) or 1×10^{-3} mol dm^{-3} Ox (receptor). Constant composition could be assumed for the droplet, and mass transport only had to be considered for the receptor phase.

Communication 9/04641K

Spatially close porphyrin pair linked by the cyclic peptide Gramicidin S

Toru Arai,*[a] Naoki Maruo,[a] Yuko Sumida,[a] Chie Korosue[a] and Norikazu Nishino*[b]

[a] *Department of Applied Chemistry, Faculty of Engineering, Kyushu Institute of Technology, Tobata, Kitakyushu, Japan, 804-8550. E-mail: arai@che.kyutech.ac.jp*

[b] *Institute for Fundamental Research of Organic Chemistry, Kyushu University, Higashi, Fukuoka, Japan, 812-8581*

Received (in Cambridge, UK) 7th April 1999, Accepted 23rd June 1999

Two porphyrins were attached to the cyclic decapeptide Gramicidin S and its analogs *via* the side chain amide bonds and the solvent-dependent molecular structure was characterized by various spectroscopic methods.

Since the elucidation of a natural system with a number of tetrapyrroles,[1] such porphyrin assemblies have attracted much attention. To understand the function of the multi-porphyrin systems, many porphyrin arrays with different linker architecture have been studied as models.[2] So far, the porphyrin units have often been connected by tight linkers which determine their distance and orientation.[2b–d] However, a peptide-linked porphyrin array may be interesting because of its likeness to the natural system with a flexible peptide moiety.[3] The flexible linker may afford a porphyrin array wherein structural changes reflect its surroundings such as solvents.

Gramicidin S [*cyclo*(-Val-Orn-Leu-D-Phe-Pro-)$_2$, GS, Fig. 1] is a natural cyclic decapeptide with a pair of antiparallel β-sheets and two β-turns.[4] GS has often been modified without changing its rigid cyclic conformation in various solvents.[4b,c] The incorporation of porphyrins to the Orn residues facing each other may afford a defined porphyrin dimer. Here we report the syntheses and the spectroscopic characterisation of the porphyrin array attached on this rigid cyclic decapeptide and its analogs.

The cyclic decapeptides with side chain Z-protection (**1a**, **2a** and **3a**) were synthesized *via* the cyclisation–cleavage method on the oxime resin in 74–84% yield.[4c] After Z-deprotection with H_2–Pd/C, 5-(*p*-carboxyphenyl)-10,15,20-tritolylporphyrin (2 equiv.) was coupled with PyBOP–HOBt in 70–84% yield. The products with two porphyrins (**1b**, **2b** and **3b**) were characterized with FAB-HIMS and ^{1}H NMR (1D and 2D) spectra.

In the ^{1}H NMR spectrum of **2b** in DMSO-d_6, the α-amide NH signals appeared at δ 8.93 (D-Phe), 8.80 (Leu), 8.50 (Orn) and 7.30 (Val) at 303 K (data not shown). Both the chemical shifts and their temperature dependency (−8.3, −2.6, −4.5 and −2.0 ppb K^{-1}, respectively) were close to those of GS.[4c] These facts suggested the intramolecular hydrogen bonding between the NH and CO groups of Leu and Val residues (see Fig. 1), *i.e.* the conformational similarity of **3b** to GS. The attachment of porphyrins on the Orn positions did not change the peptide conformation. Such phenomena were also confirmed in the ^{1}H NMR study in $CDCl_3$.

The striking feature of the ^{1}H NMR spectrum of **2b** was that the tolyl groups of porphyrins appeared as two sets of doublets, δ 8.06/7.61 (4H each) and δ 7.79/7.23 (8H each) [Fig. 2(*a*)]. The methyl signals of the tolyl groups also appeared as two sets, δ 2.66 (6H) and 2.39 (12H). Compared with the monomeric porphyrin [Fig. 2(*b*)], apparently four tolyl groups among six in **2b** were high field shifted probably because of the ring current effect of the other porphyrin. The tolyl group near the other porphyrin (10-position, the inner tolyl groups in Fig. 3) may be high field shifted, but those at the 15- and 20- positions may be not. The tolyl signals at δ 7.79 and 7.23 were broad at 303 K [Fig. 2(*a*)] and were sharp at 333 K (data not shown), which implied restricted rotation of the porphyrin ring along the porphyrin–peptide axis. The signals of the 10- and 20-positions might be averaged and showed a broadened signal in the higher field. These facts suggest that the two porphyrins are spatially close. Fig. 3 shows the molecular structure of **2b** (bis-zinc complex) built by CAChe® MM2, adopting the crystal structure for the peptide moiety.[4a,5] This model also suggests that the two porphyrins are spatially close, and moreover, the left-twisted chiral orientation of the porphyrins (see below).

In CH_2Cl_2 **1b**, **2b** and **3b** (1.6 μM concentration, determined by the amino acid analysis) showed strong CD signals (data not shown), for instance **2b**, $[\theta]_{min}$ and $[\theta]_{max}$ at 424 and 416 nm ($[\theta]_M$ = −168 000 and 97 000 deg cm^2 dmol^{-1}, respectively). These CD signals were assigned to the split Cotton effects *via* the exciton coupling of the two porphyrins.[6] The (−+) sign of the couplets indicated the left-twisted orientation of the porphyrins, which was also suggested by the CAChe® calculation (Fig. 3). The intensity of the CD signals were **1b** < **2b** > **3b**. The drastic difference between **2b** (Orn) and **3b** (Lys) suggested that the flexible Lys side chains caused the loose structure of **3b**.

The Cotton effect for the porphyrins on GS was solvent-dependent (Fig. 4). The CD spectra of **2b(Zn$_2$)** in toluene (1.6 μM) showed a split Cotton effect at 435, 427 and 418 nm ($[\theta]_M$ = −951 000, 1275 000 and −234 000 deg cm^2 dmol^{-1}). The CD signals were weaker in other solvents, for instance in MeOH, $[\theta]_{430}$ = −803 000 and $[\theta]_{422}$ = 594 000 deg cm^2 dmol^{-1}. The intensity of the Cotton effect was in the order toluene > MeOH > trimethyl phosphate > TFE > CH_2Cl_2 > pyridine. These facts may indicate that the two

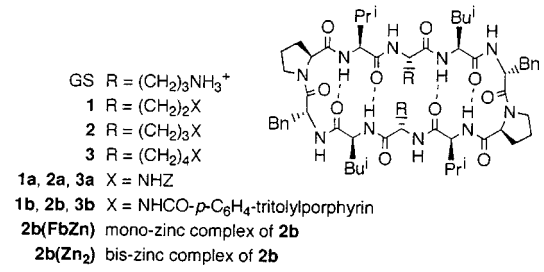

Fig. 1 Structure of Gramicidin S (GS) and its analogs.

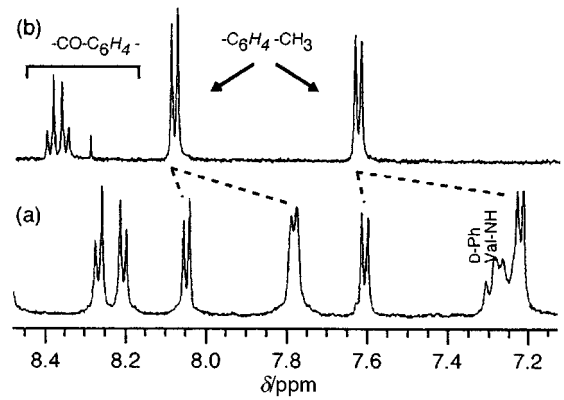

Fig. 2 ^{1}H NMR spectra of (*a*) **2b** and (*b*) 5-(*p*-methoxycarbonylphenyl)-10,15,20-tritolylporphyrin in DMSO-d_6 (303 K).

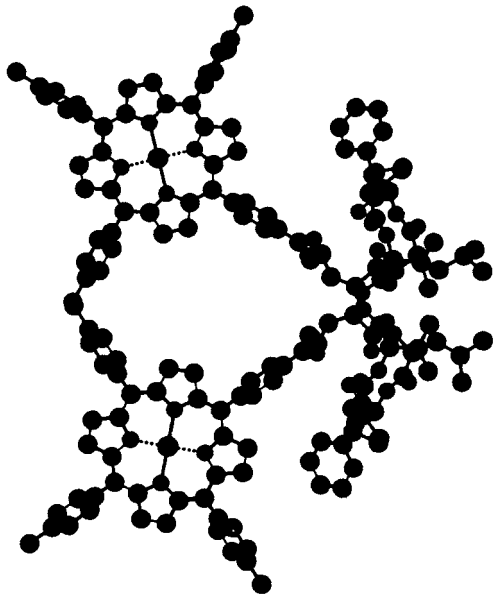

Fig. 3 CAChe® MM2 generated structure of **2b(Zn$_2$)**.

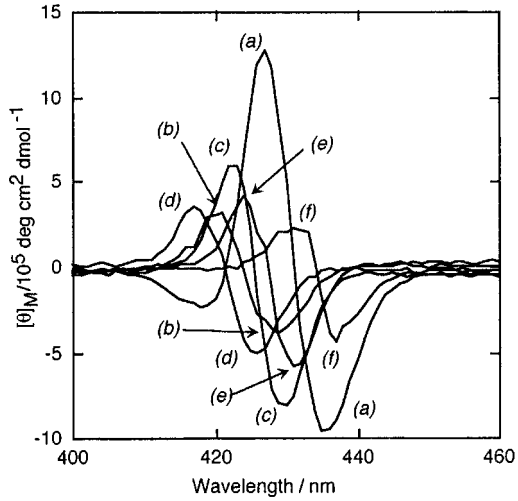

Fig. 4 CD spectra (1.6 μM for peptide) of **2b(Zn$_2$)** in (*a*) toluene, (*b*) CH_2Cl_2, (*c*) MeOH, (*d*) TFE, (*e*) trimethyl phosphate and (*f*) pyridine.

porphyrins in **2b(Zn$_2$)** were in close proximity in toluene, and the distance differed in the solvents. The different assembling ability of porphyrins in these solvents might cause different CD in the solvents, probably because of the different stabilization effect of the solvent for the π–π interaction. The details of the π–π interaction of the porphyrins are not clear yet, however, an electrostatic model may account for the tendency for porphyrin assembly in nonpolar solvents.[7] The UV spectra also supported the different orientation of the two porphyrins in these solvents. The λ_{max} of **2b(Zn$_2$)** in toluene (424 nm) was a little red-shifted from that of zinc tetratolylporphyrin (421 nm), which might be interpreted by the edge-to-edge interaction of the two π-systems.[8] However, such a shift of the λ_{max} was not observed in the other solvents investigated in the CD study, probably because of the weak interaction of the porphyrins.

Anyway, the porphyrins on GS showed different CD, *i.e.* different orientations in various solvents. This interesting fact was further confirmed by steady-state fluorescent spectrometry.[2a,3a] For this purpose, **2b(FbZn)** with one free-base porphyrin and one zinc porphyrin was synthesized. GS with different side-chain protection (Z and Fmoc) was synthesized in the same way as **2a**. After selective Z-deprotection by TFA–thioanisole–*m*-cresol (75% yield),[9] 5-(*p*-carboxyphenyl)-10,15,20-tritolylporphyrin was coupled using PyBOP–HOBt (quantitative). Then, Fmoc was removed with piperidine and zinc 5-(*p*-carboxyphenyl)-10,15,20-tritolylporphyrinate was coupled. After HPLC purification, **2b(FbZn)** was isolated in 60% yield (2 steps), and characterized with FAB-HIMS, HPLC and ^{1}H-NMR. The visible spectrum of **2b(FbZn)** (data not shown) was close to the average of **2b** (bis free-base) and **2b(Zn$_2$)**, suggesting no interaction of the two porphyrins in **2b(FbZn)** in the Q-state. However, the Soret band was somewhat broadened, suggesting a weak interaction in the B-state.[2a]

Upon exciting **2b(FbZn)** in toluene at 552 nm, the emission appeared at 608, 655 and 723 nm with an intensity ratio of 14:58:28. The ratio of ε_{552} of **2b** (bis free-base) and **2b(Zn$_2$)** was 40:60, *i.e.* 40% of the excitation light at 552 nm was absorbed by the free-base component of **2b(FbZn)** and 60% by the zinc porphyrin. From the comparison with the fluorescence spectra of **2b** (λ_{em} = 655, 719 nm, 74:26) and **2b(Zn$_2$)** (λ_{em} = 608, 652 nm, 46:54), intramolecular quenching of the excited state zinc porphyrin by the free-base porphyrin was suggested. The energy transfer from excited Zn porphyrin to free-base smoothly occurred intramolecularly, because these two porphyrins were in close proximity. The quenching efficiency was calculated to be *ca.* 82%. The same experiment performed in CH_2Cl_2 showed that 65% of the energy of the excited zinc porphyrin in **2b(FbZn)** was quenched by the free-base porphyrin. This semi-quantitative fluorescence experiment might suggest that the orientation of porphyrins differs in solvents, as suggested by CD and UV spectroscopy. However, the different energy transfer efficiencies in toluene and in CH_2Cl_2 could be due to a single solvent effect, as one of the reviewers pointed out.

We thank Professor Hideo Akisada at Kyushu Kyoritsu University for CD measurements. The molecular modeling study was partially done by Dr Masako Fujiwara at JOEL, which is gratefully acknowledged.

Notes and references

1 G. McDermott, S. M. Prince, A. A. Freer, A. M. Hawthornthwaite-Lawless, M. Z. Papiz, R. J. Cogdell and N. W. Isaacs, *Nature*, 1995, **374**, 517.

2 (*a*) R. L. Brookfield, H. Ellul, A. Harriman and G. Porter, *J. Chem. Soc., Faraday Trans. 2*, 1986, **82**, 219; (*b*) H. Kurreck and M. Huber, *Angew. Chem., Int. Ed. Engl.*, 1995, **34**, 849; (*c*) A. Osuka, N. Mataga and T. Okada, *Pure Appl. Chem.*, 1997, **69**, 797; (*d*) S. I. Yang, R. K. Lammi, J. Seth, J. A. Riggs, T. Arai, D. Kim, D. F. Bocian, D. Holten and J. S. Lindsey, *J. Phys. Chem. B*, 1998, **102**, 9426 and references cited therein.

3 (*a*) H. Tamiaki, K. Nomura and K. Maruyama, *Bull. Chem. Soc. Jpn.*, 1993, **66**, 3062; (*b*) T. Arai, K. Takei, N. Nishino and T. Fujimoto, *Chem. Commun.*, 1996, 2133; (*c*) H. Y. Liu, J. W. Huang, X. Tian, X. D. Jiao, G. T. Luo and L. N. Ji, *Chem. Commun.*, 1997, 1575.

4 (*a*) G. Némethy and H. A. Sheraga, *Biochem. Biophys. Res. Commun.*, 1984, **118**, 643; (*b*) N. Nishino, T. Arai, J. Hayashida, H. I. Ogawa, H. Yamamoto and S. Yoshikawa, *Chem. Lett.*, 1994, 2435; (*c*) T. Arai, T. Imachi, T. Kato, H. I. Ogawa, T. Fujimoto and N. Nishino, *Bull. Chem. Soc. Jpn.*, 1996, **69**, 1383.

5 To construct the molecular model of **2b(Zn)$_2$**, the structure of GS [ref. 4(*a*)] was first taken into MolSkop®, then translated to the CAChe software.

6 X. Huang, B. H. Rickman, B. Borhan, N. Berova and K. Nakanishi, *J. Am. Chem. Soc.*, 1998, **120**, 6185 and references cited therein. See also ref. 4(*b*).

7 C. Hunter, *From Simplicity to Complexity in Chemistry–and Beyond*, ed. A. Müller, A. Dress and F Vögtle, Vieweg, 1996, pp. 113–126.

8 M. Kasha, H. R. Rawls and M. A. El-Bayoumi, *Pure Appl. Chem.*, 1965, **11**, 371; T. Nagata, A. Osuka and K. Maruyama, *J. Am. Chem. Soc.*, 1990, **112**, 3054.

9 H. Yajima, Y. Minamitake, S. Funakoshi, Y. Hirai and T. Nakajima, *Chem. Pharm. Bull.*, 1981, **29**, 1752.

Communication 9/02774B

ChemComm

Catalytic enantioselective addition of enol silanes to ketomalonate mediated by C_2-symmetric bisoxazoline Lewis acid complexes

Frank Reichel, Xiangming Fang, Sulan Yao, Marina Ricci and Karl Anker Jørgensen*

Center for Metal Catalyzed Reactions, Department of Chemistry, Aarhus University, DK-8000 Aarhus C, Denmark. E-mail: kaj@kemi.aau.dk

Received (in Cambridge, UK) 22nd March 1999, Accepted 22nd June 1999

A catalytic enantioselective addition reaction of silyl enol ethers to ketomalonate in the presence of C_2-symmetric copper(II) bisoxazolines as catalysts is presented; the reaction has been studied for different ligands and substrates under various reaction conditions and proceeds in good yield and with ee's > 90% and a procedure for the preparation of an optically active hydroxy acid is shown.

C_2-Symmetric copper(II) bisoxazoline Lewis acid complexes have proven to be highly enantioselective catalysts for a variety of different organic reactions. Such reactions include addition to dicarbonyl compounds[1] where they promote Diels–Alder,[2] hetero-Diels–Alder,[3] Mukaiyama aldol[4] and carbonyl ene reactions.[3a,5] Recently, it has been shown that copper(II) bisoxazolines can catalyze the reaction of ketomalonate with conjugated dienes leading to chiral CO_2 synthons and 1,4-disubstituted cyclohex-2-enes in good yields and ee's > 90%.[1b,6] It was proposed that the reaction proceeded *via* a five-membered ring intermediate with ketomalonate coordinated to the metal center through the reacting carbonyl and one of the two ester carbonyls.[6] This communication presents the first catalytic enantioselective addition of silyl enolates **1** to ketomalonate **2** with high ee in the presence of C_2-symmetric bisoxazoline Lewis acid complexes as the catalysts [eqn. (1)].

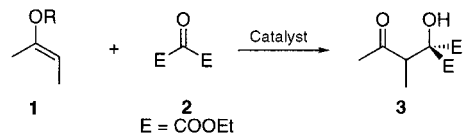

(1)

1 **2** (E = COOEt) **3**

Thus, the preparation of highly functionalised molecules such as **3** is achieved in high enantiomeric purity. Compound **3** may be regarded as the starting point for the preparation of valuable compounds such as β-keto and β-hydroxy esters or polyhydroxylated compounds.[7] It should also be mentioned that Evans *et al.*[8] in a very recent paper showed that copper bisoxazolines can also catalyze the enantioselective Michael addition of silylketene acetals to alkylidene malonates. Thus, we were prompted to present our recent results for the reaction outlined in eqn. (2).

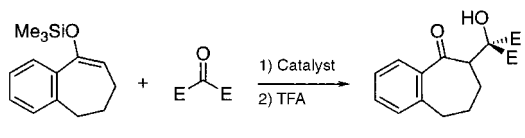

(2)

1a **2** **3a**

The reaction of the silyl enol ether **1a** with ketomalonate **2** has been investigated in order to study the potential of the bidentate and tridentate bisoxazoline-type ligands **4a–c**, **5a**,**b** in combination with $Cu(OTf)_2$ and $Zn(OTf)_2$ as the Lewis acid as enantioselective catalysts.† The yield and ee of **3a** are presented in Table 1.

The results in Table 1 show that both copper(II) and zinc(II) as the Lewis acids in the combination with the various ligands **4a–c**, **5a**,**b** are able to catalyze the reaction of the silyl enol ether

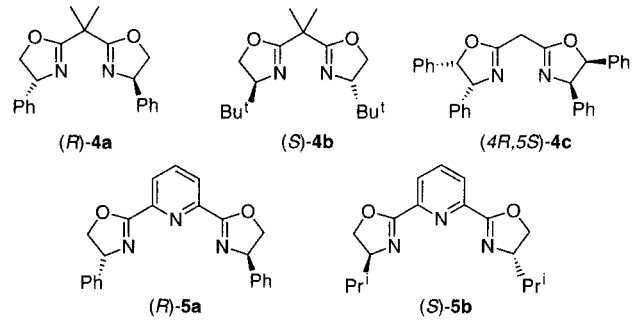

1a with ketomalonate **2**. However, the yield and ee of **3a** are very dependent on the Lewis acid and ligand applied. The highest yields and ee's are obtained with the (*R*)-**4a**-$Cu(OTf)_2$ and (4*R*,5*S*)-**4c**-$Cu(OTf)_2$ (entries 2, 4), where 99 and 94% isolated yield, and 67 and 70% ee, respectively, are obtained. Applying the same ligand, but changing the Lewis acid to zinc(II) leads to a reduction in both yield and ee of **3a** (entry 1). It is notable that changing the chiral ligand from the phenyl-substituted bisoxazoline (*R*)-**4a** to the *tert*-butyl-substituted (*S*)-**4b** and $Cu(OTf)_2$ as the Lewis acid leads to a significant reduction in the ee of **3a** as only 1% ee is obtained (entry 3). The application of the tridentate bisoxazoline ligands **5a**,**b** gives only moderate yield of **3a** accompanied with very low ee's (entries 5,6).

The promising results for the reaction of the silyl ether **1a** with ketomalonate **2** prompted us to investigate the influence of the choice of anions, solvents and temperature on the reaction course. The results are presented in Table 2 and it appears that the reaction is dependent on the solvent, temperature and anion. A fast reaction takes place at room temperature with high isolated yield and 77% ee in Et_2O as the solvent (entries 1–3), while at −10 °C longer reaction times are required to achieve good yield and the best results are obtained in Et_2O and Bu^{t}OMe where 86 and 83% ee are obtained, respectively (entries 5, 6). Changing the anion to hexafluoroantimonate causes a dramatic decrease in ee of **3a** (entry 7). Reducing the reaction temperature to −78 °C improves the ee up to 93% (entry 8). The chiral ligand (4*R*,5*S*)-**4c** is also a promising ligand and similar good yield and high ee are obtained as using (*R*)-**4a**-$Cu(OTf)_2$ as the catalyst (entries 9, 10).

Table 1 The reaction of silyl enol ether **1a** with ketomalonate **2** in the presence of the chiral ligands **4a–c**, **5a**,**b** in combination with $Cu(OTf)_2$ and $Zn(OTf)_2$ as Lewis acid in CH_2Cl_2 at room temperature

Entry	Catalyst	Yield[a] **3a** (%)	Ee[b] (%)
1	(*R*)-**4a**-$Zn(OTf)_2$	65	43
2	(*R*)-**4a**-$Cu(OTf)_2$	99	67
3	(*S*)-**4b**-$Cu(OTf)_2$	87	1
4	(4*R*,5*S*)-**4c**-$Cu(OTf)_2$	94	70
5	(*R*)-**5**-$Zn(OTf)_2$	58	3
6	(*S*)-**5b**-$Zn(OTf)_2$	48	0

[a] Isolated yield. [b] Determined by chiral HPLC.

Table 2 The reaction of silyl enol ether **1a** with ketomalonate **2** in the presence of the chiral ligands (*R*)-**4a** and (*R*)-**4c** in combination with Cu^{II} salts (10 mol%) in various solvents and different temperatures

Entry	Catalyst	Solvent	*T*/°C	*t*/h	Yield[a] **3a** (%)	Ee[b] (%)
1	(*R*)-**4a**-$Cu(OTf)_2$	CH_2Cl_2	rt	1	99	67
2	(*R*)-**4a**-$Cu(OTf)_2$	Et_2O	rt	1	89	77
3	(*R*)-**4a**-$Cu(OTf)_2$	THF	rt	1	81	71
4	(*R*)-**4a**-$Cu(OTf)_2$	CH_2Cl_2	−10	40	80	78
5	(*R*)-**4a**-$Cu(OTf)_2$	Et_2O	−10	40	81	86
6	(*R*)-**4a**-$Cu(OTf)_2$	Bu^tOMe	−10	40	77	83
7	(*R*)-**4a**-$Cu(SbF_6)_2$	CH_2Cl_2	−10	40	89	37
8	(*R*)-**4a**-$Cu(OTf)_2$	Et_2O	−78	75	88	93
9	(4*R*,5*S*)-**4c**-$Cu(OTf)_2$	CH_2Cl_2	−10	45	94	70
10	(4*R*,5*S*)-**4c**-$Cu(OTf)_2$	Et_2O	−10	40	76	86

[a] Isolated yield. [b] Determined by chiral HPLC.

The reaction has been studied for a series of silyl enol ethers **1a**–**g** reacting with ketomalonate **2** in the presence of (*R*)-**4a** in combination with $Cu(OTf)_2$ or $Zn(OTf)_2$ and the results are presented in Table 3.

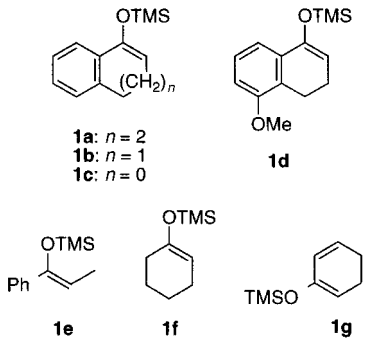

The reactions generally proceed with high isolated yields for the various substrates; for the cyclic aromatic silyl enol ethers **1a**,**b**,**d**, high ee's were obtained (Table 3, entries 1, 3, 6), whereas for the five membered analogue **1c**, the ee is reduced to 58% (entry 5). Furthermore, it appears from the results for **1b**,**c** that zinc(II) also can be used as the Lewis acid, however the ee is lower in these reactions (entries 2, 4). For the aromatic acyclic silyl enol ether **1e** the reaction proceeds also very well with very high isolated yield and ee (entry 7). The cyclic aliphatic silyl enol ether **1f** reacts also smoothly with ketomalonate **2** in the presence of (*R*)-**4a**-$Cu(OTf)_2$ as the catalyst giving the corresponding adduct in good yield and with up to 60% ee (entry 8), whereas the conjugated silyl enol ether **1g** only leads to the corresponding product in moderate yield and ee by using (*R*)-**4a**-$Cu(OTf)_2$ as the catalyst, while high yield and a racemic compound is obtained when (*R*)-**4a**-$Zn(OTf)_2$ is the catalyst (entries 9, 10).

The potential of the reaction is shown by the reduction, followed by oxidative cleavage of the ester groups in **3b** [eqn. (3)] giving the corresponding hydroxy acid in good yield and maintaining the ee obtained in the catalytic step.[9a] These reactions lead also to an assignment of the absolute configuration of the chiral center formed in the catalytic reaction.[9b]

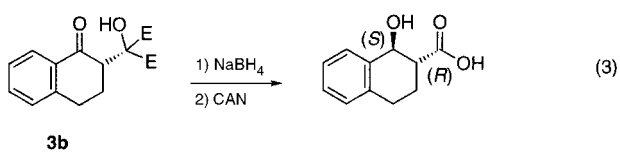

3b (3)

In conclusion we have presented a novel catalytic enantioselective addition reaction of different silyl enol ethers to ketomalonate catalyzed by copper(II) bisoxazoline complexes giving highly functionalized optically active compounds.

This work was made possibly by a grant from The Danish National Research Foundation.

Table 3 The reaction of silyl enol ethers **1a**–**g** with ketomalonate **2** in the presence of (*R*)-**4a**-$Cu(OTf)_2$ or (*R*)-**4a**-$Zn(OTf)_2$ (10 mol%) as the catalyst in Et_2O as the solvent

Entry	Substrate	*T*/°C	*t*/h	Yield[a] (%)	Ee[b] (%)
1[c]	**1a**	−78	75	88	93
2[d,e]	**1b**	−10	42	81	77
3[c]	**1b**	−78	75	91	86
4[d,e]	**1c**	−10	12	91	45
5[c]	**1c**	−78	75	82	58
6[c]	**1d**	−78	65	90	85
7[c]	**1e**	−78	65	95	90
8[c]	**1f**	−78	75	80	60
9[c]	**1g**	rt	18	26	36
10[d]	**1g**	rt	18	96	1

[a] Isolated yield. [b] Determined by chiral HPLC. [c] Catalyst (*R*)-**4a**-$Cu(OTf)_2$. [d] Catalyst (*R*)-**4a**-$Zn(OTf)_2$. [e] CH_2Cl_2 as the solvent.

Notes and references

† *Representative procedure*: $Cu(OTf)_2$ (18.1 mg, 0.05 mmol) and the ligand (*R*)-**4b** (17.6 mg, 0.0525 mmol) were placed in a flame dried Schlenk tube and dried under high vacuum for 1–2 h. Et_2O (1.5 ml) was added and the suspension was stirred for 1 h. Subsequently **2** (76 μl, 0.5 mmol) was added and the mixture was placed in a dry ice–acetone bath and after 30 min **1a** (232 mg, 1.0 mmol) was added. Stirring was continued for 75 h followed by addition of TFA–CH_2Cl_2 (10%, 1 ml). After 30 min TLC showed completion of hydrolysis and the solvent was removed. The residue was purified by FC (20% EtOAc in light petroleum) to afford **3a** (147 mg, 0.44 mmol, 88%) as a colourless oil with 93% ee, determined by chiral HPLC using a Chiralcel OJ column (5% Pr^iOH in hexane, 0.7 ml min^{-1}); $[\alpha]_D^{rt}$ −23.6 (*c* 0.008 g ml^{-1}, $CHCl_3$). δ_H 7.72 (dd, *J* 8.2, 1.1, 1H, arom.), 7.41 (dt, *J* 8.8, 1.5, 1H, arom.), 7.29 (t, *J* 7.2, 1H, arom.), 7.20 (d, *J* 7.1, 1H, arom.), 4.40 (br s, 1H, OH), 4.34–4.20 (m, 4H, CH_2), 3.86 (dd, *J* 11.0, 3.8, 1H, C(O)CHC), 3.12–2.86 (m, 2H, CH_2), 2.17–1.64 (m, 4H, CH_2), 1.28 (t, *J* 7.1, 3H, CH_3), 1.14 (t, *J* 7.1, 3H, CH_3) δ_C 204.4, 170.2, 169.0, 141.6, 137.9, 132.5, 129.9, 129.0, 126.7, 81.3, 62.7, 62.6, 53.5, 32.8, 25.0, 23.7, 14.1, 13.9.

1 (*a*) A. K. Ghosh, P. Mathivanen and J. Cappiello, *Tetrahedron: Asymmetry*, 1998, **9**, 1; (*b*) K. A. Jørgensen, M. Johannsen, S. Yao, H. Audrain and J. Thorhauge, *Acc. Chem. Res.*, 1999, **32**, 605.

2 See *e.g.* (*a*) E. J. Corey, N. Imai and H. Zhang, *J. Am. Chem. Soc.*, 1991, **113**, 728; (*b*) D. A. Evans, S. J. Miller and T. Letcka, *J. Am. Chem. Soc.*, 1993, **115**, 6469; (*c*) D. A. Evans, J. Murry, P. Matt, R. D. Norcross and S. J. Miller, *Angew. Chem., Int. Ed. Engl.*, 1995, **34**, 798.

3 See *e.g.* (*a*) M. Johannsen and K. A. Jørgensen, *J. Org. Chem.*, 1995, **60**, 5979; (*b*) M. Johannsen, S. Yao and K. A. Jørgensen, *Chem. Commun.*, 1997, 2169; (c) D. A. Evans and J. S. Johnson, *J. Am. Chem. Soc.*, 1998, **120**, 4895; (*d*) S. Yao, M. Johannsen, H. Audrain, R. Hazell and K. A. Jørgensen, *J. Am. Chem. Soc.*, 1998, **120**, 8599; (*e*) J. Thorhauge, M. Johannsen and K. A. Jørgensen, *Angew. Chem., Int. Ed.*, 1998, **37**, 2404; (*f*) D. A. Evans, E. J. Olhava, J. S. Johnson and J. M. Janey, *Angew. Chem., Int. Ed.*, 1998, **37**, 3554.

4 See *e.g.* D. A. Evans, M. C. Kozlowski, J. A. Murry, C. S. Burgey, K. R. Campos, B. T. Connell and R. J. Staples, *J. Am. Chem. Soc.*, 1999, **121**, 669 and references therein.

5 D. A. Evans, C. S. Burgey, N. A. Paras, T. Vojkovsky and S. W. Tregay, *J. Am. Chem. Soc.*, 1998, **120**, 5824.

6 S. Yao, M. Roberson, F. Reichel, R. G. Hazell and K. A. Jørgensen, *J. Org. Chem.*, in the press.

7 See *e.g.* (*a*) J. R. March, *Advanced Organic Chemistry*, 5th edn., Wiley, New York, 1992; (*b*) S. Benetti, R. Romagnoli, C. D. Risi, G. Spalluto and V. Zanirato, *Chem. Rev.*, 1995, **95**, 1065.

8 D. A. Evans, T. Rovis, M. C. Kozlowski and J. S. Tedrow, *J. Am. Chem. Soc.*, 1999, **121**, 1994.

9 (*a*) R. G. Salomon, S. Roy and M. F. Salomon, *Tetrahedron Lett.*, 1988, **29**, 769; (*b*) A. Schoofs, J. P. Guetté and A. Horeau, *Bull. Soc. Chim. Fr.*, 1976, 1215.

Communication 9/02227I

ChemComm

Covalent adhesion; organic reactivity at a solid–solid interface through an inter-bead Diels–Alder reaction†

Iain P. Thomas, James A. Ramsden, Tibor Z. Kovacs and John M. Brown

Dyson Perrins Laboratory, South Parks Road, Oxford, UK OX1 3QY. E-mail: john.brown@chemistry.ox.ac.uk

Received (in Liverpool, UK) 26th February 1999, Accepted 18th June 1999

Polystyrene resin beads carrying respectively maleimide and anthracene groups attached to extended side-chains adhere to one another in a manner consistent with an inter-bead cycloaddition reaction.

We reported earlier on the synthesis of modified polymers based on cross-linked polystyrene where *ca.* 60% of the arene rings bore a long alkyl side-chain possessing terminal functionality.[1] The quality of ^{13}C NMR spectra observed for the solvent-swollen polymer and in particular the high degree of mobility deduced from the ^{13}C T_1 relaxation times indicated a fluid-like polymer where the functional groups were readily accessible. In addition, their effective concentration is in the 2–2.5 mM region. This led us to consider the possibility for reaction at the interface between two polymers of this type, each carrying a different reactive entity. There are interesting precedents for employing an intermolecular Diels–Alder reaction as a probe for the reaction environment, or immobilisation;[2] the reaction is a formal addition to give a single product, and it is relatively insensitive to solvent polarity.[3]

Synthesis of the desired polymers was accomplished according to Scheme 1. For the dienophilic component, the maleimide functionality was introduced in a one-step sequence whereby the alcohol **1a** was reacted with *N*-(chlorocarbonylmethyl)maleimide, giving **2**.[4] First attempts at forming a polymer-linked diene involved attachment of chlorodimethylcyclopentadienylsilane[5] (in the expectation of forming a regiochemically defined product) but were not quantitative. A more successful approach involved reaction of alcohol **1a** with 9-(2-chlorocarbonylethyl)-10-methylanthracene[6] from which resin **3** was obtained. For control experiments, the saturated succinimide **4** and fumarate ester **5** were synthesised using related methods. A staining procedure was adapted by synthesis of the dienophilic dye **6** prepared from Disperse Red 1 which was shown to selectively stain the resin diene **3** bright red[7] (1% solution, 1 h, THF), and to leave the dienophilic resin **2** unaffected under the same conditions. It was confirmed by ^{13}C NMR that the desired polymers had been synthesised without significant side-reactions and also that the staining procedure introduced an insignificant number of additional linkages into resin **3**. It were further confirmed by ^{13}C NMR that diene resin **3** reacted with maleimide to form the adduct **8** and dienophile resin **2** reacted with cyclopentadiene to form the adduct **7**. Both cycloadditions were complete by ^{13}C NMR. Since there is a rapid intermolecular Diels–Alder reaction between maleimide and 9,10-dimethylanthracene,[8] these polymer-bound entities provided a suitable test for investigation of interfacial reactivity.

Solvent effects on the aggregation of resin beads were explored first. Alcohol **1a** and its silyl ether **1b** were suspended in a range of solvents; the former aggregated in toluene or cyclohexane, the latter in ethanol (weakly) or DMF, indicating the inverse relationship between functional group polarity and disposition to aggregation in a given solvent. Further experiments demonstrated that all the resins **2**, **3** and **5** possessing unsaturated chains were aggregated in cyclohexane and fully dispersed in DMF. On this basis a protocol for the desired inter-bead Diels–Alder reaction was established. Approximately equal quantities of stained resin **3** and resin **2** were briefly sonicated together and then stood in toluene or cyclohexane. After 20 h there was considerable aggregation which persisted on transfer to suspension in DMF. On standing longer the degree of aggregation increased after the same treatment, and after an extended period agglomeration was observed.

Two more quantitative approaches were then attempted. Samples of resins **2** and **3** were mixed by sonication as before, centrifuged together for a defined period (0–75 min, 6500 rpm), suspended in the minimum quantity of DMF (centrifugation was not necessary in order to observe the described phenomena, but shortened the timescale). After completion the suspension was transferred to water on a microscope slide, causing considerable dispersal of aggregates, and observed by microscopy. The following observations were made, facilitated by the staining of the diene with maleimide **6** before reaction.

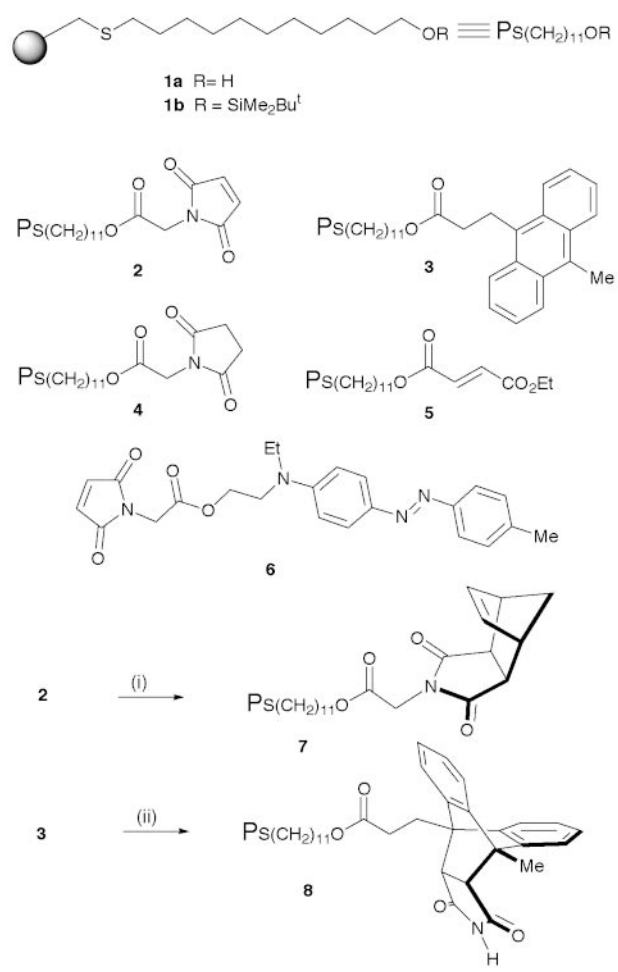

Scheme 1 *Reagents*: (i) neat cyclopentadiene, rt, 3 d; (ii) xs. maleimide, C_7H_8, rt, 6 d.

† A colour version of Fig. 1 is available as supplementary data from the RSC web site, see http://www.rsc.org/suppdata/cc/1999/1507/

Table 1 Analysis of bead–bead contacts after centrifugation in DMF and resuspension in water

	No. of beads		No. of contacts							
t/min	Diene **3**	Dienophile **2**	**3**–**3**	**2**–**2**	**2**–**3**	Total beads	No. in aggregation	Total contacts[a]	Statistical **2**–**3**	Actual **2**–**3**
0	213	445	43	54	96	658	273	193	0.438	0.497
30	700	1051	77	109	449	1751	780	635	0.480	0.707
75	703	1119	233	155	832	1822	1006	1220	0.487	0.682

[a] Includes single and multiple contacts.

(a) The extent of aggregation and the average size of aggregates increased with time; without mechanical intrusion the proportion of **2**:**3** (heterotopic) contacts was significantly higher than statistical, the proportion of **2**:**2** and **3**:**3** (homotopic) contacts likewise significantly lower than statistical expectation. Results are recorded in Table 1.

(b) When either resins **2** or **3** was subjected to the same treatment separately, no aggregation phenomena were observed.

(c) The nature of the interface was distinct for **2**:**3** contacts when compared to **2**:**2** or **3**:**3** contacts. For the latter, the point of contact was not defined, so that two or three beads made visible rolling movements, the stable state of most trimers being triangular. In contrast, association between beads **2** and **3** occurred at a fixed point and the interaction was stable (Fig. 1). Alternating linear tetramers were observed, but rarely higher states of linear aggregation. These aggregates could move freely maintaining their inter-bead vectors. By carrying out the staining procedure *after* inter-bead reaction, it was verified that heterotopic interactions (**2**:**3**) were uniquely responsible for the distinctive stable linear trimers and tetramers.

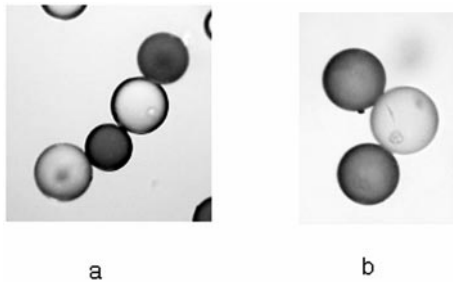

Fig. 1 Reaction of diene beads **3**, stained with Disperse Red to 1% of accessible functionality (dark spheres), with dienophile **2** in DMF (light spheres). Aggregates were located by microscopy after dispersal in water.

(d) Aggregates were not observed in control experiments involving the succinimide-capped resin **4** together with resin **3**, where complete dispersal to individual beads was observed on transfer to a polar medium.

(e) Aggregates formed in DMF were not broken down by exposure to maleimide (1 M in DMF, 20 min).

Although these aggregates were robust enough to be mechanically manipulated, their fragility is evident from the loss of adhesion after evaporation of all solvent DMF and attendant shrinkage of the beads.

Although the definitive explanation must await further studies at the nanochemical level, these experiments are best interpreted through the operation of a cycloaddition reaction occurring between diene and dienophile on separate beads, in the manner of Scheme 2. The beads remain undistorted, so that the extent of reaction is small. For a hard contact of a pair of beads 10^5 nm diameter in a solvent (DMF) of molecular volume 0.13 nm^3, the contact area is 7500 nm^3, with respectively 7×10^3 diene and 8×10^3 dienophile moieties in the surface segment. With long alkyl chains attached to an spatially irregular polymer backbone the surface of the bead will be rough at molecular dimensions, permitting reaction over a greater surface area than this. Since the activation free energy of the retro-Diels–Alder reaction is about 190 kJ mol^{-1},[10] each cycloaddition provides an interparticle bond of strength 3×10^{-19} J. Many bonding events are likely to be necessary to overcome shear forces.

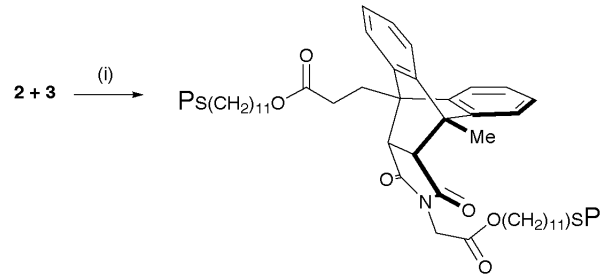

Scheme 2 Suspend in DMF, sonicate 1–2 min, centrifuge 0–75 min, 5000 rpm.

There are few precedents for a well-defined reacting system with the components confined to different surfaces. A reasonable analogy can be made with the work of Sasaki and Maeda,[11] who studied peptide–peptide interactions with one component bound to magnetic polystyrene beads and the other bound to 5 μm controlled pore glass beads. Recent work of Whitesides and co-workers has been concerned with surface adhesion of micromachined objects through controlled hydrophobic or hydrophilic character of surfaces.[12] Our aims are to develop these present observations and define the scope and limitations of solid–solid interfacial chemistry.

We thank EPSRC for an award under the ROPA Scheme. Dr Colin Bain and Mr Peter Breed made helpful comments. We thank referees for valuable comments.

Notes and references

1 J. M. Brown and J. A. Ramsden, *Chem. Commun.*, 1996, 2117.
2 M. Marty, Z. Clyde-Watson, L. J. Twyman, M. Nakash and J. Sanders, *Chem. Commun.*, 1998, 2265; B. Wang and I. O. Sutherland, *Chem. Commun.*, 1997, 1495; M. N. Yousaf and M. Mrksich, *J. Am. Chem. Soc*., 1999, **121**, 4286.
3 F. Fringuelli and A. Taticchi, *Dienes in the Diels–Alder Reaction*, Wiley, New York, 1990.
4 J. E. T. Corrie and D. R. Trentham, *J. Chem. Soc., Perkin Trans. 1*, 1995, 1993.
5 D. W. Carpenetti, L. Kloppenburg, J. T. Kupec and J. L. Petersen, *Organometallics*, 1996, **15**, 1572.
6 J. L. Adelfang and G. H. Daub, *J. Am. Chem. Soc.*, 1958**, 80**, 1405.
7 D. Lowik, M. D. Weingarten, M. Broekema, A. J. Brouwer, W. C. Still and R. Liskamp, *Angew. Chem., Int. Ed.*, 1998, **37**, 1846, for a recent example of staining with this dye.
8 A. Mielert, C. Braig, J. Sauer, J. Martelli and R. Sustmann, *Liebigs Ann. Chem.*, 1980, 954; J. Fleischauer, A. N. Assad, W. Schleker and H.-D. Scharf, *Liebigs Ann. Chem.*, 1981, 306. The bimolecular rate constant for maleimide plus 9,10-dimethylanthracene is 2.5×10^{-2} L mol^{-1} s^{-1} at 25 °C in $CHCl_3$.
9 J. N. Israelachvili, *Intermolecular and Surface Forces*, 2nd edn., Academic Press, London, 1992.
10 M. Taagepera and E.R. Thornton, *J. Am. Chem. Soc*., 1972, **94**, 1168 gives $\Delta H^{\ddagger}$ = 49. 1 kcal mol^{-1}, $\Delta S^{\ddagger}$ = 12 e.u. for the retro-Diels–Alder reaction of 9,10-ethanoanthracene.
11 S. Sasaki, M. Takagi, Y. Tanaka and M. Maeda, *Tetrahedron Lett*., 1996, **37**, 85.
12 T. L. Breen, J. Tien, S. Oliver, T. Hadzic and G. M. Whitesides, *Science*, 1999, **284**, 948; I. S. Choi, N. Bowden and G. M. Whitesides, *J. Am. Chem. Soc.*, 1999, **121**, 1754; J. Tien, T. L. Breen and G. M. Whitesides, *J. Am. Chem. Soc.*, 1998, **120**, 12670; W. Huck, J. Tien and G. M. Whitesides, *J. Am. Chem. Soc.*, 1998, **120**, 8267.

Communication 9/01643K

ChemComm

Catalytically self-threading polyrotaxanes

Dönüs Tuncel and Joachim H. G. Steinke*

Department of Chemistry, Imperial College of Science, Technology and Medicine, South Kensington, London, UK SW7 2AY. E-mail: j.steinke@ic.ac.uk

Received (in Cambridge, UK) 14th April 1999, Accepted 24th June 1999

A mainchain polyrotaxane is formed in which polymerisation and rotaxane formation occur simultaneously, due to the presence of the catalytically-active self-threading macrocycle cucurbituril.

Exerting increasing architectural control in the synthesis of polymers is key to the development of new materials.[1] This has been exemplified in the case of dendrimers where for the first time truly single entity synthetic polymers have been prepared.[2] The convergent approach in particular highlights how a well-established synthetic concept from one area of chemistry (protection/deprotection chemistry) can have a tremendous impact on another one (polymer synthesis). In a similar vein we describe in this communication a unique route for the synthesis of structurally perfect mainchain polyrotaxanes (Fig. 1).

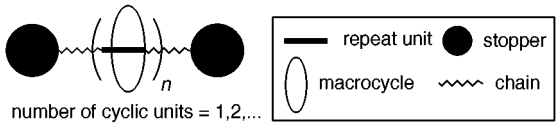

Fig. 1 A perfect polyrotaxane.

Polyrotaxanes represent a relatively recent addition to the repertoire of polymer architectures. Seminal work by Gibson,[3] Stoddart,[4] Harada[5] and Wenz,[6] and more recently Kim,[7] has produced a wealth of polyrotaxane structures and identified key synthetic parameters.[8] Earlier work was limited to the statistical synthesis of mainchain polyrotaxanes, but the current state-of-the-art uses directed (templated) strategies applied to the synthesis of mainchain, sidechain and hyperbranched polyrotaxanes and polypseudorotaxanes.[9,10] Perfect linear mainchain and networked polyrotaxanes have also been prepared, albeit in the solid-state only.[11]

Here we would like to add to the repertoire of polyrotaxane syntheses. In our approach polymerisation and rotaxane formation occur simultaneously to yield a perfectly threaded polyrotaxane due to the presence of cucurbituril, a macrocycle that catalyses 1,3-dipolar cycloadditions. Cucurbituril has also been used recently by Meschke *et al.* as the statistically threaded macrocyclic component in an interfacial condensation polymerisation.[12]

There are principally three ways in which to ensure that each polymer repeat unit is threaded by an integer number of cyclic units: (i) to polymerise a preformed rotaxane monomer, (ii) to select a polymer backbone that can bind strongly and selectively to a suitably chosen macrocycle, or (iii) to ensure that during the polymerisation step each added monomer contains an integer number of cyclic units. We opted for the third alternative by employing cucurbituril as macrocyclic component (Fig. 2). It was established by Mock *et al.*[13] in the 1980s that cucurbituril is capable of catalysing 1,3-dipolar cycloadditions in an enzyme-like fashion (Fig. 2).

The bond forming process requires the complexation of an ammonium azido and an ammonium alkyne compound to each of the carbonyl-fringed portals of cucurbituril. Complexation is accompanied by the displacement of solvent molecules from the hydrophilic interior of the macrocycle. The resulting complex is slightly strained. The release of this strain is responsible for the catalytic effect of cucurbituril on the cycloaddition reaction leading to an acceleration by a factor of 10^5.[14]

We decided to utilise this intriguing reaction for the synthesis of polyrotaxanes since each cycloaddition reaction catalysed by cucurbituril not only leads to a chemical bond but also to the self-threading of the macrocyclic catalyst. From a polymer synthesis point of view this means that each additional repeat unit added to a polymer chain is inevitably accompanied by the threading of exactly one cyclic unit.

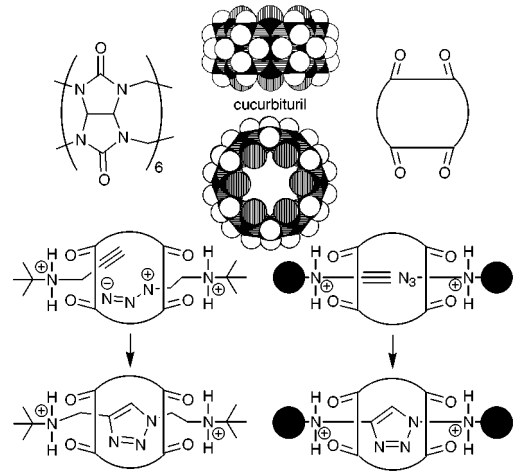

Fig. 2 1,3-Dipolar cycloaddition catalysed by cucurbituril.

Cucurbituril was synthesised according to a literature procedure.[15] The required diazide and dialkyne monomers have been synthesised efficiently as shown in Fig. 3. Monomer A was synthesised by treating **1** with propargylamine (propargyl = prop-2-ynyl), followed by formation of the dihydrochloride salt in 86% overall yield. The synthesis of monomer B also started from **1**, reacting first with 2-aminoethanol. Subsequent treatment with $SOCl_2$, followed by substitution with sodium azide and formation of the dihydrochloride salt gave monomer B in 4 steps and 39% overall yield.

The preparation of model compounds synthesised from monomer A and B with 2 equivalents of a corresponding *tert*-butylamine-derived mono-azido and mono-alkyne compound in the presence of cucurbituril yielded [3]rotaxanes in 88% and 67% yield respectively (for NMR see Fig. 5). The correspond-

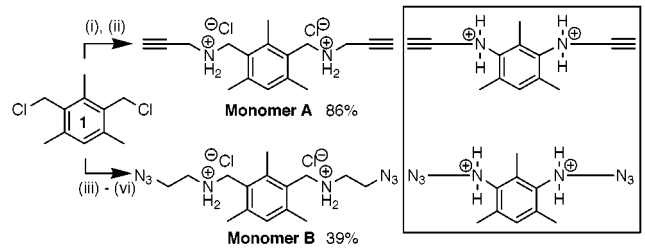

Fig. 3 Synthesis of monomers A and B. (i) $NH_2CH_2C{\equiv}CH$, neat, 0 °C → rt, 16 h, 100% (crude), (ii) 1 M HCl in Et_2O, rt, 86%, (iii) $NH_2CH_2CH_2OH$, neat, 5 h, 150–160 °C, 66%, (iv) $SOCl_2$, $CHCl_3$, 5 h, rt, 70%, (v) NaN_3, H_2O, 75 °C, 16 h, 87%, (vi) 1 M HCl in Et_2O, rt, 96%.

ing [2]rotaxane, first prepared by Mock *et al.*[14] was obtained in 76% yield. Polymerisation was carried out at room temperature by dissolving equimolar amounts of monomer A and monomer B in acidified water followed by the addition of 2 equivalents of cucurbituril (Fig. 4).

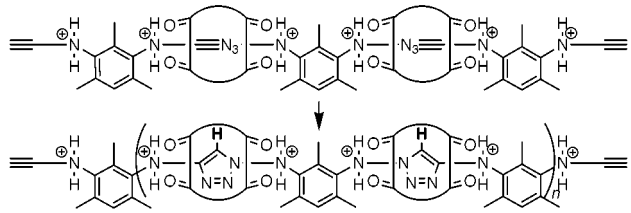

Fig. 4 Synthesis of a perfect mainchain polyrotaxane.

The reaction was followed by ^{1}H-NMR. Comparison of the relative intensities of the triazole proton to phenyl proton indicated the formation of possibly dimers (ratio 1 : 2) within the first 24 h of the reaction. After an additional 24 h the ratio had changed to a value close to 1 : 1. Longer reaction times had no bearing on the reaction outcome. Precipitation of the aqueous solution into acetone resulted in a white precipitate which was filtered, washed and dried *in vacuo* (yield: 68%). ^{1}H- and ^{13}C-NMR (^{13}C data of the corresponding carbon in brackets) are in agreement with the proposed structure. The crucial appearance of the triazole proton is documented in Fig. 5 and compared with a [3]rotaxane[16] and [2]rotaxane model compound (*vide infra*).

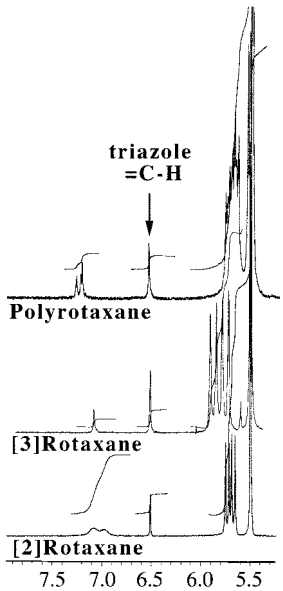

Fig. 5 ^{1}H-NMR overlay of the triazole region of the polyrotaxane and a [3][16] and [2]rotaxane model compound.

The triazole proton located inside the cavity of cucurbituril has a chemical shift of 6.54 ppm (122.7 ppm) which is further confirmed through the model [2]rotaxane and [3]rotaxane (Fig. 5). In an unprotonated triazole model compound the same proton appears at 7.52 ppm (120.8 ppm) and is shifted even further downfield in the same compound at 8.56 ppm (130.5 ppm) upon its diprotonation (formation of the dihydrochloride salt). Furthermore in the absence of cucurbituril polymerisation has not been observed. GPC data in DMF were obtained after anion exchange (Cl^- to PF_6^-) gave a M_n value of 5100 and a M_w value of 9000 based on polystyrene standards. MALDI-TOF showed very broad peak clusters and the reason for this is not known. Peak maxima are spaced by about *m/z* 1350 (molar masses of the repeat units are 1324.14 and 1386.17) with an average value close to 6000. ^{1}H-NMR allows an estimate of the molecular weight by comparing the integration of the triazole proton with the one located on the benzene ring. A ratio of 0.9 (triazole) to 1 translates into a molecular weight of about 13000. We have not been able to precisely establish the charge state of the polyrotaxane in our ES-MS measurements. Indications so far are of a molar mass of about 10000. Finally small angle light scattering measurements were attempted but have been unsuccessful because a reliable d*n*/d*c* value could not be obtained (maybe due to concentration dependent aggregation effects). Additional evidence for the formation of a polyrotaxane was also found in its solubility behaviour. Cucurbituril and the polyrotaxane are both soluble in acidic aqueous media, but *only* cucurbituril dissolves in a saturated solution of sodium chloride as shown by Kim.[17] Dissolution of cucurbituril in water through the presence of a sodium salt requires accessibility of the carbonyl portals to which sodium cations are complexed. This has become impossible (*vide infra*) once cucurbituril has been incorporated into a mainchain polyrotaxane architecture.

We have presented the first solution synthesis of a perfect mainchain polyrotaxane. Investigations are in progress to reveal mechanistic details of the polymerisation itself and to apply our approach to more complex polymer architectures.

We would like to thank the EPSRC for providing an IPSI project studentship for D. T. Thanks are also due to Dr Welham of the University of London ULIRS service for running MALDI-TOF spectra, Dr Ball for providing us with ES mass spectrometry data and the EPSRC RAPRA service for GPC characterisation data.

Notes and references

1 (*a*) J. R. Ebdon and G. C. Eastmond (Eds.), *New methods of polymer synthesis*. Vol. 2., Blackie, 1995; (*b*) the entire issue, *Top. Curr. Chem.*, 1998, **197**.
2 (*a*) D. A. Tomalia, A. M. Naylor and W. A. Goddard, *Angew. Chem., Int. Ed. Engl.*, 1990, **29**, 138; (*b*) L. J. Hobson and R. M. Harrison, *Curr. Opin. Solid State Mater. Sci.*, 1997, **2**, 683.
3 C. G. Gong and H. W. Gibson, *Curr. Opin. Solid State Mater. Sci.*, 1997, **2**, 647.
4 S. A. Nepogodiev and J. F. Stoddart, *Chem. Rev.*, 1998, **98**, 1959.
5 A. Harada, *Adv. Polym. Sci.*, 1997, **133**, 141.
6 (*a*) G. Wenz, M. B. Steinbrunn and K. Landfester, *Tetrahedron*, 1997, **53**, 15575; (*b*) G. Wenz, *Angew. Chem., Int. Ed. Engl.*, 1994, **33**, 803.
7 D. Whang and K. Kim, *J. Am. Chem. Soc.*, 1997, **119**, 451.
8 H. W. Gibson, M. C. Bheda and P. T. Engen, *Prog. Polym. Sci.*, 1994, **19**, 843.
9 C. G. Gong and H. W. Gibson, *Macromol. Chem. Phys.*, 1998, **199**, 1801.
10 R. K. Castellano and J. Rebek, *J. Am. Chem. Soc.*, 1998, **120**, 3657.
11 D. Whang, Y.-M. Jeon and K. Kim, *Chem. Lett.*, 1996, 503.
12 C. Meschke, H. J. Buschmann and E. Schöllmeyer, *Polymer*, 1999, **40**, 945.
13 W. L. Mock, *Top. Curr. Chem.*, 1995, **175**, 1.
14 W. L. Mock, T. A. Irra, J. P. Websiec and M. Adhya, *J. Org. Chem.*, 1989, **54**, 5302.
15 R. Behrend, E. Meyer and F. Rusche, *Liebigs Ann. Chem.*, 1905, **339**, 1.
16 [3]rotaxane = Monomer A reacted with two *tert*-butyl azido stoppers.
17 Y.-M. Jeon, J. Kim, D. Whang and K. Kim, *J. Am. Chem. Soc.*, 1996, **118**, 9790.

Communication 9/02990G

ChemComm

Low temperature structural analysis of a TDAE·C_{60} crystal

Bakhyt Narymbetov,*[a]† Hayao Kobayashi,[a] Madoka Tokumoto,[b] Ales Omerzu[c] and Dragan Mihailovic[c]

[a] *Institute for Molecular Science, Okazaki 444, Japan. E-mail: narymbetov@ims.ac.jp*
[b] *Electrotechnical Laboratory, 1-1-4 Umezono, Tsukuba, Ibaraki 305, Japan*
[c] *Jozef Stefan Institute, Jamova 39, 1000 Ljubljana, Slovenia*

Received (in Cambridge, UK) 1st April 1999, Accepted 30th June 1999

X-Ray single crystal diffraction studies of TDAE·C_{60} were performed at low temperature and its crystal structure could be solved and analysed on the basis of diffraction data obtained at 7–11 K.

The discovery of organic ferromagnetism in TDAE·C_{60} by Allemand *et.al.*,[1] where TDAE is tetrakis(dimethylamino)-ethylene, with a transition temperature of about 16 K aroused considerable interest in this compound, since it has the highest T_c of any known molecular ferromagnet without transition metal atoms. A number of possible models, such as itinerant ferromagnetism, superparamagnetism, spin-glass like ground state, and spin-canted weak ferromagnetism have been proposed [1–6] to explain its magnetic behavior at low temperatures. However, despite intensive studies of TDAE·C_{60}, a detailed crystal structure based on single crystal diffraction data has not been published until now. The first structural characterization of TDAE·C_{60} crystals was conducted on X-ray powder diffraction data by Stephens *et.al.*,[7] on the basis of which it has been shown that TDAE·C_{60} is a 1:1 charge-transfer complex and that the structure has a *C*-centered monoclinic unit cell. The space group was determined as *C2/m* (or non-centric subgroups *Cm* and *C*2). However, a more recent X-ray study of single crystals suggests a space group of symmetry *C2/c* with a doubling of the unit cell size in the *c*-direction and with TDAE shifted along the *b*-axis by about 0.02 Å perpendicular to the *c*-axis.[6] A determination of the crystal structure at room temperature is complicated because, as is well known, in most materials based on fullerenes the C_{60} molecules rotate rapidly or have orientational disorder at room temperature. In TDAE·C_{60} crystals the fullerene molecules also rotate at room temperature and freeze out below 150 K,[6] so it is hard to localize carbon atom positions of the molecule in this temperature range.

We have carried out an X-ray single crystal diffraction study of TDAE·C_{60} compound at low temperatures down to 7 K. As was shown by EPR measurements the freshly grown, unannealed single crystals are found to be ordered antiferromagnetically below 10 K[6,8] and do not show a ferromagnetic transition.

For crystal growth we used the diffusion method, originally developed in the 1970s for the crystallization of organic charge-transfer salts.[9] C_{60} (Hoechst, gold grade) and TDAE (Aldrich, 95% pure) were used without further purification. The solvent (toluene) was distilled under argon atmosphere and transferred into a glove-box (O_2 concentration < 1 ppm). A toluene solution of C_{60} (2 mg ml^{-1}) and a mixture of toluene and TDAE (3:1) were prepared inside the glove-box and poured separately into the two compartments of a growing cell separated by fritted glass. The cell was carefully closed and maintained at 8 °C. After six months the crystal growth was completed. The cell was then transferred back to a glove-box, and the crystals were extracted from it, washed with hexane and dried.

The full set of diffraction patterns for structural analysis were obtained using a Weissenberg type X-ray imaging plate at 160, 30, 7 and 11 K. The structure was solved and refined based on the space group *C*2/*c* for the set of data obtained at 7 K. The same structural parameters were used as initial values for analyzing the intensity arrays collected at other temperatures.

The crystal structure for TDAE·C_{60} at 160 K shows the presence of significant molecular disorder, with rapid oscillation of the carbon atoms of the C_{60} molecules around the *b*-axis. This is expressed by the large values of the thermal coefficients for the atoms. Even at the lowest temperatures, the values of B_{eq} remain high, which testifies to the presence of some degree of disorder in the structure. It seems that the degree of orientational ordering depends on the cooling time below 50 K and structural parameters with relatively low thermal coefficients were obtained for data collected at 11 K after cooling at that temperature for about 4 h.‡

There are four chemically equivalent $C_{60}\cdot C_2(NC_2H_6)_4$ units per unit cell. Projections of the structure along the *b* and *c* crystallographic axes are shown in Fig. 1. The packing of the unit cell shows that C_{60} anions are located at inversion centers with the coordinates (0.5, 0, 0), (0, 0.5, 0), (0.5, 0, 0.5) and (0,

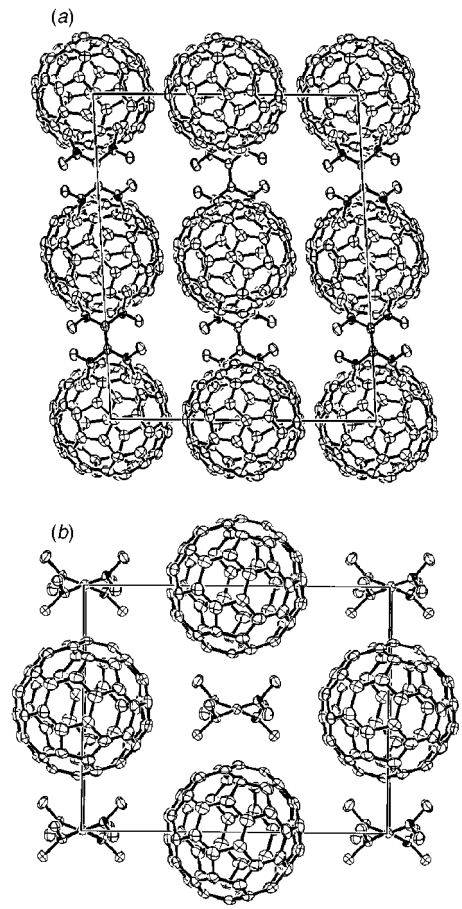

Fig. 1 Projections of the C_{60}·TDAE crystal structure (ORTEP-III, 50% probability) at 11 K along the (*a*) *b*-axis and (*b*) *c*-axis.

† Permanent address: Complex Institute of Natural Sciences, Karakalpak branch of Uzbek Academy of Science, Nukus, Karakalpakstan, 742000 Uzbekistan.

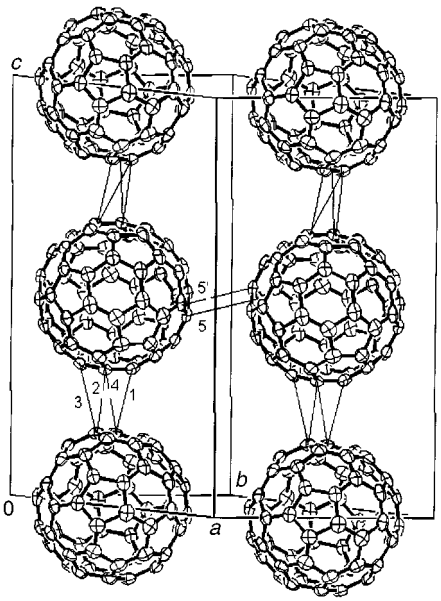

Fig. 2 Shortest $C_{60}\cdots C_{60}$ contacts along the [001] and [1$\bar{1}$0] directions: (1) C(16)–C(16') = 3.369(6), (2) C(24)–C(24') = 3.082(6), (3) C(24)–C(28') = 3.373(4), (4) C(16)–C(24') = 3.479(4), (5,5') C(3)–C(14') = 3.471(4) Å.

0.5, 0.5). The centers of gravity of the C=C double bonds of the TDAE units are at the two-fold axes and the molecules are located at positions (0, −0.0022, 0.25), (0, 0.0022, 0.75), (0.5, 0.4978, 0.25) and (0.5, 0.5022, 0.75), with the double bonds parallel to the *c*-axis.

The C_{60} molecules form a chain along the *c*-axis with the shortest distance between molecular centers equal to 9.915 Å at that temperature. There are several short contacts between adjacent fullerene molecules along the chain: 3.082(6), 3.369(6) and 3.373(4) Å. The intermolecular separation between C_{60} molecules within the *ab* plane is 10.223 Å and there is a short contact [3.471(4) Å] in the [1$\bar{1}$0] crystallographic direction, while in the [110] direction all distances are more than 3.60 Å. The $C_{60}\cdots C_{60}$ type short contacts are shown by dashed lines in Fig. 2.

The C–C bonds in the six-membered rings (6:6) of the C_{60} molecule vary from 1.369(5) to 1.409(5) Å, and in the five-membered rings (5:6) they fall in the range 1.433(4)–1.490(4) Å. In the previous reports[10–16] it was noticed that on going from the neutral molecule C_{60} to the C_{60}^{n-} (n = 1–6) anions, the mean 6:6 ring junction bond length tends to increase [1.355(9) Å (for C_{60})[12] → 1.389(3) Å (C_{60}^{-})[13] → 1.399(2) Å (C_{60}^{2-})[10]], while the mean 5:6 bond tends to decrease [1.467(21) → 1.449(3) → 1.446(2) Å].§ The trend of increasing 6:6 bond lengths and descreasing 6:5 bond lengths in the series C_{60} → C_{60}^{n-} with increasing n is consistent with successive additions of electrons to the t_{1u} LUMO of C_{60}.[10,16] The mean 6:6 and 5:6 bond lengths in TDAE·C_{60} are 1.389(5) and 1.453(5) Å, respectively. These values are close to those of C_{60}^{-} and also C_{60} in the molecular complexes [Fe(C_5H_5)$_2$]C_{60} [1.387(6) and 1.450(6) Å][14] and TPDP(C_{60})$_2$(CS_2)$_4$ [1.381(6) and 1.451(6) Å].[11]

Two symmetrical parts of the TDAE molecule are twisted about the C=C double bond and the dihedral angle between the planes formed by the symmetrically equivalent N–C–N group of atoms is equal to 41.7°. The central C–C bond length is 1.408(6) Å, and distances from the central C atoms to the N atoms of the N(CH_3)$_2$ groups are equal to 1.372(3) and 1.369(3) Å. The N–C type bond lengths within the N(CH_3)$_2$ groups are 1.454(4)–1.461(3) Å. The obtained configurations of TDAE are in reasonable agreement with predictions,[17] which testifies to a charge state of TDAE of +1. There are several short distances between atoms of C_{60} molecule and methyl groups of TDAE. The two contacts, 3.401(4) and 3.482(4) Å, show that there is close interaction between C_{60} and TDAE.

Low temperature X-ray single crystal diffraction studies have allowed access to detailed structural characteristics of an unannealed sample of TDAE·C_{60}. On the basis of this analysis it has been shown that there are very short contacts (3.082 Å) between adjacent C_{60} molecules along the chain of fullerene molecules as well as the presence of close interactions between C_{60} and TDAE.

Notes and references

‡ *Crystal data* at 11 K: $C_{70}N_4H_{24}$, monoclinic, space group *C2/c* (No.15), a = 15.890(8), b = 12.867(7), c = 19.83(3) Å, β = 93.6(2)°, V = 4046(5) Å^3, Z = 4, M = 920.99, D_c = 1.51 g cm^{-3}, F(000) = 1888, Monochromated Mo-Kα radiation, λ = 0.71069 Å, μ = 0.89 cm^{-1}. Data collection was carried out using an Imaging Plate system (rotating anode) equipped with a liquid helium cooling device. 3309 reflections with $I > 3\sigma(I)$ were used in refinement. Atomic parameters were refined *via* a full-matrix least-squares procedure with anisotropic temperature factors. Hydrogen atoms were located from a difference Fourier map and refined with isotropic thermal coefficients equivalent to that for the bonded carbon atom. Final parameters were: R = 0.078, R_w = 0.076, S = 4.36, 370 variables, 3309 observed reflections (4874 unique reflections), max./min. peak in final diff. map = +0.56 / −0.47 e Å^{-3}. CCDC 182/1309. See http://www.rsc.org/suppdata/cc/1999/1511/ for crystallographic data in .cif format.

§ All the averaged values of bond lengths given there were obtained *via* single crystal structure analysis at low temperatures, and their accuracies allow for bond length analysis.

1 P. M. Allemand, K. C. Khemani, A. Koch, F. Wudl, K. Holczer, S. Donovan, G. Grüner and J. D. Thompson, *Science*, 1991, **253**, 301.
2 K. Tanaka, A. A. Zakhidov, K. Yoshizawa, K. Okahara, T. Yamabe and K. Yakushi, *Phys. Rev. B*, 1993, **47**, 7554.
3 P. Venturini, D. Mihailovic, R. Blinc, P. Cevc, J. Dolinsek, D. Abramic, B. Zalar, H. Oshio, P. M. Allemand, A. Hirsch and F. Wudl, *Int. J. Mod. Phys. B*, 1992, **6**, 3947.
4 K. Tanaka, T. Sato, K. Yoshizawa, K. Okahara, T. Yamabe and M. Tokumoto, *Chem. Phys. Lett.*, 1995, **237**, 123.
5 M. Tokumoto, Y. S. Song, K. Tanaka, T. Sato and T. Yamabe, *Solid State Commun.*, 1996, **97**, 349.
6 R. Blinc, K. Pokhodnia, P. Cevc, D. Arčon, A. Omerzu, D. Mihailovic, P. Venturini, L. Golič, Z. Trontelj, J. Lužnik, Z. Jegličič and J. Pirnat, *Phys. Rev. Lett.*, 1996, **76**, 523.
7 P. W. Stephens, D. Cox, J. W. Lauher, L. Mihaly, J. B. Wiley, P.-M. Allemand, A. Hirsch, K. Holczer, Q. Li, J. D. Thompson and F. Wudl, *Nature*, 1992, **335**, 331.
8 A. Mrzel, P. Cevc, A. Omerzu and D. Mihailovic, *Phys. Rev. B*, 1996, **53**, R2922.
9 H. Anzai, *J. Cryst. Growth*, 1975, **33**, 185; M. L. Kaplan, *J. Cryst. Growth*, 1975, **33**, 161.
10 P. Paul, Z. Xie, R. Bau, P. D. W. Boyd and C. A. Reed, *J. Am. Chem. Soc.*, 1994, **116**, 4145.
11 B. Zh. Narymbetov, S. S. Khasanov, L. V. Zorina, L. P. Rozenberg, R. P. Shibaeva, D. V. Konarev and R. N. Lyubovskaya, *Crystallogr. Rep.*, 1997, **42**, 783 (translated from *Kristallografiya*, 1997, **42**, 851).
12 S. Liu, Y.-J. Lu, M. M. Kappes and J. A. Ibers, *Science*, 1991, **251**, 408.
13 W. C. Wan, X. Liu, G. M. Sweeney and W. E. Broderick, *J. Am. Chem. Soc.*, 1995, **117**, 9580.
14 J. D. Grane, P. B. Hitchcock, H. W. Kroto, R. Taylor and D. R. M. Walton, *J. Chem. Soc., Chem. Commun.*, 1992, 1764.
15 A. C. Duggan, J. M. Fox, P. F. Henry, S. J. Heyes, D. E. Laurie and M. J. Rosseinsky, *Chem. Commun.*, 1996, 1191.
16 K. M. Allen, W. I. F. David, J. M. Fox, R. M. Ibberson and M. J. Rosseinsky, *Chem. Mater.*, 1995, **7**, 764.
17 K. I. Pokhodnia, J. Papavassiliou, P. Umek, A. Omerzu and D. Mihailovic, *J. Chem. Phys.*, 1999, **110**, 3606.

Communication 9/02647I

ChemComm

Unexpected polymeric string formation between Ag(I) and a homoleptic thioether cage: synthesis and crystal structure of [R,R′-S_6tricosane] and {[Ag(R,R′-S_6hexacosane)]TsO}$_\infty$

Roger Alberto,*[a] Daniela Angst,[a] Ulrich Abram,[b] Kirstin Ortner,[b] Thomas A. Kaden[c] and August P. Schubiger[a]

[a] *Center for Radiopharmacy, Paul Scherrer Institute, CH-5232 Villigen, Switzerland. E-mail: ariel@aci.unizh.ch*
[b] *Forschungszentrum Rossendorf, Institute of Radiochemistry, D-01062 Dresden, Germany*
[c] *Department of Inorganic Chemistry, University of Basel, CH-5067 Basel, Switzerland*

Received (in Basel, Switzerland) 29th April 1999, Accepted 13th June 1999

The large cavity homoleptic thioether cages [R,R′-S_6tricosane] (1-hydroxymethyl-9-methyl-3,7,11,15,18,22-hexathiabicyclo[7.7.7]tricosane) (1) and [R,R'-S_6hexacosane] (1-hydroxymethyl-10-methyl-3,8,12,17,20,25-hexathiabicyclo-[8.8.8]hexacosane) (2) have been synthesized and the structures of 1 and of the complex {[Ag(2)]TsO}$_\infty$ have been elucidated, the latter showing a polymeric string structure with Ag^+ coordinated by three different cages.

The radionuclide ^{111}Ag has excellent decay properties for applications in radioimmunotherapy.[1] For applications of the labile Ag(I) in organisms, this metal center has to be efficiently shielded in order to prevent transchelation from cancer specific antibodies to serum proteins. For this purpose, a number of thia- and thia-aza macrocycles of various ring size providing high selectivity and/or stability have been prepared for Ag(I).[2–6] However, although the corresponding silver complexes are of relatively high thermodynamic stability,[7] Ag(I) was found to transchelate rapidly to other coordinating sites in serum. Ligand exchange at d^{10} metal centers often occurs *via* an associative or interchange associative mechanism.[8] Only efficient shielding of Ag^+ might allow the protection of Ag(I) against incoming ligands. We therefore prepared thio-cages with large cavities in order to encapsulate Ag^+ and to profit from the well known high kinetic stability of the corresponding metal complexes.[9]

Although a number of homoleptic thio-cages have been published, their coordination chemistry is far less well investigated than that of their aza- or thia-aza-homologues. The only structurally characterized inclusion complex of a homoleptic thio-cage is that of Co(II) and ligand **4**. Additionally, a similar structure of the Co(III) complex with ligand **3** has been concluded from ^{1}H NMR measurements.[10,11] We have prepared the two cages **1** and **2** by a novel route and investigated their coordination chemistry with Ag(I) (Scheme 1).

The syntheses presented here are principally different from published methods but also involve adaption of the conventional synthesis for macrocyclic thioethers with a Cs_2CO_3 mediated ring closure step.[11] The -SH groups are located on the larger fragment of the [1+1] bicyclisation, whereas the leaving groups are on the small cap. The yields for such bicyclisations are relatively high and reach up to 30%. The hydroxymethyl groups have been attached to allow subsequent covalent binding of **1** or **2** to proteins. Ligand **3** was prepared according to the same procedure. Reaction yield, rate of formation and behaviour of **3** are very similar to **1**. ^{1}H NMR data of **3** are in full agreement with the published ones.[10]

Structure optimization of **1** by simple molecular modelling calculations predicts a structure with predominant *exo*-orientation of the lone pairs which is confirmed by the X-ray structure of **1** (Fig. 1).[12]

The structure of **3** was determined as well. The basic framework of the two ligands is essentially the same, showing that the influence of the functional group is negligible in regard to the orientation of the lone pairs.

Although no X-ray structure of a metal complex with **1** has been described to date, the ^{1}H NMR spectrum of the Co(III) complex of **3** clearly shows the metal center to be encapsulated.[13] Since Co(III) forms highly inert complexes, rapid transchelation between different donors, resulting in a fully symmetrical ^{1}H NMR spectrum, can be excluded (even on the NMR timescale). Thus, **1** and **3** are able to reorganize their conformation from *exo*- to *endo*-sulfur lone-pairs, as required for inclusion of the metal. Obviously, the relatively small Co(II) ion is able to penetrate a 16-membered ring of **1** and to coordinate additionally to the sulfur atoms of the bicyclic backbone (oxidation to Co(III) was done after inclusion). The highly symmetrical ^{1}H NMR spectrum rationalizes an octahedral coordination geometry.

Ag(I) is much larger than Co(II) (ionic radii 129 *vs*. 89 pm) and probably not able to penetrate the formal 16-membered ring in **1**. This assumption is supported by the X-ray structure of the Ag(I) complex with [16]aneS_4 recently published.[14] This ligand coordinates only through one sulfur to Ag(I) resulting in a three dimensional polymer. In contrast, the X-ray structure analysis of [Ag([18]aneS_6)]$^+$ clearly demonstrated that, when the ring is enlarged, the Ag^+ can slip inside and the ligand wraps around it.[15]

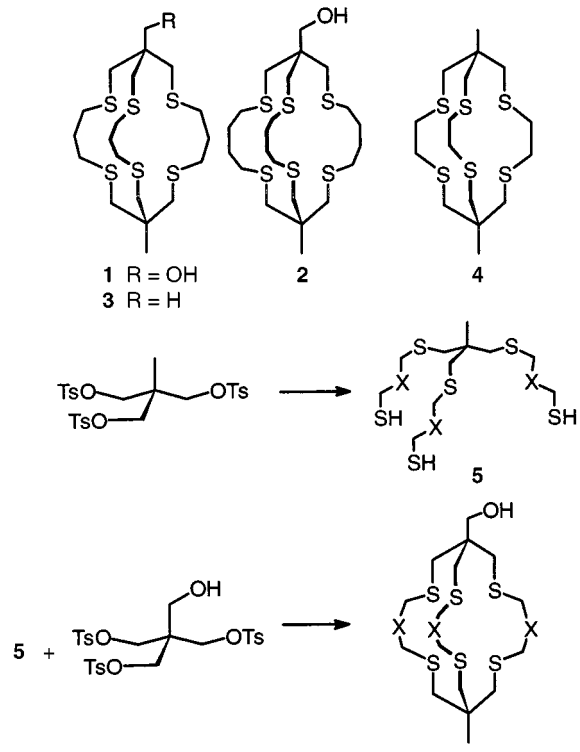

Scheme 1

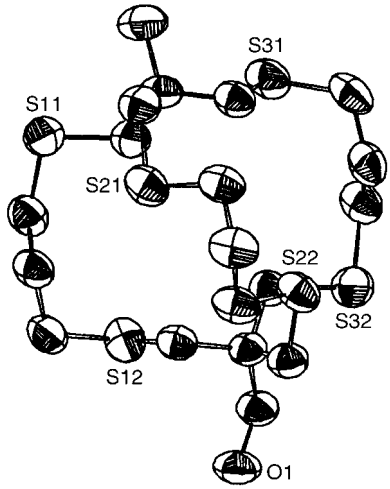

Fig. 1 ORTEP plot of (1-hydroxymethyl-9-methyl-3,7,11,15,18,22-hexathiabicyclo[7.7.7]tricosane) (**1**).

We have enlarged the propylene backbone in **1** to butylene in **2**. Molecular modelling calculations gave a reasonable coordination geometry for $[Ag(\mathbf{2})]^+$ without significant steric interactions between hydrogen atoms from the backbone or from the cap. The ^{1}H NMR of **2** shows 6 signals. Complexation with different Ag^+ salts shifts the resonances by about 0.1 ppm towards lower field but leaves the pattern unchanged. The exhibition of 6 different H's indicates either an inclusion of the metal ion (pseudo-symmetry retained) or a fast fluxionality between different coordination sites.

Several modes of external coordination can be expected, *i.e.* by one, two, three or four sulfur atoms from one ring in the bicyclic ligand which is known in the literature for tridentate thio crowns where Ag^+ is found to bind at least to two different macrocycles.[16] X-Ray structure analysis exhibits an unexpected polymeric string structure (Fig. 2). Three cages are coordinated to one Ag(I) center by one thioether ligand atom. Thus, each cage is coordinated to three Ag^+ atoms. The distorted tetrahedral geometry around the Ag^+ center is completed by the coordination of one counter-ion (tosylate).[17] The highly symmetrical ^{1}H NMR spectrum thus comes from a fast exchange between the different coordinating sites.

Monodentate coordination only is unexpected. Analysis of the solid state structure of **1** or calculated models of **2** reveals that preorganization could favour bidentate external coordination by two sulfur atoms from two different backbones under formation of a six-membered chelate in **1** or in **2**. Six-membered chelates with Ag(I) and sulfur are disfavoured compared to five-membered rings.[18] Indeed, the Cambridge Crystallographic Database does not contain any Ag(I) complex with a six-membered thioether chelate. However, a number of crown thioethers with propylene backbones were found to coordinate in a monodentate fashion to Ag(I) resulting in comparable polymeric structures as in $[Ag(\mathbf{2})]^+$.[5,14,16]

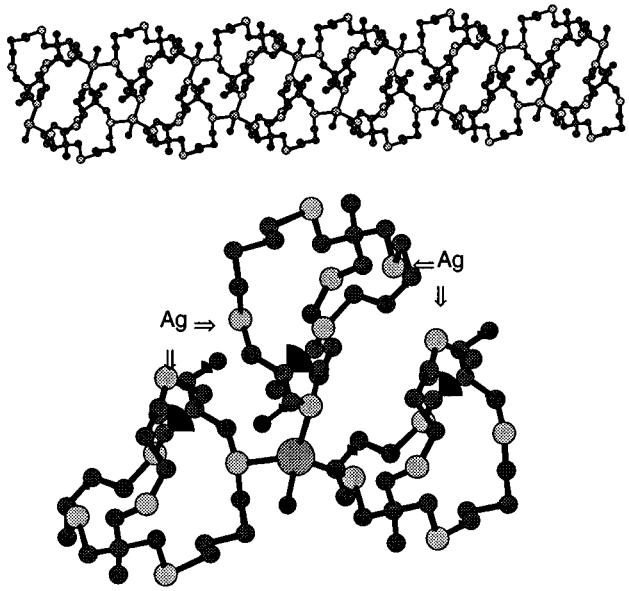

Fig. 2 Part of the polymeric string structure of $\{[Ag(\mathbf{2})]TsO\}_\infty$. The coordinated tosylate anions are omitted for clarity (above). Excerpt of the structure, depicting three cages coordinated to one Ag^+ (below).

To exclude the possibility that the product is a kinetic intermediate and to overcome high reorganization energies for the encapsulation, we exposed $[Ag(\mathbf{2})]^+$ to ultrasound or microwave heating. In neither case was it possible to obtain a 1:1 complex of Ag^+ encapsulated in cage **2**.

In the case of radioactive ^{111}Ag, where the metal concentrations are extremly low, similar behaviour was not observed. Chromatographic investigations (the only possible analytical method) exhibits only free $^{111}Ag^+$, demonstrating the low ability of a monodentate thioether to compete with coordinating solvents.

Although thio-cages can kinetically stabilise labile metal centers, their coordination chemistry, in particular with late transition metals, is not routine. The steric requirements and the electronic properties of a metal center demand a perfectly tailored framework of backbones and donor atoms.

Notes and references

1 P. A. Schubiger, R. Alberto and A. Smith, *Bioconjugate Chem.*, 1996, **7**, 165.

2 T. Gyr, H. R. Mäcke and M. Hennig, *Angew. Chem., Int. Ed. Engl.*, 1997, **109**, 2869.

3 R. Alberto, W. Nef, A. Smith, Th. A. Kaden, M. Neuburger, M. Zehnder, A. Frey, U. Abram and P. A. Schubiger, *Inorg. Chem.*, 1996, **11**, 3420.

4 J. A. R. Hartman, E. J. Hintsa and S. R. Cooper, *J. Chem. Soc., Chem. Commun.*, 1984, 386.

5 A. J. Blake and M. Schröder, *Adv. Inorg. Chem.*, 1990, **35**, 1 and references cited therein.

6 A. J. Blake, M. A. Halcrow and M. Schröder, *J. Chem. Soc., Dalton Trans.*, 1992, 2803.

7 L. D. Pettit and H. K. J. Powell, *IUPAC Stability Constants Database*, Academic Software, 1994.

8 H. Diebler, *Pure Appl. Chem.*, 1969, **20**, 93.

9 B. Dietrich, J. M. Lehn and J. P. Sauvage, *J. Chem. Soc., Chem. Commun.*, 1970, 1055; L. R. Gahan, T. W. Hambley, A. M. Sargeson and M. R. Snow, *Inorg. Chem.*, 1982, **21**, 2699; A. M. Sargeson, *Pure Appl. Chem.*, 1986, **58**, 1511 and references cited therein.

10 P. Osvath and A. M. Sargeson, *J. Chem. Soc., Chem. Commun.*, 1993, 40.

11 J. Bute and R. M. Kellog, *J. Org. Chem.*, 1981, **46**, 4481; R. E. Wolf Jr., J. R. Hartman, L. A. Ochrymowycz and S. R. Cooper, *Inorg. Synth.*, 1989, **25**, 122.

12 *Crystal data* for **1**: $C_{19}H_{36}OS_6$, MW = 472.84, colourless plates, monoclinic, $P2_1/c$, a = 18.186(4), b = 26.587(4), c = 10.255(2) Å, β = 101.16(1)° , V = 4864(1) Å^3, Z = 8, 9737 reflections, 5657 with $F > 2\sigma(F)$ used for refinement: R = 0.0553, wR_2 = 0.1381.

13 P. Osvath, A. M. Sargeson, B. W. Skelton and A. H. White, *J. Chem. Soc., Chem. Commun.*, 1991, 1036.

14 A. J. Blake, W.-S. Li, V. Lippolis and M. Schröder, *Chem. Commun.*, 1997, 1943.

15 A. J. Blake, R. O. Gould, A. J. Holder, T. I. Hyde and M. Schröder, *Polyhedron*, 1989, **4**, 513.

16 H.-J. Küppers, K. Wieghardt, Y.-H. Tsay, C. Krüger, B. Nuber and J. Weiss, *Angew. Chem., Int. Ed. Engl.*, 1987, **6**, 575; P. J. Blower, J. A. Clarkson, S. C. Rawle, J. R. Hartman, R. E. Wolf, R. Yagbasan, S. G. Bott and S. R. Cooper, *Inorg. Chem.*, 1989, **28**, 4040.

17 *Crystal data* for **2**: $C_{29}H_{49}AgO_4S_7$, MW = 793.97, monoclinic, $P2_1/c$, a = 10.707(4), b = 17.737(4), c = 19.081(8) Å, β = 103.61(2)°, V = 3522(2) Å^3, Z = 4, μ(Mo-Kα) = 0.1020 cm^{-1}, 5807 reflections, 1661 with $F > 2\sigma(F)$ used for refinement: R = 0.0695, wR_2 = 0.0671. CCDC 182/1329. See http://www.rsc.org.suppdata/cc/1999/1513/ for crystallographic data in .cif format.

18 R. E. Wolf Jr., J. R. Hartman, J. M. E. Storey, B. M. Foxman and S. R. Cooper, *J. Am. Chem. Soc.*, 1987, **109**, 4328.

Communication 9/03455B

Structural isomerization of cyclopropane: a new mechanism through propylidene

Holger F. Bettinger,[a] Jonathan C. Rienstra-Kiracofe,[a] Brian C. Hoffman,[a] Henry F. Schaefer III,[a] John E. Baldwin[b] and Paul v. R. Schleyer*[a]

[a] *Center for Computational Quantum Chemistry, The University of Georgia, 1004 Cedar Street, Athens, GA, 30602-2556, USA. E-mail: schleyer@paul.chem.uga.edu*

[b] *The Department of Chemistry, Syracuse University, Syracuse, New York 13244-4100, USA.*

Received (in Corvallis, OR, USA) 4th March 1999, Accepted 20th May 1999

***Ab initio* coupled cluster methods indicate that the isomerization of cyclopropane to propene (E_a = 64–66 kcal mol^{-1} experimentally) might involve two different mechanisms: the barrier for the newly proposed pathway through propylidene is only slightly higher ($\Delta E^{\ddagger}$ = 66.6 kcal mol^{-1}) than that of the traditional trimethylene route ($\Delta E^{\ddagger}$ = 64.2 kcal mol^{-1}).**

Even though cyclopropane (**1**) and propene (**2**) have comparable thermodynamic stabilities (8 kcal mol^{-1} in favor of **2**),[1] a remarkably high activation energy of approximately 65 kcal mol^{-1} hampers their interconversion.[2–9] Both concerted and stepwise mechanisms have been considered for this isomerization.[3,5,10–14] The stepwise pathway (A in Scheme 1) involving trimethylene (**3**) has generally been favored since Benson[11] presented arguments against a concerted reaction: his estimated barrier for such a process was significantly higher than the activation energy determined experimentally.[5] However, the most recent computational study purported to have located a transition state 'connected to cyclopropane and propylene without an intermediate.'[14] We examine another path (B in Scheme 1) involving carbene **4** as an intermediate which apparently has not been considered for the parent rearrangement, although carbene pathways have been implicated in more elaborate systems.[15]

The singlet biradical **3** is assumed to be involved in the geometrical and the 'optical' (*i.e.* enantiomeric) isomerization of appropriately labeled cyclopropanes,[16–30] but has only been observed recently *via* femtosecond laser spectroscopy. The extremely rapid ring closure to **1** limits the lifetime of **3** to 120 fs.[29]

Although the [1,2]-H shift *via* **TS1** is the rate determining step in the **1** → **2** isomerization *via* **3**, the **3** to **2** rearrangement has not been studied as comprehensively as the **1** ⇌ **3** process. A barrier of approximately 5 kcal mol^{-1} was estimated for the **3** → **2** [1,2]-H shift.[13] This was based both on the experimental finding that the structural isomerization of **1** at 480 °C is approximately an order of magnitude slower than the **1** ⇌ **3** process (ΔE_a = 3.7 kcal mol^{-1})[31] and on the theoretical barrier of less than 1 kcal mol^{-1} for the **3** → **1** reaction.[18–20]

Fan *et al.*[13] recently computed pathway A (Scheme 1) at various levels, but found good agreement with the experimental activation energies for the overall **1** → **2** reaction (64–66 kcal mol^{-1})[2–9] only at UB3LYP/6-31G**//UMP2/6-31G** (66.1 kcal mol^{-1}). However, the **3** → **2** barrier *via* **TS1** was 9.5 kcal mol^{-1}, indicating that the computed energy of the trimethylene intermediate might be somewhat too low. Doubleday obtained a zero point corrected barrier of 6.9 kcal mol^{-1} for the **3** → **2** [1,2]-H shift reaction at MR-CISD//CASSCF(4,4).[22] Dubnikova and Lifshitz[14] reported a transition structure at UB3LYP/cc-pVDZ which is very similar to Doubleday's TS1 for the **3** → **2** reaction; however, their intrinsic reaction coordinate (IRC) computation was not able to locate intermediate **3** and was said to connect **TS1** to **1** and **2** directly.[14] This result is the only evidence in favor of a concerted process, but may be an artifact due to the inadequacy of density functional methods for closed shell biradicals.

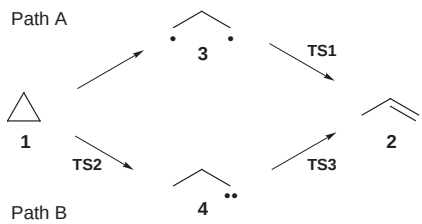

Scheme 1 Ring opening of cyclopropane (**1**) *via* trimethylene (**3**) (Path A) or propylidene (**4**) (Path B) to propene (**2**).

We now propose a new possibility. Our *ab initio* data† suggest a carbene mechanism (path B in Scheme 1) involving propylidene (**4**) to be competitive energetically to the traditional trimethylene (**1** → **3** → **2**) pathway A.

A transition state (**TS2**, 66.6 kcal mol^{-1} above **1**) for the endothermic ring opening of **1** leads directly to propylidene (**4**, Fig. 1). The carbene obtained from this reaction is in conformation **4a** (66.5 kcal mol^{-1}), where the divalent carbon center is stabilized by the adjacent C2–C3 bond through hyperconjugation and by interaction with the methyl CH bond (analogous stabilizations have been reported for related carbocations).[34,35] Isomer **4b**, oriented in a conformation favoring CH hyperconjugation, is slightly lower in energy (1.5 kcal mol^{-1}). The [1,2]-H shifts in acyclic alkylcarbenes are well known to be very facile.[36–38] Indeed, only an very small barrier (0.07 kcal mol^{-1} *via* **TS3**), which disappears after the CCSD/DZP ZPVE correction, is predicted for the **4b** → **2** rearrangement.

In addition to **TS1**, Doubleday obtained a structure very similar to **TS2** previously at the CASSCF(4,4) level.[22] However, his intrinsic reaction coordinate (IRC) computation at CASSCF(4,4) with a modified 6-31G* basis set indicated that his **TS2**-like transition structure connects **3** and **4**. In contrast to Doubleday's report, our CASSCF(4,4)/TZ2P IRC clearly shows that **TS2** is not connected to **3** but rather joins **1** to **4a**

Table 1 Relative energies, zero-point corrected relative energies (in parentheses), and zero-point vibrational energies of C_3H_6 stationary points.

Species	CCSD/DZP	CCSD/TZ2P	CCSD(T)/TZ2P[a]	ZPVE[b]/ kcal mol^{-1}
1	0	0	0	52.1
2	−7.2 (−8.7)	−8.4 (−9.9)	−9.2 (−10.7)	50.6
4a	70.9 (68.2)	69.8 (67.1)	69.2 (66.5)	49.4
4b	69.3 (65.6)	68.8 (65.1)	68.7 (65.0)	48.4
TS1	79.7 (73.9)	78.6 (72.8)	70.0 (64.2)	46.3
TS2	72.0 (68.9)	71.1 (68.0)	69.7 (66.6)	49.0
TS3	70.9 (66.3)	69.7 (65.1)	68.8 (64.2)	47.5

[a] Single point energies employing the CCSD/TZ2P geometries. [b] Computed at the CCSD/DZP level; not scaled. The imaginary vibrational frequency of transition structures is ignored.

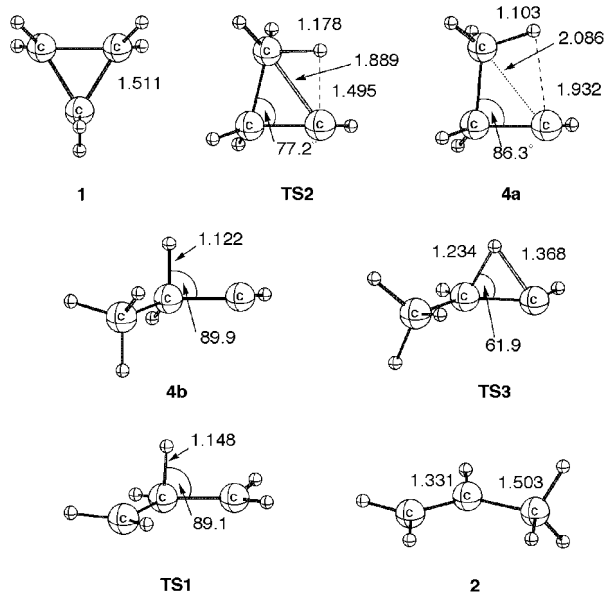

Fig. 1 Geometries of C_3H_6 stationary points optimized at the CCSD/TZ2P level of theory. All distances are in Å, all angles in degrees.

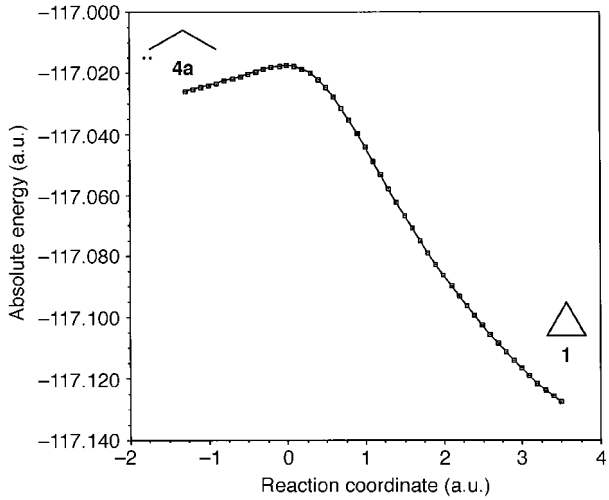

Fig. 2 The intrinsic reaction coordinate for the propylidene (**4a**) to cyclopropane (**1**) reaction *via* **TS2**.

(Fig. 2). The dominating initial mode along the path towards **1** is the migration of the H atom approximately in the ring plane. This motion is accompanied by a shortening of the C1–C3 distance and a decrease of the C1–C2–C3 angle leading ultimately to **1**.

We restricted our investigation to the highest point along path A, *i.e.* the transition structure (**TS1**) for the [1,2]-H shift from **3** to **2**. The analyses of the CCSD wave function (small T_1 diagnostic value of less than 0.02) as well as that of CISD (the Hartree–Fock configuration has a coefficient of 0.93) indicate that **TS1** should be computed reliably using coupled cluster methods. We find that **TS1** is 64.2 kcal mol^{-1} above **1**, and therefore 2.4 kcal mol^{-1} lower in energy than **TS2**. This difference is significantly smaller than that reported by Doubleday [5.5 kcal mol^{-1} in favor of **TS1**] at the MRCI/VTZ(2d,p)//CASSCF(4,4)/VTZ(2d,p) level. Our more extensive computations suggest that the carbene mechanism for the rearrangement of **1** to **2** has a zero-point corrected barrier of 66.6 kcal mol^{-1} which agrees with the barrier deduced experimentally (64–66 kcal mol^{-1}).[2–9] Hence, the carbene pathway might compete energetically with the trimethylene mechanism (64.2 kcal mol^{-1}). As experimental data have been discussed traditionally in terms of the latter mechanism,[5,11] additional investigations of the rearrangement of appropriately labeled cyclopropanes to propenes are desirable.

This work was supported by the U.S. Department of Energy.

Notes and references

† This study employed double-ζ and triple-ζ basis sets augmented with one [DZP, α_p(H) = 0.75, α_d(C) = 0.75] or two [TZ2P, α_p(H) = 1.5 and 0.375, α_d(C) = 1.5 and 0.375] sets of polarization functions. Single point energy computations at the CCSD(T)/TZ2P level employed the CCSD/TZ2P geometries.[32] In addition the geometry of **TS2** was optimized with the complete active space SCF method and the TZ2P basis set [CASSCF(4,4)/TZ2P] (ref. 33). Harmonic vibrational frequencies were computed *via* finite differences of analytic gradients at CCSD/DZP, and, for **TS2**, *via* analytic second derivatives at CASSCF/TZ2P.

1 J. B. Pedley and J. Rylance, Sussex-N.P.L. Computer Analysed Thermochemical Data: Organic and Organometallic Compounds, University of Sussex, 1977.
2 M. Trautz and K. Winkler, *J. Prakt. Chem.*, 1922, **104**, 53.
3 T. S. Chambers and G. B. Kistiakowsky, *J. Am. Chem. Soc.*, 1934, **56**, 399.
4 H. O. Pritchard, R. G. Sowden and A. F. Trotman-Dickenson, *Proc. R. Soc. London, Ser. A*, 1953, **217**, 563.
5 B. S. Rabinovitch, E. W. Schlag and K. B. Wiberg, *J. Chem. Phys.*, 1958, **28**, 504.
6 E. W. Schlag and B. S. Rabinovitch, *J. Am. Chem. Soc.*, 1960, **82**, 5996.
7 W. E. Falconer, T. F. Hunter and A. F. Trotman-Dickenson, *J. Chem. Soc.*, 1961, 609.
8 H. Furue and P. D. Pacey, *Can. J. Chem.*, 1982, **60**, 916.
9 U. Hohm and K. Kerl, *Ber. Bunsenges. Phys. Chem.*, 1990, **94**, 1414.
10 N. B. Slater, *Proc. R. Soc. London Ser. A*, 1953, **218**, 224.
11 S. W. Benson, *J. Chem. Phys.*, 1961, **34**, 521.
12 K. Jug, *Theor. Chim. Acta*, 1976, **42**, 303.
13 K.-N. Fan, Z.-H. Li, W.-N. Wang, H.-H. Huang and W. Huang, *Chem. Phys. Lett.*, 1997, **277**, 257.
14 F. Dubnikova and A. Lifshitz, *J. Phys. Chem. A*, 1998, **102**, 3299.
15 S. F. Sellers, T. C. Klebach, F. Hollowood, M. Jones and P. v. R. Schleyer, *J. Am. Chem. Soc.*, 1982, **104**, 5492.
16 R. Hoffmann, *J. Am. Chem. Soc.*, 1968, **90**, 1475.
17 J. A. Horsely, Y. Jean, C. Moser, L. Salem, R. M. Stevens and J. S. Wright, *J. Am. Chem. Soc.*, 1972, **94**, 279.
18 Y. Yamaguchi, H. F. Schaefer and J. E. Baldwin, *Chem. Phys. Lett.*, 1991, **185**, 143.
19 S. J. Getty, E. R. Davidson and W. T. Borden, *J. Am. Chem. Soc.*, 1992, **114**, 2085.
20 J. E. Baldwin, Y. Yamaguchi and H. F. Schaefer, *J. Phys. Chem.*, 1994, **98**, 7513.
21 D. A. Hrovat, S. Fang, W. T. Borden and B. K. Carpenter, *J. Am. Chem. Soc.*, 1997, **119**, 5253.
22 C. Doubleday, *J. Phys. Chem.*, 1996, **100**, 3520.
23 C. Doubleday, K. Bolton and W. L. Hase, *J. Am. Chem. Soc.*, 1997, **119**, 5251.
24 C. Doubleday, K. Bolton and W. L. Hase, *J. Phys. Chem. A*, 1998, **102**, 3648.
25 A. Skancke, D. A. Hrovat and W. T. Borden, *J. Am. Chem. Soc.*, 1998, **120**, 7079.
26 W. R. Roth, T. Wasser and M. Boenke, *Liebigs Ann./Rec.*, 1997, 1323.
27 F. Tian, S. B. Lewis, M. D. Bartberger, W. R. Dolbier and W. T. Borden, *J. Am. Chem. Soc.*, 1998, **120**, 6187.
28 E. M. Goldfield, *Faraday Discuss. Chem. Soc.*, 1998, **110**, 185.
29 S. Pedersen, J. L. Herek and A. H. Zewail, *Science*, 1994, **266**, 1359.
30 J. E. Baldwin, in *The Chemistry of the Cyclopropyl Group*, ed. Z. Rappoport, Wiley, New York, 1995, vol. 2, ch. 9.
31 E. V. Waage and B. S. Rabinovitch, *J. Phys. Chem.*, 1972, **76**, 1695.
32 ACES II is a program product of the Quantum Theory Project, University of Florida, J. F. Stanton *et al*. Integral packages included are VMOL (J. Almlöf and P. R. Taylor); VPROPS (P. R. Taylor); ABACUS (T. U. Helgaker, H. J. A. Jensen, P. Jørgensen, J. Olsen and P. R. Taylor).
33 GAUSSIAN 94, Revision C.3, M. J. Frisch *et al.*, Gaussian, Inc., Pittsburgh, PA, 1995.
34 J. W. M. Carneiro, P. v. R. Schleyer, W. Koch and K. Raghavachari, *J. Am. Chem. Soc.*, 1990, **12**, 4064.
35 P. Buzek, P. v. R. Schleyer, S. Sieber, W. Koch, J. W. Carneiro, H. Vancik and E. D. Sunko, *J. Chem. Soc., Chem. Commun.*, 1991, 671.
36 H. F. Schaefer, *Acc. Chem. Res.*, 1979, **12**, 288.
37 J. D. Evanseck and K. N. Houk, *J. Phys. Chem.*, 1990, **94**, 5518.
38 D. A. Modarelli and M. S. Platz, *J. Am. Chem. Soc.*, 1993, **115**, 470.

Communication 9/01886G

Synthesis and properties of a novel phosphodiester analogue, nucleoside boranophosphorothioate

Jinlai Lin and Barbara Ramsay Shaw*

Paul M. Gross Chemical Laboratory, Department of Chemistry, Duke University, Durham, North Carolina 27708-0346, USA. E-mail: brs@chem.duke.edu

Received (in Corvallis, OR, USA) 8th February 1999, Accepted 28th April 1999

The first boranophosphorothioate [$(RO)_2P(S)(BH_3)^-$] mimic of a phosphodiester compound, dithymidine boranophosphorothioate, has been synthesized; while it is water soluble, this new analogue is more lipophilic and nuclease resistant than natural nucleoside phosphodiesters [$(RO)_2P(O)(O)^-$] and phosphorothioates [$(RO)_2P(S)(O)^-$].

Novel oligonucleotide analogues are currently attracting attention as probes in biochemistry and molecular biology[1] and as possible therapeutic agents against cancer and viral diseases.[2] An impressive variety of these analogues[3] have been developed as potential therapeutic drugs for 'antisense' and 'antigene' targeting of specific genes to modulate their expression.[4] Of these modified oligonucleotides, the nucleoside phosphorothioates[5] and nucleoside boranophosphates[6] (Fig. 1) are among the most promising because they are resistant to nucleases and support RNase H induced cleavage[7] of the complementary messenger RNA. Nearly a dozen phosphorothioate oligonucleotides are now in clinical trials.[8] By structurally combining the phosphorothioate and boranophosphate backbones, we have created a new phosphodiester analogue, the boranophosphorothioate, $[S{=}P{-}BH_3]^-$, wherein the two nonbridging oxygen atoms of a phosphodiester group are replaced with a sulfur atom and borane group.

Here, we report the first example of a novel boranophosphorothioate compound, specifically the dithymidine boranophosphorothioate, its synthesis and properties.

The general procedure for the synthesis of dinucleoside boranophosphorothioates is outlined in Scheme 1. 5′-*O* Fluorenylmethoxycarbonyl (Fmoc)-thymidine[9] was phosphitylated with $(Pr^i_2N)_2PCl$ catalyzed by DMAP to give **1**. Phosphite **1** was treated *in situ* with 3′-*O*-acetylthymidine and tetrazole in DMF to give **2**. To the above mixture, 4-nitrophenol and tetrazole in DMF were added to yield **3**, which was then treated with excess $BH_3{\cdot}SMe_2$ complex to afford the phosphite–borane **4** with ^{31}P NMR signal at δ_P 116.6 (br). Dry **4** was reacted with Li_2S to give **5** (broad ^{31}P NMR signal at δ_P 161.0) which was converted to **6** with conc. NH_4OH–MeOH (1 : 1) at room temperature. The crude mixture was purified by ion-exchange column chromatography on QA-52 (HCO_3^-) cellulose to give **6** as the ammonium salt and isolated by HPLC. The overall yield of dithymidine boranophosphorothioate **6** (T^SpBT) was about 28%. Successful separation of the two diastereomers (R_P and S_P) of **6** was achieved by reverse-phase HPLC. The first eluted isomer T^SpBT I (**6a**) and the second eluted isomer T^SpBT II (**6b**) were characterized by ^{31}P and ^1H NMR.[10] The Li_2S method used above should be applicable to the synthesis of other boranophosphorothioates including $[^{35}S{=}P{-}BH_3]^-$ phosphodiesters.

In oligodeoxynucleotides (ODN), the replacement of a nonbridging oxygen atom in the natural phosphodiester linkage by S^-, Me or BH_3^- imparts resistance to nucleases that cleave DNA.[6f,g,11] For instance, the non-ionic methylphosphonates (Me-ODN) are highly resistant[11c] to phosphodiesterases; the

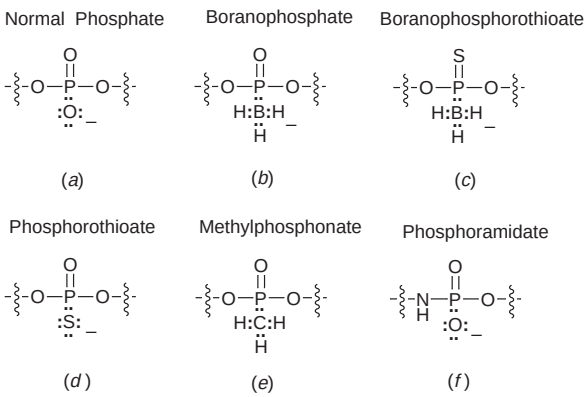

Fig. 1 Structurally and/or electronically similar internucleotide linkages and their abbreviations: (*a*) normal phosphate [O=P–O$^-$], (*b*) boranophosphate [O=P–BH$_3^-$], (*c*) boranophosphorothioate [S=P–BH$_3^-$], (*d*) phosphorothioate [O=P–S$^-$], (*e*) methylphosphonate [O=P–Me], (*f*) phosphoramidate. Placement of the negative charge does not necessarily reflect the actual spatial location of charge in the molecule.

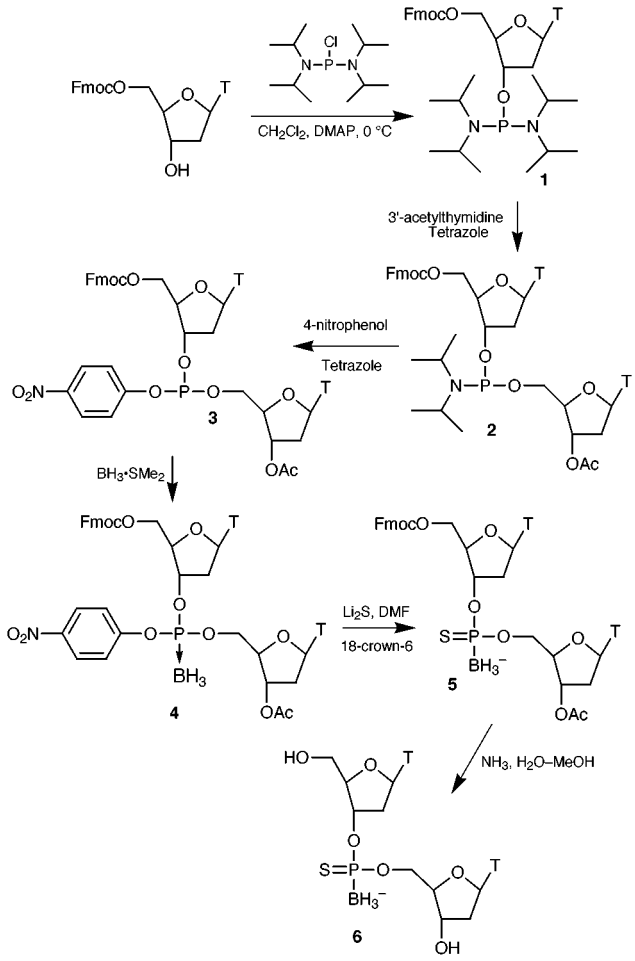

Scheme 1

Table 1 Special properties of $[S{=}P{-}BH_3]^-$ backbone relative to natural and other phosphodiester backbone analogues

Property	$[O{=}P{-}O]^-$	$[O{=}P{-}S]^-$	O=P–Me	$[O{=}P{-}BH_3]^-$	$[S{=}P{-}BH_3]^-$
Nuclease resistance	—	+	++	+	++
Lipophilicity	—	+	+++	+	++
RNase H activity	+	+	—	+	N.D.

anionic phosphorothioates (S^--ODN) can be hydrolyzed by phosphodiesterase I, but with a much lower rate[11d] than O^--ODN. Boranophosphates (BH_3^--ODN) are even more resistant[6g] to certain phosphodiesterases than S^--ODN. This nuclease resistance, together with the ability to form stable duplex structures with DNA or RNA, has led to broad trials of S^-- and Me-ODN as agents for regulating gene expression *in vitro* and *in vivo*.[4] By combining aspects of both the charged $[O{=}P{-}S]^-$ and the non-ionic O=P–Me into a $[S{=}P{-}BH_3]^-$ hybrid phosphodiester linkage, it was anticipated that the resulting compound may exhibit greater nuclease resistance and other unique or potentially useful properties. The BH_3 moiety in $[S{=}P{-}BH_3]^-$ is isoelectronic with oxygen and isosteric with the Me group in O=P–Me, but imparts a negative charge to the backbone, like S^- in $[O{=}P{-}S]^-$. By virtue of the larger volume of the BH_3 group and its lack of lone pair electrons, we expect that $[S{=}P{-}BH_3]^-$ oligonucleotides should be more lipophilic than $[O{=}P{-}S]^-$ oligonucleotides. The new $[S{=}P{-}BH_3]^-$-ODN, which is a hybrid backbone of S^--ODN and BH_3^--ODN, has some special properties summarized in Table 1.

The boranophosphorothioate group is very stable towards basic or acidic hydrolysis. The diastereomers, T^Sp^BT I and T^Sp^BT II, were each dissolved in 100 mM AcOH–NH_4OH pH 3 or pH 11 buffer and incubated for 24 h at 37 °C. No hydrolyzed or degraded products were detected *via* HPLC.

The boranophosphorothioate internucleotide linkage in dimer **6** is quite stable towards cleavage by both snake venom phosphodiesterase (SVPDE) and bovine spleen phosphodiesterase (BSPDE). Under conditions where the natural dithymidine phosphate (TpT) was > 99% cleaved by SVPDE, both T^Sp^BT I and T^Sp^BT II were > 99% stable. Similarly, with BSPDE, while TpT was > 96% cleaved, T^Sp^BT I and T^Sp^BT II were > 98 and 97% stable, respectively.

The $[S{=}P{-}BH_3]^-$ dimers carry a full negative charge and are water soluble, yet are intermediate between normal phosphates and methylphosphonates in lipophilicity. In partitioning experiments,[12] T^Sp^BT was 320- and 18-fold more lipophilic than natural TpT and Tp^BT (dithymidine boranophosphate) accordingly.

The $[S{=}P{-}BH_3]^-$ nucleotidic linkage is the only non-bridging disubstituted chiral phosphodiester with a negative charge. This property coupled with ready synthesis of isotopic $[^{35}S{=}P{-}BH_3]^-$ compounds from Li_2S^* ($S^* = {}^{35}S$) could make this linkage very useful for elucidating the stereochemical course of phosphoryl and nucleotidyl transfer reactions and at the same time probing whether one or two non-bridging oxygens are necessary in these reactions.

To summarize, we have synthesized a totally new type of modified phosphodiester analogue, in which the two non-bridging oxygen atoms of a phosphodiester group have been replaced with a sulfur atom and borane group. The analogue has been placed in a nucleic acid and the resulting dithymidine boranophosphorothioate diastereomers shown to be stable under a broad range of pH conditions and highly resistant to enzymatic cleavage relative to natural DNA. Based on partitioning into octanol, the boranophosphorothioates may exhibit a greater membrane permeability than the O-oligonucleotides, yet maintain nuclease resistance like the methylphosphonates. The novel combination of high lipophilicity, reasonable water solubility and nuclease resistance could be extremely useful for drug design;[13] the $[S{=}P{-}BH_3]^-$ linkage instead of $[O{=}P{-}O]^-$ may enable the compounds to penetrate the plasma membrane and to enter cells.

Thus, synthesis of the first $[S{=}P{-}BH_3]^-$ phosphodiester analogue offers the possibility of preparing an entirely new and intriguing class of compounds, including modified nucleotides and nucleic acids. Their similarity to natural nucleic acids and unique properties such as high lipophilicity and resistance to enzymatic cleavage, in conjunction with their potential utility as molecular probes for the study of stereochemical aspects of enzymatic and nonenzymatic reactions and as carriers of ^{10}B in boron neutron capture therapy (BNCT)[14] for the treatment of cancer, make the $[S{=}P{-}BH_3]^-$ linkage a promising candidate for further mechanistic, diagnostic and therapeutic applications.

We thank Drs Dmitri S. Sergueev, Vladimir Rait and Zinaida Sergueeva and Mr Kaizhang He for their suggestions and help. This work was supported by grants 1R01-GM57693-01 from NIH and DE-FG05-97ER62376 from DOE to B. R. S. and is in partial fulfillment of requirements (J. L.) for a PhD at Duke University.

Notes and references

1 F. Eckstein, *Angew. Chem., Int. Ed. Engl.*, 1983, **22**, 423.
2 *Antisense Therapeutic: Progress and Prospect*, ed. G. L. Trainor, ESCOM Science Publishers, The Netherlands, 1996, pp. 1–85.
3 M. Egli, *Angew. Chem., Int. Ed. Engl.*, 1996, **35**, 1894; E. Uhlmann and A. Peyman, *Chem. Rev.*, 1990, **90,** 543.
4 S. T. Crooke and C. F. Bennett, *Annu. Rev. Pharmacol. Toxicol.*, 1996, **36**, 107.
5 F. Eckstein, *Annu. Rev. Biochem.*, 1985, **54**, 367.
6 (*a*) A. Sood, B. R. Shaw and B. F. Spielvogel, *J. Am. Chem. Soc.*, 1990, **112**, 9000; (*b*) J. Tomasz, B. R. Shaw, K. Porter, B. F. Spielvogel and A. Sood, *Angew. Chem., Int. Ed. Engl.*, 1992, **31**, 1373; (*c*) B. R. Shaw, J. Madison, A. Sood and B. F. Spielvogel, *Methods Mol. Biol.*, 1993, **20**, 225; (*d*) H. Li, C. Hardin and B. R. Shaw, *J. Am. Chem. Soc.*, 1996, **118**, 6606; (*e*) K. W. Porter, J. D. Briley, B. R. Shaw, *Nucleic Acids Res.*, 1997, **25**, 1611; (*f*) F. Huang, A. Sood, B. F. Spielvogel and B. R. Shaw, *J. Biomol. Struct. Dynam.*, 1993, **10**, a078; (*g*) D. S. Sergueev and B. R. Shaw, *J. Am. Chem. Soc.*, 1998, **120**, 9417.
7 V. Rait and B. R. Shaw, *Antisense Nucleic Acid Drug Dev.*, 1999, **9**, 53; B. R. Shaw, in Papers from the 5th Annual International Conference on Antisense: DNA and RNA Based Therapeutics. IBC, Southborough, MA, 1998, pp. 1–8; RNase H activity was mentioned by Higson *et al.* (A. P. Higson, A. Sierzchala, H. Brummel, Z.-G. Zhao and M. H. Caruthers, *Tetrahedron Lett.*, 1998, **39**, 3899), but no data were shown.
8 S. Agrawal, *Trends Biotechnol.*, 1996, **14**, 376.
9 C. Lehmann, Y.-Z. Xu, C. Christodoulou, Z.-K. Tan and M. J. Gait, *Nucleic Acids Res.*, 1989, **17**, 2379.
10 *Selected data* for **6** $\delta_H(D_2O$, 400 MHz) 7.56, 7.52, 7.50, 7.47 (4s, 1H, H6), 6.18–6.05 (m, 2H, H1′), 4.85–4.72 (m, 1H, H3′), 4.44–4.34 (m, 1H, H3′), 4.00 (m, 2H, H4′), 3.94–3.59 (2m, 4H, H5′), 2.38–2.14 (2m, 4H, H2′), 1.77, 1.75, 1.74, 1.71 (4s, 6H, 5-CH_3), 0.68–—0.44 (br, 3H, BH_3); $\delta_P(D_2O)$ 160.1 (br); λ_{max}/nm 267; *m/z* (FAB$^-$) 559.16 (M^-) [Calc. for $C_{20}H_{29}O_{10}N_4BPS$, 559.1435 (M^-), found, 559.1421]; HPLC conditions: Waters Delta Pak C18-300 Å, 15 μ, 7.8 × 300 mm column; eluants were 18% MeOH and 82% 20 mM KH_2PO_4 (pH 7.0); flow rate, 3.0 ml min^{-1}; t_R (**6a**) = 28.69 min, t_R (**6b**) = 32.52 min.
11 (*a*) P. S. Sarin, S. Agrawal, M. P. Civéira, J. Goodchild, T. Ikeuchi and P. C. Zamecnik, *Proc. Natl. Acad. Sci. USA*, 1988, **85**, 7448; (*b*) D. M. Tidd, *Anticancer Res.*, 1990, **10**, 1169; (*c*) K. L. Agarwal and F. Riftina, *Nucleic Acids Res.*, 1979, **6**, 3009; (*d*) P. M. J. Burgers and F. Eckstein, *Biochemistry*, 1979, **18**, 592.
12 Partition coefficients, defined as the ratio of concentration in octan-1-ol to that in water, were 2.8×10^{-2}, 1.6×10^{-3} and 8.7×10^{-5} for T^Sp^BT (mixture of diastereomers), Tp^BT (dithymidine boranophosphate), and TpT respectively. The partition coefficient of T^Sp^BT was 320 times greater than that of TpT.
13 C. McGuigan, D. Cahard, A. Salgado, E. De Clercq and J. Balzarini, *Antiviral Chem. Chemother.*, 1996, **7**, 31.
14 M. F. Hawthorne, *Angew. Chem., Int. Ed. Engl.*, 1993, **32**, 950.

Communication 9/01157I

ChemComm

A novel two-electron mixed-valence Ir(II)–Ir(0) complex

Alan F. Heyduk and Daniel G. Nocera*

Department of Chemistry, Massachusetts Institute of Technology, 6-335, 77 Massachusetts Avenue, Cambridge, MA 02139-4307, USA. E-mail: nocera@mit.edu

Received (in Bloomington, IN, USA) 26th March 1999, Accepted 24th June 1999

An Ir^{II}–Ir^{0} mixed-valence complex, $Ir_2\{MeN[P(OEt^{F3})_2]_2\}_3Cl_2$ (OEt^{F3} = OCH_2CF_3), has been prepared by treatment of $Ir_2Cl_2(cod)_2$ with 3 equiv. of $MeN[P(OEt^{F3})_2]_2$; donor ligands ($CNBu^t$ and PEt_3) add to the binuclear core, which provides a novel platform for the multielectron activation of small molecule substrates.

Few ligand systems are able to support the intramolecular disproportionation of a symmetric binuclear metal core. The bis(difluorophosphino)methylamine (dfpma) ligand,[1] $CH_3N(PF_2)_2$, therefore, is distinguished by its ability to drive the conversion of binuclear $Rh^{I}(\mu\text{-}X_2)Rh^{I}$ (X = Cl, Br or I) dimers to two-electron mixed-valence X_2Rh^{II}–Rh^{0} complexes.[2] When a long-lived excited state can be incorporated into the electronic structure of the two-electron mixed-valence center, controlled multielectron photoreactivity may be achieved.[3] For instance, we have recently accomplished a four-electron photoreaction among discrete molecular species, for the first time, by using a dσ* excited state to interconvert among $Rh(0,0)_2(dfpma)_3(L)_2$, $Rh(II,0)_2(dfpma)_3X_2(L)$ and $Rh(II,II)_2(dfpma)_3X_4$ (L = PF_3, η^1-dfpma or PPh_3).[4] By spanning reduced LRh^{0}–$Rh^{0}L$ and oxidized X_2Rh^{II}–$Rh^{II}X_2$ brethren, the X_2Rh^{II}–$Rh^{0}L$ complex sustains the multielectron reactivity of the Rh_2 dfpma system. This multielectron design strategy is general as long as a two-electron mixed-valence complex can be stabilized with respect to its symmetric congener.

With the understanding that M^{n+2}–M^{n} complexes are a keystone to multielectron photoreactivity, we sought to expand the concept of two-electron mixed valency to other transition metals. Our initial attempts focused on iridium, for which Ir^{0}–Ir^{II} cores are unknown.[5] Efforts to use the dfpma ligand to develop a parallel chemistry to that of Rh, however, were met with frustration as mixtures of Ir^{I} monomers and various oligomerization products were obtained. Introduction of more sterically demanding OR substituents on P could avoid these problematic reactions while providing us with the additional flexibility of tuning the electronic properties[6] of the two-electron mixed-valence core by R substitution. As we now report, an excursion into Ir chemistry with the bidentate diphosphazane, $MeN[P(OEt^{F3})_2]_2$ (OEt^{F3} = OCH_2CF_3), successfully afforded two-electron mixed-valence compounds and not the oligomers that plague Ir dfpma chemistry.

Addition of $HOEt^{F3}$ to a cold Et_2O solution of $MeN(PCl_2)_2$[1,7] and NEt_3 results in the formation of $MeN[P(OEt^{F3})_2]_2$ in good yields.[8] $Ir_2Cl_2(cod)_2$ was treated with 3 equiv. of the ligand in CH_2Cl_2 at room temperature. The solution immediately turned yellow and then slowly darkened to orange–brown. Over several days, a fine green powder precipitated from the reaction solution. Single crystals of the compound, which analyzes as $Ir_2\{MeN[P(OEt^{F3})_2]_2\}_3Cl_2$ (**1**),† were obtained from saturated CH_2Cl_2 solutions of **1** at 22 °C.

X-Ray diffraction analysis of **1** reveals the unsymmetrical coordination sphere of the Ir^{0}–Ir^{II} binuclear core displayed in Fig. 1.‡ In a structural departure from Rh–dfpma chemistry, two of the three bidentate ligands adopt a bridging coordination mode with the third ligand binding as a chelate. The Ir^{0} center possesses a trigonal bipyramidal coordination geometry that is typical for d^9 metals composing a binuclear core.[2,9] Two equatorial sites of the Ir^{0} center are coordinated by phosphites from the bridging $MeN[P(OEt^{F3})_2]_2$ ligands with the third equatorial site occupied by one end of a chelating $MeN[P(OEt^{F3})_2]_2$ ligand. The other end of the chelating ligand resides at an axial coordination site of the Ir^{0} center. The apical position of the square pyramid that defines the coordination geometry about the neighboring Ir^{II} center is reciprocally capped by the Ir^{0} center. Two *cis*-equatorial sites are occupied by phosphites from the bridging ligands, while the other two equatorial sites are occupied by chloride ligands. An Ir–Ir bond distance of 2.7871(8) Å is typical of singly bonded binuclear iridium complexes.[10]

Although **1** shows little solubility in non-coordinating solvents, the 16-e^- Ir^{II} center readily receives donor ligands at its open coordination site, rendering more soluble derivatives. Addition of $CNBu^t$ or PEt_3 to suspensions of **1** in CH_2Cl_2 results in the rapid dissolution of the solid to form bright yellow solutions.† Pale yellow crystals of the $CNBu^t$ (**2**) and PEt_3 (**3**) derivatives were obtained upon the addition of pentane to reaction solutions that had been concentrated by solvent evaporation. Ligand occupation of the vacant axial site of the Ir^{II} center of **1** is confirmed by an X-ray crystal structure of **2**.‡ Excepting changes along the P_{ax}–Ir^{0}–Ir^{II}–L axis, the X-ray crystal structure of **2**, is very similar to that of **1**.

As determined from ^1H and ^{31}P NMR spectroscopy, the solid state coordination geometries of **1**–**3** are preserved in solution. Whereas the methylene protons of the ligand's OCH_2CF_3 group are not well resolved, two distinct resonances in a 2 : 1 ratio are observed for the methyl groups of both the bridging and chelating $MeN[P(OEt^{F3})_2]_2$ ligands. The integration ratios for the protons of $CNBu^t$ and PEt_3 in **2** and **3**, respectively, compared to those of the proton resonances of $MeN[P(OEt^{F3})_2]_2$ establish the incorporation of only one ligand into the diiridium coordination sphere. The ^{31}P NMR spectra presented in Fig. 2 reveal congruent solution structures for **1**–**3**. Two signals at δ *ca.* 46 and 95 are maintained in each of the spectra, consistent with the preserved equatorial arrangement of phosphites in **1**–**3**. The resonance at δ 46 is assigned to the P(5) phosphite of the Ir^{0} equatorial plane and the resonance at δ 95

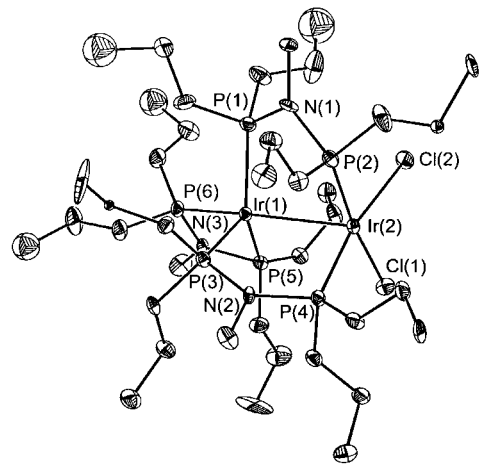

Fig. 1 ORTEP representation of **1**, with fluorine atoms omitted for clarity. Thermal ellipsoids are drawn at the 25% probability level.

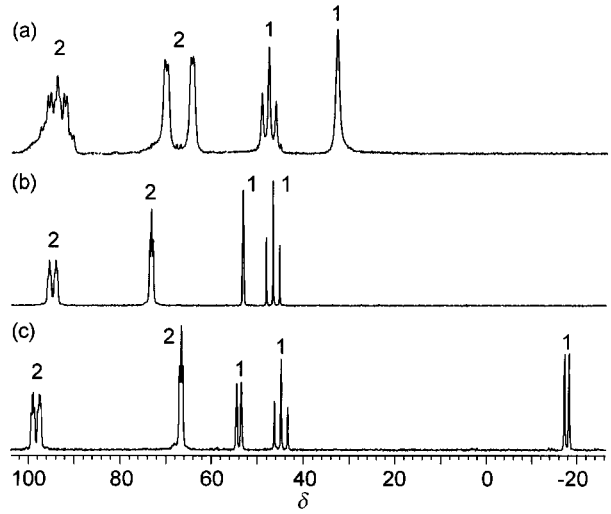

Fig. 2 ^{31}P NMR (121.488 MHz) of the two-electron mixed-valence compounds (a) **1**, (b) **2** and (c) **3** in CD_3CN, referenced to an external 85% H_3PO_4 standard. The relative integration values are indicated for each phosphorus resonance.

is consistent with the P(2)/P(4) equatorial phosphites coordinated to the Ir^{II} center. Conversely, differences are observed for the resonance associated with the axial phosphite [P(6)]. The high frequency shift of the P(6) resonance from δ 32.7 in **1** to δ 52.5 and 53.3 in **2** and **3**, respectively, is in accordance with the structural perturbations induced by the presence of the donor ligand in the axial coordination site of Ir^{II}. The observed increase in the Ir^0–P_{ax} bond distance [*d*(Ir(1)–P(6)) = 2.238(6) Å in **2** *vs* *d*(Ir(1)–P(6)) = 2.206(4) Å in **1**] upon coordination of the donor ligand is expected to result in decreased $Ir^0 \rightarrow P_{ax}$ π-backbonding and consequently a shift of the axial phosphite resonance to higher frequency. The $^3J(P_{ax},PEt_3)$ coupling for **3**, and its absence in **1** and **2**, follows logically from the coordination of a phosphorus donor ligand along the metal–metal bond. The only other significant difference in the three spectra of Fig. 2 is the collapse of the resonances at δ 64.7 and 70.5 of **1**, assigned to the remaining Ir^0 phosphites [P(1) and P(3)], to give triplet signals at δ 72.5 and 66.0 for **2** and **3**, respectively.

Initial investigations of the reactivity of the Ir^{II}–Ir^0 compounds suggest a facile oxidative-addition chemistry. Suspensions of **1** in CH_2Cl_2 yield homogeneous, yellow solutions upon the introduction of H_2, I_2, HCl and $PhICl_2$. As exemplified by the reaction between **1** and $PhICl_2$, the addition products are consistent with the presence of an $Ir^I \rightarrow Ir^{III}$ dative bond, with both metals assuming an octahedral coordination geometry. The NMR spectrum of the isolated product, $Ir_2\{MeN[P(OEt^{F3})_2]_2\}_3Cl_4$, shows that the coordination of the bridging and chelating phosphites remains unchanged. In contrast to **1**, reactions of **2** and **3** with strong oxidants proceed sluggishly and not at all with H_2. This arrested reactivity of the latter complexes suggests that ligand dissociation should precede the oxidative-addition of substrates when the diiridium core is coordinatively saturated.

Previous reactivity studies of bimetallic complexes indicate that the presence of two-electron mixed valence cores inhibit oxidation–reduction chemistry.[11] Thus, our observation that the mixed-valence Ir^{II}–Ir^0 core undergoes facile redox conversions is noteworthy. Current investigations are continuing to explore the structure, spectroscopy and reactivity of the Ir^{II}–Ir^0 compounds and their addition products.

The authors thank Dr William M. Davis for assistance with the solution of the X-ray crystal structures. The National Science Foundation Grant CHE-9817851 funded this research.

Notes and references

† *Experimental Procedures:* **1**: in a nitrogen atmosphere, 734 mg (1.51 mmol) of $MeN[P(OEt^{F3})_2]_2$ was added to a solution of 331 mg (0.493 mmol) of $Ir_2Cl_2(cod)_2$ (Strem) dissolved in 15 mL of CH_2Cl_2. The mixture was stirred at room temp. for 24 h during which a dark precipitate formed. A green powder precipitated from solution over several days. The solid was collected by filtration, washed with 5 mL of C_6H_6 and three 5 mL aliquots of pentane and then dried *in vacuo* to yield 590 mg (62%) of the analytically pure product. $C_{27}H_{33}Cl_2F_{36}Ir_2N_3O_{12}P_6$; found: C, 17.06; H, 1.65; N, 2.29; P, 9.63; requires: C, 16.92; H, 1.74; N, 2.19; P, 9.70%. ^{1}H NMR (CD_3CN, 300 MHz, TMS) δ 2.576 (t, 10.5 Hz, 3 H), 2.763 (s, 6 H), 4.0–5.5 (m, 24 H). ^{31}P NMR (CD_3CN, 121 MHz, 85% H_3PO_4) δ 32.710 (s), 47.665 (dd, 299, 292 Hz), 64.702 (m), 70.509 (m), 94.002 (m). UV–VIS (CH_2Cl_2) λ_{max}/nm (ε/dm^3 mol^{-1} cm^{-1}): 271 (11 400), 348 (1090), 402 (1480), 509 (140).

2: in an N_2 atmosphere, a few drops of $CNBu^t$ were added to a suspension of **1** (201 mg, 0.105 mmol) in 8 mL of CH_2Cl_2 at room temperature. The solution immediately turned yellow and all the solid dissolved. After a few hours the solvent volume was reduced to 2 mL and 10 mL of pentane was added. Cooling the solution to −35 °C over 24 h resulted in the formation pale yellow crystals exhibiting a plate morphology. Yield 155 mg (74%). $C_{32}H_{42}Cl_2F_{36}Ir_2N_4O_{12}P_6$; found: C, 19.30; H, 2.18; N, 2.86; requires: C, 19.22; H, 2.12; N, 2.80%. ^{1}H NMR (CD_3CN, 300 MHz, TMS) δ 1.510 (s, 9 H), 2.494 (dd, 12.3, 9.0 Hz, 3 H), 2.730 (dt, 9.0, 3.6 Hz, 6 H), 4.15−4.95 (m, 24 H). ^{31}P NMR (CD_3CN, 121 MHz, 85% H_3PO_4) δ 46.056 (t, 290 Hz), 52.509 (s), 72.530 (t, 75.4 Hz), 93.960 (dm, 290 Hz). UV–VIS (CH_2Cl_2) λ_{max}/nm (ε/dm^3 mol^{-1} cm^{-1}): 302 (13 400).

3: in an N_2 atmosphere, PEt_3 (19 mg, 0.160 mmol) was added to **1** (102 mg, 0.053 mmol) in 10 mL of CH_2Cl_2 at room temperature. The solution immediately turned yellow and all the solid dissolved. The solution was concentrated and 10 mL of pentane was added. Cooling to −35 °C overnight caused a yellow microcrystalline solid to precipitate from solution. Yield 87 mg (81%). $C_{33}H_{48}Cl_2F_{36}Ir_2N_3O_{12}P_7$; found: C, 19.58; H, 2.55; N, 2.12; requires: C, 19.22; H, 2.12; N, 2.80%. ^{1}H NMR (CD_3CN, 300 MHz, TMS) δ 1.230 (dt, 13.2, 7.6 Hz, 9 H), 2.114 (dq, 7.4, 7.5 Hz, 6 H), 2.559 (dd, 11.7, 8.7 Hz, 3 H), 2.648 (m, 6 H), 4.040 (m, 2 H), 4.29–4.87 (m, 18 H), 5.010 (m, 4 H). ^{31}P NMR (CD_3CN, 121 MHz, 85% H_3PO_4) δ: −18.189 (dd, 205 Hz, 18.8 Hz), 44.238 (t, 288 Hz), 53.340 (d, 208 Hz), 65.967 (t, 71.4 Hz), 97.496 (dm, 291 Hz).

‡ *Crystal data*: **1**: $C_{27}H_{29}Cl_2F_{36}Ir_2N_3O_{12}P_6$, M = 1912.65, monoclinic, space group $C2/c$, a = 22.6597(5), b = 12.8038(2), c = 40.1310(6) Å, β = 92.4210(10)°, U = 11632.8(4) Å^3, Z = 8, D_c = 2.184 g cm^{-3}, T = 183(2) K, μ = 4.996 mm^{-1}, $wR2$ = 0.1441 (8322 independent reflections), $R1$ = 0.0669 [$I > 2\sigma(I)$]. C(8), C(14) and the CF_3 group of C9 were disordered between two positions. The fluorine atoms on C(5) and C(7) were placed in an idealized, tetrahedral geometry.

2: $C_{32.5}H_{43}Cl_3F_{36}Ir_2N_4O_{12}P_6$, M = 2042.28, monoclinic, space group $P2_1/n$, a = 13.0879(2), b = 54.4519(9), c = 18.4318(3) Å, β = 101.1890(10)°, U = 12885.9(4) Å^3, Z = 8, D_c = 2.105 g cm^{-3}, T = 183(2) K, μ = 4.558 mm^{-1}, $wR2$ = 0.1787 (18440 independent reflections), $R1$ = 0.0892 [$I > 2\sigma(I)$]. The asymmetric unit contains two chemically identical, but crystallographically different molecules; the CF_3 groups were generated in an idealized, tetrahedral geometry then refined anisotropically. CCDC 182/1301.

1 J. F. Nixon, *J. Chem. Soc. A*, 1968, 2689.
2 J. I. Dulebohn, D. L. Ward and D. G. Nocera, *J. Am. Chem. Soc.*, 1988, **110**, 4054; 1990, **112**, 2969; J. Kadis, Y.-g. K. Shin, J. I. Dulebohn, D. L. Ward and D. G. Nocera, *Inorg. Chem.*, 1996, **35**, 811.
3 C. M. Partigianoni and D. G. Nocera, *Inorg. Chem.*, 1990, **29**, 2033; C. M. Partigianoni, C. Turró, T. L. C. Hsu, I. J. Chang and D. G. Nocera, *Adv. Chem. Ser.*, 1993, **238**, 147; D. G. Nocera, *Acc. Chem. Res.*, 1995, **28**, 209; T. L. C. Hsu, S. A. Helvoigt, C. M. Partigianoni, C. Turró and D. G. Nocera, *Inorg. Chem.*, 1995, **34**, 6186; D. S. Engebretson, E. Graj, G. E. Leroi and D. G. Nocera, *J. Am. Chem. Soc.*, 1999, **121**, 868.
4 A. F. Heyduk, A. M. Macintosh and D. G. Nocera, *J. Am. Chem. Soc.*, 1999, **121**, 5023.
5 The Cambridge Structure Database (CSD) was searched, as were the Science Citation Index and Chemical Abstracts using the key words 'iridium' and 'mixed-valence.'
6 C. A. Tolman, *Chem. Rev.*, 1977, **77**, 313.
7 R. B. King and J. Gimeno, *Inorg. Chem.*, 1978, **17**, 2390.
8 A. L. Odom, A. F. Heyduk and D. G. Nocera, manuscript in preparation.
9 M. A. Bennett and D. J. Patimore, *Inorg. Chem.*, 1971, **10**, 2387; R. B. King, M. Chang and M. G. Newton, *J. Organomet. Chem.*, 1985, **296**, 15.
10 B. R. Sutherland and M. Cowie, *Inorg. Chem.*, 1984, **23**, 2324; C. P. Kubiak, C. Woodcock and R. Eisenberg, *Inorg. Chem.*, 1980, **19**, 2733.
11 B. Bosnich, *Inorg. Chem.*, 1999, **38**, 2554; D. G. McCollum and B. Bosnich, *Inorg. Chim. Acta*, 1998, **270**, 13.

Communication 9/02487E

Isopropyl *tert*-butyl ether from crude acetone streams

John F. Knifton,* Pei-Shing E. Dai and John M. Walsh

Shell Chemical Company,PO Box 1380, Houston, TX 77251-1380, USA. E-mail: jfknifton@shellus.com

Received (in Bloomington, IN) 19th March 1999, Accepted 22nd June 1999

Isopropyl *tert*-butyl ether may be prepared from crude acetone streams through a combination of selective hydrogenation and *tert*-butyl alcohol etherification.

Methyl *tert*-butyl ether (MTBE) has in recent years been under severe environmental pressure[1] and refiners have been examining alternative gasoline blending stocks, including *tert*-amyl methyl ether (TAME), ethyl *tert*-butyl ether (ETBE), *etc*.[2,3] Of the fuel ethers seriously being considered, isopropyl *tert*-butyl ether (IPTBE) has the triple advantages[3] (see Table 1) of (i) highest octane blending values, (ii) lowest oxygen content and (iii) low vapor pressure. However, until now the only route to IPTBE was through the acid-catalyzed etherification of isobutene (oftentimes in short supply) with isopropyl alcohol (propan-2-ol, IPA) [eqn. (1)].[4,5] We have developed an alternative route to IBTBE from crude acetone streams, making it a co-product of propylene oxide (PO) manufacture. Propylene epoxidation with *tert*-butyl hydroperoxide produces PO plus *tert*-butyl alcohol commercially [eqn. (2)], with significant quantities of acetone as a secondary by-product.[6] We have demonstrated,[7] and report herein, that IPTBE can be made in good yield *via* (i) selective hydrogenation of the crude acetone (Me_2CO) by-product stream to give isopropanol [eqn. (3)] and (ii) isopropyl alocol etherification with the *tert*-butyl alcohol co-product to yield IPTBE plus water [eqn. (4)].

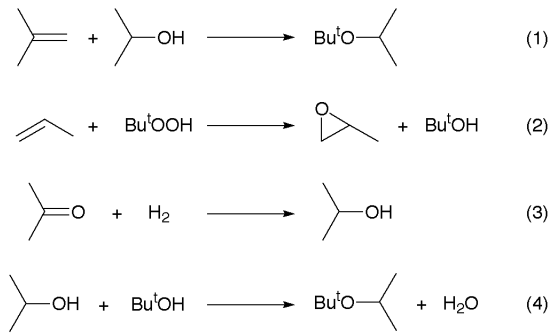

Typically, low-value acetone by-product streams from propylene oxide manufacture comprise 20–80% Me_2CO, but also contain significant quantities of MeOH, *tert*-butyl alcohol (tBA), and allyl *tert*-butyl peroxide (ATBP), as well as detectable quantities of HCO_2H, AcOH, plus their ester derivatives, such as *tert*-butyl formate (tBF).[6] Selective hydrogenation of a 61.7% acetone stream in a continuous, upflow, reactor system containing a nickel, copper, chromium bulk-metal catalyst (72% Ni), at 160 °C, is illustrated in Table 2. Near quantitative (99%) acetone conversion levels are achieved at liquid hourly space velocities (LHSVs) of 0.5, with IPA as the major product. Selectivity to IPA is typically in the range of 76–80 mol%. Critical features of this selective hydrogenation are (i) catalyst activity may be sustained for extended periods without loss of performance and (ii) any ATBP or *tert*-butyl hydroperoxide fractions present in this crude acetone feed are quantitatively converted to more innocuous alcohols, *e.g. tert*-butyl alcohol, without causing catalyst deactivation.

Table 1 Typical properties of fuel ethers[a]

	MTBE	ETBE	TAME	IPTBE
Octane blending value (R + M)/2	110	112	105	113
Oxygen content (wt%)	18.2	15.7	15.7	13.8
Vapor pressure neat Rvp (37.8 °C)	7.8	4.0	2.5	2.5

[a] Data taken from references 2 and 3.

Etherification of the IPA intermediate with added tBA to give IPTBE [eqn. (4)] has also been demonstrated in continuous, upflow, reactor systems using three classes of acidic, large-pore, zeolites:[7] Zeolite Beta, transition metal-modified β-zeolites, and dealuminized Y-zeolites.

IPTBE is typically generated in near quantitative molar selectivities (on the basis of IPA converted) in the crude liquid products under mild etherification conditions. Fig. 1 illustrates IPTBE syntheses from the crude IPA stream of Table 2, plus added tBA (IPA:tBA mole ratio 1:1.6), using an acidic β-zeolite catalyst (80% Beta, 20% alumina binder, in $\frac{1}{16}$″ diameter extruded form), over a reactor temperature range of 40 to 100 °C. At 60–80 °C the estimated IPA conversion level is moderate (*ca*. 12%) and the crude liquid effluent comprises 7–8 wt% IPTBE. However, IPTBE molar selectivity on the basis of tBA converted is below 50% with this crude feedstock, due to

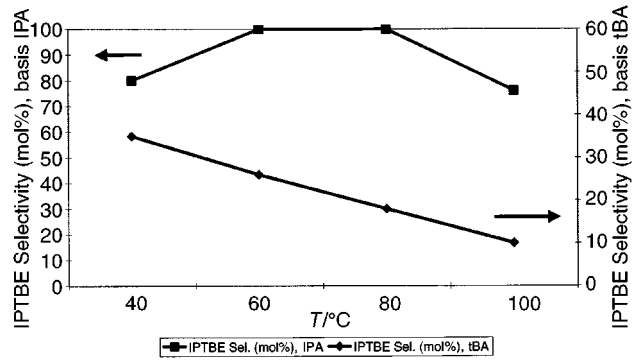

Fig. 1 Crude IPA etherification to IPTBE with tBA. IPTBE molar selectivity basis IPA and tBA converted.

Table 2 Crude acetone hydrogenation to isopropyl alcohol

				Composition (%)					
Catalyst	*T*/°C	LHSV	Sample	Me_2CO	IPA	MeOH	tBA	tBF	ATBP
			Feed	61.7	0.1	13.9	16.7	0.1	3.3
Ni-2715	160	0.5[a]	Product[b]	0.8	48.3	15.8	30.8	< 0.1	< 0.1

[a] Hydrogen feed rate, 90 l h^{-1}; total pressure, *ca*. 35 bar. [b] Product composition maintained for 200 h.

Table 3 Isopropyl alcohol etherification to isopropyl *tert*-butyl ether

				Composition (%)						
Catalyst	*T*/°C	LHSV	Sample	IPTBE	MTBE	IPA	tBA	MeOH	C4H8	C8H16
			Feed		0.1	11.3	81.2	3.4		
Pt/Beta zeolite	60	0.25	#1	5.9	4.2	9.3	68.3	1.3	6.6	0.5
	80	0.25	#2	5.5	5.9	9.1	61.1	0.8	10	2.9
Pd/Beta zeolite			Feed			11.3	82.2	2.1		
	60	0.25	#1	6.1	4.3	9.3	67.7	1.2	6.7	0.6
	80	0.25	#2	5.4	6.2	9.5	60.6	0.7	9.7	3

[a] Designations as per Table 2.

Table 4 Standard enthalpy and entropy changes for IPTBE syntheses

IPTBE Synthesis Route	ΔH/kcal mol^{-1}	ΔS/cal mol^{-1} K^{-1}
IPA + iso-C_4H_8 → IPTBE	−6.1[a]	−17.1[a]
	−5.5[b]	−14.4[b]
IPA + tBA → IPTBE + H_2O	−0.4[c]	−7.0[c]

[a] From reference 4. [b] From reference 5. [c] This work, ideal gas conditions (298 K, 1.0 atm).

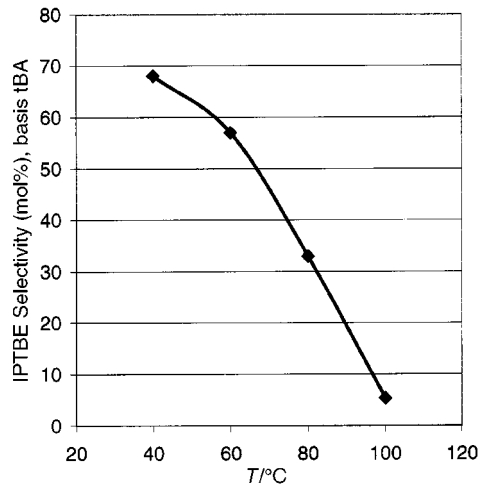

Fig. 2 Pure IPA etherification to IPTBE with tBA.

competing tBA dehydration and oligomerization to isobutene and diisobutene, as well as the formation of smaller quantities of MTBE through etherification. It is noteworthy, nevertheless, that the β-zeolite catalyst does maintain etherification activity and good IPTBA molar selectivity with this crude hydrogenated Me_2CO feedstock for extended periods.[7]

Very similar product distributions were realized when using transition metal-modified β-zeolite catalysts—particularly β-zeolites modified with platinum, palladium, and nickel. These data are illustrated in Table 3 for the non-aqueous product fraction, when starting with the same crude IPA feed stream of Table 2, but adding additional tBA (IPA:tBA molar feed ratio 1:5.8). The transition metal-modified β-zeolites were selected for study here, on the basis of our earlier observations that they provide superior performance in related service, *e.g.* MTBE production from Bu^{t}OH–MeOH mixtures,[8] as well as in ETBE synthesis.[9] Significantly poorer etherification performance was generally realized with the dealuminized Y-zeolites.[7]

Liquid-phase IPTBE synthesis from IPA–tBA mixtures [eqn. (4)] is essentially thermoneutral—see Table 4—in contrast to IPTBE from isobutene [eqn. (1)].[4,5] Isolating and purifying (99%) the intermediate IPA from Table 2, and running etherification with close to stoichiometric quantities of tBA, provides measurably higher IPTBE selectivities over this temperature range (see Fig. 2, IPA:tBA feed ratio 1:1.6) and fewer competing reactions. However, etherifications conducted much above 100 °C lead to the formation of diisopropyl ether as a dominant product.[10]

Continuing improvements in this technology are under investigation, particularly in the area of an integrated, one-step, route to C-3 ethers from crude acetone streams plus tBA.[11]

The authors wish to thank Mr Melvin Stockton for experimental excellence.

Notes and references

1 See: *Chem. Eng. News*, May 5, 1997, 54; *ibid*., Dec. 2, 1996, 14; *ibid*., Nov. 23, 1998, 30.
2 W. J. Piel, *Fuel Reformulation*, March/April 1994, **4**, 28.
3 W. J. Piel, *Fuel Reformulation*, November/December 1992, **2**, 34.
4 J. A. Linnekoski, A. O. I. Krause, A. Holman, M. Kjetsa and K. Moljord, *Appl. Catal.*, 1998, **174**, 1.
5 A. Calderon, J. Tejero, J. F. Izquierdo, M. Iborra and F. Cunill, *Ind. Eng. Chem. Res.*, 1997, **36**, 896.
6 Stanford Research Institute PERP Report 2E, 'Propylene Oxide', August 1994.
7 J. F. Knifton, E. L. Yeakey and P. E. Dai, US Patent 5449838, 1995.
8 J. F. Knifton and P. E. J. Dai, US Patent 5364981, 1994.
9 P. E. Dai, R. J. Taylor, J. F. Knifton and B. R. Martin, US Patent 5476972, 1995.
10 J. F. Knifton and P. E. Dai, *Catal. Lett*., 1999, **57**, 193.
11 R. J. Taylor, P. E. Dai, J. F. Knifton and B. R. Martin, US Patent 5637778, 1997.

Communication 9/02458A

Electrocatalytic reduction of dioxygen to water by tren-capped porphyrins, functional models of cytochrome *c* oxidase†

David Ricard,[a] Bruno Andrioletti,[a] Maurice L'Her*[b] and Bernard Boitrel*[a]

[a] *Université de Bourgogne/LSEO, UMR-CNRS 5632, 6, boulevard Gabriel, 21000 Dijon, France. E-mail: bboitrel@satie.u-bourgogne.fr*

[b] *Université de Bretagne Occidentale/Faculté des Sciences, UMR-CNRS 6521, B.P. 809, 29285 Brest CEDEX, France. E-mail: maurice.lher@univ-brest.fr*

Received (in Basel, Switzerland) 23rd April 1999, Accepted 21st June 1999

Two different tren-capped porphyrins—in which the two metals, iron and copper, are more or less off-centered—are shown to be efficient catalysts for the reduction of O_2 to H_2O; surprisingly, their iron-only complexes are shown to be even more effective 4e$^-$ catalysts when adsorbed on a graphite electrode.

The biological reduction of dioxygen to water is an essential reaction that produces energy in the mitochondria. The protein that drives this reaction, the cytochrome *c* oxidase (C*c*O), is the terminal enzyme of the respiratory chain. Additionally, this reaction is coupled with proton translocation across the inner membrane, for the synthesis of ATP.[1] The design and synthesis of new functional analogs is absolutely critical for the understanding of the structural features required for this reaction. This area has been reviewed several times[2] and in particular through the application of 'cofacial metallodiporphyrin' models.[3] The first biomimetic model of C*c*O with a copper complex covalently bound above the porphyrin in a well-defined geometry was reported five years ago.[4] In 1995, the X-ray analysis of bovine heart oxidase[5] revealed that the Cu_B was 4.5 Å from the Fe_{a3} and 1 Å away from the normal axis of the heme iron position. These observations led us to design the 'Arbor' porphyrins,[6] a new series of biomimetic models based on tren [tris(2-aminoethyl)amine] capped porphyrins and for which we have already pointed out that the secondary amino groups could be crucial for the interaction with dioxygen.[7] Since the description of the 'Arbor' porphyrins, several compounds closely related to them have recently appeared in the literature but in both cases with a tri-alkylated cap.[8,9] Until a few months ago,[10] the only biomimetic models having catalytic activity were a cobalt(II) porphyrin associated with a copper(I) triazacyclononane[11] and a copper(I) imidazole-picket iron(II) porphyrin.[12] We report herein our observations about the reduction reaction of dioxygen catalyzed by two different, but still related, model compounds (Scheme 1), for which the relative position of the two metal centers is precisely tuned. The coordination site of the copper ion is highly dependent on the number of 'linker arms' which attach the tripodal cap to the porphyrin core. Compound **4** was obtained by grafting the tren molecule on a chloroacetamido picket porphyrin, leading to a ligand in which the cap is more off-centered and closer to the porphyrin than in model **3** (where a Michael acceptor was used). To the best of our knowledge, this is the first series of two Fe/Cu model complexes differing only in the relative position of copper *vs*. iron, achieved in this work not only by the use of two different linkers but also by a specific strategy that consists in using a non-protected tren molecule.

The synthetic routes to the two different final complexes are shown in Scheme 1. The atropisomer $\alpha\alpha\alpha\alpha$ of the *meso*-(tetra-*o*-aminophenyl)porphyrin (TAPP)—or its singly acetylated derivative—was acylated by either chloroacetyl chloride or acryloyl chloride. These acylations lead to either the three chloroacetyl or the four acryloyl picket porphyrins, which are eventually used in the iron insertion reaction. The capping reaction is carried out on the iron complexes, before copper insertion, to avoid any possible cross-metallation. Then, an excess of nitrogenous base (1,2-dimethylimidazole) is added to stabilize the iron(II) as a five coordinate complex. By combining two crucial structural features: a) the distance between the two coordination sites and b) the off-centering of the two metals, it might be possible to know if one of these two compounds is more efficient than the other one for O_2 electroreduction.

Among the four possible ligands that could be synthesized (3 or 4 linkers and one or two methylene groups), the two studied complexes **3** and **4**‡ (which are the most different compounds in terms of Fe–Cu distance and relative positions of the two metal centers) were found to be active catalysts for the four electron reduction of dioxygen in aqueous solution. This has been assessed by rotating ring-disk voltammetry. Experiments have been performed at pH = 6.86 ($HPO_4^{2-}/H_2PO_4^-$ buffer), an acidity level close to the physiological pH at which cytochrome

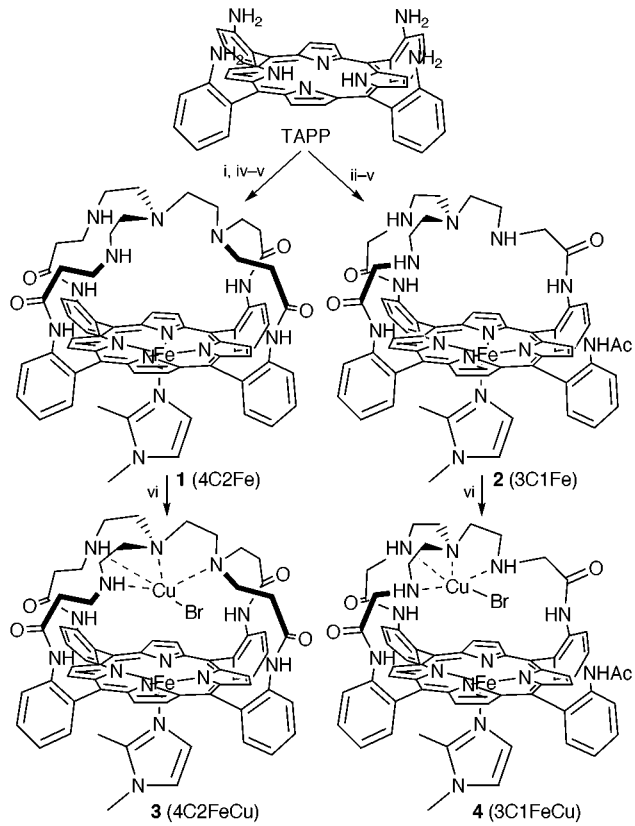

Scheme 1 *Reagents and conditions*: (i) CH_2=CHCOCl, NEt_3, THF; (ii) CH_3COCl, NEt_3, THF, 0 °C; (iii) $ClCH_2COCl$, NEt_3, THF; (iv) $FeBr_2$, 2,6-lutidine, THF, 55 °C; (v) tren, MeOH, 50 °C; (vi) CuBr, CH_3CN, 60 °C.

† Further experimental and spectroscopic data are available from the RSC web site, see http://www.rsc.org/suppdata/cc/1999/1523/

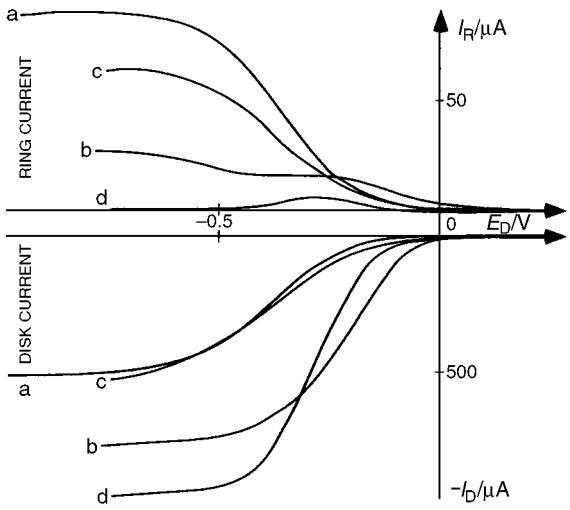

Fig. 1 Rotating ring-disk voltammetry for O_2 reduction; graphite disk impregnated with **1** or **3**. pH = 6.86; N_r = 250 rpm; reference: SCE; $P(O_2)$ = 1 atm; potential of the platinum ring-electrode: 0.8 V. a: bare graphite electrode. b,c: first and third consecutive voltammogram after coating with **3** (4C2FeCu). d: after coating with **1** (4C2Fe).

c oxidase operates; however, as dicobaltbisporphyrins require acidic media for the 4e$^-$ reduction, the catalytic efficiencies of **3** and **4** have also been tested at low pH (0.1 M $HClO_4$).

As illustrated for **3** (Fig. 1), models **4** and **3** have identical effects on the reduction of O_2 at pH 6.86, when adsorbed on the graphite disk. The reduction waves for the first scan (curve b) begin at −0.1 V and have almost the same limiting current. From comparison with the dioxygen reduction on a bare edge-plane graphite electrode (curve a), it can be concluded that the number of electron exchanged per O_2 molecule is 2.8. The production of H_2O_2 is detected at the platinum ring (ring current, curve b) almost immediately at the beginning of O_2 reduction, which means that the two and four electron reduction processes occur simultaneously. A second and third scan with the same electrode (curve c) show that the catalyst is degraded, as proved by the lower reduction current. When the electrode is in contact with an aqueous acidic solution (0.1 M $HClO_4$), O_2 reduction starts at a higher potential (0.1 V); the 4e$^-$ process occurs also under these conditions but the catalytic efficiency is lost more rapidly than in the neutral medium. The number of electrons for the electrocatalytic reduction of O_2, measured as described above, is only apparent as the catalyst is degraded during the reduction. Surprisingly, changes in the structure of the molecule do not seem to significantly affect the activity of these models of cytochrome *c* oxidase. The first hypothesis which explains the loss of activity could be the leaching of copper from its rather labile complex. The second could be the decoordination of the fifth ligand of the iron. These two structural features have been presented as essential to the catalytic activity in related biomimetic models.[11] However, catalysts **1** and **2**, the respective analogs of **3** and **4** without copper, cleanly catalyze the 4e$^-$ reduction, as shown for **1** in Fig. 1 (curve d). This simple test has never been reported even for close structural models bearing imidazole pickets.[8,12]

These experimental observations led us to several conclusions. Firstly, the loss of activity that occurs during the O_2 reduction is not due to the decoordination of the copper ion in contact with aqueous media as the iron-only compounds are even more efficient catalysts. The second conclusion derived from this study is that the fifth ligand does not need to be covalently bound to the porphyrin.

The fact that the iron catalysts are efficient for the reduction of dioxygen to water excludes the formation of a μ-peroxo intermediate between iron and copper atoms as a prerequisite for O_2 activation, as it has been postulated.[1a,d] However, it is compatible with a peroxo derivative, probably protonated.[2b] In the case of the enzyme, Yoshikawa *et al*. have suggested that this hydroperoxo complex is formed by addition of a proton delivered by Tyr 244.[13] In the case of the present model compounds, whether the proton transfer from the solution to the peroxo entity is mediated by the tren cap, or these secondary amino groups stabilize the hydroperoxo complex, are questions that could not receive proper answers in this preliminary work.

In conclusion, this new series of catalysts are efficient and selective for the electroreduction of dioxygen to water, without copper in the tripodal cap. This is in favor of the formation of a hydroperoxo complex rather than a μ-peroxo complex. Surprisingly, these results seem to be in contradiction with what has already been reported for related model compounds.[9] This difference of reactivity could be explained by structural differences; more explicitly, the existence of secondary amino groups in our compounds. These are certainly protonated when the compounds are in an aqueous environment at pH 6.86. Indeed, it would be of great interest to know if iron-only models such as the imidazole picket porphyrin of Holm[8] or its analog with an intramolecular nitrogen base described by Collman[12] are also efficient 4e$^-$ catalysts or not. It should however be stressed that these conclusions have been reached by the observation of molecules adsorbed on a graphite electrode in contact with water, a situation different from the environment of the active site of the enzyme. This study is presently in progress with other new molecules, to investigate if these tren-capped porphyrins represent a particular case or if this unexpected reactivity is general for iron–copper cytochrome *c* oxidase models.

Notes and references

‡ *Selected data* for complex **1** obtained after step (iv) in Scheme 1: 64%. HRMS (LSIMS): *m/z* 1091.4132 calc. for $C_{62}H_{59}N_{12}O_4Fe$ [M − H]$^+$, found 1091.4160. For **1** before the capping reaction: 90%; δ_H(500 MHz, pyridine-d_5, 323 K) 8.82 (d, *J* 7.0, 4H, arom.), 8.74 (s, 8H, β-pyr.), 8.23 (large s, 4H, -NHCO), 7.98 (d, *J* 7.0, 4H, arom.), 7.77 (t, *J* 7.5, 4H, arom.), 7.47 (t, *J* 7.5, 4H, arom.), 5.90 (d, *J* 17.0, 4H, –CH=), 5.17 (m, 4H, =CH_2), 5.06 (m, 4H, =CH_2). For **3**: HRMS (LSIMS): *m/z* 1169.3299 calc. for $C_{62}H_{58}N_{12}O_5FeCu$ [M$^{+\bullet}$], found 1169.3324. For **4**: Before copper insertion, HRMS (LSIMS): *m/z* 1036.3586 calc. for $C_{58}H_{52}N_{12}O_4Fe$ [M$^{+\bullet}$], found 1036.3527. For more extensive experimental details, see Note †.

1 (*a*) B. G. Malmström, *Chem. Rev.*, 1990, **90**, 1247; **(b)** M. X. Calhoun, J. W. Thomas and R. B. Gennis, *TIBS*, 1994, 325; (*c*) R. Gennis and S. Ferguson-Miller, *Science*, 1995, **269**, 1063; (*d*) S. Ferguson-Miller and G. T. Babcock, *Chem. Rev.*, 1996, **96**, 2889.

2 (*a*) R. H. Holm, *Pure Appl. Chem.*, 1995, **67**, 217; (*b*) S. Fox, A. Nanthakumar, N. Wei, N. N. Murthy and K. D. Karlin, *Pure Appl. Chem.*, 1993, **65**, 2335.

3 (*a*) J. P. Collman, P. S. Wagenknecht and J. E. Hutchison, *Angew. Chem., Int. Ed. Engl.*, 1994, **33**, 1537; (*b*) J. P. Collman, N. H. Hendricks, C. R. Leidner, E. Ngameni and M. L'Her, *Inorg. Chem.*, 1988, **27**, 387.

4 J. P. Collman, P. C. Herrmann, B. Boitrel, X. M. Zhang, T. A. Eberspacher, L. Fu, J. L. Wang, D. L. Rousseau and E. R. Williams, *J. Am. Chem. Soc.*, 1994, **116**, 9783.

5 T. Tsukihara, H. Aoyama, E. Yamashita, T. Tomizaki, H. Yamaguchi, K. Shinzawa-Itoh, R. Nakashima, R. Yaono and S. Yoshikawa, *Science*, 1995, **269**, 1069.

6 B. Andrioletti, B. Boitrel and R. Guilard, *J. Org. Chem.*, 1998, **63**, 1312.

7 D. Ricard, B. Andrioletti, B. Boitrel and R. Guilard, *New J. Chem.*, 1998, 1331.

8 J. O. Baeg and R. H. Holm, *Chem. Commun.*, 1998, 571.

9 J. P. Collman, *Inorg. Chem.*, 1997, **36**, 5145.

10 J. P. Collman, L. Fu, P. C. Herrmann, Z. Wang, M. Rapta, M. Broring, R. Schwenninger and B. Boitrel, *Angew. Chem., Int. Ed.*, 1998, **37**, 3397.

11 J. P. Collman, L. Fu, P. C. Herrmann and X. Zhang, *Science*, 1997, **275**, 949.

12 J. P. Collman, M. Rapta, M. Broring, L. Raptova, R. Schwenninger, B. Boitrel, L. Fu and M. L'Her, *J. Am. Chem. Soc.*, 1999, **121**, 1387.

13 S. Yoshikawa, K. ShinzawaItoh, R. Nakashima, R. Yaono, E. Yamashita, N. Inoue, M. Yao, M. J. Fei, C. P. Libeu, T. Mizushima, H. Yamaguchi, T. Tomizaki and T. Tsukihara, *Science*, 1998, **280**, 1723.

Communication 9/03257F

ChemComm

An efficient synthesis of CMP-3-fluoroneuraminic acid

Michael D. Burkart, Stéphane P. Vincent and Chi-Huey Wong*

Department of Chemistry and The Skaggs Institute for Chemical Biology , The Scripps Research Institute, 10550 N. Torrey Pines Road, La Jolla, CA 92037, USA. E-mail: wong@scripps.edu

Received (in Corvallis, OR, USA) 27th April 1999, Accepted 23rd June 1999

CMP-3-fluoroneuraminic acid, a useful mechanistic probe for sialyltransferases, has been efficiently synthesized using recent fluorination and phosphorylation techniques from a sialic acid glycal.

Sialic acids displayed on the surface of mammalian cells are involved in many cell–surface interactions including cell–cell recognition processes, cell adhesion, and viral receptor recognition.[1,2] Sialyltransferases are the enzymes responsible for transfer of sialic acid from cytidine 5′-monophospho-*N*-acetylneuraminic acid (CMP-Neu5Ac) to a growing oligosaccharide, often terminating the series at the non-reducing end.[3] We recently synthesized the nucleotide phosphate sugars of fucose and galactose fluorinated α to the anomeric carbon that demonstrated significant competitive inhibition against the respective fucosyl- and galactosyl-transferase enzymes. These results, together with isotope studies, are indicative of substantial oxocarbenium ion transition state structure.[4,5] The effect of fluorine is attributed to its strong electron-withdrawing nature which destabilizes formation of positive charge within the carbohydrate ring. Though several substrate analog inhibitors have recently been designed to effectively inhibit α(2,6)-sialyltransferase,[6–9] a cationic transition state structure has not yet been demonstrated in mechanistic studies. Only solvolysis of CMP-Neu5Ac has been shown to display a finite sialyl cation species.[10] Additionally, *N*-acetyl-3-fluoroneuraminic acid (3F-Neu5Ac) alone serves as a competitive inhibitor of bacterial and viral sialidases.[11–13] Therefore, a fluorinated CMP-Neu5Ac derivative would be expected to inhibit sialyltransferases as a non-reactive mechanism-based inhibitor if the enzyme catalyzes formation of a cationic transition state species in the donor glycon. Such inhibition by a fluorinated substrate analog would extend the cationic transition state phenomenon to sialyltransferase enzymes, as has been demonstrated with other glycosyltransferases. Here we describe the synthesis of cytidine 5′-monophospho-*N*-acetyl-3-fluoroneuraminic acid **1**, which employs a fluorine subsituent α to the anomeric carbon on the neuraminic acid, and demonstrate its competitive inhibition of α(2,6)-sialyltransferase in the presence of CMP-Neu5Ac.

Previous syntheses of *N*-acetyl-3-fluoroneuraminic acid have relied upon fluorination of the glycal of peracetyl-*N*-acetylneuraminic acid methyl ester **2** with XeF_2–BF_3•OEt_2[12] or molecular fluorine.[13] The reported overall yield of this method gives less than 20% of the fluorinated monosaccharide in several steps from the sialic acid methyl ester. With the recent development of a one-pot, high-yielding fluorination technique using F–TEDA–CH_2Cl•$2BF_4$ (Selectfluor), the 2-hydroxy-3-fluoro protected monosaccharide **3** is available in 80% yield from the glycal.[14] Unlike previous methods, the fluorinated product retains all protecting groups from the glycal starting material, leaving a deprotected hydroxy at the anomeric position that is ready for selective chemical modification. This technique uniquely solves problems associated with the synthesis of **1**, as 3F-Neu5Ac is not a substrate of CMP-Neu5Ac synthase (EC 2.7.7.43), which converts Neu5Ac and cytidine-5′-triphosphate to CMP-Neu5Ac.[15] Hence, synthesis of the fluorinated CMP-Neu5Ac derivative must proceed *via* chemical methods. Conveniently, an improved synthesis of CMP-Neu5Ac and its conjugates was recently published enumerating a four step strategy from the 2-OH protected monosaccharide.[16] Combination of these two techniques with a new method to synthesize the glycal are reported here to synthesize **1**.

The known protected sialic acid glycal **2** was prepared directly from the peracetylated neuraminic acid (Scheme 1).[17] The described procedure utilizing TMSOTf in MeCN[18] led generally to a mixture of glycal **2** (65%) along with the 2,3-dehydro-4,5-oxazoline **2a**.[19,20] We found that the use of a catalytic amount of PPh_3HBr[21] in place of TMSOTf gave **2** in nearly quantitative yield (96%) without detectable cyclized product.

The glycal **2** was fluorinated with F–TEDA–BF_4 following the general glycal fluorination procedure in DMF and H_2O (Scheme 2).[14] Purification by silica gel chromatography yields **3** in 80% yield (3 : 1 F_{ax}/F_{eq}). The 2-*O*-acetylated derivative of this molecule and the fully deacetylated 3-fluoro-Neu5Ac have been previously characterized and were demonstrated to contain β anomeric configuration based upon no ^{13}C–^{19}F coupling between C1 and F3.[13] For this reason as well as an established anomeric effect for sialic acid[22] and the yield of only one stereoisomer from this reaction, we concluded **3** to be in the pure β form.

Compound **3** (F_{ax}) was condensed with phosphoramidite **6**[16] in MeCN followed by quench with Et_3N. The product was purified by Dowex LH-20 size-exclusion chromatography in MeCN to give the protected phosphite **4** in 54% yield.[23] Anomeric stereochemistry was determined to retain β configuration by ^{13}C–^{19}F coupling between C1 and F3 (0 Hz) and by the chemical shift of H3 deviating less than 0.1 ppm from **3**. Anomerization is well known to give rise to significant chemical shift at H3.[24] Furthermore, only one stereochemical isomer was isolated.

The phosphite **4** was oxidized to the phosphate with *tert*-butyl hydroperoxide and deprotected with $Pd(PPh_3)_4$ and Pr^i_2NH. Silica gel chromatography gave **5** in 72% yield.[25] Deprotection of the methyl ester with NaOMe in MeOH was followed by immediate size-exclusion chromatography in water. The product was deacetylated with 1 M NaOH and subsequently purified

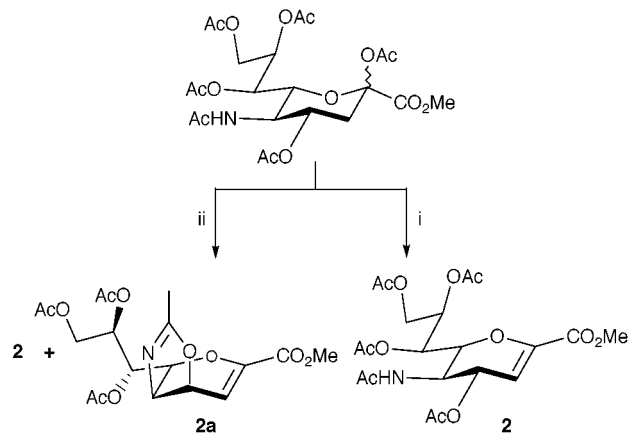

Scheme 1 *Reagents and conditions*: i, PPh_3HBr, MeCN, 96%; ii, TMSOTf, MeCN.

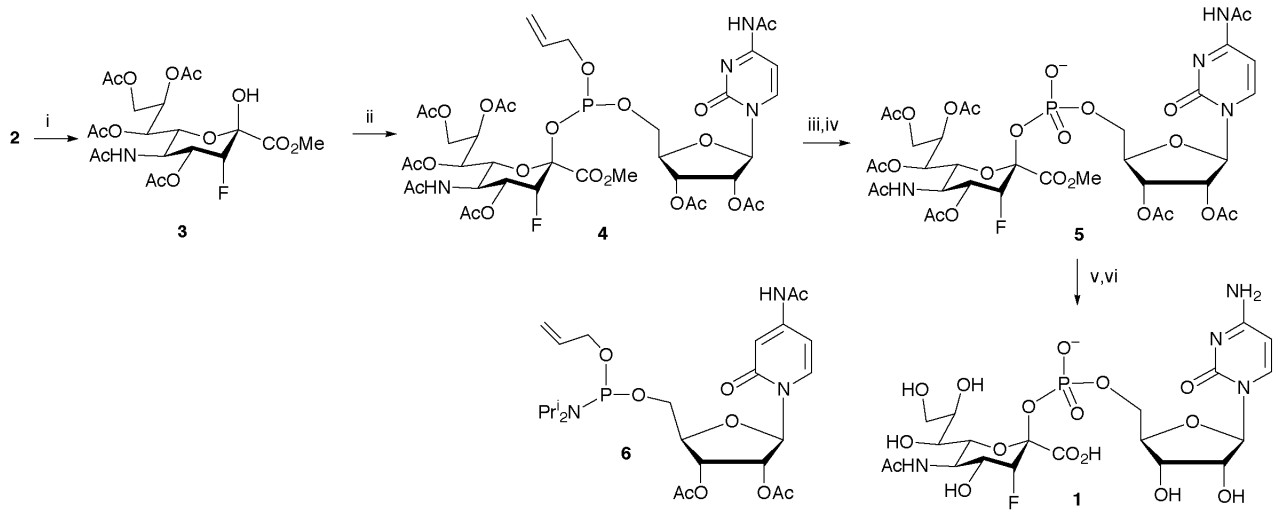

Scheme 2 *Reagents and conditions*: i, Selectfluor, DMF–H_2O (3 : 1), 60 °C, 80%; ii, **6**, 1*H*-tetrazole, MeCN, −78 °C→room temp., 60%; iii, Bu^{t}OOH, Et_3N; iv, $Pd(PPh_3)_4$, Pr^i_2NH, 72% for 2 steps; v, NaOMe, MeOH; vi, NaOH, 80% for 2 steps.

by aqueous size-exclusion chromatography to provide **1** in 80% yield over two steps.[26]

Compound **1** was assayed as an inhibitor of α(2,6)-sialyltransferase (Calbiochem, San Diego, CA) using standard radioisotopic assay procedures. These results show that **1** competes with CMP-Neu5Ac for the enzyme with K_i = 5.7 ± 1.2 μM.[27] Compared to the K_m for CMP-Neu5Ac of 15 μM, this result is consistent with a transition state structure containing considerable oxocarbenium ion characteristic.[5]

Notes and references

1 M. von Itztein and R. J. Thomson, *Curr. Med. Chem.*, 1997, **4**, 185.
2 S. Kelm and R. Schauer, *Int. Rev. Cytol.*, 1997, **175**, 137.
3 A. Harduin-Lepers, M. A. Recchi and P. Delannoy, *Glycobiology*, 1995, **5**, 741.
4 T. Hayashi, B. Murray, R. Wang and C.-H. Wong, *Bioorg. Med. Chem.*, 1997, **5**, 497.
5 B. W. Murray, V. Wittmann, M. D. Burkart, S.-C. Hung and C.-H. Wong, *Biochemistry*, 1997, **36**, 823.
6 B. Muller, C. Schaub and R. R. Schmidt, *Angew. Chem., Int. Ed.*, 1998, **37**, 2893.
7 B. Muller, T. J. Martin, C. Schaub and R. R. Schmidt, *Tetrahedron Lett.*, 1998, **39**, 509.
8 Y. Kajihara, H. Hashimoto, H. Kodama, T. Wakabayashi and K. Sato, *J. Carbohydr. Chem.*, 1993, **12**, 991.
9 Y. Kajihara, K. Kodama, T. Wakabayashi, K. Sato and H. Hashimoto, *Carbohydr. Res.*, 1993, **247**, 179.
10 B. A. Horenstein and M. Bruner, *J. Am. Chem. Soc.*, 1996, **118**, 10371.
11 T. Hagiwara, I. Kijima-Suda, T. Ido, H. Ohrui and K. Tomita, *Carbohydr. Res.*, 1994, **263**, 167.
12 C. R. Petrie, III., M. Sharma, O. D. Simmons and W. Korytnyk, *Carbohydr. Res.*, 1989, **186**, 326.
13 T. Nakajima, H. Hori, H. Ohrui, H. Meguro and T. Ido, *Agric. Biol. Chem.*, 1988, **52**, 1209.
14 M. D. Burkart, Z. Zhang, S.-C. Hung and C.-H. Wong, *J. Am. Chem. Soc.*, 1997, **119**, 11743 for synthesis of **3**.
15 J. L.-C. Liu, G.-J. Shen, Y. Ichikawa, J. F. Rutan, G. Zapata, W. F. Vann and C.-H. Wong, *J. Am. Chem. Soc.*, 1992, **114**, 3901.
16 M. D. Chappell and R. L. Halcomb, *J. Am. Chem. Soc.*, 1997, **119**, 3393 for synthesis and application of **6**.
17 A. Marra and P. Sinay, *Carbohydr. Res.*, 1989, **190**, 317.
18 K. C. Nicolaou, C. W. Hummel and Y. Iwabuchi, *J. Am. Chem. Soc.*, 1992, **114**, 3126.
19 V. Kumar, J. Kessler, M. E. Scott, B. H. Pathwarden, S. W. Tannenbaum and M. Flashner, *Carbohydr. Res.*, 1981, **94**, 123.
20 E. Schreiner, E. Zbiral, R. G. Kleineidam and R. Schauer, *Liebigs Ann. Chem.*, 1991, **1991**, 129.
21 V. Bolitt, C. Mioskowski, S.-G. Lee and J. R. Falck, *J. Org. Chem.*, 1990, **55**, 5812.
22 H. Ogura, K. Furuhata, H. Saito, G. Izumi, M. Itoh and Y. Shitori, *Chem. Lett.*, 1984, 1003.
23 *Selected data* for **4**: δ_H(400 MHz, $CDCl_3$) 8.95 (s, 1H), 7.66 (*J* 7.2, 1H), 7.60 (d, *J* 10, 1H), 7.45 (*J* 7.6, 1H), 5.95–5.84 (m, 1H), 5.73 (*J* 3.4, 1H), 5.67-5.62 (m, 3H), 5.52–5.55 (m,, 1H), 5.30 (dd, *J* 1.5, 17.1, 1H), 5.20–5.16 (m, 2H), 5.06 (d, *J* 2.2, 51.6, 1H), 4.67 (d, *J* 2.6, 12.0, 1H), 4.41–4.33 (m, 6H), 4.22–4.18 (m, 2H), 4.09 (dd, *J* 8.5, 12.1, 1H), 3.81 (s, 3H), 2.22 (s, 3H), 2.19 (s, 3H), 2.10 (s, 3H), 2.07 (s, 3H), 1.96 (s, 3H), 1.91 (s, 3H), 1.85 (s, 3H); δ_F (376 MHz, $CDCl_3$) −180.40 (dd).
24 U. Dabrowski, H. Friebolin, R. Brossmer and M. Supp, *Tetrahedron*, 1979, **48**, 4637.
25 *Selected data* for **5**: δ_H(400 MHz, $CDCl_3$) 8.33 (d, *J* 6.0, 1H), 7.38 (d, *J* 5.8, 1H), 6.33 (d, *J* 4.9, 1H), 5.53–5.43 (m, 3H), 5.29 (dd, *J* 9.3, 11.5, 1H), 5.03 (d, *J* 50.2, 1H), 4.80 (dd, *J* 2.6, 12.1, 1H), 4.53 (dd, *J* 10.5, 21.0, 1H), 4.48–4.43 (m, 1H), 4.29–4.21 (m, 3H), 3.82 (s, 3H), 2.22 (s, 3H), 2.16 (s, 3H), 2.10 (s, 3H), 2.08 (s, 3H), 2.04 (s, 3H), 1.99 (s, 3H), 1.86 (s, 3H); δ_F(376 MHz, $CDCl_3$) −179.80 (dd); LRMS (M + Cs) calc. for $C_{35}H_{45}FN_4O_{23}PCs$, 1073; found 1073.
26 *Selected data* for **1**: δ_H(400 MHz, $CDCl_3$) 7.96 (d, *J* 7.7, 1H), 6.06 (d, *J* 7.7, 1H), 5.83 (d, *J* 4.4, 1H), 4.23 (t, *J* 5.0, 1 H), 4.19 (t, *J* 4.7, 1H), 4.16 (m, 2H), 4.13 (m, 1H), 4.08–4.01 (m, 2H), 3.97 (dd, *J* 9, 11.7, 1H), 3.76 (m, 2H), 3.72 (dd, *J* 2.5, 11.9, 1H), 3.47 (dd, *J* 6.44, 1.7, 1H), 3.29 (d, *J* 9.1, 1H), 1.90 (s, 3H), 1.90 (d, *J* 40, 1H); δ_F(376 MHz, $CDCl_3$) −194.02 (dd, *J* 11.0, 49.0); LRMS (M + Na) calc. for $C_{20}H_{30}FN_4O_{16}PNa$, 655.1276; found 655.
27 J. Weinstein, U. deSousa-e-Silva and J. C. Paulson, *J. Biol. Chem.*, 1982, **257**, 13825.

Communication 9/03362I

ChemComm

Urea–picoline *N*-oxide (4:2) cocrystal: an unusual channel inclusion compound

Veneta Videnova-Adrabińska* and Elżbieta Janeczko

Institute of Inorganic Chemistry and Metallurgy of Rare Elements, Wrocław University of Technology, 23 Smoluchowskiego St. 50 370 Wrocław, Poland. E-mail: veneta@ichn.ch.pwr.wroc.pl

Received (in Oxford, UK) 26th April 1999, Accepted 28th June 1999

The crystal structure of urea–picoline *N*-oxide cocrystal reveals urea channel formation in which two independent picoline *N*-oxide molecules are stacked with their charge-transfer axes aligned approximately at 60° toward the crystallographic *b*-axis.

In the classical urea inclusion compounds[1–3] the host structure comprises an extensive hydrogen-bonded array of urea molecules, giving rise to parallel chains (with an internal diameter of 5.3–5.7 Å) within which the guest molecules are densely packed. The X-ray structural characterisation confirmed that the vast majority of urea inclusion compounds are incommensurate, that is no small integers m and n exist to satisfy $mc_h = nc_g$, where c_h and c_g are the host and guest repeat distance along the channel axis. Unusual inclusion compounds are formed by urea and sebaconitrile[4] (6 urea:1 guest) and undecane-2,10-dione (9 urea:1 guest),[5] in which additionally hydrogen-bond interactions appear between the host and the guest molecules. Urea also forms many inclusion compounds with the incorporation of other molecular species as additional building blocks of their hydrogen-bonded host lattices as for example halides and pseudohalides, planar oxoanions, dihydrogen orthoborate $BO(OH)_2$ and allophanate ion $NH_2CONHCO_2^-$, spirocyclic pentaborate anion $[B_5O_6(OH)_4]^-$, and tetra-*n*-propylammonium halides.[6] Thus far, with the exception of urea inclusion complexes with trioxane,[7] undecan-5-one[8] and with certain short-chain α,ω-dihaloalkanes and dicarboxylic acids,[9] virtually all urea inclusion compounds are incommensurate, where the repeat distance of host and guest along the channel is a common factor, and the guest molecules pack within van der Waals contact of each other. In some cases, particularly at low temperatures, the host structure becomes slightly distorted from the conventional hexagonal tunnel structure, but the repeat length along the channel axis is uniformly close to the standard value of 11.0 Å.[2] If a guest species cannot be accommodated by the conventional hexagonal channel, it is ordinarily not included within urea,[10] and either separate phases or specific cocrystals[11] are formed. Recent reviews[12,13] summarise the present level of understanding of the structural and dynamic properties of urea and thiourea channel inclusion compounds.

We now report the X-ray single crystal structure† of a novel channel inclusion compound formed by urea and picoline *N*-oxide molecules (4 urea:2 guest). Nice transparent rectangular plates of significant sizes were obtained by the slow evaporation method from a methanol solution of urea and picoline *N*-oxide (T_m 146–148 °C).‡ The crystal structure comprises two independent picoline *N*-oxide molecules, each lying on a mirror plane, and four independent urea molecules forming host channels in which the guests are imbedded. The IR spectra§ of the crystal are qualitatively different from the spectra of the substituents and reflect the formation of a hydrogen-bonded network, substantially different from that in the urea crystal. The splitting of the ring C–C and C–H modes in the regions 1450–1500 cm^{-1}, 1150–1250 cm^{-1}, 1000–1050 cm^{-1} and 750–760 cm^{-1}, as well as of the CH_3 stretching and deformation modes (3000–3130 cm^{-1} and 1370–1460 cm^{-1}), reflects the presence of two independent picoline *N*-oxide molecules. On the other hand, the significant changes (band broadening, multiplication and wavenumber shift) observed in the regions of νNH_2 and δNH_2 modes (3450–3000 and 1600–1700 cm^{-1}) are consequential to the hydrogen-bond modification in the new channel arrays. However, the most spectacular changes are observed in the region 750–500 cm^{-1}, where several new bands appear, each of which is doubly split. This region is not well understood now and requires further investigation, but it very probably has something to do with the formation of hydrogen bonds toward the picoline O21 oxygen atom.

The 1D hydrogen-bonded arrays are extended explicitly through $N–H_{syn}\cdots O{=}C$. Each pair of urea molecules assigned as U1–U3 and U2–U4 (related *via* screw rotation along the *z*-axis) form hydrogen-bonded ring motifs $R_2^2(8)$ which are further propagated to form molecular tapes running along the *a*-crystallographic axis. Distortions from planarity allow for mutual topological, geometrical and sterical adaptation and recognition of the hydrogen-bond donor and acceptor sites, left unused in the tape formation, in order to zip each two neighbouring tapes at 1/2a, 3/2a, 5/2a, *etc.* *via* four $N–H_{anti}\cdots O$ bonds with the resultant formation of a strongly folded 2D hydrogen-bond arrangement of the host lattice (see Chart 1a).

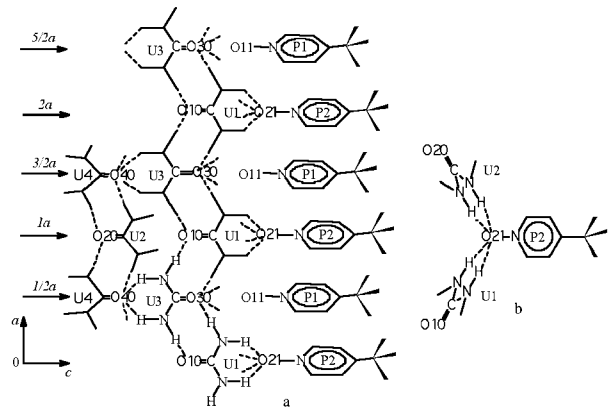

Chart 1

The dihedral angle between the zipped tapes is *ca.* 120°. The fourfold accessibility of O30 and O40 for hydrogen bonds is a rare phenomenon, so far noted only in urea crystals. This fact suggests that the two electron pairs on the urea oxygen are delocalised on a cone surface. The four hydrogen bonds toward the urea O30 and O40 adapt a pyramidal configuration. The other two oxygens O10 and O20 from U1 and U2 are imbedded in the tapes and are not accessible for additional hydrogen bonds.

The two independent picoline *N*-oxide molecules assigned as P1 and P2 are stacked in the host channels of urea with a repeat distance of 3.55 Å between the aromatic ring planes and densely fill the empty space. However, the bound mechanism toward the host lattice is diverse for the guests P1 and P2. Four $N–H_{anti}$ donors from U1 and U2 project the O21 atoms located on P2 in order to form four hydrogen bonds with a pyramidal configuration (see Chart 1b). The dihedral angle between the planes of two pairs of hydrogen bonds toward O21, donated by U1 and U2 is 120°. Thus, each two neighbouring tapes are hinged on the P2 molecules at 1a, 2a, 3a *etc.*, completing the 3D hydrogen-bonded network (Chart 1 and Table 1). The three-dimensional

Table 1 Hydrogen bond geometries and hydrogen bond patterns in urea picoline *N*-oxide (4:2) cocrystal

Hydrogen bonds	D–H···A/ Å	H···A/ Å	Symmetry operator
host interactions			
U1–U3 tape			
N30–H1(N30)···O10	2.920(9)	2.05(4)	*x*, *y*, *z* 2 − *x*, *y*, *z*
N10–H1(N10)···O30	2.991(9)	2.04(8)	*x*, *y*, *z*
U2–U4 tape			
N20–H1(N20)···O40	3.016(9)	2.17(4)	*x*, *y*, *z*
N40–H1(N40)···O20	2.926(9)	2.12(4)	*x*, *y*, *z* 2 − *x*, *y*, *z*
U3–U4 intertape			
N40–H2(N40)···O30	3.021(5)	2.15(4)	*x*, −1 + *y*, *z* 1 − *x*, −1 + *y*, *z*
N30–H2(N30)···O40	2.969(5)	2.15(4)	1 − *x*, 2 −*y*, − 5 + *z*
host–guest interactions			
N20–H2(N20)···O21	2.994(5)	2.24(3)	*x*, *y*, *z* 2 − *x*, *y*, *z*
N10–H2(N10)···O21	2.994(5)	2.25(4)	*x*, *y*, *z* 2 − *x*, *y*, *z*

crystal structure can be considered as consisting of urea channels running along the *a*-axis, in which the P2 molecules are hydrogen-bond fixed perpendicularly to the urea chains, padlocking large cavities where the other guests P1 are simply trapped. Despite the similar geometry of both guest molecules, the topology of the host lattice dictates different including mechanism and the P1 molecules intercalate (at 1/2a, 3/2a *etc*.) between the P2 molecules residing the empty spaces in between. The acceptor site O11 on the P1 molecule is imbedded in the O10 and O20 electron rich environment, lacking free hydrogen-bond donors. However, neither the repulsive forces between the P1 guests and U host lattice nor the dipole–dipole interactions between the P1 and P2 are strong enough to overcome the hydrogen bond interactions confining the cavity size. So, the P1 molecules, though not specifically bonded to the host, are only free to some librational motions. The sublimation process in the temperature range 100–140 °C may be explained with a partial breaking of the hydrogen bond lattice and leaving of the P1 molecules. As a result of this unusual channel inclusion mechanism, both guest molecules P1 and P2 are aligned almost in the same way in the host lattice (see Fig. 1). Their charge-transfer (CT) axes are directed approximately at 60° toward the optical *b*-axis, which is very close to the optimal molecular orientation for bulk phase-matching in the *mm*2 space group.[14] The crystal passes positively a second harmonic generation test yielding a signal 1.5 times higher than that of urea.

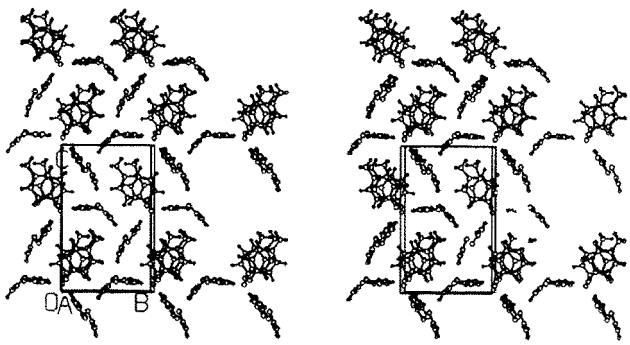

Fig. 1

Notes and references

† *Crystal data*: $C_8H_{15}O_3N_5$, M_r = 229.24 g mol^{-1}, white prism, (0.60 × 0.50 × 0.30 mm), orthorhombic, space group $Pmc2_1$ (no. 26) a = 7.09(3), b = 10.065(3), c = 16.267(4) Å, V = 1162(6) Å^3, Z = 4, D_c = 1.311 Mg m^{-3}, T = 297 K, $F(000)$ = 488, μ(Mo-Kα) = 0.096 mm^{-1}; 3055 measured reflections ($20.28 < 2\theta < 47.14°$), 1649 unique reflections (R_{int} = 0.017); refinement on F for 1139 observed reflections ($I > 2.00\ \sigma(I)$), and 210 variable parameters, R = 0.043, wR = 0.048. CCDC 182/1306. See http://www.rsc.org/suppdata/cc/1999/1527/ for crystallographic data in .cif format.

‡ The crystal sublimes at temperatures higher than 100 °C and melts at 146–148 °C. At 170 °C it starts to boil.

§ Solid state IR spectra were measured on a Nicolet FT-IR spectrometer as Nujol mulls.

1 A. E. Smith, *Acta Crystallogr*., 1952, **5**, 224.

2 K. D. M. Harris and J. M. Thomas, *J. Chem Soc*., *Faraday Trans*., 1990, **86**, 2985; K. D. M. Harris and M. D. Hollingsworth, *Proc. R. Soc. London, Ser. A*, 1990, **431**, 245.

3 K. D. M. Harris, S. P. Smart and M. D. Hollingsworth, *J. Chem. Soc., Faraday Trans*., 1991, **87**, 3423.

4 M. D. Hollingsworth, B. D. Santarsiero and K. D. M. Harris, *Angew. Chem., Int. Ed. Engl*., 1994, **33**, 649.

5 M. E. Brown and M. D. Hollingsworth, *Nature*, 1995, **376**, 323.

6 T. C. W. Mak and R. K. McMullan, *J. Inclusion Phenom*., 1988, **6**, 473; Q. Li, W. H. Yip and T. C. W. Mak *J. Inclusion Phenom*., 1995, **23**, 233; T. C. W. Mak, W. H. Yip and Q. Li, *J. Am. Chem. Soc*., 1995, 117, 11995; Q. Li and T. C. W. Mak, *Supramol. Chem*., 1996, **8**, 73; Q. Li and T. C. W. Mak, *Supramol. Chem*., 1997, **8**, 73; Q. Li and T. C. W. Mak, *Acta Crystallogr., Sect. B*, 1998, **54**, 180.

7 R. Claude, R. Clement and A. Dworkin, *J. Chem Thermodyn*., 1977, **9**, 1199; R. Clement, C. Mazieres and L. Guibe, *J. Solid State Chem*., 1972, **5**, 436.

8 M. D. Hollingsworth and C. R. Goss, *Mol. Cryst. Liq. Cryst*., 1992, **219**, 43.

9 J. Otto, *Acta Crystallogr., Sect. B*, 1972, **28**, 543; A. E. Aliev, S. P. Smart, I. J. Shanon and K. D. M. Harris, *J. Chem. Soc., Faraday Trans*., 1996, **92**, 2179; V. Videnova-Adrabińska, *The Hydrogen Bond as a Design Element of the Crystal Architecture. Crystal Engineering*, TUW, Wrocław, Poland, 1994.

10 K. Takemoto and N. Sonoda, in *Inclusion Compounds*, vol. 2, ed. J. L. Atwood, J. E. Davies and D. D. MacNicol, Academic Press, Orlando, FL, USA, 1984, p. 47.

11 M. D. Hollingsworth, B. D. Santarsiero, H. Oumar-Mahamat and C. J. Nichols, *Chem. Mater*., 1991, **3**, 23; X. Zhao, Y.-L. Chang, F. W. Fowler and J. W. Lauher, *J. Am. Chem. Soc*., 1990, **112**, 6627; V. Videnova-Adrabińska, *J. Mater. Chem*., 1995, **5**, 2309; *J. Mol. Struct*., 1996, **374**, 199.

12 K. D. M. Harris, *J. Mol. Struct*., 1996, **374**, 241.

13 M. D. Hollingsworth and K. D. M. Harris, in *Comprehensive Supramolecular Chemistry*, vol. 6, ed. J. L. Atwood, J. E. D. Davies, D. MacNicol, F. Vögtle, F. Toda and R. Bishop, Pergamon, Oxford, 1996.

14 Bulk-phase matching is defined by the angle α between the CT axis and the principle dielectric axis. For more information see: J. Zyss and J. L. Oudar, *Phys. Rev*., 1982, **A26**, 2028; J. Zyss and D. S. Chemla, in *Nonlinear Optical Properties of Organic Molecules and Crystals*, vol. 1, ed. D. S. Chemla and J. Zyss, 1987, Academic Press. For optimal molecular orientations and phase-matching configurations see Figure 16 and Table XIV therein.

Communication 9/03602D

Single-electron reduction of C_{60} with a carbon radical: formation of the Crystal Violet cation–fulleride ion salt†

Toshikazu Kitagawa,* Yangsoo Lee and Ken'ichi Takeuchi*

Department of Energy and Hydrocarbon Chemistry, Graduate School of Engineering, Kyoto University, Sakyo-ku, Kyoto 606-8501, Japan. E-mail: kitagawa@scl.kyoto-u.ac.jp

Received (in Cambridge, UK) 17th May 1999, Accepted 5th July 1999

Whereas many carbon radicals are known to add to C_{60}, the reaction of Crystal Violet radical $\mathbf{1}^{\bullet}$ with C_{60} resulted in single-electron transfer, leading to a carbocation–carbanion salt $\mathbf{1}^{+}C_{60}^{\bullet-}$: the product was isolated as microcrystalline powder and was characterized by EPR, VIS-NIR and NMR spectroscopy.

The addition of radicals to buckminsterfullerene (C_{60}) to give fullerenyl radicals constitutes a well-known and characteristic reaction. The addition of reactive carbon-centered radicals, such as alkyl, benzyl and haloalkyl radicals and some heteroatom-centered radicals, to C_{60} has been reported to produce $RC_{60}^{\bullet}$ as well as multiple-addition fullerenyl radicals.[1] The high affinity of C_{60} toward radicals has been demonstrated by its ability to absorb up to 34 methyl radicals,[2] 15 benzyl radicals,[2] 11 phenyl radicals,[3] and 16 perfluoroethyl radicals.[4] Another possibility in the reaction of an alkyl radical with C_{60} is electron transfer from the radical to C_{60}. Such a reaction, which, to the best of our knowledge, has not been reported, would be expected to occur if the reducing power of the radical is sufficiently strong to reduce C_{60}. We report herein the single-electron reduction of C_{60} with the Crystal Violet radical $\mathbf{1}^{\bullet}$ and the isolation of the product $\mathbf{1}^{+}C_{60}^{\bullet-}$ as a solid (Scheme 1).

For stoichiometric single-electron transfer from a carbon-centered radical $R^{\bullet}$ to C_{60} without a subsequent redox or chemical process, the following requirements must be fulfilled. First, the oxidation potential of $R^{\bullet}$ must be more negative than the first reduction potential of C_{60} (−1.09 V *vs.* Fc/Fc^{+}),[5] but not more negative than the second reduction potential (−1.48 V *vs.* Fc/Fc^{+}).[5] Considering the effective delocalization of the positive charge in $\mathbf{1}^{+}$ over three nitrogen atoms, one would expect that the corresponding radical $\mathbf{1}^{\bullet}$ would be readily oxidized. Cyclic voltammetry for $\mathbf{1}^{+}I^{-}$ indicates that the $\mathbf{1}^{\bullet}/\mathbf{1}^{+}$ redox couple has a potential of −1.19 V *vs.* Fc/Fc^{+} in PhCN, which is midway between the first and second reduction potentials, thus allowing a complete single-electron reduction to give $C_{60}^{\bullet-}$ but no further electron transfer to C_{60}^{2-}.[6] Secondly, the ions produced by the electron transfer, R^{+} and $C_{60}^{\bullet-}$, should be sufficiently stable so as not to react with each other. Although carbocations and carbanions have a strong tendency to combine to form neutral molecules, we have earlier reported that a highly stabilized carbocation with a $pK_{R^{+}}$ of 7.29–13.6 and a carbanion whose conjugate acid has a pK_a of 5.7–5.9 can, in fact, coexist in solution and in the solid state, without cation–anion coordination.[8] The reported $pK_{R^{+}}$ of $\mathbf{1}^{+}$ (9.36[9]) and the pK_a of the conjugate acid of $C_{60}^{\bullet-}$ (3.4–9.0[10]) led to the prediction that these ions are sufficiently stable to allow the formation of a stable salt, $\mathbf{1}^{+}C_{60}^{\bullet-}$, rather than a neutral radical, $\mathbf{1}$–$C_{60}^{\bullet}$. In addition, the formation of such a bond would be severely hindered, because of the repulsion between the aromatic rings of $\mathbf{1}^{+}$ and the fullerene cage.

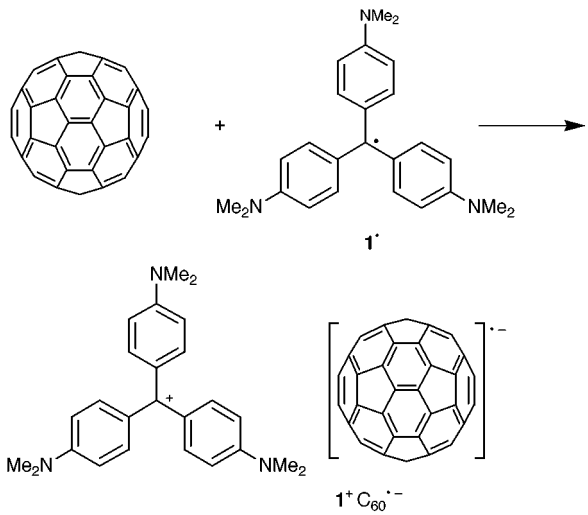

Scheme 1

Radical $\mathbf{1}^{\bullet}$ can be quantitatively generated by the reduction of the Crystal Violet cation $\mathbf{1}^{+}$ with zinc.[11] Unlike the unsubstituted triphenylmethyl radical, this radical does not dimerize but persists in solution.[12] All the procedures for the preparation of $\mathbf{1}^{+}C_{60}^{\bullet-}$ and spectroscopic analysis of the product were carried out under degassed conditions using a glass apparatus connected to a high-vacuum line ($< 10^{-4}$ mmHg). The apparatus contains two chambers, one for the preparation of $\mathbf{1}^{\bullet}$ and the other for the reduction of C_{60}. The two chambers are separated by a sintered glass frit, and to the latter is connected a tube or a cell for spectroscopic analysis of the product. In a typical experiment, $\mathbf{1}^{\bullet}$ was prepared by the treatment of anhydrous Crystal Violet iodide (2.05 mg) with zinc powder (93 equiv.) in 0.1 ml of pyridine. The zinc iodide was precipitated as the pyridine complex by diluting the reaction mixture with hexane (1.2 ml). The resulting red solution of $\mathbf{1}^{\bullet}$ was then transferred to the other chamber, which contained a CS_2 solution (5 ml) of C_{60} (2.86 mg, 0.97 equiv.). The salt $\mathbf{1}^{+}C_{60}^{\bullet-}$ was immediately precipitated from the mixed solution as red–brown microcrystalline powder, which was collected on the sintered glass frit and washed three times with small amounts of CS_2. Elemental analysis of the crystals[13] showed a nitrogen content of 3.50%, a value close to that calculated for $\mathbf{1}^{+}C_{60}^{\bullet-}$ (3.84%), consistent with the 1:1 molar ratio of the Crystal Violet moiety and the C_{60} component.

The EPR spectrum for a powder sample showed a broad single line (g = 1.999, peak-to-peak width 2.9 mT at 20 °C). The signal intensity, relative to a known amount of external standard, 4-hydroxy-TEMPO, indicated that the solid contained 90 ± 10% of the theoretical amount of unpaired spins. A THF solution of the solid material showed spectra typical of the fullerene anion (Fig. 1). A broad signal (peak-to-peak width *ca.* 9 mT) with a superimposed spike (peak-to-peak width 1 mT, g = 2.000) was observed at room temperature; the former became narrower with decreasing temperature. These observations are all in agreement with the behavior of the $C_{60}^{\bullet-}$ signal reported earlier.[14,15]

A ^{1}H NMR spectrum, taken in CD_2Cl_2, showed the presence of $\mathbf{1}^{+}$ and the corresponding alcohol **1**–OH in 41:59 molar ratio.

† Experimental details and the ^{1}H NMR data for $\mathbf{1}^{+}C_{60}^{\bullet-}$ are available as supplementary data from the RSC web site, see http://www.rsc.org/suppdata/cc/1999/1529/

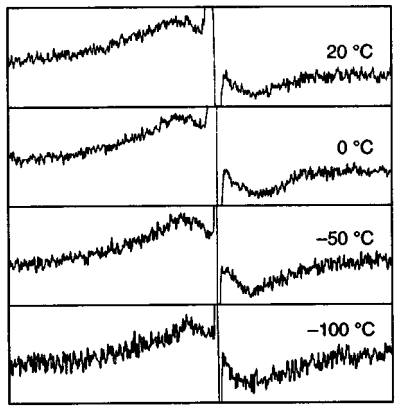

Fig. 1 X-Band EPR spectra of $\mathbf{1}^{+}C_{60}^{\bullet-}$ in THF recorded at 0.6 mW microwave power, 0.4 mT modulation and 50 mT sweep width.

The signals of $\mathbf{1}^{+}$ were significantly broadened, probably due to the paramagnetism of $C_{60}^{\bullet-}$. Hydrolysis by a trace amount of water in the solvent appears to be responsible for the formation of alcohol, indicating that the salt $\mathbf{1}^{+}C_{60}^{\bullet-}$ is extremely moisture-sensitive. This is in contrast to the fact that the other Crystal Violet salts, *e.g.* $\mathbf{1}^{+}Cl^{-}$, are stable in water. The difference may be explained by the higher basicity of $C_{60}^{\bullet-}$ compared with Cl^{-} and the dimerization of the resulting radical $HC_{60}^{\bullet}$ (Scheme 2).[16]

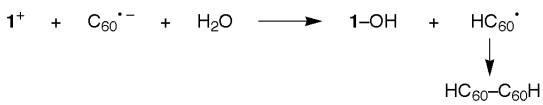

Scheme 2

The VIS-NIR spectrum of a THF solution of $\mathbf{1}^{+}C_{60}^{\bullet-}$ exhibited absorption maxima which were characteristic of $\mathbf{1}^{+}$ and $C_{60}^{\bullet-}$ at 593 and 1074 nm, respectively (Fig. 2). The latter absorption band had a substructure identical with that reported for $C_{60}^{\bullet-}$.[15,17] Based on the molar absorptivity of $\mathbf{1}^{+}$ at 593 nm (1.05×10^{5} M^{-1} cm^{-1}) and assuming a 1 : 1 composition of $\mathbf{1}^{+}$ and $C_{60}^{\bullet-}$,[18] the molar absorptivity of $C_{60}^{\bullet-}$ at 1074 nm was calculated to be 1.96×10^{4} M^{-1} cm^{-1}, which is comparable with reported values of $1.20–2.00 \times 10^{4}$ M^{-1} cm^{-1}.[15c,17] The observed absorption line shape is in agreement with the sum of the independently measured absorptions of $\mathbf{1}^{+}$ and $C_{60}^{\bullet-}$. No significant decay of absorbance was observed, indicating the absence of charge recombination. Charge-transfer type interaction is also unlikely, since no absorption band indicative of a charge-transfer complex was observed.

The above experiments clearly demonstrated that C_{60} undergoes single-electron reduction by an electron-rich, sterically protected radical $\mathbf{1}^{\bullet}$. The product, $\mathbf{1}^{+}C_{60}^{\bullet-}$, is stable both in solution and in the solid state, providing a new isolated carbocation–carbanion salt. Thus, the possibility of electron-transfer in the reaction of organic radicals to C_{60} has been demonstrated as an alternative to the addition to C_{60}, which is usually observed for reactive radicals.

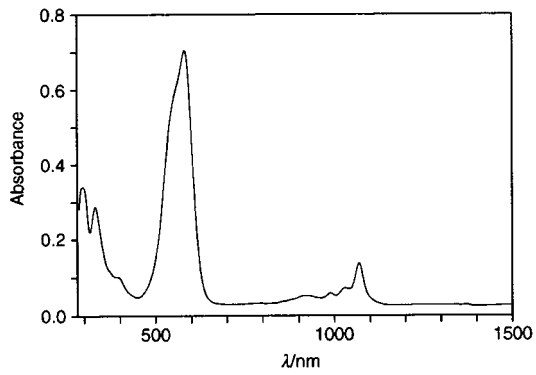

Fig. 2 VIS–NIR absorption spectrum of $\mathbf{1}^{+}C_{60}^{\bullet-}$ in THF at 25 °C.

This work was supported by a grant from the Asahi Glass Foundation and a Grant-in-Aid for Scientific Research on Priority Areas (A) from the Ministry of Education, Science, Sports and Culture, Japan.

Notes and references

1 For reviews, see J. R. Morton, F. Negri and K. F. Preston, *Acc. Chem. Res.*, 1998, **31,** 63; R. Taylor, in *The Chemistry of Fullerenes*, ed. R. Taylor, World Scientific, Singapore, 1995, ch. 13; A. Hirsch, *The Chemistry of the Fullerenes*, Thieme, Stuttgart, 1994, ch. 6.
2 P. J. Krusic, E. Wasserman, P. N. Keizer, J. R. Morton and K. F. Preston, *Science*, 1991, **254**, 1183.
3 P. J. Krusic, E. Wasserman, B. A. Perkinson, B. Malone, E. R. Holler, Jr., P. N. Keizer, J. R. Morton and K. F. Preston, *J. Am. Chem. Soc.*, 1991, **113**, 6724.
4 P. J. Fagan, P. J. Krusic, C. N. McEwen, J. Lazar, D. H. Parker, N. Herron and E. Wasserman, *Science*, 1993, **262**, 404.
5 Half-wave potentials, measured in 1,2-dichlorobenzene: T. Kitagawa, T. Tanaka, Y. Takata, K. Takeuchi and K. Komatsu, *Tetrahedron*, 1997, **53**, 9965.
6 As a control experiment, the reaction of the tris(2,6-dimethoxyphenyl)methyl radical (ref. 7) and C_{60} was examined under the same conditions as above. As expected from the oxidation potential of this radical (−0.49 V *vs.* Fc/Fc^{+} in PhCN), which is more positive than the first reduction potential of C_{60}, no reaction was observed.
7 M. J. Sabacky, C. S. Johnson, Jr., R. G. Smith, H. S. Gutowsky and J. C. Martin, *J. Am. Chem. Soc.*, 1967, **89**, 2054.
8 T. Tanaka, T. Kitagawa, K. Komatsu and K. Takeuchi, *J. Am. Chem. Soc.*, 1997, **119,** 9313; K. Takeuchi, T. Kitagawa, A. Miyabo, H. Hori and K. Komatsu, *J. Org. Chem.*, 1993, **58**, 5802; K. Komatsu, H. Akamatsu, S. Aonuma, Y. Jinbu, N. Maekawa and K. Takeuchi, *Tetrahedron*, 1991, **47**, 6951; K. Okamoto, T. Kitagawa, K. Takeuchi, K. Komatsu, T. Kinoshita, S. Aonuma, M. Nagai and A. Miyabo, *J. Org. Chem.*, 1990, **55**, 996.
9 R. J. Goldacre and J. N. Phillips, *J. Chem. Soc.*, 1949, 1724.
10 M. E. Niyazymbetov, D. H. Evans, S. A. Lerke, P. A. Cahill and C. C. Henderson, *J. Phys. Chem.*, 1994, **98**, 13 093; D. E. Cliffel and A. J. Bard, *J. Phys. Chem.*, 1994, **98**, 8140.
11 E. Weitz, L. Müller and K. Dinges, *Chem. Ber.*, 1952, **85,** 878.
12 An EPR spectrum of a hexane solution of $\mathbf{1}^{\bullet}$ (1.1×10^{-3} M), which exhibited a signal intensity corresponding to 90 ± 10% of the theoretical value, confirmed the absence of any significant dimerization.
13 Calc. for $C_{85}H_{30}N_{3}$: C, 93.39; H, 2.77; N, 3.84. Found for the freshly prepared salt: C, 90.01; H, 2.23; N, 3.50%. Although the C, H, N values are close to the expected values, the total of these elements was only 96%, suggesting a reaction with molecular oxygen and/or water during the analysis.
14 R. Subramanian, P. Boulas, M. N. Vijayashree, F. D'Souza, M. T. Jones and K. M. Kadish, *J. Chem. Soc., Chem. Commun.*, 1994, 1847; D. Dubois, M. T. Jones and K. M. Kadish, *J. Am. Chem. Soc.*, 1992, **114**, 6446; P.-M. Allemand, G. Srdanov, A. Koch, K. Khemani, F. Wudl, Y. Rubin, F. Diederich, M. M. Alvarez, S. J. Anz and R. L. Whetten, *J. Am. Chem. Soc.*, 1991, **113,** 2780.
15 (*a*) M. M. Khaled, R. T. Carlin, P. C. Trulove, G. R. Eaton and S. S. Eaton, *J. Am. Chem. Soc.*, 1994, **116**, 3465; (*b*) J. Stinchcombe, A. Pénicaud, P. Bhyrappa, P. D. W. Boyd and C. A. Reed, *J. Am. Chem. Soc.*, 1993, **115**, 5212; (*c*) A. J. Schell-Sorokin, F. Mehran, G. R. Eaton, S. S. Eaton, A. Viehbeck, T. R. O'Toole and C. A. Brown, *Chem. Phys. Lett.*, 1992, **195,** 225.
16 J. R. Morton, K. F. Preston, P. J. Krusic, S. A. Hill and E. Wasserman, *J. Am. Chem. Soc.*, 1992, **114**, 5454.
17 T. Kato, T. Kodama and T. Shida, *Chem. Phys. Lett.*, 1993, **205,** 405; G. A. Heath, J. E. McGrady and R. L. Martin, *J. Chem. Soc., Chem. Commun.*, 1992, 1272; D. R. Lawson, D. L. Feldheim, C. A. Foss, P. K. Dorhout, C. M. Elliott, C. R. Martin and B. Parkinson, *J. Electrochem. Soc.*, 1992, **139,** L68.
18 Trace amounts of water in THF may also cause partial hydrolysis, which gives rise to **1**–OH. However, the 1 : 1 ratio would be retained, since the same amount of $C_{60}^{\bullet-}$ would be converted to HC_{60}–$C_{60}H$. **1**–OH and HC_{60}–$C_{60}H$ would be expected to have only a weak ($\varepsilon < 10^{3}$) absorption at wavelengths above 500 nm.

Communication 9/03911B

Synthesis and characterization of 'calixsalens': a new class of macrocyclic chiral ligands

Zengmin Li and Chet Jablonski*

Department of Chemistry, Memorial University of Newfoundland, St. John's, Newfoundland, Canada A1B 3X7. E-mail: cjablons@morgan.ucs.mun.ca

Received (in Corvallis, OR, USA) 4th January 1999, Accepted 7th June 1999

Template directed reaction of dialdehydes and (*R*,*R*)- or (*S*,*S*)-1,2-diaminocyclohexane affords a practical route to chiral, metal-free macrocyclic salen dimers which have a novel calixarene-like structure and show catalytic activity for enantioselective epoxidation of unfunctionalized alkenes in the presence of Mn^{III}–NaOCl (aq.).

Chiral Schiff base ligands are efficient chiral auxiliaries for a wide range of enantioselective epoxidations.[1] Our search strategy for new asymmetric catalysts, particularly for asymmetric epoxidation of unfunctionalized alkenes,[1–4] has focussed on development of chiral macrocycles bearing two salen-based metal binding sites[5] which can act co-operatively[6a,7] within an enzyme-like chiral cavity. This approach is based on the expectation that non-covalent interactions,[8] which are the sole determinants of stereochemical outcome for enantioselective reactions of unfunctionalized substrates,[2a,9] can be maximized within a chiral host–guest paradigm.[6] The macrocycles reported herein are simple chiral salen dimers (Scheme 1) containing two tetradentate metal binding sites coupled by one- or four-atom linking groups which determine ring size.

The 26- or 32-membered salen macrocycles **5** and **6** were synthesized by template-induced cyclization (Scheme 1) of *trans*-(*R*,*R*) or *trans*-(*S*,*S*)-1,2-diaminocyclohexane and an appropriate dialdehyde (**3a**–**d** or **4**), prepared from the corresponding aldehydes.[10] Three products, identified as the dimer **5d** (*m/z* 893), along with the corresponding trimer (*m/z* 1339) and tetramer, were isolated from condensation of dialdehyde **3d** and *trans*-(*R*,*R*)-(−)-1,2 diaminocyclohexane. Two major products were obtained from cyclization of **3a**–**c** with the (*R*,*R*)-diamine. The higher TLC R_f product in each case was confirmed to be macrocyclic dimer **6a**–**c** (*m/z* 668, 725 and 837). Relatively simple and similar ^{1}H NMR spectra of the dimer and the corresponding trimer or tetramer suggested a highly symmetric structure. ^{13}C NMR revealed seven low field signals assigned to the four equivalent imine C=N carbons and six of the twenty-four aromatic carbons of **5a**–**d**. Consistent with overall D_2 symmetry, four (**5a**), five (**5b**) or six (**5c**,**d**) high field ^{13}C NMR signals were observed for the remaining carbon atoms.

A single crystal X-ray study† of **5a**·DMF confirms the D_2 symmetric structure (Fig. 1) inferred from solution spectroscopy. The four benzene rings of **5a**·DMF form a well-defined cavity and adopt a 1,3-dialternate conformation with a striking calixarene-like[11] structure, hence we have introduced the name 'calixsalen' to describe these macrocycles. The two opposing face-to-face benzene rings are nearly coplanar and lie 7.57 Å apart and, as a consequence of the preferred 1,3-dialternate conformation, the hydroxy groups are twisted away from the 'salen' plane so that hydrogen-bonding between adjacent OH groups is precluded.

In contrast, the ambient temperature 500 MHz ^{1}H NMR spectrum of the 32-membered salen macrocycle **6**, obtained as a single TLC band from cyclization of **4** with the (*R*,*R*)-diamine (*cf.* Scheme 1), showed four imine signals (8.12, 8.10, 8.09 and 8.07 ppm) in a ratio of 2:4:8:30 which were assigned to four slowly-interconverting conformers. NMR and mass spectral (*m/z* 761) evidence are consistent with the dimeric structure **6**. ^{13}C NMR showed two imine carbon signals (164.74, 164.51 ppm) in an approximate ratio of 10:30 corresponding to the two most stable conformers. Eleven pairs of ^{13}C resonances for the two major conformers, tentatively assigned as the D_2 symmetric 1,3-alternate and C_2 symmetric 1,2-alternate conformers in slow exchange, were observed. Although a maximum of eleven ^{13}C resonances are expected for the D_2 symmetric 1,3-alternate conformation, the 1,2-alternate or any of the remaining

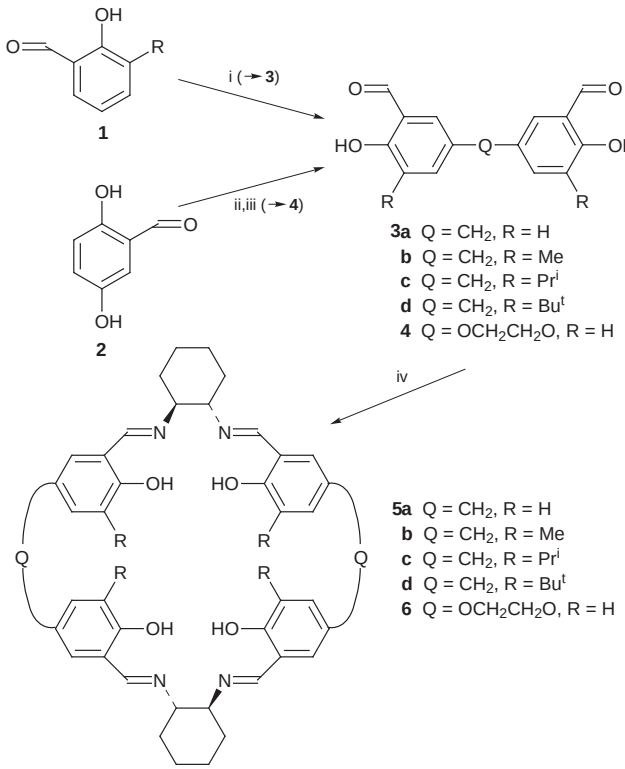

Scheme 1 *Reagents and conditions*: i, $(CH_2O)_3$, H_2SO_4, AcOH, 70 °C; ii, NaH, $(TsOCH_2)_2$; iii, HCl; iv, 1,2-diaminocyclohexane, $Ba(ClO_4)_2$, MeOH–THF.

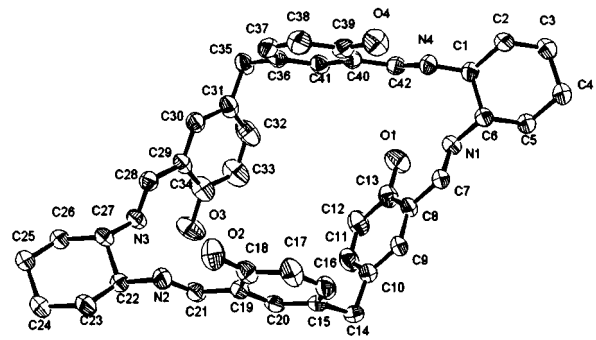

Fig. 1 ORTEP representation (30% ellipsoids) for **5a**·DMF (DMF and hydrogen atoms removed for clarity).

conformations should show a total of 22 resonances. We conclude that some degree of flexibility, made possible by the ethylene glycol links, establishes a second, time-average C_2 axis. Warming to 55 °C results in collapse of the two ^{13}C imine resonances into a single peak at 165.04 ppm, possibly as a result of 1,3-alternate ↔ 1,2-alternate exchange which becomes fast on the NMR time scale.

Although the solid state conformation of **5a**·DMF appears ill-disposed to provide two tetradentate salen coordination sites, reaction with Mn^{III} salts is facile. Addition of a solution of $Mn(OAc)_3$ to solutions of the salen dimers **5** or **6** caused an immediate colour change from yellow to deep brown. An electrospray mass spectrum of a methanolic solution of the dark brown product obtained by treatment of **5d** with $Mn(OAc)_3$ showed strong peaks at *m/z* 1093 [(**5d** −4H)Mn_2·2MeOH·CH_2O]$^+$, 1063 [(**5d** −4H)Mn_2·2MeOH]$^+$, 1045 [(**5d** −4H)Mn_2·HCO_2H]$^+$, 999 [(**5d** −4H)Mn_2]$^+$ and 893 [**5d**]$^+$, consistent with the formation of a bimetallic complex.

Preliminary tests of the brown Mn^{II} macrocyclic salen complexes as catalysts for the epoxidation of styrene, the most challenging enantioselective version of this type of reaction thus far,[12] were conducted at room temperature (23 °C) using NaOCl (aq) as terminal oxidant (Scheme 2). Both ring-opened chloromethyl ether and epoxide products were obtained with modest enantioselectivity (Scheme 2) in methanolic solvent. Chemoselectivity responds to the steric requirements of the R groups**.** For example, *tert*-butyl substituted macrocycle **5d** gave epoxide : chloro ether in the ratio 100 : 3 but only one product (85–87% chemical yield), identified as 1-phenyl-1-chloro-2-methoxy ethane by mass spectrometric analysis and comparison of NMR data with 1-phenyl-1-methoxy-2-chloroethane (obtained through direct chlorination of styrene in MeOH), was isolated in the presence of unsubstituted dimer **5a** or **6**. Interestingly, both epoxide and chlorinated products (chloro ether or chlorohydrin) in a ratio of 10 : 1 are obtained with catalyst **5b** (R = CH_3).

The ring opened products obtained were uniquely *anti*-Markownikoff, hence Scheme 2 may have some important synthetic applications.[13] Reversed regioselective chlorination of alkenes has previously been observed in alkoxychlorination of allylamines with Wacker type catalysts[14] but Markownikoff addition was found for all other alkenes tested.

Unlike mononuclear salen catalysts,[2a] the enantioselectivity of the macrocyclic Mn^{III}–calixsalen systems reported in this work appears unrelated to the steric requirements of the R groups on the *ortho* position of the phenol in the salen frame (Scheme 2). We therefore speculate that the observed enantioselectivity is controlled by host–guest intra-cavity interactions.

The dimanganese complex isolated from ligand **5d**, which unlike that from **5a** was soluble in CH_2Cl_2, allows direct comparison of the enantioselectivity of the bimetallic calixsalen complexes reported in this work with the well characterized Jacobsen catalysts. Aqueous NaOCl oxidation of styrene in the presence of the brown dimanganese complex of **5d** in CH_2Cl_2 gave only epoxide product with 52% ee in 63% isolated chemical yield at 25 °C. This result compares favourably with the best value of 59% ee at 23 °C in CH_2Cl_2 for a mononuclear Mn^{III} salen catalyst reported by Jacobsen.[12]

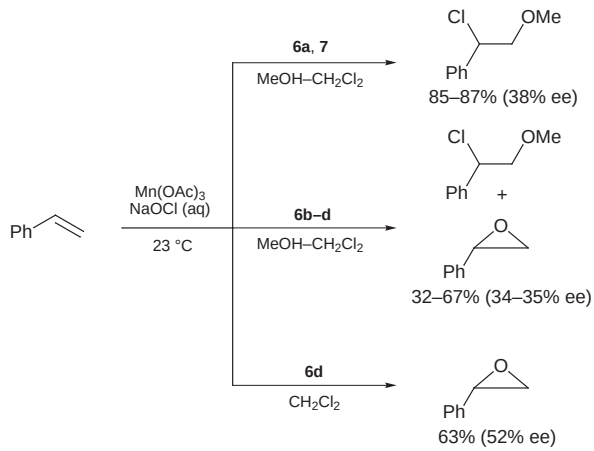

Scheme 2

C. J. acknowledges the Natural Science and Engineering Council of Canada (NSERC) for a grant in aid of research. Z. L. acknowledges Memorial University for financial support. We thank Professor M. McGlinchey and MacMaster University for 500 MHz NMR data reported for compound **6** and Mr David Miller, Memorial University Crystallography Laboratory, for determination of the molecular structure of **5a**.

Notes and references

† *Crystal data* for **6a**: $C_{42}H_{40}O_4N_4$·DMF, yellow, monoclinic, space group $P2_1/c$ (#14), a = 14.640(3), b = 25.679(4), c = 11.045(6) Å, β = 81.97(2)°, V = 4112(4) Å^3, Z = 4, 5858 unique reflections, R = 0.077, R_w = 0.045, GOF = 1.80. CCDC 182/1289.

1 W. Zhang and E. N. Jacobsen, *J. Org. Chem.*, 1991, **56**, 2296; S. H. Zhao, P. R. Ortiz, B. A. Keys and K. G. Davenport, *Tetrahedron Lett.*, 1996, **37**, 2725; P. J. Pospisil, D. H. Carsten and E. N. Jacobsen, *Chem. Eur. J.*, 1996, **2**, 974; T. Hamada, T. Fukuda, H. Imanishi and T. Katsuki, *Tetrahedron*, 1996, **52**, 515; T. Nagata, K. Imagawa, T. Yamada and T. Mukaiyama, *Bull. Chem. Soc. Jpn.*, 1995, **68**, 1455; K. D. S. Bernardo, A. Robert, F. Dahan and B. Meunier, *New J. Chem.*, 1995, **19**, 129; T. Kuroki, T. Hamada and T. Katsuki, *Chem. Lett.*, 1995, 339; K. G. Rasmussen, D. S. Thomsen and K. A. Jorgensen, *J. Chem. Soc., Perkin Trans. 1*, 1995, 2009; I. Fernández, J. R. Pedro and R. Delasalud, *Tetrahedron*, 1996, **52**, 12 031.

2 (*a*) E. N. Jacobsen, in *Catalytic Asymmetric Synthesis*, ed. I. Ojima, VCH, New York, 1993, p. 159; (*b*) J. P. Collman, X. Zhang, V. J. Lee, E. S. Uffelman and J. I. Brauman, *Science*, 1993, **261**, 1404; (*c*) V. Schurig and F. Betschinger, *Chem. Rev.*, 1992, **92**, 873; (*d*) T. Katsuki, *Coord. Chem. Rev.*, 1995, **140**, 189.

3 K. B. M. Janssen, I. Laquiere, W. Dehaen, R. F. Parton, I. F. J. Vankelecom and P. A. Jacobs, *Tetrahedron: Asymmetry*, 1997, **8**, 3481.

4 B. B. De, B. B. Lohray, S. Sivaram and P. K. Dhal, *J. Polym. Sci. Part A: Polym. Chem.*, 1997, **35**, 1809.

5 H. Brunner and H. Schiessling, *Angew. Chem., Int. Ed. Engl.*, 1994, **33**, 125; C. Fraser, R. Ostrander, A. L. Rheingold, C. White and B. Bosnich, *Inorg. Chem.*, 1994, **33**, 324; C. Fraser and B. Bosnich, *Inorg. Chem.*, 1994, **33**, 338; F. C. J. M. van Veggel, W. Verboom and D. Reinhoudt, *Chem. Rev.*, 1994, **94**, 279.

6 (*a*) J. M. Lehn, *Angew. Chem., Int. Ed. Engl.*, 1988, **27**, 89; (*b*) H. L. Anderson and J. K. Sanders, *J. Chem. Soc., Perkin Trans. 1*, 1995, 2223; (*c*) A. J. Kirby, *Angew. Chem., Int. Ed. Engl.*, 1996, **35**, 707.

7 P. Scrimin, P. Tecilla, U. Tonellato and A. Veronese, *Molecular Design and Bioorganic Catalysis*, ed. C. S. Wilcox and A. D. Hamilton, Kluwer, Dordrecht, 1996, p. 211.

8 D. J. Cram, *Angew. Chem., Int. Ed. Engl.*, 1988, **27**, 1009.

9 R. W. Quan, Z. Li and E. N. Jacobsen, *J. Am. Chem. Soc.*, 1996, **118**, 8156.

10 G. Casiraghi, G. Casnati, M. Corina, A. Pochini, G. Puglia, G. Sartori and R. J. Ungaro, *J. Chem. Soc., Perkin Trans. 1*, 1978, 318; C. S. Marvel and N. Tarköy, *J. Am. Chem. Soc.*, 1957, **79**, 6000; A. R. van Doorn, R. Shaafstra, M. Bos, S. Harkema, J.-V. Erden, W. Verboom and D. N. Reinhoudt, *J. Org. Chem.*, 1991, **56**, 6083.

11 C. Wieser, C. B. Dieleman and D. Matt, *Coord. Chem. Rev.*, 1997, **165**, 93.

12 M. Palucki, P. J. Pospisil, W. Zhang and E. N. Jacobsen, *J. Am. Chem. Soc.*, 1994, **116**, 9333.

13 A. El-Qisairi, O. Hamed and P. M. Henry, *J. Org. Chem.*, 1998, **63**, 2790; J. Y. Lai, F. S. Wang, G. Z. Guo and L. X. Dai, *J. Org. Chem.*, 1993, **58**, 6944; H. Nakamura, M. Sekido, M. Ito and Y. Yamamoto, *J. Am. Chem. Soc.*, 1998, **120**, 6838.

14 J. Y. Lai, X. X. Shi and X. Dai, *J. Org. Chem.*, 1992, **57**, 3485.

Communication 9/00018F

New weakly coordinating counter anions for high activity polymerisation catalysts: $[(C_6F_5)_3B–CN–B(C_6F_5)_3]^-$ and $[Ni\{CNB(C_6F_5)_3\}_4]^{2-}$

Simon J. Lancaster, Dennis A. Walker, Mark Thornton-Pett and Manfred Bochmann*

School of Chemistry, University of Leeds, Leeds, UK LS2 9JT. E-mail: m.bochmann@chem.leeds.ac.uk

Received (in Basel, Switzerland) 11th May 1999, Accepted 29th June 1999

The new borate $[CPh_3]^+[CN\{B(C_6F_5)_3\}_2]^-$ and the anionic isocyanoborate complex $[Ni\{CNB(C_6F_5)_3\}_4]^{2-}$ are readily accessible in one-pot reactions and act as a highly efficient activators for metallocene polymerisation catalysts; turnover numbers of up to 53 000 s^{-1} appear to be the highest reported so far for ethene polymerisation catalysts.

The basicity of the counter anion X^- in cationic metal alkyl complexes $[L_nMR]^+X^-$ is known to be one of the most important factors that determine the ability of these complexes to act as catalysts for the polymerisation of alkenes.[1,2] Research has been directed at reducing the nucleophilicity of such anions as far as possible, for example by increasing steric hindrance in borate and aluminate anions, such as $[B(C_6F_4SiR_3)_4]^-$, $[MeB(2\text{-}C_6F_4C_6F_5)_3]^-$, $[FA1(2\text{-}C_6F_4C_6F_5)_3]^-$,[3] or by using halogenated carboranes such as $[CB_{11}H_6Cl_6]^-$ and $[CB_{11}HF_{11}]^-$.[4,5] Since the synthesis of such anions requires a very substantial preparative effort, for practical purposes $[B(C_6F_5)_4]^-$ and $[MeB(C_6F_5)_3]^-$ are most widely used.

An alternative strategy for reducing the nucleophilicity of borate anions is to distribute the negative charge over more than one boron atom. Such borate anions can be made by reacting $B(C_6F_5)_3$ with anions which can act as bridging groups. Thus the reaction of $B(C_6F_5)_3$ with KCN in Et_2O followed by treatment with Ph_3CCl in CH_2Cl_2 gives rise to $[CPh_3]^+[(C_6F_5)_3B–CN–B(C_6F_5)_3]^-$ **1** (Scheme 1). The synthesis is best conducted as a one-pot procedure.

As an activator for metallocene-based polymerisation catalysts, compound **1** has several practical advantages over the commonly employed $[CPh_3][B(C_6F_5)_4]$.[6] The synthesis of $[B(C_6F_5)_4]^-$ requires the use of hazardous LiC_6F_5 which is prone to detonate on warming above −20 °C;[7] yields of $Li[B(C_6F_5)_4]$ tend to be variable, $[CPh_3][B(C_6F_5)_4]$ is frequently very difficult to crystallise and purify and is air sensitive. By contrast, $B(C_6F_5)_3$ is commercially available and can be made by safe alternative routes,[8] it is readily converted into **1** in high yield, the product crystallises very easily, and we found that crystalline **1** can be exposed to air for weeks without any visible signs of deterioration.

The crystal structure of **1** is shown in Fig. 1.† The anion is related to the borohydride $[H_3B–CN–BH_3]^-$ but gives a slightly higher ν_{CN} stretching frequency (**1**: 2305 cm^{-1}; $[CN(BH_3)_2]^-$: 2260 cm^{-1}).[9] The serendipitous formation of $[Ph_3B–CN–BPh_3]^-$ has also been reported (ν_{CN} 2255 cm^{-1});[10] this anion was however found to be prone to dissociation into BPh_3 and $[Ph_3BCN]^-$. The higher Lewis acidity of $B(C_6F_5)_3$ evidently makes such a dissociation less facile.

Another type of anion with even more extensively delocalised charges is represented by metal complexes of the isocyanoborate anion, accessible from $B(C_6F_5)_3$ and metal cyanides. For example, the reaction with $K_2[Ni(CN)_4]$ gives off-white microcrystalline $K_2[Ni\{CNB(C_6F_5)_3\}_4]$ which on treatment with Ph_3CCl in dichloromethane affords orange **2a** (ν_{CN} 2234 cm^{-1}) (Scheme 1), while metathesis with $[HNMe_2Ph]Cl$ leads to colourless crystals of $[HNMe_2Ph]_2[Ni\{CNB(C_6F_5)_3\}_4]\cdot Me_2CO$ **2b** (ν_{CN} 2239 cm^{-1}). The crystal structure confirms the square geometry of the anion in **2a** (Fig. 2).†

The suitability of **1** and **2a** as activators for metallocene polymerisation catalysts was tested at 1 bar and under pressure at temperatures up to *ca*. 100 °C using *rac*-$Me_2Si(indenyl)_2ZrMe_2$ **3** and Cp_2ZrMe_2 **4** as standard test metallocenes. The results are collected in Table 1; for comparison the literature data for other high-activity catalysts have also been included.

Activity tests at 1 bar are frequently used to assess catalyst performance, and short reaction times are thought to prevent mass-transport limitations.[3] However, exposing mixtures of **1** and **3** to ethene at 1 bar resulted in the instantaneous formation of polymer films on the surface of the rapidly stirred liquid which impeded feed gas diffusion. Higher pressure was therefore employed to reduce mass transport problems. At 7 bar ethene pressure and 5 μmol **1** at a starting temperature of 20 °C in toluene, a significant reaction exotherm raised the temperature to > 60 °C, and ethene polymerisation was found to be so rapid that after about 2 min gas take-up stopped because the

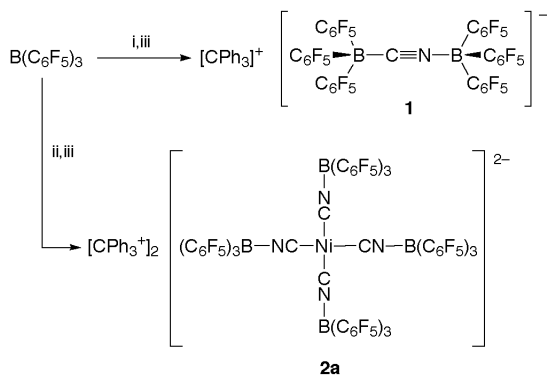

Scheme 1 *Reagents and conditions*: i, KCN, Et_2O, room temp.; ii, $K_2[Ni(CN)_4]$, Et_2O; iii, Ph_3CCl, CH_2Cl_2.

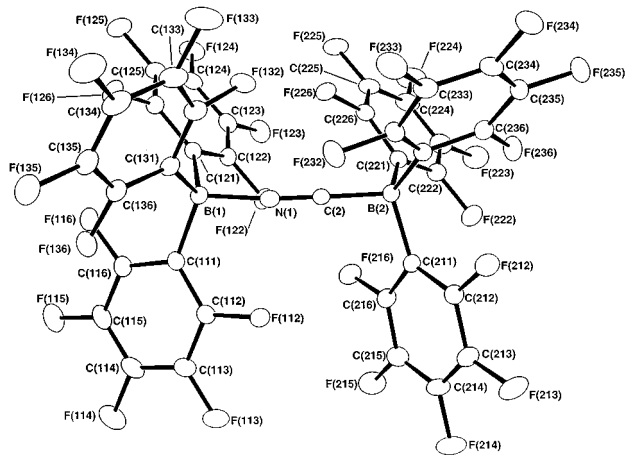

Fig. 1 Structure of the anion in **1**. Selected bond lengths (Å) and angles (°): N(1)–C(2) 1.144(2), N(1)–B(1) 1.593(2), C(2)–B(2) 1.583(2); C(2)–N(1)–B(1) 173.55(14), N(1)–C(2)–B(2) 174.50(14), N(1)–B(1)–C(111) 108.41(11), N(1)–B(1)–C(121) 103.76(11), N(1)–B(1)–C(131) 104.75(11).

Table 1 Ethene polymerisation results

Run	Metallocene (μmol)	Activator (μmol)	$AlBu^i_3$/μmol	Ethene/bar	T/°C	t/min	Polymer yield/g	Productivity[a]	$10^3\ M_w$	M_w/M_n	Ref.
1	**3** (2.5)	**1** (2.5)	—	1[b]	60	0.5	0.423	20.4	n.d.	—	[c]
2	**3** (2.5)	**1** (2.5)	500	1[b]	25	0.5	0.375	18.1	206	4.5	[c]
3	**4** (5)	**1** (5)	—	1[b]	25	1.0	0.523	6.3	310	3.6	[c]
4	**4** (10)	**2a** (5)	—	1[b]	25	2.0	0.433	1.3	n.d.	—	[c]
5	**3** (1)	**1** (0.2)	1000	7[d]	60	4	71.1	760	94.7	2.1	[c]
6	**3** (5)	MAO (Al:Zr 1000:1)	—	7[d]	60	6	74.0	21	n.d.	—	[c]
7	**4**	MAO (67 000:1)		8	90	360		283			13
8	(C_2H_4)(fluorenyl)$_2ZrCl_2$	MAO (500:1)		14	100	60		352	401	2.1	14

[a] In 10^6 g PE{(mol M) h bar}$^{-1}$. [b] In 50 cm^3 toluene. [c] This work. [d] In 3 L toluene.

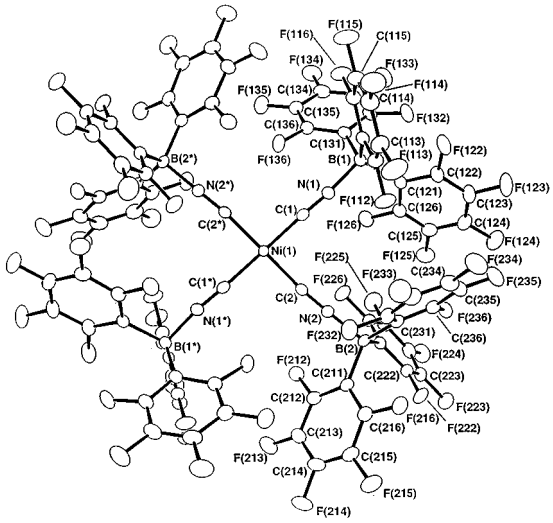

Fig. 2 Structure of the anion in **2a**. Selected bond lengths (Å) and angles (°): Ni–C(1) 1.855(2), Ni–C(2) 1.862(2), N(1)–B(1) 1.574(2), C(1)–N(1) 1.145(2); C(1)–Ni–C(2) 87.15(7), C(1)–Ni–C(2*) 92.85(7), Ni–C(1)–N(1) 176.5(2), C(1)–N(1)–B(1) 174.8(2), N(1)–B(1)–C(111) 103.65(14).

autoclave was filled with swollen polymer. Polymerisations in a 5-l autoclave at the reduced activator concentration of 6.7×10^{-8} M and an initial temperature of 60 °C proceeded so rapidly that the rate of feed gas delivery could not keep pace with gas consumption; the pressure dropped to *ca*. 2 bar and only recovered after 4 min when the amount of polymer formed prevented effective gas take-up. Under these conditions, a turnover number of 53 000 s^{-1} was observed. This figure represents a lower limit estimate and is to our knowledge the highest activity for an ethene polymerisation catalyst reported in the literature so far. Mixtures of **4** and **2a** also showed a good activity of $>10^6$ g PE {(mol Zr) h bar}$^{-1}$.

The activity of a catalyst may be due to several factors: (i) the ligand influence on the rate of chain propagation, (ii) the concentration of active centres generated by the activator, (iii) the position of the equilibrium between active species and dormant states, (iv) the rate of irreversible deactivation of the active centre. When assessing catalysts, it is often tacitly assumed that (i) is the most important factor, and hence the search for new catalysts concentrates on ligand design.[11] The results reported here show that at least equally large variations in catalyst activity are achieved by varing the mode of activation: under closely comparable conditions, activation of **3** with **1**/$AlBu^i_3$ gives a catalyst which is 36 times more active than **3**/MAO (entries 5 and 6).[12]

This work was supported by the Engineering and Physical Sciences Research Council.

Notes and references

† *Crystal data*: compound **1**: $C_{56}H_{15}B_2F_{30}N$, M = 1293.31, triclinic, space group $P\bar{1}$, a = 13.3342(2), b = 14.8405(2), c = 15.8631(2) Å, α = 116.4370(6), β = 90.9440(7), γ = 113.6410(5)°, V = 2501.10(6) Å^3, Z = 2, D_c = 1.717 g cm^{-3} μ = 0.178 mm^{-1}. 9800 independent reflections were collected (R_{int} = 0.0304) (Nonius KappaCCD diffractometer, Mo-Kα, 150 K) solved by direct methods (SHELXS-97)[15] and refined by full-matrix least squares (SHELXL-97)[16] on F^2 of all unique data to R_1 = 0.0355 [8664 observed data with $F^2 > 2\sigma(F^2)$], wR_2 = 0.0972 (all data), S = 1.034. Compound **2a**: $C_{114}H_{30}B_4F_{60}N_4Ni{\cdot}2CH_2Cl_2$, M = 2867.22, monoclinic, space group $P2_1/c$, a = 12.0340(1), b = 14.6297(1), c = 31.8468(3) Å, β = 100.6920(6)°, V = 5509.41(8) Å^3, Z = 2, D_c = 1.728 g cm^{-3} μ = 0.430 mm^{-1}. 10807 independent reflections were collected (R_{int} = 0.0540), solved by direct methods (SHELXS-97) and refined by full-matrix least squares (SHELXL-97) on F^2 of all unique data to R_1 = 0.0344 [9064 observed data with $F^2 > 2\sigma(F^2)$], wR_2 = 0.0857 (all data), S = 1.006.

CCDC 182/1312. See http://www.rsc.org/suppdata/cc/1999/1533/ for crystallographic files in .cif format.

1 M. Bochmann and L. M. Wilson, *J. Chem. Soc., Chem. Commun*., 1986, 1610; R. F. Jordan, C. S. Bajgur, C. S. Willett and B. Scott, *J. Am. Chem. Soc*., 1986, **108**, 7410; H. W. Turner, *Eur. Pat. Appl*., EP 0277004, 1988; M. Bochmann, A. J. Jaggar and J. C. Nicholls, *Angew. Chem., Int. Ed. Engl*., 1990, **29**, 780; A. D. Horton and J. H. G. Frijns, *Angew. Chem., Int. Ed. Engl*., 1991, **30**, 1152; M. Bochmann, *Angew. Chem., Int. Ed. Engl*., 1992, **31**, 1181.

2 X. Yang, C. L. Stern and T. J. Marks, *Organometallics*, 1991, **10**, 840.

3 L. Jia, X. Yang, C. L. Stern and T. J. Marks, *Organometallics*, 1997, **16**, 842; Y. X. Chen, M. V. Metz, L. Li, C. L. Stern and T. J. Marks, *J. Am. Chem. Soc*., 1998, **120**, 6287; L. Li and T. J. Marks, *Organometallics*, 1998, **17**, 3996.

4 C. A. Reed, *Acc. Chem. Res*., 1998, **31**, 133.

5 A. J. Lupinetti and S. H. Strauss, *Chemtracts—Inorg. Chem*., 1998, **11**, 565 and references therein.

6 J. A. Ewen and M. J. Elder, *Eur. Pat. Appl*., EP 0426637, 1990; J. C. W. Chien, W. M. Tsai and M. D. Rausch, *J. Am. Chem. Soc*., 1991, **113,** 8570; M. Bochmann and S. J. Lancaster, *J. Organomet. Chem*., 1992, **434**, C1.

7 A. N. Chernega, A. J. Graham, M. L. H. Green, J. Haggitt, J. Lloyd, C. P. Mehnert, N. Metzler and J. Souter, *J. Chem. Soc., Dalton Trans*., 1997, 2293.

8 J. L. W. Pohlmann and F. E. Brinckmann, *Z. Naturforsch., Teil B*, 1965, **20**, 5.

9 R. C. Wade, E. A. Sullivan, J. R. Berschield and K. F. Purcell, *Inorg. Chem*., 1970, **9**, 2146.

10 C. M. Giandomenico, J. C. Dewan and S. J. Lippard, *J. Am. Chem. Soc*., 1991, **103**, 1407.

11 G. J. P. Britovsek, V. C. Gibson and D. F. Wass, *Angew. Chem., Int. Ed*., 1999, **38**, 429; H. G. Alt and E. Samuel, *Chem. Soc. Rev*., 1998, **27**, 323.

12 High activities with AlR_3/[CPh_3][$B(C_6F_5)_4$] initiator systems in propene polymerisations have been observed: J. C. W. Chien, W. Song and M. D. Rausch, *J. Polym. Sci., Part A: Polym. Chem*., 1994, **32**, 2387.

13 W. Kaminsky, M. Miri, H. Sinn and R. Woldt, *Makromol. Chem., Rapid. Commun*., 1983, **4**, 417.

14 H. G. Alt, W. Milius and S. J. Palackal, *J. Organomet. Chem*., 1994, **472**, 113.

15 G. M. Sheldrick, *Acta Crystallogr., Sect. A*, 1990, **46**, 467.

16 G. M. Sheldrick, SHELXL-97 Program for refinement of crystal structures, University of Göttingen, 1997.

Communication 9/03788H

Ligand properties of 1*H*-diphosphirenes and diphosphirenylium salts towards iron carbonyl fragments

Didier Bourissou, Yves Canac, Heinz Gornitzka, Antoine Baceiredo and Guy Bertrand*

Laboratoire d'Hétérochimie Fondamentale et Appliquée, UPRESA-5069-CNRS, Université Paul Sabatier, 118 route de Narbonne, F-31062 Toulouse Cédex, France. E-mail: gbertran@ramses.ups-tlse.fr

Received (in Cambridge, UK) 14th June 1999, Accepted 7th July 1999

Treatment of η¹-[1,3-bis(diisopropylamino)-1*H*-diphosphirene]tetracarbonyl iron 2 with trifluoromethanesulfonic acid affords the binuclear [3-diisopropylaminodiphosphirenylium salt] iron complex 5, which reacts with diisopropylamine giving the opened binuclear iron complex 3.

The chemistry of phosphorus-containing three-membered rings has attracted considerable attention over the last 15 years.[1] In the diphosphorus-containing series,[2] the 1*H*-diphosphirenes **A**[3] and diphosphirenium salts **B**[4] were discovered in the early 1990s. More recently, we have described the synthesis and reactivity of P-functionalized 1*H*-diphosphirenes **A** and diphosphirenylium salts **C** (Scheme 1) as tungsten carbonyl complexes.[5] Here, we report the ligand behavior of heterocycles **A** and **C** towards iron carbonyl fragments, including the unprecedented cleavage of the P–P bond of the ring framework.

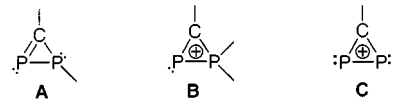

Scheme 1 1*H*-diphosphirene **A**, diphosphirenium cation **B** and diphosphirenylium cation **C**.

The η¹-iron tetracarbonyl complex **2** was readily obtained in 85% yield by treatment of **1** with 1 equiv. of $Fe_2(CO)_9$ (Scheme 2). The end-on coordination of the σ³-P was unequivocally established by comparing the spectroscopic data for **2**† with those of the related η¹-tungsten pentacarbonyl complexes.[5,6]

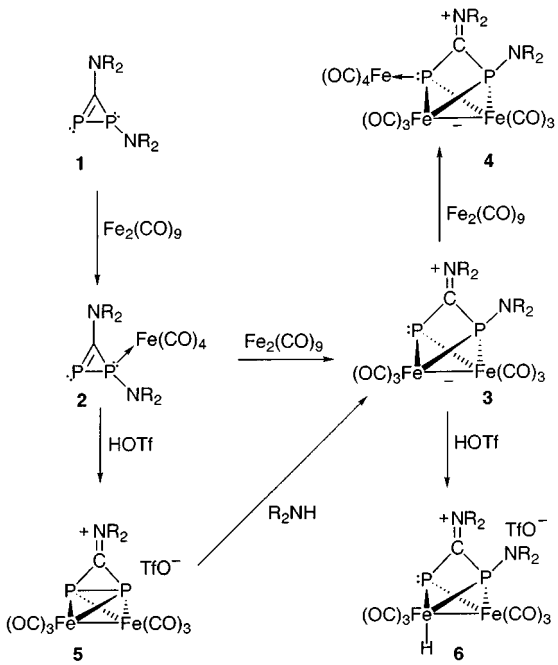

Scheme 2 R = Pr^i, Tf = CF_3SO_2.

Addition of 1 equiv. of $Fe_2(CO)_9$ to **2** afforded the binuclear complex **3**, which was isolated in 42% yield as red crystals. The low-field AB system (δ 125.5 and 122.4, J_{PP} 85 Hz) observed in the ^{31}P NMR spectrum for **3** strongly suggests that the three-membered ring has been opened, although the value of the J_{PP} coupling constant remains large. The cleavage of the P–P bond was confirmed by an X-ray diffraction study‡ (Fig. 1), the P···P distance (P1–P2 2.62 Å) being much longer than that of a classical P–P single bond (2.20–2.35 Å).[7] The structure of **3** consists of a 1,3-diphosphorus chain bridging a metal–metal bonded $Fe_2(CO)_6$ unit (Fe1–Fe2 2.61 Å), both phosphorus atoms being bonded to both iron atoms (P1–Fe1 2.21 Å, P1–Fe2 2.22 Å, P2–Fe1 2.29 Å, P2–Fe2 2.33 Å).[8] The N2P1C1N1P2 skeleton is perfectly planar (maximum deviation from the best plane: 0.036 Å), and the C1–N1 bond length [1.298(9) Å] is in the range expected for a CN double bond, implying that the positive charge has shifted to the nitrogen atom. P1 can be regarded as a typical phosphido phosphorus atom, while P2 is a three-coordinate phosphorus atom with a strongly pyramidal geometry (sum of the angles: 243.3°) suggesting its potential for coordination of an additional transition-metal fragment. Indeed, when **3** was treated with an excess of $Fe_2(CO)_9$ in THF solution, after two days at room temperature, the trinuclear complex **4** was isolated as red crystals in 70% yield (Scheme 2). The spectroscopic data observed for **4** are very similar to those of **3**,† and the structure of **4** has been confirmed by an X-ray diffraction study.‡ The introduction of the $Fe(CO)_4$ fragment on P2 does not result in dramatic geometric modifications. In

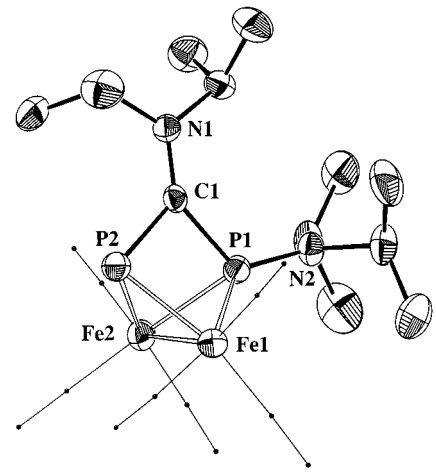

Fig. 1 Thermal ellipsoid diagram (30% probability) of **3** showing the atom numbering scheme. All the carbonyl groups have been omitted, and the isopropyl groups have been simplified. Selected bond lengths (Å) and angles (°): C(1)–N(1) 1.298(9), C(1)–P(1) 1.811(7), C(1)–P(2) 1.841(7), P(1)–N(2) 1.671(7), P(1)–Fe(1) 2.206(2), P(1)–Fe(2) 2.222(2), P(2)–Fe(1) 2.294(3), P(2)–Fe(2) 2.329(3), Fe(1)–Fe(2) 2.613(2); N(1)–C(1)–P(1) 137.9(6), N(1)–C(1)–P(2) 130.4(5), P(1)–C(1)–P(2) 91.4(3), C(1)–P(1)–N(2) 121.1(3), C(1)–P(1)–Fe(1) 94.1(3), C(1)–P(1)–Fe(2) 87.9(2), N(2)–P(1)–Fe(1) 134.3(2), N(2)–P(1)–Fe(2) 131.3(3), Fe(1)–P(1)–Fe(2) 72.31(8), C(1)–P(2)–Fe(1) 90.5(2), C(1)–P(2)–Fe(2) 84.0(2), Fe(1)–P(2)–Fe(2) 68.81(1).

particular, the P···P distance is still long (2.58 Å), and the N2P1C1N1P2 fragment remains planar with the supplementary iron centre Fe3 in the same plane (maximum deviation from the best plane: 0.044 Å). Therefore, in contrast to that observed in the coordination sphere of tungsten (end-on coordination *via* both phosphorus lone pairs of **1**),[5] the binuclear iron complex **3** formally results from the insertion of a $Fe_2(CO)_6$ fragment into the P–P bond of **1**, which leaves a phosphorus lone pair available for coordination to a third metal fragment.

Surprisingly, treatment of the 1*H*-diphosphirene mononuclear complex **2** with 2 equiv. of trifluoromethanesulfonic acid at −78 °C led to the diphosphirenylium binuclear complex **5**§ (Scheme 2). The presence of a $Fe_2(CO)_6$ fragment in **5** was unambiguously established from the mass spectrum [*m/z* 454 (M^+) and 426 ($M - CO)^+$], while the cationic three-membered ring structure was apparent from the high-field ^{31}P NMR (s, δ −139.8) and low-field ^{13}C NMR (t, δ 218.2 J_{PC} 93.1 Hz) signals. Interestingly, **5** was not formed when the binuclear iron complex **3** was reacted with trifluoromethanesulfonic acid. Instead, protonation of an iron centre occurred leading to the iron carbonyl hydride **6**.†

Although the mechanism of the reaction of **2** with triflic acid remains obscure, it is quite clear that the formation of the binuclear complex **5** involves a metallic disproportionation process. To achieve an 18-electron configuration for each iron atom in **5**, the three-membered ring must act as a six-electron ligand (*via* the P=P bond and the lone pair of both phosphorus atoms). This coordination mode is similar to that observed in [*cis*-$P_2Bu^t_2$]·[$Fe_2(CO)_6$],[9] but it necessarily implies that in **5** both phosphorus centres have an unusual inverted tetrahedral geometry.[10]

Finally, we investigated the reactivity of this new diphosphirenylium salt complex. Using diisopropylamine, the neutral binuclear complex **3** was obtained in quantitative yield. Therefore, nucleophilic attack occurs at the highly electrophilic phosphorus atom as observed for the tungsten complexes,[5] but simultaneous cleavage of the P–P bond is observed for the iron complex.

Notes and references

† *Selected spectroscopic data* for **2**–**6**: **2**, $\delta_P(C_6D_6$, 32 MHz) −53.0 (d, J_{PP} 195 Hz, $PNPr^i_2$), 52.6 (d, J_{PP} 195 Hz, σ^2-P); $\delta_C(C_6D_6$, 100 MHz) 195.4 (dd, J_{PC} 83.6, 34.0 Hz, PCP), 214.7 (d, $^2J_{PC}$ 23.1 Hz, CO). **3**, mp 160–162 °C; $\delta_P(C_6D_6$, 32 MHz) 122.4 (d, J_{PP} 85 Hz, $PNPr^i_2$), 125.5 (d, J_{PP} 85 Hz, σ^3-P); $\delta_C(C_6D_6$, 100 MHz) 214.0 (s, CO), PCP was not observed; CIMS (NH_3) 555 (MH^+). **4**, mp 176–178 °C; $\delta_P(C_6D_6$, 32 MHz) AB system 145.7 and 151.0 (J_{PP} = 29 Hz); $\delta_C(C_6D_6$, 100 MHz) 213.0 (s, CO), 217.1 (d, J_{PC} 13.3 Hz, CO), PCP was not observed; CIMS (NH_3) 723 (MH^+). **5**, $\delta_P(C_6D_6$, 32 MHz) −139.8; $\delta_H(CDCl_3$, 200 MHz) 4.44 (spt, $^3J_{HH}$ 6.1 Hz, 2H, CHN); $\delta_C(CDCl_3$, 100 MHz) 61.5 (s, CHN), 119.9 (q, $^1J_{CF}$ 310 Hz, CF_3), 200.1 (m, CO), 218.2 (t, J_{PC} 93.1 Hz, PCP). **6**, $\delta_P(CDCl_3$, 32 MHz) 111.5 (m, J_{PP} 92, J_{PH} = 46.6, 14.3 Hz, $PNPr^i_2$), 140.0 (dd, J_{PP} 92, J_{PH} 8.3 Hz, σ^3-P); $\delta_H(CDCl_3$, 200 MHz) −19.0 (dd, J_{PH} 46.6, 8.3 Hz, 1H, FeH). Satisfactory elemental analyses have been obtained for compounds **2**, **3** and **4**.

‡ *Crystallography*: data for **3** and **4** were collected at low temperatures using an oil-coated shock-cooled crystal[11] on a Stoe-IPDS with Mo-Kα (λ = 0.71073 Å) radiation. The structures were solved by direct methods using SHELXS-97[12] and refined with all data on F^2 using SHELXL-97.[13] All non-hydrogen atoms were refined anisotropically. The hydrogen atoms of the molecules were geometrically idealized and refined using a riding model. A numerical absorption correction was employed, min./max. transmissions for **3** are 0.4325/0.5682 and for **4** 0.7035/0.8889. Refinement of an inversion twin parameter[14] [x = 0.49(2), where x = 0 for the correct absolute structure and +1 for the inverted structure] confirmed a racemic twinning of **3**.

Crystal data: **3**: $C_{19}H_{28}Fe_2N_2O_6P_2$, M = 554.07, monoclinic, space group $P2_1/n$, a = 9.885(2), b = 18.173(3), c = 20.3360(5) Å, β = 99.85(2)°, V = 2606.9(9) Å^3, Z = 4, F(000) = 1144, D_c = 1.412 g cm^{-3}, μ(Mo-Kα) = 1.269 mm^{-1}, 4 < 2θ < 46°, 3493 reflections, 287 parameters, R_1 = 0.0693, wR_2 = 0.1942.

4: $C_{23}H_{28}Fe_3N_2O_{10}P_2$, M = 721.96, orthorhombic, space group *Pbca*, a = 15.7039(4), b = 19.5502(4), c = 20.3360(5) Å, β = 90°, V = 6243.4(3) Å^3, Z = 8, F(000) = 2944, D_c = 1.536 g cm^{-3}, μ(Mo-Kα) = 1.529 mm^{-1}, 4 < 2θ < 46°, 4287 reflections, 370 parameters, R_1 = 0.0513, wR_2 = 0.1233. CCDC 182/1321. See http://www.rsc.org/suppdata/cc/1999/1535/ for crystallographic files in .cif format.

§ The ^{31}P NMR spectrum showed only one singlet corresponding to complex **5**, while the ^1H and ^{13}C NMR spectra revealed the presence of diisopropylammonium trifluoromethane sulfonate.

1 F. Mathey, *Chem. Rev.*, 1990, **90**, 997.
2 D. Bourissou and G. Bertrand, *Acc. Chem. Res.*, in press.
3 E. Niecke, R. Streubel, M. Nieger and D. Stalke, *Angew. Chem., Int. Ed. Engl.*, 1989, **28**, 1673; D. Bourissou, Y. Canac, M. I. Collado, A. Baceiredo and G. Bertrand, *Chem. Commun.*, 1997, 2399.
4 F. Castan, A. Baceiredo, J. Fischer, A. De Cian, G. Commenges and G. Bertrand, *J. Am. Chem. Soc.*, 1991, **113**, 8160; M. Soleilhavoup, Y. Canac, A. M. Polozov, A. Baceiredo and G. Bertrand, *J. Am. Chem. Soc.*, 1994, **116**, 6149; M. Soleilhavoup, A. Baceiredo, F. Dahan and G. Bertrand, *J. Chem. Soc., Chem. Commun.*, 1994, 337; Y. Canac, M. Soleilhavoup, L. Ricard, A. Baceiredo and G. Bertrand, *Organometallics*, 1995, **14**, 3614; Y. Canac, A. Baceiredo, H. Gornitzka, D. Stalke and G. Bertrand, *Angew. Chem., Int. Ed. Engl.*, 1995, **34**, 2677; Y. Canac, A. Baceiredo, W. W. Schoeller, D. Gigmes and G. Bertrand, *J. Am. Chem. Soc.*, 1997, **119**, 7579.
5 D. Bourissou, Y. Canac, M. I. Collado, A. Baceiredo and G. Bertrand, *J. Am. Chem. Soc.*, 1997, **119**, 9923; D. Bourissou, Y. Canac, H. Gornitzka, C. Marsden, A. Baceiredo and G. Bertrand, *Eur. J. Inorg. Chem.*, in press.
6 F. Mercier, L. Ricard, F. Mathey and M. Regitz, *J. Chem. Soc., Chem. Commun.*, 1991, 1305; R. Streubel, L. Ernst, J. Jeske and P. G. Jones, *J. Chem. Soc., Chem. Commun.*, 1995, 2113.
7 *CRC Handbook of Chemistry and Physics*, ed. D. R. Lide, CRC Press, Boca Raton, FL, 1992, S. 9-1.
8 Related complexes featuring di- and tri-phosphorus chains have been reported: R. B. King, F.-J. Wu and E. M. Holt, *Inorg. Chem.*, 1986, **25**, 1733; R. B. King, F.-J. Wu and E. M. Holt, *J. Am. Chem. Soc.*, 1988, **110**, 2775; R. B. King, F.-J. Wu and E. M. Holt, *Inorg. Chem.*, 1988, **27**, 1241; Y. W. Li, M. G. Newton, N. K. Bhattacharyya and R. B. King, *Inorg. Chem.*, 1992, **31**, 2069; Y. W. Li, M. G. Newton and R. B. King, *Inorg. Chem.*, 1993, **32**, 5720.
9 H. Vahrenkamp and D. Wolters, *Angew. Chem., Int. Ed. Engl.*, 1983, **22**, 154.
10 For inverted geometries at carbon centres, see for example: K. B. Wiberg, *Acc. Chem. Res.*, 1984, **17**, 379; K. B. Wiberg and S. T. Waddell, *J. Am. Chem. Soc.*, 1990, **112**, 2194.
11 D. Stalke, *Chem. Soc. Rev.*, 1998, **27**, 171.
12 G. M. Sheldrick, *Acta Crystallogr., Sect. A*, 1990, **46**, 467.
13 G. M. Sheldrick, Program for Crystal Structure Refinement, Universität Göttingen, 1997.
14 H. D. Flack, *Acta Crystallogr., Sect. A*, 1983, **39**, 876.

Communication 9/04747F

Synthesis of a cyclodextrin azo dye [3]rotaxane as a single isomer

Michael R. Craig,[a] Tim D. W. Claridge,[a] Michael G. Hutchings[b] and Harry L. Anderson*[a]

[a] *Department of Chemistry, University of Oxford, Dyson Perrins Laboratory, South Parks Road, Oxford, UK OX1 3QY. E-mail: harry.anderson@chem.ox.ac.uk*

[b] *BASF plc, PO Box 4, Earl Road, Cheadle Hulme, Cheshire, UK SK8 6QG*

Received (in Liverpool, UK) 29th March 1999, Revised 28th June 1999, Accepted 30th June 1999

Azo coupling between 2,6-dimethylphenol and aqueous 4,4′-bis(diazonio)azobenzene chloride in the presence of α-cyclodextrin yields an azo dye [3]rotaxane as a single stereoisomer, with the 2,3-rims of both cyclodextrins pointing outwards.

As part of a project on the encapsulation of chromophores,[1] we recently reported[1b] that reaction of 4,4′-bis(diazonio)azobenzene chloride **1** with aqueous β-naphthol **2** in the presence of

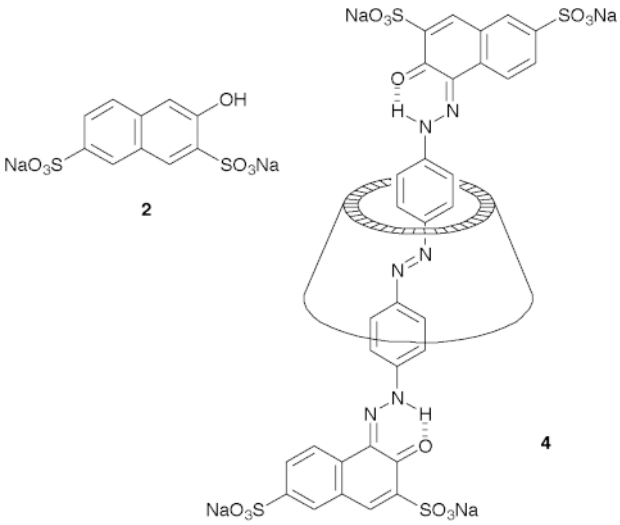

α-cyclodextrin (α-CD) **3** yields the azo dye [2]rotaxane **4**. Here we present the unexpected discovery that, when this reaction is carried out using 2,6-dimethylphenol **5** instead of β-naphthol **2**, the main product is the [3]rotaxane **6** (Scheme 1). The [2]rotaxane **7** and the unencapsulated dye **8** are also formed. To the best of our knowledge this is the first report of a cyclodextrin [3]rotaxane[2] (previous [3]rotaxanes have been made from crown ethers[3] and cyclophanes;[1a,c,4] polyrotaxanes have also been prepared using cyclodextrins[5]). α-Cyclodextrin has a narrow 6-rim (with primary OH groups) and a wider 2,3-rim (with secondary OH groups). There are three possible relative orientations of the cyclodextrin units in **6**, but, remarkably, this [3]rotaxane is formed as a single stereoisomer.

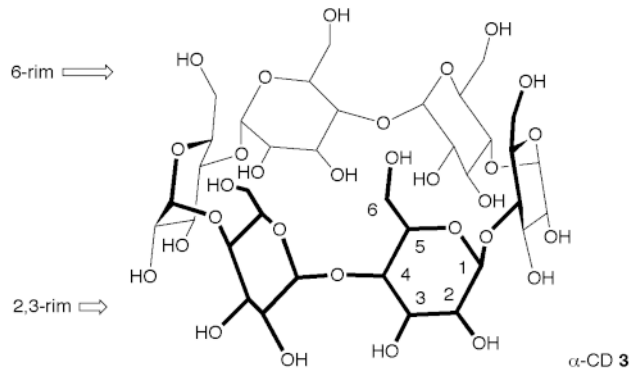

The three products of the reaction shown in Scheme 1 were separated by column chromatography on silica, eluting with 25% aqueous ammonia–butanone–*n*-propanol (1:1:1). Traces of [2]rotaxane **7**, dumbbell **8** and free α-CD **3** can be removed from the [3]rotaxane **6** by ultrafiltration; **6** is retained by a cellulose ultrafiltration membrane (1000 nominal molecular weight limit†), whereas the other components wash through.

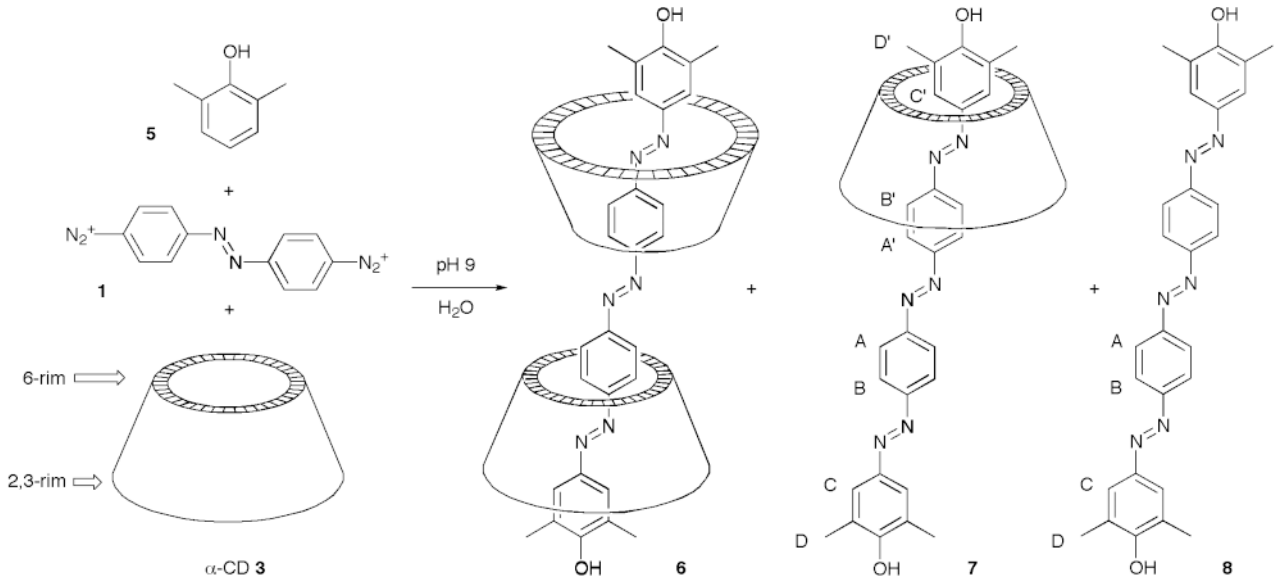

Scheme 1

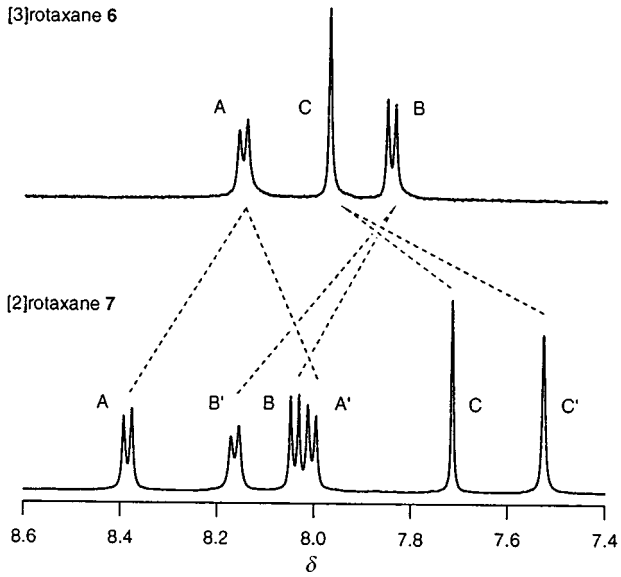

Fig. 1 Aromatic regions of the ^{1}H NMR spectra (DMSO-d_6, 340 K, 500 MHz) of [2]rotaxane **7** and [3]rotaxane **6**.

The isolated yields of **6** and **7** are 12 and 9%, respectively, and the [3]rotaxane can be prepared on a 0.5 g scale using this technique.

The [2]rotaxane and [3]rotaxane were thoroughly authenticated by ^{1}H and ^{13}C NMR, and mass spectrometry.‡ Their ^{1}H NMR spectra were assigned using 2D techniques. The aromatic regions of these spectra are shown in Fig. 1. In the [2]rotaxane, all the resonances of the azo dye dumbbell are split, as expected, due to the inequivalence of the rims of the cyclodextrin, leading to six aromatic signals (H_A–H_C are nearer the 2,3-rim and H_A–$H_{C'}$ are nearer the 6-rim). This type of splitting is not observed in the spectra of the [3]rotaxane, which has only three aromatic resonances (H_A–H_C). This shows that the two α-CD units are either 6-rim-to-6-rim or 2,3-rim-to-2,3-rim; these possibilities were distinguished using 1D gradient NOESY experiments. Strong NOEs are observed from the methyl protons (H_D) to positions on the 2,3-rim of the α-CD (H-3, OH-3 and OH-2), proving that it is the 6-rim-to-6-rim isomer, as depicted in Scheme 1. The reasons for exclusive formation of this isomer are being investigated. Surprisingly, NOE experiments on the [2]rotaxane, in DMSO-d_6, show that it prefers the conformation shown in Scheme 1, with the 6-rim near the end of the chromophore. The two methyl signals, H_D and $H_{D'}$, are almost coincident, and cannot be selectively inverted, however when both methyl resonances are inverted, the dominant NOEs are to H-6, H-6′ and H-5; an NOE is also observed to H-3, but it is about half as large as those to H-6, H-6′ and H-5. Strong NOEs are also observed from $H_{C'}$ to H-6, H-6′ and H-5, whereas H_C shows only a weak NOE to H-3 (about four times smaller than those from $H_{C'}$ to H-6, H-6′ and H-5). The cyclodextrin shuttles rapidly along the dumbbell on the NMR timescale at room temperature, but it shows a distinct preference for the A′–D′ end near the 6-rim.

Yoshida has shown that azo dyes derived from 2,6-dimethylphenol do not easily slip through the cavity of α-CD,[6] but we were initially uncertain as to whether this end-group would be large enough to yield a stable rotaxane. No unthreading[3f,7] of **6** and **7** has been observed in solution at temperatures up to 100 °C, but when **6** was heated to 120 °C in DMSO-d_6 for a week, ^{1}H NMR showed about 15% of the material unthreaded to give **7** and α-CD **3**. This corresponds to a unimolecular rate constant for unthreading of about 10^{-7} s^{-1} and a free energy barrier ($\Delta G^{\ddagger}$) of 147 kJ mol^{-1} at 120 °C, which indicates that the half-life for unthreading at room temperature is probably more than 10^5 years.

This direct route to a [3]rotaxane encapsulated azo dye, in one step from readily available materials, will facilitate investigations into the consequences of chromophore encapsulation, and into the photochemistry of these rotaxanes.[8]

This work was generously supported by the EPSRC and BASF plc.

Notes and references

† Amicon YM1 membrane, from Millipore Ltd.

‡ *Selected data* for **6**: δ_H(330 K, DMSO-d_6) 2.39 (12H, s, H_D), 3.27 (12H, d, H-2), 3.44 (12H, t, H-6′), 3.47 (12H, t, H-4), 3.65 (12H, t, H-3), 3.73 (24H, m, H-5 and H-6), 4.21 (12H, t, OH-6), 4.75 (12H, d, H-1), 5.00 (12H, d, OH-3), 5.14 (12H, d, OH-2), 7.83 (4H, d, H_B), 7.96 (4H, s, H_C), 8.14 (4H, d, H_A); δ_C(330 K, DMSO-d_6) 15.93, 59.77, 70.94, 72.08, 72.87, 81.48, 101.93, 122.05, 123.81, 124.18, 124.47, 145.20, 151.73, 153.79, 157.44; λ_{max}/nm (log ε) (DMSO) 454 (4.8); *m*/*z* (MALDI TOF) 2446.3 (M + Na)$^+$ (Calc. for $C_{100}H_{146}N_6O_{62}\cdot 12H_2O$: C, 45.5; H, 6.5; N, 3.2. Found C, 45.6; H, 6.8; N, 3.2%). For **7**: δ_H(300 K, DMSO-d_6) 2.28 (6H, s, H_D or $H_{D'}$), 2.29 (6H, s, H_D or $H_{D'}$), 3.15 (6H, m, H-2), 3.26 (6H, m, H-6′), 3.36 (6H, t, H-4), 3.52 (12H, m, H-6 and H-3), 3.61 (6H, d, H-5), 4.34 (6H, t, OH-6), 4.67 (6H, d, H-1), 5.23 (6H, d, OH-3), 5.28 (6H, d, OH-2), 7.48 (2H, s, $H_{C'}$), 7.76 (2H, s, H_C), 7.96 (2H, d, $H_{A'}$), 8.00 (2H, d, H_B), 8.12 (2H, d, $H_{B'}$), 8.34 (2H, d, H_A); δ_C(300 K, DMSO-d_6) 16.50, 16.53, 59.92, 71.63, 72.45, 73.32, 82.09, 102.30, 122.54, 123.48, 123.60, 123.64, 123.95, 125.00, 125.24, 125.41, 145.34 (2C), 152.39, 152.67, 153.55, 153.95, 158.12 (2C); λ_{max}/nm (log ε) (DMSO) 439 (4.8); *m*/*z* (MALDI TOF) 1473.5 (M + Na)$^+$.

1 (*a*) S. Anderson and H. L. Anderson, *Angew. Chem., Int. Ed. Engl.*, 1996, **35**, 1956; (*b*) S. Anderson, T. D. W. Claridge and H. L. Anderson, *Angew. Chem., Int. Ed. Engl.*, 1997, **36**, 1310; (*c*) S. Anderson, R. T. Aplin, T. D. W. Claridge, T. Goodson III, A. C. Maciel, G. Rumbles, J. F. Ryan and H. L. Anderson, *J. Chem. Soc., Perkin Trans. 1*, 1998, 2383; (*d*) S. Anderson, W. Clegg and H. L. Anderson, *Chem. Commun.*, 1998, 2379 and 2773.

2 S. A. Nepogodiev and J. F. Stoddart, *Chem. Rev.*, 1998, **98**, 1959.

3 (*a*) A. G. Kolchinski, N. W. Alcock, R. A. Roesner and D. H. Busch, *Chem. Commun.*, 1998, 1437; (*b*) P. R. Ashton, P. T. Glink, J. F. Stoddart, P. A. Tasker, A. J. P. White and D. J. Williams, *Chem. Eur. J.*, 1996, **2**, 729; (*c*) P. R. Ashton, P. T. Glink, J. F. Stoddart, S. Menzer, P. A. Tasker, A. J. P. White and D. J. Williams, *Tetrahedron Lett.*, 1996, **37**, 6217; (*d*) D. B. Amabilino, P. R. Ashton, M. Belohradsky, F. M. Raymo and J. F. Stoddart, *J. Chem. Soc., Chem. Commun.*, 1995, 747; (*e*) J.-C. Chambron, V. Heitz and J.-P. Sauvage, *J. Am. Chem. Soc.*, 1993, **115**, 12 378; (f) P. R. Ashton, M. Belohradsky, D. Philp, N. Spencer and J. F. Stoddart, *J. Chem. Soc., Chem. Commun.*, 1993, 1274.

4 T. Dünnwald, R. Jäger and F. Vögtle, *Chem. Eur. J.*, 1997, **3**, 2043; F. Vögtle, T. Dünnwald, M. Händel, R. Jäger, S. Meier and G. Harder, *Chem. Eur. J.*, 1996, **2**, 640.

5 I. Yamaguchi, K. Osakada and T. Yamamoto, *J. Am. Chem. Soc.*, 1996, **118**, 1811; A. Harada, J. Li and M. Kamachi, *J. Am. Chem. Soc.*, 1994, **116**, 3192; G. Wenz and B. Keller, *Angew. Chem., Int. Ed. Engl.*, 1992, **31**, 197; A. Harada, J. Li and M. Kamachi, *Nature* (*London*), 1992, **356**, 325.

6 N. Yoshida, *J. Chem. Soc., Perkin Trans. 2*, 1995, 2249.

7 A. P. Lyon, N. J. Barton and D. H. Macartney, *Can. J. Chem.*, 1998, **76**, 843; P. R. Ashton, I. Baxter, M. C. T. Fyfe, F. M. Raymo, N. Spencer, J. F. Stoddart, A. J. P. White and D. J. Williams, *J. Am. Chem. Soc.*, 1998, **120**, 2297; I. T. Harrison, *J. Chem. Soc., Chem. Commun.*, 1972, 231.

8 H. Murakami, A. Kawabuchi, K. Kotoo, M. Kunitake and N. Nakashima, *J. Am. Chem. Soc.*, 1997, **119**, 7605.

Communication 9/02494H

A conjugated triple strand porphyrin array

G. Scott Wilson and Harry L. Anderson*

Department of Chemistry, University of Oxford, Dyson Perrins Laboratory, South Parks Road, Oxford, UK OX1 3QY. E-mail: harry.anderson@chem.ox.ac.uk

Received (in Liverpool, UK) 17th May 1999, Accepted 30th June 1999

A conjugated tetrapyridylporphyrin dimer has been synthesised, which binds two metalloporphyrin dimers to form a triple strand array; formation of this supramolecular assembly holds both components in planar conformations, increasing the conjugation.

The unusual electronic and optical properties of conjugated porphyrin oligomers make them appealing materials for a variety of potential applications.[1] We are interested in controlling the behaviour of these materials through the formation of non-covalent arrays.[2] Self-assembly offers a way of controlling the conformation, and thus indirectly controlling the π-overlap and conjugation. The reversible formation of multi-strand arrays could also be used to control the synthesis of these covalent units, *via* template-directed coupling and even self-replication. Here we present the synthesis of a conjugated tetrapyridylporphyrin dimer **1**, which binds a zinc porphyrin dimer **2**[3] to form double and triple strand arrays (Scheme 1), changing the conformation and conjugation of both components.

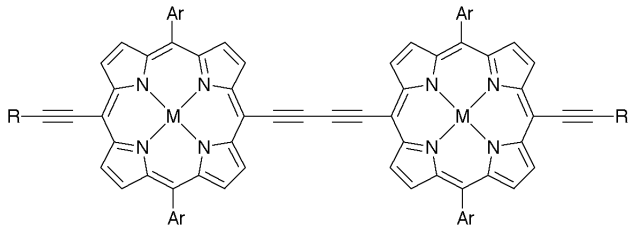

1 M = H_2, Ar = 4-pyridyl, R = Si(*n*-C_6H_{13})$_3$
2 M = Zn, Ar = 3,5-$Bu^t_2C_6H_3$, R = Si(*n*-C_6H_{13})$_3$

The key intermediate in the synthesis of tetrapyridylporphyrin dimer **1** is 5,15-bis(4-pyridyl)-10,20-bis(triisopropylsilylethynyl)porphyrin **7** (Scheme 2). Attempts to prepare **7** by condensation of pyridine-4-carbaldehyde and *meso*-alkynyl dipyrromethanes, and also by reaction of acetylenic aldehydes with *meso*-pyridyl dipyrromethane, were unsuccessful.[4] We eventually prepared **7** using *meso*-bromination[5] and Stille coupling,[2d,6] as shown in Scheme 2. *meso*-Bromination of 5,15-dialkynylporphyrins is difficult due to competing β-substitution and alkyne addition. The electron-withdrawing alkynes deactivate the porphyrin ring towards bromination, but this effect can be overcome by inserting an electropositive metal into the macrocycle.[5a] Bromination of free-base **5**, or its zinc complex, with NBS gave complex mixtures of products, whereas the magnesium complex reacted cleanly at both *meso*-positions, to give the dibromoporphyrin **6**. Stille coupling with 4-(trimethylstannyl)pyridine worked efficiently with the zinc complex of **6**, giving **7** in 83% yield. Triisopropylsilyl groups were used to protect the alkynes during the synthesis of **7**, and were subsequently changed to trihexylsilyls in **1**, to increase the solubility. Compound **1** was prepared from **7** by protecting group manipulation and Glaser–Hay coupling.[7]

UV-visible titrations showed that dimers **1** and **2** form a stable 1 : 2 complex in CH_2Cl_2. When ligand **1** is added to **2**, the spectrum evolves with several sharp isosbestic points, indicating clean formation of the **1**·$\mathbf{2}_2$ complex (Scheme 1). The titration has a well defined end-point at 1 : 2 stoichiometry and the stability constant of **1**·$\mathbf{2}_2$ is too high to determine accurately ($\alpha K_1^2 \approx 10^{16}$–$10^{19}$ M^{-2}). The UV-visible spectrum of **1**, the **2**·(pyridine)$_2$ complex (scaled ×2) and **1**·$\mathbf{2}_2$ are compared in

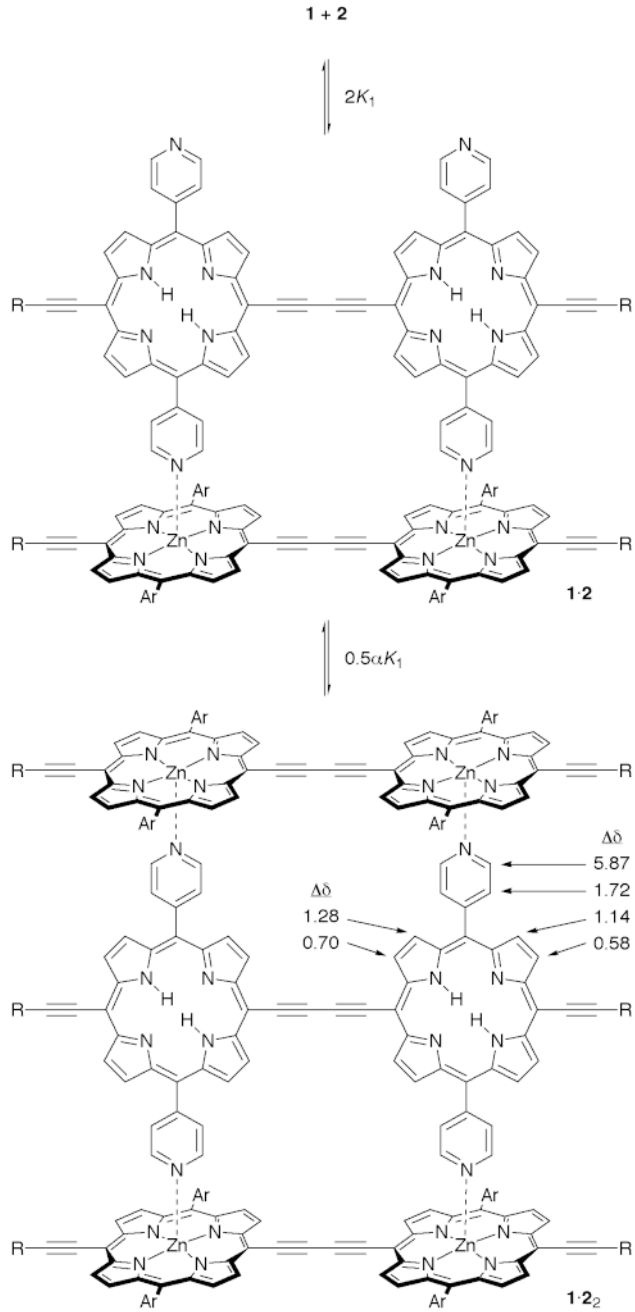

Scheme 1 Coordination of **1** and **2** gives **1**·**2** and **1**·$\mathbf{2}_2$. Selected complexation induced shifts are marked on **1**·$\mathbf{2}_2$, in ppm up-field relative to free **1** (equilibrium constants: $\alpha = 1.8 \pm 0.3$ and $K_1 \approx 10^8$–10^9 M^{-1} in CH_2Cl_2 at 298 K).

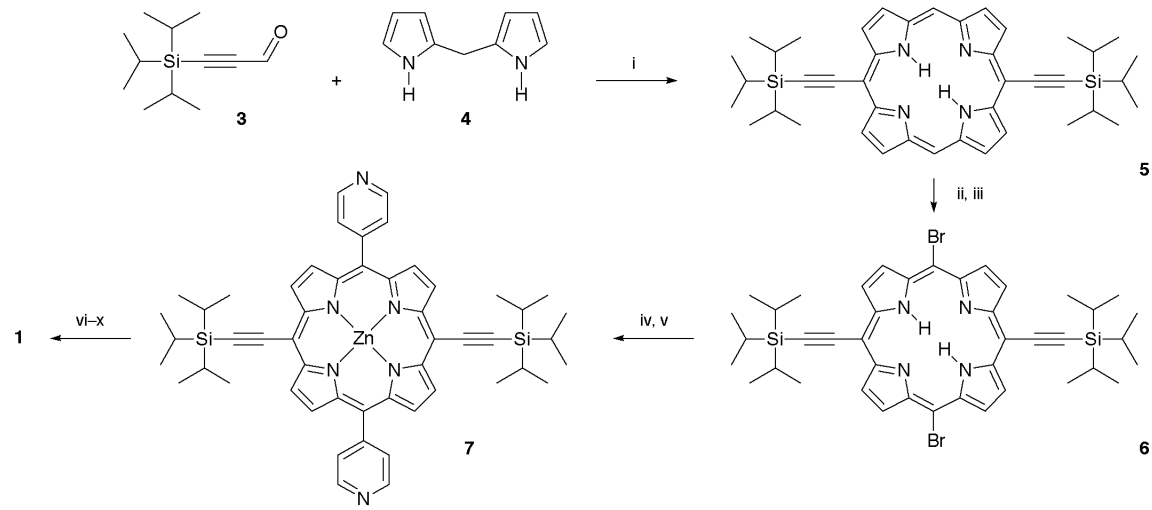

Scheme 2 *Reagents and conditions:* i, $BF_3{\cdot}OEt_2$, then DDQ, 31%; ii, MgI_2, 97%; iii, NBS then TFA, 59%; iv, $Zn(OAc)_2$, 92%; v, 4-(trimethylstannyl)pyridine, Pd_2dba_3, PPh_3, LiCl, PhMe, 83%; vi, TBAF (2 equiv.), 97%; vii, LiHMDS then $(n\text{-}C_6H_{13})_3SiCl$ (1 equiv.), 26%; viii, CuCl, TMEDA, CH_2Cl_2, air, 91%; x, TFA, 94%.

Fig. 1(*a*)–(*c*). If the conformations of dimers **1** and **2** were to remain unchanged when they form **1**·$\mathbf{2}_2$, then spectrum (*c*) would be the sum of spectra (*a*) and (*b*); clearly this is not the case. Formation of the triple strand array is accompanied by an increased splitting in the Soret band (B_x and B_y) and an increased red-shift in the Q_x band, both of which indicate increased conjugation, due to increased planarity. The absorption bands at 460 and 680 nm, which decrease when **1** and **2** bind together, can be attributed to less conjugated conformations with large porphyrin–porphyrin dihedral angles.

^{1}H NMR titrations (in CD_2Cl_2 or $CDCl_3$ at 298 K) confirm that **2** forms a 2:1 complex with **1**. When up to half an equivalent of ligand **1** is added to **2**, the system is in slow exchange. Sharp well-resolved signals are observed for free **2** and for the **1**·$\mathbf{2}_2$ complex, but there is no sign of **1**·**2**, nor of free **1**. Complete assignment of the ^{1}H NMR spectrum of **1**·$\mathbf{2}_2$ was made possible by the observation of NOEs from one of the β-pyrrole doublets to the trihexylsilyl end groups. The selected complexation-induced shifts marked on Scheme 1 support the proposed triple-strand geometry. When more than half an equivalent of **1** is added to **2**, the system goes into fast exchange. An equilibrium is established between **1**·$\mathbf{2}_2$ and **1**·**2**, which shifts gradually towards **1**·**2** as the concentration of **1** is increased. Analysis of this binding isotherm shows that the cooperativity coefficient α is 1.8 ± 0.3. The fact that there is positive cooperativity ($\alpha > 1$) confirms that formation of the **1**·**2** complex tends to hold the ligand unit **1** in a coplanar conformation, increasing its affinity for a second molecule of **2**.

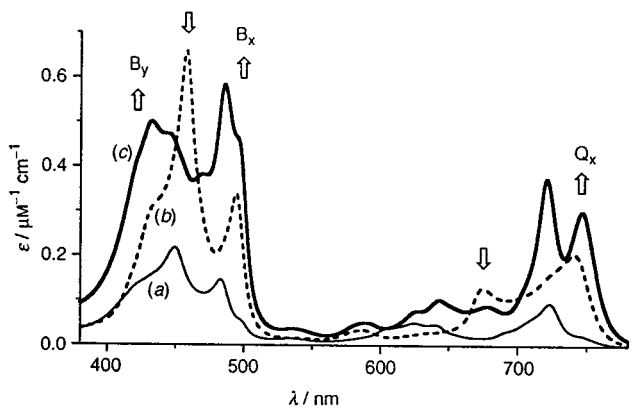

Fig. 1 Electronic absorption spectra of (*a*) **1**, (*b*) the **2**·(pyridine)$_2$ complex and (*c*) **1**·$\mathbf{2}_2$ in CH_2Cl_2. Spectrum (*b*) was recorded in the presence of excess pyridine and is scaled ×2 to facilitate comparison with (*c*). Arrows highlight regions of increased or decreased absorption in the **1**·$\mathbf{2}_2$ complex.

There has been some debate about the conformational properties of alkyne-linked conjugated porphyrin dimers such as **1** and **2**.[1b,2a,3,8] The results reported here demonstrate that these dimers explore a range of torsional angles in solution, and that non-covalent self-assembly can be used to hold them co-planar, to maximise the electronic coupling. A detailed analysis of the ^{1}H NMR and electronic spectra of structures such as **1**, **2** and **1**·$\mathbf{2}_2$ may enable us to elucidate the distribution of dihedral angles. The ability to control this conformational equilibrium should result in materials with enhanced non-linear optical behaviour.

This work was generously supported by the EPSRC. We thank the EPSRC mass spectrometry service (Swansea) for FAB mass spectra.

Notes and references

1 (*a*) H. L. Anderson, S. J. Martin and D. D. C. Bradley, *Angew. Chem., Int. Ed. Engl.*, 1994, **33**, 655; (*b*) V. S.-Y. Lin, S. G. DiMagno and M. J. Therien, *Science*, 1994, **264**, 1105; (*c*) G. E. O'Keefe, J. J. Halls, C. A. Walsh, G. J. Denton, R. H. Friend and H. L. Anderson, *Chem. Phys. Lett.*, 1997, **276**, 78; (*d*) B. Jiang, S.-W. Yang, D. C. Barbini and W. E. Jones Jr., *Chem. Commun.*, 1998, 213; (*e*) D. P. Arnold, G. A. Heath and D. A. James, *New J. Chem.*, 1998, 1377.

2 (*a*) H. L. Anderson, *Inorg. Chem.*, 1994, **33**, 972; (*b*) X. Chi, A. J. Guerin, R. A. Haycock, C. A. Hunter and L. D. Sarson, *J. Chem. Soc., Chem. Commun.*, 1995, 2563; (*c*) S. Anderson, H. L. Anderson, A. Bashall, M. McPartin and J. K. M. Sanders, *Angew. Chem., Int. Ed. Engl.*, 1995, **34**, 1096; (*d*) R. T. Stibrany, J. Vasudevan, S. Knapp, J. A. Potenza, T. Emge and H. J. Schugar, *J. Am. Chem. Soc.*, 1996, **118**, 3980; (*e*) K. Funatsu, T. Imamura, A. Ichimura and Y. Sasaki, *Inorg. Chem.*, 1998, **37**, 1798; (*f*) J. N. H. Reek, A. P. H. J. Schenning, A. W. Bosman, E. W. Meijer and M. J. Crossley, *Chem. Commun.*, 1998, 11; (*g*) C. M. Drain, F. Nifiatis, A. Vasenko and J. D. Batteas, *Angew. Chem., Int. Ed.*, 1998, **37**, 2344.

3 P. N. Taylor, J. Huuskonen, G. Rumbles, R. T. Aplin, E. Williams and H. L. Anderson, *Chem. Commun.*, 1998, 909.

4 G. S. Wilson and H. L. Anderson, *Synlett*, 1996, 1039.

5 (*a*) R. Schlözer and J.-H. Fuhrhop, *Angew. Chem., Int. Ed. Engl.*, 1975, **14**, 363; (*b*) L. R. Nudy, H. G. Hutchinson, C. Schieber and F. R. Longo, *Tetrahedron*, 1984, **40**, 2359.

6 S. G. DiMagno, V. S.-Y. Lin and M. J. Therien, *J. Am. Chem. Soc.*, 1993, **115**, 2513.

7 P. N. Taylor, A. P. Wylie, J. Huuskonen and H. L. Anderson, *Angew. Chem., Int. Ed.*, 1998, **37**, 986.

8 V. S.-Y. Lin and M. J. Therien, *Chem. Eur. J.*, 1995, **1**, 645; R. Stranger, J. E. McGrady, D. P. Arnold, I. Lane and G. A. Heath, *Inorg. Chem.*, 1996, **35**, 7791.

Communication 9/03883C

ChemComm

Synthesis of the first complex with acetonine as ligand: the first crystal structure of an acetonine derivative

José Vicente,* María Teresa Chicote, Rita Guerrero and M. Carmen Ramírez de Arellano†

Grupo de Química Organometálica,‡ Departamento de Química Inorgánica, Facultad de Química, Universidad de Murcia, Apartado 4021, Murcia, 30071 Spain. E-mail: jvs@fcu.um.es

Received (in Cambridge, UK) 15th June 1999, Accepted 8th July 1999

The complex $[Au(acetonine)_2]ClO_4$ (3·ClO_4) (acetonine = 2,2,4,4,6-pentamethyl-2,3,4,5-tetrahydropyrimidine) is obtained by bubbling NH_3 through an acetone solution containing equimolar amounts of $NaClO_4$ and [AuCl(tht)] (tht = tetrahydrothiophene); the crystal structure of 3·ClO_4 was determined by X-ray crystallography.

We have recently reported the synthesis of $[Au(NH_3)_2]Cl$ (**1**·Cl) by reacting [AuCl(tht)][1] (tht = tetrahydrothiophene) with NH_3 in acetone (Scheme 1).[2] The reaction of **1**·Cl with $TlCF_3SO_3$ or $AgClO_4$ gives, respectively, **1**·CF_3SO_3 or **1**·ClO_4. The latter two complexes react with acetone to give the first acetiminogold(I) complexes $[Au(NH{=}CMe_2)_2]X$ (**2**·CF_3SO_3,[3] **2**·ClO_4, Scheme 1) while **1**·Cl neither reacts with acetone nor with $NaClO_4$ in acetone, probably due to its low solubility in this solvent. In an attempt to prepare **1**·ClO_4 in a one-pot reaction, using $NaClO_4$ instead of $AgClO_4$, we bubbled NH_3 through an acetone solution containing equimolar amounts of [AuCl(tht)] and $NaClO_4$. However, a suspension formed from which a small amount of **1**·Cl was removed, and from the resulting solution the complex $[Au(acetonine)_2]ClO_4$ (**3**·ClO_4) (acetonine = 2,2,4,4,6-pentamethyl-2,3,4,5-tetrahydropyrimidine) was isolated in 88% yield (Scheme 1).

Acetonine was first characterized by Bradbury *et al.*[4] in 1947, based on its molecular refraction and its reduction and hydrolysis products. It has been reported to form among the decomposition products of acetimine $NH{=}CMe_2$,[5] but it is most frequently obtained from the reaction of acetone with ammonia; many attempts to improve its synthesis have recently been reported (most of them patents). Thermal or photochemical activation, as well as a wide variety of catalysts have been used.[6–13] Acetonine finds its main use in its reaction with acetone to give 2,2,6,6-tetramethyl-4-oxopiperidine (triacetonamine)[9,11,14–17] which is an attractive intermediate for the synthesis of pharmaceutical products, pesticides, photostabilizers for polymers *etc.*[18] With so much work devoted to acetonine and its derivatives we were rather surprised to find that neither a single acetonine complex of any element nor X-ray studies on acetonine itself or any substituted acetonine had been reported.

In the reaction of NH_3, [AuCl(tht)] and $NaClO_4$ leading to **3**·ClO_4, neither **1**·ClO_4 nor **2**·ClO_4 were detected. We have independently proved that these two complexes react with acetone solutions of NH_3 to give **3**·ClO_4 (Scheme 1) which could explain their absence among the reaction products, if they were formed. These results suggest that acetonine forms from the reaction of NH_3 with acetone and replaces tht in [AuCl(tht)]. The displacement of Cl^- by ClO_4^- (from [AuCl(tht)] or from the possible intermediate [AuCl(acetonine)], or even from the non-isolated **3**·Cl) is crucial in the formation of **3**·ClO_4 because, as mentioned above, in the absence of $NaClO_4$, [AuCl(tht)] and NH_3 react in acetone to give **1**·Cl. It is likely that in the latter reaction the insolubility of **1**·Cl prevents the substitution of NH_3 by acetonine to give **3**·Cl or [AuCl(acetonine)]. This and previous studies,[2,3] show the complexity of acetone solutions of NH_3 from which it is possible to isolate coordination compounds with NH_3, $NH{=}CMe_2$ and acetonine ligands.

The crystal structure of **3**·ClO_4 was determined by X-ray crystallography (Fig. 1).§ The structure consists of centrosymmetric $[Au(acetonine)_2]^+$ cations and perchlorate anions forming a chain through hydrogen bonds [N2···O2 3.26(1) Å, H2···O2 2.46(4) Å, N2–H2···O2 157(5)°]. In Fig. 1 the packing diagram along the *c* axis and the hydrogen bonds are shown. Although the gold atoms are in a chain there are no aurophilic interactions (Au···Au 5.921 Å). In the acetonine ring the C2–C1–N1–C4–N2 fragment is planar (mean deviation 0.0052 Å) and makes an angle of 44.7° with the C2–C3–N2 plane. The Au–N bond distance found in **3**·ClO_4 [2.040 (5) Å] is similar to those found in **2**·CF_3SO_3[3] [2.017(5), 2.018(2) Å] or other complexes containing Au–N(sp^2) bonds (range 1.985–2.07 Å).[19,20] The bond distances in the acetonine rings are similar to those found in compounds with the same hybridization and bond order.[21] ^1H and ^{13}C NMR spectra of **3**·ClO_4 show that the coordination of the gold center to the iminic nitrogen atom is maintained in solution, as no chiral centers seem to be present and one pair of Me groups show a change of chemical shift upon complexation [$\delta(Me)_{complex} - \delta(Me)_{acetonine}$] greater [0.57 ppm; asigned to methyls on C(6)] than the other one [0.09 ppm; asigned to methyls on C(4)].¶

This work was supported by DGES (PB-97/1047). R. G. and M. C. R. A. are grateful to Ministerio de Educación y Cultura (Spain) for Grants.

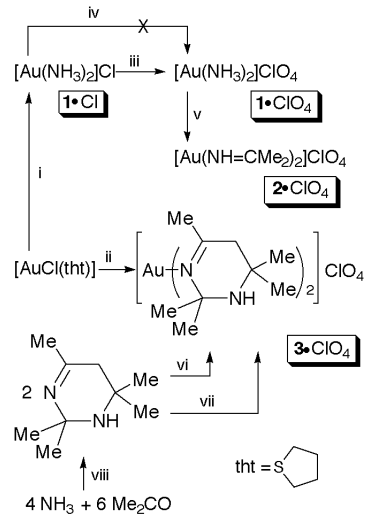

Scheme 1 *Reagents*: i, + 2 NH_3 − tht; ii, + 4 NH_3 + 6 Me_2CO + $NaClO_4$ − 6 H_2O − NaCl − tht; iii, + $AgClO_4$ − AgCl; iv, + $NaClO_4$; v, + 2 Me_2CO − 2 H_2O; vi, + $[Au(NH_2)_2]ClO_4$ − 2 NH_3; vii, + $[Au(NH{=}CMe_2)_2]ClO_4$ − $HN{=}CMe_2$; viii, − 6 H_2O.

† Present address: Departamento de Química Orgánica, Facultad de Química, Universidad de Valencia, 46100 Valencia, Spain. E-mail: mcra@fcu.um.es

‡ WWW: http://www.scc.um.es/gi/gqo/

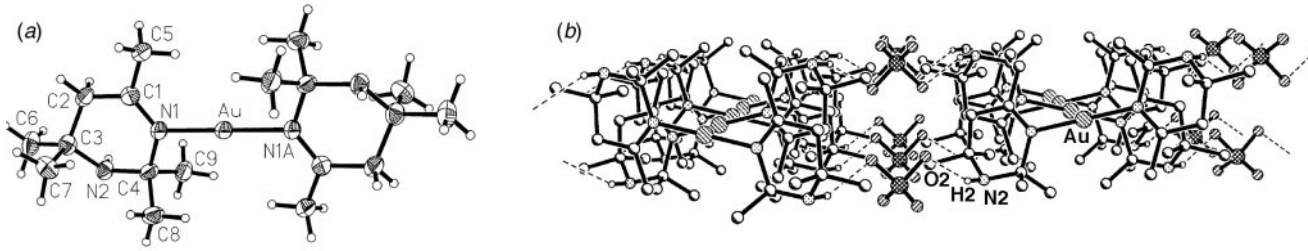

Fig. 1 (*a*) Crystal structure of the cation **3** showing the atom numbering scheme. Selected bond lengths (Å) and angles (°): Au–N1 2.040(5), N1–C1 1.297(8), C1–C2 1.502(8), C2–C3 1.528(7), C3–N2 1.469(7), N2–C4 1.474(7), C4–N1 1.510(7), N1–C1–C2 122.1(5), C1–C2–C3 112.6(5), C2–C3–N2 108.0(4), C3–N2–C4 118.3(4), N2–C4–N1 113.6(4), C4–N1–C1 122.6(5). (*b*) Packing diagram along the *c* axis of compound **3**·ClO_4 showing hydrogen bonds.

Notes and references

§ *Crystal data* for **3**·ClO_4: $C_{18}H_{36}AuClN_4O_4$, 0.48 × 0.40 × 0.02 mm, monoclinic, *C*2/*c*, a = 15.871 (2), b = 14.707 (2), c = 11.841 (2) Å, β = 123.910 (6)°, V = 2293.8 (5) Å^3, Z = 4, ρ_{calc} = 1.752 Mg m^{-3}, $2\theta_{max}$ = 50.0°, Mo-Kα radiation, λ = 0.71073 Å, ω-scans, T = 173(2) K, 3514 reflections measured, 1514 reflections observed [$I < 2\sigma(I)$], all 2009 independent reflections included in the refinement, R_{int} = 0.0383, absorption correction based on Ψ-scans (μ = 6.560 mm^{-1}, min./max. transmission = 0.140/0.732), the structure was solved by the heavy atom method and refined on F^2 using SHELXS86 and SHELXL93 (G. M. Sheldrick, University of Göttingen, Germany), 133 parameters, the N–H hydrogen was found on the difference Fourier synthesis and refined using an N–H distance restraint, other hydrogen atoms were refined as rigid methyl groups or using a riding model, the perchlorate anion is disordered over two sites, $R1$ [$I > 2\sigma(I)$] = 0.0287, $wR2$ (all reflections) = 0.0811, $\Delta\rho_{max}$ = 1.405 e Å^{-3} (at *ca*. 1 Å from the Au atom). CCDC 182/1322. See http://www.rsc.org/suppdata/cc/1999/1541 for crystallographic data in .cif format.

¶ Acetonine was isolated from an acetone solution of NH_3 by removing the solvent at room temperature. δ_H(300 MHz, $CDCl_3$) 1.12 [s, 6H, C(4)*Me*], 1.38 [s, 6H, C(2)*Me*], 1.87 (s, 2 H, CH_2), 1.96 [s, 3H, C(6)*Me*].

1 R. Usón, J. Laguna and J. Vicente, *J. Organomet. Chem.*, 1977, **131**, 471.
2 J. Vicente, M. T. Chicote, R. Guerrero, P. G. Jones and M. C. Ramírez de Arellano, *Inorg. Chem.*, 1997, **36**, 4438.
3 J. Vicente, M.-T. Chicote, M.-D. Abrisqueta, R. Guerrero and P. G. Jones, *Angew. Chem., Int. Ed. Engl.*, 1997, **36**, 1203.
4 R. B. Bradbury, N. C. Hancox and H. H. Hatt, *J. Chem. Soc.*, 1947, 1394.
5 K. Findeisen, H. Heitzer and K. Deehnicke, *Synthesis*, 1981, 702.
6 G. Goemar, M. Bernhardt and W. Haubold (Leuna-Werke A.-G.), DE 4,216,056, 1993 (*Chem. Abstr.*, 1994, **120**, 245138a).
7 A. Balogh, J. Durmis, K. M., J. Sabados, M. Collak, M. Magura and M. Holko, Cs 235,379, 1987 (*Chem. Abstr.* 1988, **108**, 167494z).
8 R. Ballardini, V. Borzatta, M. T. Gandolfi and R. Scrima, *Res. Discl.*, 1993, **354**, 701.
9 K. Sasaki, O. M. and K. Myake (Sumitomo Chemical Co), JP 07,291,931, 1995 (*Chem. Abstr.*, 1996, **124**, 202290j).
10 G. Shimada (Daicel Chemical Industries, Ltd.), JP 03,188,066, 1989 (*Chem. Abstr.*, 1992, **116**, 41319t).
11 Y. Fukuda (Kyowa Yuka Kk), JP 05,117,242, 1991 (*Chem. Abstr.*, 1993, **119**, 180817d).
12 I. Dragutan, S. Serban, P. Obloja, D. Nistor and V. Dragutan (Combinatul Petrochimic, Pitesti), Rom. RO 96,131, 1987 (*Chem. Abstr.*, 1990, **113**, 172048q).
13 I. Dragutan, S. Servan, P. Obloja, D. Nistor and V. Dragutan (Combinatul Petrochimic, Pitesti), Rom. RO 96,132, 1987 (*Chem. Abstr.*, 1990, **113**, 212011f).
14 M. Inaba and Y. Inui (Mitsubishi Petrochemical Co., Ltd.), JP 01,233,271, 1989 (*Chem. Abstr.*, 1990, **112**, 55627w).
15 R. Kinishi and M. Kasagi (Yoshitomi Pharmaceutical Industries, Ltd.), JP 62,132,859, 1985 (*Chem. Abstr.*, 1987, **107**, 198104f).
16 K. Sakanashi and Y. Azaki (Yoshitomi Pharmaceutical Industries, Ltd.), JP 62,167,763, 1987 (*Chem. Abstr.*, 1988, **108**, 150314t).
17 R. Kinishi (Yoshitomi Pharmaceutical Industries, Ltd.), JP 63,10,761, 1988 (*Chem. Abstr.*, 1988, **109**, 92800f).
18 Z. Ma, Q. Huang and J. M. Bobbit, *J. Org. Chem.*, 1993, **58**, 4837.
19 W. Schneider, A. Bauer and H. Schmidbaur, *J. Chem. Soc., Dalton Trans.*, 1997, 415; W. Schneider, A. Bauer, A. Schier and H. Schmidbaur, *Chem. Ber.*, 1997, **130**, 1417.
20 W. Schneider, K. Angermaier and H. Schmidbaur, *Z. Naturforsch., Teil B*, 1996, **51**, 801.
21 F. H. Allen, O. Kennard, D. G. Watson, L. Brammer, A. G. Orpen and R. Taylor, *J. Chem. Soc., Perkin Trans. 1*, 1987, S1.

Communication 9/04777H

Fully substituted cyclooctatetraenes assembled by the [4 + 4] cross coupling of two different diene units: a shunting strategy of Wilke's metallacyclopentadiene coupling mechanism†

Yoshihiko Yamamoto, Tatsuya Ohno and Kenji Itoh*

Department of Molecular Design and Engineering, Graduate School of Engineering, Nagoya University, Chikusa, Nagoya 464-8603, Japan. E-mail: itohk@apchem.nagoya-u.ac.jp

Received (in Cambridge, UK) 8th June 1999, Accepted 1st July 1999

The first regio- and chemo-selective synthesis of fully substituted cyclooctatetraenes from two or three different alkynes was achieved using the cross-coupling between 1,4-dicuprabuta-1,3-dienes and 1,4-diiodobuta-1,3-dienes.

Since Reppe's historical discovery of his cyclooctatetraene (COT) synthesis from acetylene,[1] the nickel-catalyzed cyclotetramerization of alkynes leading to COTs has been extensively studied from both synthetic and mechanistic points of view.[2] The catalytic reactions, however, are generally limited to the parent and terminal acetylenes, and the reaction of monosubstituted alkynes gave the 1,2,4,6-, 1,2,4,7- and 1,3,5,7-substituted isomers depending on the alkyne employed rather than on the nature of the catalyst. Moreover, the concomitant formation of other oligomers and polymers of alkynes is also a problem for the catalytic methods.

Forty years after Reppe's discovery of the Ni-catalyzed COT synthesis,[1] Wilke proposed a fascinating mechanism: two nickelacyclopentadienes generated from four molecules of acetylene couple together to form COT.[3] Based on this proposal, we postulated that highly substituted COTs **1** might be chemo- and regio-selectively synthesized if the selective coupling between two different independently prepared metallacycles is possible. In order to realize such an idea, the cross-coupling of 1,4-dicuprabuta-1,3-dienes **2** with 1,4-diiodobuta-1,3-dienes **3** was investigated instead of the direct coupling of the parent metallacyclopentadiene counterparts **4** and **5** (Scheme 1).[4] The vinylcopper reagents **2** can be prepared by the transmetallation of the corresponding zirconacyclopentadienes **4** as reported by Takahashi and coworkers.[5] The bifunctional electrophile, diiodides **3**, can be readily obtained from the corresponding titanacyclopentadienes **5** and iodine according to the Tamao–Sato procedure.[6]

At the outset, we examined the coupling of an isolated bicyclic zirconacyclopentadiene **6**[7] with a cyclic diiodide **7a**.

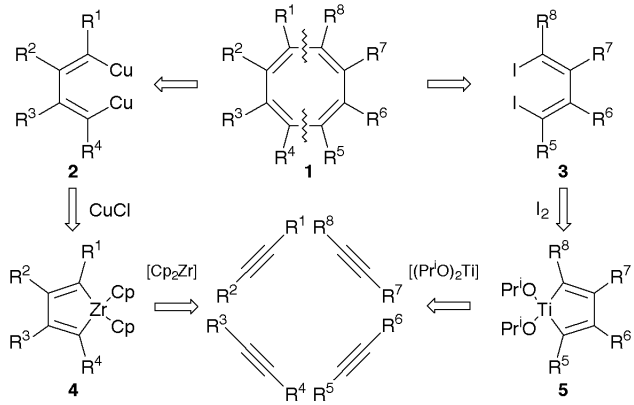

Scheme 1

† Experimental and spectral data for **9** and **12a–f** are available from the RSC web site, see http://www.rsc.org/suppdata/cc/1999/1543/

Interestingly, both diene units **6** and **7a** were prepared from a common precursor, 4-oxa-1,7-bis(trimethylsilyl)hepta-1,6-diyne. In the presence of 3 equiv. of 1,3-dimethyl-3,4,5,6-tetrahydro-2(1*H*)-pyrimidone (DMPU), equimolar amounts of **6** and **7a** were treated with 2.1 equiv. of CuCl in THF at 50 °C for 15 h. The usual work-up followed by chromatographic separation gave a symmetrically substituted coupling product **9**[8] in 56% yield (Scheme 2). Its structure was confirmed based on the following spectral data: in its ^{1}H NMR spectra, only one singlet of the four trimethylsilyl groups was observed at δ 0.27, indicative of **9** having a highly symmetrical structure. This was also supported by its ^{13}C NMR spectra, in which only two sp^2 signals were observed at δ 116.3 and 143.3 together with a signal of the trimethylsilyl groups and a signal of the methylene carbon α to the ether oxygen at δ −0.6 and 70.1, respectively. Nonaromatic COT is known to exist in a tub shape rather than in a planar structure.[9] This is also true for **9**; the expected **8** isomerized to the thermodynamically more favorable tub-shaped isomer **9**. This was deduced by the absorption of its methylene protons α to the ether oxygen being observed as a couple of doublets with a geminal coupling constant J = 16.5 Hz.

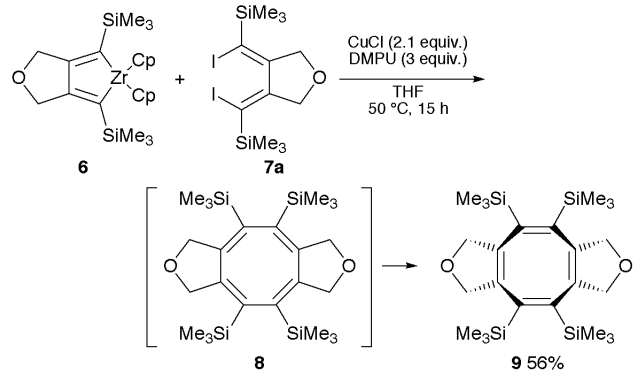

Scheme 2

The cyclic structure of **7a** plays a critical role in the present coupling; an acyclic diiodide **10** gave no coupling product under the same reaction conditions. This is attributed to the conformational flexibility of its butadiene moiety. The diiodobutadiene moiety fixed as the s-*cis* form in **7a** is required for the cross coupling, whereas acyclic **10** may mainly exist in the s-*trans* form in order to avoid steric repulsion between the two iodine atoms (Scheme 3).

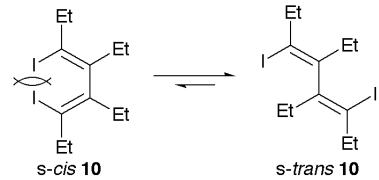

Scheme 3

Based on these results, we next examined the generality of this approach (Table 1). According to established methods,[5] unstable zirconacycles[10] were converted into the corresponding dicopper reagents **11a**–**d** without isolation. In the presence of DMPU, the diiodide **7a** was reacted with **11a**[11] at ambient temperature for 1 h to afford the desired coupling product **12a**[8] in high yield (88%). In the same manner, a cyclic dicopper **11b** derived from deca-2,8-diyne gave a tricyclic product **12b**[8] in 52% yield. In contrast, the coupling of a tetraphenyl-substituted dicopper **11c** required higher temperature. The reaction of **11c** with **7a** was carried out at 50 °C for 1 h to afford **12c**[8] in 56% yield. Similarly, an unsymmerical dicopper **11d**, prepared from hex-3-yne and oct-4-yne, gave the corresponding unsymmetrical COT **12d**[8] in 79% yield. In addition to the furan derivative **7a**, a cyclopentane **7b** and a pyrrolidine **7c** can be used as the diiodide units. The reaction with dicopper **11a** gave **12e**[8] and **12f**[8] in 65 and 41% yields, respectively.

Table 1 Cross coupling of dicoppers **11a**–**d** with diiodides **7a**–**c**[a]

Dicopper	Diiodide	Conditions	Product and yield[b]
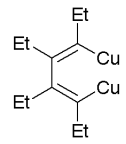 **11a**	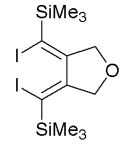 **7a**	rt, 1 h	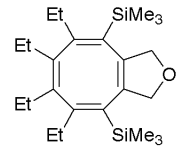 **12a** 88%
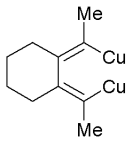 **11b**	**7a**	rt, 1 h	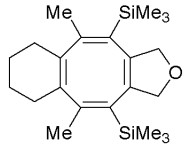 **12b** 52%
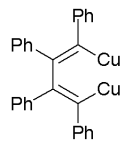 **11c**	**7a**	50 °C, 1 h	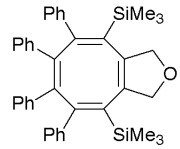 **12c** 56%
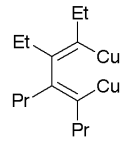 **11d**	**7a**	rt, 1 h	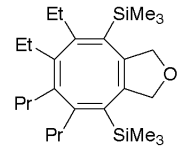 **12d** 79%
11a	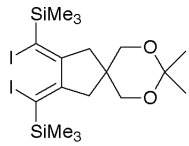 **7b**	50 °C, 20 h	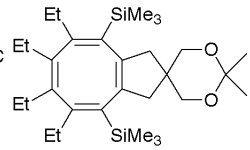 **12e** 65%
11a	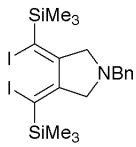 **7c**	rt, 20 h	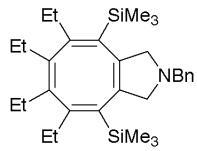 **12f** 41%

[a] Zirconacyclopentadiene (1 mmol), **7** (0.5 mmol), CuCl (2.1 mmol), DMPU (3 mmol), THF (5 ml). [b] Isolated yields based on **7**.

In addition to the furan derivative **7a**, a cyclopentane **7b** and a pyrrolidine **7c** can be used as the diiodide units. The reaction with dicopper **11a** gave **12e**[8] and **12f**[8] in 65 and 41% yields, respectively.

In conclusion, we successfully developed a novel strategy to assemble fully substituted COTs by imitating Wilke's coupling mechanism of two metallacyclopentadiene moieties for the prototype Ni-catalyzed COT synthesis. This approach allows us to synthesize fully substituted unsymmetrical COTs with complete chemo- and regio-selectivity from 1,4-dicuprabuta-1,3-dienes and 1,4-diiodobuta-1,3-dienes as different diene units.

We gratefully acknowledge financial support in the form of a Grant-in-Aid (09305059 and 10132222) from the Ministry of Education, Science Sports and Culture, Japan.

Notes and references

1 W. Reppe, O. Schlichting, K. Klager and T. Toepel, *Justus Liebigs Ann. Chem.*, 1948, **560**, 1.

2 P. W. Jolly, in *Comprehensive Organometallic Chemistry*, ed. G. Wilkinson, F. G. A. Stone and E. W. Abel, Pergamon, London, 1982, vol. 8, p. 649.

3 G. Wilke, *Pure Appl. Chem.*, 1978, **50**, 677.

4 The Ni-mediated homo-coupling of a 1,4-dilithiobuta-1,3-diene was reported, see: C. J. Lawrie, K. P. Gable and B. K. Carpenter, *Organometallics*, 1989, **8**, 2274.

5 CuCl-Mediated cross-coupling of zirconacyclopentadienes, see: T. Takahashi, M. Kotora, K. Kasai and N. Suzuki, *Organometallics*, 1994, **13**, 4183; T. Takahashi, R. Hara, Y. Nishihara and M. Kotora, *J. Am. Chem. Soc.*, 1996, **118**, 5154; M. Kotora, C. Umeda, T. Ishida and T. Takahashi, *Tetrahedron Lett.*, 1997, **38**, 8355; T. Takahashi, W.-H. Sun, Y. Liu, K. Nakajima and M. Kotora, *Organometallics*, 1998, **17**, 3841; T. Takahashi, Z. Xi, A. Yamazaki, Y. Liu, K. Nakajima and M. Kotora, *J. Am. Chem. Soc.*, 1998, **120**, 1672.

6 S. Yamaguchi, R.-Z. Jin, K. Tamao and F. Sato, *J. Org. Chem.*, 1998, **63**, 10 060.

7 F. Mohamadi and M. M. Spees, *Organometallics*, 1992, **11**, 1398.

8 All new compound were characterized according to their ^{1}H and ^{13}C NMR and mass spectra.

8 O. Bastiansen, L. Hedberg and K. Hedberg, *J. Chem. Phys.*, 1957, **27**, 1311.

9 E. Negishi, S. J. Holmes, J. M. Tour, J. A. Miller, F. E. Cederbaum, D. R. Swanson and T. Takahashi, *J. Am. Chem. Soc.*, 1989, **111**, 3336; Z. Xi, R. Hara and T. Takahashi *J. Org. Chem.*, 1995, **60**, 4444.

10 Although only 1 equiv. is required, 2 equiv. of **11** were used to ensure the complete consumption of **7**.

Communication 9/04556B

ChemComm

A novel double-strand helical motif in a two-dimensional polymeric complex of silver(I) perchlorate with benzo[*e*]acephenanthrylene

Megumu Munakata,*[a] Gui Ling Ning,[b] Yusaku Suenaga,[a] Kunihisa Sugimoto,[a] Takayoshi Kuroda-Sowa[a] and Masahiko Maekawa[a]

[a] *Department of Chemistry, Kinki University, Kowakae, Higashi-Osaka, Osaka 577-8502, Japan. E-mail: munakata@chem.kindai.ac.jp*

[b] *School of Chemical Engineering, Dalian University of Technology, Dalian, China. E-mail: jxsui@nmemc.gov.cn*

Received (in Cambridge, UK) 18th May 1999, Accepted 29th June 1999

A 2-D double-strand helical complex with a strand of polycyclic aromatic hydrocarbons and a strand of silver(I) perchlorate has been isolated and crystallographically characterised.

Polymetallic helical complexes are of special interest because of their structural similarities to nucleic acids. They are also intrinsically interesting for their potential applications in the fields of supramolecular chemistry, asymmetric catalysis, and nonlinear optical materials.[1–3] Very often, these helicates are prepared by the coordination of metal ions to tailored polydentate organic strands, such as oligopyridines and some optically active organic ligands, in which nitrogen or oxygen atoms always serve as binding units along the strand.[1–6] In contrast, we report an unprecedented 2-D double-strand helical polymer synthesized from a polycyclic aromatic hydrocarbon (PAH), benzo[*e*]acephenanthrylene (bpa), and silver(I) perchlorate. It was proven in our earlier studies that metal complexes with planar PAH ligands have a tendency to form decker-like or multilayer architectures.[7–9] To our surprise, the planar bpa can lead to the formation of a helical structure with a sheet network. Here we present our results showing how the bpa molecules are self-assembled and wrapped about the flexible silver(I) ions to construct a unique double-strand helical architecture. Some physicochemical properties of the complex are also discussed.

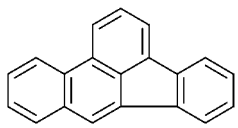

benzo[*e*]acephenanthrylene (bpa)

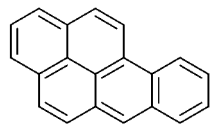

benzo[*a*]pyrene (L)

The reaction of bpa with $AgClO_4$ in toluene leads to formation of the complex $[Ag_4(bpa)_3(ClO_4)_4]$ **1**.† The X-ray structural determination‡ reveals a two-dimensional framework constructed from cation–π interactions of Ag^I with bpa. While there are two crystallographically independent Ag^I cations, both of them have a similar pseudotetrahedral environment comprising two C=C π-bonds from two aromatic groups and two oxygen atoms from two perchlorate anions (taking the C=C group as one ligand) (Fig. 1). The Ag–O and Ag–C distances range from 2.402(6) to 2.69(1) Å, and 2.412(6) to 2.755(6) Å, respectively. The next closest contact between silver and carbon is 2.867(8) Å, well beyond the limits from 2.40 to 2.76 Å observed in the reported silver(I) aromatic complexes.[7] On the other hand, the aromatic ligand also involves two different coordination modes, one displaying μ-di-η^2 coordination with two metal ions above and below the aromatic plane, and the other exhibiting a μ-tri-η^2 motif with three metal centers on the same side of the aromatic plane. Furthermore, these aromatic ligands are coordinated to the silver(I) ions by wrapping about them to construct a double-helical chain with the silver(I) perchlorate groups in one strand and the μ-tri-η^2 aromatic ligands in the other (Fig. 2). The period of the helix is equal to the crystallographic *a* axis (14.11 Å). In addition, each μ-di-η^2 bpa moiety functions as a linkage bridging two adjacent helical chains *via* the Ag^I ions. This results in extended interactions of the double-strand helical chains to form the two-dimensional framework shown in Fig. 3.

The most significant structural feature presented here is the interesting arrangement of bpa molecules and unusual coordination of the silver ions forming a unique helical structure. As established in the literature,[2] for most helicates the governing factor of the structure is that the organic ligand is shaped into one strand and contains several binding units, such as N or O, along the strand allowing the recognition and coordination of the metal ions. By comparison, the organic strands in complex **1** are self-assembled *via* π–π interactions at the overlapped portion of two adjacent μ-tri-η^2 bpa molecules, with a shortest interplanar separation of 3.52 Å. On the other hand, the flexible silver(I) ions, linked by perchlorate anions, exhibit a special spiral structure, being bound both to these stacked aromatic strands forming the helical chains and to the μ-di-η^2 bpa molecules exhibiting a sheet framework. Such a structural feature, to the best of our knowledge, has not been described before. There is only one example in the literature describing a helical structure of a polycyclic aromatic hydrocarbon, $[Ag_4(L)_2(ClO_4)_4(toluene)_2]$ (L = benzo[*a*]pyrene), where no stacking interactions were observed along the organic strand, and the double-helical chains are formed by aromatic π–π interactions *via* interweaved strands of polycycles.[7]

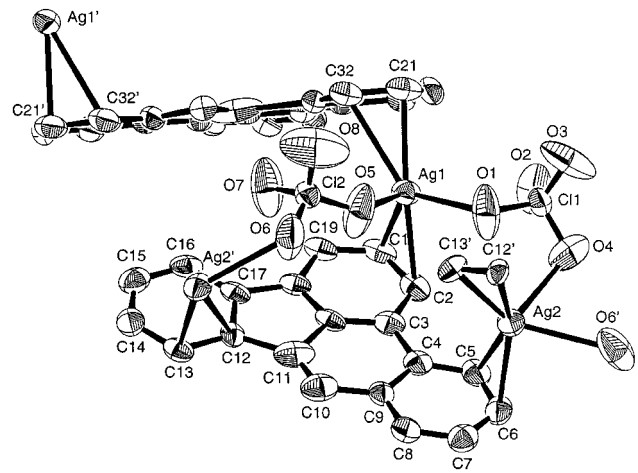

Fig. 1 Structure and partial labeling of $[Ag_4(bpa)_3(ClO_4)_4]$. Selected bond lengths (Å) and angles (°): Ag(1)–O(1) 2.452(7), Ag(1)–O(5) 2.402(6), Ag(1)–C(1) 2.502(6), Ag(1)–C(2) 2.555(6), Ag(1)–C(21) 2.446(7), Ag(1)–C(32) 2.720(7), Ag(2)–O(4) 2.69(1), Ag(2)–O(6) 2.532(8), Ag(2)–C(5) 2.622(7), Ag(2)–C(6) 2.454(6), Ag(2)–C(12) 2.755(6), Ag(2)–C(13) 2.412(6); O(1)–Ag(1)–O(5) 77.2(2), O(1)–Ag(1)–C(1) 125.0(3), O(1)–Ag(1)–C(21) 106.0(3), O(5)–Ag(1)–C(1) 118.9(3), O(5)–Ag(1)–C(21) 105.6(3), C(1)–Ag(1)–C(21) 116.8(2), O(4)–Ag(2)–O(6) 72.5(2), O(4)–Ag(2)–C(6) 104.7(3), O(4)–Ag(2)–C(13) 110.5(3), O(6)–Ag(2)–C(6) 86.3(3), O(6)–Ag(2)–C(13) 130.0(3), C(6)–Ag(2)–C(13) 135.2(3).

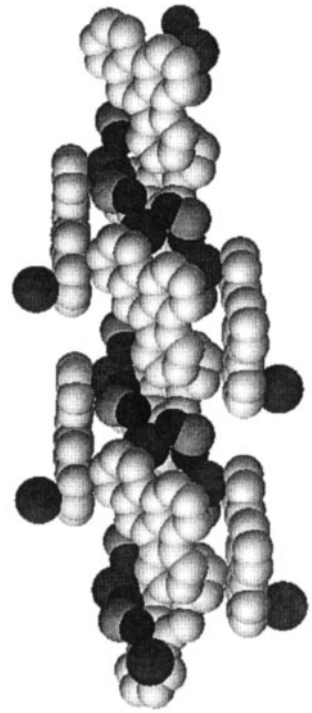

Fig. 2 Space-filling model of the double-strand helical structure of **1**.

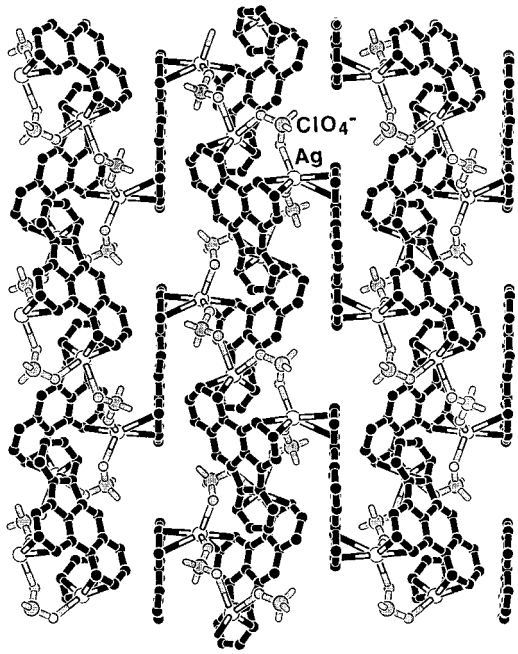

Fig. 3 Two-dimentional sheet framework of **1**.

The compound is soluble in most common organic solvents. It is reasonably stable in ambient daylight for 1 week, but shows slight moisture sensitivity under atmospheric conditions. The UV–VIS absorption spectrum of the free ligand bpa in toluene (2.5×10^{-4} M) displays an intense absorption around 350 nm, indicative of a $\pi \rightarrow \pi^*$ transition.[10] Upon complexation to Ag(I), the transition does not change significantly, probably due to the dissociation of the complex in solution. The electrical conductivity of the complex and its free ligand bpa was measured *via* the silver-coated two-probe technique with compacted pellets and showed that complex **1** displays semiconducting behavior with a σ value of 1.1×10^{-4} S cm^{-1}, whereas the bpa free ligand is non-conducting at room temperature.

It is obvious that helicates can sometimes be obtained from non-stranded polycyclic aromatic hydrocarbons through stacking interactions. Although structural control in this new system is rather difficult compared with the conventional polydentate strand-like organic ligands,[1,2] once structural control and molecular programming have been significantly explored and improved, the very interesting motifs isolated may broaden our insight into the helicate research field and introduce a novel perspective in the area of supramolecular chemistry. Further studies are directed toward the development of the structure-predicting process in this area with the aim of exploring the intrinsic nature and design of other novel helicate frameworks.

This work was partly supported by a Grant-in-Aid for Science Research [Nos. 10440201 and 10016743 (priority areas)] from the Ministry of Education, Science, Culture and Sports, Japan.

Notes and references

† To a solution of benzo[*e*]acephenanthrylene (25.2 mg, 0.1 mmol) in 1 ml of toluene was added $AgClO_4$ (84 mg, 0.4 mmol). After about 20 min of stirring, the resultant colorless solution was introduced into a 7 mm diameter glass tube and layered with *n*-hexane as a diffusion solvent. The glass tube was sealed under Ar and wrapped with aluminium foil. After standing at room temperature for 3 days yellow brick-like crystals were obtained (calc. for $C_{60}H_{36}Cl_4Ag_4O_{16}$: C, 45.39; H 2.27. Found: C, 44.96; H, 2.31%). **CAUTION:** Perchlorate salts of metal complexes with organic ligands are potentially explosive. Suitable care should be taken during the synthesis.

‡ *Crystal data* for **1**: $C_{60}H_{36}Cl_4Ag_4O_{16}$, M = 1586.22, orthorhombic, space group *Pbcn* (#60), a = 14.114(1), b = 18.0670(7), c = 20.8589(4) Å, V = 5319.0(4) Å^3, Z = 4, D_c = 1.981 g cm^{-3}, μ(Mo-Kα) = 17.24 cm^{-1}, F(000) = 3120.00, T = 293(2) K, 6044 reflections collected (Quatum CCD diffactometer), 3628 unique reflections, R_1 = 0.060 (3628 reflections), wR = 0.158. The μ-di-η^2 bpa molecule was analyzed as disordered such that there is a mirror plane bisecting the longer molecular axis. CCDC 182/1308. See http://www.rsc.org/suppdata/cc/1999/1545/ for crystallographic data in .cif format.

1 M. Munakata, L. P. Wu and T. Kuroda-Sowa, *Adv. Inorg. Chem.*, 1999, **46**, 173.
2 C. Piguet, G. Bernardinelli and G. Hopfgartner, *Chem. Rev.*, 1997, **97**, 2005.
3 P. Comba, A. Fath, T. W. Hambley, A. Kühner, D. T. Richens and A. Viefort, *Inorg. Chem.*, 1998, **37**, 4389.
4 K. A. Hirsch, S. R. Wilson and J. S. Moore, *Inorg. Chem.*, 1997, **36**, 2960.
5 G. Baum, E. C. Constable, D. Fenske, C. E. Housecroft and T. Kulke, *Chem. Commun.*, 1999, 195.
6 L. Carlucci, G. Ciani, D. M. Proserpio and A. Sironi, *Inorg. Chem.*, 1998, **37**, 5941.
7 M. Munakata, L. P. Wu, T. Kuroda-Sowa, M. Maekawa, Y. Suenaga, G. L. Ning and T. Kojima, *J. Am. Chem. Soc.*, 1998, **120**, 8610.
8 L. P. Wu, G. L. Ning and M. Munakata, *Coord. Chem. Rev.*, in the press.
9 M. Munakata, L. P. Wu, G. L. Ning, T. Kuroda-Sowa, M. Maekawa and Y. Suenaga, *J. Am. Chem. Soc.*, 1999, **121**, 4968.
10 C. Piguet, G. Bernardinelli, B. Bocquet, A. Quattrpni and A. F. Williams, *J. Am. Chem. Soc.*, 1992, **114**, 7440.

Communication 9/03941D

ChemComm

Solid-phase synthesis of pyrrolidines employing a cyclisation–cleavage strategy

Richard C. D. Brown* and Martyn Fisher

Department of Chemistry, University of Southampton, Highfield, Southampton, UK SO17 1BJ.
E-mail: rcb1@soton.ac.uk

Received (in Liverpool, UK) 20th May 1999, Accepted 28th June 1999

The solid-phase synthesis of several pyrrolidines has been realised utilising imino-Sakurai and palladium-catalysed cyclisation–cleavage reactions as key steps.

The development of solid-phase combinatorial and multiple parallel synthesis methods has stimulated considerable interest in the design of new linkers and cleavage strategies which are suitable for the release of small molecules from the solid support.[1–4] Linkers or cleavage conditions which activate a polymer-bound molecule towards nucleophilic cleavage can be particularly useful providing an additional point of variability in the released compounds,[4] or allowing the formation of a ring upon cleavage.[4,5] Here we describe the development of a novel nucleophile-cleavable linker that is sufficiently robust to survive a multi-step reaction sequence, yet can be cleaved under mild conditions with incorporation of a nucleophile.

Several linkers which rely upon the palladium-catalysed cleavage of allylic systems have been reported, releasing carboxylic acids or amines (through an intermediate carbamic acid) from the resin.[6–9] We imagined that a reversed allylic linker would provide a mild means of generating electrophilc π-allyl palladium species which could be trapped with heteroatom- or carbon-centred nucleophiles to release cyclic **2** or acyclic **3** products from the solid phase (Scheme 1).

In order to demonstrate the viability of a palladium-catalysed cyclisation–cleavage reaction we chose to investigate the solid-phase synthesis of pyrrolidines **4** (Scheme 2).[10,11] A key intermediate is the homoallylic amine **5** which could be derived from the reaction of a resin-bound allylic nucleophile with an imine.[11–13] The presence of an ester group in the linker meant that the reactivity of the allyl metal component would have to be attenuated, leading us to consider the use of an allylic silane as the immobilised nucleophile.

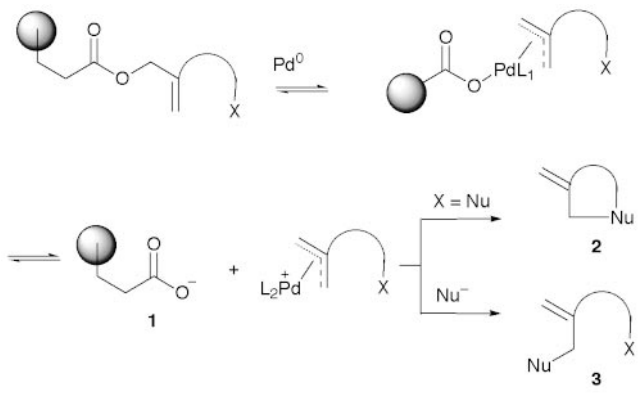

Scheme 1

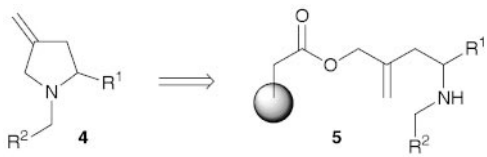

Scheme 2

Before attempting any solid-phase work the analogous solution chemistry was investigated (Scheme 3). 2-Hydroxymethyl-3-trimethylsilylpropene **6** was esterified with 2-methyl-3-phenylpropanoyl chloride to give the allylic silane **7a**. Addition of **7a** to the preformed *N*-acyl imine **8** provided a satisfactory yield of the homoallylic amine **9a**. Attempted cyclisation of either the Boc-protected homoallylic amine **9a** or the corresponding deprotected primary amine failed using 10 mol% $Pd(acac)_2$ with 15 mol% diphenylphosphinoethane (dppe). However, deprotection and reductive alkylation of **9a** provided secondary amine **10a** which when subjected to the same cyclisation conditions afforded the desired pyrrolidine **11** in 35% yield. Although some of the yields in the solution pyrrolidine synthesis were rather low, we were sufficiently satisfied with the overall approach to carry out further optimisation on the solid phase.

Solid phase synthesis of pyrrolidine **11** started with a carboxyethylated polystyrene resin† **1** which was prepared in three steps from Merrifield resin. The 2-hydroxymethyl-3-trimethylsilylpropene **6** was immobilised under standard carbodiimide coupling conditions using an excess of DMAP to prevent the well-known side reaction leading to a resin-bound *N*-acylurea. The imino-Sakurai reaction required some optimisation, turning out to be the most challenging step in the solid-phase reaction sequence. The effect of changing several reaction parameters including reaction time, amount of *N*-acylimine and the amount of Lewis acid was investigated. The efficiency of the reaction was measured by reduction of the ester linkage followed by purification of the cleaved alcohol **12** and quantification (Scheme 4). Our results are shown in Table 1. Optimum conditions required a large excess of the *N*-acylimine **8** and an excess of $BF_3{\bullet}OEt_2$ relative to the resin-bound allylsilane **7b** (entry 7), providing significantly better yield of the homoallylic amine than was achieved in the analogous reaction in solution.

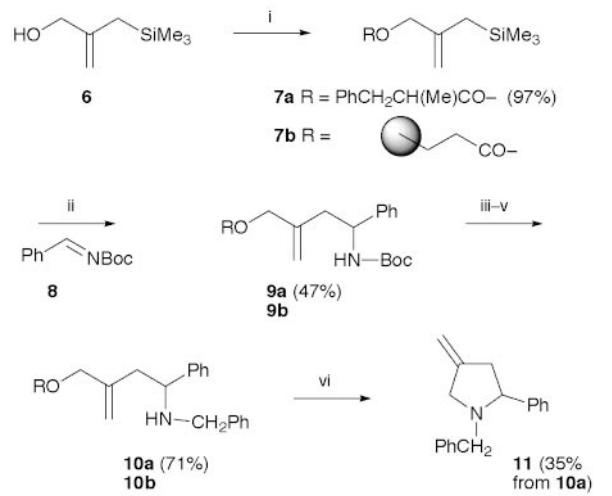

Scheme 3 *Reagents and conditions*: i, 1,3-diisopropylcarbodiimide, DMAP, CH_2Cl_2, **1**; or 2-methyl-3-phenylpropionyl chloride, CH_2Cl_2, pyridine; ii, $BF_3{\bullet}OEt_2$, CH_2Cl_2; iii, TFA, CH_2Cl_2; iv, PhCHO, AcOH, CH_2ClCH_2Cl; v, $Me_4NB(OAc)_3H$, CH_2ClCH_2Cl; vi, $Pd(acac)_2$, dppe, THF, Δ.

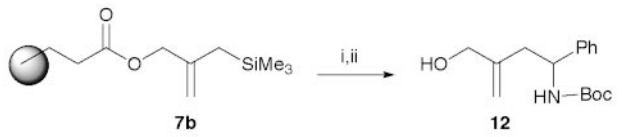

Scheme 4 *Reagents and conditions*: i, **8**, BF_3•OEt_2, CH_2Cl_2; ii, $LiBH_4$, MeOH (1 equiv.), THF.

Table 1 Effect of reaction parameters on yield

Entry	Molar ratio[a] of *N*-acylimine **8**	Molar ratio[a] of BF_3•OEt_2	Reaction time/h	Yield[a] (%)
1	8	12	12	16
2	8	4	12	25
3	15	8	12	61
4	15	8	28	49
5	23	8	12	70
6	23	8	3	70
7	23	4	3	70

[a] The yield represents the amount of purified isolated alcohol **12** relative to the loading of the carboxylated resin **1**. Molar ratios are also based upon the loading of the carboxylated resin **1**.

Removal of the carbamate protecting group from **9b** and a two-step reductive alkylation using benzaldehyde gave the resin-bound cyclisation precursor **10b**, which was also quantified by reductive cleavage from the resin. Initial attempts to perform the cyclisation–cleavage reaction of **10b** gave the desired heterocycle **11** in low yield, even when a large quantity of palladium complex was employed. However, efficient catalytic cyclisation-cleavage was achieved by employing a three-fold excess of the dppe ligand relative to palladium (10 mol% based upon the loading of the carboxylated resin **1**), returning an excellent yield of the desired pyrrolidine **11**.‡

In order to demonstrate the scope of the palladium-catalysed cyclisation–cleavage reaction, pyrrolidines **11** and **13**–**17** were synthesised.§ In all instances the desired pyrrolidine was obtained, furthermore the purity of the crude product, except in the case of **13**, was judged to be high by inspection of the ^1H NMR spectra. Notably, the crude pyrrolidines **11**, **13**–**17** were

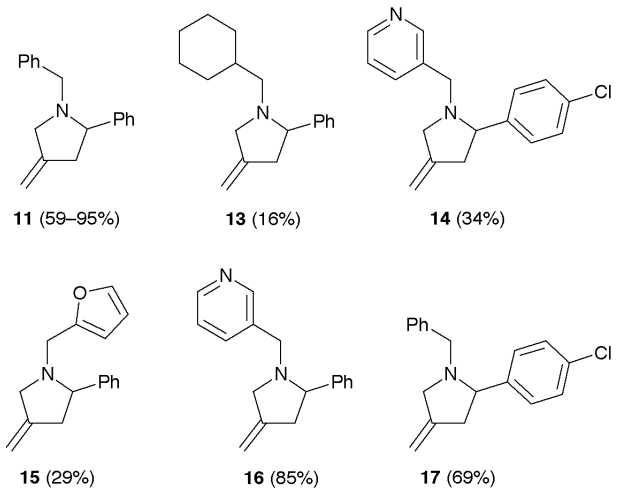

cleaner than their acyclic precursors which were released from the resin by reductive cleavage of **18** using $LiBH_4$. This significant result suggests that the cyclisation–cleavage reaction acts as an in-built quality control step, favouring the release of

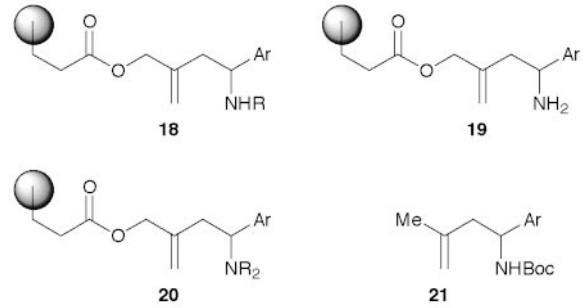

the desired product over the release of by-products from earlier steps. To test this theory further, several of the possible by-products from the deprotection–reductive alkylation sequence **9b**, **19** and **20** were subjected to the cyclisation–cleavage reaction conditions. No significant quantity of material was released from any of the resins **9b**, **19** or **20**. Interestingly, treatment of the resin **9b** recovered from the attempted palladium-catalysed cleavage with $LiBH_4$ in THF afforded a reduced product **21** in 80% yield rather than the expected allylic alcohol **12**.

In summary, the viability of a palladium-catalysed cyclisation–cleavage reaction has been demonstrated by the solid-phase synthesis of pyrrolidines **11** and **13**–**17**. This strategy should also be amenable to the solid-phase synthesis of other heterocyclic and carbocyclic compounds. Intermolecular palladium-catalysed nucleophilic cleavage, using $LiBH_4$ as a source of hydride, is also possible releasing substituted propene derivatives such as **21**.

We wish to thank the Royal Society for a University Research Fellowship (R. C. D. B.), and the EPSRC for a QUOTA studentship (M. F.). We wish to acknowledge the use of the EPSRC's Chemical Database Service at Daresbury.[14]

Notes and references

† Merrifield resin was heated with the sodium salt of diethyl malonate at 60 °C for 14 h. Hydrolysis was carried out in refluxing THF–2 M KOH (9:1). Finally, decarboxylation in THF–HCl gave the desired carboxyethylated polystyrene **1**.

‡ Yields have been calculated based on the loading of the carboxylated polystyrene resin **1**.

§ All reactions were carried out on at least a 50 μM scale with respect to the loading of the carboxylated polystyrene resin **1**. All products were purified by flash chromatography and gave satisfactory analytical data.

1 S. Booth, P. H. H. Hermkens, H. C. J. Ottenheijm and D. C. Rees, *Tetrahedron*, 1998, **54**, 15 385.
2 R. C. D. Brown, *J. Chem. Soc., Perkin Trans. 1*, 1998, 3293.
3 H.-M. Eggenweiler, *Drug Discovery Today*, 1998, **3**, 552.
4 I. W. James, *Tetrahedron*, 1999, **55**, 4855.
5 J. H. van Maarseveen, *Comb. Chem. High Throughput Screening*, 1998, **1**, 185.
6 F. Guibé, O. Dangles, G. Balavoine and A. Loffet, *Tetrahedron Lett.*, 1989, **30**, 2641.
7 K. Kaljuste and A. Undén, *Tetrahedron Lett.*, 1996, **37**, 3031.
8 H. Kunz and B. Dombo, *Angew. Chem., Int. Ed. Engl.*, 1988, **27**, 711.
9 X. Zhang and R. A. Jones, *Tetrahedron Lett.*, 1996, **37**, 3789.
10 B. M. Trost and P. J. Bonk, *J. Am. Chem. Soc.*, 1985, **107**, 1778.
11 B. M. Trost and C. M. Marrs, *J. Am. Chem. Soc.*, 1993, **115**, 6636.
12 S. J. Veenstra and P. Schmid, *Tetrahedron Lett.*, 1997, **38**, 997.
13 W. J. N. Meester, F. Rutjes, P. H. H. Hermkens and H. Hiemstra, *Tetrahedron Lett.*, 1999, **40**, 1601.
14 D. A. Fletcher, R. F. McMeeking and D. Parkin, *J. Chem. Inf. Comput. Sci.*, 1996, **36**, 746.

Communication 9/04135D

Pyrolysis reactions of 4-nonafluorobiphenyl prop-2-enyl ether: a remarkable rearrangement reaction

Andrei S. Batsanov, Gerald M. Brooke,* Darren Holling and Alan M. Kenwright

Chemistry Department, Science Laboratories, South Road, Durham, UK DH1 3LE.
E-mail: g.m.brooke@durham.ac.uk

Received (in Liverpool, UK) 21st April 1999, Accepted 9th July 1999

The formation of the unexpected bicyclic compound 16 *via* the pyrolytic isomerisation of 4-nonafluorobiphenyl prop-2-enyl ether 8 can be rationalised by invoking the intermediacy of a rare retro-cyclisation reaction of the internal Diels–Alder adduct 12 (from the Claisen intermediate 9) to a tethered ketene 18, recyclisation *via* the alternative mode to 17 and its subsequent transformation.

In some earlier work[1] the thermolysis of pentafluorophenyl prop-2-enyl ether **1** *in vacuo* at 137–141 °C over 13 days was shown to give **3**, one of the two possible intramolecular Diels–Alder adducts from the intermediate Claisen rearrangement compound **2**. Under FVP conditions at 365 °C and 0.05 mmHg through a silica tube packed with silica wool, **1** gave the cyclohexa-2,5-dienone **4** *via* **2** followed by a classical Cope rearrangement,[2] while under even more forcing conditions at 440 °C and 0.001 mmHg the fluorovinyl compound **5** was isolated, formed by the decomposition of **3** and loss of HF.[3] In a separate FVP experiment at 480 °C and 0.05–0.1 mmHg, **1** was also shown to be converted into the bicyclic compound **7**, the formation of which was rationalised by invoking the decomposition of the other possible intramolecular Diels–Alder adduct **6**, formed from **2**.[4] All these reactions are summarised in Scheme 1 which also shows the original objective of the present work: namely, the investigation of the pyrolysis of the closely related 4-nonafluorobiphenyl prop-2-enyl ether **8** to ascertain whether **10**, an expected intermediate from the Claisen rearrangement intermediate **9**, would undergo two further possible rearrangements to give the novel isomer **11**; to our knowledge, no Cope rearrangement has ever been described in which one moiety in a 3,3-sigmatropic reaction is an aromatic ring. In the event, no isomerisation of **8** to either **10** or **11** occurred, but a much more interesting rearrangement reaction was discovered.

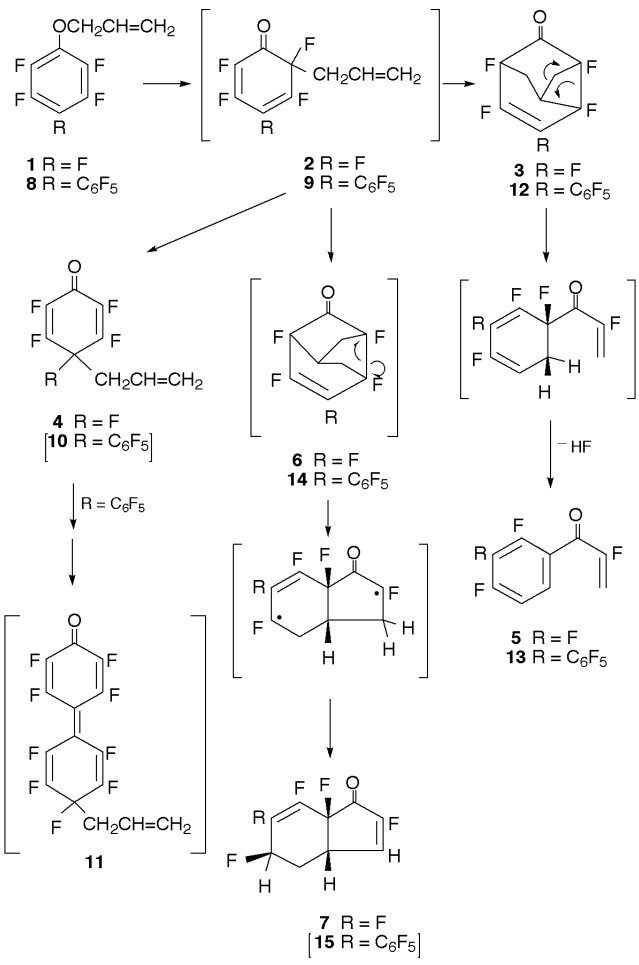

Scheme 1

The starting ether **8**, readily accessible from 4-hydroxynonafluorobiphenyl,[5] was subjected to FVP at 350 °C and 0.01 mmHg as before to give a complex mixture of products among which was **12** (13% isolated yield), the structure of which was determined by X-ray crystallography† (Fig. 1). When the pyrolysis of the ether **8** was carried out at 420 °C and 0.01 mmHg, more than 90% of the crude product was shown by ^{19}F NMR spectroscopy to contain three major products in the proportions shown, which were separated by chromatography on silica using light petroleum (bp 40–60 °C)–Et_2O (95 : 5 v/v): 4-hydroxynonafluorobiphenyl (46%); the fluorovinyl compound **13** (24%) (identified unequivocally by ^{1}H, ^{19}F and ^{19}F–^{19}F COSY NMR spectroscopy); and a compound isomeric with the starting material, possessing a CHF functionality (readily identified by ^{1}H NMR spectroscopy as a doublet, $J_{H,F}$ 49 Hz) (30%). Not all of the ^{1}H and ^{19}F NMR characteristics of this latter product were in agreement with the expected bicyclic

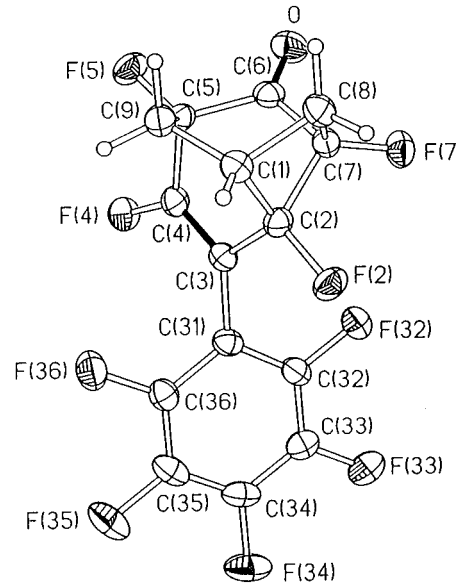

Fig. 1 Molecular structure of **12** (50% displacement ellipsoids; double bonds shown in black).

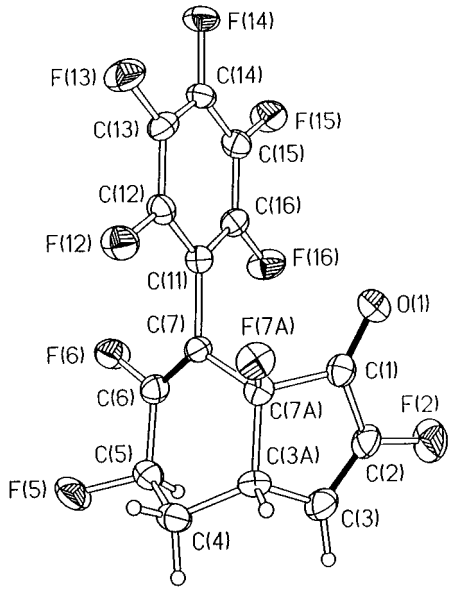

Fig. 2 Molecular structure of **16** (50% displacement ellipsoids; double bonds shown in black).

compound **15** which would have been formed if the Diels–Alder adduct **14** had been produced directly from the Claisen intermediate **9** by analogy with the mechanism proposed earlier for the formation of **7** from **1** *via* **2** and then **6**. The material was shown by X-ray crystallography† to have the structure **16** (Fig. 2) which enabled all the NMR data to be rationalised.

The formation of compound **16** (a racemate, but having the enantiomeric structure shown in Scheme 2 when formed from **12** with the configuration given), isomeric with the starting material **8**, poses an intriguing mechanistic problem since the Diels–Alder adduct **14** must not have been formed from **9** during the reaction; the precursor to **16** has to be **17**, the basic skeleton of which is identical with **14** but having the alkenic F and R groups interchanged. The formation of the unexpected intermediate tricyclic compound **17** can be rationalised most simply on the basis of a retro-Diels–Alder reaction of **12** to give the cyclohexa-2,4-dienylmethyl fluoroketene **18**—a very rare[6] reaction type—followed by the alternative intramolecular Diels–Alder cyclisation as shown in Scheme 2. Intermolecular (4 + 2) π reactions of ketenes to form six-membered *carbocyclic* rings[7] are uncommon, but an intramolecular process of this type has been recorded.[8]

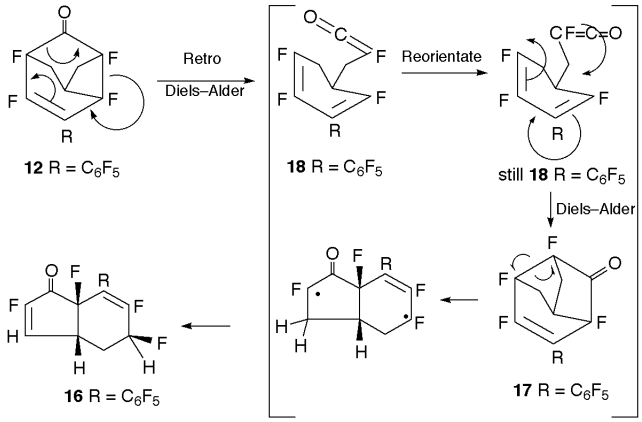

Scheme 2

The present work begs the question: *why* do the complex molecular dynamics involved in the rearrangement of **12** to **17** take place in preference to the direct formation of **14** having the same basic carbon skeleton? We have no real answer to this question but models show that the formation of structures **6**[4] and **14** from **2** and **9** respectively are sterically more demanding than for the formation of compounds **3** and **12**, which were isolated under milder conditions. Consequently, even the formation of **7** is likely to proceed *via* this new molecular rearrangement reaction.

Notes and references

† *Crystal data* for **12**: $C_{15}H_5F_9O$, M = 372.2, monoclinic, space group $C2/c$ (No. 15), a = 21.242(3), b = 6.219(2), c = 20.254(2) Å, β = 93.05(1)°, U = 2671.8(8) Å, Z = 8, D_c = 1.851 g cm^{-3}, μ = 1.84 mm^{-1}, T = 150 K, 3080 reflections (2394 unique) with $2\theta \leqslant 150°$, 247 variables, R_1 = 0.037 and wR_2 = 0.098 on 1926 data with $I \geqslant 2\sigma(I)$, max. residual $\Delta\rho$ = 0.25 e Å^{-3}. For **16**: $C_{15}H_5F_9O$, M = 372.2, monoclinic, space group $P2/c$ (No. 13), a = 13.446(2), b = 11.033(1), c = 19.249(1) Å, β = 108.41(1)°, U = 2709.4(5) Å, Z = 8, D_c = 1.825 g cm^{-3}, μ = 1.81 mm^{-1}, T = 150 K, 5009 reflections (4172 unique) with $2\theta \leqslant 135°$, 492 variables, R_1 = 0.046 and wR_2 = 0.100 on 3238 data with $I \geqslant 2\sigma(I)$, max. residual $\Delta\rho$ = 0.23 e Å^{-3}. X-Ray experiments were performed on a Rigaku AFC6S 4-circle diffractometer (Cu-Kα radiation, $\bar{\lambda}$ = 1.54184 Å, $2\theta/\omega$ scan mode); structure solution (direct methods) and least-squares refinement (non-H atoms anisotropic, all H refined isotropically, against F^2 of all data) with SHELX-97 software (G. M. Sheldrick, University of Göttingen, Germany, 1997); CCDC 182/1326. See http://www.rsc.org/suppdata/cc/1999/1549/ for crystallographic data in .cif format.

1 G. M. Brooke and D. H. Hall, *J. Fluorine Chem.*, 1982, **20**, 163.
2 G. M. Brooke, *Tetrahedron Lett.*, 1971, 2377.
3 G. M. Brooke and D. H. Hall, *J. Chem. Soc., Perkin Trans. 1*, 1976, 1463.
4 G. M. Brooke, *J. Chem. Soc., Perkin Trans. 1*, 1974, 233.
5 M. W. Buxton, R. H. Mobbs and D. E. M. Wotton, *J. Fluorine Chem.*, 1972/73, **2**, 231.
6 D. J. Pollart and H. W. Moore, *J. Org. Chem.*, 1989, **54**, 5444; T. T. Tidwell, *Ketenes*, Wiley, New York, 1995.
7 J. A. Hyatt and P. W. Raynolds, *Org. React.*, 1994, **45**, 159.
8 T. Miyashi, H. Kawamoto, T. Nakajo and T. Mukai, *Tetrahedron Lett.*, 1979, 155.

Communication 9/03209F

Photocatalytic epoxidation of propene by molecular oxygen over highly dispersed titanium oxide species on silica

Hisao Yoshida,* Chizu Murata and Tadashi Hattori

Department of Applied Chemistry, Graduate School of Engineering, Nagoya University, Nagoya 464-8603, Japan. E-mail: yoshidah@apchem.nagoya-u.ac.jp

Received (in Oxford, UK) 17th June 1999, Accepted 2nd July 1999

Highly dispersed titanium oxide species on silica prepared by the sol-gel method catalyse selective epoxidation of propene by molecular oxygen upon photoirradiation.

Propene epoxidation is of industrial importance. The mixed oxide of Ti and Si has been recognized as a catalyst for the epoxidation of olefins with hydroperoxides and is employed industrially to produce propene oxide (PO) from propene.[1] TS-1, titanium-containing crystalline silica, is known to catalyse epoxidation of propene using H_2O_2.[2] However, employing oxygen as oxidant would be the most economical way of carrying out the oxidation.[1] The discovery of catalysts for the epoxidation of propene by molecular oxygen is highly desirable. One of the most promising systems for this reaction should be photocatalysis on silica-supported systems, since PO was obtained as a product over Nb/SiO_2,[3] Mg/SiO_2 and even over bare amorphous silica[4,5] with significant selectivity. However, the PO yield in these systems was still low, and it is not clear whether the reaction proceeds catalytically or not.

In the present study, we prepared highly dispersed titanium oxide species on silica by two methods, impregnation and sol-gel methods, and examined their photocatalytic activity for propene epoxidation using molecular oxygen.

Amorphous silica was prepared from $Si(OEt)_4$ by the sol-gel method followed by calcination in a flow of air at 773 K for 5 h.[6] The bulk titanium oxide employed was a Japan Reference Catalyst (JRC-TIO-4; equivalent to P-25). A silica-supported titanium oxide sample containing 0.1 mol% Ti (Ti/Ti + Si), referred to as T/S(0.1), was prepared by the impregnation method.† A TiO_2–SiO_2 mixed oxide sample containing 0.34 mol% Ti, T-S(0.34), was prepared by the sol-gel method.‡ The Ti content was determined by inductively coupled plasma (ICP) measurements. A diffuse reflectance UV-VIS absorption spectrum of the sample *in vacuo* was recorded at room temperature with a JASCO V-570 spectrophotometer after the same pretreatment as for the photoreaction test.

Before the photoreaction, the samples were heated in air up to 673 K, and then evacuated. Subsequently the samples were treated with 100 Torr oxygen (1 Torr = 133.3 N m^{-2}) at 673 K for 1 h, followed by evacuation at 673 K for 1 h.§ The photooxidation of propene was carried out in a closed reaction vessel made of quartz (123.6 cm^3) for 2 h. The temperature of the catalyst bed was elevated by *ca.* 20 K from room temperature by the photoirradiation. The reactants were propene (100 μmol, 15 Torr) and oxygen (200 μmol, 30 Torr). The catalyst (200 mg) was spread on the flat bottom (12.6 cm^2) of the vessel. A 200 W Xe lamp was used as the light source. Products in the gas phase and products desorbed by photoirradiation for 1 h were analyzed separately by gas chromatography, followed by analysis of the desorbed products by heating at 573 K. The results presented here are the sum of each product yield. The products were propene oxide (PO), propanal (PA), acetone (AC), acrolein (AL), acetaldehyde (AA), alcohols (MeOH, EtOH and Pr^iOH), hydrocarbons (ethene and butenes; HC) and CO and CO_2 (CO_x).

Fig. 1 shows diffuse reflectance UV-VIS spectra of the samples. Bare silica showed no large absorption band [Fig. 1(*a*)], while bulk TiO_2 showed a large absorption band below the band gap [Fig. 1(*d*)]. Both T/S(0.1) and T-S(0.34) exhibited a narrow band centred at *ca.* 210 nm [Fig. 1(b),(*c*)] which is assigned to the ligand-to-metal charge transfer band of highly dispersed tetrahedral titanium species.[7] This means that T/S(0.1) and T-S(0.34) consist of predominantly highly dispersed tetrahedral titanium species on silica.

Table 1 shows the results of photooxidation of propene by molecular oxygen on the samples. Bare silica (entry 1) exhibited almost the same conversion (1.53%) and propene oxide selectivity (22.3%) as previously reported.[4,5] The conversion to CO_x was not significant. Other major by-products are AC, AL and AA. Bulk TiO_2 (entry 2) showed high photooxidation activity; the conversion of propene was 14.1% when irradiated for 1 h (half of the standard irradiation time). However, the

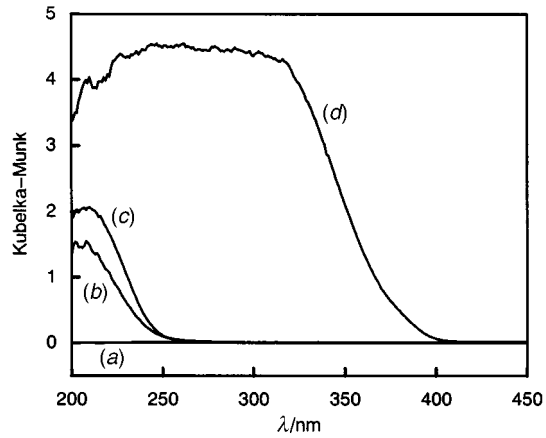

Fig. 1 Diffuse reflectance UV-VIS spectra of (*a*) silica, (*b*) T/S(0.1), (*c*) T-S(0.34) and (*d*) TiO_2.

Table 1 Results of the photooxidation of propene

Entry	Sample	BET surface area/ $m^2\ g^{-1}$	Irradiation time/h	Conversion of propene (%)	PO yield (%)	Selectivity (%)							
						PO	PA	AC	AL	AA	Alcohol	HC	CO_x
1	SiO_2	558	2	0.7	0.2	27.1	1.4	26.7	8.9	16.8	6.0	8.8	4.3
2	TiO_2	34	1	14.1	0.0	0.0	0.0	1.3	0.0	0.8	0.0	1.7	96.2
3	T/S (0.1)	477	2	9.1	3.7	40.8	3.3	11.3	4.2	24.5	3.6	2.3	10.0
4	T-S (0.34)	423	2	9.2	5.3	57.5	2.7	5.8	1.2	21.1	0.0	5.1	6.6

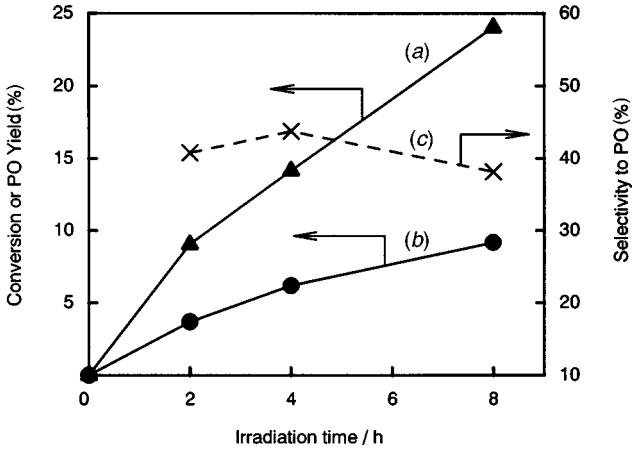

Fig. 2 Time course of (*a*) propene conversion, (*b*) PO yield and (*c*) PO selectivity in the photooxidation of propene by molecular oxygen on T/S(0.1).

major product (96.2%) was CO_x; no propene oxide was observed.

On the other hand, the silica-supported titania sample T/S(0.1) (entry 3) exhibited higher selectivity to PO (40.8%) than bare silica and bulk TiO_2. The conversion of propene on T/S(0.1) was much higher than on bare silica, while selectivity to CO_x was considerably lower than bulk TiO_2. Therefore, it was found that dispersed titanium oxide on silica has a moderate ability to produce PO from propene and molecular oxygen upon photoirradiation.

T-S(0.34) prepared by the sol-gel method showed almost the same conversion as T/S(0.1); therefore, an accurate comparison of product selectivity was allowed. Obviously the PO selectivity on T-S(0.34) was higher than that on T/S(0.1); it was also higher than the selectivities previously reported in the literature.[3–5] The conversion to CO_x was also suppressed more than that of T/S(0.1). It is thus indicated that T-S(0.34) has excellent properties for this photoepoxidation; sol-gel methods should be advantageous for producing active sites for selective photoepoxidation of propene using molecular oxygen.

Fig. 2 presents the time course of propene conversion, PO yield and PO selectivity in the photooxidation on T/S(0.1). The conversion of propene and yield of PO increased with increasing irradiation time. The selectivity was not affected significantly by the conversion at least until a conversion of 24.1%. After 8 h photoirradiation, the yield of PO achieved was 9.2% of the initial amount of propene. The amount of PO produced was 9.2 μmol, and the calculated amount of titanium ions in the reactor was 3.33 μmol. Even if all the titanium ions were active sites, the turnover number¶ would be 2.8, indicating that the photoepoxidation of propene on titanium oxide species on silica proceeded catalytically. This is the first report of the catalytic photooxidation of propene to propene oxide by molecular oxygen.

In conclusion, highly dispersed titanium oxide species were found to catalyse the photooxidation of propene to propene oxide by molecular oxygen at room temperature. The selectivity to propene oxide on titanium oxide species on silica was affected by the preparation method; the sol-gel method was superior to conventional impregnation methods. Titania–silica prepared by the sol-gel method in the present study showed higher selectivity to propene oxide than those previously reported in the literature. It is expected that fine-tuning of the preparation method, the amount of titanium oxide and the reaction conditions should further enhance their activities.

This work was supported by a Grant-in-aid from the Ministry of Education, Science, Art, Sports and Culture, Japan.

Notes and references

† Calcined silica was impregnated by aqueous solutions of ammonium titanyl oxalate, dried at 383 K for 12 h and calcined at 773 K in a flow of air for 5 h.

‡ A mixture of $Si(OEt)_4$, EtOH, H_2O and HNO_3 (1, 3.8, 1, and 0.085 mol, respectively) was stirred at 353 K for 3 h and cooled down to room temperature. An Pr^iOH solution of titanium isopropoxide was added dropwise and stirred at 293 K for 2 h, followed by very slow addition of an aqueous solution of HNO_3 [1 and 0.085 mol respectively, the amount of this acid solution was equivalent to that of $Si(OEt)_4$ used]. Two weeks later, the obtained gel was heated at a rate of 0.2 K min^{-1} up to 338 K and dried for 5 h. After drying for an additional 5 h at 373 K, the TiO_2–SiO_2 mixed oxide was obtained by calcination at 773 K in a flow of air for 8 h.

§ This treatment temperature was lower than that of the previous reports (refs. 4,5) because low temperature (673 K, even room temperature) was found to be sufficient to activate the sample.

¶ Turnover number is defined as (the amount of produced PO)/(the amount of catalytic active sites).

1 B. Notari, *Adv. Catal.*, 1996, **41**, 253.
2 M. G. Clerich, G. Bellussi and U. Romano, *J. Catal.*, 1991, **129**, 159.
3 T. Tanaka, H. Nojima, H. Yoshida, H. Nakagawa, T. Funabiki and S. Yoshida, *Catal.Today*, 1993, **16**, 297.
4 H. Yoshida, T. Tanaka, M. Yamamoto, T. Funabiki and S. Yoshida, *Chem. Commun.*, 1996, 2125.
5 H. Yoshida, T. Tanaka, M. Yamamoto, T. Yoshida, T. Funabiki and S. Yoshida, *J. Catal.*, 1997, **171**, 351.
6 S. Yoshida, T. Matsuzaki, T. Kashiwazaki, K. Mori and K. Tarama, *Bull. Chem. Soc. Jpn.*, 1974, **47**, 1564.
7 S. Bordiga, S. Coluccia, C. Lamberti, L. Marchese, A. Zecchina, F. Boscherini, F. Buffa, F. Genoni, G. Leofanti, G. Petrini and G. Vlaic, *J. Phys. Chem.*, 1994, **98**, 4125.

Communication 9/04886C

ChemComm

Intramolecular C–H···O hydrogen bonding reduces cation complexation strength in a fluorescent crown ether

Stephen L. De Wall, Eric S. Meadows, Leonard J. Barbour and George W. Gokel*

Bioorganic Chemistry Program and Department of Molecular Biology and Pharmacology, Washington University School of Medicine, 600 S. Euclid Avenue, Campus Box 8103 St. Louis, MO 63110, USA.
E-mail: ggokel@molecool.wustl.edu

Received (in Columbia, MO, USA) 6th April 1999, Accepted 20th May 1999

Complexes of the fluorescent crown ether, *N,N*-bis(9-anthrylmethyl)-4,13-diaza-18-crown-6, with NaI_3 and KSCN reveal the presence of intramolecular C–H···O hydrogen bonds that appear to control conformation and lead to reduced cation binding affinity.

For more than a decade, the fluorescent properties of macrocycles have proved fascinating.[1] A hope has been that fluorescent residues appended to macrocycles would afford lariat ethers[2] that could function as cation sensors.[3] Indeed, de Silva and de Silva demonstrated 'fluorescent signaling' in *N*-(9-anthrylmethyl)aza-15-crown-5 and -18-crown-6 nearly 15 years ago.[4] Anthracene has proved particularly popular as the fluorescent element. It has, for example, been incorporated into crowns and cryptands used as probes of phospholipid membrane fluidity.[5] It has been attached to one crown, to two crowns, and *via* the 9- and 10-positions of a single molecule to a macrocycle to afford proton sensors.[6] Two anthracenes incorporated into a macrocycle[7] and two anthracenes attached to a crown afforded a crown–cryptand photoswitch.[8] Anthracene has also been incorporated as the fluorescent element for sensing Cu^{2+} ions[9] and D-glucosamine.[10] Very recently, Kubo, Ishige and Sakurai have prepared and studied *N,N′*-bis(9-anthrylmethyl)-4,13-diaza-18-crown-6 **1** for use as a fluorescent cation sensor. In the latter case, some cation binding selectivity and cation-induced fluorescence change were observed, but the results were generally modest. This is surprising for such a widely used and strongly fluorescent residue. We now report the first solid state structures of **1** bound by either Na^+ or K^+. Intimate C–H···O hydrogen bonding between the sidearm and macrorings clearly decrease the ability of **1** to form stable cation complexes and, in turn, diminish their utility as sensors.

Compound **1** was prepared by heating commercial 9-chloromethylanthracene, 4,13-diaza-18-crown-6,[11] and Na_2CO_3 in MeCN for 72 h. Crystallization from toluene afforded **1** as yellow needles (68%, mp 195–196 °C).[12] Kubo and co-workers report **1** in 90% yield as yellow needles (from $CHCl_3$) having mp 189–190 °C. The NaI_3 complex of **1** was isolated from a mixture of **1** and NaI (1:1) in THF that was not protected from the air. The rhombohedral crystals obtained (dark yellow to brown) had the stoichiometry **1**·NaI_3·$(THF)_2$ and decomposed on melting, presumably with loss of THF, at *ca.* 215 °C. A projection of the complex is shown in Fig. 1.

There are several notable features about this complex. First, the macroring is in the D_{3d} conformation, as expected. The average Na^+–O distance is 2.46 Å and the Na^+–N distances are 3.03 and 2.92 Å. These values are typical for diaza-18-crown-6 Na^+ complexes. The sidearms are in the *anti* conformation, one being above, and the other below, the mean plane of the macroring heteroatoms. The *anti* orientation of the anthryl sidearms effectively excludes the anion from the cation's solvation sphere. It is especially interesting that the two (disordered) THF molecules (normally excellent donors) found in the crystal lattice do not coordinate the cation. Since the macroring is essentially planar, it is reasonable to expect the apical position(s) to be occupied by donor groups. Either I_3^- or THF or a combination of the two could fill the void above and below the macrocycle but neither does. Instead, the space is filled by anthracene.

There are two especially close contacts between C–H bonds and electronegative elements. The first involves the hydrogen atoms on anthracene's 1-position (α-position). The C···O distances are 3.54 (θ = 152.7°) and 3.58 Å (θ = 156.7°). If the aromatic C–H bonds are 0.95 Å long, this makes the average H-bond distance ~2.7 Å from the nearest macroring oxygen atom. The second type of close contast is a C···I interaction observed between one (but not the other) of the anthracene 2-positions (β-positions) and the proximal terminus of I_3^- (3.79 Å) and has a C–H–I bond angle of *ca.* 140°. In contrast, the shortest distance between Na^+ and any iodine atom or either THF oxygen is ⩾6 Å. There are also anthracene–crown C···N contacts apparent in both structures (3.17–3.39 Å range) but the contact angles (113–117°) make their overall importance unclear.

The K^+ complex of **1** was isolated from a mixture of **1** and KSCN (1:1), dissolved in $CHCl_3$–EtOH (1:1 v/v). The colorless, rhombohedral crystals had the stoichiometry **1**·KSCN·$(EtOH)_2$. Interactions analogous to those observed in the Na^+ complex of **1** are apparent here. The average K–O distance for the macroring contacts is 2.73 Å and the average K–

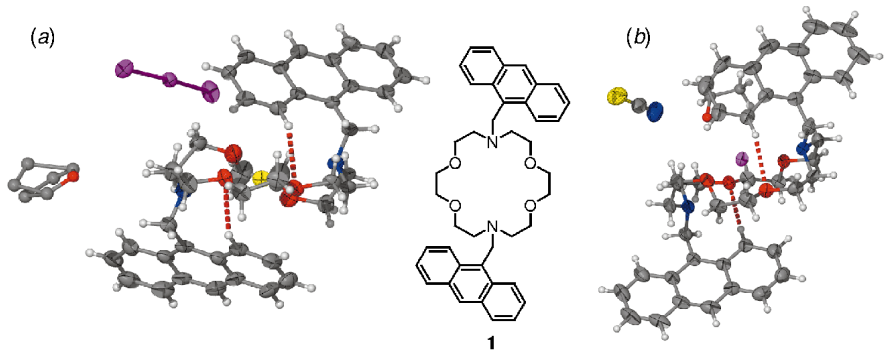

Fig. 1 Solid state structures of **1** complexed by (*a*) NaI_3 and (*b*) KSCN. In each case, one of two disordered solvent molecules has been deleted for clarity. Dotted lines indicate C–H···O contacts. Thermal ellipsoids are shown at 50% probability.

N distance is 3.20 Å. We also note a contact between the oxygen of one EtOH molecule and K^+ (K–O) that is 2.71 Å, essentially identical to the macroring K–O interactions. The anthracene C–H to macroring oxygen contacts (C···O, similar to those observed for **1**·Na^+) are 3.58 (θ = 177.5°) and 3.63 Å (155.5°). Carbon-3 of one anthracene is 4.12 Å from the sulfur atoms of SCN^- and the C–H···S angle is 151.3°.

Other data are worthy of note. The transannular N↔N separation in **1**·NaI_3 is 5.93 Å and in **1**·KSCN is 6.11 Å. The latter value is similar to those reported for other K^+ complexes of diaza-18-crown-6 derivatives.[13] In contrast, the transannular span for the Na^+ complex is considerably larger than the value of 5.10 Å reported for *N*,*N*′-bis(2-hydroxyethyl)-4,13-diaza-18-crown-6.[13]

Kubo *et al.*[14] have titrated **1** with either Na^+ or K^+ and used fluorescence changes to determine complexation constants. They have found that in MeOH–$CHCl_3$ (9 : 1 v/v), log K_s (Na^+) for **1** is 2.70 and log K_s (K^+) is 3.29. They do not report values in the more commonly used solvent: anhydrous MeOH. The poor solubility of **1** in MeOH prevented us from measuring log K_s in this solvent.

Several observations clearly indicate that unusual interactions occur in the Na^+ and K^+ complexes of **1**. One of the most obvious is the low cation binding constant. In anhydrous MeOH solution, *N*,*N*′-dibenzyl-4,13-diaza-18-crown-6 (**2**) was found to have the following cation complexation constants: log K_s (Na^+) = 2.72 and log K_s (K^+) = 3.38. It is well known that cation complexation constants diminish with increasing polarity of the solvent.[15] It is expected, therefore, that complexation constants determined in a $CHCl_3$–MeOH mixture would be greater than in more polar MeOH. In fact, the binding constants are *lower* by a small factor (1.2- to 1.4-fold). This suggests that in MeOH, log K_s would be significantly lower for **1** than for **2**.

In previous studies, we found a clear correlation between the complexed cation's coordination number and the metal–heteroatom donor group distances.[13] As the coordination number increased, the M^+–O distance increased. Indeed, our data correlated well with the values published by Shannon.[16] Thus, metal-ion-to-oxygen distances for six-coordinated Na^+ and K^+ should be, respectively, 2.42 and 2.78 Å. (Considering the EtOH interaction in **1**·KSCN, the latter value could be 2.86 Å). In fact, the average distances observed are, respectively, 2.47 and 2.73 Å. The predicted M^+–N distances are 2.52 and 2.62 Å for Na^+ and K^+. The observed average distances are 2.97 and 3.20 Å. The M^+–O distances are approximately as expected for six-coordinated Na^+ and K^+, but the M^+–N lengths are remarkably long. This suggests that the cation's interaction with macroring nitrogen is weaker than expected and may be compensated by other, less obvious interactions.

The most remarkable feature of these two structures is the short C–H···O contacts observed between the anthracene α-hydrogen and a proximate macroring oxygen. Desiraju has recently discussed the occurrence of such interactions.[17] The four close contacts observed for the interaction noted above are in the range (designated *D*) of 3.54–3.62 Å and exhibit C–H···O angles from 152.7–177.5°. Desiraju has noted that '*D* values span the range 3.00–4.00 Å' and has further stated that 'linear bonds ($150 < \theta < 180$°) are structurally significant.' Clearly, all of these putative contacts fall within the 'significant' range by both criteria. Moreover, the molecules that possess these remarkable contacts are unusually poor cation binders. The excellent fluorescent potential of the anthryl residue should thus be weighed against its potential to interfere with complexation when considered as the sensor element in fluorescent signaling cation complexers.

We thank the NIH (GM-36262) and the NSF (CHE-9805840) for grants that supported this work. We are also grateful for an American Chemical Society fellowship, funded by Procter and Gamble, to E. S. M. We appreciate helpful discussions with Professors Nigam Rath and Jonathan Steed.

Notes and references

1 H.-G. Löhr and F. Vögtle, *Acc. Chem. Res.*, 1985, **18**, 65.
2 G. W. Gokel and J. E. Trafton, *Cation Binding by Lariat Ethers*, in *Cation Binding by Macrocycles*, ed. Y. Inoue and G. Gokel, Marcel Dekker, New York, 1990, pp. 253–310; G. W. Gokel, *Chem. Soc. Rev.*, 1992, **21**, 39; G. W. Gokel and O. F. Schall, *Lariat Ethers*, in *Comprehensive Supramolecular Chemistry*, ed. G. Gokel, Pergamon, Oxford, 1996, vol. 1, pp. 97–152.
3 *Fluorescent Chemosensors for Ion and Molecule Recognition*, ed. A. W. Czarnik, *ACS Symp. Ser.* ACS, Washington, DC, 1993, vol. 538.
4 A. P. de Silva and S. A. de Silva, *J. Chem. Soc., Chem. Commun.*, 1986, 1709.
5 U. Herrmann, B. Tümmler, G. Maas, P. K. T. Mew and F. Vögtle, *Biochemistry*, 1984, **23**, 4059; B. Tümmler, U. Herrmann, G. Maas and H. Eibl, *Biochemistry*, 1984, **23**, 4068.
6 R. A. Bissell, E. Calle, A. P. deSilva, S. A. deSilva, H. Q. N. Gunaratne, J.-L. Habib-Jiwan, S. L. A. Peiris, R. A. D. D. Rupasinghe, T. K. S. D. Samarasinge, K. R. A. S. Sandanayake and J.-P. Soumillon, *J. Chem. Soc., Perkin Trans. 2*, 1992, 1559.
7 D. Marquis, J.-P. Desvergne and H. Bouas-Laurent, *J. Org. Chem.*, 1995, **60**, 7984.
8 J. H. R. Tucker, H. Bouas-Laurent, P. Marsau, S. W. Riley and J.-P. Desvergne, *Chem. Commun.*, 1997, 1165.
9 G. DeSantis, L. Fabbrizzi, M. Licchelli, C. Mangano, D. Sacchi and N. Sardone, *Inorg. Chim. Acta*, 1997, **257**, 69.
10 C. R. Cooper and T. D. James, *Chem. Commun.*, 1997, 1419.
11 V. J. Gatto, S. R. Miller and G. W. Gokel, *Org. Synth.*, 1989, **68**, 227.
12 Combustion analysis: Calc. for $C_{42}H_{46}N_2O_4$: C, 78.47; H, 7.21; N, 4.36%. Found: C, 78.44; H, 7.34; N, 4.28%.
13 R. D. Gandour, F. R. Fronczek, V. J. Gatto, C. Minganti, R. A. Schultz, B. D. White, K. A. Arnold, D. Mazzocchi, S. R. Miller and G. W. Gokel, *J. Am. Chem. Soc.*, 1986, **108**, 4078.
14 K. Kubo, R. Ishige and T. Sakuri, *Heterocycles*, 1998, **48**, 347.
15 D. M. Dishong and G. W. Gokel, *J. Org. Chem.*, 1982, **47**, 147.
16 R. D. Shannon, *Acta Crystallogr., Sect. A*, 1976, **32**, 751.
17 G. R. Desiraju, *Acc. Chem. Res.*, 1996, **29**, 441.

Communication 9/02676B

ChemComm

1- and 2-Naphthylmethyl sidearms of isomeric bibracchial lariat ethers significantly affect alkali metal cation complexation

Eric S. Meadows, Stephen L. De Wall, Leonard J. Barbour and George W. Gokel*

Bioorganic Chemistry Program and Department of Molecular Biology and Pharmacology, Washington University School of Medicine, 660 S. Euclid Avenue, Campus Box 8103 St. Louis, MO 63110 USA.
E-mail: ggokel@molecool.wustl.edu

Received (in Columbia, MO) 20th April 1999, Accepted 23rd June 1999

Derivatives of 4,13-diaza-18-crown-6 having benzyl or isomeric naphthylmethyl sidearms have significantly different solid state structures and show differences in cation complexation strengths.

During the more than three decades since Pedersen reported the first crown ethers,[1] these remarkable cation binders have been studied in exquisite detail. Numerous structural studies have established their conformations when unbound or when complexed by a variety of alkali and alkaline earth metal cations as well as by numerous other cationic and even neutral species. The now well-established chemistry of macrocycles[2] is exhibiting utility in the development of supramolecular systems.[3] As more complicated structures are designed, unanticipated properties occasionally emerge. Understanding such unusual effects is critical for achieving the desired properties in supramolecular structures that incorporate crowns as modules. We have recently reported the first definitive evidence for arene participation in the complexation of sodium and potassium cations.[4] In a second study, the indolylethyl sidearms[4] that bound Na^+ or K^+ were replaced by 9-anthrylmethyl.[5] In the latter case,[5] the intercession of C–H···O hydrogen bonding affected complexation geometry and cation binding strength. We now report the results of a study involving isomeric aromatic sidearms and the effect they have on complexation geometry and cation binding strength.

N,*N*′-Bis(1-naphthylmethyl)-4,13-diaza-18-crown-6, **1**, and its isomer *N*,*N*′-bis(2-naphthylmethyl)-4,13-diaza-18-crown-6, **2**, were prepared by alkylation (48 h reflux) of diaza-18-crown-6[6] using either 1-chloro- or 2-bromomethylnaphthalene in $CH_3CH_2CH_2CN$ in the presence of KI and Na_2CO_3. Compound **2** was obtained as a thick yellow oil that crystallized from hexanes and then EtOH to give light yellow prisms (76%, mp 92–93 °C).[7]

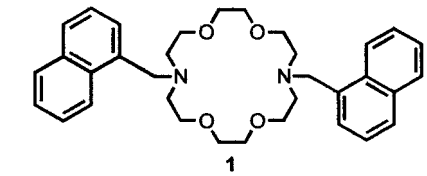

1

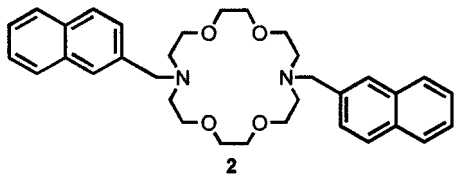

2

Kubo and coworkers have recently reported the preparation of **1** as part of a program to develop fluorescent cation sensors.[8] The fluorescent properties of **1** allowed them to determine cation complexation constants. They reported that log K_s values in anhydrous MeOH for Na^+ and K^+ complexation by **1** were 2.09 and 3.27, respectively. This compares with binding constants determined for *N*,*N*′-dibenzyl-4,13-diaza-18-crown-6 (**3**) as follows: log K_s (Na^+) = 2.68 and log K_s (K^+) = 3.38. There is a 1.3-fold difference in the K^+ binding constant but a larger, ~4-fold, difference in the Na^+ binding constant. We have independently determined the binding constant for **1** and find log K_s (Na^+) to be 2.32 ± 0.26. While this 1.7-fold difference is more in line with related compounds, K_s is still lower than expected. A complexation constant determination for previously unreported **2** gave a log K_s value of 2.68 ± 0.10. For calibration, **3** was re-examined and log K_s (Na^+) was found to be 2.71, identical within experimental error to the previously reported value (see above) and to the binding constant for **2**.

Although the complexation constant differences are not major, the variation between isomers **1** and **2** is striking. We thus determined the solid state structures of the two Na^+ complexes in the hope that differences observed there might help to account for the binding variation. The structures of **1**·Na^+ and **2**·Na^+ are shown in Fig. 1(*b*),(*d*). Kubo and coworkers have reported the structure **1** in the absence of any cation (not shown).[8a] The previously unreported structure of **3**·NaI is shown in Fig. 1(*a*). For comparison, the structure we reported a number of years ago for **3**·KSCN is shown in Fig. 1(*c*).[9]

It is worth noting at the outset that the reported structure[8a] of uncomplexed **1** (not shown) is similar to many other unbound 18-membered macrocycles. The conformation of **1** is planar and the methylene groups adjacent to each macroring nitrogen atom are rotated inward in a typical free macrocycle conformation. The naphthyl groups are clearly turned away from the macroring. Kubo comments that 'the naphthalene ring of [**1**] is close to the N atom of the crown ether; the distance between C1 and N1 is 2.505 Å, shorter than the sum (3.05 Å) of their van der

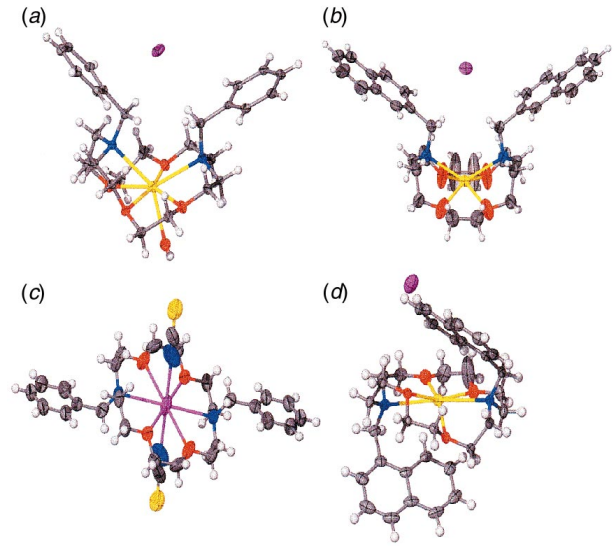

Fig. 1 (*a*) Structure of dibenzyl sodium complex, **3**·NaI. (*b*) Structure of bis(2-naphthyl) sodium complex, **2**·NaI. (*c*) Structure of **3**·KSCN (see ref. 9). (*d*) Structure of bis(1-naphthyl) sodium complex, **1**·NaI.

Waals radii.'[8a] The authors note only that intramolecular charge transfer between these atoms may be favorable.

The structures of **2** and **3** complexing NaI are both unusual but identical in essential features. In both cases the macrocycle is bowed upward with the nitrogen atoms at the peaks. This contraction reduced the N↔N separation from ~5.5–6 Å to ~4.5 Å. Likewise, the sidearm methylenes are separated by 4.02 Å and the sidearm methylene hydrogens across the ring from each other are separated by 2.76 Å and 3.41 Å, respectively. The *syn* 2-naphthyl residues mirror each other through a symmetry plane that intersects Na^+ and I^-. The bowed macroring conformation is also observed for the bis(benzyl)crown complex, **3**·NaI.

The **3**·NaI complex [Fig. 1(*a*)] differs significantly from the structure of **3**·KSCN [Fig. 1*c*)]. In the latter, the macrocycle is in the expected D_{3d} conformation, the M^+–O and M^+–N contacts are as expected, and the apical positions are occupied by SCN anions. In fact, the structure of **3**·KSCN is typical of 18-membered ring crown complexes that lack sidearms.

In contrast to the situation with **2**·NaI [Fig. 1(*b*)], the isomeric complex **1**·NaI [Fig. 1(*d*)] has an *anti*, rather than *syn*, arrangement of the 1-naphthyl sidearms. Although the macroring is far from planar, the N↔N separation is a more typical 5.9 Å. One of the naphthalene α-hydrogens is separated from the nearest macroring oxygen atom by only 2.67 Å (C···O distance = 3.56 Å). The adjacent β-hydrogen is 2.99 Å from the adjacent macroring nitrogen atom and that C–H is only 3.31 Å from iodide. These close contacts suggest significant C–H···X hydrogen bonding interactions.[10] The presence of C–H···O contacts in complexes of **1** and their absence in complexes of **2** may help to account for differences in cation binding strengths observed for these isomeric host molecules. The arene-sidearm to ring C–H···O contacts observed for **1** correspond well with those noted for the structurally related anthrylmethyl derivative previously reported.[5]

The dibenzyl- and dinaphthyldiaza-18-crown-6 derivatives reveal unexpected complex structures. The **1**·NaI complex does not appear to be stabilized by π-stacking interactions but rather by a variety of C–H···X contacts that define sidearm and, in turn, macroring conformation. The **1**·NaI complex exhibits the geometry noted above and **1** also exhibits reduced cation binding affinity, a pattern observed in previous studies from this laboratory.[5,11] Two factors may contribute to the decreased binding ability of **1** compared to **2** or **3**. First, complexes of **1** may require more complete desolvation of the cation than do complexes of **2** or **3** because of the 1-naphthyl sidearms' steric requirements compared to either benzyl or 2-naphthyl. Second, the C–H···O interactions that we observe in the complex of **1** may be able to organize the naphthyl sidearms over the macrocycle in the unbound state, therefore blocking access by the cation. It seems reasonable that both cation binding and release may be directly affected by these sidearm interactions. Our previous study of the 9-anthrylmethyl sidearmed compound,[5] which is closely related to **1**, shows a similar result for a similar geometrical situation. Ultimately, resolution of the contributory factors will require a thermodynamic study so that entropic and enthalpic contributions to ΔG and, in turn, to K_s can be appreciated. For now, it is important to note that such significant differences in conformational and binding behavior occur with isomeric host molecules.

We thank the NIH (GM-36262) and the NSF (CHE-9805840) for grants that supported this work. We are also grateful for an American Chemical Society Division of Organic Chemistry fellowship, funded by Procter and Gamble, to E. S. M.

Notes and references

1 C. J. Pedersen, *J. Am. Chem. Soc.*, 1967, **89**, 7017.
2 (*a*) H. Hiraoka, *Crown compounds: their characteristics and applications*, Elsevier, Amsterdam, 1982; (*b*) G. W. Gokel, *Crown ethers and cryptands*, Royal Society of Chemistry, Cambridge, 1991, vol. 3; (*c*) B. G. Cox and H. Schneider, *Coordination and Transport Properties of Macrocyclic Compounds in Solution*, Elsevier, Amsterdam, 1992; (*d*) B. Dietrich, P. Vout and J.-M. Lehn, *Macrocyclic Chemistry*, VCH, Weinheim, 1993.
3 (*a*) T. M. Fyles, D. Loock and X. Zhou, *J. Am. Chem. Soc.*, 1998, **120**, 2997; (*b*) M. T. Fyfe and J. F. Stoddart, '(Supra) molecular systems based on crown ethers and secondary diakylammonium ions,' in *Advances in Supramolecular Chemistry*, vol. 5, ed. G. W. Gokel, JAI Press, Stamford, CT, 1999, pp. 1–54; (*c*) K. N. Houk, S. Menzer, S. P. Newton, F. M. Raymo, J. F. Stoddart and D. J. Williams, *J. Am. Chem. Soc.*, 1999, **121**, 1479.
4 S. L. De Wall, E. S. Meadows, L. J. Barbour and G. W. Gokel, *J. Am. Chem. Soc.*, 1999, **121**, 5613.
5 S. L. De Wall, E. S. Meadows, L. J. Barbour and G. W. Gokel, *Chem. Commun.*, 1999, 1553.
6 V. J. Gatto, S. R. Miller and G. W. Gokel, *Org. Synth.*, 1989, **68**, 227.
7 *Selected data* for **2**: δ_H(acetone-d_6) 7.85 (m, 4H), 7.59 (d, 2H, *J* 8.7), 7.46 (m, 4H), 3.86 (s, 4H), 3.65 (t, 8H, *J* 5.7), 3.57 (s, 8H), 2.84 (t, 8H, *J* 6.0). Anal. Calcd for $C_{34}H_{42}N_2O_4$: C, 75.25; H, 7.80; N, 5.16%. Found: C, 75.16; H, 7.90; N, 5.11%.
8 (*a*) K. Kubo, R. Ishige, N. Kato, E. Yamamoto and T. Sakurai, *Heterocycles*, 1997, **45**, 2365; (*b*) K. Kubo, R. Ishige and T. Sakuri, *Heterocycles*, 1998, **48**, 347.
9 K. A. Arnold, A. M. Viscariello, M. Kim, R. D. Gandour, F. R. Fronczek and G. W. Gokel, *Tetrahedron Lett.*, 1988, 3025.
10 G. R. Desiraju, *Acc. Chem. Res.*, 1996, **29**, 441.
11 E. S. Meadows, S. L. De Wall, P. W. Salama, E. Abel and G. W. Gokel, *Supramol. Chem.*, 1999, **10**, 163.

Communication 9/03162F

Multiple morphologies of aggregates from block copolymers containing glycopolymer segments

Zi-Chen Li, Yu-Zeng Liang and Fu-Mian Li*

Department of Polymer Science and Engineering, College of Chemistry, Peking University, Beijing 100871, China. E-mail: fmli@chemms.chem.pku.edu.cn

Received (in Cambridge, UK) 25th June 1999, Accepted 6th July 1999

Multiple morphologies of aggregates (micelle-like spheres, vesicles, tubules) from well-defined polystyrene-*b*-poly[(2-β-D-glucopyranosyloxy)ethyl acrylate] (PS-*b*-PGEA) diblock copolymers in diluted aqueous solutions were observed by transmission electron microscopy.

Block copolymers have been investigated vigorously as building units for highly ordered molecular aggregates. It has been shown that when diblock copolymers are dissolved in a solvent which is selective for one of the blocks, colloidal size aggregates or micelles can form as a result of the association of the insoluble blocks.[1–3] Recent reports on rigid-coil diblock copolymers reveal that highly asymmetric diblock copolymers can self-assemble into highly ordered supramolecular architectures with special optical and electrical or encapsulation properties.[4,5] Ordered aggregates from other types of diblock copolymers have also been reported by Armes *et al.*[6] Amphiphilic AB block copolymers are a very important type of block copolymer that show various applications in which the combination of hydrophobic and hydrophilic properties of these materials may be utilized. It has been shown recently by Eisenberg *et al.* that special amphiphilic block copolymers can form stable aggregates of variable morphologies, namely, spheres, rods, vesicles *etc.*, in aqueous solution. Polystyrene (PS) based copolymers, PS-*b*-poly(acrylic acid) (PS-*b*-PAA), PS-*b*-poly(ethylene oxide) (PS-*b*-PEO) and PS-*b*-poly(4-vinylpyridine) (PS-*b*-P4VPy) with various compositions have been extensively investigated.[7] Several factors, including the copolymer composition, the initial copolymer concentration and the nature of the common solvent, have been found to be essential to control the aggregate morphologies. The morphologies are normally studied by observation with a transmission electron microscope (TEM).

In the recent past, increasing attention has been paid to synthetic polymers substituted with pendant saccharide moieties (so called glycopolymers) as biological recognition signals.[8–10] Studies on the synthesis of block copolymers containing glycopolymers as hydrophilic segments and the aggregates formed therefrom in aqueous media are few, especially for block copolymers with controlled molecular weight and narrow molecular weight distribution.[11–13] Recent developments in atom transfer radical polymerization (ATRP) have made it possible to synthesize well-defined block polymers very easily.[14] By using this initiation system, we have successfully synthesized a series of well-defined amphiphilic block copolymers with PS as the hydrophobic block and poly(2-β-D-glucopyranosyloxy)ethyl acrylate) as the hydrophilic one (PS-*b*-PGEA).[15]† The aim of our study is to use these amphiphilic copolymers to construct ordered molecular aggregates and then to use them as models for the study of cell–lectin interactions. Here, we report our preliminary results on the multiple morphologies formed from these amphiphilic block copolymers in aqueous media. The block copolymers used in this study are summarized in Table 1.

To study the aggregation behavior of these new block copolymers in water, a known amount of the completely dried block copolymer sample was dissolved in a common solvent of the two blocks, such as DMF, dioxane *etc.*, to obtain solutions

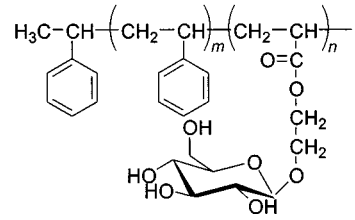

PS-*b*-PGEA

with different concentrations (0.5–5 wt%). While vigorously stirring the solution, water was added at a rate of 0.2–0.3 wt% every 10 s. When *ca.* 6 wt% of water was added, the clear solution became turbid. The addition of water was continued until 25 wt% of water had been added. Then the sample was put into a dialysis bag (molecular weight cut: 10000) and dialyzed against distilled water for 4 days to remove the organic solvents. To observe the morphologies of these aggregates under TEM, one drop of the diluted suspension was put onto a carbon-coated copper grid, and was negatively stained with uranyl acetate. The observation was conducted with a JEOL 100 CXII transmission electron microscope operated at 100 kV.

Multiple morphologies of aggregates from these PS-*b*-PGEA block copolymer are obtained by using different solvents or changing the initial copolymer concentration. When DMF was used as solvent, small spheres were observed for a large range of initial copolymer concentration for these three PS-*b*-PGEA diblock copolymers as listed in Table 1. One of the typical pictures is shown in Fig. 1(*a*). It can be seen that the spheres are of low polydispersity and their average diameters are *ca.* 25 nm. The small spheres belong to the normal 'crew cut' micelles.[7] The largest initial copolymer concentrations of PS_{88}-*b*-$PGEA_4$, PS_{101}-*b*-PGEA7 and PS_{55}-*b*-$PGEA_9$ in DMF that form spheres in water are 2.5, 3.2 and 4.0 wt% respectively. Above these concentrations, large compound micelles coexisted with the crew cut micelles that were normally observed.

Vesicles were obtained for these three PS-*b*-PGEA block copolymers in other solvents. Fig. 1(*b*) shows a typical example of the vesicular structure obtained from PS_{88}-*b*-$PGEA_4$ in dioxane. The vesicular nature is evidenced by a higher transmission in the center of the aggregates than around their periphery in the TEM pictures. When the initial concentration of PS_{88}-*b*-$PGEA_4$ is within the range of 2.0–4.0 wt%, predominant

Table 1 A summary of the molecular weight, polydispersities and copolymer compositions of PS-*b*-PGEA

Copolymers[a]	GEA content/ mol%	M_n[b]/ g mol^{-1}	M_w/M_n[b]
PS_{88}-*b*-$PGEA_4$	4.3	9 700	1.18
PS_{101}-*b*-$PGEA_7$	6.5	13 000	1.28
PS_{55}-*b*-$PGEA_9$	14.1	8 300	1.24

[a] Degree of polymerization of polystyrene block was determined by GPC; PGEA chain length was determined by measuring the ^{1}H NMR spectra of the copolymer precursor in $CDCl_3$. [b] As determined by GPC in DMF (RI detector, calibrated with polystyrene standards).

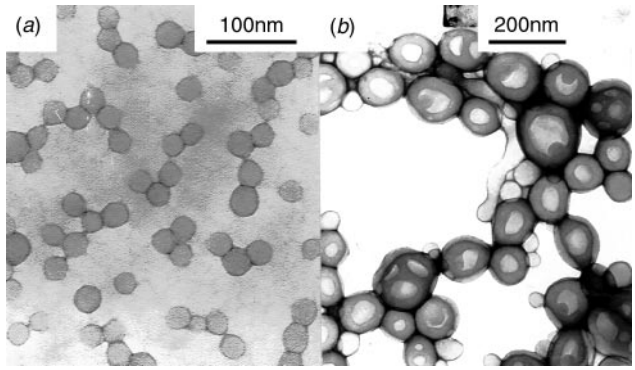

Fig. 1 TEM pictures of (*a*) PS_{101}-*b*-$PGEA_7$ aggregates in DMF (the initial copolymer concentration was 2.0 wt%) and (*b*) PS_{88}-*b*-$PGEA_4$ aggregates in dioxane (the initial copolymer concentration was 3.0 wt%).

vesicular structures were detected, however, there were also a few small spheres and occasionally short cylinders. Most of the vesicles are single-room and coexist with some two- or multiple-room ones. The sizes of the vesicles are very polydisperse with the outer diameters ranging from 100 to 200 nm. The vesicles formed from PS_{55}-*b*-$PGEA_9$ in dioxane (3.5 wt%) were irregular in shape and coexisted with tubular aggregates as shown in Fig. 2(*a*). The overall sizes of vesicle vary very much. The outer diameter ranges from 100 to 300 nm. PS_{101}-*b*-$PGEA_7$ did not yield vesicles in dioxane, however, it formed primarily single-room vesicles in dioxane–DMF (1 : 1, v/v, 2.5–4.0 wt%). The outer diameter of the vesicles ranges from 250 to 500 nm. The present results indicated that the sizes of the vesicles were sensitive to the solvent and the initial copolymer concentration, however, the wall thickness of the vesicle was very uniform and independent of the size of vesicles.

More interestingly, PS_{55}-*b*-$PGEA_9$ also formed tubular structures in dioxane as shown in Fig. 2(*c*). The wall thickness of the tubules is equal to the wall thickness of the vesicles [Fig. 2(*a*)]. The tubular aggregates have not been found for the other two PS-*b*-PGEA copolymers. When the initial copolymer concentration in dioxane is 2.5–3.0 wt%, vesicles are predominate, and when the concentration is 3.0–4.0 wt%, tubules coexisted with vesicles. The morphologies shown in Fig. 2(*b*) are the intermediate shape of vesicles and tubules, which can usually be obtained from a 3.5 wt% dioxane solution. This suggests the transition of morphologies from vesicles to tubules upon increasing the initial copolymer concentration.

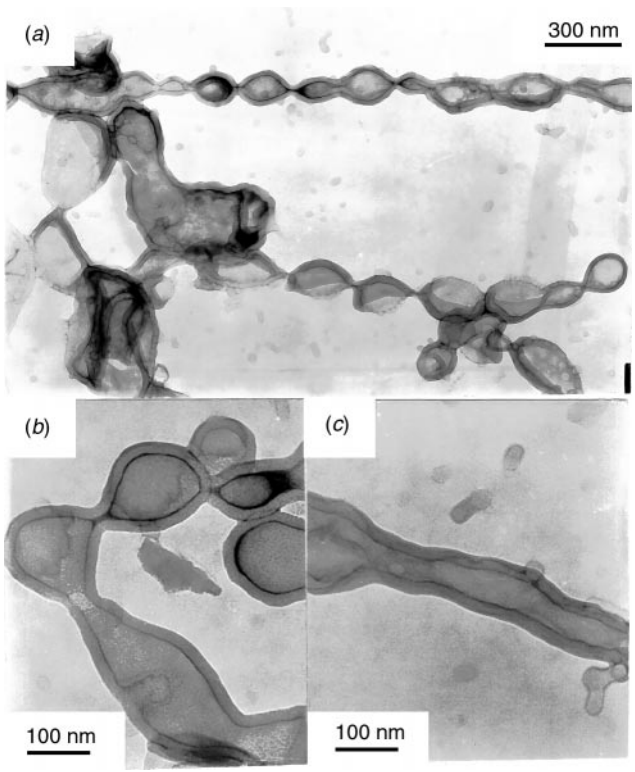

Fig. 2 TEM pictures of PS_{55}-*b*-$PGEA_9$ aggregates in dioxane. The initial copolymer concentrations were (*a*) 2.5, (*b*) 3.5 and (*c*) 4.0 wt%.

Besides the above-mentioned morphologies, other aggregates of PS-*b*-PGEA, such as large compound micelles (LCMs) and large compound vesicles (LCVs) were also observed. Their diameters range from 100 nm to 2 μm. It is also worth noting that the spheres and vesicles formed from the present block copolymers tend to connect with each other. This might be caused by hydrogen bond interactions between the PGEA blocks that constitute the outer surface of the aggregates.

In conclusion, PS-*b*-PGEA belongs to a novel class of amphiphilic AB block copolymers, exhibiting interesting aggregation behavior in aqueous medium. Several morphologies of aggregates, such as micelle-like spheres, vesicles and tubules have been observed from PS-*b*-PGEA block copolymers with different compositions. The morphologies are also found to be dependent on the solvent, and the initial copolymer concentration. These aggregates will be used as models to study cell–lectin recognition.

We wish to thank the National Natural Science Foundation of China and the Ministry of Education of China for financial support.

Notes and references

† PS-*b*-PGEA was synthesized as follows: First, styrene was polymerized with 1-phenylethyl bromide, CuBr and 2,2′-bipyridine in chlorobenzene at 110 °C for 20 h (conversion was about 90%) and the bromo-terminated polystyrene (Br-PS) was isolated by precipitation from MeOH. The dried sample was then used as a macroinitiator for the polymerization of the second monomer. In the second step, the OH protected monomer [2-(2′,3′,4′,6′-tetra-*O*-acetyl-β-D-glucopyranosyloxy)ethyl acrylate (AcGEA)] was polymerized with a pre-determined amount of CuBr, 2,2′-bipyridine and the macroinitiator to obtain the block copolymers, PS-*b*-PAcGEA. The precursor block copolymer was deprotected to the target amphiphilic block copolymer by treatment with a dilute solution of freshly prepared MeONa in a mixed solvent of anhydrous MeOH and $CHCl_3$ at room temperature. The final product was further purified by extraction with cyclohexane and water repeatedly to remove the homopolymers. IR and NMR analysis confirmed the quantitative deprotection without any degradation of the polymer main chain.

1 Z. Tuzar and P. Krattochvil, in *Surface and Colloidal Science*, ed. E. Matijevic, Plenum, New York, 1993, vol. 15, pp. 1–83.
2 V. Moffit, K. Khougaz and A. Eisenberg, *Acc. Chem. Res.*, 1996, **29**, 95.
3 F. L. Baines, S. P. Armes, N. C. Billingham and Z. Tuzar, *Macromolecues*, 1996, **29**, 8151.
4 I. Stupp, V. LeBonheur, K. Walker, S. Li, K. E. Huggins, M. Keser and A. Amstutz, *Science*, 1997, **276**, 384.
5 S. A. Jenekhe and X. L. Chen, *Science*, 1998, **279**, 1903.
6 V. Burun, N. C. Billingham and S. P. Armes, *J. Am. Chem. Soc.*, 1998, **120**, 11 818, 12 135; 1999, **121**, 4288.
7 L. Zhang and A. Eisenberg, *Science*, 1995, **268**, 1728; K. Yu and A. Eisenberg, *Macromolecules*, 1996, **29**, 6359; L. Zhang and A. Eisenberg, *Polym. Adv. Technol.*, 1998, **9**, 677.
8 G. Wulff, J. Schmid and T. Venhoff, *Macromol. Chem. Phys.*, 1996, **197**, 259.
9 K. Kobayashi, A. Tsuchida, T. Usui and T. Akaike, *Macromolecules*, 1997, **30**, 2016.
10 Y. Qiu, T. Zhang, M. Ruegsegger and R. E. Merchang, *Macromolecules*, 1998, **31**, 165.
11 K. Yamada, K. Yamaoka, M. Minoda and T. Miyamoto, *J. Polym. Sci., Polym. Chem. Ed.*, 1997, **35**, 255.
12 K. Ohno, Y. Tsujii and T. Fukuda, *J. Polym. Sci., Polym. Chem. Ed.*, 1998, **36**, 2473.
13 M.-P. Labeau, H. Cramail and A. Deffieux, *Macromol. Chem. Phys.*, 1998, **199**, 335.
14 J.-S. Wang and K. Matyjaszewski, *J. Am. Chem. Soc.*, 1995, **117**, 5614; A. Muhlebach, S. G. Gaynor and K. Matyjaszewski, *Macromolecules*, 1998, **31**, 6046.
15 Y. Z. Liang, Z. C. Li and F. M. Li, manuscript in preparation.

Communication 9/05114G

Photochemical reaction of *ortho*-formylbenzyltrialkylstannanes for the generation of α-oxy-*o*-quinodimethane

Hiroshi Sano,* Daisuke Asanuma and Masanori Kosugi

Department of Chemistry, Faculty of Engineering, Gunma University, Kiryu, Gunma 376-8515, Japan.
E-mail: sano@chem.gunma-u.ac.jp

Received (in Cambridge, UK) 18th June 1999, Accepted 6th July 1999

Irradiation of *o*-formylbenzyltrialkylstannanes in benzene gives α-trialkylstannoxy-*o*-quinodimethanes which are trapped with dienophiles at room temperature to afford cycloadducts with high stereoselectivities, while the corresponding silane and germane gave a different type of *o*-quinodimethane and moderate stereoselectivities in cycloadditions.

o-Quinodimethane intermediates are a useful synthetic tool for the synthesis of condensed cyclic compounds and numerous methods for the generation of the intermediates have been developed.[1] We previously reported new methods for the generation of *o*-quinodimethanes from tin precursors utilizing the high leaving ability of the tributylstannyl cation and radical.[2] In the course of our studies, we focused our attention on the photochemical generation of *o*-quinodimethane intermediates utilizing the characteristics of Group 14 organometallic compounds, since it is known that facile generation of α-hydroxy-*o*-quinodimethanes was achieved by irradiation of *o*-tolualdehyde *via* a photoenolisation process involving a 1,5-hydrogen shift.[3] We present here our investigation on the photoreactions of *o*-formylbenzyltrialkyl-stannanes, -silane and -germane in the presence of dienophiles.

The tin precursors **1c**,**d** were easily prepared from *o*-methylbenzyl alcohol in two steps by a method previously reported,[2b] and the corresponding timethylsilyl and tributylgermyl derivatives **1a**,**b** were prepared in a similar way. First, these precursors were irradiated in a benzene solution at room temperature to give the corresponding *o*-quinodimethane intermediates, which were trapped *in situ* with dimethyl fumarate (Scheme 1 and Table 1).

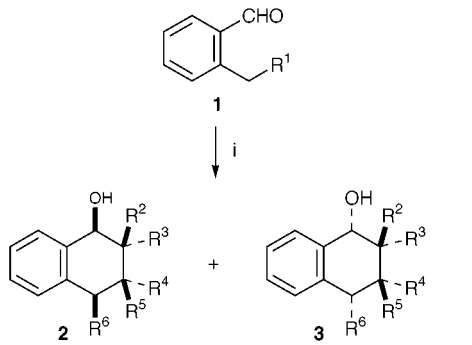

a $R^1 = SiMe_3$, $R^2 = R^4 = CO_2Me$, $R^3 = R^5 = H$, $R^6 = SiMe_3$
b $R^1 = GeBu_3$, $R^2 = R^4 = CO_2Me$, $R^3 = R^5 = H$, $R^6 = GeBu_3$
c $R^1 = SnMe_3$, $R^2 = R^4 = CO_2Me$, $R^3 = R^5 = R^6 = H$
d $R^1 = SnBu_3$, $R^2 = R^4 = CO_2Me$, $R^3 = R^5 = R^6 = H$
e $R^1 = SnBu_3$, $R^2 = COMe$, $R^3 = R^4 = R^5 = R^6 = H$
f $R^1 = SnBu_3$, $R^2 = CO_2Me$, $R^3 = R^4 = R^5 = R^6 = H$
g $R^1 = SnBu_3$, R^2–R^5 = -CO-N(Me)-CO-, $R^3 = R^4 = R^6 = H$
h $R^1 = SnBu_3$, R^2–R^5 = -CO-N(Ph)-CO-, $R^3 = R^4 = R^6 = H$

Scheme 1 *Reagents and conditions*: i, dienophile (3 equiv.), *hν*, PhH, room temp.

Table 1 Photoreaction of **1** with dienophiles

1	Dienophile	Cycloadduct	Yield(%) (**2**:**3**)
1a	Dimethyl fumarate	**2a** + **3a**	35 (71:29)
1b	Dimethyl fumarate	**2b** + **3b**	45 (53:47)
1c	Dimethyl fumarate	**2c** + **3c**	36 (>99:1)
1d	Dimethyl fumarate	**2d** + **3d**	48 (>99:1)
1d	Dimethyl maleate	**2d** + **3d**	35 (>99:1)
1e	Methyl vinyl ketone	**2e** + **3e**	38 (>99:1)
1f	Methyl acrylate	**2f** + **3f**	21 (>99:1)
1g	*N*-methylmaleimide	**2g** + **3g**	25 (>99:1)
1h	*N*-phenylmaleimide	**2h** + **3h**	51 (>99:1)

It has been reported that cycloaddition of α-hydroxy-*o*-quinodimethane with dimethyl fumarate gave the corresponding cycloadduct as a mixture of two stereoisomers (1,2-*cis* and 1,2-*trans*) in a 74:26 ratio.[4] Compounds **1a**,**b** also showed similar selectivities. When **1a** was irradiated with dimethyl fumarate, the cycloadduct having a trimethylsilyl group on the benzylic position was isolated as a mixture of two stereoisomers in a 71:29 ratio; **1b** gave a similar result. In these reactions, it is obvious that a 1,5-hydrogen shift proceeds upon photolysis to give *o*-quinodimethane intermediates (**A** in Fig. 1) followed by trapping with the dienophile to afford the cycloadducts **2a**(+**3a**) and **2b**(+**3b**) , respectively.

In the case of stannanes **1c**,**d**, however, the corresponding cycloadducts **2c**(+**3c**) and **2d**(+**3d**) involved no stannyl groups and the stereoselectivity was extremely high.[5] In a control experiment, it was observed that when 1-hydroxy-4-tributylstannyl-1,2,3,4-tetrahydronaphthalene was irradiated under similar conditions, most of the compound was recovered without loss of the stannyl group. This observation suggests that the formation of **2c**(+**3c**) and **2d**(+**3d**) does not proceed *via* an α-hydroxy-α′-trialkylstannyl-*o*-quinodimethane such as **A** in Fig. 1. The plausible reactive intermediate would be α-trialkylstannoxy-*o*-quinodimethane **B** (Fig. 1) .

That is, it is conceivable that a 1,5-shift of the stannyl group proceeded to give **B**,[6] which was trapped with the dienophile to give 2,3-dimethoxycarbonyl-1-trialkylstannoxy-1,2,3,4-tetrahydronaphthalene followed by destannylation to give the hydroxy compounds.[7] Furthermore, the present high stereoselectivities in the cycloadditions can be rationalized by supposing the existence of the intermediate **B**. When **B** approaches the dimethyl fumarate, the 1,2-*cis endo* addition **C** would be a favored pathway, since the 1,2-*trans exo* addition **D**

$R^1 = SiMe_3$, $GeBu_3$ — **A**

$R^1 = SnMe_3$, $SnBu_3$ — **B**

Fig. 1 The structure of *o*-quinodimethanes generated from the silane and geramane (**A**) and the stannane (**B**).

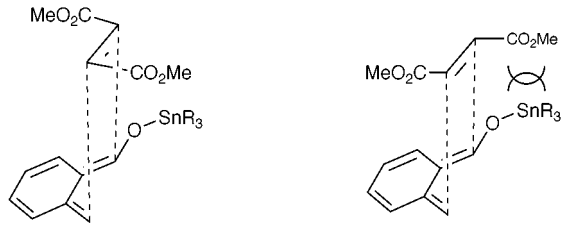

C D

Fig. 2 Transition states for the cycloaddition of *o*-quinodimethane with dimethyl fumarate: 1,2-*cis endo* addition (**C**); 1,2-*trans exo* addition (**D**).

suffers from steric repulsion between the trialkylstannyl group and the ester group (Fig. 2).

We next examined the photoreaction of *o*-formylbenzyltributylstannane with various dienophiles, as shown in Table 1. It is noted that the cycloadditions proceeded with exclusive formation of the 1,2-*cis* isomers in all cases. That dimethyl maleate gave the same cycloadduct (2,3-*trans*) as in the case of dimethyl fumarate could be explained by the following facts. It is known that dimethyl maleate isomerizes to dimethyl fumarate under irradiation conditions, and it is also known that dimethyl fumarate is a more reactive dienophile than dimethyl maleate in Diels–Alder reaction.[8]

In summary, we have shown that the generation of α-trialkylstannoxy-*o*-quinodimethanes was achieved *via* 1,5-shift of the stannyl group by irradiation of *o*-formylbenzyltrialkylstannanes, and the stereoselectivities of the cycloadditions with dienophiles were extremely high, whereas other precursors without a stannyl group undergo a 1,5-hydrogen shift and showed moderate selectivities in the cycloadditions.

This work was supported by a Grant-in-aid for Scientific Research from the Ministry of Education, Science, Sports and Culture, Japan.

Notes and references

1 For review: N. Martin, C. Seoane and M. Hanack, *Org. Prep. Proced. Int.*, 1991, **23**, 237.
2 (*a*) H. Sano, H. Ohtsuka and T. Migita, *J. Am. Chem. Soc.*, 1988, **110**, 2014; (*b*) H. Sano, K. Kawata and M. Kosugi, *Synlett*, 1993, 831; (*c*) H. Sano, H. Mashio, T. Nakayama and M. Kosugi, *Tetrahedron Lett.*, 1996, **37**, 8891.
3 For review: P. G. Sammes, *Tetrahedron*, 1976, **32**, 405.
4 J. L. Charlton and S. Maddaford, *Can. J. Chem.*, 1993, **71**, 827.
5 *Selected data* for **2c**: δ_H 2.37 (d, *J* 5.1, 1H), 2.89 (dd, *J* 11.7, 16.6, 1H), 3.12 (dd, *J* 3.4, 11.7, 1H), 3.21 (dd, *J* 5.5, 16.6, 1H), 3.39 (dt, *J* 3.5, 11.7, 1H), 5.12 (dd, *J* 3.5, 5.1, 1H), 7.10–7.40 (m, 4H).
6 A similar 1,5-shift of a boron group upon the generation of *o*-quinodimethanes has been reported: G. Kanai, N. Miyaura and A. Suzuki, *Chem. Lett.*, 1993, 845.
7 It seems that the destannylation proceeded during the irradiation, since the trialkylstannoxy compound could not be detected after the reaction.
8 W. Carruthers, *Some Modern Methods of Organic Synthesis*, 2nd edn., Cambridge University Press, Cambridge, 1978, p. 164.

Communication 9/04872C

New type of metal squarates. Magnetic and multi-temperature X-ray study of di-hydroxy(μ_6-squarato)manganese†

Dmitrii S. Yufit,*[a] Daniel J. Price,[b] Judith A. K. Howard,[a] Siegfried O. H. Gutschke,[b] Annie K. Powell[b] and Paul T. Wood[b]

[a] *Department of Chemistry, University of Durham, Durham, UK DH1 3LE. E-mail: d.s.yufit@dur.ac.uk*
[b] *School of Chemical Sciences, University of East Anglia, Norwich, UK NR4 7TJ*

Received (in Oxford, UK) 16th April 1999, Accepted 9th July 1999

A new type of crystal packing with μ_6-bridged squarate anions has been found in the structure of $Mn_2(OH)_2(C_4O_4)$ 1 during magnetic and X-ray single crystal diffraction measurements performed over a wide range of temperatures; the unit cell parameters for the crystal remain remarkably unchanged in the interval from 10 to 120 K.

We are currently investigating the use of solvothermal synthesis to generate materials with extended metal–ligand networks,[1] particularly ones displaying cooperative magnetic effects. As part of this study we have prepared $Mn_2(OH)_2(C_4O_4)$ **1** from the hydrothermal reaction of NaOH, $H_2C_4O_4$ and $MnCl_2$ at 220 °C. A study of the magnetic behaviour of this compound‡ is consistent with canted antiferromagnetic ordering below 32 K (Fig. 1). Compound **1** obeys the Curie–Weiss law in the paramagnetic region, and fitting the data in the range $70 \leqslant T/K \leqslant 300$ gives a Weiss constant of −52(1) K. Below 32 K a very small but significant spontaneous magnetisation of 13 cm^3 G mol^{-1} is observed, which corresponds to a canting angle φ_m = 0.03° for a two-sublattice model. This type of ordering can be caused by either single ion anisotropy or antisymmetric exchange coupling.[2] The former is a product of the interaction of spin–orbit coupling with a low-symmetry crystal field whilst the latter is also caused by spin–orbit coupling and is due to its modification of the exchange interaction. The weakness of spin–orbit coupling in octahedral high-spin Mn(II) means that canting is rare for this ion in comparison to those such as high-spin Co(II) which display large spin–orbit couplings. Both single-ion anisotropy and antisymmetric exchange have been invoked to account for the observed spin canting in Mn(II) phthalocyaninate[3] and $Mn(CO_3)$[4] respectively. Although the single ion anisotropy for Mn(II) is generally small[5] the distorted Mn environment (see below) and unusual yellow colour of this material are evidence for its existence. Regardless of the magnitude of any single ion anisotropy, the presence of crystallographic inversion centres in the solid state between hydroxy bridged manganese(II) ions means that the axes of anisotropy will be collinear. This precludes single-ion anisotropy as the source of spin canting, unless there is significant structural change accompanying the magnetic phase transition. Therefore it was important to obtain structural data at a temperature as close to the magnetic phase transition as possible. In order to follow possible structural changes during the magnetic phase transition, we collected single crystal X-ray data§ for **1** at 120, 40, 20 and 10 K (well below T_c) using an *Fddd* diffractometer.[6]

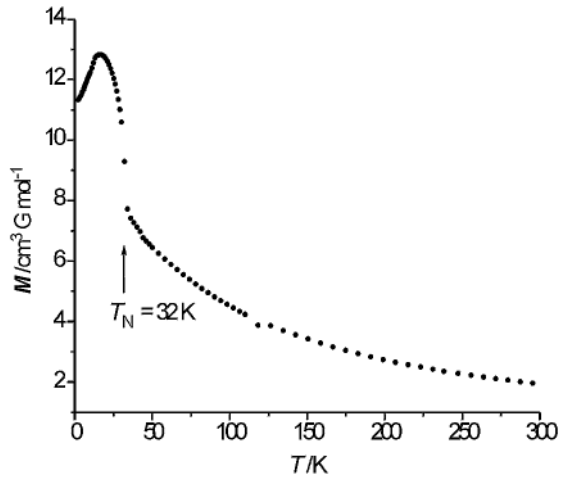

Fig. 1 The static magnetic susceptibility of a powdered sample of **1** in an applied field of 100 G in the temperature range 2 to 300 K.

† Electronic supplementary information (ESI) available: magnetic susceptibility measurement results; crystal data at various temperatures. See http://www.rsc.org/suppdata/cc/1999/1561

Squarate complexes of transition metals are well known, not least as materials with unusual magnetic and optoelectronic properties. The new interest in these compounds arose with the development of crystal engineering of organometallic compounds.[7] It was found that the structures of metal squarates contain a complex network of hydrogen bonds, usually there are channels in the structure, $C_2O_4^{2-}$ dianions form stacks and the coordination of the first row transition metals is close to octahedral with squarate ligands in mutually *trans* positions. Depending on the stoichiometry the squarate can be a terminal, μ- or μ_4- bridged ligand. In a recent review,[8] three types of aqua squarates were analyzed and their structural relationship was discussed.

The structure of **1** is remarkably different from those of the aqua squarates, which are chemically closely related to **1**. As in all previously known squarates of Mn the metal center has an octahedral coordination (Fig. 2), but in **1** the octahedron is severely distorted. The coordination mode is unusual: there are not two or four, but three μ-squarate ligands, which are not in the usual mutual *trans* positions but occupy the adjacent vertices (fac) of the octahedron. The squarate dianions occupy special positions in the center of symmetry and adopt the usual geometry for $C_4O_4^{2-}$ with delocalized C–C and C–O bonds and almost perfect D_{4h} symmetry. The slight difference in C–O bond lengths is the result of different crystal environments and bonding for O(1) and O(2). Indeed, atom O(1) is μ-bridged between two Mn atoms and O(2) is bonded to one Mn atom and accepts a hydrogen bond from the hydroxy group. Therefore each squarate dianion in structure **1** is connected to 6 metal atoms and is a μ_6-ligand. We are not aware of any other observations of such bonding of squarate anions.

In spite of the unusual coordination, the squarate anions in **1** maintain the usual tendency to form stacks. In **1** the stacks are formed along the short *a* axis and the distance between the planes of the anions is about 3.1 Å. The angle between the planes of the anions in adjacent stacks is 35.2°. The Mn(OH) chains are located between the stacks (Fig. 3).

As mentioned above, the aqua squarate complexes of transition metals usually have a number of hydrogen bonds. Complex **1** contains just one independent H atom and the cations and anions have to be linked together by Mn–O bonds.

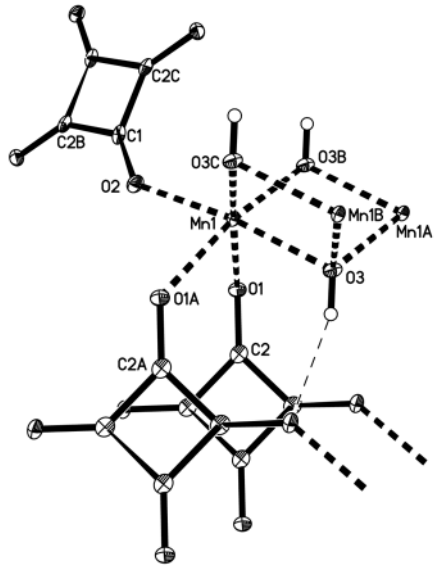

Fig. 2 Fragment of the crystal packing of **1** showing the coordination of the metal atom (thermal ellipsoids are at 70% probability level). Bond lengths (Å) at 10 K: Mn(1)–O(1) 2.3653(9), Mn(1)–O(1A) 2.264(1), Mn(1)–O(2) 2.1374(7), Mn(1)–O(3) 2.1820(7), Mn(1)–O(3B) 2.1132(9), Mn(1)–O(3C) 2.1297(8), O(1)–C(2) 1.2617(9), O(2)–C(1) 1.252(1), C(1)–C(2′) 1.467(1) and C(1)–C(2″) 1.468(1).

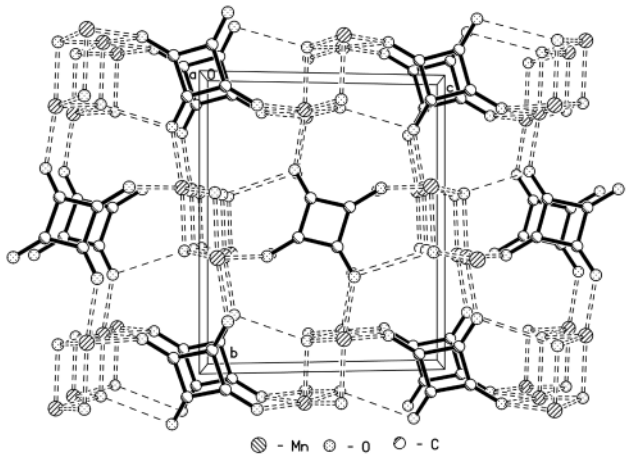

Fig. 3 Crystal packing of **1** (view along *a*). H-atoms omitted for clarity. Mn–O bonds are shown as double-dashed and H-bonds as single-dashed lines.

The only hydrogen bond in the structure links the hydroxy group with the O(2) carbonyl oxygen atom of the squarate anion. The result is a much closer crystal packing of **1** without substantial channels or cavities. This fact is probably the reason for the remarkable thermal behaviour of compound **1**: the crystal is virtually 'unshrinkable' from room temperature down to 10 K: in this range the unit cell volume changes from 295.5(1) to 292.9(1) Å^3—less than 1%.

At all temperatures studied the Mn–O, O–C and C–C distances are constant in the range 2–3σ. There is a slight tendency towards the contraction of the shortest Mn···Mn distance from 3.2055(6) Å at 120 K to 3.1974(6) Å at 10 K, and the Mn(1)–O3–Mn(1B) angle from 96.18(7)° to 95.72(2)°. These changes happen progressively across the whole range of temperatures studied and obviously are the result of thermal contraction rather than of a structural phase transition.

Since there is no apparent change in the symmetry of the crystallographic unit cell on passing through the magnetic phase transition, we can draw the conclusion that the source of the canting is an antisymmetric exchange interaction. Importantly this shows that **1** may be used as a model system in which the canting can unequivocally be ascribed to one type of anisotropy. Many of the types of magnetic behaviour which are the subject of considerable current interest, such as single molecule magnets, metamagnets and spin-flop phases, canted ferro- and antiferromagnets, are caused by different sources of anisotropy. Hence we hope that the title compound will provide an insight into antisymmetric exchange that can be used as a component in much-needed reliable magnetostructural correlations.

Financial support from EPSRC is gratefully acknowledged.

Notes and references

‡ The static magnetic susceptibility measurements were made between 2 and 300 K in an applied field of 100 G on a Quantum Design MPMS SQUID magnetometer. Data have been deposited as electronic supplementary information (http://www.rsc.org/suppdata/cc/1999/1561).

§ *Crystal data* for **1**, $C_4H_2Mn_2O_6$, M = 255.94, F(000) = 248, μ = 4.29 mm^{-1}, monoclinic, space group $P2_1/c$, Z = 2. At 10 K a = 3.3760(7), b = 10.268(2), c = 8.575(2) Å, β = 99.82(3)°, U = 292.9(1) Å^3, D_c = 2.902 g cm^{-1}. The crystal data at 20, 45, 120 and 293 K are available as electronic supplementary information (http://www.rsc.org/suppdata/cc/1999/1561) as well as the results of the refinements. All the data were collected from the same single crystal on a *Fddd* four circle diffractometer equipped with an APD-202 Displex cryogenic refrigerator and a Bruker AXS rotating anode generator with graphite-monochromated Mo-Kα radiation (λ = 0.71073 Å). The structure was solved by direct methods and refined by full-matrix least-squares on F^2 (SHELXL-93). For the 10 K data final $R(F^2)$ = 0.0234 for all 2588 reflections. CCDC 182/1328. See http://www.rsc.org/suppdata/cc/1999/1561 for crystallographic files in .cif format.

Microanalysis: found C 18.7%, H 0.7%; calculated for $C_4H_2O_6Mn_2$: C, 18.8%, H, 0.8%.

1 (*a*) S. O. H. Gutschke, A. M. Z. Slawin and P. T. Wood, *J. Chem. Soc., Chem. Commun.*, 1995, 2197; (*b*) S. O. H. Gutschke, M. Molinier, A. K. Powell, R. E. P. Winpenny and P. T. Wood, *Chem. Commun.*, 1996, 823; (*c*) S. O. H. Gutschke, M. Molinier, A. K. Powell and P. T. Wood, *Angew. Chem., Int. Ed. Engl.*, 1997, **36**, 991; (*d*) M. Molinier, D. J. Price, P. T. Wood and A. K. Powell, *J. Chem. Soc., Dalton Trans.*, 1997, 4061; (*e*) S. O. H. Gutschke, D. J. Price, A. K. Powell and P. T. Wood, *Angew. Chem., Int. Ed.*, 1999, **38**, 1088.

2 T. Moriya, in *Magnetism, Vol. 1*, ed. G. T. Rado and H. Suhl, Academic Press, New York, 1963, p. 85.

3 S. Mitra, A. K. Gregson, W. E. Hatfield and R. R. Weller, *Inorg. Chem.*, 1983, **22**, 1729.

4 A. S. Borovik-Romanov and M. P. Orlova, *J. Exp. Theor. Phys. (USSR)*, 1956, **31**, 579.

5 R. L. Carlin, *Magnetochemistry*, Springer-Verlag, Berlin, 1986.

6 R. C. B. Copley, A. E. Goeta, C. W. Lehmann, J. C. Cole, D. S. Yufit, J. A. K. Howard and J. M. Archer, *J. Appl. Crystallogr.*, 1997, **30**, 413.

7 D. Braga and F. Grepioni, *Chem. Commun.*, 1998, 911.

8 C-R. Lee, C-C. Wang and Y. Wang, *Acta Crystallogr., Sect. B*, 1996, **52**, 966.

Communication 9/03032H

ChemComm

Topological control in coordination polymers by non-covalent forces

Gemma Guilera and Jonathan W. Steed*

Department of Chemistry, King's College London, Strand, London, UK WC2R 2LS. E-mail: jon.steed@kcl.ac.uk

Received (in Columbia, MO, USA) 20th April 1999, Accepted 23rd June 1999

Reaction of Zn^{2+} salts with the terephthalate dianion results in a herringbone motif coordination polymer; the orientation of the terephthalate spacer ligands and the coordination geometry about the Zn^{2+} ion is crucially dependent on hydrogen bonding to ancillary ligands; replacement of coordinated water with ethylenediamine results in marked changes to the polymer orientation without disruption of the fundamental features of the material.

A key objective in the emerging field of crystal engineering is the control and manipulation of weak interactions in order to tune the properties of the bulk material.[1–6] Potential applications of such studies include the preparation of new non-linear optical materials, design of porous solids with novel inclusion or reactivity properties (*e.g.* for use in separation science and heterogeneous catalysis, particularly in stereo- or enantiospecific synthesis) and new sensor materials and coatings.[7–11] The vast majority of current work centres around the controlled assembly of donor and acceptor building blocks (particularly involving hydrogen bond acid–base pairs, *e.g.* nucleobases[12]) in order to generate an entirely 'supramolecular polymer', *i.e.* a material held together solely by non-covalent interactions. While such systems can be remarkably robust,[12] such an approach is fundamentally limited by the intrinsic strength of the constituent interactions, which are markedly weaker than covalent or ionic bonds, although our recent work has focussed on the importance of such interactions.[13–16] With this in mind, we have begun a programme of research aimed at the construction of molecular coordination polymers of low dimensionality in which mechanical strength is imparted by strong coordinate bonds, while admitting scope for weaker, lateral interactions which might enable the material to be tuned in the same way as in more conventional crystal engineered solids. We now report the results of simple, proof of principle studies, which demonstrate how an inherently robust coordination polymeric framework may be manipulated by weak interactions.

In attempting to prepare coordination polymers we were struck by the utility of avoiding the need for counter anions which must *inter alia* disrupt the solid state packing and give rise to additional cation–anion interactions which might be difficult to control.[17] Accordingly we have chosen to examine the reactions of divalent metal cations with the terephthalate dianion, (tph^{2-}, **1**) in the expectation of generating a neutral polymeric material. We chose initially relatively labile Zn^{2+} (as nitrate or acetate salts) in the hope of generating reaction products under thermodynamic control. The structure of zinc acetate itself, $Zn(O_2CMe)_2{\cdot}2H_2O$, consists of two essentially bidentate acetate ligands and two water molecules engaging in intra- and intermolecular hydrogen bonding interactions.[18] We reasoned that replacement of acetate with terephthalate would result in an analogous structure consisting of both a polymer chain and ancillary aqua ligands which would exert additional control over the polymer geometry by means of strong hydrogen bonding interactions. Consistent with expectation, an excellent yield of crystalline material of stoichiometry $[Zn(tph)]{\cdot}2H_2O$ **2** was deposited within 24 h. This material was characterised by low temperature X-ray crystallography† (100 K) and proved to consist of the desired coordination polymer, Fig. 1. The compound consists of approximately tetrahedral

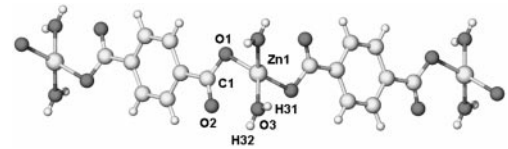

Fig. 1 XSeed[21] view of the coordination polymer $[Zn(H_2O)_2(\mu\text{-}O,O'\text{-}tph)]_\infty$ **2**. Selected bond lengths (Å): Zn(1)–O(1) 2.0049(15), Zn(1)–O(2) 2.5500(16), Zn(1)–O(3) 1.9855(18) Å.

Zn^{2+} centres linked by a herringbone pattern of tph^{2-} spacers aligned approximately along the crystallographic *a/c* diagonal. The tph ligands are essentially monodentate with Zn–O(1) 2.0049(15) Å, however the Zn–O(2) distance of 2.5500(16) Å suggests a non-negligible interaction with the uncoordinated oxygen, which may be described as a semi-chelating coordination mode.[19] The two water molecules within the coordination sphere of the metal cation engage in two distinct hydrogen bonded interactions, which, together, are responsible for the conformation of the polymer. In the crystallographic *b* direction, perpendicular to the direction of chain propagation, the metal cations stack precisely on top of one another and are linked in an eight membered hydrogen bonded ring [R_2^2 (8) in graph set notation[20]] involving the water hydrogen atom H31 attached to O3 and the coordinated oxygen atoms of the tph ligand, Fig 2(a). In addition, lateral hydrogen bonds involving the second unique water hydrogen atom H32 and the uncoordinated terephthalate oxygen atoms link one chain to those adjacent in R_2^2 (12) hydrogen bonded sets, Fig. 2(b). The aryl

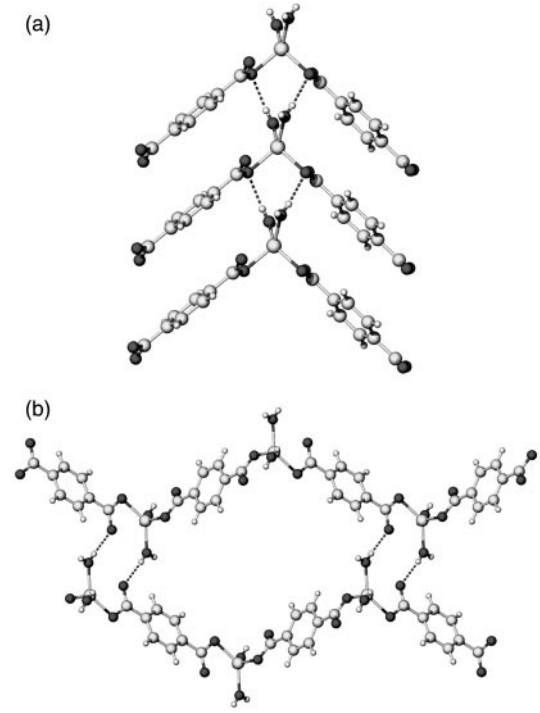

Fig. 2 (a) Stacking of $[Zn(H_2O)_2(\mu\text{-}O,O'\text{-}tph)]_\infty$ **2** in the *b* direction *via* R_2^2 (8) hydrogen bonded sets,[20] O···O 2.776(2) Å, (b) lateral R_2^2 (12) motifs which link one polymeric chain to those adjacent, O···O 2.699(3) Å.

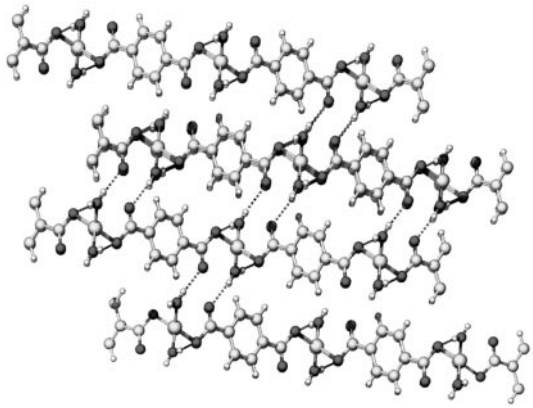

Fig. 3 Crystal packing in **2**.

rings of the tph ligands stack in an offset fashion perpendicular to the *b* direction, *ca.* 3.7 Å apart. The overall crystal packing is shown in Fig. 3.

Clearly the presence of two labile water molecules within the Zn^{2+} coordination sphere, playing only an indirect part in the polymeric chain, suggests that they might be replaced by other ligands with different hydrogen bonding characteristics. This should influence, *via* hydrogen bonding, the geometry of the coordination polymer. Hence we carried out the reaction of Zn^{2+} salts with Na_2tph in the presence of 1 equivalent of ethylenediamine (en). This resulted in the formation of an exactly analogous coordination polymer, $[Zn(en)(\mu\text{-O,O'-tph})]_\infty$ **3**, in which the two water molecules have been replaced by a single, chelating en ligand. Fascinatingly, the X-ray crystal structure of this material† reveals the same essential features of the coordination geometry and herringbone packing of the polymer observed in **2** despite the greatly different characteristics of the en ancillary ligand. As in **2**, the Zn^{2+} centres stack precisely along the crystallographic *b* direction. However, in **3** there is no possibility of the propagating R_2^2 (8) hydrogen bonded links because of the steric bulk of the ethylene spacer and this is reflected in the dramatic expansion of the crystallographic *b* axis from 5.00 to 7.25 Å. One of the amine protons on each donor atom is thus unable to take part in any hydrogen bonding. The NH_2 functions are, however, capable of engaging in lateral interactions from one chain to another in the same fashion as **2** to give twelve-membered hydrogen bonded rings, Fig. 4. The most obvious consequence of the reduction in inter-chain connectivity is the dramatic reorientation of the aryl groups of the tph ligands such that in **3** they are approximately parallel with the crystallographic *b* direction, as opposed to perpendicular, as in **2**. This has the curious consequence both of disrupting the π-stacking interactions seen for **2** *and* changing the coordination mode of the tph ligands from 'semi-chelating', to entirely unidentate, with a non-bonded Zn–O(2) distance of 2.931(3) Å, compared to 2.5500(16) Å in **2** and a shortening of the Zn–O(1) bond length to 1.947(3) Å. Since it is the non-coordinated tph oxygen atom O(2) which is involved as a hydrogen bond acceptor in both cases it is clear that the accommodation of the lateral hydrogen bonds plays a much more significant role in determining the overall structure than factors such as weak interactions of O(2) with the zinc centre and π-stacking.

The key to the future potential of this system clearly lies in the robustness of the one dimensional coordination polymeric chain and its ability to tolerate other ancillary ligands. In order to explore the phase space of the Zn^{2+}–tph^{2-} system a large variety of reactions between these two components were set up with mole ratios of 1 : 1 up to 1 : 4 in a range of solvents and with a range of Zn^{2+} salts. Compound **2** was formed in excellent yield in every case (as determined by solid state IR spectroscopy and measurement of unit cell dimensions) except for one occasion in which the reaction of hydrated zinc acetate with Na_2(tph) in water in a 1 : 1 ratio gave a mixture of **2** and a further product of formula $[Zn(H_2O)(tph)]_\infty$ **4**. Compound **4** is a highly cross-linked polymer involving coordination of all four tph oxygen atoms, each to a different trigonal bipyramidal Zn^{2+} centre (aqua ligand equatorial). The structure is based on a ladder arrangement of puckered eight-membered $Zn_2O_4C_2$ rings. Thermogravimetric analysis of **2** indicates stepwise loss of the two aqua ligands at 168 and 192 °C, respectively, suggesting the possible conversion of **2** into **4**. Full details of this system will be reported fully in a separate paper.

We thank the EPSRC and King's College London for funding of the diffractometer system and the Nuffield Foundation for the provision of computing equipment. Grateful acknowledgement is also given to the ULIRS Thermochemistry service at UCL.

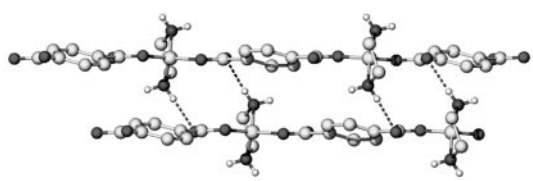

Fig. 4 Lateral R_2^2 (12) motifs in $[Zn(en)(\mu\text{-O,O'-tph})]_\infty$ **3**, N···O 2.984(5) Å (CH hydrogen atoms omitted for clarity). Note the second NH proton does not take part in any hydrogen bonds.

Notes and references

† *Crystal data*: **2**: $C_8H_8O_6Zn$, M = 265.51, monoclinic, space group $C2/c$, a = 14.9503(8), b = 5.0031(4), c = 12.1617(11) Å, β = 103.647(6)°, U = 883.99(12) Å^3, D_c = 1.995 Mg m^{-3}, Z = 4, μ = 27.84 cm^{-1}, T = 100(2) K, Reflections measured: 8316, unique data: 1010 (R_{int} = 0.069), parameters: 78, $R1$ [$F^2 > 2\sigma(F^2)$] = 0.0310, $wR2$ (all data) = 0.0802.

3: $C_{10}H_{12}N_2O_4Zn$, M = 289.59, monoclinic, space group $P2/n$, a = 5.6508(11), b = 7.2496(14), c = 13.179(3) Å, β = 100.468(2)°. U = 530.90(18) Å^3, D_c = 1.812 Mg m^{-3}, Z = 2, μ = 23.17 cm^{-1}, T = 100(2) K, Reflections measured: 2189, unique data: 1212 (R_{int} = 0.078), parameters: 87, $R1$ [$F^2 > 2\sigma(F^2)$] = 0.0511, $wR2$ (all data) = 0.1297.

CCDC 182/1299. See http://www.rsc.org/suppdata/cc/1999/1563/ for crystallographic data in .cif format.

1 D. Braga, L. Maini and F. Grepioni, *Angew. Chem., Int. Ed.*, 1998, **37**, 2240.
2 M. J. Zaworotko, *Chem. Soc. Rev.*, 1994, **23**, 283.
3 D. Braga, A. Angeloni, L. Maini, A. W. Götz and F. Grepioni, *New J. Chem.*, 1999, **23**, 17.
4 G. R. Desiraju, *Angew. Chem., Int. Ed. Engl.*, 1995, **34**, 2311.
5 G. R. Desiraju, *Acc. Chem. Res.*, 1996, **29**, 441.
6 V. R. Thalladi, B. S. Goud, V. J. Hoy, F. H. Allen, J. A. K. Howard and G. R. Desiraju, *Chem. Commun.*, 1996, 401.
7 M. D. Hollingsworth, M. E. Brown, A. C. Hillier, B. D. Santarsiero and J. D. Chaney, *Science*, 1996, **273**, 1355.
8 O. M. Yaghi, G. Li and H. Li, *Nature*, 1995, **378**, 703.
9 O. König, H.-B. Bürgi, T. Armbuster, J. Hulliger and T. Weber, *J. Am. Chem. Soc.*, 1997, **119**, 10632.
10 *Comprehensive Supramolecular Chemistry*, ed. J. L. Atwood, J. E. D. Davies, D. D. MacNicol and F. Vögtle, Pergamon, Oxford, 1996.
11 H. Li, M. Eddaoudi, T. L. Groy and O. M. Yaghi, *J. Am. Chem. Soc.*, 1998, **120**, 8571.
12 P. Brunet, M. Simard and J. D. Wuest, *J. Am. Chem. Soc.*, 1997, **119**, 2737.
13 J. W. Steed and K. Johnson, *J. Chem. Soc., Dalton Trans.*, 1998, 2601.
14 J. W. Steed, P. C. Junk and B. J. McCool, *J. Chem. Soc., Dalton Trans.*, 1998, 3417.
15 J. W. Steed and P. C. Junk, *J. Chem. Soc., Dalton Trans.*, 1999, 2141.
16 H. Hassaballa, J. W. Steed, P. C. Junk, and M. R. J. Elsegood, *Inorg. Chem.*, 1998, **37**, 4666.
17 R.-G. Xiong, S. R. Wilson and W. Lin, *J. Chem. Soc., Dalton Trans.*, 1998, 4089.
18 J. W. Steed and P. C. Junk, unpublished work.
19 C. C. Addison, N. Logan, S. C. Wallwork and C. D. Garner, *Quart. Rev. Chem. Soc.*, 1971, **25**, 289.
20 J. Bernstein, R. E. Davis, L. Shimoni and N.-L. Chang, *Angew. Chem., Int. Ed. Engl.*, 1995, **34**, 1555.
21 L. J. Barbour, 'XSeed', University of Missouri–Columbia, 1999.

Communication 9/03163D

ChemComm

Seven-coordinate Mn^{2+} ions in $[Mn(15\text{-crown-}5)(H_2O)_2]^{2+}$ as luminescent probes for dynamic supramolecular events†

Howard O. N. Reid,[a] Ishenkumba A. Kahwa,*[a] Andrew J. P. White[b] and David J. Williams[b]

[a] *Chemistry Department, University of the West Indies, Mona Campus, Kingston 7, Jamaica. E-mail: ikahwa@uwimona.edu.jm*

[b] *Chemical Crystallography Laboratory, Department of Chemistry, Imperial College of Science, Technology and Medicine, South Kensington, London, UK SW7 2AY*

Received (in Columbia, MO, USA) 12th May 1999, Accepted 23rd June 1999

Spectra and temperature dependent decay rates of emission from $[Mn(15\text{-crown-}5)(H_2O)_2]^{2+}$ ions anchored by a network of O–H···Br···H–O bonds in two- and one-dimensional supramolecular arrays of $\{[Mn(15\text{-crown-}5)(H_2O)_2][TlBr_5]\}_n$ 1 and $\{[Mn(15\text{-crown-}5)(H_2O)_2]Br_2\}_n$ 2 demonstrate the potential efficacy of manganese(II) ions as luminescent probes for supramolecular dynamics.

The good response of the manganese(II) $^4T_1(^4G)$ state to changing ligand field strength and symmetry as well as the high sensitivity of luminescence techniques, such as time resolved luminescence spectroscopy, make the $Mn^{2+}[^4T_1(^4G)\rightarrow{}^6A_1]$ emission attractive as a potential diagnostic tool for coordination characteristics of divalent metal ions.[1,2] Besides classical four- and six-coordinate oxide and halide species,[3] $Mn^{2+}[^4T_1(^4G)\rightarrow{}^6A_1]$ emission was recently shown to occur in well defined seven- and eight-coordinate environments[4] thereby expanding the range of Mn^{2+} coordination environments accessible by luminescence techniques. Herein we demonstrate the diagnostic efficacy of the $Mn^{2+}[^4T_1(^4G)\rightarrow{}^6A_1]$ emission by probing the behaviour of coordinated H_2O in response to thermal tuning of the structural rigidity of $[Mn(15\text{-crown-}5)(OH_2)_2]^{2+}$ cations anchored in two- and one-dimensional supramolecular arrays of $\{[Mn(15\text{-crown-}5)(H_2O)_2][TlBr_5]\}_n$ **1**[4] and $\{[Mn(15\text{-crown-}5)(H_2O)_2]Br_2\}_n$ **2**.[5]

Compounds **1**[4] and **2**[5] were prepared as described previously, whilst compound **3** was obtained by a procedure similar to that used for **2** but with D_2O and CH_3OD replacing H_2O and CH_3OH respectively. X-Ray analysis‡ shows compound **1** to be composed of two-dimensional corrugated sheets of $[TlBr_5]^{2-}$ anions and $[Mn(15\text{-crown-}5)(OH_2)_2]^{2+}$ cations cross-linked *via* O–H···Br hydrogen bonds (Fig. 1). The symmetry at the seven-coordinate manganese centre is crystallographically imposed C_{2h} with the two symmetry related aqua ligands lying on the mirror plane. The 15-crown-5 component is disordered, having four resolved symmetry-imposed partially overlapping orientations. The $[TlBr_5]^{2-}$ dianion has crystallographic C_{2v} symmetry, adopting a slightly distorted trigonal bipyramidal geometry; the equatorial Tl–Br bonds subtend angles of 116.43(5), 116.43(5) and 127.15(10)° and the axial bonds an angle of 175.36(9)°, and there is a very marked asymmetry between the axial [2.883(2) Å] and the equatorial [2.540(2) and 2.552(3) Å] bond lengths. The anion geometry observed here {the first reported structural characterisation of $[TlBr_5]^{2-}$} differs markedly from that observed in the only two reported examples of the closely related anion $[TlCl_5]^{2-}$, both of which are slightly distorted square pyramidal with only small asymmetries in the bond lengths.[6] A $[Br\cdots TlBr_4]^{2-}$ species was reported recently.[7]

In contrast, the structure of **2** comprises one-dimensional chains of $[Mn(15\text{-crown-}5)(OH_2)_2]^{2+}$ cations linked by pairs of O–H···Br hydrogen bonds to the Br^- anions.[5]

In the light of these structural results, it was interesting to determine if this difference in structural rigidity would translate into contrasts in the ability of H_2O to quench $Mn^{2+}[^4T_1(^4G)\rightarrow{}^6A_1]$ emission from the $[Mn(15\text{-crown-}5)(H_2O)_2]^{2+}$ cations of **1** and **2**. The excitation and luminescence spectra of dihydrates **1** and **2** were too weak to measure reliably on the LS5B spectrometer.§ We thus sought to prepare deuterates of **1** and **2**, namely $[Mn(15\text{-crown-}5)(D_2O)_2][TlBr_5]$ and $[Mn(15\text{-crown-}5)(D_2O)_2]Br_2$, since D_2O vibrations are much less effective quenchers. However, impracticably large amounts of the CH_3OD–CH_2Cl_2 mixed solvent system were required for the deuteration of **1** and thus its synthesis was abandoned. Crystals of $[Mn(15\text{-crown-}5)(D_2O)_2]Br_2$ **3** are readily prepared and upon microscopic examination were found to have a morphology similar to that of **2**. The emission and excitation spectra of seven-coordinate manganese(II) in $[Mn(15\text{-crown-}5)(D_2O)_2]^{2+}$ are shown in Fig. 2(b). These are the first pure spectra for seven-coordinate Mn^{2+}; the excitation spectrum reported in ref. 4 is contaminated by transitions of the sensitizing $MnBr_4^{2-}$ anion.

Comparison of the spectra of $[Mn(15\text{-crown-}5)(D_2O)_2]^{2+}$ [Fig. 2(b)], $[Mn(12\text{-crown-}4)_2]^{2+}$ [Fig. 2(c)], classical $[MnBr_4]^{2-}$ [Fig. 2(d)], $[MnBr_3]^-$ [Fig. 2(a)] and the previously reported[8] absorption spectrum of species $[MnBr(Me_6tren)]^+$ reveals major variations in emission and excitation/absorption spectral profiles for Mn^{2+} ions in coordination numbers 7, 8, 4, 6 and 5 respectively. Luminescence techniques may thus be informative in probing such common Mn^{2+} coordination sites[9] in a wide range of materials including phosphors,[3] polymers,[10] industrial minerals,[11] biomolecules and potential MRI contrast agents for which the behaviour of the Mn–OH_2 linkage is crucial.[12]

To establish whether the decay rates of $Mn^{2+}[^4T_1(^4G)\rightarrow{}^6A_1]$ emission from the seven-coordinate Mn(II) centre in [Mn(15-

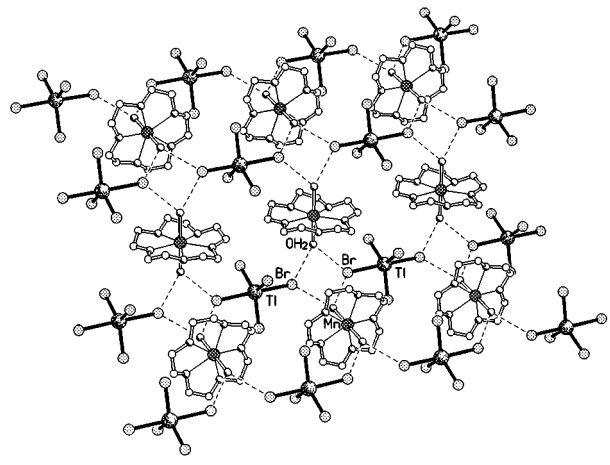

Fig. 1 Part of one of the corrugated hydrogen bonded sheets of $[TlBr_5]^{2-}$ anions and $[Mn(15\text{-crown-}5)(H_2O)_2]^{2+}$ cations in the structure of **1**. The O···Br distances are all 3.25 Å.

† Dedicated to Dr Earle V. Roberts in celebration of his service to the Department of Chemistry, University of the West Indies, Mona Campus.

crown-5)$(H_2O)_2]^{2+}$ are sensitive enough to allow the detection of dynamic supramolecular lattice events we compared the luminescence decay dynamics of compounds **1**–**3**. The absorption energy of the broad $Mn^{2+}[^4T_1(^4G)\leftarrow{}^6A_1]$ transition ($\lambda_{max} \approx 520$ nm) of [Mn(15-crown-5)$(H_2O)_2]^{2+}$ [Fig. 2(b)] overlaps well with the second harmonic of Nd:YAG lasers (532 nm). Our powerful Nd:YAG laser§ was thus used to directly excite the $Mn^{2+}[^4T_1(^4G)]$ energy level in complexes **1**–**3**; a broad emission centered at *ca.* 590 nm [Fig. 2(b)] was observed in each case. The temperature dependence (10–320 K)§ of this emission revealed remarkable similarities between the behaviour of the more rigid two-dimensional hydrate **1** and that of the one-dimensional deuterate **3**, with both of these differing dramatically from the behaviour of the one-dimensional hydrate **2**. For $T < 100$ K, compounds **1** and **3** exhibit similar double exponential luminescence decay kinetics with a common minor short-lived temperature independent emission (component A) decaying at *ca.* 1×10^3 s^{-1}. The major emission comes from a marginally temperature dependent and much longer-lived component (decay rate is *ca.* 7×10 s^{-1} at 10 K) with phonon type thermal barriers of *ca.* 2.1×10^2 and 2.7×10^2 cm^{-1} for **1** and **3** respectively. By sharp contrast, compound **2** exhibits temperature independent perfectly double exponential decay behaviour for $T < 160$ K. Besides the common minor component A (decay rate *ca.* 1.1×10^3 s^{-1}), compound **2** features a major very short-lived emission (decay rate *ca.* 7.0×10^3 s^{-1}).

These observations we believe can be rationalised as follows: the sharply contrasting behaviour between the two one-dimensional compounds **2** and **3** is due to the more efficient quenching of the $Mn^{2+}[^4T_1(^4G)\rightarrow{}^6A_1]$ emission by H_2O in **2** compared to the weak quenching action of D_2O in **3**. The similarity of the behaviour of **1** and **3** however, can be explained by considering the rigidity of the two-dimensional O–H···Br···H–O bonds in **1** which hinders the vibrational motions of the coordinated H_2O molecules of [Mn(15-crown-5)$(H_2O)_2]^{2+}$. At low temperature vibrational restrictions in **1** appear to be so severe that the normal quenching effect of the aqua ligands is stopped and hence the similarity in the decay behaviour of hydrate **1** and deuterate **3**. The thermal barrier of *ca.* 210 cm^{-1} is in this case the energy needed to distort the lattice of **1** and allow some vibrational freedom for the H_2O molecules which triggers quenching of the $Mn^{2+}[^4T_1(^4G)\rightarrow{}^6A_1]$ emission by those coordinated H_2O molecules. To our knowledge, this is the first example of thermal tuning of the luminescence quenching action of H_2O molecules, in particular, one in which supramolecular manipulations are employed.

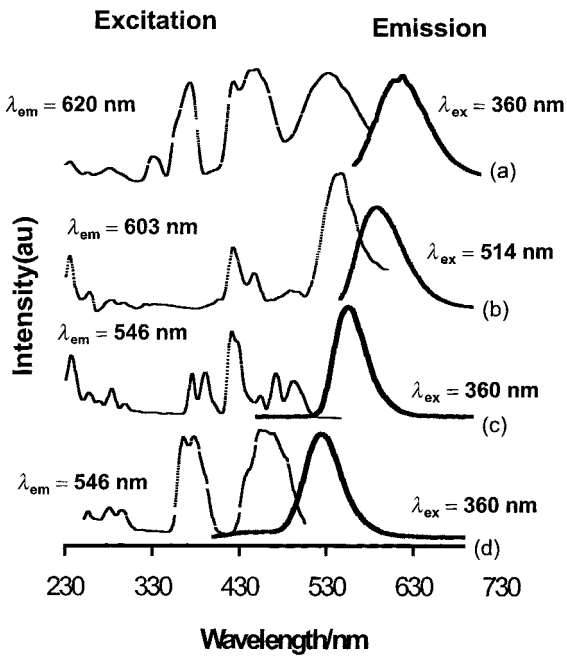

Fig. 2 Excitation and emission spectra of manganese(II) in (T_d = delay time; T_g = gating time): (a) six-coordination, $[NMe_4][MnBr_3]$ (293 K; T_d = 1.00 ms, T_g = 1.00 ms); (b) seven-coordination, $[\{Mn(15\text{-crown-}5)(D_2O)_2\}Br_2]_n$ **3** (77 K; T_d = 0.01 ms, T_g = 5.00 ms); (c) eight-coordination, $[Mn(12\text{-crown-}4)_2][NMe_4]_2[MnBr_4]_x[ZnBr_4]_{2-x}$ (77 K; T_d = 12.0 ms, T_g = 0.5 ms); (d) four-coordination, $[NMe_4]_2[MnBr_4]$ (293 K; T_d = 1.00 ms, T_g = 1.00 ms).

We thank the University of the West Indies (UWI) for a demonstratorship to HONR and the Inter-American Development Bank-UWI development programme (R&D Project #29) for funds used to purchase the powerful Nd:YAG laser and the helium refrigerator. We also thank the TMRU (UWI) for use of the LS5B luminescence spectrometer and Mr S. Logan for help with setting up the laser induced luminescence facilities.

Notes and references

‡ *Crystal data*: **1**: $[C_{10}H_{24}O_7Mn][TlBr_5]$, M = 915.2, orthorhombic, space group *Pmma* (no. 51), a = 15.879(3), b = 10.122(3), c = 7.109(1) Å, V = 1142.5(5) Å^3, Z = 2 (the cation and anion have crystallographic C_{2h} and C_{2v} symmetries respectively), D_c = 2.660 g cm^{-3}, μ(Mo-Kα) = 163.6 cm^{-1}, $F(000)$ = 842, T = 293 K; yellow blocks, 0.40 × 0.33 × 0.30 mm, Siemens P4/PC diffractometer, ω-scans, 1102 independent reflections. The structure was solved by direct methods and, because of the severe disorder (see text) only the oxygen atom of the aqua ligand and the manganese, thallium and bromine atoms were refined anisotropically using full matrix least squares based on F^2 to give R_1 = 0.054, wR_2 = 0.132 for 850 independent observed absorption corrected reflections [$|F_o| > 4\sigma(|F_o|)$, $2\theta \leqslant 50°$] and 92 parameters. Full structural details of compound **2** will be reported elsewhere.[5] CCDC 182/1305. See http://www.rsc.org/suppdata/cc/1999/1565/ for crystallographic files in .cif format.

§ Luminescence and excitation spectra were recorded using a LS5B Perkin Elmer Fluorescence spectrometer that is essentially similar to the one described earlier.[13] The luminescence decay rates were measured using a Continuum Powerlite 8000 YAG laser and an electronic and computational set up which was described previously.[13] The Powerlite 8000 YAG laser generates *ca.* 600 mJ pulses (5–8 ns) of the second harmonic at 532 nm but minimum light intensities required to obtain decay curves of satisfactory signal:noise ratios were used. Variable temperature measurements (8–320 K) were done using an APD Cryogenics Inc. CSW-202 Displex helium refrigerator system with the sample in contact with cryocon conducting grease.

1 U. Lanver and G. Lehman, *J. Lumin.*, 1978, **17**, 225.
2 J. C. Hempel, R. A. Palmer and M. C. Yang, *J. Chem. Phys.*, 1976, **64**, 4314.
3 N. S. Fender, F. R. Fronczek, V. John, I. A. Kahwa and G. L. McPherson, *Inorg. Chem.*, 1997, **36**, 5539; M. M. de Lucas and F. Rodriguez, *J. Phys.: Condens. Matter.*, 1989, **11**, 4251; D. T. Palumbo and J. J. Brown, *J. Electrochem.*, 1971, **118**, 1159; D. T. Palumbo and J. J. Brown, *J. Electrochem.*, 1970, **117**, 1185; L. E. Shea, R. K. Dalta and J. J. Brown, *J. Electrochem. Soc.*, 1994, **141**, 1950; B. T. Collins and M. Ling, *J. Electrochem. Soc.*, 1993, **140**, 1752; L. DeMarsh, *SMPTE J.*, 1993, 1095.
4 H. O. N. Reid, I. A. Kahwa, A. J. P. White and D. J. Williams, *Inorg. Chem.*, 1998, **37**, 3868.
5 H. O. N. Reid, I. A. Kahwa, J. T. Mague and G. L. McPherson, *Acta Crystallogr. Sect. C*, 1999, submitted.
6 M. A. James, M. B. Millikan and B. D. James, *Main Group Met. Chem.*, 1991, **14**, 1; M. A. James, J. A. C. Clyburne, A. Linden, B. D. James, J. Liesegang and V. Zuzich, *Can. J. Chem.*, 1996, **74**, 1490.
7 M. A. Liden, M. A. James, M. B. Millikan, L. M. Kivlighon, A. Petridis and B. D. James, *Inorg. Chim. Acta*, 1999, **284**, 215.
8 M. Ciampolini, *Structure Bonding* (*Berlin*), 1969, **6**, 78.
9 C. E. Holloway and M. Melnik, *Rev. Inorg. Chem.*, 1996, **16**, 101.
10 R. Breslow, *J. Chem. Educ.*, 1998, **75**, 705; R. H. Holm, P. Kennepohl and E. Solomon, *Chem. Rev.*, 1996, **96**, 2239.
11 V. V. Bakhterev and I. V. Solomonov, *Inorg. Mater.* (*Transl. Neorg. Mater.*), 1995, **31**, 526; O. V. Kononov and I. V. Nesterov, *Mineral. Geokhim. Vol'framovykh Mestorozhd., Tr. Vses. Soveshch. 3rd*, 1995, p. 364; E. Loh, *Am. Mineral.*, 1975, **60**, 79.
12 J. A. Cowan, *Chem. Rev.*, 1998, **98**, 1067; R. B. Lauffer, *Chem. Rev.*, 1987, **87**, 901.
13 A. S. Gajadhar-Plummer, I. A. Kahwa, A. J. P. White and D. J. Williams, *Inorg. Chem.*, 1999, **38**, 1745.

Communication 9/03808F

Effect of the end-groups upon delocalisation in polymethines: the first crystallographically characterised bond-alternated cyanine

Stephen Barlow,†[a] Lawrence M. Henling,[a] Michael W. Day[a] and Seth R. Marder*[abc]

[a] *Beckman Institute, 139-74, California Institute of Technology, Pasadena, CA 91125, USA*
[b] *Jet Propulsion Laboratory, California Institute of Technology, Pasadena, CA 91109, USA*
[c] *Department of Chemistry, University of Arizona, Tucson, AZ 85721, USA*

Received (in Oxford, UK) 14th May 1999, Accepted 23rd June 1999

The reorganisation energy associated with the end groups may be used to influence the localisation behaviour of cyanines; thus, the 1,3-bis(ruthenocenyl)allylium cation is markedly unsymmetrical in the crystal structure of its hexafluorophosphate salt, with the positive charge localised on one ruthenium, whereas the analogous iron species is delocalised and has approximate C_5 symmetry.

Concepts of resonance lead to the expectation that typical polymethine cations or anions (cyanines) should have symmetrical structures, intermediate between two unsymmetrical extreme resonance structures [Figure 1(a)]. Numerous reported crystal structures[1] confirm that typical cyanines are indeed symmetrical delocalised systems with equalised C–C bond lengths. However, extrapolation of the properties of a typical cyanine to infinite chain length[2] affords a one-dimensional zero-band-gap material, which should be subject to a Peierls distortion.[3] If the end groups can stabilise the overall positive or negative charge, this distortion is predicted to result in a bond-alternated structure resembling *one* of the extreme structures in Fig. 1(a); the two structures are now related by an equilibrium arrow.[4–7] To date the only experimental evidence for a Peierls-distorted cyanine is for the compound shown in Fig. 1(b); the solution structure was shown to be unsymmetrical by comparison of its IR and UV–VIS–NIR spectra with those of symmetrical delocalized shorter chain homologues.[8]

Although previous studies have distinguished between end groups which stabilise the overall charge and those which do not,[7] the possibility of different charge-stabilising end groups controlling the length at which localisation occurs does not seem to have been discussed in detail. It has been noted[8,9] that Peierls-distorted cyanines are analogous to class II mixed-valence compounds, whilst typical cyanines are analogous to class III species. The placement of a compound in the Robin and Day classification[10] depends on the interplay of the electronic coupling between the two extreme localised structures, V, and the vertical reorganisation energy of Marcus theory, λ.[11] In a polymethine, V will be influenced by the length and planarity of the polymethine chain, whilst λ will have contributions from interconverting the end groups (for example: the Me_2N^+= and Me_2N– geometries in a cyanine such as that in Fig. 1(a); analogous to the Ru^{II} and Ru^{III} coordination geometries in the mixed-valence Creutz–Taube ion[11]), as well as from the polymethine bridge itself, where the sense of the bond-length alternation must be inverted. In a typical cyanine, the end group effect is limited to changing a few bond lengths. We chose to investigate the Group 8 metallocenes as end groups with potentially different reorganisation energy characteristics: a carbocation α to a metallocene is stabilised through resonance contributions from the [(η^6-fulvene)(η^5-cyclopentadienyl)-metal] cation,[12] which has significantly different geometry from the parent metallocene,[13] especially when the metal is ruthenium[14] or osmium.[15]

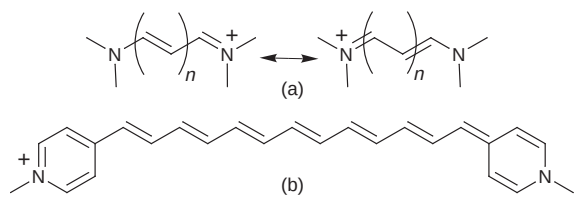

Fig. 1 Representations of (a) the extreme unsymmetrical resonance structures for a typical cyanine and (b) the Peierls-distorted cyanine reported by Tolbert and Zhao.[8]

We synthesised a range of 1,3-bis(metallocenyl)allylium salts, $[Mc(CH)_3Mc']^+[X]^-$ {Mc = Mc′ = ferrocenyl (Fc), **1**; Mc = Mc′ = 2,3,4,5,1,2,3,4-octamethyl-1-ferrocen-1-yl (Fc″), **2**; Mc = Mc′ = ruthenocenyl (Rc), **3**; Mc = Fc, Mc′ = Rc, **4**; X = PF_6, **a**; X = BF_4, **b**}. Single crystal X-ray diffraction showed the cations in **1a**‡ and **2a**[16] to be essentially symmetrical with equalised C–C bonds in the allylium bridges, as might be expected by analogy with the previously described structure of closely related cyclopentadienyl(1,3-diferrocenyl-1-ylium-pentalenyl)iron tetrafluoroborate.[17] In contrast, we found the structure of **3a**‡ to be much less symmetrical (Fig. 2), although the packing diagrams for **1a** and **3a** are rather similar. The structural parameters for the Ru1 ruthenocene are similar to those for previously reported examples of ruthenocene-stabilised carbocations; *i.e.* it is essentially fully distorted to an [(η^6-fulvene)(η^5-cyclopentadienyl)ruthenium] cation structure. Thus, the Ru1–C11 bond length of 2.381(3) Å may be compared with 2.270(3) Å for the corresponding distance in $[Cp^*Ru(\eta^6\text{-}C_5Me_4CH_2)]^+[BPh_4]^-\cdot CH_2Cl_2$ **5**;[14] similarly the Ru1–C_{ring} distances fall in the range 2.089(2)–2.234(2) Å, whilst those for **5** fall in the range 2.066(3)–2.274(3) Å. In the $[Rc(CH)_3Rc]^+$ cation of **3a**, the α-carbon C11 is bent towards Ru1 such that the C10–C11 bond makes an angle of 38.2° with the C6–10 plane; the corresponding angle in **5** is 40.4°. The dimensions of the Ru2 ruthenocene are typical for a 'normal' ruthenocene; thus, the Ru2–C_{ring} distances for **3a** fall in the range 2.167(2)–2.194(3) Å, whilst those for *E*-1,2-dimethyl-1,2-diruthenocenylethylene[18] and ruthenocene itself[19] fall in the

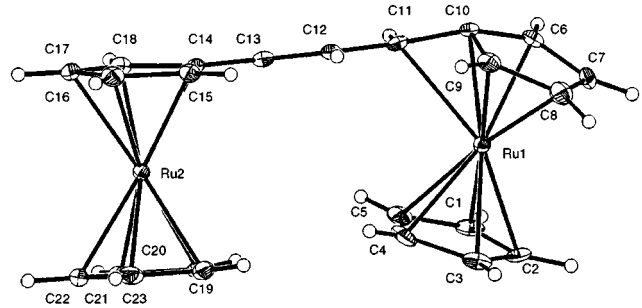

Fig. 2 View of the $[Rc(CH)_3Rc]^+$ cation in the crystal structure of its hexafluorophosphate salt, **3a**, showing the atomic numbering scheme; non-hydrogen atoms are represented by 50% thermal ellipsoids, whilst hydrogen atoms are shown as spheres of arbitrary radius.

† Present address: Inorganic Chemistry Laboratory, University of Oxford, South Parks Road, Oxford, UK OX1 3QR.

ranges 2.171(3)–2.216(3) and 2.181(2)–2.188(2) Å respectively. The α-carbon, C13, is *not* bent towards Ru2 and the Ru2–C13 distance is 3.237(3) Å. The structure of **3a** also shows considerable bond length alternation in the allylium bridge; the C(11)–C(12) bond length is 1.443(4) Å, whilst the C(12)–C(13) bond length is 1.343(4) Å.[20]

The structure of **3a** is the first crystal structure of a nominally symmetrical cyanine adopting an unsymmetrical bond-alternated structure. Indeed, the only previously reported Peierls-distorted cyanine is the much longer species shown in Fig. 1(b). One question that now arises is whether the unsymmetrical structure of the cation in **3a** is due to solid-state (crystal-packing) effects. However, *all* previous cyanine structures *are* symmetrical, despite a great variety of counterions and packing motifs. Moreover, the similarity in the packing of **1a** and **3a** suggests the differences in molecular structure are due to internal electronic, rather than external crystal-packing, effects.[21] We believe that the origin of these electronic effects is the larger reorganisation energy of the ruthenium system; the structural differences between ruthenocene and [(η^6-fulvene)-(η^5-cyclopentadienyl)ruthenium] cation are much greater than for the analogous iron species. To further investigate this question we studied the **3** cation in solution.[22] Symmetrical and unsymmetrical forms of cyanines are expected to have vibrational modes of different energies; calculations support this expectation for $[NH_2(CH)_nNH_2]^+$ (n = 19, 25).[23] The differences should be most readily detected in the stretches associated with the multiple bonding of the polymethine bridge. **3a** (1609 cm^{-1} in KBr, 1598 cm^{-1} in CH_2Cl_2) and **3b** (1603 cm^{-1} in KBr, 1603 cm^{-1} in CH_2Cl_2) both show a strong IR band which we assign to the multiple bond stretch; neither ruthenocene nor [(η^6-fulvene)(η^5-cyclopentadienyl)ruthenium] cations[24] show absorptions in the same region. The same band is also present in Raman spectra (1609 and 1601 cm^{-1} for **3a** in KBr and CH_2Cl_2, respectively). The insensitivity of the band to the counter ion, or the medium, implies that the structure of the **3** cation is the same in crystals of both its tetrafluoroborate and hexafluorophosphate salts, and in CH_2Cl_2 solution. Moreover, the IR evidence implies that the structure of the **3** cation most closely resembles that of the **4** cation (1598 cm^{-1} in KBr for **4a**), which is unsymmetrical both formally and electronically (according to ^1H–^1H coupling constants), and is somewhat different from those of the **1** (1558 and 1558 cm^{-1} for **1a** in KBr and CH_2Cl_2 respectively) and **2** (1538 and 1542 cm^{-1} for **2a** in KBr and CH_2Cl_2 respectively) cations (which have been shown to be symmetrical in the crystal structures of their hexafluorophosphate salts).

In conclusion, we believe that the large reorganisation energy associated with the ruthenocene / [(η^6-fulvene)(η^5-cyclopentadienyl)ruthenium] system has enabled us to characterise a bond-alternated cyanine at an unprecedentedly short chain length. We have presented the first crystal structure of a Peierls-distorted bond-alternated cyanine; vibrational spectroscopy suggests the cyanine is also unsymmetrical in solution. Control of the reorganisation energy in this way may be a useful design principle for the synthesis of other charge-localised cyanines, which have potential optical and electronic applications.

Support from the National Science Foundation and Air Force Office of Scientific Research (AFOSR) at Caltech is gratefully acknowledged. The research described in this paper was performed in part by the Jet Propulsion Laboratory (JPL) California Institute of Technology, as part of its Center for Space Microelectronics Technology and was supported by the Ballistic Missile Defense Initiative Organization, Innovative Science and Technology Office through an agreement with the National Aeronautics and Space Administration (NASA). We thank Kenneth Calgren for his assistance with Raman measurements and Dr Paul Roussel for assistance with low temperature NMR experiments.

Notes and references

‡ Single crystals of **1a** and **3a** were grown by layering dichloromethane solutions with diethyl ether. Diffraction data were acquired at 85 K using an Enraf-Nonius CAD-4 diffractometer, employing Mo-Kα radiation (0.71073 Å). Structures were solved by direct methods using SHELXS97;[25] full-matrix least-squares refinement on F^2 against all reflections was carried out using SHELXL97.[25]

Crystal data: for **1a**, $C_{23}H_{21}F_6Fe_2P$, M = 554.07, orthorhombic, a = 14.420(3), b = 12.267(2), c = 24.062(5) Å, V = 4256.3(14) $Å^3$, space group *Pbcn*, Z = 8, μ = 1.499 mm^{-1}, 9150 reflections measured, 3752 unique (R_{int} = 0.034); the final R indices (for all data) were $R1$ = 0.101 and $wR2$ = 0.1327. Fourier maps revealed disorder, whereby there is a minor alternative orientation of the cation related to the major orienation by rotation about an axis perpendicular to the plane of the bridging group and passing through the central atom of the bridge. However, this could not be satisfactorily modelled and is, therefore, not included in the reported structure.

For **3a**; $C_{23}H_{21}F_6PRu_2$, M = 644.51, monoclinic, a = 26.409(6), b = 15.004(3), c = 11.970(3) Å, β = 113.83(2)°, V = 4338.6(17) $Å^3$, space group $C2/c$, Z = 4, μ = 1.526 mm^{-1}, 10256 reflections measured, 3818 unique (R_{int} = 0.014); the final R indices (for all data) were $R1$ = 0.0238 and $wR2$ = 0.0491.

CCDC 182/1296. See http://www.rsc.org/suppdata/cc/1999/1567/ for crystallographic files in .cif format.

1 D. L. Smith, *Photogr. Sci. Eng.*, 1974, **18**, 309 and references therein.
2 S. Dähne and R. Radegalia, *Tetrahedron*, 1971, **27**, 3673.
3 R. E. Peierls, *Quantum Theory of Solids*, OUP, Oxford, 1955.
4 C. Kuhn, *Synth. Met.*, 1991, **41**–**43**, 3681.
5 J. S. Craw, J. R. Reimers, G. B. Bacskay, A. T. Wong and N. S. Hush, *Chem. Phys.*, 1992, **167**, 77.
6 L. M. Tolbert and M. E. Ogle, *Synth. Met.*, 1992, **51**, 391.
7 In contrast, when the end groups do not electronically stabilise the charge, as in the case of phenyl-terminated polymethine anions, the distorted cyanine is predicted to retain its symmetry, but with the charge no longer being delocalised onto the end groups.[6]
8 L. M. Tolbert and X. Zhao, *J. Am. Chem. Soc.*, 1997, **119**, 3253.
9 S. F. Nelsen, H. Q. Tran and M. A. Nagy, *J. Am. Chem. Soc.*, 1998, **120**, 298.
10 M. B. Robin and P. Day, *Adv. Inorg. Chem. Radiochem.*, 1967, **10**, 247.
11 C. Creutz, *Prog. Inorg. Chem.*, 1983, **30**, 1.
12 W. E. Watts, in *Comprehensive Organometallic Chemistry*, ed. G. Wilkinson, F. G. A. Stone and E. W. Abel, Pergamon, London, 1988.
13 U. Behrens, *J. Organomet. Chem.*, 1979, **182**, 89.
14 A. I. Yanovsky, Y. T. Struchkov, A. Z. Kreindlin and M. I. Rybinskaya, *J. Organomet. Chem.*, 1989, **369**, 125.
15 M. I. Rybinskaya, A. Z. Kreindlin, Y. T. Struchkov and A. I. Yanovsky, *J. Organomet. Chem.*, 1989, **359**, 233.
16 S. Barlow, L. M. Henling, M. W. Day, W. P. Schaefer and S. R. Marder, manuscript in preparation.
17 J. Lukasser, H. Angleitner, H. Schottenberger, H. Kopacka, M. Schweiger, B. Bildstein, K.-H. Ongania and K. Wurst, *Organometallics*, 1995, **14**, 5566.
18 C.-F. Chiu, M. Song, B.-H. Chen and K. S. Kwan, *Inorg. Chim. Acta*, 1997, **266**, 73.
19 P. Seiler and J. D. Dunitz, *Acta Crystallogr., Sect. B*, 1980, **36**, 2946.
20 The bond length alternation in **1a** is insignificant, although the large values for the appropriate bond lengths [1.469(10) and 1.461(10) Å] are artefacts of unmodelled disorder in the structure.
21 The inherently unsymmetrical **4a** is isomorphous with **3a**.[16]
22 The **3** cation appears symmetrical on the NMR timescale at room temperature [as does the cation shown in Fig. 1(b)]; low temperature studies (to –85 °C, 500 MHz for ^1H and 125 MHz for ^{13}C) also give no unambiguous evidence for localisation. UV–VIS solvatochromism studies are also inconclusive; symmetrical **1** and **2**, and unsymmetrical **4** all show similar behaviour to **3**.
23 J. R. Reimers and N. S. Hush, *Chem. Phys.*, 1993, **176**, 407.
24 M. Sato, Y. Kawata, A. Kudo, A. Iwai, H. Saitoh and S. Ochiai, *J. Chem. Soc., Dalton Trans.*, 1998, 2215.
25 G. M. Sheldrick, SHELXS97 and SHELXL97, Programs for Crystallography, University of Göttingen, Germany, 1997.

Communication 9/03868J

A novel heterometallic alkoxide: lithium–potassium *tert*-butoxide $[(Bu^tO)_8Li_4K_4]$

William Clegg,[a] Allison M. Drummond,[b] Stephen T. Liddle,[a] Robert E. Mulvey*[b] and Alan Robertson[b]

[a] *Department of Chemistry, University of Newcastle, Newcastle upon Tyne, UK NE1 7RU*
[b] *Department of Pure and Applied Chemistry, University of Strathclyde, Glasgow, UK G1 1XL. E-mail: r.e.mulvey@strath.ac.uk*

Received (in Cambridge, UK) 16th June 1999, Accepted 8th July 1999

Synthesised from its homonuclear components in the presence of the Lewis base TMEDA, the title heteronuclear alkoxide crystallises in an unsolvated TMEDA-free form; its novel breastplate-like $Li_4K_4O_8$ cage structure, which undergoes an exchange process in arene solution as determined by dynamic NMR spectroscopic studies, displays a planar K_4 arrangement in marked contrast to the tetrahedral K_4 arrangement found in homonuclear $[(Bu^tOK)_4]$.

The chemistry of metal alkoxides has gained greater significance in recent years primarily because of the demand for technologically important oxide materials: metal alkoxides serve as excellent precursors to oxide-based electronic and ceramic materials by sol–gel and MOCVD processes.[1,2] Group 1 alkoxides command additional attention due to their role in two-component 'superbases',[3] epitomised by 'BuLi·Bu^{t}OK', which are utilised widely in synthetic chemistry. As part of our continuing development of hetero-s-block metal chemistry, we have a particular interest in synthesising alkoxides that contain a mixture of Group 1 metals. Having recently reported the octalithium–dipotassium mixed oxide–alkoxide $[(Bu^tOLi)_6(Bu^tOK)_2(Li_2O)\cdot 2TMEDA]$,[4] the cage structure of which is built around an O^{2-} core, we subsequently directed our efforts towards synthesising a pure, oxide-free, analogue. These studies have afforded the new solvent-free heterometallic tetralithium–tetrapotassium alkoxide, $[(Bu^tO)_8Li_4K_4]$, **1**. Herein we report its synthesis, novel molecular structure, and dynamic NMR spectral data in arene solution.

Whilst many bimetallic alkoxides containing an alkali metal in combination with a less electropositive (p- or d-block) metal have been synthesised by direct reaction of the component homonuclear alkoxides,[5] this strategy has not been used previously as an entry into mixed alkali metal alkoxides. We have found it to be successful here for the synthesis of **1**. To elaborate, in a Schlenk tube under an argon atmosphere, a mixture of Bu^{t}OLi (4 mmol) and Bu^{t}OK (2 mmol) in toluene (5 ml) solution was heated to 70–80 °C for 20 min. On cooling to room temperature, the solution was treated with dried TMEDA (4 mmol) and stirred for 2 h. All solvent was then removed *in vacuo* to leave an oily pale yellow residue. Almost complete dissolution was achieved by the subsequent addition of hexane (5 ml). After filtering, the resulting solution was cooled to −26 °C for 48 h, at which time colourless crystals of **1** were obtained (yield, based on consumption of Bu^{t}OK, 65%). These crystals can be distinguished from their homonuclear components by a simple melting point analysis (*i.e.*, 242 °C, *cf.*, Bu^{t}OLi, decomp. > 250 °C;[6] Bu^{t}OK, 256–258 °C[7]). The synthesis of **1** proved reproducible on changing the Bu^{t}OLi: Bu^{t}OK reaction stoichiometry to 1 : 1 to match that found in the crystal. It is noteworthy that no TMEDA is present in **1** even though it was available in the reaction mixture. This contrasts with the situation encountered in the aforementioned $[(Bu^tOLi)_6(Bu^tOK)_2(Li_2O)\cdot 2TMEDA]$, and its rubidium relative $[\{(Bu^tOLi)_5(Bu^tORb)_4(Li_2O_2)\cdot 2TMEDA\}_\infty]$.[8] The compositions and structures of these solvates are presumably largely dictated by the templating action of their core dianion, O^{2-} or O_2^{2-}. An alternative structure building principle must operate in the absence of such templates; hence it is no surprise that the metal stoichiometry in **1** (4Li : 4K) is very different to that in the mixed-anion alkoxides (8Li : 2K or 7Li : 4Rb). Why such oxygen-based contaminants, and different ones at that, appear in the TMEDA solvates but not in **1** when the same routine 'inert-atmosphere' conditions were used in all three cases is not clear at present. Less efficient drying and degassing, leading to adventitious moisture or oxygen participation, is an obvious possibility, but more complex chemistry may be at work. In this regard, it is germane to note that the formation of another heterometallic oxo-alkoxide of potassium, $[(Pr^iO)_{10}(O)K_4Zr_2]$,[9] is thought to involve C–O bond scission from Pr^{i}OM units.

Possessing exact crystallographic C_s (*m*) symmetry, the molecular structure of **1**† (Fig. 1) displays a distinctive breastplate-like, sixteen vertex $Li_4K_4O_8$ core (Fig. 2). The crystallographic mirror plane runs through Li(1), Li(2), O(1), O(2), O(3), O(4) in the body of the cage, and C(1), C(4), C(7),

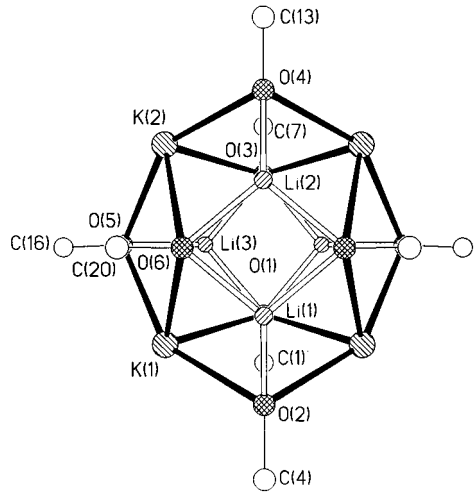

Fig. 1 Molecular structure of **1** with unique atoms labelled (not methyl C). Hydrogen atoms and methyl C atoms have been omitted for clarity. Bonds to K are filled, to Li hollow, to C single line.

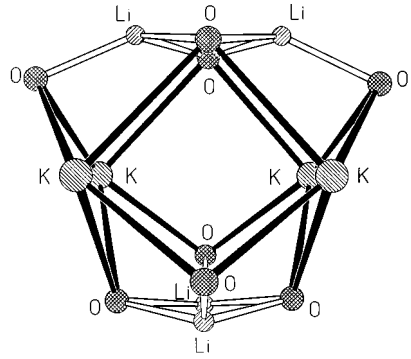

Fig. 2 Sixteen-vertex $O_8Li_4K_4$ 'breastplate' core of **1**.

C(10) outside the body. The molecular symmetry is essentially D_{2d} (42*m*), with Fig. 1 viewed along the S_4 axis. There are 14 MOMO faces: 8(LiOKO), 4$(KO)_2$ and 2$(LiO)_2$ types. The Li(3)O(1)Li(3A)O(3) 'neck' and Li(1)O(6)Li(2)O(6A) 'waist' rings lie almost orthogonal to each other. A plane of $4K^+$ cations occupies the 'midriff' position. These large cations form the apex of tetragonal pyramidal KO_4 coordination polyhedra. The smaller Li^+ cations form the apex of trigonal pyramidal LiO_3 coordination polyhedra. Half of the O centres [O(2)O(4), O(5)O(5A)] coordinate to 3 metal cations (1Li/2K), while the other half [O(1)O(3), O(6)O(6A)] coordinate to 4 metal cations (2Li/2K). The alkyl foliage completes the structure.

Intriguingly, whilst **1** is formally a 1:1 stoichiometric composite of lithium *tert*-butoxide and potassium *tert*-butoxide, it has a unique structure not made from contiguous fragments of the homonuclear structures $[(Bu^tOLi)_6]$[10] and $[(Bu^tOK)_4]$.[7] From a comparison with the homonuclear structures the major reorganisation behind the heterometallic construction has taken place at the 'softer' K^+ centres. First, together they make up a K_4 plane. Second, they occupy the higher (four) coordinate sites which are organised asymmetrically in two short and two long K–O bonds (mean values: 2.463 Å and 2.815 Å, respectively). This contrasts markedly with the tetrahedral K_4 arrangement and symmetrical μ_3-K–O bonding (mean length, 2.623 Å) found in the cubane $[(Bu^tOK)_4]$. Furthermore, there are no planar $(KO)_n$ rings in **1** like those observed in other cocomplexes of potassium *tert*-butoxide such as $[\{(cyNLi)_3Sb\}_2(Bu^tOK)_3{\cdot}x$-(toluene)][11] or $[\{[PhN(H)]_2(Bu^tO)LiNaK{\cdot}(TMEDA)_2\}_2]$.[12] There has been only one previous report of a planar K_4 substructure in the aforementioned $[(Pr^iO)_{10}(O)K_4Zr_2]$,[9] but this is not strictly analogous as here the four cations are fixed in place by an O^{2-} ligand at its centre. Contrary to the situation for K^+, the Li^+ cations have not had to compromise from their optimum μ_3-bonding role adopted in $[(Bu^tOLi)_6]$ in forming heterometallic **1** [range of Li–O bond lengths, 1.815(3)–1.919(3) Å]. This reflects the 'harder', more strongly polarising character of the smaller alkali metal. Given the strength of Li–O bonding it is perhaps surprising that a larger fragment of $[(Bu^tOLi)_6]$ has not been retained in **1**, *cf.* the tetrameric unit in $[(Bu^nLi{\cdot}Bu^tOLi)_4]$[13] and the hexameric unit in $[(Bu^tOLi)_{10}(LiOH)_6]$.[14] The fact that **1** formally contains only dimeric $(Bu^tOLi)_2$ fragments suggests that the Lewis base TMEDA may be involved in the mechanism of the reaction without appearing in the final product. Another factor in the construction of **1** is the coordinative flexibility of the alkoxide ligands. Exclusively μ_3-bonded in the homonuclear precursors, they exhibit both μ_3- and μ_4-bonding modes here. Following the expected trend, the μ_4-O centres form longer bonds (mean: to Li, 1.915 Å; to K, 2.875 Å) than their μ_3-O counterparts (mean: to Li, 1.811 Å; to K, 2.643 Å).

The ^{1}H NMR (400 MHz) spectrum of **1** in [$^2H_8$]toluene solution at 295 K reveals two singlet resonances (at 1.25 and 1.31 ppm) in a 1:1 ratio. Assuming the sixteen-vertex cage structure is retained these resonances can be assigned to the two distinct types (μ_3- or μ_4-bonded) of butoxide ligand present (there are four of each type). This receives support from the corresponding ^{13}C NMR (100.6 MHz) spectrum which shows a pair of CH_3 (36.09 and 36.55 ppm) and a pair of $(CH_3)_3C$ resonances (66.79 and 67.11 ppm). A variable-temperature ^{1}H NMR study reveals only one resonance at elevated temperatures with coalescence occurring at 312(±1) K, while the two resonances remain distinct but progressively broaden at lower temperatures down to 183 K. This data is consistent with the exchange of Bu^tO^- ligands between three-coordinate and four-coordinate sites. From the limiting chemical shift difference of 27(±2) Hz, a rate constant k of 60 s^{-1} can be estimated[15] for the uncoupled exchanging protons: this corresponds to a free energy of activation, $\Delta G^{\ddagger}$, of 65.9 kJ mol^{-1}. The variable-temperature spectra also contain trace amounts of an unknown protic impurity (having chemical shifts of 1.54 and 1.50 ppm at 273 K) which is not involved in the dynamic process.

Perhaps the most interesting aspect of **1** is its remarkable structural similarity to a series of heterobimetallic Group 15–Group 1 or Group 11 imido cage species (*e.g.*, $[\{As_2(N\text{-}Cy)_4\}_2Na_4]$);[16] this development, which will be elaborated upon in a full account of this work, may have its origin in the isoelectronic relationship between RO^- and RN^{2-}.

Finally, in view of the relationship of Bu^tOK to the superbasic reagent '$BuLi{\cdot}Bu^tOK$' as alluded to earlier, it will be of future interest to probe the interaction of BuLi with the new heterometallic alkoxide.

We thank the EPSRC for financial support.

Notes and references

† *Crystal data* for **1**: $C_{32}H_{72}K_4Li_4O_8$, M = 769.1, monoclinic, space group $P2_1/m$, a = 11.5194(6), b = 17.1506(10), c = 13.0058(7) Å, β = 110.166(2)°, U = 2412.0(2) Å^3, Z = 2, D_c = 1.059 g cm^{-3}, μ = 0.41 mm^{-1} (Mo-Kα, λ = 0.71073 Å), T = 160 K; R ($F^2 > 2\sigma$) = 0.0324, R_w (F^2, all data) = 0.0880, for 4372 unique data (10325 measured, R_{int} = 0.0192, $2\theta < 50°$, CCD diffractometer) and 266 refined parameters, including three-fold disorder of the C(7) *tert*-butyl group. Programs: standard Bruker AXS control and integration software and SHELXTL. CCDC 182/1324. See http://www.rsc.org/suppdata/cc/1999/1569/ for crystallographic files in .cif format.

1 D. C. Bradley, *Chem. Rev.*, 1989, **89**, 1317.
2 W. A. Herrmann, N. W. Huber and O. Runte, *Angew. Chem.*, 1995, **106**, 2371; *Angew. Chem. Int. Ed. Engl.*, 1995, **34**, 2187.
3 A. Mordini, in *Advances in Carbanion Chemistry*, ed. V. Snieckus, JAI Press, London, 1992, vol. 1, p. 1.
4 F. M. Mackenzie, R. E. Mulvey, W. Clegg and L. Horsburgh, *Polyhedron*, 1998, **17**, 993.
5 R. C. Mehrotra, A. Singh and S. Sogani, *Chem. Soc. Rev.*, 1994, **23**, 215; M. Veith, S. Mathur and C. Mathur, *Polyhedron*, 1998, **17**, 1005.
6 M. H. Chisholm, S. R. Drake, A. A. Naiini and W. E. Streib, *Polyhedron*, 1991, **10**, 805.
7 M. H. Chisholm, S. R. Drake, A. A. Naiini and W. E. Streib, *Polyhedron*, 1991, **10**, 337.
8 W. Clegg, A. M. Drummond, R. E. Mulvey and S. T. Liddle, *Chem. Commun.*, 1998, 2391.
9 B. A. Vaartstra, W. E. Streib and K. G. Caulton, *J. Am. Chem. Soc.*, 1990, **112**, 8593.
10 H. Huml, *Czech. J. Phys.*, 1965, **B15**, 699; R. D. Thomas, S. G. Bott, P. W. Gravelle and H. D. Nguyen, Abstracts of papers of the American Chemical Society, 1998, vol. 215, no. pt. 1, pp. 291-INOR.
11 D. Barr, A. J. Edwards, M. A. Paver, P. R. Raithby, M.-A. Rennie, C. A. Russell and D. S. Wright, *Angew. Chem.*, 1995, **107**, 1088; *Angew. Chem., Int. Ed. Engl.*, 1995, **34**, 1012.
12 F. M. Mackenzie, R. E. Mulvey, W. Clegg and L. Horsburgh, *J. Am. Chem. Soc.*, 1996, **118**, 4721.
13 M. Marsch, K. Harms, L. Lochmann and G. Boche, *Angew. Chem.*, 1990, **102**, 334; *Angew. Chem., Int. Ed. Engl.*, 1990, **29**, 308.
14 C. Lambert, F. Hampel, P. v. R. Schleyer, M. G. Davidson and R. Snaith, *J. Organomet. Chem.*, 1995, **487**, 139.
15 H. Friebolin, *Basic One- and Two-Dimensional NMR Spectroscopy*, 3rd edn., Wiley-VCH, Weinheim, 1998, p. 301.
16 A. Bashall, M. A. Beswick, E. A. Harron, A. D. Hopkins, S. J. Kidd, M. McPartlin, P. R. Raithby, A. Steiner and D. S. Wright, *Chem. Commun.*, 1999, 1145 and refs. therein.

Communication 9/04800F

Preparation and characterisation of a highly active bimetallic (Pd–Ru) nanoparticle heterogeneous catalyst†

Robert Raja,[ab] Gopinathan Sankar,[b] Sophie Hermans,[a] Douglas S. Shephard,[a] Stefan Bromley,[b] John Meurig Thomas*[b] and Brian F. G. Johnson*[a]

[a] *Department of Chemistry, University of Cambridge, Lensfield Road, Cambridge, UK CB2 1EW*
[b] *Davy Faraday Research Laboratory, Royal Institution of Great Britain, 21 Albemarle Street, London, UK W1X 4BS*
E-mail: dawn@n.ac.uk

Received (in Liverpool, UK) 15th February 1999, Accepted 9th July 1999

The mixed-metal carbonylate cluster $[Pd_6Ru_6(CO)_{24}]^{2-}$ was used as a single-source precursor in the synthesis of a highly active hydrogenation catalyst (stoichiometry PdRu) which has been characterised by electron microscopy and X-ray absorption spectroscopy: PdRu readily hydrogenates alkenes and naphthalene (the latter predominantly to *cis*-decalin) under mild conditions

Bimetallic nanoparticle catalysts occupy a position of high prominence in modern heterogeneous catalysis, especially for reactions of petrochemical significance.[1–3] Published reports[4–9] on such catalysts, typified by Pt–Re, Ir–Sn, Pt–Ru, Ag–Ru and Cu–Ru, reveal that enhanced catalytic performance apparently arises from the synergy between the component elements at the nanoscale which is absent in solid solutions of the two bulk metals.

In this communication we show that a single-source, mixed-metal cluster carbonylate precursor yields (by gentle thermolysis) a uniform distribution of discrete nanoparticles (*ca*. 17 Å diameter) of a Pd–Ru bimetallic catalyst encapsulated within the pores (*ca*. 30 Å diameter) of mesoporous silica. This catalyst is highly active in the hydrogenation of linear alkenes and significantly more so than two other bimetallic catalysts also prepared from single-source carbonylate precursors, Ag_3Ru_{10}[7] and Cu_4Ru_{12}.[9] Moreover, the Pd–Ru catalyst described here is capable of hydrogenating naphthalene under relatively mild conditions.

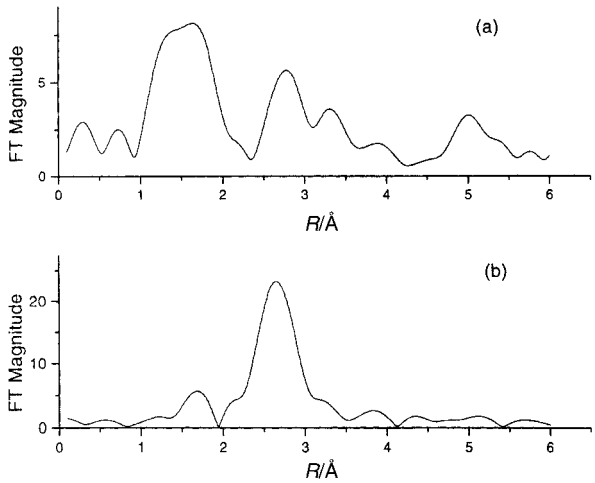

Fig. 1 (a) Fourier transform of the Pd K-edge EXAFS data (effectively a radial distribution function) for the mixed-metal carbonylate ion $[Pd_6Ru_6(CO)_{24}]^{2-}$ precursor dispersed inside the mesopores of the MCM-41 silica. (b) The corresponding transform for the dispersed precursor after gentle thermolysis (see text). The resulting cluster (see Fig. 2) has an average metal–metal (Pd–Ru and Pd–Pd) distance that peaks at 2.73 Å and the average co-ordination number is 5.3.

† Electronic supplementary information (ESI) available. See http://www.rsc.org.suppdata/cc/1999/1571.

The anionic molecular precursor $[Pd_6Ru_6(CO)_{24}]^{2-}$, **1**, was synthesised as described[10] previously; and isolated as its NEt_4^+ salt. This particular precursor was selected for a variety of reasons including its solubility, stoichiometry, adsorbability at, and dispersion across, the silanol rich[11,12] interior surfaces of the mesoporous silica support (MCM-41), as well as the ease with which it sheds its cloak of carbonyl groups during mild thermal treatment. Of prime importance also was our wish to design a bimetallic catalyst in which a metal (Pd) that readily takes up hydrogen is juxtaposed with one (Ru) that has a strong tendency to bind arenes. A Pd–Ru catalyst should therefore function effectively in the hydrogenation of aromatic molecules.

The methodology for its preparation and encapsulation into the mesopores is essentially that used in our earlier work[7,9] on Ag–Ru and Cu–Ru bimetallic nanocrystals. Retention of the structural integrity of the mixed-metal cluster carbonylate inside the mesoporous silica was deduced from *in situ* spectroscopic analysis, both infra red[9] (Nujol mull) and X-ray absorption using a specially designed cell.[13,14] The respective data sets showed the same structural features as those of the cluster when dispersed in homogeneous solution (tetrahydrofuran as solvent). The characteristic IR absorption peaks were somewhat broadened and slightly shifted (*ca*. 3 cm^{-1}) to lower energy upon encapsulation. Precise structural information (Ru–Ru, Pd–Pd and Ru–Pd distances and associated co-ordination numbers), retrieved from EXAFS analyses for Ru and Pd K-absorption edges, was in good accord with that obtained from the single-crystal X-ray structure[10] of Et_4N^+ salts of the anion **1**.

When the encapsulated carbonylate **1** was heated (10^{-4} Torr) for 1 h, at 180 °C, the sample changed colour from brown to

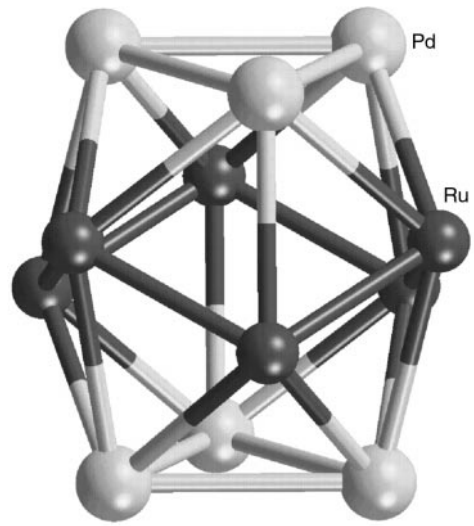

Fig. 2 Schematic diagram of the Pd_6Ru_6 cluster derived from an EXAFS analysis of the Ru and Pd K-edge X-ray absorption spectra (it is difficult to distinguish scattering by Pd atoms from that by Ru atoms).

Table 1 Hydrogenation of olefins—comparison of catalysts

Substrate (mass/g)	Catalyst	Solvent	Reaction time/h	Residual H_2 pressure/bar	Conv. (%)	TOF/ h^{-1}	Product distribution (mol%)		
							n-Hexane	*cis*-Hex-2-ene	*trans*-Hex-2-ene
Hex-1-ene	Pd_6Ru_6/MCM-41	—	4	1	99	4954	68	22	9
(≈ 50 g)	Cu_4Ru_{12}/MCM-41	—	4	8	56	2805	51	30	19
	Ru_6/MCM-41	—	4	15	13	325	14	42	45
			24	13	19	277	10	36	53
	Pd/MCM-41	—	4	18	6	250	6	45	48
			24	16	14	196	5	33	63
	No Catalyst	—	24	17	7	—	—	32	67
							n-Dodecane	*cis*-Dodec-2-ene	*trans*-Dodec-2-ene
Dodec-1-ene	Pd_6Ru_6/MCM-41	—	4	3	88	2202	63	29	7
(≈ 50 g)	Cu_4Ru_{12}/MCM-41	—	4	7	35	877	54	32	13
							cis-Decalin	*trans*-Decalin	Others
Naphthalene	Pd_6Ru_6/MCM-41	CH_3CN	8	12	19	50	86	4	9
(≈ 8 g)		Hexadecane	8	10	7	19	50	34	15
		Hexadecane[a]	8	20	0			No Reaction	
	Cu_4Ru_{12}/MCM-41	CH_3CN	8	18	0.8	2	—	—	100
		Hexadecane	8	20	0			No Reaction	

Reaction conditions: catalyst = 20 mg; T = 373 K; starting H_2 pressure = 20 bar; solvent ≈ 55 g; [a] 200 ppm of sulfur was added in the form of benzothiophene.

black; the IR carbonyl stretching region gradually disappeared; and the atomic structure of the mixed-metal cluster, as seen by details of the XANES and EXAFS, changed dramatically (Fig. 1). High-resolution transmission electron microscopy (HRTEM) revealed[15] that the Pd–Ru bimetallic nanoparticles were of uniform size (*ca*. 17 Å diameter) and spatially well distributed within the pores of the siliceous support.

The catalytic performance in alkene hydrogenation of the Pd–Ru nanoparticles is compared in Table 1 with those of similarly prepared (and sized) Cu_4Ru_{12} bimetallic nanoparticles. The kinetics of hydrogenation of hex-1-ene and dodec-1-ene reveal that the Pd_6Ru_6 catalysts showed a higher selectivity for n-hexane (or n-dodecane) than Cu_4Ru_{12}. The Pd_6Ru_6 catalyst is more active than Cu_4Ru_{12} for the hydrogenation of hex-1-ene (≈2 times) and dodec-1-ene (≈2.5 times). For comparison, a monometallic Ru_6 cluster was encapsulated in MCM-41 and a Pd/MCM-41 catalyst was prepared following a literature procedure,[16] and both were tested for the hydrogenation of hex-1-ene employing the same reaction conditions. It is very clear from Table 1 that the bimetallic catalysts are far superior in performance (% conversion) than their monometallic analogues and more importantly yield a higher selectivity for hydrogenated products, suggesting a possible synergism between the two bimetallic nanoparticles. The Pd_6Ru_6 catalyst was more effective than Cu_4Ru_{12} in the hydrogenation of naphthalene and higher conversions were obtained when acetonitrile was used as a solvent. Other solvents such as hexadecane showed a lower preference for the production of *cis*-decalin. The solid catalyst may be recycled without any significant decrease in activity or selectivity. This was done by filtering off the solvent–product mixture and recharging the Parr reactor with fresh material[17] (see Table 1 for reaction conditions). Unsurprisingly,[1–3] the introduction of ≈200 ppm of sulfur in the reaction mixture completely poisons the catalyst.

Surveys by electron-stimulated energy dispersive X-ray emission[17] of the Pd–Ru nanocatalyst particles after their use in four consecutive test runs showed that there was no segregation of the two components of the bimetallic catalyst. Moreover, annular dark field (*Z*-contrast) high-resolution microscopy showed[15] that there was no evidence of coalescence or sintering of the nanoparticles during catalytic use. Guided by energy-minimisation procedures[18] using density-functional theory computations, we have arrived at the EXAFS model for the structure of the bimetallic cage shown in Fig. 2.

We thank Professor C. R. A. Catlow for invaluable assistance. We also thank the EPSRC for a rolling grant to J. M. T., a ROPA award funding S. B. and a regular one to B. F. G. J., the Commissioners of the 1851 Royal Exhibition for an award to R. R., the European Commission for a grant to S. H., and the Royal Society and Peterhouse for a Research Fellowship to D. S. S. G. S. was funded partly by J. M. T.'s rolling grant and the CCRL Daresbury Laboratory, to whom we are grateful.

Notes and references

1 J. H. Sinfelt, *Int. Rev. Phys. Chem.*, 1988, **7**, 281.
2 C. N. Satterfield, *Heterogeneous Catalysis in Industrial Practice*, 2nd edn., McGraw Hill, New York, 1991.
3 J. M. Thomas and W. J. Thomas, *Principles and Practice of Heterogeneous Catalysis*, Wiley-VCH, Weinheim, 1997.
4 M. S. Nasher, A. I. Frenkel, D. L. Adler, J. R. Shapley and R. G. Nuzzo, *J. Am. Chem. Soc.*, 1997, **119**, 7760.
5 M. Ichikawa, *Adv. Catal.*, 1992, **38**, 283.
6 B. C. Gates, *Chem. Rev.*, 1995, **95**, 511.
7 D. S. Shephard, T. Maschmeyer, B. F. G. Johnson, J. M. Thomas, G. Sankar, D. Ozkaya, W. Zhou and R. D. Oldroyd, *Angew. Chem., Int. Ed. Engl.*, 1997, **36**, 2242.
8 D. M. Somerville and J. R. Shapley, *Catal. Lett.*, 1998, **52**, 123.
9 D. S. Shephard, T. Maschmeyer, G. Sankar, J. M. Thomas, D. Ozkaya, B. F. G. Johnson, R. Raja, R. D. Oldroyd and R. G. Bell, *Chem. Eur. J.*, 1998, **4**, 1214.
10 E. Brivio, A. Ceriotti, R. D. Pergola, L. Garlaschelli, F. Domartin, M. Marassero, M. Sansoni, P. Zanello, F. Laschi and B. T. Heaton, *J. Chem. Soc., Dalton Trans.*, 1994, 3237.
11 J. M. Thomas, *Faraday Discuss.*, 1996, **105**, 1.
12 T. Maschmeyer, F. Rey, G. Sankar and J. M. Thomas, *Nature*, 1995, **37**, 159.
13 J. M. Thomas, *Chem. Eur. J.*, 1997, **3**, 1557.
14 I. J. Shannon, J. M. Thomas, G. Sankar, T. Maschmeyer, M. Sheehy, D. Madill and R. D. Oldroyd, *Catal. Lett.*, 1997, **44**, 23.
15 D. Ozkaya, W. Zhou, J. M. Thomas, P. A. Midgeley, V. J. Keast and S. Hermans, *Catal. Lett.*, in press.
16 C. P. Mehnert and J. Y. Ying, *Chem. Commun.*, 1997, 2215.
17 R. Raja and J. M. Thomas, *Chem. Commun.*, 1998, 1841.
18 S. Bromley, C. R. A. Catlow *et al.*, in preparation.

Communication 9/01263J

A simple route to synthesise nanodimensional CdSe–CdS core–shell structures from single molecule precursors

Neerish Revaprasadu,[a] M. Azad Malik,[a] Paul O'Brien*[a] and Gareth Wakefield[b]

[a] *Department of Chemistry, Imperial College of Science, Technology and Medicine, South Kensington, London, UK SW7 2AZ. E-mail: p.obrien@ic.ac.uk*

[b] *Department of Engineering Science, University of Oxford, Parks Road, Oxford, UK OX1 3PJ*

Received (in Oxford, UK) 10th March 1999, Accepted 5th July 1999

Highly mono-dispersed CdSe–CdS core–shell nanoparticles have been prepared by a novel method in which [Cd{Se_2CNMe(^{n}Hex)}$_2$] (250 °C for 30 min) and [Cd{S_2CNMe(^{n}Hex)}$_2$] (250 °C for a further 30 min) are thermolysed in tri-*n*-octylphosphine oxide (TOPO) in a 'one pot' synthesis; the core–shell structure has been characterized by electronic spectroscopy, photoluminescence, X-ray diffraction and electron microscopy (SAED, SEM and TEM).

Unique physical and chemical properties due to quantum confinement effects have been reported for a wide range of semiconductor nanoparticles.[1–6] Whilst many studies have focused on the relationship between particle size and optical behavior, the control of the surface chemistry is still a challenge to chemists. The presence of localized surface trap sites (defects) due to the high surface-to-volume ratio has made surface modification a necessity. Passivation of the surface has been achieved by organic ligands such as thiopyridine,[7] thiolates,[8] and 2,2′-bypyrimidine.[9] Core–shell structures such as Si–SiO_2,[10] CdS–$Cd(OH)_2$,[11] CdSe–ZnS,[12] CdSe–ZnSe,[13,14] CdS–HgS–CdS[15] and CdSe–CdS[16–18] are examples of inorganic passivation. These systems normally show an increase in photoluminescence efficiency and reduced fluorescence lifetimes.

We report the synthesis of a CdSe–CdS core–shell structure using the precursors [Cd{Se_2CNMe(Hex)}$_2$] and [Cd{S_2CNMe(Hex)}$_2$] for the CdSe core and CdS shell, respectively.† In a typical synthesis, [Cd{Se_2CNMe(Hex)}$_2$] (0.8 g) was dissolved in tri-*n*-octylphosphine (TOP) (15 ml). This solution was then injected into hot (250 °C) tri-*n*-octylphosphine oxide (TOPO) (20 g) and kept at this temperature for 30 min to give CdSe. To prepare the core–shell structure a solution of [Cd{S_2CNMe(Hex)}$_2$] (0.5 g) in TOP (10 ml) was injected into the deep red reaction mixture. The reaction was allowed to proceed for a further 30 min and the resulting solution was cooled to *ca*. 70 °C. Methanol was then added and a flocculant precipitate formed which was separated by centrifugation. CdS and CdSe nanocrystals were also synthesized as described previously.[19]

The absorption spectra for CdS, CdSe and CdSe–CdS nanoparticles are shown in Fig. 1.‡ The band edge (652 nm; 1.90 eV) of the CdSe–CdS structure is red shifted (22 nm, 0.02 eV) as compared to the CdSe nanocrystals (630 nm; 1.96 eV). This red shift is indicative of the formation of the core–shell structure. The overall shape of the spectrum is similar to that of CdSe, however a slight sharpening of the features at 535 and 613 nm is observed which may suggest a narrower size distribution. Photoluminescence (PL, λ_{ex} = 400 nm) shows an emission maximum close to the absorption band edge in both CdSe (585 nm) and the core–shell (622 nm) nanocrystals (Fig. 1), an observation consistent with the observed absorption spectra. The intensity of the emission maximum is considerably increased in the core–shell structure as compared to the parent materials.[10–17]

The X-ray diffraction pattern‡ of CdSe–CdS shows broad peaks along the (110), (103) and (112) planes which are assigned to the hexagonal phase of CdSe (Fig. 2) suggesting that the diffraction is predominantly due to the CdSe core. The sharp X-ray pattern§ indicates epitaxial growth of the shell. This also accounts for the slight shift in the peaks to higher 2θ values in the core–shell structure since the epitaxy requires that the lattice parameters are the same for both core and shell and hence will be between those for CdS and CdSe, as is observed. Similarly, in the SAED,‡ a pattern intermediate between that for CdS and that for CdSe was observed, as expected (Fig. 2). The reflections for the (002), (100) and (101) planes shown in the hexagonal CdS diffraction pattern are not visible in the CdSe and CdSe–CdS patterns owing to broadening of the peak in the region 2θ

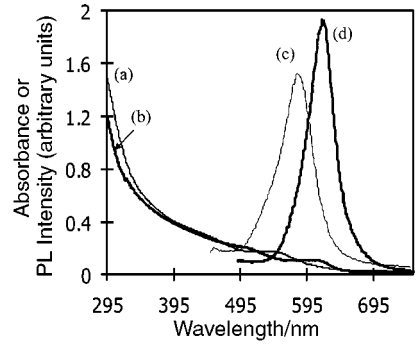

Fig. 1 Absorption spectra of (a) CdSe–CdS, (b) CdSe and photoluminescence spectra (λ_{ex} = 400 nm) of (c) CdSe, (d) CdSe–CdS.

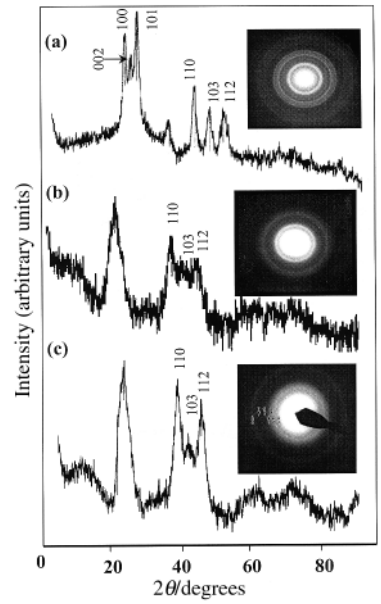

Fig. 2 XRD and SAED patterns showing the hexagonal phase for (a) CdS, (b), CdSe and (c) CdSe–CdS.

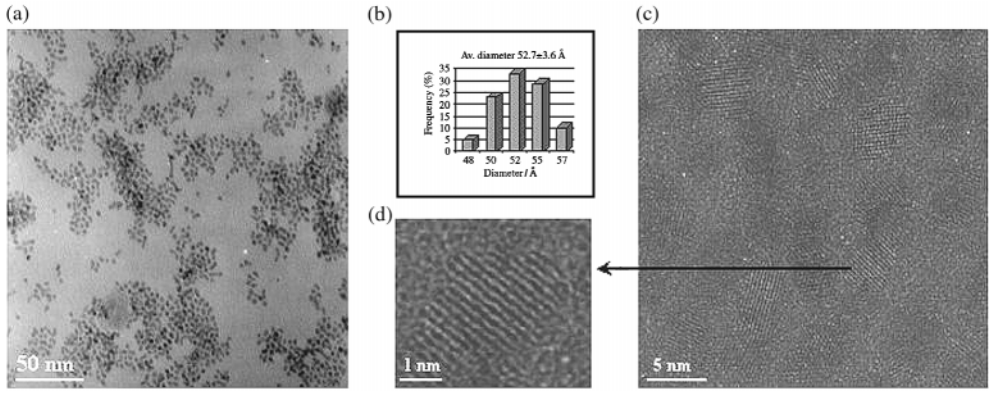

Fig. 3 CdSe–CdS core–shell nanocrystals: (a) TEM image, (b) particle size histogram, (c) HRTEM image, (d) HRTEM image of a single quantum dot (*ca.* 5.3 nm in diameter).

≈ 20–25°. The X-ray data may be consistent with a core–shell structure or with the formation of a composite but the composite would give blue shifts in the emission and absorption maxima. A red shift clearly shows the presence of the core–shell structure.

TEM images‡ show well defined, spherical CdSe–CdS particles (Fig. 3) with an average size of 53 ± 3.6 Å. The average size of the bare CdSe nanoparticles is 45 Å which indicates an increase of 8 Å due to the CdS shell in the core–shell nanoparticles. The crystallinity of the core–shell structure is confirmed by an HRTEM image (Fig. 3) which shows clear lattice fringes for the CdSe core (hexagonal phase).

HRTEM‡ showed lattice spacings intermediate between those for CdSe and CdS as is observed by SAED and X-ray patterns. As expected, no interface can be observed by HRTEM between the CdSe core and the CdS shell. The EDAX pattern and ICP analysis‡ confirmed the presence of Cd, Se and S in the CdSe–CdS nanoparticles. The peak for phosphorus in each case was due to the capping of the particles by TOPO which was further confirmed by a shift in the IR band (from 1146 to 1120 cm^{-1}, P=O) for TOPO.

Highly monodispersed CdSe–CdS core–shell nanoparticles have been prepared by a novel route involving thermolysis in TOPO using $[Cd\{Se_2CNMe(^nHex)\}_2]$ and $Cd\{S_2CNMe(^nHex)\}_2]$ as single molecule precursors in a one-pot synthesis. This route is a simple and convenient route to produce reasonable quantities of high quality, monodispersed core–shell nanoparticles. The precursors are easy to synthesize and store and give high yields of TOPO capped quantum dots.

P. O'B. is the Sumitomo/STS Professor of Materials Chemistry. We thank the EPSRC for a grant supporting work on single molecule precursors for quantum dots. N. R. is supported by a Royal Society/FRD development program between ICSTM and UZULU.

Notes and references

† The compounds were prepared by adaptations of the literature method[20,21] and fully characterised by NMR, mass spectometry, microanalysis and IR spectroscopy.

‡ A Philips PU 8710 spectrophotometer was used to perform the optical measurements for which the samples were placed in silica cuvettes (1 cm path length). For photoluminescence spectroscopy a Spex FluoroMax instrument with a xenon lamp (150 W) and a 152 P photomultiplier tube as a detector was used to measure the photoluminescence of the particles. Measurements were carried out on samples with an optical density of 0.1 at 400 nm, also the excitation wavelength. Good spectra were obtained with the slits set at 2 nm and an integration time of 1 s. The samples were placed in quartz cuvettes (1 cm path length). X-Ray diffraction studies were performed using secondary graphite-monochromated Cu-Kα radiation (40 kV) on a Philips X'Pert Materials Research Diffractometer (MRD, R. Sweeney, IC). Measurements were taken using a glancing angle incidence detector at an angle of 3°, for 2θ values in the range 20–60° in steps of 0.04° with a count time of 1 s. For electron microscopy a JEOL 2000 FX MK 1 electron microscope operated at 200 kV with an Oxford Instrument AN 10000 EDS analyser was used for the conventional TEM (transmission electron microscopy) images. Selected area electron diffraction (SAED) patterns were obtained using a JEOL 2000 FX MK2 electron microscope operated at 200 kV. The samples for TEM and SAED were prepared by placing a drop of a dilute solution of sample in toluene on a copper grid (400 mesh, agar). The excess solvent was wicked away with a paper tip and the sample allowed to dry completely at room temperature. EDAX (energy dispersion analytical X-rays) was performed on samples deposited by evaporation on glass substrates using a JEOL JSM35CF scanning electron microscope. ICPAES analyses (Cd, Se, S) were recorded on an ARL instrument, Geology Department, Imperial College.

§ The X-ray diffraction pattern of the CdS particles gave peaks with the following observed *d* values (% relative intensity, *hkl*): of 3.55 Å (76, 100), 3.35 Å (52, 002), 3.16 Å (100, 101), 2.06 Å (43, 110) and 1.90 Å (26, 103) corresponding to the hexagonal cadmium sulfide *cf.* 3.57 Å (62, 100), 3.36 Å (91, 002), 3.16 Å (100, 101), 2.45 Å (29, 102), 2.07 Å (48, 110) and 1.90 Å (50, 103) {ASTM}. For CdSe: 3.50 Å (100, 002), 2.13 Å (80, 110), 1.84 Å (50, 112) and 1.96 Å (48, 103) corresponding to the hexagonal phase *cf.* 3.51 Å (70, 002), 2.15 Å (85, 110), 1.83 Å (50, 112) and 1.98 Å (70, 103) {ASTM}. For the CdSe–CdS core–shell: 3.50 Å (100, 002), 2.15 Å (85, 110), 1.83 Å (66, 112), 1.98 Å (60, 103) corresponding to the hexagonal phase *cf.* 3.51 Å (70, 002), 2.15 Å (85, 110), 1.83 Å (50, 112) and 1.98 Å (70, 103) {ASTM}.

1 A. Henglein, *Chem. Rev*., 1989, **89**, 1861.
2 M. L. Steigerwald and L. E. Brus, *Acc. Chem. Res*., 1990, **23**, 183.
3 Y. Wang and N. Herron, *J. Phys. Chem*., 1991, **95**, 525.
4 H. Weller, *Adv. Mater*., 1993, **5**, 88.
5 L. E. Brus, *Appl. Phys. A*, 1991, **53**, 495.
6 L. E. Brus, *J. Phys. Chem*., 1994, **98**, 3577.
7 H. Noglik and W. J. Pietro, *Chem. Mater*., 1994, **6**, 1593.
8 J. E. Katari, V. L. Colvin and A. P. Alivisatos, *J. Phys. Chem*., 1994, **98**, 4109.
9 T. Trindade, X. Zhang and P. O'Brien, *Chem. Mater*., 1997, **9**, 523.
10 W. L. Wilson, P. F. Szajowski and L. E. Brus, *Science*, 1993, **262**, 1242.
11 L. Spanel, M. Haase, H. Weller and A. Henglein, *J. Am. Chem. Soc*., 1987, **109**, 5649.
12 M. Danek, K. F. Jensen, C. B. Murray and M. G. Bawendi, *Chem. Mater*., 1996, **8**, 173.
13 M. A. Hines and P. Guyot-Sionnest, *J. Phys. Chem.*, 1996, **100**, 468.
14 A. R. Kortan, R. Hull, R. L. Opila, M. G. Bawendi, M. L. Steigerwald, P. J. Carrol and L. E. Brus, *J. Am. Chem. Soc*., 1990, **112**, 1327.
15 A. Mews, A. Eychmuller, M. Giersig, D. Schooss and H. Weller, *J. Phys. Chem*., 1994, **98**, 934.
16 X. Peng, M. C. Schlamp, A. V. Kadavanich and A. P. Alivisatos, *J. Am. Chem. Soc*., 1997, **119**, 7019.
17 Y. Tian, T. Newton, N. A. Kotov, D. M. Guldi and J. H. Fendler, *J. Phys. Chem*., 1996, **100**, 8927.
18. U. Banin, M. Bruchez, A. P. Alivisatos, T. Ha, S. Weiss and D. S. Chemla, *J. Chem. Phys*., 1999, **110**, 1195.
19 B. Ludolph, M. A. Malik, N. Revaprasadu and P. O'Brien, *Chem. Commun.*, 1998, 1849.
20 P. O'Brien, D. J. Otway and J. R. Walsh, *Adv. Mater. CVD*, 1997, **3**, 227.
21 M. Chunggaze, J. McAleese, P. O'Brien and D. J. Otway, *Chem. Commun*., 1998, 833.

Communication 9/01969C

ChemComm

Dynamic combinatorial libraries of pseudo-peptide hydrazone macrocycles

Graham R. L. Cousins, Sally-Ann Poulsen and Jeremy K. M. Sanders*

Cambridge Centre for Molecular Recognition, University Chemical Laboratory, Lensfield Road, Cambridge, UK CB2 1EW. E-mail: jkms@cam.ac.uk

Received (in Cambridge, UK) 21st May 1999, Accepted 5th July 1999

Combinatorial libraries of pseudo-peptide hydrazone macrocycles are formed from amino acid-derived building blocks equipped with hydrazide and aldehyde functionalities; a series of experiments confirm that hydrazone formation is reversible and that the libraries are genuinely dynamic.

Dynamic combinatorial libraries (DCLs) are emerging as interesting systems for the identification of new catalyst, host and guest molecules.[1] In a DCL the connections between building blocks are reversible and in flux: they may be covalent or non-covalent, and are continuously being made and broken. The composition of a DCL is dependent on the environment, in that the addition of a template which selectively binds one member may bias the equilibrium towards that member. Many different reversible reactions have been proposed for the purpose of DCL generation, but none has yet been shown to be ideal.[1–3] Here we report that transimination of hydrazones, a reaction that occurs at room temperature in the presence of a mild acid catalyst (Scheme 1),[4] is a promising candidate for the generation of DCLs. Relative to simple imines (Schiffs bases), hydrazides are expected to have the advantage of greater stability and the potential for peptide-like hydrogen bonding.[5]

The amino acid-derived building blocks **1**–**4**, each comprising a protected aldehyde moiety and a hydrazide functionality on an amino acid core, were synthesised by standard routes.† Proline features prominently in these monomers because its frequent occurrence in protein β-turns[6] led us to expect that it would give a propensity for the formation of macrocyclic products. Phenylalanine and phenylglycine, components of the other monomers, possess 'chemically inert' side chains, ideal for preliminary investigations.

Cyclisation of the monomers **Fm**, **Pm**, **PFm** and **PBm** is performed by the addition of 50 μl of TFA to a 5 mM solution of monomer in CH_2Cl_2; TFA catalyses both dimethoxy acetal deprotection to the free aldehyde and hydrazone exchange (Scheme 2).‡ The low concentration of monomer directs formation of cyclic oligomers; linear polymers are likely to be formed at higher concentrations. Electrospray mass spectrometry (ES-MS) analysis of reaction solutions of any one of **Pm**, **PFm** or **PBm** reveals the formation of a range of oligomeric macrocyclic species.§ After 2 h there is no evidence of free protected or deprotected linear monomer, and more significantly, no evidence for linear oligomeric products. Under these conditions **Pm** affords cyclic dimer through to cyclic heptamer; cyclic dimer to cyclic nonamer are observed for **PBm**, and finally **PFm** exhibits cyclic dimer through to cyclic hexamer. Monomer **Fm** showed no formation of identifiable oligomeric species; all of the monomer was consumed but the products were largely insoluble and presumably polymeric.

Combinatorial libraries of great diversity are rapidly achieved by the treatment of a solution of two or more monomers with TFA. For example, a solution of **PBm** and **PFm**, when treated with TFA, yields a library of 75 readily

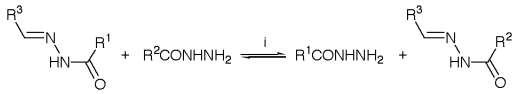

Scheme 1 *Reagents and conditions*: i, Dilute acid.

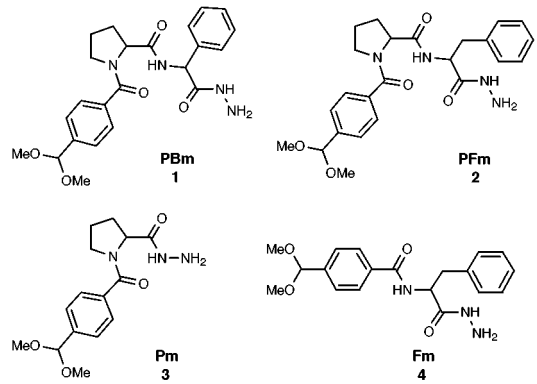

detected macrocyclic species; other products may well be formed in lower concentrations. Importantly, all possible combinations of monomers are detected from cyclic dimer through to cyclic undecamer. Cyclic oligomers of hexamer and above are observed as the doubly-charged species in the range *m/z* 200–2000, and gratifyingly, hexamers, octamers and decamers of odd numbers of each of the two monomers exhibit unique doubly-charged masses, which interdigitate between those signals due to the mono-charged cyclic trimers, tetramers and pentamers respectively (Fig. 1).

The cyclisation of **Pm**, **PFm** and **PBm** in the presence of TFA gives a very diverse macrocyclic library; for example, 14 out of the 15 possible tetramer compositions are detected by ES-MS. In this experiment > 30 product compositions are identified within the sensitivity range of the spectrometer, including dimers, trimers, tetramers and pentamers. These spectra underestimate the number of products formed: doubly charged higher oligomeric species are not observed, perhaps because as the number of possible products increases, their concentration may decrease. This analysis also neglects sequence isomers, which are not detectable by conventional MS.

Mixing experiments performed with monomers **Fm** and **Pm** highlighted the role played by proline in inducing the formation of cyclic species. **Fm** under the cyclisation conditions does not afford any detectable cyclic species, but when **Pm** is introduced mixed cyclic species are observed as well as homo-**Pm** cyclic species. Thus, **Fm** may be incorporated into DCLs but will not stand alone in pseudo-peptide macrocycle formation.

The dynamic reversibility of hydrazone formation is illustrated by two simple experiments. If solutions of macrocycles generated from two different monomers, and containing no free monomer, are mixed, then libraries of the mixed macrocyclic species are observed. The final composition is identical to that observed by mixing the monomers prior to treatment with TFA. It follows that the mixed cyclic species must be the result of

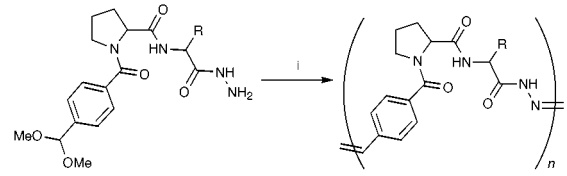

Scheme 2 *Reagents and conditions*: i, TFA, CH_2Cl_2, RT.

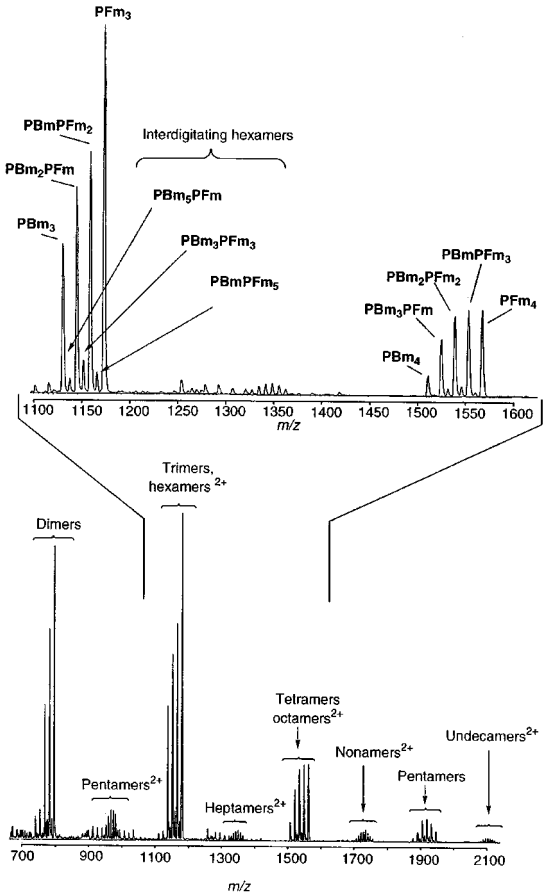

Fig. 1 ES-MS spectrum for the mixed cyclisation of **PBm** and **PFm**.

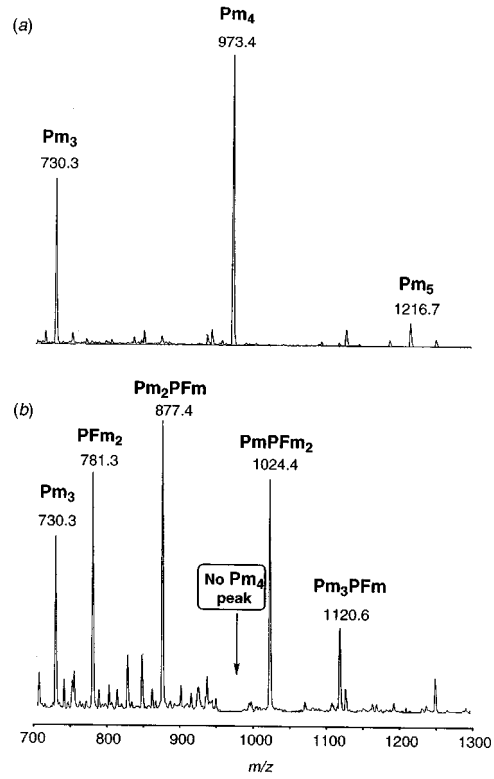

Fig. 2 (*a*) ES-MS spectrum demonstrating cyclisation of **Pm** in the presence of TFA after 2 h. (*b*) ES-MS spectrum of the same reaction mixture recorded 4 h after **PFm** was added. Note the absence of a peak at *m/z* 973 for $\mathbf{Pm}_4$.

homo-oligomer fragmentation and subsequent hydrazone formation. More elegantly, in a second experiment, **Pm** was cyclised in the presence of TFA. To the solution containing preformed macrocyclic **Pm** oligomers was added a 5 mM solution of **PFm**. ES-MS analysis showed the preferential formation of mixed products, with complete loss of *m/z* 973 ($\mathbf{Pm}_4$) and 1216 ($\mathbf{Pm}_5$), present in the solution prior to the addition of **PFm** (Fig. 2). Indeed $\mathbf{Pm_4}$ is the only tetramer not observed in the three monomer library. This preference for mixed species is in marked contrast to the self-sorting of homo-oligomers that we previously observed in relatively rigid alkaloid-derived libraries under transesterification conditions.[3]

The ability to 'switch off' the reaction is of fundamental importance to the success of any DCL. Two separate cyclisation solutions, one of **PFm** and the other of **PBm**, were each treated with 1.5 equiv. of Et_3N relative to the amount of TFA. The solutions were stirred for 15 min before being combined. ES-MS analysis after 2 h showed no formation of mixed cyclic species, demonstrating that in the absence of acid no exchange of hydrazones occurs. Even after 36 h no mixed products are observed. Upon addition of an excess of TFA the exchange reaction is restarted and within a few hours the same distribution of cyclic products is observed as if the reaction had been initiated from a mixture of two protected monomers.

These results demonstrate the applicability of hydrazone chemistry to the generation of DCLs. In conjunction with amino acid-derived building blocks, this chemistry allows for the rapid, and potentially automated, generation of libraries of pseudo-peptide macrocycles which are under thermodynamic control. The mild conditions of hydrazone exchange offer reason to be optimistic that efficient template binding will bias the libraries to receptors with good binding characteristics. The rewards may include a rapid evolution of pseudo-peptide macrocycles as catalysts and host or guest molecules.

We thank the BBSRC, Royal Society and Ethyl Corporation (UK) for financial support, M. Simpson for preliminary experiments and P. Lukeman and S. Rowan for helpful discussions.

Notes and references

† Monomers were synthesised from carboxybenzaldehyde dimethoxy acetal, Cbz-proline and commercially available amino acid methyl esters using standard peptide chemistry. The notation is derived from the single letter notation for amino acids with **B** assigned to phenylglycine.

‡ The general procedure for cyclisation experiments entailed dissolution of monomers in freshly distilled CH_2Cl_2 and the addition of 50 μl of TFA. All were carried out on a 5–10 mg scale at a concentration of 5 mM. The reactions were stirred at room temperature for 2 h before ES-MS analysis. This deprotection–cyclisation chemistry is compatible with a range of solvents including DMSO and MeCN and aqueous mixtures of these solvents.

§ Electrospray mass spectra were recorded on a Micromass Quattro-LC triple quadrapole apparatus fitted with a *z*-spray electrospray source. The electrospray soucre was heated to 100 °C and the sampling cone voltage (V_c) was 65 V. Samples were prepared by removal of 200 μl of crude reaction mixture and dilution in 200 μl of THF. Samples were introduced into the mass spectrometer source with an LC pump (Shimadzu LC-9A LC pump) at a rate of 4 μl min^{-1} of MeCN–H_2O (1:1). Calibration was performed using protonated horse myoglobin. Scanning was performed from *m/z* 300 to 2100 in 8 s and several scans were summed to obtain the final spectrum which was processed using MassLynx V3.0 software.

1 For a review, see A. Ganesan, *Angew. Chem., Int. Ed.*, 1998, **37**, 2828.
2 J. K. M. Sanders, *Chem. Eur. J.*, 1998, **4**, 1378; P. A. Brady and J. K. M. Sanders, *Chem. Soc. Rev.*, 1997, **26**, 327.
3 S. J. Rowan, P. S. Lukeman, D. J. Reynolds and J. K. M. Sanders, *New J. Chem.*, 1998, 1015; S. J. Rowan, D. G. Hamilton, P. A. Brady and J. K. M. Sanders, *J. Am. Chem. Soc.*, 1997, **119**, 2578.
4 *The Chemistry of the Carbon–Nitrogen Double Bond*, ed. S. Patai, Interscience, London, 1970.
5 E. Cabezas and A. C. Satterthwait, *J. Am. Chem. Soc.*, 1999, **121**, 3862.
6 T. E. Creighton, *Proteins, Structures and Molecular Properties*, Freeman, New York, 1984.

Communication 9/04091I

A macromolecular Gd(III) complex as pH-responsive relaxometric probe for MRI applications

Silvio Aime,*[a] Mauro Botta,[b] Simonetta Geninatti Crich,[a] Giovanni Giovenzana,[c] Giovanni Palmisano[d] and Massimo Sisti[e]

[a] *Dipartimento di Chimica I.F.M., Università di Torino, via P. Giuria 7, -10125 Torino, Italy. E-mail: aime@silver.ch.unito.it*
[b] *Dipartimento di Scienze e Tecnologie Avanzate, Università del Piemonte Orientale 'Amedeo Avogadro', corso Borsalino 54, 1-15100 Alessandria, Italy*
[c] *Dipartmento di Chimica Organica ed Industriale, Università di Milano, Viale Venezian 21, 1-20133 Milano, Italy*
[d] *Dipartimento di Science Mediche, Università del Piemonte Orientale, V.le Ferrucci 33, 1-28100 Novara, Italy*
[e] *Dipartimento Scienze CC.FF.MM., Università dell'Insubria, Via Lucini 3, 1-22100 Como, Italy*

Received (in Basel, Switzerland) 18th January 1999, Accepted 14th June 1999

The ability of the paramagnetic macromolecular complex $(GdDO3ASQ)_{30}$-Orn_{114} to enhance the water proton relaxation rate has been found to be a function of pH; this behaviour is related to the structural changes occurring in the polypeptide upon protonation of the side-chain NH_2 groups.

Magnetic resonance imaging (MRI) is a powerful diagnostic technique based on the acquisition of images which are topological representations of NMR parameters, including the T_1 and T_2 of water protons. Contrast agents (CAs) for MRI are mainly represented by Gd(III) chelates whose high paramagnetism causes a marked increase of the water proton relaxation rates in the bodily regions where they distribute.[1–3] The effectiveness of a Gd(III) complex as a CA is measured by the relaxivity, r_{1p}, which represents the net increment of the water proton relaxation rate in a 1 mmol l^{-1} solution of the paramagnetic solute. The development of a second generation of Gd(III) based CAs stems from systems endowed either with higher relaxivities or with an improved ability to act as reporters of their biochemical environment. Among the various possibilities, the availability of a pH-sensitive Gd(III) chelate appears particularly interesting since it is known that increased glycolytic activity may cause a significant pH decrease in the extracellular region of certain tumours.[4] At the magnetic fields usually employed in MRI (0.5–1.5 T) the relaxivity of a Gd(III) chelate is mainly determined by the molecular reorientational time τ_r.[5] Thus a means of assaying pH may be pursued by designing systems whose molecular mobility is a function of pH. It is well established that the structures of poly(amino acid)s like polylysine and polyornithine are strongly dependent upon the pH of the solution. In fact, at acidic pHs, the repulsion among positively charged amino groups induces the occurrence of a highly flexible structure whereas at basic pHs the formation of intra-chain hydrogen bonds yields the formation of an α-helix resulting in an overall rigidity of the macromolecular system.

On this basis a novel macromolecular system has been recently synthesised, containing thirty Gd(III) chelates bound to a poly(amino acid) chain made of 114 ornithine residues. Since it has been recently reported that squaric esters readily react with amines,[6] we exploited this finding by using the squaric acid moiety as a linker between the tetraazamacrocyclic structure of DO3A and the amino groups of the polyornithine chain (Scheme 1).[7] In addition to acting as linker between the poly(amino acidic) chain and the DO3A ligand, the squaric acid moiety may participate in the coordination of the Gd(III) ion through the oxygen atom of the carbonyl group. Such a reaction scheme has some advantage with respect to that previously reported for $(GdDTPA)_n$-Lys_m.[8] In fact, the synthesis of the latter system implies the use of the bifunctional DTPA bis-anhydride which leads to undesirable intra- and inter-molecular cross-linking reactions with a consequent reduction of the thermodynamic stability of the metal complexes.[9] The use of a monoreactive chelate derivative allows a controlled and specific activation of the amino groups in the poly(amino acid) macromolecule.

At acidic pH the unreacted amino groups in $(GdDO3ASQ)_{30}$-Orn_{114} are protonated and highly hydrated, thus they tend to stay as far apart as possible. The paramagnetic moieties too maintain a relatively high degree of mobility along the lateral chain of each substituted ornithine and the molecular reorientation of the complex only in part 'feels' the large size of the whole macromolecule. The progressive deprotonation of the $-NH_3^+$ groups occurring with the increase of pH induces a 'rigidification effect' due to the formation of intramolecular hydrogen bonds between adjacent peptidic linkages. The progressive changes in the overall structure of $(GdDO3ASQ)_{30}$-Orn_{114} are reflected in the relaxivity parameter as shown in Fig. 1. At pH < 4 r_{1p} has a constant values of *ca.* 23 mM^{-1} s^{-1} which is about five times higher than the r_{1p} value normally found for related monomeric Gd(III) complexes. The increase of the pH of the solution causes a linear increase of r_{1p} which reaches the value of 32 mM^{-1} s^{-1} at pH 8. Further increase of pH above this value does not cause any change in the observed relaxivity. To check that the observed behaviour is a con-

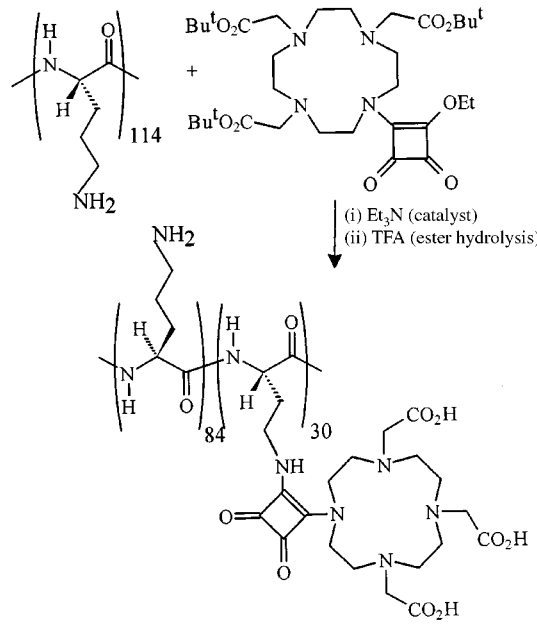

Scheme 1

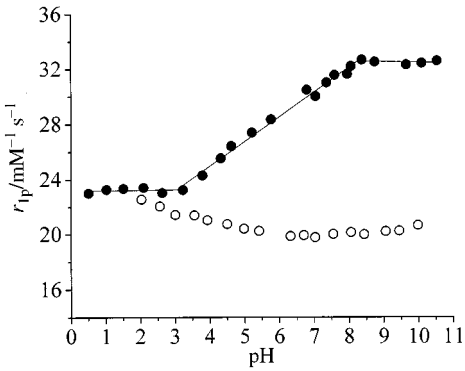

Fig. 1 pH dependence of r_{1p} values for $(GdDO3ASQ)_{30}$-Orn_{114} (●) and $(GdDO3ASQ)_{50}$-Orn_{50} (○). The latter system has been chosen because its molecular weight is similar to that of $(GdDO3ASQ)_{30}$-Orn_{114}.

sequence of a change in τ_r, the $1/T_1$ dependence on the Larmor frequency (ω_0) (NMRD profile) has been measured at three pH values (Fig. 2). The shape of the NMRD profile of Gd(III) chelates, as measured on a field-cycling relaxometer over the frequency range from 0.01 to 50 MHz, is determined by a number of parameters including the number of water molecules in the inner coordination sphere, the molecular reorientational time (τ_r), the exchange lifetime of the coordinated water (τ_m), the electronic relaxation time (τ_s), and the Gd-bound water proton distance (r).[5] The NMRD profiles of paramagnetic macromolecular systems show a characteristic hump in the 20–35 MHz region whose height is determined by the relative ratio of τ_s to τ_r.[10] In fact, in the low frequency range r_{1p} is determined primarily by τ_s whose value, being field dependent, increases steadily with ω_0 causing an increase of the observed r_{1p}. As τ_s becomes longer than τ_r, the observed r_{1p} is determined by the latter parameter and the $1/T_1$ dispersion takes place. As shown in Fig. 2, a significant increase in the height of the relaxivity peak in the 20–35 MHz region occurs as the pH of the solution passes from 4.5 to 8.5. This behaviour is consistent with an increase of τ_r with pH. Furthermore, the increase in pH also induces an increase in relaxivity at low magnetic field strength. Such behaviour, which is reminiscent of that observed upon formation of macromolecular adducts between a paramagnetic Gd(III) chelate and HSA,[2] has been accounted for in terms of an additional contribution to the overall relaxivity arising from water molecules surrounding the complex and those belonging to the hydration layers of the macromolecule. We take this finding as further evidence of structure formation in the polypeptide chain upon deprotonation of the -NH_3^+ side chain groups.

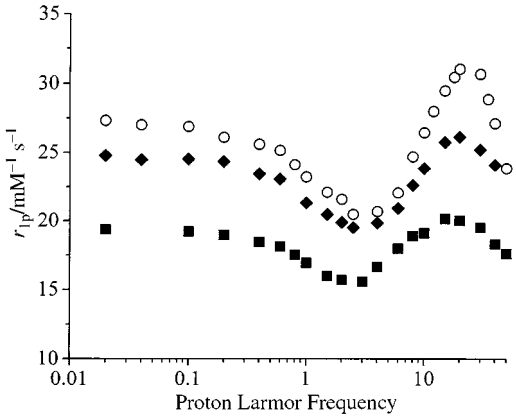

Fig. 2 $1/T_1$ NMRD profiles (298 K) of $(GdDO3ASQ)_{30}$-Orn_{114} (1 mM) at pH 4.5 (■), 7 (◆) and 8.5 (○) respectively.

The role of the free amino groups on the macromolecule in determining the dependence of r_{1p} upon the pH of the solution is clearly assessed by compairing the pH dependence of r_{1p} for $(GdDO3ASQ)_{30}$-Orn_{114} and r_{1p} of a related system containing no free NH_2 groups (Fig. 1). Such a system has been obtained by following an analogous procedure to that used for $(GdDO3ASQ)_{30}$-Orn_{114} but with a higher DO3A ester : poly-(amino acid) ratio.[7] Clearly, the lower r_{1p} values shown by the saturated conjugate indicate that, in this system, the chelates moieties undergo larger motions than in $(GdDO3ASQ)_{30}$-Orn_{114}. It is likely that the steric requirements of the bulky chelates do not allow the poly(amino acid) chain to adopt, at basic pHs, a compact α-helix structure as occurs for the partially substituted derivative. Rather, the flexibility of the main chain is transfered to the side-chains bearing the paramagnetic chelates which, in turn, are responsible for the partial 'quenching' of the relaxivity potentially expected for systems of this size.

In summary $(GdDO3ASQ)_{30}$-Orn_{114} is an interesting macromolecular MRI agent whose high relaxivity is made strongly pH dependent through structural changes which limit the internal mobility of the chelate moieties. The pH range at which r_{1p} changes fits better the physiological values than that recently observed for another macrocyclic Gd(III) complex whose pH-dependent r_{1p} is the result of variations in its hydration sphere.[11] Furthermore it appears to provide an alternative MRI route to recently reported procedures for the determination of the extracellular pH of tumours based on ^1H, ^{19}F or ^{31}P probe molecules, known to have pH-dependent MR properties which titrate in the physiological range.[12,13]

Notes and references

‡ Synthesis of $(GdDO3ASQ)_{30}$-Orn_{114}. The triester (1,4,7,10-tetraazacyclododecane-1,4,7-triacetic acid, tri-*tert*-butyl ester) is reacted with diethyl squarate in ethanol, overnight at room temperate (RT) to yield the DO3A5Q ligand. The synthesis of the polyornithine conjugate is pursued by reacting the latter compound and the poly(amino acid) (at the molar ratio of *ca.* 30 : 1) at RT for 72 h in ethanol (in the presence of triethylamine as catalyst). Finally hydrolysis of *tert*-butyl ester groups is carried out with TFA. The complexation was carried out by adding a stoichiometric amount of $GdCl_3$ to the aqueous solution of the polyornithine conjugate at neutral pH and at RT. The eventual excess of free Gd(III) ions is easily removed by centrifugation of the solution brought to basic pH. All new compounds exhibited satisfactory spectral and elemental analysis. The CD spectra between 200 and 250 nm of $polyOrn_{114}$ and of $(GdDO3ASQ)_{30}$-Orn_{114} appear similar, indicating that the conformation of the polypeptide backbone is unaltered upon partial conjugation of lateral amino groups to squaric acid moieties.

1 J. A. Peters, J. Huskens and D. J. Raber, *Prog. Nucl. Magn. Reson. Spectrosc.*, 1996, **28**, 283.
2 S. Aime, M. Botta, M. Fasano and I. Terreno, *Chem. Soc. Rev.*, 1997, **26**, 1.
3 D. Parker and J. A. G. Williams, *J. Chem. Soc., Dalton Trans.*, 1996, 3613.
4 J. A. Meyer, *Am. Surg.*, 1974, **179**, 88.
5 S. H. Koenig and R. D. Brown III, *Prog. Nucl. Magn. Reson. Spectrosc.*, 1990, **22**, 487.
6 L. F. Tietze,C. Schroter, S. Gabius, U. Brinck, A. Goerlach-Graw and H. J. Gabius, *Bioconjugate Chem.*, 1991, **2**, 48.
7 S. Aime, M. Botta, S. Geninatti Crich, G. Giovenzana, G. Palmisano and M. Sisti, *Bioconjugate Chem.*, 1999, **10**, 192.
8 P. F. Sieving, A. D. Watson and M. R. Rocklage, *Bioconjugate Chem.*, 1990, **1**, 65.
9 A. D. Sherry, W. P. Cacheris and K. T. Kuan, *Magn. Reson. Med.*, 1988, **8**, 180.
10 R. B. Lauffer, *Chem. Rev.*, 1987, **87**, 901.
11 J. Hall, R. Häner, S. Aime, M. Botta, S. Faulkner, D. Parker and A. S. de Sousa, *New J. Chem.*, 1998, 627.
12 R. J. Gillies, Z. Liu and Z. Bhujwalla, *Am. J. Physiol.*, 1994, C195.
13 Y. Aoki, K. Akagi, Y. Tanaka, J. Kawai and M. Takahashi, *Invest. Radiol.*, 1996, **31**, 680.

Communication 9/00499H

Giant self-contained metallosupramolecular entities

Dirk G. Kurth,* Frank Caruso* and Corinna Schüler

Max-Planck-Institute of Colloids and Interfaces, D-14424 Potsdam, Germany.
E-mail: dirk.kurth@mpikg-golm.mpg.de; frank.caruso@mpikg-golm.mpg.de

Received (in Cambridge, UK) 25th June 1999, Accepted 9th July 1999

We present an approach to fabricate very large, soluble, self-contained metallosupramolecular entities employing a template-directed strategy based on charged nanoparticles: consecutive deposition of negatively charged macromolecules and positively charged metallosupramolecular coordination polyelectrolytes is exploited to assemble the metallosupramolecular components on the nanoparticles.

Self-assembly provides an efficient approach to create large supramolecular architectures through non-covalent interactions, bypassing problems associated with stepwise covalent synthetic methodologies.[1] In recent years, metal ion mediated self-assembly has been intensely investigated as a means to construct complex structures. Two dominant metallosupramolecular architectures can be identified. The first involves closed, self-contained (solution) architectures of well-defined shape and nanometer size with a small number of components, a representative example being the cage-type architectures of polytopic bipyridine ligands, 6-PhHat and Cu^{I} or Ag^{I} ions.[2] The other class consists of infinite solid-state architectures, as in crystals of 1,2-di(4-pyridyl)ethane and Fe^{II} ions.[3] Complementarity and metal ion–ligand interactions are the dominating assembly principles for the spatial organization of the components.

Metal ion containing assemblies are expected to exhibit novel physicochemical properties such as optical, magnetic, electrochemical and catalytic functions, similar to a variety of proteins bearing multi-metal active sites.[4] In order to integrate active functional units into operating molecular based materials and devices, existing assembly methodologies have to be improved and new methods need to be developed. To date, it has not been possible to construct metallosupramolecular assemblies that bridge the gap between closed cage-type structures (few components) and extended solid-state architectures (infinite number of components). Here, we present a template-directed strategy to fabricate metallosupramolecular entities that contain a very large, yet finite, number of components which remain in solution. To achieve this goal, two types of interaction that operate on two different length scales are utilized. At the molecular level, metal ion mediated interactions generate the supermolecules. Primarily electrostatic interactions effect self-assembly of single layers at the mesoscopic level. The concept of template-directed self-organization is analogous to biological processes; for instance, spontaneous assembly of protein segments along an RNA strand generates the tobacco mosaic virus.[5]

Terpyridine transition metal ion complexes were found to present an array of interesting electronic, photonic, magnetic and reactive properties.[6] Recently, Kurth *et al.* showed that metal ion mediated self-assembly of the ditopic ligand 1,4-bis(2,2′:6′,2″-terpyridin-4′-yl)benzene with transition metal ions results in the formation of metallosupramolecular coordination polyelectrolytes (MEPE).[7] Using the layer-by-layer technique, consecutive deposition of the positively charged MEPE and oppositely charged polyelectrolytes results in well-defined multilayers.[8] This facile method relies on electrostatic interactions of oppositely charged macromolecules. The resulting films present a periodic architecture of active supramolecular components. Thin films with functional components and a well-defined architecture provide an interesting class of advanced materials or devices with tailored properties.

Here, we extend this concept to produce self-contained, yet large metallosupramolecular entities by using nanometer-size templates, namely nanoparticles. In contrast to the previously mentioned methods, this approach offers the following advantages: (i) a large number of active components can be assembled in an easy and inexpensive way; (ii) different functional units can be easily combined within one layer or along the radial direction in order to tailor the properties of the final entity; (iii) the final entity remains in solution (in contrast to crystalline solids); and (iv) the total number of components is readily controlled through the size of the template and the number of layers deposited. A simplified scheme of our approach is shown in Fig. 1.

As templates we employed cetyltrimethylammonium-stabilized, positively charged polystyrene (PS) latices with an average diameter of 73 ± 14 nm (determined from light scattering).[9] Consecutive adsorption of sodium polystyrene-

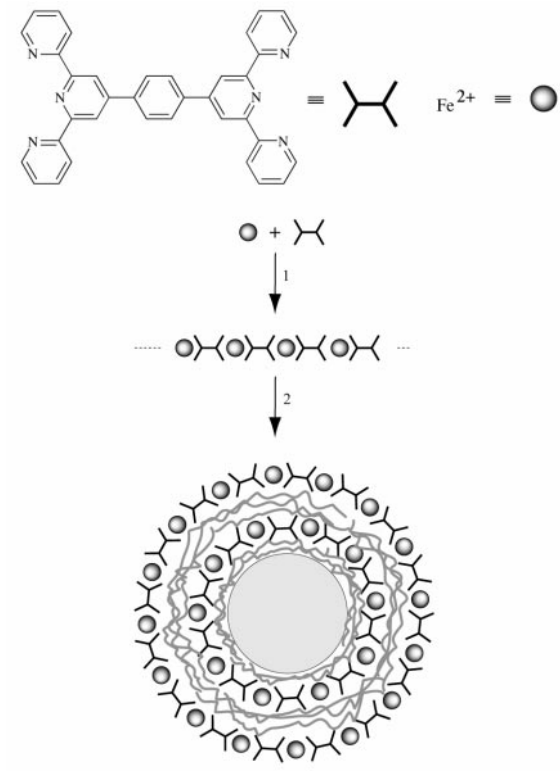

Fig. 1 Two different types of interactions at two different length scales are operative in generating giant, self-contained metallosupramolecular entities (bottom). Metal ion coordination is operative at the molecular level to produce the supermolecules (step 1). Electrostatic interactions are employed to assemble single layers of charged macromolecules on charged nanoparticles at the mesoscopic length scale (step 2). Using PS latices with a diameter of 73 nm, each layer contains approximately 7600 metal ions and ligands; multilayer sheaths with a total of 53 000 components per nanoparticle were created by consecutive deposition of PSS and Fe^{II}–MEPE. The counterions are omitted for clarity; the configurations of the polymers are simplified and the molecules are not drawn to scale.

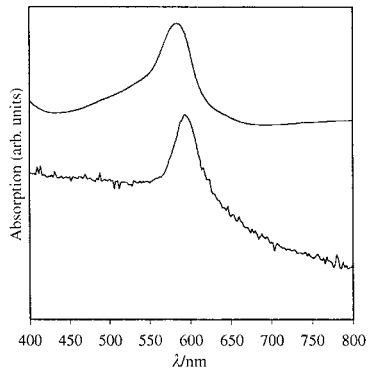

Fig. 2 UV/vis absorption (arbitrary units) spectrum of Fe^{II}–MEPE in aqueous solution (top) and of the coated Fe^{II}–MEPE nanoparticles (bottom). The UV/vis spectrum of the Fe^{II}–MEPE coated nanoparticles was corrected for particle background scattering.

sulfonate (PSS) and Fe^{II}–MEPE results in multilayers on the PS latices.[10] Repeated centrifugation and washing of the PS latices removes excess polyelectrolyte.

Evidence for the deposition of PSS/Fe^{II}–MEPE multilayers on the PS latices is obtained by visual inspection: upon deposition, the PS latices turn blue, the characteristic color of Fe^{II}–MEPE. A representative UV/vis absorption spectrum of the coated PS latices and of Fe^{II}–MEPE in aqueous solution is shown in Fig. 2. The band at 583 nm is characteristic of the Fe^{II}–terpyridine complex; it is associated with a metal-to-ligand charge transfer transition. In the case of the coated PS latices, this band is observed at 593 nm.The red shift is attributed to the different polarity within the multilayer polyelectrolyte film and is characteristic of PSS/Fe^{II}–MEPE layers.

Layer-by-layer growth is confirmed by successful recharging of the particle surface with each deposition cycle. The neat PS latices have a positive ζ-potential of +60 mV. Deposition of PSS reverses the sign of the ζ-potential (approximately −42 mV). Subsequent deposition of Fe^{II}–MEPE results in a positive ζ-potential (app. +18 mV).[11] The ζ-potential for deposition of 14 PSS/Fe^{II}–MEPE layers is summarized in Fig. 3. Alternating ζ-potentials are characteristic of regular multilayer growth on colloidal templates.[12]

Additional evidence for the adsorption of Fe^{II}–MEPE on the particles is provided by energy dispersive X-ray analysis measurements, which clearly show the presence of Fe^{II} on the Fe^{II}–MEPE/PSS-coated particles. Preliminary TEM experiments reveal that PS latices coated with PSS/Fe^{II}–MEPE multilayers have a rougher surface than the uncoated nanocolloids. This is attributed to the linear, rigid-rod type shape of Fe^{II}–MEPE.

A single metallosupramolecular component consisting of one ligand and one metal ion occupies roughly a surface area of 1.2 × 1.8 nm^2. Based on the surface area of *ca.* 17 000 nm^2 per nanoparticle, one particle can accommodate approximately 7600 metallosupramolecular components in one layer. Since up to 7 Fe^{II}–MEPE layers were assembled, a total of 53 000 metal

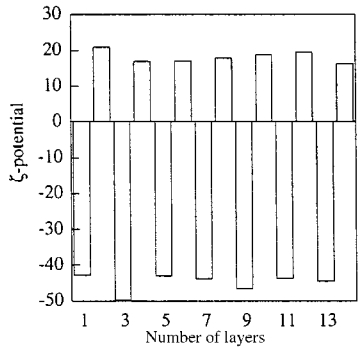

Fig. 3 ζ-potential of alternating layers of PSS (negative values) and Fe^{II}–MEPE (positive values) on PS latices. Alternating ζ-potential values confirm layer-by-layer growth of PSS/Fe^{II}–MEPE multilayers on colloidal templates.

ions and ligands are confined on a single particle. This number can be readily increased, simply by carrying out extra deposition cycles.

Due to the non-covalent nature of the coordination bond, the metal ion–ligand union is labile and subject to exchange processes. Adding chelating agents, like phenanthroline or salicylic acid, to a solution of Fe^{II}–MEPE results in discoloration of the solution. This is due to disassembly of the Fe^{II}–terpyridine bond. In contrast to the solution species, PSS/Fe^{II}–MEPE multilayers show a much greater stability under these conditions: no color change was detected by UV/vis spectroscopy even after prolonged exposure to chelating agents. Apparently, the adsorption of the charged macromolecules at multiple contact points reduced the degrees of freedom of the Fe^{II}–MEPE to such an extent that removal of a single component becomes strongly hindered.

The template-directed approach based on nanoparticles presented here opens a novel entry to stable dispersed metallosupramolecular entities with a large number of active components. Ongoing research in our laboratories suggests that this approach is generally applicable to the construction of other 'giant', dispersed metallosupramolecular entities. Due to the facile and efficient layer-by-layer method, different active components can be assembled in each layer, thus opening avenues to construct complex functional materials and devices (*e.g.* with vectorial properties). The fact that these entities remain in solution makes them potential candidates for various technological applications. Stimulus-responsive ligands could trigger the release of the metal ions, similar to neuronal action.[13] After removal of the template, the remaining shell constitutes an internal, separated micro-compartment.[14] Motion of the shell may be induced by electrochemical switching of the metal ion coordination geometry. In addition, the permeability of the shell may be controlled with an electrochemical stimulus.

This study was supported by the Max-Planck-Society. Helmuth Möhwald is acknowledged for valuable discussions. The authors thank Christa Stolle and Markus Schütte for the preparation of Fe^{II}–MEPE.

Notes and references

1 J.-M. Lehn, *Supramolecular Chemistry*, VCH, Weinheim, 1995.
2 For reviews see: P. N. W. Baxter, in *Comprehensive Supramolecular Chemistry*, ed. J. L. Atwood, J. E. D. Davies, D. D. MacNicol and F. Vögtle, Pergamon, Oxford, 1996, p. 165; M. Fujita, *ibid.*, p. 253; E. C. Constable, *ibid.*, p. 213.
3 J. A. Real, E. Andrés, M. C. Muños, M. Julve, T. Granier, A. Bousseksou and F. Varret, *Science*, 1995, **268**, 265. For a review, see S. R. Batten and R. Robson, *Angew. Chem., Int. Ed.*, 1998, **37**, 1461.
4 P. M. Harrison, P. D. Hempstead, P. J. Artymiuk and S. Andrews, *Met. Ions Biol. Syst.*, 1998, **35**, 435.
5 A. Klug, *Angew. Chem.*, 1983, **95**, 579.
6 V. Balzani and F. Scandola, *Supramolecular Photochemistry*, Ellis Horwood, New York, 1991.
7 M. Schütte, D. G. Kurth, M. R. Linford, H. Cölfen and H. Möhwald, *Angew. Chem., Int.Ed.*, 1998, **37**, 2891.
8 G. Decher, *Science*, 1997, **277**, 1232.
9 K. Landfester, N. Bechthold, F. Tiarks and M. Antonietti, *Macromolecules*, 1999, **32**, 2679.
10 PSS/Fe–MEPE multilayers were prepared as follows: 1 ml of a 1 mg ml^{-1} aqueous PSS (M_w 1100, Polymer Standards Service, Mainz, Germany) solution (containing no additional salt) was added to ~10^{10} particles dispersed in 0.5 ml of water. The solution was occasionally stirred for 15 min. The solution was centrifuged at 40 000*g* for 15 min, the supernatent was removed and the pellet redispersed in water. The procedure was repeated three times to remove excess polyelectrolyte. Additional layers were deposited in identical fashion.
11 F. Caruso E. Donath and H. Möhwald, *J Phys. Chem. B*, 1998, **102**, 2011.
12 F. Caruso, H. Lichtenfeld, E. Donath and H. Möhwald, *Macromolecules*, 1999, **32**, 2317.
13 S. Shinkai, in *Cation Binding by Macrocycles*, ed. Y. Inoue and G. W. Gokel, Marcel Dekker, New York and Basel, 1990, p. 397.
14 F. Caruso, C. Schüller and D. G. Kurth, submitted for publication in *Chem. Mater*.

Communication 9/05115E

ChemComm

Lithium naphthalenide induced reductive cleavage of α,β-epoxy ketones: an efficient procedure for the preparation of β-hydroxy ketones

Renata Jankowska,[a] George L. Mhehe[b] and Hsing-Jang Liu*[a]†

[a] *Department of Chemistry, University of Alberta, Edmonton, Alberta, Canada, T6G 2G2*
[b] *Department of Chemistry, University of Dar-Es-Salaam, PO Box 35061, Dar-Es-Salaam, Tanzania*

Received (in Cambridge, UK) 10th June 1999, Accepted 6th July 1999

Lithium naphthalenide presents itself as a mild and efficient reagent for the cleavage of α,β-epoxy ketones to give the corresponding β-hydroxy ketones in good yields.

β-Hydroxy ketones and the closely related 1,3-diol group are important functionalities, which are found in prostaglandins,[1] taxol and congeners,[2] and many other interesting natural products. β-Hydroxy ketones are commonly prepared by an aldol condensation reaction[3] or by reductive cleavage of an α,β-epoxy ketone. The aldol process proved to be highly useful for the preparation of 'acyclic' β-hydroxy ketones. For cyclic β-hydroxy ketones, however, this method cannot be generally applied efficiently due to the lack of stereo- and regio-control in general, side reactions such as the intermolecular aldol, and further reactions (*e.g.* dehydration) of the desired products. Many reagents have been found to be effective for the reductive cleavage of α,β-epoxy ketones, which are readily accessible from conjugated enones and allylic alcohols with stereocontrol and possible asymmetric induction, including alkali metal in liquid ammonia,[4] zinc in acetic acid,[5] samarium diiodide,[6] aluminium amalgam,[7] chromous salts in alcohol,[8] organoselenium borate complex,[9] sodium hydrogen telluride,[10] sodium iodide in conjunction with sodium acetate,[11] and the combination of palladium, formic acid and triethylamine.[12] It has also been shown that the reductive cleavage can be carried out electrochemically.[13] The yields of the desired β-hydroxy ketones, however, are often inconsistent by the use of many of the existing procedures. This is mainly because of the intrinsic instability of the β-hydroxy ketone system which may undergo facile dehydration or retro-aldol reaction even under weakly acidic or basic conditions at somewhat higher temperature over somewhat longer reaction time. Herein we describe an efficient and apparently general procedure for the reductive cleavage of α,β-epoxy ketones to the corresponding β-hydroxy ketones under very mild conditions, which minimize the side reactions.

The new procedure, which is operationally simple, makes use of lithium naphthalenide (LN) as the reducing agent. This reagent, which can be easily prepared as a stable stock solution by mixing equal parts of lithium metal and naphthalene in THF at room temperature,[14] was found to be highly effective for the selective cleavage of the α,β-epoxy ketone system.‡ In a typical experiment, a solution of epoxy ketone **1** (49 mg, 0.32 mmol) in THF (2 ml) was added to a 0.34 M solution of LN in THF (2.8 ml) at −78 °C. The resulting solution was stirred at −78 °C under an atmosphere of argon for 10 min. Then water (1 ml) was added, and the resulting solution was allowed to warm up to room temperature, diluted with water (4 ml) and extracted with Et_2O (15 ml). Usual work-up of the ethereal solution gave the β-hydroxy ketone **2** in 78% yield after flash chromatography on silica gel (prewashed with a 1% solution of Et_3N in hexanes), eluting with a 15% solution of EtOAc in hexanes containing a small amount of Et_3N (5 drops in 100 ml of solution). The generality of this procedure is evident from the results obtained for a number of α,β-epoxy ketones examined (Table 1). In all cases, products were obtained in synthetically useful yields, many of which are superior to those obtained using other reducing agents. For example, the reduction of epoxide **3** derived from (*R*)-carvone was found to be ineffective with samarium diiodide.[6] With lithium in liquid ammonia, it gave only 35% yield of the desired product **4**.[4b] In the present case with LN, a considerably higher yield of **4** (62%) was realized. As another example, many attempts previously made to introduce the β-hydroxy ketone moiety to steroidal compounds often met with undesirable results.[4c,d,8] Again, by the use of LN under the described conditions, two isomeric steroidal epoxy ketones (entries 8 and 9) were readily reduced to the corresponding β-hydroxy ketones.

In light of its generality, operational simplicity, good yield in product formation, and the mild reaction conditions under which many functional groups are known to be unaffected towards LN,[14] the aforementioned procedure promises to be a method of choice for the synthesis of β-hydroxy ketones *via* reductive cleavage of the corresponding epoxy ketones. As illustrated by the following experimental results, this procedure can be extended to facilitate the preparation of α,α-disubstituted β-hydroxy ketones *via* alkylation of the ensuing enolate produced from the reductive cleavage of the epoxy ring and of 2,2-disubstituted 1,3-diones by subsequent oxidation. Treatment of epoxy ketone **3** with LN in tetrahydrofuran under the standard conditions (*vide supra*) for 30 min, followed by addition of MeI (5 equiv.) and warming up to room temperature resulted in the formation of β-hydroxy ketone **5** in 70% yield.

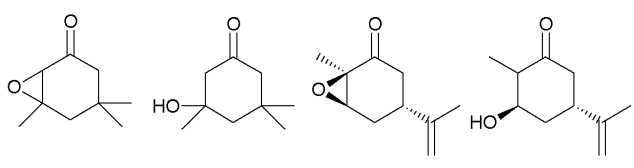

1 **2** **3** **4**

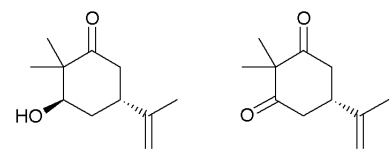

5 **6**

When hydroxy ketone **5** was subjected to oxidation [PCC (5 equiv.), CH_2Cl_2, 20 °C, 8 h], diketone **6** was formed in 78% yield.

We are grateful to the Natural Sciences and Engineering Research Council of Canada and the University of Alberta for financial support and to the University of Dar-Es-Salaam for granting a sabbatical leave to G. L. M.

† Present address: Department of Chemistry, National Tsing Hua University, Hsinchu, Taiwan 30043, R.O.C. E-mail: hjliu@chem.nthu.edu.tw

Table 1 Reductive cleavage of α,β-epoxy ketones with lithium naphthalenide to the corresponding β-hydroxy ketones

Entry	α,β-Epoxy ketone[a]	*t*/min	Product	Yield[b] (%)	Entry	α,β-Epoxy ketone[a]	*t*/min	Product	Yield[b] (%)
1	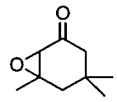	10	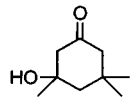	78	6	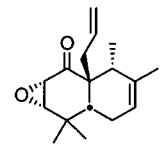	20	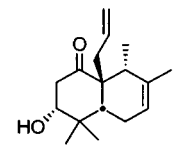	88
2		15	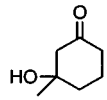	78					
3	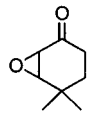	15	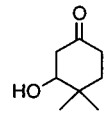	71	7	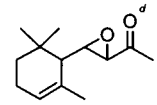	60	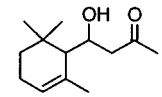	65[d]
4	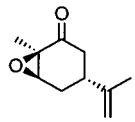	30	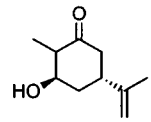	62[c]	8	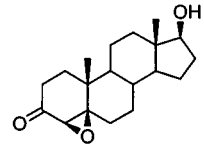	30[e]	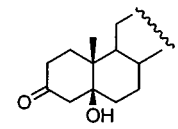	77
5	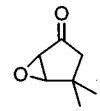	25	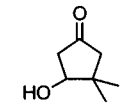	68	9	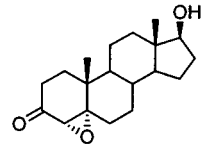	30[e]	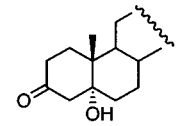	87

[a] The α,β-epoxy ketones used for the present study were prepared by treatment of the corresponding enones with LiOH (0.5 equiv.), 30% H_2O_2 (1.5–2.0 equiv.) in MeOH (4 ml per 1 mmol of enone) at room temperature for 0.5–2 h. [b] Yields are for isolated products. [c] An inseparable mixture of two diastereomers was obtained in a ratio of 11 : 1. The stereochemistry of these compounds remains to be determined. [d] A single stereoisomer was obtained. Its stereochemistry remains to be determined. [e] In each of these cases, 4 equiv.of LN was used.

Notes and references

‡ The reductive cleavage of epoxides derived from alkenes with aromatic radical anions has been studied previously by Bartmann (ref. 15) and Cohen *et al*. (ref. 16). To the best of our knowledge, however, this procedure has never been applied to α,β-epoxy ketones to facilitate the preparation of 1,3-ketols.

1 B. Samuelsson, *Angew. Chem., Int. Ed. Engl.*, 1983, **22**, 805.
2 R. G. Powell, R. W. Miller and C. R. Smith, *J. Chem. Soc., Chem. Commun.*, 1979, 102.
3 A. T. Nielsen and W. J. Houlihan, *Org. React.*, 1968, **16**, 1; T. Mukaiyama, *Org. React.*, 1982, **28**, 203.
4 (*a*) P. A. Grieco, M. Nishizawa, S. D. Burke and N. Marinovic, *J. Am. Chem. Soc.*, 1976, **98**, 1612; (*b*) J. D. McChesney and T. N. Thompson, *J. Org. Chem.*, 1985, **50**, 3473; (*c*) D. H. R. Barton, R. H. Hesse, M. M. Pechet and E. Rizzardo, *J. Am. Chem. Soc.*, 1973, **95**, 2748; (*d*) H. Hirschmann and M. A. Daus, *J. Org. Chem.*, 1959, **24**, 1114.
5 K. Yamakawa and K. Nishitani, *Chem. Pharm. Bull.*, 1976, **24,** 2810.
6 G. A. Molander and G. Hahn, *J. Org. Chem.*, 1986, **51**, 2596.
7 W. P. Schneider, G. L. Bundy and F. H. Lincoln, *J. Chem. Soc., Chem. Commun.*, 1973, 254.
8 C. H. Robinson and R. Henderson, *J. Org. Chem.*, 1972, **37**, 565; W. Cole and P. L. Julian, *J. Org. Chem*., 1954, **19**, 131.
9 M. Mikyashita, T. Suzuki, M. Hoshino and A. Yoshikoshi, *Tetrahedron*, 1997, **53**, 12469.
10. A. Osuka, K. Taka-Oka and H. Suzuki, *Chem. Lett.*, 1984, 271.
11 H. Paulsen, K. Eberstein and W. Koebernick, *Tetrahedron Lett.*, 1974, 4377.
12. S. Torii, H. Okumoto, S. Nakayasu and T. Kotani, *Chem. Lett.*, 1989, 1975.
13 E. L. Shapiro and M. J. Gentles, *J. Org. Chem.*, 1981, **46**, 5017.
14 H. J. Liu, J. Yip and K. S. Shia, *Tetrahedron Lett.*, 1997, **38**, 2253.
15 E. Bartmann, *Angew. Chem., Int. Ed. Engl*., 1986, **25**, 653.
16 T. Cohen, I. H. Jeong, B. Mudryk, M. Bhupathy and M. A. Awad, *J. Org. Chem.*, 1990, **55**, 1528.

Communication 9/04646A

Nickel-catalysed enantioselective hydrovinylation of styrenes in liquid or supercritical carbon dioxide

Andreas Wegner and Walter Leitner*

Max-Planck-Institut für Kohlenforschung, Kaiser-Wilhelm-Platz 1, 45470 Mülheim an der Ruhr, Germany. E-mail: leitner@mpi-muelheim.mpg.de

Received (in Cambridge, UK) 16th June 1999, Accepted 14th July 1999

Compressed (liquid or supercritical) CO_2 is an environmentally benign reaction medium for the highly efficient regio-, chemo- and enantio-selective nickel-catalysed hydrovinylation of styrenes and it allows for catalyst recycling and selective removal of the product from the reaction mixture.

The formation of carbon–carbon bonds is a fundamental operation in synthetic organic chemistry. There is a great demand for catalytic C–C coupling reactions that allow a high level of chemo-, regio- and stereo-selectivity and can be carried out under environmentally friendly conditions. A very efficient catalytic carbon–carbon bond forming reaction is the transition metal catalysed co-dimerisation of alkenes with ethene yielding 3-substituted but-1-enes (hydrovinylation).[1] The hydrovinylation reaction is particularly intriguing because both starting materials are incorporated entirely in the product and the resulting double bond can be used for further transformations to highly functionalised molecules. Wilke *et al.* introduced the (η^3-allyl)nickel(II) complex **3** (containing a unique chiral 1,2-substituted 1-azaphospholene ligand) as a catalyst precursor for the asymmetric hydrovinylation of aromatic olefins (Scheme 1).[1,2] Complex **3** catalyses the enantioselective hydrovinylation of styrenes at extremely high rates and with unrivalled chemo-, regio- and enantio-selectivity, but it needs to be activated by an excess of highly flammable $Et_3Al_2Cl_3$. Furthermore, the reaction requires temperatures below −60 °C and the use of toxicologically disreputable CH_2Cl_2 as a solvent.

In order to overcome these drawbacks, we investigated the hydrovinylation with complex **3** in liquid and supercritical CO_2 as an alternative solvent.[3,4] The reaction proceeded smoothly using $Et_3Al_2Cl_3$ as the co-catalyst, but ees were disappointingly low (Table 1). We also observed some corrosion of the stainless steel high pressure reactor under these conditions, and therefore tried to replaced the aggressive Lewis acid by weakly co-ordinating anions which are easier to handle and non-corrosive under the reaction conditions. Unfortunately, no catalytic activity was observed using TfO^- or $[Al(O(CH_2)_2C_6F_{13})_4]^-$ as co-catalysts. The use of $[Al(OC(Ph)(CF_3)_2)_4]^-$ led to an active catalytic system but reactivity and stereoselectivity were low. Finally, we were pleased to find that the use of tetrakis[3,5-bis(trifluoromethyl)phenyl]borate (BARF) yields a catalytic system that is comparable to $Et_3Al_2Cl_3$ in activity and chemoselectivity but gives far better ees.† The use of BARF activates **3**, increases the thermal stability of the catalyst, and provides sufficient solubility of the active species in liquid and supercritical CO_2,[5] thus allowing the reaction to proceed close to and beyond the critical point of pure CO_2 (T_c = 31 °C, P_c = 73 atm, d_c = 0.468 g cm^{-3}). The 4-substituted styrenes **1b**,**c** were also successfully reacted with ethene in liquid and supercritical CO_2 to yield **2b**,**c** in high yield and with high ee. We note that **2c** is a key intermediate in a potential route to the non-steroidal anti-inflammatory drug Ibuprofen™.[1]

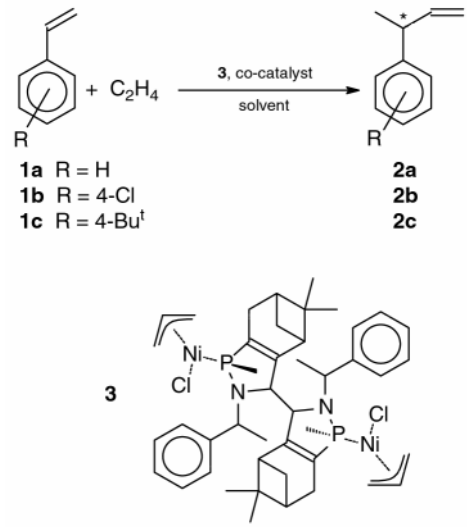

Scheme 1

Table 1 Enantioselective hydrovinylation of styrenes **1a–c** in CO_2[a]

Substrate/ product	Co-catalyst	*T*/°C	Conversion[b] (%)	Selectivity[b,c] (%)	Ee of **2**[b] (%)
1a/**2a**	$Cl_3Al_2Et_3$	1	> 99	92.9	70.2 (*R*)
1a/**2a**	TfO^-	40	< 1.0	—	—
1a/**2a**	$[Al(O(CH_2)_2C_6F_{13})_4]^-$	22	0	—	—
1a/**2a**	$[Al(OC(Ph)(CF_3)_2)_4]^-$	22	35	94.3	76.0 (*R*)
1a/**2a**	BARF	1	> 99	88.9	86.2 (*R*)
1a/**2a**	BARF	23	> 99	71.4	85.6 (*R*)
1a/**2a**	BARF	40	> 99	74.9	83.6 (*R*)
1a/**2a**	BARF	35[d]	> 99	38.9	91.6 (*R*)
1b/**2b**	BARF	40	> 99	80.5	81.0 (−)
1b/**2b**	BARF	24	> 99	87.0	81.3 (−)
1c/**2c**	BARF	35[e]	> 99	44.4	89.4 (*R*)
1c/**2c**	BARF	20[e]	75.8	71.4	76.6 (*R*)

[a] For standard reaction conditions see note †. [b] Determined by GC analysis. [c] Fraction of **2** in product mixture. Typical by-products were 2-phenylbut-2-enes and hydrovinylation products of **2**. [d] Reaction time 30 min. [e] Reaction time 50 min.

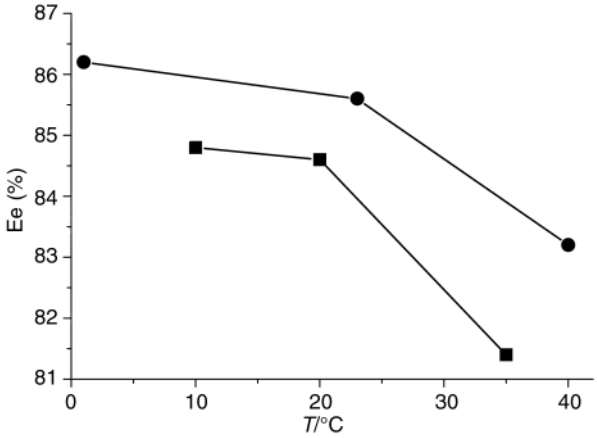

Fig. 1 Enantiomeric excess of **2a** obtained from hydrovinylation using the **3**–NaBARF catalyst in (●) CO_2 and (■) CH_2Cl_2 at different temperatures.

In hydrovinylation, the positive 'BARF effect' on the thermal stability of catalyst is not limited to $scCO_2$ as a solvent.[6] This anion can also be used as co-catalyst with **3** for the hydrovinylation of **1a** in CH_2Cl_2 and, at temperatures above 0 °C, proves to be superior to $Et_3Al_2Cl_3$ in terms of enantioselectivity (84.8 *vs.* 70.2% at 1 °C) with similar chemo- and regioselectivities. However, a comparison of the solvents CO_2 and CH_2Cl_2 reveals that enantioselectivity is generally better in CO_2 (Fig. 1). Chemoselectivity for **2a** is also considerably higher in CO_2 at elevated temperatures; 57.2% selectivity for **2a** are observed in CH_2Cl_2 at 35 °C compared to 74.9% in $scCO_2$ at 40 °C, with complete conversion in both cases.

In $scCO_2$, the catalyst formed from **3** and NaBARF exhibits remarkable stability as demonstrated in an experiment at 40 °C where a **1a**:Ni ratio of 10 000:1 was used (Fig. 2). With an initial turnover frequency of greater than 1300 h^{-1}, a total turnover number of 5000 (corresponding to 50% conversion) was achieved. This result is quite remarkable because previously reported turnover numbers for other nickel-catalysed reactions in the presence of $scCO_2$ were below 22.[7] A catalyst formed from [Ni(cod)$_2$] and PEt_3 was found to be highly susceptible to ligand oxidation in $scCO_2$, resulting in the formation of nickel carbonyls and the corresponding phosphinoxides.[7c] In the experiment shown in Fig. 2, the desired product **2a** was formed with extremely high chemoselectivity and no other products could be detected by NMR or GC analyses. The ee of 79.8% was only slightly lower than in experiments leading to complete conversion of **1a**.

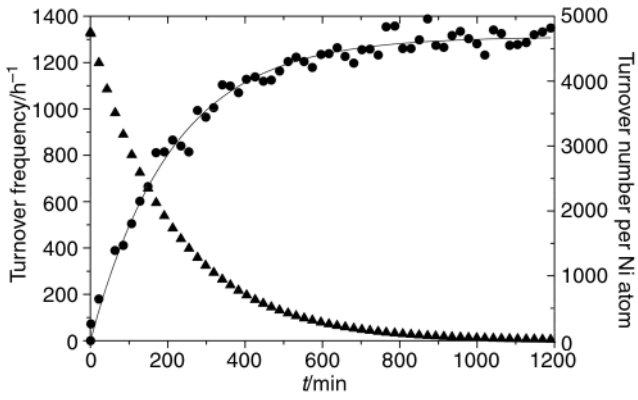

Fig. 2 (●) Turnover number of hydrovinylation of **1a** in the presence of **3**–NaBARF (**1a**:Ni = 10.000) in CO_2 at 40 °C. (▲) Turnover frequencies, derived from the first derivative of the least-squares fit of the turnover number data.

Another intriguing feature of our new procedure for hydrovinylation is the difference in product distribution of the condensate collected from the cold trap and the residue in the high pressure vessel. If the reactor was vented at temperatures above T_c of pure CO_2, the trap content was considerably enriched with **2a** (*e.g.* 81.0 *vs.* 60.5% in the residue) and contained less of the by-products formed from isomerisation and hydrovinylation of **2a**. This finding indicates that it is possible to remove **2a** selectively from the reaction mixture with CO_2. Additionally, the catalyst can be easily recycled after venting and removal of all volatiles *in vacuo*. At a reaction temperature of 22 °C, the ee was minimally reduced (from 83.4% at the beginning down to 79.8%), but some loss in activity was observed (from > 99% conversion down to 33% conversion of **1a**) in four subsequent runs.

In summary, we obtained highly promising results performing enantioselective nickel-catalysed hydrovinylation in liquid and supercritical CO_2. The attractive prospects for catalyst recycling and selective removal of the product encourage our ongoing efforts to explore CO_2 as a solvent for enantioselective catalysis.

This work was supported by the Max-Planck-Gesellschaft, the Deutsche Forschungsgemeinschaft (Gerhard-Hess-Programm) and the Fonds der Chemischen Industrie. We thank Professor G. Wilke for his encouragement in this project and for stimulating discussions.

Notes and references

† In a typical experiment, a stainless steel high pressure reactor (V = 27 cm^3) equipped with thick-wall glass windows, a PTFE stirring bar, a bore hole for a thermocouple, and needle and ball valves was charged with NaBARF (33.4 mg, 35.5×10^{-3} mmol) under argon. A dosing unit containing a solution of **3** (5.4 mg, 6.3×10^{-3} mmol) in **1a** (450 mg, 4.37 mmol) was connected to the reactor through the closed ball valve and pressurised with CO_2 (7.1 g). The reactor was filled through the needle valve with ethene (1.1 g, 39.3 mmol) and CO_2 (14.6 g) using a compressor. The reaction mixture was then warmed to 40 °C, while the dosing unit was heated to 60 °C. Opening the ball valve started the reaction, which was allowed to proceed for 15 min. The reactor contents were then vented through a trap cooled to −55 °C. The products were collected separately from the trap and the reactor by extraction with Et_2O or acetone and analysed by GC and NMR.

1 For a review, see P. W. Jolly and G. Wilke, *Applied Homogenous Catalysis with Organic Compounds 2*, ed. B. Cornils and W. A. Herrman, Wiley-VCH, Weinheim, 1996, p. 1024.
2 G. Wilke and J. Monkiewicz, DOS 3 618 169, Priority 30.05.86; *Chem. Abstr.* 1988, **109**, P6735.
3 *Chemical Synthesis Using Supercritical Fluids*, ed. P. G. Jessop and W. Leitner, Wiley-VCH, Weinheim, 1999.
4 For recent reviews, see P. G. Jessop, T. Ikariya and R. Noyori, *Science*, 1995, **269**, 1065; D. A. Morgenstern, R. M. LeLacheur, D. K. Morita, S. L. Borkowsky, S. Feng, G. H. Brown, L. Luan, M. F. Gross, M. J. Burk and W. Tumas, *Green Chemistry*, ed. P. T. Anastas and T. C. Williamson, ACS Symp. Ser. 626, American Chemical Society, Washington DC, 1996, p. 132; P.G. Jessop, T. Ikariya and R. Noyori, *Chem. Rev.*, 1999, **99**, 475; M. Poliakoff, S. M. Howdle and S. G. Kazarian, *Angew. Chem., Int. Ed. Engl.*, 1995, **34**, 1275.
5 For the use of BARF in other enantioselective metal-catalysed reactions in $scCO_2$, see: J. Burk, S. Feng, M. F. Gross and W. Tumas, *J. Am. Chem. Soc.*, 1995, **117**, 8277; S. Kainz, A. Brinkmann, W. Leitner and A. Pfaltz, *J. Am. Chem. Soc.*, 1999, **121**, 6421.
6 For the use of BARF to activate less selective hydrovinylation catalysts in conventional solvents, see: N. Nomura, J. Jin, H. Park and T. V. RajanBabu, *J. Am. Chem. Soc.*, 1998, **120**, 459.
7 (*a*) M. T. Reetz, W. Könen and T. Strack, *Chimia*, 1993, **47**, 493; (*b*) E. Dinjus, R. Fornika and M. Scholz, *Chemistry Under Extreme or Non-Classical Conditions*, ed. R. van Eldik and C. D. Hubbard, Wiley, New York, 1996, p. 219; (*c*) U. Kreher, S. Schebesta and D. Walther, *Z. Anorg. Allg. Chem.*, 1998, **624**, 602.

Communication 9/04799I

ChemComm

Incorporation of dimethyldodecylammonium chloride functionalities onto poly(propylene imine) dendrimers significantly enhances their antibacterial properties

Chris Zhisheng Chen,[a] Nora C. Beck Tan[b] and Stuart L. Cooper*[a]†

[a] *Department of Chemical Engineering, University of Delaware, Newark, DE 19716 USA. E-mail: cooper@iit.edu*
[b] *Polymers Research Branch, US Army Research Laboratory, APG, MD 21005-5069 USA*

Received (in Columbia, MO, USA) 11th June 1999, Accepted 6th July 1999

Dimethyldodecylammonium chloride functionalized poly(propylene imine) generation 3 dendrimers have been synthesized and proven to have strong antibacterial properties.

The novel architecture of dendrimers[1–6] provides a very high number of functional groups in a compact space. Thus, it is reasonable to expect that these novel molecules will play a major role in materials whose performance depends on high local concentration, such as drugs or antimicrobial agents. Presently, there are few reports in this field. In this work, DSM Astramol™ poly(propylene imine) (PPI) dendrimers have been successfully used to synthesize dendritic biocides, which are shown to be over two orders of magnitude more potent than their small molecule counterpart, *n*-dodecyltrimethylammonium chloride (DTAC), against *Escherichia coli*.

Quaternary ammonium compounds (QACs) have been widely used as disinfectants. They are effective biocidal agents when they possess an alkyl chain with at least eight carbon atoms. Although the exact mechanism of their antimicrobial action is still unclear, it is mostly attributed to cell membrane disruption, their ability to increase cell permeability, and their possible effects on proteins.[7] Since biocidal action requires interactions with the cell membrane, it will be influenced by both the size of the molecules and the functional group density. Larger molecules tend to have a lower permeation rate through the cell membranes, and thus are less efficient. Therefore, dendritic biocides need to counterbalance the negative side of their bulkier size to be very effective. The antibacterial actions against Gram-positive and Gram-negative bacteria are also different since they have different cell structures. The purpose of this study was to synthesize novel dendritic biocides by converting the surface groups of dendrimers to quaternary ammonium functionalities and to test their biocidal capability. The target biocides not only carry 16 quaternary ammonium groups per molecule but also possess a polycationic structure, which is well-known to increase the permeability of cell membranes and thus aid the killing process.[8]

Commercially available poly(propylene imine) (PPI) dendrimers were used in this study. These dendrimers are well-characterized by various techniques.[9–11] The purity of PPI dendrimers has also been investigated by electrospray mass spectrometry.[12] To synthesize these dendritic biocides, the peripheral primary amine groups of PPI generation 3 dendrimers [DAB-dendr-$(NH_2)_{16}$] were reacted with 2-chloroethyl isocyanate to yield pendent chloroethyl groups.[13,14] Urea protons (CO-NH-CO) were observed at δ 6.72 (^{1}H NMR, $CDCl_3$) and carbonyl carbons (CO-NH-CO) were observed at δ 158.7 (^{13}C NMR, 15% in $CDCl_3$). The modified dendrimers were subsequently quaternized by dimethyldodecylamine to give the dimethyldodecylammonium chloride functionalized dendrimers (Scheme 1).[15] A five-fold excess of dimethyldodecylamine was used to facilitate the reaction and to prevent inter-

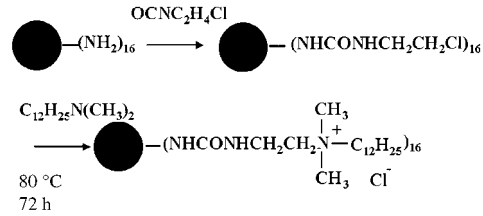

Scheme 1 Synthesis of dimethyldodecylammonium chloride functionalized PPI generation 3 dendrimers (the filled circle represents a complete dendrimer molecule except for the end groups).

dendrimer quaternization. Two different carbons in the methyl groups were clearly identified with ^{13}C NMR. The methyl groups connected directly with nitrogen were observed at δ 51.1 while the methyl carbon in the dodecyl groups was observed at δ 13.8. FTIR analysis also showed C–H saturation at 2930.4 cm^{-1}, C=O at 1639.9 cm^{-1}, N–H bend at 1562.3 cm^{-1} and N–H stretch at 3297.9 cm^{-1}. The final product was obtained as a yellow solid in 70% yield. It is very soluble in alcohol and $CHCl_3$, and slightly soluble in water. Although MALDI data for a similar amphiphilic dendrimer structure have been published,[2] our effort to collect MALDI-TOF data was not successful, probably because the sample was extremely hygroscopic and the hydrophobic chains were hard to ionize. The nomenclature used is D3C1NC12, which denotes dimethyldodecyl (C12) ammonium (N) chloride (C1) functionalized PPI generation 3 dendrimers (D3).

The antibacterial properties of D3C1NC12 against Gram-negative *E. coli* were determined by a bioluminescence method.[16–18] Bioluminescence is observed under normal growth conditions for the recombinant *E. coli* strain TV 1048. Whenever the bacteria are in a biocidal environment, the light-off response corresponds to the toxic effect of the biocide.[19] Fig. 1 shows typical data for the bioluminescence experiment. The result is expressed as the sample bioluminescence normalized to a control (without biocide) *vs.* time. The reduction of luminescence quantitatively shows the antibacterial properties of the

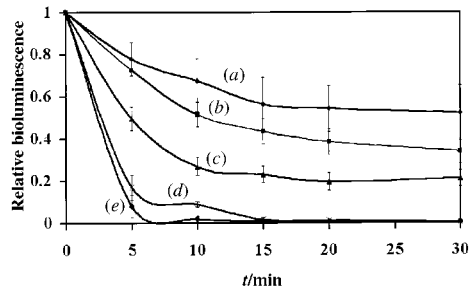

Fig. 1 Time course of the relative bioluminescence of *E. coli* in contact with D3C1NC12: (*a*) 4, (*b*) 8, (*c*) 12, (*d*) 16 and (*e*) 20 μg ml^{-1}. The temperature of experiments was maintained at 30 °C, the optimal temperature for the growth of strain TV 1048. The dendrimer biocides were added to bacterial suspensions with an optical density at 600 nm at 0.2. The data shown are the average of three experiments.

† Current address: Illinois Institute of Technology, E1 Room 117, 10 West 32nd Street, Chicago, IL 60616 USA.

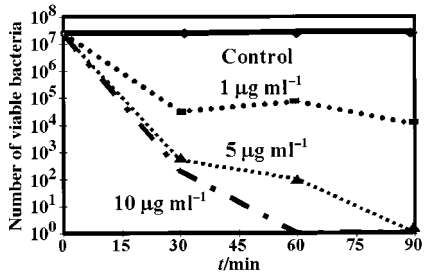

Fig. 2 Biocidal effect of D3C1NC12 on *S. aureus* in suspension tests (10% Tween 80 was used as a neutralizer).

sample. At 4 μg ml^{-1}, the dendrimer inhibited the growth of *E. coli*, but the bacteria could adjust to the environmental stress and survive. At higher concentrations (20 μg ml^{-1}), the bioluminescence decreased very rapidly and was reduced to an undetectable level in 15 min, indicating a strong biocidal effect. In the control experiment, the bioluminescence of the bacteria did not change significantly (5%) if the same concentration of pure PPI generation 3 dendrimers was added (data not shown).

To quantify the level of the biocidal effect of the cationic dendrimer and to compare it to its small molecule counterpart, the *n*-dodecyltrimethylammonium chloride (DTAC) EC_{50} value was determined. EC_{50} is defined as the concentration of the compound which causes a 50% reduction of the bioluminescence in a certain time period. EC_{50} concentrations were determined by interpolation of the bioluminescence against concentration curves at a specific time. A lower EC_{50} indicates a more toxic compound. The EC_{50} of D3C1NC12 is about 12 μg ml^{-1} at 5 min while the EC_{50} of DTAC is about 2000 μg ml^{-1}. The dendrimer architecture increases the potency of DTAC against *E. coli* over 100 times.

Conventional linear or branched polymeric QACs have been investigated for many potential applications.[20–23] Interestingly, it is not enhanced efficiency but low toxicity to humans and the absence of foaming that are often cited as their special features.[7] Compared to conventional linear or branched polymers, dendrimers offer a large number of functional groups in a compact space. These chemical functionalities of the dendrimer biocides are presumably exposed on the surface, while a significant portion of them will be trapped on the interior of random-coil linear polymers. Therefore, the increased potency of dendritic biocides results from their novel dendritic architecture. These biocides could possibly achieve enhanced antimicrobial properties along with low toxicity and the absence of foaming. QACs are not very effective on Gram-negative bacteria such as *E. coli* because they have a complex outer membrane structure that effectively keeps out the antibacterial agents. The combination of their high functional group density and increasing permeability due to their polycationic structure allow dendritic biocides to reach and disrupt cell membranes and eventually lead to cell death. This explanation is supported by the analysis of the bioluminescence data, which give a dilution coefficient of 1.8. The dilution coefficient is similar to the reaction order in chemical kinetics. It represents the change in activity brought about by different concentrations. The higher the dilution coefficient, the more rapidly the antimicrobial agent loses its activity. The dilution coefficient of the novel dendrimer biocides falls into the range of conventional QACs (1–2.5), implying a similar mode of action.[24]

To verify that the biocidal effects of D3C1NC12 were not bacteria dependent, its antibacterial properties against Gram-positive *Staphylococcus aureus* were investigated by suspension tests.[25] Fig. 2 shows that D3C1NC12 inhibited the growth of *S. aureus* at levels as low as 1 μg ml^{-1} and effectively killed them at 10 μg ml^{-1} in 60 min. Similar results have been reported for DTAC.[7] This demonstrates the strong potency of dendritic biocides on typical Gram-positive *S. aureus*.

We have demonstrated that it is feasible to synthesize highly potent dendrimer-based antibacterial agents. The novel dendritic biocides are over two orders of magnitude more potent than their small molecule counterparts against Gram-negative bacteria. They are also very effective against Gram-positive bacteria. The dendritic architecture greatly enhances the effectiveness of common quaternary ammonium disinfectants.

The authors would like to acknowledge Dr Prasad Dhurjati (University of Delaware), Tina K. Van Dyk and Dr Robert LaRossa (DuPont Company) for the use of *E. coli* strain TV1048 and Steve Bai (University of Delaware) for assistance with NMR.

Notes and references

1 A. P. H. J. Schenning, C. Elissen-Roman, J. Weener, M. W. P. L. Baars, S. J. van der Gaast and E. W. Meijer, *J. Am. Chem. Soc.*, 1998, **120**, 8199.
2 S. Stevelmans, J. C. M. van Hest, J. F. G. A. Jansen, D. A. F. J. van Boxtel, E. M. M. de Brabander-van den Berg and E. W. Meijer, *J. Am. Chem. Soc.*, 1996, **118**, 7398.
3 G. R. Newkome, C. N. Moorefield and F. Vögtle, *Dendritic Macromolecules: Concepts, Syntheses, Perspectives*, VCH, Weinheim, Germany, 1996.
4 G. R. Newkome, *Advances in Dendritic Macromolecules*, JAI, Greenwich, CT, 1995, vol. 2.
5 D. A. Tomalia, A. M. Naylor and W. A. Goddard III, *Angew. Chem., Int. Ed. Engl.*, 1990, **29**, 138.
6 J. Issberner, R. Moors and F. Vögtle, *Angew. Chem., Int. Ed. Engl.*, 1994, **33**, 138.
7 S. Block, *Disinfection, Sterilization and Preservation*, 3rd edn., Lea and Febiger, Philadelphia, 1983.
8 T. J. Franklin and G. A. Snow, *Biochemistry of Antimicrobial Actions*, 4th edn., Chapman and Hall, London, 1987.
9 E. M. M. de Brabander-van den Berg, *Angew. Chem., Int. Ed. Engl.*, 1993, **32**, 1308.
10 G. J. M. Koper, M. H. P. van Genderen, C. Elissen-Roman, M. W. P. L. Barrs, E. W. Meijer and M. Borkovec, *J. Am. Chem. Soc.*, 1997, **119**, 6512.
11 R. Scherrenberg, B. Coussens, P. van Vliet, G. Edouard, J. Brackman and E. de Brabander, *Macromolecules*, 1998, **31**, 456.
12 J. C. Hummelen, J. L. J. van Dongen and E. W. Meijer, *Chem. Eur. J.*, 1997, **3**, 1489.
13 G. R. Newkome, C. D. Weis, C. N. Moorefield, G. R. Baker, B. J. Childs and J. Epperson, *Angew. Chem., Int. Ed.*, 1998, **37**, 307.
14 G. Oertel, *Polyurethane handbook*, 2nd edn., Hanser, Munich, 1993.
15 R. J. Goddard and S. L. Cooper, *Macromolecules*, 1995, **28**, 1390.
16 A. J. Walker, S. A. A. Jassim, J. H. Holah, S. P. Denyer and G. S. A. B. Stewart, *FEMS Microbiol. Lett.*, 1992, **91**, 251.
17 A. M. Hibma and S. A. A. Jassim, *Int. J. Food Microbiol.*, 1996, **33**, 157.
18 T. K. Van Dyk, W. R. Majarian, K. B. Konstantinov, R. M. Young, P. S. Dhurjati and R. A. LaRossa, *Appl. Environ. Microbiol.*, 1994, **60**, 1414.
19 C. Z. Chen, J. T. Oh, P. Dhurjati, T. K. VanDyk, R. A. LaRossa and S. L. Cooper, *Transactions of the Society for Biomaterials*, San Diego, CA, 1998, vol. 21, p. 269.
20 J. Hazziza-Laskar, N. Nurdin, G. Helary and G. Sauvet, *J. Appl. Polym. Sci.*, 1993, **50**, 651.
21 M. Ghosh, *Polym. News*, 1988, **13**, 71.
22 T. Ikeda and S. Tazuke, *Macromol. Chem. Rapid Commun.*, 1983, **4**, 459.
23 A. Rembaum, *J. Appl. Polym. Sci. Appl. Polym. Symp.*, 1973, **22**, 299.
24 C. H. Collins, M. C. Allwood, S. F. Bloomfield and A. Fox, *Disinfectants: Their use and evaluation of effectiveness*, Academic Press, London, 1981.
25 P. Broxton, P. M. Woodcock and P. Gilbert, *J. Appl. Bacteriol.*, 1983, **54**, 345.

Communication 9/04662C

Unique polymers *via* radical diene cyclization: polyspironorbornanes and their application to 193 nm microlithography

Robert P. Meagley, Dario Pasini, Linus Y. Park and Jean M. J. Fréchet*

Department of Chemistry, University of California, Berkeley, CA 94720-1460, USA.
E-mail: frechet@cchem.berkeley.edu

Received (in Corvallis, OR, USA) 25th March 1999, Accepted 23rd June 1999

The design of novel alkylated norcamphor derivatives that undergo cyclopolymerization is explored; the resulting polymers incorporate suitable functional groups for chemical amplification and show excellent imaging characteristics under lithographic exposure at 193 nm.

The rapid advance in the miniaturization of microelectronic devices requires the development of new imageable polymeric materials for 193 nm microlithography.[1] Highly sensitive, chemically amplified resists for 248 nm microlithography were described in the early 1980s,[2] and have been used commercially for more than a decade. They operate on the basis of acid-catalyzed deprotection of a polymer in a process that renders the final product soluble in aqueous base.[3] The next generation of resists for 193 nm lithography requires much structural redesign to obtain optical transparency at 193 nm while preserving the etch resistance normally afforded by aromatic rings.

Acrylic and methacrylic acids[4] have been suggested for this application due to their good transparency but their dry-etch resistance is limited. Since a high carbon to hydrogen (C/H) ratio is required to confer etch resistance[5] to the polymeric structure, several carbon-rich, chemically amplified resist materials have recently been described.[6,7] Here, we present a novel synthetic approach for the construction of carbon-rich polymers *via* the cyclopolymerization[8] of suitably modified difunctional monomers.

In earlier work, Marvel *et al.*,[9] and later Mathias *et al.*,[10] have described the free radical polymerization of diacrylates to afford soluble cyclopolymers with virtually complete cyclization. We have now designed bifunctional acrylic-like monomers, incorporating both (i) *tert*-butyl esters as imageable functionalities for chemical amplification, and (ii) carbon-rich cage moieties for etch resistance. A suitable commercially available building block is racemic norcamphor. It can be alkylated *via* its enolate using *tert*-butyl 2-(bromomethyl)acrylate **1** to give the monosubstituted product **2** in good yield (Scheme 1).† This alkylation, as shown by 2D ^{1}H NMR spectroscopy, proceeds diastereoselectively, the *endo* face of the norbornene structure being less sterically hindered and more suitable for reaction with the bromide. The disubstituted monomer **3** could also be obtained under the same reaction conditions, although incomplete conversion of the starting monosubstituted camphor derivative **2** into **3** was observed, probably due to attack of the alkylating agent on the more sterically hindered *exo* face.

Isolation of pure monomer **3** required careful purification of the crude product by flash column chromatography. The structure of **3** was determined by standard spectrometric techniques and confirmed by X-ray crystallographic analysis. The ketone functionality of **3** could be selectively reduced with KBH_4 in MeOH to afford alcohol monomer **4** in good yields.

Monomers **3** and **4** undergo smooth cyclopolymerization under free-radical conditions in deoxygenated solvents to give the cyclopolymerized products **6** and **7**, respectively (in up to 88% yield after precipitation from MeOH). The resulting polymers were soluble in a variety of organic solvents, and IR and NMR spectroscopic analyses revealed the absence of residual alkene groups in the two polymers, thus confirming that virtually complete cyclization had been achieved. Interestingly,

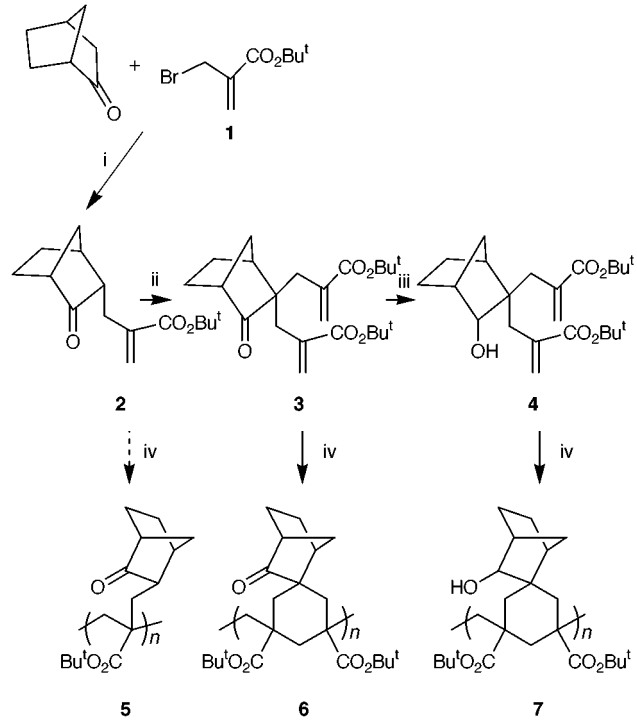

Scheme 1 *Reagents and conditions*: (i) NaOBu^t, THF, 0 °C, 70%; (ii) **1**, NaOBu^t, THF, 0 °C, 50%; (iii) KBH_4, MeOH, 0 °C, 50%; (iv) AIBN, solvent, 70 °C, 30 h.

the monosubstituted camphor derivative **2** did *not* polymerize under standard free radical conditions, probably as a result of the extreme steric hindrance that adjacent camphor derivatives would experience within the backbone of polymer **5**.

Differential scanning calorimetry analysis of polymers **6** and **7** showed no transitions below the decomposition temperature of the polymer, which occurs at *ca.* 240 °C and results from the thermolysis of the *tert*-butyl esters. Thermogravimetric analysis data for the polymers were in close agreement with the observed and calculated weight losses for the thermolysis of the *tert*-butyl ester functionalities. As can be seen in Table 1, variations in

Table 1 Cyclopolymerization of monomers **3** and **4** under free radical conditions

Monomer	Conc./mol dm^{-3}	Solvent	Additive/mol% AIBN	Additive/mol% Thiol	M_n[a]	M_w[a]	PDI[b]
3	1.8	benzene	2	0	35 600	64 000	1.8
3	1.2	benzene	2	0	10 200	17 500	1.7
4	2	Bu^{t}OH	2	0	34 200	57 700	1.7
4	1.2	Bu^{t}OH	9	0	7 600	12 900	1.7
4	1.2	benzene	2	3	28 600	44 900	1.6
4	1.2	benzene	2	6	14 900	22 800	1.5

[a] Molecular weights determined by size exclusion chromatography relative to polystyrene standards. [b] Polydispersity index.

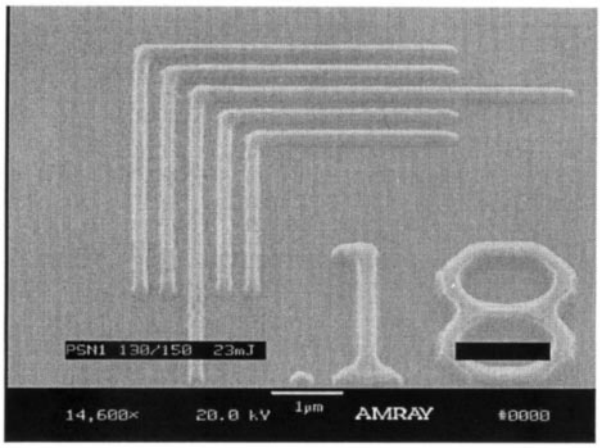

Fig. 1. Electron micrograph of 180 nm nested features obtained from films of polymer **6** and a photoacid generator after exposure to a 193 nm stepper.

monomer or initiator concentrations, solvent, or the use of dodecanethiol as a chain transfer agent,[11] brought about considerable variations in the molecular weight distribution. Control of molecular weight is useful for such polymers since low molecular weight polymers are often desirable for lithographic applications at 193 nm.

Camphor-derived polymers **6** and **7** produced high quality films on silicon wafers. Nevertheless, the absorbance of films of polymer **6** at 193 nm (A = 0.66 per μm of film thickness) was found to be relatively high. The corresponding polymer **7**, free of ketone or olefin moieties, showed a greatly reduced absorbance at 193 nm (A = 0.23 μm^{-1}). Films prepared from polymer **6** bearing ketone functionalities and 10 wt% of a photoacid generator[12] showed clearing doses in the order of 10 mJ cm^{-2}. Similar films prepared from polymer **7** and 5 wt% photoacid generator required doses of *ca.* 15 mJ cm^{-2}. This confirms that the removal of the somewhat basic ketone functionalities, in addition to lowering the absorbance of the films, contributes to enhance the photospeed of the corresponding resist formulations. Images with feature sizes of 0.18 μm (Fig. 1) and lower could be obtained. This study demonstrates the feasibility and flexibility of a cyclopolymerization protocol that allows the rapid adjustment of 'carbon density' within the polymeric structure for applications such as nanolithography. All of these bis-olefinic monomers cyclopolymerize readily and preliminary experiments suggest they can also be used in copolymerizations with a variety of co-monomers. We are currently pursuing further optimization of the fundamental design of these materials as well as of their imaging properties.

Funding by SEMATECH is acknowledged with thanks. This work was carried out in collaboration with Professor C.G. Willson at the University of Texas-Austin. We thank Professor Willson and his group, as well as Dr J. Byers of SEMATECH and the IBM Almaden Lithography Group, for assistance in the 193 nm imaging experiments.

Notes and references

† *Selected data* for **2**: $\delta_H(CDCl_3)$ 6.12 (s, 1H; C=C*H*), 5.46 (s, 1H; C=C*H*), 2.57 (m, 2H; norcamphor), 2.39 (br s, 1H; norcamphor), 2.16 (dd, 1H; norcamphor), 2.0–1.6 (m, 5H; norcamphor), 1.6–1.3 [m, 11H; norcamphor and $C(CH_3)_3$]; $\delta_C(CDCl_3)$ 218.7, 166.0, 140.1, 125.2, 80.8, 52.7, 49.6, 38.6, 34.6, 31.1, 28.0, 27.9, 23.9. For **3**: $\delta_H(CDCl_3)$ 6.13 (s, 2H; C=C*H*), 5.60 (s, 1H; C=C*H*), 5.49 (s, 1H; C=C*H*), 2.71 (dd, 2H; norcamphor), 2.6–2.1 (m, 5H; norcamphor), 1.9–1.3 [m, 23H; norcamphor and $C(CH_3)_3$]; $\delta_C(CDCl_3)$ 219.1, 167.1, 166.5, 139.4, 138.8, 127.1, 125.1, 80.8, 80.7, 54.4, 49.8, 44.2, 34.9, 34.1, 32.1, 28.0, 27.9, 24.9, 23.8. (calc. for $C_{23}H_{34}O_5$: C 70.7, H 8.7; found: C 70.7, H 8.8%). For **4**: $\delta_H(CDCl_3)$ 6.08 (s, 1H; C=C*H*), 6.05 (s, 1H; C=C*H*), 5.56 (s, 1H; C=C*H*), 5.51 (s, 1H; C=C*H*), 3.89 (br s, 1H; C*H*OH), 2.6–2.1 (m, 6H; norcamphor), 1.7–1.1 [m, 25H; norcamphor and $C(CH_3)_3$]; $\delta_C(CDCl_3)$ 167.9, 167.6, 140.4, 139.8, 126.1, 124.8, 80.5, 80.5, 77.6, 46.6, 44.6, 43.2, 38.4, 33.8, 30.2, 30.2, 27.9, 25.0, 18.8 (calc. for $C_{23}H_{36}O_5$: C 70.4, H 9.2; found: C 70.6, H 9.1%). For polymer **6**: TGDTA analysis: 235 °C; calc. loss 29%, found 31%; ν_{max}(KBr)/cm^{-1} 2980, 1740, 1720, 1450, 1370, 1250, 1150, 850, 750; $\delta_H(CDCl_3)$ 3–1 (br s) (calc. for $(C_{23}H_{34}O_5)_n$: C 70.7, H 8.7; found: C 70.6, H 8.7%). For polymer **7**: TGDTA analysis: 238 °C; calc. loss 29%, found 29%; ν_{max}(KBr)/cm^{-1} 3460, 2950, 1720, 1455, 1370, 1250, 1150, 850; $\delta_H(CDCl_3)$ 4.5–3.5 (br s), 3–1 (br s).

1 Semiconductor Industry Association (SIA), *The National Technology Roadmap for Semiconductors*, San Jose, CA, 1997.
2 J. M. J. Fréchet, E. Eichler, H. Ito and C. G. Willson, *Polymer*, 1983, **24**, 995; H. Ito, C. G. Willson and J. M. J. Fréchet, *US Pat.* 4,491,628, 1985; C. G. Willson, H. Ito, J. M. J. Fréchet, T. G. Tessier and F. M. Houlihan, *J. Electrochem. Soc.*, 1986, **133**, 181.
3 S. A. MacDonald, C. G. Willson and J. M. J. Fréchet, *Acc. Chem. Res.*, 1994, **27**, 151.
4 R. R. Kunz, R. D. Allen, W. D. Hinsberg and G. M. Wallraff, *Proc. SPIE*, 1993, **1925**, 167; R. D. Allen, G. M. Wallraff, W. D. Hinsberg, W. E. Conley and R. R. Kunz *J. Photopolym. Sci. Technol.*, 1993, **6**, 575; R. R. Kunz, S. C. Palmateer, A. R. Forte, R. D. Allen, G. M. Wallraff, R. A. DiPietro and D. C. Hofer, *Proc. SPIE*, 1996, **2724**, 365.
5 H. Gokan, S. Esho and Y. Ohnishi, *J. Electrochem. Soc.*, 1983, **130**, 143.
6 F. M. Houlihan, T. I. Wallow, O. Nalamasu and E. Reichmanis, *Macromolecules*, 1997, **30**, 6517; S.-J. Choi, Y. Kang, D.-W. Jung, C.-G. Park and J.-T. Moon, *Proc. SPIE*, 1997, **3049**, 104; U. Okoroanyanwu, T. Shimokawa, J. Byers and C. G. Willson, *Chem. Mater.*, 1998, **10**, 3319; U. Okoroanyanwu, J. Byers, T. Shimokawa and C. G. Willson, *Chem. Mater.*, 1998, **10**, 3328.
7 Q. J. Niu and J. M. J. Fréchet, *Angew. Chem., Int. Ed.*, 1998, **37**, 667.
8 G. B. Butler, *Encyclopedia of Polymer Science and Engineering*, ed. J. I. Kroschwitz, Wiley, New York, 1986, vol. 4, p. 543.
9 C. S. Marvel and R. D. West, *J. Am. Chem. Soc.*, 1957, **79**, 5771.
10 L. J. Mathias, *Trends Polym. Sci.*, 1996, **10**, 330; L. J. Mathias, R. M. Warren and S. Huang, *Macromolecules*, 1991, **24**, 2036; T. Tsuda and L. J. Mathias, *Macromolecules*, 1993, **26**, 6359.
11 F. Jahanzad, M. Kazemi, S. Sajjadi and F. Taromi, *Polymer*, 1993, **34**, 3542.
12 Preliminary screening of photoacid generators showed triphenylsulfonium or diphenyliodonium nonafluorobutanesulfonate salts to give the best results in terms of resolution and sensitivity. The relative rate of etching of formulations containing polymer **6** in comparison to the commercial resist APEX was 1.25 (124 sccm HBr, 100 sccm Cl_2).

Communication 9/02405K

Unexpected formation of β-lactams and penem isosteres from mesoionics: sequential ring-opening–rearrangement of [3 + 2] cycloadducts

Martín Avalos,*[a] Reyes Babiano,[a] Pedro Cintas,[a] Michael B. Hursthouse,[b] José L. Jiménez,[a] Mark E. Light,[b] Ignacio López[a] and Juan C. Palacios[a]

[a] *Departamento de Química Orgánica, Facultad de Ciencias, Universidad de Extremadura, E-06071 Badajoz, Spain. E-mail: mavalos@unex.es*

[b] *Department of Chemistry, University of Southampton, Highfield, Southampton, UK SO17 1BJ*

Received (in Liverpool, UK) 28th May 1999, Accepted 9th July 1999

A novel and simple method has been developed to obtain penem analogs with biologically interesting functionalities, which combines aromatic aldehydes with thioisomünchnones, a readily available class of mesoionic heterocycles.

Mesoionics, five-membered aromatic heterocycles that cannot be represented by Lewis forms not involving charge separation, constitute a large and heterogeneous family of masked dipoles.[1] Their [3 + 2] cycloadditions have proven to be a fertile methodology, often encompassing the preparation of naturally-occurring products.[2] The versatility of these synthons can be exemplified in the case of 1,3-thiazolium-4-olates (thioisomünchnones) which have been converted into six-,[3] five-[4] and three-membered[5] functionalized rings by reaction with different dipolarophiles.

In contrast to what was expected, the reactions of 2-aminothioisomünchnones, such as **1** and **2**, with aromatic aldehydes yielded β-lactams, which have hitherto been unknown for this type of mesoionics. These condensations were conducted in anhydrous benzene at reflux and gave rise to a monocyclic β-lactam skeleton in moderate to good yields and without by-products (Scheme 1, Table 1). Besides the crucial importance of β-lactams as antimicrobial agents,[6] monocyclic azetidin-2-ones are potential inhibitors of elastase enzymes.[7] An additional feature of the structures arising from the above-mentioned coupling is the presence of a sulfur-containing side chain, the structural motif encountered in other penem antibiotics such as penicillins and cephalosporins.[8]

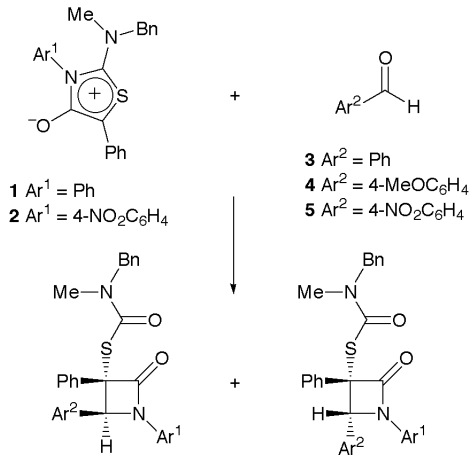

Scheme 1

Table 1 Synthesis of β-lactams **6**–**11**

Mesoionic	Aldehyde	*t*/h	Yield (%)[a]		*cis*:*trans*[b]
1	**3**	4	**6a** (41)	**6b** (34)	65:35
1	**4**	10	**7a** (54)	**7b** (20)	70:30
1	**5**	3	**8a** (—)[c]	**8b** (30)	59:41
2	**3**	1	**9a** (35)	**9b** (25)	57:43
2	**4**	6	**10a** (29)	**10b** (20)	60:40
2	**5**	1	**11a** (42)	**11b** (25)	58:42

[a] Yields of the pure isolated *cis* and *trans* isomers. [b] The *cis*:*trans* ratio was determined by ^{1}H NMR (400 MHz). [c] Not isolated.

In every case, β-lactams were formed as a mixture of *cis*- and *trans*-isomers (with respect to the orientation of aryl substituents at C-3 and C-4) and the *cis*:*trans* ratio was established by ^{1}H NMR of crude samples.† Individual diastereomers could be separated either by fractional crystallization or preparative chromatography. Furthermore, the structure of compound *cis*-**7a** was unequivocally confirmed by single-crystal X-ray diffraction analysis (Fig. 1).‡

A plausible rationale to account for the formation of β-lactams is shown in Scheme 2. The tandem process involves first a [3 + 2] cycloaddition in which thioisomünchnone plays the role of the dipole to produce a transient cycloadduct which undergoes a spontaneous C–N bond cleavage, followed by a rearrangement under the reaction conditions. The first step may also be rationalized assuming the stereoelectronic effect provided by the lone pair of the *N*,*N*-dialkylamino nitrogen *via* an intramolecular elimination. The pyramidal configuration of this nitrogen may bring the lone-pair orbital into an *anti* disposition with the leaving group, which competes favorably with the alternative carbon–sulfur scission. The resulting zwitterionic intermediate would largely be stabilized by resonance effects of the substituents on the charged atoms. The

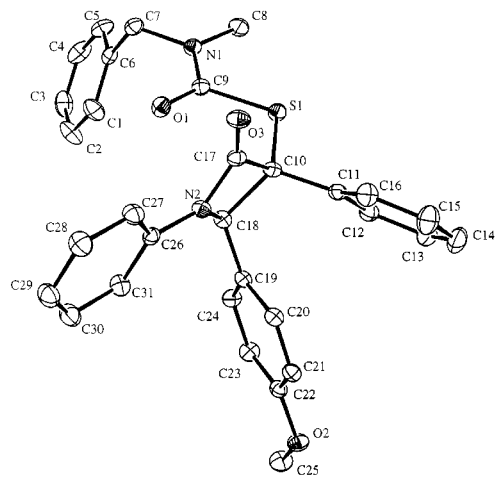

Fig. 1 Solid-state structure of compound **7a**.

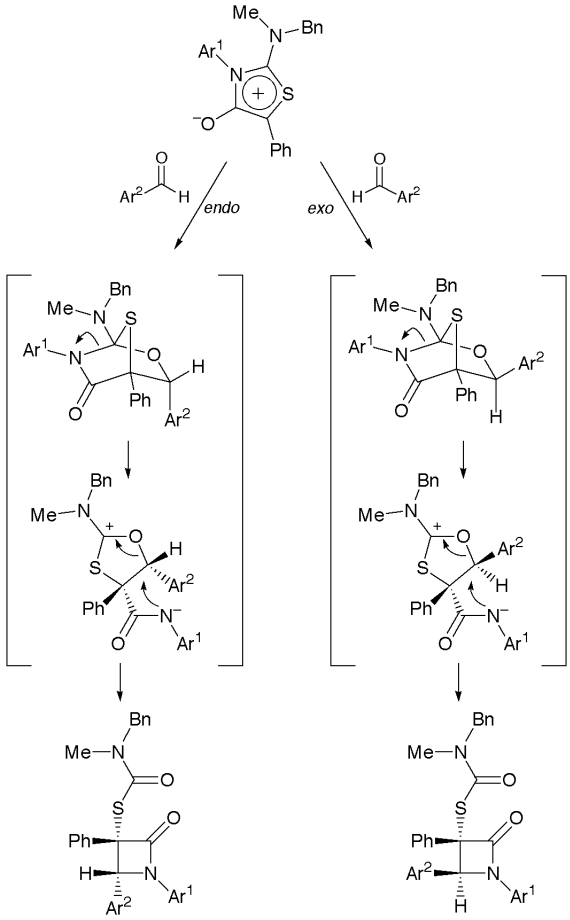

Scheme 2

formation of *cis*- and *trans*-diastereomers results from *exo* and *endo* approaches to the mesoionic ring.

It is fair to say that another mesoionic system, 1,3-oxazolium-5-olate, denoted colloquially as münchnone and containing an azomethine ylide dipole, also affords β-lactams by reaction with imines.[9] This formal [2 + 2] cycloaddition has been rationalized assuming that münchnones exist in equilibrium with their ketene-type valence tautomers, which would ultimately be the reactive species. However, there is no spectroscopic evidence of such tautomers, albeit this might be accounted for by a weak equilibrium in solution or a very short lifetime of the latter species. Since β-lactams have now been obtained from thioisomünchnones, for which putative valence tautomers would otherwise lead to a different four-membered ring (Scheme 3), the hypothesis of ketene reagents for münchnone cycloadditions should be revisited. In fact, it is also plausible for a stepwise reaction mechanism combining a [3 + 2] cycloaddition and rearrangement to afford the desired β-lactams. Even though further studies are required, our results represent a step in a direction that has been overlooked. It thus seems likely that münchnones do not behave like ketenes, a belief held for almost three decades.

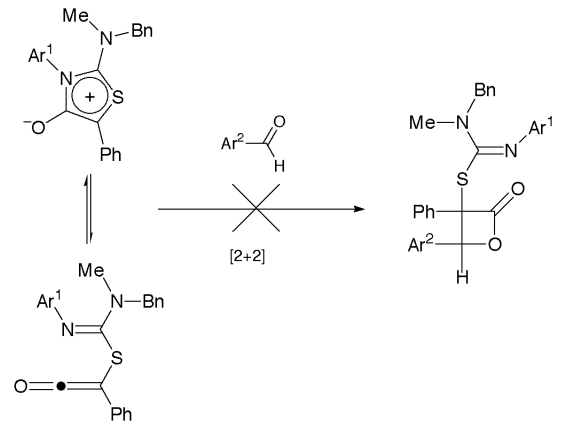

Scheme 3

To sum up, a concise and novel approach to β-lactams has been developed. The strategy may provide an exciting and growing interest in mechanistic and synthetic chemistry with mesoionic systems.

Financial support by grants from the Spanish Ministry of Education and Culture (DGICYT, PB95-0259) and the Junta de Extremadura-Fondo Social Europeo (IPR98-A064 and IPR98-C040) is gratefully acknowledged.

Notes and references

† *Selected data* for **6a**: recrystallized from EtOH, mp 147 °C; δ_H(400 MHz, $CDCl_3$) 7.90–6.80 (m, Ar), 5.89 (s, H-4), 4.54 (m, Ph-CH_2), 2.89 (br s, N-CH_3); δ_C(100 MHz, $CDCl_3$) 166.3 (S-CO-N), 164.6 (C-2), 137.7, 136.2, 134.5, 133.5, 129.0, 128.7, 128.6, 128.3, 128.2, 128.0, 127.9, 127.6, 127.2, 124.1, 117.8 (Ar), 69.0 (C-4), 68.3 (C-3), 53.9, 51.9 (Ph-CH_2, two resonances due to restricted rotation), 34.3 (N-CH_3) (Calc. for $C_{30}H_{26}N_2O_2S$: C, 75.29, H, 5.48, N, 5.85, S, 6.70; found: C, 75.18, H, 5.51, N, 5.89, S, 6.65%). For **6b**: recrystallized from CH_2Cl_2–EtOAc–Et_2O, mp 203 °C; δ_H(400 MHz, $CDCl_3$) 7.91–6.78 (m, Ar), 5.83 (s, H-4), 4.13 (d, Ph-CH_2), 2.55 (s, N-CH_3); δ_C(100 MHz, $CDCl_3$) 164.1 (S-CO-N), 163.5 (C-2), 137.6, 137.2, 135.7, 133.7, 129.1, 129.0, 128.4, 128.3, 128.0, 127.7, 127.4, 126.9, 124.1, 117.5 (Ar), 69.7 (C-4), 66.6 (C-3), 52.6 (Ph-CH_2), 34.1 (N-CH_3) (Calc. for $C_{30}H_{26}N_2O_2S$: C, 75.29, H, 5.48, N, 5.85, S, 6.70; found: C, 75.02, H, 5.44, N, 5.86, S, 6.82%).

‡ *Crystal data* for *cis*-**7a**: $C_{31}H_{28}N_2O_3S$, M_r = 508.6, T = 150(2) K, monoclinic, space group $P2_1/c$, a = 11.3385(3), b = 22.6660(7), c = 10.2516(4) Å, β = 92.1722(18)°, V = 2632.75(15) Å^3, ρ_{calc} = 1.283 g cm^{-3}, μ = 0.158 mm^{-1}, Z = 4, reflections collected: 24655, independent reflections: 5299 (R_{int} = 0.0633), final R indices [$I > 2\sigma(I)$]: $R1$ = 0.0443, $wR2$ = 0.1031, R indices (all data): $R1$ = 0.0675, $wR2$ = 0.1171. CCDC 182/1327. See http://www.rsc.org/suppdata/cc/1999/1589 for crystallographic data in .cif format.

1 W. D. Ollis and C. A. Ramsden, *Adv. Heterocycl. Chem.*, 1976, **19**, 1; C. G. Newton and C. A. Ramsden, *Tetrahedron*, 1982, **38**, 2965; W. D. Ollis, S. P. Stanforth and C. A. Ramsden, *Tetrahedron*, 1985, **41**, 2239.
2 K. T. Potts, in *1,3-Dipolar Cycloaddition Chemistry, Vol. 2*, ed. A. Padwa, Wiley, New York, 1984, pp. 1–82; M. H. Osterhout, W. R. Nadler and A. Padwa, *Synthesis*, 1994, 123.
3 P. Areces, M. Avalos, R. Babiano, L. González, J. L. Jiménez, J. C. Palacios and M. D. Pilo, *Carbohydr. Res.*, 1991, **222**, 99; M. Avalos, R. Babiano, M. J. Diánez, J. Espinosa, M. D. Estrada, J. L. Jiménez, A. López-Castro, M. M. Méndez and J. C. Palacios, *Tetrahedron*, 1992, **48**, 4193; C. O. Kappe, K. Peters and E.-M. Peters, *J. Org. Chem.*, 1997, **62**, 3109.
4 M. Avalos, R. Babiano, A. Cabanillas, P. Cintas, M. J. Diánez, M. D. Estrada, J. L. Jiménez, A. López-Castro, J. C. Palacios and S. P. Garrido, *J. Chem. Soc., Chem. Commun.*, 1995, 2213; M. Avalos, R. Babiano, A. Cabanillas, P. Cintas, F. J. Higes, J. L. Jiménez and J. C. Palacios, *J. Org. Chem.*, 1996, **61**, 3738.
5 P. Areces, M. Avalos, R. Babiano, L. González, J. L. Jiménez, M. M. Méndez and J. C. Palacios, *Tetrahedron Lett.*, 1993, **34**, 2999.
6 *The Chemistry of β-Lactams*, ed. M. I. Page, Blackie, London, 1992; *The Organic Chemistry of β-Lactams*, ed. G. I. Georg, VCH, New York, 1993.
7 P. D. Edwards and P. R. Bernstein, *Med. Res. Rev.*, 1994, **14**, 127; O. A. Mascaretti, C. E. Boschetti, G. O. Danelon, E. G. Mata and O. A. Roveri, *Curr. Med. Chem.*, 1995, **1**, 441.
8 R. J. Simonds, *Chemistry of Biomolecules—An Introduction*, The Royal Society of Chemistry, Cambridge, 1992, pp. 216–258.
9 E. Funke and R. Huisgen, *Chem. Ber.*, 1971, **104**, 3222.

Communication 9/04333K

ChemComm

Efficient ruthenium–TEMPO-catalysed aerobic oxidation of aliphatic alcohols into aldehydes and ketones

Arné Dijksman, Isabel W. C. E. Arends and Roger A. Sheldon*

Laboratory for Organic Chemistry & Catalysis, Department of Biotechnology, Delft University of Technology, Julianalaan 136, 2628 BL Delft, The Netherlands. E-mail: secretariat-ock@stm.tudelft.nl

Received (in Liverpool, UK) 30th March 1999, Accepted 3rd June 1999

The combination of $RuCl_2(PPh_3)_3$ and TEMPO affords an efficient catalytic system for the aerobic oxidation of a broad range of primary and secondary (aliphatic) alcohols at 100 °C, giving the corresponding aldehydes and ketones, respectively, in >99% selectivity in all cases.

The oxidation of primary and secondary alcohols into their corresponding aldehydes and ketones, respectively, plays a central role in organic synthesis.[1] Traditionally, such transformations have been performed with stoichiometric quantities of inorganic oxidants, such as chromium(VI) compounds.[2] The quest for effective catalytic systems that use clean, inexpensive primary oxidants, such as molecular oxygen or hydrogen peroxide, *i.e.* a 'green method' for converting alcohols to carbonyl compounds on an industrial scale, remains an important challenge.[3]

Ruthenium compounds have been extensively investigated[4] as catalysts for alcohol oxidations using a variety of primary oxidants, *e.g.* iodosobenzene,[5] *N*-methylmorpholine *N*-oxide,[6] *tert*-butyl hydroperoxide,[7] hypochlorite,[8] bromate[9] or a combination of oxygen and an aldehyde.[10] Ruthenium compounds, *e.g.* $RuCl_2(PPh_3)_3$,[11a] trinuclear ruthenium complexes[11b] and Ru-hydrotalcite,[11c] have also been shown to catalyse the oxidation of alcohols using oxygen as the sole oxidant, but the scope was generally limited to activated alcohols, *i.e.* allylic and benzylic alcohols.

A few ruthenium-based systems for the catalytic aerobic oxidation of non-activated aliphatic alcohols (Scheme 1) are known.[12] For example, ruthenium complexes in combination with hydroquinone as cocatalyst,[12b,c] and tetrapropylammonium perruthenate (TPAP), either as such[12d] or supported on an ion exchange resin,[12e] catalyse the reaction in Scheme 1. Two heterogeneous ruthenium catalysts, the improved Ru/Co-hydrotalcite[12f] and Ru/CeO_2,[12g] have also been described. Besides ruthenium, a few other metals, *e.g.* palladium,[13] cobalt[14] and copper,[3,15] have also been shown to catalyse the reaction in Scheme 1. However, all reported systems require relatively large quantities of catalyst (5–10 mol%) and/or additives, *i.e.* cocatalyst (10–20 mol%) and drying agents (2 equiv.), to achieve their activity.

The stable free radical 2,2′,6,6′-tetramethylpiperidine *N*-oxyl (TEMPO) catalyses the oxidation of alcohols by positive halogen compounds, *e.g.* hypochlorite, hypobromite and trichloroisocyanuric acid.[16,17] In this reaction, the corresponding oxoammonium salt is the active oxidant. The hydroxylamine, which is formed, is reoxidised by the positive halogen compound. Alternatively, the use of TEMPO in combination with copper salts and oxygen as primary oxidant was reported by Semmelhack.[18] However, this system was effective only with easily oxidised benzylic and allylic alcohols, simple primary and secondary alcohols being largely unreactive.

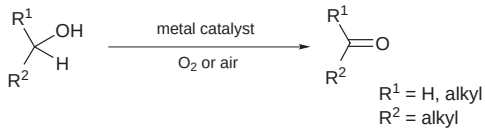

Scheme 1

Based on the various systems described above, we reasoned that the combination of ruthenium and TEMPO would likely lead to an efficient catalytic system for the aerobic oxidation of alcohols. For our initial experiments, we selected octan-2-ol as the test substrate and allowed it to react in PhCl with catalytic quantities of $RuCl_2(PPh_3)_3$ in the presence of TEMPO and oxygen. The results of these studies are collected in Table 1.

A typical reaction was carried out as follows: octan-2-ol (15.0 mmol; 1.96 g), *n*-hexadecane (internal standard; 3.0 mmol; 0.69 g), $RuCl_2(PPh_3)_3$[19] (0.225 mmol; 215.7 mg) and TEMPO[20] (0.675 mmol; 105.5 mg) were dissolved in 30 ml of PhCl and heated in a high-pressure reactor (10 bar) under a nitrogen atmosphere to 100 °C. The nitrogen atmosphere was replaced by a continuous stream (10 ml min^{-1}) of an oxygen–nitrogen mixture (8:92; v/v) and the mixture was stirred for 7 h. Octan-2-ol conversion and octan-2-one selectivity were determined using GC-analysis (50 m × 0.53 mm CP-WAX 52 CB column).

As can be seen from Table 2, $RuCl_2(PPh_3)_3$ alone is a poor catalyst for the oxidation of octan-2-ol to octan-2-one (entry 1). On the other hand, addition of TEMPO, which itself is not active as catalyst, to $RuCl_2(PPh_3)_3$ leads to a substantial increase in activity (entry 2). The use of PhCl as solvent is not essential and was chosen merely to simplify the GC analysis. Toluene can also be employed and even better results were obtained in neat octan-2-ol (entry 4). In this case, the same absolute conversion (15 mmol) was achieved within 1 h compared to the 9–16 h needed in PhCl (entries 2 and 3). Other ruthenium compounds were also tested. $RuCl_3$ gave lower rates and $RuCl_2(bipy)_2$ and $RuCl_2(DMSO)_4$ were completely unreactive. The turnover frequency (TOF) of our system in the oxidation of octan-2-ol is 9 h^{-1} and is superior to the most active ruthenium system

Table 1 Aerobic ruthenium–TEMPO catalysed oxidation of octan-2-ol[a]

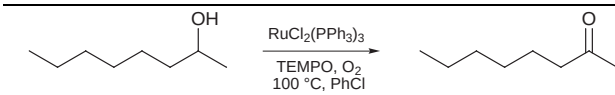

Entry	Substrate : catalyst ratio	*t*/h	Conversion (%)[b]	Selectivity (%)[b]
1[c]	67	7	10	> 99
2	67	7	95	> 99
		9	100 (90)[e]	> 99
3	100	7	78	> 99
		16	100 (91)[e]	> 99
4[d]	625	1	8.5	> 99
		5	17	> 99
		22	38	> 99

[a] *Reaction conditions:* 15 mmol substrate, Ru : TEMPO = 1 : 3, 30 ml PhCl, 10 ml min^{-1} O_2–N_2 (8 : 92; v/v), P = 10 bar, T = 100 °C; [b] Conversions and selectivities based on GC results using *n*-hexadecane as internal standard. [c] No TEMPO. [d] Neat octan-2-ol as solvent, [e] Isolated yield after distillation under reduced pressure.

Table 2 Ruthenium–TEMPO-catalysed aerobic oxidation of several alcohols[a]

Entry	Substrate	Product	*t*/h	Conversion (%)[b]
1	Octan-2-ol	octan-2-one	7	95
2[c]	Octan-1-ol	octanal	7	85
3	Octan-3-ol	octan-3-one	7	85
4[d]	Adamantan-2-ol	adamantan-2-one	7	92
5	Cyclooctanol	cyclooctanone	7	85
6[e]	$Me_2C{=}CHCH_2OH$	$Me_2C{=}CHCHO$	7	96
7[e]	Geraniol	geranial	7	91
8[d]	PhMeCHOH	PhAc	7	91
9[d]	BnOH	PhCHO	5	100
10[d]	$3\text{-}MeOC_6H_4CH_2OH$	$3\text{-}MeOC_6H_4CHO$	4	100
11[d]	$4\text{-}MeOC_6H_4CH_2OH$	$4\text{-}MeOC_6H_4CHO$	3	100
12[d]	$4\text{-}MeC_6H_4CH_2OH$	$4\text{-}MeC_6H_4CHO$	4	100
13[d]	$4\text{-}O_2NC_6H_4CH_2OH$	$4\text{-}O_2NC_6H_4CHO$	7	68

[a] *Reaction conditions:* 15 mmol substrate, 1.5 mol% $RuCl_2(PPh_3)_3$, 4.5 mol% TEMPO, 30 ml PhCl, 10 ml min^{-1} O_2–N_2 (8:92; v/v), P = 10 bar, T = 100 °C. [b] Conversions based on GC results (selectivity >99% in all cases) using *n*-hexadecane as internal standard. [c] 2 mol% $RuCl_2(PPh_3)_3$, 5 mol% TEMPO and O_2 atmosphere. [d] 1 mol% $RuCl_2(PPh_3)_3$ and 3 mol% TEMPO. [e] O_2 atmosphere.

described in the literature, *i.e.* TPAP,[12d] which in our hands gave a TOF of 5.5 h^{-1} for octan-2-ol.

The use of $RuCl_2(PPh_3)_3$–TEMPO as catalyst for the aerobic oxidation of alcohols was then applied to a range of representative alcohols. As can be seen from Table 2, octan-1-ol is oxidised selectively into octanal (entry 2). TEMPO not only accelerates the oxidation of octan-1-ol, but also completely suppresses the over-oxidation of octanal to octanoic acid. Attempted oxidation of octanal under the same reaction conditions, in the presence of TEMPO, gave no reaction in one week. On the other hand, without TEMPO octanal was converted completely to octanoic acid within 1 h. Besides primary alcohols, secondary, cyclic, allylic and benzylic alcohols also undergo smooth oxidation (selectivity in all cases >99%) into the corresponding ketones and aldehydes (entries 3–13).

In competition experiments, the Ru–TEMPO system displayed a selectivity for primary *versus* secondary alcohols. When an equimolar mixture of octan-1-ol and octan-2-ol was used, 80% of the octan-1-ol was converted, in 7 h, to octanal, whereas only 10% of the octan-2-ol was oxidised to octan-2-one. For an equimolar mixture of BnOH and PhMeCHOH, after 3 h, respectively 90 and 5% conversion was obtained. The preference for primary alcohols is analogous to results obtained with other ruthenium systems, which involve an oxidative dehydrogenation mechanism.

In summary, we have discovered that $RuCl_2(PPh_3)_3$–TEMPO is an effective catalyst for the aerobic oxidation of non-activated aliphatic alcohols and a broad range of other alcohols to aldehydes and ketones, thus providing an environmentally benign method for these synthetically important transformations. To the best of our knowledge this is one of the most reactive catalysts reported to date for the aerobic oxidation of (aliphatic) alcohols. We are currently investigating the mechanistic details of this interesting catalytic system.

We gratefully acknowledge IOP (Innovation-Oriented Research Program) for financial support and Johnson Matthey Inc. for their donation of $RuCl_3$ hydrate.

Notes and references

1 R. A. Sheldon and J. K. Kochi, in *Metal-Catalysed Oxidations of Organic Compounds*, Academic Press, New York, 1981; S. V. Ley, J. Norman, W. P. Griffith and S. P. Marsden, *Synthesis*, 1994, 639; M. Hudlicky, in *Oxidations in Organic Chemistry*, ACS: Washington, DC, 1990 and references cited therein.
2 G. Cainelli and G. Cardillo, in *Chromium Oxidations in Organic Chemistry*, Springer, Berlin, 1984.
3 I. E. Marko, P. R. Giles, M. Tsukazaki, S. M. Brown and C. J. Urch, *Science*, 1996, **274**, 2044.
4 T. Naota, H. Takaya and S.-I. Murahashi, *Chem. Rev.*, 1998, **98**, 2599 and references cited therein.
5 P. Müller and J. Godoy, *Tetrahedron Lett.*, 1981, **22**, 2361.
6 W. P. Griffith, S. V. Ley, G. P. Whitcombe and A. D. White, *J. Chem. Soc., Chem. Commun.*, 1987, 1625; K. Vijayasri, J. Rajaram and J. C. Kuriacose, *J. Mol. Catal.*, 1987, **39**, 203.
7 W.-H. Fung, W.-Y. Yu and C.-M. Che, *J. Org. Chem.*, 1998, **63**, 2873; M. Tanaka, T.-A. Kobayashi and T. Sakakura, *Angew. Chem.*, 1984, **96**, 519.
8 T. Sugiura, T. Sacki, S. Matsumoto and Y. Shizume, *Jap. Pat.*, 1986, 61,289,053 [86,289,053]; *Chem Abstr.*, 1987, **106**, 175781g.
9 S. Giddings and A. J. Mills, *J. Org. Chem.*, 1988, **53**, 1103; A. J. Bailey, W. P. Griffith, S. I. Mostafa and P. A. Sherwood, *Inorg. Chem.*, 1993, **32**, 268.
10 S.-I. Murahashi, T. Naota and N. Hirai, *J. Org. Chem.*, 1993, **58,** 7318.
11 (*a*) M. Matsumoto and S. Ito, *J. Chem. Soc., Chem. Commun.*, 1981, 907; (*b*) C. Bilgrien, S. Davis and R. S. Drago, *J. Am. Chem. Soc.*, 1987, **109**, 3786; (*c*) K. Kaneda, T. Yamashita, T. Matsushita and K. Ebitani, *J. Org. Chem.*, 1998, **63**, 1750.
12 (*a*) R. Tang, S. E. Diamond, N. Neary and F. Mares, *J. Chem. Soc., Chem. Commun.*, 1978, 562; (*b*) A. Hanyu, E. Takezawa, S. Sakaguchi and Y. Ishii, *Tetrahedron Lett.*, 1998, **39**, 5557; (*c*) G.-Z. Wang, U. Andreasson and J.-E. Bäckvall, *J. Chem. Soc., Chem. Commun.*, 1994, 1037; (*d*) I. E. Marko, P. R. Giles, M. Tsukazaki, I. Chellé-Regnaut, C. J. Urch and S. M. Brown, *J. Am. Chem. Soc.*, 1997, **119**, 12 661; (*e*) B. Hinzen, R. Lenz and S. V. Ley, *Synthesis*, 1998, 977; (*f*) T. Matsushita, K. Ebitani and K. Kaneda, *Chem. Commun.*, 1999, 265; (*g*) F. Vocanson, Y. P. Guo, J. L. Namy and H. B. Kagan, *Synth. Commun.*, 1998, **28**, 2577.
13 T. Nishimura, T. Onoue, K. Ohe and S. Uemura, *Tetrahedron Lett.*, 1998, **39**, 6011.
14 T. Iwahama, S. Sukaguchi, Y. Nishiyama and Y. Ishii, *Tetrahedron Lett.***,** 1998, **36**, 6923.
15 I. E. Marko, A. Gautier, I. Chellé-Regnaut, P. R. Giles, M. Tsukazaki, C. J. Urch and S. M. Brown, *J. Org. Chem.*, 1998, **63**, 7576.
16 A. E. J. de Nooy, A. C. Besemer and H. van Bekkum, *Synthesis* 1996, 1153 and references cited therein; C.-J. Jenny, B. Lohri and M. Schlageter, *Eur. Pat.*, 1997, 0775684A1; M. R. Leanna, T. J. Sowin and H. E. Morton, *Tetrahedron Lett.*, 1992, **33**, 5029; T. Inokuchi, S. Matsumoto, T. Nishiyama and S. Torii, *J. Org. Chem.*, 1990, **55**, 462.
17 T. Miyazawa and T. Endo, *J. Org. Chem.*, 1985, **50**, 3930; E. G. Rozantsev and V. D. Sholle, *Synthesis*, 1971, 190; J. M. Bobbitt and M. C. L. Flores, *Heterocycles*, 1988, **27**, 509.
18 M. F. Semmelhack, C. R. Schmid, D. A. Cortés and C. S. Chou, *J. Am. Chem. Soc.*, 1984, **106**, 3374.
19 $RuCl_2(PPh_3)_3$ was prepared according to: R. Holm, *Inorg. Synth.*, 1970, **12**, 238.
20 TEMPO was purchased from the Aldrich Chemical Co. and used without further purification.

Communication 9/02594D

Making cyclic RNAs easily available

Miriam Frieden, Anna Grandas and Enrique Pedroso*

Departament de Química Orgànica, Facultat de Química, Universitat de Barcelona, Martí i Franquès 1-11, 08028 Barcelona, Spain. E-mail: pedroso@admin.qo.ub.es

Received (in Cambridge, UK) 17th June 1999, Accepted 13th July 1999

A simple solid-phase procedure allows cyclic oligoribonucleotides to be obtained as long as the linear precursor attached to the support has a 2′-deoxyribonucleoside or a 2′-*O*-methylribonucleoside at the 3′-end.

Some of the smallest oligoribonucleotides with known biological activity are cyclic molecules. For instance, c(GG) is an activator of cellulose synthase in *Acetobacter xilinum*,[1] and c(UU) and c(AU) are inhibitors of the DNA dependent RNA polymerase of *E. coli*.[2] At the other end of the scale, large cyclic RNAs are formed in the splicing processes of ribonucleic acids in certain organisms[3] and viroids have circular single stranded RNA as their genomic material.

The structure of cyclic RNAs has been determined either by X-ray diffraction[4] or by NMR[5] only for very small molecules. Cyclic RNAs may be useful models for the study of a variety of RNA structural motifs,[6] such as hairpin loops, which could bring new insights into the structure–function relationship of ribonucleic acids.

In spite of their wide potential applications, few efforts have been dedicated so far to the development of chemical methods for the preparation of cyclic oligoribonucleotides. The synthesis of cyclic dinucleotides[7] and tetranucleotides[8,9] has been reported using the phosphotriester[7,8] or the H-phosphonate[9] methods in solution, whereas a solid-phase method has been employed for the preparation of cytidine homooligomers.[10] Larger cyclic RNAs have been obtained either by template-directed chemical[11] or enzymatic[12] ligation, and by rolling circle transcription and self-processing of circular DNA oligonucleotides encoding hairpin ribozymes.[13]

We have recently described a straightforward solid-phase procedure for obtaining small to medium-sized cyclic oligodeoxyribonucleotides.[14] The main advantage of the method is that, after the cyclization and cleavage reactions, non-cyclized chains, polymers and other by-products remain attached to the solid matrix. Therefore, fairly pure crude products are obtained, regardless of the size of the circles and the sometimes low cyclization yields. Scheme 1 shows the key steps in the extension of this methodology to the preparation of cyclic RNA. Synthesis of the ribonucleotide-resin **1** and chain elongation by the phosphite-triester approach using 2-cyanoethyl (CNE) phosphoramidites yields the oligonucleotide-resin **2** which, upon cyclization with 1-mesitylenesulfonyl-3-nitro-1,2,4-triazole (MSNT), affords **3**. After oximate cleavage of **3** and deprotection the cyclic RNA is obtained.

The choice of a suitable 2′-OH protecting group is the most crucial decision in RNA synthesis. It is well documented that the last step of the synthesis must be the deprotection of the 2′-hydroxy functions to avoid strand cleavage or 3′–5′ to 2′–5′ migration of the phosphodiester linkages.[15] The commonly used TBDMS group was discounted because of its lack of stability towards the oximate cleavage treatment.[16] Early elimination of the TBDMS group of the ribonucleoside directly attached to the support may result in the above mentioned undesirable side reactions.

For this reason, we turned our attention to the acid-labile 1-(2-fluorophenyl)-4-methoxypiperidin-4-yl group (Fpmp),[17] whose stability to oximate was confirmed using 2′-*O*-Fpmp-uridine (data not shown). However, to our surprise, the first attempts to prepare small cyclic RNAs (2- to 6-mer) employing the Fpmp group were completely unsuccessful: very low yields and impure crude products were obtained. We reasoned that the key difference with respect to cyclic DNA synthesis was the presence of the bulky 2′-*O*-Fpmp group at the 3′-end of **2** that may be hindering the cyclization reaction. In order to test the validity of this assumption, three nucleotide resins **1** having differently hindered phosphate groups were prepared as previously described[14] on an NH_2-TentaGel™ resin, **1a** (B′ = T, R′ = H), **1b** (B′ = U, R′ = OMe) and **1c** (B′ = U, R′ - OFpmp), and their homogeneity was assessed by gel-phase ^{31}P NMR.† On these nucleotide-resins a series of dinucleotides were assembled, cyclized, cleaved and deprotected.‡ Nucleoside sequences, yields and mass spectrometric data are indicated in Table 1 (entries 1 to 5). These results clearly indicate that the lowest yields were obtained when the nucleotide-resin **1c** was employed (entries 4 and 5). In fact, c(UU) could not be isolated from the complex crude mixture, whilst the rest of the cyclic dinucleotides were easily purified by C18-HPLC chromatography and unequivocally characterized by mass spectrometry and enzymatic digestion.[14] Particularly striking is the difference in yield between the two syntheses of c(UT) [= c(TU)] (entries 3 and 4): much lower yield was obtained from the most hindered resin **1c** than from **1a**, thus demonstrating that steric hindrance in the vicinity of the 3′ terminus phosphate of linear precursor **2** plays a key role. Nevertheless, comparing the results of entries 4 and 5 we can assert that the rest of the chain has a non-negligible effect. Most probably, it hinders the dinucleotide in attaining a reactive conformation.

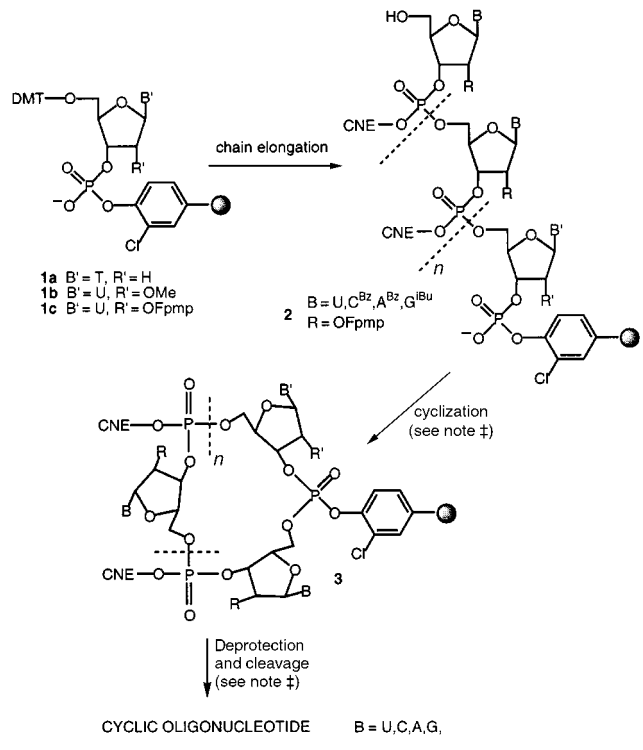

Scheme 1

Table 1 Synthesized cyclic oligoribonucleotides

Entry	Oligonucleotide-resin	Cyclic oligonucleotide	Crude yield (%)	Purity (%) (HPLC)	Mass spectrometry	
					calc.	found
1	T-T-**R**	c(TT)	50	>90	608.09	608.29[b]
2	T-U_{OMe}-**R**	c(TU_{OMe})	43	>90	624.08	624.20[b]
3	U_{OFpmp}-T-**R**	c(UT)	48	>90	610.07	610.39[b]
4	T-U_{OFpmp}-**R**	c(TU)	14	80	610.07	610.39[b]
5	U_{OFpmp}-U_{OFpmp}-**R**	c(UU)	3	—	612.09	—
6	UUU-T-**R**[a]	c(UUUT)	19	75	1222.12	1222.14[c]
7	CUC-T-**R**[a]	c(CUCT)	33	69	1220.15	1222.20[c]
8	UUUUU-T-**R**[a]	c(UUUUUT)	7	57	1834.17	1834.76[c]
9	UGCUUGC-T-**R**[a]	c(UGCUUGCT)	20	70	2523.49	2521.39[c]
10	UAUAG-U_{OMe}-**R**[a]	c(UAUAGU_{OMe})	5	80[d]	1935.57	1933.56[c]
11	UAGCA-U_{OMe}-**R**[a]	c(UAGCAU_{OMe})	4	80[d]	1934.26	1932.84[c]

[a] Ribonucleosides were 2′-*O*-Fpmp protected. [b] Electrospray MS. [c] MALDI-TOF MS. [d] Estimated by PAGE.

The synthesis of some larger circles was undertaken to further evaluate the possibilities of the method. Several cyclic oligoribonucleotides were obtained at the 1–2 μmol scale from resins **1a** and **1b**. Results are shown in Table 1 (entries 6 to 11). The cyclic products were submitted to Sephadex G-10 gel filtration and HPLC or PAGE purification, and were characterized as above.

Yields of crude products are generally lower than those typically obtained in the synthesis of cyclic DNA. The low yield obtained for c(U_5T) (entry 8) and the difference in yield between the two cyclic tetramers (entries 6 and 7) reflect the difficulty in getting high and reproducible yields in the cyclization reaction with MSNT. A 2′-*O*-methylribonucleotide at the 3′ end of the linear precursor seems to have a negative effect on the cyclization yield of the hexamers (entries 10, 11), which was not observed for a dinucleotide (entry 2). The homogeneity of the crude products detached from the resin is also slightly lower than in cyclic DNA synthesis. However, a major HPLC peak or PAGE band is always obtained, thus allowing easy purification of the circle and showing that the key advantage of the method is preserved.

In conclusion, cyclic RNA can be obtained provided that the linear precursor attached to the support has a 2′-deoxyribonucleoside or a 2′-*O*-methylribonucleoside at the 3′ end. Such single modification in the sequence of the cyclic RNAs should have little relevance for many purposes. For instance, enzymatically circularized hammerhead ribozymes containing non-nucleoside linkers have been shown to display increased biological activity and reduced divalent metal ion requirement.[18]

Work is in progress to prepare larger, 'all-ribonucleoside' cyclic RNAs by circumventing the problem of the steric hindrance at the 3′ end phosphate.

This work was supported by the Ministerio de Educación (DGES, grant PB97-941) and the Generalitat de Catalunya (Centre de Referència de Biotecnologia and SGR98-1).

Notes and references

† *Selected* ^{31}P *NMR data* (121.4 MHz, $CDCl_3$) for **1a**: δ_P −5.12. For **1b**: δ_P −6.99. For **1c**: δ_P −6.90.

‡ Oligonucleotide chains were assembled using 5′-*O*-DMT-nucleoside 3′-cyanoethylphosphoramidites (2′-*O*-Fpmp-protected, when required) and tetrazole for the coupling step, and Bu^tOOH for the oxidation. Conditions for the cyclization reaction are: 0.15 M MSNT in pyridine, three treatments (4 h + 4 h + overnight) with 20 equiv. MSNT each. Conditions for the deprotection and cleavage reactions are: (i) Et_3N–pyridine (1:1), 3 × 1 h; (ii) 0.2 M tetramethylguanidinium *syn*-pyridine-2-aldoximate in dioxane–water (1:1), 4 h + 4 h + overnight with 50 equiv. oximate; (iii) conc. aqueous NH_3, 55 °C, 12 h; (iv) 0.5 M AcONa, pH 4, 12 h, and then neutralization with 3 M Tris·HCl, pH 8.

1 P. Ross, H. Weinhouse, Y. Aloni, D. Michaeli, P. Weinberger-Ohana, R. Mayer, S. Braun, E. de Vroom, G. A. van der Marel, J. H. van Boom and M. Benziman, *Nature*, 1987, **325**, 279.
2 C.-Y. L. Hsu and D. Dennis, *Nucleic Acids Res.*, 1982, **10**, 5637.
3 A. J. Zaug, P. J. Grabowski and T. R. Cech, *Nature*, 1983, **301**, 578; T. R. Cech, *Annu. Rev. Biochem.*, 1990, **59**, 543.
4 M. Egli, R. V. Gessner, L. D. Williams, G. J. Quigley, G. A. van der Marel, J. H. van Boom, A. Rich and C. A. Frederick, *Proc. Natl. Acad. Sci. U.S.A.*, 1990, **87**, 3235.
5 M. M. W. Mooren, S. S. Wijmenga, G. A. van der Marel, J. H. van Boom and C. W. Hilbers, *Nucleic Acids Res.*, 1994, **22**, 2658.
6 G. L. Conn and D. E. Draper, *Curr. Opin. Struct. Biol.*, 1998, **8**, 278.
7 C.-Y. L. Hsu, D. Dennis and R. A. Jones, *Nucleosides Nucleotides*, 1985, **4**, 377.
8 E. de Vroom, H. J. G. Broxterman, L. A. J. M. Sliedregt, G. A. van der Marel and J. H. van Boom, *Nucleic Acids Res.*, 1988, **16**, 4607; C. Sund, P. Agback and J. Chattopadhyaya, *Tetrahedron*, 1991, **47**, 9659.
9 C. B. Reese and Q. Song, *Nucleic Acids Res.*,1999, **27**, 963.
10 L. De Napoli, A. Galeone, L. Mayol, A. Messere, G. Piccialli and C. Santacroce, *J. Chem. Soc., Perkin Trans. 1*, 1993, 747; L. De Napoli, A. Galeone, L. Mayol, A. Messere, D. Montesarchio and G. Piccialli, *Bioorg. Med. Chem.*, 1995, **3**, 1325.
11 S. Wang and E. T. Kool, *Nucleic Acids Res.*, 1994, **22**, 2326.
12 T. Pan, R. R. Gutell and O. C. Uhlenbeck, *Science*, 1991, **254**, 1361; C. Y. Chen and P. Sarnow, *Science*, 1995, **268**, 415.
13 A. M. Diegelman and E. T. Kool, *Nucleic Acids Res.*, 1998, **26**, 3235.
14 E. Alazzouzi, N. Escaja, A. Grandas and E. Pedroso, *Angew. Chem., Int. Ed. Engl.*, 1997, **36**, 1506.
15 M. A. Morgan, S. A. Kazakov and S. M. Hecht, *Nucleic Acids Res.*, 1995, **23**, 3949.
16 K. K. Ogilvie, N. Y. Theriault, J.-M. Seifert, R. T. Pon and M. J. Nemer, *Can. J. Chem.*, 1980, **58**, 2686.
17 M. V. Rao, C. B. Reese, V. Schehlmann and P. S. Yu, *J. Chem. Soc., Perkin Trans. 1*, 1993, 43; D. C. Capaldi and C. B. Reese, *Nucleic Acids Res.*, 1994, **22**, 2209.
18 L. Wang and D. E. Ruffner, *Nucleic Acids Res.*, 1998, **26**, 2502; *J. Am. Chem. Soc.*, 1998, **120**, 7684.

Communication 9/04851K

ChemComm

Formation of cyclooctatetraenes from zirconacyclopentadienes

Tamotsu Takahashi,*[a] Wen-Hua Sun[a] and Kiyohiko Nakajima[b]

[a] *Catalysis Research Center and Graduate School of Pharmaceutical Sciences and CREST, Science and Technology Corporation (JST) Hokkaido University, Sapporo 060-0811, Japan. E-mail: tamotsu@cat.hokudai.ac.jp*

[b] *Department of Chemistry and CREST, Science and Technology Corporation (JST), Aichi University of Education, Kariya, Aichi 448-8542, Japan*

Received (in Cambridge, UK) 8th April 1999, Accepted 6th July 1999

Treatment of zirconacyclopentadienes with 2 equiv. of CuCl at room temperature and with 1 equiv. of NBS at −78 °C selectively afforded cyclooctatetraene derivatives in good yields.

The cyclo-coupling reaction of acetylene to give cyclooctatetraene [eqn. (1)] was discovered by Reppe using the $NiBr_2$/CaC_2 system.[1] For this reaction, the mechanism most generally accepted involves the coupling of two nickellacyclopentadienes for the formation of cyclooctateteraenes.[2]

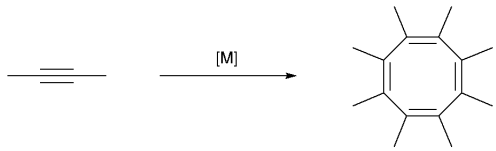

(1)

However, to the best of our knowledge, there is no report of the formation of cyclooctatetraenes from two metallacyclopentadienes [eqn. (2)].[3] This prompted us to investigate the formation of cyclooctatetraene derivatives from zirconacyclopentadienes.[4]

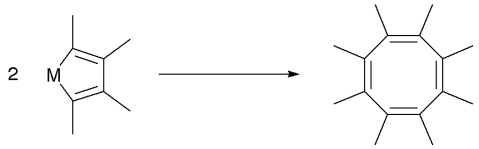

(2)

Here we report the first example of cyclooctatetraene formation from metallacyclopentadienes. Sequential treatment of zirconacyclopentadiene with 2 equiv. of CuCl and 1 equiv. of NBS afforded cyclooctatetraenes as described in Scheme 1.†

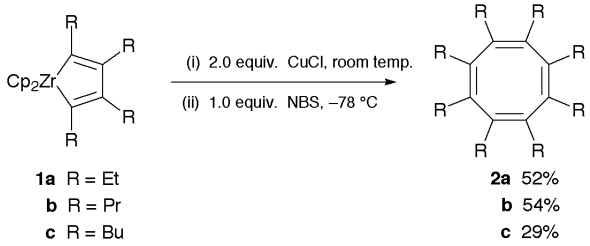

Scheme 1

A typical procedure is as follows. Tetraethylzirconacyclopentadiene **1a** in THF was treated with 2 equiv. of CuCl at room temperature for 1 h. After the mixture was cooled to −78 °C, 1 equiv. of NBS was added, and the resulting mixture was stirred for 3 h at −78 °C. The product, octaethylcyclooctatetraene **2a**, was obtained in 52% yield.

In order to prepare the cyclooctatetraenes from zirconacyclopentadienes, we designed two reactions, namely, (i) a coupling reaction of **4** with **5** and (ii) a coupling reaction of two molecules of **6**. Reaction of **4** with **5** did not give **2**, and it was not a clean reaction. As already reported,[5] the complex **3** produced cyclobutadienes in good to high yield when it was treated with CuCl. Therefore, the formation of **6** has been

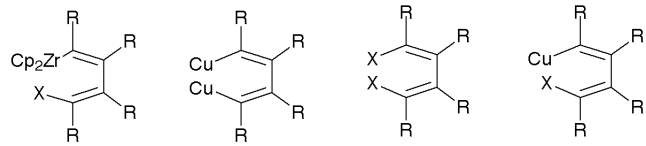

3 X = I or Br **4** **5** X = I or Br **6** X = I or Br

proposed although **6** was not detected. In the reaction a dimer of the cyclobutadienes, tricyclo[4.2.0.$0^{2,5}$]octa-3,7-diene, was obtained as the major product at room temperature. Only a trace amount of cyclooctatetraene was detected in this reaction. This suggested that at room temperature the intramolecular coupling of **6** was faster than the intermolecular coupling. However, we expected that the reaction rate of the intramolecular coupling of **6** would be significantly decreased at low temperature due to steric crowding. In this case, the intermolecular coupling would be the major reaction. Since transmetalation of the Zr–C bond of **3** to a Zr–Cu bond requires room temperature conditions, the complex **6** could not be formed from **3** at low temperature. Therefore, we used monobromination of **4** with 1 equiv. of NBS to produce **6** at low temperature, since it proceeds at −78 °C.

A mixture of tricyclooctadienes and cyclooctatetraenes was obtained as expected when the reaction was carried out at −30 °C. Reflux of the mixture of the two products in THF did not change the ratio. This clearly indicates that rearrangement of tricyclooctadienes to cyclooctatetraenes did not occur. As shown in Scheme 1, cyclooctatetraenes were obtained in good yield at −78 °C as the major product. An X-ray study was carried out to verify the structure of **2b**.‡

On the basis of these results, the following mechanism is plausible (Scheme 2). In the first step, transmetallation of

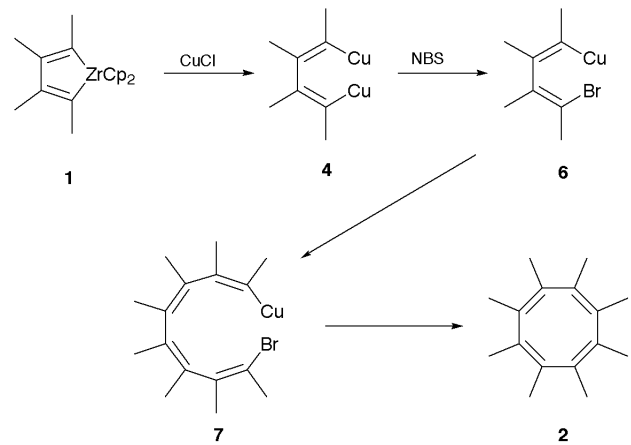

1 **4** **6** **7** **2**

Scheme 2

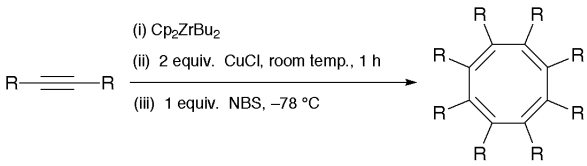

Scheme 3

zirconacyclopentadiene with CuCl gives dicopper intermediate **4**. Addition of 1 equiv. of NBS to **4** leads to monobromination at −78 °C giving **6**. The intermediate **6** undergoes intermolecular coupling to form **2** *via* **7**.

It is noteworthy that the formation of cyclooctatetraene derivatives can be performed in one pot from the starting acetylene as follows. For example, to a mixture of 1 mmol of Cp_2ZrCl_2 and 5 ml of THF was added 2 mmol of BuLi at −78 °C. The mixture was stirred for 1 h at −78 °C and then 2 mmol of hex-3-yne was added. The reaction mixture was gradually warmed to room temperature and tetraethylzirconacyclopentadiene **1a** was formed. The same procedure described above for **1a** can then be used (Scheme 3).

Notes and references

† *Selected data* for **2a**: $\delta_H(CDCl_3, Me_4Si)$ 0.94 (t, *J* 7.5, 24H), 1.99–2.10 (m, 16H); $\delta_C(CDCl_3, Me_4Si)$ 14.24, 23.58, 138.39. HRMS for $C_{24}H_{40}$: calc. 328.3128, found 328.3132. For **2b**: $\delta_H(CDCl_3, Me_4Si)$ 0.87 (t, *J* 7.3, 24H), 1.17–1.29 (m, 8H), 1.30–1.44 (m, 8H), 1.85–2.00 (m, 16H); $\delta_C(CDCl_3, Me_4Si)$ 14.88, 22.86, 33.58, 137.68. HRMS for $C_{32}H_{56}$: calc. 440.4379, found 440.4391. For **2c**: $\delta_H(CDCl_3, Me_4Si)$ 0.89 (t, *J* 7.0, 24H), 1.21–1.37 (m, 32H), 1.94–1.98 (m, 16H); $\delta_C(CDCl_3, Me_4Si)$ 14.01, 23.44, 30.94, 31.93, 137.71. HRMS for $C_{40}H_{72}$: calc. 552.5630, found 552.5638.

‡ *Crystal data* for **2b**: $C_{32}H_{56}$, M = 440.80, triclinic, space group $P\bar{1}$ (No. 2), a = 9.5552(2), b = 9.5131(3), c = 17.1505(9) Å, α = 88.553(4), β = 83.021(3), γ = 87.903(2)°, U = 1546.0(1) Å^3, Z = 2, D_c = 0.95 g cm^{-3}, μ(Cu-Kα) = 3.53 cm^{-1}, 6676 measured reflections, 3160 reflections with $I > 3\sigma(I)$, R = 0.053. CCDC 182/1315. See http://www.rsc.org/suppdata/cc/1999/1595/ for crystallographic data in .cif format.

1 W. Reppe, O. Schlichting, K. Klager and T. Toepel, *Justus Liebigs Ann. Chem.*, 1948, **560**, 1.

2 G. Wilke, *Pure Appl. Chem.*, 1978, **50**, 677; R. E. Colborn and K. P. C. Vollhardt, *J. Am. Chem. Soc.*, 1986, **108**, 5470; C. J. Lawrie, K. P. Gable and B. K. Carpenter, *Organometallics*, 1989, **8**, 2274; J. J. Eisch, J. E. Galle, A. A. Aradi and M. P. Boleslawski, *J. Organomet. Chem.*, 1986, **312**, 399.

3 D. Lloyd, *The Chemistry of Conjugated Cyclic Compounds*, Wiley, Chichester, 1990, p. 21; P. Auchter-Krummel and K. Muellen, *Angew. Chem., Int. Ed. Engl.*, 1991, **30**, 1003; D. B. Grotjahn, in *Comprehensive Organometallic Chemistry II*, ed. W. Edard, E. W. Abel, F. G. A. Stone and G. Wilkinson, Pergamon, Oxford, 1995, vol. 12, p. 747; P. W. Jolly, in *Comprehensive Organometallic Chemistry*, ed. G. Wilkinson, F. G. A. Stone and E. W. Abel, Pergamon, London, 1982, vol. **8**, p. 649; M. Lautens, W. Klute and W. Tam, *Chem. Rev.*, 1996, **96**, 49; P. M. Maitlis, *J. Organomet. Chem.*, 1980, **200**, 161.

4 For a recent review on the preparation and reactions of zirconacyclopentadienes, see T. Takahashi, Z. Xi and M. Kotora, *Res. Dev. Pure Appl. Chem.*, 1998, 2 and references therein.

5 H. Ubayama, W.-H. Sun, Z. Xi and T. Takahashi, *Chem Commun.*, 1998, 1931.

Communication 9/02788B

High-yield synthesis of a chiroporphyrin by hydrogen bond-directed cyclisation

Céline Pérollier,[a] Jacques Pécaut,[a] René Ramasseul,[a] Robert Bau[b] and Jean-Claude Marchon*[a]

[a] *Laboratoire de Chimie de Coordination, Service de Chimie Inorganique et Biologique, Département de Recherche Fondamentale sur la Matière Condensée, CEA-Grenoble, 38054 Grenoble, France. E-mail: jcmarchon@cea.fr*
[b] *Department of Chemistry, University of Southern California, Los Angeles, California 90089-0744, USA*

Received (in Basel, Switzerland) 24th May 1999, Accepted 29th June 1999

A new chiroporphyrin is prepared in 60% yield using complementary intramolecular hydrogen-bonding interactions between *N*-acylurea substituents to direct the cyclisation of the tetrapyrrolic intermediate; similar hydrogen-bond assistance by carboxylic acid functions is suggested for cyclisation of hydroxymethylbilane to uroporphyrinogen I.

Esters and disubstituted amides of (1*R*, 3*S*)-(−)-2,2-dimethyl-3-formylcyclopropane-1-carboxylic acid **1** [also called (1*R*, *cis*)-caronaldehyde or biocartol][1,2] are valuable building blocks for the synthesis of porphyrins bearing chiral *meso*-cyclopropyl groups. These chiroporphyrins are obtained as the D_2-symmetric α,β,α,β atropisomer exclusively by classical condensation reaction between the formyl group and pyrrole in modest yield (2–20%). We have shown recently that their manganese(III) complexes are competent catalysts in the asymmetric epoxidation[3] and aziridination[4] of aromatic alkenes. We have also found that the ruthenium(II) and cobalt(III) complexes of tetramethylchiroporphyrin (derived from the methyl ester of **1**) display multipoint binding of axial ligands such as alcohols,[5] amines[6] and amino alcohols:[7] in addition to the metal–ligand interaction, the host–guest bonding array involves two convergent ester carbonyl groups which act as hydrogen bond *acceptors* on each face and are instrumental in ligand enantioselection. In order to obtain a new type of chiroporphyrin bearing both hydrogen bond *donors* and *acceptors*, we have now synthesized the *N*-acylurea **2** by reaction of **1** with DCC, and the corresponding chiroporphyrin. To our surprise, the amphoteric nature of **2** led to an unprecedented high yield of chiroporphyrin **3** (60%), presumably by directing cyclisation of the porphyrinogen intermediate *via* intramolecular hydrogen bonding.

Compound **2** was previously obtained as a side-product (18%) in esterification reactions of **1** catalyzed by DCC–DMAP, and it has been characterised as an *N*-acylurea on the basis of its ^{1}H and ^{13}C NMR spectra.[1] Without competing alcohol or amine reactant, reaction between **1**, 1.2 equiv. of DCC and 1.2 equiv. of Et_3N in DMF, followed by workup and purification by silica gel chromatography (CH_2Cl_2–EtOAc 9 : 1) affords **2** in 50% yield (Scheme 1). The structure assignment was confirmed by X-ray crystallography† (Fig. 1). Notable features of the stereochemistry of **2** are the planarity of the disubstituted amide and urea moieties, and the near orthogonality of the two corresponding planes. The urea is flanked by two sterically bulky cyclohexyl substituents, yet its C11–O12 group is able to interact with the N13–H group of a neighbouring molecule in the crystal, resulting in a chain of strong head-to-tail N–H···O=C–N–H···O=C hydrogen bonds (N13A···O12, 2.889 Å; H13···O12, 1.937 Å; N13A–H···O12, 170.6°) along the *c* axis. There is no hydrogen bond to the amide carbonyl group C8–O9.

After the classical condensation reaction between **2** and pyrrole, subsequent aromatisation of the porphyrinogen intermediate[8] with DDQ and neutralisation with Et_3N, the purple color and nearly clean porphyrin UV–visible spectrum of the reaction mixture came as a surprise. In fact, the D_2-symmetric free base porphyrin **3** was obtained in an unprecedented yield of 60% after purification by silica gel chromatography with CH_2Cl_2–MeOH mixtures. For comparison, a similar condensation reaction carried out on the related *N*-ethyl-*N*-phenyl amide of **1** led only to a 12% yield of chiroporphyrin.[9] Isolation of the abundant porphyrinogen intermediate of **3** was attempted, but this compound was still contaminated with linear oligopyrrole side-products after silica gel chromatography and single crystals could not be obtained. Crystals of the nickel(II)-substituted derivative of **3** were successfully grown from a DMSO solution.

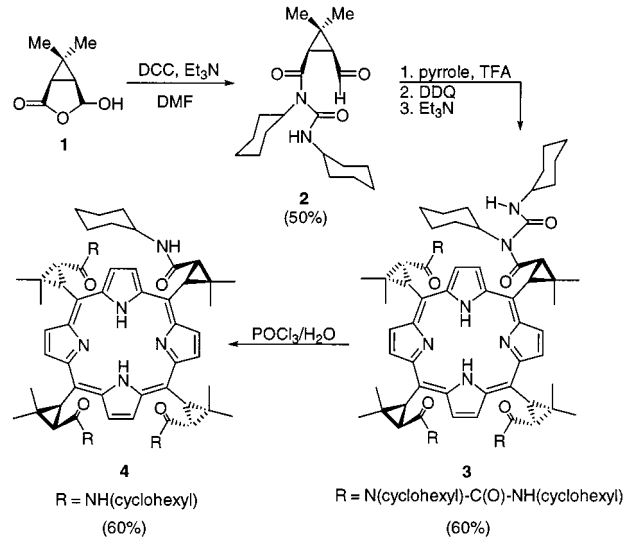

Scheme 1

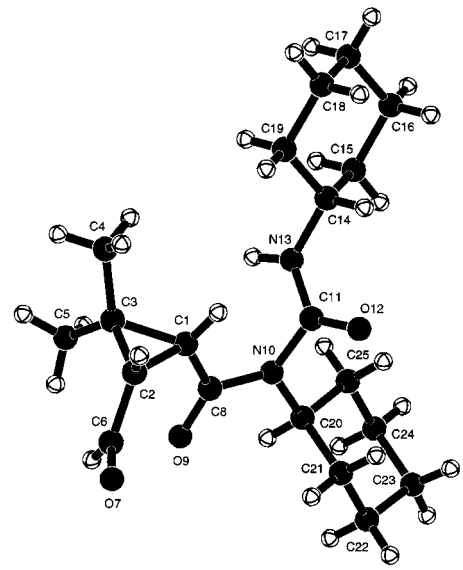

Fig. 1 Molecular structure of **2** showing the planar amide (C1–C8–O9–N10–C11–C20) and urea (N10–C11–O12–N13–C14) moieties, and the near orthogonality of the two corresponding planes (dihedral angle around N10–C11: 76.4°).

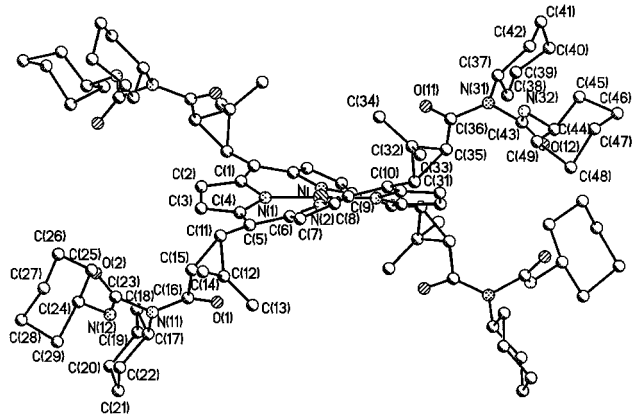

Fig. 2 ORTEP view (30% probability) of the molecular structure of Ni-**3** showing the conformations of the *N*-acylurea substituents with inward oriented amide carbonyl (O1, O11) and urea N–H (N12, N32) groups, and the absence of intramolecular hydrogen bonds.

The X-ray structure of Ni-**3**† (Fig. 2) shows a highly ruffled α,β,α,β porphyrin with inward oriented amide carbonyl and urea N–H groups, and indicates that the distance between two opposite α or β substituents is too large to allow any intramolecular hydrogen bonding interaction. However, examination of a molecular model of the porphyrinogen intermediate suggests that conformations in which the opposite *meso* groups on each face are close enough to allow double hydrogen bonding between the urea N–H donor and amide C=O acceptor groups[10] are accessible. We conclude that the self-complementary nature of the *N*-acylurea substituent of **2** leads to a preorganised, quadruply hydrogen-bonded tetrapyrrole intermediate in which the close proximity of the two reactive end groups directs intramolecular cyclisation[11] and leads to a high yield of porphyrinogen [Fig. 3(*a*)].

The carboxylic acid function is another classical example of self-complementary hydrogen-bonding groups, and it is tempting to speculate that the carboxylic acid substituents on the β-pyrrolic positions of porphobilinogen may serve the function of

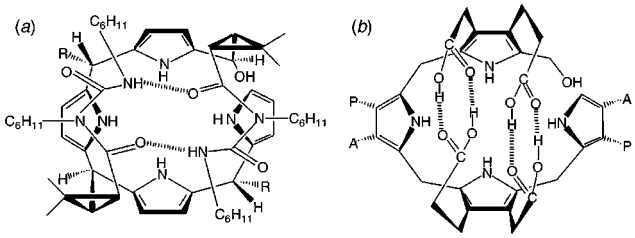

Fig. 3 (*a*) The conformation of the tetrapyrrole intermediate, preorganised by hydrogen bonding between self-complementary *N*-acylurea substituents, which leads to a high yield of porphyrinogen and to a 60% yield of **3**. For the sake of clarity, only the H-bonding pattern on the top face is shown, and each of the two H-bonded *meso* substituents on the bottom face is abbreviated as R. (*b*) Proposed hydrogen-bond assistance by carboxylic acid functions in the cyclisation of hydroxymethylbilane to uroporphyrinogen I. For the sake of clarity, the double hydrogen bond between each of the opposite acetic (A) and propionic (P) substituent pairs on the lower face has been omitted.

directing the spontaneous macrocyclisation of the hydroxymethylbilane tetrapyrrole to uroporphyrinogen I [Fig. 3(*b*)].[12]

Finally, the high yield synthesis of **3** from a readily accessible *N*-acylurea derivative of **1** makes this macrocycle a convenient precursor of other chiroporphyrins, as exemplified by the preparation of the tetra-*N*-cyclohexylamide **4** by $POCl_3$-induced cleavage of the ureido groups,[13] which will be described elsewhere.

Notes and references

† *Crystal data* for **2**: $C_{20}H_{32}N_2O_3$, M_r = 348.5, orthorhombic, a = 10.861(2), b = 20.595(3), c = 8.948(2) Å, U = 2001.5(6) Å^3, T = 163 K, space group $P2_12_12_1$, Z = 4, μ(Cu-Kα) = 0.615 mm^{-1}, 1574 reflections measured, 1425 unique, of which 1273 with $F > 4.0\,\sigma(F)$ were used in all calculations, R_1 = 0.0608 [$I > 2\sigma(I)$], wR_2 = 0.1553, GOF = 1.19. For Ni-**3**: $C_{96}H_{132}N_{12}O_8Ni{\bullet}5C_2H_6SO{\bullet}3H_2O$, M = 2085.53, tetragonal, $a = b$ = 15.091(3), c = 63.54(2) Å, U = 14472(6) Å^3, T = 193 K, space group $P4_32_12$, Z = 4, μ(Mo-Kα) = 0.257 mm^{-1}, 46236 reflections measured, 10825 unique (R_{int} = 0.3052), of which 2864 with $F > 4.0\,\sigma(F)$ were used in all calculations, R_1 = 0.1192 [$I > 2\sigma(I)$], wR_2 = 0.2614, GOF = 1.004, Flack index 0.04(5). The relatively poor quality of the data set collected for Ni-**3**, as judged from the large R_{int} value, probably contributes to the large final R factors. CCDC 182/1314. See http://www.rsc.org/suppdata/cc/1999/1597/ for crystallographic data in .cif format.

1 M. Veyrat, L. Fantin, S. Desmoulins, A. Petitjean, M. Mazzanti, R. Ramasseul, J.-C. Marchon and R. Bau, *Bull. Soc. Chim. Fr.*, 1997, **134**, 703.
2 C. Pérollier, J. Pécaut, R. Ramasseul and J.-C. Marchon, *Bull. Soc. Chim. Fr.*, 1997, **134**, 517.
3 M. Veyrat, O. Maury, F. Faverjon, D. E. Over, R. Ramasseul, J.-C. Marchon, I. Turowska-Tyrk and W. R. Scheidt, *Angew. Chem., Int. Ed. Engl.*, 1994, **33**, 220; C. Pérollier, J. Pécaut, R. Ramasseul and J.-C. Marchon, *Inorg. Chem.*, 1999, in the press.
4 J.-P. Simonato, J. Pécaut, W. R. Scheidt and J.-C. Marchon, *Chem. Commun.*, 1999, 989.
5 M. Mazzanti, M. Veyrat, R. Ramasseul, J.-C. Marchon, I. Turowska-Tyrk, M. Shang and W. R. Scheidt, *Inorg. Chem.*, 1996, **35**, 3733.
6 D. Toronto, F. Sarrazin, J. Pécaut, J.-C. Marchon, M. Shang and W. R. Scheidt, *Inorg. Chem.*, 1998, **37**, 526.
7 J.-P. Simonato, J. Pécaut and J.-C. Marchon, *J. Am. Chem. Soc*., 1998, **120**, 7363.
8 J. S. Lindsey and R. W. Wagner, *J. Org. Chem.*, 1989, **54**, 828.
9 C. Pérollier, *Doctoral Thesis*, Université Joseph Fourier, Grenoble, 1998.
10 For structurally characterised examples of strong dimerisation *via* complementary hydrogen bonding between urea N–H donors and amide C=O acceptors, see: F. H. Beijer, R. P. Sijbesma, H. Kooijman, A. L. Spek and E. W. Meijer, *J. Am. Chem. Soc*., 1998, **120**, 6761.
11 For reviews of hydrogen-bonded self-assembling complexes, see: D. S. Lawrence, T. Jiang and M. Levitt, *Chem. Rev.*, 1995, **95**, 2229; M. M. Conn and J. Rebek, Jr., *Chem. Rev.*, 1997, **97**, 1467. For a previous example of macrocyclisation directed by hydrogen bonding, see: F. J. Carver, C. A. Hunter and R. J. Shannon, *J. Chem. Soc., Chem. Commun.*, 1994, 1277.
12 For a recent review of heme biosynthesis, see: A. R. Battersby and F. J. Leeper, *Top. Curr. Chem.*, 1998, **195**, 143. For structurally characterised uroporphyrinogen derivatives, see: G. Sawitzki and H. G. von Schnering, *Angew. Chem., Int. Ed. Engl*., 1976, **15**, 552; C. Lehmann, B. Schweizer, C. Leumann and A. Eschenmoser, *Helv. Chim. Acta*, 1997, **80**, 1421.
13 S. Avramovici-Grisaru and S. Sarel, *Nouv. J. Chim.*, 1982, **6**, 455.

Communication 9/04134F

ChemComm

exo-Glycal approaches to *C*-linked glycosyl amino acid synthesis

Andrew D. Campbell,[a] Duncan E. Paterson,[a] Tony M. Raynham[b] and Richard J. K. Taylor[a]*

[a] *Department of Chemistry, University of York, Heslington, York, UK YO10 5DD. E-mail: rjkt1@york.ac.uk*
[b] *Roche Discovery Welwyn, Welwyn Garden City, Hertfordshire, UK AL7 3AY*

Received (in Cambridge, UK) 22nd June 1999, Accepted 8th July 1999

Two novel routes to *C*-linked glycosyl amino acids are described; the first involves elaboration of an *exo*-glycal and subsequent Ramberg–Bäcklund rearrangement of a sulfone intermediate to give, after functional group manipulation, a protected *C*-glycosyl serine, while the second uses hydroboration–Suzuki coupling of the same *exo*-glycal to produce ultimately the corresponding *C*-glycosyl asparagine analogue.

Glycopeptides and glycoproteins are of great current interest from the viewpoints of structure elucidation, molecular recognition, biological function and chemical synthesis.[1] Replacement of the glycosidic oxygen by carbon gives the corresponding *C*-glycoside analogues (glycopeptidomimetics), compounds which are particularly valuable for biological studies because of their hydrolytic stability. The recent publications in this area[1,2] prompt us to disclose our own results. We have recently established that the Ramberg–Bäcklund rearrangement of *S*-glycoside dioxides provides a versatile route to di-, tri- and tetra-substituted *exo*-glycals[3] which are themselves useful intermediates for the preparation of more elaborate *C*-glycosides.[4] Scheme 1 illustrates this methodology with a glucose-derived sulfone: the Meyers variant[5] of the Ramberg–Bäcklund rearrangement is used to convert the sulfones **1** directly into the corresponding *exo*-glycals **2** or **3** without competing 1,2-glycal formation. We have gone on to apply this methodology to the synthesis of *C*-linked disaccharides such as β,β-*C*-trehalose and methyl *C*-gentiobioside.[6]

We now report the application of this methodology to the construction of *C*-linked glycopeptidomimetics. Initial studies (Scheme 2) were concerned with the synthesis of the *C*-glucosyl serine analogue **9**. The key starting material, iodide **4**, was readily prepared from *exo*-glycal **2** by stereoselective 9-BBN hydroboration–oxidation[7] followed by iodination.[6] Thiol **6** was the required coupling partner. We were surprised to discover that this useful building block had not been reported previously but it was easily obtained from the Garner aldehyde (*S*)-**5**[8] by reduction followed by Mitsunobu displacement using thioacetic acid and then treatment with sodium methoxide.† Alkylation of thiol **6** using iodide **4** followed by oxidation of the resulting sulfide produced sulfone **7** {$[\alpha]_D$ −30.1 (*c* 0.57, $CHCl_3$) [HRMS (FAB+): Found: 838.3601. $C_{46}H_{57}NO_{10}SNa$ requires 838.3608 (0.9 ppm error)]}. This sulfone was then treated under Chan's tandem halogenation–Ramberg–Bäcklund conditions[5b] to produce the *E*-alkene **8** (*J* 15.6 Hz) in 37% unoptimised yield. Alkene reduction was efficiently achieved using diimide generated *in situ* and the amino acid was unmasked using a one-pot hydrolysis–oxidation procedure.[9] Diazomethane esterification gave the target *C*-glycosyl serine derivative **9** {$[\alpha]_D$ −8.2 (*c* 1.45, $CHCl_3$) [HRMS (FAB+): Found: 762.3614. $C_{44}H_{53}NO_9Na$ requires 762.3618 (0.6 ppm error)]}.

The second target was the *C*-glycosyl asparagine analogue **12** depicted in Scheme 3. In principle, this compound could be made *via* the methodology outlined in Scheme 2 simply by using the higher homologue of iodide **4**[6] or of thiol **6**. However, we decided to investigate an alternative approach based on the Suzuki coupling procedure developed by Johnson and Johns[10] but not previously applied to *C*-glycosyl amino acid synthesis (Scheme 3). For this route we required vinyl iodide **10** which has been described but *via* a rather lengthy route.[11] An improved route to **10** was developed: treatment of the Garner aldehyde (*R*)-**5**‡ with $CHI_3/CrCl_2$[12] produced **10** exclusively as the *E*-isomer {$[\alpha]_D$ −80.8 (*c* 1.76, $CHCl_3$); lit.,[11] −75.3 (*c* 1.9, $CHCl_3$)}. Hydroboration of *exo*-glycal **2** followed by Suzuki coupling with vinyl iodide **10** gave alkene **11** in moderate yield but with complete control over 'anomeric' configuration and alkene geometry (*J* 15.5 Hz). Diimide reduction followed by treatment with Jones' reagent and then diazomethane, as before,

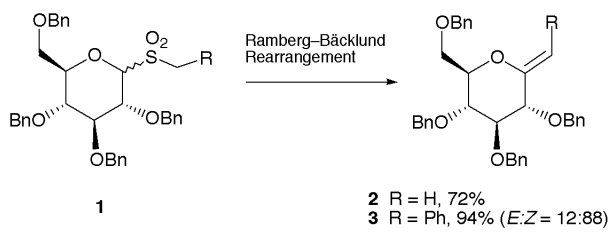

Scheme 1

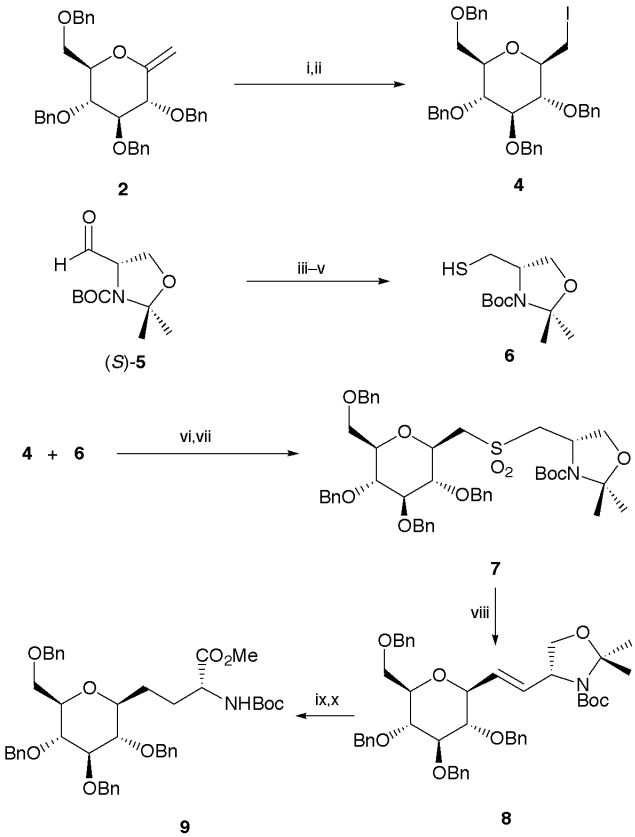

Scheme 2 *Reagents and conditions*: i, 9-BBN, then H_2O_2, NaOH; ii, PPh_3, imidazole, I_2, 80% (ref. 6); iii, $NaBH_4$; iv, PPh_3, diisopropyl azodicarboxylate, AcSH; v, NaOMe, 38% for 3 steps; vi, K_2CO_3, MeCN–MeOH, reflux; vii, MCPBA, Na_2HPO_4, 66% for 2 steps; viii, CBr_2F_2, KOH–Al_2O_3, Bu^{t}OH, 60 °C, 37%; ix, $TsNHNH_2$, NaOAc, 85 °C, 82%; x, Jones' reagent (1 M), then CH_2N_2, 60%.

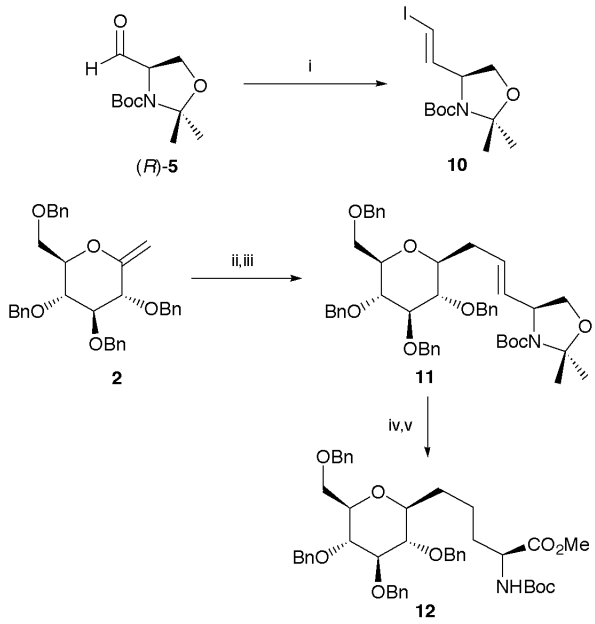

Scheme 3 *Reagents and conditions*: i, CHI_3, $CrCl_2$, THF, 60%; ii, 9-BBN; iii, **10**, $PdCl_2(dppf)\cdot CHCl_3$, aq. K_3PO_4, DMF, 48%; iv, $TsNHNH_2$, NaOAc, 85 °C, 78%; v, Jones' reagent (1 M), then CH_2N_2, 56%.

gave the protected *C*-glycosyl amino acid **12** in good yield. All data correlated well with those reported in a previous synthesis of **12** by Dondoni *et al.*[2a] {*e.g.* $[\alpha]_D$ +6.25 (*c* 0.8, $CHCl_3$); lit.,[2a] +6.2 (*c* 0.7, $CHCl_3$) [HRMS (FAB+): Found: 776.3783. $C_{45}H_{55}NO_9Na$ requires 776.3775 (1.2 ppm error)]} and thus confirmed the expected[7,10] β-selectivity of the hydroboration step.

In summary, we have devised two new, versatile routes to glycopeptidomimetics which join together the individual sugar and amino acid units to produce exclusively β-stereoisomers at the 'anomeric' centre. We have also established that the Ramberg–Bäcklund rearrangement of *S*-glycoside dioxides is a general procedure which can be utilised for the synthesis of *exo*-glycals,[3] *C*-linked disaccharides,[6] and now in this work, *C*-linked glycosyl amino acids. We are currently optimising the above procedures and extending the methodology to more challenging targets.

We are grateful to the BBSRC and the University of York for studentships (A. D. C. and D. E. P., respectively). We would also like to thank Roche Discovery Welwyn for CASE support (A. D. C.).

Notes and references

† All new compounds were fully characterised spectroscopically and by HRMS/elemental analysis.

‡ The enantiomeric Garner aldehyde (*R*)-**5** was used in this route because full data is available for diastereoisomer **12**.

1 For a comprehensive review, see C. M. Taylor, *Tetrahedron*, 1998, **54**, 11317.
2 For more recent work in this area, see (*a*) A. Dondoni, A. Marra and A. Massi, *J. Org. Chem.*, 1999, **64**, 933; (*b*) R. N. Ben, A. Orellana and P. Arya, *J. Org. Chem.*, 1998, **63**, 4817; D. Urban, T. Skrydstrup and J.-M. Beau, *Chem. Commun.*, 1998, 955; (*c*) T. Fuchss and R. R. Schmidt, *Synthesis*, 1998, 753; (*d*) F. Burkhart, M. Hoffmann and H. Kessler, *Angew. Chem., Int. Ed. Engl.*, 1997, **36,** 1191.
3 F. K. Griffin, P. V. Murphy, D. E. Paterson and R. J. K. Taylor, *Tetrahedron Lett.*, 1998, **39**, 8179; see also P. S. Belica and R. W. Franck, *Tetrahedron Lett.*, 1998, **39**, 8225.
4 M.-L. Alcaraz, F. K. Griffin, D. E. Paterson and R. J. K. Taylor, *Tetrahedron Lett.*, 1998, **39**, 8183.
5 (*a*) C. Y. Meyers, A. M. Malte and W. S. Matthews, *J. Am. Chem. Soc.*, 1969, **91**, 7510; (*b*) T.-L. Chan, S. Fong, Y. Li, T.-O. Man and C. D. Poon, *Chem. Commun.*, 1994, 1771.
6 F. K. Griffin, D. E. Paterson and R. J. K. Taylor, *Angew. Chem., Int. Ed.*, 1999, in the press.
7 T. V. RajanBabu and G. S. Reddy, *J. Org. Chem.*, 1986, **51**, 5458.
8 P. Garner and J. M. Park, *J. Org. Chem.*, 1987, **52**, 2361; A. D. Campbell, T. M. Raynham and R. J. K. Taylor, *Synthesis*, 1998, 1707.
9 A. Dondoni, A. Marra and A. Massi, *Tetrahedron*, 1998, **54**, 2827.
10 C. R. Johnson and B. A. Johns, *Synlett*, 1997, 1406.
11 G. Reginato, A. Mordini and M. Caracciolo, *J. Org. Chem.*, 1997, **62**, 6187.
12 K. Takai, K. Nitta and K. Utimoto, *J. Am. Chem. Soc.*, 1986, **108**, 7408.

Communication 9/05014K

Unusual chromatic properties observed from polymerized dipeptide diacetylenes

Qun Huo, Shaopeng Wang, Aurélien Pisseloup, Deepali Verma and Roger M. Leblanc*

Center for Supramolecular Science and Department of Chemistry, University of Miami, PO Box 249118, Coral Gables, FL 33124, USA. E-mail: rml@umiami.ir.miami.edu

Received (in Columbia, MO, USA) 1st June 1999, Accepted 1st July 1999

The chromatic properties of a few dipeptide polydiacetylenes were found to change dramatically with very slight structural variations of dipeptides, leading to the proposal of a non-coplanar packing model to explain the chromatic behavior of polydiacetylenes.

In 1993 Charych *et al.* reported the development of a direct colorimetric detection method of influenza virus based on the chromatic change of polydiacetylene Langmuir–Blodgett films.[1] This work provided a new possibility for diagnostic applications, and the chromatic property of polydiacetylenes has caused extensive attention since then. However, up until now, the precise molecular mechanism of the blue to red color change or transition remains unclear.

At the present time, it is generally accepted that the chromatic difference is based on the difference in the effective π-electron delocalization length along the polymer backbone. The blue form of polydiacetylene, which absorbs light at around 640 nm in the red region, is believed to have a more effective π-electron conjugation length, whereas the red form of polydiacetylene, which absorbs light at around 540 nm in the blue region, has a shorter π-electron conjugation length.[2] However, conflicting explanations for what causes the difference of the effective π-electron conjugation length have been put forward. A model which was generally accepted during the past years attributes the less effective π-electron conjugation of red form polydiacetylenes to conformational disorder or the entangling of the side chains.[3] However, this side chain disorder model is facing more and more challenges from new experimental observations. Recent investigations by FT-IR, electron diffraction[4] and atomic force microscopy[5] have shown that the side chains of red form polydiacetylenes are actually also in an ordered conformation.

Cheng and Stevens reported that the chromatic properties of polydiacetylene liposomes functionalized with amino acids such as Glu, Gln and His as polar moieties were affected by the pH of the aqueous solution.[6] The chromatic change upon pH value variation is attributed to the repulsive Coulombic interactions developed on the surface due to ionization of the amino acid head groups. As a result, the head groups must rearrange themselves to a staggered non-coplanar packing to accommodate the new charge distribution. The staggered non-coplanar packing of diacetylene lipids leads to the formation of a non-linear red form polydiacetylene backbone when irradiated, yet the alkyl chains attached to polydiacetylene backbone remain in their well-ordered conformation.

In the meantime, our recent study of hydrogen bonding effects on the polymerization and chromatic properties of a triaminotriazine diacetylene lipid has led us to the same conclusion.[7] In order for two different diacetylene lipids to attain stable intermolecular hydrogen bonding, the two lipids were packed into a staggered non-coplanar packing mode in the mixed monolayer, leading to the observation of only red form polydiacetylene films.

We now report experimental evidence which further supports this mechanism. Four dipeptides, GlyGly, AlaGly, ValGly and PheGly, were attached to pentacosa-10,12-diynoic acid (PDA) through solid phase peptide synthesis. The four dipeptide

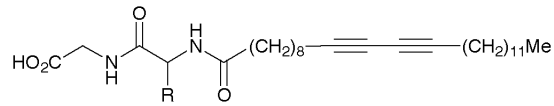

PDA-GlyGly-OH R = H
PDA-AlaGly-OH R = Me
PDA-ValGly-OH R = Pr^i
PDA-PheGly-OH R = Bn

diacetylene lipids have the same molecular skeleton structure, except that they have different hydrophobic side groups on the second amino acid residue. While PDA-GlyGly-OH has no side group, PDA-AlaGly-OH has a methyl side group, PDA-ValGly-OH has an isopropyl side group and PDA-PheGly-OH has a benzyl side group. The surface pressure–area isotherm measurements have shown that the four lipids formed stable monolayers at the air-water interface (Fig. 1). The limiting molecular areas of PDA-GlyGly-OH, PDA-AlaGly-OH, PDA-ValGly-OH and PDA-PheGly-OH are 23, 32, 36 and 40 $Å^2$ $molecule^{-1}$, respectively, which are proportional to the size of the second amino acid side groups in the dipeptides.

The dipeptide Langmuir films were irradiated with UV light (254 nm) at a surface pressure of 20 mN m^{-1} on a pure water subphase (pH 5.80). The *in situ* UV-Vis absorption spectra of the monolayers with different irradiation times are presented in Fig. 2. Tremendous chromatic differences were observed from the four polymerized dipeptide lipid monolayers, despite the very slight structural differences between these molecules. While the PDA-GlyGly-OH monolayer exhibits a typical blue absorption band with a maximum absorption around 640 nm, the polymerization of PDA-AlaGly-OH, PDA-ValGly-OH and PDA-PheGly-OH monolayers leads to the appearance of polymer absorption bands at 570 (purple form), 535 (red form) and 525 nm (red–yellow form), respectively.

The only difference between these peptide amphiphiles is the size of the hydrophobic side groups on the second amino acid residue. It has been reported previously that dipeptide GlyGly derivatized lipids with single hydrophobic alkyl chains tend to form β-sheet structures at the air-water interface, due to strong

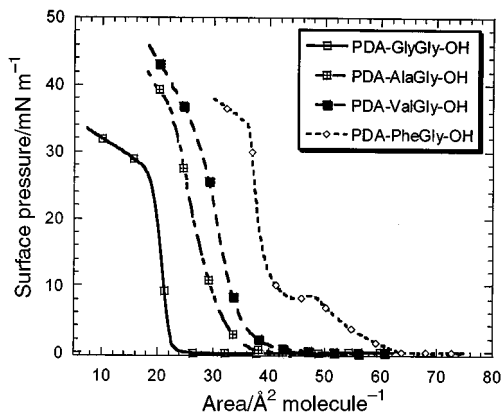

Fig. 1 The surface pressure–area isotherms of the dipeptide diacetylene lipids at the air-water interface.

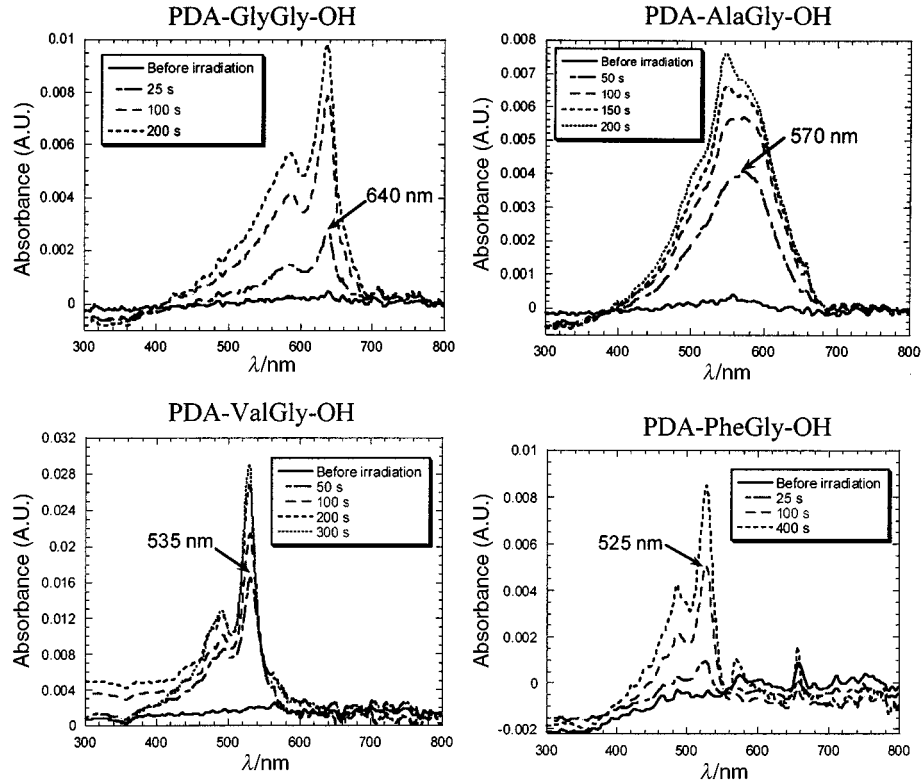

Fig. 2 The UV-Vis absorption spectra of polymerized dipeptide diacetylene monolayers with different irradiation times.

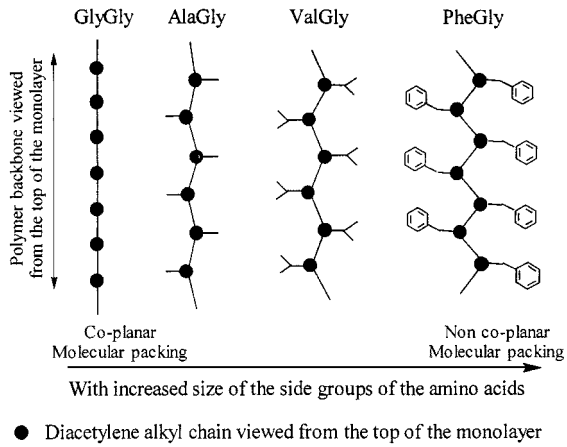

Fig. 3 An illustration of the decreased linearity of the polydiacetylene backbone due to the non-coplanar packing of diacetylene lipids with the increased size of the side groups on the dipeptides.

hydrogen bonding between the GlyGly polar moieties.[8] We believe that the PDA-GlyGly-OH lipids also formed a β-sheet structure at the air-water interface and the lipid alkyl chains are packed in a coplanar mode. As a result, the polymerization of the coplanar diacetylene groups leads to the formation of a linear blue form polydiacetylene backbone, as shown in Fig. 3.

In the case of PDA-AlaGly-OH, due to the presence of a methyl group as a side group on the dipeptide, steric hindrance does not allow the formation of a perfect β-sheet structure. The PDA-AlaGly-OH lipids are obliged to adopt a staggered non-coplanar packing mode. With this staggered non-coplanar packing of diacetylene lipids, the photoirradiation leads to the formation of a non-linear zigzag red form polydiacetylene backbone, as illustrated in Fig. 3. With increased size of the side groups on the amino acid residues, as in the case of PDA-ValGly-OH and PDA-PheGly-OH, the linearity of the polymer backbone is further decreased, leading to a shift of the absorption band towards lower wavelength.

Theoretical calculations have shown that very slight rotations around the C–C bonds of the polymer backbone (5°) are enough to produce a dramatic decrease in the π–π electron conjugation length.[9] When the non-coplanar packed monolayer is polymerized, the C–C single bonds must rotate away from the linear backbone to accommodate the non-coplanar packing of the lipids. Even a slight deviation of lipids from coplanar packing may introduce enough rotations of C–C bonds to produce large chromatic differences, as observed from the four dipeptide lipids. In the meantime, the alkyl side chains attached to the polymer backbone remain in their well-ordered conformation without being disturbed by the slight structural change of the polydiacetylene backbone.

This work was supported by the Charles E. Culpeper Foundation.

Notes and references

1 D. H. Charych, J. O. Nagy, W. Spevak and M. D. Bednarski, *Science*, 1993, **261**, 585.
2 H. Eckhardt, D. S. Boudreaux and R. R. Chance, *J. Chem. Phys.*, 1986, **85**, 4116; Y. Tomioka, N. Tanaka and S. Imazeki, *J. Chem. Phys.*, 1989, **91**, 5694.
3 N. Mino, H. Tamura and K. Ogawa, *Langmuir*, 1991, **7**, 2336; A. A. Deckert, J. C. Horne, B. Valentinr, L. Kiernan and L. Fallon, *Langmuir*, 1995, **11**, 1257.
4 K. Kuriyama, H. Kikuchi and T. Kajiyama, *Langmuir*, 1998, **14**, 1130.
5 A. Lio, A. Reichert, D. J. Ahn, J. O. Nagy, M. Salmeron and D. H. Charych, *Langmuir*, 1997, **13**, 6524.
6 Q. Cheng and R. C. Stevens, *Langmuir*, 1998, **14**, 1974.
7 Q. Huo, K. C. Russell and R. M. Leblanc, *Langmuir*, 1999, **15**, 3972.
8 X. Cha, K. Ariga and T. Kunitake, *Bull. Chem. Soc. Jpn.*, 1996, **69**, 163.
9 B. J. Orchard and S. K. Tripathy, *Macromolecules*, 1986, **19**, 1844; V. Dobrosavljevic and R. M. Stratt, *Phys. Rev. B*, 1987, **35**, 2781.

Communication 9/04332B

Electrochemically controlled self-complexation of cyclodextrin–viologen conjugates

Armen Mirzoian and Angel E. Kaifer*

Center for Supramolecular Science and Department of Chemistry, University of Miami, Coral Gables, FL 33124-0431, USA. E-mail: akaifer@umiami.ir.miami.edu

Received (in Columbia, MO, USA) 21st May 1999, Accepted 6th July 1999

Self-complexation of cyclodextrin–viologen conjugates can be controlled electrochemically through changes in the oxidation states of the viologen subunits as well as chemically when competing water-soluble hosts or guests are added to solutions of the conjugates.

The phenomenon of intermolecular self-complexation has attracted considerable interest in supramolecular chemistry.[1,2] A compound must possess suitably located complementary (host and guest) sites to recognize itself and form intermolecular complexes in solution. Depending on the spatial relationship between the host and guest sites of the self-complementary monomer units, different superstructures can be predicted, from cyclic dimers to polymer-like, extended acyclic ones.[3–5] Of course, intramolecular self-complexation is also possible in molecules with enough flexibility.[6] Here we report the first example of electrochemically-driven,[7] intermolecular self-complexation. Specifically, we describe a series of cyclodextrin–viologen conjugates that exhibit remarkable intermolecular self-recognition triggered by the two-electron reduction of their viologen subunits.

We have recently reported on the binding interactions between the hosts β-cyclodextrin (β-CD) and its heptakis(2,6-*O*-dimethyl) analog (DM-β-CD) and a series of viologens (*N*,*N*′-disubstituted 4,4′-bipyridinium derivatives) designed to enhance their water solubility in any of their three oxidation states.[8,9] We have shown that while the oxidized forms of the viologen derivatives are not bound by the CD hosts, the two-electron reduced forms give rise to very stable inclusion complexes.[9] The intermediate one-electron reduced forms are only weakly bound by β-CD. Based on these findings, we reasoned that compounds containing covalently linked β-CD and viologen subunits should undergo self-complexation upon two-electron reduction. Therefore, we prepared the series of cyclodextrin–viologen conjugates $\mathbf{1}^{2+}$–$\mathbf{3}^{2+}$ by alkylation of their precursor $\mathbf{4}^{+}$.[10]

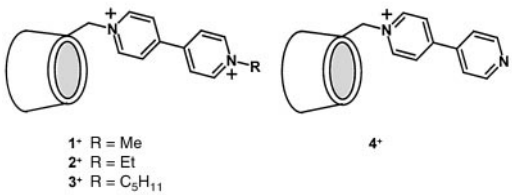

As anticipated, the electrochemical behavior of $\mathbf{1}^{2+}$–$\mathbf{3}^{2+}$ is dominated by the two reversible, one-electron reductions of their viologen residues.[11] Fig. 1 (solid line) shows a typical voltammogram for $\mathbf{2}^{2+}$ in 0.5 M phosphate buffer (pH = 7) solution. Half-wave potential values for $\mathbf{1}^{2+}$–$\mathbf{3}^{2+}$ and $\mathbf{4}^{+}$ are collected in Table 1. In aqueous media the cathodic voltammetric behavior of most viologens is affected by the precipitation on the electrode surface of their more hydrophobic, reduced forms.[12–14] In contrast, the CD–viologen conjugates $\mathbf{1}^{2+}$–$\mathbf{3}^{2+}$ exhibit (at concentrations around 1 mM) two reversible voltammetric reduction waves, free from any precipitation effects, due to the solubilizing effect of the appended CD moieties. On the other hand, we found that the electrochemical behavior of the CD–viologen conjugates is strongly concentration dependent. The second reduction wave of $\mathbf{1}^{2+}$–$\mathbf{3}^{2+}$ broadens and shifts to more positive potentials (Fig. 1, dotted line) at concentrations above 1 mM. In control experiments, other highly water-soluble viologens lacking covalently appended CD residues did not show this type of concentration dependent behavior.[15] Furthermore, the changes observed in the second reduction waves of $\mathbf{1}^{2+}$–$\mathbf{3}^{2+}$ at concentrations above 1 mM are similar to those observed for water-soluble viologens in the presence of added β-CD.[9] We thus conclude that compounds $\mathbf{1}^{2+}$–$\mathbf{3}^{2+}$ undergo intermolecular self-complexation upon two-electron reduction of the viologen subunit (Scheme 1). The intermolecular character of these self-complexation processes is clearly evidenced by the observed concentration dependence. To further verify that the presence in the same molecule of viologen and β-CD subunits is responsible for self-complexation, we performed several experiments using independent guest or host molecules. Fig. 2 shows the voltammetric behavior of a solution containing 7.3 mM $\mathbf{3}^{2+}$ (solid line) clearly

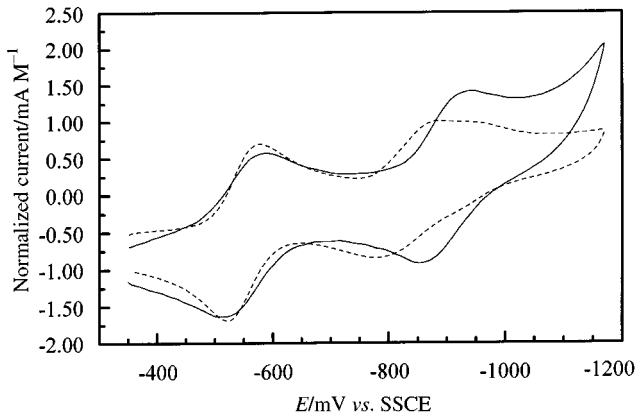

Fig. 1 Normalized cyclic voltammograms (0.1 V s^{-1}) of 0.15 (solid line) and 6.7 mM solutions of $\mathbf{2}\cdot Cl_2$ in 0.5 M pH 7 phosphate buffer.

Table 1 Half-wave potentials ($E_{1/2}$) and peak-to-peak splittings (ΔE_p) measured for the cyclodextrin–viologen conjugates in 0.5 M phosphate buffer (pH 7) solution

Cationic compound	$E_{1/2}^1$/V (ΔE_p/mV)[a]	$E_{1/2}^2$/V (ΔE_p/mV)[b]
$\mathbf{1}^{2+}$	−0.573 (80)	−0.933 (90)[c]
$\mathbf{2}^{2+}$	−0.555 (60)	−0.911 (65)[d]
$\mathbf{3}^{2+}$	−0.524 (65)	−0.934 (75)[e]
$\mathbf{4}^{+}$	−0.908 (70)[f]	—

[a] Half-wave potentials for the first one-electron reduction of the bipyridinium subunit (V^{2+}/V^{+}). The value in parenthesis represents the potential difference between the cathodic and anodic peak potentials measured by cyclic voltammetry at a scan rate of 0.100 V s^{-1}. [b] Same for the second one-electron reduction of the bipyridinium subunit (V^{+}/V). [c] 1.2 mM. [d] 0.15 mM. [e] 7.3 mM (potential data for the free compound obtained after adding excess of competing guest). [f] 0.22 mM.

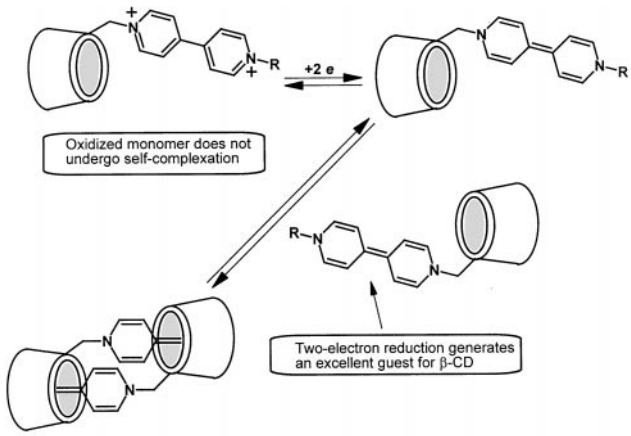

Scheme 1

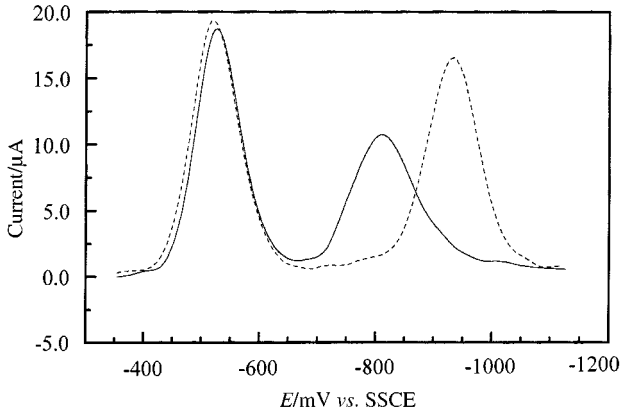

Fig. 2 Square wave voltammograms of a 7.3 mM solution of **3**·Cl_2 in 0.5 M pH 7 phosphate buffer in the absence (solid line) and presence (dotted line) of 8.7 mM adamantane-1-carboxylic acid (ACA). Data recorded using a potential step of 4 mV, pulse amplitude of 25 mV, and frequency of 15 Hz.

exhibiting the broadening and anodic shifting of the second reduction wave which is associated with the self-complexation of the reduced form **3**. Addition of adamantane-1-carboxylic acid, an excellent guest for β-CD hosts,[16] has a profound effect on the second reduction wave (dotted line), which returns to the potential region and to the appearance that it had at concentrations ⩽1 mM. Thus, adamantane-1-carboxylic acid disrupts self-complexation by competing with the reduced viologen subunits for the available CD cavities.

Similarly, voltammograms of the investigated CD–viologen conjugates exhibit large changes in the presence of heptakis(2,6-*O*-dimethyl)-β-cyclodextrin (DM–β-CD). In this case, the addition of the DM–β-CD host leads to a greater anodic shift for the second reduction waves of $\mathbf{1}^{2+}$–$\mathbf{3}^{2+}$, as the added host increases the CD-bound fraction of the reduced viologen subunits (voltammograms not shown). Thus, the observed voltammetric results clearly reveal that the self-complexation of the CD–viologen conjugates upon two-electron reduction (**1**–**3**) can be disrupted by addition of competing CD guests or free CDs. Based on previous electrochemical and spectroscopic studies on the complexation of CD hosts with the viologen guests we estimate the association constant of observed intermolecular complexes to be 10^3 to 10^4 M^{-1}.[17]

A final issue that must be addressed is the mode of assembly exhibited by the CD–viologen conjugates. Are they interacting face-to-face to yield dimeric structures (as shown in Scheme 1) or face-to-tail to produce oligomeric aggregates formed by a larger number of monomers? An unequivocal answer to this question will require additional physicochemical characterization of fully isolated reduced complexes. This task has proven to be a very difficult one due to extreme air sensitivity of the reduced viologen species.[11] Park and coworkers,[10c] however, demonstrated formation of face-to-face dimers in solution upon photochemically-induced, one-electron reduction of related CD–viologen conjugates. Our data also suggest face-to-face dimerization, since face-to-tail complexation should yield bulky insoluble aggregates in solution, which we have never observed, upon two-electron reduction of the viologen moieties. Entropic considerations similarly suggest that formation of small cyclic dimeric complexes is more favorable than aggregation to yield large assemblies.

In summary, we have prepared a series of three CD–viologen conjugates that exhibit concentration-dependent voltammetric behavior. This behavior is clearly indicative of intermolecular self-complexation upon two-electron reduction of the pendant viologen subunits.

The authors are grateful to the National Science Foundation (to A. E. K., CHE-9633434) for the generous support of this work.

Notes and references

1 J. M. Lehn, *Supramolecular Chemistry: Concepts and Perspectives*, VCH, Weinheim, 1995.
2 M. M. Conn and J. Rebek, *Chem. Rev.*, 1997, **97**, 1647.
3 N. Yamaguchi, D. S. Nagvekar and H. W. Gibson, *Angew. Chem., Int. Ed.*, 1998, **37**, 2361.
4 (*a*) D. Metzafos, A. Terzis, A. W. Coleman and C. de Rango, *Carbohydr. Res.*, 1996, **282**, 125; (*b*) A. Ueno, T. Kuwabara, A. Nakamura and F. Toda, *Nature*, 1992, **356**, 136; (*c*) R. C. Petter, J. S. Salek, C. T. Sikorski, G. Kumaravel and F. T. Lin, *J. Am. Chem. Soc.*, 1990, **112**, 3860.
5 P. R. Ashton, I. W. Parsons, F. M. Raymo, J. F. Stoddart, A. J. P. White, D. J. Williams and R. Wolf, *Angew. Chem., Int. Ed.*, 1998, **37**, 1913; J. Bugler, N. A. J. M. Somerdijk, A. J. W. G. Visser, A. van Hoek, R. J. M. Nolte, J. F. J. Engbersen and D. Reinhoundt, *J. Am. Chem. Soc.*, 1999, **121**, 28; P. R. Ashton, I. Baxter, S. J. Cantrill, M. C. T. Fyfe, P. T. Glink, J. F. Stoddart, A. J. P. White and D. J. Williams, *Angew. Chem., Int. Ed.*, 1998, **37**, 1294; J. L. Sessler, A. Andrievsky, P. A. Gale and V. Lynch, *Angew. Chem., Int. Ed. Engl.*, 1996, **35**, 2782.
6 For a recent example, see: M. B. Nielsen, S. B. Nielsen and J. Becher, *Chem. Commun.*, 1998, 475.
7 For reviews on the use of electrochemical reactions to control host–guest complexation, see: A. E. Kaifer, *Acc. Chem. Res.*, 1999, **32**, 62; P. L. Boulas, M. Gómez-Kaifer and L. Echegoyen, *Angew. Chem., Int. Ed.*, 1998, **37**, 216.
8 A. Mirzoian, PhD Dissertation, University of Miami, 1998.
9 A. Mirzoian and A. E. Kaifer, *Chem. Eur. J.*, 1997, **3**, 1052.
10 Compounds $\mathbf{1}^{2+}$–$\mathbf{3}^{2+}$ were synthesized by reaction of $\mathbf{4}^{+}$ with the corresponding alkyl iodide in DMF. In turn, $\mathbf{4}^{+}$ was prepared by the reaction of mono-6-deoxy(*p*-tolylsulfonyl)-β-CD [ref. 4(*c*)] with excess 4,4′-bipyridine. Compounds $\mathbf{1}^{2+}$–$\mathbf{3}^{2+}$ were isolated as dichloride salts (yields 12–38%) after size exclusion chromatography (Biogel P-2 column) and ion exchange (Amberlite IRA 401). All compounds were characterized by ^{1}H NMR (400 MHz), UV–VIS spectroscopy and MALDI-TOF mass spectrometry. Compounds $\mathbf{1}^{2+}$ and $\mathbf{2}^{2+}$, as well as related CD–viologen conjugates, have been synthesized previously using different methodology: (*a*) Y. Du, A. Nakamura and F. Toda, *Bull. Chem. Soc. Jpn.*, 1990, **63**, 3351; (*b*) Y. Du, A. Nakamura and F. Toda, *J. Inclusion Phenom.*, 1991, **10**, 443; (*c*) J. W. Park, N. H. Choi and J. H. Kim, *J. Phys. Chem.*, 1996, **100**, 769; (*d*) H. Ikeda, Y. Du, A. Nakamura and F. Toda, *Chem. Lett.*, 1991, 1495; (*e*) J. W. Park, J. H. Kim, B. K. Hwang and K. W. Park, *Chem. Lett.*, 1994, 2075; (*f*) K. K. Park and S. Y. Han, *Tetrahedron Lett.*, 1997, **38**, 4231.
11 C. Bird and A. T. Kuhn, *Chem. Soc. Rev.*, 1981, **10**, 49.
12 A. E. Kaifer and A. J. Bard, *J. Phys. Chem.*, 1985, **89**, 4876.
13 P. A. Quintela and A. E. Kaifer, *Langmuir*, 1987, **3**, 769.
14 P. Quintela, A. Diaz and A. E. Kaifer, *Langmuir*, 1988, **4**, 663.
15 Viologens modified with hydrophilic side chains were used in this experiment along with the highly water soluble methylviologen. See ref. 9.
16 L. A. Godínez, L. Schwartz, C. M. Criss and A. E. Kaifer, *J. Phys. Chem. B*, 1997, **101**, 3376.
17 T. Matsue, T. Kato, U. Akiba and T. Osa, *Chem. Lett.*, 1985, 1825; A. Díaz, P. A. Quintela, J. M. Schuette and A. E. Kaifer, *J. Phys. Chem.*, 1988, **92**, 3537; A. Yasuda, H. Mori and J. Seto, *J. Appl. Electrochem.*, 1987, **17**, 567; M. Kodaka and T. Fukaya, *Bull. Chem. Soc. Jpn.*, 1986, **59**, 2032.

Communication 9/04095A

Self-patterned H-bond supramolecular self-assembly

Y. W. Cao, X. D. Chai,*[a] T. J. Li,[a] Jim Smith[b] and DeQuan Li*[b]

[a] *Department of Chemistry, Jilin University, Changchun, 10023, P. R. China*
[b] *Los Alamos National Laboratory, Chemical Sciences and Technology Division (CST-4), and Center for Materials Science, Los Alamos, NM 87545, USA. E-mail: dequan@lanl.gov*

Received (in Columbia, MO, USA) 6th April 1999, Accepted 1st June 1999

Barbituric acid and melamine derivatives self-assembled into highly ordered structures from the molecular scale (~ 3 Å) to geometric patterns on a macroscale (~ 0.5 mm).

Supramolecular self-assembly is a fascinating process in which hierarchical organization from the molecular level to the mesoscale and macroscale is spontaneously established. Mesoscale ordered domains have been observed before,[1] but formation of well-defined patterns up to the macroscale is rare. Given knowledge of chemical functionalities, it is widely accepted that one cannot accurately predict the spontaneously organized structures by design, from intuition, or from physical principles. Here we attempt to understand the relationship between self-assembled structures and molecular functionalities using SEM, TEM, X-ray, and IR spectroscopy. Hydrogen bonding has long been employed as a powerful tool to organize molecules in the solid state[2] and on air/water interfaces.[3] H-bonded networks in barbituric acid and melamine systems[4] are intriguing because of their structural resemblance to the base pairs of DNA. We synthesized new derivatives of barbituric acid and melamine which formed highly organized molecular self-assemblies exhibiting order from the molecular scale (0.3 nm) to the macroscale (0.5 mm). This shows that macrostructures and macropatterns may be controlled by molecular functionalities.

The melamine and barbituric derivatives **1** and **2** were studied, along with **3** with a single barbituric acid for

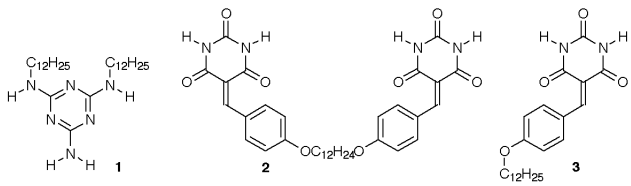

comparison. Supramolecular assemblies were prepared by mixing **2** and **1** in a molar ratio of 1:2 in dried DMF (~ 0.2–1 mM), followed by heating the solution to 50 °C for 24 h.[5] Samples were prepared by simply drop-casting the homogeneous solution onto various substrates such as glass, carbon, gold and germanium. These substrates were chosen to meet the requirements of various analytical techniques, for example, gold and carbon for electron microscopy and germanium for infrared spectroscopy.

The $\mathbf{2}\cdot\mathbf{1}_2$ supramolecular system was linked with six complementary H-bonds (~ 30 kcal mol^{-1}), which is the minimum number that nature requires to precisely transfer information from DNA to RNA (triplet base pairs or codons).[6] The formation of our supramolecular self-assemblies is driven primarily by the interplay of encoded six H-bonds, and secondarily by hydrophobic chain–chain interactions, π–π interactions, and functional group–substrate interactions. The zigzag H-bond network in the $\mathbf{2}\cdot\mathbf{1}_2$ system was verified with IR measurements carried out in the internal (total) reflection at the center of the flat surface of a Ge hemisphere. First, the shifts of carbonyl, amide, and amino infrared bands confirm the formation of six-fold zigzag H-bonds between **2** and **1**.[7] Secondly, the carbonyl vibrations at the 2,6-position (1675 cm^{-1}) of the barbituric acid are insensitive to polarization because of their structural arrangement. However, the carbonyl vibrations at the 4-position (1733, 1705 cm^{-1}; *para* to ylidine substitution) are strong in p-polarization but weak in s-polarization. This polarization effect proves that the 4-position C=O bond is mostly perpendicular to the surface, suggesting that the extended H-bonded networks are parallel to the surface. Finally, the low CH_2 vibration frequencies (υ = 2916 and υ_s = 2849 cm^{-1}) indicate that the hydrocarbon chains are highly crystalline;[8] this order is rather long range (> μm) as shown by the constant CH_2 vibrational frequencies when the IR beam is changed from grazing incidence (75°) to near-normal incidence (20°). While **2** is replaced with **3**, no such long-range order was observed; both CH_2 vibration frequencies incresed by ~ 5 cm^{-1} from 75 to 20°, indicating that the alkyl chains become more disordered away from the Ge substrate.

Bright-field transmission electron microscopy (TEM) indicated that these systems consist of layered structures with very long, linear 'ribbons' (width = ~ 322–644 Å) as the secondary building blocks. High-resolution TEM and electron diffraction (Fig. 1) revealed that the layered structure had four different periodicities of d = 2.6, 3.7, 4.0 and 4.6 Å in the plane of the substrate. Small-angle X-ray diffraction of $\mathbf{2}\cdot\mathbf{1}_2$ on silicon yielded the first-order Bragg diffraction peak at 2θ = 1.334°, which proved that $\mathbf{2}\cdot\mathbf{1}_2$ formed multilayers with a d-spacing of c = 66.2 Å along surface normal. This value agrees quite well with a d-spacing of c = ~ 65 Å generated from a 3D molecular model. These results also support the IR observation that the $\mathbf{2}\cdot\mathbf{1}_2$ system is a layered structure with extended H-bonded networks parallel to the substrate surface. The TEM and X-ray results are consistent with the proposed supramolecular structure illustrated in Fig. 2. Fig. 2(*a*) describes that the distance between barbituric acids or melamines is 9.8 Å[9] and their nearest neighbor in the next sheet is 4.3 Å away at an angle of 70°. This packing (Fig. 2) of the extended H-bond networks can explain all the observed d-spacing values;[10] they are (1) the periodicity along the H-bond network $d(1,-1) = a \sin 60° =$ 4.6 Å, and (2) the stacking distance between H-bond networks $d(1,1) = b \sin 32.5° =$ 4.0 Å and between phenyl rings in **2**

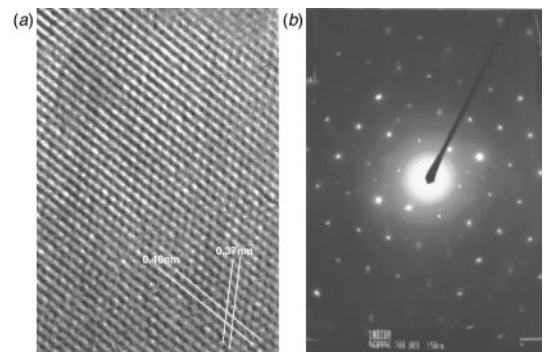

Fig. 1 (*a*) A high-resolution TEM image of the $\mathbf{2}\cdot\mathbf{1}_2$ multilayer supramolecular self-assembly on a carbon-coated copper grid. The four d = 2.6, 3.7, 4.0 and 4.6 Å. (*b*) An electron diffraction pattern of the same $\mathbf{2}\cdot\mathbf{1}_2$ system confirms the d-spacing values of 2.6, 3.7, 4.0 and 4.6 Å.

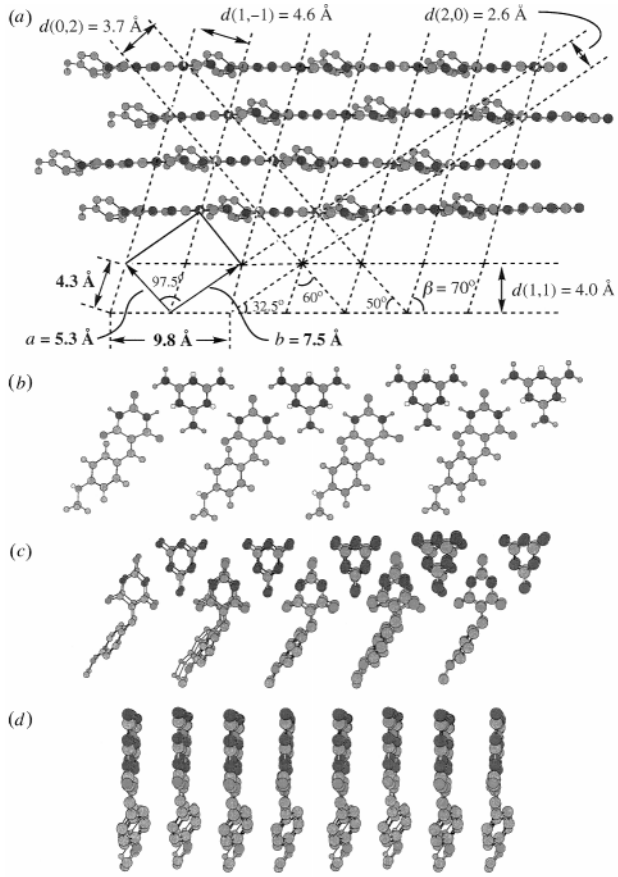

Fig. 2 (*a*) Proposed **2**·**1**$_2$ crystal lattice structure which explains the observed *d*-spacing values. (*b*) Side view of the H-bond networks, *d*(1,−1) = 4.6 Å. (*c*) Stacking along the phenyl ring direction, *d*(0,2) = 3.7 Å. (*d*) End view of H-bond networks, distance between H-bond sheets is *d*(1,1) = 4.0 Å.

d(0,2) = 3.7 Å, and *d*(2,0) = 2.6 Å. Molecular modeling of steric interactions between the 2,6-position oxygen atoms and the *ortho* position hydrogen atoms on the phenyl ring gives a dihedral angle between these two stacking planes of 49° [Fig. 2(*a*),(*c*)]. This angle corresponds to the 50° angle observed in high-resolution TEM between *d*(0,2) = 3.7 Å phenyl–phenyl planes and *d*(1,1) = 4.0 Å barbituric–melamine planes.

In Fig. 3(*a*), we observed that the amplified molecular information was expressed as very long straight lines with a line width between 3 and 4 μm and a length exceeding 0.1 mm. Furthermore, the amplified molecular information stored in the chemical units also generated well-defined angular structures of 60 and 70° through intermolecular interactions. These features may result from much interplay of secondary interactions including the H-bond, ribbon packing, and the alkyl chain interaction/tilt. When we substituted **3** for **2**, no such pattern was observed [Fig. 3(*b*)]. This fact suggests that the template effect from the gold substrate is not a dominant factor in the formation of these specific geometric structures because **3** has all the chemical functional groups that **2** has. Furthermore, these lines are hierarchical and built from smaller dot-like units (0.5–2 μm) which are also observed in the SEM image. The SEM micrograph clearly shows that there is a strong tendency to form such long-range ordered patterns that are governed by the information encoded in the molecular structures. These results imply that molecular building blocks can be programmed to spontaneously assemble into prescribed structures according to a molecular blueprint, a process needed in materials by design. In the **2**·**1**$_2$ system, we have employed H-bonding interactions and hydrophobic associations to generate microscale straight lines and angles on gold surfaces. The ability to generate pattern on the microscale through tuning of the molecular functionality is important because it allows formation of unique structures without utilizing external lithographic tools.

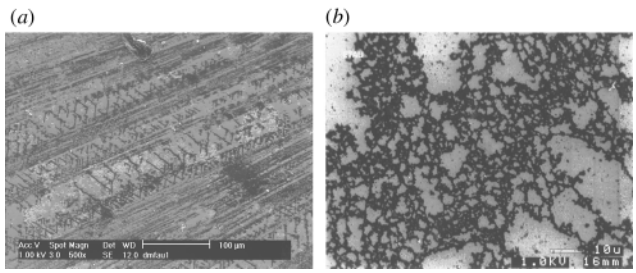

Fig. 3 (*a*) SEM images of **2**·**1**$_2$ systems on gold surfaces. The **2**·**1**$_2$ self-assemblies are darker, and they form extremely long lines (> 0.5 mm) and micron-size angles. These geometric features are constructed from secondary plate-like units, which are also observed in the micrograph. (*b*) The SEM image of the **3**·**1** system on gold surfaces shows random network structures. Note that the **3**·**1** system has all the functionalities of the **2**·**1**$_2$ system. The only difference is that the two barbituric acid groups are linked together in the **2**·**1**$_2$ system.

In conclusion, we have demonstrated that molecular design can lead to order on the microscale, mesoscale, and macroscale. The results show that H-bonding effects are the major driving forces in our systems, compared to hydrophobic interactions and van der Waals forces. The perfect match of six pairs of H-bonds induces the system to spontaneously organize into highly ordered hierarchical architectures manifested as micro-wide straight lines with 60 and 70° angles.

The authors at Los Alamos National Laboratory acknowledge the support of Laboratory Directed Research and Development and Center of Materials Science. The authors at Jilin University are grateful for support from National Climbing B Project and the National Science Foundation of China.

Notes and references

1 R. P. Andres, J. D. Bielefeld, J. I. Henderson, D. B. Janes, V. R. Kolagunta and C. P. Kubiak, *Science*, 1996, **273**, 1690; D. Q. Li, M. A. Rathner, T. J. Marks, C. Zhang, J. Yang and G. K. Wong, *J. Am. Chem. Soc.*, 1990, **112**, 7389; G. E. Poirier and E. D. Pylant, *Science*, 1996, **272**, 1145; X. Yang, D. McBranch, B. I. Swanson and D. Q. Li, *Angew. Chem., Int. Ed. Engl.*, 1996, **35**, 538; R. Maoz, S. Matlis, E. Dimasi, B. M. Ocko and J. Sagiv, *Nature*, 1996, **384**, 150; V. R. Pedireddi and C. N. R. Rao, *J. Am. Chem. Soc.*, 1999, **121**, 1752.

2 D. Gurrera, L. D. Taylor and J. C. Warner, *Chem. Mater.*, 1994, **6**, 1293; E. Fan, C. Vicent, S. J. Geib and A. D. Hamilton, *Chem. Mater.*, 1994, **6**, 1113.

3 T. M. Bohanon, S. Denzinger, R. Fink, W. Paulus, H. Ringsdorf and M. Weck, *Angew. Chem., Int. Ed. Engl.*, 1995, **34**, 58.

4 J. A. Zerkowski and G. M. Whitesides, *J. Am. Chem. Soc.*, 1994, **116**, 4298; J. M. Lehn, M. Mascal, A. Decian and J. Fischer, *J. Chem. Soc., Chem. Commun.*, 1990, 479.

5 Y. W. Cao, PhD Thesis, Jilin University, Changchun, PRC, 1996.

6 A. Krasnopoler, N. Kizhakevariam and E. M. Stuve, *J. Chem. Soc., Faraday Trans.*, 1996, **92**, 2445; M. W. Feyereisen, D. Feller and D. A. Dixon, *J. Phys. Chem.*, 1996, **100**, 2993.

7 **2** has amide N–H vibrations at 3217 (vs), 3143 (sh) and 3049 (sh) cm^{-1} and carbonyl C=O absorption bands at 1754 (sh), 1740 (sh), 1724 (s), 1692 and 1668 cm^{-1}. The stretching bands for amino groups in **1** are observed at 3450 (m), 3342 (m), 3271 (m) and 3164 (m) cm^{-1}, and the N–H deformation bands appear at 1671 (sh) and 1627 (sh) cm^{-1}. Upon self-assembly, the N–H vibrations become weak and shift to 3329–3259 (br) and 3138–3126 cm^{-1}; the carbonyl vibrations change to new positions at 1733 (sh), 1705 (s) and 1675 (s) cm^{-1}.

8 C. W. Sheen, J.-X. Shi, J. Martensson, A. N. Parikh and D. L. Allara, *J. Am. Chem. Soc.*, 1992, **114**, 1514; D. L. Allara, S. V. Atre, C. A. Elliger and R. G. Snyder, *J. Am. Chem. Soc.*, 1991, **113**, 1852; R. G. Nuzzo, L. H. Dubois and D. L. Allara, *J. Am. Chem. Soc.*, 1990, **112**, 558.

9 J. A. Zerkowski, J. C. Macdonald, C. T. Seto, D. A. Wierda and G. M. Whitesides, *J. Am. Chem. Soc.*, 1994, **116**, 2382.

10 M. Mascal, P. S. Fallon, A. S. Batsanov, B. R. Heywood, S. Champ and M. Colclough, *J. Chem. Soc., Chem. Commun.*, 1995, 805; M. Mascal, N. M. Hext, R. Warmuth, M. H. Moore and J. P. Turkenburg, *Angew. Chem., Int. Ed. Engl.*, 1996, **35**, 2204.

Communication 9/02674F

ChemComm

Synthesis, structure and inclusion properties of 1,4,15,18-tetrahydro-1,4,15,18-tetraoxodibenzo[*b*,*h*]tetraphenylene†

Xiao-Ping Yang,‡ Da-Ming Du,§ Qi Li,¶ Thomas C. W. Mak‖ and Henry N. C. Wong*

Department of Chemistry, The Chinese University of Hong Kong, Shatin, New Territories, Hong Kong, China

Received (in Cambridge, UK) 24th May 1999, Accepted 24th June 1999

The new host molecule 1,4,15,18-tetrahydro-1,4,15,18-tetraoxodibenzo[*b*,*h*]tetraphenylene forms inclusion complexes with specific guest molecules, exhibiting two distinctly different types of host lattices whose construction is dictated by intermolecular, face-to-face π··π interactions between benzoquinone rings across inversions centres.

Recent advances in crystal engineering[1] have generated a large variety of fascinating supramolecular frameworks which rely on non-covalent bonding interactions[2,3] for their self-organization. The geometry of the π-stacking motif is of particular interest since Burley and Petsko[4] have identified two important orientations for aromatic–aromatic interactions, namely face-to-face and edge-to-face interactions, in their survey of protein crystal structures.[5]

Our investigation of the host–guest chemistry of tetraphenylene **1**[6] and its benzo-fused derivatives, *e.g.* **2**[6d] and **3**,[6c] revealed that a secondary molecular C_2 axis passing through the

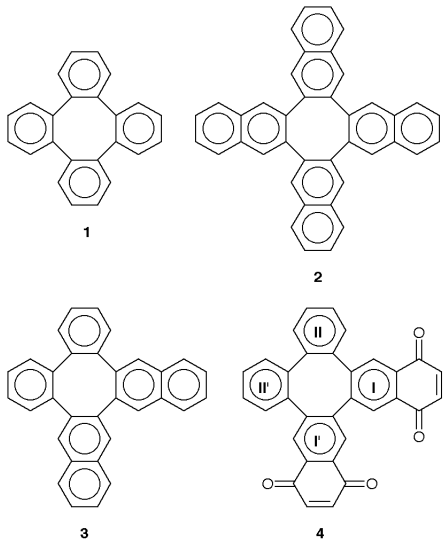

centres of a pair of opposite carbon–carbon single bonds, which gives tetraphenylenes their twisted shapes, would be a prerequisite component of inclusion behaviour.[6a,b,7] In order to substantiate this presumption and to enhance the inclusion capacity of the otherwise non-polar tetraphenylenes, namely **1**, **2** and **3**, we decided to undertake the design of a functionalized oxo derivative of **3**. Here we report the synthesis and "guest-specific" clathrate inclusion property of 1,4,15,18-tetrahydro-1,4,15,18-tetraoxodibenzo[*b*,*h*]tetraphenylene (**4**).

As can be seen in Scheme 1, the synthesis of bis-quinone **4** began with dehydrobromination of the known dibromide **5**[8] with Bu^{t}OK in the presence of freshly generated 4,7-dimethoxyisobenzofuran (**6**).[9] This reaction presumably proceeded through a cyclodienediyne intermediate[8] which underwent intermolecular Diels–Alder reaction with the reactive isobenzofuran **6**. In this way, **7** was obtained in 53% yield as the major product after careful chromatographic separation. Low-valent titanium deoxygenation[10] of **7** then produced the tetramethoxy compound **8** in 79% yield. On oxidation with silver(II) oxide and nitric acid in dioxane, **8** was smoothly converted to the desired product **4** in 60% yield.

A mixture of toluene–xylene–mesitylene (1:1:1 v/v/v) was added to a solution of **4** in CH_2Cl_2, and the resulting solution allowed to stand at room temperature for several days, after which crystals of **4**·$C_6H_3Me_3$ appeared in the form of yellow prisms. Slow evaporation of a solution of **4** in hexane–EtOAc (1:1 v/v) yielded yellow plate-like crystals of **4**·C_6H_{14}. Recrystallisation of **4** in EtOAc–AcOH (1:1 v/v) gave yellow prismatic crystals of **4**·AcOH. Yellow crystals of **4**·C_6H_{12} in the form of prisms were obtained from evaporation of a solution of **4** in cyclohexane–EtOAc (1:1 v/v).

Host **4** exhibits selective inclusion behaviour toward aromatic solvents: it does not form any crystalline adduct with either pyridine or benzene, and it selectively includes mesitylene from an equivolume mixture of toluene–*p*-xylene–mesitylene, forming a 1:1 crystalline complex. Among potential guests of the aliphatic type, only *n*-hexane and AcOH (as a hydrogen-bonded cyclic dimer) have been found to form 1:1 crystalline inclusion compounds with **4**. In the case of saturated ring systems, cyclohexane readily forms a 1:1 complex with **4**, but THF does not.

X-Ray analysis** has shown that the 1,4,15,18-tetrahydro-1,4,15,18-tetraoxodibenzo[*b*,*h*]tetraphenylene host molecule (**4**) has normal molecular dimensions and exhibits structural features common to the four inclusion compounds: a crystallographic C_2 axis†† passes through the midpoints of two opposite

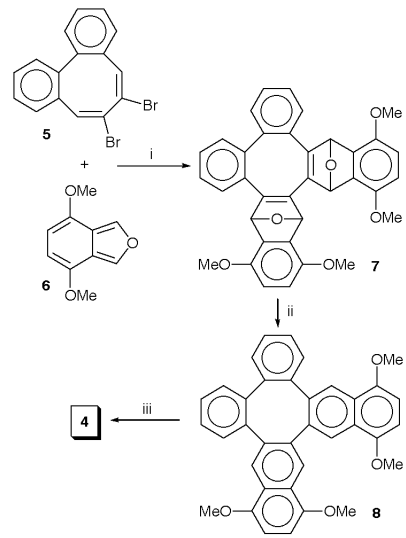

Scheme 1 *Reagents and conditions:* i, Bu^{t}OK, THF (53%); ii, $TiCl_4$, $LiAlH_4$, Et_3N, THF, reflux (79%); iii, AgO, HNO_3, dioxane (60%).

† Dedicated to Professor Peter J. Garratt on the occasion of his retirement.

‡ On leave of absence from Liaoning Normal University, Dalian, China.

§ On leave of absence from Shandong University, Jinan, China.

¶ On leave of absence from Beijing Normal University, Beijing, China.

‖ To whom correspondence concerning crystallography should be addressed.

Table 1 Selected structural parameters of inclusion complexes of 1,4,15,18-tetrahydro-1,4,15,18-tetraoxodibenzo[*b*,*h*]tetraphenylene (**4**)

	Dihedral angle between rings (°) in host molecule		Intermolecular π··π interaction between pair of adjacent benzoquinone rings	
Inclusion complex	I–I′	II–II′	*d*, interplanar spacing/Å	*D*, centroid-to-centroid distance/Å
4·Mesitylene	56.1	62.7	3.476	3.728
4·Hexane	67.1	63.3	3.581	3.909
4·Acetic acid	73.2	65.0	3.426	3.926
			3.508	3.825
4·Cyclohexane	69.7	65.3	3.441	3.883

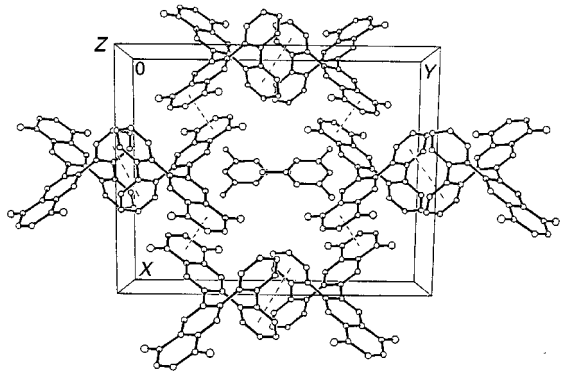

Fig. 1 Crystal structure of **4**·mesitylene (1:1) showing the packing of mesitylene guest molecules arranged in a zigzag column along an open channel running parallel to the *c* axis. The centroid-to-centroid distances between pairs of π··π interacting rings are represented by broken lines.

carbon–carbon single bonds in the central cyclooctatetraene ring, which is tub-shaped with C–C and C=C bonds alternating around it. The naphthoquinone rings I and I′ and the benzene rings II and II′ are disposed alternately above and below the mean plane of the molecule, and the dihedral angles between pairs of rings of the same kind are listed in Table 1. The resulting molecular configuration of **4** enables it to function as an efficient host for a wide range of guest molecules.

Complexes **4**·$C_6H_3Me_3$ and **4**·C_6H_{14} are isostructural with the same host framework and differ only in regard to the enclosed guest molecules. As shown in Fig. 1, the host molecules are connected by intermolecular face-to-face π··π interactions[11] between pairs of centrosymmetrically-related benzoquinone rings to form a zigzag chain running parallel to the [1 0 1] direction. The contact between these rings is described by two geometric parameters, namely the interplanar spacing *d* and the centroid-to-centroid distance *D*, as listed in Table 1. In an analogous manner, similar but much weaker π··π interactions between benzene rings across inversion centres (d = 4.341, D = 4.389 Å) give rise to another type of zigzag chain running parallel to the *c* axis. The three-dimensional host lattice resulting from these two systems of inter-connected chains contains open channels running parallel to the *c* axis, which accommodate the mesitylene guest molecules in a zigzag fashion.

Compounds **4**·AcOH and **4**·C_6H_{12} have essentially the same type of sandwich-like crystal structure although they belong to different space groups. In each case the host molecules are linked by π··π interactions between benzoquinone rings across centres of symmetry to form an infinite chain. Such chains are aligned side by side to constitute a layer, but there is no significant interaction between them. The chains are orientated in different directions, [0 1 $\bar{1}$] in **4**·AcOH and [1 0 $\bar{1}$] in **4**·C_6H_{12}, and the separations between adjacent chains are almost equal, being 8.19 and 8.13 Å, respectively.

In **4**·AcOH, two centrosymmetrically-related guest molecules are linked by a pair of O–H··O hydrogen bonds to form a cyclic dimer, in which all non-hydrogen atoms are almost coplanar (mean deviation 0.026 Å). These dimers are accommodated in voids and sandwiched between layers of host molecules whose mean planes correspond to the (100) series of planes. In a similar manner, the disordered cyclohexane guest molecules in **4**·C_6H_{12} are sandwiched between pairs of host layers that match the (010) planes. The difference in size of the guest molecules is reflected in the interplanar spacings of the host layers, which are 8.83 and 9.65 Å, respectively.

This work was fully supported by a grant from the Research Grants Council of the Hong Kong Special Administrative Region, China (Project Ref. No. CUHK 456/95P). D.M.D. and X.P.Y. acknowledge with thanks the award of Croucher Foundation Visitorships by the Croucher Foundation (Hong Kong).

Notes and references

** *Crystal data* for **4**·mesitylene: $C_{32}H_{16}O_4$·C_9H_{12}, M = 584.6, monoclinic, space group *C*2/*c*, (No. 15), a = 15.359(1), b = 19.181(2), c = 10.616(1) Å, β = 101.12(1)°, V = 3068.8(4) Å^3, Z = 4, F(000) = 1224, D_c = 1.265 Mg m^{-3}, μ(Mo-Kα) = 0.081 mm^{-1}, 2450 unique data, final R_1 = 0.081, wR_2 = 0.229 for 2304 observed data [$I > 2\sigma(I)$]. For **4**·hexane: $C_{32}H_{16}O_4$·C_6H_{14}, M = 550.6, monoclinic, space group *C*2/*c* (No. 15), a = 15.807(2), b = 18.590(3), c = 10.590(2) Å, β = 100.55(1)°, V = 3059.3(8) Å^3, Z = 4, F(000) = 1160, D_c = 1.195 Mg m^{-3}, μ(Mo-Kα) = 0.077 mm^{-1}, 2386 unique data, final R_1 = 0.063, wR_2 = 0.191 for 2109 observed data [$I > 2\sigma(I)$]. For **4**·AcOH: $C_{32}H_{16}O_4$·$C_2H_4O_2$, M = 524.5, triclinic space group *P*$\bar{1}$ (No. 2), a = 9.345(2), b = 10.121(3), c = 14.498(2) Å, α = 98.65(1), β = 101.23(1), γ = 101.23(1)°, V = 1293.7(5) Å^3, Z = 2, F(000) = 544, D_c = 1.346 Mg m^{-3}, μ(Mo-Kα) = 0.093 mm^{-1}, 3480 unique data, final R_1 = 0.069, wR_2 = 0.186 for 2906 observed data [$I > 2\sigma(I)$]. For **4**·cyclohexane: $C_{32}H_{16}O_4$·C_6H_{12}, M = 548.6, monoclinic, space group *P*2/*n* (No. 13), a = 10.498(3), b = 9.646(2), c = 14.687(3) Å, β = 101.08(1)°, V = 1459.6(5) Å^3, Z = 2, F(000) = 576, D_c = 1.248 Mg m^{-3}, μ(Mo-Kα) = 0.080 mm^{-1}, 2415 unique data, final R_1 = 0.072, wR_2 = 0.219 for 2411 observed data [$I > 2\sigma(I)$]. Both host and guest molecules in **4**·$C_6H_3Me_3$, **4**·C_6H_{14} and **4**·C_6H_{12} occupy sites of symmetry 2. The cyclohexane guest molecule in **4**·C_6H_{12} was found to be two-fold disordered with a C_2 axis passing through a pair of carbon atoms. CCDC 182/1304.
†† The C_2 axis is non-crystallographic in the case of **4**·AcOH. See http://www.rsc.org/suppdata/cc/1999/1607 for crystallographic data in .cif format.

1 G. R. Desiraju, *Crystal Engineering*: *The Design of Organic Solids*, Elsevier, Amsterdam, 1989; *The Crystal as a Supramolecular Entity*, ed. G. R. Desiraju, Wiley, Chichester, 1996; G. R. Desiraju, *Chem. Commun.*, 1997, 1453.
2 A. J. Blake, N. R. Champness, S. S. M. Chung, W.-S. Li and M. Schröder, *Chem. Commun.*, 1997, 1005; N. N. L. Madhavi, A. K. Katz, H. L. Carrell, A. Nangia and G. R. Desiraju, *Chem. Commun.*, 1997, 1953.
3 T. Steiner, E. B. Starikov, A. M. Amado and J. J. C. Teixeira-Dias, *J. Chem. Soc., Perkin Trans. 2*, 1995, 1321.
4 S. K. Burley and G. A. Petsko, *Science*, 1985, **229**, 23.
5 A. D. Hamilton in *Supramolecular Chemistry*, ed. V. Balzani and L. De Cola, Kluwer, Dordrecht, 1992, pp. 137–144.
6 (*a*) T. C. W. Mak and H. N. C. Wong, *Top. Curr. Chem.*, 1987, **140**, 141; (*b*) T. C. W. Mak and H. N. C. Wong, in *Comprehensive Supramolecular Chemistry*, ed. D. D. MacNicol, F. Toda and R. Bishop, Pergamon, Oxford, 1996, pp. 351–369; (*c*) Y.-M. Man, T. C. W. Mak and H. N. C. Wong, *J. Org. Chem.*, 1990, **55**, 3214; (*d*) H. N. C. Wong, Y.-M. Man and T. C. W. Mak, *Tetrahedron Lett.*, 1987, **28**, 6359.
7 T.-L. Chan, T. C. W. Mak and J. Trotter, *J. Chem. Soc., Perkin Trans. 2*, 1980, 672; M. Czugler and A. Kálmán, *J. Mol. Struct.*, 1981, **75**, 29.
8 H. N. C. Wong and F. Sondheimer, *J. Org. Chem.*, 1980, **45**, 2438.
9 B. A. Keay, H. P. Plaumann, D. Rajapaksa and R. Rodrigo, *Can. J. Chem.*, 1983, **61**, 1987.
10 H. Hart and G. Nwokogu, *J. Org. Chem.*, 1981, **46**, 1251; Y. D. Xing and H. N. C. Wong, *J. Org. Chem.*, 1982, **47**, 140; H. N. C. Wong, *Acc. Chem. Res.*, 1989, **22**, 145.
11 C. A. Hunter, *Chem. Soc. Rev.*, 1994, 101.

Communication 9/04144C

Dinuclear lanthanum complex catalyzes the hydrolysis of a phosphate diester with unprecedented speed

Paul E. Jurek and Arthur E. Martell*

Department of Chemistry, Texas A and M University, College Station, Texas 77842-3012, USA.
E-mail: martell@mail.chem.tamu.edu

Received (in Bloomington, IN, USA) 23rd October 1998, Accepted 12th July 1999

The dihydroxo dilanthanum macrocyclic complex hydrolyzes bis(*p*-nitrophenyl) hydrogen phosphate (BNP) with a remarkably high rate constant and a unique third-order dependence on the concentration of the dinuclear complex.

Restriction endonucleases are enzymes that hydrolyze the phosphate diester bonds of DNA with great specificity and high turnover numbers.[1] A small molecule that could recognize a specific DNA sequence and catalyze the rapid hydrolysis of the phosphate diester bond would be an invaluable research tool. Multinuclear metal complexes have been known to hydrolyze phosphate diesters[2] and are models for a number of phosphodiesterases that contain multinuclear active sites.[3] This work reports a defined dinuclear lanthanum(III) complex that can hydrolyze a phosphate diester (BNP) with unprecedented speed. This complex also has the unique feature that the hydrolysis of BNP is third-order with respect to the concentration of the dinuclear La^{3+} complex, $[LLa_2]$.

The ligand L was synthesized according to literature procedures.[4] Potentiometric experiments were performed by

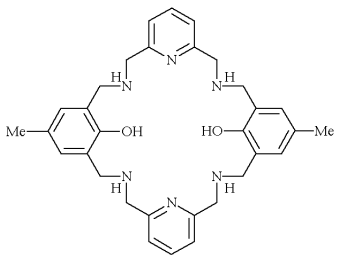

L

means of a well-defined method[5] to determine stability constants for the mono- and di-nuclear La^{3+} complexes (Table 1). The pK_a of a water bound to the mononuclear complex [LLa] is 11.15, while the pK_a of a water bound to the dinuclear complex $[LLa_2]$ is 7.75. The fact that the pK_a is lowered by 3.40

Table 1 Stability constants for the formation of mono- and di-nuclear La^{3+} complexes with the ligand L. T = 35 °C, μ = 0.10 M KCl, 3:1 EtOH–H_2O solution pK_as of L, under the same conditions: 12.95, 12.84, 8.24, 7.39, 5.76 and 4.38

Equilibrium	Log K
[LLa]/[L][La]	18.52
[LHLa]/[LH][La]	14.48
$[LH_2La]/[LH_2][La]$	9.31
$[LH_3La]/[LH_3][La]$	6.23
$[LH_4La]/[LH_4][La]$	3.56
[LLa(OH)][H]/[LLa]	11.15
$[LLa_2]/[LLa][La]$	6.67
$[LLa_2(OH)][H]/[LLa_2]$	7.75
$[LLa_2(OH)_2][H]/[LLa_2(OH)]$	10.03
$[LLa_2(OH)_3][H]/[LLa_2(OH)_2]$	11.17

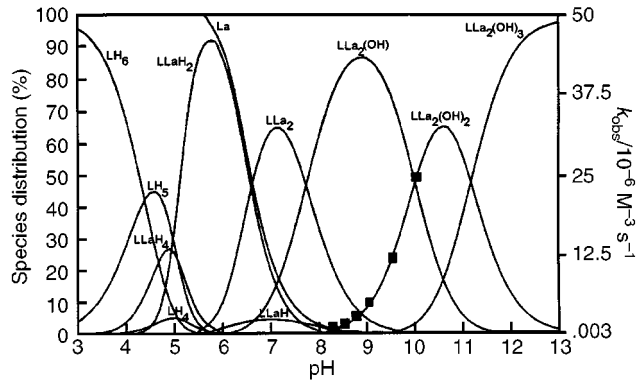

Fig. 1 Species distribution diagram for a system containing a 1:2 ratio L to La^{3+}. Observed third-order rate constants are denoted by (■).

pH units implies that the water is bridging the two La^{3+} ions. The pK_a of the second water bound to the dinuclear complex is 10.03, so this water also forms a bridge between the two La^{3+} ions.

In Fig. 1 the prevalence of the various dinuclear μ-hydroxy species can be seen. In the pH range 6–8 the rate constants are easily measurable, but relatively small in magnitude. The graph clearly shows that the rate constants follow the formation of the dinuclear dihydroxo complex $[LLa_2(OH)_2]$. When $[LLa_2]_{TOT}$ = $[BNP]_{INIT}$ = 0.5 mM, it would take 5.0 days for one turnover at pH 7.[6] It would take only 27 min for one turnover at pH 9 and a mere 6 min at pH 10. It is not clear why the dihydroxo complex is more effective than the monohydroxo complex $[LLa_2(OH)]$. There is at least one other example in the literature of a dinuclear macrocyclic complex where the active catalyst for hydrolyzing BNP is the dihydroxo complex and not the analogous monohydroxo species.[2a] The reason may simply be that the second hydroxo ligand is better positioned for nucleophilic attack than the initial hydroxo complex that forms.

Within the concentration range studied, the reaction is first-order with respect to $[BNP]_{INIT}$. However, analysis of the data in Table 2 shows that the reaction is an unusual third-order with respect to the concentration of the dinuclear species $[LLa_2]_{TOT}$. Consequently, the rate law is given by eqn. (1).

$$\text{Rate} = k_{obs}[LLa_2]^3_{TOT}[BNP]_{INIT} \quad (1)$$

A reaction may appear to have an unusual catalyst dependence if there is an unexpected equilibrium at the concentration at which the kinetic trials were measured as opposed to the

Table 2 Dependence of the rate of BNP hydrolysis on the concentration of $[LLa_2]_{TOT}$

pH	$[LLa_2]_{TOT}$/M	$[BNP]_{INIT}$/M	Rate/10^8 M s^{-1}
8.25	0.000728	0.000531	24
8.25	0.000486	0.000539	7.3
8.25	0.000244	0.000518	0.81

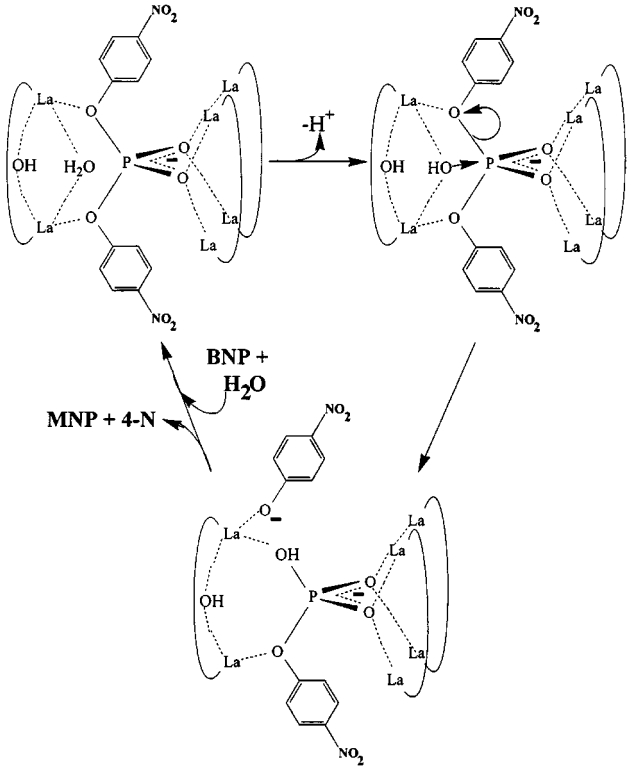

Scheme 1 Proposed mechanism for BNP hydrolysis by $[LLa_2(OH)_2]$. For simplicity, the ligand has been drawn as a curved line and the coordinated hydroxides of the two rightmost $[LLa_2(OH)_2]$ species were not included.

concentration at which the potentiometric experiments were performed. To test this hypothesis the stability constants were measured over a large concentration range. The stability constants at various concentrations agreed to within experimental error. Thus this aggregation of three $[LLa_2]$ molecules, required to satisfy the third-order rate law dependence, occurs only in the presence of substrate.

A proposed mechanism is shown in Scheme 1. Two dinuclear La^{3+} complexes coordinate the partially negatively charged phosphate oxygens. The third dinuclear La^{3+} complex coordinates both ester groups and attacks the phosphorus center with one of its bridging hydroxide nucleophiles. A *p*-nitrophenolate group (4-N) is displaced and the monophosphate ester (MNP) is generated. The products are displaced and the $[LLa_2]$ complex molecules coordinate another incoming substrate. The active catalyst $[LLa_2(OH)_2]$ is regenerated by the loss of a proton from a coordinated water. Hydrolysis is fast because there are three dinuclear La^{3+} complexes withdrawing electron density from the phosphorus center. This makes that phosphorus center extremely susceptible to nucleophilic attack from the coordinated hydroxide nucleophile.

This work describes the formation of the first defined dinuclear La^{3+} complex capable of hydrolyzing phosphate diesters. The catalysis occurs at such an unprecedented rate that it takes only 6 min for one turnover at pH 10. The rate constant *versus* pH profile clearly shows the most efficient catalyst is the dinuclear dihydroxo complex $[LLa_2(OH)_2]$. The unique third-order dependence on $[LLa_2]_{TOT}$ is the most probable reason for the high rate constants that are observed. The high rate constants and third-order concentration dependence holds much promise for future work of hydrolyzing DNA on a practical time scale.

Notes and references

1 R. J. Roberts and D. Macelis, *Nucleic Acids Res.*, 1993, **21**, 3125.
2 (*a*) C. Bazzicalupi, A. Bencini, A. Bianchi, V. Fusi, C. Giorgi, P. Paoletti, B. Valtancoli and D. Zanchi, *Inorg. Chem.*, 1997, **36**, 2784; (*b*) W. H. Chapman and R. Breslow, *J. Am. Chem. Soc.*, 1995, **117**, 5462; (*c*) T. Koike, M. Inoue, E. Kimura and M. Shiro, *J. Am. Chem. Soc.*, 1996, **118**, 3091; (*d*) M. Wall, R. C. Hynes and J. Chin, *Angew. Chem., Int. Ed. Engl.*, 1993, **32**, 1633; (*e*) M. J. Young and J. Chin, *J. Am. Chem. Soc.*, 1995, **117**, 10577; (*f*) C. Duboc-Toia, S. Ménage, J.-M. Vincent, M. Averbuch-Pouchot and M. Fontecave, *Inorg. Chem.*, 1997, **36**, 6148.
3 L. S. Beese and T. A. Steitz, *EMBO J.*, 1991, **10**, 25; D. Kostrewa and F. K. Winkler, *Biochemistry*, 1995, **34**, 683; E. Hough, L. K. Hansen, B. Birknes, K. Jynge, S. Hansen, A. Hordvik, C. Little, E. Dodson and Z. Derewends, *Nature*, 1989, **338**, 357; A. Volbeda, A. Lahm, F. Sakiyama and D. Suck, *EMBO J.*, 1991, **10**, 1607; S. M. Callahan, N. W. Cornell and P. V. Dunlap, *J. Biol. Chem.*, 1995, **270**, 17627.
4 Z. Wang, J. Reibenspies and A. E. Martell, *Inorg. Chem.*, 1997, **36**, 629.
5 A. E. Martell and R. J. Motekaitis, *Determination and Use of Stability Constants*, 2nd edn., VCH, New York, 1992.
6 A k_{cat} value of 0.0004 s^{-1} was measured at pH 7.0 by using $[LLa_2]_{TOT}$ = 5.0 mM and $[BNP]_{INIT}$ = 0.5 mM. The rate enhancement over spontaneous hydrolysis is 1.2×10^7. A k_{cat} value at pH 10.0, with the concentrations just described, is too fast to measure by our method. By extrapolation, it calculates to $k_{cat} = 0.32\ s^{-1}$ which is one turnover every 3–4 s. This is a rate enhancement of 1.2×10^8.

Communication 9/00860H

Typeset and printed by Black Bear Press Limited, Cambridge, England

ChemComm
FEATURE ARTICLE

Combinatorial and rapid screening approaches to homogeneous catalyst discovery and optimization

Robert H. Crabtree

Yale Chemistry, PO Box 208107, 225 Prospect St., New Haven, CT 06520-8107, USA

Received (in Bloomington, IN, USA) 3rd February 1999, Accepted 29th March 1999

Rapid screening and combinatorial chemistry are expected to influence the way homogeneous catalysts are discovered and developed.

Homogeneous catalyst discovery owes at least as much to empirical testing as to mechanistic understanding, because structure/function relationships are either obscure or not readily predictable for most catalysts. Once an initial lead catalyst has been identified—either in current experimental work in one's own laboratory or in the literature—incremental changes in the ligand set, often guided by simple mechanistic considerations, are then made to bring the activity, selectivity or scope of the catalyst up to useful levels. Since each new potential catalyst is normally separately prepared and purified, then assayed, progress is relatively slow. In our own early studies, an iridium catalyst that is highly active for the hydrogenation of tri- and tetra-substituted alkenes was only found after a year, even though only 6–12 complexes were assayed. Activity proved to be poor in then-standard solvents and only when a weakly coordinating solvent, CH_2Cl_2, was used did high activity emerge.[1] At that time CH_2Cl_2 was considered inadvisable for homogeneous hydrogenation because of its oxidising character. This emphasizes the point that a new catalyst may need to be assayed under non-standard conditions, where rapid screening methods could prove useful.

Robert H. Crabtree was educated at New College Oxford with Malcolm Green, studied for his PhD with Joseph Chatt at Sussex University and spent four years in Paris at the Natural Products Institute of the CNRS, the French national laboratory.

In 1977 he came to the US as an Assistant Professor at Yale, where he is now Professor of Chemistry. He has been A. P. Sloan Foundation Fellow and Dreyfus Teacher-Scholar, received the ACS and RSC prizes for organometallic chemistry and is past Chair of the Division of Inorganic Chemistry of ACS. He has also received the Mack Award in Chemistry, Ohio State University, been an H. C. Brown Lecturer at Purdue University, Esso Distinguished Lecturer at the University of Toronto, Albright and Wilson lecturer at Warwick University, and visiting Professor at the University of Toulouse.

He has been involved in C–H activation chemistry, including oxidative addition and mercury photosensitized pathways and more recently, C–F bond activation. In hydride chemistry, he contributed to the development of dihydrogen complexes, including the development of physical methods for their detection, and developed the chemistry of hydrogen bonding in inorganic chemistry. He discovered halocarbon and HF complexes. Early work on hydrogenation led to a homogeneous hydrogenation catalyst with useful properties. He has also been involved in the bioinorganic chemistry of nickel and manganese, most recently in functional modelling of photosynthetic water oxidation.

With the advent of combinatorial chemistry,[2] a new strategy is currently emerging that may accelerate the pace of homogeneous catalyst discovery and development. It combines parallel synthesis of a broad range of catalysts, the catalyst library, with a rapid and preferably parallel assay, the rapid screen. When perfected, this procedure is expected to greatly accelerate the rate at which catalysts are discovered or improved although the area is still in its earliest phases. Another potential advantage of making screening much easier is that complexes that do *not* appear promising candidates can also be assayed, leading to the possibility that unexpected classes of catalyst may be found. One recent example,[3] discovered by conventional means, shows that an important class of catalyst for alkene polymerization long escaped discovery in spite of intense activity in the field, in this case because, being based on a late metal, it defied expectations based on what later proved to be oversimplified mechanistic arguments. For a decade or more in the development of alkene polymerization catalysis, it was thought that commercially useful polymer molecular weights in alkene polymerization would only be obtained with early metal catalysts. Late metals were considered to be too prone to β-elimination and would therefore only form oligomers at best. In spite of intense activity in the polymerization area, highly active late metal complexes were only discovered very recently. They prove to have usefully different properties from their early metal counterparts. This example shows how the influence of inappropriately generalised mechanistic ideas can sometimes hold back advance in catalysis research by creating artificial conceptual barriers to innovation.

Combinatorial ideas have already made a strong impact in drug discovery, are becoming established in organic chemistry, and are now beginning to enter homogeneous catalysis. In addition to speeding catalyst discovery and development they are likely to change homogeneous catalysis in a number of ways. The convenience of polystyrene-bead-based combinatorial solid phase synthesis and on-bead testing of catalysts may emphasize the area of supported homogeneous catalysis.[4a] Solid phase organic synthesis (SPOS) allows certain types of reactions to be carried out particularly easily, including ones not possible in solution, so we may be led to envisage ligands not currently in the lexicon of the catalysis chemist.

Combinatorial chemistry

Combinatorial chemistry involves three steps: the rapid parallel synthesis of a library of many compounds of related structure, the parallel testing of these compounds for a desired property by an appropriate assay, and the identification of the compounds, called 'hits', that show the best desired properties. In this way, chemical structural diversity can be thought of as a multi-dimensional space probed by the combinatorial method. Once an initial hit has been identified in the initial broad library, a new library may be constructed that probes a smaller region of diversity space around the intial hit. Combinatorial chemistry

can therefore be considered as an artificially accelerated evolution process but with human rather than natural selection as its motor.

Merrifield's[4b] solid phase synthesis of polypeptides (1963) on polystyrene beads was the first step on the road to the new ideas. In a Merrifield synthesis, the growing polypeptide chain is anchored to a polystyrene bead and extended one amino acid residue at a time using appropriate reagents; final cleavage gives the desired polypeptide. The method can readily be automated. The advantage of the solid phase is that the steps can be pushed to high yield using an excess of reagents and the growing polypeptide can be separated at each step simply by filtering the beads and washing. The availability of this procedure led to the concept of replacing a specific amino acid residue reagent, as is normally used in a specific chain-extension step, by a mixture of reagents, leading to a mixture of compounds in the final product. By having fixed amino acid residues at most sites but variable residues at a few sites, an unprecedentedly large degree of diversity could be obtained rather easily within a class of closely related polypeptides. Suitable procedures were then developed to assay for the desired ligand binding properties and identify which sequence is responsible for binding.

The next conceptual step was the recognition by Bunin and Ellman[5] that the same sort of diversity could be created by SPOS for non-peptide organic compounds, where the substituent groups on a central motif were permuted. The method was first applied to benzodiazepines, where four different substituents could be independently varied.

From this, it is a short step to the idea of creating a diverse library of potential ligands on a set of beads, binding a reactive metal complex to the supported ligand and assaying the resulting bead for catalytic activity. This and related ideas are being developed at the moment, both in academia and in such industrial companies as Symyx.[6]

Rapid screening of catalysts

High throughput screening (HTS) in the pharmaceutical industry became so efficient by the early 1990s that it made the synthesis of drug candidates the rate determining step in the drug discovery process and directly encouraged the adoption of combinatorial synthesis.[7] In the catalyst area, neither HTS methods nor combinatorial synthesis had been applied until very recently, so both have had to be developed together.

Assays reported to date can be either parallel or non-parallel: in a parallel assay, all the data are collected at one, but in a non-parallel assay, each data point is obtained independently, one at a time, by conventional methods. It is clearly more efficient to screen a combinatorial catalyst library with a parallel HTS screen than with conventional GC or HPLC, although the availability of automatic sampling could modify this conclusion. Continuous assays have the advantage of allowing monitoring of a reaction in real time; others require some action to be taken to gather the data, such as taking a sample, in which case the method is discontinuous. Methods are also likely to vary in their quantitative value, going from a purely qualitative indication to a detailed quantitative analysis of all species present. They also vary very considerably in sophistication going from low to high tech. The former are generally easier to apply but the latter will be advantageous for automation. There will probably eventually be a hierarchy of such HTS assays, but the initial screen is likely often to be that for activity, because without sufficient activity, no catalyst, however selective, is likely to be useful.

Perhaps the simplest is our own continuous, parallel assay[8] based on a reactive dye **1** that bleaches when a catalytic reaction, such as hydrosilation, takes place. The assay is carried out in a glove bag or glove box on a Teflon block drilled with 70 reaction wells. This allows us to continuously monitor a large set of catalysts until a 'hit' (the most active catalyst) is registered by the dye bleaching in one of the reaction wells. We needed a dye that would not have potentially interfering reactive groups, hence the choice of a ferrocenyl group as electron donor and of a pyridinium as acceptor; the bulky benzylic tail is needed to make the dye conveniently soluble. When the reactive C=C or C=N bond is saturated, the electronic connection between donor and acceptor is broken and the absorption coefficient of the material drops by a factor of *ca*. 100. The starting dye must absorb intensely [ε(EtOAc) = 12 600, **1a**; 5200, **1b**] so as to mask any catalyst color and to be a sensitive indicator. Some quantitative data can be obtained: an initial bleaching time, t_i, corresponds to the first observable color change relative to a control well and a final time, t_f, corresponds to complete bleaching. Other work indicated that t_i corresponds to *ca*. 40% dye conversion and t_f to *ca*. 95%. A long induction time therefore translates to a long t_i, and high activity after induction to a short value of $t_f - t_i$. Recording the data proved possible using a digital camera.

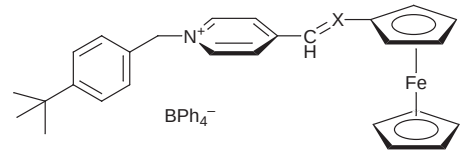

1a X = CH
1b X = N

As an initial test, we applied the method to a library of conventional catalysts, some of which were known to be active while others had never been considered for hydrosilation. The results showed that such well known species as $RhCl(PPh_3)_3$ are very active catalysts for **1**–Ph_2SiH_2, but, unexpectedly, that among the most active of all was a palladacycle never previously tried for hydrosilation. For reasons that are not yet clear, the dyes are activated substrates and react much faster than conventional ones, like stilbene, but the relative order of activity of different catalysts seems to be preserved between dye-substrates and conventional ones. Controls demonstrated that catalyst, silane and substrate are all required for reaction to occur. Fig. 1 shows the result of a typical run.

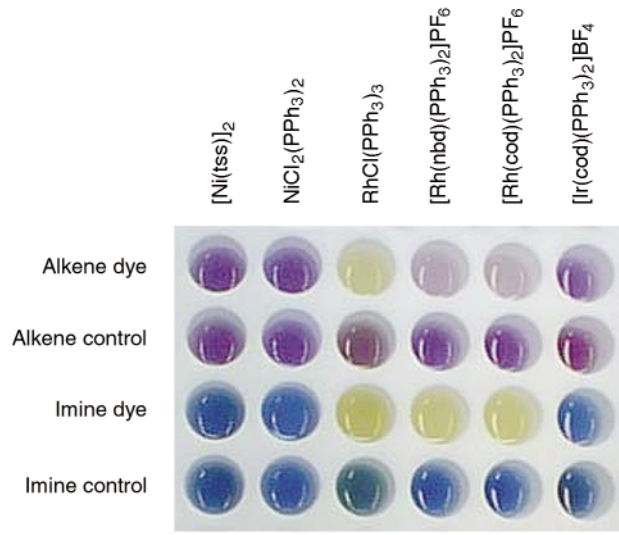

Fig. 1 Results of a typical run using the dyes **1a**,**b** to screen the catalysts identified in the figure for hydrosilation with Ph_2SiH_2.

The heat output of a catalytic reaction has been used by several groups as a continuous, parallel assay for activity. For example, Morken and coworkers[9] used an IR camera to record heat output. This was used to assay a simple polypeptide catalyst library on polystyrene beads that catalysed an exothermic ester hydrolysis in one case and in another the catalysts were homogeneous Mn, Cr and Co complexes for epoxide

opening. Each hit appeared as a bright spot on the image (Fig. 2) as the result of that bead having a temperature estimated to be *ca*. 1 °C above that of the reaction medium. Some differentiation of the spots by relative intensities was possible. Heterogeneous catalyst arrays can be analyzed in the same way.[10]

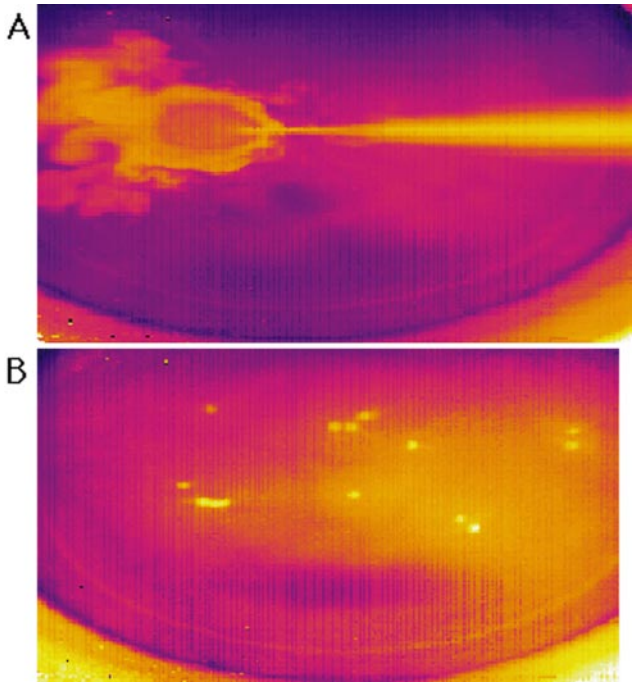

Fig. 2 Results of Morken's IR camera screening method. The more highly catalytically active beads appear bright because of the heat output from the reaction. (A) Thermographic image during addition of acetic anhydride to a chloroform mixture of ethanol, triethylamine and polystyrene bead-supported 4-aminopyridine. (B) As in (A), but after 15 s, showing bright beads. The illustrations were kindly provided by Professor Morken.

Hartwig and coworkers[11] have reported an interesting discontinuous fluorescence screen in which a series of forty conventional homogeneous $Pd(dba)_2$ + L (L = phosphine and diphosphine) catalysts were assayed for activity for coupling of an aryl halide with an alkene (Heck reaction). The aryl halide component was grafted onto cross-linked polystyrene and catalytically coupled with a soluble alkene bearing a powerfully fluorescent coumarin group (Fig. 3). At the end of the catalytic

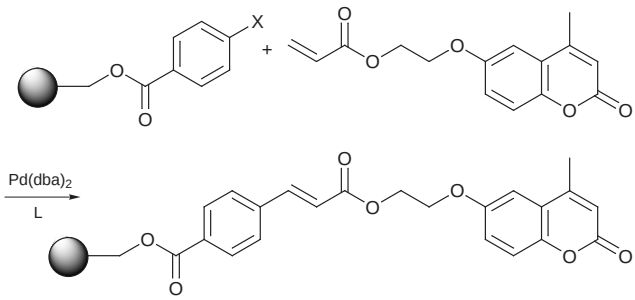

Fig. 3 The principle of Hartwig's[11] fluorescence screen of forty conventional homogeneous $Pd(dba)_2$ + L (L = phosphine and diphosphine, dba = dibenzylidene acetone) catalysts for activity in coupling of an aryl halide with an alkene (Heck reaction).

reaction the polymer beads were isolated by filtration and their fluoroescence assayed visually as low, moderate or high. Greater catalyst activity for a conventional homogeneous reaction using the same catalyst was shown to correlate quite well with the catalysts that gave the strongest fluorescence in the rapid assay. For example, the L = PBu^t_3 catalyst was identified as one of the most active.

Copeland and Miller[12] have proposed a method in which the catalytic reaction of eqn. (1) was followed by fluorescence: the acid released in the acyl transfer step protonates the dye precursor **2** [eqn. (2)] and turns on the fluorescent response.

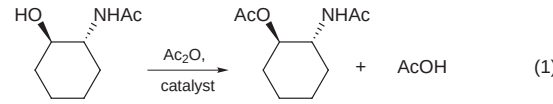

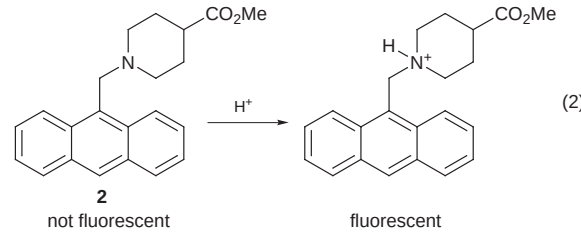

Using an automated fluorescent plate reader allowed quantitative, parallel intensity data to be obtained in solution on a 96-well plate, allowing comparison in triplicate of seven catalysts at three different loadings. The data were good enough to allow the kinetics to be followed. As described in more detail below, the same method was also applied to assaying a small catalyst library on polystyrene beads.

In an extremely sophisticated continuous parallel assay, proposed by Senkan,[13] resonance-enhanced multi-photon ionization techniques were used in connection with the evaluation of a heterogeneous catalyst library. A big advantage is that the method allows the products to be directly analyzed and selectivity data to be obtained. Catalyst libraries have also been evaluated by the conventional discontinuous, non-parallel methods of GC and HPLC.[14]

Asymmetric reactions pose special problems because a catalyst may be efficient only for one class of substrate but mediocre for others. To help solve this problem, Kagan[15] has proposed a discontinuous screening of the products from the reduction of multiple substrates from a one-pot reaction. The results for borane reduction of seven ketones with a chiral oxazaborolidene catalyst, where enantiomeric excesses were highly substrate-dependent, were comparable to those from conventional single substrate reactions on the individual ketones, suggesting only limited cross-talk took place between parallel reactions. Assay was by HPLC analysis with a chiral column.

Libraries of catalysts

A wide variety of methods[2] have been used for implementing combinatorial strategies in other fields but we will only discuss methods that have been applied to transition metal chemistry. The types of libraries that can be considered are just as varied as the types of assays. Libraries, which may be soluble or polymer-bound, may consist of preformed catalysts or of ligands that are active without metal ions or are converted to the catalytically active form by loading a suitable metal-containing precursor *in situ*. Catalysts can be highly solvent-sensitive, so varying the solvent can be useful. A study by Burgess *et al.*[16] illustrates the use of HTS to identify the best ligand/metal/solvent combination for a carbene insertion into a C–H bond [eqn. (3)]. In all, seven different metal ions, five chiral ligands and four solvents were studied using HPLC with an autosampler for determination of the diastereoisomer ratio. Each distinct combination was run in one well of a 96-well microtitre plate. Silver ion, previously not generally considered as a suitable catalyst, was shown to be very effective.

Having described the principal known catalyst assays, we move to the types of catalyst libraries that have been considered to date. These can be soluble or polymer-bound and either conventional or combinatorial. Although using a rapid parallel

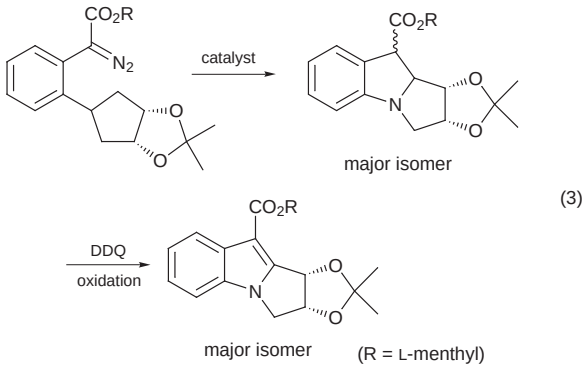

(3)

assay with a large combinatorial library is ultimately likely to be the most effective strategy for catalyst discovery, semiclassical approaches like conventional screening of combinatorial libraries or rapid screening of conventional catalysts are likely to be useful in certain situations.

A set of conventional homogeneous metal catalysts, such as was used in a study discussed above,[8] constitutes one of the simplest soluble libraries, and can be useful when the best combination of metal and ligand type is sought in the initial stage of an investigation. Once these have been chosen, the natural next step would be to vary the ligand set using parallel synthesis. Solid phase organic synthesis (SPOS) being so widely used for polymer-bound library synthesis, many catalysts are likely to be most conveniently synthesized on beads. Extensive literature on SPOS is available[17] but some discussion is appropriate here. Merrifield's original 2% cross-linked styrene–divinylbenzene copolymer is one current recognized standard, because it swells in many organic solvents, thus allowing reagents access to the interior of the bead, yet it does not dissolve and has substantial thermal stability. The material is partially chloromethylated to form the base resin used in SPOS. The level of chloromethylation determines the maximum achievable loading of the resin. A linker is normally employed to provide the starting point for the organic synthetic steps proper and to introduce a spacer group so that the reactive functionality is held somewhat apart in space from the polymer itself. The organic synthesis then proceeds on the linker. High yields are required in each step if good overall yields are to be obtained. Many standard organic reactions have been found to go well on solid phase and an excess of reagents can often be used to drive these reactions to high yield. Finally, the product may be cleaved from the resin, if a cleavable linker has been chosen, or used directly on-bead, although full characterization may not be possible if this alternative is chosen. Other related resins, such as Wang resin,[2] have also proved useful in catalysis studies.

A small library of four purely organic peptide-like catalysts has been assayed for acyl transfer catalytic activity with Miller's fluorescence assay [eqn. (1) and (2)].[12] In this case, the catalyst and the sensor were both grafted onto a Wang resin, each bead containing only a single type of catalyst. Once exposed to the substrates, acid was formed within the individual beads by the catalytic reaction. The resulting fluorescence [eqn. (2)] was detected visually with a microscope. Similar relative activities were observed between soluble and bead-bound versions of the same catalyst.

While not catalytic, Jacobsen's[18] combinatorial syntheses of a peptide-like library having metal-ligating properties illustrates how standard[2] 'split-and-pool' techniques can be used to introduce diversity into a ligand library. In such a synthesis, different batches of beads receive different initial residues in the first step of a parallel synthesis, and are then pooled together. The beads are then split so each batch can be subjected to a synthesis step that attaches a different residue in the second position. The beads are once again pooled and the procedure repeated until all the residues have been added. The final pool contains beads that have every permutation of possible sequences. The Still[19] encoding procedure was used by which a covalently bond organic tagging compound was grafted onto each type of bead to allow the ligand present on that bead type to be identified *via* MS detection of the tag after cleavage. Finally, the beads were assayed for their ability to bind Ni(II) *vs.* Fe(III). Colorimetric detection of metal binding provided the required assay.

Solid phase synthesis of a ligand and loading a metal to make a catalyst precursor poses no particular difficulty, but cleavage of a reactive catalyst from the bead is not likely to be possible without degradation of the complex, so it is likely that the ligands will be characterized on an aliquot of the bead sample before metal binding and catalysts will normally be assayed on-bead. For a valid comparison of two bead-catalysts for activity, it is not necessary to know exactly how many of the purported active sites really are active, but all the beads in the study must have approximately the same proportion of active sites. That beads that prove to be most active contain active sites is certain, but it may be very hard to rule out the possibility that one of the inactive or barely active beads would have been extremely active if the desired complex had been formed as intended. At a severely practical level one could say that this does not matter—a catalyst that cannot be made is not of practical interest. On a theoretical level, however, such an outcome would severely perturb any structure–activity relationships one was hoping to extract and therefore lead to erroneous conclusions. From the point of view of improving our understanding of catalysis, these structure–activity relationships are likely to be the most important general points that emerge from combinatorial catalysis and it remains to be seen how reliable these will be. Direct comparison of bead catalyst data with data from the solution analogues will not necessarily give reliable information, because we will not know whether to ascribe any deviation to improper synthesis of the active catalyst on the bead or to catalyst–polymer interactions.

One technical problem that can be readily addressed is the possibility of slow diffusion of the catalytic reagents into and products out of the bead could mask activity differences. To distinguish such differences between catalysts we need the catalyst turnover, not the diffusion steps, to be rate-limiting. This is most readily achieved, we find, by limiting the loading of the resin. Instead of using commercially chloromethylated resin, we therefore have made our own; the appropriate level may need to be determined for each case. This problem may be general. We also need a solvent that efficiently swells the polymer to allow rapid substrate access and product departure; the observed rate needs to reflect the rate of the catalytic and not the diffusion steps.

Assuming we use a suitable assay for picking the bead-bound catalyst with the properties that best correspond to what is needed, we are faced with a significant choice: do we try to make a homogeneous analogue of the successful catalyst or do we continue to use the bead-bound version in later work. The advantage of the homogeneous version is that it can be fully characterized and it is more amenable to full mechanistic studies. The successful ligand may be much harder to make by conventional methods than by SPOS, however, but this problem is unlikely to be serious. The most severe problem is that the activity and selectivity of the catalyst may well be very different in going from the bead-bound to the soluble forms; many examples of big differences in chemistry between soluble and polymer phase are known. As an example of a typical difference that might be expected to affect catalytic activity, a polymer-bound catalyst is unlikely to be as easily able to dimerize as a soluble version, and it may also interact with the linker or backbone polymer in some way. Not enough is known to be able to tell how big a problem this will prove to be, but it is already clear that solution and bead-bound catalysts do show significant differences. A significant dependence on the nature of the

polymer support and differences between bead-bound and the corresponding homogeneous catalyst in solution have already been seen for Jacobsen's epoxidation catalyst.[20] On the other hand, Hoveyda studied this specific problem and found generally good agreement between the selectivities of bead-bound and solution phase catalysts in the particular case studied.

We have prepared a diverse monophosphine library[21] of the type **P**–C_6H_4PRR' (**P** = polymer) on cross linked polystyrene by the route shown in Fig. 4 and loaded it with [M(diene)-

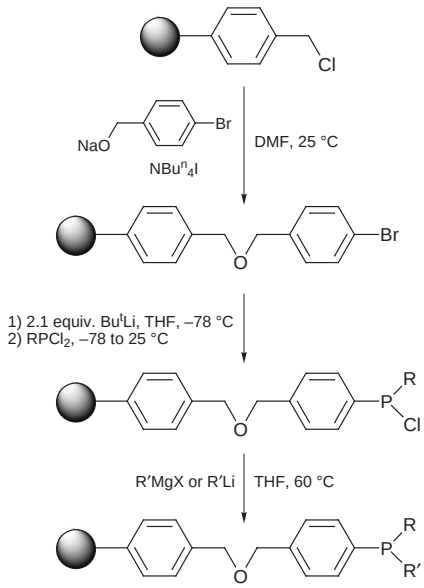

Fig. 4 The synthetic route to the generalized phosphine library of ref. 21.

$(py)_2]PF_6$, (M = Rh, Ir; py = pyridine). The two resulting sublibraries were assayed for hydrosilation activity with dyes **1a**,**b** following the prior[8] procedure to find the best supported catalysts. The resulting activities followed a different phosphine dependence for Ir *vs*. Rh and for alkene dye *vs*. imine dye, so catalysts selective for either alkene or imine could be identified. Structure/activity trends were weakly marked. The best catalyst of all had M = Ir, R = Ph and R′ = 1-naphthyl, but only rapidly reduced the alkene dye and the Rh analogue was rather slow for both dyes, an unexpected combination given the other trends seen. A combinatorial search may be particularly useful in situations such as this were the existence of ill-defined trends makes it hard to design a good catalyst.

Limitations

These methods are likely to have a number of significant limitations. Not all catalytic problems will be readily susceptible to the rapid screening-combinatorial approach. Bead-bound catalysts may also differ strongly from their soluble analogues in certain cases, making correlations between the two types of systems very difficult. Bead bound catalysts are difficult to characterize, and so one may not always be able to tell for sure why any particular bead-catalyst is poorly active—it could be that the catalyst is inherently poorly active or that the intended complex was not properly formed on the bead or that a catalyst dimerization only possible in free solution is required for activity. Careful controls and reliable analysis of the materials for metal content will be needed. Different solvents are expected to swell the polymer to different extents, resulting in rate differences that are unrelated to what would be seen in solution. We typically check, for example, that the unmodified starting resin does not take up metal and act as a catalyst in the absence of covalently attached ligand groups and that typical high activity resins have similar metal analyses to medium and low-activity resins. Even more than in traditional catalyst work, care will be needed in interpreting the results of combinatorial studies.

Combinatorial methods are unlikely to displace traditional characterization and mechanistic work. Indeed, these methods may enrich mechanistic studies by making structure–activity relationships available over a much wider range of structures than is usual in traditional studies. They may also help correct mechanistic misconceptions based on examining too small an amount of data.

Combinatorial methods could potentially be applied to any inorganic, organometallic, or bioinorganic problem where a suitable assay can be devised. For example, functional modelling of enzyme active sites has proved very challenging by traditional approaches. They also seem suitable for determining what coordination or organometallic structures can bind, or selectively bind, particular classes of ligand; in many cases, these ligands could be covalently bound to dyes for easy visualization. This approach might also help in determining the resting state of catalysts. For example, in hydrosilation, the silane might be tagged with a red dye and the alkene with a blue one. In such a case, catalyst beads that bound silane but not alkene would be red, silane but not alkene, blue, and if both were bound the beads would be expected to appear purple.

Future developments

There are already initial indications that other areas of inorganic chemistry than homogeneous catalysis are also likely to benefit from combinatorial methods. Mallouk *et al.*[22] have shown how they can be applied to finding electrochemical oxidation catalysts, for example, and they have also been used for materials synthesis, such as finding a superior luminescent material.[23]

Although the area of combinatorial chemistry and rapid screening is very new as applied to inorganic chemistry, it has already made a significant impact. The challenge now is to develop methods to apply it to a variety of problems to see how widely they are applicable. Care will be needed to characterize the resulting materials and to check the reliability of the data obtained by comparison with traditional approaches on selected materials. There are so many different ways these ideas could be embodied, that the effort will require ingenuity combined with a close attention to practicality and care in interpretation.

Acknowledgements

I am grateful to the US Dept. of Energy, Catalytica Corp. and Mitsubishi Oil Co. for funding, Jennifer Loch, Alyssa White, Matthew Torres and Alan Cooper for unpublished data and the other coworkers mentioned in the citations for their work on the problem.

Notes and references

1 R. H. Crabtree, *Acc. Chem. Res.*, 1979, **12**, 331.
2 S. R. Wilson and A. W. Czarnik, *Combinatorial Chemistry*, Wiley, New York, ed. J. Szostak, *Chem. Rev.*, 1997, **97**, 347 (Special issue on combinatorial chemistry).
3 C. M. Killian, D. J. Tempel, L. K. Johnson and M. Brookhart, *J. Am. Chem. Soc.*, 1996, **118**, 11 664.
4 (*a*) F. R. Hartley, *Supported Metal Complexes. A New Generation of Catalysts*, Riedel, Dordrecht, 1985; (*b*) R. B. Merrifield, *J. Am. Chem. Soc.*, 1963, **85**, 2149.
5 B. A. Bunin and J. Ellman, *J. Am. Chem. Soc.*, 1992, **114**, 10 997.
6 B. Jandeleit and W. H. Weinberg, *Chem. Ind.*, 1998, **19**, 795; W. H. Weinberg, B. Jandeleit, K. Self and H. Turner, *Curr. Opin. Solid State Mater. Sci.*, 1998, **3**, 104.
7 J. K. Borchardt, *Today's Chemist at Work*, 1998, **7**(10), 35.
8 A. C. Cooper, L. H. McAlexander, D.-H. Lee, M. T. Torres and R. H. Crabtree, *J. Am. Chem. Soc.*, 1998, **120**, 9971.
9 S. J. Taylor and J. P. Morken, *Science*, 1998, **280**, 267. See also: M. T. Reetz, M. H. Becker, K. M. Kühling and A. Holzwarth, *Angew. Chem., Int. Ed.*, 1998, **37**, 2647; F. C. Moates, M. Somani, J. Annamalai, J. T.

Richardson, D. Luss and R. C. Wilson, *Ind. Eng. Chem. Res.*, 1996, **35**, 4801.
10 A. Holzwarth, P. W. Schmidt and W. E. Maier, *Angew. Chem., Int. Ed.*, 1998, **37**, 2644.
11 K. H. Shaughnessy, P. Kim and J. H. Hartwig, *J. Am. Chem. Soc.*, 1999, **121**, 2123.
12 G. T. Copeland and S. J. Miller, *J. Am. Chem. Soc.*, 1999, **121**, 4306.
13 S. M. Senkan, *Nature*, 1998, **394**, 350.
14 M. S. Sigman and E. N. Jacobsen, *J. Am. Chem. Soc.*, 1998, **120**, 4901.
15 H. B. Kagan, *J. Organomet. Chem.*, 1998, **567**, 3; X. Gao and H. B. Kagan, *Chirality*, 1998, **10**, 120.
16 K. Burgess, H.-J. Lim, A. M. Porte and G. A. Sulikowski, *Angew. Chem., Int. Ed.*, 1996, **35**, 220.
17 J. S. Früchtel and G. Jung, *Angew. Chem., Int. Ed.*, 1996, **35**, 17; R. Epton, *Innovation and Perspectives in Solid Phase Synthesis*, Intercept, Andover, 1992.
18 M. B. Francis, N. S. Finney and E. N. Jacobsen, *J. Am. Chem. Soc.*, 1996, **118**, 8983.
19 M. H. J. Ohlmeyer, R. N. Swanson, L. W. Dillard, J. C. Reader, G. Asouling, R. Kobayashi, M. Wigler and W. C. Still, *Proc. Natl. Acad. Sci.*, 1993, **90**, 10 922.
20 L. Canali, E. Cowan, H. Deleuze, C. L. Gibson and D. C. Sherrington, *Chem. Commun.*, 1998, 2561.
21 A. C. Cooper, J. A. Loch and R. H. Crabtree, *J. Am. Chem. Soc.*, submitted; A. C. Cooper, J. A. Loch, A. White and R. H. Crabtree, unpublished data.
22 T. E. Mallouk, E. Reddington, C. Pu, K. L. Ley and E. S. Smotkin, *Ext. Abstr., Fuel Cell Seminar, Orlando, FL*, 1996, p. 686.
23 R. F. Service, *Science*, 1997, **277**, 474; E. Danielson, J. H. Golden, E. McFarland, C. M. Reaves, W. H. Weinberg and X. D. Wu, *Nature*, 1997, **389**, 944.

Paper 9/01022J

Lanthanide organometallic chemistry based on the porphyrinogen skeleton: acetylene and ethylene bridging praseodymium and neodymium $\eta^5:\eta^1:\eta^5:\eta^1$-bonded to *meso*-octaethylporphyrinogen

Elisa Campazzi, Euro Solari, Rosario Scopelliti and Carlo Floriani*

Institut de Chimie Minérale et Analytique, BCH, Université de Lausanne, CH-1015 Lausanne, Switzerland. E-mail: carlo.floriani@icma.unil.ch

Received (in Basel, Switzerland) 19th May 1999, Accepted 8th July 1999

The reaction of *meso*-octaethylporphyrinogen–lanthanide complexes, [{($\eta^5:\eta^1:\eta^5:\eta^1$-$Et_8N_4$)M}Na(thf)$_2$] [M = Pr, Nd], with $NaC_{10}H_8$ in an ethylene or acetylene atmosphere leads to the isolation of dimeric species, where the metals are bridged by the $[C_2H_4]^{2-}$ and $[C_2]^{2-}$ anions.

Porphyrinogen tetraanions provide a unique binding cavity for electron deficient metals, *e.g.* early transition metals.[1] Such metals can exploit the $\eta^5:\eta^3:\eta^1$ bonding mode of each of the pyrrolyl anions according to the metal charge and electronic requirements. In addition, the electron-rich pyrrolyl anions can function as binding countercations in the structure.[1,2] Although the organometallic chemistry of divalent lanthanides[3] is largely confined to Sm(II)[4–6] and, to a lesser extent, Yb(II)[7] and Eu(II),[3] and based on cyclopentadienyl ligands,[4,5] it has been possible, using *meso*-octaethylporphyrinogen as an ancillary ligand, to generate the oxidation state (II) for lanthanides which are usually not available in this oxidation state,[8] and to make them very reactive in the presence of appropriate substrates.

The reduction of complexes **1**[9] and **2**[9] with sodium metal in the presence of 18-crown-6 led to the isolation of the dimetalla-ethane-like skeleton, where each lanthanide ion is supported by the porphyrinogen tetraanion. It is important that the reaction is carried out in the presence of 18-crown-6 because of its beneficial effect on crystallization and the higher stability of the ethylene complex in case of the ion-separated form. A particularly interesting synthetic route to complexes **3** and **4**† is the replacement of N_2 by ethylene from complexes **5**[9] and **6** (Scheme 1).[9] Such a replacement was successful when it was carried out in the presence of 18-crown-6. The solvation of the alkali countercations, though often neglected, can be, in some of the polynuclear compounds like those reported here, a determining factor on the energetics of the reaction. Complexes **3** and **4** have been obtained under such experimental conditions (see synthetic procedures) which rule out any reversible binding of ethylene to the metal in complexes **3** and **4**.

The structure of the anion in complex **4**‡ is shown in Fig. 1 along with selected structural parameters. The porphyrinogen moieties display a saddle-shaped conformation with the metals being $\eta^5:\eta^1:\eta^5:\eta^1$ bonded to them. The solvation of the two sodium cations linked to the dimetallic tetraanion is provided by two adjacent pyrrole moieties, which act, at the same time, as η^5 ligands for the lanthanide and η^1 for the sodium and *vice versa*; solvation is completed by two THF molecules.[2] The other sodium cations are bonded together by a dioxane, and they both complete their coordination spheres with an 18-crown-6 and a THF molecule. The C–C bond distance [C37–C37′, 1.49(2) Å] tells us that the original ethylene has been converted into a 1,2-dimetalla-ethane moiety. The M–C bond distances [M–C37, 2.497(7); M–C25, 2.790 Å][10] however, when compared with those of olefin complexes from the literature,[5,10] leave the possibility of assuming a μ-$\eta^2:\eta^2$-bonding mode for the bridging $[C_2H_4]$ fragment. The metals in complexes **3** and **4** are in the oxidation state (III) according to the magnetic moments, which are very close to those of the starting complexes **1** and **2**.

When the same synthetic method was applied to the reaction of **1** and **2** in the presence of acetylene, deprotonation of the substrate occurred instead of reduction of the metal, leading to **7**† and **8** (Scheme 1). The resulting acetylido complex **7**‡ is shown in Fig. 2 with selected structural parameters. The dimer

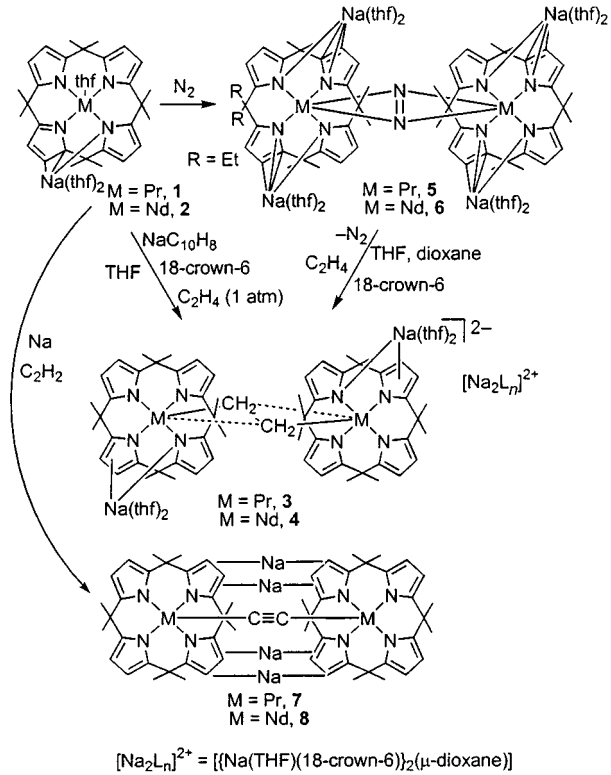

Scheme 1

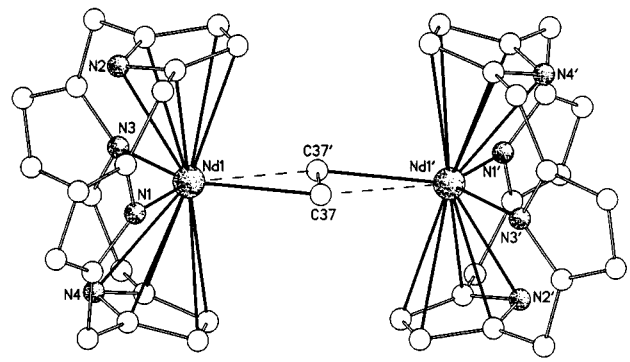

Fig. 1 A view of complex **4**. Selected bond distances (Å): Nd(1)–η^5(Pyr)$_{av}$ 2.584(4), Nd(1)–η^1(Pyr)$_{av}$ 2.564(7), Nd(1)–C(37) 2.497(7), Nd(1)–C(37′) 2.790(7), C(37)–C(37′) 1.49(2). η^5(Pyr)$_{av}$ indicates the centroid. Prime indicates a transformation of $-x, -y, -z$. (*meso*-Ethyl groups omitted for clarity).

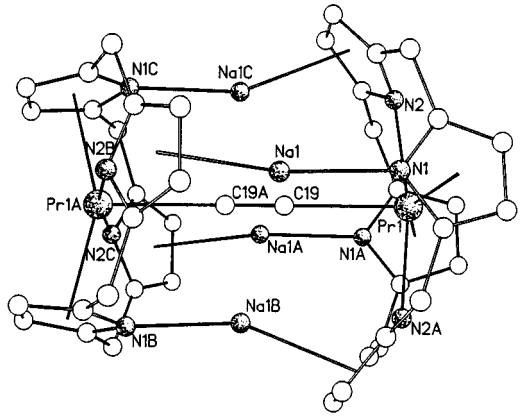

Fig. 2 A view of complex **7**. Selected bond distances (Å): Pr(1)–η⁵(Pyr) 2.492(1), Pr(1)–η¹(Pyr) 2.408(2), Na(1)–η⁴(Pyr) 2.612(2), Na(1)–η¹(Pyr) 2.376(2), Pr(1)–C(19) 2.670(4), C(19)–C(19A) 1.250(8). η⁵(Pyr) indicates the centroid. Letters A, B and C indicate symmetry operations of $-x + 1/2$, $-y + 1/2$, z; y, $-x + 1/2$, $-z + 1/2$; $-y + 1/2$, x, $-z + 1/2$, respectively. (*meso*-Ethyl groups omitted for clarity).

has C_4 symmetry and the porphyrinogen, in the saddle-shaped conformation, displays an $\eta^5:\eta^1:\eta^5:\eta^1$ bonding mode. The two metal–porphyrinogen moieties are bridged by the C_2^{2-} μ-$\eta^2:\eta^2$-bonded anion [C–C, 1.250(8) Å]. The rather long M–C bond distances [2.670(4) Å][11] account for the high coordination number of the metals when bonded to the *meso*-octaalkylporphyrinogen tetraanion.[1,2] The C_2^{2-} anion is an appropriate spacer determining the cavity inside which are bound four Na cations, which are sandwiched by the two metalla-porphyrinogen moieties.[2d] Each Na is alternately bonded η^1 and η^4 to the two metalla-porphyrinogens, which assure complete solvation of all four alkali metal cations without the help of any additional solvent.[2]

The methodology reported in this paper represents a new entry into the organometallic chemistry of lanthanides for a number of issues: (i) the use of non-conventional ancillary ligands; (ii) the possibility to exploit the high reactivity of transient Ln(II) derivatives, *i.e.* for those metals which are not stable in this oxidation state; and (iii) the possibility to form M–C σ bonds readily directly from olefins and alkynes.

Notes and references

† *Synthesis of* **4**. The addition of 18-crown-6 (2.61 g, 9.87 mmol) to a sky-blue suspension of **2** in THF (130 cm³) caused the formation of a sky-blue solution. The addition of sodium metal (0.124 g, 5.38 mmol) under a C_2H_4 atmosphere did not cause any change until a small amount of naphthalene was added (0.172 g, 1.34 mmol). After 2 h a green suspension was obtained and was kept at room temperature until the complete disappearance of sodium metal. The solvent was evaporated to 10 cm³, then pentane (40 cm³) was added (5.3 g, 44%). Crystals appropriate for X-ray analysis were obtained from refluxing THF in the presence of a small amount of dioxane. (Found: C, 60.15; H, 8.25; N, 4.28. **4**·(18-crown-6)$_2$(THF)$_8$(dioxane), $C_{134}H_{220}N_8Na_4Nd_2O_{22}$ requires C, 60.15; H, 8.29; N, 4.19%). μ_{eff} = 3.18 μ_B at 298 K. The magnetic susceptibility was measured with an MPMS5 SQUID susceptometer. Complex **4** was obtained equally well from the reaction of **6** with ethylene in the presence of 18-crown-6. *Synthesis of* **7**. Sodium metal (0.089 g, 3.85 mmol) was added to a yellow suspension of **1** (2.94 g, 3.48 mmol) in THF (130 cm³) under an acetylene atmosphere. The sodium reacted within 24 h at room temperature. Some white solid was filtered out and the solvent evaporated to dryness. The solid residue was collected using pentane (2.20 g, 72%). (Found: C, 61.40; H, 7.54; N, 6.23. **7**·4THF, $C_{90}H_{128}N_8Na_4Pr_2O_4$ requires C, 61.43; H, 7.33; N, 6.37%). μ_{eff} = 2.61 μ_B at 298 K. Crystals for X-ray analysis were obtained from refluxing benzene, as **7**·4C_6H_6.

‡ *Crystal data for* **4**: $C_{90}H_{132}N_8Na_2Nd_2O_4$·$C_{36}H_{72}Na_2O_{16}$·2$C_4H_8O$, M = 2675.62, triclinic, space group $P\bar{1}$, a = 15.530(3), b = 15.847(4), c = 16.647(5) Å, α = 113.08(3), β = 111.51(2), γ = 95.86(2)°, V = 3358.8(15) Å³, Z = 1, D_{calc} = 1.323 g cm^{-3}, F(000) = 1420, λ(Mo-Kα) = 0.71070 Å, μ = 0.846 mm^{-1}; crystal dimensions 0.31 × 0.22 × 0.17 mm. Diffraction data were collected on a mar345 Image Plate Detector at 143 K. For 6344 observed reflections [$I > 2\sigma(I)$] and 767 parameters the final $R1$ index is 0.0842 ($wR2$ = 0.2489 for 8475 independent reflections). For **7**: $C_{74}H_{96}N_8Na_4Pr_2$·4C_6H_6, M = 1783.80, tetragonal, space group $P4_2/n$, a = 15.2320(10), c = 18.729(2) Å, V = 4345.4(6) Å³, Z = 2, D_{calc} = 1.363 g cm^{-3}, F(000) = 1852, λ (Mo-Kα) = 0.71070 Å, μ = 1.179 mm^{-1}; crystal size 0.38 × 0.31 × 0.24 mm. Diffraction data were collected on a mar345 Image Plate Detector at 143 K. For 3239 observed reflections [$I > 2\sigma(I)$] and 255 parameters the final $R1$ index is 0.0303 ($wR2$ = 0.0971 for 3801 independent reflections). CCDC 182/1333. See http://www.rsc.org/suppdata/cc/1999/1617/ for crystallographic files in .cif format.

1 (*a*) D. Jacoby, C. Floriani, A. Chiesi-Villa and C. Rizzoli, *J. Am. Chem. Soc.*, 1993, **115**, 3595; (*b*) D. Jacoby, S. Isoz, C. Floriani, A. Chiesi-Villa and C. Rizzoli, *J. Am. Chem. Soc.*, 1995, **117**, 2793; (*c*) C. Floriani, in *Stereoselective Reactions of Metal-Activated Molecules*, ed. H. Werner and J. Sundermeyer, Vieweg, Wiesbaden, 1995, pp. 97–106; (*d*) D. Jacoby, S. Isoz, C. Floriani, K. Schenk, A. Chiesi-Villa and C. Rizzoli, *Organometallics*, 1995, **14**, 4816; (*e*) S. Isoz, C. Floriani, K. Schenk, A. Chiesi-Villa and C. Rizzoli, *Organometallics*, 1996, **15**, 337; (*f*) E. Solari, F. Musso, C. Floriani, A. Chiesi-Villa and C. Rizzoli, *J. Chem. Soc., Dalton Trans.*, 1994, 2015; (*g*) D. Jacoby, S. Isoz, C. Floriani, A. Chiesi-Villa and C. Rizzoli, *J. Am. Chem. Soc.*, 1995, **117**, 2805; (*h*) C. Floriani, *Pure Appl. Chem.*, 1996, **68**, 1; (*i*) R. Crescenzi, E. Solari, C. Floriani, N. Re, A. Chiesi-Villa and C. Rizzoli, *Organometallics*, 1999, **18**, 606.

2 (*a*) S. De Angelis, E. Solari, C. Floriani, A. Chiesi-Villa and C. Rizzoli, *Angew. Chem., Int. Ed. Engl.*, 1995, **34**, 1092; (*b*) S. De Angelis, E. Solari, C. Floriani, A. Chiesi-Villa and C. Rizzoli, *Organometallics*, 1995, **14**, 4505; (*c*) G. Solari, E. Solari, C. Floriani, A. Chiesi-Villa and C. Rizzoli, *Organometallics*, 1997, **16**, 508; (*d*) C. Floriani, E. Solari, G. Solari, A. Chiesi-Villa and C. Rizzoli, *Angew. Chem., Int. Ed.*, 1998, **37**, 2245; (*e*) L. Bonomo, O. Dandin, E. Solari, C. Floriani and R. Scopelliti, *Angew. Chem. Int. Ed.*, 1999, **38**, 913.

3 G. B. Deacon and Q. Shen, *J. Organomet. Chem.*, 1996, **506**, 1 and references therein.

4 (*a*) W. J. Evans, D. K. Drummond, L. R. Chamberlain, R. J. Doedens, S. G. Bott, H. Zhang and J. L. Atwood, *J. Am. Chem. Soc.*, 1988, **110**, 4983; (*b*) W. J. Evans and D. K. Drummond, *J. Am. Chem. Soc.*, 1988, **110**, 2772; (*c*) W. J. Evans and D. K. Drummond, *J. Am. Chem. Soc.*, 1989, **111**, 3329; (*d*) W. J. Evans, J. T. Leman, J. W. Ziller and S. I. Khan, *Inorg. Chem.*, 1996, **35**, 4283; (*e*) W. J. Evans, T. A. Ulibarri, L. R. Chamberlain, J. W. Ziller and D. Alvarez, Jr., *Organometallics*, 1990, **9**, 2124; (*f*) W. J. Evans and D. K. Drummond, *Organometallics*, 1988, **7**, 797; (*g*) W. J. Evans, R. A. Keyer, G. W. Rabe, D. K. Drummond and J. W. Ziller, *Organometallics*, 1993, **12**, 4664.

5 (*a*) R. D. Ernst and T. J. Marks, *J. Organomet. Chem.*, 1987, **318**, 29; (*b*) R. D. Ernst, *J. Organomet. Chem.*, 1990, **392**, 51; (*c*) R. D. Rogers and L. M. Rogers, *J. Organomet. Chem.*, 1990, **380**, 51; 1991, **416**, 201; 1992, **442**, 83; 1992, **442**, 225; (*d*) T. J. Marks and R. D. Ernst, in *Comprehensive Organometallic Chemistry*, ed. G. Wilkinson, F. G. A. Stone and E. W. Abel, Pergamon, Oxford, 1982, vol. III, ch. 21; (*e*) F. T. Edelmann, in *Comprehensive Organometallic Chemistry II*, ed. E. W. Abel, F. G. A. Stone and G. Wilkinson, Pergamon, Oxford, 1995, vol. 4, ch. 2; (*f*) M. Ephtrikhine, *Chem. Rev.*, 1997, **97**, 2193; (*g*) H. Schumann, J. A. Meese-Marktscheffel and L. Esser, *Chem. Rev.*, 1995, **95**, 865.

6 Samarium has been complexed to the same kind of macrocycle in: J. L. Song and S. Gambarotta, *Angew. Chem., Int. Ed. Engl.*, 1995, **34**, 2141; J. Jubb and S. Gambarotta, *J. Am. Chem. Soc.*, 1994, **116**, 4477.

7 (*a*) D. J. Schwartz, G. E. Ball and R. A. Andersen, *J. Am. Chem. Soc.*, 1995, **117**, 6027; (*b*) D. J. Schwartz and R. A. Andersen, *Organometallics*, 1995, **14**, 4308.

8 For a very interesting approach in the field, see: M. C. Cassani, D. J. Duncalf and M. F. Lappert, *J. Am. Chem. Soc.*, 1998, **120**, 12958.

9 E. Campazzi, E. Solari, C. Floriani and R. Scopelliti, *Chem. Commun.*, 1998, 2603.

10 W. J. Evans, T. A. Ulibarri and J. W. Ziller, *J. Am. Chem. Soc.*, 1990, **112**, 219; 2314 and references therein.

11 (*a*) W. J. Evans, G. W. Rabe and J. W. Ziller, *J. Organomet. Chem.*, 1994, **483**, 21; (b) W. J. Evans, R. A. Keyer and J. W. Ziller, *Organometallics*, 1993, **12**, 2618.

Communication 9/04032C

Catalyst poisoning by methyl groups

Peter Albers,*[a] Hubert Angert,[a] Günter Prescher,[a] Klaus Seibold[a] and Stewart F. Parker[b]

[a] *Degussa-Hüls AG, P.O. Box 1345, D-63403 Hanau, Germany. E-mail: Dr_Peter.Albers@degussa.de*
[b] *ISIS Facility, Rutherford Appleton Laboratory, Chilton, Didcot, UK OX11 0QX*

Received (in Cambridge, UK) 23rd June 1999, Accepted 12th July 1999

Palladium catalysts which showed premature deactivation under technical conditions were studied by means of inelastic incoherent neutron scattering (INS) spectroscopy revealing the cause of the poisoning to be a surface-bound methyl group.

During investigations on deactivation phenomena on catalysts from various industrial applications, macroscopic samples (many kilograms each) of spent palladium catalysts were isolated because of their peculiar behaviour. These catalysts were used for the partial hydrogenation of C=C structures in the ring systems of aromatic and polyaromatic molecules and for the hydrogenation of C=O groups to C–OH groups of functionalized aromatic and polyaromatic systems.† Conventional analytical methods for catalyst characterisation did not give any clear evidence for the presence of coke, inorganic contaminants or chemical poisons (carbon monoxide, sulfidic species) which are the most common causes of premature deactivation. Hydrogen absorption/desorption isotherms did not reveal anomalous properties or atypical hysteresis effects compared to literature data,[1,2] nor did electron microscopy studies show any unusual particle growth or sintering effects. When comparing the compositions of active and deactivated catalysts by elemental analysis, there was no correlation between the total amount of residual carbonaceous species and the catalytic activity. Surface spectroscopy by means of energy dispersive X-ray microanalysis, time-of-flight secondary ion mass spectrometry, and X-ray photoelectron spectroscopy did not result in the identification of any critical surface contamination involved. The signals of residual amounts of adsorbed solvent molecules were observed predominantly.

Vibrational spectroscopy has been extensively used for the characterisation of surface species on metal single crystal surfaces[3] and supported metal catalysts.[4] However, finely divided metal particles of catalysts absorb electromagnetic radiation from the infrared through the visible. As a result, Raman spectroscopy, using either visible or near-infrared excitation, and infrared spectroscopy were both unsuccessful. This problem could uniquely be circumvented by the use of inelastic neutron scattering spectroscopy. For neutrons the scattering is determined by the total scattering cross-section and the amplitude of vibration. For palladium the large mass (106.4 u) and small cross-section (4.48 barns, 1 barn = 1×10^{-28} m^2) mean that the palladium is largely transparent to neutrons. In contrast, the incoherent scattering cross-section for hydrogen is huge (79.90 barns) and together with its light mass (1.007 u) has the result that the scattering is dominated by hydrogenous motions.

The normalized INS spectra‡ of a deactivated catalyst before and after extraction with acetone (24 h, afterwards dried *in vacuo*) are shown in Fig. 1 together with the spectrum of the corresponding active catalyst after extraction with acetone under exactly the same conditions. In its original condition—as obtained from the technical application—the catalyst surface is still covered by a variety of adsorbed species consisting of polyaromatic molecules which are mainly residual amounts of solvent molecules [Fig. 1(a)]. After extraction, the broad background due to these solvent molecules or other adsorbed organic species is removed from the spectrum but a series of strong, sharp peaks remain [Fig. 1(b)] which are completely absent on the corresponding active catalyst [Fig. 1(c)]. Note that the same peaks are present in the "as-received" sample before clean-up.

The most striking feature of the spectrum is its simplicity: there are remarkably few bands. This implies either a highly symmetric structure with many degenerate modes or a small molecule. The intense 302 cm^{-1} feature suggested a methyl torsion, so a model consisting of a methyl group in an on-top site (see inset in Fig. 2) was used as the basis for a CLIMAX[5] analysis of the spectrum. The excellent fit shown in Fig. 2 was obtained. The quality of the fit is not dependent on the precise geometry of the model; small changes in bond angles or distances do not make any significant difference. The critical factors are the number of atoms and their spatial arrangement, thus a surface methylene group gives a different pattern. The only modification necessary was to increase the mass of the outer Pd atoms by a factor of 10 (*i.e.* to 1060 u) to mimic the

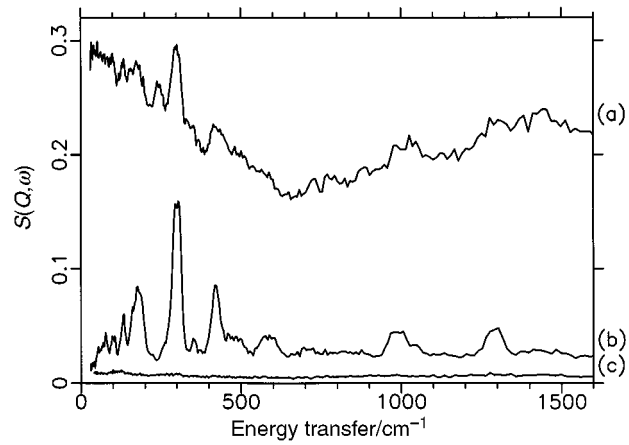

Fig. 1 INS spectra of palladium catalysts. Deactivated catalyst before (a) and after (b) extraction. Active catalyst after extraction (c).

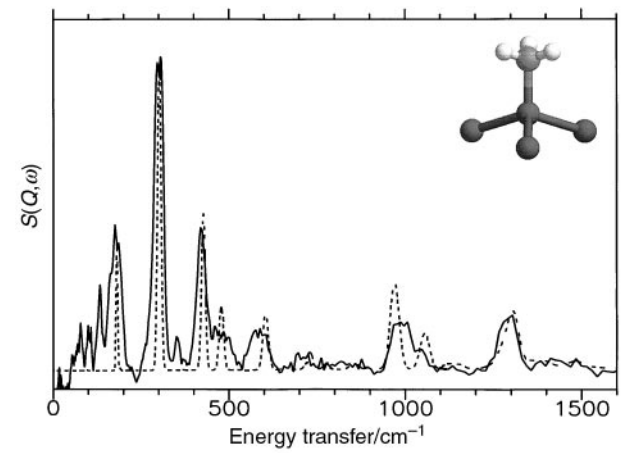

Fig. 2 Comparison of the INS spectrum of the deactivated catalyst (solid line) and the results from the CLIMAX analysis of the spectrum (dashed line).

Table 1 Observed bands (cm^{-1}) and assignments for MCH_3 in C_{3v} symmetry

Literature					
Typical[6]	$CH_3Mn(CO)_5$[7,8]	$CH_3Ni(111)$[9]	$CH_3Pt(111)$[10]	Present work	Assignment
				74w	Bulk Pd phonon
				100w	νPd–Pd (A_1)
				133w	Bulk Pd phonon
				179s	νPd–Pd (E)
				265sh	Bulk Pd phonon
				301vs	CH_3 torsion (A_2)
				353w	$2 \times \nu$Pd–Pd (E)
				420s	δPd–C (E)
400–700	420	370	520	484w	νM–CH_3 (A_1)
				580m	$2 \times CH_3$ torsion (A_2)
				699w	CH_3 torsion (A_2) + δPd–C (E)
700–950	783		820	973m	CH_3 rock (E)
1100–1300	1184	1220	1180	1013sh	δCH_3 (A_1)
1350–1400	1420	1360	1410	1287m	δCH_3 (E)

ν = stretch, δ = bend, s = strong, m = medium, w = weak, v = very, br = broad, sh = shoulder

inertia of the catalyst surface. Only the band at 179 cm^{-1} was affected by this procedure. Table 1 lists all the observed bands and their assignments as well as some literature comparisons.[6–10] The assignments for the fundamentals are taken from the literature. It should be noted that the frequencies for the methyl vibrations differ significantly from those typical of organic molecules, this is well documented. The assignments for the overtones and combinations come from the CLIMAX fit. The assignment to surface bound methyl groups is also supported by a recent density functional calculation[11] that indicated CH_3 on Pd(111) was stable to dehydrogenation and preferentially adsorbed in the on-top site, as observed here. Additional computer simulation experiments on the spectral features of ethyl, methylidyne, methylene and ethylidyne groups revealed that the only fit with reasonable quality and chemically reasonable frequencies was obtained for a surface methyl group.

The sharpness of the peaks suggests that the methyl groups are bound to the topmost atomic layer of the catalyst and the intensities suggest that macroscopic amounts of CH_3–Pd species are present. Comparing the normalized intensities of the CH_3–Pd signals for several deactivated samples showed an excellent correlation of these intensities with the degree of catalyst deactivation. The large quantity of bound methyl groups presumably caused a modified surface polarity by their sp^3 centres inhibiting the adsorption of sp^2 type reactants on the catalyst surface and, therefore, significantly lowered the catalyst performance by a surface blocking effect. The CH_3–Pd species at the surfaces of the deactivated catalysts were observed to be quite stable in air and quite resistant to repeated solvent extraction or hydrogenation/dehydrogenation experiments under ambient conditions.

It seems remarkable that on the surfaces of finely divided, deactivated catalysts from large scale technical applications very well defined, simple molecular structures can reproducibly be found at a macroscopic scale which hitherto have only been detected in surface science experiments on metal single crystals. This example illustrates that the gap[12] between surface science and technical catalysis, which is considered to complicate the translation of results from experiments on low surface area materials at low pressures on the one hand into the field of applied catalysis on high surface area materials at ambient or high pressures on the other, may, in some cases, not be as large as is believed.

We would like to express our gratitude to the Rutherford Appleton Laboratory for access to the neutron beam facilities of ISIS. Degussa-Hüls AG is thanked for support of the measurements.

Notes and references

† The hydrogenation reactions were carried out in conventional gas/liquid reactor systems with suspended catalyst and internal recycle at temperatures between 60 °C and 90 °C, hydrogenation pressures between 1.5 and 3 bar. At reactant concentrations of 10–15% the degree of hydrogenation was adjusted to 60–70% yielding product concentrations of about 7–10% of hydrogenated products for further processing. The spent catalyst samples exhibited less than 10% of their regular hydrogenation activity. Usually they show excellent activity over extended times of use under varying conditions.

‡ 25 g samples of the palladium catalysts were put into thin walled aluminium cans which were evacuated to 10^{-6} mbar to remove volatile adsorbed species. INS spectra were recorded at 20 K using the INS spectrometer TFXA (Time Focused Crystal Analyzer) at the ISIS pulsed neutron scattering facility (Rutherford Appleton Laboratory, Chilton, UK).

1 F. A. Lewis, *The Palladium Hydrogen System*, Academic Press, London 1967, pp. 23–30.
2 E. Wicke and H. Brodowsky, in *Hydrogen in Metals II*, ed. G. Alefeld, and J. Völkl, *Top. Appl. Phys.*, Springer, Berlin, 1978, vol. 29, p. 73 and refs. cited therein.
3 F. Zaera, *Chem. Rev.*, 1995, **95**, 2651.
4 J. L. G. Fierro, *Stud. Surf. Sci. Catal. B*, 1990, **57**, 67.
5 G. J. Kearley, *Nucl. Instrum. Methods Phys. Res., Sect. A*, 1995, **354**, 53.
6 K. Nakamoto, *Infrared and Raman Spectra of Inorganic and Coordination Compounds, Part B*, Wiley Interscience, New York, 5th edn., 1997, p. 258.
7 M. A. Andrews, J. Eckert, J. A. Goldstone, L. Passell and B. Swanson, *J. Am. Chem. Soc.*, 1983, **105**, 2262.
8 G. P. McQuillan, D. C. McKean, C. Long, A. R. Morrison and I. Torto, *J. Am. Chem. Soc.*, 1986, **108**, 863.
9 M. B. Lee, Q. Y. Yang and S. T. Ceyer, *J. Chem. Phys.*, 1987, **87**, 2724.
10 M. A. Henderson, G. E. Mitchell and J. M. White, *Surf. Sci.*, 1987, **184**, L325.
11 J.-F. Paul and P. Sautet, *J. Phys. Chem. B*, 1998, **102**, 1578.
12 H. P. Bonzel, *Surf. Sci.*, 1977, **68**, 236.

Communication 9/05034E

ChemComm

First evidence for radical anions in metathesis catalysis

Valia Amir-Ebrahimi,[a] James G. Hamilton,[a] Jane Nelson,[a] John J. Rooney,[a] Jillian M. Thompson,[a] Andrew J. Beaumont,[b] A. Denise Rooney[b] and Charles J. Harding[c]

[a] *School of Chemistry, The Queen's University, Belfast, UK BT9 5AG*
[b] *Chemistry Department, National University of Ireland, Maynooth, Kildare, Ireland*
[c] *Chemistry Department, The Open University, Milton Keynes, UK MK7 6AA. E-mail: c.j.harding@open.ac.uk*

Received (in Cambridge, UK) 9th June 1999, Accepted 5th July 1999

The Grubbs' catalyst, $(PCy_3)_2RuCl_2$(=CHPh), generates persistent radical anions on treatment with π-acceptors such as *p*-benzoquinones and a remarkably wide range of dienes and even simple alkenes.

In the course of an investigation of the metathesis polymerisation of several norbornadiene derivatives catalysed by $(PCy_3)_2RuCl_2$(=CHPh) (**1**), we have noted[1] that 2,3-bis(ethoxycarbonyl)norbornadiene is slow to react even though it polymerises rapidly using $RuCl_3{\cdot}nH_2O$ as catalyst. Dias and Grubbs[2] previously remarked on the reluctance of 2,3-bis(trifluoromethyl)norbornadiene to polymerise, so there is here a hint that those dienes which are also Michael acceptors may chelate to **1** in the di-*endo* mode *via* a charge transfer interaction which retards normal initiation and/or propagation. Furthermore there is a very recent report[3] that **1** is also a very good catalyst for methyl methacrylate polymerisation. This led us to conclude that **1** may be capable of reducing a variety of π-acceptors in solution to radical anions. We therefore decided to investigate, by EPR analysis, the presence of radical anions generated from strong π-acceptors such as tetrahydro- (**2**), tetrafluoro- (**3**), tetrachloro- (**4**) and dichlorodicyano-*p*-benzoquinone (**5**).

When 0.5 cm^3 of a (1–5) $\times$ 10^{-3} M solution of **1** in CH_2Cl_2 is mixed with 0.5 cm^3 of a solution of the of π-acceptor [(5–10) $\times$ 10^{-2} M] in the same solvent under argon at room temperature, EPR spectra are observed which persist for many hours.† Each diene generates a different EPR spectrum centred close to the free spin value, (g ~ 2.005, typical of radical anions) and bearing no resemblance to Ru^{III}-centred EPR signals in general[4] or to Ru^{III}-bound alkenes in particular.[5]

Using **2** we observed immediate strong well-resolved EPR signals (Fig. 1) that decay over a period of hours. The spectrum consists of a triplet of triplet of triplets, arising from coupling to three pairs of spin ½ nuclei, presumably the protons H_A and H_B (see **I**) together with the ^{31}P nuclei of the catalyst.

The EPR spectrum from **3** under these conditions is complex; on preliminary analysis, two distinct overlapping patterns of six and eight lines suggesting the existence of more than one radical species. When **1** is replaced by (phen)$Ru(CO)_2Cl_2$ (**6**) as donor, however, addition of **3** gave a weak simple 1:2:1 triplet which was stable over several hours (Fig. 2). By way of contrast, the addition of Grubbs' catalyst **1** to **4** generated a very strong doublet, while with **6**, **4** generated only a very intense singlet. The behaviour of **6** with benzoquinone is different in nature from anything so far observed in this work. The initial weak complex signal evolves into a relatively intense five-line metal-centred signal due to coupling to two equivalent N atoms from the phen ligand, similar to those found previously[6] for electrochemically generated Ru-centred radical anions.

The most striking result occurred on addition of norbornadiene **7** to **1**. An intense sharp triplet (Fig. 3) is observed, which decays only by some 50% over 24 h. We believe this signal can be explained by delocalisation of unpaired spin over *one* alkene moiety, as represented by **I**.

On treatment with **1**, norbornene and cyclopentene afford similar but much weaker triplets, while benzonorbornadiene gives a similar triplet following on the disappearance of an initial short-lived doublet of around the same g value. We are, as yet, unable to assign these spectra.

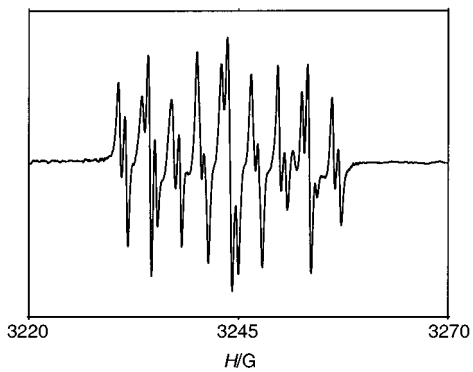

Fig. 1 EPR spectrum of Grubbs' catalyst **1** (1×10^{-3} M) with benzoquinone **2** (1×10^{-1} M), recorded in CH_2Cl_2 at 20 °C, showing the 1:2:1:2:4:2:1:2:1 triplets. g = 2.0048; A_1 = 4.8 G, A_2 = 1.6 G, A_3 = 0.4 G.

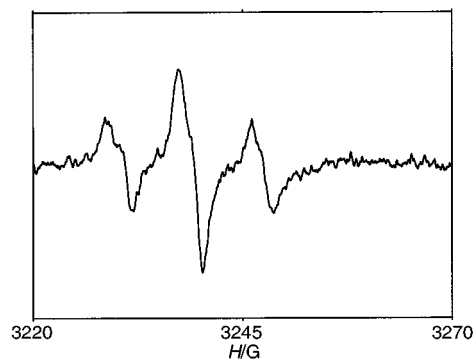

Fig. 2 EPR spectrum of **6** (5×10^{-3} M) with tetrafluorobenzoquinone **3** (5×10^{-2} M), recorded in CH_2Cl_2 at 20 °C. g = 2.0075; A = 8.6 G.

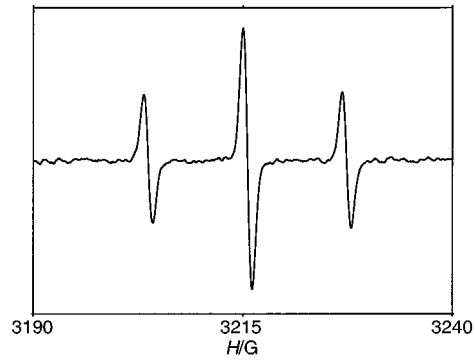

Fig. 3 EPR spectrum of **1** (1×10^{-3} M) with norbornadiene **7** (2×10^{-1} M), recorded in CH_2Cl_2 at 20 °C. g = 2.0064; A = 12.0 G.

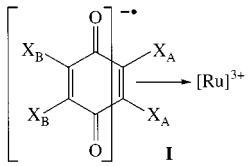

I

The presence of **2**, **3** or **4** enhances the activity of the Grubbs catalyst without changing the *cis* content of the polynorbornadiene (16%) as found using **1** alone. Similar results have also been obtained[7] when **4** is used as a cocatalyst with mesityl-$Mo(CO)_3$ for phenylacetylene and norbornene polymerisations.

Several major points arise from this work.

(i) Species **1** is remarkably effective at forming radical anions even from simple olefins.

(ii) The spectrum generated by treatment of **2** with **1** indicates the loss of equivalence of the four protons in the benzoquinone radical anion,[8] a consequence of the η^2-binding of **2** to the Ru^{II} centre as in **I**. Following π-donation from the coordinated C=C moiety, electron transfer takes place from the ruthenium cation to the uncoordinated C=C group. In this way the inequivalence of the X_B and X_A sets in Fig. 1 and 2 is explained; in Fig. 2, indeed, the F_A set is seen to be EPR silent.

(iii) The mechanism of initiation and perhaps even propagation of the metathesis reaction involves radical anions even for simple alkenes in accordance with eqns. (1) and (2). In support

$$\mathbf{1} + \text{alkene} \rightarrow [\mathbf{1}\text{–}\eta^2\text{-alkene}] \quad (1)$$

$$[\mathbf{1}\text{–}\eta^2\text{-alkene}] + \text{alkene} \rightarrow [\mathbf{1}\text{–}\eta^2\text{-alkene}]^{\bullet+} + [\text{alkene}]^{\bullet-} \quad (2)$$

of this we note that norbornadiene, which may act *in lieu* of two alkene molecules and chelate as in **I**, generates a more intense signal than norbornene and also initiates polymerisation far more efficiently. This suggests that in metathesis the substrate itself may act as a cocatalyst by virtue of radical anion formation, as supported by the cocatalytic effect noted above for quinones **2, 3** and **4**. While there is evidence for involvement of anion radicals in the initiation step, we do not know whether this extends to the [2 + 2] cycloaddition propagation step. Should this prove to be so, it raises very fundamental questions about the exact theoretical nature (concerted or otherwise) of the key step.‡

(iv) Not only is the EPR technique now seen as a valuable novel probe in metathesis reactions but it can also be employed for a wide variety of organometallic systems and other catalytic processes where the presence of suitable π-acceptors may also act as important promoters. With the objective of identifying, *via* detailed assignment of their spectra, the radical anions observed in this work, we plan experiments to replace by ^2H both olefinic H atoms and the α-H atom of the carbene ligand. We also intend to examine the behaviour of more recent analogues of **1**, which lack the phosphine ligands.[9] The elucidation of the nature and reactivity of the radical anions involved should assist in the design of improved catalysts for metathesis.

Notes and references

† EPR spectra were recorded at X-band frequencies in liquid CH_2Cl_2 at room temperature. No signals were observed from solutions of **1** in the absence of added substrates.

‡ We have now found that **1** polymerises α-methylstryrene and simultaneously generates EPR-active species. This information, together with the knowledge that Grignard reagents also catalyse free radical addition polymerisation (ref. 10) and metathesis polymerisation of norbornene (ref. 11), suggests a novel mechanism based on metalla-radicals.

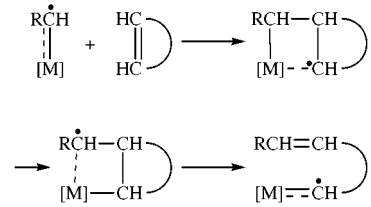

We believe that a metalla-carbenium ion mechanism is responsible when the most acidic metathesis catalysts are used, but the new metalla-radical scheme applies using **1** or when Mg-based catalysts (Grignard reagents) are active.

1 V. Amir-Ebrahimi, D. G. Corry, J. G. Hamilton, J. J. Rooney and J. M. Thompson, *Macromolecules*, submitted for publication.
2 E. L. Dias and R. H. Grubbs, *Organometallics*, 1998, **17**, 2758.
3 F. Simal, A. Demenceau and A. F. Noels, *Angew. Chem., Int. Ed.*, 1999, **38**, 538.
4 R. DeSimone, *J. Am. Chem. Soc.*, 1973, **95**, 6237.
5 M. A. Bennett, G. A. Heath, D. R. Hockless, I. Kovacik and A. C. Willis, *Organometallics*, 1997, **17**, 5767.
6 J. Fees, W. Kaim, M. Moscherosch, W. Matheis, J. Klima, M. Krejcik and S. Zalis, *Inorg. Chem.*, 1993, **32**, 167.
7 M. Belen Mula, A. J. Beaumont, K. O. Doyle, M. L. Gallaher and A. D. Rooney, *J. Mol. Catal.*, in the press.
8 B. Ventakaran and G. R. Fraenkel, *J. Chem. Phys.*, 1955, **23**, 577.
9 T. Westkamp, W. E. Schattenmann, M. Spiëgler and W. Herzmann, *Angew. Chem., Int. Ed.*, 1998, **37**, 2490.
10 J. Bovey, *J. Polym. Sci.*, 1960, **44**, 173.
11 P. Buchacher, W. Fischer, K. D. Aichholzen and F. Stelzen, *J. Mol. Catal. A*, 1997, **115**, 163.

Communication 9/04619D

ChemComm

Palladium complexes of phosphine functionalised carbosilane dendrimers as catalysts in a continuous flow membrane reactor†

Debby de Groot,[a] Eva B. Eggeling,[b] Janine C. de Wilde,[a] Huub Kooijman,[c] Richard J. van Haaren,[a] Alexander W. van der Made,[d] Anthony L. Spek,[c] Dieter Vogt,[b] Joost N. H. Reek,[a] Paul C. J. Kamer[a] and Piet W. N. M. van Leeuwen*[a]

[a] *Institute of Molecular Chemistry, University of Amsterdam, Nieuwe Achtergracht 166, 1018 WV Amsterdam, The Netherlands. E-mail: pwnm@anorg.chem.uva.nl*
[b] *Institute of Inorganic Chemistry and Catalysis, Eindhoven University of Technology, Post Office Box 513, 5600 MD Eindhoven, The Netherlands*
[c] *Bijvoet Center for Biomolecular Research, Crystal and Structural Chemistry, University of Utrecht, Padualaan 8, 3584 CH Utrecht, The Netherlands*
[d] *Shell International Chemicals BV Amsterdam, Badhuisweg 3, 1031 CM Amsterdam, The Netherlands*

Received (in Cambridge, UK) 4th June 1999, Accepted 15th July 1999

Phosphine functionalised carbosilane dendrimers have been synthesised and their palladium complexes used as catalysts in the allylic alkylation reaction performed in a continuous flow membrane reactor.

Since Vögtle and co-workers synthesised branched structures in 1978,[1] much research has been devoted to the synthesis and investigation of dendrimeric molecules.[2] One of the main applications of dendrimers[2h,i] is in catalysis,[3] allowing easy recycling of the homogeneous catalyst by means of nanofiltration.[4] Here we report the synthesis of phosphine functionalised carbosilane dendrimers and their use as catalysts in a continuous process.

We have chosen carbosilane dendrimers[5] as a backbone for our catalytic system because of their catalytic inertness. A previous report describes the synthesis of these dendrimers.[6] The second generation dendrimer is a white solid and crystals suitable for X-ray analysis were grown from a diethyl ether–methanol solution.‡ The structure (Fig. 1a) shows that the molecule crystallised with all the bonds in a zigzag conformation. This dendrimer has a calculated molecular volume of 2414 Å^3, which is anticipated to be large enough for separation from a reaction mixture by nanofiltration.

The phosphine functionalised carbosilane dendrimers were synthesised by hydrosilylation of the double bonds of the various generations (G_0, G_1, G_2) with chlorodimethylsilane or dichloromethylsilane followed by reaction with lithium methyldiphenylphosphine–TMEDA[7] (Scheme 1).§ All the phosphine functionalised dendrimers were obtained as wax-like solids. Characterisation by ^{1}H and ^{31}P-{^{1}H} NMR and MALDI-TOF MS shows that the P-functionalised dendrimers were obtained in at least 95% purity. The dendrimer with seventy-two phosphine groups could not be prepared, probably because of surface congestion.

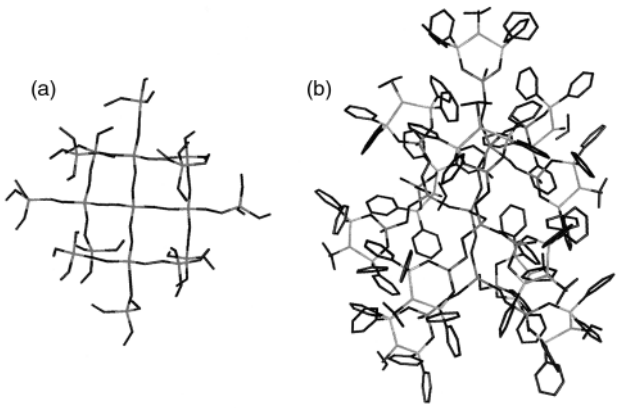

Fig. 1 Crystal structure of the second generation dendrimer (a) and a modelled structure of the Pd(allyl) complex of **8** (b). Hydrogens and counterions have been omitted for clarity. [See Electronic Supplementary Information (ESI) for a colour version of this figure (Si in red, C in dark blue, Pd in green, P in yellow)].

† Electronic supplementary information (ESI) available: full colour version of Fig. 1. See http://www.rsc.org/suppdata/cc/1999/1623/

Dendrimers **7** and **8** have four and twelve endgroups, respectively, each containing a chelating bidentate phosphine ligand. The endgroups of dendrimers **4**, **5** and **6** contain monodentate phosphine ligands. Allylpalladium complexes of these dendrimers were synthesised by reaction with [(η^3-C_3H_7)PdCl]$_2$. According to ^{1}H and ^{31}P-{^{1}H} NMR the phosphine dendrimers **7** and **8** co-ordinate in a bidentate way resulting in well defined Pd complexes, while the monodentate phosphine dendrimers give rise to a mixture of products.

All the Pd(allyl) dendrimer complexes were used as catalysts in the allylic alkylation reaction of allyl trifluoroacetate and sodium diethyl methylmalonate yielding diethyl allylmethylmalonate. The reaction was first carried out *via* a batch process. All the dendrimeric catalysts showed a very high activity. Using a substrate–Pd ratio of 2000 the yield after 30 min was over 80%, and only small differences in reaction rates were observed for the different catalysts.¶ The fact that the activity did not decrease with increasing generation indicates that all active sites act as independent catalysts. From molecular modelling (Fig. 1b) it was clear that indeed all the Pd(allyl) groups reside at the outer surface of the dendrimer and should be easily accessible to

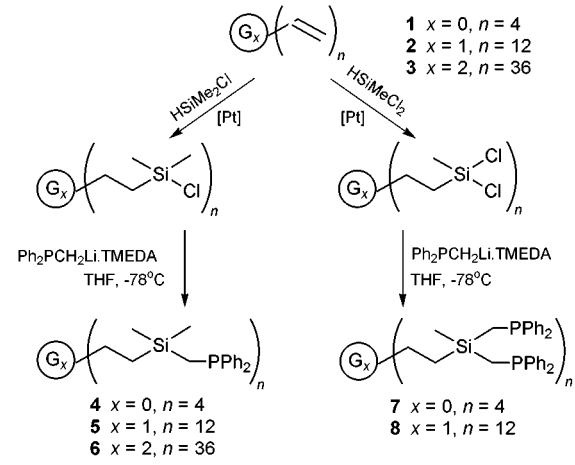

Scheme 1 Synthesis of phosphine functionalised carbosilane dendrimers.

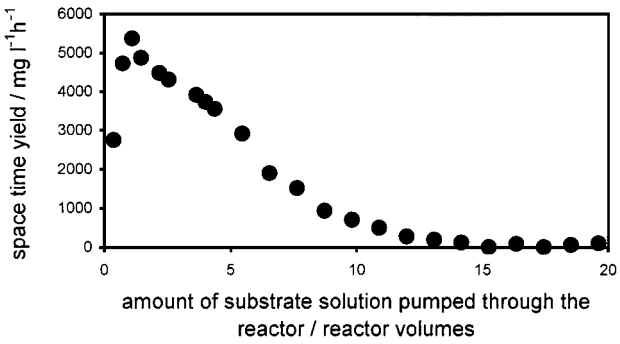

Fig. 2 Space time yield *versus* amount of solvent pumped through the reactor of the continuous allylic alkylation reaction in a membrane reactor.‡‡

the nucleophile. Addition of a second portion of substrate after nearly full consumption of the sodium diethyl methylmalonate (over 90%) showed that the catalyst remained active.

These novel dendrimeric catalysts were studied in a continuous process using a membrane reactor.‖ A solution of allyl trifluoroacetate and sodium diethyl methylmalonate in THF (including *n*-decane as an internal standard) was pumped through the reactor. The allylpalladium complex of the largest dendrimer with bidentate phosphines (**8**) was used as a catalyst.**

In Fig. 2 the space time yield is plotted as a function of the amount of solvent (expressed in reactor volumes) pumped through the reactor. The reaction started immediately after addition of the catalyst and reached its maximum space time yield after one reactor volume. The space time yield slowly dropped to zero after *ca.* 15× the reactor volume of substrate solution had been pumped through the reactor. Regarding the size of the catalyst, this decrease was unexpectedly rapid. The retention in the membrane reactor of the second generation dendrimer (molecular volume: 2414 Å^3), which is much smaller than the Pd catalyst (calculated molecular volume: ≈7600 Å^3 (Fig. 1)), was determined to be 98.1%. Using this number the decrease in catalyst activity is calculated to be only 25% after flushing the reactor fifteen times. The observed decrease in catalyst activity is therefore ascribed to decomposition†† of the palladium compound and not to loss of the dendrimeric catalyst. This is in agreement with the observation that samples taken from the product flow were not catalytically active, indicating that no active catalyst had gone through the membrane.

In conclusion, carbosilane dendrimers functionalised with diphenylphosphine groups at the periphery have been synthesised and characterised. Palladium complexes of these dendrimers have been used as catalysts in the allylic alkylation reaction. It has been shown that these dendrimeric catalysts can be used in a continuous process using a membrane reactor. Current work is aiming at the enhancement of the stability of these catalysts, and the exploration of these systems in other reactions.

This work was supported in part (A. L. S.) by the Council for Chemical Sciences of the Netherlands Organisation for Scientific Research (CW-NWO).

Notes and references

‡ *Crystal data* for **3**: $C_{104}H_{172}Si_{17}$, M_r = 1899.96, triclinic, space group $P\bar{1}$, a = 17.2970(4), b = 19.5782(4), c = 22.2298(5) Å, α = 106.1813(15), β = 108.1431(15), γ = 106.6735(14)°, V = 6268.0(2) Å^3, Z = 2, μ(Mo-Kα) = 0.2 mm^{-1}, 80242 reflections measured, 14833 independent, R_{int} = 0.1352, (1.6° < θ < 24.1°, T = 150 K). Only Si atoms were refined with anisotropic displacement parameters. The outside of the molecule shows considerable dynamic disorder, which gives rise to high displacement parameters and unrealistic geometries. No satisfactory disorder models could be obtained. Mild distance restraints were introduced for the most unrealistic parameters. *wR*2 = 0.2949, *R*1 = 0.1369, *S* = 0.886, −0.38 < $\Delta\rho$ < 0.78 e Å^{-3}. CCDC 182/1331. See http://www.rsc.org/suppdata/cc/1999/1623/ for crystallographic files in .cif format.

§ *Selected data* for **4**: ^{1}H NMR ($CDCl_3$): δ 7.5 (m, 16H, ArH), 7.3 (m, 24H, ArH), 1.40 (s, 8H, SiCH_2P), 0.26 (s, 16H, SiCH_2CH_2Si), −0.10 (s, 24H, SiCH_3). ^{31}P-{^{1}H} NMR ($CDCl_3$): δ −20.8. Dendrimers **5** and **6** have similar NMR spectra. For **7**: ^{1}H NMR ($CDCl_3$): δ 7.5–7.1 (m, 80H, ArH), 1.26 (s br, 16H, SiCH_2P), 0.19 (m, 16H, SiCH_2CH_2Si), −0.29 (s br, 12H, SiCH_3). ^{31}P-{^{1}H} NMR ($CDCl_3$): δ −22.5. Dendrimer **8** has similar NMR spectra.

¶ Room temperature, solvent: THF, [allyl trifluoroacetate] = 50 mM, [diethyl methylmalonate] = 25 mM, [Pd] = 12.5 μM.

‖ Koch/SelRO MPF-60 NF membrane, Koch Membrane Systems, Düsseldorf, Germany, molecular weight cut-off (MWCO) = 400 Daltons.

** Room temperature, reactor volume: 20 ml, solvent: THF, [allyl trifluoroacetate] = 50 mM, [diethyl methylmalonate] = 25 mM, [Pd] = 12.5 μM, flow rate: 44 ml h^{-1}.

†† Much higher turnover numbers can be reached in a batch reactor compared to the membrane reactor, showing that in the membrane reactor new problems are introduced that are not related to the dendrimeric catalyst.

‡‡ The space time yield has been corrected for the background reaction.

1 E. Buhleier, W. Wehner and F. Vögtle, *Synth. Commun.*, 1978, 155.
2 Reviews on dendrimers: (*a*) H.-B. Mekelburger, W. Jaworek and F. Vögtle, *Angew. Chem., Int. Ed. Engl.*, 1992, **31**, 1571; (*b*) D. A. Tomalia and H. D. Durst, *Top. Curr. Chem.*, 1993, **165**, 193; (*c*) J. Issberner, R. Moors and F. Vögtle, *Angew. Chem., Int. Ed. Engl.*, 1994, **33**, 2413; (*d*) D. Gudat, *Angew. Chem., Int. Ed. Engl.*, 1997, **36**, 1951; (*e*) H. Frey, C. Lach and K. Lorenz, *Adv. Mater.*, 1998, **10**, 279; (*f*) R. J. Puddephatt, *Chem. Commun.*, 1998, 1055; (*g*) J.-P. Majoral and A.-M. Caminade, *Chem. Rev.*, 1999, **99**, 845; (*h*) D. K. Smith and F. Diederich, *Chem. Eur. J.*, 1998, **4**, 1353; (*i*) M. Fischer and F. Vögtle, *Angew. Chem., Int. Ed.*, 1999, **38**, 884.
3 (*a*) J. W. J. Knapen, A. W. van der Made, J. C. de Wilde, P. W. N. M. van Leeuwen, P. Wijkens, D. M. Grove and G. van Koten, *Nature*, 1994, **372**, 659; (*b*) P. Bhyrappa, J. K. Young, J. S. Moore and K. S. Suslick, *J. Am. Chem. Soc.*, 1996, **118**, 5708; (*c*) K. Matyjaszewski, T. Shigemoto, J. M. J. Fréchet and M. Leduc, *Macromolecules*, 1996, **29**, 4167; (*d*) D. Seebach, R. E. Marti and T. Hintermann, *Helv. Chim. Acta*, 1996, **79**, 1710; (*e*) M. T. Reetz, G. Lohmer and R. Schwickardi, *Angew. Chem., Int. Ed. Engl.*, 1997, **36**, 1526; (*f*) I. Morao and F. P. Cossío, *Tetrahedron Lett.*, 1997, **38**, 6461; (*g*) H. Brunner, *J. Organomet. Chem.*, 1995, **500**, 39.
4 (*a*) U. Kragl and C. Dreisbach, *Angew. Chem., Int. Ed. Engl.*, 1996, **35**, 642; (*b*) N. J. Hovestad, E. B. Eggeling, H. J. Heidbüchel, J. T. B. H. Jastrzebski, U. Kragl, W. Keim, D. Vogt and G. van Koten, *Angew. Chem.*, 1999, **38**, 1655.
5 (*a*) L.-L. Zhou and J. Roovers, *Macromolecules*, 1993, **26**, 963; (*b*) D. Seyferth, D. Y. Son, A. L. Rheingold and R. L. Ostrander, *Organometallics*, 1994, **13**, 2682; (*c*) B. Alonso, I. Cuadrado, M. Morán and J. Losada, *J. Chem. Soc., Chem. Commun.*, 1994, 2575; (*d*) H. Frey, K. Lorenz, R. Mülhaupt, U. Rapp and F. J. Mayer-Posner, *Macromol. Symp.*, 1996, **102**, 19; (*e*) E. V. Getmanova, T. B. Chenskaya, O. B. Gorbatsevich, E. A. Rebrov, N. G. Vasilenko and A. M. Muzafarov, *React. Funct. Polym.*, 1997, **33**, 289.
6 A. W. van der Made and P.W.N.M van Leeuwen, *J. Chem. Soc., Chem. Commun.*, 1992, 1400.
7 N. E. Schore, L. S. Benner and B. E. LaBelle, *Inorg. Chem.*, 1981, **20**, 3200.

Communication 9/04455H

Pyridine analogue of macrocyclic polyyne $C_{58}H_4N_2$ as a precursor to diazafullerene $C_{58}N_2$

Yoshito Tobe,*[a] Hironobu Nakanishi,[a] Motohiro Sonoda,[a] Tomonari Wakabayashi[b] and Yohji Achiba[c]

[a] *Department of Chemistry, Faculty of Engineering Science, Osaka University, Toyonaka, Osaka 560-8531, Japan. E-mail: tobe@chem.es.osaka-u.ac.jp*
[b] *Division of Chemistry, Graduate School of Science, Kyoto University, Kyoto 606-8502, Japan*
[c] *Department of Chemistry, Tokyo Metropolitan University, Hachioji, Tokyo 192-0397, Japan*

Received (in Cambridge, UK) 29th June 1999, Accepted 14th July 1999

(1,3,5)Pyridinophanes having [4.3.2]propellatriene units were synthesized as precursors to macrocyclic polyyne $C_{58}H_4N_2$; diazafullerene anion $C_{58}N_2^-$ was detected in the laser desorption mass spectrum of the pyridinophanes.

Increasing interest has been focused on heterofullerenes, in which one or several carbon atoms of the fullerene cage are replaced by heteroatoms. Regarding azafullerenes, Wudl and Hirsch reported mass spectral detection of monoazafullerene cation $C_{59}N^+$, which was generated by the fragmentation of precursors manipulated from C_{60}.[1] Subsequently, isolation of its stable derivatives such as $C_{59}NH$, $C_{59}NR$ (R = $CHPh_2$, Ar) was reported from the same groups.[2] Rao reported the formation of azafullerenes $C_{59}N$ to $C_{56}N_4$ together with nitrogen-containing carbon clusters such as $C_{70}N_2$, $C_{59}N_6$, $C_{59}N_4$ and $C_{59}N_2$ in the soot produced by contact arc vaporization of graphite in the presence of N_2 or NH_3.[3] The closed shell azafullerenes having an even number of nitrogen atoms, $C_{60-n}N_n$ (n = 2, 4 and 6), are isoelectronic with the di-, tetra- and hexa-anions of C_{60}, respectively, and are predicted to be reasonably stable.[4] However, selective formation of such azafullerenes has not been achieved so far experimentally.

Recently we synthesized (1,3,5)cyclophane **1** fused by [4.3.2]propellatriene units, as precursors to polyyne-bridged macrocycle $C_{60}H_6$ **2**.[5] The laser-desorption mass spectra of **1** exhibited not only the negative ion corresponding to $\mathbf{2}^-$ but also C_{60} ions in both positive and negative modes. Rubin obtained similar results using a cyclobutenedione derivative related to **1**.[6] The formation of C_{60} from **2** can be explained in terms of the zipping-up cyclization of the polyyne chain accompanying the loss of hydrogen atoms.[7] As an extension of this method to the synthesis of azafullerenes, we report here the synthesis of pyridinophane **3** and its regioisomer **4** which would serve as precursors to polyyne $C_{58}H_4N_2$ **5** and **6**, respectively.[8] We detected the $C_{58}N_2$ anion in the laser desorption mass spectrum of **3** and **4**.

The Corey–Fuchs ethynylation[9] of dichloroformylpyridine **7**[10] afforded **8** which was converted to triethynylpyridine **9**† by the Sonogashira coupling[11] with trimethylsilylacetylene (Scheme 1). Tris(bromoethynyl)pyridine **10** derived from **9** by treatment with NBS and $AgNO_3$ was coupled with mono-(triisopropylsilyl)-protected diethynyl[4.3.2]propellatriene **11**[5] using Pd^0–Cu^I catalyst[12] to afford the tripod **12**.† After removal of the protective group, oxidative coupling of **13** under high-dilution conditions gave a mixture of pyridinophanes **3** and **4**† as a light-sensitive yellow solid.[13]

The positive mode laser desorption time-of-flight mass spectrum of **3** and **4** exhibited only indane fragments. Fig. 1 shows the negative mode laser desorption mass spectrum of **3** and **4**. The prominent peak due to $\mathbf{5}^-$ and $\mathbf{6}^-$, *i.e.* $C_{58}H_4N_2^-$, was observed at *m/z* 728 together with those of $C_{58}H_4N_2$(indane)$^-$ at *m/z* 846 and $C_{58}H_4N_2$(indane)$_2^-$ at *m/z* 964 formed by the successive loss of the indane fragments. More importantly, as shown in the inset of Fig. 1, the peak due to the $C_{58}N_2$ anion was indeed observed at *m/z* 724, albeit in relatively low

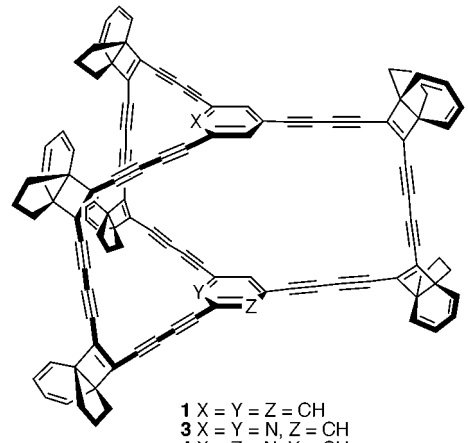

1 X = Y = Z = CH
3 X = Y = N, Z = CH
4 X = Z = N, Y = CH

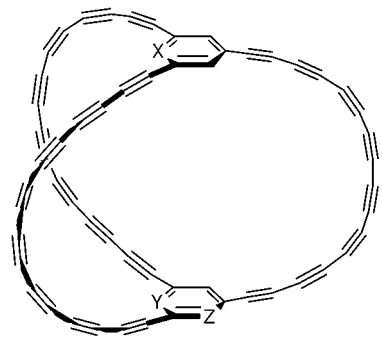

2 X = Y = Z = CH
5 X = Y = N, Z = CH
6 X = Z = N, Y = CH

intensity, which represents the first observation of diazafullerene formed in a size selective manner. It seems likely that the conversion of $C_{58}H_4N_2^-$ to $C_{58}N_2^-$ takes place in a stepwise fashion, since intermediate species such as $C_{58}H_3N_2^-$ and $C_{58}H_2N_2^-$ were detected. Observation of such dehydrogenation from the aromatic pyridine derivative $C_{58}H_4N_2^-$ manifests itself as the fullerene-like structure of the $C_{58}N_2$ anion.[14]

A relatively high yield of C_{60}^- was reported for the transformation of $C_{60}H_6$ to C_{60}.[5,6] The relatively inefficient conversion of $C_{58}H_4N_2$ to $C_{58}N_2$ in the present work is ascribed to the thermodynamic and kinetic lability of diazafullerene.[4] Indeed, Fig. 1 shows a strong peak due to CN^- which must be extruded from $C_{58}N_2$ or its precursors. Moreover, anions $C_{57}N^-$ and C_{56}^- formed by the loss of neutral CN from $C_{58}N_2^-$ are detected as shown in the inset of Fig. 1, even though it is well-documented that the internal temperature of negative ions is relatively low.[15]

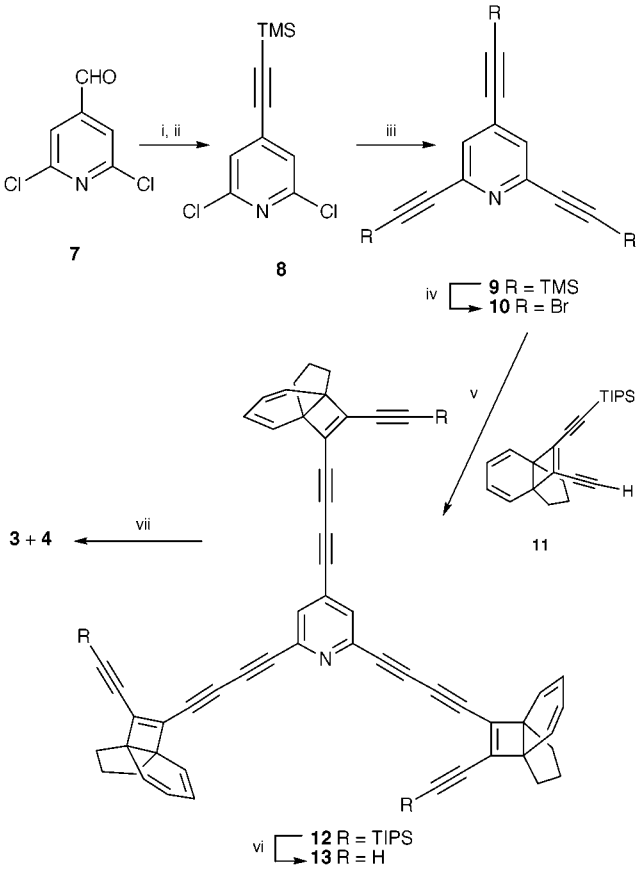

Scheme 1 *Reagents and conditions*: i, CBr_4, PPh_3, CH_2Cl_2, 0 °C, 76%; ii, LDA, THF, 0 °C, then Me_3SiCl, 89%; iii, trimethylsilylacetylene, $Pd(PPh_3)_4$, CuI, Pr^i_2NH, THF, 73%; iv, NBS, $AgNO_3$, acetone, 77%; v, $Pd(dba)_3{\cdot}CHCl_3$, CuI, pentamethylpiperidine, benzene, 61%; vi, Bu_4NF, AcOH, THF; vii, $Cu(OAc)_2$, pyridine, 12%.

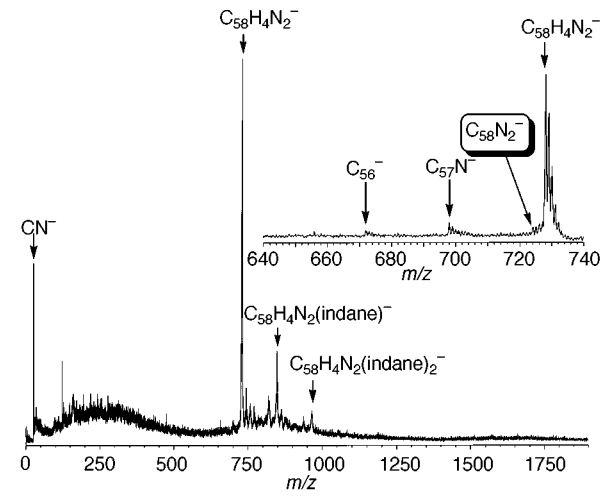

Fig. 1 Negative mode laser desorption time-of-flight mass spectrum of **3** + **4**. Liquid paraffin was used as a matrix and the third harmonic of a Nd:YAG laser (355 nm, typically 3 MW cm^{-2} with a 7 ns duration) was employed for simultaneous desorption and ionization.

In summary, we synthesized pyridinophanes **3** and **4** which served as precursors to polyyne $C_{60}H_4N_2$ **6** and **7** and detected diazafullerene anion $C_{58}N_2^-$ in the laser desorption mass spectrum of **3** and **4**.

This work was supported by Grants-in-Aid from the Ministry of Education, Science, Sports and Culture of Japan. The authors are grateful to Professor Aihara for providing us with his results on the estimation of the kinetic stability of azafullerenes.

Notes and references

† *Selected data* for **9**: mp 78–80 °C; ν(KBr)/cm^{-1} 2163; δ_H(300 MHz, $CDCl_3$) 0.24 (27H, s), 7.40 (2H, s); δ_C(75 MHz, $CDCl_3$) −0.44, −0.40, 96.1, 100.6, 101.5, 102.6, 128.3, 132.0, 143.3. For **10**: decomp. 159 °C; ν(KBr)/cm^{-1} 2195; δ_H(300 MHz, $CDCl_3$) 7.37; δ_C(75 MHz, $CDCl_3$) 53.7, 58.2, 76.3, 78.5, 128.8, 132.0, 143.2. For **12**: mp 97–99 °C; ν(KBr)/cm^{-1} 2201, 2136, 2124; δ_H(300 MHz, $CDCl_3$) 1.09 (63H, br s), 1.18–1.33 (6H, m), 1.41–1.53 (3H, m), 1.55–1.67 (3H, m), 1.93–2.01 (6H, m), 5.78–5.92 (12H, m), 7.41 (2H, s); δ_C(75 MHz, $CDCl_3$) 11.2, 18.6, 18.7, 32.8, 33.0, 56.3, 56.7, 56.9, 75.4, 75.8, 77.2, 77.7, 78.4, 80.2, 80.7, 98.3, 98.4, 101.0, 101.4, 122.0, 122.1, 128.1, 128.2, 129.2, 129.5, 131.2, 138.2, 138.7, 143.1. For **3** + **4**: decomp. 128 °C; ν(KBr)/cm^{-1} 2205; δ_H(300 MHz, $CDCl_3$) 1.19–1.34 (12H, m), 1.38–1.52 (6H, m), 1.59–1.62 (6H, m), 1.90–2.01 (12H, m), 5.90–5.92 (12H, m), 7.36–7.41 (4H, m); λ_{max}(benzene)/nm (log ε) 369 (4.85), 393 (4.82), 428 (4.65).

1 J. C. Hummelen, B. Knight, J. Pavlovich, R. González and F. Wudl, *Science*, 1995, **269**, 1554; I. Lamparth, B. Nuber, G. Schick, A. Skiebe, T. Grösser and A. Hirsch, *Angew. Chem., Int. Ed. Engl.*, 1995, **34**, 2257.

2 M. Keshavarz-K., R. González, R. G. Hicks, G. Srdanov, V. I. Srdanov, T. G. Collins, J. C. Hummelen, C. Bellavia-Lund, J. Pavlovich, F. Wudl and K. Holczer, *Nature*, 1996, **383**, 147; C. Bellavia-Lund, R. González, J. C. Hummelen, R. G. Hicks, A. Sastre and F. Wudl, *J. Am. Chem. Soc.*, 1997, **119**, 2946; B. Nuber and A. Hirsch, *Chem. Commun.*, 1996, 1421.

3 T. Pradeep, V. Vijayakrishnan, A. K. Santra and C. N. R. Rao, *J. Phys. Chem.*, 1991, **95**, 10 564.

4 Z. Chen, K. Ma, Y. Pan, X. Xhao, A. Tang and J. Feng, *J. Chem. Soc., Faraday Trans.*, 1998, **94**, 2269; J. Aihara, unpublished results.

5 Y. Tobe, N. Nakagawa, K. Naemura, T. Wakabayashi, T. Shida and Y. Achiba, *J. Am. Chem. Soc.*, 1998, **120**, 4544.

6 Y. Rubin, T. C. Parker, S. J. Pastor, S. Jalistagi, C. Boulle and C. L. Wilkins, *Angew. Chem., Int. Ed.*, 1998, **37**, 1226.

7 Y. Rubin, *Chem. Eur. J.*, 1997, **3**, 1009; U. H. F. Bunz, Y. Rubin and Y. Tobe, *Chem. Soc. Rev.*, 1999, **28**, 107; Y. Tobe, *Advances in Strained and Interesting Organic Molecules*, ed. B. Halton, JAI Press, Stamford, 1999, vol. 7, p. 153.

8 There are many possible isomers for **3** and **4** due to the orientation of the propellane units. Only one of the isomers of **3** and **4** are depicted in this paper for clarity.

9 E. J. Corey and P. L. Fuchs, *Tetrahedron Lett.*, 1972, 3769.

10 R. Graf and A. Weinberg, *J. Prakt. Chem.*, 1932, **134**, 180.

11 For a review; K. Sonogashira, *Comprehensive Organic Synthesis*, ed. B. M. Trost and I. Fleming, Pergamon, Oxford, 1991, vol. 3, p. 521.

12 C. Cai and A. Vasella, *Helv. Chim. Acta*, 1995, **78**, 2053.

13 There are so many possible isomers for the oxidative coupling product of **13** that it is not possible to determine the ratio of **3** and **4** nor even confirm whether it is indeed a mixture of the two by spectroscopic and chromatographic techniques.

14 Only one isomer, 1,49-diazafullerene, would result from the $C_{58}N_2$ isomer **5**, while two isomers, 1,49- and 1,60-diaza derivatives, would be formed from **6**, provided that the cyclization of the polyyne chain takes place without bond breaking through a transition state with minimal bond angles of the alkyne chains as depicted in ref. 7.

15 K. Kaizu, M. Kohno, S. Suzuki, H. Shiromaru, T. Moriwaki and Y. Achiba, *J. Phys. Chem.*, 1997, **106**, 9954.

Communication 9/05207K

ChemComm

Novel oxo-peroxo molybdenum(VI) complexes incorporating 8-quinolinol: synthesis, structure and catalytic uses in the environmentally benign and cost-effective oxidation method of methyl benzenes: $Ar(CH_3)_n$ (n = 1, 2)

Ratna Bandyopadhyay,[a] Sudeb Biswas,[a] Subhadra Guha,[b] Alok K. Mukherjee[b] and Ramgopal Bhattacharyya*[a]

[a] *Department of Chemistry, Jadavpur University, Calcutta-700032, India*
[b] *Department of Physics, Jadavpur University, Calcutta-700032, India*

Received (in Cambridge, UK) 3rd June 1999, Accepted 14th July 1999

A hitherto unknown distorted pentagonal bipyramidal complex, $[MoO(O_2)(QO)_2]$, very efficiently catalyses homogeneous liquid phase oxidation of methylbenzenes, *viz.* toluene and *o*- and *p*-xylenes to benzoic acid, phthalic acid and *p*-toluic acid respectively, using H_2O_2 and O_2 as oxidants.

Oxo-peroxo molybdenum complexes[1] catalytically oxidise a variety of organic substrates,[2] *viz.* alkenes, alcohols, amides and nitro compounds *etc.*, *via* homogeneous as well as heterogeneous routes.[3] However, homogeneous liquid-phase hydrocarbon oxidation is rare.[4] In this communication, besides reporting two new oxo-peroxo molybdenum(VI) compounds, *viz.* $MoO(O_2)_2{\cdot}2QOH$ (**1**) and $[MoO(O_2)(QO)_2]$ (**2**) (QOH = 8-quinolinol),† and elucidating the structure of **2** by X-ray crystallography,‡ we also report and substantiate that **2** is the catalyst precursor and **1** the active catalyst in the homogeneous and selective oxidation of toluene, *o*-xylene and *p*-xylene to benzoic acid, phthalic acid and *p*-toluic acid respectively, under very mild conditions, with an impressive yield and turnover number and smooth catalyst recovery technique. This can be regarded as one of the most inexpensive, environmentally benign and industrially feasible methods of oxidising methylbenzenes (which are very important by-products in coal-tar distillation and petroleum cracking) to the corresponding carboxylic acids, which have many uses in the chemical and pharmaceutical industries.

The structure of **2** consists of discrete monomeric units of $[MoO(O_2)(QO)_2]$ (QO = 8-quinolinolate anion), and disordered CH_2Cl_2 molecules held in the lattice. The geometry around the Mo atom can be best described as distorted pentagonal bipyramidal (Fig. 1) with the axial sites being occupied by the oxo (O5) and a phenolate oxygen (O1) ligands. The other phenolate oxygen (O2), two N atoms (N1,N2) of the bidentate QO^- ligands and the η^2-peroxo moiety (O3,O4) define the equatorial plane with the Mo atom being displaced by 0.175(1) Å from the equatorial plane towards the oxo oxygen. The two essentially planar five-membered chelate rings (Mo, O1, C8, C9, N1 and Mo, O2, C17, C18, N2) are approximately orthogonal to each other,‡ the dihedral angle between the least square planes through the ring atoms is 81.0(1)°. The bond distance and angles (Fig. 1) correspond well to those of other seven coordinate molybdenum oxo-peroxo complexes.[5]

Empirically **1** contains two atoms of oxygen and two atoms of hydrogen more than **2**. During crystallization or oxidation the yellow solution of **1** changes to orange and displays a UV-Vis spectrum which is identical to that of **2**; **2** is actually deposited from this orange solution. When in isolation **2** reacts with an excess ($Mo:H_2O \approx 1:4$) of H_2O_2 to yield **1** (this is also observed under a UV-Vis probe). Analytical and infrared data (see Notes and references) indicate that **1** may be formulated as $MoO(O_2)_2{\cdot}2QOH$ (**1**) or $MoO(O_2)(QO)_2{\cdot}H_2O_2$ (**1a**). However, preliminary rate data show that the conversion of **1** to **2** at room temperature is rather slow which is not compatible with its formulation as **1a**. Moreover, when **1** (but not **2**) is treated with $FeCl_3$ solution, a deep green colour appears instantaneously due to the formation of $[Fe(QO)_3]$. Also, the $\{MoO(O_2)_2\}$ moiety is formed readily.[6] Hence, it appears that, albeit putatively, **1** is correctly formulated. Interestingly, **1** reacts§ with toluene to give benzoic acid (72%), with *o*-xylene to give phthalic acid (55%) and with *p*-xylene to give *p*-toluic acid (61%) (all were confirmed using the undepressed mixed melting point, and the superimposability of the IR and NMR spectra with those of the respective authentic acids as well as their methyl esters), with **2** produced also. The reaction with toluene is shown by eqn. (1) as

$$MoO(O_2)_2{\cdot}2QOH + C_6H_5{-}CH_3 + O_2 \rightarrow C_6H_5COOH + [MoO(O_2)(QO)_2] + 2H_2O \quad (1)$$

a representative case. These observations led to the prediction that **2** may be the catalyst precursor and **1** the active catalyst in the oxidation of methylbenzenes. This has been excellently verified by observing that **2** in a catalytic concentration furnishes the same oxidations (Table 1) in refluxing acetonitrile in the presence of H_2O_2 and a brisk bubble of dioxygen/air. The yield is reduced when only H_2O_2 is used as the oxidant, and trace when exclusively O_2 is used. The data in Table 1, suggest that the catalytic process may be shown as Scheme 1. Table 1 shows that the use of an excess of H_2O_2 imparts a negative effect on the catalytic oxidation, even in the double additive case. The reason for this is at present obscure. When H_2O_2 is used as the sole oxidant, it may undergo disproportionation ($H_2O + O_2$) under the catalytic influence of **2**, and the O_2 produced is utilized to drive the reaction in a similar fashion as in the twin reagent case. This hypothesis is supported by the fact that the process needs a much greater amount of H_2O_2 than is necessary in the double additive method.

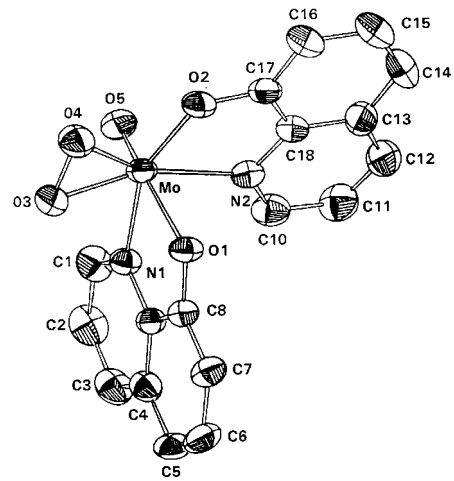

Fig. 1 An ORTEP view of $[MoO(O_2)(QO)_2]$ **2** with selected bond distances (Å) and angles (°): Mo–O1, 2.037(3); Mo–O3, 1.933(3); Mo–O5, 1.685(3); Mo–N2, 2.269(3); Mo–O2, 1.993(3); Mo–O4, 1.925(3); Mo–N1, 1.441(4); O3–Mo–O4, 43.86(13); O2–Mo–N2, 75.36(12); O1–Mo–N1, 74.87(11); O1–Mo–O5, 156.25(14); O3–Mo–N2, 159.72(13).

Table 1 Oxidation of methylbenzenes by H_2O_2 and O_2 catalysed by $[MoO(O_2)(QO)_2]$[a]

Substrate[b]	Time/h	Oxidant[c]	Product[d]	Yield[e] (%)	Turnover no.[f]
$C_6H_5CH_3$ (A)	6	H_2O_2 (0.038) + O_2	 (D)	95	1310
A	10	H_2O_2 (0.076)	D	72	1019
A	10	H_2O_2 (0.190) + O_2	D	15	21
o-$C_6H_4(CH_3)_2$ (B)	6	H_2O_2 (0.038) + O_2	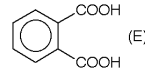 (E)	76	1047
B	10	H_2O_2 (0.076)	E	55	757
p-$C_6H_4(CH_3)_2$ (C)	6	H_2O_2 (0.038) + O_2	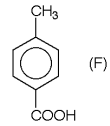 (F)	88	1221
C	10	H_2O_2 (0.076)	F	60	832

[a] **2** is the catalyst precursor (1.15×10^{-5} moles used in each case), while **1** is the active species. No oxidation occurs without using **2** (or **1**, though much less efficiently). [b] 0.016 mol used in each case. [c] Figures in parentheses indicate mol of H_2O_2. Rate of flow of O_2 = one bubble per second. [d] See footnote ¶. [e] Based on mol of substrates used. Temp = reflux, solvent = acetonitrile. [f] Is defined here as the ratio of the number of mol of product obtained to the number of mol of catalyst used, in 1 batch.

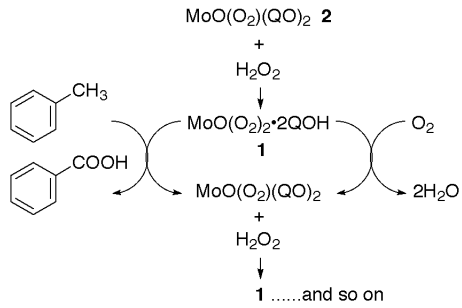

Scheme 1

It is extremely satisfying to note that the recovered catalyst in the double additive process can be used again to oxidize a new batch of the corresponding methylbenzenes showing similar catalytic efficiency, but from the third batch onwards the efficiency falls to a marked extent. Interestingly no oxidation occurs if benzoquinone is added to the reaction medium, and a 98% yield (*vs.* 30% without AIBN) is obtained after only 3 h reflux when using AIBN [azobis(isobutyronitrile)], indicating that the oxidation proceeds *via* a radical mechanism. All these aspects will be detailed in due course.

Data collection for X-ray crystallography was done from RSIC, Bose Institute, Calcutta. We thank the Alexander von Humboldt-Foundation, Germany for the donation of the IR spectrophotometer used and UGC and CSIR, New Delhi, for financial support.

Notes and references

† **1** was synthesised by dissolving MoO_3 in 30% H_2O_2 and adding an acetic acid solution of QOH at 1:2 molar ratio. Yield 80%. IR (KBr) ν/cm^{-1}: (Mo=O) 960; (O–O) 860, 910(sh);[7] (O–H) 3080 (b, H-bonded); Electronic spectrum of **1**, λ/nm: {QOH → $MoO(O_2)_2$ CT} 355, {O_2^{2-} → Mo(VI) LMCT} 375 (sh). **2** was obtained by slow crystallization of **1** from CH_2Cl_2–hexane or CH_3CN–Et_2O, yield 60%. IR (KBr) ν/cm^{-1}: (Mo=O) 945; (O–O) 920; vibrations of QO^- comparable to those of $[MoO_2(QO)_2]$[8] where QO^- is bidentate;[9] electronic spectrum, λ/nm: {QO^- → Mo(VI) LMCT} 400;[10] {O_2^{2-} → Mo(VI) LMCT} 375 (sh). Satisfactory elemental analyses (C,H,N,Mo) were obtained for all the isolated complexes.

‡ *Crystal data* for **2**: $[MoO(O_2)(QO)_2]$, $C_{19}H_{14}Cl_2N_2O_5Mo$, M = 517.16, orange, triclinic, space group $P\bar{1}$, a = 9.791(1) Å, b = 10.643(1) Å, c = 10.964(2) Å, α = 117.70(2)°, β = 90.14(1)°, γ = 105.08(1)°, V = 966.5 (3) Å^3, T = 293(2) K, Z = 2, λ = 0.71093 Å, D_c = 1.777 g cm^{-3} D_m = 1.73 g cm^{-3}, μ(Mo-Kα) = 0.990 mm^{-1}. 3359 observed [$I > 2\sigma(I)$] reflections. Enraf Nonius CAD4 diffractometer. Mo-Kα, R_1 = 0.0414, wR_2 = 0.1190 and GOF on F^2 = 1.099. Structure solved and refined by Patterson (SHELXS86) and successive Fourier and full matrix least squares (SHELXL93) methods. CCDC 182/1330. See http://www.rsc.org/suppdata/cc/1999/1627/ for crystallographic files in .cif format.

§ In three different experiments **1** (0.05 g; 0.15 mmol) and (a) toluene (0.01 g; 0.11 mmol), (b) *o*-xylene (0.012 g; 0.11 mmol) and (c) *p*-xylene (0.012 g; 0.11 mmol) were separately dissolved in acetonitrile (15 ml), refluxed for 4 h and then cooled. In the case of toluene the resulting mixture was evaporated to dryness, the mass extracted with diethyl ether and the extract shaken with aqueous bicarbonate. On acidifying the aqueous layer, benzoic acid was obtained. In the cases of *o*- and *p*-xylenes the respective products separated out on standing the solutions after CH_3CN reflux.

¶ **2** and (a) toluene, (b) *o*-xylene, (c) *p*-xylene were separately dissolved in acetonitrile (15 ml) and 30% H_2O_2 (4 ml; 38 mmol) was added. The resulting solution was refluxed for 6 h under bubbling dioxygen, cooled, acetonitrile expelled, aqueous remains treated with diethyl ether and the separated catalyst filtered from the aqueous solution. The ether extract was treated with aqueous bicarbonate and the aqueous layer was acidified to obtain benzoic acid. For phthalic acid (b) and *p*-toluic acid (c), after evaporating off the CH_3CN the aqueous layer was subjected to CH_2Cl_2 extraction to separate the catalyst. The aqueous portion was then concentrated using a rotary evaporator to get the respective acids. All the acids obtained were chromatographically and analytically pure.

1 M. H. Dickman, *Chem. Rev.*, 1994, **94**, 569.
2 H. Mimoun, in *Comprehensive Co-ordination Chemistry*, ed. G. Wilkinson, R. D. Gillard and J. A. McCleverty, Pergamon Press, Oxford, 1987, vol. 6, and references therein; F. P Ballistreri, A. Bazzo, G. A. Tomaselli and R. M. Toscano, *J. Org. Chem.*, 1992, **57**, 7074; M. K. Trost and R. G. Bergman, *Organometallics*, 1991, **10**, 1172.
3 K. T. Queeney, D. A.Chen and C. M. Friend, *J. Am. Chem. Soc.*, 1997, **119**, 6945 and references therein.
4 J. M. Aubry and S. Bouttemy, *J. Am. Chem. Soc.*, 1997, **119**, 5286.
5 N. M. Gresley, W. P. Griffith, B. C. A. Parkin, J. P. While and D. J. Williams, *J. Chem. Soc., Dalton Trans.*, 1996, 2039; P. K. Chakraborty, S. Bhattacharya, C. G. Pierpont and R. Bhattacharyya, *Inorg. Chem.*, 1992, **31**, 3573.
6 F. A. Cotton, G. Wilkinson, C. A. Murillo and M. Bochmann, *Advanced Inorganic Chemistry*, 6th edn., John Wiley and Sons, New York, 1999, p. 955.
7 S. E. Jacobson, R. Mares and F.Mares, *Inorg. Chem.*, 1978, **17**, 3061; M. T. H. Tarafder and N. S. Islam, *Polyhedron*, 1992, **11**, 795.
8 P. C. H. Mitchell, *Quart. Rev.* (*London*) 1966, **20**, 103; R Bhattacharyya and S. Ghosh, *Indian. J. Chem. A*, 1991, **30**, 35.
9 T. Venkataraman and K. S. Nagaraja, *Polyhedron*, 1992, **2**, 185.
10 C. Djordjevic, B. C. Puryear, N. Vuletic, C. J. Abett and S. J. Sheffield, *Inorg. Chem.*, 1988, **27**, 2926.

Communication 9/04440J

ChemComm

An uncommon bonding mode of a familiar ligand: a molybdenum complex with a four-electron donor chelating η^3-PPh_3 ligand, and its structural determination using synchrotron radiation

Tan-Yun Cheng, David J. Szalda† and R. Morris Bullock*

Chemistry Department, Brookhaven National Laboratory, Upton, New York 11973-5000, USA. E-mail: bullock@bnl.gov

Received (in Bloomington, IN, USA) 15th June 1999, Accepted 8th July 1999

A crystallographic study using synchrotron radiation shows that a C=C bond of one phenyl group of a PPh_3 ligand bonds to Mo in $[Cp(CO)_2(PPh_3)Mo]^+$, resulting in an unusual bonding mode in which PPh_3 functions as a chelating four-electron donor ligand.

The triphenylphosphine ligand occupies a prominent role in organometallic chemistry and homogeneous catalysis. The traditional mode of bonding of PPh_3 is as a two-electron donor through the lone pair on the phosphorus atom. We have prepared a new complex in which PPh_3 functions as a chelating four-electron donor ligand, with a C=C bond of one phenyl group bonding to the metal. A structural determination by X-ray crystallography was carried out using synchrotron radiation. Weak C–F···H–C interactions are found between C–F groups on the $BAr'_4{}^-$ [Ar′ = 3,5-bis(trifluoromethyl)phenyl] counterion and ligand C–H groups on the cationic molybdenum complex.

Hydride transfer from $Cp(CO)_2(PPh_3)MoH$ to $Ph_3C^+BF_4^-$ gives $Cp(CO)_2(PPh_3)MoFBF_3$.[1] In this reaction and many others reported by Beck and co-workers, the 16-electron metal cation resulting from removal of hydride is captured by a weakly coordinating counterion such as BF_4^-.[2] We recently measured the kinetics of this and several related hydride transfer reactions using stopped-flow techniques.[3] We have found that a completely different product results when hydride abstraction from $Cp(CO)_2(PPh_3)MoH$ is carried out using a counterion that is much more weakly coordinating than BF_4^-. Reaction of $Ph_3C^+BAr'_4{}^-$ with $Cp(CO)_2(PPh_3)MoH$ at −30°C led to the isolation of a new complex (**1**) in 84% yield [eqn. (1)].[4]

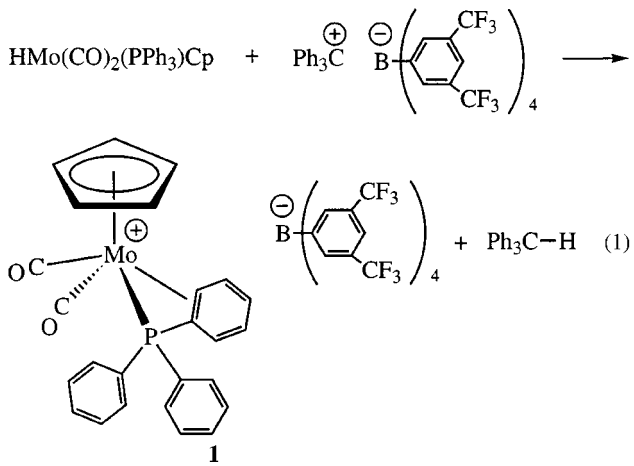

1

The ^{13}C NMR spectrum of **1** at −60 °C exhibits a doublet (J_{CP} = 29 Hz) at δ 81.5 and another doublet (J_{CP} = 12 Hz) at δ 90.0. These resonances are assigned as the *ipso* and *ortho* carbons of one of the C=C bonds of the Ph ring. The significant upfield shift of these carbons from the other aromatic carbons (δ 120 –135) suggests that one C=C bond of the ring is coordinated to the molybdenum, as indicated in eqn. (1).

Remarkable progress has been made recently in the design and utility of large, weakly coordinating counterions.[5] A serious drawback often encountered is the difficulty of obtaining single crystals that are large enough and that diffract well. Initial attempts to obtain a crystal structure of **1** using a conventional X-ray diffractometer suffered from an insufficient number of observed data to enable a complete refinement. The use of a high intensity source of X-rays, such as a synchrotron, can provide sufficient scattering to obtain a reliable structural determination. The crystal structure of **1** was successfully solved and refined[6] using data collected from a beamline at the National Synchrotron Light Source at Brookhaven. A significant advantage of using a synchrotron source of X-rays is that small crystals are suitable; the crystal we used had dimensions of 0.02 × 0.08 × 0.08 mm. The use of synchrotron radiation may offer advantages for single crystal diffraction studies of other complexes of large, weakly coordinating counterions, as well as other complexes for which only small crystals suitable for diffraction can be obtained.

The ORTEP diagram in Fig. 1 shows that the Mo is located out of the plane of the arene ring. The distortion of the PPh_3 ligand is evidenced by the acute Mo–P–C(31) angle of 73.0(3)°, compared to angles of 117.8(3)° and 131.3(4)° for the other two Mo–P–C bonds. The dihedral angle between the Mo–C–C plane and the plane of the phenyl ring is 62°. The bond distances of the Ph ring bonded to Mo show some evidence of localization of C=C and C–C bonds. Similar structural parameters were found

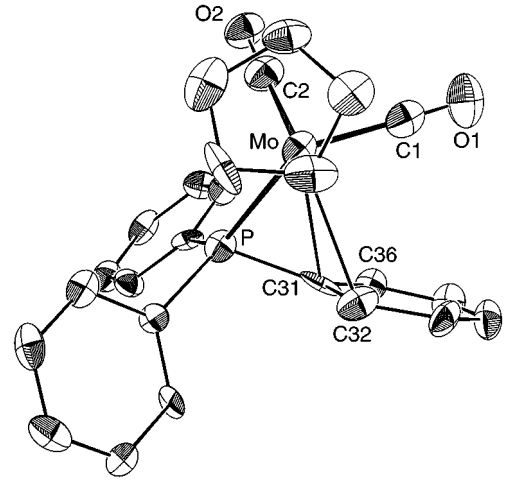

Fig. 1 ORTEP diagram of **1** showing 50% probability ellipsoids. Selected bond lengths (Å) and angles (°): Mo–C(2) 1.968(12); Mo–C(1) 1.99(2); Mo–P 2.429(3); Mo–C(31) 2.566(9); Mo–C(32) 2.645(9); C(31)–C(32) 1.418(13); C(31)–C(36) 1.445(14); C(32)–C(33) 1.424(14); C(33)–C(34) 1.361(14); C(34)–C(35) 1.404(13); C(35)–C(36) 1.368(13); C(2)–Mo-C(1) 79.7(5); C(2)–Mo–P 83.8(3); C(1)–Mo–P 115.7(3).

† Research Collaborator at Brookhaven National Laboratory. Permanent Address: Department of Natural Sciences, Baruch College, New York, NY 10010, USA.

in other M(η^2-arene) complexes, such as Cp*(PMe_3)Rh(η^2-phenanthrene),[7] Cp*(NO)Ru(η^2-naphthalene),[8] and $[(NH_3)_5Os(\eta^2$-naphthalene)$]^{2+}$.[9] An η^2-C=C bond of a *p*-tolyl group was shown to be bound to tungsten in a series of bimetallic compounds where the *p*-tolyl group was part of a bridging alkylidene in a W[μ-C(*p*-tolyl)(R)]Pd moiety.[10]

In several previously reported examples where a metal bonds to the phenyl group of a $PPhR_2$ ligand, the CH bond of the arene interacts with the metal in an η^2-CH agostic[11] interaction, rather than the η^2-C=C bonding found here. Structurally characterized phosphine complexes with agostic C–H interactions include $Pd(PPh^tBu_2)_2$,[12] $RhHCl(SiCl_3)(PPh_3)_2$,[13] $RuCl_2(PPh_3)_3$,[14] and $PdI_2(PPhMe_2)_2$.[15] These η^2-CH agostic complexes have conspicuous structural differences that contrast with η^2-arene complexes: the metal is normally nearly coplanar with the arene ring (dihedral angle of < 15° between M–C–C and arene planes) and the M–P–C angles are typically 111–114° rather than the acute Mo–P–C(31) angle of 73.0(3)° noted above. Although it has been suggested[11] that $[Rh(PPh_3)_3]^+$ [16] has an agostic interaction, its structural features (Rh–P–C angle of 75.6(5)°; dihedral angle of 59° between Rh–C–C and arene planes) are much more similar to those found in **1**. Accordingly, we suggest that $[Rh(PPh_3)_3]^+$ [16] has an η^2-arene interaction, rather than agostic, and we believe that these structural criteria will be diagnostic in distinguishing between agostic and η^2-arene interactions in other complexes. Other than complex **1** reported here and $[Rh(PPh_3)_3]^+$ which we interpret as having an η^2-CH arene interaction, we are not aware of other examples where a PPh_3 ligand bonds to a metal as a four-electron donor in an η^3-bonding mode. There are, however, examples of η^2-C=C bonds in Ru complexes with chelating diphosphine ligands BINAP[17] or MeO-BIPHEP.[18] These diphosphines are bridged by substituted-biphenyl groups.

The structural determination of **1** reveals a series of weak C–F···H–C interactions, with over twenty F···H distances in the range of 2.6–3.0 Å. The presence of F···H–C interactions[19] has been observed in a variety of compounds recently,[20] though their assignment as hydrogen bonds is not without controversy.[21]

Although **1** was isolated as a pure solid, it decomposes slowly at room temperature (several days in CD_2Cl_2 solution or a few months as a solid). The weak C=C bond of **1** is readily and cleanly displaced by ligands such as CH_3I and H_2O. Further spectroscopic and structural studies of these compounds will be reported.

This research was carried out at Brookhaven National Laboratory under contract DE-AC02-98CH10886 with the US Department of Energy and was supported by its Division of Chemical Sciences, Office of Basic Energy Sciences. We thank Dr. Jonathan C. Hanson for assistance with the use of Beamline X7B at the National Synchrotron Light Source.

Notes and references

1 K. Sünkel, H. Ernst and W. Beck, *Z. Naturforsch., Teil B*, 1981, **36**, 474.
2 W. Beck and K. Sünkel, *Chem. Rev.*, 1988, **88**, 1405.
3 (*a*) T.-Y. Cheng, B. S. Brunschwig and R. M. Bullock, *J. Am. Chem. Soc.*, 1998, **120**, 13121; (*b*) T.-Y. Cheng and R. M. Bullock, *J. Am. Chem. Soc.*, 1999, **121**, 3150.
4 Selected spectroscopic data for **1**: ^{1}H NMR (CD_2Cl_2, −60 °C): the signals for BAr'_4^- (δ 7.74 and 7.53) overlapped with the signals of PPh_3 (δ 7.82 –7.20), δ 6.12 (br t, 1 H, C*H*, $^3J_{HH} \approx {}^3J_{PH}$ = 6.9 Hz), 5.62 (s, 5 H, *Cp*). ^{13}C{^{1}H} NMR (CD_2Cl_2, −60 °C): δ 237.0 (d, J_{CP} = 24.8, *C*O), 231.4 (s, *C*O), 94.4 (s, *Cp*), 90.0 (d, J_{CP} = 11.8 Hz, *o*-C of P*Ph*Ph$_2$), 81.5 (d, J_{CP} = 28.6 Hz, *ipso*-C of P*Ph*Ph$_2$). ^{31}P{^{1}H} NMR (CD_2Cl_2, −60 °C): δ 37.6 (s). IR (CH_2Cl_2): ν(CO) 2009 (s), 1939 (s) cm^{-1}.
5 S. H. Strauss, *Chem. Rev.*, 1993, **93**, 927.
6 *Crystal data* for **1**·toluene: $C_{64}H_{40}BF_{24}MoO_2P$, M = 1434.68, monoclinic; space group $P2_1/n$, a = 15.371(2) Å, b = 24.095(2) Å, c = 17.319(2) Å, β = 106.67(2)°, V = 6144.8(12) Å^3, Z = 4, ρ(calc) = 1.551 g cm^{-3}, $2\theta_{max}$ = 74°, λ = 1.100 Å, image plates with ψ scans, Fourier absorption correction, T = 95(2) K, 18041 reflections collected, 5504 independent reflections, heavy atom solution, full-matrix least-squares refinement on F^2, 674 parameters, R_1 = 0.0738, wR_2 = 0.1899. All non-hydrogen atoms were refined using anisotropic thermal parameters except for the carbon atoms of the BAr'_4^- anion. CCDC 182/1325. See http://www.rsc.org/suppdata/cc/1999/1629/ for crystallographic files in .cif format.
7 R. M. Chin, L. Dong, S. B. Duckett, M. G. Partridge, W. D. Jones and R. N. Perutz, *J. Am. Chem. Soc.*, 1993, **115**, 7685.
8 C. D. Tagge and R. G. Bergman, *J. Am. Chem. Soc.*, 1996, **118**, 6908.
9 M. D. Winemiller, B. A. Kelsch, M. Sabat and W. D. Harman, *Organometallics*, 1997, **16**, 3672.
10 A. Macchioni, P. S. Pregosin, P. F. Engel, S. Mecking, M. Pfeffer, J.-C. Daran and J. Vaissermann, *Organometallics*, 1995, **14**, 1637.
11 M. Brookhart, M. L. H. Green and L.-L. Wong, *Prog. Inorg. Chem.*, 1988, **36**, 1.
12 S. Otsuka, T. Yoshida, M. Matsumoto and K. Nakatsu, *J. Am. Chem. Soc.*, 1976, **98**, 5850.
13 K. W. Muir and J. A. Ibers, *Inorg. Chem.*, 1970, **9**, 440.
14 S. J. La Placa and J. A. Ibers, *Inorg. Chem.*, 1965, **4**, 778.
15 (*a*) N. A. Bailey, J. M. Jenkins, R. Mason and B. L. Shaw, *Chem. Commun.*, 1965, 237; (*b*) N. A. Bailey and R. Mason, *J. Chem. Soc. (A)*, 1968, 2594.
16 (*a*) Y. W. Yared, S. L. Miles, R. Bau and C. A. Reed, *J. Am. Chem. Soc.*, 1977, **99**, 7076; (*b*) C. B. Knobler, T. B. Marder, E. A. Mizusawa, R. G. Teller, J. A. Long, P. E. Behnken and M. F. Hawthorne, *J. Am. Chem. Soc.*, 1984, **106**, 2990.
17 D. D. Pathak, H. Adams, N. A. Bailey, P. J. King and C. White, *J. Organomet. Chem.*, 1994, **479**, 237.
18 (*a*) N. Feiken, P. S. Pregosin, G. Trabesinger and M. Scalone, *Organometallics*, 1997, **16**, 537. (b) N. Feiken, P. S. Pregosin, G. Trabesinger, A. Albinati and G. L. Evoli, *Organometallics*, 1997, **16**, 5756.
19 L. Shimoni and J. P. Glusker, *Struct. Chem.*, 1994, **5**, 383.
20 (*a*) L. Brammer, W. T. Klooster and F. R. Lemke, *Organometallics*, 1996, **15**, 1721; (*b*) D. J. Teff, J. C. Huffman and K. G. Caulton, *Inorg. Chem.*, 1997, **36**, 4372.
21 J. D. Dunitz and R. Taylor, *Chem. Eur. J.*, 1997, **3**, 89.

Communication 9/05092B

ChemComm

Wavelength dependent photochemistry of an iron–arene organometallic photoinitiator: a quantitative study of the photoreactivity†

Vladimír Jakúbek and Alistair J. Lees*

Department of Chemistry, State University of New York at Binghamton, Binghamton, New York 13902-6016, USA. E-mail: alees@binghamton.edu

Received (in Bloomington, IN, USA) 18th May 1999, Accepted 12th July 1999

The quantitative photochemistry of the widely used cationic photoinitiator complex, [CpFe(η⁶-isopropylbenzene)]PF_6, has been investigated in several different solvents as a function of exciting wavelength in the 355–683 nm region; the photoefficiency results reveal that the system exhibits a strong wavelength dependence following excitation into its ligand field (LF) manifold and that the photochemistry does not occur solely from the lowest lying LF triplet excited state.

In recent years the [CpFe(η⁶-arene)]X system (Cp = η^5-C_5H_5; arene = benzene, toluene, hexamethylbenzene, naphthalene, anthracene, pyrene; X = BF_4, PF_6, SbF_6, AsF_6, CF_3SO_3) has been shown to be an effective cationic photoinitiator in the polymerization of epoxides,[1] dicyanate esters,[2] pyrrole,[3] styrene,[4] dioxolenes[5] and acrylates.[4,6] Consequently, complexes such as [CpFe(η⁶-ipb)]PF_6 (ipb = isopropylbenzene) are used widely in industrial polymerization processes, including the manufacture of printed circuit boards[7] and other coating applications.[8] A number of detailed studies of the photochemistry of [CpFe(η⁶-arene)]X have been carried out and the influence of several parameters (substitution on Cp ligand and nature of arene, counter ion and solvent) on the photoefficiency have revealed that the reactivity involves arene dissociation *via* an initial ring slippage mechanism.[1,9]

Despite the importance of this system our knowledge of the quantitative photochemistry has been restricted. All investigations to date have employed excitation at 436 nm to avoid any light absorption by the entering ligand. At this wavelength the lowest lying ligand field (LF) absorption manifold is populated and it has been assumed that the quantum efficiency for intersystem crossing is unity and that the reactivity occurs exclusively from a lowest energy LF triplet state (a^3E_{1g}).[9a] Recently we have developed a photokinetic procedure that enables one to study in detail the wavelength dependence of the photoreactivity in systems where there are inner filter absorbances.[10] Here, we report an investigation of [CpFe(η⁶-ipb)]PF_6 in various solvents; quantitative results have been obtained over a wide range of excitation wavelengths and they clearly show that the photochemistry does not occur solely from the lowest energy triplet excited LF state.

The UV-visible absorption spectrum of [CpFe(η⁶-ipb)]PF_6 in dichloromethane is shown in Fig. 1a and irradiations have been performed at 355, 458, 488, 514, 632 and 683 nm. Excitation in the 458–514 nm region results in population of the lowest lying LF singlet band (a^1E_{1g}).[9] Excitation at 355 nm results in population of an upper lying LF singlet band ($^1E_{2g}$) and may also involve some absorption into the long-wavelength tail of a higher lying ligand-to-metal charge transfer (LMCT) transition.[9,11] Excitation at 632 and 683 nm directly populates the LF triplet excited state of the complex (a^3E_{1g}),[9a] notwithstanding the extremely low absorbance in this region (in acetone, λ_{max} = 650 nm, ε = 3.2 M^{-1} cm^{-1}).

Fig. 1b illustrates UV-visible absorption spectra that have been recorded during the 458 nm photolysis of [CpFe(η⁶-ipb)]PF_6 in deoxygenated acetone solution containing an excess concentration (0.05 M) of scavenging phen (phen = 1,10-phenanthroline) ligand. Photolysis experiments have been performed at 355 and 683 nm with a Nd:YAG laser (the latter excitation wavelength utilized a Raman shift of the laser line), at 458, 488 and 514 nm with an Ar^+ laser and at 632 nm with a He–Ne laser. The spectral sequence depicted in Fig. 1b is representative of those obtained at any of the excitation wavelengths studied and in each case the reaction involves an exceptionally clean conversion to the $[Fe(phen)_3]^{2+}$ photoproduct (λ_{max} = 510 nm), according to eqn. (1).[9a] It was determined that the photochemistry was uncomplicated by any thermal processes or secondary photoreactions under these experimental conditions.

$$[CpFe(\eta^6\text{- ipb})]PF_6 \xrightarrow[0.05\ M\ phen]{h\nu} [Fe(phen)_3]^{2+} + ipb + PF_6^- + Cp^- \quad (1)$$

Absolute photochemical quantum efficiencies (ϕ_{cr}) have been obtained for the arene dissociation reaction of [CpFe(η⁶-

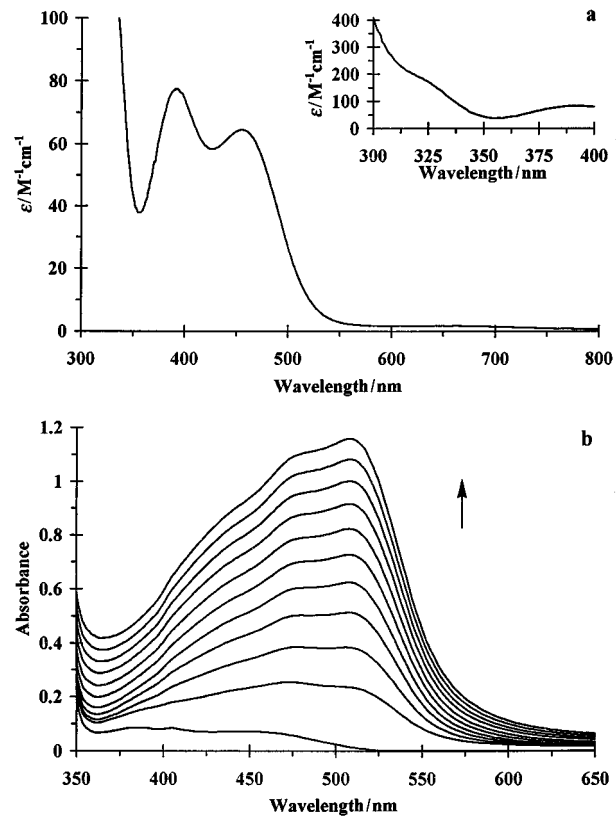

Fig. 1 (a) UV-visible absorption spectra of [CpFe(η⁶-ipb)]PF_6 in dichloromethane at 293 K. (b) UV-visible absorption spectral changes accompanying the 458 nm photolysis of 1 × 10^{-3} M [CpFe(η⁶-ipb)]PF_6 in deoxygenated acetone containing 0.05 M phen at 293 K. Spectra are depicted following 1 min time intervals; initial spectrum was recorded prior to irradiation.

† Dedicated to the memory of Dr Stephen J. Fuerniss who died suddenly on October 31, 1998.

Table 1 Absolute photochemical quantum efficiencies (ϕ_{cr}) for the arene dissociation reaction of [CpFe(η^6-ipb)]PF_6 in various solutions following excitation at several wavelengths[a,b]

	ϕ_{cr}					
Solvent	355 nm	458 nm	488 nm	514 nm	632 nm	683 nm
Dichloromethane	0.33(0.02)	0.25(0.001)	0.29(0.003)	0.20(0.003)		0.066(0.002)
Acetonitrile	0.66(0.07)	0.64(0.01)	0.62(0.01)	0.49(0.007)	0.20(0.01)	0.15(0.002)
Acetone	0.61(0.03)	0.66(0.01)	0.65(0.01)	0.49(0.008)		0.14(0.004)
Nitromethane	—[c]	0.72(0.01)	0.72(0.006)	0.55(0.003)		0.17(0.002)
1,2-Dichloroethane	0.25(0.02)	0.21(0.001)	0.22(0.002)	0.17(0.002)		0.051(0.002)

[a] Errors estimated at ±5%; values in parentheses represent the standard deviations from at least five measurements. [b] phen Concentration is 0.05 M in each case. [c] Value was not obtained due to solvent absorption.

ipb)]PF_6 following excitation at each of the above irradiation wavelengths. These values were determined by our previously reported procedure which accounts for inner filter effect absorbances due to the entering ligand.[10] Such a method is much more accurate than the procedure used earlier (in which ϕ_{cr} values were obtained over a small percentage of reaction[9c]) and it has also facilitated measurement of ϕ_{cr} data at both short and long excitation wavelengths. When phen is present in excess concentration it is understood to act solely as a scavenging ligand and not affect the reaction kinetics.[9c] For each excitation wavelength, the predicted linearity of the data, according to the photokinetic procedure,[10] was indeed observed in plots of $\ln[(A_t - A_\infty)/(A_0 - A_\infty)]$ *versus* $\int_{t_0}^{t_i}[(1 - 10^{-A_{tot}})/A_{tot}]dt$, where A_0, A_t and A_∞ are the absorbance values of the photoproduct at 510 nm during the irradiation, and A_{tot} is the total absorbance at various irradiation times t. This confirms that there is only one light step in the photochemistry. Time-resolved absorption spectra obtained for this system have also indicated that the initial photochemistry is extremely rapid (picosecond timescale) and that subsequent ligand scavenging is a much slower dark process ($k_{bimol} \approx 10^5$–10^8 M^{-1} s^{-1}).[1,9b]

The determined absolute photochemical quantum efficiencies for the arene dissociation reaction of [CpFe(η^6-ipb)]PF_6 are shown in Table 1. In each case, the phen concentration was kept constant and in excess (0.05 M) in order to make a fair comparison across all of the excitation wavelengths. The ϕ_{cr} results reveal strong dependence on the exciting wavelength for each solvent studied. The arene dissociation reaction clearly proceeds very efficiently following excitation in the 355–514 nm region into either of the two lowest lying LF singlet states, whereas this process is much less effective upon long-wavelength excitation in the 632–683 nm region following direct population of the LF triplet state. The observed wavelength dependence of ϕ_{cr} demonstrates unequivocally that the reaction does not occur solely from the lowest energy triplet level. If the quantum efficiency for intersystem crossing from the lowest lying singlet excited state (a^1E_{1g}) to the triplet reactive state (a^3E_{1g}) was unity[9a] then the determined ϕ_{cr} values would represent the processes from the lowest energy triplet state and would be independent of excitation wavelength. One possibility is that in the [CpFe(η^6-ipb)]PF_6 complex the lowest lying singlet (a^1E_{1g}) and triplet (a^3E_{1g}) LF states have distinct photoreactive pathways. Recently, independent photochemical routes occurring from lowest energy singlet and triplet excited states have been identified in $W(CO)_5$(py) and $W(CO)_5$(pip) (py = pyridine, pip = piperdine),[12] $W(CO)_4$(en) (en = ethylenediamine)[13] and $CpMn(CO)_3$.[14] Another possibility is that the photoreactivity arises exclusively from the singlet level (a^1E_{1g}) and the long wavelength photochemistry proceeds *via* thermal activation from the triplet (a^3E_{1g}) state.

Additionally, the ϕ_{cr} results in Table 1 show a significant solvent dependence for each excitation wavelength with higher ϕ_{cr} values being obtained in more polar solvents. The lower ϕ_{cr} values in solvents with low relative permittivities are understood to be caused by ion-pair formation of [CpFe(η^6-ipb)]$^+$ PF_6^- and the subsequent participation of the counter ion in the photochemical mechanism. Previously, time-resolved experiments have indicated that the close interaction of the counter ion results in a separate pathway involving a longer lived ring slipped (η^4-arene) reaction intermediate.[9b,c] Such long lived intermediates give additional opportunity for the arene ligand to undergo a reverse ring slippage ($\eta^4 \rightarrow \eta^6$), thereby lowering the ϕ_{cr} values. Currently, a number of solvent effects on the photochemical mechanism are under further investigation.

This study represents the first one in which the photochemistry of the [CpFe(η^6-arene)]X system has been investigated quantitatively at different excitation wavelengths. The results illustrate that the photoreaction is extremely efficient in the UV and visible regions, particularly if polar solvents are employed. Moreover, it is noteworthy that the photochemistry can be effectively performed throughout the visible spectrum making it possible to use a variety of laser excitation sources; indeed, the triplet state can be populated directly at 683 nm. The wavelength dependence of the photochemistry reveals that the reactivity does not solely derive from the lowest triplet state, as previously assumed. The strong wavelength dependence in this system will certainly have a major influence on future photoinitiator applications in coatings and moldings, in holography and lithography, in the manufacture of liquid-crystal display devices and protective films for optical devices, and in dentistry.[1–8]

We are grateful to the US DOE (Grant DE-FG02-89ER14039) for support of this research.

Notes and references

1 K. M. Park and G. B. Schuster, *J. Organomet. Chem.*, 1991, **402**, 355.
2 (*a*) T. G. Kotch, A. J. Lees, S. J. Fuerniss, K. I. Papathomas and R. Snyder, *Polym. Mater. Sci. Eng.*, 1992, **66**, 462; (*b*) T. G. Kotch, A. J. Lees, S. J. Fuerniss and K. I. Papathomas, *Chem. Mater.*, 1995, **7**, 801.
3 J. F. Rabek, J. Lucki, M. Zuber, B. J. Qu and W. F. Shi, *Polymer*, 1992, **33**, 4838.
4 P. Wang, Y. Shen, S. Wu, E. Adamczak, L. Linden and J. F. Rabek, *J. Macromol. Sci. Pure Appl. Chem. A*, 1995, **32**, 1973.
5 C. Bolln, H. Frey and R. Muelhaupt, *J. Polym. Sci. Part A: Polym. Chem.*, 1995, **33**, 587.
6 G. Eisele, J. P. Fouassier and R. Reeb, *Angew. Makromol. Chem.*, 1996, **239**, 169.
7 A. Reiser, *Photoreactive Polymers: The Science and Technology of Resists*, Wiley-Interscience, New York, 1989.
8 N. Pietschmann and H. Schulz, *Coating*, 1996, **29**, 270.
9 (*a*) A. M. Nair, J. L. Schrenk and K. R. Mann, *Inorg. Chem.*, 1984, **23**, 2633; (*b*) D. R. Chrisope, K. M. Park and G. B. Schuster, *J. Am. Chem. Soc.*, 1989, **111**, 6195; (*c*) K. R. Mann, A. M. Blough, J. L. Schrenk, R. S. Koefod, D. A. Freedman and J. R. Matachek, *Pure Appl. Chem.*, 1995, **67**, 95 and references therein.
10 A. J. Lees, *Anal. Chem.*, 1996, **68**, 226.
11 (*a*) J.-R. Hanon, D. Astruc and P. Michaud, *J. Am. Chem. Soc.*, 1981, **103**, 758; (*b*) G. Gamble, P. A. Grutsch, G. Ferrandi and C. Kutal, *Inorg. Chim. Acta*, 1996, **247**, 5.
12 C. Moralejo and C. H. Langford, *Inorg. Chem.*, 1991, **30**, 567.
13 R. S. Panesar, N. Dunwoody and A. J. Lees, *Inorg. Chem.*, 1998, **37**, 1648.
14 H. Yang, M. C. Asplund, K. T. Kotz, M. J. Wilkens, H. Frei and C. B. Harris, *J. Am. Chem. Soc.*, 1998, **120**, 10 154.

Communication 9/03975I

A stable and recyclable supported aqueous phase catalyst for highly selective hydroformylation of higher olefins†

Albertus J. Sandee, Vincent F. Slagt, Joost N. H. Reek, Paul C. J. Kamer and Piet W. N. M. van Leeuwen*

Institute of Molecular Chemistry, University of Amsterdam, Nieuwe Achtergracht 166, 1018 WV Amsterdam, The Netherlands. E-mail: pwnm@anorg.chem.uva.nl

Received (in Basel, Switzerland) 17th May 1999, Accepted 5th July 1999

A highly regioselective supported aqueous phase hydroformylation catalyst is presented that is completely and conveniently separated from the products and reused in numerous consecutive catalytic cycles.

Hydroformylation is one of the mildest and cleanest methods to produce aldehydes and is therefore widely applied in the petrochemical industry. The cleanest and most important industrial hydroformylation process is the aqueous biphasic process, developed by Ruhrchemie, affording a straightforward separation of the organic products from the catalyst. The applicability of this system, however, is strictly limited to substrates that are slightly water soluble, such as propene and but-1-ene.[1] The industrial hydroformylation of higher olefins is carried out in a single, organic phase and the catalyst is separated by distillation, which may result in catalyst decomposition. Distillation techniques are not suitable for the production of heavier products or fine chemicals because of the high boiling points of the products.

An interesting novel concept of catalyst immobilisation is the supported aqueous phase catalyst (SAPC).[2] In this system the catalyst is immobilised in a thin water layer adhered within the pores of a high-surface-area silicate.[3] Using this system higher alkenes can be converted at a relatively high rate without metal leaching. The regioselectivity, however, towards the linear aldehyde of the reported systems thus far is very low and surprisingly little has been reported on the recyclability and stability of these systems.[4] Virtually all SAP hydroformylation catalysts described in literature are based on rhodium, cobalt or platinum/nickel complexes with TPPTS as the ligand.[5,6] Only in a single case were sulfonated diphosphines examined.[7] Diphosphines with a large P–M–P bite angle have a beneficial influence on the regioselectivity of homogeneous hydroformylation catalysts.[8,9] We recently reported on the synthesis of a water-soluble ligand with a large bite angle: the disodium salt of 2,7-bissulfonate-4,5-bis(diphenylphosphino)-9,9-dimethylxanthene (Sulfoxantphos) (**A**) and its use in biphasic hydroformylation reactions.[10] The high regioselectivity obtained with this ligand stimulated us to investigate its performance as an SAPC.

It was shown that the rhodium hydride HRh(**A**)$(CO)_2$ (**1**), the precursor to the active species in hydroformylation reactions, was formed quantitatively under a CO–H_2 (1:1) atmosphere in DMSO-d_6.[10] When **1** is exposed to 1 bar of CO it completely transforms to the rhodium dimer [Rh(**A**)(CO)(μ-CO)]$_2$ (**2**) (Scheme 1), which was isolated and characterised by means of NMR, FT-IR and FAB-MS.[11] The ^{31}P NMR spectrum of **2** is consistent with an AA′BB′XX′ spin system ($^1J_{RhP}$ = 129, 135, 155 and 164 Hz, $^2J_{RhP}$ = 8 Hz, $^1J_{PP}$ = 18 Hz, $^3J_{PP}$ = 2 and 5 Hz, see Fig. 1). The equilibrium between **1** and **2** can be forced completely to either side by changing the hydrogen pressure.[12] A similar experiment in D_2O revealed that the formation of both **1** and **2** is much slower under aqueous conditions. The *in situ* formation of **2** on CPG-240 was, however, clearly observed using NMR techniques.‡

† Electronic Supplementary Information (ESI) available: experimental details. See http://www.rsc.org/suppdata/cc/1999/1633/

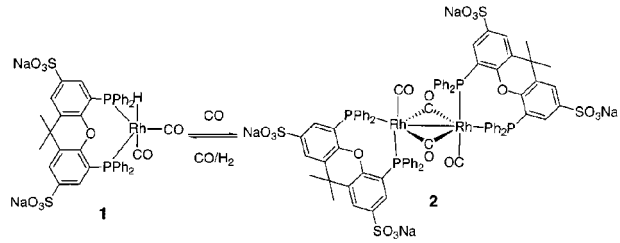

Scheme 1 Equilibrium between rhodium hydride and carbonyl-bridged dimeric species.

Both the novel Rh(**A**)/SAPC and the known Rh(TPPTS)/SAPC were studied in the hydroformylation of oct-1-ene.§ Rh(**A**)/SAPC is very selective towards the linear aldehyde; a linear to branched aldehyde ratio of 40:1 was obtained. This is an increase in regioselectivity, compared to Rh(TPPTS)/SAPC, of a factor of at least 10 (Table 1, entries 1 and 11). This proves that **A** plays a key role in the regulation of the regioselectivity in the hydroformylation of immobilised homogeneous catalysts.

The rate of hydroformylation of oct-1-ene using Rh(**A**)/SAPC at 80 °C in toluene as the co-solvent was found to be low (*ca.* 1 turnover per hour; Table 1, entries 1 and 2). When the catalysis was performed in pure oct-1-ene, however, the rate increased to a turnover rate of 15 per hour (Table 1, entry 1 and 3). Interestingly, this large concentration dependence was not found for Rh(TPPTS)/SAPC (Table 1, entries 11 and 12). We also found a 5-fold increase on performing the catalysis at 100 °C (turnover rates of 55 and 160 per hour, entries 9 and 13). Under optimised conditions the activities of Rh(**A**)/SAPC and Rh(TPPTS)/SAPC are competitive while the high selectivity of the former catalyst is retained.

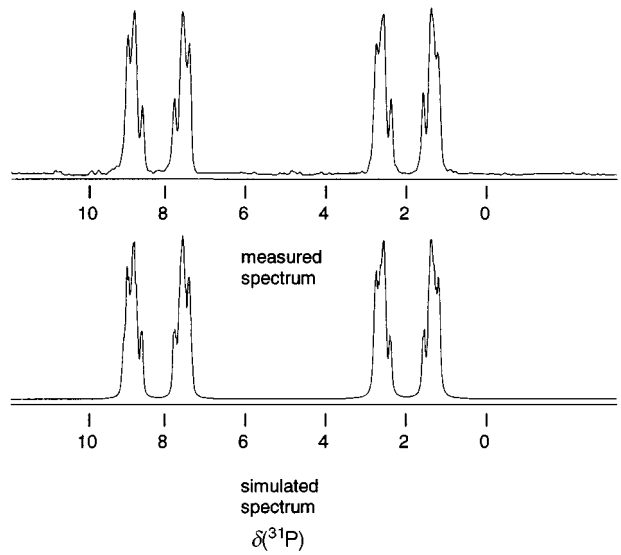

Fig. 1 Observed and calculated ^{31}P NMR spectrum of [Rh(Sulfoxantphos)(μ-CO)(CO)]$_2$ **2**.

Table 1 Results from the hydroformylation of oct-1-ene at 80–100 °C and 50 bar $CO–H_2$ (1:1).

Entry	Catalyst [cycle][a]	Conversion after 24 h (%)	TOF[b]	Linear to branched ratio[c]	Alkene isomerisation[c] (%)	Linear aldehyde[c] (%)
1	Rh(**A**) [1]	7	1	38	1.9	95.6
2	Rh(**A**) [2]	28[d]	1	44	5.7	92.2
3	Rh(**A**) [3][e]	14	15	46	5.0	93.0
4	Rh(**A**) [4][e]	14	14	42	8.7	89.2
5	Rh(**A**) [5][e]	12	14	40	8.5	89.3
6	Rh(**A**) [6][e]	10	13	40	7.7	90.0
7	Rh(**A**) [7][e]	24[f]	10	39	7.3	90.3
8	Rh(**A**) [8][g]	37	44	31	7.0	90.1
9	Rh(**A**) [9][g]	46	55	31	4.1	92.9
10	Rh(**A**) [10][g]	48	55	27	5.8	90.7
11	Rh(TPPTS) [1]	20	15	3	7.4	67.2
12	Rh(TPPTS) [2][e]	3	30	3	12.3	67.2
13	Rh(TPPTS) [3][g]	17	160	3	7.3	70.5
14	Rh(TPPTS) [4][g]	90[f]	146	2	52.6	33.9

[a] Ligand to rhodium ratio is 10 for Rh(**A**) and 20 for Rh(TPPTS), catalysis performed at 80 °C and 50 bar $CO–H_2$ in 15 ml toluene as a co-solvent using 1 ml of oct-1-ene. [b] Average turnover frequencies were calculated as (mol aldehyde/mol catalyst)$^{-1}$ h^{-1}. [c] Determined by means of GC analysis using decane as an internal standard. [d] Conversion after 96 h. [e] Catalysis performed in 15 ml oct-1-ene at 80 °C. [f] Conversion after 72 h. [g] Catalysis performed in 15 ml oct-1-ene at 100 °C.

The product/catalyst separation efficiency of the SAPCs was examined on performing recycling experiments (Table 1). Rh(**A**)/SAPC could be recycled numerous times without deterioration of the catalyst performance (entries 1–10). The selectivity towards the linear aldehyde remained high during all experiments and the decrease in rate of hydroformylation was very small (at 100 °C we even observed a small increase in rate in successive runs).¶ This indicates that ligand **A** retains the rhodium quantitatively on the support which is confirmed by rhodium analysis on the product by means of ICP-AES. No traces of rhodium were detected in the product phase of any of the SAPC experiments (detection limit 1 ppm). In contrast, Rh(TPPTS)/SAPC showed a drop in catalyst performance after three catalytic runs (Table 1, entries 11–14). In the fourth cycle, over 50% of the oct-1-ene isomerised and the linear-to-branched ratio decreased to 2. The Rh(**A**)/SAPC is thus far more robust then the TPPTS based SAPC; Rh(**A**)/SAPC could be recycled over at least three weeks, showing no deterioration of the catalyst performance whereas under similar conditions Rh(TPPTS)/SAPC showed a strong reduction in hydroformylation performance after three days.

Importantly, Rh(**A**)/SAPC is stable in the absence of substrate as it can be transformed into the dimer [Rh(**A**)(μ-CO)(CO)]$_2$ which is stable over weeks when properly stored under 1 bar of CO. The reversible switching between the catalytically active species **1** and the stable dimeric species **2** did not influence the catalytic performance in at least four consecutive runs.‖

We can conclude that the introduction of rigid bidentate diphosphines with a large 'natural' bite angle in the supported aqueous phase catalysis improves the regioselectivity towards the linear aldehyde enormously compared to the SAPCs known thus far. Moreover, the application of Sulfoxantphos in SAP catalysed hydroformylation gives rise to a significant improvement of the sustainability of the system. To the best of our knowledge this supported aqueous phase catalyst is the first example of an immobilised homogeneous catalyst that is highly selective and robust and shows no metal leaching in numerous consecutive catalytic runs.

This work was sponsored by the Innovation Oriented Research Program (IOP-katalyse). We thank J. Elgersma for performing the Rh analyses.

Notes and references

‡ For more experimental details see Electronic Supplementary Information (ESI).

§ The recycling experiments were performed as follows. A stainless steel 50 ml autoclave, equipped with a mechanical stirrer, a substrate vessel, a cooling spiral and a sample outlet, was charged with 1 g of SAPC containing (1) 1×10^{-4} mol **A**; (2) 1×10^{-5} mol Rh(acac)(CO)$_2$ and (3) 4% (m/m) water on CGP-240 in 10 ml toluene. The suspension was incubated for 1 h at 80 °C under 20 bar $CO–H_2$ (1:1). A mixture of 1 ml oct-1-ene and 1 ml decane in 3 ml toluene was added and the $CO–H_2$ pressure was brought to 50 bar. The mixture was stirred for 24 h. The autoclave was cooled to 15 °C and the pressure was reduced to 2 bar. With the small overpressure the liquid was slowly removed from the catalyst with a 1.2 mm syringe. After the catalyst was washed with 5 ml toluene, 10 ml of toluene was added and the pressure was brought to 20 bar. Finally the mixture was heated to 80 °C and the next cycle was performed.

¶ We also observed this increase in rate of hydroformylation in successive catalytic runs in the biphasic Rh(**A**) system (ref. 10). We suggest that at this temperature the remaining catalytically inactive species are slowly transformed into the active form (the inactive species is most probably the carbonyl bridged rhodium dimer).

‖ The procedure described above is extended as follows. After a catalytic run was performed the reaction medium was cooled to 90 °C the $CO–H_2$ (1:1) pressure was removed and 20 bar of CO was introduced. The mixture was slowly cooled to 20 °C and stirred for 4 h. The liquid was subsequently removed from the catalyst by means of a syringe. The catalyst was washed with CO-saturated toluene and the next cycle proceeded after the reaction mixture was pressurised with 50 bar of $CO–H_2$.

1 E. G. Kuntz, *Chemtech*, 1987, 570.
2 J. P. Arhancet, M. E. Davis, J. S. Merola and B. E. Hanson, *Nature*, 1989, **339**, 454.
3 M. E. Davis, *Chemtech*, 1992, 498.
4 J. P. Arhanchet, M. E. Davis and B. E. Hanson, *J. Catal.*, 1991, **129**, 100.
5 W. A. Herrmann and C. W. Kohlpainter, *Angew. Chem., Int. Ed. Engl.*, 1993, **32**, 1524.
6 M. S. Anson, M. P. Leese, L. Tonks and J. M. J. Williams, *J. Chem. Soc., Dalton Trans.*, 1998, 3529.
7 I. Tóth, I. Guo and B. E. Hanson, *J. Mol. Catal.*, 1997, **116**, 217.
8 C. P. Casey, G. T. Whiteker, M. G. Melville, L. M. Petrovich, J. A. Gavey and D. R. Powell, *J. Am. Chem. Soc.*, 1992, **114**, 5535.
9 M. Kranenburg, Y. E. M. van der Burgt, P. C. J. Kamer, P. W. N. M. van Leeuwen, K. Goubitz and J. Fraanje, *Organometallics*, 1995, **14**, 3081; L. A. van der Veen, M. D. K. Boele, F. R. Bregman, P. C. J. Kamer, P. W. N. M. van Leeuwen, K. Goubitz, J. Fraanje, H. Schenk and C. Bo, *J. Am. Chem. Soc.*, 1998, **120**, 11 616.
10 M. Schreuder Goedheijt, P. C. J. Kamer and P. W. N. M. van Leeuwen, *J. Mol. Catal.*, 1998, **134**, 243.
11 B. R. James, D. Mahajan, S. J. Rettig and G. M. Williams, *Organometallics*, 1983, **2**, 1452.
12 A. Castellanos-Paéz, S. Castillón, C. Claver, P. W. N. M. van Leeuwen and W. G. J. de Lange, *Organometallics*, 1998, **17**, 2543.

Communication 9/03916C

Protein film cryovoltammetry: demonstrations with a 7Fe ([3Fe–4S] + [4Fe–4S]) ferredoxin

James P. McEvoy and Fraser A. Armstrong*

Inorganic Chemistry Laboratory, Department of Chemistry, Oxford University, South Parks Road, Oxford, UK OX1 3QR. E-mail: fraser.armstrong@chem.ox.ac.uk

Received (in Cambridge, UK) 22nd April 1999, Accepted 29th June 1999

Low-temperature protein film voltammetry, demonstrated here by studies of Fe–S clusters in the 7Fe ferredoxin from *Thermoplasma acidophilum*, offers a novel way to investigate active site redox reactions, allowing resolution of complex transformations and transient states, and providing an immediate and sensitive gauge of solvent effects.

Protein film voltammetry (PFV) is proving to be a powerful method of investigating biological redox-active sites.[1,2] The protein sample is adsorbed onto a suitable electrode surface as an electroactive film, and its electron transfer and coupled processes are probed as functions of potential and time. Signals obtained from a minuscule quantity of sample (monolayer coverage or less, equating to pmol cm^{-2}) lead to the detection and characterization of labile active sites and deconvolution of complex reaction sequences. The potential may be cycled at rates > 100 V s^{-1}, accessing coupled reactions occurring on the sub-millisecond time scale. Here we report an important extension of PFV in which the sample is easily and reversibly transferred to a cryosolvent. Details of redox chemistry are revealed across a wide sub-zero temperature range, and transient states can be trapped at slow (< 100 mV s^{-1}) scan rates. The approach draws together several areas, notably cryoenzymology,[3] enzymes in organic solvents[4] and cryovoltammetry.[5]

We demonstrate the concept with experiments on a 7Fe ferredoxin (Fd). These proteins contain a [3Fe–4S] and a [4Fe–4S] cluster, and have been extensively characterized. They display distinctive voltammetry with a unique combination of characteristics, both simple and complex, that can be identified and correlated with behavior established under more conventional conditions.[6–10] The ferredoxin from *Thermoplasma acidophilum* (*Ta*),[11] MW *ca.* 16 kDa, which also contains a single Zn atom, is related structurally to the previously studied ferredoxin isolated from *Sulfolobus acidocaldarius*.[9,10,12,13]

The redox reactions of interest are shown in Scheme 1. The [4Fe–4S] cluster undergoes only one redox transition (2+/+), referred to in PFV as signal B′, while the [3Fe–4S] cluster exhibits more complex behavior. The '+' and '0' oxidation levels (whose interconversion gives rise to signal A′) are well characterized[8,9,14] and a further two electrons are taken up in a chemically reversible process (signal C1′) to produce an unusual all-Fe(II) cluster.[10] It has been shown[13] that this hyper-reduced state is capable of undergoing a rapid and reversible two-electron–two-proton oxidation (signal C2′), the immediate oxidized product of which reverts to the normal '0' state within a second at 273 K unless re-reduced within this time. The C′ signals are due to *cooperative* two-electron transfers (as revealed by the narrow voltammetric peak shapes),[15] making it likely that this novel cluster reaction involves disulfide coupling instead of Fe-based redox transitions.

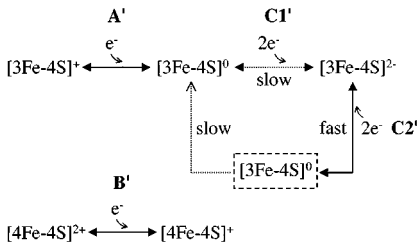

Scheme 1 Redox transitions of the [3Fe–4S] and [4Fe–4S] clusters in *Thermoplasma acidophilum* ferredoxin. The transition between alternative states of $[3Fe–4S]^0$ is also shown, with the metastable form capable of very rapid $2e^-$–$2H^+$ transfer indicated by the dashed box. Proton transfers are not included.

Fig. 1 shows voltammograms, scan rate 20 mV s^{-1}, obtained from a film of *Ta* Fd formed on a pyrolytic graphite edge (PGE) electrode in aqueous solution[16] and then transferred to a cell containing 70% v/v methanol–water (pH* = 7.4 at 273 K[17]), the temperature of which could be varied down to 188 K.[3a] The potential range engages only the $[3Fe–4S]^{+/0}$ couple, to provide the simplest test of the system. At 273 K the oxidation and reduction peaks of signal A′ are nearly symmetrical and the reduction potential $E^{\circ\prime}$ is −297 ± 10 mV, compared with −250 mV obtained under the same conditions in aqueous electrolyte. Experiments with 60% v/v ethane-1,2 diol–water gave similar results with $E^{\circ\prime}$ = −276 mV. The electroactive coverage, *ca.* 55 × 10^{-12} mol cm^{-2} based on geometric electrode area, is as expected for a very densely packed monolayer on an ideal flat surface.[1b] As the temperature is lowered, $E^{\circ\prime}$ increases (linearly with temperature, as expected), the peak separation increases to reflect slower interfacial electron transfer, and the peaks broaden slightly. In the limit of a Nernstian system, half-height peak widths should decrease from 83 mV at 273 K to 60 mV at 198 K.[15] However, the expected sharpening was not observed even if a very slow scan rate (2 mV s^{-1}) was used; reductive and oxidative peak widths at 273 K were 86 and 90 mV respectively, with peak separation 7 mV, whereas at 198 K these broadened

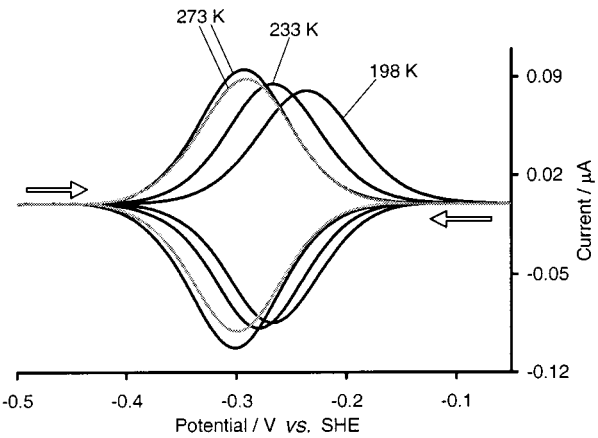

Fig. 1 Background-subtracted cyclic voltammograms obtained from a single film of *Thermoplasma acidophilum* ferredoxin adsorbed on a PGE electrode (coated from ice-cold aqueous solution) and transferred to a 70 : 30 methanol–water electrolyte, showing the temperature dependence of the $[3Fe–4S]^{+/0}$ couple. Each scan was conducted at 20 mV s^{-1} and started from the oxidative limit. The film was cooled from 273 to 233 and then to 198 K, before re-warming to 273 K (final voltammogram shown in grey). The cell solution (pH* = 7.4 as measured at 273 K) contained 0.1 M NaCl, 20 mM HEPES buffer and 200 μg ml^{-1} polymyxin B sulfate. Chunky arrows indicate the direction of scanning.

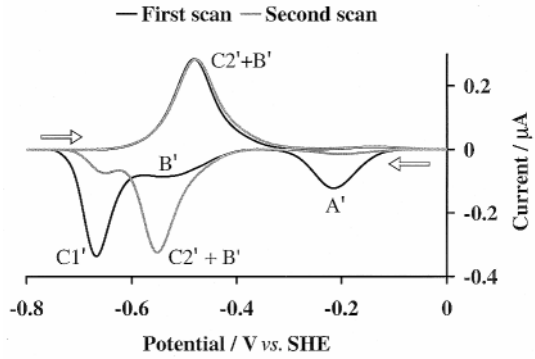

Fig. 2 Background-subtracted cyclic voltammograms showing the first cycle (black) and the second (grey) obtained from a film of *Thermoplasma acidophilum* ferredoxin (coated from aqueous solution) adsorbed on a PGE electrode in 70:30 methanol–water electrolyte at 198 K. The scan was conducted at 40 mV s^{-1} and started from an oxidative poise. The cell solution, pH* = 5.0 as measured at 273 K, contained 0.1 M NaCl, 20 mM acetate buffer and 200 μg ml^{-1} polymyxin B sulfate. Arrows indicate direction of scanning.

slightly to 90 and 96 mV, with a modest 23 mV peak separation.[18] Warming to 273 K almost completely restores the voltammetry measured at the start of the experiment (*ca.* 1 h previously).[19]

Fig. 2 shows the voltammetry obtained across a wide potential range, engaging all the redox couples shown in Scheme 1 to provide a more demanding test. The solution acidity (pH* = 5.0 at 273 K) parallels conditions used to reveal the novel cooperative two-electron couple at ambient temperatures in aqueous electrolyte.[13] In the first cycle, started from an oxidative poise, the reduction peaks correspond to $[3Fe–4S]^{+/0}$ (A′ is at a higher potential than in Fig. 1 because pH* is below p*K*[16]), $[4Fe–4S]^{2+/+}$ (B′, somewhat broader than A′), and $[3Fe–4S]^{0/2-}$ (C1′, narrow and intense). The A′:B′:C1′ peak area ratio is 1:1.1:1.8, close to that expected. The subsequent oxidative scan is dominated by one large signal in the position expected for a superposition of B′ and C′. Notably, the oxidation peak of signal A′ has almost vanished; the second reductive scan also reveals very little A′ and is dominated instead by the new couple C2′. As reported recently, the immediate product of two-electron oxidation of $[3Fe–4S]^{2-}$ is an alternative '0' state which cannot be oxidized rapidly to $[3Fe–4S]^{+}$. Poising for sufficient time at potentials higher than the $[3Fe–4S]^{+/0}$ couple restores almost completely the voltammetry of the first cycle. At 245 K this requires *ca.* 3 min, whereas at 273 K the metastable '0' species is too short-lived to be detected below 1 V s^{-1}.[13]

The behavior of this system therefore mimics that observed in fast-scan experiments at ambient temperatures in pure aqueous media. We conclude that extremely small samples of protein, immobilized on an electrode, can be introduced conveniently and reversibly into cryosolvents—in effect, an instantaneous microscopic dialysis—and studied at low temperatures. Convoluted and multi-step redox reactions are retarded to allow deconvolution and detection of intermediates at conventional scan rates. Other proteins respond similarly well to this technique, and we are currently extending its application to enzymes.

We are grateful to Professors Richard Cammack and Dieter Oesterhelt for providing a sample of *Thermoplasma acidophilum* ferredoxin, and Dr Michael Honeychurch for helpful discussions. This research was supported by the UK Engineering and Physical Sciences Research Council, and by the Royal Society.

Notes and references

1 F. A. Armstrong, H. A. Heering and J. Hirst, *Chem. Soc. Rev.*, 1997, **26**, 169; J. Hirst and F. A. Armstrong, *Anal. Chem.*, 1998, **70**, 5062.

2 For recent articles describing different aspects of the voltammetry of protein films, see, for example: A. E. Kasmi, J. M. Wallace, E. F. Bowden, S. M. Binet and R. J. Linderman, *J. Am. Chem. Soc.*, 1998, **120**, 225; J. L. Kong, Z. Q. Lu, Y. M. Lvov, R. Z. B. Desamero, H. A. Frank and J. F. Rusling, *J. Am. Chem. Soc.*, 1998, **120**, 7371.

3 (*a*) P. Douzou, *Cryobiochemistry*, Academic Press, New York, 1977; (*b*) A. L. Fink and M. A. Geeves, in *Contemporary Enzyme Kinetics and Mechanism*, Academic Press, New York, 1983, p. 173; (*c*) F. Travers and T. Barman, *Biochim.*, 1995, **77**, 937.

4 A. M. Klibanov, *Trends Biochem. Sci.*, 1989, **14**, 141.

5 G. K. Rowe, M. T. Carter, J. N. Richardson and R. W. Murray, *Langmuir*, 1995, **11**, 1797.

6 F. A. Armstrong, J. N. Butt and A. Sucheta, *Methods Enzymol.*, 1993, **227**, 479.

7 J. N. Butt, F. A. Armstrong, J. Breton, S. J. George, A. J. Thomson and E. C. Hatchikian, *J. Am. Chem. Soc.*, 1991, **113**, 6663; J. N. Butt, S. E. J. Fawcett, J. Breton, A. J. Thomson and F. A. Armstrong, *J. Am. Chem. Soc.*, 1997, **119**, 9729.

8 B. Shen, L. L. Martin, J. N. Butt, F. A. Armstrong, C. D. Stout, G. M. Jensen, P. J. Stephens, G. N. La Mar, C. M. Gorst and B. K. Burgess, *J. Biol. Chem.*, 1993, **268**, 25928; J. Hirst, J. L. C. Duff, G. N. L. Jameson, M. A. Kemper, B. K. Burgess and F. A. Armstrong, *J. Am. Chem. Soc.*, 1998, **120**, 7085.

9 J. L. Breton, J. L. C. Duff, J. N. Butt, F. A. Armstrong, S. J. George, Y. Pétillot, E. Forest, G. Schäfer and A. J. Thomson, *Eur. J. Biochem.*, 1995, **233**, 937.

10 J. L. C. Duff, J. L. J. Breton, J. N. Butt, F. A. Armstrong and A. J. Thomson, *J. Am. Chem. Soc.*, 1996, **118**, 8593.

11 S. Wakabayashi, N. Fujimoto, K. Wada, H. Matsubara, L. Kerscher and D. Oesterhelt, *FEBS Lett.*, 1983, **162**, 21; T. Iwasaki, T. Suzuki, T. Kon, T. Imai, A. Urushiyama, D. Ohmori and T. Oshima, *J. Biol. Chem.*, 1997, **272**, 3453.

12 T. Fujii, Y. Hata, M. Oozeki, H. Moriyama, T. Wakagi, N. Tanaka and T. Oshima, *Biochemistry.*, 1997, **36**, 1505.

13 J. Hirst, G. N. L. Jameson, J. W. A. Allen and F. A. Armstrong, *J. Am. Chem. Soc.*, 1998, **120**, 11994.

14 S. J. George, A. J. M. Richards, A. J. Thomson and M. G. Yates, *Biochem. J.*, 1984, **224**, 247; M. K. Johnson, D. E. Bennett, J. A. Fee and W. V. Sweeney, *Biochim. Biophys. Acta*, 1987, **911**, 81; P. J. Stephens, G. M. Jensen, F. Devlin, T. V. Morgan, C. D. Stout and B. K. Burgess, *Biochemistry*, 1991, **30**, 3200; C. D. Stout, *J. Biol. Chem.*, 1993, **268**, 25920; Z. G. Hu, D. Jollie, B. K.Burgess, P. J. Stephens and E. Münck, *Biochemistry*, 1994, **33**, 14475.

15 E. Laviron, in *Electroanalytical Chemistry*, ed. A. J. Bard, Marcel Dekker, New York, 1982, **12**, 53.

16 The methodology was based on that described in ref. 6. Polymyxin B sulfate (200 μg ml^{-1}) was present as co-adsorbate in both the aqueous electrode-coating solution and the cryosolvent cell solution (usually 70% v/v methanol; Prolabo > 99%) with 0.1 M NaCl buffered by HEPES at pH* 7.4 or acetate at pH* 5.0. The aqueous saturated calomel reference electrode (SCE) with internal salt bridge was held in a Luggin side arm filled with cryosolvent but maintained at room temperature with a water jacket. Values of pH and pH* [see: ref. 3(*a*), and R. G. Bates, *Determination of pH: Theory and Practice*, Wiley, New York, 1973] were measured with glass pH electrode at 273 K, without corrections. Cell anaerobicity was maintained by purging with Ar. Temperatures were controlled by immersing the cell compartment in a stirred ethanol bath, to which was added dry ice or frozen ethanol, and measured (±1 K) with a thermometer after 10 min equilibration. Background currents were subtracted using an in-house analysis program (Dr H. A. Heering).

17 Measurements of the $[3Fe–4S]^{+/0}$ couple between pH* 4 and 9 (recorded at 273 K) showed that, over the full temperature range studied, the p*K* for protonation of $[3Fe–4S]^{0}$ remains significantly lower than the pH* used in measuring the voltammetry for Fig. 1, thus ruling out the possibility that $E^{\circ\prime}$ varies trivially as a result of pH* changes. Values obtained were: at 273 K (aqueous) p*K* = 5.6, at 273 K (70% v/v methanol) p*K* = 6.7, at 198 K (70% v/v methanol) p*K* = 6.8 (an apparent value since pH* is measured at 273 K).

18 The peak broadening observed as the temperature is lowered is not due to increased uncompensated resistance (*iR*); like irreversible electrode kinetics, *iR* effects are associated with large increasaes in peak separation. See: L. Roullier and E. Laviron, *J. Electroanal. Interfacial Electrochem.*, 1983, **157**, 193.

19 Peak potentials were completely restored although peak areas were *ca.* 10% smaller than measured at the start of the experiment.

Communication 9/03222C

A fluorescent probe for the detection of NAD(P)H

Carl A. Roeschlaub, Nicola L. Maidwell, M. Reza Rezai and Peter G. Sammes*

Molecular Probes Unit, Department of Chemistry, School of Physical Sciences, UNIS, Guildford, Surrey, UK GU2 5XH. E-mail: p.sammes@surrey.ac.uk

Received (in Cambridge, UK) 22nd June 1999, Accepted 16th July 1999

NAD(P)H may be monitored by using reduction to release the fluorophore umbelliferone from a precursor conjugate with a quinoxalinium salt.

NADH and its phosphate ester NADPH are ubiquitous reducing agents in nature. In rapidly proliferating cervical cancer cells the turnover of NAD(P)H is greater than in normal cells and thus it can be used as a general biological marker for cancer.[1] A potential fluorescent probe for the detection of these aberrant cells has been described[2] that uses the reduction of the weakly-fluorescent dye resazurin **1** to the fluorescent derivative

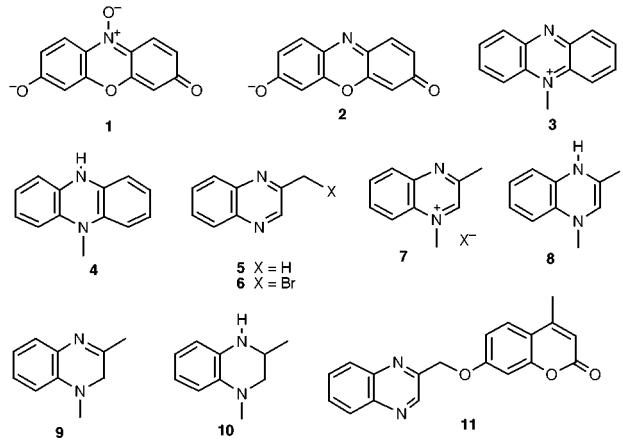

resorufin **2**. A disadvantage of this system is that direct reduction of resazurin to resorurufin does *not* occur and the reaction has to be 'catalysed' by an electron carrier such as phenazinium methosulfate **3** or an enzyme such as diaphorase.[3] The mechanism of this reduction has been investigated[2] and, for the catalyst phenazinium methosulfate, shown to proceed *via* initial formation of the dihydrophenazine derivative **4**, which is extremely unstable and rapidly undergoes further redox reactions.

NAD(P)H is also co-produced by a number of enzyme-based redox systems, such as glucose-6-phosphate dehydrogenase[4] and is used in a number of enzyme linked immunosorbent assays (ELISA).[5] In these assays a catalyst has also to be used, often another enzyme such as diaphorase, to act as the electron carrier in conjunction with either resazurin, reduced to the fluorescent resorufin,[3] or of a leuco-dye, such as a tetrazolium salt, which is reduced to the corresponding, highly coloured formazan.[6]

In order to avoid the need for these two-component systems involving an electron carrier, conjugation of a masked fluorophore to a reducible heteroaromatic system was considered, in which the reduction would unmask the fluorophore. After studying several systems we focused on use of derivatives of the quinoxalinium system. 2-Methylquinoxaline **5** was found to react regioselectively with methylating agents, such as MeI and MeOTf, to produce the corresponding 1,3-dimethylquinoxalinium salt **7**.† Reduction of these salts with NADH at pH 7.5 rapidly produces a dihydro compound. Whilst mechanistic studies with NADH predict that this will be the 1,4-dihydro isomer **8**,[7] this was not obtained since it efficiently tautomerises to the 1,2-dihydro isomer **9,** isolated in high yield (> 90%). In contrast to the dihydrophenazine **4,** the dihydroquinoxaline **9** is relatively stable, although, upon exposure to air it is oxidised to give a variety of highly coloured products. It is to be noted that both **4** and **8** are both formally anti-aromatic and this undoubtedly contributes to their chemical reactivity. Reduction of the salt **7** can also be effected with $NaBH_4$, although with an excess of this reagent, over-reduction to give the tetrahydroquinoxaline **10** was observed. None of **10** was observed upon reduction of **7** with NADH.

Because of its bimolecular nature, the rate of reduction of the quinoxalinium salt **7** by NADH is concentration dependent. At concentrations in the micromolar range the reduction takes several hours to complete but at millimolar concentrations reaction is complete within seconds.

In order to generate a useful fluorescent probe, 2-methylquinoxaline **5** was brominated at the methyl group, using NBS, and the bromomethyl compound **6** then conjugated with umbelliferone **16** to produce the derivative **11**. Methylation of this base with MeOTf afforded the triflate salt **12**. Neither of the compounds **11** nor **12** showed any significant fluorescence.

Reduction of the salt **12** with NADH was effected by adding a solution of the salt to a stirred solution of NADH at pH 7.5 and immediately re-measuring the emission spectrum. A signal corresponding to that of free umbelliferone **16** formed almost immediately. That this was due to liberated umbelliferone **16** was also confirmed by TLC and direct isolation; in a quantitative experiment > 85% **16** could be extracted from the solution. In the absence of NADH no formation of umbelliferone **16** was observed, confirming that the liberation was a direct consequence of reduction by NADH.

The fate of the quinoxalinium moiety has also been explored. Reduction is assumed to give, initially, the 1,4-dihydro intermediate **13**. Rather than tautomerising, in the manner observed for the conversion of the unsubstituted quinoxalinium salt (**7** to **8** to **9**), to give **14**, which has not been observed, elimination of umbelliferone occurs to give the quinoxalinium

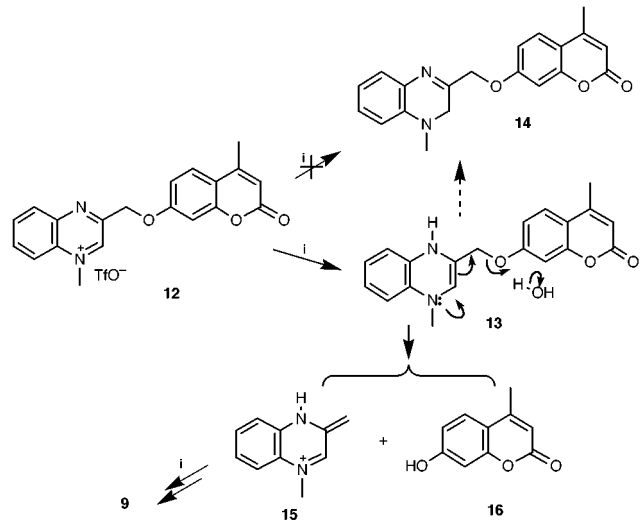

Scheme 1 *Reagents and conditions*: i, NADH, pH 7.5.

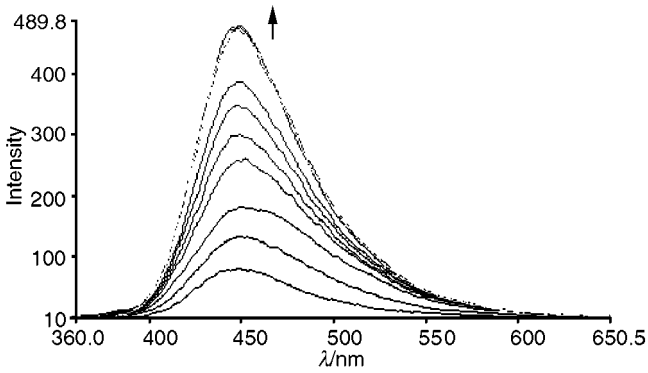

Fig. 1 Increase in emission with time; scans at 2 min. intervals; maximum reached in < 24 min. See text for conditions.

tautomer **15**, which then reforms the quinoxalinium species **7**, followed by a second NADH reduction step to produce the imine **9**, which has also been isolated and characterised (see Scheme 1).

Fig. 1 shows the results of a typical reaction. The increase of umbelliferone **16** fluorescence is obtained by mixing a solution of the salt **12** at 1×10^{-4} mol dm^{-3} with NADH at 1×10^{-3} mol dm^{-3} in TRIS buffer at pH 7.5, taking aliquots at 2 min intervals and diluting 100-fold in buffer (to give a sample at 1×10^{-6} mol dm^{-3}) before measuring the fluorescence spectrum, (λ_{ex} 350 nm), monitoring the umbelliferone emission peak at λ_{em} 450 nm. Under these conditions reduction is observed in under 24 min. Control fluorescence measurements on pure umbelliferone, in the presence of 1 equiv. of the imine **7,** indicate that release of the umbelliferone from the salt **12** is quantitative.

We thank the EPSRC for support of this work and the EPSRC National Mass Spectrometry Service Centre, Swansea, Wales, for accurate mass measurements.

Notes and references

† All new compounds gave satisfactory microanalyses and/or accurate mass measurements.

1 S. K. Jonas, C. Benedetto, A. Flatman, L. Micheletti, C. Riley, P. A. Riley, D. Spargo, M. Zonca and T. F. Slater, *Br. J. Cancer*, 1992, **66**, 185.
2 L. P. Candeis, D. P. S. MacFarlane, S. L. W. McWhinnie, N. L. Maidwell, C. A. Roeschlaub, P. G. Sammes and R. Whittlesey, *J. Chem. Soc., Perkin Trans. 2*, 1998, 2333.
3 D. B. Cook and C. H. Self, *Clin. Chem.*, 1993, **39**, 965.
4 H. Shah, A. M. Saranko, M. Harkonen and H. Adlercreutz, *Clin. Chem.*, 1984, **30**, 185.
5 For a review see A. Voller and D. E. Bidwell, *Enzyme Immunoassays*, in *Alternative Immunoassays*, ed. W. P. Collins, Wiley, Chichester, 1985, pp. 77–86.
6 E. Seidler, *The Tetrazolium-Formazan System: Design and Histochemistry*, in *Progress in Histochemistry and Cytochemistry*, Gustav Fischer Verlag, Stuttgart, 1991, vol. 24, pp. 1–86.
7 G. Blankenhorn, in *Pyridine Nucleotide Dependent Dehydrogenases*, ed. H. Sund, W. de Gruyter & Co., Berlin, 1997, pp. 185–205.

Communication 9/04971A

Steering non-centrosymmetry into the third dimension: crystal engineering of an octupolar nonlinear optical crystal

Venkat R. Thalladi,[a] Roland Boese,*[a] Sophie Brasselet,[b] Isabelle Ledoux,[b] Joseph Zyss,*[b] Ram K. R. Jetti[c] and Gautam R. Desiraju*[c]

[a] *Institut für Anorganische Chemie, FB 8, Universität-GH Essen, Universitätsstrasse 5-7, D-45177 Essen, Germany. E-mail: boese@structchem.uni-essen.de*

[b] *Département de Physique, École Normale Supérieure de Cachan, 61, Avenue du Président Wilson, 94235 Cachan Cedex, France. E-mail: zyss@lpqm.ens-cachan.fr*

[c] *School of Chemistry, University of Hyderabad, Hyderabad 500 046, India. E-mail: grdch@uohyd.ernet.in*

Received (in Cambridge, UK) 7th June 1999, Accepted 16th July 1999

The ability of CH_3 groups to form helical chains of C–H···π interactions with phenyl rings leads to polar stacking of trigonal octupolar networks in a substituted triazine, and therefore to three-dimensional non-centrosymmetry.

Structural control in the third dimension continues to be one of the most sought-after goals in crystal engineering.[1,2] We have recently reported that a family of *sym*-triaryloxytriazines **1** lend themselves well, *via* dimeric Piedfort units (PU) **2**, to the adoption of trigonal two-dimensional networks **3** (Scheme 1).[3] This disymmetric network stacks in a parallel or anti-parallel fashion to give, respectively, **4** and **5**. Arrangement **4** meets the requirements of crystalline octupolar nonlinear optical (NLO) behaviour[4] and is seen in compound **1a**. A number of other derivatives **1b-f** crystallise in arrangement **5**, that is, they do not display Second Harmonic Generation (SHG). The undesirable anti-parallel stacking in these cases may be attributed to the steric bulk of Cl, Br and CH_3 substituent groups located in the *meta* position of the phenoxy rings.

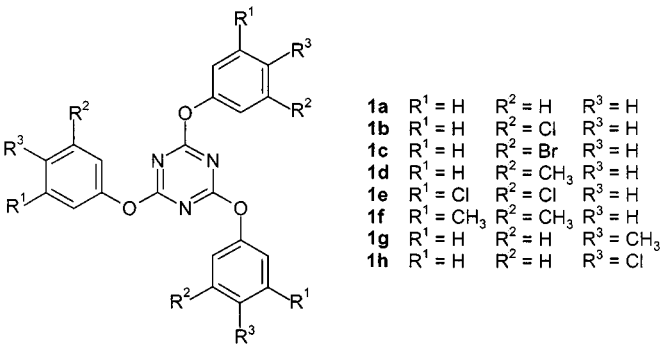

We had explored variations in the *meta* substituent, arguing that tampering with the *ortho* H-atoms of the phenoxy rings would disturb the formation of the PU itself, while the *para* H-atom was needed for the C–H···π interactions that are implicated in the formation of trigonal network **3**.[3] Here, we show that 2,4,6-tris(4-methylphenoxy)-1,3,5-triazine **1g** adopts a non-centrosymmetric packing because the *para* CH_3 substituent can form C–H···π interactions with an orientation that sustains three-dimensional chirality.

Single crystals of **1g** suitable for X-ray diffraction (non-centrosymmetric space group *R*3*c*) were grown from slow evaporation of an *o*-xylene solution.† The molecules are positioned on three-fold axes and retain their molecular symmetry in the crystal. Successive *c*-glide related molecules are stacked and are interconnected by C–H···O (*D*, 3.57 Å, *d*, 2.64 Å; *θ*, 143°)‡ and C–H···N (3.46 Å, 2.43 Å, 160°) hydrogen bonds to form the D_3-symmetric PUs. The trigonal assembly of D_3-PUs generates an octupolar network structure parallel to (001) as shown in Fig. 1.

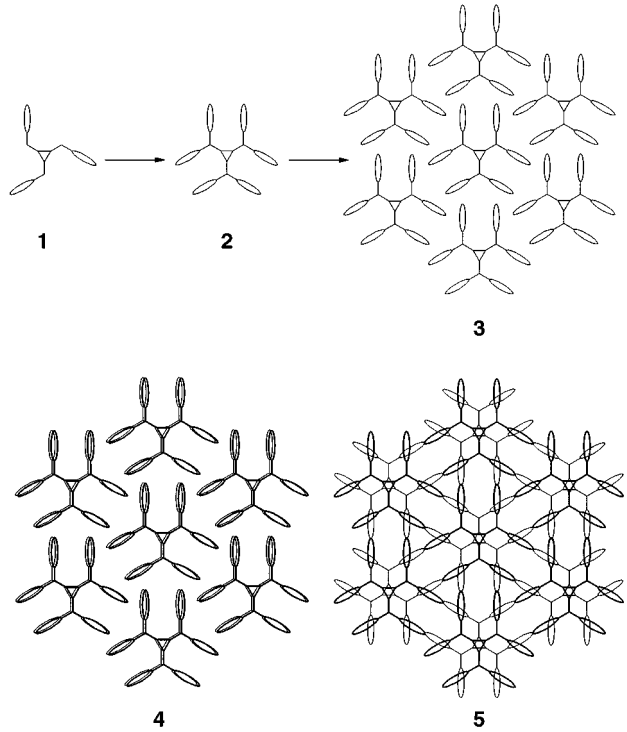

Scheme 1

The *para* CH_3 groups participate in C–H···π interactions[5] (*D*, 3.60 Å, *d*, 2.77 Å; *θ*, 133°) that link interlayer D_3-PUs. This ability of the CH_3 groups to form C–H···π interactions coupled with fact that the C–H vectors are bent with respect to the plane of the trigonal network allows these groups to link with molecules in the third dimension.[6] Fig. 2 shows that the C–H···π interactions are arranged around 3_1 and 3_2-axes and that they extend to the third dimension in a helical manner. Any two adjacent helices have opposite handedness, but the chains of C–H···π interactions always run along [001]. Thus all C–H···π helices have the *same* polarity. Consequently, successive layers are compelled to stack in an eclipsed manner leading to bulk non-centrosymmetry.

It is of interest to note that, in triazines **1b**–**f**, the peripheral aryloxy rings are inclined perpendicular to the central heterocyclic ring (with an inclination angle of 89–92°) whereas they are inclined at a much shallower angle in **1g** (67°).§ The C–H···O and C–H···N bonds become shorter and linear with such flattening and as such are more effective. Additionally, the central rings in **1g** are stacked at a separation of 3.30 Å. This is much shorter when compared to the stacking found in triazines **1a**–**f** (3.6–4.0 Å). In summary, the CH_3 groups not only maintain the eclipsed stacking of the layers but also reinforce

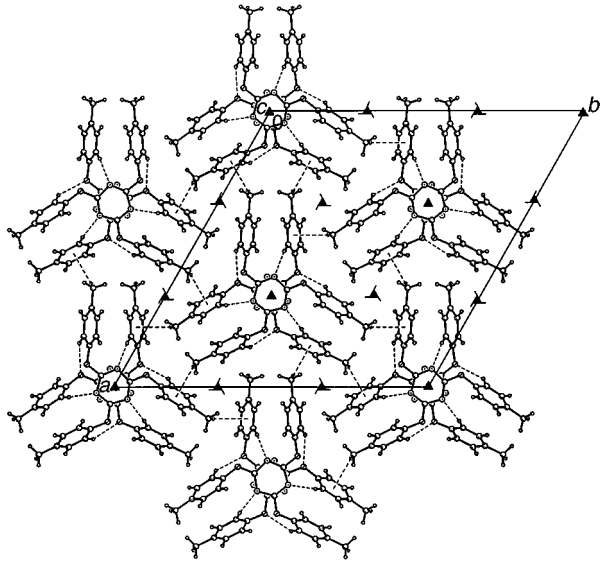

Fig. 1 Octupolar trigonal network structure in **1g**. The 3-fold, 3_1- and 3_2-axes are indicated. Notice the C–H···O and C–H···N hydrogen bonds within a D_3-PU. Notice that the C–H···π interactions extend to the third dimension in a helical manner around 3_1- and 3_2-axes.

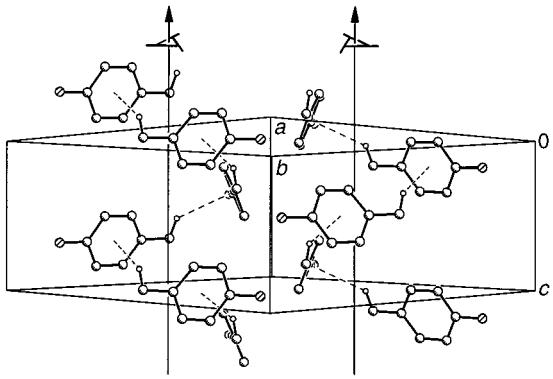

Fig. 2 Helical arrangement of C–H···π hydrogen bonds in triazine **1g** (several atoms deleted). Note that the two helices have opposite handedness but that they run in the same direction, [00$\bar{1}$].

other interactions which are important for effective three-dimensional packing.

The non-centrosymmetric nature of **1g** was confirmed by a powder SHG signal at 1.064 μm which is ~1 × KDP. Due to the weak donor property of the methyl group, the quadratic hyperpolarisability of **1g** may be assumed to be very close to that of **1a**. Indeed there is evidence for the equivalence of the unsubstituted and *para*-methyl substituted aromatic rings towards quadratic effects in NLO.[7] One can further infer[8] a rough estimate of the crystalline *d* susceptibility, assuming the oriented gas model[9] with optimal cos(3θ) projection factors corresponding to a fully eclipsed stacking,[8] and assuming a cubic order Lorentz–Lorentz local field correction factor of 3.5 corresponding to a realistic value of 1.6 for the index of refraction. This simplified model is known to be reliable and leads in the present case to a magnitude of 120×10^{-9} esu comparable to that of *N*-4-nitrophenyl-L-prolinol, a prototype crystal often used as a standard.[10] The comparatively modest powder SHG signal of **1g** may be related to absence of phase-matching at the 1.06 μm fundamental wavelength used by us. Alternatively, a noticeably small average grain size may prevent any benefit from a cumulative phase-matching in a non-resonant configuration considering that the coherence length must be significantly larger than the grain size.

The structure of **1g** is also important from a different perspective. Usually, Cl and CH_3 groups can be interchanged with no structural change when these groups contribute merely to the close packing.[11] However, in this case the corresponding chloro triazine **1h** forms an entirely different structure that is stabilised by trimeric Cl_3 supramolecular synthons.[3] This emphasizes the fact that the CH_3 and Cl groups in **1g** and **1h** respectively play structurally distinct roles and that they are involved in interactions specific to the functional groups.

This work demonstrates that the weak C–H···π interactions may be employed to achieve third dimensional control of a crystal structure, which leads in the present case to an interesting physical property, namely crystalline octupolar NLO with a remarkably large estimated *d* coefficient. In tribenzylisocyanurate[12] and in **1a**, bulk non-centrosymmetry was not designed and is not easily extendable to other examples. This is not so in the present case, where the preferred C–H···π interactions clearly discriminate in favour of a polar packing. Our continued interest in this family of compounds stems from their transparency in the blue region and from their possible utilization in unphase-matched thin film configurations for short pulse NLO.[8]

V. R. T. thanks the AvH Foundation for providing a post-doctoral fellowship. R. B. thanks the DFG and the FCI and R. K. R. J. and G. R. D. thank the DST for financial support (SP/S1/G-19/94).

Notes and references

† *Crystal data* for **1g**: $C_{24}H_{21}N_3O_3$, M = 399.44, rhombohedral, space group *R*3*c*, *a* = 23.576(3), *c* = 6.5913(8) Å, *V* = 3172.9(7) Å^3, *Z* = 6, λ = 0.71073 Å, *T* = 223(2) K, μ = 0.084 mm^{-1}, 750 independent reflections (R_{int} = 0.142), *R* = 0.058, wR_2 = 0.127. CCDC 182/1337. See http://www.rsc.org/suppdata/cc/1999/1639/ for crystallographic data in .cif format.

‡ The C–H bond lengths are always neutron-normalised to 1.083 Å.

§ A similar shallow inclination is also observed in **1a** which is also non-centrosymmetric, see ref. 3.

1 A. Nangia and G. R. Desiraju, *Acta Crystallogr., Sect. A*, 1998, **54**, 934; G. R. Desiraju, *Curr. Opin. Solid State Mater. Sci.*, 1997, **2**, 451.
2 Y. Aoyama, K. Endo, T. Anzai, Y. Yamaguchi, T. Sawaki, K. Kobayashi, N. Kanehisa, H. Hashimoto, Y. Kai and H. Masuda, *J. Am. Chem. Soc.*, 1996, **118**, 5562.
3 V. R. Thalladi, S. Brasselet, H. C. Weiss, D. Bläser, A. K. Katz, H. L. Carrell, R. Boese, J. Zyss, A. Nangia and G. R. Desiraju, *J. Am. Chem. Soc.*, 1998, **120**, 2563.
4 J. Zyss, *J. Chem. Phys.*, 1993, **98**, 6583; J. Zyss and I. Ledoux, *Chem. Rev.*, 1994, **94**, 77; S. Brasselet and J. Zyss, *J. Opt. Soc. Am. B.*, 1998, **15**, 257.
5 G. R. Desiraju and T. Steiner, *The Weak Hydrogen Bond in Structural Chemistry and Biology*, Oxford University Press, 1999, pp. 122–201; M. Nishio, M. Hirota and Y. Umezawa, *The CH/π Interaction: Evidence, Nature and Consequences*, Wiley-VCH, New York, 1998; N. N. L. Madhavi, A. K. Katz, H. L. Carrell, A. Nangia and G. R. Desiraju, *Chem. Commun.*, 1997, 1953.
6 For a non-centrosymmetric structure obtained from a C_3-symmetrical molecule *via* herringbone and CH_3···aryl interactions, see B. S. Hammes, D. Ramos-Maldonado, G. P. A. Yap, A. L. Rheingold, V. G. Young Jr. and A. S. Borovik, *Coord. Chem. Rev.*, 1998, **174**, 241. However the CH_3···aryl interactions observed here are much weaker (C···aryl centroid distance is 4.45 Å).
7 C. R. Moylan and C. A. Walsh, *Nonlinear Opt.*, 1993, **6**, 113.
8 J. Zyss, S. Brasselet, V. R. Thalladi and G. R. Desiraju, *J. Chem. Phys.*, 1998, **109**, 658; S. Brasselet and J. Zyss, *J. Nonlinear Phys. Mater.*, 1996, **5**, 4; J. Zyss and S. Brasselet, *J. Nonlinear Phys. Mater.*, 1998, **7**, 397.
9 J. L. Oudar and J. Zyss, *Phys. Rev. A*, 1982, **26**, 2016.
10 J. Zyss, J. F. Nicoud and A. Coquillay, *J. Chem. Phys.*, 1984, **81**, 4160.
11 G. R. Desiraju and J. A. R. P. Sarma, *Proc. Ind. Acad. Sci., Chem. Sci.*, 1986, **96**, 599.
12 V. R. Thalladi, S. Brasselet, D. Bläser, R. Boese, J. Zyss, A. Nangia and G. R. Desiraju, *Chem. Commun.*, 1997, 1841.

Communication 9/04490F

An organic sensitizer within Ti-zeolites as photocatalyst for the selective oxidation of olefins using oxygen and water as reagents

Ana Sanjuán,[a] Mercedes Alvaro,[a] Avelino Corma*[b] and Hermenegildo García*[b]

[a] *Departamento de Química, Universidad Politécnica de Valencia, Camino de Vera s/n, 46022 Valencia, Spain*
[b] *Instituto de Tecnología Química CSIC-UPV, Universidad Politécnica de Valencia, Avda. de los Naranjos s/n, 46022 Valencia, Spain. E-mail: hgarcia@qim.upv.es*

Received (in Liverpool, UK) 2nd June 1999, Accepted 14th July 1999

A new positive photocatalytic system comprising an organic dye within the micropores of a titanium zeolite is able to effect the catalytic dihydroxylation of alkenes using water and molecular oxygen as reagents; the dye acts as an antenna to absorb the energy of visible light, generating hydroxyl radicals from water; subsequently, the OH˙ radicals react with olefins in the presence of oxygen to form allylic hydroperoxides that in the presence of the Ti atoms of the zeolite promote the epoxidation of the alkene.

Photocatalysis applies the energy of light to effect chemical reactions. The energy of a blue photon (λ = 400 nm) is 71 kcal $\times$ mol^{-1}, enough to overcome most of the activation barriers of chemical reactions. Compounds considered chemically inert, such as water, may become reactive under photocatalytic conditions.

Up to now, photocatalysis has been almost exclusively limited to the degradation of pollutants in aqueous media,[1] but *positive* photocalysis being applied to the synthesis of organic compounds is more scarce.[2] Herein, we report a positive photocatalytic system that comprises 2,4,6-triphenylpyrylium ion (TP^+) encapsulated within the voids of tridirectional large-pore zeolites that absorbs visible light, transforming it into chemical energy. A second Ti catalytic site located in the walls of these molecular sieves promotes oxidation of an alkene using as reagent the hydroperoxides generated *in situ* in the photochemical process (Fig. 1).

Zeolites are crystalline aluminosilicates whose structure contains strictly uniform cavities and channels of molecular dimensions called micropores.[3] The zeolite host cooperates in the success of the overall process, playing several crucial roles. Thus, TP^+ is not stable in H_2O where it undergoes rapid hydrolysis to 1,3,5-triphenylpent-2-ene-1,5-dione. This prevents the direct use of this sensitizer in aqueous media. In contrast, when encapsulated inside the cages of zeolites (TP-Z), the confined space provided by the host impedes the reaction of the heterocycle because it involves bulkier intermediates that simply would not fit in. As result, when entrapped inside the zeolite micropores TP^+ is completely stable in the presence of

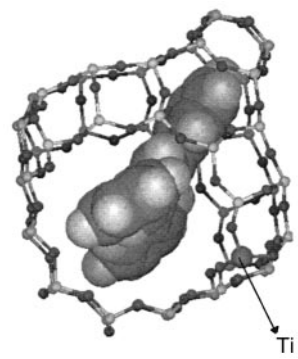

Fig. 1 Molecular modeling structure of TP,Ti-Zeolite bifunctional photocatalyst. The bulky TP^+ acting as light harvester is entrapped inside the zeolite cavities. The Ti atoms are bonded to the framework of the zeolite.

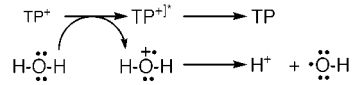

Scheme 1

H_2O. In addition, the zeolite pores provide a polar reaction medium favorable for the initial photoinduced electron transfer between TP^+ excited state and water (Scheme 1). This oxidation transforms inert water into chemically agressive hydroxyl radicals. Evidence for the formation of OH˙ in this system has been previously obtained by laser flash photolysis.[5] In addition, trapping of OH˙ by 5,5-dimethyl-1-pyrroline *N*-oxide leads to a persistent N-centered radical detectable by conventional EPR spectroscopy.

Normally, OH˙ radicals would destroy any organic photosensitizer. However, in the case of the TP-Z system, the restricted reaction cavity prevents this OH˙ attack. In fact, no bleaching of TP^+ was observed after an operation time of 100 h. Furthermore, the final product of the OH˙ chemistry in the TP-Z irradiation of pure water is H_2O_2, indicative of OH˙ coupling [eqn. (1)].

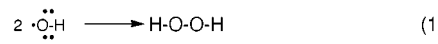

(1)

Eqn. (1) is well-established in the γ-radiolysis of H_2O[6] but never occurs when there are alternate waste channels for OH˙ radicals. Fig. 2 shows an illustrative time-conversion plot for the concentration of H_2O_2 under these conditions.

The ability of TP-NaY sensitizer to generate a constant concentration of H_2O_2 has been exploited here for the epoxidation of styrene using titaniumsilicalite (TS-1) as co-catalyst, whereby styrene oxide is formed [eqn. (2)]. However,

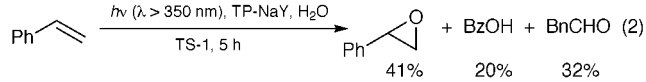

(2)

the low photostationary concentration of H_2O_2 determines that the epoxidation step takes hours. This allows the occurrence of concomitant photochemical reactions leading to by-products (mainly benzoic acid and 2-phenylacetaldehyde).

This limitation was overcome by using TP-Z as a continuous source of OH˙ radicals to generate *in situ* organic hydroperoxides formed through hydrogen abstraction and subsequent trapping of the carbon-centered radical by O_2. Thus, when cyclohexene was present during the irradiation of a H_2O–MeCN slurry with TP-Z photocatalyst, 3-hydroperoxycyclohexene was formed (Scheme 2). This was confirmed by addition of PPh_3 after the photocatalytic irradiation. PPh_3 reacts quantitatively with organic hydroperoxides giving rise to the corresponding alcohol plus $Ph_3P{=}O$. The yield of hydroperoxycyclohexene can be quantitatively determined by iodometric titrations or, alternatively, by the amount of $Ph_3P{=}O$ formed. Control experiments showed that the direct reaction of cyclohexene with TP^+ in its excited state does not occur, in agreement with the high cyclohexene oxidation potential (2.14 V *vs.* SCE).

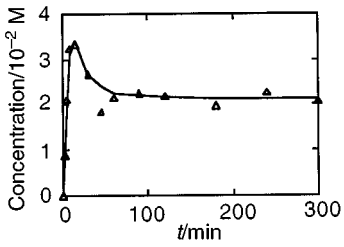

Fig. 2 Hydrogen peroxide concentration profile upon irradiation (visible light, $\lambda > 350$ nm) of TP-NaY (100 mg) in water.

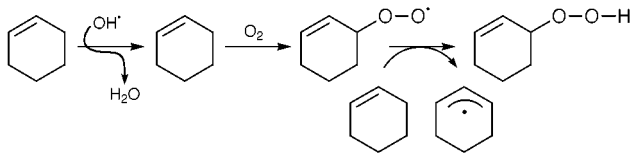

Scheme 2

Large pore Ti molecular sieves are efficient catalysts for the selective epoxidation of alkenes by organic hydroperoxides.[7] We have exploited the ability of TP-NaY to generate a significant concentration of hydroperoxides from light and H_2O–O_2 and coupled it with the subsequent epoxidation converting the whole process in a one-pot reaction.

Two different strategies have been explored. The simplest one consists in using a mechanical mixture of two molecular sieves, one containing TP^+ as photocatalyst and the second one having Ti atoms as epoxidation sites. Table 1 summarizes the results that have been achieved using a system containing a mixture of TP-NaY and Ti-β or Ti-MCM-41.[7–10] The major difference between the latter two epoxidation catalysts is the geometry and dimensions of the internal voids, both having in common their relative hydrophocity that favors the preferential adsorption of organic compounds.[7] The structure of β zeolite defines a tridirectional network of oval cages (11 Å major axis) while MCM-41 is formed by an array of hexagonal channels (30 Å diameter).

In agreement with the chemical literature,[7] Al-free Ti-MCM-41 was found more active than Al-free Ti-β. The higher activity of Ti-MCM-41 is easily rationalized based on the larger dimensions of its pores that suit better to the size of the reagents involved in the process. When the TP-NaY/Tiβ mixture was reused in a second and third experiment with fresh feed a notable loss of activity was observed (see Table 1, footnotes *c* and *d*). However, this decay in the efficiency of the photocatalytic mixture is not caused by the bleaching of TP^+ since no changes were observed in the characteristic UV/vis absorption of the solid. Rather, it is more likely that the deactivation is due to blocking of the pores by oligomers or bleaching of Ti atoms out of the Ti-β framework.

Table 1 Results after 4 h irradiation (125 W Hg lamp through Pyrex) at room temperature of cyclohexene (2 ml) in a mixture of MeCN (2 ml)–H_2O (1 ml) in the presence of the corresponding photocatalyst (500 mg, 4% loading of TP^+)

	Products/mg		
Photocatalyst[a]	cyclohexane-1,2-diol	cyclohex-2-enol	cyclohex-2-enone
TP-NaY[b]	1.5	6.8	13.9
TP-NaY/Ti-β	10.9	23.7	16.8
TP-NaY/Ti-β[c]	4.5	13.9	13.8
TP-NaY/Ti-β[d]	2.2	13.6	7.4
TP-NaY/Ti-MCM-41	13.4	17.6	18.7
TP, Ti-β	20.2	39.7	11.5

[a] Blank controls under Ar atmosphere, in the dark or in the absence of TP-Y did not lead to any product. [b] In the absence of Ti-containing co-catalyst. [c] Second run reusing TP-NaY/Ti-β with fresh reagents. [d] Third run reusing TP-NaY/Ti-β with fresh reagents.

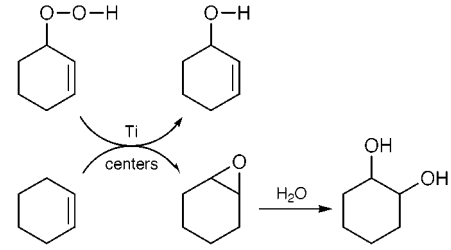

Scheme 3

On the other hand, according to Scheme 3, cyclohex-2-enol and cyclohexane-1,3-diol would be concurrently formed in the oxidation step while cyclohex-2-enone would arise from the subsequent overoxidation of cyclohex-2-enol.

Even though the TP-NaY/Ti-zeolite mixtures act as photocatalysts, their activity and selectivity are far from optimal. In order to increase the efficiency of the overall photocatalytic reaction, a fully-integrated approach was explored. It consists of the preparation of a single bifunctional photocatalyst that contains the two centers necessary for the process in the closest possible proximity. For this purpose, we have carried out the ship-in-a-bottle synthesis of TP^+ in a Ti-Beta zeolite following the procedure reported for zeolite Y.[9] As can be seen in Table 1, the efficiency of the overall dihydroxylation process is almost doubled using this novel TP, Ti-β photocatalyst compared to the mechanical mixture of the two separate components. This higher activity of TP,Ti-β for the production of cyclohexane-1,2-diol can be understood as a consequence of the spatial arrangement of the sites that reduces the chances for undesirable decomposition of hydroperoxy cyclohexene.

To establish a valid comparison of the efficiency of the TP, Ti-β photocatalysis, the autooxidation of cyclohexene (2 ml) initiated by azoisobutyronitrile (30 mg) was also carried in MeCN (2 ml) in the presence of Ti-β (200 mg) bubling air through the solution. After 5 h reaction, only 4.5 mg of cyclohexane-1,2-diol was formed. This value is smaller than those achieved with the TP,Ti-β photocatalysis (see Table 1).

Even though further improvements are still needed, herein we have shown that TP,Ti-β acts as a new *positive* photocatalytic system that by using photons promotes the dihydroxylation of cyclohexene using water and oxygen as reagents. The overall process occurs within the pores of zeolites, whose rigid structure embeds and protects the active centers, cooperating in the process in a way reminiscent of the quaternary structure of enzymes around a prostetic group.

Notes and references

1 O. Legrin, E. Oliveros and A. M. Braun, *Chem. Rev.*, 1993, **93**, 671.
2 L. Cermenati, C. Richter and A. Albini, *Chem. Commun.*, 1998, 805.
3 *Introduction of Zeolite Science and Practice*, ed. H. van Bekkum, E. M. Flanigen and J. C. Jansen, Elsevier, Amsterdam, 1991.
4 M. A. Miranda and H. García, *Chem. Rev.*, 1994, **94**, 1063.
5 A. Sanjuán, M. Alvaro, G. Aguirre, H. García and J. C. Scaiano, *J. Am. Chem. Soc.*, 1998, **120**, 7351.
6 M. Fattahi, C. Houeelevin, C. Ferradini and P. Jacquier, *Radiat. Phys. Chem.*, 1992, **40**, 167.
7 T. Blasco, M. A. Camblor, A. Corma, P. Esteve, J. M. Guil, A. Martínez, J. A. Perdigón-Melón and S. Valencia, *J. Phys. Chem. B*, 1998, **102**, 75.
8 TP-NaY was obtained by submitting TP-HY (ref. 9) to exhaustive Na^+ exchange with aqueous Na_2CO_3. Ti-β was prepared by the novel OH^- free procedure (ref. 7). Ti-MCM-41 was prepared as reported (ref. 10).
9 A. Corma, V. Fornés, H. García, M. A. Miranda, J. Primo and M. J. Sabater, *J. Am. Chem. Soc.*, 1994, **116**, 2276.
10 A. Corma, M. T. Navarro, J. Pérez-Pariente, and F. Sánchez, *Stud. Surf. Sci. Catal.*, 1994, **84**, 69.

Communication 9/04519H

Novel hydrogen bonding ring motifs in a model peptide: crystal and molecular conformation

Ashwani K. Thakur, Ashish and Raghuvansh Kishore*

Institute of Microbial Technology, Sector 39-A, Chandigarh - 160 036, India. E-mail: kishore@imtech.ernet.in

Received (in Cambridge, UK) 14th June 1999, Accepted 16th July 1999

The crystal molecular structure of a model peptide, Boc-Ile-Thr-NH_2, unexpectedly revealed two unusual intramolecularly hydrogen bonded ring motifs, *i.e.* an intraresidue main-chain to main-chain interaction (N_i–H···O=C_i) and an interresidue 'newly discovered' side-chain to main-chain interaction (N_i–H···O_i^{γ}Thr), across a polar proteinogenic residue.

The design, synthesis and identification of peptide backbone secondary structural features, stabilised by intramolecularly hydrogen bonding (H-bonding) ring motifs, are of paramount significance since they are targets of *de novo* design, and they also serve as powerful molecular tools for probing the problems of structure–function relationships, protein folding and thermodynamic stabilities.[1] For example, α-bend, β-bend and γ-bend secondary structures, which are frequently observed in proteins and polypeptides and are stabilised by single intramolecular H-bonding interactions, constitute 13-membered (C_{13}-form), 10-membered (C_{10}-form) and 7-membered (C_7-form) ring motifs respectively, and have been the subject of intense conformational investigations over three decades.[2]

The fully extended *intraresidue* H-bonded secondary structure, *i.e.* N_i–H···O=C_i interaction, often referred to as a C_5-structure, constitutes the smallest possible intramolecularly H-bonded conformation across an α-amino acid. Ideally, this five-membered ring is characterised by the backbone torsion angles: $\phi \approx \psi \approx \pm 180$ (±20°) in the Ramachandran map.[3] The conformational characteristics available for this structural motif across proteinogenic residues are extremely rare and poorly understood, presumably due to the non-availability of suitable conformational models. As an attempt to investigate systematically the conformational characteristics of the secondary structure element,[4] we describe here the first unambiguous X-ray diffraction analysis and molecular conformation of this fully extended intramolecularly H-bonded structure, across a chiral proteinogenic residue in a simple model peptide, Boc-Ile-Thr-NH_2 **1**.† In addition to the C_5-interaction, the analysis also revealed the existence of a newly discovered six-membered ring motif stabilised by a main-chain to side-chain H-bond (*i.e.* N_{i+1}–H···O_i^{γ}) interaction, and provided further insight into the folding behaviour of the two ring motifs.[5]

A perspective view of the molecular conformation observed for **1** in the solid state is shown in Fig. 1 and the relevant torsional angles are listed in Table 1. The most surprising feature of the molecular conformation is the observation of an *intramolecular* H-bond between the Thr N2–H and C15=O5 groups. This H-bond results in the formation of a pentagonal ring motif, the 'C_5-structure'. This structure is characterised by the significantly extended backbone torsion angles (ϕ = −163.5°, ψ = +175.6°) and H-bond geometric parameters [bond distance d(N···O) = 2.566 Å, d(H···O) = 2.166 Å, bond angle (N–H···O) = 108.01° and the planarity of the hydrogen bond torsion angle (N_i–H···O=C_i) = 12.4°] (Fig. 2a). The apparent unusual degree of conformational rigidity, imposed by steric effects arising from the exposed amphiphilic C^{β} of the Thr side-chain, appears to be the primary cause of the strong conformational preferences, influencing the location of the Thr side-chain and the secondary-structure-dependent preferred rotation about the C^{α}–C^{β} bond in favour of a C_5-structure.

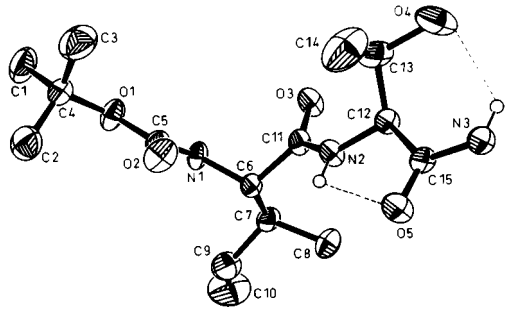

Fig. 1 An ORTEP representation of the molecular structure of Boc-Ile-Thr-NH_2, in the solid state. The thermal ellipsoids are shown at the 40% probability level. Intramolecular H-bonds are indicated by dashed lines.

Table 1 Selected torsion angles (°) for Boc-Ile-Thr-NH_2 **1**

Torsion angle	Ile	Thr
ϕ	−89.7	−163.4
ψ	129.4	175.6
χ_1	170.3,[a] −67.2	−167.8,[b] 69.3
χ_2	163.6	—
ω[c]	179.4	171.3

[a] Torsion angles: N1–C6–C7–C8 = 170.3°; [b] N2–C12–C13–O4 = −167.8°. [c] The C-terminal amide bond, ω_{i+1}, torsion angle C12–C15–N3–H3D = 179.9°.

Another important structural feature of **1** is the influence of the C_5-structural parameters on the unusual energetically unfavourable rotameric distribution of the Thr side-chain.[6] Interestingly, a shift of the Thr C^{α}–C^{β} torsion angle towards a rarely observed *trans* conformation ($\chi_1 \approx -167.8°$) clearly favours the formation of a novel six-membered H-bonded ring motif between the main-chain amide N3–H group and the $O4^{\gamma}$ atom of the Thr side-chain, *i.e.* N_{i+1}–H···O_i^{γ} Thr, interaction. The geometric parameters [d(H···O) = 2.288 Å, d(N···O) = 2.854 Å, bond angle N–H···O = 123.51°, H-bond torsion angle (N_{i+1}–H···O_i^{γ}–C^{β}) = −17.7°] characterise the newly discovered ring motif[5] across a chiral proteinogenic residue (Fig. 2b). In **1**, besides the planarity of the C-terminal amide bond, *i.e.* ω_{i+1}, the set of torsional angles (ψ_i = +175.6° and χ_1 = 167.8°)

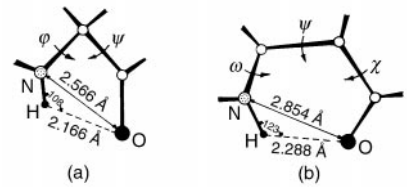

Fig. 2 The geometric characteristics of the two H-bonded ring motifs across the Thr residue: (a) the C_5-structure, N_i–H···O=C_i, main-chain to main-chain interaction; (b) the six-membered ring, N_{i+1}–H···O_i^{γ}Thr, side-chain to main-chain interaction. Relevant torsion angles are marked. Intramolecular H-bonds are indicated by dashed lines. Interacting oxygen and hydrogen atoms are indicated by large and small black circles, respectively.

of the preceding i^{th} residue appear to be the key determinants for the conformational preferences. The topological considerations of the significantly extended torsion angles, $\psi \approx \chi_1 \approx \pm 180$ (±20°), of the Thr residue may not allow the N–H group to approach the O^{γ} atom, precluding the formation of a normal five-membered H-bonding (*i.e.* N_i–H···$O_i{}^{\gamma}$ Thr) interaction. Therefore, an extended backbone ψ torsion angle, in addition to the *trans* χ_1 torsion angle of the i^{th} residue, appears to be the stringent requirement for the juxtaposition of the interacting atoms (N_{i+1}–H···$O_i{}^{\gamma}$) in order to form a six-membered ring across a chiral proteinogenic Thr or Ser residue.[5] In the crystal packing each molecule participates, as a donor or as an acceptor, in the formation of a complex network of intermolecular hydrogen bonding interactions, particularly those involving the Thr and the *trans*-carboxamide NHs. All these interactions probably contribute to the stability of the crystal molecular conformation.

The observation of a rare C_5-interaction across a chiral proteinogenic residue is indeed very interesting since, to date, extensively investigated derivatives and homopeptides incorporating achiral non-proteinogenic $C^{\beta\beta'}$ symmetrically disubstituted Gly residues alone have indicated strong preferences for this structure.[7] Although in these cases the reported average geometric parameters for the C_5-structure are in excellent agreement with those observed for **1**, the conformationally informative τ(N–C^{α}–C′) bond angle of the Thr residue (τ = 106.89°), contrary to our expectation, is not markedly reduced to an average value ≈103°. These results are distinctly inconsistent with the previous results and clearly suggest that the significant narrowing of the τ value may not be mandatory for an effective C_5-interaction, at least across chiral proteinogenic residue(s).

One- and two-dimensional ^{1}H NMR spectroscopic results provided unequivocal evidence, largely consistent with the crystal structure analysis, that in the compact state peptide **1** adopts an intramolecularly H-bonded C_5-structure in solution.[4] However, because of exchange effects (rotation about the C–N bond) the moderately low temperature coefficient ($\Delta\delta/\Delta T \approx -3.66 \times 10^{-3}$ ppm K^{-1}) value obtained for one of the C-terminal primary amide N–H groups was not interpreted as indicative of its involvement in an intramolecular H-bonding interaction stabilising the six-membered ring motif.[4,8] The thermodynamic characteristics of the two stable ring motifs, in a poorly interacting hydrophobic environment, were investigated to gain further insight into their folding–unfolding behaviour. Assuming a two-state process (an equilibrium between intramolecularly H-bonded and non-H-bonded states), the thermodynamic parameters deduced from van't Hoff plots of the variable temperature ^{1}H NMR data indicate that although both the H-bonded ring motifs are enthalpically favoured and entropically disfavoured, among both the ring sizes the more strained five-membered ring is relatively less preferred enthalpically while more favoured entropically (unpublished data).[4,8]

The results of the conformational analysis of **1** indicate that the C_5-structural motif, across an α-amino acid having oxygen atoms(s) in the γ-positions, may facilitate the formation of another six-membered H-bonded ring motif, *i.e.* an N_{i+1}–H···$O_i{}^{\gamma}$ interaction. The variations in the torsional angles ($\phi_i \approx \psi_i$ and $\psi_i \approx \chi_i \approx \omega_{i+1}$) of the five- and six-membered ring motifs, respectively, may characterise the geometric and thermodynamic parameters. It is worth stressing that the combined effect of the two specific ring motifs originating from the chiral moiety, on the molecular conformation appears to be the significant planar arrangement. The marked influence of the main-chain conformational preferences on the side-chain geometry (or *vice versa*) may indicate that χ_1 constrained amino acid derivatives can be exploited as structural tools for *de novo* design of relatively more rigid ring motifs for investigating unexplored structural and functional properties of bioactive molecules. From these observations we are also inclined to suggest that unlike reverse turn structures, the occurrence of such 'flat ring motifs' in proteins and polypeptides may not necessarily be responsible for the chain reversal.

In conclusion, this communication establishes the surprising existence of two fascinating ring motifs, stabilised by intramolecular H-bonding interactions across a chiral proteinogenic residue, and may argue for their intrinsic stabilities. The analysis of conformation-directing effects indicates that unexplored unique local, short range interactions (similar to the Asx-turn motif) might be accessible to small linear peptides incorporating residue(s) bearing a C^{β}-sterogenic centre with short polar side-chain(s). Unambiguous experimental characterisation, in solution as well as in the crystalline state, of the newly described H-bonded topologies are of fundamental importance and may provide an opportunity to examine their occurrence in the highly refined protein data bank; this may further enhance our understanding of polypeptide/protein conformations. Finally, such well defined H-bonded peptide templates/motifs may promise a 'bright future in biochemical and materials science applications.'[9]

This work was supported by a grant from the DBT Government of India. The authors wish to acknowledge the use of the National Diffractometer Facility (DST), New Delhi, for data collection. R. K. is grateful to the Director for his consistent encouragement. This is IMTech communication number 02/99.

Notes and references

† Peptide **1** was synthesised by employing solution phase procedures. A single crystal suitable for an X-ray diffraction study was grown from a methanol solution. The crystal data were collected at 293 K on CAD4 Enraf-Nonius diffractometer with graphite monochromated Cu-Kα radiation (λ = 1.5418 Å) using ω–2θ scan mode. *Crystal data for* **1**: $C_{15}H_{28}N_3O_5$, M = 332.42, orthorhombic, $P2_12_12_1$, colourless needles measuring 1.1 × 0.7 × 0.25 mm^3, a = 8.040(4), b = 12.582(7), c = 18.128(7) Å, $\alpha = \beta = \gamma$ = 90°, V = 1839.7(8) Å^3, Z = 4. The structure was solved by direct methods using SHELXS-97.[10] The structure was refined by full matrix least-squares on F^2 by using SHELXL-97.[11] Final R = 0.0548 [$I > 2\sigma(I)$], R_w = 0.1605. All non hydrogen atoms were refined anisotropically. All hydrogen atoms were placed in idealised positions with assigned isotropic parameters. CCDC 182/1338. See http://www.rsc.org/suppdata/cc/1999/1643/ for crystallographic files.

1 E. N. Baker and R. E. Hubbard, *Prog. Biophys. Mol. Biol.*, 1984, **44**, 97; T. E. Creighton, *Proteins: Structures and Molecular Principles*, 2nd edn., Freeman, New York, 1993; *Peptides: Synthesis Structure and Applications*, ed. B. Gutte, Academic Press, New York, 1995; V. Munõz, P. A. Thompson, J. Hofrichter and W. A. Eaton, *Nature*, 1997, **390**, 196; S. H. Gellman, *Acc. Chem. Res.*, 1998, **31**, 173.

2 C. M. Vankatachalam, *Biopolymers*, 1968, **6**, 1425; *Tetrahedron Symposia-in-Print No. 50*, 1993, **49**, 3433; B. V. V. Prasad and P. Balaram, *CRC Crit. Rev. Biochem.*, 1984, **16**, 307; G. D. Rose, L. M. Gierasch and J. A. Smith, *Adv. Protein Chem.*, 1985, **37**, 1; D. J. Tobias and C. L. Brooks, *Biochemistry*, 1991, **30**, 6059; J. Rizo and L. M. Gierasch, *Annu. Rev. Biochem.*, 1992, **61**, 387.

3 G. N. Ramachandran and V. Sasisekharan, *Adv. Protein Chem.*, 1968, **23**, 283.

4 Ashish and R. Kishore, *Tetrahedron Lett.*, 1997, **38**, 2767; Ashish and R. Kishore, *FEBS Lett.*, 1997, **417**, 97.

5 W. M. Wolf, M. Stasiak, M. T. Leplawy, A. Bianco, F. Formaggio, M. Crisma and C. Toniolo, *J. Am. Chem. Soc.*, 1998, **120**, 11 558.

6 J. Janin, S. Wodak, M. Levitt and B. Maigret, *J. Mol. Biol.*, 1978, **125**, 357; E. Benedetti, G. Morelli, G. Nemethy and H. A. Scheraga, *Int. J. Peptide Protein Res.*, 1983, **22**, 1; J. W. Ponder and F. M. Richards, *J. Mol. Biol.*, 1987, **193**, 775; R. L. Dunbrack Jr. and M. Karplus, *J. Mol. Biol.*, 1993, **230**, 543; P. Chakrabarti and D. Pal. *Protein Eng.*, 1998, **8**, 631.

7 C. Toniolo and E. Benedetti, in *Molecular Conformation and Biological Interactions: G. N. Ramachandran Festschift*, ed. P. Balaram and S. Ramaseshan, Indian Academy of Sciences, Bangalore, India, 1991, p. 511; C. Toniolo, *Janssen Chim. Acta*, 1993, **11**, 10.

8 K. Wüthrich, *NMR in Biological Peptides and Proteins*, North Holland, Amsterdam, 1967; R. Kishore and P. Balaram, *Indian J. Chem.*, 1984, **23B**, 1137.

9 M. Crisma, F. Formaggio, C. Toniolo, T. Yoshikawa and T. Wakamiya, *J. Am. Chem. Soc.*, 1998, **121**, 3272.

10 G. M. Sheldrick, SHELXS-97, A program for crystal structure solution, *Acta Crystallogr., Sect. A*, 1990, **46**, 467.

11 G. M. Sheldrick, SHELXL-97, University of Göttingen, 1997.

Communication 9/04711E

ChemComm

A tetranuclear aluminium hydrazide derivative with a ladder-type structure

Joel S. Silverman, Colin D. Abernethy, Richard A. Jones* and Alan H. Cowley*

Department of Chemistry and Biochemistry, The University of Texas at Austin, Austin, Texas 78712, USA. E-mail: cowley@mail.utexas.edu

Received (in Columbia, MO, USA) 20th May 1999, Accepted 15th July 1999

The reaction of $(Me_2NAlH_2)_3$ with excess H_2NNMe_2 affords $[Al_4(NHNMe_2)_6(NNMe_2)_4]$; the compound possesses an Al_4N_4 ladder-shaped core.

The renewed interest in group 13 hydrazides can be attributed to two driving forces. Firstly, since hydrazide ligands are potentially multi-functional they can promote the formation of novel rings, cages, and polymers featuring group 13–nitrogen linkages. Secondly, group 13 hydrazides could play an important role as precursors to group 13 nitrides. The most successful current approach to the deposition of such nitrides involves the thermal reaction of the respective metal alkyl with ammonia.[1] Unfortunately, the requisite reaction temperatures are somewhat high (> 900 °C) and lower thermal budgets are desirable to obviate such problems as thermal stresses and stoichiometry losses in the resulting films. Hydrazine[2] and dimethylhydrazine[3] have been suggested as alternative, lower temperature nitrogen delivery sources thus rendering the investigation of group 13 hydrazides an attractive proposition.

Despite being known since 1961,[4] structural information on aluminium hydrazides is confined to that of the dimer, $[Me_2Al\{\mu\text{-}N(H)NMe_2\}]_2$.[5] Moreover, it was only in 1995 that $[Et_2Ga\{\mu\text{-}N(H)NPh_2\}]_2$, the first gallium hydrazide, was prepared.[6] More recent interest has focused on the construction of cage and ring structures from group 13 hydrazides, two important examples of which are $[MeGaN(H)NPh]_4$[7] and an octa-aluminium analogue of a calix[4]pyrrole which features four five-membered AlN_3C rings connected by Me_2Al bridges.[8] Herein, we describe the synthesis and structural assay of a novel tetra-aluminium hydrazide derivative that possesses a ladder-type core.[9] A further distinguishing feature of the present work is that the replacement of a trialkylalane by $(Me_2NAlH_2)_3$[10] as the aluminium source results in lower reaction temperatures.

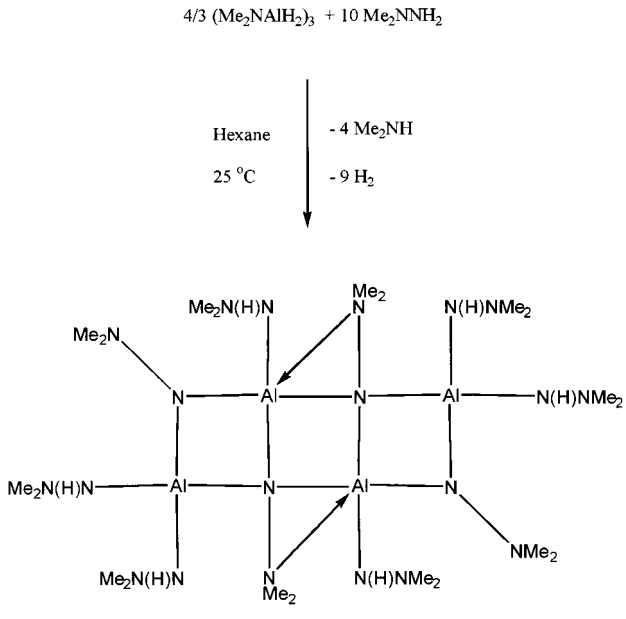

1

Scheme 1

The reaction of $(Me_2NAlH_2)_3$ with an excess of 1,1-dimethylhydrazine in hexane solution at 25 °C is exothermic and results in the evolution of hydrogen and dimethylamine (Scheme 1). Following filtration of the reaction mixture, cooling of the filtrate to −20 °C resulted in the formation of colourless crystals of **1**.† Mass spectroscopic assay indicated a composition of $C_{20}H_{67}Al_4N_{20}$ for **1** (HRMS: calc. for $(M + H)^+$, 695.512; found, 695.513) and this was in accord with combustion analysis data. Unfortunately, it was not possible to deduce the structure of **1** using ^1H, ^{13}C, and ^{27}Al NMR data† at this stage, hence an X-ray diffraction experiment became necessary.‡

Compound **1** crystallizes in the triclinic space group $P\bar{1}$ with $Z = 2$ (for an asymmetric unit of formula $[Al_2\{NHNMe_2\}_3\{NNMe_2\}_2]$. The crystalline state comprises an array of tetranuclear molecules. $[Al_4\{NHNMe_2\}_6\{NNMe_2\}_4]$ and there are no unusually short intermolecular contacts. As illustrated in Fig. 1, the Al_4N_4 skeleton of **1** adopts a ladder-type arrangement that consists of three fused four-membered Al_2N_2 rings. The

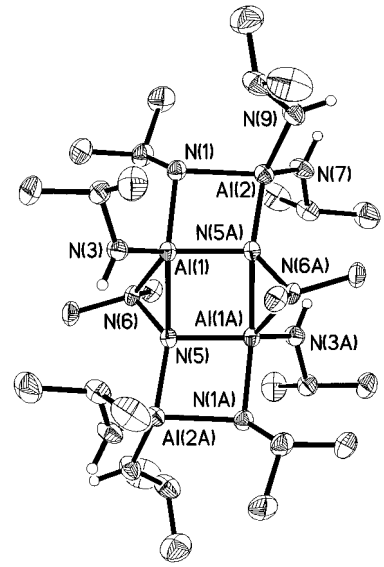

Fig. 1 Molecular structure of **1** showing the atom numbering scheme.Some hydrogen atoms have been eliminated for clarity. Selected bond distances (Å) and angles (°): Al(1)–N(5) 2.091(3), Al(1)–N(5A) 1.877(2), Al(1)–N(6) 1.957(2), N(5)–N(6) 1.488(3), Al(1)–N(3) 1.787(3) Al(1)–N(1) 1.959(3), Al(2)–N(1) 1.973(2), N(1)–N(2) 1.467(3), Al(2)–N(5A) 1.860(2), N(5A)–Al(1)–N(5) 89.43(10), N(3)–Al(1)–N(5A) 128.09(12), N(1)–Al(1)–N(5) 142.17(10), N(6)–Al(1)–Al(1A) 74.08(8), N(1)–Al(1)–N(3) 107.29(11), N(3)–Al(1)–N(6) 110.90(11), N(5A)–Al(1)–N(6) 113.73(10), N(5A)–Al(1)–N(1) 83.09(10), N(6)–Al(1)–N(1) 107.68(10), N(3)–Al(1)–N(5) 106.43(11), N(6)–Al(1)–N(5) 42.97(9) N(3)–Al(1)–Al(1A) 128.29(10), N(5A)–Al(1)–Al(1A) 47.77(8), N(1)–Al(1)–Al(1A) 120.32(8), N(5)–Al(1)–Al(1A) 41.67(6), N(3)–Al(1)–Al(2) 128.06(9), N(5A)–Al(1)–Al(2) 39.70(8), N(6)–Al(1)–Al(2) 118.41(8), N(1)–Al(1)–Al(2) 43.39(7), N(5)–Al(1)–Al(2) 120.18(7) Al(1A)–Al(1)–Al(2) 81.99(4) N(6)–N(5)–Al(2A) 132.2(2), N(6)–N(5)–Al(1A) 122.9(2), Al(2A)–N(5)–Al(1A) 100.16(11), N(6)–N(5)–Al(1) 63.72(13), Al(2A)–N(5)–Al(1) 141.68(13), Al(1A)–N(5)–Al(1) 90.57(10), N(7)–Al(2)–N(9) 105.46(13), N(7)–Al(2)–N(5A) 116.80(12), N(9)–Al(2)–N(5A) 122.14(12), N(7)–Al(2)–N(1) 121.93(12), N(9)–Al(2)–N(1) 106.76(12), N(5A)–Al(2)–N(1) 83.14(10).

central such ring, which resides on a crystallographic inversion centre, is essentially rectangular with bond angles of 89.43(10) and 90.57(10)° at aluminium and nitrogen, respectively, and a difference of *ca.* 0.2 Å in the Al–N bond distances. In turn, the central Al_2N_2 moiety is flanked on either side by a fused three-membered AlN_2 ring formed by N → Al dative bonding from hydrazide lone pairs. As a consequence, the coordination numbers of Al(1) and Al(1A) are both five. In a formal sense, there are four Al–N σ-bonds (Al(1)–N(5) 2.091(3) Å; Al(1)–N(5A) 1.877(2) Å; Al(1)–N(3) 1.787(2) Å, Al(1)–N(1) 1.959(3) Å and one N → Al dative bond (Al(1)–N(6) 1.957(2) Å) at each aluminium centre. The average Al–N bond distance of 1.934(3) Å is close to that reported for $[Me_2Al\{\mu\text{-}N(H)NMe_2\}]_2$ (1.955(3) Å), the only aluminium hydrazide structurally characterized previously.[5] The bond angles within the AlN_5 coordination sphere range from 42.97(9)° (N(5)–Al(1)–N(6)) to 142.17(10)° (N(1)–Al(1)–N(5)); at best, the geometry can be described as highly distorted trigonal bipyramidal. Not unexpectedly, the geometries at N(5) and N(5A) show a marked departure from the ideal tetrahedral angle and range from 63.72(13)° for Al(1)–N(5)–N(6) to 132.2(2)° for Al(2A)–N(5)–N(6). The outer four-membered Al_2N_2 rings are somewhat rhomboid; however, there is a wide scatter in the Al–N bond distances and intra-ring angles (Fig. 1 caption). The average Al–N bond distance of 1.917(3) Å for the outer Al_2N_2 rings is shorter than that for the inner ring (1.934(3) Å). The geometries at Al(2) and N(1) are distorted tetrahedral and pyramidal, respectively. Overall, the geometry of the Al_4N_4 core of **1** is somewhat similar to that reported[11] for a lithium salt of composition $C_{52}H_{78}Al_4Li_2N_4$.

Ex post facto, the NMR data for **1** can be interpreted satisfactorily and indicate the integrity of the ladder-type structure in solution. Thus, two aluminium environments are evident in the ^{27}Al NMR spectrum and the methyl groups on N(6) and N(6A) are anisochronous. The observation of four, rather than three, $N(H)NMe_2$ environments may be due to the presence of rotational isomers.

We thank the Science and Technology Center Program of the National Science Foundation and the Robert A. Welch Foundation for financial support.

Notes and references

† *Experimental procedures*: **1**: An excess of Me_2NNH_2 (4.0 ml, 3.12 g, 53 mmol) was added dropwise *via* syringe to a stirred solution of $(H_2AlNMe_2)_3$[10] (1.0 g, 4.6 mmol) in hexane (75 ml) at 25 °C. After stirring for 1 h, an initial precipitate of white powdery **1** was isolated by filtration (0.5 g, 21%). The clear, colourless filtrate was stored at −20 °C resulting in a second crop of **1** (0.65 g, 27%) as X-ray quality crystals that were used for the acquisition of spectroscopic and analytical data. In subsequent experiments, total yields as high as 66% have been obtained. Mp 192–193 °C. HRMS: calc. for $C_{20}H_{67}Al_4N_{20}$ [*i.e.* $(M + H)^+$] 695.512; found, 695.513. ^1H NMR (300.15 MHz, C_6D_6) δ 1.72 (s, 2H, H–N), 1.75 (s, 2H, H–N), 2.50 (s, 12H, C1, C2/C5, C6), 2.56 (s, 24H, C7, C8, C9, C10), 2.58 (s, 12H, C1, C2/C5, C6), 2.90 (s, 6H, C3/C4), 3.04 (s, 6H, C3/C4), 3.08 (s, 2H, H–N), 3.66 (s, 2H, H–N). $^{13}C\{^1H\}$ NMR (75.14 MHz, C_6H_6) δ 51.29 (C3/C4), 52.98 (C1, C2/C5, C6), 53.20 (C3/C4), 54.66 (C1, C2/C5, C6), 55.28 (C7, C8, C9, C10). ^{27}Al NMR (78.21 MHz, C_6D_6) δ 62.7 (br); 96.7 (br). Anal. Calc. for $C_{20}H_{66}Al_4N_{20}$; C, 34.51; H, 9.63. Found: C, 33.78; H, 9.33%.

‡ *Crystal data*: **1**: $C_{20}H_{66}Al_4N_{20}$, M = 694.88, triclinic, space group $P\bar{1}$, a = 9.1066(3), b = 10.8316(7), c = 11.8213(8) Å; α = 69.101(3), β = 70.496(4), γ = 78.967(4)°, U = 1023.36(10) Å^3, Z = 2, D_c = 1.127 g cm^{-3}, T = 213(2) K, μ = 0.154 mm^{-1}, wR_2 = 0.1275 (4139 independent reflections), R = 0.0566 ($I > 2\sigma(I)$)]. CCDC 182/1334. See http://www.rsc.org/suppdata/cc/1999/1645/ for crystallographic files in .cif format.

1 (*a*) H. Amano, N. Sawaki and I. Akasaki, *Appl. Phys. Lett.*, 1986, **48**, 353; (*b*) S. Nakamura, *Appl. Phys. Lett.*, 1991, **58**, 2021; (*c*) M. Asif Khan, J. N. Kuznia, D. T. Olson and R. Kaplan, *J. Appl. Phys.*, 1993, **73**, 3108; (*d*) K. G. Fertitta, A. L. Holmes, J. G. Neff, F. J. Ciuba and R. D. DuPuis, *Appl. Phys. Lett.*, 1994, **65**, 1823.

2 (*a*) S. Fujieda, M. Mizuta and Y. Matsumoto, *Jpn. J. Appl. Phys.*, 1987, **26**, 2067; (*b*) M. Mizuta, S. Fujieda, Y. Matsumoto and T. Kawamura, *Jpn. J. Appl. Phys.*, 1986, **25**, L945.

3 (*a*) H. Okumara, S. Misawa and S. Yoshida, *Appl. Phys. Lett.*, 1991, **59**, 1058; (*b*) S. Yoshida, H. Okumura, S. Misawa and E. Sakuma, *J. Cryst. Growth*, 1992, **267**, 50; (*c*) H. Okumura, S. Yoshida, S. Misawa and E. Sakuma, *J. Cryst. Growth*, 1992, **120**, 114; (*d*) S. Miyoshi, K. Onabe, N. Ohkouchi, H. Yaguchi, R. Ito, S. Fukatsu and Y. Shiraki, *J. Cryst. Growth*, 1992, **124**, 439.

4 N. R. Fetter and B. Bartocha, *Can. J. Chem.*, 1961, **39**, 2001.

5 Y. Kim, J. H. Kim, J. E. Park, H. Song and J. T. Park, *J. Organomet. Chem.*, 1997, **545**, 99.

6 D. A. Neumayer, A. H. Cowley, A. Decken, R. A. Jones, V. Lakhotia and J. G. Ekerdt, *Inorg. Chem.*, 1995, **34**, 4698.

7 D. W. Peters, M. P. Power, E. D. Bourret and J. Arnold, *Chem. Commun.*, 1998, 753.

8 V. C. Gibson, C. Redshaw, A. J. P. White and D. J. Williams, *Angew. Chem., Int. Ed.*, 1999, **38**, 961.

9 For other ladder structures see, for example: (*a*) R. J. Wehmschulte and P. P. Power, *J. Am. Chem. Soc.*, 1997, **119**, 8387; (*b*) M. M. Banaszak Holl, P. T. Wolczanski, D. Proserpio, A. Bielecki and D. B. Zax, *Chem. Mater.*, 1996, **8**, 2468; (*c*) J. A. Zubieta and J. J. Zuckerman, *Prog. Inorg. Chem.*, 1978, **24**, 251.

10 R. Ehrlich, *Inorg. Chem.*, 1970, **9**, 146.

11 S. Horchler, E. Parisini, H. W. Roesky, H.-G. Schmidt and M. Noltemeyer, *J. Chem. Soc., Dalton Trans.*, 1997, 2761.

Communication 9/04046C

ChemComm

Structures of $[Co(II)(L)(NO_3)(HOCH_3)_n]BPh_4$ (n = 4, 5) complexes (L = *cis,cis*-1,3,5-triaminocyclohexane-based ligand): structural 'snapshots' of anion binding to a metal centre

Clive J. Boxwell and Paul H. Walton*

Department of Chemistry, University of York, Heslington, York, UK YO10 5DD. E-mail: phw@york.ac.uk

Received (in Cambridge, UK) 16th June 1999, Accepted 15th July 1999

The crystal structures of $[Co(II)(L)(NO_3)(HOCH_3)_n]BPh_4$ {L = *cis,cis*-1,3,5-tri[(4-*tert*-butylphenyl)propenylideneamino]cyclohexane} complexes demonstrate the role of solvent molecules in the stabilisation of anions within a solvated cavity: the structures can be compared with bicarbonate binding in the active site of carbonic anhydrase.

Small molecule metal complexes have long been used successfully to mimic the immediate metal coordination sphere of metal ions in metalloproteins. Some of the most successful model complexes, especially models of myoglobin,[1] have attempted to model not only the metal and its surrounding ligands but also other active site features. Such models have the potential to provide chemical clues about the mechanistic roles of these features which are remote from the immediate metal coordination sphere. Of late, we have been interested in preparing small molecule complexes which mimic both primary and secondary coordination spheres of the metal ion in the zinc-containing metalloenzyme human carbonic anhydrase II (CA). CA (and its catalytically competent Co(II)-substituted form) is of significant interest since it catalyses the hydration of carbon dioxide at near diffusion-limited rates. The enzyme's active site can be described as a 15 Å deep cleft with a metal ion coordinated by three histidine residues at the 'bottom' of the cleft. There are several amino acid residues remote from the primary coordination sphere of the metal which are critical in maintaining the high catalytic efficiency of the enzyme.[2] Another feature of the active site are chains of hydrogen-bonded water molecules extending from the metal to the 'top' of the cavity; studies show that the active site water molecules have important roles to play in proton transfer and in substrate binding.[3] To model these remote active site features in a synthetic complex requires a ligand design which combines an N_3 face-capping coordination geometry with a rigid 'superstructure', *e.g.* derivatised cyclodextrins[4] and derivatised tris-pyrazolylborate complexes.[5]

We have previously reported the use of propenylidene derivatives of *cis,cis*-triaminocyclohexane ligands (abbreviation: protach) in the modelling of CA.[6] The protach ligand system provides a face-capping N_3 coordination environment on one 'face' of the metal and surrounds the other 'face' with a rigid, hydrophobic superstructure (Fig. 1). We have shown that this superstructure is capable of encapsulating several solvent molecules, modelling the solvated active site cavity seen in CA.[7] In this paper we report two new structures using the protach-based ligand system (4-*tert*-butylphenylprotach). These structures exhibit different degrees of nitrate solvation within the structures' cavities. One structure shows the nitrate coordinated to the metal centre [cobalt(II)], whereas the other structure of the same metal–ligand complex—crystallised under different conditions—shows the nitrate solvated by methanol molecules at the 'top' of the cavity.

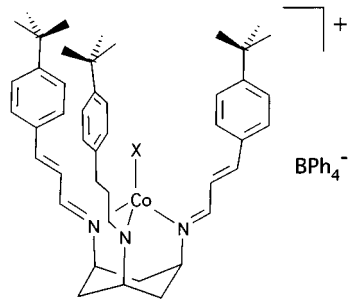

Fig. 1 Metal ligand complex used in this study (X = NO_3).

Condensation of 4-*tert*-butylcinnamaldehyde with *cis*-1,3,5-triaminocyclohexane gave the ligand *cis,cis*-1,3,5-tri[(4-*tert*-butylphenyl)propenylideneamino]cyclohexane (L) in 58% yield. Addition of L to $Co(NO_3)_2{\cdot}6H_2O$ in CH_2Cl_2–CH_3OH (*ca.* 10/90 v/v) solution gave, after slow evaporation of the solvent, crystals of $[Co(L)(HOCH_3)_3](NO_3)(HOCH_3)_2(BPh_4)$ **1** in 65% yield. Repeating the procedure with CH_2Cl_2–CH_3OH (*ca.* 30/70 v/v) solution gave crystals of $[Co(L)(NO_3)(HOCH_3)](HOCH_3)_3(CH_2Cl_2)_2(BPh_4)$ **2** in 74% yield. Satisfactory analyses were obtained for the fully desolvated complexes of **1** and **2**. The crystals of both **1** and **2** rapidly lost all solvent *in vacuo*.

The structures of **1** and **2** were determined by single crystal X-ray diffraction.† The structure of **1** (Fig. 2) shows the cobalt atom in a near octahedral co-ordination geometry, with L co-ordinating in the expected face-capping fashion. The phenylpropenylidene 'arms' of the ligand form a rigid cavity around the metal's remaining co-ordination sites, which are occupied by three methanol molecules. All three co-ordinated methanol molecules are involved in hydrogen bonding with either other methanol molecules or the nitrate anion in the cavity. The OH groups of two coordinated methanol molecules, O(2) and O(3),

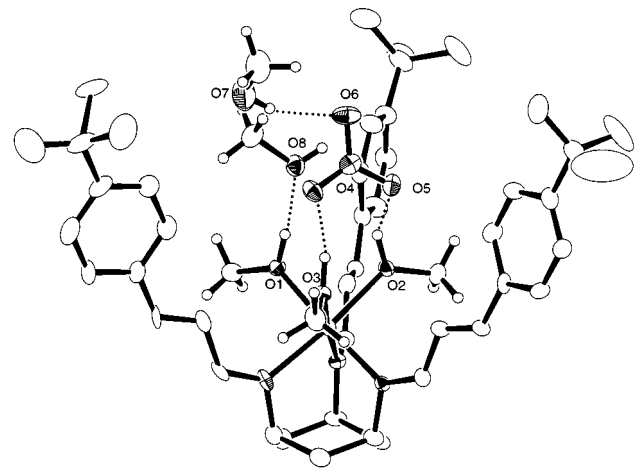

Fig. 2 ORTEP[9] representation of **1** (30% probability ellipsoids). Co(1)–O(1) 2.140(6), Co(1)–O(3) 2.134(6), Co(1)–O(2) 2.161(6), O(1)···O(8) 2.690(9) Å, O(1)–H(1)···O(8) 144.7°, O(2)···O(5) 2.769(9) Å, O(2)–H(2)···O(5) 140.2°, O(3)···O(4) 2.672(9) Å, O(2)–H(2)···O(5) 164.2°, O(7)···O(6) 3.055(12) Å, O(7)–H(7)···O(6) 168.2°, O(8)···O(5)* 3.005(9) Å, O(8)–H(8)···O(5)* 161.5°, Tetraphenylborate anion and hydrogen atoms on L are not shown for clarity.

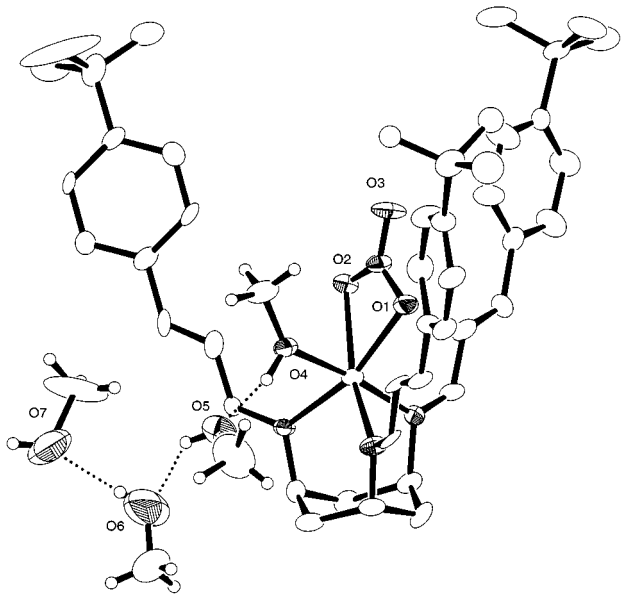

Fig. 3 ORTEP[9] representation of **2** (30% probability elipsoids). Co(1)–O(1) 2.145(11), Co(1)–O(2) 2.244(9), Co(1)–O(4) 2.153(11), O(4)···O(5) 2.602(18) Å, O(4)–H(4)···O(5) 168.3°, O(5)···O(6) 2.73(2) Å, O(5)–H(5)···O(6) 145.1°, O(6)···O(7) 2.54(3) Å, O(6)–H(6)···O(7) 136.2°. Tetraphenylborate anion, dichloromethane molecules and hydrogen atoms on L are not shown for clarity.

are hydrogen-bonded to two oxygen atoms of the nitrate, O(5) and O(4) respectively. The third nitrate oxygen atom, O(6), is hydrogen-bonded to two further methanol molecules, O(7) and O(8)*, at the 'top' of the cavity. The third coordinating methanol molecule, O(1), is hydrogen-bonded to another methanol molecule, O(8); this methanol molecule forms a hydrogen bond to an oxygen of the nitrate anion, O(6)*, of an adjacent asymmetric unit. Accordingly, the two cobalt complex cations form a pseudo-dimer. A tetraphenylborate anion completes the structure.

The structure of **2** (Fig. 3) shows the cobalt atom in a near octahedral co-ordination geometry with L co-ordinating in a face-capping fashion. As before, the phenyl propenylidene 'arms' of the ligand form a rigid cavity around the metal ion's remaining co-ordination sites, which are occupied by the oxygen atom of one methanol molecule and an η^2-nitrate. The oxygen atom of the coordinated methanol molecule, O(4), is hydrogen-bonded to a chain of three further hydrogen bonded methanol molecules, O(5), O(6) and O(7). The nitrate anion is not involved in any hydrogen bonding. A tetraphenylborate anion and two dichloromethane solvent molecules complete the structure. The cobalt coordination geometry matches closely with that of cobalt in the structure of Co-substituted CA (HCO_3^-); in the protein structure the cobalt has a bidentate bicarbonate ligand (analogous to nitrate in the model complex) and a water molecule occupying the sixth coordination site (analogous to methanol).[8]

The structures of **1** and **2** demonstrate the ability of the complexes to encapsulate solvent molecules. These solvent molecules are involved in extensive hydrogen-bonding interactions. It appears that by controlling the concentration of methanol in the crystallising solvent it is possible to control the degree of methanol incorporation in the complexes; this is a powerful tool to study the effects of solvent on the solvation of anions within the cavity of the complex. Comparison of the two structures (see Fig. 4) shows two possible structural 'snapshots' of nitrate binding to cobalt through a shell of solvent molecules. The structure of **1** illustrates one possible stage along the binding pathway in which the nitrate ion forms hydrogen-bond interactions with coordinated solvent molecules. There are

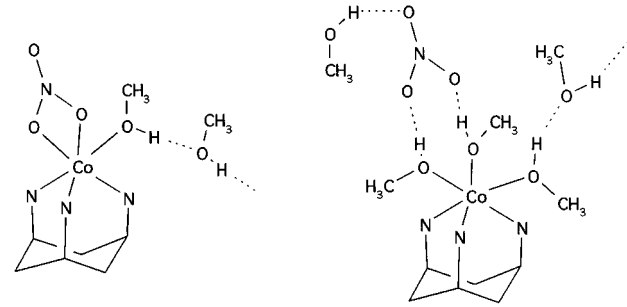

Fig. 4 Schematic comparison of nitrate–metal interactions in **1** (right) and **2** (left). Phenylpropenylidene groups, tetraphenylborate anions and dichloromethane molecules are not shown for clarity.

parallels between our models and the binding of bicarbonate in the Co-substituted form of CA. By analogy it is possible that the transfer of bicarbonate in and out of the active site is stabilised by similar hydrogen-bond interactions between metal-bound water molecules and bicarbonate. Such interactions could be important in facilitating rapid transfer of bicarbonate in and out of the hydrophobic active site. In other words, bicarbonate binding through a hydrophobic active site can be achieved without extensive desolvation of the bicarbonate, and also binding can be achieved with relatively little reorganisation of solvent molecules.

C. J. B. acknowledges the EPSRC for the provision of a maintenance grant.

Notes and references

† *Crystal data* for **1**: $C_{74}H_{97}BCoN_4O_8$, M = 1240.30, a = 16.491(8), b = 19.048(11), c = 12.838(6) Å, α = 98.79(5), β = 97.26(4), γ = 114.35(4)°, V = 3549(3) Å^3, triclinic, space group $P\bar{1}$, (no. 2), Z = 2, T = 150 K, final $R1$ = 0.063, $wR2$ = 0.225 for 8918 reflections, GoF (on F^2) = 1.023, Δ/σ (max.) = 0.00.

Crystal data for **2**: $C_{75}H_{97}BCl_4CoN_4O_7$, M = 1378.11, a = 10.393(4), b = 16.811(5), c = 21.737(5) Å, β = 97.21(2)°, V = 3768(2) Å^3, monoclinic, space group $P2_1$ (no. 4), Z = 2, T = 150 K, final $R1$ = 0.064, $wR2$ = 0.232 for 5138 reflections, GoF (on F^2) = 1.025, Δ/σ (max.) = 0.00.

Both structures were solved using direct methods with SHELXS. Full matrix refinement on F^2 with SHELXL 93.[10] Hydrogen atoms involved in hydrogen bonding were placed in fixed positions near appropriate peaks in a Fourier difference map. CCDC 182/1332. See http://www.rsc.org/suppdata/cc/1999/1647/ for crystallographic files in .cif format.

1 See: M. Momenteau and C. A. Reed, *Chem. Rev.*, 1994, **94**, 659, and references therein.
2 See: S. Toba, G. Colombo and K. M. Merz Jr., *J. Am. Chem. Soc.*, 1999, **121**, 2290, and references therein.
3 D. N. Silverman and S. Lindskog, *Acc. Chem. Res.*, 1988, **21**, 30.
4 I. Tabushi and Y. Kuroda, *J. Am. Chem. Soc.*, 1984, **106**, 4580.
5 C. Kimblin, W. E. Allen and G. Parkin, *J. Chem. Soc., Chem. Commun.*, 1995, 1813; R. Alsfasser, M. Ruf, S. Trofimenko and H. Vahrenkamp, *Chem. Ber./Recueil*, 1993, **126**, 703.
6 B. Greener, M. H. Moore and P. H. Walton, *Chem. Commun.*, 1996, 27.
7 L. Cronin, B. Greener, M. H. Moore and P. H. Walton, *J. Chem. Soc., Dalton Trans.*, 1996, 3337.
8 K. Håkansson and A. Wehnert, *J. Mol. Biol.*, 1992, **228**, 1212.
9 C. K. Johnson, ORTEP, Report ORNL-5138, Oak Ridge National Laboratory, Oak Ridge, TN, 1976.
10 G. M. Sheldrick, SHELXS86, program for crystal structure determination, University of Göttingen, 1986; P. T. Beurskens, G. Admiraal, G. Beurskens, G. Bosman, W. P. Garcia-Granda, R. O. Gould, J. M. M. Smits and C. Smykalla, the DIRDIF program system, technical report of the crystallographic laboratory, University of Nijmegen, 1992; G. M. Sheldrick, SHELXL 93, program for crystal structure refinement, University of Göttingen, 1993.

Communication 9/04802B

ChemComm

Deboronation of *ortho*-carborane by an iminophosphorane: crystal structures of the novel carborane adduct *nido*-$C_2B_{10}H_{12}\cdot HNP(NMe_2)_3$ and the borenium salt $[(Me_2N)_3PNHBNP(NMe_2)_3]_2O^{2+}(C_2B_9H_{12}^-)_2$

Matthew G. Davidson, Mark A. Fox,* Thomas G. Hibbert, Judith A. K. Howard, Angus Mackinnon, Ivan S. Neretin and Kenneth Wade

Chemistry Department, Durham University Science Laboratories, South Road, Durham, UK DH1 3LE. E-mail: m.a.fox@durham.ac.uk

Received (in Cambridge, UK) 16th April 1999, Accepted 20th July 1999

The structures of the adduct *nido*-$C_2B_{10}H_{12}\cdot HNP(NMe_2)_3$ and the borenium salt $[(Me_2N)_3PNHBNP(NMe_2)_3]_2O^{2+}(C_2B_9H_{12}^-)_2$, both obtained from 1,2-$C_2B_{10}H_{12}$ and $HNP(NMe_2)_3$, were determined by X-ray crystallography; the adduct represents the first structurally determined carborane of its type, a possible intermediate in the well known conversion of *closo*-1,2-$C_2B_{10}H_{12}$ into the *nido*-7,8-$C_2B_9H_{12}^-$ anion by bases.

The *closo*-icosahedral carboranes $C_2B_{10}H_{12}$ have an extensive (3-dimensional aromatic) chemistry with implications for neutron scavenging, for materials (thermally stable or conducting or otherwise electroactive oligomers and polymers), for metal extraction, supramolecular chemistry and catalysis.[1] Remarkably resilient to heat and oxidising agents, they are known to have one very important degradation reaction, being susceptible to nucleophilic attack by a select few powerful Lewis bases (*e.g.* alkoxides, fluoride, amines)[2–5] which can remove one of their BH units, formally as BH^{2+}, leaving *nido*-shaped $C_2B_9H_{11}^{2-}$ (or $C_2B_9H_{12}^-$) anionic residues that can strongly bind metal ions to their open C_2B_3 faces,[6] useful for metal-extraction and catalytic applications. However, although such base deboronations have been known for 35 years, details of their mechanisms have remained elusive. Here, we describe work that sheds light on the mechanism, reporting the X-ray structural characterization of an adduct $C_2B_{10}H_{12}\cdot HNP(NMe_2)_3$ **2**, formed in the nucleophilic attack by the new deboronating base $HNP(NMe_2)_3$ on *ortho* carborane, 1,2-$C_2B_{10}H_{12}$ **1**. We also show that the hitherto unknown monoboron cation $(Me_2N)_3PNHB[NP(NMe_2)_3]_2^+$ is a later product of the same reaction, and that the dication $[(Me_2N)_3PNHBNP(NMe_2)_3]_2O^{2+}$ is an unexpected product if traces of water are present.

Iminotris(dimethylamino)phosphorane $HNP(NMe_2)_3$ is very effective in the conversion of *closo*-$C_2B_{10}H_{12}$ **1** into *nido*-7,8-$C_2B_9H_{12}^-$. Several NMR-scale reactions of carborane **1** with dry $HNP(NMe_2)_3$ in anhydrous deuterated toluene at varying temperatures (−20 to 20 °C), ratios (carborane : base 1 : 10 to 10 : 1) and concentrations (0.1 to 0.01 M) were monitored by ^{11}B NMR spectroscopy. We found that boron peaks corresponding to a carborane intermediate were best observed using a 1 : 1 ratio mixture of low concentration (0.01 M) at room temperature after only two minutes reaction time. The peaks observed arising from the intermediate at 34.8 (br), −18.2 (d) and −27.8 (d) ppm accounted for only 2% of the total boron peak intensities (the major carborane is **1** with peaks at −2.0, −8.7, −13.2 and −14.4 ppm at this stage) and disappeared rapidly to peaks corresponding to the carborane anion, $C_2B_9H_{12}^-$.[4] This anion was observed by multinuclear NMR spectroscopy accompanied by a 1 : 1 mixture of the cation $H_2NP(NMe_2)_3^+$ **3** and the novel protonated tris(imino)-borane $(Me_2N)_3PNHB[NP(NMe_2)_3]_2^+$ **4** respectively (Scheme 1).†

A preparative scale reaction was carried out to allow structural characterization of the products. Under nitrogen, slow addition of dry $HNP(NMe_2)_3$ (1.78 g, 10 mmol) in anhydrous toluene (15 ml) to a solution of **1** (1.44 g; 10 mmol) in toluene (15 ml) resulted in the formation of a crystalline product (*ca.* 0.03 g) overnight. Although this product was identified by boron NMR spectroscopy as a mixture of **1** and 7,8-$C_2B_9H_{12}^-$ in solution, an X-ray structural determination on a crystal selected from the material revealed a carborane adduct $C_2B_{10}H_{12}\cdot HNP(NMe_2)_3$ **2** (Fig. 1).‡ The volume of the decanted solution was halved by solvent removal *in vacuo* and, after standing for a week at room temperature, the crystals formed were identified by NMR as the salt $H_2NP(NMe_2)_3^+$ (7,8-$C_2B_9H_{12}^-$) **3** (0.32 g) and confirmed by an X-ray structural determination.‡ The mother liquor was cooled to −20 °C to yield a white solid identified by NMR spectroscopy as the protonated tris(imino)borane salt **4** (0.43 g).

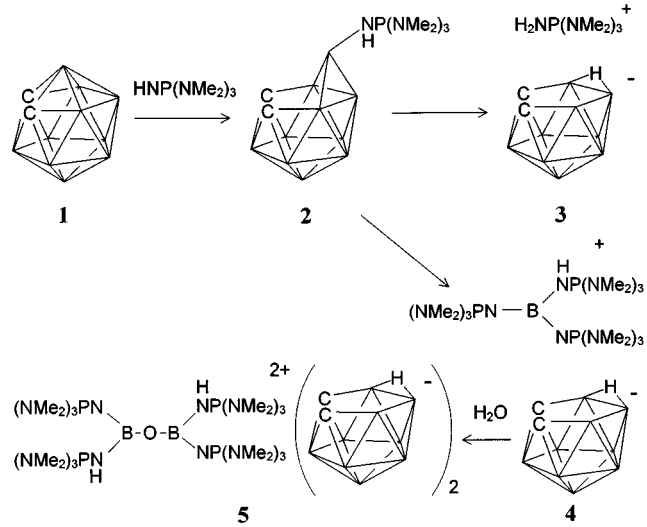

Scheme 1

Calculated (GIAO HF/6-31G*) boron NMR shifts§ generated from the X-ray geometry of the carborane adduct **2** show good agreement with the intermediate observed in the NMR-scale reactions once masking of certain peaks by the starting carborane **1** is taken into account. This suggests that adduct **2** is the first structurally characterized intermediate in the well known conversion of *closo*-1,2-$C_2B_{10}H_{12}$ **1** into *nido*-7,8-$C_2B_9H_{12}^-$. As revealed by the X-ray structure of **2**, the first step of the *closo–nido* conversion is the attachment of the base to the most positively charged boron atom near the two neighbouring carbon atoms which pivots about B(10), cleaving the two B–C bonds and stretching the two B–B bonds to B(9) and B(11). The structure of adduct **2** may be contrasted with the hydrogen-bonded structures of $C_2B_{10}H_{12}\cdot OP(NMe_2)_3$ and $C_2B_{10}Cl_{10}H_2\cdot OSMe_2$ adducts.[7]

As expected from simple skeletal-electron counting rules for a 12-vertex 28 skeletal electron *nido* geometry, the cluster framework of carborane **2** is viewed as a 13-vertex *closo*-deltahedron with a 5-coordinate vertex removed.[8] Positions of

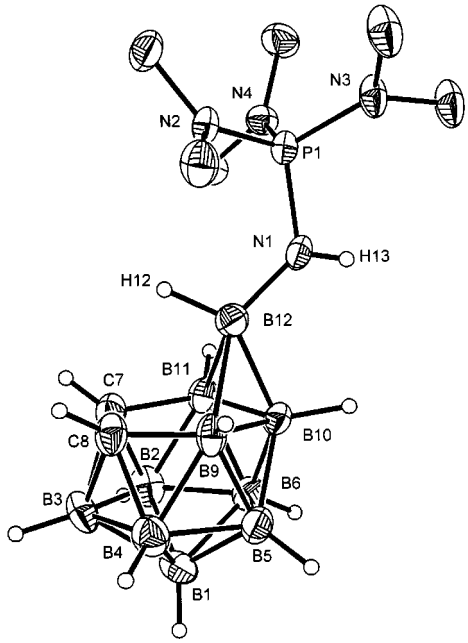

Fig. 1 Molecular structure of adduct **2** (50% ellipsoids; methyl hydrogens omitted for clarity). Important interatomic distances (Å) are: P(1)–N(1) 1.651(3), N(1)–H(13) 0.75(4), N(1)–B(12) 1.506(6), B(12)–H(12) 1.18(4), C(7)–C(8) 1.530(6), C(7)–B(11) 1.654(6), C(8)–B(9) 1.651(6), B(12)–B(10) 1.761(6), B(12)–B(9) 2.099(6), B(12)–B(11) 2.091(6), B(10)–B(9) 1.779(6), B(10)–B(11) 1.802(6). Selected angle (°): P–N(1)–B(12) 127.3(3).

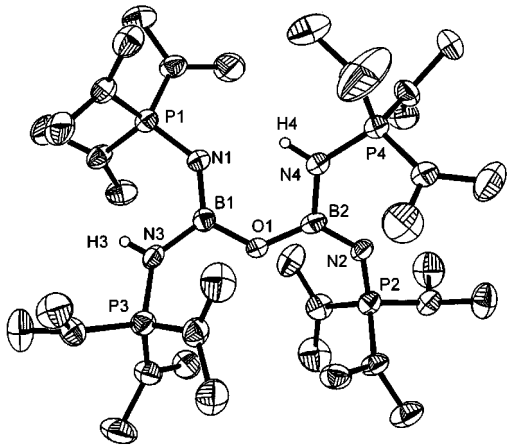

Fig. 2 Molecular structure of cation in **5** (50% ellipsoids; methyl hydrogens omitted for clarity). Important interatomic distances (Å) are: B(1)–N(1) 1.402(6), B(1)–N(3) 1.463(5), B(1)–O(1) 1.373(5), B(2)–N(2) 1.389(5), B(2)–N(4) 1.464(6), B(2)–O(1) 1.416(5), N(1)–P(1) 1.555(3), N(2)–P(2) 1.554(3), N(3)–P(3) 1.630(4), N(4)–P(4) 1.614(3).

the cage carbons in the carborane adduct **2** were conclusively determined by an *ab initio* optimization of a model of $C_2B_{10}H_{12}{\cdot}HNP(NH_2)_3$ at the HF/6-31G* level of theory where both theoretical and experimental geometries are nearly identical. These carbon placements are supported by a similar cage geometry observed in the *nido*-C_2B_{10} moiety of the two-cage anion $[PhCB_{10}H_{10}CB_{10}H_{10}C_2HPh]^-$ structurally characterized by X-ray crystallography.[9]

During attempts to obtain suitable crystals of the salt **4** containing the cation $(Me_2N)_3PNHB[NP(NMe_2)_3]_2^+$ from toluene, a single crystal was characterized by an X-ray study‡ as a salt **5** containing the dication $[(Me_2N)_3PNHBNP(NMe_2)_3]_2O^{2+}$ (Fig. 2). The oxygen atom apparently arose from inadequately dried toluene. According to bond order calculations¶ (AM1) carried out on the structure of the dication $[RN(RNH)BOB(NHR)(NR)]^{2+}$ there is strong BN π bonding within each RN(RNH)B unit to the imino (NR) residue, much less to the imine (RNH) residue, though evidently sufficient to ensure planarity of the $(PN)_2BO$ unit.

Our work suggests that the formation of an adduct $C_2B_{10}H_{12}{\cdot}L$, with an expected *nido*-structure, is the first step in the deboronation of *ortho*-carborane by $HNP(NMe_2)_3$ and presumably other Lewis bases L. Further studies, both experimental and theoretical, will be needed to clarify the later steps.

We are grateful to the EPSRC (M. A. F.), BNFL (T. G. H.) and Durham University (Sir Derman Christopherson Fellowship to J. A. K. H. and studentship to A. M.) for financial support.

Notes and references

† NMR data for cation of **3**: δ_P (d_8-toluene; standard 85% H_3PO_4) 43.2, δ_H 2.33 [*J*(PH) 10 Hz, CH_3] δ_C 36.7 [*J*(PC) 18 Hz, CH_3]; for cation of **4**: δ_P 40.2 (br, 1P), 23.6 (br, 2P), δ_B (standard $BF_3{\cdot}Et_2O$), 22.3 (s), δ_H 2.46 [^{3}*J*(PH) 10 Hz, 18H, CH_3], 2.43 [*J*(PH) 10 Hz, 36H, CH_3], δ_C 37.1 [*J*(PC) 18 Hz], 36.8 [*J*(PC) 18 Hz].

‡ *Crystal data* for **2**: $C_8H_{31}B_{10}N_4P$, M = 322.44, orthorhombic, space group *Pbca* (no. 61), a = 10.799(2), b = 17.252(4), c = 20.326(4) Å, U = 3786.9(13) Å^3, Z = 8, D_c = 1.131 g cm^{-3}, μ = 0.141 mm^{-1}, F(000) = 1376, T = 153(2) K, 25525 reflections (4337 unique), $2\theta \leqslant 55°$, R_1 = 0.077 (2221 data $I > 2\sigma(I)$), $wR(F^2)$ = 0.187, GOF (obs) = 1.053. For **3**: $C_8H_{32}B_9N_4P$, M = 312.64, monoclinic, space group $P2_1/n$ (no. 14), a = 11.580(2), b = 13.182(3), c = 12.385(2) Å, β = 91.88(5)°, U = 1889.5(6) Å^3, Z = 4, D_c = 1.099 g cm^{-3}, μ = 0.140 mm^{-1}, F(000) = 672, T = 150(2) K, 14804 reflections (4992 unique), $2\theta \leqslant 58°$, R_1 = 0.0435 (4283 data $I > 2\sigma(I)$), $wR(F^2)$ = 0.118, GOF(obs) = 1.085. All NMe_2 groups of the cation are disordered. For **5**: $C_{28}H_{98}B_{20}N_{16}P_4O$, M = 1015.30, orthorhombic, space group $P2_12_12_1$ (no. 19), a = 14.105(3), b = 16.529(3), c = 25.563(5) Å, U = 5960(2) Å^3, Z = 4, D_c = 1.132 g cm^{-3}, μ = 0.168 mm^{-1}, F(000) = 2184, T = 150(2) K, 44070 reflections (16579 unique), $2\theta \leqslant 61°$, R_1 = 0.062 (5792 data $I > 2\sigma(I)$), $wR(F^2)$ = 0.138, GOF (obs) = 0.893. The absolute configuration was determined; Flack parameter −0.04(9). CCDC 182/1339. See http://www.rsc.org/suppdata/cc/1999/1649/ for crystallographic files in .cif format.

§ Calculated (GIAO HF/6-31G*) ^{11}B NMR data for **2**: δ 35.7 (B12), −6.3 (B5,6), −6.6 (B2,4), −13.9 (B3), −15.4 (B9,11), −18.3 (B10), −24.0 (B1).

¶ Calculated (AM1) bond orders for **5** (π bond order in parentheses): B(1)–O(1) 1.029 (0.207), B(1)–N(1) 1.311 (0.441), B(1)–N(3) 0.829 (0.086), B(2)–O(1) 0.932 (0.152), B(2)–N(4) 0.920 (0.129), B(2)–N(2) 1.317 (0.444).

1 J. Plešek, *Chem. Rev.*, 1992, **92**, 269 and references therein; M. F. Hawthorne, in *Advances in Boron Chemistry*, ed. W. Siebert, The Royal Society of Chemistry, Cambridge, 1997, p. 261 and references therein.
2 R. A. Wiesboeck and M. F. Hawthorne, *J. Am. Chem. Soc.*, 1964, **86**, 1642; L. I. Zakharkin and V. N. Kalinin, *Tetrahedron Lett.*, 1965, **7**, 407.
3 M. F. Hawthorne, D. C. Young, P. M. Garrett, D. A. Owen, S. G. Schwerin, F. N. Tebbe and P. A. Wegner, *J. Am. Chem. Soc.*, 1968, **90**, 862; L. I. Zakharkin and V. S. Kirillova, *Bull. Acad. Sci. USSR Div. Chem. Sci.* (*Engl. Transl.*), 1975, 2484.
4 H. Tomita, H. Luu and T. Onak, *Inorg. Chem.*, 1991, **30**, 812.
5 M. A. Fox, J. A. H. MacBride and K. Wade, *Polyhedron*, 1997, **16**, 2499; M. A. Fox and K. Wade, *Polyhedron*, 1997, **16**, 2517.
6 N. N. Greenwood and A. Earnshaw, *Chemistry of the Elements*, 1st edn., Pergamon, Oxford, 1984, p. 209 and references therein; J. Plešek and S. Heřmánek, *Inorg. Synth.*, 1984, **22**, 231 and references therein.
7 M. G. Davidson, T. G. Hibbert, J. A. K. Howard, A. Mackinnon and K. Wade, *Chem. Commun.*, 1996, 2285; A. I. Yanovskii, Yu. T. Struchkov, L. E. Vinogradova and L. A. Leites, *Bull. Acad. Sci. USSR, Div. Chem. Sci.* 1983, 1988.
8 F. Meyer, J. Muller, P. Paetzold and R. Boese, *Angew. Chem., Int. Ed. Engl.*, 1992, **31**, 1227 and references therein.
9 L. I. Zakharkin, G. G. Zhigareva, A. V. Polyakov, A. I. Yanovskii and Y. T. Struchkov, *Bull. Acad. Sci. USSR, Div. Chem. Sci.* (*Engl. Transl.*), 1987, 798.

Communication 9/03030A

Synthesis, X-ray structure, and hydrolytic chemistry of the highly potent antiviral polyniobotungstate A-α-$[Si_2Nb_6W_{18}O_{77}]^{8-}$

Gyu-Shik Kim,† Huadong Zeng, Jeffrey T. Rhule, Ira A. Weinstock† and Craig L. Hill*

Department of Chemistry, Emory University, 1515 Pierce Drive, Atlanta, GA 30322, USA. E-mail: chill@emory.edu

Received (in Bloomington, IN, USA) 14th May 1999, Accepted 5th July 1999

Potently antiviral polyniobotungstates have been structurally characterized; the dimer A-α-$[Si_2Nb_6W_{18}O_{77}]^{8-}$ cleaves cleanly to the monomer A-α-$[SiNb_3W_9O_{40}]^{7-}$ within 1 min in aqueous solution buffered at physiological (neutral) pH establishing that the monomer and not the dimer is pharmacologically relevant.

In recent years, several classes of early transition-metal oxygen-anion clusters or polyoxometalates (POMs) have been documented to exhibit antiviral properties.[1] The size, shape and functional group complementarity of these nanometer-sized inorganic compounds and key enzymatic targets, including the active sites of HIV-1 reverse transcriptase[2] and HIV-1 protease,[3] is substantial. This fact coupled with the growing ability to systematically vary the physical and electronic structures and other properties of POMs,[4] has increased interest in POMs as potential antiviral agents. The double-Keggin POMs of formula A-α- or A-β-$[Si_2Nb_6W_{18}O)_{77}]^{8-}$ (**1**) are as promising as any of the 200+ POMs investigated to date as antiviral agents. The A-β isomer was first prepared by Finke and Droege in 1984,[5] and subsequently shown by our group and others to strongly inhibit a number of viruses including HIV-1, HIV-2, respiratory syncytial virus (RSV) and several strains of influenza and herpes while being essentially non-toxic in mammals.[6] The A-α isomer, A-α-$[Si_2Nb_6W_{18}O_{77}]^{8-}$ (A-α-**1**) has comparable pharmacological profiles (therapeutic indices) to A-β-**1**.[1] Despite the interest in A-α- and A-β-**1**, the structure or hydrolytic form of these dimers in aqueous solution under physiological conditions has never been characterizaed. We report here, that the dimers (A-α- or A-β-**1**) are not present under physiological conditions, because cleavage to the corresponding monomers is thermodynamically and kinetically favorable at serum pH values. We focus here on the A-α system for which X-ray structures of both A-α-**1** and its corresponding monomer A-α-$[SiNb_3W_9O_{40}]^{7-}$ (A-α-**2**) have been obtained. The A-β system exhibits effectively identical aqueous speciation chemistry.

The organic-solvent-soluble tetrabutylammonium (TBA) salt of **1** (A-α-TBA**1**) can be prepared by the peroxide-bisulfite method that Finke and Droege used to make the analogous TBA salt of the A-β isomer.[7] Efforts to use this method[7] to obtain water-soluble forms of either isomer of **1** were hampered by co-precipitation of sulfate-salt byproducts. This problem was overcome in two ways: by selective precipitation using K^+ and Cs^+ salts under carefully controlled conditions and by use of a new sulfate-free synthesis. Selective precipitation was accomplished by adding saturated methanolic solutions of either CsCl (8 equiv.) or of CF_3CO_2K (10 equiv. of neat CF_3CO_2H followed by 24 equiv. of methanolic CF_3CO_2K) to 10 mM acetonitrile solutions of A-α-TBA**1**. Powders of the respective salts obtained were washed with methanol, followed by acetonitrile, to remove excess salts. The Cs^+ salt, (A-α-Cs**1**),‡ was obtained in 90% yield based on A-α-TBA**1**. The K^+ salt (34% yield from A-α-TBA**1**) was partially hydrolyzed by reversible cleavage of one of the three Nb–O–Nb μ-O linkages:‡ subsequent dissolution in 1.0 M HCl and passage of the solution through a Dowex-50 proton exchange resin gave the free-acid form of recondensed **1**, A-α-$H_8[Si_2Nb_6W_{18}O_{77}]$ (A-α-H**1**)‡ in effectively quantitative yield.

The Cs^+ salt of A-α-**1** was also prepared by direct condensation of the monomeric triperoxoniobium precursor A-α-$[Si(NbO_2)_3W_9O_{37}]^{7-}$: a yellow solution of A-α-$Cs_7[Si(NbO_2)_3W_9O_{37}]$ [12 mM in 2.0 M HCl(aq)] was refluxed until it was colorless and CsCl (22 equiv.) was added to give A-α-Cs**1** in 86% yield. Reflux of a yellow acetonitrile solution of A-α-$(TBA)_4H_3[Si(NbO_2)_3W_9O_{37}]$ in the presence of HCl followed by diffusion of diethyl ether into the reaction mixture gave X-ray quality crystals of A-α-TBA**1**§ in 74% yield. The solid state (KBr pellet) IR spectra of all the A-α-**1** salts prepared using these methods exhibit strong Nb–O–Nb bands in the 680–700 cm^{-1} region; the spectra of the monomer, A-α-**2**,‡ does not.

X-Ray crystal structures¶ of A-α-TBA**1** and the A-α-Cs**2** confirm the A-α-isomeric assignments. The structure of A-α-**1** with principal bond distances and angles is given in Fig. 1. Bond valence sum calculations[8] indicate that all the niobium atoms in both A-α-**1** and A-α-**2** are in the +5 oxidation state, a result consistent with the NMR spectra (both POMs are diamagnetic). The 'double Keggin' structure in **1** is known in three other structurally characterized POMs: A-α-$[H_9Si_2Cr^{III}_6W_{18}O_{77}]^{11-}$,[9] a tri-μ-hydroxo compound, and A-β-$[Si_2Ti_6W_{18}O_{77}]^{14-}$,[10] and A-α-$[Ge_2Ti_6W_{18}O_{77}]^{14-}$,[11] both tri-μ-oxo compounds.

With both the dimer, A-α-**1**, and monomer, A-α-**2**, structurally characterized in both the solid state and in solution, the pH-dependent aqueous speciation chemistry of these POMs and the form present at physiological (neutral) pH was readily established. It is well documented that various bases cleave the Nb–O–Nb unit in both metal oxide materials[12] and POMs.[5,13] A combined pH–conductometric titration of A-α-H**1** confirmed that 14 equiv. of hydroxide were required to arrive at the inflection point. This is consistent with eqns. (1) and (2) and the

$$H_8Si_2Nb_6W_{18}O_{77} + 8\ OH^- \rightarrow Si_2Nb_6W_{18}O_{77}^{8-} + 8\ H_2O \quad (1)$$

$$Si_2Nb_6W_{18}O_{77}^{8-} + 6\ OH^- \rightarrow 2\ SiNb_3W_9O_{40}^{7-} + 3\ H_2O \quad (2)$$

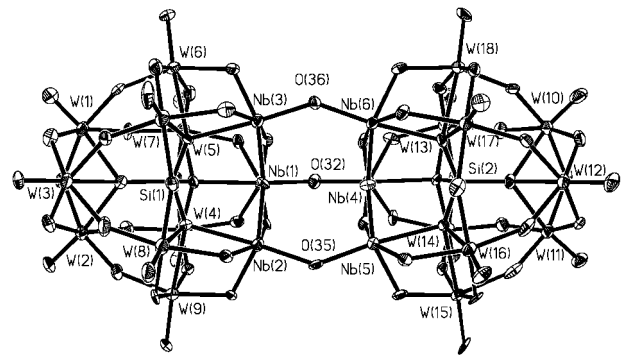

Fig. 1 The ORTEP drawing of A-α-$[Si_2Nb_6W_{18}O_{77}]^{8-}$. Selected bond lengths (Å) and angles (°): Nb(1)–O(32) 1.904(12), Nb(2)–O(35) 1.915(12), Nb(3)–O(36) 1.893(11), Nb(4)–O(32) 1.922(12), Nb(5)–O(35) 1.907(12), Nb(6)–O(36) 1.919(12), Nb(1)–O(32)–Nb(4) 136.6(7), Nb(5)–O(35)–Nb(2) 137.3(6), Nb(3)–O(36)–Nb(6) 137.1(7).

† Permanent addresses: (G.-S. K.); Department of Science Education, Kangwon National University, 192-1 Hyoja-2-dong, Chunchon, 200-701 South Korea. E-mail: gskim@cc.kangwon.ac.kr. (I. A. W.); U.S. Forest Service, Forest Products Laboratory, One Gifford Pinchot Dr, Madison, WI 53705. E-mail: iaweinst@facstaff.wisc.edu.

fact that **1** is a tri-μ-oxo dimer in acidic aqueous solution. Examination of A-α-**1** and A-α-**2** by both ^{183}W NMR and FTIR in D_2O buffered at pD 7.0 using 3 different systems, *N*-[2-hydroxyethyl]piperazine-*N*′-[2-ethanesulfonic acid] (HEPES), 3-[*N*-morpholino]propanesulfonic acid (MOPS), or phosphate, indicated that only monomer, A-α-**2**, was present in all cases. While these measurements indicated the thermodynamic instability of the dimer relative to the monomer at physiological pH, they did not provide the rate of dimer cleavage, the issue of most relevance to the use of A-α-**1** as an antiviral agent. Unfortunately, overlapping absorbances or instrument-limited acquisition times rendered all the obvious spectroscopic techniques, including FTIR on aqueous buffer solutions, inadequate to assess the rate. However, it was determined that the Nb–O–Nb stretching region of the mid-IR could be used to follow this hydrolytic cleavage process provided D_2O was used as the solvent. Dimer cleavage was assessed by adding 0.156 g (0.0303 mmol) of A-α-**1** to 3.00 mL of 0.609 M MOPS buffer in D_2O to give a clear, colorless solution with a pD of 7.0. An aliquot of this solution was added to an AgBr IR solution cell and the spectrum, obtained in < 1 min showed that no dimer Nb–O–Nb band remained. The same experiments using 0.609 M HEPES or phosphate buffer in place of MOPS yielded the same results. ^{183}W NMR and FTIR established that when the pH of the hydrolyzed neutral solution was decreased to 0, A-α-**1** was re-formed in very high yield (Fig. 2). The corresponding experiments with the A-β system gave analogous results and, in neither system was Baker–Figgis (α–β) isomerisation[14] observed.

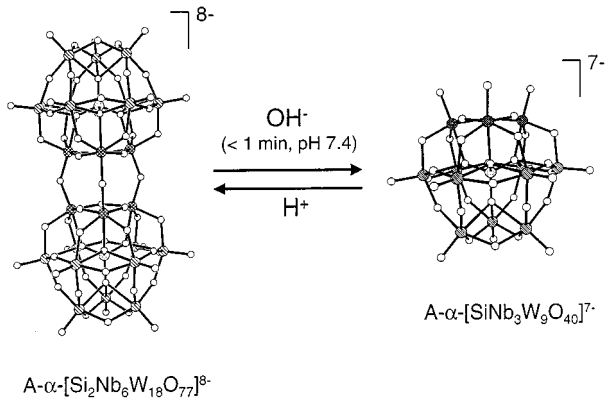

Fig. 2 Summary of dimer–monomer interconversions [eqn, (2) is the balanced reaction].

In summary, the tri-μ-oxo linkages in the double Keggin complexes, A-α-**1** or A-β-**1**, are cleaved quickly and with effectively quantitative selectivity to the corresponding monomers at physiological pH. In consequence, it is highly unlikely that the double Keggin POM structure accounts for any of the extensive biological data reported for these complexes.

This work was supported by the National Institutes of Health (R01 AI32903-04A1), and the Molecular Design Institute (Office of Naval Research, grant N00014-95-1-1116). We thank Dr Don VanDerveer (Georgia Inst. Tech.) for collecting the X-ray data.

Notes and references

‡ A-α-Cs**1**: anal. Calc. for $Cs_8[Si_2Nb_6W_{18}O_{77}]\cdot 18H_2O$: H, 0.55; Cs, 16.3; Nb, 8.52; W, 50.6. Found: H, 0.50; Cs, 16.3; Nb, 8.31; W, 50.6%. FTIR (KBr): 687s, *ν*(Nb–O–Nb). FT Raman (solid): 984vs, 910w, 860(sh).

α-K dimer: unlike **1**, which contains three μ-oxo Nb–O–Nb linkages between the Keggin $SiNb_3W_9$ units, the K^+ dimer contains two μ-oxo linkages, which results in *syn* and *anti* orientations between the two $SiNb_3W_9$ units. Anal. Calc. for $K_{10}[Si_2Nb_6W_{18}O_{78}]\cdot 25H_2O$: H, 0.84; K, 6.50; Nb, 9.27; W, 55.0. Found: H, 0.83; K, 6.68; Nb, 8.98; W, 54.6%. ^{183}W NMR (lithiated 0.07 M in D_2O, pD = 0.4 with DCl; ref. 2.0 M Na_2WO_4 in D_2O): *syn*-di-μ-dimer, δ −99.0 (4W), −119.3 (4W), −128.7 (4W), −130.0 (2W), −146.4 (4W) (80 mol%), *anti*-di-μ-dimer, δ −101.2 (4W), −111.3 (2W), −125.4 (4W), −130.8 (4W), −143.6 (4W) (20 mol%). FTIR (KBr): 683s, *ν*(Nb–O–Nb). FT Raman (solid): 983vs, 904w.

A-α-H**1**: Anal. Calc. for $H_8[Si_2Nb_6W_{18}O_{77}]\cdot 20H_2O$: H, 0.87; Nb, 10.0; W, 59.9. Found: H, 0.78; Nb, 9.83; W, 59.6%. FTIR (KBr): 683s, *ν*(Nb–O–Nb). FT Raman (solid): 989vs, 903w. ^{183}W NMR (0.08 M in D_2O, $[D^+]$ = 1.2 M with DCl; ref. 2.0 M Na_2WO_4 in D_2O): δ −124.1 (6W), −141.2 (12W).

A-α-Cs**2**: anal. Calc. for $Cs_7SiNb_3W_9O_{40}\cdot 10H_2O$: Cs, 25.2; Nb, 7.54; W, 44.8. Found: Cs, 24.7; Nb, 7.40; W, 45.0%. FTIR (KBr): 1003w, 963m, 905s, 778vs, 538m. ^{183}W NMR (0.08 M in D_2O, pD = 6.0 with LiOH, ref. 2.0 M Na_2WO_4 in D_2O): δ −106.8 (6W), −148.7 (3W).

§ A-α-TBA**1**·Et_2O: anal. Calc. for $C_{100}H_{228}N_6Si_2Nb_6W_{18}O_{77}$: C, 17.96; H, 3.44; N, 1.26; Si, 0.84; Nb, 8.34; W, 49.5. Found: C, 17.92; H, 3.37; N, 1.36; Si, 0.67; Nb, 8.43; W, 49.7%. FTIR (KBr): 688s, *ν*(Nb–O–Nb). FT Raman (solid): 988vs, 973m, 921 (sh), 909w, 885(sh). FAB-MS: *m*/*z* (intensity), [assignment]: 5410 (28), $[M + Q + 6H]^-$ 4709 (100), $[M + 7H - 2WO_3]^-$; 4496 (64), $[M + 7H - W_3O_8]^-$; 4275 (47), $[M + 7H - W_4O_{10}]^-$; 4070 (35), $[M + 7H - W_5O_{12}]^-$; 3836 (24), $[M + 7H - W_6O_{15}]^-$. ^{183}W NMR (0.2 M in 1 : 1 CD_3CN–DMF; ref. 2.0 M Na_2WO_4 in D_2O): δ −110.30 (6W), −130.45 (12W).

¶ *Crystal data*: A-α-TBA**1**·Et_2O: $C_{100}H_{228}Nb_6O_{78}Si_2W_{18}$, M = 6685.81, orthorhombic, space group $Pca2_1$, a = 29.4854(3), b = 20.3867(3), c = 28.4247(10) Å, V = 17086.4(3) Å^3, D_c = 2.57 g cm^{-3}, T = 293 K, Z = 4, F(000) = 12232, μ(Mo-Kα) = 12.540 mm^{-1}, Siemens SMART CCD, 87737 reflections measured, 28106 unique (R_{int} = 0.0895) which were used in all calculations. The final R_1 = 0.0506 and wR_2 = 0.1107.

A-α-Cs**2**·$4H_2O$: $Cs_6H_9Nb_3O_{44}SiW_9$, M = 3471.98, tetragonal, space group $P4_2/ncm$, a = 21.0827(4), c = 10.4262(3) Å, V = 4634.2(2) Å^3, D_c = 4.99 g cm^{-3}, T = 293 K, Z = 4, μ(MoKα) = 27.726 mm^{-1}, Siemens SMART CCD, 38780 reflections measured, 2944 unique (R_{int} = 0.0828) which were used in all calculations. The final R_1 = 0.0363 and wR_2 = 0.0991. The 3 Nb and 9 W atoms are statistically distributed among the 12 positions in the Keggin unit due to a crystallographically imposed 2/*m* symmetry passing through Si atom. CCDC 182/1313. See http://www.rsc.org/suppdata/cc/1999/1651/ for crystallographic files in .cif format.

1 J. T. Rhule, C. L. Hill, D. A. Judd and R. F. Schinazi, *Chem. Rev*., 1998, **98**, 327.
2 S. G. Sarafianos, U. Kortz, M. T. Pope and M. J. Modak, *Biochem. J*., 1996, **319**, 619.
3 C. L. Hill, D. A. Judd, J. Tang, J. Nettles and R. F. Schinazi, *Antiviral Res*., 1997, **34**, A43.
4 M. T. Pope and A. Müller, *Angew. Chem., Int. Ed. Engl*., 1991, **30**, 34; *Chem. Rev*. (special issue on polyoxometalates), ed. C. L. Hill, 1998, **98**, 1–390.
5 R. G. Finke and M. W. Droege, *J. Am. Chem. Soc*., 1984, **106**, 7274.
6 N. Yamamoto, D. Schols, E. De Clercq, Z. Debyser, R. Pauwels, J. Balzarini, H. Nakashima, M. Baba, M. Hosoya, R. Snoeck, J. Neyts, G. Andrei, B. A. Murrer, B. Theobald, G. Bossard, G. Henson, M. Abrams and D. Picker, *Mol. Pharm.*, 1992, **42**, 1109; G. Kim, D. A. Judd, C. L. Hill and R. F. Schinazi, *J. Med. Chem*., 1994, **37**, 816; L. Ni, F. D. Boudinot, S. G. Boudinot, G. W. Henson, G. E. Bossard, S. A. Martelucci, P. W. Ash, S. P. Fricker, M. C. Darkes, B. R. C. Theobald and R. F. Schinazi, *Antimicrob. Agents Chemother*., 1994, **38**, 504; D. L. Barnard, C. L. Hill, T. Gage, J. E. Matheson, J. H. Huffman, R. W. Sidwell, M. I. Otto and R. F. Schinazi, *Antiviral Res*., 1997, **34**, 27; J. H. Huffman, R. W. Sidwell, D. L. Barnard, A. Morrison, M. J. Otto, C. L. Hill and R. F. Schinazi, *Antiviral Chem. Chemother*., 1997, **8**, 75.
7 R. G. Finke and M. W. Droege, *J. Am. Chem. Soc*., 1984, **106**, 7274.
8 N. E. Brese and M. O'Keeffe, *Acta. Crystallogr., Sect. B*., 1991, **47**, 192.
9 K. Wassermann, R. Palm, H.-J. Lunk, J. Fuchs, N. Steinfeldt and R. Stoesser, *Inorg. Chem*., 1995, **34**, 5029.
10 Y. Lin, T. J. R. Weakley, B. Rapko and R. G. Finke, *Inorg. Chem*., 1993, **32**, 5095.
11 T. Yamase, T. Ozeki, H. Sakamoto, S. Nishiya and A. Yamamoto, *Bull. Chem. Soc. Jpn*., 1993, **66**, 103.
12 F. Fairbrother, *The Chemistry of Niobium and Tantalum*, Elsevier, 1967.
13 V. W. Day, W. G. Klemperer and C. Schwartz, *J. Am. Chem. Soc*., 1987, **109**, 6030; M. W. Droege and R. G. Finke, *J. Mol. Catal*., 1991, **69**, 323; M. K. Harrup, G.-S. Kim, H. Zeng, R. P. Johnson, D. VanDerveer and C. L. Hill, *Inorg. Chem*., 1998, **37**, 5550.
14 I. A. Weinstock, J. J. Cowan, E. M. G. Barbuzzi, H. Zeng and C. L. Hill, *J. Am. Chem. Soc*., 1999, **121**, 4608.

Communication 9/03983J

Ag nanoparticles synthesised in template-structured mesoporous silica films on a glass substrate

Yuri Plyuto,†[a] Jean-Marc Berquier,*[a] Catherine Jacquiod[a] and Christian Ricolleau[b]

[a] *Laboratoire CNRS, Saint-Gobain 'Surface du Verre et Interfaces', UMR 125, B.P. 135, 39 quai Lucien Lefranc, 93303 Aubervilliers, France. E-mail: jean-marc.berquier@sgr.saint-gobain.com*

[b] *Laboratoire de Minéralogie, Cristallographie, UMR 7590, Université Paris VII—D. Diderot, tour 16, 4 place Jussieu, 75252 Paris Cedex 05, France*

Received (in Oxford, UK) 11th June 1999, Accepted 21st July 1999

Ag nanoparticles have been synthesised within a mesoporous template-structured silica film by a chemical route which includes ion-exchange with $Ag(NH_3)_2^+$ followed by reduction.

Thin films of surfactant-templated mesoporous metal oxides have been recently the focus of numerous studies.[1–6] In particular, a sol–gel-based dip-coating method for the rapid synthesis of continuous hexagonal and cubic mesoporous silica films has been developed.[3] The remarkable physico-chemical properties of these advanced materials (mesoporosity, unidimensional channels, preferable orientation with respect to the supporting substrate) are very promising for applications in membrane-based separation, catalysis and sensors. Here, we demonstrate a new potential of such films. Namely, we show that Ag nanoparticles can be chemically synthesised in the pores of mesoporous silica films deposited on glass substrates. To the best of our knowledge this development constitutes a novel application of mesoporous coatings which has, so far, not yet been described in the literature. However different applications of Ag nanoparticles have already initiated the development of numerous approaches for their elaboration, modification and incorporation into the surface layer of various materials *via* sol–gel processing,[7] melt-quenching,[8] electron beam lithography,[9] magnetron cosputtering,[10] ion-exchange,[11] ion-implantation,[12] or covalent linkage to self-assembled monolayers.[13]

Mesoporous silica films were synthesised using a precursor solution prepared in accordance with the published procedure[3] by addition of CTAB cationic surfactant [cetyltrimethylammonium bromide, $Me(CH_2)_{15}N^+Me_3Br^-$] to a silica sol with molar ratio 1 $Si(OC_2H_5)_4$: 22 C_2H_5OH : 5 H_2O : 0.004 HCl. The CTAB concentration in the final solution was 0.06 M, this reagent being essential for the formation of mesoporous silica films consisting of hexagonally packed one-dimensional channels adjacent to the air–film interface and shorter-range structural ordered channels in the core of the film.[3] The transparent and continuous films of *ca.* 100 nm thickness were deposited on Pyrex slides by dip-coating (10 cm min^{-1} withdrawal rate) at room temperature. Calcination in air at 400 °C (heating rate 1 °C min^{-1}) for 10 h resulted in films whose XRD patterns [Fig. 1(a) and (c)] are in accord with the formation of a mesophase with a $d(100)$ value of *ca.* 3.05 nm (assuming a hexagonal phase with a unit cell constant a = 3.52 nm).

For incorporation of silver, Pyrex slides covered with the calcined mesoporous silica films were contacted for 15 s with an aqueous solution of $[Ag(NH_3)_2]NO_3$ (prepared by dropwise addition of 28% NH_3(aq) to 0.05 M aqueous $AgNO_3$ leading to the formation of a clear colourless solution), rinsed thoroughly with deionised water and dried in a stream of nitrogen at room temperature. For the reduction of silver, the as-synthesised samples were treated in an H_2–N_2 (5% H_2) flow at different temperatures (heating rate 5 °C min^{-1}) for 1 h.

† On leave from the Institute of Surface Chemistry, National Academy of Sciences of Ukraine, Pr. Nauki 31, Kiev 252022, Ukraine.

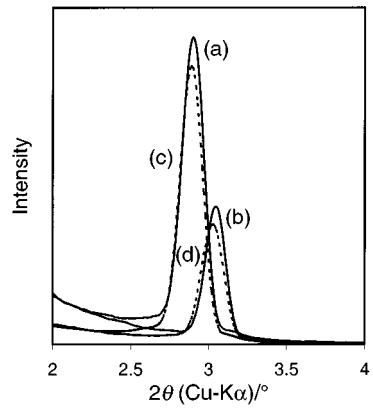

Fig. 1 XRD patterns of two Pyrex substrates with mesoporous silica films after calcination at 400 °C. Before/after [(a)/(b)] contact with an aqueous solution of $[Ag(NH_3)_2]$ NO_3 and subsequent reductive treatment at 400 °C. Before/after [(c)/(d)] contact with an ammoniacal solution and subsequent reductive treatment at 400 °C.

The presence of Ag^+ ions in the mesoporous film after contact with the solution of $[Ag(NH_3)_2]NO_3$ was detected by XPS. X-Ray photoelectron spectra of the as-synthesised samples reveal the presence of intense Ag $3d_{3/2}$ and Ag $3d_{5/2}$ peaks at 374.5 and 368.4 eV, respectively, characteristic for Ag^+.[14] It is reasonable to suggest the following ion-exchange mechanism of silver incorporation into the mesoporous film [eqn. (1)], as a consequence of deprotonation of hydroxy groups

$$Si–OH + Ag(NH_3)_2^+ = Si–OAg(NH_3)_2 + H^+ \quad (1)$$

at the pore surface.[6] Assuming a uniform distribution of Ag^+ ions in the film, their concentration was estimated from the integral intensities of Ag 3d (374.5–368.4 eV) and Si 2p (103.8 eV) envelopes and the atomic sensitivity factors of Ag and Si.[14,15] The experimental I_{Ag}/I_{Si} ratio was close to 3.3 which corresponds to an Ag/Si atomic ratio of 0.17 or to *ca.* 10 wt.% of silver in the mesoporous silica film.

The as-synthesised samples were colourless [Fig. 2(a)] while a yellowish colour appeared after reductive treatment at 100 °C and the intensity of the absorption peak at *ca.* 410–435 nm progressively increased up to 500 °C [Fig. 2(b)–(f)]. The presence of this peak is consistent with the surface plasmon resonance of Ag nanoparticles[8] which are formed upon reduction. The position and the width of the plasmon resonance peak can give information about the average diameter of the nanoparticles. The observed blue shift of the plasmon resonance peak from 435 to 410 nm and the decrease of its width [Fig. 2(b)–(f)] can be related to the increase of the average particle diameter when the reductive treatment continues.[8]

In the X-ray photoelectron spectrum of the sample reduced at 400 °C, the I_{Ag}/I_{Si} ratio was 1.2. This decrease in comparison with the value observed in the as-synthesised sample indicates aggregation of the Ag atoms upon reductive treatment.[16] The formation of the Ag nanoparticles commences with reduction of

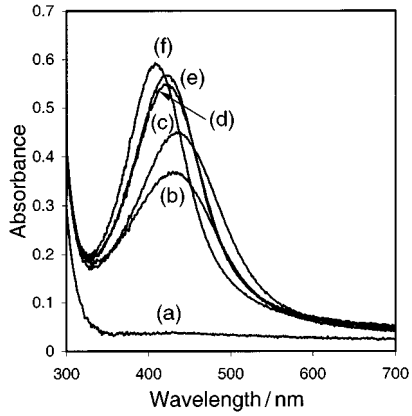

Fig. 2 UV–VIS spectra of a Pyrex slide covered with calcined mesoporous silica film after contacting with an aqueous solution of $[Ag(NH_3)_2]NO_3$ and drying in air (a), and subsequent reductive treatment at 100 °C (b), 200 °C (c), 300 °C (d), 400 °C (e) and 500 °C (f).

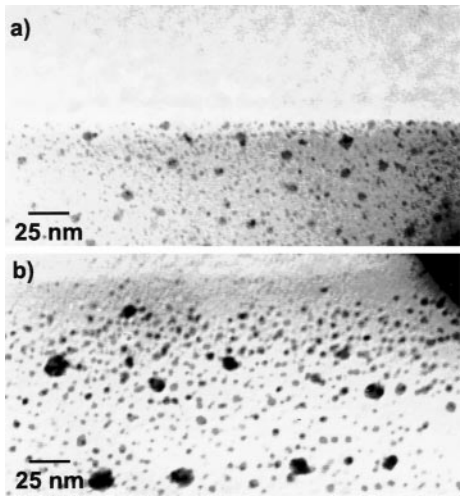

Fig. 3 Transmission electron micrographs of the calcined mesoporous silica film observed in cross-section view after one (a) and three (b) contacts with an aqueous solution of $[Ag(NH_3)_2]NO_3$ and subsequent reductive treatment at 400 °C.

Ag^+ to Ag^0 atoms which migrate within the silica mesoporous matrix.

The sample reduced at 400 °C was also characterised by transmission electron microscopy (TEM) [Fig. 3(a)]. Two types of Ag nanoparticles of different diameter can be distinguished. The first consists in nanoparticles of an almost spherical shape and of 3 nm average diameter while the second type is characterised by an average diameter of 6–7 nm. The existence of two sizes may be ascribed to the presence of defects, such as locally coalesced pores or walls. All particles are well separated from each other and are homogeneously and randomly distributed in the mesoporous silica matrix except in the vicinity of the external surface where ordering of Ag nanoparticles parallel to the surface is clearly seen. This ordering can reasonably be attributed to the preferable parallel orientation of the pore channels in the upper part of the film.[3] This supports the idea that the periodicity of the porous matrix can at least partially control the spatial arrangement of the nanoparticles.

As can be seen from Fig. 1(a) and (b), contact of the calcined sample with the $[Ag(NH_3)_2]NO_3$ solution followed by reductive treatment results in the partial shrinkage of the initial film (decrease of the 1-dH mesophase unit cell constant from *ca.* 3.52 to 3.35 nm). Also, a decrease of the peak intensity at constant width is observed which reveals a decrease of the volumic fraction of the ordered mesoporous domains. In order to ascertain if these effects are connected with the formation of Ag nanoparticles, a sample covered with the calcined film was treated according to the above procedure except that the ammoniacal solution did not contain $AgNO_3$ [Fig. 1(c) and (d)]. Comparing the positions and the relative intensities of the XRD peaks in Fig. 1 it can be concluded that similar modifications occurred for contact with both solutions. This means that both effects are connected with the chemical interaction of the mesoporous silica film with the ammoniacal solution rather than with the formation of Ag nanoparticles. Condensation of the silica framework promoted by ammonia has been reported previously.[4]

Since the organisation of the silica mesoporous film was maintained upon incorporation of Ag nanoparticles, it appeared possible to increase the silver concentration inside the pores. A progressive increase of the intensity of the surface plasmon resonance peak of Ag nanoparticles at 425 nm was indeed observed when the sample was successively contacted with $[Ag(NH_3)_2]NO_3$ solution and subjected to reductive treatment at 400 °C twice and three times.

The sample subjected to three consecutive ion-exchanges and reduction at 400 °C has been characterised by TEM [Fig. 3(b)]. As for the once only treated sample, two types of Ag nanoparticles are observed. Most are of almost spherical shape having an average diameter reaching 5 nm predominate while only a few larger Ag nanoparticles of an average diameter approaching 11 nm are present. The particles are well separated from each other and are homogeneously distributed in the mesoporous silica matrix. It appears that the particles diameter is not limited by the pore size.

In order to clarify whether the possibility of fabrication of Ag nanoparticles in mesoporous silica film relates to its unique structure, a silica film was dip-coated on a Pyrex substrate in the same manner from a precursor solution containing all reactants except CTAB. In this case of a non-mesoporous silica film no evidence of formation of Ag nanoparticles was observed.

Notes and references

1 H. Yang, A. Kuperman, N. Coombs, S. Mamiche-Afara and G. A. Ozin, *Nature*, 1996, **379**, 703.
2 M. Ogawa, *Chem. Commun.*, 1996, 1149.
3 Y. Lu, R. Ganguli, C. A. Drewien, M. T. Anderson, C. J. Brinker, W. Gong, Y. Guo, H. Soyez, B. Dunn, M. H. Huang and J. I. Zink, *Nature*, 1997, **389**, 364.
4 A. Sellinger, P. M. Weiss, A. Nguyen, Y. Lu, R. A. Assink, W. Gong and C. J. Brinker, *Nature*, 1998, **394**, 256.
5 P. Yang, D. Zhao, D. I. Margolese, B. F. Chmelka and G. D. Stucky, *Nature*, 1998, **396**, 152.
6 J.-M. Berquier, L. Teyssedre and C. Jacquiod, *J. Sol–Gel. Sci. Technol.*, 1998, **13**, 739.
7 G. De, A. Licciulli, C. Masarro, L. Tapfer, M. Catalano, G. Battaglin, C. Meneghini and P. Mazzoldi, *J. Non-Cryst. Solids*, 1996, **194**, 225.
8 H. Itoigawa, T. Kamiyama and Y. Nakamura, *J. Non-Cryst. Solids*, 1997, **220**, 210.
9 M. X. Yang, D. H. Gracias, P. W. Jacobs and G. A. Somorjai, *Langmuir*, 1998, **14**, 1458.
10 B. Wang and L. Zhang, *Appl. Surf. Sci.*, 1999, **140**, 227; I. Tanahashi, M. Yoshida, Y. Manabe and T. Tohda, *J. Mater. Res.*, 1995, **10**, 362.
11 M. Dubiel, S. Brunsch, U. Kolb, D. Gutwerk and H. Bertagnolli, *J. Non-Cryst. Solids*, 1997, **220**, 30; G. De Marchi, F. Gonella, P. Mazzoldi, G. Battaglin, E. J. Knystautas and C. Meneghini, *J. Non-Cryst. Solids*, 1996, **196**, 79.
12 A. L. Stepanov, D. E. Hole, A. A. Bukharaev, P. D. Townsend and N. I. Nurgazizov, *Appl. Surf. Sci.*, 1998, **136**, 298; T. S. Anderson, R. H. Magruder III, D. L. Kinser, J. E. Wittig, R. A. Zuhr and D. K. Thomas, *J. Non-Cryst. Solids*, 1998, **224**, 299.
13 K. Bandyopadhyay, V. Patil, K. Vijayamohanan and M. Sastry, *Langmuir*, 1997, **13**, 5244.
14 J. F. Moulder, W. F. Stickle, P. E. Sobol and K. D. Bomben, *Handbook of X-Ray Photoelectron Spectroscopy*, ed. J. Chastain, Perkin-Elmer Corp., Eden Prairie, MN, 1992.
15 *Practical Surface Analysis*, ed. D. Briggs and M. P. Seah, John Wiley and Sons, Chichester, vol. 1, 1990.
16 F. P. J. M. Kerkhof and J. A. Moulijn, *J. Phys. Chem.*, 1979, **83**, 1612.

Communication 9/04681J

Structural variability of the active site of Fe-only hydrogenase and its hydrogenated forms

Ian Dance

School of Chemistry, University of New South Wales, Sydney 2052, Australia. E-mail: I.Dance@unsw.edu.au

Received (in Cambridge, UK) 12th May 1999, Accepted 21st July 1999

Density functional calculations show that the (cys-S)-(CO)(CN)FeS_2(μ-CO)Fe(CO)(CN) active site of the Fe-only hydrogenase from *Clostridium pasteurianum* is redox ambivalent and stereochemically flexible at the CO and S bridges, and at the Fe atoms, and with bound hydrogen: the fundamentals of probable mechanisms are revealed.

The hydrogenase enzymes, which catalyse the reaction $H_2 \rightleftharpoons 2H^+ + 2e^-$, occur as the FeNi-enzymes which mainly oxidise H_2,[1–3] and as the Fe-only enzymes which mainly reduce hydrons H^+.[1,4,5] Crystal structures of both types have been reported recently,[6–12] and reveal the presence of biologically unusual CO and CN ligands at the active sites. In particular, the active site of Fe-hydrogenase from *Clostridium pasteurianum* (CpI)[9] contains an Fe_2 site, **I**, in which two Fe atoms are each coordinated by one CO and one CN^- ligand, and bridged by two S atoms and one CO ligand, as shown in Fig. 1: **I** is linked by bridging cysteine to a cubanoid Fe_4S_4(S-cys)$_4$ cluster at the end of an evident electron transfer pathway. Assignment and differentiation of the CO and CN^- ligands in **I** is from the IR data[13] coupled with the occurrence of two hydrogen bonds from surrounding protein.[14]

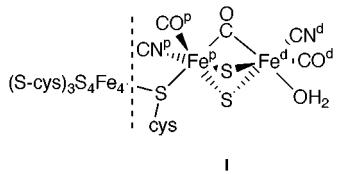

I

Fig. 1 The Fe_2 site **I** as revealed crystallographically for the Fe hydrogenase from *Clostridium pasteurianum*.[9] The Fe atoms and their ligands are labelled as proximal (Fe^p) and distal (Fe^d) to the Fe_4S_4 cluster.

The Fe_2 site **I** is considered to control hydron reduction, the simplest of chemical reactions, but **I** is unprecedented in chemistry. I have investigated the key questions—redox states, stereochemical flexibility, electronic structure, binding of H^+, H and H_2, and mechanism—by density functional calculations† on $[(CH_3S)(CO)(CN)FeS_2(\mu\text{-}CO)Fe(CO)(CN)]^z$, **II**, in which CH_3S^- replaces the cysteine at Fe^p.

Molecule **II** has two low-energy stereochemical variables: (1) the bridging CO ligand can easily swing like a gate between Fe^p and Fe^d; (2) the two bridging S atoms can be separate (at *ca.* 3.3 Å, symbolised S/S), or bonded (S–S, at *ca.* 2.1 Å). Both of these variables are evident in the results shown in Scheme 1, which shows the energies and barrierless transformations of six isomers at three possible redox levels specified by the total charge *z*. The small energy associated with shifts of the CO bridge is evident in the energies of **4** and **5**: $E(\mathbf{4}^{-2}) = E(\mathbf{5}^{-2})$; $E(\mathbf{4}^{-1}) = E(\mathbf{5}^{-1}) + 3$ kcal mol^{-1}; $\mathbf{4}^0$ transforms to $\mathbf{5}^0$ without a barrier. The CO gate shifts left to right for both the S/S (**3** → **2**) and S–S (**6** → **5**) structures, because Fe^d would otherwise be only four-coordinate. Note the small energy differences between isomers with and without S–S bonding: $\mathbf{5}^{-1}$ with an S–S bond is within 7 kcal mol^{-1} of $\mathbf{2}^{-1}$, while for charge –2 the energy difference between **5** and **2** is only 2 kcal mol^{-1}. There are substantial stereochemical changes at Fe^p and Fe^d concomitant with changes in the bridge.

Similar results are found for a model with OH_2 bound to Fe^d. In particular, isomer **1–OH$_2$** as observed in the crystal[9] transforms to isomer **5–OH$_2$** with S–S bonding. There is good agreement between the other bond distances observed and calculated (in parentheses) for **5–OH$_2$**: Fe–Fe 2.62 (2.63); Fe–S

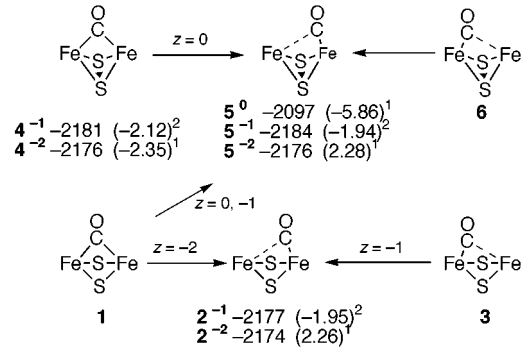

Scheme 1 Relationships between six isomers of $[(CH_3S)(CO)(CN)FeS_2$-(CO)Fe(CO)(CN)]^z, **II**. In these diagrams the CH_3S, terminal CO and CN ligands are omitted; superscripts are the charges *z*. The numbers listed for each minimum are the total energy (kcal mol^{-1}, relative to free atoms) and the (energy/eV)^{population} of the HOMO. Arrows identify barrierless exergonic transformations.

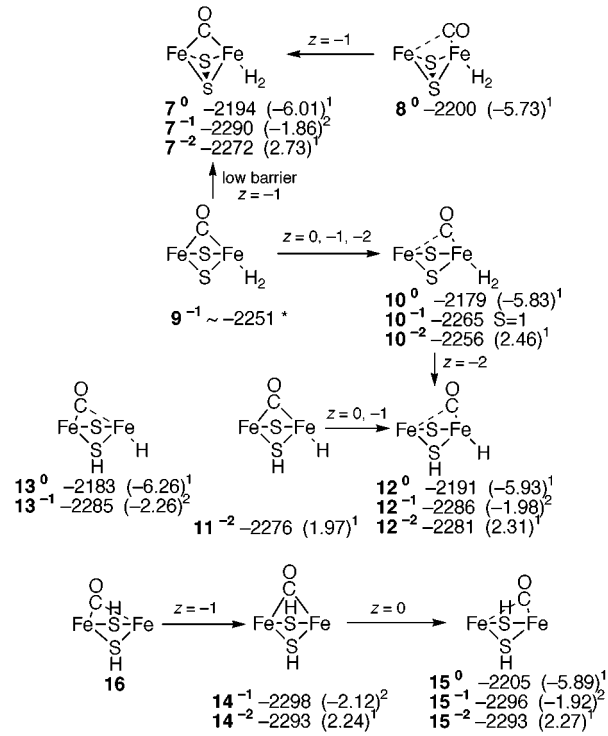

Scheme 2 Isomers of **II** plus two H atoms: diagrams are simplified and information summarised as for Scheme 1. **7**, **8**, **9** and **10** have Fe–H_2 coordination; **11**, **12** and **13** contain SH and Fe–H; **14**, **15** and **16** have $(SH)_2$. * Close-lying electronic states.

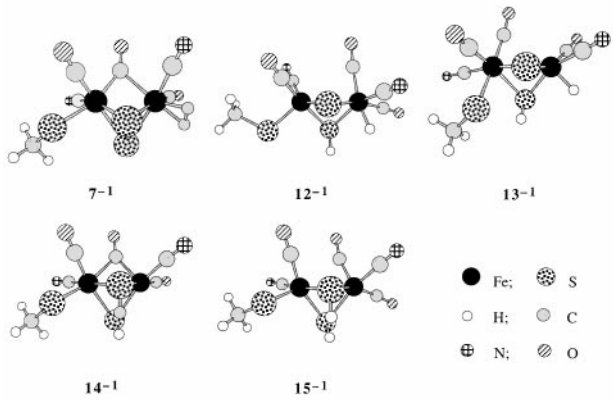

Fig. 2 Optimised structures for five isomers containing 2H, with similar energies but very different bonding patterns, and variations in the coordination stereochemistry at Fe.

2.32–2.34 (2.31–2.39); Fe–SCH_2 2.38 (2.38); Fe-(μ-CO) 2.04–2.10 (1.95–2.03) Å.

What about the redox levels? For $\mathbf{2}^{-1}$ with an $(S^{2-})_2$ bridge the formal oxidation states are $(Fe^{III})_2$ and the doubly occupied HOMO is at −1.95 eV. Reduction to $\mathbf{2}^{-2}$ raises the HOMO to positive energy (Scheme 1). In contrast, $\mathbf{5}^{-1}$ with an $(S_2)^{2-}$ bridge is formally $(Fe^{II})_2$ with the HOMO at −1.95 eV, and $\mathbf{5}^0$ (Fe^{II}, Fe^{III}) has its HOMO at a normal energy of −5.86 eV. In this context it is significant that the Fe_2 hydrogenase from *Desulfovibrio desulfuricans* has a dithiolate bridge $^-SCH_2CH_2CH_2S^-$,[12] and the NiFe hydrogenases have bis-cysteine bridges $(RS^-)_2$,[6–8,10,11] all of which involve redox levels like **5**, not **2**. Extra electron density in the bridging region of CpI[9] could be a dithiolate bridge,[18] or partial occurrence of a S_2^{2-} bridge.

What happens when the active site binds H^+ (at S), H (at S and/or Fe), or H_2 (at Fe)? Scheme 2 displays structures, energies and electronic states of isomers for the model **II** + 2H. Dihydrogen binds to Fe^d, although weakly. The least stable isomer is **9** (*i.e.* the crystal structure with H_2 bound at Fe^d in place of OH_2), which is stabilised by a CO gate shift right (to **10**). In its reduced state $\mathbf{9}^{-2}$ undergoes a mechanistically significant barrierless transfer of one H atom from H_2–Fe to form SH (→ $\mathbf{12}^{-2}$). There is a low barrier for the exergonic S–S bond formation in $\mathbf{9}^{-1}$ (→ $\mathbf{7}^{-1}$). A significant result is that chemically different isomers in Scheme 2 have very similar energies: examples are: $\mathbf{15}^{-1}$ −2296 [$(SH)_2$, CO-right], $\mathbf{14}^{-1}$ −2293 [$(SH)_2$, CO-sym], $\mathbf{7}^{-1}$ −2290 [S–S, Fe–H_2, CO-sym], $\mathbf{12}^{-1}$ −2286 [SH, Fe–H, CO-right], $\mathbf{13}^{-1}$ −2285 [SH, Fe–H, CO-left] kcal mol^{-1}. The calculated geometries of these are presented in Fig. 2, which also emphasises the stereochemical flexibility at Fe^p and Fe^d.

The main conclusion is that the unusual active site of this Fe-only hydrogenase possesses a relatively flat potential energy surface for geometrical change at Fe, CO, S, and bound H. The species in Scheme 2, and others not shown, can be combined in various ways as mechanisms to be calculated in further detail. It is likely that the mechanism involves the following fundamentals:

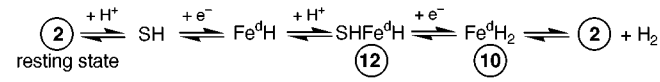

This research is supported by the Australian Research Council and the University of NSW.

Notes and references

† BLYP functional, numerical basis sets, spin restricted and unrestricted, in the program DMol, as described previously.[15–17]

1 M. W. W. Adams, *Biochim. Biophys. Acta*, 1990, **1020**, 115.
2 S. P. J. Albracht, *Biochim. Biophys. Acta*, 1994, **1118**, 167.
3 M. Frey, *Struct. Bonding*, 1998, **90**, 97.
4 M. W. W. Adams and E. I. Stiefel, *Science*, 1998, **282**, 1842.
5 R. Cammack, *Nature*, 1999, **397**, 214.
6 A. Volbeda, M.-H. Charon, C. Piras, E. C. Hatchikian, M. Frey and J. C. Fontecilla-Camps, *Nature*, 1995, **373**, 580.
7 J. C. Fontecilla-Camps, M. Frey, E. Garcin, C. Hatchikian, Y. Montet, C. Piras, X. Vernede and A. Volbeda, *Biochimie*, 1997, **79**, 661.
8 Y. Higuchi, T. Yagi and N. Yasuoka, *Structure*, 1997, **5**, 1671.
9 J. W. Peters, W. N. Lanzilotta, B. J. Lemon and L. C. Seefeldt, *Science*, 1998, **282**, 1853.
10 E. Garcin, X. Vernede, E. C. Hatchikian, A. Volbeda, M. Frey and J. C. Fontecilla-Camps, *Structure*, 1999, **7**, 557.
11 Y. Higuchi, H. Ogata, K. Miki, N. Yasuoka and T. Yagi, *Structure*, 1999, **7**, 549.
12 Y. Nicolet, C. Piras, P. Legrand, C. E. Hatchikian and J. C. Fontecilla-Camps, *Structure*, 1999, **7**, 13.
13 A. J. Pierek, M. Hulstein, W. Hagen and S. P. J. Albracht, *Eur. J. Biochem.*, 1998, **258**, 572.
14 I. Dance, unpublished results.
15 I. G. Dance, in *Transition Metal Sulfur Chemistry: Biological and Industrial Significance*, ed. E. I. Stiefel and K. Matsumoto, American Chemical Society, Washington DC, USA, 1996, pp. 135–152.
16 I. G. Dance, *J. Biol. Inorg. Chem.*, 1996, **1**, 581.
17 I. Dance, *Chem. Commun.*, 1998, 523.
18 J. W. Peters, personal communication, 1999.

Communication 9/03803E

Hydrodechlorination of chlorinated hydrocarbons over metal–carbon composite catalysts prepared by a modified carbothermal reduction method

N. Lingaiah, Md. A. Uddin, A. Muto and Yusaku Sakata*

Department of Applied Chemistry, Faculty of Engineering, Okayama University, Okayama, 700-8530, Japan. E-mail: yssakata@cc.okayama-u.ac.jp

Received (in Cambridge, UK) 25th May 1999, Accepted 19th July 1999

A highly stable and active Pd–Fe carbon composite catalyst system for hydrodechlorination of chlrohydrocarbons is obtained by a novel modified carbothermal reduction method using ion exchange resins.

Chlorinated hydrocarbons are one of the most widespread and persistent toxic pollutants. The disposal of these organic wastes is a vital environmental issue. Among the several methods proposed for their destruction, catalytic hydrodechlorination (HDC) is of increasing interest because it excludes the formation of more toxic compounds such as dioxins and has a comparatively low reaction temperature.[1–3] Noble metals are the catalysts of choice for this reaction, which is carried out in either the liquid or the gas phase. Chlorobenzene is usually studied as a model compound for the HDC reaction since it represents the halogen species found in many organic wastes. Deactivation of the catalyst by HCl produced during the reaction is a commonly encountered problem.[4] The development of highly stable and active catalysts for this reaction remains as a challenging task. Recently, more attention has been focused on bimetallic catalysts over monometallic catalysts in order to improve longevity and activity.[5] However, it has been reported that the use of bimetallic catalysts instead of monometalic ones can result in a decrease of HDC activity.[6]

In this work we report for first time the preparation of Pd and Pd–Fe carbon composite catalysts by a novel modified carbothermal reduction (CTR) method, and their activity in chlorobenzene HDC. We have been developing a modified carbothermal reduction (CTR) method to prepare highly dispersed and thermally stable metal or metal compound-based carbon composite catalysts.[7] In the CTR process, first an organic ion exchange resin is exchanged with the required metal ions, followed by thermal treatment in the temperature range 500–800 °C. Since the metallic ions adsorbed on the resin are highly dispersed, the catalysts prepared by this method are highly dispersed.

In the preparation of the catalysts, first the required amounts of aqueous solutions of Pd and Fe ($PdCl_2$ and $Fe(NO_3)_3$ precursors used respectively) were added to a commercial chelate type of ion exchange resin (spherical granules) under constant stirring with a magnetic rod. The stirring was continued for about six hours then the solution was filtered and the metal exchanged resin dried at room temperature for about 12 h. The dried samples were then subjected to carbothermal reduction at 800 °C in an N_2 flow (300 ml min^{-1}) for 3 h. After CTR the catalysts retained their spherical shape but were reduced in size.

The catalyst tests were performed in a fixed bed microreactor at atmospheric pressure as described elsewhere.[8]

The physical characteristics of the catalysts along with their compositions are shown in Table 1, which shows that the surface areas and pore volumes are increased in the bimetallic catalysts in comparison with the corresponding monometallic catalysts. In monometallic catalysts pore blocking due to segregation during the CTR process might be the cause of the decrease in these values. The presence of Fe in the bimetallic catalysts may result in a reduction of the Pd segregation.

The XRD pattern of monometallic Pd/C shows peaks arising from metallic Pd. In bimetallic catalysts, the addition of more iron leads to the formation of Fe_3C. In the monometallic Fe/C catalyst, most of the iron exists as Fe_3C.

The HDC of chlorobenzene over mono- (Pd, Fe) and bimetallic (Pd–Fe/C) catalysts resulted in the formation of benzene as the only organic product. Percentage conversion values obtained after the catalysts reached steady state conditions at a reaction temperature of 150 °C are presented in Fig. 1. Note that the monometallic Pd/C catalyst shows very low activity at steady state conditions. The Fe/C catalyst does not show any activity in this reaction. In the bimetallic Pd–Fe/C catalysts the addition of Fe to Pd leads to a substantial increase in the activity, even though Fe is inactive for this reaction. The increased activity of the bimetallic catalysts relative to the monometallic catalysts is in contrast to earlier findings, where a decrease in activity in the cases of bimetallic Pd–Sn, Pd–Rh and Pd–Fe catalysts due to the second metal diluting the catalyst surface was reported.[6,9]

Preparation by the CTR method may result in a different morphology of the catalyst surface. SEM–EDX images of Pd and Fe for a cross-sectional view of a cylindrical granule of the bimetallic 2Pd–2Fe/C catalyst are shown in Fig. 2. It can be seen from Fig. 2(a) that the majority of the Pd is present on the surface whereas most of the iron [Fig. 2(b)] is dispersed inside the catalyst particle. During the CTR the Pd might be

Table 1 Physical characteristics of the mono- and bimetallic Pd–Fe carbon composite catalysts

Catalyst code	Fe content/ g g_{cat}^{-1}	Pd content/ g g_{cat}^{-1}	S_{BET}/m^2 g^{-1}	V_p/ml g_{cat}^{-1}	XRD Peak
2Pd	0	0.069	140	0.071	Fe, Fe_3C
4Pd	0	0.11	209	0.149	Pd
2Pd2Fe	0.036	0.068	331	0.331	Pd
2Pd4Fe	0.079	0.06	333	0.334	Pd
2Pd8Fe	0.111	0.054	370	0.377	Pd, Fe, Fe_3C
2Fe	0.29	0	200	0.327	Pd, Fe, Fe_3C

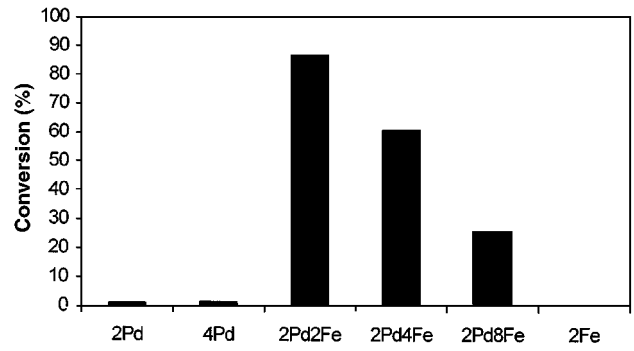

Fig. 1 Hydrodechlorination of chlorobenzene on monometallic Pd and Fe and bimetallic Pd–Fe carbon composite catalysts (reaction temperature: 150 °C; space velocity: 7680 h^{-1}).

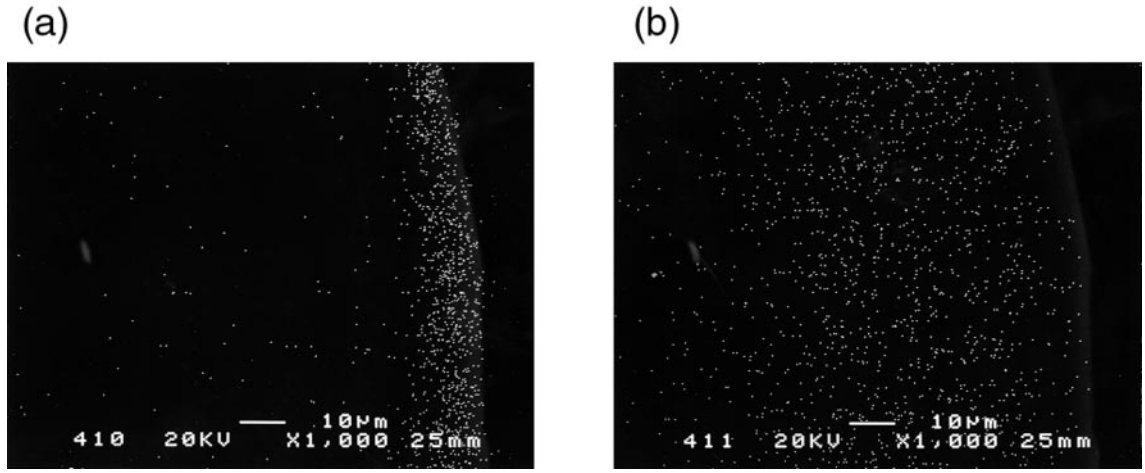

Fig. 2 SEM-EDX images of a cross-sectional view of a spherical granule of the 2Pd–2Fe/C catalyst [(a): EDX of Pd; (b): EDX of Fe].

transported to the surface. Similar behavior has been observed for other bimetallic catalysts.

Wunder and Phillips,[10] in their studies on Pd–Fe supported on graphite, proposed that the iron exists on the surface and the Pd in the bulk. In conventional methods of preparation the iron is present initially as hematite which is later reduced to magnetite and metallic iron during the catalyst runs. During this process most of the iron migrates to the surface.

The TEM data show that in the case of the monometallic Pd/C catalyst the Pd forms large clusters (particle size about 56 nm). The low values of BET surface area and pore volume also suggest the aggregation of Pd. TEM of the bimetallic 2Pd2Fe/C catalyst depicts highly dispersed small particles (about 14 nm) of the bimetallic ensembles. The surface migration of Pd and the formation of small Pd–Fe bimetallic particles may be responsible for the substantial increase in activity in the bimetallic catalysts.

Upon the addition of more Fe to Pd a decrease in activity in the conversion of chlorobenzene was observed. In the high Fe containing catalyst 2Pd–8Fe/C it also observed from SEM–EDX of Pd and Fe that the Pd is present on the surface, similar to other catalysts, but the density of Fe in the catalyst is high, diluting the Pd. Another reason for the low activity reported earlier is that the less active metal Fe, which is present in large amounts, migrates to the surface in the HCl atmosphere generated during the reaction.[6]

Comparisons were made of the highly active 2Pd–2Fe/C catalyst with a catalyst prepared by a conventional impregnation method, with a similar composition, on carbon. The results show that the bimetallic catalyst prepared by modified CTR method possesses higher activity (87% conversion) than the catalyst prepared by the the conventional method (53% conversion).

The advantage of the CTR method over conventional methods of preparation for carbon based catalysts is that the metal ions are well dispersed on the ion exchange resin and this leads to the formation of bimetallic ensembles from a single step, whereas in conventional methods there is a need for separate treatments to obtain the bimetallic ensembles.

This method of preparation can be applied to the preparation of a variety of mono- and bimetallic carbon composite catalysts with varying metal contents.

Time on stream analysis results for 2Pd/C and 2Pd–2Fe/C catalysts, at a reaction temperature of 200 °C, are shown in Fig. 3. It can be seen that the activity of monometallic 2Pd/C steadily decreased with time, whereas the bimetallic 2Pd–2Fe/C catalyst exhibited fairly constant conversion throughout the period of study. The bimetallic catalysts prepared by the modified CTR method revealed high activity with higher stability in the HDC reaction.

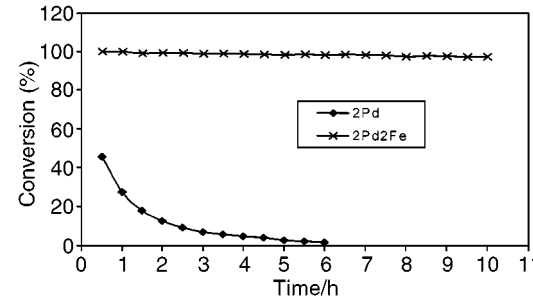

Fig. 3 Hydrodechlorination of chlorobenzene: time on stream analysis (reaction temp: 200 °C; space velocity: 7680 h^{-1}).

Notes and references

1 E. N. Balko, E. Zybylski and F. Von Trentini, *Appl. Catal. B.*, 1993, **2**, 1.
2 F. Gioia, E. J. Gallagher and V. Familetti, *J. Haz. Mater.*, 1994, **38**, 277.
3 A. Gampine and D. P. Eyman, *J. Catal.*, 1998, **179**, 315.
4 B. Coq, G. Ferrato and F. Figueras, *J. Catal.*, 1986, **101**, 434.
5 A. G. Fendler, D. Richard and P. Gallezot, *Stud. Surf. Sci. Catal.*, 1998, **41**, 171.
6 P. Bodnaviuk, B. Coq, G. Ferrato and F. Figueras, *J.Catal.*, 1989, **116,** 459.
7 Y. Sakata, A. Muto, Md. Azhar Uddin and K. Harino, *J. Mater. Chem.*, 1996, **6**, 1241.
8 P. S. Sai Prasad, N. Lingaiah, P. Kanta Rao, F. J. Berry and L. Smart, *Catal. Lett.*, 1995, **35**, 345.
9 N. Lingaiah, Ph.D thesis, Osmania University, Hyderabad, India, 1995
10 R. W. Wunder and J. Phillips, *J. Phys. Chem.*, 1996, **100**, 14 430.

Communication 9/04170B

Synthesis and crystal structure of $Li[\{Ca_7(\mu_3\text{-}OH)_8I_6(thf)_{12}\}_2(\mu\text{-}I)]\cdot 3THF$, a unique H-bound dimer of a Ca_7-cluster on the way to sol–gels

Katharina M. Fromm*

University of Geneva, Sciences II, 30, Quai Ernest-Ansermet, CH-1211 Geneva 4, Switzerland.
E-mail: Katharina.Fromm@chiam.unige.ch

Received (in Cambridge, UK) 8th June 1999, Accepted 23rd July 1999

In analogy to transition metal clusters, a mixed ligand Ca-cluster, consisting of two Ca_7-units linked *via* H-bonds, has been synthesised and structurally characterised, its thermal decomposition leading to the formation of sol–gels is also described.

In recent years, alkaline earth metal compounds have been increasingly studied owing to their application in different research fields, especially in the search for new precursors for superconductors and complex metal oxides. In this context, inorganic polymers of different dimensionality have been structurally characterised.[1] Furthermore, the synthesis of alkaline earth metal alkoxides has led to higher aggregated cage compounds such as the dimer $[IBa(BHT)(THF)_3]_2\cdot 2THF$,[2] (BHT = $OC_6H_2Bu^t_2$-2,6-Me-4), the cubane like compounds $[Ba(\mu_3\text{-}OBu^t)(OBu^t)(Bu^tOH)_2]_4$,[3] and $[Mg_4(\mu_3\text{-}OMe)_4(OMe)_4(MeOH)_8]$,[4] the large cluster $[Ca_9(OCH_2CH_2OMe)_{18}(HOCH_2CH_2OMe)_2]$[5] or the CO_3^{2-}-insertion product $[Mg_9(\mu_5\text{-}CO_3)(O_2COMe)_8(\mu_3\text{-}OMe)_8(MeOH)_{13}]\cdot MeOH\cdot C_7H_8$.[6] Anionic N-donor ligands also yield clusters such as the THF-solvated hexamer $[(THF)MgNPh]_6$[7] or the solvent free cubane $[BaNP(NMe_2)_2NP(NMe_2)_2NSiMe_3]_4$.[8] The presence of alkoxy- or N-donor-groups and the resulting possibility of oxolation, that is the formation of oxygen bridges by hydrolysis, makes them potential precursors for sol–gel synthesis.

This work reports on the synthesis of a Ca_7-cluster forming dimers by hydrogen bonding [eqn. (1)].

$$CaI_2 + (Bu^nLi)_{1.1}(LiOH) \xrightarrow{THF,\ -(Bu^nLi)_m(LiI)_n} Li[\{Ca_7(\mu_3\text{-}OH)_8I_6(thf)_{12}\}_2(\mu\text{-}I)]\cdot 3THF \quad \mathbf{1} \quad (1)$$

The reaction of CaI_2 in THF with a hexane solution containing Bu^nLi and LiOH yields the ionic cage compound $Li[\{Ca_7(\mu_3\text{-}OH)_8I_6(THF)_{12}\}_2(\mu\text{-}I)]\cdot 3THF$ **1**.† Colorless prismatic crystals suitable for single crystal analysis which crystallise in the trigonal space group $R(\bar{3})$ (No. 148) were obtained by cooling a THF solution to –20 °C.‡ Attempts to synthesise **1** from the reaction of CaI_2 with LiOH failed probably owing to the stability and low solubility of the latter in THF. However, it has been shown that some mixed-anion compounds $(RLi)_m(XLi)_n$ (R = alkyl; X = halide, hydroxide or alkoxide) are synthetically useful reagents owing to their enhanced reactivity compared to the pure components RLi or XLi.[9] In the synthesis of **1**, partial hydrolysis of a Bu^nLi solution obviously leads to a soluble mixed-anion compound which was titrated to be 1.1 M in Bu^nLi and 1 M in LiOH. With this reagent, the synthesis of **1** is reproducible with yields of up to 87%. Addition of further equivalents of $(Bu^nLi)_m(LiOH)_n$, leads to the formation of sol–gels, fewer equivalents lower the yield of **1**.

This cluster compound is synthesised in a similar way as for transition metal clusters. For the latter, a reaction scheme includes, for instance, a metal chloride as metal source, a chalcogenide reagent such as $Se(SiMe_3)_2$ and a ligand compound to protect the outer cluster sphere, the driving force being the formation of a stable, volatile side product $SiMe_3Cl$. For **1**, CaI_2 is used as the metal source with $(Bu^nLi)_m(LiOH)_n$ as the reagent to form LiI and also as bridging ligand source. LiI is partially included in the structure of **1**. The ligands which complete the outer coordination sphere are provided by THF and part of the iodide. Unreacted Bu^nLi and LiI remain in solution, mainly forming the species $(Bu^nLi)_1(LiI)_1$ as determined by titration.

The molecule consists of two neutral Ca_7-clusters of composition $[Ca_7(\mu_3\text{-}OH)_8I_6(THF)_{12}]$ **1a**, linked together by μ-bridging iodide ions which form hydrogen bonds to an OH-group of each cluster unit (Fig. 1). To the best of the author's knowledge, this structural feature is unique for an alkaline earth metal cluster compound with mixed ligands.

The structure of the Ca_7-subunits can be described as two $(Ca–O)_4$ heterocubanes sharing a vertex or as a body-centered Ca-icosahedron with the outer six-membered Ca-ring missing. An alternative description is that of two Ca_4-tetrahedra sharing a vertex, each of the eight triangular faces of the two tetrahedra being μ_3-bridged by a hydroxy anion. The central calcium atom

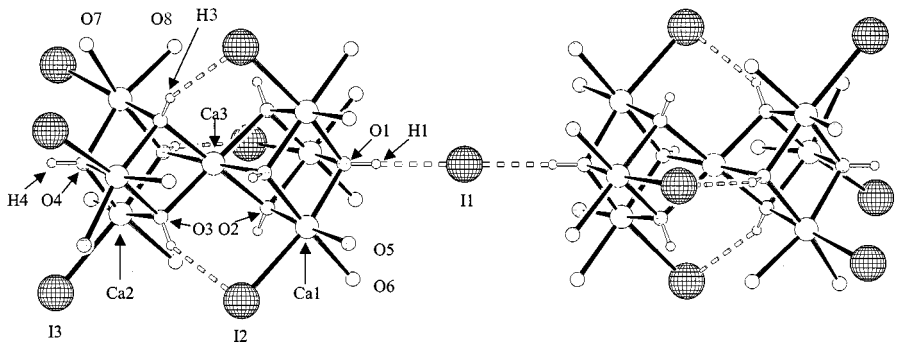

Fig. 1 Crystal structure of **1** along the horizontal C_3 axis passing through Ca3, O1, H1 and I1. Selected bond lengths (Å) and angles (°): Ca1–I2 3.151(1), Ca2–I3 3.147(1), Ca1–O2 2.312(5), Ca1–O1 2.354(4), Ca1–O5 2.413(6), Ca1–O6 2.411(6), Ca1–Ca3 3.557(2), Ca1–Ca1 3.592(3), Ca2–O3 2.322(5), Ca2–O4 2.346(4), Ca2–O8 2.425(7), Ca2–O7 2.438(7), Ca2–Ca3 3.553(3), Ca2–Ca2 3.595(3), Ca3–O3 2.365(5), Ca3–O2 2.388(5), H1–I1 2.68(2), H3–I2 2.87(7); I2–Ca1–Ca3 87.17(5), I2–Ca1–Ca1 131.40(5)–133.93(5), I3–Ca2–Ca3 145.59(6), I3–Ca2–Ca2 100.69(6)–138.28(4), Ca3–Ca1–Ca1 59.68(3), Ca1–Ca1–Ca1 (Ca2–Ca2–Ca2) 60.0, Ca3–Ca2–Ca2 59.61(3), Ca2–Ca3–Ca2 60.77(6), Ca1–Ca3–Ca2 178.87(4), O1–H1–I1 180, O3–H3–I2 149.12.

Ca3 is placed on a three fold axis (0, 0, *z*; *c*) and features an octahedral coordination sphere of six OH-groups as next neighbours. At a longer distance range, it is surrounded by six Ca-atoms, Ca1, Ca2 and their symmetry equivalents, in form of a trigonal antiprism. The Ca–Ca-distances within the tetrahedra lie between 3.553(3) and 3.594(3) Å. Ca1 and Ca2 of the Ca_7-cluster also reach coordination number six, their coordination spheres being completed by three terminal ligands, two THF molecules and one iodide anion per calcium. The Ca–I distances are 3.154(2) Å (Ca1-I2) and 3.147(2) Å (Ca2-I3) and thus only slightly longer than in $CaI_2(THF)_4$ [Ca–I 3.106(2) Å] or ICa(clox)$(THF)_4$ [Ca–I 3.108(3) Å; clox = $OCPh_2CH_2C_6H_4Cl$-4],[2] and correspond to the sum of the Shannon ionic radii [Ca^{2+}(coord. 6) 1.00 Å, I^- 2.20 Å].[10] Ca–O bond lengths to the terminally bound THF-molecules in the range of 2.414(6) to 2.433(7) Å are observed, corresponding to literature data [Ca–O(THF) 2.33–2.454 Å].[2] The Ca–O(OH) distances can be divided into the shorter Ca–O bond lengths Ca1–O and Ca2–O and their symmetry equivalents [2.312(5)–2.354(4) Å] and the longer Ca–O bond lengths of the central Ca3-atom to the hydroxy groups [2.366(5)–2.393(5) Å]. They correspond, on average, to the Shannon ionic radii sum (2.35 Å). The hydroxy groups act as μ_3-ligands.

The threefold axis through Ca3 also passes through O4 and O1 (0, 0, *z*; *c*) and the μ-iodide ligand I1 which, additionally, is placed on an inversion center (0, 0, 0; *a*). Hydrogen bonding occurs along this threefold axis between the two Ca_7-clusters [I1–O1 3.682(6) Å, I1–H1 2.70(7) Å; H–I–H 180° (due to symmetry).] Other H-bonds are formed within the Ca_7-cluster between I2 and H3 [2.89(6) Å], slightly longer than that above as is also the case for the corresponding I2–O3 distance [3.771(6) Å] and the O3–H3–I2 angle is bent to 149.26°. H–I-hydrogen bonds described in the literature are of the same order of magnitude, such as in [*trans*-$(py)_4Mg(OH_2)_2]I_2\cdot$2py with I–O(H) 3.438(7)–3.669(9) Å (2.4–2.7 Å),[11] or in [$Mg(HOMe)_6]I_2\cdot$2tmeda with I–O 3.377(5)-4.209(5) Å and [(tmeda)$SrI_2(HOMe)_3]\cdot$0.5tmeda with I–O(H) 3.516(9)–3.555(7) Å (2.5–3.0 Å).[12] The IR spectrum of **1** in Nujol on CsI plates shows a sharp band for free OH at 3640 cm^{-1} (O4–H4, O2–H2), along with broader bands at 3550, 3300 and 3200 cm^{-1}, indicating hydrogen bonding.

μ_3-Capped Ca_3-triangles as in **1** can be found in the alkoxide aggregate $[Ca_9(OCH_2CH_2OMe)_{18}(HOCH_2CH_2OMe)_2]$[5] in which the coplanar Ca-atoms occupy octahedral holes between two close-packed oxygen layers. A similar tetrahedral feature as in the building units for **1** was found in [Ba(μ$_3$-OBu^t)(OBu^t)(Bu^{t}OH)$_2$]$_4$,[3] where the tetrahedron is formed by Ba-atoms, and the triangle capping OH-groups are formally replaced by OBu^t. The same ligand (OBu^t and Bu^{t}OH) acts as a terminal ligand on the alkaline earth metal, whereas in **1**, different ligands are found on almost every position. Another tetrahedrally built compound is the solvent free [{BaNP(NMe$_2$)$_2$NP(NMe$_2$)$_2$NSiMe$_3$}$_4$] which consists of a RN-capped Ba-tetrahedron and forms, on hydrolysis, a white gel of composition $Ba(OH)_2\cdot xH_2O$. **1** is soluble in THF or other solvents and may also act as a precursor for sol–gels. The capping hydroxy groups can undergo elimination of water with the hydroxy groups of neighbouring cluster molecules, forming oxo bridges between the clusters. This oxolation leads to gels in the classical way. Isolated and washed crystals of **1** decompose in THF after heating to form a white gel. Furthermore, the crystals lose solvent after a short period of time, and thermal treatment (DTA and thermogravimetry) shows the elimination of all the THF at 70 °C followed by water at 110 °C. Other polymerisation mechanisms are envisageable, such as elimination of terminally bound THF and saturation of the thus empty coordination site on calcium by a terminal iodide ligand of a neighbouring molecule to yield a μ-I-bridge, or elimination of iodide by addition of an excess of Bu^{n}Li. Further investigations on the use of **1** as a sol–gel precursor are under way.

This work was financed by the Swiss National Foundation and the University of Geneva. I am grateful to Professor A. F. Williams for his support, Dr H. Goesmann, University of Karlsruhe, Germany and Dr G. Bernardinelli, University of Geneva, for reflection data collection, H. Lartigue for DTA and thermogravimetric measurements, E. Rivara-Minten for ^{7}Li-NMR and M. Martin, University of Geneva, for ICP-MS measurements.

Notes and references

† CaI_2 was dried under vacuum at 200 °C and the reaction carried out under nitrogen atmosphere. The solution of (Bu^{n}Li)$_m$(LiOH)$_n$ in hexane was obtained by partial hydrolysis of a commercially available, upconcentrated 2.1 M solution of Bu^{n}Li in hexane. A Gilman's titration of the solution revealed concentrations of 1.1 M in Bu^{n}Li and 1 M in LiOH.

0.45 g (1.53 mmol) of CaI_2 were dissolved in 20 ml freshly dried and distilled THF to give a light yellow solution. At room temperature, 1.4 ml of a hexane solution containing 1.1 M Bu^{n}Li (1.54 mmol) and 1 M LiOH (1.4 mmol) was added dropwise to the stirred solution. After two days at room temperature, the colorless solution was cooled to −25 °C to give colorless crystals of **1** within 24 h. Yield: 87% (for CaI_2). Satisfactory analysis for Ca, I, C and H. The presence of Li in **1** was determined by ICP-MS and ^{7}Li NMR, giving a signal at δ 1.83 in d_8-THF (LiCl in D_2O as standard). IR (CsI, Nujol) (cm^{-1}): 3640m, 3550s, 3300s, 3200s, 2900vs (Nujol), 1500vs (Nujol), 1370s (Nujol), 1340s (Nujol), 1290s, 1240s, 1180vs, 1050vs, 910vs, 665vs, 575s, 360s, 280m, 240m.

‡ *Single crystal data* for **1**: $C_{112}H_{240}O_{44}LiCa_{14}I_{13}$, M = 4508.90, rhombohedral, space group $R\bar{3}$ (No. 148), a = 21.592(3), c = 36.839(7) Å, V = 14874(4) Å^3, Z = 6, D_c = 1.521 Mg m^{-3}, $F(000)$ = 6723, T = 200 K, λ = 0.71073 Å, μ(Mo-Kα) = 2.450 mm^{-1}, 4.5 < 2θ < 53.86°, 7166 reflections of which 7166 unique and 7161 observed, 296 parameters refined, GOF (on F^2) = 1.026, $R1$ = 0.065, $wR2$ = 0.1677 for $I > 2\sigma(I)$ and $R1$ = 0.1190, $wR2$ = 0.2061 for all data.

Crystals of **1** were measured on an ENRAF-NONIUS four-circle diffractometer at 200 K. The data collection was performed on a crystal of 0.2 × 0.15 × 0.08 mm and an absorption correction was applied by analytical integration. The structure was solved with direct methods and refined by full matrix least squares on F^2 with the SHELX-97 package.[13] Slight disorder was observed for the THF molecules bound to Ca, while severe disorder was observed for the free solvent. All heavy atoms of the cluster could be refined anisotropically. Owing to the presence of heavy atoms such as iodine, the positions of the hydrogen atoms could not be determined and were thus calculated. The Li cation could not be localised in the single crystal structure due to the fact that it is either placed on a special position with a site occupation factor of 1/3 or else disordered, probably coordinated to some free THF. However, the presence of lithium was established by inductively coupled plasma mass spectrometry analysis (ICP-MS Hewlett Packard 4500) of isolated and washed single crystals which were dissolved in dilute HNO_3. CCDC 182/1345. See http://www.rsc.org/suppdata/cc/1999/1659/ for crystallographic files in .cif format.

1 K. M. Fromm, *Angew. Chem.*, 1997, **109**, 2876; *Angew. Chem., Int. Ed. Engl.*, 1997, **36**, 2799.
2 K. F. Tesh, D. J. Burkey and T. P. Hanusa, *J. Am. Chem. Soc.*, 1994, **116**, 2409.
3 B. Borup, J. A. Samuels, W. E. Streib and K. G. Caulton, *Inorg. Chem.*, 1994, **33**, 994.
4 Z. A. Starikova, A. I. Yanovsky, E. P. Turevskaya and N. Ya. Turova, *Polyhedron*, 1997, **16**, 967.
5 S. C. Goel, M. A. Matchett, M. Y. Chiang and W. E. Buhro, *J. Am. Chem. Soc.*, 1991, **113**, 1844.
6 V. C. Arunasalam, I. Baxter, J. A. Darr, S. R. Drake, M. B. Hursthouse, K. M. Abdul Malik and D. M. P. Mingos, *Polyhedron*, 1998, **17**, 5; 641.
7 T. Hascall, K. Ruhlandt-Senge and P. P. Power, *Angew. Chem.*, 1994, **106**, 350; *Angew. Chem., Int. Ed. Engl.*, 1994, **33**, 356; W. J. Grigsby, T. Hascall, J. J. Ellison, M. M. Olmstead and P. P. Power, *Inorg. Chem.*, 1996, **35**, 3254.
8 S. K. Pandey, A. Steiner, H. W. Roesky and D. Stalke, *Angew. Chem.*, 1993, **105**, 625; *Angew. Chem., Int. Ed. Engl.*, 1993, **32**, 596.
9 C. Lambert, F. Hampel, P. von Ragué Schleyer, M. G. Davidson and R. Snaith, *J. Organomet. Chem.*, 1995, **487**, 139 and references therein.
10 R. D. Shannon, *Acta Crystallogr., Sect. A.*, 1976, **32**, 751.
11 D. L. Kepert, B. W. Skelton, A. F. Waters and A. H. White, *Aust. J. Chem.*, 1996, **49**, 47.
12 A. F. Waters and A. H. White, *Aust. J. Chem.*, 1996, **49**, 87.
13 G. M. Sheldrick, SHELX-97, University of Göttingen, Göttingen, 1997.

Communication 9/04560K

Novel columnar mesogen with octupolar optical nonlinearities: synthesis, mesogenic behavior and multiphoton-fluorescence-free hyperpolarizabilities of subphthalocyanines with long aliphatic chains†

Seok Ho Kang,[a] Yoon-Sok Kang,[b] Wang-Cheol Zin,[b] Geert Olbrechts,[c] Kurt Wostyn,[c] Koen Clays,*[c] Andre Persoons[c] and Kimoon Kim*[a]

[a] *National Creative Research Initiative Center for Smart Supramolecules, Department of Chemistry, Pohang University of Science and Technology, San 31 Hyojadong, Pohang 790-784, South Korea. E-mail: kkim@postech.ac.kr*

[b] *Department of Materials Science and Engineering, Pohang University of Science and Technology, San 31 Hyojadong, Pohang 790-784, South Korea*

[c] *Laboratory of Chemical and Biological Dynamics, Center for Research on Molecular Electronics and Photonics, Department of Chemistry, University of Leuven, Celestijnenlaan 200D, B-3001 Leuven, Belgium. E-mail: koen.clays@fys.kuleuven.ac.be*

Received (in Cambridge, UK) 26th May 1999, Accepted 19th July 1999

Novel subphthalocyanines with long thioalkyl chains exhibit hexagonal columnar mesophases at room temperature; their inherent first hyperpolarizability values (β) measured by hyper-Rayleigh scattering (HRS) with fluorescence suppression are (189 ± 30) × 10^{-30} esu at 1300 nm.

The unique supramolecular architectures of the columnar mesophases[1] have many potential applications in molecular devices.[2] Among columnar liquid crystals, bowl-shaped liquid crystals[3] have attracted considerable attention as potential ferroelectric and/or second-order nonlinear optical (NLO) materials because of their polar organization in the liquid crystalline phases.

Subphthalocyanines (SubPcs) are cone-shaped macrocycles composed of three isoindoline units with a boron inside.[4] They have been used as intermediates for the synthesis of unsymmetrical phthalocyanine (Pc) derivatives.[5] Furthermore, their unique 14 electron π-conjugated system with C_3 symmetry allows them to exhibit large molecular hyperpolarizabilities, mainly due to octupolar contributions.[6]

In our efforts to discover new columnar liquid crystals,[7] we became interested in SubPcs as potential columnar mesogens with NLO properties. Although liquid crystalline Pcs have been studied extensively,[8] there is no report on SubPc derivatives exhibiting liquid crystalline phases. Herein we report syntheses and mesogenic behavior of SubPcs containing long thioalkyl chains. Since molecular hyperpolarizabilities of SubPcs have been overestimated due to their strong fluorescence,[6a] here we also report their hyperpolarizabilities measured by hyper-Rayleigh scattering (HRS) using flurorescence suppression techniques.[9]

Subphthalocyanines containing thioalkyl groups **2a**–**d** were synthesized in two steps as shown in Scheme 1. Reaction of 1,2-dichloro-4,5-dicyanobenzene with alkanethiols ($C_nH_{2n+1}SH$; n = 10, 12, 16 and 18) yields 4,5-bis(alkylthio)phthalonitrile, cyclotrimerization of which in the presence of BCl_3 produces the desired products.‡

SubPcs **2a**–**d** show enantiotropic liquid crystalline behavior as revealed by differential scanning calorimetry (DSC), polarizing optical microscopy, and X-ray diffraction. The phase behavior of these compounds is summarized in Table 1. Compounds **2a** (n = 10) and **2b** (n = 12) exhibit mesomorphic behavior at room temperature. Upon heating, the transition from mesophase to isotropic liquid occurs at 90.9 and 86.1 °C for **2a** and **2b**, respectively. For these compounds, melting or crystallization peaks are not observed in the DSC scan, even down to −40 °C. As usual, the melting temperature increases while the clearing point decreases with increasing side chain length. For example, **2c** (n = 16) shows a phase transition from crystalline to mesophase near room temperature and transforms into an isotropic liquid at 75 °C. Furthermore, **2d** (n = 18) is a solid at room temperature and melts at 43 °C to form a mesophase which turns into an isotropic liquid phase at 70 °C. These compounds have good thermal stability as they decompose above 250 °C.

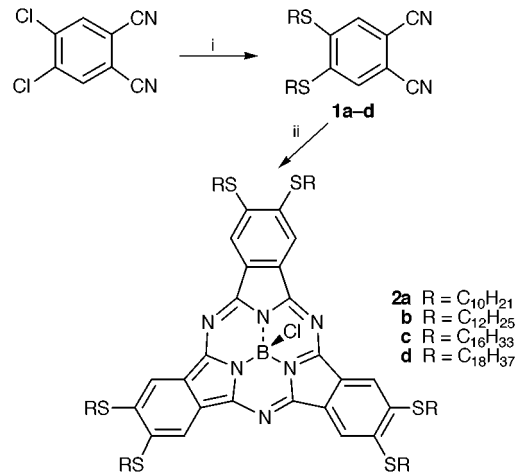

Scheme 1 *Reagents and conditions*: i, RSH, K_2CO_3, DMSO; ii, BCl_3, 1-chloronaphthalene.

Table 1 Optical and thermal properties of the compounds **2a**–**d**[a]

	T/°C (ΔH/J g^{-1})	
Compound	Heating	Cooling
2a (n = 10)	D_{hd} 90.9 (0.29) I	I 79.6 (0.28) D_{hd}
2b (n = 12)	D_{hd} 86.1 (0.68) I	I 70.5 (1.31) D_{hd}
2c (n = 16)	K 27.2 (13.42) D_{hd} 75.3 (0.35) I	I 67.6 (0.61) D_{hd} 20.9 (10.36) K
2d (n = 18)	K 43.4 (21.80) D_{hd} 70[b] I	I 63[b] D_{hd} 36.6 (0.53) K 33.6 (9.56) K′

[a] Transition temperatures and enthalpies of transition were determined by DSC (scan rate 10 °C min^{-1}). K, K′ = crystalline phase; D_{hd} = hexagonal columnar phase; I = isotropic phase. [b] Transition observed only by microscopy.

† Experimental and spectral data for **2a**–**d** are available from the RSC web site, see http://www.rsc.org/suppdata/cc/1999/1661/

In polarizing optical microscopy, **2a**–**d** in mesophases exhibit pseudo-focal conic textures, which are characteristic of columnar mesophases. Except for **2d**, these textures are maintained at room temperature, demonstrating the stability of the liquid crystalline phases at room temperature. To obtain information on the structures of **2a**–**d** in the mesophases, X-ray diffraction studies were carried out using synchrotron radiation. The X-ray pattern (Fig. 1) of the mesophase of **2c** at room temperature shows an intense peak and two weak peaks in the small-angle region with reciprocal Bragg spacings in a ratio $1:\sqrt{3}:2$. These peaks were assigned to the (100), (110) and (200) reflections of a hexagonal arrangement with a lattice constant a = 33.02 Å. In the wide-angle region a broad halo at 4.43 Å is observed, which is related to the liquid-like correlations between the molten aliphatic chains. Similar X-ray diffraction patterns are observed for other compounds in their mesophases. It is not clear how the cone-shaped molecules are arranged in the mesophase. However, as previously suggested in bowl-shaped mesogens, the cones may be stacked in a head-to-tail fashion to form a polar column which in turn forms a hexagonal array with random polarity.

We measured the molecular first hyperpolarizabilities (β) of **2a**–**c** using HRS techniques.[10] Regardless of the alkyl chain length these compounds have a strong absorption band at ~602 nm and an intense emission at ~612 nm. Since they are highly fluorescent, high-frequency demodulation of multiphoton fluorescence was used to retrieve their fluorescence-free first hyperpolarizability values. A detailed description of the experimental set-up is given elsewhere.[9a] The measurements were performed in $CHCl_3$ solution. Disperse Red 1 was used as the external reference with $\beta = 54 \times 10^{-30}$ esu at 1300 nm.[9c] The inherent fluorescence-free first hyperpolarizability values for **2a**–**c** are the same within the experimental uncertainties: $(189 \pm 30) \times 10^{-30}$ esu at 1300 nm. Using a three-level model,[11] the dispersion-free β value (β_0) was calculated to be $(21 \pm 3) \times 10^{-30}$ esu. These results are in good agreement with the recently reported β value of 40×10^{-30} esu at 1460 nm and β_0 value of 10×10^{-30} esu for a similar SubPc compound.[6b]

In summary, we have synthesized liquid crystalline SubPcs exhibiting hexagonal columnar mesophases at room temperature. Since they are highly fluorescent, their inherent first hyperpolarizability values were measured by HRS using fluorescence suppression techniques. In the mesophases, the cone-shaped molecules appear to be stacked in a head-to-tail fashion to form a polar column which in turn forms a hexagonal array with random polarity. Despite the nonlinearity/transparency trade-off that appears better for dipolar that for octupolar chromophores,[12] the incorporation of dipolar chromophores into stable macroscopic ensembles has been hampered by strong antiparallel dipolar interactions, leading to centrosymmetric arrangements with zero bulk susceptibility. The polar organization of these SubPcs in the liquid crystalline phase will results in a thermodynamically stable non-zero second order susceptibility. The next challenging goal is to align all the columns with the same polarity to achieve large ferroelectricity and second order bulk susceptibility. We are currently working along this line.

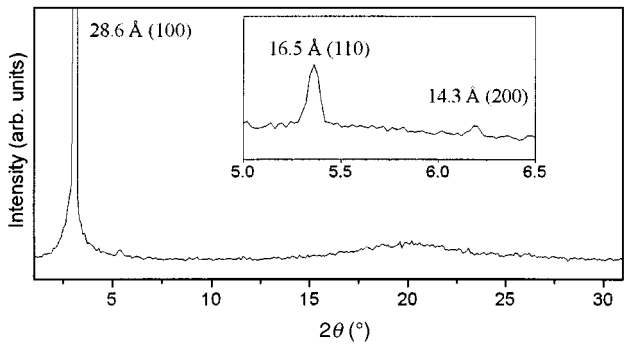

Fig. 1 X-Ray diffraction pattern of **2c** taken at room temperature.

This work was supported by the Creative Research Initiative Program of the Korean Ministry of Science and Technology and by research grants from the Fund for Scientific Research - Flanders (FWO-V) (G.0338.98 and G.0407.98), the Belgian government (IUAP P4/11, 'Supramolecular Chemistry and Supramolecular Catalysis'), the University of Leuven (GOA/95/01). G. O. is a Research Assistant and K. C. is a Senior Research Associate of the FWO-V. The X-ray measurements were performed at the Pohang Accelerator Laboratory (Beamline 3C2).

Notes and references

‡ All the compounds have been fully characterized by ^{1}H NMR, UV-VIS, IR and mass spectrometry and gave satisfactory elemental analyses. *Selected data* for **2a**: Compound **1a** (2.13 g, 4.50 mmol) was dissolved in 1-chloronaphthalene (4 ml) under Ar. After cooling of the solution in an ice bath a solution of BCl_3 (1.5 ml, 1.5 mmol, 1 M solution in *n*-heptane) was added. The mixture was stirred at 0 °C for 10 min and then heated to 100 °C for 4 h. After cooling to room temperature, the mixture was diluted with acetone. The crude product was isolated by filtration and purified by column chromatography on silica gel using CH_2Cl_2 as eluent (0.30 g, 14%); δ_H($CDCl_3$, 300 MHz) 0.88 (t, 18H), 1.59 (m, 84H), 1.89 (m, 12H), 3.31 (m, 12H), 8.51 (s, 6H); δ_C($CDCl_3$, 75 MHz) 14.52, 23.09, 28.86, 29.56, 29.72, 29.74, 29.96, 30.01, 32.31, 34.08, 119.91, 128.69, 141.23, 149.53; ν_{max}(KBr)/cm^{-1} 2955, 2924, 2853, 2360, 2342, 1597, 1462, 1419, 1368, 1080, 979; λ_{max}($CHCl_3$)/nm (log ε) 602 (5.00), 558 (4.50), 415 (4.53), 389 (4.52), 306 (4.85); Fluorescence (excitation was at 360 nm, $CHCl_3$): λ_{max}/nm 613, 504; *m*/*z* (FAB-MS) 1463 $[M+H]^+$ (Calc. for $C_{84}H_{132}BClN_6S_6$: C, 68.88; H, 9.08; N, 5.74. Found: C, 68.48; H, 9.18; N, 5.48%). Compounds **2b**–**d** were synthesized by the same method as **2a**.

1 S. Chandrasekar, in *Advances in Liquid Crystals*, ed. G. H. Brown, Academic Press, New York, vol. 5, 1982; S. Chandrasekar, *Liq. Cryst.*, 1993, **14**, 3.
2 J. Simmerer, B. Glusen, W. Paulus, A. Kettner, P. Schuhmacher, D. Adam, K. H. Etzbach, K. Siemensmeyer, J. H. Wendorff, H. Ringsdorf and D. Haarer, *Adv. Mater.*, 1996, **8**, 815; E. J. Osburn, A. Schmidt, L. K. Chau, S. Y. Chen, P. Smolenyak, N. R. Armstrong and D. F. O'Brian, *Adv. Mater*., 1996, **8**, 815; C.-Y. Liu, H.-L. Pan, M. A. Fox and A. J. Bard, *Science*, 1993, **261**, 897.
3 J. Malthete and A. Collet, *J. Am. Chem. Soc.*, 1987, **109**, 7544; G. Cometti, E. Dalcanale, A. Du vosel and A.-M. Levelut, *J. Chem. Soc., Chem. Commun.*, 1990, 163; J. Malthete, *Adv. Mater*., 1994, **6**, 315; B. Xu and T. M. Swager, *J. Am. Chem. Soc.*, 1993, **115**, 1159; B. Xu and T. M. Swager, *J. Am. Chem. Soc.*, 1995, **117**, 5011.
4 M. Geyer, F. Plenzig, J. Rauschnabel, M. Hanack, B. del Rey, A. Sastre and T. Torres, *Synthesis*, 1996, 1139; N. Kobayashi, *J. Porphyriyns Phthalocyanines*, in the press.
5 N. Kobayashi, R. Kondo, S. Nakajima and T. Osa, *J. Am. Chem. Soc.*, 1990, **112**, 9640; A. Weitemeyer, H. Kliesch and D. Wohrle, *J. Org. Chem.*, 1995, **60**, 4900; A. Sastre, B. del Rey and T. J. Torres, *J. Org. Chem.*, 1996, **61**, 8591.
6 (*a*) A. Sastre, T. Torres, M. A. Diaz-Garcia, F. Agullo-Lopez, C. Dhenaut, S. Brasselet, I. Ledoux and J. Zyss, *J. Am. Chem. Soc.*, 1996, **118**, 2746; (*b*) B. del Rey, U. Keller, T. Torres, G. Rojo, F. Agullo-Lopez, S. Nonell, S. Marti, S. Brasselet, I. Ledoux and J. Zyss, *J. Am. Chem. Soc.*, 1998, **120**, 12 808.
7 S. J. Kim, S. H. Kang, K.-M. Park, H. Kim, W.-C. Zin, M.-G. Choi and K. Kim, *Chem. Mater*., 1998, **10**, 1889; S. H. Kang, M. Kim, H.-K. Lee, Y.-S. Kang, W.-C. Zin and K. Kim, *Chem. Commun.*, 1999, 93.
8 J. Simon and P. Bassoul, in *Phthalocyanines: Properties and Applications*, ed. C. C. Leznoff and A. B. P. Lever, VCH, Weinheim, 1992, vol. 2, ch. 6.
9 (*a*) G. Olbrechts, R. Strobbe, K. Clays and A. Persoons, *Rev. Sci. Instrum.*, 1998, **69**, 2233; (*b*) K. Clays, G. Olbrechts, T. Munters, A. Persoons, O.-K. Kim and L.-S. Choi, *Chem. Phys. Lett.*, 1998, **293**, 337; (*c*) G. Olbrechts, K. Wostyn, K. Clays and A. Persoons, *Opt. Lett.*, 1999, **24**, 403.
10 E. Hendrickx, K. Clays and A. Persoons, *Acc. Chem. Res.*, 1998, **31**, 675.
11 J. Zyss, T. Chauvan, C. Dhenaut and I. Ledoux, *Chem. Phys.*, 1993, **177**, 281.
12 S. Stadler, R. Dietrich, G. Bourhill and Ch. Bräuchle, *Opt. Lett.*, 1996, **21**, 251.

Communication 9/04254G

Highly regio- and enantio-selective rhodium-catalysed asymmetric hydroformylation without organic solvents

Giancarlo Franciò† and Walter Leitner*

Max-Planck-Institut für Kohlenforschung, Kaiser-Wilhelm-Platz 1, 45470 Mülheim an der Ruhr, Germany. E-mail: leitner@mpi-muelheim.mpg.de

Received (in Liverpool, UK) 25th May 1999, Accepted 15th July 1999

High enantioselectivity and unprecedented high regioselectivity without the need for hazardous organic solvents are achieved in rhodium-catalysed asymmetric hydroformylation with the perfluoroalkyl-substituted ligand (*R,S*)-3-H^{2}F^6-BINAPHOS, whereby the substitution pattern of the ligand is crucial for its successful use in compressed carbon dioxide and for the increased regioselectivity.

Asymmetric hydroformylation using chiral transition metal catalysts is an efficient and well established strategy for the synthesis of functionalised non-racemic organic compounds, providing for example viable routes to important anti-inflammatory drugs starting from simple vinyl arenes.[1] The chiral phosphine/phosphite ligand (*R,S*)-BINAPHOS **4a** allows rhodium-catalysed asymmetric hydroformylation of vinyl arenes **1a**–**c** with outstanding levels of enantiocontrol (Scheme 1).[2] However, the regioselectivity towards the chiral branched aldehydes **2a**–**c** is less satisfactory (88% for **2a**) even under carefully optimised conditions, leading to considerable amounts of linear aldehydes **3a**–**c** as undesired by-products. Furthermore, the established protocols require the use of ecologically and toxicologically hazardous organic solvents, especially benzene, representing another major drawback in light of the potential practical application of the methodology.

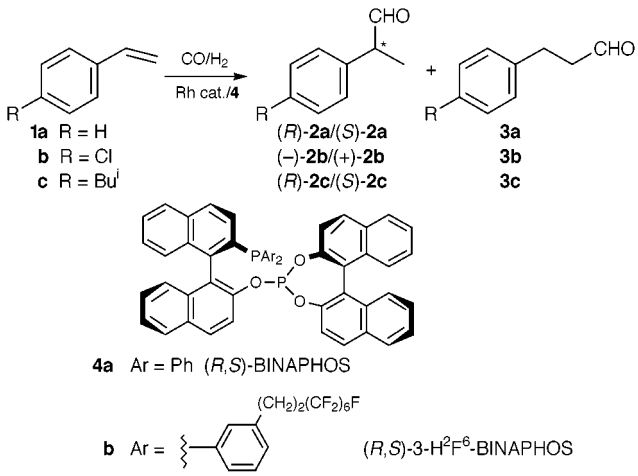

Scheme 1

We now report that the use of the new perfluoroalkyl-substituted derivative (*R,S*)-3-H^{2}F^6-BINAPHOS **4b**[3] allows rhodium-catalysed hydroformylation of vinyl arenes (Scheme 1) to be carried out in compressed (liquid or supercritical) carbon dioxide as a solvent with similar catalytic activity and the same level of enantiocontrol as **4a**, resulting at the same time in unprecedented high regioselectivity for the branched aldehydes. The high regioselectivity originates from the ligand substitution pattern and is retained also during hydroformylations in other solvents or even in the neat substrate.

Supercritical carbon dioxide ($scCO_2$) has gained increasing interest as an environmentally friendly solvent with unique properties for chemical synthesis in general[4] and metal-catalysed reactions in particular.[5] Non-enantioselective hydroformylation has been achieved in $scCO_2$,[6–10] and there are also examples of highly enantioselective catalytic reactions in this medium.[11,12] These promising results encouraged us[9] and others[10c] to apply $scCO_2$ as a reaction medium for asymmetric hydroformylation as well. However, it soon became apparent that **4a** cannot be used efficiently in $scCO_2$, owing to its low solubility in this medium.[9]

We have shown recently that the low solubility of aryl-phosphorous ligands and their metal complexes in $scCO_2$ can be overcome by fixation of perfluoroalkyl substituents $(CH_2)_x(CF_2)_yF$ at the aryl rings.[8a] Following this approach, we set out to synthesise the fluoroalkyl-substituted (*R,S*)-3-H^{2}F^6-BINAPHOS **4b** and its rhodium complex [(**4b**)Rh(acac)] **5b**. The fluoroalkyl substituents were introduced *via* the bisaryl phosphonic acid **7**, which was obtained in a one-pot procedure from the *meta*-substituted aryl bromide **6**[13] (Scheme 2). Crystallisation from pentane provided **7** as a white solid in 63% yield.[14] The remaining route to **4b** was a modified version of the original synthesis of **4a** giving a similar overall yield. The $^{31}P\{^1H\}$ NMR data of the phosphine/phosphite ligand **4b** and its rhodium complex **5b** are almost identical to those reported for the unsubstituted parent compounds **4a** and **5a**.[2,14]

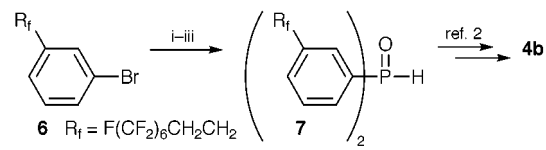

Scheme 2 *Reagents and conditions*: i, BuLi, Et_2O, −30 °C, then 30 min at 0 °C; ii, $(NEt_2)PCl_2$, Et_2O, −30 °C; iii, conc. HCl.

In contrast to **4a**, the perfluoroalkyl-substituted ligand **4b** allows highly efficient asymmetric hydroformylation of styrene **1a** using compressed CO_2 as the reaction medium (Table 1, entries 5–9).‡ The isomer (*R*)-**2a** was formed preferentially with ees between 90 and 94% under various reaction conditions. Quantitative conversion (> 98%) of **1a** could be achieved in less than 16 h at a substrate-to-rhodium ratio of 1000 : 1 and a reaction temperature of 60 °C. Somewhat longer reaction times were required at lower temperatures or lower catalyst loadings. Most remarkably, a very high regioselectivity of 93–96% was achieved consistently for the formation of **2a**.

Similar results were obtained using **4b** in the asymmetric hydroformylation of the substituted vinyl arenes **1b**,**c**. Substrate **1b** bearing an electron-withdrawing chloride substitutent in the *para* position was hydroformylated with a modest enantiomeric excess of 88% ee, but the regioselectivity was again high (92%, entry 12). Substrate **1c**, the precursor for the hydroformylation route to ibuprofen, was hydroformylated with excellent enantioselectivities of up to 93% and an unprecedented high regioselectivity of 96% for **2c** (entries 13, 14).

† Current address: Giancarlo Franciò, Dipartimento di Chimica Inorganica, Chimica Analitica e Chimica Fisica, Universitá di Messina, Salita Sperone 31, I-98166 Vill. S. Agata, Messina, Italy.

Table 1 Rhodium-catalysed asymmetric hydroformylation of vinyl arenes **1a–c**[a]

Entry	Substrate	S/Rh	Ligand	L/Rh	Solvent	d (CO_2)[b] /g cm^{-3}	T/°C	$P_{H_2/CO}$ /bar	P_{tot} /bar	t/h	Conversion (%)	Regioselectivity[c] (%)	Ee (%)
1[d]	**1a**	2000	**4a**	4	Benzene	—	60	100	—	43	> 99	88	94 (*R*)
2	**1a**	2000	**4b**	4	Benzene	—	60	100	—	17	> 99	92.7	90.6 (*R*)
3	**1a**	1000	**4b**	4	Hexane	—	40	100	—	46	42.0	95.7	90.0 (*R*)
4	**1a**	2000	**4b**	4	Neat	—	60	100	—	12	> 99	94.1	90.6 (*R*)
5	**1a**	2000	**4b**	3	CO_2	0.681	40	40	178	66	75.4	94.8	93.6 (*R*)
6	**1a**	1000	**4b**	2	CO_2	0.596	60	20	156	16	> 99	92.5	90.4 (*R*)
7	**1a**	1000	**4b**	2	CO_2	0.596	60	60	242	16	97.6	93.0	92.0 (*R*)
8	**1a**	1000	**4b**	2.4	CO_2	0.460	36	40	123	62	91.6	94.8	91.8 (*R*)
9	**1a**	1000	**4b**	2.4	CO_2	0.80	31	40	115	62	96.5	95.6	91.8 (*R*)
10[d]	**1b**	2000	**4a**	4	Benzene	—	60	100	—	34	> 99	87	93 (−)
11	**1b**	1000	**4b**	2	CO_2	0.580	40	40	150	15	89.0	91.9	88.4 (−)
12[d]	**1c**	300	**4a**	4	Benzene	—	60	100	—	66	> 99	88	92 (*R*)
13	**1c**	1000	**4b**	2	CO_2	0.531	40	40	146	16	> 99	95.5	90.1 (*R*)
14	**1c**	1000	**4b**	2	CO_2	0.81	29	40	115	43	61.2	96.1	92.8 (*R*)

[a] See note ‡. [b] Density derived from weighed amount of CO_2 and reactor volume for $T > T_c$. [c] Defined as **2**/(**2** + **3**); hydrogenation or other side reactions were insignificant. [d] Data taken from ref. 2(*a*) for comparison.

It is important to note that the positive results achieved with ligand **4a** are *independent* of the phase behaviour of the reaction mixture. At temperatures ≥40 °C and CO_2 densities of $d \geq 0.59$ g cm^{-3}, the reaction mixtures with substrate **1a** were homogeneous by visual inspection and no phase separation was observed throughout the reaction. At T = 36 °C and d = 0.46 g cm^{-3}, *i.e.* in close vicinity to the critical point of pure CO_2 (T_c = 31.1 °C, d_c = 0.466 g cm^{-3}) the formation of small droplets was detected during the latter stages of the reaction. A liquid phase was present throughout the reaction at T = 31 °C. With substrate **1c**, the reaction occurred smoothly and with high selectivity at temperatures above or below T_c of pure CO_2.

The most striking feature of Table 1 is clearly the remarkably increased regioselectivity observed with **4b** as compared to **4a**. In order to distinguish solvent effects[6a,8b] from ligand effects,[15] we carried out control experiments with **4b** in typical organic solvents and in the neat substrate. Excellent regio- and enantioselectivities were observed in all cases (entries 2–4) demonstrating that the higher regioselectivity of the system **4b**/CO_2 compared to **4a**/benzene is mainly due to the ligand substitution pattern rather than the reaction medium.

In summary, we have accomplished the first synthesis of a highly complex ligand containing perfluoroalkyl substituents. The ligand (*R*,*S*)-3-H^{2}F^6-BINAPHOS **4b** allows for the first time efficient and highly regio- and enantio-selective hydroformylation of vinyl arenes using compressed CO_2 as an environmentally and toxicologically benign solvent. Particularly in the case of the practically most important substrate **1c**, the selectivities and reaction rates with ligand **4b** in compressed CO_2 compare favourable to those reported previously using **4a** in benzene under similar conditions. The successful use of CO_2 as a reaction medium raises the attractive possibility of applying our recently developed protocols for catalysis and extraction using supercritical carbon dioxide (CESS process).[8b,12,16] The evaluation of the scope and limitations of this approach and spectroscopic investigations of the rhodium complexes under catalytic conditions are under way.

This work was supported by the Max-Planck-Society, the Deutsche Forschungsgemeinschaft (Gerhard-Hess-Award to W. L.) and the University of Messina (Exchange Fellowship to G. F.). Gifts of chemicals form Celanese GmbH and Degussa AG are gratefully acknowledged. We thank Professor K. Nozaki for fruitful discussions and Professor I. Ojima for a preprint of ref. 10(*c*). Special thanks are due to Professor F. Faraone, University of Messina, for his encouragement in this project.

Notes and references

‡ Hydroformylation experiments were carried out in a window-equipped stainless-steel high-pressure reactor (V = 10 cm^{-3}). Complex **5b** and the ligand **4b** were charged as THF solutions in the reactor under argon. After stirring for 5 min, the solvent was removed *in vacuo* and the substrate was introduced. The reactor was pressurised with a 1:1 mixture of CO and H_2 and then filled with a weighed amount of CO_2 by means of a compressor. The reaction mixture was heated and stirred with a PTFE stirring bar for the desired reaction time. After cooling to 0 °C, the reactor was carefully vented and the products were collected by extraction of the reactor content with toluene for NMR and GC analysis.

1 G. Consiglio, *Catalytic Asymmetric Synthesis*, ed. I. Ojima, VCH, Weinheim, 1993, p. 273; F. Agbossou, J.-F. Carpentier and A. Mortreux, *Chem. Rev.*, 1995, **95**, 2485.
2 (*a*) K. Nozaki, H. Takaya and T. Hiayama, *Top. Catal.*, 1997, **4**, 175; (*b*) K. Nozaki, N. Sakai, S. Mano, T. Higashijima, T. Horiuchi and H. Takaya, *J. Am. Chem. Soc.*, 1997, **119**, 4413.
3 For the nomenclature of fluoroalkyl-substituted aryl phosphines see ref. 8(*a*).
4 *Chemical Synthesis Using Supercritical Fluids*, ed. P. G. Jessop and W. Leitner, Wiley-VCH, Weinheim 1999; E. Dinjus, R. Fornika and M. Scholz, *Chemistry under Extreme or Non-Classical Conditions*, ed. R. van Eldik and C. D. Hubbard, Wiley, New York, 1996, p. 219.
5 P. G. Jessop, T. Ikariya and R. Noyori, *Science*, 1995, **269**, 1065; D. A. Morgenstern, R. M. LeLacheur, D. K. Morita, S. L. Borkowsky, S. Feng, G. H. Brown, L. Luan, M. F. Gross, M. J. Burk and W. Tumas, *Green Chemistry*, ed. P. T. Anastas and T. C. Williamson, *ACS Symp. Ser. 626*, American Chemical Society, Washinton DC, 1996, p. 132; P. G. Jessop, T. Ikariya and R. Noyori, *Chem. Rev.*, 1999, **99**, 475.
6 (*a*) J. W. Rathke, R. J. Klingler and T. R. Krause, *Organometallics*, 1991, **10**, 1350; (*b*) Y. Guo and A. Akgerman, *Ind. Eng. Chem. Res.*, 1997, **36**, 4581.
7 P. G. Jessop, T. Ikariya and R. Noyori, *Organometallics*, 1995, **14**, 1510.
8 (*a*) S. Kainz, D. Koch, W. Baumann and W. Leitner, *Angew. Chem., Int. Ed. Engl.*, 1997, **36**, 1628; (*b*) D. Koch and W. Leitner, *J. Am. Chem. Soc.*, 1998, **120**, 13 398.
9 S. Kainz and W. Leitner, *Catal. Lett.*, 1998, **55**, 223.
10 (*a*) I. Bach and D. J. Cole-Hamilton, *Chem. Commun.*, 1998, 1463; (*b*) D. R. Palo and C. Erkey, *Ind. Eng. Chem. Res.*, 1999, **38**, 2163; (*c*) I. Ojima, M. Tzamarioudaki, C.-Y. Chuang, D. M. Iula and Z. Li, *Catalysis of Organic Reactions*, ed. F. E. Herkes, Dekker, New York, 1998, p. 333; (*d*) A. Banet, D. R. Paige, A. M. Stuard, I. R. Chadbond, E. G. Hope and J. Xiao, *11th International Symposium on Homogeneous Catalysis*, St. Andrews, 1998, p. 252.
11 M. J. Burk, S. Freng, M. F. Gross and W. Tumas, *J. Am. Chem. Soc.*, 1995, **117**, 8277; J. Xiao, S. C. A. Nefkens, P. G. Jessop, T. Ikariya and R. Noyori, *Tetrahedron Lett.*, 1996, **37**, 2813.
12 S. Kainz, A. Brinkmann, W. Leitner and A. Pfaltz, *J. Am. Chem. Soc.*, 1999, **121**, 6421; A. Wegner and W. Leitner, *Chem. Commun.*, 1999, 1583.
13 S. Kainz, Z. Luo, D. P. Curran and W. Leitner, *Synthesis*, 1998, 1425.
14 *Selected data* for **7**: $\delta_H(CD_2Cl_2)$ 7.94 (d, J_{PH} 482); $\delta_P(CD_2Cl_2)$ 21.3 (s). For **4b**: $\delta_P(CD_2Cl_2)$ −13.3 (P^1, d, $J_{P^1P^2}$ 27.7), 146.5 (P^2, d, $J_{P^1P^2}$ 27.7). For **5b**: $\delta_P(CD_2Cl_2)$ 48.1, dd, (P^1 J_{RhP^1} 172.9, $J_{P^1P^2}$ 84.0), 161.5 (P^2, dd J_{RhP^2} 330.1, $J_{P^1P^2}$ 84.0) P^1 = phosphine P, P^2 = phosphite P.
15 C. P. Casey, E. L. Paulsen, E. W. Beutenmüller, B. R. Proft, B. A. Matter and D. R. Powell, *J. Am. Chem. Soc.*, 1999, **121**, 63.
16 A. Fürstner, D. Koch, K. Langemann, W. Leitner and C. Six, *Angew. Chem., Int. Ed. Engl.*, 1997, **36**, 2466.

Communication 9/04281D

Remarkable Lewis acid mediated enhancement of enantioselectivity during free-radical reductions by simple chiral non-racemic stannanes

Dainis Dakternieks,[a] Kerri Dunn,[a] V. Tamara Perchyonok[b] and Carl H. Schiesser*[b]

[a] *Centre for Chiral and Molecular Technologies, Deakin University, Geelong, Victoria, Australia, 3217*
[b] *School of Chemistry, The University of Melbourne, Parkville, Victoria, Australia, 3052. E-mail: c.schiesser@chemistry.unimelb.edu.au*

Received (in Cambridge, UK) 14th June 1999, Accepted 16th July 1999

Additions of 1 equiv. of achiral and chiral Lewis acids to free-radical reduction reactions involving (1*S*,2*S*,5*R*)-menthyldiphenyltin hydride 1, bis[(1*S*,2*S*,5*R*)-menthyl]-phenyltin hydride 2, bis[1*S*,2*S*,5*R*)-menthyl][8-(*N*,*N*-dimethylamino)naphthyl]tin hydride 3, bis[(1*R*,2*S*,5*R*-menthyl]{1-(*S*)-*N*,*N*-dimethylaminoethyl]phenyl}tin hydride 4 or 3α-dimethylstannyl-5α-cholestane 5 result in remarkable increases in enantioselectivity.

Despite there being numerous reports of free-radical reactions proceeding with diastereocontrol,[1,2] there are relatively very few examples of free-radical reactions which proceed with genuine enantiocontrol.[2] The majority of examples that demonstrate enantioselective outcomes involve the use of chiral auxiliaries and, as a result, are further examples of diastereoselectivity in free-radical chemistry.[1,2] Of the remaining few reports, the introduction of asymmetry in the substrate through the use of chiral Lewis acid mediation,[3,4] and in the reagent through the use of chiral ligands on the tin atom in suitably constructed stannanes[5–8] have been the methods of choice for achieving enantioselectivity in radical chemistry.

Our approach to the development of synthetically useful chiral stannanes primarily involves the judicious choice of ligand from the multitude of compounds available in the natural chiral pool. Here we report that significant improvements in enantioselectivity during asymmetric reductions involving chiral non-racemic stannanes are achieved by the addition of Lewis acids.

(1*S*,2*S*,5*R*)-Menthyldiphenyltin hydride **1**, bis[(1*S*,2*S*,5*R*)-menthyl)phenyltin hydride **2** and 3α-dimethylstannyl-5α-cholestane **5** were prepared previously within our group.[9] The remaining hydrides **3** and **4** were prepared by reaction of the appropriate aryllithium with bis[(1*S*,2*S*,5*R*)-menthyl]phenyltin chloride followed by $LiAlH_4$ reduction.[9,10] Substrates chosen for this work include bromides **6** (X = Br) employed by Metzger and co-workers in their recent study[8] and the ketone **7** used by Curran and Nanni;[6] in this manner a direct comparison with previous work is possible.

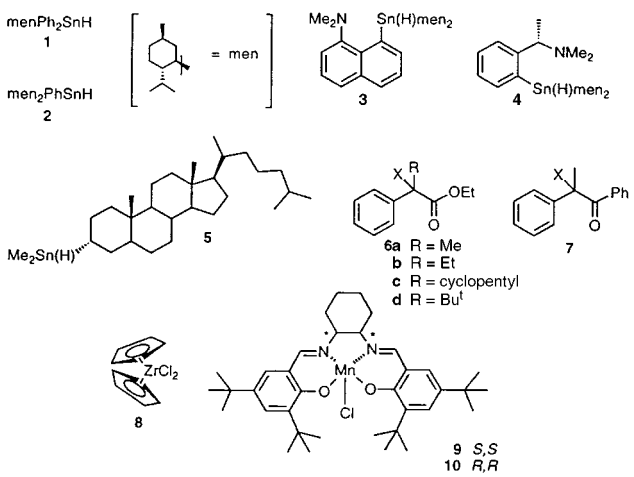

In this study, reductions were carried out at concentrations of approximately 0.1 M of the substrate in to which 1.0 equiv. of the Lewis acid† of choice and 1.1 equiv. of the stannane were added in toluene at −78 °C, initiated using 9-BBN.[11] Reactions were carried out until TLC analysis indicated the absence of starting material (*ca.* 1–2 h) at which time the reaction mixtures were examined by chiral-phase gas chromatography (GC)‡ and the percentage conversion and enantiomeric ratios determined by integration of the signals corresponding to the mixture of reduced compounds **6** and **7** (X = H) against an internal standard (either octane or undecane). Reduced compounds **6** and **7** (X = H) were identified by comparison of their GC retention times with those of the authentic compounds. The absolute configuration of the dominant isomer in each case was assigned by comparison with the GC retention times of the (*S*)-products **6** and **7** prepared and resolved following literature procedures.[12]

Table 1 lists enantioselectivity data for the model substrates **6** and **7** reacting with bis[(1*S*,2*S*,5*R*)-menthyl]phenyltin hydride **2** at −78 °C in toluene in the absence of any additive and in the presence of 1 equiv. of BF_3, zirconocene dichloride **8**, (*S*,*S*)-(−)- and (*R*,*R*)-(+)-*N*,*N*′-bis(3,5-di-*tert*-butylsalycidene)-1,2-diaminocyclohexanemanganese(III) chloride **9** or **10**.[13]

Inspection of Table 1 reveals some interesting features which aid in our understanding of the factors which goven the

Table 1 Enantioselectivities observed for reactions involving bis-[(1*S*,2*S*,5*R*)-menthyl]phenyltin hydride **2** in toluene at −78 °C[a]

Entry	Substrate	Lewis acid	Ee[a] (%)	Conversion[b] (%)
1	**6a**	None	2	80
2	**6a**	BF_3	32	64
3	**6a**	**8**	36	58
4	**6a**	**9**	60	81
5	**6a**	**10**	55	59
6	**6b**	None	4	81
7	**6b**	BF_3	20	68
8	**6b**	**8**	46	52
9	**6b**	**9**	86	75 (71)[c]
10	**6b**	**10**	84	69
11	**6c**	None	9	81
12	**6c**	BF_3	30	79
13	**6c**	**8**	35	74
14	**6c**	**9**	80	82 (70)[c]
15	**6c**	**10**	78	75
16	**6d**	None	6	82
17	**6d**	BF_3	10	76
18	**6d**	**8**	60	68
19	**6d**	**9**	80	72
20	**6d**	**10**	83	52
21	**7**	None	16	81
22	**7**	BF_3	12	69
23	**7**	**8**	52	92
24	**7**	**9**	52	76
25	**7**	**10**	50	60

[a] All reductions gave the (*S*)-product. [b] GC conversion. [c] Isolated yield.

Table 2 Enantioselectivities observed for reactions involving zirconocene dichloride **8** and (*S*,*S*)-(−)-*N*,*N*′-bis(3,5-di-*tert*-butylsalycidene)-1,2-diaminocyclohexanemanganese(III) chloride **9** and its enantiomer **10** in toluene at −78 °C

Entry	Substrate	Lewis acid	Stannane	Ee (%)	Yield[a] (%)
1	**6a**	**8**	**1**	36 (*S*)	59
2	**6a**	**8**	**3**	38 (*S*)	77
3	**6a**	**8**	**5**	60 (*S*)	82
4	**6a**	**9**	**1**	60 (*S*)	82
5	**6a**	**9**	**4**	90 (*R*)	73 (68)[e]
6	**6a**	**9**	**5**	34 (*S*)	58
7	**6b**	**8**	**1**	42 (*S*)	51
8	**6b**	**8**	**3**	52 (*S*)	79
9	**6b**	**8**	**5**	54 (*S*)	54
10	**6b**	**9**	**2**	70 (*S*)	78
11	**6b**	**9**	**4**	72 (*S*)	68
12	**6b**	**9**	**5**	62 (*S*)	67
13	**6b**	**10**[b]	*ent*-**2**[c]	86 (*R*)	72
14	**6c**	**9**	**4**	96[d] (*S*)	75 (67)[c]
15	**6d**	**8**	Bu_3SnH	0 (—)	—
16	**6d**	**8**	**1**	58 (*S*)	63
17	**6d**	**8**	**3**	62 (*S*)	87
18	**6d**	**8**	**5**	76 (*S*)	96
19	**6d**	**9**	Bu_3SnH	8 (*S*)	—
20	**6d**	**9**	**1**	72 (*S*)	74
21	**6d**	**9**	**4**	80 (*S*)	76
22	**6d**	**9**	**5**	82 (*S*)	72 (68)[e]
23	**7**	**8**	**1**	50 (*S*)	68
24	**7**	**8**	**3**	56 (*S*)	62
25	**7**	**8**	**5**	42 (*S*)	79
26	**7**	**9**	**1**	58 (*S*)	81
27	**7**	**9**	**3**	46 (*S*)	85
28	**7**	**9**	**4**	62 (*S*)	74
29	**7**	**9**	**5**	52 (*S*)	72

[a] GC conversion. [b] The enantiomer of **9**. [c] Bis[(1*R*,2*R*,5*S*)-menthyl]phenyltin hydride. [d] See footnote ¶. [e] Isolated yield.

stereochemical outcome in the reactions of interest. Firstly, a Lewis acid is crucial in obtaining reasonable enantioselectivities. Experiments carried out in the absence of these Lewis acids give significantly poorer ees. For example, addition of 1 equiv. of BF_3 to the reaction involving **6b** (X = Br) results in an increase in enantioselectivity from 4 to 20%. Increasing Lewis acid bulk results in further increases; 46% ee is observed with the addition of zirconocene dichloride **8**, while addition of **9** results in a remarkable improvement in ee to a value of 86%. It is interesting to note that the (*S*)-isomer of the product dominates in all of the reductions listed in Table 1. It is also important to note, when the reduction of **6b** (X = Br) was repeated with the enantiomer of **2**, bis[(1*R*,2*R*,5*S*)-menthyl]phenyltin hydride, in the presence of **10**, (*R*)-**6b** (X = H) was obtained with an ee of 86% under the same reaction conditions.

Despite the obvious benefit derived by the presence of the Lewis acid, chirality transfer appears to originate with the ligand on tin because the achiral Lewis acid **8** itself has a remarkable effect on the stereochemistry of the reaction in question. In addition, both enantiomeric forms of *N*,*N*′-bis(3,5-di-*tert*-butylsalicylidene)-1,2-diaminocyclohexanemanganese(III) chloride, namely **9** and **10**, result in enantioselectivities within a few percent of each other and with the same enantiomeric form of the reduced substrate dominating.

Table 2 lists the effect that different stannanes have on the observed enantioselectivities at −78 °C for reactions involving Lewis acids **8**, **9** and (for one example) **10**. It should be noted that the achiral stannane, tributyltin hydride, reacts with **6d** (X = Br) in the presence of Lewis acids **8** and **9** to afford **6d** (X = H) with 0 and 8% ee, respectively. The former result is expected; the latter result demonstrates, one again, that chirality in the stannane is more important than that in the Lewis acid.

The reader's attention is drawn to the numerous examples provided in Tables 1 and 2 where the observed enantioselectivity exceeds 80% and the two examples (entries 5 and 14, Table 2) of ees ⩾ 90%. These results are significant as they represent the highest-ever reported enantioselectivities in stannane reduction chemistry,[1,4,14]§ the 96% ee observed for the reaction of **6c** (X = Br) with **4** in the presence of **9** being truly remarkable; indeed, this result exceeds the highest ee achieved in any free-radical reaction.[1,15,16] We believe that, consistent with previous models proposed to account for diastereoselective outcomes in radical reactions,[1–4] the profound increases in enantioselectivity observed upon addition of the Lewis acids in this study are a result of the significant increases in steric bulk[17] associated with the ester group during coordination of the carbonyl moiety of the boron or metal centre in BF_3, **8**–**10**.

In order to explore the synthetic utility of the use of these reagents and catalysts, we repeated the reduction of several substrates in the presence of **9** (entries 9, 14 in Table 1; 5, 14, 22 in Table 2). We were delighted to isolate the reduction products **6** (X = H) in 67–71% yield after workup and chromatography; GC analysis provided ees as listed.¶

We are currently exploring immobilisation of these chiral reagents onto polymer support and the use of catalytic chiral stannane reductions. We thank the Australian Research Council for financial support.

Notes and references

† The use of less than 1.0 equiv. results in noticeably lower ees, while greater amounts provide no increases in ee.

‡ Enantioselectivities were determined by gas chromatographic analyses of the reaction mixtures using a chiral trifluoroacteylated γ-cyclodextrin (Chiraldex™ G-TA, 30 m × 0.25 mm) capillary column purchased from Alltech.

§ To the best of our knowledge, the value of 61% reported by Hoshino and co-workers represents the previous record, see ref. 1, 4, 13. Roberts has reported recently some enantioselective hydrosilation reactions which proceed with ees approaching 95%, see ref. 16.

¶ 96% ee for entry 14 in Table 2 represents a GC-determined lower limit.

1 For excellent reviews, see: D. P Curran, N. A. Porter and B. Giese, *Stereochemistry of Radical Reactions*, VCH, Weinheim, 1995; W. Smadja, *Synlett*., 1994, 1; N. A. Porter, B. Giese and D. P. Curran, *Acc. Chem. Res.*, 1991, **24**, 296.
2 M. Sibi and N. A. Porter, *Acc. Chem. Res.*, 1999, **32**, 163.
3 For early examples, see: Y. Guindon, C. Yoakim, R. Lemieux, L. Boisvert, D. Delorme and J.-F. Lavellée, *Tetrahedron Lett.*, 1990, **31**, 2845; Y. Guindon, J.-F. Lavallée, M. Llinas-Brunet, G. Horner and J. Rancourt, *J. Am. Chem. Soc.*, 1991, **113**, 9701.
4 For a comprehensive review, see: P. Renaud and M. Gerster, *Angew. Chem., Int. Ed.*, 1998, **37**, 2563.
5 H. Schumann, B. Pachaly and B. C. Schütze, *J. Organomet. Chem.*, 1984, **265**, 145.
6 D. P. Curran and D. Nanni, *Tetrahedron: Asymmetry*, 1996, **7**, 2417.
7 M. Blumenstein, K. Schwartzkopf and J. O. Metzger, *Angew. Chem., Int. Ed. Engl.*, 1997, **36**, 235.
8 K. Schwartzkopf, M. Blumenstein, A. Hayen and J. O. Metzger, *Eur. J. Chem.*, 1998, 177.
9 D. Dakternieks, K. Dunn, D. J. Henry, C. H. Schiesser and E. R. T. Tiekink, *Organometallics*, in press; C. H. Schiesser and M. A. Skidmore, *Phosphorus Sulfur Silicon Relat. Elem.*, in press.
10 J. B. T. H. Jastrzebski, G. van Koten, K. Goubitz, C. Arlen and M. Pfeffer, *J. Organomet. Chem.*, 1983, **246**, C75; G. van Koten and J. B. T. H. Jastrzebski, *Tetrahedron*, 1989, **45**, 569.
11 V. T. Perchyonok, C. H. Schiesser, *Tetrahedron Lett.*, 1998, **39**, 5437.
12 A. Campbell and S. Kenyon, *J. Chem. Soc.*, 1946, 25; C. Aaron, D. Dull, S. L. Schmiegel, D. Jaeger, J. Ohashi and H. S. Mosher, *J. Org. Chem.*, 1967, **32**, 2797; F. A. A. Elhafez and D. J. Cram, *J. Am. Chem. Soc.*, 1952, **74**, 5846.
13 Jacobson's catalyst: E. N. Jacobsen, W. Zhang, A. R. Muci, J. R. Ecker and L. Deng, *J. Am. Chem. Soc.*, 1991, **113**, 7063.
14 M. Murakata, H. Tsutsui and O. Hoshino, *J. Chem. Soc., Chem. Commun.*, 1995, 481.
15 M. Murakata, T. Jono, Y. Mizuno and O. Hoshino, *J. Am. Chem. Soc.*, 1997, **119**, 11 713.
16 M. B. Haque, B. P. Roberts and D. A. Tocher, *J. Chem. Soc., Perkin Trans. 2*, 1998, 2881.
17 D. Dakternieks, D. J. Henry and C. H. Schiesser, *J. Phys. Org. Chem.*, 1999, **12**, 233.

Communication 9/04700J

A linear metal string $[Cr_7(\mu_7\text{-teptra})_4Cl_2]$ complex with delocalized heptachromium(II) multiple bonds (teptraH_3 = tetrapyridyltriamine)

Yu-Hua Chen, Chung-Chou Lee, Chih-Chieh Wang, Gene-Hsiang Lee, Shie-Yang Lai, Feng-Yin Li, Chung-Yuan Mou and Shie-Ming Peng*

Department of Chemistry, National Taiwan University, Taipei, Taiwan. E-mail: smpeng@chem35.ch.ntu.edu.tw

Received (in Cambridge, UK) 22nd June 1999, Accepted 21st July 1999

A heptachromium(II) metal chain helically wrapped by four all-*syn* type teptra^{3-} ligands with delocalized Cr^{II}–Cr^{II}–Cr^{II}–Cr^{II}–Cr^{II}–Cr^{II} multiple bonds is found in the complex $[Cr_7(\mu_7\text{-teptra})_4Cl_2]$. The band structure of a hypothetical one-dimensional chromium string based on this structure is calculated and shows metallic behavior for the string structure.

The bonding interaction of the metal string in oligonuclear linear metal chain complexes, which have the potential as molecular metal-wires is an important and exciting topic.[1–12] Bonding information and the electronic configurations of metal centers on oligonuclear metal complexes from trinuclear metal complexes with *syn–syn* bis(α-pyridyl)amido (dpa) ligand $[M_3(\mu_3\text{-dpa})_4X_2]$, (M = Cu,[1] Ni,[2] Co,[3,6] Cr,[7] Ru,[4] Rh[4]) and from pentanuclear metal complexes with all-*syn* tris(α-pyridyl)diamido (tpda) ligand $[M_5(\mu_5\text{-tpda})_4X_2]$, (M = Ni,[5,8] Co,[5,8] Cr[10,11]) have been described and discussed in detail. Although the Ni–Ni bond order is zero, the Ni–Ni distance altered predictably from 2.379(2) Å for the terminal one to 2.307(1) Å for the intermediate one and to 2.220(2) Å for the innermost one in the heptanickel $[Ni_7(\mu_7\text{-teptra})_4Cl_2]$ complex.[12] The next target of study is the linear oligochromium(II) complexes with a strong Cr–Cr bond (bond order 1.5). In this system, the Cr–Cr distances are found to be 2.36(1) Å in trichromium $[Cr_3(\mu_3\text{-dpa})_4Cl_2]$,[7] and 2.284(1) and 2.2405(8) Å in pentachromium $[Cr_5(\mu_5\text{-tpda})_4Cl_2]$.[11] Here we report the synthesis and structure of the heptachromium(II) metal string complex, $[Cr_7(\mu_7\text{-teptra})_4Cl_2]$, and the band structure of a hypothetical one-dimensional metal string based on the structure of this complex.

The title compound, $[Cr_7(\mu_7\text{-teptra})_4Cl_2]$, was synthesized by using anhydrous $CrCl_2$ and teptraH_3 ligand as the starting materials and naphthalene as the solvent under an argon atmosphere.† Bu^{t}OK was used as a base to deprotonate the amine groups of the teptraH_3 ligand. The teptraH_3 ligand was synthesized in the same manner as previously reported.[13,14] The crystal structure of $[Cr_7(\mu_7\text{-teptra})_4Cl_2]$ is shown in Fig. 1.‡ The space group of the title compound is $P2_1/c$ with a whole molecule and six THF molecules in an asymmetric unit. The structure is essentially identical to those of $[Ni_7(\mu_7\text{-teptra})_4X_2]$, (X = Cl^-, NCS^-)[9,12] with the linear heptachromium chain being wrapped helically by four all-*syn* type teptra^{3-} ligands. The complex exhibits an approximate D_4 symmetry. According to our structural analysis, the Cr–Cr bond lengths are symmetrically distributed in the range 2.211(2)–2.291(2) Å. Logically, the bonding mode in the Cr^{II}_7 unit favors a delocalized arrangement (**I**) over a localized arrangement (**II**).

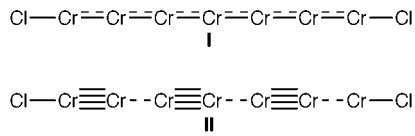

However, our study shows that the inner chromium ions (Cr(2)–Cr(6)) have anisotropic ellipsoidal structures with a larger thermal parameter in the direction of the metal axis.

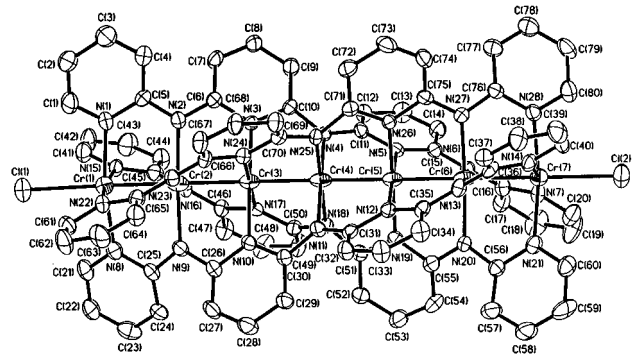

Fig. 1 Crystal structure of $[Cr_7(\mu_7\text{-teptra})_4Cl_2]$ (ORTEP side view). Atoms are shown as 30% vibrational thermal ellipsoids. Pertinent bond lengths (Å) and angles (°): Cr(1)–Cr(2) 2.291(2), Cr(2)–Cr(3) 2.243(2), Cr(3)–Cr(4) 2.211(2), Cr(4)–Cr(5) 2.215(2), Cr(5)–Cr(6) 2.243(2), Cr(6)–Cr(7) 2.280(2), Cr(1)–$N_{av.}$ 2.113(8), Cr(2)–$N_{av.}$ 2.026(7), Cr(3)–$N_{av.}$ 2.051(7), Cr(4)–$N_{av.}$ 2.025(6), Cr(5)–$N_{av.}$ 2.054(7), Cr(6)–$N_{av.}$ 2.024(7), Cr(7)–$N_{av.}$ 2.113(8), Cr(1)–Cl(1) 2.557(3), Cr(7)–Cl(2) 2.544(3), Cl(1)–Cr(1)–Cr(2) 178.6(1), Cr(1)–Cr(2)–Cr(3) 179.35(9), Cr(2)–Cr(3)-Cr(4) 179.74(9), Cr(3)–Cr(4)–Cr(5) 179.58(9), Cr(4)–Cr(5)–Cr(6) 179.79(8), Cr(5)–Cr(6)–Cr(7) 179.7(1), Cr(6)–Cr(7)–Cl(2) 179.6(1).

Although they still have reasonable values (av. U_{11}, U_{22}, U_{33} are 0.078, 0.041, 0.033, respectively), the disordered form of **II** can not be completely excluded. Three types of Cr–Cr bond lengths, with small differences among them, are observed. The averaged values of the bond length are 2.286(2) Å for the terminal Cr–Cr bonds, 2.243(2) Å for the intermediate Cr–Cr bonds and 2.213(2) Å for the innermost Cr–Cr bonds. A comparison of the Cr–Cr distances among the tri-, penta-, and heptachromium(II) complexes are shown in Fig. 2. All of the Cr–Cr distances in $[Cr_7(\mu_7\text{-teptra})_4Cl_2]$ are shorter than those in $[Cr_3(\mu_3\text{-dpa})_4Cl_2]$ (2.36(1) Å),[7] and are comparable with 2.284(1) Å of the terminal Cr–Cr bond, and 2.2405(8) Å of the inner Cr–Cr bond in $[Cr_5(\mu_5\text{-tpda})_4Cl_2]$. In a previous report,[12] the probability of

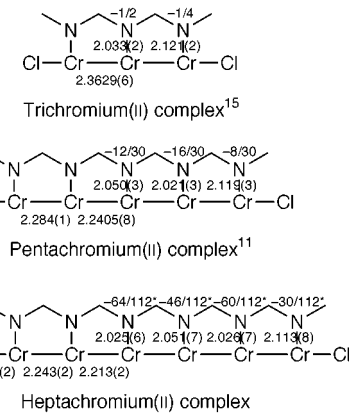

Fig. 2 Comparisons of Cr–Cr and Cr–N distances among tri-, penta- and heptachromium(II) complexes. *: Probability of negative charge distribution on the N atoms according to 112 resonance structures.

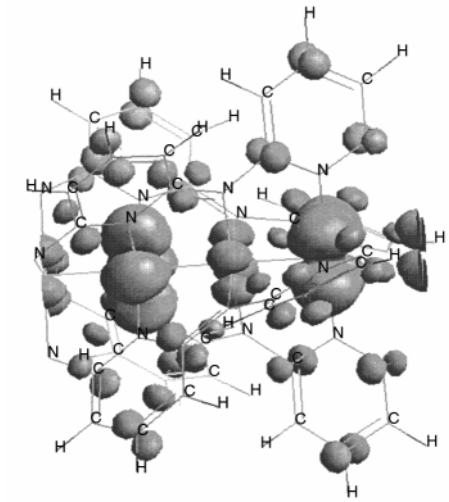

Fig. 3 The HOMO orbital of the $[Cr_4(\mu_4\text{-dpda})_4]_n$ chain.

negative charge distribution on the seven N atoms by 112 resonance structures are shown to be −30/112, −60/112, −46/112, and −64/112 from the terminal N atom to the central N atom, respectively (Fig. 2). This charge distribution is qualitatively similar to the calculated net atomic charges obtained from EHMO and Gaussian/DFT calculations.[12] The results indicate that the bond length of the Cr–N bond should depend on the bonding interaction between the N and Cr atoms. The larger the negative charge is on the N atom, the stronger is the Cr–N bond and the shorter is the Cr–N bond distance. This prediction is proven directly from the Cr–N distances obtained from structural analyse. In Fig. 2, the two terminal Cr–N bond distances are obviously the longest. The Cr–N bond distance neighboring the terminal Cr–N bond and the central Cr–N bond distance are the shortest. This result is in good agreement with the prediction based on the charge distributions.

The electronic band structure of the molecular polynuclear metal-wire is calculated for a hypothetical infinite one-dimensional metal-wire created by extending the length of the linear metal complex. In light of the D_4 symmetry of the metal complex, $[Cr_7(\mu_7\text{-teptra})_4Cl_2]$, a model metal-wire is constructed with $[Cr_4(\mu_4\text{-dpda})_4]_n$ (dpda = dipyridyldiamido moiety) taken from the crystal structure of the $[Cr_7(\mu_7\text{-teptra})_4Cl_2]$, as the repeat unit. The molecular structure of this model is then optimized and the band structure is calculated.§ The results indicate that the linear complex is a metal since the Fermi level is located within the HOMO band and there is thus no band gap. The HOMO orbital (Fig. 3) of this hypothetical metal-wire is delocalized and mainly constitutes of the d_{xy} and the $d_{x^2-y^2}$ orbitals of chromium and the p orbitals of carbon in the $dpda^{2-}$ ligands. The LUMO is localized on the chromium chain, and is composed of the d_{z^2} orbital of chromium. This model shows that the chromium metal-wire can likely serve as a conducting wire in, for example, nanostructure applications.

In summary, we have demonstrated a seven-centered metal multiple bonding scheme for early transition metal ions. The variations of the M–M distances in the Ni_7 system with a weak antiferromagnetic interaction and in the Cr_7 system with a strong M–M bonding have been described and compared. In both cases, the M–M distances converge to *ca.* 2.22 Å. Studies on the application of metal string complexes as molecular metal-wires are in progress.

The authors thank the National Science Council of the Republic of China for financial support. The authors also thank the National Center for High-performance Computing (NCHC) for providing computational facilities.

Notes and references

† *Preparation and characterization of* $[Cr_7(\mu_7\text{-teptra})_4Cl_2]$. Anhydrous $CrCl_2$ (1.40 g, 11.4 mmol) and $teptraH_3$ (1.00 g, 2.8 mmol) were placed in an Erlenmeyer flask, and naphthalene (10 g) was added under nitrogen in a glove box. The mixture was heated (about 160–180 °C) for 20 h under argon. Then a solution of potassium *tert*-butoxide (1.04 g, 9.3 mmol) in *tert*-butyl alcohol (10 mL) was added dropwise. The mixture was refluxed for 18 h continuously. After the mixture had cooled, hexane was added to wash out naphthalene. The remaining solid was extracted with CH_2Cl_2 and recrystallized from DMF–THF. Deep brown crystals were obtained. (Yield: 40%), IR (KBr) ν/cm^{-1} = 1600, 1580, 1546 (C=C). UV/Vis (CH_2Cl_2) λ_{max}/nm (ε/dm^3 mol^{-1} cm^{-1}) = 285 (1.79 × 10^5), 338 (1.28 × 10^5), 409 (1.36 × 10^5), 503 (1.34 × 10^4); 534 (1.14 × 10^4), 745 (1.44 × 10^4). MS(FAB): *m*/*z* (%) 1844 (85) $[M]^+$, 1809 (100) $[M - Cl]^+$, 1721 (21) $[Cr_6(\mu_6\text{-teptra})_4]^+$.

‡ *Crystal data* for $[Cr_7(\mu_7\text{-teptra})_4Cl_2]$•6THF, $Cr_7Cl_2N_{28}C_{104}H_{104}O_6$, M = 2277.05, monoclinic, space group $P2_1/c$, a = 35.2674(2), b = 15.0195(3), c = 19.6563(4) Å, β = 98.615(1)°, V = 10276.9(3) Å^3, D_c = 1.472 g cm^{-3}, Z = 4, μ = 0.834 mm^{-1}. The crystal was sealed in a capillary with the mother liquor since it cracked immediately after leaving the solution. Data were collected on a SMART CCD diffractometer with graphite-monochromated Mo-Kα radiation at 295 K. SADABS absorption correction (T_{min} 0.65 and T_{max} 0.83), a total of 38720 reflections were measured and 13181 unique reflections (2θ < 45°, R_{int} = 0.0514) were used in the refinement. Full-matrix least-square refinement on F^2 (1070 variables) converged to $R(F)$ = 0.103 and $R(wF^2)$ = 0.265 (I > 2σ(I)) and $R(F)$ = 0.145 and $R(wF^2)$ = 0.297 (all data). The THF molecules were refined using 'similarity restraints' in SHELXTL. CCDC 182/1340. See http://www.rsc.org/suppdata/cc/1999/1667/ for crystallographic files in .cif format.

§ *Computational details*. The *ab initio* quantum mechanical calculations were performed with CASTEP 3.9 code.[16,17] Gradient-corrected density functional theory[18,19] (DFT) is used to calculate the electronic ground state of the system. We expand the valence electronic wavefunctions in plane waves up to a 290 eV cut-off and represent the nuclei and core electrons by ultrasoft pseudopotentials. Details of the computational study of the molecular metal-wire for Ni, Co, and Cr complex chains will be published in a separate paper.

1 (*a*) L. P. Wu, P. Field, T. Morrisey, C. Murphy, P. Nagle, B. Hathaway, C. Simmons and P. Thornton, *J. Chem. Soc., Dalton Trans.*, 1990, 3835; (*b*) G. J. Pyrka, M. El-Mekki and A. A. Pinkerton, *J. Chem. Soc., Chem. Commun.*, 1991, 84.
2 S. Aduldecha and B. Hathaway, *J. Chem. Soc., Dalton Trans.*, 1991, 993.
3 E. C. Yang, M. C. Cheng, M. S. Tsai and S. M. Peng, *J. Chem. Soc., Chem. Commun.*, 1994, 2377.
4 J. T. Sheu, C. C. Liu, I. Chao, C. C. Wang and S. M. Peng, *Chem. Commun.*, 1996, 315.
5 S. J. Shieh, C. C. Chou, G. H. Lee, C. C. Wang and S. M. Peng, *Angew. Chem., Int. Ed. Engl.*, 1997, **36**, 56.
6 (*a*) F. A. Cotton, L. M. Daniels and G. T. Jordan IV, *Chem. Commun.*, 1997, 421; (*b*) F. A. Cotton, L. M. Daniels, G. T. Jordan IV and C. A. Murillo, *J. Am. Chem. Soc.*, 1997, **119**, 10 377.
7 (*a*) F. A. Cotton, L. M. Daniels, C. A. Murillo and I. Pascual, *J. Am. Chem. Soc.*, 1997, **119**, 10 223; (*b*) F. A. Cotton, L. M. Daniels, C. A. Murillo and X. Wang, *Chem. Commun.*, 1998, 39.
8 C. C. Wang, W. C. Lo, C. C. Chou, G. H. Lee, J. M. Chen and S. M. Peng, *Inorg. Chem.*, 1998, **37**, 4059.
9 S. Y. Lai, Z. W. Lin, Y. H. Chen, C. C. Wang, G. H. Lee, M. H. Yang, M.-k. Leung and S. M. Peng, *J. Am Chem. Soc.*, 1999, **121**, 250.
10 F. A. Cotton, L, M. Daniels, C. A. Murillo and X. Wang, *J. Chem. Soc., Dalton Trans.*, 1999, 517.
11 H. C. Chang, J. T. Li, C. C. Wang, T. W. Lin, H. C. Lee, G. H. Lee and S. M. Peng, *Eur. J. Inorg. Chem.*, 1999, 1243–1251.
12 S. Y. Lai, C. C. Wang, Y. H. Chen, C. C. Lee, Y. H. Liu and S. M. Peng, *J. Chin. Chem. Soc.*, 1999, **46**, 477.
13 M. H. Yang, T. W. Lin, C. C. Chou, H. C. Lee, H. C. Chang, G. H. Lee, M. k. Leung and S. M. Peng, *Chem. Commun.*, 1997, 2279.
14 S. Wagaw and S. L. Buchwald, *J. Org. Chem.*, 1996, **61**, 7240.
15 J. T. Li, G. H. Lee and S. M. Peng, unpublished results.
16 M. C. Payne, M. P. Teter, D. C. Allan, T. A. Arias, T. A. Johannopoulos and J. Johannopoulos, *Rev. Mod. Phys.*, 1992, **64**, 1045.
17 Cerius^2 User Guide, Molecular Simulations, San Diego, CA, 1997.
18 P. Hohenberg and W. Kohn, *Phys. Rev.*, 1964, **136**, B864.
19 W. Kohn and L. J. Sham, *Phys. Rev.*, 1965, **140**, A1133.

Communication 9/05001I

ChemComm

A two-dimensional organic–inorganic material constructed from copper-dipyridylamine and vanadate chains: [Cu(dpa)VO_3]†

Robert L. LaDuca, Jr.,*[a] Robert Finn[b] and Jon Zubieta*[b]

[a] *Department of Chemistry, Syracuse University, Syracuse, NY 13244 USA. E-mail: jazubiet@mailbox.syr.edu*
[b] *Department of Chemistry and Physics, King's College, Wilkes-Barre, PA 18711 USA*

Received (in Bloomington, IN, USA) 26th March 1999, Accepted 7th July 1999

The hydrothermal reaction of a mixture of $CuCl_2$, $NaVO_3$, 4,4′-dipyridylamine (dpa) and Et_4NOH in water yields [Cu(dpa)VO_3], a material constructed from one-dimensional $\{VO_2O_{2/2}\}_n^{n-}$ chains and $\{Cu(dpa)\}_n^{n+}$ chains linked into a two-dimensional framework.

The inorganic oxides are characterized by diverse physical properties, resulting in applications to areas as diverse as heavy construction and microelectronics.[1] The widespread interest in inorganic oxide/organic hybrid materials reflects the potential exploitation of these phases for tailoring the structures and properties of oxides. The dramatic influence of organic components on oxide structures has been demonstrated for materials as diverse as biomineralized systems,[2] zeolites,[3] mesoporous compounds of the MCM-41 class,[4] organically templated oxometal phosphates and phosphonates,[5,6] and molybdenum oxides.[7]

Layered inorganic oxides constitute a diverse subclass of the oxides and include clays, layered double hydroxides,[8] and transition metal phosphates and phosphonates.[9, 10] As an extension of our investigations of organically templated metal oxides,[7] we recently described a new class of materials which contain amine-templated transition or post-transition metal cations situated between or decorating the surface of vanadium oxide layers, the VOXI class of materials.[11, 12] In elaborating this chemistry, the role of polymeric cations constructed from geometrically constrained organonitrogen ligands bridging first row transition metal centers on the structures of vanadium oxides has been addressed. The versatility of such polymeric coordination complex cations in providing one-, two-, or three-dimensional substructures suggested that these structural motifs could be exploited as scaffolding for directing the architecture of the vanadium oxide anion component. This expectation has been realized in the preparation of [Cu(dpa)VO_3] (**1**), a two-dimensional material composed of linked $\{Cu(dpa)\}_n^{n+}$ and $\{VO_2O_{2/2}\}_n^{n-}$ one-dimensional chains.

Compound **1** is formed as orange needles in 25% yield‡ in the hydrothermal reaction of $CuCl_2$, $NaVO_3$, 4,4′-dipyridylamine, Et_4NOH, and H_2O in the mole ratio 1:2:2:1:1500 at 160 °C for 72 h. Hydrothermal techniques are now well established for the preparation of materials from relatively insoluble and unreactive precursors. Advantages include enhanced rates of solvent extraction of solids and crystal growth from solution and the ability to overcome differential solubilities of organic and inorganic components. The judicious choice of reaction conditions and precursors 'directs' the self-assembly of metastable phases which are not accessible by other synthetic routes.

The infrared spectrum of **1** exhibits a strong band at 910 cm^{-1} associated with ν(V=O) and a series of bands in the 1050–1450 cm^{-1} range attributed to the ligand. Thermogravimetric analysis exhibits a weight loss of *ca.* 50% in the range 350–420 °C corresponding to loss of the ligand.

As shown in Fig. 1, the structure of **1**§ consists of a two-dimensional covalent network constructed from the linking of $\{Cu(dpe)\}_n^{n+}$ and $\{VO_2O_{2/2}\}_n^{n-}$ chains. The anionic component consists of a buckled chain of corner-sharing $\{VO_4\}$ tetrahedra. Three distinct $\{Cu(dpa)\}_n^{n+}$ chain types provide charge balance and serve to decorate the periphery of the vanadate chains or to bridge the chains into the network structure.

The first polymeric cation chain type (A), shown in Fig. 2, runs parallel to the vanadate chains with the Cu(I) sites bonded to a vanadate oxygen at every fifth vanadium site of the anionic chain, forming a ladderlike double chain motif with the side rails provided by the {V–O–V–} and {Cu–dpe–Cu–} chains and the rungs by the {Cu–O–V} linkages. This architecture also results in an unusual twenty-two membered ring motif of approximate dimensions 11.5 × 3.3 Å. The copper site exhibits $\{CuN_2O\}$ distorted trigonal planar geometry.

These mixed metal double chains are interconnected into a network structure through parallel $\{Cu(dpa)\}_n^{n+}$ chains running at 73° to the axes of the vanadate chains. There are two types of these parallel chains. The first (B) consists of pairs of adjacent $\{Cu(dpa)\}_n^{n+}$ chains which exhibit tetrahedral $\{CuN_2O_2\}$ sites. These cationic chains are orientated with respect to the vanadate

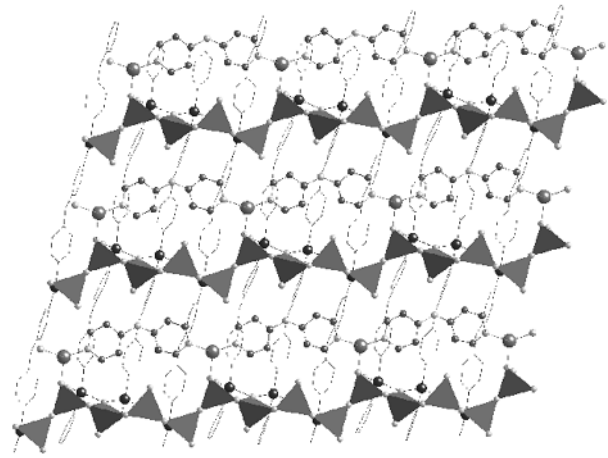

Fig. 1 A view of a single layer of [Cu(dpa)VO_3] (**1**) parallel to the crystallographic *a* axis, showing the crisscross network motif. The vanadium sites are illustrated in polyhedral representation. Copper sites of the (A) chains are grey spheres while the copper atoms of the (B) double chains are black spheres. The copper centers of the (C) chains are masked by the vanadate tetrahedra. Selected bond lengths (Å): chain (A): Cu1–O2, 2.106(4); Cu1–N21, 1.925(5); Cu1–N23, 1.933(5); chain (B): Cu2–N11, 1.931(5); Cu2-N13, 1.936(5); Cu2–O4, 2.122(4); Cu2–O9, 2.357(4); Cu3–N3, 1.975(5); Cu3–N1, 1.988; Cu3–O10, 2.204(4); Cu3-O9, 2.223; chain (C): Cu4–N33, 1.906(5); Cu4–N31, 1.927(5); Cu4–O11, 2.054(4).

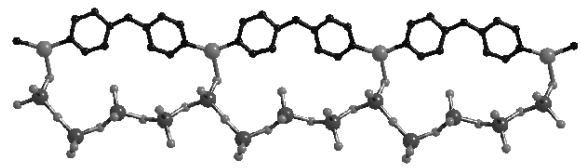

Fig. 2 A view of the double chain formed by fused $\{VO_3\}_n^{n-}$ and parallel $\{Cu(dpa)\}_n^{n+}$ chains.

† Electronic Supplementary Information (ESI): Colour versions of Figs. 1 and 4, see: http://www.rsc.org/suppdata/cc/1999/1669/

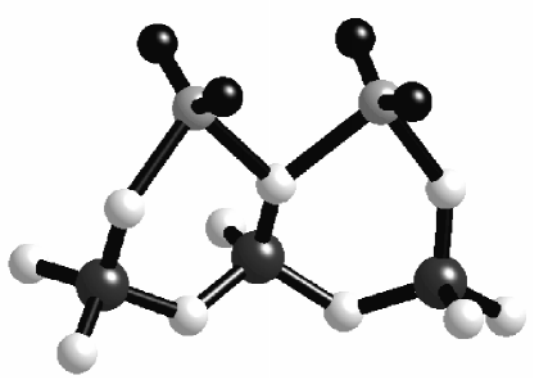

Fig. 3 The $\{V_3Cu_2O_{12}N_4\}$ cluster formed by the interaction of the vanadate chain and the $\{Cu(dpa)\}_n^{n+}$ double chains in the crisscross network.

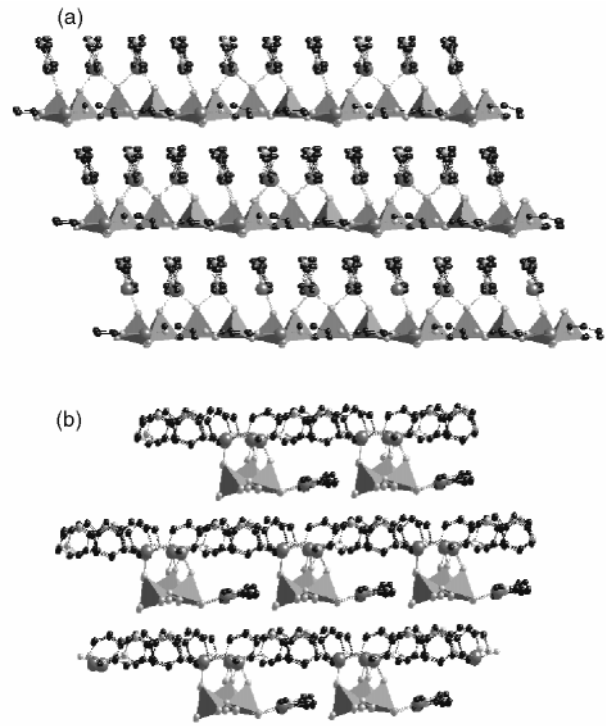

Fig. 4 (a) A view of the structure parallel to the (B) type double chains, showing the alternation of (B) double chains and (C) chains. (b) A view of the stacking of layers parallel to the crystallographic *c* axis, showing the location of (A) chains within the slots formed by vanadate chains and the (B) and (C) chains of neighboring layers. The amine of the (A) chain exhibits hydrogen bonding to an oxo group of the adjacent intralamellar vanadium oxide chain: N32···O7, 2.71 Å. The amines associated with the (B) and (C) chains exhibit interlamellar hydrogen bonding to the adjacent layer: N2···O5, 2.89 Å; N12···O3, 2.85 Å; N22···O1, 2.76 Å.

chains so as to bridge Cu sites on adjacent chains through the oxo group of one vanadate tetrahedron of the anionic chain. The consequence of this arrangement of submotifs is the unusual pentanuclear $\{Cu_2V_3\}$ oxo-bridged cluster shown in Fig. 3.

The buckling of vanadate chain results in a translation by one polyhedral edge length of $\{Cu(dpa)\}_n^{n+}$ chains adjacent to the oxo-bridged pairs, as shown in Figs. 1 and 4. When viewed parallel to this third chain motif (C), the alternation of $\{Cu(dpa)\}_n^{n+}$ paired chains and single chains is apparent. The Cu site of this chain type exhibits distorted $\{CuN_2O\}$ trigonal planar geometry.

The interconnection of these one-dimensional substructures results in the crisscross network pattern shown in Fig. 1. When viewed parallel to the vanadate chain, as in Fig. 4(b), the distinctiveness of the $\{Cu(dpa)\}_n^{n+}$ chain types is highlighted, as well as the unusual architecture of the layer repeat pattern. The $\{Cu(dpa)\}_n^{n+}$ chains designated (A) occupy cavities bordered by adjacent $\{VO_3\}_n^{n-}$ parallel chains, the (B) and (C) type $\{Cu(dpa)\}_n^{n+}$ chains of the same layer and those of an adjacent layer. The folding of the (A) chains into the intralamellar slots results in strong hydrogen bonding between the amine group and the oxo groups of the adjacent vanadate chain.

The preparation of compound **1** emphasizes the power of hydrothermal techniques in the isolation of organic–inorganic oxide materials. Furthermore, the structure of the resulting hybrid solid illustrates the observation that both metal and ligand have significant structure-directing influences on the vanadium oxide substructure which adapts to maximize covalent and noncovalent interactions with the coordination complex cation. In this respect, it is noteworthy that previously described examples of vanadium oxide–inorganic complex hybrid materials which exploited mononuclear coordination complex subunits exhibit two-dimensional vanadate substructures exclusively. In contrast, the coordination complex polymer of **1** directs the vanadate substructure into a one-dimensional type. Thus, while the structure-directing role of the polymeric cation is evident, the chemistry of the organic–inorganic interface is complex and remains largely unmapped, rendering predictability of structures a goal yet to be achieved.

This work was supported by NSF grant CHE 9617232.

Notes and references

‡ The crystals coprecipitate with an amorphous powder. Compound **1** is readily separated from the powder by exploiting its greater density in water. Satisfactory elementary analyses were obtained.

§ *Crystal data*: $C_{40}H_{36}Cu_4O_{12}N_{12}V_4$, M_w = 1334.73, triclinic *P*1, a = 11.0353(3), b = 11.2938(3), c = 11.4311(4) Å, α = 81.612(1), β = 65.755(1), γ = 61.907(1)°, V = 1143.96(6) Å^3, Z = 1, D_{calc} = 1.937 g cm^{-3}, T = 160 K; structure solution and refinement based on 6010 reflections converged at $R1$ = 0.0434, $wR2$ = 0.0828. CCDC 182/1335.

1 A. J. Cheetham, *Science*, 1994, **264**, 794 and references therein.
2 S. Mann, *J. Chem. Soc., Dalton Trans.*, 1997, 3953, and references therein.
3 M. L. Occelli and H. C. Robson, *Zeolite Synthesis*, American Chemical Society, Washington DC, 1989.
4 C. T. Kresge, M. E. Leonowitz, W. J. Roth, J. C. Vartuli and J. S. Beck, *Nature*, 1992, **359**, 710.
5 R. C. Haushalter and L. A. Mundi, *Chem. Mater.*, 1992, **4**, 31.
6 M. I. Khan, L. M. Meyer, R. C. Haushalter, C. L. Schwietzer, J. Zubieta and J. L. Dye, *Chem. Mater.*, 1996, **8**, 43.
7 P. J. Zapf, R. C. Haushalter and J. Zubieta, *Chem. Mater.*, 1997, **9**, 2019; P. J. Zapf, C. J. Warren, R. C. Haushalter and J. Zubieta, *Chem. Commun.*, 1997, 1543; P. J. Zapf, R. P. Hammond, R. C. Haushalter and J. Zubieta, *Chem. Mater.*, 1998, **10**, 1366; D. Hagrman, P. J. Zapf and J. Zubieta, *Chem. Commun.*, 1998, 1283; D. Hagrman, R. C. Haushalter and J. Zubieta, *Chem. Mater.*, 1998, **10**, 361.
8 W. Jones and M. Chibwe, in *Pillared Layered Structures*, ed. I. V. Mitchell, Elsevier, London, 1990.
9 A. Clearfield, *Comments Inorg. Chem.*, 1990, **10**, 89.
10 M. I. Khan and J. Zubieta, *Prog. Inorg. Chem.*, 1995, **43**, 1.
11 Y. Zhang, J. R. D. DeBord, C. J. O'Connor, R. C. Haushalter, A. Clearfield and J. Zubieta, *Angew. Chem., Int. Ed. Engl.*, 1996, **35**, 989.
12 P. J. Ollivier, J. R. D. DeBord, P. J. Zapf, J. Zubieta, L. M. Meyer, C.-C. Wang, T. E. Mallouk and R. C. Haushalter, *J. Solid State Chem.*, in press.

Communication 9/02451D

The reaction of difluorodioxirane with caesium trifluoromethoxide

Qun Huang and Darryl D. DesMarteau*

Department of Chemistry, Box 341905, Clemson University, Clemson, S.C. 29634-1905, USA. E-mail: fluorin@clemson.edu

Received (in Corvallis, OR, USA) 17th May 1999, Accepted 19th July 1999

The reaction of difluorodioxirane with caesium trifluoromethoxide in the presence of CsF forms $CF_3OOC(O)F$ and the new compounds $CF_3O(OCF_2O)_nOC(O)F$ (n = 1 ~ 3); ^{13}C labeling shows that the dioxirane undergoes ring opening at the O–O bond.

Dioxiranes are powerful oxygen transfer reagents which have been studied extensively over the last twenty years.[1–3] Epoxidations, heteroatom oxidations and C–H insertion reactions are the most investigated reactions of dioxiranes. The heteroatom oxidations are generally explained by an S_N2 type attack of the heteroatom lone pair (A:) on the dioxirane peroxide bond [eqn. (1)].[4]

(1)

The mechanism is based on the fact that oxygen-type nucleophiles catalytically decompose dioxiranes with evolution of molecular oxygen [eqn. (2)].[5]

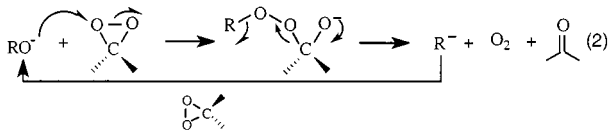

(2)

Until now, no peroxide related product has been detected in these reactions. Our recent investigation of difluorodioxirane **1** chemistry provides direct evidence of this mechanism.

Difluorodioxirane is one of the most stable dioxiranes known. The first successful synthesis of **1** was based on the reaction of its isomer fluorocarbonyl hypofluorite [FC(O)OF] with ClF in the presence of CsF.[6]† As expected, **1** is a powerful oxidant and can undergo reactions that are typical of dioxiranes. It readily transfers oxygen to alkenes, forming epoxides and COF_2 in high yield.[6] Beside this, little is known about the reactivity of **1**. Here we report a very unusual result from the reaction of **1** with COF_2 in the presence of CsF.

Difluorodioxirane was originally prepared by passing a 1:1 (v/v) mixture of FC(O)OF and ClF over a CsF catalyst.[6] We have improved this method by using Cl_2 and the new catalyst KHF_2.‡ A 1:1 (v/v) mixture of FC(O)OF and Cl_2 passed through a Teflon tube containing the new catalyst KHF_2 provided **1** in moderate but higher yields (30–50%) [eqn. (3)]. Also the dioxirane **1** prepared by this procedure is easily purified by vacuum fractional condensation as a mixture of **1** (70–90%) and COF_2 (10–30%). The mechanism of this reaction is assumed to be the same as previously proposed.[6]

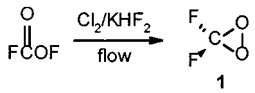

(3)

1

The O–O bond length in **1** is 157.6 pm, and is the longest O–O bond ever calculated and measured.[7] The relatively weak O–O bond should be easily broken but to date no direct evidence was available for this. Recent studies on the reaction of **1** with COF_2 in the presence of CsF show that dioxirane reacts by ring opening at the O–O bond [eqn. (4)].

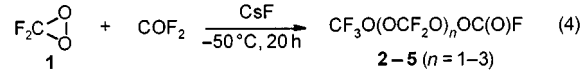

(4)

2–5 (n = 1–3)

We were able to show that the reaction occurred at the oxygen atom of the difluorodioxirane by using ^{13}C labeled COF_2 [eqn. (5)].§¶

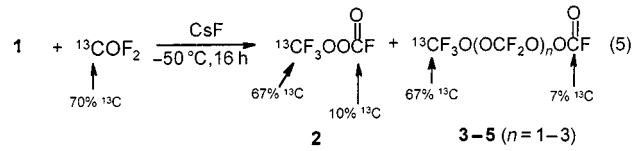

(5)

2 **3–5** (n = 1–3)

A reasonable mechanistic proposal is given in Scheme 1. The well-known trifluoromethoxy anion is first formed by the reaction of carbonyl fluoride with caesium fluoride.[8] Then an S_N2-type attack of this anion on the dioxirane peroxide bond occurs to give $CF_3OOCF_2O^-$, which loses fluoride to form **2**,[9] or reacts further with the dioxirane to form the new oligomeric peroxides **3**–**5**. The ^{13}C distribution in the products makes it clear that the predominate reaction is the attack of CF_3O^- on the dioxirane at oxygen and not at the more electropositive carbon. Previously we had suggested[10] that reaction of **1** with CsF might form CF_3OO^- and **2** could then be formed by reaction with COF_2. However this path would lead to the ^{13}C label in the carbonyl group, contrary to what is observed. The small amount of ^{13}C present in the carbonyl carbon arises from secondary reactions of the products, which have been confirmed by additional ^{13}C labeling experiments. These results will be described in a future publication.

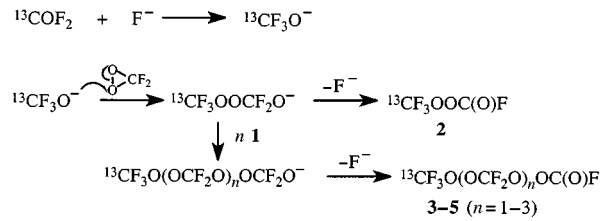

Scheme 1

Remarkably the ^{19}F chemical shifts for **2**–**5** can be assigned from a mixture of the compounds. The NMR data is presented in Fig. 1 for pure **2** and **3** and for **4** and **5** taken from a mixture of **3**–**5**. Compound **2** is unequivocally identified by comparison with known samples prepared by other routes. For **3**–**5** the chemical shifts for the CF_3OO and the $OOCF_2OO$ groups are characteristic and show a large shift relative to CF_3O and OCF_2O functions in fluorocarbon ethers. While the chemical shift differences between **2**–**5** are small, at 188 MHz all the signals except the C(O)F are separated and the expected peak integration for each compound is observed. Finally ^{19}F bound to ^{13}C and ^{12}C exhibits substantial isotopic shifts in the ^{19}F NMR in addition to the large $^1J_{F-^{13}C}$ coupling, making it trivial to discern the presence of ^{13}C.

A variety of other novel fluorocarbon peroxides can be formed by related reactions with other nucleophiles and the

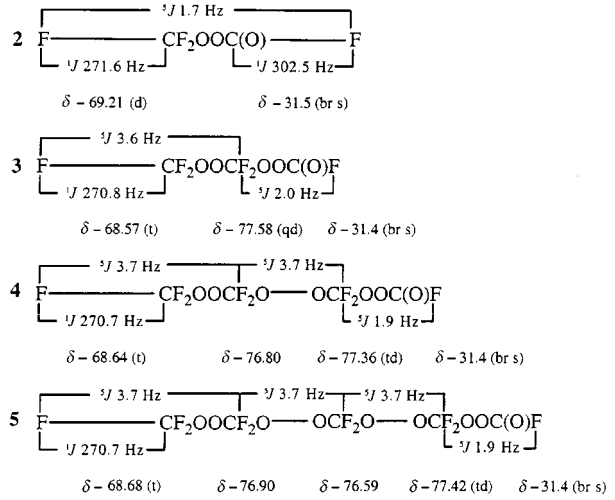

Fig. 1 ^{19}F NMR data for **2**–**5** (CCl_4 solvent, $CFCl_3$ reference, external D_2O lock, 188 MHz). Data for **4** and **5** come from a mixture of **3**–**5**.

chemistry of difluorodioxirane is proving to be quite extraordinary.

We are grateful to Ausimont SPA (Italy) for financial support of this work and to W. Navarrini of Ausimont for technical support.

Notes and references

† **CAUTION!** The chemicals employed in this work are hazardous and should only be used by experienced personnel familiar with the safe handling of toxic strong oxidizers.

‡ In a typical reaction a mixture of equimolar amounts (0.5–3.0 mmol) of FC(O)OF and Cl_2 at 23 °C were passed at reduced pressure through a Teflon FEP tube (35 × 1 cm outer diameter) containing 20 g of pelletized KHF_2 catalyst. The calculated flow rate of the mixture through the tube was 0.37 $cm^3\ s^{-1}$. The effluent exited into a trap cooled to −196 °C and under dynamic vacuum. The gases condensed at −196 °C were vacuum distilled several times through traps at −145 and −196 °C. This procedure gave **1** in the −196 °C trap, contaminated with a small amount of COF_2. *Selected data* for **1**: −92.4 (s), δ_F −20.7 (d, $^1J_{C-F}$ = 283.3) δ_C 119.5 (t). The original report of the ^{19}F NMR data in ref. 6 is in error.

§ Two 500 ml ss cylinders fitted with ss valves were connected to the vacuum line through a PFA tee closed by an ss valve. The cylinders were evacuated and one was filled with 7 mmol of fluorine gas and the other with 7 mmol of ^{13}CO (99%^{13}C). At 22 °C, the cylinders valves were then opened to the closed and evacuated tee in the order fluorine/^{13}CO. After 4 h, the contents of the two cylinders were passed through the tee into a trap cooled to −196 °C under dynamic vacuum. Unreacted F_2 and ^{13}CO passed through the −196 °C trap and through a soda lime scrubber. The contents of the −196 °C trap were then passed through −140 and −196 °C traps under dynamic vacuum to give pure $^{13}COF_2$ (3.5 mmol, 50%) in the −196 °C trap. *Selected data* for $^{13}COF_2$: δ_C 133.8 (t); δ_F −20.7 (d, $^1J_{C-F}$ 311.3); ν_{max}/cm^{-1} 1882.1, 1208.2, 957.9, 749.5, 648.6.

¶ The reactions of **1** with COF_2 and $^{13}COF_2$ were carried out in a 150 ml ss cylinder which contained 2 g of dry powdered CsF. Compound **1** (0.3 mmol) and carbonyl fluoride (0.3 mmol) were then vacuum transferred into the cylinder cooled to −196 °C. The mixture was then allowed to warm to −50 °C over 1 h and remained at −50 °C for 16–20 h. The products were separated by vacuum fractional condensation through traps at −90, −110, −130 and −196 °C. The −90 °C fraction consisted of **3**, **4** and **5** (0.03 mmol), the −110 °C fraction consisted of **3** (0.03 mmol), the −130 °C fraction consisted of **2** (0.07 mmol) and the −196 °C fraction consisted of COF_2 (0.3 mmol). Compounds **2**–**5** were identified by NMR (see Fig. 1) and IR. *Selected data* for **2**: δ_C 122.6 (q, CF_3, $^1J_{C-F}$ 271.6); 141.2 [d, C(O)F, $^1J_{C-F}$ 302.9]; ν_{max}/cm^{-1} 1874, 1254, 1209, 1153, 1005, 930, 750, 614.

1 R. W. Murray, *Chem. Rev.*, 1989, **89**, 1187.
2 R. Curci, A. Dinoi and M. F. Rubino, *Pure Appl. Chem.*, 1995, **67**, 811.
3 W. Adam and A. Smerz, *Bull. Soc. Chim. Belg.*, 1996, **105,** 581.
4 W. Adam and D. Golsh, *Angew. Chem., Int. Ed. Engl.*, 1993, **32**, 737.
5 A. Lange and H. Brauer, *J. Chem. Soc., Perkin Trans. 2*, 1996, 805.
6 A. Russo and D. D. DesMarteau, *Angew. Chem., Int. Ed. Engl.*, 1993, **32,** 905.
7 H. Burger, P. Weinrath, G. A. Arguello, B. Julicher, H. Willner, D. D. DesMarteau and A. Russo, *J. Mol. Spectrosc.*, 1994, **167,** 607.
8 W. B. Farnham, B. E. Smart, W. J. Middleton, J. C. Calabrese and D. A. Dixon, *J. Am. Chem. Soc.* 1985, **107**, 4565.
9 D. D. DesMarteau, *Inorg. Chem.*, 1970, **9,** 2179.
10 A. Russo and D. D. DesMarteau, *Inorg. Chem.*, 1995, **34,** 6221.

Communication 9/04090K

ChemComm

New reactions of cyclic sulfoxides under Pummerer conditions

R. Alan Aitken,* Lawrence Hill, Philip Lightfoot† and Neil J. Wilson

School of Chemistry, University of St. Andrews, North Haugh, St. Andrews, Fife, UK KY16 9ST.
E-mail: raa@st-and.ac.uk

Received (in Cambridge, UK) 18th June 1999, Accepted 20th July 1999

Reaction of the dihydrotetrathiafulvalene monosulfoxide 3 with TFAA results both in deoxygenation to give 1 and rearrangement to give the isomer 8, whose X-ray structure is presented; the corresponding disulfoxide 4 similarly rearranges to give 20.

We recently described the direct construction of norbornane-fused dihydrotetrathiafulvalenes such as **1** by reaction of norbornene with Bu_3P, CS_2 and acetylenic esters such as DMAD.[1] Although such dihydro-TTFs have shown some promise as potential electron donors,[2] the fully unsaturated analogues **2** would clearly be of more interest. We describe here our attempts to convert **1** into **2** which have led to the discovery both of a novel deoxygenation reaction of the sulfoxide **3** under Pummerer conditions and of its unexpected rearrangement to give the isomeric spiro compound **8**.

We decided to adopt a Pummerer approach since this has been successfully applied in the introduction of unsaturation into TTF type systems,[3] although we were aware that the rather strained nature of the expected intermediate **5** might cause some problems. Compound **1** was readily oxidised to its monosulfoxide **3** (55%) using 1 equiv. of MCPBA (Scheme 1), while use of an excess of the reagent gave the disulfoxide **4** (89%).‡ It is interesting to note that no further oxidation occurs in this system and examination of molecular models shows that introduction of oxygen on the face of the dithiolane ring *cis* to the norbornane function is sterically impossible. Both **3** and **4** were obtained as single diastereomers as shown with S=O *trans* to the norbornane function. When the sulfoxide **3** was treated with 1.1 equiv. of TFAA in CH_2Cl_2 either with or without added Hünig's base, evaporation of the reaction mixture followed by chromatography afforded two products. The first of these (38%) was readily identified as the starting dihydro-TTF **1**. Analytical and spectroscopic examination‡ of the second product (42%) revealed that it was an isomer of **3** with most of the original functionality still present, but the ^{13}C NMR signals due to the C=C double bond between the four sulfurs had been replaced by signals at δ_C 189.5 and 82.2. Its structure was finally confirmed by a single-crystal X-ray diffraction study to be the novel spiro tetrathio-orthooxalate **8** (Fig. 1).§

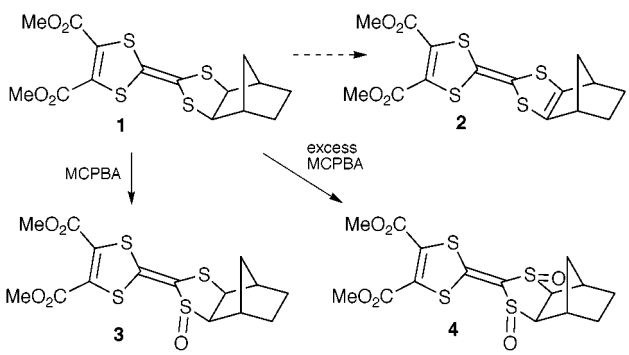

Scheme 1

† To receive correspondence regarding the X-ray structure (e-mail: pl@st-and.ac.uk).

A possible mechanism which accounts for the formation of both **1** and **8** *via* a common intermediate is shown in Scheme 2. In this the key step is participation of the dithiole ring in the initially formed salt **6** leading to a 1,2-shift of the trifluoroacetoxy group to give **7**. Although intramolecular migration of the trifluoroacetoxy group as shown seems quite likely, we cannot exclude the intermediacy of a dication, as shown, in the conversion of **6** into **7**. Attack of the trifluoroacetate at oxygen either in **6** or **7** would then give trifluoroacetyl peroxide and **1**, while the more conventional attack at CO in **7** leads to rearrangement to give **8** and regenerate the TFAA. No evidence was obtained for the formation of trifluoroacetyl peroxide but this is known to be an extremely unstable substance which rapidly decomposes to gaseous products at room temperature.[4] Although this is a completely new reaction in the dihydro-TTF system, there are a few analogous rearrangements which may all be represented as **9** going to **10** where D is an electron donor (Scheme 3). Thus, Ogura and Tsuchihashi found that treatment of the enamines **11** with Ac_2O gave the rearranged products **12**,[5] and the same authors later described the conversion of **13** into **14** with HCl gas in Bu^tOH.[6] The air oxidation of the highly reactive dithiadiazafulvalene **15** to give a low yield of a product formulated as **16**[7] also falls within the same category, as does the recently reported conversion of **17** into **18** by treatment with TFAA followed by hydrolysis.[8]

In view of these results it was of great interest to examine the behaviour of the disulfoxide **4** since the expected intermediate **19**, analogous to **7**, might rearrange with migration of either the sulfoxide sulfur to give **20** or the sulfide sulfur to give the isomer **21** containing the elusive α-keto sulfoxide functionality (Scheme 4). To the best of our knowledge no compound containing the C–C(=O)–S(=O)–C function has ever been isolated, since all attempts at generation in solution by *S*-oxidation of thioesters have resulted in rearrangement to the carboxylic–sulfenic anhydrides C–C(=O)–O–S–C which then react further.[9] In the event, treatment of **4** with 1.1 equiv. of TFAA afforded a rearranged product (42%) whose spectroscopic data‡ were more in keeping with the structure **20**, and

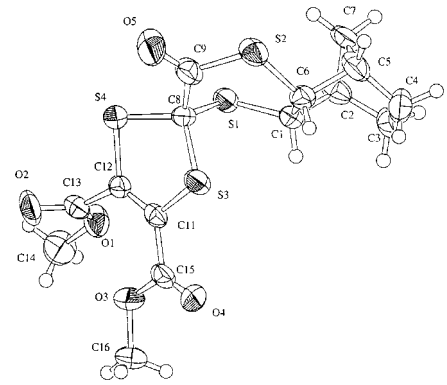

Fig. 1 X-Ray structure of the spiro compound **8**. Selected bond lengths (Å) and angles (°): S(1)–C(1) 1.816(10), S(1)–C(8) 1.834(9), S(2)–C(6) 1.821(10), S(2)–C(9) 1.76(1), C(9)–O(5) 1.21(1), C(9)–C(8) 1.51(1), C(8)–S(3) 1.828(9), C(8)–S(4) 1.825(9), S(3)–C(11) 1.761(9), S(4)–C(12) 1.756(9), C(11)–C(12) 1.31(1); C(1)–S(1)–C(8) 99.8(4), C(6)–S(2)–C(9) 108.6(5), C(8)–S(3)–C(11) 92.7(4), C(8)–S(4)–C(12) 92.4(4).

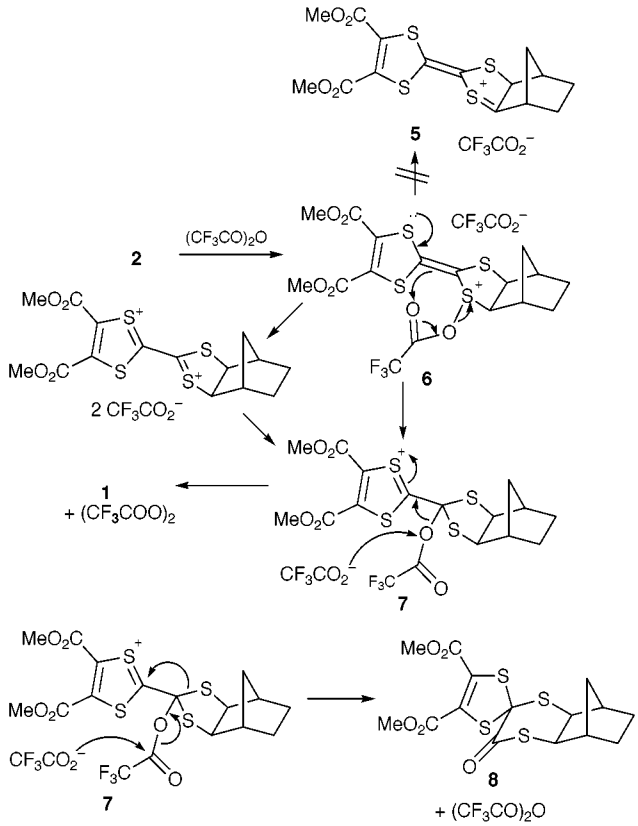

Scheme 2

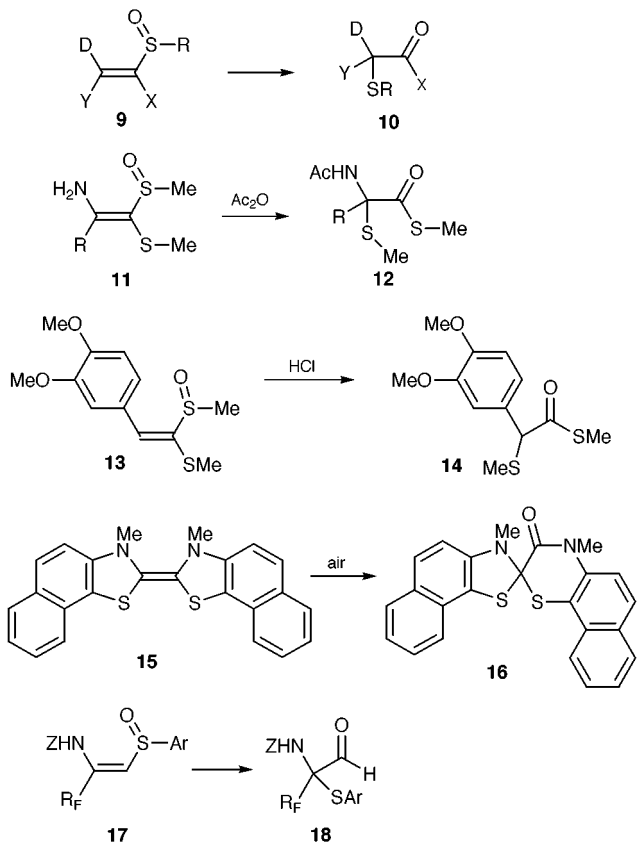

Scheme 3

this was confirmed by the observation that oxidation of **8** with MCPBA gave an identical product.

Finally, in a further attempt to convert **1** into **2**, it was treated with the well established dehydrogenating agent DDQ, and to our surprise this also afforded **8** (37%). In this case we believe

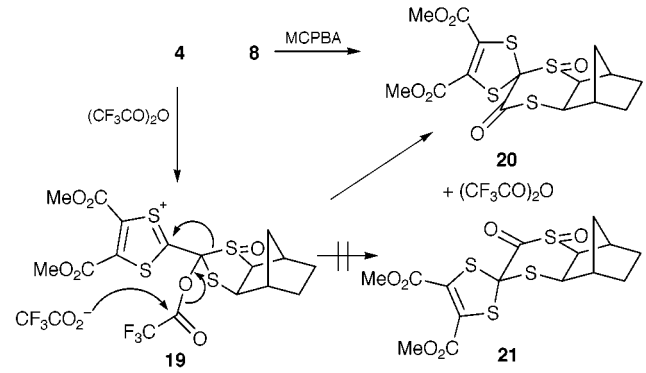

Scheme 4

the mechanism to involve a series of single electron transfer steps with the oxygen in the product being provided by adventitious water, which also serves to reduce the DDQ.

We thank EPSRC for their generous support of this work (Research Grant J 38895).

Notes and references

‡ New compounds gave satisfactory microanalytical and spectroscopic data. *Selected data* for **3**: δ_H 4.00 and 3.33 (2 H, AB pattern of d, *J* 7.2, 1.5), 3.85 (6 H, s), 2.75 (1 H, m), 2.40 (1 H, m), 1.8–1.6 (2 H, m), 1.46 (1 H, half AB pattern of m, *J* 11) and 1.4–1.2 (2 H, m); δ_C 159.6 (2 × CO_2Me), 133.1 (2 × C=C), 120.4, 112.6, 81.5 (CH–SO), 59.2 (CHS), 54.0 (2 × Me), 44.2 and 38.7 (2 × CH), 34.0, 28.7 and 27.5; *m/z* 404 (M^+, 20%), 388 (M^+–O, 10), 310 (40) and 262 (100). For **4**: δ_H 4.08 (2 H, d, *J* 2), 3.92 (6 H, s), 2.86 (2 H, m), 1.8–1.6 (2 H, m), 1.4–1.2 (3 H, m) and 0.85 (1 H, half AB pattern of m, *J* 12); δ_C 158.6 (2 × CO_2Me), 133.6 (2 × C=C), 128.3, 118.9, 83.8 (2 × CH–SO), 54.2 (2 × Me), 38.7, 36.2 and 28.0. For **8**: δ_H 3.99 (1 H, half AB pattern of d, *J* 7.3, 1.5), 3.84 and 3.83 (each 3 H, s), 3.80 (1 H, half AB pattern of d, *J* 7.3, 1.8), 2.35–2.15 (3 H, m), 1.75 (2 H, m) and 1.5–1.35 (3 H, m); δ_C 189.5 (S–CO), 160.8 and 160.2 (2 × CO_2Me), 133.8 and 125.3 (2 × C=C), 82.2 (spiro C), 54.3 (CHS), 53.4 and 53.3 (2 × Me), 48.8 (CHS), 45.9 and 40.4 (2 × CH), 34.9 (CH–CH_2–CH), 29.4 and 27.3. For **20**: δ_H 4.15 and 3.89 (2 H, AB pattern, *J* 8), 3.86 (3 H, s), 3.82 (3 H, s), 3.12 (1 H, br s), 2.40 (1 H, br s), 2.26 and 1.52 (2 H, AB pattern, *J* 11), 1.95–1.85 (2 H, m) and 1.6–1.45 (2 H, m); δ_C 185.9 (S–CO), 159.4 and 158.9 (2 × CO_2Me), 133.7 and 124.8 (2 × C=C), 91.3 (spiro C), 59.5 (CHS), 53.6 and 53.5 (2 × Me), 46.0, 43.4, 38.4, 35.5 (CH–CH_2–CH), 29.7 and 27.7.

§ *Crystal data* for **8**: $C_{15}H_{16}S_4O_5$, *M* = 404.53, colourless block, crystal dimensions 0.40 × 0.40 × 0.30 mm, monoclinic, space group $P2_1/a$ (#14), *a* = 9.321(8), *b* = 15.481(5), *c* = 12.756(7) Å, β = 105.06(5)°, *V* = 1777(1) Å^3, *Z* = 4, D_c = 1.512 Mg m^{-3}, *T* = 293 K, *R* = 0.095, R_W = 0.092 for 2278 reflections with $I > 3\sigma(I)$ and 218 variables. Data were collected on Rigaku AFC7S diffractometer with graphite-monochromated Mo-Kα radiation (λ = 0.71069 Å). The structure was solved by direct methods (SIR92) and refined using full-matrix least-squares methods. CCDC 182/1342. See http://www.rsc.org/suppdata/cc/1999/1673/ for crystallographic data in .cif format.

1 R. A. Aitken, L. Hill and P. Lightfoot, *Tetrahedron Lett.*, 1997, **38**, 7927.
2 J. Yamada, Y. Amano, S. Takasaki, R. Nakanishi, K. Matsumoto, S. Satoki and H. Anzai, *J. Am. Chem. Soc.*, 1995, **117**, 1149; J. Yamada, S. Takasaki, M. Kobayashi, H. Anzai, N. Tajima, M. Tamura, Y. Nishio and K. Kajita, *Chem. Lett.*, 1995, 1069.
3 M. Sato, N. C. Gonnella and M. P. Cava, *J. Org. Chem.*, 1979, **44**, 930.
4 W. H. Gumprecht and R. H. Dettre, *J. Fluorine Chem.*, 1975, **5**, 245.
5 K. Ogura and G. Tsuchihashi, *J. Am. Chem. Soc.*, 1974, **96**, 1960.
6 K. Ogura, Y. Ito and G. Tsuchihashi, *Bull. Chem. Soc. Jpn.*, 1979, **52**, 2013.
7 H.-W. Wanzlick, H.-J. Kleiner, I. Lasch, H. U. Füldner and H. Steinmaus, *Liebigs Ann. Chem.*, 1967, **708**, 155.
8 P. Bravo, M. Crucianelli, G. Fronza and M. Zanda, *Synlett*, 1996, 249; A. Volonterio, M. Zanda, P. Bravo, G. Fronza, G. Cavicchio and M. Crucianelli, *J. Org. Chem.*, 1997, **62**, 8031.
9 T. Kumamoto and T. Mukaiyama, *Bull. Chem. Soc. Jpn.*, 1968, **41**, 2111; M. J. Sousa Lobo and H. J. Chaves das Neves, *Tetrahedron Lett.*, 1978, 2171. For a review, see K. Schank and F. Werner, *Liebigs Ann. Chem.*, 1979, 1977.

Communication 9/04882K

ChemComm

When is a polymorph not a polymorph? Helical trimeric O–H···O synthons in *trans*-1,4-diethynylcyclohexane-1,4-diol

Clair Bilton,[a] Judith A. K. Howard,*[a] N. N. Laxmi Madhavi,[b] Ashwini Nangia,[b] Gautam R. Desiraju,*[b] Frank H. Allen[c] and Chick C. Wilson[d]

[a] *Department of Chemistry, University of Durham, South Road, Durham, UK DH1 3LE. E-mail: j.a.k.howard@durham.ac.uk*
[b] *School of Chemistry, University of Hyderabad, Hyderabad 500 046, India. E-mail: grdch@uohyd.ernet.in*
[c] *Cambridge Crystallographic Data Centre, 12 Union Road, Cambridge, UK CB2 1EZ*
[d] *ISIS Department, CLRC Rutherford Appleton Laboratory, Chilton, Didcot, Oxon, UK OX11 0QX*

Received (in Oxford, UK) 18th June 1999, Accepted 22nd July 1999

Two polymorphs (A and B) of *trans*-1,4-diethynylcyclohexane-1,4-diol represent a unique example of the simultaneous occurrence of both conformational polymorphism and conformational isomorphism, while a pseudopolymorphic monohydrate is closely related.

Definitions of *polymorphism*, the existence of two or more different crystal structures for the same compound,[1] and *pseudopolymorphism*, the existence of one or more solvated crystalline forms of the same compound,[2] are in common usage. Similarly, the existence of different conformations of the same molecule in crystals have been distinguished[3] by the terms *conformational polymorphism*, the occurrence of different conformers in different polymorphic structural modifications, and *conformational isomorphism*, the occurrence of different conformers in the same crystal structure. Here we describe two structural polymorphs and one pseudopolymorph of *trans*-

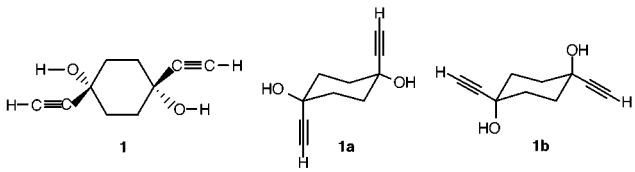

1,4-diethynylcyclohexane-1,4-diol **1**, in which the simultaneous occurrence of both conformational polymorphism and conformational isomorphism are the key distinguishing features of the crystal structures, and also provide a unique test of existing definitions.

Our studies of **1** were prompted by recent interest[4] in

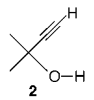

structures containing the *gem*-hydroxyethynyl fragment **2**. As well as the expected O–H···O hydrogen bonds, arrays of C–H···O, O–H·π and C-H··π interactions (π = ethynyl, phenyl), sometimes stabilised by cooperativity, frequently dominate the crystal packing. This variety of interactions leads to considerable structural diversity amongst the > 90 structures containing **2** that are already available in the Cambridge Structural Database (CSD).[5] Simple mono-alcohols exhibit two types of O–H···O aggregates (chains and rings), but even here there is no predominant motif. Thus, the available evidence suggests that structures containing **2** are strongly influenced by the remaining portion of the molecule, prompting us to investigate the crystal structure of compound **1**, in which competitive effects are minimised so that the intrinsic hydrogen-bonding preferences of **2** may be more clearly discerned.

Diol **1** was synthesised by adding TMSC≡C-Li to cyclohexane-1,4-dione and hydrolysis of the TMS groups by KOH. The unwanted *cis*-isomer was separated by repeated recrystallisations from EtOAc. Further recrystallisation of pure *trans*-**1** yielded crystals of two modifications, **A** and **B**, in the same flask. We find that both forms crystallise in space group $P\bar{1}$ with $Z = 3$,† both structures have three symmetry-independent half-molecules occupying distinct inversion centres, and both structures assemble around a spine of helical, cooperatively assisted, trimeric motifs formed *via* O–H···O bonds [**A**: Fig. 1(*a*), **B**: Fig. 1(*b*); *d*(O···H) = 1.70–1.76 Å, θ (O–H···O) = 163–177° over both structures, H-atom positions neutron-normalised). However, Fig. 1(*a*) shows that form **A** contains two molecules of conformer **1a** in which the hydroxy groups are diequatorial, while the third molecule has the diaxial OH conformation (**1b**). Fig. 1(*b*) shows that the reverse is true in form **B**: two molecules have diaxial OH groups (**1b**) and the third has the diequatorial OH conformation (**1a**). Interestingly, form **B** is 3% more efficiently packed than form **A** but this is compensated for by the better O–H···O hydrogen bonds in form A (mean *d* = 1.715 A *vs.* 1.745 in form **B**).

Amazingly, a third crystalline form was isolated from the same flask and characterised by both low-temperature X-ray and neutron diffraction.† Form **C** ($P2_1/c$, $Z = 4$) was shown to be a 1:1 hydrate of the diequatorial OH conformer **1a**, and the crystal structure maintains the helical O–H···O trimer *via* the assembly of two symmetry-independent half-molecules of **1a** and one O–H donor from a water molecule [Fig. 1(*c*), *d* = 1.64–1.80 Å, θ = 164–177°]. The second O–H donor of the water molecule interlinks inversion-related trimers (*d* = 1.91 Å, θ = 174°). In effect, the water molecule replaces the axial OH group in form **A** so that the trimeric O-H···O hydrogen-bonded helical spine is the dominant recurring pattern in all three crystalline forms of **1**.

It would appear that the presence of both conformers is required for the formation of the robust helical trimeric synthon in the unsolvated polymorphs, a supposition that is reinforced by the crystal structure of *trans*-cyclohexane-1,4-diol **3**.[6] The

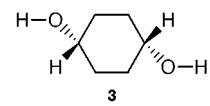

diol **3** also contains the helical O–H···O trimer and crystallises in space group $P2_1/n$ with 1.5 molecules per asymmetric unit. The molecule in general positions has diequatorial OH groups, while the molecule on an inversion centre has diaxial OH groups. The O–H···O trimer is then formed by two diequatorial and one diaxial conformer, as in form **A** of **1**.

Why is it that both conformers are required for trimer formation in forms **A** and **B** of **1**, and in the diol **3**? It may be that the simultaneous presence of inversion centres (arising from the molecular structures of **1** and **3**), and the 3- or 3_1-axes that could arise if the trimer formed from three *identical* conformers of **1**

or **3**, would impose significant constraints on the packing efficiency. It appears that these constraints are alleviated by the presence of both conformers in forming the trimeric H-bonded synthon. There are no clear or simple ways of supporting or refuting this conjecture. Nevertheless, we note that the CSD contains no examples of single-conformation cyclohexane-1,4-diols that form O–H···O trimers, but that single-conformation alicyclic diols do form such trimers (around 3_1-axes), but only where the molecules do not have additional inversion symmetry. These arguments provide a rationale for the ready incorporation of water in form **C** as a replacement for the 'other' conformer of **1**.

In summary, the structures described above have a number of important implications. (i) This is the first example (to the best of our knowledge) in which the phenomena of conformational polymorphism and conformational isomorphism are observed simultaneously, revealing a new and unforeseen facet of polymorphism. Specifically, **A** or **B** when taken individually exhibit conformational isomorphism while the pair when taken together exhibit conformational polymorphism. (ii) The definition of forms **A** and **B** of **1** as polymorphs and form **C** as a pseudopolymorph can be viewed as somewhat subjective. If **1a** and **1b** are considered as rapidly equilibrating conformers of **1**, then the accepted definitions hold. However, if **1a** and **1b** are viewed as distinct molecular species, then forms **A** and **B** are simply binary crystals of 2:1 and 1:2 stoichiometry, and form **C** is a hydrate of **1a**. (iii) The isolation of three concomitant crystalline modifications of **1** suggest that the energy differences between them are small (1–2 kcal mol^{-1}) and that crystal forces influence the molecular conformation. The polymorph formation is not kinetically controlled and the three forms are stable over time. (iv) The recurrence of the O–H···O helical trimer in structures of **1** and **3** confirms that this is a robust supramolecular synthon which is insensitive to a change in substitution from ethynyl (in **1**) to the much smaller H-atom (in **3**). The extent to which a molecular structure can be perturbed without changing the structure-determining synthons in its crystal structure is a contemporary theme in crystal engineering. (v) The structures of the three forms of **1** resemble the structures of simple diols much more closely that they resemble structures of other *gem*-alkynols, in which there is considerable interference between the stronger O–H···O hydrogen bonds and weaker interactions (C–H···O, O–H·π, C–H··π) that involve the alkyne C–H and π-density. Further structural and computational studies of other *gem*-alkynols are in progress to shed more light on the role of this functional group in crystal packing.

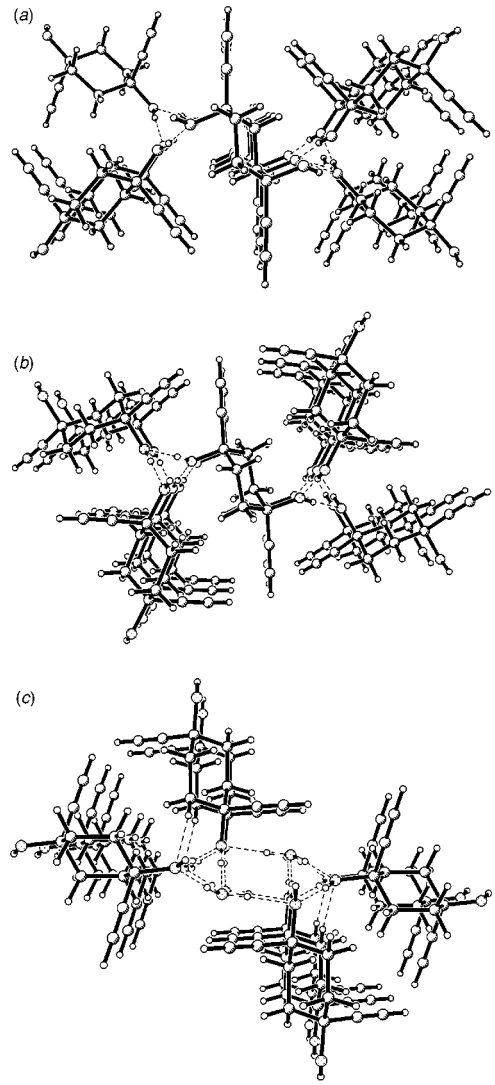

Fig. 1 Perspective views of the crystal structures of (*a*) form **A** of **1**, (*b*) form **B** of **1**, and (*c*) the monohydrated form **C** of **1**, showing the common helical O–H···O trimeric synthon and the conformations adopted by **1**.

Notes and references

† *Crystal data* for form **A** of **1**: $C_{10}H_{12}O_2$, M = 164.20, triclinic, a = 6.2074(3), b = 10.0187(5), c = 11.5666(5) Å, α = 103.005(2), β = 93.424(2), γ = 94.572(2)°, U = 696.41(6) Å^3, T = 150 K, space group $P\bar{1}$, Z = 3, μ(Mo-Ka) = 0.081 mm^{-1}, block shaped crystals, size 0.5 × 0.4 × 0.4 mm. Data were collected on a Bruker SMART-CCD detector, 5564 total reflections of which 3618 were independent, 3027 observed [$I > 2\sigma(I)$]. The structure was refined against F^2 with 235 parameters, $R1$ [$I > 2\sigma(I)$] = 0.0409. For form **B** of **1**: $C_{10}H_{12}O_2$, M = 164.20, triclinic, a = 6.4140(2), b = 9.6367(3), c = 11.7852(4) Å, α = 105.689(2), β = 101.838(1), γ = 94.736(1)°, U = 678.98(4) Å^3, T = 150 K, space group $P1$, Z = 3, μ(Mo-Ka) = 0.083 mm^{-1}, block shaped crystals, size 0.3 × 0.25 × 0.25 mm. Data were collected on a Bruker SMART-CCD detector, 4754 total reflections of which 3061 were independent, 2554 observed [$I > 2\sigma(I)$]. The structure was refined against F^2 with 235 parameters, $R1$ [$I > 2\sigma(I)$] = 0.0461. For monohydrated form **C** of **1**: $C_{10}H_{12}O_2.H_2O$, M = 182.20, monoclinic, a = 9.925(2), b = 6.1343(12), c = 16.725(3) Å, β = 104.12(3)°, U = 987.5(3) Å^3, T = 150 K, space group $P2_1/c$, Z = 4, μ = 0.226 mm^{-1}, rectangular crystals, size 2 × 2 × 1.5 mm. Data were collected on the SXD single crystal diffractometer at ISIS, 9863 total reflections of which 2661 were independent, 2659 observed [$I > 2\sigma(I)$]. The structure was refined against F^2 with 244 parameters, $R1$ [$I > 2\sigma(I)$] = 0.0888. CCDC 182/1343. See http://www.rsc.org/suppdata/cc/1999/1675/ for crystallographic data in .cif format.

1 T. L. Threlfall, *Analyst*, 1995, **120**, 2435.
2 A. Nangia and G. R. Desiraju, *Chem. Commun.*, 1999, 605; V. S. S. Kumar, S. S. Kuduva and G. R. Desiraju, *J. Chem. Soc., Perkin Trans. 2*, 1999, 1069.
3 J. Bernstein, in *Organic Solid State Chemistry*, ed. G. R. Desiraju, Elsevier, London, 1987, pp. 471–518.
4 G. R. Desiraju and T. Steiner, *The Weak Hydrogen Bond in Structural Chemistry and Biology*, OUP, Oxford, 1999, pp. 175–185.
5 F. H. Allen, J. E. Davies, J. J. Galloy, O. Johnson, O. Kennard, C. F. Macrae, E. M. Mitchell, G. F. Mitchell, J. M. Smith and D. G. Watson, *J. Chem. Inf. Comput. Sci.*, 1991, **31**, 187.
6 T. Steiner and W. Saenger, *J. Chem. Soc., Perkin Trans. 2*, 1998, 371.

Communication 9/05025F

ChemComm

Structure determination of a steroid directly from powder diffraction data†

Benson M. Kariuki,[a] Katerina Psallidas,[a] Kenneth D. M. Harris,*[a] Roy L. Johnston,[a] Robert W. Lancaster,[b] Susan E. Staniforth[b] and Simon M. Cooper[b]

[a] *School of Chemistry, University of Birmingham, Edgbaston, Birmingham, UK B15 2TT. E-mail: k.d.m.harris@bham.ac.uk*

[b] *Glaxo Wellcome Research and Development, Gunnels Wood Road, Stevenage, Hertfordshire, UK SG1 2NY*

Received (in Cambridge, UK) 14th June 1999, Accepted 14th July 1999

We report the determination of the crystal structure of a new polymorph of the pharmaceutical material fluticasone propionate, which is obtained as a microcrystalline powder by a supercritical crystallization procedure; the structure was solved directly from powder diffraction data using our Genetic Algorithm technique (in which a population of trial structures evolves through well-defined procedures for mating, mutation and natural selection) and refined using Rietveld refinement techniques.

Single crystal X-ray diffraction is without question the most powerful tool for elucidating crystal and molecular structures. However, the requirement for single crystal samples imposes a natural limitation on the scope of this technique, as many materials of interest cannot be prepared as single crystals of sufficient size and quality, but are instead available only as microcrystalline powders. Such materials include many industrially important solids, such as pigments, pharmaceuticals and catalysts, as well as many materials of biological importance. Here we report progress in the structure determination of one such material—a new polymorph of the steroid fluticasone propionate, which is important with regard to its pharmaceutical applications—using a Genetic Algorithm technique developed recently for solving crystal structures directly from *powder* diffraction data.

Fluticasone propionate ($C_{25}H_{31}F_3O_5S$; FP) is a potent synthetic anti-inflammatory steroid which suppresses inflammation of the bronchial passages in the lungs. When formulated as an inhaled product (under the trademark‡ Flixotide™ or

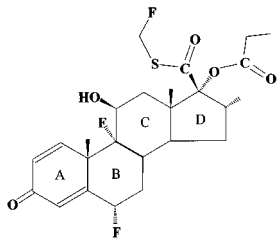

Flovent™), the anti-inflammatory action of FP treats the underlying inflammatory component of asthma. FP also has an indication in an intra-nasal form for rhinitis, where it is marketed under the trademark‡ Flixonase™. It has a superior therapeutic index to beclomethasone dipropionate (BDP).

FP is known to exist in two polymorphic forms. Form 1 can be obtained by crystallization from a variety of solvents (typically acetone), and the crystal structure of form 1 has been determined previously[1] from single crystal X-ray diffraction (and also confirmed as part of our current research by structure determination from powder diffraction data using the techniques discussed below). In attempts to produce crystals of FP of controlled size and morphology for pharmaceutical applications, crystallization in a supercritical fluid medium (with EtOH or acetone as solvent) was carried out, and was found to yield a new polymorph (form 2). As form 2 was obtained only by the supercritical crystallization method, yielding polycrystalline powder samples, structural characterization of form 2 could not be carried out by single crystal X-ray diffraction. Here we report the determination of the crystal structure of form 2 of FP directly from powder X-ray diffraction data.

Although traditional techniques[2–4] for structure solution from powder diffraction data have been applied successfully in several cases, these techniques have certain intrinsic limitations[3] and organic molecular crystals represent a particularly challenging case. For this reason, there has been much recent interest in the development of new methods for solving crystal structures directly from powder diffraction data, leading *inter alia* to a new generation of 'direct-space' approaches that are particularly suited for molecular crystals. The direct-space strategy[5,6,3] is based on sampling trial crystal structures in direct space, with the 'quality' of each trial structure assessed by comparing the powder diffraction pattern calculated for the trial structure and the experimental powder diffraction pattern. In our work, this comparison is made using the profile *R*-factor R_{wp},[3,5] which considers the whole digitized intensity profile and thus implicitly takes care of peak overlap. In effect, the structure solution process involves searching a hypersurface $R_{wp}(\mathbf{X})$ to find the best structure solution (lowest R_{wp}), where $\{\mathbf{X}\}$ represents the variables that define the trial structures. In the case of one molecule in the asymmetric unit, the variables in $\{\mathbf{X}\}$ represent the position $\{x, y, z\}$, orientation $\{\theta, \phi, \psi\}$ and intramolecular geometry (specified by variable torsion angles $\{\tau_1, \tau_2, \ldots \tau_n\}$) of the molecule. In general, the bond lengths and bond angles (and any known torsion angles) are fixed in the calculation, and are taken either from standard values for the type of molecule under study or from the known geometries of similar molecules. Methods used to search *R*-factor hypersurfaces to locate the global minimum (structure solution) within direct-space structure solution strategies have included Monte Carlo,[5,7,8] simulated annealing[6,9,10] and Genetic Algorithm (GA)[11–15] techniques. Here we focus on the application of our GA method, details of which are described in ref. 12. In this approach, a population of trial structures is allowed to evolve subject to the normal rules and operations (mating, mutation and natural selection) that govern evolutionary systems.

The powder X-ray diffraction pattern of form 2 of FP was recorded at 22 °C in transmission mode on a Siemens D5000 diffractometer, using Ge-monochromated Cu-Kα_1 radiation and a linear position-sensitive detector covering 8° in 2θ. The total 2θ range was 5° to 60°, measured over 12 h in steps of 0.02°. The powder X-ray diffraction pattern was indexed by the program ITO.[16] [The lattice parameters following Rietveld refinement (see below) are: a = 23.2434(9), b = 13.9783(5), c = 7.6510(3) Å.] Systematic absences are consistent with space group $P2_12_12_1$, and density considerations suggest that there is one molecule in the asymmetric units.§

In the GA structure solution calculation (using the program GAPSS,[17,12]), all non-hydrogen atoms of the FP molecule were used (to define the asymmetric unit). The tetracyclic ring system

† Fractional coordinates for the non-hydrogen atoms in the final crystal structure of form 2 of FP are available from the RSC web site, see http://www.rsc.org/suppdata/cc/1999/1677/

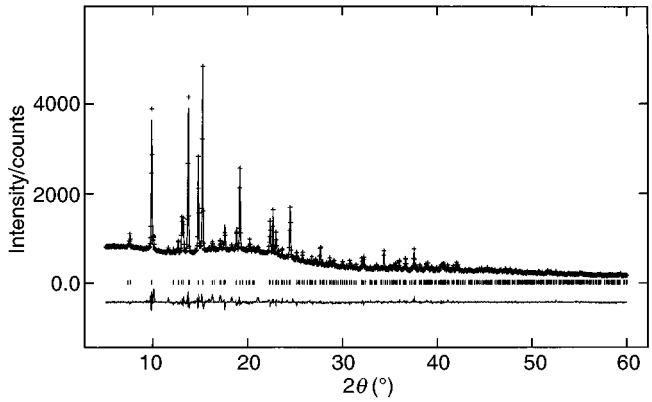

Fig. 1 Experimental (+), calculated (solid line) and difference (lower line) powder X-ray diffraction profiles for the Rietveld refinement of form 2 of FP. Reflection positions are marked. The calculated powder diffraction profile is for the final refined crystal structure, details of which are given in the supplementary material. See note †.

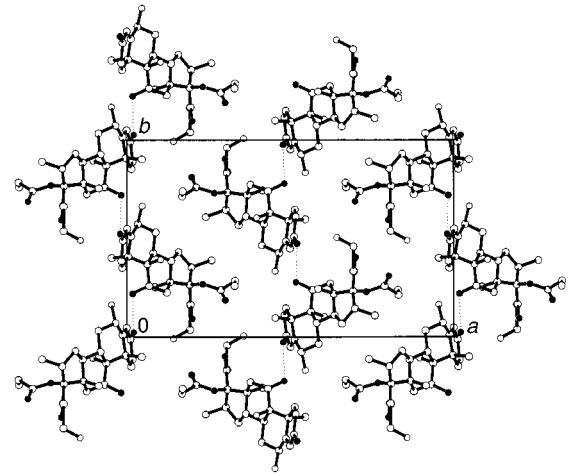

Fig. 2 Final refined crystal structure of form 2 of FP (hydrogen atoms not shown) viewed along the *c*-axis. Dashed lines indicate hydrogen bonding interactions.

was considered as a rigid unit, comprising one planar six-membered ring (designated A), two six-membered rings in chair conformation (B and C), and a five-membered ring in an envelope conformation (D). The side-groups attached to the D ring were considered as flexible units, with their conformations defined by six variable torsion angles. Thus, the GA calculation involved 12 degrees of freedom $\{x, y, z, \theta, \phi, \psi, \tau_1, \tau_2, \ldots \tau_6\}$. Bond lengths and angles were taken from known structures of other steroid molecules and from other information on standard molecular geometries.[18] The GA calculation involved the evolution of 60 generations of a population of 100 structures. In each generation, 200 offspring (involving 100 pairs of parents) and 10 mutations were considered. For mating and mutation, each of the 12 variables was considered as an independent gene. In carrying out a given mating operation between two parents to generate two offspring, the 12 variables from each parent were combined and distributed between the two offspring, with no restriction on the combination of variables allowed to pass from a given parent to a given offspring. In carrying out the mutation procedure on a selected structure, six variables were selected at random, and a new random value was assigned to each of the selected variables.

The best structure solution (lowest R_{wp} in the final generation) was taken as the starting structural model for Rietveld refinement using the GSAS program package.[19] The positions of all non-hydrogen atoms were refined, with standard geometric restraints applied to bond lengths and angles. A common isotropic displacement parameter was refined (final U_{iso} = 0.050 Å^2), and in the final stages a preferred orientation parameter was refined. The final Rietveld refinement (Fig. 1; Table 1) gave R_{wp} = 4.8% and R_p = 3.3%.

In the crystal structure of form 2 of FP (Fig. 2), the molecules form stacks along the *c*-axis with adjacent molecules related by translation. Zig-zag chains of molecules related by the 2_1 screw operation along the *b*-axis are linked by C–O–H···O=C hydrogen bonds involving the hydroxy group (C ring) and carbonyl group (A ring) of adjacent molecules (O···O, 2.8 Å; C–O···O, 110°). This structure provides interesting similarities and contrasts with the structure of form 1 of FP.[1] Both structures contain similar hydrogen-bonded chains (described above along the *b*-axis in form 2), but differ in the structural relationship between adjacent chains of this type; in form 2, adjacent chains are anti-parallel (related by a 2_1 axis), whereas in form 1, adjacent chains are parallel to each other (related by translation).

It is clear that knowledge of the structure of form 2 of FP provides a basis for understanding differences in the properties of forms 1 and 2, including those relating to pharmaceutical applications of these materials. This opportunity has arisen through the present-day ability to solve molecular crystal structures of moderate complexity directly from powder diffraction data.

We are grateful to Glaxo Wellcome plc and the EPSRC for financial support.

Notes and references

‡ Flixotide™, Flovent™ and Flixonase™ are trademarks of the Glaxo Wellcome group of companies.

§ *Note added in response to a referee:* Form 2 of FP transforms to form 1 between *ca.* 154 and 165 °C which then subsequently melts (with decomposition) between *ca.* 279 and 291 °C. The densities at ambient temperature are: form 1, 1.33 g cm^{-3} (measured), 1.34 g cm^{-3} (calculated); form 2, 1.34 g cm^{-3} (calculated).

1 Glaxo Wellcome plc, unpublished results.
2 L. B. McCusker, *Acta Crystallogr., Sect. A*, 1991, **47**, 297.
3 K. D. M. Harris and M. Tremayne, *Chem. Mater.*, 1996, **8**, 2554.
4 D. M. Poojary and A. Clearfield, *Acc. Chem. Res.*, 1997, **30**, 414.
5 K. D. M. Harris, M. Tremayne, P. Lightfoot and P. G. Bruce, *J. Am. Chem. Soc.*, 1994, **116**, 3543.
6 J. M. Newsam, M. W. Deem and C. M. Freeman, *Accuracy in Powder Diffraction II*; *NIST Special Publ. No. 846*, 1992, p. 80.
7 D. Ramprasad, G. P. Pez, B. H. Toby, T. J. Markley and R. M. Pearlstein, *J. Am. Chem. Soc.*, 1995, **117**, 10 694.
8 M. Tremayne, B. M. Kariuki and K. D. M. Harris, *Angew. Chem., Int. Ed. Engl.*, 1997, **36**, 770.
9 Y. G. Andreev, P. Lightfoot and P. G. Bruce, *Chem. Commun.*, 1996, 2169.
10 W. I. F. David, K. Shankland and N. Shankland, *Chem. Commun.*, 1998, 931.
11 B. M. Kariuki, H. Serrano-González, R. L. Johnston and K. D. M. Harris, *Chem. Phys. Lett.*, 1997, **280**, 189.
12 K. D. M. Harris, R. L. Johnston and B. M. Kariuki, *Acta Crystallogr., Sect. A*, 1998, **54**, 632.
13 P. Calcagno, B. M. Kariuki, K. D. M. Harris, D. Philp and R. L. Johnston, *Angew. Chem., Int. Ed. Engl.*, 1999, **38**, 831.
14 K. Shankland, W. I. F. David and T. Csoka, *Z. Kristallogr.*, 1997, **212**, 550.
15 K. Shankland, W. I. F. David, T. Csoka and L. McBride, *Int. J. Pharm.*, 1998, **165**, 117.
16 J. W. Visser, *J. Appl. Crystallogr.*, 1969, **2**, 89.
17 R. L. Johnston, B. M. Kariuki and K. D. M. Harris, *GAPSS*, Genetic Algorithm for Powder Structure Solution, University of Birmingham, 1997.
18 F. H. Allen, O. Kennard, D. G. Watson, L. Brammer, A. G. Orpen and R. Taylor, *J. Chem. Soc., Perkin Trans. 2*, 1987, S1.
19 A. C. Larson and R. B. Von Dreele, Los Alamos Lab. Report No. LA-UR-86-748, 1987.

Communication 9/04702F

Towards the Loewenstein limit (Si/Al = 1) in thermally stable mesoporous aluminosilicates

Saúl Cabrera,[a] Jamal El Haskouri,[a] Sagrario Mendioroz,[b] Carmen Guillem,[a] Julio Latorre,[a] Aurelio Beltrán-Porter,[a] Daniel Beltrán-Porter,[a] M. Dolores Marcos*[a] and Pedro Amorós*[a]

[a] *Institut de Ciència dels Materials de la Universitat de València (I.C.M.U.V.), PO Box 2085, 46071-València, Spain. E-mail: pedro.amoros@uv.es; loles.marcos@uv.es*

[b] *Instituto de Catálisis y Petroleoquímica, Campus Universidad Autónoma, Cantoblanco, 28049-Madrid, Spain*

Received (in Oxford, UK) 14th June 1999, Accepted 23rd July 1999

The use of complexing agents to generate polynuclear precursor species containing both Al and Si allows the synthesis of thermally stable mesoporous aluminosilicates including solely tetrahedrally coordinated aluminium, in which the Si/Al ratio can be modulated down to a minimum Si/Al value of 1.06(4).

A great part of fine chemicals production is dependent on high surface Al–Si mixed oxides or zeolites which act as catalysts or serve as catalyst supports.[1–3] After the discovery of silica-based MCM-41 mesoporous derivatives,[4] a key scientific objective has been the attainment of increasing content of tetrahedral Al in the framework of materials of this type to achieve higher Brønsted acidity and thus improved catalytic activity. Different direct surfactant-assisted synthetic procedures related to that of MCM-41[5–8] or, alternatively, post-synthesis reactions[9] have been explored with this aim. Indeed, the use as principal reagent of $Al_4Si_4(OH)_8O_{12}^{4-}$ cube-like molecular polyanions (*i.e.* by incorporating the optimal Si/Al = 1 molar ratio into the precursor) led to a mesostructured material with high Al content.[5] Unfortunately, surfactant removal led to a collapse of the pore system together with partial conversion of tetrahedral Al centers into octahedral ones. In general, the best results have been obtained by reproducing the MCM-41 synthesis in the presence of an Al source. As far as we know, stable mesoporous solids prepared through surfactant-assisted procedures having the largest contents of tetrahedral Al are those reported by Luan *et al.*[6] (Si/Al = 2.5) and Borarde and Clearfield[7] (Si/Al = 2), who used $Al_2(SO_4)_3$ and $NaAlO_2$, respectively. This notwithstanding, as stated by Hamdan *et al.*,[8] the outcome of direct synthesis of Al containing MCM-41 depends strongly on the nature of the Al source used, which often leads to irreproducible results.

We report here a new direct and reproducible procedure that provides thermally stable mesoporous aluminosilicate molecular sieves in which the Al content in the framework can be modulated down to a minimum Si/Al value of 1.06(4), very close to the ideal molar ratio of 1 (compatible with the presence of mainly tetrahedrally coordinated Al centers).[10]

Aluminium rich mesoporous materials of the MCM-41 type have been synthesized using CTABr as surfactant in $TEAH_3$–water (CTABr = cetyltrimethylammonium bromide, $TEAH_3$ = triethanolamine). A typical preparation leading to the Si/Al = 1.06 mesoporous aluminosilicate can be described as follows: a mixture of TEOS (7.2 mL, 0.033 mol) and $Al(OBu^s)_3$ (8.4 mL, 0.033 mol) was added to a solution containing $TEAH_3$ (30 mL, 0.226 mol) and 1.32 g (0.03 mol) of NaOH in 2 mL of water, and heated at 190 °C for 10 min [TEOS = tetraethylorthosilicate, $Al(OBu^s)_3$ = aluminium *sec*-butoxide]. The resulting solution was cooled to 50 °C, and CTABr (6.5 g, 0.018 mol) in 180 mL of water was added while stirring. The mixture was allowed to age for 5 days at room temperature, resulting in the formation of a white solid. This was then filtered off washed with ethanol and air dried. To obtain the final mesoporous material, the as-synthesized solid, which is mesostructured, was calcined at 500 °C for 5 h under air to eliminate the surfactant. Table 1 summarises the main synthesis variables and physical data corresponding to some selected samples. All the samples were analyzed and characterized by electron probe microanalysis (EPMA), (Philips SEM-515 instrument), XRD techniques (Seifert 3000TT diffractometer using Cu-Kα radiation), TEM (Philips CM10 microscope), ^{29}Si and ^{27}Al MAS NMR (Varian Unity-300 spectrometer), and N_2 adsorption–desorption isotherms (Micromeritics ASAP2010 analyzer). Moreover, fast atom bombardment (FAB) analysis of the precursor solutions was been performed to gain insight into the role of $TEAH_3$.

EPMA analysis shows that all the samples are chemically homogeneous with a regular distribution of aluminium and silicon atoms throughout the inorganic walls. Hence, the solids can be considered as monophasic products. The Si/Al molar ratio in the final material is very close to that present in the mother-liquor, indicating that there is no preferential incorporation of aluminium or silicon into the final net.

XRD pattern resolution of mesoporous materials is poorer than for purely siliceous MCM-41 solids. This fact indicates a degree of loss of the typical hexagonal order observed for MCM-41 solids. Hence, the pore packing motif can be better described as disordered hexagonal, as confirmed by TEM micrographs (Fig. 1).

Previous ^{27}Al NMR results indicate that Al containing MCM-41 solids may include octahedrally coordinated aluminium atoms, with a degree of controversy about their extra- or intra-framework nature. Thus, on the basis on 2-D NMR data, Janicke *et al.*[11] have recently concluded that both four- and six-coordinate Al centers can coexist in the inorganic walls. In any case, it seems clear that Al atoms in octahedral environments do

Table 1 Selected synthetic and physical data for some mesoporous aluminosilicates samples

Sample	Si/Al (Precursor)	Si/Al[a] (Solid)	δ^b	d_{100}/Å	a^c/Å	Pore size/Å	Pore wall thickness/Å	Surface area/ $m^2\ g^{-1}$
1	∞	∞	−113.3	37.5	43.3	25.6	17.7	1118
2	14.0	8.17(3)	−105.0	38.5	44.5	25.0	19.5	985
3	5.0	4.51(6)	−97.8	38.5	44.5	21.5	23.0	832
4	1.0	1.06(4)	−87.9	41.8	48.3	20.0	28.3	430

[a] Values averaged from EPMA of *ca.* 40 different particles, (statistical esds in parenthesis). [b] ^{29}Si MAS NMR chemical shifts. [c] Calculated cell parameter values assuming an MCM-41 type hexagonal cell.

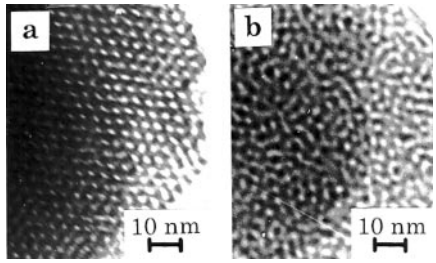

Fig. 1 TEM micrographs of (a) sample 1 (Si/Al = ∞) and (b) sample 4 [Si/Al = 1.06(4)].

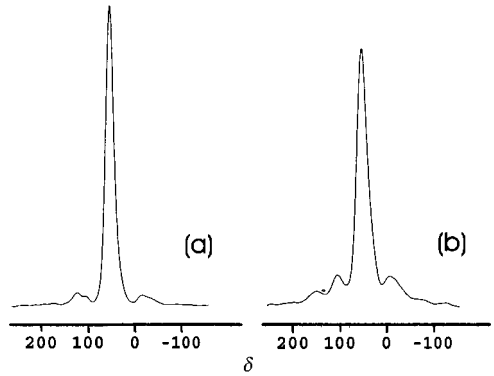

Fig. 2 ^{27}Al MAS NMR spectra of sample 4 [Si/Al = 1.06(4)]. (a) mesostructured; (b) mesoporous. Small signals at either side of the main one are due to the spinning of the sample (side bands).

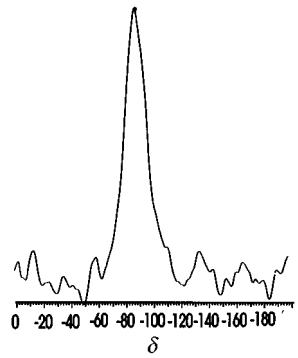

Fig. 3 ^{29}Si MAS NMR spectrum of mesoporous sample 4 [Si/Al = 1.06(4)].

not contribute to the Brønsted acidity. The ^{27}Al MAS NMR spectra of all mesostructured or mesoporous materials reported here show essentially only one resonance signal at δ *ca.* 55 (Fig. 2), which is characteristic of tetrahedral Al. The small signals at either side of the main signal are due to the spinning of the sample (side bands) as they move equally when changing the spinning frequency. A remarkable fact is that neither dealumination nor conversion from tetrahedral into octahedral aluminium occurs as a consequence of surfactant removal. ^{29}Si MAS NMR spectra for all samples show a very strong and broad signal whose center shifts from δ −113 for pure siliceous MCM-41 materials to δ −87.9 for sample 4 (Fig. 3) (see Table 1). In this last case, the displacement of the signal is in accordance with the resonance of Q^4 (4Al) and Q^3 (3Al) Si environments. The broadness of the signal may be a consequence of resonances of other minor Si environments such as Q^4 (3Al) and other Q^3 sites, similarly to results reported in ref. 5. Thus, both ^{27}Al and ^{29}Si MAS NMR results are in good accordance with the Si/Al = 1.06 molar ratio calculated from EPMA analysis.

All samples show one well defined step in their N_2 adsorption isotherms. According to previous observations, incorporation of Al leads to significant decreases in BET surface area and pore size (Table 1). Despite this, the high surface area, porosity and thermal stability characteristic of the parent mesoporous silicas, are retained even for the highest Al content [Si/Al = 1.06(4)]. An estimation of the pore wall dimensions can be made from XRD and porosity data. As shown in Table 1, the pore wall thickness increases (17.7–28.3 Å) with Al content and probably leads to the materials' high thermal stability.

A preliminary mass-spectral analysis (FAB) carried out on TEOS–Al(OBu^s)$_3$–TEAH$_3$ mixtures, prior to surfactant addition, indicates the presence of entities of different nuclearity in which triethanolamine must displace the initial alkoxide anions from the metallic coordination spheres and give rise to more hydrolysis stable complexes when water is added [TEAH$_{3-n}$-(TEASi)$_n$ (n = 1–3); Al(TEA)]. Although MS FAB analysis cannot differentiate between Si and Al in polynuclear species, taking into account the similar affinity of both Si and Al towards coordination of TEA,[12] mixed molecular precusor species can be envisaged, *e.g.* Si$_{3-n}$Al$_n$ (TEA)$_{4-n}$(TEAH)$_n$ (n = 1,2) This fact indicates that Al and Si are essentially mixed to a nearly atomic level in the precursor solution, and explains the high chemical homogeneity observed both in the mesostructured and in the final mesoporous solids.

In summary, this work demonstrates that it is possible to increase, in a continuous way, the Al content in MCM-41-like mesoporous materials up to virtually a 1/1 Si/Al molar ratio, the maximum possible for an aluminosilicate without formation of Al–O–Al links. Taking into account the ready formation of stable monomeric and polynuclear species, the role played by triethanolamine can be viewed as a 'hydrolysis retarding agent' for both Si and Al. This allows a balance between the hydrolysis and condensation reactions affecting the inorganic species and the self-assembling processes between the resulting inorganic fragments and the organic surfactant. Moreover, by leading to an intimate mixture of Al and Si in the mother-liquor, the presence of triethanolamine favours chemical homogeneity and hence the thermal stability of the resulting materials. In this context, complexing agents such as triethanolamine appear invaluable and highly promising tools for the preparation of new mesoporous materials.

This research was supported by D.G.E.S. under grant PB95-1094. J. E. H. and S. C. thank the A.E.C.I. for doctoral grants.

Note added at proof: During the revision of this work a paper describing low silica Al-MCM-41 materials has appeared (M. T. Janicke *et al., Chem. Mater*., 1999, **11**, 1342)

Notes and references

1 A. Sayari, *Chem. Mater.*, 1996, **8**, 1840.
2 A. Corma, *Chem. Rev.*, 1997, **97**, 2373.
3 J. Y. Ying, C. P. Mehnert and M. S. Wong, *Angew. Chem., Int. Ed.*, 1999, **38**, 56.
4 C. T. Kresge, M. E. Leonowicz, W. J. Roth, J. C. Vartuli and J. S. Beck, *Nature*, 1992, **359**, 710.
5 G. Fu, C. A. Fyfe, W. Schwieger and G. T. Kokotailo, *Angew. Chem., Int. Ed. Engl.*, 1995, **34**, 1499.
6 Z. Luan, C. F. Cheng, W. Zhou and J. Klinowski, *J. Phys. Chem.*, 1995, **99**, 1018.
7 R. B. Borarde and A. Clearfield, *Catal. Lett.*, 1995, **31**, 267.
8 H. Hamdan, S. Endud, H. He, M. Nazlan Mohd Muhih and J. Klinowski, *J. Chem. Soc., Faraday Trans.*, 1996, **92**, 2311.
9 R. Mokaya and W. Jones, *Chem. Commun.*, 1998, 1839.
10 W. Loewenstein, *Am. Mineral.*, 1954, **39**, 92.
11 M. T. Janicke, C. C. Landry, S. C. Christiansen, D. Kumar, G. D. Stucky and B. F. Chmelka, *J. Am. Chem. Soc.*, 1998, **120**, 6940.
12 R. M. Laine, D. R. Treadwell, B. L. Mueller, C. R. Bickmore, K. F. Waldner and T. R. Hinklin, *J. Mater. Chem.*, 1996, **6**, 1441.

Communication 9/04762J

Al K-edge XANES study for the quantification of aluminium coordinations in alumina

Ken-ichi Shimizu,*[a] Yuko Kato,[a] Tomoko Yoshida,[b] Hisao Yoshida,*[a] Atsushi Satsuma[a] and Tadashi Hattori[a]

[a] *Department of Applied Chemistry, Graduate School of Engineering, Nagoya University, Chikusa-ku, Nagoya 464-8603, Japan*

[b] *Center for Integrated Research in Science and Engineering, Nagoya University, Chikusa-ku, Nagoya 464-8603, Japan*

Received (in Oxford, UK) 27th May 1999, Accepted 26th July 1999

Curve fitting analysis of Al K-edge XANES is employed as a novel characterization method for the quantitative estimation of tetrahedral and octahedral Al in various aluminas.

Transition aluminas, such as γ-Al_2O_3, formed by partial dehydration of aluminium hydrates have been of catalytic importance.[1] It is well established that the catalytic property of aluminas depends strongly on their local structure.[1] However, because of their poor crystallinity, accurate structures of the transition aluminas are not known except for θ-Al_2O_3, in which Al atoms are equally distributed between tetrahedral and octahedral sites of the spinel.[2] ^{27}Al MAS NMR can be used to distinguish several Al atoms with different local structures, and quantification of Al coordination has been successful for crystalline materials.[3] However, for amorphous alumina, its application to quantitative structural analysis is difficult owing to a large quadrupolar interaction.[4] A conventional tool for determining Al distribution in catalytic alumina is desirable. X-Ray absorption spectroscopy (EXAFS/XANES) is another method for investigating local structure.[5–8] In general, EXAFS is popular for quantitative structural analysis, while XANES is less so. Considering the fact that XANES can potentially reflect the local site symmetry around X-ray absorbing atoms, and that the intensity of XANES spectra is higher than EXAFS oscillations, it can be a valuable tool for quantitative analysis if a proper method of analysis is established. Recently, we have succeeded in using Ga K-edge XANES analysis for the quantification of tetrahedral/octahedral Ga atoms in gallium oxides.[7,8] In this study, Al K-edge XANES analysis is applied for the quantitative determination of tetrahedral and octahedral Al atoms in transition aluminas.

Mordenite-type aluminosilicate (JRC-Z-HM15,[9] SiO_2/Al_2O_3 = 15) containing Al atoms in the zeolite framework was supplied from the Catalysis Society of Japan. θ-Al_2O_3 was prepared by calcining γ-Al_2O_3 (JRC-ALO-4[10] supplied from the Catalysis Society of Japan) at 1273 K for 12 h. Boehmite (γ-AlO_2H) was prepared by hydrolysis of aluminium(III) triisopropoxide, followed by drying at 393 K for 12 h. A series of aluminas with various phases were prepared by calcining boehmite in air at various temperatures (673–1773 K) for 2 h. The crystal phases of these samples were confirmed by X-ray diffraction and are given in Table 1. The diffraction pattern of the alumina sample calcined at 1773 K corresponds to that of pure α-Al_2O_3 (corundum).

Al K-edge X-ray absorption spectra were measured on BL-7A at UVSOR with a ring energy of 750 MeV and a stored current of 70–220 mA in a mode of total electron yields. An YB_{66} double crystal monochromator was used, and the absolute energy scale was calibrated to a negative glitch due to the Y L_3 peak of YB_{66} at 2080.0 eV.[11] The monochromator scanning step width was 0.01°, which corresponds to *ca.* 0.3 eV at 1560 eV.

Fig. 1 shows the normalised Al K-edge XANES spectra of alumina samples together with those of model compounds containing AlO_4 tetrahedra (mordenite) and AlO_6 octahedra (corundum and boehmite). It is known in the literature that a clear distinction can be made between the XANES spectra of AlO_4 and AlO_6; a white line peak at 1566 eV is characteristic of AlO_4 compounds, while peaks at 1568 and 1572 eV are characteristic of AlO_6 compounds.[12,13] In this study, it was confirmed that a single peak at 1566 eV due to AlO_4 appeared in the spectrum of mordenite, while a peak at 1568 eV and a broad peak at *ca.* 1571–1572 eV due to AlO_6 appeared in the spectra of corundum and boehmite. In addition, the edge positions of AlO_6 compounds were *ca.* 2 eV higher than those of AlO_4 compounds. For the transition alumina samples calcined in the temperature range 673–1273 K and θ-Al_2O_3, XANES spectra exhibited three distinguishable peaks due to AlO_4 (1566 eV) and AlO_6 (1568 and 1572 eV). Clearly, the relative intensity of the 1566 and 1568 eV peaks differs from sample to sample. This observation is similar to that observed in our previous study of Ga K-edge XANES, where the relative intensity of white line peaks due to GaO_4 and GaO_6 varied with Ga distribution in the samples.

To estimate the ratio of Al atoms in tetrahedral and octahedral sites in transition aluminas, curve fitting analysis of XANES spectra[6] was carried out. Fig. 2 shows the deconvoluted spectrum of θ-Al_2O_3 as an example. Following the method in

Table 1 Parameters of deconvoluted peaks in XANES spectra of aluminium oxide

Sample (calcn. temp.[a]/K)	Crystal phase	AlO_4 tetrahedra/eV		AlO_6 octahedra/eV		Third peak/eV		AlO_4 : AlO_6 ratio[b]
		Position	Area	Position	Area	Position	Area	
θ-Al_2O_3	θ	1565.4	2.6	1567.7	2.6	1571.2	5.0	50 : 50
393	boehmite	1565.5	0.6	1567.8	3.5	1571.4	15.6	15 : 85
673	boehmite (+γ)	1565.5	2.1	1567.6	3.4	1571.3	7.2	38 : 62
873	γ	1565.6	2.2	1567.5	2.9	1571.3	6.3	43 : 57
1073	γ	1565.6	3.3	1567.6	3.8	1571.3	8.3	47 : 53
1173	γ	1565.5	3.2	1567.5	3.9	1571.3	8.2	45 : 55
1273	α + θ	1565.5	1.5	1567.7	4.0	1571.5	6.5	27 : 73
1773	α (corundum)	1565.5	0.5	1567.7	5.3	1571.8	5.7	9 : 91

[a] Calcination temperature. [b] Ratio of the area of AlO_4 peak : AlO_6 peak. The analytical error is estimated to be ±4%.

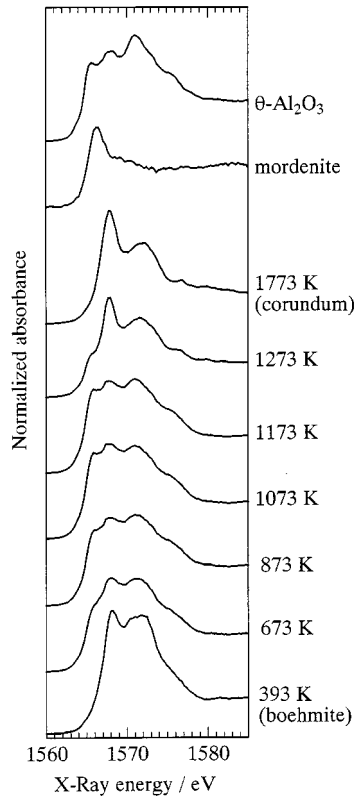

Fig. 1 Al K-edge XANES spectra of alumina samples calcined at various temperatures and of reference compounds.

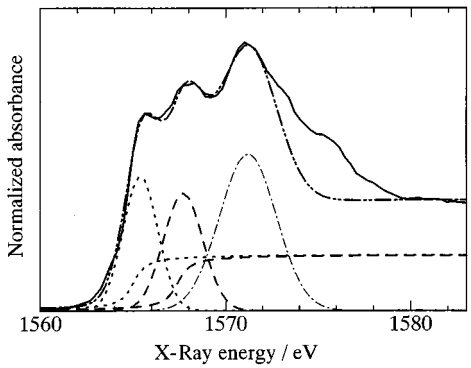

Fig. 2 Al K-edge XANES spectrum of θ-Al_2O_3 (—) and the simulated spectrum (-···-), which is composed of two sets of Gaussian and one arctangent function (dotted and broken) and a Gaussian function (-··-).

our previous study,[7,8] the analysis was performed on the assumption that absorptions due to AlO_4 (1566 eV) and AlO_6 (1568 eV) are expressed by a set of Gaussian and arctangent functions. As for the third peak (at 1572 eV), it is likely, from a comparison of the spectra of AlO_6 compounds (corundum and boehmite) that the relative intensity of the 1568 eV peak to the 1571–1572 eV peak is not constant. Considering the suggestion that this peak can include multiple scattering contributions,[14] it was not employed for the quantitative analysis in this study, and was tentatively expressed by a Gaussian function. Thus, the best parameters, *i.e.*, the exact peak energy, and the peak area of each Gaussian were determined so as to simulate the original spectra in the range 1560–1572 eV and are listed in Table 1. The positions of the first and the second Gaussian peaks were centered at 1565.5 ± 0.1 and 1567.7 ± 0.2 eV, which were almost identical to those of AlO_4 and AlO_6 model compounds, respectively, within experimental error. For θ-Al_2O_3, the ratio of the areas of the 1566 and 1568 eV peaks was determined to be 50 : 50 with an analytical error of ±4%. This value is in good agreement with that derived from X-ray diffraction analysis,[2] which suggests that the ratio of AlO_4 to AlO_6 in the samples can

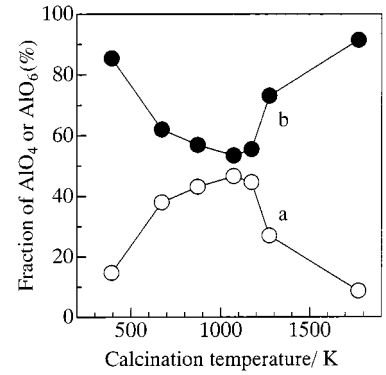

Fig. 3 Fraction of AlO_4 tetrahedra (a) and AlO_6 octahedra (b) in alumina samples as a function of calcination temperature.

be estimated quantitatively from the ratio of each Gaussian peak area.

The percentage of AlO_4 and AlO_6 was estimated by using the above method for a series of aluminas and is plotted as a function of calcination temperature (Fig. 3). The results show that the ratio of AlO_4 to AlO_6 is a function of the calcination temperature. For aluminium hydrate (boehmite), as expected, AlO_6 octahedra are predominant. As the calcination temperature is increased to 1073 K, the fraction of AlO_4 increases to a value of 47%, and then decreases at higher calcination temperatures. For the sample calcined at 1773 K, which is classified as α-Al_2O_3 (corundum), AlO_6 octahedra are again predominant. Thus, it is shown that XANES analysis is helpful for a better understanding of the effect of calcination conditions on the Al cation distribution in transition aluminas.

In conclusion, curve fitting analysis of Al K-edge XANES is shown to be a novel characterisation method for the quantitative estimation of Al coordination states (tetrahedra and octahedra) in alumina samples. This method will now be used for quantitative estimation of Al coordination states in unknown aluminium oxides.

Notes and references

1 H. Knozinger and P. Ratnasamy, *Catal. Rev.-Sci. Eng.*, 1978, **17**, 31; C. Morterra and G. Magnacca, *Catal. Today*, 1996, **27**, 497.
2 R.-S. Zhou and R. L. Snyder, *Acta Crystallogr., Sect. B*, 1991, **47**, 617.
3 D. Massiot, C. Bessda, J. P. Coutures and F. Taulelle, *J. Magn. Reson.*, 1990, **90**, 231.
4 G. Kunath-Fandrei, T. J. Bastow, J. S. Hall, C. Jager and M. E. Smith, *J. Phys. Chem.*, 1995, **99**, 15138.
5 J. C. J. Bart, *Adv. Catal.*, 1986, **34**, 203.
6 S. Yoshida and T. Tanaka, in *X-Ray Absorption Fine Structure for Catalysts and Surfaces*, ed. Y. Iwasawa, World Scientific, Singapore, 1996, ch. 8.
7 K. Nishi, K. Shimizu, M. Takamatsu, H. Yoshida, A. Satsuma, T. Tanaka, S. Yoshida and T. Hattori, *J. Phys. Chem. B*, 1998, **102**, 10190.
8 K. Shimizu, M. Takamatsu, K. Nishi, H. Yoshida, A. Satsuma, T. Tanaka, S. Yoshida and T. Hattori, *J. Phys. Chem. B*, 1999, **103**, 1542.
9 T. Hattori, H. Matsumoto and Y. Murakami, *Stud. Surf. Sci. Catal.*, 1987, **31**, 815.
10 Y. Murakami, *Stud. Surf. Sci. Catal.*, 1983, **16**, 775.
11 T. Kinoshita, Y. Takata, T. Matsukawa, H. Aritani, S. Matsuo, T. Yamamoto, M. Takahashi, H. Yoshida, T. Yoshida, Y. Ufktepe, K. G. Nath, S. Kimura and Y. Kitajima, *J. Syncrotron Rad.*, 1998, **5**, 726.
12 D. A. McKeown, G. A. Waychunas and G. E. Brown Jr., *J. Non-Cryst. Solids*, 1985, **74**, 349.
13 D. Cabaret, P. Sainctavit, P. Ildefonse and A.-M. Flank, *J. Phys.: Condens. Matter.*, 1996, **8**, 3691.
14 D. Li, G. M. Bancroft, M. E. Fleet, X. H. Feng and Y. Pan, *Am. Mineral.*, 1995, **80**, 432.

Communication 9/04286E

Electrochemically controlled micropatterning of immobilised species on functionalised electrode interfaces

Charlotte S. Hadyoon,[ab] Andrew Glidle,[a] David G. Morris[b] and Jonathan M. Cooper*[a]

[a] *Department of Electronics and Electrical Engineering, University of Glasgow, Glasgow, Scotland, UK G12 8QQ. E-mail: jmcooper@elec.gla.ac.uk*

[b] *Department of Chemistry, University of Glasgow, Glasgow, Scotland, UK G12 8QQ*

Received (in Oxford, UK) 15th June 1999, Accepted 19th July 1999

The reactivity of an activated ester group in a suitably functionalised electrodesposited conducting polymer can be modulated electrochemically, providing a mechanism for the patterning of immobilised species at discrete electrodes.

Conducting polymer matrices have previously been used extensively for the immobilisation of active biological species including enzymes and DNA fragments,[1] as well as other ligand binding species, including *e.g.* crown ethers.[2] One advantage of the technique concerns the ability to electrodeposit the polymer matrix in specific, electronically addressable arrays, thereby providing the possibility of selective immobilisation of different species at different places within an electrode array (*i.e.* to pattern a bound species). Under these circumstances the polymer matrix must either be deposited sequentially,[3] with intervening coupling reactions, or sequentially activated,[4] for example by light passing through a photolithographic mask.

When considering the various methods that can be used for biomolecule immobilisation at a biosensor interface, reaction between a polymer-bound activated ester and a nucleophilic amine (*e.g.* a biomolecule) has a number of advantages, including minimisation of side reactions and high reaction yields. We now describe a method of promoting or inhibiting the immobilisation of such a species onto a suitably functionalised conducting polymer matrix, involving the (simple) use of an applied electrochemical potential to modulate the reactivity of an activated ester group. We demonstrate this by using electrochemistry, XPS and FTIR spectroscopy to characterise the immobilisation of two model species, hexylamine and 2-ferrocenyl ethylamine ($FcCH_2CH_2NH_2$). These complementary surface-sensitive techniques allow us to investigate both the interfacial and bulk properties of the polymer.

The activated polymer investigated in this study is derived from the pentafluorophenyl ester of 3-pyrrolylpropionic acid (PFP). Thin films of this polymer are prepared by electropolymerisation of the monomer at potentials in excess of 1.0 V (*vs.* Ag/AgCl) in MeCN.[5] Electrochemical doping and undoping of the polymer occurs at 0.75 V, a potential which is significantly higher than the 0.65 V required to dope the unactivated parent polymeric species, poly(3-pyrrolylpropionic acid). This shift in redox potential suggests that the energy levels in the conjugated polymer backbone are perturbed either by electronic distributions in the carbonyl region of the N-pendant group, or more probably by steric effects concomitant with the bulkier side group.[6] Here, we explore the possibility that changes *induced* in the distribution of electrons in the polymer backbone, brought about by electrochemical oxidative doping and undoping, could influence the reactivity of the pendant group activated ester.

Doped and undoped films of poly(PFP) were immersed in DMSO solutions containing a nucleophilic amine species and the results of the experiments, described below, indicate that the rates of both aminolysis and hydrolysis are significantly reduced when oxidatively doped poly(PFP) is exposed to nucleophile-containing solutions. To assist in evaluating the extent of aminolysis of poly(PFP), 2-ferrocenylethylamine, a redox centre containing moiety, was used as a model nucleophile, due to its characteristic electrochemical and Fe(2p) XPS spectroscopic signature. The redox peaks at *ca.* 0.42 V in the cyclic voltammograms of Fig. 1(*a*), due to the Fc/Fc^+ couple, illustrate the degree of coupling which occurs upon holding a poly(PFP) electrode in a 1 mM 2-ferrocenylethylamine solution at 0 V. When the poly(PFP) electrode is held in the 2-ferrocenylethylamine solution at 0.77 V, there is a complete absence of these redox peaks, [Fig. 1(*b*)]. Fig. 1(*c*) shows the voltammogram arising from an electrode previously held in the doped state in the $FcCH_2CH_2NH_2$ solution, after reimmersion, following undoping, in the nucleophile containing solution. These results clearly show the immobilisation of ferrocene species into the polymer matrix is inhibited by maintaining the polymer in a doped state, and furthermore, that the reactivity is restored following undoping of the polymer.

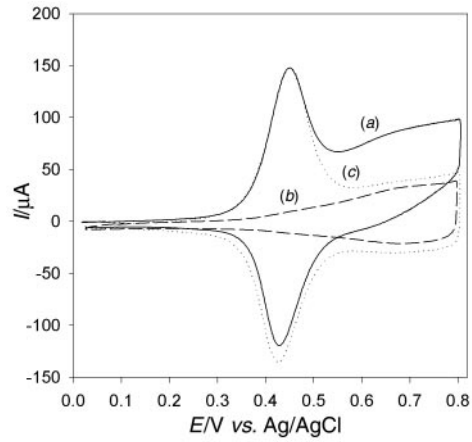

Fig. 1 Cyclic voltammagrams of poly(PFP) films in MeCN after immersion in DMSO solutions containing 1 mM $FcCH_2CH_2NH_2$ for 3 min under various conditions of electrochemical control: (*a*) electrode held at 0 V; (*b*) electrode held at 0.77 V; (*c*) electrode initially held at 0.77 V in $FcCH_2CH_2NH_2$/DMSO solution for 3 min, and then held at 0 V in same solution for 3 min. Electrode areas 1 cm^2; scan rate 20 mV s^{-1}; supporting electrolyte 0.1 M tetraethylammonium perchlorate, for both MeCN and DMSO solutions.

The RAIRS spectra of Fig. 2(*a*)–(*c*) are of a poly(PFP) film [Fig. 2(*a*)], together with poly(PFP) electrodes which have been held in $FcCH_2CH_2NH_2$ solutions at either 0 [Fig. 2(*b*)] or 0.77 V [Fig. 2(*c*)]. These confirm that for the polymer held at 0 V, the ferrocene species becomes covalently attached *via* an amide linkage (loss of the fluorophenyl ester peak at 1790 cm^{-1}, and the subsequent appearance of amide I and amide II peaks at 1650 and 1570 cm^{-1}). The small change from the as-deposited spectrum, for the doped polymer which has been immersed in the nucleophile containing solution at 0.77 V [Fig. 2(*b*)], indicates the activated ester functionality is not lost following maintenance of polymer in the oxidised state. This observation is consistent with the cyclic voltammetry of Fig. 1(*c*) corre-

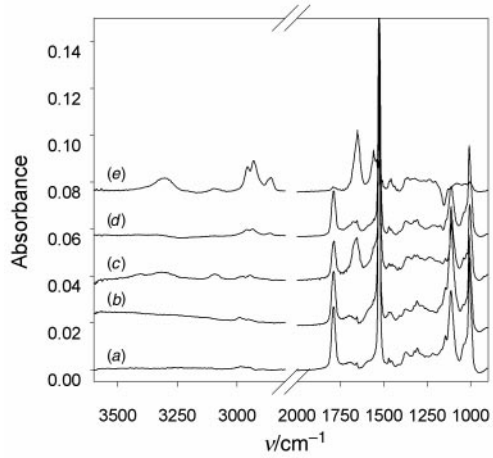

Fig. 2 RAIRS spectra for poly(PFP) films polymerised on evaporated gold electrodes, after immersion in amine containing solutions whilst holding at specified electrochemical potentials (spectra offset for clarity): (*a*) as prepared poly(PFP) film; (*b*) oxidatively doped film immersed in 1 mM $FcCH_2CH_2NH_2$/DMSO for 3 min; (*c*) undoped film immersed in 1 mM $FcCH_2CH_2NH_2$/DMSO for 3 min; (*d*) oxidatively doped film immersed in 0.5 mM hexylamine/DMSO for 3 min; (*e*) undoped film immersed in 0.5 mM hexylamine/DMSO for 3 min.

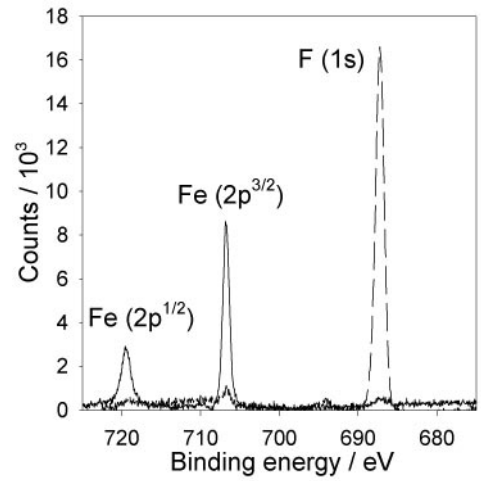

Fig. 3 F(1s) and Fe(2p) XPS spectra of poly(PFP) films after immersion in DMSO solutions containing 1 mM $FcCH_2CH_2NH_2$ and 0.1 M tetraethylammonium perchlorate for 5 min; (---) electrode held at 0.77 V; (—) electrode held at 0 V.

sponding to immobilisation of $FcCH_2CH_2NH_2$ into a previously 'inhibited' polymer film. The short reaction times used for the samples illustrated in Fig. 2 show that partial substitution is possible, if desired; however complete substitution is readily achieved simply by increasing the immersion time. Notably, coupling inhibition in the doped polymer can be maintained for >30 min.

The Fe(2p) and F(1s) XPS spectra of Fig. 3 corroborate the results of Figs. 1 and 2, and show that the amount of ferrocene in the surface layers of the film following immersion of the modified electrode at 0.77 V in the ferrocene ethylamine solution is *ca.* 5% of that found in a fully reacted film, giving a patterning selectivity of 20:1 in this unoptimised system. This low level could not directly be inferred from the lack of signal in the corresponding cyclic voltammogram (Fig. 1) since physisorbed, or partitioned, $FcCH_2CH_2NH_2$ may have exhibited poor electronic communication with the poly(PFP) matrix.

Since $FcCH_2CH_2NH_2$ is in the positively charged, oxidised state at 0.77 V, to investigate whether this coupling inhibition was a consequence of permselectivity effects in the oxidised, cationic membrane, similar potential-dependent coupling experiments were performed with the strong nucleophile, hexylamine. Hexylamine is unoxidised at these potentials (and also uncharged) and thus its permeation into the polymer is not restricted by similar permselectivity effects as may operate for $FcCH_2CH_2NH_2$. As expected, the redox voltammograms of the hexylamine-substituted poly(PFP) show the doping/undoping process now occurs at a lower potential (*ca.* 0.6 V). Figs. 2(*c*) and (*d*) show the RAIRS spectra for poly(PFP) electrodes held in either the undoped or oxidatively doped state respectively whilst immersed in hexylamine–DMSO solutions. These spectra indicate a complete reaction occurs with the undoped poly(PFP) (appearance of amide bands and C–H stretch at 2850 cm^{-1} arising from the alkyl chain) and a limited reaction for polymer films poised in the doped state. It was also noted that coupling inhibition persisted after removal of the applied potential following doping of the polymer at 0.77 V.

Furthermore, it has been found that hydrolysis in basic semi-aqueous MeCN, DMF or DMSO solutions can also be inhibited for *ca.* 30 min by electrode polarisation at 0.77 V. This extended duration compares to less than 5 min for complete hydrolysis when the electrode is held at 0 V, and, as a consequence, this technique may suitable for the nucleophilic coupling of biological species from semi-aqueous organic solvents. Furthermore, using an electrochemical assay to determine the degree of aminolysis by either $FcCH_2CH_2NH_2$ or hexylamine it has been possible to demonstrate selective patterning of $FcCH_2CH_2NH_2$ on a photolithographically fabricated microelectrode, followed by coupling of hexylamine to an adjacent (10 μm separation) polymer modified electrode (at which $FcCH_2CH_2NH_2$ coupling had previously been inhibited).

A functionalised, conjugated polymer film is physically a complex environment and the results to date do not establish a mechanism for the inhibition of these aminolysis and hydrolysis reactions, other than its independence of significant charge permselectivity control. Further mechanistic possiblities which are being investigated include: (i) changes in the bonds strengths in the activated ester group induced by electronic band changes in the conducting polymer backbone associated with doping and undoping; (ii) hindrance of nucleophile attack at the activated ester group induced by molecular conformational changes associated with doping and undoping the polymer backbone; and (iii) changes in the membrane's internal ionic strength associated with doping inhibiting the ingress of hydrophobic nucleophiles.

The authors wish to acknowledge Dr Graham Beamson (Daresbury) for assistance in the acquisition of XPS spectra, the Leverhulme Trust, EU Research Project 'BICEPS' and EPSRC for the provision of both a studentship and their funding through CCLRC of XPS facilities at RUSTI, Daresbury Laboratory, UK.

Notes and references

1 F. Garnier, H. KorriYoussoufi, P. Srivastava, B. Mandrand and T. Delair, *Synth. Met.*, 1999, **100**, 89.
2 H. Youssoufi, M. Hmyene, A. Yassar and F. Garnier, *J. Electroanal. Chem.*, 1996, **406**, 187.
3 L. Rozsnyai and M. Wrighton. *Langmuir*, 1995, **11**, 3913.
4 F. Britland, P. Clark, P. Connolly and G. Moores, *Exp. Cell Res.*, 1992, **198**, 124.
5 C. J. Pickett and K. Ryder, *J. Chem. Soc., Dalton Trans.*, 1994, 2181.
6 J. Roncali, H. Korri, R. Garreau, F. Garnier and M. Lemaire. *J. Chem. Soc., Chem. Commun.*, 1990, 414.

Communication 9/04765D

Supramolecular dendritic solubilisation of a hydrophilic dye and tuning of its optical properties

David K. Smith

Department of Chemistry, University of York, Heslington, York, UK YO10 5DD. E-mail: dks3@york.ac.uk

Received (in Cambridge, UK) 17th May 1999, Accepted 23rd July 1999

Dendritic peptides with a carboxylic acid at the focal point of the branched structure specifically solubilise a polybasic aromatic dye, the microenvironment and optical properties of which are controlled by the size (generation) of the branched peptide.

The development and investigation of the unique properties of functional dendrimers is a research area of intense current activity.[1] The preparation of dendrimers, however, requires considerable synthetic input and consequently, supramolecular dendrimer chemistry and self-assembling systems are of increasing interest.[2,3] There have been extensive investigations of the use of spherical dendrimers for the supramolecular solubilisation of dyes,[4] which are ideal optical probes of the branched environment. It has also been shown that a dendritic shell can generate a unique microenvironment deep within its branched architecture, modulating optical properties,[5] as well as behaviour such as redox chemistry, molecular recognition and catalysis.[6] Here a new approach to the supramolecular dendritic solubilisation of a hydrophilic dye is reported. Rather than using spherical dendrimers,[4] individual dendritic branches with a functional group at the focal point are used for the supramolecular encapsulation process. Furthermore, the encapsulated dye experiences a unique microenvironment,[5] with its optical properties being dendritically tuned by the extent of the branching assembled around it.

Dendritic branches **1**–**3** were constructed in a solution phase approach, starting from protected L-lysine building blocks.[7] All dendritic branches were fully characterised and monodisperse as proven by electrospray mass spectrometry and analytical gel permeation chromatography (Shodex gel). It was proposed that these dendritic branches containing a free carboxylic acid unit at the focal point should interact with molecules containing basic amine sites through the formation of a hydrogen bonded (acid–base) complex with potential proton transfer.[8] A hydrophilic dye containing amine groups, proflavine **4**, was of great interest as a putative guest. It is intensely coloured and possesses interesting luminescence properties, which assist in monitoring the uptake of the dye by the dendritic branch. Furthermore, its optical behaviour is dependent on the microenvironment in which it is located and this allows the effect of supramolecular dendritic encapsulation to be quantified.[5]

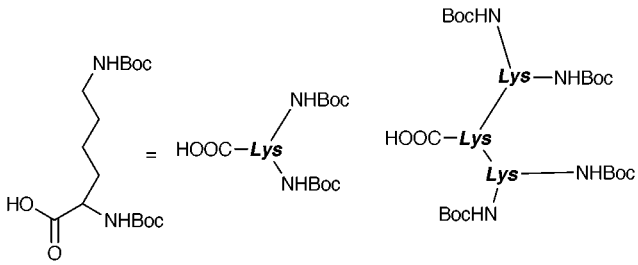

First Generation Branch **1** Second Generation Branch **2**

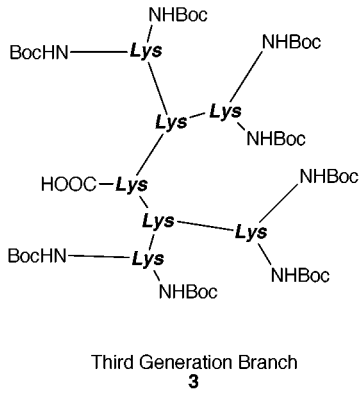

Third Generation Branch **3**

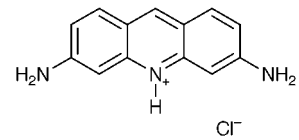

Proflavine hydrochloride **4**

Solid-liquid extraction (solubilisation) experiments were performed using 2 ml of a solution of dendritic branch in CH_2Cl_2 (13.0 mM) and solid proflavine **4** (20 mg). The mixture was stirred at ambient temperature for 24 h, filtered through a pad of Biobeads gel in a pipette, which was washed with additional solvent, and the resultant solution made up to 5 ml in a volumetric flask. This solution was then analysed using UV-visible and fluorescence spectroscopy to assess the degree of dye uptake.

Each of dendritic branches **1**–**3** solubilised a small but significant quantity of the solid hydrophilic proflavine dye **4** into the apolar CH_2Cl_2 solution, as was clear from UV-visible spectroscopy (Table 1), with the dye molecule exhibiting an absorption maximum around 450 nm. In CH_2Cl_2 without dendritic branch present, however, no uptake was observed and the solution remained colourless. The effect of other additives (13.0 mM) was also investigated. AcOH led to no significant uptake of the dye (a simple carboxylic acid is not effective), whilst the methyl ester of **2** also exhibited no uptake (the dendritic branch without a carboxylic acid group at the focal point is not effective). Stearic acid ($C_{17}H_{35}CO_2H$) also did not solubilise the dye (a long unbranched hydrophobic chain is not effective). It therefore seems clear that the carboxylic acid group and the dendritic branching act cooperatively, solubilis-

Table 1 UV-Visible and fluorescence spectroscopic data after proflavine uptake by the dendritic branches, **1**–**3**

	UV-Visible data		Fluorescence data	
Dendritic branch	Peak maximum/nm	Relative absorption intensity	Emission peak maximum/nm	Relative emission intensity
1	446	1.0	505	1.0
2	448	2.25	503	2.10
3	450	13.7	500.5	7.85

ing proflavine **4** into apolar CH_2Cl_2, presumably *via* the formation of supramolecular interactions between acid and amine groups within the dendritic environment.†

Furthermore, the optical properties of proflavine differ in a progressive manner: as the branched molecule becomes larger, increasing quantities of the dye are solubilised into CH_2Cl_2. This effect is particularly marked between second and third generation branches. This would be consistent with a model in which the hydrophilic dye becomes encapsulated within a branched environment, shielding it from bulk solvent and enhancing its solubility in the hydrophobic solvent phase.[4c–f]

In addition, the UV-visible absorption maximum of proflavine is dependent on the size of the dendritic branch. For branch **1**, this maximum is at 446 nm, whilst for branch **2** it absorbs at 448 nm and for branch **3** it has shifted to 450 nm. These results agree with binding studies performed by Seel and Vögtle on proflavine using an acidic endoreceptor in which the absorption maximum of proflavine shifted bathochromically on encapsulation.[9] The absorption maximum of proflavine is dependent on the protonation state of the molecule, with more highly protonated proflavine absorbing at longer wavelength.[10] It is possible that as the size of the dendritic branch increases, the degree of proton transfer from carboxylic acid to amine accompanying dendritic encapsulation increases. This would agree with theoretical studies,[11] which indicate that carboxylic acid–amine interactions are favoured in a low dielectric (*i.e.* CH_2Cl_2 solvent) whilst carboxylate–ammonium interactions (with proton transfer) are only favoured in a higher dielectric (*i.e.* that generated by the larger polypeptide dendritic branches).

Fluorescence investigations provided further insight (Table 1). On excitation at 450 nm, a proflavine emission peak was observed at 505 (**1**), 503 (**2**) and 500.5 nm (**3**). Interestingly, the relative intensities of these emissions increase less markedly than the intensities of the associated UV-visible absorptions. This would indicate that for the larger dendritic branches there is a greater degree of fluorescence quenching. This once again illustrates the dendritic microenvironment experienced by proflavine.

These results clearly show for the first time that, like their spherical dendrimer counterparts,[4c–f] individual dendritic branches with suitable functionalisation at the focal point can non-covalently solubilise a hydrophilic dye. Furthermore, the optical properties of the encapsulated dye indicate that it experiences a unique microenvironment[5a] as a consequence of supramolecular encapsulation.[5b,9] This has implications for the future design of functional branched systems, as some of the time-consuming covalent synthesis may be avoided. Investigations in this laboratory are currently targeting the synthesis of well-defined aggregates.[3] In addition, dendritic control of a wide variety of molecular function, and the application of assembled branched architectures to the problems of drug encapsulation and delivery,[12] are of considerable interest.

D. K. S. acknowledges the support of the University of York in initiating this new research programme.

Notes and references

† The complex still has low solubility, which has thus far prevented an accurate analysis of its stoichiometry, but studies are in progress with other hydrophilic dyes and in different solvents to ascertain how many branches interact with the dye, and hence fully characterise these dendritic aggregates.

1 For reviews of dendrimer chemistry see: G. R. Newkome, C. N. Moorefield and F. Vögtle, *Dendritic Molecules: Concepts, Syntheses, Perspectives*, VCH, Weinheim, 1996; H.-F. Chow, T. K.-K. Mong, M. F. Nongrum and C.-W. Wan, *Tetrahedron*, 1998, **54**, 8543; O. A. Matthews, A. N. Shipway and J. F. Stoddart, *Prog. Polym. Sci.*, 1998, **23**, 1.

2 For general reviews of supramolecular dendrimer chemistry see: F. W. Zeng and S. C. Zimmerman, *Chem. Rev.*, 1997, **97**, 1681; V. V. Narayanan and G. R. Newkome, *Top. Curr. Chem.*, 1998, **197**, 20.

3 For reports of self assembling dendrimers see: S. C. Zimmerman, F. Zeng, D. E. C. Reichert and S. V. Kolotuchin, *Science*, 1996, **271**, 1095; V. Percec, W.-D. Cho, P. E. Mosier, G. Ungar and D. J. P. Yeardley, *J. Am. Chem. Soc.*, 1998, **120**, 11 061; Y. Wang, F. Zeng and S. C. Zimmerman, *Tetrahedron Lett.*, 1997, **31**, 5459; M. Kawa and J. M. J. Fréchet, *Chem. Mater.*, 1998, **10**, 286. For a general review see: T. Emrick and J. M. J. Fréchet, *Curr. Opin. Colloid Interface Sci.*, 1999, **4**, 15.

4 For reports of spherical dendrimers solubilising dyes see: (*a*) G. R. Newkome, C. N. Moorefield, G. R. Baker, M. J. Saunders and S. H. Grossman, *Angew. Chem., Int. Ed. Engl.*, 1991, **30**, 1178; (*b*) C. J. Hawker, K. L. Wooley and J. M. J. Fréchet, *J. Chem. Soc., Perkin Trans. 1*, 1993, 1287; (*c*) J. F. G. A. Jansen, E. M. M. de Brabander-van den Berg and E. W. Meijer, *Science*, 1994, **266**, 1226; (*d*) S. Stevelmans, J. C. M. van Hest, J. F. G. A. Jansen, D. A. F. J. van Boxtel, E. M. M. de Brabander-van den Berg and E. W. Meijer, *J. Am. Chem. Soc.*, 1996, **118**, 7398; (*e*) M. W. P. L. Baars, P. E. Froehling and E. W. Meijer, *Chem. Commun.* 1997, 1959; (*f*) A. I. Cooper, J. D. Londono, G. Wignall, J. B. McClain, E. T. Samulski, J. S. Lin, A. Dobrynin, M. Rubinstein, A. L. C. Burke, J. M. J. Fréchet and J. M. DeSimone, *Nature*, 1998, **389**, 368.

5 (*a*) C. J. Hawker, K. L. Wooley and J. M. J. Fréchet, *J. Am. Chem. Soc.*, 1993, **115**, 4375; (*b*) S. Mattei, P. Seiler, F. Diederich and V. Gramlich, *Helv. Chim. Acta*, 1995, **78**, 1904; (*c*) C. Devadoss, P. Bharathi and J. S. Moore, *Angew. Chem., Int. Ed. Engl.*, 1997, **36**, 1633.

6 D. K. Smith and F. Diederich, *Chem. Bur. J.*, 1998, **4**, 1353 and references therein.

7 R. G. Denkewalter, J. Kolc and W. J. Lukasavage, *US Pat.*, 4 289 872, 1981, assigned to Allied Corp; J. P. Tam, *Proc. Natl. Acad. Sci. U.S.A.*, 1988, **85**, 5409.

8 Such acid–base interactions have recently been used for complexation both on the surface and in the interior of spherical PAMAM dendrimers: V. Chechik, M. Zhao and R. M. Crooks, *J. Am. Chem. Soc.*, 1999, **121**, 4910; L. J. Twyman, A. E. Beezer, R. Esfand, M. J. Hardy and J. C. Mitchell, *Tetrahedron Lett.*, 1999, **40**, 1743.

9 C. Seel and F. Vögtle, *Angew. Chem., Int. Ed. Engl.*, 1991, **30**, 442.

10 K. Yamaoka and M. Shimadzu, *Bull. Chem. Soc. Jpn.*, 1983, **56**, 55.

11 T. Liljefors and P.-O. Norrby, *J. Am. Chem. Soc.*, 1997, **119**, 1052.

12 The application of branched molecules to the field of drug delivery is an area of intense current activity, see: K. Uhrich, *Trends Polym. Sci.*, 1997, **5**, 388 and references therein.

Communication 9/03934A

A surface-modified functional liposome capable of binding to cell membranes

Nobuhiro Yagi,[ab] Yoshikatsu Ogawa,[a] Masato Kodaka,*[a] Tomoko Okada,[a] Takenori Tomohiro,[a] Takeo Konakahara[b] and Hiroaki Okuno[a]

[a] *Biomolecules Department, National Institute of Bioscience and Human-Technology, 1-1 Higashi, Tsukuba, Ibaraki 305-8566, Japan. E-mail: kodaka@nibh.go.jp*

[b] *Faculty of Industrial Science and Technology, Science University of Tokyo, 2641 Yamazaki, Noda, Chiba 278-8510, Japan*

Received (in Cambridge, UK) 1st July 1999, Accepted 19th July 1999

A liposome including the lipopeptide RGD-C4A2, whose surface is modified by a GRGDS-repeating peptide ligand, is found to bind to NIH3T3 cells *via* the interaction between the peptide ligand and the membrane receptor.

Liposomes have been extensively examined as potential carriers of drugs,[1] proteins[2] and DNA[3–5] for drug delivery systems (DDS), in spite of their nonspecificity of delivery due to entrapment by reticuloendothelial systems.[6] We present here a new functional liposome (RGD liposome) whose surface is modified with a high density of peptide chains. Lipopeptide **RGD-C4A2** composed of peptide and lipid parts was synthesized in advance by a method similar to that previously reported,[7,8]† and was then incorporated into the liposome bilayer membrane when the liposome was prepared using the freeze-thaw method.[9]‡ **RGD-C4A2** has a five-times repeated GRGDS sequence, which is the same as the cell adhesion sequence of fibronectin,[10] and therefore is thought to bind to the cell membrane receptor.

The peptide ligand extruded from the RGD liposome into the aqueous phase was expected to bind specifically to an anti-peptide antibody. We therefore confirmed using immunoelectron microscopy[11,12]§ that the peptide ligand was actually placed in the outer aqueous phase. Experimentally,gold colloidal particles were clearly observed on the surface of the liposome when **RGD-C4A2** was located in the liposome membrane, while they were rarely seen in the control liposome.

We applied flow cytometry to evaluate the binding between RGD liposomes and the NIH3T3 cell line (Fig. 1).¶ NIH3T3 was established from mouse fibroblasts, had normal cell-like properties, and was thought to have fibronectin receptors and bind to the present modified liposome. It is worth noting that RGD liposome/NIH3T3 [Fig. 1(*c*)] gave greater fluorescence intensity than either the NIH3T3 alone [Fig. 1(*a*)] or the control liposome/NIH3T3 [Fig. 1(*b*)]. This indicates that the RGD liposome can bind to the cells to a greater degree than the control liposome. We undertook an inhibition experiment to confirm that the peptide chain of **RGD-C4A2** participates in the binding to NIH3T3. The fluorescence intensity was actually reduced by 34.8% in the presence of the free peptide, H-Trp-(Gly-Arg-Gly-Asp-Ser)$_5$-NH$_2$ [Fig. 1(*d*)]. This strongly suggests that the binding between the RGD liposome and the NIH3T3 cell takes place *via* the interaction between the peptide chain of **RGD-C4A2** and the membrane receptor of NIH3H3.

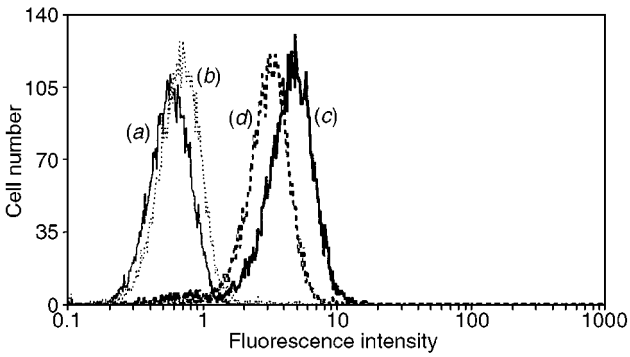

Fig. 1 Flow cytometry of (*a*) NIH3T3 only, (*b*) NIH3T3 + control liposome, (*c*) NIH3T3 + RGD-liposome and (*d*) NIH3T3 + RGD liposome + H-Trp-(Gly-Arg-Gly-Asp-Ser)$_5$-NH$_2$.

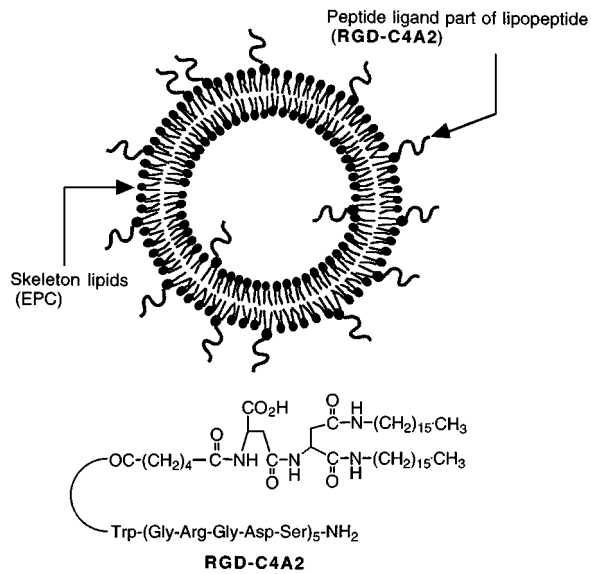

Viruses have been used as vectors in the field of gene therapy.[13] In spite of their prominent function as drug carriers, problems endangering vital functions have not yet been completely solved and thus their clinical use is still limited. Compared to viruses, however, liposomes are superior in safety and reproducibility if only the problem of specificity can be solved. Many trials have been made to give liposome the binding specificity to cells. For example, the liposome surface has been equipped with a glycolipid,[14] transferrin[15] or an antibody[16,17] as a binding anchor to cells. Among various ligand candidates, peptides seem the most appropriate for the present purpose, since information about amino acid sequences and corresponding receptors is easily available and the synthetic methods are also well established.[18] In ordinary methods such as the 'succinimide method',[16] proteins or peptides are reacted with amino groups of specific lipid molecules already incorporated into lipid bilayer membranes. However, it is very difficult to modify the surface of liposomes at high density by this ordinary method, because the reactivity is reduced owing to the steric repulsion between the liposome membrane and the protein or peptide ligand fragments. In contrast to the succinimide method, our new technique was highly efficient in incorporating the lipopeptide in the liposome membrane, *viz.* more than 90% of the added **RGD-C4A2** was introduced into the liposome.

In conclusion, we have succeeded in preparing a liposome whose surface is modified by peptide chains at high density. This liposome has been shown to bind to the membrane receptor of NIH3H3 cells using the peptide ligand on its surface. This method may open a way to wide application of liposomes for clinical use.

We thank Dr Kazunori Kawasaki, Dr Toku Kanaseki and Ms Rena Kawai of the National Institute of Bioscience and Human-Technology for assisting with the electron microscopy.

Notes and references

† *Selected data* for **RGD-C4A2**: $\delta_H(D_2O)$ 7.34–7.60 (m, 2H, Trp), 7.19 (s, 1H, Trp), 6.98–7.14 (m, 2H, Trp), 4.68–4.82 (m, 6H, CH), 4.28–4.50 (m, 10H, CH), 3.75–4.12 (m, 30H, Ser-CH_2, Gly-CH_2), 3.21 (m, 10H, Arg-$CH_2CH_2CH_2N$), 2.74–2.94 (m, 10H, Asp-CH_2), 2.04–2.34 (m, 4H, $COCH_2$), 1.54–1.98 (m, 20H, Arg-$CH_2CH_2CH_2N$), 1.36–1.54 (m, 4H, $NHCH_2CH_2$), 1.27 (s br, 52H, $2(CH_2)_{13}CH_3$), 0.88 (t, 6H, $2CH_2CH_3$, *J* 6.6); MALDI-TOFMS: calc. 3369.8 (MH^+), found: 3370. Retention time in HPLC (YMC-Pack ODS-AM, 4.6 × 250 mm, eluant: 0.08% aq. TFA–MeCN from 100 : 0 to 50 : 50 over 30 min, flow rate: 0.8 ml min^{-1}): 17.4 min.

‡ After **RGD-C4A2** was dissolved in 10 μl of 20% AcOH, 100 μl of egg phosphatidylcholine (EPC)–chloroform solution (5 μmol ml^{-1}) was added. These two separated phases became homogeneous after addition of a few drops of MeOH. The solvent was evaporated under reduced pressure to form a thin lipid film on the wall of a test tube. This film was left *in vacuo* for at least 12 h to thoroughly remove the solvent. Hank's buffer solution (pH 7.2) (1 ml) was added to the thin lipid film, which was vortexed for 5 min at room temperature and subjected to repeated (7 times) freezing (−196 °C) and thawing (70 °C). The solution was then extruded 5 times through a polycarbonate membrane (pore size: 0.1 μm).

§ An antibody against H-Cys-Trp-(Gly-Arg-Gly-Asp-Ser)$_5$-NH_2 [one cysteine residue was added to H-Trp-(Gly-Arg-Gly-Asp-Ser)$_5$-NH_2] was prepared by an ordinary method from a female New Zealand white rabbit using KLH (Keyhole Limpet, Hemocyanin)-conjugated Cys-Trp-(Gly-Arg-Gly-Asp-Ser)$_5$-NH_2. After labeling the modified liposome by the prepared primary antibodies and a secondary antibody (goat anti-rabbit IgG), the samples were negatively stained with uranyl acetate, stabilized by perpendicular carbon evaporation, and observed under a transmission electron microscope.

¶ To the lipopeptide (0.1 μmol) dissolved in 20% AcOH (10 μl) was added a chloroform solution containing EPC (1.6 μmol), cholesterol (Ch) (0.4 μmol) and *N*-(fluorescein-5-thiocarbamoyl)-1,2-dihexadecanoyl-*sn*-glycero-3-phosphoethanolamine (FITC-PE) (0.02 μmol). A few drops of MeOH were added to make the solution homogeneous and the modified liposome was prepared in a similar manner as described above. After the liposome and NIH3T3 cells had been incubated at 37 °C for 30 min, the cells were washed by centrifugation (1000 rpm, 3 min) at 37 °C, twice with Dulbecco's modified Eagle's medium (DMEM) and once with CMF-PBS. The cells were then suspended in 1.0 ml of CMF-PBS containing BSA (0.1%) and sodium azide (0.1%), and the fluorescence emitted from the cells was measured on the flow cytometer.

1 J. Cannor and L. Huang, *Cancer Res.*, 1986, **46**, 3431.
2 P. Briscoe, I. Caniggia, A. Graves, B. Benson, L. Huang, A. K. Tanswell and B. A. Freeman, *Am. J. Physiol.*, 1995, **268**, L374.
3 C. Ropert, C. Malvy and P. Couvreur, *Pharm. Res.*, 1993, **10**, 1427.
4 E. G. Holmberg, Q. R. Reuer, E. E. Geisert and J. L. Owens, *Biochem. Biophys. Res. Commun.*, 1994, **201**, 888.
5 D. D. Lasic, H. Strey, M. C. A. Stuart, R. Podgornik and P. M. Frederik, *J. Am. Chem. Soc.*, 1997, **119**, 832.
6 N. Higashi and J. Sunamoto, *Biochim. Biophys. Acta*, 1995, **1243**, 386.
7 Y. Ogawa, T. Tomohiro, Y. Yamazaki, M. Kodaka and H. Okuno, *Chem. Commun.*, 1999, 823.
8 Y. Ogawa, H. Kawahara, N. Yagi, M. Kodaka, T. Tomohiro, T. Okada, T. Konakahara and H. Okuno, *Lipids*, 1999, **34**, 387.
9 U. Pick, *Arch. Biochem. Biophys.*, 1981, **212**, 186.
10 M. D. Pierschbacher and E. Ruoslahti, *Nature*, 1984, **309**, 30.
11 J. Zhao, S. Kimura and Y. Imanishi, *Biochim. Biophys. Acta*, 1996, **1282**, 249.
12 D. F. Hulser, B. Rehkopf and O. Traub, *Exp. Cell Res.*, 1997, **233**, 240.
13 M. J. Cooper, M. Lippa, J. M. Payne, G. Hatzivassiliou, E. Reifenberg, B. Fayazi, J. C. Perales, L. J. Morrison, D. Templeton, R. L. Piekarz and J. Tan, *Proc. Natl. Acad. Sci. U.S.A.*, 1997, **94**, 6450.
14 I. Eggens, B. Fenderson, T. Toyokuni, B. Dean, M. Stroud and S. Hakomori, *J. Biol. Chem.*, 1989, **264**, 9476.
15 P. Afzelius, E. J. F. Demant, G. H. Hansen and P. B. Jensen, *Biochim. Biophys. Acta*, 1989, **979**, 231.
16 F. J. Martin and D. Papahadjopoulos, *J. Biol. Chem.*, 1982, **257**, 286.
17 F. J. Martin and W. L. Hubbell and D. Papahadjopoulos, *Biochemistry*, 1981, **20**, 4229.
18 B. Merrifield, *Biopolymers*, 1995, **37**, 3.

Communication 9/05322K

A new family of amorphous molecular materials showing large photorefractive effect

Qing Wang, Liming Wang, Haythem Saadeh and Luping Yu*

Department of Chemistry and James Franck Institute, The University of Chicago, 5735 S. Ellis Avenue, Chicago, IL 60637, USA. E-mail: lupingyu@midway.uchicago.edu

Received (in Corvallis, OR, USA) 15th June 1999, Accepted 19th July 1999

A novel series of amorphous molecular materials containing carbazole and methine dyes have been synthesized and characterized for photorefractive applications.

In recent years, functional molecular materials exhibiting nonlinear optical, electroluminescent, ferromagnetic and photoconducting properties have been sought for practical applications.[1–4] These materials possess excellent processibility, transparency and can be efficiently purified by many well-known techniques such as chromatography. The versatility of structural modification offers a unique opportunity to meet additional challenges, for example, designing multifunctional materials that could simultaneously possess several properties. Photorefractive (PR) materials are such multifunctional materials that combine photoconductivity and nonlinear optical (NLO) response to modulate the refractive index of the medium.[5] Due to their potential applications in holographic optical data storage and real-time optical processing, various classes of organic PR materials including polymers,[6–8] liquid crystals[9] and organic glasses[10,11] have been explored. Herein, we report a novel series of amorphous molecular materials based on carbazole and methine dyes, which exhibit very interesting charge-transfer complex formation and large PR responses.

The synthetic route is shown in Scheme 1, where carbazole was chosen as the photoconductive component for hole transport. Condensation of aldehyde **3** with electron withdrawing groups yielded methine dye as the NLO chromophores. The molecules synthesized (compound **4**) thus possess dual functions: photoconductivity and second-order NLO activity.

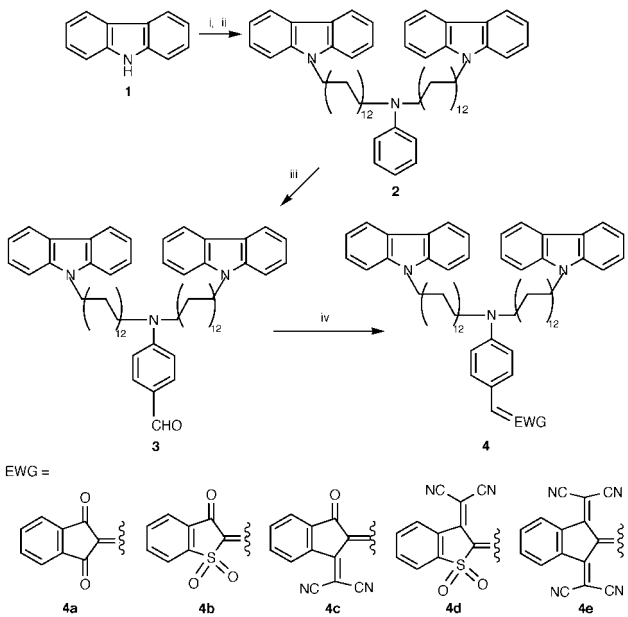

Scheme 1 *Reagents and conditions*: i, $Br(CH_2)_{12}Br$, NaH; ii, aniline, K_2CO_3; iii, $POCl_3$, DMF; iv, EWG, EtOH.

The long aliphatic chain was introduced to prevent the materials from crystallization and help resulting compounds remain amorphous at room temperature. The structures of the compounds were confirmed by microanalysis and by spectroscopic methods.[12] The thermal properties of the compounds are summarized in Table 1, which indicated the low T_g nature of the materials. These compounds were found to readily form amorphous films, as evidenced by differential scanning calorimetry (DSC), polarizing microscopy and X-ray diffraction. The amorphous films made from these compounds are very stable in an ambient atmosphere for over a year up to the present time and no crystallization phenomenon was observed even on further heating. The UV/vis spectra of compound **4** in CH_2Cl_2 display two intense bands. The one at around 347 nm can be attributed to the carbazole moiety, while the other is due to the NLO chromophore. As also shown in Table 1**,** increasing acceptor strength by replacing carbonyl groups with sulfonyl and dicyanovinyl groups results in a bathochromic shift in the corresponding chromophores. It is interesting to note that in solid UV/vis spectra, new long-wavelength absorption bands were observed in addition to the peaks from chromophore and carbazole. The intensity of these new peaks varies as a function of temperature. As the temperature increases, the absorbance decreases and finally becomes zero at around 75 °C. These new bands were assigned to the formation of charge-transfer complexes (CTC) between the carbazole and electron withdrawing groups because it was observed that when compound **2** was mixed with electron acceptors in CH_2Cl_2 solution, an intense coloration with new long-wavelength absorption peaks developed immediately. For example, CTC bands at 492 and 690 nm were observed for compounds **4b** and **4c** respectively. These new absorption bands enable us to photoexcite the materials mainly through the charge-transfer complex at a longer wavelength. It is worth mentioning that additional photosensitizers, such as 2,4,7-trinitrofluoren-9-one (TNF), are needed in most reported composite PR materials containing a carbazole moiety.[13] The system reported here shows all necessary functions for PR response in single molecules.

Photocurrent measurements indicated these materials are photoconductive and a second harmonic generation signal was observed as a function of an external field. The PR nature of these molecular materials was verified in two-beam coupling measurements. In this experiment, two coherent laser beams (*p*-polarized) intersect inside the sample to write a holographic

Table 1 The properties of carbazole containing amorphous molecules

Compound	T_g/°C[a]	T_d/°C[a]	λ_{max}/nm[b]	ε_{max}/l mol^{-1} cm^{-1}[b]
4a	9	292	491	48 900
4b	10	282	492	59 100
4c	13	211	570	49 000
4d	7	228	602	59 300
4e	6	205	628	18 300

[a] The glass transition temperature (T_g) and the decomposition temperature (T_d) were determined by DSC, 10 °C min^{-1}. [b] Measured in CH_2Cl_2.

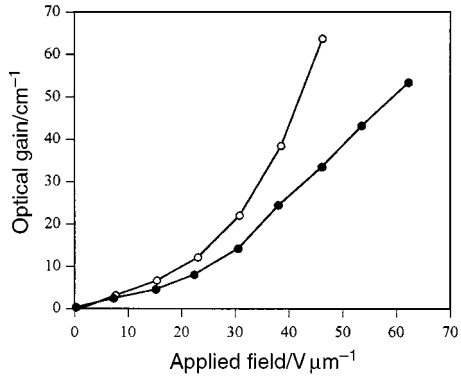

Fig. 1 Photorefractive optical gain of compound **4b** (○) and compound **4c** (●) as a function of the applied field.

grating. It is known that this grating has a non-zero phase shift with respect to the light intensity pattern. An asymmetric energy exchange between the two beams, characterized by the two-beam coupling gain coefficient Γ, can be observed.[5] A further note is that in this experiment, the normal of the sample surface needs to be tilted 52 °C to yield a projection of the grating wave vector along the poling axis. The films for PR characterization were prepared by sandwiching the melt of compounds between two glass substrates coated with indium-tin oxide. The thickness of films is about 128 μm, maintained by a polyimide spacer. Some preliminary results performed on compound **4b** and **4c** are presented in Fig. 1. Compound **4b** was measured with a He-Ne laser (632.8 nm), while compound **4c** was excited by a diode laser with a wavelength of 780 nm. As the applied field increased, the intensity of one beam increased, while that of the second beam decreased. When the electric field was turned off, the intensities returned to their original levels and no energy exchange was observed. The strong field dependence of the optical gain reflects the field dependence of both the quantum yield of photogeneration of charge carriers and the second-order NLO response. For compound **4b**, at a field of 46 V μm^{-1}, an optical gain value of 65.4 cm^{-1} was achieved. The absorption coefficient of the material was only 1.4 cm^{-1}, thus giving us a net optical gain of 64 cm^{-1}. For compound **4c,** we have obtained a PR gain of 53 cm^{-1} by applying a field of 62 V μm^{-1}, whereas the absorption coefficient was 4.3 cm^{-1}. The index grating recorded in the material was further tested by a weaker, counter-propagating probe beam (*p*-polarized) in the four wave mixing experiments. The diffraction efficiency η is calculated as the intensity ratio of the diffracted signal to the probe beam. It was observed that the diffraction efficiency also had a strong dependence on the applied field and reached 17% for compound **4b** and 9% for compound **4c** at E = 42 V μm^{-1}.

In summary, a new series of multifunctional amorphous molecules has been synthesized and characterized for photorefractive applications. Selecting different electron acceptor groups affords control not only of electrooptic effects but also of charge generating characteristics of the resulting materials. This approach opens the way for an extension of PR sensitivity to near-IR or even IR regions, which is very interesting for applications in telecommunication. Moreover, the synthetic flexibility and simplicity of this molecular system offer great possibilities for structural modifications to further improve performance or match the laser wavelength for the application desired. Extensive work based on this system is now under way.

We gratefully acknowledge the financial support of the National Science Foundation and Air Force Office of Scientific Research. This work also benefited from the support of the NSF MERSEC program at the University of Chicago.

Notes and references

1 T. Noda and Y. Shirota, *J. Am. Chem. Soc*., 1998, **120**, 9714.
2 M. Thelakkat and H. Schmidt, *Adv. Mater*., 1998, **10**, 219.
3 K. Naito and A. Miura, *J. Phys. Chem*., 1993, **97**, 6240.
4 Y. Shirota, K. Moriwaki, S. Yoshikawa, T. Ujike and H. Nakano, *J. Mater. Chem*., 1998, **8**, 2579.
5 *Photorefractive Materials and Their Applications*, ed. P. Gunter and J. P. Huignard, Springer-Verlag, Berlin, 1988, vol. I and II.
6 W. E. Moerner and S. M. Silence, *Chem. Rev*., 1994, **94**, 127.
7 L. P. Yu, W. K. Chan, Z. H. Peng and A. Gharavi, *Acc. Chem. Res*., 1996, **29**, 13.
8 W. Li, A. Gharavi, Q. Wang and L. P. Yu, *Adv. Mater.*, 1998, **10**, 927.
9 G. P. Wiederrecht, B. A. Yoon and M. R. Wasielewski, *Adv. Mater*., 1996, **8**, 535.
10 P. M. Lundquist, R. Wortmann, C. Geletneky, R. J. Twieg, M. Jurich, V. Y. Lee, C. R. Moylan and D. M. Burland, *Science*, 1996, **29**, 13.
11 Q. Wang, A. Gharavi, W. Li and L. P. Yu, *Polym. Prepr*., 1997, **38**(2), 508.
12 *Selected data* for **4b**: $\delta_H(CDCl_3)$ 1.24–1.37 (m, 36H, alkyl), 1.55 (m, 4H, alkyl protons), 1.85 (t, *J* 7.32, 4H, arom), 3.36 (t, *J* 7.74, 4H, CH_2N), 4.28 (t, *J* 7.19, 4H, CH_2Ar), 6.69 (d, *J* 8.97, 2H, arom), 7.23 (t, *J* 7.31, 4H, arom), 7.38 (d, *J* 8.08, 4H, arom), 7.45 (m, 5H, arom), 7.75 (t, *J* 7.89, 1H, arom), 7.81 (t, *J* 7.85, 1H, arom), 7.91 (s, 1H, vinyl), 7.98 (d, *J* 8.05, 2H, arom), 8.03 (d, *J* 8.10, 1H, arom), 8.09 (d, *J* 7.79, 4H, arom) (Calcd. for $C_{63}H_{74}N_3O_3S_1$: C, 79.42; H, 7.77; N, 4.41. Found: C, 79.34; H, 7.79; N, 4.34%).
13 Y. Zhang, R. Burzynski, S. Ghosal and M. K. Casstevens, *Adv. Mater*., 1996, **8**, 111.

Communicaion 9/04767K

ChemComm

Chemoselectivity and enantiocontrol in catalytic intramolecular metal carbene reactions of diazo acetates linked to reactive functional groups by naphthalene-1,8-dimethanol

Michael P. Doyle,* Doina G. Ene, David C. Forbes and Thomas H. Pillow

Department of Chemistry, University of Arizona, Tucson, Arizona, USA. E-mail: mdoyle@u.arizona.edu

Received (in Corvallis, OR, USA) 3rd June 1999, Accepted 14th July 1999

The use of chiral dirhodium(II) carboxamidate catalysts for metal carbene transformations of diazo acetates linked to a reactive functionality through naphthalene-1,8-dimethanol produces chemoselective and enantioselective reaction either at the remote functionality or by addition to the 1,2-position of the naphthalene ring; enantioselectivities up to 84% ee have been obtained for the Büchner reaction.

Considerable mechanistic and synthetic interest has been directed recently to the Büchner reaction.[1,2] Catalytic intramolecular cycloaddition has been pursued with vigor since dirhodium(II) catalysts were employed,[3,4] but there have been few reports that provided evaluation of the Büchner reaction in competitive processes.[5,6] Similarly, only two reports have documented enantiocontrol in this transformation from the use of chiral catalysts.[3,7] In our ongoing investigations of enantiocontrol in catalytic intramolecular metal carbene transformations, we have discovered two reacting systems that offer catalyst-controlled chemoselectivity and the highest levels of enantiocontrol yet achieved in aromatic cycloaddition reactions.

We investigated the influence of catalyst on the partitioning of the metal carbene derived from **1** between products **2** and **3**. The diazo acetate linked to a propargyl group through a naphthalene-1,8-dimethanol (**1**) was prepared by standard methods in good overall yield. Consistent with recently reported results for macrocyclic cyclopropenation,[8] treatment of **1** with $Rh_2(OAc)_4$ produced macrocyclic cyclopropene **2** in 69% isolated yield. However, the application of chiral catalysts to this system resulted not only in **2** but also in the aromatic cycloaddition product **3**. Indeed, use of $Rh_2(4R\text{-MEOX})_4$ gave **3** in 66% overall yield and in 73% ee. The norcaradiene structure for **3** was confirmed spectrally and is consistent with results obtained with a structurally analogous diazo ketone.[9] Results obtained with a representative selection of chiral catalysts are presented in Table 1.

As is evident in these data, the catalyst has a definite but, in this system, unpredictable influence on chemoselectivity. The selectivity achieved with chiral dirhodium(II) carboxamidate catalysts is not uniform. Also, since reactivity of the catalysts generally finds $CuPF_6$–**4** to be comparable to $Rh_2(S\text{-TBPRO})_4$, with both of them much more reactive than the chiral dirhodium(II) carboxamidates, chemoselectivity appears to respond here to a subtle combination of electronic and steric effects. In any case, proper choice of catalyst allows the selection of either **2** or **3**.

The competition between ylide formation and aromatic cycloaddition was also evaluated. By investigating the design potential of the naphthalene-1,8-dimethanol linker for ylide formation–[2,3]-sigmatropic rearrangement,[10] we discovered similar results to those reported in Table 1. The synthesis of **5** was accomplished in good yield. Treatment with $Rh_2(S\text{-TBPRO})_4$ caused the sole production of [2,3]-sigmatropic rearrangement (Scheme 1) product **7** in 82% yield (6% ee).[11] In contrast, use of $Rh_2(4S\text{-MEOX})_4$ gave aromatic cycloaddition product **8** exclusively in 55% isolated yield (84% ee). The use of $CuPF_6$–**4** gave a 20:80 mixture of **7** (44% ee) and **8** (76% ee).

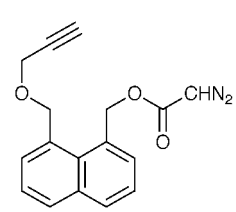

1

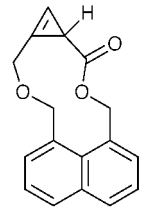

2

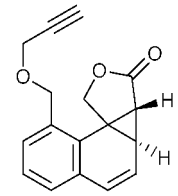

3

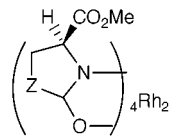

$Rh_2(4S\text{-MEOX})_4$ Z = O
$Rh_2(5S\text{-MEPY})_4$ Z = CH_2
$Rh_2(4S\text{-MPPIM})_4$ Z = $NCOCH_2CH_2Ph$

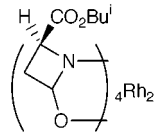

$Rh_2(4S\text{-IBAZ})_4$

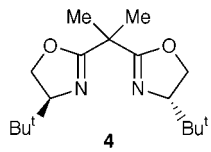

4

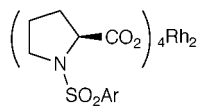

$Rh_2(S\text{-TBPRO})$
(Ar = *p*-$Bu^tC_6H_4$)

To determine the effectiveness of these catalysts for aromatic cycloaddition on the basic naphthalene system, **9** was treated with a selection of catalysts from Table 1. Aromatic cycloaddition product **10** was produced[12] in high isolated yield in each case (% **10**, % ee): $Rh_2(4R\text{-MEOX})_4$ (76% yield, 56% ee); $Rh_2(5S\text{-MEPY})_4$ (72% yield, 42% ee); $Rh_2(4S\text{-IBAZ})_4$ (87% yield, 81% ee); $Cu(MeCN)_4PF_6$–**4** (83% yield, 42% ee). Thus,

Table 1 Products from catalytic diazo decomposition of **1**[a]

Catalyst	Isolated yield (%)[b]	Relative yield (%)		Ee (%)	
		2	**3**	**2**	**3**
$Rh_2(OAc)_4$	69	100	0	—	—
$Rh_2(4R\text{-MEOX})_4$	66	0	100	—	73
$Rh_2(5S\text{-MEPY})_4$	74	54	46	62	10
$Rh_2(4S\text{-MPPIM})_4$	74	83	17	15	—
$Rh_2(4S\text{-IBAZ})_4$	74	68	32	51	65
$Cu(MeCN)_4PF_6$–**4**	72	14	86	—	59
$Rh_2(S\text{-TBPRO})_4$	72	98	2	11	—

[a] Reactions were performed in refluxing CH_2Cl_2 using 1.0 mol% catalyst. [b] Yield of **2** + **3** after chromatography.

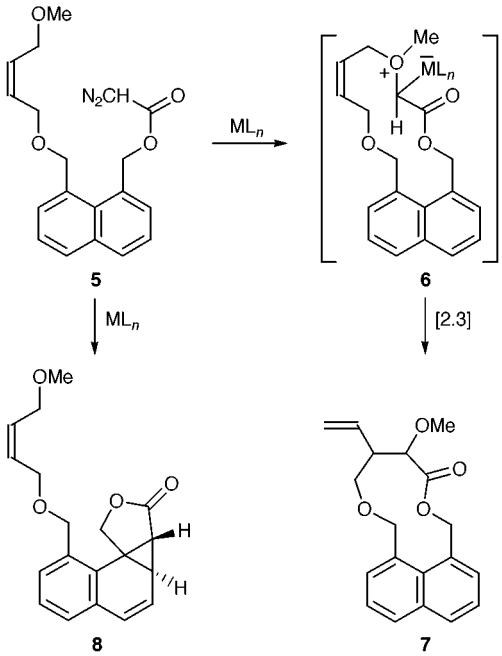

Scheme 1

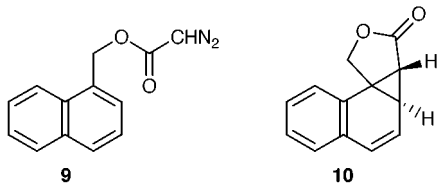

in this case, $Rh_2(4S\text{-IBAZ})_4$ is superior even to $Rh_2(MEOX)_4$ catalysts for highly enantioselective aromatic cycloaddition.

The composite of results demonstrates that the more reactive catalysts favor reactions that occur at remote functional groups rather than at the nearby naphthalene. This selectivity characterizes alkyne addition and ylide formation and should also be evident in other addition and association reactions. Furthermore, the enantiomeric excess for aromatic cycloaddition in these naphthalene systems is the highest yet reported.

We are grateful to the National Science Foundation and to the National Institutes of Health (GM-46503) for their support of this research.

Notes and references

1 P. Manitto, D. Monti, S. Zanzola and G. Speranza, *Chem. Commun.*, 1999, 543; P. Manitto, D. Monti, S. Zanzola and G. Speranza, *J. Org. Chem.*, 1997, **62**, 6658.

2 C. J. Moody, S. Miah, A. M. Z. Slawin, D. J. Mansfield and I. C. Richards, *J. Chem. Soc., Perkin Trans. 1*, 1998, 4967; A. R. Maguire, N. R. Buckley, P. O'Leary and G. Ferguson, *J. Chem. Soc., Perkin Trans. 1*, 1998, 4077.

3 M. P. Doyle, M. A. McKervey and T. Ye, *Modern Catalytic Methods for Organic Synthesis with Diazo Compounds*, Wiley, New York, 1998, ch. 6.

4 J. C. Morris, L. N. Mander and D. C. R. Hockless, *Synthesis*, 1998, 455.

5 A. Padwa, D. J. Austin, A. T. Price, M. A. Semones, M. P. Doyle, M. N. Protopopova, W. R. Winchester and A. Tran, *J. Am. Chem. Soc.*, 1993, **115**, 8669; M. P. Doyle, M. S. Shanklin and H. Q. Pho, *Tetrahedron Lett.*, 1988, **29**, 2639.

6 A. G. H. Wee, B.-S. Liu and L. Zhang, *J. Org. Chem.*, 1992, **57**, 4404.

7 M. Kennedy, M. A. McKervey, A. R. Maguire and G. H. P. Roos, *J. Chem. Soc., Chem. Commun.*, 1990, 361.

8 M. P. Doyle, D. G. Ene, C. S. Peterson and V. Lynch, *Angew. Chem., Int. Ed.*, 1999, **38**, 700.

9 P. Manitto, D. Monti and G. Speranza, *J. Org. Chem.*, 1995, **60**, 484.

10 M. P. Doyle, D. C. Forbes, M. M. Vasbinder and C. S. Peterson, *J. Am. Chem. Soc.*, 1998, **120**, 7653.

11 Only one product was observed by GC and NMR analyses and, based on results reported in ref. 10, this product is assumed to be the *erythro* isomer.

12 Enantiomeric excesses for **3**, **8** and **10** were determined with baseline separation on a WHELK-O column operated at 2 ml min^{-1} in hexanes–Pr^iOH (9 : 1). *Selected data* for **10**: δ_H(300 MHz, $CDCl_3$) 7.51 (d, *J* 7.1, 1H), 7.39–7.22 (m, 3H), 6.53 (d, *J* 9.5, 1H), 6.34 (dd, *J* 9.5, 4.6, 1H), 5.13 (d, *J* 9.5, 1H), 4.35 (d, *J* 9.5, 1H), 2.45 (dd, *J* 4.6, 2.4, 1 H), and 1.08 (d, *J* 2.4, 1H); δ_C(75 MHz, $CDCl_3$) 176.5, 133.1, 130.7, 128.9, 128.3, 128.2, 127.5, 124.7, 124.1, 69.2, 34.2, 30.9 and 21.2; $\nu_{max}(CHCl_3)$/cm^{-1} 1789 and 1752; mp 82–84 °C (Calc. for $C_{13}H_{10}O_2$: C, 78.77; H, 5.08. Found: C, 77.95; H, 5.14%).

Communication 9/04530I

ChemComm

A novel approach to site-specifically platinated oligonucleotides applying combinations of nucleobase protecting groups

Robert J. Heetebrij, Reynier A. Tromp, Gijs A. van der Marel, Jacques H. van Boom and Jan Reedijk*

Leiden Institute of Chemistry, Gorlaeus Laboratories, Leiden University, PO Box 9502, 2300 RA Leiden, The Netherlands. E-mail: reedijk@chem.leidenuniv.nl

Received (in Cambridge, UK) 1st June 1999, Accepted 14th July 1999

Platination of a properly protected oligonucleotide followed by deprotection represents a new method for the synthesis of site-specific platinum-modified nucleic acids; N7 platination of 2′-deoxyguanosine can be circumvented by introducing a bulky protective group at the O6 position.

Since the discovery of the cytotoxic activity of cisplatin, *cis*-$[Pt(NH_3)_2Cl_2]$, much effort has been directed towards elucidating the mechanism of action of this drug. At present it is generally accepted[1] that intracellular damage occurs by coordination of cisplatin to DNA, causing a profound spatial disturbance and destabilisation of the double-helix leading to inhibition of DNA replication. It is well-established now that the intrastrand 1,2-GG (G = guanine) crosslink is the predominant platinum–DNA adduct. Moreover, other adducts such as 1,2-AG and 1,3-GXG adducts, as well as interstrand GG crosslinks, have also been observed.[2]

The molecular mechanistic aspects of platinum antitumour drugs are commonly investigated by elucidation of the 3D structures of platinum adducts of oligonucleotides.[3] In addition, selectively platinated oligonucleotides are required in fairly large amounts for applications in new therapeutic strategies like gene modulation *via* antisense and antigene methodologies.[4] The construction of selectively platinated DNA adducts by modification of an unprotected oligonucleotide with a platinum complex is often hampered by lack of selectivity of the platination reaction. Consequently the available range of DNA–Pt crosslinks to be studied is rather limited.

One approach to overcome these problems entails the use of platinum-bound mononucleotides[5] in the synthesis of platinum adducts by automated DNA synthesis following an H-phosphonate coupling approach. However, the recovery of site-specifically platinated oligonucleotides was rather disappointing. Recently, an automated DNA synthesis based on phosphoramidite chemistry of Ru^{II} and Os^{II} modified oligonucleotides was published.[6] This methodology leads to higher yields, but has been limited to coordinatively saturated complexes covalently linked to the nucleobase *via* polypyridine ligands.

Lippert *et al.*[7] showed that coordination of M^{II}(dien) (M = Pd,Pt) towards N6′,N6′,N9-trimethyladenine solely occurs at N3. The latter finding implies that platination at the N7 position of guanosine can be prevented by the introduction of a sterically demanding protective group at the O6 position of the guanine moiety. Consequently, it was to be expected that platination would be inhibited by N2,O6 protection, while N7 platination would be allowed in the case of N2 protection.

In order to substantiate the viability of the aforementioned hypothesis, we first examined the influence of the N2 protecting group on the course of the platination (Fig. 1). To this end we compared the traditionally used[8a] diphenylacetyl (DPA) group in **1a** with the more mildly removable[8b,c] di-*n*-butylaminomethylene (DNB) group in **1b**. For reasons of solubility the platination experiments were carried out in DMF-d_7–D_2O (80:20) mixtures and using [Pt(dien)Cl]Cl.† The reaction between [Pt(dien)Cl]Cl and **1a** and **1b** at 37 °C, monitored by ^{1}H NMR (see Fig. 2), clearly reveals that N7 platination occurs. Surprisingly the 2-*N*-DNB protected guanine derivative **1b** proved to be roughly two-fold more reactive towards $[Pt(dien)]^{2+}$ than the 2-*N*-DPA protected derivative **1a**. The latter observation might be explained by electronic effects of the amidine group in **1b**, as well as by stacking of the diphenyl group in **1a**, thereby reducing the accessibility of N7. A detailed study on these effects is currently being performed.

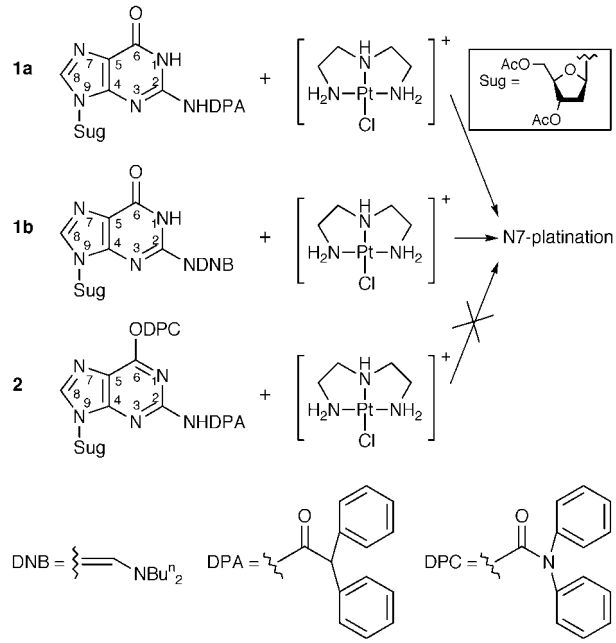

Fig. 1 Structures of 2′-deoxy-3′,5′-*O*-acetylated guanosine model compounds differing in base-protection and their (absence of) reactivity towards [Pt(dien)Cl]Cl.

The diphenylcarbamoyl (DPC) group[9] was selected to protect O6 of the guanine base giving, in combination with a diphenylacetyl (DPA) group at the N2 position, compound **2**. It can be seen in Fig. 2 that N7 platination of the N2,O6 protected derivative **2** is completely prevented.

Additional evidence for retardation of N7 platination was found by comparing the reactivity of *trans*-$[Pt(NH_3)_2Cl(DMF\text{-}d_7)]BF_4$ towards 2-*N*-(isobutyryl)-2′-deoxyguanosine (2-*N*-Bu^i-dG)‡ and 6-*O*-(diphenylcarbamoyl)-2-*N*-(diphenylacetyl)-2'-deoxyguanosine (6-*O*-DPC-2-*N*-DPA-dG). At room

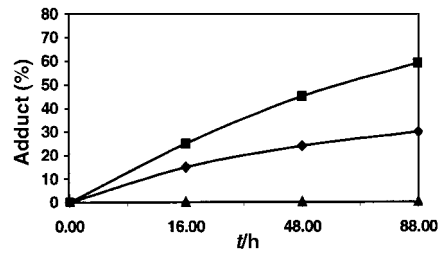

Fig. 2 Observed product formation during the reaction between [Pt(dien)Cl]Cl and (◆) **1a**, (■) **1b** and (▲) **2** in a 1:1 ratio at 4 mM concentration in DMF-d_7–D_2O (8:2 v/v) at 37 °C.

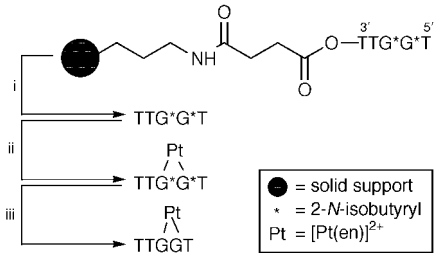

Scheme 1 *Reagents and conditions* i, NH_3–H_2O, (room temp., 15 min; ii, $[Pt(en)Cl(H_2O)]NO_3$, pH 6.0, 50 °C, 16 h; iii, NH_3–H_2O, 50 °C, 16 h.

temperature in DMF-d_7 with a slight excess of the platinum species, platination of 2-*N*-Bu^i-dG at N7, as gauged by ^{1}H NMR, went to completion within 1 h. No significant amount of platinated 6-*O*-DPC-2-*N*-DPA-dG could be observed under the same conditions. In the reaction of a 1 : 1 mixture of 2-*N*-Bu^i-dG and 6-*O*-DPC-2-*N*-DPA-dG with 1.1 equiv. of *trans*-$[Pt(NH_3)_2Cl(DMF\text{-}d_7)]BF_4$, only the downfield shifted H8 and H1′ resonances of the 2-*N*-Bu^i-dG derivative are observed, implying selective N7 platination for the 2-*N*-protected guanosine derivative in this competitive system.

The additional role of the electronic and/or steric effect of the protecting group at the exocyclic amine upon the reaction kinetics of N7 platination would allow a synergistic effect in our approach of protecting group directed selectivity enhancement.

Implementation of the latter results in the synthesis of selectively platinated oligonucleotides requires an effective platination of a N2-protected oligonucleotide. Therefore, the fully protected and immobilised pentamer d(TTGGT), having 2-*N*-Bu^i protection of the guanine bases and a β–cyanoethyl protection of the phosphate, which lacks strong competing nucleobase binding sites besides the 1,2-GG motif, was selected as a test system for maximisation of the product yield. The protected pentamer was obtained *via* routine automated DNA synthesis using controlled-pore glass (CPG) as the solid support. The platination of this immobilised pentamer by $[Pt(en)]^{2+}$ to form the 1,2-GG adduct was investigated. Platination experiments were performed under various conditions. Anion-exchange analysis on the platinated and deprotected sequence reveals that only 50–60% platinated pentanucleotide was obtained in this heterogeneous $[Pt(en)]^{2+}$/oligo-support system (data not shown). To increase the yield of platinated oligonucleotide, an alternative approach was followed (see Scheme 1) in which the oligonucleotide was cleaved from the support leaving the isobutyryl groups at the N2 position of the guanines intact.§ Subsequent platination of the base-protected pentamer by $[Pt(en)Cl(H_2O)]^+$, followed by removal of 2-*N*-Bu^i groups by aminolysis, provided a platination efficiency which was nearly quantitative. This can be attributed to both the homogeneity of this system, and loss of β-cyanoethyl phosphate protection (by the ammonia treatment) affording a negatively-charged backbone, thus allowing nucleophilic attack by the N7 and also electrostatic interaction between Pt and the target, as well as an increased hydrophilicity. Moreover, the observed stability of the [Pt(en){d(TTGGT)-N7(3),N7(4)}] adduct under prolonged ammonia exposure allows the use of more base-stable protecting groups like DPA and Bu^i at N2 within this, protective-group forced, platination strategy.

In summary, a promising new synthetic strategy utilising G building blocks with O6 protecting groups to prevent platination and G building blocks bearing amidine and acyl type N2 protection at the predetermined site for the bifunctional Pt-lesion has been presented. The general applicability of our approach to the synthesis of site-specifically platinated oligonucleotides is currently under investigation.

The authors wish to thank Professor Dr B. Lippert, Fachbereich Chemie Universität Dortmund, Germany, for scientific contributions and helpful discussions on the manuscript. This work was performed in the frame of the BIOMED project BMHA-CT97-2485. The authors wish to thank Johnson & Matthey (Reading, UK) for their generous loan of K_2PtCl_4.

Notes and references

† [Pt(dien)Cl]Cl, $[Pt(en)Cl_2]$ and *trans*-$[Pt(NH_3)_2Cl_2]$ were synthesized according to literature procedures, (ref. 10); the latter two were converted into the reactive species $[Pt(en)Cl(DMF)]NO_3$ and *trans*-$[Pt(NH_3)_2Cl(DMF\text{-}d_7)]BF_4$ by treatment with 1 equiv. of $AgNO_3$ or $AgBF_4$, respectively, in DMF and DMF-d_7. The protected mononucleosides **1a** and **1b** and 2-*N*-(isobutyryl)-2′-deoxyguanosine were synthesized according to procedures adapted from the literature (ref. 8), 6-*O*-protected nucleoside **2** was synthesized by a procedure analogous to Robbins *et al.* (ref. 9). ^{1}H and ^{195}Pt NMR measurements were performed on a Bruker WM 300 spectrometer. Internal calibration was based on the methyl groups of DMF in the case of ^{1}H NMR measurements and externally on K_2PtCl_6 for ^{195}Pt NMR measurements. Platination reactions of the protected mononucleosides and [Pt(dien)Cl]Cl were performed at a 4 mM concentration of both reactants in a DMF-d_7–D_2O mixture (80 : 20 v/v) at 37 °C. Calculations were performed by relative integration (estimated error 10%) of H8 and H1′ proton signals of both reaction products and starting materials during the reaction.

‡ Reaction of 2-*N*-(isobutyryl)-2′-deoxyguanosine at 4 mM concentration with 1.1 equiv. of *trans*-$[Pt(NH_3)_2Cl(DMF\text{-}d_7)]BF_4$ in DMF-d_7 showed a downfield shift of the H8 proton from δ 8.29 to δ 9.01 and from δ 6.30 to δ 6.38 for the H1′ proton.

§ The model oligonucleotide d(TTGGT) was assembled using an automated Gene Assembler (Pharmacia). Stepwise elongation of thymidine, immobilized by a 3′-*O*-succinyl bond to controlled pore glass (CPG), was carried out using standard synthesis protocols. The immobilised pentamer was washed thoroughly with MeCN and dried *in vacuo*. Cleavage conditions, for removal of the protected oligonucleotide from CPG matrix (*i.e.* hydrolysis of the succinyl linker) by treatment with NH_3–H_2O (25%) at room temperature, were established by analytical reversed phase HPLC (Lichrosphere® C_{18} column, starting buffer of 5% MeCN in TEAA (pH 7), 100 mM, to 75% MeCN in Et_4NOAc buffer). Deprotected species started to appear upon exposure times exceeding 20 min. For platination experiments a 1 mM stock solution of protected pentamer in H_2O was prepared and used immediately in reactions with $[Pt(en)Cl(H_2O)]NO_3$ (0.5 mM at pH 6.0). After reaction was allowed to proceed for 16 h at 50 °C, excess NH_3–H_2O (25%) was added and deprotection performed for 16 h at 50 °C, the reaction mixture was concentrated *in vacuo* and redissolved for analysis by anion exchange FPLC (APB MonoQ® HR 5/5 column, gradient from starting eluent 0.01 M NaOH to 1.2 M NaCl in 0.01 M NaOH).

1 J. Reedijk, *Chem. Commun.*, 1996, 801.
2 A. M. J. Fichtinger-Schepman, J. L. Van der Veer, J. H. J. Den Hartog, P. H. M. Lohman and J. Reedijk, *Biochemistry*, 1985, **24**, 707.
3 P. M. Takahara, A. C. Rosenzweig, C. A. Frederik and S. J. Lippard, *Nature*, 1995, **377**, 649; D. Yang, S. S. G. E. van Boom, J. Reedijk, J. H. van Boom and A. H.-J. Wang, *Biochemistry*, 1995, **34**, 12 912; A. Gelasco and S. J. Lippard, *Biochemistry*, 1998, **37**, 9230; J. M. Teuben, C. Bauer, A. J.-H. Wang and J. Reedijk, *Biochemistry*, in the press.
4 R. Dalbiès, D. Payet and M. Leng, *Proc. Natl. Acad. Sci. U.S.A.*, 1994, **91**, 8147; C. Colombier, B. Lippert and M. Leng, *Nucleic Acids Res.*, 1996, **24**, 4519; E. Bernal-Méndez, J.-S. Sun, F. Gonzalez-Vilchez and M. Leng, *New. J. Chem.*, 1998, 1479.
5 J. Schliepe, U. Berghoff, B. Lippert and D. Cech, *Angew. Chem., Int. Ed. Engl.*, 1996, **35**, 646; R. Manchanda, S. U. Dunham and S. J. Lippard, *J. Am. Chem. Soc.*, 1996, **118**, 5144; U. Berghoff, K. Schmidt, M. Janik, G. Schröder and B. Lippert, *Inorg. Chim. Acta*, 1998, **269**, 135.
6 D. J. Hurley and Y. Tor, *J. Am. Chem. Soc.*, 1998, **120**, 2194; S. I. Khan, A. E. Beilstein and M. W. Grinstaff, *Inorg. Chem.*, 1999, **38**, 418.
7 C. Meiser, B. Song, E. Freisinger, M. Peilert, H. Sigel and B. Lippert, *Chem. Eur. J.*, 1997, **3**, 388.
8 For some examples of synthetic approaches to the 2-*N*-protected 2′-deoxyguanosines, see: (*a*) C. H. M. Verdegaal, P. L. Jansse, J. F. M. de Rooij, G. A. van der Marel and J. H. van Boom, *Recl. Trav. Chim. Pays-Bas*, 1981, **100**, 200; (*b*) L. J. McBride, R. Kierzek, S. L. Beaucage and M. H. Carruthers, *J. Am. Chem. Soc.*, 1986, **108**, 2040; (*c*) B. C. Froehler and M. D. Matteucci, *Nucleic Acids Res.*, 1983, **11**, 8031.
9 R. Zou and M. J. Robbins, *Can. J. Chem.*, 1987, **65**, 1436; M. J. Robbins, R. Zou, Z. Guo and S. F. Wnuk, *J. Org. Chem.*, 1996, **61**, 9207.
10 G. W. Watt and W. A. Cude, *Inorg. Chem.*, 1968, **7**, 335; A. Pasini, C. Caldirola, S. Spinelli and M. Valsecchi, *Synth. React. Inorg. Met.-Org.Chem.*, 1993, **23**, 1021; G. B. Kauffman and D. O. Cowan, *Inorg. Synth.*, 1963, **7**, 239.

Communication 9/04365I

ChemComm

Synthesis and X-ray structure of $[(THF)K(C_5H_4CH_2CH_2PPh_2)]_\infty$: a structurally characterized heavier alkali metal phosphane complex

Hans H. Karsch,* Volker W. Graf and Manfred Reisky

Anorganisch-chemisches Institut der Technischen Universität München, Lichtenbergstr. 4, D-85747 Garching, Germany. E-mail: Hans.H.Karsch@lrz.tu-muenchen.de

Received (in Cambridge, UK) 12th March 1999, Revised manuscript received 12th July, Accepted 26th July 1999

Reaction of spiro[2.4]hepta-4,6-diene with $KPPh_2$ in THF gives $K(C_5H_4CH_2CH_2PPh_2)$ 1, which crystallizes from THF and shows coordination of a neutral phosphane functionality to potassium.

Stable complexes with phosphorus to alkali metal bonds are obtained with anionic phosphane type ligands like phosphanides {*e.g.* $[KPHMes^*]_\infty$,[1] $[K_3(THF)\{PH(Mes)\}_3]_\infty$,[2] $[K(THF)P(SiMe_3)_2]$[3]}. In these complexes phosphorus is of the σ^2, λ^3-type. So far there is no example for coordination of a neutral phosphane (σ^3, λ^3) to a heavier alkali metal center (K, Rb, Cs)[4] with one remarkable exception: In $[\{(Bu^tP)_2H\}K\bullet pmdeta]_2$ (pmdeta = *N*,*N*,*N*′,*N*′,*N*″-pentamethyldiethylenetriamine), a 'secondary coordinative interaction' of the neutral phosphorus to potassium is defined, containing a long K–P interaction of 3.658 (3) Å. This phosphorus is directly attached to a neighbouring phosphanide P-atom,[5] formally introducing the negative charge on the ligand. This resembles the situation in phosphanomethanides, where a carbanion enhances the donor capacity of the adjacent neutral phosphorus atom to an extent, that a variety of phosphane complexes including very electropositive metals (alkali, alkaline earth, lanthanide metals) have successfully been synthesized.[6]

In contrast, in alkyl substituted cyclopentadienyl ligands with an additional phosphane functionality in the side chain ('anionic phosphane ligands') the negative charge is well separated from the phosphane donor functionality. Nevertheless these anionic ligands likewise bind to electropositive metal centers. Remarkable results have been obtained in the field of lanthanide chemistry.[7]

The additional phosphane functionality, in contrast to 'simple' cyclopentadienyl derivatives, provides a labile and hence reversible coordination to metal centers, thus combining coordinative 'protection' with enhanced reactivity and therefore is of great interest for catalytic reactions, particularly when combined with transition or lanthanide metal centers. Lithium derivatives[7,8*a*] have been used to transfer the anionic phosphanoalkyl cyclopentadienide moiety to these metals,[7] but derivatives of the heavier alkali metals often have advantages in salt separation from the reaction mixtures.

We report here the synthesis and the solid state structure of $[(THF)K(C_5H_4CH_2CH_2PPh_2)]_\infty$ **1**, the first molecular example exhibiting a coordinative interaction of a neutral phosphane donor with a heavier organo alkali metal center.

Phosphanoethyl substituted cyclopentadienides $\{M[C_5H_4(CH_2)_2PR_2]$, M = Li, Na,} are best prepared by reaction of the corresponding phosphanide with spiro[2.4]hepta-4,6-diene.[8] Anionic lithium and sodium compounds with R = Ph, Pr^i, Bu^t,[8] Me[7] are known, but not structurally characterized. The complex $K[C_5H_4(CH_2)_2PPh_2]$† was synthesized by reaction of spiro[2.4]hepta-4,6-diene with $KPPh_2$ in THF (Scheme 1).

Scheme 1

In the $^{31}P\{^1H\}$ NMR spectrum (dioxane-d^8) only one singlet at δ −13.27 is detected. The signal remains unchanged upon varying the temperature. This result indicates that the compound is not involved in dynamic processes but there is no indication of the actual species present in solution. In particular, the kind of ligation around potassium and the degree of association remains unknown.

The crystal structure‡ of $[(THF)K(C_5H_4CH_2CH_2PPh_2)]_\infty$ consists of polymeric zigzag chains [Fig. 1(a)] as, for example, in CpK,[9] $CpK\bullet Et_2O$,[10] $Cp^*K\bullet 2Py$[11] and $(C_5H_4SiMe_3)K$.[12]

The potassium atom is surrounded by two cyclopentadienyl rings in an η^5 fashion. The $K–Cp_{center}$ distances are 2.821(2) (intramolecular) and 2.792(2) Å ($K\text{-}Cp_{center}$ distance to the next molecule) [Fig. 1(b)], *i.e.* the 'intermolecular' distance is shorter than the 'intramolecular' one. Therefore, the ligand $CpCH_2CH_2PPh_2^-$ can be regarded a bridging rather than a chelating ligand.

These values can be compared with the $K–Cp_{center}$ distance in the coordination polymers of KCp [mean 2.816(3) Å][9] and

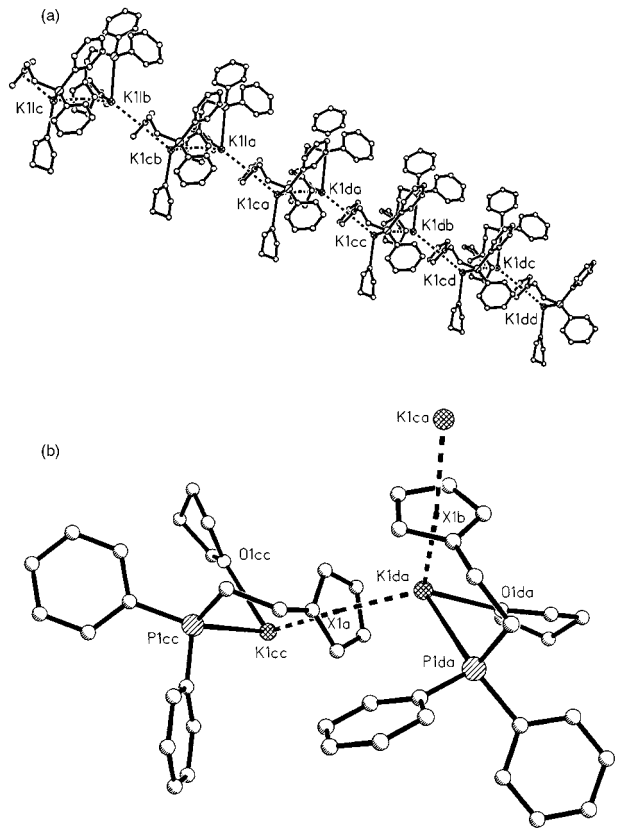

Fig. 1 Structure of $[(THF)K(C_5H_4CH_2CH_2PPh_2)]_\infty$ **1** (a) Polymer chain; (b) detail of the structure. Selected bond lengths (Å) and angles (°):K1da–P1da 3.320(2), K1da–O1da 2.708(2), K1da–X1a 2.792(2), K1da–X1b 2.821(2); P1d–K1da–O1da 88.75(4), P1d–K1da–X1a 123.90(5), O1da–K1da–X1a 109.32(4), O1da–K1da–X1b 126.7(6), K1da–X1a–K1cc 173.10(4); X: centroids of the Cp-rings.

KCp*•2Py (mean 2.79 Å).[11] An unique feature of the solid state structure is the additional P–K bond due to an intramolecular coordination of the alkyl phosphano functionality. The P–K distance of 3.320(2) Å is only slightly longer than in the phosphanide compounds $[Bu^t_2SiFK(THF)_2PC_6H_2Me_3]_2$[13] [3.230(1)], $[K_3(THF)_2\{PH(Mes)\}_3]_\infty$[2] [3.368(1), 3.397(1), 3.453(1), 3.306(2) Å], $[\{(Bu^tP)_2H\}K•pmdeta]_2$[5] [3.251(2) Å], $[KPH(2,4,6\text{-}Bu^t_3C_6H_2]_\infty$[2] [shortest distance 3.271(2), longest distance 3.357(2) Å] and $[K(THF)P(SiMe_3)_2]_\infty$[3] [3.317(7) Å], but considerably shorter (0.332 Å) than the only other K–P distance involving a neutral phosphane donor as mentioned earlier[5].

In **1** the K–Cp_{center}–K angle is 173.1(4)° and the Cp_{center}–K–Cp_{center} angle amounts to 126.7°. To complete the coordination sphere one molecule of THF is coordinated to potassium. The K–O distance of 2.708(2) Å lies in the expected range for a K–O interaction {2.781(2) in $[K(THF)P(SiMe_3)_2]_\infty$}.[3]

The first organopotassium compound with an additional potassium–phosphorus bond presented here establishes the first example of a potassium to phosphorus bond exhibiting a 'normal' bond length and involving a neutral phosphane donor and is the first structurally characterized alkali metal cyclopentadienide with a phosphanoalkyl side chain. All other known molecules with potassium phosphorus bonds contain phosphanide ligands. Particularly noteworthy is the fact that the potassium–phosphorus bond is formed even on precipitation from THF solution, *i.e.* this bonding can successfully compete with a potassium–THF interaction. As in many other K–Cp compounds a polymeric zigzag chain of alternating cyclopentadienyl groups and potassium atoms is adopted in the solid state structure of **1**.

Notes and references

† To a solution of 0.041 mol (9.1 g) $KPPh_2$ in 150 ml of THF 0.041 mol (3.59 g) spiro[2.4]hepta-4,6-diene in 20 ml of THF were added by means of a pipette. After stirring the reaction mixture for 12 h at room temperature the solvent was removed and the product was washed three times with pentane. After drying the residue, 8.9 g (68%) of a colorless solid were obtained. Decomp. 181 °C; correct elemental analysis.

^{1}H NMR (dioxane-d^8, room temp., 400 MHz) δ 1.76 (m, 4H, CH_2CH$_2$O), 2.21 (m, 2H, CpCH$_2$CH_2PPh$_2$), 3.52 (m, 2H, CpCH_2CH$_2$PPh$_2$), 3.62 (m, 4H, CH$_2$CH_2O), 5.29 (s, 4H, C$_5H_4$CH$_2$CH$_2$), 7.19–7.44 (10H, phenyl);^{13}C{^{1}H} NMR (dioxane-d^8, room temp., 100.4 MHz) δ 26.16 (s, *C*H$_2$CH$_2$O), 26.93 (d, $^2J_{CP}$ 15.6 Hz, *C*H$_2$CH$_2$PPh$_2$), 31.83 (d, $^1J_{CP}$ 10.1 Hz, *C*H$_2$P), 67.57 (s, CH$_2$*C*H$_2$O), 104.11 (s, CH$_2$*C*CH), 121.1 (d,$^3J_{CP}$ 11.0 Hz, *ipso*-C), 128.92 (d, $^3J_{CP}$ 6.4 Hz, C3, phenyl), 129.01 (s, C4, phenyl), 133.64 (d, $^2J_{CP}$ 18.4 Hz, C2, phenyl), 140.57 (d, $^1J_{CP}$ 13.8 Hz, *ipso*-C, phenyl); ^{31}P{^{1}H} NMR (dioxane-d^8, room temp., 161.7 MHz) δ −13.27 (s).

‡ Colorless crystals of $[(THF)K(C_5H_4CH_2CH_2PPh_2)]_\infty$ precipitate on concentrating a solution of $K[C_5H_4(CH_2)_2PPh_2]$ in THF. *Crystal data* for $C_{23}H_{26}KOP$: M = 388.51, monoclinic, space group $P2_1/c$, a = 10.432(1), b = 19.929(1), c = 10.026(1) Å, β = 90.56(1)°, U = 2084.3(3) Å^3, T = 199 K, Z = 4, μ = 0.340 mm^{-1} 4763 reflections measured, 4528 independent. The final $wR(F^2)$ was 0.085 (all data). The structure was solved by direct methods and refined by full-matrix least squares on F^2(SHELXL-93).[14] CCDC 182/1349. See http//www.rsc.org/suppdata/cc/1999/1695/ for crystallographic files in .cif format.

1 G. W. Rabe, G. P. Yap and A. L. Rheingold, *Inorg. Chem.*, 1997, **36**, 1990.
2 C. Frenzel, P. Jörchel and E. Hey-Hawkins, *Chem. Commun.*, 1998, 1363.
3 U. Englich, K. Hassler, K. Ruhland-Senge and F. Uhlig, *Inorg. Chem.*, 1998, **37**, 3532.
4 J. D. Smith, *Adv. Organomet. Chem.*, 1998, **43**, 267.
5 M. A. Beswick, A. D. Hopkins, L. C. Kerr, M. E. Mosquera, J. S. Palmer, P. R. Raithby, A. Rothenberger, D. Stalke, A. Steiner, A. E. Wheatley and D. S. Wright, *Chem. Commun.*, 1998, 1527.
6 H. H. Karsch, *Russ. Chem. Bull.*, 1993, **42**, 1937; H. H. Karsch, G. Ferazin, H. Kooijman, O. Steigelmann, A. Schier, P. Bissinger and W. Hiller, *J. Organomet. Chem.*, 1994, **482**, 151; H. H. Karsch, A. Appelt, J. Riede and G. Müller, *Angew. Chem.*, 1986, **98**, 832; *Angew. Chem., Int. Ed. Engl.*, 1986, **25**, 832; H. H. Karsch and M. Reisky, *Eur. J. Inorg. Chem.*, 1998, 905.
7 H. H. Karsch, V. Graf, E. Witt and M. Reisky, *Eur. J. Inorg. Chem.*, 1998, 1403; H. H. Karsch, V. Graf and M. Reisky, to be submitted.
8 (*a*) R. T. Kettenbach, W. Bonrath and H. Butenschön, *Chem. Ber.*, 1993, **126**, 1657; (*b*) T. Kauffmann, J. Ennen, H. Lhotak, A. Rensing, F. Steinseifer and A. Woltermann, *Angew. Chem.*, 1980, **92**, 321.
9 R. E. Dinnebier, U. Behrens and F. Olbrich, *Organometallics*, 1997, **16**, 3855.
10 V. Jordan, U. Behrens, F. Olbrich and E. Weiss, *J. Organomet. Chem.*, 1996, **517**, 81.
11 G. Rabe, H. W. Roesky, D. Stalke, F. Pauer and G. M. Sheldrick, *J. Organomet. Chem.*, 1991, **403**, 11.
12 P. Jutzi, W. Leffers, B. Hampel, S. Pohl and W. Saak, *Angew. Chem.*, 1987, **99**, 563; *Angew. Chem., Int. Ed. Engl.*, 1987, **26**, 583.
13 M. Andrianarison, D. Stalke and U. Klingebiel, *Chem. Ber.*, 1990, **123**, 71.
14 SHELXL-93: G. M. Sheldrick, C. Krüger and R. Goddard, *Crystallographic Computing 3*, Oxford Univ. Press 1985, p. 175; G. M. Sheldrick, *Program for Refinement of Crystal Structures*, University of Göttingen, 1993; N. Walker and D. Stuart, *Acta Crystallogr., Sect. A*, 1983, **39**, 158.

Communication 9/04248B

ChemComm

Electron induced modification of the surface electrochemical properties of diamond electrodes

Christiaan H. Goeting,[a] Frank Marken,[a] Chris Salter,[b] Richard G. Compton[a] and John S. Foord*[a]

[a] *Physical and Theoretical Chemistry Laboratory, University of Oxford, Oxford, UK OX1 3QZ. E-mail: John.Foord@chem.ox.ac.uk*

[b] *Department of Materials, University of Oxford, Oxford, UK OX1 3PH*

Received (in Cambridge, UK) 30th June 1999, Accepted 23rd July 1999

A novel method has been developed to modify the surface properties of boron-doped CVD diamond electrodes by electron stimulated desorption (ESD) of hydrogen and oxygen from as grown diamond surfaces allowing the selective electrochemical silver deposition on the areas not irradiated with electrons.

Boron-doped CVD diamond is a very promising material in areas such as electrochemistry and electronics owing to very useful properties, such as extreme hardness, chemical inertness, very high electrical and heat conductivity and negative electron affinity (NEA) when hydrogen terminated. In this study, results are presented on the effect of the electron stimulated desorption of hydrogen and oxygen from boron-doped diamond surfaces on the electrochemical characteristics, monitored by the silver deposition on areas irradiated and not irradiated with high energy electrons in a scanning electron microscope (SEM). A correlation between changes in electron affinity and electrochemical activity is observed.

Highly conductive boron-doped diamond films were deposited on 5 mm diameter tungsten substrates from a gaseous feed of diborane and 1% methane in hydrogen using a hot filament assisted CVD reactor as described previously.[1] The boron-doped diamond surface was irradiated by an electron beam of an energy ranging from 1 to 25 keV and a current density ranging from *ca.* 93 mA cm^{-2} to 60 A cm^{-2} at a background pressure of *ca.* 10^{-6} mbar at room temperature. SEM images of treated and untreated areas after electrochemical deposition of silver on the surface of the boron-doped diamond are presented in Fig. 1. An interesting feature shown in the SEM images is the well defined dark irradiated area in contrast to the much brighter surroundings. In a XPS study, Cui *et al.*[2] reported electron beam stimulated desorption of hydrogen from single crystal diamond (111) surfaces. They showed that H-terminated diamond has a negative electron affinity (NEA) of $\chi = -1.27$ eV and that electron irradiation desorbed the terminal hydrogen as a function of time giving the diamond surface a positive electron affinity of $\chi = +0.4$ eV (less brightness in SEM images) without graphitising the surface. NEA materials such as hydrogenated diamond when irradiated with energetic electrons, exhibit very high secondary electron emission.[3] Hence, the darker feature shown on the SEM image can be attributed to lower secondary electron emission and is therefore indicative of a hydrogen depleted diamond surface. Interestingly, in the backscatter mode no shading is observed. The backscatter electrons have much higher energy than secondary electrons and so are insensitive to the energy barrier which exists at the surface. This is consistent with a surface modification involving a change in χ.

Based on the work by Cui *et al.*[2] it is proposed that the electron beam irradiation desorbs hydrogen from a well defined area with a resolution approximating that of the electron beam (*ca.* 0.5 nm) from the hydrogen terminated diamond surface. Energy dispersive X-ray spectrometry (EDX) was performed in order to estimate the oxygen concentration of the irradiated area compared to the surrounding surface. Although EDX is not highly surface sensitive, a comparison clearly indicates that the electron irradiated area, after the silver deposition process, exhibits a very low O/C ratio (O below the signal to noise level) and therefore had practically no oxygen functionalities on the surface. The O/C peak area ratio in the EDX spectrum for the area not irradiated was significantly higher with a value of *ca.* 5%. It can be concluded that the electron beam actively removes hydrogen, oxygen, and probably other impurities from the surface.

In order to study the effect of the electron beam on the electrochemical characteristics of the surface of the boron-doped diamond, silver was deposited electrochemically. Fig. 2 shows cyclic voltammograms for three consecutive potential cycles with a scan rate of 0.1 V s^{-1} for the reduction/oxidation

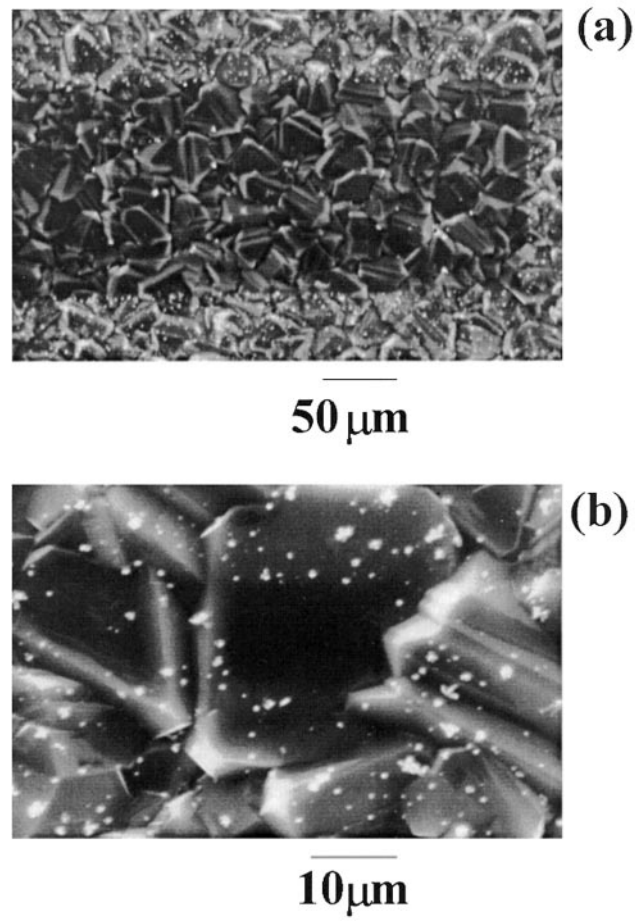

Fig. 1 SEM images of boron-doped diamond electrode surfaces after electrochemical deposition of silver from 1mM $AgNO_3$ in aqueous 0.1 M HNO_3 at a potential of $E = +0.17$ V *vs.* SCE (deposition time 3 min, irradiated with electrons of (a) an energy of 1 keV and a current density of *ca.* 93 mA cm^{-2} for 30 min and (b) an energy of 25 keV and a current density of *ca.* 60 A cm^{-2} for 5 min).

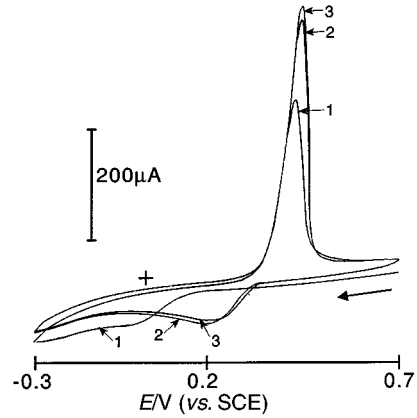

Fig. 2 Three consecutive cyclic voltammograms recorded with a scan rate of 0.1 V s^{-1} for the reduction/oxidation of 1mM $AgNO_3$ in aqueous 0.1 M HNO_3 at a 5 mm diameter boron-doped diamond electrode ('+' indicates zero current).

of 1 mM $AgNO_3$ in aqueous 0.1 M HNO_3 at the surface treated boron-doped diamond electrode. On the first forward scan starting from +0.7 V *vs.* SCE to negative potentials the nucleation process starts at *ca.* 0.0 V *vs.* SCE followed by growth at more negative potentials. On the reverse scan a characteristic stripping response is observed indicative for dissolution of the metallic silver into solution. These observations are in accord with a recent study by Vinokur *et al.*[4] A closer look at the stripping peak reveals an asymmetric tailing indicating that the dissolution is slow and not complete. The second and third scan show a reduction peak at a significantly more positive potential in agreement with silver growth on the silver nuclei already present from the previous scan. The silver remaining on the diamond surface after the stripping process could also be verified by SEM and XPS measurements.[5] This incomplete oxidation of deposits on diamond has been reported for Ag[4,5] and Pb[6,7] but is not yet fully understood.

After recording the cyclic voltammograms, silver was deposited on the electron beam treated diamond surface from a solution of 1 mM $AgNO_3$ in aqueous 0.1 M HNO_3 by applying a potential of $E = +0.17$ V *vs*. SCE [Fig. 1(a) and (b)] and of $E = -0.3$ V *vs*. SCE (not shown) for periods of 3 min. The SEM image clearly shows that there is a high density of silver deposition in the unexposed area while in the darker electron irradiated area hardly any deposition occurred. However, when the deposition potential was set to more negative potentials, silver deposition was detected also in the areas exposed to the electron beam. Fig. 1(b) shows an SEM image which reveals a dark *ca.* 200 μm^2 irradiated area on a single (100) crystallite face without any silver deposition. The selectivity of the electron induced surface modification is such that even single diamond crystallites may be patterned and partly covered with silver. Hydrogenating highly resistive non-doped diamond is known to induce p-type surface conductivity.[8] However, the diamond samples are highly boron-doped making it very conductive and therefore, it can be assumed that the observed effect is a surface effect, and not a localised change in (surface) conductivity. A possibly related patterning effect has been observed after photo-treatment and electro-deposition of copper.[9]

The present study shows that diamond surfaces can be modified selectively and with high spatial resolution using a focussed electron beam and that metallic silver can be selectively deposited on the unexposed diamond surface. It is proposed that electron irradiation desorbs hydrogen, oxygen, and impurities from the as grown diamond surface yielding a surface of more positive electron affinity and lower activity towards silver nucleation and growth. It is widely accepted that oxygen functionalities play an important role in the surface activity of diamond electrodes. The selectivity towards the metal deposition can be improved by optimising the doses of electron irradiation and hence the level of dehydrogenation. Even the surface structure can be manipulated[2] to give hydrogen rich (1×1), hydrogen poor (1×1), hydrogen poor (2×1), or hydrogen free reconstructed (2×1) by controlling the level of dehydrogenation and the electron affinity may be fine tuned between $\chi = -1.27$ eV and +0.40 eV.

In conclusion, the electron stimulated modification of diamond surfaces may offer potential benefits in a wide range of applications, such as selective metal deposition, fabrication of microelectrodes and sensors, cold cathodes, and patterned field emitters.

Notes and references

1 C. H. Goeting, J. S. Foord, F. Marken and R. G. Compton, *Diamond Rel. Mater*., 1999, **8**, 824.
2 J. B. Cui, R. Graupner, J. Ristein and L. Ley, *Diamond Rel. Mater.*, 1999, **8**, 748.
3 H. J. Hopman, J. Verhoeven, P. K. Bachmann, H. Wilson and R. Kroon, Poster Presentation, *9th European Conference on Diamond, Diamond-like Materials, Nitrides and Silicon Carbides*, Crete, Greece, September 13th–18th, 1998.
4 N. Vinokur, B. Miller, Y. Avyigal and R. Kalish, *J. Electrochem. Soc.*, 1999, **146**, 125.
5 C. H. Goeting, J. S. Foord, F. Marken and R. G. Compton, in preparation.
6 M. Awada, J. W. Strojek and G. M. Swain, *J. Electrochem.Soc*., 1995, **142**, L42.
7 C. H. Goeting, F. Jones, J. S. Foord, J. C. Eklund, F. Marken, R. G. Compton, P. R. Chalker and C. Johnston, *J. Electroanal. Chem*., 1998, **442**, 207.
8 H. J. Looi, L. Y. S. Pang, A. B. Molloy, F. Jones, J. S. Foord and R. B. Jackman, *Diamond Rel. Mater*., 1998, **7**, 550.
9 S. Yoshihara, K. Shinozaki, T. Shirakashi, K. Hashimoto, D. A. Tryk and A. Fujishima, *Electrochim. Acta*, 1999, **44**, 2711.

Communication 9/05275E

Stereodifferentiation and base-pair selectivity in the binding of Δ and Λ cationic lanthanide complexes to $[(CG)_6]_2$, $[(AT)_6]_2$ and CT-DNA

Linda J. Govenlock,[a] Céline E. Mathieu,[a] Christine L. Maupin,[c] David Parker,*[a] James P. Riehl,[c] Giuliano Siligardi[b] and J. A. Gareth Williams[a]

[a] *Department of Chemistry, University of Durham, South Road, Durham, UK DH1 3LE*
[b] *Department of Pharmacy, King's College London, Manresa Road, London, UK SW3 6LX*
[c] *Department of Chemistry, Michigan Technological University, Houghton, Michigan 4993 11295 USA*

Received (in Cambridge, UK) 26th May 1999, Accepted 28th July 1999

Metal- and ligand-based luminescence, absorption and circular dichroism difference spectroscopy signal the extent and nature of binding of enantiopure Δ and Λ cationic lanthanide complexes to $[(CG)_6]_2$ and $[(AT)_6]_2$.

Whilst there have been many reports probing the interaction of the aqua lanthanide ions with nucleotides and DNA using NMR[1] and luminescence methods,[2] no studies have appeared in which the binding of well defined chiral lanthanide complexes has been defined. Following the characterisation of the cationic, enantiomeric lanthanide complexes of ligands (*RRR*)-MeL[1a] and (*SSS*)-MeL[1b],[3] we report herein preliminary binding studies with calf-thymus DNA and the oligonucleotides $[(CG)_6]_2$ and $[(AT)_6]_2$.† These lanthanide complexes possess complementary properties allowing their interaction with chiral polyanions to be studied, including the absorption and fluorescence emission behaviour of the phenanthridinium unit and the intensity, polarisation and lifetime of the lanthanide emission.[4]

The absorption spectrum of each complex was monitored as a function of added oligonucleotide or DNA, at pH 7.4 in low added salt (Fig. 1 and Table 1). For the complexes with $[(CG)_6]_2$ and calf thymus (CT)-DNA isosbestic points were observed at 302 and 378 nm, with pronounced hypochromism in the bands at 320 and 370 nm and a red-shift, accompanied by formation of a long wavelength tail beyond 400 nm. For complexes with $[(AT)_6]_2$, changes in intensity were much smaller and the long wavelength tail and isosbestic point at 378 nm were absent. The observed hypochromism and concomitant red shifts are often associated with intercalative binding,[5] and are consistent here with a preferred charge transfer interaction involving the more electron-rich C and G bases and the positively-charged phenanthridinium unit.

The fluorescence of the *N*-alkylphenanthridinium moiety was monitored at 408 nm, as a function of added DNA, following excitation at the isosbestic point. Quenching of fluorescence was observed, as is often found when planar aromatic fluorophores bind to DNA, arising from charge transfer-catalysed non-radiative deactivation of the singlet excited state. Quenching of the long-lived europium emission (*e.g.* at 594 nm) was also observed and mirrored the decrease in the fluorescence intensity. No significant change in the lifetime of the metal emission was observed, from its value of 0.55 ms in water in the absence of DNA,[4] ruling out any direct quenching of the metal excited state by photoinduced electron transfer from the DNA bases.

Intrinsic binding constants, *K*, and site sizes *n*′ (per mole of duplex) were estimated using the method of McGhee and von Hippel[6] (Table 1). Values obtained for the model intercalators ethidium bromide and *N*-ethylphenanthridinium iodide were measured under the same conditions. Strongest binding of the Eu complexes was observed to $[(CG)_6]_2$ with one complex bound per three base pairs on average, and the Δ isomer bound slightly more strongly than the Λ. With Δ-$[EuL^{1a}]^{4+}$, binding affinity to $[(AT)_6]_2$ was over 50 times weaker than to $[(CG)_6]_2$ (with a reduced site density, suggestive of a weaker intercalative interaction) , and in this case the Λ isomer bound more strongly ($\Delta\Delta G$ = 4 kJ mol^{-1}). The effect of increasing the salt concentration (10, 50 and 100 mM NaCl) was also examined for

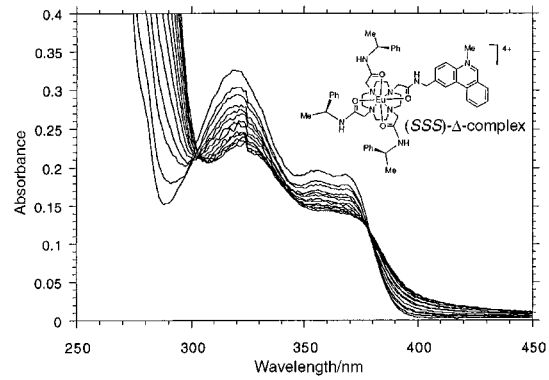

Fig. 1 UV-absorbance spectra for (*SSS*)-Δ-$[Eu(MeL^{1b})]^{4+}$ (23.6 μM) upon addition of increasing concentrations of $[CG)_6]_2$ (0–12.9 μM) in buffered aqueous solution (HEPES 10 mM, pH 7.4, NaCl 10 mM, 293 K).

Table 1 Intrinsic binding constants (*K*), site sizes (*n*′) and degree of hypochromism measured for complexes of $[(CG)_6]_2$ and $[(AT)_6]_2$ with Δ$[LnL^{1a}]^{4+}$ and Λ$[LnL^{1b}]^{4+}$ (298 K, 10 mM HEPES pH 7.4, 10 mM NaCl)

Complex	10^{-5} K^a/dm^3 mol^{-1} duplex^{-1}	n'^a/(duplex)$^{-1}$	% hypochromism at 320 (370) nm
Δ-$[EuL^{1a}]^{4+}$/$[(CG)_6)]_2$	87	3.98	35 (27)[c]
Λ-$[EuL^{1b}]^{4+}$/$[(CG)_6]_2$[b]	36	3.96	33 (28)[c]
Δ-$[EuL^{1a}]^{4+}$/$[(AT)_6]_2$	1.6	1.52	13 (10)
Λ-$[EuL^{1b}]^{4+}$/$[(AT)_6]_2$	8.0	1.82	15 (12)
N-ethylphenanthridinium iodide/$[(AT)_6]_2$	< 0.3	n.d.	11 (10)
ethidium bromide/$[(CG)_6)]_2$	31	2.26	n.a.
N-ethylphenanthridinium iodide/$[(CG)_6)]_2$	6.8	3.88	32 (10)

[a] Typically [LnL] = 10–20 μM; data from luminescence intensity changes[d] with added oligonucleotide were analysed by the method of McGhee and von Hippel;[6] an approximate analysis of the more limited CD data gave similar values. [b] In 50 mM NaCl, $K = 7.2 \times 10^5$ and $n' = 2.0$ and in 100 mM NaCl, $K = 2.8 \times 10^5$ ($n' = 1.9$). [c] Very similar spectra were observed for Δ/Λ-Eu complexes binding to calf-thymus DNA (42% CG). [d] Limiting changes in fluorescence intensity ratio (I_{free}/I_{bound}) were 55 for Δ-Eu/$[(CG)_6]_2$ and 2 for Λ-Eu/$[(AT)_6]_2$.

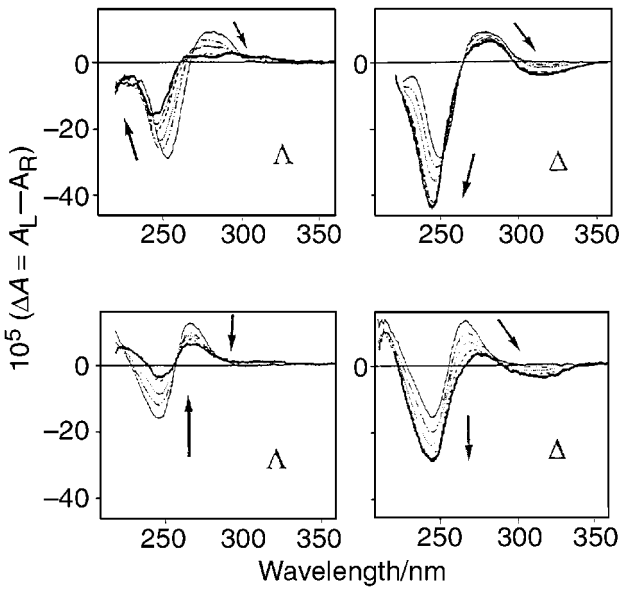

Fig. 2 Near-UV region CD spectrum of $[(CG)_6]_2$ (upper) and $[(AT)_6]_2$ (lower) in buffered aqueous. solution (10 mM HEPES, NaCl 10 mM) and in the presence of increasing ratios of Λ(0, 0.50, 0.99, 1.96, 2.91, 4.76, 7.41) and Δ-$[EuL^1]^{4+}$ (0, 0.49, 0.97, 1.92, 2.86, 3.77, 4.67) (left and right respectively). In each case, the CD spectrum of the complex itself at the same concentration has been subtracted.

Λ-$[EuL^{1b}]^{4+}$ /$[(CG)_6]_2$: only modest reductions in overall affinity were found (Table 1), ruling out the possibility of a predominantly electrostatic binding interaction.

The interaction of the europium complexes with the oligonucleotides has also been examined by circular dichroism difference spectroscopy, adding the complex to a fixed concentration of the oligonucleotide. In the near-UV region, the CD spectra of $[(CG)_6]_2$ and $[(AT)_6]_2$ show the features characteristic of *B*-DNA;[7] these gross features persisted even after addition of a substantial excess of the Eu complexes (Fig. 2) ruling out the $B \rightarrow Z$ transition which can occur in the presence of a highly charged metal complex.[2] In the 220–260 and 290–340 nm regions, the CD changes for a given oligonucleotide were markedly dependent upon the chirality of the complex, and changed in the opposite sense for each pair of diastereoisomeric complexes. In particular, in the 290–340 nm region, the observed changes for the Λ isomer titration were at least 50% less than those for the Δ isomer. Control experiments, examining CD difference spectra following addition of the tripositive C_4 symmetric parent complexes (*i.e.* lacking the phenanthridinium moiety) to $[(CG)_6]_6$ and $[(AT)_6]_2$, revealed only *very* small changes in ellipticity (< 6% of the change seen with $[EuL^{1a}]^{4+}$). The difference CD spectra obtained with $[EuL^{1a}]^{4+}$ and CT-DNA were almost identical to those obtained with $[(CG)_6]_2$.

In the visible region (Fig. 3), the CD signals arise exclusively from the phenanthridinium chromophore. For the unbound enantiomeric Eu complexes, weak, mirror image CD spectra were observed in this region. Upon binding to both $[(CG)_6]_2$ and to $[(AT)_6,]_2$, a positive induced CD at *ca.* 370 nm was observed for each enantiomer and qualitatively similar changes were noted with increasing oligo concentration. This suggests that the chirality of the oligonucleotide binding site must be similar for both $[(CG)_6]_2$ and $[(AT)_6]_2$ as the induced CD is *independent* of complex handedness.

The stoichiometry of the oligonucleotide–Eu complex binding was further investigated using the method of continuous variation, by plotting the CD intensity at a single wavelength *vs.* the mole fraction of the complex. Discontinuities at 0.5 and 0.67

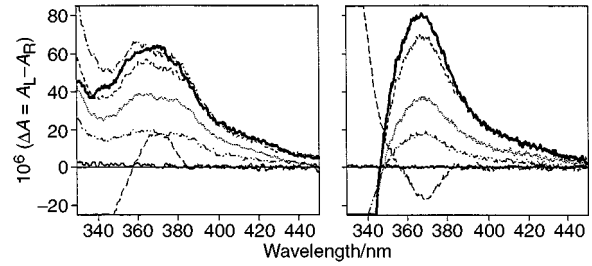

Fig. 3 Visible region CD spectra of $[(CG)_6]_2$ in the presence of increasing ratios of the Λ (left) and Δ (right) enantiomers of the Eu complex (Λ ratios shown are 0.50, 0.99, 1.96, 2.81 and 7.1; Δ: 0.49, 0.98, 1.92, 2.83), showing the long wavelength region where signals arise only from the phenanthridinium group. The CD spectrum of the complex at the same concentration has been subtracted in each case; spectra of the complexes in the absence of DNA are shown for reference (---------).

were found, consistent with stepwise formation of 1:1 and 2:1 complexes for both $[(AT)_6]_2$ and $[(CG)_6]_2$ binding.

In conclusion, the absorbance and fluorescence changes of the phenanthridinium moiety upon binding to $[(CG)_6]_2$ and CT-DNA, together with the relatively weak induced CD at 370 nm, are all consistent with a binding interaction predominantly involving intercalation. Binding to $[(AT)_6]_2$ is over 50 times weaker with Δ-$[EuL^{1a}]^{4+}$ and any intercalation is much less pronounced; the very similar spectral (CD, absorbance) changes observed with CT-DNA (42% CG) accord with this base-pair selectivity. AT-Rich sequences are believed to favour metal complex binding at the minor groove when the handedness of the complex is complementary to that of the right-handed helix.[8] Thus the stereodifferentiation observed in the interaction of the Eu complexes with $[(AT)_6]_2$ could arise from preferential minor-groove binding of the **Λ** isomer.

We thank EPSRC and the National Chiroptical Centre for support and the Royal Society for a Leverhulme Trust Senior Research Fellowship (D. P.).

Notes and references

† $(CG)_6$ is an abbreviation for $(dC–dG)_6$, which exists as a duplex in aqueous media.

1 C. D. Barry, A. C. T. North, J. A. Glasel, R. J. P. Williams and A. V. Xavier, *Nature*, 1971, **232**, 236.
2 P. K.-L. Fu and C. Turro, *J. Am. Chem. Soc*., 1999, **121**, 1; Y.-X. Ci , Y.-Z. Li and X.-J. Liu, *Anal. Chem*., 1995, **67**, 1785; P. C. Ionannou and T. K. Christopoulos, *Anal. Chem*., 1998, **70**, 698; S. L. Klakamp and W. deW. Horrocks, *Biopolymers*, 1990, **30**, 33; M. D. Topal and J. R. Fresco, *Biochemistry*, 1980, **19**, 5531.
3 We have used CPL spectroscopy to establish that the (*SSS*)-L^{1b} complexes of Eu, Tb and Yb possess the Δ configuration. The Yb complex possesses a reduced helicity about the metal centre (*ca*. 29 *vs*. 40° for Eu/Tb), associated with its twisted square-anti-prismatic solution structure. VT-Proton NMR studies have confirmed that > 97% of one isomeric species exists in solution in each case: for a related example, see A. S. Batsanov, A. Beeby, J. I. Bruce, J. A. K. Howard, A. M. Kenwright and D. Parker, *Chem. Commun.*, 1999, 1011.
4 D. Parker, P. K. Senanayake and J. A. G. Williams, *J. Chem. Soc., Perkin Trans. 2*, 1998, 2129.
5 V. A. Bloomfield, D. M. Crothers and I. Tinoco, *Physical Chemistry of Nucleic Acids*, Harper and Row, New York, 1974.
6 J. D. McGhee and P. H. von Hippel, *J. Mol. Biol*., 1974, **86**, 469.
7 Strictly speaking there is evidence that $[(dA–dT)_6]_2$ may exist as an alternating structure termed 'wrinkled D': A. Rich, A. Nordheim and A. H.-J. Wang, *Annu. Rev. Biochem.*, 1984, **53**, 791; S. Arnott, R. Chandreasekaran, D. W. L. Hukins, P. J. C. Smith and L. Watts, *J. Mol. Biol*., 1974, **88**, 523; R. Chandrasekaran and S. Arnott, *in Landolt-Bornstein New Series VII/1b*, ed. W. Saenger, Springer-Verlag, New York, 1989, pp. 31–70.
8 J. K. Barton, *Science*, 1986, **233**, 727; N. Grover, N. Gupta and H. H. Thorp, *J. Am. Chem. Soc*., 1992, **114**, 3390.

Communication 9/04257A

Structure and reactions of a metallacyclic complex containing a remarkably long uranium–carbon bond

Rita Boaretto, Paul Roussel, Andrew J. Kingsley, Ian J. Munslow, Christopher J. Sanders, Nathaniel W. Alcock and Peter Scott*

Department of Chemistry, University of Warwick, Coventry, UK CV4 7AL. E-mail: peter.scott@warwick.ac.uk

Received (in Basel, Switzerland) 11th May 1999, Accepted 17th July 1999

The intramolecular metalation of a β-silyl methyl group in [U{N(CH$_2$CH$_2$NSiMe$_2$Bu^t)$_3$}(CH$_2$Ph)] occurs rapidly, despite the conformational demands of the triamidoamine ligand, to produce a highly strained metallacycle (U–C *ca.* 2.75 Å); this complex reacts cleanly with a range of carbon and other acids to give, for example, an alkynyl with a bent (156°) U–C≡C unit.

Intramolecular C–H activation of ligands is relatively common among early actinide complexes, including those containing bulky alkyls,[1] amides,[2] phosphides[3] and phenoxides.[4] Molecular models suggested that triamidoamine[5] [(RNCH$_2$CH$_2$)$_3$N)]$^{3-}$ complexes of metals with large van der Waals radii would be less prone to such reactions because of conformational restrictions (*vide infra*), and might instead undergo *inter*molecular reactions with hydrocarbons. With this in mind we set out to synthesise species such as [{(RNCH$_2$CH$_2$)$_3$N}MR′] (M = U, Th; R′ = H, alkyl). While we have prepared a wide range of triamidoamine complexes containing bonds between the early actinides and other elements,[6] the synthesis of M–C σ bonds proved troublesome. For example, reactions of the uranium and thorium chlorides [{(RNCH$_2$CH$_2$)$_3$N}MCl] (R = SiMe$_3$) and related compounds with a wide variety of metal alkyls led to the formation of intractable yellow mixtures. More recently however we have shown that the bulkier triamidoamine (where R = SiMe$_2$Bu^t, henceforth NN′$_3$), forms much more synthetically useful complexes with the f elements.[7,8] Use of this ligand has allowed us to isolate an extremely reactive and structurally fascinating metallacyclic uranium complex which is an excellent starting material for the synthesis of other organometallic compounds.

Treatment of [U(NN′$_3$)I][7] **1** with a stoichiometric amount of lithium or potassium alkyl in pentane afforded brown solutions from which extremely air-sensitive orange–brown crystals of **2** were isolated by filtration and cooling to −30 °C (Scheme 1). This product was the same irrespective of the alkylating agent used, although optimum yields (71% isolated) were obtained by use of lithium neopentyl or potassium benzyl in toluene. When this latter reaction was performed in an NMR tube and monitored by ^{1}H NMR spectroscopy, smooth and quantitative conversion of **1** to **2** with co-production of toluene was observed within minutes at ambient temperature. Interestingly, the presumed intermediate species [U(NN′$_3$)CH$_2$Ph] immediately decomposed to the metallacycle **2** and was not detected. The rapidity of this reaction is quite surprising; by comparison, conversion of the titanium[9] and molybdenum[10] triamidoamines [{(Me$_3$SiNCH$_2$CH$_2$)$_3$N}TiBu^s] and [{(Me$_3$SiNCH$_2$CH$_2$)$_3$N}MoH] to their respective metallacycles occurs only slowly and at elevated temperatures. Similarly, Andersen's metallacycle [U{N(SiMe$_3$)$_2$}$_2${N(SiMe$_3$)(CH$_2$SiMe$_2$)}] is produced by thermolysis of [U{N(SiMe$_3$)$_2$}$_3$X] (X = H, Me).[2]

Single crystals of **2** were grown from a saturated solution of the pure compound in pentane and the molecular structure (Fig. 1) was determined by X-ray crystallography.† The U–C(108) distance of 2.752(11) Å is significantly longer than any other U–C σ-bond hitherto recorded; the usual range is *ca.* 2.4–2.55 Å,[12] although distances of *ca.* 2.60 Å have been measured in complexes of chelating phosphorus ylids.[13] The metallacyclic phosphide [Cp*$_2$U(CH$_2$SiMe$_2$PSiMe$_3$)][3] and amide [Cp*$_2$Th$_2$(CF$_3$SO$_3$)$_3$(NSiMe$_3$)(CH$_2$SiMe$_2$NSiMe$_3$)][14] contain M–C–Si–N rings similar to that in **2** but the M–C distances of 2.415(20) and 2.43(5) Å are well within the range observed for their acyclic counterparts. Schrock's (triamidoamine)molybdenum metallacycle[10] adopts a similar conformation to **2**, but the Mo–C bond is only *ca.* 0.08 Å longer than those in acyclic alkyls.

An important feature of the structure of **2** is the orientation of the SiMe$_2$ groups at Si(12) and Si(13) which bring one methyl group from each, C(114) and C(119), toward the otherwise open face of the uranium centre. The non-bonded U–C distances of 3.056(14) and 3.218(10) Å, respectively, are consistent with the presence of C–H→U agostic interactions.[15] The maximum deviations of any atom from the least-squares planes [U, N(12), Si(12), C(114)], [U, N(13), Si(13), C(119)] and [U, N(11), Si(11), C(108)] are 0.08, 0.05 and 0.06 Å respectively.

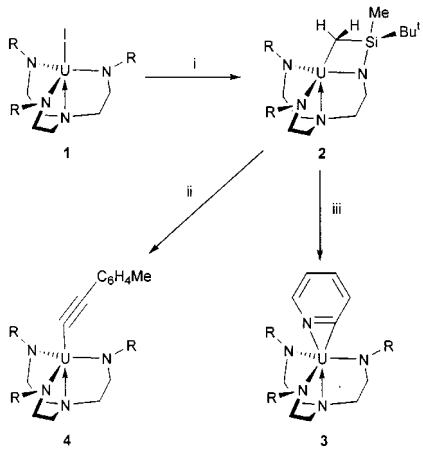

Scheme 1 Synthesis of complexes **2**–**4**. *Reagents and isolated yields*: i, KPh, toluene, 71%; ii, *p*-methylphenylacetylene, pentane, 80%; iii, pyridine, pentane, recrystallisation from hexamethyldisiloxane, 80%.

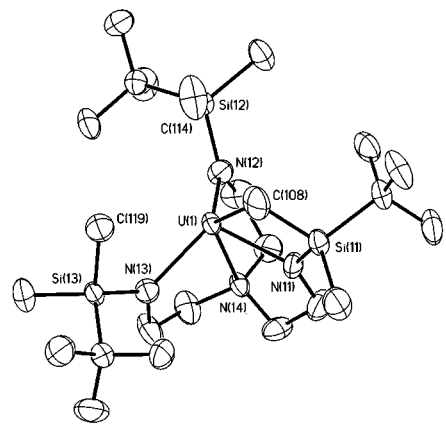

Fig. 1 Thermal ellipsoid plot of the molecular structure of **2**; hydrogen atoms omitted.

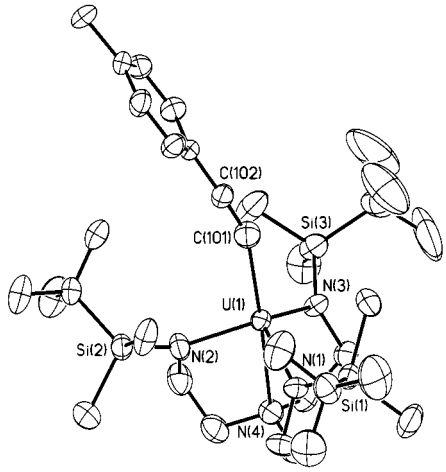

Fig. 2 Thermal ellipsoid plot of the molecular structure of **4**; hydrogen atoms omitted.

The ^{1}H NMR spectrum of **2** recorded in d_8-toluene contains a total of 22 peaks indicating that the product is chiral. Of these, 20 peaks are readily assigned to methyl and *tert*-butyl groups or diastereotopic methylene protons in the ligand backbone. Relatively broad peaks, at δ −35.34 and −52.34 are assigned to the Si–CH_2–U group on the basis of a selective deuteration study.‡ Other spectroscopic and analytical data are also in accord with the structure proposed for **2**.

The metallacycles [{$(Me_3Si)_2N$}$_2$M{$N(SiMe_3)(SiMe_2CH_2)$}] (M = U, Th) have been used extensively as starting materials for a wide range of complexes.[16] Accordingly, we have found that **2** reacts cleanly with acids HX under very mild conditions to form a range of U–X bonds with concomitant regeneration of the symmetric triamidoamine framework.

Reactions of **2** with trimethylamine hydrochloride, diethylamine and Bu^{t}OH give the complexes [(NN_3')UCl], [(NN_3')U(NEt_2)][7] and [(NN_3')U(OBu^t)][17] in essentially quantitative yields. Similarly, reaction of **2** with pyridine proceeds rapidly at room temperature to give the brown crystalline η^2-pyridyl complex **3** and *p*-methylphenylacetylene gives the yellow–green alkynyl [$(NN_3')(\eta^1$-C≡CC_6H_4Me)] **4**.

The molecular structure of **4** is shown in Fig. 2. The angle U–C(101)–C(102) of 156.4(6)° is significantly lower than the range found for the few structurally characterised non-bridging alkynyls of the f elements (170–176°).[18] Perhaps the alkynyl uranium fragment in **4** bends in order to allow for increased U–C π-overlap. We are currently investigating this and other related phenomena.

Hence, although the conformational constraints of the triamidoamine ligand do not prevent intramolecular C–H activation of the somewhat acidic β-silyl methyl groups in [U(NN'_3)R], the metallacycle **2** thus formed is an excellent starting material for the generation of a range of highly crystalline organometallic complexes of uranium.

P. S. wishes to thank EPSRC for a Project Studentship and SmithKline Beecham for a CASE award (to C. J. S.), Pfizer (UK) Ltd for a CASE award to I. J. M., Universitá degli Studi di Ferrara for support of R. B., and BNFL for both a CASE award (to P. R.) and postdoctoral fellowship (to A. J. K.). We thank EPSRC and Siemens Analytical Instruments for grants in support of the diffractometer.

Notes and references

† *Crystal data*: $C_{24}H_{56}N_4Si_3U$ **2**: M = 723.03, triclinic, space group $P\bar{1}$, a = 12.7602(5), b = 13.3286(5), c = 13.3902(5) Å, α = 119.3350(10), β = 109.0980(10), γ = 92.8980(10)°, U = 1813.56(12) Å^3 (by least squares refinement on 9181 reflection positions), T = 180(2) K, Z = 2, μ(Mo-Kα) = 4.590 mm^{-1}, 11113 reflections measured, 8070 unique (R_{int} = 0.0296), R_1 [for 6567 reflections with $I > 2\sigma(I)$] = 0.0459, wR_2 = 0.1206.

$C_{33}H_{64}N_4Si_3U$ **4**: M = 839.18, monoclinic, space group $P2_1/c$, a = 17.3244(10), b = 12.7945(10), c = 18.6257(15) Å, β = 97.7090(10)°, U = 4091.2(5) Å^3 (by least squares refinement on 7606 reflection positions), T = 180(2) K, Z = 4, μ(Mo-Kα) = 4.080 mm^{-1}, 24202 reflections measured, 9593 unique (R_{int} = 0.0922), R_1 [for 8001 reflections with $I > 2\sigma(I)$] = 0.0559, wR_2 = 0.1533. Data were collected on a Siemens SMART CCD. The structures were solved by direct methods with additional light atoms found by Fourier methods. Atoms N(13) and C(119) in **2** were refined anisotropically.

CCDC 182/1350. See http://www.rsc.org/suppdata/cc/1999/1701/ for crystallographic files in .cif format.

‡ Addition of dry D_2 to a sample of **2** in toluene-d^8 leads to deuteration at ambient temperature over a period of hours of all $SiMe_2$ groups and the metallacyclic CH_2 *via* sequential σ-bond metathesis reactions. Andersen's metallacycle is fully deuterated under these conditions. See ref. 2.

1 C. M. Fendrick and T. J. Marks, *J. Am. Chem. Soc.*, 1986, **108**, 425.
2 S. J. Simpson, H. W. Turner and R. A. Andersen, *Inorg. Chem.*, 1981, **20**, 2991.
3 S. W. Hall, J. C. Huffman, M. M. Miller, L. R. Avens, C. J. Burns, D. S. J. Arney, A. F. England and A. P. Sattelberger, *Organometallics*,1993, **12**, 752.
4 D. L. Clark, S. K. Grumbine, B. L. Scott and J. G. Watkin, *Organometallics*, 1996, **15**, 949.
5 R. R. Schrock, *Acc. Chem. Res.*, 1997, **30**, 99; J. G. Verkade, *Acc. Chem. Res.*, 1993, **26**, 483.
6 P. Roussel, P. B. Hitchcock, N. D. Tinker and P. Scott, *Chem. Commun.*, 1996, 2053; P. Scott and P. B. Hitchcock. *J. Chem. Soc., Chem. Commun.*, 1995, 579; P. Scott and P. B. Hitchcock, *J. Chem. Soc., Dalton Trans.*, 1995, 603.
7 P. Roussel, N. W. Alcock, R. Boaretto, A. J. Kingsley, I. J. Munslow, C. J. Sanders and P. Scott, *Inorg. Chem.*, in press.
8 P. Roussel and P. Scott, *J. Am. Chem. Soc.*,1998, **120**, 1070; P. Roussel, N. W. Alcock and P. Scott, *Inorg. Chem.*, 1998, **37**, 3435.
9 C. C. Cummins, R. R. Schrock and W. M. Davis, *Organometallics*, 1992, **11**, 1452.
10 R. R. Schrock, S. W. Seidel, N. C. Mösch-Zanetti, K.-Y. Shih, M. B. O'Donoghue, W. M. Davis and W. M. Reiff, *J. Am. Chem. Soc.*, 1997, **119**, 11 876.
11 G. Perego, M. Cesari, F. Farina and G. Lugli, *Acta Crystallogr., Sect. B*, 1976, **32**, 3034; P. G. Edwards, R. A. Andersen and A. Zalkin, *Organometallics*, 1984, **3**, 293; J. L. Stewart and R. A. Andersen, *J. Chem. Soc., Chem. Commun.*, 1987, 1846; M. Wedler, F. Knosel, F. T. Edelmann and U. Behrens, *Chem. Ber.*, 1992, **125**, 1313.
12 R. E. Cramer, S. Roth, F. Edelmann, M. A. Bruck, K. C. Cohn and J. W. Gilje, *Organometallics*, 1989, **8**, 1192.
13 R. J. Butcher, D. L. Clark, S. K. Grumbine and J. G. Watkin, *Organometallics*, 1995, **14**, 2799.
14 M. Müller, V. C. Williams, L. H. Doerrer, M. A. Leech, S. A. Mason, M. L. H. Green and K. Prout, *Inorg. Chem.*, 1998, **37**, 1315; see also citation in ref. 4.
15 S. J. Simpson and R. A. Andersen, *J. Am. Chem. Soc.*, 1981, **103**, 4063; A. Dormond, A. el Bouadili and C. Moise, *J. Chem. Soc., Chem. Commun.*, 1985, 914; A. Dormond, A. A. Aalti, A. el Bouadili and C. Moise, *Inorg. Chim. Acta*, 1987, **139**, 171; D. M. Barnhart, D. L. Clark, S. K. Grumbine and J. G. Watkin, *Inorg. Chem.*,1995, **34**, 1695; D. M. Barnhart, D. L. Clark, J. C. Gordon, J. C. Huffman and J. G. Watkin, *Inorg. Chem.*, 1995, **34**, 5416; D. M. Barnhart, D. L. Clark, J. C. Gordon, J. C. Huffman and J. G. Watkin, *Inorg. Chem.*, 1994, **33**, 3939; D. L. Clark and J. G. Watkin, *Inorg. Chem.*, 1993, **32**, 1766; J. M. Berg, D. L. Clark, J. C. Huffman, D. E. Morris, A. P. Sattelberger, W. E. Streib, W. G. Vandersluys and J. G. Watkin, *J. Am. Chem. Soc.*, 1992, **114**, 10 811.
16 P. Roussel, P. B. Hitchcock, N. D. Tinker and P. Scott, *Inorg. Chem.*,1997, **36**, 5716.
17 J. L. Atwood, C. F. Hains Jnr., M. Tsutsui and A. E. Gebala, *J. Chem. Soc., Chem. Commun.*, 1973, 452; J. L. Atwood, M. Tsutsui, N. Ely and A. E. Gebala, *J. Coord. Chem.*, 1976, **5**, 209; W. J. Evans, T. A. Ulibarri, L. R. Chamberlain, J. W. Ziller and D. Alvarez Jnr., *Organometallics*, 1990, **9**, 2124; W. J. Evans, R. A. Keyer and J. W. Ziller, *Organometallics*, 1993, **12**, 2618; W. J. Evans, G. W. Rabe and J. W. Ziller, *J. Organomet. Chem.*, 1994, **21**, 483.

Communication 9/03783G

Evaluation of the relative Lewis acidities of lanthanoid(III) compounds by tandem mass spectrometry

Hideyuki Tsuruta,[a] Kentaro Yamaguchi*[b] and Tsuneo Imamoto*[a]

[a] *Department of Chemistry, Faculty of Science, Chiba University, Yayoi-cho, Inage-ku, Chiba 263-8522, Japan*
[b] *Chemical Analysis Center, Chiba University, Yayoi-cho, Inage-ku, Chiba 263-8522, Japan.*
E-mail: yamaguchi@cac.chiba-u.ac.jp

Received (in Cambridge, UK) 9th July 1999, Accepted 29th July 1999

The Lewis acidities of five series of lanthanoid(III) compounds are evaluated based on their competitive dissociation observed by tandem mass spectrometry.

The reactivity of lanthanoid compounds is of considerable interest in synthetic organic chemistry and has been studied for the past two decades.[1,2] Although mass spectrometry has been used mainly for organic structure elucidation,[3] tandem mass spectrometry has been applied recently to evaluate the reactivities of organic compounds.[4] Here, we use this method for the investigation of reactivities of lanthanoid compounds.

Trivalent lanthanoid compounds such as $CeCl_3$, $Yb(OTf)_3$ and $Sc(OTf)_3$ are frequently employed as reagents or catalysts, which owing to their high Lewis acidities, interact with carbonyl or imine functionalities in organic compounds.[1,2,5–9] The intrinsic chemical properties of lanthanoid compounds, however, including their reactivity, still remains unclear. A quantitative evaluation of their Lewis acidities is essential for the development of new reagents and catalysts, as well as for a comprehensive understanding of their reactivities. Herein, we report a direct method for the evaluation of the Lewis acidities of lanthanoid compounds by the use of tandem mass spectrometry (MS).[10]

We have observed an extremely reproducible fragmentation of precursor ions derived from a series of lanthanoid(III) triflate complexes, using collision-activated decomposition (CAD) in tandem MS. Moreover, the intensity ratio of the ion due to the loss of the triflate group to that from the loss of a coordinating ligand such as hexamethylphosphoramide (Fig. 1), shows significant differences among the lanthanoid(III) compounds studied. This suggested to us that the stability of these product ions directly reflects the electronic properties of each central element a view strongly supported by recent kinetic studies using MS for thermochemical measurements.[4,11]

A total of 48 compounds consisting of three series of lanthanoid complexes, $M(OTf)_3(hmpa)_4$ (hmpa = hexamethylphosphoramide), $M(OTf)_3(tepo)_4$ (tepo = triethylphosphine oxide) and $M(OTf)_3(tmp)_4$ (tmp = trimethyl phosphate), (M = Sc, Y, La, Ce, Pr, Nd, Sm, Eu, Gd, Tb, Dy, Ho, Er, Tm, Yb or Lu) were synthesized. The tandem MS measurements were performed with four-sector (EB/EB) equipment, JMS-700T (JEOL), using Xe as the collision gas with a variable collision cell voltage of 0.5–3.0 kV. FAB with NBA as a matrix was used for ionization.

In all hmpa complexes, the fragment ion $[M(OTf)_2(hmpa)_2]^+$ is the base peak. This ion was selected as the parent ion for the CAD experiments. The FAB MS fragment ion spectrum of $[Er(OTf)_2(hmpa)_2]^+$ is shown in Fig. 2 as a representative example. In this fragment ion spectrum, we focused our attention on $[ErF(OTf)(hmpa)_2]^+$ and $[Er(OTf)_2(hmpa)]^+$, obtained by loss of OTf and hmpa, respectively. The logarithmic ratio of the ion intensities, $\ln\{[MF(OTf)(hmpa)_2]^+/[M(OTf)_2(hmpa)]^+\}$,† show significant differences with M (Fig. 3).

Upon loss of OTf, a fluoride ion remains attached to the central atom. Retention of fluoride has been ascribed to the strong affinity of Ln(III) for fluoride, and it has been previously reported that the thermal decomposition of $Ln(OTf)_3$ affords LnF_3.[12] The overall fragmentation scheme of the complexes studied involves the competitive loss of (OTf − F), and the loss of a ligand connected to the central atom such as hmpa (see Fig. 2). Any difference in the ratio of the two fragment ions reflects the electronic property of the lanthanide in terms of the affinity between the metal and oxygen or fluorine rather than any steric contribution. Observation of a discontinuity at gadolinium (Fig. 4) as a result of its electronic state also supports this theory. The properties of a given lanthanide, *i.e.* its Lewis acidity, can thus be evaluated using tandem MS.

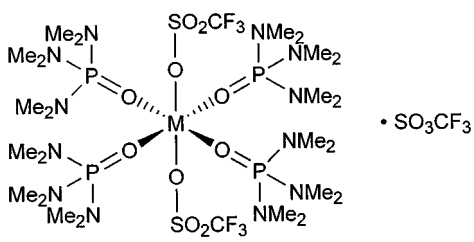

Fig. 1 Chemical structure of $M(OTf)_3(hmpa)_4$.

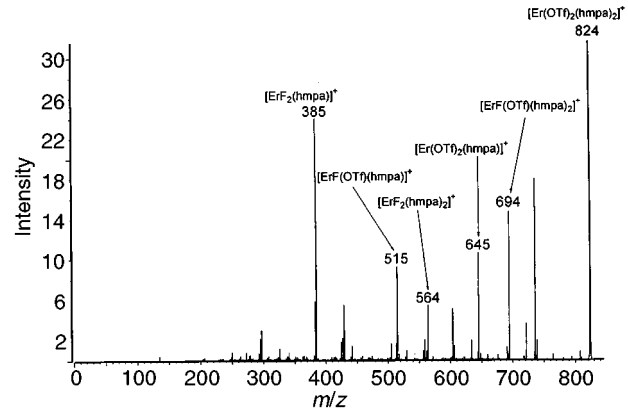

Fig. 2 MS/MS spectrum of $[Er(OTf)_2(hmpa)_2]^+$ (m/z = 824).

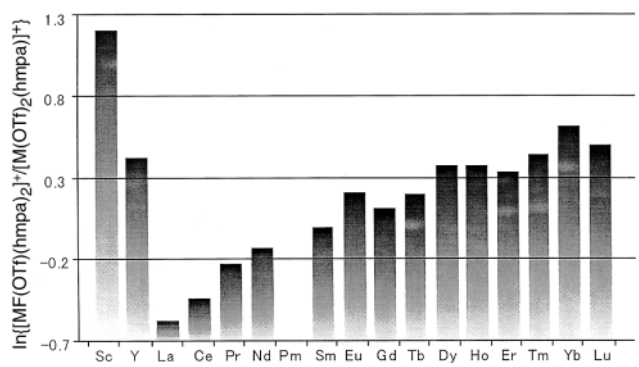

Fig. 3 MS/MS ion peak ratio, $\ln\{[MF(OTf)(hmpa)_2]^+/[M(OTf)_2(hmpa)]^+\}$.

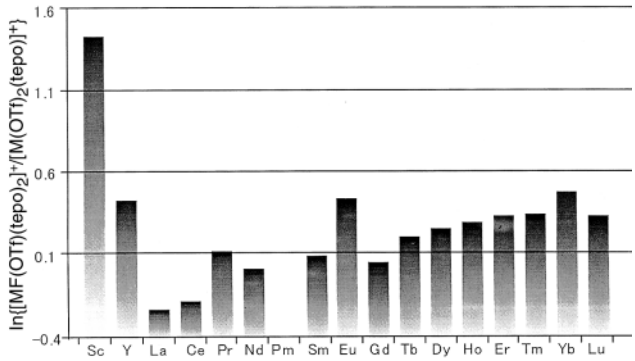

Fig. 4 MS/MS ion peak ratio, ln{[MF(OTf)(tepo)$_2$]$^+$/[M(OTf)$_2$(tepo)]$^+$}.

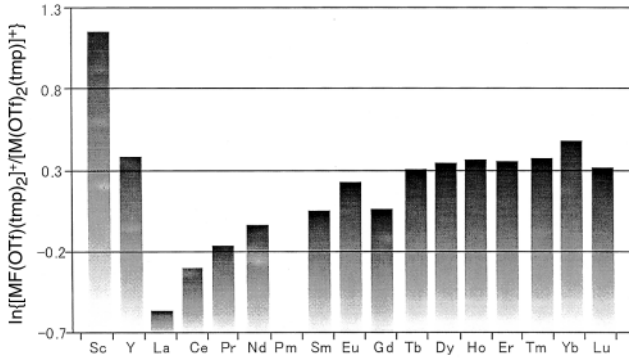

Fig. 5 MS/MS ion peak ratio, ln{[MF(OTf)(tmp)$_2$]$^+$/[M(OTf)$_2$(tmp)]$^+$}.

Two other series of rare earth complexes, M(OTf)$_3$(tepo)$_4$ and M(OTf)$_3$(tmp)$_4$, exhibit similar results. The corresponding intensity ratios for ln{[MF(OTf)(tepo)$_2$]$^+$/[M(OTf)$_2$(tepo)]$^+$} obtained from [M(OTf)$_2$(tepo)$_2$]$^+$ as the parent ion, and for ln{[MF(OTf)(tmp)$_2$]$^+$/[M(OTf)$_2$(tmp)]$^+$} from [M(OTf)$_2$(tmp)$_2$]$^+$ are illustrated in Fig. 4 and 5, respectively.

The oxophilicity of lanthanoids was also observed by the measurement of the competitive loss of OTf and tepo from [M(OTf)$_2$(tepo)$_4$]$^+$ to give [M(OTf)$_2$(tepo)$_3$]$^+$ or [M(OTf)$_2$-(tepo)$_2$]$^+$. The values of ln{[M(OTf)$_2$(tepo)$_3$]$^+$/[M(OTf)$_2$-(tepo)$_2$]$^+$} for the lanthanoid(III) metals were as follows Sc: 1.55, Y: 1.45, La: 1.40, Ce: 1.42, Pr: 1.42, Nd: 1.40, Sm: 1.43, Eu: 1.45, Gd: 1.41, Tb: 1.43, Dy: 1.46, Ho: 1.42, Er: 1.43, Tm: 1.45, Yb: 1.52, Lu: 1.42. Additionally, pure oxophilicity was estimated using [MCl$_2$(tepo)$_3$]$^+$ in which the effect of fluorine is not involved and the values of ln{[MCl$_2$(tepo)$_2$]$^+$/[MCl$_2$(tepo)]$^+$} were as follows: Sc: 2.37, Y: 1.87, La: 1.36, Ce: 1.37, Pr: 1.41, Nd: 1.49, Sm: 1.68, Eu: nd., Gd: 1.72, Tb: 1.76, Dy: 1.80, Ho: 1.84, Er: 1.87, Tm: 1.91, Yb: 2.09, Lu: 1.97.

The data presented in Figs. 3–5 and above, clearly demonstrate that Sc has the largest quotient followed by Yb.[13]† This is consistent with the exceptionally high catalytic activity of both Sc(III) and Yb(III) compounds in many Lewis acid-promoted reactions. Identical results were derived from experiments for complexes of other ligands such as dimethylsulfoxide and dimethylpropyleneurea. The high Lewis acidity of Sc(III) and Yb(III) is mainly ascribed to their small ionic radii. The higher acidity of Yb(III) relative to Lu(III) may originate from an incomplete number of electrons (thirteen) in the 4f orbital which has a tendency to become filled (f^{14}) which renders Yb(III) more electron-attractive than Lu(III). Other important observations of lanthanoid(III) behavior such as the gadolinium break and tetrad effects are also observed in these results.

In summary, using tandem mass spectrometry we have successfully evaluated the relative Lewis acidities of lanthanoid(III) compounds. The application of this methodology to other related compounds is in progress.

This work was supported by 'Research for the Future' Program JSPS-RFTF96P00304 from the Japanese Society for the Promotion of Science.

Notes and references

† The ratio of the rate constant k_1 (OTf loss) and k_2 (ligand loss) can be determined from the abundance of two product ions, [MF(OTf)(ligand)$_2$]$^+$ and [M(OTf)$_2$(ligand)]$^+$. Therefore, ln(k_1/k_2) gives a measure of the affinity for each central atom. See ref. 4, pp. 378–381.

‡ These facts are consistent with the data obtained from X-ray crystallographic analysis of a series of hmpa-coordinated lanthanoid triflates. The Sc and Yb complexes show relatively long P–O bond lengths towards hmpa. It is reasonable to consider that such P–O bond elongations are due to the relatively strong Lewis acidity of Sc^{3+} and Yb^{3+}.

1 G. A. Molander, in *Comprehensive Organic Synthesis*, ed. B.M. Trost, Pergamon, Oxford, 1991, vol. 1, ch. 1.9.
2 T. Imamoto, *Lanthanides in Organic Synthesis*, Academic Press, London, 1994.
3 E. De Hoffmann, J. Charette and V. Stroobant, *Mass Spectrometry; Principles and Applications*, John Wiley, New York, 1996.
4 R. G. Cooks and P. S. H. Wong, *Acc. Chem. Res.*, 1998, **31**, 378.
5 T. Imamoto, in *Comprehensive Organic Synthesis*, ed. B. M. Trost, Pergamon, Oxford, 1991, vol. 1, ch. 1.8.
6 S. Kobayashi, *Synlett*, 1994, 689.
7 S. Kobayashi, *Pure Appl. Chem.*, 1988, **70**, 1019.
8 A. Sella and J. G. Brennan, *Organometallics.*, 1998, **26**, 28.
9 S. Kobayashi, *Eur. J. Org. Chem.*, 1999, **1**, 15.
10 K. L. Busch, G. L. Glish and S. A. McLuckey, *Mass Spectrometry/Mass Spectrometry: Techniques and Applications of Tandem Mass Spectrometry*, VCH, New York, 1988.
11 R. G. Cooks, J. S. Patrick, T. Kotiaho and S. A. McLuckey, *Mass Spectrom. Rev.*, 1994, **13**, 278.
12 N. Yanagihara, S. Nakamura and M. Nakayama, *Chem. Lett.*, 1995, 555.
13 T. Imamoto, M. Nishiura, Y. Yamanoi, H. Tsuruta and K. Yamaguchi, *Chem. Lett.*, 1996, 875.

Communication 9/05569J

ChemComm

A new route to incompletely condensed silsesquioxanes: acid-mediated cleavage and rearrangement of (c-$C_6H_{11})_6Si_6O_9$ to C_2-[(c-$C_6H_{11})_6Si_6O_8X_2$]

Frank J. Feher,* Frank Nguyen, Daravong Soulivong and Joseph W. Ziller

Department of Chemistry, University of California, Irvine, CA 92697-2025, USA. E-mail: f.j.feher@uci.edu

Received (in Bloomington, IN, USA) 18th May 1999, Accepted 19th July 1999

Acid-mediated cleavage and rearrangement of (c-$C_6H_{11})_6Si_6O_9$ 1 by triflic acid (TfOH) and methanesulfonic acid (MsOH) produces good yields of C_2-[(c-$C_6H_{11})_6Si_6O_8X_2$] (4a, X = OTf; 4b, X = MsO), which reacts with water, $LiNMe_2$ and LiC≡CPh to afford C_2-[(c-$C_6H_{11})_6Si_6O_8(OH)_2$] 5, C_2-[(c-$C_6H_{11})_6Si_6O_8(NMe_2)_2$] 8 and C_2-[(c-$C_6H_{11})_6Si_6O_8(CCPh)_2$] 9; silylation of 5 with $ClSiMe_2H$–Et_3N produces C_2-[(c-$C_6H_{11})_6Si_6O_8(OSiMe_2H)_2$] 6, while reaction of 5 with HBF_4·OMe_2–BF_3·OEt_2 produces C_2-[(c-$C_6H_{11})_6Si_6O_8F_2$] 7, which also reacts with $LiNMe_2$ and LiC≡CPh to afford 8 and 9.

Incompletely condensed polyhedral silsesquioxanes are versatile precursors to a wide range of Si–O and Si–O–M frameworks,[1a,b] including precursors to hybrid organic–inorganic polymers.[1c] Until recently, the pool of incompletely condensed silsesquioxanes available in synthetically useful quantities was quite limited.[2] Our discovery that fully condensed $[RSiO_{3/2}]_n$ frameworks, such as (c-$C_6H_{11})_6Si_6O_9$ **1** and (c-$C_6H_{11})_8Si_8O_{12}$ **2**, can be selectively cleaved by strong acids provides access to many useful new incompletely condensed frameworks.[3] However, the synthesis of difunctional silsesquioxane frameworks with well defined structures is relatively difficult and there are strong incentives for developing practical routes to other compounds. Here, we report the syntheses of several new frameworks derived from acid-mediated cleavage and rearrangement of readily available (c-$C_6H_{11})_6Si_6O_9$ **1**.[2a,b] These difunctional frameworks have excellent potential as precursors to more elaborate Si–O frameworks because their unique C_2-symmetric $Si_6O_8X_2$ skeleton can undergo nucleophilic substitution reactions without producing complex mixtures of diastereomers.

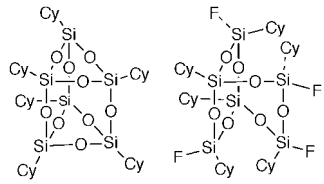

1 **3**

Framework **1** reacts with many strong acids to afford products resulting from cleavage of both Si_3O_3 rings. When the acid is HBF_4·OMe_2–BF_3·OEt_2, cleavage of Si–O is irreversible, and the major product is a C_2-symmetric tetrafluoride (*i.e.* **3**) derived from the substitution of two framework O atoms by four F atoms with inversion of stereochemistry at all Si centers.[3a] Both Si_3O_3 rings are also cleaved upon reaction of **1** with CF_3SO_3H (TfOH) or $MeSO_3H$ (MsOH), but the products from these reactions are not $R_6Si_6O_7(OSO_2R)_4$ frameworks analogous to **3**. Instead, the reactions of **1** with TfOH and MsOH both produce difunctional $R_6Si_6O_8(OSO_2R)_2$ derivatives resulting from selective cleavage and rearrangement of the Si–O framework.

The reaction of **1** with TfOH (5 equiv., $CDCl_3$, 25 °C, 15 min) occurs quickly upon mixing to produce several new Si-containing products. The major product, which is present in *ca.* 85% yield, exhibits three resonances with equal integrated intensities in the ^{29}Si NMR spectrum (δ −60.30, −61.10 and −61.44). All three of these resonances appear upfield from the ^{29}Si resonance for **1** (δ −56.23) and significantly downfield from the region characteristic of Si_4O_4 rings in relatively unstrained, fully condensed cyclohexylsilsesquioxanes (δ −65 to −70). Similar results are observed for the reaction of **1** with MsOH (5.2 equiv., $CDCl_3$, 70 °C, 5 h).† Numerous attempts to obtain crystalline samples of these products were unsuccessful because both compounds are extremely soluble in all solvents with which they do not react. However, **4a** and **4b** are the only structures consistent with our characterization data, and the formation of these compounds seems certain based on the reaction chemistry outlined below.

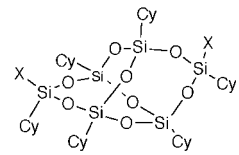

4a	X =	OTf
4b		OMs
5		OH
6		$OSiMe_2H$
7		F
8		NMe_2
9		CCPh

The hydrolysis of triflate-substituted silsesquioxanes can be accomplished cleanly to produce either of two stereochemical outcomes.[3b,c] Direct hydrolysis with water occurs with complete inversion of stereochemistry, while indirect hydrolysis *via* sequential treatment with aniline and aqueous HCl occurs with complete net retention of stereochemistry at Si. For **4a** and **4b**, which possess C_2-symmetric $R_6Si_6O_8X_2$ frameworks, hydrolysis with inversion or retention produces the same compound, namely disilanol **5**.‡ (Hydrolysis with inversion at one Si and retention at the other produces the enantiomer of **5**.) The structure of **5** was assigned on the basis of compelling spectroscopic data and confirmed by a single crystal X-ray diffraction study.§ As illustrated in Fig. 1, disilanol **5** crystallizes as discrete molecules with O3 and O5 located on a crystallographic C_2 axis of rotation. All bond distances and angles fall within their accepted ranges, but the Si–O–Si bond angles within the Si_4O_4 rings of **5** are more acute than those observed in the Si_4O_4 rings of **2**. In fact, the average Si–O–Si angle for **5** is only 142°, which is in the range of average Si–O–Si angles defined by **1** (133°)[4a] and **2** (149.5°).[4b] In light of the correlation between Si–O–Si bond angles and ^{29}Si chemical shifts for fully condensed polyhedral silsesquioxanes,[5] the relatively deshielded ^{29}Si resonances for **4a**, **4b** and **5** can be easily rationalized. (The ^{29}Si chemical shifts for **1** and **2** are δ −56.23 and −68.6, respectively.)

The availability of **4a**, **4b** and **5** provides access to a wide range of difunctional silsesquioxane frameworks. For example, silylation of **5** with $ClSiMe_2H$–Et_3N produces **6**, while reaction of **5** with HBF_4·OMe_2–BF_3·OEt_2[6] produces difluoride **7**. Subsequent reactions of **7** with $LiNMe_2$ and LiC≡CPh afford **8** and **9**, which can also be prepared by reacting **4a** or **4b** with $LiNMe_2$ and LiC≡CPh.¶ Although there are strong preferences for either complete retention or complete inversion of stereochemistry at Si for all of these nucleophilic substitution reactions,[4b,6,7] the stereochemical consequences are irrelevant with a C_2-symmetric $R_6Si_6O_8X_2$ framework (*vide supra*). The isolation of pure compounds is therefore relatively easy and isolated yields for all of these reactions are generally good.

The formation of **4a** and **4b** during the reactions of **1** with TfOH and MsOH requires the competitive formation of an Si_4O_4 ring under conditions where fused Si_3O_3/Si_4O_4 rings are cleaved selectively and Si–OH groups are converted into Si–OTf or Si–OMs groups. Both of these processes, as well as most

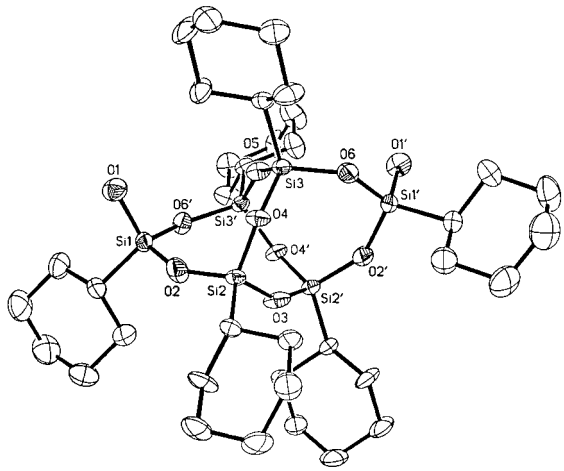

Fig. 1 ORTEP plot of **5** with thermal ellipsoids plotted at the 50% probability level. Selected distances (Å) and angles (°): Si1–O1 1.632(3), Si1–O2 1.620(2), Si1–O6′ 1.632(2), other Si–O 1.615–1.634; O1–Si1–O2 110.15(14), O1–Si1–O6′ 109.89(12), O2–Si2–O3 109.57(11), O2–Si2–O4 108.26(13), O3–Si2–O4 108.21(12), O4–Si3–O5 108.91(12), O4–Si3–O6 108.40(12), O5–Si3–O6 108.42(9), Si1–O2–Si2 147.60(16), Si2–O3–Si2′ 146.6(2), Si2–O4–Si3 133.76(14), Si3–O5–Si3′ 151.7(2), Si3–O6–Si1′ 137.57(14).

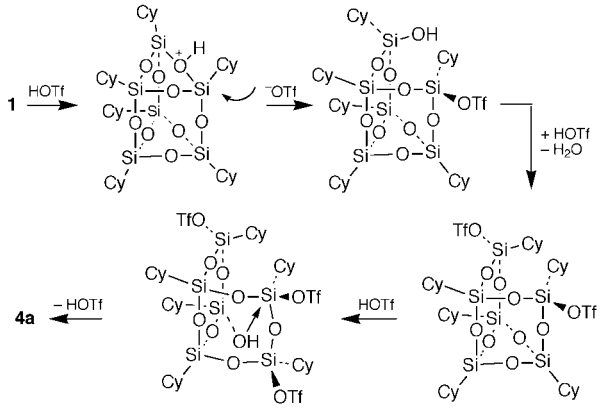

Scheme 1

nucleophilic substitution reactions of triflate-substituted silsesquioxanes, are known to occur with complete inversion of stereochemistry at Si.[4b,7] It is therefore likely that **4a** and **4b** are produced by the mechanism proposed in Scheme 1; a mechanistically similar process occurs during the reaction of **2** with TfOH.[3c] The release of ring strain in the Si–O framework is an important driving force for this process. Another important driving force is the formation of water, which is prevented from reacting with **4a** or **4b** by protonation with excess strong acid.

In conclusion, reactions of **1** with TfOH and MsOH both produce $R_6Si_6O_8(OSO_2R)_2$ derivatives resulting from selective cleavage and rearrangement of the $R_6Si_6O_9$ framework. These new compounds exhibit a rich reaction chemistry and provide access to a wide range of new Si–O frameworks.

This work was supported by the National Science Foundation and Air Force Research Laboratory (Edwards AFB).

Notes and references

† Frameworks **4a** and **4b** were prepared by reacting **1** (0.5 mM) with TfOH (5 equiv., 25 °C, 15 min) or MsOH (5.2 equiv., 50 °C, 5 h) in $CHCl_3$ (5 mL). Excess acid and water produced by the reaction were removed using an excess of 4 Å molecular sieves. Evaporation of the solvent (25 °C, 0.1 Torr) affords crude **4a** or **4b** as a pale yellow microcrystalline solid. The mass yield is practically quantitative, but the purity of **4a** and **4b** is only 80–90% as judged by ^{29}Si, ^{13}C and ^{1}H NMR spectroscopy. Both **4a** and **4b** react quickly with traces of water and are extremely soluble in all solvents with which they do not react; both compounds were used without further purification. For **4a**: $^{13}C\{^1H\}$ NMR (125 MHz, $CDCl_3$, 25 °C): δ 27.18, 26.90, 26.48, 26.27, 26.13, 26.10, 25.83, 25.69, 25.57 (CH_2), 23.05, 22.44, 22.03 (2:2:2 for CH). $^{29}Si\{^1H\}$ NMR (99 MHz, $CDCl_3$, 25 °C): δ −60.30, −61.10, −61.44 (2:2:2). MS (70 eV, 200 °C, relative intensity): *m*/*z* 1092 (M^+, 2%), 1009 {$[M - C_6H_{11}]^+$, 100%}. For **4b**: $^{13}C\{^1H\}$ NMR (125 MHz, $CDCl_3$, 25 °C): δ 39.15 (CH_3), 26.99, 26.93, 26.87, 26.83, 26.79, 26.28, 26.18, 26.03, 26.02, 25.83, 25.79, 25.63 (CH_2), 23.07, 22.33, 22.06 (2:2:2 for CH). $^{29}Si\{^1H\}$ NMR (99 MHz, $CDCl_3$, 25 °C): δ −61.43, −61.63, −61.80 (2:2:2). MS (70 eV, 200 °C, relative intensity): *m*/*z* 970 {$[M - CH_3]^+$, 28%}, 901 {$[M - C_6H_{11}]^+$, 95%}.

‡ Disilanol **5** was prepared by the hydrolysis of **4a** or **4b** in diethyl ether. The conversion of **4a**/**4b** to **5** is essentially quantitative as judged by ^{1}H, ^{13}C and ^{29}Si NMR spectroscopy; the isolated yield after recrystallization from CCl_4 is typically 40%. For **5**: ^{1}H NMR (500 MHz, $CDCl_3$, 25 °C): δ 2.32 (br s, SiOH, 2H), 1.73 (br m, 30H), 1.22 (br m, 30H), 0.80 (br m, 6H). $^{13}C\{^1H\}$ NMR (125 MHz, $CDCl_3$, 25 °C): δ 27.46, 27.35, 27.27, 26.75, 26.70, 26.65, 26.47, 26.45, 26.27, 26.21 (CH_2), 23.63, 22.86, 22.67 (2:2:2 for CH). $^{29}Si\{^1H\}$ NMR (99 MHz, $CDCl_3$, 25 °C): δ −55.24, −61.73, −61.94 (2:2:2). MS (70 eV, 200 °C, relative intensity): *m*/*z* 745 ($[M - C_6H_{11}]^+$, 100%). M.p. (DSC) = 187 °C.

§ *Crystal data* for **5**: $C_{36}H_{68}O_{10}Si_6$, M = 829.44, orthorhombic, space group *Aba*2, a = 22.7887(12), b = 9.4184(5), c = 20.441(10) Å, V = 4387.3(4) Å^3, T = 158 K, Z = 4, D_c = 1.256 Mg m^{-3}, μ = 0.241 mm^{-1}, $F(000)$ = 1792, λ = 0.71073 Å, crystal dimensions: 0.40 × 0.33 × 0.10 mm, 3.58 ≤ 2θ ≤ 56.6°; of the 13586 collected reflections, 4665 are independent, and these were used for the refinement of 237 parameters; R_1 = 0.0489, wR_2 = 0.1033 with $R_1 = \Sigma||F_o| - |F_c||/\Sigma|F_o|$ and $wR_2 = (\Sigma w(F_o^2 - F_c^2)^2/\Sigma w(F_o^2)^2)^{0.5}$. CCDC 182/1354.

¶ *Selected characterization data*: for **6**: ^{1}H NMR (500 MHz, $CDCl_3$, 25 °C): δ 4.74 (dq, *J* 2.77, 0.88 Hz, 2H), 1.74 (br m, 30H), 1.24 (br m, 30H), 0.78 (br m, 4H), 0.70 (br m, 2H), 0.22 (dd, *J* 2.77, 0.92 Hz, 12H). $^{13}C\{^1H\}$ NMR (125 MHz, $CDCl_3$, 25 °C): δ 27.58, 27.44, 27.39, 26.86, 26.77, 26.56, 26.53, 26.37, 26.35 (CH_2), 24.20, 23.01, 22.89 (CH, 2:2:2), 0.59 (CH_3). $^{29}Si\{^1H\}$ NMR (99 MHz, $CDCl_3$, 25 °C): δ −5.43, −62.32, −62.55, −64.29 (1:2:2:2). MS (70 eV, 200 °C, relative intensity): *m*/*z* 861 {$[M - C_6H_{11}]^+$, 100%}, 943.5 (M^+, 5%). For **7**: ^{1}H NMR (500 MHz, $CDCl_3$, 25 °C): δ 1.73 (br m, 30H), 1.29 (br m, 30H), 0.87 (br m, 6H). $^{13}C\{^1H\}$ NMR (125 MHz, $CDCl_3$, 25 °C): δ 27.27, 27.23, 27.18, 26.63, 26.62, 26.57, 26.27, 26.13, 25.98, 25.95 (CH_2), 22.59, 22.36 (s for CH, 2:2), 21.99 (d for CH, *J* 23.72 Hz). $^{29}Si\{^1H\}$ NMR (99 MHz, $CDCl_3$, 25 °C): δ −61.75 (d, *J* 273 Hz), −61.35, −61.67 (2:2:2). MS (70 eV, 200 °C, relative intensity): *m*/*z* 749 {$[M - C_6H_{11}]^+$, 100%}. For **8**: ^{1}H NMR (500 MHz, $CDCl_3$, 25 °C): δ 2.49 (s, 12H), 1.71 (br m's, 30H), 1.24 (br m's, 30H), 0.75 (br m's, 6H). $^{13}C\{^1H\}$ NMR (125 MHz, $CDCl_3$, 25 °C): δ 37.08, 27.78, 27.51, 27.47, 27.04, 26.99, 26.80, 26.70, 26.52 (CH_2), 24.70, 23.21, 23.06 (s for CH, 2:2:2). $^{29}Si\{^1H\}$ NMR (99 MHz, $CDCl_3$, 25 °C): δ −46.38, −62.48, −62.66 (2:2:2). MS (70 eV, 200 °C, relative intensity): *m*/*z* 799 {$[M - C_6H_{11}]^+$, 100%}, 882 (M^+, 22%). For **9**: ^{1}H NMR (500 MHz, $CDCl_3$, 25 °C): δ 7.49 (d, *J* 1.49 Hz, 2H), 7.47 (d, *J* 1.86 Hz, 2H), 7.33 (4H), 7.31 (2H), 1.72 (br m, 30H), 1.25 (br m, 30H), 0.85 (br m, 6H). $^{13}C\{^1H\}$ NMR (125 MHz, $CDCl_3$, 25 °C): δ 132.21, 128.78, 128.14, 122.63 (s for aromatic C), 102.56, 89.66, 27.41, 27.35, 27.32, 26.82, 26.75, 26.66, 26.37, 26.25, 25.78 (CH_2), 26.13, 22.75, 22.64 (s for CH, 2:2:2). $^{29}Si\{^1H\}$ NMR (99 MHz, $CDCl_3$, 25 °C): δ −47.98, −61.18, −61.28 (2:2:2). MS (70 eV, 200 °C, relative intensity): *m*/*z* 913 {$[M - C_6H_{11}]^+$, 100%}.

1 (*a*) F. J. Feher and T. A. Budzichowski, *Polyhedron*, 1995, **14**, 3239; (*b*) P. G. Harrison, *J. Organomet. Chem.*, 1997, **542**, 141; (*c*) J. J. Schwab and J. D. Lichtenhan, *Appl. Organomet. Chem.*, 1998, **12**, 707.

2 (*a*) J. F. Brown and L. H. Vogt, *J. Am. Chem. Soc.*, 1965, **87**, 4313; (*b*) F. J. Feher, D. A. Newman and J. F. Walzer, *J. Am. Chem. Soc.*, 1989, **111**, 1741; (*c*) T. W. Hambley, T. Maschmeyer and A. F. Masters, *Appl. Organomet. Chem.*, 1992, **6**, 253; (*d*) F. J. Feher, T. A. Budzichowski, R. L. Blanski, K. J. Weller and J. W. Ziller, *Organometallics*, 1991, **10**, 2526; (*e*) J. F. Brown, *J. Am. Chem. Soc.*, 1965, **87**, 4317; (*f*) M. Unno, K. Takada and H. Matsumoto, *Chem. Lett.*, 1998, 489; (*g*) O. I. Shchegolikhina, V. A. Igonin, Y. A. Molodtsova and Y. A. Pozdniakova, *J. Organomet. Chem.*, 1998, **562**, 141.

3 (*a*) F. J. Feher, D. Soulivong and G. T. Lewis, *J. Am. Chem. Soc.*, 1997, **119**, 11 323; (*b*) F. J. Feher, D. Soulivong and A. E. Eklund, *Chem. Commun.*, 1998, 399; (*c*) F. J. Feher, D. Soulivong and F. Nguyen, *Chem. Commun.*, 1998, 1279.

4 (*a*) H. Behbehani, B. J. Brisdon, M. F. Mahon and K. C. Molloy, *J. Organomet. Chem.*, 1994, **469**, 19; (*b*) F. J. Feher, unpublished results.

5 E. Rikowski and H. C. Marsmann, *Polyhedron*, 1997, **16**, 3357.

6 F. J. Feher, S. H. Phillips and J. W. Ziller, *J. Am. Chem. Soc.*, 1997, **119**, 3397.

7 F. J. Feher, S. Soulivong, F. Nguyen and J. W. Ziller, *Angew. Chem., Int. Ed.*, 1998, **37**, 2663.

Communication 9/03984H

Robust and catalytically active mono- and bis-Pd-complexes of the 'Trost modular ligand'

Craig P. Butts, John Crosby, Guy C. Lloyd-Jones* and Susanna C. Stephen

School of Chemistry, Cantock's Close, Bristol, UK BS8 1TS. E-mail: guy.lloyd-jones@bris.ac.uk

Received (in Cambridge, UK) 20th July 1999, Accepted 29th July 1999

A catalytically active, bimetallic Pd–allyl complex of the Trost modular ligand, for which X-ray crystallography reveals a tetradentate ('POPO') coordination mode, induces a memory effect in Pd-catalysed allylic alkylation.

Asymmetric Pd-catalysed allylic alkylation[1] has recently enjoyed much attention and has undoubtedly joined the ranks of the 'benchmark reactions' by which new chiral ligands are tested and compared. Under the appropriate conditions, the modular ligand systems of Trost,[2] *e.g.* (*R*,*R*)-**1**, have proved to be remarkably enantioselective for a range of allylic alkylations, particularly the more demanding small cyclic substrates such as **2**→**3**.[3]

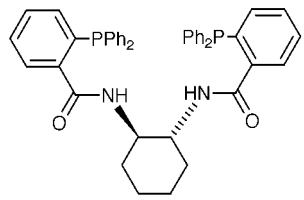

(*R*,*R*)-**1**

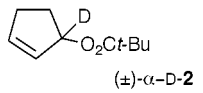

(±)-α-D-**2**

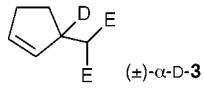

(±)-α-D-**3**

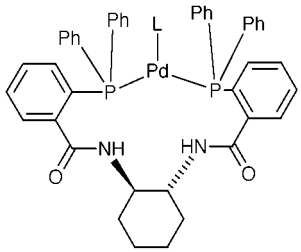

L = η^3 or η^2 ligand *etc.*

(*R*,*R*)-**4**

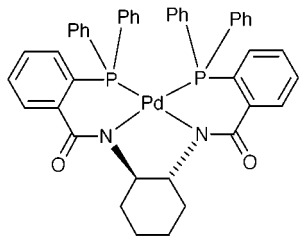

(*R*,*R*)-**5**

Knowledge of the mode(s) of coordination of **1** to palladium is essential in any mechanistic explanation of such high selectivities and it has generally been assumed that there is bidentate diphosphine chelation ('P,P') to Pd throughout the catalytic cycle† as in **4**.[4] However, to date, there have been no reports of the isolation or *in situ* characterisation of catalytic intermediates—which are readily converted to catalytically inert **5**.[5]

In recent investigations[6] of 'memory effects'[7] in the Pd-catalysed conversion of **2** to **3**, we suggested that a (P,L)-complexation mode (L = non-P ligand) could be responsible for the memory effect with mismatched **2** and '[**1**–Pd]'. Powerful memory effects are sometimes observed with other (P,L) ligands[6c,7c] and we noted that an amide carbonyl in **1** could act as 'L'. However, although we observed no memory effect with ligand **6**,[6a] ligands **7** and **8** are reported to give low and reversed ees (as compared to **1**) in the reaction of **2**.[4]

These latter results have in fact been taken as evidence that P,P-bidentate coordination of **1** is essential and that amide

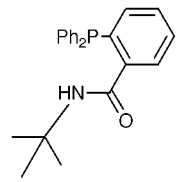

6

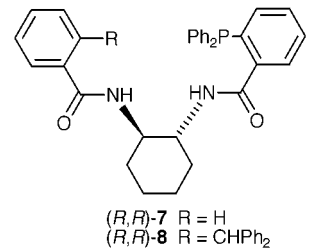

(*R*,*R*)-**7** R = H
(*R*,*R*)-**8** R = $CHPh_2$

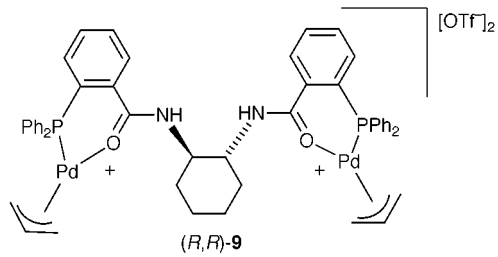

(*R*,*R*)-**9**

carbonyl coordination (P,O) is not important in the catalytically active species.[8] Herein we describe air- and shelf-stable, catalytically active, Pd-complexes of **1**. We also show that P,O coordination of **1** can give rise to a highly active catalyst and a significant memory effect.

Non-complexed ligand **1** was crystallised from hot acetonitrile. The single crystal X-ray structure is presented in Fig. 1.‡ Notable is the latent tendency of **1** to present P and O donors on opposite faces of the elongated structure. Reaction of **1** with 1 equivalent of halide-free $[Pd(allyl)(MeCN)_2][OTf]$ in CH_2Cl_2 then evaporation gave a pale yellow powder. Combustion analysis and ES-MS§ were fully consistent with a complex of stoichiometry [Pd(allyl)(**1**)][OTf]. However, despite many attempts at crystallisation, amorphous powders were always obtained and X-ray structural analysis remained elusive. Furthermore, ^1H and ^{13}C NMR spectra (CD_2Cl_2 or 3:1 d_8-THF–CD_2Cl_2, 26 °C) were very broad and complicated. Nonetheless, all of the allyl–Pd signals disappeared rapidly on addition of a slight excess of $[NaCH(CO_2Me)_2]$ and cleanly gave allyl–$CH(CO_2Me)_2$ (> 95%, ^1H NMR).[9]

In the solid state, the mixture of complexes is air- and shelf-stable (for years) and serves as a very convenient pro-catalyst

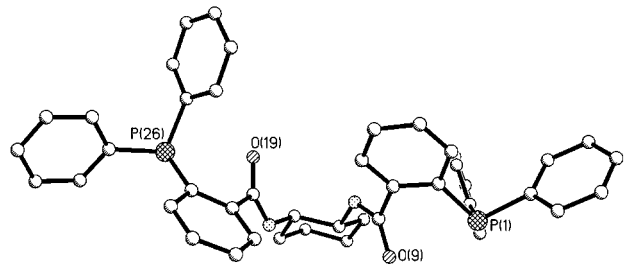

Fig. 1 The molecular structure of **1**. One and one half molecules occupy the unit cell. The half molecule and all hydrogens and solvent (MeCN) are omitted for clarity.

for asymmetric allylation of **2**.¶ Also, like the conventional 'Pd-**1**' catalysts generated *in situ* under chloride-free conditions,[6b] the pro-catalyst mixture also effects powerful kinetic resolution with (*S*)-**2** reacting over twenty-fold faster than (*R*)-**2** with $[NaCH(CO_2Me)_2]$ in THF.

When the ratio of Pd/ **1** was raised (*i.e.* ⩾1) evidence for P,O coordination was obtained. Thus, analytically pure $[Pd_2(allyl)_2(\mathbf{1})][(OTf)_2]$ **9** (mp 203 °C) was prepared as yellow–green prisms by addition of 2 equivalents of [Pd(allyl)(MeCN)$_2$][OTf] to **1** in $CHCl_3$ (99.9% yield on a 1.1 g scale). The single crystal X-ray structure of **9** which displays P,O-coordination to two Pd–allyl moieties is shown in Fig. 2.‡ This complex was also catalytically active and 2.5 mol% effected ⩾90% conversion of α-[^{2}H]-**2** to α,γ-[^{2}H]-**3** in < 60 s (22 °C, THF).‖ Importantly, the P,O complexation mode induced a moderate α-memory effect: both enantiomers of substrate giving a *ca.* 57 : 43 (±1) ratio of α-[^{2}H]-**3**/γ-[^{2}H]-**3** [83–86% isolated yield after chromatography, ^{2}H and ^{13}C NMR analysis with (+)-Eu(hfc)$_3$] and a global enantioselectivity of *ca.* 2% ee (*R*).

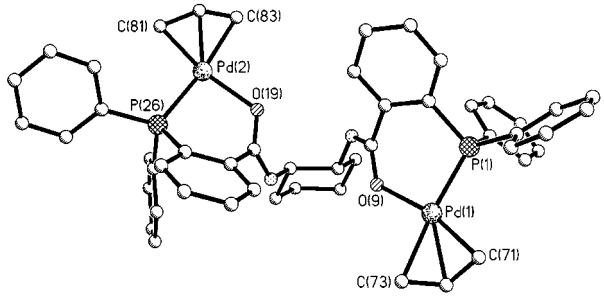

Fig. 2 The molecular structure of dication **9**. Hydrogens and triflate counter ions are omitted for clarity. Selected bond lengths (Å) and angles(°): Pd–P 2.279(2) 2.289(2), Pd–O 2.097(4), 2.109(4), Pd–C(71/81) 2.052(8)/2.086(7), Pd–C(73/83) 2.27(8)/2.191(7); P–Pd–O 89.90(11), 89.82(12), C–Pd–C 67.4(4), 69.5(3).

^{1}H, ^{13}C and ^{31}P NMR (CD_2Cl_2, 25 °C) of complex **9** indicated a single quasi-symmetrical species was present in solution (δ_P 24.8). Five unique π-allyl ^{1}H NMR signals with only one of the two allylic carbons *trans*-related to P (J_{CP} 27.3 Hz) indicated apparent allyl rotation was slow at the NMR time scale. Furthermore, the concentration independent 2.34 ppm downfield chemical shift of the N–H amide protons (δ 8.84) relative to free **1** confirmed the bis-(P,O)-complexation mode in solution. A moderate ion current corresponding to $[Pd_2(allyl)_2(\mathbf{1})]^{2+}$ (*m*/*z* 492) was observed on ES-MS analysis {a substantial proportion of the complex loses $[Pd(allyl)]^+$ and $[Pd(allyl)_2]^+$ (*m*/*z* 147 and 188) to give $[Pd(allyl)(\mathbf{1})]^+$}. When 1 equivalent of **1** was added, ^{31}P NMR and ES-MS analysis indicated complete reaction of **1** and $[Pd_2(allyl)_2(\mathbf{1})]^{2+}$ to give '$[Pd(allyl)(\mathbf{1})]^+$' suggesting a thermodynamically more favoured (P,P) binding mode in the latter species.[9]

In conclusion, reaction of **2** catalysed by the fully characterised complex **9** in which there is a bis-P,O-coordination mode (X-ray and NMR) proceeds with a significant α-memory effect in both manifolds (*R*- and *S*-**2**) and gives racemic **3**. However, with a Pd : **1** ratio of 1 : 1 a number of P,P-complexes are generated. These are active for *asymmetric* allylic alkylation with $[NaCH(CO_2Me)_2]$, effect powerful kinetic resolution and, consistent with earlier work, only demonstrate a memory effect with the mismatched enantiomer of **2**.[6a]

Generous donations from the Zeneca Strategic Research Fund and Pfizer Ltd are gratefully acknowledged. S. C. S thanks the University of Bristol for a Postgraduate Scholarship.

Notes and references

† To the best of our knowledge, published evidence for P,P-coordination of **1** is limited to the reaction of $Pd_2(dba)_3{\cdot}CHCl_3$ with **1** (**1**/Pd = 2) which gives an AB ^{31}P NMR spectrum (δ 24.9, 22.5; J_{PP} 14.6 Hz) and free **1** (δ −9) see ref. 4.

‡ *Crystal data:* for **1**: $C_{68.46}H_{60}N_{4.23}O_3P_3$, M = 1082.83, orthorhombic, space group $P2_12_12$, a = 17.8937(5), b = 31.1163(9), c = 10.8869(3) Å; V = 6061.7(3) Å^3, Z = 4, μ = 0.147 mm^{-1}, T = 173(2) K. Data (38625 total, 13780 unique, R_{int} = 0.0753). Final R_1 = 0.0587 for all 7876 data with $F^2 > 2\sigma(F^2)$]. For $[Pd(C_3H_5)_2(\mathbf{1})_2][O_3SCF_3]_2$ **9**: $C_{52}H_{50}F_6N_2PdO_8P_2S_2$, M = 1283.8, orthorhombic, space group $P2_12_12_1$, a = 16.9797(2), b = 17.594(3), c = 18.052(3) Å; V = 5392.7(14) Å^3, Z = 4, μ = 0.878 mm^{-1}, T = 123(2) K. Data (40417 total, 12202 unique, R_{int} = 0.0470). Final R_1 = 0.051 for all 9638 data with $F^2 > 2\sigma(F^2)$].

CCDC 182/1356. See http://www.rsc.org/suppdata/cc/1999/1707/ for crystallographic data in .cif format.

§ The major ion current (> 90%) corresponded to $[(Pd(allyl)(\mathbf{1}))]^+$ (*m*/*z* = 837), or oligomers, and there was no free **1**, reference **1**: $[\mathbf{1} + H]^+$, *m*/*z* = 691.

¶ In all literature reports, 'Pd–**1**' catalysts are generated *in situ* (1–1.5 equiv. **1** and Pd^{II} or Pd^0). Identical results are obtained with [Pd(allyl)(**1**)][OTf] as pro-catalyst [adding chloride, if required, see ref. 6(*b*)].

‖ The reaction mixture remained bright yellow (no palladium black) for up to 2 h after ⩾98% consumption of substrate (< 10 min), reinforcing the conclusion that **1** can function as a bis-bidentate ligand for Pd^{II} and Pd^0.

1 G. Consiglio and R. M. Waymouth, *Chem. Rev.*, 1989, **89**, 257; C. G. Frost, J. Howarth and J. M. J. Williams, *Tetrahedron: Asymmetry*, 1992, **3**, 1089; B. M. Trost and D. L. Van Vranken, *Chem. Rev.*, 1996, **96,** 395.

2 B. M. Trost, *Acc. Chem. Res.*, 1996, **29**, 355.

3 For examples of other ligands that effect high ee in this substrate class see: G. Helmchen, S. Kudis, P. Sennhenn and H. Steinhagen, *Pure Appl. Chem.*, 1997, **69**, 513; P. Dierkes, S. Ramdeehul, L. Barloy, A. De Cian, J. Fischer, P. C. J. Kamer, P. W. N. M. van Leeuwen and J. A. Osborn, *Angew. Chem. Int. Ed.*, 1998, **37**, 3116; A. Saitoh, M. Misawa and T. Morimoto, *Tetrahedron: Asymmetry*, 1999, **10**, 1025.

4 B. M. Trost, B. Breit and M. G. Organ, *Tetrahedron Lett.*, 1994, **35**, 5817.

5 For leading references and the current working model, see: B. M. Trost and F. D. Toste, *J. Am. Chem. Soc.*, 1999, **121**, 4545.

6 (*a*) G. C. Lloyd-Jones and S. C. Stephen, *Chem. Eur. J.*, 1998, **4**, 2539; (*b*) G. C. Lloyd-Jones and S. C. Stephen, *Chem. Commun.*, 1998, 2321; (*c*) P. Kočovský, Š. Vyskočil, I. Císařová, J. Srjbal, I. Tišlerová, M. Smrčiná, G. C. Lloyd-Jones, S. C. Stephen, C. P. Butts, M. Murray and V. Langer, *J. Am. Chem. Soc.*, 1999, in press.

7 (*a*) B. M. Trost and R. C. Bunt, *J. Am. Chem. Soc.*, 1996, **118**, 235; (*b*) J.-C. Fiaud and J. L. Malleron, *Tetrahedron Lett.*, 1981, **22**, 1399; (*c*) T. Hayashi, M. Kawatsura, Y. Uozumi, *J. Am. Chem. Soc.* 1998, **120**, 1681.

8 See ref. 5 and B. M. Trost and D. E. Patterson, *J. Org. Chem.*, 1998, **63**, 1339.

9 Prior to (and after) addition of $[NaCH(CO_2Me)_2]$ the ^{31}P NMR spectrum indicated the presence of many complexes whose relative abundance were time-dependent. A much more complete and detailed report of our NMR, kinetic and other studies on this complex mixture will be published in due course.

Communication 9/05851F

Solid state organisation of C_{60} by inclusion crystallisation with triptycenes†

E. Marc Veen,[a] Peter M. Postma[b] Harry T. Jonkman,[b] Anthony L. Spek,[c] and Ben L. Feringa*[a]

[a] *Department of Organic and Molecular Inorganic Chemistry, University of Groningen, Nijenborgh 4, 9747 AG Groningen, The Netherlands. E-mail: b.l.feringa@chem.rug.nl*

[b] *Department of Solid State Physics, Materials Sciences Center, University of Groningen, Nijenborgh 4, 9747 AG Groningen, The Netherlands,*

[c] *Bijvoet Center for Biomolecular Research, Crystal and Structural Chemistry, Utrecht University, Padualaan 8, 3584 CH Utrecht, The Netherlands*

Received (in Cambridge, UK) 4th June 1999, Accepted 22nd July 1999

Triptycene and azatriptycene act as concave receptor molecules for C_{60}, resulting in the solid state organisation of C_{60} in a layered and a hexagonal pattern, respectively.

Fullerenes are of considerable interest in the design of novel materials as the strong electron acceptor properties associated with C_{60} result in intriguing optical and semiconductor phenomena.[1] The controlled organisation of C_{60} in stacks or arrays by crystal engineering and host–guest chemistry plays a decisive role in these efforts.[2,3] The solid state structures of a number of inclusion complexes and supramolecular arrays of fullerenes have been reported in recent years.[4,5] An emerging structural feature in controlling the delicate host–guest interactions is geometrical complementarity of the globular C_{60} guest and dish or saddle shaped host molecules.[2,5,6] Here we report a simple method to achieve the solid state organisation of C_{60} by inclusion crystallisation with triptycene. In addition a change in organisation, by modification at a single position in the host molecule, as shown by X-ray analysis of the inclusion complexes was observed.

We envisioned that the combination of star-shaped triptycenes, with three concave faces, and C_{60} with its convex surface might lead to self-assembly as shown in Scheme 1.

The inclusion complex of C_{60} and triptycene **1** was obtained as dark red crystals from a hot *o*-xylene solution, by slow evaporation of part of the solvent over several days. NMR, IR and chromatographic analysis established an inclusion complex of C_{60}, triptycene and *o*-xylene. X-Ray structure analysis confirmed the composition in a 1:2:2 ratio respectively. The molecular structure is shown in Fig. 1(*a*).‡

The inclusion complex has centric [monoclinic space group *P*2(1)/*c*] symmetry in the solid state. The fullerene molecules pack in an approximate hexagonal close packed sphere pattern parallel to the *bc*-plane with translation vectors 9.9958(11) (= *b*-axis) and 10.1468(11) Å [= $\frac{1}{2}$(*b*+*c*)].

The packing arrangement is shown in Fig. 2. Adjacent triptycenes stack in an antiparallel fashion generating two concave surfaces in opposite directions. Each C_{60} is capped by two molecules of **1** [Fig. 1(*a*)] and the closest distance between the two flanking arene groups of each triptycene (dihedral angle 120°) and C_{60} of approximately 3.27 Å§ is significantly shorter than those reported for calixarene and related complexes (3.51–3.62 Å).[6]

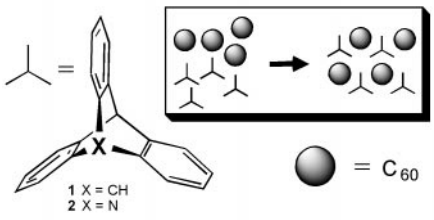

Scheme 1

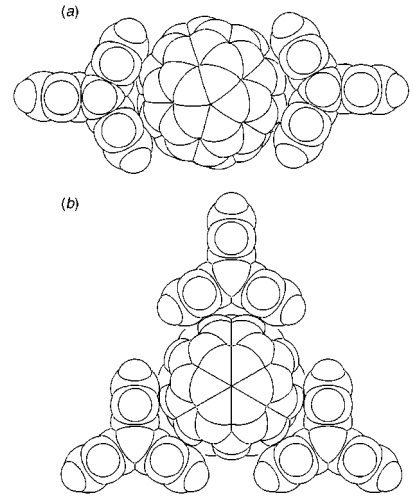

Fig. 1 (*a*) Moleculer structure of C_{60} and triptycene (**1**) (*o*-xylene omitted for clarity). (*b*) Molecular structure of C_{60} and azatriptycene (**2**).

The C_{60} molecules are arranged in sheets composed of one-dimensional strands in the *bc*-plane to achieve a close packing of spheres in the sheets. The shortest $C_{60}\cdots C_{60}$ separation of 3.08 Å¶ is close to that found in other linear strands.[2] Each sheet is separated by a double layer of antiparallel oriented triptycenes and *o*-xylenes with the latter filling voids between the

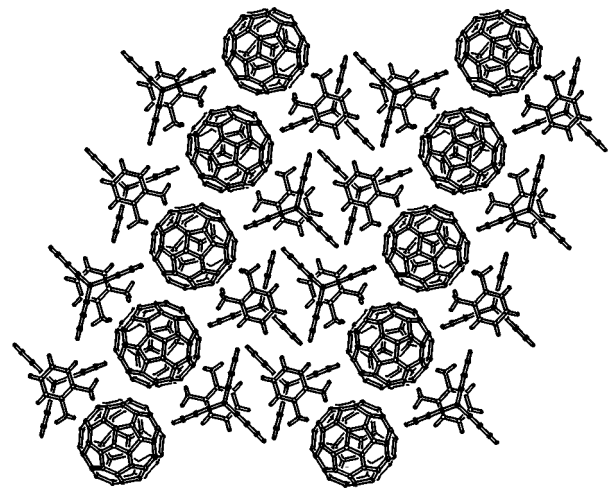

Fig. 2 Packing arrangement for the complex of C_{60}, *o*-xylene and triptycene.

† Colour versions of Figs. 1–3 are available from the RSC web site, see http://www.rsc.org/suppdata/cc/1999/1709/

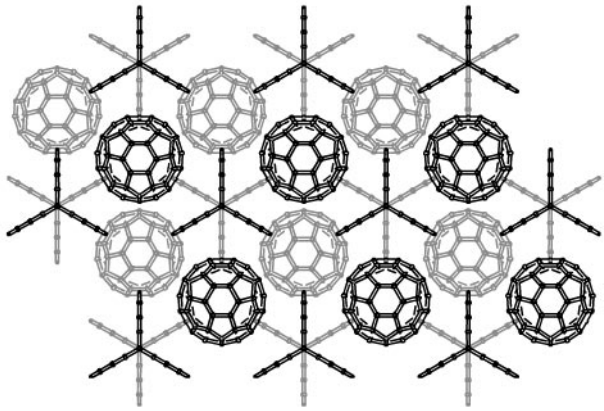

Fig. 3 Packing arrangement for the complex of C_{60} and azatriptycene.

triptycenes in this double layer. The nearest neighbour C_{60} molecules in two adjacent layers are 18.58 Å apart.

As the rigid concave triptycene has a favourable receptor shape to allow the formation of supramolecular arrays of C_{60} its molecular architecture might be suitable to change the assembly formation by modifying in the host–guest interactions. Introduction of a nitrogen atom at a bridgehead position, as is the case in azatriptycene **2**,[8] was envisioned to enhance additional electrostatic interactions in the host–guest system.

Slow evaporation of part of the solvent (*o*-xylene) from a hot solution of a 1 : 1 mixture of C_{60} and azatriptycene **2** resulted in dark red crystals of the inclusion complex suitable for X-ray analysis. The molecular structure is shown in Fig. 1(*b*).‖ The hexagonal unit cell contains two C_{60} molecules and two azatriptycenes. The fullerene molecule is rotationally disordered but as each C_{60} is flanked by three molecules of **2** [Fig. 1(*b*)], whose positions are exactly determined in the crystal lattice, and as a result of the space group symmetry, the position of each fullerene is well defined.

The C_{60} molecules assemble in the hexagonal close packing pattern with each azatriptycene embracing three C_{60} molecules and each C_{60} embraced by three azatriptycene. Capping of a C_{60} molecule by three molecules of **2** results in six concave surfaces at the periphery of this ensemble which interact with a further six fullerene molecules leading to the anticipated arrangement in each layer.

The translation period in the *ab*-packing plane amounts to 13.464(1) Å (= *a*-axis). Layers are separated by 6.349(1) Å (= 1/2 *c*-axis). The closest C–C contact between both molecular species amounts to 3.40(2) Å.

The packing arrangement is shown in Fig. 3. The azatriptycenes are arranged in one-dimensional strands parallel to the *c* axis in a head-to-tail arrangement. The C_9 carbon and the central nitrogen atom of neighbouring azatriptycenes are at a distance of 3.76 Å. Each molecule of **2** in a single strand is rotated 60° with respect to its neighbour, and as a consequence each set of three concave faces in the hexagonal arrangement in a particular layer, due to a single molecule of **2**, is rotated 60° with respect to the next layer. The hexagonal packing of the C_{60} spheres is evident if one realises that the 'pillars' of the azatriptycenes generate the voids in which a C_{60} molecule in one layer is positioned exactly between six C_{60} molecules in the two adjacent layers.

The shortest intermolecular C_{60} distance (C_{60} molecules in different layers) is approximately 2.97 Å¶ which is similar to that found in the inclusion complex of C_{60} and *p*-bromocalix-[4]arene propyl ether.[2] The centre–centre distance of the azatriptycenes in one layer is 13.464(1) Å. The remarkable propensity of triptycenes to change the self-assembly of C_{60} and the fascinating structures obtained in this way are intriguing in view of the design of new host–guest systems and materials based on fullerenes.** Studies along these lines using functionalised triptycenes are in progress.

Financial support by the Dutch National Science Foundation (NWO) is gratefully acknowledged.

Notes and references

‡ *Crystal data* for complex with **1**: $C_{60}\cdot2(C_{20}H_{14})\cdot2(C_8H_{10})$, M = 1441.54, dark red plate, space group $P2(1)/c$, a = 19.767(2), b = 9.9958(10), c = 17.661(2) Å, β = 109.882(10)°, Z = 2, V = 3281.6(6) Å^3, D_c = 1.459 g cm^{-3}, μ = 0.1 mm^{-1}, λ = 0.71073 Å, T = 150 K, θ_{max} = 25.3°. A hemisphere of reflections (11766) was scanned and averaged [R(int) = 0.15] into a unique set of 5988 reflections [2080 of which with $I > 2\sigma(I)$]. The structure was solved by direct methods (SIR97) and refined on F^2 using SHELXL97. Two sets of bond restraints were introduced in order to restrain 5-6 and 6-6 bond types. The restraints refined to 1.462(4) and 1.347(6) Å, respectively. Hydrogen atoms were introduced at calculated positions and refined riding on their carrier atoms. The displacement parameters for the C_{60} atoms display the common flat disk characteristics. Convergence was reached at R_1 = 0.0947, wR_2 = 0.261, S = 1.00, 5988 reflections, 527 parameters, 45 restraints, $-0.43 < \Delta_r < 0.64$ e Å^{-3}.

§ As a consequence of the dihedral angle of 120° in **1** and **2** the closest distance is with the C–C carbon atoms at the periphery of the (aza)-triptycenes.

¶ Based on the mean atom-to-atom diameter of C_{60} of approximately 7.07 Å (ref. 7).

‖ *Crystal data* for complex with **2**: $C_{60}\cdot C_{19}H_{13}N$, M = 975.90, dark red block, space group $P6(3)mc$ (no. 186), $a = b$ = 13.4643(11), c = 12.6983(9) Å, Z = 2, V = 1993.6(3) Å^3, D_c = 1.626 g cm^{-3}, μ = 0.1 mm^{-1}, λ = 0.71073 Å, T = 150 K, θ_{max} = 27.5°. A hemisphere of reflections (6587) was scanned and averaged (R_{int} = 0.069) into a unique set of 909 reflections [711 of which with $I > 2\sigma(I)$]. Three space groups are consistent with the observed systematic extinctions [$P6(3)mc$, P-62c and $P6(3)/mmc$]. Interpretable (partial) results (with SHELXS97 and SIR97) were obtained in both $P6(3)mc$ and its centrosymmetric counterpart $P6(3)/mmc$. In both cases it was clear that the C_{60} moiety is severely orientationally disordered. The model presented here is based on the refinement (with SHELXL97) of a restrained C_{60} 'order-model' in $P6(3)mc$. The restraint for 5-6 bonds refined to 1.480(8) Å and for 6-6 bonds to 1.290(14) Å. The unrestrained geometry of the azatriptycene is satisfactory along with the associated anisotropic displacement parameters. The anisotropic displacement parameters of the C_{60} atoms show the common flat disc shape (some non-positive definite). Hydrogen atoms were taken into account at calculated positions. Since the current refinement was stable (R_1 = 0.0861, wR_2 0.272, S = 1.05, $-0.60 < \Delta_r < 0.65$ e Å^{-3}) in the non-centrosymmetric symmetry space group description, no further attempts were made to refine a less attractive disorder model (for both moieties) required for the description in the related centrosymmetric space group. CCDC 182/1344. See http://www.rsc.org/suppdata/cc/1999/1709/ for crystallographic data in .cif format.

** The effects of C_{60}–triptycene interactions or kinetics of crystal packing on the solid state arrangement need further investigation.

1 P.-M. Allemand, A. Koch, F. Wudl, Y. Rubin, F. Diederich, M. M. Alvarez, S. J. Anz and R. L. Whetten, *J. Am. Chem. Soc.*, 1991, **113**, 1050.

2 L. J. Barbour, G. W. Orr and J. L. Atwood, *Chem. Commun.*, 1998, 1901 and references cited therein.

3 G. R. Desiraju, *Crystal Engineering: The Design of Organic Solids*, Elsevier, Amsterdam, 1989.

4 J. L. Atwood, G. A. Koutsantonis, and C. L. Raston, Nature, 1994, **368**, 229; M. F. Meidine, P. B. Hitchcock, H. W. Kroto, R. Taylor and D. R. M. Walton, *Chem. Commun.*, 1992, 1534; R. M. Williams and J. W. Verhoeven, *Recl. Trav. Chim. Pays-Bas*, 1992, **111**, 531; A. Ikeda, M. Yoshimura and S. Shinkai, *Tetrahedron Lett.*, 1997, **38**, 2107; C. L. Raston, J. L. Atwood, P. J. Nichols and I. B. N. Sudria, *Chem. Commun.*, 1996, 2615; N. S. Isaacs, P. J. Nichols, C. L. Raston, C. A. Sandova and D. J. Young, *Chem. Commun.*, 1997, 1839; T. Haino, M. Yanase and Y. Fukazawa, *Angew. Chem., Int. Ed. Engl.*, 1997, **36**, 259.

5 C. L. Raston, in *Comprehensive Supramolecular Chemistry* ed. J. L. Atwood, Pergamon, Oxford, 1996, ch. 22, p. 777.

6 O. Ermer, *Helv. Chim. Acta*, 1991, **74**, 1339; T. Haino, M. Yanase and Y. Fukazawa, *Tetrahedron Lett.*, 1997, **38**, 3739; R. E. Douthwaite, M. L. H. Green, S. J. Heyes, M. J. Rosseinsky and J. F. C. Turner, *J. Chem. Soc., Chem. Commun.*, 1994, 1367; D. V. Konarev, E. F. Valeev, Y. L. Slovokhotov, Y. M. Shul'ga and R. N. Lyubovskaya, *J. Chem. Res. (S)*, 1997, 442; B. Kräutler, T. Müller, J. Maynollo, K. Gruber, C. Kratky, P. Ochsenbein, D. Schwarzenbach and H.-B. Bürgi, *Angew. Chem., Int. Ed. Engl.*, 1996, **35**, 1204; P. D. Croucher, J. M. E. Marshall, P. J. Nichols and C. L. Raston, *Chem. Commun.*, 1999, 193; K. Tsubaki, K. Tanaka, T. Kinoshita and K. Fuji, *Chem. Commun.*, 1998, 895.

7 J. S. Lui, Y. Lu, M. M. Kappes and J. A. Ibers, *Science*, 1991, **254**, 408.

8 G. Wittig and G. Steinhoff, *Anal. Chem.*, 1964, **21**, 676; G. Wittig and G. Steinhoff, *Angew. Chem.*, 1963, **75**, 453.

Communication 9/04457D

Fabrication of a covalently attached self-assembly multilayer film *via* H-bonding attraction and subsequent UV-irradiation

Jinyu Chen and Weixiao Cao*

College of Chemistry and Molecular Engineering, Peking University, Beijing 100871, China. E-mail: wxcao@263.net

Received (in Cambridge, UK) 12th July 1999, Accepted 27th July 1999

A photosensitive ultrathin film has been fabricated from a diazo resin (DR) and phenol–formaldehyde resin (PR) *via* hydrogen bonding, covalent bonds are formed UV irradiation giving a covalently linked ultra-thin film; as a consequence the stability of the film towards polar solvents increases dramatically.

Recently a self-assembly technique to form ultra-thin films *via* H-bonding attraction was developed by Zhang *et al.*[1] and Stockman and Rubner.[2] However, such H-bonding attraction is very weak, which leads to the films being readily destroyed in polar solvents. In this contribution, we report a new multilayer film fabricated from a diazo-resin (DR) and phenol–formaldehyde resin (PR) formed *via* H-bonding attraction between N^+N: of DR and –OH of PR in methanol. It has been confirmed that under UV irradiation, following the decomposition of the diazonium group, that covalent bonds form in the film structure and the stability of the film towards polar solvents is substantially increased. To our knowledge, this is the first report of the formation of stable ultra-thin films from a precursor film formed *via* hydrogen bonding attraction.

DR was prepared according to the method described elsewhere.[3] PR, a polycondensation product of 4-*tert*-butylphenol and formaldehyde, ($M_w \approx 2600$, Chemical Agent Factory, Zheng-zhe City, Huinan Province, P.R. China) was used as received. The films were prepared at room temperature in the dark. A fresh quartz wafer (fused silica), which was modified with a monolayer of *N*-[3-(trimethoxysilyl)propylethylenediamine according to ref. 4, was used as substrate. The quartz wafer was first immersed in a methanol solution of polyvinylpyrrolidone (PVP) (1 mg ml^{-1}) for 5 min. After rinsing with methanol and drying, the wafer was immersed in a methanol solution of PR (1 mg ml^{-1}) for 5 min followed, after rinsing with methanol by immersion in a methanol solution of DR (0.2 mg ml^{-1}) for 5 min. The wafer was then rinsed again with methanol and air dried. In each cycle of immersion into PR and DR solutions, a bilayer of PR–DR is formed on both sides of the quartz wafer.

UV–VIS spectra were recorded on a UV–VIS spectrophotometer (Shimadzu 2100) which was used to monitor the self-assembly process of the fabrication as shown in Fig. 1. Peaks at 384 and 284 nm are assigned to the absorptions of diazonium group of DR and the phenyl group of PR. Results show that the absorbance increases uniformly in the assembly process and indicates that the step-by-step fabrication is smooth. The inset plot shows the linear relationship of the absorbance at 384 nm (or 284 nm) with the number of bilayers. Unfortunately, this multilayer film is unstable in the presence of polar solvents. For example, upon immersion of a multilayer film (14 bilayers) deposited on a quartz wafer in DMF for 10 min, most of the layer (> 90%, as calculated from the decreased absorbance at 384 nm) was destroyed. This result shows that the stability towards polar solvents of multilayer films formed *via* H-bonding attraction is poorer than for films formed by electrostatic attraction.[5,6]

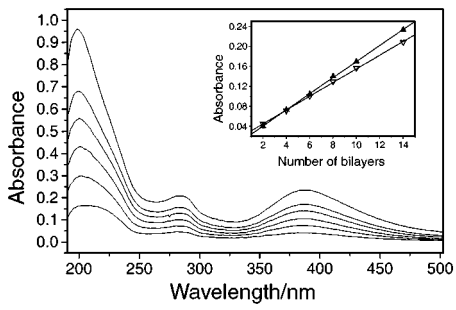

Fig. 1 UV–VIS spectra of multilayer films from PR and DR with various numbers of bilayers; bilayer number (bottom to top): 2, 4, 6, 8, 10, 14; Inset: absorbance at 384 nm (▲) and at 284 nm (▽).

It is known that DR decomposes readily under UV-irradiation or upon heating. Fig. 2 shows the photodecomposition of a 14 bilayer film under UV-irradiation (230 μW cm^{-2}). The inset of Fig. 2 drawn from the absorbance at 384 nm shows that this reaction follows first order reaction kinetics under the experimental conditions. The absorption at 284 nm (Ph–O–Ph absorption) increased with a decrease of the absorbance at 384 nm ($-N_2^+$ group absorption), which indicates the formation of the Ph–O–Ph ether bond. The conversion of the H-bond to a covalent bond (Ph–O–Ph) is shown in Scheme 1.

The stability of the film towards polar solvents increases dramatically upon exposure of the films towards UV radiation.

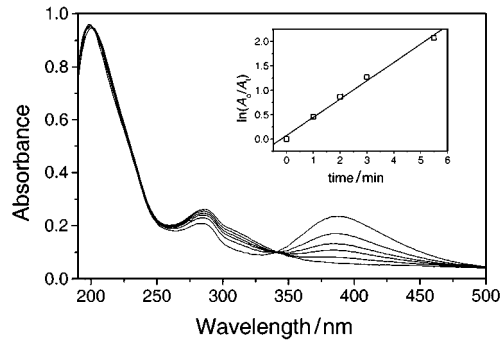

Fig. 2 UV–VIS spectra of a 14 bilayer film irradiated for different times (irradiation intensity = 230 W cm^{-2}). Irradiation time (min) 0, 1, 2, 3, 5.5, 20 min. Inset: absorbance at 384 nm.

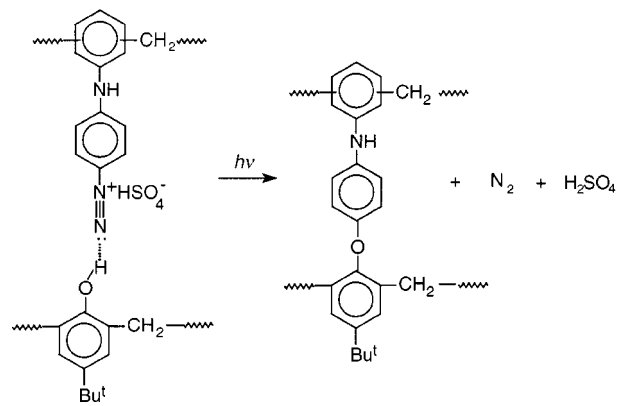

Scheme 1 The photoreaction of DR and PR in a self-assembled film.

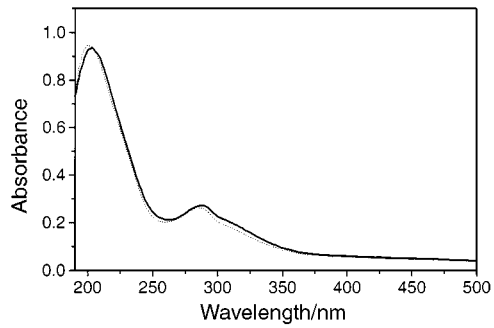

Fig. 3 UV–VIS spectra of a 14 bilayer film before (----) and after (—) etching in DMF for 10 h at 25 °C.

For example after irradiation for 20 min, the film was then immersed in DMF at 25 °C for 10 h with no decrease in absorbance (Fig. 3) being observed. This shows that the film is very stable towards polar solvents after UV irradiation.

To verify the assembly driving force is from the formation of a hydrogen bond between N^+N of DR and –OH or PR rather than NH of DR and –OH of PR, we studied PVP as an H-acceptor and DR as an H-donor in an attempt to prepare a layer-by-layer film, but this was unsuccessful. It can thus be assumed that the NH group of DR does not form a H-bond with PVP although the latter is a strong H-acceptor.

To further verify the formation of a hydrogen bond and subsequent reaction in the film upon UV irradiation, a film with 20 bilayers was fabricated on a CaF_2 wafer from DR and PR and its IR spectrum (not shown) recorded. A broad peak at 3251.0 cm^{-1} and a peak at 1371.4 cm^{-1} indicate the OH group of the PR is in an associated state. A peak at 2155.9 cm^{-1} is assigned to the stretching vibration of the diazonium group which is shifted by 11 cm^{-1} as compared with the free-molecule (2167 cm^{-1}).[5] Both observations indicate formation of an H-bond between N^+N: and OH. The film was then exposed to UV irradiation for 20 min at 230 μW cm^{-2} and the IR spectra (not shown) were recorded again. The broad peak at 3251.0 cm^{-1} was found to be weakened with both the peak at 1371.4 cm^{-1} and the absorption of the diazonium group (at 2155.9 cm^{-1}) dissappearing. This result indicates that after exposure to UV light the original H-bond has been destroyed.

In conclusion, *via* hydrogen bond attraction between the diazonium group of DR and the hydroxy group of PR and subsequent UV-irradiation, an ultra-thin film which is stable towards polar solvents was fabricated from DR and PR by a self-assembly technique.

The authors greatly appreciate the NSFC for financial support of this work.

Notes and references

1 L.-Y. Wang, Z.-Q. Wang, X. Zhang and J.-C. Shen, *Macromol. Rapid Commun.*, 1997, **18**, 509.
2 W. B. Stockton and M. F. Rubner, *Macromolecules*, 1997, **30**, 2717.
3 C. Zhao, J.-Y. Chen and W.-X. Cao, *Angew. Makromol. Chem.*, 1998, **259**, 77.
4 T. M. Cooper, A. L. Campbell and R. L. Crane, *Langmuir*, 1995, **11**, 2713.
5 J.-Q. Sun, T. Wu, Y.-P. Sun, Z.-Q. Wang, X. Zhang, J.-C. Shen and W.-X. Cao, *Chem. Commun.*, 1998, 1853.
6 J.-Y. Chen, L. Huang, L.-M. Ying, G.-B. Luo, X.-S. Zhao, W.-X. Cao, *Langmuir*, 1999, in press.

Communication 9/05629G

ChemComm

A novel catalytic approach to the chemical detoxification of P-ester nerve agents

Wendy Y. Mills, Rebecca M. Kissling and Michel R. Gagné*

Department of Chemistry CB#3290, University of North Carolina, Chapel Hill, NC 27599, USA. E-mail: mgagne@unc.edu

Received (in Corvallis, OR, USA) 27th May 1999, Accepted 23rd July 1999

An effective method for the destruction of P-based nerve agent simulants using the ester interchange reaction is described; depolymerization of polycarbonate in the presence of aryl phosphinates and KOBu^t (5 mol%) leads to a net breakdown of the toxic constituents of the simulants while immobilizing each component as a polymer end group; the data suggest that application of this approach to the destruction of nerve agents such as VX may be fruitful.

Chemical warfare agents such as VX [*S*-2-(diisopropylamino)-ethyl *O*-ethyl methylphosphonothioate] are polar organic liquids at ambient conditions.[1] Given the current stockpile of these agents (thousands of tons in the US alone), efficient and safe methods for their destruction present a scientifically challenging and important research problem. Currently, methods for their destruction rely on incineration or chemical neutralization. Each of these methods, however, have attendant disadvantages as they produce hazardous fumes or byproducts that may still be highly toxic. To address some of these issues, we have recently initiated experiments utilizing ester interchange to disassemble (*i.e.* detoxify) the key subunits of these agents, while simultaneously immobilizing them for subsequent safe disposal.

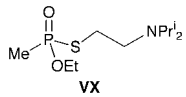

VX

We have previously reported that alkali-metal alkoxide clusters catalyze the ester interchange reaction under mild conditions and at high rates (up to 10^6 turnovers h^{-1}) [eqn. (1)].[2] As an extension of this original observation we have additionally demonstrated that (i) phosphonates are highly susceptible to ester interchange [eqn. (2)],[3] and (ii) diaryl carbonate (DAC) interchange can be used to depolymerize high molecular weight (MW) bisphenol A polycarbonate (PC) with subsequent control over polymer end groups [eqn. (3)].[4] The reaction rates for the former processes are also rapid and turnover frequencies as high as 1.5×10^6 h^{-1} have been measured. A key consideration in the successful application of this methodology is a matching of the pK_as for the two interchanging esters, *i.e.* the two ester leaving groups must be similarly competent.

Our data therefore suggest that, given a suitable interchange partner, VX should be capable of swapping its toxic amino thiolate side chain for a less toxic one. pK_a considerations indicate that thioesters (*e.g.* AcSEt) or aryl esters (*e.g.* AcOAr) should be suitable.[5] Since VX derivatives containing simple non-functionalized side chains like SEt are toxic and can be volatile, polymeric non-sulfur containing side chains might be ideal detoxification products from both a toxicity and volatility perspective. Therefore, in analogy to the depolymerization process, utilization of VX or a VX simulant as a breakdown agent for PC should effectively destroy the agent while immobilizing the toxic components as polymer end groups (Scheme 1). The additional entropic driving force associated with a polymer breakdown protocol should additionally maximize the chemical potential for P-ester destruction.

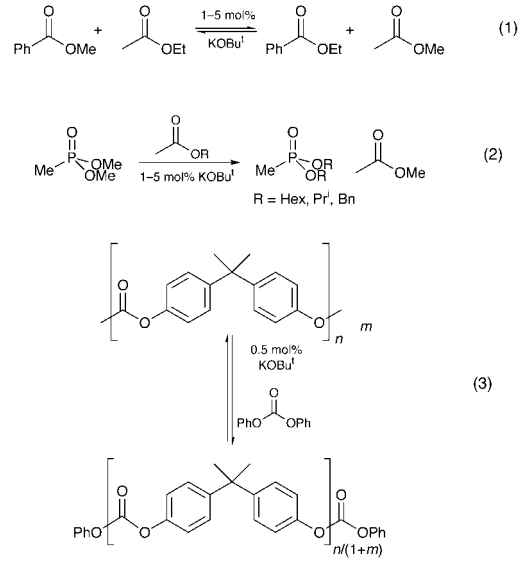

To test this hypothesis, two model VX simulants (naphthyl diphenylphosphinate **1** and phenyl diphenylphosphinate **2**) were each allowed to interchange with diphenyl carbonate (DPC) [eqn. (4)], cyclic PC (CPC)[6] and linear PC (LPC)[7] in the presence of 5 mol% KOBu^t as shown in Scheme 1. Some of the expected products from the reaction are also highlighted in Scheme 1. Under a dry argon atmosphere the desired phosphinates and carbonate were dissolved in THF and, after catalyst addition, were stirred for 30 min at room temperature. The polymer-based reactions were subsequently worked up by precipitation into a 10-fold excess of MeOH; the collected polymeric precipitates were then analyzed by GPC (Table 1) and ^{31}P NMR (*vide infra*). The amount of unreacted phosphinate in the filtrate was obtained by solvent removal and quantitative HPLC analysis (Table 1).[8] The relative amount of carbonate to phosphinate functional groups in the starting mixture was varied (10 : 1, 20 : 1 and 50 : 1) to determine its effect on simulant conversion. As expected, increasing ratios of carbonate drove the reactions forward, especially in the cases of CPC and LPC (entries 1–10). With ratios of 50 : 1, CPC and LPC reactions yielded residual amounts of **2** that were too low to accurately measure using our HPLC assay. Optimized breakdown conditions required 5 mol% of KOBu^t; lower catalyst loadings or the use of NaOBu^t or LiOBu^t gave inferior results. Most surprising were the attenuated changes in the residual phosphinate observed using DPC as the carbonate source. Longer reaction times before quenching indicated that the DPC breakdown experiments had not yet reached equilibrium (Table 1, entries 11–13). For example, quenching the reactions in entry 11 after 6 h led to 5.3% residual **1**.[9] The polymeric breakdown experiments apparently reach a final state more rapidly (< 30 min) than DPC-based protocols, as later quenching did not

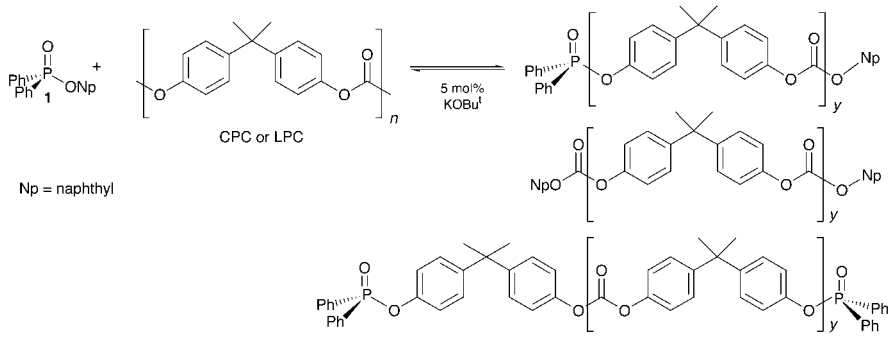

Scheme 1

Table 1 HPLC and GPC analysis data[a]

Entry	Carbonate	Phosphinate	Substrate ratio[b]	Unreacted[c] (%)	M_n[d]	M_w	PDI
1	CPC	**1**	10:1	5.3	2497	3541	1.42
2	CPC	**1**	20:1	2.1	3182	4982	1.57
3	CPC	**1**	50:1	0.95	3773	6313	1.67
4	CPC	**2**	10:1	6.2	2504	3553	1.42
5	CPC	**2**	20:1	1.1	2842	4254	1.50
6	LPC	**1**	10:1	5.3	2214	3353	1.52
7	LPC	**1**	20:1	2.4	2531	3922	1.55
8	LPC	**1**	50:1	0.9	2989	4959	1.66
9	LPC	**2**	10:1	5.3	2217	3166	1.43
10	LPC	**2**	20:1	1.4	2633	4102	1.56
11	DPC	**1**	10:1	6.8–8.3[e]	—	—	—
12	DPC	**1**	20:1	3.5–6.1[e]	—	—	—
13	DPC	**1**	50:1	3.1–4.9[e]	—	—	—

[a] Catalyst loadings were at the 5 mol% level with respect to total carbonate and phosphinate functionalities; reactions were carried out in THF and were each quenched after 30 min. [b] Ratios refer to the relative quantities of carbonate and phosphinate functionalities. [c] Residual amounts of phosphinate reflect an average of at least two runs. [d] Corrections for the MW of PC utilized the universal calibration method (K_{PS} = 0.013, K_{PC} = 0.039, α_{PS} = 0.71 and α_{PC} = 0.70, see ref. 11 [e] Ranges reflect non-equilibrium ratios (see text).

affect the amount of residual **1**. While we are confident that 10:1 and possibly 20:1 polymer experiments reach a true equilibrium state,[10] we suspect that the 50:1 cases do not. Unfortunately the low phosphinate concentrations in the residues do not allow us to determine whether catalyst death occurs before a true equilibrium is reached. Clearly, low phosphinate concentrations can be achieved with these experimental conditions.

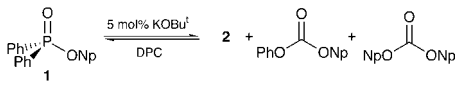

(4)

In addition to preparative protocols, *in situ* ^{31}P NMR experiments to monitor the transfer of the phosphorus-containing fragment from the simulant to the polymer were also undertaken. The naphthyl phosphinate **1** proved particularly useful in this regard as its conversion to product was readily observed by the 0.5–1 ppm upfield shift of its resonance upon substitution of an oligomeric substituent for ONp. The amount of unreacted phosphinate in these experiments closely matched those data obtained on preparative scales. ^{31}P NMR spectra of the precipitated polymers showed only a singlet shifted slightly upfield from the starting material. Spiking of these samples with either **1** or **2** confirmed that no starting material was present in the MeOH precipitate and that quantifying unreacted simulant in the filtrate is a valid protocol for assessing overall destruction.

In summary, by combining two separate methodologies, one for the synthesis of phosphonates and the other for the breakdown of polycarbonates, a potentially useful method for the destruction of toxic chemical warfare agents has been revealed. The salient features of this approach are the low levels of simulant remaining after reaction and the safe immobilization of the simulant constituents as polymer end groups.

We gratefully acknowledge the United States Army Research Office (DAAG55-98-1-0257) for funding of this research. We also wish to thank Dr D. B. Priddy Jr. at Bayer AG, Krefeld Germany, for kindly providing a generous sample of CPC.

Notes and references

1 Y. C. Yang, *Acc. Chem. Res.*, 1999, **32**, 109; Y. C. Yang, J. A. Baker, and J. R. Ward, *Chem. Rev.*, 1992, **92**, 1729.
2 M. G. Stanton and M. R. Gagné, *J. Am. Chem. Soc.*, 1997, **119**, 5075; M. G. Stanton and M. R. Gagné, *J. Org. Chem.*, 1997, **62**, 8240.
3 R. M. Kissling and M. R. Gagné, *J. Org. Chem.*, 1999, **64**, 1585.
4 M. R. Korn and M. R. Gagné, *Macromolecules*, 1998, **32**, 4023.
5 In DMSO, the pK_a of butanethiol and naphthol are 17.0 and that of phenol is 18.0, see: F. G. Bordwell, *Acc. Chem. Res.*, 1988, **21**, 456.
6 M_n = 852; DP = 3.4, PDI = 1.37. See: D. J. Brunelle, E. P. Boden and T. G. Shannon, *J. Am. Chem. Soc.*, 1990, **112**, 2399.
7 The linear PC was prepared by first dissolving it into THF, filtering it, precipitating it into an excess of MeOH, and finally drying *in vacuo* at 50 °C (M_n = 14 330; DP = 55; PDI = 1.99).
8 Chromatograms were obtained on a Hewlett-Packard 1100 LC instrument using a cyano-terminated silica gel column (LiChrosphere 100CN) for **1**, and a silica gel column (DYNAMAX 60A) for **2**. For **1**, filtrate samples were run at 1 ml min^{-1} in THF–hexanes (3:7 v/v) with a gradient elution of 0.5% THF min^{-1} for 10 min. For **2**, filtrate samples were run at 1 ml min^{-1} in THF–hexanes (45:55 v/v). A UV diode array detector was used for analysis.
9 As expected, no net reaction is observed with **2** and DPC.
10 Monitoring reactions *in situ* by ^{31}P NMR while sequentially adding aliquots of catalysts indicated that after reaching *ca.* 5% conversion (10:1 case), additional catalyst did not change the amount of unreacted phosphinate. Similar observations were noted for the 20:1 experiments.
11 M. Kurata and Y. Tsunashima, *Viscosity–Molecular Weight Relationships and Unperturbed Dimensions of Linear Chain Molecules*, in *Polymer Handbook*, 3rd edn., ed. J. Brandrup and E. H. Immergut, Wiley-Interscience, New York, 1989, ch. VII, pp. 1–60.

Communication 9/04328D

Prochiral selectivity and deuterium kinetic isotope effect in the oxidation of benzyl alcohol catalyzed by chloroperoxidase

Enrico Baciocchi,*[a] Osvaldo Lanzalunga[b] and Laura Manduchi[a]

[a] *Dipartimento di Chimica, Università 'La Sapienza', Rome, Italy. E-mail: baciocchi@axcasp.caspur.it*
[b] *Dipartimento di Chimica and Centro CNR di Studio sui Meccanismi di Reazione, Università 'La Sapienza', Rome, Italy*

Received (in Liverpool, UK) 26th May 1999, Accepted 23rd July 1999

The chloroperoxidase-catalyzed oxidation of benzyl alcohol exhibits a very high prochiral selectivity, involving only the cleavage of the *pro-S* C–H bond.

The mechanistic aspects of the reactions catalyzed by chloroperoxidase (CPO), a hemoprotein isolated from the fungus *Caldariomyces fumago*, are attracting continuous interest as this enzyme is able to catalyze the H_2O_2-promoted oxidation of a large variety of organic compounds.[1] There is general consensus that in all cases the active oxidant is an iron(IV) oxo complex porphyrin IX (P) radical cation [$P^{+\cdot}$–Fe^{IV}=O], also indicated as compound I, formed by reaction of the resting enzyme with H_2O_2 [eqn. (1)].[1d,2]

$$P\text{–}Fe^{III} + H_2O_2 \rightarrow \underset{\text{Compound I}}{P^{+\cdot}\text{–}Fe^{IV}\text{=O}} + H_2O \qquad (1)$$

Here we report on a kinetic and products study of the oxidation of benzyl alcohol **1** and the enantiomeric and racemic forms of α-monodeuterated benzyl alcohol (**1**-*d*). The results obtained have shown that the process is characterized by an extremely high prochiral selectivity, providing us with useful information about the reaction mechanism.

The racemic [α-$^2H_1$]benzyl alcohol [(±)-**1**-*d*)] and the two enantiomers (*R*)- and (*S*)-[α-$^2H_1$]benzyl alcohol [(*R*)-**1**-*d* and (*S*)-**1**-*d*, respectively] were reacted with H_2O_2 in H_2O at pH 6 (0.1 M phosphate buffer), in the presence of CPO (2 nmol for 10 mmol of H_2O_2). In each case, the molar ratio between PhCDO and PhCHO produced in the reaction was measured by GC-MS and/or ^{1}H NMR, the two methods giving very similar results. The results are reported in Table 1. The kinetic parameters K_m and k_{cat} for the CPO-catalyzed oxidation of deuterated and undeuterated benzyl alcohols were obtained, as usual, by measuring the initial rates of formation of benzaldehyde at different concentrations of substrate (Lineweaver–Burk plots). These values are collected in Table 2.

Table 1 Oxidations of [α-$^2H_1$]benzyl alcohols with H_2O_2 catalyzed by CPO[a]

Substrate	Yields (%)[b]	PhCDO/PhCHO[c]
(*S*)-[α-^{2}H]benzyl alcohol	58	< 0.1
(*R*)-[α-^{2}H]benzyl alcohol	68	> 30
(±)-[α-^{2}H]benzyl alcohol	47	2.0

[a] The alcohol (0.1 ml of a solution 0.5 M in CD_3CN) and CPO (Sigma) (2 nmol) were magnetically stirred in 5 ml of 0.1 M phosphate buffer pH 6.0 at 25 °C, H_2O_2 (200 μl, 0.5 M) was then slowly added in 1 h *via* a syringe pump. After extraction with $CDCl_3$ reaction mixtures were analyzed by ^{1}H NMR, GC and GC-MS. Benzaldehyde and [α-$^2H_1$]benzaldehyde were the only products formed. [b] Yields are with respect to the starting material. Average of at least three determinations, the error is ±10%. [c] Molar ratio measured *via* GC-MS by the ratio between the corrected signal intensities of the two molecular ions at *m/z* 107 and 106. Average of at least three determinations, the error is ±10%. Similar values were obtained by ^{1}H NMR considering that the signal of the benzylic protons *ortho* to the carbonyl is due to the sum of the two products (PhCHO + PhCDO) and that of the aldehydic proton derives from PhCHO.

By looking at the data in Table 1, a very remarkable observation is that from (*S*)-**1**-*d* practically only PhCHO is produced, whereas the oxidation of its enantiomer (*R*)-**1**-*d* leads almost exclusively to PhCDO. Comparable amounts of deuterated and undeuterated benzaldehydes form instead from the racemic alcohol (±)-**1**-*d*.

These results clearly indicate that in the oxidation of (*S*)-**1**-*d* the bond broken is almost exclusively the C-D bond, whereas the oxidation of (*R*)-**1**-*d* involves almost exclusively the cleavage of the C–H bond. Thus, the ratio between the k_{cat} values for (*R*)-**1**-*d* (C–H bond cleavage) and (*S*)-**1**-*d* (C–D bond cleavage), reported in Table 2, should provide us with a lower limit for the *intrinsic* kinetic deuterium isotope effect of the reaction (k_H/k_D).[3] A value of 2.8 is obtained which is slightly smaller than those (3.3, 3.5) found in the benzylic hydroxylation of *p*-methylanisole.[1i] It therefore seems possible to suggest a similar mechanism for the two processes, *i.e.* the oxidation of benzyl alcohol catalyzed by CPO should involve the transfer of a hydrogen atom to the ferryl oxygen of the iron oxo complex (Scheme 1, path a).[5] An α-hydroxy carbon radical and the iron hydroxy complex P–Fe^{IV}–OH form. They may lead to the hydrated form of benzaldehyde directly (oxygen rebound, Scheme 1, path b) or stepwise with formation of the intermediate α-hydroxybenzyl cation (Scheme 1, path c and d). A similar sequence has also been proposed for the oxidation of benzyl alcohol catalyzed by cytochrome P-450.[6]

The possibility of an electron transfer mechanism facilitated by the aromatic ring seems unlikely since the value of k_H/k_D is significantly higher than that (1.8) determined in the oxidation of racemic **1**-*d* induced by the genuine one-electron oxidant $SO_4^{-\cdot}$.[7]

The data presented in Table 1 also allow some speculation concerning the orientation of the substrate in the enzyme active site. In particular, it can be suggested that the substrate binds to the enzyme orienting the C–D bond of the *S* enantiomer, and the

Table 2. Steady-state kinetic constants for the chloroperoxidase catalyzed oxidation of benzyl alcohols by H_2O_2

Substrate	K_m/mM[a]	k_{cat}/s^{-1}[a]
1	1.3 ± 0.1	17.2 ± 0.7
(*S*)-**1**-**d**	1.1 ± 0.1	6.6 ± 0.4
(*R*)-**1**-**d**	1.6 ± 0.1	18.7 ± 0.9

[a] Obtained from a Lineweaver–Burk plot. The initial rates for the formation of benzaldehyde were determined spectrophotometrically at 25 °C and pH 6 following the increase of absorbance at 280 nm.

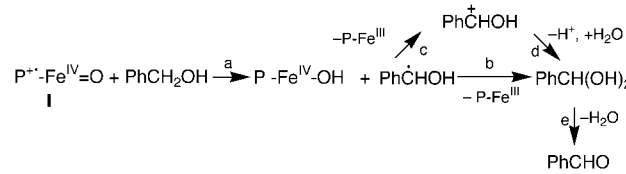

Scheme 1

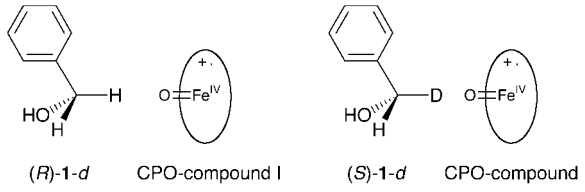

Fig. 1 Proposed orientation of (*R*)-**1**-*d* and (*S*)-**1**-*d* with respect to the iron oxo complex in the CPO active site.

C–H bond of the *R* enantiomer, towards the oxygen of the active oxidant, as illustrated in Fig. 1.

It follows that the oxidation of benzyl alcohol catalyzed by CPO should be characterized by a very high prochiral selectivity with *only* the *pro-S* hydrogen [Fig. 2(*a*)] involved in the process. An additional very interesting notation is that the same spatial orientation as that observed for the oxidation of benzyl alcohol appears to be also required in the CPO-induced oxidation of ethylbenzene, which accordingly has been reported to produce (*R*)-1-phenylethanol,[1j,8] exclusively [Fig. 2(*b*).

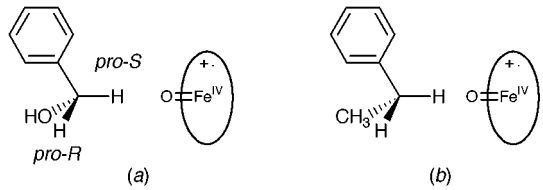

Fig. 2 Proposed orientation of (*a*) benzyl alcohol and (*b*) ethylbenzene with respect to the iron oxo complex in the CPO active site.

Thus, it would seem that in the oxidation of benzyl alcohol the OH group does not play any specific role with respect to the spatial orientation assumed by the substrate in the enzyme reacting pocket. Accordingly, the orientation appears not to change when OH is replaced by a Me group. Probably, the interaction of the aromatic ring with the side chains of Phe 103 and/or Phe 186 plays the major role in this respect. Both Phe 103 and Phe 186 are situated at the bottom of the opening of the CPO substrate-binding pocket and have been suggested to be of fundamental importance in establishing hydrophobic interactions with organic substrates.[9] Theoretical calculations to test this hypothesis are under way.

Thanks are due to the National Council of Research (CNR) and the Ministry for the University and Scientific and Technological Research (MURST) for financial support.

Notes and references

1 (*a*) S. Kobayashi, M. Nakano, T. Kimura and A. P. Schaap, *Biochem. Biophys. Res. Commun*., 1986, **135**, 166; (*b*) S. Kobayashi, M. Nakano, T. Kimura and A. P. Schaap, *Biochemistry*, 1987, **26**, 5019; (*c*) P. R. Ortiz de Montellano,Y. S. Choe, G. DePillis and C. E. Catalano, *J. Biol. Chem*, 1987, **262**, 11641; (*d*) B. W. Griffin, in *Peroxidases in Chemistry and Biology*, ed. J. Everse, K. E. Everse and M. B. Grisham, CRC Press, Boca Raton, 1991, vol. II, pp. 85–137; (*e*) S. Colonna, N. Gaggero, L. Casella, G. Carrea and P. Pasta, *Tetrahedron: Asymmetry*, 1992, **3**, 95; (*f*) L. Casella, M. Gullotti, R. Ghezzi, S. Poli, T. Beringhelli, S. Colonna and G. Carrea, *Biochemistry*, 1992, **31**, 9451;. (*g*) O. Okazaki and F. P. Guengerich, *J. Biol. Chem*., 1993, **268**, 1546; (*h*) L. Casella, S. Poli, M. Gullotti, C. Selvaggini, T. Beringhelli and A. Marchesini, *Biochemistry*, 1994, **33**, 6377; (*i*) V. P. Miller, R. A. Tschirret-Guth and P. R. Ortiz de Montellano, *Arch. Biochem. Biophys*., 1995, **319**, 333; (*j*) A. Zaks and D. R. Dodds, *J. Am. Chem. Soc*., 1995, **117**, 10419; (*k*) P. H. Toy, M. Newcomb and L. P. Hager, *Chem. Res. Toxicol*., 1998, **11**, 816; (*l*) S. Hu and L. P. Hager, *J. Am. Chem. Soc*., 1999, **121**, 872.

2 J. H. Dawson, *Science*, 1988, **240**, 433; M. C. R. Franssen and H. C. Van der Plas, *Adv. Appl. Microbiol*., 1992, **37**, 41.

3 Actually, k^R_{cat}/k^S_{cat} is a measure of the intrinsic deuterium isotope effect only if the rate of release of the product from the enzyme–product complex is not kinetically significant. If this condition does not hold, the intrinsic deuterium isotope effect is expected to be larger than k^R_{cat}/k^S_{cat} (ref. 4).

4 *Reaction Rates of Isotopic Molecules*, ed. L. Melander and W. H. Saunders, Wiley, New York, 1980, ch. 10, pp. 297–305.

5 However, a concerted oxygen insertion, as suggested by the use of radical probe substrates [ref. 1(*j*), (*k*)], might also be compatible with the observed intrinsic k_H/k_D values.

6 A. D. N. Vaz and M. J. Coon, *Biochemistry*, 1994, **33**, 6442. Interestingly, in this paper an intramolecular kinetic isotope effect of 2.6 was determined in the oxidation of [α-$^2H_1$]benzyl alcohol induced by purified rabbit liver cytochrome P450 2B4, using only the racemic monodeuterated benzyl alcohol. In preliminary experiments we have found significantly different values of the observed intramolecular kinetic deuterium isotope effect in the phenobarbital induced rat liver microsomal oxidation of (*R*)-**1**-*d* and (*S*)-**1**-*d* (1 and 4, respectively).

7 (±)-**1**-*d* was reacted with $SO_4^{\bullet-}$ (from $Ti^{III}/K_2S_2O_8$ or γ-radiolysis/$K_2S_2O_8$) in H_2O at pH 6 (0.1 M phosphate buffer). From the molar ratio between PhCDO and PhCHO produced in the reaction, measured by GC-MS, a k_H/k_D value of 1.8 was calculated.

8 The *pro-R* hydrogen in ethylbenzene corresponds to the *pro-S* hydrogen in benzyl alcohol.

9 M. Sundaramoorthy, J. Terner and T. L. Poulos, *Structure*, 1995, **3**, 1367.

Communication 9/04327F

ChemComm

New products in an old reaction: isomeric products from H_2 addition to Vaska's complex and its analogues

Sarah K. Hasnip,[a] Simon B. Duckett,*[a] Christopher J. Sleigh,[a] Diana R. Taylor,[b] Graham K. Barlow[b] and Mike J. Taylor[b]

[a] *Department of Chemistry, University of York, Heslington, York, UK YO10 5DD. E-mail: sbd3@york.ac.uk*
[b] *BP Amoco Chemicals, BP Chemicals Limited, Salt End, Hull, UK HU12 8DS*

Received (in Cambridge, UK) 12th July 1999, Accepted 29th July 1999

***para*-Hydrogen enhanced NMR signals aid detection of minor isomers of complexes $IrH_2(L)_2(CO)Cl$ (L = PPh_3, PMe_3, PPh_2Cl and $AsPh_3$) containing magnetically inequivalent hydride ligands that are produced *via* addition across the L–Ir–L axis of $Ir(L)_2(CO)Cl$: in the case of L = PPh_3, reaction with CO and H_2 is shown to yield the substitution product $IrH_2(CO)_2(PPh_3)Cl$ which reacts further *via* HCl transfer to form $IrH(CO)(PPh_3)_2Cl_2$ and thereby enables the detection of $IrH_3(CO)_2(PPh_3)$.**

It has been shown that the addition of H_2 enriched in the *para* spin state to a transition metal centre leads to greatly enhanced hydride signals in associated ^{1}H NMR spectra.[1] This phenomenon is a powerful tool available to characterise minor reaction products such as *all-cis* $Ru(H)_2(CO)_2(PMe_3)_2$[2] and investigate hydrogenation kinetics.[3] The addition of H_2 to Vaska's complex,[4] *trans*-$Ir(CO)(PPh_3)_2Cl$ **1a**, and its analogues has been the subject of much investigation and it is currently accepted that, in general, addition proceeds exclusively over the OC–Ir–Cl axis. However, calculations by Sargent and Hall[5] revealed that H_2 addition over the OC–Ir–Cl axis rather than the P–Ir–P axis is favoured by 9.5 kJ mol^{-1} in the case of $Ir(CO)(PMe_3)_2Cl$. Furthermore, calculations indicate that increasing the π-accepting nature of the phosphine will favour H_2 addition across the P–Ir–P axis. Here, we describe studies that test this prediction by monitoring reactions of $Ir(L)_2(CO)Cl$ (L = PPh_3, PMe_3, PPh_2Cl and $AsPh_3$) with *para*-hydrogen (*p*-H_2).

It has already been shown that when a solution containing *cis*,*trans*-$IrH_2(CO)(PPh_3)_2Cl$ **2a** is examined by ^{1}H NMR spectroscopy the corresponding hydride resonances are polarised (**2a**, 0.1 mmol dm^{-3}, toluene-d_8, 343 K and 3 atm *p*-H_2).[6] Under these conditions, H_2 addition is reversible, and exchange leads to hydride signal enhancements that are 11 fold. At 298 K the hydride resonances of **2a** are unaffected by the presence of *p*-H_2 because exchange is suppressed. However, when the reaction of **1a** with *p*-H_2 is monitored by NMR spectroscopy, *in-situ*, the dihydride products are detected as they form and prior to spin population relaxation. In the corresponding ^{1}H spectrum polarised hydride resonances are detected for **2a**, and a second previously unreported species, as shown in Fig. 1(a). The enhanced resonance of this minor product is only visible when **1a** is reacting with *p*-H_2 and the associated signals decay away rapidly. Furthermore, the extra hydride resonance arises from a second order spin system with magnetically distinct hydrides.[6,7] The ^{31}P and ^{13}C chemical shifts and the multiplicities of the hydride, phosphine and carbonyl resonances of this product, located *via* a series of 2D NMR experiments, are consistent with their origin in *cis*,*cis*-$IrH_2(CO)(PPh_3)_2Cl$ **3a**. This product is formed by H_2 addition over the P–Ir–P axis of **1a**, as shown in Scheme 1.† At 295 K, the difference in hydride signal intensities of **2a** and **3a** was determined by the application of a pulse sequence involving a 90° ^{1}H pulse, a pulsed field gradient, a 100 ms delay, and a 45° ^{1}H read pulse. This procedure enables the instantaneous observation of the ratio of **2a**:**3a** by suppressing signals from pre-formed materials and suggests the ratio of **2a** to **3a** is ≈ 100 if similar enhancements are assumed for each species. There is no evidence to suggest that these two species interconvert on the NMR time scale.

In order to test the generality of this reaction pathway we repeated this procedure with $Ir(CO)(L)_2Cl$ [L = PMe_3 **1b**, Fig. 1(*b*) and L = $AsPh_3$ **1c**]. In both these cases dihydride products corresponding to addition over the Cl–Ir–CO and L–Ir–L axes of *trans*-$IrCl(L)_2(CO)$ are detected. The spectral features of the PMe_3 products **2b** and **3b** are similar to those of their PPh_3 analogues.† However, hydride resonances for both these species are visible at 333 K for extended periods. The failure to observe **3b** with normal hydrogen suggests that while both **2b** and **3b** are accessible by H_2 addition to **1b**, both are able to reductively eliminate H_2 at 333 K, otherwise **3b** would become a significant reaction product.

When the reaction with L = $AsPh_3$ is monitored with normal hydrogen, two isomers, *cis*,*trans*-$IrH_2(CO)(AsPh_3)_2Cl$ **2c** (with hydride resonances at δ −7.11 and −18.91) and *cis*,*cis*-$IrH_2(CO)(AsPh_3)_2Cl$ **3c** (hydride δ −9.62) are detected in the ratio 1:2.85, respectively, at 295 K.† After five days the ratio became 1:0.1, this suggests that addition over the As–Ir–As

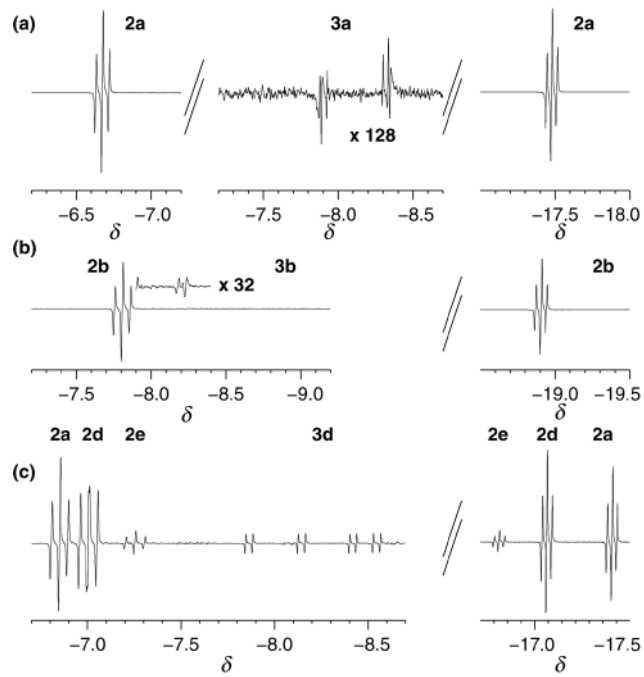

Fig. 1(a) ^{1}H NMR spectrum (400 MHz, 295 K) of a 0.1 mM solution of **1a** in benzene-d_6 under 3 atm of *p*-H_2. The weak second order resonance arises from *cis*,*cis*-$IrH_2(CO)(PPh_3)_2Cl$ **3a**. (b) ^{1}H NMR spectrum (400 MHz, 333 K) of a 0.1 mM solution of **1b** in benzene-d_6 under 3 atm of *p*-H_2 with resonances due to **2b** and **3b** indicated. (c) ^{1}H NMR spectrum (400 MHz, 333 K) of a 0.1 mM solution of **2a** in benzene-d_6 in the presence of a four-fold excess of PPh_2Cl under 3 atm of *p*-H_2 showing resonances due to **2a**, **2d**, **2e** and **3d**.

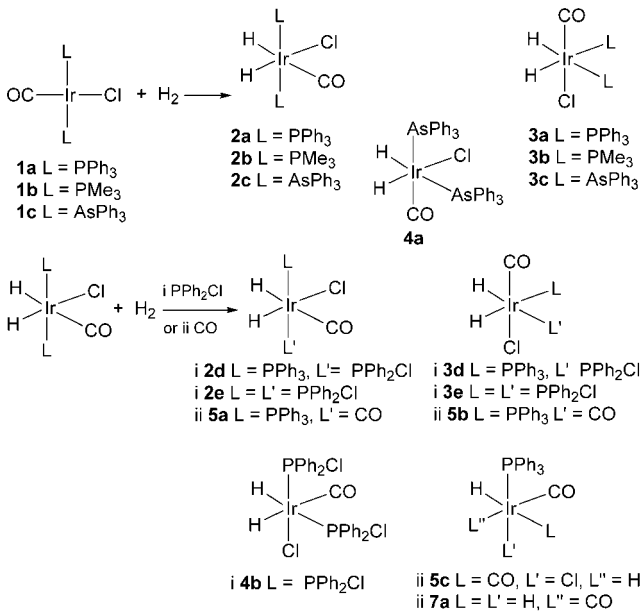

Scheme 1 Species observed in the reactions of a series of chlorocarbonylbis(phosphine)iridium(I) and dihydridochlorocarbonylbis(phosphine)-iridium-(III) complexes under *p*-H_2.

axis is kinetically preferred while addition over the OC–Ir–Cl axis leads to the thermodynamic product. Product **2c** was characterised by 2D NMR methods at 333 K where the rate of H_2 exchange is fast and the *p*-H_2 signal enhancements are long-lived.† The structure of the *cis,cis* product **3c** was confirmed by ^{13}C labelling experiments, ^1H integral measurements, and the presence of two ν(IrH) modes at 2083 and 2115 cm^{-1} in the corresponding IR spectrum.

Interestingly, a third *p*-H_2 enhanced isomer, **4a**, was detected at 338 K in the ^1H NMR spectrum that was not previously visible [Fig. 1(c)]. The chemical shifts of the hydride resonances of this product, δ −11.70 and −18.50, suggest hydride locations *trans* to CO or arsine, and *trans* to chloride, respectively. NOE measurements revealed that the hydride ligand of **4a** which resonates at δ −11.70 is close in space to a single set of *ortho*-phenyl protons (δ 7.65) while that which is *trans* to chloride is adjacent to two different sets (δ 7.65 and 7.60). **4a** therefore contains two inequivalent arsine ligands. When a ^{13}CO labelled sample was examined, the δ −11.70 signal showed a small ^1H–^{13}CO coupling of 3.4 Hz indicating that the hydride is *trans* to arsine rather than CO. In the NOE experiment, no interconversion between **2c**, **3c** and **4a** was observed which suggests that the most probable route to formation of the minor isomer **4a** is H_2 addition over the OC–Ir–As axis of the *cis* isomer of $Ir(CO)(AsPh_3)_2Cl$ (Scheme 1).

A sample containing a four-fold excess of PPh_2Cl relative to **2a** was examined to test the π-accepting role of the phosphine [Fig. 1(c)]. While this spectrum contains no resonances that can be assigned to trisphosphine species, signals corresponding to the hydride resonances of mono- and bis-phosphine exchange products (**2d**, **2e**, Scheme 1) containing *cis* hydrides and *trans* phosphines were readily assigned. Furthermore, resonances for the *cis,cis* isomers **3d** and **3e** were present in significantly higher proportions than those seen in the reaction with **1a** described above. Significantly, by virtue of the mixed phosphines, **3d** contains inequivalent hydride ligands which resonate at δ −8.13 and −8.34 with the resonances having doublet of doublet of doublet multiplicities consistent with *trans* and *cis* phosphine connections. This product is formed by H_2 addition across the P–Ir–P axis of $Ir(CO)(PPh_3)(PPh_2Cl)Cl$. Weak signals due to **4b** were also present.† Ultimately the signals of all these species disappear, and the major hydride resonances are associated with the bisphosphine carbonyl dichloride monohydride complexes **6a** and **6b**.[8] Complex **6a** is also observed in the reaction chemistry of **1a** when both CO and *p*-H_2 are present. Under these conditions, three isomers of $IrH_2(CO)_2(PPh_3)Cl$, **5a**, **5b** and **5c** and the *fac-trans* isomer of $IrH_3(CO)_2(PPh_3)$ **7a** are detected as *p*-H_2 enhanced products (Scheme 1).[9] These observations are consistent with HCl transfer from $IrH_2(CO)_2Cl(PPh_3)$ to **1a**, followed by H_2 addition to yield the dicarbonyl trihydride product.

Here we have demonstrated that H_2 addition to a series of iridium(I) carbonyl complexes based on $Ir(CO)(PPh_3)_2Cl$ involves a minor reaction pathway where addition proceeds across the P–Ir–P axis. We also show that in the presence of mixtures of CO and H_2, $IrH_2(CO)(PPh_3)_2Cl$ and the phosphine substitution product $IrH_2(CO)_2Cl(L)$ are detected in addition to HCl transfer products and a series of trihydride complexes.

Financial support from the EPSRC (Spectrometer, C. J. S. and S. K. H.), BP Chemicals (CASE award S. K. H.), the Royal Society, NATO and Bruker UK, and discussions with Professor R. N. Perutz, and Dr R. J. Mawby are gratefully acknowledged.

Notes and references

† *Selected spectroscopic data* at 400.13 MHz (^1H) and 161.45 MHz (^{31}P) and 100.2 MHz (^{13}C) in benzene-d_6 (couplings Hz): **2a**: ^1H, δ −6.64 {H, *J*(PH) 18.8, *J*(HH) −5.7}, −17.48 {H, *J*(PH) 13.7, *J*(HH) −5.7}; ^{31}P, δ 8.4. **2b**: ^1H, δ −7.80 {H, *J*(PH) 20.8, *J*(HH) −5.2}, −18.90 {H, *J*(PH) 14.7, *J*(HH) −5.2}, ^{31}P, δ −41.1; ^{13}C, δ 183.0 {CO}. **2c** (296 K): ^1H, δ −7.11 {H, *J*(COH) 44.5, *J*(HH) −5.0}, −18.91 {H, *J*(CH) 3.7, *J*(HH) −5.0}; ^{13}C, δ 177.2 {CO, s}. **2d** ^1H, δ −6.81 {H, *J*(PH) 14.4, *J*(PH) 14.7, *J*(HH) −4.7}, −16.99 {H, *J*(PH) 17.3, *J*(PH) 17.3, *J*(HH) −4.7}, ^{31}P, δ 9.0 {PPh_3, *J*(PP) 398.6}, 66.2 {PPh_2Cl, *J*(PP) 398.6}, ^{13}C, δ 176.3 {CO, *J*(PC) 7.9}. **2e** ^1H, δ −7.24 {H, *J*(PH) 20.3, *J*(COH) 44.0, *J*(HH) −5.0}, −16.73 {H, *J*(PH) 15.0, *J* (COH) 3.5, *J*(HH) −5.0}; ^{31}P, δ 65.1; ^{13}C, δ 174.8 {CO, *J*(PC) 7.9}. **3a** (295 K): ^1H, δ −8.10 {m, second order}; ^{31}P, δ −5.9; ^{13}C, δ 167.1 {CO}. **3b** (333 K): ^1H δ −8.15 {m, second order}; ^{31}P δ −7.98, ^{13}C, δ 173.37 {CO}. **3c** (296 K): ^1H, δ −9.62 {H, *J*(COH) 6.4}; ^{13}C δ 165.7 {CO, s}. **3d**: ^1H, δ −8.13 {H, *J*(PH) 222.4, *J*(PH) 15.0, *J*(HH) −1.8}, −8.34 {H, *J*(PH) 160.8, *J*(PH) 15.9, *J*(HH) −1.8}; ^{31}P, δ −4.0 {PPh_3, *J*(PP) 28.5}, 65.2 {PPh_2Cl, *J*(PP) 28.5}; ^{13}C, δ 165.3 {CO, *J*(PC) 6}. **3e**: ^1H, δ −8.37 {m, second order}; ^{31}P, δ 62.9. **4a** (338 K): ^1H, δ −11.70 {H, *J*(COH) 3.4, *J*(HH) −5.9}, −18.50 {H, *J*(CH) 4.7, *J*(HH) −5.9}; ^{13}C, δ 170.3 {CO, s}. **4b**: ^1H, δ −7.52 {H, *J*(PH) 16, *J*(PH) 23, *J*(CH) 48, *J*(HH) −2.9}, −9.50 {H, *J*(PH) 202.2, *J*(PH) 23.0, *J*(CH) 4.4, *J*(HH) −2.9}; ^{31}P, δ 65.3 {PPh_2Cl, br}; ^{13}C, δ 174 {CO}. **5a**: ^1H, δ −7.42 {H, *J*(PH) 14.5, *J*(COH) 56.9 and 7, *J*(HH) −7}, −8.37 {H, *J*(PH) 162.0, *J*(COH) 5, *J*(HH) −7}; ^{31}P, δ −5.7; ^{13}C, δ 169.8 {CO, *J*(PC) 8}, 161.7 {CO, *J*(PC) 123}. **5b**: ^1H, δ −7.97 {H, *J*(PH) 17.4, *J*(COH) 45.5 and 6, *J*(HH) −5}, −16.51 {H, *J*(PH) 16.0, *J*(COH) 2.8, *J*(HH) −5}; ^{31}P, δ 5.2 {*J*(PC) 123.4}; ^{13}C, δ 170.8 {CO, *J*(PC) 8}, 166.1 {CO, *J*(PC) 123}. **5c**: ^1H, δ −8.09 {H, *J*(PH) 18.8, *J*(COH) 57.2 and 6}. **6a** (333 K): ^1H, δ −14.60 {H, *J*(PH) 11.6, *J*(COH) 5.2}; ^{31}P, δ −2.9 {*J*(PC) 7.9}; ^{13}C, δ 163.2 {CO}. **6b**: ^1H, δ −14.22 {H, td, *J*(PH) 12.3, *J*(COH) 5.0}, ^{31}P, δ −3.0 {P, PPh_3, *J*(PP) 456}, 55.7 {P, PPh_2Cl, *J*(PP) 456}, ^{13}C, δ 162.3 {CO}. **7a**: ^1H, δ −8.8 {H, *J*(PH) 136.9, *J*(HH) 2.7}, −9.7 {H, *J*(PH) 121.6, *J*(HH) −2.4}: δ_p 43.2.

1 C. R. Bowers and D. P. Weitekamp, *J. Am. Chem. Soc.*, 1987, **109**, 5541; R. Eisenberg, *Acc. Chem. Res.*, 1991, **24**, 110; J. Natterer and J. Bargon, *Prog. Nucl. Magn. Reson. Spectrosc.*, 1997, **31**, 293; C. J. Sleigh and S. B. Duckett. *Prog. Nucl. Magn. Reson. Spectrosc.*, 1999, **34**, 71.
2 S. B. Duckett, C. L. Newell and R. Eisenberg, *J. Am. Chem. Soc*., 1994, **116**, 10 548; S. B. Duckett and R. Eisenberg, *ibid*., 1993, **115**, 5292; S. B. Duckett, R. J. Mawby and M. G. Partridge, *Chem. Commun*., 1996, 383; P. D. Morran, S. A. Colebrooke, S. B. Duckett, J. A. B. Lohmann and R. Eisenberg, *J. Chem. Soc., Dalton. Trans*., 1998, 3363.
3 P. Hubler, R. Giernoth, G. Kummerle and J. Bargon, *J. Am. Chem. Soc*., 1999, **121**, 5311.
4 L. Vaska and M. F. Wernke, *Trans. N. Y. Acad. Sci*., 1971, **33**, 80; P. B. Chock and J. Halpern, *J. Am. Chem. Soc*., 1966, **88**, 3511; R. Ugo, A. Pasini and S. Cenini, *ibid*., 1972, **94**, 7364.
5 A. L. Sargent and M. B. Hall, *Inorg. Chem*., 1992, **31**, 317.
6 B. A. Messerle, C. J. Sleigh, M. G. Partridge and S. B. Duckett, *J. Chem. Soc., Dalton Trans*., 1999, 1429. C. J. Sleigh, S. B. Duckett, and B. A. Messerle, *Chem. Commun*., 1996, 2395; S. B. Duckett, C. L. Newell and R. Eisenberg, *J. Am. Chem. Soc*., 1993, **115**, 1156.
7 S. B. Duckett, G. K. Barlow, M. G. Partridge and B. A. Messerle, *J. Chem. Soc., Dalton Trans*., 1995, 3427.
8 R. A. Vanderpool and H. B. Abrahamson, *Inorg. Chem*., 1985, **24**, 2985.
9 S. K. Hasnip, S. B. Duckett, D. R. Taylor and M. J. Taylor, *Chem. Commun*., 1998, 923.

Communication 9/05590H

ChemComm

Intramolecular Michael addition of benzylamine to sugar derived α,β-unsaturated ester: a new diastereoselective synthesis of a higher homologue of 1-deoxy-L-*ido*-nojirimycin

Vijaya N. Desai, Nabendu N. Saha and Dilip D. Dhavale*

Department of Chemistry, Garware Research Centre, University of Pune, Pune - 411 007, India.
E-mail: ddd@chem.unipune.ernet.in

Received (in Cambridge, UK) 6th July 1999, Accepted 23rd July 1999

The diastereoselective intramolecular Michael addition of the benzylamine generated *in situ* from hemiacetal 3 leads to the lactone 4a with the required homoazasugar ring skeleton; reduction of the lactone functionality and removal of the protecting groups afford 1-deoxy-L-*ido*-homonojirimycin.

Naturally occurring polyhydroxylated piperidine alkaloids such as nojirimycin and mannonojirimycin are glycosidase inhibitors of great potential therapeutic value.[1] In order to examine the structure–activity relationship, a number of synthetic analogues of nojirimycin have been synthesised and evaluated for glycosidase inhibition in the treatment of various diseases such as diabetes, cancer, AIDS and viral infections. This includes synthesis of 6-deoxynojirimycin,[2a] 1-deoxynojirimycin,[2b] *N*-alkyl nojirimycin[2c] and *N*-linked disaccharide units.[2d] In recent years, preparation and evaluation of homoazasugars with a CH_2 homologation either at C-1 or in the C-5 side chain and nojirimycin with D and L sugar derivatives have received much attention.[3] As a part of our continuing efforts in the synthesis of nojirimycin analogues[4] we report herewith the synthesis of a one carbon higher (in the C-5 side chain) homologue of 1-deoxy-L-*ido*-nojirimycin **6**. We envisioned that the removal of the 1,2-*O*-isopropylidene in the D-glucose derived α,β unsaturated ester **2** (Scheme 1) followed by reductive amination at the anomeric carbon and concomitant intramolecular conjugate addition should lead to the homoazasugar ring skeleton. Reduction of the ester group and removal of the protecting groups should lead the target molecule. Although the intramolecular Michael addition of amines to α,β-unsaturated carbonyl compounds is widely utilized in the synthesis of polyhydroxylated pyrrolidenes and piperidine derivatives,[5] its application to the homoazasugars is highly restricted.[6]

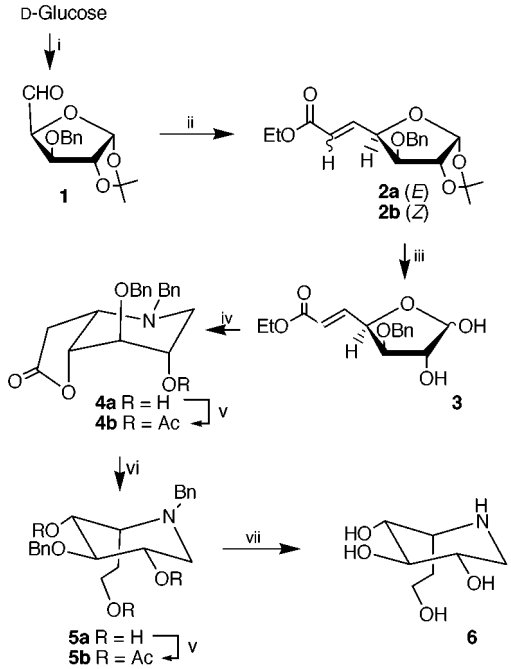

Scheme 1 *Reagents and conditions* i, ref 8; ii, PPh_3CHCO_2Et (1.3 equiv.), MeCN, reflux, 2 h; iii, TFA–H_2O (3:2), rt, 2 h; iv, $BnNH_2$ (1.0 equiv.), $NaCNBH_3$ (2.0 equiv.), AcOH (0.2 equiv.), MeOH, −78 °C, 2 h, rt, 24 h; v, Ac_2O, pyridine, DMAP, rt, 24 h; vi, LAH (3.0 equiv.), dry THF, 0 °C to rt, 2 h; vii, 10% Pd/C, HCO_2NH_4, MeOH, reflux, 1 h.

Our synthetic route involves **2** as the starting compound, which was prepared in high yield from D-glucose. Thus, the Wittig reaction[7] of α-D-*xylo*-pentodialdose[8] **1** with PPh_3CHCO_2Et gave an isomeric mixture of **2** (*E*:*Z* = 73:27) which was separated by chromatography to afford **2a** (*E*, 64%) and **2b** (*Z*, 24%). The cleavage of acetonide group in **2a** afforded hemiacetal **3** (anomeric mixture, α:β = 7:3) with an exclusively *E* geometry at the double bond.† The one pot reaction of **3** with $BnNH_2$ (1.0 equiv.) in the presence of catalytic amounts of AcOH in MeOH followed by treatment with $NaCNBH_3$ afforded a lactone **4a** as the only isolable product (Scheme 1). Thus, the overall three step transformation presumably involves amine as the primary reaction product which undergoes concomitant intramolecular Michael addition and domino[9] lactonisation to yield diastereoselective formation of **4a** in 79% yield. The lactone **4a** was acetylated with Ac_2O in pyridine to give **4b** (78%).‡ The spectroscopic and analytical data obtained for **4a** and **4b** were in full accord with the assigned structures.§ The configuration at C-5 and conformation of **4a** and **4b** were determined from their high field ^1H NMR spectra based on the coupling constant values. The initial geometry ensures that, in the product, the substituents at C-2, C-3 and C-3, C-4 should be *trans*. The low values of $J_{3,2}$ (~6.4 Hz) and $J_{3,4}$ (~4.3 Hz) indicate that the protons at these carbons are equatorial and the substituents are axial. This suggests that the bicyclic lactones have the $^1C_4$ conformation. The small value of $J_{5,4}$ (~5.3 Hz) along with the axial orientation of the C-4 hydroxy group suggests that the C-5 substituent is equatorial with the (5*S*) configuration. This confirms that the six membered piperidine ring is *cis* fused with the lactone ring.

The diastereoselective formation of **4a** can be explained by considering the transition states **A** and **B** (Fig. 1). In general, the stereoelectronic and steric factors often play an integral role in affecting the stereochemical outcome of the intramolecular Michael addition reactions.[10] However we believe that, under the reaction conditions of borohydride reductive amination and *in situ* Michael addition, the complexation of boron with nitrogen and the C-2 and C-4 hydroxy groups determines the

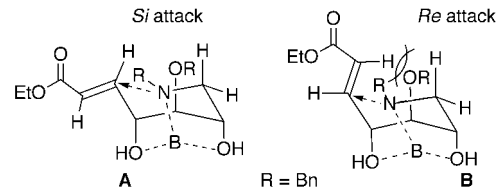

Fig. 1

amine addition.[5] Thus, the complexation of the boron with the C-2,4 hydroxy and amine groups holds the nitrogen atom in such a way that the preferred *Si* face attack at the diastereotopic β-carbon atom, as shown in transition state **A** (Fig. 1), leads to the formation of **4a**.¶ However, transition state **B** (Fig. 1), in which *Re* face attack leads to the formation of the other isomer, is destabilised due to the non-bonded interactions of the α-olefinic hydrogen with the C-1 axial hydrogen and C-3 *O*-benzyl group.

In the subsequent steps, lactone **4a** was reduced with LAH in Et_2O, and the primary alcohol **5a** (colorless solid, 84%) thus obtained was peracetylated to afford **5b** (80%).‖ In the ^{1}H NMR spectra of **5a** and **5b**, H-3 showed a double doublet with large coupling constants ($J_{2,3}$ and $J_{3,4}$ ~ 8.8 Hz).§ This indicated the axial–axial relationship of H-3 with H-2 and H-4, confirming the change in conformation of piperidine ring from $^1C_4$ to $^4C_1$. Finally, removal of the benzyl groups in **5a** was achieved in one step using HCO_2NH_4 and 10% Pd/C in MeOH to give 1-deoxy-L-*ido*-homonojirimycin **6** (90%). The ^{1}H and ^{13}C NMR spectra and analytical data are in agreement with the proposed structure with the $^4C_1$ conformation.§

In conclusion, the one pot reaction sequence of introduction of amine functionality and concomitant intramolecular conjugate addition to D-glucose derived α,β-unsaturated ester provides a unique strategy for the synthesis of homoazasugars. Easy availability of starting materials, mild reaction conditions, high diastereoselectivity and good yields make the route attractive and indicate that it could operate on a gram scale. Work is in progress to study the intermolecular Michael addition of amines to **2** and its applications to the synthesis of homoazasugars and indolizidine alkaloids.

We are thankful to AICTE, New Delhi, for the financial support, TIFR Bombay for high resolution NMR spectra and to UGC, New Delhi, for the JRF to V. N. D. We are grateful to Professor M. S. Wadia for helpful discussions.

Notes and references

† As indicated from the ^{1}H NMR spectrum, the cleavage of the acetonide group either in the isomeric mixture **2** or in **2b** (*Z*-isomer) with TFA–H_2O afforded hemiacetal **3** (α:β = 7:3) with exclusively *E* geometry. Acid catalysed $Z \rightarrow E$ isomerisation has been reported (ref. 11).

‡ Our attempts to isolate either the diastereomer or other products in pure form were unsuccessful. The ^{1}H NMR spectrum of the crude mixture indicated the presence of signals (< 10%) corresponding to an ethyl group. This could be the uncyclised open ester with (5*S*) configuration. Lactone **4a** was easily removed from the mixture by column chromatography followed by recrystallisation. The other diastereomer could not be detected even though the subsequent transformations were conducted without separation of **4a**. For example the direct acetylation of crude mixture of **4a** with Ac_2O and DMAP in pyridine gave **4b** as the only isolable product in 88% yield.

¶ This argument would be valid even if lactonisation precedes Michael addition.

‖ The direct reduction of crude mixture **4a** with LAH followed by peracetylation afforded **5b** in 68% yield.

§ *Selected data* for **4a**: white solid, mp 95 °C, $[\alpha]_D$ = +38.45 (*c* 0.5, $CHCl_3$); ν_{max}(Nujol)/cm^{-1} 3500–3300 (OH), 1770 (C=O); δ_H($CDCl_3$, 300 MHz) 2.33 (1H, dd, *J* 6.9, 11.9, 1_a-H), 2.42 (1H, dd, *J* 6.4, 16.7, 6_a-H), 2.53 (1H, brd, exchanges with D_2O, OH), 2.81 (1H, dd, *J* 6.0, 16.7, 6_e-H), 2.98 (1H, dd, *J* 2.9, 11.9, 1_e-H), 3.44 (1H, d, *J* 13.4, NC*H*$_2$Ph), 3.46 (1H, ddd, *J* 5.3, 6.0, 6.4, 5-H), 3.63 (1H, dd, *J* 4.3, 6.8, 3-H), 3.73 (1H, d, *J* 13.4, NC*H*$_2$Ph), 3.90 (1H, m, 2-H), 4.54 (1H, d, *J* 11.7, OC*H*$_2$Ph), 4.72 (1H, dd, *J* 4.3, 5.3, 4-H), 4.77 (1H, d, *J* 11.7, OC*H*$_2$Ph), 7.26–7.37 (10H, m, Ar-H); δ_C($CDCl_3$, 125 MHz) 31.6, 49.9, 58.2, 58.7, 66.5, 72.9, 76.1, 76.9, 127.6, 127.8, 127.9, 128.4, 128.5, 128.6, 136.7, 137.3, 175.2 (Calc). for $C_{21}H_{23}NO_4$: C, 71.37; H, 6.56. Found: C, 71.62; H, 6.77%). For **4b**: white solid, mp 89–90 °C; $[\alpha]_D$ +38.68 (*c* 0.4, $CHCl_3$); ν_{max}(Nujol)/cm^{-1} 1783 (C=O), 1742 (C=O); δ_H($CDCl_3$, 300 MHz) 2.01 (3H, s, C*H*$_3$), 2.48 (1H, dd, *J* 6.6, 16.8, 6_a-H), 2.62 (1H, dd, *J* 5.9, 12.5, 1_a-H), 2.65 (1H, dd, *J* 6.6, 16.8, 6_e-H), 2.80 (1H, dd, *J* 3.7, 12.5, 1_e-H), 3.43 (1H, d, *J* 14.0, NC*H*$_2$Ph), 3.58 (1H, q, *J* 6.6, 5-H), 3.74 (1H, dd, *J* 6.2, 6.9, 3-H), 3.78 (1H, d, *J* 14.0, NC*H*$_2$Ph), 4.52 (1H, dd, *J* 6.6, 6.9, 4-H), 4.68 (1H, d, *J* 11.7, OC*H*$_2$Ph), 4.76 (1H, d, *J* 11.7, OC*H*$_2$Ph), 4.93 (1H, m, 2-H), 7.24–7.37 (10H, m, Ar-H); δ_C($CDCl_3$, 125 MHz) 21.0, 31.0, 48.4, 57.4, 58.6, 69.4, 73.2, 75.7, 80.1, 127.7, 127.8, 128.0, 128.41, 128.5, 128.6, 137.0, 137.6, 170.3, 174.6 (Calc. for $C_{23}H_{25}NO_5$: C, 69.85; H, 6.37. Found: C, 69.72; H, 6.15%). For **5a**: white solid, mp 105–107 °C, $[\alpha]_D$ −3.66 (*c* 0.5, $CHCl_3$); ν_{max}(Nujol)/cm^{-1} 3500–3050, 3453, 3200 (OH); δ_H($CDCl_3$, 300 MHz) 1.87–1.92 (2H, m, 6-H), 2.20–2.55 (3H, br, exchanges with D_2O, OH), 2.68–2.77 (2H, m, 1-H), 3.10 (1H, ddd, *J* 6.11, 4.8, 5.9, 5-H), 3.49 (1H, t, *J* 8.8, 3-H), 3.65–3.70 (2H, m, 7-H, NC*H*$_2$Ph), 3.73–3.77 (1H, m, 7-H), 3.83 (1H, d, *J* 13.2, NC*H*$_2$Ph), 3.84–3.90 (1H, m, 2-H), 3.92 (1H, dd, *J* 4.8, 8.8, 4-H), 4.78 (1H, d, *J* 11.7, OC*H*$_2$Ph), 4.85 (1H, d, *J* 11.7, OC*H*$_2$Ph), 7.25–7.40 (10H, m, Ar-H); δ_C ($CDCl_3$, 125 MHz) 26.6, 50.7, 58.2, 61.2, 62.0, 69.1, 69.9, 74.4, 82.8, 127.4, 127.7, 127.9, 128.5, 128.6, 138.3, 138.5 (Calc. for $C_{21}H_{27}NO_4$: C, 70.56; H, 7.61. Found: C, 70.36; H, 7.89%). For **5b**: thick liquid; $[\alpha]_D$ −15.60 (*c* 0.35, $CHCl_3$); ν_{max}(neat)/cm^{-1} 1736 (C=O); δ_H($CDCl_3$, 300 MHz) 1.80–1.88 (2H, m, 6-H), 1.92 (3H, s, C*H*$_3$), 1.95 (3H, s, C*H*$_3$), 2.01 (3H, s, C*H*$_3$), 2.61 (1H, dd, *J* 10.6, 13.5, 1_a-H), 2.93 (1H, dd, *J* 5.5, 13.5, 1_e-H), 3.20–3.24 (1H, m, 5-H), 3.71 (1H, t, *J* 9.9, 3-H), 3.82 (1H, d, *J* 13.2, NCH_2Ph), 3.89 (1H, d, *J* 13.2, NCH_2Ph), 3.95–4.10 (2H, m, 7-H), 4.67 (2H, s, OCH_2Ph), 5.06–5.14 (1H, m, 2-H), 5.23 (1H, dd, *J* 5.5, 9.9, 4-H), 7.21–7.36 (10H, m, Ar-H); δ_C ($CDCl_3$, 125 MHz) 21.0(s), 23.7, 46.9, 55.0, 58.4, 62.2, 71.0, 71.8, 74.6, 78.6, 127.5, 128.4, 128.7, 138.5, 169.9(s), 171.0 (Calc. for $C_{27}H_{33}NO_7$: C, 67.06; H, 6.88. Found: C, 66.83; H, 6.84%. For **6**: foamy solid, mp 132–135 °C; $[\alpha]_D$ −13.85 (*c* 0.8, H_2O); ν_{max}(KBr)/cm^{-1} 3336, 3062, 1216, 1094; δ_H(D_2O, 300 MHz) 1.62–1.78 (2H, m, 6-H), 2.62 (1H, dd *J* 8.2, 13.6, 1_a-H), 2.88 (1H, dd *J* 4.2, 13.6, 1_e-H), 3.04–3.18 (1H, m, 5-H), 3.40–3.76 (5H, m, 2-H, 3-H, 4-H, 7-H); δ_C(D_2O, 125 MHz) 30.9, 46.7, 55.1, 62.1, 73.2, 74.5, 75.3 (Calc. for $C_7H_{15}NO_4$: C, 47.44; H, 8.53. Found: C, 47.25; H, 8.74%).

1 A. B. Hughes and A. J. Rudge, *Nat. Prod. Rep.*, 1994, **11**, 135; P. Sears and C.-H. Wong, *Chem. Commun.*, 1998, 1161;

2 (*a*) A. Defoin, H. Sarazin and J. Streith, *Helv. Chim. Acta*, 1996, **79**, 560 and references therein; (*b*) U. M. Lindstrom and P. Somfai, *Tetrahedron Lett.*, 1998, **39**, 7173; A. J. Rudge, I. Collins, A. B. Holmes and R. Baker, *Angew. Chem., Int. Ed. Engl.*, 1994, **33**, 2320; (*c*) C. R. R. Matos, R. S. C. Lopes and C. C. Lopes, *Synthesis*, 1999, 571; Y. Yoshikuni, *Agric. Biol. Chem.*, 1988, **52**, 121; (*d*) L. Sun, P. Li, N. Amankulor, W. Tang, D. W. Landry and K. Zhao, *J. Org. Chem.*, 1998, **63**, 6472.

3 Y. Suhara and K. Achiwa, *Chem. Pharm. Bull.*, 1995, **43**, 414; C. Herdeis and T. Schiffer, *Tetrahedron*, 1996, **52**, 14745; C.-H. Wong, L. Provencher, J. A. Porco Jr., S.-H. Jung, Y.-F. Wang, L. Chen, R. Wang and D. H. Steensma, *J. Org. Chem.*, 1995, **60**, 1492; A. Defoin, H. Sarazin and J. Streith, *Tetrahedron*, 1997, **53**, 13769; 1997, **53**, 13 783.

4 D. D. Dhavale, V. N. Desai, M. D. Sindkhedkar, R. S. Mali, C. Castellari and C. Trombini, *Tetrahedron: Asymmetry*, 1997, **8**, 1475; D. D. Dhavale, N. N. Saha and V. N. Desai, *J. Org. Chem.*, 1997, **62**, 7482.

5 S. Saito, S. Matsumoto, S. Sato, M. Inaba and T. Moriwake, *Heterocycles*, 1986, **24**, 2785; K. Shishido, Y. Sukegawa and K. Fukumoto, *J. Chem. Soc., Perkin Trans. 1*, 1987, 993; T. Wakabayashi and M. Saito, *Tetrahedron Lett.*, 1977, 93; C. Schneider and C. Borner, *Synlett*, 1998, 652; M. G. Banwell, C. T. Bui, H. T. T. Pham and G. W. Simpson, *J. Chem. Soc., Perkin Trans. 1*, 1996, 967; R. A. Bunce, C. J. Peeples and P. B. Jones, *J. Org. Chem.*, 1992, **57**, 1727; M. Hirama, T. Shigemoto, Y. Yamazaki and S. Ito, *J. Am. Chem. Soc.*, 1985, **107**, 1797.

6 F. Compernolle, G. Joly, K. Peeters, S. Toppet, G. Hoornaert, A. Kilonda and B. Bila, *Tetrahedron*, 1997, **53**, 12 739; A. Kilonda, F. Compernolle, S. Toppet and G. J. Hoornaert, *Tetrahedron Lett.*, 1994, **35**, 9047;

7 D. Tulshian, R. J. Doll, M. F. Stansberry and A. T. McPhail, *J. Org. Chem.*, 1991, **56**, 6819.

8 M. L. Wolfrom and S. Hanessian, *J. Org. Chem.*, 1962, **27**, 1800.

9 L. F. Tietze, *Chem. Rev.*, 1996, **96**, 115; L. F. Tietze and U. Beifuss, *Angew. Chem., Int. Ed. Engl.*, 1993, **32**, 131.

10 R. D. Little, M. R. Masjedizadeh, O. Wallquist and J. I. McLoughlin, *Org. React.*, 1995, **47**, 315.

11 *Stereochemistry of alkenes*, in *Stereochemistry of Organic Compounds*, ed. E. L. Eliel, S. H. Wilen and L. N. Mander, Wiley, New York, 1994, p. 579.

Communication 9/05440E

New synthesis of pyridoacridines based on an intramolecular aza-Diels–Alder reaction followed by an unprecedented rearrangement†

Juan M. Cuerva,‡ Diego J. Cárdenas and Antonio M. Echavarren*

Departamento de Química Orgánica, Universidad Autónoma de Madrid, Cantoblanco, 28049 Madrid, Spain. E-mail: anton.echavarren@uam.es

Received (in Liverpool, UK) 24th June 1999, Accepted 29th July 1999

The synthesis of pyridoacridines related to the ascididemins can be performed by an intramolecular aza-Diels–Alder cycloaddition of an α,β-unsaturated hydrazone to a quinone followed by an unprecedented rearrangement to yield benzo- or pyrido-[*b*]acridine-6,11-diones.

Pyridoacridine alkaloids of marine origin, such as amphimedine and the ascididemins (**1a**–**c**),[1] have attracted much attention due to their structural novelty and cytotoxic properties.[2,3] Strategies based on Diels–Alder azacycloadditions are amongst the most conceptually simple and potentially general approaches for the synthesis of these heterocycles.[2,4] However, the practical realisation of these schemes has been hampered by the lack of suitable reactivity of 4-substituted 1-azadienes towards 1,4-quinones.[4–6]

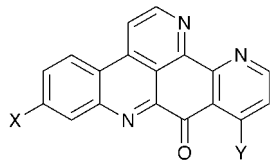

1a X = Y = H
b X = Br, Y = H
c X = H, Y = OH

Herein we report a new approach for the synthesis of heterocycles **2a**–**b**[7,8] related to the ascididemins (**1a**–**c**) based on an intramolecular aza-Diels–Alder reaction of 1-dimethylamino-1-azadienes[9] followed by an unprecedented rearrangement which occurs under oxidative conditions. The bond connectivity achieved between azadiene **3**[4] and 1,4-naphthoquinones **4a**,**b** in the cycloaddition–rearrangement is shown in Scheme 1. This scheme is formally equivalent to an intermolecular cycloaddition of diene **3** with the corresponding 1,2-naphthoquinones.

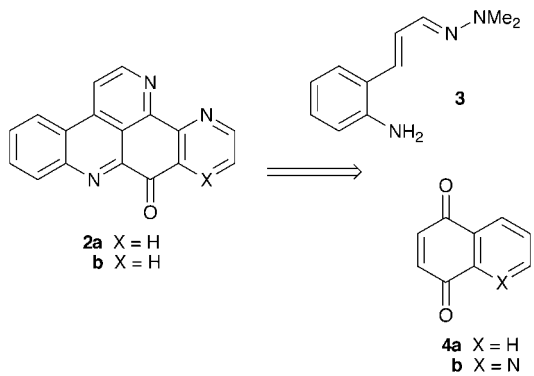

2a X = H
b X = H

3

4a X = H
b X = N

Scheme 1

† Dedicated to Professor José Elguero on the occasion of his 65th birthday.

‡ Current address: Departamento de Química Orgánica, Facultad de Química, Universidad de Granada, Spain.

The intramolecular cycloaddition of **5a**–**c** was examined as part of a projected synthesis of the alkaloid meridine[1c,10] and related compounds (Scheme 2). These aminoquinones were readily available by the addition of the aniline **3**[3] to **4a** or **4b** in MeOH at 23 °C the presence of $CeCl_3 \cdot 7H_2O$ (0.1 equiv) (70% for **4a**, 48% for **4b**).[11] On the other hand, a hydroxy group in the position 4 of quinolinequinone directs the nucleophilic attack of aniline derivatives allowing the synthesis of adducts **5d**–**e** with the opposite regioselectivity.[12]

After much experimentation, the desired cycloadditions were realised by trifluoroacetylation of the amines of **5a**,**b** (NaH, TFAA, 3 equiv. each, THF, 23 °C) followed by replacement of THF by CH_2Cl_2 and addition of excess TFA (23 °C, 1 h) to furnish quinones **6a** (45%) and **6b** (47%),[13] respectively. Under these conditions, the intermediate cycloadducts, which could not be isolated, suffer elimination of the trifluoroacetamides to form the quinone chromophores.

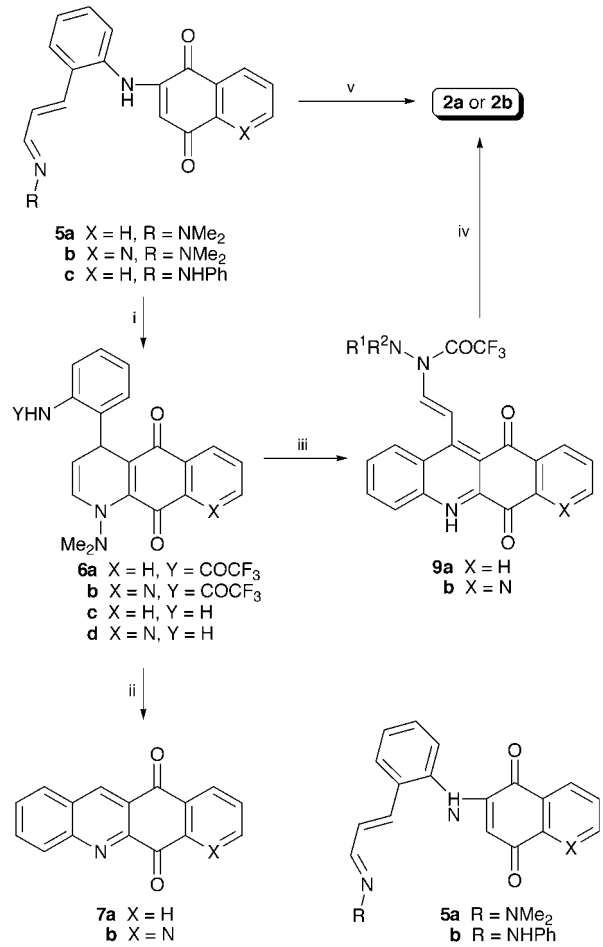

5a X = H, R = NMe_2
b X = N, R = NMe_2
c X = H, R = NHPh

6a X = H, Y = $COCF_3$
b X = N, Y = $COCF_3$
c X = H, Y = H
d X = N, Y = H

9a X = H
b X = N

7a X = H
b X = N

5a R = NMe_2
b R = NHPh

Scheme 2

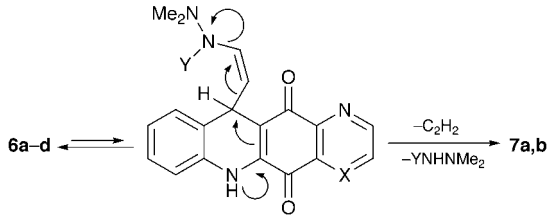

Scheme 3

Much to our surprise, **6a** was cleanly transformed into tetracycle **7a**[14] by heating with acid (1:1 10% aq HCl–1,4-dioxane, reflux; 94%). Quinone **7a** could also be obtained directly from **5a** by thermolysis (xylene, reflux; 55%) or by treatment with TFA (23 °C; 68%).[15] Under these latter conditions, heterocyclic quinone **7b** was similarly obtained from **5b** (66%).[13] Scheme 3 suggests a possible mechanism for these remarkable transformations in which the dimethylhydrazine and two carbons are lost under relatively mild conditions. Accordingly, a 6-*endo-trig* cyclization of the trifluoroacetamide (from **6a**,**b**) or the amine (*via* **6c**,**d** formed *in situ* from **5a**,**b**) onto the quinone double bond with concomitant (or subsequent) transacylation would lead to intermediates **8**, which may undergo aromatization to form a pyridine ring by a Grob-type fragmentation to give acetylene and the hydrazine derivative. The first step of this process, nucleophilic addition–elimination on a quinone, is somewhat reminiscent of the so-called mitomycin rearrangement.[16]

According to the hypothetical equilibrium of Scheme 3, oxidation of intermediate **8** could yield a precursor of tetracycles related to the ascididemins (**1**). In the event, treatment of **6a**,**b** with excess MnO_2 in CH_2Cl_2 at 23 °C smoothly led to tetracycles **9a**,**b** in quantitative yield as single isomers. The rearrangement also takes place in the presence of DDQ or CAN as the oxidants. A *trans* configuration was assigned for the alkenyl portion of these derivatives on the basis of a vicinal coupling constant of 15.5 Hz. However, the configuration around the enamine nitrogen was not rigorously assigned. Reaction of **9a**,**b** with NH_4Cl and NaOAc in EtOH under refluxing conditions gave pentacyclic **2a**[4] (93%) and **2b** (84%).[13] After examining several hydrazone and oxime derivatives,[17] we found that thermolysis of phenylhydrazone **5c** directly furnished **2a** (refluxing xylene, 40%), probably through intermediate **10a**. In fact, related tetracyclic derivative **10b** could be isolated in 54% yield by thermolysis of **5b** in xylene.

In summary, a highly concise synthesis of heterocycles **2a**,**b** has been developed based on an intramolecular aza-Diels–Alder cycloaddition followed by a novel rearrangement in which the aminoaryl formally undergoes a 1,2-shift.

This work was supported by the DGES (Project PB97-0002-C2-02). We acknowledge the Instituto Biomar, S.A., for the data in ref. 3.

Notes and references

1 Isolation: (*a*) Ascididemin: J. Kobayashi, J. Cheng, H. Nakamura, Y. Ohizumi, Y. Hirata, T. Sasaki, T. Ohta and S. Nozoe, *Tetrahedron Lett.*, 1988, **29**, 1177; (*b*) 2-bromoascididemin (2-bromoleptoclidinininone): J. J. Bloor and F. J. Schmitz, *J. Am. Chem. Soc.* 1987, **109**, 6134; 11-Hidroxyascididemin (*c*): F. Schmitz, F. S. DeGuzman, M. B. Hossain and D. van der Helm, *J. Org. Chem.*, 1991, **56**, 804.

2 Reviews: T. F. Molinski, *Chem. Rev.*, 1993, **93**, 1825; B. S. Davidson, *Chem. Rev.* 1993, **93**, 1771; A. M. Echavarren, in *Advances in Nitrogen Heterocycles*, ed. C. J. Moody, JAI Press, Greenwich, 1996, vol. 2. ch. 5.

3 Indeed, we have found that analogue **2b** is highly cytotoxic *in vitro* to mouse lymphoma (P-388), human lung carcinoma (A-549), human colon carcinoma (HT-29), and human melanoma (MEL-28) (IC_{50} values of 0.01, 0.0012, 0.005 and 0.0025 μg ml^{-1}, respectively).

4 A. M. Echavarren, *J. Org. Chem.*, 1990, **55**, 4255.

5 J. M. Cuerva and A. M. Echavarren, *Synlett*, 1997, 173; M. C. Carreño, J. M. Cuerva, Ribagorda and A. M. Echavarren, *Angew. Chem., Int. Ed.*, 1999, **38**, 1449.

6 The first step of a synthesis of the alkaloid meridine is a Diels–Alder cycloaddition of the nitro analogue of **3** which proceeds in low yield (6%): Y. Kitahara, F. Tamura and A. Kubo, *Chem. Pharm. Bull.* 1994, **42**, 1363; S. Nakahara, Y. Tanaka and A. Kubo, *Heterocycles*, 1996, **43**, 2113; a similar reaction was used for the synthesis of cistodamine: Y. Kitahara, F. Tamura and A. Kubo, *Tetrahedron Lett.* 1997, **38**, 4441. Alternative synthesis of aromatized adducts: P. Molina, A. Pastor and M. Villaplana, *Tetrahedron* 1995, **51**, 1265.

7 Previous synthesis of **2a**: J. R. Peterson, J. K. Zjawiony, S. Liu, C. D. Hupfford, A. M. Clark and R. D. Rogers, *J. Med. Chem.*, 1992, **35**, 4069.

8 Synthesis of another regioisomer of **1a** and **2b**: E. Gómez-Bengoa and A. M. Echavarren, *J. Org. Chem.*, 1991, **56**, 3497.

9 Intramolecular cycloaddition of 1-dimethylamino-1-azadienes: N. Bushby, C. J. Moody, D. A. Riddick and I. R. Waldron, *Chem. Commun.*, 1999, 793; R. E. Dolle, W. P. Armstrong, A. N. Shaw and R. Novelli, *Tetrahedron Lett.*, 1988, **29**, 6349.

10 P. J. McCarthy, T. P. Pitts, G. P. Gunawardana, M. Kelly-Borges and S. A. Pomponi, *J. Nat. Prod.*, 1992, **55**, 1664.

11 Hydrazones **5c**–**e** were obtained in three steps by: (i) reaction of the quinolinequinone with *o*-aminocinnamol ($CeCl_3 \cdot 7H_2O$, MeOH, 23 °C); (ii) oxidation of the allyl alcohol to the aldehyde with PCC or MnO_2; (iii) condensation of the aldehyde with the hydrazine.

12 By using the reaction pathway outlined in Scheme 2, adducts **5d**–**e** could be converted into 11-hydroxyascididemin (**1c**).

13 Yield based on unrecovered starting material.

14 A. Ettienne and A. Staehelin, *Bull. Soc. Chim. Fr.*, 1954, 748; V. Zanker and F. Mader, *Chem. Ber.*, 1960, **93**, 850. 2-Chloro derivative: M. Prato, G. Scorrano, M. Stivanello, P. Tecilla and V. Lucchini, *Gazz. Chim. Ital.*, 1987, **117**, 325.

15 Quinone **5a** was quantitatively converted into **7a** and *N*,*N*-dimethylhydrazine at 50–55 °C (3:1 benzene-d_6–TFA-*d* solution, sealed NMR tube). In addition, a small signal at 1.8 ppm attributable to dissolved acetylene was also observed.

16 M. Kono, Y. Saitoh, K. Shirahata, Y. Arai and S. Ishii, *J. Am. Chem. Soc.*, 1987, **109**, 7224; T. Fukuyama and L. Yang, *J. Am. Chem. Soc.*, 1987, **109**, 7881; T. Fukuyama and L. Yang, *J. Am. Chem. Soc.*, 1989, **111**, 8303.

17 The methoxime and diphenylhydrazone analogues of **5a** afforded **7a** after being treated with TFA.

Communication 9/05234H

Anthracene-linked calix[4]pyrroles: fluorescent chemosensors for anions

Hidekazu Miyaji,[a] Pavel Anzenbacher Jr,[a] Jonathan L. Sessler,*[a] Ellen R. Bleasdale[b] and Philip A. Gale*[b]†

[a] *Department of Chemistry and Biochemistry, The University of Texas at Austin, Austin, Texas 78712-1167, USA*
[b] *Department of Chemistry, University of Oxford, Inorganic Chemistry Laboratory, South Parks Road, Oxford, UK OX1 3QR*

Received (in Cambridge, UK) 24th June 1999, Accepted 27th July 1999

Fluorescent anthracene–calix[4]pyrrole conjugates 2, 4 and 5 have been synthesized; these receptors can detect the presence of anions (*e.g.* F^-, Cl^-, $H_2PO_4^-$) by a significant quenching of their fluorescence.

The selective detection of guest species by redox[1] or photoactive[2] host molecules is a challenging area of supramolecular chemistry that has attracted increasing interest in the last few years. In spite of this, optical sensors for anions are still relatively rare.[3–7] We have recently discovered that calix[4]pyrroles, a class of molecule known for over a century, are effective anion binding agents in solution and in the solid state.[8–10] Our first attempt at using the calixpyrrole moiety as a sensor involved attaching redox active ferrocene moieties to the calixpyrrole skeleton *via* amide linkages and studying perturbations in the ferrocene/ferrocenium redox couple on addition of anionic guests.[11] Substantial changes occurred in the electrochemical properties of these materials but these changes were unpredictable and difficult to rationalize. We therefore decided to investigate whether calix[4]pyrrole, when combined with a fluorescent reporter group, would act as an optical sensor for anions. Here we report the synthesis a series of compounds **2**, **4** and **5** that contain a calix[4]pyrrole anion binding site linked to a fluorescent anthracene moiety.

In order to minimise the distance between the anion binding site and the fluorophore (and also provide a conjugated bond pathway between them), a new calix[4]pyrrole-monoacid precursor **1** was prepared using a modification of the procedure used previously to prepare a homologous calix[4]pyrrole ester derivative.[12] Specifically, *meso*-octamethylcalix[4]pyrrole[13] was dissolved with stirring in dry THF under an argon atmosphere, and the flask cooled to −78 °C. A solution of BuLi in hexanes (4.0 equiv.) was added dropwise to the calix[4]pyrrole solution and, after 30 min, solid CO_2 was added. The reaction was stirred for a further 3 h at −78 °C and then allowed to warm to room temperature. The solvent was removed and the residue was suspended in water. The suspension was filtered to remove unreacted *meso*-octamethylcalix[4]pyrrole and the solution was acidified with perchloric acid, whereupon calix[4]pyrrole acid **1** precipitated out as a white powder. Recrystallisation from acetone–water by slow evaporation produced colourless crystals of the mono-acid **1** in 6.8% yield. The anthracene-linked calix[4]pyrrole **2** was prepared by activation of calix[4]pyrrole acid **1** with DCC and hydroxybenzotriazole hydrate (HOBt) in DMF followed by treatment with commercially available 1-aminoanthracene. Purification by column chromatography afforded compound **2** in 34% yield (Scheme 1).

Compound **4** was prepared by coupling calixpyrrole monoacid **3**[12,14] with 1 equiv. of 1-aminoanthracene using the benzotriazol-1-yloxytris(dimethylamino)phosphonium hexafluorophosphate (BOP) amide coupling reagent (1.1 equiv.) in DMF in the presence of excess Et_3N. After removal of DMF, the calixpyrrole–anthracene conjugate **4** was isolated as a yellow foam by column chromatography in 63% yield. Compound **5** was prepared in an analogous manner by coupling compound **3** with 9-aminomethylanthracene.[15] Compound **5** was isolated by column chromatography as a yellow foam in 51% yield.

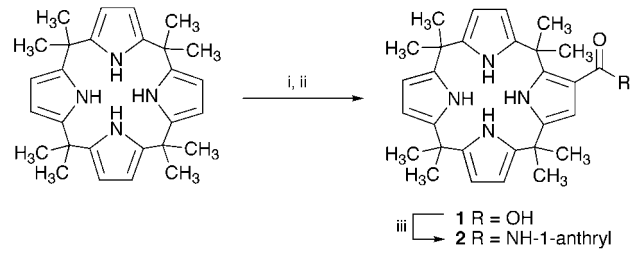

Scheme 1 *Reagents and conditions*: i, BuLi (4 equiv.), THF; ii, CO_2; iii, 1-aminoanthracene, DCC, HOBt, DMF.

Initial complexation studies were conducted using ^{1}H NMR titration techniques. Aliquots of the tetrabutylammonium salts of the putative anionic guests (0.1 mol dm^{-3}) were added to a solution of compound **2**, **4** or **5** (0.01 mol dm^{-3}) in CD_3CN and the shift of the calix[4]pyrrole NH proton noted after each addition. Significant downfield shifts of the pyrrole NH protons were observed upon addition of anions, consistent with the formation of calixpyrrole–anion hydrogen bonds. In the presence of fluoride anions, the NMR spectrum broadened considerably, making a determination of the stability constant impossible by this method. However, analysis of the remaining titration data using the EQNMR[16] computer program revealed that the compounds form 1 : 1 receptor:anion complexes with chloride, dihydrogen phosphate and bromide anions. The resulting stability constants are shown in Table 1.

Fluorescence quenching experiments were carried out by addition of solutions of anions (tetrabutylammonium fluoride, chloride, bromide, dihydrogenphosphate or hydrogensulfate) to

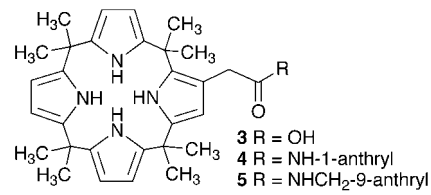

Table 1 Stability constants of compounds **2**, **4** and **5** with various anions in the form of tetrabutylammonium salts determined by ^{1}H NMR titration in CD_3CN; errors < 15%

	log *K* in CD_3CN		
Anion	**2**	**4**	**5**
F^-	[a]	[a]	[a]
Cl^-	> 4	> 4	> 4
Br^-	3.59	3.00	2.63
$H_2PO_4^-$	> 4[b]	3.50	3.08
HSO_4^-	2.77	[c]	[c]

[a] NH resonance broadened precluding a determination of this value using NMR spectroscopic methods. [b] Stability constant determined by following pyrrole CH resonance. [c] Weak interaction $K < 20$ M^{-1}.

† Present address: Department of Chemistry, University of Southampton, Southampton, UK SO17 1BJ. E-mail: philip.gale@soton.ac.uk

Table 2 Stability constants for compounds **2**, **4** and **5** with various anions (as tetrabutylammonium salts) in CH_3CN and CH_2Cl_2 as determined from fluorescence quenching analyses at 25 °C. Compound **2** excited at 378 nm, emission λ_{max} at 446 nm, compound **4** excited at 393 nm, emission λ_{max} at 429 nm and compound **5** excited at 387 nm, emission λ_{max} at 418 nm. Errors are estimated to be < 15%

	log *K* in CH_2Cl_2			log *K* in CH_3CN		
Anion	**2**	**4**	**5**	**2**	**4**	**5**
F^-	4.94	4.52	4.49	5.17	4.69	4.69
Cl^-	3.69	2.96	2.79	4.87	3.81	3.71
Br^-	3.01	[a]	[a]	3.98	2.86	[a]
$H_2PO_4^-$	4.20	3.56	[a]	4.96	3.90	[a]

[a] Quenching insufficient to provide an accurate stability constant value.

50 μM solutions of compounds **2**, **4** and **5** in CH_2Cl_2 or CH_3CN. Excitation and λ_{max} (emission) values for the three compounds are given in the footnote to Table 2. Significant fluorescence quenching was observed upon addition of tetrabutylammonium fluoride to compounds **2**, **4** and **5**. For example, the fluorescence spectra of compound **2** obtained as a function of added fluoride anion are shown in Fig. 1.

Quenching was also observed in varying degrees upon addition of other anions to receptors **2**, **4** and **5**. This is illustrated in Fig. 2(*a*) which shows the effects of different anions on the fluorescence of compound **2** in CH_2Cl_2. In this instance it can be seen that, on a per molar basis, the addition of fluoride anion causes the greatest fluorescence quenching, followed by the addition of dihydrogenphosphate and chloride anions. Using these quenching data and standard Scott plot analyses,[17] association constants were calculated for receptors **2**, **4** and **5** interacting with fluoride, chloride, bromide and dihydrogenphosphate anions (Table 2). In general, good agreement was observed between these K_a values and those obtained using NMR analyses. However, several of the flourescence-derived plots exhibited biphasic behaviour. This

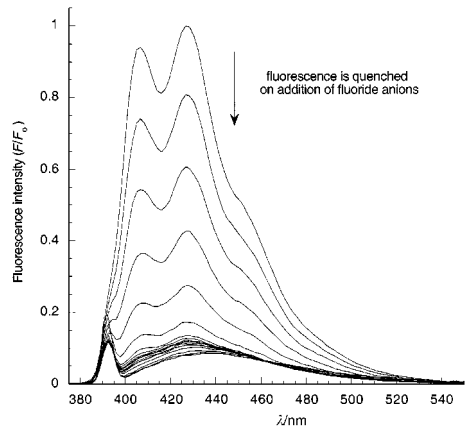

Fig. 1 Fluorescence spectra of calixpyrrole **2** in CH_2Cl_2 (0.05 mM) excited at 378 nm showing the changes induced upon the addition of increasing quantities of tetrabutylammonium fluoride.

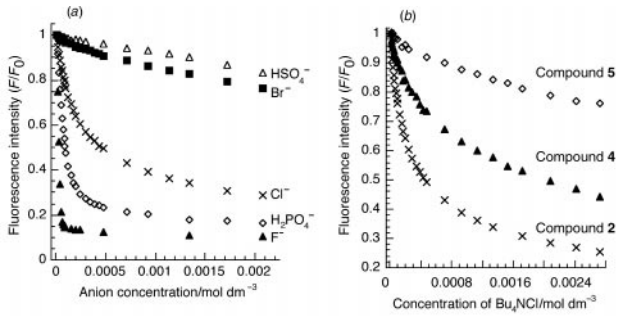

Fig. 2 (*a*) The quenching effect of various anions on compound **2** and (*b*) the fluorescence quenching effect of chloride anions on compounds **2**, **4** and **5**.

may be due to aggregation of the anthracene moieties, coordination of the anion to the amide moiety,[11] oligomerisation of dihydrogenphosphate anions[18] or heavy atom effects,[2] and is currently the topic of further investigation.

Control experiments were carried out with anthracene. At an anthracene concentration of 50 μM in CH_2Cl_2, there was no significant fluorescence quenching observed on addition of fluoride and chloride anions. On the other hand it was found that bromide and iodide acted to quench fluorescence in concentrations between 100 to 1000 mM (presumably due to the heavy atom effect).[2] No significant quenching was observed on addition of dihydrogenphosphate or hydrogensulfate anions to these control anthracene solutions.

A comparison of the quenching caused by chloride at the respective λ_{max} (emission) is shown for each of receptors **2**, **4** and **5** in Fig. 2(*b*). It can be clearly seen that chloride quenches the fluorescence of compound **2** most efficiently and compound **5** least efficiently. This trend may be related to the structure of the receptors and to their affinity for anions. The stability constants of the receptors with chloride follow the trend **2** > **4** > **5** (*cf.* Table 2). Further, the distance between the anthracene fluorophore and the anion-binding site increases in the order **2** < **4** < **5**. Finally, compound **2** has a conjugated bond pathway linking the fluorophore and anion-binding site of the calixpyrrole providing an electronic communication pathway between them, whereas compounds **4** and **5** do not. It might therefore be expected that fluorescence quenching is most efficient in compound **2** and least efficient in compound **5**.

In summary, a series of calixpyrrole–anthracene conjugate compounds have been synthesized that possess conjugated (compound **2**) and unconjugated bond pathways of different lengths (compounds **4** and **5**) between the calix[4]pyrrole anion binding site and the anthracene reporter group. The fluorescence of these receptors is quenched significantly in the presence of certain anionic guests. Compounds **2**, **4** and **5** thus represent prototypical calix[4]pyrrole based-fluorescent anion sensing agents.

This work was supported by the National Institutes of Health (Grant GM58907 to J. L. S.), the Texas Advanced Research Program (Grant No.3658 to J. L. S.) and by a Royal Society University Research Fellowship to P. A. G.

Notes and references

1 P. D. Beer, P. A. Gale and Z. Chen, *J. Chem. Soc., Dalton Trans.*, 1999, 1897.
2 A. P. de Silva, H. Q. N. Gunaratne, T. Gunnlaugsson, A. J. M. Huxley, C. P. McCoy, J. T. Rademacher and T. E. Rice, *Chem. Rev.*, 1997, **97**, 1515 and references cited therein.
3 A.W. Czarnik, *Acc. Chem. Res.*, 1994, **27**, 302.
4 R. S. Dickens, T. Gunnlaugsson, D. Parker and R. D. Peacock, *Chem. Commun*., 1998, 1643.
5 L. Fabbrizzi, I. Faravelli, G. Francese, M. Licchelli, A. Perotti and A. Taglietti, *Chem. Commun.*, 1998, 971.
6 P. D. Beer, *Chem. Commun.*, 1996, 689 and references cited therein.
7 A. Metzger and E. V. Anslyn, *Angew. Chem., Int. Ed.*, 1998, **37**, 649.
8 P. A. Gale, J. L. Sessler, V. Král and V. Lynch, *J. Am. Chem. Soc.*, 1996, **118**, 5140.
9 P. A. Gale, J. L. Sessler and V. Král, *Chem. Commun.*, 1998, 1.
10 J. L. Sessler, A. Andrievsky, P. A. Gale and V. Lynch, *Angew. Chem., Int. Ed. Engl.*, 1996, **35**, 2782.
11 J. L. Sessler, A. Gebauer and P. A. Gale, *Gazz. Chim. Ital.*, 1997, **127**, 723.
12 P. A. Gale, J. L. Sessler, W. E. Allen, N. A. Tvermoes and V. Lynch, *Chem. Commun*., 1997, 665.
13 A. Baeyer, *Ber. Dtsch. Chem. Ges.*, 1886, **19**, 2184.
14 J. L. Sessler, P. A. Gale and J. W. Genge, *Chem. Eur. J.*, 1998, **4**, 1095.
15 H. Weizman, O. Ardon, B. Mester, J. Libman, O. Dwir, Y. Hadar, Y. Chen and A. Shanzer, *J. Am. Chem. Soc.*, 1996, **118**, 12368.
16 M. J. Hynes, *J. Chem. Soc., Dalton Trans.*, 1993, 311.
17 K. A. Connors, *Binding Constants: the measurement of molecular complex stability*, Wiley, New York, 1987.
18 F. Chu, L. S. Flatt and E. V. Anslyn, *J. Am. Chem. Soc.*, 1994, **116**, 4194; V. Jubian, A. Veronese, R. P. Dixon and A. D. Hamilton, *Angew. Chem., Int. Ed. Engl.*, 1995, **34**, 1237.

Communication 9/05054J

New synthesis of a useful C3 chiral building block by a heterogeneous method: enantioselective hydrogenation of pyruvaldehyde dimethyl acetal over cinchona modified Pt/Al_2O_3 catalysts

Béla Török,[a] Károly Felföldi,[b] Katalin Balázsik[a] and Mihály Bartók[ab]

[a] *Organic Catalysis Research Group of the Hungarian Academy of Sciences, József Attila University, H-6720 Szeged, Dómtér 8, Hungary. E-mail: bartok@chem.u.szeged.hu*

[b] *Department of Organic Chemistry József Attila University, H-6720 Szeged, Dómtér 8, Hungary. E-mail: bartok@chem.u.szeged.hu*

Received (in Cambridge, UK) 14th June 1999, Accepted 20th July 1999

The first satisfactory application of the heterogeneous cinchona-modified Pt catalyst system for the synthesis of a C3 chiral building, namely, the highly enantioselective (up to 96.5% ee) hydrogenation of pyruvaldehyde dimethyl acetal to lactaldehyde dimethyl acetal is described.

The increasing use of chiral compounds has raised the profile of asymmetric synthesis, in particular the environmentally more friendly heterogeneous enantioselective hydrogenations.[1] One of them, the cinchona alkaloid-modified platinum catalyst system, was found to be effective in the hydrogenation of α-keto esters and keto acids.[1] The chiral hydrogenation of ethyl pyruvate provides excellent (up to 97% ee) enantioselectivity using presonicated cinchonidine–Pt/Al_2O_3 catalysts under mild hydrogen pressure.[2] In recent years new substrates have also been studied such as unsaturated carboxylic acids,[3–5] ketoamides,[6] pyruvic acid oxime,[7] ethyl nicotinate[8] and trifluoromethyl ketones.[9] Unfortunately, the optical yields in these latter cases are far from excellent.

The major thrust of our work was to widen the type of substrates in the Pt–cinchona catalyzed hydrogenations. Here, we report a new successful enantioselective ketone hydrogenation over cinchona-modified Pt/Al_2O_3 catalyst, namely, the asymmetric hydrogenation of pyruvaldehyde dimethyl acetal. This compound is a very frequently used synthon equivalent in synthetic organic chemistry for the preparation of chiral *O*-protected α-hydroxy aldehydes.[10] The enantioselective hydrogenation of the target compound and its further transformation to a valuable synthon are shown in Scheme 1.

Pyruvaldehyde dimethyl acetal itself has already been reduced to the corresponding hydroxy derivatives by rhodium complexes,[11] boranes[12] or by enzymatic methods.[13] Although each method is satisfactory, in cost or simplicity they cannot be compared to the cinchona modified Pt-catalyzed hydrogenations.

In this study two Pt/Al_2O_3 catalysts (Engelhard 4759 and 40655) were used while the modifiers [cinchonidine (CD) and cinchonine (CN)] and the substrate [Pyruvaldehyde dimethyl acetal (PDA)] were all Fluka products. The hydrogenations were performed in an atmospheric batch reactor or in a Berghof Bar 45 autoclave at 20 °C as described previously.[2] Product identification was carried out by GC-MS (HP5890 GC-HP5970MSD) and ^{1}H NMR spectroscopy (Bruker AM400), while the enantiomeric excesses (ee (%) = ($|[R] - [S]|$) × 100/($[R] + [S]$)] were monitored by chiral gas chromatography (HP 5890 GC-FID, 30 m long Lipodex-A capillary column). The ee values were reproducible to within 1%.

According to our recent observations[2] two catalysts, the well-known reference catalyst E4759 and a second 5% Pt/Al_2O_3 catalyst (E40655), which was highly efficient in the enantioselective hydrogenation of ethyl pyruvate, were tested in the hydrogenation of PDA. Taking into account the fact that in the literature many solvents have been applied, some common solvents were tested in an atmospheric system to find the most suitable medium for the hydrogenation of PDA. Although in toluene or EtOH the enantioselectivity is only moderate (up to 66% with CD and 25% with CN), using AcOH as solvent the results are comparable to those obtained with ethyl pyruvate[1,2] using both modifiers. The results obtained in AcOH including reaction rates and optical yields are summarized in Table 1.

Since the ethyl pyruvate hydrogenation produces higher optical yields under elevated hydrogen pressures the effect of hydrogen pressure on the present system was also studied. The optical yields obtained in different solvents are plotted as a function of the hydrogen pressure in Fig. 1.

According to the ee data the enantioselectivity seems to be strongly solvent dependent. It was found that the application of

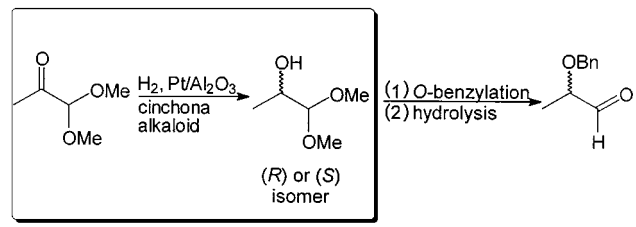

Scheme 1

Table 1 Enantioselective hydrogenation of pyruvaldehyde dimethyl acetal over 5% Pt/Al_2O_3 catalysts (E4759, E40655) under 1 bar hydrogen pressure and at 20 °C in AcOH

Entry	Substrate/ml	Catalyst	Modifier[a]	Rate/mol g^{-1} min^{-1}	Configuration	Ee (%)
1	0.27	E4759	CD	0.79	*R*	93.2[b]
2	0.27	E4759	CN	0.61	*S*	88
3	0.27	E40655	CD	0.81	*R*	96.5[b]
4	0.27	E40655	CN	0.72	*S*	88
5	1.35	E40655	CD	0.77	*R*	93
6	2.70	E40655	CD	0.75	*R*	93
7	0.27	E4759	—	0.20	racemic	0

[a] CD = cinchonidine, CN = cinchonine. [b] Average of three experiments.

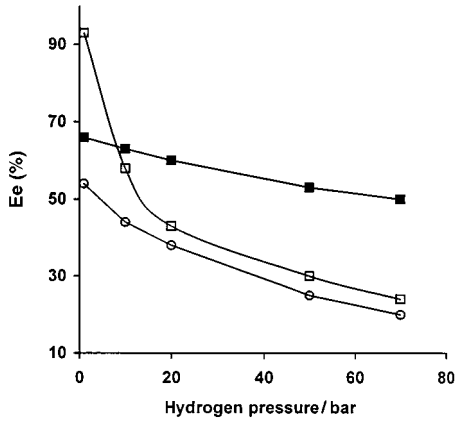

Fig. 1 Enantiomeric excess *vs.* hydrogen pressure for the enantioselective hydrogenation of pyruvaldehyde dimethyl acetal over a 5% Pt/Al_2O_3 (E4759)–cinchonidine catalyst system in different solvents at 20 °C: (□) AcOH, (■) EtOH and (○) toluene.

both CD and CN provides the best optical yields in AcOH at low hydrogen pressures. In our opinion this significant solvent dependence is a result of the weaker adsorption of PDA in the case of toluene (6π electrons *versus* 2π electrons), while using EtOH the substrate can form a semi-acetal with the solvent as pointed out for ethyl pyruvate.[1] As the data show, the increase in hydrogen pressure resulted in monotonically decreasing enantioselectivities in each solvent. However, this decrease is more pronounced in AcOH and toluene than in EtOH, for which only a slight decrease was observed.

Although E4759 provided excellent results [93% for the (*R*)-isomer], however, the other catalyst (E40655) produced even higher enantioselectivity; the highest ee obtained is 96.5% for the (*R*)-isomer. The (*S*)-isomer can be prepared in 88% optical purity in the presence of the E4759 catalyst. In this way, both enantiomers can be prepared in excellent optical purity, and no further optimization is needed. Although this work is basically of an experimental nature, the kinetic data indicate that the mechanism is most likely similar to that proposed in the case of ethyl pyruvate. The modified reactions all take place at higher rates than the nonmodified one (Table 1, compare all entries to entry 7), indicating a ligand accelerated mechanism. As a result, the highest enantioselectivity was obtained at the highest reaction rate (entry 3), however, explaining the roles of geometrical and electronic factors is not possible at this level of the study.

It should be mentioned that the above listed results were obtained on a microscale level. Taking into account the potential of the optically active product the scale up the reaction was also studied in order to isolate the hydroxy acetal. The results of the scale up experiments are also shown in Table 1 (compare entries 3, 5 and 6). After the hydrogenation was complete (see entry 6), the product mixture was poured into NaOH solution and the hydroxy acetal was extracted with Et_2O. After solvent evaporation, 2.1 g (78% yield) of the (*R*)-product was isolated. Further purification by distillation resulted in a product of 99.9% chemical (GC) and 93% optical purity [(*R*)-enantiomer]. The (*S*)-isomer can also be isolated in the same way.

The present study provides the first experimental proof that species other than α-keto acids and α-keto esters (including the cyclic ketopantolactone) can be hydrogenated with excellent optical yields over cinchona-modified platinum catalysts. Since the synthetic importance of chiral hydroxy aldehydes as useful chiral building blocks is well-known this new, environmentally friendly method for their preparation may even widen their applications.

In conclusion, the cinchona-modified Pt/Al_2O_3 catalytic system was found to be effective in the enantioselective hydrogenation of a 2-keto aldehyde derivative, providing the opportunity to still widen the practical applications and potential of this unique and important catalytic system.

Financial support (AKP97-4 2,4) is highly appreciated.

Notes and references

1 A. Baiker and H.-U. Blaser, in *Handbook of Heterogeneous Catalysis*, ed. G. Erlt, H. Knözinger and J. Weitkamp, Wiley-VCH, New York, 1997, vol. 5, p. 2422.
2 B. Török, K. Felföldi, G. Szakonyi, K. Balázsik and M. Bartók, *Catal. Lett.*, 1998, **52**, 81.
3 T. J. Hall, P. Johnston, W. A. H. Vermeer, S. R. Watson and P. B. Wells, *Stud. Surf. Sci. Catal.*, 1996, **101**, 221.
4 K. Borszeky, T. Mallat and A. Baiker, *Catal. Lett.*, 1996, **41**, 199.
5 Y. Nitta, Y. Ueda and T. Imanaka, *Chem. Lett.*, 1994, 1095.
6 G. Z. Wang, T. Mallat and A. Baiker, *Tetrahedron: Asymmetry*, 1997, **8**, 2133.
7 K. Borszeky, T. Mallat, R. Aeschiman, W. B. Schweizer and A. Baiker, *J. Catal.*, 1996, **161**, 451.
8 H.-U. Blaser, H. Hönig, M. Studer and C. Wedemeyer-Exl, *J. Mol. Catal. A*, 1999, **139**, 253.
9 T. Mallat, M. Bodmer and A. Baiker, *Catal. Lett.*, 1997, **44**, 95.
10 R. S. Atkinson, *Stereoselective Synthesis*, Wiley, Chichester, 1995; J. Fetter, F. Bertha, M. Kajtár-Peredy, K. Lempert and A. Sápi, *J. Chem. Res.*, 1997, (*S*) 118; (*M*) 0725.
11 M. Takahashi, T. Morimoto and K. Achiwa, *Chem. Lett.*, 1987, 855.
12 B. T. Cho and Y. S. Chun, *Tetrahedron: Asymmetry*, 1994, **5**, 1147.
13 C.-H. Wong, D. G. Druckhammer and H. M. Sweers, *J. Am. Chem. Soc.*, 1985, **107**, 4028.

Communication 9/04694A

ChemComm

Enantioselective hydrogenation of α-keto acetals with cinchona modified Pt catalyst

Martin Studer,* Stefan Burkhardt and Hans-Ulrich Blaser

Scientific Services, Novartis Service AG., R-1055.616, CH-4002 Basel, Switzerland.
E-mail: martin.studer@sn.novartis.com

Received (in Cambridge, UK) 25th June 1999, Accepted 20th July 1999

The enantioselective hydrogenation of a variety of α-keto acetals to the corresponding α-hydroxy acetals with Pt catalysts modified with cinchonidine derivatives is described with ees up to 97% and high reaction rates, and the influence of the substrate structure, the modifier and the reaction conditions (catalyst, solvent, temperature, pressure, modifier concentration) was investigated in some detail.

Modified heterogeneous catalysts for enantioselective hydrogenation are of interest, both from a theoretical and practical point of view.[1] Up to now only two efficient catalyst systems are known with enantioselectivities of 90% or higher. Most notable are the tartrate modified Raney nickel catalysts with ees of up to 98% for β-keto esters and for β-diketones[2–4] and the cinchona modified Pt catalysts for the hydrogenation of α-keto esters with ees up to 98%.[5-7] Even though recently some progress in expanding the substrate scope of the Pt–cinchona catalysts has been reported,[8–11] only a few of the new substrates are hydrogenated with ees > 60% or are of synthetic relevance. Here we describe the enantioselective hydrogenation of α-keto acetals to the corresponding α-hydroxy acetals with cinchona modified Pt catalysts with ees up to 97% and high rates. The influence of substrate structure, the modifier and the reaction conditions (catalyst, solvent, temperature, pressure, modifier concentration) were investigated. While there are some literature reports of the enantioselective reduction of α-keto acetals,[12–15] the Pt–cinchona catalysts shows clear advantages with respect to selectivity, activity and simplicity for the synthesis of interesting chiral synthons.

The results of a rather broad variation of the α-keto acetal structure, using Pt/Al_2O_3 in presence of 10,11-dihydrocinchonide (HCd) in toluene or 9-methoxy-HCd (MeOHCd) in AcOH are summarized in Table 1. Obviously, α-keto acetals are extraordinarily suitable substrates for the cinchona modified Pt catalysts with respect to both enantioselectivity and activity. The highest ee and rate values were obtained with two pyruvaldehyde acetals (entries 1 and 2). Compared to ethyl pyruvate, the ees were slightly higher (ee up to 96% for ethyl pyruvate), and the rates somewhat lower (up to 400 mmol g^{-1} min^{-1} for ethyl pyruvate). The addition of the modifier led to a rate acceleration of the order of ten, also comparable to ethyl pyruvate. Other aliphatic and aromatic α-keto acetals with low bulkiness gave very high ees, but with significantly lower rates (entries 5,7,9–11). Significantly lower ees and very much lower rates were observed for keto acetals with more bulky R especially with larger R′ moieties. Aromatic and aliphatic ethers as well as esters and amides are tolerated and do not affect the enantioselectivity very much (entries 10–13). α-Keto ketals (entries 14,15) are hydrogenated very slowly and with negligible induction.

The effect of the modifier/solvent combination and of different Pt catalysts was studied for pyruvaldehyde dimethyl acetal and other substrates (for selected results see Table 2). The best results were always observed either with MeOHCd in AcOH or with HCd in toluene, while EtOH usually gave both lower enantioselectivities and rates. The reaction rates of the modified and the unmodified system were compared for HCd in EtOH. In most cases, ligand accelerated catalysis was observed. The best catalyst was a 5% Pt/Al_2O_3 catalyst, JMC 94 (Johnson Matthey), which in our hands also had the best performance with ethyl pyruvate. Several alumina and silica supported Pt catalysts from several catalyst manufacturers were compared; while the rates differed by a factor of up to 4, all catalysts gave ees of ⩾93% with pyruvaldehyde dimethyl acetal and MeOHCd in AcOH.

For the model reaction with pyruvaldehyde dimethyl acetal, the influence of hydrogen pressure, temperature and substrate and modifier concentration were investigated, with results similar to those obtained for ethyl pyruvate.[16,17] The most notable difference was the influence of the hydrogen pressure. In contrast to ethyl pyruvate, ees ⩾ 94% were observed at 1 bar (increasing to 96% at pressures between 2 and 140 bar), and the rate showed a half order dependence on hydrogen pressure. The substrate concentration had only a small effect on the enantioselectivity (94% at 0.4 M, 96% at 2.8 M and 80% in neat substrate at 8 M) while the rate was affected very strongly: 25 mmol g^{-1}

Table 1 Variation of ketone structure[a]

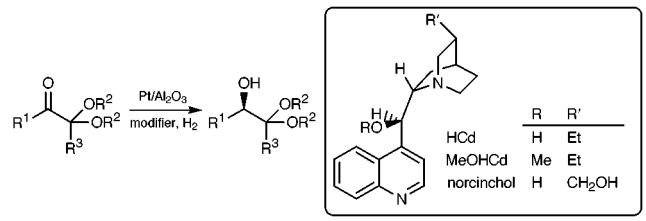

Entry	R^1	R^2	R^3	Ee (%)	Rate/mmol g^{-1} min^{-1}
1[b]	Me	Me, Me	H	96	53
2[c]	Me	$(CH_2)_3$	H	97	42
3[d]	Me	Et, Et	H	91	5.8
4[e]	Me	Bu, Bu	H	85	1.8
5[f,g]	Ph	Me, Me	H	89	1.5
6[b,g]	Ph	Et, Et	H	81	0.5
7[h]	Pr	Me, Me	H	93	4
8[g,c]	Bu[i]	Me, Me	H	62	< 0.1
9[h]	$PhCH_2CH_2$	Me, Me	H	93	15
10[c]	$PhO(CH_2)_3$	Me, Me	H	93	5
11[c]	$EtO(CH_2)_3$	Me, Me	H	92	5
12[c,g,i]	$Me_2NOC(CH_2)_2$	Me, Me	H	80	0.7
13[c,i]	$MeO_2C(CH_2)_2$	Me, Me	H	50	< 0.1
14[b]	Me	Me, Me	Me	< 10%	< 0.1
15[b]	Ph	Me, Me	Ph	< 10%	< 0.1

[a] Conditions: all hydrogenations were carried out as described in ref. 17. Typically, 1–2 g substrate, 5% Pt/Al_2O_3 (JMC type 94, 2 h pretreated with H_2 at 400 °C), 5–50 mg MeOHCd, 15–20 ml AcOH, 60 bar, 25 °C. All ees and conversions were determined by GLC (Beta-dex 110, Supelco hydrogen carrier) or by HPLC (Chiracel OD, 95% hexane and 5% Pr^iOH). All new substrates and products gave satisfactory analytical results (^{13}C, ^1H, and MS). [b] Substrate from Fluka. [c] Substrate synthesised according to literature methods. [d] Substrate synthesized from substrate in entry 1 using H^+ and EtOH. [e] Substrate synthesized from substrate in entry 1 using H^+ and BuOH. [f] Substrate synthesized from substrate in entry 6 using H^+ and MeOH. [g] Reaction in toluene using HCd. [h] Ee estimated. [i] Substrate not very pure.

Table 2 Effect of solvent, modifier structure and catalyst type (selected results)[a]

Solvent/modifier	Catalyst	Ee % (*R*)	Rate/mmol g^{-1} min^{-1}
AcOH/MeOHCd	1	96.5	41
AcOH/MeOHCd	2	96	23
AcOH/MeOHCd	3	94	12
AcOH/MeOHCd	4	93	33
Propanoic acid/MeOHCd	1	96	50
AcOH/norcinchol	1	83	26
AcOH/HCd	1	82	28
Toluene/HCd	1	79	5.7
EtOH/HCd	1	61	8.4
EtOH/MeOHCd	1	35	—
EtOH/none	1	−1.1	1.3

[a] Conditions: 2 ml pyruvaldehyde dimethyl acetal, 50 mg catalyst, 5 mg modifier, 25 °C, 60 bar, 20 ml solvent. Catalyst 1 was 5% Pt/Al_2O_3, JMC 94 (Johnson Matthey), catalyst 2 was 5% Pt/Al_2O_3, E 4759 (Engelhard), catalyst 3 was 5% Pt/Al_2O_3, F 213XR/D (Degussa), catalyst 4 was 5% Pt/SiO_2, 98993 (Heräus), all 2 h pretreated with H_2 at 400 °C.

min^{-1} at 0.4 M and 119 mmol g^{-1} min^{-1} at 2.8 M, decreasing to 36 mmol g^{-1} min^{-1} at 8 M. The dependence of ee and rate on the temperature was studied between 10 and 50 °C. While the ee was almost constant (97 and 96%), the rate strongly increased between 10–30 °C. At temperatures above 30 °C, a decrease in both ee and rate was observed. Most likely, the modifier is either desorbed from the catalyst surface or hydrogenated at higher temperature. Fig. 1 shows the dependence of ee and rate on the MeOHCd concentration. Both curves had a similar shape, as was observed for ethyl pyruvate in toluene,[16] and could be modeled with a simple kinetic model assuming reversible but strong adsorption of the modifier on the Pt surface. As expected, the ee values are rather low at low modifier concentration if the reaction is run to high conversion, most likely because the modifier is hydrogenated and thereby made ineffective during the course of the reaction.

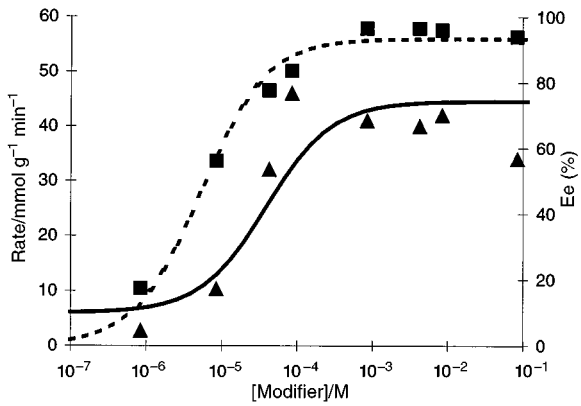

Fig. 1 Dependence of ee and rate on modifier concentration: (▲) observed rate, (—) calculated rate, (■) observed ee and (---) calculated ee. Calculated curves according to ref. 11. Pyruvaldehyde dimethyl acetal (2 ml), AcOH (18 ml), 5% Pt/Al_2O_3 (50 mg) (JMC type 94, 2 h pretreated with H_2 at 400 °C), 25 °C, 60 bar.

Enantiomerically enriched α-hydroxy acetals are interesting synthons and can be transformed into a variety of chiral building blocks (*e.g.* 1,2 diols, α-hydroxy acids, 1,2 amino alcohols) as shown in Scheme 1. While the oxidation to (*R*)-ethyl lactate was rather difficult and required the protection of the OH group, the reduction could be easily accomplished after hydrolysis of the acetal. No significant racemisation was observed. With a boronic acid derivative and a secondary amine, it was also possible to synthesize amino alcohols with high diastereoselectivity according to ref. 18.

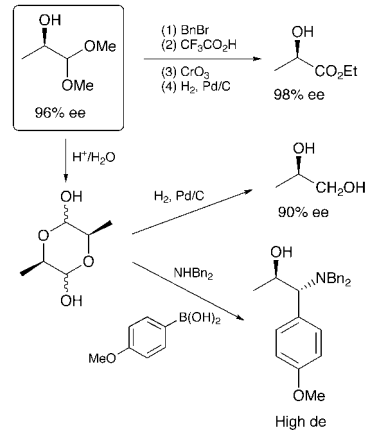

Scheme 1

From all the results presented above, we conclude that the Pt–cinchona catalyzed hydrogenation of α-keto acetals is very similar to the well studied reaction of α-keto acid derivatives:[1] the most likely mode of action is that the adsorbed ketone interacts with the N_1 atom of the adsorbed cinchona modifier, probably *via* a hydrogen bridge, resulting in both a rate acceleration and the preferential addition of hydrogen from the *si* side of the keto group to produce (*R*)-α-hydroxy acetals.[17] Concerning the requirements for a suitable substrate for this chiral catalyst system we in principle confirm the postulate of Mallat *et al.*[9] that an electron-withdrawing group α to the C=O can lead to good ees. However, if we consider the results for methoxy acetone (best ee 12%), trifluoroacetophenone (56%) and the α-hydroxy acetals (97%), it is obvious that there is no clear correlation between the electronic character of the carbon α to the ketone and the enantioselectivity. The presence of either a second C=O or of a $CH(OR)_2$ group in the α-position is especially beneficial to obtain both very high ees and acceptable reaction rates. For this fact there is as yet no convincing explanation available.

We thank Professor M. Bartok for his co-operation for the back-to-back publication (see preceding article).

Notes and references

1 H. U. Blaser, H. P. Jalett, M. Müller and M. Studer, *Catal. Today*, 1997, **37**, 441.
2 S. Nakagawa, T. Sugimura and A. Tai, *Chem. Lett.*, 1997, 589.
3 A. Tai, K. Ito and T. Harada, *Bull. Chem. Soc. Jpn.*, 1981, **54** 223.
4 A. Tai, T. Kikukawa, T. Sugimura, Y. Inoue, S. Abe, T. Osawa, S. Fujii and T. Harada, *Bull. Chem. Soc. Jpn.*, 1994, **67**, 2473.
5 H. U. Blaser, H. P. Jalett and J. Wiehl, *J. Mol. Catal.*, 1991, **68**, 215.
6 X. Zuo, H. Liu and M. Liu, *Tetrahedron Lett.*, 1998, **39**, 1941.
7 B. Török, K. Felfödi, G. Szakonyi, K. Balazsik and M. Bartok, *Catal. Lett.*, 1998, **52**, 81.
8 W. A. H. Vermeer, A. Fulford, P. Johnston and P. B. Wells, *J. Chem. Soc., Chem. Commun.*, 1993, 1053.
9 T. Mallat, M. Bodmer and A. Baiker, *Catal. Lett.*, 1997, **44**, 95.
10 G. Z. Wang, T. Mallat and A. Baiker, *Tetrahedron: Aysmmetry*, 1997, **8**, 2133.
11 M. Studer, V. Okafor and H. U. Blaser, *Chem. Commun.*, 1998, 1053.
12 B. T. Cho and Y. S. Chun, *Tetrahedron: Asymmetry*, 1994, **5**, 1147.
13 H. Takahashi T. Morimoto and K. Achiwa, *Chem. Lett.*, 1987, 855.
14 J. Peters, T. Zelinski, T. Minuth and M. R. Kula, *Tetrahedron: Asymmetry*, 1993, **4**, 1683.
15 C. H. Wong, D. G. Drueckhammer and H. M. Sweers, *J. Am. Chem. Soc.*, 1985, **107**, 4028.
16 H. U. Blaser, M. Garland and H. P. Jalett, *J. Catal.*, 1993, **144**, 569.
17 H. U. Blaser, H. P. Jalett, M. Garland, M. Studer, H. Thies and A. Wirth-Tijani, *J. Catal.*, 1998, **173**, 282.
18 N. A. Petasis and I. A. Zavialov, *J. Am. Chem. Soc.*, 1998, **120**, 11 798.

Communication 9/05113I

Simultaneous conversion of methane and carbon dioxide to aromatics over silica supported chromium-based catalysts

Hui Zhang[ab] and Yuan Kou*[a]

[a] *College of Chemistry and Molecular Engineering, Peking University, Beijing 100871, China. E-mail: yuankou@pku.edu.cn*

[b] *Lanzhou Institute of Chemical Physics, Chinese Academy of Sciences, Lanzhou 730000, China*

Received (in Cambridge, UK) 14th June 1999, Accepted 29th June 1999

Simultaneous activation of methane and carbon dioxide to aromatics (SAMCA) over sodium-modified silica supported chromium-based catalysts is reported.

In this decade, much attention has been paid to the aromatization of methane under non-oxidative conditions following the early work conducted by Bragin *et al.*[1] Effective catalysts and mechanisms have been recently reviewed.[2,3] Molybdenum oxide supported on HZSM-5 zeolite seems to be a uniquely effective catalyst system for the aromatization of methane under non-oxidative conditions.[2–6] However, understanding the interaction of methane with the surfaces greatly depends upon various observations. It appears, in general, that reduction and/or carbidation of Mo species over Mo/ZSM-5 catalyst plays a key role in the activation of methane to produce initial C_2 products, and the primary intermediates are then further oligomerized to benzene on the B-acid sites within the channels of ZSM-5 zeolite.[2,3,6] Recently, we have found that sodium-modified silica supported chromium-based catalysts exhibit considerable activity for the simultaneous activation of methane and carbon dioxide to aromatics (SAMCA). This is the first investigation, to our knowledge, to use non-zeolite supported oxide catalysts for the non-free-oxygen activation of methane to produce benzene and toluene in the presence of large amounts of carbon dioxide.

The catalysts were prepared as follows. CR18, as a typical example, is described in detail. Given amounts of Cr_2O_3 (0.35 g) and/or $(NH_4)_2Cr_2O_7$ (the molar ratio of Cr_2O_3 to $(NH_4)_2Cr_2O_7$ is 2:1) and $NaNO_3$ (0.89 g) were slurried with silica sol (42 wt% water, 45 g) for 3 h, and then dried overnight at 120 °C. Several samples with different metal loadings and different Cr(III)/Cr(VI) ratios were prepared by controlling the concentration of the sol. The resulting samples were calcined at 500 °C for 4 h and then at 800 °C for 4 h. All of the calcined catalyst samples were crushed and sieved to 26–55 mesh. The XPS spectrum in the Cr 2p region for the catalyst CR18 revealed a strong peak at a binding energy of 579.0 eV and a shoulder of this peak at a binding energy of 576.6 eV corresponding to Cr(VI) $2p_{3/2}$ and Cr(III) $2p_{3/2}$, respectively. The ratio of Cr(VI)/Cr(III) in CR18 on the basis of the XPS peak area is 5:1.

The catalytic runs were carried out at a pressure of 0.4 MPa in a fixed-bed vertical-flow stainless steel reactor mounted inside a tube furnace. The amount of the catalyst charged in the reactor was 1.0 g. The catalyst was pretreated in highly pure nitrogen (99.99%) at 840 °C for 30 min. Then, the reactant gas mixture ($CH_4:CO_2$ = 7:5) was introduced at a flow rate of 22 ml min^{-1}. When the support (SiO_2) was used as a catalyst alone, the reaction results also indicated small amounts of aromatics (yield < 0.07%, see Table 1). Isotopic trace experiments were carried out under the same conditions but at a pressure of 0.3 MPa. Pure $^{13}CO_2$ obtained from $Ba^{13}CO_3$ was pressurized to 0.3 MPa by high pressure CH_4 and CO_2 to give a CH_4/CO_2 molar ratio of 7/5. The relative partial pressure of $^{13}CO_2$ in the CO_2 mixture was calculated to be 1/3.

The products in the effluent stream were analyzed by an online GC equipped with a Hayesep Q column (TCD,H_2 as carrier) for CO, CH_4, CO_2 and C_1–C_3, 13X and 5A sieve columns (TCD, Argon as carrier) for H_2, CH_4 and CO, and a quartz capillary column coated with SE-54 (FID) for benzene and toluene. Both methane and carbon dioxide were 99.995% pure.

Operating parameters significantly influence the activity of the catalyst in the SAMCA reaction. Fig. 1(a) shows that both the aromatics yield and the selectivity are increased by increasing the reaction temperature. The yield and the selectivity of aromatics are also found to go through maxima at a contact time of 0.79 h g l^{-1}, indicating that deep oxidation may occur when the contact time is > 0.79 h g l^{-1}.

Fig. 1(b) shows the effect of the CH_4/CO_2 molar ratio on the selectivities and the yields at 840 °C. Both the selectivity and the yield of aromatics are enhanced with an increasing proportion of CH_4 in the reactant mixture, and reach a maximum at a CH_4/CO_2 molar ratio of 1.4. However, the selectivity to C_{2+} hydrocarbons essentially remains constant for CH_4/CO_2 molar ratios of > 1.1. When the molar ratio of CH_4/CO_2 is < 0.5 or > 2.5, both C_{2+} hydrocarbons and aromatics are difficult to detect. It is of note that the yields of C_{2+}

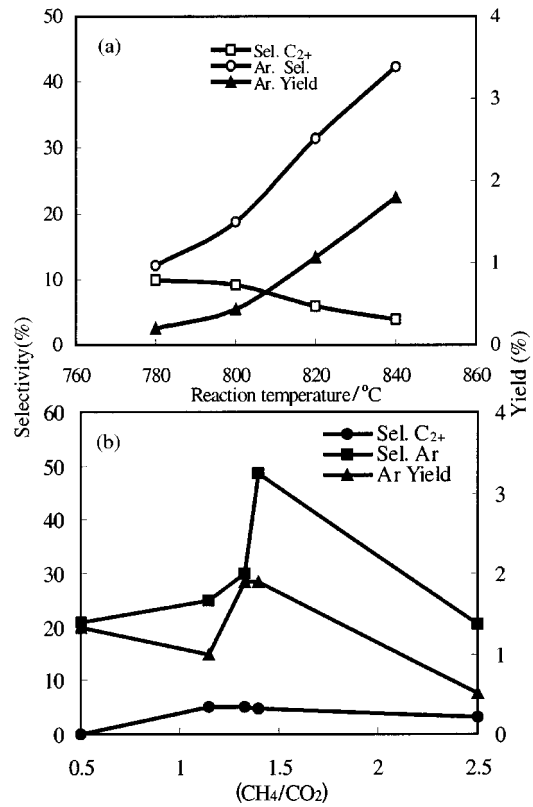

Fig. 1 Effect of operating parameters on the activity of the catalyst 5 wt% Na–7.5 wt% Cr/SiO_2 in SAMCA. (a) Effect of reaction temperature (0.4 MPa, 0.79 h g l^{-1}, CH_4/CO_2 = 7:5) and (b) effect of CH_4/CO_2 molar ratio (0.4 MPa, 0.79 h g l^{-1}, 840 °C).

Table 1 Catalytic performances of a series of chromium-based catalysts in the SAMCA reaction[a]

Catalyst	Cr (wt%)	Na (wt%)	S_{BET}/ $m^2\ g^{-1}$	$V/cm^3\ g^{-1}$	Conversion		Selectivity			Aromatics yield (%)
					CH_4	CO_2	C_2^+	Ar[b]	CO	
SiO_2	0	0	204.48	46.8	0.9	5.1	11.9	7.6	80.4	0.07
CR16	7.5	0	202.44	46.17	2.7	21.4	0.0	23.7	76.3	0.6
CR17	7.5	2	10.05	2.29	2.4	10.6	4.1	38.4	57.5	0.9
CR18	7.5	5	3.35	0.76	3.8	16.0	4.8	48.7	46.5	1.9
CR19	7.5	10	1.87	0.43	4.0	7.1	4.1	41.2	54.7	1.7
CR7[c]	11.4	2	9.80	2.11	1.4	13.5	3.6	1.8	94.6	0.03
CR8[d]	8.9	2	10.12	2.19	2.3	16.6	4.0	30.7	65.3	0.7
CR15[e]	7.5	10	2.11	0.51	1.9		30.5	5.2	64.2	0.1
CR10[e]	7.5	2	9.51	2.13	2.1		23.1	2.2	74.7	0.05

[a] *Reaction conditions*: 0.4 MPa, 840 °C, 20–23 ml min^{-1}, CH_4/CO_2 = 7/5. [b] Benzene + toluene. [c] Na–Cr(III)/SiO_2. [d] Na–Cr(VI)/SiO_2. [e] CH_4 feed only.

hydrocarbons and aromatics are very low when only methane is fed into the reaction mixture as demonstrated by the results for CR10 and CR15 in Table 1.

Variation of the Cr^{3+}/Cr^{6+} ratio in the preparation of the catalyst precursors has a considerable effect on the activity of the catalyst in SAMCA. The reaction results obtained from a series of chromium-based catalysts are presented in Table 1. Over the Cr_2O_3/SiO_2 catalyst (CR7 in Table 1), the dominant product is carbon monoxide (94.6%) although C_{2+} and aromatics are detectable. This situation is very similar to the results over a Cr_2O_3 catalyst reported by Asami *et al.*[7] except that they observed no aromatics.[7] However, addition of Cr^{VI} to the Cr_2O_3/SiO_2 catalyst led to significantly increased SAMCA reactivity. In particular, over the catalyst containing a 2 : 1 molar ratio of Cr^{3+} to Cr^{6+} and modified with 5 wt% sodium promoter (CR18), CH_4 conversion reaches 3.8%, while selectivity to aromatics increases to 48.7%. By comparison, when only Cr^{VI} species are present on the fresh catalyst surface (CR8), the CH_4 conversion decreases to 2.6%, and the selectivity to aromatics also decreased to 13.9%. Interestingly, when the highest selectivity to aromatics is obtained over CR18 (5 wt% Na and 2 : 1 molar ratio of Cr^{3+} to Cr^{6+}), the selectivity to CO is at a minimum, and the molar ratio of benzene to CO is *ca.* 1 : 1. In this case, small amounts of H_2 were observed at a CO/H_2 molar ratio of 3. However, after being on-stream for 6 h, the catalyst CR18 shows behavior more closely resembling that of Cr_2O_3 (CR7). Correspondingly, XPS analysis of the quenched catalyst indicates the Cr(III) $2p_{3/2}$ peak only. As proposed previously,[8–10] it is highly probable that mixing of octahedral and tetrahedral site-symmetries on the surface of the supported oxide catalyst presents catalytically active sites for the SAMCA reaction.

Asami *et al.* have proposed the reaction given by eqn. (1) to explain the formation of ethene:[7]

$$2CH_4 + 2CO_2 \rightarrow C_2H_4 + 2CO + 2H_2O \quad (1)$$

We tentatively suggest a subsequent additional step here to explain the formation of benzene for SAMCA in which the CO molecules can be obtained from either reaction (1) or the partial reduction of CO_2 in the hydrogen atmosphere.

$$2C_2H_4 + 3CO \rightarrow C_6H_6 + CO_2 + H_2O \quad (\Delta G = -183.2\ kJ\ mol^{-1}\ at\ 840\ °C) \quad (2)$$

In order to confirm whether CO_2 participates in the formation of benzene, isotopic trace experiments using $^{13}CO_2$ in CH_4 and CO_2 co-feed have been carried out under a pressure of 0.3 MPa. The $^{13}CC_5H_6$ species, which was not observed by using the normal CH_4–CO_2 mixture as the feed gas, is identified by a peak at *m/z* 79.17 in the online mass spectrum (Fig. 2), indicating that the carbon in CO_2 demonstrably takes part in the construction of the benzene ring.

Despite their low reactivity, this work has demonstrated that methane and carbon dioxide can be simultaneously activated. The reaction producing aromatics over silica supported chromium-based catalysts is accompanied by an induction period of *ca.* 20 minutes. Ethene, as the primary intermediate, is necessary for the formation of benzene, however, the definate requirement of zeolite channels as proposed based on the Mo/ZSM-5 system is questioned. This research may therefore lead to some new insights on the mechanism for the aromatization of methane.

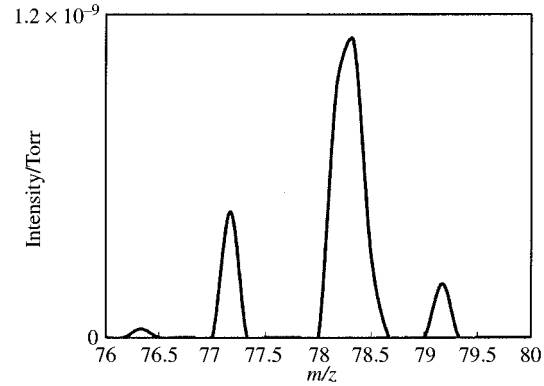

Fig. 2 MS spectra of the products formed in the SAMCA reaction with $^{13}CO_2$-labelled reactant.

Further work is in progress, not only to carry out the reaction on a larger experimental scale, but also to elucidate the nature of the mixed site-symmetry/oxidation state catalysts by XAFS analysis.

We greatly appreciate Professor Shikong Shen at Beijing Petroleum University for his helpful suggestions and discussions. We thank Drs Changchun Yu and Chunyi Li for experimental assistance.

Notes and references

1 A. V. Bragin, T. V. Vasina, A. V. Preobrazhenskii and K. M. Minachev, *IZV. Akad. Nauk. SSSR Ser. Khim.*, 1989, **3**, 750.
2 D. Wang, M. Rosynek and J. H. Lunsford, *J. Catal.*, 1997, **169**, 347.
3 J. Zhang, M. Long and R. Howe, *Catal. Today*, 1998, **44**, 293.
4 Y. Xu, S. Liu, L. Wang, M. Xie and X. Guo, *Catal. Lett.*, 1995, **30**, 135.
5 L. Chen, L. Lin, Z. Xu, X. Li and T. Zhang, *J. Catal.*, 1995, **157**, 190.
6 Y. Shu, Y. Xu, S. Wong, L. Wang and X. Guo. *J. Catal.*, 1997, **170**, 11.
7 K. Asami, T. Fujita, K. I. Kusakabe, Y. Nishiyama and Y. Ohtsaka, *Appl. Catal. A*, 1995, **126**, 245.
8 H. Zhang, J. Niu and Y. Kou, T. Tanaka and S. Yoshida, *J. Solid State Chem.*, 1998, **137**, 325.
9 Y. Kou and H. Wang, *5th China–Japan Bilateral Symposium on Effective Utilization of Carbon Resources (EUCR-V) Proceedings*, Chengdu, China, 1997, p. 5.
10 H. Zhang and Y. Kou, *5th China–Japan Bilateral Symposium on Effective Utilization of Carbon Resources (EUCR-V) Proceedings*, Chengdu, China, 1997, p. 137.

Communication 9/04753K

ChemComm

Synthesis, structure and reactivity of the hexaphospha-titanocene, bis-(η^5-3,5-di-*tert*-butyl-1,2,4-triphosphacyclopentadienyl)titanium(II)

F. Geoffrey N. Cloke,* John R. Hanks, Peter B. Hitchcock and John F. Nixon*

School of Chemistry, Physics and Environmental Science, University of Sussex, Brighton, UK BN1 9QJ. E-mail: J.Nixon@sussex.ac.uk

Received (in Cambridge, UK) 7th July 1999, Accepted 26th July 1999

The novel, fully structurally characterised, 14e-titanocene [Ti(η^5-($P_3C_2Bu^t_2$)$_2$] made by (i) cocondensation of titanium vapour with the phosphaalkyne Bu^tCP (ii) reaction of Bu^tCP with [Ti(η^6-C_6H_5Me)$_2$] at −78 °C or (iii) by heating $TiCl_n$ with $n(KP_3C_2Bu^t_2)$ (n = 2, 3) in toluene at 110 °C, undergoes an unusual [2+2] cycloaddition reaction with Bu^tCP to give [Ti(η^5-$P_3C_2Bu^t_2$)(η^3-η^2-$P_4C_3Bu^t_3$)].

Despite several attempts by different workers using a variety of routes, isolation and structural characterisation of a monomeric, (non C–H activated), titanocene has failed owing to the high reactivity of the carbene-equivalent [Ti(η^5-C_5H_5)$_2$] unit. The addition of neutral ligands such as CO, N_2, PF_3, PMe_3, C_2H_4 and bulky ethynes facilitated isolation of derivatives of [Ti(η^5-C_5H_5)$_2$] and [Ti(η^5-C_5Me_5)$_2$],[1–7] however, the use of bulky substitutents on the cyclopentadienyl rings proved less successful until the very recent report of [Ti(η^5-Cp^s)$_2$] [Cp^s = $C_5Me_4(SiMe_2Bu^t)$] by Lawless and coworkers[8]

Previously[9,10] we showed that cocondensation of the phosphaalkyne Bu^tCP with transition metal vapours affords a wide variety of organometallic compounds of which those containing the di- and tri-phosphorus substituted cyclopentadienyl rings are by far the most common. We now report that cocondensation of titanium atoms with Bu^tCP yields the first example of a phosphorus substituted titanocene which has been fully characterised and its molecular structure established by a single crystal X-ray diffraction study.

Cocondensation of electron beam generated[11] titanium atoms with an excess of Bu^tCP at 77 K (i) affords the hexaphospha-titanocene complex [Ti(η^5-$P_3C_2Bu^t_2$)$_2$] **1** (*ca.* 2.5% after work up, based on titanium) (Scheme 1). **1**, which was obtained as dark-red air and moisture-sensitive crystals by sublimation (180 °C, 1 × 10^{-5} mbar) followed by recrystallisation from pentane (−20 °C)† can also be prepared, in slightly better yield (ii) by adding an excess of Bu^tCP to a pentane solution of [Ti(η^6-C_6H_5Me)$_2$] at −78 °C or in moderate (*ca.* 30%) yield (iii) by heating $TiCl_n$ with $n(KP_3C_2Bu^t_2)$[12] (n = 2, 3) in toluene at 110 °C.

A single crystal X-ray diffraction study‡ (Fig. 1) confirms the formulation of **1** and shows it to be a slightly bent, monomeric sandwich compound (angle between the planes of the two $P_3C_2Bu^t_2$ rings = 16.05°; centroid–Ti–centroid angle = 173.9°). The rings are approximately planar, with the *tert*-butyl groups staggered so as to minimize inter-ring interactions and the phosphorus atoms lying slightly above the plane containing the carbons. Although several phosphorus-containing sandwich compounds are known, the only other reported hexaphospha-metallocene structures are for Cr, Fe and Ru[13–15] although there also exists an unpublished Mn structure.[16] As expected, the metal to ring-centroid distances steadily decrease in the series [M(η^5-$P_3C_2Bu^t_2$)$_2$] (M = Ti, Cr, Mn, Fe), as the size of the metal decreases (Ti 1.942, Cr 1.815, Mn 1.710, Fe 1.687 Å). A similar trend in metal–ring distances has been observed and rationalised in the analogous metallocenes [M(η^5-C_5H_5)$_2$] (M = V, Cr, Fe).[17–20] The [M(η^5-$P_3C_2Bu^t_2$)$_2$] complexes all have slightly bent sandwich structures with centroid–metal–centroid angles of 173.5° (Cr), 173.2° (Fe), 171.0° (Mn). Since the 18e Fe and Ru compounds and the 16e Cr compound would be expected to have parallel rings, the slight distortion has been attributed to the steric effect of the *tert*-butyl groups being unable to fully intermesh. As expected, the pentaphosphametallocenes, [M(η^5-$P_3C_2Bu^t_2$)(η^5-$P_2C_3Bu^t_3$)] (M = V, Fe)[10,14] have essentially parallel rings as here the *tert*-butyl groups can fully intermesh.

Only limited structural comparisons can be made between **1** and other titanocenes because the parent titanocene is not monomeric but exists instead as various dimers.[1] Likewise, although decamethyltitanocene [Ti(η^5-C_5Me_5)$_2$] is monomeric, (in equilibrium with a C–H activated species), no structural data are available.[1] The X-ray structure of the very recently synthesised [Ti(η^5-Cp^s)$_2$] shows that the two rings are planar, staggered and exactly parallel, with the $SiMe_2Bu^t$ substituents rotated by 180° with respect to each other.[8] The metal–centroid distance [2.014(8)Å] is larger than that determined for **1** [1.942(2) Å], presumably either because of the more sterically demanding Cp^s ligand and/or the stronger bonding of the phosphorus substituted cyclopentadienyl rings.[9] The exactly parallel nature of the two Cp^s rings is also presumably due to steric factors. Although **1** has a $3d^2$ electronic configuration, it is found to be diamagnetic. At room temperature the ^1H,

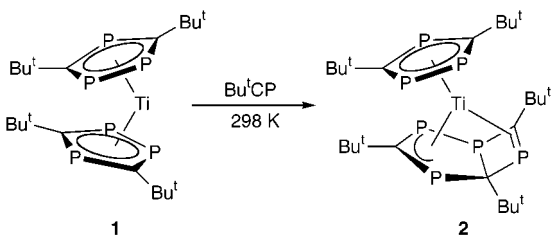

Scheme 1

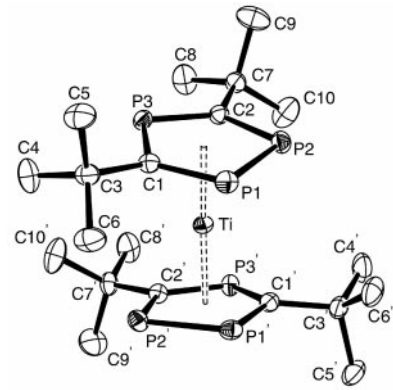

Fig. 1 Molecular structure of [Ti(η^5-$P_3C_2Bu^t_2$)$_2$], **1**. Selected distances (Å) and angles(°): Ti–M(1) 1.942(2), Ti–C(1) 2.354(2), Ti–C(2) 2.470(2), Ti–P(1) 2.477(1), Ti–P(2) 2.535(1), Ti–P(3) 2.637(1), P(1)–C(1) 1.790(2), P(1)–P(2) 2.167(1), P(2)–C(2) 1.784(2), P(3)–C(2) 1.739(2), P(3)–C(1) 1.764(2), C(1)–P(1)–P(2) 97.84(7), C(2)–P(2)–P(1) 98.72(7), C(2)–P(3)–C(1) 99.92(10), P(3)–C(1)–P(1) 121.47(12), P(3)–C(2)–P(2) 121.74(12), M(1)–Ti–M(1)′ 173.9(1), angle between the least-squares planes of the two rings 16.05(0.07). M(1) and M(1)′ refer to the centroids of the two rings.

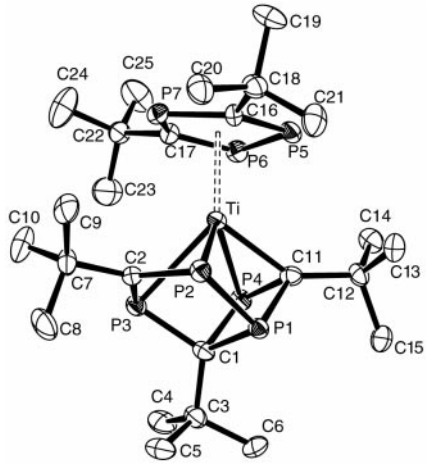

Fig. 2 Molecular structure of [Ti(η^5-$P_3C_2Bu^t_2$)(η^3-η^2-$P_4C_3{}^tBu_3$)] **2**. Selected distances (Å): Ti–M(1) 2.120(6), Ti–C(2) 2.503(6), Ti–C(11) 2.210(6), Ti–C(16) 2.465(5), Ti–C(17) 2.663(6), Ti–P(2) 2.472(2), Ti–P(3) 2.662(2), Ti–P(4) 2.577(2), Ti–P(5) 2.609(2), Ti–P(6) 2.673(3), Ti–P(7) 2.709(2), C(1)–P(1) 1.876(5), P(1)–P(2) 2.216(2), P(2)–C(2) 1.790(5), C(2)–P(3) 1.752(5), P(3)–C(1) 1.831(6), P(1)–C(11) 1.858(5), C(11)–P(4) 1.828(5), P(4)–C(1) 1.909(5). M(1) refers to the centroid of the ring P(5)C(16)P(7)C(17)P(6).

$^{13}C\{^1H\}$ and $^{31}P\{^1H\}$ NMR spectra§ are all sharp (and temperature invariant over the range 185–385 K) and indicate that in solution the two $P_3C_2Bu^t_2$ rings are equivalent and that there is no inter-ring coupling. This is in contrast to the iron and ruthenium analogues which exhibit fluxional behaviour and inter-ring coupling constants of 53 Hz (Fe) and 37.4 Hz (Ru).[13,14]

Decamethyltitanocene forms dinitrogen complexes (some reversibly), and although **1** does not react with dinitrogen, it readily undergoes addition reactions with CO or ^{t}BuNC to give the 16e and 18e complexes [Ti(η^5-$P_3C_2Bu^t_2$)$_2$L] (L = CO) and [Ti(η^5-$P_3C_2Bu^t_2$)$_2$L$_2$] (L = CO, Bu^tNC) respectively, which will be reported in detail elsewhere.[21] However, with an excess of Bu^tCP the novel red–brown 14e-complex [Ti(η^5-$P_3C_2Bu^t_2$)(η^3:η^2-$P_4C_3Bu^t_3$)] **2** is formed as a result of an unusual [2+2] cycloaddition with a P=C bond of *one* of the η^5-$P_3C_2Bu^t_2$ rings of **1** (Scheme 1). No reaction is observed in an analagous experiment with Bu^tCN. The molecular structure of **2**, determined by a single crystal X-ray diffraction study,‡ is shown in Fig. 2. The titanium is attached in an η^5-fashion to the one remaining $P_3C_2Bu^t_2$ ring and η^3:η^2- ligated to the new $P_4C_3Bu^t_3$ moiety. The $^{31}P\{^1H\}$ NMR spectrum of **2** exhibits the expected seven different resonances and the ^1H NMR spectrum contains the expected five singlets.§

The mechanism of formation of **2** from **1** might involve the intermediacy of an η^1- (or less likely η^2-ligated) Bu^tCP complex and the subsequent η^5- to η^3-ring slippage of one of the $P_3C_2Bu^t_2$ facilitating a [2+2] cycloaddition with the resulting uncoordinated P=C bond leading to the product **2**. Interestingly, although **2** can be sublimed (170 °C, 1×10^{-5} mbar) with only slight decomposition to **1**, it was not isolated from the original cocondensation experiment.

To our knowledge, the only related metallocene ring addition reactions previously reported concern nickelocene and fluoroalkenes or an activated norbornadiene however no structural data are available for comparison.[22,23]

We thank Dr A. Abdul-Sada for recording the mass spectrum of **1** and the EPSRC for financial support (for J. R. H.).

Notes and references

† $C_{20}H_{36}P_6Ti$: MS (EI, 70 eV), *m/z* 510 (100%) (M^+), 57 (8%) (Bu^{t+}) with the expected isotope pattern. Elemental analysis: C, 47.08 (46.57), H, 7.11 (7.15%).

‡ *Crystal data:* for **1**: $C_{20}H_{36}P_6Ti$, M = 510.2, orthorhombic, space group $C222_1$ (no. 20), a = 11.632(6), b = 16.114(5), c = 13.920(4) Å, U = 2609(2) Å^3; Z = 4, D_c = 1.30 Mg m^{-3}, T = 173(2) K. Data were obtained with an Enraf-Nonius CAD4 diffractometer using Mo-Kα radiation, λ = 0.71073 Å, (μ = 0.70 mm^{-1}), on a crystal of dimensions 0.4 × 0.4 × 0.2 mm; 2112 unique reflections were measured for $2 < 2\theta < 30°$ and 2035 reflections with $I > 2\sigma(I)$ were used in the refinement. The final residuals were R = 0.025, $wR2$ = 0.062 for $I > 2\sigma(I)$. Hydrogen atoms were refined isotropically. The molecule lies on a crystallographic two fold rotation axis.

For **2**: $C_{25}H_{45}P_7Ti$, M = 610.3, triclinic, space group $P\bar{1}$(no.2), a = 10.299(5), b = 11.910(6), c = 14.230(10) Å, α = 86.48(5), β = 71.00(5), γ = 68.75(4)°, U = 1535(2)Å^3; Z = 2, D_c = 1.32 Mg m^{-3}, T = 173(2) K. Data were obtained with an Enraf-Nonius CAD4 diffractometer using Mo-Kα radiation, λ = 0.71073 Å, (μ = 0.66 mm^{-1}), on a crystal of dimensions 0.4 × 0.3 × 0.05 mm; 5362 unique reflections were measured for $2 < 2\theta < 25°$ and 4021 reflections with $I > 2\sigma(I)$ were used in the refinement. The final residuals were R = 0.077, $wR2$ = 0.196 for $I > 2\sigma(I)$.

CCDC 182/1348. See http://www.rsc.org/suppdata/cc/1999/1731/ for crystallographic files in .cif format.

§ NMR for **1** (d_8-toluene, 298 K). ^1H (300.13 MHz): δ 0.18 (s, 36 H, Ti{$P_3C_2[C(CH_3)_3]_2$}$_2$). $^{13}C\{^1H\}$ (75.47 MHz): δ 35.2 (d, $^2J_{CP}$ 7 Hz, Ti{$P_3C_2[C(CH_3)_3]_2$}$_2$), 42.6 (d, $^2J_{CP}$ 18 Hz, Ti{$P_3C_2[C(CH_3)_3]_2$}$_2$). $^{31}P\{^1H\}$ (121.49 MHz): d 342.5 (t, 1P, $^2J_{PP}$ 44.2 Hz, PPC*P*C), 386.0 (d, 2P, $^2J_{PP}$ = 46.7 Hz, *PP*CPC).

NMR for **2** (d_6-benzene, 298 K). ^1H (300.13 MHz): δ 1.05 (s, 9 H) 1.29 (s, 9 H), 1.38, 1.40 [2s (overlapping) 18 H], 1.67 (s, 9 H). $^{31}P\{^1H\}$ (121.49 MHz): $\delta_{P(1)}$ −60.3 (ddd, $^1J_{P(1)P(2)}$ 290, $^2J_{P(1)P(3)}$ 12, $^2J_{P(1)P(4)}$ 12 Hz), $\delta_{P(2)}$ 309 (dd, $^1J_{P(1)P(2)}$ 290, $^2J_{P(2)P(3)}$ 40 Hz), $\delta_{P(3)}$ 98.7 (dddd, $^2J_{P(2)P(3)}$ 40, $^2J_{P(3)P(4)}$ 32, $^2J_{P(3)P(1)}$ 12, $^2J_{P(3)P(5)}$ = 5 Hz), $\delta_{P(4)}$ 283.9 (dddd of m, $^2J_{P(4)P(6)}$ 70, $^2J_{P(4)P(3)}$ 32, $^2J_{P(4)P(5)\text{ or }P(1)}$ 14, $^2J_{P(4)P(1)\text{ or }P(5)}$ = 12, plus other *ca.* 5 Hz inter-ring couplings), $\delta_{P(5)}$ 260.8 [dd, $^1J_{P(5)P(6)}$ 430, $^2J_{P(5)P(7)}$ 50, $^2J_{P(5)P(4)}$ 12 Hz (inter-ring)], $d_{P(6)}$ 301.3 [dd, $^1J_{P(6)P(5)}$ 430, $^2J_{P(6)P(7)}$ 52, $^2J_{P(6)P(4)}$ 70 Hz (inter-ring)], $\delta_{P(7)}$ 225.2 (dd, $^2J_{P(7)P(6)}$ = 50, $^2J_{P(7)P(5)}$ 50 Hz).

1 G. P. Pez and J. N. Armor, *Adv. Organomet. Chem.*, 1981, **19**, 1.
2 R. D. Sanner, D. M. Duggan, T. C. McKenzie, R. E. Marsh and J. E. Bercaw, *J. Am. Chem. Soc.*, 1976, **98,** 8358.
3 B. H. Edwards, R. D Rogers, D. J. Sikora, J. L. Atwood and M. D. Rausch, *J. Am. Chem. Soc.*, 1983, **105**, 416.
4 L. B. Kool, M. D. Rausch, H. G. Alt, M. Herberhold, U. Thewalt and B. Wolf, *Angew. Chem., Int. Ed. Engl.*, 1985, **24**, 394.
5 S. A. Cohen, P. R. Auburn and J. E. Bercaw, *J. Am. Chem. Soc.*, 1983, **105,** 1136.
6 V. Varga, K. Mach, M. Polásek, P. Sedmera, J. Hiller, U. Thewalt and S. I. Troyanov, *J. Organomet. Chem.*, 1996, **506**, 241.
7 V. V. Burlakov, A. V. Polyakov, A. I Yanovsky, Y. T. Struchkov, V. B. Shur, M. E. Vol'pin, U. Rosenthal and H. Görls, *J. Organomet. Chem.*, 1994, **476,** 197.
8 P. B. Hitchcock, F. M. Kerton and G. A. Lawless, *J. Am. Chem. Soc.*, 1998, **120**, 10 264.
9 K. B. Dillon, F. Mathey and J. F. Nixon, *Phosphorus: The Carbon Copy*, John Wiley and Sons, Chichester 1998 and references therein.
10 F. G. N. Cloke, K. R. Flower, P. B. Hitchcock and J. F. Nixon, *J. Chem. Soc., Chem. Commun.*, 1995, 1659.
11 F. G. N. Cloke and M. L. H. Green, *J. Chem. Soc., Dalton Trans.*, 1981, 1938.
12 C. Callaghan, G. K. B. Clentsmith, F. G. N. Cloke, P. B. Hitchcock, J. F. Nixon and D. M. Vickers, *Organometallics*, 1999, **18**, 793.
13 P. B. Hitchcock, J. F. Nixon and R. M. Matos, *J. Organomet. Chem.*, 1995, **490**, 155.
14 R. Bartsch, P. B. Hitchcock and J. F. Nixon,. *J. Chem. Soc., Chem. Commun.*, 1987, 1146.
15 R. Bartsch, P. B. Hitchcock and J. F. Nixon,. *J. Organomet. Chem.*, 1988, **356**, C1.
16 U. Zenneck, personal communication.
17 R. D Rogers, J. L. Atwood, D. Foust and M. D. Rausch, *J. Cryst. Mol. Struct.*, 1981, **11**, 183.
18 K. R Flower and P. B. Hitchcock, *J. Organomet. Chem.*, 1996, **507**, 275.
19 P. Seiler and J. Dunitz, *Acta Crystallogr., Sect. B.*, 1979, **35**, 1069.
20 A. Haaland, *Acc. Chem. Res.*, 1978, **12**, 415.
21 F. G. N. Cloke, J. R. Hanks, P. B. Hitchcock and J. F. Nixon, papers in preparation.
22 M. Dubeck, *J. Am. Chem. Soc.*, 1960, **82**, 6193.
23 D. W. McBride, R. L. Pruett, E. Pitcher and F. G. A. Stone *J. Am. Chem. Soc.*, 1962, **84**, 497.

Communication 9/05469C

ChemComm

Synthesis of amino-sugars using the directed dihydroxylation reaction

Timothy J. Donohoe,* Kevin Blades and Madeleine Helliwell†

Department of Chemistry, The University of Manchester, Oxford Road, Manchester, UK, M13 9PL. E-mail: t.j.donohoe@man.ac.uk

Received (in Cambridge, UK) 22nd June 1999, Accepted 29th July 1999

The synthesis of protected forms of two amino-sugars, talosamine 1 and allosamine 2, is described; the *syn, syn* stereochemistry at C-2, C-3 and C-4 was controlled by the use of a hydrogen-bonding directed dihydroxylation reaction using stoichiometric and catalytic OsO_4; proof of the relative stereochemistry of the allosamine series was obtained through an X-ray crystal structure of a protected derivative.

2-Amino-sugars are the key constituents of a variety of naturally occurring polysaccharides. We are interested in the synthesis of two of the rarer amino-sugars, talosamine and allosamine: *N*-acetyltalosamine has been isolated from both bovine and ovine cartilage,[1] whilst *N*-acetylallosamine is the repeat unit in the sugar portion of allosamidin[2] (which is an interesting chitinase inhibitor).

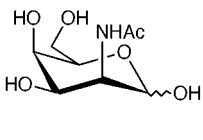

N-acetyl-D-talosamine
1

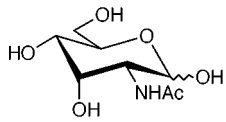

N-acetyl-D-allosamine
2

We have recently described that combination of OsO_4 with an amine (usually TMEDA) produces a reagent which dihydroxylates allylic amides: efficient hydrogen bonding between the oxidant and the allylic amide means that the stereoselectivity observed is contra-steric and therefore opposite to that obtained under standard oxidation conditions.[3] Examination of talosamine and allosamine reveals that they both have *syn,syn* stereochemistry at C2–C4 and so are ideally configured for synthesis *via* our chemistry.

Our synthesis of *N*-acetyl talosamine began with tri-*O*-acetyl-D-glucal, which was converted into the allylic trichloroacetamide **5** using standard chemistry (Scheme 1).[4] Compounds **3**, **4** and **5** are formed as mixtures of anomers (9 : 1) and the major one was separated and is shown for clarity. The dihydroxylation of **5** was then examined under a variety of conditions to investigate ways of forming the *syn,syn* isomer which corresponds to the talosamine series. As can be observed from Scheme 1, oxidation under standard Upjohn conditons (step viii) gave predominantly the *syn,anti* isomer (this corresponds to the altrose series of amino sugars) as expected. However, use of OsO_4 and TMEDA at low temperature was successful in completely reversing the facial bias of this molecule and provides the *syn,syn* isomer with complete stereoselectivity (as measured by ^1H NMR spectroscopy, step ix) and excellent yield. The relative stereochemistry of the adducts shown in Scheme 1 was proven by correlation to a compound of known configuration (*vide infra*). Note that the products from the stoichiometric and catalytic oxidations are slightly different; the acidic work-up used with stoichiometric OsO_4 removes the TBDMS group at C-6; the resulting triol was then peracetylated with Ac_2O in order to expedite isolation.

† Author to whom correspondence regarding the crystallography should be addressed.

We then turned our attention to allosamine **2** and proceeded to prepare allylic amide **9** by a process analogous to that described earlier (Scheme 2).[5]‡ The modified conditions reported by Isobe and co-workers were crucial to success in the Overman rearrangement.[6] The oxidation of **9** (again the major anomer was isolated and is shown for clarity) proved to be most interesting. In this case the standard Upjohn reaction was moderately *syn* selective for the allosamine isomer (step vi). Unfortunately the addition of TMEDA to OsO_4 only marginally improved the *syn* selectivity of the oxidation, (step vii). Occasionally, our attempts to use TMEDA/OsO_4 for directing the dihydroxylation reaction have been frustrated by either electrostatic or steric repulsion between the substrate and the oxidant.[7] In such cases we have found that addition of a monodentate amine (quinuclidine is best) to OsO_4 can give better *syn* stereoselectivity *via* a hydrogen bonding process; this was indeed the case (step viii), and the selectivity attainable was now high enough to be synthetically useful. The reagent formed during this reaction is not as effective a hydrogen bond acceptor as OsO_4/TMEDA but can give higher levels of *syn* stereoselectivity, presumably as a consequence of its reduced steric bulk. One of the advantages of using a monodentate amine promoter in the dihydroxylation reaction is that the process can be made catalytic in osmium by using the amine as its

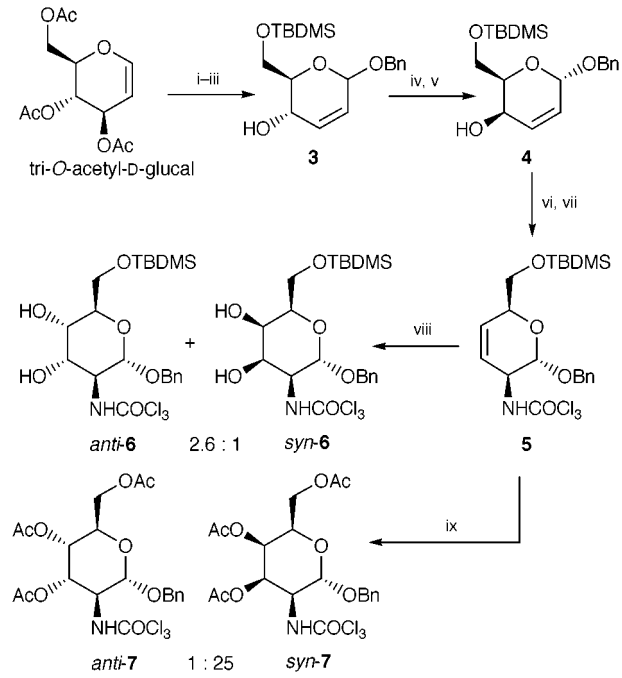

Scheme 1 *Reagents and conditions*: i, BnOH (1.1 equiv.), $BF_3{\cdot}OEt_2$ (0.1 equiv.), CH_2Cl_2, −20 °C room temp., 1 h, 98%; ii, K_2CO_3 (0.5 equiv.), MeOH–H_2O (4 : 1), room temp., 1 h, 93%; iii, TBDMSCl (1.1 equiv.), Et_3N (2.2 equiv.), CH_2Cl_2, room temp., 24 h, 74%; iv, PPh_3 (4.0 equiv.), $PhCO_2H$ (4.0 equiv.), DEAD (4.0 equiv.), THF, 0 °C, 2 h, 88%; v, NaOMe (0.5 equiv.), MeOH, room temp., 86%; vi, DBU (1.2 equiv.) CCl_3CN (1.3 equiv.), CH_2Cl_2, −20 °C–room temp., 97%; vii, xylene, cat. K_2CO_3, Δ, 18 h, 93%; viii, NMO (1.5 equiv.), cat. OsO_4, acetone–H_2O (4:1), room temp., 77%; ix, TMEDA (1.05 equiv.), OsO_4 (1.05 equiv.), CH_2Cl_2, −78 °C–room temp., then MeOH–HCl, then Ac_2O, 89%.

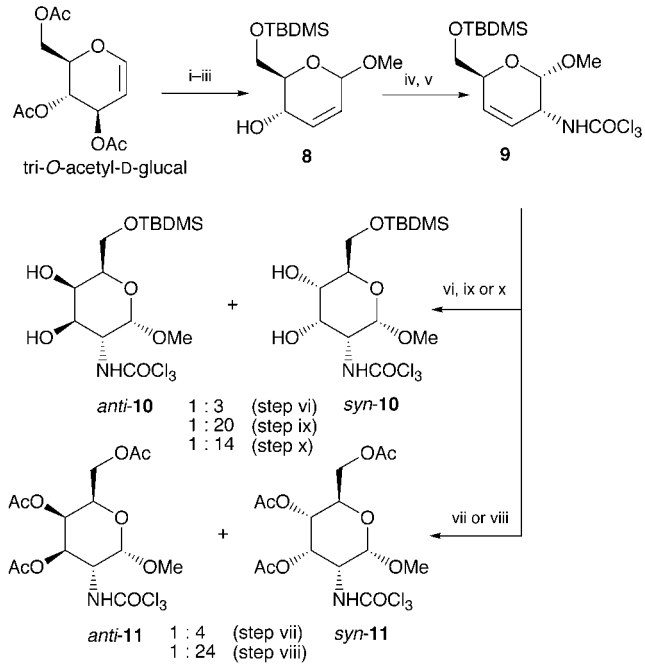

Scheme 2 *Reagents and conditions*: i, MeOH (1.1 equiv.), $BF_3{\cdot}OEt_2$ (0.5 equiv.), toluene, −20 °C–room temp., 1 h, 89%; ii, K_2CO_3 (0.5 equiv.), MeOH–H_2O (4:1), room temp., 1 h, 92%; iii, TBDMSCl (1.1 equiv.), Et_3N (2.2 equiv.), CH_2Cl_2, room temp., 24 h, 91%; iv, DBU (1.2 equiv.), CCl_3CN (1.3 equiv.), CH_2Cl_2, −20 °C–room temp., 98%; v, Ph_2O, cat. K_2CO_3, 195 °C, 3 h, 64%; vi, NMO (1.5 equiv.), cat. OsO_4, acetone–H_2O (4:1), room temp., 75%; vii, TMEDA (1.05 equiv.), OsO_4 (1.05 equiv.), CH_2Cl_2, −78 °C–room temp., then MeOH–HCl, then Ac_2O, 92%; viii, quinuclidine (1.1 equiv.), OsO_4 (1.05 equiv.), CH_2Cl_2, −78 °C–room temp., then MeOH–HCl, then Ac_2O, 90%; ix, quinuclidine *N*-oxide (2.0 equiv.), cat. OsO_4, CH_2Cl_2, room temp., 80%; x, $Me_3NO{\cdot}2H_2O$ (1.5 equiv.), cat. OsO_4, CH_2Cl_2, room temp., 87%.

corresponding *N*-oxide (with sufficient water added to allow the catalytic cycle to turn over). So, the use of quinuclidine *N*-oxide (2 equiv.)[8] and *catalytic* OsO_4 (5 mol%) with approximately 4 equiv. of water, also gave an excellent level of *syn* stereoselectivity (step ix). This novel oxidising system gave better stereoselectivity than that observed by using trimethylamine *N*-oxide as a reoxidant (step x).[9]

The relative stereochemistry of the allosamine series of compounds was proven by an X-ray crystal structure on the benzylidine protected derivative **12** (Fig. 1).§

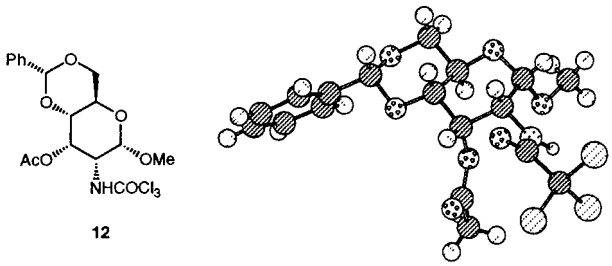

Fig. 1 X-Ray structure of **12**.

As amino-sugars frequently occur in nature as their *N*-acetyl derivatives, we removed the trichloroacetyl group and added an acetyl functionality. This was accomplished readily in a two stage, one pot process (Scheme 3).¶ Compound **14** prepared by this route is known in the literature[10] and displayed characteristics identical to those previously reported (^{1}H NMR, $[\alpha]_D$); this correlation proves the stereochemistry of the talosamine series described in Scheme 1.

To conclude, we have prepared protected forms of two naturally occurring and rare amino-sugars, talosamine and allosamine: both compounds are available in high yield and with excellent levels of stereoselectivity. These derivatives are ideally configured for further elaboration into polysaccharides and work is continuing in this direction. Moreover, we have

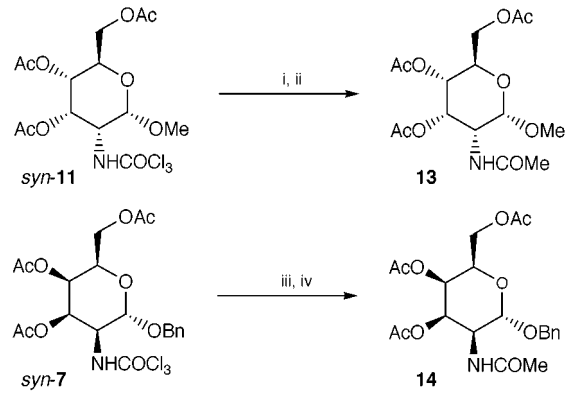

Scheme 3 *Reagents and conditions*: i, NaOH, EtOH, 10 min; ii, Ac_2O, cat. DMAP, pyridine, 24 h, 82%; iii, NaOH, EtOH, 10 min; iv Ac_2O, cat. DMAP, pyridine, 24 h, 86%.

introduced a novel oxidising system, using quinudidine *N*-oxide, which is capable of dihydroxylating certain allylic amides with hydrogen-bonding control‖ and which uses *catalytic* OsO_4.

We wish to thank the EPSRC (K. B.) and Zeneca Pharmaceuticals (Strategic Research Fund) for financial support.

Notes and references

‡ A similar strategy has been adopted previously for the synthesis of allosamine. However, the reported route is troubled by both a low yielding Overman rearrangement (30%) and oxidation with RuO_4 (50%).

§ *Crystal data* for $C_{18}H_{20}NO_7Cl_3$ **12**: M = 468.70, orthorhombic, a = 12.862(7), b = 27.763(6), c = 6.007(4) Å^3, T = 296 K, space group $P2_12_12_1$ (no. 19), Z = 4, μ(Cu-Kα) = 4.225 mm^{-1}, 2179 independent reflections which were used in all calculations. The final $\omega R(F^2)$ was 0.1554 (all data). $R(F)$ was 0.0499 using 1703 reflections with $I > 2\sigma(I)$. The structure was solved using direct methods and developed using difference Fourier techniques, then refined by full matrix least-squares on F^2. CCDC 182/1357.

¶ *Selected data* for **13**: $[\alpha]_D$ +69 (*c* 5.33, EtOH); δ_H(300 MHz; $CDCl_3$) 5.83 (d, 1H, *J* 9.3), 5.51 (dd, 1H, *J* 3.0, 3.5), 4.97 (dd, 1H, *J* 3.0, 10.2), 4.68 (d, 1H, *J* 4.4), 4.48 (ddd, 1H, *J* 3.5, 4.4, 9.3), 4.30-4.15 (m, 3H), 3.42 (s, 3H), 2.16 (s, 3H), 2.09 (s, 3H), 1.99 (s, 3H) 1.97 (s, 3H); δ_C (75 MHz; $CDCl_3$) 170.6, 170.4, 169.2, 169.0, 97.6, 68.3, 66.0, 63.0, 62.1, 55.7, 47.4, 23.0, 20.9, 20.6, 20.4. For **14**: $[\alpha]_D$ +72 (*c* 0.80, $CHCl_3$); δ_H(300 MHz; $CDCl_3$) 6.39 (d, 1H, *J* 9.6), 5.40 (m, 1H), 5.34 (dd, 1H, *J* 3.5, 4.5), 4.91 (d, 1H, *J* 1.1), 4.68 (d, 1H, *J* 11.6), 4.54 (d, 1H, *J* 11.6), 4.48 (dddd, 1H, *J* 9.6, 4.7, 1.1, 1.1), 4.27 (ddd, 1H, *J* 7.1, 6.2, 1.3), 4.12 (ABX, 2H, J_{AB} 11.1, J_{AX} 6.2 J_{BX} 7.1), 2.18 (s, 3H), 2.07 (s, 3H), 2.03 (s, 3H) 1.99 (s, 3H); δ_C(75 MHz; $CDCl_3$) 170.3, 169.4, 169.4, 168.9, 136.2, 128.5, 128.1, 128.0, 99.1, 69.8, 67.7, 66.5, 64.7, 61.7, 48.5, 23.4, 20.6, 20.5.

‖ Oxidation of **5** with quinuclidine *N*-oxide under the conditions described in Scheme 2 gave a 1:1 mixture of stereoisomers. However, other allylic amides do give *syn* selective results using this oxidant; details will be reported in due course.

1 M. J. Crumpton, *Nature*, 1957, **180**, 605; R. Heyworth and P. G. Walker, *Proc. Int. Congr. Biochem. 4th*, 1958, **1**, 7.
2 See, D. J. Kassab and B. Ganem, *J. Am. Chem. Soc*., 1999, **64**, 1782 and references therein.
3 T. J. Donohoe, K. Blades, P. R. Moore, J. J. G. Winter, M. Helliwell and G. Stemp, *J. Org. Chem*., 1999, **64**, 2980; T. J. Donohoe, P. R. Moore, M. J. Waring and N. J. Newcombe, *Tetrahedron Lett.*, 1997, **38**, 5027; for early studies in this area see: H. C. Kolb, M. S. VanNieuwenhze and K. B. Sharpless, *Chem. Rev*., 1994, **94**, 2483.
4 K. Takeda, E. Kaji, Y. Konda, N. Sato, H. Nakamura, N. Miya, A. Morizane, Y. Yanagisawa, A. Akiyama, S. Zen and Y. Harigaya, *Tetrahedron Lett*., 1992, **33**, 7145.
5 T. Sugai, H. Okazaki, A. Kuboki and H. Ohta, *Bull. Chem. Soc. Jpn*., 1997, **70**, 2535.
6 T. Nishikawa, M. Asai, N. Ohyabu and M. Isobe, *J. Org. Chem*., 1998, **63**, 188.
7 T. J. Donohoe, K. Blades, M. Helliwell, M. J. Waring, and N. J. Newcombe, *Tetrahedron Lett.*, 1998, **39**, 8755.
8 I. A. O'Neil, J. Y. Q. Lai and D. Wynn, *Chem. Commun*., 1999, 59.
9 G. Poli, *Tetrahedron Lett*., 1989, **30**, 7385; T. J. Donohoe, R. Garg and P. R. Moore, *Tetrahedron Lett*., 1996, **37**, 3407; T. J. Donohoe, P. R. Moore and R. L. Beddoes, *J. Chem. Soc., Perkin Trans. 1*, 1997, 43.
10 A. Banaszek and W. Karpiesiuk, *Carbohydr. Res.*, 1994, **251**, 233.

Communication 9/04991F

ChemComm

Photodegradation of aryl sulfonamides: *N*-tosylglycine

Roger R. Hill,* Graham E. Jeffs, David R. Roberts and Sharon A. Wood

Department of Chemistry, The Open University, Milton Keynes, UK, MK7 6AA. E-mail: r.r.hill@open.ac.uk

Received (in Cambridge, UK) 2nd July 1999, Accepted 2nd August 1999

Continuing uncertainty about pathways and consequences of the photolability of aryl sulfonamides is partly resolved by the results of comprehensive product analysis in the photolysis of aqueous *N*-tosylglycine, which indicate that intramolecular electron or hydrogen transfer (according to conditions) promote the widely reported S–N cleavage and reveal the nature of subsequent and competing processes.

Aryl sulfonamides are of topical interest photochemically for two reasons: as photolabile pharmaceutical compounds[1] and as photolabile protected amines, peptides and proteins, the latter attracting continuing study[2] despite subsequent results[3] detracting from their early promise.[4] Regulatory demands for increasingly detailed stability data[5] contrast with rudimentary knowledge of the photochemistry of existing sulfonamide drugs, and prompt increasing attention to those in development. The variable and generally unsatisfactory results of attempted photodeprotections have been attributed to side reactions that can be reduced in some cases by structural modification[3] or the addition of further reagents,[6] but remain largely unknown.

In a continuing study of the photochemistry of peptide derivatives,[7,8] we have monitored products during the photolysis of aqueous *N*-tosylglycine (**1**) and, observing a high mass balance early in the reaction, are able to propose a sequence of events that both explains the product distributions and implicates processes that may direct photolytic outcomes with other aryl sulfonamides.

Photolyses were carried out under nitrogen with 10^{-2} mol dm^{-3} aqueous solutions of *N*-tosylglycine, either unadjusted (pH 3) or adjusted to pH 9 with NaOH, in quartz tubes and using a carousel surrounding a 400 W medium pressure mercury arc as previously described.[7] Products were identified by diagnostic chromatographic comparison with standards and quantified by HPLC[9] (formaldehyde and glyoxylic acid as DNP derivatives; glycine as AccQ.Tag® derivative by fluorescence detection[10]) and gas electrode analysis (CO_2 and NH_3).[7]

The data in Table 1 are consistent with the sequence of reactions in Scheme 1 (shown for 7% reaction at pH 9), which also accords collectively with several earlier observations of sulfonamide photochemistry reported separately.[3] Reaction (i) indicates a cyclic abstraction of H–C_α and reaction (ii) suggests β-homolysis of a bond known to be involved in the $\pi \rightarrow \pi^*$ state of analogous carboxamides[11] and dimerization of the comparatively stable amido-methylene radical.[7] The major route, reaction (iii), reflects the known behaviour of excited aryl sulfonamides as electron acceptors,[12] and generates an intermediate from which observed products are derived by loss of CO_2 alone [reaction (iv)] or with concomitant S–N cleavage [reaction (vi)], and, more speculatively, *via* cyclizations and hydrolysis [reactions (v) and (vii)]. Such processes would require particular orbital alignments, so product distribution would be determined largely by the conformations available in the short-lived intermediates.

Table 1 Product distributions (mol%) in the photolysis of *N*-tosylglycine

	7% reaction[a]		20% reaction[b]	
Product	pH 3	pH 9	pH 3	pH 9
NH_3	47	49	50	49
CO_2	34	80	32	87
TsH[c]	28	68	31	62
HCHO	29	51	29	35
$OHCCO_2H$	13	7	8	4
TsOH	19	7	6	3
$H_3N^+CH_2CO_2^-$	13	—[d]	8	—
$TsNH_2$	5	7	3	5
$TsNHCH_3$	0	8	1	6
$(TsNHCH_2)_2$[e]	14	9	8	5
Mass balance[f]	80	> 90	60	60

[a] Error < ± 4. [b] Error < ± 2. [c] Standard: Li salt (98%), Sigma-Aldrich Ltd. [d] Not measured. [e] Standard tosylation of diamine, mp 161 °C (lit., 160 °C). [f] According to Scheme 1 (see text); error < ± 11 and < ± 6 at 7 and 20% reaction, respectively.

The percentage assigned to each route in Scheme 1 corresponds with the observed yield values of uniquely associated products. The accumulated values implicated for coproducts formed in more than one route [CO_2 (68%), NH_3 (58%) and TsH (58%)] are in fair agreement with those observed, and would be more so if the value for HCHO reflected some losses, directly or indirectly, by the unassigned reducing capacity available from reaction (ii). The latter would, in any case, account for loss of some material and this is incorporated in the mass balance data of Table 1. Scheme 1 is also supported by product correlations (*e.g.* TsH *vs.* NH_3, r^2 = 0.998, slope 1.1; TsH *vs.* HCHO + glyoxylic acid, r^2 = 0.984, slope = 0.9) and by the main differences in outcome when the substrate is not ionized. In that case, lower yields of principal products by reaction (iii) are consistent with the need for H-atom transfer,[13] making other pathways, including reactions (i) and (ii), slightly more competitive. The lack of $TsNHCH_3$ and the enhanced yield of TsOH may be associated with the inability to generate the sulfonyl group directly in reactions (iv) and the easier hydrolysis anticipated for the protonated intermediate in reactions (vii), respectively. While quantitation at 20% conversion is intrinsically more accurate, the scope for complication by secondary processes is increased. The data remain consistent with Scheme 1, however.

It would appear from these results that electron or hydrogen-atom transfer to the sulfonyl group will be prominent in the photochemistry of aryl sulfonamides, with β-homolysis a

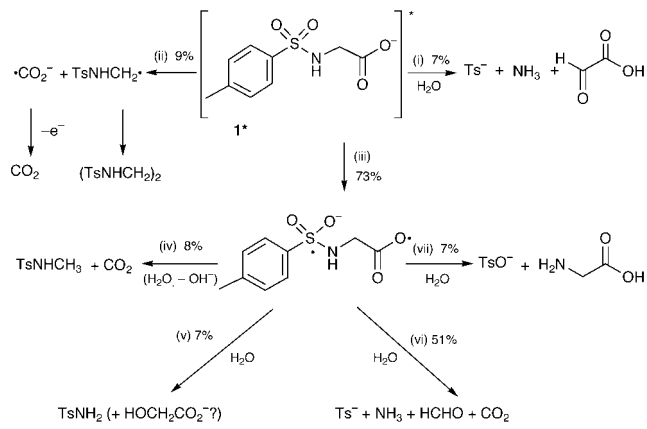

Scheme 1

significant competing process. The availability of diverse pathways subsequently suggests that a search among such derivatives for photoremoveable protecting groups is unlikely to be productive and that their use for this purpose may be best pursued with cathodic deprotection strategies in mind.[14] The photochemical strategy is flawed by the capacity of the oxidized component of the charge-separated intermediates to promote highly competitive alternative degradation.

We thank Central Research, Pfizer Ltd (Sandwich) for financial support for this work and Mrs J Burrage for technical assistance.

Notes and references

1 (*a*) *Drugs: Photochemistry and Photostability*, ed. A. Albini and E. Fasani, Royal Society of Chemistry, London, 1998; (*b*) *Photostability of Drugs and Drug Formulations*, ed. H. H. Tonnesen, Taylor and Francis, London, 1996.
2 G. Papageorgiou and J. E. T. Corrie, *Tetrahedron*, 1999, **55**, 237.
3 J. A. Pincock, in *Handbook of Photochemistry and Photobiology*, ed. W. M. Horsepool and P.-S. Song, CRC Press, Boca Raton, 1995, p. 757; J. E. T. Corrie and G. Papageorgiou, *J. Chem. Soc., Perkin Trans. 1*, 1996, 1583.
4 L. D'Souza, *Science*, 1968, **160**, 882.
5 Ref. 1(*a*), p. 66.
6 T. Hamada, A. Nishida and O. Yonemitsu, *Tetrahedron Lett.*, 1989, **30**, 4241.
7 R. R. Hill, J. D. Coyle, D. Birch, E. Dawe, G. E. Jeffs, D. Randall, I. Stec and T. M. Stevenson, *J. Am. Chem. Soc.*, 1991, **113**, 1805.
8 R. R. Hill, C. W. Richenberg and D. R. Roberts, *J. Photochem. Photobiol. A: Chem.*, 1996, **97**, 109; R. R. Hill, G. E. Jeffs, F. Banaghan, T. McNally and A. R. Werninck, *J. Chem. Soc., Perkin Trans. 2*, 1996, 1595.
9 Waters Millenium System with diode array detection; Phenomenex Luna 5 mm C18 column; gradient elution using water, 0.1 mol dm^{-3} phosphoric acid and MeCN.
10 C. van Wandelen and S. A. Cohen, *J. Chromatogr.*, 1997, **763**, 11.
11 G. Sieler, R. Schweitzer-Sterner, J. S. W. Holtz, V. Pajcini and S. A. Asher, *J. Phys. Chem. B*, 1999, **103**, 372; C.M. Brenemen and L.W. Weber, *Can. J. Chem.*, 1996, **74**, 1271.
12 G. Jones, L. N. Lu, H. Fu, C. W. Farahat, C. Oh, S. R. Greenfield, D. J. Gosztola and M. R. Wasielewski, *J. Phys. Chem. B*, 1999, **103**, 572.
13 Closely analogous to that observed in the photolytic decarboxylation of phthalimido amino acids: A.G. Griesbeck, *Chimia*, 1998, **52**, 272.
14 R. Kossai, B. Emir, J. Simonet and G. Mousset, *J. Electroanal. Chem.*, 1989, **270**, 253.

Communication 9/05358A

Stereoselective total synthesis of (±)-fragranol by $TiCl_4$ promoted [2+2] cycloaddition of allyl-*tert*-butyldiphenylsilane and methyl methacrylate†

Hans-Joachim Knölker,*[a] Gerhard Baum,[b] Oliver Schmitt[a] and Günter Wanzl[a]

[a] *Institut für Organische Chemie, Universität Karlsruhe, Richard-Willstätter-Allee, 76131 Karlsruhe, Germany. E-mail: knoe@ochhades.chemie.uni-karlsruhe.de*

[b] *Institut für Anorganische Chemie, Universität Karlsruhe, Engesserstraße, 76128 Karlsruhe, Germany.*

Received (in Liverpool, UK) 21st June 1999, Accepted 22nd July 1999

A stereoselective total synthesis of the monoterpenoid alcohol (±)-fragranol has been accomplished utilizing a $TiCl_4$ promoted [2 + 2] cycloaddition of allyl-*tert*-butyldiphenylsilane and methyl methacrylate as the key step.

1 **2**

The monoterpenoid alcohol fragranol **1** was isolated in 1973 by Bohlmann and co-workers from the roots of *Artemisia fragrans* Willd.[2] The diastereoisomeric grandisol **2** is a sex pheromone of the male cotton boll weevil *Anthonomus grandis* Boheman and other beetles.[3] Because of their structural features and biological activity both compounds represent important targets for novel procedures directed towards the total synthesis of four-membered ring natural products.[4] Over the past years we developed a novel synthetic methodology for the stereoselective construction of cyclobutanes by $TiCl_4$ promoted [2 + 2] cycloaddition of allylsilanes and acrylic esters.[5] We now report the stereoselective total synthesis of fragranol **1** which is the first application of this strategy to the total synthesis of a natural product.[6]

The $TiCl_4$ promoted [2 + 2] cycloaddition of allyl-*tert*-butyldiphenylsilane **4** and methyl methacrylate **3** afforded the two diastereoisomeric silylmethylcyclobutanes *anti*-**5** and *syn*-**5** along with the silylcyclopentane **6** in a total yield of 84% and a ratio of 14 : 2 : 1 (Scheme 1).‡ The structural and stereochemical assignments were based on comparison of the ^{13}C NMR data with those of our previous studies.[5a] After chromatography the major isomer *anti*-**5** was crystallized in pure form out of this mixture and structurally confirmed by X-ray crystallography (Fig. 1).§

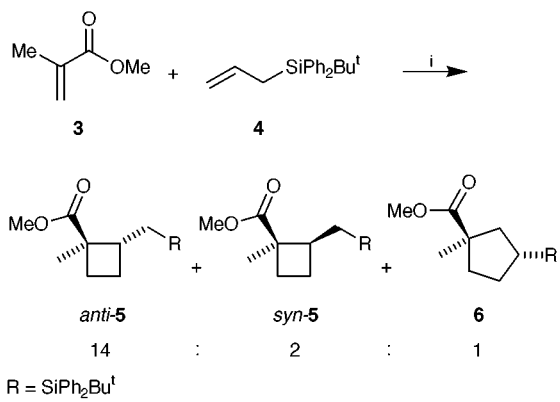

Scheme 1 *Reagents and conditions*: i, $TiCl_4$, CH_2Cl_2, 40 °C, 4 d (84%, ratio *anti*-**5** : *syn*-**5** : **6** = 14 : 2 : 1), then crystallization from this mixture afforded selectively *anti*-**5** (67%).

† See ref. 1.

For the projected total synthesis the silyl group had to be converted into a hydroxy group. We have recently shown that by modifaction of the Fleming–Tamao oxidation[7] sterically hindered silyl groups, like triphenylsilyl, diisopropylphenylsilyl and *tert*-butyldiphenylsilyl, can be transformed to hydroxy groups.[8] Using these conditions the *tert*-butyldiphenylsilyl derivative *anti*-**5** was first converted to the *tert*-butyldifluorosilyl derivative **7** and then to the alcohol **8** (Scheme 2). The next task was to transform the hydroxymethyl group into the isopropenyl group present in the natural product. For the oxidation of the hydroxy to the formyl group we required reaction conditions which avoided an epimerization at the stereogenic center. Swern oxidation[9] and oxidation with the Dess–Martin periodinane reagent[10] provided good yields, however to a large extent with epimerization. Treatment of **8** with tetrapropylammonium perruthenate (TPAP)[11] provided a yield of 94% for the aldehydes *anti*-**9** and *syn*-**9** which were obtained in a ratio of 13 : 1.

Chemoselective addition of methyltitanium triisopropoxide[12] at the formyl group at −10 °C afforded the alcohol **10** as a 1 : 1 mixture of two diastereoisomers (Scheme 3). A further oxidation with TPAP[11] provided in 94% yield the methyl ketone **11** without epimerization at the chiral center. Wittig reaction using methylenetriphenylphosphorane gave the isopropenyl derivative **12** which was reduced to the alcohol **13** by $LiAlH_4$. Finally, a homologation of the primary alcohol was required. For this purpose the alcohol **13** was transformed to the aldehyde **14** by Swern oxidation.[9] Wittig reaction using methoxymethyltriphenylphosphonium bromide/sodium amide[13] followed by hydrolysis of the resulting enol ether afforded the homologated

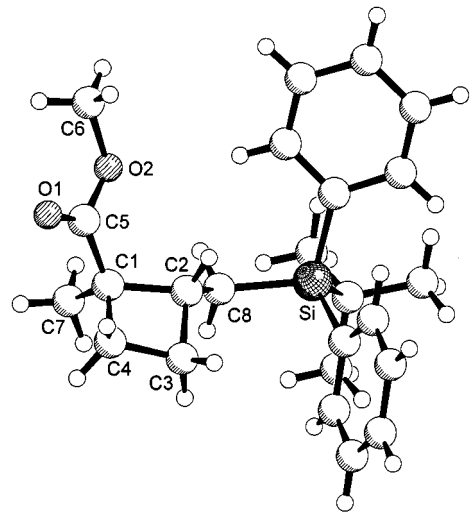

Fig. 1 Molecular structure of *anti*-**5** in the crystal. Selected bond lengths (Å): C(1)–C(2) 1.570(3), C(2)–C(3) 1.538(3), C(3)–C(4) 1.532(3), C(1)–C(4) 1.541(4), C(1)–C(5) 1.507(4), C(1)–C(7) 1.516(4), C(2)–C(8) 1.525(3), C(8)–Si 1.883(2).

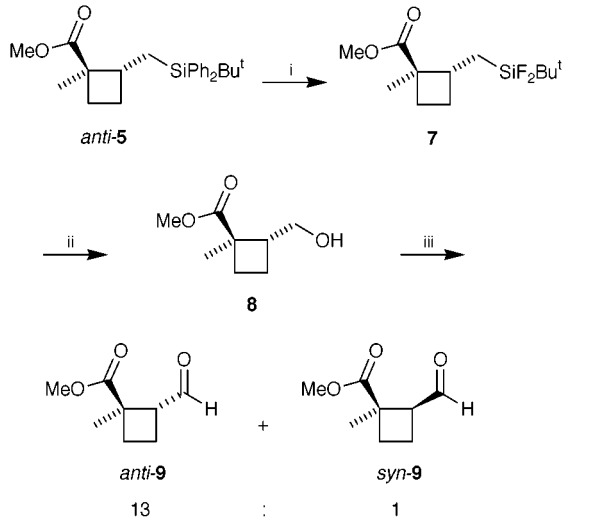

Scheme 2 *Reagents and conditions*: i, BF_3·2 HOAc, CH_2Cl_2, 40 °C, 4 h (87%); ii, H_2O_2, KF, $NaHCO_3$, THF–MeOH (1:1), 25 °C, 24 h (51%); iii, TPAP (cat.), NMO, powdered 4 Å molecular sieves, CH_2Cl_2, 0 to 25 °C, 2 h (94%, ratio *anti*-**9**:*syn*-**9** = 13:1).

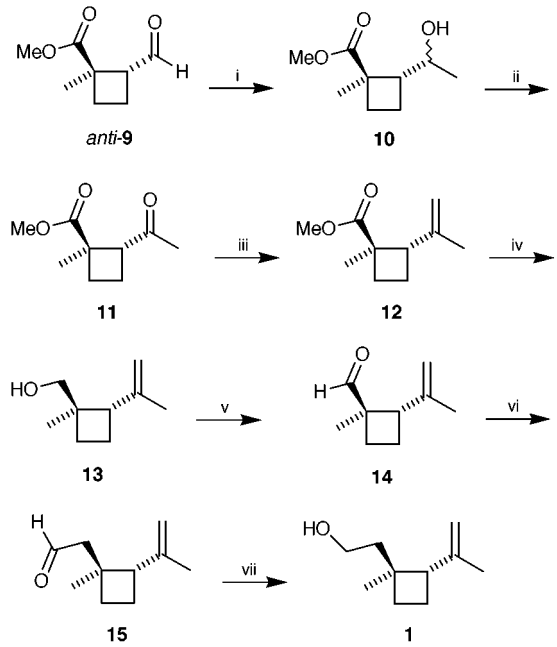

Scheme 3 *Reagents and conditions*: i, $MeTi(OP^ir)_3$, CH_2Cl_2, −10 to 25 °C, 14 h (70%); ii, TPAP (cat.), NMO, powdered 4 Å molecular sieves, CH_2Cl_2, 0 to 25 °C, 2 h (94%); iii, $Ph_3P{=}CH_2$, THF, 0 to 25 °C, 2 h (65%); iv, $LiAlH_4$, THF, 0 to 25 °C, 12 h (99%); v, $(COCl)_2$, DMSO, CH_2Cl_2, Et_3N, −78 °C, 20 min (84%); vi, $MeOCH_2Ph_3P^+Br^-$, $NaNH_2$, Et_2O, −20 to 25 °C, 12 h, then TFA–H_2O (4:1), Et_2O, 25 °C, 12 h (78%); vii, $LiAlH_4$, Et_2O, 0 °C, 10 min (93%).

aldehyde **15** which on reduction with $LiAlH_4$ provided (±)-fragranol **1**. The spectral data of our synthetic fragranol (IR, ^{1}H NMR, ^{13}C NMR, MS and HRMS)¶ were in full agreement with those reported for the natural product.[2,6]

The present synthesis *via* the [2 + 2] cycloaddition of allyl-*tert*-butyldiphenylsilane **4** afforded fragranol in 11 steps and 7% overall yield based on methyl methacrylate **3**. It has been demonstrated for the first time that the Lewis acid promoted cycloaddition of allyl-*tert*-butyldiphenylsilane followed by our modified Fleming–Tamao oxidation represents a powerful new tool in natural product synthesis.

Financial support of this project was provided by the Deutsche Forschungsgemeinschaft (Kn 240/5-3) and the Fonds der Chemischen Industrie. We thank Dr John, Wacker-Chemie GmbH, Burghausen, for a generous gift of *tert*-butylchlorodiphenylsilane.

Notes and references

‡ *Synthesis* of *anti*-**5**: A solution of methyl methacrylate **3** (3.37 g, 33.7 mmol, 3.6 ml) in dry CH_2Cl_2 (30 ml) was added to a stirred solution of $TiCl_4$ (6.92 g, 36.5 mmol, 4 ml) in dry CH_2Cl_2 (50 ml) under argon at room temperature. After addition of a solution of allyl-*tert*-butyldiphenylsilane **4** (13.6 g, 48.5 mmol) in dry CH_2Cl_2 (30 ml) the reaction mixture was heated at reflux for 4 days. The mixture was hydrolyzed by addition of aq. NH_4Cl, the organic layer was separated, the aqueous layer was extracted three times with CH_2Cl_2 and the combined organic layers were dried over $MgSO_4$. Evaporation of the solvent and flash chromatography (hexane–Et_2O 20:1) of the residue on silica gel afforded a mixture of *anti*-**5**, *syn*-**5** and **6** (10.8 g, 84%, ratio 14:2:1). Crystallization out of this oil over a period of 14 days provided the cyclobutane *anti*-**5** (8.6 g, 67%) as colorless crystals, mp 65 °C; δ_H (400 MHz, $CDCl_3$) 1.04 (s, 9 H), 1.12–1.27 (m, 3 H), 1.33 (s, 3 H), 1.44 (m, 2 H), 2.10 (dt, *J* 9.0, 10.8, 1 H), 2.70 (dddd, *J* = 12.4, 10.3, 8.4, 2.1, 1 H), 3.67 (s, 3 H), 7.31–7.41 (m, 6 H), 7.63 (m, 4 H); δ_C (100 MHz, $CDCl_3$)11.43 (CH_2), 16.99 (CH_3), 18.11 (C), 25.29 (CH_2), 27.83 (3 CH_3), 28.62 (CH_2), 37.47 (CH), 46.75 (C), 51.44 (CH_3), 127.37 (2 CH), 127.52 (2 CH), 128.96 (CH), 129.00 (CH), 134.26 (C), 135.26 (C), 135.95 (2 CH), 136.04 (2 CH), 177.94 (C=O) (calc. for $C_{24}H_{32}O_2Si$: C, 75.74; H, 8.47; found: C, 75.65; H, 8.35%).

§ *Crystal data* for *anti*-**5**: $C_{24}H_{32}O_2Si$, *M* = 380.59, orthorhombic, space group $P2_12_12_1$, *a* = 7.900(3), *b* = 14.751(5), *c* = 18.956(6) Å, *U* = 2209.0(13) Å^3, *Z* = 4, D_c = 1.144 g cm^{-3}, μ = 0.121 mm^{-1}, *T* = 200(2) K, Mo-Kα (λ = 0.71073 Å), 10267 reflections collected, 4228 unique (R_{int} = 0.0912), 249 parameters; STOE IPDS area detector. The structure was solved by direct methods (SHELXS-97) and refined by full-matrix least-squares on F^2 (SHELXL-97). R_1 [$I > 2\sigma(I)$] = 0.0523, wR_2 = 0.1392, absolute structure (Flack parameter): χ = −0.10(14). CCDC 182/1352. See http://www.rsc.org/suppdata/cc/1999/1737/ for crystallographic data in .cif format.

¶ *Spectral data* for **1**: ν_{max} (film)/cm^{-1} 3352 (br), 3080, 2960, 2931, 2870, 1646, 1455, 1378, 1283, 1182, 1161, 1054, 886; δ_H (500 MHz, $CDCl_3$) 0.92 (s, 3 H), 1.41 (m, 1 H), 1.64 (s, 3 H), 1.67 (br s, 1 H), 1.72–1.84 (m, 4 H), 1.97 (m, 1 H), 2.56 (m, 1 H), 3.67 (m, 2 H), 4.61 (s, 1 H), 4.82 (q, *J* 1.5, 1 H); δ_C (125 MHz, $CDCl_3$): 19.46 (CH_3), 19.73 (CH_2), 23.02 (CH_3), 30.23 (CH_2), 40.93 (C), 46.64 (CH_2), 50.52 (CH), 59.79 (CH_2), 109.77 (CH_2), 145.58 (C); *m*/*z* (35 °C): 154 (M^+, 0.2), 139 (2), 136 (1), 123 (2), 121 (6), 109 (43), 107 (11), 69 (17), 68 (100), 67 (41) (calc. for $C_{10}H_{18}O$: 154.1358, found: 154.1349).

1 Part 16 of Cycloadditions of Allylsilanes. Part 15: H.-J. Knölker, R. Graf, P. G. Jones and O. Spieß, *Angew. Chem.*, 1999, **111**, 2742; *Angew. Chem., Int. Ed.*, 1999, **38**, 2583.
2 F. Bohlmann, C. Zdero and U. Faass, *Chem. Ber.*, 1973, **106**, 2904.
3 J. H. Tumlinson, D. D. Hardee, R. C. Gueldner, A. C. Thompson, P. A. Hedin and J. P. Minyard, *Science*, 1969, **166**, 1010 and references cited in 4(*c*).
4 (*a*) J. A. Katzenellenbogen, *Science*, 1976, **194**, 139; (*b*) K. Mori, in *The Total Synthesis of Natural Products*, ed. J. ApSimon, Wiley, New York, 1981, vol. 4, p. 1; (*c*) K. Mori, in *The Total Synthesis of Natural Products*, ed. J. ApSimon, Wiley, New York, 1992, vol. 9, p. 303.
5 (*a*) H.-J. Knölker, G. Baum and R. Graf, *Angew. Chem.*, 1994, **106**, 1705; *Angew. Chem., Int. Ed. Engl.*, 1994, **33**, 1612; (*b*) review: H.-J. Knölker, *J. Prakt. Chem.*, 1997, **339**, 304; (*c*) H.-J. Knölker, E. Baum and O. Schmitt, *Tetrahedron Lett.*, 1998, **39**, 7705.
6 For previous total syntheses of fragranol, see: D. Kim, Y. K. Lee, Y. M. Jang, I. O. Kim and S. W. Park, *J. Chem. Soc., Perkin Trans. 1*, 1990, 3221; S. Yamazaki, H. Fujitsuka, F. Takara and T. Inoue, *J. Chem. Soc., Perkin Trans. 1*, 1994, 695; T. Martin, C. M. Rodriguez and V. S. Martin, *Tetrahedron: Asymmetry*, 1995, **6**, 1151 and references cited therein.
7 Reviews: I. Fleming, *Chemtracts: Org. Chem.*, 1996, **9**, 1; K. Tamao, in *Advances in Silicon Chemistry*, JAI Press, Greenwich (CT), 1996, vol. 3, p. 1; G. R. Jones and Y. Landais, *Tetrahedron*, 1996, **52**, 7599.
8 H.-J. Knölker and G. Wanzl, *Synlett*, 1995, 378; H.-J. Knölker, P. G. Jones and G. Wanzl, *Synlett*, 1998, 613.
9 A. J. Mancuso and D. Swern, *Synthesis*, 1981, 165; T. T. Tidwell, *Synthesis*, 1990, 857.
10 D. B. Dess and J. C. Martin, *J. Org. Chem.*, 1983, **48**, 4155; D. B. Dess and J. C. Martin, *J. Am. Chem. Soc.*, 1991, **113**, 7277.
11 W. P. Griffith and S. V. Ley, *Aldrichim. Acta*, 1990, **23**, 13; S. V. Ley, J. Norman, W. P. Griffith and S. P. Marsden, *Synthesis*, 1994, 639.
12 M. T. Reetz, J. Westermann, R. Steinbach, B. Wenderoth, R. Peter, R. Ostarek and S. Maus, *Chem. Ber.*, 1985, **118**, 1421; B. Weidmann and D. Seebach, *Helv. Chim. Acta*, 1980, **63**, 2451.
13 G. Wittig, W. Böll and K.-H. Krück, *Chem. Ber.*, 1962, **95**, 2514.

Communication 9/05019A

ChemComm

The first isolation of an alkoxy-*N*,*N*-dialkylaminodifluorosulfane from the reaction of an alcohol and DAST: an efficient synthesis of (2*S*,3*R*,6*S*)-3-fluoro-2,6-diaminopimelic acid

Andrew Sutherland and John C. Vederas*

Department of Chemistry, University of Alberta, Edmonton, Alberta, Canada T6G 2G2.
E-mail: john.vederas@ualberta.ca

Received (in Corvallis, OR, USA) 15th June 1999, Accepted 14th July 1999

During improvement of the synthesis of (2*S*,3*R*,6*S*)-3-fluoro-2,6-diaminopimelic acid 3, a potent inhibitor of DAP epimerase, a stable alkoxy-*N*,*N*-dialkylaminodifluorosulfane 9 was isolated from the reaction of alcohol 6 with DAST

Emergence of multi-drug resistant bacteria has intensified efforts to develop new antibiotics that disrupt microbial cell wall synthesis.[1] Several studies have shown that inhibitors of the biosynthesis of diaminopimelic acid (DAP),[2] the key crosslinking amino acid in the peptidoglycan cell wall of Gram negative bacteria, possess antibiotic activity.[3] An important enzyme in this pathway, L,L-diaminopimelate epimerase, interconverts L,L-DAP **1** and *meso*-DAP **2** without the aid of any detectable metals or cofactors (Scheme 1). The mechanism has been suggested to be an unusual 'two-base' process that employs a thiolate as a general base and a thiol as a general acid.[4] We have previously shown that β-fluoro-DAP stereoisomers are potent inhibitors of DAP epimerase that can act as probes to help define substrate conformation in the enzyme active site.[5] Continued interest in the mechanism of this enzyme and recent crystallographic studies on an inactive form of this protein[4b] encouraged us to improve the synthesis[5] of pure β-fluoro-DAP isomers. We now report an efficient preparation of (2*S*,3*R*,6*S*)-3-fluoro-2,6-diaminopimelic acid **3** and the first isolation of an alkoxy-*N*,*N*-dialkylaminodifluorosulfane from the reaction of an alcohol with DAST.

The original synthesis of β-fluoro-DAP involved an aldol reaction between a Schöllkopf bis-lactim ether[6] and a glutamate semialdehyde to afford an alcohol, which was fluorinated using diethylaminosulfur trifluoride (DAST).[5] However, the reactive nature of the oxazolidinone protecting group on the glutamate semialdehyde lowered yields and made extensive purification of the intermediates obligatory. A recent synthesis[7] of *N*,*N*-di-Boc glutamate semialdehyde **5**, a versatile intermediate,[8] suggested its application to the troublesome aldol condensation. Addition of **5** to the anion of (3*S*)-3,6-dihydro-2,5-dimethoxy-3-(1-methylethyl)pyrazine **4**[6] gave a 3:1 mixture of two inseparable diastereomeric alcohols **6** and **7** in 73% yield (Scheme 2).† Treatment of **6** and **7** with freshly distilled DAST permitted isolation of only the dehydrated compound **8**, which is presumably formed by base elimination of the activated intermediate **9**. By accident we found that this dehydration could be suppressed by using DAST contaminated with water. The presence of a trace amount of water causes the release of HF and results in the stabilisation of the activated intermediate, thereby allowing the preparation of the fluoro derivative **10** as a single diastereomer in 52% yield with only trace amounts of the dehydrated product **8** (7%). In some cases carbocation rearrangements accompanying the DAST preparation of alkyl fluorides have implied a mixed S_N1 and S_N2 mechanism,[9] but formation of **10** with complete inversion of stereochemistry from alcohol **6** indicates an S_N2 reaction. Surprisingly, the modified conditions permit the isolation of alkoxy-*N*,*N*-dialkylaminodifluorosulfane **9** as a single diastereomer in 12% yield.

Compound **9** is unexpectedly stable to column chromatography and amenable to characterisation,‡ although it does decompose after several weeks at room temperature. Alkoxy-

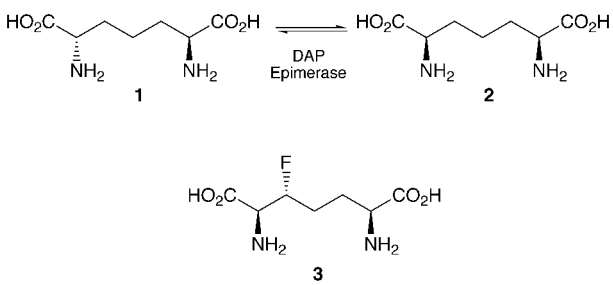

Scheme 1

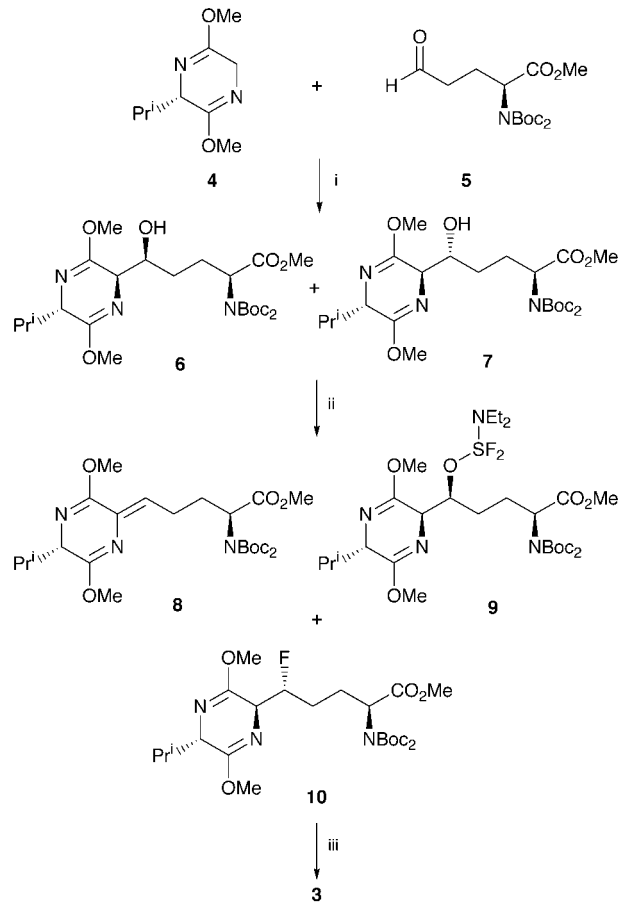

Scheme 2 *Reagents and conditions*: i, BuLi, THF, −78 °C, 73%, **6**:**7** (3:1); ii, DAST, CH_2Cl_2, −78 °C, **8** (7%), **9** (12%), **10** (52%); iii, 6 M HCl, Δ, 71%.

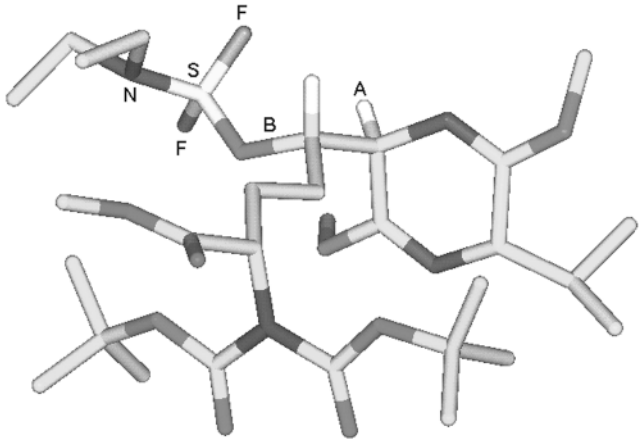

Fig. 1 A model of **9** representing a possible minimum energy conformation calculated using InsightII (MSI). Although elimination to give **8** can occur, in this geometry the orientation of hydrogen A and the cleaving bond B is disfavoured for a facile E2 process. An S_N2 reaction to cleave bond B is also sterically hindered. Only two adjacent hydrogens (white) are shown for clarity.

N,*N*-dialkylaminodifluorosulfanes are postulated as intermediates in the DAST fluorination of alcohols,[10] and the transient existence of these compounds has previously been inferred from ^{19}F NMR studies.[11] Although Markovskii *et al.* have reported the formation of analogous compounds having a perfluoroalkoxy group by reaction of polyfluoroalkyl trimethylsilyl ethers[12] with dialkylaminosulfur trifluorides, the fluoroalkyl groups obstruct elimination or substitution reactions. Preparation of **9** by reaction of an alcohol and DAST represents the first isolation of such a compound which in principle can readily undergo such decomposition. The unusual stability of **9** may be due to the steric crowding provided by nearby substituents (Fig. 1), including the two Boc groups, since DAST reactions with closely-related β-hydroxy-DAP derivatives bearing an *N*-Cbz substituted oxazolidinone[5] do not permit isolation of the corresponding intermediate.

Treatment of **9** with 1.0 equiv. of TBAF in an attempt to prepare **10** results in elimination to give **8**. Minor alcohol **7** could be recovered in quantitative yield as a single stereoisomer from the 'wet' DAST reaction of a mixture of **6** and **7**, thereby indicating that only alcohol **6** reacts to generate inverted fluoro derivative **10**. Molecular modeling of the two alcohols using InsightII (MSI) suggests that the alcohol functionality of **7** is more sterically crowded than **6**, which may account for the observed kinetic resolution. To complete the synthesis of (2*S*,3*R*,6*S*)-3-fluoro-2,6-diaminopimelic acid, the fluoro derivative **10** was hydrolysed with hydrochloric acid to give the desired β-fluoro-DAP **3** in 71% yield after cellulose chromatography. Further studies on synthesis of fluoro-DAP isomers and other DAP analogues[13] are in progress.

Financial support from the Natural Sciences and Engineering Research Council of Canada and the Alberta Heritage Foundation for Medical Research (Fellowship to A. S.) are gratefully acknowledged.

Notes and references

† Compound **4** is available from Merck Schuchardt (Hohenbrunn, Germany).

‡ *Selected data* for **9**: $[\alpha]_D^{26}$ −54.4 (*c* 0.2, $CHCl_3$); ν_{max}($CHCl_3$ cast)/cm^{-1} 2872 (CH), 1749, 1698 (C=O), 1459, 1436, 1382, 1367, 1240, 1146, 1123, 782 (SF); δ_H(300 MHz, $CDCl_3$) 0.64 [3H, d, *J* 6.6, C*H*$_3$(CH$_3$)CH], 1.02 [3H, d, *J* 6.6, CH$_3$(C*H*$_3$)CH], 1.13 [6H, t, *J* 7.8, N(CH$_2$C*H*$_3$)$_2$], 1.40–1.50 [19H, m, (CO$_2$Bu^t)$_2$ and OCHC*H*H], 1.69 (1H, m, NCHC*H*H), 1.90 (1H, m, NCHCH*H*), 2.26 [2H, m, (CH$_3$)$_2$C*H* and OCHCH*H*], 3.16 [4H, q, *J* 7.8, N(C*H*$_2$CH$_3$)$_2$], 3.64 (3H, s, OMe), 3.69 (6H, s, 2 × OMe), 3.89 (1H, t, *J* 3.5, (CH$_3$)$_2$CHC*H*], 4.21 (1H, t, *J* 3.5, NC*H*COMe), 4.28 (1H, ddd, *J* 8.3, 5.9, 2.6, NCHC*H*O), 4.81 [1H, dd, *J* 9.6, 6.1, C*H*N(CO$_2$Bu^t)$_2$]; δ_C(100 MHz, $CDCl_3$) 13.8 [N(CH$_2$*C*H$_3$)$_2$], 16.7 [(*C*H$_3$)CH$_3$CH], 19.0 [(CH$_3$)*C*H$_3$CH], 26.8 (OCH*C*H$_2$), 28.0 [OC(*C*H$_3$]$_3$), 29.0 (NCH*C*H$_2$), 31.2 [(CH$_3$)$_2$*C*H], 36.7 [N(*C*H$_2$CH$_3$)$_2$], 52.2, 52.3, 52.7 (O*C*H$_3$), 58.4 [(CH$_3$)$_2$CH*C*H], 59.4 (N*C*HCOMe), 60.7 [*C*HN(CO$_2$Bu^t)$_2$], 77.4 (NCH*C*HO), 83.1 [O*C*(CH$_3$)$_3$], 152.0, 160.5, 165.5, 171.0 (C=O); δ_F(376 MHz, $CDCl_3$) −123.02 (d, *J* 13.5, S*F*F), −123.07 (d, *J* 13.5, S*F*F) [Found (ES): [MH]$^+$, 671.3499. $C_{29}H_{52}N_4O_9SF_2$ requires [MH]$^+$, 671.3501].

1 T. D. H. Bugg and C. T. Walsh, *Nat. Prod. Rep*., 1992, **9**, 199.
2 R. J. Cox, *Nat. Prod. Rep*., 1996, **13**, 29; G. Scapin and J. S. Blanchard, *Adv. Enzymol. Relat. Areas Mol. Biol*., 1998, **72**, 279.
3 See for example: D. A. Berges, W. E. DeWolf Jr., G. L. Dunn, S. F. Grappel, D. J. Newman, J. J. Taggart and C. Gilvarg, *J. Med. Chem*., 1986, **29**, 89; J. G. Kelland, L. D. Arnold, M. M. Palcic, M. A. Pickard and J. C. Vederas, *J. Biol Chem*., 1986, **261**, 13 216; L. K. P. Lam, L. D. Arnold, T. H. Kalantar, J. G. Kelland, P. M. Lane-Bell, M. M. Palcic, M. A. Pickard and J. C. Vederas, *J. Biol Chem*., 1988, **263**, 11 814.
4 (*a*) C. W. Koo and J. S. Blanchard, *Biochemistry*, 1999, **38**, 4416; (b) M. Cirilli, R. Zheng, G. Scapin and J. S. Blanchard, *Biochemistry*, 1998, **37**, 16 452.
5 M. H. Gelb, Y. Lin, M. A. Pickard, Y. Song and J. C. Vederas, *J. Am. Chem. Soc*., 1990, **112**, 4932.
6 U. Groth and U. Schollkopf, *Synthesis*, 1983, 673.
7 J. M. Padron, G. Kokotos, T. Martin, T. Markidis, W. A. Gibbons and V. S. Martin, *Tetrahedron: Asymmetry*, 1998, **9**, 3381.
8 A. Sutherland, J. F. Caplan and J. C. Vederas, *Chem. Commun*., 1999, 555.
9 M. Hudlicky, *Org. React*., 1988, **35**, 513.
10 W. J. Middleton, *J. Org. Chem*., 1975, **40**, 574.
11 T. J. Tewson and M. J. Welch, *J. Org. Chem*., 1978, **43**, 1090.
12 L. N. Markovskii, L. S. Bobkova and V. E Pashinnik, *Zh. Org. Khim*., 1981, **17**, 1699 (English edition).
13 Y. Gao, P. Lane-Bell and J. C. Vederas, *J. Org. Chem*., 1998, **63**, 2133.

Communication 9/04821I

The synthesis of ethenyl bifunctional reagents containing a sulfone moiety and zirconium by the abnormal addition of $Cp_2Zr(H)Cl$ to internal acetylenic sulfones

Xian Huang* and De-Hui Duan

Department of Chemistry, Zhejiang University (Xixi Campus), Hangzhou Zhejiang 310028, P.R. China. E-mail: Huangx@mail.hz.zj.cn

Received (in Cambridge, UK) 9th June 1999, Accepted 27th July 1999

Ethenyl bifunctional reagents containing a sulfone moiety and zirconium are prepared by the abnormal addition of $Cp_2Zr(H)Cl$ to internal acetylenic sulfones.

Acetylenic sulfones have been used extensively in organic synthesis as activated acetylene equivalents. They can take part in cycloadditions,[1] Michael additions[2] and alkylative desulfonylation reactions.[3] Surprisingly, little attention has been paid to their hydrometalation reactions. On the other hand, *via* the hydrozirconation of alkynes, many bifunctional ethenyl reagents have been synthesized containing elements such as selenium and zirconium,[4] tellurium and zirconium,[5] silicon and zirconium,[6] tin and zirconium,[7] zinc and zirconium[8] and boron and zirconium.[9] Apparently, no efforts have been focused on the bifunctional ethenyl reagent containing sulfur and zirconium. We now report that we have successfully synthesized sulfonyl-substituted alkenylzirconocene compounds *via* the hydrozirconation of internal acetylenic sulfones. Unexpectedly, the products of *anti*-addition of $Cp_2Zr(H)Cl$ to the acetylene are observed.

Phenylacetylenic sulfones **1a**–**c** were synthesized in good yields according to the method of Suzuki.[10] Hydrozirconation of the acetylenic sulfones with 1.2 equiv. of $Cp_2Zr(H)Cl$ in THF for 5 min at room temperature gave a clear yellow solution. Unique *E*-vinyl sulfones **3a**–**c** or *E*-β-deuterovinyl sulfones **4a**–**c** were obtained respectively after hydrolysis or deuterolysis (Scheme 1 and Table 1).† The *E*-olefin geometry was verified by the coupling constant ($^3J_{HH}$ = 15.4 Hz) of the vicinal olefinic protons. In addition, the product melting points are also identical to those previously reported.[11] The olefinic proton of every deuterovinyl sulfone presents a single peak at δ 6.84, which shows that the deuterium atom must be attached to the β-position of the sulfonyl group. Thus the (*Z*)-β-sulfonylalkenylzirconocene compounds **2** are produced in the hydrozirconation reaction (Scheme 1).

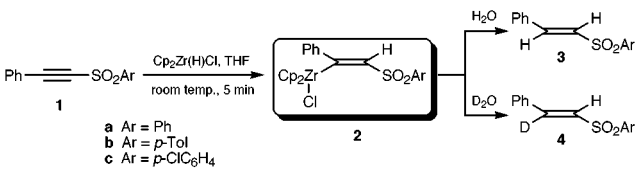

Scheme 1

Table 1 Yields and melting points for **3a**–**c** and **4a**–**c**

Compound	Ar	Yield (%)[a]	Mp/°C
3a	Ph	72	74.5–75.5
3b	*p*-Tol	69	126–121
3c	*p*-ClC_6H_4	70	82–84
4a	Ph	70	73.5–75
4b	*p*-Tol	73	118–120
4c	*p*-ClC_6H_4	68	82–83

[a] Yields of pure compounds.

Hex-1-ynyl *p*-tolyl sulfone was synthesized in two steps according to the method of Truce.[12] After hydrozirconation–hydrolysis, a mixture of *E* and *Z* vinyl sulfones (*E*:*Z* = 2.9:1) was obtained (Scheme 2). Its ^{1}H NMR spectrum (300 MHz) exhibits a doublet of triplets at δ 6.97 (*E*-H_b, *J* 15.1, 6.8 Hz) and multiple peaks at δ 6.20–6.32 [including *E*-H_a, (dt, *J* 15.1, 1.4 Hz) and *Z*-H_a + H_b (ABX_2 system, J_{AB} 11.1 Hz, J_{AX} 6.5 Hz)]. Further proof is also provided by the ^{1}H NMR signals for two kinds of methylenic protons [δ 2.67 (q, 0.52 H, *J* 7.7, 6.5 Hz, *Z*-CH_2) and 2.25 (dq, 1.48 H, *J* 7.4, 6.8, 1.4 Hz, *E*-CH_2)]. The proportion of the *E*:*Z* mixture was estimated *via* the integral areas of the two kinds of methylenic protons. After the parallel experiment of hydrozirconation–deuterolysis, a mixture of two regio- and stereo-isomers (*E*:*Z* = 3:1 by ^{1}H NMR) was obtained (Scheme 2). Its ^{1}H NMR spectrum exhibits a triplet at δ 6.97 (*E*-H_b), a single peak at δ 6.26 (*Z*-H_a), a triplet at δ 2.68 (*Z*-CH_2) and a quartet at δ 2.25 (*E*-CH_2). These results show that two types of alkenylzirconocene compounds **2d** (**I** and **II**) are generated in the hydrozirconation reaction.

Compounds **2** were reacted with various electrophiles (Table 2). NCS, NBS and I_2 (2.5 equiv.) reacted with **2a** to give β-halo vinyl sulfones. Using the method, we can access *Z*-β-halo vinyl sulfones, whose configurations were identified by comparisons with authoritative data.[13] Thus this approach complements the addition of sulfonyl halides to acetylenes, which provides either an *E* and *Z* mixture[13] or only the *E* isomer.[12] Carbon–carbon bond formation also occurred readily with various carbon electrophiles. Reactions with carboxylic acid chlorides afforded (*Z*)-β-sulfonyl α,β-unsaturated ketones. The cross-coupling with allyl bromide provided (*E*)-penta-1,4-dienyl sulfone. Their configurations were affirmed by H–H 2D NOSEY spectra (300 MHz). As is expected, the reaction of **2d** with BzCl afforded two isomers.

There are some regiochemical and stereochemical issues associated with the addition of $Cp_2Zr(H)Cl$ across unsymmetrical acetylenic sulfones. Based on the different substituents (Bu or Ph) on the acetylene bond, α- (major) or β-sulfonyl alkenylzirconocene compounds are obtained respectively. The different regiochemistry could be ascribable to the dissimilarity of the polarizing ability of the two groups to the C≡C triple bond and the long-distance π,π-interaction of the phenyl and bicyclopentadienyl groups.

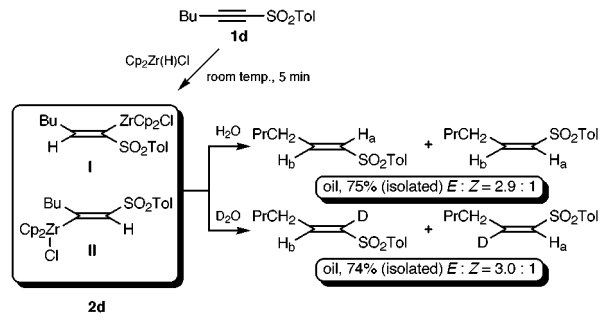

Scheme 2

Table 2 Reaction of **2a** and **2d** with electrophiles

2	E–X	Product	Isolated yield (%)
2a	NCS	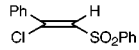	57
2a	NBS	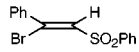	63
2a	I_2	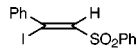	56
2a	BzCl[a]	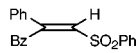	65
2a	AcCl[a]	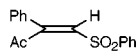	70
2a	$H_2C{=}CHCH_2Br$[b]	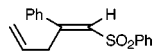	51
2d	BzCl[a]	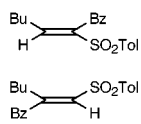	45 28

[a] Reaction conditions: CuBr (0.5 equiv.), acid chlorides (1.05 equiv.), THF, 25 °C, 2 h. [b] Reaction conditions: $Pd(PPh_3)_4$ (5 mol%), allyl bromide (1.05 equiv.), 40 °C, 3 h.

In conclusion, bifunctional ethenyl reagents containing sulfone and zirconium moieties are prepared by the abnormal addition of $Cp_2Zr(H)Cl$ to internal acetylenic sulfones. The addition reactions usually generate vinyl sulfone compounds, which can be exploited for further synthetic elaboration.[14] Currently a more thorough study is being carried out in our laboratory.

Project 29772007 is supported by the National Natural Science Foundation of China; this work is also supported by the Laboratory of Organometallic Chemistry, Shanghai Instituted of Organic Chemistry, Academia Sinica.

Notes and references

†All new compounds were characterized *via* IR, ^1H NMR (300 MHz), EI-MS and elemental analysis.

1 D. F. Huang and T. Y. Shen, *Tetrahedron Lett.*, 1993, **34**, 4477; D. J. Hlasta and J. H. Ackerman, *J. Org. Chem.*, 1994, **59**, 6184.
2 W. E. Truce and B. W. Onken, *J. Org. Chem.*, 1975, **40**, 3200; V. Fiandanese, G. Marchese and F. Naso, *Tetrahedron Lett.*, 1978, 5131.
3 J. J. Eisch, B. Shafii, J. D. Odom and A. L. Rheingold, *J. Am. Chem. Soc.*, 1990, **112**, 1847; E. J. Corey, P. Da Silva Jardine and T. Mohri, *Tetrahedron Lett.*, 1988, **29**, 6409.
4 L. S. Zhu, Z. Z. Huang and X. Huang, *J. Chem. Res. (S)*, 1996, 112; M. J. Dabdoub, M. L. Begnini and P. G. Guerrero Jr., *Tetrahedron*, 1998, **54**, 2371.
5 J. W. Sung, W. B. Jang and D. Y. Oh, *Tetrahedron Lett.*, 1996, **37**, 7537.
6 I. Hyla-Kryspin, R. Gleiter, C. Kruger, R. Zwettler and G. Erker, *Organometallics*, 1990, **9**, 517.
7 B. H. Lipshutz, R. Keil and J. C. Barton, *Tetrahedron Lett.*, 1992, **33**, 5861.
8 C. E. Tucker and P. Knochel, *J. Am. Chem. Soc.*, 1991, **113**, 9888.
9 L. Deloux, E. Skrzypczak-Janjkun, B. V. Cheesman and M. Srebnik, *J. Am. Chem. Soc.*, 1994, **116**, 10 302.
10 H. Suzuki and H. Abe, *Tetrahedron Lett.*, 1996, **37**, 3717.
11 G. Cardillo, D. Savoia and A. Umani-Ronchi, *Synthesis*, 1975, 453; L. K. Liu, Y. Chi and K. Y. Jen, *J. Org. Chem.*, 1980, **45**, 406; G. H. Posner and D. J. Brunelle, *J. Org. Chem.*, 1972, **37**, 3547.
12 W. E. Truce and G. C. Wolf, *J. Org. Chem.*, 1971, **36**, 1727.
13 Y. Amiel, *J. Org. Chem.*, 1971, **36**, 3691; 1974, **39**, 3867.
14 N. S. Simpkins, *Tetrahedron*, 1990, **46**, 6951.

Communication 9/04620H

ChemComm

A stereoselective synthesis of (−)-tetrahydrolipstatin

Arun K. Ghosh* and Chunfeng Liu

Department of Chemistry, University of Illinois at Chicago, 845 W. Taylor Street, Chicago, Illinois 60607, USA

Received (in Corvallis, OR, USA) 4th June 1999, Accepted 21st July 1999

A stereoselective synthesis of (−)-tetrahydrolipstatin has been accomplished utilizing olefin metathesis of an acrylate ester as the key step.

Tetrahydrolipstatin **1**, a member of the lipstatin class of β-lactone microbial agents, is a potent and irreversible inhibitor of pancreatic lipase.[1] The lipase enzyme is responsible for the digestion of fat in the diet of humans.[2] The strained β-lactone functionality of **1** is critical to its lipase inhibitory properties. The inactivation mechanism involves an irreversible acylation of the active site serine residue of pancreatic lipase by the β-lactone moiety.[3] Recent clinical studies have revealed that treatment with **1** along with diet modifications have led to sustained weight loss in humans.[4] Indeed, Hoffman-La Roche Laboratories have now introduced (−)-tetrahydrolipstatin under the trade name Xenical® as an anti-obesity agent. The important biological properties along with its unique structural features have stimulated interest in the synthesis of **1** and its structural variants.[5] Herein we report an asymmetric synthesis of (−)-tetrahydrolipstatin. The key synthetic strategy involves a stereoselective construction of a *syn*-1,3-diol synthon by olefin metathesis, stereoselective epoxidation and regioselective epoxide reduction followed by its elaboration to **1**.

As depicted in Scheme 1, we planned to construct the β-lactone ring from the corresponding β-hydroxy acid derivative **2**. The elaboration of the *syn*-1,3-diol functionality and stereoselective introduction of the C-2 alkyl chain in **2** would be achieved from the α,β-unsaturated δ-lactone **3**. The intermediate **3** would be derived from ring-closing metathesis of the corresponding acrylate ester **4**. Recently, a number of convenient syntheses of various α,β-unsaturated γ- and δ-lactones have been reported involving ring closing metathesis of acrylates utilizing Grubbs' catalyst.[6] The broad synthetic utility of Grubbs' catalyst is now well established.[7] The key starting material, homoallylic alcohol **5** was prepared in multigram quantities by Keck's enantioselective allylation of dodecanal employing a catalytic amount (10 mol%) of (*R*)-BINOL and $Ti(OPr^i)_4$ to furnish **5** in 90% yield.[8] The optical purity of the alcohol **5** [92% ee, $[\alpha]_D^{23}$ −6.3 (*c* 1.23, $CHCl_3$)] was obtained by formation of the Mosher ester and ^{19}F NMR analysis.[9] Reaction of **5** with acryloyl chloride (1.2 equiv.) and Et_3N (3 equiv.) in the presence of a catalytic amount of DMAP in CH_2Cl_2 provided the acrylate ester **4** in 91% yield after silica gel chromatography (Scheme 2). Olefin metathesis of **4** with commercially available Grubbs' catalyst (10 mol%) in the presence of $Ti(OPr^i)_4$ (0.3 equiv.) in refluxing CH_2Cl_2 (0.007 M solution) for 15 h afforded the α,β-unsaturated δ-lactone **3** in 93% yield. Consistent with our earlier report, exposure of acrylate ester **4** to Grubbs' catalyst (10 mol%) in CH_2Cl_2 for 15 h in the absence of $Ti(OPr^i)_4$ resulted in low conversion of lactone **3** (50% by ^1H NMR) with a substantial amount of unreacted starting material remaining.[6b] Epoxidation of lactone **3** was carried out with alkaline H_2O_2 in MeOH at 23 °C for 1 h. Acidification, extractive work-up followed by azeotropic removal of the water by heating in benzene furnished the epoxide **6** as a single isomer. Epoxidation of **3** proceeded stereoselectively from the less hindered β-face.[10] Exposure of epoxide **6** to PhSeSePh and $NaBH_4$ in Pr^iOH at 0 °C in the presence of AcOH resulted in regioselective reduction of the epoxide to afford the β-hydroxy-lactone **7** in 83% yield (from **3**) after silica gel chromatography.[11] Thus, the sequence of reactions involving olefin metathesis, stereoselective epoxidation and regioselective epoxide reduction constitute an effective protocol for the *syn*-1,3-diol synthon **9**. For introduction of the C-2 alkyl chain, attempted direct alkylation of the β-hydroxy-lactone **7** under a variety of reaction conditions was unsuccessful. Therefore, the elaboration of the C-2 side chain was carried out by an alternate route using Seebach's asymmetric alkylation of β-hydroxy esters.[12]

The β-hydroxy lactone **7** was first protected as a TBDMS ether **8** by treatment with TBDMSCl and Pr^i_2NEt in DMF at

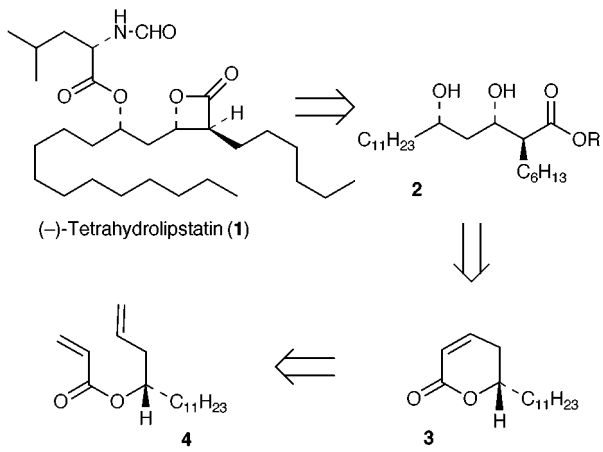

Scheme 1

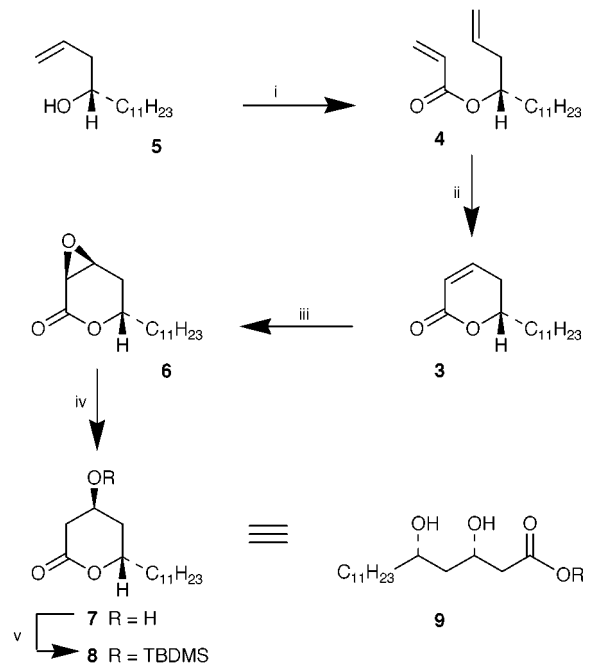

Scheme 2 *Reagents and conditions*: i, CH_2=CHCOCl, Et_3N, DMAP, 23 °C (91%); ii, $(PCy_3)_2Cl_2Ru$=CHPh (10 mol%), $Ti(OPr^i)_4$ (0.3 equiv.), CH_2Cl_2, 40 °C (93%); iii, aq. NaOH, H_2O_2, 23 °C; iv, PhSeSePh, $NaBH_4$, Pr^iOH, AcOH, 0 °C (83%); v, TBDMSCl, Pr^i_2NEt, DMF, 25 °C (98%).

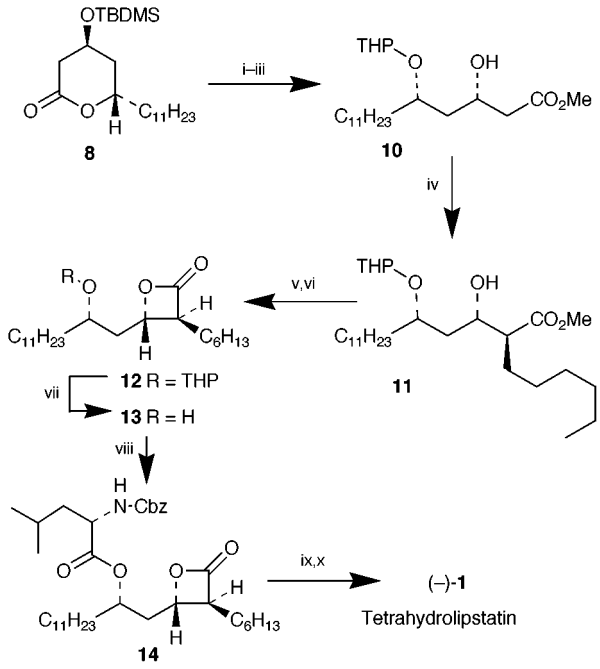

Scheme 3 *Reagents and conditions*: i, Et_3N, MeOH, 23 °C, 12 h (75%); ii, DHP, PPTS, 8 h; iii, Bu_4NF, THF, AcOH, 25 °C, 5 h (60% from **7**); iv, LDA, HMPA, $C_6H_{13}I$, THF, −78 to 0 °C, 6 h (70% conversion, 85%); v, aq. LiOH, 25 °C, 12 h, H^+; vi, $PhSO_2Cl$, Py, 0 °C, 8 h (84% from **11**); vii, PPTS, EtOH, reflux, 3 h (90%); viii, Cbz-Leu, DCC, DMAP (95%); ix, H_2, Pd-C, 12 h; x, AcOCHO, THF, 25 °C, (87%).

23 °C for 12 h. Lactone **8** was converted to β-hydroxy ester **10** in a three step sequence involving (i) opening of the lactone ring by exposure to Et_3N in MeOH at 23 °C for 12 h, (ii) protection of the resulting δ-hydroxy methyl ester as THP ether, and (iii) removal of the TBDMS group by treatment with Bu_4NF in THF in the presence of AcOH at 23 °C for 5 h (60% from **7**). The C(2) hexyl side chain was then introduced by an asymmetric alkylation of the β-hydroxy ester **10** (Scheme 3). Thus, methyl ester **10** was treated with LDA (2.2 equiv.) in the presence of HMPA (5 equiv.) in THF at −78 °C and the reaction mixture was warmed to −50 °C for 2 h. The resulting dianion was cooled to −78 °C and reacted with hexyl iodide (2 equiv.) at −78 to 0 °C for 6 h to afford the alkylated product **11** in 85% yield (based upon 30% recovery of starting material). The removal of the THP ether group in **11** revealed excellent diastereoselectivity (ratio 22:1 by ^{13}C NMR).[13] The stereochemical course of such alkylation processes has been well-established previously.[12]

Saponification of ester **11** with aqueous LiOH followed by exposure of the resulting acid to $PhSO_2Cl$ in pyridine at 0 °C for 8 h, as described by Barbier and Schneider, afforded the β-lactone **12** in 84% yield (from **11**).[5k] The removal of the THP group by treatment with PPTS in EtOH at reflux furnished the (5*S*)-hydroxy β-lactone **13** [$[\alpha]_D^{23}$ −14.4 (*c* 1.2, $CHCl_3$)] as a single isomer. Attempted esterification with *N*-formylleucine under a variety of conditions failed to provide satisfactory results. To complete the synthesis, *N*-formylleucine was introduced by an alternate protocol as described by Uskokovic *et al.*[5g] Esterification of **13** with Cbz-leu and DCC in the presence of DMAP provided the Cbz derivative **14** in 95% yield.[14] Catalytic hydrogenation of **14** over 10% Pd-C followed by *N*-formylation of the resulting amine with formic acetic anhydride in THF at 23 °C for 1 h furnished the synthetic (−)-tetrahydrolipstatin **1** [$[\alpha]_D^{23}$ −33.8, (*c* 1.4, $CHCl_3$); lit.,[1] $[\alpha]_D^{23}$ −34.45, (*c* 1, $CHCl_3$)]. Spectral data (IR and 400 MHz ^1H NMR) for the synthetic tetrahydrolipstatin are identical to those reported for the natural product.[1]

In summary, an asymmetric synthesis of (−)-tetrahydrolipstatin has been accomplished. A number of key features of this synthesis are noteworthy; a Keck enantioselective allylation of dodecanal, olefin metathesis of an acrylate ester to an unsaturated δ-lactone, elaboration of this lactone to a *syn*-1,3-diol synthon and Seebach's asymmetric alkylation of a β-hydroxy ester.

Financial support for this work was provided by the National Institutes of Health (GM 55600).

Notes and references

1 E. K. Weibel, P. Hadvary, E. Hochuli, E. Kupfer and H. Lengsfeld, *J. Antibiot.*, 1987, **40**, 1081; P. Hadvary, H. Lengsfeld and H. Wolfer, *Biochem. J.*, 1988, **256**, 357.

2 S. Hogan, A. Fleury, P. Hadvary, H. Lengsfeld, M. K. Meier, J. Triscari and A. C. Sullivan, *Int. J. Obes.*, 1987, **11**, 35 (suppl. 3).

3 P. Hadvary, W. Sidler, W. Meister, W. Vetter and H. Wolfer, *J. Biol. Chem.*, 1991, **266**, 2021.

4 M. L. Drent and E. A. van der Veen, *Obes. Res.*, 1995, **3** (suppl. 4), 623S.

5 (*a*) I. Paterson and V. A. Doughty, *Tetrahedron Lett.*, 1999, **40**, 393; (*b*) I. Fleming and N. J. Lawrence, *J. Chem. Soc., Perkin Trans. 1*,, 1998, 2679; (*c*) B. Giese and M. J. Roth, *J. Braz. Chem. Soc.*, 1996, **7**, 243; (*d*) A. Pommier, J. M. Pons, P. J. Kocienski and L. Wong, *Synthesis*, 1994, 1294; (*e*) S. Hanessian, A. Tehim and P. Chen, *J. Org. Chem.*, 1993, **58**, 7768; (*f*) S. C. Case-Green, S. G. Davies and C. J. R. Hedgecock, *Synlett*, 1991, 781; (*g*) N. K. Chadha, A. D. Batcho, P. C. Tang, L. F. Courtney, C. M. Cook, P. M. Wovkulich and M. R. Uskokovic, *J. Org. Chem.*, 1991, **56**, 4714; (*h*) I. Fleming and N. J. Lawrence, *Tetrahedron Lett.*, 1990, **31**, 3645; (*i*) J. Pons and P. J. Kocienski, *Tetrahedron Lett.*, 1989, **30**, 1833; (*j*) P. Barbier and F. Schneider, *J. Org. Chem.*, 1988, **53**, 1218; (*k*) P. Barbier and F. Schneider, *Helv. Chim. Acta*, 1987, **70**, 196; (*l*) P. Barbier, F. Schneider and U. Widmer, *Helv. Chim. Acta*, 1987, **70**, 1412.

6 (*a*) K. C. Nicolaou, R. M. Rodriguez, H. J. Mitchell and F. L. van Delft, *Angew. Chem., Int. Ed.*, 1998, **37**, 1874; (*b*) A. K. Ghosh, J. Cappiello and D. Shin, *Tetrahedron Lett.*, 1998, **39**, 4651; (*c*) J. Cossy, D. Bauer and V. Bellosta, *Tetrahedron Lett.*, 1999, **40**, 4187 and references cited therein.

7 For recent reviews, see: D. L. Wright, *Curr. Org. Chem.*, 1999, **3**, 211; R. H. Grubbs and S. Chang, *Tetrahedron*, 1998, **54**, 4413; S. K. Amstrong, *J. Chem. Soc., Perkin Trans. 1*, 1998, 371; (*d*) M. Schuster and S. Blechert, *Angew. Chem., Int. Ed. Engl.*, 1997, **36**, 2037 and references cited therein.

8 G. E. Keck, K. H. Tarbet and L. S. Geraci, *J. Am. Chem. Soc.*, 1993, **115**, 8467; G. E. Keck and D. Krishnamurthy, *Org. Synth.*, 1997, **75**, 12.

9 J. A. Dale, D. L. Dull and H. S. Mosher, *J. Org. Chem.*, 1969, **34**, 2543.

10 S. Takano, Y. Shimazaki, Y. Sekiguchi and K. Ogasawara, *Synthesis*, 1989, 539.

11 M. Miyashita, T. Suzuki and A. Yoshikoshi, *Tetrahedron Lett.*, 1987, **28**, 4293; M. Miyashita, M. Hoshino, T. Suzuki and A. Yoshikoshi, *Chem. Lett.*, 1988, 507.

12 D. Seebach, J. Aebi and D. Wasmuth, *Org. Synth.*, 1985, **63**, 109.

13 Alkylation of the corresponding β-hydroxy ester containing an *anti*-δ-benzyloxy group proceeded with excellent diastereoselectivity (40:1). [ref. 5(*e*)]. Thus, the stereochemistry of the remote alkoxy group has little influence on the stereochemical outcome of this alkylation process.

14 All new compounds gave satisfactory spectroscopic and analytical results.

Communication 9/04533C

New method for the synthesis of α-substituted tetrahydrofuran-2-methanols through diastereoselective addition of THF to aldehydes mediated by Et_3B in the presence of air

Takehiko Yoshimitsu,* Maki Tsunoda and Hiroto Nagaoka*

Meiji Pharmaceutical University, Noshio, Kiyose, Tokyo 204-8588, Japan. E-mail: takey@my-pharm.ac.jp

Received (in Cambridge, UK) 14th June 1999, Accepted 26th July 1999

The tetrahydrofuranyl radical, generated from THF with Et_3B in the presence of air, was found to react with aldehydes *threo*-selectively to afford α-substituted tetrahydrofuran-2-methanols, the common structural motifs of biologically active acetogenin polyketides, in moderate yields.

α-Substituted tetrahydrofuran-2-methanols **1** and **2** are common structural units present in acetogenins that possess important biological properties, such as antineoplastic and immunosuppressive activity.[1] Numerous attempts have thus been made to

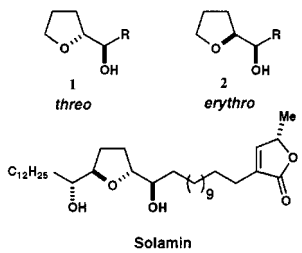

elaborate these structural units,[2–4] but the direct addition of tetrahydrofuranyl synthons to aldehydes is a rare case of a carbon–carbon bond-forming reaction in the convergent synthesis of acetogenins.[5,6] The authors have accordingly established a new method for the stereoselective synthesis of **1** through the addition of tetrahydrofuranyl radical **3** generated from THF with Et_3B in the presence of air[7] to aldehydes **4**, thereby facilitating the construction of core structural motifs of acetogenins (Scheme 1). To the best of our knowledge, the

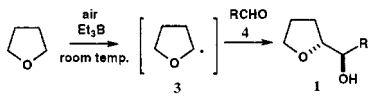

Scheme 1

radical addition of THF to aldehydes to give *threo*-α-substituted tetrahydrofuran-2-methanols **1** stereoselectively is presented in this paper for the first time.[8]

The results of the addition of THF to 4-methoxybenzaldehyde **4a**, mediated by Et_3B either in the presence or absence of air at room temperature, are listed in Table 1.†‡

The radical reaction in the presence of air, which is necessary for radical initiation,[7,9] proceeded *threo*-selectively (*ca.* 90 : 10) to afford alcohols (**1a** and **2a**) along with unchanged aldehyde **4a**. It should be emphasized that the continuous admission of air greatly enhanced the efficiency of the reaction. The chemical yield was also increased by additional amounts of reagents, but it was not significantly improved by prolonged reaction time. Its

Table 1 Radical reaction of THF with 4-methoxybenzaldehyde **4a**[a]

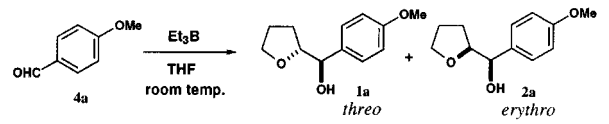

	Reagents/equiv.				
Entry	Et_3B	THF	*t*/h	Yield (%)[f]	**1a**:**2a**[g]
1[b]	3	31	12	42 (37)	91:9
2[b]	3	31	36	44 (38)	90:10
3[c]	3	31	12	4 (81)	88:12
4[bd]	1	10	12	11 (70)	90:10
5[be]	3	31	12	1 (99)	93:7

[a] Unless otherwise stated, aldehyde (1.0 mmol) and 1.0 M THF solution of Et_3B (3.0 ml) were used. [b] Air was introduced through a syringe needle with a balloon (*ca.* 10–20 ml h^{-1}). [c] The reaction was carried out under argon. [d] Aldehyde (1.0 mmol) and 1.0 M THF solution of Et_3B (1.0 ml) were used [e] Galvinoxyl (0.3 equiv.) added. [f] Isolated yields: yields of recovered aldehyde **4a** are given in parentheses. [g] Ratio determined from the ^1H NMR spectrum of the diastereomeric mixture.

Table 2 Radical reaction of THF with aldehydes **4**[a]

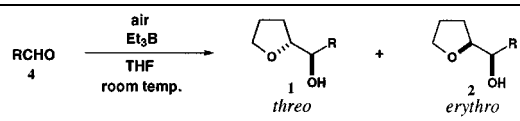

	Reagents/equiv.						
Entry	Et_3B	THF	*t*/h	**4**	R	Yield (%)[b]	**1**:**2**[c]
1	3	31	12	**4a**	4-$MeOC_6H_4$	42 (37)	91:9
2	3	31	17	**4b**	1,3-benzodioxol-5-yl	47 (38)	89:11
3	3	31	12	**4c**	Ph	44 (21)	85:15
4	3	31	12	**4d**	2-BrC_6H_4	45 (20)	71:29
5	3	31	12	**4e**	$C_{12}H_{25}$	37 (—)[d]	62:38
6	3	31	12	**4f**	c-C_6H_{11}	32 (—)[d]	54:46[e]

[a] Aldehydes (1.0 mmol) and 1.0 M THF solution of Et_3B (3.0 ml) were used. Air was introduced through a syringe needle with a balloon (*ca.* 10–20 ml h^{-1}). [b] Isolated yields: yields of recovered aldehydes **4** are given in parentheses. [c] Ratio determined from the ^1H NMR spectrum of the diastereomeric mixture or based on isolated yields of the corresponding acetates derived from the crude products. [d] Unreacted aldehyde **4** was not recovered. [e] Stereochemistry of the major isomer yet to be determined.

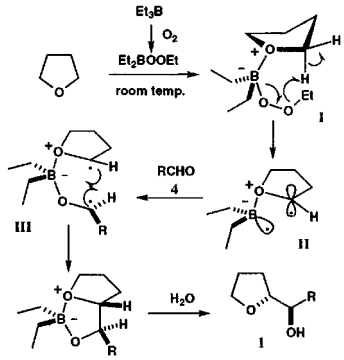

Scheme 2

inhibition by radical inhibitors such as galvinoxyl[10] clearly indicated that the reaction proceeds *via* a radical mechanism (entry 5 in Table 1). The radical reaction was also applied to representative aldehydes **4b**–**f**.

Table 2 demonstrates the general applicability of the present method to various aldehydes, though in only moderate yields.[11] The *threo*-selectivity of the addition was generally high for aromatic aldehydes, and low to moderate in the cases of aliphatic and *ortho*-substituted aromatic aldehydes (entries 4, 5 and 6 in Table 2).§ The reasons for the stereochemical outcome remain unclear but a transition state (**III**) in which boron atoms tether radical **3** to aldehydes **4** may be reasonably assumed (Scheme 2).[12]

In summary, a new method has been established for the stereoselective synthesis of *threo*-α-substituted tetrahydrofuran-2-methanols **1** by addition of tetrahydrofuranyl radical **3**, generated from THF with Et_3B in the presence of air, to aldehydes **4**. This method is quite easy to conduct and readily provides access to common structural motifs of biologically important acetogenins. It may thus be considered a superior means for the synthesis of these natural products. The mechanism of the reaction and potential applications to total synthesis of acetogenins are presently under investigation.

Notes and references

† Representative procedure: To 4-methoxybenzaldehyde **4a** (136 mg, 1.0 mmol) was added 1.0 M Et_3B in THF (3.0 ml, 3.0 mmol) at room temperature. The mixture was stirred at the same temperature with continuous bubbling of air through a syringe needle with a balloon (flow rate; 10–20 ml h^{-1}) for 12 h. The mixture was treated with AcOH and then extracted with CH_2Cl_2, and washed with sat. $NaHCO_3$. The organics were dried over $MgSO_4$. Following solvent evaporation, the residue was purified by column chromatography on silica gel (EtOAc–hexane 1:2) to afford a colorless solid consisting of α-(4-methoxyphenyl)tetrahydrofuran-2-methanols (88 mg, 42%) as a diastereomixture (**1a**:**2a** = 91:9) and unreacted aldehyde **4a** (51 mg, 37%).

‡ The relative configuration of the major adducts **1** was unambiguously determined by comparison of ^{1}H NMR spectral data with those of authentic *threo*-alcohols prepared by dihydroxylation of (*E*)-allyl tosylate **5**.

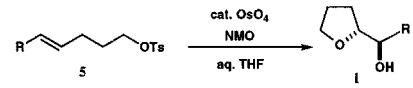

§ Satisfactory analytical (high-resolution mass) and spectral (IR, ^{1}H NMR, and MS) data were obtained for new compounds.

1 F. Q. Alali, X.-X. Liu and J. T. McLaughlin, *J. Nat. Prod.*, 1999, **62**, 504; A. Cave, B. Figadere, A. Laureno and D. Cortes, in *Progress in the Chemistry of Natural Products*, ed. W. Hery, G. W. Kirby, R. E. Moore, W. Steglich and C. Tamm, Springer, New York, 1997, vol. 70, p. 81; L. Zeng, Q. Ye, N. H. Oberlies, G. Shi, Z.-M. Gu, K.He and J. L. McLaughlin, *Nat. Prod. Rep.*, 1996, 275.

2 B. Figadere and A. Cave, in *Studies in Natural Products Chemistry*, ed. Atta-ur-Rahman, Elsevier, Amsterdam, 1996, vol. 18, p. 193; B. Figadere, *Acc. Chem. Res.*, 1995, **28**, 359; U. Koert, *Synthesis*, 1995, 115; R. Hoppe and H.-D. Scharf, *Synthesis*, 1995, 1447.

3 Recent syntheses (after 1998); Z. Ruan and D. R. Mootoo, *Tetrahedron Lett.*, 1999, **40**, 49; S.-T. Jan, K. Li, S. Vig, A. Rudolph and F. M. Uckun, *Tetrahedron Lett.*, 1999, **40**, 193; S. Takahashi and T. Nakata, *Tetrahedron Lett.*, 1999, **40**, 723; Y. Mori, T. Sawada and H. Furukawa, *Tetrahedron Lett.*, 1999, **40**, 731; L. Lemee, A. Jegou and A. Veyrieres, *Tetrahedron Lett.*, 1999, **40**, 2761; P. Li, J. Yang and K. Zhao, *J. Org. Chem.*, 1999, **64**, 2259; A. Sinha, S. C. Sinha, S. C. Sinha and E. Keinan, *J. Org. Chem.*, 1999, **64**, 2381; Q. Yu, Z.-J. Yao, X.-G. Chen and Y.-L. Wu, *J. Org.Chem.*, 1999, **64**, 2440; S. Hanessian and T. A. Grillo, *J. Org. Chem.*, 1998, **63**, 1049; H. Zang, M. Seepersaud, S. Seepersaud and D. R. Mootoo, *J. Org. Chem.*, 1998, **63**, 2049; S. E. Schaus, J. Branat and E. N. Jacobsen, *J. Org. Chem.*, 1998, **63**, 4876; J. A. Marshall and H. Jiang, *J. Org. Chem.*, 1998, **63**, 7066.

4 J. B. Gale, J.-G. Yu, X. E. Hu, A. Khare, D. K. Ho and J. M. Cassady, *Tetrahedron Lett.*, 1993, **34**, 5847; Y. Morimoto and T. Iwai, *J. Am. Chem. Soc.*, 1998, **120**, 1633; F. E. McDonald, T. B. Towne and C. C. Schultz, *Pure Appl. Chem.*, 1998, **70**, 355; M. Champdore, M. Lasalvia and V. Piccialli, *Tetrahedron Lett.*, 1998, **39**, 9781.

5 F. Zanardi, L. Battistini, G. Rassu, L. Pinna, M. Mor, N. Culeddn and G. Casiraghi, *J. Org. Chem.*, 1998, **63**, 1368; B. Figadere, J.-F. Peyrat and A. Care, *J. Org. Chem.*, 1997, **62**, 3428.

6 T. Cohen and M.-T. Lin, *J. Am. Chem. Soc.*, 1984, **106**, 1130.

7 Precedents of the reaction of tetrahydrofuranyl radical with olefins; H. C. Brown and M. M. Midland, *Angew. Chem., Int. Ed. Engl.*, 1972, **11**, 692; A. J. Clark, S. Rooke, T. J. Sparey and P. C. Tayler, *Tetrahedron Lett.*, 1996, **37**, 909.

8 A ketone–THF coupling reaction, mediated by SmI_2 and iodobenzene, has been reported; H. B. Kagan, J. L. Namy and P. Girard, *Tetrahedron Suppl. No. 1*, 1981, **37**, 175; J. Inanaga, M. Ishikawa and M. Yamaguchi, *Chem. Lett.*, 1987, 1485.

9 A. Suzuki, *J. Synth. Org. Chem. Jpn.*, 1971, **29**, 995.

10 G. W. Kabalka, H. C. Brown, A. Suzuki, S. Honma, A. Arase and M. Itoh, *J. Am. Chem. Soc.*, 1970, **92**, 710.

11 Yields not yet optimized.

12 A recent report on multiple roles of Et_3B as radical initiator and Lewis acid: H. Miyabe, M. Ueda, N. Yoshioka and T. Naito, *Synlett*, 1999, 465.

Communication 9/04745J

ChemComm

[Tris(*o*-iminosemiquinone)cobalt(III)]—a radical complex with an $S_t = {}^3/_2$ ground state

Cláudio Nazari Verani, Stefan Gallert, Eckhard Bill, Thomas Weyhermüller, Karl Wieghardt* and Phalguni Chaudhuri*

Max-Planck-Institut für Strahlenchemie, Stiftstraße 34-36, D-45470 Mülheim an der Ruhr, Germany. E-mail: chaudh@mpi-muelheim.mpg.de

Received (in Basel, Switzerland) 11th May 1999, Accepted 2nd August 1999

Owing to their topology, three iminosemiquinone radical ligands couple in a ferromagnetic fashion, mediated by a low-spin Co(III) ion.

The realization of the widespread occurrence of radicals in enzyme catalysis has triggered considerable interest and research activity in metal–radical interactions.[1–10] Additionally, investigations relating organic radicals bound to metal ions are relevant to the field of 'molecular magnets'.[11,12]

In earlier reports[13–15] the $Ga(SQ)_3$ complex (SQ = 3,5-di-*tert*-butyl-1,2-semiquinonato) was characterized, both structurally and spectroscopically, and was found to exhibit a weak ferromagnetic exchange interaction ($J = +7.8$ cm^{-1}) between the three $S = {}^1/_2$ coordinated semiquinone ligands, mediated by a metal centre with empty d orbitals. In pursuit of our interest in coordinated radicals,[16] we now report a compound containing three *ortho*-iminosemiquinone radicals bound to a diamagnetic metal ion, low-spin Co(III), and exhibiting much stronger ferromagnetic interactions than those reported for similar systems.[17]

Treatment of anhydrous $CoCl_2$ in the presence of air with 3 equiv. of the N,O-chelating ligand H_2L in acetonitrile yielded a deep blue solution, which on addition of NEt_3 turned deep green.

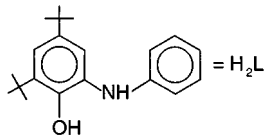

The green solution was refluxed for 0.5 h, followed by stirring at room temperature for an additional 5 h. Slow evaporation of the clear solution afforded X-ray quality deep brown crystals of **1** (yield: 65%).

The most noteworthy features in the IR spectrum of **1** are the absence of both N–H and O–H modes and the appearance of two medium intense ν(CN) bands at 1588, 1577 cm^{-1} and a very strong ν(C–O) band at 1433 cm^{-1}. Optical spectra of **1** in solvents such as MeCN, THF and $CHCl_3$ consist of a series of intense bands and shoulders; in particular two extremely intense absorptions at low energies are noteworthy: λ/nm (ε/M^{-1} cm^{-1}) (MeCN) 881(2628), 668(2510); ($CHCl_3$) 902(20300), 676(16400); (THF) 910(16170), 675(13050). The intensity and its dependence on the solvent suggest that allowed electronic transitions of a CT nature dominate the spectra. The intensity of these bands decreases with time indicating the unstable nature of the radicals in solution. Cyclic voltammetric experiments exhibit four quasi-reversible one-electron redox waves for **1** in CH_2Cl_2 [0.1 M $NBu^n{}_4PF_6$]: $E^1{}_{1/2} = 0.196$, $E^2{}_{1/2} = -0.363$, $E^3{}_{1/2} = -0.933$ and $E^4{}_{1/2} = -1.320$ V *vs.* Fc^+–Fc. The first three redox potentials are associated with three ligand centred redox processes and $E^4{}_{1/2}$ must be assigned to the Co(III)–Co(II) couple.

The single crystal X-ray structure of **1** (Fig. 1)† shows that the first coordination sphere of cobalt has a C_2 axis passing through O(2)–Co(1)–N(3); the ligands have lost their aminohydrogen atoms. The structure determination unambiguously shows that cobalt is hexa-coordinated to three deprotonated ligands, each of which contains an iminosemiquinone radical anion, hence indicating a formal +3 oxidation state at the cobalt centre. Thus the distances C3–C4, C5–C6, C23–C24, C25–C26, C43–C44 and C46–C45 at 1.37 ± 0.01 Å are significantly shorter than the other C–C distances in the original phenol ring, 1.43 + 0.01 Å. Correspondingly, the imino C=N bonds at 1.345 ± 0.005 Å are shorter than the C–N bonds to the aniline rings, 1.420 ± 0.005 Å. Similar asymmetric electron density distribution in *ortho*-iminosemiquinone has been observed previously.[16*a*] Secondary structural confirmation of the intermediate reduction level of the ligand comes from the C–O bond distances, 1.304 ± 0.004(av.), which are much shorter than the 1.35 Å expected of a catechol.[18] They are in the range of those found for other first-row metal semiquinone complexes.[19] The Co–O and Co–N bond distances at 1.88 ± 0.01(av.) and 1.93 ± 0.01(av.) Å, respectively, are in accord with the low-spin description of the cobalt centre.

Magnetic data (SQUID) with $B = 1$ T for a polycrystalline sample of **1** are displayed in Fig. 2 as μ_{eff} *vs.* *T*. On lowering the temperature, μ_{eff} (3.16 μ_B at 290 K) increases monotonically approaching a maximum around 15 K with a value of 3.71 μ_B,

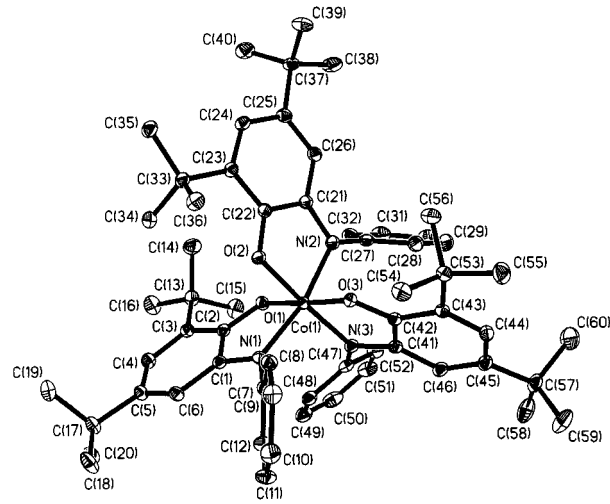

Fig. 1 Structure of the neutral complex CoL_3 **1** with selected bond lengths (Å) and angles (°): Co(1)–O(1) 1.878(1), Co(1)–N(1) 1.937(1), Co(1)–O(2) 1.896(1), Co(1)–N(2) 1.946(1), Co(1)–O(3) 1.889(1), Co(1)–N(3) 1.918(1), O(1)–C(2) 1.307(2), N(1)–C(1) 1.350(2), O(2)–C(22) 1.300(2), N(1)–C(7) 1.419(2), O(3)–C(42) 1.305(2), N(2)–C(21) 1.342(2), N(2)–C(27) 1.425(2), N(3)–C(41) 1.348(2), N(3)–C(47) 1.423(2), C(1)–C(6) 1.425(2), C(1)–C(2) 1.438(2), C(2)–C(3) 1.424(2), C(3)–C(4) 1.379(2), C(4)–C(5) 1.434(2), C(5)–C(6) 1.373(2), C(21)–C(26) 1.432(2), C(21)–C(22) 1.435(2), C(22)–C(23) 1.429(2), C(23)–C(24) 1.379(2), C(24)–C(25) 1.436(2), C(25)–C(26) 1.366(2), C(41)–C(46) 1.428(2), C(41)–C(42) 1.440(2), C(42)–C(43) 1.427(2), C(43)–C(44) 1.383(2), C(44)–C(45) 1.430(2), C(45)–C(46) 1.369(2); C(1)–N(1)–C(7) 121.2(1), C(47)–N(3)–C(41) 122.3(1), C(21)–N(2)–C(27) 119.7(1).

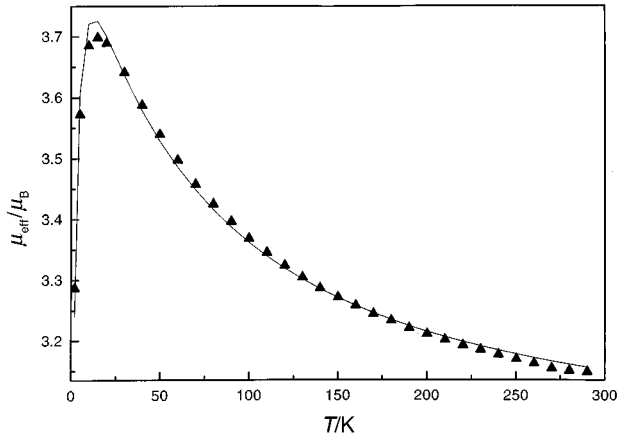

Fig. 2 A plot of μ_{eff} *vs.* T for **1**. The solid line represents the simulation of the experimental data.

which is close to the spin-only value for $S_t = 3/2$, expected as the ground state for three ferromagnetically coupled iminosemiquinone radicals. Below 15 K there is a decrease in μ_{eff}, which reaches a value of 3.30 μ_B at 2 K due to saturation effects and/or intermolecular antiferromagnetic interactions. A full-matrix diagonalization approach[20] was employed to fit the experimental data. We have found that the experimental data could not be fitted with only one 'J' as satisfactorily as with two 'J' values. Two exchange coupling constants have to be considered for the simulation based on the Hamiltonian

$$H = -2J(S_1 \bullet S_2 + S_2 \bullet S_3) - 2J_{13}(S_1 \bullet S_3)$$

with $S_1 = S_2 = S_3 = 1/2$ and the best fit shown as the solid line in Fig. 2 yields $J = J_{12} = J_{23} = +9.1$ cm^{-1}, $J_{13} = +59.5$ cm^{-1}, $g_1 = g_2 = g_3 = 2.005$ (fixed), TIP $= 100 \times 10^{-6}$ cm^3 mol^{-1} (fixed). Thus the quartet ground state is separated from the first doublet state by 27 cm^{-1} owing to the exchange interactions.

The quartet ground state is stabilized by the topology of the three magnetic orbitals of the iminosemiquinone radicals. In an idealized C_2 symmetry the three π*-magnetic orbitals are orthogonal to each other, thus rationalizing the observed ferromagnetic coupling. The superexchange mechanism is most probably mediated by the metal 3d π-orbitals. A rationale for the relative strengths of the two 'J' values might be sought in the orthogonality of the planes of the three ligands including the central cobalt in the coordination polyhedron. The dihedral angle between the two ligand planes containing O2 and O3 is 92.7°, accounting for the stronger coupling J_{13}. On the other hand, the dihedral angles between the planes containing O1 and O3 (79.4°) and between the planes containing O1 and O2 (82.8°) deviate significantly from 90°, thus rendering an appreciable antiferromagnetic contribution to the overall coupling. As a result the latter couplings, $J = J_{12} = J_{23}$, are weaker than the former one J_{13}.

The results reported here show that much larger ferromagnetic coupling can be achieved with suitably designed organic radicals by using appropriate diamagnetic acceptors. A novel tris(iminosemiquinone)metal(III) complex is described that can provide a suitable basis for further research in a systematic way, especially on the electronic properties of other metal(III)–radical complexes.

C. N. V. thanks DAAD (Bonn) for a fellowship. The experimental skill of Frau D. Schweiger is thankfully acknowledged.

Notes and references

† *Crystal data:* $C_{60}H_{75}N_3O_3Co$, monoclinic, space group $P2_1/n$, a = 15.043(1), b = 13.953(1), c = 27.594(2) Å, β = 103.62(2)°, V = 5629.0(7) Å^3, Z = 4, D_c = 1.115 g cm^{-3}, T = 100(2) K, $F(000)$ = 2028, λ(Mo-Kα) = 0.71073 Å, μ = 0.348 mm^{-1}. Brown–black crystal, size 0.66 × 0.59 × 0.39 mm, Siemens SMART CCD, 53106 reflections collected. Structure solution by using the Siemens ShelXTL software package (G. M. Sheldrick, Universität Göttingen) from 16129 independent reflections; full-matrix least-squares refinement on F^2, using 16074 and 622 parameters, refinement converged at R_1 = 0.042 and R_2 = 0.064 (all data).

CCDC 182/1362. See http://www.rsc.org/suppdata/cc/1999/1747/ for crystallographic files in .cif format.

1 J. Stubbe, *Annu. Rev. Biochem.*, 1989, **58**, 257.
2 P. A. Frey, *Chem. Rev.*, 1990, **90**, 1343.
3 *Metalloenzymes involving amino acid-residue and related radicals*, ed. H. Sigel and A. Sigel, Marcel Dekker, New York, 1994, vol. 30.
4 J. Z. Pedersen and A. Finazzi-Agro, *FEBS Lett.*, 1993, **325**, 53.
5 R. C. Prince, *Trends Biochem. Sci.*, 1988, **13**, 152.
6 G. T. Babcock, M. Espe, C. Hoganson, N. Lydakis-Simantiris, J. McCracken, W. Shi, S. Styring, C. Thommos and K. Warncke, *Acta Chem. Scand.*, 1997, **51**, 533.
7 M. Fontecave and J.-L. Pierre, *Bull. Soc. Chim. Fr.*, 1996, **133**, 653.
8 D. P. Goldberg and S. J. Lippard in *Mechanistic Bioinorganic Chemistry*, ed. H. Holden Thorp and V. L. Pecoraro, *Advances in Chemistry*, Series 246, American Chemical Society, Washington DC 1995, p. 61.
9 J. Stubbe and W. A. van der Donk, *Chem. Rev.*, 1998, **98**, 705.
10 R. H. Holm and E. I. Solomon, Guest Editors, *Chem. Rev.*, 1996, **96**, No. 7.
11 *Magnetic Molecular Materials*, ed. D. Gatteschi, O. Kahn, J. S. Miller and F. Palacio, Kluwer, Dordrecht, 1991.
12 O. Kahn, *Adv. Inorg. Chem.*, 1995, **43**, 179.
13 A. I. Prokof'ev, N. N. Bubnov, S. P. Solodovnikov and M. I. Kabachnik, *Dokl. Chem.* (*Engl. Transl.*), 1979, **245**, 178.
14 A. Ozarowski, B. R. McGarvey, A. El-Hadad, Z. Tian, D. G. Tuck, D. J. Krovich and G. C. DeFotis, *Inorg. Chem.*, 1993, **32**, 841.
15 D. M. Adams, A. L. Rheingold, A. Dei and D. N. Hendrickson, *Angew. Chem., Int. Ed. Engl.*, 1993, **32**, 391.
16 For example: (*a*) P. Chaudhuri, M. Hess, T. Weyhermüller and K. Wieghardt, *Angew. Chem., Int. Ed.*, 1999, **38**, 1095; (*b*) A. Sokolowski, E. Bothe, E. Bill, T. Weyhermüller and K. Wieghardt, *Chem. Commun.*, 1996, 1671.
17 S. Bruni, A. Caneschi, F. Cariati, C. Delfs, A. Dei and D. Gatteschi, *J. Am. Chem. Soc.*, 1994, **116**, 1388 and references therein.
18 S. R. Sofen, D. C. Ware, S. R. Cooper and K. N. Raymond, *Inorg. Chem.*, 1979, **18**, 234.
19 (*a*) C. G. Pierpont and C. W. Lange, *Prog. Inorg. Chem.*, 1994, **41**, 331; (*b*) C. G. Pierpont and R. M. Buchanan, *Coord. Chem. Rev.*, 1981, **38**, 45.
20 This program was developed by V. Staemmler, F. Birkelbach and C. Krebs, Bochum, 1997.

Communication 9/03778K

ChemComm

Synthesis and characterization of π-conjugated oligomers that contain metal-to-ligand charge transfer chromophores†

Kevin D. Ley, Yiting Li, Jodie V. Johnson, David H. Powell and Kirk S. Schanze*

Department of Chemistry, University of Florida, PO Box 117200, Gainesville, FL 32611-7200, USA. E-mail: kschanze@chem.ufl.edu

Received (in Columbia, MO, USA) 30th April 1999, Accepted 20th July 1999

The synthesis and characterization of a series of *p*-phenyleneethynylene oligomers that contain the 2,2′-bipyridine-5,5′-diyl moiety is reported; metallation of the oligomers with $Re^{I}(CO)_5Cl$ and $Ru(bpy)_2Cl_2$ yields the corresponding $(L)Re(CO)_3Cl$ and $(L)Ru(bpy)_2^{2+}$ complexes.

π-Conjugated oligomers and polymers are of interest due to unique optical and electronic properties which enable their use as the active medium in optical, electronic, optoelectronic and chemical sensing devices.[1,2] We recently synthesized and characterized the photophysical properties of a series of π-conjugated polymers that incorporate a metal–bipyridine (bpy) chromophore directly into the backbone of a poly(phenyleneethynylene) (PPE) polymer.[3] The metal–organic polymers exhibit several interesting properties, including a decreased band-gap compared to the unmetallated polymer and a long-lived photoluminescence believed to arise from the metal-to-ligand charge transfer (MLCT) state. In an effort to better understand the optical properties of the metal–organic π-conjugated materials, we set out to prepare a series of monodisperse PPE-based metal–organic oligomers as models for the structurally related polymers.[4] Accordingly we have synthesized oligomers **1**–**4**, along with the corresponding metal complex derivatives, **Re-1**–**Re-4** and **Ru-1**–**Ru-4**. The present report describes the synthesis and optical absorption data for this new series of oligomers.

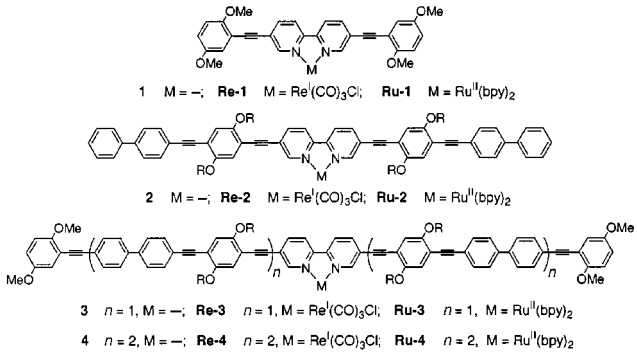

Preparation of series **1**–**4** required an iterative strategy that uses Pd-mediated (Sonogashira)[5] coupling chemistry to extend the PPE backbone outward from a 2,2′-bipyridine-5,5′-diyl 'core'. In order to implement this strategy a suitably functionalized 'monomer' unit that contains a protected terminal acetylene or a protected (or masked) aryl iodide was required. Other groups had previously reported application of the TMS group to protect terminal acetylenes and/or the 1-aryl-3,3-diethyltriazene function as a masked aryl iodide in the synthesis of mono-disperse PPE oligomers.[2a–d] The 1-aryl-3,3-diethyltriazene masking group was deemed unsuitable for our needs owing to the possibility that the bipyridyl nitrogens would react with the electrophile (MeI) that is used in the aryltriazene to aryl iodide conversion step. Although the TMS group seemed suitable for protecting the terminal acetylene, preliminary synthetic efforts aimed at preparing a monomer which contained an aryl iodide and a TMS-protected acetylene were thwarted due to the difficulty of separating the desired product from unreacted starting materials and by-products. The chromatographic separation is difficult (if not impossible) because the starting materials, the by-products and the desired product are all non-polar and therefore have similar solubility and comparable R_f values.

We finally discovered that the 2-hydroxypropan-2-yl (2-HP) protecting group[6] would allow us to readily prepare and purify multigram quantities of monomer **6** (Scheme 1), which features a protected terminal acetylene and a reactive aryl iodide.‡ Thus, in a two-step, one-pot procedure 4,4′-diiodobiphenyl was reacted with TMSC≡CH and then with 2-methylbut-3-yn-2-ol to afford **5a**. The 2-HP protecting group in **5a** allows this compound to be separated from the reaction by-products by silica chromatography. The separation is facile because the by-products have significantly higher R_f values compared to **5a** owing to the polar 2-HP protecting group. Selective removal of the TMS group from **5a** with KOH–MeOH afforded mono-protected compound **5b**. Monomer **6** was obtained by coupling **5b** with 1 equiv. of 1,4-diiodo-2,5-dioctadecyloxybenzene. Here again the polarity of the 2-HP protecting group in **6** allowed this material to be easily separated from the reaction by-products, affording the pure compound in 28% yield after chromatography.

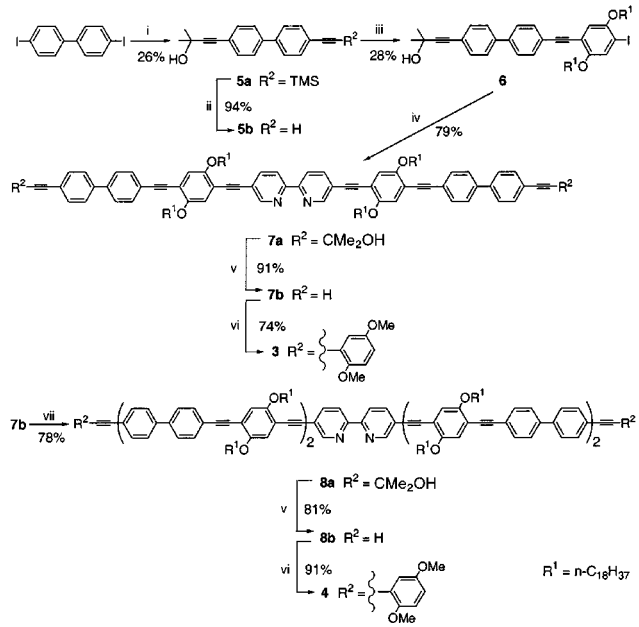

Scheme 1 *Reagents and conditions*: i, TMSC≡CH (1 equiv.), Pd/Cu (cat.), heat, 3 h, then $HC{\equiv}CCMe_2OH$ (excess), heat, 3 h; ii, KOH, THF–MeOH; iii, 1,4-diiodo-2,5-dioctadecyloxybenzene (1 equiv.), Pd/Cu (cat.); iv, 5,5′-diethynyl-2,2′-bipyridine (0.5 equiv.), Pd/Cu (cat.); v, KOH, toluene, reflux; vi, 2-iodo-1,4-dimethoxybenzene (2 equiv.), Pd/Cu (cat.); vii, **6** (2 equiv.), Pd/Cu (cat.).

† Details of the synthesis and characterization of the oligomers is available from the RSC web site, see http://www.rsc.org/suppdata/cc/1999/1749/

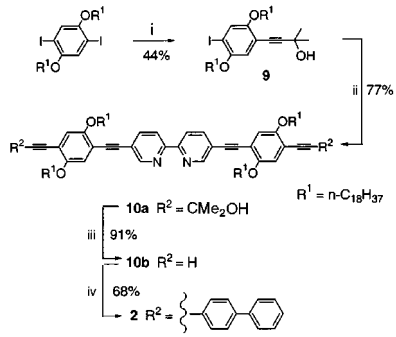

Scheme 2 *Reagents and conditions*: i, HC≡CCMe$_2$OH (1 equiv.), Pd/Cu (cat.); ii, 5,5′-diethynyl-2,2′-bipyridine (0.5 equiv.), Pd/Cu (cat.); iii, KOH, toluene, reflux; iv, 4-bromobiphenyl, Pd/Cu (cat.).

Once **6** was available in multigram quantities, synthesis of the desired oligomers proceeded rapidly. Thus, reaction of 2 equiv. of **6** with 5,5′-diethynyl-2,2′-bipyridine[7] produces **7a**, which is subsequently deprotected by KOH, toluene and heat to afford **7b**. Endcapping of **7b** with 2-iodo-1,4-dimethoxybenzene affords **3**, and subsequent metallation of **3** with Re(CO)$_5$Cl in toluene or Ru(bpy)$_2$(CF$_3$SO$_3$)$_2$ in THF–acetone yields **Re-3** and **Ru-3**, respectively. A further iterative sequence beginning with coupling of **7b** with 2 equiv. of **6** followed by deprotection and endcapping affords oligomer **4**.

As shown in Scheme 2, **2** was synthesized by a different approach that also relies upon the use of the 2-HP protecting group. First, 1,4-diiodo-2,5-dioctadecyloxybenzene was coupled with 1 equiv. of 2-methylbut-3-yn-2-ol to produce **9**. This compound was readily separated from unreacted starting material owing to the polar 2-HP function. Reaction of 2 equiv. of **9** with 5,5′-diethynyl-2,2′-bipyridine afforded **10a**, which was deprotected to **10b** by KOH, toluene and heat. Finally, **10b** was coupled with 4-bromobiphenyl to produce **2** which is subsequently metallated to afford **Re-2** or **Ru-2**.

Fig. 1 compares the UV-visible absorption spectra of the free oligomers with those of the corresponding (L)Re(CO)$_3$Cl and (L)Ru(bpy)$_2^{2+}$ complexes. The free oligomers all feature two absorption bands in the 300–500 nm region. The lowest energy band is assigned to the long-axis polarized π,π* (HOMO → LUMO) transition, while the second band is assigned to the short-axis polarized π,π* transition. The low energy band red-shifts considerably from **1** to **2**, but the position and bandshape of the transition remains relatively constant in **2**–**4**, indicating that the bandgap of the oligomers is defined early in the series. This observation contrasts with observations made on PPE oligomers that contain phenylene repeats (as opposed to the biphenyl and bipyridyl repeats present in **1**–**4**), in which the bandgap continues to decrease for 10 or more repeat units.[2b,d,f] This suggests that the poor electronic coupling between the non-coplanar phenyl (and pyridyl) rings in the biphenyl and bipyridyl units in **2**–**4** restricts the conjugation length.

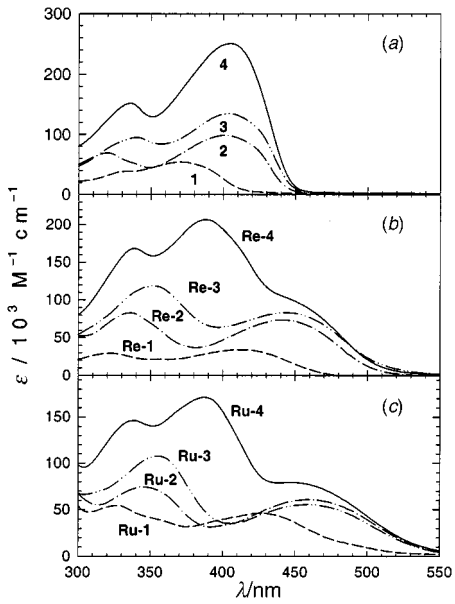

Fig. 1 Absorption spectra of oligomers: (*a*) **1**–**4** in THF solution; (*b*) **Re-1**–**Re-4** in THF solution; (*c*) **Ru-1**–**Ru-4** in CH_2Cl_2 solution.

Comparison of the spectra of **Re-1**–**Re-4** with those of the corresponding free oligomers demonstrates that metallation induces a substantial red-shift of the lowest π,π* absorption. The oscillator strength of the low energy band is large, but relatively constant throughout the series **Re-1**–**Re-4**. The low-energy band likely arises from a long-axis polarized π,π* transition localized predominantly on the chromophore defined by the bis(dioctadecyloxyphenylethynyl)-capped bipyridine segment. The transition is red-shifted because metallation forces the bipyridyl unit into a planar conformation, thereby effectively increasing the conjugation length.[4d] In addition to this effect, the electrophilic metal center likely decreases the LUMO energy and consequently decreases the HOMO–LUMO gap. An important point is that the dπ (Re) → π* (bpy-oligomer) MLCT transition, which is expected to arise in the 400–500 nm region (with $\varepsilon \approx 10^3$–10^4 M^{-1} cm^{-1}), is likely buried under the considerably more intense ligand-centered π,π* transition.

The spectra of the Ru^{II} complexes **Ru-1**–**Ru-4** are also dominated by the π,π* transitions of the ligand; in fact, these bands have approximately the same λ_{max} and ε in the Ru^{II} and Re^{I} complexes. A distinct shoulder is observed ($\lambda \approx 485$ nm, $\varepsilon \approx 8000$ M^{-1} cm^{-1}) in the spectrum of **Ru-1** which is very likely the dπ (Ru) → π* (**1**) MLCT transition. A similar MLCT band is not observed in the spectra of **Ru-2**–**Ru-4** because it is obscured by the more intense π,π* transition that occurs at a lower energy in these oligomers.

In conclusion, we have applied an iterative method to synthesize a series of mono-disperse PPE-based metal–organic oligomers. Ongoing spectroscopic and photophysical studies demonstrate that the oligomers are excellent models for structurally related bipyridine-containing poly(*p*-phenyleneethynylene) polymers.

We are grateful to the National Science Foundation (Grant No. CHE 99-01862) for support of this work.

Notes and references

‡ Godt and co-workers recently reported the use of the hydroxymethyl (HM) moiety as a protecting group for terminal acetylenes in the synthesis of PPE oligomers [ref. 2(*f*)].

1 For leading reviews on π-conjugated polymers see: *Handbook of Conducting Polymers*, ed. T. A. Skotheim, R. L. Elsenbaumer and J. R. Reynolds, Marcel Dekker, New York, 2nd edn., 1998; H. Bassler and L. J. Rothberg, *Chem. Phys.*, 1998, **227**, 1; A. Kraft, A. C. Grimsdale and A. B. Holmes, *Angew. Chem., Int. Ed.*, 1998, **37**, 402; A. D. Schlüter and G. Wegner, *Acta Polym.*, 1993, **44**, 59.

2 (*a*) J. M. Tour, *Chem. Rev.*, 1996, **96**, 537; (*b*) L. R. Jones, J. S. Schumm and J. M. Tour, *J. Org. Chem.*,1997, **62**, 1388; (*c*) J. S. Moore, *Acc. Chem. Res.*, 1997, **30**, 402; (*d*) M. Moroni, J. LeMoigne and S. Luzzati, *Macromolecules*, 1994, **27**, 562; (*e*) U. Ziener and A. Godt, *J. Org. Chem.*, 1997, **62**, 6137; (*f*) H. Kukula, S. Veit and A. Godt, *Eur. J. Org. Chem.*, 1999, 277.

3 K. D. Ley, C. E. Whittle, M. D. Bartberger and K. S. Schanze, *J. Am. Chem. Soc.*, 1997, **119**, 3423; K. D. Ley and K. S. Schanze, *Coord. Chem. Rev.*, 1998, **171**, 287; K. A. Walters, K. D. Ley and K. S. Schanze, *Chem. Commun.*, 1998, 1115.

4 (*a*) Z. Peng and L. Yu, *J. Am. Chem. Soc.*, 1996, **118**, 3777; (*b*) S. C. Rasumssen, D. W. Thompson, V. Singh and J. D. Peterson, *Inorg. Chem.*, 1996, **35**, 3449; (*c*) Z. Peng, A. Gharavi and L. Yu, *J. Am. Chem. Soc.*, 1997, **119**, 4622; (*d*) B. Wang and M. R. Wasielewski, *J. Am. Chem. Soc.*, 1997, **119**, 12; (*e*) L. X. Chen, W. J. H. Jäger, M. P. Niemczyk and M. R. Wasielewski, *J. Phys. Chem. A*, 1999, **103**, 4341.

5 K. Sonogashira, in *Comprehensive Organic Synthesis*, ed. B. M. Trost and I. Fleming, Pergamon, Oxford, 1991, vol. 3, p. 521.

6 L. Della Ciana and A. Haim, *J. Heterocycl. Chem.*, 1984, **21**, 607; S. J. Havens and P. M. Hergenrother, *J. Org. Chem.*,1985, **50**, 1763.

7 V. Grosshenny, F. M. Romero and R. Ziessel, *J. Org. Chem.*, 1997, **62**, 1491.

Communication 9/03476E

Dideoxygenated calix[4]arene crown-6 ethers enhanced selectivity for caesium over potassium and rubidium

Richard A. Sachleben,*[a] Agathe Urvoas,[a] Jeffrey C. Bryan,[a] Tamara J. Haverlock,[a] Benjamin P. Hay[b] and Bruce A. Moyer[a]

[a] *Oak Ridge National Laboratory, PO Box 2008, MS-6119/4500S, Oak Ridge, TN 37831, USA. E-mail: sik@ornl.gov*
[b] *Pacific Northwest National Laboratory, PO Box 999/MS KI-83, Richland, WA 99352, USA.*

Received (in Columbia, MO, USA) 2nd December 1998, Revised 6th July 1999, Accepted 6th July 1999

Calix[4]arene crown-6 ethers derived from dideoxygenated calix[4]arene exhibit enhanced extraction selectivity for caesium over potassium; the crystal stucture of the uncomplexed calix[4]arene monobenzocrown-6 ether exists in the 1,3-alt conformation in the solid state.

Calixarenes[1] have been taking on an increasingly important role in host–guest chemistry, in large part because they can provide a well-organized platform for the attachment of pendant functional groups.[2,3] The incorporation of a calix[4]arene (**1** in Scheme 1) moiety into crown ethers[4] has been used to develop powerful, highly selective ionophores for alkali metal cations,[5,6] the properties of which are often dependent on the conformation adopted by the calixarene. Whereas diethoxycalix[4]arene crown-4 ether in the cone conformation exhibits high sodium selectivity,[7] diethoxycalix[4]arene crown-5 ether in the 1,3-alternate conformation exhibits selectivity for K^+ over Na^+ exceeding that of Valinomycin.[8] Furthermore, 1,3-alt calix[4]arene crown-6 ethers exhibit high caesium binding[9,10] with selectivities for Cs^+/Na^+ of *ca.* 10^4–10^5,[9–11] a property which has led to their study for the selective removal of caesium from nuclear fuel reprocessing wastes.[12,13] However, Cs/K selectivities are only *ca.* 80–600, which is of concern since the wastes may contain as much as 1 M K^+ in a typical matrix containing 5–7 M Na^+, but only 10^{-6}–10^{-3} M Cs.[14] Having undertaken an effort to develop extractants with improved Cs/K selectivity, we have synthesized three new calix[4]arene crown-6-ethers (**3a**–**c** in Scheme 1)† derived from di-dehydroxylated calix[4]arene **2a**,[15] which exhibit Cs^+/Rb^+ and Cs^+/K^+ selectivities significantly greater than that of comparable 1,3-dialkoxycalix[4]arene crown-6-ethers **4a**–**c**.

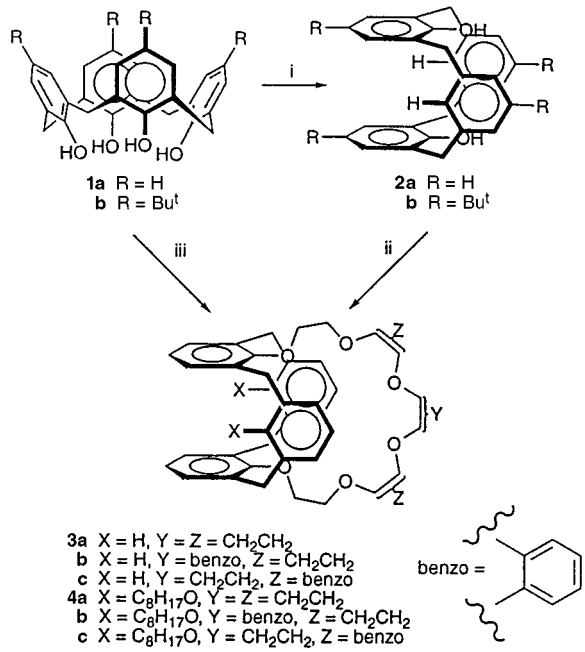

Scheme 1 *Reagents and conditions*: i, $(EtO)_2PHO$, CCl_4, Et_3N, toluene, 0 °C, then K, NH_3 (liquid); ii, $(TsOCH_2CH_2O\text{-}Z\text{-}O)_2Y$, Cs_2CO_3, MeCN; iii, $C_8H_{17}I$, K_2CO_3, MeCN, then $(TsOCH_2CH_2O\text{-}Z\text{-}O)_2Y$, Cs_2CO_3, MeCN.

Competitive extractions of alkali metal nitrates by the six calix[4]arenes **3a**–**3c** and **4a**–**c** were performed essentially as described previously,[14] with the organic phase consisting of 0.025 M of calixarene crown ether in 1,2-dichloroethane and the aqueous phase consisting of a mixture of alkali metal nitrates: 1.00 M $LiNO_3$, 1.00 M $NaNO_3$, 0.100 M KNO_3, 0.0020 M $RbNO_3$ and 0.0011 M $CsNO_3$. Metal ion concentrations were determined for both phases, from which distribution ratios $D_M = [M^+]_{organic}/[M^+]_{aqueous}$ were calculated directly. Caesium was analyzed by γ spectrometry, while lithium, sodium, potassium and rubidium were analyzed, subsequent to stripping of the organic phase with 1.0 mM HNO_3, by inductively coupled plasma atomic emission spectroscopy. From the data given in Table 1, it can be seen that in each case where the calixarene is changed from dioctyloxycalix[4]arene **4a**–**c** to the dihydrocalix[4]arene **3a**–**c** the extraction strength for caesium, expressed in terms of D_{Cs}, decreases by roughly an order of magnitude. However, an even larger decrease is observed for the extraction of the other alkali metals, to the point for K^+ and Rb^+ where no extraction was measured. This is despite the fact that the aqueous phase used in these experiments contained significantly higher concentrations of Li^+, Na^+, K^+ and Rb^+ than Cs^+. As a consequence, selectivity for extraction of caesium (as expressed by $S_{Cs/M} = D_{Cs}/D_M$) increases. Since only upper limits are available for the extraction of Rb^+ and K^+ by calix[4]arene crown ethers **3a**–**c**, the magnitude of the selectivity increase as compared to **4a**–**d** can only be assigned a lower limit. Even so, the observed trends provide evidence that improved extraction selectivity for Cs^+ can be obtained by appropriate modification of the calixarene portion of calix[4]-arene crown-6 ethers.

Table 1 Calix[4]arene crown-6 ethers used in this study, their distribution ratios (D_M) for the extraction of alkali metal nitrates from water to 1,2-dichloroethane at 25 °C, and the corresponding selectivities (S) for Cs^+ ions over Li^+, Na+, K^+ and Rb^+ ions [a]

Extractant	D_{Cs}	D_{Rb} ($S_{Cs/Rb}$)	D_K ($S_{Cs/K}$)	$D_{Na}/10^{-5}$ ($S_{Cs/Na}$)	$D_{Li}/10^{-5}$ ($S_{Cs/Li}$)
3a	0.403	—[b] (> 58)	—[b] (> 4200)	2.17 (23000)	1.90 (32000)
3b	0.383	—[b] (> 54)	—[b] (> 4000)	—[b] (> 150000)	—[b] (> 660000)
3c	0.116	—[b] (> 17)	—[b] (> 1200)	—[b] (> 47000)	—[b] (> 200000)
4a	3.65	0.180 (20)	0.0152 (240)	22.0 (17000)	2.98 (120000)
4b	4.04	0.214 (19)	0.0141 (290)	3.9 (100000)	0.99 (> 450000)
4c	1.61	0.178 (9.0)	0.0125 (130)	—[b] (> 640000)	0.97 (170000)

[a] All values are the average of two determinations. [b] Lower limits on measurement of distribution ratios: $D_{Li} = 5.8 \times 10^{-7}$, $D_{Na} = 2.5 \times 10^{-6}$, $D_K = 9.6 \times 10^{-5}$, $D_{Rb} = 0.0070$.

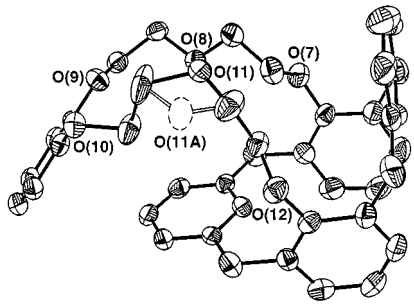

Fig. 1 ORTEP drawing (50% probability elipsoids) of **5b**. For clarity only one molecule from the asymmetric unit is displayed, hydrogen atoms are omitted, and only oxygen atoms are labeled. The minor disorder component (O11A) is represented with a dashed boundary ellipsoid.

Since previous studies have shown that the 1,3-alternate conformation is preferred for high caesium binding and selectivity[9] and that calixarenes bearing substituents smaller than ethoxy are conformationally mobile,[16] we considered the conformational preferences of these new compounds. The crystal structure of **3b** (Fig. 1)‡ reveals that this compound crystallizes with two molecules in the crystallographic asymmetric unit, with the calix[4]arene portions of both molecules clearly in the 1,3-alt conformation. The calix[4]arene crown-6-ethers **3a–c** exhibit room temperature ^{1}H NMR ($CDCl)_3$ where the Ar-CH_2-Ar resonances of the calixarene appear as a pair of doublets at $\delta \sim 4.2$ and ~ 3.7 with a coupling constant of ~ 15.5 Hz, while the intraannular proton on the deoxygenated aromatic ring is found upfield at $\delta \sim 6.0$. Grynszpan and Biali[17] interpreted the upfield shift of the corresponding proton in **2b** in terms of shielding by the two phenolic rings in the 1,3-alt conformation, whereas the positions and coupling constants of the calixarene methylenes are more consistent with the report by Ting *et al.*[15] where the 'unsubstituted phenyl rings can rotate freely'. The calixarene methylene carbon of **3b** was observed at δ 35.3, similar to the values reported to be observed for the 1,3-alternate conformers in conformationally immobile calix-[4]arenes.[18] We performed VT-NMR on **3b** in $CDCl_3$ and observed a decrease in the separation between the pair of doublets assigned to the calixarene methylene resonances, from 216 to 187 Hz ($\Delta\delta$ = 29 Hz), when the temperature was decreased from 340–220 K, consistent with rapid conformational interconversion which shows upon lowering the temperature. Conversely, in toluene-d_8, the separation between this pair of doublets decreased, from 340 to 298 Hz ($\Delta\delta$ = 42 Hz), when the temperature was *increased* from 170 to 370 K, suggesting a slow conformational interconversion which speeds up with increasing temperature. However, coalescence was not achieved even when a solution of **3b** was heated to 500 K in nitrobenzene-d_5. In $(CD_2Cl)_2$, $\Delta\delta \approx 0$ over the temperature range 240–340 K. Consequently, the solution conformation cannot be assigned to the calixarene portion of **3b** based on these results.

The results reported here have significant ramifications, not only in the effort to develop more highly selective extractants, but also in understanding the conformational and electronic factors which contribute to the remarkable ionophoric properties of calixarenes and calix[4]arene crown ethers. Efforts in this area are the subject of ongoing investigations.

This research was sponsored by the Environmental Management Science Program, Offices of Energy Research and Environmental Management, U.S. Department of Energy, under contract DE-AC05-960R22464 with Oak Ridge National Laboratory, managed by Lockheed Martin Energy Research Corporation.

Notes and references

† ^{1}H NMR and ^{13}C NMR data were consistent with the assigned structures for all new compounds.

‡ *Crystal data* for **5b**: $C_{42}H_{42}O_6$, 642.8 g mol^{-1}, triclinic, a = 10.634(3), b = 17.432(4), c = 19.578(4) Å, α = 70.959(17), β = 89.846(17), γ = 77.52(2)°, V = 3340.6(13) Å^3, T = 173(2) K, $P\bar{1}$, Z = 4, μ = 0.084 mm^{-1}, refinement of F^2, final $wR2$ = 0.117, on all 8182 independent reflections. CCDC 182/1353. See http://www.rsc.org/suppdata/cc/1999/1751 for crystallographic data in .cif format.

1 C. David Gutsche, *Calixarenes, Monographs in Supramolecular Chemistry*, ed. J. F. Stoddard, The Royal Society of Chemistry, Cambridge, 1989, vol. 1; *Calixarenes, A Versatile Class of Macrocyclic Compounds*, ed. J. Vicens and V. Böhmer, Kluwer, Dordrecht, 1991.
2 S. Shinkai, *Tetrahedron*, 1993, **49**, 8933.
3 P. Timmerman, W. Verboom and D. N. Reinhoudt, *NATO ASI Ser. Ser. E*, 1996, **320**, 245.
4 C. Alfieri, E. Dradi, A. Pochini, R. Ungaro and G. D. Andreetti, *J. Chem. Soc., Chem. Commun.*, 1983, 1075.
5 P. J. Dijkstra, J. A. Brunink, K.-E. Bugge, D. N. Reinhoudt, S. Harkema, R. Ungaro, F. Ugozzoli and E. Ghidini, *J. Am. Chem. Soc.*, 1989, **111**, 7567; E. Ghidini, F. Ugozzoli, R. Ungaro, S. Harkema, A. A. El-Fadl and D. N. Reinhoudt, *J. Am. Chem. Soc.*, 1990, **112**, 6979.
6 Z. Asfari, S. Wenger and J. Vicens, *J. Inclusion Phenom.*, 1994, **19**, 137.
7 H. Yamamoto and S. Shinkai, *Chem. Lett.*, 1994, 1115.
8 A. Casnati, A. Pochini, R. Ungaro, C. Bocchi, F. Ugozzoli, R. J. M. Egberink, H. Struijk, R. Lugtenberg, F. de Jong and D. N. Reinhoudt, *Chem. Eur. J.*, 1996, **2**, 436.
9 R. Ungaro, A. Casnati, F. Ugozzoli, A. Pochini, J.-F. Dozol, C. Hill and H. Rouquette, *Angew. Chem.*, 1994, **106**, 1551; A. Casnati, A. Pochini, R. Ungaro, F. Arnaud, S. Fanni, M.-J. Schwing, R. J. M. Egberink, R. Lugtenberg, F. de Jong and D. N. Reinhoudt, *J. Am. Chem. Soc.*, 1995, **117**, 2767.
10 C. Hill, J.-F. Dozol, V. Lamare, H. Rouquette, S. Eymard, B. Tournois, J. Vicens, Z. Asfari, C. Bressot, R. Ungaro and A. Casnati, *J. Inclusion Phenom.*, 1994, **19**, 399; Z. Asfari, C. Bressot, J. Vicens, C. Hill, J.-F. Dozol, H. Rouquette, S. Eymard, V. Lamare and B. Tournois, *Anal. Chem.*, 1995, **67**, 3133.
11 V. Lamare, J.-F. Dozol, F. Ugozzoli, A. Casnati and R. Ungaro, *Eur. J. Org. Chem.*, 1998, **8**, 1559; J. F. Dozol, N. Simon, V. Lamare, H. Rouquette, S. Eymard, B. Tournois, D. DeMarc and R.-M. Macias, *Sep. Sci. Technol.*, in the press.
12 J.-F. Dozol, Z. Asfari, C. Hill and J. Vicens, FR 2698362 (*Chem. Abstr.*, 1994, **121**, 189685); J.-F. Dozol, H. Rouquette, R. Ungaro and A. Casnati, WO 9424138 (*Chem. Abstr.*, 1995, **122**, 239730).
13 B. A. Moyer, P. V. Bonnesen, R. A. Sachleben and D. J. Presley, WO 9912878 (*Chem. Abstr.*, 1999, **130**, 214967).
14 T. J. Haverlock, P. V. Bonnesen, R. A. Sachleben and B. A. Moyer, *Radiochim. Acta*, 1997, **76**, 103.
15 Compound **2a** was prepared in the manner previously reported for **2b**: Y. Ting, W. Verboom, L. C. Groenen, J.-D. van Loon and D. N. Reinhoudt, *J. Chem. Soc., Chem. Commun.*, 1990, 1432; F. Grynszpan, Z. Goren and S. E. Biali, *J. Org. Chem.*, 1991, **56**, 532.
16 C. D. Gutsche, D. Dhawan, J. A. Levine, K. H. No and L. J. Bauer, *Tetrahedron*, 1983, **39**, 409.
17 F. Grynszpan and S. Biali, *Tetrahedron Lett.*, 1991, **32**, 5155.
18 C. Jaime, J. de Mendoza, P. Prados, P. M. Nieto and C. Sanchez, *J. Org. Chem.*, 1991, **56**, 3372. These authors report that the ^{13}C chemical shifts are relatively insensitive to the substituents at the 1 and 4 positions of the aromatic rings.

Communication 9/05682C

A facile route to 3,7-*cis*-disubstituted cycloocta-1,5-diene-1,2,5,6-tetracarboxylates through photochemical [2 + 2]cycloaddition of 3-substituted cyclobutene-1,2-dicarboxylates and thermal isomerization†

Hisayuki Watanabe,*[a] Yasuyuki Nakajima,[a] Michiaki Adachi,[a] Hiroyasu Hotta,[a] Kazutaka Arai,[a] Yoshiyasu Baba,[b] Carole Noutary,[b] Satsuki Ichikawa,[b] Tetsuo Kusumoto[b] and Tamejiro Hiyama*[c]

[a] *Central Research Institute, Nissan Chemical Industries Ltd., 722-1 Tsuboicho, Funabashi, Chiba 274-8507, Japan. E-mail: watanabeh@nissanchem.co.jp*

[b] *Sagami Chemical Research Center, 4-4-1 Nishiohnuma, Sagamihara, Kanagawa 229-0012, Japan.*

[c] *Department of Material Chemistry, Graduate School of Engineering, Kyoto University, Yoshida, Kyoto 606-8501, Japan*

Received (in Cambridge, UK) 18th May 1999, Accepted 29th July 1999

Photochemical dimerization of 3-substituted cyclobutene-1,2-dicarboxylates followed by thermal isomerization gives regio- and stereo-selectively 3,7-*cis*-disubstituted cycloocta-1,5-diene-1,2,5,6-tetracarboxylates.

Cyclooctanoids have been attracting great interest in the fields of agricultural and pharmaceutical chemistry because of their unique structures and biological activities. For example, natural product Zopfiellin[1] was isolated very recently. Synthetic

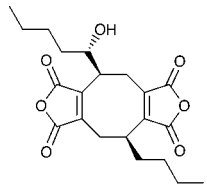

Zopfiellin

methods for cyclooctanoids have been studied over the last few decades.[2] We also reported a route to cyclooctanoids *via* bromination of tetramethyl cycloocta-1,5-diene-1,2,5,6-tetracarboxylate followed by alkylation with organocopper reagents to give rise to regio- and stereo-selectively 3,7-*cis*-disubstitution of the tetraester.[3] This method, however, was restricted to primary alkyl groups due mainly to the low reactivity of secondary and tertiary alkylcopper reagents.

Accordingly, we considered that introduction of bulky groups such as secondary, tertiary and substituted alkyls before eight-membered ring formation would be favorable. In addition, [2 + 2]cycloaddition of cyclobutene looked attractive for eight membered ring formation. Although the synthetic scheme has precedents,[4] we felt it necessary to study carefully the stereochemical and regiochemical outcome of cyclooctanoid synthesis.

Herein we demonstrate that [2 + 2]cycloaddition is widely applicable to the synthesis of eight-membered ring compounds, especially highly substituted ones, as shown in Scheme 1. Although the dimerization ring opening route is limited to symmetrical cyclooctadiene systems, we considered it important to first establish a reliable synthetic route to cyclooctanoids containing various functional groups. We envisaged that dimeric [2 + 2]cycloaddition of cyclobutene **i** would afford a mixture of tricyclo[4.2.0.0]octanes **ii** which might thermally isomerize to 3,7-*cis*-disubstituted cycloocta-1,5-diene derivative **iii**, a precursor of bisanhydride **1** closely related to Zopfiellin. After many experiments, we were pleased to find that this new synthetic route worked. Many 3,7-*cis*-disubstituted cycloocta-1,5-diene derivatives, including those substituted by secondary and tertiary alkyl groups, could be synthesized regio- and stereo-selectively by this method.

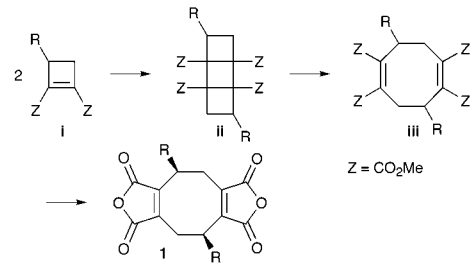

Scheme 1

Key starting materials **2** were prepared from readily available terminal olefins according to the route shown in Scheme 2.[5] Yields of **2** based on the respective olefins are summarized in Table 1. In addition to **2** with a primary alkyl group, those with a secondary or tertiary alkyl group were prepared in good to high yields. Vinyl, bromo and acetoxy groups did not interfere with the reaction (**2g**–**k**). Trimethylsilylmethyl-substituted cyclobutene **2l** was accessible, albeit in a lower yield.

Photochemical dimerization of 3-substituted cyclobutene-1,2-dicarboxylates **2** proceeded smoothly to afford isomeric mixtures of tricyclo[4.2.0.0]octanes, which upon thermal iso-

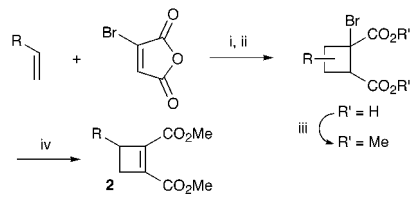

Scheme 2 *Reagents and conditions*: i, *hν*, Ph_2CO, MeCN; ii, aq. Na_2CO_3, then aq. HCl; iii, H_2SO_4, MeOH; iv, DBU, $CHCl_3$.

Table 1 Synthesis of 3-substituted cyclobutene-1,2-dicarboxylates **2**

R	Products	Yield (%)[a]	R	Products	Yield (%)[a]
Pr	**2a**	57	$CH{=}CH_2$	**2g**	24
C_6H_{13}	**2b**	43	CH_2CH_2Br	**2h**	39
Pr^i	**2c**	50	CH_2OAc	**2i**	35
Bu^s	**2d**	23[b]	CH_2CH_2OAc	**2j**	38
CHMePr	**2e**	51[b]	CH(OAc)Bu	**2k**	16[b]
Bu^t	**2f**	25	CH_2SiMe_3	**2l**	15

[a] Isolated overall yields. [b] Diastereomeric mixture (1 : 1).

† Dedicated to Professor Michinori Ōki on the occasion of his 70th birthday.

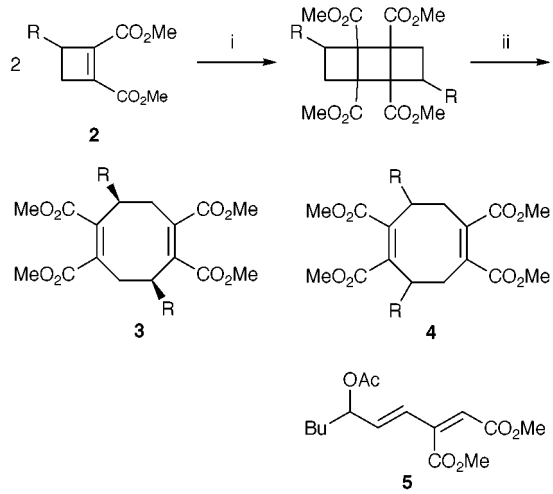

Scheme 3 *Reagents and conditions*: i, *hν*, Ph_2CO, MeCN; ii, xylene, reflux; iii, aq. NaOH,MeOH, then aq. HCl.

Table 2 Transformation of **2** to **3**

R	Products	Yield (%)[a]	R	Products	Yield (%)[a]
Pr	**3a**	48	CH=CH_2	**3g**	—[c]
C_6H_{13}	**3b**	49	CH_2CH_2Br	**3h**	38
Pr^i	**3c**	34	CH_2OAc	**3i**	31
Bu^s	**3d**	37[b]	CH_2CH_2OAc	**3j**	20
CHMePr	**3e**	22[b]	CH(OAc)Bu	**3k**	—[d]
Bu^t	**3f**	5	CH_2SiMe_3	**3l**	34

[a] Isolated overall yields are given. [b] Inseparable isomeric mixture. [c] Unidentified compounds were obtained. [d] Compound **5** was obtained.

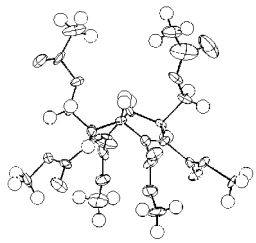

Fig. 1 X-Ray crystallography of **3i**.

merization gave 3,7-*cis*-disubstituted cycloocta-1,5-diene-1,2,5,6-tetracarboxylates **3** as described in Scheme 3.

The results with **2a-l** are listed in Table 2. The possible regioisomer, 3,8-disubstituted cyclooctadiene **4**, was not isolated in all cases. In addition to **2a**, secondary alkyl substituted cyclobutenes **2c**, **2d** and **2e** were smoothly converted into **3c**, **3d** and **3e**, respectively.[6] *tert*-Butyl-substituted cyclooctadiene **3f** was also obtained but in 5% yield. Although **2g** (R = vinyl) gave unidentified compounds, **2h** (R = CH_2CH_2Br), **2i** (R = CH_2OAc) and **2j** (R = CH_2CH_2OAc) were transformed to cyclooctadienes **3h**, **3i** and **3j**, respectively, in moderate yields. These are potential precursors for further elaboration of side chains. The stereochemistry of **3i**[7] was proved to be 3,7-*cis* by X-ray crystallography (Fig. 1). Unexpected product **5** (13%) *in lieu* of **3k** was formed from cyclobutene **2k**. Similarly **2l** was converted into **3l**.

Regio- and stereo-selective formation of **3** is worthy of note. We consider that the dimerization of 3-substituted cyclobutene-1,2-dicarboxylates **2** would take place through diagonal aggregates due to steric repulsion to afford a single regioisomer of the bicyclo[4.2.0.0]octane tetracarboxylates which, upon heating, give thermodynamically favorable 3,7-*cis*-disubstituted cyclooctadienes **3**.

Dipropyl- and diisopropyl-substituted cyclooctadiene tetraesters **3a** and **3c** were converted into the corresponding bisanhydrides **1a**[8,9] (Fig. 2) and **1c** by alkaline hydrolysis and

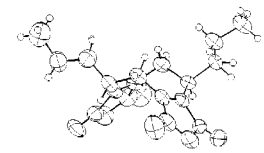

Fig. 2 X-Ray crystallography of **1a**.

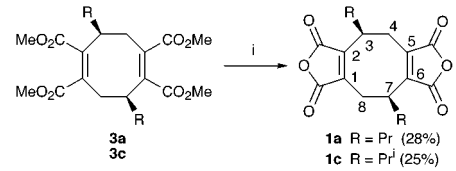

Scheme 4 *Reagents and conditions*: i, aq. NaOH,MeOH, then aq. HCl.

subsequent acidification (Scheme 4). Fungicidal activities of **1a** and **1c** were shown to be close to that of Zopfiellin.[9]

In summary, we have disclosed that facile photochemical [2 + 2]cycloaddition of 3-substituted cyclobutene-1,2-dicarboxylates followed by thermal isomerization affords regio- and stereo-selectively 3,7-*cis*-disubstituted cycloocta-1,5-diene-1,2,5,6-tetracarboxylates in moderate to good yields. Further mechanistic study of the regio- and stereo-selectivity of this new synthetic strategy is in progress.

We are grateful to the Analytical Chemistry Division of Nissan Chemical Industries Ltd. for analytical support.

Notes and references

1 T. Watanabe, K. Yasumoto, M. Murata, M. Tagawa, H. Narushima, T. Furusato, M. Kuwahara, M. Hanaue and T. Seki, *Jpn. Kokai Tokkyo Koho*, 1994, JP 06-184157, EP 582267, US 5346919; *Chem. Abstr.*, 1994, **121**, 7432t.

2 N. A. Petasis and M. A. Patane, *Tetrahedron*, 1992, **48**, 5757.

3 Y. Baba, C. Noutary, S. Ichikawa, T. Kusumoto, H. Watanabe, M. Adachi, H. Hotta, Y. Nakajima, K. Arai and T. Hiyama, *Synlett*, 1997, 1393.

4 *Houben Weyl*, **4/5a**, 344–345, 352, 500–501; E. Vogel, O. Roos and K.-H. Disch, *Justus Liebigs Ann. Chem.*, 1962, **653**, 55; D. Bellus, K. Bredow, H. Sauter and G. D. Weis, *Helv. Chim. Acta*, 1973, **56**, 3004; K. I. Booker-Milburn, F. D. Jimenez and A. Sharpe, *Synlett*, 1995, 735.

5 J. D. White, M. P. Dillon and R. J. Butlin, *J. Am. Chem. Soc.*, 1992, **114**, 9673.

6 Products **3d** and **3e** formed as inseparable mixtures of isomers due to asymmetric carbons of side chains.

7 *Crystal data* for $C_{22}H_{28}O_{12}$ **3i**: M = 484.00, monoclinic, $C2/c$, a = 16.866(3), b = 10.100(2), c = 14.408(3) Å, β = 93.43(2)°, U = 2450.0(8) Å^3, T = 298 K, Z = 4, μ(Cu-Kα) = 1.009 mm^{-1}, 1980 reflections measured, 1873 unique (R_{int} = 0.065), R = 0.114, R_w = 0.117. *Selected data* for **3i**: $\delta_H(CDCl_3)$ 2.07 (s, 6H), 2.62 (dd, J_1 = 14.2, J_2 6.3, 1H), 3.15 (t, J 14.0, 1H), 3.28–3.38 (m, 1H), 3.74 (s, 6H), 3.76 (s, 3H), 4.24 (dd, J_1 11.2, J_2 4.9, 1H), 4.31 (dd, J_1 11.2, J_2 6.1, 1H); *m/z* (FAB) 485 (M^{+}+1), 453, 425, 411.

8 The stereochemistry of **1a** was confirmed to be 3,7-*cis* by X-ray crystallography, and further suggested the stereoselectivity of this route. *Crystal data* for $C_{18}H_{20}O_6$ **1a**: M = 332.00, monoclinic, $P2_1/a$, a = 11.987(3), b = 13.131(3), c = 11.801(2) Å, β = 112.97(2)°, U = 1710.2(7) Å^3, T = 298 K, Z = 4, μ(Cu-Kα) = 0.7686 mm^{-1}, 2542 reflections measured, 1486 unique (R_{int} = 0.160), R = 0.098, R_w = 0.119. CCDC 182/1355. See http://www.rsc.org/suppdata/cc/1999/1753/ for crystallographic data in .cif format. *Selected data* for **1a**: $\delta_H(CDCl_3)$ 0.98 (t, J 7.2, 6H), 1.41–1.50 (m, 4H), 1.58–1.67 (m, 2H), 1.74–1.83 (m, 2H), 2.91–3.05 (m, 6H).

9 M. Adachi, Y. Nakajima, H. Watanabe, H. Hotta, K. Arai, M. Tagawa, M. Futagawa, T. Furusato, H. Ohya, Y. Baba, C. Noutary, S. Ichikawa, T. Kusumoto and T. Hiyama, 'The 21st IUPAC International Symposium on The Chemistry of Natural Products,' Chinese Chem. Soc., Beijing, 1998, p. 169. Zopfiellin and its analogs **1a** and **1c** exhibit fungicidal activity at 100 ppm (*in vitro*) against *Botorytis cinerea*. Detailed results of the assay will be reported elsewhere.

Communication 9/03942B

Anion recognition and luminescent sensing by new ruthenium(II) and rhenium(I) bipyridyl calix[4]diquinone receptors

Paul D. Beer,*[a] Vadim Timoshenko,[a] Mauro Maestri,*[b] Paolo Passaniti[b] and Vincenzo Balzani[b]

[a] *Department of Chemistry, Inorganic Chemistry Laboratory, University of Oxford, South Parks Road, Oxford, UK OX1 3QR. E-mail: paul.beer@chem.ox.ac.uk*

[b] *Dipartimento di Chimica 'G. Ciamician', Universita di Bologna, via Selmi 2, 1-40126 Bologna, Italy*

Received (in Cambridge, UK) 30th June 1999, Accepted 2nd August 1999

New ruthenium(II) and rhenium(I) bipyridyl calix[4]diquinone receptors have been prepared and shown to selectively bind and sense acetate anions *via* remarkable luminescent emission intensity retrieval effects.

Anionic species are well known to play numerous fundamental roles in biological and chemical processes and their detrimental effects as environmental pollutants is of growing concern.[1] In view of this there is intense current interest being shown in the design and syntheses of receptors that are proficient at detecting anions in solution.[2] By incorporating redox- and photo-active transition metal inorganic signalling probes into various acyclic, macrocyclic and calixarene ligand frameworks we have produced a series of selective spectral and electrochemical responsive reagents for anions.[2a,3] For example, using the ruthenium(II) bipyridyl luminescent reporter moiety the selective sensing of dihydrogen phosphate has been demonstrated with lower[4] and upper rim[5] ruthenium(II) bipyridyl calix[4]arene receptor systems. In an effort to construct a novel type of switchable and selective luminescent sensitive receptor for anions we report here the synthesis of new ruthenium(II) and rhenium(I) bipyridyl calix[4]diquinone receptors which selectively bind and sense acetate anions *via* remarkable emission intensity retrieval effects.

The condensation of the lower rim 1,3-bis(chlorocarbonyl) substituted *p-tert*-butylcalix[4]arene **1**[6] with 2 equiv. of mono-Boc protected 1,2-diaminoethane[7] followed by HCl gave **2** in 68% yield. The reaction of **3**[8] with **2** in the presence of Et_3N in dry CH_2Cl_2 under high dilution conditions afforded the [1 + 1] product **4** in 44% yield together with the [2 + 2] dimer in 20% yield. $Tl(O_2CCF_3)_3$ in TFA[9] was used to oxidise **4** and produce the new bipyridyl bridged calix[4]arene-diquinone **5** in 68% yield (Scheme 1). Complexation reactions with $(bipy)_2RuCl_2{\cdot}2H_2O$ followed by NH_4PF_6, and $Re(CO)_5Cl$ gave the new receptors L^1 and L^2 in 81 and 79% respective yields. Analogous high yielding complexation reactions with **4** produced the new lower rim calix[4]arene derivatives L^3 and L^4.

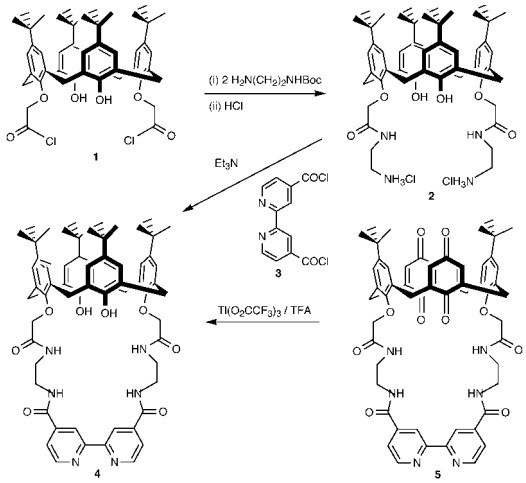

Scheme 1

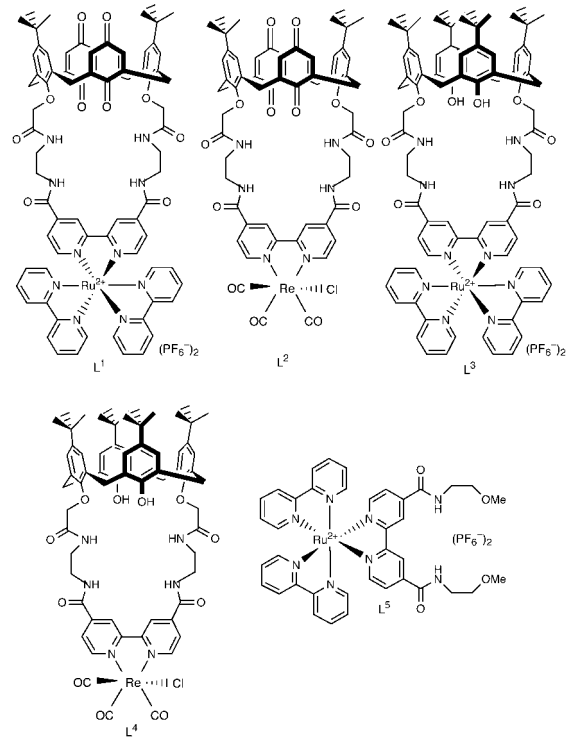

The addition of Bu_4NOAc, Bu_4NCl and $Bu_4N(H_2PO_4)$ to DMSO-d_6 ^{1}H NMR solutions of L^1–L^4 resulted in significant perturbations of most notably the respective amide and 3,3′-bipyridyl receptor protons by up to $\Delta\delta$ = 0.95 ppm. The resulting titration curves all suggested a 1:1 receptor:anion stoichiometry. The computer program EQNMR[10] was used to determine the stability constants from the ^{1}H NMR titration data, and the results are summarised in Table 1, which includes for comparison purposes stability constant data for acyclic receptor L^5.[13] It is evident that the topological nature of a receptor's calix[4]arene/calix[4]diquinone cavity and the bipyridyl coordinated charged ruthenium(II)/neutral rhenium(I) transition metal centre have a major effect on the anion thermodynamic stability and on the selectivity preference that a particular receptor exhibits. Compared to acyclic receptor L^5, L^1–L^4 form significantly stronger anion complexes with AcO^- and Cl^-, and

Table 1 Stability constants of receptors with anions in DMSO-d_6

	K^a/M^{-1}		
Receptor	Cl^-	AcO^-	$H_2PO_4^-$
L^1	1050	9990	215
L^2	255	1790	160
L^3	840	4060	240
L^4	435	760	185
L^5	150	350	1300

[a] Errors < 10%; T = 298 K.

weaker complexes with $H_2PO_4^-$. The AcO^- > Cl^- > $H_2PO_4^-$ selectivity trend displayed by L^1–L^4 contrasts acyclic L^5 selectivity preference $H_2PO_4^-$ > AcO^- > Cl^-. It is noteworthy that the AcO^- stability constant magnitudes are significantly larger for the calix[4]diquinone-containing receptors L^1 and L^2 when compared to the calix[4] arene receptors L^3 and L^4. Electrostatic considerations can account for the neutral rhenium(I) receptors forming relatively weaker anion complexes in contrast to the charged ruthenium(II) analogues.

Preliminary absorption and emission investigations displayed in Table 2, reveal that these receptors behave like the parent $[Ru(bpy)_3]^{2+}$ and $[Re(bpy)(CO)_3Cl]$ complexes.

As expected,[11,12] the heteroleptic nature of the ruthenium receptors leads to two metal–ligand charge transfer (MLCT) transitions, Ru→bpy-macrocycle and Ru→bpy; the former lies at slightly lower energy than the Ru→bpy ones because of the presence of the electron-withdrawing carbonyl amide substituents on the bpy-macrocycle ligand. As a consequence, for L^1 and L^3 the absorption band around 450 nm is broader and the emission band is red-shifted compared to that of $Ru(bpy)_3^{2+}$. The low emission yield exhibited by L^1 is expected since it is well known that quinones efficiently quench the luminescence emission of $Ru(bpy)_3^{2+}$ *via* an oxidative (intramolecular[13] or intermolecular[14]) electron transfer mechanism. In our case an intermolecular quenching process can be ruled out because of the low receptor concentration used; thus an intramolecular quenching mechanism is operative and a rate constant of 3×10^7 s^{-1} can be calculated on the basis of the lifetimes of Ru–calix[4]arene L^3 and Ru–calix[4]diquinone L^1.

Table 2 also shows that the rhenium receptors exhibit red-shifts of the lowest energy absorption and emission bands compared to the reference $[Re(bpy)(CO)_3Cl]$ complex.[15] Again the carbonyl amide substituents on the bpy-macrocycle ligand can explain the energy decrease of the MLCT excited state involved in the absorption (^{1}MLCT) or in the emission (^{3}MLCT) process. An excited state quenching process *via* intramolecular electron transfer is also expected for the Re–calix[4]diquinone receptor L^2 since the redox properties[15] of the excited Re^I moiety are quite similar to those of the excited Ru^{II} complexes. On the basis of the luminescence lieftimes of Re–calix[4]arene L^4 and Re–calix[4]diquinone L^2 a value of 7×10^7 s^{-1} can be calculated for the rate constant of the intramolecular quenching.

The addition of Bu_4NOAc and Bu_4NCl was found to dramatically affect the luminescence spectrum of all the receptors, the only exception being an insensitive response with L^2 and Cl^- in DMSO solution. While the Ru–calix[4]arene receptor L^3 exhibits an emission decrease, the other receptors L^1, L^2 and L^4 display a marked emission retrieval upon anion addition. In particular, AcO^- addition to MeCN solutions of L^1 caused a remarkable intensity increase of up to 500% concomitant with a slight blue shift of the emission maximum (Fig. 1). A notable 60% intensity increase was observed on Cl^- addition

Table 2 Absorption and emission data of the four receptors and of the reference compounds

	Absorption[a]		Emission[a]		
Compound	λ/nm[b]	ε/dm^3 mol^{-1} cm^{-1}	λ/nm[c]	τ/ns[d]	Φ_{em}[e]/10^{-3}
$[Ru(bpy)_3]^{2+}$	452	14 000	615	180	—
L^3	472	9 300	654	510	30
L^1	475	11 000	660	30[f]	1.0
$[Re(CO)_3bpyCl]$[g]	384		615	50	—
L^4[h]	393	4 200	675	21	2.0
L^2[h]	385	4 600	685	8.5	0.5

[a] Room temperature, air equilibrated MeCN solutions, unless otherwise noted. [b] Wavelength of the lowest energy absorption band. [c] Corrected wavelength of the emission band. [d] Luminescence emission lifetime values (±10%). [e] Luminescence emission quantum yield values (±30%). [f] A longer decay is also present as a minority component (see ref. 13). [g] CH_2Cl_2, ref. 15. [h] DMSO.

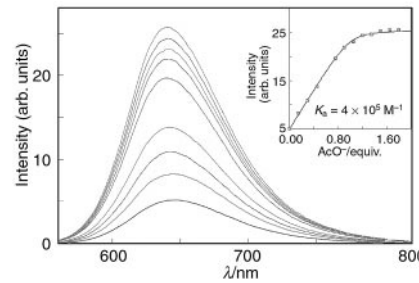

Fig. 1 Emission spectral variations upon titration of MeCN solution of L^1 (1.1×10^{-4} M) with Bu_4NOAc.

to L^1. Results obtained from Cl^- and AcO^- titrations of L^1 and L^3 in CD_3CN are consistent with a receptor–anion complex of 1:1 stoichiometry with stability constant magnitudes $>10^4$ M^{-1}, larger than the ^{1}H NMR determined values in DMSO-d_6, reflecting the less competitive CD_3CN solvent medium. The anion induced enhancement of the luminescence intensity in the case of Ru–calix[4]diquinone complex L^1 is clearly due to a significant decrease in the electron transfer rate constant, indicating that the anion binding decreases the interaction between the ruthenium(II) bipyridyl centre and the quinone moieties. In the case of Cl^- addition to Ru–calix[4]arene L^3 the intensity decrease matches the decrease in the emission lifetime (−25%) indicating that, at least in this case, anion binding favours the non-radiative decay processes.†

In summary the new ruthenium(II) and rhenium(I) bipyridyl calix[4]diquinone receptors selectively bind and optically sense AcO^- anions by overcoming intramolecular quenched luminescence and retrieving an anion induced emission.

We thank the Leverhulme Trust for a postdoctoral fellowship (V. T.) and the EPSRC for use of the mass spectrometry service at the University of Wales, Swansea.

Notes and references

† Whilst this work was in progress, Harriman *et al.* reported ruthenium(II) bipyridyl methylene appended calix[4]diquinones that sense alkali metal cations; A. Harriman, M. Hissler, P. Jost, G. Wipff and R. Ziessel; *J. Am. Chem. Soc.*, 1999, **121**, 14.

1 F. P. Schmidtchen and M. Berger, *Chem. Rev.*, 1997, **97**, 1609; P. D. Beer and D. K. Smith, *Progr. Inorg. Chem.*, 1997, **46**, 1; J. L. Atwood, K. T. Holman and J. W. Steed, *Chem. Commun.*, 1996, 1401.
2 (*a*) P. D. Beer, *Acc. Chem. Res.*, 1998, **31**, 71; (*b*) A. P. de Silva, H. Q. N. Guarantee, T. Gunnlaugsson, A. J. Huxley, C. P. McCoy, J. T. Rademacher and T. R. Rice, *Chem. Rev.*, 1997, **97**, 1515.
3 P. D. Beer, *Chem. Commun.*, 1996, 689; P. D. Beer and J. Cadman, *New J. Chem.*, 1999, **23**, 347.
4 F. Szemes, D. Hesek, Z. Chen, S. W. Dent, M. G. B. Drew, A. J. Goulden, A. R. Graydon, A. Greive, R. J. Mortimer, T. Wear, J. S. Weightman and P. D. Beer, *Inorg. Chem.*, 1996, **35**, 5868.
5 P. D. Beer, M. G. B. Drew, D. Hesek, M. Shade and F. Szemes, *Chem. Commun.*, 1996, 2161.
6 M. A. McKervey, E. M. Collins, E. Madigan, M. B. Moran, M. Owens, G. Ferguson and S. J. Harris, *J. Chem. Soc., Perkin Trans. 1*, 1991, 3137.
7 A. P. Kropcho and C. S. Knell, *Synth. Commun.*, 1990, **20**, 2559.
8 C. P. Whittle, *J. Heterocycl. Chem.*, 1977, **14**, 191.
9 P. A. Reddy, R. P. Kashyap, W. H. Watson and C. D. Gutsche, *Isr. J. Chem.*, 1992, **32**, 89.
10 M. J. Hynes, *J. Chem. Soc., Dalton Trans.*, 1993, 311.
11 P. D. Beer, F. Szemes, V. Balzani, C. M. Salà, M . G. B. Drew, S. W. Dent and M. Maestri, *J. Am. Chem. Soc.*, 1997, **119**, 11 864.
12 M. Maestri, N. Armaroli, V. Balzani, E. C. Constable and A. M. W. Cargill Thompson, *Inorg. Chem.*, 1995, **34**, 2759.
13 V. Goulle, A. Harriman and J.-M. Lehn, *J. Chem. Soc., Chem. Commun.*, 1993, 1034.
14 A. Vlcek and F. Bolletta, *Inorg. Chim. Acta*, 1983, **76**, L227.
15 K. Kalyanasundaram, *Photochemistry of Polypyridine and Porphyrin Complexes*, Academic Press, London, 1992.

Communication 9/05277A

ChemComm

A new stereoselective approach to the manzamine alkaloids

Iain Coldham,*[a] Simon J. Coles,[b] Katherine M. Crapnell,[a] Joan-Carles Fernàndez,[a] Thomas F. N. Haxell,[a] Michael B. Hursthouse,[b] Jonathan D. Moseley[c] and Alan B. Treacy[a]

[a] *School of Chemistry, University of Exeter, Stocker Road, Exeter, UK EX4 4QD. E-mail: i.coldham@exeter.ac.uk*
[b] *EPSRC National Crystallography Service, Department of Chemistry, University of Southampton, Southampton, UK SO17 1BJ*
[c] *Zeneca Pharmaceuticals, Avlon Works, Severnside Site, Bristol, UK BS10 7SJ*

Received (in Liverpool, UK) 9th June 1999, Accepted 28th July 1999

The key step in a new, stereoselective approach to the manzamine alkaloids involves an intramolecular azomethine ylide cycloaddition reaction, which forms rings B and C simultaneously, together with three new chiral centres; this has allowed a rapid access to the core ABC ring system of manzamine A.

The manzamine and related alkaloids consist of a structurally complex polycyclic ring system, typified by manzamine A **1**.[1]

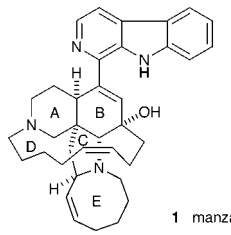

1 manzamine A

Manzamine A was the first of the family to be isolated in 1986 and, together with other manzamine alkaloids isolated from various marine sponges, has been shown to possess significant antileukemic and antibacterial properties.[1,2] The fascinating molecular structure and the promising biological activity of manzamine A has led to a number of synthetic endeavors in this area.[3] Recently the groups of Winkler[4] and Martin[5] have reported the synthesis of manzamine A, ircinol A and ircinal A. The key step in these syntheses makes use of a [2 + 2] (followed by ring expansion) or [4 + 2] cycloaddition reaction to set up ring B. Other [4 + 2] cycloaddition or cyclization strategies have been reported.[6] Our own efforts have centred on a [3 + 2] azomethine ylide cycloaddition reaction[7] to set up ring C. This approach seems ideally suited to access the manzamine alkaloids as an intramolecular cycloaddition reaction would allow, in a single step, the simultaneous formation of not only ring C but also ring B, together with all three chiral centres within ring C. Literature precedent[7,8] suggested that the azomethine ylide cycloaddition reaction would proceed to give the desired stereochemical arrangement found within the manzamine alkaloids. Herein we report a successful model study using this strategy.

The conversion of commercially-available arecoline **2** (Scheme 1) to the corresponding *N*-Boc derivative **3** has been reported by Olofson and co-workers.[9] Reduction of the ester **3** with $LiAlH_4$ gave the alcohol **4**. Use of the Johnson–Claisen rearrangement[10] with triethyl orthoacetate gave a rapid access to the piperidine **5**, containing the *exo*-methylene unit required for the key cycloaddition reaction. As an alternative route, reduction of arecoline and Johnson–Claisen rearrangement gave the corresponding *N*-methyl derivative **7**. Replacement of the *N*-Me for the *N*-Boc group in derivative **7** provided the desired compound **5**, although the yields in each step were more variable using this latter route.

The ester **5** was reduced to the corresponding alcohol **8** using $LiAlH_4$ (Scheme 2). Conversion of the alcohol **8** to the iodide

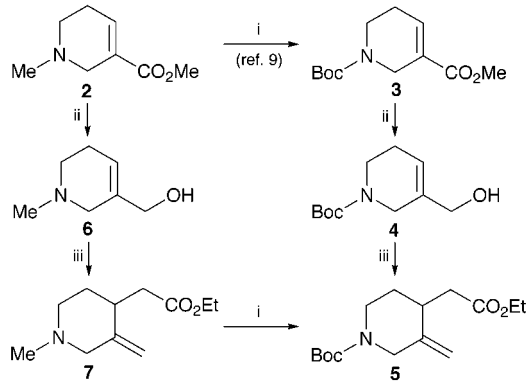

Scheme 1 *Reagents and conditions*: i, MeCH(Cl)OCOCl, PhMe, heat, then MeOH, heat, then Boc_2O, CH_2Cl_2, Et_3N, 81% from **2**, 79% from **7**; ii, $LiAlH_4$, THF, 0 °C, 95% from **3**, 99% from **2**; iii, $MeC(OEt)_3$, xylene, 2,4-dinitrophenol, heat, 71% from **4**, 39–87% from **6**.

9 was accomplished *via* the corresponding bromide. The iodide **9** was found to be a better electrophile than the bromide towards the deprotonated dithiane **10**. Addition of the dithiane gave the ester **11**, which contained the required carbon framework for rings A and B of manzamine A. Reduction of the ester **11** and oxidation gave the aldehyde **12** needed for the key cycloaddition reaction.

Our initial studies towards the formation of the ABC ring system of manzamine A have centred on the condensation of the secondary amine sarcosine ethyl ester **13** with the aldehyde **12**. Formation of the azomethine ylide (Fig. 1) and intramolecular cycloaddition leads to the generation of the pyrrolidine ring C, together with simultaneous formation of ring B. A single diastereomeric product **14** was obtained† which consisted of the

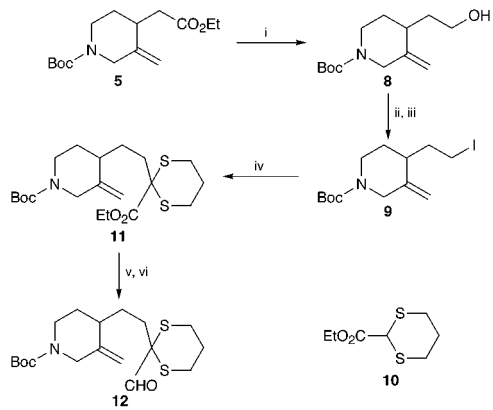

Scheme 2 *Reagents and conditions*: i, $LiAlH_4$, THF, 0 °C, 85%; ii, CBr_4, Ph_3P, CH_2Cl_2; iii, NaI, acetone, 96% over two steps; iv, BuLi, THF, HMPA, **10** followed by addition of **9**, −78 °C to room temp., 82%; v, $LiAlH_4$, THF, 0 °C, 92%; vi, $(COCl)_2$ (2.2 equiv.), DMSO, CH_2Cl_2, −60 °C then Et_3N, 70%.

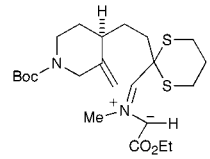

Fig. 1 Azomethine ylide formed from the condensation of **12** and **13**.

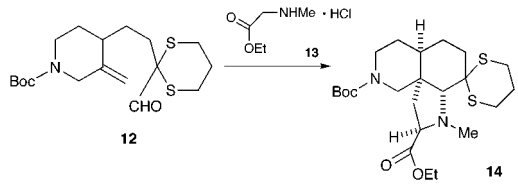

Scheme 3 *Reagents and conditions*: i, Pr^i_2NEt, PhMe, heat, 24 h, 45%.

desired ABC ring system of the manzamine alkaloids (Scheme 3). The stereochemical assignment could not be verified by NMR spectroscopy due to overlapping signals. Hydrolysis of the *N*-Boc group (TFA, CH_2Cl_2) gave rise to the corresponding secondary amine in which the peaks in the ^1H NMR spectrum were better resolved, but not to the extent required for NOE studies. The problem was solved by single crystal X-ray spectroscopic studies (Fig. 2)‡ of the *N*-Boc derivative **14**, which confirmed the structure and the relative stereochemistry of the cycloaddition product. The *cis* ring junction is favoured between rings A and B and between rings B and C. A possible ylide stereochemistry and orientation for cycloaddition is shown in Fig. 1.

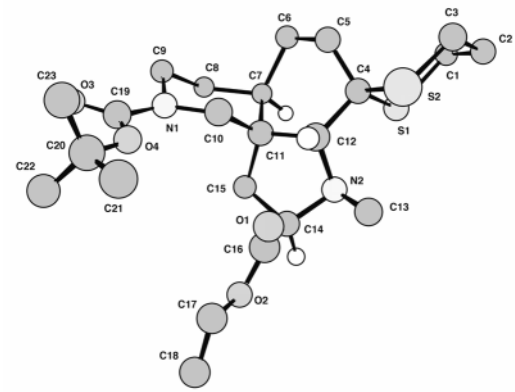

Fig. 2 X-Ray structure of the cycloadduct **14**.

In conclusion, we have demonstrated a short and efficient route to the core ABC ring system of the manzamine alkaloids. The key step is a stereocontrolled intramolecular azomethine ylide cycloaddition reaction, which sets up two new rings (rings B and C) and three new chiral centres (controlled by the existing chiral centre) in a single transformation. Further work to extend this chemistry to the preparation of more advanced intermediates of the manzamine alkaloids and to complete the total synthesis is in progress.

We thank the EPSRC for funding (to A. B. T. and K. M. C.), the Spanish Government (Ministerio de Educación y Cultura) for a postdoctoral fellowship and the University of Exeter for further support (to J.-C. F.), Zeneca Pharmaceuticals for a CASE award (to K. M. C.) and support through the Strategic Research Fund and Pfizer Ltd for an unrestricted grant.

Notes and references

† *Cycloaddition of the aldehyde* **12**: The aldehyde **12** (139 mg, 0.39 mmol), sarcosine ethyl ester hydrochloride **13** (90 mg, 0.59 mmol) and Pr^i_2NEt (0.12 cm^3, 0.7 mmol) in dry toluene (2.0 cm^3) were heated under reflux using a Dean–Stark trap. After 24 h, the solvent was removed under reduced pressure and the residue was purified by column chromatography on silica gel, eluting with light petroleum (bp 40–60 °C)–EtOAc (5:1) to give the amine **14** (82 mg, 45%) as needles; R_f 0.59 [light petroleum (bp 40–60 °C)–EtOAc (3:1)]; mp 140–142 °C; ν_{max}(neat)/cm^{-1} 1735 (C=O, ester) and 1685 (C=O, carbamate); δ_H(400 MHz, $CDCl_3$) 1.26 (3H, t, *J* 7.0), 1.24–2.17 (11H, m), 1.41 (9H, s), 2.57 (2H, br t, *J* 12.5), 2.74–2.91 (1H, m), 2.82 (1H, s), 2.85 (3H, s), 2.95 (1H, t, *J* 12.5), 2.97–3.16 (1H, m), 3.26 (1H, t, *J* 12.5), 3.50–3.76 (3H, m), 4.10–4.16 (2H, m); δ_C(100 MHz, $CDCl_3$, broad) 14.3, 22.0, 25.8, 25.9, 26.5, 27.6, 28.4, 29.8, 33.9, 38.9, 39.1, 47.1, 50.9, 55.9, 60.0, 65.1, 73.5, 79.3, 155.1, 173.9 (Found: M^+ 470.2263. $C_{23}H_{38}N_2O_4S_2$ requires *M*, 470.2273); *m/z* 470 (45%, M^+), 414 (24, M − C_4H_8), 397 (100, M − OBu^t), 369 (20, M − CO_2Bu^t), 341 (98) (Found: C, 58.63; H, 8.17; N, 5.67. $C_{23}H_{38}N_2O_4S_2$ requires C, 58.72; H, 8.08; N, 5.96%).

‡ *Crystal data* for **14**: $C_{23}H_{38}N_2O_4S_2$, M_r = 470.67, triclinic space group *P*, *a* = 9.891(2), *b* = 10.419(3), *c* = 13.574(3) Å, α = 67.91(3), β = 74.89(3), γ = 87.88(3)°, *U* = 1248.4(4) $Å^3$, *Z* = 2, D_c = 1.252 g cm^{-3}, μ = 0.244 mm^{-1}, *F*(000) = 508, crystal size 0.15 × 0.15 × 0.05 mm. Data were collected at 293 K on a Nonius KappaCCD area detector diffractometer, at the window of a Nonius FR591 rotating anode [λ(Mo-Kα) = 0.71073 Å]. Combined φ and ω scans, with a frame increment of 2.0°, gave 100% completeness to θ_{max} = 22.5° (index ranges $-10 \leqslant h \leqslant 10$, $-11 \leqslant k \leqslant 11$, $-14 \leqslant l \leqslant 14$). A correction was applied to account for absorption effects by means of comparing equivalent reflections, using the program SORTAV (ref. 11) (transmission factors = 0.995 / 0.912). A solution was obtained *via* direct methods and refined (ref. 12) by full-matrix least-squares on F^2, with hydrogens included in idealised positions. 3267 unique data were produced from 19877 measured reflections (R_{int} = 0.0968). 285 parameters refined to R_1 = 0.0556 and wR_2 = 0.1348 [$I > 2\sigma(I)$] (R_1 = 0.0931 and wR_2 = 0.1593 for all data), with residual electron densities of 0.342 and −0.308 e $Å^{-3}$. CCDC 182/1358. See http://www.rsc.org.suppdata/cc/1999/1757/ for crystallographic data in .cif format.

1 R. Sakai, T. Higa, C. W. Jefford and G. Bernardinelli, *J. Am. Chem. Soc.*, 1986, **108**, 6404; H. Nakamura, S. Deng, J. Kobayashi, Y. Ohizumi, Y. Tomotake, T. Matsuzaki and Y. Hirata, *Tetrahedron Lett.*, 1987, **28**, 621.

2 R. Sakai, S. Kohmoto, T. Higa, C. W. Jefford and G. Bernardinelli, *Tetrahedron Lett.*, 1987, **28**, 5493; T. Ichiba, R. Sakai, S. Kohmoto, G. Saucy and T. Higa, *Tetrahedron Lett.*, 1988, **29**, 3083; M. Tsuda, K. Inaba, N. Kawasaki, K. Homna and J. Kobayashi, *Tetrahedron*, 1996, **52**, 2319; I. I. Ohtani, T. Ichiba, M. Isobe, M. Kelly-Borges and P. J. Scheuer, *J. Am. Chem. Soc.*, 1995, **117**, 10 743; F. Kong and R. J. Andersen, *Tetrahedron*, 1995, **51**, 2895; J. Rodríguez, B. M. Peters, L. Kurz, R. C. Schatzman, D. McCarley, L. Lou and P. Crews, *J. Am. Chem. Soc.*, 1993, **115**, 10 436; D. Watanabe, M. Tsuda and J. Kobayashi, *J. Nat. Prod.*, 1998, **61**, 689.

3 For reviews, see M. Tsuda and J. Kobayashi, *Heterocycles*, 1997, **46**, 765; N. Matzanke, R. Gregg and S. Weinreb, *Org. Prep. Proced. Intl.*, 1998, **30**, 1; E. Magnier and Y. Langlois, *Tetrahedron*, 1998, **54**, 6201.

4 J. D. Winkler and J. M. Axten, *J. Am. Chem. Soc.*, 1998, **120**, 6425.

5 S. F. Martin, J. M. Humphrey, A. Ali and M. C. Hillier, *J. Am. Chem. Soc.*, 1999, **121**, 866.

6 For recent studies, see H. Uchida, A. Nishida and M. Nakagawa, *Tetrahedron Lett.*, 1999, **40**, 113; D. I. MaGee, M. L. Lee and A. Decken, *J. Org. Chem.*, 1999, **64**, 2549; S. M. Li and S. Yamamura, *Tetrahedron*, 1998, **54**, 8691; J. E. Baldwin, T. D. W. Claridge, A. J. Culshaw, F. A. Heupel, V. Lee, D. R. Sping, R. C. Whitehead, R. J. Boughtflower, I. M. Mutton and R. J. Upton, *Angew. Chem., Int. Ed.*, 1998, **37**, 2661; A. Kaiser, X. Billot, A. Gateau-Olesker, C. Marazano and B. C. Das, *J. Am. Chem. Soc.*, 1998, **120**, 8026.

7 A. Padwa, in *Comprehensive Organic Synthesis*, ed. B. M. Trost and I. Fleming, Pergamon, Oxford, 1991, vol. 4, p. 1069; P. A. Wade, in *Comprehensive Organic Synthesis*, ed. B. M. Trost and I. Fleming, Pergamon, Oxford, 1991, vol. 4, p. 1111.

8 See, for example P. N. Confalone and E. M. Huie, *J. Am. Chem. Soc.*, 1984, **106**, 7175; P. N. Confalone and R. A. Earl, *Tetrahedron Lett.*, 1986, **27**, 2695; L. M. Harwood and I. A. Lilley, *Tetrahedron Lett.*, 1993, **34**, 537; R. Grigg, V. Savic and M. Thornton-Pett, *Tetrahedron*, 1997, **53**, 10 633.

9 R. A. Olofson, J. T. Martz, J.-P. Senet, M. Piteau and T. Malfroot, *J. Org. Chem.*, 1984, **49**, 2081.

10 W. S. Johnson, L. Werthemann, W. R. Bartlett, T. J. Brocksom, T.-T. Li, D. J. Faulkner and M. R. Petersen, *J. Am. Chem. Soc.*, 1970, **92**, 741; for a Johnson–Claisen rearrangement with a 3-(hydroxyalkyl)tetrahydropyridine derivative, see M. Amat, M.-D. Coll, J. Bosch, E. Espinosa and E. Molins, *Tetrahedron: Asymmetry*, 1997, **8**, 935 and references therein.

11 R. H. Blessing, *Acta Crystallogr., Sect. A*, 1995, **51**, 33; R. H. Blessing, *J. Appl. Crystallogr.*, 1997, **30**, 421.

12 G. M. Sheldrick, SHELXL-97. Program for the refinement of crystal structures. University of Göttingen, 1997.

Communication 9/04667D

ChemComm

Self-assembly of monopyrazolylporphyrins by hydrogen bonding in solution

Chusaku Ikeda,* Noriko Nagahara, Eiko Motegi, Naoki Yoshioka and Hidenari Inoue

Department of Applied Chemistry, Keio University, Kohoku-ku, Yokohama 223-8522 Japan. E-mail: c05351@educ.cc.keio.ac.jp

Received (in Cambridge, UK) 7th June 1999, Accepted 28th July 1999

The self-associated structures of two noble *meso*-(monopyrazolyltritolyl)porphyrins synthesized *via* their NH-protected precursors have been studied by ^{1}H NMR, FT-IR and ESI MS measurements; *meso*-(pyrazol-4-yl)porphyrin and *meso*-(3,5-dimethylpyrazol-4-yl)porphyrin form a dimer and a tetramer, respectively, in solution due to intermolecular hydrogen bonding between pyrazole units.

In recent years there has been considerable interest in the construction of porphyrin assemblies of well-organized shape for molecular photonic devices such as artificial light harvesting systems.[1] A self-assembling strategy *via* reversible non-covalent bonding has received much attention and several attempts have been made recently to prepare supramolecular porphyrin arrays.[2–4] Hydrogen bonding is a very useful means of constructing molecular assemblies because it can fix molecules in a particular geometry by virtue of its directionality. Indeed, there are some reports in which assemblies of hydrogen bonded porphyrins have been constructed in both solution[3] and the solid state.[4] The elegance of these systems involves utilizing simple building blocks to establish a well-defined architecture. It is important to prepare novel and simple building blocks for hydrogen bonding which may realize more versatile porphyrin assemblies. In this context, five-membered diazole rings, particularly pyrazole, have been focused on because they have both hydrogen donor and acceptor sites in adjacent positions which can build up a self-complementary hydrogen-bonded assembly. It is well-known that 3,5-disubstituted pyrazoles form a dimer, a cyclic trimer and a cyclic tetramer in the solid state and/or in solution,[5] which motivated us to examine the self-association of pyrazolylporphyrins.

Here we report novel self-assembled dimers and tetramers of porphyrins having 1*H*-pyrazol-4-yl and 3,5-dimethyl-1*H*-pyrazol-4-yl groups, respectively, at the *meso*-position. Porphyrin **2** and **4** were prepared by the conventional Adler–Longo

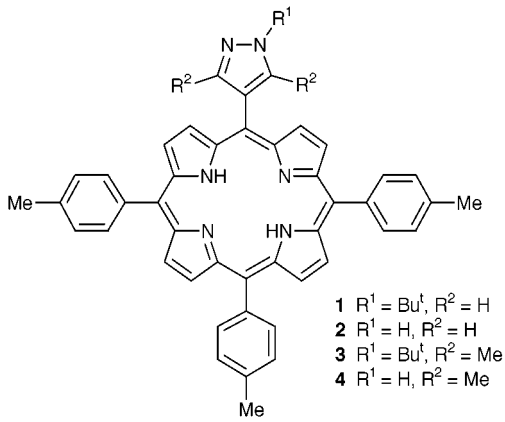

condensation[6] *via* their pyrazole-NH protected precursors **1** (13%) and **3** (8%) followed by removal of the *tert*-butyl groups in refluxing formic acid to afford the desired porphyrins in moderate yields (81% for **2** and 85% for **4**).

The IR spectra of **2** and **4** recorded in $CDCl_3$ showed strong concentration dependencies. The sharp ν(NH) at 3463 cm^{-1} assignable to pyrazole NH stretching 'free' from hydrogen bonding was weakened upon increasing the concentration, while the broad pyrazole-NH···(N) hydrogen-bonded vibration began to be observed around 3200 cm^{-1} above *ca*. 10^{-2} M. These spectral changes indicate that the formation of hydrogen bonds between pyrazole rings at higher concentrations[7] leads to the porphyrin assemblies. The ESI mass spectra using $CHCl_3$ as eluent showed a peak at *m/z* 1294.1 for **2** and *m/z* 2699.5 for **4**. These two peaks correspond to a dimer of **2** (MW = 1293.6 g mol^{-1}) and a tetramer of **4** (MW = 2699.4 g mol^{-1}), respectively. The peaks of the porphyrin oligomers almost disappeared upon addition of a protic solvent such as MeOH to the eluent, which strongly supports the suggestion that the porphyrin self-assembly is formed by intermolecular hydrogen bonding. In order to confirm the self-assembly of pyrazolylporphyrins, ^{1}H NMR dilution experiments were carried out in $CDCl_3$. In **2** and **4**, appreciable concentration dependencies were observed for the chemical shifts of the pyrazole ring protons, though the pyrazole NH peaks were too broad to be detected under the present experimental conditions.† The proton signal showing the largest concentration dependency was that nearest to the pyrazole NH group, *i.e*. the pyrazole-H3 or -H5 proton of **2** and the pyrazole 3,5-methyl protons of **4**. The magnitude of the dilution shift ($\Delta\delta$) of these protons was 0.033 ppm (downfield shift) for **2** and 0.059 ppm (upfield shift) for **4** upon dilution from 10$^{-3.7}$ to 10$^{-1.5}$ M. These dilution shifts are relatively small but apparently larger than $\Delta\delta$ in the presence of MeOH ($\Delta\delta_{max}$ = 7 × 10^{-3} ppm in $CDCl_3$–CD_3OD = 7:3) and $\Delta\delta$ observed for the corresponding NH-protected **1** and **3** ($\Delta\delta_{max}$ = 6 × 10^{-3} ppm) in $CDCl_3$. The above comparison of ^{1}H NMR spectra has revealed that the concentration depend-

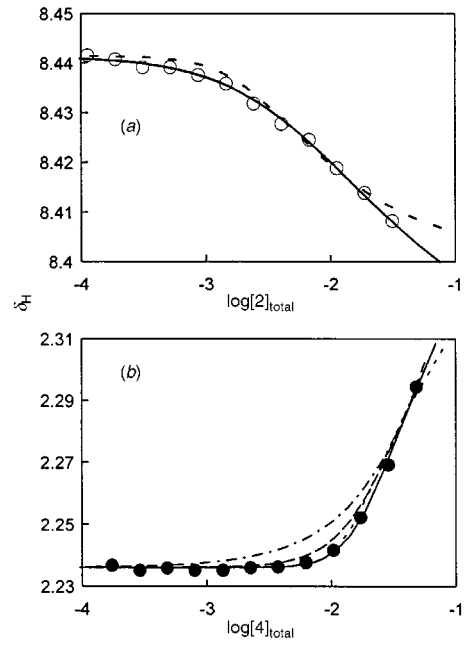

Fig. 1 Curve fitting analysis of ^{1}H NMR dilution shifts in pyrazolylporphyrins: (*a*) (○) pyrazole 3,5-H of **2**, (——) dimer model, (– – –) trimer model; (*b*) (●) pyrazole 3,5-methyl of **4**, (–·–·–·–) dimer model (– – –) trimer model, (——) tetramer model, (·····) pentamer model.

encies observed in **2** and **4** are due to the formation of hydrogen bonds between pyrazole units rather than any other type of aggregation.‡ In order to estimate the possible structure of the association, the dilution curves (at 295 K in $CDCl_3$) were fitted to the models for an equivalent *n*-merization process using nonlinear least-square fitting.[8] The dilution curve for **2** fits well the optimized dimer model throughout the concentration range, but the best-fit trimer model deviates substantially from the experimental data (Fig. 1). On the other hand, the experimental data for **4** fit the tetramer model while they do not obey the dimer, trimer or pentamer model (Fig. 1). The combined ESI MS, IR and NMR results demonstrate that **2** forms a dimer $[\mathbf{2}]_2$

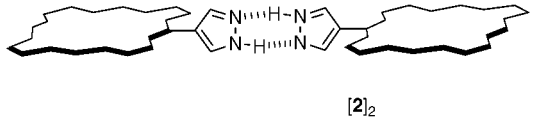

$[\mathbf{2}]_2$

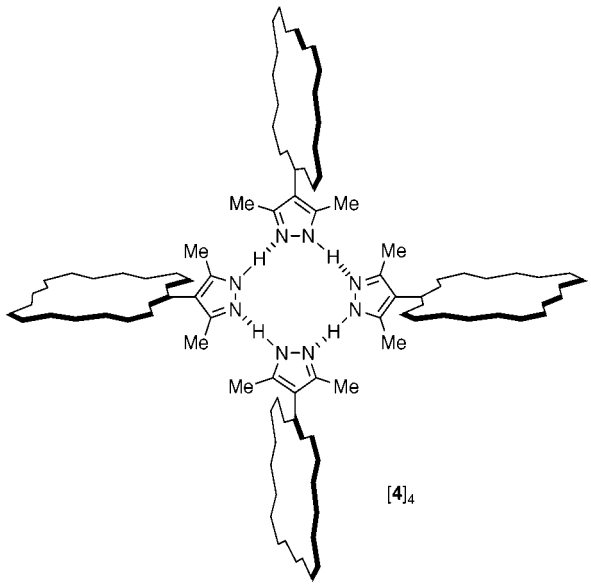

$[\mathbf{4}]_4$

and **4** a cyclic tetramer $[\mathbf{4}]_4$ in $CHCl_3$. There is a report that the hydrogen bonded pyrazole dimer is less stable than the trimer or tetramer.[9] However, porphyrin **2**, in which the rotational barrier of the pyrazole ring is very low,§ seems to prefer the dimer structure (based on molecular modeling), as the aryl groups at the 10 and 20 positions might cause steric hindrance in the case of a co-planer geometry of the pyrazole ring with the porphyrin plane in the trimer or tetramer model. The dimerization constant, $K_2 = 39\ M^{-1}$, obtained from the curve fitting of **2**, is roughly comparable to that in the 2-pyridone system.[10] The tetramerization constant of **4** (K_4) is estimated to be $9.3 \times 10^3\ M^{-3}$ from the curve fitting, which is much larger than that of the hydroxy analogue (*e.g.* phenol).[11] The unique associated structure of the cyclic square is expected to be an interesting building block for porphyrin architecture. Studies in the solid state as well as in solution of pyrazolyl-porphyrins with more than two pyrazole rings, and their metal complexes are currently underway.

We are grateful to Professor Taira Imamura and Mr Kenji Watabe at Hokkaido University and Mr Yutaka Takahashi, JEOL Co., for their help with the ESI mass spectrometry.

Notes and references

† This is probably due to the electronic quadrupole moment of the nitrogen atom and/or the equilibrium of hydrogen bonding. In the case of pyrazole itself the NH proton can be observed only above *ca.* 10^{-1} M in $CDCl_3$.
‡ The possibility of π–π stacking was excluded because no broadening of the ^1H NMR signals was observed.
§ The rotational barrier of the pyrazole ring in **2** is much lower than that of the *p*-tolyl group: the calculated values are *ca*. 130 and 420 kcal mol^{-1} for the 3,5-unsubstituted pyrazole and the *p*-tolyl groups, respectively (MMX force field).

1 M. R. Wasielewski, *Chem. Rev.*, 1992, **92**, 435; M. D. Ward, *Chem. Soc. Rev.*, 1997, **26**, 365; R. W. Wagner, T. E. Johnson and J. S. Lindsey, *J. Am. Chem. Soc.*, 1996, **118**, 11 166; G. Mcdermott, S. M. Prince, A. A. Freer, A. M. Hawthornthwaite-Lawless, M. Z. Papiz, R. J. Cogdell and N. W. Isaacs, *Nature*, 1995, **374**, 517.
2 M. R. Johnston, M. J. Gunter and R. N. Warrener, *Chem.Commun.*, 1998, 2739; N. N. Gerasimchuk, A. A. Mokhir and K. R. Rodgers, *Inorg. Chem.*, 1998**,** **37**, 5641; K. Funatsu, T. Imamura, A. Ichimura and Y. Sasaki, *Inorg. Chem.*, 1998**,** **37**, 1798; H. Tamiaki, *Coord. Chem. Rev.*, 1996, **148**, 183.
3 J. L. Sessler, B. Wang and A. Harriman, *J. Am. Chem. Soc.*, 1995, **117**, 704; C. M. Drain, K.C. Russell and J. M. Lehn, *Chem. Commun.*, 1996, 337.
4 K. Kobayashi, M. Koyanagi, K. Endo, H. Masuda and Y. Aoyama, *Chem. Eur. J.*, 1998, **4**, 417; P. Bhyrappa, S. R. Wilson and K. S. Suslick, *J. Am. Chem. Soc.*, 1997, **119**, 8492.
5 A. Baldy, J. Elguero, R. Faure, M. Pierrot and E. J. Vincent, *J. Am. Chem. Soc.*, 1985, **107**, 5290; F. A. Parrilla, G. Scherer, Hans-Heinrich Limbach, M. C. Foces-Foces, F. H. Cano, J. A. S. Smith, C. Toiron and J. Elguero, *J. Am. Chem. Soc.*, 1992, **114**, 9657; J. Elguero, F. H. Cano, C. Foces-Foces, A. L. Llamas-Saiz, H.-H. Limbach, F. Aguilar-Parrilla, R. M. Claramunt and C. López, *J. Heterocycl. Chem.*, 1994, **31**, 695; S. N. Vinogradov and M. Kilpatrick, *J. Phys. Chem.*, 1964, **68**, 181.
6 R. G. Little, J. A. Anton, P. A. Loach and J. A. Ibers, *J. Heterocycl. Chem.*, 1975, **12**, 343; A. C. Chan, J. Dalton and L. R. Milgrom, *J. Chem. Soc., Perkin Trans. 1*, 1984, 1483.
7 D. M. W. Anderson, J. L. Duncan and F. J. C. Rossotti, *J. Chem. Soc.*, 1961, 140; E. Grech, Z. Malarski and L. Sobczyk, *Spectrochim. Acta.*, 1992, **48A**, 519.
8 M. R. Ghadiri, C. Soares and C. Choi, *J. Am. Chem. Soc.*, 1992, **114**, 825; W. F. DeGrado and J. D. Lear, *J. Am. Chem. Soc.*, 1985, **107**, 7684; K. A. Connor, *Binding Constants*, Wiley, New York, ch. 5, 1987.
9 D. M. W. Anderson, J. L. Duncan and F. J. C. Rossotti, *J. Chem. Soc.*, 1961, 140.
10 Y. Ducharme and J. D. Wuest, *J. Org. Chem.*, 1988, **53**, 5789; S. C. Zimmerman and B. F. Duerr, *J. Org. Chem.*, 1992, **57**, 2215.
11 M. Saunders and J. B. Hyne, *J. Chem. Phys.*, 1958, **29**, 1319.

Communication 9/04513I

ChemComm

Intermolecular reactions of indol-2-yl radicals: a new route to 2-substituted indoles

Andrea Fiumana and Keith Jones*

School of Applied Chemistry, Kingston University, Penrhyn Road, Kingston-upon-Thames, Surrey, UK KT1 2EE. E-mail: keith.jones@kingston.ac.uk

Received (in Liverpool, UK) 22nd June 1999, Accepted 22nd July 1999

The generation of indol-2-yl radicals and their addition to a variety of radical acceptors to prepare 2-substituted indoles is presented.

The intermolecular reaction of alkyl radicals has been extensively studied and forms a useful method for the creation of new carbon–carbon bonds under mild conditions[1] and with the potential for stereocontrol.[2] Exploration of the more reactive aryl radicals has been centred almost exclusively on their intramolecular reactions and this has provided a powerful approach to a variety of polycyclic compounds.[3] Radicals derived from heteroaromatic systems have been much less extensively explored despite the fact that heteroaromatic rings form the basis of many natural products and synthetically-derived bioactive molecules.[4] However, the literature contains only vague reference to the intermolecular reactions of aryl radicals.[5] We now disclose the results of our studies on the intermolecular reactions of radicals derived from 2-haloindoles as a method for the regiospecific formation of carbon–carbon bonds to the 2-position of indoles.

The generation of 2-lithioindoles using either an activating group attached to the indole nitrogen or the *in situ* activation of Bergman[6] and Katritzky[7] provides a method for reaction at C-2 but under extremely basic conditions. Alternatively, 2-haloindoles can be coupled with a variety of unsaturated carbon centres using palladium chemistry.[8] We have previously reported on the cyclisation reactions of radicals derived from 2-bromoindoles[9] and we wished to explore the possibility of trapping these radicals in an intermolecular sense. A range of 2-haloindole substrates were synthesised as shown in Scheme 1. Thus treatment of indole under Bergman conditions with either a brominating agent or iodinating agent gave 2-bromo- and 2-iodo-indole in 96 and 84% yields, respectively. Under similar conditions, 5-methoxyindole gave the 2-iodo derivative in 38% yield, whilst 3-methylindole gave 2-iodo-3-methylindole in 41% yield. Finally, 2-iodoindole was reacted with phenylsulfonyl chloride and base to give the *N*-phenylsulfonylindole in 95% yield, and 2-bromoindole was reacted with di-*tert*-butyl dicarbonate to give the *N*-Boc derivative in 98% yield.

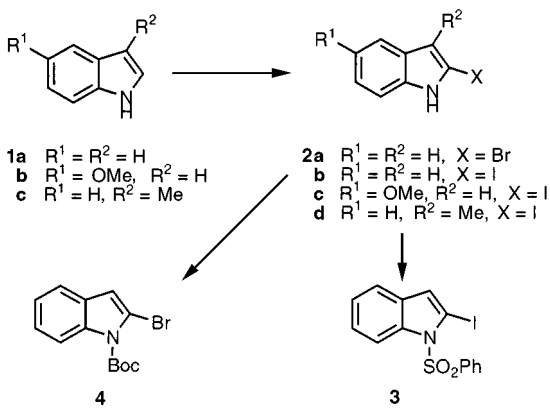

Scheme 1

Initially, a range of these substrates were reacted under various conditions to explore the generation and intermolecular trapping of the indol-2-yl radical. Acrylonitrile, which is an excellent acceptor for nucelophilic alkyl radicals, was used as the trapping reagent. Reaction of either bromo- or iodo-indoles using tributyltin hydride (TBTH) at low concentration or delivered by syringe pump consistently gave reduced indole as product. The use of hexabutylditin instead of TBTH led to little or no reaction. Using a different strategy, the reaction of the 2-haloindoles with allyltributylstannane[10] was explored, but no 2-allylindoles could be detected. At this stage, the catalytic TBTH conditions developed by Stork and Sher were investigated.[11] The reaction of 2-iodoindole with tributyltin chloride and $NaCNBH_3$ in Bu^tOH using AIBN as initiator and acrylonitrile as the radical trap gave 2-(2-cyanoethyl)indole in 30% yield. Having found suitable conditions, a range of 2-haloindoles and electron-deficient alkenes were reacted together and the results are presented in Scheme 2 and Table 1.†

With the exception of 2-iodo-3-methylindole, which gave only traces of the desired adducts by GC-MS, all 2-iodoindole substrates reacted under these conditions. Acrylonitrile proved in each case to be the best radical acceptor, with an acceptable yield of 37% for the reaction with *N*-phenylsulfonyl-2-iodoindole. Modest yields were obtained for the reactions with *N*-unsubstituted indoles, illustrating this important feature of radical reactions. Acrylate esters also proved to be reasonable radical acceptors, giving the appropriate 3-indole-substituted propionates in poor to modest yields. In the simplest case of 2-iodoindole, phenyl vinyl sulfone gave the desired adduct in 25% yield, although with other iodoindoles only reduction of the indole was observed. The effect of indole substituents is interesting. The *N*-phenylsulfonyl and the 5-methoxy group seem to have little effect on the reactions with acrylonitrile and acrylate esters, but the reaction with phenyl vinyl sulfone only works in the case of an unsubstituted indole. However, the 3-methyl group on the indole seems to shut down the intermolecular radical pathway almost completely. This is

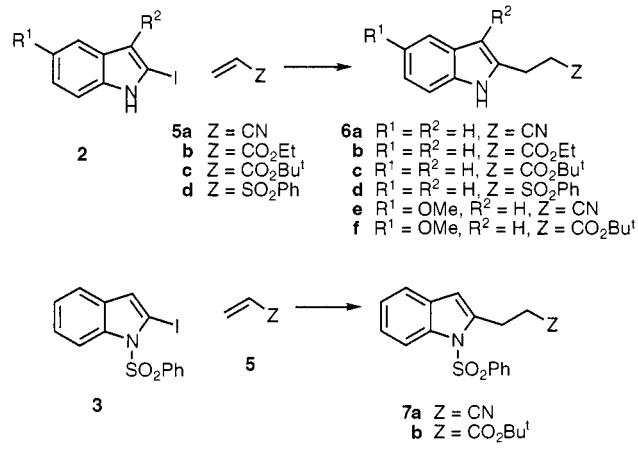

Scheme 2

Table 1 Reaction of 2-iodoindoles with electron-deficient alkenes

Indole	Alkene	Product	Yield (%)
2b	**5a**	**6a**	30
2b	**5b**	**6b**	25
2b	**5c**	**6c**	18
2b	**5d**	**6d**	25
3	**5a**	**7a**	37
3	**5c**	**7b**	28
3	**5d**		reduction[a]
2c	**5a**	**6e**	25
2c	**5c**	**6f**	23
2c	**5d**		reduction[a]
2d	**5a**		trace[b]
2d	**5b**		trace[b]
2d	**5c**		trace[b]

[a] No addition product could be detected by GC-MS, only the de-iodinated product was isolated. [b] No addition product could be isolated, but it was detected in very low yield by GC-MS.

presumably caused by the increase in steric hinderance close to the radical centre and must reflect the sensitive nature of these reactions to the reaction conditions and the exact radical precursor and acceptor. The balance between intermolecular addition to the alkene, intermolecular reaction with TBTH (leading to reduction) and the radical chain breaking down (leading to starting material) is clearly delicate. The critical nature of the halogen abstracted to form the indolyl radical is demonstrated by the lack of any addition product using 2-bromoindoles as radical precursors.

Having achieved some success in the reaction of indol-2-yl radicals with electron-deficient alkenes, attention was turned to the reaction with *tert*-butyl isocyanide.[12] 2-Cyanoindoles have been shown to be useful in directing radical addition to indoles[13] but their synthesis generally requires multi-step sequences or an indole ring synthesis. Using the catalytic TBTH method and *tert*-butyl isocyanide the results shown in Scheme 3 and Table 2 were obtained. 2-Iodoindole and 2-iodo-5-methoxyindole gave 37 and 40% yields of cyanoindoles, respectively, whilst 2-iodo-3-methylindole again proved to be a significantly poorer substrate. Interestingly, *N*-phenylsulfonyl-2-iodoindole gave rise to mainly reduced product along with a small amount of the de-sulfonylated 2-cyanoindole. Investigation of the reaction

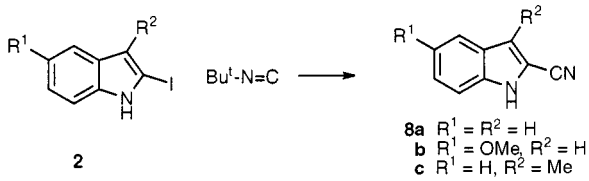

Scheme 3

Table 2 Reaction of 2-iodoindoles with *tert*-butyl isocyanide

Indole	Product	Yield (%)
2b	**8a**	38
2c	**8b**	40
2d	**8c**	10
3	*N*-Phenylsulfonylindole	90
	2-Cyanoindole	trace

mixture by GC-MS revealed the presence of *tert*-butyl phenyl sulfone, suggesting that the *tert*-butyl radical generated is able to cleave the N–S bond. This suggests a possible radical method for desulfonylation of *N*-sulfonyl indoles but a trial reaction using *tert*-butyl bromide as the source of *tert*-butyl radicals indicated that it is necessary to generate the *tert*-butyl radicals in the vicinity of the *N*-sulfonyl group to achieve the bond cleavage, providing some evidence for a cyclic mechanism (Fig. 1).

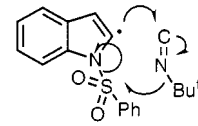

Fig. 1

In summary, we have demonstrated that, under appropriate conditions, indol-2-yl radicals can be generated from 2-iodoindoles, and they undergo addition to electron-deficient alkenes and addition of the cyano group from *tert*-butyl isocyanide in moderate yields. The fact that *N*-protection is not required for these reactions is a useful feature.

We should like to acknowledge financial support from Kingston University, and Dr John Storey for helpful discussions.

Notes and references

† *Typical procedure* for the radical additions: A mixture of 2-iodoindole (0.50 g, 2.06 mmol), Bu_3SnCl (56 μl, 0.206 mmol), $NaCN{\cdot}BH_3$ (0.259 g, 4.12 mmol), ethyl acrylate (4.46 ml, 20.6 mmol) and AIBN (0.033 g, 0.2 mmol) in degassed Bu^{t}OH (40 ml) was prepared and immediately refluxed for 5 h under nitrogen. After cooling, the Bu^{t}OH was removed under reduced pressure. The residue was dissolved in Et_2O (20 ml) and washed with 20% aq. NH_3 (3 × 20 ml), brine (3 × 20 ml), dried over $MgSO_4$ and concentrated *in vacuo*. The residue was chromatographed (3:1 CH_2Cl_2–hexane; R_f 0.45) to give a solid which was recrystallized from hexane–Et_2O to give 3-(1*H*-indol-2-yl)propionic acid ethyl ester **6b** (0.125 g, 28%) as white needles, mp 83–85 °C (lit.,[14] 84–85 °C).

1 B. Giese, *Angew. Chem., Int. Ed. Engl.*, 1985, **24**, 553.
2 D. P. Curran, N. A. Porter and B. Giese, *Stereochemistry of Radical Reactions: Concepts, Guidelines and Synthetic Applications*, VCH, New York, 1995.
3 D. P. Curran, *Synthesis*, 1988, 417 and 489; D. P. Curran, C. P. Jasperse and T. L. Fevig, *Chem. Rev.*, 1991, **91**, 1237; B. Giese, B. Kopping, T. Gögel, J. Dickhaut, G. Thoma, K. J. Kulicke and F. Trach, *Org. React.*, 1996, **48**, 301.
4 A. Nadin and T. Harrison, *Tetrahedron Lett.*, 1999, **40**, 4073; K. Jones and M. L. Escudero-Hernandez, *Tetrahedron*, 1998, **54**, 2275.
5 B. Giese and J. A. González-Gómez, unpublished work cited in ref. 1.
6 J. Bergman and L. Venemalm, *J. Org. Chem.*, 1992, **57**, 2495.
7 A. R. Katritzky and K. Akutagava, *Tetrahedron Lett.*, 1985, **26**, 5935.
8 S. S. Labadie and E. Teng, *J. Org. Chem.*, 1994, **59**, 4250.
9 A. P. Dobbs, K. Jones and K. T. Veal, *Tetrahedron Lett.*, 1995, **36**, 4857; A. P. Dobbs, K. Jones and K. T. Veal, *Tetrahedron*, 1998, **54**, 2149.
10 G. E. Keck, E. J. Enholm, J. B. Yates and M. R. Wiley, *Tetrahedron*, 1985, **41**, 4079.
11 G. Stork and P. M. Sher, *J. Am. Chem. Soc.*, 1986, **108**, 303.
12 G. Stork and P. M. Sher, *J. Am. Chem. Soc.*, 1983, **105**, 6765.
13 C.-C. Yang, H.-T. Chang and J.-M. Fang, *J. Org. Chem.*, 1993, **58**, 3100.
14 E. V. Sadanandan, C. P. Srinivasan and M. Vedachalam, *Indian J. Chem., Sect. B*, 1993, **32**, 481.

Communication 9/05024H

ChemComm

Highly efficient palladium catalyst system for addition of trihydrosilanes to acetylenes and its application to thermally stable polycarbosilane synthesis

Hiroshi Yamashita* and Yuko Uchimaru

National Institute of Materials and Chemical Research, Tsukuba, Ibaraki 305-8565, Japan.
E-mail: yamashita@home.nimc.go.jp

Received (in Cambridge, UK) 25th June 1999, Accepted 29th July 1999

Regio- and stereo-selective mono-, di- and tri-alkenylation of trihydrosilanes with monoynes proceeded smoothly with a Pd–PCy_3 catalyst, while the reaction of phenylsilane with 1,4-diethynylbenzene provided a thermally stable and blue light emissive polycarbosilane.

Transition metal-catalysed hydrosilylation is a versatile reaction affording useful organosilicon derivatives.[1] Addition of trihydrosilanes to acetylenes is expected to give C=C and/or Si–H bond-containing alkenylsilanes utilisable as new synthetic reagents, monomers for silicon polymers *etc.*[2] However, in our hands conventional Pt catalysts such as Speier's (H_2PtCl_6) and Karstedt's ($Pt_2(dvs)_3$, dvs = $[(H_2C{=}CH)Me_2Si]_2O$) systems have proved to be inefficient (*vide infra*).[3,4] Through a survey of group 10 metal complexes we have found that a Pd–PCy_3 system is highly active for the reaction. In addition, the catalysis affords the first successful example of polymerisation of a trihydrosilane with diynes providing polycarbosilanes with unique thermal and optical properties.[5]

Thus, when a mixture of phenylsilane (**1a**, 0.20 mmol) and oct-1-yne (**2a**, 1 equiv.) in benzene-d_6 (0.05 ml) was treated with a benzene-d_6 (0.10 ml) solution of $Pd_2(dba)_3$ (1 mol% Pd) and PCy_3 (P/Pd = 2) at room temperature for 15 min, (*E*)-2- and 1-hexylvinylsilane [**3a**(β) and **3a**(α), respectively] were formed with high linear selectivity (β : α = 94 : 6) and in good combined yields (80%) (≥98% conversion of **2a**; Scheme 1, Table 1, run 1).† The formation of the *Z* isomer of **3a**(β) and diphenylsilane (a redistribution byproduct from **1a**) was negligible according to NMR analysis. A small amount of dialkenylsilane **4a** (9%) was also formed with recovery of **1a** (8%). In contrast, previously reported $RhCl(PPh_3)_3$[3] was not effective under the present conditions [yield of **3a** = 29% (β : α = 73 : 27)]. Conventional H_2PtCl_6 and $Pt_2(dvs)_3$ catalysts also resulted in much lower yields [3% (β : α = 5 : 1) and 14% (81 : 19), respectively]. In the cases of $RhCl(PPh_3)_3$[3] and $Pt_2(dvs)_3$, unfavorable diphenylsilane formation (10 and 20%, respectively) was also observed. The Pd–PCy_3 system was very active, and only 0.01 mol% Pd effectively converted ≥98% of **2a** after heating at 60 °C for 3 h (run 2). Di- and tri-alkenylation took place cleanly by controlling the charged amount of **2a**; using 2 or 3 equiv. of **2a** respectively provided **4a** or **5a**, each in > 90% yield (runs 3 and 4). These reactions proceeded regioselectively, yielding **4a**(β_2) and **5a**(β_3) with linear alkenyl moieties as the major products.

Besides **2a**, phenylacetylene (**2b**, 1 equiv.) also readily reacted with **1a** to give the corresponding mono- and di-alkenylsilane (**3b**, 75%; **4b**, 13%) with predominant formation of the linear regioisomers (run 5). Aromatic acetylene **2b** was much more reactive than **2a**, and even 0.01 mol% Pd catalyst completed the reaction after 3 h at room temperature (run 6). Dialkenylsilane **4b** was obtained in a high yield (83%) by using 2 equiv. of **2b** (run 7). Likewise, hexylsilane (**1b**) underwent smooth mono- and di-alkenylation with **2b** (runs 8 and 9).

Instead of $Pd_2(dba)_3$–PCy_3, $PdCl_2(PCy_3)_2$ could be used as well, although the reaction was slower; the yields of **3b** and **4b** in the reaction of **1a** and **2b** were respectively 20 and ≤2 (room temp., 15 min) and 75 and 12% (40 °C, 2 h). Other Pd–trialkylphosphine catalysts were also active, albeit in lower efficiency; the yields of **3b** and **4b** (40 °C, 2 h) were 63 and 5

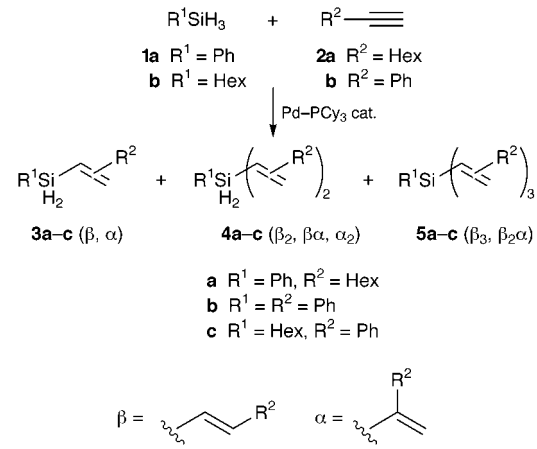

Scheme 1

Table 1 Pd-catalysed hydrosilylation of trihydrosilanes **1** with acetylenes **2**[a]

				Yield[b] (%)		
Run	**1**	**2** (**2**/**1**)	Conditions	**3** (β : α)	**4** (β_2 : βα : α_2)	**5**(β_3 : $\beta_2\alpha$)
1	**1a**	**2a** (1)	r.t., 15 min	80 (94 : 6)	9 (9 : 1 : 0)	0
2[c]	**1a**	**2a** (1)	60 °C, 3 h	81 (93 : 7)	9 (9 : 1 : 0)	0
3	**1a**	**2a** (2)	40 °C, 6 h	4 (9 : 1)	92 (87 : 14 : 0)	≤2
4	**1a**	**2a** (3)	40 °C, 6 h	0	4 (9 : 1 : 0)	92 (86 : 14)
5	**1a**	**2b** (1)	r.t., 15 min	75 (79 : 21)	13 (7 : 3 : 0)	0
6[c]	**1a**	**2b** (1)	r.t., 3 h	77 (77 : 23)	12 (7 : 3 : 0)	0
7	**1a**	**2b** (2)	r.t., 15 min	8 (7 : 3)	83 (63 : 32 : 5)	≤2
8	**1b**	**2b** (1)	r.t., 15 min	63 (74 : 26)	17 (2 : 1 : 0)	0
9	**1b**	**2b** (2)	r.t., 5 h	4 (7 : 3)	86 (60 : 35 : 5)	≤2

[a] **1** (0.20 mmol), **2** (0.20–0.60 mmol), $Pd_2(dba)_3$–PCy_3 (dba = dibenzylideneacetone, Cy = cyclohexyl, P/Pd = 2) (0.002 mmol Pd), C_6D_6 (0.15 ml). [b] Based on **1** (estimated by NMR and/or GC). [c] 0.00002 mmol Pd.

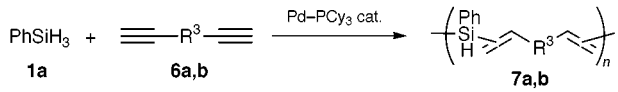

1a 6a,b 7a,b

a $R^3 = -(CH_2)_5-$
b R^3 = 1,4-phenylene

Scheme 2

$[PdCl_2(PBu^i{}_3)_2]$, 47 and 5 $[PdCl_2(PEt_3)_2]$ and 34 and 5% $[PdCl_2(PBu_3)_2]$. Accordingly, the Pd^0–PCy_3 system is the best catalyst among the Pd complexes examined.

Since acetylenes **2** (2 equiv.) react with **1a** cleanly, C=C–SiH–C=C linkage-containing polycarbosilanes can be readily prepared. Thus, treatment of a mixture of **1a** (0.20 mmol) and nona-1,8-diyne (**6a**, 1 equiv.) with the Pd–PCy_3 catalyst (0.1 mol% Pd) in benzene-d_6 (0.15 ml) at 40 °C for 4 h gave a new polymer (**7a**) with one Si–H bond being intact nearly quantitatively (by ^{1}H NMR, Scheme 2).‡ The molecular weight M_w (M_w/M_n) was estimated by GPC (polystyrene standards) to be 29 000 (3.1). The vinylic moieties in the C=C–SiH–C=C linkages were assigned by ^{1}H NMR to be VL × 2 (VL = vinylene) and VL + VD (VD = vinylidene) in the ratio of 88 : 12. Similarly, the use of 1,4-diethynylbenzene (**6b**) (0.1 mol% Pd cat., 40 °C, 1 h) yielded **7b** with phenylene rings (≥95% NMR yield; M_w = 49 000, M_w/M_n = 4.8; VL × 2 : VL + VD : VD × 2 = 63 : 33 : 4 for the vinylic moieties).

Polymers **7** have reactive C=C and Si–H bonds, and cross-linking between them easily proceeds to form thermally stable polymeric materials. Thus, heating a cast film of **7b** on a glass plate at 100 °C for 2 h under vacuum formed a hard film that was nearly insoluble in toluene, $CHCl_3$ and THF. The mp was > 300 °C and thermogravimetric analysis revealed considerably high T_{d_1} and T_{d_5} values (1 and 5% weight loss temperatures, 444 and 504 °C, respectively, under N_2) and a good char yield (78% at 980 °C). This suggests that **7b** is utilisable for manufacturing heat-resistant materials and/or SiC ceramics. In addition, **7b** has interesting light-emitting properties; a film of **7b** exhibited intense blue emission on irradiation with a UV lamp, and a THF solution of **7b** [λ_{max} in UV: 308 nm (ε = 2.2 × 10^4)] showed photoluminescence with λ_{max} = 445 and 466 nm (excitation at 393 nm).[6]

To summarize, the Pd–PCy_3 catalyst is demonstrated to be highly efficient for hydrosilylation of acetylenes with trihydrosilanes and applicable to the synthesis of polycarbosilanes, which are promising as new functional materials. Extension of the substrates and application of the resulting polycarbosilanes are under way.

Notes and references

† All the major alkenylsilanes **3**–**5** were purified by preparative TLC (or GPC) and identified by their NMR, (HR)MS and/or IR spectra; for the ^{1}H NMR data [$\delta_H(C_6D_6$, 300 MHz)] of the characteristic SiH signals of **3** and **4**, **3a**(β): 4.78 (d, *J* 3.1); **3a**(α): 4.75 (s); **4a**(β_2): 5.05 (t, *J* 2.9); **4a**(βα): 5.01 (d, *J* 3.4); **3b**(β): 4.88 (d, *J* 3.2); **3b**(α): 4.98 (s); **4b**(β_2): 5.33 (t, *J* 2.9); **4b**(βα): 5.44 (d, *J* 3.0); **4b**(α_2): 5.60 (s); **3c**(β): 4.29 (q, *J* 3.5); **3c**(α): 4.40 (t, *J* 3.7); **4c**(β_2): 4.74 (quint, *J* 3.3); **4c**(βα): 4.84 (q, *J* 3.5); **4c**(α_2): 4.93 (t, *J* 3.8). Relatively large *J* values (18–19 Hz) between the vinylene protons for **3**–**5** suggest *E* stereochemistry.

‡ In separate 0.50 mmol scale reactions in benzene preparative GPC gave purified **7a** (M_w = 20 000, M_w/M_n = 3.0, 88% yield) and **7b** (M_w = 23 000, M_w/M_n = 3.7, 80%), which were fully characterised by NMR, IR and microanalysis. *Selected data* for **7a**: $\delta_H(C_6D_6$, 300 MHz) 1.0–1.6 [br m, $=CC(CH_2)_3$], 1.9–2.4 (br m, $=CCH_2$), 5.06 [d, *J* ~3, (VL)(VD)SiH], 5.12 [br t-like, $(VL)_2SiH$], 5.66 (d, *J* ~2, SiC=CH^aH^b), 5.8–6.0 (br m, SiCH= and SiC=CH^aH^b), 6.35 (br dt, *J* 18.5 and 6.1, SiCH=C*H*), 7.1–7.4 and 7.6–7.9 (each br m, C_6H_5); ν_{max}(film)/cm^{-1} 2142 (Si-H). For **7b**: $\delta_H(C_6D_6)$ 5.3–5.4 [br m, $(VL)_2SiH$], 5.4–5.5 [br m, (VL)(VD)SiH], 5.6–5.7 [br m, $(VD)_2SiH$], 5.7–5.9 and 6.1–6.3 (each br m, $SiC=CH_2$), 6.5–6.8 (br m, SiCH=), 7.0–7.9 (br m, SiCH=C*H*, C_6H_5 and C_6H_4); ν_{max}(film)/cm^{-1} 2126 (Si-H).

1 *Comprehensive Handbook on Hydrosilylation*, ed. B. Marciniec, Pergamon, Oxford, 1992; I. Ojima, Z. Li and J. Zhu, in *The Chemistry of Organic Silicon Compounds, Vol. 2*, ed. Z. Rappoport and Y. Apeloig, Wiley, Chichester, 1998, p. 1687.

2 T.-Y. Luh and S.-T. Liu, in *The Chemistry of Organic Silicon Compounds, Vol. 2*, ed. Z. Rappoport and Y. Apeloig, Wiley, Chichester, 1998, p. 1793.

3 $RhCl(PPh_3)_3$-catalysed addition of phenylsilane to RC≡CH (R = Ph, Hex) was reported, although byproduct (diphenylsilane) was also formed in the case of R = Hex. J. B. Baruah K. Osakada and T. Yamamoto, *J. Mol. Catal. A: Chem.*, 1995, **101**, 17.

4 Organolanthanide-catalysed hydrosilylation of internal acetylenes with phenylsilane has recently been reported. H. Schumann, M. R. Keitsch, J. Winterfeld, S. Mühle and G. A. Molander, *J. Organomet. Chem.*, 1998, **559**, 181 and references cited therein.

5 For recent intriguing examples of hydrosilylation polymerisation or cross-linking with monohydrosilyl groups, see (*a*) B. Boury, R. J. P. Corriu, D. Leclercq, P. H. Mutin, J.-M. Planeix and A. Vioux, *Organometallics*, 1991, **10**, 1457; (*b*) Y. Pang, S. Ijadi-Maghsoodi and T. J. Barton, *Macromolecules*, 1993, **26**, 5671; (*c*) G.-H. Wang, M.-W. Chen and W. P. Weber, *Chem. Mater.*, 1993, **5**, 1651; (*d*) R.-M. Chen, Z. B. Deng, G. Sun, S.-T. Lee and T.-Y. Luh, *Polym. Prepr.*, 1998, **39**, 89; (*e*) J. Hu and D. Y. Son, *Macromolecules*, 1998, **31**, 4645 and references cited therein.

6 For photo- and/or electro-luminescence of arylene- and vinylene-containing silicon polymers, H. K. Kim, M.-K. Ryu and S.-M. Lee, *Macromolecules*, 1997, **30**, 1236; ref. 5(*d*).

Communication 9/05128G

ChemComm

A selection of short peptides that interact with a porphyrin as a small target by immobilized phage display

Junji Kawakami,[ab] Takehisa Kitano[a] and Naoki Sugimoto*[ab]

[a] *Department of Chemistry, Faculty of Science, Konan University, 8-9-1 Okamoto, Higashinada-ku, Kobe 658-8501, Japan. E-mail: sugimoto@konan-u.ac.jp*

[b] *High Technology Research Center, Konan University, 8-9-1 Okamoto, Higashinada-ku, Kobe 658-8501, Japan*

Received (in Cambridge, UK) 19th April 1999, Accepted 29th July 1999

Porphyrin H_2TMpyP binding peptides were selected from a phage displayed pentapeptide library that was immobilized onto a solid phase and, as a result, a binding motif that binds to the porphyrin in the same way as a motif obtained by our previous combinatorial chemistry was revealed.

Two methods, combinatorial chemistry and phage display, are used to obtain novel interactions between polypeptides or proteins and desired target molecules. Combinatorial chemistry can select functional molecules from complete libraries of molecules of five or fewer amino acids.[1] On the other hand, phage display can deal with huge libraries and use cDNA libraries for a selection, so that this method is suitable for high molecular weight molecules such as proteins, although some deviation of the libraries occurs because of codon usage by the host cells.[2,3] From such properties, combinatorial chemistry has been used to obtain small functional peptides,[4] while phage display has been applied to epitope mapping of proteins or antibody selection *in vitro*.[5,6]

However, binding motifs obtained *via* the two methods do not always correspond with each other.[7] For example, Maruyama *et al.* specified two epitopes of human galectin-3 *via* a λ phage display system, but the epitopes were not similar to the motifs selected by combinatorial chemistry.[8] The discrepancy may be due to the difference of the selection procedures, *i.e.* an immobilized library and a free target are used for combinatorial chemistry, while a free library and an immobilized target have been used for phage display so far.[9] Here we have carried out a peptide selection against a porphyrin [5,10,15,20-tetrakis(*N*-methylpyridinium-4-yl)-21*H*,23*H*-porphine; H_2TMpyP] which was a small target molecule of our combinatorial chemistry study reported previously,[4] using a new phage display selection method with an immobilized library and the free target porphyrin as for the combinatorial chemistry selection.

A random pentapeptide library displayed on a phage was constructed[10] and used for peptide selection with H_2TMpyP. The library can contain up to 20^5 ($= 3.2 \times 10^6$) individual peptides with different sequences. The phage library was immobilized on nitrocellulose filters as follows, instead of immobilization of the target (the commonly used method for a selection using a phage display system).[9] The recombinant phages were incubated with an *Escherichia coli* TG1 (*supE*) fresh culture and spread on 2×YT agar plates.[11] The spread phages on the plates were transferred onto nitrocellulose filters. The filters were blocked with 1% bovine serum albumin in PBT buffer[12] for 2 min and washed with PBT buffer for 2 min. Then the filters were incubated with 10 μM H_2TMpyP in 2×SSC buffer[12] for 12 h and washed with 2×SSC for 4 min. Porphyrin binding phages on the filters were detected *via* emission of the porphyrin at 656 nm. As a result, four plaques with very strong signals, corresponding to the four phages shown in Fig. 1, were specified by the assay with H_2TMpyP from over 1×10^7 plaques. The four plaques were amplified and their phagemids were sequenced by the dideoxy method. The translated amino acid sequences of the introduced random region at the N-terminus of the pIII coat protein of the four phages were His-Ala-Ser-Tyr-Ser (HASYS), Arg-Ala-Ser-Ser-Leu (RASSL), Arg-Leu-Tyr-Val-Arg (RLYVR) and Leu-Pro-Tyr-Ala-Thr (LPYAT). Every phage displayed a peptide with aromatic amino acids or Arg on the pIII protein. Equal amounts of phage particles of the four positive phages were blotted on a nitrocellulose filter and incubated with H_2TMpyP. The HASYS phage that displayed aromatic His and Tyr was the tightest binder of all, as shown in Fig. 1, with a K_a of about 10^5 M^{-1}.

We obtained previously a porphyrin binding peptide Tyr-Ala-Gly-Tyr (YAGY) that interacted with H_2TMpyP by a sandwiching interaction from a combinatorial library.[4] Molecular modeling was carried out to anticipate the interaction between the HASYS phage and H_2TMpyP. A crystal structural study of the N-terminus domain of the pIII protein[13] suggested that the structure of an expressed peptide in a fusion protein was not influenced by the pIII coat protein and was flexible. Thus we carried out the molecular modeling of an N-terminus tridecapeptide of the pIII protein Ala-Ala-Gln-Leu-Ala-His-Ala-Ser-Tyr-Ser-Ala-Ala-Ala containing the HASYS sequence. 120 conformations of the tridecapeptide–H_2TMpyP complex were generated after a simulated annealing from 0 to 1000 K. Although the two molecules were dissociated during the annealing in about half of the conformations, H_2TMpyP was stacked in the space between the side chains of His and Tyr in all the remaining conformations. The energies of these complexes were minimized and over two thirds of the minimized structures corresponded to the structure shown in Fig. 2. As a result, a cognate sandwiching[14,15] interaction, as in the case of YAGY, was suggested to be a suitable way for the HASYS peptide to interact with H_2TMpyP. Many natural proteins use a His residue to interact with a porphyrin,[16,17] however, the imidazole ring of the His stands perpendicular to the porphyrin ring. In this case, the vertical conformation was suggested to be unstable by molecular modeling, probably because the porphyrin H_2TMpyP used as the target molecule did

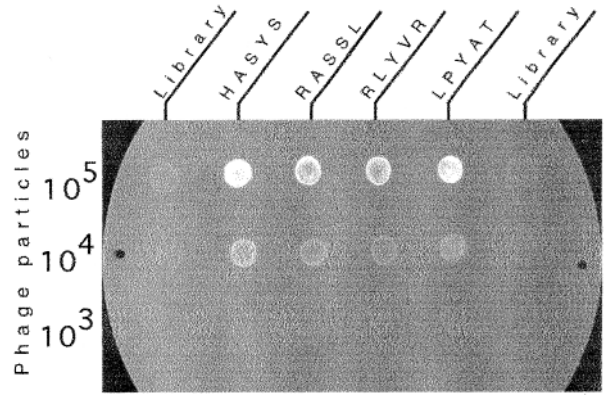

Fig. 1 Binding of the positive phages to H_2TMpyP visualized by fluorescence of the H_2TMpyP. After the selection, equal amounts of phage particles of the four positive phages (HASYS, RASSL, RLYVR, LPYAT) were blotted on a nitrocellulose filter and incubated with H_2TMpyP. Library is the phage before the selection.

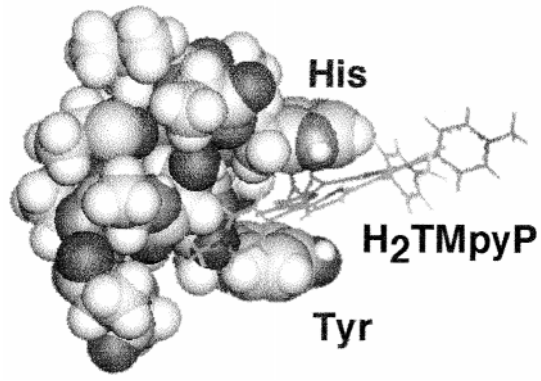

Fig. 2 Proposed structure of the HASYS–H_2TMpyP complex drawn with a molecular modeling calculation using QUANTA97/CHARMm23.2. The energy of the complex was minimized by the adopted basis set Newton–Raphson method. All calculations were performed on a Silicon Graphics Indigo2 workstation running IRIX 5.3.

not have a metal in its center. Consequently, the HASYS peptide should interact with H_2TMpyP by means of a sandwiching interaction in the same manner as the H_2TMpyP–YAGY interaction, as shown in Fig. 2. The YAGY peptide was selected from a biased combinatorial library in which two aromatic amino acids were inserted into positions *i* and *i*+3 or *i*+4.[4] The fact that the same sandwiching interaction was revealed from a completely random library suggests that the stacking between aromatic amino acids and a porphyrin is the most profitable manner for a short peptide to interact with a porphyrin.

In a few cases of selection, only with a protein as the target molecule, common motifs were revealed from the two methods, combinatorial chemistry and phage display. Bianchi *et al.* obtained a very similar consensus from a phage library and a combinatorial library for a binding motif to monoclonal immunoglobulin,[18] and many streptavidin binding phages selected from a phage library with 36 random amino acids[19] contained a similar sequence to one of the consensus sequences picked from a combinatorial pentapeptide library.[1] In both the cases, the target molecule was very large and the obtained interaction was very strong. When a small target is used, as in the present study, such a strong binding with enough energy for anchoring a phage to the target molecule cannot be expected because the available interactions are restricted. So, a high background may hinder simple and efficient selection by the normal phage display system with an immobilized small target.[8] Consequently our system, which binds free H_2TMpyP (MW 1364) to a solid support *via* the interaction between a porphyrin and a phage, is superior to a system that binds a free phage with a 10^4 times greater mass than the porphyrin by the same interaction.

In summary, we have succeeded in obtaining the same peptide motif that binds to a small target H_2TMpyP from both combinatorial chemistry and phage display with an immobilized phage library. Our results suggest that the immobilized phage display system is a promising method for identifying functional short peptides that interact with a small target.

This work was supported in part by Grants-in-Aid from the Ministry of Education, Science, Sports and Culture, Japan and a Grant from the 'Research for the Future' Program of the Japan Society for the Promotion of Science.

Notes and references

1 K. S. Lam, S. E. Salmon, E. M. Hersh, V. J. Hruby, W. M. Kazmierski and R. J. Knapp, *Nature*, 1991, **354**, 82.
2 G. P. Smith and V. A. Petrenko, *Chem. Rev*., 1997, **97**, 391.
3 G. P. Smith, *Science*, 1985, **228**, 1315.
4 N. Sugimoto and S. Nakano, *Chem. Lett*., 1997, 939.
5 M. Baca, T. S. Scanlan, R. C. Stephenson and J. A. Wells, *Proc. Natl. Acad. Sci. U.S.A.*, 1997, **94**, 10 063.
6 T. J. Vaughan, J. K. Osbourn and P. R. Tempest, *Nat. Biotechnol*., 1998, **16**, 535.
7 J. Ellman, B. Stoddard and J. Wells, *Proc. Natl. Acad. Sci. U.S.A.*, 1997, **94**, 2779.
8 I. Kuwabata, H. Maruyama, Y. G. Mikawa, R. I. Zuberi, F. T. Lui and I. N. Maruyama, *Nat. Biotechnol*., 1998, **15**, 74.
9 B. Levitan, *J. Mol. Biol*., 1998, **277**, 893.
10 Oligonucleotides $TGGCC(NNK)_5GC$ and $GGCCGC(MNN)_5$-GGCCAGCT (N = A/G/C/T, K = G/T and M = A/C, respectively) were synthesized on a solid support by employing the phosphoramidite method. The deblocked free oligonucleotides were kinated and annealed to form a duplex with the restricted end of *Sfi* I and *Not* I. The synthesized duplex was ligated to the *Sfi* I and *Not* I sites of a filamentous phagemid vector pCANTAB5E (Pharmacia). The introduced artificial codons lead to successive five random amino acids in an N-terminus region of a surface protein, pIII. An amber suppresser *Escherichia coli* TG1 was transformed by the phagemid and recombinant phages were collected from the overnight culture medium after infection of a helper phage M13KO7.
11 J. Sambrook, E. F. Feritsch and T. A. Maniatis, *Molecular cloning*: *a laboratory manual*, 2nd edn., Cold Spring Harbor Laboratory, Cold Spring Harbor, N.Y., 1989.
12 PBT buffer contains 137 mM NaCl, 8.1 mM $Na_2HPO_4{\cdot}12H_2O$, 2.68 mM KCl, 1.47 mM KH_2PO_4, 0.05% (v/v) Tween 20, pH 7.4. 2×SSC buffer contains 300 mM NaCl, 30 mM sodium citrate, pH 7.0.
13 J. Lubkowski, F. Henneckle, A. Plückthun and A. Wlodawer, *Nat. Struct. Biol.*, 1998, **5**, 140.
14 Y. Aoyama, J. Otsuki, Y. Nagai, K. Kobayashi and H. Toi, *Tetrahedron Lett*., 1992, **33**, 3775.
15 J. Otsuki, K. Kobayashi, H. Toi and Y. Aoyama, *Tetrahedron Lett*., 1993, **34**, 1945.
16 S.-R. Yeh and D. L. Rousseau, *Nat. Struct. Biol*., 1998, **5**, 222.
17 K. A. Gray, P. L. Dutton and F. Daldal, *Biochemistry*, 1994, **33**, 723.
18 E. Bianchi, A. Folgori, A. Wallace, M. Nicotra, S. Acali, A. Phalipon, G. Barbato, R. Bazzo, R. Cortese, F. Felicil and A. Pessi, *J. Mol. Biol*., 1995, **247**, 154.
19 B. K. Kay, N. B. Adey, Y. S. He, J. P. Manfredi, A. H. Mataragnon and D. M. Fowlkes, *Gene*, 1993, **128**, 59.

Communication 9/03083B

ChemComm

meso-Tetraarylporphyrins as dipolarophiles in 1,3-dipolar cycloaddition reactions

Ana M. G. Silva, Augusto C. Tomé, Maria G. P. M. S. Neves, Artur M. S. Silva and José A. S. Cavaleiro*

Department of Chemistry, University of Aveiro, 3810-193 Aveiro, Portugal. E-mail: jcavaleiro@dq.ua.pt

Received (in Liverpool, UK) 21st June 1999, Accepted 21st July 1999

***meso*-Tetraarylporphyrins participate, as dipolarophiles, in 1,3-dipolar cycloaddition reactions with azomethine ylides to yield novel chlorins and isobacteriochlorins.**

Recently we have shown that peripheral double bond(s) of the porphyrin nucleus can participate in Diels–Alder reactions.[1] The results of that work prompted us to investigate the behaviour of the porphyrins in other pericyclic reactions, namely in 1,3-dipolar cycloadditions with azomethine ylides.

A very simple approach to the generation of azomethine ylides involves the reaction of an aldehyde with an α-amino acid: the *in situ* thermal decarboxylation of the resulting imine gives the corresponding 1,3-dipole. Lately these transient species are being used extensively for the functionalization of fullerene C_{60}.[2]

Here we report that azomethine ylides react with *meso*-tetraarylporphyrins to give, in good yields, pyrrolidine-fused chlorins and isobacteriochlorins.

Based on our previous results on the relative reactivities of the arylporphyrins in Diels–Alder reactions, we decided to use *meso*-tetrakis(pentafluorophenyl)porphyrin **1** as a dipolarophile in the reaction with azomethine ylide **2** (Scheme 1). A toluene (5 ml) solution of **1** (22 mg), *N*-methylglycine (4 mg, 2 equiv.) and paraformaldehyde (3.4 mg, 5 equiv.) was heated at reflux for 5 h under a nitrogen atmosphere. TLC of the reaction mixture showed that about half of the starting porphyrin was converted into two new products. Further portions of *N*-methylglycine (4 mg) and paraformaldehyde (3.4 mg) were then added and the resulting mixture was refluxed for another 5 h. The solvent was evaporated and the compounds were separated by column chromatography using a gradient of $CHCl_3$–light petroleum. The first fraction to be collected was the unchanged starting porphyrin (4.4 mg; 20%), then a chlorin (14.2 mg; 61%) and, finally, one isobacteriochlorin (2.8 mg; 11%) were eluted.

For the main product, the ^{1}H, ^{19}F and ^{13}C NMR and mass spectra, and its elemental analysis, are in agreement with structure **3**; also the UV-Vis spectrum of this compound is typical of a chlorin (λ_{max} = 652 nm).† The ^{1}H NMR spectrum of **3** shows, in the aliphatic region, a singlet at δ 2.21, corresponding to the N-CH_3 protons, and two multiplets at δ 2.52–2.56 and 3.11–3.16, corresponding to the methylene protons. Another multiplet at δ 5.24–5.27 was assigned to the resonance of the two β-pyrrolic protons of the reduced ring. In the aromatic region, four of the six β-pyrrolic protons appear as two doublets at δ 8.40 and 8.71 (*J* 4.9 Hz) and a singlet at δ 8.48 for the other two. The ^{19}F NMR spectrum of **3** shows two sets of equivalent pentafluorophenyl rings.‡ The mass spectrum of the minor product shows that it is a bis-adduct [$(M+H)^+$ = 1089]. On the basis of our previous results on the bis-addition of *o*-quinodimethanes to porphyrins we expected that this compound could be a bacteriochlorin. Surprisingly, its UV-Vis spectrum shows that it is an isobacteriochlorin (λ_{max} = 546 and 588 nm). In order to increase the amount of the bis-adduct, the chlorin **3** (21 mg) was treated with *N*-methylglycine and paraformaldehyde in refluxing toluene. After 40 h, and successive additions of small portions of the 1,3-dipole precursors, most of the chlorin was converted into bis-adducts (Scheme 2). Purification of the reaction mixture by preparative TLC gave several fractions. The one with higher R_f was the unchanged chlorin **3** (6.8 mg). The next two fractions (very small amounts) correspond to diasterioisomeric bacteriochlorins, on the basis of their mass [$(M+H)^+$ = 1089] and UV-Vis spectra (λ_{max} = 732 nm). The following fraction was the main product (8.3 mg); it is identical with the isobacteriochlorin previously obtained. The next fraction was also an isobacterio-

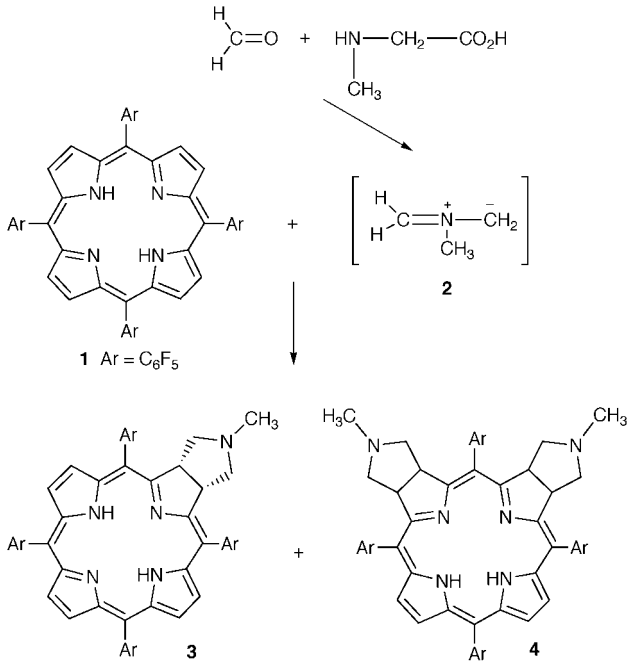

Scheme 1

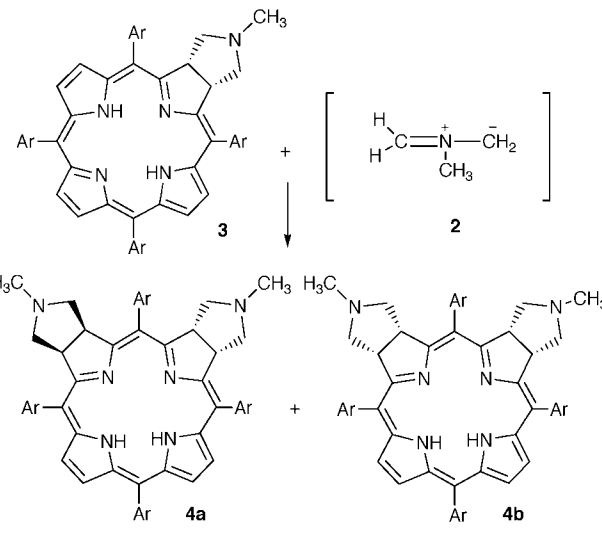

Scheme 2

chlorin, but in a much smaller amount (1.2 mg) than the previous one. The last fraction (the one with lower R_f) was also obtained in small amount and was shown by MS (parent ion at *m/z* 1146) to be a 'tris-adduct'.

The formation of two isomeric isobacteriochlorins and two bacteriochlorins is not surprising since in the bis-adducts the two pyrrolidine rings can be in a '*cis*' or '*trans*' configuration. It is evident from the results of this experiment that the formation of the bis-adducts is regio- and stereo-selective, yielding mainly one of the four possible isomers. By analysis of the ^{1}H, ^{19}F, ^{13}C and 2D COSY and HETCOR NMR spectra of the two isobacteriochlorins we were able to establish their structures and configurations: the main product has structure **4a** and the minor one has structure **4b**. In the ^{1}H NMR spectra of these compounds, in addition to the expected aliphatic and aromatic proton resonances, a broad singlet appears at δ 4.12 for **4a** and at δ 4.08 for **4b**, corresponding to two protons in each case. These signals disappear after shaking with deuterium oxide and thus were assigned to the N*H* proton resonances.§ The ^{19}F NMR spectra of compounds **4a** and **4b** gave us important information for the establishment of the structure of these compounds as isobacteriochlorins. If the products were bacteriochlorins, then, due to the symmetry of the two possible diastereomers, all the pentafluorophenyl rings should be equivalent and only two signals would be expected for each group of *o*- and *m*-fluorine atoms, which is not the case. However, for the two possible diastereomers of isobacteriochlorin **4** three sets of non-equivalent pentafluorophenyl rings were expected, in the proportion 1:2:1, which is the case observed for compounds **4a** and **4b**. This fact is confirmed, in both isomers, by the integral values of the *p*-fluorine atoms (1F:2F:1F) in their ^{19}F NMR spectra. From the spectrum of compound **4b** we can conclude that: (i) the resonances attributed to the two *o*-fluorine atoms of the 5-phenyl ring are very different from each other (δ −133.32 and −137.62, 1F each), and the former have a quite different environment relative to all of the other fluorine atoms in the molecule; (ii) the phenyl rings at positions 10 and 20 are equivalent but again, in each ring, the two *o*-fluorine atoms are not equivalent (δ −136.66 and −139.73, 2F each); and (iii) the two *o*-fluorine atoms in the 15-phenyl ring are also not equivalent but have a similar environment (δ −139.26 and −139.53, 1F each). These results are only compatible with the structure of an isobacteriochlorin having a '*cis*' configuration. The ^{19}F NMR spectrum of compound **4a** shows that its structure must be more symmetrical than **4b**, since only four signals (δ−136.98, −137.16, −139.27 and −139.67) are observed for the *o*-fluorine atoms: one signal for the two *o*-F atoms in the 5-phenyl ring, two signals for the two non-equivalent *o*-F atoms in the equivalent 10- and 20-phenyl rings, and one signal for the two *o*-F atoms in the 15-phenyl ring. This spectrum is only compatible with the structure of an isobacteriochlorin having a '*trans*' configuration.

Table 1 Comparative reactivity and product yields of *meso*-tetraarylporphyrins with azomethine ylides

		Yield (%)	
meso-Aryl group	*t*/h	Monoadduct	Bis-adducts
C_6F_5	10	61	11
2,6-$C_6H_3Cl_2$	35	26	6
Ph	50	12	not observed

In order to find the effect of the substituents in the *meso*-aryl groups, we performed the same type of reaction (porphyrin, *N*-methylglycine and paraformaldehyde in refluxing toluene) with two other porphyrins. The results are presented in Table 1. It is evident from the results that the presence of electron-withdrawing atoms in the aryl groups increase the reactivity of the porphyrin towards azomethine ylides.

Work is in progress in our laboratory to extend these studies to other azomethine ylides and to other families of 1,3-dipoles.

Thanks are due to the University of Aveiro and to FCT, Portugal, for funding the Research Unit 62/94, the Praxis/2/2.1/QUI/145 Project and a Ph.D. grant (A. M. G. Silva).

Notes and references

†*Selected data* for **3**: $\lambda_{max}(CHCl_3)$/nm [log (ε/10^3 dm^3 mol^{-1} cm^{-1})] 405 (5.29), 505 (4.26), 598 (3.77), 652 (4.72); *m/z* (LSIMS) 1032 $(M + H)^+$ (calc. for $C_{47}N_{17}N_5F_{20}$: C, 54.72; N, 6.79; H, 1.66; found: C, 54.69; N, 6.49; H, 2.10%).

‡ It is important to note that, for each pentafluorophenyl group, the two *o*-F and the two *m*-F are non-equivalent (they are coupled to each other, $^4J \sim 8$ Hz). This may result from the lack of free rotation of the pentafluorophenyl groups.

§ Similar chemical shift values (δ 2.98–3.65 ppm) were reported for N*H* protons of other isobacteriochlorins (ref. 3).

1 A. C. Tomé, P. S. S. Lacerda, M. G. P. M. S. Neves and J. A. S. Cavaleiro, *Chem. Commun*., 1997, 1199.

2 M. Maggini, G. Scorrano and M. Prato, *J. Am. Chem. Soc*., 1993, **115**, 9798; T. Da Ros, M. Prato, F. Novello, M. Maggini and E. Banfi, *J. Org. Chem*., 1996, **61**, 9070; S. R. Wilson, Y. Wang, J. Cao and X. Tan, *Tetrahedron Lett*., 1996, **37**, 775.

3 C. K. Chang, *Biochemistry*, 1980, **19**, 1971; A. M. Stolzenberg, L. O. Spreer and R. H. Holm, *J. Am. Chem. Soc.*, 1980, **102**, 364.

Communication 9/05016G

Typeset and printed by Black Bear Press Limited, Cambridge, England

ChemComm
FEATURE ARTICLE

Oligomeric porphyrin arrays

M. Graça H. Vicente, Laurent Jaquinod and Kevin M. Smith*

Department of Chemistry, University of California, Davis, Davis CA 95616, USA. E-mail: kmsmith@ucdavis.edu

Received (in Cambridge, UK) 23rd March 1999, Accepted 14th May 1999

The field of synthesis and physical characterization of oligomeric porphyrin arrays has been the subject of intense research in recent years. Some of these systems present unique physical and optical properties which reflect the extent of electronic interaction between the monomers in the array, and determines their potential applications in chemistry, physics, and biology. General synthetic approaches to a multitude of porphyrin arrays, including directly linked *meso-meso*, *meso*-β, and β-β compounds, oligoporphyrins with fused π-systems, and arrays bearing rigid or flexible spacers, developed by us and by others, are described. X-Ray structures of representative compounds are presented.

Introduction

Procedures for the synthesis and functionalization of monomeric porphyrin molecules have advanced to the stage that almost any porphyrin can be obtained using available methodology.[1] Many research groups have now moved to the development of syntheses of porphyrin analogues and to the construction of multiporphyrin arrays which can either mimic natural systems, or can be used as molecular-level devices for advanced technological tasks. Interest in porphyrin arrays as model systems to mimic the vital functions of photosynthetic reaction centers and antenna systems has increased significantly in recent years. Considerable work has been reported in the field of oligoporphyrins, and we will illustrate the most general approaches by discussing some recent developments to which our own group has contributed.

Porphyrin arrays are potential precursors in building electron- and energy-transfer molecular devices; they are also robust and efficient catalysts for the multielectron redox transformations of small molecules and for the oxidation of organic substrates.[2] For all of the uses mentioned above it is important that the individual molecules within an array communicate with each other, otherwise the whole will be no better than the sum of the components and the array cannot behave with enhanced effectiveness. For effective electronic communication between adjacent porphyrins, the geometry, distance, and orientation between components of rigid porphyrin arrays are usually to be considered, though, in the area of molecular recognition such rigidity is not essential.[3] The nature of the bridges between porphyrin components, the extent of steric interactions (if any), and the connectivity of the porphyrin components directly affect the photophysical properties of covalently linked systems. The present Feature Article reports on recent work carried out in our UC Davis laboratories, and places this within the context of related research from other groups.

In the first part of this Article we concentrate on methodology we have developed to use the so-called McMurry reaction for construction of dimeric porphyrin arrays. These include cofacial bisporphyrins and bischlorins, symmetrical and unsymmetrical systems linked by ethene, stilbene, styryl, and hexatriene linkages, as well as planar fully congugated systems, and directly *meso-meso* linked dimers. After that, we discuss porphyrin oligomers derived from other synthetic approaches, leading to structures containing fused π-systems, orthogonal π-systems and supramolecular arrays.

Bridged and cofacial porphyrin oligomers

It seems clear that, at least for the reaction center in bacterial photosynthesis,[4a] cofacial π–π interacting tetrapyrrole chromophores are essential for charge separation, the first step in photosynthesis. Likewise, such interactions are vital in light-harvesting systems.[4b] A simple model of the special pair in such reaction centers would be two cofacially disposed porphyrins with a *meso-meso* alkene tether possessing a *cis* orientation (*e.g.* **1**). Prior to our work, two approaches had been investigated to provide such face-to-face dimers: (1) compounds linked on one side by a rigid aromatic spacer [the PacMan porphyrins of C. K. Chang (*vide infra*)], and (2) compounds with two or more flexible strapping units. Synthetic routes to these kinds of compounds are usually laborious, requiring multiple steps, and provide only low yields of the targeted compounds. Our methodology for the synthesis of cofacial bisporphyrins is based on the low-valent titanium-induced reductive coupling [$TiCl_3(DME)_{1.5}$/Zn-Cu couple] of *meso*-formyl-metalloporphyrins, which are conveniently prepared by Vilsmeier formylation of metalloporphyrins.[5] In the McMurry reaction a mixture of both the *cis*- and the *trans*-bisporphyrins is generally produced.[6,7] That the *cis* compound (presumably the least stable geometrical isomer) is produced at all is something of a surprise; presumably the strong intramolecular face-to-face π-stacking of the metalloporphyrin pinacol intermediate results in the formation of the kinetic cofacial *cis*-dimers, which can be converted into the stable thermodynamic extended *trans*-dimers by heating (to 120 °C for several hours) or photochemically. *Cis-trans* isomerization of ethene-linked bisporphyrins is also observed in acidic conditions and occurs more readily for the metal-free compounds.[7,8] The nature of the central metal ion is a determinant of the relative amounts of the *cis*- and *trans*-bisporphyrins obtained in this reaction, since it significantly affects the extent of macrocyclic π–π stacking prior to the formation of the ethene bond. In the cofacial arrangement (Fig. 1) the two macrocycles are almost parallel, the distance between the two metal centers is 5.36 Å (for the Ni/Zn heterodimer), and substantial macrocyclic overlap occurs as a result of the π–π interaction between the two macrocycles. The ^{1}H NMR spectra of diamagnetic *cis*-bisporphyrins typically show downfield shifts for the ethylenic protons (between 9.0 and 9.5 ppm), diastereotopic methylene proton signals, and substantial upfield shifts of the *meso* protons adjacent to the ethylene bridge; this supports a similar stacking of the porphyrin units in solution as in the solid state. In contradistinction, the extended *trans*-bisporphyrins (*e.g.* **2**) display a simplified ^{1}H NMR spectrum with the ethylene protons at 7.7 ppm, and the *meso* protons at 9.5 ppm; the X-ray structure of a bis-Ni *trans*-dimer **2** is shown in Fig. 2. In the optical spectrum the Soret band of the *cis*-porphyrins typically appears blue-shifted relative to the Soret of the corresponding extended *trans*-isomers. The *cis*- and *trans*-isomers also display distinct solubility differences; the *cis*-bisporphyrins are generally more soluble in organic solvents than are the *trans*-compounds, which facilitates their chromato-

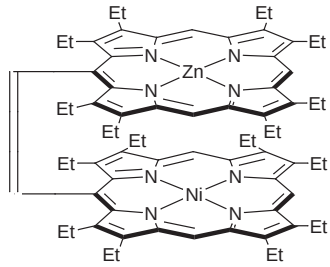

1

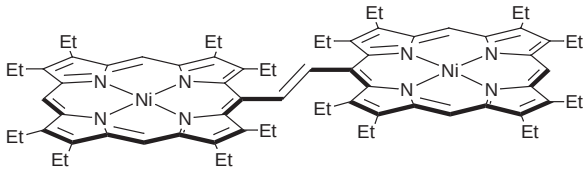

2

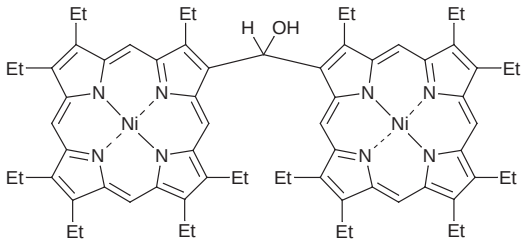

3

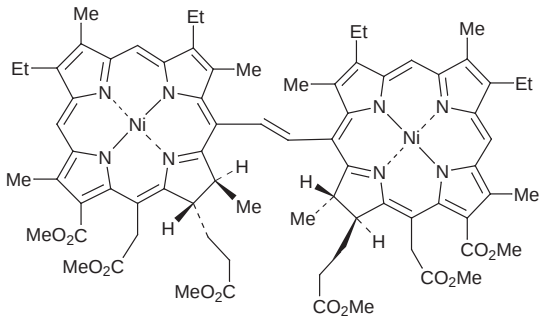

4

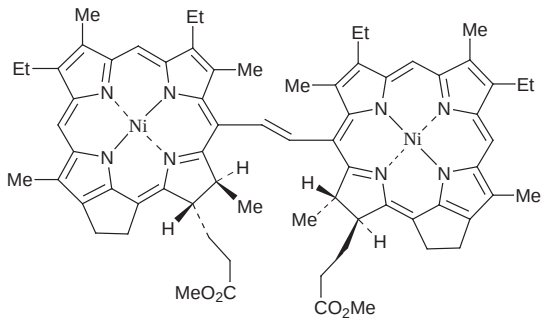

5

graphic separation. Pure metal-free *trans*-ethene-1,2-bisporphyrins have also been obtained by oxidation of the corresponding ethanebisporphyrins in refluxing acetic acid.[9] The free-base

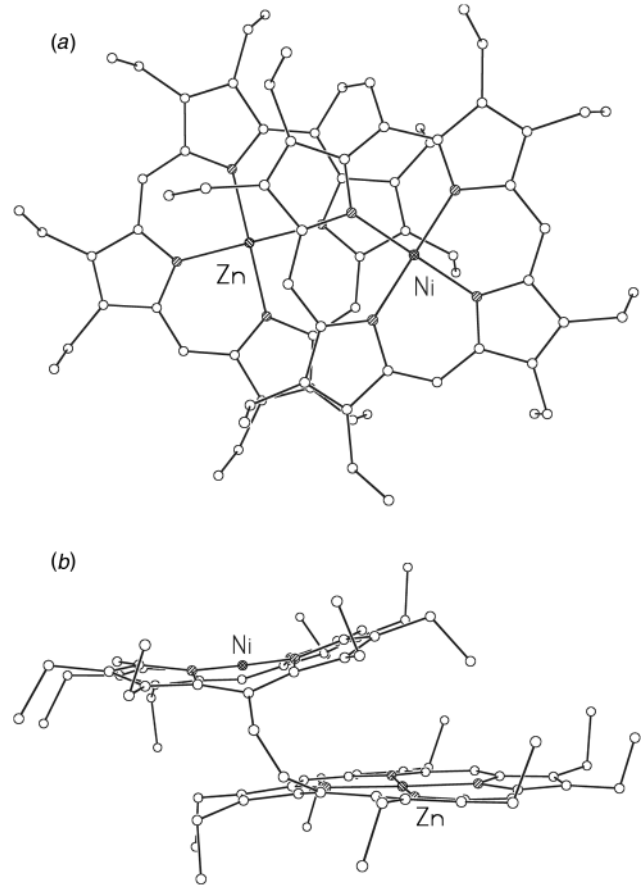

Fig. 1 Molecular structure of heterobimetallic [Ni^{II}][Zn^{II}] *cis*-ethene dimer **1** (hydrogen atoms not shown); (*a*) top view, (*b*) side view.

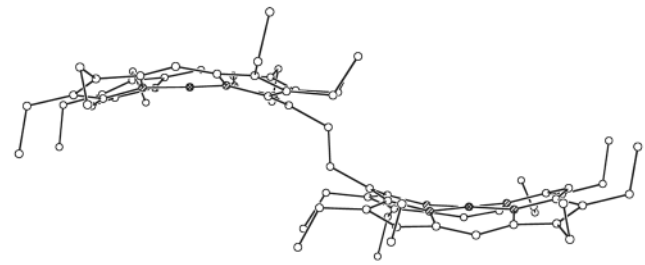

Fig. 2 Molecular structure of bis-Ni^{II} *trans*-ethene dimer **2** (hydrogen atoms not shown).

dimer can be selectively metalated to afford a series of monometallic, and homo- and hetero-bimetallic bisporphyrins.[10] The reductive coupling of *meso*-(2-formylvinyl)metalloporphyrins and metallochlorins analogously produces the corresponding dimers, linked by three conjugated carbon–carbon double bonds.[5]

Under the same reductive coupling conditions, a β-formylmetalloporphyrin produced a hydroxymethylene-bridged dimer **3** by loss of one of the formyl groups,[6] although a β-formylmetallochlorin formed the expected ethene-linked bischlorin. The crystal structure of **3** (Fig. 3) displays a skewed arrangement of the two macrocycles, the two planes of the four nitrogens form an angle of 77.3°, and the distance between the two metal centers is 8.08 Å. The reductive coupling of *meso*-formylmetallochlorins containing bulky propionate ester substituents resulted in the selective formation of the *trans*-bischlorins (such as **4**), which because of steric interactions did not significantly isomerize to the corresponding *cis*-products even upon heating in acetic acid.[11] Aerial oxidation of **4** in refluxing toluene–acetic acid led to the formation of the corresponding *trans*-bisporphyrin, as well as a porphyrin-chlorin hetero-dimer; under the same conditions bischlorin **5** selectively produced the corresponding *cis*-bisporphyrin.

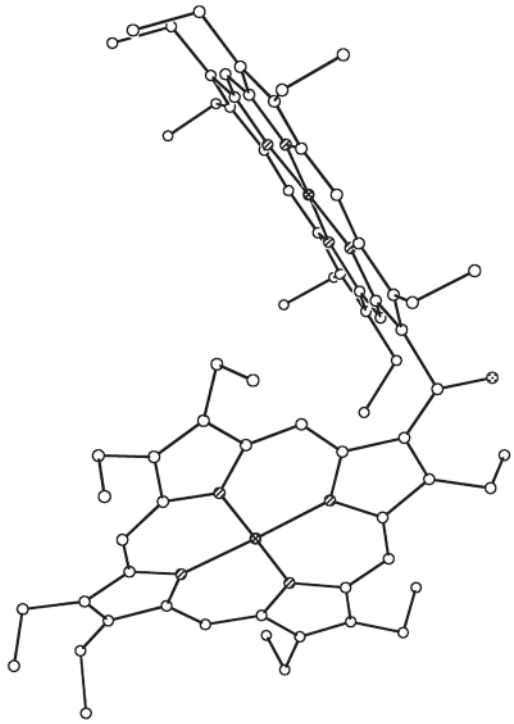

Fig. 3 Molecular structure of bis-Ni^{II} porphyrinyl alcohol **3** (hydrogen atoms not shown).

Syntheses of symmetrical cofacial bisporphyrins containing rigid aromatic bridges, such as 1,2-phenylene, biphenylene and anthracene (the so-called PacMan series), have been accomplished by stepwise condensation of aromatic dialdehydes with a 2-unsubstituted pyrrole, followed by reaction of the α-unsubstituted aromatic-linked bis(dipyrromethane) with a 1,9-diformyldipyrromethane.[12,13] Both symmetrical and unsymmetrical cofacial bisporphyrins are most conveniently prepared by initial monoprotection of the dialdehyde bridge, followed by condensation with pyrrole and an aromatic aldehyde to afford an aldehyde-protected porphyrin. This, upon deprotection and a second cyclization, produces homo- and hetero-bisporphyrins.[14,15] The syntheses of cofacial bisporphyrins bearing two amide bridges,[16] and larger host cavities with four strapping units,[17] have also been reported.

Another successful application of the McMurry methodology involves the synthesis of symmetric stilbene-linked bisporphyrins (*e.g.* **6**). The key intermediate is a stilbene-linked bis(dipyrromethane), produced by reductive dimerization of a 5-(*p*-formylphenyl)dipyrromethane, which upon MacDonald-type condensation with a 1,9-diformyldipyrromethane affords symmetric bisporphyrins such as **6**.[18,19] In yet another approach, these systems were obtained, albeit in lower yield, by reductive coupling of metalloporphyrins bearing a *meso*-(*p*-formylphenyl) substituent.[18,20] The latter methodology yielded both *cis*- and *trans*-stilbene-linked systems.

The synthesis of symmetrical bisporphyrins linked at the *meso* positions by an aryl group usually involves a stepwise

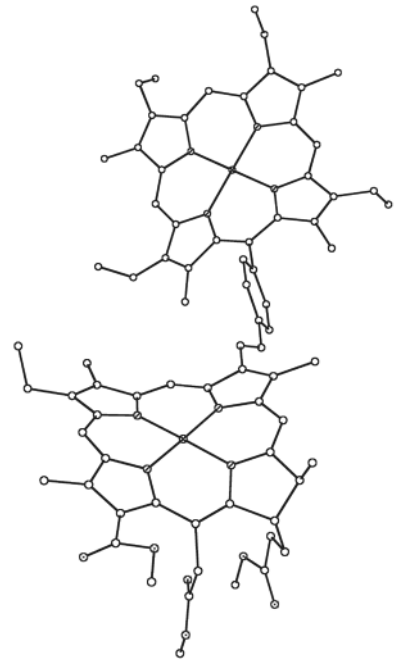

Fig. 4 Molecular structure of Ni^{II} porphyrin–Ni^{II} chlorin heterodimer **7** (hydrogen atoms not shown).

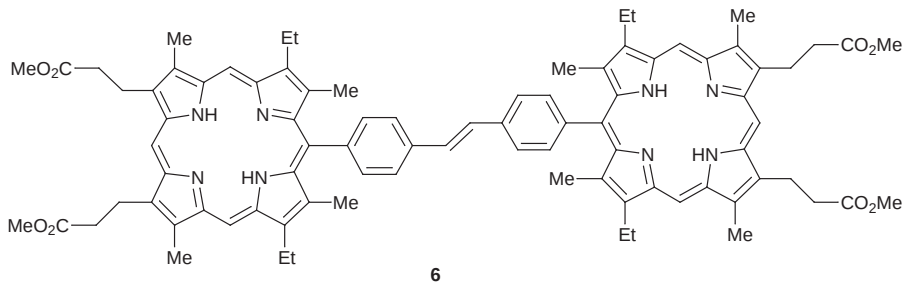

6

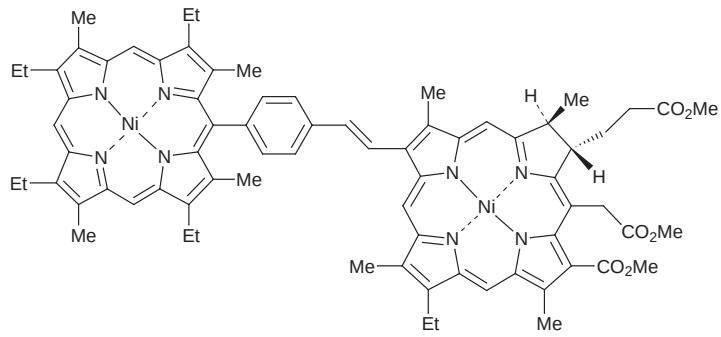

7

methodology, from intermediate aryl-linked α-unsubstituted bis(dipyrromethanes), which are in turn obtained from the condensation of formyl-substituted aromatic units with 2-unsubstituted pyrroles.[21,22] The preparation of symmetrical phenyl-linked bisporphyrins has also been accomplished, by acid-catalyzed condensation of a porphyrin bearing a *meso*-formylphenyl substituent with an excess of pyrrole and benzaldehyde;[23,24] in the presence of a large excess of pyrrole, a *meso*-[(*p*-formylphenyl)triphenyl]porphyrin was reported to produce a pentaporphyrin in 1% yield.[24] Unsymmetrical dimers and porphyrin-chlorin systems can be obtained from low-valent titanium-promoted heterocouplings of formyl-substituted porphyrins and chlorins, although a statistical mixture of all possible homo- and hetero-dimers is generally produced. When a 2:1 mixture of nickel(II) 3-formylchlorin-e_6 trimethyl ester and a *meso*-(*p*-formylphenyl)porphyrin was coupled under the McMurry conditions, the corresponding bisporphyrin and bischlorin were obtained in 6 and 42% yields, respectively, along with the porphyrin-chlorin dimer **7**, in 41% yield.[18] The crystal structure of **7** (Fig. 4) shows the *trans* arrangement of the two macrocycles, and a bow-shaped structure for this molecule with an angle between the two N_4 planes of 35.7°. Unsymmetrical bisporphyrins, such as **8**, linked at the *meso* positions by aromatic groups are generally synthesized as shown in Scheme 1;[18] the key intermediate is an unsymmetrical bis(dipyrromethane) bearing both benzyl and ethyl ester groups which are selectively cleaved and reacted with a dipyrromethane, in a stepwise manner. Phenyl-linked unsymmetrical dimers have been synthesized by reaction of a *meso*-(formylphenyl)porphyrin with a 2-unsubstituted pyrrole, followed by condensation with a dipyrromethane,[25] or by mixed condensation.[26] Bisporphyrins bound by several *trans*-stilbene linkages have also been synthesized from the corresponding poly(benzyl sulfone)-linked bisporphyrins *via* the Ramberg–Bäcklund reaction.[27] A β-substituted porphyrin methylphosphonium salt has been used as a building block for the synthesis of porphyrin arrays, linked by butadiene, styryl, and diethenylphenylene bridges, and consisting of up to nine porphyrin units.[28]

Other syntheses of *meso*-*meso*, *meso*-β or β-β linked porphyrin arrays take advantage of metal-mediated cross-coupling methodologies and the ease with which β- or *meso*-haloporphyrins are prepared. Alkynyl-bridged porphyrin arrays, obtained *via* the Pd^0 cross-coupling of a small set of ethynyl- and halo-porphyrin building blocks display large porphyrin–porphyrin excitonic and electronic couplings far exceeding those of other porphyrin-to-porphyrin aromatic, aliphatic or vinylic linkages.[29] *meso*-Ethynyl bridges are most efficient to conjugatively connect porphyrins. Glazer–Hay oxidative coupling of 5,15-diethynylporphyrin afforded polymeric materials absorbing in the near IR region and exhibiting strong third-order non-linear optical behavior.[30] Construction of *meso*-alkynylaryl

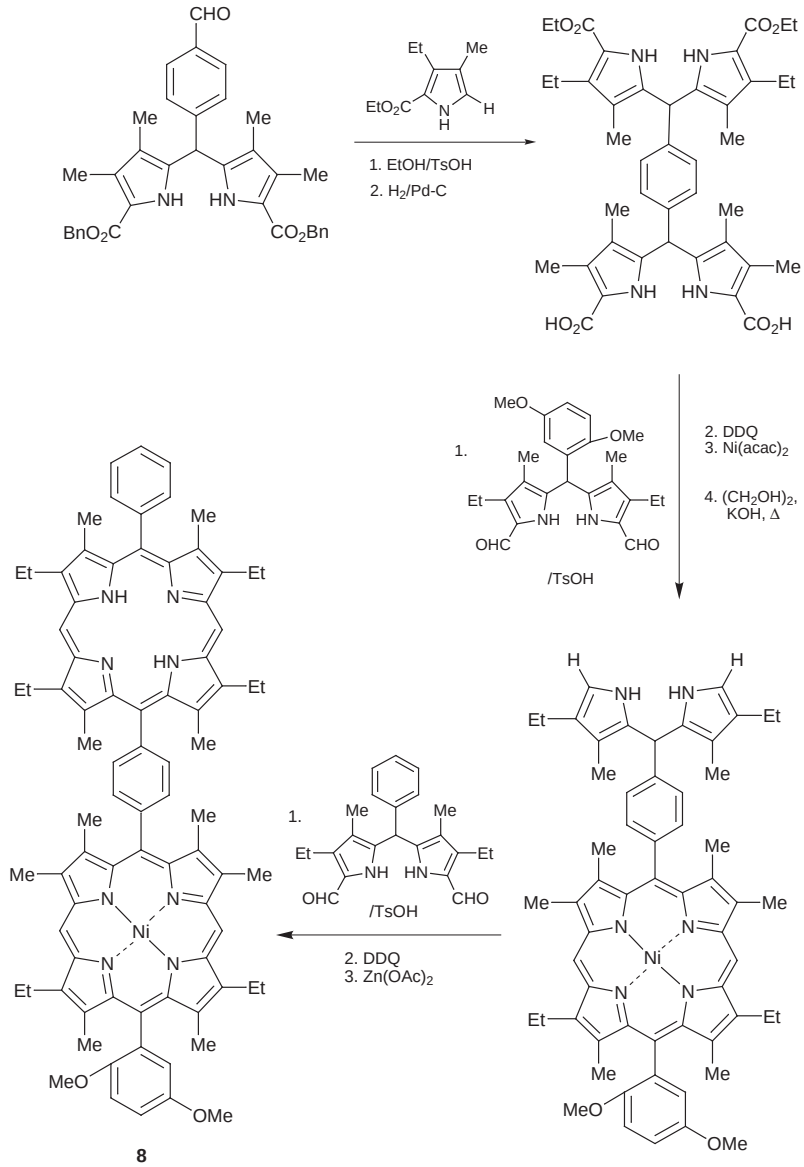

8

Scheme 1

linked oligoporphyrins relied also on a small set of (halo- and ethynyl-phenyl)porphyrin building blocks and iterative cross-coupling reactions. A variety of molecular structures have been obtained, as exemplified by the preparation of a square macrocyclic array of four mutually coplanar porphyrins from the palladium catalyzed reaction of zinc(II) 5,10-di(*p*-ethynylphenyl)-15,20-dimesitylporphyrin with 5,10-di(*p*-iodophenyl)-15,20-dimesitylporphyrin in the presence of $As(Ph)_3$.[31] Positive coupling of linear *m*-ethynylaryl functionalized porphyrins with copper(I) chloride/air in the presence of pyridine-based templates yielded butadiyne bridged dimeric or tetrameric cyclic species.[32]

Porphyrin oligomers with orthogonal π-systems

The low-valent titanium coupling reaction provides a synthetic route to directly linked *meso-meso* bisporphyrins (*e.g.* **9**). Dipyrrol-2-yl ketone smoothly undergoes reductive coupling in the presence of pyridine, affording tetra(pyrrol-2-yl)ethene, which upon tetraformylation under the Vilsmeier conditions, followed by MacDonald-type condensation with a 1,9-di-unsubstituted dipyrromethane, produced bisporphyrin **9** (Scheme 2).[33] The crystal structure of **9** (Fig. 5) shows an orthogonal arrangement of the two directly linked macrocycles; the dihedral angle between the two porphyrin planes was found to be 83.9° (crystallization from CH_2Cl_2–methanol) or 64.3° (crystallization from THF–hexane), the difference probably due to variable lattice packing. The optical spectrum of **9** exhibits a large splitting of the Soret band ($\Delta\lambda$ = 36 nm) which reveals excitonic coupling[34] indicating substantial electronic interaction between the two macrocycles, despite their orthogonal arrangement. Directly *meso-meso* linked bisporphyrins and trisporphyrins have also been obtained by reaction of a *meso*-formyl β-unsubstituted porphyrin with a 1,9-di-unsubstituted dipyrromethane,[35] and by electrochemical or Ag^I-promoted oxidative coupling of 5,15-diarylporphyrins.[36] The latter approach also produced higher oligomers, which can be separated by size exclusion chromatography. The one-electron oxidations are usually performed on the Zn^{II} complexes, which readily form the π-cation radical intermediates, and the reaction mechanism probably involves subsequent nucleophilic attack by a neutral zinc(II) porphyrin. The chemical oxidation is usually accomplished with $AgPF_6$ at room temperature, and addition of iodine was reported to accelerate the coupling reaction. The electrochemical oxidation generally uses a platinum net as the working electrode;[37] electrochemical oxidations performed on the free-base porphyrin, and on the Cu^{II}, Pd^{II} and Ni^{II} complexes regioselectively produced *meso*-β linked bisporphyrins.[38] The electrochemical oxidation of zinc(II)octaethylporphyrin in the presence of an excess of 4,4′-bipyridine led to the production of a pentaporphyrin, *via* a *meso*-tetra(4,4′-bipyridinium)porphyrin intermediate.[39]

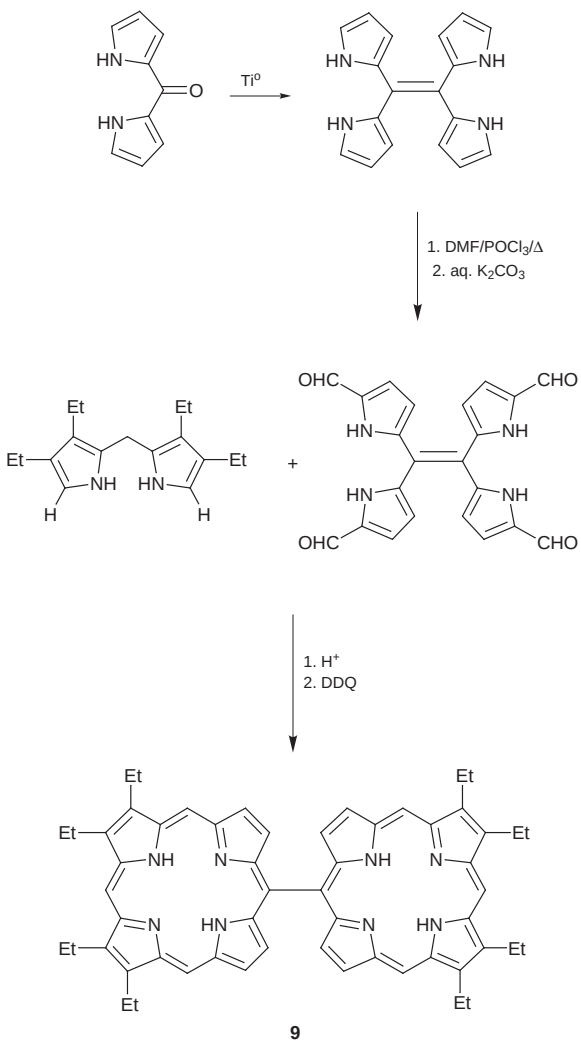

9

Scheme 2

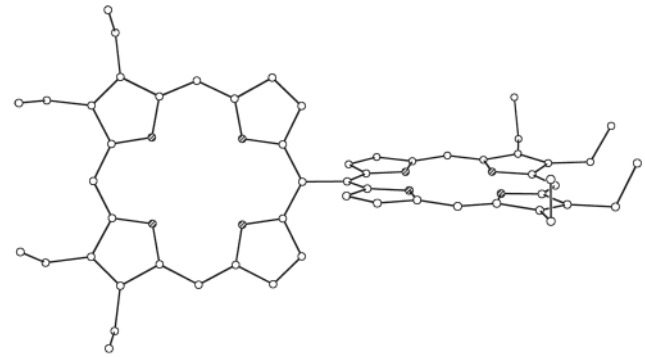

Fig. 5 Molecular structure of free-base *meso-meso* linked dimer **9** (hydrogen atoms not shown). Dihedral angle is 83.9°.

Directly *meso*-β linked porphyrin-chlorin dimers have been obtained by mixed condensation of methyl pyropheophorbide *d*, *o*-methylbenzaldehyde, and a 1,9-di-unsubstituted dipyrromethane.[40] We have developed a related synthetic route to porphyrin-chlorin dimers by stepwise condensation of a β-formylchlorin with a 2-unsubstituted pyrrole, *via* a chlorin-dipyrromethane intermediate.[41] Dimer **10** was produced from the condensation of a pyropheophorbide *a*-dipyrromethane with a 1,9-diformyldipyrromethane, whereas trimer **11** resulted from condensation of β-formylpyropheophorbide *a* with a 1,9-di-unsubstituted dipyrromethane. A dimer was also produced from the latter reaction, presumably by cleavage of the strained C_β–C_{meso} bridge at the pyropheophorbide *a*-porphodimethene oxidation step.

Porphyrin oligomers with fused π-systems

Relatively few oligoporphyrin arrays in which individual porphyrin rings are bridged by coplanar aromatic bridges have been prepared. Such rigid coplanar arrays should display pronounced electronic interactions between metal centers *via* overlap of their d(π) orbitals with the conjugated π-system of the porphyrins. The McMurry reaction, applied to chlorophyll derivatives containing an exocyclic cyclopentanone ring, produces fully conjugated bischlorins.[42] The metal-free compound **12** was obtained from the zinc complex monomer by performing the McMurry reaction in the presence of pyridine, followed by demetalation with TFA. The crystal structure of **12** (Fig. 6) shows that the molecule is essentially planar, forming an angle of 2.2° between the two planes of the N_4 atoms. These bischlorin systems show substantial hyperchromic and bathochromic shifts ($\Delta\lambda$ *ca.* 90–100 nm) of the long-wavelength absorption band in their optical spectra when compared with the precursor monomers, a result of their extended π-electronic delocalization (Fig. 7).

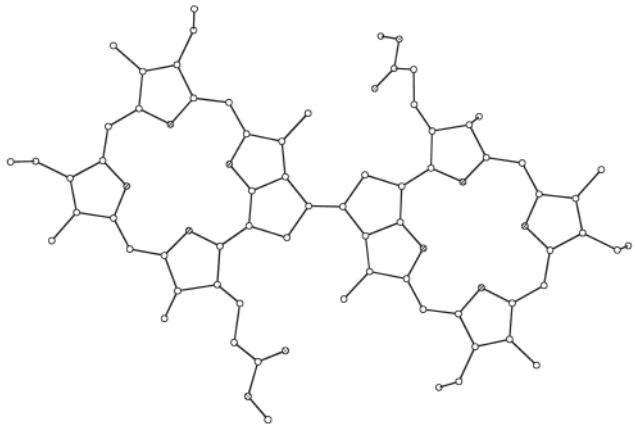

Fig. 6 Molecular structure of planar free-base bis-chlorin **12** (hydrogen atoms not shown).

Crossley and co-workers developed an approach to laterally extended oligoporphyrins sharing up to three 1,4,5,8-tetraazaanthracene units.[43] Linear and bent tris-porphyrins and a tetrakis-porphyrin were prepared by condensing porphyrin-2,3-diones and porphyrin-2,3,12,13- or -2,3,7,8-tetraones with aromatic *ortho*-diamines or 1,2,4,5-tetraamines in refluxing toluene. A bis-tetrabenzoporphyrin in which two benzoporphyrins share a fused benzene ring has been obtained by cross-condensation of pyromellitic dipotassium diimide and potassium *tert*-butylphthalimide at 320 °C.[44] Our approach to related arrays sharing a common benzene ring was based on the participation of *meso*-tetraarylporphyrins as dienophiles in Diels–Alder type reactions with highly activated dienes, such as those generated *in situ* by thermal extrusion of SO_2 from fused aromatic sulfones. Refluxing a solution of *meso*-tetraphenylporphyrin and excess ethyl 1,1-sulfolano[3,4-*c*]pyrrole-2-carboxylate in 1,2,4-trichlorobenzene gave tetraphenylchlorin **13** as an enantiomeric mixture.[45] Oxidation with DDQ and subsequent zinc(II) insertion afforded the corresponding zinc(II) 2*H*-isoindoloporphyrin. Reduction of the ester group of this porphyrin with $LiAlH_4$ produced the alcohol which, upon acid-catalyzed tetramerization and oxidation with *p*-chloranil, gave a cyclohexadiene annulated pentaporphyrin. This pentamer could be further aromatized with excess DDQ to afford a conjugated

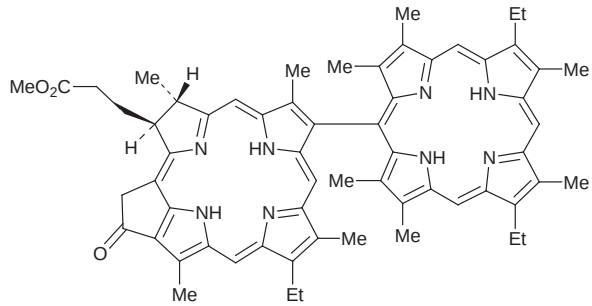

10

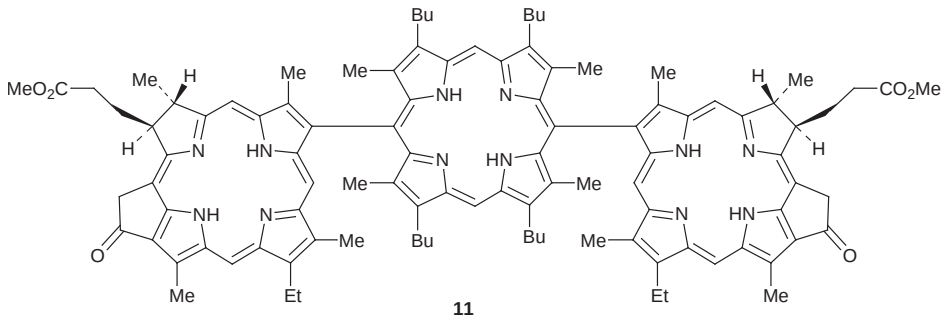

11

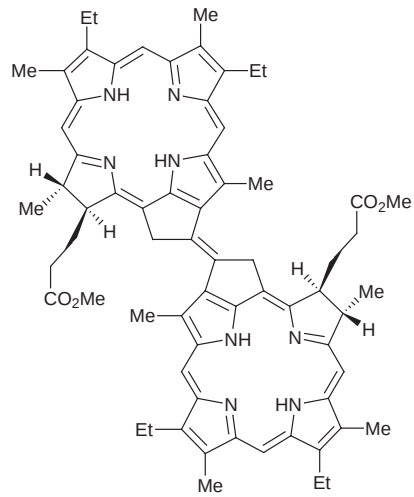

12

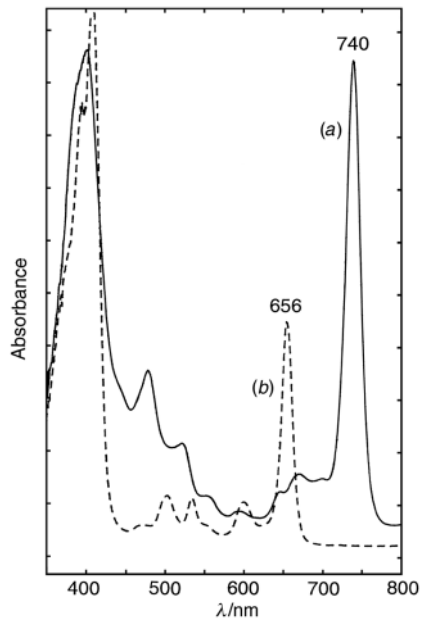

Fig. 7 Optical spectrum, in CH_2Cl_2, of (*a*) bis-chlorin **12** and (*b*) its monomeric pyropheophorbide precursor.

pentaporphyrin **14**, displaying a long-wavelength absorption band at 774 nm. In order to further enhance the interporphyrin communication, we prepared a novel modular β-β′ building block, *i.e.* pyrrolo[3,4-*b*]porphyrin, by applying the [3 + 2] cycloaddition of nitroalkenes with isocyanoacetates[46] to metallo-2-nitrotetraphenylporphyrins (2-NO_2TPPs). We took advantage of the strong ability of the nitro group to activate a tetraarylporphyrin towards Michael addition and its propensity to act as leaving group. Thus, refluxing Ni(2-NO_2TPP) with methyl isocyanoacetate and two equiv. of DBU in THF–Pr^iOH led, as a result of an *in situ* transesterification reaction with Pr^iOH, to the formation of the first β-fused pyrroloporphyrin, as its isopropyl ester **15**. Fig. 8 shows the X-ray structure of pyrroloporphyrin **15**. Use of benzyl alcohol in place of Pr^iOH yielded advantageously the pyrroloporphyrin benzyl ester **16**. Reaction of Ni(2-NO_2TPP) with *tert*-butyl isocyanoacetate (in THF–Bu^tOH) gave (in addition to pyrroloporphyrin *tert*-butyl ester) naphthochlorin **17**. Attempted crystallization of **17** afforded a β-β′ naphthochlorin dimer (**18**).[47] Despite the direct β-β′ bond, the macrocycles were nearly coplanar, exhibiting an interplanar angle of 30.1° (Fig. 9). The macrocyclic overlap was limited to one pyrrolic subunit of each naphthochlorin monomer, displaying a marked similarity to the special pair in the bacterial photosynthetic reaction center. The π-radical dimerization of **17** could be promoted by benzoyl peroxide in refluxing benzene to afford **18** in higher yield. When Zn(2-NO_2TPP) was subjected to the Barton–Zard conditions

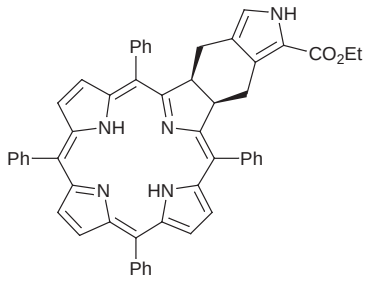

13

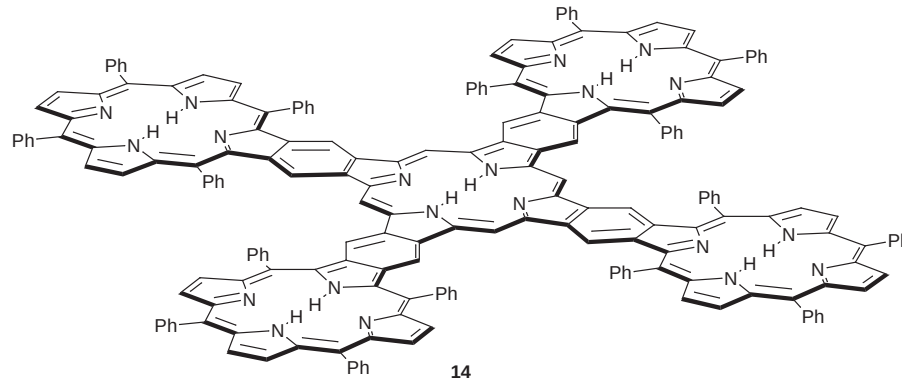

14

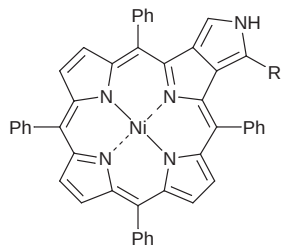

15 R = CO_2Pr^i
16 R = CO_2Bz
20 R = H

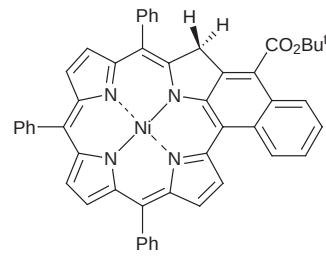

17

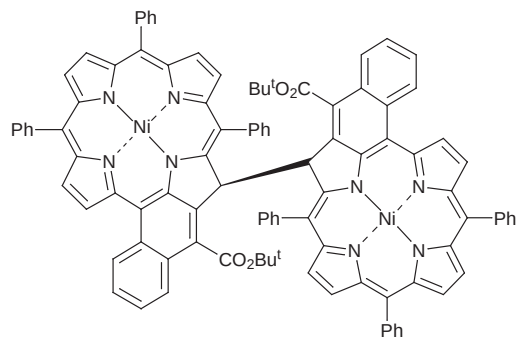

18

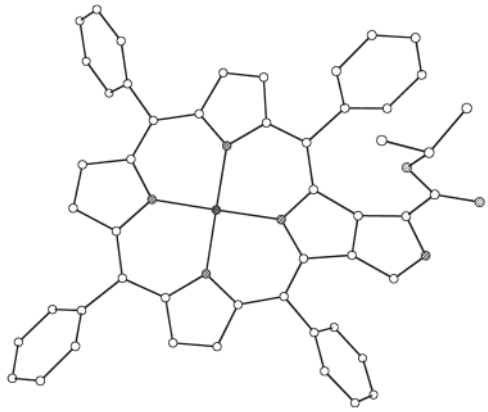

Fig. 8 Molecular structure of Ni^{II} pyrroloporphyrin **15** (hydrogen atoms not shown).

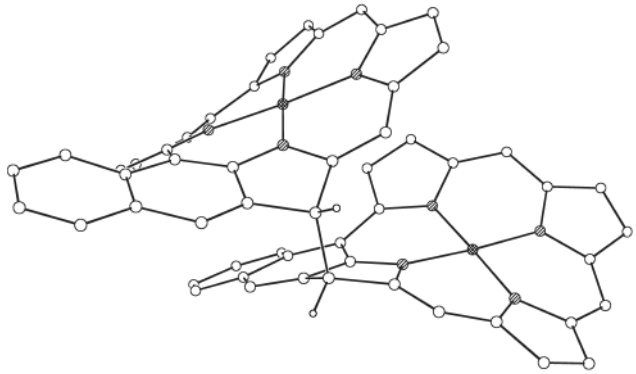

Fig. 9 Molecular structure of Ni^{II} naphthochlorin dimer **18**; ester functions, non-fused phenyl rings, and hydrogen atoms (with the exception of those associated with the direct dimer link) have been omitted for clarity.

Fig. 10 Molecular structure of aggregated Zn^{II} cyclopropyl-annulated chlorin **19** (hydrogen atoms not shown).

($NCCH_2CO_2Et$, Pr^iOHTHF, DBU), no pyrroloporphyrin was formed; instead a cyclopropyl-annulated chlorin was isolated with an *endo* configuration with regard to the isocyanide group.[48] This zinc(II) chlorin self-assembled with isocyanide axially coordinated to the central zinc(II) ions, affording **19** (crystal structure shown in Fig. 10). Isolation of this cyclopropylchlorin prompted our development of a new methodology for dihydroporphyrin synthesis based on the Michael addition of active methylene compounds to 2-NO_2TPPs.[49] A Diels–Alder cycloaddition of di(2-phenylethyl) acetylenedicarboxylate with an *N*-(*tert*-butoxycarbonyl)pyrrolo[3,4-*b*]porphyrin gave, after cleavage of the Boc group and subsequent zinc(II) insertion, the

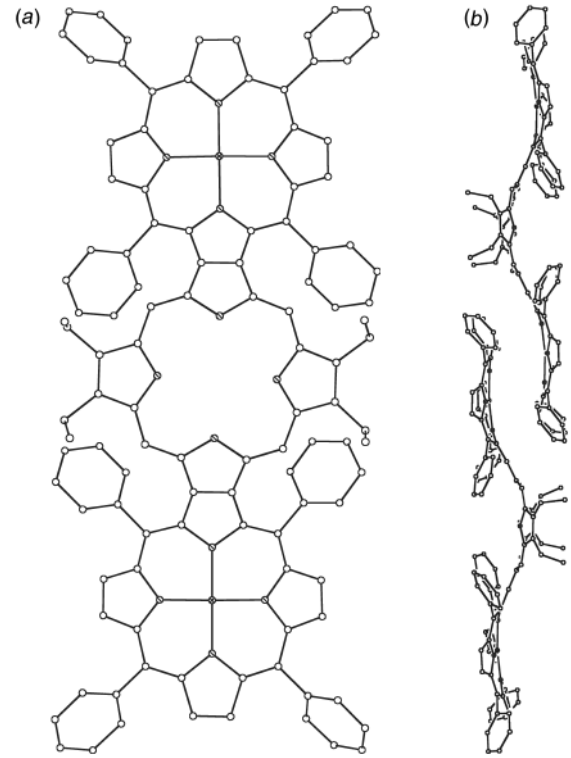

Fig. 11 Molecular structure of $[Ni^{II}][H_4^{2+}][Ni^{II}]$ fused trimer **21**·$(HCl)_2$ (hydrogen atoms not shown); (*a*) top view, (*b*) side view of two molecules illustrating the π–π interactions observed in the crystal packing.

corresponding zinc(II) 7-azabicyclo[2.2.1]heptadiene porphyrin.[50] In the solid state, a non-covalent cyclic hexameric array was obtained wherein each zinc(II) porphyrin was coordinated to the fused azabicyclo group of an adjoining porphyrin unit. Hydrogenolysis of pyrroloporphyrin benzyl ester **16** using 20% palladium(II) hydroxide on carbon and cyclohexene as the hydrogen donor afforded the green di-α-unsubstituted pyrroloporphyrin **20**.[51] Under non-acidic conditions, 2,5-bis(trimethylammoniomethyl)-3,4-diethylpyrrole reacted with **20** in refluxing methanol–THF in the presence of $K_3Fe(CN)_6$/air to afford the first β-β′-directly-fused porphyrin trimer **21**.[52] This novel compound possesses a large fully-delocalized aromatic network which could possibly give rise to metallic type conduction. The molecular structure of **21**·$(HCl)_2$ was confirmed by X-ray crystallography (Fig. 11). Protonation of the central porphyrin facilitated the crystal packing by enabling intermolecular π–π stacking to occur only between terminal porphyrins, thus giving rise to independent linear rods of fused porphyrins. The porphyrin trimer has an edge-to-edge span of 27.0 Å and an intramolecular distance between metals of 16.16 Å. The most notable feature in the absorption spectra of **21** and a related β-β′ fused dimer [obtained from cross condensation of **20**, pyrrole and 2,5-bis(trimethylammoniomethyl)-3,4-diethylpyrrole] is an intense Q band at 715 nm or at 652 nm for the fused dimer, reminiscent of a bacteriochlorin (or chlorin) type visible spectrum [see optical spectrum of **21**·$(HCl)_2$ on the cover of this Issue]. Demetalation of **21** gave a stable metal-free porphyrin trimer which undergoes two reversible, spectroscopically distinct protonation steps. As shown by X-ray crystallography, protonation takes place first on the two bookend moieties to yield a green tetraprotonated species.[53] The two inner hydrogen atoms of the central porphyrin were located on the non-fused diethylpyrrolic moieties. Upon addition of excess acid a red hexaprotonated species was obtained which featured a split Soret band (429, 510 nm) and two broad Q bands (664, 820 nm). The metal free trimeric fused porphyrin shows a very intense fluorescence band with a maximum at 775 nm. The very short Stokes shift observed could lead, by analogy with the monomeric porphyrin, to the attribution of this band to the lowest π–π* transition. Such an intense band is quite rare in the 750–900 nm range, so

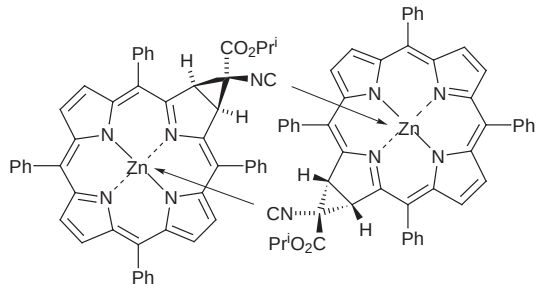

19

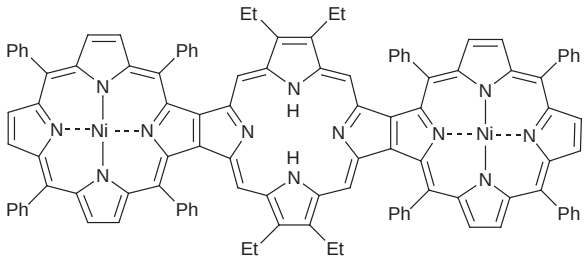

21

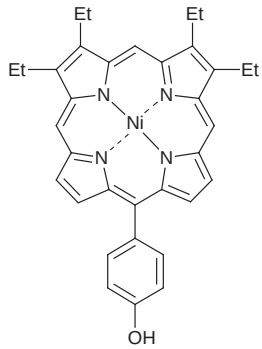

22

the fused trimer could be a good reference for measuring quantum yields in this spectral region.[53]

Supramolecular arrays

Spontaneous generation of higher order structures is a major goal in supramolecular chemistry, and self-assembly concepts have been widely applied to rigid polynucleating porphyrin-based ligands in order to mimic light harvesting and electron transport systems. Many photoactive supramolecular assemblies are based upon the peripheral coordination of *meso*-pyridyl groups to transition metals[54] or on their coordination to the central metal ion of a porphyrin.[55] As a recent example, a palladium mediated peripheral assembly of twenty one components [*i.e.* four di(4-pyridyl)porphyrins, four tri(4-pyridyl)porphyrins, one tetra(4-pyridyl)porphyrin and twelve $PdCl_2$ units] resulted in a nonameric square planar porphyrin array.[54] Self-assembled arrays occur through the coordination of the central metal ion by a β-functional group afforded head-to-tail dimeric,[48,56] trimeric,[57] hexameric[50] or polymeric species.[56] Other supramolecular analogues of the photosynthetic special pair have been prepared by inducing the intermolecular aggregation of two tetra(alkylammonio)porphyrins *via* binding their ammonium moieties within the cavities of four ditopic crown ethers.[58] Multiple hydrogen bonding has been employed in the construction of organized porphyrin arrays,[59] but their low kinetic stability ultimately limit their study as well as their use. In the case of double decker or triple decker metal-

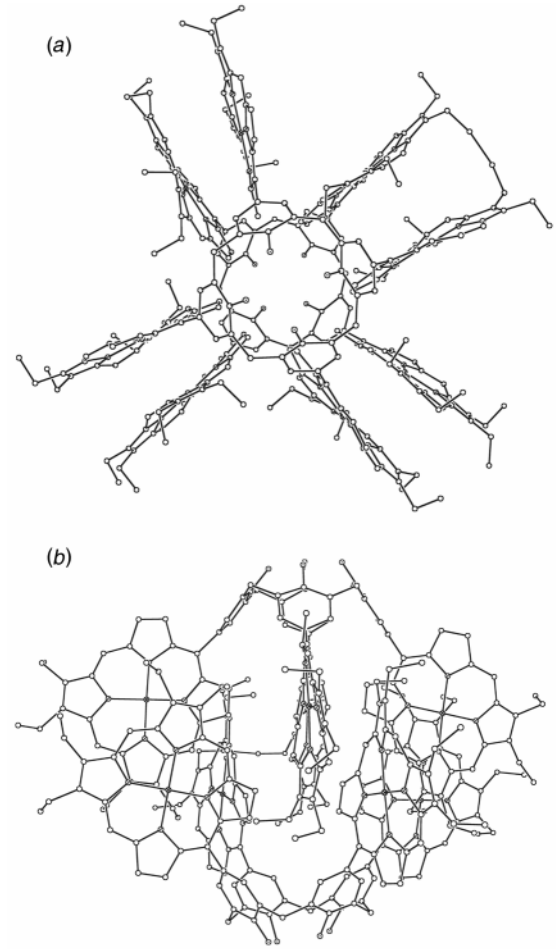

Fig. 12 Molecular structure of aggregated Ni^{II} calix[4]arenoporphyrin (**23**) dimer (hydrogen atoms not shown); (*a*) top view, (*b*) side view.

loporphyrinoids, the coordinated metal ions, usually from the lanthanide series, act as the bridging units.[60]

The design of complex three dimensional arrays *via* the use of building blocks displaying electronic and structural information enticing a covalent self-assembly process is less common. We felt that applying known macrocylization reactions to suitably functionalized porphyrinoids could lead to covalent supramolecular assemblies which are stable, both thermodynamically and kinetically. Our approach to the construction of such arrays with highly organized cavities was based on the redox reactivity of 15-substituted oxophlorins,[61] or the use of a *covalent template* strategy (since up to eight new covalent bonds could be formed in a predefined manner) based on the condensation of phenolic porphyrins into a calix[*n*]arene molecular platform.[62]

Combination of calix[4]arenes, which possess strong ion binding properties, with an organized array of pH-dependent photoactive chromophores can lead to the development of efficient sensor agents. Condensation of a *meso*-(*p*-hydroxyphenyl)porphyrin with formaldehyde under selective alkaline conditions may potentially afford calix[4], [6] or [8]arenoporphyrins. We first targeted a calix[4]arenoporphyrin and adopted the Zinke–Cornforth procedure with minor modifications. To minimize steric congestion among adjacent porphyrins and to increase the solubility of the final product, a porphyrin with unsubstituted β-positions on its upper half and β-ethyl groups on its lower half was targeted. Vilsmeier bisformylation of 5-(*p*-methoxyphenyl)dipyrromethane in refluxing CH_2Cl_2 gave the corresponding 1,9-diformyldipyrromethane, which upon acidic condensation with 2,3,7,8-tetraethyldipyrromethane afforded *p*-(12,13,17,18-tetraethylporphyrin-5-yl)anisole in moderate yield. This MacDonald-type (*i.e.* '2 + 2') condensation was successful only when the β-unsubstituted upper moiety bore the bridging formyl groups. After BBr_3 demethylation and metalation of the nitrogen core, *p*-substituted phenol **22** was obtained

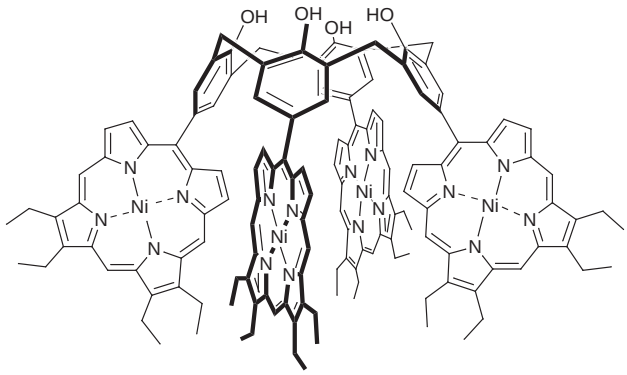

23

and refluxed in dioxane in the presence of NaOH and formaldehyde, affording mono- and di-benzyl alcohol porphyrins. The crude mixture was then refluxed in diphenyl ether to give the calix[4]arenoporphyrin **23** (purified on Sephadex). The calix[4]arenoporphyrin adopted the cone conformation, a motif prevalent in calix[4]arenes which is stabilized by a cyclic array of intramolecular hydrogen bonds among OH groups. For the solid state, this was shown by X-ray diffraction studies. Figure 12 shows the interactions which exist between two neighboring molecules of calix[4]arenoporphyrin and fully explains the preferential cone conformation over other possible conformations such as the 1,2- or 1,3-alternate. It is apparent that the preference for the cone conformation is related more to a unique π-stabilized dimerization process rather than intramolecular hydrogen bonding at the phenolic head of the molecule; very strong π-stacking interactions are the key feature in the molecular recognition of two calix[4]arenoporphyrin molecules leading to a unique non-covalent cogwheeled array of eight porphyrins. Although an AB type pattern for the benzylic methylene protons characteristic of a fixed cone conformation was not clearly identified, the broad NMR signals, which were only marginally temperature dependent, attest of the persistence of such an aggregated dimeric form in solution. Functionalization of the upper rim and a decrease in hydrogen bonding could favor an aggregation network based on a 1,3-alternate conformation.

Our second strategy toward the synthesis of covalent supramolecular arrays relied on the propensity of oxophlorins (5-oxyporphyrins) to form, upon light induced aerial oxidation, fairly stable π-neutral radicals in which dimerization results in the formation of a carbon–carbon bond between two sp^3 *meso* carbons, sited opposite to the carbonyl group (*i.e.* at the 15-position).[63] In order to alter the oxidation potential, the spin distribution of the π-neutral radical, and the dimerization process, we synthesized 15-substituted oxophlorins, *via* a '2 + 2' condensation of 1,9-diformyldipyrroketones with 5-substituted (ethyl, aryl, porphyrin-5-yl, corrol-10-yl) dipyrromethanes in acid.[61] The ethyl substituent induced a steric stabilization of a novel non-aromatic, non-redox active tautomeric species of oxophlorins (*i.e.* 15-iso-oxophlorin) because the resulting loss in aromatic stabilization is largely overcome by a decrease in the steric congestion at the 15-position introduced by a sp^3 hybridized carbon atom.[61] Upon complexation with zinc(II), these 15-iso-oxophlorins formed a doubly oxo-bridged head to tail dimer, placing the two macrocycles within π–π contact. Formation of the π-neutral radical of 15-substituted oxophlorins with air occurred spontaneously in solution in the case of electron-donating substituents and led to the formation of dimeric species. The presence of two

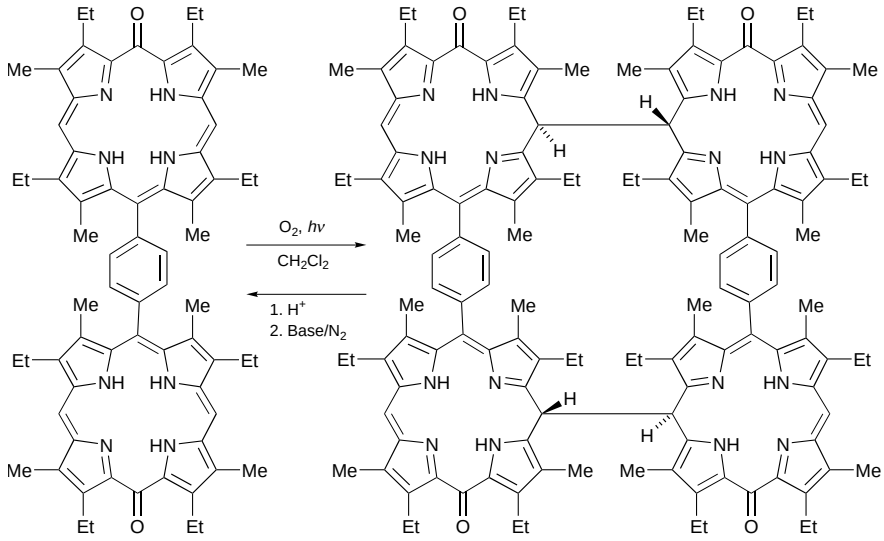

24 **25**

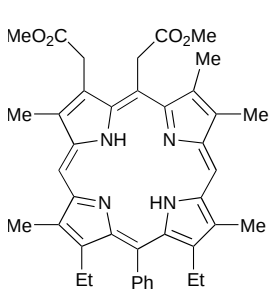

26

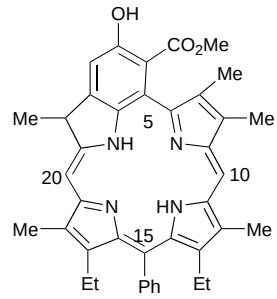

27

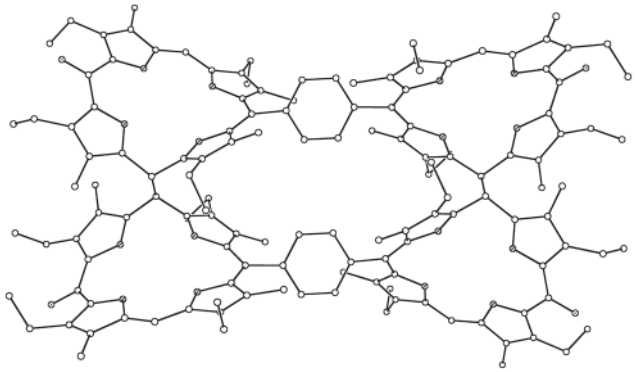

Fig. 13 Molecular structure of dimerized bis-oxophlorin **25** (hydrogen atoms not shown).

regioisomers (with regard to the orientation of the carbonyl groups) resulting from the dimerization demonstrated that 15-substituted oxophlorins dimerize at the 10,10′-positions. Although no attempts were made to separate these regioisomers, spontaneous resolution occurred during the growth of individual single crystals, as shown by the molecular structures of ethyl and phenyl 15-substituted dimers. Introduction of electron-withdrawing groups such as a pentafluorophenyl efficiently minimizes the spontaneous formation of oxophlorin π-radicals. Radical formation could be mediated with a mild oxidant such as $K_3Fe(CN)_6$ in THF, and 15-(pentafluorophenyl)oxophlorins were shown to dimerize with this kind of encouragement, in high yield.

Having established the redox activity of 15-substituted oxophlorins, we used their self-assembly to prepare various tetrameric arrays of chromophores.[61] Bis-oxophlorin **24** was prepared by condensation of 1,9-diformyldipyrroketone with a symmetrical 1,4-bis(dipyrromethan-5-yl)benzene in TFA. A daylight-induced oxidative coupling of bis-oxophlorin **24** afforded, in very high yield, a cyclic macromolecule **25** consisting of four iso-oxophlorin-like subunits arranged in a stereochemically unique *trans*,*trans*,*trans* fashion at the bridging 10,10′-positions (Fig. 13). The molecular structure of **25** showed an overall helical structure with disordered molecules of *n*-hexane fitting into the groove of the helix (not shown). The stereochemistry of the self-assembly process of the achiral components can be controlled by the insertion of a methoxy group at the 10-position of the bis-oxophlorin precursor (when prepared in MeOH–CH_2Cl_2, TsOH) resulting in a tetrameric array possessing a "stepped" structure with a *trans*,*cis*,*trans* orientation at the 10,10'-bridges. Whereas aromatic porphyrins display extremely shielded central nitrogen protons, these iso-oxophlorin species have an interrupted conjugation pathway and feature ^{1}H NMR peaks characteristic of a non-aromatic chromophore, with D_2O/Et_3N exchangeable NH peaks around 13 ppm. Addition of acid (TFA) to all these dimeric and tetrameric species reverses quantitatively the oligomerization process to form the oxophlorin dications as shown by the clean isosbestic points in spectrophotometric studies and by X-ray crystallography. Neutralization drives again the oxidative self-assembly. This overall process involves a very facile redox couple. Owing to the reversible, high yielding self-assembly behaviour of these oxophlorin species, we term this strategy *radical capture* and stress that it represents a unique approach towards the design and synthesis of covalently linked supramolecular assemblies. To further explore radical processes as a generic strategy, we turned our attention to adjacent *meso*,β-bis(methoxycarbonylmethyl)porphyrins.[64] Such porphyrins (*e.g.* **26**) when adsorbed on CH_2Cl_2-moistened silica gel gave the Dieckmann-like cyclized β-keto ester **27** which dimerized at the 20-position *via* the intermediacy of a delocalized π-radical. Any porphyrinoid system that possesses structural features which can efficiently form a stabilized π-radical (*e.g.* the carbonyl oxygen in oxophlorins, or the phenolic moiety in **27**) should undergo oxidative chemistry leading potentially to oligoporphyrin arrays.

Conclusions

It seems clear, from the work of our group and others, that past dramatic advances in the synthesis of monomeric porphyrin systems have brought us to the point where combination strategies for preparation of oligomeric porphyrin arrays are now not only possible, but are being actively exploited. When one combines the unparalleled redox, photochemical, spectroscopic, metal chelation/ligand binding, and catalytic properties of our favorite chromophore with the potential for assembling these molecules to give interactive arrays, one can only conclude that the future for research in this area is unbounded.

Acknowledgements

The research from UC Davis reported in this review was generously supported by the National Science Foundation (CHE-96-23117) and the National Institutes of Health (HL-22252). We are grateful to Dr Daniel J. Nurco for preparation of the Figures presented in this review.

Notes and references

1 K. M. Smith, in *The Porphyrin Handbook*, ed. K. M. Kadish, K. M. Smith and R. Guilard, Academic Press, Burlington, MA, 1999, in the press.
2 J. P. Collman, *Inorg. Chem.*, 1997, **36**, 5145.
3 A. Hamilton, J.-M. Lehn and J. L. Sessler, *J. Am. Chem. Soc.*, 1986, **108**, 5158; V. Kral, A. Andrievsky and J. L. Sessler, *J. Chem. Soc., Chem. Commun.*, 1995, 2349.
4 (*a*) J. P. Allen, G. Feher, T. O. Yeates, D. C. Rees, J. Deisenhofer, H. Michel and R. Huber, *Proc. Natl. Acad. Sci. U.S.A.*, 1986, **83**, 8589; (*b*) G. McDermott, S. M. Prince, A. A. Freer, A. M. Hawthorne-Lawless, M. Z. Papíz, R. J. Cogdell and N. W. Isaacs, *Nature (London)*, 1995, **374**, 517; J. Koepke, X. Hu, C. Muenke, K. Schulten and H. Michel, *Structure*, 1996, **4**, 581.
5 M. G. H. Vicente and K. M. Smith, *J. Org. Chem.*, 1991, **56**, 4407.
6 M. O. Senge, K. R. Gerzevske, M. G. H. Vicente, T. P. Forsyth and K. M. Smith, *Angew. Chem. Int. Ed. Engl.*, 1993, **32**, 750.
7 M. O. Senge, M. G. H. Vicente, K. R. Gerzevske, T. P. Forsyth and K. M. Smith, *Inorg. Chem.*, 1994, **33**, 5625.
8 G. V. Ponomarev, V. V. Borokov, K. Sugiura, Y. Sakata and A. M. Shul'ga, *Tetrahedron Lett.*, 1993, **34**, 2153.
9 A. M. Shul'ga and G. V. Ponomarev, *Khim. Geterotsikl. Soedin.*, 1988, 276.
10 T. E. Clement, D. J. Nurco and K. M. Smith, *Inorg. Chem.*, 1998, **37**, 1150.
11 L. Jaquinod, D. J. Nurco, C. J. Medforth, R. K. Pandey, T. P. Forsyth, M. M. Olmstead and K. M. Smith, *Angew. Chem., Int. Ed. Engl.*, 1996, **35**, 1013.
12 C. K. Chang and I. Abdalmuhdi, *Angew. Chem., Int. Ed. Engl.*, 1984, **23**, 164; C. K. Chang and I. Abdalmuhdi, *J. Org. Chem.*, 1983, **48**, 5388.
13 J. P. Collman, J. E. Hutchison, M. A. Lopez, A. Tabard, R. Guilard, W. K. Seok, J. A. Ibers and M. L'Her, *J. Am. Chem. Soc.*, 1992, **114**, 9869; R. Guilard, M. A. Lopez, A. Tabard, P. Richard, C. Lecomte, S. Brandes, J. E. Hutchison and J. P. Collman, *J. Am. Chem. Soc.*, 1992, **114**, 9877.
14 A. Osuka, S. Nakajima, T. Nagata, K. Maruyama and K. Toriumi, *Angew. Chem., Int. Ed. Engl.*, 1991, **30**, 582.
15 J. P. Collman, D. A. Tyvoll, L. L. Chng and H. T. Fish, *J. Org. Chem.*, 1995, **60**, 1926.
16 J. P. Collman, P. Denisevich, Y. Konai, M. Marrocco, C. Koval and F. C. Anson, *J. Am. Chem. Soc.*, 1980, **102**, 6027; S. S. Eaton, G. R. Eaton and C. K. Chang, *J. Am. Chem. Soc.*, 1985, **107**, 3177.
17 K. H. Neumann and F. Vögtle, *J. Chem. Soc., Chem. Commun.*, 1988, 520; M. Kreysel and F. Vögtle, *Synthesis*, 1992, 733.
18 R. Paolesse, R. K. Pandey, T. P. Forsyth, L. Jaquinod, K. R. Gerzevske, D. J. Nurco, M. O. Senge, S. Licoccia, T. Boschi and K. M. Smith, *J. Am. Chem. Soc.*, 1996, **118**, 3869.
19 R. K. Pandey, T. P. Forsyth, K. R. Gerzevske, J. J. Lin and K. M. Smith, *Tetrahedron Lett.*, 1992, **33**, 5315.
20 R. Cosmo, C. Kautz, K. Meerholz, J. Heinze and K. Müllen, *Angew. Chem., Int. Ed. Engl.*, 1989, **28**, 604.
21 J. L. Sessler, J. Hugdahl and M. R. Johnson, *J. Org. Chem.*, 1986, **51**, 2838; J. L. Sessler, M. R. Johnson, S. E. Creager, J. C. Fettinger and J. A. Ibers, *J. Am. Chem. Soc.*, 1990, **112**, 9310.
22 D. Heiler, G. McLendon and P. Rogalskyj, *J. Am. Chem. Soc.*, 1987, **109**, 604.

23 I. Tabushi and T. Sasaki, *Tetrahedron Lett.*, 1982, **23**, 1913.
24 O. Wennerström, H. Ericsson, I. Raston, S. Svensson and W. Pimlott, *Tetrahedron Lett.*, 1989, **30**, 1129.
25 K. Maruyama, T. Nagata, N. Ono and A. Osuka, *Bull. Chem. Soc. Jpn.*, 1989, **62**, 3167.
26 A. Osuka, S. Marumo, K. Maruyama, N. Mataga, Y. Tanaka, S. Taniguchi, T. Okada, I. Yamazaki and Y. Nishimura, *Bull. Chem. Soc. Jpn.*, 1995, **68**, 262.
27 N. Ono, H. Tomita and K. Maruyama, *J. Chem. Soc., Perkin Trans. 1*, 1992, 2453.
28 A. K. Burrell and D. L. Officer, *Synlett*, 1998, 1297.
29 V. S.-Y. Lin and M. J. Therien, *Chem. Eur. J.*, 1995, **1**, 645.
30 H. L. Anderson, S. J. Martin and D. D. C. Bradley, *Angew. Chem., Int. Ed. Engl.*, 1994, **33**, 655.
31 R. W. Wagner, J. Seth, S. I. Yang, D. Kim, D. F. Bocian, D. Holten and J. S. Lindsey, *J. Org. Chem.*, 1998, **63**, 5042.
32 S. Anderson, H. L. Anderson and J. K. M. Sanders, *J. Chem. Soc., Perkin Trans. 1*, 1995, 2247.
33 R. G. Khoury, L. Jaquinod and K. M. Smith, *Chem. Commun.*, 1997, 1057.
34 H. L. Anderson, *Inorg. Chem.*, 1994, **33**, 972.
35 K. Susumu, T. Shimidzu, K. Tanaka and H. Segawa, *Tetrahedron Lett.*, 1996, **37**, 8399.
36 A. Osuka and H. Shimidzu, *Angew. Chem., Int. Ed. Engl.*, 1997, **36**, 135.
37 T. Ogawa, Y. Nishimoto, N. Yoshida, N. Ono and A. Osuka, *Chem. Commun*., 1998, 337.
38 T. Ogawa, Y. Nishimoto, N. Yoshida, N. Ono and A. Osuka, *Angew. Chem., Int. Ed*., 1999, **38**, 176.
39 L. Ruhlmann, S. Lobstein, M. Gross and A. Giraudeau, *J. Org. Chem.*, 1999, **64**, 1352.
40 M. R. Wasielewski, D. G. Johnson, M. P. Niemczyk, G. L. Gaines III, M. P. O'Neil and W. A. Svec, *J. Am. Chem. Soc.*, 1990, **112**, 6482.
41 G. Zheng, R. K. Pandey, T. P. Forsyth, A. N. Kozyrev, T. J. Dougherty and K. M. Smith, *Tetrahedron Lett.*, 1997, **38**, 2409.
42 L. Jaquinod, M. O. Senge, R. K. Pandey, T. P. Forsyth and K. M. Smith, *Angew. Chem., Int. Ed. Engl.*, 1996, **35**, 1840.
43 M. J. Crossley, L. J. Govenlock and J. K. Prashar, *J. Chem. Soc., Chem. Commun.*, 1995, 2379.
44 N. Kobayashi, M. Numao, R. Kondo, S.-I. Nakajima and T. Osa, *Inorg. Chem.*, 1991, **30**, 2241.
45 M. G. H. Vicente, M. T. Cancilla, C. B. Lebrilla and K. M. Smith, *Chem. Commun.*, 1998, 2355.
46 D. H. R. Barton, J. Kervagoret and S. Z. Zard, *Tetrahedron*, 1990, **46**, 7587.
47 B. Krattinger, D. J. Nurco and K. M. Smith, *Chem. Commun.*, 1998, 757.
48 L. Jaquinod, C. Gros, M. M. Olmstead, M. Antolovitch and K. M. Smith, *Chem. Commun.*, 1996, 1475.
49 K. M. Shea, L. Jaquinod and K. M. Smith, *J. Org. Chem.*, 1998, **63**, 7013.
50 S. Knapp, J. Vasudevan, T. J. Emge, B. H. Arison, J. A. Potenza and H. J. Schugar, *Angew. Chem., Int. Ed.*, 1998, **37**, 2368.
51 C. Gros, L. Jaquinod, R. G. Khoury, M. M. Olmstead and K. M. Smith, *J. Porphyrins Phthalocyanines*, 1997, **1**, 201.
52 L. Jaquinod, O. Siri, R. G. Khoury and K. M. Smith, *Chem. Commun.*, 1998, 1261.
53 L. Prodi, L. Jaquinod, R. Paolesse, D. J. Nurco and K. M. Smith, unpublished results.
54 C. M. Drain, F. Nifiatis, A. Vasenko and J. D. Batteas, *Angew. Chem., Int. Ed.*, 1998, **37**, 2344.
55 K. Funatsu, T. Imamura, A. Ichimura and Y. Sasaki, *Inorg. Chem.*, 1998, **37**, 4986.
56 J. Wojaczynski and L. Latos-Grazynski, *Inorg. Chem.*, 1996, **35**, 4812.
57 A. K. Burrel, D. L. Officer, D. C. W. Reid and K. Y. Wild, *Angew. Chem., Int. Ed.*, 1998, **37**, 114.
58 M. C. Feiters, M. C. T. Fyfe, M.-V. Martinez-Dia, S. Menzer, R. J. M. Nolte, J. F. Stoddart, P. J. M. van Kan and D. J. Williams, *J. Am. Chem. Soc.*, 1997, **119**, 8119.
59 C. M. Drain, K. C. Russel and J.-M. Lehn, *Chem. Commun.*, 1996, 337.
60 D. Chabach, A. Decian, J. Fischer and R. Weiss, *Angew. Chem., Int. Ed. Engl.*, 1996, **35**, 898.
61 R. G. Khoury, L. Jaquinod, D. J. Nurco, R. K. Pandey, M. O. Senge and K. M. Smith, *Angew. Chem., Int. Ed. Engl.*, 1996, **35**, 2496; R. G. Khoury, L. Jaquinod, R. Paolesse and K. M. Smith, *Tetrahedron*, 1999, **55**, 6713.
62 R. G. Khoury, L. Jaquinod, K. Aoyagi, M. M. Olmstead, A. J. Fisher and K. M. Smith, *Angew. Chem., Int. Ed. Engl.*, 1997, **36**, 2497.
63 A. L. Balch, B. C. Noll, S. M. Reid and E. P. Zovinka, *J. Am. Chem. Soc.*, 1993, **115**, 2531.
64 R. T. Holmes, J. J. Lin, R. G. Khoury, C. P. Jones and K. M. Smith, *Chem. Commun.*, 1997, 819.

Paper 9/02334H

ChemComm

A quantitative UV–VIS probe of enantioselectivity in metalloporphyrin catalyzed oxygenation using aluminium model complexes

James P. Collman,* Zhong Wang, Christian Linde, Lei Fu, Louis Dang and John I. Brauman*

Department of Chemistry, Stanford University, Stanford, California 94305-5080, USA.
E-mail: jpc@chem.stanford.edu

Received (in Bloomington, IN, USA) 24th May 1999, Accepted 29th July 1999

UV–VIS spectroscopy is used to study the selective binding of enantiomeric pairs of chiral epoxides to an αααββ binaphthyl-strapped Al porphyrin; the binding selectivity correlates to the enantioselectivity in the epoxidation of alkenes catalyzed by its Fe analog.

Catalytic asymmetric epoxidation and hydroxylation constitute appealing strategies for synthesizing optically active organic compounds.[1] Much effort has been devoted to the design and preparation of catalysts with novel chiral structures in order to generate good enantioselectivity. Although efficient methods have been developed for asymmetric epoxidation of allylic alcohols,[2] enantioselective epoxidation of unfunctionalized alkenes and hydroxylation of simple alkanes, in general, have been less successful.[3] Owing to the lack of directing functional groups, only weak non-bonding interactions can be used to induce enantioselectivity in oxygenation of unfunctionalized alkenes and alkanes. Evaluating the energy differences of these weak interactions and predicting the enantioselectivity have been virtually impossible.

A paramagnetic NMR relaxation technique was recently used to study the complexation of epoxides to a chiral Cu porphyrin,[4] and correlation was found between the favorable mode of epoxide binding and the direction of chiral induction in the epoxidation. This experiment suggested that the transition state of oxygen transfer in metalloporphyrin-catalyzed epoxidations resembles the product epoxide bound to the metalloporphyrin. However, this method provides no information on the *degree* of chiral induction (*i.e.* the enantiomeric excess of the epoxidation reaction), which is critical for evaluating the efficiency of a chiral catalyst and designing systems with improved selectivity. Herein we present the first quantitative method to probe enantioselectivity in metalloporphyrin-catalyzed oxygenations, by studying the complexation of oxygenation products to an aluminium porphyrin using UV–VIS spectroscopy. This method allows for quantitative measurement of the binding constants of a pair of epoxide or alcohol enantiomers to the Al center. The relative binding selectivity correlates to the enantioselectivity observed in Fe porphyrin catalyzed epoxidation and hydroxylation.

Porphyrins H_2–**1**, Al–**1** and Fe–**1** (Fig. 1) were synthesized by condensing the corresponding ααββ-tetrakis(*o*-aminophenyl)-porphyrin with a binaphthyl diacid chloride. The Fe complex efficiently catalyzes the epoxidation of unfunctionalized alkenes with high enantioselectivity for simple terminal alkenes.[5] The ^{1}H NMR spectrum of Al–**1** shows two sets of resonances for the protons on the two sides of the porphyrin, reflecting a five-coordinate Al center and the resulting disruption of C_2 symmetry. Reversible binding of O or N ligands to this complex gives a distinct red shift in the Q-band region of UV–VIS spectra. This is a useful feature that allows us to conduct ligand titrations and to measure the complexation constants for different ligands.[6] The UV–VIS titration with enantiomerically pure (*S*)- and (*R*)-styrene oxides† in CH_2Cl_2 shows that Al–**1** preferentially binds (*S*)-styrene oxide, which is the major enantiomer obtained in Fe–**1** catalyzed epoxidation of styrene. The binding constants of (*S*)- and (*R*)-styrene oxide to Al–**1** are K_S = 14 dm^3 mol^{-1} and K_R = 1 dm^3 mol^{-1} [eqn. (1) and (2)].‡

This suggests that the (styrene oxide)–Al–**1** complex is a good transition state analog of the Fe–**1** catalyzed epoxidation of styrene (Scheme 1), and that the factors governing the enantioselective binding of Al–**1** are also responsible for the facial selectivity in Fe–**1** catalyzed epoxidations.

It is significant that enantiopure samples are not necessary for this method because the binding constants for two enantiomers can be determined by performing a series of measurements using samples of varying enantiomeric purities.§ For example, the formal binding constants (K_{obs}) can be obtained with (1*R*,2*S*)/(1*S*,2*R*) = 50/50 (racemic), 70/30, and 90/10 mixtures of (1*R*,2*S*)- and (1*S*,2*R*)-*cis*-β-methylstyrene oxide. The binding constants for pure (1*R*,2*S*)- and (1*S*,2*R*)-isomers are calculated to be 0.22 and 0.96 dm^3 mol^{-1}, respectively. The more

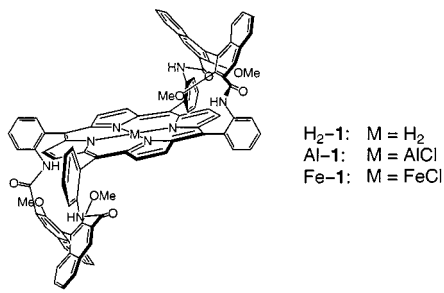

Fig. 1 Binaphthyl-strapped porphyrins.

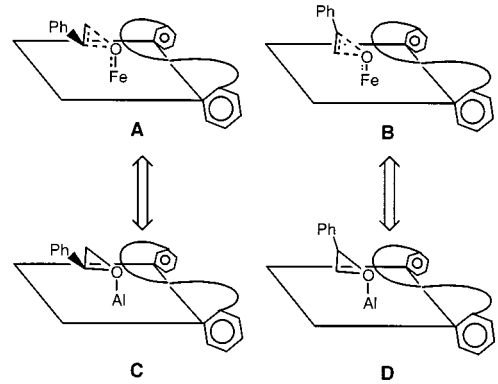

Scheme 1 Epoxide–Al–**1** complexes as epoxidation transition state analogs: **A** proposed epoxidation transition state forming (*S*)-styrene oxide (favored); **B** transition state forming (*R*)-styrene oxide (disfavored); **C** (*S*)-styrene oxide–Al–**1** complex (more stable) and **D** (*R*)-styrene oxide–Al–**1** complex (less stable). The S curve is the schematic designation of the chiral (*R*)-binaphthyl group.

Table 1 Comparison of the enantioselectivities in Al–**1** complexation and Fe–**1** catalyzed epoxidation[a]

Epoxidation product	Binding to Al–**1**		Fe–**1** catalyzed epoxidation	
	(*S*/*R*)	$\Delta\Delta G^\circ_{R-S}$/ kcal mol^{-1}	(*S*/*R*)	$\Delta\Delta G^\ddagger_{R-S}$/ kcal mol^{-1}
Styrene oxide	14.0 ± 1.7	1.56 ± 0.07	4.71 ± 0.35	0.92 ± 0.04
2-Naphthyl oxirane	4.5 ± 0.5	0.89 ± 0.06	2.43 ± 0.12	0.53 ± 0.04
cis-β-Methyl styrene oxide	4.4 ± 0.5[b]	0.88 ± 0.07	2.33 ± 0.12[b]	0.50 ± 0.04
trans-β-Methyl styrene oxide	3.2 ± 0.3[c]	0.69 ± 0.06	1.67 ± 0.08[c]	0.30 ± 0.03

[a] UV titration and epoxidation were both conducted at 298 K in CH_2Cl_2. [b] *S*/*R* = (1*S*,2*R*)/(1*R*,2*S*). [c] *S*/*R* = (1*S*,2*S*)/(1*R*,2*R*).

favorably bound enantiomer, (1*S*,2*R*)-epoxide, is again the major isomer formed in the Fe–**1** catalyzed epoxidation. The complexation constants of *cis*-β-methylstyrene oxides to Al–**1** are significantly smaller than those of styrene oxides, suggesting that steric exclusion is a major factor governing the enantiofacial selectivity in the epoxide binding. Table 1 compares the selectivities ($S/R = K_S/K_R$) of a number of epoxides obtained in ligand binding studies and Fe–**1** catalyzed epoxidations,¶ as well as the corresponding free energy differences $\Delta\Delta G^\circ$ and $\Delta\Delta G^\ddagger$, for binding and reactivity respectively. These data show that the selectivities in epoxide to Al–**1** complexation and Fe–**1** catalyzed epoxidation are in agreement, *i.e.* greater binding selectivity correlates to higher enantioselectivity in the epoxidation. A plot of $\Delta\Delta G^\ddagger$ against $\Delta\Delta G^\circ$ shows an excellent linear correlation (Fig. 2), demonstrating that the epoxide–metalloporphyrin complex can serve as a transition state model for metalloporphyrin catalyzed epoxidations.[7] The slope of *ca.* 0.6 suggests that the interaction in the epoxidation transition state is slightly less than that in the Al complex. More significantly, the quantitative correlation allows us to use Al porphyrin complexes to screen different chiral structures and substrates and predict the *degree* of enantioselectivity of epoxidation before conducting the actual reaction.

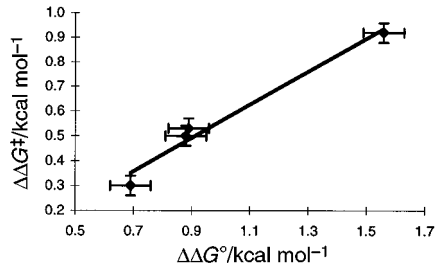

Fig. 2 Linear correlation between $\Delta\Delta G^\ddagger$ and $\Delta\Delta G^\circ$.

We have also applied this method to model the Fe porphyrin catalyzed asymmetric hydroxylation with chiral alcohol-bound Al complexes. Enantiomerically pure (*R*)- and (*S*)-*sec*-phenethyl alcohol have been used as model compounds to study ethylbenzene hydroxylation. Binding studies show that (*R*)-*sec*-phenethyl alcohol coordinates to Al–**1** more strongly than the (*S*)-alcohol by a factor of 2.1 (K_R = 16.0 dm^3 mol^{-1}, K_S = 7.4 dm^3 mol^{-1}). When we carried out the actual hydroxylation of ethylbenzene with Fe–**1** as the catalyst, we found that (*R*)-alcohol is formed preferentially, giving an enantiomeric excess of 20%. Although more data are needed to verify the correlation between the alcohol binding and hydroxylation, the qualitative agreement suggests that this UV–VIS technique can be a useful method to study the mechanism and enantioselectivity of metalloporphyrin catalyzed hydroxylation.[8,9]

In summary, we have demonstrated a UV–VIS spectroscopic method to probe the enantioselectivity in catalytic asymmetric oxygenation reactions. This technique quantifies the differential binding of enantiomers to a chiral metalloporphyrin; it not only can be used to measure the selectivity in enantiomer binding and compute the relative energy differences involved, but also can be applied to screen and predict the stereoselectivity of catalysts before carrying out the reaction. We believe the application of this technique to related fields will have a significant impact in chiral ligand design and catalyst development.

We thank the NSF (Grant No. CHE-9612725) for financial support. We also thank the Mass Spectrometry Facility, University of California, San Francisco, supported by the NIH (Grant Nos. RR 04112 and RR 01614). C. L. thanks the Royal Institute of Technology, Sweden, for a research fellowship. L. D. thanks the Bing Foundation for a summer scholarship.

Notes and references

† Aluminium porphyrin catalyzed polymerization of propylene oxide and ethylene oxide has been reported (T. Aida and S. Inoue, *Macromolecules*, 1981, **14**, 1166). However, in our experiment, no polymerization of styrene oxide was observed: both Al–**1** and styrene oxide can be recovered quantitatively after the UV titration. This is probably due to the hindered porphyrin structure which substantially slows down the polymerization or oligomerization.

‡ We have attempted to use NMR titration to determine the binding constants, but we were not able to observe distinct chemical shift changes at room temperature because of the relatively small binding constants and rapid ligand exchange on the NMR time-scale.

§ In a system involving a mixture of *R*- and *S*-ligands, the formal binding constant $K_{obs} = K_R R + K_S (1\text{-}R)$ where *R* is the percentage/100 of *R* enantiomer in the mixture. The binding constants of pure *R* and *S* isomers K_R and K_S can thus be calculated from the formal binding constants of two different samples:

$K_S = (K_{obs}'R'' - K_{obs}''R')/(R''\% - R')$

$K_R = [K_{obs}'(1 - R'') - K_{obs}''(1 - R')]/(R' - R'')$

¶ Catalyst modification occurs during Fe–**1** catalyzed epoxidation, resulting in a rise of ee in the early stages of reaction.[5] We have taken the *initial* enantioselectivities of the epoxidation, which better reflect the stereoselectivity of the original Fe catalyst.

1 I. Ojima, *Catalytic Asymmetric Synthesis*, VCH, New York, 1993; R. A. Sheldon, *Chirotechnology*, Marcel Dekker, New York, 1993.
2 K. B. Sharpless, *Janssen Chim. Acta*, 1988, **6**, 3; M. G. Finn and K. B. Sharpless, in *Asymmetric Synthesis*, ed. J. D. Morrison, Academic Press, New York, 1985, vol. 5, p.193; W. Adam and M. J. Richter, *Acc. Chem. Res.*, 1994, **27**, 57.
3 T. Katsuki, *J. Mol. Catal. A: Chem.*, 1996, **113**, 87; E. N. Jacobsen, *Asymmetric Catalytic Epoxidation of Unfunctionalized Olefins*, in *Catalytic Asymmetric Synthesis*, ed. I. Ojima, VCH, New York, 1993, pp. 159–202; Y. Tu, Z. Wang, M. Frohn, M. He, H. Yu, Y. Tang and Y. Shi, *J. Org. Chem.*, 1998, **63**, 8475; V. Schurig and F. Betschinger, *Chem. Rev.*, 1992, **92**, 873; J. T. Groves and P. Viski, *J. Org. Chem.*, 1990, **55**, 3628.
4 J. T. Groves, S. J. Crowley and K. V. Shalyaev, *Chirality*, 1998, **10**, 106.
5 J. P. Collman, Z. Wang, A. Straumanis, M. Quelquejeu and E. Rose, *J. Am. Chem. Soc.*, 1999, **121**, 460.
6 H. Tsukube, H. Furuta, A. Odani, Y. Takeda, Y. Kudo, Y. Inoue, Y. Liu, H. Sakamoto and K. Kimura, in *Comprehensive Supramolecular Chemistry*, ed. J. E. D. Davies and J. A. Ripmeester, Pergamon, Oxford, 1996, vol. 8, p. 426.
7 J. T. Groves, Y. Han and D. V. Engen, *J. Chem. Soc., Chem. Commun.*, 1990, 436; C. Linde, B. Åkermark, P.-O. Norrby and M. Svensson, *J. Am. Chem. Soc.*, 1999, **121**, 5083.
8 J. I. Manchester, J. P. Dinnocenzo, L. Higgins and J. P. Jones, *J. Am. Chem. Soc.*, 1997, **119**, 5069.
9 P. H. Toy, M. Newcomb and P. F. Hollenberg, *J. Am. Chem. Soc.*, 1998, **120**, 7719.

Communication 9/04141I

Bimodal pore systems in non-ionically templated [Si]-MSU-X mesoporous silica through biomimetic synthesis in weakly ionic solutions

Stephen A. Bagshaw

Advanced Materials Group, Industrial Research Limited, PO Box 31-310, Lower Hutt, New Zealand.
E-mail: s.bagshaw@irl.cri.nz

Received (in Cambridge, UK) 14th June 1999, Accepted 3rd August 1999

Non-ionically templated [Si]-MSU-1 mesoporous silicas have been prepared in weakly ionic sodium salt solutions from a non-ionic silica precursor and exhibit highly symmetric bimodal mesopore systems and demonstrate the immense flexibility of the non-ionic templating system.

Innovation in the synthesis of inorganic structures with novel and improved synthesis routes and structures is an area of intense international scientific and technological research. Ever since the disclosure of the M41S family of materials[1] in 1992, a veritable explosion of research effort has occurred in the area of macromolecular and micelle templating syntheses of mesostructured materials.[2] A considerable number of different synthesis approaches have now been developed, all of which possess strong philosophical similarities but are both chemically and mechanistically diverse.[3]

One of the major post M41S advances has been the discovery that non-ionic alkyl polyethylene oxide (PEO) surfactants and block co-polymers can template regular inorganic structures.[4–9] The N^0I^0,[4,5] $N^0/N^+X^-I^+$[6,7] and $N^0M^+I^-$[6] non-ionic templating routes appear to offer significant advantages over other assembly pathways. These include reproduction of structures reported in cationic systems[7] and novel structures, thicker pore walls and economic and environmental cost benefits of near ambient temperature, neutral pH and low cost, non-toxic and recoverable templates.

Biomimetic vesicular structures can form when the ionic strength of the non-ionic surfactant solution is raised from that of the pure aqueous solution through modification of the PEO–H_2O hydrogen bonding. To date such structures have only been exploited for inorganic phase formation through the application of diamine bolaform surfactants.[10] Here, we have simultaneously created biomimetic vesicle structures along with regular micelles from non-ionic alkyl-PEO surfactants in dilute electrolyte solutions† and thereby used these to direct the assembly of novel mesostructured silicas. We report, for the first time, the synthesis of inorganic silica structures that exhibit bimodal pore systems with pore diameters in the size range 3.0–9.0 nm.

Powder X-ray diffraction patterns (XRD) of a hydrothermally treated [Fig. 1(a)] and then calcined [Fig. 1(b)] sample synthesised in the presence of NaCl can be compared to XRD patterns of regular MSU-X materials.[5] The latter generally display single d_{100} reflections indicative of uniform worm-like mesopores with no long range periodicity. Two strong major reflections are observed in conjunction with a number of minor reflections at higher angles. An initial hypothesis was that these reflections were due to reflections from a novel two- or three-dimensional pore structure. Further analysis however modified this hypothesis and suggested a structure simultaneously possessing two distinct pore arrangements.

The formation of a novel structure type was supported by N_2 sorption isotherms (Fig. 2) which clearly display two distinct capillary condensation steps.[11] BJH model analysis of a material prepared in NaCl solution provides two pore diameter maxima at 3.4 and 5.2 nm (Table 1). Hysteresis is observed in the desorption branch which also exhibits two distinct, but less well separated, desorption steps. The suggestion is therefore, that two interconnected pore systems are present and that the desorption hysteresis suggests a three-dimensional pore structure.

Scanning electron micrographs (SEM) indicate elementary particles of *ca.* 0.5 μm that exhibit a general spherical morphology and some evidence for the formation of rounded extrusion-like particles. Secondary particles are aggregates of *ca.* 10–15 μm diameter. Confirmation of a double pore system was obtained from transmission electron micrographs (TEM) (Fig. 3). The micrographs show regions of extended lamellar-like features with low curvature, regions of highly ordered pores in hexagonal symmetry and regions of less ordered worm-like pore symmetry. This suggests that both vesicular and micellar aggregation types co-exist in these systems.

The effects on the synthesis of [Si]-MSU-1 materials in the presence of Na^+ electrolytes can be separated into two different effects. In the case of H^+ cation addition[6,7] some authors have proposed that the template becomes protonated and should thus

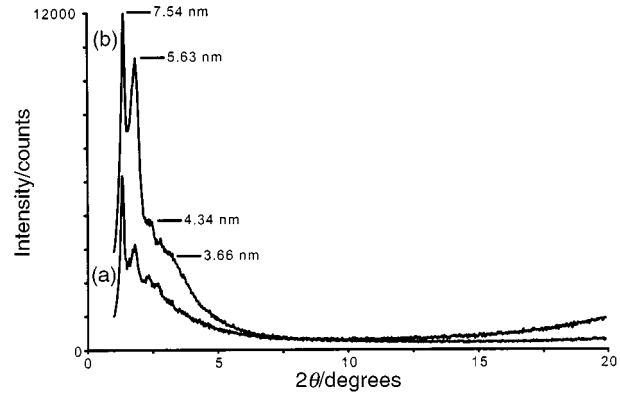

Fig. 1 XRD patterns of Brij 97 templated [Si]-MSU-1 prepared in the presence of NaCl: (a) hydrotreated at 100 °C for 72 h and (b) hydrotreated and calcined at 600 °C for 4 h.

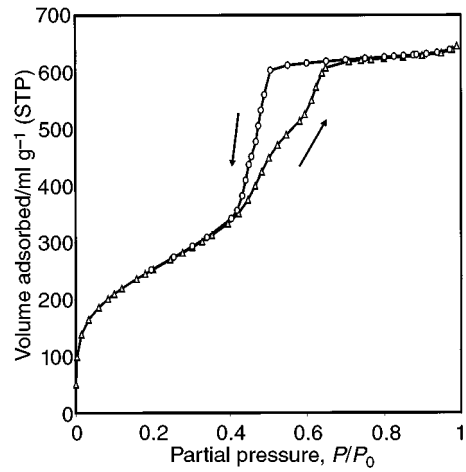

Fig. 2 Nitrogen adsorption–desorption isotherms of hydrotreated and calcined [Si]-MUS-1 prepared in the presence of NaCl.

Table 1 Properties of [Si]-MSU-1 silica samples prepared in the presence of dilute electrolytes

[Si]MSU-1 sample[a]	Electro-lyte[b]	d_{h00}[c]/nm	Pore diameter[d]/ nm	Surface area[e]/ $m^2\ g^{-1}$	Pore volume[f]/ ml g^{-1}
1	NaF	9.2, 5.3	8.7	520	1.2
2	NaCl	7.5, 5.6	5.2, 3.4	900	1.0
3	NaBr	7.9, 5.8	5.6, 3.6	810	1.1
4	NaI	8.7, 5.8	8.0	500	1.3
5	$NaSO_4$	8.5, 6.0	6.2, 3.8	880	1.2
6	$NaNO_3$	7.8, 6.0	5.8, 4.5	730	1.1
7	NaOAc	8.5, 4.9	6.7	900	1.4

[a] All samples templated with Brij 97 oleyl-EO_{10} non-ionic surfactant. [b] Sodium salts added at 5 mol% w.r.t Si. [c] ±0,1 nm [d] Pore diameters (±0.1 nm) calculated using the BJH cylinder model. (This model has recently been shown to underestimate pore diameters by up to 20%).[13] [e] Surface areas (±10 $m^2\ g^{-1}$) calculated with the BET model. [f] Pore volumes (±0.1 ml g^{-1}) calculated from $P/P_0 = 0.98$.

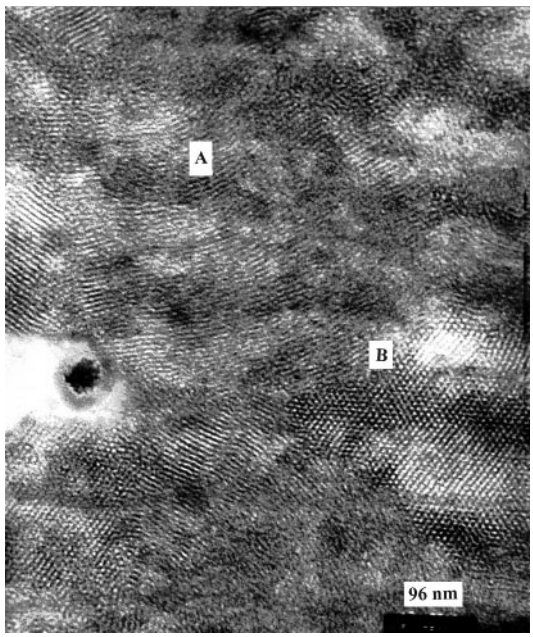

Fig. 3 Representative TEM of hydrotreated and calcined [Si]-MSU-1 prepared in the presence of NaCl showing (A) extended curved lamellar and (B) hexagonally ordered mesopores.

be labelled $N^+X^-I^+$.[7] In the system presented here, the pH of the reaction medium remains neutral and thus the assembly pathway is a true ion mediated non-ionically templated $N^0X^{+/-}I^0$ pathway. We suggest that the Na^+ cations induce the formation of vesicular systems through 'coordination' of PEO head groups, conformation extension and surface curvature decrease thereby forming vesicles. As the Na^+ concentration is 40 mol% with respect to R-PEO and each R-PEO contains 10 EO groups, only 4–8 mol% of the R-PEO surfactant will be fully Na^+ coordinated (assuming one Na^+ per one or two EO groups). Thus the remaining 96–92 mol% R-PEO surfactant will be in the normal state with regular PEO conformations forming regular micelles with greater surface curvature.

The second electrolyte effect is that of the anion which modifies not only the interaction of the tetraethyl orthosilicate (TEOS) silica precursor with the template head-group, but also the rate of hydrolysis and condensation of the TEOS. The effect of different anions in the $N^0X^{+/-}I^0$ pathway is to cause subtle changes to the final form of the mesostructures beyond the template aggregation modification caused by the cation. Fluoride addition has been previously reported[5] and remains a special case. The F^- ion possesses special chemistry that leads to very rapid TEOS condensation,[11] very small elementary particles, decreased micelle curvature and hence larger pore diameters.[5] The strong F^-/TEOS interaction appears to override any cation effects and a single pore system is formed. The other halides Cl^-, Br^- and I^- show decreasing rates of TEOS hydrolysis with increasing ionic radius. The oxy-anions SO_4^{2-}, NO_3^- and OAC^- show varying separation of the diameters of the two pore systems again with increasing ionic radius and decreasing ionisation (Table 1). ^{29}Si MAS NMR spectra indicate that anions with greater ionisation constant (*e.g.* F^-, Cl^-, SO_4^{2-}) induce more extensive hydrolysis of the TEOS and therefore more condensed and stable silica structures. Possible coordination effects by oxy-anions have not as yet been fully considered.

The results briefly outlined here provide further indications of the immense flexibility of the non-ionic alkyl-PEO templating system. They show that simple engineering of the chemistry in the synthesis medium can have profound effects on the templating mechanism and resultant porous products. This is further indication that the technological future of mesoporous materials development will lie within the PEO templating system. The exact nature of the templating system remains to be established. An investigation of the complete mechanisms through which different electrolytes (*i.e.* hard and soft cations and anions) modify the templating process is currently under investigation and will be discussed in a future contribution.

This work has been performed as part of a research contract with the New Zealand Foudnation for Science Research and Technology, contract number CO 8512.7. The author thanks Karen Reader of the Victoria University of Wellington Electron Microscopy facility for expert TEM analysis.

Notes and references

† *Experimental*: In a typical $N^0X^-I^0$ [Si]-MSU-X synthesis, a non-ionic polyethylene oxide surfactant was dissolved in distilled water at 7.5 wt%. In this study, Brij 97 (oleyl EO_{10}) surfactant was used exclusively. The temperature of the surfactant solution was raised to 40 ± 2 °C and TEOS was added under stirring to an Si: surfactant molar ratio of 8 : 1 and stirred for a predetermined time. The electrolyte, dissolved in a minimum of water was then added to the surfactant–TEOS solution at 5 mol% with respect to Si (*i.e.* 0.4 mol% w.r.t. PEO, 0.04 mol% w.r.t EO). The mixture was stirred at moderate rate, while the temperature was held at 40 ± 2 °C, over 36 h ensuring that the total aqueous volume was maintained. The white precipitate obtained was recovered by filtration, washed with distilled water and dried in air at room temperature. The dried samples were then hydrothermally treated by dispersing in distilled water and heating in a sealed polypropylene bottle at 100 °C for 72 h. The hydrothermally treated samples were recovered by filtration and dried in air at room temperature. The template was removed from the products by calcination at 600 °C in air over 4 h at a heating rate of 2 °C min^{-1}.

1 C. T. Kresge, M. E. Leonowicz, W. J. Roth, J. C. Vartuli and J. S. Beck, *Nature*, 1992, **359**, 710.
2 A. Corma, *Chem. Rev.*, 1997, **97**, 2373.
3 U. Ceisla and F. Schüth, *Microporous Mesoporous Mater.*, 1999, **27**, 131.
4 S. A. Bagshaw, E. Pouzet and T. J. Pinnavaia, *Science*, 1995, **269**, 1242.
5 E. Prouzet and T. J. Pinnavaia, *Angew. Chem., Int. Ed. Engl.*, 1997, **36**, 516.
6 S. A. Bagshaw, T. Kemmitt and N. B. Milestone, *Microporous Mesoporous Mater.*, 1998, **22**, 419.
7 D. Zhao, J. Feng, Q. Huo, N. Melosh, G. H. Freidrikson, B. F. Chmelka and G. D. Stucky, *Science*, 1998, **279**, 548.
8 S. A. Bagshaw, *Chem. Commun.*, 1999, 271.
9 L. Sierra and J.-L. Güth, *Microporous Mesoporous Mater.*, 1999, **27**, 243.
10 P. T. Tanev and T. J. Pinnavaia, *Science*, 1996, **271**, 1267.
11 S. J. Gregg and K. S. W. Sing, *Adsorption, Surface Area and Porosity*, Academc Press, London, 1982.
12 C. J. Brinker and G. W. Scherer, *Sol–Gel Science: The Physics and Chemistry of Sol–Gel Processing*, Academic Press, San Diego, 1990.
13 A. Galarneau, D. Desplantier, R. Dutartre and F. Di Renzo, *Microporous Mesoporous Mater.*, 1999, **27**, 297.

Communication 9/04751D

The first efficient bovine serum albumin catalyzed asymmetric oxidation of tertiary amines to the corresponding *N*-oxides *via* kinetic dynamic resolution

Stefano Colonna,[a] Nicoletta Gaggero,*[a] Józef Drabowicz,*[b] Piotr Łyżwa[b] and Marian Mikołajczyk[b]

[a] *Centro CNR and Istituto di Chimica Organica della Facolta di Farmacia, Universita degli Studi di Milano, via Venenzian 21, 2-133 Milano, Italy. E-mail: colonna@imiucca.csi.unimi.it*

[b] *Center of Molecular and Macromolecular Studies, Polish Academy of Sciences, 90-363 Łódź, Sienkiewicza 112, Poland. E-mail: draj@bilbo.cbmm.lodz.pl*

Received (in Cambridge, UK) 12th July 1999, Accepted 27th July 1999

Unsymmetrical teriary amines were oxidized with a few oxidants in the presence of bovine serum albumin to give the corresponding *N*-oxides of the highest optical purity ever reported (up to 66%) for the reaction of asymmetric oxidation of amines *via* their kinetic dynamic resolution.

During the last three decades chiral sulfoxides **1**[1] and phosphine oxides **2**[2] have found widespread application in the stereochemistry of heteroorganic compounds and especially in asymmetric synthesis. In a sharp contrast, the nitrogen analogues of **1** and **2**, *i.e.* chiral tertiary amine *N*-oxides **3**, are much

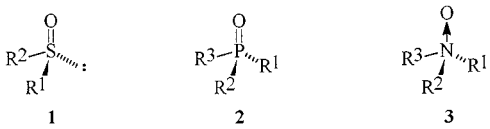

1 **2** **3**

less known and without practical use in asymmetric synthesis. This results mainly from the fact that access to optically active tertiary *N*-oxides is very limited[3] in comparison to the sulfur and phosphorus analogues. Until now a few optically active tertiary *N*-oxides of high optical purity have been obtained *via* classical resolution of the corresponding racemates. At the beginning of this century Meisenheimer[4] resolved some asymmetric *N*,*N*-dialkylarylamine oxides *via* diasteromeric salts with α-bromocamphoric acid and tartaric acids. More recently, the enantiomers of *N*-methyl-*N*-phenyl-4-methylcyclohexylamine *N*-oxide[5] and *N*-methyl-*N*-neopentyl-4-methylcyclohexylamine *N*-oxide[6] were resolved using (−)-dibenzoyltartaric acid. Very recently, Toda *et al.*[7] reported nonclassical resolution of some asymmetric *N*,*N*-dialkylarylamine *N*-oxides with optically active host compounds. Simultaneously a report[8] appeared on partial resolution of the enantiomers of *N*-benzyl-*N*-methylpropynylamine *N*-oxide using the chiracal OD and chiralpark AD CPS columns.

Asymmetric oxidation of unsymmetrical tertiary amines has also been used for the preparation of optically active *N*-oxides. However, all the reported procedures gave the required oxidation products in very low optical yield. Thus, when *N*-methyl-1,2,3,4-tetrahydroquinoline was treated[9] with percamphoric acid at −70 °C in $CHCl_3$ the corresponding *N*-oxide obtained as the hydrochloride had an ee value of only 0.6%. Similar oxidation of a series of *N*-alkyl-*N*-methylanilines produced *N*-oxides with germinal optical rotation.[10] (+)-*N*-*trans*-crotyl-*N*-ethyl-*p*-toluidine *N*-oxide having an ee of 16% was derived from the parent amine by oxidation with dibenzoyl-L-pertartaric acid.[11]

As part of our program involving biologically-mediated reactions of prochiral heteroorganic substrates[12] we became interested in the asymmetric protein catalyzed oxidation of unsymmetrical tertiary amines **4** to the corresponding optically active *N*-oxides **3**.

Our interest in this oxidation results not only from the still existing need for an efficient procedure for the preparation of optically active *N*-oxides, but mainly from the fact that this conversion fulfils at least one of the conditions which characterise an ideal dynamic kinetic resolution procedure.[13] Indeed the starting material enantiomers (tertiary amines) are always in equilibrium due to a very fast pyramidal inversion on the stereogenic nitrogen atom of the substrates.

Here we report that a number of optically active *N*-oxides **3** of considerably higher enantiomeric excess than these reported until now were obtained from the direct oxidation of the corresponding amines **4** in the presence of bovine serum albumin (BSA) [eqn. (1)]. BSA, the most abundant protein in

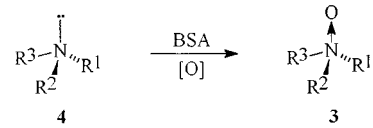

4 **3** (1)

blood plasma, acts as a transport protein and forms adducts with various kinds of hydrophoboic compounds.[14] Effective discrimination of the substituents bonded to the nitrogen atom in amine **4** should be achievable by fixing the amine in the chiral environment of BSA, thus making asymmetric induction in the subsequent oxidation possible. Here we report that BSA can be used in catalytic amounts to afford the corresponding optically active *N*-oxides. The reactions were carried out by stirring at room temperature a heterogeneous mixture of substrate (1 mmol) and oxidant (2 mmol) in the presence of BSA (0.05 mmol; the molecular weight of the BSA was taken as 66 000) in a borate buffer solution (pH 9). (These conditions were found to afford the highest enantioselectivity in the BSA—catalyzed sulfoxidation of functionalized sulfides.[12])

The results collected in Table 1 show the oxidations always produced optically active *N*-oxides in chemical yields ranging from 10% to quantitative. It should be noted that in many cases, when chemical yields are low, a substantial amount of the starting amine was recovered during the chromatographic purification of the crude reaction products. The extent of asymmetric induction was determined by ^{1}H NMR spectroscopy using optically active *tert*-butylphenylphosphinothioic acid as a chiral solvating agent.[15] Analysis of the ee values indicates that optically active *N*-oxides of high opitcal purity (*ca.* 65%) were produced in two cases (**3d** and **3e**).

Modest enantiomeric excesses were observed in other cases. In general higher selectivity is observed with increased length of the alkyl chain of *N*-alkyl-*N*-methylbenzylamine *N*-oxides. The highest ee values in the oxidation with $NaIO_4$ were observed for *n*-butyl oxide **3d** (64.6%) and *n*-pentyl homologue **3e** (63.5%). Similar behaviour has already been observed in the BSA catalyzed sulfoxidation of sulfides with $NaIO_4$[12*a*] and dioxiranes.[12*b*] In this context it was interesting to check the influence of the nature of the oxidant on the stereochemical outcome of the oxidation of amines to *N*-oxides. As a model compound amine **4e** was selected. Analysis of the observed relationship indicates that the stereoselectivity change dramatically with MCPBA as oxidant instead of $NaIO_4$, the ees being

Table 1 The bovine serum albumin catalyzed oxidation of tertiary amines $R^1R^2R^3N$ **4** to the corresponding *N*-oxides, $R^1R^2R^3N \rightarrow O$ **3**

Amine						*N*-Oxide			
4	R^1	R^2	R^3	Oxidant	*t*/h	**3**	Yield (%)	$[\alpha]_{589}$[a]	Ee[b] (%)
4a	Me	Bn	Et	$NaIO_4$	48	**3a**	35[c]	−2.5	20.0
4b	Me	Bn	Pr	$NaIO_4$	24	**3b**	30[c]	−3.9	48.5
4c	Me	Bn	Pr^i	$NaIO_4$	24	**3c**	30[c]	−3.6	41.7
4d	Me	Bn	Bu	$NaIO_4$	24	**3d**	30[c]	−4.9	64.6
4e	Me	Bn	C_5H_{12}	$NaIO_4$	42	**3e**	87	−4.8	63.5
4e	Me	Bn	C_5H_{12}	Oxone	72	**3e**	40	−3.0	40.0
4e	Me	Bn	C_5H_{12}	H_2O_2	72	**3e**	100	−7.1	66.8
4e	Me	Bn	C_5H_{12}	MCPBA	72	**3e**	100	+0.5	4.0
4f	Me	Bn	C_7H_{15}	$NaIO_4$	48	**3f**	83	−2.5	48.0
4g	Me	Ph	Et	$NaIO_4$	72	**3g**	25[c]	−3.2	18.0[d]
4h	Me	Ph	Pr	$NaIO_4$	72	**3h**	13[c]	−4.1	44.0
4h	Me	Ph	Pr	MCPBA	24	**3h**	48[c]	+0.7	10.0
4i	Me	Ph	C_5H_{12}	$NaIO_4$	72	**3i**	24	−2.1	28.0
4j	Me	*p*-Tol	Et	$NaIO_4$	60	**3j**	35[c]	−3.2	24.0[e]

[a] All rotations were measured in $CHCl_3$. [b] Determined by ^1H NMR spectroscopy with *tert*-butylphenylphosphinothioic acid as a chiral solvating agent (ref. 15). [c] Substantial amount (20–30%) of the starting amine was recovered during chromatographic purification of the produced *N*-oxide. [d] Maximum value reported for this *N*-oxide is $[\alpha]_D$ +16.4 ($CHCl_3$) (ref. 7). [e] Maximum value reported for this *N*-oxide is $[\alpha]_D$ +13.0 ($CHCl_3$) (ref. 7).

4 and 63.5%, respectively. This shows the great sensitivity of this method to changes in the reaction conditions.

In conclusion we would like to stress that although our method did not always give very high stereoselectivity, it constitutes the first procedure for effective asymmetric oxidation of unsymmetrical amines to the corresponding *N*-oxides. It also constitutes the first example of a dynamic kinetic resolution procedure, which is based on the inherent ability of the substrate enantiomers to be in equilibrium under the reaction conditions. The results presented above demonstrate moreover that the use of a catalytic amount of BSA is not limited to the oxidation of prochiral organosulfur derivatives, but can be extended to substrates containing other heteroatoms. Work is in progress to extend the applicability of this dynamic kinetic resolution procedure and to determine the absolute configuration at the nitrogen stereogenic center in the formed optically active *N*-oxides by spectroscopic techniques.

Partial financial support by the Polish Committee of Scientific Research (Grant No. 3T09A 077 14 to J. D.) is gratefully acknowledged.

Notes and references

1 M. Mikołajczyk, J. Drabowicz and P. Kiełbasiński, *Chiral Sulfur Reagents: Application in Asymmetric and Stereoselective Synthesis*, CRC Press, Boca Raton, 1997.
2 M. K. Pietrusiewicz and M. Zabłocka, *Chem. Rev.*, 1994, **94**, 1375.
3 F. A. Davis and J. R. H. Jenkins, in *Asymmetric Synthesis*, ed. J. D. Morrison, Academic Press, New York, 1983, vol. 4, pp. 346–351.
4 J. Meisenheimer, *Chem. Ber.*, 1908, **41**, 3966; J. Meisenheimer, *Ann.*, 1928, **428**, 252.
5 G. Berti and G. Belluci, *Tetrahedron Lett.*, 1964, 3853.
6 S. Goldberg and F. L. Lam, *J. Am. Chem. Soc.*, 1969, **94**, 5113.
7 F. Toda, K. Mori, Z. Stein and I. Goldberg, *Tetrahedron Lett.*, 1989, **30**, 1841.
8 M. R. Hadley, E. Švidlenka, L. A. Damani, H. G. Oldham, J. Tribe, P. Camilleri and A. J. Hutt, *Chirality*, 1994, **6**, 91.
9 J. D. Morrison and K. P. Long, unpublished results cited in J. D. Morrison and H. S. Mosher, *Asymmetric Organic Reactions*, ACS, Washington, p. 367.
10 K. Lang, *Diss. Abstr. Int. B*, 1970, **31**, 3926.
11 M. Moriwaki, Y. Yamamoto, J. Oda and Y. Inonye, *J. Org. Chem.*, 1976, **41**, 300.
12 (*a*) S. Colonna, S. Banfi, R. Annunziata and L. Casella, *J. Org. Chem.*, 1986, **51**, 891; (*b*) S. Colonna, N. Gaggero, M. Leone and P. Pasta, *Tetrahedron*, 1991, **47**, 8385; (*c*) M. Chiari, C. Ettori, P. G. Righetti, S. Colonna, N. Gaggero and A. Negri, *Electrophoresis*, 1991, **12**, 376.
13 For a recent application of the dynamic kinetic resolution strategy to asymmetric conversions, see M. M. Jones and J. M. J. Williams, *Chem. Commun.*, 1998, 2519.
14 U. Krugah-Hansen, *Pharmacol. Rev.*, 1981, **33**, 17.
15 J. Drabowicz, B. Dudiński, M. Mikołajczyk, S. Colonna and N. Gaggero, *Tetrahedron: Asymmetry*, 1997, **8**, 2267.

Communication 9/05594K

Asymmetric epoxidation of alkenes catalysed by chromium binaphthyl Schiff base complex supported on MCM-41

Xiang-Ge Zhou,[a] Xiao-Qi Yu,[a] Jie-Sheng Huang,[a] Shou-Gui Li,[b] Lian-Sheng Li[b] and Chi-Ming Che*[a]

[a] *Department of Chemistry, The University of Hong Kong, Pokfulam Road, Hong Kong. E-mail: cmche@hkucc.kku.hk*

[b] *Department of Chemistry, Jilin University, Changchun 130023, P.R. China*

Received (in Cambridge, UK) 1st July 1999, Accepted 27th July 1999

A chromium(III) binaphthyl Schiff base complex immobilised on modified MCM-41 is an effective catalyst for asymmetric epoxidation of unfunctionalised alkenes and gave significantly higher ee than the free complex.

The heterogenisation of homogeneous catalysts, which endows the homogeneous systems with attractive features such as easy product separation and catalyst recovery, constitutes a rapidly expanding research area.[1–5] Chief among various types of heterogenised catalysts are the metal complexes immobilised onto solid supports such as molecular sieves,[2,3] ion-exchange resins[4] and polymer membrance.[5] Although such immobilisation can sometimes enhance the activity of homogeneous catalysts, a common problem encountered in asymmetric catalysis is a decrease of enantioselectivity upon heterogenisation.[6] Indeed, all the heterogenised catalysts developed very recently for epoxidation of unfunctionalised alkenes exhibit considerably lower[7–10] or no higher[5,11] enantioseletivity than their homogeneous counterparts. Herein we report the alkene epoxidation with PhIO catalysed by a chromium binaphthyl Schiff base complex immobilised on MCM-41,[2] which demonstrates that the heterogenisation of a homogeneous catalyst can result in an increase of enantioselectivity for epoxidation of unfunctionalised alkenes.

The preparation of the heterogenised chromium Schiff base complex is depicted in Scheme 1.† Species **2** was characterised by IR and FAB mass spectroscopy as well as elemental analysis.‡ Based on the structures of the iron and manganese complexes,[12] the size of **2** is estimated to be 14 Å. Treatment of **2** with MCM-41(m),[13] a modified MCM-41 having a pore size of 36 Å, in CH_2Cl_2 readily led to immobilisation of **2** on the support.§ The catalyst thus obtained is designated as **2**–MCM-41(m), as indicated in Scheme 1. By varying the amount of **2** used in the immobilisation reaction, **2**–MCM-41(m) having four different contents of **2**, namely, 0.5, 0.8, 1.8 and 3.6 wt% determined on a POEMS ICP spectrometer, was obtained. The X-ray diffraction patterns of these catalysts all resemble that of MCM-41 as well as that of MCM-41(m), indicating that, after the above immobilisation treatments, the mesoporous structure of this support remains undisrupted and the molecules of **2** should be dispersed on the surface of the support. On the other hand, the FT-Raman spectrum of **2**–MCM-41(m) is similar to that of **2** if the bands belonging to MCM-41(m) are excluded. This suggests that **2** remains intact in the heterogenised catalysts.

Since the chromium centre in **2** is either five-coordinate or six-coordinate with a substitutionally labile water molecule, immobilisation of **2** onto MCM-41(m) could be readily achieved through coordination of the chromium ion to a terminal NH_2 group of the surface-bound tether *via* simple addition or ligand substitution reactions, as in the case of our recent immobilisation of ruthenium porphyrins onto the same support.[13] As might be expected, attempts to immobilise **2** onto the unmodified MCM-41, which lacks the above mentioned NH_2 groups, have failed.

The epoxidation of a series of unfunctionalised alkenes with PhIO catalysed by **2**–MCM-41(m) was carried out in toluene for 12–36 h by using 20 mg of the catalyst, 0.1 ml of substrate and 16 mg of PhIO. The reactions were monitored by GC until completion. The results are summarised in Table 1. Besides epoxides, some minor side products such as benzaldehyde or its derivatives were also detected by GC. Efforts were first directed to optimise the content of **2** in the catalysis with *p*-chlorostyrene as substrate. As is obvious from entries 1–3 and 9 in Table 1, both the yield and ee of the corresponding epoxide increase with the content of **2** until it reaches 1.8%. However, a further increase of the content of **2** results in a decrease of the yield and ee. Therefore, we used **2**–MCM-41(m) containing 1.8% of **2** for all further studies. The effect of temperature was investigated. Interestingly, a temperature decease of 20 °C led to very little change in either the yield or ee (entries 3 and 8), in contrast to the catalysis involving free **2**, in which the ee markedly increased with a decrease in temperature (entries 10 and 11). The reusability of **2**–MCM-41(m) was also examined. After the epoxidation reaction was complete, the catalyst could be recovered simply by filtration followed by washing with CH_2Cl_2. Entries 4–7 give the results obtained for reusing

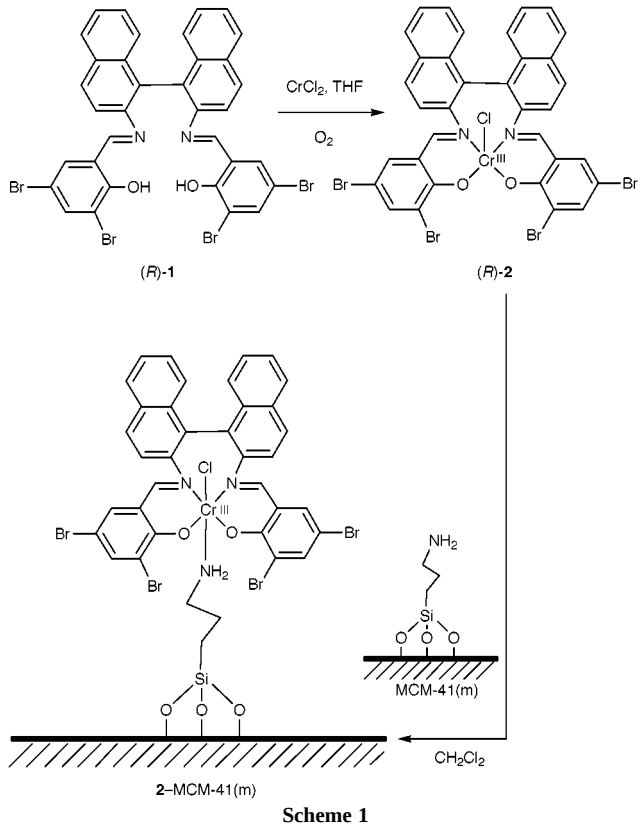

Scheme 1

Table 1 Asymmetric epoxidation of alkenes with PhIO catalysed by **2**–MCM-41(m).[a] The results obtained by using free **2**[b] (entries 10, 11, 17, 18) with *p*-chlorostyrene and *cis* β-methylstyrene are also listed

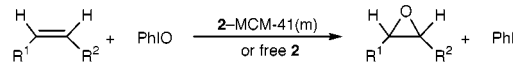

	Substrate						
Entry	R^1	R^2	Content of **2**/wt%[c]	Yield (%)[d]	Ee (%)[e]	TON	*T*/°C
1	4-ClC_6H_4	H	0.5	36	57 (*R*)	254	20
2	4-ClC_6H_4	H	0.8	42	60 (*R*)	162	20
3	4-ClC_6H_4	H	1.8	59	65 (*R*)	104	20
4[f]	4-ClC_6H_4	H		62	66 (*R*)	109	20
5[g]	4-ClC_6H_4	H		62	68 (*R*)	109	20
6[h]	4-ClC_6H_4	H		23	49 (*R*)	40	20
7[i]	4-ClC_6H_4	H		21	20 (*R*)	37	20
8	4-ClC_6H_4	H	1.8	61	67 (*R*)	110	0
9	4-ClC_6H_4	H	3.6	55	58 (*R*)	52	20
10[j]	4-ClC_6H_4	H		30	48 (*R*)	30	20
11[j]	4-ClC_6H_4	H		48	63 (*R*)	48	0
12	Ph	H	1.8	38	55 (*R*)	67	20
13	4-$CF_3C_6H_4$	H	1.8	31	63 (*R*)	55	20
14	4-FC_6H_4	H	1.8	32	56 (*R*)	56	20
15	–CH_2CH_2-1,2-C_6H_4–		1.8	26	42 (1*R*,2*S*)	46	20
16	Ph	Me	1.8	32[k]	73[l] (1*R*,2*S*)	56	20
17[j]	Ph	Me		43[k]	54[l] (1*R*,2*S*)	43	20
18[j]	Ph	Me		52[m]	62[l] (1*R*,2*S*)	52	0

[a] All reactions were performed in toluene by using 20 mg of catalyst, 0.1 ml of substrate, and 16 mg of PhIO. This gives, for example, 0.56 mol% of **2** relative to PhIO for the 1.8% content of **2**. [b] Reaction conditions: identical to those for **2**–MCM-41(m) except 1 mol% of **2** (relative to PhIO) was used. [c] The content of **2** in **2**–MCM-41(m) was determined on a POEMS ICP spectrometer. [d] Determined by GC based on the PhI formed. [e] Determined by GC with chiral column. [f] First, [g] second, [h] third, and [i] fourth reuse of **2**–MCM-41(m) containing 1.8% of **2**. After these reuses, a total of 2–3% of Cr had leached into solution. [j] Free **2** was used instead of **2**–MCM-41(m). [k] The ratio of *cis*:*trans* = 66:31. [l] *cis* Isomer. [m] The ratio of *cis*:*trans* = 91:9.

2–MCM-41(m) up to four times. Notably, this catalyst could be reused at least two times with a total turnover number of 322 (entries 3–5) without a decrease in enantioselectivity. In contrast, a recently reported Mn–MCM-41–salen catalyst suffered from a loss of enantioselectivity of 40% ee when reused for the first time.[10] Extension of the above epoxidation reaction to other substrates also gave moderate to relatively high ees at room temperature (entries 12–16). The highest ee (73%) was obtained for *cis*-β-methylstyrene (entry 16).

Surprisingly, the heterogenised **2** exhibits significantly higher enantioselectivity than free **2** under identical conditions (entry 3 *vs.* 10 or 16 *vs.* 17). For example, with *cis*-β-methylstyrene as substrate, the ee increased by as much as *ca.* 20% upon immobilisation of **2** onto MCM-41(m) (entries 16 and 17). As the support MCM-41(m) showed negligible catalytic activity toward these oxidation reactions, the increase in chiral recognition could arise from the enhanced stability of the chromium complex upon immobilisation. Alternatively, it could also result from the unique spatial environment constituted by both the chiral binaphthyl Schiff base ligand and the surface of the support. To make clear which environment, inside or outside the channels, is responsible for the enhancement of chiral induction, we immobilised **2** on another modified MCM-41 designated as MCM-41(m-in), whose external surface was passivated with Ph_2SiCl_2, thus placing the same surface-bound tether containing the terminal NH_2 groups as in MCM-41(m) inside the channels only.[14] Under the same conditions with *p*-chlorostyrene as substrate, both **2**–MCM-41(m-in) and **2**–MCM-41(m), having similar content of **2**, afforded the corresponding epoxide in almost the same yield and ee. This shows that the environment inside the channels of the support leads to the enhancement in the chiral induction.

We acknowledge support from The University of Hong Kong and the Hong Kong Research Grants Council.

Notes and references

† *Preparation* of **2**: A mixture of anhydrous chromium(II) chloride (1 mmol) and **1** (1 mmol) in THF (20 ml) was stirred under argon at room temperature for 3 h, leading to a color change from brown to green. The mixture was then left open to the air for 3 h to allow full oxidation of chromium(II) to chromium(III). After removal of the solvent, the residual solid was recrystallised from CH_2Cl_2–hexane to give the desired product as a green solid. Yield: 70%.

‡ *Spectral data* for **2**: ν_{max}(KBr)/cm^{-1}) 3443, 1603, 1507, 1430, 1302, 1207, 1160, 1072, 820, 751, 715, 688, 539; *m/z* (FAB MS) 893 (M^+), 858 ([M − Cl]$^+$) (Calc. for $C_{34}H_{18}N_2O_2Br_4CrCl\cdot 2H_2O$: C, 43.89; H, 2.37; N, 3.01. Found: C, 43.71; H, 2.58; N, 3.21%). The ^{1}H NMR spectrum of **2** is featureless due to its paramagnetism.

§ *Preparation* of **2**–*MCM-41(m)*: A mixture of **2** and MCM-41(m) (100 mg) in CH_2Cl_2 (10 ml) was stirred at room temperature for 2 h. The solid product was then collected by filtration, thoroughly washed with CH_2Cl_2, and dried under vacuum.

1 D. Brunel, N. Bellocq, P. Sutra, A. Cauvel, M. Laspéras, P. Moreau, F. D. Renzo, A. Galarneau and F. Fajula, *Coord. Chem. Rev.*, 1998, **178–180**, 1085.
2 J. Y. Ying, C. P. Mehnert and M. S. Wong, *Angew. Chem., Int. Ed.*, 1999, **38**, 56.
3 A. Choplin and F. Quignard, *Coord. Chem. Rev.*, 1998, **178–180**, 1679.
4 D. R. Leanord and J. R. Lindsay Smith, *J. Chem. Soc., Perkin Trans 2*, 1991, 25.
5 I. F. J. Vankelecom, D. Tas, R. F. Parton, V. V. de Vyver and P. A. Jacobs, *Angew. Chem., Int. Ed. Engl.*, 1996, **35**, 1346.
6 R. Noyori, *Asymmetric Catalysis in Organic Synthesis*, Wiley, New York, 1994, ch. 8, p. 346.
7 B. B. De, B. B. Lohray, S. Sivaram and P. K. Dhal, *Tetrahedron: Asymmetry*, 1995, **6**, 2105.
8 F. Minutolo, D. Pini, A. Petri and P. Salvadori, *Tetrahedron: Asymmetry*, 1996, **7**, 2293.
9 M. J. Sabater, A. Corma, A. Domenech, V. Fornés and H. García, *Chem. Commun.*, 1997, 1285.
10 P. Piaggio, P. McMorn, C. Langham, D. Bethell, P. C. Bulman-Page, F. E. Hancock and G. J. Hutchings, *New J. Chem.*, 1998, 1167.
11 S. B. Ogunwumi and T. Bein, *Chem. Commun.*, 1997, 901.
12 M.-C. Cheng, M. C.-W. Chan, S.-M. Peng, K.-K. Cheung and C.-M. Che, *J. Chem. Soc., Dalton Trans.*, 1997, 3479.
13 C.-J. Liu, W.-Y. Yu, S.-G. Li and C.-M. Che, *J. Org. Chem.*, 1998, **63**, 7364,
14 D. S. Shephard, W. Zhou, T. Maschmeyer, J. M. Matters, C. L. Roper, S. Parsons, B. F. G. Johnson and M. J. Duer, *Angew. Chem., Int. Ed.*, 1998, **37**, 2719.

Communication 9/05313A

ChemComm

Enantioselective hydroxylation of benzylic C–H bonds by D_4-symmetric chiral oxoruthenium porphyrins†

Rui Zhang, Wing-Yiu Yu, Tat-Shing Lai and Chi-Ming Che*

Department of Chemistry, The University of Hong Kong, Pokfulam Road, Hong Kong. E-mail: cmche@hku.hk

Received (in Cambridge, UK) 21st May 1999, Accepted 20th July 1999

A D_4-symmetric chiral dioxoruthenium(VI) porphyrin can effect stoichiometric and catalytic enantioselective hydroxylation of benzylic C–H bonds to give enantioenriched aryl alcohols, the highest ee of 76% being attained in the catalytic oxidation of 4-ethyltoluene with 2,6-dichloropyridine *N*-oxide as terminal oxidant; the oxidations proceed *via* a rate-limiting H-atom abstraction to germinate a benzylic radical intermediate.

Despite significant advances in asymmetric alkene epoxidations,[1] the development of protocols for highly enantioselective hydroxylations of saturated C–H bonds has met with limited success. Groves and Viski first described the catalytic enantioselective benzylic C–H bond hydroxylations using a chiral iron porphyrin catalyst.[2] Recently, with the use of chiral Mn(salen) catalysts, ethylbenzene can be oxidized enantioselectively to 1-phenylethanol in 22% yield and 53% ee.[3] We herein describe a highly enantioselective benzylic C–H bond hydroxylation based on oxoruthenium complexes supported by a D_4-symmetric chiral porphyrin.

The [Ru^{II}(Por*)(CO)(EtOH)] and [Ru^{VI}(Por*)O_2] complexes {H_2Por* = 5,10,15,20-tetrakis[(1*S*,4*R*,5*R*,8*S*)-1,2,3,4,5,6,7,8-octahydro-1,4:5,8-dimethanoanthracen-9-yl]-porphyrin} were prepared by the literature methods.[4] In a

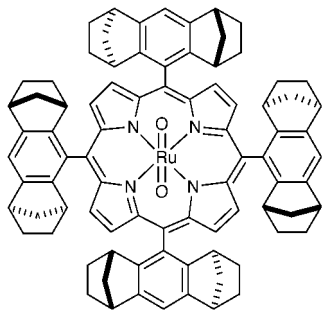

[Ru^{VI}(Por*)O_2]

degassed CH_2Cl_2 solution (containing 2% w/w pyrazole), an excess of ethylbenzene reacted with [Ru^{VI}(Por*)O_2] to afford a mixture of 1-phenylethanol (32%) and acetophenone (33%) at room temperature; the (*S*)-1-phenylethanol was obtained in 45% ee (Table 1, entry 1). This features the first well-characterized chiral oxo-metal complex capable of hydroxylating saturated C–H bonds enantioselectively. Similarly, the stoichiometric oxidations of substituted ethylbenzenes, 2-ethylnaphthalene, indane and tetrahydronaphthalene by [Ru^{VI}(Por*)O_2] also furnished enantioenriched (*S*)-alcohols, and the oxidation of 2-ethylnaphthalene registered the highest ee of 58% ee (Table 1, entry 7). In all cases, a bis-pyrazolato-ruthenium(IV) porphyrin, [Ru^{IV}(Por*)$(pz)_2$], was isolated in > 85% yield at the end of the oxidation.

† Experimental and kinetic data, including UV-vis spectral traces, dual-parameter Hammett correlation studies and representative chiral GLC chromatograms, are available from the author at the address given above.

Under pseudo-first order conditions, the ethylbenzene oxidation by [Ru^{VI}(Por*)O_2] in 1,2-dichloroethane (with 2% w/w Hpz) exhibited isosbestic UV-vis spectral changes from Ru^{VI} to Ru^{IV} porphyrin (isosbestic points at 350, 415 and 444 nm). At 313 K, the second-order rate constant (k_2) is $(7.7 \pm 0.4) \times 10^{-4}$ dm^3 mol^{-1} s^{-1}. The second-order rate constants for the oxidation of *para*-substituted ethylbenzenes had been measured, and a linear dual-parameter Hammett correlation between log k_{rel} [$k_{rel} = k_2$(4-substituted ethylbenzene)/k_2(ethylbenzene)] and the $\sigma_{JJ}^{\cdot}$ and σ_p^+ constants[5] was established: log k_{rel} = + (0.57 ± 0.04) $\sigma_{JJ}^{\cdot}$ − (0.36 ± 0.01) σ_p^+ (R = 0.99; $|\rho_{JJ}^{\cdot}/\rho^+|$ = 1.58),† consistent with a rate-limiting benzylic radical intermediate formation. The primary kinetic isotope effect (k_H/k_D) for the oxidation of ethylbenzene-d_{10} was found to be 8.9 (313 K), in accord with a rate-limiting step involving substantial C–H bond cleavage.[6]

A catalytic quantity of either [Ru^{II}(Por*)(CO)(EtOH)] or [Ru^{VI}(Por*)O_2] can effect hydroxylation of ethylbenzene using 2,6-dichloropyridine *N*-oxide (Cl_2pyNO) as terminal oxidant to produce (*S*)-1-phenylethanol in 62% yield and 72% ee at 25 °C (Table 1, entry 1). More importantly, the catalytic reactions afforded the alcohols in much higher enantioselectivity. Benzene is the solvent of choice, while the use of CH_2Cl_2 led to a lower ee of 62% (Table 1, entry 1). Likewise, other *para*-substituted ethylbenzenes were oxidized to their (*S*)-1-arylethanols in 62–76% ee and 28–72% yields under the ruthenium-catalyzed conditions (entries 2–6). Notably, the catalytic asymmetric 2-ethylnaphthalene oxidation afforded 1-naphthylethanol in 75% ee and 66% yield (Table 1, entry 7). In all cases, only alcohols and ketones were formed, and the combined alcohol and ketone yields have a mass balance of 98% of the amount of substrate consumed.

The effect of *para*-substituents on the chiral ruthenium porphyrin-catalyzed asymmetric hydroxylation of ethylbenzenes has been examined. Both electron-donating and -withdrawing substituents can promote the reaction, and the relative rate constants (log k_{rel}), established by competitive experiments, correlate linearly with the $\sigma_{JJ}^{\cdot}$ and σ_p^+ substituent constants:[5] log k_{rel} = + (0.78 ± 0.05) $\sigma_{JJ}^{\cdot}$ − (0.71 ± 0.02) σ_p^+ (R = 0.99, $|\rho_{JJ}^{\cdot}/\rho^+|$ = 1.1, Fig. 1). A primary kinetic isotope effect (k_H / k_D) of 11.2 (298 K) was found for the catalytic oxidation of ethylbenzene-d_{10}.

It is known that ruthenium porphyrin-catalyzed alkane oxidations using 2,6-dichloropyridine *N*-oxide proceed through a reactive oxoruthenium intermediate.[7] Thus, the high ee observed in the catalytic ethylbenzene hydroxylations would suggest that the chiral 'Ru=O' intermediate should preferentially abstract the *pro-S* hydrogen atom of ethylbenzene, if a hydrogen atom abstraction mechanism is operative.[2a] Because oxidation of benzyl alcohol by reactive oxoruthenium complexes involves a rate-limiting C–H bond cleavage analogous to the hydroxylation of aromatic hydrocarbons,[6d,8] the (*S*)-isomer of racemic 1-phenylethanol is expected to be more readily oxidized to acetophenone, leaving an excess of (*R*)-1-phenylethanol. However, when racemic 1-phenylethanol (1 mmol) was subjected to the ruthenium-catalyzed conditions {[Ru^{II}(Por*)(CO)(EtOH)] (0.5 μmol) and Cl_2pyNO (3 mmol) in C_6H_6}, we found that only a 4% excess of (*R*)-1-phenylethanol and 97% yield of acetophenone were produced at 42% alcohol

Table 1 Enantioselective oxoruthenium mediated benzylic hydroxylations

			$[Ru^{VI}(Por^*)O_2]$[a]			$[Ru^{II}(Por^*)(CO)(EtOH)] + Cl_2pyNO$[e]				
Entry	Substrate	Product	Alcohol yield (%)[b]	Ee (%)	Ketone yield (%)[c]	*t*/h	Conv. (%)	Alcohol yield (%)[f]	Ee (%)	Ketone yield (%)[f] (total turnovers)
1		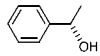	32 30[d]	45 (*S*) 37 (*S*)[d]	33 34[d]	12 12[g]	13 10[g]	62 67[g]	72 (*S*) 62 (*S*)[g]	37 (112) 32[g]
2	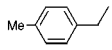	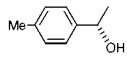	31	51 (*S*)	32	30	20	72	76 (*S*)	24 (224)
3	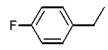	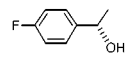	36	58 (*S*)	30	10	11	60	72 (*S*)	38 (129)
4	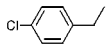	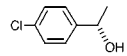	35	55 (*S*)	31	18	23	28	74 (*S*)	70 (262)
5	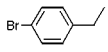	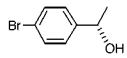	27	41 (*S*)	34	8	14	63	74 (*S*)	36 (164)
6	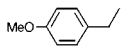	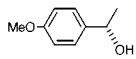	44	55 (*S*)	26	8	15	65	62 (*S*)	32 (190)
7	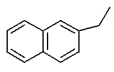	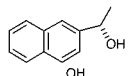	32	58 (*S*)	31	20	15	62	75 (*S*)	38 (168)
8			48	9 (*S*)	25	6	54	65	12 (*S*)	34 (551)
9			47	18 (*S*)	24	2	42	60	12 (*S*)	40 (475)

[a] Stoichiometric oxidation: to a degassed CH_2Cl_2 solution (2 cm^3) containing pyrazole (0.05 g) and alkane (1.0 mmol) was added $[Ru^{VI}(Por^*)O_2]$ (30 μmol) under argon; the mixture was then stirred at room temperature for 12 h. The ruthenium complex was removed by filtration through a short alumina column. After addition of 1,4-dichlorobenzene as internal standard, aliquots were analyzed by GLC for product identification and quantification. [b] Yields were based on the ruthenium oxidant used. [c] The ketone yields were calculated based on a stoichiometric ratio of oxidant-to-ketone = 2:1. [d] In C_6H_6. [e] Catalytic oxidations: a mixture of alkane (0.5 mmol), $[Ru^{II}(Por^*)(CO)(EtOH)]$ (0.5 μmol) and Cl_2pyNO (0.55 mmol) was stirred in dry and degassed C_6H_6 (5 cm^3). Aliquots were analyzed by chiral capillary GC equipped with J & W scientific Cyclodex-B or B-PM chiral column for quantification and ee determination. [f] Yields were based on the amount of alkane consumed. [g] In CH_2Cl_2.

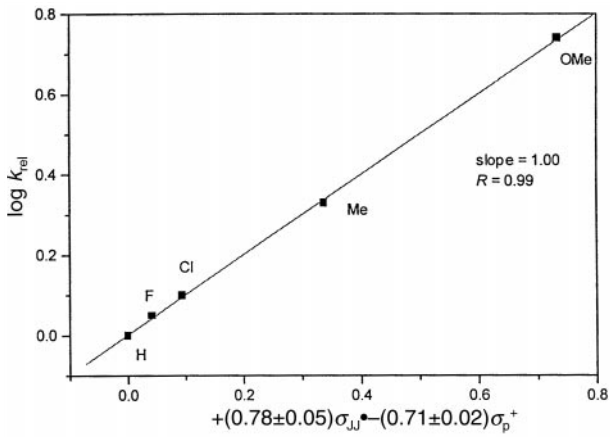

Fig. 1 Dual-parameter Hammett correlation for the ruthenium catalyzed enantioselective hydroxylation of *para*-substituted ethylbenzenes (*p*-YC_6H_4Et; Y = MeO, Me, F, Cl and H).

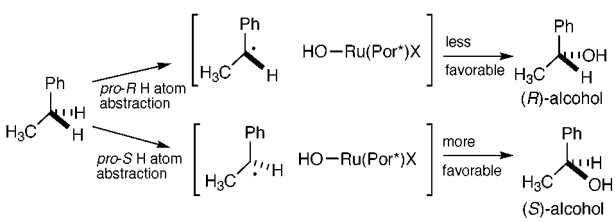

Scheme 1

consumption. The low degree of kinetic resolution for the catalytic (±)-1-phenylethanol oxidation is in constrast to the high ee of the catalytic ethylbenzene hydroxylation reactions. Assuming an oxygen rebound mechanism (Scheme 1),[9] we postulate that the production of enantioenriched alcohols may arise from the preferential collapse of the benzylic radical on the *pro-S* face *versus* the *pro-R* face at the oxygen atom rebound step, due to the good fit of the substrate into the chiral cavity.

We acknowledge financial support from The University of Hong Kong, the Hong Kong Research Grants Council and the Hong Kong University Foundation.

Notes and references

1 E. N. Jacobsen, in *Comprehensive Organometallic Chemistry II*, ed. G. Wilkinson, F. G. A. Stone, E. W. Abel and L. S. Hegedus, Pergamon, New York, 1995, vol. 12, ch. 11.1; T. Katsuki, *Coord. Chem. Rev.*, 1995, **140**, 189; D. Yang, Y.-C. Yip, M.-W. Tang, M.-K. Wong, J.-H. Zheng and K.-K. Cheung, *J. Am. Chem. Soc.*, 1996, **118**, 491; D. Yang, X.-C. Wang, M.-K. Wong, Y.-C. Yip and M.-W. Tang, *J. Am. Chem. Soc.*, 1996, **118**, 11 311.

2 (*a*) Enantioselectivity of 77% was reported for the catalytic asymmetric hydroxylation of (*S*)-(1-deuterioethyl)benzene, see: J. T. Groves and P. Viski, *J. Am. Chem. Soc.*, 1989, **111**, 8537; (*b*) J. T. Groves and P. Viski, *J. Org. Chem.*, 1990, **55**, 3628.

3 K. Hamachi, R. Irie and T. Katsuki, *Tetrahedron Lett.*, 1996, **37**, 4979.

4 T.-S Lai, R. Zhang, K.-K. Cheung, H.-L. Kwong and C.-M. Che, *Chem. Commun.*, 1998, 1583; T.-S. Lai, H.-L. Kwong, R. Zhang and C.-M. Che, *J. Chem. Soc., Dalton Trans.*, 1998, 3559; A. Berkessel and M. Frauenkron, *J. Chem. Soc., Perkin Trans. 1*, 1997, 2265.

5 X.-K. Jiang, *Acc. Chem. Res.*, 1997, **30**, 283.

6 (*a*) C.-M. Che, C. Ho and T.-C. Lau, *J. Chem. Soc., Dalton Trans.*, 1991, 1259; (*b*) C. Ho, W.-H. Leung and C.-M. Che, *J. Chem. Soc., Dalton Trans.*, 1991, 2933; (*c*) C.-M. Che, W.-T. Tang, K.-Y. Wong and C.-K. Li, *J. Chem. Soc., Dalton Trans.*, 1991, 3277; (*d*) W.-C. Cheng, W.-Y. Yu, C.-K. Li and C.-M. Che, *J. Org. Chem.*, 1995, **60**, 6840.

7 J. T. Groves, M. Bonchio, T. Carofiglio and K. Shalyaev, *J. Am. Chem. Soc.*, 1996, **118**, 8961; C.-J. Liu, W.-Y. Yu and C.-M. Che, *J. Org. Chem.*, 1998, **63**, 7364; Z. Gross and S. Ini, *Inorg. Chem.*, 1999, **38**, 1446.

8 C.-M. Che, W.-T. Tang, W.-O. Lee, K.-Y. Wong and T.-C. Lau, *J. Chem. Soc. Dalton Trans.*, 1992, 1551; L. Roecker and T. J. Meyer, *J. Am. Chem. Soc.*, 1987, **109**, 746.

9 J. T. Groves and G. A. McClusky, *J. Am. Chem. Soc.*, 1976, **98**, 859; J. T. Groves and P. Viski, *J. Am. Chem. Soc.*, 1989, **111**, 8537.

Communication 9/04100A

Regioselective 1,2-insertion of Ru into the C–S bond in 3-substituted thiophenes

Jose Giner Planas, Masafumi Hirano and Sanshiro Komiya*

Department of Applied Chemistry, Faculty of Technology, Tokyo University of Agriculture and Technology, 2-24-16 Nakacho, Koganei, Tokyo 184-8588, Japan. E-mail: komiya@cc.tuat.ac.jp

Received (in Cambridge, UK) 15th July 1999, Accepted 6th August 1999

Reactions of [Ru(cod)(cot)] 1 [cod = cycloocta-1,5-diene, cot = cycloocta-1,3,5-triene] with 3-acetyl(or formyl)thiophene and 2-acetyl(or formyl) thiophene in the presence of depe [1,2-bis(diethylphosphino)ethane] lead to completely regioselective 1,2- or 1,5-insertion into the C–S bond giving the new thiaruthenacycles [Ru(SCR=CHCR′=CH)(depe)$_2$] [R = H, R′ = COMe (2a); R = H, R′ = CHO (2b); R = COMe, R′ = H (3a); R = CHO, R′ = H (3b)], respectively.

The study of coordination and reactivity of transition metal complexes with thiophene derivatives[1] is an area of increasing interest with regard to the hydrodesulfurization (HDS) reaction of fossil fuels.[2] In this sense, electron-withdrawing substituents at the 2- or 3-position of thiophene were reported to facilitate the insertion of Rh into the less congested C–S bond.[3] In addition, when small metal fragments were used, mixtures of the 1,2- and 1,5-insertion products were generally obtained.[4] We wish to report here the completely regioselective 1,2- or 1,5-insertion reactions of [Ru(cod)(cot)] **1** with thiophenes having an electron-withdrawing substituent at the 3- or 2-position, respectively, in the presence of depe.

3-Acetylthiophene reacted with **1** in the presence of 2 equiv. of depe in toluene at room temperature for 12 h to give [Ru{SCH=CHC(COMe)=CH}(depe)$_2$] **2a**[5] in 72% yield, as a yellow solid [eqn. (1)].

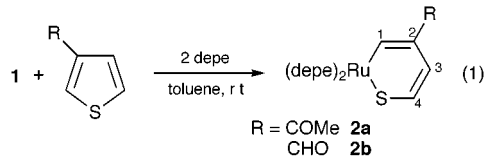

The ^{31}P{^{1}H} NMR spectrum of **2a** shows an AMNX spin system at δ 54.8, 48.5, 45.5 and 28.8 for four different phosphorous nuclei, and the ^{1}H NMR spectrum exhibits resonances for the thiaruthenacycle protons at δ 10.73 (H^1), 6.61 (H^3) and 5.90 (H^4). 3-Formylthiophene reacted in a similar way giving [Ru{SCH=CHC(CHO)=CH}(depe)$_2$] **2b** in 68% yield [eqn. (1)]. The molecular structure of **2b** was established by X-ray structure analysis (Fig. 1).[6] The ORTEP drawing clearly shows that ring cleavage occurred at the C–S bond close to the substituent in spite of the steric repulsion. The six-membered ring defined by Ru, S, C1, C2, C3 and C4 atoms is basically planar, with no atom deviating by more than 0.1 Å from their mean plane. Furthermore, the C–C distances for C1–C2, C2–C3 and C3–C4 of 1.371(9), 1.44(1) and 1.33(1), respectively, indicate bond alternation suggesting a localized diene structure.

It is remarkable that the regioselective 1,2-insertion of the very bulky Ru(depe)$_2$ fragment takes place into the C–S bond of the 3-substituted thiophene, suggesting that the electronic effect is the major controlling factor in the selectivity of the insertion.

In contrast to the above results, **1** reacted with 2-acetylthiophene to give the 1,5-insertion product [Ru{SC(COMe)=CHCH=CH}(depe)$_2$] **3a**[7] in 84% yield, as a red solid (eqn. 2).

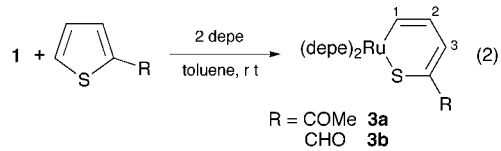

The ^{1}H NMR of **3a** shows resonances for the thiaruthenacycle protons at δ 8.36 (H^1), 7.98 (H^3) and 7.39 (H^2). Detailed analysis of coupling constants by homo-decoupling techniques indicated that protons H^1 and H^2 are coupled with the P nuclei (J_{H^1P} 18.0, 3.3 Hz and J_{H^2P} 12.3, 3.0 Hz) and between them ($J_{H^1H^2}$ 12.0 Hz), but H^3 only displays coupling with H^2 ($J_{H^2H^3}$ 7.5 Hz). A dtd resonance at δ 169.6 for C^1 in the ^{13}C{^{1}H} NMR spectrum of **3a** provides strong evidence for the formulation of the C–S insertion product. In addition, spectroscopic data of **3a** are comparable with those for the known thiaferracycle [Fe{SC(COMe)=CHCH=CH}(depe)$_2$] in which insertion also takes place into the C^5–S bond,[8] away from the substituent at the 2-position. 2-Formylthiophene reacted giving also the 1,5-insertion product [Ru{SC(CHO)=CHCH=CH}(depe)$_2$] **3b** in 36% yield [eqn. (2)]. Thus, the steric effect seems to be predominant in 2-substituted thiophenes. It is noteworthy that neither 2,5-dimethyl-3-acetylthiophene nor alkyl-substituted thiophenes reacted under the same reaction conditions.[9]

Reactions of **2a**, **b** and **3a** with MeI followed by treatment with NaBPh$_4$ gave exclusively the S-methylated cationic adducts [Ru(SCH$_3$CR=CHCR′=CH)(depe)$_2$][BPh$_4$] [R = H, R′ = COMe (**4a**); R = H, R′ = CHO (**4b**); R = COMe, R′ = H (**5a**)].[10] The molecular structure of **5a** has been unequivocally

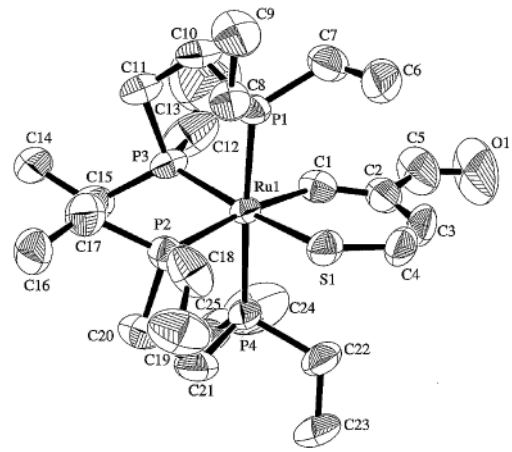

Fig. 1 An ORTEP drawing of **2b** with the numbering scheme. The hydrogen atoms are omitted for clarity. Selected bond distances (Å) and angles (°): Ru1–C1, 2.049(6), Ru1–S1 2.427(2), C1–C2 1.371(9), C2–C3 1.44(1), C3–C4 1.33(1), C4–S1 1.715(8); S1–Ru1–C1 90.3(2), Ru1–S1–C4 110.4(3), S1–C4–C3 130.9(6), C4–C3–C2 127.4(7), C3–C2–C1 126.9(7), C2–C1–Ru1 133.4(5).

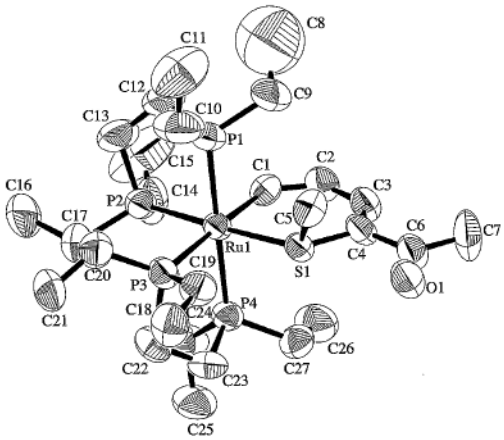

Fig. 2 An ORTEP drawing of **5a** with the numbering scheme. The tetraphenylborate anion and hydrogen atoms are omitted for clarity. Selected bond distances (Å) and angles (°): Ru1–C1, 2.044(9), Ru1–S1 2.423(2), C1–C2 1.38(1), C2–C3 1.44(1), C3–C4, 1.37(1) C4–S1 1.739(9); S1–Ru1–C1 89.3(2), Ru1–S1–C4 115.0(3), S1–C4–C3 124.6(7), C4–C3–C2 128.9(9), C3–C2–C1 129.1(8), C2–C1–Ru1 132.8(6).

determined by single-crystal X-ray structure analysis (Fig. 2).[6]

The ORTEP drawing of **5a** also supports that 1,5-insertion takes place in the 2-substituted thiophene. The thiaruthenacycle ring in **5a** is also planar (highest deviation from the best mean plane is 0.07 Å) with a localized diene structure of the C1–C2–C3–C4 linkage.

In all cases, except for **3b**, the formation of the thiaruthenacycles was very clean and no other side-products were observed when the reactions were followed by ^{1}H and ^{31}P{^{1}H} NMR.

The present Ru-promoted C–S bond cleavage of thiophenes may be essentially interpreted by the mechanism reported by Harris and Jones.[11] Thus, thiophene coordinates to the metal through the sulfur atom, followed by attack of the metal on the adjacent carbon atom *via* donation into the C–S antibonding orbital. As previously reported for a Rh complex,[3] electron-withdrawing substituents on the thiophene facilitate the C–S bond cleavage and, in fact, that is what we observed for Ru since alkylthiophenes did not react in our system. The preferred insertion of Ru into the C–S bond close to the substitutents in **2a** and **2b** can be interpreted in terms of the large coefficient on C^2 in the LUMO of these thiophenes bearing electron-withdrawing substituents.[12]

In conclusion, for the first time, electronic effects were found to be predominant in 3-substituted thiophenes leading exclusively to 1,2-insertion of Ru into the C–S bond, whereas steric effects become much more important in 2-substituted thiophenes affording only 1,5-insertion products.

This study was partially supported by the Ministry of Education, Science, Sports, and Culture, Japan and NEDO.

Notes and references

1 W. D. Jones, D. A. Vicic, R. M. Chin, J. H. Roache and A. W. Myers, *Polyhedron*, 1997, **16**, 3115; R. J. Angelici, *Polyhedron*, 1997, **16**, 3073; C. Bianchini and A. Meli, *Acc. Chem. Res.*, 1998, **31**, 109; C. Bianchini, D. Masi, A. Meli, M. Peruzzini, F. Vizza and F. Zanobini, *Organometallics*, 1998, **17**, 2495.

2 H. Topsoe, B. S. Clausen and F. E. Massoth, *Hydrotreating Catalysis*, Springer-Verlag, Berlin, 1996; R. R. Chianelli, M. Daage and M. J. Ledoux, *Adv. Catal.*, 1994, **40**, 177.

3 C. Bianchini, M. V. Jimenez, A. Meli and F. Vizza, *Organometallics*, 1995, **14**, 3196.

4 L. Dong, S. B. Duckett, K. F. Ohman and W. D. Jones, *J. Am. Chem. Soc.*, 1992, **114**, 151; W. D. Jones and L. Dong, *J. Am. Chem. Soc.*, 1991, **113**, 559; I. E. Buys, L. D. Field, T. W. Hambley and A. E. D. McQueen, *J. Chem. Soc., Chem. Commun.*, 1994, 557.

5 As a typical example, spectroscopic and analytical data of **2a**: Found: C, 48.33; H, 8.64; S, 5.09. Calc. for $C_{26}H_{54}OP_4RuS$: C, 48.81; H, 8.51; S, 5.01%. ^{1}H NMR (300 MHz, CD_3OD): δ 10.73 (br d, $^3J_{HP}$ 18.0 Hz, 1 H, H^1), 6.61 (dd, $^3J_{HH}$ 10.0, $^4J_{HH}$ 1.8 Hz, 1H, H^3), 5.90 (t, $^3J_{HH}$ 10.0, $^4J_{HP}$ 10.0 Hz, 1H, H^4), 2.25 (s, 3H, $COCH_3$), 2.2–0.8 (m, 48H, 2 depe). ^{31}P{^{1}H} NMR (121 MHz, CD_3OD), AMNX spin system: δ 54.8 (td, J 20.0, 16.0 Hz, 1P, eq-P *trans* to S), 48.5 (dt, J 329.4, 20.0 Hz, 1P, ap-P), 45.5 (ddd, J 329.4, 22.0, 17.0 Hz, 1P, ap-P), 28.8 (dt, J 20.0, 16.0 Hz, 1P, eq-P *trans* to C). Selected ^{13}C{^{1}H} NMR (75.5 MHz, CD_3OD): δ 200.8 (dtd, $^2J_{CP}$ 57.3, 15.0, 8.0 Hz, C^1), 196.1 (d, $^3J_{CP}$ 8.3 Hz, C^4). IR(KBr, cm^{-1}): 1615 ($\nu_{C=O}$).

6 *Crystal data*: for $C_{26}H_{52}OP_4RuS$ **2b**: M = 625.71, *monoclinic*, space group $P2_1/n$ (no. 14), a = 10.638(5), b = 15.753(5), c = 18.502(4) Å, β = 99.22(2)°, V = 3060(1) Å^3, T = 293 K, Z = 4, μ(Mo-Kα) = 8.06 cm^{-1}, $R(R_w)$ = 0.043(0.045) for 3792 reflections. For $C_{51}H_{77}OP_4RuSB$ **5a**: M = 974.0, monoclinic, space group $P2_1/c$ (no. 14), a = 11.485(5), b = 24.678(5), c = 18.369(4) Å, β = 95.22(3)°, V = 5184(2) Å^3, T = 293 K, Z = 4, μ(Mo-Kα) = 5.00 cm^{-1}, $R(R_w)$ = 0.068(0.081) for 6755 reflections. Single crystals of both **2b** and **5a** were recrystallised from acetone and mounted in a glass capillary. Both structures were solved using heavy atom Patterson methods and refined by full-matrix least squares on F. CCDC 182/1364. See http://www.rsc.org/suppdata/cc/1999/1793/ for crystallographic data in .cif format.

7 As a typical example, spectroscopic and analytical data of **3a**: Found: C, 48.10; H, 9.24; S, 4.85. Calc. for $C_{26}H_{54}OP_4RuS$: C, 48.81; H, 8.51; S, 5.01%. ^{1}H NMR (300 MHz, C_6D_6): δ 8.36 (ddq $^3J_{HP}$ 18.0, 3.0, $^3J_{HH}$ 12.0 Hz, 1H, H^1), 7.98 (d, $^3J_{HH}$ 7 Hz, 1H, H^3), 7.39 (tdt, $^4J_{HP}$ 12.3, 3.0, $^3J_{HH}$ 7.5 Hz, 1H, H_2), 2.86 (s, 3H, $COCH_3$), 2.5–0.5 (m, 48H, 2depe). ^{31}P{^{1}H} NMR (121 MHz, C_6D_6), AMNX spin system: δ 53.6 (td, J 20.7, 13.8 Hz, 1P, eq- *trans* to S), 46.7 (dt, J 371.4, 21.0 Hz, 1P, ap-P), 43.3 (ddd, J 371.4, 19.1, 15.2 Hz, 1P, ap-P), 30.3 (dt, J 17.0, 15.0 Hz, 1P, eq-P *trans* to C). Selected ^{13}C {^{1}H} NMR (75.5 MHz, C_6D_6): δ 199.2 (d, $^3J_{CP}$ 7.5 Hz, C^4), 169.6 (dtd, $^2J_{CP}$ 57.3, 16.8, 9.8 Hz, C^1). IR(KBr, cm^{-1}): 1636 ($\nu_{C=O}$).

8 T. Morikita, M. Hirano, A. Sasaki and S. Komiya, *Inorg. Chim. Acta*, 1999, **291**, 341.

9 Thiophenes investigated: 2-methyl-, 3-methyl- and 2,5-dimethylthiophene.

10 As a typical example, selected spectroscopic and analytical data of **5a**: Found: C, 62.52; H, 8.00; S, 3.85. Calc. for $C_{51}H_{77}BOP_4RuS$: C, 62.89; H, 7.97; S, 3.29%. ^{1}H NMR (300 MHz, acetone-d_6): δ 9.78 (ddq, $^3J_{HP}$ = 16.0, 4.6, $^3J_{HH}$ 12.0 Hz, 1H, H^1), 7.88 (d, $^3J_{HH}$ 7.8 Hz, 1H, H^3), 7.00–6.90 (m, 1H, H^2), 2.45 (d, J 2.4 Hz, 3H, SCH_3), 2.37 (s, 3H, $COCH_3$). ^{31}P{^{1}H} NMR (121 MHz, acetone-d_6), AMNX spin system: δ 54.5 (ddd, J 29.0, 19.4, 16.5 Hz, 1P, eq-P *trans* to S), 48.1 (dt, J 244.3, 19.4 Hz, 1P, ap-P), 44.3 (ddd, J 244.3, 29.0, 14.6 Hz, 1P, ap-P), 29.5 (ddd, J 19.4, 17.0, 14.6 Hz, 1P, eq-P *trans* to C). IR(KBr, cm^{-1}): 1643 ($\nu_{C=O}$). Molar electric conductivity in acetone: Λ = 7.99 S cm^2 mol^{-1}.

11 (*a*) S. Harris and R. R. Chianelli, *J. Catal.*, 1984, **86**, 400; (*b*) L. Dong, S. B. Duckett, K. F. Ohman and W. D. Jones, *J. Am. Chem. Soc.*, 1992, **114**, 151.

12 Preliminary semiempirical calculations were carried out on 3-acetyl- and 3-formyl-thiophene using the MOPAC program in the Cache calculation package. Coefficients for C^2 and C^5 were −0.62 and −0.40 for 3-acetyl thiophene and −0.63 and −0.41 for 3-formyl thiophene, respectively.

Communication 9/05748J

ChemComm

TEMPO oxidations with a silica-supported catalyst

Carsten Bolm* and Thomas Fey

Institut für Organische Chemie der RWTH Aachen, Professor-Pirlet-Straße 1, D-52056 Aachen, Germany. E-mail: carsten.bolm@oc.rwth-aachen.de

Received (in Cambridge, UK) 14th July 1999, Accepted 29th July 1999

Silica-supported 1-hydroxy-2,2,6,6-tetramethylpiperidine (SG-TMP-OH) was successfully applied as a recyclable catalyst in the oxidation of various alcohols.

Aminoxyl† radicals are well-established catalysts for the oxidation of alcohols.[1] Typically, such oxidations are carried out in the presence of 1 mol% of catalyst and a stoichiometric amount of a terminal oxidant such as bleach,[2] sodium chlorite,[3] sodium bromite,[4] *tert*-butyl hypochlorite,[5] *N*-chlorosuccinimide,[6] MCPBA,[7] [bis(acetoxy)iodo]benzene,[8] or oxygen in combination with a high-valent metal salt.[9] Furthermore, electrochemical reoxidation of the catalyst is possible.[10]

Especially for large scale oxidations, the TEMPO–bleach protocol introduced by Anelli *et al.*[2] appears most useful.[11] Although usually a small quantity of the catalyst is sufficient for an efficient transformation, it is still desirable to develop improved work-up conditions which allow simple product isolation as well as catalyst separation and recycling.[12] We envisaged that both requirements could be realised by using a polymer-supported aminoxyl radical. Usually TEMPO-catalysed reactions afford the desired carbonyl compounds in high yields without the formation of significant amounts of by-product, and thus catalyst separation and product isolation could easily be accomplished by simple filtration and phase separation followed by evaporation of the organic solvent (Scheme 1).

Although several polymer-bound aminoxyl radicals have already been synthesised,[13] only a very few of them were applied as oxidation catalysts.[13*a–d*] To the best of our knowledge, none of them has been studied under the conditions mentioned above. Due to several publications concerning the application of polymer-supported oxidation reagents and catalysts,[14] and based on our own expertise in the use of heterogenised alkaloids in the Sharpless dihydroxylation reaction,[14*g*,15] we focused our attention on the attachment of the TEMPO precursor 1-hydroxy-4-oxo-2,2,6,6-tetramethylpiperidine (**2**)[16] onto silica. The synthesis of **3** (SG-TMP-OH) was accomplished by reductive amination of **2** with commercially available aminopropyl-functionalised support (Scheme 2).[17]‡ The resulting solid was carefully washed with hot MeOH using a Soxhlet extractor for several days in order to ensure complete removal of non-chemically bounded hydroxypiperidine derivatives from the surface.

SG-TMP-OH **3** was then applied as catalyst in the oxidation of various alcohols according to the Anelli protocol (Table 1).[2*a*]§ As shown by quantitative GC analysis, aldehydes and ketones were formed in high yields from the corresponding primary and secondary alcohols, respectively. Both benzylic and aliphatic substrates react equally well.

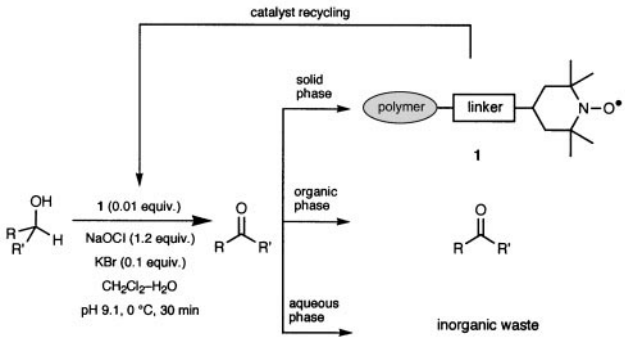

Scheme 1

In order to study the selectivity profile in the oxidation of primary and secondary alcohols, we performed competition experiments using equimolar mixtures of both. Entries 8 and 9 of Table 1 show a high selectivity towards the oxidation of the primary alcohols, which resembles the known behaviour of the unsupported TEMPO catalyst.[19] Thus, the corresponding aldehydes of nonan-1-ol and benzyl alcohol were formed in 96 and 92% yield, respectively, whereas the oxidation of the secondary alcohols nonan-2-ol and 1-phenylethanol occured in low yield only (1 and 3%, respectively). In addition, as in catalysed oxidations with TEMPO itself,[2*c*] no racemisation of optically active compounds occured (entry 10).

We finally investigated the possibility of recycling the catalyst. Therefore, the silica-bound TEMPO derivative was recovered by filtration after the reaction and reapplied in a sequence of oxidations using nonan-1-ol as substrate. The results illustrated in Fig. 1 show that even after 10 subsequent runs the catalyst activity remained high. In both substrate conversion and product yield only a minor decrease was observed, proving the high efficiency of the catalyst recovery.

In conclusion, we have demonstrated that silica-supported TEMPO is an excellent catalyst for the oxidation of alcohols, affording the corresponding carbonyl derivatives in high yields. Primary alcohols are selectively oxidised in the presence of

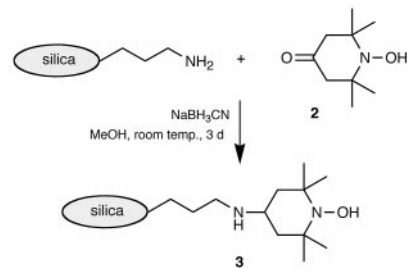

Scheme 2

Table 1 TEMPO oxidation of various alcohols to the corresponding aldehydes and ketones with silica-supported catalyst **3**[*a*]

Entry	Substrate	Yield (%)[*b*]
1	Benzyl alcohol	92 (75)
2	Heptan-1-ol	90
3	Octan-1-ol	88
4	Nonan-1-ol	90 (85)
5	Dodecan-1-ol	81
6	Nonan-2-ol	65
7	1-Phenylethanol	91
8	Nonan-1-ol/nonan-2-ol	96/1
9	Benzyl alcohol/1-phenylethanol	92/3
10	*(S)*-2-Methylbutan-1-ol[*c*]	60

[*a*] Oxidation experiments conducted following the protocol in note §. [*b*] Yields were determined by quantitative GC analysis using decane or dodecane as internal standard. Values in parentheses are isolated yields. [*c*] The ee of 95% remained unchanged (ref. 18).

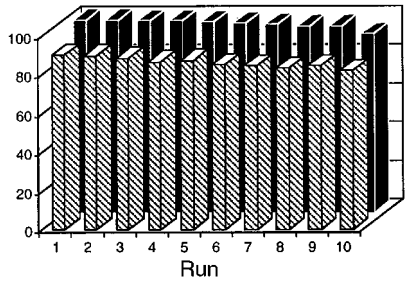

Fig. 1 Yields [hatched (%)] and conversions [black (%)] in consecutive oxidation reactions of nonan-1-ol when using silica-supported catalyst **3**.

secondary substrates. Optically active starting materials can be used without racemisation. Finally, the catalyst was shown to be stable under the reaction conditions, thus allowing it to be recycled without significant loss of activity.

This research was supported by the Katalyseverbund NRW and the Fonds der Chemischen Industrie.

Notes and references

† CAS nomenclature = nitroxyl.

‡ Aminopropyl-functionalised silica was purchased from Aldrich. According to the distributor's information the degree of functionalisation is approximately 1.0 mmol g^{-1}.

§ *General procedure* for the oxidation of alcohols with SG-TMP-OH **3** as catalyst: The reaction was performed in a glass tube with a cooling mantle. The bottom of the tube was equipped with a ceramic filter plate and a stopcock allowing easy separation of the supported catalyst from the reaction mixture by filtration. In this vessel was placed 9.2 mg of SG-TMP-OH **3** (8 μmol based on complete functionalisation; degree of functionalisation = 0.87 mmol g^{-1}). Then a CH_2Cl_2 solution (2 ml) of the alcohol (0.4 M) and decane or dodecane (0.12 M; as internal standard) was added followed by an aqueous solution (0.16 ml) of KBr (0.5 M). After the cooling of the reaction mixture to 0 °C, 2.7 ml of aq. NaOCl (diluted to a final concentration of 0.37 M and buffered by the addition of $NaHCO_3$ to a pH of 9.1) was added. Then, the reaction mixture was vigorously shaken for 30 min. After filtration, the organic phase was separated, dried over $MgSO_4$, and the product composition was analysed by means of GC [ultra-2-column (Hewlett Packard)]. The filtered solid was washed five times with water, MeOH and CH_2Cl_2 (2 ml each), air-dried, and reused as such. Preparative runs were carried out on a five-fold scale, and the reaction time was extended to 1 h. After filtration the organic layer was separated, and the aqueous phase was extracted with CH_2Cl_2 once. The combined organic phases were dried over $MgSO_4$, the solvent was removed *in vacuo*, and the crude product purified by column chromatography on silica gel with CH_2Cl_2 as eluent.

1 For reviews see: A. E. J. de Nooy, A. C. Besemer and H. van Bekkum, *Synthesis*, 1996, 1153; J. M. Bobbitt and M. C. L. Flores, *Heterocycles*, 1988, **27**, 509; early observations: E. G. Rozantsev and V. D. Sholle, *Synthesis*, 1971, 401.

2 (*a*) P. L. Anelli, C. Biffi, F. Montanari and S. Quici, *J. Org. Chem.*, 1987, **52**, 2559; (*b*) P. L. Anelli, S. Banfi, F. Montanari and S. Quici, *J. Org. Chem.*, 1989, **54**, 2970; (*c*) P. L. Anelli, F. Montanari and S. Quici, *Org. Synth.*, 1990, **69**, 212.

3 M. Zhao, J. Li, E. Mano, Z. Song, D. M. Tschaen, E. J. J. Grabowski and P. J. Reider, *J. Org. Chem.*, 1999, **64**, 2564.

4 T. Inokuchi, S. Matsumoto, T. Nishiyama and S. Torii, *J. Org. Chem.*, 1990, **55**, 462.

5 F. Melvin, A. McNeill, P. J. F. Henderson and R. B. Herbert, *Tetrahedron Lett.*, 1999, **40**, 1201.

6 J. Einhorn, C. Einhorn, F. Ratajczak and J.-L. Pierre, *J. Org. Chem.*, 1996, **61**, 7452.

7 J. A. Cella, J. A. Kelley and E. F. Kenehan, *J. Org. Chem.*, 1975, **40**, 1860; J. A. Cella, J. P. McGrath, J. A. Kelley, O. ElSoukkary and L. Hilpert, *J. Org. Chem.*, 1977, **42**, 2077; J. A. Cella, J. A. Kelley and E. F. Kenehan, *J. Chem. Soc., Chem. Commun.*, 1974, 943; S. D. Rychnovsky and R. Vaidyanathan, *J. Org. Chem.*, 1999, **64**, 310.

8 A. De. Mico, R. Margarita, L. Parlanti, A. Vescovi and G. Piancatelli, *J. Org. Chem.*, 1997, **62**, 6974.

9 M. F. Semmelhack, C. R. Schmid, D. A. Cortés and C. S. Chou, *J. Am. Chem. Soc.*, 1984, **106**, 3374; T. Miyazawa and T. Endo, *J. Mol. Catal.*, 1985, **32**, 357.

10 M. F. Semmelhack, C. S. Chou and D. A. Cortés, *J. Am. Chem. Soc.*, 1983, **105**, 4492; T. Inokuchi, S. Matsumoto and S. Torii, *J. Org. Chem.*, 1991, **56**, 2416; Y. Kashiwagi, Y. Yanagisawa, F. Kurashima, J.-i. Anzai, T. Osa and J. M. Bobbitt, *Chem. Commun.*, 1996, 2745; Y. Yanagisawa, Y. Kashiwagi, F. Kurashima, J.-i. Anzai, T. Osa and J. M. Bobbitt, *Chem. Commun.*, 1996, 1043.

11 R. Siedlecka, J. Skarzewski and J. Mlochowski, *Tetrahedron Lett.*, 1990, **31**, 2177; M. R. Leanna, T. J. Sowin and H. E. Morton, *Tetrahedron Lett.*, 1992, **33**, 5029; T. S. Straub, *J. Chem. Educ.*, 1991, **68**, 1048; N. J. Davis and S. L. Flitsch, *Tetrahedron Lett.*, 1993, **34**, 1181; C. Palomo, J. M. Aizpurua, C. Cuevas, R. Urchegui and A. Linden, *J. Org. Chem.*, 1996, **61**, 4400; G. Tong, J. W. Perich and R. B. Johns, *Tetrahedron Lett.*, 1990, **31**, 3759.

12 For a review on that topic: D. P. Curran, *Angew. Chem., Int. Ed.*, 1998, **37**, 1174.

13 (*a*) T. Miyazawa and T. Endo, *J. Polym. Sci., Polym. Chem. Ed.*, 1985, **23**, 2487; (*b*) T. Miyazawa and T. Endo, *J. Mol. Catal.*, 1988, **49**, L31; (*c*) A. Deronzier, D. Lìmosin and J.-C. Moutet, *Electrochim. Acta*, 1987, **32**, 1643; (*d*) T. Osa, U. Akiba, I. Segawa and J. M. Bobbitt, *Chem. Lett.*, 1988, 1423; (*e*) F. MacCorquodale, J. A. Crayston, J. C. Walton and D. J. Worsfold, *Tetrahedron Lett.*, 1990, **31**, 771; (*f*) C. Amiel, B. Sebille, H. Hommel and A. P. Legrand, *J. Colloid Interface Sci.*, 1994, **165**, 236; (*g*) A. W. Bosman, R. A. J. Janssen and E. W. Meijer, *Macromolecules*, 1997, **30**, 3606.

14 Selected recent examples of oxidations with polymer-supported reagents and catalysts: (*a*) J. A. Elings, R. Ait-Meddour, J. H. Clark and D. J. Macquarrie, *Chem. Commun.*, 1998, 2707; (*b*) B. Hinzen and S. V. Ley, *J. Chem. Soc., Perkin Trans. 1*, 1997, 1907; (*c*) B. Hinzen, R. Lenz and S. V. Ley, *Synthesis*, 1998, 977; (*d*) L. Canali, E. Cowan, H. Deleuze, C. L. Gibson and D. C. Sherrington, *Chem. Commun*., 1998, 2561; (*e*) J. K. Karjaleinen, O. E. O. Hormi and D. C. Sherrington, *Tetrahedron: Asymmetry*, 1998, **9**, 1563; (*f*) L. Canali and D. C. Sherrington, *Chem. Soc. Rev*., 1999, **28**, 85; (*g*) F. Minutolo, D. Pini, A. Petri and P. Salvadori, *Tetrahedron: Asymmetry*, 1996, **7**, 2293; (*h*) C. Bolm, and A. Gerlach, *Eur. J. Org. Chem.*, 1998, 21 and references therein.

15 C. Bolm, A. Maischak and A. Gerlach, *Chem. Commun.*, 1997, 2353.

16 Compound **2** was synthesised as described in C. M. Paleos and P. Dais, *J. Chem. Soc., Chem. Commun.*, 1977, 345.

17 The reductive amination was carried out with an excess of the carbonyl compound analogously to the synthesis of 4-amino-TEMPO from 4-oxo-TEMPO: G. M. Rosen, *J. Med. Chem.*, 1974, **17**, 358.

18 The ee of the product was determined by GC [Lipodex-A (Macherey-Nagel), 50 m × 0.25 mm, 100 kPa H_2, 30 °C] after its reduction to the corresponding alcohol.

19 Some mechanistic aspects concerning this phenomenon are discussed in A. E. J. de Nooy, A. C. Besemer and H. van Bekkum, *Tetrahedron*, 1995, **51**, 8023.

Communication 9/05683A

Platinum-catalyzed hydrosilylation of C_{60}: synthesis of a novel fullerene–siloxane polymer

Michael L. Miller[a] and Robert West*[b]

[a] *Department of Chemistry, Utica College, 1600 Burrstone Road, Utica, NY 13502-4892, USA*
[b] *Department of Chemistry, University of Wisconsin, 1101 University Avenue, Madison, Wisconsin 53706, USA. E-mail: west@chem.wisc.edu*

Received (in Columbia, MO, USA) 30th April 1999, Accepted 27th July 1999

The hydrosilylation of buckminsterfullerene with the oligomer poly(methylhydridomethyloctylsiloxane) produced a soluble, oxidation-resistant fullerene–siloxane copolymer, in which the siloxane oligomer is multiply attached to the C_{60} moiety by covalent Si–C bonds essentially encapsulating the fullerene cage.

With the development of a method for the preparation of macroscopic amounts of buckminsterfullerene, the chemistry of this closed shell molecule has been extensively investigated.[1,2] Finding useful chemical applications for C_{60}, however, has been met with limited success, partly due to its low solubility in common organic solvents.[3] Thus, much of the organic chemistry involving this molecule focuses on the synthesis, isolation, and characterization of its derivatives. It is hoped that some of these compounds will find useful application due to their increased solubility and unique electronic properties.

In 1991 Fagan *et al.* published the synthesis of C_{60}-η^2-bis(triphenylphosphine)platinum, the first fullerene–metal complex.[4] This landmark paper has led to further developments in fullerene–metal chemistry.[5] In addition, since platinum is the favored catalyst for hydrosilylation, it raised the possibility that C_{60} might be derivatized by R_3SiH addition reactions.[6] We report the metal catalyzed hydrosilylation of C_{60} with poly(methylhydridomethyloctylsiloxane), MHMO, and characterization of the product, an unusual fluid.[7]

The original goal of this research was to synthesize a siloxane copolymer with pendant C_{60} units. C_{60} was synthesized using a modified graphite evaporation apparatus and was purified by continuous column chromatography.[8,9] The reaction of pure C_{60} with 2.1 equiv. of MHMO ($M_w \approx 1470$; 3.1 Si–H/chain), and 0.05 equiv. of the platinum catalyst, (divinyltetramethyldisiloxane)platinum(0), afforded a shiny, black oil **1** in 83% yield (Scheme 1).† Product **1** was relatively viscous and displayed a low molecular weight, low dispersion pattern using size exclusion chromatographic analysis with an estimated molecular weight of *ca.* 4000 (Fig. 1). **1** was readily soluble in tetrahydrofuran, toluene, benzene, chloroform and carbon disulfide; slightly soluble in hydrocarbons such as hexane, cyclohexane and 3-methylpentane; and insoluble in water and alcohols. In contrast to many fullerenes and fullerene derivatives, **1** was resistant to air oxidation.[10] The IR absorption spectrum of the purified compound showed no absorption in the 2100–2300 cm^{-1} region, indicating the absence of any Si–H functionality.

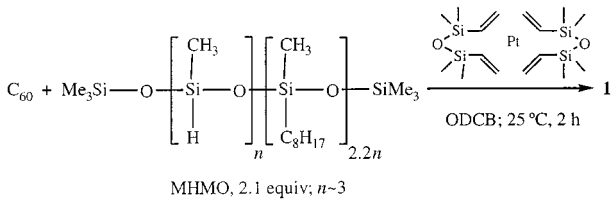

Scheme 1

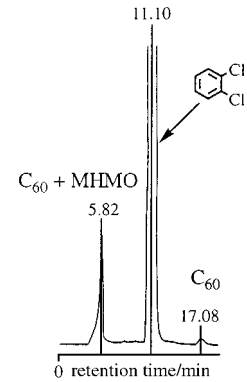

Fig. 1 GPC chromatograph of the reaction mixture after 1 h; a small amount of unreacted C_{60} is still present.

The UV–VIS spectra of the product and of unreacted C_{60} in THF are shown in Fig. 2. The strongest absorption band observed in the spectrum of unreacted C_{60} (λ = 256 nm) has completely disappeared in the absorption profile of **1**, with a coincident increase in the intensity of the band at λ = 220 nm. The intensity of the absorption at λ = 333 nm is also reduced. These changes are characteristic of a highly derivatized C_{60} moiety, where more than two π-bonds of the fullerene cage have been reduced.[11]

The ^{1}H NMR spectra of unreacted MHMO and of the product are shown in Fig. 3.‡ The upfield signals in both spectra can be unambiguously assigned to alkyl substituents, shifted by < 0.05 ppm on going from the siloxane copolymer to the product. In the ^{1}H NMR spectrum of unreacted MHMO, a characteristic Si–H resonance is found at δ 5.18. In the product this is replaced by a resonance at δ 3.99 which we attibute to hydrogen attached to the fullerene cage.[13] Integration of this signal with an internal standard suggests the incorporation of 5.9 protons per fullerene–siloxane adduct.

Analysis of the MALDI mass spectrum indicated an average parent ion mass of 3650 au. The C_{70}–siloxane adduct was also observed when a mixture of C_{60} and C_{70} was used. (Fig. 4).

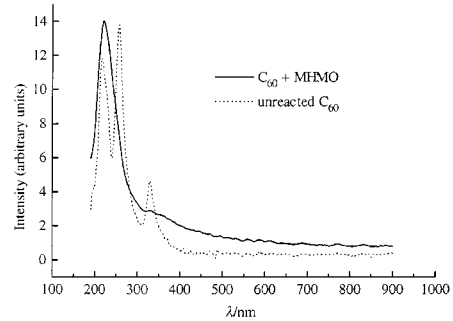

Fig. 2 UV–VIS absorption spectra of **1** (THF) and of C_{60} (toluene).

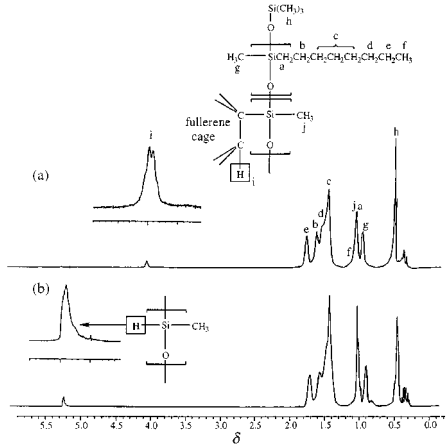

Fig. 3 ^{1}H NMR spectra (500 MHz; [$^2H_6$]benzene) with designations of H and C atoms for tentative assignment of ^{1}H and ^{13}C NMR resonances. (a) polymer **1** and (b) poly(methylhydridomethyloctylsiloxane).

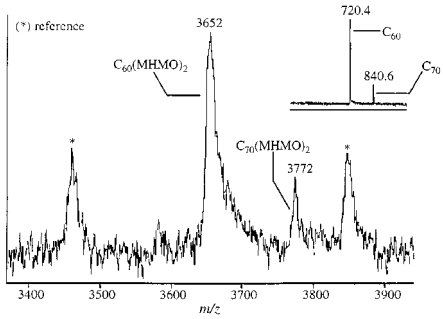

Fig. 4 MALDI mass spectrum of **1**. Inset: unreacted C_{60}/C_{70} mixture.

The analytical and spectroscopic data for **1** are inconsistent with the anticipated pendant structure. The molecular weight determination indicates that **1** is a 2:1 adduct of the siloxane copolymers with C_{60}. The lack of Si–H bonds in the product suggests that every Si–H silicon atoms in the polymer becomes attached to the fullerene cage. We propose a structure in which the C_{60} moiety is surrounded and essentially encapsulated by two siloxane molecules, both multiply attached. A hypothetical representation of the structure is shown in Fig. 5. The sharp GPC peak and unusual resistance to air oxidation are also consistent with the proposed structure of this hybrid siloxane–fullerene fluid. The fullerene ^{13}C resonances are also highly indicative of a reduced fullerene cage.

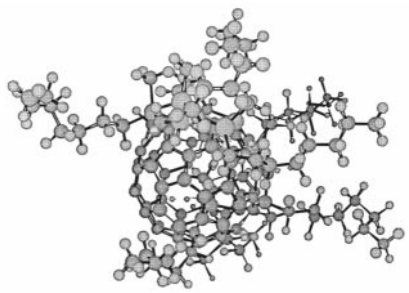

Fig. 5 A schematic representation of 'shrink-wrapped' fullerene. One of the siloxane adducts has been removed to reveal the C_{60} moiety.

The order of the addition of the platinum catalyst was found to be important.[14] If buckminsterfullerene was allowed to stir with the platinum complex before the addition of the poly(alkylhydridosiloxane), an insoluble precipitate would form; this precipitate, which we suppose to be a platinum–fullerene adduct, was unreactive towards the poly(alkylhydridosiloxane) and greatly reduced the overall yield of **1**.

This research was supported by a grant from the National Science Foundation.

Notes and references

† *Reagents and conditions*: MHMO polymer was obtained from Gelest, Inc. Chloroplatinic acid ($H_2PtCl_4·6H_2O$), Aldrich, was used without further purification and stored under argon with refrigeration. The tetramethyldivinyldisiloxane platinum(0) complex was prepared by the reaction of chloroplatinic acid and 1,1,3,3-tetramethyl-1,3-divinylsiloxane $(CH_2{=}CHSiMe_2)_2O$ (Gelest) to yield a 16 wt% platinum solution.

All experiments were carried out with Schlenk techniques under a dry argon atmosphere. All solvents were distilled immediately before use. NMR: Bruker AM-500 instrument, the solvent was used as an internal standard, with TMS as an external standard: [$^2H_6$]benzene (δ_H 7.15), CS_2 (δ_C 198), $CDCl_3$ (δ_{Si}). IR: Mattson FTIR spectrometer (KBr plates, neat). GPC analysis: Waters Associates LC system {Shodex KF-802 column; THF: flow rate, 1.0 ml min^{-1}; UV detector, (λ = 254 nm)}. UV–VIS: Perkin Lambda Array 3840 spectrometer (THF).

Synthesis of **1**: in a typical experiment, MHMO siloxane copolymer (130 mg, 0.087 mmol) was added to divinyldisiloxane Pt catalyst (2.5 mg, 0.013 mmol) dissolved in 5 ml degassed *o*-dichlorobenzene. The solution was stirred for 15 min at which point the clear, colorless mixture had become straw-yellow. A clear, purple solution of C_{60} (30 mg, 0.042 mmol) in 24 ml of benzene was added. The reaction mixture immediately darkened and became opaque. After stirring for 2.75 h at 25 °C, the mixture was loaded onto an activated silica gel column and the amber-colored fraction was collected using benzene–MeOH (9:1) solution as the mobile phase (under 7.5 psi N_2). Some black, insoluble material remained on the column head. Removal of the solvent afforded 122 mg (80%) of a dark brown oil (**1**). GPC analysis indicated that no unreacted C_{60} remained in the product. The material was then characterized as previously described. Exposure of **1** to air for several months led to no change in its spectra or its solubility.

‡ *NMR spectra*: see Fig. 3 for identification. Most resonances are multiplets. δ_H, a, 0.91, b, 1.58, c, 1.36; d, 1.42; e, 1.64 f; 0.96; g, 0.84; h, 0.42; i, 3.99; j, 0.94. δ_C a, 21.7; b, 4.52; c, d, 27.5–34.8; e, 20.0; f, 9.9; g, j, 23.5, 23.6; h, −3.0; C_{60}, 125.5–147.5.[12] δ_{Si}, Me_3Si, −5.9; (*n*-octyl)SiMe, −24.9; $MeSiC_{60}$, 6.2.

1 W. Krätschmer, L. D. Lamb, K. Fostiropoulos and P. R. Huffman, *Nature*, 1990, **347**, 359.

2 Some representative chemistry: Diels–Alder reactions: S. H. Hoke II, J. Molstad, D. Dilettato, M. Jay, D. Carlson, B. Kahr and G. Cooks, *J. Org. Chem.*, 1992, **57**, 5069; Carbene addition: T. Suzuki, Q. Li, K. Khemani and F. Wudl, *J. Am. Chem. Soc.*, 1992, **114**, 7301; Silylene addition: T. Akasaka, W. Ando, K. Kobayashi and S. Nagase, *J. Am. Chem. Soc.*, 1993, **115**, 1605; Fullerene containing organic polymers: D. Roy and R. Assink, *J. Am. Chem. Soc.*, 1992, **114**, 3977.

3 D. Parker, P. Wurz, K. Chatterjee, K. R. Lykke, J. E. Hunt, M. J. Pellin, J. C. Hemminger, D. M. Gruen and L. M. Stock, *J. Am. Chem. Soc.*, 1991, **113**, 7499.

4 P. J. Fagan, J. C. Calabrese and B. Malone, *J. Am. Chem. Soc.*, 1991, **113**, 9408.

5 A. L. Balch, J. W. Lee, B. C. Noll and M. Olmstead, *J. Am. Chem. Soc.*, 1992, **114**, 10 984; R. W. Koefod, M. F. Hudgens and J. R. Shapley, *J. Am. Chem. Soc.*, 1991, **113**, 8957.

6 For a review: I. Ojima, in *The Chemistry of Organic Silicon Compounds*, ed. S. Patai and S. Rappoport, Wiley Publishers, Chichester, 1989, part 2, ch. 25.

7 MHMO: $Me_3SiO[SiMe(H)O]_n[SiMe(n\text{-octyl})O]_{2.2n}SiMe_3$; $n \approx 3$.

8 P. Bhyrappa, A. Penicaud, M. Kawamoto and C. A. Reed, *J. Chem. Soc., Chem. Commun.*, 1992, 936.

9 F. Wudl, A. S. Koch and K. C. Khemani, *J. Org. Chem.*, 1991, **56**, 4543.

10 R. Taylor, M. P. Barrow and T. Drewello, *Chem. Commun.*, 1998, 2497.

11 R. West, K. Oka, H. Takahashi, M. Miller and T. Gunji, in *Inorganic and Organometallic Polymers II: Advanced Materials and Intermediates*, ed. P. Wisian-Neilson, H. R. Allcock and K. J. Wynne, ACS Symp. Ser. 572, Washington DC, 1994, pp. 92–101.

12 ^{13}C resonances for substituted C_{60} are typically found in the region δ 130–150, see: H. Okamura, K. Miyazono, M. Minoda and T. Miyamoto, *Macromol. Rapid Commun.*, 1999, **20**, 41; G. A. Burley, P. A. Keller, S. G. Pyne and G. E. Ball, *Chem. Commun.*, 1998, 2539.

13 A recent paper reports ^{1}H chemical shifts for hydrogenated fullerenes to lie in the range δ 2.5–4.5: A. S. Lobach, A. A. Perov, A. I. Reov, O. S. Roshchupkina, V. A. Tkacheva and A. N. Stepanov, *Russ. Chem. Bull.*, 1997, **46**, 641.

14 F. O. Stark, J. R. Falender and A. P. Wright, in *Comprehensive Organometallic Chemistry*, ed. G. Wilkinson, F. G. A. Stone and E. W. Abel, Pergamon, New York, 1982, vol. 2, ch. 9.3.

Communication 9/03477C

Silylacetylene dendrimers: synthesis and characterization

Tsukasa Matsuo, Kumiko Uchida and Akira Sekiguchi*

Department of Chemistry, University of Tsukuba, Tsukuba, Ibaraki, 305–8571, Japan.
E-mail: sekiguch@staff.chem.tsukuba.ac.jp

Received (in Cambridge, UK) 25th June 1999, Accepted 5th August 1999

The first silylacetylene dendrimers (1G and 2G) with alternating silicon–acetylene units [(SiC≡C)$_n$] have been synthesized and characterized by spectroscopic methods; the X-ray structure of 1G is reported.

Nanochemistry is a rapidly expanding field that is concerned with the synthesis, characterization and properties of structures of nanosize dimensions.[1] Dendrimers with a regular, three-dimensional, tree-like structure have attracted much attention as well-defined nanosize compounds. In the past 10 years, there has been increasing interest in the synthesis and properties of dendritic molecules.[2] Phenylacetylene dendrimers and related compounds are well known as a class of dendrimers containing acetylene units.[3] However, there are no published studies on dendrimers with alternating E (E = CR, SiR *etc.*) and carbon–carbon triple bonds [(EC≡C)$_n$], due to the instability of polyacetylene derivatives.[4] We report here the structurally defined nanoscale synthesis of the first silylacetylene dendrimers with alternating silicon–acetylene units [(SiC≡C)$_n$] up to the second generation with 22 silicon atoms and 21 acetylene units.

All of the previously characterized silicon-containing dendrimers, *e.g.* carbosilane dendrimers,[5] siloxane dendrimers[6] and polysilane dendrimers,[7] have been made solely by the divergent method. However, the divergent method is not suitable for silylacetylene dendrimers due to the problem of the deprotection step. Thus, we have applied a convergent method for the unprecedented synthesis of silylacetylene dendrimers.

The preparation of the silylacetylene dendrimers starts with the synthesis of the chlorosilanes **2** and **6**.† First, $MeHSiCl_2$ was reacted with (trimethysilyl)ethynylmagnesium bromide in Et_2O

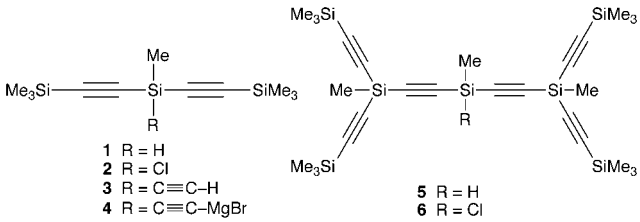

to give diyne **1** in 76% yield. Then, the Si–H moiety of **1** was converted to a Si–Cl moiety (**2**) using catalytic $PdCl_2$ in CCl_4 (85%). Next, **2** was reacted with ethynylmagnesium bromide to yield triyne **3** in 87% yield. After treatment of ethylmagnesium bromide with **3**, the resulting Grignard reagent **4** was added to $MeHSiCl_2$ to produce hexayne derivative **5** in 79% yield. Finally, the Si–H moiety of **5** was converted to a Si–Cl moiety (**6**) in CCl_4 using benzoyl peroxide (BPO) (52% yield).

As a core part, triyne Grignard reagent **7** was prepared from triethynylmethylsilane[8] with 3 equiv. of ethylmagnesium bromide in THF. Species **1G** was isolated as colorless crystals by the reaction of **7** with 3 equiv. of dendron **2** in THF (48% yield, Scheme 1). Crystallization from benzene afforded fine crystals of **1G** containing three molecules of benzene. However, these crystals quickly become opaque when removed from the mother liquor.

The molecular structure of **1G**·3C_6H_6 and the packing of the molecule in the crystal's unit cell are shown in Figs. 1 and 2, respectively.‡ There are three independent molecules in the unit cell, and the crystal structure possesses a crystallographic three-fold axis. Unlike previously reported dendrimers, **1G** has a nearly planar structure due to the rigid linear acetylene units, with a diameter of about 2 nm. The two molecules of **1G** lie in an alternating fashion to produce layers, in which the dendritic arms of these two molecules are arranged to give a staggered conformation through the core Si–Me bond. The benzene molecules fill spaces between the layers. The C–C triple bond

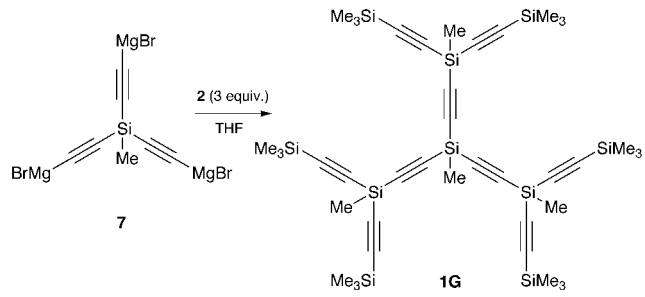

Scheme 1

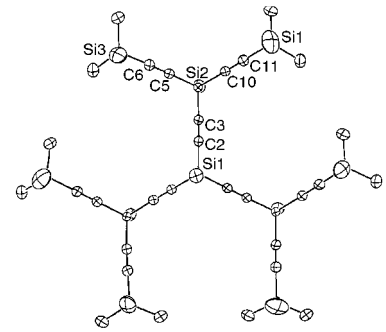

Fig. 1 Structure of **1G**·3C_6H_6 (hydrogen atoms are omitted for clarity). Selected bond distances (Å) and angles (°) are: Si1–C2 1.831(5), Si2–C3 1.835(5), Si2–C5 1.827(5), Si2–C10 1.828(5), Si3–C6 1.851(5), Si4–C11 1.849(5), C2–C3 1.205(6), C5–C6 1.208 (7), C10–C11 1.211(7); Si1–C2–C3 178.3(5), Si2–C3–C2 177.3(4), Si2–C5–C6 177.5(5), Si2–C10–C11 178.3(5), Si3–C6–C5 179.7(5), Si4–C11–C10 179.7(5).

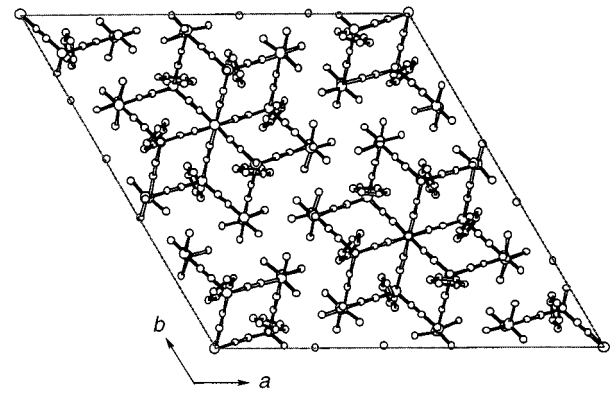

Fig. 2 Perspective view of **1G**·3C_6H_6 from the direction of the *c* axis.

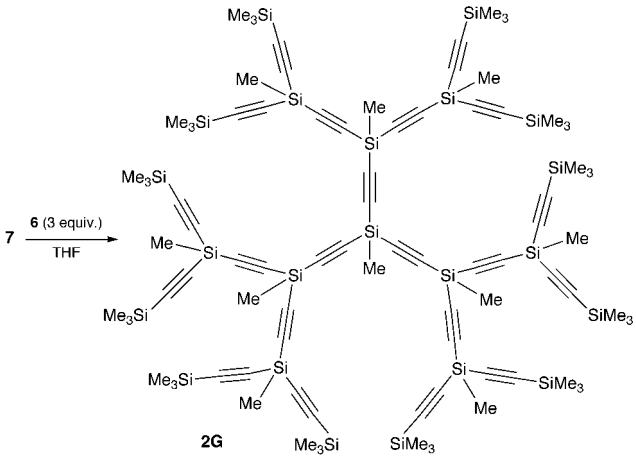

Scheme 2

lengths are 1.205(6)–1.211(7) Å [av 1.208(7) Å], and the Si–C (sp) single bond lengths are 1.827(5)–1.851(5) Å [av. 1.837(5)Å]. The bond angles of the acetylene units [Si–C(sp)–C(sp)] are almost linear {177.3(4)–179.7(5)° [av. 178.5(5)°]}.

Dendrimer **2G** was obtained as a colorless glassy solid by the reaction of **7** with 3 equiv. of dendron **6** in THF (18% yield, Scheme 2).§ The structure of **2G** was characterized by NMR spectroscopy and matrix-assisted laser desorption/ionization time-of-flight (MALDI-TOF) mass spectrometry. The MALDI-TOF mass spectrum showed an intense ion peak at 1836.8 ($M + Na^+$), in agreement with the formula $C_{88}H_{138}Si_{22} + Na^+$. In the ^{29}Si NMR spectrum, four sets of signals were observed at δ −68.3, −66.5, −66.3 and −17.4. The signal appearing at δ −17.4 is assignable to the terminal trimethylsilyl groups. The other three signals at higher field are assignable to triethynyl-substituted silicon atoms. The ^{13}C NMR showed eight resonances of sp carbon atoms; δ 108.3 (3 C) and 108.6 (3 C) for the innermost acetylene carbons, δ 107.6 (6 C) and 110.1 (6 C) for the middle acetylene carbons, and δ 106.22 (6 C), 106.23 (6 C) 117.3 (6 C), and 117.4 (6 C) for the outermost acetylene carbons. Assignments of these ^{13}C resonances were made on the basis of peak intensities. Four sets of methyl groups were also found in the ^{13}C NMR spectrum; the core SiMe at δ −0.2 (1 C), the adjacent branched SiMe at δ −0.3 (3 C), the next adjacent branched SiMe at δ 1.0 (6 C), and the peripheral $SiMe_3$ at δ −0.55 (18 C) and −0.53 (18 C). The outermost two (trimethylsilyl)ethynyl groups are diastereotopic.

The polyyne dendrimers (**1G** and **2G**) are thermally stable up to 200 °C. However, they are highly sensitive to both acidic and alkaline conditions, and the Si–C(sp) bonds are easily cleaved. In the UV-VIS spectrum of **2G**, two absorption bands are observed at 210 (ε = 28900) and 219 nm (ε = 15300), whose intensities are about three times larger than those of **1G**, at 210 (ε = 10700) and 219 nm (ε = 5200).

This work was supported by Grants-in-Aid for Scientific Research (Nos. 09239101, 10304051, 1113321, 11166209) from the Ministry of Education, Science and Culture of Japan, and TARA (Tsukuba Advanced Research Alliance) fund.

Notes and references

† A THF solution of ethylmagnesium bromide (30 ml, 24 mmol) was added to triethynylmethylsilane (0.91 g, 7.7 mmol) in THF (10 ml) to produce the Grignard reagent of the triyne. Bis(trimethylsilylethynyl)methylchlorosilane **2** (6.00 g, 25 mmol) in THF (30 ml) was added to the THF solution of the resulting Grignard reagent **7**, and the mixture was stirred overnight. Usual workup followed by Kugelrohr distillation gave **1G** as colorless crystals (180–190 °C/0.2 mmHg). Yield 48% (3.05 g), mp 115–118 °C; δ_H(300 MHz, $CDCl_3$) 0.18 (s, 54H, CH_3), 0.47 (s, 9H, CH_3), 0.52 (s, 3H, CH_3); δ_C(75.5 MHz, $CDCl_3$) −0.4 (CH_3), 0.5 (CH_3), 1.0 (CH_3), 105.5 (C), 106.9 (C), 109.4 (C), 117.0 (C); δ_{Si}(59.6 MHz, $CDCl_3$) −69.0, −67.3, −17.4 [calc. (MALDI): 850.8 ($M + Na^+$), found: 850.8].

‡ *Crystal data* for **1G**·3 C_6H_6: $C_{40}H_{66}Si_{10}\cdot 3C_6H_6$, M = 1062.17, trigonal, a = 31.061(1), c = 12.566(1) Å, V = 10499.3(3) Å^3, T = 180 K, space group = $P3$, Z = 6, ρ_{calc} = 1.008 g cm^{-3}. Diffraction data were collected on a Mac Science DIP2030K Image Plate Diffractometer employing graphite-monochromatized Mo–Kα radiation (λ = 0.71073 Å). The final R factor was 0.054 (R_w = 0.051) for 7207 reflections with $I > 3\sigma(I)$. Single crystals of **1G**·3 C_6H_6 were obtained by crystallization from benzene, mounted in a glass capilary tube and transferred to the cold gas stream of the diffractometer. The structure was solved by the direct method and refined by the full-matrix least-squares method. CCDC 182/1363. See http://www.rsc.org/suppdata/cc/1999/1799/ for crystallographic data in .cif format.

§ *Spectral data* for **2G**: δ_H(500 MHz, C_6D_6) 0.029 (s, 54H, CH_3), 0.034 (s, 54H, CH_3), 0.10 (s, 9H, CH_3), 0.23 (s, 3H, CH_3), 0.41 (s, 18H, CH_3); δ_C(125 MHz, C_6D_6) −0.55 (CH_3), −0.53 (CH_3), −0.3 (CH_3), −0.2 (CH_3), 1.0 (CH_3), 106.22 (C), 106.23 (C), 107.6 (C), 108.3 (C), 108.6 (C), 110.1 (C), 117.3 (C), 117.4 (C); δ_{Si}(59.6 MHz, C_6D_6) −68.3, −66.5, −66.3, −17.4; [calc. (MALDI): 1836.9 ($M + Na^+$), found 1836.8].

1 G. A. Ozin, *Adv. Mater.*, 1992, **4**, 612.
2 For recent reviews of dendrimers, see: G. R. Newkome, C. N. Moorefield and F. Vögtle, *Dendritic Molecules. Concepts, Syntheses, Perspectives*, VCH, Weinheim 1996; J.-P. Majoral and A.-M. Caminade, *Chem. Rev.*, 1999, **99**, 845; M. Fischer and F. Vögtle, *Angew. Chem., Int. Ed.*, 1999, **38**, 884.
3 Z. Xu and J. S. Moore, *Angew. Chem., Int. Ed. Engl.*, 1993, **32**, 246; Z. Xu and J. S. Moore, *Angew. Chem., Int. Ed. Engl.*, 1993, **32**, 1354; Z. Xu, M. Kahr, K. L. Walker, C. L. Wilkins and J. S. Moore, *J. Am. Chem. Soc.*, 1994, **116**, 4537; T. Kawaguchi, K. L. Walker, C. L. Wilkins and J. S. Moore, *J. Am. Chem. Soc.*, 1995, **117**, 2159; D. J. Pesak, J. S. Moore and T. E. Wheat, *Macromolecules*, 1997, **30**, 6467.
4 P. J. Stang and F. Diederich, *Modern Acetylene Chemistry*, VCH, Weinheim 1995.
5 A. W. van der Made and P. W. N. M. van Leeuwen, *J. Chem. Soc., Chem. Commun.*, 1992, 1400; D. Seyferth, D. Y. Son, A. L. Rheingold and R. L. Ostrander, *Organometallics*, 1994, **13**, 2682; B. Alonso, I. Cuadrado, M. Morán and J. Losada, *J. Chem. Soc., Chem. Commun.*, 1994, 2575; S. W. Krska and D. Seyferth, *J. Am. Chem. Soc.*, 1998, **120**, 3604.
6 E. A. Rebrov, A. M. Muzafarov, V. S. Papkov and A. A. Zhdanov, *Dokl. Akad. Nauk SSSR.*, 1989, **309**, 376; H. Uchida, Y. Kabe, K. Yoshino, A. Kawamata, T. Tsumuraya and S. Masamune, *J. Am. Chem. Soc.*, 1990, **112**, 7077; L. J. Mathias and T. W. Carothers, *J. Am. Chem. Soc.*, 1991, **113**, 4043.
7 J. B. Lambert, J. L. Pflug and C. L. Stern, *Angew. Chem., Int. Ed. Engl.*, 1995, **34**, 98; A. Sekiguchi, M. Nanjo, C. Kabuto and H. Sakurai, *J. Am. Chem. Soc.*, 1995, **117**, 4195; J. B. Lambert, J. L. Pflug and C. L. Stern, *Organometallics*, 1998, **17**, 4904.
8 U. Krüerke, *J. Organomet. Chem.*, 1970, **20**, 83.

Communication 9/05107D

Oxidation of methyl groups in the reaction of sulfur homopolyatomic cations with acetonitrile: formation and crystal structure of the novel trithietanylium ring

T. Stanley Cameron,[a] Andreas Decken,[b] Min Fang,[b] Simon Parsons,[c] Jack Passmore*[b] and Dale J. Wood[b]

[a] *Department of Chemistry, Dalhousie University, Halifax, Nova Scotia, Canada B3H 4J3.*
[b] *Department of Chemistry, University of New Brunswick, Fredericton, New Brunswick, Canada E3B 6E2. E-mail: passmore@unb.ca*
[c] *Department of Chemistry, University of Edinburgh, King's Buildings, West Mains Road, Edinburgh, Scotland, UK EH9 3JJ*

Received (in Cambridge, UK) 21st May 1999, Accepted 16th July 1999

RCN (R = C_6F_5, Me) reacts with $S_n(AsF_6)_2$ (n = 4, 8) in liquid SO_2 to give the corresponding 3,5-disubstituted-1,2,4 thiadiazoles, and also, in the MeCN case, the tricyclic trication 4 containing the trithietanylium -$\overline{CSSS}^+$ and 1,2,3-dithiazolium -$\overline{CSSNCH}^+$ rings formed by the oxidation of methyl groups by sulfur homopolyatomic cations.

The isolation of stable soluble salts of the homopolyatomic cations of groups16 and 17[1] has allowed the exploration of their chemistry, leading to new classes of compounds.[2] Reactions of sulfur cations with F_3CCCCF_3 and CF_3CN gave the new radical cations $F_3C\overline{CSSSSCCF_3}^{+\cdot}$ **1** and $F_3C\overline{CNSSS}^{+\cdot}$ quantitatively,[3]

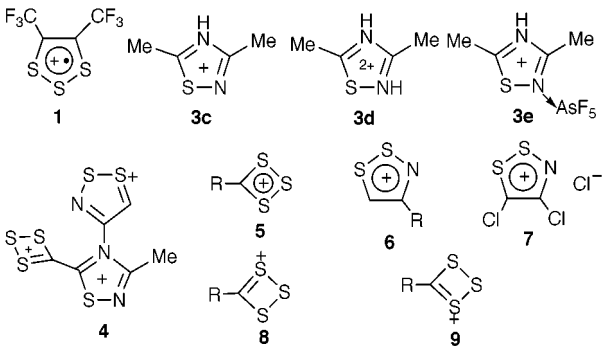

and with dicyanogen the diradical $^{+\cdot}\overline{SSSNCCNSSS}^{+\cdot}$.[4] In an attempt to probe the generality of such reactions, we found that with C_6F_5CN, **2a** and **2b** were obtained, and with MeCN, derivatives of **3a** were formed. This furnishes a new, simple, high yield synthetic route to 3,5-disubstituted 1,2,4-thiadiazoles from nitriles with relatively low ionisation energies.[5]

The reaction of an equal molar mixture of $S_4(AsF_6)_2$ and $S_8(AsF_6)_2$ with MeCN gives the AsF_6^- salt of **4**, as well as AsF_6^- salts of **3c**, **3d** and **3e**. Species **4** contains the trithietanylium ring **5**, the first example of the -$\overline{CXXX}^+$ (X = O, S, Se, and Te) heterocyclic ring system, and a 1,2,3-dithiazolium ring **6**, formed by the oxidation of the methyl groups by sulfur cations and transfer of the protons to **3a** (Scheme 1). This reaction is reminiscent of the oxidation of $ArCH_3$ to $ArCO_2H$ by strong oxidising reagents.[6] The synthesis of the chloride of **5** (R = Ph) has been claimed,[7] but no structural evidence has been reported. Fused derivatives of **6**, Herz salts, are well known,[8] and recently, the X-ray structure of **7** (Appel's salt) was determined.[9]

The structures of **2b**† and the AsF_6^- salts of **3c**,‡ **3e**§ and **4**¶ were determined by X-ray crystallography. Species **4** dimerises by weak electrostatic interactions [S(5)–N(4a) 2.946(6) Å]. The centrosymmetric dimer is shown in Fig. 1. All rings are planar, and calculated (at MPW1PW91/6-31G* level)‖ distances and

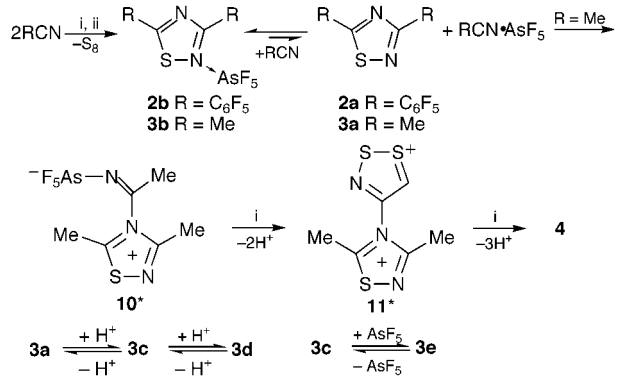

Scheme 1 *Reagent and condition*: i, $S_n(AsF_6)_2$ (n = 4 or 8); ii, liquid SO_2. * = Proposed intermediates.

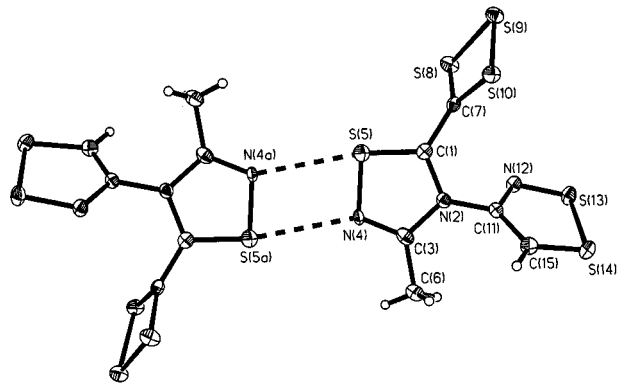

Fig. 1. ORTEP of **4** drawn at the 50% probability level. Selected bond lengths (Å), and angles (°); calculated results (MPW1PW91/6–31G*) are given in parentheses and in bold. C(1)–N(2) 1.377(7) (**1.367**), N(2)–C(3) 1.384(8) (**1.417**), C(3)–N(4) 1.332(8) (**1.300**), N(4)–S(5) 1.676(5) (**1.630**), S(5)–C(1) 1.663(6) (**1.697**), C(3)–C(6) 1.500(9) (**1.484**), C(1)–C(7) 1.450(8) (**1.451**), C(7)–S(8) 1.686(6) (**1.703**), S(8)–S(9) 2.046(2) (**2.064**), S(9)–S(10) 2.057(2) (**2.067**), S(10)–C(7) 1.692(6) (**1.705**), N(2)–C(11) 1.443(7) (**1.430**), C(11)–N(12) 1.335(7) (**1.319**), N(12)–S(13) 1.579(5) (**1.600**), S(13)–S(14) 2.041(2) (**2.063**), S(14)–C(15) 1.664(6) (**1.669**), C(15)–C(11) 1.398(8) (**1.409**); C(1)–N(2)–C(3) 111.1(5) (**111.8**), N(2)–C(3)–N(4) 115.2(5) (**113.4**), C(3)–N(4)–S(5) 109.2(4) (**112.3**), N(4)–S(5)–C(1) 94.3(3) (**94.4**), S(5)–C(1)–N(2) 110.0(4) (**108.2**), C(1)–N(2)–C(11) 122.0(5) (**126.1**), C(11)–N(2)–C(3) 126.6(5) (**122.1**), N(2)–C(3)–C(6) 122.6(6) (**124.3**), C(6)–C(3)–N(4) 122.2(6) (**122.4**), S(5)–C(1)–C(7) 123.3(4) (**122.0**), N(2)–C(1)–C(7) 126.7(5) (**129.8**), C(1)–C(7)–S(8) 124.9(4) (**123.2**), S(8)–(C7)–S(10) 107.0(3) (**106.6**), C(7)–S(8)–S(9) 85.3(2) (**85.4**), S(8)–S(9)–S(10) 82.86(8) (**82.8**), S(9)–S(10)–C(7) 84.8(2) (**85.2**), S(10)–C(7)–C(1) 127.4(4) (**129.5**), C(11)–N(12)–S(13) 115.5(4) (**116.5**), N(12)–S(13)–S(14) 98.2(2) (**97.5**), S(13)–S(14)–C(15) 93.0(2) (**92.4**), S(14)–C(15)–C(11) 114.4(4) (**115.4**), C(15)–C(11)–N(12) 118.9(5) (**118.2**), N(2)–C(11)–N(12) 116.9(5) (**118.6**), C(15)–C(11)–N(2) 124.2(5) (**123.2**).

Table 1 Observed[a] and calculated[b] (in parentheses) ^{1}H and ^{13}C NMR chemical shifts of **3a** derivatives

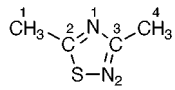

Deriv-ative	δ_H C1-H	C4-H	N1-H	N2-H	δ_C C1	C2	C3	C4
3a	2.73 (2.69)	2.53 (2.47)	—	—	15.4 (18.6)	187.9 (196.6)	173.3 (182.0)	17.4 (19.7)
3c	3.07 (3.05)	2.75 (2.89)	12.33 (9.69)	—	14.3 (16.0)	192.9 (205.0)	164.3 (173.5)	15.5 (16.9)
3d[c]	3.50 (3.85)	3.35 (3.66)	13.21 (10.50)	12.93 (10.10)	17.0 (21.1)	196.1 (214.4)	170.9 (185.3)	15.6 (19.5)
3e[c]	3.39 (3.09)	3.24 (3.47)	12.74 (9.47)	—	15.8 (16.6)	193.7 (202.7)	169.0 (175.6)	16.3 (18.3)

[a] Chemical shifts were obtained at −70 °C in liquid SO_2, using $NH_4(AsF_6)$ (δ_H 5.80) or MeCN·AsF_5 (δ_H 2.67, δ_C 110.7) as internal standards. [b] Isotropic NMR shielding tensors were calculated at the MPW1PW91/6-311G(2DF)//MPW1PW91/3-21G* level and referenced against calculated TMS values. [c] ^{1}H and ^{13}C chemical shifts were assigned based on HMQC and HMBC experiments at −70 °C.

bond angles are in good agreement with the values derived from the X-ray structure. The structure of the observed 1,2,4-thiadiazolium ring fragment in **4** does not differ significantly from that in **3c** and **3e**. Although the $-\overline{CSSS}^+$ ring is formally related to the 6π square planar S_4^{2+} ring,[1] the cyclobutadiene dianion,[10] and 1,2-dithietes,[11] it can be represented by the valence bond structures **8** and **9**, consistent with the average Pauling bond orders of 1.35 (C–S) and 1.06 (S–S).

C_6F_5CN (3.283 g; 17.00 mmol) reacted with $S_4(AsF_6)_2$[12] (2.198 g; 4.344 mmol) in SO_2 (11.917 g) in a two-bulb Pyrex glass vessel incorporating a medium sintered-glass frit (apparatus and techniques given in ref. 12). After 3 days, insoluble S_8 (FT-Raman), OSF_2, AsF_3 (gas phase IR and ^{19}F NMR), 5.136 g of a mixture of **2a** (elemental analysis, ^{19}F NMR) and **2b** (elemental analysis, ^{19}F NMR, X-ray crystal structure, MS, IR and FT-Raman), and $S_n(AsF_6)_2$ ($n \approx 19$) (colour, EPR) were identified.**

The AsF_6^- salts of **3c**, **3e** and **4** were prepared by the reaction of MeCN (0.5108 g; 12.443 mmol) and an equal molar mixture of $S_n(AsF_6)_2$ (n = 4, 8) [prepared by the reaction of S_8 (1.0222 g; 31.878 mmol) and AsF_5 (2.6668 g; 15.694 mmol) in SO_2 (12.991 g)][3] for about 15 days under strictly anhydrous conditions.[12] The overall molar ratio of MeCN, $S_4(AsF_6)_2$ and $S_8(AsF_6)_2$ was 4:1:1. After slowly removing the solvent and washing out the most soluble products (minor), the obtained mixture contained significant amounts of white needle-like crystals of the AsF_6^- salt of **3e** and dark red brick-like crystals of the AsF_6^- salt of **4**. The mixture was dissolved in SO_2, leaving insolubles (including the AsF_6^- salt of **4** and S_8), and the obtained solubles were identified as a mixture of the AsF_6^- salts of **3c**, **3d** and **3e** by multinuclear NMR studies, here and in related studies. Observed and calculated NMR results are in reasonable agreement (Table 1). OSF_2 and AsF_3 (^{19}F NMR) and minor amounts of deprotonated species (*in situ* ^{13}C studies) were also identified. The formation of S_8 indicates that sulfur cations were reduced during the deprotonation process of the methyl groups. In a related reaction of $S_4(AsF_6)_2$ and **3a**,†† crystals of the AsF_6^- salt of **3c** were obtained and the X-ray crystal structure determined.

Hitherto the chemistry of homopolyatomic sulfur and selenium cations has been restricted to hydrogen-free compounds with the exception of a preliminary report of the reaction of E_n^{2+} (E = S, Se, n = 4, 8) with alkanes and toluene giving products that included sulfides and selenides.[13] This work suggests an extensive novel organic chemistry of homopolyatomic cations of group 16, presently under investigation.

We thank Dr Ingo Krossing for valuable advice on the theoretical calculations, Dr Larry Calhoun (UNB) for his assistance with numerous NMR experiments, Dr J. Britten (McMaster University) for X-ray data collection on species **3e** AsF_6 and **4** $(AsF_6)_3$, and NSERC for an operating grant (J. P.).

Notes and references

† *Crystal data* for **2b**: $C_{14}AsF_{15}N_2S$, M = 588.14, monoclinic ($C2/c$), a = 11.967(4), b = 12.268(4), c = 24.076(5) Å, β = 96.66(3)°, U = 3511(2) Å^3, D = 2.225 g cm^{-3}, T = 293(2) K, F(000) = 2256, Z = 8, μ = 2.216 mm^{-1}, 6593 reflections measured, 3093 independent reflections, $R1$ ($wR2$) = 0.0538 (0.1347).

‡ *Crystal data* for **3c** AsF_6: $C_4H_7AsF_6N_2S$, M = 304.10, orthorhombic, space group *Pbca*, a = 11.874(3), b = 12.617(3), c = 13.005(3) Å, U = 1948.3(9) Å^3, Z = 8, D = 2.073 g cm^{-3}, T = 150(2) K, F(000) = 1184, μ = 3.757 mm^{-1}. 3649 reflections measured, 1725 independent reflections, $R1$ ($wR2$) = 0.0433 (0.0737).

§ *Crystal data* for **3e** AsF_6: $C_4H_7As_2F_{11}N_2S$, M = 474.04, orthorhombic, space group *Pnma*, a = 14.746(3), b = 8.023(2), c = 11.034(2) Å, U = 1305.4(5) Å^3, Z = 4, D = 2.412 g cm^{-3}, T = 210(2) K, F(000) = 904, μ = 5.402 mm^{-1}. 13468 reflections measured, 1502 independent reflections, $R1$ ($wR2$) = 0.0262 (0.0615).

¶ *Crystal data* **4** $(AsF_6)_3$: $C_6H_4As_3F_{18}N_3S_6$, M = 877.24, monoclinic, space group $P2_1/n$, a = 13.9666(1), b = 10.6426(1), c = 16.5839(1) Å, β = 111.285(1)°, U = 2296.90(3) Å^3, Z = 4, D = 2.537 g cm^{-3}, T = 153 K, F(000) = 1672, μ = 5.034 mm^{-1}. 24701 reflections measured, 5200 independent reflections, $R1$ ($wR2$) = 0.0593 (0.1499). The hydrogen atoms were found in difference Fourier maps and included into the refinement by a riding model. CCDC 182/1336. See http://www.rsc.org/suppdata/cc/1999/1801/ for crystallographic data in .cif format.

‖ All calculations were performed with GAUSSIAN 98W. (ref. 14). MPW1PW91 is a hybrid HF-DFT method. (ref. 15). Calculated distances and angles and observed values are in good agreement for **3c** and **3e**.

** Similar results were obtained from reaction of C_6F_5CN with an equal molar mixture of $S_n(AsF_6)_2$ (n = 4, 8).

†† Species **3a** was synthesised according to ref. 16.

1 N. Burford, J. Passmore and J. C. P. Sanders, in *From Atoms to Polymers, Isoelectronic Analogies*, VCH, Florida, 1989, p. 53 and references therein; S. Brownridge, I. Krossing, J. Passmore, H. D. B. Jenkins and H. K. Roobottom, *Coord. Chem. Rev*., 1999, in the press and references therein.
2 T. Klapötke and J. Passmore, *Acc. Chem. Res.*, 1989, **22**, 234; S. Parsons and J. Passmore, *Acc. Chem. Res.*, 1994, **27**, 101.
3 T. S. Cameron, R. C. Haddon, S. M. Mattar, S. Parsons, J. Passmore and A. P. Ramirez, *J. Chem. Soc., Dalton Trans.*, 1992, 1563; T. S. Cameron, R. C. Haddon, S. M. Mattar, S. Parsons, J. Passmore and A. P. Ramirez, *Inorg. Chem.*, 1992, **31**, 2274.
4 G. D. Enright, J. R. Morton, J. Passmore, K. F. Preston, R. C. Thompson and D. J. Wood, *Chem. Commun.*, 1996, 967.
5 D. J. Wilkins and P. A. Bradley, in *Comprehensive Hetereocyclic Compounds II*, Pergamon, Oxford, 1996, vol. 4, p. 307.
6 H. T. Clarke and E. R. Taylor, *Org. Synth.*, 1948, **Coll. Vol. 2**, 135.
7 E. Campaine, M. Pragnell and F. Haaf, *J. Heterocyc. Chem.*, 1968, **5**, 141.
8 L. I. Khmelnitski and O. A. Rakitin, in *Comprehensive Hetereocyclic Compounds II*, Pergamon, Oxford, 1996, vol. 4, p. 409.
9 S. Rabe and U. Müller, *Z. Kristallogr. New Cryst. Struct.*, 1999, **214**, 68.
10 P. J. Garratt and R. Zahler, *J. Am. Chem. Soc.*, 1978, **100**, 7753.
11 J. Nakayama, K. S. Choi, I. Akiyama and M. Hoshino, *Tetrahedron Lett.*, 1993, **34**, 115.
12 M. P. Murchie, R. Kapoor, J. Passmore, G. Schatte and T. Way, *Inorg. Synth.*, 1997, **31**, 102.
13 A. M. Rosan, *J. Chem. Soc., Chem. Commun.*, 1985, 377.
14 GAUSSIAN 98W, Revision A.3, Gaussian, Inc., Pittsburgh PA, 1998.
15 C. Adamo and V. Barone, *J. Chem. Phys.*, 1998, **108**, 664.
16 G. Kresze, A. Maschke, R. Albrecht, K. Bederke, H. P. Patzschke, H. Smalla and A. Trede, *Angew. Chem., Int. Ed. Engl.*, 1962, **1**, 89.

Communication 9/04107I

ChemComm

A new nonionic surfactant pathway to mesoporous molecular sieve silicas with long range framework order

Wenzhong Zhang, Brian Glomski, Thomas R. Pauly and Thomas J. Pinnavaia*

Department of Chemistry and Center for Fundamental Materials Research, Michigan State University, East Lansing, MI 48824-1322, USA. E-mail: pinnavai@cem.msu.edu

Received (in Oxford, UK) 16th June 1999, Accepted 2nd August 1999

Mesoporous molecular sieve silicas with ordered structures are formed from tetraethylorthosilicate (I^0) in a new reaction pathway based on nonionic $R(EO)_nH$ surfactants (N^0) and denoted $(N^0M^{n+})I^0$, wherein electrostatic forces are introduced into the assembly process through $-(EO)_nH$ complexation of small metal cations (M^{n+} = Li^+, Co^{2+}, Ni^{2+}, Mn^{2+} and Zn^{2+}).

The long-range structures of mesoporous molecular sieve silicas and other metal oxides are determined in part by the pathways used to assemble the polymerizable inorganic reagent at the surface of the structure-directing supramolecular micelle.[1] Assembly pathways that utilize electrostatic charge matching between ionic surfactants (S^+ or S^-) and inorganic reagents (I^+ or I^-) typically afford hexagonal, cubic or lamellar structures that minimize the electrostatic energy.[2,3] In contrast, coulombic forces are absent in pathways that exclusively utilize H bonding interactions between electrically neutral surfactants (S^0) and inorganic reagents (I^0).[4] Consequently, S^0I^0 pathways and related N^0I^0 pathways based on non-ionic polyethylene oxide surfactants,[5] afford disordered framework structures with wormhole-like channel motifs.[6]

Electrically neutral assembly pathways offer several attractive features for the preparation of mesoporous molecular sieve silicas.[4,5] For instance, assembly can be carried-out at near-neutral pH and relatively low reaction temperatures (20–65 °C). Also, recovery of the surfactant by simple solvent extraction can be achieved without sacrificing the surface areas and pore size fidelity obtained through charge matching pathways. In addition to these processing advantages, the pore branching and, especially, the complementary textural porosity associated with wormhole frameworks, can improve catalytic reactivity by facilitating access to reactive sites in the framework.[7] Nevertheless, long range order is desirable for certain electronic and photonic applications where structural periodicity can be important.[8]

In the present work we describe the synthesis of ordered silica mesostructures without sacrificing the processing advantages of neutral surfactant assembly. Our approach is based on a new pathway, denoted $(N^0M^{n+})I^0$, in which hydrogen bonds are formed between a cationic metal complex form of a nonionic (N^0) polyethylene oxide surfactant of the type $R(EO)_nH$ and the electrically neutral inorganic precursor (I^0). The complexation of small M^{n+} cations by the EO groups of N^0 brings the assembly process under electrostatic control and forms ordered mesostructures in much the same way as the recently reported acid-mediated $N^0(H^+X^-)I^+$ pathway,[9] except that strong acid conditions are avoided.

As shown by the representative X-ray powder diffraction pattern in Fig. 1A, one-dimensional hexagonal mesostructures were formed upon hydrolysis of tetraethylorthosilicate (TEOS) at 25–65 °C in the presence of Brij 56 [$C_{16}H_{33}(EO)_{10}H$], Triton X-100[$C_8H_{17}(C_6H_4)(EO)_{10}H$], and Tergitol 15-S-12 and the chloride salts of Co^{2+}, Ni^{2+}, Mn^{2+} and Zn^{2+} as structure modifiers at a reaction stoichiometry of H_2O/Si = 85, N^0/Si = 0.04–0.07 and M^{2+}/N^0 = 0.5–2.0. All of these structure-modifying cations are known to form complexes with polymeric EO units.[10] For each modifier, a hexagonal mesostructure was indicated by the presence of at least three XRD lines that could be indexed as 100, 110 and 200 reflections (*cf.*, Fig. 1A). Consequently, these one-dimensional hexagonal framework structures are analogous to MCM-41[2] and SBA-3 silicas[3] in long range order. In the absence of the metal ion salts, only wormhole structures with a single broad diffraction line were formed.

The incorporation of lithium chloride into the reaction mixtures also yielded hexagonal mesostructures. Interestingly, however, metals such as Fe^{3+}, Cr^{3+} and Rh^{3+} afforded only wormhole structures. The inability of these latter cations to induce long range electrostatic order presumably is related to their formation of polynuclear oxocations[11] under near neutral conditions of pH and the inability of these large ions to form stable complexes with the $(EO)_n$ segment of the N^0 surfactant.

Decreasing the divalent metal ion concentration in the reaction mixture to M^{2+}/N^0 values in the range 0.10–0.20 results in an ordered structure different from the one-dimensional hexagonal frameworks described above. Fig. 2 provides a representative TEM image and an electron diffraction pattern for this new structure in comparison with the hexagonal framework formed by $(N^0M^+)I^0$ assembly. The deviation from a hexagonal structure most likely is associated with a change in the surfactant packing parameter upon decreasing the average charge on the surfactant head group through metal ion complexation. Similar TEM images and electron diffraction patterns have been reported for electrostatically assembled cage–like frameworks with 3D hexagonal symmetry,[12] as well as for cubic and faulted 3D hexagonal–cubic structures.[13] The X-ray powder diffraction patterns of the products formed at lower M^{2+}/N^0 values contain only a single, well-resolved line (*cf.*, Fig. 1B), which precludes a definitive structural assignment. Nevertheless, the TEM and electron diffraction properties

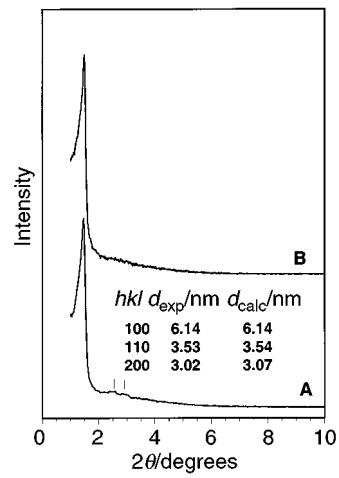

Fig. 1 XRD patterns of silica molecular sieves formed through $(N^0M^{n+})I^0$ assembly at 45 °C: (A) the product assembled at a Co^{2+}/Brij 56 ratio of 0.50; (B) the product formed at a Co^{2+}/Brij 56 ratio of 0.12. The N^0/Si ratio was 0.04 in both cases and the samples were calcined at 600 °C. Analogous patterns were obtained for solvent-extracted products.

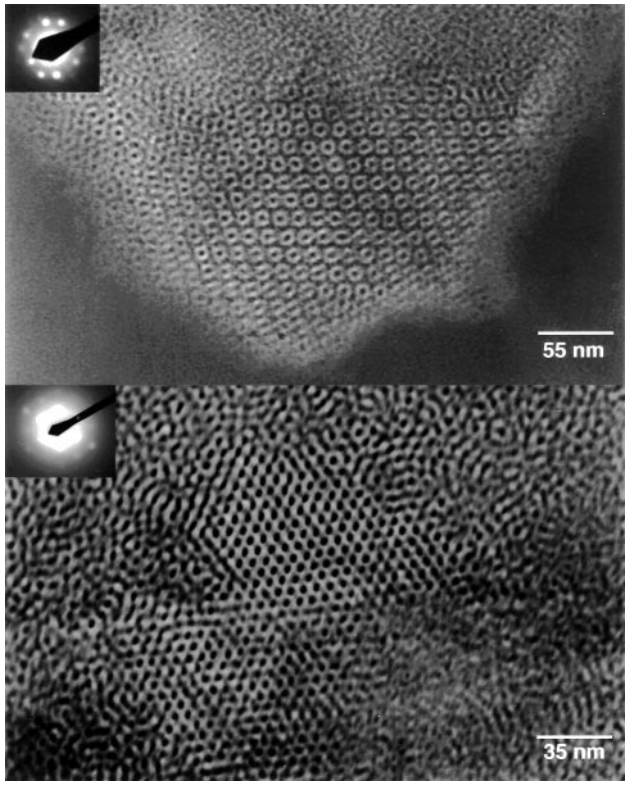

Fig. 2 TEM images and electron diffraction patterns (insets) of the silica mesostructures assembled at Co^{2+}/Brij 56 ratios of 0.50 (lower image) and 0.12 (upper image).

closely resemble the faulted 3D hexagonal–cubic structures recently observed for silica films on glass,[12] and we tentatively favor this type of 3D faulted structure.

The N^0 surfactant is easily removed from the ordered mesostructures by ethanol extraction or by calcination. Moreover, the solvent-extracted products are free of both framework metal ions and the structure-mediating metal salt. These observations are consistent with our proposed $(N^0M^{n+})I^0$ pathway, wherein hydrogen bonds are formed between the uncomplexed EO oxygen atoms of the cationic (N^0M^{n+}) complex and the silanol protons of the hydrolyzed I^0 precursor. Charge balance at the surfactant–silica interface is achieved through ion pairing with the counter anions of the metal salt. However, the anion does not play a direct structure-directing role, because the same structures are obtained regardless of the type of anion (chloride, nitrate, or acetate) used in the assembly process.

Fig. 3 shows N_2 adsorption–desorption isotherms for representative mesostructures formed in the presence of Brij 56 and Co^{2+} as the structure modifier. Pore necking in the 3D faulted structure, as suggested by the cage-like pore structure of the upper TEM image of Fig. 2, is verified by the hysteresis loop associated with the filling and emptying of the framework void space. Little or no hysteresis is observed for the one-dimensional hexagonal structure, as expected. The BET surface areas, pore volumes, and Horvath–Kawazoe pore diameters for the 3D faulted structure are 1103 $m^2\ g^{-1}$, 1.06 $cm^3\ g^{-1}$ and 6.0 nm, respectively. The corresponding values for the hexagonal mesostructures are 937 $m^2\ g^{-1}$, 0.68 $cm^3\ g^{-1}$ and 4.3 nm. These textural parameters are comparable to those for mesoporous silica molecular sieves obtained through conventional electrostatic assembly pathways. Future studies will examine the framework crosslinking and hydrothermal stability of these ordered silicas in comparison to silicas formed through other electrostatic pathways.

In conclusion, we have shown that long range structural order can be introduced through complex formation of the N^0 surfactant with small metal ions at M^{n+}/N^0 ratios in the range 0.1–2.0 and near-neutral pH. In comparison, acid mediated pathways that use comparable amounts of protons rather than complexable metal ions have been shown previously to yield only wormhole structures.[14] In order to assemble ordered silica frameworks through acid mediation of EO–based nonionic surfactants, much higher H^+/N^0 ratios, typically in the range 30–600, are needed to introduce structural order.[9] The new $(N^0M^{n+})I^0$ pathway reported here offers a promising alternative approach for introducing electrostatic forces and long range structural order into the assembly process while avoiding the need for high acid concentrations. It also avoids the need for high surfactant concentrations and liquid crystal templating (casting) as a means of generating ordered frameworks.[15]

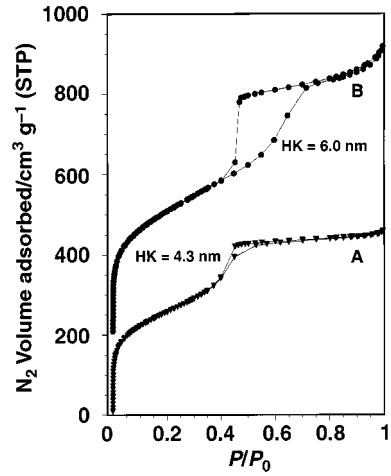

Fig. 3 N_2 adsorption–desorption isotherms for the silica mesostructures assembled at Co^{2+}/Brij 56 ratios of 0.50 (lower isotherm) and 0.12 (upper isotherm). The upper isotherm is offset by 200 $cm^3\ g^{-1}$ for clarity.

The support of this work by NSF-CRG grants CHE-9633798 and −9903706 is gratefully acknowledged.

Notes and references

1 P. Behrens, *Angew. Chem., Int. Ed. Engl*., 1996, **35**, 515.
2 C. T. Kresge, M. E. Leonowicz, W. J. Roth, J. C. Vartuli and J. S. Beck, *Nature*, 1992, **359**, 710.
3 (*a*) Q. Huo, D. I. Margolese, U. Ciesla, D. G. Demuth, P. Feng, T. E. Gier, P. Sieger, A. Firouzi, B. F. Chmelka, F. Schüth and G. D. Stucky, *Chem. Mater*., 1994, **6**, 1176; (*b*) Q. Huo, D. I. Margolese and G. D. Stucky, *Chem. Mater*., 1996, **8**, 1147.
4 P. T. Tanev and T. J. Pinnavaia, *Science*, 1995, **267**, 865.
5 S. A. Bagshaw, E. Prouzet and T. J. Pinnavaia, *Science*, 1995, **269**, 1242.
6 W. Zhang, T. R. Pauly and T. J. Pinnavaia, *Chem. Mater*., 1997, **9**, 2491.
7 T. J. Pinnavaia and W. Zhang, *Stud. Surf. Sci. Catal*., 1998, **117**, 23.
8 K. Hoffmann, D. Prescher and F. Marlow, *J. Inf. Rec. Mater*., 1998, **24**, 191.
9 D. Zhao, Q. Huo, J. Feng, B. F. Chmelka and G. D. Stucky, *J. Am. Chem. Soc*., 1998, **120,** 6024.
10 M. B. Armand, in *Polymer Electrolyte Review - 1*, ed. J. R. MacCallum and C. A. Vincent, Elsevier Applied Science, London and New York, 1987, p. 1; F. E. Bailey Jr. and J. V. Koleske, in *Alkylene Oxides and Their Polymers*, Marcel Dekker, New York, 1990.
11 J. Livage, M. Henry and C. Sanchez, *Prog. Solid State Chem*., 1988, **18**, 259.
12 Q. Huo, R. Leon, P. M. Petroff and G. D. Stucky, *Science*, 1995, **268**, 1324.
13 Y. Lu, R. Ganguli, C. A. Drewien, M. T. Anderson, C. J. Brinker, W. Gong, Y. Guo, H. Soyez, B. Dunn, M.H. Huang and J. I. Zink, *Nature*, 1997, **389**, 364.
14 S. Bagshaw, T. Kemmitt and N. B. Milestone, *Microporous Mesoporous Mater*., 1998, **22**, 419.
15 G. S. Attard, J. C. Glyde and C. G. Goltner, *Nature*, 1995, **378**, 366.

Communication 9/04803K

ChemComm

Characterization of 2,6-$Trip_2H_3C_6GaCl_2$, $\{2,6\text{-}Trip_2H_3C_6InCl(\mu\text{-}Cl)\}_2$ and $\{2,6\text{-}Trip_2H_3C_6GaCl(\mu\text{-}OH)\}_2$ (Trip = 2,4,6-triisopropylphenyl)

Brendan Twamley and Philip P. Power*

Department of Chemistry, University of California, Davis, One Shields Avenue, Davis, CA 95616 USA. E-mail: pppower@ucdavis.edu

Received (in Cambridge, UK) 25th May 1999, Accepted 26th July 1999

The spectroscopy and structures of the title compounds show that the analogous species described previously were probably contaminated by OH^- at the Cl^- positions.

A recent paper in this journal reported the terphenyl gallium and indium dichlorides $\{2,6\text{-}Trip_2H_3C_6MCl_2\}_2$ (M = Ga or In; Trip = $C_6H_2Pr^i_3$-2,4,6) which were described as having halide bridged dimeric structures.[1] Unusually, the bridging metal chloride distances [Ga–μ-Cl 2.198(5) Å, In–μ-Cl 2.235(4) Å] were shorter than those to the terminal chlorides [Ga-Cl(terminal) 2.230(5) Å, In–Cl(terminal) 2.448(7) Å]. This differs from other halide bridged structures, including the related $\{2,6\text{-}Mes_2H_3C_6MCl_2\}_2$ (Mes = $C_6H_2Me_3$-2,4,6; M = Ga, In) dimers,[2] where the M–μ-Cl distances are longer than the terminal ones.[3] The M–μ-Cl bonds also differed by only 0.037 Å in spite of the different sizes of Ga and In.† Furthermore, the cell constants for these compounds resemble those reported for $\{2,6\text{-}Trip_2H_3C_6Al(Cl)_{0.68}(H)_{0.32}(\mu\text{-}OH)\}_2{\cdot}2C_6H_6$, which arose *via* contamination of the product (presumably by H_2O) during the synthesis of the halide $\{2,6\text{-}Trip_2H_3C_6AlCl_2\}_2$ from $\{2,6\text{-}Trip_2H_3C_6AlH_2\}_2$.[4] We hypothesized that the short 'Ga–Cl' and 'In–Cl' distances might be due to contamination of the μ-Cl positions by OH^-. We resolved to isolate the terphenyl metal dihalides under the rigorous exclusion of moisture, and to react these dihalide products with H_2O in order to synthesize the hydroxides deliberately.

Reaction of $2,6\text{-}Trip_2H_3C_6Li(OEt_2)$[5] and $GaCl_3$ in Et_2O gave, initially, $2,6\text{-}Trip_2H_3C_6GaCl_2(OEt_2)$ **1a** as colorless crystals‡ which were characterized by spectroscopy. Its structure probably resembles that reported for $2,6\text{-}Mes_2H_3C_6AlCl_2(OEt_2)$.[4] Recrystallization of **1a** from hot hexane yielded $2,6\text{-}Trip_2H_3C_6GaCl_2$ **1b**,‡ whose crystal structure shows that, unlike the earlier compound,[1] it is monomeric (Fig. 1).§ The Ga atom has distorted trigonal planar coordination with Ga–Cl 2.113(4) and 2.124(3) Å and Ga–C 1.930(8) Å. These are similar to those in the only other three-coordinate, monomeric aryl gallium dichloride, Mes^*GaCl_2[6] (Mes* = $C_6H_2Bu^t_3$-2,4,6) which was characterized by two groups who reported the bond distances: Ga–C 1.935(4) Å (av.), Ga–Cl 2.157(1) Å (av.); Ga–C 1.953(13) Å, Ga–Cl 2.212(4) Å.

The reaction of $2,6\text{-}Trip_2H_3C_6Li(OEt_2)$[5] with $InCl_3$ gave $\{2,6\text{-}Trip_2H_3C_6InCl_2\}_2$ **2** which was characterized by spectroscopy‡ and X-ray diffraction.§ There is ^1H NMR evidence that an Et_2O adduct of **2** (similar to **1a**) is formed, but dissociation of Et_2O is readily effected by recrystallization from hexane. It crystallizes as a centrosymmetric dimer (Fig. 2) whose structural details differ markedly from those previously reported.[1] Notably, the distance of 2.5239(7) Å is *ca.* 0.28 Å longer than the In–μ-Cl lengths 2.236(4) and 2.233(4) Å given earlier.[1] Also, the terminal In–Cl distance in **2**, 2.3341(12) Å, is *ca.* 0.11 Å shorter than the published In–Cl(terminal) distance, 2.448(7) Å. The In–C and In–Cl distances in **2** are in agreement with those in other halide bridged In compounds, *e.g.* $\{2,6\text{-}Mes_2H_3C_6InCl_2\}_2$,[2] In–μ-Cl 2.519(2), 2.514(2) Å, In–Cl(terminal) 2.344(3) Å; $\{In(CH_2CMe_3)(CH_2SiMe_3)Cl\}_2$,[3d] In–μ-Cl 2.659(3), 2.572(3) Å.

To show that the original structure of '$\{2,6\text{-}Trip_2H_3C_6GaCl_2\}_2$'[1] could have been contaminated with OH^- at the bridging positions, H_2O was added to **1b** in THF.‡ Crystals of $\{2,6\text{-}Trip_2H_3C_6GaCl(\mu\text{-}OH)\}_2{\cdot}2C_6H_6$ **3** have cell parameters which resemble those of '$\{2,6\text{-}Trip_2H_3C_6GaCl_2\}_2$'[1] and $\{2,6\text{-}Trip_2H_3C_6Al(Cl)_{0.68}(H)_{0.32}(\mu\text{-}OH)\}_2{\cdot}2C_6H_6$.[4] It has a centrosymmetric OH^- bridged structure with terminal Ga–Cl bonds (Fig. 3).§ The Ga–μ-O distances, 1.932(4) and 1.906(4) Å, are close to those in related OH^- bridged compounds, *e.g.* $\{2,4,6\text{-}(CF_3)_3H_2C_6GaCl(\mu\text{-}OH)\}_2$,[7] Ga-O 1.903(4), 1.895(4) Å; $\{Mes_2Ga(\mu\text{-}OH)\}_2{\cdot}THF$,[8] Ga–O 1.949(2) Å; $\{[(Me_3Si)_2CH]_2Ga(\mu\text{-}OH)\}_2$,[9] Ga–O 1.963(4), 1.976(4) Å. The terminal Ga–Cl and Ga–C distances, 2.1465(19) and 1.949(5) Å, in **3** are similar to those in **1b** and related compounds.

The data for **1b**, **2** and **3** lead to the following conclusions: (a) $2,6\text{-}Trip_2H_3C_6GaCl_2$ **1b** is a monomer owing to the large size of the C_6H_3Trip-2,6 ligand and the dimeric structure of the In compound **2** is due to the larger size of In which reduces steric crowding and permits association; (b) the dimeric structure of **3** results from contamination of the μ-Cl^- ligands by OH^-, and since the originally reported short 'Ga–Cl' and 'In–Cl' distances lie about halfway between those expected for bridging

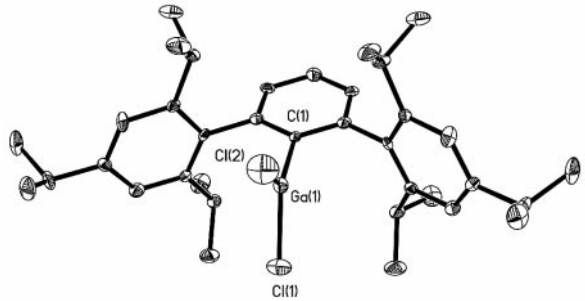

Fig. 1 Drawing of **1b** (30% probability). H atoms not shown. Selected bond lengths (Å) and angles: Ga(1)–C(1) 1.930(8), Ga(1)–Cl(1) 2.124(3), Ga(1)–Cl(2) 2.113(4); C(1)–Ga(1)–Cl(1) 124.0(3), C(1)–Ga(1)–Cl(2) 127.5(3), Cl(1)–Ga(1)-Cl(2) 108.54(14).

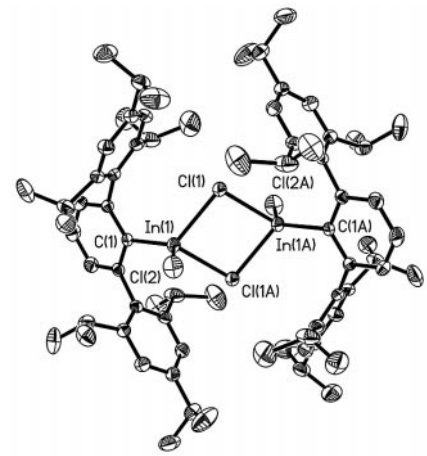

Fig. 2 Drawing of **2** (30% probability). H atoms not shown. Selected bond lengths (Å) and angles (°): In(1)–C(1) 2.145(3), In(1)–Cl(1) 2.5239(7), In(1)–Cl(2) 2.3341(12); C(1)–In(1)–Cl(2) 128.19(9), C(1)–In(1)–Cl(1) 119.01(6), Cl(2)–In(1)–Cl(1) 98.51(2), In(1)–Cl(1)–In(1A) 96.85(3).

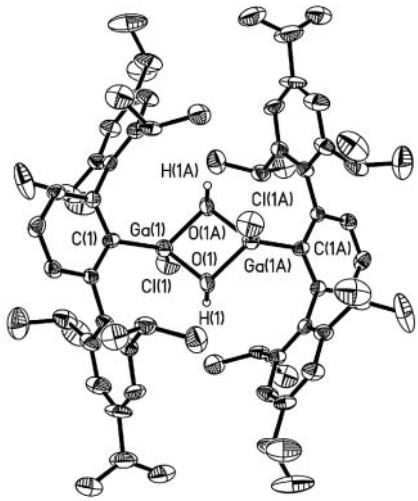

Fig. 3 Drawing of the structure of **3** (30% probability). H atoms not shown. Selected bond lengths (Å) and angles (°): Ga(1)–C(1) 1.949(5), Ga(1)–O(1) 1.932(4), Ga(1)–(O1A) 1.906(4), Ga(1)–Cl(1) 2.1465(19); C(1)–Ga(1)–Cl(1) 126.23(17), Ga(1)–O(1)–Ga(1A) 99.94(19), O(1A)–Ga(1)–Cl(1) 104.33(14).

M–OH and M–Cl (M = Ga, In) bonds, the contamination of the μ–Cl^- positions by OH^- ions is 50% which is sufficient to produce the apparent 'dimerization'; (c) the M–Cl distances in both **1b** and **2** are normal, and there is no shortening in the bridging In–Cl distance which is *ca*. 0.29 Å longer than the terminal In–Cl bond.

We note that the hydrolysis of related organogallium compounds to give Ga–OH products has been investigated in detail,[8,10] and the susceptibility of **1b** and **2** to hydrolysis agrees with these studies. The ability of OH^- ligands to occupy Cl^- sites bears some similarity to the bond stretch isomerism controversy where 'short' M–Cl (or 'long' M–O) bonds were shown to be a result of occupancy of the same site by different percentages of the O or Cl atoms rather than a new type of bonding isomerism.[11]

Notes and references

† The effective ionic radius of four coordinate Ga^{3+} is 0.47 Å and that of In^{3+} is 0.62 Å: R. D. Shannon, *Acta Crystallogr., Sect. A*, 1976, **32**, 751.

‡ *Experimental*: **1a**: under anaerobic and anhydrous conditions, 2,6-$Trip_2H_3C_6Li{\cdot}OEt_2$ (7.90 g, 14 mmol) in Et_2O (40 mL) at 0 °C was added dropwise (0.5 h) to freshly sublimed $GaCl_3$ (2.47 g, 14 mmol) in Et_2O (20 mL) at *ca*. −78 °C. The mixture was stirred at *ca*. −78 °C (3 h) before warming to *ca*. 20 °C. After stirring for 2 d, the solvent was removed and the residue was extracted with hexane (80 mL) and filtered (Celite). Concentration to incipient crystallization (*ca*. 40 mL) and cooling to *ca*. −25 °C yielded colorless crystals of **1a**, 7.60 g, 78%. Anal. calc. (found) for $C_{40}H_{59}Cl_2GaO$: C, 68.98 (68.53), H, 8.54 (8.91)%. ^{1}H NMR (300 MHz, C_6D_6) δ 0.82 [t, 6H, $(CH_3CH_2)_2O$], 1.15 [d, 12H, *o*-CH(CH_3)$_2$, $^3J_{HH}$ 6.6 Hz], 1.29 [d, 12H, *p*-CH(CH_3)$_2$, $^3J_{HH}$ 6.9 Hz], 1.53 [d, 12H, *o*-CH(CH_3)$_2$, $^3J_{HH}$ 6.0 Hz], 2.88 [sept, 2H, *p*-C*H*$(CH_3)_2$, $^3J_{HH}$ 6.6 Hz], 3.14 [q, 4H + 4H, $(CH_3CH_2)_2O$ + *o*-C*H*$(CH_3)_2$, J_{HH} 6.9 Hz], 7.19–7.28 [m, 7H, *p*-C_6H_3, *m*-Trip (7.24, s), *m*-C_6H_3]; ^{13}C{^{1}H} NMR (75 MHz, C_6D_6) δ 14.3 [($CH_3CH_2)_2O$], 23.1 [*p*-CH(CH_3)$_2$], 24.4 [*o*-CH(CH_3)$_2$], 26.2 [*o*-CH(CH_3)$_2$], 31.1 [*o*-C*H*$(CH_3)_2$], 34.8 [*p*-C*H*$(CH_3)_2$], 66.1 [$(CH_3CH_2)_2O$)], 121.0 (*m*-Trip), 128.2 (*p*-C_6H_3), 130.1 (*m*-C_6H_3), 138.8 (*ipso*-Trip), 147.4 (*p*-Trip), 147.8 (*o*-Trip), 148.8 (br, *o*-C_6H_3), the *ipso* C resonance was not observed. **1b**: **1a** (6.5 g, 0.93 mmol) in hexane (100 mL) was concentrated to *ca*. 50 mL. The precipitates were redissolved by heating and **1b** crystallized on standing at *ca*. 20 °C. Yield 5.0 g, 87%. Mp 230 °C sweats, 244 °C partial melt, 258–260 °C complete melt. Anal. calc. (found) for $C_{36}H_{49}Cl_2Ga$: C, 69.47 (68.90), H, 7.94 (8.11)%. IR ν_{Ga-Cl} 400s, 330s br cm^{-1}; ^{1}H NMR (300 MHz, C_6D_6) δ 1.06 [d, 12H, *o*-CH(CH_3)$_2$, $^3J_{HH}$ 6.9 Hz], 1.26 [d, 12H, *p*-CH(CH_3)$_2$, $^3J_{HH}$ 6.9 Hz], 1.42 [d, 12H, *o*-CH(CH_3)$_2$, $^3J_{HH}$ 6.9 Hz], 2.84 [sept, 2H, *p*-C*H*$(CH_3)_2$, $^3J_{HH}$ 6.9 Hz], 2.94 [sept, 4H, *o*-C*H*$(CH_3)_2$, $^3J_{HH}$ 6.9 Hz], 7.17–7.24 [m, 7H, *p*-C_6H_3, *m*-Trip (7.21, s), *m*-C_6H_3]; ^{13}C{^{1}H} NMR (75 MHz, C_6D_6) δ 22.5 [*p*-CH(CH_3)$_2$], 24.3 [*o*-CH(CH_3)$_2$], 26.3 [*o*-CH(CH_3)$_2$], 31.1 [*o*-C*H*$(CH_3)_2$], 34.8 [*p*-C*H*$(CH_3)_2$], 121.8 (*m*-Trip), 128.3 (*p*-C_6H_3), 129.1 (*m*-C_6H_3), 137.8 (*ipso*-Trip), 146.8 (*p*-Trip), 147.3 (*o*-Trip), 150.3 (*o*-C_6H_3), 171.6 (*ipso*-C_6H_3). **2**: A solution of 2,6-$Trip_2H_3C_6Li{\cdot}OEt_2$ (3.95 g, 7.02 mmol) in Et_2O (40 mL) was added to a suspension of $InCl_3$ (1.55 g, 7.02 mmol) in Et_2O (20 mL) at *ca*. −78 °C. The mixture was stirred at ca. −78° C (1 h), before warming to *ca*. 20 °C, and stirred overnight. The solvent was removed and the residue was extracted with hexane (100 mL), and filtered (Celite). The pale yellow solution was concentrated to *ca*. 20 mL and heated to redissolve the precipitates. Standing at *ca*. 20 °C afforded colorless crystalline **2**, 3.74 g, 80%. Mp 160 °C opaque, 226 °C sweats, 236–238 °C melt. Anal. calc. (found) for $C_{72}H_{98}Cl_4In_2$: C, 64.78 (64.01), H, 7.39 (8.2)%. IR ν_{In-Cl} 335s br cm^{-1}; ^{1}H NMR (300 MHz, C_6D_6) δ 1.05 [d, 24H, *p*-CH(CH_3)$_2$, $^3J_{HH}$ 6.6 Hz], 1.36 [d, 24H, *o*-CH(CH_3)$_2$, $^3J_{HH}$ 6.9 Hz], 1.44 [d, 24H, *o*-CH(CH_3)$_2$, $^3J_{HH}$ 6.9 Hz], 2.90 [m, 12H, *p*-C*H*$(CH_3)_2$ + *o*-C*H*$(CH_3)_2$, $^3J_{HH}$ 6.6 Hz], 7.11 (t, 2H, *p*-C_6H_3, $^3J_{HH}$ 7.5 Hz), 7.21 (s, 8H, *m*-Trip), 7.22 (d, 4H, *m*-C_6H_3, $^3J_{HH}$ 13.2 Hz); ^{13}C{^{1}H} NMR (75 MHz, C_6D_6) δ 23.1 [*p*-CH(CH_3)$_2$], 24.4 [*o*-CH(CH_3)$_2$], 26.2 [*o*-CH(CH_3)$_2$], 31.0 [*o*-CH(CH_3)$_2$], 34.9 [*p*-C*H*$(CH_3)_2$], 121.8 (*m*-Trip), 128.9 (*p*-C_6H_3), 129.8 (*m*-C_6H_3), 138.5 (*ipso*-Trip), 147.1 (*p*-Trip), 148.1 (*o*-Trip), 149.8 (*o*-C_6H_3), *ipso* C resonance not observed. **3**: H_2O (33 μL, 1.85 mmol) was added to **1b** (1.15 g, 1.85 mmol) in THF (40 mL) at *ca*. 0 °C and stirred (2 d). The solvent was removed under reduced pressure and the residue was extracted with C_6H_6 (40 mL), filtered (Celite) and concentrated to *ca*. 10 mL. The solution was cooled to *ca*. 5 °C (2 weeks) to afford **3** as colorless crystals, 1.08 g, 90%. Anal. calc. (found) for $C_{72}H_{100}Cl_2Ga_2O_2$: C, 71.59 (72.31); H, 8.34 (8.62)%. Mp 215 °C sweats, 227–229 °C melt. IR ν_{OH} 3440br, 3200br, ν_{Ga-Cl} 380s, 330s br cm^{-1}; ^{1}H NMR (300 MHz, $CDCl_3$) δ 0.94 [d, 24H, *o*-CH(CH_3)$_2$, $^3J_{HH}$ 6.9 Hz], 1.13 [d, 24H, *o*-CH(CH_3)$_2$, $^3J_{HH}$ 6.6 Hz], 1.17 [d, 24H, *p*-CH(CH_3)$_2$, $^3J_{HH}$ 6.75 Hz], 2.58 [sept, 8H, *o*-C*H*$(CH_3)_2$, $^3J_{HH}$ 6.75 Hz], 2.815 (sept, 4H, *p*-C*H*$(CH_3)_2$, $^3J_{HH}$ 6.9 Hz], 4.00 (s, br 2H, OH), 6.97 (s, 8H, *m*-Trip), 7.10 (d, 4H, *m*-C_6H_3, $^3J_{HH}$ 7.5 Hz), 7.31 (t, 2H, *p*-C_6H_3, $^3J_{HH}$ 7.5 Hz); ^{13}C{^{1}H} NMR (75 MHz, $CDCl_3$) δ 22.6 [*p*-CH(CH_3)$_2$], 24.1 [*o*-CH(CH_3)$_2$], 25.7 [*o*-CH(CH_3)$_2$], 30.5 [*o*-C*H*$(CH_3)_2$], 34.4 [*p*-C*H*$(CH_3)_2$], 120.9 (*m*-Trip), 127.9 (*p*-C_6H_3), 128.9 (*m*-C_6H_3), 137.8 (*ipso*-Trip), 146.6 (*p*-Trip), 147.4 (*o*-Trip), 149.2 (*o*-C_6H_3), *ipso C* resonance not observed.

§ *Crystal data* at 130 K for **1b** and 299 K for **2** and **3**, with Mo-Kα (λ = 0.71073 Å) radiation: **1b**: $C_{36}H_{49}Cl_2Ga$, M = 622.37, orthorhombic, space group *Pbcm*, a = 11.069(2), b = 12.170(2), c = 25.275(5) Å, V = 3404.8(12) Å^3, Z = 4, D_c = 1.214 Mg m^{-3}, μ = 0.987 mm^{-1}, scan type ω scans, θ range 1.6–22.50°. GoF on F^2 0.999 for 2287 unique observed data and 190 parameters, R_1 = 0.0676, wR_2 = 0.1096. **2**: $C_{72}H_{98}Cl_4In_2$, M = 1334.94, orthorhombic, space group *Cmca*, a = 25.6540(13), b = 21.2270(11), c = 12.7609(6) Å, V = 6949.0(6) Å^3, Z = 4, D_c = 1.276 Mg m^{-3}, μ = 0.855 mm^{-1}, scan type ϕ and ω scans, θ range 1.92–29.00°. GOF on F^2 1.058 for 4706 unique observed data and 203 parameters, R_1 = 0.0418, wR_2 = 0.0691. **3**·$2C_6H_6$: $C_{84}H_{112}Cl_2Ga_2O_2$, M = 1364.08, monoclinic, space group $P2_1/c$, a = 14.2605(10), b = 15.9037(10), c = 18.0905(12) Å, β = 108.613(2)°, V = 3888.2(4) Å^3, Z = 2, D_c = 1.165 Mg m^{-3}, μ = 0.805 mm^{-1}, scan type ϕ and ω scans, θ range 1.75–22.50°. GOF on F^2 1.017 for 5074 unique observed data and 419 parameters, R_1 = 0.0620, wR_2 = 0.1037.

CCDC 182/1347. See http://www.rsc.org/suppdata/cc/1999/1805/ for crystallographic files in .cif format.

1 J. Su, X.-W. Li, and G.H. Robinson, *Chem. Commun.*, 1998, 2015.
2 G. H. Robinson, X.-W. Li and W. T. Pennington, *J. Organomet. Chem.*, 1995, **501**, 399; R. C. Crittendon, X.-W. Li, J. Su and G. H. Robinson, *Organometallics*, 1997, **16**, 2443.
3 *E.g.* (*a*) O. T. Beachley, R. B. Hallock, H. M. Zhang and J. L. Atwood, *Organometallics*, 1985, **4**, 1675; (*b*) R. D. Schluter, H. S. Isom, A. H. Cowley, D. A. Atwood, R. A. Jones, F. Olbrich, S. Corbelin and R. J. Lagow, *Organometallics*, 1994, **13**, 4058; (*c*) M. B. Power, W. M. Cleaver, A. W. Apblett, A. R. Barron and J. W. Ziller, *Polyhedron*, 1992, **11**, 477; (*d*) M. F. Self, A. T. McPhail, L. J. Jones III, R. L. Wells and J. C. Huffman, *Polyhedron*, 1994, **13**, 199.
4 R. J. Wehmschulte, W. J. Grigsby, B. Schiemenz, R. A. Bartlett and P. P. Power, *Inorg. Chem.*, 1996, **35**, 6694.
5 B. Schiemenz and P. P. Power, *Organometallics*, 1996, **15**, 958.
6 (*a*) M. A. Petrie, P. P. Power, H. V. Rasika Dias, K. Ruhlandt-Senge, K. M. Waggoner and R. J. Wehmschulte, *Organometallics*, 1993, **12**, 1086; (*b*) S. Schulz, S. Pusch, E. Pohl, S. Dielkus, R. Herbst-Irmer, A. Meller and H. W. Roesky, *Inorg. Chem.*, 1993, **32**, 3343.
7 R. D. Schluter, H. S. Isom, A. H. Cowley, D. A. Atwood, R. A. Jones, F. Olbrich, S. Corbelin and R. J. Lagow, *Organometallics*, 1994, **13**, 4058.
8 J. Storre, A. Klemp, H. W. Roesky, H.-G. Schmidt, M. Noltemeyer, R. Fleischer and D. Stalke, *J. Am. Chem. Soc.*, 1996, **118**, 1380.
9 W. Uhl, I. Hahn, M. Koch and M. Layh, *Inorg. Chim. Acta*, 1996, **249**, 33.
10 C. Schnitter, H. W. Roesky, T. Albers, H.-G. Schmidt, C. Ropken, E. Parisini and G. M. Sheldrick, *Chem. Eur. J.*, 1997, **3**, 1783.
11 G. Parkin, *Acc. Chem. Res.*, 1992, **25**, 455; G. Parkin, *Chem. Rev.*, 1993, **93**, 887.

Communication 9/04212A

First example of B–C bond cleavage in the BAr_F ($B[C_6H_3(CF_3)_2\text{-}3,5]_4$) anion mediated by a transition metal species, *trans*-$[(Ph_3P)_2Pt(Me)(OEt_2)]^+$

Wayde V. Konze, Brian L. Scott and Gregory J. Kubas*

Chemical Science and Technology Division, MS J514, Los Alamos National Laboratory, Los Alamos, NM 87545, USA. E-mail: kubas@lanl.gov

Received (in Bloomington, IN, USA) 22nd March 1999, Revised version received 26th July 1999, Accepted 28th July 1999

The first example of transition metal-mediated decomposition of the widely used BAr_F anion (BAr_F = $B[C_6H_3(CF_3)_2\text{-}3,5]_4$) has been accomplished by mild heating of the cationic platinum complex *trans*-$[(Ph_3P)_2Pt(Me)(OEt_2)]^+(BAr_F)^-$ in low-coordinating solvents to form the diarylated product *trans*-$(Ph_3P)_2Pt(Ar_F)_2$ in good yield, thus demonstrating that such non-interacting anions can react with electrophilic transition metal complexes.

The incorporation of non-coordinating, low-interacting anions for the stabilization of reactive transition metal cations has proven to be very useful for carrying out interesting bond-cleavage reactions, catalytic polymerization reactions and for stabilizing weakly coordinating ligands.[1] In order for these reactions to be successful, the anion must not coordinate to the vacant site, and must not react with the metal center. The BAr_F ($B[C_6H_3(CF_3)_2\text{-}3,5]_4$) anion has been used widely in this respect because of its ease of preparation and extremely robust character toward a variety of reactive transition metal cations.[2] Recently, however, the BAr_F anion was found to coordinate to various metal complexes in either η^3-, η^4- or η^6-fashion,[3] indicating that this anion can coordinate to suitable transition metal fragments.

Although the non-fluorinated BPh_4^- anion has been shown to be relatively reactive, displaying a marked tendency to act as a phenylating agent toward transition metal cations,[4] there have been no reported examples of arylation reactions between the BAr_F anion and transition metal centers. We herein report the first example of the reaction of the BAr_F anion with a transition metal cation in the complex *trans*-$[(Ph_3P)_2Pt(Me)(OEt_2)]^+(BAr_F)^-$ **1a**, which decomposes to form the diarylated complex *trans*-$(Ph_3P)_2Pt(Ar_F)_2$ **2** under mild conditions.

The complex *trans*-$[(Ph_3P)_2Pt(Me)(OEt_2)]^+(BAr_F)^-$ **1a** was prepared by reacting $(Ph_3P)_2Pt(Me)_2$ with $[H(OEt_2)_2]^+BAr_F^-$ in Et_2O at room temperature. Compound **1a** is stable in Et_2O solution for several weeks at −30 °C, and is stable indefinitely at −30 °C as an isolated solid. However, when **1a** was placed in benzene and allowed to stand at room temperature for 5 days, the compound *trans*-$(Ph_3P)_2Pt(Ar_F)_2$ **2** formed as colorless crystals [eqn. (1)].† The reaction was also more conveniently

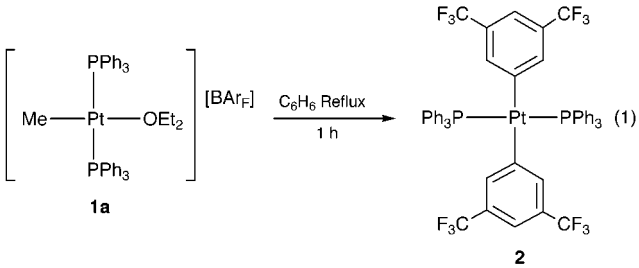

1a **2** (1)

carried out by refluxing **1a** in toluene for 20 min. Complex **2** was characterized by elemental analysis, ^1H NMR and $^{31}P\{^1H\}$ NMR,† and the structure was determined by X-ray diffraction studies.‡ A characteristic feature of the ^1H NMR spectrum of **2** is the downfield shift of the Ar_F resonances and the change in relative peak heights; the BAr_F anion has peaks at δ 7.73 and 7.58 in a 2:1 ratio, while the coordinated Ar_F group in **2** exhibits peaks at δ 8.25 and 8.05 in a 1:2 ratio. The molecular structure of **2** (Fig. 1) shows that the platinum is in a square planar environment, with the bis(trifluoromethyl)phenyl groups located *trans* to each other and at an angle of 72.6° to the plane defined by Pt(1), P(1), P(1A), C(19) and C(19A).‡

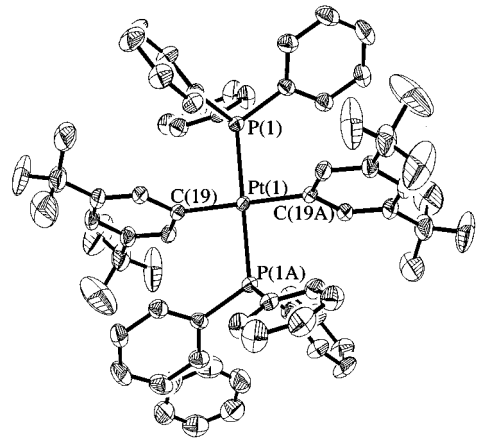

Fig. 1 Molecular structure of **2** showing the atom numbering scheme (50% probability ellipsoids). Selected bond distances (Å) and angles (°): Pt(1)–C(19) 2.083(2), Pt(1)–P(1) 2.3180(5), C(19)–Pt(1)–P(1) 91.73(6), C(19)–Pt(1)–P(1A) 88.27(6).

The formation of **2** entails the net transfer of two 3,5-bis(trifluoromethyl)phenyl groups from the BAr_F anion to the platinum center, constituting the first example of aryl group transfer from the BAr_F anion. Although this reaction is unprecedented for the BAr_F anion, similar reactions have been carried out with the BPh_4 anion; the metathesis reaction [eqn. (2)] of $[(PhMe_2P)_2Pt(Me)(solv)]^+$ with $NaBPh_4$ results in the

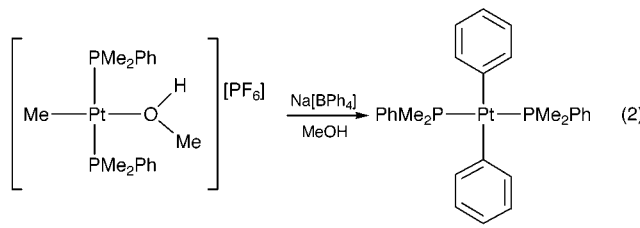

(2)

formation of the neutral bis(phenyl)platinum derivative $(PhMe_2P)_2Pt(Ph)_2$.[5] It was determined from these studies that weakly bound ligands (*e.g.*, $F_2C{=}CFH$) in place of the coordinated solvent molecules enhanced the phenylation reaction. In a separate study,[6] the mechanism of phenyl transfer from the BPh_4 anion to the dicationic platinum species $[Pt(solv)_2(L)_2]^{2+}$ (L = PMe_3, PEt_3, PPh_3; solv = H_2O, MeOH) to form $[Pt(Ph)(solv)(L)_2]^+$ was investigated. It was found that

the actual phenylating species is BPh_3, which was formed from proton-induced decomposition of the BPh_4 anion to form BPh_3 and PhH. The coordinated solvent molecules in $[Pt(solv)_2(L)_2]^{2+}$ were assumed to be acidic enough to cause the decomposition of the BPh_4 anion. It is doubtful that a similar mechanism is occurring in the decomposition of **1a**, as the coordinated Et_2O molecule does not contain acidic protons which could cause the decomposition of the BAr_F anion. Instead, this reaction most likely proceeds through an initial step that involves electrophilic attack of the platinum cation on one of the aryl groups of the BAr_F anion. The fate of the methyl ligand is not known, but no methane was evolved during the reaction.

In order to determine the effects of the ligands on the arylation reaction, both the coordinated solvent and the phosphine ligands were varied in **1a**. Complexes containing both coordinated MeCN and MeOH were prepared by dissolving **1a** in MeCN and MeOH, respectively, and precipitating out *trans*-$[(Ph_3P)_2Pt(Me)(NCMe)]^+(BAr_F)^-$ **1b** and *trans*-$[(Ph_3P)_2Pt(Me)(MeOH)]^+$ $(BAr_F)^-$ **1c** as solids.† The ^{1}H NMR spectrum of **1b** was almost identical to the known compound *trans*-$[(Ph_3P)_2Pt(Me)(NCMe)]^+(BF_4)^-$,[7] and exhibited a singlet at δ 1.157 corresponding to coordinated MeCN, which disappeared when CD_3CN was added. Complex **1c** exhibited a signal at δ 2.684 corresponding to coordinated MeOH, which disappeared when CD_3OD was added. When **1b** was refluxed in either benzene or toluene under identical conditions to that of **1a**, there was no evidence for formation of **2**. However, when **1c** was refluxed in toluene under identical conditions, **2** formed in roughly the same yield as from the reaction of **1a**. Evidently, the more weakly bound Et_2O and MeOH ligands allow the aryl group transfer to occur in order to form **2**, while the more stongly bound MeCN ligand prevents this reaction from taking place.

In order to examine the effects of the phosphine ligand on the aryl group transfer, the complexes *trans*-$[(Pr^i_3P)_2Pt(Me)(OEt_2)]^+(BAr_F)^-$ **1d** and *trans*-$[(Et_3P)_2Pt(Me)(OEt_2)]^+(BAr_F)^-$ **1e** were synthesized analogously to the preparation of **1a**. After refluxing **1d** in toluene for several hours, there was no evidence of B–C bond cleavage. However, the less sterically encumbered **1e** reacted after refluxing for 10 min in benzene. A mixture of platinum complexes formed which could not be identified, but clear crystals were obtained from benzene which were characterized by X-ray diffraction to be $B[C_6H_3(CF_3)_2\text{-}3,5]_3$ **3**, the structure of which has not been previously reported.‡ Although this reaction gave different results than the decomposition of **1a**, it still indicates that B–C cleavage takes place with this more basic, less steric phosphine. Evidently, bulky phosphines do not allow this reaction to take place, which is consistent with the transition metal cation attacking the bulky BAr_F anion.

The aryl group transfer from the BAr_F anion to the platinum metal center in *trans*-$[(Ph_3P)_2Pt(Me)(OEt_2)]^+(BAr_F)^-$ **1a** represents the first example of a transition metal-mediated decomposition of the normally non-interacting BAr_F anion and serves to alert those who use this anion to the possibility of its reactivity. The mechanism of this reaction is unclear, but we have found that the coordinated solvent must be a weak ligand (Et_2O, MeOH), the solvent for the decomposition reaction must be non-coordinating, and the phosphine ligands must not be too bulky in order for this reaction to proceed. Preliminary results indicate that analogs of **1a** containing isocyanides instead of phosphines allow similar B–C bond cleavage reactions to proceed immediately at room temperature. These results indicate that the initial step of this reaction is electrophilic attack of the platinum cation on an aryl group of the BAr_F anion, which is consistent with the fact that both a sterically accessible metal center and a weakly occupied coordination site are necessary for aryl group transfer to occur.

Notes and references

† *Experimental procedures*: **1a:** to a stirred Et_2O solution (10 mL) of $[H(OEt_2)_2]^+BAr_F^-$ (0.135 g, 0.133 mmol) at room temp. was added $(Ph_3P)_2Pt(Me)_2$ (0.100 g, 0.133 mmol) as a solid. Evolution of methane began immediately, and after 5 min the solution was clear and colorless. The volume was reduced to 3 mL, and 10 mL of hexanes was then added. The volume was reduced to *ca.* 8 mL and placed in a −30 °C freezer for 1 day to obtain a white, crystalline solid. The filtrate was decanted off, the solids were washed with 3 × 5 mL of hexanes at −30 °C and dried under vacuum to give **1a** (0.195 g, 87%). ^{1}H NMR (CD_2Cl_2, −80 °C): δ 7.73 (s, 8H, BAr_F), 7.21–7.62 (34H, Ph + BAr_F), 3.53 (br, 4H, ether CH_2), 1.16 (t, J_{HH} = 7.05 Hz, 6H, ether CH_3), 0.73 (t, J_{HP} 6.75, J_{HPt} 71.0 Hz, 3H, Pt–Me). ^{31}P{^{1}H} NMR (CD_2Cl_2, −80 °C): δ 31.3 (s, J_{PPt} 3195 Hz). Anal. Calc. for $C_{75}H_{55}BF_{24}OP_2Pt$: C, 52.44; H, 3.32. Found: C, 52.43; H, 3.59%.

1b and **1c:** complex **1a** (0.100 g, 0.0598 mmol) was dissolved in 10 mL of either MeCN (for **1b**) or MeOH (for **1c**) at room temp. and stirred for 15 min. The solvent was removed under vacuum, the oily residue was dissolved in 2 mL of CH_2Cl_2 and 15 mL of hexanes was then added. After cooling overnight at −30 °C, off-white crystals formed which were isolated by removing the filtrate and drying under vacuum to give **1b** (0.0905 g, 92%) or **1c** (0.0854 g, 90%). For **1b**: ^{1}H NMR (CD_2Cl_2, 25 °C): δ 7.53–7.75 (42H, Ph + BAr_F), 1.16 (br, 3H, MeCN), 0.28 (t, 3H, J_{HP} 7.05, J_{HPt} 78.3 Hz, Pt–Me). ^{31}P{^{1}H} NMR (CD_2Cl_2, 25 °C): δ 27.2 (s, J_{PPt} 3008 Hz). Anal. Calc. for $C_{71}H_{48}BF_{24}NP_2Pt$: C, 52.03; H, 2.95; N, 0.85. Found: C, 52.41; H, 3.04; N, 0.84%. For **1c**: ^{1}H NMR (CD_2Cl_2, 25 °C): δ 7.53–7.75 (42H, Ph + BAr_F), 2.68 (br, 3H, CH_3OH), 0.612 (t, 3H, J_{HP} 6.90, J_{HPt} 87.6 Hz, Pt–Me). ^{31}P{^{1}H} NMR (CD_2Cl_2, 25 °C): δ 32.4 (s, J_{PPt} 3114 Hz). Anal. Calc. for $C_{70}H_{49}BF_{24}OP_2Pt$: C, 51.58; H, 3.03. Found: C, 51.63; H, 3.03%.

2: complex **1a** (0.200 g, 0.120 mmol) was dissolved in toluene (5 mL) and heated to reflux for 20 min. The solution turned orange during this time. The solution was cooled, the solvent was removed under vacuum and 5 mL of MeOH was added. The mixture was cooled to −30 °C for 4 h, the white precipitate was collected on a frit, washed with cold MeOH and dried in vacuum to yield pure **2** (0.0875 g, 63%). ^{1}H NMR (CD_2Cl_2, 25 °C): δ 8.25 (s, 2H, BAr_F), 8.05 (s, 4H, BAr_F), 7.35–7.18 (30H, Ph). ^{31}P{^{1}H} NMR (CD_2Cl_2, 25 °C): δ 20.6 (s, J_{PPt} 2998 Hz). Anal. Calc. for $C_{52}H_{36}F_{12}P_2Pt$: C, 54.51; H, 3.17. Found: C, 54.47; H, 3.28%.

‡ *Crystal data*: for **2**: $C_{52}H_{36}F_{12}P_2Pt{\cdot}2\ C_6H_6$, M = 1302.05, triclinic, space group $P\bar{1}$, a = 11.3973(6), b = 11.4539(5), c = 12.8260(6) Å, α = 105.675(1), β = 111.466(1), γ = 103.393(1)°, V = 1394.5(1) Å^3, Z = 1, T = 203 K, μ = 2.654 mm^{-1}, wR_2 = 0.0473 (5227 independent reflections), R = 0.0186 [$I > 2\sigma(I)$].

3: $C_{24}H_9BF_{18}$, M = 650.12, triclinic, space group $P\bar{1}$, a = 9.5433(9), b = 11.656(1), c = 12.775(1) Å, α = 100.544(2), β = 110.146(1), γ = 97.299(2)°, V = 1283.4(2) Å^3, Z = 2, T = 203 K, μ = 1.89 cm^{-1}. The final refinement (5459 reflections collected, 4206 independent) included anisotropic temperature factors on all non-hydrogen atoms and converged to R_1 = 0.0628 and wR_2 = 0.1820.

CCDC 182/1365. See http://www.rsc.org/suppdata/cc/1999/1807/ for crystallographic files in .cif format.

1 S. H. Strauss, *Chem. Rev.*, 1993, **93**, 927.
2 M. Brookhart, B. Grant and A. F. Volpe, *Organometallics*, 1992, **11**, 3920; See also: M. D. Butts, B. L. Scott and G. J. Kubas, *J. Am. Chem. Soc.*, 1996, **118**, 11831; P. J. Alaimo, B. A. Arndtsen and R. G. Bergman, *J. Am. Chem. Soc.*, 1997, **119**, 5269; M. W. Holtcamp, L. M. Henling, M. W. Day, J. A. Labinger and J. E. Bercaw, *Inorg. Chim. Acta*, 1998, **270**, 467.
3 J. Powell, A. Lough and T. Saeed, *J. Chem. Soc., Dalton Trans.*, 1997, 4137.
4 M. Aresta, E. Quaranta and I. Tommasi, *New J. Chem.*, 1997, **21**, 595.
5 H. C. Clark and J. D. Ruddick, *Inorg. Chem.*, 1970, **9**, 1226; H. C. Clark and L. E. Manzer, *Inorg. Chem.*, 1971, **10**, 2699.
6 K. Siegmann, P. S. Pregosin and L. M. Venanzi, *Organometallics*, 1989, **8**, 2659.
7 R. A. Michelin, M. Mozzon, P. Berin, R. Bertani, F. Benetollo, G. Bombieri and R. J. Angelici, *Organometallics*, 1994, **13**, 1341.

Communication 9/02274K

Extremely selective $Mg(ClO_4)_2$ mediated removal of Bpoc/Ddz moieties suitable for the solid phase peptide synthesis of thioxo peptides

Dirk Wildemann, Mario Drewello, Gunter Fischer and Mike Schutkowski*

Max-Planck Research Unit 'Enzymology of Protein Folding', Weinbergweg 22a, Halle, Germany. E-mail: schutkowski@enzyme-halle.mpg.de

Received (in Cambridge, UK) 13th July 1999, Accepted 3rd August 1999

$Mg(ClO_4)_2$ in organic solvents acts as an extremely mild reagent for repetitive Bpoc/Ddz deprotection during solid phase peptide synthesis even in the presence of the acid labile thioxo amide moiety with excellent yields.

Peptide backbone modification by replacement of an amide moiety by a thioamide moiety (thioxylation)† has attracted attention in recent years for several reasons. On one hand receptor interactions of thioxylated analogues of biologically active peptides may be more selective or more potent than their parent compounds and on the other hand enhanced stability against enzymatic action could be shown for various proteolytic enzymes.[1] The introduction of a thioamide moiety is a nearly isologous substitution for an amide moiety[2] but biological studies have shown that the behavior of such modified compounds is unpredictable.[3] Nevertheless, a thioxo peptide bond provides an extraordinary backbone label for peptides and proteins introducing special spectroscopic and photochemical properties into the molecule with minimal variation of the constitution.

Regarding thioxo peptide synthesis the deprotection of the widely used side-chain protecting groups in the presence of thioxo peptide bonds is problematic because of the sensitivity of these groups toward acids. Acidolytic Boc deprotection of thioxo peptides led in most cases (depending on the sequence) to unsatisfactory yields between 10 and 65%.[4] Besides dethioxylation the thioxylated products often undergo thiazolone formation, a side reaction similar to the Edman degradation.[5]

Moreover, thioxo peptides are sensitive to the repetitive treatment with base necessary for the removal of the Fmoc protecting group, resulting in epimerized peptide derivatives. To circumvent these limitations we developed a method which can be used for both conventional peptide synthesis in the liquid phase and for solid phase peptide synthesis (SPPS) of thioxo peptides. It exclusively uses Lewis acids for both removal of the temporary 2-(biphenyl-4-yl)propan-2-yloxycarbonyl (Bpoc) or 2-(3,5-dimethoxyphenyl)propan-2-yloxycarbonyl (Ddz) protecting groups and final detachment/side-chain deprotection.

We disclosed that $SnCl_4$ is a powerful reagent for Boc deprotection in the presence of the acid-sensitive thioxo moiety.[6] In a more systematic investigation we found that Lewis acids like $Mg(ClO_4)_2$ in MeCN or $ZnCl_2$ in THF‡ are extremely mild and selective reagents for Bpoc/Ddz removal without damage of the thioxo peptide bond. This method is suitable in SPPS using extremely acid labile resins like Sieber- and Rink-amide and SASRIN® resins. The Bpoc deprotection of thioxo peptides utilising $Mg(ClO_4)_2$ in MeCN at 50 °C is fully compatible with side-chain Boc protection.[7] The thioxo moiety of Ala-Ala-Ala-Pro-ψ[CS-NH]Phe-NH-Np§ is completely stable under these conditions even after 5 weeks. We were able to synthesize the thioxylated model polyproline II helix **7** on a Sieber-amide resin using Ddz protected proline for chain elongation¶ and Bpoc-Pro-thioxo-6-nitrobenzotriazolide (Bpoc-Pro-TNB) for thioacylation‖ of resin-bound pentaproline. Detachment from the support using $ZnCl_2$-Et_2O complex in CH_2Cl_2** yielded thioxo peptide **7** in 72% yield after HPLC purification. Additionally, we synthesized bovine β-Casomorphine(1-5) amide **2** using the Fmoc strategy for preparation of the tripeptide Phe-Pro-Gly on a Sieber-amide resin, switching to Bpoc-Pro-TNB for introduction of the thioxo amide moiety and selective Bpoc-deprotection using $Mg(ClO_4)_2$ in MeCN. After acylation of the thioxo tetrapeptide with Boc-Tyr(OtBu), simultaneous Boc/OtBu-deprotection and detachment from the resin was successful using $ZnCl_2$–Et_2O complex. Moreover, we prepared the biologically active thioxo peptides endomorphine **3** and allanthoin **4** (Scheme 2) in a similar manner (Table 1).

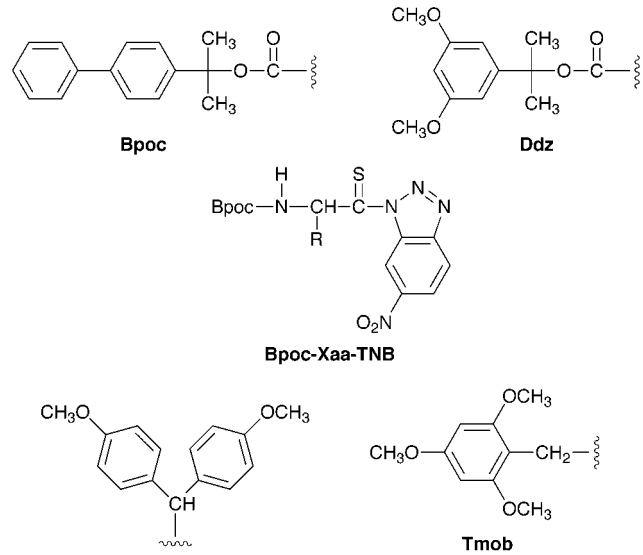

The synthesis of the thioxo bradykinins **5** and **6** (Table 1) was successful starting from Fmoc-Arg(Boc)$_2$-SASRIN® resin and using Boc-Arg(Boc)$_2$ for final acylation of the resin-bound thioxo octapeptides. Side-chain deprotection–detachment with $ZnCl_2$–Et_2O complex yielded thioxo peptides in excellent yields and purity. The widely used Pmc/Pbf and Trt protecting groups are relatively stable against $ZnCl_2$-Et_2O complex. Therefore we preferred the trimethoxybenzyl (Tmob) and 4,4′-Dimethoxydityl (Dod) groups for side-chain protection of Gln (peptide **10**) and Asn (peptide **8**), respectively, and double Boc protection of the guanidino function of Arg to overcome these limitations. To test this method in a more sophisticated reaction we synthesized the fully protected thioxylated RNAse A fragment Boc–Lys(Boc)-Glu(OtBu)-Thr(tBu)-Ala-ψ[CS-NH]Ala-Ala-Lys(Boc)-Phe-Glu(OtBu) on SASRIN® resin and treated it with $ZnCl_2$–Et_2O complex for 10 h at room temperature. The major product corresponds to the expected thioxo peptide **9** as demonstrated by MALDI mass spectrometry. Finally, we synthesized the complete RNAse A derived thioxo S-peptide **10** using this new method. The main product (30%) of the complex mixture was **10** but in all other oligopeptides derived from incomplete couplings a thioxo moiety has been detected by the charateristic UV-band at 280 nm. This suggests that no dethioxylation had taken place. We repeated the synthesis of **10** using Fmoc-(FmocHmb)Ala and Fmoc-Asp-(2,2-dimethyl)oxazolidine-4-carboxylic acid at

Table 1 $ZnCl_2$–Et_2O complex mediated final deprotection–detachement of thioxo peptides synthesized on solid supports with Bpoc or Ddz as temporary protecting group

Entry	Final product	Yield (%)	$[M + H]^+$ calc.	$[M + H]^+$ found
1	Ala-Ala-Ala-Pro-ψ[CS-NH]Phe-NH-Np	83	607.24	607.5[a]
2	Tyr-Pro-ψ[CS-NH]Phe-Pro-Gly-NH_2	87	595.29	595.1[a]
3	Tyr-ψ[CS-N]Pro-Phe-Phe-NH_2	74	588.28	588.5[a]
4	Gly-Gly-Ser-Leu-ψ[CS-NH]Tyr-Ser-Phe-Gly-Leu-NH_2	71	915.45	915.5[a]
5	Arg-Pro-Pro-Gly-Phe-Ser-ψ[CS-N]Pro-Phe-Arg	62	1076.56	1076.2[b]
6	Arg-Pro-ψ[CS-N]Pro-Gly-Phe-Ser-Pro-Phe-Arg	68	1076.56	1076.1[b]
7	Ac-Pro-Pro-Pro-Pro-Pro-Pro-ψ[CS-N]Pro-Pro-Pro-Pro-Pro-NH_2	72	1143.63	1143.7[a]
8	Arg-Asn-Lys-His-Ile-Arg-Thr-ψ[CS-N]Pro-Phe-Lys-NH_2	71	1311.75	1312.4[b]
9	Lys-Glu-Thr-Ala-ψ[CS-NH]Ala-Ala-Lys-Phe-Glu	79	1010.52	1010.7[ab]
10	Lys-Glu-Thr-Ala-ψ[CS-NH]Ala-Ala-Lys-Phe-Glu-Arg-Gln-His-Nle-Asp-Ser-Ser-Thr-Ser-Ala-Ala	63	2163.53	2163.7[b]

[a] Characterized by ESI mass spectrometry. [b] Characterized by MALDI mass spectrometry.

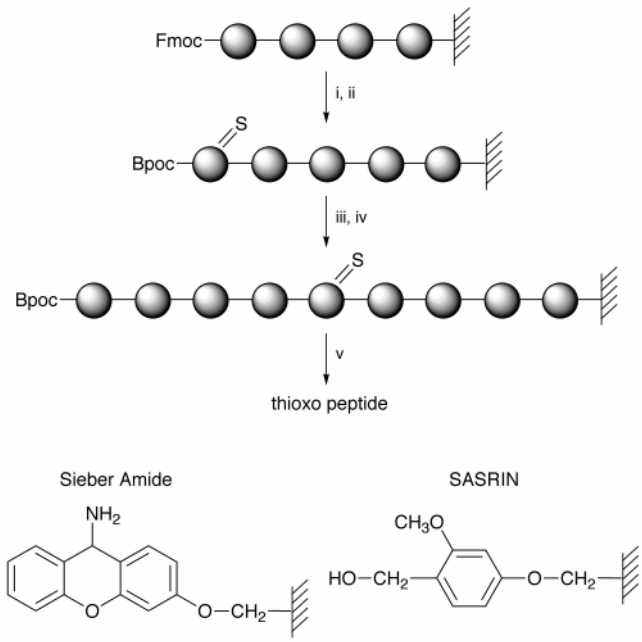

Scheme 1 *Reagents and conditions*: i, piperidine–DMF; ii, Bpoc-Xaa-TNB, DMF; iii, $Mg(ClO_4)_2$ MeCN or $ZnCl_2$/THF; iv, peptide synthesis using Bpoc for temporary protection; v, $ZnCl_2$–Et_2O complex, CH_2Cl_2.

positions 19 and 14–15, respectively, yielding **10** in 63% after final treatment with $ZnCl_2$–Et_2O complex and HPLC purification.

In conclusion, we have demonstrated that this novel deprotection scheme (Scheme 1) is an extraordinarily mild method for the SPPS of peptide derivatives containing acid and/or base sensitive functionalities. Linear thioxo peptides, which are known to be difficult to synthesize in a positionally predetermined manner, can now be prepared in good yields without epimerization.

We thank Dr A. Schierhorn and M. Kipping for mass spectroscopic measurements and Dr U. Reimer for NMR measurements. We are grateful to Thomas Schumann for atomic emission spectroscopic measurements. We gratefully acknowledge B. Hökelmann and I. Kunze for excellent technical assistance.

Notes and references

† For naming C=S the prefix 'thiono' has been frequently used in place of 'thioxo', however the IUPAC nomenclature committee recommends the use of 'thioxo'.

‡ Other Lewis acids that were investigated include ZnI_2, $Zn(AcO)_2$, $Zn(ClO_4)_2$, $MgCl_2$, $SnCl_2$, $SnBr_4$, $SnCl_4$, $Sn(AcO)_4$, $Cs(F_3CCO_2)$, $AlCl_3$ and $Ti(OPr^i)_4$. In the case of ZnI_2, $Zn(AcO)_2$, $Zn(ClO_4)_2$ and $MgCl_2$ the deprotection of Bpoc was promoted with a selectivity of at least 2000 over Boc deprotection but proceeds with sluggish kinetics. We preferred $Mg(ClO_4)_2$ due to its relative low cost, the weakly interacting counterion, its good solubility in organic solvents like MeCN, and its ease of removal.

§ Alterations of a peptide bond are represented by the ψ nomenclature system. *Pure Appl. Chem.*, 1984, **5b**, 595.

¶ The resin bound Bpoc-protected peptide derivative was treated with 10 equiv. $Mg(ClO_4)_2$ in MeCN at 50 °C for 3 h. The next acylation step in the case of SPPS was performed after extensive washing with MeCN and re-swelling in DMF. Using this method in liquid phase synthesis precipitation of the crude product with Et_2O was sufficient for removal of the deprotecting reagent.

‖ The thioxylated Bpoc-protected amino acid 6-nitrobenzotriazolides were synthesized according to a modified procedure from the literature (M. A. Shalaby, C. W. Grote and H. Rapoport, *J. Org. Chem.*, 1996, **61**, 9045).

** We preferred $ZnCl_2$–Et_2O complex for the final treatment of the resin bound thioxo peptide because of its convenient handling and because there are no difficulties with precipitation of insoluble materials complicating HPLC purification. For simultaneous detachment–side-chain deprotection we incubated the peptide resin with 2.2 M $ZnCl_2$–Et_2O complex in CH_2Cl_2 for 10 h at room temperature. After filtration the solvent was removed and the resulting slurry was re-dissolved in THF and the desired thioxo peptide was precipitated with Et_2O. Final purification using HPLC gave pure thioxo peptides. Investigation of these peptides using atomic emission spectroscopy demonstrated that the Zn^{2+} content is within the normal range (below 180 μg g^{-1}). Additionally, we were able to remove *tert*-butyl and benzyl protecting groups from the phosphate moiety in the presence of thioxo peptide bonds using this method, allowing the synthesis of side-chain phosphorylated thioxo peptides.

1 (*a*) For a review, see T. Hoeg-Jensen, *Phosphorus Sulfur Silicon Relat. Elem.*, 1996, **108**, 257; (*b*) M. Schutkowski, M. Jakob, G. Landgraf, I. Born, K. Neubert and G. Fischer, *Eur. J. Biochem.*, 1997, **245**, 381; (*c*) S. Yao, R. Zutshi and J. Chmielewski, *Bioorg. Med. Chem. Lett.*, 1998, **8**, 699.

2 R. Bardi, A. M. Piazzesi, C. Toniolo, O. E. Jensen, R. S. Omar and A. Senning, *Biopolymers*, 1988, **27**, 747.

3 (*a*) D. Seebach, S. Y. Ko, H. Kessler, M. Köck, M. Reggelin, P. Schmieder, M. Walkinshaw, J. Bölsterli and D. Bevec, *Helv. Chim. Acta*, 1991, **74**, 1953; (*b*) M. Schutkowski, S. Wöllner and G. Fischer, *Biochemistry*, 1995, **34**, 13016; (*c*) H. Morita, Y. S. Yun, K. Takeya, H. Itokawa and O. Shirota, *Bioorg. Med. Chem.*, 1997, **5**, 631; (*d*) H. Morita, Y. S. Yun, K. Takeya and H. Itokawa, *Heterocycles*, 1998, **47**, 391; (*e*) J. Lehmann, A. Linden and H. Heimgartner, *Tedrahedron*, 1998, **98**, 8721.

4 F. S. Guziec and L. M. Wasmund, *J. Chem. Res. (M)*, 1989**,** 1301; B. Zacharie, G. Sauve and C. Penney, *Tetrahedron* 1993, **49**, 10489; ref. 1(*a*) and 3(*b*). However, there are some reports of successful deprotection by the usual methods: D. W. Brown, M. M. Campell and C. V. Walker, *Tetrahedron*, 1983, **39**, 1075; B. D. Sherman and A. F. Spatola, *J. Am. Chem. Soc.*, 1990, **112**, 433.

5 D. W. Brown, M. M. Campbell, M. S. Chambers and C. V. Walker, *Tetrahedron Lett.*, 1987, **28**, 2171; K. Clausen, M. Thorsen, S. O. Lawesson and A. F. Spatola, *J. Chem. Soc., Perkin Trans. 1*, 1984, 785.

6 R. Frank and M. Schutkowski, *Chem. Commun.*, 1996, 2509.

7 J. A. Stafford, M. F. Brackeen, D. S. Karanewsky and N. L. Valvano, *Tetrahedron Lett.*, 1993, **34**, 7873

Communication 9/05678E

Regio- and enantio-selective Heck reactions of aryl and alkenyl triflates with the new chiral ligand (*R*)-BITIANP

Lutz F. Tietze,*[a] Kai Thede[a] and Franco Sannicolò[b]

[a] *Institut für Organische Chemie der Universität Tammannstraße 2, D-37077 Göttingen, Germany. E-mail: ltietze@gwdg.de*

[b] *Dipartimento di Chimica Inorganica, Metallorganica e Analitica, Università di Milano, Via Venezian 21, I-20133 Milano, Italy*

Received (in Liverpool, UK) 29th June 1999, Accepted 29th July 1999

The Heck reaction of dihydrofuran 3 with aryl triflates 4 and 6a–d and alkenyl triflate 8 in the presence of the chiral ligand (*R*)-BITIANP 1 provides the 2-substituted 2,3-dihydrofurans 5a, 7a–d and 9, respectively, with complete regioselectivity, high enantioselectivity (86–96% ee) and good yields (76–93%).

One of the main objectives in modern synthetic organic chemistry is the catalytic enantioselective formation of C–C bonds. In this respect, the Heck reaction[1]—the Pd^0 catalyzed coupling of an aryl or alkenyl halide or triflate with an alkene—is a highly versatile procedure since it tolerates several functional groups. In the years since the first enantioselective Heck reactions in 1989, published by Shibasaki[2] and Overman,[3] several novel chiral ligands have been developed which give high enantioselectivities and which have been used in natural product syntheses.[4] However, one of the problems encountered in the use of chiral ligands, especially in intermolecular Heck reactions, is the often low reactivity of the formed Pd complexes.[5] Therefore it is important to develop novel ligands and show their applicability in C–C bond formation. Here we report on the use of the new chiral ligands (*R*)-(+)-2,2′-bis(diphenylphosphino)-3,3′-bi(benzo[*b*]thiophene) [(*R*)-BITIANP] **1** and (+)-4,4′-bis(diphenylphosphino)-2,2′,5,5′-tetramethyl-3,3′-bithiophene [(+)-TMBTP] **2** in Heck reactions; ligand **1** has been employed with great success in the hydrogenation of C–C and C–O bonds,[6] whereas ligand **2** has not been used so far for enantioselective transformations.

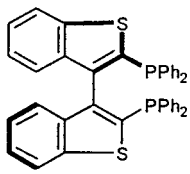

1

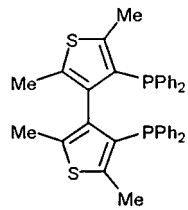

2

To allow a comparison with other chiral ligands we investigated the Heck reactions of dihydrofuran **3** with the triflates **4**, **6a–d** and **8**. In principle, the Heck reaction of dihydrofuran **3** with phenyl triflate **4** leads to the two isomers **5a** and **5b** (Scheme 1). Using BINAP[7] the regioselectivity is rather low, whereas with a substituted MeO-BIPHEP[8] ligand a 22:1 ratio of **5a** and **5b** was obtained, and with chiral phosphinooxazolines[9] only **5b** is obtained.[10]

We have now shown that the Heck reaction of **3** and **4** in DMF at 90 °C using Pd_2dba_3·dba and the new chiral ligand **1** employing a Pd ligand ratio of 1:2 and 1,8-bis(dimethylamino)-naphthalene (proton sponge) as the base affords **5a** exclusively in 84% yield and 91% ee within 18 h (Table 1, entry 1).† Similar results were obtained using Pr^i_2NEt as base (entry 2); however, with THF as solvent at 70 °C the transformation was less selective and much slower. Even after 7 days the reaction was not complete (entry 3). Interestingly, (*R*)-BINAP as chiral ligand using the best conditions found for the transformation with **1** gave **5a** with a 3:1 regioselectivity and only 42% ee (entry 4). The use of the second new ligand (+)-TMBTP **2** was only marginally successful. Here the regioisomer **5b** was obtained preferentially, but with very poor ee values (entries 5–7).

In the presence of the ligand (*R*)-BITIANP **1**, other phenyl triflates **6a–d** containing either an electron-withdrawing or an electron-donating group also reacted with high regio- and enantio-selectivities (Scheme 2, Table 2). In addition alkenyl triflates could be transformed successfully; thus, the Pd catalyzed reaction of cyclohex-1-enyl triflate **8** with dihydrofuran **3** provides exclusively the dihydrofuran derivative **9** within 13 h with good yield and high enantioselectivity.

The described Heck reactions with the new chiral ligand (*R*)-BITIANP **1** have shown that this ligand has an excellent potency and may serve as a useful alternative to the ligands

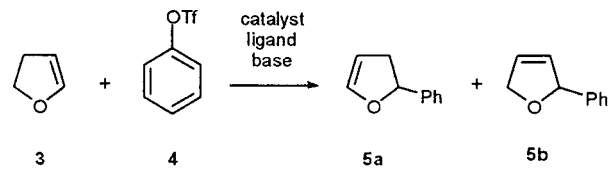

3 **4** **5a** **5b**

Scheme 1

Table 1 Enantioselective Heck reactions of **3** and **4** providing **5a** and **5b**

	Pd_2dba_3·dba/ mol%	Ligand (mol%)	Base (equiv.)	Solvent	*T*/°C	*t*	Conversion[a] (**4**:**5a** + **5b**)	Ratio[a] **5a**:**5b**	Yield (%) **5a**	Yield (%) **5b**	Ee (%)[b] **5a**	Ee (%)[b] **5b**
1	3	BITIANP **1** (12)	PS (3)[c]	DMF	90	18 h	<1:100	100:<1	84	—	91	
2	3	BITIANP **1** (12)	Pr^i_2 NEt (3)	DMF	90	20 h	<1:100	100:<1	90	—	90	
3	5	BITIANP **1** (10)	Pr^i_2NEt (3)	THF	70	7 d	16:84	7:1	62	—	80	
4	3	BINAP (12)	PS (3)[c]	DMF	90	18 h	<1:100	3:1	58	20	42	33
5	5	TMBTP **2** (10)	Pr^i_2NEt (3).	DMF	90	3 d	<1:100	1:2	27	58	4	2
6	5	TMBTP **2** (10)	Pr^i_2NEt (3)	THF	70	4 d	1:22	3:1	54	19	14	10
7	5	TMBTP **2** (10	PS (3)[c]	C_6H_6	70	4 d	1:26	6:1	73	12	4	0

[a] Determined by GC. [b] Determined by chiral GC. [c] PS = Proton sponge = 1,8-bis(dimethylamino)naphthalene.

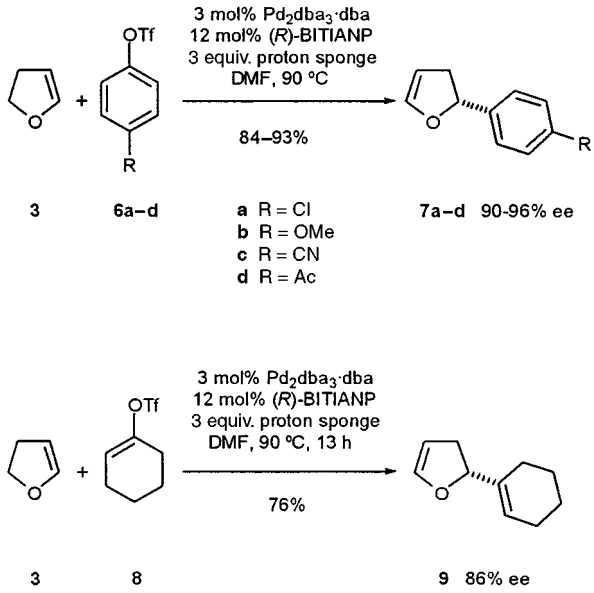

Scheme 2

Table 2 Enantioselective Heck reaction with the aryl triflates **4**, **6a–d** and the alkenyl triflate **8**

Entry	R	Substrate	Product	*t*/h	Yield (%)	Ee (%)[a]
1	H	**4**	**5a**	18	84	91
2	Cl	**6a**	**7a**	18	87	94
3	MeO	**6b**	**7b**	18	84	90
4	CN	**6c**	**7c**	24	91	96
5	MeCO	**6d**	**7d**	24	93	95
6	—	**8**	**9**	13	76	86

[a] Determined by chiral GC.

described by Hayashi,[7] Pfaltz,[9] Pregosin[8] and Shibasaki[5] with the special advantage of high reactivity.

The work was supported by the Deutsche Forschungsgemeinschaft (SFB 416) and the Fonds der Chemischen Industrie. We thank the Degussa AG for a generous gift of precious metals and Dr S. Console, Chemi SpA, Italy, for a gift of the ligands.

Notes and references

† Typical experimental procedure: A mixture of Pd_2dba_3·dba (7.6 mg, 6.63 μmol, 3 mol%), (*R*)-BITIANP **1** (16.8 mg, 26.5 μmol, 12 mol%) and 1,8-bis(dimethylamino)naphthalene (142.1 mg, 0.663 mmol, 3 equiv.) in dry and degassed DMF (5 ml) was stirred for 0.5 h at 40 °C until an orange solution was formed. Then **4** (50.0 mg, 0.221 mmol) and **3** (77.5 mg, 1.105 mmol, 5 equiv.) were added and the mixture was stirred for 18 h at 90 °C until the reaction was complete [GC analysis; SGE BPX-5% phenyl (equiv.) polysilphenylene-siloxane, 50 m, 60–160 °C, 5 °C min^{-1}, 50 kPa: t_R = 8.8 min (**4**), t_R = 15.1 min (**5a**)]. The red solution was filtered through a batch of silica gel, eluted with Et_2O (100 ml), concentrated, diluted with the same volume of water and extracted with Et_2O (3 × 30 ml). The organic layers were combined, washed with water and brine and dried over Na_2SO_4. Removal of the solvent *in vacuo* and purification of the residue by column chromatography (silica gel, 2 × 25 cm, light petroleum–CH_2Cl_2 3:1) gave (*R*)-(−)-**5a** (27.0 mg, 84%) as a colourless oil, $[\alpha]_D$ −61.5 (*c* 2.30, $CHCl_3$, 20 °C, 91% ee according to GC). GC [octakis(6-*O*-methyl-2,3-di-*O*-pentyl)-γ-cyclodextrin (50% in OV 1701 w/w), 25 m, 70–100 °C, 1 °C min^{-1}, 50 kPa]: 13.1 min (*S*)-**5a**, 14.4 min (*R*)-**5a**.

1 Reviews: M. Shibasaki, C. D. J. Boden and A. Kojima, *Tetrahedron*, 1997, **53**, 7371; E. Negishi, C. Coperet, S. Ma, S.-Y. Liou and F. Liu, *Chem. Rev.*, 1996, **96**, 365; W. Cabri and I. Candiani, *Acc. Chem. Res.*, 1995, **28**, 2; A. de Meijere and F. E. Meyer, *Angew. Chem., Int. Ed. Engl.*, 1994, **33**, 2379; H.-G. Schmalz, *Nachr. Chem. Tech. Lab.*, 1994, **42**, 270; R. F. Heck, *Palladium Reagents in Organic Synthesis*, Academic Press, London, 1985.
2 Y. Sato, M. Sodeoka and M. Shibasaki, *J. Org. Chem.*, 1989, **54**, 4738.
3 N. E. Carpenter, D. J. Kucera and L. E. Overman, *J. Org. Chem.*, 1989, **54**, 5846.
4 L. F. Tietze and T. Raschke, *Liebigs Ann. Chem.*, 1996, 1981; L. F. Tietze and T. Raschke, *Synlett*, 1995, 597; T. Ohshima, K. Kagechika, M. Adachi, M. Sodeoka and M. Shibasaki, *J. Am. Chem. Soc.*, 1996, **118**, 7108; L. E. Overman, *Pure Appl. Chem.*, 1994, **66**, 1423.
5 S. Y. Cho and M. Shibasaki, *Tetrahedron Lett.*, 1998, **39**, 1773.
6 P. Antognazza, T. Benincori, E. Brenna, E. Cesarotti, L. Trimarco and F. Sannicolò, EP 0770085 to Chemi SpA (*Chem. Abstr.*, 1996, **124**, 317487w); T.Benincori, E. Brenna, F. Sannicolò, L. Trimarco, P. Antognazza, E. Cesarotti, F. Demartin and T. Pilati, *J. Org. Chem.*, 1996, **61**, 6244.
7 F. Ozawa, A. Kubo, Y. Matsumoto and T. Hayashi, *Organometallics*, 1993, **12**, 4188; F. Ozawa, Y. Kobatake and T. Hayashi, *Tetrahedron Lett.*, 1993, **34**, 2505.
8 G. Trabesinger, A. Albinati, N. Feiken, R. W. Kunz, P. S. Pregosin and M. Tschoerner, *J. Am. Chem. Soc.*, 1997, **119**, 6315.
9 O. Loiseleur, M. Hayashi, N. Schmees and A. Pfaltz, *Synthesis*, 1997, 1338; O. Loiseleur, P. Meier and A. Pfaltz, *Angew. Chem., Int. Ed. Engl.*, 1996, **35**, 200.
10 For further investigations about Heck reactions with dihydrofurans, see K. K. Hii, T. D. W. Claridge and J. M. Brown, *Angew. Chem., Int. Ed. Engl.*, 1997, **109**, 984; S. Hillers and O. Reiser, *Chem. Commun.*, 1996, 2197; S. Hillers, S. Sartori and O. Reiser, *J. Am. Chem. Soc.*, 1996, **118**, 2087.

Communication 9/05309C

ChemComm

The diastereoselective cycloaddition of vinyl ethers with isomünchnones

Sergey N. Savinov and David J. Austin*

Department of Chemistry, Yale University, 225 Prospect St., New Haven, CT 06520-8107 USA. E-mail: david.austin@yale.edu

Received (in Corvallis, OR, USA) 28th April 1999, Accepted 14th July 1999

Complete diastereoselective product formation in the intermolecular 1,3-dipolar cycloaddition of isomünchnones with alkyl vinyl ethers is reported.

The 1,3-dipolar cycloaddition reaction is a powerful pericyclic process, leading to the concomitant formation of two carbon–carbon bonds in a single transformation.[1] While intramolecular cycloaddition reactions have been vigorously applied to natural product synthesis,[2] the intermolecular cycloaddition reaction suffers from a lack of diastereoselectivity,[3–5] resulting in diminished synthetic utility. During our efforts to utilize this reaction in the synthesis of biomimetic probes,[6,7] we discovered that the intermolecular cycloaddition of vinyl ethers with isomünchnones proceeds with complete diastereoselectivity (Scheme 1). Here we describe this unprecedented selectivity and explore the potential of vinyl ethers as dipolarophiles.

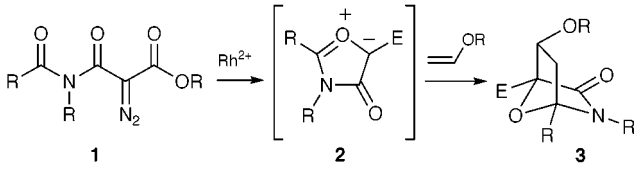

1 **2** **3**

Scheme 1

We sought to investigate the 1,3-dipolar cycloaddition reaction as the principal component of our synthetic approach in the construction of a rigid bicyclic framework for molecular recognition. Mesoionic species such as isomünchnones (**2**) have been reported to undergo highly selective and mild pericyclic chemistry.[8,9] When formed from α-diazo imide precursors (**1**), with rhodium(II) mediated catalysis,[10,11] these 1,3-dipoles provide the possibility of a rapid and convergent construction of a heterocyclic system (**3**, E = CO_2Me) that would be well suited for the presentation of a wide variety of functional groups, in a highly dense array.

Although the isomünchnones are a well-studied class of 1,3-dipoles,[5] the selectivity of the intermolecular isomünchnone cycloaddition has primarily been explored with symmetric, electron-deficient dipolarophiles such as *N*-phenylmaleimide, tetracyanoethylene, fumarates, maleates and dimethyl acetylenedicarboxylate.[5,9] Only one example of an intermolecular isomünchnone cycloaddition with a monoactivated, electron-deficient olefin has been reported.[12] We therefore sought to explore the reactivity of various unsymmetric, monoactivated alkenes. The vinyl ethers, being a diverse and readily available set of substrates,[13] represented a good candidate functionality for this study. Treatment of α-diazo imides **4** or **5** with a catalytic amount of rhodium(II) perfluorobutyramidate [Rh_2(pfbm)$_4$], in the presence of various dipolarophiles (Table 1), led to the isolation of a single diastereomer in each case (**6**–**15**). The relative stereochemistry of compound **7** was verified by X-ray crystallographic structure analysis.[14]

For every dipolarophile evaluated, *endo* orientation of the alkoxy functionality was maintained. [15,16] Moreover, the steric properties of this substituent do not appear to influence either product yield or reaction rate. Even sterically demanding groups, such as *tert*-butyl (entry 6) and trimethylsilyl (entry 7), were accommodated with little variation in yield or rate. In order to evaluate the relative rates for β-substituted vinyl ethers, 1-methoxyoct-1-ene was tested (entries 8 and 9). When the starting *E*:*Z* ratio of the dipolarophile was 1:9, the *anti*:*syn* product distribution was 24:72 (entry 8). A starting *E*:*Z* ratio of 3:2 provided an 80:20 *anti*:*syn* product distribution (entry 9). When the *anti*:*syn* distribution of products is normalized according to the original *E*:*Z* ratio (74:26 and 72:28, in entries 8 and 9, respectively), the cycloaddition preference for the *E* isomer becomes apparent. β-Disubstituted vinyl ether (entry 10) provides the same extent of diastereoselectivity as the less sterically congested dipolarophiles. This result is remarkable, considering the high functional density of the cycloadduct (**15**) obtained *via* this cycloaddition.

Table 1 Reaction of isomünchnones with electron-donating dipolarophiles

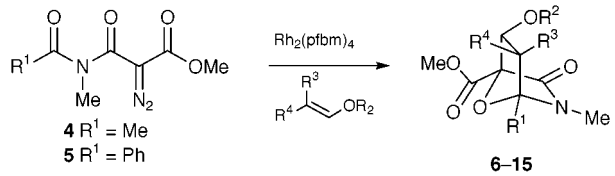

4 R^1 = Me
5 R^1 = Ph

6–15

Entry	R^1	R^2	R^3	R^4	Product	Yield (%)
1[a]	Me	Et	H	H	**6**	> 98
2[a]	Ph	Et	H	H	**7**	> 98
3[a]	Me	Bn	H	H	**8**	> 98
4[a]	Me	Cy	H	H	**9**	> 98
5[a]	Me	Ph	H	H	**10**	> 98
6[a]	Me	Bu^t	H	H	**11**	> 98
7[a]	Me	$SiMe_3$	H	H	**12**	> 98
8[b,d]	Me	Me	*n*-hexyl	H	**13**	95[f]
	Me	Me	H	*n*-hexyl	**14**	
9[b,e]	Me	Me	*n*-hexyl	H	**13**	97[f]
	Me	Me	H	*n*-hexyl	**14**	
10[c]	Me	Isopentyl	Me	Me	**15**	82

[a] 80 °C, benzene, 20 min. [b] 100 °C, benzene, 30 min. [c] 130 °C, chlorobenzene, 1 h. [d] 5 equiv. of dipolarophile with an *E*:Z ratio of 1:9 was used in this experiment. [e] 5 equiv. of dipolarophile with an E:Z ratio of 3:2 was used in this experiment. [f] Overall yield.

In order to evaluate whether our observed selectivity is steric or electronic in nature, we investigated the intermolecular cycloaddition of dipole precursor **4** with 2-methoxypropene, an *ipso*-substituted vinyl ether (Scheme 2). Interestingly, the reaction proceeded only at relatively high temperature (130 °C) and after prolonged exposure (8 h), to yield a 1:3 *exo*:*endo* ratio of the diastereomers **16** and **17**.[17] A similar reduction in rate has been reported with ketene acetals, which topologically resemble the *ipso*-substituted 2-methoxypropene.[12] Their low

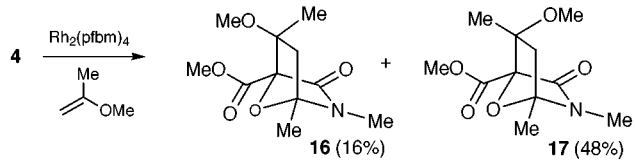

16 (16%) **17** (48%)

Scheme 2

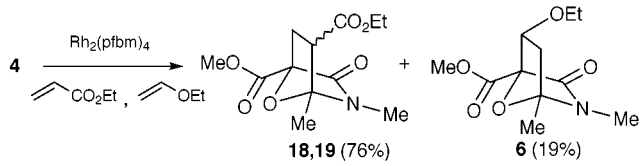

Scheme 3

reactivity was attributed to the existence of a large HOMO–LUMO gap between the dipole and dipolarophile.[12,18] The dramatic decrease in reaction rate for these disubstituted dipolarophiles, compared to the vinyl ethers described in Table 1, supports a steric involvement in diastereoselectivity. Whether this effect is purely steric or stereoelectronic in nature is ambiguous, since there still appears to be a preference for the *endo*-product (**17**).

Frontier Molecular Orbital theory has successfully rationalized both the rates and regioselectivity of most 1,3-dipolar cycloaddition reactions.[19] The fact that isomünchnones can undergo cycloaddition with both electron-rich and electron-deficient dipolarophiles is a defining feature of dipoles which readily proceed through a type II process.[1] This remarkable and useful behavior may be understood in terms of a small HOMO–LUMO energy gap.[1,5,20] We sought to further evaluate the electronic preference of isomünchnones while minimizing the steric bias on the dipolarophile. For this reason, α-diazo imide **4** was treated with $Rh_2(pfbm)_4$ in the presence of an equimolar amount of ethyl acrylate and ethyl vinyl ether at 60 °C, which resulted in a 4 : 1 mixture of cycloaddition products (Scheme 3). This comparable reactivity indicates similar FMO energetics for both electron-rich and electron-deficient dipolarophiles in the isomünchnone cycloaddition.

A pattern of diastereoselectivity for the cycloaddition of isomünchnones with vinyl ethers is apparent and appears to be controlled by the electron-donating ether functionality. Relative cycloaddition rates for these dipolarophiles are summarized in Scheme 4. Dipolarophile reactivity does not seem to be directly correlated with the extent of substitution on the alkene, but rather the placement of substitution on the alkene.

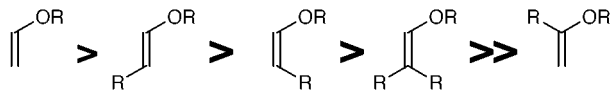

Scheme 4

In summary, we have demonstrated the diastereoselectivity of the intermolecular 1,3-dipolar cycloaddition of isomünchnones with vinyl ethers. The general nature of this diastereoselectivity is unprecedented for this class of dipoles.[5,15,20] In addition, dipolarophiles of diverse topologies have been shown to provide a synthetically feasible entry into [2.2.1] bicyclic heterocycles, in a controlled manner. Future effort in this area will include the investigation of potential stereoelectronic factors for this selective cycloaddition and expansion of the scope of vinyl ethers as dipolarophiles in the 1,3-dipolar cycloaddition reaction.

Financial support was provided by Yale Corporation. S. N. S. thanks Boehringer-Ingelheim for a summer research fellowship. The authors would like to thank Dr Susan de Gala for obtaining the crystal structure of compound **7**.

Notes and references

1 *1,3-Dipolar Cycloaddition Chemistry*, ed. A. Padwa, Wiley, New York, 1984, vol. 1.
2 P. A. Wender, R. M. Keenan and H. Y. Lee, *J. Am. Chem. Soc.*, 1987, **109**, 4390; W. G. Dauben, J. Dinges and T. C. Smith, *J. Org. Chem.*, 1993, **58**, 7635; J. P. Marino, M. H. Osterhout and A. Padwa, *J. Org. Chem.*, 1995, **60**, 2704; T. M. Heidelbaugh, B. Liu and A. Padwa, *Tetrahedron Lett.*, 1998, **39**, 4757.
3 A. Padwa, and S. F. Hornbuckle, *Chem. Rev.*, 1991, **91**, 263.
4 A. Padwa and K. E. Krumpe, *Tetrahedron*, 1992, **48**, 5385.
5 M. H. Osterhout, W. R. Nadle and A. Padwa, *Synthesis*, 1994, 123.
6 D. L. Whitehouse, K. H. Nelson, S. N. Savinov and D. J. Austin, *Tetrahedron Lett.*, 1997, **38**, 7139.
7 D. L. Whitehouse, K. H. Nelson, Jr., S. N. Savinov, R. S. Lowe and D. J. Austin, *Bioorg. Med. Chem.*, 1998, **6**, 1273.
8 T. Ibata, M. Hamaguchi and H. Kiyohara, *Chem. Lett.*, 1975, 21.
9 M. Hamaguchi and T. Ibata, *Chem. Lett.*, 1975, 499.
10 M. E. Maier and K. Evertz, *Tetrahedron Lett.*, 1988, **29**, 1677.
11 A. Padwa, D. L. Hertzog and R. L. Chinn, *Tetrahedron Lett.*, 1989, **30**, 4077.
12 A. Padwa and D. L. Hertzog, *Tetrahedron*, 1993, **49**, 2589.
13 Dipolarophiles used were either commercially available or synthesized using previously described procedures. G. Dujardin, S. Rossignol and E. Brown, *Tetrahedron Lett.*, 1995, **36**, 1653; P. A. Grieco, J. D. Clark and C. T. Jagoe, *J. Am. Chem. Soc.*, 1991, **113**, 5488; P. G. Gassman and S. J. Burns, *J. Org. Chem.*, 1988, **53**, 5574; R. D. Miller and D. R. McKean, *Tetrahedron Lett.*, 1982, **23**, 323.
14 *Crystal data* for **7**: C_{16} $H_{19}NO_5$, M = 305.33, orthorhombic, a = 9.066(2), b = 9.841(4), c = 17.138(3) Å, U = 1529(1) Å^3, T = 273 K, space group $P2_12_12_1$ (no. 19), Z = 4, μ(Mo-Kα) = 1.9 mm^{-1}, 1811 reflections measured, 1116 unique [$I > 3.00\sigma(I)$] which were used in all calculations. The final $wR(F^2)$ was 0.057 (all data). A single pale yellow prism crystal of **7**, having approximate dimensions 0.29 × 0.43 × 0.48 mm, was mounted on a glass fiber and collected on an Enraf-Nonius CAD-4 diffractometer using the ω–2θ scan technique. The structure was solved using direct methods, and the non-hydrogen atoms were refined anisotropically by full-matrix least-squares on F^2. CCDC 182/1341.
15 For a recent description of *exo*/*endo* facial selectivity and nomenclature of isomünchnones see: A. Padwa and M. Prein, *J. Org. Chem.*, 1997, **62**, 6842.
16 In each case, only a single diastereomer could be detected by ^{1}NMR spectroscopy, suggesting a >96:4 diastereoselectivity. The structural analysis for cycloadducts **6** and **8**–**15** was extrapolated by correlating corresponding ^{1}H NMR chemical shift data with compound **7**, whose structure was determined crystallographically.
17 Characterization of diastereoselectivity was made on the basis of a NOESY spectral correlation between the *exo*-methyl and the methyl ester of compound **17**.
18 I. Fleming, *Frontier Orbitals and Organic Chemical Reactions*, Wiley-Interscience, New York, 1976.
19 R. Huisgen, *Angew. Chem., Int. Ed. Engl.*, 1963, **2**, 633; R. Sustmann, *Tetrahedron Lett.*, 1971, 2717; R. Sustmann and H. Trill, *Angew. Chem., Int. Ed. Engl.*, 1972, **9**, 838; K. N. Houk, *Acc. Chem. Res.*, 1975, **8**, 361.
20 M. D.Weingarten, M. Prein, A. T. Price, J. P. Snyder and A. Padwa, *J. Org. Chem.*, 1997, **62**, 2001.

Communication 9/03381E

Effect of competing π-donor N-bound ligands on structure and bonding. Synthesis and structure of tungsten organoimido nitrido complexes

Caroll E. Pohl-Ferry, Joseph W. Ziller and Nancy M. Doherty*

Department of Chemistry, University of California, Irvine, CA 92697-2025, USA. E-mail: nmdohert@uci.edu

Received (in Bloomington, IN, USA) 26th July 1999, Accepted 4th August 1999

Tungsten organoimido nitrido compounds, $[W_2(N)(NR)_2Cl_5]_3$ (R = Et, C_6H_4Me-*p*), form in high yield in the reactions of $W(NR)Cl_4$ with $N(SiMe_3)_3$ and adopt structures in solution and the solid state consisting of chloro-bridged trimers of mononitrido-bridged di(organoimidotungsten) units with an unusual geometry that allows maximum π-donation from the imido and nitrido ligand set.

The nitride ion, N^{3-}, is a simple ligand that can be incorporated into a variety of environments in transition-metal compounds.[1–4] We have been interested in the nitrido ligand as a bridging group to link transition metals in new polynuclear, oligomeric and polymeric species.[5–9] To do so, it is necessary to establish control over bridging *versus* terminal structures in metallonitride compounds. Simple models of bonding suggest that competing π-donor ligands could be used to favor formation of nitrido-bridged structures. We report here, the synthesis and structure of two tungsten organoimido nitrido compounds, that support this idea. To our knowledge, these represent the first examples of *organo*imido nitrido transition-metal compounds, although compounds containing both the nitrido and parent imido (NH) ligand, especially clusters, are known,[10–15] and polynuclear haloimido nitrido complexes have been reported.[16,17]

$[W_2(N)(NEt)_2Cl_5]_3$ **1** and $[W_2(N)(NC_6H_4Me\text{-}p)_2Cl_5]_3$ **2** are isolated in high yield from the 2:1 reaction of the appropriate tungsten organoimido chloro compound with $N(SiMe_3)_3$.† ^1H NMR monitoring of the reaction indicates quantitative formation of **1** or **2** and $ClSiMe_3$ according to the stoichiometry in eqn. (1).

$$6\ W(NR)Cl_4(L) + 3\ N(SiMe_3)_3 \rightarrow [W_2(N)(NR)_2Cl_5]_3 + 9\ ClSiMe_3 + 6\ L \quad (1)$$

1 (R = Et L = none)
2 (R = C_6H_4Me-*p* L = OEt_2)

Compound **1** is a yellow air-sensitive solid while **2** is a purple air-sensitive solid. Single crystal X-ray diffraction studies indicate that **1** and **2** adopt solid state structures consisting of chlorobridged trimers of linear mononitrido-bridged ditungsten units (Figs. 1 and 2).‡ Solution studies indicate that the trimeric structure persists in dichloromethane. The ^1H NMR spectrum of **1** shows a single ethylimido signal with diastereotopic methylene protons consistent with the dissymmetry of the trimeric structure, and a molecular weight measurement of **2** confirms its trimeric nature in solution.§

The cyclic structures of **1** and **2** contain six approximately octahedral tungsten atoms each coordinated to one bridging nitrido ligand, one terminal organoimido ligand, and one terminal plus three bridging chloro ligands (Figs. 1 and 2). The $W–N_{nitrido}$ distances and $W–N_{nitrido}–W$ angles are consistent with tungsten–nitrogen double bonds in a W=N=W unit.[1,4] The $W–N_{imido}$ distances and $W–N_{imido}–C$ angles indicate tungsten–nitrogen triple bonds in an essentially linear W≡NR.[4,18] The W–Cl distances follow an understandable pattern, with $W–Cl_{terminal}$ distances (average 2.33 Å for **1**, 2.32 Å for **2**) shorter than $W–Cl_{bridging}$ distances that, in turn, vary with the *trans* ligand. Specifically, the $W–Cl_{bridging}$ distances increase on

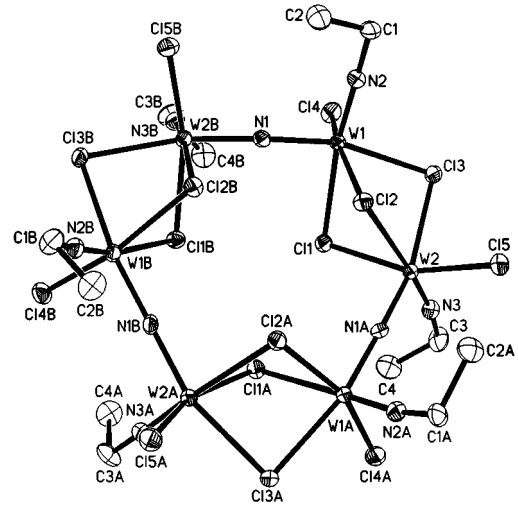

Fig. 1 Structural drawing of **1** with 50% probability thermal ellipsoids for non-hydrogen atoms. Selected bond distances (Å) and angles (°): For W=N=W, W(1)–N(1) 1.833(5), W(2B)–N(1) 1.849(5), W(1)–N(1)–W(2B) 174.5(3). For W≡NR, W(1)–N(2) 1.726(6), W(2)–N(3) 1.732(6), W(1)–N(2)–C(1) 168.6(5), W(2)–N(3)–C(3) 172.0(5). For $W–Cl_{bridging}$, W(1)–Cl(1) 2.631(2), W(1)–Cl(2) 2.443(2), W(1)–Cl(3) 2.552(2), W(2)–Cl(1) 2.452(2), W(2)–Cl(2) 2.641(2), W(2)–Cl(3) 2.546(2). For $W–Cl_{terminal}$, W(1)–Cl(4) 2.332(2), W(2)–Cl(5) 2.336(2).

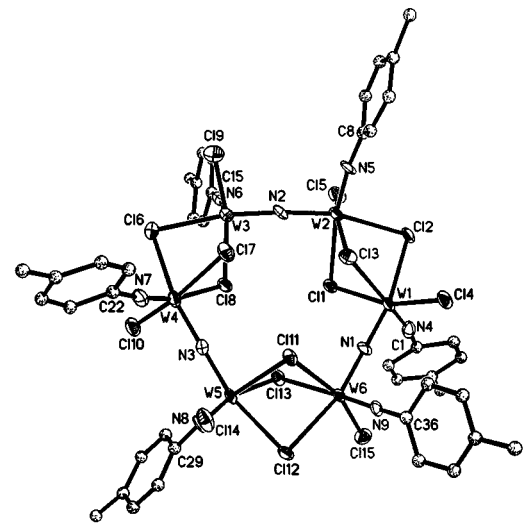

Fig. 2 Structural drawing of **2** with 50% probability thermal ellipsoids for non-hydrogen and non-carbon atoms. Selected bond distances (Å) and angles (°): For W=N=W: W(1)–N(1) 1.841(11), W(2)–N(2) 1.851(11), W(3)–N(2) 1.818(11), W(4)–N(3) 1.832(11), W(5)–N(3) 1.840(11), W(6)–N(1) 1.831(11), W(1)–N(1)–W(6) 175.3(7), W(2)–N(2)–W(3) 175.2(8), W(4)–N(3)–W(5) 175.0(8). For W≡NR: W(1)–N(4) 1.727(13), W(2)–N(5) 1.752(12), W(3)–N(6) 1.723(13), W(4)–N(7) 1.731(14), W(5)–N(8) 1.726(11), W(6)–N(9) 1.747(10), W(1)–N(4)–C(1) 167.6(10), W(2)–N(5)–C(8) 171.9(11), W(3)–N(6)–C(15) 171.0(12), W(4)–N(7)–C(22) 172.9(12), W(5)–N(8)–C(29) 176.2(10), W(6)–N(9)–C(36) 178.0(10).

going from W–Cl bonds *trans* to the terminal chloride (average 2.45 Å for **1** and **2**), to *trans* to the doubly bonded bridging nitride (average 2.55 Å for **1** and **2**), to *trans* to the triply bonded organoimido ligand (average 2.64 Å for **1**, 2.62 Å for **2**), consistent with the *trans* effects of these groups.

Of particular interest is the orientation of the two organoimido ligands in each $W_2(N)(NR)_2$ unit. The organoimido ligands are *cis* to the bridging nitrido ligand and at (RN)WW(NR) torsion angles of 105.3° for **1** and 95.2–98.9° for **2**. This nearly orthogonal orientation of the two triply bonded organoimido ligands at $W^{VI}(N)W^{VI}$ allows the complex to achieve maximum electron donation from the ligand set (each tungsten has an 18-electron count) and maximum nitrogen–tungsten π-bonding. This unusual geometry indicates that **1** and **2** may be viewed as inorganic analogs of allene with localized perpendicular π-bonds to the central atom (Fig. 3), as has also been noted for $[(\eta\text{-}C_5Me_5)W(NO)(CH_2CMe_3)](\mu\text{-}N)[(\eta\text{-}C_5Me_5)W(O)Cl]$ and $[(\eta\text{-}C_5Me_5)Mo(NO)(CH_2SiMe_3)](\mu\text{-}N)[(\eta\text{-}C_5Me_5)Mo(O)(CH_2SiMe_3)]$.[19] This is in sharp contrast with the many previously reported M=N=M compounds that are best described by delocalized three-center π-bonding.[20]

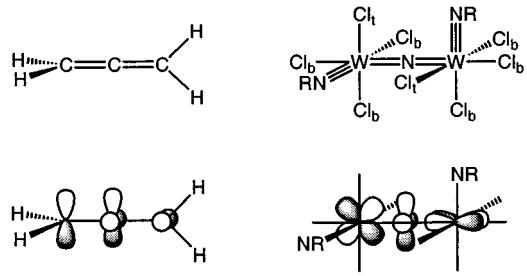

Fig. 3 Comparison of π-bonding to the central atom in allene and in the $W_2(N)(NR)_2$ unit.

Organoimido and nitrido ligands are both multiply bonding nitrogen-bound species, as terminal ligands they have similar demands for the empty π-symmetry orbitals at early transition metals, and both are capable of bridging between two or more metals. However, in a compound containing both these ligands, the nitrido should have advantages over the organoimido in a bridging position because it is sterically less demanding and a more flexible donor, able to adopt a number of different bridging structures. This is borne out by the synthesis and structures of **1** and **2**. Extension of this work to other early transition metals and the synthesis and study of 1:1:1 organoimido–nitrido–metal compounds are being explored in our laboratory.

We gratefully acknowledge support of this work by the National Science Foundation (CHE 93-21196 & 97-12775).

Notes and references

† For $[W_2(N)(NEt)_2Cl_5]_3$ **1**: a solution of $W(NEt)Cl_4$ (0.802 g, 2.17 mmol) and $N(SiMe_3)_3$ (0.250 g, 1.07 mmol) in toluene (50 mL) was stirred with heating at 90 °C under vacuum for 24 h. The solvent and volatiles were removed under reduced pressure, and the resulting solids were crystallized from dichloromethane–pentane (1:1) affording yellow crystalline **1** (0.574 g, 83%). For $[W_2(N)(NC_6H_4Me\text{-}p)_2Cl_5]_3$ **2**: a solution of $W(NC_6H_4Me\text{-}p)Cl_4\cdot Et_2O$ (2.00 g, 3.96 mmol) and $N(SiMe_3)_3$ (0.462 g, 1.98 mmol) in toluene (50 mL) was stirred with heating at 90 °C under vacuum for 24 h. The solids produced in the reaction were collected by filtration and recrystallized from dichloromethane affording purple crystalline **2** (1.32 g, 87%).

‡ *Crystal data*: for **1**: $C_{12}H_{30}Cl_{15}N_9W_6$, rhombohedral, $P\bar{3}$, a = 21.108(2), b = 21.108(2) Å, c = 16.258(3) Å, $\alpha = \beta = 90$, $\gamma = 120°$, Z = 6. Intensity data were collected at 158 K on a Siemens P4 rotating-anode diffractometer *via* a 2θ–ω scan technique in the range $2.56 < \theta < 27.50°$ using Mo-Kα radiation, λ = 0.71073 Å. All 3351 data were corrected for absorption, μ = 17.417 mm^{-1}, and for Lorentz and polarization effects. The structure was solved by direct methods (SHELXTL) and refined on F^2 by full-matrix least-squares techniques. Hydrogen atoms were included using a riding model. At convergence, $wR2 = [\Sigma w(F_o^2 - F_c^2)^2/\Sigma w(F_o^2)^2]^{1/2} = 0.0765$ and GOF = 1.039 for 127 variables refined against all 3123 unique data; $R1 = \Sigma||F_o| - |F_o||/\Sigma|F_o| = 0.0266$ for those 2521 data with $F_o > 4.0\sigma(F_o)$. For **2**: $C_{42}H_{42}Cl_{15}N_9W_6$, triclinic, $P\bar{1}$, a = 10.140(2), b = 15.796(2), c = 22.529(2) Å, α = 87.921(10), β = 86.200(15), γ = 78.862(14)°, Z = 2. Intensity data were collected at 158 K on a Siemens P4 rotating-anode diffractometer *via* a θ–2θ scan technique in the range $4.0 < 2\theta < 55.0°$ using Mo-Kα radiation, λ = 0.71073 Å. All 17128 data were corrected for absorption, μ = 10.33 mm^{-1}, and for Lorentz and polarization effects. The structure was solved by direct methods (SHELXTL) and refined by full-matrix least-squares techniques; the quantity minimized was $\Sigma w(F_o - F_c)^2$. Hydrogen atoms were included using a riding model. Three carbon atoms in the tolyl ring attached to N(5) are disordered and were included with two components each; four carbon atoms in the tolyl ring attached to N(6) exhibited high thermal motion, however, the probable disorder could not be fit to a reasonable model.At convergence, $R_F = \Sigma||F_o| - |F_c||/\Sigma|F_o| = 0.055$, $R_{wF} = [\Sigma w(|F_o| - |F_c|)^2/\Sigma w|F_o|^2]^{1/2} = 0.083$, and GOF = 2.82 for 451 variables refined against those 11817 data with $|F_o| > 6.0\sigma(|F_o|)$. CCDC 182/1369.

§ *Spectroscopic data*: for **1**: ^{1}H NMR (CD_2Cl_2): δ 1.56 (t, J 7 Hz, 3H), 6.27 (13-line non-first-order pattern at 500 MHz observation frequency, 2H). IR (neat): 2983, 2934, 2853, 1679, 1447, 1423, 1373, 1313, 1279, 1107, 1066, 1003, 949, 863, 826, 796, 613, 342, 294 cm^{-1}. For **2**: ^{1}H NMR (CD_2Cl_2): δ 7.42 (d, J 8 Hz, 2H), 7.23 (d, J 8 Hz, 2H), 2.87 (s, 3H). IR (neat): 2924, 2856, 1679, 1587, 1490, 1439, 1410, 1350, 1221, 1170, 1115, 1023, 1010, 954, 818, 787, 738, 645, 546, 442, 350, 295 cm^{-1}. MW calc. for $C_{42}H_{42}Cl_{15}N_9W_6$: 2307.8, found ($CH_2Cl_2$) 2403. Anal. Calc. for $C_{42}H_{42}Cl_{15}N_9W_6$: C, 21.86; H, 1.83; N, 5.46. Found: C, 22.13; H, 1.82; N, 5.43%.

1 K. Dehnicke and J. Strähle, *Angew. Chem., Int. Ed. Engl.*, 1992, **31**, 955.
2 K. Dehnicke and J. Strähle, *Angew. Chem., Int. Ed. Engl.*, 1981, **20**, 413.
3 C. E. Housecroft, in *Inorganometallic Chemistry*, ed. T. P. Fehlner, Plenum, New York, 1992, ch. 3, sect. 4.1, pp. 100–115.
4 W. A. Nugent and J. M. Mayer, *Metal–Ligand Multiple Bonds*, Wiley, New York, 1988.
5 S. C. Critchlow, M. E. Lerchen, R. C. Smith and N. M. Doherty, *J. Am. Chem. Soc.*, 1988, **110**, 8071.
6 K. L. Sorensen, M. E. Lerchen, J. W. Ziller and N. M. Doherty, *Inorg. Chem.*, 1992, **31**, 2678.
7 T. S. Haddad, A. Aistars, J. W. Ziller and N. M. Doherty, *Organometallics*, 1993, **12**, 2420.
8 C. Newton, K. D. Edwards, J. W. Ziller and N. M. Doherty, *Inorg. Chem.*, in press.
9 See also, C. M. Jones and N. M. Doherty, *Polyhedron*, 1995, **14**, 81.
10 C. F. Gibson and L. F. Dahl, *Organometallics*, 1988, **7**, 543.
11 H. W. B. Roesky and M. Noltemeyer, *Angew. Chem., Int. Ed. Engl.*, 1989, **28**, 754.
12 M. B. Banaszak Holl and P. T. Wolczanski, *J. Am. Chem. Soc.*, 1992, **114**, 3854.
13 D. Ostermann and H. Jacobs, *J. Alloys Compd.*, 1994, **206**, 15.
14 M. T. Benson, J. C. Bryan, A. K. Burrell and T. R. Cundari, *Inorg. Chem.*, 1995, **34**, 2348.
15 K. K. H. Lee and W. T. Wong, *Inorg. Chem.*, 1996, **35**, 5393.
16 K. Dehnicke, E. Schweda and J. Strähle, *Z. Naturforsch., Teil B*, 1984, **39**, 1114.
17 D. Fenske, T. Godemeyer and K. Dehnicke, *Z. Naturforsch., Teil B*, 1988, **43**, 12.
18 D. E. Wigley, *Prog. Inorg. Chem.*, 1994, **42**, 239.
19 J. D. Debad, P. Legzdins, R. Reina, M. A. Young, R. J. Batchelor and F. W. B. Einstein, *Organometallics*, 1994, **13**, 4315.
20 R. A. Wheeler, R. Hoffmann and J. Strähle, *J. Am. Chem. Soc.*, 1986, **108**, 5381.

Communication 9/06037E

Facile synthesis of well-defined water-soluble polymers *via* atom transfer radical polymerization in aqueous media at ambient temperature

X.-S. Wang, S. F. Lascelles, R. A. Jackson and S. P. Armes*

School of Chemistry, Physics and Environmental Science, University of Sussex, Falmer, Brighton, UK BN1 9QJ. E-mail: s.p.armes@sussex.ac.uk

Received (in Oxford, UK) 14th June 1999, Accepted 5th August 1999

Monomethoxy-capped oligo(ethylene oxide) methacrylate (OEGMA) is readily polymerised in aqueous media by atom transfer radical polymerisation at 20 °C using various initiators; the resulting OEGMA polymers and macromonomers were obtained in high yield (> 95%) within short reaction times and polydispersities were as low as 1.12.

Atom transfer radical polymerisation (ATRP) which is applicable to both styrenic and (meth)acrylate monomers and is remarkably tolerant of functional groups.[1,2] With regard to hydrophilic monomers, recent ATRP publications describe: (i) the polymerisation of 2-hydroxyethyl acrylate in aqueous media at 90 °C;[3] (ii) the (co)polymerisation of 2-(dimethylamino)ethyl methacrylate either in bulk or in non-aqueous media[4] and (iii) the polymerisation of sodium methacrylate at 90 °C.[5] In this latter example polymerisation was slow and incomplete: yields of only 70–80% were obtained after 21 h. Herein we describe the efficient, well-controlled polymerisation of monomethoxy-capped oligo(ethylene oxide) methacrylate (OEGMA) *via* ATRP in aqueous media at 20 °C. Excellent yields (> 95%) are obtained in short reaction times (< 0.5 h) even at 20 °C. Moreover, vinyl functional initiators can be used to prepare well-defined OEGMA macromonomers.

Our ATRP formulation was based on that described by Matyjaszewski's group.[1] The transition metal catalyst was Cu^{I}Cl and the ligand was 2,2′-bipyridine (bpy). Initiator **1** was synthesised according to a literature procedure.[5,6] A typical ATRP synthesis was carried out as follows (Scheme 1). Initiator

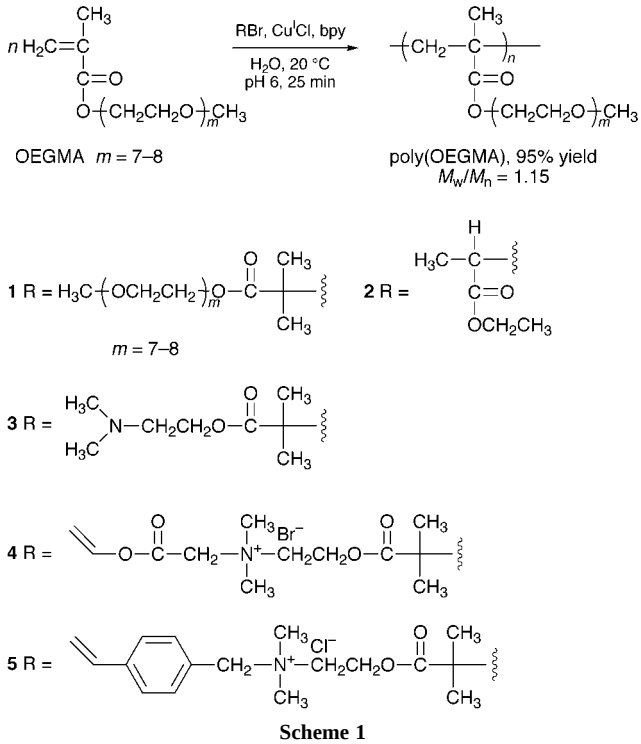

Scheme 1

1 (232 mg, 0.54 mmol, 1 equiv.) was dissolved in 5 ml of doubly distilled de-ionised water. To this degassed solution was added the bpy ligand (211 mg, 1.08 mmol, 2 equiv.), followed by Cu^{I}Cl (53 mg, 0.54 mmol, 1 equiv.). OEGMA monomer (9.70 g, 23 mmol, 42 equiv.) was added to this reaction mixture using a double-tipped needle and the solution was de-gassed using a nitrogen stream for 10–30 min with continuous stirring at 20 °C. The reaction solution became dark brown and much more viscous, indicating the onset of polymerisation; exotherms of 5–10 °C were typically observed. After 0.5 h, THF (50 ml) was added to the reaction solution, followed by excess $MgSO_4$ (15 g) to absorb the water. After filtration, the THF solution of poly(OEGMA) was passed through an alumina column to remove residual catalyst. THF was then removed under vacuum, yielding off-white polymers.

Molecular weight distributions were assessed using GPC (THF eluent; PMMA standards; RI detector). Polymer molecular weights, polydispersities and yields are summarised in Table 1. Conversion of OEGMA to polymer was monitored by ^{1}H NMR spectroscopy: Fig. 1(*a*) illustrates the progressive reduction of monomer vinyl signals at δ 5.4–5.8, accompanied by a concomitant increase in poly(OEGMA) signals (*e.g.* at δ 3.8–4.0). Fig. 1(*b*) shows a typical conversion *vs.* time curve derived from the NMR spectra. High conversions of monomer to polymer were obtained in short reaction times and the consumption of monomer followed first order kinetics, as expected. Narrow polydispersities (M_w/M_n < 1.12–1.30), indicative of a living polymerisation, were obtained for initiators **1**, **2** and **4**. At present we have no explanation for the somewhat higher polydispersities obtained with initiator **3**.

Overlapping peaks prevented discrimination between the NMR signals due to the oligo(ethylene oxide) initiator **1** and the OEGMA residues. However, inspection of the ^{1}H NMR spectra ($CDCl_3$ or D_2O) of the cleaned-up polymers prepared using initiators **2** and **4** confirmed the presence of the initiator, as expected. The peak integral of the NMR signal assigned to the α-proton of **2** at δ 2.1–2.2 (or to the azamethylene protons of **4** at δ 4.6) was compared to that due to the ethylene oxide protons of the OEGMA residues at δ 3.8–4.0 in order to determine the degree of polymerisation of the OEGMA chains by end-group analysis. Such calculations yielded number-average molecular weights (M_n) which were in excellent agreement with those expected from the corresponding monomer/initiator ratios (see Table 1). Moreover, in the case of initiator **4**, well-defined vinyl acetate-capped macromonomers were obtained, which are expected to be useful reactive stabilisers for poly(vinyl acetate) latex syntheses. Facile synthetic routes to such well-defined hydrophilic macromonomers are very rare in the literature, although similar selectivity has been reported by Matyjaszewski's group for the preparation of hydrophobic polystyrene-based macromonomers by ATRP utilizing a vinyl chloroacetate initiator.[7] Our attempts to prepare the analogous styrene-capped macromonomers using initiator **5** under the same conditions were not successful. High molecular weights and broad polydispersities were obtained (see Table 1), which suggests insufficient selectivity: the styrenic end-groups probably copolymerise with the OEGMA even at 20 °C.

Table 1 A summary of the molecular weights and polydispersities of various OEGMA-based polymers synthesised using ATRP in aqueous media at 20 °C. Synthesis conditions: [initiator] = 0.54–2.14 mmol; initiator : $Cu^{I}Cl$: bpy was 1 : 1 : 2 in all experiments

			M_n			
Initiator	*t*/h	Conversion (%)	Target	^{1}H NMR	GPC	M_w/M_n
1	0.5	> 99[a]	8500	—	6500[b]	1.12
1	0.5	> 99[a]	16300	—	9700[b]	1.17
2	2.0	> 99[a]	11200	10600	6000[b]	1.17
3	8.0	> 99[a]	2400	2500	3500[c]	1.38
3	0.5	> 99[a]	5100	5300	4700[c]	1.42
4	1.0	> 99[a]	14600	14500	9700[c]	1.21
4	0.5	98	5000	4900	5500[c]	1.30
5	2.0	> 99[a]	18700		31500[c]	1.86
5	0.5	98	6000		15000[c]	1.89

[a] No residual monomer signal detected in ^{1}H NMR spectrum. [b] THF eluent; PMMA standards. [c] Aqueous eluent; PEO standards.

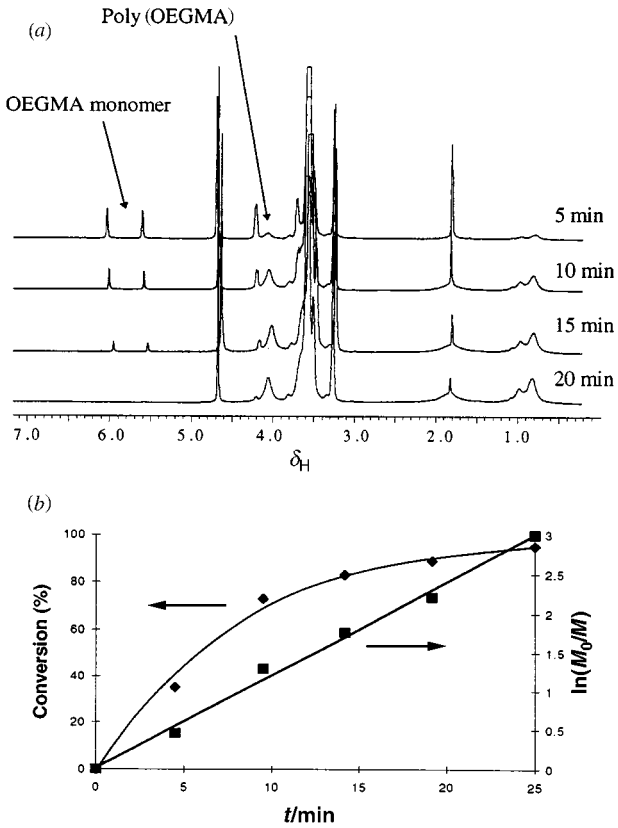

Fig. 1 (*a*) Evolution of ^{1}H NMR spectra (D_2O) for the homopolymerisation of OEGMA by ATRP at 20 °C in aqueous media using initiator **1**, (*b*) Typical conversion *vs*. time curve derived from the ^{1}H NMR spectra: (◆) conversion and (■) ln (M_o/M).

As far as we are aware, there have been no previous reports of rapid ATRP in aqueous media at ambient temperature. However, ATRP of hydrophobic monomers at ambient temperature is well-documented. Haddleton *et al*. described[8] the relatively slow bulk polymerisation of methyl methacrylate at 25 °C, with 92% conversion requiring a reaction time of 20 h. In contrast, Matyjaszewski and co-workers reported[9] the rapid bulk polymerisation of methyl acrylate at 22 °C. In this latter case it was shown that the choice of ligand for the Cu^{I} catalyst was critical for efficient polymerisation: much slower rates were obtained with a dialkyl-substituted bipyridine ligand than for a multifunctional ligand, hexamethylated tris[2-(dimethylamino)ethyl]amine. The same research group has also shown[10] that solvent polarity can be an important parameter in ATRP. Thus the rate of polymerisation of *n*-butyl acrylate in polar solvents such as ethylene carbonate was unexpectedly faster than that observed for bulk polymerisation, even though the monomer and initiator concentrations were significantly higher in the latter case. This observation was attributed to the mononuclear nature of the Cu^{I} catalyst. Since water is a very polar solvent, it is perhaps understandable that the ATRP of hydrophilic monomers such as OEGMA is particularly fast in aqueous media, even at room temperature. We also note that the $Cu^{I}[bpy]_2$ catalyst is more likely to be mononuclear in aqueous media, with more complex binuclear halo-bridged structures being formed in non-aqueous media.[11] One referee believes that the rapid ATRP of OEGMA described herein is due to complexation of the ethylene oxide residues to the Cu catalyst. We believe that this hypothesis is unlikely because we observe similar rates of polymerization for the ATRP of unrelated monomers such as sodium 4-vinylbenzoate.[12] The second referee pointed out that, since OEGMA is a sterically hindered monomer, its rate coefficient for termination may be anomalously low; similar observations have been recently reported for *n*-dodecyl methacrylate.[13] This would be consistent with the apparent lack of termination observed even at high conversions (see Fig. 1). This referee also suggested that the Cu–Cl bond may be more easily cleaved in water than in non-aqueous media. Thus the rate of deactivation would be reduced and faster polymerisations would ensue.

In summary, ATRP of OEGMA is facile and well-controlled under environmentally-friendly conditions; this discovery has considerable potential for commercial exploitation.

We thank the EPSRC for financial support. We also thank the referees for their comments.

Notes and references

1 J.-S. Wang and K. Matyjaszewski, *Macromolecules*, 1995, **28**, 7901; J.-S. Wang and K. Matyjaszewski, *J. Am. Chem. Soc.*, 1995, **117**, 5614; T. E. Patten and K. Matyjaszewski, *Adv. Mater*., 1998, **10**, 901.
2 D. M. Haddleton, C. Waterson, P. J. Derrick, C. B. Jasieczek and A. J. Shooter, *Chem. Commun.*, 1997, 683.
3 S. Coca, C. B. Jasieczek, K. L. Beers and K. Matyjaszewski, *J. Polym. Sci., Polym. Chem. Ed*., 1998, **36**, 1417.
4 X. Zhang, J. H. Xia and K. Matyjaszewski, *Macromolecules*, 1998, **31**, 5167; X. Zhang and K. Matyjaszewski, *Macromolecules*, 1999, **32**, 1763.
5 E. J. Ashford, V. Naldi, R. O'Dell, N. C. Billingham and S. P. Armes, *Chem. Commun*., 1999, 1285.
6 K. Jankova, X. Y. Chen, J. Kops and W. Batsberg, *Macromolecules*, 1998, **31**, 538.
7 K. Matyjaszewski, K. L. Beers, A. Kern and S. G. Gaynor, *J. Polym. Sci., Polym. Chem. Ed*., 1998, **36**, 823.
8 D. M. Haddleton, D. Kukulj, D. J. Duncalf, A. M. Heming and A. J. Shooter, *Macromolecules*, 1998, **31**, 5201.
9 J. H. Xia, S. G. Gaynor and K. Matyjaszewski, *Macromolecules*, 1998, **31**, 5958.
10 K. Matyjaszewski, Y. Nakagawa and C. B. Jasieczek, *Macromolecules*, 1998, **31**, 1535.
11 S. Kitagawa and M. Munakata, *Inorg. Chem*., 1981, **20**, 2261.
12 X.-S. Wang, R. A. Jackson and S. P. Armes, submitted.
13 M. Buback and C. Kowollik, *Macromolecules*, 1999, **32**, 1445.

Communication 9/04691G

Mechanism for isomerization of *n*-hexane over sulfated zirconia: role of hydrogen

Jean-Claude Duchet,*[a] Denis Guillaume,[a] Agnès Monnier,[a] Jacob van Gestel,[a] Georges Szabo,[b] Pedro Nascimento[b] and Sebastien Decker[b]

[a] *Catalyse et Spectrochimie, UMR CNRS 6506, ISMRA-Université, 14050 Caen, France. E-mail: duchet@ismra.fr*
[b] *CERT, Total Raffinage Distribution, 76700 Harfleur, France*

Received (in Cambridge, UK) 20th July 1999, Accepted 9th August 1999

The complex influence of hydrogen on *n*-hexane isomerization over sulfated zirconia enriched with platinum has been kinetically modelled with a simple three parameter rate equation derived from a mechanism involving Lewis sites and hydride species.

Sulfated zirconias are acidic catalysts which are able to isomerize linear alkanes at low temperature.[1,2] In practice, hydrogen is added to the isomerization unit in order to saturate the aromatics contained in the C_5–C_6 fraction and to prevent coking of the platinum enriched catalyst. Some authors attribute participation of hydrogen in isomerization *via* activation on platinum by creating either Brønsted acid sites[3,4] or hydride species accelerating the desorption of the carbenium ions.[5,6] In the literature, analysis of the influence of hydrogen has been limited to low hydrogen pressures.[6,7] Here we report the influence of hydrogen over a wide range of partial pressures (0.5–4.5 MPa) independently of the hexane pressure (0.1–0.5 MPa). Insight into the isomerization mechanism is obtained from the kinetic treatment of the data.

The catalyst was prepared as follows: zirconium hydroxide was precipitated from an aqueous solution of zirconium oxychloride by ammonium hydroxide. The dry material was sulfated with 0.5 M H_2SO_4, and then crystallised at 923 K. The sulfur content amounted to 2.0 wt%. Platinum was loaded at 0.3 wt% by impregnation with an H_2PtCl_6 solution and the final catalyst was calcined at 753 K. The catalyst was activated in the reactor at 623 K for 2 h in a dry air stream and contacted with flowing hydrogen at 423 K during 1 h. Dry *n*-hexane (0.1, 0.3 or 0.5 MPa) was vaporised in a dry hydrogen–helium mixture at 5 MPa total pressure and 423 K. The hydrogen partial pressure was varied from 0.5 to 4.5 MPa. Conversions were kept low to calculate initial rates.

The reaction was not observed without hydrogen owing to rapid deactivation. With hydrogen, the catalyst was stable for > 1 week and cracking was negligible. The distribution among isomers showed that 2-methylpentane, 3-methylpentane and 2,3-dimethylbutane were primary products formed in their thermodynamic ratio. The formation of 2,2-dimethylbutane was a consecutive reaction. The distribution was not influenced by hydrogen partial pressure.

The variation of the isomerization rate with hydrogen pressure is shown in Fig. 1. At a given hexane pressure, the rate strongly increases up to a maximum, then slowly decreases. The position of the maximum was shifted from 0.3 to 1.5 MPa pressure of hydrogen with increasing hexane pressure in the range 0.1–0.5 MPa. The reaction order with respect to *n*-hexane was slightly lower than unity at low hydrogen pressure, and reached unity beyond the maximum.

Any proposed mechanism should account for the change in reaction order for hydrogen, from positive to negative, so yielding a maximum isomerization rate. Kinetic modelling was used to infer the reaction sequence.

The maximum activity with hydrogen pressure has scarcely been reported in the literature dealing with isomerization of light alkanes over acidic catalysts. A classical metal–acid bifunctional mechanism has been developed on platinum–zeolite catalysts operating at 523 K. The detrimental effect of hydrogen was easily interpreted by the dehydrogenation step of the hydrocarbon into an alkene. However, further dehydrogenation into a diene is required to account for a positive effect at low hydrogen pressure, so yielding a maximum in the curves.[8] We found that the corresponding rate equation completely failed to fit our data in the whole range of hexane pressure. Indeed, a classical bifunctional metal–acid mechanism is improbable at 423 K. The alkene concentration is likely to be too low, and the catalyst more likely operates by an acidic mechanism. The acidity of sulfated zirconia is generally attributed to Brønsted sites[9] and accordingly, carbenium ions are formed *via* carbonium intermediates. However, reaction sequences based on this first step did not yield satisfactory rate equations. On the other hand, Lewis sites are readily created during the activation of sulfated catalysts at 923 K.[9] We propose a mechanism involving Lewis sites in which hydride abstraction from *n*-hexane (RH) on coordinatively unsaturated zirconium atoms creates carbenium ions which adsorb on Lewis basic sites (bridged oxygen atoms). The adsorbed carbenium ions are then rapidly isomerized and finally desorbed by the hydride species (Scheme 1). The isomerization step is not rate-limiting, as shown by the thermodynamic distribution of primary isomers.

This scheme is fully consistent with the poisoning effect of water adsorbed on Lewis sites. The closed sequence isomerizes

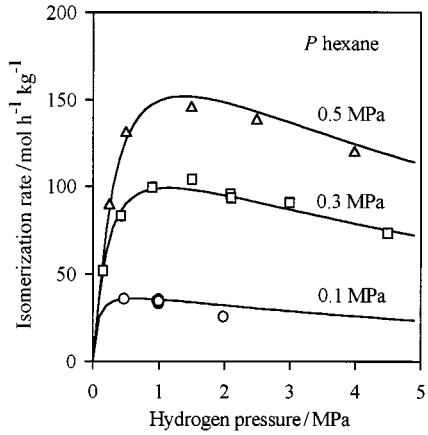

Fig. 1 Isomerization of *n*-hexane at 423 K and 5 MPa as a function of hydrogen pressure.

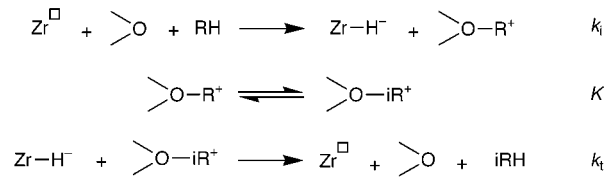

Scheme 1 Isomerization sequence.

n-hexane in the absence of hydrogen but the catalyst rapidly deactivates by coking. Hydrogen prevents this coking.

The influence of hydrogen on the isomerization rate may be rationalised by a second sequence (Scheme 2) involving platinum. Molecular hydrogen is homolytically dissociated on the metal and the hydrogen atoms migrate by spillover to the sulfated zirconia where they are converted into hydride species (Zr–H$^-$) and protons (O–H$^+$).

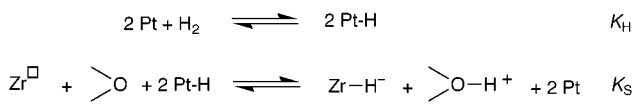

Scheme 2 Hydrogen sequence.

In this manner, hydrogen increases the concentration of hydride species, accelerates the desorption of carbenium ions and thus the overall rate. This explains the positive order at low hydrogen pressure, while the decrease in activity at higher hydrogen partial pressure is simply owing to a competition between protons and carbenium species.

Kinetic treatment of this sequence yielded the rate eqn. (1)

$$r = \frac{kP_{RH}}{\left\{1 + \alpha P_H + \frac{\beta P_{RH}}{\alpha P_H}\right\}^2} \quad (1)$$

with $k = Lk_i$ (L = number of adsorption sites), where $\alpha = K_H K_S$, $\beta = (k_i/(k_t)[1 + (1/K)]$, P_H = pressure of hydrogen and P_{RH} = pressure of hexane.

Besides the rate constant k, which is related to the number of sites, two parameters, α and β, characterise the catalyst. Parameter α is associated with the sequence combining the capacity of platinum to adsorb hydrogen (K_H) and the transfer of hydrogen by spillover to the coordinatively unsatured zirconium and to the oxygen sites of the sulfated zirconia (K_S). The spillover is determined by the zirconia surface. The second parameter β is representative of the strength of the sulfated zirconia sites in the isomerization sequence.

The curves on the Fig. 1 were obtained after optimisation of the kinetic parameters. The fit is very satisfactory over the whole range of hexane pressure. This model has the advantage of involving two independent parameters that can be used as a guide to improve the catalysts. For instance, the hydrogen pressure at maximum isomerization rate is inversely proportional to α. Thus, to minimise the hydrogen pressure, α should be increased, either by increasing the platinum efficiency or the spillover rate.

The above mechanism demonstrates the importance of hydrogen in isomerization. For the first time, a complete reaction sequence is proposed, that offers a very good alternative for the classical bifunctional mechanism. Such a mechanism opens perspectives in the interpretation of the influence of hydrogen on various reactions.

Notes and references

1 K. Arata, *Adv. Catal.*, 1990, **37**, 165.
2 X. Song and A. Sayari, *Catal. Rev.-Sci. Eng.*, 1996, **38**, 329.
3 K. Ebitani, J. Konishi and H. Hattori, *J. Catal.*, 1991, **130**, 257.
4 T. Shishido and H. Hattori, *Appl. Catal. A: Gen.*, 1996, **146**, 157.
5 E. Iglesia, S. L. Soled and G. M. Kramer, *J. Catal.*, 1993, **144**, 238.
6 R. A. Comelli, Z. R. Finelli, S. R. Vaudagna and N. R. Fígoli, *Catal. Lett.*, 1997, **45**, 227.
7 E. Iglesia, D. G. Barton, S. L. Soled, S. Miseo, J. E. Baumgartner, W. E. Gates, G. A. Fuentes and G. D. Meitzner, *Stud. Surf. Sci. Catal.*, 1996, **101**, 533.
8 M. Guisnet, V. Fouche, M. Belloum, J. P. Bournonville and C. Travers, *Appl. Catal.*, 1991, **71**, 295.
9 T. Yamaguchi, *Appl. Catal.*, 1990, **61**, 1.

Communication 9/05855I

ChemComm

Efficient transfer hydrogenation of alkynes and alkenes with methanol catalysed by hydrido(methoxo)iridium(III) complexes

Kazuhide Tani,* Aika Iseki and Tsuneaki Yamagata

Department of Chemistry, Graduate School of Engineering Science, Osaka University, Toyonaka, Osaka 560-8531, Japan. E-mail: tani@chem.es.osaka-u.ac.jp

Received (in Cambridge, UK) 15th July 1999, Accepted 10th August 1999

Hydrido(methoxo)iridium(III) complexes, [{Ir(H)(diphosphine)}$_2$(μ-OMe)$_2$(μ-Cl)]$^+$Cl$^-$ [diphosphine = (*R*)-BINAP **2a or = 2,2′-bis(diphenylphosphino)-1,1′-biphenyl (BPBP) **2b**] catalysed transfer hydrogenation of alkynes with methanol to give *trans*-alkenes selectively; plausible reaction pathways are also proposed.**

Catalytic transfer hydrogenation of unsaturated compounds using organic hydrogen donors such as alcohols and formic acid has widely been studied as an attractive method of reduction owing to its operational simplicity and environmentally friendly properties of the hydrogen donors.[1] Although methanol could be an exceedingly useful source of hydrogen from many viewpoints,[2] only a few reports of its use in homogeneous catalysis are available.[2,3] In addition, in contrast to the transfer hydrogenation of ketones, that of simple alkynes and alkenes by homogeneous catalysis remains relatively undeveloped.[3b,d,4] Here, we report efficient selective catalytic transfer hydrogenation of alkynes to *trans*-alkenes with soluble iridium complexes by using methanol as a hydrogen donor.

Recently we have reported that [IrCl(diphosphine)]$_2$ [diphosphine = BINAP **1a**, or 2,2′-bis(diphenylphosphino)-1,1′-biphenyl (BPBP) **1b**][5] carrying a peraryldiphosphine readily activates methanol at ambient temperature to give iridium(III) hydrido(methoxo) complexes, [{IrCl(H)(diphosphine)}$_2$(μ-Cl)(μ-OMe)$_2$]Cl [diphosphine = BINAP **2a** or BPBP **2b**].[6] In the course of the study concerning the reactivity of complexes **2** we have found that these hydrido(methoxo) complexes serve as efficient catalyst precursors for reduction of alkynes to give *trans*-alkenes using methanol as a source of hydrogen. Over-hydrogenation to alkanes was also observed. Hydrogenation proceeded in toluene–methanol (1:1, v/v) solution under fairly mild conditions at 80 °C in the presence of a catalytic amount of **2** [eqn. (1)].[7]

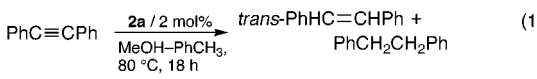

(1)

The results are summarized in Table 1. After 18 h with catalyst **2a**, diphenylacetylene was consumed completely to give 83% *trans*-stilbene and 17% 1,2-diphenylethane. Formation of *cis*-stilbene was not detected. When the reaction was stopped after 1 h, the conversion of diphenylacetylene was 29% and 12% *trans*-stilbene and 16.5% *cis*-stilbene were obtained, accompanied with 0.5% 1,2-diphenylethane. Reaction after 2 h gave the *trans*-alkene as the main product with 52% conversion. Although the reaction also proceeded under reflux > 36 h were required before complete consumption of diphenylacetylene. Hydrogenation of *trans*-stilbene gave 29% of 1,2-diphenylethane after 18 h, whereas hydrogenation of *cis*-stilbene gave the alkane in 39% yield, with almost all starting *cis*-stilbene being isomerised to *trans*-stilbene. Thus, *cis*-stilbene was hydrogenated faster than *trans*-stilbene and isomerisation of the *cis*-alkene to the *trans*-alkene proceeded much faster than its hydrogenation to the alkane in the presence of the iridium catalyst. The rate difference of the reduction between the *cis* and the *trans* isomers may reflect the difference of their binding constants,[8] resulting in high selectivity for the *trans*-alkene in the product. In other words, the initial hydrogenation product of diphenylacetylene should be *cis*-stilbene, which is isomerised to *trans*-stilbene by the iridium catalyst under the reaction conditions. Diphosphine complexes **1** can also be employed as the catalyst precursor for transfer hydrogenation. Interestingly, ethanol or propan-2-ol, generally more favorable sources of hydrogen,[2] were far less effective for the present transfer hydrogenation, and ketones were poor substrates. Acetophenone was hydrogenated in only 32% yield to give phenethyl alcohol with **2a** in toluene–methanol at 80 °C after 18 h. When the transfer hydrogenation was conducted in CD_3OD–toluene (1:1) using **2a** as a catalyst precursor, the deuterium contents of the olefinic as well as the methylene hydrogens of the products amounted to 100%. For the reaction performed in a CH_3OD–toluene (1:1), however, the corresponding values were 43 and 41%, respectively, as determined by 500 MHz ^{1}H NMR spectroscopy and GC–MS. Thus, during transfer hydrogenation hydrogens of both CH_3 and OH groups of methanol were incorporated in the products.

From the solid residue obtained from the catalytic reduction product of 1-phenylpropyne with methanol using complex **2a** as a catalyst precursor after removing all volatile materials *in*

Table 1 Transfer hydrogenation of alkynes and alkenes with MeOH catalysed by **1** and **2**[a]

Substrate	Catalyst	*t*/h	Conversion (%)	*trans*-Alkene (%)	*cis*-Alkene (%)	Alkane (%)
PhC≡CPh	**2a**	1	29	12	16.5	0.5
	2a	2	52	36	14.5	1.5
	2a	18	100	83	0	17
	2b	18	100	90	0	10
PhC≡CMe	**2a**	18	100	50	0	50
	1a	18	100	60	3	37
	1a[b]	18	25	3	22	0
	1b[c]	18	95	63	20	12
trans-PhCH=CHPh	**2a**	18	29	71	0	29
cis-PhCH=CHPh	**2a**	18	> 99	60	< 1	39
$Me(CH_2)_4C{\equiv}C(CH_2)_4Me$	**2a**	48	100	nd[d]	nd[d]	nd[d]

[a] [Substrate] = 0.5 M, [Substrate]:[Ir$^+$] = 25:1, solvent: MeOH–toluene (1:1), reaction temperature = 80 °C. Yields and conversion were determined by GLC, ^{1}H NMR and GC-MS. [b] Solvent: EtOH–toluene (1:1). [c] Solvent: Pr^{i}OH–toluene (1:1). [d] nd = not determined. Mixtures of dodecenes and dodecane were detected by GC–MS.

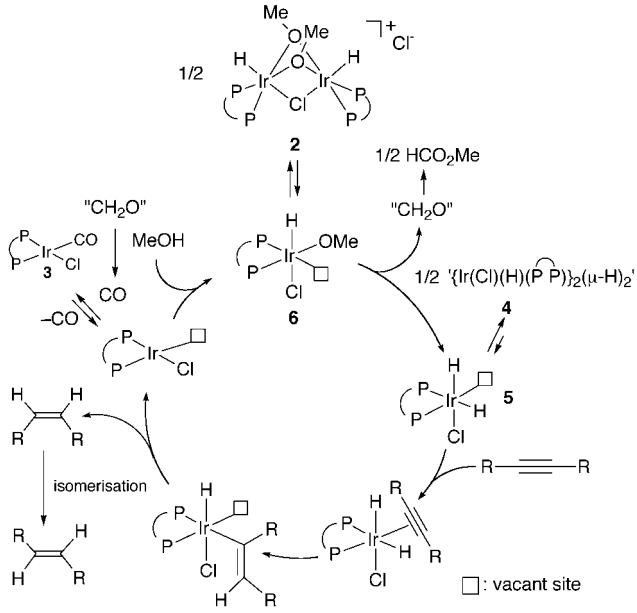

Scheme 1

vacuo, two iridium complexes, IrCl(CO)(BINAP) **3**[9] (major) and '{Ir(Cl)(H)(BINAP)}$_2$(μ-H)$_2$' **4** (minor),[10] were isolated. Although complex **3** showed comparable catalytic activity to that of **2a** for the transfer hydrogenation of diphenylacetylene, complex **4** was far less efficient. Methyl formate, the Tishchenko product of the by-product formaldehyde, was also detected by GC–MS in the reaction mixture. Based on these experimental results, we propose a plausible reaction pathway of the transfer hydrogenation of alkynes as well as alkenes and the isomerisation of alkenes catalysed by complex **2** (Scheme 1).[11] The real catalyst may be a nascent mononuclear dihydride species such as **5**, which dimerises to give the catalytically inactive dimer **4**. The possibility that coordination of alkyne to the monomeric hydrido(methoxo)complex **6** is the first step followed by hydride insertion to give a methoxo(vinyl) complex, however, can not be eliminated, though such species could not be detected by NMR of the reaction mixture of complex **2a** and diphenylacetylene.

This work was partly supported by the Grant-in Aid for Scientific Research from the Ministry of Education, Science, Sports, and Culture of Japan. BINAP was a generous gift from Takasago Perfumery Co. Ltd.

Notes and references

1 For reviews see: R. A. W. Johnstone, A. H. Wilbi and I. D. Entwisth, *Chem. Rev.*, 1985, **85**, 129; G. Brieger and T. J. Nestricle, *Chem. Rev.*, 1974, **74**, 563; R. Noyori and S. Hashiguchi, *Acc. Chem. Res.*, 1997, **30**, 97.

2 T. A. Smith and P. M. Maitlis, *J. Organomet. Chem.*, 1985, **289**, 385.

3 (*a*) J. C. Bailar and H. Itatani, *J. Am. Chem. Soc.*, 1967, **89**, 1592, 1600; *J. Am. Oil Chem. Soc.*, 1967, **43**, 377; 1967, **44**, 147; (*b*) H. Imai, T. Nishiguchi and K. Fukuzumi, *J. Org. Chem.*, 1974, **39**, 1622; (*c*) T. A. Smith and P. M. Maitlis, *J. Organomet. Chem.*, 1984, **269**, C7; (*d*) D. Milstein, *J. Mol. Cat.*, 1986, **36**, 387.

4 K. Tani, N. Ono, S. Sakamoto and F. Sato, *J. Chem. Soc., Chem. Commun.*, 1993, 386; B. M. Trost and R. Braslau, *Tetrahedron Lett.*, 1989, **30**, 4657; M. E. Vol'pin, V. P. Kukolev, V. O. Chernyshev and I. S. Kolomnikov, *Tetrahedron Lett.*, 1971, 4435. Stoichiometric transfer hydrogenation of diphenylacetylene to *trans*-stilbene with ethanol mediated by 'Ir(PPh$_3$)$_2$H$_3$' has been reported: R. Zanella, F. Canziani and M. J. Graziani, *J. Organomet. Chem.*, 1974, **67**, 449. For transfer hydrogenation of activated alkenes, see: M. Saburi, M. Ohnuki, M. Ogasawara, T. Takahashi and Y. Uchida, *Tetrahedron Lett.*, 1992, **39**, 5783; H. Brunner and W. Leitner, *Angew. Chem., Int. Ed. Engl.*, 1988, **27**, 1180.

5 T. Yamagata, A. Iseki and K. Tani, *Chem. Lett.*, 1997, 1215.

6 K. Tani, A. Iseki and T. Yamagata, *Angew, Chem., Int. Ed.*, 1998, **37**, 3381; *Angew, Chem.*, 1998, **110**, 3590.

7 Catalytic transfer hydrogenation: an alkyne (2 mmol) and complex **2** (0.04 mmol) were dissolved in a mixture of methanol (2 mL) and toluene (2 mL) in a glass ampoule under argon and sealed under reduced pressure at −197 °C. The ampoule, placed in a steel pipe, was heated at 80 °C for 18 h. The reaction products were analyzed by GLC, ^{1}H NMR and GC–MS.

8 J. P. Collman, L. S. Hegedus, J. R. Norton and R. G. Finke, *Principles and Applications of Organotransition Metal Chemistry*, University Science Books, Mill Valley, CA, 1987, p. 531.

9 Complex **3**: orange powder. Anal. Calc. for $C_{45}H_{32}ClIrOP_2$: C, 61.53; H, 3.67. Found: C, 61.42; H, 3.84%; Mp > 120 °C (decomp.); MS (FAB) *m/z* 878 (M^+), 850 (M^+ − CO); IR 1986 (film, ν_{CO}), 304w cm^{-1} (Nujol, ν_{Ir-Cl}); δ_P($CDCl_3$, 121 MHz) 16.5 (d, *J* 28 Hz), 22.7 (d, *J* 28 Hz); δ_C($CDCl_3$, 75 MHz) 180.7 (dd, *J* 11, 123 Hz, *C*O). Complex **3** can be quantitatively prepared from the reaction of **1** and CO.

10 Complex **4**: yellowish orange powder, IR (Nujol) 2279 (ν_{Ir-H_t}), *ca.* 1620w br cm^{-1} (ν_{Ir-H_b}); δ_H($CDCl_3$, 300 MHz) −22.38 (dd, *J* 15, 21 Hz, Ir–H$_t$) and −11.57(tt, *J* 8, 64 Hz, Ir–H$_b$); δ_P($CDCl_3$, 121.5 MHz) 3.6 (dd, *J* 9, 10 Hz) and 5.9 (dd, *J* 9, 10 Hz); MS (FAB): group of peaks centered at *m/z* 1703 resembling the simulated pattern for (M^+ − 1) (M = $C_{88}H_{68}{}^{35}Cl_2{}^{193}Ir_2P_2$). Although complex **4** could not be isolated as a pure state, on the basis of these spectral data we tentatively propose the structure '{Ir(H)(Cl)(BINAP)}$_2$(μ-H)$_2$'. Complex **4** can also be obtained as the main product by pyrolysis of complex **2a** at 80 °C in methanol–toluene.

11 For isomerisation as well as hydrogenation of alkenes, the same dihydride **5** can also act as a catalyst. Insertion of *cis*-alkene into Ir–H and subsequent β-hydrogen elimination from the hydrido(alkyl) complex gives *trans*-alkene and **5**, or reductive elimination from the hydrido(alkyl) complex gives alkane and 'Ir(diphosphine)Cl', respectively.

Communication 9/05765J

Sulfide accumulation and sensing based on electrochemical processes in microdroplets of N^1-[4-(dihexylamino)phenyl]-N^1,N^4,N^4-trihexyl-1,4-phenylenediamine

Frank Marken,*[a] Alastair Blythe,[a] Richard G. Compton,[a] Steven D. Bull[b] and Stephen G. Davies[b]

[a] *Physical and Theoretical Chemistry Laboratory, Oxford University, South Parks Road, Oxford, UK OX1 3QZ. E-mail: Frank@physchem.ox.ac.uk*

[b] *Dyson Perrins Laboratory, Oxford University, South Parks Road, Oxford, UK OX1 3QY*

Received (in Cambridge, UK) 30th June 1999, Accepted 10th August 1999

Electroanalytical sulfide detection *via* oxidation of N^1-[4-(dihexylamino)phenyl]-N^1,N^4,N^4-trihexyl-1,4-phenylene diamine (DPTPD) deposited in form of microdroplets onto basal plane pyrolytic graphite electrodes immersed in aqueous 0.1 M $NaClO_4$ containing sulfide is proposed to be associated with two consecutive reversible one electron processes accompanied by ClO_4^- uptake, sulfide accumulation, and formation of a methylene blue derivative.

Voltammetric experiments at microdroplets of electrochemically active materials deposited on suitable types of electrode surfaces in form of an organic oil have recently been shown to result in unique electrochemical characteristics.[1,2] An organic redox system such as phenylenediamine can be made highly insoluble in aqueous media by introducing several hexyl chains into the molecular structure. With this kind of derivatisation the resulting material shows as a further useful property an extremely low tendency to crystallise or freeze into a solid glass. Surprisingly, the liquid nature of the material at room temperature remains even after oxidation and the associated uptake of anions from the solution phase to achieve charge neutrality. The material resulting from this type of redox process, a room temperature ionic liquid, is of considerable interest for electrochemical applications requiring ion accumulation and/or ion conduction.

Redox processes in microdroplets of organic oils proceed *via* exchange of anions with the surrounding solution phase and for chemically reversible processes, such as the first oxidation of tetrahexylphenylenediamine,[1] the ion exchange process has been shown to be very fast. Usually the most hydrophobic anion crosses from the aqueous into the organic liquid phase most readily. In cases in which secondary chemical processes are coupled to the redox process much more complicated conditions arise. Voltammograms become chemically irreversible and products mix with the original oil phase or escape into the aqueous solution phase. The presence of a product with a redox potential different to that of the starting material may interfere with the mass and charge transport in the microdroplet and therefore considerably change the voltammetric characteristics. The rate of the chemical follow up step is a crucial parameter which determines whether (i) the redox process can be driven to completion before reaction or (ii) the chemical step is fast and directly proceeds thereby effectively stopping any charge transport by electron hopping in the zone close to the electrode.

In the present study a novel redox system, N^1-[4-(dihexylamino)phenyl]-N^1,N^4,N^4-trihexyl-1,4-phenylenediamine (DPTPD, structure **I**) is deposited in form of microdroplets onto basal plane pyrolytic graphite electrodes, immersed in aqueous electrolyte media, and used in voltammetric experiments. A key feature of this type of molecule is its ability in the presence of sulfide to undergo a nucleophilic substitution reaction at the aromatic rings to yield phenothiazine type derivatives.[3] This type of process is known as the 'methylene blue reaction'[4] and used for the selective and highly sensitive analytical determination of traces of sulfide with *N*,*N*-dimethylphenylenediamine and a chemical oxidant, Fe^{3+}. The preliminary work described here is aimed at coupling the highly selective chemical sulfide detection method *via* the methylene blue process to the electrochemical process in the microdroplet deposit at the electrode surface.

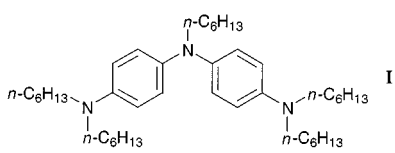

I

DPTPD deposited onto a basal plane pyrolytic graphite electrode surface and immersed into aqueous 0.1 M $NaClO_4$ undergoes two well defined and reversible oxidation processes shown in Fig. 1. Based on the comparison of the amount of material deposited, 1.7×10^{-9} M corresponding to 0.17 mC per electron transferred, and the charge under the first and second oxidation responses (combined 0.34 ± 0.03 mC), the processes may be identified as the first and the second oxidation of DPTPD [eqn. (1) and (2)]. For this amount of deposit present on the surface of the graphite electrode the charge under the voltammetric response for the oxidation (Fig. 1) is essentially independent of the scan rate over the range of 1–100 mV s^{-1} and therefore a nearly complete conversion of the material even at moderately fast scan rate appears to be possible. However, the lack of symmetry in the observed voltammetric responses[5] suggests that mass transport effects are present and affect the shape. Voltammetric data are summarised in Table 1. The comparison of the voltammetric characteristics with results obtained for the oxidation of THPD under similar conditions[1] suggests that DPTPD is chemically much more stable in the dicationic oxidation state because of delocalisation of the

$$DPTPD_{oil} + ClO_4^-{}_{solution} \rightleftharpoons [DPTPD^+ClO_4^-]_{oil} + e^- \quad (1)$$

$$[DPTPD^+ClO_4^-]_{oil} + ClO_4^-{}_{solution} \rightleftharpoons [DPTPD^{2+}(ClO_4^-)_2]_{oil} + e^- \quad (2)$$

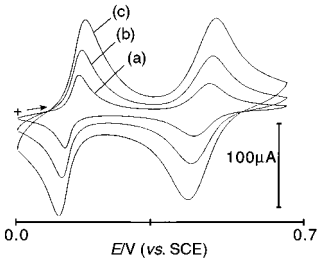

Fig. 1 Cyclic voltammograms obtained for the oxidation of 1.7×10^{-9} mol DPTPD deposited onto a 4.9 mm diameter basal plane pyrolytic graphite electrode and immersed in aqueous 0.1 M $NaClO_4$. The third cycle from a multicycle experiment is shown for scan rates of (a) 20, (b) 50 and (c) 100 mV s^{-1}.

Table 1 Voltammetric data for the oxidation of 1.7×10^{-9} mol DPTPD deposited onto a 4.9 mm diameter basal plane pyrolytic graphite electrode and immersed in aqueous 0.1 M $NaClO_4$

Scan rate/ V s^{-1}	E_p^{ox}/ V(*vs.* SCE)	I_p^{ox}/ μA	E_p^{red}/ V (*vs.* SCE)	I_p^{red}/ μA	ΔE^a/ mV	$E_{1/2}{}^b$/ V (*vs.* SCE)	ΔE_{hh}/ mV
First oxidation process: $DPTPD^{0/+}$							
0.02	0.158	44	0.124	−44	34	0.141	66
0.05	0.165	75	0.116	−80	49	0.140	80
0.10	0.173	109	0.110	−124	63	0.141	100
Second oxidation process: $DPTPD^{+/2+}$							
0.02	0.498	34	0.457	−28	41	0.477	120
0.05	0.505	68	0.452	−62	53	0.478	133
0.10	0.515	113	0.444	−106	71	0.480	165

[a] Peak-to-peak separation of the voltammetric responses associated with oxidation and the reduction. [b] The half wave potential, $E_{1/2}$, corresponds to the mid-potential given by $1/2(E_p^{ox} + E_p^{red})$.

positive charge over both aromatic rings (see structure **I**). Changes in shape or width at half height, ΔE_{hh}, of the voltammetric response, may be interpreted as a measure of the interaction of redox centres in the organic oil.[6] The wider peak for the second oxidation process is consistent with a better mixing or repulsive interaction in the regular solution model[7] of the $DPTPD^{2+}$ and $DPTPD^{+}$ containing ionic liquids compared to the mixing of the $DPTPD^{+}$ containing ionic liquid and the neutral oil.

The experiment shown in Fig. 1 has been conducted with 1.7×10^{-9} mol deposit. It can be calculated, based on the geometric area of the electrode and a hypothetic density of DPTPD of 0.5 g cm^{-3}, that this amount corresponds to a layer of *ca.* 57 nm height. However, owing to the surface morphology of the basal plane pyrolytic graphite microdroplets of *ca.* 0.1 μm size are anticipated. Changing the amount of deposited material causes a corresponding change in the charge under the voltammetric signals, although for high coverages corresponding to a layer of more than *ca.* 1 μm height the time for the redox process to go to completion becomes long (several minutes).

When the concentration of the supporting electrolyte is changed or other types of anion such as nitrate are used characteristic changes in form of shifts in the reversible potential, $E_{1/2}$, following the same trend observed in earlier studies are detected. However, in the presence of SH^- ions, the voltammetric response for the oxidation of DPTPD changes dramatically. Fig. 2 shows voltammetric responses for the oxidation of a deposit of 4.2×10^{-9} mol DPTPD on a 4.9 mm diameter basal plane pyrolytic graphite electrode immersed in aqueous 0.1 M $NaClO_4$ containing 2 mM HS^-. It can be seen that the main response at $E_{1/2}$ = 0.14 V *vs.* SCE drastically changes over consecutive potential cycles. A new broad response at E_p^{ox} = *ca.* 0.3 V *vs.* SCE can be detected on the first positive scan of a multi-cycle voltammogram and a product response gradually appears at $E_{1/2}$ = *ca.* −0.1 V *vs.* SCE. Qualitatively, the rate at which the change in the voltammogram occurs depends on the concentration of sulfide present in the solution phase and the experimental conditions such as the scan rate.

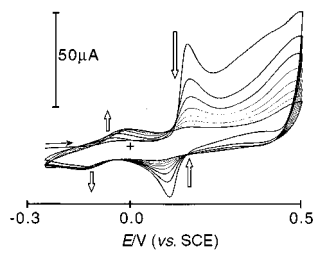

Fig. 2 Cyclic voltammograms obtained for the oxidation of 3.4×10^{-9} mol DPTPD deposited onto a 4.9 mm diameter basal plane pyrolytic graphite electrode and immersed in aqueous 0.1 M $NaClO_4$ containing 2 mM HS^- (scan rate: 20 mV s^{-1}).

Based on the known redox chemistry of dimethylphenylenediamine[4] it is proposed that the product of the chemical reaction step in the microdroplet is a hexyl derivative of methylene blue (PHPD, structure **II**). A hypothesis for the overall mechanism of

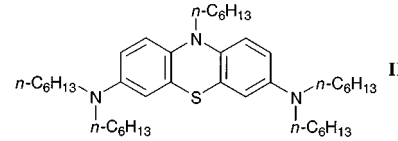

II

this reaction, which involves DPTPD in the monocationic state, is given in eqn. (3). The voltammetric response associated with the formation of the product with $E_{1/2}$ = *ca.* −0.1 V *vs.* SCE may be proposed to result from the reversible one electron redox process given in eqn. (4). The range of organic oils giving room

$$[DPTPD^{+}ClO_4^{-}]_{oil} + HS^{-} \rightarrow [PHPD^{+}ClO_4^{-}]_{oil} + 3\ H^{+} + 4\ e^{-} \quad (3)$$

$$[PHPD^{+}ClO_4^{-}]_{oil} + e^{-} \rightleftharpoons PHPD_{oil} + ClO_4^{-} \quad (4)$$

temperature ionic liquids can be easily extended by derivatising the core redox molecule with long chain alkyl groups and chemical systems of high analytical value can be employed. The novel electroanalytical procedure based on sulfide accumulation in oil microdroplets by ion-exchange and selective detection by a chemical reaction sequence promises to combine high selectivity and sensitivity and is open to the use of combined spectroelectroanalytical techniques.

F. M. thanks the Royal Society for the award of a University Research Fellowship and New College, Oxford, for a Stipendiary Lectureship in Physical Chemistry.

Notes and references

† The redox active reagent N^1-[4-(dihexylamino)phenyl]-N^1,N^4,N^4-trihexyl-1,4-phenylenediamine (DPTPD) was prepared *via* refluxing N^1-[4-aminophenyl]-1,4-phenylenediamine (200 mg) with sodium hydride (192 mg, 8 equiv.) and hexyl bromide (1.32 g, 8 equiv.) in DMF (20 ml) at 90 °C for 12 h. The crude reaction mixture was purified by pouring into water (20 ml), extracted with ethyl acetate (3×20 ml), dried ($MgSO_4$), and the solvent removed in vacuum, and the resulting crude oil purified by chromatography over silica gel (2% Et_2O–98% hexane) to afford the title compound (142 mg) pure in 23% yield. ^1H NMR(d^8-toluene,200 MHz); 0.87 (15H, br t), 1.15 (30H, br), 1.48 (8H, br), 1.65 (2H, br), 3.10 (8H, br t), 3.55 (2H, br t), 6.61 (4H, br d), 6.95 (4H, br d); *m/z* (CI) 620 (M + 1); HRMS, calc. for $C_{42}H_{74}N_3$ 620.5883, found 620.5891.

Electrochemical experiments were conducted in a conventional three-electrode cell with a 4.9 mm diameter basal plane pyrolytic graphite working electrode, a gold wire counter electrode and a saturated calomel (SCE, Radiometer, Kopenhagen) reference electrode. A potentiostat (Autolab PGSTAT 20, Ecochemie, Netherlands) was used for cyclic voltammetric experiments. The procedure for the deposition of DPTPD microdroplets on the surface of the basal plane pyrolytic graphite electrode was based on evaporation of a solution of 0.1 mM DPTPD in acetonitrile. Solutions were degassed with argon (Pureshield, BOC) for at least 15 min prior to experiments. All studies were carried out at 20 ± 2 °C.

1 F. Marken, R. D. Webster, S. D. Bull and S. G. Davies *J. Electroanal. Chem.*, 1997, **437**, 209.
2 F. Marken, R. G. Compton, C. H. Goeting, J. S. Foord, S. D. Bull and S. G. Davies, *Electroanalysis*, 1998, **10**, 821.
3 L. Gustafsson, *Talanta*, 1960, **4**, 227 and references therein.
4 See, for example: W. J. Williams, *Handbook of Anion Determination*, Butterworths, London, 1979.
5 See for example: A. J. Bard and L. R. Faulkner, *Electrochemical Methods*, Wiley, New York, 1980, p. 523.
6 B. J. McClelland, *Statistical Thermodynamics*, Chapman and Hall, London, 1973.
7 See for example: R.G. Compton, M.E. Laing, A. Ledwith and I. Abu-Abdoun, *J. Appl. Electrochem.*, 1988, **18**, 431 and references therein.

Communication 9/05278J

Intramolecular alkylation of an α-sulfinyl vinylic carbanion without loss of optical purity: a novel access to chiral cyclic vinylic sulfoxides

Naoyoshi Maezaki, Mayuko Izumi, Sachiko Yuyama, Chuzo Iwata and Tetsuaki Tanaka*

Graduate School of Pharmaceutical Sciences, Osaka University, 1-6 Yamadaoka, Suita, Osaka 565-0871, Japan. E-mail: t-tanaka@phs.osaka-u.ac.jp

Received (in Cambridge, UK) 1st July 1999, Accepted 9th August 1999

Novel cyclisation *via* intramolecular α-alkylation of vinylic sulfoxides was studied and cyclic vinylic sulfoxides of various ring sizes (5–7) were synthesised from both (*E*)- and (*Z*)-isomers without loss of optical purity.

1-Alkenyl aryl sulfoxides are deprotonated at the α-position and generate vinylic carbanion species, which react with a variety of electrophiles such as alkyl halides, epoxides, aldehydes and ketones.[1] This methodology is very useful for the synthesis of substituted vinylic sulfoxides, which can be transformed into a variety of functional groups and which also have potential use for asymmetric reactions.[2] However, research on the intermolecular reactions of α-lithio vinylic sulfoxides has revealed two problems: (i) contamination of the geometric isomer by isomerisation of its olefin moiety, and (ii) racemisation of the stereogenic center on the sulfur atom during isomerisation.[3] During the course of our research on the reaction of α-sulfinyl carbanions,[4] we have become interested in intramolecular α-alkylation of vinylic sulfoxides, which, to the best of our knowledge, has never been discussed in the literature (Scheme 1). This reaction has two advantages. (i) Not only (*E*)-isomers but also (*Z*)-isomers could be cyclised into the same product *via* rapid isomerisation; this would then provide a cyclic vinylic sulfoxide. Therefore, neither selective preparation of the geometric isomers nor their separation is required. (ii) The loss of enantiomeric excess is expected to be overcome since the intramolecular reaction is generally milder than the corresponding intermolecular version, due to the reduced decrease in the entropy of the intramolecular system.

Here we report a novel cyclisation *via* intramolecular alkylation of α-sulfinyl vinylic carbanions generated from (*E*)- and (*Z*)-isomers; this process provides cyclic vinylic sulfoxides without a subsequent loss of optical purity.

We began our study employing (*E*,*R*)-6-iodohex-1-en-1-yl *p*-tolyl sulfoxide (*E*)-**1a**. On treatment of (*E*)-**1a** with LDA (1.5 equiv.) in THF at −78 °C, rapid cyclisation proceeded to give cyclohex-1-enyl *p*-tolyl sulfoxide **2** in 82% yield; neither elimination of iodide nor the rearrangement of the double bond to the β,γ-position was observed (Table 1, entry 1). The corresponding bromide (*E*)-**1b** also afforded **2** in a comparable yield (79%) (entry 2). On the other hand, the tosylate and mesylate analogues caused the production of many products and therefore resulted in poor results (entries 3 and 4). Variation of the additive, base and solvent used did not improve the yield (entries 5–13).

Next, we examined cyclisation of ω-iodo vinylic sulfoxides (*E*)-**1e**,**f** with different chain lengths. Five- to seven-membered rings were formed in a good yield (79–82%; Table 2, entries 1–3). However, an eight-membered ring could not be formed even under highly dilute conditions (0.001 M), yielding instead many unidentified products together with the dimer **6** (22%) (entry 4). Then, we focused on the intramolecular alkylation of (*Z*)-isomers. As expected, cyclisation of (*Z*)-**1a**,**e**,**f** proceeded *via* isomerisation of their olefin geometry followed by cyclisa-

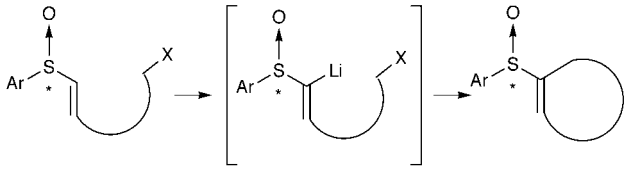

Scheme 1

Table 1 Intramolecular alkylation of α-sulfinyl vinyl carbanion[a]

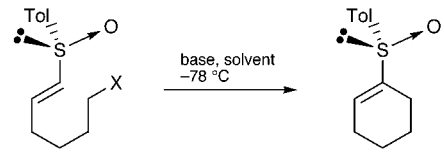

(*E*)-**1a**–**d** **2** Tol = *p*-MeC_6H_4

Entry	Substrate (X)	Base	Additive	Solvent	Yield (%)[b]
1	**1a** (I)	LDA	—	THF	82
2	**1b** (Br)	LDA	—	THF	79
3	**1c** (OTs)	LDA	—	THF	24
4	**1d** (OMs)	LDA	—	THF	complex
5	**1a** (I)	LDA	HMPA	THF	55
6	**1a** (I)	LDA	TMEDA	THF	62
7	**1a** (I)	LICA[c]	—	THF	75
8	**1a** (I)	LTMP[d]	—	THF	65
9	**1a** (I)	NaHMDS	—	THF	complex
10	**1a** (I)	KHMDS	—	THF	complex
11	**1a** (I)	LDA	—	DME	39
12	**1a** (I)	LDA	—	Et_2O	10
13	**1a** (I)	LDA	—	toluene	21

[a] The substrate was treated with 1.5 equiv. of the base at −78 °C under N_2. [b] Isolated yield. [c] LICA = lithium cyclohexylisopropylamide. [d] LTMP = lithium 2,2,6,6-tetramethylpiperidide.

Table 2 Cyclisation of (*E*)- and (*Z*)-**1** and optical purities of the products[a]

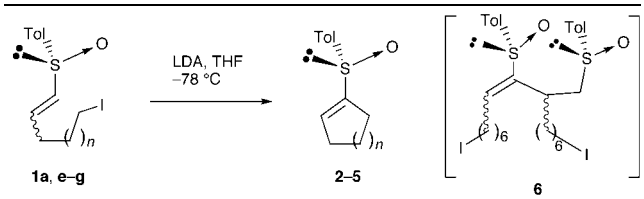

1a, **e**–**g** **2**–**5** **6**

Entry	Substrate	Product	*n* (ring size)	Yield (%)[b]	$[\alpha]_D$	Ee[c]
1	(*E*)-**1e**	**3**	1 (5)	81	+57	98
2	(*E*)-**1a**	**2**	2 (6)	82	+9	98
3	(*E*)-**1f**	**4**	3 (7)	79	+10	—
4	(*E*)-**1g**	**5**	4 (8)	0	—	—
5	(*Z*)-**1e**	**3**	1 (5)	66	+57	96
6	(*Z*)-**1a**	**2**	2 (6)	71	+9	98
7	(*Z*)-**1f**	**4**	3 (7)	64	+10	—

[a] The substrate was treated with 1.5 equiv. of the base at −78 °C under N_2. [b] Isolated Yield. [c] Determined by chiral HPLC.

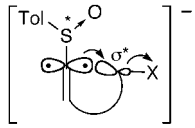

Fig. 1 Reaction mechanism.

tion to give **2**–**4**, respectively, in moderate yield (64–71%; entries 5–7).

Posner reported that α-deprotonation of optical pure (*E*,*R*)-undec-1-en-1-yl *p*-tolyl sulfoxide followed by reprotonation produced no racemisation, whereas similar treatment of the corresponding (*Z*)-isomer produced racemisation (*ca.* 30% loss of optical purity).[3] Therfore, the specific rotations of the cyclised products of intramolecular alkylation from the (*E*)- and (*Z*)-isomers were compared. The cyclic vinylic sulfoxides from the (*Z*)-isomers have almost the same specific rotations as those from the corresponding (*E*)-isomers. Furthermore, the products **2** and **3** prepared from (*E*)- and (*Z*)-ω-iodo vinylic sulfoxides **1a** and **1e** were confirmed to be highly optically pure (≥96% ee) by chiral HPLC (Daisel Chiralcel OB). As we expected, racemisation did not occur appreciably during (*Z*)- to (*E*)-isomerisation with the intramolecular alkylation of α-lithio vinylic sulfoxides.

The mechanism of racemisation in the α-carbanion of the (*Z*)-vinylic sulfoxide has not been revealed. However, the results of Posners' experiments indicate that racemisation occurs during isomerisation because no racemisation occurs in the corresponding reaction of the (*E*)-isomer. This means that the intramolecular alkylation of the (*Z*)-isomer is not a stepwise reaction involving isomerisation and cyclisation. We assumed the concerted mechanism shown in Fig. 1, wherein the σ*-orbital of the internal C–X bond participates in the olefin isomerisation by accepting the carbanion extending through the sp^2 carbon and assists the isomerisation.[1c,5] This interaction with the internal electrophile would prevent the racemisation of the sulfoxide.

A typical experimental procedure is described for the reaction of 7-iodohept-1-en-1-yl tolyl sulfoxide with LDA. A solution of the iodide **1f** (43 mg, 0.12 mmol) in dry THF (2.3 ml) was added to a solution of LDA (1.5 equiv.) [prepared from Pr^i_2NH (25 μl, 0.18 mmol) and 1.58 M BuLi in hexane (115 μl, 0.18 mmol) in dry THF (2.3 ml)]. The solution was stirred at −78 °C under N_2. After 30 min, the reaction was quenched with saturated aqueous NH_4Cl and extracted with EtOAc. The extract was washed with brine prior to drying and solvent evaporation. The crude sample was purified by preparative TLC on silica gel with hexane–EtOAc (2 : 1) to give cyclohex-1-enyl *p*-tolyl sulfoxide (22 mg, 79%).

In summary, we found a ring-forming reaction *via* intramolecular alkylation of the α-lithio vinylic sulfoxides, which proceeded in moderate to good yield. Interestingly, even vinylic sulfoxides with (*Z*)-configuration were cyclised *via* rapid isomerisation; no racemisation occurred at the sulfur atoms. Further study of this method of cyclisation is currently underway.

Notes and references

1 (*a*) R. R. Schmidt, H. Speer and B. Schmid, *Tetrahedron Lett.*, 1979, 4277; (*b*) G. H. Posner, P.-W. Tang and J. P. Mallamo, *Tetrahedron Lett.*, 1978, **42**, 3995; (*c*) H. Okamura, Y. Mitsuhira, M. Miura and H. Takei, *Chem. Lett.*, 1978, 517.

2 Review: M. C. Carreño, *Chem. Rev.*, 1995, **95**, 1717.

3 G. H. Posner, in *Asymmetric Synthesis*, ed. J. D. Morrison, Academic Press, New York, 1983, vol. 2A, pp. 225–241; G. H. Posner, J. P. Mallamo and K. Mirua, *J. Am. Chem. Soc.*, 1981, **103**, 2886.

4 N. Maezaki, A. Sakamoto, T. Tanaka and C. Iwata, *Tetrahedron: Asymmetry*, 1998, **9**, 179; N. Maezaki, A. Sakamoto, M. Soejima, I. Sakamoto, Y.-X. Li, T. Tanaka, H. Ohishi, K. Sakaguchi and C. Iwata, *Tetrahedron: Asymmetry*, 1996, **7**, 2787 and references cited therein.

5 Concomitant isomerisation–alkylation of an α-sulfinyl carbanion on an sp^3 carbon has been reported, see: G. Chassaing, R. Lett and A. Marquet, *Tetrahedron Lett.*, 1978, 471.

Communication 9/05320D

Regioselective modification of the sugar moiety in pyrimidine nucleosides *via* a 4′,5′-dehydro-2′,3′-anhydrouridine intermediate

Kosaku Hirota,* Hideki Takasu, Yoshie Tsuji and Hironao Sajiki

Laboratory of Medicinal Chemistry, Gifu Pharmaceutical University, Mitahora-higashi, Gifu 502-8585, Japan. E-mail: hirota@gifu-pu.ac.jp

Received (in Cambridge, UK) 12th July 1999, Accepted 9th August 1999

3′-Substituted pyrimidine nucleoside derivatives are obtained in moderate to high yields by the reaction of 1-(2′,3′-anhydro-5′-deoxy-4′,5′-didehydro-α-L-*erythro*-pentofuranosyl)uracil with nucleophiles without the formation of the corresponding 2′-adduct.

Nucleosides modified in the sugar moiety have become important components of both chemotherapeutic agents, as potential antimetabolites,[1] and synthetic oligonucleotide probes.[2] From a synthetic point of view, it is desirable to develop a common key intermediate. 2′,3′-Anhydro-β-D-lyxo-

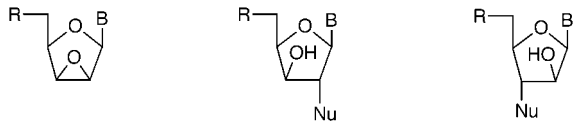

1 **2** **3**

furanosyl pyrimidine nucleosides **1** first synthesized by Fox *et al.*[3] are versatile building blocks, which through a nucleophilic ring-opening reaction can function as precursors of enantiomerically pure and biologically interesting pyrimidine nucleoside derivatives, and a number of reports for the application of **1** have appeared in the literature.[4] However, it is well known that the nucleophilic addition of **1** gave a mixture of 2′- and 3′-adducts (**2** and **3**) in most cases.

During our studies on the nucleophilic modification of 2′,3′-epoxy derivatives **1** and related compounds, we have discovered that the treatment of 2′,3′-epoxy-5′-iodouridine **4**[3c] with MeONa afforded 4′,5′-dehydro-5′-deoxy-3′-methoxy derivative **5a** in 96% yield as the sole product (Scheme 1). The possible reaction intermediates, 1-(2′,3′-anhydro-5′-deoxy-4′,5′-didehydro-α-L-*erythro*-pentofuranosyl)uracil **6** and 5′-iodo-3′-methoxy derivative **7**, were prepared. The epoxide **6** reacted regioselectively with MeONa to give the corresponding 3′-adduct **5a** in 80% yield *via* regiospecific nucleophilic attack of the methoxide anion at the highly reactive allylic 3′-position of **6**. On the other hand, only 2′,5′-anhydro derivative **8** was accessible from 5′-iodo-3′-methoxy derivative **7** without the formation of **5a** (Scheme 1).

We have now worked out an efficient synthetic method for the epoxide **6**, possessing contiguous enol ether and epoxide moieties in the molecule, which acts as a prominent precursor for a variety of 3′-adducts **5** and that can be incorporated into 3′-modified pyrimidine nucleosides. The synthesis of 2′,3′-anhydrouridine **6** was achieved in 92% yield by the reaction of **4** with LiHMDS (2.2 equiv.) in dry DMF (0 °C, 4 h). The efficiency of **6** as the precursor of the modified sugar moiety was demonstrated in the nucleophilic addition using various nucleophiles (Table 1). With the exception of two examples (Table 1, entries 1 and 2), which needed reflux temperatures for the completion of the reaction, all other additions were achieved at room temperature, and the yields of the 3′-adduct **5** were in the range of 52–81%. In the reaction with NaN_3 or PhSH as a comparatively soft nucleophile, 5′-adduct (**9g** or **9h**)[5] was also formed as a side product (3 or 11% yield) *via* S_N2' addition[6] together with a major product, the 3′-adduct (**5g** or **5h**).

In addition, when Et_2AlCN was used as a nucleophile, isomerized product **11** was obtained in 58% yield due to the activation of 3′-hydrogen of intermediate **10** by the strong electron-withdrawing cyano group (Scheme 2).

Next, we examined the hydroboration reaction of **5a**, aiming to convert it into the 5′-hydroxy derivatives **12** and **13**. When **5a** was refluxed with 18 equiv. of BH_3–THF in dry THF and then subsequently treated with H_2O_2–NaOH, the α-isomer **12** was obtained as the major product (53%) together with the β-isomer

Table 1 Nucleophilic addition to **6**

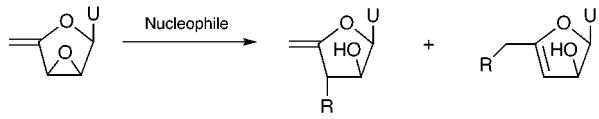

6 **5** **9**

Entry	Nucleophile	Solvent[a]	*t*/h	R	Product	Yield (%)[b] **5**	**9**
1	MeONa	MeOH[c]	2	OMe	**a**	80	ND[d]
2	Me_3Al	CH_2Cl_2[c]	12	Me	**b**	81	ND[d]
3	$BnNH_2$	CH_2Cl_2	24	NHBn	**c**	81	ND[d]
4	$NaCH(CO_2Me)_2$	MeOH	12	$CH(CO_2Me)_2$	**d**	69	ND[d]
5	BzOH[e]	CH_2Cl_2	1	OBz	**e**	61	ND[d]
6	BzSH[e]	CH_2Cl_2	48	SBz	**f**	52	ND[d]
7	NaN_3	DMF	3	N_3	**g**	63	3
8	PhSH	Et_3N	1	SPh	**h**	80	11

[a] Unless otherwise noted, the reactions were carried out at room temperature. [b] Isolated yields after chromatographic separation; all the reaction products were fully characterized by elemental analysis and spectroscopic data. [c] The reactions were carried out under reflux conditions. [d] Not detectable. [e] Reactions were performed in the presence of Et_3N as base.

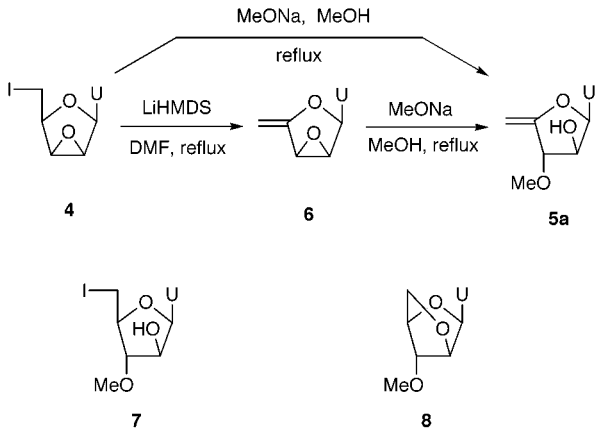

Scheme 1

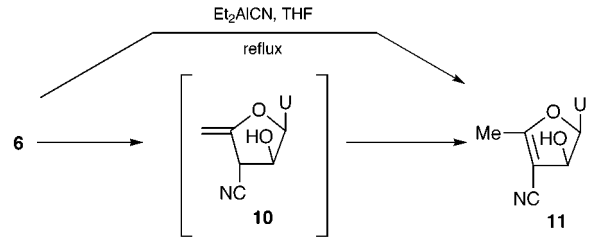

Scheme 2

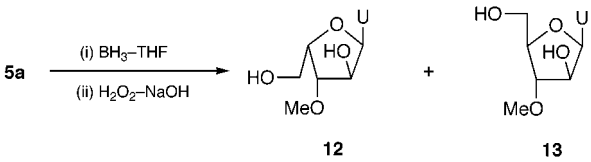

Scheme 3

13 as a minor product (17%) (Scheme 3). This isomer ratio may be interpreted by invoking the steric hindrance effects of the methoxy group at the 3′-position.

In conclusion, we have developed a regioselective method for the synthesis of 3′-substituted pyrimidine nucleoside derivatives **5**, **11**, **12** and **13** using 1-(2′,3′-anhydro-5′-deoxy-4′,5′-didehydro-α-L-*erythro*-pentofuranosyl)uracil **6** as a key intermediate without the formation of the corresponding 2′-adduct. The results presented herein provide a novel entry into a variety of sugar-modified pyrimidine nucleosides.

Notes and references

1 C. Perigaud, G. Gosselin and J.-L. Imbach, *Nucleosides Nucleotides*, 1992, **11**, 903; L. R. Townsend, *Chemistry of Nucleosides and Nucleotides*, Plenum, New York, 1988; A. Matsuda, *J. Synth. Org. Chem. Jpn.*, 1990, **48**, 907; H. Maag, R. M. Rydzewski, M. J. McRoberts, D. Crawford-Ruth, J. P. H. Verheyden and E. J. Prisbe, *J. Med. Chem.*, 1992, **35**, 1440; M.-J. Camarasa, M.-J. Perez-Perez, A. San-Felix, J. Balzarini and E. De Clercq, *J. Med. Chem.*, 1992, **35**, 2721; M.-J. Perez-Perez, A. San-Felix, J. Balzarini, E. De Clercq and M.-J. Camarasa, *J. Med. Chem.*, 1992, **35**, 2988.

2 T. L. Ruth, *Oligonucleotides and Their Analogues*, IRL Press, London, 1991; B. Giese, P. Imwinkelried and M. Petretta, *Synlett*, 1994, 1003 and references therein.

3 (*a*) J. F. Cordington, R. Fecher and J. J. Fox, *J. Am. Chem. Soc.*, 1960, **82**, 2794; (*b*) N. C. Chang, J. H. Burchanel, R. Fecher, R. Duschinsky and J. J. Fox, *J. Am. Chem. Soc.*, 1961, **83**, 4060; (*c*) J. F. Cordington, R. Fecher and J. J. Fox, *J. Org. Chem.*, 1962, **27**, 163.

4 K. Minamoto, Y. Yamano, Y. Matsuoka, K. Watanabe, T. Hirata and S. Eguchi, *Nucleosides Nucleotides*, 1992, **11**, 457; J. P. Horwits, J. Chua, M. A. D. Rooge, M. Noel and I. L. Klundt, *J. Org. Chem.*, 1966, **31**, 205; T. Sasaki, K. Minamoto and K. Hattori, *Tetrahedron*, 1974, **30**, 2689; D. H. Hollenberg, K. A. Watanabe and J. J. Fox, *J. Med. Chem.*, 1977, **20**, 113; G. Kowollik and P. Z. Langen, *Z. Chem.*, 1975, **15**, 147; P. Herdewijin, A. Van Aerschot and L. Kerremans, *Nucleosides Nucleotides*, 1989, **8**, 65; H. M. Misra, W. P. Gati, E. E. Kraus and L. I. Wiebe, *J. Heterocycl. Chem.*, 1984, **21**, 773; J.-T. Haung, L.-C. Chen, L. Wang, M.-H. Kim, J. A. Warshaw, D. Armstrong, Q.-Y. Zhu, T.-C. Chou, K. A. Watanabe and J. J. Fox, *J. Med. Chem.*, 1991, **34**, 1640; U. Reichman, D. H. Hollenberg, C. K. Chu, K. A. Watanabe and J. J. Fox, *J. Org. Chem.*, 1976, **41**, 2042; C. F. Hunnel and R. P. Carty, *Nucleosides Nucleotides*, 1983, **2**, 249; M. E. Perlman and K. A. Watanabe, *Nucleosides Nucleotides*, 1989, **8**, 145; D. Habich and W. Barth, *Synthesis*, 1988, 943; A. Mate, J. B. Hobbs, D. C. Scopes and R. F. Newton, *Tetrahedron Lett.*, 1985, **26**, 97; M. Ashwell, A. S. Jones and R. T. Walker, *Nucleic Acids Res.*, 1987, **15**, 2157; T. R. Webb, H. Mitsuya and S. Broder, *J. Med. Chem.*, 1988, **31**, 1475; M. J. Bamford, P. L. Coe and R. T. Walker, *J. Med. Chem.*, 1990, **33**, 2494; K. Hamaguchi, H. Tanaka, H. Maeda, Y. Itoh, S. Saito and T. Miyasaka, *J. Org. Chem.*, 1991, **56**, 5401; P. Wigerinck, A. V. Aerschot, G. Janssen, P. Claes, J. Balzarini, E. De Clercq and P. Herdewijin, *J. Med. Chem.*, 1990, **33**, 868; X. Ariza, J. Garces and J. Vilarrasa, *Tetrahedron Lett.*, 1992, **33**, 4069; I. L. Doerr, J. F. Cordington and J. J. Fox, *J. Org. Chem.*, 1965, **30**, 467.

5 V. Dalla and P. Pale, *Tetrahedron Lett.*, 1996, **37**, 2781.

6 J. A. Marshall, *Chem. Rev.*, 1989, **89**, 1503.

Communication 9/05608D

Preparation of mesoporous tin oxide for electrochemical applications

Fanglin Chen and Meilin Liu*

School of Materials Science and Engineering, Georgia Institute of Technology, Atlanta, GA 30332-0245, USA. E-mail: meilin.liu@mse.gatech.edu

Received (in Bloomington, IN, USA) 24th May 1999, Accepted 9th August 1999

Mesoporous tin oxide stable up to 500 °C has been prepared for the first time using both cationic and neutral surfactants.

Following the discovery of the MCM family of mesoporous silicates using the supramolecular templating approach,[1] mesoporous materials have attracted considerable attention because of their remarkably large surface areas and narrow pore size distributions, which make them ideal candidates for catalysts, molecular sieves, and as electrodes in solid-state ionic devices. A number of related synthetic strategies have been developed and a variety of materials, in terms of both composition and structure, have been prepared.[2–4]

Tin oxide is a wide-energy-gap semiconductor and has been widely used as a catalyst for oxidation of organic compounds, and for applications such as solid-state gas sensors, rechargeable Li-batteries, and optical electronic devices. The success in many of these applications relies critically on the preparation of crystalline SnO_2 with uniform nanosize pore structure. Consequently, the synthesis of thermally stable mesoporous SnO_2 is of great importance.

To date, several preparative approaches utilizing a supramolecular templating mechanism have been reported for the preparation of mesoporous tin oxide.[5–7] Upon removal of the surfactant, however, the mesoporous structures were destroyed; in other words, the preparation of mesoporous SnO_2 without the support of a surfactant has not yet been achieved. For example, upon hydrolysis of $SnCl_4$ in the presence of sodium dioctylsulfosuccinate (AOT, an anionic surfactant), Rao and Ulagappan[5] obtained a mesoporous SnO_2–AOT material with an average pore size of 3.2 nm. Attempts to remove the surfactant either by calcination at *ca.* 400 °C or by solvent extraction, however, resulted in collapse of the mesoporous structure. Similarly, upon hydrolysis of $SnCl_4$ in the presence of sodium dodecyl sulfonate (another anionic surfactant), Qi *et al.*[6] obtained mesoporous tin oxide with an average pore size of 4.1 nm. Again, the mesostructure collapsed when the surfactant was removed at 400 °C. Starting with tin isopropoxide and tetradecylamine (a neutral surfactant), Pinnavaia and coworkers[7] obtained mesoporous tin oxide with an average pore size of 5.6 nm. The mesoporous structure was stable up to 350 °C, but was destroyed upon calcination at 400 °C and the surface area was greatly reduced.

For electrochemical applications such as gas sensors, however, thermal stability of a mesoporous structure at high temperatures and without the support of a surfactant is critical for high catalytic reactivity, fast charge and mass transport, and long-term microstructural stability and durability. Thus, the objective of this study was to develop synthesis procedures for the preparation of mesoporous SnO_2, stable at high temperatures (> 400 °C), without the support of a surfactant. We have explored both neutral (S^0I^0) and electrostatic (S^+I^-) templating approaches to prepare mesoporous SnO_2.

In the neutral templating approach,† tetradecylamine (a neutral primary amine) was used as the surfactant (S^0) or structure director and tin isopropoxide as the inorganic precursor (I^0). Fig. 1 shows X-ray diffraction (XRD) patterns of the as-synthesized product and the mesostructured SnO_2 after calcination at 500 °C for 2 h. While the as-synthesized product showed a sharp diffraction peak at low angle (characteristic of a mesostructured material), the calcined sample displayed only a very broad diffraction peak. However, TEM analysis indicated that the calcined solid was indeed mesoporous; the short-range hexagonal order can be seen from the TEM images shown in Fig. 2. The average *d*-spacings of the as-synthesized and the as-calcined mesostructures are 4.8 and 3.4 nm, respectively, as calculated from the positions of the XRD peaks, which are also consistent with the pore sizes as determined from the TEM micrographs. Thermogravimetric analysis of the as-synthesized tin oxide mesoporous powder under N_2 flow indicated that the weight loss occurred between 200 and 500 °C, probably resulting from the decomposition of the surfactant and subsequent removal of the carbon residue. There was no detectable weight loss above 500 °C, indicating that the amine surfactant was completely removed from the mesoporous SnO_2 structure upon calcination at 500 °C for 2 h. Thus, we have obtained mesoporous SnO_2 (without the support of a surfactant) which is stable up to 500 °C.

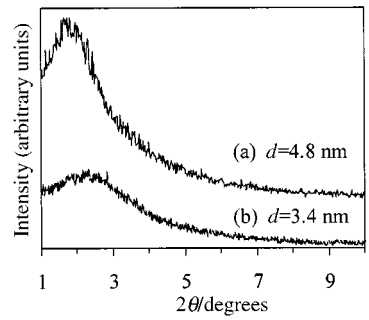

Fig. 1 XRD patterns of tin oxide synthesized *via* a neutral templating approach: (a) as-synthesized and (b) after calcination at 500 °C for 2 h.

In the electrostatic templating approach, cetyltrimethylammonium bromide (CTAB) was used as the structure director (S^+) and $[Sn(OH)_6]^{2-}$ used as the inorganic precursor (I^-).‡ This approach is similar to that employed by Suib and coworkers.[8]§ Fig. 3 shows the XRD patterns of the as-synthesized product and the mesostructured SnO_2 after calcination at 500 °C for 2 h. A sharp diffraction peak at small angle corresponding to the (100) diffraction was observed in both cases. Small peaks due to the (110) and (200) reflections are also observable before and after the removal of the surfactant.

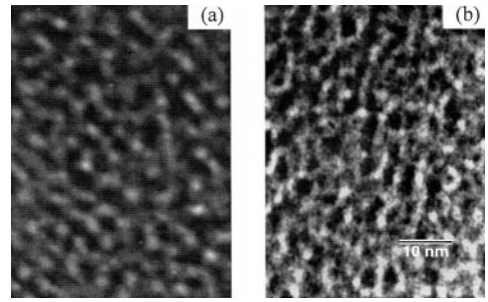

Fig. 2 Representative TEM micrographs of tin oxide synthesized *via* a neutral templating approach: (a) as-synthesized and (b) after calcination at 500 °C for 2 h.

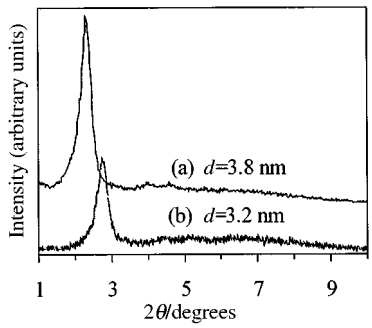

Fig. 3 XRD patterns of tin oxide synthesized *via* an electrostatic templating approach: (a) as-synthesized and (b) after calcination at 500 °C for 2 h.

The average *d*-spacings of the (100) layers in the as-synthesized and calcined SnO_2 mesostructures are 3.8 and 3.2 nm, respectively, as determined from the peak positions in the XRD patterns. Thermogravimetric analysis of the as-synthesized tin mesoporous powder under an N_2 flow showed that most of the weight loss occurred below 500 °C, implying that the surfactant could be removed from the mesoporous SnO_2 structure upon calcination at 500 °C for 2 hours. Fig. 4 shows the TEM images of the mesoporous SnO_2 before and after surfactant removal.

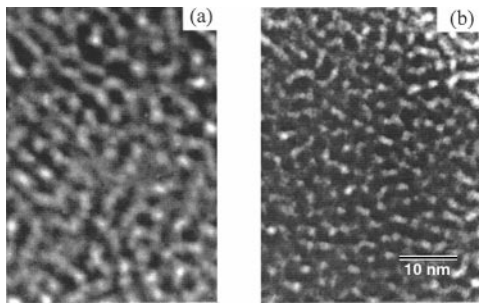

Fig. 4 Representative TEM micrographs of tin oxide synthesized *via* an electrostatic templating approach: (a) as-synthesized and (b) after calcination at 500 °C for 2 h.

In both approaches, the (100) peak shifts to slightly larger angles after removal of the surfactant, indicating that the mesostructure (and hence the pore size) contracted slightly upon surfactant removal. After calcination at 500 °C for 2 h, the BET surface area of the mesoporous SnO_2 from the neutral templating approach is *ca.* 107 $m^2\ g^{-1}$ and that from the electrostatic templating approach is *ca.* 143 $m^2\ g^{-1}$. The measured surface areas are much smaller than those for MCM-type materials (usually $> 500\ m^2\ g^{-1}$), implying that some of the pores are closed and are not accessible to BET measurement. It is clear, however, that the electrostatic templating approach is better than the neutral templating approach for the preparation of mesoporous SnO_2 with well organized structure (as revealed by XRD and TEM) and large surface area.

The major challenge in obtaining mesoporous oxides is to preserve the mesoporous structures while the surfactant is being removed. In order to avoid the collapse of the mesostructure, it is necessary to form a rigid three-dimensional inorganic framework based on Sn–O–Sn bonding before surfactant removal. In this study, it is believed that Sn–O–Sn bonds are formed during the aging process through water- or alcohol-condensation. Once a condensed 3-D mesoporous network is formed, its essential mesoporous features are likely to be preserved upon surfactant removal at 500 °C. Although there is no direct evidence to prove the formation of the Sn–O–Sn network during the aging process, we believe that this is a critical step to successful preservation of the mesoporous structure during surfactant removal. The detailed mechanism of formation of mesoporous SnO_2 structures which are stable at high temperatures is still under investigation.

Preliminary testing of a CO_2 gas sensor based on the mesoporous SnO_2 from the electrostatic templating approach showed a response time of 110 s when the gas was switched from CO_2 to air, which is seven times faster than CO_2 gas sensors based on nanosized SnO_2 powders derived from a sol–gel process (response time *ca.* 750 s[9]). Currently, the processing conditions are being further optimized to reduce the pore diameters or increase the surface area in an effort to enhance the sensitivity and speed of response of gas sensors based on mesoporous SnO_2. Further, the cycling behavior and reversible capacities of mesoporous SnO_2 used as an electrode in lithium batteries are still under investigation and will be reported in due course.

This work was supported by National Science Foundation (Award No. DMR-9357520) and by Georgia Tech Research Corporation.

Notes and references:

† 3.0 g of tin isopropoxide and 0.36 g of 1-tetradecylamine were added to 80 ml of propan-2-ol and stirred to form a homogeneous solution. This solution was kept under water-saturated air at room temp. for 48 h prior to loading to an autoclave and being kept at 80 °C for 24 h. The precipitate was then filtered off, washed with water and ethanol and then refluxed in ethanol for 10 h. The dried product was crushed into a powder and calcined at 500 °C in static air for 2 h.

‡ 10 g of $SnCl_4$ was dissolved in 30 ml distilled deionized water (DDW) and heated to 75 °C. 6.2 g of NaOH dissolved in 15 ml DDW was added to the $SnCl_4$ solution under vigorous stirring to form $Sn(OH)_4$. The pH of the solution was maintained at *ca.* 10. Then 6.7 g of CTAB was dissolved in 45 ml DDW and this solution was added to the $Sn(OH)_4$ solution. The mixture was stirred at 75 °C for 30 min and then loaded in an autoclave kept at 75 °C for 24 h. It was then aged at 90 °C for 24 h. After cooling to room temperature, the precipitate was recovered by filtration on a Buchner funnel, washed with water and dried. The as-synthesized product was then calcined in air at 500 °C for 2 h.

§ Starting from $MnCl_2$ and CTAB, Suib and coworkers[8] synthesized mesoporous manganese oxide structures which were reported to be stable up to 1000 °C. They proposed that an electrostatic interaction was established between $[Mn(OH)_6]^{4-}$ and the positively charged surfactant head group (CTA^+). Owing to the similarity between $[Sn(OH)_6]^{2-}$ and $[Mn(OH)_6]^{4-}$, it was thought that this approach was applicable to the preparation of mesoporous SnO_2.

1 C. T. Kresge, M. E. Leonowicz, W. J. Roth, J. C. Vartuli and J. S. Beck, *Nature* (*London*), 1992, **359**, 710.
2 Q. Huo, D. I. Margolese, U. Ciesla, D. G. Demuth, P. Feng, T. E. Gier, P. Sieger, A. Firouzi, B. F. Chmelka, F. Schuth and G. D. Stucky, *Chem. Mater*., 1994, **6**, 1176.
3 A. Sayari and P. Liu, *Microporous Mater*., 1997, **12**, 149.
4 J. Y. Ying, C. P. Mehnert and M. S. Wong, *Angew. Chem. Int. Ed*., 1999, **38**, 56.
5 N. Ulagappan and C. N. R. Rao, *Chem. Commun*., 1996, 1685.
6 L. Qi, J. Ma, M. Cheng and Z. Zhao, *Langmuir*, 1998, **14**, 2579.
7 K. G. Severin, T. M. Abdel-Fattah and T. J. Pinnavaia, *Chem. Commun*., 1998, 1471.
8 Z.-R. Tian, W. Tong, J.-Y. Wang, N.-G. Duan, V. V. Krishnan and S. L. Suib, *Science*, 1997, **276**, 926.
9 G. Zhang and M. Liu, *Sens. Actuators B*, submitted.

Communication 9/04142G

ChemComm

Two-electron photoelimination reactions from edge-sharing bioctahedral dimolybdenum(III) complexes

Bradford J. Pistorio and Daniel G. Nocera*

Department of Chemistry, 6-335, Massachusetts Institute of Technology, 77 Massachusetts Avenue, Cambridge, MA 02139-4307, USA. E-mail: nocera@MIT.edu

Received (in Bloomington, IN, USA) 24th May 1999, Accepted 9th August 1999

Dimolybdenum(III) edge-sharing bioctahedral (ESBO) complexes, $Mo_2X_6(dtbppm)_2$ [dtbppm = *bis*(di(4-*tert*-butylphenyl)phosphinomethane), X = Cl, Br, I], photoreact when irradiated with near-UV light, cleanly producing the corresponding quadruple metal–metal bonded complexes, $Mo_2X_4(dtbppm)_2$.

Metal complexes in electronic excited states typically exhibit one-electron oxidation–reduction chemistry. Conversely, the small molecule activation processes of most energy conversion schemes encompass multielectron transformations. This discontinuity between the intrinsic redox stoichiometries of electronic excited states and the reactions that they are targeted to thermodynamically drive has prompted us to explore conceptually new excited state reaction pathways, extending beyond the single electron. A strategy occupying our recent efforts is predicated on the chemistry of two-electron mixed-valence excited states. As one-electron mixed valence complexes promote single electron transfer reactions, a two-electron mixed valence complex can promote reactions in two-electron steps at the individual metal centers of the bimetallic core.[1] In one approach we have shown that excitation of quadruply bonded metal–metal (M^4M) dimers pairs two electrons in a d_{xy} orbital localized, for the most part, at one center of the bimetallic core with a corresponding two-electron hole at the other metal center.[2] The resultant $^+M–M:^-$ zwitterion (formally, a $M^{III}M^{I}$ intermediate for M = Mo and W) exhibits reactivity that establishes it as an excited state analog of Vaska's complex;[3] $M_2X_4(PP)_2$ (M = Mo, W; X = halide; PP = bridging phosphine) complexes undergo two-electron photoadditions of substrates to yield M^{III}_2 complexes with edge-sharing bioctahedral (ESBO) geometries.[4,5] An extensive reaction chemistry of the past decade shows these ESBO photoproducts to be inert, especially when metal–halide bonds compose the core.[6] This stability has hampered the construction of cyclic reaction schemes based on $M^{II}M^{II} \leftrightarrow M^{III}M^{III}$ photoreactivity. Accordingly, we became interested in developing the two-electron photoreduction chemistry of ESBO complexes. We now report the photoactivation of the metal–halogen bonds of the ESBO framework and subsequent two-electron photoconversion of $Mo_2X_6(PP)_2$ to $Mo_2X_4(PP)_2$.

Early efforts to investigate ESBO photochemistry were hampered by the limited solubility of $Mo_2X_6(PP)_2$ compounds in common solvents possessing moderate dielectric constants. We overcame this problem by introducing *tert*-butyl groups at the *para* position of the phenyl rings of bis(diphenyl)phosphinomethane (dppm). Reaction of $Cl_2PCH_2PCl_2$ with 12 equiv. of Bu^t-4-PhMgBr in diethyl ether at –78 °C under the N_2 atmosphere of a glove box, followed by procedures standard to a Grignard work-up, afforded bis(di-(4-*tert*-butylphenyl)-phosphinomethane) (dtbppm), which was recrystallized from acetonitrile: yield, 89%.† The introduction of the dtbppm ligand onto bimetallic cores proceeds smoothly according to literature procedures.[7] Treatment of $Mo_2(O_2CMe)_4$ with 4 equiv. of Me_3SiX and 2.2 equiv. of dtbppm in THF resulted in conversion to $Mo_2X_4(dtbppm)_2$, which was recrystallized from pentane and benzene.† Halogen oxidation of $Mo_2X_4(dtbppm)_2$ produced paramagnetic $Mo_2X_6(dtbppm)_2$ in good yields.† The electronic absorption spectra of the $Mo_2X_4(dtbppm)_2$ and $Mo_2X_6(dtbppm)_2$ complexes‡ are similar to those of their dppm counterparts,[7c,8] with only slight differences observed in absorption maxima and intensities. Fig. 1 shows the evolution of the absorption profiles for the photolysis of $Mo_2X_6(dtbppm)_2$ in THF. Each photoreaction behaves similarly. The initial spectrum, which is maintained indefinitely in the absence of light, promptly changes when THF solutions of the compound and a non-coordinating base such as 2,6-lutidine (2,6-dimethylpyridine) are irradiated with light in the blue and UV spectral regions. Well anchored isosbestic points maintained throughout the irradiation attest to a clean and quantitative photoreaction. With the appearance of the final absorption spectrum, no additional changes are observed with continued irradiation. For each photolysis reaction shown in Fig. 1, a single product is isolated with electronic absorption and $^{31}P\{^1H\}$ NMR spectra identical to those of independently prepared $Mo_2X_4(dtbppm)_2$ complexes. The photochemistry proceeds in THF only when carried out in the presence of at least a 2 equiv. excess of 2,6-lutidine (per equiv. of metal complex), though the photoconversion efficiency is independent of the concentration of base to excesses of 10^4 equiv. These results are consistent with THF acting as an *in situ* trap of

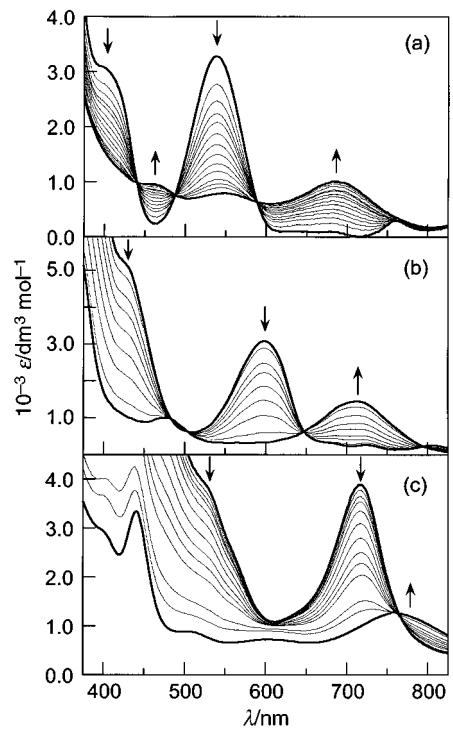

Fig. 1 The absorption profiles demonstrate the conversion of THF solutions of $Mo_2X_6(dtbppm)_2$ (*ca.* 10^{-5} M) in the presence of 20 equiv. of 2,6-lutidine at 0 °C: (a) X = Cl (λ_{exc} > 335 nm), (b) X = Br (λ_{exc} > 335 nm), and (c) X = I (λ_{exc} > 495 nm). The arrows indicate the disappearance of $Mo_2X_6(dtbppm)_2$ and appearance of $Mo_2X_4(dtbppm)_2$. Spectra were recorded over the span of 12 h for (a) and (c) and 2 h for (b).

Table 1 Product quantum yields for $Mo_2X_6(dtbppm)_2$ photolysis at selected excitation wavelengths

	$10^2\phi_p[Mo_2X_6(dtbppm)_2]^a$		
λ_{exc}/nm	X = Cl	Br	I
312	1.4(2)	0.38(4)	—
335	0.0012(1)	0.010(1)	—
365	0.0045(5)	0.0036(4)	—
405	0.00045(4)	0.0010(1)	—
470	—	—	0.0090(9)
510	—	—	0.0013(1)

[a] The quantum yield experiments were performed in THF at 0 °C containing 2,6-lutidine in 20 equiv. excess of $Mo_2X_6(dtbppm)_2$. The $Mo_2I_4(dtbppm)_2$ photoproduct decomposes when $\lambda_{exc} < 436$ nm.

photoeliminated X, arising from the susceptibility of the weak C_α–H bonds of THF toward atom abstraction.[9] In support of this contention, NMR spectra of photolyzed solutions exhibit a broad high frequency signal at δ 16.8 and a sharp methyl resonance at δ 2.9 of 2,6-lutidinium halide ($lutH^+X^-$); independently prepared lutidinium bromide exhibits a resonance at δ 16.3 for the acid proton and δ 2.96 for the methyl groups in $CDCl_3$. Moreover, integration of these resonances establish a stoichiometry of 2 equiv. of HX produced per equiv. of $Mo_2X_6(dtbppm)_2$ photoreagent to establish the following photoprocess of eqn. (1).

$$Mo_2X_6(dtbppm)_2 \xrightarrow[THF,\ lut]{h\nu} Mo_2X_4(dtbppm)_2 + 2\ lutH^+X^- \quad (1)$$

Table 1 lists the product appearance quantum yields (ϕ_p) for selected irradiation wavelengths. Quantum yields are high for near-UV excitation, but they decrease precipitously as λ_{exc} is moved into the visible spectral region. Moreover, the wavelength onset of this decrease red shifts along the series Cl < Br < I. A parallel shift of the near-UV absorption profiles (2900 and 5100 cm^{-1} red shift upon substitution of chloride by bromide and bromide by iodide, respectively) indicates that the action spectra are governed by the population of ligand-to-metal charge transfer states. Though no definitive assignments have been forthcoming in the absence of detailed spectroscopic investigation, computation[10] and experiment[11] identify the low-energy absorption profile of Fig. 1 to be derived largely from d and p metal-based orbitals with some halide character resulting from X p_π-mixing. The intense absorptions to higher energy are due to the Mo_2X_6 σ-framework, comprising metal in-plane π orbitals admixed with X p_σ-orbitals. Depopulation of these metal–halide σ-orbitals (and population of the correspondingly σ* orbitals) will result in significant disruption of the Mo_2X_6 equatorial framework, accounting for the high photoconversion efficiencies associated with near-UV excitation.

Photoelimination from oxidized cores of $M^{\underline{n}}M$ complexes has only previously been observed for the alkyl ligands axially coordinated to a pre-established $W^{III}{}_2L_6$ core.[12] In view of the preponderance of ESBO compounds in multiply bonded metal–metal chemistry, the photochemistry reported here provides a general framework in which to develop multielectron photoredox schemes based on $M^{\underline{n}}M$ photoreagents. Recent work in our group shows that metal–halide bonds are susceptible to photochemical activation along reaction pathways featuring two-electron mixed-valence species.[1b] Is the same M^+–$M:^-$ two-electron mixed valence zwitterion, responsible for promoting $M^{\underline{4}}M$ photoaddition reactions,[3–5] facilitating ESBO photoelimination chemistry? Alternatively, disproportionation of a photogenerated $Mo^{II}Mo^{III}$ complex could also lead to the observed photochemistry. In ongoing work, we are addressing such mechanistic issues by investigating the ESBO photochemistry with transient absorption and Raman spectroscopy, with the aim of directly establishing the precise nature of the photointermediate that leads to ESBO activation.

We are indebted to Ann M. Macintosh for her initial efforts on $Mo_2X_6(dppm)_2$ photochemistry. The National Science Foundation Grant CHE-9817851 funded this research.

Notes and references

† *Selected Data* for dtbppm: mp, 180–183 °C. Calc. for $C_{41}H_{54}P_2$: C, 80.88; H, 8.94; P, 10.18. Found: C, 80.72; H, 9.08; P, 10.25%. ^1H NMR (acetone-d_6), δ 1.24 (s), 2.90 (s), 7.50 (m); $^{31}P\{^1H\}$ NMR ($CDCl_3$, ext. 85% H_3PO_4) δ −24.1 (s).

For $Mo_2X_4(dtbppm)_2$: $^{31}P\{^1H\}$ NMR (C_6D_6, ext. 85% H_3PO_4) δ 15.24 (s), 16.94 (s), 13.64 (s) for X = Cl, Br and I, respectively.

For $Mo_2X_6(dtbppm)_2$: pink $Mo_2Cl_6(dtbppm)_2$ was obtained by oxidation with $PhICl_2$ in CH_2Cl_2, 95% yield. Calc. for $C_{82}H_{108}Mo_2P_4Cl_6$: C, 60.71; H, 6.71. Found: C, 60.85; H, 6.85%. $Mo_2Br_6(dtbppm)_2$ and $Mo_2I_6(dtbppm)_2$ were obtained by oxidation with Br_2 and I_2, respectively, in benzene. X = Br (pine green), 92% yield. Calc. for $C_{82}H_{108}Mo_2P_4Br_6$: C, 52.14; H, 5.76. Found: C, 52.21; H, 5.85. X = I (sepia), 85% yield. Calc. for $C_{82}H_{108}Mo_2P_4I_6$: C, 45.37; H, 5.01. Found: C, 45.08; H, 5.16%.

‡ Absorption spectra were recorded in THF. Absorption coefficients were determined from Beer–Lambert plots constructed from absorption measurements recorded at 5–7 different concentrations. Each experiment was repeated and in all cases the measured ε value was accurate to three significant figures. λ_{max}/nm (ε/$dm^3\ mol^{-1}\ cm^{-1}$) for $Mo_2X_4(dtbppm)_2$, X = Cl: 340 (5720), 460 (740), 694 (1550); X = Br: 369 (3110), 448 (1100), 713 (1760); X = I: 442 (7500), 496 (1570), 600 (440), 772 (2540). λ_{max}/nm (ε/$dm^3\ mol^{-1}\ cm^{-1}$) for $Mo_2X_6(dtbppm)_2$, X = Cl: 288 (17200), 335 (11400), 400 (3190), 540 (3400), 750 (300); X = Br: 311 (13000), 371 (13300), 425 (4520), 600 (3400); X = I: 296 (27200), 352 (12400), 424 (10200), 467 (6440), 524 (4300), 718 (4200).

1 (*a*) D. G. Nocera, *Acc. Chem. Res*., 1995, **28**, 209; (*b*) A. F. Heyduk, A. M. Macintosh and D. G. Nocera, *J. Am. Chem. Soc*., 1999, **121**, 5023.

2 D. S. Engebretson, J. M. Zaleski, G. E. Leroi and D. G. Nocera, *Science*, 1994, **265**, 759; D. S. Engebretson, E. Graj, G. E. Leroi and D. G. Nocera, *J. Am. Chem. Soc*., 1999, **121**, 868.

3 C. M. Partigianoni, C. Turró, T. L. C. Hsu, I—J. Chang and D. G. Nocera, *Photosensitive Metal–Organic Systems; Mechanistic Principles and Applications*, ed. C. Kutal and N. Serpone, Adv. Chem. Ser. 238, American Chemical Society, Washington, D.C., 1993, pp. 147–163.

4 C. M. Partigianoni and D. G. Nocera, *Inorg. Chem*., 1990, **29**, 2033.

5 T. L. C. Hsu, S. A. Helvoigt, C. M. Partigianoni, C. Turró and D. G. Nocera, *Inorg. Chem.*, 1995, **34**, 6186.

6 F. A. Cotton and R. A. Walton, *Multiple Bonds between Metal Atoms*, Oxford University Press, New York, 1993; F. A. Cotton, *Polyhedron*, 1987, **6**, 667; R. A. Walton, *Polyhedron*, 1989, **8**, 1689; R. Poli and H. D. Mui, *Inorg. Chem*., 1991, **30**, 65.

7 (*a*) M. L. H. Green, G. Parkin, J. Bashkin, J. Fail and K. Prout, *J. Chem. Soc., Dalton Trans*., 1982, 2519; (*b*) F. L. Campbell III, F. A. Cotton and G. L. Powell, *Inorg. Chem.*, 1984, **23**, 4222; (*c*) F. A. Cotton, K. R. Dunbar and R. Poli, *Inorg. Chem*., 1986, **25**, 3700.

8 F. A. Cotton, L. M. Daniels, K. R. Dunbar, L. R. Favello, C. J. O'Connor and A. C. Price, *Inorg. Chem.*, 1991, **30**, 2509.

9 J. Fossey and D. Lefort, *Free Radicals in Organic Chemistry*, John Wiley & Sons: New York, 1995.

10 S. Shaik, R. Hoffmann, C. Fisel and R. H. Summerville, *J. Am. Chem. Soc*., 1980, **102**, 4555; F. A. Cotton, M. P. Diebold, C. J. O'Connor and G. L. Powell, *J. Am. Chem. Soc*., 1985, **107**, 7438; F. A. Cotton and X. Feng, *Int. J. Quantum Chem.*, 1996, **58**, 671; R. Poli and R. C. Torralba, *Inorg. Chim. Acta*, 1993, **212**, 123.

11 J. M. Canich, F. A. Cotton, L. M. Daniels and D. B. Lewis, *Inorg. Chem.*, 1987, **26**, 4046; A. R. Chakravarty, F. A. Cotton, M. P. Diebold, D. B. Lewis and W. J. Roth, *J. Am. Chem. Soc.*, 1986, **108**, 971.

12 M. H. Chisholm, D. L. Clark, J. C. Huffman, W. G. Van Der Sluys, E. M. Kober, D. L. Lichtenberger and B. E. Bursten, *J. Am. Chem. Soc*., 1987, **109**, 6796; M. H. Chisholm, *Pure Appl. Chem*., 1991, **63**, 665.

Communication 9/04143E

α-$[NH_3(CH_2)_5NH_3]SnI_4$: a new layered perovskite structure

Jun Guan, Zhongjia Tang and Arnold M. Guloy*

Department of Chemistry and Texas Center for Superconductivity, University of Houston, Houston, Texas 77204-5641, USA. E-mail: aguloy@uh.edu

Received (in Bloomington, IN, USA) 15th February 1999, Revised manuscript received 29th June 1999, Accepted 30th July 1999

The synthesis and crystal structure of new organic–inorganic layered material, α-$[NH_3(CH_2)_5SnI_4$, is reported, which features an unprecedented <330>-terminated layered perovskite structure.

Much attention has been devoted to the synthesis and characterization of organic–inorganic multilayered perovskites owing to the tunability of their structural features.[1–5] The physical and structural properties of these compounds can be fine tuned by substituting or tailoring the organic layers or by modulating the thickness of the perovskite inorganic slabs. Applications of layered perovskite materials involve the development of functional electronic, magnetic and optoelectronic materials.[2,6,7] Several examples of conducting layered perovskites generally exhibit a trend from semiconducting to metallic behavior with increasing 'thickness' of perovskite layers (*n*).[8] This was demonstrated with the synthesis of a family of organic-based layered halide perovskites, $(C_4H_9NH_3)_2(CH_3NH_3)_{n-1}Sn_nI_{3n+1}$.

Layered perovskite structures can be derived by terminating the three dimensional cubic perovskite structure along different crystal faces.[9] Among the variety of metal oxides with layered perovskite structures, the common terminating planes are <001>, <110> and <111>. In layered organic–inorganic perovskites the ability to control the termination of perovskite sheets through the proper choice of organic cations was demonstrated by the synthesis of $[NH_2C(I)=NH_2]_2(CH_3NH_3)_{m-1}Sn_mI_{3m+2}$.[5] In contrast to the $(C_4H_9NH_3)_2(CH_3NH_3)_{n-1}Sn_nI_{3n+1}$ family, which consists of <001>-terminated perovskite layers, this structural class of Sn(II) iodides contains perovskite layers terminated along the <110> planes. Furthermore, the family of <110>-terminated Sn(II) iodide layered perovskites were found to be more conducting than their <001>-terminated analogs. This strongly suggests that termination of the perovskite layers provides an added flexibility in tuning the electronic properties of these layered materials.

Another structural element that modulates the properties of these mica-like materials is the dimensionality of the organic layers. Reducing the organic bilayers in the above mentioned perovskites into single layers may be achieved by using α,ω-substituted diamines, thereby increasing the interlayer coupling within the material.[1c,3b] Eliminating hydrophobic interactions in the organic bilayers leads to improved crystallization and mechanical strength while maintaining the two-dimensionality of the electronic structure. Herein, we report the synthesis and crystal structure of α-$[NH_3(CH_2)_5NH_3]SnI_4$ which consists of single layers of 1,5-pentanediammonium ions and an unprecedented inorganic layered perovskite.

α-$[NH_3(CH_2)_5NH_3]SnI_4$ **1** Was prepared by reacting SnI_2 (2 mmol), CH_3NH_3I (1 mmol) and $[NH_3(CH_2)_5NH_3]I_2$ (1 mmol) in concentrated HI (3 ml) solution. The HI solution of the organic and tin iodides was prepared at room temperature and heated to 120 °C. The resulting red solution was slowly cooled to 20 °C resulting in the formation of dark-red prismatic-column crystals. The dark-red air stable crystals were preserved in the mother liquor and were found to be of compound **1**. As a general precaution, all reactions were carried out under a nitrogen atmosphere and all solvents were degassed before use. The addition of CH_3NH_3I in the synthesis of **1** is crucial. Analogous reactions without CH_3NH_3I result in the formation of an orange–red polymorph, β-$[NH_3(CH_2)_5NH_3]SnI_4$, which features the commonly observed <001>-terminated $[SnI_4^{2-}]$ single perovskite sheets, as in K_2NiF_4.[10] The 'templating' role of $CH_3NH_3^+$ is presumably related to the stabilization and formation of the perovskite structure, as in $CH_3NH_3SnI_3$, and allows for its termination into layers along different crystallographic planes. Chemical analysis on several crystals of **1** confirmed the stoichiometry obtained from the structural refinement. Incorporation of CH_3NH_3I results in the formation of higher order layered perovskites $[NH_3(CH_2)_5NH_3](CH_3NH_3)_xSn_{1+x}I_{3x+1}$ (x = 1–3).[10] IR spectra recorded from thin disks of α-$[NH_3(CH_2)_5NH_3]SnI_4$, in the range 500–4000 cm^{-1}, feature characteristic IR bands (C–H at 3000–3180 and 1455 cm^{-1}, and N–H at 3430–3500 cm^{-1}) associated with 1,5-pentanediammonium ions. Measurement of the UV absorption spectra of a thin pressed disk of **1**, in the range 200–800 nm at 30 °C, shows a sharp absorption peak centered at 571 nm, in contrast to that observed at 560 nm in <001>-terminated β-$[NH_3(CH_2)_5NH_3]SnI_4$. Thermal measurements indicate that compound **1** and β-$[NH_3(CH_2)_5NH_3]SnI_4$, melt incongruently at 167 and 190 °C, respectively.

Compound **1** crystallizes in the orthorhombic space group *Pbcn*.[11] The asymmetric unit consists of three SnI_4^{2-} units (part of a layer of corner-sharing octahedra), and three $[NH_3(CH_2)_5NH_3]^{2+}$ ions. The orthorhombic crystal structure contains organic diammonium cations sandwiched between parallel corrugated sheets, $[SnI_2I_{4/2}^{2-}]$, of corner-shared tin(II) iodide octahedra. The tin layers can be built-up from $Sn^{II}I_6$ octahedra linked *via* corners into nominal zigzag chains, in the manner –*cis*–*trans*–*trans*–*cis*–*trans*–*trans*–, along the crystallographic *a*-axis. Adjacent parallel chains are further linked through their *trans*-vertices along the *b*-axis forming single corrugated $[SnI_4^{2-}]$ sheets along the *ab*-plane. The corrugated sheets are stacked along the crystallographic *c*-axis resulting in interlayer sites defined by eight terminal iodine atoms. The 1,5-pentanediammonium ions are located within the nearly orthorhombic interlayer sites forming single organic layers in contrast to the bilayers found in the monoamine compounds, $(RNH_3)_2SnI_4$. The $[SnI_4^{2-}]$ layer in compound **1** may be described as a combination of the <001> and <110> terminations and hence considered as the first member of the family of <330>-terminated layered perovskites.[9a] To our knowledge, the remarkable mixed *cis*–*trans* <330>-terminated perovskite layers is unprecedented in metal oxide and halide perovskite structures.

The unprecedented inorganic sheets feature two types of SnI_6 octahedra, namely, *trans*- and *cis*-shared, as shown in Fig. 1. The relatively long Sn–I bonds, 3.464(1) Å, in the *cis*-iodine bridges reflect the significant steric effects present in the *cis* conformation of the SnI_6 octahedra. The bond angles in both types of SnI_6 octahedra are slightly distorted from the ideal geometry as expected in low-order layered perovskite structures.[4,5,12] These bond angle distortions and the Sn–I bond distance inequalities are reflected in the 'twists' and 'buckles' of the inter-octahedral linkages and may be attributed to hydrogen-bonding and the stereochemical activity of the Sn(II) $5s^2$ lone pairs.[12]

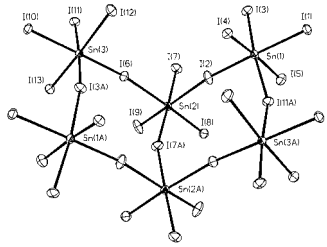

Fig. 1 ORTEP representation of the asymmetric unit of < 330 > -terminated $[SnI_4^{2-}]$ layer. Bond distances (Å): (a) around Sn(1): I(1) 3.307(1), I(2) 3.072(I), I(3) 3.116(2), I(4) 3.010(1), I(5) 3.217, I(11A) 3.217(2); (b) around Sn(2): I(2) 3.429(1), I(6) 3.464(1), I(7) 3.110(2), I(8) 2.961(1), I(9) 2.961(1), I(7A) 3.159(2); (c) around Sn(3): I(6) 3.113(1), I(10) 3.257(1), I(11) 3.154(2), I(12) 3.332(1), I(13) 2.994(1), I(3A) 3.155(2). Ellipsoids are drawn at 50% probability.

Close inspection of the organic–inorganic heterostructure in **1** reveals important characteristics. The $[NH_3(CH_3)_5NH_3]^{2+}$ ions lie between the corrugated sheets of $[SnI_4^{2-}]$ within two types of interlayer sites formed by terminal iodides of the single perovskite sheets, as shown in Fig. 2. These are sites formed between *trans*-SnI_6 octahedral units of adjacent layers, and sites formed by adjacent *cis*-SnI_6 units. In the *trans* interlayer sites, both $-NH_3$ ends of the cation are directed near the center of the 'bay' formed by four terminal iodines on each inorganic layer. The diammonium ions within the smaller *cis* interlayer sites are crowded into the 'open bay' area of these sites by close contacts with terminal iodines. The spatial environment of the different interlayer sites can be correlated with the N–N distances between the terminal nitrogen of the dications. The N–N distances are 6.10(2) and 6.65(2) Å for the dications in the *trans* sites, and 5.18(2) Å in the *cis*-sites. The N–N distances of the same diammonium ions in the interlayer sites of < 001 > -terminated β-$[NH_3(CH_2)_5NH_3]SnI_4$ range from 5.98(2) to 6.12(2) Å.[10] The variation in the observed N–N distances indicates significant differences in the conformation of the organic dications within the different interlayer sites in **1**. Moreover, steric effects present in the *cis* interlayer sites of **1** are reflected in the short N–N distances and the observed molecular shape of the diammonium ions which may be attributed to the torsional rotations around the chain backbone. Hence, formation of the unusual *cis*-SnI_6 linkage is related to a 'recognition' of the different conformations of the organic diammonium ions. The conformational differences of the cations are manifested by the differences in the C–H bands of the IR spectra of both polymorphs. The IR spectrum of the β-form features broader C–H bands (2860–3180 cm^{-1}) than those of the α-form, reflecting larger changes in the dipole moments and decreased steric restrictions on the C–H vibrations of the conformers in the β-form.[13] The thermodynamic stability and lower steric effects present in the

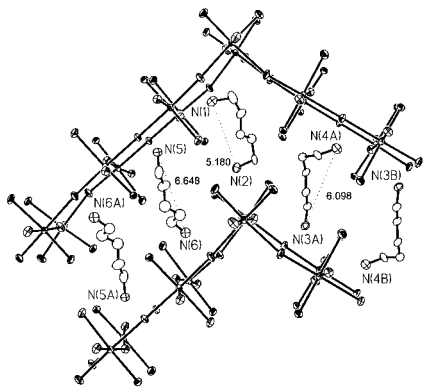

Fig. 2 ORTEP representation of the packing of 1,5-pentanediammonium ionds betwen two < 330 > -terminated $[SnI_4^{2-}]$ layers in compound **1**. Dashed lines represent distances between α- and ω-N atoms. Ellipsoids are drawn at 50% probability.

< 001 > -terminated β-form may be correlated to its higher melting point and density (ρ_β = 3.055 g cm^{-3}) compared to the < 330 > -terminated α-form (ρ_α = 3.035 g cm^{-3}). Band structure calculations on the two layered structures indicate that the < 330 > -terminated sheets have a smaller band gap than the < 100 > -terminated layer in accord with the UV absorption spectra.[4,14] The optical absorption attributed to transitions from Sn 5s and I 5p derived valence states to mainly Sn 5p conduction bands.

The control of the layer termination of the inorganic component is significantly dictated by cooperative non-covalent organic–inorganic interactions, as well as by the stereochemistry of the organic moieties. These provide additional fine variables in tuning the structure and electronic properties of layered organic–inorganic perovskites. The synthesis of **1** demonstrates the unusual structural chemistry exhibited by layered organic-based Sn(II) iodide perovskites.

This material is based in part on work supported by the Robert A. Welch Foundation, MRSEC Program of the National Science Foundation (Award Number DMR-9632667), and the State of Texas through the Texas Center for Superconductivity.

Notes and references

1 (*a*) L. J. de Jongh and A. R. Miedema, *Adv. Phys.*, 1974, **23**, 1; (*b*) G. F. Needham, R. D. Willet and H. F. Franzen, *J. Phys. Chem.*, 1984, **88**, 674; (*c*) P. Day, *Philos. Trans. R. Soc. London A*, 1985, **314**, 145; (*d*) T. Ishihara, J. Takahashi and T. Goto, *Phys. Rev. B*, 1990, **42**, 11 099; (*e*) J. Calabrese, N. L. Jones, R. L. Harlow, D. Thorn and Y. Wang, *J. Am. Chem. Soc.*, 1991, **113**, 2328.

2 G. C. Papavassiliou, I. B. Koutselas, A. Terzis and M. H. Whangbo, *Solid State Commun.*, 1994, **91**, 695; G. C. Papavassiliou, in *Nanophase Materials*, ed. G. C. Hadjipanayis and R. W. Siegel, Kluwer Academic Publishers, Dordrecht, The Netherlands, 1994, pp. 493–502 and references therein.

3 B. Tieke and G. Wegner, *Angew. Chem., Int. Ed. Engl.*, 1984, **20**, 687.

4 D. B. Mitzi, C. A. Feild, W. T. A. Harrison and A. M. Guloy, *Nature*, 1994, **369**, 467.

5 D. B. Mitzi, S. Wang, C. A. Feild, C. A. Chess and A. M. Guloy, *Science*, 1995, **267**, 1473.

6 J. G. Bednorz and K. A. Mueller, *Z. Phys. B*, 1986, **64**, 189.

7 A. J. Millis, B. I. Shraiman and R. Mueller, *Phys. Rev. Lett.*, 1996, **77**, 175.

8 R. J. Cava, *Phys. Rev. B: Condens. Matter*, 1992, **46**, 14 101.

9 (*a*) A. J. Jacobson, in *Chemical Physics of Intercalation II*, ed. P. Bernier, J. E. Fischer, S. Roth and S. A. Solin, Plenum Press, New York, 1993, pp. 117–139 and references therein; (*b*) C. N. R. Rao and B. Raveau, *Transition Metal Oxides*, Wiley-VCH, New York, 2nd edn., 1998, pp. 38–220.

10 J. Guan, Z. Tang and A. M. Guloy, unpublished work.

11 Single crystal X-ray analysis, using a Siemens SMART diffractometer equipped with a CCD detector was carried out at −50 °C. Monochromatized Mo-Kα radiation was used to collect a hemisphere of data. Empirical absorption correction was applied and redundant reflections were averaged. Laue photos and systematic absences unambiguously indicated the space group to be *Pbcn*. The final cell constants are: a = 30.255(2), b = 12.352(7), c = 25.6706(14) Å, V = 9593.0(5) Å^3. Other relevant crystallographic data are: M = 730.49, Z = 24, μ = 9.291 mm^{-1}, $2\theta_{max}$ = 48.40°; total data collected, 44333; independent reflections, 8381; observed reflections ($> 3\sigma_I$), 7618; total variables, 309. The final R indices, [$I > 4\sigma(I)$]: $R1$ = 0.0506, $wR2$ = 0.1282; (all data): $R1$ = 0.0691, $wR2$ = 0.1432. The structure was solved by direct methods and refined by full-matrix least-squares calculations. Thermal parameters of all non-hydrogen atoms were treated anisotropically. Five carbon sites (C3, C4, C13, C14, C15) exhibited conformational disorder and were refined based on a rotational disorder model. All hydrogen atoms were treated with a riding model (dC–H = dN–H = 0.89 Å, U_{iso} = 0.050). CCDC 182/1361.

12 S. Wang, D. B. Mitzi, C. A. Feild and A. M. Guloy, *J. Am. Chem. Soc.*, 1995, **117**, 5297.

13 E. L. Eliel, *Stereochemistry of Carbon Compounds*, McGraw-Hill, Singapore, 1962, pp. 124–179.

14 J. del Hoyo, MS thesis, University of Houston, USA, 1997.

Communication 9/05323I

ChemComm

The first bridged 9,10-bis(1,3-dithiol-2-ylidene)-9,10-dihydroanthracene derivatives: strained redox-active cyclophanes

Terry Finn, Martin R. Bryce,* Andrei S. Batsanov and Judith A. K. Howard

Department of Chemistry, University of Durham, Durham, UK DH1 3LE. E-mail: m.r.bryce@durham.ac.uk

Received (in Cambridge, UK) 22nd July 1999, Accepted 16th August 1999

The reaction of anthraquinone and the dianion of bis(1,3-dithiolyl)diphosphonate reagents 2 and 3 afford the cyclophane derivatives 4 and 5, the cyclic voltammetry and X-ray crystal structures of which are reported.

There is considerable current interest in polycyclic ring systems which fold to form concave clefts[1] or saddle-like surfaces.[2] In this context the 9,10-bis(methylene)-9,10-dihydroanthracene building block has received limited attention, although crystallographic and theoretical studies have shown that bulky substituents attached to the methylene sites enforce a folding of the central anthracenediylidene ring into a boat conformation, and, hence, the molecule adopts a saddle shape.[3] Bis(1,3-dithiole) substituents placed at these methylene sites, *e.g.*

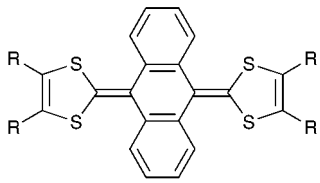

1a R = Me
b R = SMe

compound **1**,[3b] provide especially interesting electron donors with extended π-conjugation;[4] they are characterised by a single, two-electron redox wave to yield a thermodynamically stable dication at E^{ox} *ca.* +0.40 V (*vs.* Ag/AgCl) in the cyclic voltammogram (CV).[3a–c,4b,5] Methyl substituents slightly lower the oxidation potential relative to methylsufanyl substituents (*cf.* compounds **1a** and **1b**).

We have now incorporated this structural moiety into cyclophane structures,[6] and herein we report the synthesis and characterisation of the first bridged 9,10-bis(methylene)-9,10-dihydroanthracene derivatives, *viz.* compounds **4** and **5**. The synthesis of **4** and **5** was achieved by a two-fold olefination reaction, under high dilution conditions, of anthraquinone using reagents **2** and **3** (Scheme 1),[7] which were deprotonated by LDA at −78 °C, following literature precedents for other 1,3-dithiole phosphonate ester reagents.[8] Compounds **4** and **5**† were isolated as single isomers, and the *cis* configuration was confirmed by X-ray structure analysis.‡

Compound **4** gave a mixture of amber block- and needle-like crystals, which were characterised as monoclinic (α) and orthorhombic (β) polymorphs, respectively, of *cis*-**4**. Two symmetrically independent molecules in the β-**4** structure adopt very similar conformations (Fig. 1), while that of α-**4** is significantly different. In each case, the conformation of the hexamethylene bridge is rather strained and asymmetric: torsion angles around the C–C bonds range from 144 to 180° in β-**4** and from 58 to 176° in α-**4**, where two methylene groups are disordered. The bridge aggravates the U-bend of the bis(dithiolylidene)benzoquinone system: the dihedral angle between the outer S(1)C(16)C(17)S(2) and S(3)C(19)C(20)S(4) moieties is reduced from 77° in non-bridged molecule **1**[3b] to 54° in β-**4** and to only 46° in α-**4**, mostly through increased folding of both dithiole rings along the S(1)···S(2) and S(3)···S(4) vectors (24 and 13° respectively in α-**4**, 24 and 20° in β-**4**, *vs.* 17 and 8° in

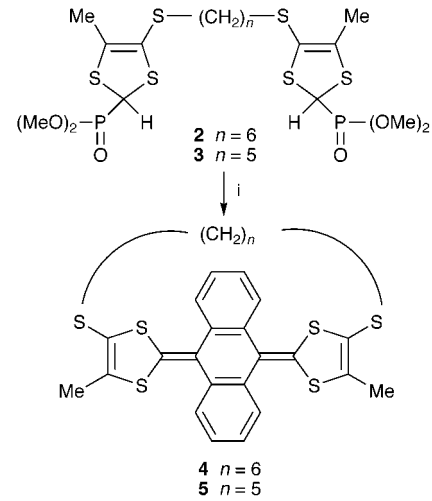

2 *n* = 6
3 *n* = 5

4 *n* = 6
5 *n* = 5

Scheme 1 *Reagents and conditions*: i, LDA (2.2 equiv.), anthraquinone, THF, −78 °C, 30 min, then raise to 20 °C.

1b). On the other hand, folding of the anthracene system along the C(9)···C(10) vector in**4** (37–40°) remains the same as in **1b** (38°).

The structure of **5** contains two independent molecules, one of which shows disorder that can be rationalised as either a varying degree of molecular bending or a rocking of the molecule as a whole. In the other (ordered) molecule (Fig. 2) the pentamethylene bridge adopts a nearly all-*trans* conformation (C–C–C–C torsion angles 164–177°) and enhances the folding of the anthracene moiety (by 43.4°) and both dithiole rings (by 29.4 and 22.6°), thus narrowing the dihedral angle between the S(1)C(16)C(17)S(2) and S(3)C(19)C(20)S(4) planes to 34.7°. The cavity is essentially empty in the solid state structures of both **4** and **5**.

The solution electrochemistry of compounds **4** and **5** was studied by cyclic voltammetry and differential pulse voltammetry. Both compounds display an irreversible two-electron oxidation wave at E^{ox} +0.69 V (compound **4**) and +0.74 V (compound **5**) [*vs.* Ag/AgCl, electrolyte $Bu_4N^+ClO_4^-$ (0.1 M),

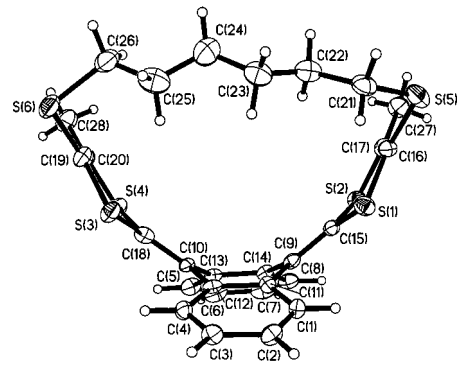

Fig. 1 Molecular structure of **4** in the β-polymorph (30% displacement ellipsoids).

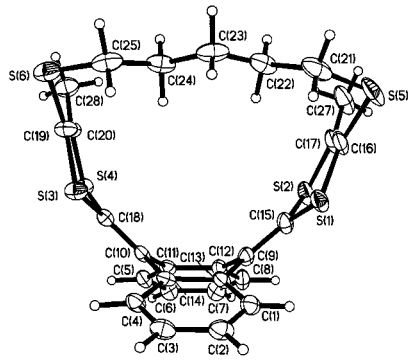

Fig. 2 Molecular structure of **5** (50% displacement ellipsoids).

MeCN, room temperature, scan rate 100 mV s^{-1}], *i.e.* the oxidation wave of the bridged systems **4** and **5** shows a significant positive shift (ΔE^{ox} *ca.* 300 mV) compared to the non-bridged analogues, *e.g.* **1**,[3b] recorded under the same conditions. This is explained by the rigidity of **4** and **5** (imparted by the bridge) restricting the conformational change which is known to accompany oxidation of the 9,10-bis(1,3-dithiol-2-ylidene)-9,10-dihydroanthracene system.[3a] The slightly higher oxidation potential of **5** compared to **4** (ΔE^{ox} 50 mV) is also consistent with oxidation becoming progressively harder as the strain in the system increases, as observed previously for strained tetrathiafulvalenes.[9] A second oxidation wave is observed at E^{ox} +1.0 V. Simulation of the data suggest an ECE process where dication formation is followed by a chemical reaction to form a new electroactive species, which gives rise to the oxidation wave at more positive potentials. The UV-Vis absorption spectra of **4** and **5** display a significant blue shift in the two longest wavelength bands compared to the non-bridged analogues [λ_{max} (MeCN) **1a**:[3b,8] 235, 369, 433 nm; **4**: 264, 356, 416 nm; **5**: 264, 352, 412 nm]. The further small blue shift (4 nm) for these two bands in compound **5** compared to **4** is again consistent with the more folded structure of **5**.

In summary, double olefination reactions of anthraquinone have afforded novel bridged 9,10-bis(methylene)-9,10-dihydroanthracenes, paving the way for studies on a new family of conformationally strained cyclophanes with interesting redox and structural properties.

We thank the EPSRC for funding, Dr R. Kataky for assistance with the electrochemical studies and Dr A. J. Moore for helpful discussions.

Notes and references

† Both compounds **4** and **5** gave mass spectrometric and elemental analytical data consistent with their structures. *Selected data* for **4**: yellow crystals, 22% yield; mp 286–288 °C (decomp.); $\delta_H(CDCl_3)$ 1.11 (m, 4H), 1.32 (m, 4H), 2.10 (s, 6H), 2.23 (m, 2H), 2.68 (m, 2H), 7.35 (m, 6H), 7.49 (m, 2H). For **5**: yellow crystals, 10% yield; mp 294–296 °C (darkens at 250 °C); $\delta_H(CDCl_3)$ 0.85 (m, 2H), 1.12 (m, 4H) 1.97 (s, 6H), 2.17 (m, 2H), 2.61 (m, 2H), 7.30 (m, 6H), 7.36 (m, 2H).

‡ Crystals of **4** and **5** for X-ray analysis were grown from MeCN–CH_2Cl_2. X-Ray experiments were performed with a SMART CCD area detector (Mo-K_α radiation, λ = 0.71073 Å). Absorption corrections by numerical integration, structure solutions by direct methods and least-squares refinement against F^2 of all data were performed using SHELX-97 programs (G. M. Sheldrick, University of Göttingen, Germany, 1997); CCDC 186/1377. See http://www.rsc.org/suppdata/cc/1999/1835/ for crystallographic data in .cif format.

Crystal data for α-**4**: $C_{28}H_{26}S_6$, M = 554.85, monoclinic, space group $P2_1/c$ (No. 14), T = 295 K, a = 18.139(2), b = 11.041(1), c = 14.406(2) Å, β = 109.05(1)°, U = 2727.1(5) Å^3, Z = 4, D_c = 1.351 g cm^{-3}, μ = 0.52 mm^{-1}, 24278 reflections (6247 unique) with $2\theta \leqslant 55°$, 384 variables, R = 0.035 on 4325 data with $I \geqslant 2\sigma(I)$, $wR(F^2)$ = 0.092, max. residual $\Delta\rho$ = 0.22 e Å^{-3}; C(25) and C(26) are disordered over two positions (A and B) with occupancies 82.3 and 17.7(6)%. For β-**4**: orthorhombic, space group $Pna2_1$ (No. 33), T = 295 K, a = 19.231(2), b = 9.520(1), c = 30.089(3) Å, U = 5509(1) Å^3, Z = 8, D_c = 1.338 g cm^{-3}, μ = 0.51 mm^{-1}, 31379 reflections (9683 unique) with $2\theta \leqslant 50°$, 384 variables, R = 0.049 on 5758 data with $I \geqslant 2\sigma(I)$, $wR(F^2)$ = 0.099, max. residual $\Delta\rho$ = 0.22 e Å^{-3}; absolute polarity determined from anomalous X-ray scattering [Flack parameter –0.15(9)]. For **5**: $C_{27}H_{24}S_6$, M = 540.82, triclinic, space group $P\bar{1}$ (No. 2), T = 120 K, a = 10.944(4), b = 14.591(5), c = 16.924(7) Å, α = 71.18(1), β = 89.65(2), γ = 85.66(1)°, U = 2550(2) Å^3, Z = 4, D_c = 1.409 g cm^{-3}, μ = 0.55 mm^{-1}, 23433 reflections (11538 unique) with $2\theta \leqslant 55°$, 678 variables, R = 0.048 on 7045 data with $I \geqslant 2\sigma(I)$, $wR(F^2)$ = 0.104, max. residual $\Delta\rho$ = 0.46 e Å^{-3}.

1 Review : J. Rebek, *Angew. Chem., Int. Ed. Engl*., 1990, **29**, 245.
2 K. Yamamoto, H. Sonobe, H. Matsbara, M. Sato, S. Okamoto and K. Kitaura, *Angew. Chem., Int. Ed. Engl*., 1996, **35**, 69; P. D. Croucher, J. M. E. Marshall, P. J. Nichols and C. L. Raston, *Chem. Commun*., 1999, 193; J. Tellenbröker and D. Kuck, *Angew. Chem., Int. Ed*., 1999, **38**, 919.
3 (*a*) M. R. Bryce, A. J. Moore, M. Hasan, G. J. Ashwell, A. T. Fraser, W. Clegg, M. B. Hursthouse and A. I. Karaulov, *Angew. Chem., Int. Ed. Engl*., 1990, **29**, 1450; (*b*) A. S. Batsanov, M. R. Bryce, M. A. Coffin, A. Green, R. E. Hester, J. A. K. Howard, I. K. Lednev, N. Martín, A. J. Moore, J. N. Moore, E. Ortí, L. Sánchez, M. Savíron, P. M. Viruela, R. Viruela and T.-Q. Ye, *Chem. Eur. J*., 1998, **4,** 2580; (*c*) N. Martín, L. Sánchez, C. Seoane, E. Ortí, P. M. Viruela and R. Viruela, *J. Org. Chem*., 1998, **63**, 1268; (*d*) A. de Meijere, Z. Z. Song, A. Lansky, S. Hyuda, K. Rauch, M. Noltmeyer, B. König and B. Knieriem, *Eur. J. Org. Chem*., 1998, 2289.
4 (*a*) Review: Y. Yamashita and M. Tomura, *J. Mater. Chem*., 1998, **8**, 1933; (*b*) C. Boulle, O. Desmars, N. Gautier, P. Hudhomme, M. Cariou and A. Gorgues, *Chem. Commun*., 1998, 2197.
5 M. R. Bryce, M. A. Coffin, M. B. Hursthouse, A. I. Karaulov, K. Müllen and H. Scheich, *Tetrahedron Lett*., 1991, **32**, 6029.
6 F. Diederich, *Cyclophanes*, Royal Society of Chemistry, Cambridge, 1991.
7 Reagents **2** and **3** were synthesised by analogy with literature analogues: P. Hascoat, D. Lorcy, A. Robert, K. Boubekeur, P. Batail, R. Carlier and A. Tallec, *J. Chem. Soc., Chem. Commun*., 1995, 1229.
8 A. J. Moore and M. R. Bryce, *J. Chem. Soc., Perkin Trans. 1*, 1991, 157.
9 T. K. Hansen, T. Jørgensen, F. Jensen, P. H. Thygesen, K. Christiansen, M. B. Hursthouse, M. E. Harman, M. A. Malik, B. Girmay, A. E. Underhill, M. Begtrup, J. D. Kilburn, K. Belmore, P. Roepstorff and J. Becher, *J. Org. Chem*., 1993, **58**, 1359; C. Wang, M. R. Bryce, A. S. Batsanov and J. A. K. Howard, *Chem. Eur. J*., 1997, **3**, 1679.

Communication 9/05938E

New efficient blue light emitting polymer for light emitting diodes

Wang-Lin Yu,[ab] Jian Pei,[ab] Yong Cao,[bc] Wei Huang*[a] and Alan J. Heeger*[bc]

[a] *Institute of Materials Research and Engineering, National University of Singapore, Singapore 119260, Republic of Singapore*
[b] *Institute for Polymers and Organic Solids, University of California at Santa Barbara, Santa Barbara, CA 93106-5090, USA. E-mail: ajh@physics.ucsb.edu*
[c] *UNIAX Corporation, 6780 Cortona Drive, Santa Barbara, CA 93117, USA*

Received (in Columbia, MO, USA) 6th July 1999, Accepted 9th August 1999

The synthesis, by the Suzuki coupling reaction, of a novel soluble blue light emitting polymer, poly{(9,9-dihexyl-2,7-fluorene–*alt*-*co*-[2,5-bis(decyloxy)-1,4-phenylene]} (PDHFDDOP) is reported. PDHFDDOP exhibits photoluminescence (PL quantum efficiency of 40% in neat films) and electroluminescence (EL) with deep blue emission.

The design and synthesis of light emitting polymers have received attention in the last decade following the discovery of EL in conjugated polymers and the development of polymer light emitting diodes (PLEDs) as a display technology.[1–4] Although the three primary colors have been demonstrated in PLEDs, only red (orange) and green PLEDs have sufficient efficiencies and lifetimes to be of commercial value.[3,4] Thus, to achieve full color polymer emissive displays, there is a need for stable blue-emitting conjugated polymers with high photoluminescence efficiency.

The first blue PLED was fabricated from poly(*para*-phenylene) (PPP),[5] which is not soluble in its conjugated form. Subsequently, soluble substituted PPPs were synthesized and high external EL quantum efficiencies were demonstrated.[6] However, low molecular weight and poor stability have limited the application of blue-emitting conjugated polymers. Blue EL has also been demonstrated in poly(*para*-phenylene vinylene) derivatives,[7] 3,4-disubstituted polythiophenes,[8] copolymers with and without non-conjugated segments,[9,10] and other structures.[11,12] Recently, the 9,9-disubstituted polyfluorenes have drawn attention as efficient blue-emitting polymers.[13–16]

We report here, the synthesis of a new blue light emitting conjugated polymer and preliminary data which characterize the emission from this polymer. As depicted in Scheme 1, poly{(9,9-dihexyl-2,7-fluorene)–*alt*-*co*-[2,5-bis(decyloxy)-1,4-phenylene]} (PDHFDDOP) comprises alternating fluorene and phenylene units. The long hydrocarbon chains at the fluorene bridge ('9') methylene and on the phenylene ring ensure the solubility of the polymer. PDHFDDOP was synthesized through the Suzuki coupling reaction.[17] The monomer 9,9-dihexylfluorene-2,7-bis(trimethylene boronate) **I**, was synthesized from 2,7-dibromofluorene **a** as starting material.† The monomer 1,4-dibromo-2,5-bis(decyloxy)benzene **II**, was prepared from hydroquinone by reaction with 1-bromodecane in a solution of NaOEt in ethanol, followed by bromination. Polymerization was performed in a refluxing toluene/aqueous potassium carbonate solution (2 M) containing 1.0–1.5 mol% of $Pd(PPh_3)_4$ under vigorous stirring for 48 h. The polymer was isolated by pouring the reaction mixture into methanol. After being purified and dried under dynamic vacuum at room temperature, the polymer was obtained as a white solid with the yield of *ca*. 85%. The structure was confirmed by NMR and elemental analysis.‡

PDHFDDOP readily dissolves in solvents, such as THF, chloroform, toluene and xylene. Uniform colorless films were prepared with thicknesses of *ca*. 750 Å on quartz and ITO coated glass substrates by spin coating from solution in toluene (3%) at a spin rate of 1500 rpm. Upon exposure to UV radiation, the films emitted intense blue fluorescence. The UV–VIS

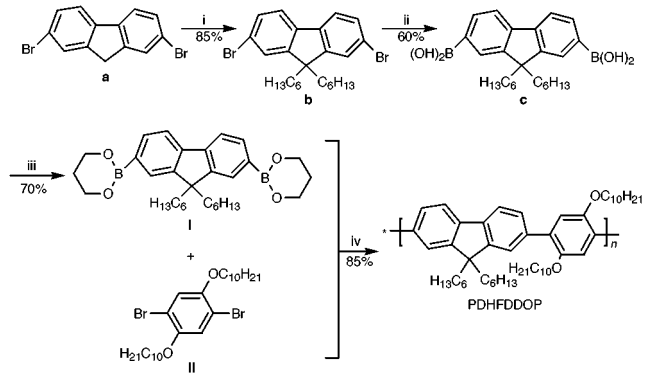

Scheme 1 *Reagents and conditions*: i, 1-bromohexane, 50% NaOH aqueous solution, TBACl, 80 °C; ii, (1) Mg, THF, (2) $B(OMe_3)_3$, THF, −78 °C to room temp., 48 h, (3) H_2SO_4 (5% in ice); iii, Propane-1,3-diol, toluene, reflux, 3 h; iv, Toluene/aqueous potassium carbonate solution (2 M), $Pd(PPh_3)_4$, reflux, 48 h.

absorption and PL spectra obtained from the films on quartz are displayed in Fig. 1. The PL spectrum of poly(9,9-dihexyl-2,7-fluorene) (PDHF) is also given in Fig. 1 for comparison. The PL spectrum of PDHFDDOP has a maximum at 420 nm with a well defined vibronic feature at 448 nm. The emission peaks in the blue are very similar to those of PDHF. However, PDHF also emits at longer wavelengths (486, 534 nm). This longer wavelength emission is common in 9,9-disubstituted polyfluorenes and has been attributed to interchain excimer formation.[13,16] By contrast, the PL spectrum of PDHFDDOP does not include the longer wavelength components. The absolute PL efficiency of PDHFDDOP in neat films, as measured in an integrating sphere at room temperature, was found to be *ca*. 40%.

Cyclic voltammetry (CV) was performed with a polymer film on a glassy carbon disc working electrode (*ca*. 0.2 cm^2) using a platinum wire as counter electrode and a silver wire as a quasi-reference electrode (electrochemical potential *ca*. 0.01 V *vs*.

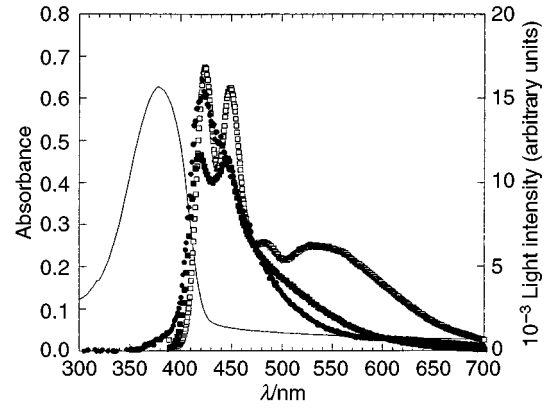

Fig. 1 Absorption (○), photoluminescence (■) and electroluminescence (●) spectra of PDHFDDOP. The photoluminescence spectrum of PDHF (□) is also given for comparison.

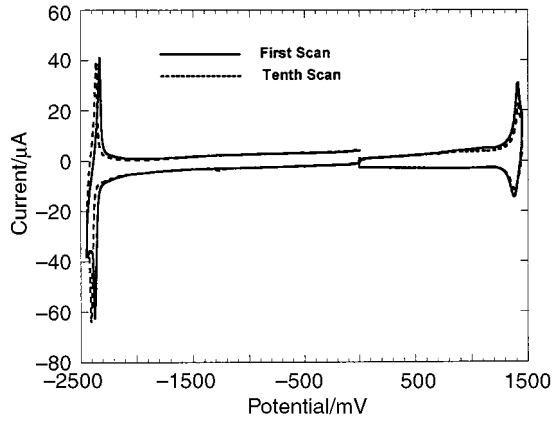

Fig. 2 Cyclic voltammograms of PDHFDDOP recorded from the first scan (——) and the tenth scan (– – – –) in a solution of $TBAPF_6$ (0.10 mol L^{-1}) in MeCN at room temp. Scan rate = 40 mV s^{-1}.

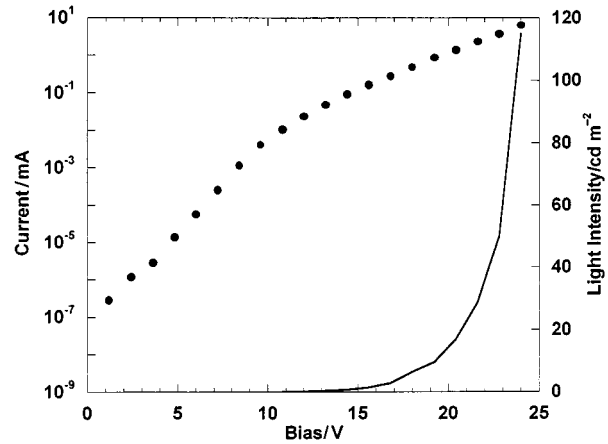

Fig. 3 Light output and *I–V* characteristics of a device in the ITO|PVK|PDHFDDOP|Ca configuration.

SCE). The data are shown in Fig. 2. Both the oxidative and the reductive reactions are reversible. The onset of reduction occurs at *ca*. −1.78 V above which the cathodic current quickly increases, and a cathodic peak appears at −2.38 V. A corresponding re-oxidation peak appears at −2.33 V. The n-doping potential, $E_{Red}^{1/2}$, is −2.36 V. For oxidation, the onset potential is *ca*. 1.22 V and an anodic peak occurs at 1.42 V with the corresponding re-reduction peak at 1.37 V. The oxidation potential, $E_{Ox}^{1/2}$, is 1.39 V. The difference between the p- and n-doping onset potentials is 3.00 V, implying that the π–π* band gap of the polymer is 3.00 eV; the same as the value determined from the onset of optical absorption. The HOMO and LUMO energy levels of the polymer were estimated from the p- and n-doping onset potentials[18] to be 5.66 and 2.62 eV, respectively. As shown in Fig. 2, after ten scans for the same polymer film, both the potentials and the current intensities of the redox peaks remain almost unchanged.

EL devices with the configuration of ITO|PVK (900 Å)|PDHFDDOP (750 Å)|Ca were fabricated, where PVK is poly(*N*-vinylcarbazole). Because of the low HOMO energy of PDHFDDOP, 5.66 eV below vacuum there is a large energy barrier for hole injection from ITO into the polymer layer. Here we use PVK as hole transporting layer. A typical device emits visible blue light at *ca*. 10 V forward bias (ITO wired positive) and reaches the brightness of 115 cd m^{-2} for a bias of 23.8 V. This gives an efficiency of 0.34 cd A^{-1} and a luminosity of 0.045 lm W^{-1}. The maximum external quantum efficiency was 0.60%. The current and light output characteristics are given in Fig. 3. The EL spectrum is displayed in Fig. 1. As noted for other polymer LED devices,[11] the HOMO level of PL (6.1 eV below vacuum) causes a large barrier for hole injection. Nevertheless, the external quantum efficiency is three times higher than that of the blue polymer LED device of 9,9-dioctylpolyfluorene, in which a polymeric triphenyldiamine is used as hole transporting layer and the thickness of the emissive polymer layer has been optimized.[14]

In summary, a new light emitting polymer, poly{(9,9-dihexyl-2,7-fluorene)–*alt*-*co*-[2,5-bis(decyloxy)-1,4-phenylene]}, has been synthesized. The polymer emits deep blue light without longer wavelength components in the emission spectrum. Relatively high PL and EL efficiences have been demonstrated. Improved EL performance, lower operating voltage and higher efficiency can be expected by further improving the hole-injection. The results demonstrate that this new polymer is a promising candidate for blue-emitting polymer LEDs.

W. Y. was supported by the Institute for Materials Research and Engineering, Singapore. Research at UCSB was supported by NSF-DMR9730126.

Notes and references

† The reaction of 2,7-dibromofluorene with 1-bromohexane in 50% NaOH aqueous solution in the presence of tetrabutylammonium chloride at 80 °C afforded 2,7-dibromo-9,9-dihexylfuorene **b** as white crystals after purification by recrystallization from ethanol. 2,7-Dibromo-9,9-dihexylfuorene **b** was treated with magnesium (turnings) in THF to form the Grignard reagent. The Grignard reagent solution was slowly dropped into a sitrred solution of trimethyl borate in THF at −78 °C. The mixture was stirred at −78 °C for 2 h and then at room temperature for two days. The reaction mixture was then poured into crushed ice containing sulfuric acid (5%) while stirring. The mixture was extracted with diethyl ether and the combined extracts were evaporated to give a white solid. Recrystallization of the crude product from hexane–acetone (80 : 20) afforded pure 9,9-dihexylfuorene-2,7-diboronic acid **c** as a white solid. The diboronic acid **c** was then reacted with propane-1,3-diol in toluene under reflux to produce monomer **I**.

‡ PDHFDDOP, ^{1}H NMR ($CDCl_3$, 200 MHz) δ 7.80 (d, 2H), 7.74 (s, 2H), 7.58 (d, 2H), 7.14 (s, 2H), 3.99 (t, 4H), 2.05 (br, 4H), 1.72 (t, 4H), 1.50–0.97 (m, 44H), 0.82 (t, 12H). Anal. Found: C, 84.50; H, 10.59. Calc. for $C_{51}H_{76}O_2$: C, 84.94; H, 10.62%.

1 J. H. Burroughes, D. D. C. Bradley, A. R. Brown, R. N. Marks, K. Mackay, R. H. Friend, P. L. Burn and A. B. Holmes, *Nature (London)*, 1990, **347**, 539.
2 A. Kraft, A. C. Grimsdale and A. B. Holmes, *Angew. Chem., Int. Ed.*, 1998, **37**, 402.
3 R. H. Friend, R. W. Gymer, A. B. Holmes, J. H. Burroughes, R. N. Marks, C. Taliani, D. D. C. Bradley, D. A. Dos Santos, J. L. Bredas, M. Logdlund and W. R. Salaneck, *Nature (London)*, 1999, **397**, 121.
4 A. J. Heeger, *Solid State Commun.*, 1998, **107**, 673.
5 G. Grem, G. Leditzky, B. Ullrich and G. Leising, *Adv. Mater.*, 1992, **4**, 36.
6 Y. Yang, Q. Pei and A. J. Heeger, *J. Appl. Phys.*, 1996, **79**, 934.
7 A. W. Grice, A. Tajbakhsh, P. L. Burn and D. D. C. Bradley, *Adv. Mater.*, 1997, **9**, 1174.
8 M. R. Andersson, M. Berggren, O. Inganas, G. Gustafsson, J. C. Gustafsson-Carlberg, D. Selse, T. Hjertberg and O. Wennerstrom, *Macromolecules*, 1995, **28**, 7525.
9 F. Garten, A. Hilberer, F. Cacialli, E. Esselink, Y. van Dam, B. Schlatmann, R. H. Friend, T. M. Klapwijk and G. Hadziioannou, *Adv. Mater.*, 1997, **9**, 127.
10 C. Hosokawa, N. Kawasaki, S. Sakamoto and T. Kusumoto, *Appl. Phys. Lett.*, 1992, **61**, 2503.
11 I. D. Parker, Q. Pei and M. Marrocco, *Appl. Phys. Lett.*, 1994, **65**, 1272.
12 W. Huang, H. Meng, W.-L. Yu, J. Gao and A. J. Heeger, *Adv. Mater.*, 1998, **10**, 593.
13 Q. Pei and Y. Yang, *J. Am. Chem. Soc.*, 1996, **118**, 7416.
14 A. W. Grice, D. D. C. Bradley, M. T. Bernius, M. Indasekaran, W. W. Wu and E. P. Woo, *Appl. Phys. Lett.*, 1998, **73**, 629.
15 S. Janietz, D. D. C. Bradley, M. Grell, C. Giebeler, M. Inbasekaran and E. P. Woo, *Appl. Phys. Lett.*, 1998, **73**, 2453.
16 M. Kreyenschmidt, G. Klaerner, T. Fuhrer, J. Ashenhurst, S. Karg, W. D. Chen, V. Y. Lee, J. C. Scott and R. D. Miller, *Macromolecules*, 1998, **31**, 1099.
17 N. Miyaura and A. Suzuki, *Chem. Rev.*, 1995, **95**, 2457.
18 M. D. de Leeuw, M. M. J. Simenon, A. B. Brown and R. E. F. Einerhand, *Synth. Met.*, 1997, **87**, 53.

Communication 9/05482K

ChemComm

Photochemical incorporation of *N*-benzylidene(phenyl)amine into the complex [{Ti(η^5-C_5Me_5)(η-O)}$_3$(μ_3-CH)] as a model of the titanium oxide surface†

Pilar Gómez-Sal, Avelino Martín, Miguel Mena,* María del Carmen Morales and Cristina Santamaría

Departamento de Química Inorgánica, Universidad de Alcalá, E-28871 Alcalá de Henares, Madrid, Spain. E-mail: mmena@inorg.alcala.es

Received (in Basel, Switzerland) 25th June 1999, Accepted 9th August 1999

The photochemical incorporation of PhCH=NPh to the metal oxide model [{TiCp*(μ-O)}$_3$(μ$_3$-CH)] (Cp* = η^5-C_5Me_5) occurs by breaking of the C=N imine bond and formation of μ-imido and σ-alkenyl groups on the [Ti_3O_3] core; the crystal structure of the obtained product, [{TiCp*(μ-O)}$_3$(μ-NPh)(CH=CHPh)], was determined by X-ray diffraction.

Ti_3O_3(μ$_3$-CR) systems are surface models suitable for examination of both the cooperative interaction between metal centres maintained in close proximity and the chemistry of alkylidyne groups on a metallic oxide support. Recently we have described that the reactions under mild conditions of carbon monoxide and isocyanides with [{TiCp*(μ-O)}$_3$(μ$_3$-CR)] complexes proceed *via* insertion into the μ$_3$-alkylidyne units.[1] However, the incorporation of ketones follows other pathways and the experimental data support the insertion of carbonyl groups, R_2C=O, into the Ti–H bond of the *in situ* formed [{TiCp*(μ-O)}$_3$(μ-C=CH_2)(H)] intermediate to give alkoxide–vinylidene derivatives [{TiCp*(μ-O)}$_3$(μ-C=CH_2)($OCHR_2$)].[2] Here, we present the preliminary result observed from the photochemical treatment of the trinuclear titanium derivative [TiCp*(μ-O)}$_3$(μ$_3$-CH)] **1**[3] with *N*-benzylidene(phenyl)amine.

When a solution of **1** and PhCH=NPh in hexane was irradiated for 45 h the alkenylimido complex [{TiCp*(μ-O)}$_3$(CH=CHPh)(μ-NPh)] **2** (Scheme 1) was obtained in good yield.‡ The ^{1}H NMR spectrum of compound **2** shows two signals in a 2:1 ratio for the Cp* ligands in accord with C_s symmetry in solution, and supports the presence of a *trans*-styryl group ($^3J_{HH}$ 18.3 Hz).‡ This ligand is σ-bonded to the titanium atom in accord with the observation in the ^{13}C NMR spectrum of a doublet of doublets at δ 190.4 (^1J 126.0, ^2J 2.5 Hz) and a doublet of multiplets at δ 140.2 (^1J 154.4 Hz) corresponding to C_α and C_β resonances, respectively. A band of medium intensity at 1581 cm^{-1} in the IR spectrum is assigned to the alkenyl carbon–carbon double bond.

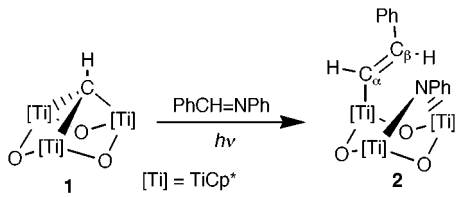

Scheme 1

An X-ray diffraction study of **2** reveals (Fig. 1)§ a *trans*-alkenyl group on one titanium atom and a phenyl imido moiety bridging the other two titanium atoms in a *syn–syn* disposition.

The styrene environment is planar with a Ti(2)–C(41) bond length of 2.127(9) Å, similar to those observed for Ti–C(sp^3) bonds in alkyl titanium complexes [TiCp*Me_3] (av. 2.10 Å),[4a] [{TiCp*Me}$_3$(μ-O)$_3$] (av. 2.09 Å),[4b] [{Ti_4Cp*$_4Me_2$}(μ-O)$_5$] (2.11 Å),[4c] [{TiCp*(μ-O)}$_3$(μ$_3$-CMe)] (av. 2.11 Å),[4d] [{TiCp*(μ-O)}$_3$(CH_2CH=CHMe)$_3$] (av. 2.13 Å)[4e] or Ti–C(sp^2) in alkenyl biscyclopentadienyl derivatives.[5] Within the styryl group, the C(41)–C(42) bond length [1.320(12) Å] is within the range for a C=C double bond.[6]

On the opposite side of the molecule, the Ti(1), Ti(3), N(13) and O(13) atoms form a distorted square (see Fig. 1), almost perpendicular to the Ti(1)–Ti(2)–Ti(3) and phenyl [C(51)–C(56)] planes. The N(13) atom shows a planar environment with Ti–N distances of 1.957(6) and 1.948(6) Å, close to the value of 1.91 Å (av.) found in [TiCp*(NMe_2)$_3$][7] and also to that of 1.939 Å reported in the cubane structure [{Ti_4Cp*$_4$}(μ$_3$-N)$_4$].[8] The average Ti–O bond distance (1.84 Å)[9] and Ti–ring centroid distance (2.06 Å) are comparable to those in the literature for the titanium organometallic oxides [{TiCp*(μ-O)}$_3$$X_3$] (X = Me,[4b] Cl,[10] Br[11]).

A reasonable proposal for this reaction (Scheme 2) involves imine insertion into one of the three titanium–carbon(alk-

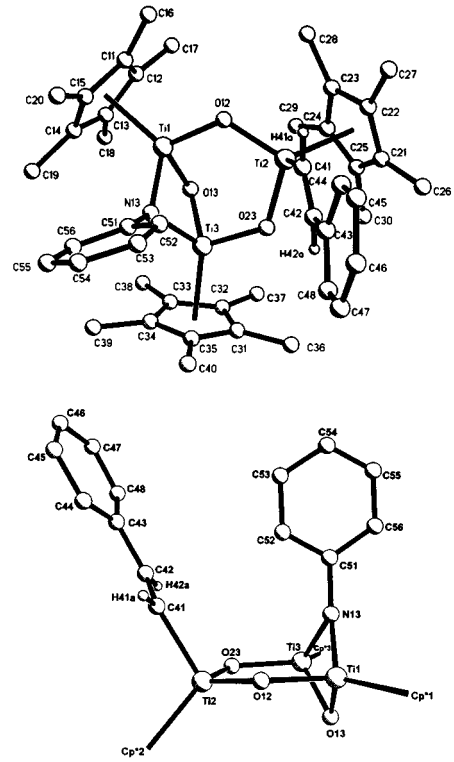

Fig. 1 Molecular structure of [{Ti(η^5-C_5Me_5)(μ-O)}$_3$(CH=CHPh)(μ-NPh)] **2**. Selected lengths (Å) and angles (°): Ti–Cp* 2.06(av.), Ti–O 1.84(5)(av.), Ti(2)–C(41) 2.127(9), C(41)–C(42) 1.32(1), Ti(1)–N(13) 1.957(6), Ti(3)–N(13) 1.948(6); O(12)–Ti(1)–O(13) 102.4(2), O(12)–Ti(1)–N(13) 101.4(2), O(13)–Ti(1)–N(13) 84.8(2), O(12)–Ti(2)–O(23) 106.6(2), O(12)–Ti(2)–C(41) 105.4(3), O(23)–Ti(2)–C(41) 100.2(3); O(13)–Ti(3)–O(23) 100.7(2), O(13)–Ti(3)–N(13) 84.5(2), O(23)–Ti(3)–N(13) 102.5(3), Ti(1)–N(13)–Ti(3) 88.7(3), Ti(2)–O(12)–Ti(1) 122.7(3), Ti(1)–O(13)–Ti(3) 95.6(2), Ti(2)–O(23)–Ti(3) 123.7(3). Cp* is the centroid of the C_5Me_5 ring.

† Dedicated to Alexander von Humboldt on the occasion of his commemorative year 1999.

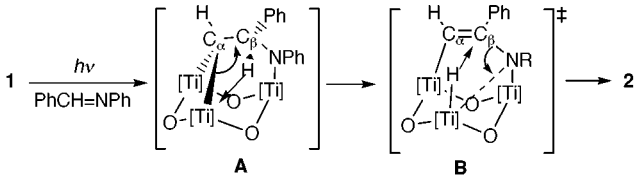

Scheme 2

ylidyne) bonds to generate the species **A** which was not detected. β-Hydrogen elimination[2] would then give a hydride–enamine intermediate **B** while subsequent carbon–nitrogen bond rupture, transfer of hydrogen from titanium to the β-carbon and formation of a nitrogen–titanium bond, would afford the σ-alkenyl-μ-imido complex **2**. However, we can not exclude the possibility that the conversion of **A** to **2** could occur directly by a concerted pathway.

To our knowledge, this observed behaviour is comparable only to the alkylidene/imine metathesis-like reactions reported by Rocklage and Schrock,[12] and by Cantrell and Meyer[13] for mononuclear niobium, tantalum and molybdenum alkylidene complexes. In our case the metathesis-like process occurs on the Ti_3O_3 surface with the cooperative participation of the three metal atoms and opens new perspectives in trinuclear titanium chemistry. Further studies of this process with other imines are in progress and the results will be published in due course.

The authors thank the financial support from the DGES (PB96-0672).

Notes and references

‡ *Preparation* of **2**: *N*-benzylidene(phenyl)amine (0.356 g, 197 mmol) was added to a solution of **1** (1.0 g, 164 mmol) in 60 mL of hexane. The reaction mixture was irradiated at room temp. for 45 h with a UV lamp. The final reddish solution was concentrated and cooled to obtain red crystals of **2**. Yield: 0.90 g (*ca*. 75%). Anal. Calc. for $C_{44}H_{57}NO_3Ti_3$, (*M* = 791.64): C, 66.76; H, 7.26; N, 1.77. Found: C, 67.28; H, 7.69; N, 1.72%. Selected NMR data (*δ*, *J*/Hz): ^{1}H (500 MHz, C_6D_6, 25 °C, TMS): 1.95 (s, 30H, C_5Me_5), 2.09 (s, 15H, C_5Me_5), 8.04 (d, 1H, ^3J 18.3, –C*H*=CHPh), 6.84 (d, 1H, ^3J 18.3, –CH=C*H*Ph); ^{13}C{^{1}H} (125 MHz, C_6D_6, 25 °C, TMS): 11.7, 12.20 (C_5*Me*$_5$), 122.6, 122.5 (*C*$_5$Me$_5$), 140.2 (dm, ^1J 154.4, –CH=*C*HPh), 158.9, (C_{ipso}, μ-NPh), 190.4 (dd, ^1J 126.0, ^2J 2.5, –*C*H=CHPh). IR (KBr, cm^{-1}): *ν* 3052w, 2913s, 1581m, 1542w, 1488w, 1440s, 1375s, 1245s, 1024m, 898s, 759w, 729s, 688s, 397s. EI mass spectrum *m/z* 792 (M^+, 11%).

§ Single crystals of **2** were obtained by slow cooling of a hexane solution. *Crystal data* for **2**: $C_{44}H_{57}NO_3Ti_3$, *M* = 791.61, triclinic, space group $P\bar{1}$, *a* = 11.4865(1), *b* = 12.559(1), *c* = 16.049(1) Å, *α* = 87.64(1), *β* = 89.82(1), *γ* = 82.87(1)°, *V* = 2295.3(3) Å^3, *Z* = 2, D_c = 1.145 g cm^{-3}; *F*(000) = 836. *λ* = 0.71073 Å, *μ*(Mo-K*α*) = 0.544 mm^{-1}. The data were collected on an Enraf Nonius CAD4 diffractometer. Intensity measurements were performed by *ω*–*θ* scans in the range 6 < 2*θ* < 44° at 19 °C on a crystal of dimensions 0.45 × 0.40 × 0.38 mm. Of the 5916 measured reflections, 5577 were independent; largest minimum and maximum in the final difference Fourier synthesis: −0.415 and 1.422 e Å^{-3}, *R*1 = 0.077 and *wR*2 = 0.251 [for 4025 reflections with $F > 4\sigma(F)$]. The structure was solved by direct methods (SHELXS-97) and refined by least-squares against F^2 (SHELXL-97). CCDC 182/1374. See http://www.rsc.org/suppdata/cc/1999/1839/ for crystallographic data in .cif format.

1 R. Andrés, M. Galakhov, M. P. Gómez-Sal, A. Martín, M. Mena and C. Santamaría, *Chem. Eur. J.*, 1998, **4**, 1206.
2 M. Galakhov, M. Mena and C. Santamaría, *Chem. Commun.*, 1998, 691.
3 R. Andrés, M. Galakhov, A. Martín, M. Mena and C. Santamaría, *J. Chem. Soc., Chem. Commun.*, 1995, 551; R. Andrés, Thesis Doctoral, Universidad de Alcalá, Madrid, 1995.
4 (*a*) R. Blom, K. Rypdal, M. Mena, P. Royo and R. Serrano, *J. Organomet. Chem.*, 1990, **391**, 47; (*b*) S. G. Blanco, M. P. Gómez-Sal, S. M. Carreras, M. Mena, P. Royo and R. Serrano, *J. Chem. Soc., Chem. Commun.*, 1986, 1572; (*c*) P. Gómez-Sal, A. Martín, M. Mena and C. Yélamos, *Inorg. Chem.*, 1996, **35**, 242; (*d*) R. Andrés, M. Galakhov, A. Martín, M. Mena and C. Santamaría, *Organometallics*, 1994, **13**, 2159; (*e*) R. Andrés, M. Galakhov, M. P. Gómez-Sal, A. Martín, M. Mena and C. Santamaría, *J. Organomet. Chem.*, 1996, **526**, 135.
5 G. S. Herrmann, H. G. Alt and U. Thewalt, *J. Organomet. Chem.*, 1990, **393**, 83; R. Beckhaus, I. Strauss and T. Wagner, *J. Organomet. Chem.*, 1994, **464**, 155; R. Beckhaus, J. Sang, J. Oster and T. Wagner, *J. Organomet. Chem.*, 1994, **484**, 179; R. Beckhaus, J. Sang, T. Wagner and B. Ganter, *Organometallics*, 1996, **15**, 1176; J. J. Eisch, A. M. Piotrowski, S. K. Brownstein, E. J. Gabe and F. L. Lee, *J. Am. Chem. Soc.*, 1985, **107**, 7219; R. Beckhaus, M. Wagner and R. Wang, *Z. Anorg. Allg. Chem.*, 1998, **624**, 277.
6 J. March, *Advanced Organic Chemistry. Reactions, Mechanism, and Structure*, John Wiley & Sons, Inc., New York, 1985.
7 A. Martín, M. Mena, C. Yélamos, R. Serrano and P. R. Raithby, *J. Organomet. Chem.*, 1991, **467**, 79.
8 P. Gómez-Sal, A. Martín, M. Mena and C. Yélamos, *J. Chem. Soc., Chem. Commun.*, 1995, 2185.
9 Although all the Ti–O distances are similar, the Ti–O–Ti angles present very different values if they form the distorted square (95.6°) or the rest of the core (123°).
10 T. Carofiglio, C. Floriani, A. Sgamellotti, M. Rosi, A. Chiesi-Villa and C. Rizzoli, *J. Chem. Soc., Dalton Trans.*, 1992, 1081.
11 S. I. Troyanov, V. Varga and K. Mach, *J. Organomet. Chem.*, 1991, **402**, 201.
12 S. M. Rocklage and R. R. Schrock, *J. Am. Chem. Soc.*, 1982, **104**, 3077.
13 G. K. Cantrell and T. Y. Meyer, *J. Am. Chem. Soc.*, 1998, **120**, 8035.

Communication 9/05129E

The use of M41S materials in chiral HPLC

Carla Thoelen, Kris Van de Walle, Ivo F. J. Vankelecom and Pierre A. Jacobs*

Katholieke Universiteit Leuven, Faculty of Agricultural and Applied Biological Sciences, Centre for Surface Chemistry and Catalysis, Kardinaal Mercierlaan 92, B-3001 Heverlee, Leuven, Belgium.
E-mail: pierre.jacobs@agr.kuleuven.ac.be

Received (in Cambridge, UK) 7th June 1999, Accepted 16th August 1999

Siliceous MCM-41 and MCM-48, covalently linked with the chiral selector (*R*)-naphthylethylamine, have been evaluated as supports in chiral HPLC and show for several racemates higher separation factors than for a stationary phase based on amorphous silica.

Since the discovery of MCM-41 and MCM-48 in 1992, much research has been reported on their use in the field of catalysis, where their mesoporosity is beneficial for the conversion of large substrates.[1–3] These mesoporous molecular sieves are characterized by a high specific surface area in combination with highly ordered pores. These pores are one-dimensional in the case of MCM-41 in contrast to the three-dimensional network of MCM-48. Furthermore, the pore size of these materials can be tuned between 15 and 100 Å. In the domain of heterogeneous chiral catalysis, an extensively growing research area owing to the increasing demand for enantiomerically pure products, these mesoporous materials provide interesting supports for the development of new chiral catalysts.[4,5] Recently, in chromatographic separation techniques such as GC and HPLC, the use of non-functionalized MCM-41 has also been reported.[6,7] In chiral HPLC however, M41S materials were, up till now, not investigated in terms of their performance as supports in spite of their numerous advantages.

In this study, three chiral stationary phases (CSPs) with (*R*)-naphthylethylamine [(*R*)-NEA] as chiral selector were synthesized starting from amorphous silica, Si-MCM-41 and Si-MCM-48, respectively. MCM-41 and MCM-48 were prepared following a hydrothermal synthesis procedure.[8] They were characterized by XRD, SEM and sorption measurements. In both cases, the BET area appeared to be *ca.* 1000 $m^2\ g^{-1}$. The particle sizes of the resulting MCM-41 and MCM-48 are 5–15 μm and 0.1–0.5 μm, respectively. After silylation of the pore walls with aminopropyltriethoxysilane, these materials as well as Lichrosorb-NH_2 (Merck, 10 μm particle size), a reference for amorphous silica, were coupled with (*R*)-NEA (Fig. 1). This was done using succinic acid as a spacer molecule, according to the literature procedure.[9]

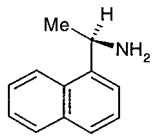

Fig. 1 Chiral selector used: (*R*)-naphthylethylamine.

Thermogravimetric analysis (TGA) revealed the amount of chiral selector on the supports: 0.06, 0.24 and 0.23 mmol (*R*)-NEA per gram of Lichrosorb-NH_2, MCM-41 and MCM-48, respectively. With the same technique, these functionalized materials were found to be thermally stable up to 130 °C. Moreover, because the selector is linked covalently, the materials are stable in all common solvents.

In order to compare the performance of the MCM-41 based CSP with the performance of the phase based on amorphous silica, two manually packed columns (10 cm) were tested in chiral HPLC experiments (Table 1) for their chiral recognition ability towards three racemates (Fig. 2). The higher separation factors achieved with MCM-41 as support are very promising. The resolution and efficiency, however, are quite poor, but can be improved by applying the slurry packing technique. Therefore in the following step, a slurry packed column of MCM-41 was tested on the same racemates (Table 2) and the study was extended to MCM-48, for which the three-dimensional pore structure might further improve the chromatographic separation.

The chiral stationary phase based on MCM-41 is characterized by 3–4 fold higher retention factors for the tested racemates than that based on amorphous silica. This is in accordance with their difference in specific area (Lichrosorb-NH_2: 300 $m^2\ g^{-1}$, MCM-41: 1000 $m^2\ g^{-1}$), leading to a higher coverage with chiral selector. This also explains the excellent separation factors achieved. An augmentation of the separation factor by 40% was obtained for DNB–NEA by using the column based on MCM-41 instead of that based on amorphous silica.

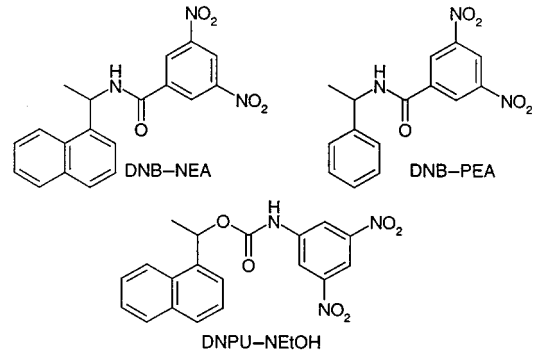

Fig. 2 Tested racemates: dinitrobenzoyl derivatives of naphthylethylamine (DNB–NEA) and phenylethylamine (DNB–PEA), dinitrophenylurethane derivative of naphthylethanol (DNPU–NEtOH).

Table 1 Chromatographic performance of manually packed Lichrosorb-NH_2 and Si-MCM-41 based CSPs[a]

	Lichrosorb-NH_2 (manually packed)					Si-MCM-41 (manually packed)				
Component	k_S	k_R	α	N	R_s	k_S	k_R	α	N	R_s
DNB–NEA	1.36	2.96	2.18	447	2.68	4.50	13.78	3.06	74	1.88
DNB–PEA	1.37	2.10	1.53	429	1.38	4.41	8.28	1.88	58	0.92
DNPU–NEtOH	1.21	1.41	1.17	—[b]	—[b]	3.30	3.97	1.20	—[b]	—[b]

[a] Mobile phase: *n*-hexane–1,2-dichloroethane–ethanol (40 : 12 : 3), flow rate: 0.6 ml min^{-1}, UV detection (254 nm), k = retention factor, α = separation factor, N = plate number, R_s = resolution. [b] Peak width determination was impossible owing to poor peak resolution.

Table 2 Chromatographic performance of slurry packed Si-MCM-41 and Si-MCM-48 based CSPs[a]

	Si-MCM-41 (slurry packed)					Si-MCM-48 (slurry packed)				
Component	k_S	k_R	α	N	R_s	k_S	k_R	α	N	R_s
DNB–NEA	3.31	10.44	3.16	136	2.50	3.48	9.11	2.62	605	4.7
DNB–PEA	3.34	6.47	1.93	117	1.32	3.47	5.92	1.71	680	2.76
DNPU–NEtOH	2.51	3.16	1.26	—[b]	—[b]	2.46	3.02	1.23	667	0.94

[a] Mobile phase: *n*-hexane–1,2-dichloroethane–ethanol (40 : 12 : 3), flow rate: 0.6 ml min^{-1}, UV detection (254 nm), k = retention factor, α = separation factor, N = plate number, R_s = resolution. [b] Peak width determination was impossible owing to poor peak resolution.

The resolution and particularly the efficiency are poor owing to the large peak widths. Peak tailing prevents accurate determination of the peak widths. Nevertheless, MCM-41 seems to be a promising support material because of the high separation factors in combination with a good analysis time (< 30 min for the strongest retained component) and very acceptable inlet pressures (100 bar). Moreover, the mobile phase used was optimized for the amorphous silica CSP, so probably further improvements can be made for the column based on MCM-41 by changing the composition of the mobile phase.

By using slurry packed columns of MCM-41 and MCM-48 based CSPs, band broadening, which is disadvantageous to the efficiency, can be reduced owing to the formation of a more uniformly packed bed. Comparing Tables 1 and 2, both the resolution and the efficiency of the separation with MCM-41 are clearly improved by use of this packing method; the efficiency of the column was doubled. The use of MCM-48 as support leads to further improvement with the efficiencies increasing by a factor of six, owing to a faster mass transfer through the three-dimensional pore system. Separations performed on this material show very good resolution and efficiency, and only slightly lower separation factors (the separation factor decreases by < 20% compared to the use of MCM-41 as support). Band broadening is substantially reduced and peak symmetry is improved. The nature of the pore system together with the smaller particle dimensions and the narrower particle size distribution can account for the successful separation with MCM-48. On both columns, based on either MCM-41 or MCM-48, a whole range of racemates are currently being tested. No loss of chromatographic performance was observed with time illustrating the stability of the materials towards repeated cycles of guest exchange.

In conclusion, the first utilization of M41S materials as supports in chiral HPLC is reported. Both MCM-41 and MCM-48 show high retention and separation factors for the tested racemates and are very promising for liquid chromatography. These results, in combination with good analysis times and very acceptable inlet pressures, make these HPLC columns successful analytical instruments. Excellent resolution and efficiency could be achieved with MCM-48. Columns based on MCM-41 show good resolution, but the efficiency should be further improved by a better control of the particle size distribution. The influence of pore size and selector loading on chromatographic performance is under current investigation for both M41S materials.

This research is done within the framework of an IUAP–PAI grant from the Federal Government. C. T. thanks the Flemish Fund of Scientific Research (F. W. O.) for a grant as aspirant research fellow. I. F. J. V. is indebted to the F.W.O. for a fellowship as postdoctoral research assistant.

Notes and references

1 C. T. Kresge, M. E. Leonowicz, W. J. Roth, J. C. Vartuli and J. S. Beck, *Nature (London)*, 1992, **359**, 710.
2 J. S. Beck, J. C. Vartuli, W. J. Roth, M. E. Leonowicz, C. T. Kresge, K. D. Schmitt, C. T-W. Chu, D. H. Olson, E. W. Sheppard, S. B. McCullen, J. B. Higgins and J. L. Schlenker, *J. Am. Chem. Soc*., 1992, **114**, 10834.
3 A. Corma, *Chem. Rev.*, 1997, **97**, 2373.
4 J. M. Thomas, T. Maschmeyer, B. F. G. Johnson and D. S. Shephard, *J. Mol. Catal. A: Chem.*, 1999, **141**, 139.
5 S. O'Brien, J. Tudor, T. Maschmeyer and D. O'Hare, *Chem. Commun.*, 1997, **19**, 1905.
6 M. Raimondo, G. Perez, M. Sinibaldi, A. De Stefanis and A. A. G. Tomlinson, *Chem. Commun.*, 1997, 1343.
7 M. Grün, A. A. Kurganov, S. Schacht, F. Schüth and K. K. Unger, *J. Chromatogr.*, 1996, **740**, 1.
8 J. Lujano, Y. Romero and J. Carrazza, *Zeolites: A Refined Tool for Designing Catalytic Sites, Proceedings of International Zeolite Symposium*, ed. L. Bonneviot and S. Kaliaguine, Québec, Canada, Elsevier Science, 1995, p. 149.
9 N. Ôi, M. Nagase and T. Doi, *J. Chromatogr.*, 1983, 111.

Communication 9/04487F

Reactions of water soluble iron(II) and cobalt(II) porphyrins with nitric oxide. Implications for the reactivity of NO and biologically relevant metal centers

Leroy E. Laverman and Peter C. Ford*

Department of Chemistry, University of California, Santa Barbara, California 93106, USA.
E-mail: ford@chem.ucsb.edu

Received (in Bloomington, IN, USA) 6th April 1999, Accepted 4th August 1999

The entropies and volumes of activation ($\Delta S^{\ddagger}_{on}$ and $\Delta V^{\ddagger}_{on}$) for the fast reactions ($k_{on} > 10^9$ dm^3 mol^{-1} s^{-1}) reaction of NO with the water soluble iron(II) porphyrin complexes Fe^{II}(TPPS) [TPPS = tetrakis(4-sulfonatophenyl)porphinato] and Fe^{II}(TMPS) [TMPS = tetrakis(sulfonatomesityl)porphinato] are small and positive indicating that these reactions are dominated by the diffusion processes as is the analogous formation of the cobalt(II) complex Co^{II}(TPPS)(NO).

Nitric oxide has important and diverse roles in mammalian biology including cytotoxic immune response and intracellular signaling.[1] Under physiological conditions the principal targets for NO are metal centers, primarily iron, the best documented being the ferroheme center in soluble guanylyl cyclase (sGC).[2] NO may also have roles as an inhibitor of metalloenzymes such as catalase,[3] nitrile hydrase[4] and cytochrome oxidase,[5] as the vasodilator released from the salivary ferriheme protein of a blood sucking insect[6] and in blood pressure regulation by hemoglobin.[7] However, despite numerous rate measurements for NO reactions with ferro- and ferri-heme centers,[8] there has been little quantitative study to deduce the bimolecular mechanisms by which NO undergoes coordination to metal porphyrin centers [eqn. (1)].

$$M(por)_{aq} + NO \underset{k_{off}}{\overset{k_{on}}{\rightleftharpoons}} M(por)(NO)_{aq} \quad (1)$$

To address this deficiency, we have initiated studies on the temperature and hydrostatic pressure effects for the 'on' and 'off' reactions with water soluble iron(II) and iron(III) porphyrins in aqueous solutions as simple models for ferro- and ferriheme proteins {M = Fe^{II} or Fe^{III}; por = TPPS [tetrakis(4-sulfonatophenyl)porphinato anion] or TMPS [tetrakis(sulfonatomesityl)porphinato anion]}.[9] From these data, one can extract the activation parameters $\Delta H^{\ddagger}_{on}$, $\Delta S^{\ddagger}_{on}$ and $\Delta V^{\ddagger}_{on}$ in order to gain insight into the nature of the transition state(s) of the rate limiting step(s). Here we describe results for the 'on' reaction of the ferroheme complexes Fe^{II}(TPPS) **I** and Fe^{II}(TMPS) **II** in aqueous solutions and compare these to the analogous reaction for the cobalt(II) porphyrin Co^{II}(TPPS) **III**.

Fig. 1 shows the difference spectrum obtained by subtracting the absorbance spectrum of aqueous Fe^{II}(TPPS)(NO) and NO (1.7 mM) from that recorded subsequent to a 355 nm laser pulse recorded with a CCD camera (50 ns delay, 100 ns gate width).[10] This is in exact agreement with the difference between the spectra of **I** and Fe^{II}(TPPS)(NO) according to eqn. (1). The transient absorption changes decayed back to baseline and no permanent photoproducts were spectrally apparent (Fig. 1, inset).

The k_{obs} values obtained by exponential fits of these data are independent of the observation wavelength. According to relaxation kinetics, $k_{obs} = k_{on}[NO] + k_{off}$, and correspondingly plots of k_{obs} *vs.* [NO] are linear with slopes equal to k_{on} with values of (1.47 ± 0.05) × 10^9 and (1.04 ± 0.08) × 10^9 dm^3 mol^{-1} s^{-1} for **I** and **II**, respectively, in 298 K phosphate buffered (pH 7.0) aqueous solutions. The intercepts of such plots should equal k_{off}, but since equilibrium constants for Fe^{II}(por)(NO) formation ($K_1 = k_{on}/k_{off}$) are very large, k_{off} values could not be determined by extrapolation. Independent measurements in this laboratory give the upper limit estimate $k_{off} < 2$ s^{-1} for **I**.[11]

Temperature effects on the k_{on} values for **I** and **II** were evaluated from linear plots of k_{obs} *vs.* [NO] for at least six NO concentrations at each temperature. Eyring plots gave straight lines from which were extracted the values for $\Delta H^{\ddagger}_{on}$ and $\Delta S^{\ddagger}_{on}$. For **I** these were 24 ± 3 kJ mol^{-1} and 12 ± 10 J mol^{-1} K^{-1} and for **II** these were 26 ± 6 kJ mol^{-1} and 16 ± 20 J mol^{-1} K^{-1}, respectively.

Hydrostatic pressure (*P*) effects were evaluated by determining k_{on} from plots of k_{obs} *vs.* [NO] for individual *P* ranging from 0.1 to 250 MPa. Plots of ln(k_{on}) *vs. P* were linear and activation volumes were calculated according to $\Delta V^{\ddagger}_{on} = -RT[d\ln(k_{on})/dP]_T$.[12] The respective $\Delta V^{\ddagger}_{on}$ values obtained for **I** and **II** were 5.0 ± 1.0 and 2.2 ± 0.6 cm^3 mol^{-1}.

The measured rate constants k_{on} for NO binding to ferrohemes range over many orders of magnitude, from 8.3 dm^3 mol^{-1} s^{-1} for Cyt^{II} (Cyt^{II} = Fe^{II}cytochrome *c*) to 1.5 × 10^9 dm^3 mol^{-1} s^{-1} for **I** at ambient temperature.[8] Ferrohemes may be six-coordinate in the presence of an excess of strong field ligands such as pyridine or imadazole but tend to be coordinatively unsaturated otherwise. In wet toluene or dichloromethane, the model ferroheme Fe^{II}(TtButPP) {TtButPP = [(N-*tert*-butylcarbamoyl)phenyl]porphyrin} was found to bind H_2O only weakly.[13] Furthermore, ferroheme proteins tend to be five-coordinate unless a strong field ligand such as CO, O_2 or CN^- occupy an axial site, in which case the Fe^{II} is six-coordinate, although in the case of Cyt^{II} the Fe^{III} is six-coordinate with histidine and cysteine thiolate ligands in the axial site.[14] It does not appear coincidental that Cyt^{II} is extremely slow in its reaction with NO. While the exact coordination environments of **I** and **II** have not been explicitly determined in buffered aqueous media, analogy to the above and other examples clearly suggests that water is a weak field ligand for these ferrohemes which are likely to be effectively five-coordinate in solution.

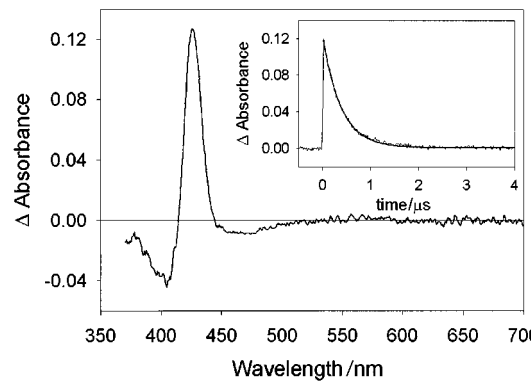

Fig. 1 The transient absorbance spectrum of aqueous Fe^{II}(TPPS)(NO) recorded 50 ns after pulsed laser excitation at 355 nm. Inset: decay of absorbance at 425 nm following a laser pulse, $k_{obs} = 2.7 \times 10^6$ s^{-1}.

Our earlier study[9] of the temperature and hydrostatic pressure effects on the rates of NO binding with the ferriheme analogs Fe^{III}(TPPS) **III** and Fe^{III}(TMPS) **IV** demonstrated very large and positive values for both $\Delta V^{\ddagger}_{on}$ and $\Delta S^{\ddagger}_{on}$. Such behaviour is a signature for a mechanism where $Fe^{III}NO$ bond formation is preceded by ligand dissociation, in this case from the hexacoordinate ferriheme complexes $Fe^{III}(por)(H_2O)_2$. In contrast, the $\Delta S^{\ddagger}_{on}$ and $\Delta V^{\ddagger}_{on}$ values determined for the iron(II) species **I** and **II** are much smaller while, correspondingly, the k_{on} values are three orders of magnitude faster.

The kinetics of ligand binding to ferrohemes have led to a proposed scheme[15] in which an encounter pair is formed before bond formation occurs, *i.e.*

$$Fe^{II}(por) + L \underset{k_{-d}}{\overset{k_d}{\rightleftharpoons}} \{Fe^{II}(por) \| L\} \xrightarrow{k_a} Fe^{II}(por)(L) \qquad (2)$$

In this model, k_d is the rate constant for formation of the encounter pair by diffusion, k_{-d} is that for diffusion of the reactants apart, and k_a represents that for formation of the Fe–L bond. If the steady state approximation is made with respect to the encounter pair {Fe(por)‖ L}, then,

$$k_{on} = \frac{k_d k_a}{k_{-d} + k_a} \qquad (3)$$

and to a first approximation,

$$\Delta V^{\ddagger}_{on} = \Delta V^{\ddagger}_{d} + \Delta V^{\ddagger}_{a} - RT\left(\frac{d \ln (k_a + k_{-d})}{dP}\right)_T \qquad (4)$$

The two limiting cases are ones in which ligand binding is activation controlled or in which the reaction is diffusion controlled. In the former $k_d \gg k_a$, thus

$$\Delta V^{\ddagger}_{on} = \Delta V^{\ddagger}_{d} + \Delta V^{\ddagger}_{a} - \Delta V^{\ddagger}_{-d} \qquad (5)$$

The difference $\Delta V^{\ddagger}_{d} - \Delta V^{\ddagger}_{-d}$ is the volume difference between a contact pair and a solvent separated pair. While unknown, this can be assumed to be small when L is uncharged. The principal contributor to $\Delta V^{\ddagger}_{on}$ thus becomes $\Delta V^{\ddagger}_{a}$, which would be expected to be negative if Fe^{II}(por) is five coordinate (since this step involves bond formation).[12]

In the other limiting case, $k_a \gg k_{-d}$ and $\Delta V^{\ddagger}_{on} \cong \Delta V^{\ddagger}_{d}$. Activation volumes for diffusion limited reactions ($\Delta V^{\ddagger}_{d}$) in various solvents are generally positive owing to pressure induced increases in viscosity. In the present case, the $\Delta V^{\ddagger}_{on}$ values measured for **I** and **II** (5.0 and 2.2 $cm^3\ mol^{-1}$, respectively) are somewhat larger than expected from a diffusion limited rate in water[16] but are much smaller than found for the ferriheme analogs.[9] This suggests that k_{on} is largely dominated by the diffusional terms. Indeed the rates for reaction of NO with **I** and **II** are within an order of magnitude of the diffusion limit in water ($k_d \approx 10^{10}\ dm^3\ mol^{-1}\ s^{-1}$ at 298 K).[17]

A similar analysis of $\Delta S^{\ddagger}$ gives $\Delta S^{\ddagger}_{on} \cong \Delta S^{\ddagger}_{d}$, if $k_a \gg k_{-d}$. The activation entropy $\Delta S^{\ddagger}_{d}$ for diffusion in water is small and positive; a value of *ca.* 34 $J\ mol^{-1}\ K^{-1}$ can be calculated according to Eyring and coworkers.[18] In this context, the measured $\Delta S^{\ddagger}_{on}$ values for **I** and **II** (12 and 16 $J\ mol^{-1}\ K^{-1}$, respectively) are further argument for a diffusion dominated process.

We have also determined the temperature effects on the kinetics of the reaction of Co^{II}(TPPS) with NO to give Co^{II}(TPPS)(NO). Notably the behavior of this system is quite similar to that of the Fe^{II} analog with $k_{on} = 2.3 \pm 0.1 \times 10^9\ (dm^3\ mol^{-1}\ s^{-1})$ at 298 K, $\Delta H^{\ddagger}_{on} = 28 \pm 2\ kJ\ mol^{-1}$ and $\Delta S^{\ddagger}_{on} = 28 \pm 7\ J\ mol^{-1}\ K^{-1}$. Hence, the kinetics of the 'on' reaction for Co^{II}(TPPS) can also be concluded to be dominated by diffusion processes.

For nitric oxide to be important in intracellular signaling at the sub-μM concentrations generated *in vivo*,[19] the reactions of NO with ferroheme proteins must have very high second order rate constants in order to compete with other processes leading to NO depletion. The present study demonstrates that activation parameters for the reactions of NO with the water soluble Fe(II) porphyrin complexes **I** and **II** are consistent with the small and positive values of $\Delta V^{\ddagger}_{on}$ and $\Delta S^{\ddagger}_{on}$ expected for diffusion limited (or nearly limited) processes in solution. These results experimentally support the intuitive notion that the nearly diffusion limited rates for NO reaction with iron(II) hemes is due to vacant or extraordinarily labile coordination sites at those metal centers.

This work was supported by the National Science Foundation (CHE 9726889).

Notes and references

1 L. J. Ignarro, G. M. Buga, K. S. Wood and R. E. Byrns, *Proc. Natl. Acad. Sci. USA*, 1987, **84**, 9265; S. Moncada, R. M. J. Palmer and E. A. Higgs, *Pharmacol. Rev.*, 1991, **43**, 109; P. L. Feldman, O. W. Griffith and D. J. Stuehr, *Chem. Eng. News*, 1993, **71**, 26.

2 J. N. Burstyn, A. E. Yu, E. A. Dierks, B. K. Hawkins and J. H. Dawson, *Biochemistry*, 1995, **34**, 5896; S. Kim, G. Deinum, M. T. Gardner, M. M. Marletta and G. T. Babcock, *J. Am. Chem. Soc.*, 1996, **118**, 8769.

3 G. C. Brown, *Eur. J. Biochem.*, 1995, **232**, 188.

4 T. Noguchi, J. Honda, T. Nagamune, H. Sasabe, Y. Inoue and I. Endo, *FEBS Lett.*, 1995, **358**, 9.

5 M. W. J. Cleeter, J. M. Cooper, V. M. Darley-Usmar, S. Moncada and A. H. Scapira, *FEBS Lett.*, 1994, **345**, 50.

6 J. M. C. Ribiero, J. M. H. Hazzard, R. H. Nussenzveig, D. E. Champange and F. A. Walker, *Science*, 1993, **260**, 539.

7 J. S. Stamler, L. Jia, J. P. Eu, T. J. McMahon, I. T. Demchenko, J. Bonaventura, K. Gernert and C. A. Piantadosi, *Science*, 1997, **276**, 2034.

8 R. J. Morris and Q. H. Gibson, *J. Biol. Chem.*, 1980, **255**, 8050; M. Hoshino, K. Ozawa, H. Seki and P. C. Ford, *J. Am. Chem. Soc.*, 1993, **115**, 9568; T. G. Traylor, D. Magde, J. Marsters, K. Jongeward, G. Wu and K. Walda, *J. Am. Chem. Soc.*, 1993, **115**, 4808; E. Chiancone, R. Elber, W. E. Royer, Jr., R. Regan and Q. H. Gibson, *J. Biol. Chem.*, 1993, **268**, 5711; M. Hoshino, L. E. Laverman and P C. Ford, *Coord. Chem. Rev.*, 1999, **187**, 75.

9 L. E. Laverman, M. Hoshino and P. C. Ford, *J. Am. Chem. Soc.*, 1997, **119**, 12 663.

10 Laser flash photolysis experiments were performed using instrumentation described by D. R. Crane and P. C. Ford, *J. Am. Chem. Soc.*, 1991, **113**, 8510. Samples were prepared in 50 mM phosphate buffer at pH 7.0 in a specially designed cuvette and degassed by four freeze–pump–thaw cycles. Ferroheme complexes were prepared by addition of sodium dithionite to solutions of the respective Fe^{II} species under inert atmosphere. After degassing, the samples were allowed to equilibrate for >45 min at the desired P_{NO} and T before data collection. Rate constants were drawn from the averages of several kinetics traces.

11 This was done by using dithionite to trap NO spontaneously released from Fe^{II}(TPPS)(NO).

12 *Inorganic High Pressure Chemistry*, ed. R. van Eldik, Elsevier Science Publishers, Amsterdam, 1986; T. G. Traylor, J. Luo, J. A. Simon and P. C. Ford, *J. Am. Chem. Soc.*, 1992, **114**, 4340.

13 L. Leondiadis, M. Momenteau and A. Desbois, *Inorg. Chem.*, 1992, **31**, 4691.

14 T. Takano and R. E. Dickerson, *J. Mol. Biol.*, 1981, **153**, 79.

15 E. J. Rose and B. M. Hoffman, *J. Am. Chem. Soc.*, 1983, **105**, 2866.

16 E. F. Caldin, *Fast Reactions in Solution*, J. Wiley and Sons, New York, 1964, p. 12.

17 W. D. Turley and H. W. Offen, *J. Phys. Chem.*, 1984, **88**, 3605.

18 S. Glasstone, K. J. Laidler and H. Eyring, in *The Theory of Rate Processes*, ed. L. P. Hammett, McGraw Hill, New York and London, 1941, p. 225.

19 T. Malinski and C. Czuchajowski, in *Methods in Nitric Oxide Research*, ed. M. Feelish and J. S. Stamler, J. Wiley and Sons, Chichester, England, 1966, ch. 22 and references therein.

Communication 9/02725I

ChemComm

Stereoselective bromohydrin formation from β-hydroxy sulfoxides mediated by the pendant sulfoxide†‡

Sadagopan Raghavan,* M. Abdul Rasheed, Suju C. Joseph and A. Rajender

Organic Division I, Indian Institute of Chemical Technology, Hyderabad 500 007, India. E-mail: purush101@hotmail.com

Received (in Cambridge, UK) 2nd June 1999, Accepted 12th August 1999

Regio- and stereo-selective bromohydrin formation promoted by a neighbouring sulfinyl moiety is disclosed.

The development of new and efficient methods for regio- and stereo-selective synthesis of biologically active compounds is an active area of research.[1] Our interest in the synthesis of polyhydroxylated sulfoxides and sulfides, *e.g.* Mannostatin A and B, has focussed initially on the stereoselective introduction of chiral centres in appropriate acyclic precursors.

It is well-known that sulfoxides may participate as neighbouring groups in a number of reactions.[2] Sulfoxide group participation in halohydrin formation from cyclic[3] and simple acyclic olefins[4] has been demonstrated, but its potential to produce highly functionalised products with stereochemical control at two adjacent centres in substituted acyclic systems remains unexplored. Here we report the formation of bromohydrins from acyclic β-hydroxy-γ,δ-unsaturated sulfoxides (Scheme 1). The unsaturated β-hydroxy sulfoxide precursors shown in Table 1 were prepared as an epimeric mixture in equimolar proportion and good yield[5] by condensing the lithium anion of (*R*)-(+)-methyl *p*-tolyl sulfoxide[6] **1** with the appropriate aldehydes[7] **2** (Scheme 2). The isomeric hydroxy sulfoxides [(R_S, S_C) and (R_S, R_C)] were separated[8] by chromatography and their configuration assigned unambiguously by comparison of coupling constants for the protons directly bonded to the carbon in the β-hydroxy sulfoxide moiety.[9]

The unsaturated β-hydroxy sulfoxides were reacted with NBS and water in toluene at ambient temperature to afford the bromohydrins in moderate to high stereoselectivity in good yield. Use of solvents like THF, MeCN and CH_2Cl_2 were not satisfactory. The sulfoxide group was envisaged to function as a pendant nucleophile and attack the intermediate bromonium ion, resulting in formation of a cyclic sulfonium salt which could then be hydrolysed by water to afford the bromohydrin (Scheme 3).[4] It is well known that hydrolysis of sulfoxonium salts proceeds with clean inversion on sulfur. Hence in effect the configuration on sulfur would get inverted.[3,10]

As Table 1 indicates, the reaction is general for a variety of γ,δ-unsaturated sulfoxides. According to the literature precedent[11] the reaction of **6a** with NBS is expected to afford **7a** as the predominant product. Contrary to the above expectation the outcome was a 1 : 1 mixture of **7a** and **8a**. The phenyl group in

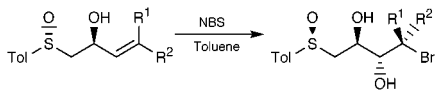

Scheme 1

Table 1 Regio- and stereo-selectivity of bromohydrin formation[a]

β-Hydroxy sulfoxide	Products: *Anti* (C-2/C-3)	Products: *Syn* (C-2/C-3)	Yield (%) (*anti* : *syn*)
3a $R^1 = R^2 = H$ **6a** $R^2 = H$, $R^1 = CH_2OTBDPS$	**4a** **7a**	**5a** **8a**	80 (<5:>95)[b] 82 (1:1)[c]
9a $R^2 = H$, $R^1 = Ph$ **12a** $R^1 = H$, $R^2 = Ph$	**10a** **13a**	**11a** **14a**	75 (2:1)[cd] 78 (1:2)[cd]
3b $R^1 = R^2 = H$ **6b** $R^2 = H$, $R^1 = CH_2OTBDPS$	**4b** **7b**	**5b** **8b**	75 (<5:>95)[b] 80 (2:3)[c]
9b $R^2 = H$, $R^1 = Ph$ **12b** $R^1 = H$, $R^2 = Ph$	**10b** **13b**	**11b** **14b**	75 (<5:>95)[bd] 85 (>95:<5)[b]

[a] All reactions were carried out on a 0.25 mmol reaction scale at a concentration of 0.20 M in toluene in the presence of 1.2 equiv. of NBS and 1.7 equiv. of H_2O. [b] Only one isomer was observed in the crude NMR spectrum of the product mixture. [c] Ratio of the isomers determined after separation of the isomers. [d] 10–25% of the product resulting from non-participation of the sulfinyl moiety also observed.

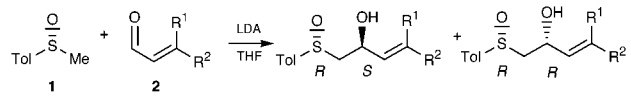

Scheme 2

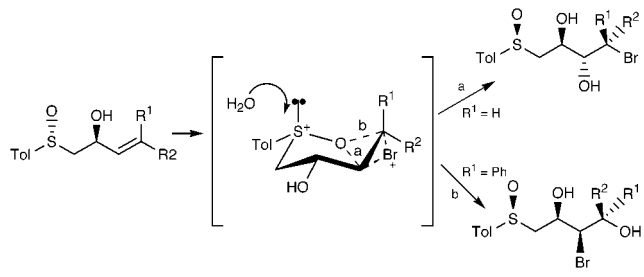

Scheme 3

† IICT Communication No. 4301.

‡ Experimental and spectral data for species described in this paper are available from the RSC web site, see http://www.rsc.org/suppdata/cc/1999/1845/

the sulfoxides **9a**, **9b**, **12a** and **12b** directs nucleophilic attack on the intermediate bromonium ions to C-4 to afford, regioselectively, products from 6-*endo* opening.[12] It is also apparent that the (R_S, R_C) isomers react to yield products more stereoselectively than the corresponding (R_S, S_C) isomers.

The stereochemical assignments were made by ^{13}C and ^{1}H NMR analysis of the spectra of the acetonides derived from the bromohydrins. The use of ^{13}C NMR data for acetonides of 1,3-diols and 1,2-diols for predicting their relative configurations has been reported by Rychnovsky and co-workers[13] and Dana and co-workers,[14] respectively. The coupling constants of protons on the carbon bearing the hydroxy and bromine in the six-membered ring acetonides reveal stereospecific *trans* addition to the double bond of **9** and **12**.[15] There are ample precedents for overall stereospecific *trans* addition to the double bond with respect to the olefin geometry in a similar reaction, *viz.* halolactonisation.[11] Similarly stereospecific *trans* addition to the double bond should be operative with **3** and **6** also. The sulfoxide group is known to deshield protons in which the S=O bond and the C–H bond are in a 1,3-parallel orientation.[16] The proton on C-2 of the acetonides derived from **5b**, **7b**, **8b**, **11b** and **13b** would occupy a 1,3-parallel orientation, while the proton on C-2 for the isomers **5a**, **7a**, **8a**, **11a** and **13a** would be almost orthogonal to the sulfoxide. A comparison of the chemical shifts for the protons on C-2 of the isomeric sulfoxides supports the configuration assigned to sulfur.

In conclusion, even though the product distribution often shows regio- and stereo-selectivity in a predictable way, striking anomalies are observed which underscore the influence of the sulfoxide group and its configuration on the outcome of the reaction. Experiments bearing on the mechanistic reasons for the observed stereoselectivity will be discussed in a later paper.

Notes and references

1 G. Helmchen, R. W. Hoffmann, J. Mulzer and E. Schaumann, *Stereoselective Synthesis, Houben-Weyl Methods of Organic Chemistry*, Georg Thieme Verlag, Stuttgart, 1996, Workbench Edition E 21, vols. 1–10.

2 K. Narasaka, Y. Ichikawa and H. Kubota, *Chem Lett*., 1987, 2139; *The Chemistry of Sulphones and Sulphoxides*, ed. S. Patai, Wiley, New York, 1988, pp. 345–346.

3 F. Montanari, R. Danieli, H. Hogeveen and G. Maccagnani, *Tetrahedron Lett*., 1964, 2685.

4 D. R. Dalton, V. P. Dutta and D. C. Jones, *J. Am. Chem. Soc*., 1968, **90**, 5468.

5 All new compounds gave satisfactory analytical and spectral data.

6 G. Solladie, J. Hull and A. Girardin, *Synthesis*, 1987, 173.

7 G. I. Tsuchihashi, S. Iriuchijima and M. Ishibashi, *Tetrahedron Lett*., 1972, 4605; N. Kunieda, M. Kinoshita and J. Nokami, *Chem Lett*., 1977, 289; D. R. Williams, J. G. Phillips, F. H. White and J. C. Huffman, *Tetrahedron*, 1986, **42**, 3003; S. G. Pyne and G. Boche, *J. Org. Chem*., 1989, **54**, 2663.

8 The β-hydroxy sulfoxides **3** and **12** were separated as their silyl ethers followed by cleavage with Bu_4NF.

9 M. C. Carreno, T. L. Garcia Ruano, A. M. Martin, C. Pedregal, J. H. Rodrigues, A. Rubio, J. Sanchez and G. Solladie, *J. Org. Chem*., 1990, **55**, 2120 and references cited therein; C. A. Kingsbury and R. A. Auerbach, *J. Org. Chem*., 1971, **36**, 1737.

10 A. D. Westwell, M. Thornton Pett and C. M. Rayner, *J. Chem. Soc., Perkin Trans. 1*, 1995, 847; B. M. Trost and M. Fray, *Tetrahedron Lett*., 1988, **29**, 2163.

11 A. R. Chamberlin, M. Dezube, P. Dussalt and M. C. McMills, *J. Am. Chem. Soc*., 1983, **105**, 5819.

12 M. M. Midland and R. L. Holtermann, *J. Org. Chem*., 1981, **46**, 1227 and references cited therein; G. Belluci, G. Berti, R. Bianchini, G. Ingrosso and E. Mastrorilli, *Gazz. Chim. Ital*., 1976, **106**, 955 and references cited therein.

13 S. D. Rychnovsky and D. J. Skalitzky, *Tetrahedron Lett*., 1990, **31**, 945.

14 G. Dana and H. Danechpajouh, *Bull. Soc. Chim. Fr*., 1980, 395.

15 For instance, the coupling constants for the protons H_a and H_b in **15** is 1.5 Hz, while in **16** it is 9.52 Hz.

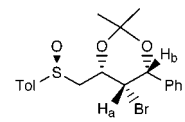

15

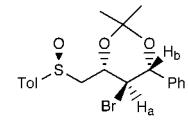

16

16 P. Sohar, *Nuclear Magnetic Resonance Spectroscopy*, CRC Press, Florida, 1983, vol. 1, p. 34; A. B. Foster, T. D. Inch, M. H. Qadir and J. M. Webber, *J. Chem. Soc., Chem. Commun*., 1968, 1086.

Communication 9/04420E

2-Propanephosphonic acid anhydride (T3P)-mediated segment coupling and head-to-tail cyclization of sterically hindered peptides

Jana Klose,[a] Michael Bienert,[a] Christoph Mollenkopf,[b] Detlef Wehle,[b] Chong-wu Zhang,[c] Louis A. Carpino[c] and Peter Henklein*[d]

[a] *Institute of Molecular Pharmacology, A.-Kowalke-Str. 4, 10315 Berlin, Germany*
[b] *Clariant GmbH, Frankfurt-Hoechst, Germany*
[c] *Department of Chemistry, University of Massachusetts, Amherst, MA 01003, USA*
[d] *Department of Biochemistry, Humboldt-University, Hessische Str. 3-4, 10115 Berlin, Germany. E-mail: peter.henklein@charite.de*

Received (in Liverpool, UK) 22nd June 1999, Accepted 3rd August 1999

In the course of comparing the effectiveness of an HOAt-derived coupling reagent (HAPyU) and a phosphonic acid-based condensation agent (T3P) by cyclization of model sequences, we found that T3P was a superior reagent with regard to conversion of the linear peptide into the stereochemically intact cyclic monomer when sterically hindered amino acids are found at the cyclization site.

Although the stepwise coupling of urethane-protected amino acids in peptide chemistry normally causes no problems with regard to loss of configuration at the reactive carboxy residue, head-to-tail cyclizations of short peptide chains having the all-L-configuration (*e.g.* penta- and hexa-peptides) or the corresponding segment condensation often remain problematic.[1c,2] For this reason, such systems represent good models for evaluating the usefulness of newly developed coupling methods. HOBt- and, more importantly, HOAt-derived coupling reagents,[3] have been evaluated and recommended as efficient tools for solving some of the most intractable problems such as reaction rate, degree of epimerization, and extent of oligomerization.[4]† Various authors have compared the efficiency of condensation reagents derived from HOBt (*e.g.* TBTU, HBTU), HOAt (*e.g.* HATU, HAPyU) and phosphoric and phosphonic acids (*e.g.* DPPA, T3P[5]) in cyclization reactions and have confirmed the superiority of the HOBt-[6] and, especially, HOAt-based reagents[4] with regard to these problems.

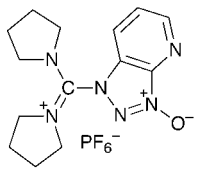

HAPyU

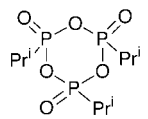
T3P

For peptide cyclization involving sterically hindered α,α-dialkyl- or *N*-methyl-amino acids at the *N*-terminal position there has been little systematic effort to uncover the important factors which influence the efficiency of the cyclization process. For loss of configuration during ordinary segment coupling it has long been known that increasing steric hindrance in the amino component correlates with increasing loss of configuration.[7] In the case of cyclization of the four possible linear precursors which lead to cyclo(Aib-Phe-D-Pro-Ala), only the isomer bearing N-terminal Ala gave the cyclopeptide in significant amount (44%).[8] The other three isomers cyclized in only trace amounts (2–3%), suggesting that factors other than steric effects at the N-terminal position are important. Although some investigators have deliberately avoided attempting cyclization at an N-Me amino acid, for example in the case of cyclosporin,[9] others have reported effective depsipeptide cyclization at N-terminal sites occupied by MeLeu (oxime ester, > 48%;[10] BOP-Cl, 87%[11]) or MeVal (acid chloride, 25%[12]). Since none of these previously reported systems involved the difficult all-L-configuration, the present study was initiated.

In the course of segment condensation studies leading to the ACP decapeptide (acyl carrier protein 74-65) one of us (P. H.) showed the effectiveness of 2-propanephosphonic acid anhydride (T3P) as a condensation reagent. This result, along with Wenger's demonstration[9] that T3P and the BOP reagent were equally effective in the cyclosporin case (65% cyclization), led to a reexamination of the T3P reagent in segment condensations and head-to-tail cyclizations of all-L-pentapeptides, especially those bearing sterically hindered amino acids at the cyclization site. Whereas comparison of HAPyU, a reagent which we had previously shown to be one of the most effective coupling reagents for peptide cyclization,[4] and T3P in ordinary [2 + 1] segment condensations in the presence of Pr^i_2NEt for the model tripeptide Z-Phe-Val-Pro-NH_2 showed far more epimerization for the T3P case (29.7 *vs.* 10.8%) along with a lower yield (58.6 *vs.* 88.8%), upon substitution of the more hindered H-Aib-NH_2 for H-Pro-NH_2 the loss of configuration for T3P, while significant, was substantially less than for HAPyU (14.6 *vs.* 41.1%) (Table 3).‡ However, under the normal conditions for HAPyU reactions, the T3P reaction was extremely slow.

In order to evaluate the cyclization utility of T3P, we studied the ring closure of several linear pentapeptides (model peptides **1**, **4**–**7** and thymopoietin-derived sequences **2** and **3**) by analytical HPLC using T3P and HAPyU as condensation reagents. For pentapeptide **1** optimization studies were carried out with T3P under various reaction conditions (temperature,

1 AANMeAAA
2 R(Ac)KAVY [SP5]
3 R(Ac)K(Hmb)AVY [(Hmb)Ala[3]-SP5]
4 AibAAAA
5 (*N*-Me)AAAAA
6 (*N*-Me)FAAAA
7 (Tmob)AAAAA

Table 1 AA(*N*-Me)AAA cyclization in DMF (after 24 h reaction)

Entry	Coupling reagent	P:B:CR[a]	Yield (%) all-L-CM[b]	AA(*N*-Me)-AAa CM[b]	all-L-CD[c]
1	HAPyU	1:3:1.1	55	1.6	33
2	T3P	1:6:5	70	2.9	5
3[d]	T3P	1:6:5	65	2.2	10
4	T3P	1:6:1.5	73	9.3	7
5	T3P	1:3:1.5	66	10	8
6[e]	T3P	1:6:5	52	5.9	16

[a] P = linear peptide, B = base (Pr^i_2NEt), CR = coupling reagent; 10^{-3} M. [b] Cyclic monomer. [c] Cyclic dimer. [d] Temperature at the beginning of the reaction = 0 °C. [e] 10^{-2} M.

Table 2 Cyclization of N-terminally sterically hindered peptides in DMF

	Yield (%) after 80 h			
	HAPyU cyclization[a]		T3P cyclization[b]	
Sequence	all-L-CM[c]	epimerized CM[c,d]	all-L-CM[c]	epimerised CM[c,d,e]
AibAAAA	22	64	38	2
(*N*-Me)AAAAA	4	69	24	5
(*N*-Me)FAAAA	1	87	15	6
(Tmob)AAAAA	13	59	6	22

[a] For conditions, see Table 1, entry 1. [b] For conditions, see Table 1, entry 2. [c] Cyclic monomer. [d] Due to C-terminal epimerisation of the all-L precursor during reaction. [e] After 80 h, 40–60% linear peptide (both epimerized and unepimerized) was still detectable.

concentration, excess of reagent and base) and the results compared with the best results previously obtained with HAPyU. In the case of all peptides which lack a sterically demanding amino acid in the N-terminal position (Table 1), differences between T3P- and HAPyU-mediated reactions are not significant, although for the cyclization of AA(*N*-Me)AAA at 10^{-3} M concentration, regardless of reaction conditions, T3P gives a higher yield of the all-L-cyclic monomer than the corresponding HAPyU reagent (Table 1). Under the best conditions T3P led to a level of epimerization (2.2%) which is only slightly higher than that observed with HAPyU (1.6%). For the T3P case, the degree of epimerization appears to depend more on the excess of condensation reagent and concentration rather than an excess of base (Table 1). The rate of T3P-mediated cyclization is comparable to that previously observed for HAPyU; after approximately 2 min the reaction is about 90% complete in all cases. In accordance with previous results for HAPyU (J. Klose, unpublished) T3P-induced cyclization at lower temperatures leads to significantly enhanced cyclodimerization (Table 1). The cases of SP5 and (Hmb)Ala[3]-SP5 are very similar for the two activators in that comparable amounts of all-L-cyclic monomer are formed with T3P leading to somewhat less epimerization (data not shown). In all three cases significantly larger amounts of the undesired all-L-cyclodimer is formed for the HAPyU system.

Whereas for these cyclization reactions involving relatively unhindered amino acids no clear superiority of T3P can be shown, the situation is drastically different in the case of cyclization *via* peptide bond formation at a sterically hindered amino acid (Table 2). Here, HAPyU-mediated cyclization yields almost exclusively the C-terminally epimerized cyclic monomer (59–87%).§ In contrast, T3P-promoted reactions yield the desired all-L-cyclic monomer as the major product, even though the overall yield of cyclic product is not high due to the sluggishness of the reaction, which was allowed to proceed for 80 h. Even at that point cyclization was incomplete. As expected, the tendency to give the all-L-cyclic monomer is lower the more hindered is the N-terminal substituent (increasing from **4** to **7**) and formation of all-L-cyclic product fails almost completely for the sterically most demanding Tmob-residue. The differences observed with regard to C-terminal stereomutation are reminiscent of the differences seen in comparison of HBTU and HAPyU or HATU, where the former leads to extensive C-terminal epimerization.[2,4]

In summary, the data presented show that T3P is at least as effective as HAPyU in the relatively demanding cyclization of all-L-pentapeptides, and remarkably more efficient for systems having a sterically hindered amino acid, such as Aib, (*N*-Me)Ala and (*N*-Me)Phe, at the cyclization site. Whereas the HAPyU-promoted cyclization yields the C-terminally epimerized product almost exclusively, the use of T3P gives the stereo-retained cyclic monomer as the main product, albeit in rather low yield.

Table 3 [2 + 1] Segment condensation of Z-Phe-Val-Aib-NH_2[a]

Coupling reagent (equiv.)	Base (equiv.)	Residue yield[b] (%)	LD (%)[c]	Yield of LL-, LD-tripeptide[d] (%)
HATU (1)	Pri_2NEt (2)	82.9	40.3	100
HATU (1)	TMP (2)	74.6	31.0	100
HATU (1)[e]	Pri_2NEt (2)	95.2	41.5 (LL)	100
HAPyU (1.1)	Pri_2NEt (3)	82.2	41.1	100
HAPyU (1.1)	TMP (3)	74.6	34.0	100
T3P (5)[f]	Pri_2NEt (6)	34.8	14.6	5.3
T3P (5)[f]	TMP (6)	33.3	13.1	3.1
T3P (5)[g]	Pri_2NEt (6)	48.1	22.3	3.2
T3P (5)[g]	TMP (6)	43.1	16.6	7.0
T3P (5)[f]	DMAP (6)	54.7	11.6	4.9

[a] Test couplings were carried out by adding the base to a stirred and ice-cooled solution of Z-Phe-Val-OH, H-Aib-NH_2 and the coupling reagent (each 1 equiv., 0.125 M in DMF). The mixture was stirred at 0 °C for 1 h at room temperature overnight. Work-up was carried out as described in L. A. Carpino, D. Ionescu and A. El-Faham, *J. Org. Chem.*, 1996, **61**, 2463, Table 1, footnote *a*. [b] Calculated based on the weight of the crude product. [c] Pure LL or LD peptides were co-injected onto HPLC to determine epimerization by comparison of retention times. [d] Calculated based on integration of the LL- and LD-tripeptide peaks relative to all other HPLC peaks. [e] Z-Phe-D-Val-OH was used in this case. [f] 24 h reaction time. [g] 90 h reaction time.

Notes and references

† Abbreviations: Aib = aminoisobutyric acid; DPPA = diphenylphosphoryl azide; HAPyU = 1-[3-oxido-1*H*-1,2,3-triazolo[4,5-*b*]pyridin-3-ium-1-yl(pyrrolidin-1-yl)methylene]pyrrolidinium hexafluorophosphate; HATU = *N*-[3-oxido-1*H*-1,2,3-triazolo[4,5-*b*]pyridin-3-ium-1-yl(dimethylamino)methylene]-*N*-methylmethanaminium hexafluorophosphate; HBTU = *N*-[3-oxido-1*H*-benzotriazol-3-ium-1-yl(dimethylamino)methylene]-*N*-methylmethanaminium hexafluorophosphate; Hmb = 2-hydroxy-4-methoxybenzyl; HOAt = 1-hydroxy-7-azabenzotriazole; HOBt = 1-hydroxybenzotriazole; TBTU = *N*-[3-oxido-1*H*-benzotriazol-3-ium-1-yl-(dimethylamino)methylene]-*N*-methylmethanaminium tetrafluoroborate; Tmob = 2,4,6-trimethoxybenzyl; TMP = 2,4,6-trimethylpyridine; T3P = PPA = 2-propanephosphonic acid anhydride.

‡ Segment condensations were performed as outlined in Table 3.

§ Generally, the amount of C-terminal epimerization was determined by analytical HPLC (cyclization of the authentic C-terminally D-Ala-containing analogues was carried out to give the authentic D-Ala cyclomonomers for establishment of the HPLC retention times) and examination of the products by ES-MS.

1 F. Albericio and L. A. Carpino, *Methods Enzymol.*, 1997, **289**, 104; M. Bodanszky, *Pept. Res.*, 1992, **5**, 134.
2 H. Kessler and B. Haase, *Int. J. Pept. Protein Res.*, 1992, **39**, 36; J. Dale, *Angew. Chem.*, 1966, **78**, 1070.
3 L. A. Carpino, A. El-Faham, C. A. Minor and F. Albericio, *J. Chem. Soc., Chem. Commun.*, 1994, 201; L. A. Carpino, *J. Am. Chem. Soc.*, 1993, **115**, 4397.
4 A. Ehrlich, H.-U. Heyne, R. Winter, M. Beyermann, H. Haber, L. A. Carpino and M. Bienert, *J. Org. Chem.*, 1996, **61**, 8831; K. J. Hale and J. Cai, *Chem. Commun.*, 1997, 2319.
5 H. Wissmann and H.-J. Kleiner, *Angew. Chem., Int. Ed. Engl.*, 1980, **19**, 133; P. Henklein and Ch. Mollenkopf, DE 19824449.5 A1, 1998.
6 S. Feiertag, K.-H. Wiesmüller, G. J. Nicholson and G. Jung, *Pept. 1996, Proc. Eur. Pept. Symp. 24th*, 1998, 157; K. J. Hale, C. Cai and G. Williams, *Synlett*, 1998, 149.
7 L.-A. Carpino, M. Beyermann, H. Wenschuh and M. Bienert, *Acc. Chem. Res.*, 1996, **29**, 268 (footnote 53).
8 J. Pastuszak, J. H. Gardner, J. Singh and D. H. Rich, *J. Org. Chem.*, 1982, **47**, 2982.
9 R. M. Wenger, *Helv. Chem. Acta*, 1984, **67**, 502.
10 B. H. Lee, *Tetrahedron Lett.*, 1997, **38**, 757.
11 J. Scherkenbeck, A. Plant and N. Mencke, *Tetrahedron*, 1995, **51**, 8459.
12 G. Losse and H. Raue, *Chem. Ber.*, 1968, **101**, 1532.

Communication 9/05021C

A coordination polymer based on twofold interpenetrating three-dimensional four-connected nets of 4^26^38 topology, [CuSCN(bpa)] [bpa = 1,2-bis(4-pyridyl)ethane]†

Quan-Ming Wang, Guo-Cong Guo and Thomas C. W. Mak*

Department of Chemistry, The Chinese University of Hong Kong, Shatin, New territories, Hong Kong SAR, P.R. China. E-mail: tcwmak@cuhk.edu.hk

Received (in Cambridge, UK) 24th June 1999, Accepted 17th August 1999

The novel coordination polymer [CuSCN(bpa)] [bpa = 1,2-bis(4-pyridyl)ethane] consists of two interpenetrating three-dimensional four-connected frameworks of rare 4^26^38 topology, each being constructed from the cross-linkage of infinite zigzag $[(CuSCN)_2]_\infty$ chains by bpa ligands.

The construction of coordination networks with different topological characteristics has received significant recent attention.[1] One of the rational synthetic strategies is to bind symmetrically different metal centers with bi- or multi-dentate ligands. A variety of infinitely extended frameworks, in particular those involving interpenetration,[2] have been designed on the basis of the unifying concept of a net, as elaborated by Wells over two decades ago.[3] The majority of interpenetrating 3D four-connected nets are constructed of tetrahedral or square-planar nodes. From the topological point of view, these four-connected nets can be classified as (i) diamond-related nets of 6^6 topology (all tetrahedral centers); (ii) quartz-like nets of 6^48^2-b topology or NbO-like nets of 6^48^2-a topology (all square-planar centers) and (iii) PtS-like 4^28^4 nets (equal numbers of square-planar and tetrahedral centers).[2,4] Additionally, two new types of four-connected nets of 6^58 and 7^59 topologies have been recently reported in the compounds $[Cu(bpa)_2(NO_3)_2]_n$[5] [bpa = 1,2-bis(4-pyridyl)ethane] and $[\{Cu(bpethy)_2(H_2O)_2\}\{Cu(bpethy)_2(NO_3)(H_2O)\}_2](NO_3)_4\cdot bpethy\cdot 1.33H_2O$[6] [bpethy = 1,2-bis(4-pyridyl)ethyne], respectively. Furthermore, two structures of 4^26^38-a type ($SrAl_2$-like) have been found in $[Cu(AcTCNE)]\cdot Me_2CO$[7] (AcTCNE = 1,1,2,2-tetracyanopentan-4-on-1-ide) and $[Ag(sebn)_2](PF_6)$[8] (sebn = 1,10-decanedinitrile) by Carlucci *et al*.

By combining flexible organic ligands with an uncharged inorganic motif containing a bifunctional polyatomic anion of suitable length, such as CuSCN or CuN_3, we hope to generate porous 3D coordination networks that may display varying degrees of interpenetration. Interestingly, our attempt to incorporate the bpa ligand into CuSCN resulted in a non-diamond 3D coordination polymer [CuSCN(bpa)] **1**, despite the fact that most Cu(I) coordination polymers exhibit diamond structures as this d^{10} ion naturally fulfills the role of a tetrahedral node.[9] To our knowledge, the doubly interpenetrating frameworks of unusual 4^26^38 topology in the present coordination polymer is unprecedented.

The hydrothermal reaction of CuSCN and bpa in molar ratio 1:1 at 180 °C leads to the formation of red air-stable compound **1**.‡ Single crystal X-ray analysis§ has revealed that **1** contains two interpenetating 3D nets, each individual framework being constructed from the building unit shown in Fig. 1. The Cu(1) and Cu(2) atoms are each located in a severely distorted tetrahedral environment, being coordinated by two N atoms of different bpa ligands, one thiocyanato S atom and one N atom of another thiocyanate ligand, with bond angles in the range 102.9(2)–118.9(2) and 97.6(2)–117.1(1)° at Cu(1) and Cu(2), respectively.

† Dedicated to the memory of Dr James C. N. Ma (1927–1999).

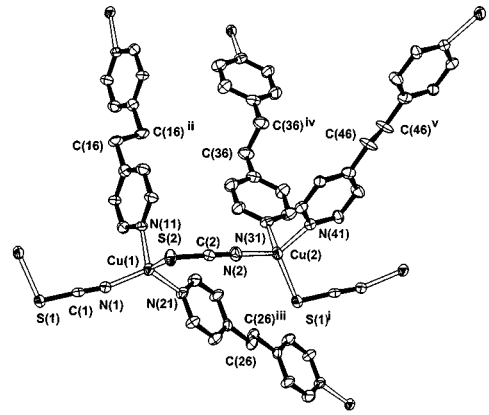

Fig. 1 The local coordination environments of Cu(I) ions in **1**; atoms are shown as 30% thermal ellipsoids. All four independent bpa ligands are located at inversion centers. Selected bond distances (Å) and angles (°): Cu(1)–N(1) 1.949(5), Cu(1)–N(21) 2.044(4), Cu(1)–N(11) 2.128(4), Cu(1)–S(2) 2.330(2), Cu(2)–N(2) 1.964(5), Cu(2)–N(41) 2.088(4), Cu(2)–N(31) 2.117(4), Cu(2)–S(1)^i 2.296(2); N(1)–Cu(1)–N(21) 118.9(2), N(1)–Cu(1)–N(11) 102.9(2), N(21)–Cu(1)–N(11) 104.8(2), N(1)–Cu(1)–S(2) 112.2(1), N(21)–Cu(1)–S(2) 108.7(1), N(11)–Cu(1)–S(2) 108.5(1), N(2)–Cu(2)–N(41) 111.1(2), N(2)–Cu(2)–N(31) 100.6(2), N(41)–Cu(2)–N(31) 97.6(2), N(2)–Cu(2)–S(1)^i, 117.1(1), N(41)–Cu(2)–S(1)^i 114.7(1), N(31)–Cu(2)–S(1)^i 113.2(1). Symmetry codes: i $x+1, y, z$; ii $-x-1, -y+1, -z+1$; iii $-x, -y, -z+1$; iv $-x, -y+1, -z+1$; v $-x+1, -y+1, -z+2$.

As shown in Fig. 2, the independent SCN^- ligands bridge Cu(1) and Cu(2) alternately to form a zigzag $[(CuSCN)_2]_\infty$ chain running parallel to the *a* direction, with bond angles Cu(1)–S(2)–C(2) 99.7(2)°, Cu(1)–N(1)–C(1) 168.1(4)° and Cu(2)–S(1)^i–C(1)^i 102.4(2)°, Cu(2)–N(2)–C(2) 167.1(4)°. Such chains are inter-connected through two bpa ligands (N21 and

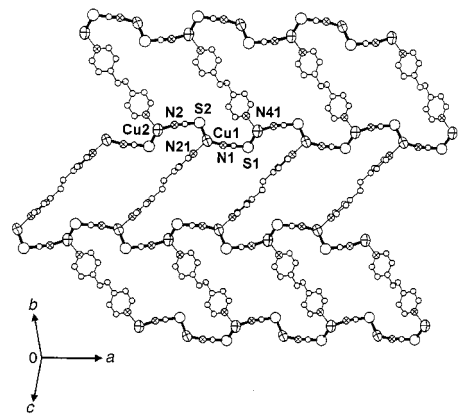

Fig. 2 A two-dimensional brick-like 6^3 network viewed along the [011] direction. Filled bonds represent $[(CuSCN)_2]_\infty$ zigzag chains running parallel to the *a* axis. The pyridyl planes of bpa N(21) and bpa N(41) make a dihedral angle of 112.7°.

N41) that bridge copper centers to generate a 2D brick-like network, which is similar to the brick-wall patterns previously reported in two-dimensional coordination compounds.[10] The pyridyl planes of bpa N21 and bpa N41 make a dihedral angle of 112.7°. Neighboring networks are further linked by the remaining bpa ligands (N11 and N31) to form a 3D framework. The dihedral angle between the pyridyl planes of bpa N11 and bpa N31 is 99.2°.

The 2D networks of 6^3 topology are stacked in an ABAB… sequence, and the mode of their linkage to build up a 3D framework is illustrated schematically in Fig. 3. It can be seen that there are three kinds of shortest circuits around every four-connected node: two 4-gons, three 6-gons and one 8-gon. Each of the resulting channels, which lie horizontally in Fig. 3, has a 10-vertex ring at its boundary. In contrast, the 6^3 nets in the $SrAl_2$-type network stack directly on top of one another so that an 8-vertex ring constitutes the boundary of each channel.[7,8]

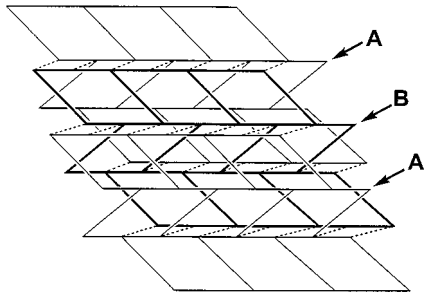

Fig. 3 Schematic representation showing the topology of a $4^2 6^3 8$ 3D network. The copper(I) ions are located at the nodes. Horizontal lines represent SCN^- ligands, inclined lines indicate bpa N(21) and N(41) ligands, and dashed lines indicate the bpa N(11) and N(31) ligands that form bridges between the 2D brick-like networks of 6^3 topology. A perspective view of a stack of three 2D networks is shown: the middle layer B (thick lines) is sandwiched between two type A layers (thin lines), and two adjacent layers are related by the translation vector ($\boldsymbol{a} + \boldsymbol{c}$).

Two 3D frameworks interpenetrate to form the crystal structure of **1**. The overall structure can alternatively be regarded as two identical 2D brick networks that interpenetrate in an inclined way, with the bridging bpa ligands (N11 and N31) occupying the voids.

The thiocyaniate ligands function as linking rods to bridge copper(I) centers to make the coordination framework of **1** a neutral one, in contrast to many common examples that are charged.[11] Several neutral Cu(I) coordination polymers have been synthesized by solution methods, for example [Cu(4,4′-bpy)Cl][12] and $[Cu_2(SCN)_2(pyz)]$ (pyz = pyrazine).[13] However, their structures are very different from **1**, as [Cu(4,4′-bpy)Cl] is built of two-fold interpenetrating 2D networks and $[Cu_2(SCN)_2(pyz)]$ has a non-interpenetrating structure. The formation of 3D frameworks depends on not only the coordination geometry at the metal centers but also the nature of the anions and the bridging ligands. In the case of **1**, the presence of four independent, centrosymmetric bpa ligands is responsible for generating the unusual framework structure.

In contrast to the extensively studied rigid ligand 4,4′-bipyridine, the flexible ligand bpa has recently attracted the interest of chemists.[5,14] The less exploited bpa ligand can adopt *gauche* and *anti* conformations, and this conformational freedom can even engender supramolecular isomerism in coordination polymers.[15] Since all four independent bpa ligands in **1** occupy $\bar{1}$ sites and exhibit the *anti* conformation, it is conceivable that other isomers may be generated in a Cu(I) system containing all *gauche* or mixed *gauche/anti* bpa ligands. Further investigation of neutral metal complexes of bpa is in progress.

This work is supported by Hong Kong Research Grants Council Earmarked Grant CUHK 4179/97P and Direct Grant A/C 2060129 of The Chinese University of Hong Kong.

Notes and references

‡ *Synthesis*: CuSCN (61 mg, 0.5 mmol), bpa (92 mg, 0.5 mmol) and 2 mL distilled water were placed in a thick-walled Pyrex tube of *ca*. 6 mL capacity, and then the mixture was frozen in liquid nitrogen. The tube was subsequently flame-sealed under vacuum and kept in a furnace at 180 °C for 24 h, and then cooled to 60 °C at 6 °C h^{-1}. From the brown powdery bulk residue, red block-like crystals of [CuSCN(bpa)] **1** were isolated in *ca.* 10% yield and washed with water. IR (KBr pellet)/cm^{-1}: 2102.9s, 2091.4s, 1605.0s, 1418.0s, 1007.6m, 825.7s, 820.7s, 761.1m, 548.1m, 535.0m. The IR spectrum of the brown powder is similar to that of **1**, except that a single peak at 2103.9 cm^{-1} appears at the position of the doublet in the spectrum of **1**. This suggests that the brown powder is a different product containing a simpler SCN^- bridging mode. Both red crystals of **1** and the brown powder are insoluble in water, MeCN and DMF.

§ *Crystal data*: [CuSCN(bpa)] **1**, $C_{13}H_{12}CuN_3S$, M = 305.86, monoclinic, space group $P2_1/c$ (no. 14), a = 10.782(2), b = 17.348(2), c = 14.084(2) Å, β = 97.405(3)°, V = 2612.4(6) Å^3, Z = 8, D_c = 1.555 Mg m^{-3}, $F(000)$ = 1248, μ(Mo-Kα) = 1.815 mm^{-1}. 11977 reflections measured, 5941 unique (R_{int} = 0.0886), final $R1$ = 0.0417, $wR2$ = 0.0759 for 2215 independent reflections [$I > 2\sigma(I)$]. Data collection was performed at 293 K on a Bruker SMART 1000 CCD diffractometer using frames of oscillation range 0.3°, with $2 < \theta < 27.5°$. CCDC 182/1379. See http://www.rsc.org/suppdata/cc/1999/1849/ for crystallographic files in .cif format.

1 R. Robson, B. F. Abrahams, S. R. Batten, R. W. Gable, B. F. Hoskins and J. Liu, in *Supramolecular Architecture*, ed. T. Bein, American Chemical Society, Washington DC, ch. 19, 1992; M. Munakata, L. P. Wu and T. Kuroda-Sowa, *Adv. Inorg. Chem.*, 1999, **46**, 173; A. J. Blake, N. R. Champness, P. Hubberstey, W.-S. Li, M. A. Withersby and M. Schröder, *Coord. Chem. Rev*. 1999, **183**, 117.

2 S. R. Batten and R. Robson, *Angew. Chem., Int. Ed*., 1998, **37**, 1460.

3 A. F. Wells, *Three-Dimensional Nets and Polyhedra*, Wiley, New York, 1977; A. F. Wells, *Further Studies of Three-Dimensional Nets*, ACA Monograph No. 8, American Crystallographic Association, 1979.

4 B. F. Abrahams, B. F. Hoskins, D. M. Michail and R. Robson, *Nature* (*London*), 1994, **369**, 727.

5 K. N. Power, T. L. Lennigar and M. J. Zaworotko, *Chem. Commun*., 1998, 595.

6 L. Carlucci, G. Ciani, P. Macchi and D. M. Proserpio, *Chem. Commun.*, 1998, 1837.

7 L. Carlucci, G. Ciani, D. M. Proserpio and A. Sironi, *Angew. Chem., Int. Ed. Engl*., 1996, **35**, 1088.

8 L. Carlucci, G. Ciani, P. Macchi, D. M. Proserpio and S. Rizzato, *Chem. Eur. J*. 1999, **5**, 237.

9 See, *e.g*. B. F. Hoskins and R. Robson, *J. Am. Chem. Soc*., 1990, **112**, 1546; L. R. MacGillivray, S. Subramanian and M. J. Zaworotko, *J. Chem. Soc., Chem. Commun*., 1994, 1325; M. Munakata, L. P. Wu, M. Yamamoto, T. Kuroda-Sowa and M. Maekawa, *J. Am. Chem. Soc.*, 1996, **118**, 3117; L. Carlucci, G. Ciani, D. M. Proserpio and A. Sironi, *J. Chem. Soc., Chem. Commun.*, 1994, 2755; A. J. Blake, N. R. Champness, S. S. M. Chung, W.-S. Li and M. Schröder, *Chem. Commun*., 1997, 1005; S. Lopez, M. Kahraman, M. Harmata and S. W. Keller, *Inorg. Chem*., 1997, **36**, 6138.

10 M. Fujita, Y. J. Kwon, O. Sasaki, K. Yamaguchi and K. Ogura, *J. Am. Chem. Soc.*, 1995, **117**, 7287; L. Carlucci, G. Ciani and D. M. Proserpio, *New J. Chem.*, 1998, 1319.

11 See, *e.g*. B. F. Abrahams, S. R. Batten, M. J. Grannas, H. Hamit, B. F. Hoskins and R. Robson, *Angew. Chem., Int. Ed.*, 1999, **38**, 1475; A. J. Blake, N. R. Champness, A. N. Khlobystov, D. A. Lemenovskii, W.-S. Li and M. Schröder, *Chem. Commun*., 1997, 2027; O. M. Yaghi, H. Li and M. O'Keeffe, *Mater. Res. Soc. Symp. Proc.*, 1997, **453**, 127.

12 O. M. Yaghi and G. Li, *Angew. Chem., Int. Ed. Engl*., 1995, **34**, 207.

13 A. J. Blake, N. R. Champness, M. Crew, L. R. Hanton, S. Parsons and M. Schröder, *J. Chem. Soc., Dalton Trans*., 1998, 1533; A. J. Blake, N. R. Brooks, N. R. Champness, L. R. Hanton, P. Hubberstey and M. Schröder, *Pure Appl. Chem.*, 1998, **70**, 2351.

14 M. Fujita, Y. J. Kwon, M. Miyazawa and K. Ogura, *J. Chem. Soc., Chem. Commun.*, 1994, 1977; C. S. Hong and Y. Do, *Inorg. Chem.*, 1998, **37**, 4470; D. Rochon, M. Andruh and R. Melanson, *Can. J. Chem.*, 1998, **76**, 1564; C. V. K. Sharma and R. D. Rogers, *Chem. Commun*., 1999, 83; M. L. Hernández, M. G. Barandika, M. K. Urtiaga, R. Cortés, L. Lezama, M. I. Arriortua and T. Rojo, *J. Chem. Soc., Dalton Trans.*, 1999, 1401.

15 T. L. Hennigar, D. C. MacQuarrie, P. Losier, R. D. Rogers and M. J. Zaworotko, *Angew. Chem., Int. Ed. Engl.*, 1997, **36**, 972.

Communication 9/05085J

ChemComm

A colourimetric calix[4]pyrrole–4-nitrophenolate based anion sensor†

Philip A. Gale,*[ab] Lance J. Twyman,*[c] Cristin I. Handlin[c] and Jonathan L. Sessler[d]

[a] *Department of Chemistry, University of Southampton, Southampton, UK SO17 1BJ. E-mail: philip.gale@soton.ac.uk*
[b] *Department of Chemistry, University of Oxford, Inorganic Chemistry Laboratory, South Parks Road, Oxford, UK OX1 3QR*
[c] *The Polymer Centre, School of Physics and Chemistry, University of Lancaster, Lancaster, UK LA1 4YA. E-mail: l.twyman@lancaster.ac.uk*
[d] *Department of Chemistry and Biochemistry, The University of Texas at Austin, Austin, Texas 78712-1167, USA*

Received (in Cambridge, UK) 15th July 1999, Accepted 19th August 1999

The intense yellow colour of the 4-nitrophenolate anion 2, in MeCN or CH_2Cl_2 solution, dissipates upon complex formation with *meso*-octamethylcalix[4]pyrrole 1; the complex may be used as a colourimetric sensor for halide anions, such as fluoride, that displace the phenolate anion thereby restoring the yellow colour, characteristic of free 4-nitrophenolate anion, to solutions containing 1, 2 and the anion in question.

The coordination chemistry of anions continues to attract increasing interest from the supramolecular chemistry community.[1–4] This is due, in no small part, to the crucial roles anions play in biological processes,[5,6] medicine,[7] catalysis[8] and molecular assembly.[9] Additionally various pollutant anions, such as pertechnetate, are believed to have deleterious effects on the environment.[10] Redox or photoactive sensor molecules have been developed that coordinate to anions and report their presence *via* changes in the physical properties of the host (such as redox potential, fluorescence or phosphorescence).[11,12] Another approach to anion detection, pioneered by Anslyn and co-workers, is the displacement assay (*i.e.* a host–anion complex that dissociates in the presence of other anions, triggering a change in the properties of the system).[13] Chemical systems that respond to the presence of anions by a colour change detectable *by eye* are extremely rare.[14] Colourimetric sensors do not require the use of a potentiostat or spectrometer to detect redox or optical perturbations and therefore have considerable advantages over other molecular sensors.[15] Here we report the formation of a new colourimetric displacement assay that is selective for halide anions over other putative anionic guest species and is extremely easy and inexpensive to make.

In 1996, we discovered that calix[4]pyrroles (*meso*-octalkylporphyrinogens), a class of molecule known for over a hundred years, can coordinate to anions such as fluoride, chloride and dihydrogen phosphate *via* the formation of pyrrole NH··· anion hydrogen bonds.[16] *meso*-Octamethylcalix[4]pyrrole **1** is particularly easy to make and can be synthesised in high yield by the acid catalysed reaction of pyrrole with acetone.[17] We decided to investigate whether the formation of a calixpyrrole–anion complex with a coloured species such as 4-nitrophenolate anion **2** would perturb the electronic properties of the anion sufficiently to produce a colour change that could be used as the basis for a colourimetric displacement assay.

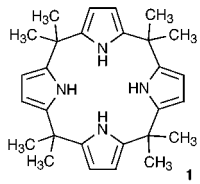

1

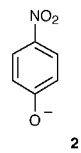

2

Initial complexation studies were conducted using ^{1}H NMR titration techniques. Aliquots of tetrabutylammonium 4-nitrophenolate[18] (0.1 mol dm^{-3}) were added to a solution of compound **1** (0.01 mol dm^{-3}) in CD_2Cl_2 and the chemical shift of the calix[4]pyrrole NH proton noted after each addition. A significant downfield shift (from δ 7.0 to 10.6) of the pyrrole NH proton was observed upon the addition of 5 equiv. of tetrabutylammonium 4-nitrophenolate, consistent with the formation of calixpyrrole–phenolate hydrogen bonds. Analysis of the titration data using the EQNMR computer program[19] revealed that *meso*-octamethylcalix[4]pyrrole forms a 1:1 complex with 4-nitrophenolate with a stability constant of 290 (± 9.7) dm^3 mol^{-1}. Previous experiments showed that fluoride and chloride bind to compound **1** with stability constants of 17 200 and 350 dm^3 mol^{-1}, respectively, under the same conditions whilst the **1**·$H_2PO_4^-$ complex has a stability constant of 97 dm^3 mol^{-1}.[16] Competition experiments with fluoride, chloride and dihydrogenphosphate anions were then conducted. A CD_2Cl_2 solution of the complex **1·2** was prepared and aliquots of tetrabutylammonium salts of the anions added. After an initial addition of 0.2 equiv. of fluoride, the NH proton resonance broadened and could not be located in the NMR spectrum. Only after addition of 1.0 equiv. of fluoride did the NH resonance reappear, further shifted downfield by over 3 ppm as compared to **1·2**, indicating the formation of a calixpyrrole–fluoride complex. In contrast, tetrabutylammonium chloride and dihydrogenphosphate produced much smaller downfield shifts of 0.78 and 0.37 ppm, respectively, upon addition of 1.0 equiv. of the anion salt.

The colourimetric properties of this complex were then studied using UV/Vis spectroscopic techniques. Addition of calix[4]pyrrole **1** (5×10^{-2} mol dm^{-3}) to a solution of tetrabutylammonium 4-nitrophenolate **2** (3.6×10^{-5} mol dm^{-3}) in CH_2Cl_2 at 25 °C caused a significant decrease in intensity of the so-called '200 nm band' at 432 nm (Fig. 1).[20]

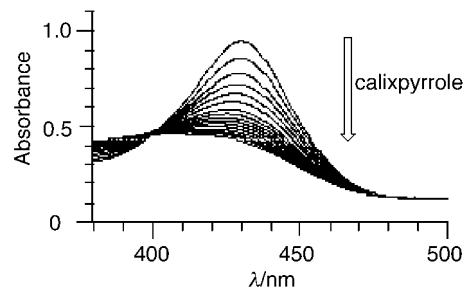

Fig. 1 Decreasing absorbance of the 4-nitrophenolate anion **2** (3.6×10^{-5} mol dm^{-3}) upon addition of calixpyrrole **1** (5×10^{-2} mol dm^{-3}) in CH_2Cl_2 at 25 °C.

† A colour picture illustrating the dissipation and reappearance of the 4-nitrophenolate yellow colour together with NMR/UV/vis titration data are available from the RSC web site, see http://www.rsc.org/suppdata/cc/1999/1851/

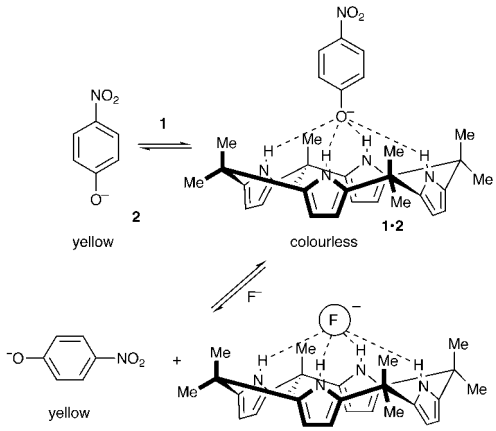

Scheme 1

Table 1 Relative absorbance values for calixpyrrole–4-nitrophenolate solutions containing equimolar concentrations of various anions.[a] Since the signal being observed is due to liberated 4-nitrophenolate anion, the larger the relative absorbance, the stronger the binding (all anions were used as their tetrabutylammonium salts)

	F^-	Cl^-	$H_2PO_4^-$	Br^-	HSO_4^-
ΔAbsorbance[b]	0.282	0.193	0.162	0.092	0.015
Relative absorbance[c]	1.0	0.68	0.57	0.33	0.05

[a] *meso*-Octamethylcalix[4]pyrrole was added to a solution of tetrabutylammonium 4-nitrophenolate (6.0×10^{-6} mol dm^{-3}) in MeCN, affording a solution that was 5.0×10^{-4} mol dm^{-3} in calixpyrrole. Solutions of tetrabutylammonium fluoride, chloride, dihydrogenphosphate, hydrogensulfate and bromide were prepared using this stock solution such that the anion concentration was 1.6×10^{-2} mol dm^{-3} in all cases. UV/vis spectra were recorded immediately after the solutions were prepared. The data were averaged over three runs (errors < 15%). [b] Calculated by measuring the difference between 490 and 430 nm. All values are corrected relative to that measured for the calix[4]pyrrole stock solution (0.03 nm). [c] Calculated relative to **1·2** + fluoride solution, *i.e.* relative absorbance = [ΔAbsorbance (anion)/ΔAbsorbance (fluoride)].

This decrease in intensity was visible to the naked eye as a yellow-to-colourless colour change and is attributed to the formation of the calixpyrrole–phenolate complex **1·2**.† Control experiments showed that addition of pyrrole to solutions of **2** (2×10^{-1} mol dm^{-3}) under the same conditions caused no decrease in the intensity of this band.

Addition of anions to solutions of **1·2** causes the yellow colour of the 4-nitrophenolate anion to return as it is displaced from the calix[4]pyrrole anion binding site (Scheme 1). Table 1 shows the relative absorbance values for solutions of **1** (5.0×10^{-4} mol dm^{-3}) and **2** (6.0×10^{-6} mol dm^{-3}) in MeCN upon addition of various anions (solution made up to 1.6×10^{-2} mol dm^{-3}). The strongest absorbance is observed upon addition of fluoride anions followed by chloride and dihydrogenphosphate anions. This trend reflects the absolute and relative affinities of *meso*-octamethylcalix[4]pyrrole for these particular anionic guests and is illustrated in Fig. 2.

The present findings serve to illustrate that calixpyrroles, such as **1**, may be used to produce anion sensors that can report the presence of anions by means of a colour change. It may therefore be possible to incorporate analogous systems into 'dip-sticks' for anion detection in the field. We are presently working to covalently attach a variety of phenolate anions and dyes to calixpyrroles in order to produce discrete molecular hosts capable of reporting anion-binding events by colour changes. The results of this work will be reported in due course.

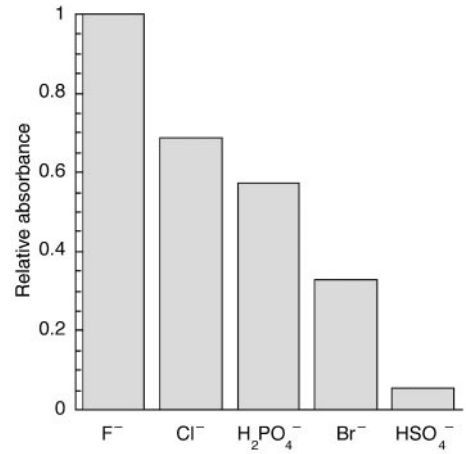

Fig. 2 Relative absorbance of solutions containing **1** (5.0×10^{-4} mol dm^{-3}), **2** (6.0×10^{-6} mol dm^{-3}) and various anions (1.6×10^{-2} mol dm^{-3}) in MeCN at 25 °C.

This work was supported by a Royal Society University Research Fellowship (to P. A. G.), a Royal Society Research Grant (to L. J. T), the University of Lancaster (L. J. T. and C. I. H.) and by the National Institutes of Health (grant GM58907 to J. L. S.) and the Texas Advanced Research Program (grant 3658-102 to J. L. S.).

Notes and references

1 P. A. Gale, *Coord. Chem. Rev.*, 1999, in the press.
2 F. P. Schmidtchen and M. Berger, *Chem. Rev.*, 1997, **97**, 1609.
3 J. L. Atwood, K. T. Holman and J. W. Steed, *Chem. Commun.*, 1996, 1401.
4 *Supramolecular Chemistry of Anions*, ed. A. Bianchi, K. Bowman-James and E. Garcia-España, Wiley-VCH, New York, 1997.
5 P. Chakrabarti, *J. Mol. Biol.*, 1993, **234**, 463.
6 B. J. Calnan, B. Tidor, S. Biancalana, D. Hudson and A. D. Frankel, *Science*, 1991, **252**, 1167.
7 J. L. Sessler, P. I. Sansom, V. Král, D. O'Connor and B. L. Iverson, *J. Am. Chem. Soc.*, 1996, **118**, 12 322.
8 J. Scheele, P. Timmerman and D. N. Reinhoudt, *Chem. Commun.*, 1998, 2613.
9 B. Hasenknopf, J. M. Lehn, B. O. Kneisel, G. Baum and D. Fenske, *Angew. Chem., Int. Ed. Engl.*, 1996, **35**, 1838.
10 P. D. Beer, P. K. Hopkins and J. D. McKinney, *Chem. Commun.*, 1999, 1273.
11 P. D. Beer, *Chem. Commun.*, 1996, 689.
12 H. Miyaji, P. Anzenbacher Jr, J. L. Sessler, E. R. Bleasdale and P. A. Gale, *Chem. Commun.*, 1999, 1723.
13 A. Metzger and E. V. Anslyn, *Angew. Chem., Int. Ed.*, 1998, **37**, 649.
14 J. L. Sessler, N. A. Tvermoes, J. Davis, P. Anzenbacher Jr., K. Jursíkova, W. Sato, D. Seidel, V. Lynch, C. B. Black, A. Try, B. Andrioletti, G. Hemmi, T. D. Mody, D. J. Magda and V. Král, *Pure Appl. Chem.*, in the press.
15 Y. Kubo, S. Maeda, S. Tokita and M. Kubo, *Nature*, 1996, **382**, 522.
16 P. A. Gale, J. L. Sessler, V. Král and V. Lynch, *J. Am. Chem. Soc.*, 1996, **118**, 5140.
17 Tetrabutylammonium 4-nitrophenolate was prepared by titrating 1 equiv. of a 0.1 mol dm^{-3} solution of tetrabutylammonium hydroxide into a stock solution of 4-nitrophenol in MeOH. The solvent was removed *in vacuo* and the residue triturated with Et_2O affording the nitrophenolate salt as a yellow powder that was dried under high vacuum and gave satisfactory spectroscopic data.
18 A. Baeyer, *Ber. Dtsch. Chem. Ges.*, 1886, **19**, 2184.
19 M. J. Hynes, *J. Chem. Soc., Dalton Trans.*, 1993, 311.
20 L. Doub and J.M. Vandenbelt, *J. Am. Chem. Soc.*, 1947, **69**, 2714; L. Doub and J. M. Vandenbelt, *J. Am. Chem. Soc.*, 1949, **71**, 2414.

Communication 9/05743I

Resolution, X-ray structure and absolute configuration of a double-stranded helical diiron(II) bis(terpyridine) complex

Gwénaël Rapenne,[a] Bradley T. Patterson,[b] Jean-Pierre Sauvage*[a] and F. Richard Keene*[b]

[a] *Laboratoire de Chimie Organo-Minérale, UMR 7513 CNRS, Université Louis Pasteur, Institut Le Bel, 4, rue Blaise Pascal, 67070 Strasbourg, France. E-mail: sauvage@chimie.u-strasbg.fr*

[b] *School of Biomedical & Molecular Sciences, James Cook University, Townsville, Queensland 4811 Australia. E-mail: Richard.Keene@jcu.edu.au*

Received (in Basel, Switzerland) 25th June 1999, Accepted 19th August 1999

A dinuclear double helix constructed around two iron(II) bis(terpyridine) centres has been resolved by preparative column chromatography, several tens of milligrams of each enantiomer were obtained, with an excellent enantiomeric excess.

In the course of the last 30 years, coordination chemistry has afforded many examples of fascinating architectures based on metal–ligand interactions.[1] Of particular interest are double-stranded helical-type complexes, exemplified by transition-metal helical complexes[2] and molecular knots[3,4] (Fig. 1). Such compounds, with their helical topography and knotted topology, are reminiscent of more complex natural structures such as DNA[4] and proteins.[5] Interestingly, a major chemical difference between a molecular trefoil knot and a double helix is that the knot will retain its chirality even after demetallation.

Helical systems are intrinsically chiral and, in metallo-helical complexes, the coordination of the first metal centre determines the chirality of the neighboring centre.[6] If the ligand is achiral, synthesis will produce a racemic mixture containing the Δ- (right-handed) and the Λ- (left-handed) double helices. In the past few years, the challenge of isolation of the chiral forms of such systems has focussed on resolution[7] or enantioselective synthetic[8,9] techniques. Only a few examples of resolved transition-metal helical complexes[10–12] and one example of a resolved knot[13] have been reported in the literature.

In our search for new optically pure transition-metal based molecular knots, we explored the use of an iron(II) bis-(2,2′:6′,2″-terpyridine) {bis-terpy} fragment in the place of the original copper(I) bis(1,10-phenanthroline) motif. This fragment successfully yielded a racemic mixture of a diiron(II) molecular knot.[14] In order to find a more general resolution method than the diastereoselective crystallization used previously for the dicopper(I) trefoil knot,[13] for the case of the diiron(II) compound we attempted a chromatographic technique which had been recently applied to the resolution of a range of cationic mono-, di- and tri-nuclear transition metal complexes.[11,12,15] Here, we report the resolution of a dinuclear iron(II) double-stranded helix and its absolute configuration determined on the basis of an X-ray crystallographic study.

A racemic mixture of the previously described[13] dinuclear iron(II) double helix $\mathbf{1}^{4+}\cdot 2SO_4^{2-}$ (Scheme 1) was absorbed onto a column (100 × 2 cm) of SP Sephadex C-25 cation exchanger and eluted with aqueous 0.075 M sodium (−)-di-*O*,*O*′-4-toluoyl-L-tartrate. After an 'effective column length' of *ca.* 6 m (achieved by recycling using a peristaltic pump), two separate bands were collected. After isolation of the separated enantiomers as the PF_6^- salts by metathesis from the solutions of eluted bands, their molar rotations were measured in acetonitrile solution and observed to be equal in magnitude and opposite in sign.

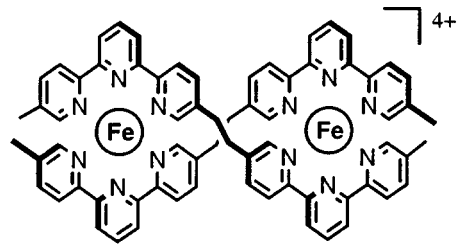

$\mathbf{1}^{4+}$

Scheme 1

The circular dichroism (CD) spectra of the enantiomers are shown in Fig. 2. As expected, they are mirror images over the whole region of the spectrum. In the visible region, $\Delta\varepsilon$ reaches a highest absolute magnitude of *ca.* 23 $dm^3\ mol^{-1}\ cm^{-1}$, which is associated with the absorption maximum of the metal-to-ligand charge transfer (MLCT) transition at 560 nm [d_π(Fe)–π^*(terpy)].†

After two months in acetonitrile solution at room temperature, no loss of any optical activity was observed, indicating high kinetic stability of the optically pure double helix. This can

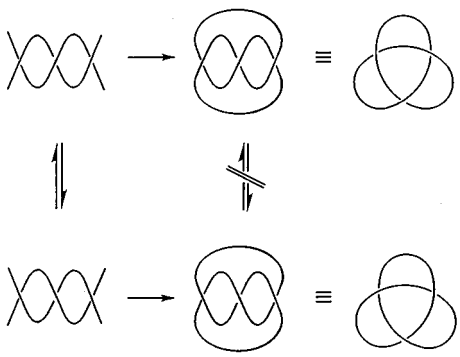

Fig. 1 From a double-stranded helix to a knot. The knotted topology makes the interconversion between both enantiomers impossible without breaking and reforming at least one chemical bond.

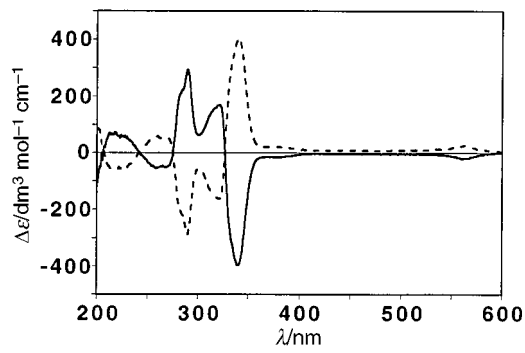

Fig. 2 Circular dichroism spectra of the enantiomers of the diiron(II) double helix in MeCN: (−)-$\mathbf{1}^{4+}\cdot 4PF_6^-$ (continuous line) and (+)-$\mathbf{1}^{4+}\cdot 4PF_6^-$ (dotted line).

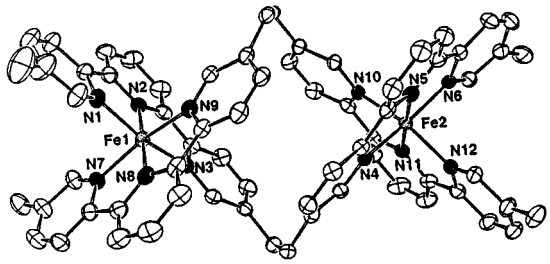

Fig. 3 Crystal structure‡ of the dextrorotatory diiron(II) double helix (+)-$\mathbf{1}^{4+}\cdot 4PF_6^-$. ORTEP representation showing the numbering scheme adopted for iron and nitrogen atoms. The solvent molecules, PF_6 anions and hydrogen atoms have been omitted and the nitrogen atoms are shown in black. Selected bond distances (Å) and angles (°) of the two pseudo-octahedral iron centres: Fe1–N1 1.990, Fe1–N2 1.899, Fe1–N3 1.992, Fe1–N7 2.008, Fe1–N8 1.869, Fe1–N9 1.981, Fe2–N4 1.963, Fe2–N5 1.872, Fe2–N6 1.976, Fe2–N10 1.981, Fe2–N11 1.902, Fe2–N12 1.966, N1–Fe1–N2 80.7, N1–Fe1–N8 99.7, N2–Fe1–N3 80.4, N2–Fe1–N7 97.4, N2–Fe1–N9 99.6, N3–Fe1–N8 99.3, N7–Fe1–N8 81.1, N8–Fe1–N9 81.9, N4–Fe2–N5 82.0, N4–Fe2–N11 99.8, N5–Fe2–N6 81.3, N5–Fe2–N10 99.7, N5–Fe2–N12 98.8, N6–Fe2–N11 97.0, N10–Fe2–N11 80.6, N11–Fe2–N12 80.9.

be compared to the mononuclear complex, $[Fe(terpy)_2]^{2+}$, which readily racemizes in solution.[16] Crystals suitable for X-ray analysis were obtained by dissolution of 14 mg of the dextrorotatory double helix (+)-$\mathbf{1}^{4+}\cdot 4PF_6^-$ in one drop of acetonitrile diluted with methanol and slow liquid diffusion of benzene. The absolute configuration of the dextrorotatory enantiomer of the double helix was determined and the X-ray crystal structure is shown in Fig. 3.

The molecule has effective D_2 symmetry, with three mutually perpendicular pseudo-twofold axes, one joining the two iron cations, another passing through the middle of the two bridges and the third being perpendicular to the others. Each ligand is twisted around the metal–metal axis in the same direction. The coordination polyhedra around each metal appeared as distorded octahedra, and it should be noted that the intramolecular Fe–Fe distance is 8.31 Å, which is larger than in the crystal obtained from a racemic mixture (7.93 Å).[14] Finally, the absolute configuration of (+)-$\mathbf{1}^{4+}\cdot 4PF_6^-$ could be determined. The two metal centres are homochiral as expected in a double-stranded helical compound where the first coordination centre induces the same chirality on the coordination of its neighbour. The *dextrorotatory* double helix corresponds to a Λ-*double helix* with the bis-terpy ligands wound in an anticlockwise fashion.

The present results demonstrate the power of the chromatographic resolution technique, although an important limitation is the requirement to have water soluble compounds. To the best of our knowledge, this is the first reported absolute configuration of an iron(II) double helix. Further developments of this work would be to achieve chromatographic resolution of the diiron(II) trefoil knot prepared recently.[14]

We thank the CNRS, the European Union and the Australian Research Council for financial support and the French Ministry of National Education for a fellowship to G. R. We are also grateful to Nathalie Kyritsakas, André De Cian and Jean Fischer for the X-ray structure.

Notes and references

† MS (HR-ES$^+$): *m*/*z* 1587.30 ([M − PF_6^-]$^+$, calc. 1587.23, uncalibrated region), 721.1362 ([M − $2PF_6^-$]$^{2+}$, calc. 721.1363), 432.4364 ([M − $2PF_6^-$]$^{3+}$, calc. 432.4360), 288.0863 ([M − $3PF_6^-$]$^{4+}$, calc. 288.0858). CD [λ/nm ($\Delta\varepsilon$/dm^3 mol^{-1} cm^{-1}), Band 1: (−)-$\mathbf{1}^{4+}\cdot 4PF_6^-$ (c = 2.80 × 10^{-5} M): 260 (−53), 268 (−51), 290 (292), 321 (169), 340 (−397), 560 (−21). Band 2: (+)-$\mathbf{1}^{4+}\cdot 4PF_6^-$ (c = 2.25 × 10^{-5}M): 260 (58), 268 (55), 290 (−289), 321 (−162), 340 (404), 560 (24). $[\alpha]_D$ band 1 −2015°, band 2 +2070°.

‡ *Crystal data* for (+)-$\mathbf{1}^{4+}\cdot 4PF_6^-$: $C_{68}H_{56}N_{12}Fe_2\cdot 4PF_6\cdot 3C_6H_6\cdot CH_3OH$, M = 1999.22, monoclinic, space group $P2_1$, a = 13.6870(2), b = 13.6560(3), c = 23.4480(5) Å, V = 4364.2 (3) Å^3, Z = 2, D_c = 1.52 g cm^{-3}, μ(Mo-Kα) = 0.512 mm^{-1}. Data were collected on a Nonius KappaCCD diffractometer using Mo-Kα graphite monochromated radiation (λ = 0.71073 Å) at 173 K. A dark red crystal of dimensions 0.20 × 0.15 × 0.10 mm was used and a total of 32515 data was collected, 2.5 < θ < 30.52°. 8706 reflections having $I > 3\sigma(I)$ were used for structure determination and refinement. The structure was solved using direct methods and refined against $|F|$. Hydrogen atoms were introduced as fixed contributors. No absorption corrections were applied. For all computations the Nonius OpenMoleN package[17] was used. The absolute structure was determined by refining Flack's x parameter: x = 0.03(0). Final results: $R(F)$ = 0.061, $Rw(F)$ = 0.077, GOF = 1.500, maximum residual electronic density = 0.707 e Å^{-3}.

CCDC 182/1385.

1 *Comprehensive Supramolecular Chemistry*, ed. J. P. Sauvage and M. W. Hosseini, Pergamon, 1996, vol. 9.
2 J. M. Lehn, A. Rigault, J. Siegel, J. Harrowfield, B. Chevrier and D. Moras, *Proc. Natl. Acad. Sci. USA*, 1987, **84**, 2565; A. F. Williams, *Chem. Eur. J.*, 1997, **3**, 15; E. C. Constable, in *Comprehensive Supramolecular Chemistry*, ed. J. P. Sauvage and M. W. Hosseini, Pergamon, 1996, vol. 9, ch. 6; J. H. Fuhrhop, G. Struckmeier and U. Thewalt, *J. Am. Chem. Soc.*, 1976, **98**, 278.
3 C. O. Dietrich-Buchecker and J. P. Sauvage, *Angew. Chem., Int. Ed. Engl.*, 1989, **28**, 189; C. O. Dietrich-Buchecker, J. Guilhem, C. Pascard and J. P. Sauvage, *Angew. Chem., Int. Ed. Engl.*, 1990, **29**, 1154.
4 C. O. Dietrich-Buchecker, G. Rapenne and J. P. Sauvage, in *Catenanes, Rotaxanes and Knots*, ed. J. P. Sauvage and C. O. Dietrich-Buchecker, Wiley-VCH, 1999, ch. 6.
5 C. Liang and K. Mislow, *J. Am. Chem. Soc.*,1995, **117**, 4201.
6 R. S. Cahn, C. Ingold and V. Prelog, *Angew. Chem., Int. Ed. Engl.*,1966, **5**, 385.
7 F. R. Keene, *Chem. Soc. Rev.*, 1998, **27**, 185.
8 W. Zarges, J. Hall, J. M. Lehn and C. Bolm, *Helv. Chim. Acta*, 1991, **74**, 1843; H. Mürner, P. Belser and A. von Zelewsky, *J. Am. Chem. Soc.*, 1996, **118**, 7989; H. Mürner, A. von Zelewsky and H. Stoeckli-Evans, *Inorg. Chem.*, 1996, **35**, 3931; M. Ziegler and A. von Zelewsky, *Coord. Chem. Rev.*, 1998, **177**, 257; U. Knof and A. von Zelewsky, *Angew. Chem., Int. Ed.*, 1999, **38**, 302; C. R. Wood, M. Benaglia, F. Cozzi and J. S. Siegel, *Angew. Chem., Int. Ed. Engl.*, 1996, **35**, 1830; E. C. Constable, T. Kulke, M. Neuburger and M. Zehnder, *New J. Chem.*, 1997, **21**, 633; E. C. Constable, T. Kulke, M. Neuburger and M. Zehnder, *Chem. Commun.*, 1997, 489.
9 F. R. Keene, *Coord. Chem. Rev.*, 1997, **166**, 121.
10 R. Krämer, J. M. Lehn, A. De Cian and J. Fischer, *Angew. Chem., Int. Ed. Engl.*, 1993, **32**, 703.
11 L. J. Charbonnière, G. Bernardinelli, C. Piguet, A. M. Sargeson and A. F. Williams, *Chem. Commun*., 1994, 1419.
12 B. Hasenknopf and J. M. Lehn, *Helv. Chim. Acta*, 1996, **79**, 1643.
13 C. O. Dietrich-Buchecker, G. Rapenne and J. P. Sauvage, *J. Am. Chem. Soc.*, 1996, **118**, 10932; G. Rapenne, C. O. Dietrich-Buchecker, J. P. Sauvage, A. De Cian and J. Fischer, *Chem. Eur. J.*, 1999, **5**, 2056.
14 G. Rapenne, C. O. Dietrich-Buchecker and J. P. Sauvage, *J. Am. Chem. Soc.*, 1999, **121**, 994.
15 D. A. Reitsma and F. R. Keene, *J. Chem. Soc., Dalton Trans.*, 1993, 2859; T. J. Rutherford, O. Van Gijte, A. Kirsch-De Mesmaeker and F. R. Keene, *Inorg. Chem.*, 1997, **36**, 4465; N. C. Fletcher, P. C. Junk, D. A. Reitsma and F. R. Keene, *J. Chem. Soc., Dalton Trans.*, 1998, 133; T. J. Rutherford and F. R. Keene, *J. Chem. Soc., Dalton Trans.*, 1998, 1155; B. T. Patterson and F. R. Keene, *Inorg. Chem.*, 1998, **37**, 645; N. C. Fletcher and F. R. Keene, *J. Chem. Soc., Dalton Trans.*, 1999, 683.
16 R. Hogg and R. G. Wilkins, *J. Chem. Soc.*, 1962, 341.
17 C. K. Fair in MoleN, An Interactive Intelligent System for Crystal Structure Analysis, Nonius, Delft, The Netherlands, 1990.

Communication 9/05135J

ChemComm

Synthesis and optical properties of water-soluble poly(*p*-phenylenevinylene)s

Zhonghua Peng,* Bubin Xu, Jianheng Zhang and Yongchun Pan

Department of Chemistry, University of Missouri-Kansas City, 5100 Rockhill Road, Kansas City, MO 64110, USA. E-mail: pengz@umkc.edu

Received (in Corvallis, OR, USA) 16th June 1999, Accepted 12th Augst 1999

A novel conjugated polymer containing carboxylic acid and 2-[2-(2-methoxyethoxy)ethoxy]ethoxy substituents which is soluble in both organic solvents and aqueous bases is synthesized.

The most common driving force for the self-assembly of conjugated polymers is aromatic π–π interaction.[1,2] The resulting π–π stacking of conjugated polymers has a profound effect on the electronic and optical properties of the bulk polymers.[3,4] Controlling the self-assembly of conjugated polymers is thus of great importance for optimizing materials properties and producing novel new materials.[3–6] Conjugated polymers with polar functional groups such as hydroxy or carboxylic acid moieties may serve this purpose.[7,8] The controllable hydrogen bonding among hydroxy or carboxylic acid group allows modification of interchain interactions, thus altering the properties of the polymer. One such example is the regioregular polythiophenes with pendent carboxylic acid side chains, which have been demonstrated to be polymer chemoselective sensors.[8]

We are interested in designing hydrogen-bonded shape-persistent polymer networks. Our ultimate goal is to achieve stable, nanoporous polymer networks with controllable and uniform pore sizes. For this purpose, the polar functional groups have to be anchored in geometrically-fixed positions, rather than on flexible side chains.[7,8] Here we report the synthesis and optical properties of a water-soluble poly(phenylenevinylene) (PPV)-based polymer, shown in Scheme 1 as Polymer II. PPV, the most extensively studied electroluminescent polymer, was chosen as the polymer backbone.[9] The hydrogen-bonding anchors, isophthalic acids,[10] are covalently bonded to the PPV backbone through oxadiazole rings arranged orthogonally to the polymer backbone, a structure which assures shape persistence during self-assembly. The rigid arm and the polymer backbone are electronically cross-conjugated to enable the electronic and optical properties of the polymer backbone to change in response to the self-assembly process.

Polymer II was synthesized by the approach outlined in Scheme 1. Starting from triethyl benzene-1,3,5-tricarboxylate **1**, oxadiazole derivative **4** was synthesized in three steps. The two alkoxy groups in **4** were converted to vinyl groups (**7**) in an approach previously reported.[11] The precursor polymer (Polymer **I**) was synthesized by the Pd-catalyzed Heck coupling reaction of **7** with dihalide **8**,[12] which was synthesized by the reaction of 2,5-diiodohydroquinone with 3,6,9-trioxadecyl toluene-*p*-sulfonate.[13]

Polymer I is soluble in THF, $CHCl_3$ and CH_2Cl_2, and insoluble in DMSO, water and aqueous bases. Its weight-average molecular weight, measured by gel-permeation chromatography (GPC) at 30 °C with polystyrene as the standard, is 91 kDa with a polydispersity of 3.2. The hydrolysis of Polymer I was performed in THF with KOBu^t as the base.[14] After hydrolysis, Polymer II shows opposite solubility characteristics to that of Polymer I. For example, Polymer II is insoluble in $CHCl_3$, slightly soluble in THF, and soluble in DMSO and dilute aqueous bases such as NaOH, NH_4OH *etc*. The structures of both polymers were confirmed by spectroscopic studies and elemental analysis.

Polymer II shows unusual solubility behavior in aqueous bases. For example, Polymer II is only soluble in aqueous NaOH solutions with limited NaOH concentration (between 2 and 0.01 M). It is insoluble in solutions with NaOH concentrations that are too high (> 3 M) or too low (< 0.001 M). The decreased solubility of Polymer II in concentrated NaOH solutions may be related to the crown ether–metal ion type of bonding between ethylene oxide side chains of different polymer chains and metal ions. Such interaction results in a less soluble polymer network.

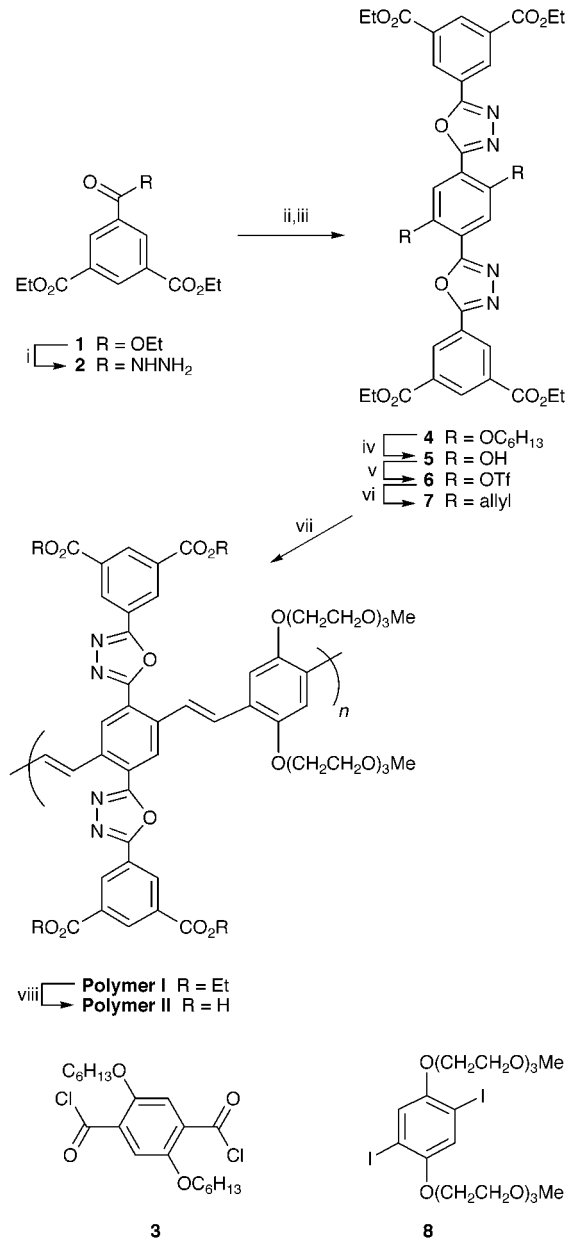

Scheme 1 *Reagents and conditions*: i, NH_2NH_2, EtOH, 52%; ii, **3**, Et_3N, $CHCl_3$, 87%; iii, $POCl_3$, 78%; iv, BBr_3, CH_2Cl_2, 93%; v, Tf_2O, pyridine, 86%; vi, tributylvinyltin, $Pd(PPh_3)_4$, 45%; vii, **8**, $Pd(OAc)_2$, P(*o*-Tol)$_3$, DMF, 90%; viii, KOBu^t. THF, quant.

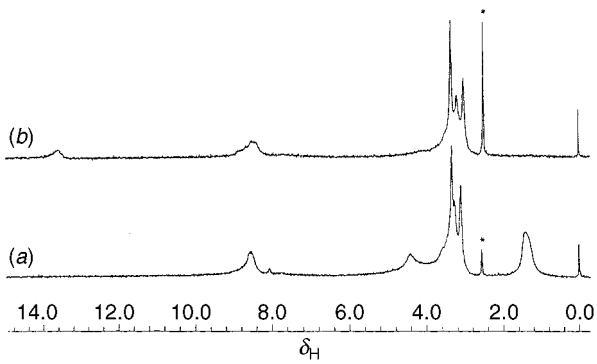

Fig. 1 ^{1}H NMR spectra of polymers (*a*) I and (*b*) II.

Fig. 1 shows the ^{1}H NMR spectra of both polymers. Before hydrolysis, Polymer I shows chemical shifts due to ester moieties at δ 4.40 and 1.5. The chemical shifts due to the ethylene oxide moieties appear between δ 3.0 and 3.7 as broad multiple peaks. The aromatic and vinyl protons are totally overlapped; only one broad peak at δ 8.6 is observed. After hydrolysis, a new peak at δ 13.5, corresponding to the carboxylic acid protons, appeared in the spectrum of Polymer II. The chemical shifts due to the ester moieties in Polymer I disappeared, indicating complete hydrolysis. Attempts to carry out the hydrolysis in acidic media such as TFA were unsuccessful.[15] It was found that, under acidic conditions, the conjugated polymer backbone was destroyed, resulting in a yellow polymer. Apparently, the acidic protons attacked the vinyl bond in the PPV backbone. The vulnerability of the vinyl bond to proton attack may be due to the partial polarization induced by the alternate electron-withdrawing and electron-donating substitution pattern of the backbones.

Polymer II also possesses good thermal stability. Differential scanning calorimetry (DSC) measurement and thermal gravimetric analysis (TGA) show that Polymer II has a decomposition temperature above 325 °C. No crosslinking process, common to the PPV backbone, is observed in the temperature range of 50–350 °C, indicating that the vinyl bonds on different polymer chains are well separated.

Fig. 2 shows the UV/Vis and fluorescence spectra of both polymers. Polymer I has two absorption peaks: *ca.* 506 nm is the absorption peak of the PPV backbone, *ca*. 310 nm can be assigned to the conjugated oxadiazole unit. After hydrolysis, the absorption of the PPV backbone is slightly blue-shifted, especially in aqueous base solutions. The maximum absorption wavelength in 1% NaOH is 484 nm.

Polymer I shows red fluorescence with an emission maximum at 615 nm. The photoluminescence quantum efficiency of Polymer I in dilute THF solutions is 3.7%. The fluorescence of Polymer II is significantly blue-shifted compared to that of Polymer I and is dependent on the choice of solvents. When a dilute DMSO solution of Polymer II was excited at 510 nm, a maximum emission at 555 nm with a shoulder at around 595 nm was observed. Polymer II in dilute NaOH solution, however, has an emission maximum at 593 nm, nearly 40 nm red-shifted compared to that of its DMSO solutions, and has a photoluminescence quantum efficiency of 4.2%.

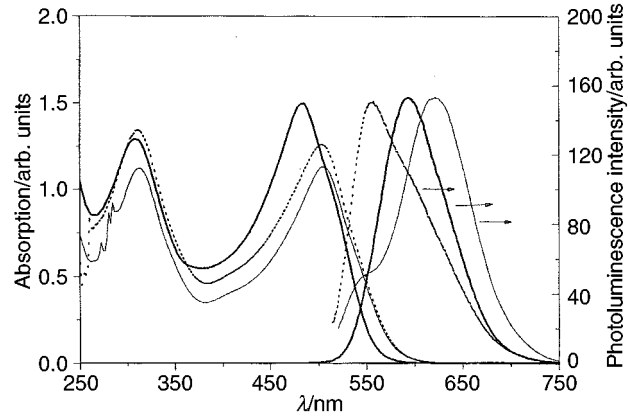

Fig. 2 Fluorescence and UV/Vis spectra of polymers I and II in solution. (*a*) I in THF, (*b*) II in 1% NaOH, (*c*) II in DMSO.

In summary, we have synthesized a novel PPV polymer containing carboxylic acid functional groups. This polymer possesses solubility in both organic solvents (DMSO) and aqueous bases (such as NaOH, NH_4OH *etc.*). The unique structure of this polymer makes it an attractive system for self-assembly studies. Its high electron affinity[11] and photoluminescence properties also warrant further study of this polymer for light-emitting diode applications, particularly as an electron-transporting layer in multilayer devices.

This work is supported by the University of Missouri-Kansas City and the University of Missouri Research Board. We thank Mr Qing Wang at the University of Chicago for the GPC measurements.

Notes and references

1 *Conjugated Polymers*, ed. J. L. Bredas and R. Silbey, Kluwer, The Netherlands, 1991.
2 T. A. Skotheim, Ed. *Handbook of Conducting Polymers I & II*, ed. T. A. Skotheim, Marcel Dekker, New York, 1986.
3 N. C. Greenham and R. H. Friend, *Solid State Phys.*, 1995, **49**, 1.
4 T.-A. Chen, X. Wu and R. D. Rieke, *J. Am. Chem. Soc.*, 1995, **117**, 233.
5 T. Bjørnholm, D. R. Greve, N. Reitzel, T. Hassenkam, K. Kjaer, P. B. Howes, N. B. Larsen, J. Bøgelund, M. Jayaraman, P. C. Ewbank and R. D. McCullough, *J. Am. Chem. Soc.*, 1998, **120**, 7643.
6 V. V. Tsukruk, *Prog. Polym. Sci.*, 1997, **22**, 247.
7 R. D. McCullough, P. C. Ewbank and R. S. Loewe, *J. Am. Chem. Soc.*, 1997, **119**, 633.
8 I. Benjamin, H. Hong, Y. Avny, D. Davidov and R. Neumann, *J. Mater. Chem*., 1998, **8**, 919.
9 A. Kraft, A. C. Grimsdale and A. B. Holmes, *Angew. Chem., Int. Ed.*, 1998, **37**, 402.
10 K. Eichhorst-Gerner, A. Stabel, G. Moessner, D. Declerq, S. Valiyaveettil, V. Enkelmann, K. Müllen and J. P. Rabe, *Angew. Chem., Int. Ed. Engl*., 1996, **35**, 1492.
11 Z. Peng and J. Zhang, *Chem. Mater*., 1999, **11**, 1138.
12 R. F. Heck, *Org. React.*, 1982, **27**, 345.
13 B. Winkler, L. Dai and A. W. H. Mau, *Chem. Mater*., 1999, **11**, 704.
14 F. C. Chang and N. F. Wood, *Tetrahedron. Lett*., 1964, 2969.
15 D. J. Pesak, J. S. Moore and T. E. Wheat, *Macromolecules*, 1997, **30**, 6467.

Communication 9/04822G

Novel generation of silacarbonyl ylides by trapping of silylene with carbonyl compounds and their cycloaddition leading to silaheterocycles

Norio Sakai, Tsuyoshi Fukushima, Satoshi Minakata, Ilhyong Ryu and Mitsuo Komatsu*

Department of Applied Chemistry, Graduate School of Engineering, Osaka University, Yamadaoka 2-1, Suita, Osaka 565-0871, Japan. E-mail: komatsu@ap.chem.eng.osaka-u.ac.jp

Received (in Cambridge, UK) 28th July 1999, Accepted 16th August 1999

The photochemical generation of silacarbonyl ylides from a silylene and carbonyl compounds and their inter- or intramolecular 1,3-dipolar cycloaddition with olefins leading to silicon heterocycles in one step was successful.

Over the past few decades the capture of a carbene with a carbonyl compound to form the corresponding carbonyl ylide has been the subject of extensive study.[1] Recently silylenes, the silicon analogues of carbenes, have attracted considerable attention in the construction of new silaheterocycles as possible new biologically active compounds and functional materials.[2] While several methods for the *in situ* generation of silylenes by photolysis have been developed,[3,4] the trapping of silylenes with aldehydes, ketones and an α-diketone leading to silaheterocycles has emerged as the result of studies on the chemical properties of silylenes.[4,5] However, specific research into the trapping of silylenes with carbonyl compounds has not been reported, nor has their application as silacarbonyl ylides in the one-step synthesis of silaheterocycles. We report herein some unprecedented examples of the 1,3-dipolar cycloaddition of photochemically generated silacarbonyl ylides, as silicon analogues of carbonyl ylides, with dipolarophiles to give silaheterocycles (Scheme 1).

The reaction of a silylene with a simple aliphatic aldehyde was investigated as an initial example. A solution of trisilane[6] **1** and acetaldehyde **2a** (100 equiv.) in hexane was irradiated at −57 °C for 40 h in a cold bath with a low pressure mercury lamp.[4] The resulting mixture was separated on a silica gel column (hexane–EtOAc = 95:5) to afford 1,4-dioxa-2-silacyclopentane **3a** in 50% yield (Scheme 2). The structure of the cycloadduct **3a** was characterized as a 1 : 2 cycloadduct of bismesitylsilylene **4** (*vide infra*) and aldehyde **2a** by spectral analysis. ^{1}H NMR observation showed that silaheterocycle **3a** was a mixture of diastereomers (*cis* : *trans* = 1 : 1), but no regioisomers such as a 1,3-dioxa-2-silacyclopentane were formed. The cycloadditions of trisilane **1** with other carbonyl compounds **2b–e** leading to 1 : 2 cycloadducts **3b–e** are summarized in Table 1.

With less bulky aldehydes such as acetaldehyde and propionaldehyde, the yields of **3** were moderate. However, when a more bulky aldehyde **2c** was employed, the yield of cycloadduct **3c** was dramatically improved to 81%. It is noteworthy that a nearly quantitative yield was observed with a non-enolizable bulky aldehyde **2d**. When acetone **2e** was employed, cycloadduct **3e** was produced in 15% isolated yield (26% by ^{1}H NMR before silica gel column separation).

Table 1 The results of the cycloaddition reactions of silylene **4** with carbonyl compounds **2a–e** leading to 1:2 cycloadducts **3a–e**[a]

	Carbonyl compounds					
Entry		R^1	R^2	equiv.	*t*/h	Yield (%)[b]
1	**2a**	Me	H	100	40	50[c]
2	**2b**	Et	H	70	24	34[c]
3	**2c**	Pr^i	H	70	20	81[c]
4	**2d**	Bu^t	H	100	17	98[c]
5	**2e**	Me	Me	100	17	15[d]

[a] Hexane solutions were irradiated at −57 °C. [b] Yield of the isolated products. [c] *cis, trans*-mixtures. [d] A large amount of enol silyl ether was detected.

The findings suggest that the silacarbonyl ylide intermediate **5** was initially generated from the silylene **4** and the carbonyl compounds **2** followed by 1,3-dipolar cycloaddition with **2** affording the cycloadduct **3**, where the aldehyde **2** plays two roles, first as a constituent of the ylide **5** and, subsequently, as a dipolarophile (Scheme 3).

Trisilane **1** was then reacted with α,β-unsaturated aldehydes in the hope of observing intramolecular cycloaddition. Contrary to our expectation, the reaction of **1** with crotonaldehyde **7** (70 equiv.) gave the intermolecular 1:2 cycloadducts 1-oxa-2-silacyclopentane **9** and 1,3-dioxa-2-silacyclopentane **10** in 27 and 25% yields, respectively (Scheme 4). The oxasilacyclo-

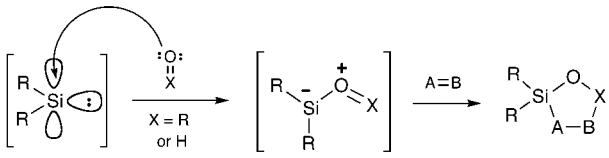

Scheme 1

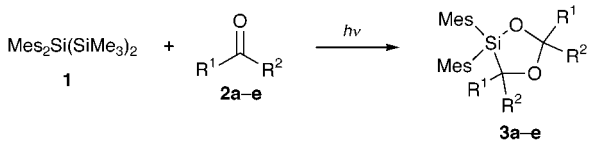

Scheme 2

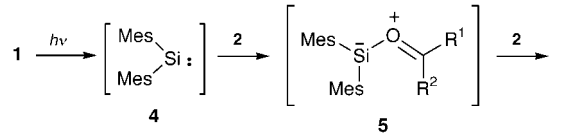

Scheme 3

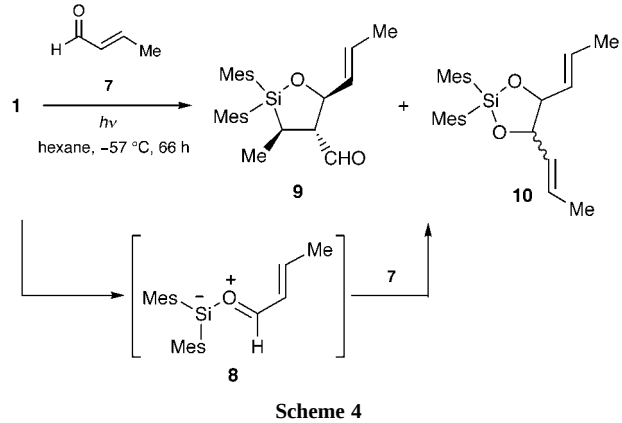

Scheme 4

pentane structure of cycloadduct **9** was determined by spectral analysis and NOE measurement of its hydrazone derivative,[7] while product **10** had the same ring system as the 1:2 cycloadduct reported for the reaction with benzaldehyde.[8] As shown in Scheme 4, the generated silacarbonyl ylide **8** was trapped by the C=C bond of aldehyde **7** to afford **9** and by the carbonyl group of **7** to give **10**. The formation of **9** represents the first example of the cycloaddition of a silacarbonyl ylide with an olefinic dipolarophile, which strongly supports our view that this type of reaction proceeds *via* the 1,3-dipolar intermediate and not *via* a siloxirane intermediate.

Intramolecular cycloaddition was successful with a non-conjugated olefinic aldehyde leading to a silicon-atom embedded bicyclic compound. Thus, a solution of trisilane **1** and 2,2-dimethylhex-5-enal **11** (45 equiv.) in hexane was irradiated at −57 °C for 20 h to afford bicyclo[3.3.0]oxasilacyclooctane **12** in 51% yield (87% by ^{1}H NMR before SiO_2 column purification) (Scheme 5).

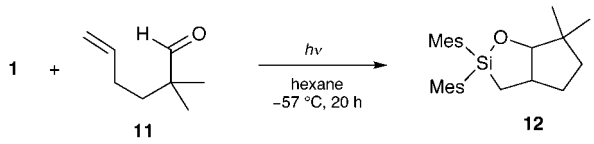

Scheme 5

Moreover, these results suggest the possibility of a three-component coupling reaction involving a silylene and two different carbonyl compounds. When a solution of trisilane **1**, pivalaldehyde **2d** (25 equiv.) and acetone **2e** (50 equiv.) in hexane was photolyzed at −57 °C for 12 h, a three-component cycloadduct **14** was successfully obtained as the major product in 37% yield along with cycloadduct **3d** in 21% yield (Scheme 6). In this three-component reaction, the 1:2 cycloadduct of silylene **4** and **2e** was not obtained at all (see entry 5, Table 1). This result implies that the generation of silacarbonyl ylide **13** from the silylene **4** and aldehyde **2d** occurred predominantly, which was followed by cycloaddition with acetone leading to **14**.

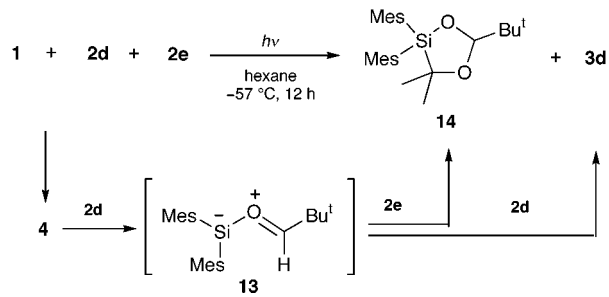

Scheme 6

Finally, the regioselectivities of the cycloadditions of silylene **4** and the aldehydes were examined by semiempirical MO calculations (PM3 method).[9] For the case of an aliphatic aldehyde such as pivalaldehyde, the orbital coefficient (−0.54) on the silicon atom is larger than that (+0.30) on the carbonyl carbon (HOMO), and the orbital coefficient (−0.64) on the carbonyl carbon of the aldehyde is larger than that (+0.47) on

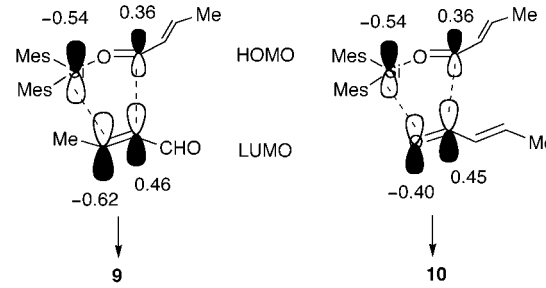

Scheme 7

oxygen (LUMO).[10] The prediction of the regiochemistry of the cycloaddition by this orbital correlation was in good agreement with the structure of the isolated 1:2 cycloadduct **3d**. In the case of aldehyde **7**, the orbital coefficient on the β-carbon in the LUMO is the largest, so that cycloaddition occurs preferentially across the C=C bond of **7** leading to cycloadduct **9** as the major product (Scheme 7). However, when the difference between the orbital coefficients is small, the regioselectivity of cycloadduct **10** appears to be controlled, not by the correlation of the coefficients, but by the strong affinity between silicon and oxygen.

Thus far, we have succeeded in the photochemical generation of novel 1,3-dipoles, silacarbonyl ylides, from a silylene and various carbonyl compounds, and their inter- or intra-molecular cycloaddition leading to silicon-embedded heterocycles in one step. The inter- and intra-molecular cycloadditions with olefins, in particular, are unprecedented.

This work was partially supported by a Grant-in-Aid for Scientific Research from Ministry of Education, Science, Sports and Culture, Japan.

Notes and references

1 A. Padwa and M. D. Weingarten, *Chem. Rev*., 1996, **96**, 223; A. F. Khlebnikov, M. S. Novikov and R. R. Kostikov, *Adv. Heterocycl. Chem*., 1996, **65**, 93; N. J. Turro and Y. Cha, *Tetrahedron Lett*., 1987, **28**, 1723; T. Ibata, M. T. H. Liu and J. Toyoda, *Tetrahedron Lett*. 1986, **27**, 4383; K. T. Potts, in *1,3-Dipolar Cycloaddition Chemistry*, ed. A. Padwa, Wiley-Interscience, New York, 1984 and references therein.
2 E. Lukevics and L. Ignatovich, *Appl. Organomet. Chem*., 1992, **6**, 113.
3 S. Masamune, Y. Hanzawa, S. Murakami, T. Bally and J. F. Blount, *J. Am. Chem. Soc*., 1982, **104**, 1150.
4 M. Ishikawa and M. Kumada, *Adv. Organomet. Chem*., 1981, **19**, 51 and references therein.
5 A. K. Franz and K. A. Woerpel, *J. Am. Chem. Soc*., 1999, **121**, 949; J. Belzner and H. Ihmels, *Adv. Organomet. Chem*., 1998, **43**, 1; J. Belzner, H. Ihmels, L. Pauletto and M. Noltemeyer, *J. Org. Chem*., 1996, **61**, 3315; W. Ando, K. Hagiwara and A. Sekiguchi, *Organometallics*, 1987, **6**, 2270; W. Ando, Y. Hamada and A. Sekiguchi, *J. Chem. Soc*., *Chem. Commun*., 1983, 952.
6 M. J. Fink, M. J. Michalczyk, K. J. Haller, R. West and J. Michl, *Organometallics*, 1984, **3**, 793.
7 M. Behforouz, J. L. Bolan and M. S. Flyynt, *J. Org. Chem*. 1985, **50**, 1186.
8 P. Jutzi, D. Eikenberg, E.-A. Bunte, A. Mohrke, B. Neumann and H.-G. Stammler, *Organometallics*, 1996, **15**, 1930.
9 Calculations were carried out with Cache MOPAC Ver. 94.1.
10 R. Sustmann, *Tetrahedron Lett*., 1971, **12**, 2717, 2721.

Communication 9/06139H

ChemComm

Triphenyleno[1,12-*bcd*:4,5-*b′c′d′*:8,9-*b″c″d″*]trithiophene: the first bowl-shaped heteroaromatic

Koichi Imamura,[a] Kazuo Takimiya,[a] Yoshio Aso[b] and Tetsuo Otsubo*[a]

[a] *Department of Applied Chemistry, Faculty of Engineering, Hiroshima University, Higashi-Hiroshima 739-8527, Japan. E-mail: otsubo@ipc.hiroshima-u.ac.jp*

[b] *Institute for Fundamental Research of Organic Chemistry, Kyushu University, Fukuoka 812-8581, Japan*

Received (in Cambridge, UK) 20th July 1999, Accepted 16th August 1999

The title compound has been synthesized, and its unique bowl-shaped molecular structure and electronic spectra have been elucidated.

The discovery of buckminsterfullerene has stimulated much interest in the chemistry of bowl-shaped polycyclic aromatic hydrocarbons, such as corannulene **1**.[1–5] Such bowl-shaped

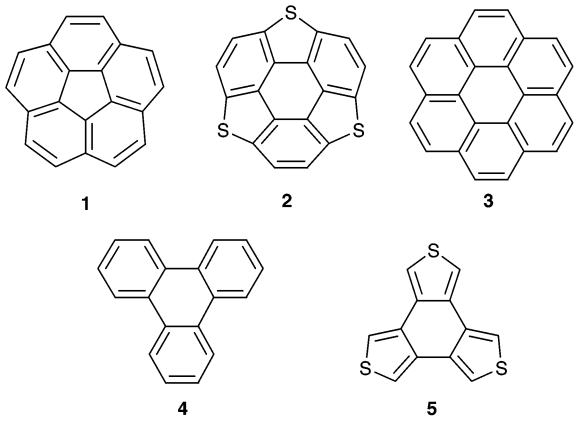

compounds can be expected to exhibit unique physicochemical properties related to the buckminsterfullerene surface. Although polycyclic heteroaromatics are of current interest for advanced materials,[6] no heteroaromatics with bowl curvature have been reported to the best of our knowledge.[7] Triphenyleno[1,12-*bcd*:4,5-*b′c′d′*:8,9-*b″c″d″*]trithiophene **2**, so far unknown, is remarkable because the electronic structure of **2** is similar to that of highly symmetrical coronene **3**. However, **2** contains severe strain in the molecular structure due to the three five-membered thiophene rings in the periphery, and accordingly, unlike planar coronene,[8] is expected to adopt a bowl-shaped structure. We now report the synthesis, molecular structure and spectroscopic properties of **2** as the first bowl-shaped heteroaromatic.

The synthesis of **2** was previously attempted by inserting sulfur bridges in the bay regions of triphenylene **4**; although the mono- and di-bridged species were successfully made, the tri-bridged species **2** was not found.[9] The difficult synthesis of **2** is presumably due to its strained structure. Our successful synthetic route is based on tribenzannulation of benzotrithiophene **5** by a flash-vacuum pyrolytic method, which was applied recently to a short access to strained aromatic systems, such as corannulene[2,4,5] and more recently to thiophene-containing heteroaromatic systems.[10] As shown in Scheme 1, **5**[11] was treated with NBS (3 equiv.) to give the tribromo derivative **6**, which was subsequently converted to the trimethylsilylethynyl derivative **7** by the Sonogashira reaction (two step yield 53%). An NMR analysis indicated that the product comprised two regioisomers **7a** and **7b** in a ratio of about 1:5. Other possible isomers which accommodate two substituent groups in the same bay region were not formed. Treatment of **7** with HCl gave the tris(chlorovinyl) compound **8**

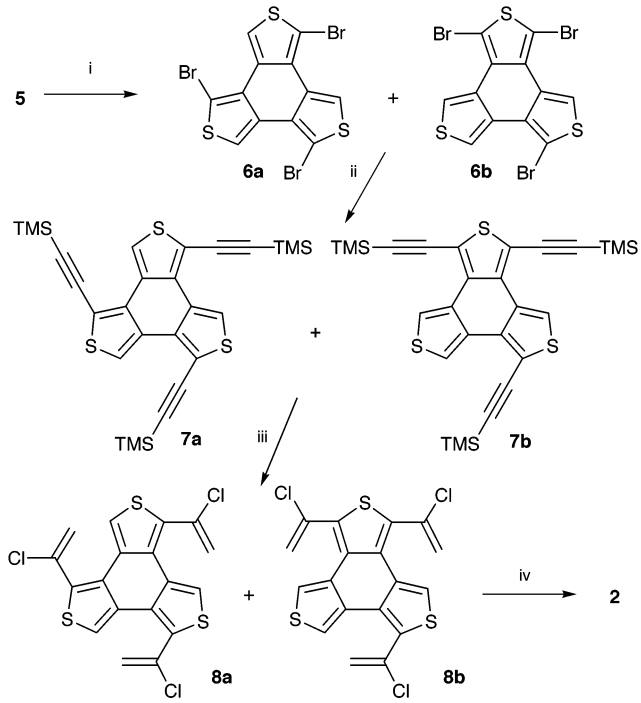

Scheme 1 *Reagents and conditions*: i, NBS (3.0 equiv.), DMF, room temp.; ii, TMSC≡CH, $Pd(PPh_3)_4$, CuI, NEt_3, reflux; iii, conc. HCl, AcOH, 80 °C; iv, 1000 °C, 0.005 Torr, N_2 flow.

(33% yield), which was then subjected to flash vacuum pyrolysis under the conditions of 1000 °C and 0.005 Torr to afford the desired compound **2** in 35% yield.†

As shown in Fig. 1, an X-ray crystallographic analysis of **2** clearly revealed that it has the expected bowl-shaped molecular structure,‡ which is somewhat shallow compared to corannulene.[12] The crystal structure belongs to the hexagonal

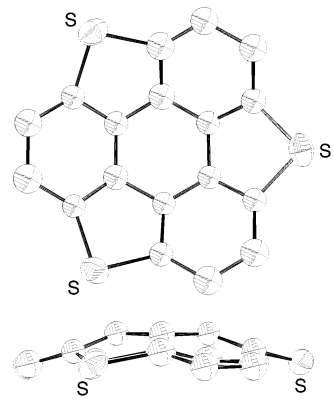

Fig. 1 Molecular structure of **2**: top view (top) and side view (bottom).

crystal system, which is very rare for the crystal structures of organic molecules. The molecules are stacked in a concave–convex fashion, unlike corannulene but like the deeper bowl-shaped aromatic hydrocarbons,[2,5] with marked intermolecular S–S contacts.

The electronic absorption spectrum of **2** in CH_2Cl_2 shows a long-wavelength vibrational α-band at λ_{max} 368 nm (log ε 3.13), which, though weak as a symmetry-forbidden transition, causes yellow coloration for **2**. In addition, there are two strong bands centered at 318 (4.42) and 245 nm (4.47), assignable to p- and β-bands, respectively. The whole absorption spectrum roughly resembles that of coronene itself,[13] supporting iso-electronic structures for both compounds. In a more detailed comparison, the respective absorption bands of **2** are somewhat blue-shifted. Coincidentally **2** demonstrates a fluorescent emission at λ_{max} 398 and 414 nm, whereas coronene fluoresces at longer wavelengths (λ_{max} 436, 456, and 482 nm).

The present work was supported by Grants-in-Aid for Scientific Research from the Ministry of Education, Science, Sports and Culture, Japan.

Notes and references

† *Selected data* for **2**: yellow fine needles from CS_2–hexane; mp > 300 °C; $\delta_H(CDCl_3)$ 8.01 (s, 6H); $\delta_C(CDCl_3)$ 122.7, 135.6, 141.0; *m/z* 318 (M^+) (Calc. for $C_{18}H_6S_3$: C, 67.89; H, 1.89. Found: C, 67.87; H, 1.97%).

‡ *Crystal data* for **2**: $C_{18}H_6S_3$, M = 318.43, hexagonal, space group $P6cc$ (no. 184), $a = b = 26.121(7)$, $c = 7.433(3)$ Å, $V = 4392(1)$ Å^3, $Z = 14$, $D_c = 1.685$ g cm^{-3}, μ(Mo-Kα) = 5.76 cm^{-1}, crystal dimensions 0.85 × 0.03 × 0.03 mm^3. The structure analysis is based on 1820 reflections ($2\theta_{max}$ = 55°), 698 observed [$I \geqslant 2\sigma(I)$], and 126 parameters. The structure was solved by direct methods (SIR92). It was refined by full-matrix least-squares (SHELXL-93) on F^2 with anisotropic temperature factors for the sulfur atoms and isotropic for the carbon atoms because the number of observed reflections is not enough to refine the structure with anisotropic temperature factors for all atoms. The hydrogen atoms were not included in the refinement. The final R was 0.085 [$I \geqslant 2\sigma(I)$]. The unit cell contains two independent molecules, and one molecule is located on a crystallographic 6-fold axis with disorder. Both molecules adopt virtually the same bowl-shaped structure. CCDC 182/1376. See http://www.rsc.org/suppdata/cc/1999/1859/ for crystallographic data in .cif format.

1 W. E. Barth and R. G. Lawtom, *J. Am. Chem. Soc.*, 1966, **88**, 380; 1971, **93**, 1730.
2 L. T. Scott, M. M. Hashemi, D. T. Meyer and H. B. Warren, *J. Am. Chem. Soc.*, 1991, **113**, 7082; L. T. Scott, *Pure Appl. Chem.*, 1996, **68**, 291; L. T. Scott, P.-C. Cheng, M. M. Hashemi, M. S. Bratcher, D. T. Meyer and H. B. Warren, *J. Am. Chem. Soc.*, 1997, **119**, 10 963; L. T. Scott, M. S. Bratcher and S. Hagen, *J. Am. Chem. Soc.*, 1996, **118**, 8743; D. M. Forkey, S. Attar, B. C. Noll, R. Koerner, M. M. Olmstead and A. L. Balch, *J. Am. Chem. Soc.*, 1997, **119**, 5766.
3 A. Borchardt, A. Fuchicello, K. V. Kilway, K. K. Baldridge and J. S. Siegel, *J. Am. Chem. Soc.*, 1992, **114**, 1921.
4 G. Zimmermann, U. Nuechter, S. Hagen and M. Nuechter, *Tetrahedron Lett.*, 1994, **35**, 4747.
5 P. W. Rabideau and A. Sygula, *Acc. Chem. Res.*, 1996, **29**, 235 and references cited therein.
6 T. Otsubo, *Synlett*, 1997, 544.
7 A few thiophene-containing [7]heterocirculenes were previously studied as examples of non-planar heteroaromatics, but their real structures have not yet been elucidated: J. H. Dopper and H. Wynberg, *J. Org. Chem.*, 1975, **40**, 1957.
8 J. M. Robertson and J. G. White, *J. Chem. Soc.*, 1945, 607.
9 L. H. Klemm, E. Hall, L. Cousins and C. E. Klopfenstein, *J. Heterocycl. Chem.*, 1989, **26**, 345.
10 K. Imamura, D. Hirayama, H. Yoshimura, K. Takimiya, Y. Aso and T. Otsubo, *Tetrahedron Lett.*, 1999, **40**, 2789.
11 H. Hart and M. Sasaoka, *J. Am. Chem. Soc.*, 1978, **100**, 4326.
12 J. C. Hanson and C. E. Nordman, *Acta Crystallogr., Sect. B*, 1976, **32**, 1147.
13 R. L. Hummel and K. Ruedenberg, *J. Phys. Chem.*, 1962, **66**, 2334; H. Gutfreund and W. A. Little, *J. Chem. Phys.*, 1969, **50**, 4468; K. Ohno, T. Kajiwara and H. Inokuchi, *Bull. Chem. Soc. Jpn.*, 1972, **45**, 996.

Communication 9/05860E

Site-specificity of bis-benzimidazole Hoechst 33258 in A-tract recognition of the DNA dodecamer duplex d(GCAAAATTTTGC)$_2$

Lee D. Higgins and Mark S. Searle*

Department of Chemistry, University of Nottingham, University Park, Nottingham, UK NG7 2RD. E-mail: mark.searle@nottingham.ac.uk

Received (in Liverpool, UK) 24th June 1999, Accepted 13th August 1999

Fluorescence titration measurements and NMR spectroscopy have identified a single molecule of Hoechst 33258 bound within the long A-tract of the dodecamer duplex d(GCAAAATTTTGC)$_2$: despite the possibility of multiple binding sites, and the apparent requirement from previous studies for the drug *N*-methylpiperazine ring to bind close to GC base pairs at the end of an A-tract (leading to an off-set asymmetric complex with this sequence), we identify a binding site that spans the central AAATTT sequence with the planar aromatic rings of the drug binding in the narrowest part of the minor groove.

The bis-benzimidazole Hoechst 33258 (H33258) binds with high affinity to the minor groove of AT rich DNA sequences.[1] Footprinting studies[2] and structural analysis of various H33258 complexes by NMR[3] and X-ray crystallography[4–6] have identified a number of key features of DNA recognition: (i) the drug binds to at least four AT base pairs, (ii) TpA steps are generally avoided, and (iii) a GC base pair is frequently accommodated at the 5′-end of the binding site. The conformation and orientation of the piperazine ring appears to account for preferential binding close to GC regions at the end of A-tracts of DNA where the wider groove has been proposed to more readily accommodate this bulky substituent.[4,5] In complexes with binding sites of only four AT base pairs (AATT)[4] the A-tract is not of sufficient length to examine this effect in detail, however, long A-tracts might enable significant site discrimination to be identified to examine the importance of the influence of the bulky *N*-methylpiperazine ring in site-specificity.

Here, we present an analysis of the interaction of H33258 with an eight AT base pair A-tract sequence within the dodecamer duplex d(GCAAAATTTTGC)$_2$ using a combination of fluorescence titration data and NMR spectroscopy to determine binding stoichiometry and site specificity within the A-tract. The sequence contains several possible high affinity sites within the A-tract (AATT, ATTT or AAAA) that could potentially complicate the analysis through multiple site occupancy with the ligand in exchange between them. Further, the A-tract is of sufficient length to accommodate two bound ligands each spanning four AT base pairs.

Fluorescence titration data were used to determine the binding stoichiometry of H33258 with the dodecamer duplex d(GCAAAATTTTGC)$_2$.[7,8] The method of continuous variation in ligand concentration (Job plot analysis) indicates a fluorescence maximum at a mole fraction of drug of 0.53, establishing a 1:1 (drug:duplex) binding stoichiometry (Fig. 1). Non-linear least-squares analysis of fractional binding saturation curves at 20 °C indicated tight binding ($\sim 10^8$ M^{-1}) in agreement with previous estimates using AATT[9] and AAATTT[7,8] containing duplexes. Despite the possibility of accommodating two drug molecules in adjacent sites, the fluorescence data indicate a single bound ligand per duplex. The fluorescence data are unlikely, however, to be able to distinguish between a number of different 1:1 binding modes in equilibrium if the ligand is bound in each case with a similar affinity.

NMR titration analysis was used to examine the possibility of multiple binding modes. In Fig. 2, the thymine methyl region of the spectrum of d(GCAAAATTTTGC)$_2$ is illustrated (1.0–2.0 ppm) for the free duplex, 0.5:1 ratio of drug:duplex and for the 1:1 complex. Addition of drug results in the four signals from the free duplex (T7, T8, T9 and T10) being replaced by a set of eight new resonances from an asymmetric 1:1 complex in which the two strands of the duplex are no longer equivalent and are in slow exchange through ligand dissociation and reassociation. We see no evidence for multiple sets of resonances that

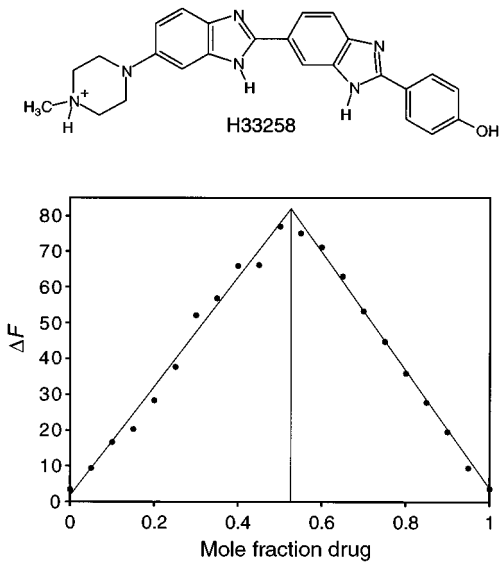

Fig. 1 Structure of H33258. Continuous variation analysis (Job plot) for binding of H33258 to d(GCAAAATTTTGC)$_2$ at pH 7.2, 100 mM NaCl and 10 mM phosphate buffer using a constant value for [ligand] + [DNA] = 0.1 μM; change in fluorescence intensity (ΔF) is plotted against mole fraction of drug. Spectra were recorded on a Perkin-Elmer Luminescence spectrometer LS 50 B at a temperature of 20 °C in 1 cm path-length polymethacrylate cuvettes using fluorescence excitation wavelengths between 330 to 360 nm and emission wavelengths from 390 to 420 nm.

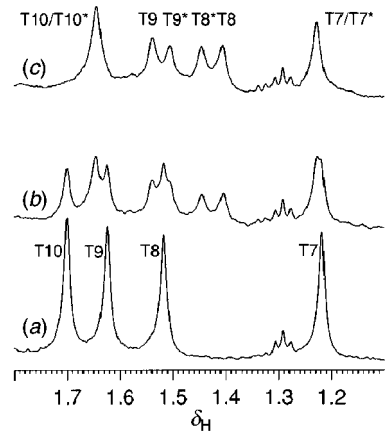

Fig. 2 ^{1}H NMR spectra (500 MHz) of the thymine methyl region (1.0–2.0 ppm) of d(GCAAAATTTTGC)$_2$: (*a*) ligand-free DNA, (*b*) drug:duplex ratio 0.5:1, and (*c*) 1:1 complex at 298 K; the two strands are distinguished by the use of asterisks, assignments are shown.

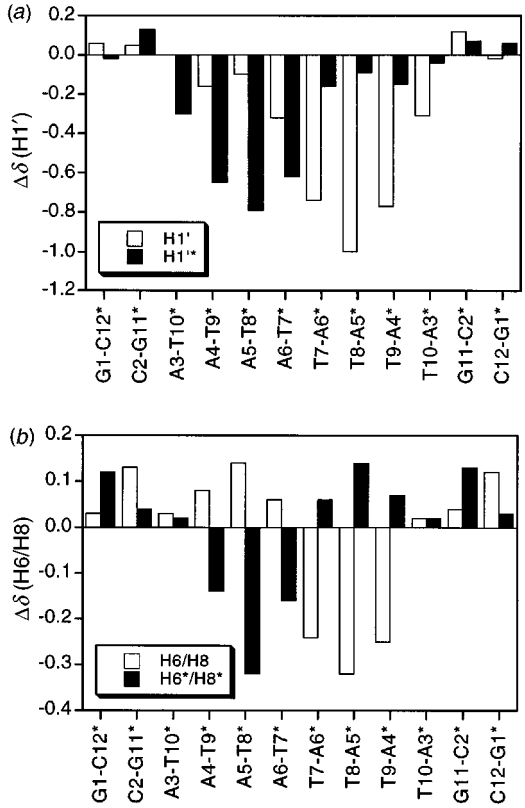

Fig. 3 Plots of drug-induced changes in ^{1}H NMR chemical shifts ($\Delta\delta = \delta_{complex} - \delta_{free}$) for (*a*) deoxyribose H1′ and (*b*) base H6/H8 for the H33258 complex with d(GCAAAATTTTGC)$_2$. The two strands of DNA read in antiparallel directions, one of which is distinguished by the use of asterisks and filled columns.

would indicate the presence of a number of slowly exchanging conformations, leading us to conclude that the drug either binds at a single high affinity site, or that the bound drug is in fast exchange between a number of overlapping sites.

To examine more closely the position of the drug within the groove we have used ^{1}H chemical shift data (assigned through 2D TOCSY and NOESY data sets) to provide an NMR 'footprint' from ligand-induced perturbations to deoxyribose H1′ and base H6/H8 resonances ($\Delta\delta = \delta_{complex} - \delta_{free}$). $\Delta\delta$ values are plotted against sequence position in Fig. 3. Many deoxyribose H1′ protons come into direct contact with the face of one or other aromatic ring of the bound ligand and experience large upfield ring current perturbations to their chemical shifts of up to 1.0 ppm. The $\Delta\delta$ values of these signals are particularly sensitive to the position of the ligand in the minor groove, with the thymine sugars showing the largest perturbations. In contrast, the effects on base H6/H8 resonances, which are located in the major groove, are smaller ($\leqslant$0.3 ppm), and probably arise from changes in base stacking interactions, but reflect the same general pattern of perturbations. The striking observation is that both sets of chemical shift perturbations suggest a highly centrosymmetric binding of the drug across the dyad axis of the duplex spanning primarily the central AAATTT sequence. The AT base pairs A3*-T10 and A3-T10* at the ends of the A-tract are relatively unperturbated by the binding interaction.

In contrast, in one X-ray structure of H33258 bound to d(CGCAAATTTGCG)$_2$,[5] containing a shorter A-tract, the drug appears to be displaced off-centre to bind across the ATTTG sequence. This binding locus is reported to accommodate the piperazine ring close to the GC base pairs at the end of the A-tract.[5] However, in a second X-ray structure with a similar AAATTT binding site the displacement is less pronounced.[6] Our data place the *N*-methylpiperazine ring within the A-tract with the bis-benzimidazole portion of the ligand binding across the AT dyad axis. Although our results seem at variance with some structural data, they do concur with some footprinting studies which also consider the interaction with longer AT tracts and which show that AATT is an unusually good binding site for H33258.[10] On a purely statistical basis, for a ligand binding site of four base pairs where there is no discrimination between sites, the central AT base pairs are expected to show the highest time-averaged site occupancy. Is a model involving fast exchange between overlapping sites consistent with the NMR data? Our preliminary analysis of intermolecular NOE data, and structural modelling, suggests that the bound ligand is restricted to a relatively small binding locus rather than shuffling between multiple (symmetrical and asymmetrical) overlapping sites. Recent studies on the binding of ammonium cations to A-tract structures,[11] together with earlier results,[12] suggest that the minor groove is at its narrowest at the centre of A_nT_n sequences. In the present context, maximising van der Waals interactions between the bound ligand and the walls of the narrowest part of the groove may be the primary determinant of A-tract site-specificity. A more detailed analysis of the structure and dynamics of this and other A-tract complexes in solution is currently in progress.

The EPSRC, the Department of Chemistry at the University of Nottingham, and the Royal Society are gratefully acknowledged for financial support. We thank John Keyte for oligonucleotide synthesis.

Notes and references

1 J. Portugal and M. J. Waring, *Biochem. Biophys. Acta*, 1988, **949**, 158.
2 K. D. Harshman and P. B. Dervan, *Nucleic Acids Res.*, 1985, **13**, 4825; A. Abu-Daya, P. M. Brown and K. R. Fox, *Nucleic Acids Res.*, 1995, **23**, 3385.
3 M. S. Searle and K. J. Embrey, *Nucleic Acids Res.*, 1990, **18**, 3753; J. A. Parkinson, J. Barber, K. T. Douglas, J. Rosamond and D. Sharples, *Biochemistry*, 1990, **29**, 10 181; A. Fede, A. Labhardt, W. Bannwart and W. Leupin, *Biochemistry*, 1991, **30**, 11 377; K. J. Embrey, M. S. Searle and D. J. Craik, *Eur. J. Biochem.*, 1993, **211**, 437; A. Fede, M. Billeter, W. Leupin and K. Wuthrich, *Structure*, 1993, **1**, 177; C. E. Bostock-Smith, C. A Laughton and M. S. Searle, *Nucleic Acids Res.*, 1998, **26**, 1660.
4 P. E. Pjura, K. Grzeskowiak and R. E. Dickerson, *J. Mol. Biol.*, 1987, **197**, 257; M.-K. Teng, N. Usman, C. A. Frederick and A. H. J. Wang, *Nucleic Acids Res.*, 1988, **16**, 2671; M. A. A. F. deC. T. Carrondo, M. Coll, J. Aymami, A. H. J. Wang, G. A. van der Marel, J. H. van Boom and A. Rich, *Biochemistry*, 1989, **28**, 7849; J. R. Quintana, A. A. Lipanov and R. E. Dickerson, *Biochemistry*, 1991, **30**, 10 294; G. R. Clark, C. J. Squire, E. J. Gray, W. Leupin and S. Neidle, *Nucleic Acids Res.*, 1996, **24**, 4882; G. R. Clark, D. W. Boykin, A. Czarny and S. Neidle, *Nucleic Acids Res.*, 1997, **25**, 1510; G. R. Clark, E. J. Gray, S. Neidle, Y.-H. Li and W. Leupin, *Biochemistry*, 1996, **35**, 13 745.
5 N. Spink, D. G. Brown, J. V. Skelly and S. Neidle, *Nucleic Acids Res.*, 1994, **22**, 1607.
6 M. C. Vega, I. Garcia Saez, J. Aymami, R. Eritja, G. A. van der Marel, J. H. van Boom, A. Rich and M. Coll, *Eur. J. Biochem.*, 1994, **222**, 721.
7 C. E. Bostock-Smith and M. S. Searle, *Nucleic Acids Res.*, 1999, **27**, 1619.
8 I. Haq, J. E. Ladbury, B. Z. Chowdhry, T. C. Jenkins and J. B. Chaires, *J. Mol. Biol.*, 1997, **271**, 244.
9 F. G. Loontiens, L. W. McLaughlin, S. Diekmann and R. M. Clegg, *Biochemistry*, 1991, **30**, 182.
10 A. Abu-Daya and K. R. Fox, *Nucleic Acids Res.*, 1997, **25**, 4962.
11 N. V. Hud, V. Sklenar and J. Feigon, *J. Mol. Biol.*, 1999, **286**, 651.
12 A. M. Burkhoff and T. D. Tullius, *Cell*, 1987, **48**, 935.

Communication 9/05232A

Palladium-catalysed borylsilylation and borylstannylative dimerization of 1,2-dienes

Shun-ya Onozawa, Yasuo Hatanaka and Masato Tanaka*

National Institute of Materials and Chemical Research, Tsukuba, Ibaraki 305-8565, Japan.
E-mail: mtanaka@home.nimc.go.jp

Received (in Cambridge, UK) 25th June 1999, Accepted 16th August 1999

A borylsilane regioselectively adds to 1,2-dienes in the presence of palladium complexes to afford high yields of alkenylboranes having allylsilane moieties, whereas a borylstannane gives a 1 : 2 telomer with 3-methylbuta-1,2-diene due to borylstannylative dimerization.

Addition reactions of metal–metal bonds to 1,2-dienes provide a straightforward route to organometallic compounds having both vinylic and allylic metal moieties, which are versatile reagents in organic synthesis.[1] Although several studies on the transition-metal-catalysed reactions of 1,2-dienes with Si–Si,[2] Sn–Sn,[3] Si–Sn,[3] Ge–Sn[4] and B–B bonds[5] have been reported, similar reactions of B–Si or B–Sn bonds have received little attention.[6,7] In the course of our investigation on the transition-metal-catalysed additions of these bonds to unsaturated organic compounds,[8,9] we have found that palladium catalysts effectively promote the reactions with 1,2-dienes, giving the corresponding adducts with extremely high regioselectivity (Scheme 1).

The following procedure is representative (Table 1, entry 1). A mixture of $Pd_2(dba)_3$ (2.5 mol%; dba = dibenzylideneacetone) and etpo as ligand [10 mol%; etpo = 4-ethyl-2,6,7-trioxa-1-phosphabicyclo[2,2,2]octane, $P(OCH_2)_3CEt$] in THF (1 ml) was heated at 80 °C for 5 min, while the color of the solution turned to green from red. To this solution were added 2-dimethylphenylsilyl-4,4,5,5-tetramethyl-2-bora-1,3-dioxacyclopentane **1** (0.33 mmol), buta-1,2-diene **2a** (1.0 mmol) and decane (30 μl; as internal standard for GC analysis), and the reaction mixture was heated at 80 °C. GC-MS analysis of the mixture indicated the complete consumption of the borylsilane **1** after 9 h and quantitative formation of a borylsilylation product **3a** (98% GC yield). It should be noted that the NMR analysis of the reaction mixture indicated the lack of formation of regioisomers like **4a**. Thus, the addition of the B–Si bond smoothly proceeded at the internal double bond of **2a**, and the boryl group was regioselectively introduced to the central carbon, leading to the exclusive formation of alkenylborane moiety. Purification of the crude product by TLC (silica gel; hexane–CH_2Cl_2 as eluent) gave analytically pure **3a** in 88% yield.†

Representative results of the reactions between **1** and various 1,2-dienes **2a–f** are summarized in Table 1. All of the products listed have exhibited satisfactory spectral data.† Under similar conditions, another monosubstituted 1,2-diene, **2b**, also underwent the borylsilylation at the internal double bond, affording **3b** in 86% yield as the sole product (entry 2). Propa-1,2-diene **2c** and sterically congested 2,4-dimethylpenta-2,3-diene **2d** effectively participated in the borylsilylation with high regioselectivity (entries 3 and 4).

The regioselectivity of the Pd–etpo-catalysed borylsilylation of 1,1-disubstituted propa-1,2-dienes was strongly influenced by the nature of substituents. For example, the reaction of 1,1-diphenylpropa-1,2-diene **2e** with **1** selectively proceeded at the terminal double bond to give **4e** in 94% yield (entry 5), whereas the borylsilylation of 3-methylbuta-1,2-diene **2f** took place at both the internal and terminal double bonds, affording a regioisomeric mixture of **3f** and **4f** with a 52 : 48 ratio (entry 6). The low regioselectivity of the latter reaction could be successfully improved by tuning the phosphorus ligands; the best result (**3f** : **4f** = 100 : 0) was achieved by using $Pd_2(dba)_3$ (2.5 mol%)–PPh_3 (10 mol%) (entry 7). The use of the $Pd_2(dba)_3$ (2.5 mol%)–PMe_3 (10 mol%) system was less effective, giving a mixture containing **3f** as major product (**3f** : **4f** = 71 : 29, entry 8).

To our surprise, the regioselectivity of this reaction completely changed when the reaction was conducted with a platinum catalyst. Thus, in the presence of a catalytic amount of $(CH_2{=}CH_2)Pt(PPh_3)_2$ (5 mol%), the B–Si bond of **1** preferentially added to the terminal double bond of **2f**, furnishing **4f** as the sole product (94% GC yield, entry 9). However, application of this catalyst to the borylsilylation of monosubstituted

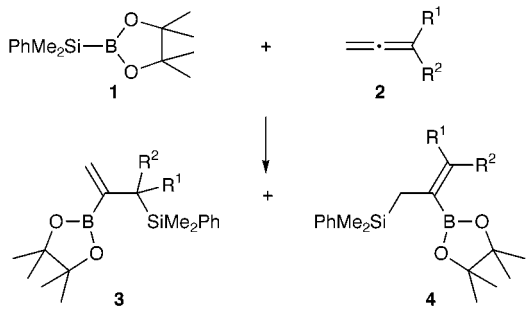

Scheme 1

Table 1 Borylsilylation of 1,2-dienes[ab]

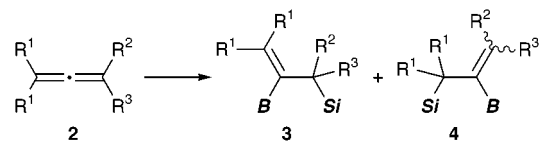

	1,2-Diene					
Entry	**2**	R^1	R^2	R^3	Yield (%)[c]	**3** : **4**[d]
1	**2a**	H	Me	H	88 (98)	100 : 0
2	**2b**	H	OMe	H	86 (93)	100 : 0
3[e]	**2c**	H	H	H	91 (96)	—
4	**2d**	Me	Me	Me	92 (94)	—
5	**2e**	H	Ph	Ph	94	0 : 100
6	**2f**	H	Me	Me	84 (85)	52 : 48
7[f]	**2f**	H	Me	Me	(90)	100 : 0
8[g]	**2f**	H	Me	Me	(90)	71 : 29
9[h]	**2f**	H	Me	Me	87 (94)	0 : 100

[a] Reaction conditions: borylsilane **1** (0.33 mmol), 1,2-dienes (1.0 mmol), catalyst $Pd_2(dba)_3$ (2.5 mol%)–etpo (10.0 mol%), THF (1 ml), 80 °C, 9 h unless otherwise noted. [b] ***Si*** = $SiMe_2Ph$, ***B*** = $B(OCMe_2)_2$. [c] Isolated yields based on the amount of the borylsilane **1**. Figures in parentheses are GC yields. [d] Determined by ^1H NMR spectroscopy. [e] A large excess of 1,2-diene was used. [f] $Pd_2(dba)_3$ (2.5 mol%)–PPh_3 (10.0 mol%) was used as catalyst. [g] $Pd_2(dba)_3$ (2.5 mol%)–PMe_3 (10.0 mol%) was used as catalyst. [h] Run in the presence of $(CH_2{=}CH_2)Pt(PPh_3)_2$ (5 mol%) at 80 °C for 3 h.

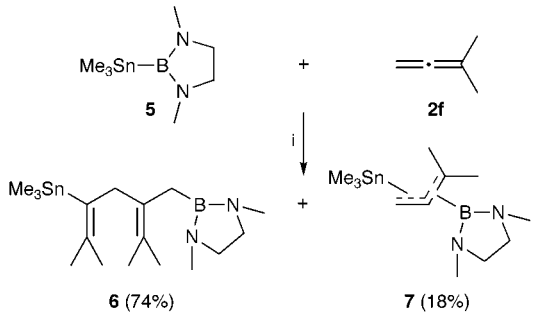

Scheme 2 *Reagents and conditions*: i, $Pd_2(dba)_3$ (2.5 mol%)–etpo (10 mol%), THF, 50 °C, 3 h.

1,2-dienes such as **2a** made the reaction sluggish, resulting in the formation of a mixture of many products.

The reactivities of borylsilanes in the present reaction were strongly influenced by the structure of the boryl group. For instance, $PhMe_2Si$–(BNMeCH_2CH_2NMe) failed to undergo the addition reaction with **2f** even at elevated temperatures (*e.g.* 110 °C) in the presence of the $Pd_2(dba)_3$–etpo system.

In contrast to the borylsilylation of 1,2-dienes, the B–Sn bond of borylstannane **5** underwent the palladium-catalysed addition reaction with 3-methylbuta-1,2-diene **2f**, predominantly yielding telomer **6** having both vinyl–Sn and allyl–B moieties (74% GC yield) along with an isomeric mixture of simple borylstannylation products **7** (18% GC yield) (Scheme 2). The reaction proceeded smoothly at 50 °C in the presence of the $Pd_2(dba)_3$–etpo system and was complete within 3 h. The purification of the reaction mixture by bulb-to-bulb distillation (116–118 °C/5.4×10^{-3} mmHg) afforded analytically pure **6** in 63% yield.† The structure of **6** was determined by NMR spectroscopy; its ^{119}Sn NMR spectrum displayed a signal at δ −49.6 assignable to tin attached to an alkenyl group.[3,4] In addition, the ^{13}C NMR spectrum showed a broad signal at δ 16.2 indicative of an allylic carbon bonded to boron. Further studies on the reaction mechanism are in progress.

In conclusion, the transition-metal-catalysed addition reaction of B–Si or B–Sn bonds to 1,2-dienes provides a selective and facile route to organometallic compounds containing both vinyl- and allyl-metal moieties. In view of the different reactivities of these metal moieties in electrophilic substitution, the products will find considerable synthetic applications for complex organic molecules.

Partial financial support from the Science and Technology Corporation (JST) through the CREST (Core Research for Evolutional Science and Technology) program is gratefully acknowledged.

Notes and references

† Selected *data* for **3a**: δ_H 0.32 and 0.34 (both s, 6H, $SiCH_3$), 1.03 (s, 12H, $OCCH_3$), 1.20 (d, *J* 7.6, 3H, CCH_3), 2.52 (q, *J* 7.6, 1H, CH), 5.52 (d, *J* 2.9, 1H, $=CH_2$), 6.24 (s, *J* 2.9, 1H, $=CH_2$), 7.18–7.24 (m, 3H, arom), 7.51–7.59 (m, 2H, aromatic); δ_C −5.3 and −3.5 ($SiCH_3$), 14.8 (CCH_3), 25.0 ($OCCH_3$), 26.8 (CH), 83.3 ($OCCH_3$), 126.3 ($=CH_2$), 127.9, 129.1, 134.6, 138.5 (arom), 145.3 (br s, =CB); δ_{Si} −1.7; δ_B 30.4. For **3b**: δ_H 0.41 and 0.45 (both s, 6H, $SiCH_3$), 0.99 and 1.01 (both s, 12H, $OCCH_3$), 3.21 (s, 3H, OCH_3), 4.28 (s, 1H, CH), 5.97 (d, *J* 4.0, 1H, $=CH_2$), 6.29 (d, *J* 4.0, 1H, $=CH_2$), 7.17–7.25 (m, 3H, arom), 7.67–7.72 (m, 2H, arom); δ_C −5.6 and −4.5 ($SiCH_3$), 24.9 and 25.0 ($OCCH_3$), 58.4 (OCH_3), 78.7 (CH), 83.3 ($OCCH_3$), 126.7 ($=CH_2$), 127.9, 129.3, 135.0, 137.8 (arom), =CB not observed; δ_{Si} −5.9; δ_B 30.0. For **3c**: δ_H 0.32 (s, 6H, $SiCH_3$), 1.02 (s, 12H, $OCCH_3$), 2.11 (s, 2H, $SiCH_2$), 5.49 (s, 1H, $=CH_2$), 6.09 (s, 1H, $=CH_2$), 7.18–7.23 (m, 3H, arom), 7.51–7.54 (m, 2H, arom); δ_C −3.0 ($SiCH_3$), 24.6 ($SiCH_2$), 24,9 ($OCCH_3$), 83.4 ($OCCH_3$), 128.0 (arom), 128.3 ($=CH_2$), 129.1, 134.3 (arom), 138.9 (br s, =CB), 139.3 (arom); δ_{Si} −4.1; δ_B 30.2. For **3d**: δ_H 0.45 (s, 6H, $SiCH_3$), 1.11 (s, 12H, $OCCH_3$), 1.27 (s, 3H, $=CCH_3$), 1.33 (s, 6H, CCH_3), 1.82 (s, 3H, $=CCH_3$), 7.18–7.21 (m, 3H, arom), 7.57–7.61 (m, 2H, arom); δ_C −3.7 ($SiCH_3$), 23.5 ($=CCH_3$), 25.5 ($OCCH_3$), 27.2 ($=CCSi$), 27.4 ($=CCH_3$), 27.8 (CCH_3), 82.9 ($OCCH_3$), 127.6, 128.9, 135.1 (arom), 136.4 ($=CMe_2$), 139.3 (arom), =CB not observed; δ_{Si} 1.7; δ_{Bi} 31.1. For **3e**: δ_H 0.39 (s, 6H, $SiCH_3$), 0.94 (s, 12H, $OCCH_3$), 2.36 (s, 2H, $SiCH_2$), 6.96–7.21 (m, 11H, arom), 7.30–7.35 (m, 2H, arom), 7.43–7.48 (m, 2H, arom); δ_C −1.5 ($SiCH_3$), 23.1 ($SiCH_2$), 24.9 ($OCCH_3$), 83.2 ($OCCH_3$), 126.7, 126.9, 127.8, 127.9, 128.5, 129.0, 130.0 (two peaks), 134.2, 140.1, 143.4, 145.9 (arom), 149.7 ($=CPh_2$), =CB not observed; δ_{Si} −2.6; δ_B 31.4. For **3f**: δ_H 0.36 (s, 6H, $SiCH_3$), 1.02 (s, 12H, $OCCH_3$), 1.30 (s, 6H, CCH_3), 5.45 (s, 1H, $=CH_2$), 6.19 (s, 1H, $=CH_2$), 7.18–7.23 (m, 3H, arom), 7.53–7.54 (m, 2H, arom); δ_C −4.8 ($SiCH_3$), 24.8 (CCH_3), 24.9 ($OCCH_3$), 29.0 ($SiCH_2$), 83.0 ($OCCH_3$), 127.1 ($=CH_2$), 127.7, 129.0, 135.2, 138.1 (arom), 149.6 (br s, =CB); δ_{Si} 1.2; δ_B 30.6. For **4f**: δ_H 0.36 (s, 6H, $SiCH_3$), 1.05 (s, 12H, $OCCH_3$), 1.52 (s, 3H, $=CCH_3$), 2.15 (s, 2H, $SiCH_2$), 2.21 (s, 3H, $=CCH_3$), 7.18–7.23 (m, 3H, arom), 7.56–7.59 (m, 2H, arom); δ_C −2.0 ($SiCH_3$), 21.2 ($SiCH_2$), 22.5 ($=CCH_3$), 24.6 ($=CCH_3$), 25.1 ($OCCH_3$), 82.7($OCCH_3$), 122.0 (br s, =CB), 127.9, 129.0, 134.2, 140.4 (arom), 145.9 [$=C(CH_3)_2$]; δ_{Si} −3.6; δ_B 30.7. For **6**: bp 116–118 °C/5.4×10^{-3} mmHg; δ_H 0.29 (s, J_{HSn} 52.1, 9H, $SnCH_3$), 1.71–1.76 (m, 11H, $3CH_3C=$ and BCH_2), 1.83 (s, J_{HSn} 12.5, 3H, $=CCH_3$), 2.57 (s, 6H, NCH_3), 2.96 (s, 4H, NCH_2), 3.22 [s, J_{HSn} 67.6, 2H, $(=C)_2CH_2$]; δ_C −7.2 (J_{CSn} 324.8, $SnCH_3$), 16.2 (br s, BCH_2), 19.8 (J_{CSn} 54.8, $=CCH_3$), 20.9 ($=CCH_3$), 21.6 (CCH_3), 28.3 (J_{CSn} 53.8, $=CCH_3$), 33.5 (NCH_3), 38.8 (J_{CSn} 50.7, CH_2), 51.8 (NCH_2), 122.5 (C), 130.9 (C), 136.8 (J_{CSn} 525.5, C), 141.3 (J_{CSn} 32.1, C); δ_B 31.7; δ_{Sn} −49.6; *m/z* (EI, 70 eV) 398 ($[M]^+$, 0.9%), 383 ($[M - Me]^+$, 5), 233 ($[M - SnMe_3]^+$, 100).

1 For the applications of alkenyl- and allyl-metals in organic synthesis, see *Comprehensive Organometallic Chemistry II*, ed. E. W. Abel, F. G. A. Stone, G. Wilkinson and A. McKillop, Pergamon, Oxford, 1995, vol. 11.
2 H. Watanabe, M. Saito, N. Sutou, K. Kishimoto, J. Inose and Y. Nagai, *J. Organomet. Chem.*, 1982, **225**, 343.
3 T. N. Mitchell and U. Schneider, *J. Organomet. Chem.*, 1991, **407**, 319.
4 T. N. Mitchell, U. Schneider and B. Fröhling, *J. Organomet. Chem.*, 1990, **384**, C53.
5 T. Ishiyama, T. Kitano and N. Miyaura, *Tetrahedron Lett.*, 1998, **39**, 2357. For the transition-metal-catalysed reactions of organoboranes with unsaturated organic compounds, see: T. B. Marder and N. C. Norman, *Top. Catal.*, 1998, **5**, 63; G. J. Irvine, M. J. G. Lesley, T. B. Marder, N. C. Norman, C. R. Rice, E. G. Robins, W. R. Roper, G. R. Whittell and L. J. Wright, *Chem. Rev.*, 1998, **98**, 2685; L.-B. Han and M. Tanaka, *Chem. Commun.*, 1999, 395.
6 S-y. Onozawa, Y. Hatanaka and M. Tanaka, presented partly at the 25th Symposium on Heteroatom Chemistry, Abstract P37, Kyoto, December 9–11th, 1998.
7 For similar selective addition of B–Si bonds to 1,2-dienes catalysed by Pd–isocyanide complexes, see: M. Suginome, Y. Ohmori and Y. Ito, presented at the 76th Annual Meeting of the Chemical Society of Japan, Abstract 1B635, Yokohama, March 28–31st, 1999.
8 S-y. Onozawa, Y. Hatanaka and M. Tanaka, *Chem. Commun.*, 1997, 1229.
9 S-y. Onozawa, Y. Hatanaka, T. Sakakura, S. Shimada and M. Tanaka, *Organometallics*, 1996, **15**, 5450; S-y. Onozawa, Y. Hatanaka, N. Choi and M. Tanaka, *Organometallics*, 1997, **16**, 5389; S-y. Onozawa, Y. Hatanaka and M. Tanaka, *Tetrahedron Lett.*, 1998, **39**, 9043.

Communication 9/05127I

Redox chemistry of cerocene: the first heterobimetallic organolanthanide complex†

Ulrike Reißmann,[a] Lutz Lameyer,[b] Dietmar Stalke,[b] Peter Poremba[a] and Frank T. Edelmann*[c]

[a] *Institut für Anorganische Chemie der Universität Göttingen, Tammannstr. 4, D-37077 Göttingen, Germany*
[b] *Institut für Anorganische Chemie der Universität Würzburg, Am Hubland, D-97074 Würzburg, Germany*
[c] *Chemisches Institut der Otto-von-Guericke-Universität Magdeburg, Universitätsplatz 2, D-39106 Magdeburg, Germany. E-mail: frank.edelmann@vst.uni-magdeburg.de*

Received (in Basel, Switzerland) 18th May 1999, Accepted 15th August 1999

The first heterobimetallic organolanthanide complex containing two different rare earth elements, $[Yb(thf)_6][Ce(cot''')_2]_2$ 2 [cot''' = η^8-1,3,6-$(Me_3Si)_3C_8H_5$], has been prepared by reacting neutral $[Ce(cot''')_2]$ with Yb metal in THF; the crystal structure of 2 consists of separated $[Yb(thf)_6]^{2+}$ and $[Ce(cot''')_2]^-$ ions.

Extensive electronic structural investigations have been carried out on neutral f-element sandwich complexes of the type $M(cot)_2$ (M = lanthanide, actinide; cot = η^8-C_8H_8).[1] The electronic structure of cerocene $[Ce(cot)_2]$ has especially been the subject of much debate for many years.[2] It is now generally accepted that cerocene and its substituted derivatives are not genuine cerium(IV) organometallics. Sophisticated *ab initio* calculations as well as recent experimental data have revealed that the oxidation state of Ce in cerocene is 3+($4f^1$) and that cerocene is best formulated as a sandwich complex containing two coordinated $(cot)^{1.5-}$ ions.[3] Despite this ambiguity in the *formal* oxidation state of cerium in neutral cerocenes, these compounds should exhibit a rich redox chemistry and serve as valuable precursors for novel sandwich complexes of the lanthanide elements. While the parent cerocene is a pyrophoric material and not readily available,[4] the recently discovered polysilylated derivative $[Ce(cot''')_2]_2$ **1** [cot''' = η^8-1,3,6-$(Me_3Si)_3C_8H_5$][5] appears to be an excellent candidate for such reactivity studies. We report here the use of **1** in the preparation of the first true heterobimetallic organolanthanide complex, *i.e.* the first organolanthanide derivative containing two different lanthanide elements in a single compound.[6]

Stirring a thf solution of **1** in the presence of an excess of $HgCl_2$-activated Yb powder (< 40 mesh) at room temp. results in a gradual colour change from deep purple to bright green, while the suspended metal powder is partially consumed [eqn. (1)].

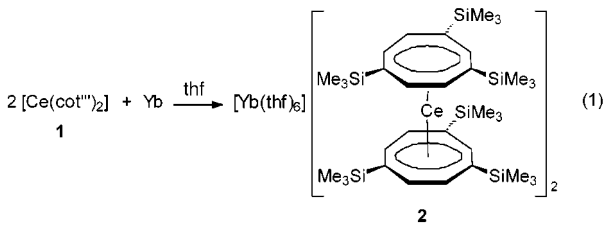

Filtration and crystallisation of the crude product from thf at −25 °C afforded the heterobimetallic ytterbium–cerium complex $[Yb(thf)_6][Ce(cot''')_2]_2$ **2** as bright green, highly air-sensitive crystals in 61% yield.‡ Obviously this product is the result of a redox reaction in which the neutral cerocene precursor **1** is reduced to the corresponding sandwich anion $[Ce(cot''')_2]^-$. The concomitant formation of Yb^{2+} is clearly evidenced by the observation of a relatively sharp ($\nu_{1/2}$ = 15 Hz) ^{171}Yb NMR signal[7] at δ 256.1. As expected, the ^{29}Si NMR spectrum exhibits two signals corresponding to the $SiMe_3$ substituents.

† Dedicated to Professor Helmut Werner on the occasion of his 65th birthday.

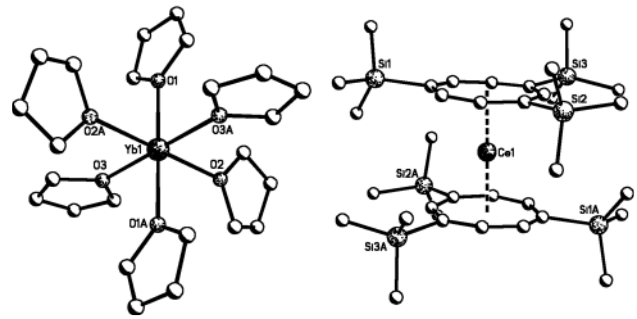

Fig. 1 Solid state structure of **1**; only the $[Yb(thf)_6]^{2+}$ cation and one of the $[Ce(cot''')_2]^-$ anions is depicted. Selected av. bond lengths (pm) and angles (°): Yb–O 237.8(5), Ce–cot_{centre} 205.3(14), Ce–C_{cot} 272(3), C–C_{cot} 141.4(11) [139.9(11)–143.6(11)], C–$SiMe_3$ 188.1(9); O–Yb–O_{cis} 87.7(2)–92.3(2,) O–Yb–O_{trans} 180, cot_{centre}–Ce–cot_{centre} 180.

X-Ray crystallography confirms the presence of the first organolanthanide complex containing two different rare earth elements in one compound (Fig. 1).§

The crystal structure of **2** consists of separated $[Yb(thf)_6]^{2+}$ cations and $[Ce(cot''')_2]^-$ anions. The mean distance between Ce and the ring centroids is 205.3(14) pm, which is in good agreement with the corresponding value in $[Li(thf)_4][Ce(cot)_2]$.[8] Quite surprisingly even the presence of six bulky trimethylsilyl substituents at the cyclooctatetraenyl rings does not lead to a significant elongation of these distances. At 237.8(5) the average Yb–O distance is practically identical to that in $[Yb(thf)_6][CPh_3]_2$ [239.0(7) pm].[9]

In the present study we have demonstrated that the readily available polysilylated cerocene derivative **1** displays an interesting redox chemistry and may thus serve as a promising precursor for the preparation of novel lanthanide organometallics.

Notes and references

‡ *Spectroscopic data* for **2**: IR (KBr): 1401w, 1307w, 1260vs, 1249vs, 1092s (sh), 1072vs, 1067vs, 1020s, 1000m (sh), 972m, 932m, 909w, 862s, 834vs, 806s (sh), 801vs, 771m, 748s, 719m, 686m, 638m, 549m, 513w, 496w, 462w cm^{-1}. ^{1}H NMR (CD_3CN): δ 3.69 (m, 24 H, THF), 2.77 (br, $\nu_{1/2}$ 68 Hz, 16 H, H-4,5,7,8), 2.45 (s br, $\nu_{1/2}$ 43 Hz, 4 H, H-2), 2.19 (s, $\nu_{1/2}$ 10 Hz, 36 H, 6-$SiMe_3$), 2.00 (s, $\nu_{1/2}$ 10 Hz, 72 H, 1,3-$SiMe_3$), 1.84 (m, 24 H, thf). ^{29}Si NMR (CD_3CN): δ −11.5 (s), −11.6 (s). ^{171}Yb NMR (thf–C_6D_6): δ 256.1 (s br, $\nu_{1/2}$ 15 Hz).

§ *Crystal data:* $C_{96}H_{184}Ce_2O_7Si_{12}Yb$. T = 153(2) K, M = 2240.79, triclinic, space group $P\bar{1}$ (no. 2), a = 1473.3(4), b = 1633.8(4), c = 1784.1(5) pm, α = 67.012(12), β = 77.86(2), γ = 75.792(13)°, V = 3.801(2) nm^3, Z = 1, D_c = 0.979 Mg m^{-3}, μ(Mo-Kα) = 1.328 mm^{-1}. A total of 13513 reflections were collected of an oil coated crystal[10] in the θ-range 4.04–22.55°, 9940 of which were independent (R_{int} = 0.0328).

Semiempirical absorption correction was applied using 423 ψ-scans.[11] The structure was solved by Patterson methods using SHELXS-93[12] and refined against F_o^2 using the full matrix least squares method with SHELXL-97.[13] An uncoordinated thf molecule was refined isotropically with a site occupation factor of 0.5. All other non-hydrogen atoms were refined anisotropically. The 1,3,6-tris(trimethylsilyl)cyclooctatetraendiide (cot‴) ligands were disordered and refined to a split occupancy of 44:56 in the case of the cot‴ coordinating Ce1 and 51:49 in the case of the cot‴ coordinating Ce2, employing 3975 bond length similarity restraints. *R*1 [$I > 2\sigma(I)$] = 0.0622, *wR*2 (all data) = 0.2049. CCDC 182/1383. See http://www.rsc.org/suppdata/cc/1999/1865/ for crystallographic files in .cif format.

1 R. G. Hayes and N. M. Edelstein, *J. Am. Chem. Soc*., 1972, **96**, 8688; A. Streitwieser, Jr., U. Müller-Westerhoff, U. G. Sonnischen, D. G. Mares, K. O. Hodgson and C. A. Harmon, *J. Am. Chem. Soc*., 1973, **95**, 8644; H.-D. Amberger, R. D. Fischer and B. Kanellakopulos, *Theor. Chim. Acta (Berlin)*,1975, **37**, 105; N. Rösch and A. Streitwieser, Jr., *J. Organomet. Chem*., 1978, **145**, 195; R. F. Dallinger, P. Stein and T. G. Spiro, *J. Am. Chem. Soc*., 1978, **100**, 7865; P. Pyykkö and L. L. Lohr, *Inorg. Chem.*, 1981, **20**, 1950; N. Rösch and A. Streitwieser, Jr., *J. Am. Chem. Soc*., 1983, **105**, 7237; N. Rösch, *Inorg. Chim. Acta*, 1984, **94**, 297; P. M. Boerrigter, E. J. Baerends and J. G. Snijders, *Chem. Phys*., 1988, **122**, 357; A. H. H. Chang and R. M. Pitzer, *J. Am. Chem. Soc*., 1989, **111**, 2500.

2 A. Streitwieser, Jr., S. A. Kinsley, J. T. Rigsbee, I. L. Fragalà, E. Ciliberto and N. Rösch, *J. Am. Chem. Soc*., 1985, **107**, 7786; T. R. Boussie, D. C. Eisenberg, J. Rigsbee, A. Streitwieser and A. Zalkin, *Organometallics*, 1991, **10**, 1922; R. D. Fischer, *Angew. Chem.*, 1994, **106**, 2253; *Angew. Chem., Int. Ed. Engl*., 1994, **33**, 2165.

3 C. S. Neumann and P. Fulde, *Z. Phys. B*, 1989, **74**, 277; M. Dolg, P. Fulde, W. Küchle, C. S. Neumann and H. Stoll, *J. Chem. Phys*., 1991, **94**, 3011; M. Dolg, P. Fulde, H. Stoll, H. Preuss, A. Chang and R. M. Pitzer, *Chem. Phys*., 1995, **195**, 71; N. M. Edelstein, P. G. Allen, J. J. Bucher, D. K. Shuh, C. D. Sofield, N. Kaltsoyannis, G. H. Maunder, M. R. Russo and A. Sella, *J. Am. Chem. Soc*., 1996, **118**, 13115.

4 A. Greco, S. Cesca and G. Bertolini, *J. Organomet. Chem.*, 1976, **113**, 321.

5 U. Kilimann, R. Herbst-Irmer, D. Stalke and F. T. Edelmann, *Angew. Chem*., 1994, **106**, 1684; *Angew. Chem., Int. Ed. Engl*., 1994, **33**, 1618.

6 H. Schumann, J. A. Meese-Marktscheffel and L. Esser, *Chem. Rev*., 1995, **95**, 865; F. T. Edelmann, in *Comprehensive Organometallic Chemistry II*, ed. E. W. Abel, F. G. A. Stone and G. Wilkinson, Pergamon Press, London, 1995, vol. 4.

7 A. G. Avent, M. A. Edelman, M. F. Lappert and G. A. Lawless, *J. Am. Chem. Soc*., 1989, **111**, 3423; J. van den Hende, P. B. Hitchcock, S. A. Holmes and M. F. Lappert, *J. Chem. Soc., Dalton Trans*., 1995, 1435.

8 U. Kilimann, M. Schäfer, R. Herbst-Irmer and F. T. Edelmann, *J. Organomet. Chem*., 1994, **469**, C10.

9 L. N. Bochkarev, N. E. Molosnova, L. N. Zakharov, G. K. Fukin, A. I. Yanovsky and Y. T. Struchkov, *J. Organomet. Chem*., 1995, **485**, 101.

10 D. Stalke, *Chem. Soc. Rev*., 1998, **27**, 171.

11 A. C. T. North, D. C. Phillips and F. S Mathews, *Acta Crystallogr., Sect. A*, 1968, **24**, 351.

12 G. M. Sheldrick, *Acta Crystallogr., Sect. A*, 1990, **46**, 467.

13 G. M. Sheldrick, Program for crystal structure refinement, Universität Göttingen, 1996.

Communication 9/03954F

$(NBu^n_4{}^+)_3[Re_6S_8Cl_6]^{3-\cdot}$: synthesis and luminescence of the paramagnetic, open shell member of a hexanuclear chalcohalide cluster redox system

Christophe Guilbaud,[a] André Deluzet,[a] Benoît Domercq,[a] Philippe Molinié,[a] Claude Coulon,[b] Kamal Boubekeur[a] and Patrick Batail*[a]

[a] *Institut des Matériaux Jean Rouxel, UMR 6502 CNRS-Université de Nantes, 2, rue de la Houssinière, 44322 Nantes, France. E-mail: patrick.batail@cnrs-imn.fr*

[b] *Centre de Recherche Paul Pascal, CNRS, Avenue Dr. Schweitzer, 33600 Pessac, France*

Received (in Cambridge, UK) 11th June 1999, Accepted 3rd August 1999

The chemical and electrochemical synthesis, X-ray crystal structure, magnetic characterization, absorption and luminescence spectra of $(NBu^n_4)_3[Re_6S_8Cl_6]$, the 23-electron cluster core member of the reversible redox couple $[Re_6S_8Cl_6]^{4-}$–$[Re_6S_8Cl_6]^{3-\cdot}$ is reported.

Amongst the series of molecular, hexanuclear sulfidohalide and sulfido cluster anions, $(NBu^n_4{}^+)_n[Re_6S_{4+n}Cl_{4-n}Cl_6]^{n-}$ (n = 1–4),[1,2] the latter tetra-anion stands out because of its unusual redox behaviour, characterised by a reversible one-electron oxidation process at the remarkably low potential of $E_{1/2}$ = 0.27 V *vs.* SCE in acetonitrile.[2] This is a salient feature since, within this set of isostructural and isoelectronic cluster anions, either no oxidation (n = 1) or reversible oxidation processes (n = 2,3) are observed albeit at the higher potential values of 0.99 (n = 2) and 1.04 (n = 3) V *vs.* SCE.[1] Both the low potential value, which qualifies $[Re_6S_8Cl_6]^{4-}$ as an electron donor comparable to tetrathiafulvalene (0.33 V *vs.* SCE in acetonitrile), and the reversible character of the redox process suggest that the paramagnetic 23-electron Re_6 cluster core anion might be isolated, an unprecedented opportunity in this chemistry of molecular forms of mineral clusters prepared by high temperature solid state synthesis.

Reactions of acetonitrile solutions of $(NBu^n_4)_4[Re_6S_8Cl_6]$[2] with $SOCl_2$, ferrocenium or $TCNQF_4$ afford crystalline precipitates the X-ray powder pattern of which differs from that of the starting material, and appears very similar to those of $(NBu^n_4)_3[Re_6S_7Cl_7]$[3,4] and $(NBu^n_4)_3[Re_6S_7(SH)Cl_6]$[2] simulated from the single crystal X-ray structure data. Thus, an excess of $SOCl_2$ (0.8 mL) was added under stirring at room temperature to a yellow solution of $(NBu^n_4)_4[Re_6S_8Cl_6]$ (263 mg, 0.1 mmol) in acetonitrile (30 mL), upon which the solution rapidly turned red. After 30 min, the solution was evaporated to dryness and the residual solid washed with water, ethanol and toluene, then dried under vacuum. Crystallisation in acetonitrile–ethanol (2:1) afforded red orange plate-like crystals (yield 221 mg, 93%).

Red single crystals were grown by anodic, constant low direct current oxidation (1.6 μA cm^{-2}) at a platinum wire electrode of a solution of 60 mg of $(NBu^n_4)_4[Re_6S_8Cl_6]$ dissolved in 12 mL THF–DMF (3:1). The solution slowly turned from yellow to pink red in the anodic compartment of the two-compartment electrocrystallization cell within a few days. The crystals harvested after 10 days lose THF molecules and recrystallisation of the latter in acetonitrile yielded high quality red orange stable single crystals which are identical to those obtained by the chemical route described above (Anal. for $C_{48}H_{108}Cl_6N_3Re_6S_8$. Calc.: C, 24.91; H, 4.75; N, 1.82; S, 11.08; Cl, 9.19. Found: C, 24.87; H, 4.61; N, 1.78; S, 11.13; Cl, 9.25%). In order to ensure that both the chemical and electrochemical syntheses were conducted on pristine $(NBu^n_4)_4[Re_6S_8Cl_6]$, with no $(NBu^n_4)_3[Re_6S_7Cl_7]$, the purity of the starting material has been qualified by X-ray powder pattern and elemental analysis.

The X-ray structure determination reveals that a single phase, formulated as $(NBu^n_4)_3[Re_6S_8Cl_6]$, is obtained by the two routes and is isostructural to triclinic $(NBu^n_4)_3[Re_6S_7Cl_7]$,[4] containing the closed shell, 24-electron cluster core trianion prepared by metathesis of solutions of $Cs_3[Re_6S_7Cl_7]$.[3] The asymmetric unit consists of two half-clusters located on inversion centres and three tetrabutylammonium cations in general positions. The analysis of the structure determined at room temperature indicates that the Re–Re bond lengths within the cluster core (Fig. 1) [$<d_{Re-Re}>$ = 2.600(1) Å] and the Re–(inner)μ_3-S bond lengths [$<d_{Re-S}>$ = 2.408(3) Å] are similar to those observed in the structure of $(NBu^n_4{}^+)_4[Re_6S_8Cl_6]^{4-}$, $<d_{Re-Re}>$ = 2.601(4) Å and $<d_{Re-S}>$ = 2.403(9) Å, respectively.[2] Of particular interest is the present opportunity to extend the structural correlation between the lengthening of the rhenium–μ-chloride distances with the increase of the net cluster anion charge revealed previously within the series of cluster anion forms with the same counter cation, $(NBu^n_4{}^+)_n[Re_6S_{4+n}Cl_{4-n}Cl_6]^{n-}$ [from 2.344(4), to 2.362(2), to 2.415(3) Å for n = 1, 2, 3, respectively).[1,4] Thus, $<d_{Re-Cl}>$ = 2.418(3) Å for $[Re_6S_8Cl_6]^{3-\cdot}$ is shorter than $<d_{Re-Cl}>$ = 2.451(4) Å determined for $(NBu^n_4{}^+)_4[Re_6S_8Cl_6]^{4-}$,[2] as expected.[1] This is also consistent with theoretical calculations for $[Re_6S_8X_6]^{4-}$ (X = Cl, Br, I) made available recently by Arratia-Perez *et al.*[5] which demonstrate that the pronounced halogen-based cluster HOMO has a large Re–(apical)halide antibonding character. In addition, $<d_{Re-Cl}>$ = 2.418(3) Å for $(NBu^n_4{}^+)_3[Re_6S_8Cl_6]^{3-\cdot}$ is identical to that obseved for the triclinic structure of $(NBu^n_4{}^+)_3[Re_6S_7Cl_7]^{3-}$ [$<d_{Re-Cl}>$ = 2.415(3) Å][4] and to that determined for $(NBu^n_4{}^+)_3[Re_6S_6(SH)Cl_7]^{3-}$ [$<d_{Re-Cl}>$ = 2.419(6) Å].[2]

The paramagnetic character of $(NBu^n_4{}^+)_3[Re_6S_8Cl_6]^{3-\cdot}$ is demonstrated both by (i) static magnetic susceptibility data, properly fitted to a Curie law down to low temperatures (C = 0.523 $cm^3\ mol^{-1}$) with a calculated effective magnetic moment (μ_{eff} = 2.045 μ_B) larger than the spin ½-only value (μ_{SO} = 1.73

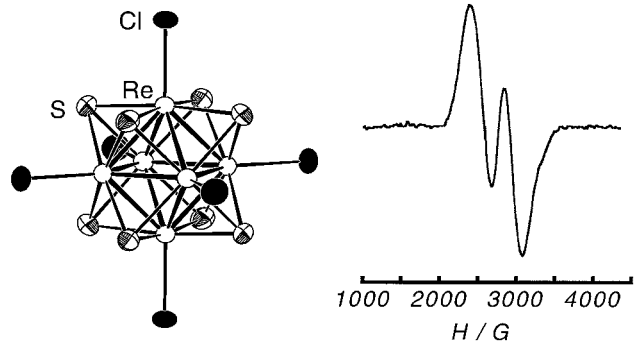

Fig. 1 Structure with thermal ellipsoids at the 50% probability level, labelling scheme and EPR spectrum of a single crystal of $(NBu^n_4)_3[Re_6S_8Cl_6]$ at 3.8 K. The two broad resonance lines with g = 2.44 and ΔH = 260 G are associated with two different orientations of the cluster in the triclinic unit cell.

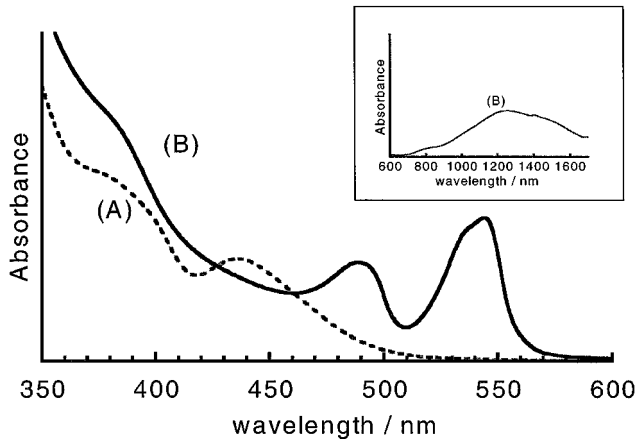

Fig. 2 Electronic absorption spectra for acetonitrile solutions ($c = 2.8 \times 10^{-4}$ M) of $(NBu^n_4)_4[Re_6S_8Cl_6]$ [(A) two poorly resolved shoulders at 335 and 380 nm and a peak of larger intensity at 436 nm ($\varepsilon_M = 8.6 \times 10^2$ dm^3 mol^{-1} cm^{-1})] and $(NBu^n_4)_3[Re_6S_8Cl_6]$ [(B), one poorly resolved shoulder (381 nm), two large peaks (489 nm, $\varepsilon_M = 8.5 \times 10^2$ dm^3 mol^{-1} cm^{-1}; 544 nm, $\varepsilon_M = 1.23 \times 10^3$ dm^3 mol^{-1} cm^{-1}) and a very wide band centred around 1250 nm (700–1750 nm, $\varepsilon_M = 4 \times 10^2$ dm^3 mol^{-1} cm^{-1})].

μ_B), a manifestation of spin–orbit coupling; and (ii) by single crystal EPR experiments ($g = 2.44$, Fig. 1). The g values for the paramagnetic hexanuclear molybdenum cluster anions $[Mo_6(X_7Q)X_6]^{2-\cdot}$ (X = Cl, Br, Q = S, Se) and $[Mo_6(Cl_6Se_2)Cl_6]^{3-\cdot}$ obtained in frozen solution at 77 K are in the range 2.05–2.23.[6,7] The higher g value observed for the present rhenium cluster is consistent with a higher spin–orbit coupling.

The UV–VIS spectrum for $(NBu^n_4{}^+)_4[Re_6S_8Cl_6]^{4-}$ in acetonitrile (Fig. 2) is essentially identical to that reported earlier by Holm and coworkers except for the absence in Fig. 2 of a weak peak at 537 nm.[2] Within the series $[Re_6S_{4+n}Cl_{4-n}Cl_6]^{n-}$, the intense absorption at 436 nm for the tetra-anion ($n = 4$) is remarkable since it is not observed for $n = 1$, 2, 3[8] and has been shown[2] to be very sensitive to the nature of the apical halide, a likely indication of ligand-to-metal charge transfer. The spectrum for acetonitrile solutions of $(NBu^n_4{}^+)_3[Re_6S_8Cl_6]^{3-\cdot}$ (Fig. 2) is strikingly different from the former. These salient differences between the spectra in Fig. 2 demonstrate that a significant change of the electronic structure of the cluster anion occurs upon the one-electron oxidation. The wide near-IR absorption band may be attributed to electronic transitions from a fully to a partially occupied metal orbital. A similar absorption band has been observed for the paramagnetic hexanuclear molybdenum clusters anions $[Mo_6(X_7Q)X_6]^{2-\cdot}$ (X = Cl, Br, Q = S, Se) and $[Mo_6(Cl_6Se_2)Cl_6]^{3-\cdot}$.[6,7]

Emission spectra for acetonitrile solutions of $[Re_6S_8Cl_6]^{4-}$ and $[Re_6S_8Cl_6]^{3-\cdot}$ are shown in Fig. 3(a) and (b), respectively, for excitations at 250 and 393 nm. As anticipated by Arratia-Pérez *et al.*,[5] the tetra-anion $[Re_6S_8Cl_6]^{4-}$ is luminescent. Altogether, the luminescence for the tetra-anion is very similar to that for the hexanuclear molybdenum(II) cluster $[Mo_6Cl_{14}]^{2-}$.[9,10] Note that the mono-, di-, and tri-anion within the chalcohalide series $[Re_6S_{4+n}Cl_{4-n}Cl_6]^{n-}$ ($n = 1$, 2, 3) do not present any such luminescence.

Strikingly, the luminescence spectra for acetonitrile solutions of $(NBu^n_4{}^+)_3[Re_6S_8Cl_6]^{3-\cdot}$ [Fig. 3(b)] exhibit emission bands which are typically more intense than those for solutions of $(NBu^n_4{}^+)_4[Re_6S_8Cl_6]^{4-}$. Time-resolved photoluminescent experiments in solution as well in the solid state are in progress in order to elucidate the nature of the excited state of the paramagnetic radical cluster anion in $(NBu^n_4{}^+)_3[Re_6S_8Cl_6]^{3-\cdot}$.

We thank P. Robin (Thomson-CSF, LCR) for assistance in optical experiments. Financial support from the CNRS, The Region Pays de Loire and the Ministry of Education (C. G. and A. D.), DGA (B. D.) is gratefully acknowledged.

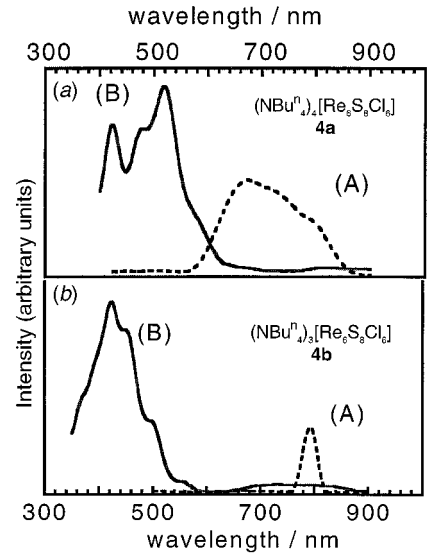

Fig. 3 (a) Luminescence spectra for an acetonitrile solution of $(NBu^n_4)_4[Re_6S_8Cl_6]$ (5×10^{-4} M) for excitations at 393 nm [(A), maximum at 660 nm] and 250 nm [(B), maxima at 418, 460 and 497 nm]. (b) Luminescence spectra for an acetonitrile solution of $(NBu^n_4)_3[Re_6S_8Cl_6]$ (1.4×10^{-4} M) for excitations at 393 nm [(A), maximum at 796 nm] and 250 nm [(B), maxima at 420, 455 and 500 nm].

Notes and references

† *Crystal structure analysis* for $(NBu^n_4)_3[Re_6S_8Cl_6]$: $C_{48}H_{108}Cl_6N_3Re_6S_8$, triclinic, space group $P\bar{1}$, $a = 12.378(1)$, $b = 17.229(1)$, $c = 18.205(2)$ Å, $\alpha = 96.39(1)$, $\beta = 106.33(1)$, $\gamma = 103.57(1)°$, $V = 3555.6(12)$ Å^3, $D_c = 2.161$ g cm^{-3}, $Z = 2$. Red–orange plate-like crystal ($0.56 \times 0.23 \times 0.02$ mm). Data were collected at 293 K on a Stoe IPDS single ϕ axis diffractometer with a 2D area detector based on imaging plate technology with Mo-Kα radiation ($\lambda = 0.71073$ Å) (250 frames recorded using the rotation method ($0 \leqslant \phi \leqslant 250°$) with $\Delta\phi = 1°$ increments, an exposure time of 5 min and a crystal-to-plate distance of 60 mm).[11] A total of 35884 reflections were collected up to $\theta = 25.8°$ of which 13220 are independent among 9098 observed [$F_o^2 > 2\sigma(F_o^2)$]. The structure solution (SHELXS-86)[12] and refinements on F_o^2 (SHELXL-97)[13] gave R(obs.) = 0.0329 [R(all) = 0.0546)] and R_w(obs.) = 0.0674 [R_w(all) = 0.0712] for 669 parameters and two restraints; min. and max. residual electron densities were 1.78 and 1.76 e Å^{-3}.

CCDC 182/1360. See http://www.rsc.org/suppdata/cc/1999/1867/ for crystallographic files in .cif format.

1 J.-C. Gabriel, K. Boubekeur and P. Batail, *Inorg. Chem.*, 1993, **32**, 2894.
2 J. R. Long, L. S. McCarthy and R. H. Holm, *J. Am. Chem. Soc.*, 1996, **118**, 4603.
3 C. B. Guilbaud, J.-C. P. Gabriel, K. Boubekeur and P. Batail, *C.R. Acad. Sci. Paris, t. 1, Ser. IIc*, 1998, 765.
4 $C_{48}H_{108}Cl_7N_3Re_6S_7$, triclinic, space group $P\bar{1}$, $a = 12.334(8)$, $b = 17.252(9)$, $c = 18.165(9)$ Å, $\alpha = 96.32(4)$, $\beta = 106.15(5)$, $\gamma = 103.55(4)°$, $V = 3545(4)$ Å^3; S. Uriel, K. Boubekeur and P. Batail, unpublished material.
5 J. Arratia-Pérez and L. Hernàndez-Acevedo, *J. Chem. Phys.*, 1999, **110**, 2529.
6 M. Ebihara, K. Toriumi and K. Saito, *Inorg. Chem.*, 1988, **27**, 13.
7 M. Ebihara, K. Toriumi, Y. Sasaki and K. Saito, *Gazz. Chim. Ital.*, 1995, **125**, 87.
8 C. B. Guilbaud, PhD Thesis, University of Nantes, France, 1998.
9 A. W. Maverick and H. B. Gray, *J. Am. Chem. Soc.*, 1981, **103**, 1298.
10 A. W. Maverick, J. S. Najdzionek, D. MacKenzie, D. G. Nocera and H. B. Gray, *J. Am. Chem. Soc.*, 1983, **105**, 1878.
11 STOE & Cie Gmbh, User's Manual V2.87, Darmstadt, Germany 1997.
12 G. M. Sheldrick, SHELXS-86, Program for Crystal Structure Solution, University of Göttingen, Germany, 1986.
13 G. M. Sheldrick, SHELXL-97, Program for Crystal Structure Refinement, University of Göttingen, Germany, 1997.

Communication 9/04669K

Synthesis of optically active bicyclic lactone building blocks using catalytic enantioselective glyoxylate-ene reaction

Nicholas Gathergood and Karl Anker Jørgensen*

Center for Metal Catalyzed Reactions, Department of Chemistry, Aarhus University, DK-8000 Aarhus C, Denmark. E-mail: kaj@kemi.aau.dk

Received (in Cambridge, UK) 12th July 1999, Accepted 13th August 1999

A new catalytic approach for the formation of optically active bicyclic lactones applying an enantioselective glyoxylate-ene reaction is presented; the catalytic reaction proceeds with formation of the two key stereogenic centers in good yield and with high diastereo- and enantio-selectivity.

The bicyclic lactones **1** are key intermediates for the preparation of a wide range of natural products and biologically active compounds.[1] The lactone **1a** is a versatile building block for the synthesis of *e.g.* brefeldin A,[2a] carbovir,[2b] sesbanimide A and B,[2c] menovilin,[2d] aristeromycin,[2e] carbodine,[2e] carboxylic nucleosides[2f] and carbocyclic analogues of polytoxins and nikkomycines.[2g]

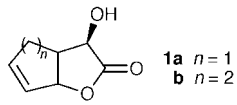

The synthesis of optically active **1a** has previously been accomplished by enzyme catalyzed kinetic resolution of the racemic compound prepared by the Diels–Alder reaction between glyoxylic acid and cyclopentadiene,[3] and more recently Helmchen *et al.* presented the preparation of **1a** using an asymmetric palladium-catalyzed allylic alkylation of 2-acetoxymalonates with cyclopent-2-enyl chloride.[4]

Here we present the first catalytic enantioselective ene reaction of cyclopentene **2a** with glyoxylate leading to a novel synthetic approach for the preparation of (+)-**1a** and by which the key stereogenic centres required for the synthesis of (+)-**1a** are formed in one step. The synthetic approach for (+)-**1a** is outlined in Scheme 1.

Recently, it has been shown that the bicyclic lactones **1b** can be prepared by a catalytic enantioselective hetero-Diels–Alder reaction of cyclohexadiene with glyoxylates catalyzed by C_2 bisoxazoline–copper(II) complexes followed by a rearrangement reaction.[5] Unfortunately, this methodology is not feasible for the reaction of cyclopentadiene with glyoxylates. However, the reaction of conjugated dienes with glyoxylates catalyzed by

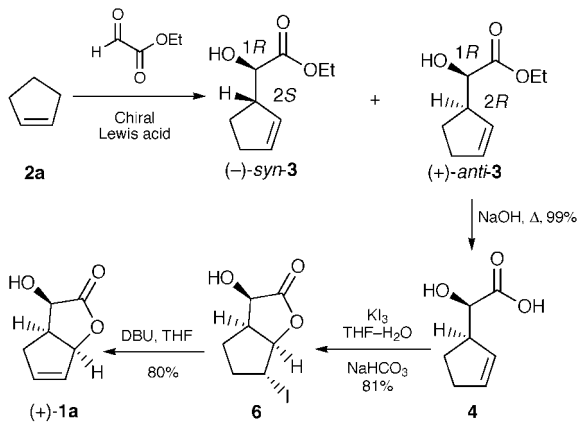

Scheme 1

C_2 bisoxazoline–copper(II) complexes gives two products, the hetero-Diels–Alder and ene products,[5a] and recently Evans *et al.*[6] developed further the latter reaction for 1,1-disubstituted alkenes, hexene and cyclohexene with high yields and enantioselectivities.

The crucial step in the total synthesis of (+)-**1a** is the catalytic ene reaction of cyclopentene **2a** with ethyl glyoxylate. This reaction has been investigated in the presence of the C_2-symmetric bisoxazoline ligands **5a**,**b** and copper(II) salts as the

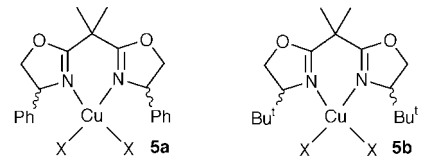

Lewis acids.† Some representative results are presented in Table 1.

The results in Table 1 show that the C_2 bisoxazoline–copper(II) complex catalyzed ene reaction of cyclopentene **2a** with ethyl glyoxylate proceed with excellent enantioselectivities for both diastereomers formed. The ligand (*S*)-**5b** gave the highest enantioinduction, with up to 98–99% ee (entries 3–5), while ligand (*R*)-**5a** gave the best diastereomeric *anti*-**3**:*syn*-**3** ratio (7.7:1) (entries 1, 6). Changing the enantiomer of the chiral ligand leads to the opposite enantiomer of *anti*-**3** (entries 1, 6), while changing the solvent to $MeNO_2$ leads to higher yield, however, a slight decrease in diastereo- and enantioselectivity (entry 7) is found. In an attempt to improve the enantioselectivity, the reaction was performed at lower temperature, but the conversion at 0 °C was very low (entry 5). An increase in the yield was achieved by increasing the catalyst loading to 25 mol%, without decreasing the diastereo- and enantio-selectivity of the products (entries 2, 6, 7). We have also investigated the enantioselective ene reactions catalyzed by (*R*)-**5a** and (*S*)-**5b** in other solvents and found that in Bu^tOMe, Et_2O and THF a lower yield of *anti*-**3** was isolated. A decrease in the diastereo- and enantio-selectivity was observed, except in Et_2O, where the *anti*-**3**:*syn*-**3** ratio was 5.1:1 with 91% ee and 89% ee

Table 1 Reaction of cyclopentene **2a** with ethyl glyoxylate in the presence of C_2-symmetric bisoxazoline–Cu^{II} salts (10 mol%) in CH_2Cl_2

					Ee (%)	
Entry	Catalyst	*T*/°C	Yield[a] (%)	*anti*-**3**:*syn*-**3**	*anti*-**3** (1*S*,2*S*)	*syn*-**3** (1*S*,2*R*)
1	(*R*)-**5a**–$Cu(OTf)_2$	25	38	7.7:1	91	89
2	(*R*)-**5a**–$Cu(OTf)_2$[b]	25	56	7.3:1	92	87
3	(*S*)-**5b**–$Cu(SbF_6)_2$[b]	25	66	2.2:1	98	97
4	(*S*)-**5b**–$Cu(SbF_6)_2$	25	55	2.8:1	98	96
5	(*S*)-**5b**–$Cu(SbF_6)_2$	0	~5	3.1:1	99	99
6	(*S*)-**5a**–$Cu(OTf)_2$[b]	25	54	7.7:1	92[c]	89[c]
7	(*S*)-**5a**–$Cu(OTf)_2$[bd]	25	72	3.9:1	83[c]	53[c]

[a] Isolated. [b] 25 mol% catalyst. [c] Opposite enantiomer compared with entry 2. [d] Solvent $MeNO_2$.

Table 2 Reaction of allyl stannane **2b** with ethyl glyoxylate in the presence of (*R*)-**5a**–$Cu(OTf)_2$ (10 mol%) in CH_2Cl_2

Entry	**2b** (equiv.)	Ethyl glyoxylate (equiv.)	*T*/°C	Yield (%)	*syn*-**3**: *anti*-**3**	Ee (%) *syn*-**3** (1*S*,2*R*)	Ee (%) *anti*-**3** (1*S*,2*S*)
1	1	2	25	98	2.2:1	24	54
2	1	10	25	99	2.4:1	43	81
3	1	10	−25	97	2.5:1	33	77
4	1	10	−78	99	2.7:1	35	69
5	2	1	25	98	2.3:1	22	24
6	2	1	−78	55	4.4:1	23	53

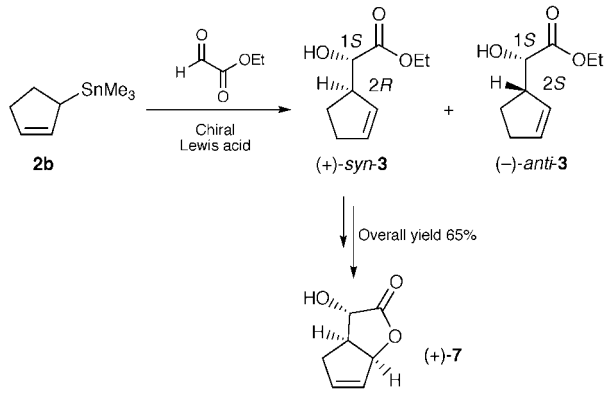

Scheme 2

for the two diastereomers, respectively. It should be noted that the absolute configuration of the ene-product *anti*-**3** is the same when using ligands (*R*)-**5a** and (*S*)-**5b** in combination with copper(II) as the Lewis acid (entries 2, 4). This phenomenon has been observed several times for these catalysts.[5,6]

From (+)-*anti*-**3** the desired bicyclic lactone (+)-**1a** can be obtained in a few steps (Scheme 1). Hydrolysis of the ester group was achieved using refluxing 3 M NaOH for 1 h giving **4** in quantitative yield. Iodolactonization of **4** using KI_3 and $NaHCO_3$ gave the iodide **6** in 81% yield. Elimination with DBU leads to (+)-**1a** in 80% yield.

By comparing the optical rotations of the bicyclic lactone **1a** to literature values[7] the absolute configuration was determined as (+)-**1a**, which leads to assignment of the absolute configuration as shown in Scheme 1.

We believed that an increase in the yield of the ene adduct could be obtained if a more active cyclopentenyl derivative was used. The allyl stannane **2b**[8] was therefore reacted with ethyl glyoxylate (Scheme 2), in the presence of C_2 bisoxazoline–copper(II) complexes; some results are presented in Table 2.

The allyl stannane **2b** was found to be more reactive than cyclopentene **2a** in the C_2 bisoxazoline–copper(II) catalyzed ene reaction with ethyl glyoxylate. At room temperature full conversion was observed in 5 min when using 2 equiv. of **2b** (entry 5). The yield for this reaction was very high, but the ee of the products was low (20% ee). When 1 equiv. of **2b** was used with 2 equiv. of ethyl glyoxylate the reaction was finished after 30 min (entry 1). The yield of the ene products *syn*-**3** and *anti*-**3** were also very good and the ee of the minor product increased to 54% ee. However the ee of the major diastereomer *syn*-**3** remained below 25% ee. By using a larger excess of ethyl glyoxylate at room temperature the ee of the major diastereomer was increased to 43% ee, with 81% ee for the minor diastereomer (entry 2). When the reaction was performed at lower temperatures (−25 and −78 °C) no improvement in the ee of the products was observed (entries 3,4). When using 1 equiv. of ethyl glyoxylate the yield was found to decrease from 98% at room temperature to 55% at −78 °C (entries 5,6). The reason for this drop in yield is attributed to the ethyl glyoxylate oligermerizing due to the extended reaction time. The ee of the major product is not dependant on the temperature of the reaction, whereas an increase from 24 to 53% ee was observed for the minor diastereomer by decreasing the temperature to −78 °C. The diastereoselectivity was also improved from 2.3:1 to 4.4:1 by reducing the temperature (entries 5,6).

The formation of (+)-*syn*-**3** in the catalytic enantioselective ene reaction using the allyl stannane **2b** as the substrate leads to a simple synthetic procedure for the formation of the other diastereomer, (+)-**7**, of (+)-**1a** in 65% overall yield as presented in Scheme 2.

In conclusion we have presented the development of highly diastereo- and enantio-selective ene reactions of cyclopentenes with ethyl glyoxylate leading to the formation of products, which in a few steps give highly attractive optically active bicyclic lactones. Work is in progress to develop this approach further.

We are indebted to The Danish National Research Foundation for financial support.

Notes and references

† *General procedure* for the catalytic ene reaction: A flame dried Schlenk tube was charged with ligand (*S*)-**5a** (84 mg, 0.25 mmol) and $Cu(OTf)_2$ (90 mg, 0.25 mmol) and stirred vigorously *in vacuo* for 1.5 h. Dry CH_2Cl_2 (3 ml) was added and the green suspension stirred until a clear solution formed (2 h). Freshly distilled ethyl glyoxylate (1.02 g, 10 mmol) in toluene (0.25 ml) was added at room temperature followed by the addition of cyclopentene **2a** (88 μl, 1.0 mmol) and stirred for 48 h. The reaction solution was purified by flash chromatography (25% Et_2O–hexane) to give *anti*-**3** in 48% yield (82 mg, 0.48 mmol). A small amount of the lower R_f diastereomer *syn*-**3** was isolated in 6% yield (10 mg, 0.06 mmol). *Selected data* for (+)-*anti*-**3**: $[\alpha]_D^{20}$ +1.25 (*c* 2.5, $CHCl_3$); $\delta_H(CDCl_3)$ 5.94 (ddd, *J* 5.5, 4.4, 2.2, 1H), 5.50 (ddd, *J* 6.1, 4.4, 2.2, 1H), 4.30–4.19 (m, 2H), 4.11 (dd, *J* 7.5, 4.5, 1H), 3.16–3.00 (m, 1H), 2.51 (d, *J* 7.5, 1H), 2.40–2.18 (m, 2H), 2.10–1.98 (m, 1H), 1.92–1.80 (m, 1H), 1.30 (t, *J* 7.2, 3H). $\delta_C(CDCl_3)$ 174.37, 135.02, 128.16, 73.11, 61.42, 49.89, 32.48, 25.85, 14.23; ν_{max}(film)/cm^{-1} 3496, 2941, 2852, 1732, 1446, 1368, 1259, 1197, 1159, 1097, 1027. (HRMS: calc. 170.0943, found 170.0945); *m*/*z* (EI) 170 (M^+), 152, 133, 123, 104, 97, 79, 76, 67 (100%); GC (Chiralsil-DEX CB, *T*. 100 °C, flow rate = 2 ml min^{-1}, retention time = 10.74 min (major, 1*R*,2*R*), 11.90 min (minor, 1*S*,2*S*). For (−)-*syn*-**3**: $[\alpha]_D^{20}$ −0.48 (*c* 3.5, $CHCl_3$); $\delta_H(CDCl_3)$ 5.89 (ddd, *J* 5.5, 4.4, 2.2, 1H), 5.66 (ddd, *J* 6.1, 4.4, 2.2, 1H), 4.31–4.20 (m, 3H), 3.20–3.10 (m, 1H), 2.75 (br s, 1H), 2.48–2.24 (m, 2H), 1.95–1.67 (m, 2H), 1.30 (t, *J* 7.1, 3H); $\delta_C(CDCl_3)$ 174.49, 133.66, 130.19, 72.37, 61.65, 49.94, 32.35, 23.41, 14.26; ν_{max}(film)/cm^{-1} 3495, 2962, 1733, 1457, 1368, 1260, 1195, 1157, 1096, 1021 (HRMS: calc. 170.0943, found 170.0944); *m*/*z* (EI) 170 (M^+), 152, 133, 123, 104, 97, 79, 76, 67 (100%). GC (Chiralsil-DEX CB, *T* 100 °C, flow rate = 2 ml min^{-1}, retention time = 12.55 min (major, 1*R*,2*S*), 13.70 min (minor, 1*S*,2*R*).

1 See *e.g.* K. C. Nicolaou and E. J. Sorensen, *Classics in Total Synthesis*, VCH, New York, 1996.
2 (*a*) V. Betina, L. Drobinica, P. Nemec and M. J. Zenanova, *J. Antibiot., Ser. A*, 1964, **17**, 93; G. Tamura, K. Ando, S. Susuki, A. Takatsuki and K. Arina, *J. Antibiot.*, 1968, **21**, 160; (*b*) R. A. MacKeith, R. McCague, H. F. Olivo, C. F. Palmer and S. M. Roberts, *J. Chem. Soc., Perkin Trans. 1*, 1993, 313; B. M. Trost and Z. Shi, *J. Am. Chem. Soc.*, 1996, **118**, 3037; (*c*) P. A. Grieco, K. J. Henry, J. J. Nunes and J. E. Matt Jr., *J. Chem. Soc., Chem. Commun.*, 1992, 368; (*d*) R. McCague, H. F. Olivo and S. M. Roberts, *Tetrahedron Lett.*, 1993, **34**, 3785; (*e*) F. Burlina, A. Favre, J. L. Fourrey and M, Thomas, *Bioorg. Med. Chem. Lett.*, 1997, **7**, 247; (*f*) H. F. Olivo and J. Yu, *Tetrahedron: Asymmetry*, 1997, **8**, 3785; (*g*) V. K. Aggarwal, N. Monterio, G. J. Tarver and S. D. Lindell, *J. Org. Chem.*, 1996, **61**, 1192.
3 A. Lubineau, A. Augé and N. Lubin, *Tetrahedron Lett.*, 1991, **32**, 7528; F. Burlina, P. Clivio, J.-F. Fourrey, C. Riche and M. Thomas, *Tetrahedron Lett.*, 1994, **35**, 8151; A. Lubineau, A. Augé, E. Grand and N. Lubin, *Tetrahedron*, 1994, **50**, 10 265.
4 S. Kudis and G. Helmchen, *Tetrahedron*, 1998, **54**, 10 449.
5 (*a*) M. Johannsen and K. A. Jørgensen, *J. Org. Chem.*, 1995, **60**, 5757; (*b*) *Tetrahedron*, 1996, **52**, 7321; (*c*) *J. Chem. Soc., Perkin Trans. 2*, 1997, 1183; (*d*) S. Yao, M. Johannsen, R. G. Hazell and K. A. Jørgensen, *J. Org. Chem.*, 1998, **63**, 118; (*e*) K. A. Jørgensen, M. Johannsen, S. Yao, H. Audrain and J. Thorhauge, *Acc. Chem. Res.*, 1999, **32**, 605.
6 D. A. Evans, C. S. Burgey, N. A. Paras, T. Vojkovsky and S. W. Tregay, *J. Am. Chem. Soc.*, 1998, **120**, 5824.
7 R. A. Mackeith, R. McCague, H. F. Olivo, C. F. Palmer and S. M. Roberts, *J. Chem. Soc., Perkin Trans. 1*, 1993, 313.
8 I. W. Muderawan, R. C. Bott and D. J. Young, *Synthesis*, 1998, 1640.

Communication 9/05637H

ChemComm

The crystal structure of 5,6,11,12,17,18-hexadehydro-1,4,7,10,13,16-hexaethynyltribenzo[*a*,*e*,*i*]cyclododecene tetrahydrofuran solvate: a case of high organization enforced by chelating alkyne C–H···O hydrogen bonding

Adam J. Matzger, Moonsub Shim and K. Peter C. Vollhardt*

Department of Chemistry, University of California at Berkeley and the Chemical Sciences Division, Lawrence Berkeley National Laboratory, Berkeley CA 94720-1460, USA. E-mail: vollhard@cchem.berkeley.edu

Received (in Columbia, MO, USA) 30th June 1999, Accepted 23rd July 1999

The crystal structure of the novel title dehydrobenzoannulene reveals supramolecular organization of the hydrocarbon around the occluded solvent molecules induced by novel multiple chelating alkyne C–H···O hydrogen bonds.

The importance of weak hydrogen bonds in the solid state has received increasing recent recognition.[1,2] Despite numerous examples of C≡C–H···Y (Y = N, O, or another electronegative atom) interactions, there appears to be no case in which two such CH bonds chelate the heteroatom. We report herein the crystal structure of 5,6,11,12,17,18-hexadehydro-1,4,7,10,13,16-hexaethynyltribenzo[*a*,*e*,*i*]cyclododecene **1**[3]

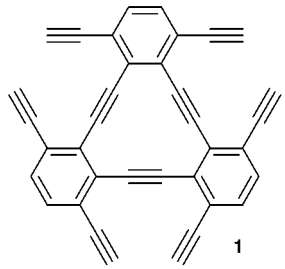

1

and the observation of THF chelation by pairs of proximal alkynyl CH bonds, the latter representing a new type of supramolecular synthon for crystal engineering.

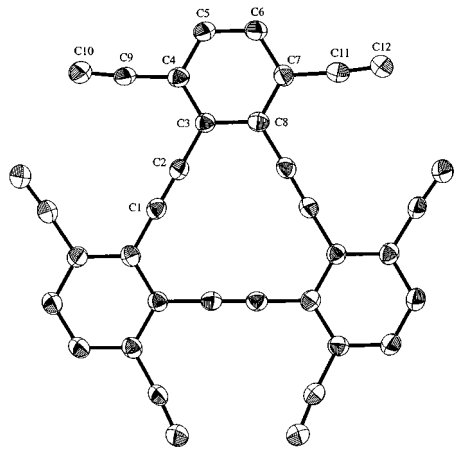

Fig. 1 Structure of **1** in the crystal. Distances (Å) and angles (°): C(1)–C(2) 1.207(3), C(1)–C(8) 1.432(3), C(2)–C(3) 1.432(3), C(3)–C(4) 1.410(3), C(3)–C(8) 1.415(3), C(4)–C(5) 1.401(3), C(4)–C(9) 1.435(3), C(5)–C(6) 1.372(3), C(6)–C(7) 1.402(3), C(7)–C(8) 1.409(3), C(7)–C(11) 1.439(3), C(9)–C(10) 1.184(3), C(11)–C(12) 1.177(3); C(2)–C(1)–(C8) 178.0(2), C(1)–C(2)–C(3) 179.0(2), C(2)–C(3)–C(4) 120.0(2), C(2)–C(3)–C(8) 120.4(2), C(4)–C(3)–C(8) 119.6(2), C(3)–C(4)–C(5) 119.6(2), C(3)–C(4)–C(9) 121.6(2), C(5)–C(4)–C(9) 118.8(2), C(4)–C(5)–C(6) 120.8(2), C(5)–C(6)–C(7) 120.9(2), C(6)–C(7)–C(8) 119.4(2), C(6)–C(7)–C(11) 118.6(2), C(8)–C(7)–C(11) 122.0(2), C(1)–C(8)–C(3) 119.9(2), C(1)–C(8)–C(7) 120.4(2), C(3)–C(8)–C(7) 119.7(2), C(4)–C(9)–C(10) 176.1(2), C(7)–C(11)–C(12) 175.6(3).

As a subunit of, and a potential precursor to, novel carbon allotropes,[4] *e.g.* graphyne,[5] the structure of dehydrobenzoannulene **1** is of particular interest. The compound crystallizes from THF as yellow needles in the space group $R\bar{3}$ (Fig. 1). In agreement with the computed geometry,† the hydrocarbon is slightly twisted in the solid state.‡ In contrast to the hexakis(cyclohexylmethyl) derivative of **1** which adopts local C_2 symmetry in the crystal,[3] the parent compound is D_3 symmetric. The absence of substituents at the alkyne termini allows for considerable planarization, a feature already evident in the electronic spectrum of **1** which resembles most closely that of the unsubstituted tribenzodehydroannulene core which is D_{3h} symmetric.[3]

The asymmetric unit contains a third of **1** which is chelating one molecule of THF, in addition to a disordered, one sixth of THF. Pairs of nonaynes and disk-like THF clusters are generated from the asymmetric unit by a 3-fold rotoinversion axis (Fig. 2). The alkyne pairs alternate with single solvent disks to give columns along the *c*-axis (Fig. 3). In projection, the latter are arranged to form a close-packed array. Each THF disk is composed of six ordered and one disordered molecule. The disorder in the latter is required, because the site symmetry is incommensurate with the molecular symmetry of THF. Each

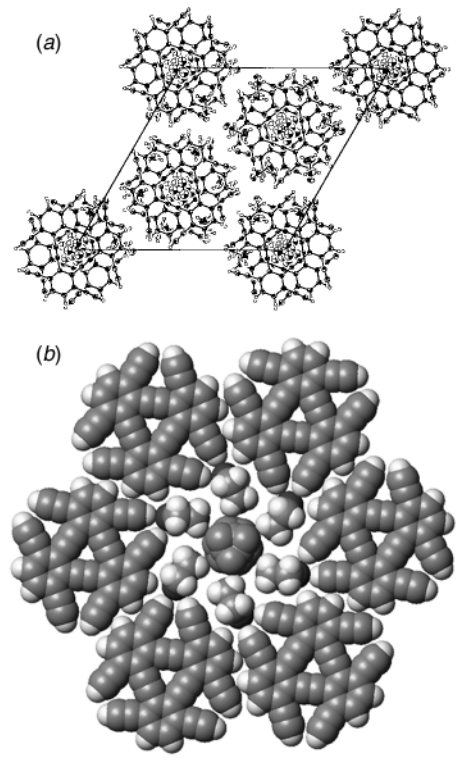

Fig. 2 (*a*) Array of **1** showing molecular packing. (*b*) Space-filling representation of a THF disk surrounded by **1**.

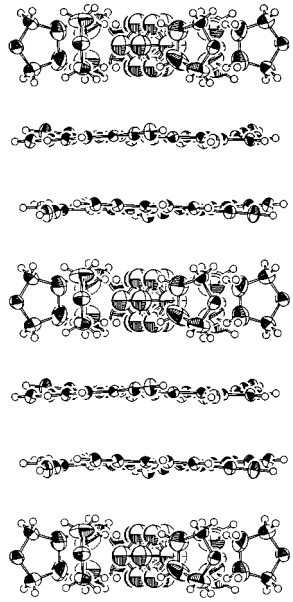

Fig. 3 Side view of a stacked column showing alternation of **1** with THF disks.

nonayne chelates three molecules of solvent in neighboring columns through two alkyne C–H···O bonds. The distances between the normalized (1.083 Å) positions of the hydrogens and the oxygen of the THF are 2.16 and 2.24 Å, respectively (C–O distances 3.22 and 3.30 Å, respectively). The corresponding respective C–H–O angles are 164.9 and 164.2°. These parameters are consistent with the assignment of these interactions as short C–H···O hydrogen bonds.[2]

Additional evidence for C–H···O hydrogen bonding was sought using infrared spectroscopy.[6] However, attempts to obtain spectra in the solid state were hampered by rapid solvent loss. In CH_2Cl_2, the alkyne CH stretching vibration was relatively unperturbed (3305 cm^{-1}) relative to that of 1,4-diethynylbenzene (3308 cm^{-1}, CCl_4).[7] However, in THF, a significant shift to lower energy (3249 cm^{-1}) was observed. Such a dramatic reduction in the CH stretching frequency is consistent with a hydrogen-bonding interaction in solution.[6]

Although examples of chelating OH···O[8] and aromatic C–H···O[9] hydrogen bonds exist, complex **1** represents the first such case for alkyne CH donors.[10]§ Furthermore, the reflection of the molecular symmetry in the organization of the solvent molecules is a stunning example of supramolecular construction in the solid state arising from weak interactions.[11] Attempts to use this property of **1** for the immobilization of a guest of appropriate symmetry are ongoing.

This work was supported by the National Science Foundation (CHE-9610430). A. J. M. thanks the Division of Organic Chemistry of the ACS for a predoctoral fellowship (sponsored by Rohm and Haas Co).

Notes and references

† MNDO-PM3 calculations using Spartan IBM version 4.1.2 predict the energies of the planar (D_{3h}) and propeller (D_3) form to be 547.81 and 547.63 kcal mol^{-1}, respectively. The computed differ from the experimental bond lengths by an average of 0.004 Å (mean absolute difference of 0.010 Å).

‡ *Crystal data* for **1**–THF solvate: $C_{50}H_{40}O_{3.5}$, M = 696.86, trigonal, a = 23.427(1), c = 12.3280(7) Å, U = 5859.5(5) $Å^3$, T = −121 °C, space group $R\bar{3}$ (no. 148), Z = 6, μ(Mo-Kα) = 0.73 cm^{-1}, 9251 reflections measured, 2353 unique (R_{int} = 0.026), 1528 reflections with $I_0 \geqslant 3\sigma(I_o)$ used in refinement, R = 0.050, R_w = 0.060. CCDC 182/1373.

§ Database analysis: Cambridge Structural Database, October 1998 update with 190307 entries, ordered and error-free crystal structures with R values < 0.010, H-atom positions normalized. Distance cutoff value: C≡C–H···O < 3.0 Å. Only eight structures having two such interactions with the same oxygen atom were found: FIXFOH, HNPRYO, JACYUH, KUZCEN, NIRBEV, TEQBOG, WETNAK, and ZODXEV. In none of these cases were the donors from the same molecule.

1 T. Steiner and G. R. Desiraju, *Chem. Commun.*, 1998, 891; T. Steiner, *Chem. Commun.*, 1997, 727; G. R. Desiraju, *Acc. Chem. Res.*, 1991, **24**, 290; 1996, **29**, 441.
2 T. Steiner, *New J. Chem.*, 1998, 1099.
3 C. Eickmeier, H. Junga, A. J. Matzger, F. Scherhag, M. Shim and K. P. C. Vollhardt, *Angew. Chem., Int. Ed. Engl.*, 1997, **36**, 2103.
4 U. H. F. Buntz, Y. Rubin and Y. Tobe, *Chem. Soc. Rev.*, 1999, **28**, 107.
5 N. Narita, S. Nagai, S. Suzuki and K. Nakao, *Phys. Rev. B*, 1998, **58**, 11 009, M. M. Haley, *Synlett*, 1998, 557.
6 B. Lutz, J. van der Maas and J. A. Kanters, *J. Mol. Struct.*, 1994, **325**, 203.
7 B. M. Kariuki, K. D. M. Harris, D. Philip and J. M. A. Robinson, *J. Am. Chem. Soc.*, 1997, **119**, 12 679.
8 For an example of intermolecular chelation of a carbonyl oxygen by a diol, see: O. Saied, M. Simard and J. D. Wuest, *J. Org. Chem.*, 1998, **63**, 3756.
9 A crystal structure revealing intramolecular chelation of a hydroxy group by aromatic CH hydrogen bonds has been reported: T. Steiner, E. B. Starikov and M. Tamm, *J. Chem. Soc., Perkin Trans. 2*, 1996, 67.
10 Chelating bis(acetylide) metal complexes of bis(2-ethynylphenyl)-ethyne are known: L. Guo, J. M. Hrabusa III, M. D. Senskey, D. B. McConville, C. A. Tessier and W. J. Youngs, *Organometallics*, 1999, **18**, 1767; L. Guo, J. D. Bradshaw, D. B. McConville, C. A. Tessier and W. J. Youngs, *Organometallics*, 1997, **16**, 1685.
11 G. R. Desiraju, *Chem. Commun.*, 1997, 1475; V. A. Russell and M. D. Ward, *Chem. Mater.*, 1996, **8**, 1654; G. R. Desiraju, *Angew. Chem., Int. Ed. Engl.*, 1995, **34**, 2328.

Communication 9/05312C

ChemComm

Convergent synthesis of (1→2)- and (1→4)-*C*-linked imino disaccharides†

Yao-Hua Zhu and Pierre Vogel*

Section de Chimie de l'Université de Lausanne, BCH, CH-1015 Lausanne-Dorigny, Switzerland.
E-mail: pierre.vogel@ico.unil.ch

Received (in Liverpool, UK) 30th June 1999, Accepted 13th August 1999

A convergent synthesis of (1→2)- and (1→4)-*C*-linked imino disaccharides was achieved by applying Nozaki–Kishi coupling of a hydroxyproline-derived carbaldehyde with isolevoglucosenone or levoglucosenone derived enol triflates.

Carbohydrate mimetics are potentially useful tools to study cellular interactions,[1] the biosynthesis of glycoproteins, the metabolism of glycoconjugates,[2] and the mechanisms of digestion.[3] Inhibitors of the enzymes involved in these processes such as the glycosidases and the glycosyltransferases are potential anti-cancer, antiviral, and antidiabetic agents, as well as insect antifeedant agents.[4] Disaccharide mimetics such as *C*-disaccharides and dideoxyiminoalditol *C*-linked to monosaccharides have emerged as a new class of specific glycosidase inhibitors and may represent non-hydrolyzable epitopes.[5–7] Recently we disclosed an efficient and versatile approach to the syntheses of (1→3)-*C*-disaccharides and (1→3)-*C*-linked imino disaccharides **5** based on the cross-aldolisation of the aldehydes **3** with the nucleophile 1,4-adducts **2** of isolevoglucosenone **1** (Scheme 1).[8,9] We report here that (1→4)- and (1→2)-*C*-disaccharides can be prepared starting from **1** and levoglucosenone **17** with **3**, respectively.

Adduct **6** of benzyl alcohol with isolevoglucosenone was enolized, without elimination of benzylate anion, on treatment with LiHMDS in 95:5 THF–HMPA at −78 °C (Scheme 2).[9] Quenching of the corresponding lithium enolate with 2-[bis(trifluoromethylsulfonyl)amino]-5-chloropyridine provided the enol triflate **7** in 87% yield.[10] Nozaki–Kishi coupling of **7** and aldehyde **8** led to allylic alcohols **9** and **10** isolated in 62 and 17% yield, respectively.[11,12]‡ Interestingly, the reaction was accelerated by ultrasound and O_2. Under N_2 atmosphere, ultrasound shortened the reaction time from 30 to 2 h. While in the presence of a catalytic amount of O_2 (5 mol% with respect to $CrCl_2$, concentration of O_2 lower than 10%), the reaction time was reduced further to less than 1 h. Moreover, O_2 suppressed the formation of **11**, resulting from H_2O quenching of the alkenylchromium species, from 36 to less than 10%.

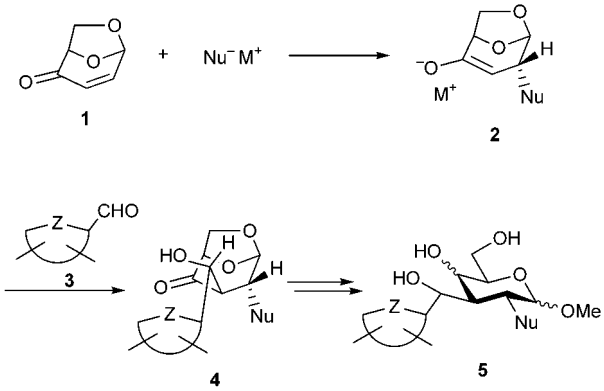

Scheme 1

† Spectral data for **15α**, **15β** and **29** are available from the RSC web site, see http://www.rsc.org/suppdata/cc/1999/1873/

Hydroboration of **9** with $BH_3{\cdot}SMe_2$ in THF at 50 °C followed by H_2O_2/NaOH work-up furnished the D-glucose derivative **12** in 57% yield. Desilylation with Bu_4NF in THF gave triol **13** (97%), which was debenzylated to give tetrol **14** (94%). Treatment of **14** in refluxing MeOH saturated with gaseous HCl for 2 days produced a 2:1 mixture of **15α** and **15β** in 83% yield.

The D-*gluco* configuration of the methyl pyranosides **15α** and **15β** was determined from their ^1H NMR spectra.[13] The configuration of the hydroxymethano linker was established by converting diol **12** into the corresponding acetonide **16** [$(MeO)_2CMe_2$, acetone, TsOH, Drierite, 25 °C, 68% yield], the structure of which was established by its NOESY and ^1H NMR spectra. The coupling constants, ^3J(H-3, H-4) = 10.9 Hz, ^3J(H-4, H-1′) = 11.2 Hz and ^3J(H-2, H-3) = 7.2 Hz, show the antiperiplanar orientation between these proton pairs. Furthermore, NOEs were observed between signals attributed to H_{syn}-6, H-2, H-4, and between those attributed to Me_{axial}, H-1′, H-3. Thus, the *Re* face of aldehyde **8** is preferred for the alkenylchromium addition, which is in accord with the Felkin–Anh Model.[14]

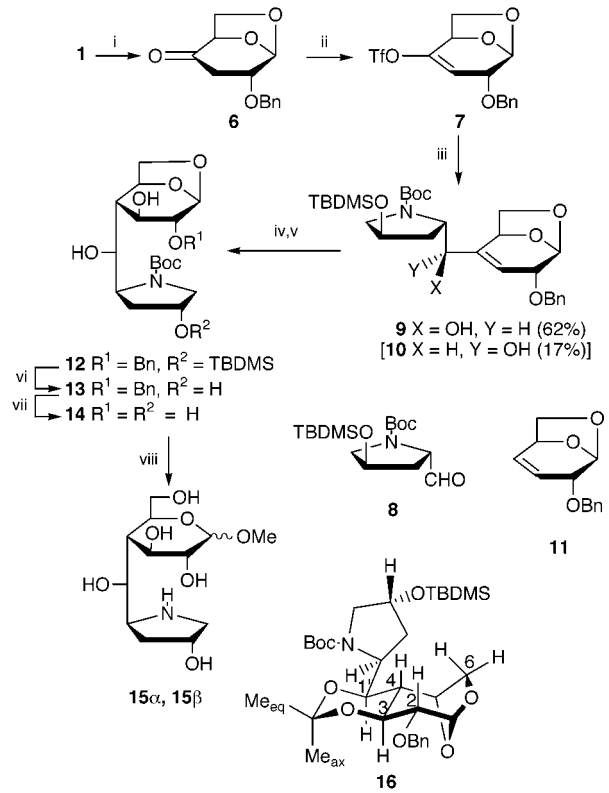

Scheme 2 *Reagents and conditions*: i, BnOH, Et_3N, 25 °C; ii, LiHMDS, HMPA–THF, 2-[bis(trifluoromethylsulfonyl)amino]-5-chloropyridine, −78 °C, 87%; iii, **8**, $CrCl_2$, $NiCl_2$, O_2, DMF, ultrasound, 25 °C; iv, $BH_3{\cdot}SMe_2$, THF, 50 °C, v, H_2O_2, NaOH, 57% for 2 steps; vi, Bu_4NF, THF, 97%; vii, H_2, 10% Pd-C, MeOH, 25 °C, 94%; viii, MeOH, HCl, reflux, 2 days, 83%.

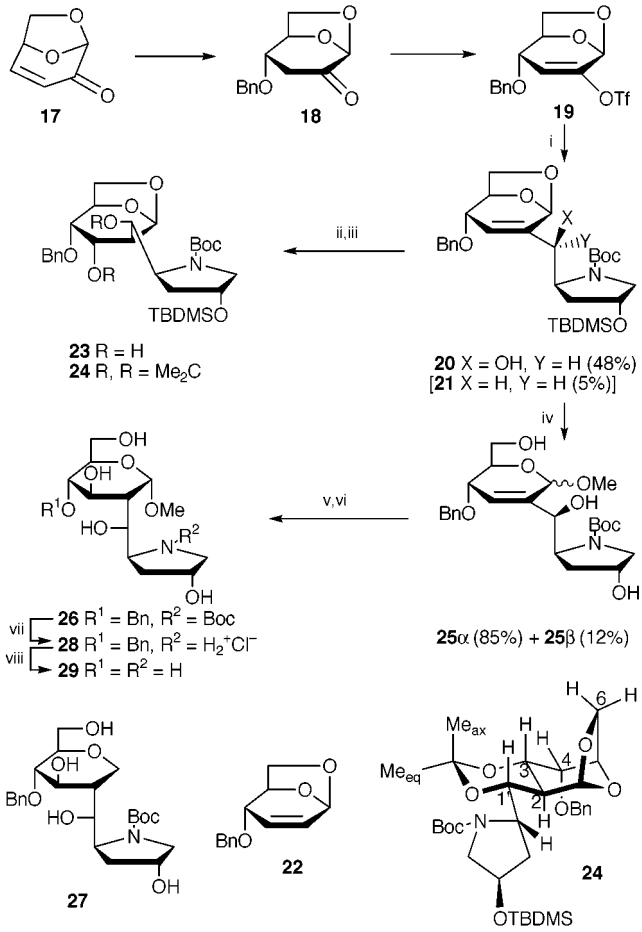

Scheme 3 *Reagents and conditions*: i, **8**, $CrCl_2$, $NiCl_2$, O_2, DMF, ultrasound, 25 °C; ii, $BH_3{\cdot}SMe_2$, THF, reflux; iii, H_2O_2, NaOH, 37% for 2 steps; iv, MeOH, TsOH, 25 °C; v, $BH_3{\cdot}SMe_2$, THF; vi, H_2O_2, NaOH, 46% for 2 steps; vii, MeOH, HCl, reflux, 92%; viii, H_2, 10% Pd-C, MeOH, 25 °C, 95%.

In parallel with the synthesis of (1→4)-*C*-disaccharides, (1→2)-*C*-disaccharides and analogues can be obtained starting from levoglucosenone **17** (Scheme 3). Benzyl alcohol adduct **18** was converted (as above) into triflate **19** in 90% yield.[15] In the Nozaki–Kishi coupling reaction, **19** was found to be less reactive than triflate **7**. It required activation with ultrasound and a catalytic amount of O_2 to react (best results with 5 mol% O_2 with respect to $CrCl_2$, 0.3 mol% $NiCl_2$). This led to alcohol **20** isolated in 48% yield, together with dehydroxylated product **21** (5% yield) and side product **22** (8% yield).‡ Hydroboration of **20** followed by oxidative work-up provided diol **23** in modest yield (37%). The ^{1}H NMR and NOESY spectra of acetonide **24** (obtained under the same conditions as those for **16**) showed coupling constants ^3J(H-2, H-3) = 10.7 Hz, ^3J(H-1′, H-2) = 10.7 Hz, ^3J(H-3, H-4) = 3.6 Hz, and NOEs between proton pairs H_{syn}-6/H-3, H-3/H-1′ H-3/Me_{axial} and H-1′/Me_{axial}. These establish the D-*altro* configuration of the anhydrohexose moiety and the (*R*) configuration of the hydroxymethano linker demonstrating again that the *Re* face of **8** was preferred for the nucleophilic addition.[16] Hydroboration took place from the *exo* face of the bicyclic system probably because of steric hindrance from the *endo* hydrogen at C6. The allylic acetal was readily opened by acidic methanolysis, which provided glycosides **25α** and **25β** isolated in 85 and 12% yield, respectively. Hydroboration of **25α** gave alcohol **26** (46%) and the anhydroglucitol derivative **27** (10%).[16] Under reflux in MeOH saturated with HCl, **28** was obtained in 92% yield. Hydrogenation liberated the (1→2)-*C*-linked imino disaccharide **29** (95%).

The stereoselective methods presented above should be applicable to the preparation of a large variety of (1→2)- and (1→4)-*C*-disaccharides and analogues employing the same starting materials as those for the synthesis of (1→3)-*C*-disaccharides, and thus make possible the exploration of their structure–activity relationships.[17]

This work was supported by the Swiss National Science Foundation. We thank also the European COST D13 action programme for encouragement.

Notes and references

‡ *Selected data* for **9**: colorless oil; $[\alpha]_D^{25}$ −107 (*c* 1.2, $CHCl_3$); δ_H(400 MHz, $CDCl_3$, 323 K) 7.38–7.25 (m, 5H, Ph), 5.54 (m, 2H, H-1, H-3), 4.76 [d, ^3J (H-5, H_{exo}-6) 3.6, H-5], 4.65 and 4.62 (2d, 2H, ^2J 11.5, PhCH_2O), 4.38 (p, ^3J 3.6, H-4′), 4.37 (m, H-1′), 4.31 (m, H-2′), 3.71 (m, 2H, H-6), 3.55 [d, ^3J(H-2, H-3) 3.9, H-2), 3.48 (d, ^2J 11.2 , H-5′a), 3.35 [dd, ^2J 11.2 , ^3J(H-4′, H-5′b) 4.2, H-5′b] 1.92 (m, 2H, H-3′), 1.48 [s, 9H, $(CH_3)_3$CO], 0.86 [s, 9H, $(CH_3)_3$CSi], 0.04 [s, 6H, $(CH_3)_3$Si]. For **20**: $[\alpha]_D^{25}$+24 (*c* 0.94, $CHCl_3$); δ_H(400 MHz, $CDCl_3$, 323 K) 7.44–7.26 (m, 5H, Ph), 5.69 (m, H-3), 5.64 (s, H-1), 4.77 [dtd, ^3J(H-5, H_{exo}-6) 6.6, ^4J(H-3, H-5) = ^3J(H-5, H_{endo}-6) = 1.7, ^3J(H-4, H-5) 1.1, H-5), 4.68 (s, 2H, PhCH_2O), 4.52 (m, H-1′), 4.32 (m, H-4′), 4.20 (m, H-2′), 3.87 (dd, ^2J 7.6, ^3J 6.6, H_{exo}-6), 3.58 [dt, ^3J(H-3, H-4) 3.9, ^3J(H-4, H-5) = ^5J (H-4, H-1′) = 1.1, H-4], 3.46 (m, H-5′a), 3.36 (dd, ^2J 11.2, ^3J 4.2, H-5′b), 3.31 (dd, ^2J 7.6 ,^3J 1.7, H_{endo}-6), 1.89 (m, 2H, H-3′), 1.49 [s, 9H, $(CH_3)_3$CO], 0.88 [s, 9H, $(CH_3)_3$CSi], 0.06 [s, 6H, $(CH_3)_2$Si].

1 See, *e.g.*: A. Varki, *Glycobiology*, 1993, **3**, 97; P. R. Crocker and T. Feizi, *Curr. Opin. Struct. Biol.*, 1996, **6**, 679; A. Varki, *Proc. Natl. Acad. Sci. U.S.A.*, 1994, **91**, 7390; K. W. Moremen, R. B. Trimble and A. Herscovics, *Glycobiology*, 1994, **4**, 113; B. Ganem, *Acc. Chem. Res.*, 1996, **29**, 340 and references cited therein.

2 R. Kornfeld and S. Kornfeld, *Annu. Rev. Biochem.*, 1985, **54**, 631; A. Lai, P. Pang, S. Kalelkar, P. A. Romero, A. Herscovics and K. W. Moremen, *Glycobiology*, 1998, **8**, 981 and references cited therein.

3 J. Marshall, *J. Adv. Carbohydr. Chem. Biochem.*, 1974, **30**, 257; D. D. Schmidt, W. Frommer, B. Junge, L. Müller, W. Wingender, E. Truscheit and D. Schefer, *Naturwissenschaften*, 1977, **64**, 535.

4 A. D. Elbein and R. J. Molyneux, in *Iminosugars as Glycosidase Inhibitors*, ed. A. E. Stütz, Wiley-VCH, Weinheim, 1999, pp. 216–251; C. W. Ekhart, M. H. Fechter, P. Hadwiger, E. Mlaker, A. E. Stütz, A. Tauss and T. M. Wrodnigg, in *Iminosugars as Glycosidase Inhibitors*, ed. A. E. Stütz, Wiley-VCH, Weinheim, 1999, pp. 253–390; M. Bols, *Acc. Chem. Res.*, 1998, **31**, 1; E. Fenouillet, M. J. Papandreou and I. M. Jones, *Virology* 1997, **231**, 89; T. Kolter, *Angew. Chem., Int. Ed. Engl.*, 1997, **36**, 1955 and references cited therein.

5 C. Pasquarello, R. Demange and P. Vogel, *Bioorg. Med. Chem. Lett.*, 1999, **9**, 793.

6 B. A. Jones, Y. T. Pan, A. D. Elbein and C. R. Johnson, *J. Am. Chem. Soc.*, 1997, **119**, 4856; K. Kraehenbuehl, S. Picasso and P. Vogel, *Helv. Chim. Acta*, 1998, **81**, 1439; M. A. Leeuwenburgh, S. Picasso, H. S. Overkleeft, G. A. van der Marel, P. Vogel and J. H. van Boom, *Eur. J. Org. Chem.*, 1999, 1185.

7 See, *e.g.*: G. D. MacLean, M. B. Bowen-Yacyshyn, J. Samuel, A. Meikle, G. Stuart, J. Nation, S. Poppema, M. Jerry, R. Koganty, T. Wong and B. M. Longenecker, *J. Immunother.*, 1992, **11**, 292; P. D. Rye, N. V. Bovin, E. V. Vlasova and R. A. Walker, *Glycobiology*, 1995, **5**, 385.

8 Y.-H. Zhu and P. Vogel, *Tetrahedron Lett.*, 1998, **39**, 31.

9 Y.-H. Zhu and P. Vogel, *J. Org. Chem.*, 1999, **64**, 666.

10 D. L. Comins and A. Dehghani, *Tetrahedron Lett.*, 1992, **33**, 6299.

11 S. Mori, T. Ohno, H, Harada, T. Aoyama and T. Shioiri, *Tetrahedron*, 1991, **47**, 5051.

12 K. Takai, M. Tagashira, T. Kuroda, K. Oshima, K. Vtimoto and H. Nozaki, *J. Am. Chem. Soc.*, 1986, **108**, 6048; D. P. Stamos, X. C. Sheng, S. S. Chen and Y. Kishi, *Tetrahedron Lett.*, 1997, **38**, 6355 and references cited therein.

13 Y. Wang, P. G. Goekjian, D. M. Ryckman, W. H. Miller, S. A. Babirad and Y. Kishi, *J. Org. Chem.*, 1992, **57**, 482.

14 F. Rübsam, S. Seck and A. Giannis, *Tetrahedron*, 1997, **53**, 2823; P. Ciapetti, M. Falorni and M. Taddei, *Tetrahedron*, 1996, **52**, 7379.

15 For the preparation of **18**, see: T. Kawai, M. Isobe and S. C. Peters, *Aust. J. Chem.*, 1995, **48**, 115.

16 J. Cossy, V. Bellosta and M. C. Müller, *Tetrahedron Lett.*, 1992, **33**, 5045.

17 An example of the synthesis of the β-*C*(1→4)glucopyranoside of 3-deoxy-D-glucose from levoglucosenone was reported by Witczak and co-workers: Z. J. Witczak, R. Chhabra and J. Chojnacki, *Tetrahedron Lett.*, 1997, **38**, 2215.

Communication 9/05310G

Lipophilic urea-functionalized dendrimers as efficient carriers for oxyanions†‡

Holger Stephan,*[a] Hartmut Spies,[a] Bernd Johannsen,*[a] Lars Klein[b] and Fritz Vögtle*[b]

[a] *Institut für Bioanorganische und Radiopharmazeutische Chemie, Forschungszentrum Rossendorf, 01314 Dresden, Germany. E-mail: h.stephan@fz.rossendorf.de*

[b] *Kekulé-Institut für Organische Chemie und Biochemie, Universität Bonn, Gerhard-Domagk-Str. 1, 53121 Bonn, Germany. E-mail: voegtle@uni-bonn.de*

Received (in Cambridge, UK) 20th July 1999, Accepted 10th August 1999

Urea-functionalized dendrimers are prepared which show very efficient phase transfer, in particular of the diagnostically relevant anions pertechnetate, perrhenate and ATP; the extractability rates are evaluated quantitatively by tracer methods; their pH dependancy allows controlled release of guest molecules from the dendrimer host.

Due to their unique topology and unusual guest-binding behaviour, dendrimers are promising reagents for use in diagnostic imaging and therapy.[1] Commercially available compounds such as poly(aminoamide) and poly(propylenimine) dendrimers have been investigated with this application in mind. At physiological pH more than 50% of the amino groups of such dendrimers are protonated, resulting in a polycation.[2] Consequently these are capable of binding anions. We are especially interested in the efficient binding of the tetrahedral oxoanion pertechnetate as a new approach to labelling organic compounds.[3] In this context dendrimers are desired having a hydrophobic periphery in order to shield the anion from hydrophilic attack. A convenient way to obtain this is reaction of the primary amino groups with alkyl and aryl isocyanates giving lipophilic polyurea-functionalized dendrimers.[4] Urea, as hydrogen bond donating moiety, is also able to stabilize the complexed anion.[5] Knowing the interaction of dendrimers with phosphate groups in oligonucleotides,[6] DNA[7] and other guests[8] we have also investigated the binding of the nucleotides AMP, ADP and ATP with the polyurea dendrimers prepared.

We report the synthesis and complexation behaviour *via* liquid–liquid extraction of various generations of these new monodisperse urea-functionalized dendrimers. Various isocyanates (hexyl, octyl, dodecyl and phenyl isocyanate) dissolved in CH_2Cl_2 [9 mmol for second generation dendrimer-$(NH_2)_8$,[9] 17 mmol for third generation dendrimer-$(NH_2)_{16}$[9]] were slowly dropped into a solution of 1 mmol poly(propylenimine) dendrimer in 150 ml of CH_2Cl_2. After stirring for 48 h at 25 °C the solvent was partially evaporated. Upon adding 40 ml of light petroleum to the remaining solution, the urea-functionalized dendrimers were precipitated. Crude products were filtered and washed with light pertroleum. The pure compounds were isolated as colourless solids in 90% yield.§

The alkyl urea-functionalized dendrimers **1**–**4** are soluble in organic solvents like $CHCl_3$ and CH_2Cl_2, a prerequisite for studying the complexation behaviour by liquid–liquid extraction.¶ On the other hand, dendrimers having phenyl urea units at the periphery are completely insoluble in these diluents. Accordingly, we have only examined the alkyl urea dendrimers. These dendritic hosts are capable of extracting pertechnetate with remarkable efficacy (Fig. 1). As expected the extractability is enhanced with decreasing pH accompanied by a higher state of protonation. Also the increasing number of potential binding sites leads to an improvement of pertechnetate extraction (generation 3 > generation 2). Introduction of hexyl and octyl

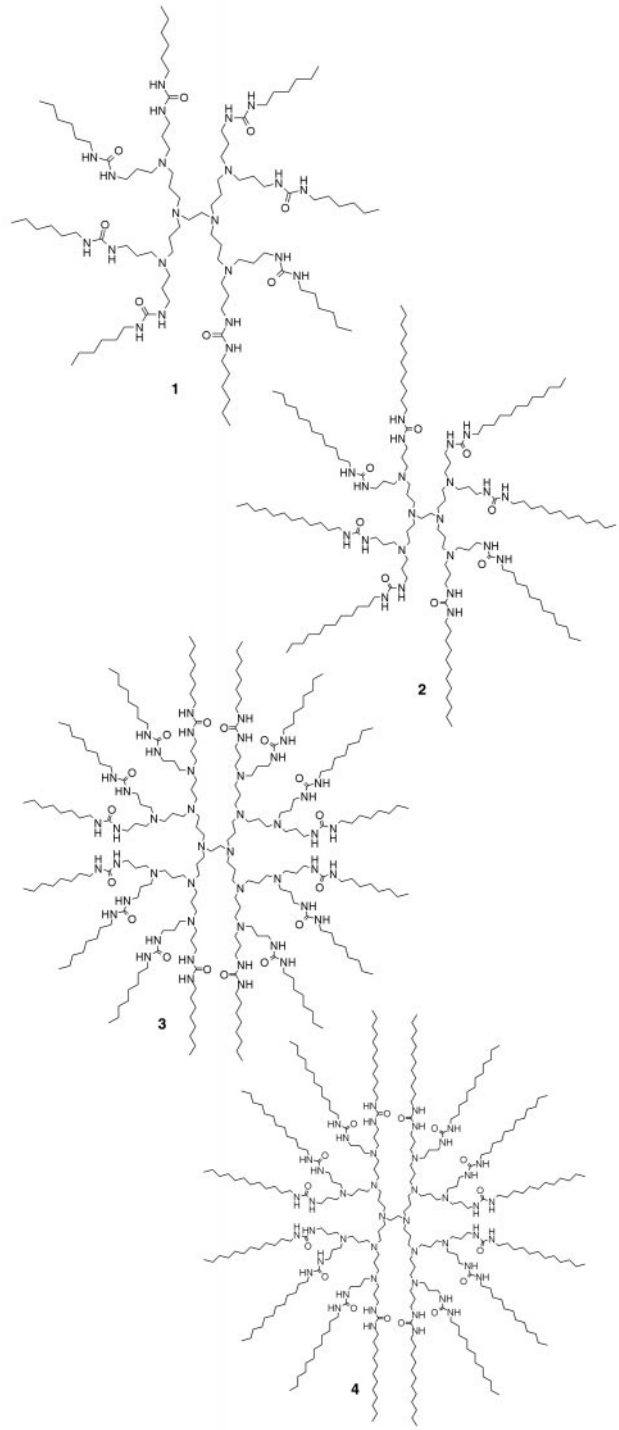

† Part of this work was presented as a poster contribution at the Seminar 'Functional Supramolecular Systems', Frankfurt (Main), Germany, June 1999.

‡ MALDI-TOF data for **3**, and **3**·$(ATP)_5$·$(H_2O)_x$ are available from the RSC web site, see http://www.rsc.org/suppdata/cc/1999/1875/

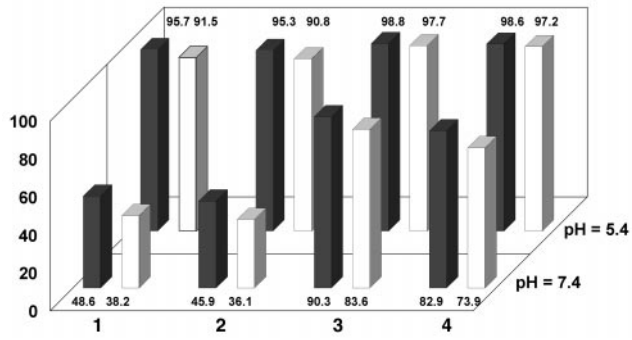

Fig. 1 Extractability of pertechnetate (grey columns) and perrhenate (white columns) with dendrimers **1**–**4**; $[KTcO_4] = [NH_4ReO_4] = 1 \times 10^{-4}$ mol dm^{-3}, pH = 5.4 (MES/NaOH buffer), pH 7.4 (HEPES/NaOH buffer), [dendrimer] $= 1 \times 10^{-3}$ mol dm^{-3} in $CHCl_3$.

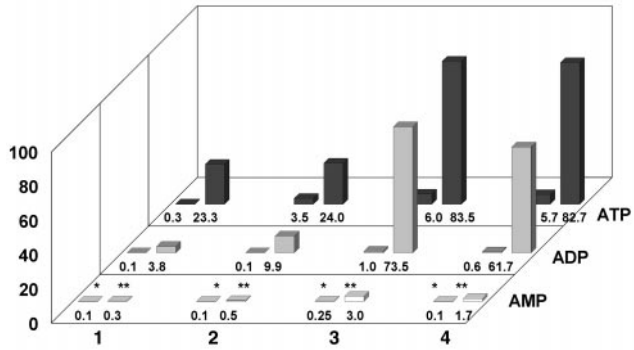

Fig. 2 Extractability of nucleotides with dendrimers **1**–**4**; [nucleotide] = 1×10^{-4} mol dm^{-3}, * = pH 7.4 (HEPES/NaOH buffer), ** = pH 5.4 (MES/NaOH buffer), [dendrimer] = 1×10^{-3} mol dm^{-3} in $CHCl_3$.

residues on the periphery of the dendrimers leads to higher distribution ratios in comparison with the dodecyl analogue. This finding is probably due to steric effects. The same trend of influence on extraction is observed for perrhenate, which is similar in size and other properties to pertechnetate. However, the efficacy is slightly decreased compared to pertechnetate extraction. This fact is also found for bimetallic cyclotriveratrylene[10] and bicyclic guanidinium hosts.[11] Differences of charge density and hydration between these two anions is probably responsible for the observed extraction behaviour.

The dendrimers investigated show also the ability to extract the highly hydrophilic nucleotide anions AMP, ADP and ATP with remarkable graduation (Fig. 2). The extraction of these anions is strongly influenced by the state of protonation and the number of binding sites in comparison to the more hydrophobic anions pertechnetate and perrhenate. The extractability of the nucleotides is enhanced with increasing number of phosphate groups, giving the order ATP > ADP > AMP. This trend meets our expectations and clearly points toward the participation of all phosphate groups in binding with the dendrimers.

As the loading capacity of the organic phase is limited, at higher concentrations of nucleotides a third phase‖ is formed during extraction. ^{31}P NMR clearly indicates that ATP is enriched in this phase. In order to obtain information about the stoichiometry of the complex extracted we utilized mass spectrometry.** Surprisingly, the MALDI-TOF mass spectrum of this complex shows one peak at *m*/*z* 6992.5, pointing to some ATP molecules being attached to the dendrimer. Considering that ATP remains hydrated†† after extraction a complex $\mathbf{3}\cdot(ATP)_5\cdot(H_2O)_x$ (with $x \approx 15$) can be postulated.

In conclusion, easily accessible urea-functionalized dendrimers are capable of binding anionic guests and transferring them to the organic phase (Table 1). The improvement of the stability of the pertechnetate complexes appears promising, and may lead to novel imaging agents. Furthermore higher generations of lipophilic dendrimers possessing anion affecting groups like (thio)ureas, amides and sulfonamides should give unusual

Table 1 Extractabilities of selected anions guests by hosts **1**–**4**

		Host–guest complex concentration/mol dm^3			
pH	Guest	**1**	**2**	**3**	**4**
7.4	$[ReO_4]^-$	38.2	36.1	83.6	73.9
	$[TcO_4]^-$	48.5	45.9	90.3	82.9
	AMP	0.1	0.1	0.25	0.1
	ADP	0.1	0.1	1.0	0.6
	ATP	0.2	3.5	6.0	5.7
5.4	$[ReO_4]^-$	91.5	90.8	97.7	97.2
	$[TcO_4]^-$	95.7	95.3	98.8	98.6
	AMP	0.3	0.5	3.0	1.7
	ADP	3.8	9.9	73.5	61.7
	ATP	23.3	24.0	83.5	82.7

complexation and distribution properties for biologically relevant guests such as oligonucleotides and nucleic acids. Another concept is the use of poly (Lewis acid) hosts, recently realized for ferrocenyl dendrimers.[12]

We thank the Sächsisches Ministerium für Wissenschaft und Kunst (Project 7533-844-98/4) for support of this work.

Notes and references

§ Compounds were fully characterised by ^{1}H and ^{13}C NMR spectroscopy and MALDI-TOF mass spectrometry.

¶ Liquid–liquid extraction studies were performed at 25 ± 1 °C in 2 cm^3 microcentrifuge tubes by mechanical shaking. The phase ratio $V_{(org)}$:$V_{(w)}$ was 1:1 (0.5 cm^3 each); the shaking period was 30 min. The extraction equilibrium was achieved during this period. All samples were centrifuged after extraction. The anion concentration in both phases was determined radiometrically using β-radiation measurement of $^{99}TcO_4^-$, $^{188}ReO_4^-$ (Amersham) and ^{14}C-labelled nucleotides (NEN Life Science Products) in a liquid scintillation counter (Tricarb 2500, Canberra-Packard). The aqueous solution was adjusted using 0.05 mol dm^3 and HEPES/NaOH buffer.

‖ Extraction of ATP (2 cm^3, 5×10^{-2} mol dm^{-3}) with **3** (1 cm^3, 5×10^{-3} mol dm^{-3} in $CHCl_3$) leads to the formation of a third phase.

** For this purpose ATP (2 cm^3, 5×10^{-3} mol dm^{-3}) is extracted from aqueous solution into $CHCl_3$ using **3** (1 cm^3, 5×10^{-3} mol dm^{-3}).

†† The ATP applied has a hydration state of 7.3.

1 D. A. Tomalia, A. M. Naylor and W. A. Goddart III, *Angew. Chem., Int. Ed. Engl.*, 1990, **29**, 138; M. Fischer and F. Vögtle, *Angew. Chem., Int. Ed.*, 1999, **38**, 884; Y. Kim and S. C. Zimmerman, *Curr. Opin. Chem. Biol.*, 1998, **2**, 733; O. A. Matthews, A. N. Shipway and J. F. Stoddart, *Prog. Polym. Sci.*, 1998, **23**, 1.

2 R. C. van Duijvenbode, M. Borkovec and G. J. M. Koper, *Polymer*, 1999, **39**, 2657; G. J. M. Koper, M. H. P. vanGenderen, C. Elissen Roman, M. W. P. L. Baars, E. W. Meijer and M. Borkovec, *J. Am. Chem. Soc.*, 1997, **119**, 6512; G. Pistolis, A. Malliaris, D. Tsiouruas and C. M. Paleos, *Chem. Eur. J.*, 1999, **5**, 1440.

3 H. Stephan, R. Berger, H. Spies, B. Johannsen and F. P. Schmidtchen, *J. Radioanal. Nucl. Chem.*, in the press.

4 G. R. Newkome, C. D. Weiss, C. N. Moorefield, B. J. Childs and J. Epperson, *Angew. Chem., Int. Ed.*, 1998, **37**, 307

5 F. P. Schmidtchen and M. Berger, *Chem. Rev.*, 1997, **97**, 1609; M. M. G. Antonisse and D. N. Reinhoudt, *Chem. Commun.*, 1998, 443.

6 S. W. Poxon, P. M. Mitchell, E. Liang and J. A. Hughes, *Drug Delivery*, 1996, **3**, 255; J. A. Hughes, A. I. Aronsohn, A. V. Avrutskaya and R. L. Juliano, *Pharm. Res.*, 1996, **13**, 404; R. DeLong, K. Stephenson, T. Loftus, M. Fisher, S. Alahari, A. Nolting and R. L. Juliano, *J. Pharm. Sci.*, 1997, **86**, 762.

7 M. X. Tang, C. T. Redemann and F. C. Szoka, Jr., *Bioconjugate Chem.*, 1996, **7**, 703; A. U. Bielinska, J. F. Kukowska-Latallo and J. R. Baker, *Biochim. Biophys. Acta*, 1997, **1352**, 180.

8 J. F. G. A. Jansen and E. W. Meijer, *J. Am. Chem. Soc.*, 1995, **117**, 4417; P. Miklis, T. Çagin and W. A. Goddard III, *J. Am. Chem. Soc.*, 1997, **119**, 7458.

9 A. Archut, G. C. Azzellini, V. Balzani, L. De Cola and F. Vögtle, *J. Am. Chem. Soc.*, 1998, **120**, 12 187.

10 J. L. Atwood, K. T. Holman and J. W. Steed, *Chem. Commun.*, 1996, 1401.

11 H. Stephan, H. Spies and F. P. Schmidtchen, unpublished work.

12 C. Valério, E. Alonso, J. Ruiz, J. C. Blais and D. Astruc, *Angew. Chem., Int. Ed.*, 1999, **38**, 1747.

Communication 9/05862A

ChemComm

Highly active and selective catalysts for the production of methyl propanoate *via* the methoxycarbonylation of ethene

William Clegg,[a] Graham R. Eastham,[b]† Mark R. J. Elsegood,[a] Robert P. Tooze,*[c] Xiao Lan Wang[c] and Keith Whiston[c]

[a] *Department of Chemistry, Bedson Building, University of Newcastle upon Tyne, Newcastle upon Tyne, UK NE1 7RU*
[b] *Department of Chemistry, University of Durham, Science Laboratories, South Road, Durham, UK DH1 3LE*
[c] *Strategic Projects Group, ICI Acrylics, PO Box 90, Wilton, Middlesbrough, UK TS90 8JE. E-mail: robert_tooze@ici.com*

Received (in Cambridge, UK) 8th July 1999, Accepted 10th August 1999

A highly active and selective catalyst for the production of methyl propanoate *via* the methoxycarbonylation of ethene is described, based on the new zero valent palladium complex L_2Pd(dba) [where L_2 = 1,2-bis(di-*tert*-butylphosphinomethyl)benzene and dba = *trans*,*trans*-dibenzylideneacetone].

The alkoxycarbonylation of alkenes is of growing importance. Eqn. (1) shows that a range of products is accessible, from high

$$CH_3OH + CO + CH_2{=}CH_2 \longrightarrow H{-}(CH_2CH_2C(=O))_nOCH_3 \quad (1)$$

molecular weight 'polyketones', which have useful properties as engineering thermoplastics,[1] to methyl propanoate [n = 1 in eqn. (1)], a potential intermediate in the manufacture of methyl methacrylate.[2] Palladium catalysts for this transformation show a marked selectivity dependence on the nature of the phosphine ligand, with monodentate phosphines generally giving methyl propanoate and bidentate phosphines giving high molecular weight co-polymers.[3] Examples of bidentate phosphines contradicting this paradigm are rare.[4]

We report here results using catalysts based on the bidentate phosphine ligand 1,2-bis(di-*tert*-butylphosphinomethyl)benzene which offer exceptional activity, selectivity and stability as ligands for methyl propanoate production.[5] This ligand has been previously described by Shaw[6] and some of its chemistry explored by Spencer;[7] however, prior to our work little structural characterisation and no catalytic studies have been reported.

Addition of this ligand to $Pd_2(dba)_3$ (dba = *trans*,*trans*-dibenzylideneacetone) gave a complex of formula L_2Pd(dba) **1** (where L_2 = the bidentate phosphine). Treatment of this

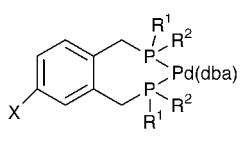

1 $R^1 = R^2 = Bu^t$, X = H
2 $R^1 = R^2 = Bu^t$, X = NO_2
3 $R^1 = R^2 = Bu^t$, X = OMe
4 $R^1 = R^2 = Pr^i$, X = H
5 $R^1 = R^2$ = Cy, X = H
6 $R^1 = R^2$ = Ph, X = H
7 $R^1 = Bu^t$, R^2 = Cy, X = H

complex with a sulfonic acid (*e.g.* MsOH) in MeOH generates a complex capable of converting ethene, CO and MeOH to methyl propanoate at a rate of 50 000 mol of product per mol of catalyst per hour with a selectivity of 99.98%. The reaction conditions are very mild (80 °C and 10 atm combined pressure of ethene and CO).[8] In our hands catalysts based on another bidentate phosphine reported to have high activity and selectivity for methyl propanoate,[4a] namely 1,3-bis(di-*tert*-butylphosphino)propane, will typically give values of 15 000 and 98% for turnover frequency and selectivity, respectively, in these batch reactions. Under continuous operation others have reported that catalysts based on PPh_3 have only modest stability, achieving 1800 turnovers on palladium.[9] Our catalyst has now also been operated under steady state conditions for extended periods, giving total turnover numbers on palladium in excess of 100 000.

Whilst functionalisation of the aryl bridge with classical electron-releasing or -withdrawing groups (MeO and NO_2) has no significant effect on catalyst performance (presumably being too remote from the palladium centre) slight modifications of the substituents on phosphorus give dramatic results (Table 1). Thus activity is reduced by a factor of 60 on going from the *tert*-butyl substituted ligand **1** to the isopropyl analogue **4**. These numbers are lower than those reported above for the preferred catalyst system due to poor mass transfer in the laboratory glass autoclave compared to that obtained in the well-agitated metal autoclave used for more detailed characterisation of the preferred system. The selectivity of the reaction also changes with ligand structure: using the tetraphenyl analogue **6** the products are a mixture of polyketone oligomers and polymers.

There has been much published about the use of the P–Pd–P bite angle in such complexes to aid the development of structure–property relationships.[10] To this end we have undertaken a detailed study of the structure of **1**, **4**, **5** and **6**. All show the expected η^2 binding of one of the alkene groups of dba and the chelating binding of the phosphine giving a trigonal planar environment around the palladium. The measured bite angle is very constant across this series and is much larger (104 *vs.* 87°) than that reported in the only other published structure of a similar compound containing dppe as the ligand.[11] For **1** this

Table 1 Comparative catalytic results for complexes **1**–**7**[a]

Complex	Activity[b]	Selectivity[c] (%)	P–Pd–P bite angle[d] (°)	Parallel pocket angle[d] (°)
1	12 000	99.9	103.9	127.7
2	11 500	99.9		
3	11 800	99.9		
4	200	20	104.3	157.9
5	200	25	103.9	150.5
6	400	20	104.6	145.4
7	500	30		

[a] *Conditions*: reactions were carried out in an identical fashion to that described in ref. 7, except that a glass Bucchi autoclave was used, agitated by means of a magnetic follower and heated by an oil bath. [b] Activity = moles of ethene consumed per mole of palladium per hour. [c] Selectivity to methyl propanoate measured by GC (details as in ref. 7), remainder oligomers and polymers. [d] Determined by X-ray crystallography, see text.

† Current address: Strategic Projects Group, ICI Acrylics, PO Box 90, Wilton, Middlesbrough, UK TS90 8JE.

appears to be at the expense of a longer Pd–P bond (2.36 *vs.* 2.29 Å). It has been argued that the observed ligand bite angle is the result of constraints imposed by the metal and ligand; here, where we have tried to eliminate many of these, the measured parameter still appears to lack sensitivity. Analysis based on the concept of parallel pocket angle[12] does show some variation. This hints that there may indeed be an optimum steric environment, dictated by the nature of the phosphine substituents rather than the bridge length, that controls single and multiple substrate insertions prior to chain termination. These arguments will be developed in a subsequent full paper.

Recognising that the likely active species is based on divalent palladium and intrigued as to why 1,2-bis(di-*tert*-butylphosphinomethyl)benzene and 1,3-bis(di-*tet*-butylphosphino)propane **8**

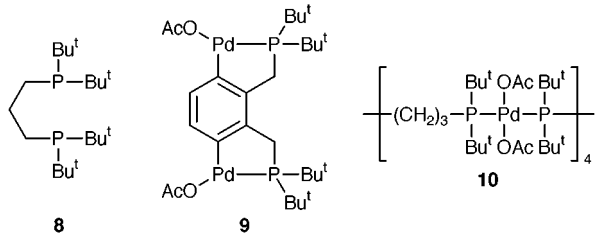

8 **9** **10**

seem unusual amongst bidentate phosphines in producing highly active catalysts selective to methyl propanoate, we have also studied the coordination chemistry of these ligands with $Pd(OAc)_2$. A standard experimental procedure was adopted whereby the ligand was added as an acetone solution to $Pd(OAc)_2$ (also in acetone solution) in equimolar proportions. The reaction mixture was stirred overnight, during which time a precipitate formed. With ligand **1** the above procedure yielded a pale green solid **9**, the spectroscopic characterisation of which is consistent with a doubly orthometallated structure.[13] Recrystallisation (from CH_2Cl_2) of the yellow–green reaction product formed when ligand **8** is added to $Pd(OAc)_2$ gives the tetrameric compound **10**, the structure of which is shown in Fig.1.‡ Inspection of the salient bond lengths and angles shows that each palladium has achieved *trans* disposition of two phosphine ligands, with the relatively long Pd–P bond lengths appropriate to this geometry. Only small deviations are observed from square planar geometry around each palladium centre.

Thus the ligands which ultimately produce catalysts with high selectivity to methyl propanoate seem loath to adopt the classical bidentate chelate structure on reaction with a source of divalent palladium; this *cis* chelate structure has been observed for 1,3-bis(diphenylphosphino)propane, the archetypal ligand for the formation of ethene–CO copolymers.[14] Whilst we are not suggesting that the compounds described here are significant catalytic intermediates, it is tempting to speculate that this reluctance to adopt *cis*-chelate structures may be related to the *cis–trans* isomerisation thought to be responsible for the production of low molecular weight materials from the analogous methoxycarbonylation reaction using PPh_3 as the ligand. This selectivity is thus thought to be driven by the thermodynamic considerations which force the phosphine ligands into a *trans* geometry, isolating the growing chain from the vacant site.[3]

G. R. E. would like to thank ICI Acrylics for the support of his PhD Studentship, and Dr Mel Kilner (University of Durham) for his guidance and encouragement. The EPSRC are also acknowledged for their support in the purchase of the diffractometer.

Notes and references

‡ *Crystal data* for **10**: $C_{92}H_{192}O_{16}P_8Pd_4 \cdot 10.5CH_2Cl_2$, M = 3119.5, orthorhombic, space group $Pca2_1$, a = 38.530(2), b = 19.1969(9), c = 20.3787(10) Å, U = 15073.2(13) Å^3, D_c = 1.375 g cm^{-3}, Z = 4, Mo-Ka radiation (λ = 0.71073 Å), μ = 0.98 mm^{-1}, T = 180 K, $R1$ = 0.0723 ($F^2 > 2\sigma$), $wR2$ = 0.1680 (all data) for 33354 unique data and 1420 parameters. Solvent molecules were restrained to have similar geometry. CCDC 182/1371. See http://www.rsc.org/suppdata/cc/1999/1877/ for crystallographic data in .cif format.

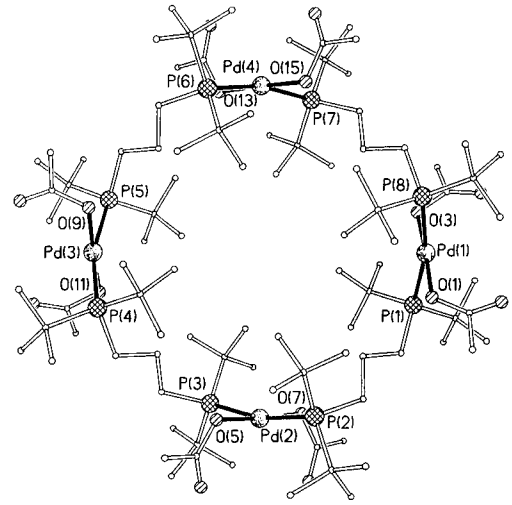

Fig. 1 Molecular structure of **10** without hydrogen atoms. Selected bond lengths (Å) and angles (°): Pd(1)–P(1) 2.382(2), Pd(1)–P(8) 2.403(2), Pd(2)–P(2) 2.397(2), Pd(2)–P(3) 2.391(2), Pd(3)–P(4) 2.394(2), Pd(3)–P(5) 2.388(2), Pd(4)–P(6) 2.397(2), Pd(4)–P(7) 2.402(2), Pd(1)–O(1) 2.024(5), Pd(1)–O(3) 2.035(5), Pd(2)–O(5) 2.039(6), Pd(2)–O(7) 2.037(5), Pd(3)–O(9) 2.044(6), Pd(3)–O(11) 2.015(6), Pd(4)–O(13) 2.039(5), Pd(4)–O(15) 2.038(5), P(1)–Pd(1)–P(8) 166.66(8), P(2)–Pd(2)–P(3) 166.58(7), P(4)–Pd(3)–P(5) 163.71(8), P(6)–Pd(4)–P(7) 166.55(8), O(1)–Pd(1)–O(3) 176.5(2), O(5)–Pd(2)–O(7) 176.5(2), O(9)–Pd(3)–O(11) 177.3(2), O(13)–Pd(4)–O(15) 177.5(2).

1 F. Garbassi, A. Sommazzi, L. Meda, G. Mestroni and A. Sciutto, *Polymer*, 1998, **39**, 1503 and references therein.
2 *Kirk-Othmer Encyclopedia of Chemical Technology*, 4th edn., Wiley, New York, 1995, vol. 16, p. 487.
3 E. Drent and P. H. Budzelaar, *Chem. Rev.*, 1996, **96**, 663.
4 (*a*) E. Drent and E. Kragtwijk (Shell), EP 0 495 548, priority date 19/11/91; (*b*) J. C. L. J. Suykerbuyk, E. Drent and P. G. Pringle (Shell), WO 98/42717, priority date 26/03/97.
5 G. R. Eastham, R. P. Tooze, X. L. Wang and K. Whiston (ICI), WO 96/19434, priority date 22/12/94.
6 C. J. Moulton and B. L. Shaw, *J. Chem. Soc., Chem. Commun.*, 1976, 365.
7 L. E. Crascall and J. L. Spencer, *J. Chem. Soc., Dalton Trans.*, 1992, 3445.
8 Typical reaction conditions: Reactions were carried out in a mechanically stirred 2 l Hastelloy autoclave, heated by external electric jacket heaters and cooled by an internal cooling coil. The palladium complex (0.01 mmol) was dissolved in deoxygenated MeOH (300 cm^3) to which was added MsOH (0.2 mmol). The resulting solution was introduced into the autoclave which had been purged and evacuated. The solution was heated to 80 °C and then an equimolar mixture of ethene and CO was admitted to a total pressure of 10 atm from a reservoir. The reaction was maintained under these conditions for 3 h. The pressure in the reservoir was recorded to give a constant indication of reaction rate. At the end of the period the autoclave was cooled, vented carefully and the contents weighed and analysed by GC using a Perkin-Elmer Autosystem XL fitted with a semi polar CPSIL 19 column, 60 m length.
9 W. G. Reman, G. B. J. De Boer, S. A. J. Van Langen and A. Nahuijsen (Shell), EP 0 411 721, priority date 01/08/89.
10 P. Dierkes and P. W. N. M. van Leeuwen, *J. Chem. Soc., Dalton Trans.*, 1999, 1519.
11 W. A. Hermann, W. R. Thiel, C. Brobmer, K. Ofele, T. Priermeier and W. Scherer, *J. Organomet. Chem.*, 1993, **461**, 51.
12 Y. Koide, S. G. Bott and A. R. Barron, *Organometallics*, 1996, **15**, 2213.
13 *Selected data* for **9**: δ_p 111.69 (s); δ_H 6.89 (br, 2H, arom), 2.94 (d, 4H, CH_2), 2.0 (s, 6H, CH_3CO), 1.35 [d, 36H, C(CH_3)$_3$]; δ_C 24.03 (s, *C*H$_3$CO), 28.85 (s, *C*H$_3$), 31.8 (d, J_{PC} 24.9, *C*H$_2$), 35.55 (d, J_{PC} 17.4, quat), 130.6 (br, arom *C*H), 143.24 (s, arom), 185.2 (s, *C*=O); ν_{max}(KBr)/cm^{-1} 1540s (C=O) (m); *m/z* (FD) 724 (80%); *m/z* (FAB + ion, NBA matrix) 605 (40%).
14 F. Benetollo, R. Bertani, G. Bombieri and L. Toniolo, *Inorg. Chim. Acta*, 1995, **233**, 5.

Communication 9/05521E

Stereospecific synthesis of chiral *N*-(ethynyl)allylglycines and their use in highly stereoselective intramolecular Pauson–Khand reactions

Bernhard Witulski* and Matthias Gößmann

Fachbereich Chemie, Universität Kaiserslautern, Erwin Schrödinger Straße, D-67663 Kaiserslautern, Germany. E-mail: Bernhard@chemie.uni-kl.de

Received (in Cambridge, UK) 21st July 1999, Accepted 2nd August 1999

The first synthesis of an enantiopure *N*-ethynylated allylglycine and its application in the intramolecular Pauson–Khand reaction, which leads to a novel highly functionalised proline derivative with complete control of stereoselectivity, is reported.

N-Functionalised 1-alkynylamides of type **A** are a new class of electronically tuneable acetylenes whose protecting group (PG)

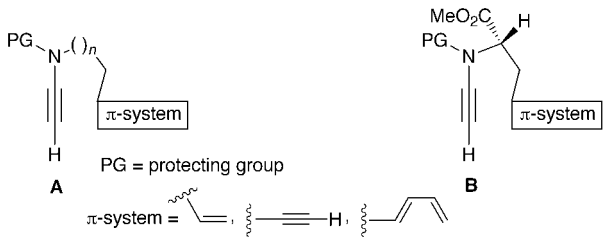

serves both in masking a secondary amine and in tuning the electron density, and hence the reactivity, of the adjacent acetylene moiety.[1] These new building blocks for organic synthesis were designed with the goal of combining the richness and diversity of the chemical reactivity of a carbon–carbon triple bond with one of the most substantial functional groups in chemistry and biology: the amino function.

Recently we described the synthesis of these novel acetylenes based on a two step sequence—ethynylation of secondary amides with trimethylsilylethynyl(phenyl)iodonium triflate[2] followed by desilylation with TBAF—and the use of the thus derived *N*-ethynylamides, whose reactivity differs significantly from those of regular ynamines,[3] in both the Pauson–Khand reaction[1] and in Rh^{I}-catalysed cyclotrimerisations.[4] Given our interest in *N*-functionalised 1-alkynylamides as versatile building blocks for nitrogen-containing heterocycles, we considered the *N*-ethynylamides **B** derived from α-amino acids as even more attractive targets, because their application in transition metal mediated cycloadditions should allow the asymmetric formation of conformationally constrained amino acids[5] and the synthesis of novel proline derivatives that are closely related to the highly potent ACE (angiotensine converting enzyme) inhibitor Ramipril.[6] Furthermore their use as alkynylogous amino acids in peptide chemistry seems to be an interesting endeavour.[7]

However, although the previously described route to *N*-functionalised 1-alkynylamides allowed some degree of functional diversity,[1,3] α-branched 1-alkynylamides could only be obtained in low yields with trimethylsilylethynyl(phenyl)iodonium triflate **3a**. Furthermore all attempts to *N*-alkynylate the α-amino acid derivatives **2a–f** with **3a** (R^2 = $SiMe_3$) failed. We assumed that the observed lack of reactivity was caused by increased steric hindrance inherent in α-branched amino acid derivatives interfering with the nucleophilic addition of the amide nitrogen to the β-carbon of the alkyne **3a** (R^2 = $SiMe_3$). The ethynyl(phenyl)iodonium triflate[8] **3b** (R^2 = H) was therefore thought to be more suitable for the intended *N*-ethynylation. Moreover its use would shorten the previously applied sequence effectively by avoiding the desilylation step and directly affording the terminal *N*-functionalised 1-alkynylamide.

With the idea of exploring the scope of the ethynylation sequence based on **3b** and developing a flexible protecting group strategy,[9] the amides **2a–f** were synthesised starting from allylglycine **1** (Scheme 1, Table 1).† Deprotonation of **2a–f** with either KHMDS in toluene or Cs_2CO_3 in DMF, followed by the addition of **3b** (1.3 equiv.) in CH_2Cl_2 at room temperature, yielded the *N*-ethynylamides **5a–d** in 70–95%.‡ A plausible mechanism for the alkyne formation embodies the *in situ* generation of the alkenylidene carbenes **4**, which immediately rearrange *via* an 1,2-H migration towards the *N*-ethynylamides **5a–d**. The observation that no 1,5-C–H insertion product was formed indicated that the migration aptitude of the hydrogen towards the carbenoid centre in **4** must have been, as anticipated,[10] significantly greater than an alternative intramolecular 1,5-C–H carbene insertion.[11] However, following

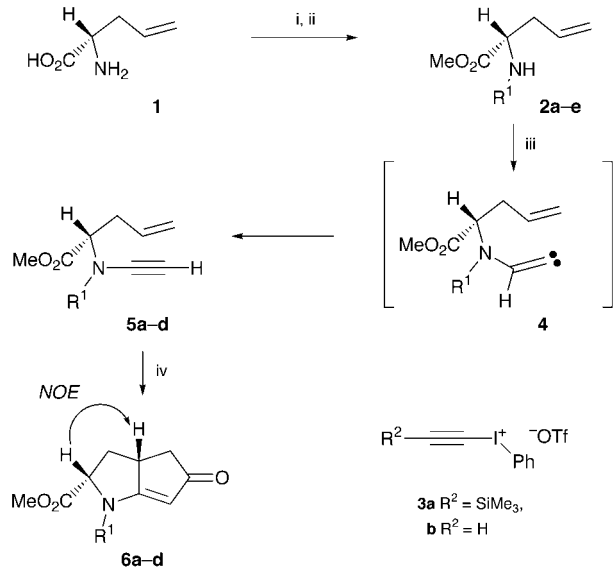

Scheme 1 *Reagents and conditions:* i, $SOCl_2$, MeOH, −10 °C, 24 h; ii, R^1Cl (for **2a–c** and **2f**) or $R^1{}_2O$ (for **2d**,**e**), Et_3N, CH_2Cl_2, 0 °C, 6–12 h, for yield of isolated **2a–f** (2 steps) see Table 1; iii, Cs_2CO_3 (1.3 equiv.), **3b** (1.3 equiv.), DMF–CH_2Cl_2, room temp., 3 h, for yield of isolated **5a–f** see Table 1; iv, $Co_2(CO)_8$ (1.1 equiv.), THF, 30 min. 0–20 °C, then NMO or Me_3NO (6 equiv.), room temp., 25 min, for yield of isolated **6a–d** see Table 1.

Table 1 Yield of isolated **2a–f**, **5a–f**, and **6a–d**†

Entry	R^1	**2**	Yield (%)	**5**	Yield (%)	**6**	Yield (%) [de (%)]
1	Ts	**2a**	88	**5a**	70	**6a**	69 [> 96]
2	2-pyridyl-SO_2	**2b**	71	**5b**	78	**6b**	69 [> 95]
3	4-$NO_2C_6H_4SO_2$	**2c**	89	**5c**	95	**6c**	35 [> 97]
4	Tf	**2d**	83	**5d**	94	**6d**	60 [> 95]
5	Boc	**2e**	80	**5e**	0	—	—
6	Ac	**2f**	94	**5f**	0	—	—

this protocol the allylglycines **2e** (R^1 = Boc) and **2f** (R^1 = Ac) could not be ethynylated with **3b** (R^2 = H) and were recovered unchanged. Obviously the increase of basicity[12] and likewise the change of nucleophilicity of the potassium salts of **2e** and **2f** prevented their addition to **3b** and instead caused its decomposition presumably initiated by deprotonation.

Gratifyingly, the application of enantiomerically pure (*S*)-**2a** [ee >98%, $[\alpha]_D$ +13 (*c* 1.0, $CHCl_3$][13] in the outlined protocol afforded enantiomerically pure *N*-(ethynyl)allylglycine methyl ester (*S*)-**5a**, testifying that *N*-ethynylation proceeded without racemisation. HPLC analysis of the crude product with a chiral stationary phase (Chiralpak AD column) stated that (*S*)-**5a** [ee >98%, $[\alpha]_D$ −60 (*c* 2.0, $CHCl_3$] was obtained essentially enantiomerically pure.[14]

Having established a short and efficient route to chiral and enantiopure *N*-ethynylated allylglycines, we tested their applicability as building blocks for the synthesis of functionalised proline derivatives *via* the intramolecular Pauson–Khand reaction.[15] Although [2+2+1] cycloadditions of **6a**–**d** could be affected at 80 °C in toluene in the presence of a stoichiometric amount of $Co_2(CO)_8$, the mild amine *N*-oxide promoted protocol developed by Schreiber was most effective with respect to yield and diastereoselectivity.[16] Treatment of **5a**–**d** with $Co_2(CO)_8$ at room temperature for 25 min and subsequent addition of either NMO or Me_3NO in CH_2Cl_2 at room temperature provided the proline derivatives **6a**–**d** in yields of 69, 69, 35 and 60%, respectively. The lower yield achieved with the sulfonamide **5c** was caused by a concurrent reduction of the 4-nitrophenylsulfonyl moiety to the corresponding aniline and led to a mixture of products. Pauson–Khand reactions with **5a**–**d** proceeded with high diastereoselectivity giving almost exclusively one single diastereomer (de >95%, determined by ^{1}H-NMR, diastereomeric pure **6a**–**d** were obtained by crystallisation).§ The structural assignment of compound **6a** was based on a combination of H, H and C, H COSY experiments and the analysis of distinct NOE relationships. The use of enantiopure (*S*)-**5a** afforded the optically active (2*S*,4*R*)-**6a** [$[\alpha]_D$ +145 (*c* 2.0, $CHCl_3$)] in 69% yield.¶

Preliminary attempts to further elaborate the obtained highly functionalised proline derivatives were successful (Scheme 2). Pauson–Khand product **6a** was stereoselectively hydrogenated on Pd-C/(H_2) to the cyclopentanone **7** in 90% yield. Luche reduction of **6a** proceeded with distinctive stereoselectivity giving exclusively the allylic alcohol **8** in 80% yield. Compound **8** was obtained as colorless crystals (mp 139–140 °C, CH_2Cl_2–pentane) after column chromatography on silica gel with CH_2Cl_2 containing 0.5% Et_3N. However, the allylic alcohol **8** being extremely sensitive to traces of acid, rearranged under H^+ catalysis with ring cleavage to the cyclopentenones **9** (2:1 mixture of two diastereoisomers).

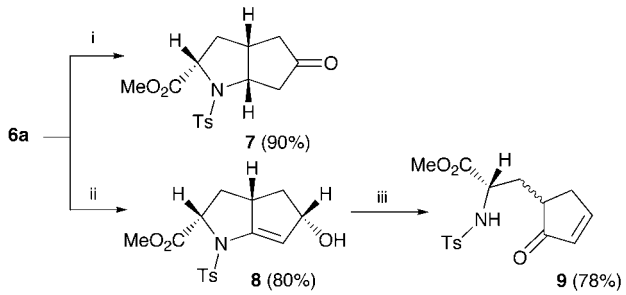

Scheme 2 *Reagents and conditions:* i, H_2 (1 atm.), (10%) Pd/C, EtOH–AcOH (1:1), room temp., 24 h; ii, $NaBH_4$ (2 equiv.), $CeCl_3 \cdot 7\ H_2O$ (1 equiv.), MeOH–CH_2Cl_2, 20 °C, 0.5 h; iii, cat. H^+, $CHCl_3$, room temp.

In conclusion, we have established a short and efficient synthesis of a first set of *N*-ethynylated amino acid derivatives and proved, for the example **2a**/**5a**, that *N*-ethynylation with the alkynyliodonium salt **3b** proceeded without detectable racemisation. Their use in the intramolecular Pauson–Khand reaction allowed the stereoselective formation of novel proline derivatives. Additional applications of *N*-alkynylated amino acids for the synthesis of conformationally constrained amino acids *via* cycloaddition strategies are part of our ongoing research.

This work was supported by the Deutsche Forschungsgemeinschaft (Wi 1696/1) and by the Fonds der Chemischen Industrie. We gratefully acknowledge the help of Dr C. Alayrac and M. Lemarié (ISMRA-Université Caen, France) with the HPLC analyses and $[\alpha]_D$ measurements. We also thank Professor Dr M. Regitz for his support.

Footnote and references

† All new compounds exhibited satisfactory spectra (^{1}H, ^{13}C NMR, IR and MS) and elemental analyses. The compounds **2b-f**, **5b**–**d**, **6b**–**d**, **8** and **9** were synthesised starting from racemic (*rac*)-**1**. The compounds **2a**, **5a**, **6a** and **7** were synthesised starting from both (*rac*)-**1** and enantiopure (*S*)-**1**.

‡ *Selected data* for (*S*)-**5a**: mp 39–40 °C (Et_2O–hexanes) (Calc. for $C_{15}H_{17}NO_4S$ (307.37): C, 58.61; H, 5.57; N, 4.56. Found: C, 58.54; H, 5.63; N, 4.61%); δ_H (400 MHz, $CDCl_3$) 7.79 (d, *J* 8.3, 2H), 7.33 (d, *J* 8.3, 2H), 5.60–5.71 (m, 1H), 5.04–5.19 (m, 2H), 4.53 (dd, *J* 9.8, 5.2, 1H), 3.57 (s, 3H), 2.84 (s, 1H), 2.54–2.74 (m, 2H), 2.45 (s, 3H).

¶ *Selected data* for (2*S*,4*R*)-**6a**: mp 132–134 °C (CH_2Cl_2–hexanes) (Calc. for $C_{16}H_{17}NO_5S$ (335.38): C, 57.30; H, 5.11; N, 4.18. Found: C, 57.01; H, 5.06; N, 4.23%); δ_H(400 MHz, $CDCl_3$) 7.81 (d, *J* 8.3, 2H), 7.36 (d, *J* 8.3, 2H), 5.67 (d, *J* 1.5, 1H), 4.64 (dd, *J* 10.3, 5.7, 1H), 3.85 (s, 3H), 2.85–2.95 (m, 1H), 2.56–2.63 (m, 1H), 2.53 (dd, *J* 17.1, 6.7, 1H), 2.45 (s, 3H), 2.21 (dd, *J* 17.1, 5.2, 1H), 1.76–1.86 (m, 1H).

§ The stereochemical course of the intramolecular Pauson–Khand reaction with the compounds **5a**–**d** follows the one previously noticed by us with other *N*-ethynylamides. See ref. 1. A detailed discussion will be presented in the full account of this study.

1 B. Witulski and T. Stengel, *Angew. Chem., Int. Ed.*, 1998, **37**, 489.
2 P. J. Stang and V. V. Zhdankin, *Chem. Rev.*, 1996, **96**, 1123.
3 G. Himbert, *Methoden Org. Chem. (Houben-Weyl)*, 1993, vol. E15, pp. 3267–3461; J. Ficini, *Tetrahedron*, 1976, **32**, 1448.
4 B. Witulski and T. Stengel, *Angew. Chem., Int. Ed.*, 1999, **38**, in the press.
5 J. Gante, *Angew. Chem., Int. Ed. Engl.*, 1994, **33**, 1699; A. E. P. Adang, P. H. H. Hermkens, J. T. M. Linders, H. C. J. Ottenheijm and C. J. van Staveren, *Recl. Trav. Chim. Pays-Bas.*, 1994, **113**, 63.
6 R. Henning, U. Lerch and H. Urbach, *Synthesis*, 1989, 265.
7 M. T. Reetz, T. J. Strack, J. Kanand and R. Goddard, *Chem. Commun.*, 1996, 733.
8 For the preparation of **3b** and its reaction with carbon nucleophiles see: M. Ochiai, T. Ito, Y. Takaoka, Y. Masaki, M. Kunishima, S. Tani and Y. Nagao, *J. Chem. Soc., Chem. Commun.*, 1990, 118; P. J. Stang, in *Modern Acetylene Chemistry*, ed. P. J. Stang and F. Diederich, VCH, Weinheim, 1995.
9 T. W. Greene and P. G. M. Wuts, *Protective Groups in Organic Synthesis*, Wiley, New York, 1991; C. Goulaouic-Dubois, A. Guggisberg and M. Hesse, *J. Org. Chem.*, 1995, **60**, 5969; T. Fukuyama, C.-K. Jow and M. Cheung, *Tetrahedron Lett.*, 1995, **36**, 6373.
10 M. M. Gallo, T. P. Hamilton and H. F. Schaefer III, *J. Am. Chem. Soc.*, 1990, **112**, 8714; W. Kirmse, *Angew. Chem., Int. Ed. Engl.*, 1997, **36**, 1164.
11 K. S. Feldman and D. A. Mareska, *J. Am. Chem. Soc.*, 1998, **120**, 4027 and references therein.
12 The pK_a values of **2a**–**e** can be estimated by comparison with the following model compounds (in DMSO): NH_3 (41), $PhSO_2NH_2$ (16.1), $CF_3SO_2NH_2$ (9.7), CH_3CONH_2 (25.5), $EtOCONH_2$ (24.8); all data taken from F. G. Bordwell, *Acc. Chem. Res.*, 1988, **21**, 456.
13 (*S*)-Allylglycine is commercially available. For its synthesis, see: Y. N. Belokon, V. I. Bakhmutov, N. I. Chernoglazova, K. A. Kochetkov, S. V. Vitt, N. S. Garbalinskaya and V. M. Belikov, *J. Chem. Soc., Perkin Trans 1*, 1988, 305.
14 Baseline separation of (*S*)-**5a** and (*R*)-**5a** from (*rac*)-**5a** could be achieved by using the Chiralpak AD column.
15 For recent reviews, see A. C. Comely and S. E. Gibson, *J. Chem. Soc., Perkin Trans 1*, 1999, 223; O. Geis and H.-G. Schmalz, *Angew. Chem., Int. Ed.*, 1998, **37**, 911; N. E. Schore, *Comprehensive Organometallic Chemistry II*, ed. L. S. Hegedus, Pergamon, 1995, vol. 12, p. 703.
16 S. Shambayati, W. E. Crowe and S. L. Schreiber, *Tetrahedron Lett.*, 1990, **31**, 5289.

Communication 9/05898B

ChemComm

Boronate-functionalized polypyrrole as a new fluoride sensing material

M. Nicolas, B. Fabre* and J. Simonet

Laboratoire d'Electrochimie Moléculaire et Macromoléculaire (Unité Mixte de Recherche n°6510 associée au CNRS), Université de Rennes 1, Campus de Beaulieu, 35042 Rennes Cedex, France. E-mail: fabre@univ-rennes1.fr

Received (in Cambridge, UK) 25th June 1999, Accepted 8th July 1999

The anodic oxidation of boronate-substituted pyrrole led to a fluoride anion-responsive electroactive polymer film.

The modification of the electrochemical response of a system in the presence of a specific ion or molecule can be considered as a recognition event. In the case where such a system is deposited onto an electrode surface, this mode of recognition can be exploited for the construction of electrochemical sensors. As an example, numerous recent reports have focused on the sensing properties towards cations of some polyether or crown ether functionalized redox-active conjugated polymers.[1–7] In contrast, anion recognition by this class of polymers derivatized with a suitable receptor has been much less developed.[8,9] We have tested a novel route to anion-responsive electrodes based on a conjugated polymer substituted by a boronate group. Here, the boron-containing moiety was used as a sensing element owing to the strong interaction of this heteroatom with hard bases like fluoride giving rise to specific orbital changes from sp^2 to more stable sp^3. So, the possible electronic and/or conformational changes induced by the boron–fluoride binding could be detected from the modification of the electrochemical response of the conjugated polymer. Although numerous boronic acid-based anion and sugar receptors have been developed by Shinkai and co-workers,[10–13] their immobilization onto an electrode surface has not been investigated so far. The incorporation of boron atoms in the backbone of conjugated polymers has already been described,[14,15] but in our case we chose to attach the boronate group to the conjugated polymer by a spacer of appropriate length.

To achieve this purpose, conjugated polymer films were electrodeposited in one step onto a platinum (diameter 1 mm) electrode surface *via* the anodic oxidation in MeCN of the functionalized pyrrole. 1-(Phenylsulfonyl)-3-vinylpyrrole was synthesized in three steps from 1-(phenylsulfonyl)pyrrole using literature procedures.[16,17] Hydroboration with diisopinocampheylborane[18] (Ipc_2BH) prepared from (+)-α-pinene and borane–dimethyl sulfide complex gave the diethyl boronate derivative (Scheme 1). Treatment with pinacol gave **1a** as a colorless oil in 23% overall yield after purification by column chromatography (CH_2Cl_2). This was deprotected electrochemically at −2.45 V (*vs.* 10^{-1} M Ag^+/Ag) using pyrene as a redox mediator to give **1b** (yield 58%).†

The electropolymerization of **1b** (10^{-2} M) was carried out in thoroughly dried MeCN containing 10^{-1} M Bu_4NPF_6 as the supporting electrolyte. The doped film was potentiodynamically electroformed with an anodic limit close to the irreversible oxidation peak potential of monomer, *e.g.* 0.75 V [Fig. 1(*a*)]. Its electrochemical response in an hydroorganic medium[19] (H_2O–MeCN) showed a stable reversible redox system at −0.11 V *vs.* SCE (ΔE_p = 40 mV at 100 mV s^{-1}) corresponding to the p-doping/undoping process [Fig. 1(*b*)]. The doping level deduced from the cyclic voltammetry curve was found to be in the range 0.20–0.30 depending on the film thickness.

The addition of KF led to the decrease of this system together with the emergence of a new redox system at −0.37 V, the magnitude of which increased with F^- concentration. For a film

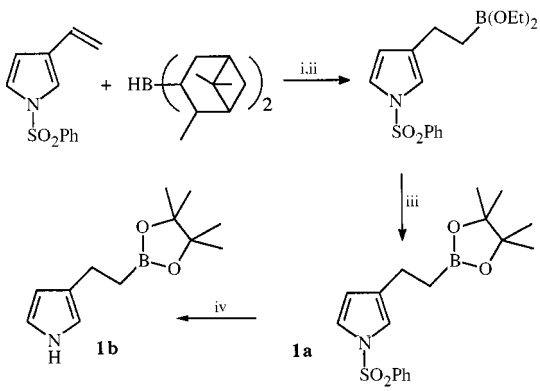

Scheme 1 *Reagents and conditions*: i, Ipc_2BH (1.2 equiv.), THF, −40 °C, then addition of the vinylated compound, room temp., 24 h; ii, acetaldehyde (10 equiv.), 0° C, 24 h; iii, pinacol (1 equiv.) in THF, room temp., 24 h; *iv*, pyrene (20%), reduction at −2.45 V (*vs.* Ag^+/Ag) in MeCN + 10^{-1} M Bu_4NClO_4.

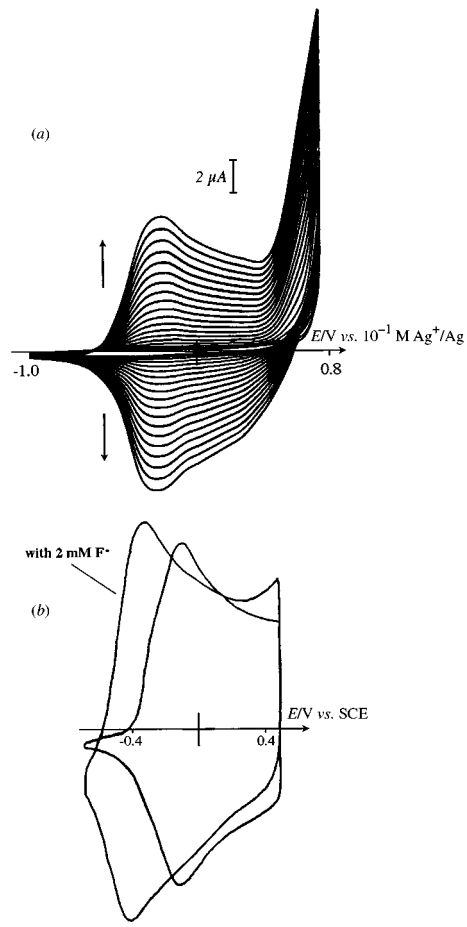

Fig. 1 (*a*) Successive cyclic voltammograms of **1b** (10^{-2} M) in MeCN + 10^{-1} M Bu_4NPF_6 (final electropolymerization charge: 70 mC cm^{-2}). (*b*) Electrochemical response of corresponding poly(**1b**) in H_2O–MeCN (1:1 v/v) + 5 × 10^{-1} M $LiClO_4$ in the absence and presence of 2 mM KF. Potential scan rate: 100 mV s^{-1}.

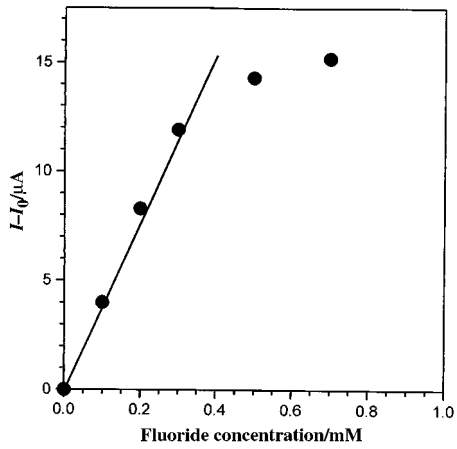

Fig. 2 Calibration curve for F^- in H_2O–MeCN (1:1 v/v) + 5×10^{-1} M $LiClO_4$ obtained with a poly(**1b**)-coated platinum (8×10^{-3} cm^2) electrode (electropolymerization charge: 280 mC cm^{-2}). I and I_o are the currents measured at −0.42 V on the voltammetric curves (100 mV s^{-1}) in the presence and absence of KF, respectively.

electropolymerized using 70 mC cm^{-2}, only the second system was observed for a large F^- concentration, *e.g.* 2 mM [Fig. 1(*b*)]. It must be pointed out that the electrochemical response of poly(**1b**) was not changed when F^- was replaced by Cl^- or Br^- up to a tested concentration of 20 mM. Moreover the interaction with F^- was specific for the boronate-containing polymer, as the voltammetric response of an unfunctionalized polymer film was found to be unmodified in the presence of this anion. Thus, all these results are consistent with a selective electrochemical recognition of F^- by poly(**1b**). The negative shift of the redox potential indicates that the F^- bound polymer was easier to oxidize. Such a result could be explained by a stabilization of F^- bound to the boron atom by the positive charges along the oxidized polymer backbone. The effect of the F^- concentration on the current intensity of the system assigned to the F^- bound polymer is shown in Fig. 2. As can be seen, an initial linear plot at low F^- concentrations (< 0.4 mM) is followed by a plateau for larger concentrations indicating that all the binding sites in the film were occupied. The slope and the linearity range of the first part were found to be dependent on the film thickness. As a matter of fact, the sensitivity to F^- was higher for thin films, as already observed for other sensory materials.[20]

Finally, this work constitutes a rare example of functionalized conducting polymer-based selective anion recognition. Some parameters, such as the film thickness, and the nature and length of the spacer arm between the monomer unit and the boron site, must be now optimized in order to obtain sensitive detection operating over a large F^- concentration range.

Drs M. Vaultier, J.-F. Pilard and G. Marchand are fully acknowledged for their help in the synthesis of monomers. The 'Région de Bretagne' is also acknowledged for a research grant to one of the authors (M. N.).

Notes and references

† *Selected data* for **1b**: $\delta_H(CDCl_3)$ 1.04 (t, 2 H), 1.15 (s, 12 H), 2.55 (t, 2 H), 6.11 (dd, 1 H), 6.48–6.60 (m, 2 H), 8.01 (s, 1 H); δ_C 21.60, 25.22, 83.38, 108.66, 114.94, 117.90, 126.74.

1 B. Fabre and J. Simonet, *Coord. Chem. Rev.*, 1998, **180**, 1211.
2 T. M. Swager, *Acc. Chem. Res.*, 1998, **31**, 201.
3 P. Bäuerle and S. Scheib, *Adv. Mater.*, 1993, **5**, 848.
4 H. Korri Youssoufi, M. Hmyene, A. Yassar and F. Garnier, *J. Electroanal. Chem.*, 1996, **406**, 187.
5 A. Ion, I. Ion, A. Popescu, M. Ungureanu, J. C. Moutet and E. Saint-Aman, *Adv. Mater.*, 1997, **9**, 711.
6 L. M. Goldenberg, I. Lévesque, M. Leclerc and M. C. Petty, *J. Electroanal. Chem.*, 1998, **447**, 1.
7 F. Sannicolo, E. Brenna, T. Benincori, G. Zotti, S. Zecchin, G. Schiavon and T. Pilati, *Chem. Mater.*, 1998, **10**, 2167.
8 P. D. Beer, *Acc. Chem. Res.*, 1998, **31**, 71.
9 M. M. G. Antonisse and D. N. Reinhoudt, *Chem. Commun.*, 1998, 443.
10 T. D. James, K. R. A. Samankumara Sandanayake and S. Shinkai, *Angew. Chem., Int. Ed. Engl.*, 1996, **35**, 1910.
11 C. R. Cooper, N. Spencer and T. D. James, *Chem. Commun.*, 1998, 1365.
12 H. Yamamoto, A. Ori, K. Ueda, C. Dusemund and S. Shinkai, *Chem. Commun.*, 1996, 407.
13 C. Dusemund, K. R. A. Samankumara Sandanayake and S. Shinkai, *J. Chem. Soc., Chem. Commun.*, 1995, 333.
14 R. J.-P. Corriu, T. Deforth, W. E. Douglas, G. Guerrero and W. S. Siebert, *Chem. Commun.*, 1998, 963.
15 N. Matsumi, K. Naka and Y. Chujo, *J. Am. Chem. Soc.*, 1998, **120**, 5112 and 10 776.
16 M. Kakushima, P. Hamel, R. Frenette and J. Rokach, *J. Org. Chem.*, 1983, **48**, 3214.
17 R. Settambolo, R. Lazzaroni, T. Messeri, M. Mazzetti and P. Salvadori, *J. Org. Chem.*, 1993, **58**, 7899.
18 I. Paterson, J. M. Goodman, M. A. Lister, R. C. Schumann, C. K. McClure and R. D. Norcross, *Tetrahedron*, 1990, **46**, 4663.
19 In water, the electroactivity of poly(**1b**) was weaker and less reversible than that exhibited in organic electrolyte, probably owing to the presence of the hydrophobic pinacol moiety.
20 See for example: A. C. Ion, J. C. Moutet, A. Pailleret, A. Popescu, E. Saint-Aman, E. Siebert and E. M. Ungureanu, *J. Electroanal. Chem.*, 1999, **464**, 24.

Communication 9/05136H

ChemComm

Pendant arm Schiff base complexes of aluminium as ethylene polymerisation catalysts

Paul A. Cameron, Vernon C. Gibson,* Carl Redshaw, John A. Segal, Michael D. Bruce, Andrew J. P. White and David J. Williams

Department of Chemistry, Imperial College, South Kensington, London, UK, SW7 2AY. E-mail: v.gibson@ic.ac.uk

Received (in Cambridge, UK) 25th June 1999, Accepted 9th August 1999

The potentially tridentate Schiff base ligands [3,5-Bu^t_2-2-(HO)C_6H_2CH=NL] 1, on reaction with Me_3Al at room temperature, afford the complexes [(3,5-Bu^t_2-2-(O)C_6H_2CH=NL)$AlMe_2$] [L = $CH_2CH_2NMe_2$ 2a, (2-PhO)C_6H_4 2b, 2-$CH_2C_5H_4N$ 2c and 8-C_9H_6N (quinoline) 2d], 2a and 2c have been characterised crystallographically; further reaction of the dimethyl compounds with $B(C_6F_5)_3$ affords the cationic systems [(3,5-Bu^t_2-2-(O)C_6H_2CH=NL)-AlMe]$^+$ 3a–d of which 3a and 3b are ethylene polymerisation catalysts.

Recent reports by Coles and Jordan[1] and ourselves[2] have revealed the potential for cationic aluminium alkyls as ethylene polymerisation catalysts. The aluminium procatalysts reported thus far are bi- and tri-dentate chelates (L) of the general form [{L}$AlMe_2$], which are synthesised by the reaction of the relevant ligand system with Me_3Al. To obtain an active catalyst system, cationic species are generated on further reaction with $B(C_6F_5)_3$ in hydrocarbon or chlorocarbon solvents. The cationic aluminium alkyls so derived display low activities as ethylene polymerisation catalysts and they produce polymers of high[1] (M_w 176000–272000) or moderate[2] (M_w 13000–23000) molecular weight. In studies directed at extending the family of cationic aluminium catalysts to N,O-Schiff base chelate ligands, we first targeted bidentate chelates *e.g.* 3,5-Bu^t_2-2-(HO)C_6H_2CH=NR (R = alkyl or aryl), which led to the isolation of a range of systems of the type [(3,5-Bu^t_2-2-(O)C_6H_2CH=NR)$AlMe_2$].[3] However attempts to obtain clean alkylaluminium cations by way of reaction with $B(C_6F_5)_3$ (in toluene or dichloromethane) were unsuccessful, always leading to a mixture of species. ^{1}H NMR spectra of the product mixtures show *inter alia* the presence of high field methyl resonances that are characteristic of (ligand)$AlMe(C_6F_5)$ species[4] formed by arylation of the Al centre by the boron reagent. In view of this undesired reactivity, the investigation was extended to Schiff base chelates bearing a pendant donor arm which it was envisaged might, through coordination, lend stability to the cationic methyl product. Here we show not only that such ligands afford stable cationic alkyl species but also that these cationic alkyls are active catalysts for ethylene polymerisation. Homogeneous olefin polymerisation catalysts hitherto described which are derived from N,O-Schiff bases are limited to complexes of transition metals, namely Ti,[5,6] Zr,[6,7] Cr[8] and Ni.[9]

The Schiff base ligands **1a**–**d** (Scheme 1) are accessible in good yields (> 80%) *via* standard imine condensation procedures. Treatment of these potentially tridentate ligands with Me_3Al in toluene at room temperature readily affords the corresponding dimethyl complexes [3,5-Bu^t-2-(O)C_6H_2CH=N-L]$AlMe_2$ **2a**–**d** with concomitant elimination of methane (Scheme 2).†

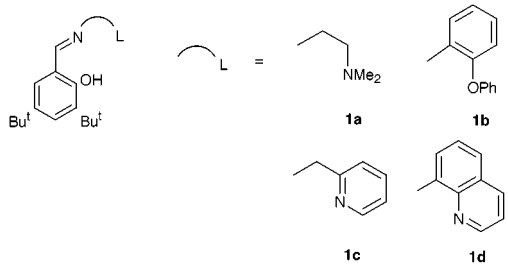

Scheme 1 Ligands **1a**–**d**.

Crystals of **2a** suitable for an X-ray structure determination‡ were grown from MeCN at room temperature. Deprotonated **1a** is seen to act as a tridentate ligand, binding to aluminium *via* the oxygen and the imino and amino nitrogen atoms [Fig. 1(a)]. The geometry at aluminium can best be described as distorted trigonal bipyramidal though with the bond to the axial amino nitrogen N(1) [2.413(5) Å] being substantially longer than that to the equatorial imino centre N(4) [1.998(4) Å]. With the exception of Al–N(1), the Al–X bonds are all clearly single in nature. These bonds, however, are noticeably longer than the corresponding linkages in the simple chelate analogues, *e.g.* {3,5-Bu^t_2-2-(O)C_6H_2CH=N(2,6-$Me_2C_6H_3$)}$AlMe_2$[3] [Al–O 1.773(3), Al–N 1.972(3), Al–Me 1.948(5), 1.959(5) Å] reflecting the presence of the additional donor in **2a** with subsequent competition for electron density. It is interesting that the aluminium atom is displaced significantly out of the equatorial plane (0.16 Å) in the direction of the ligand oxygen. The six-membered N,O chelate ring adopts a sofa conformation, the aluminium lying *ca*. 0.5 Å out of the plane of the other five atoms (which are co-planar to within 0.03 Å). The ring C=N bond has clearly retained its double bond character [N(4)–C(5) 1.294(6) Å], there being no evidence of significant delocalisation into any of the adjacent linkages. The structure of complex **2c** [Fig. 1(b)] is very similar to that of **2a**, in particular with respect to the geometry around Al, the only significant difference of note being a substantial reduction in the bond distance between the aluminium and the pyridyl nitrogen [Al–N(1) 2.254(2) Å *cf.* the dimethylamino nitrogen in **2a** [Al–N(1) 2.413(5) Å]. The remaining bond lengths and angles at aluminium do not differ significantly from those in **2a**.

The cationic complexes [(3,5-Bu^t_2-2-(O)C_6H_2CH=NL)-AlMe]$^+$ **3a**–**d** are readily generated on treatment with 1 equiv. of $[B(C_6F_5)_3]$ in CD_2Cl_2 or toluene at ambient temperature (Scheme 2) as illustrated by the ^{1}H NMR spectrum of **3a** (Fig. 2); the systems exist as free cations as opposed to the ion pairs (*i.e.* with Al···Me–B association) observed by Coles and Jordan.[1] The pendant arm is likely to stabilise the cationic aluminium centre; in its absence, as noted above, the analogous reaction with $[B(C_6F_5)_3]$ gave complicated NMR spectra corresponding to multiple products.

Complexes **2a**–**d** were combined with 1 equiv. of $B(C_6F_5)_3$ to test for ethylene polymerisation activity. Polymerisations were run with 0.25 mmol catalyst in 200 mL toluene solution under 5 bar ethylene pressure at 50 °C for 60 min. Procatalysts **2a** and

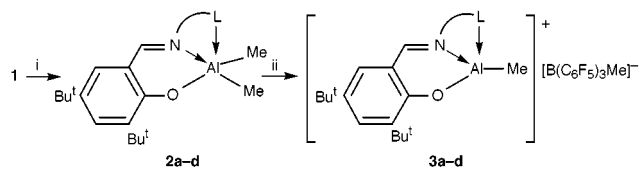

Scheme 2 *Reagents:* i. $AlMe_3$, toluene; ii, $B(C_6F_5)_3$, CD_2Cl_2 or toluene.

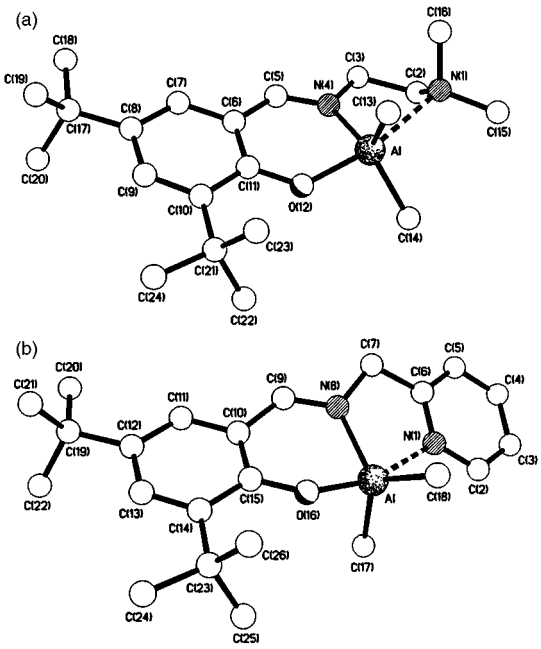

Fig. 1(a) The molecular structure of **2a**, showing the trigonal bipyramidal geometry at aluminium and the very long Al–N(amino) linkage. Selected bond lengths (Å) and angles (°): Al–N(1) 2.413(5), Al–N(4) 1.998(4), Al–O(12) 1.854(4), Al–C(13) 1.978(6), Al–C(14) 1.976(5), N(4)–C(5) 1.294(6), O(12)–Al–C(14) 96.6(2), O(12)–Al–C(13) 98.3(2), C(14)–Al–C(13) 123.7(3), O(12)–Al–N(4) 88.2(2), C(14)–Al–N(4) 116.0(2), C(13)–Al–N(4) 118.4(2), O(12)–Al–N(1) 163.0(2), C(14)–Al–N(1) 91.4(2), C(13)–Al–N(1) 89.5(2), N(4)–Al–N(1) 74.9(2). (b) Complex **2c**.

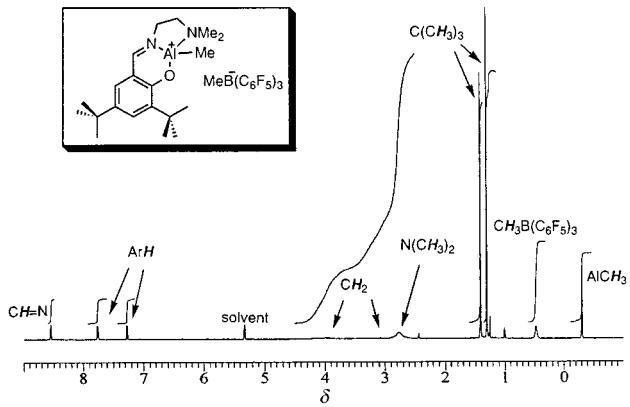

Fig. 2 ^{1}H NMR spectrum (250 MHz) of **3a**.

2b produced solid polyethylene but procatalysts **2c** and **2d** did not display any polymerisation activity. Procatalyst **2a** gave a productivity of 50 g(PE) mol^{-1} h^{-1} bar^{-1} and yielded polyethylene with M_w = 172000, M_n = 2400, whilst procatalyst **2b** gave 110 g(PE) mol^{-1} h^{-1} bar^{-1} with polymer M_w = 218000, M_n = 5200.

In contrast to our previous tridentate aluminium alkyls,[2] the present system affords higher molecular weights, as exemplified by the much higher M_w values, although the activities are similar. The results suggest that lability of the pendant donor arm, as in the cations derived from **2a**, **2b**, is an important feature of the polymerisation catalysis mechanism, providing a pathway for ethylene to approach the aluminium centre. The observation that **2c** and **2d**, which have N-heterocycles as the donor arms, did not provide active systems accords with this view as these compounds are likely to form cations with stronger donor to metal bonds (as evidenced by the significantly shorter Al–N(1) bond length in **2c** *cf.* **2a**) thereby reducing the propensity for dissociation of the coordinating arm to generate an active centre.

In summary, we have shown that Schiff base ligands are capable of stabilising cationic methylaluminium centres only when they possess an additional donor arm. We reasoned, however, that it might be possible to form cations from the analogous Schiff bases without the donor arm if a *free* donor ligand, *e.g.* THF, were added to stabilise the system. This is indeed the case, and our subsequent study of the formation of these closely related cationic species will be published elsewhere.

We thank the EPSRC for a studentship (to P. A. C.), BP-Amoco Chemicals and ICI Acrylics for financial support, and the Royal Society and the Leverhulme Trust for Fellowships (to J. A. S. and C. R.). Mr G. Audley is gratefully acknowledged for GPC measurements.

Notes and references

† Satisfactory microanalyses were obtained for compounds **2a**–**d**, cations **3a**–**d** were characterised spectroscopically. *Selected spectroscopic data* (*J*/Hz): for **2a**: ^{1}H NMR (250 MHz, C_6D_6, 298 K): δ 7.66 [d, 1H, ^4J(HH) 2.4, C_6H_2], 7.39 (s, 1H, CH=N), 6.80 [d, 1H, ^4J(HH) 2.6, C_6H_2], 2.86 [t, 2H, ^3J(HH) 6.8, CH_2CH_2], 2.08 [t, 2H, ^3J(HH) 6.2, CH_2CH_2], 1.85 [s, 6H, $N(CH_3)_2$], 1.63, [s, 9H, $C(CH_3)_3$], 1.30 [s, 9H, $C(CH_3)_3$], −0.26 (s, 6H, $AlCH_3$). For **2c**: ^{1}H NMR (C_6D_6, 298 K): δ 8.31–8.28 (m, 1H, C_5H_4N), 7.72 [d, 1H, ^4J(HH) 2.6, C_6H_2], 7.38 [t, 1H, ^4J(HH) 1.3, CH=N), 6.83 [d, 1H, ^4J(HH) 2.5, C_6H_2], 6.80 [dt, 1H, ^3J(HH) 7.7, ^4J(HH) 1.7, C_5H_4N], 6.50–6.39 (m, 1H, C_5H_4N), 6.22–6.14 (m, 1H, C_5H_4N), 3.81 (br s, 2H, CH_2), 1.76 [s, 9H, $C(CH_3)_3$], 1.38 [s, 9H, $C(CH_3)_3$], −0.15 (s, 6H, $AlCH_3$). For **3a**: ^{1}H NMR (CD_2Cl_2, 298 K): δ 8.55 (s, 1H, CH=N), 7.76 [d, 1H, ^4J(HH) 2.6, C_6H_2], 7.27 [d, 1H, ^4J(HH) 2.6, C_6H_2], 4.0 (br, CH_2CH_2), 3.0 (br, CH_2CH_2), 2.77 [br s, 6H, $N(CH_3)_2$], 1.41 [s, 9H, $C(CH_3)_3$], 1.31 [s, 9H, $C(CH_3)_3$], 0.47 (s, 3H, BCH_3), −0.31 (s, 3H, $AlCH_3$). For **3c**: ^{1}H NMR (CD_2Cl_2, 298 K): δ 8.46 (s, 1H, CH=N), 8.05 [dt, 1H, ^3J(HH) 7.9, ^4J(HH) 1.5, C_5H_4N], 8.00 [d, 1H, ^4J(HH) 2.5, C_6H_2], 7.82 [d, 1H, ^3J(HH) 5.3, C_5H_4N], 7.51 [d, 1H, ^3J(HH) 8.0, C_5H_4N], 7.20 (m, 1H, C_5H_4N), 7.20 [dt, 1H, ^3J(HH) 6.3, ^4J(HH) 1.1, C_5H_4N], 7.07 [d, 1H, ^4J(HH) 2.5, C_6H_2], 5.15 [AB q, 2H, ^3J(HH) 1.5, CH_2CH_2], 4.98 [AB q, 2H, ^3J(HH) 1.5, CH_2CH_2], 1.75 [s, 9H, $C(CH_3)_3$], 1.26 [s, 9H, $C(CH_3)_3$], 0.48 (s, 3H, BCH_3), −0.47 (s, 3H, $AlCH_3$).

‡ *Crystal data* for **2a**: $C_{21}H_{37}N_2OAl$, M = 360.5, monoclinic, space group $P2_1/c$ (no. 14), a = 10.332(2), b = 24.982(4), c = 9.729(2) Å, β = 115.98(1)°, V = 2257.4(7) Å^3, Z = 4, D_c = 1.061 g cm^{-3}, μ(Mo-Kα) = 1.00 cm^{-1}, F(000) = 792, T = 293 K, 2934 independent reflections. For **2c**: $C_{23}H_{33}N_2OAl$, M = 380.5, monoclinic, space group $P2_1/c$ (no. 14), a = 15.009(2), b = 12.207(2), c = 14.129(1) Å, β = 116.36(1)°, V = 2319.5(4) Å^3, Z = 4, D_c = 1.090 g cm^{-3}, μ(Mo-Kα) = 1.01 cm^{-1}, F(000) = 824, T = 293 K, 5299 independent reflections. Data were collected on Siemens P4/PC diffractometers using ω-scans, and the non-hydrogen atoms were refined anisotropically using full matrix least squares based on F^2 to give R_1 = 0.067 (0.054), wR_2 = 0.156 (0.136) for 1646 (3526) independent observed reflections [$|F_o| > 4\sigma(|F_o|)$, $2\theta \leq 45°$ (45°)] and 226 (245) parameters for **2a** (**2c**) respectively.

CCDC 182/1366. See http://www.rsc.org/suppdata/cc/1999/1883/ for crystallographic files in .cif format.

1 M. P. Coles and R. F. Jordan, *J. Am. Chem. Soc.*, 1997, **119**, 8125.
2 M. Bruce, V. C. Gibson, C. Redshaw, G. A. Solan, A. J. P. White and D. J. Williams, *Chem. Commun*., 1998, 2523.
3 P. A. Cameron, V. C. Gibson, C. Redshaw, G. A. Solan, A. J. P. White and D. J. Williams, manuscript in preparation.
4 B. Qian, D. L. Ward and M. L. Smith III, *Organometallics*, 1998, **17**, 3070.
5 S. Doherty, R. J. Errington, A. P. Jarvis, S. Collins, W. Clegg and M. R. J. Elsegood, *Organometallics*, 1998, **17**, 3408; J. P. Corden, W. Errington, P. Moore and M. G. H. Wallbridge, *Chem. Commun.*, 1999, 323.
6 T. Fujita, Y. Tohi, M. Mitani, S. Matsui, J. Saito, M. Nitabaru, K. Sugi, H. Makio and T. Tsutsui (Mitsui Chemicals), *Eur. Pat.*, 0874005A1, 1998.
7 E. B. Tjaden and R. F. Jordan, *Macromol. Symp.*, 1995, **89**, 231.
8 V. C. Gibson, C. Newton, C. Redshaw, G. A. Solon, A. J. P. White and D. J. Williams, *J. Chem. Soc., Dalton Trans.*, 1999, 827.
9 C. Wang, S. Friedrich, T. R. Younkin, R. T. Li, R. H. Grubbs, D. A. Bansleben and M. W. Day, *Organometallics*, 1998, **17**, 3149.

Communication 9/05120A

ChemComm

Building blocks as disposition in solution: $[\{Mo^{VI}O_3(H_2O)\}_{10}\{V^{IV}O(H_2O)\}_{20}\{(Mo^{VI}/Mo^{VI}_5O_{21})(H_2O)_3\}_{10}(\{Mo^{VI}O_2(H_2O)_2\}_{5/2})_2(\{NaSO_4\}_5)_2]^{20-}$, a giant spherical cluster with unusual structural features of interest for supramolecular and magneto chemistry†

Achim Müller,* Michael Koop, Hartmut Bögge, Marc Schmidtmann, Frank Peters and Paul Kögerler

Fakultät für Chemie der Universität, D-33501 Bielefeld, Germany. E-mail: a.mueller@uni-bielefeld.de

Received (in Cambridge, UK) 14th June 1999, Accepted 13th August 1999

The unique polyoxometalate compound $Na_{20}[\{Mo^{VI}O_3(H_2O)\}_{10}\{V^{IV}O(H_2O)\}_{20}\{(Mo^{VI}/Mo^{VI}_5O_{21})(H_2O)_3\}_{10}(\{Mo^{VI}O_2(H_2O)_2\}_{5/2})_2(\{NaSO_4\}_5)_2]\cdot xH_2O$ 1 ($x \approx 170$) shows remarkable structural features: *e.g.* (i) $\{Mo^{VI}/Mo^{VI}_5\}$-type pentagons as building blocks (being present in the relevant reaction medium as disposition), (ii) a 'magnetic ring-shaped band' built up by ten linked $\{V^{IV}_3\}$ triangles having common corners and (iii) two $\{NaSO_4\}_5$ rings encapsulated inside the cavity of an icosidodecahedron formed by twenty triangular and twelve pentagonal faces built up by ten Mo^{VI} and twenty V^{IV} centres, respectively.

The generation of a variety of extremely large complex molecular systems under one-pot reaction conditions requires variably linkable units as disposition in the related solution.[1,2] Knowledge of polyoxometalate systems allows for instance the generation and linking of pentagons of the type $\{Mo^{VI}/Mo^{VI}_5\}$, which contain a central pentagonal bipyramid sharing edges with five MoO_6 octahedra. Here we report on the isolation of a related aggregate which displays interesting structural features. The basic structure can be optimally described by referring to the faces of an icosidodecahedron (one of the thirteen Archimedean solids) spanned by ten Mo^{VI} and twenty V^{IV} centres.

If vanadyl sulfate is added to an acidified molybdate solution,‡ the compound $Na_{20}[\{Mo^{VI}O_3(H_2O)\}_{10}\{V^{IV}O(H_2O)\}_{20}\{(Mo^{VI}/Mo^{VI}_5O_{21})(H_2O)_3\}_{10}(\{Mo^{VI}O_2(H_2O)_2\}_{5/2})_2(\{NaSO_4\}_5)_2]\cdot xH_2O$ **1** ($x \approx 170$) precipitates in high yield in the presence of a high electrolyte concentration.§ Compound **1** was characterized by elemental analysis, thermogravimetric analysis for determination of the crystal water content, single crystal X-ray structure analysis¶ (including bond valence sum calculations mainly for a determination of the positions of the H atoms and the number of V^{IV} centres), electronic absorbtion as well as vibrational spectra, magnetic susceptibility and redox titrations [for the (additional) determination of the number of V^{IV} centres].

The anionic cluster **1a** has a nearly spherical shape with longest and shortest outer dimensions of 25 and 23 Å, respectively, and possesses a C_5-symmetry axis [Fig. 1(*b*)]. The structure of the anion **1a** can be best described with reference to a distorted icosidodecahedron formed by twenty triangular and twelve pentagonal faces built up by ten Mo^{VI} and twenty V^{IV} centres [see Fig. 1(*a*)]. Ten triangles spanned by the twenty V^{IV} centres form an unusual equatorial 'magnetic ring-shaped band'. The remaining ten triangles above and below this equatorial band, each formed by one V^{IV} (common to the above mentioned triangular faces) and two Mo^{VI} centres, complete the (distorted) icosidodecahedron. Whereas ten of the twelve pentagonal faces—each formed by one Mo^{VI} and four V^{IV} centres—are 'capped' by a $\{Mo/Mo_5\}$-type pentagonal unit [see Fig. 1(*a*) and consider that the earlier reported more symmetrical structure with I_h symmetry[6] contains twelve pentagonal units], the remaining two (top and bottom) faces, each spanned by five Mo^{VI} centres, are 'capped' in a similar way but show two significant differences: (i) the central pentagonal bipyramidally coordinated Mo^{VI} centre is missing and (ii) the (five) MoO_6 octahedra do not share common oxygen atoms (see Fig. 2). In addition, these five Mo^{VI} positions are under-occupied such that the occupancy factors add up to 2.5 per face [therefore referred to as the $\{Mo\}_{5/2}$ unit in the formula and in Fig. 1(*a*)].

Within the cluster cavity, ten sulfate groups (each attached *via* three oxygen atoms to three adjacent Mo^{VI} centres of each $\{Mo^{VI}/Mo^{VI}_5\}$ group) and ten Na^+ ions are encapsulated in a manner not previously observed. The Na^+ cations are located between adjacent sulfate groups thereby forming two novel

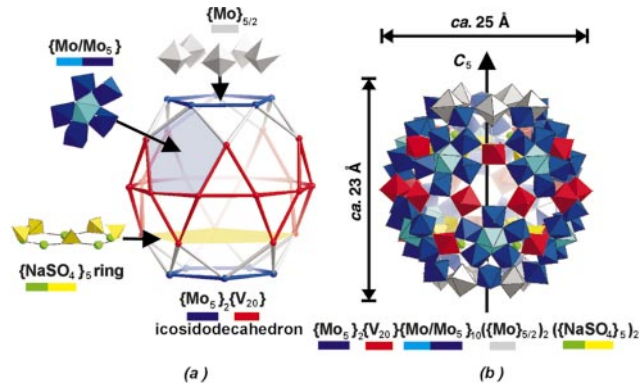

Fig. 1 (*a*) Basic framework structure of **1a** spanned by ten Mo^{VI} (blue) and twenty V^{IV} centres (red) thus forming a distorted icosidodecahedron with twenty triangles and twelve pentagons. Additional structural details shown (see text): (i) one of the $\{Mo^{VI}/Mo^{VI}_5\}$ units which cap ten of the twelve pentagonal faces (MoO_7 pentagonal bipyramid: light blue, MoO_6 octahedra: dark blue); (ii) array built up by five $MoO_4(H_2O)_2$ octahedra (see text) capping the two remaining pentagonal faces (grey); (iii) the 'magnetic ring-shaped band' formed by ten $\{V^{IV}_3\}$ triangles (red); (iv) one of the two encapsulated $\{NaSO_4\}_5$-type rings (Na atoms: green, SO_4 tetrahedra: yellow). (*b*) Polyhedral representation of the complete, nearly spherical structure of **1a** [colour code as in (*a*)].

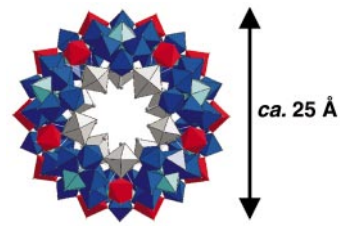

Fig. 2 Polyhedral representation of **1a** with view perpendicular to that shown in Fig. 1(*b*) (parallel to the C_5 axis).

† Disposition can be interpreted as the tendency of an object or system (here polyoxometalate solutions) to act or react in characteristic ways under certain situations (conditions); in this sense the units, such as the pentagons, which finally appear can in principle be called virtual ones.

$\{NaSO_4\}_5$ rings [Na–O(SO_3) 2.48–2.60 Å] lying above and below the equatorial ring of ten V^{IV} centres [see Fig. 1(*a*)]. Interestingly, these Na atoms possess a unique pentagonal bipyramidal coordination environment in which five of the corresponding oxygen centres belong to the cluster shell.

Although the individual metal centres all have an octahedral (or pentagonal bipyramidal) coordination geometry, the environment of some metal centres is complicated for example by disorder phenomena and can—referring to the formula—be described as follows: (i) all six Mo^{VI} centres constituting each of the ten equivalent $\{Mo^{VI}/Mo^{VI}_5\}$ groups, are surrounded by four (or five) bridging oxygen atoms; three possess a terminal oxygen atom projecting outward and a *trans*-μ_2-O atom of the tridentate sulfate ligand (see formula); two Mo centres exhibit outward projecting terminal oxygen and *trans*-OH_2 ligands; the remaining Mo centre (the type closest to the equator), possesses mainly outward projecting OH_2 ligands as well as *trans*-terminal oxygen atoms with the related disorder; (ii) all twenty V^{IV} centres have four bridging oxygen atoms but whereas the ten equatorial V^{IV} centres possess (predominantly) outward projecting OH_2 ligands and *trans*-terminal oxygen, the remaining V^{IV} centres exhibit (without the related disorder), outward projecting terminal oxygen and *trans*-OH_2 ligands; (iii) each of the five Mo^{VI} centres of the $\{Mo\}_{5/2}$ unit ($\{Mo^{VI}O_2(H_2O)_2\}_{5/2}$ part of the formula) has only two bridging (μ_2-type), and consequently four terminal ligands (two oxygen as well as two OH_2 ligands); (iv) the remaining ten Mo^{VI} centres ($\{Mo^{VI}O_3(H_2O)\}_{10}$ part of the formula) also possess disordered terminal oxygen and *trans*-OH_2 ligands; owing to the under-occupancy of the neighbouring molybdenum atoms of the $\{Mo\}_{5/2}$-type centres (occupancy factors 0.25–0.75), one or two μ_2-O atoms become terminal oxygen atoms depending on the related occupancy of the next neighbour position.

Magnetic susceptibility measurements show that χT decreases drastically from 200 to 100 K (3.4–2.3 cm^3 K mol^{-1}) indicating relatively strong antiferromagnetic exchange interactions in spite of the rather large V^{IV}–V^{IV} distances within the magnetic band (6.27–6.46 Å).

Anion **1a** is structurally similar to the inorganic superfullerene of the type $\{Mo/Mo_5\}_{12}\{Mo^V_2\}_{30}$[6] where the thirty centres (mid-points) of the $\{Mo^V\}_2$ dumb-bells span an icosidodecahedron. In this case, twelve $\{Mo^{VI}/Mo^{VI}_5\}$ pentagons cap all of the twelve faces of a distorted truncated icosahedron which is formed by the sixty atoms of the $\{Mo^V\}_2$ units. An important challenge for the future will be the apparently feasible planned synthesis of a variety of spherical clusters using the described pentagonal units.[7] In this context the encapsulation of a variety of multifunctional groups/guests as well as the integration of magnetic centres is of special interest.

The financial support of the Deutsche Forschungsgemeinschaft and the Fonds der Chemischen Industrie is gratefully acknowledged.

Notes and references

‡ $VOSO_4 \cdot 5H_2O$ (2.53 g, 10 mmol) was added under stirring to a solution of Na_2MoO_4 (2.42 g, 10 mmol) in 16.4 ml of 1.0 M hydrochloric acid. Subsequently, NaCl (1.16 g, 19.8 mmol) (which accelerates precipitation) was added to the resulting red–brown solution which was stirred under argon for 10 min before storage under exclusion of air. The red–black rhombic crystals of **1** which precipitated after 7 days were filtered off, washed with 50 ml H_2O and dried in a nitrogen stream. Yield: 0.65 g (28.6%), based on Mo (Found: Na, 3.59; S, 1.85; V, 5.29. Calc.: Na, 3.7; S, 1.72; V 5.5%). The compound is soluble in water and the resulting red solution oxidises slowly on exposure to air.

Characteristic spectroscopic data for **1**: IR ν/cm^{-1} (KBr pellet prepared under argon, 1700–400 cm^{-1}): 1197w, 1125w, 1052w [ν(S–O)]; 968m [ν(V=O)/ν(Mo=O)]; 768s, 690(sh), 631m, 571s; Raman ν/cm^{-1} (solid, KBr dilution, λ_e = 1064 nm): 944w, 880m [ν(V=O)/ν(Mo=O)]; UV–VIS λ_{max}/nm (degassed water): 498, 677 (VO^{2+} chromophore).

§ In an earlier investigation of the Mo^{VI}/V^{VI} system[3,4] it was erroneously proposed that solutions with a relative concentration Mo^{VI}/V^{IV} = 1 yield $K_2H_6[V_3Mo_3O_{19}]\cdot 7H_2O$ at pH 4.75 and the highly soluble product $H_8[V_3Mo_3O_{19}]$ at pH < 3.1. The authors assumed that both compounds would contain Lindquist-type anions.[3,5]

¶ *Crystal data* for **1**: $H_{480}Mo_{75}Na_{30}O_{550}S_{10}V_{20}$, M = 18 508.44, monoclinic, space group *C*2/*c*, a = 47.065(2), b = 43.157(2), c = 26.946(1) Å, β = 104.26°, U = 53045(4) Å^3, Z = 4, D_c = 2.318 g cm^{-3}, μ = 2.23 mm^{-1}, F(000) = 35 920, crystal size = 0.4 × 0.2 × 0.1 mm. Crystals of **1** were removed from the mother-liquor and immediately cooled to 183(2) K on a Bruker axs SMART diffractometer (Mo-Kα, graphite monochromator). A total of 155 219 reflections (1.56 < θ < 26.99°) were collected of which 57 074 unique reflections (R_{int} = 0.069) were used. An empirical absorption correction using equivalent reflections was performed with the program SADABS. The structure was solved using the program SHELXS-97 and refined using the program SHELXL-97 to R = 0.062 for 33 490 reflections with $I > 2\sigma(I)$. SHELXS/L , SADABS from G. M. Sheldrick, University of Göttingen, 1997; structure graphics with Diamond 2.1 from K. Brandenburg, Crystal Impact GbR, 1999. Because of the disorder, not all of the Na positions could be detected as is usual in the case of the said type of compounds. An initial view of the packing of the cluster anions suggested that they are linked through the $\{Mo\}_{5/2}$ units, parallel to the approximate fivefold symmetry axis. However a closer inspection of the corresponding under-occupied Mo centres, (which would correspondingly be responsible for the linking through Mo–O–Mo bridges, reveals that the anions are (probably) not connected at all. The fact that the occupancy factors of the Mo centres of adjacent anions add up to 1.0, indicating that these positions are *alternately* occupied, suggests that a connection of the clusters is improbable. The under-occupied Mo centres (occupancy factor between 0.25 and 0.75) cannot be treated as fully occupied V atoms due to the unrealistic number of terminal ligands (three including two terminal O atoms for octahedral V) and the V analysis. Additionally, as the terminal ligands are also under-occupied, fully occupied V atoms would have an incomplete coordination sphere. Furthermore the resulting necessary linkage of the clusters—owing to the full occupancy—would significantly increase the cluster charge which is impossible considering the Na analysis.

The remainder of the anion shows nearly no disorder. Only very few atoms show a O=Mo–OH_2 ↔ O=Mo–OH_2 disorder. The bond valence sums for the ordered Mo and the V positions lie in the ranges 5.8–6.1 and 4.1–4.2, respectively. Further details of the crystal structure determination may be obtained from the Fachinformationszentrum Karlsruhe, 76344 Eggenstein-Leopoldshafen, Germany (fax: (+49) 7247-808-666; E-mail: crysdata@fiz karlsruhe.de) on quoting the depository No. CSD391073.

CCDC 182/1382. See http://www.rsc.org/suppdata/cc/1999/1885/ for crystallographic files in .cif format.

1 A. Müller, H. Reuter and S. Dillinger, *Angew. Chem., Int. Ed.*, 1995, **34**, 2328; A. Müller, P. Kögerler and C. Kuhlmann, *Chem. Commun*., 1999, 1347.
2 A. Müller, F. Peters, M.T. Pope and D. Gatteschi, *Chem. Rev.*, 1998, **98**, 239; A. Müller, V.P. Fedin, C. Kuhlmann, H. Bögge and M. Schmidtmann, *Chem. Commun.*, 1999, 927.
3 D. Labonnette, *J. Chem. Res.*, 1979, (*S*) 252; (*M*) 2801.
4 S. Ostrowetsky and D. Labonnette, *Compt. Rend. (C)*, 1976, **282**, 169.
5 I. Lindquist, *Ark. Kemi*, 1953, **5**, 247.
6 A. Müller, E Krickemeyer, H. Bögge, M. Schmidtmann and F. Peters, *Angew. Chem., Int. Ed.*, 1998, **37**, 3360.
7 A. Müller, S. Sarkar, H. Bögge, M. Schmidtmann, P. Kögerler, B. Hauptfleisch, S. Q. N. Shah, A. Trautwein and V. Schünemann, *Angew. Chem., Int. Ed.*, in press.

Communication 9/04724G

Novel cavitands containing electrochemically active 4,4′-bipyridinium subunits

Carlos Peinador,[a] Esteban Román,[b] Khalil Abboud[c] and Angel E. Kaifer*[b]

[a] *Departamento de Química Fundamental e Industrial, Universidad de la Coruña, La Coruña, 15071, Spain*
[b] *Center for Supramolecular Science and Department of Chemistry, University of Miami, Coral Gables, FL 33124-0431, USA. E-mail: akaifer@umiami.ir.miami.edu*
[c] *Chemistry Department, University of Florida, Gainesville, FL 32611-7200, USA*

Received (in Columbia, MO, USA) 20th April 1999, Accepted 23rd July 1999

The synthesis and properties of a series of novel compounds containing one to five cavitand building blocks tethered by 4,4′-bipyridinium subunits is described.

Cavitands are bowl-shaped compounds that have attracted considerable attention in supramolecular chemistry as building blocks for the construction of carcerands, hemicarcerands, and other hosts.[1,2] Recently, Reinhoudt and co-workers reported the synthesis of tetrabromo cavitand **2** from **1**.[3] Here, we report the synthesis of the monobromo cavitand **3** and the utilization of the brominated cavitands **3** and **2** for the preparation of novel compounds containing several cavitand subunits interconnected by 4,4′-bipyridinium (bipy) tethers.

Treatment of **1** with 1 equiv. of NBS under reaction conditions similar to those used by Reinhoudt and co-workers[3] yields monobromo cavitand **3** as the main reaction product.[4] Reaction of **2** and **3** with excess 4,4′-bipyridine at 50 °C gives **4** or **6**, respectively, in high yield (> 90%).† Alkylation of these cavitands with MeI leads to the fully quaternized 4,4′-bipyridinium derivatives **5** and **7**, which were isolated as their PF_6^- salts after counterion exchange. Molecular modeling results obtained with **4**–**7** and single-crystal X-ray diffraction data for **4** suggest that both the partially and fully quaternized bipy subunits tend to orient themselves on or near the plane defined by the four benzylic carbons through which they are connected to the cavitand bowl. This is clearly evident in the X-ray crystal structure[5] of **4** (Fig. 1).

It is also possible to quaternize the free nitrogens in **4** or **6** by treatment with the monobromo cavitand **3**. Thus, reaction of **6** with 1 equiv. of **3** yields, after counterion exchange, the dimeric cavitand **8**. Similarly, the cruciform pentameric cavitand **9** was obtained by reaction of **4** with 4 equiv. of **3**.

The presence of partially or fully quaternized 4,4′-bipyridinium subunits confers redox properties to these compounds.[6] Their electrochemical behavior in MeCN solution was investigated using cyclic voltammetry. Each monoquaternized bipy residue exhibits a single one-electron reduction ($V^+ \rightarrow V$) and each diquaternized bipy subunit exhibits two consecutive one-electron reductions ($V^{2+} \rightarrow V^+$ and $V^+ \rightarrow V$). The half-wave potentials obtained in these experiments are given in Table 1. The voltammetric behavior of all the compounds having four reducible subunits reveals their non-interacting character, since only one wave is observed for each one of the reduction processes. The multi-electron character of some of these voltammetric waves may be responsible for the departure of the observed peak-to-peak potential differences from the theoretical values expected for Nernstian redox couples. The electrochemical behavior of **4** was strongly affected by precipitation of

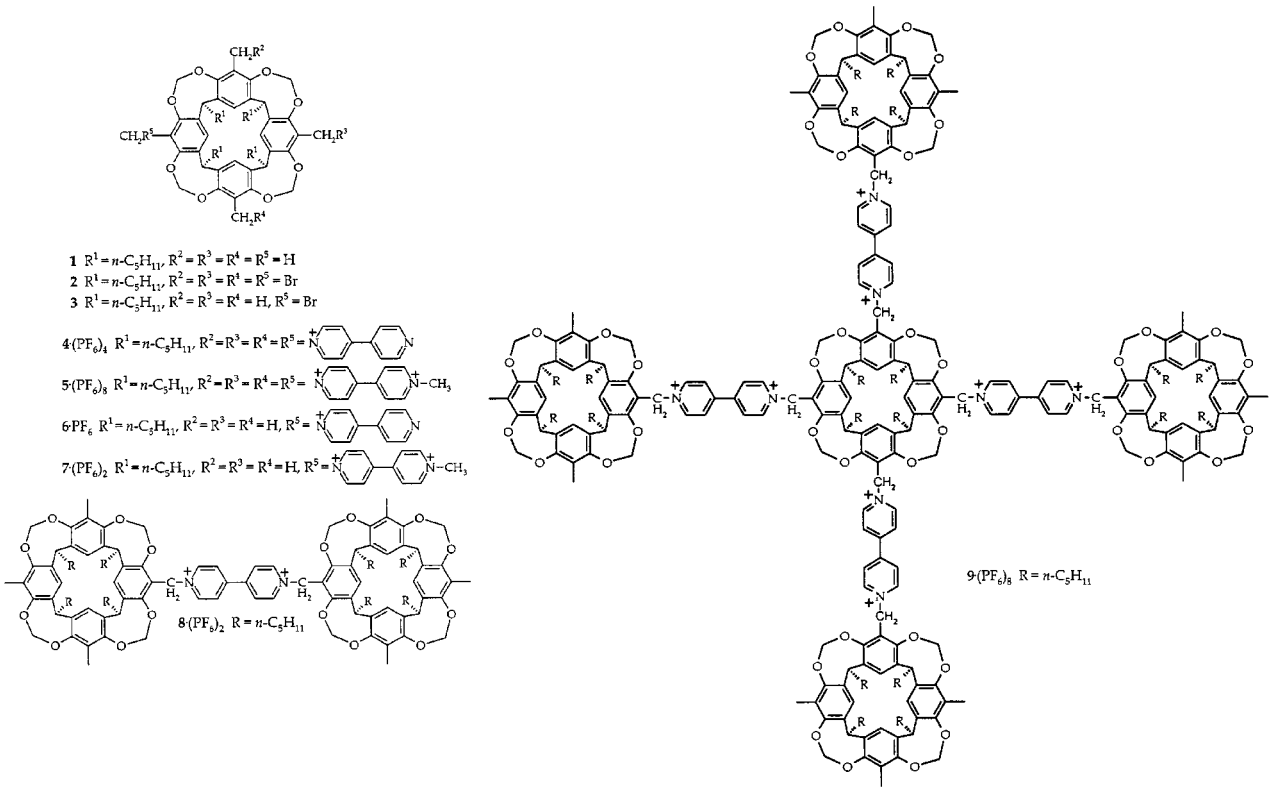

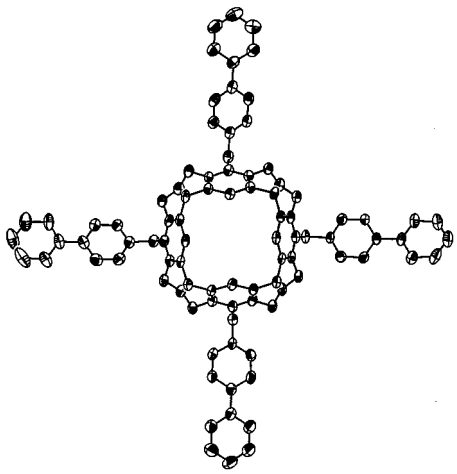

Fig. 1 X-Ray crystal structure of **4**. The four pentyl chains in the lower rim, hexafluorophosphate counterions and solvent molecules have been removed for clarity.

Table 1 Electrochemical[a] (half-wave potentials and peak-to-peak potential splittings) and spectroscopic parameters for **4**–**9**

	E/V *vs.* Ag/AgCl (ΔE_p[b]/mV)			
Cavitand	$E^1_{1/2}$	$E^2_{1/2}$	λ_{max}/nm	ε/M^{-1} cm^{-1}
4	[c]	[c]	266	88 400
5	−0.28 (87)	−0.81 (74)	257	104 000
6	−0.88 (58)	—	264	25 300
7	−0.34 (57)	−0.79 (55)	234	34 700
			250	31 200
8	−0.26 (82)	−0.82 (56)	[d]	[d]
9	[c]	[c]	251	141 000

[a] Electrochemical parameters measured with a glassy carbon working electrode immersed in 0.1 M $TBAPF_6$–MeCN solutions of **4**–**9**. [b] ΔE_p values measured at 0.1 V s^{-1}. [c] Accurate half-wave potentials could not be obtained (see text). [d] No maxima were observed in the spectrum.

the reduced form on the electrode surface. Compound **9** exhibited complicated voltammetric behavior that is currently under more detailed scrutiny.

Conceptually, these compounds provide an interesting example of covalent self-assembly. Notice that **9**, the largest compound reported here, has a molecular mass of 6138.6 daltons and a branching structure that is similar to that found in dendrimers. We are currently exploring bromination patterns for **1** that may result in different structures after reaction with 4,4′-bipyridine linkers.

The authors gratefully acknowledge the NSF (to A. E. K. CHM-9633434) for the support of this research work. C. P. is grateful to Xunta de Galicia for a postdoctoral fellowship and E. R. thanks the University of Miami for a Maytag graduate fellowship. K. A. wishes to acknowledge the NSF and the University of Florida for funding of the purchase of the X-ray equipment. The authors are grateful to Marielle Goḿez-Kaifer for conducting molecular modeling calculations with some of these compounds.

Notes and references

† All new compounds gave satisfactory elemental analyses. *Selected data* for **3**: δ_H($CDCl_3$, 400 MHz) 7.14 (s, 1H), 6.97 (s, 3H), 5.95 (d, 2H, *J* 7.14), 5.87 (d, 2H, *J* 7.14), 4.81–4.70 (m, 4H), 4.60 (s, 2H), 4.42 (d, 2H, *J* 7.14), 4.37 (d, 2H, *J* 7.14), 2.24–2.16 (m, 8H), 2.03 (s, 3H), 1.95 (s, 6H), 1.48–1.22 (m, 24H), 0.96–0.88 (m, 12H); δ_C($CDCl_3$, 100 MHz) 153.65, 153.58, 153.38, 153.32, 138.41, 138.18, 137.87, 137.06, 123.97, 123.90, 121.87, 117.32, 117.23, 99.11, 98.33, 37.05, 36.98, 32.09, 32.02, 31.59, 30.17, 30.14, 27.67, 27.61, 22.69, 22.67, 14.10, 14.07, 10.53, 10.24; *m*/*z* (FAB, NBA) 953 (MH^+); mp 242–244 °C. For **4**: δ_H(CD_3CN, 400 MHz) 8.90–8.82 (m, 16H), 8.23 (d, 8H, *J* 6.35), 7.78 (d, 8H, *J* 5.55), 7.60 (s, 4H), 6.33 (d, 4H, *J* 7.14), 5.58 (s, 8H), 4.74–4.62 (m, 8H), 2.40–2.30 (m, 8H), 1.42–1.20 (m, 24H), 0.86 (t, 12H, *J* 7.14); δ_C(CD_3CN, 100 MHz) 155.52, 154.48, 152.13, 146.29, 142.21, 139.88, 127.02, 125.53, 122.90, 121.17, 100.62, 55.51, 38.63, 32.78, 30.59, 28.25, 23.29, 14.44; *m*/*z* (FAB) 1929 ($[M - PF_6]^+$), 892 ($[M - 2\ PF_6]^{2+}$); mp 255 °C (decomp.). For **6**: δ_H(CD_3CN, 400 MHz) 8.92–8.84 (m, 4H), 8.11 (d, 2H, *J* 6.96), 8.01 (d, 2H, *J* 6.22), 7.26 (s, 1H), 6.95 (s, 3H), 6.09 (d, 2H, *J* 7.32), 5.89 (d, 2H, *J* 7.14), 5.64 (s, 2H), 4.77 (t, 2H, *J* 8.06), 4.71 (t, 2H, *J* 8.06), 4.43 (d, 2H, *J* 7.32), 4.30 (d, 2H, *J* 7.32), 2.04–2.38 (m, 8H), 2.03 (s, 9H), 1.99 (s, 9H), 1.46–1.22 (m, 24H), 0.95–0.83 (m, 12H); δ_C(CD_3CN, 100 MHz) 155.54, 154.66, 154.28, 154.06, 153.38, 152.19, 142.12, 140.79, 139.93, 139.24, 138.40, 127.01, 125.84, 125.81, 125.79, 122.88, 121.19, 119.75, 119.73, 100.47, 99.83, 55.71, 38.59, 38.51, 32.94, 32.86, 30.64, 30.46, 28.52, 28.39, 23.40, 23.36, 14.50, 14.47, 10.36, 10.33; *m*/*z* (FAB, NOBA) 1029 ($[MH - PF_6]^+$); mp 282 °C (decomp.). For **8**: δ_H($CDCl_3$, 400 MHz) 8.89 (d, 4H, *J* 6.74), 8.21 (d, 4H, *J* 6.35), 7.27 (s, 2H), 6.96 (s, 6H), 6.06 (d, 4H, *J* 7.14), 5.88 (d, 4H, *J* 7.14), 5.59 (s, 4H), 4.80–4.67 (m, 8H), 4.39 (d, 4H, *J* 7.14), 4.28 (d, 4H, *J* 7.14), 2.39–2.02 (m, 16H), 1.98 (s, 18H), 1.47–1.21 (m, 48H), 0.90 (t, 12H, *J* 6.74), 0.81 (t, 12H, *J* 6.74); δ_C($CDCl_3$, 100 MHz) 153.83, 153.37, 153.19, 153.11, 145.70, 139.81, 138.56, 137.73, 136.42, 126.77, 124.17, 123.89, 118.59, 117.13, 117.11, 99.27, 98.64, 55.40, 37.09, 37.02, 32.07, 32.00, 30.19, 29.85, 27.66, 27.58, 22.69, 22.63, 14.07, 13.96, 10.35, 10.16; *m*/*z* (MALDI-TOF) 1898 ($[M - 2PF_6]^+$); mp 282 °C (decomp.). For **9**: δ_H(CD_3CN, 400 MHz) 9.00–8.82 (m, 16H), 8.38–8.16 (m, 16H), 7.53 (s, 4H), 7.46 (s, 4H), 7.21 (s, 12H), 6.28 (br s, 4H), 6.05 (d, 8H, *J* 7.16), 5.83 (d, 8H, *J* 7.16), 5.57 (br s, 8H), 5.50 (s, 8H), 4.73–4.51 (m, 24H), 4.49 (d, 8H, *J* 7.16), 4.17 (d, 8H, *J* 7.16), 2.44–2.15 (m, 40H), 1.43–1.09 (m, 120H), 0.93–0.74 (m, 60H); δ_C(CD_3CN, 100 MHz) 154.6, 154.5, 154.2, 154, 151.2, 151.1, 147, 140.8, 139.9, 139.8, 139.2, 138.3, 128.2, 125.9, 125.8, 125.7, 120.98, 120.93, 119.7, 100.6, 100.4, 99.8, 56.3, 56.1, 38.58, 38.47, 32.92, 32.86, 30.6, 30.43, 28.5, 28.39, 29.29, 23.39, 23.34, 23.30, 14.89, 14.46, 10.36, 10.32; mp 280–282 °C (decomp.).

1 D. J. Cram and J. M. Cram, *Monographs in Supramolecular Chemistry, Vol. 4: Container Molecules and Thier Guests*, ed. J. F. Stoddart, Royal Society of Chemistry, Cambridge, 1994.
2 A. Jasat and J. C. Sherman, *Chem. Rev.*, 1999, **99**, 931.
3 H. Boerrigter, W. Verboom and D. N. Reinhoudt, *J. Org. Chem.*, 1997, **62**, 7148.
4 The reaction also produced small amounts of tribromo and dibromo derivatives that we are currently trying to prepare and isolate in larger yields.
5 *Crystal data* for **4**: $C_{104}H_{112}F_{24}N_8O_{12}P_4$, M = 2245.88, triclinic, space group $P\bar{1}$, a = 17.9704(9), b = 18.3237(9), c = 19.771(1) Å, α = 67.629(1), β = 67.447(1), γ = 78.767(1)°, V = 5550.9(5) Å^3, T = 173(2) K, Z = 2. Data were collected at 173 K on a Siemens SMART PLATFORM equipped with a CCD area detector and a graphite monochromator utilizing Mo-Kα radiation (λ = 0.71073 Å). Cell parameters were refined using up to 8192 reflections. A hemisphere of data (1381 frames) was collected using the ω-scan method (0.3° frame width). The first 50 frames were remeasured at the end of data collection to monitor instrument and crystal stability (maximum correction on I was < 1%). Absorption corrections by integration were applied based on measured indexed crystal faces. The structure was solved by the direct methods in SHELXTL5, and refined using full-matrix least-squares. The non-H atoms were treated anisotropically, whereas the methyl hydrogen atoms were calculated in ideal positions and were riding on their respective carbon atoms. Two of the R groups on the cation are disordered. They were refined in two parts each with their site occupation factors dependently refined. All four of the hexafluorophosphates are disordered and were refined with their geometries constrained to form perfect octahedra around the P atoms. The structure consists of the macrocycle cation, four hexafluorophosphates and a variety of solvent molecules most of which are disordered or partially present in the lattice. Some of the solvents identified and included in the refinement include MeCN, acetone, EtOH, MeOH and water. Because of the large lattice volumes occupied by disordered solvents, a precise formula weight could not be used but instead an approximate formula was used to reflect all that was refined. It should be noted that the refinement provided acceptable anisotropic models for the cation and four anions while all of the solvents were treated isotropically. A total of 1688 parameters, with 248 constraints, were refined in the final cycle of refinement using 14505 reflections with $I > 2\sigma(I)$ to yield R_1 and wR_2 of 8.46 and 20.58%, respectively. Refinement was done using F^2. CCDC 182/1372. See http://www.rsc.org/suppdata/cc/1999/1887/ for crystallographic data in .cif format.

See, for instance: A. Mirzoian and A. E. Kaifer, *Eur. J. Chem.*, 1997, **3**, 1052.

Communication 9/03164B

Synthesis and spectroscopic properties of a new 4-bora-3a,4a-diaza-*s*-indacene (BODIPY®) dye

Heejin Kim, Armin Burghart, Mike B. Welch, Joe Reibenspies and Kevin Burgess*

Department of Chemistry, Texas A & M University, PO Box 300012, College Station, TX 77842-3012, USA. E-mail: burgess@mail.chem.tamu.edu

Received (in Corvallis, OR, USA) 12th July 1999, Accepted 13th August 1999

The constrained dye 3 was prepared and shown to have a sharper, red-shifted, and more intense fluorescence emission than the 4,4-difluoro-4-bora-3a,4a-diaza-*s*-indacene (BODIPY®) dye 2 in which the aryl groups can rotate freely.

4,4-Difluoro-4-bora-3a,4a-diaza-*s*-indacene (BODIPY®) dyes[1] are highly fluorescent materials that have been used for several different applications.[2–5] Relatively recent efforts in our laboratories have focussed on syntheses of the new 3,5-diaryl-substituted BODIPYs of which compound **2** is typical.[6] The goal of this research was to increase the diversity of emission maxima available in the BODIPY series by introducing different substituents on the 3,5-diaryl rings. These studies were largely successful, but the 3,5-diaryl-substituted BODIPY dyes had diminished fluorescence intensities relative to similar alkyl-substituted systems. We hypothesized that this was due to dissipation of energy from an electronic excited state *via* a non-radiative process involving rotation of the aryl rings relative to the dipyrromethene core. Here we report the synthesis and investigation of the new structure **3**, work that was motivated by several considerations. First, the aryl rings in this system would not be able to spin about the aryl–pyrrole bond and this constraint could lead to enhanced fluorescence. Secondly, the ring system was completely new and might have interesting fluorescence properties. Moreover the structure should be accessible *via* demethylation of compound **1**.

A one-pot, two-step process, beginning with the dipyrromethene **1** proved to be the most convenient way to prepare compound **3** (Scheme 1).† It was isolated in high yield as a dark green solid that was stable at room temperature and to chromatography on basic alumina. The ^{11}B NMR spectrum of **2** gave a distinct triplet due to B–F coupling [δ −1.26, (t, J_{BF} = 30.6 Hz in $CDCl_3$ relative to $BF_3{\cdot}OEt_2$ external reference)], whereas the corresponding spectrum of **3** consisted of one singlet (δ −0.89).

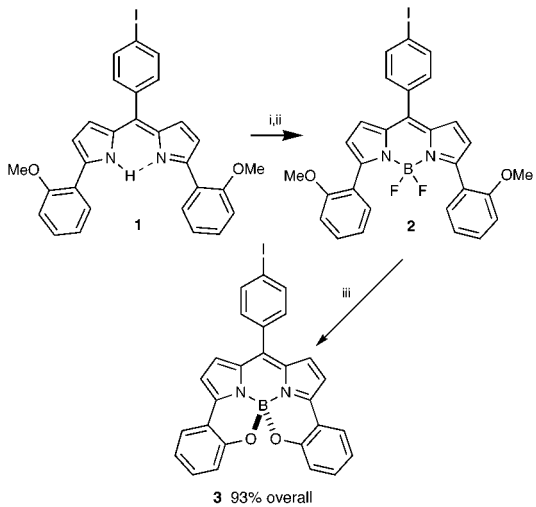

Scheme 1 *Reagents and conditions*: i, Et_3N, PhMe; ii, $BF_3{\cdot}OEt_2$, 80 °C; iii, BBr_3, O to 25 °C.

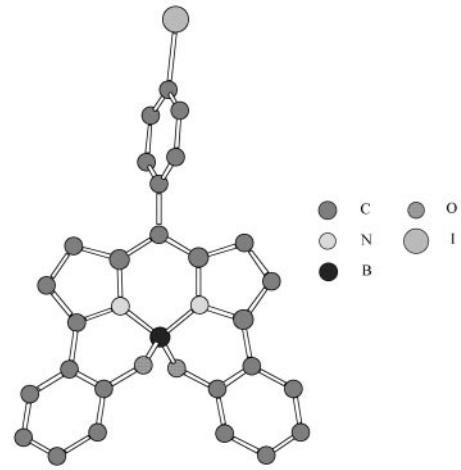

Fig. 1 Chem3D representation of **3** based on coordinates from the single crystal structure analysis.

It occurred to us that **3** is chiral, and the enantiomers of this compound might be separable at room temperature. No preparative resolution of this material has been accomplished, but HPLC analysis of pure racemic material on a Pirkle column [covalent (*S*,*S*) whelk-01 from Aldrich; Pr^{i}OH–hexanes eluant] gave two peaks. These were not baseline resolved, but they were distinct enough to indicate separation is possible.

X-Ray single crystal analysis of **3** revealed some interesting features (Fig. 1).‡ As expected, the 4-iodophenyl substituent is twisted with respect to the heterocyclic core. The tetrahedral structure of the boron in this molecule is slightly distorted. For instance, the O–B–O, N–B–N and O–B–N bond angles are 107.5, 105.5 and 115.4, respectively, showing progressively larger deviations from the perfect tetrahedral angle of 109.5°. Moreover, the torsional angles between the heterocyclic core and the 3- and 5-aryl substituents (25°) are considerably less than in the 4,4-difluoro-3,5-bis(1′-naphthyl)-BODIPY derivative (55°), whose structure was investigated recently.[7] The B–O and B–N distances are 1.47 and 1.52 Å, respectively.

Fig. 2 shows the UV absorption and fluorescence emission spectra of **2** and **3**, and some important data are presented in

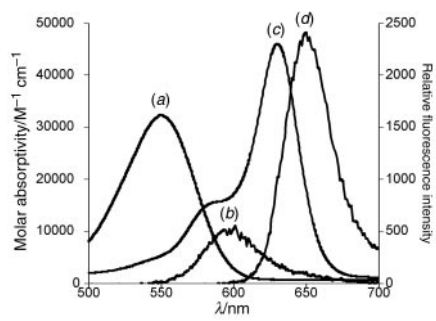

Fig. 2 Absorption (4 μM in $CHCl_3$) and fluorescence (1 μM in $CHCl_3$) spectra of **2** and **3**; (*a*) and (*b*) are absorption and fluorescence spectra of **2**; (*c*) and (*d*) are the corresponding spectra of **3**.

Table 1 Important UV and fluorescence data for **2** and **3**

	λ_{max}/nm (abs)[a]	ε/M^{-1} cm^{-1}	λ_{max}/nm (em)[a]
2	550	34 500	597
3	630	46 000	654

[a] In $CHCl_3$.

Table 1. The most striking difference between the emission spectra of **2** and **3** is that the λ_{max}(em) for the new ring system **3** is red-shifted by approximately 57 nm relative to the parent system **2**. This is probably due to extended conjugation in **3** as a result of the aryl substituents being constrained closer to planarity with the dipyrromethene nucleus. Fluorescence emission for **3** was also sharper than that of the parent BODIPY **2**; peak widths at half peak height for the emission spectra shown in Fig. 2 were 36 and 44 nm, respectively. Quantum yields for fluorescence of **2** and **3** were determined[8] in $CHCl_3$ relative to Cresyl Violet.[9] The quantum yield measured for **3** (ϕ = 0.41) is much higher than that obtained for **2** (ϕ = 0.07), validating the original premise of this work, *i.e.* that the constrained system **3** would be more fluorescent than the BODIPY system **2**.

Finally, cyclic voltammetry showed that **3** was irreversibly oxidized at a peak potential E_{pa} = +0.70 V (*vs.* ferrocene/ferrocenium at 100 mV s^{-1} in MeCN throughout), which is significantly lower than the oxidation potential of **2** (E_{pa} = +0.84 V). This implies that the rigidity of **3** allows for a more extended conjugation as compared to **2**. Both compounds are reversibly reduced at about the same potential (**3**: $E_{1/2}$ = −1.18 V, **2**: $E_{1/2}$ = −1.19 V).

In summary, the new fluorescent dye **3** gives a red-shifted, sharper fluorescence emission than the parent system **2**, and the quantum yield for its fluorescence was determined to be 5.5–6.0 times larger. It contains a unique chiral, heptacyclic core with a distorted N_2BO_2 unit. Possible applications for this new dye include studies of chiral molecular environments *via* fluorescence.

We thank Ben Lane for running the ^{11}B NMR spectra for this study, and Professor L. B.-Å. Johansson (Umeå, Sweden) for valuable discussions. Financial support for this work was provided by the NIH (HG01745) and The Robert A. Welch Foundation. A. B. thanks the Deutsche Forschungsgemeinschaft for a fellowship.

Notes and references

† *Synthesis* of **3**: Compound **2** was formed *in situ* from the corresponding dipyrromethene **1** (ref. 10) (100 mg, 0.179 mmol) in PhMe (5 ml) by addition of Et_3N (0.075 ml, 0.537 mmol), then BF_3•OEt_2 (0.113 ml, 0.896 mmol). This mixture was heated to 80 °C for 20 min to give the intermediate **2** *in situ*. The solution was cooled to 0 °C, BBr_3 (0.17 ml, 1.79 mmol) was added dropwise over 1 min, then the solution was allowed to warm to 25 °C and stirred for 5 h. The reaction mixture was filtered through Celite, concentrated and purified by column chromatography on basic alumina using 20% EtOAc–hexanes as eluant. Compound **3** was isolated as a dark green solid (90 mg, 93% yield): mp 295–296 °C; δ_H($CDCl_3$, 300 MHz) 7.89 (d, *J* 8.4, 2H), 7.77 (dd, *J* 7.8, 1.5, 2H), 7.46 (d, *J* 8.4, 2H), 7.31–7.36 (m, 2H), 7.03–7.07 (m, 2H), 7.04 (d, *J* 4.5, 2H), 6.95 (d, *J* 8.2, 2H), 6.91 (d, *J* 4.5, 2H); δ_B($CDCl_3$, 64 MHz) −0.89 (s); *m/z* (FAB) 538 (M^+); (HRMS: calc. [M^+] 538.0374, found [M^+] 538.0354).

‡ *Crystal data* for **3**: $C_{27}H_{16}BIN_2O_2$, M = 538.13, dark green crystal, triclinic, a = 8.1736(11), b = 9.2522(9), c = 15.222(2) Å, α = 97.112(10), β = 100.579(11), γ = 104.200(10)°, V = 1079.7(2) Å^3, space group $P\bar{1}$, Z = 2, D = 1.655 g cm^{-3}, μ = 1.512 mm^{-1}, F(000) = 532, λ (Mo-Kα) = 0.71073 Å. The data were collected by omega scanning techniques, at 298 K on a Siemens P4 X-ray diffractometer in the range 2.31 < Θ < 25.00°. 4078 reflections were collected, corrected for Lorentzian and polarization effects, of which 3786 were independent reflections [R(int) = 0.0371]. Structure solution by direct methods (ref. 11) and least-squares refinement of 299 parameters (ref. 12) on F^2 yielded final R indices [$I > 2\sigma(I)$]: $R(F)$ = 0.0379 $wR(F^2)$ = 0.0946; R indices (all data): $R(F)$ = 0.0406; $wR(F^2)$ = 0.0974. CCDC 182/1380.

1 A. Treibs and F.-H. Kreuzer, *Liebigs Ann. Chem.*, 1968, **718**, 208.
2 H. J. Wories, J. H. Koek, G. Lodder, J. Lugtenburg, R. Fokkens, O. Driessen and G. R. Mohn, *Recl. Trav. Chim. Pays-Bas*, 1985, **104**, 288.
3 M. Shah, K. Thangaraj, M.-L. Soong, L. T. Wolford, J. H. Boyer, I. R. Politzer and T. G. Pavlopoulos, *Heteroatom Chem.*, 1990, **1**, 389.
4 R. W. Wagner and J. S. Lindsey, *J. Am. Chem. Soc.*, 1994, **116**, 9759.
5 M. L. Metzker, J. Lu and R. A. Gibbs, *Science*, 1996, **271**, 1420.
6 L. H. Thoresen, H. Kim, M. B. Welch, A. Burghart and K. Burgess, *Synlett*, 1998, 1276.
7 A. Burghart, H. Kim, M. B. Welch, L. H. Thoresen, J. Reibenspies and K. Burgess, unpublished results.
8 J. N. Demas and G. A. Crosby, *J. Phys. Chem.*, 1971, **75**, 991.
9 D. Magde and J. H. Brannon, *J. Phys. Chem.*, 1979, **83**, 696.
10 Compound **1** was accessed *via* condensation reaction of 2-(*p*-methoxyphenyl)pyrrole and *p*-iodobenzoyl chloride. K. Burgess and L. H. Thoresen, unpublished results.
11 G. M. Sheldrick, SHELX, University of Gottingen, Germany, 1986.
12 G. M. Sheldrick, SHELXS-93, Program for Crystal Structure Refinement, University of Gottingen, Germany, 1993.

Communication 9/05739K

Synthesis, structure and redox reactions of a new crowded benzodithiolium salt: first isolation and characterization of a stable dithiolyl radical with a 7π electron framework

Satoshi Ogawa,*[a] Mieko Kikuchi,[a] Yasushi Kawai,[b] Shigeya Niizuma[c] and Ryu Sato*[a]

[a] *Department of Applied Chemistry and Molecular Science, Faculty of Engineering, Iwate University, Morioka 020-8551, Japan. E-mail: ogawa@iwate-u.ac.jp*
[b] *Institute for Chemical Research, Kyoto University, Uji, Kyoto 611-0011, Japan*
[c] *College of Humanities and Social Science, Iwate University, Morioka 020-8550, Japan*

Received (in Cambridge, UK) 30th June 1999, Accepted 9th August 1999

The molecular structure of the sterically crowded 3-(2,4,6-triisopropylphenyl)-1,2-benzodithiolium cation has been determined by crystallographic studies on the BF_4^- salt and the corresponding novel 1,2-dithiolyl radical with a 7π electron framework has been isolated by one-electron reduction.

The unusual 7π electron structure of certain five-membered rings has allowed the construction of a unique reversible one-electron redox system. Recently, we reported reversible one-electron redox couples by the use of 4,7-disubstituted benzotrichalcogenoles and found by EPR spectroscopy that their radical cation salts obtained on treatment with a one-electron oxidant had unusual 7π frameworks.[1] However, to date, dithiolyl radicals with 7π electrons have so far only been obtained in solution as unstable species by electrochemical reduction or laser flash photolysis.[2] Herein we present the synthesis and structural determination by X-ray crystallographic analysis of the new sterically crowded dithiolium salt, 3-(2,4,6-triisopropylphenyl)-1,2-benzodithiolium tetrafluoroborate **1**, and the first isolation of a stable 7π radical, 3-(2,4,6-triisopropylphenyl)-1,2-benzodithiolyl **2**, by one-electron reduction. In addition, we have succeeded in the construction of a new type of one-electron redox system between **1** and **2** by means of both chemical and electrochemical methods.

3-(2,4,6-Triisopropylphenyl)-1,2-benzodithiolium tetrafluoroborate **1** was synthesized as follows (Scheme 1). We employed commercially available thiophenol as a starting material to prepare the desired cyclic disulfide compound. 2-Mercapto-2′,4′,6′-triisopropylbenzhydrol **3** was obtained in 59% yield by *ortho* lithiation[3] of thiophenol followed by the addition of 2,4,6-triisopropylbenzaldehyde, which was readily prepared by general methods.[4] Thiolation was performed upon treatment of the benzhydrol with P_2S_5 and *in situ* cyclization of the resulting dithiol **4** was carried out in the presence of I_2/Et_3N after displacement of the solvent from toluene to CH_2Cl_2. After usual work-up, the crude product was purified by column chromatography (silica gel, *n*-hexane) to give 3-(2,4,6-triisopropylphenyl)-3*H*-1,2-benzodithiole **5** quantitatively. The corresponding dithiolium salt **1** was prepared by a two-electron oxidation of dithiole **4** with 2 equiv. of $NOBF_4$ in quantitative yield.†

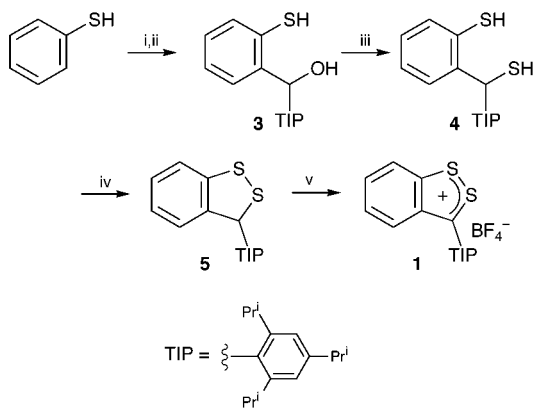

Scheme 1 *Reagents and conditions:* i, TMEDA (2.2 equiv.), BuLi (2.2 equiv.), cyclohexane, ii, 2,4,6-$Pr^i_3C_6H_2CHO$; iii, P_2S_5, toluene; iv, I_2, Et_3N, CH_2Cl_2; v, $NOBF_4$ (2.0 equiv.), THF–MeCN.

The structure of new dithiolium salt **1** has been fully characterized by physical and spectroscopic means, and its solid-state structure (recrystallized from benzene) was determined by single-crystal X-ray diffraction (Fig. 1).‡ In the solid state, the benzodithiolium unit is almost coplanar (the torsion angles $S_2S_1C_8C_7$ and $S_2C_3C_9C_4$ are 178.9 and −178.9°, respectively), with the 2,4,6-triisopropylbenzene ring very nearly orthogonal to the planar unit (the torsion angle $S_2C_3C_{10}C_{11}$ is 89°), which may arise from the steric repulsion between the bulky 2,6-isopropyl groups on benzene and the *ortho* proton on the benzene ring fused to the dithiolium ring. This conformation plays an important role in blocking radical dimerization, which is adopted *via* a cofacial alignment, resulting in the isolation of the corresponding radical (*vide infra*).

Cyclic voltammetry of **1** in MeCN at 20 °C under an Ar atmosphere exhibited well-defined reversible one-electron redox waves at $E_{1/2}$ = −0.51 V *vs.* Ag / 0.01 mol dm^{-3} $AgNO_3$.§ This result implies that dithiolium **1** provides a stable

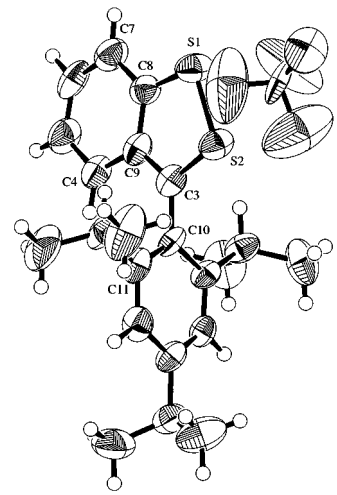

Fig. 1 ORTEP view of **1**. Benzene molecule is omitted for clarity. Selected bond lengths (Å) and angles (°): S(1)–S(2) 2.020(4), S(1)–C(8) 1.70(1), S(2)–C(3) 1.69(1), C(3)–C(9) 1.38(1), C3–C10 1.47(1), C(8)–C(9) 1.44(2); S(1)–S(2)–C(3) 97.8(4), S(2)–S(1)–C(8) 95.3(4), S(2)–C(3)–C(9) 115.0(9), S(1)–C(8)–C(9) 115.0(8), C(3)–C(9)–C(8) 116(1); S(2)–S(1)–C(8)–C(7) 178.9(10), S(2)–C(3)–C(9)–C(4) −178.9(8), S(2)–C(3)–C(10)–C(11) 89(1).

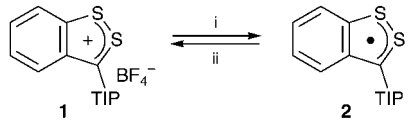

Scheme 2 *Reagents and conditions*: i, Na (1.0 equiv), THF; ii, $NOBF_4$ (1.0 equiv), THF–MeCN.

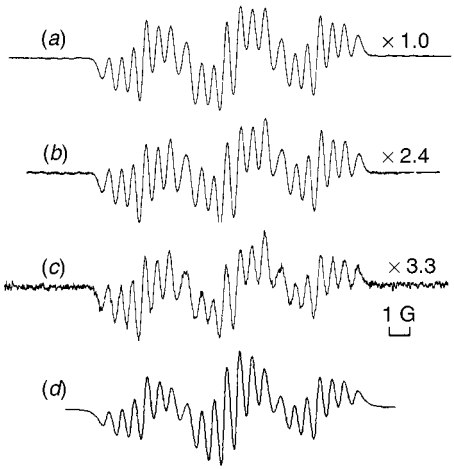

Fig. 2 VT-EPR spectra of **2** at (*a*) 18, (*b*) −50, (*c*) −81 °C, and (*d*) simulated spectrum.

neutral radical even at room temperature. The novel dithiolyl radical **2**¶ was isolated in the one-electron reduction of **1** with sodium metal in THF (Scheme 2). The structure of the first isolable dithiolyl radical **2**, a green solid, was determined by high-resolution MS and EPR spectroscopy. The EPR spectra of **2** in THF solution showed the multiple signals (g = 2.0049 G) attributable to a radical, and the a_H values were evaluated by the fitting of simulated spectra to the experiment spectrum (Fig. 2). In addition, the experimental values of the unpaired π spin density from the hyperfine splitting are in good agreement with those calculated by the simple Hückel and McLachlan's methods (Table 1). Using variable-temperature EPR spectra normalized by the Mn^{2+} on MgO standard, the intensities of the signals gradually decreased at low temperatures, but their hyperfine structure was unchanged, which suggests that the bulky substituent serves as an efficient protective group for spin-dimerization even at low temperature. Although it has not yet been possible to grow single crystals suitable for X-ray diffraction, unpaired π-electron density was delocalized over both the coplanar benzene and the five-membered heterocycle. Interestingly, the salt **2** undergoes one-electron oxidation to give **1** quantitatively by treatment with 1 equiv. of $NOBF_4$ (Scheme 2). Thus, the facile interconversion in the redox reactions of **1** and **2** has been ascribed to the unusual stabilization of the radical by the 7π electron framework.

Table 1 Unpaired spin populations (ρ^π) of **2**

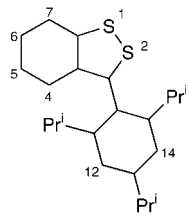

		ρ^π		
Position	Atom	Exp.	Hückel	McLachlan
1	S	—	0.146	0.210
2	S	—	0.244	0.335
3	C	0.175	0.149	0.180
4	C	0.055	0.107	0.089
5	C	0.054	0.012	−0.019
6	C	0.205	0.176	0.200
12,14	C	0.029	0.004	−0.007

Notes and references

† *Selected data* for **1**: yellow plates (CH_2Cl_2–*n*-hexane); mp 219–225 °C (decomp.) (Found C, 59.41; H, 5.90. $C_{22}H_{27}S_2BF_4$ requires C, 59.73; H, 6.15%); ν_{max}(KBr)/cm^{-1} 3449, 2959, 2871, 1593, 1458, 1431, 1380, 1084, 1035, 877, 761, 722; δ_H(400 MHz, CD_3CN) 1.02 (d, 6H, *J* 6.7, *o*-CH_3), 1.15 (d, *J* 6.7, 6H, *o*-CH_3), 1.32 (d, *J* 6.9, 6H, *p*-CH_3), 2.18 (sept, *J* 6.7, 1H, *o*-C*H*), 3.06 (sept, *J* 6.9, 1H, *p*-C*H*), 7.39 (s, 2H, *m*-Ar*H*), 7.85 (dd, *J* 8.5, 0.7, 1H, 4-Ar*H*), 7.91 (ddd, *J* 8.6, 6.8, 0.7, 1H, 6-Ar*H*), 8.30 (ddd, *J* 8.5, 6.8, 1.3, 1H, 5-Ar*H*), 8.67 (d, *J* 8.6, 1.3, 1H, 7-Ar*H*); δ_C(101 MHz, CD_3CN) 24.0 (*o*-*C*H_3), 24.1 (*o*-*C*H_3), 24.9 (*p*-*C*H_3), 32.5 (*o*-*C*H), 35.3 (*p*-*C*H), 121.5, 123.6, 126.5, 129.8, 131.3, 138.9, 143.8, 150.0, 155.4, 163.7, 197.4 (3-*C*).

‡ *Crystal data* for **1**: $C_{22}H_{27}S_2BF_4$•C_6H_6, M = 520.49, monoclinic, space group *C*2/*c* (no. 15), a = 26.387(8), b = 13.177(7), c = 19.851(7) Å, β = 122.91(2)°, U = 5794(4) Å^3, T = 293 K, Z = 8, D_c = 1.193 g cm^{-3}, μ(Cu-Kα) = 20.03 cm^{-1}, F(000) = 2192. A yellow prismatic crystal of dimensions 0.40 × 0.30 × 0.20 mm was used. 4659 reflections were measured of which 4544 were unique using a Rigaku AFC7R diffractometer with Cu-Kα radiation using ω–2θ scans. The structure was solved by direct methods (SIR92) and expanded using Fourier techniques (DIRDIF94). The non-hydrogen atoms were refined anisotropically. Hydrogen atoms were included but not refined. All calculations were performed using the teXsan crystallographic software package. The final cycle of full-matrix least-squares refinement was based on 2083 observed reflections [$I > 1.50\sigma(I)$] and 316 variable parameters with R = 0.105, R_w = 0.151. CCDC 182/1370. See http://www.rsc.org/suppdata/cc/1999/1891/ for crystallographic data in .cif format.

§ Cyclic voltammograms of **1** (2.0 mmol dm^{-3}) were measured in MeCN at 20 °C containing 0.1 mol dm^{-3} NBu_4ClO_4 as a supporting electrolyte using a glassy-carbon working electrode and Ag/0.01 mol dm^{-3} $AgNO_3$ couple in MeCN as a reference electrode; scan rate in the range from 50 to 500 mV s^{-1}.

¶ *Selected data* for **2**: green crystals (*n*-hexane); mp 76 °C (decomp.) (Found: M^+ 355.1565. $C_{22}H_{27}S_2$ requires 355.1554); X-band EPR (THF) g = 2.0049, a_{H1} = 0.461 mT, a_{H2} = 0.394 mT, a_{H3} = 0.123 mT, a_{H4} = 0.121 mT, a_{H5} = 0.065 mT.

1 S. Ogawa, T. Kikuchi, S. Niizuma and R. Sato, *J. Chem. Soc., Chem. Commun.*, 1994, 1593; S. Ogawa, T. Kikuchi, A. Sasaki, S. Chida and R. Sato, *Tetrahedron Lett.*, 1994, **35**, 5469; S. Ogawa, S. Saito, T. Kikuchi, Y. Kawai, S. Niizuma and R. Sato, *Chem. Lett.*, 1995, 321; S. Ogawa, S. Nobuta, R. Nakayama, Y. Kawai, S. Niizuma and R. Sato, *Chem. Lett.*, 1996, 757; S. Ogawa, T. Ohmiya, T. Kikuchi, Y. Kawai, S. Niizuma and R. Sato, *Heterocycles*, 1995, **43**, 321; D. Schröder, H. Schwarz, B. Löbrecht, W. Koch and S. Ogawa, *Eur. J. Inorg. Chem.*, 1998, 983.

2 C. T. Pedersen and C. Lohse, *Tetrahedron Lett.*, 1972, 5213; K. Bechgaard, V. D. Parker and C. T. Pedersen, *J. Am. Chem. Soc.*, 1973, **95**, 4373; C. T. Pedersen and C. Lohse, *Acta Chem. Scand., Ser. B*, 1975, **29**, 831.

3 G. D. Figuly, C. K. Loop and J. C. Martin, *J. Am. Chem. Soc.*, 1992, **111**, 645; E. Block, V. Eswarakrishnan, M. Gernon, G. Ofori-Okai, C. Saha, K. Tang and J. Zubieta, *J. Am. Chem. Soc.*, 1992, **111**, 658; K. Smith, C. M. Lindsay and G. J. Pritchard, *J. Am. Chem. Soc.*, 1992, **111**, 665.

4 B. B. Wayland, A. E. Sherry, G. Paszmik and A. G. Bunn, *J. Am. Chem. Soc.*, 1992, **114**, 1673.

Communication 9/05276C

Trichloroacetylhydrazones: new highly reactive alkylating agents

V. Atlan, L. El Kaim,* S. Lacroix and R. Morgentin

Laboratoire Réacteur et Processus, Ecole Nationale Superieure de Techniques Avancées, 75015 Paris, France. E-mail: elkaim@ensta.fr

Received (in Cambridge, UK) 22nd July 1999, Accepted 5th August 1999

The behavior of trichloroacylhydrazones as new highly reactive alkylating agents is disclosed; various secondary amines are alkylated within a few minutes at room temperature, and similar alkylating reductions were found with malonates.

Hydrazones are associated with a wealth of well-known reactions, such as the Wolf Kishner[1] and Shapiro[2] reactions and the Eischenmoser rearrangement.[3] In most of these fascinating reactions, loss of nitrogen is the driving force of the observed modifications. We recently reported a puzzling reaction of a class of poorly studied hydrazones, trichloroacetylhydrazones; when a number aldehyde derivatives were treated with K_2CO_3, clean conversion to 1,3,4-oxadiazoles was observed.[4] In order to have a better understanding of the behavior of these compounds, we decided to treat them in a different basic medium.

When hydrazone **1a** was treated with a large excess of morpholine in CH_2Cl_2, fast evolution of nitrogen was observed at room temperature along with the unexpected formation of the new alkylated amines **3a** and the dichloroacylamide **4a** (Scheme 1) as the only isolable compounds. The overall process from the carbonyl starting material is a reductive alkylation, as observed in the Leuckart reaction.[5] The reaction seems to be general, with ketone and aldehyde hydrazones **1** giving in a similar fashion the new alkylated amines **3** when treated with a large excess of amine **2** (Table 1). In most instances, the reaction was very clean and analysis of the crude product revealed that amines **3** and dichloroamides **4** were the only formed products; the pure amines **3** were most efficiently recovered through acid-base extraction and removal of the volatile secondary amine by evaporation. The poor isolated yield observed for **3f** was probably due to losses during evaporation of the morpholine. However, with aromatic ketones different behavior was observed when the morpholine was replaced by Et_2NH (or $Pr^i{}_2NH$); instead of the expected reduced compounds, formal oxidation of the ketone to the new α-amino hydrazone **5a** (or **5b**) occurred (Table 1).

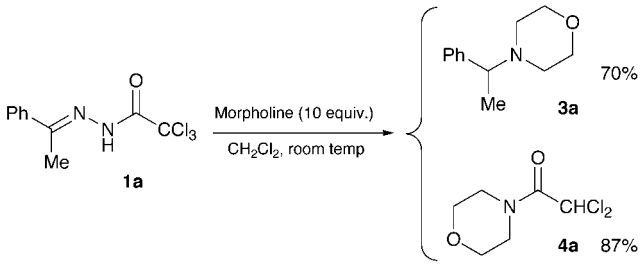

Scheme 1

Under the same conditions, primary amines also gave a fast reaction with trichloroacylhydrazones, but no alkylation compounds could be recovered from the complex product mixtures.

The use of a large excess of secondary amine could be a serious drawback for the application of this chemistry to other nucleophiles. Even if the amount of amine could be lowered, at least 1 equiv. was always lost as a trap for the dichloroacyl group. A solution to this problem was eventually given by the observation that trichloroacylhydrazones were rather unreactive in ethanolic sodium ethanolate. When hydrazone **1e** was left to react in a EtONa (4 equiv.) solution in EtOH, no change was observed after 4 h at room temperature; when the same solution was refluxed for 5 h the new oxadiazole **10a** was formed in 48% yield (Scheme 2). This behavior was similar for various hydrazones tested. We then added hydrazone **1f** to a EtONa (1.2 equiv.) solution in absolute EtOH, observed after a quarter of an hour the absence of reaction, and then added to this mixture diethyl malonate (1.2 equiv.); the evolution of nitrogen was soon observed. The reaction was left at room temperature for one day, after which the usual workup gave the alkylated

Table 1 Isolated compounds after aminolysis of hydrazones **1**

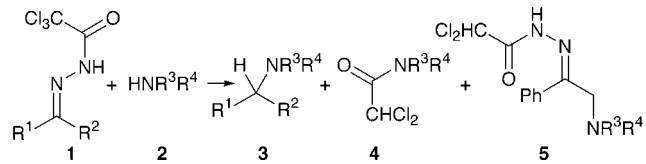

1 2 3 4 5

Hydrazone[a]			Amine			Product (% yield[b])		
1	R^1	R^2	**2**	R^3	R^4	**3**	**4**	**5**
1a	Ph	Me	**2a**	$-(CH_2)_2O(CH_2)_2-$		**3a** (70)	**4a** (87)	—
1a	Ph	Me	**2b**	$-(CH_2)_5-$		**3b** (68)	—	—
1b	$-(CH_2)_2CH{=}CHCH_2-$		**2a**	$-(CH_2)_2O(CH_2)_2-$		**3c** (89)	—	—
1b	$-(CH_2)_2CH{=}CHCH_2-$		**2c**	Et	Et	**3d** (98)	—	—
1c	Ph	H	**2a**	$-(CH_2)_2O(CH_2)_2-$		**3e** (71)	—	—
1d	$-(CH_2)_4-$		**2a**	$-(CH_2)_2O(CH_2)_2-$		**3f** (42)	—	—
1a	Ph	Me	**2c**	Et	Et	—	—	**5a** (57)
1a	Ph	Me	**2d**	Pr^i	Pr^i	—	—	**5b** (67)

[a] Yields from ketones: **1a** (64%), **1b** (50%), **1c** (75%), **1d** (65%). [b] Isolated yields.

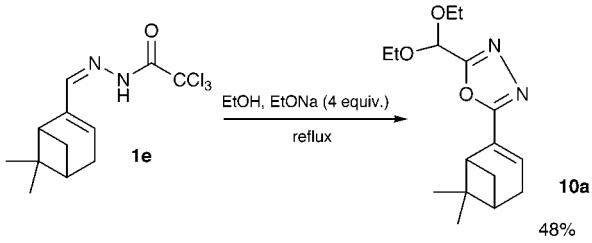

Scheme 2

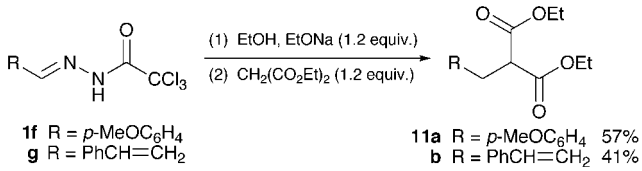

Scheme 3

malonate **11a** in 57% yield (Scheme 3). The same reaction with cinnamaldehyde hydrazone **1g** gave the new malonate **11b** in a poor 41% yield.

A reasonable mechanism for all these results is depicted in Scheme 4. The main assumption lies in a 1,5 chlorine migration from the anion. Such a migration has never been reported before but could be relevant in the results described by Yiannios *et al.* in 1968.[6] In our case the evolution of the resulting anion **6** depends on the nature of the substituted hydrazones (R = alkyl, aryl, H) and the basic conditions used in the reaction. When reprotonation of **6** is not possible (K_2CO_3, dioxane), a cyclisation to oxadiazole **10** is observed for aldehyde hydrazones giving reactive chlorides (R^1 = H, R^2 = aryl, alkenyl). When the medium is acidic enough (excess of amine and the presence of ammonium chloride salts), protonation of **6** to the α-chloroazo intermediate **7** may lead to the products through subsequent substitution and elimination reactions. With substrates sensitive to base elimination different behavior is observed: elimination of HCl from **7** (R^1 = Me, R^2 = Ph) leads

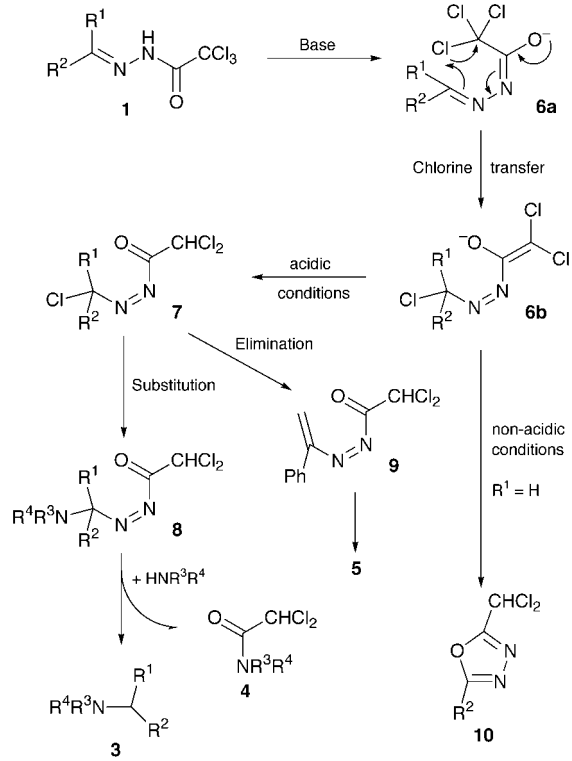

Scheme 4

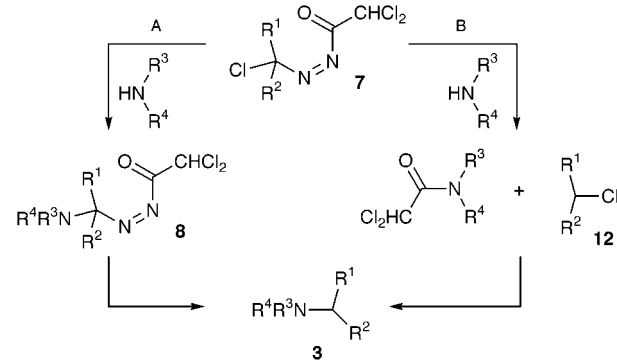

Scheme 5

to azoalkenes **9** (Scheme 4) whose chemistry has been fully explored in Michael type additions or cycloadditions with nucleophiles;[7] in our case, their reaction with Et_2NH (or Pr^i_2NH) in excess gives the observed amino hydrazone **5a** (or **5b**). This elimination is best observed with poorly nucleophilic amines; indeed highest yields were obtained with Pr^i_2NH whereas the more nucleophilic morpholine led to tertiary amine **3a**.

The acidic requirements of this reaction are stressed by the experiments conducted in EtOH. The mixture of EtONa in EtOH is not acidic enough and no reaction is observed at room temperature, however the reaction starts as soon as the slightly acidic malonate is added in the mixture.[8]

The intermediacy of chloride **12** (Scheme 5, path A) was discarded in view of the sluggish reaction observed between morpholine and chlorocyclopentane in CH_2Cl_2. After 4 h at room temperature, no formation of amine **3f** was observed; hydrazone **1** under the same conditions gives amine **3f** within 10 min, revealing the highly electrophilic properties of the intermediate involved.

Trichloroacylhydrazones certainly deserve further study to fully understand the mechanism of these reactions and exploit their full potential, yet these reductive alkylations at room temperature are most noteworthy. Whatever the structure of the active alkylating agent generated under weakly basic conditions, it is much more reactive than the related chloride and can be generated from stable starting materials with weak bases. Besides their synthetic potential underlined here trichloroacylhydrazones could find useful applications in the biological field as masked alkylating species activated after interaction with a basic site of an enzyme receptor.

Notes and references

1 R. O. Hutchins and M. K. Hutchins, *Comprehensive Organic Synthesis*, ed. I. Fleming and B. M. Trost, Pergamon, Oxford, 1991, vol. 8, pp. 327–362 and references cited therein.

2 R. M. Adlington and A. G. M. Barrett, *Acc. Chem. Res.*, 1983, **16**, 55.

3 A. Eschenmoser, D. Felix and G. Ohloff, *Helv. Chim. Acta*, 1967, **50**, 708.

4 L. El Kaim, I. Le Menestrel and R. Morgentin, *Tetrahedron Lett.*, 1998, **39**, 6885.

5 R. M. Kellogg, *Comprehensive Organic Synthesis*, ed. I. Fleming and B. M. Trost, Pergamon, Oxford, 1991, vol. 8, pp. 84–86 and references cited therein.

6 C. N. Yiannios, A. C. Hazy and J. V. Karabinos, *J. Org. Chem.*, 1968, **33**, 2076.

7 O. A. Attanasi and P. Filippone, *Synlett*, 1997, 1128.

8 Alternative intermediates such as oxadiazoles and diazo compounds can be easily proposed in the alkylation process; several analogues of these compounds have been isolated during a study on the basic treatment of the related monochloroacylhydrazones: E. C. Taylor, N. F. Haley and R. J. Clemens, *J. Am. Chem. Soc.*, 1981, **103**, 7743. The experiments conducted in EtOH are however difficult to explain with these intermediates.

Communication 9/05946F

Et_2Zn as a base: zinc enolate free from other metals significantly enhances the enantiomeric excess in palladium-catalyzed allylic alkylation

Kaoru Fuji,*[a] Naosumi Kinoshita[a]† and Kiyoshi Tanaka[b]

[a] *Institute for Chemical Research, Kyoto University, Uji, Kyoto 611-0011, Japan. E-mail: fuji@scl.kyoto-u.ac.jp*
[b] *School of Pharmaceutical Sciences, University of Shizuoka, 52-1 Yada, Shizuoka 422-8526, Japan*

Received (in Cambridge, UK) 26th July 1999, Accepted 23rd August 1999

The enantiomeric excess of palladium-catalyzed allylic alkylations was greatly increased when Et_2Zn was used as the base to generate an anion from malonates.

Et_2Zn is a widely used nucleophilic agent. Examples include the ethylation of aldehydes,[1] 1,4-addition to α,β-unsaturated carbonyl compounds,[2] preparation of the Simmons-Smith reagent[3] and the umpolung reaction of π-allylpalladium.[4] Furthermore, Et_2Zn is known to be a weak Lewis acid to which oxygen, nitrogen and halogens can coordinate.[5] To the best of our knowledge, it has not been used as a base to generate zinc enolates. These are routinely generated *in situ* by metal–metal exchange with other metal enolates. Since the other metal coexists together with zinc in the reaction medium, it is obvious that the aggregation state is quite different from that of zinc enolates free from other metals, which may affect the stereochemical outcome of the reactions. We report here a remarkable enhancement of the enantiomeric excess (ee) in a palladium-catalyzed allylic alkylation using zinc enolates free from other metals, generated with Et_2Zn as a base.

We have chosen the reaction shown in Scheme 1 as a standard reaction to evaluate the effect of zinc enolates free from other metals.[6] Et_2Zn is known to be basic enough to form a zinc alkoxide when it is mixed with an alcohol.[7] Based on the pK_a values of alcohols and the malonate, we can expect that a hydrogen of the active methylene group of dimethyl malonate will be removed by Et_2Zn. A popular chiral ligand, (*R*)-BINAP,

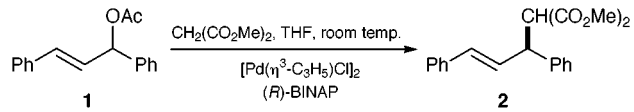

1 **2**

Scheme 1

was used for the reaction and the results are listed in Table 1. A zinc enolate prepared by metal exchange from the corresponding sodium enolate showed a considerable increase in ee, although the reactivity decreased (entries 2 and 3). A significant difference in ee was not observed between the lithium enolates and the zinc enolates generated by exchange from the lithium enolates (entries 5–8). A remarkable increase in ee was observed when the zinc enolate that was directly generated with Et_2Zn was used (entry 9). These findings indicate that the aggregation state of the zinc malonate prepared with Et_2Zn is different from that prepared by metal exchange, although it is premature to present an explanation for the increase in enantioselectivity with zinc enolate free from other metals. Temperature affects the reaction rate, but not the ee, when zinc enolate free from other metals is used (entries 9–11).

The results of allylic alkylations with various nucleophiles are listed in Table 2. Zinc enolates generally gave ees greater than those with sodium enolates at room temperature. Zinc enolates generated from malonic acid derivatives again gave comparable ees at various temperatures (entries 1,2 and 10, 11), but the ee decreased markedly at higher temperature with other enolates (entries 4, 5 and 7, 8).

Remarkably high ees were observed in the alkylation of other allylic acetates **3**–**5** and **9** with the zinc malonate (Table 3). The

Table 1 Effect of counter cation on the allylic alkylation of the racemic acetate **1** catalyzed by the Pd^0–(*R*)-BINAP giving (*S*)-**2**[a]

Entry	Base	Additive[b]	*t*/h	Yield (%)	Ee (%)
1	KH	none	5	77	59
2	NaH	none	18	75	35[c]
3	NaH	$ZnCl_2$	48	19 (58)[d]	57
4	LiH	none	64	68 (89)[d]	72
5	LDA	none	2	87	76
6	LDA	$ZnCl_2$	68	60 (71)[d]	87
7	BuLi	none	24	91	56
8	BuLi	$ZnCl_2$	42	19	53
9	$ZnEt_2$	none	39[e]	46 (72)[d]	98
10	$ZnEt_2$	none	20	84	99
11	$ZnEt_2$	none	0.5[f]	89	97
12	$ZnEt_2$	LiCl	42	67	82

[a] Reaction conditions: Allylic acetate **1** (1 equiv.), dimethyl malonate (2 equiv.), base (2 equiv.), (*R*)-BINAP (8 mol%), $[Pd(\eta^3\text{-}C_3H_5)Cl]_2$ (2 mol%) in THF at room temperature. [b] 2 equiv. [c] A 30% ee was reported under similar conditions (See ref. 8). [d] Yield in parenthesis based on the consumed starting material. [e] At 0 °C. [f] At reflux temperature.

Table 2 Allylic alkylation of the racemic acetate **1** with various nucleophiles catalyzed by the Pd^0–(*R*)-BINAP

Entry	Nucleophile	Base	*T*/°C	*t*/h	Yield (%)	Ee (%)
1	$CH_2(CO_2CH_2Ph)_2$	$ZnEt_2$	20	20	81	92
2	$CH_2(CO_2CH_2Ph)_2$	$ZnEt_2$	66[a]	1	78	95
3	$CH_2(CO_2CH_2Ph)_2$	NaH	20	2	83	0
4	$CH_2(CN)_2$	$ZnEt_2$	20	48	48	85
5	$CH_2(CN)_2$	$ZnEt_2$	66[a]	1.5	89	7
6	$CH_2(CN)_2$	NaH	20	48	33 (62)[b]	75
7	$CH_2(SO_2Ph)_2$	$ZnEt_2$	20	72	24 (44)[b]	92
8	$CH_2(SO_2Ph)_2$	$ZnEt_2$	66[a]	2	70	39
9	$CH_2(SO_2Ph)_2$	NaH	20	45	36 (60)[b]	88
10	$PhCH_2CH(CO_2Me)_2$	$ZnEt_2$	20	168	47 (53)[b]	70
11	$PhCH_2CH(CO_2Me)_2$	$ZnEt_2$	66[a]	3	92	76
12[c]	$PhCH_2CH(CO_2Me)_2$	NaH	25	211	45	0

[a] Reflux in THF. [b] Yield in parenthesis based on the consumed starting material. [c] Taken from the ref. 8.

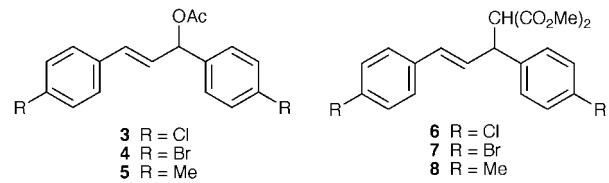

3 R = Cl
4 R = Br
5 R = Me

6 R = Cl
7 R = Br
8 R = Me

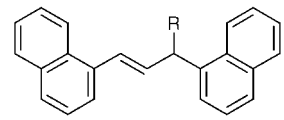

9 R = OAc
10 R = $CH(CO_2Me)_2$

† Present address: Pharmaceutical Production Department, Tokushima Second Factory, Otsuka Pharmaceutical Co., Ltd., Hiraishi Ebisuno 224-18, Kawauchi-cho, Tokushima 771-0182, Japan.

Table 3 Allylic alkylation of the racemic acetates **3**–**5** and **9** with dimethyl malonate catalyzed by Pd^0–(*R*)-BINAP

Entry	Compound	Base	*T*/°C	*t*/h	Product	Yield (%)	Ee (%)
1	**3**	$ZnEt_2$	20	20	**6**	92	97
2	**3**	$ZnEt_2$	66[a]	0.5	**6**	95	96
3	**3**	NaH	20	4	**6**	88	30
4	**4**	$ZnEt_2$	20	40	**7**	60 (65)[b]	97
5	**4**	$ZnEt_2$	66[a]	1	**7**	40	97
6	**4**	NaH	20	4	**7**	90	34
7	**5**	$ZnEt_2$	20	72	**8**	73	78
8	**5**	$ZnEt_2$	66[a]	1	**8**	91	80
9	**5**	NaH	20	4	**8**	78	19
10	**9**	$ZnEt_2$	20	48	**10**	73	88
11	**9**	$ZnEt_2$	66[a]	2	**10**	95	90
12	**9**	NaH	25	8	**10**	88	67

[a] Reflux in THF. [b] Yield in parenthesis based on the consumed starting material.

general tendency of zinc malonates described previously is observed in these cases. Thus, the zinc enolate gives greater ee than the sodium enolate and ees are not affected by differences in temperature.

In conclusion, we found that zinc malonates free from other metals can give high ees in allylic alkylations catalyzed by a palladium–(*R*)-BINAP complex. The present results suggest that zinc enolates free of other metals may be used to increase ees and/or chemical yields in other types of reactions involving enolates, although this application would be limited to highly acidic compounds.[9]

Notes and references

1 M. Kitamura, S. Suga, H. Oka and R. Noyori, *J. Am. Chem. Soc*., 1998, **120**, 9800 and references cited therein.
2 A. Alexakis, J. Vastra and P. Mangeney, *Tetrahedron Lett*., 1997, **38**, 7745 and references cited therein.
3 For a review; see A. B. Charette and J.-F. Marcoux, *Synlett*, 1995, 1197.
4 M. Kimura, Y. Ogawa, M. Shimizu, M. Sueishi, S. Tanaka and Y. Tamaru, *Tetrahedron Lett*., 1998, **39**, 6903 and references cited therein.
5 For example; H. Ozaki, A. Hirano and S. Nakahara, *Macromol. Chem. Phys*., 1995, **196**, 2099.
6 Zinc enolates of ketones free from other metals were generated from α-iodo ketones or α-iodo aldehydes with Et_2Zn; see S. Ito, H. Shinokubo and K. Oshima, *Tetrahedron Lett*., 1998, **39**, 5253.
7 M. Hayashi, K. Ono, H. Hoshimi and N. Oguni, *Tetrahedron*, 1996, **52**, 7817.
8 M. Yamaguchi, T. Shima and T. Yamagishi, *Tetrahedron*: *Asymmetry*, 1991, **2**, 663.
9 Et_2Zn was successfully used in the asymmetric Horner–Wadsworth–Emmons reaction. K. Tanaka, T. Watanabe, K. Shimamoto, P. Sahakitpichan and K. Fuji, *Tetrahedron Lett*., 1999, **40**, 6599.

Communication 9/06034K

Towards a redox-active artificial ion channel

C. D. Hall,*[a] Gregory J. Kirkovits[a] and Adam C. Hall[b]

[a] *Department of Chemistry, King's College London, Strand, London, UK WC2R 2LS. E-mail: dennis.hall@kcl.ac.uk*
[b] *Department of Biological Sciences, Mount Holyoke College, Mount Holyoke, Massachusetts, USA*

Received (in Cambridge, UK) 20th May 1999, Accepted 12th August 1999

The synthesis, characterisation and properties of an artificial ion channel containing a redox-active ferrocene unit are described.

During the last ten years substantial efforts have been made to mimic the action of natural ion channels[1] by the design and synthesis of model systems which would span natural (or artificial) lipid bilayers.[2–6] Generally speaking, the artificial channels consist of head groups (*e.g.* macrocyclic polyethers) to selectively capture specific cations, connected by long aliphatic chains designed to span the bilayers and often including a 'relay unit' which is sometimes another macrocyclic ether.[7] Alternative head groups include calixarenes[8,9] which, at least in one case,[9] support the concept of the 'billiard ball' effect, in essence, the charge repulsion theory of multiple ion transport.[10] In addition, synthetic proteins have been designed to mimic natural proteins, albeit with a single span rather than the multiple spans believed to exist in natural systems.[11] It is known that natural K^+ channels fall into two distinct categories.[12] The first is that of voltage-gated (K_v) channels which open and close ('gate') in response to the potential across the cell membrane. They have six trans-membrane domains, the fourth one of which has a positive charge every third residue and hence acts as the voltage sensor. The second category is that of the inward rectifier (K_{ir}) which consists of two trans-membrane domains connected by a loop which allows transport of K^+ ions in one direction only against the natural concentration gradient. This paper reports the synthesis, characterisation and properties of a one-domain artificial ion channel containing a redox-active centre (a ferrocene unit) in the middle of the channel to act as a 'filter'[10] and to influence the passage of cations by changing the oxidation state of the ferrocene during ion transport. The only redox-mediated channels of which we are aware are two C-terminus ferrocene derivatives of the *natural* peptide alamethicin which were shown to undergo dramatic changes in channel activity across lipid bilayers on *chemical* oxidation with excess ceric ion.[13]

The overall synthetic strategy, based on the inspirational work of Gokel *et. al.*,[2–5] was to link two macrocyclic units (as head groups) *via* long aliphatic chains to a central ferrocene unit which would also act as a cation relay. The resultant channel was designed to be approximately 30 Å long, the thickness of a typical biological membrane. The hydrophobic nature of the aliphatic chains was expected to promote lipid solubility and variation of the ring size in the head groups was expected to control cation selectivity. The precise synthetic sequence, shown in Scheme 1, afforded the target channel as a viscous orange oil in an overall yield of 16% from *N*-Boc-diaza-18-crown-6. Each compound in the synthetic sequence was purified by chromatography (Al_2O_3) and characterised by high resolution mass spectrometry and a combination of ^1H and ^{13}C NMR using DEPT (135).[14]

Cyclic voltammetry (CV) studies in MeCN as solvent with Bu_4NClO_4 (0.2 M) as the supporting electrolyte and using a glassy carbon working electrode gave rather curious results. A strong oxidation wave was observed at *+727* mV but the corresponding reduction wave failed to appear over a range of scan rates from 20–200 mV s^{-1} (Fig. 1).† Ferrocene amides of the type incorporated in the channel normally give a well-behaved electrochemical response[15] and the results suggest some sort of fast decomposition of the oxidised channel on the glassy carbon electrode or a rapid conformational change which inhibits the reduction process.‡ This feature of the electrochemistry is currently being investigated further. Introduction of two of the biologically important cations (Na^+ and Ca^{2+}) in increasing stoichiometric ratio from 1:1 to 1:10 ($L:M^{n+}$) produced perturbations of the oxidation wave and the results are shown in Table 1. During the initial additions of Na^+ (up to 1:3 stoichiometry) anodic shifts of various magnitudes were observed which is consistent with coordination of the Na^+ ion by the amide functions of the ferrocene unit. Addition of further equivalents of Na^+, however, produced a reversal of the shifts to slightly more cathodic values. It is difficult to rationalise this observation but one explanation may be that as the channel fills with cations, charge repulsion may reduce coordination by the

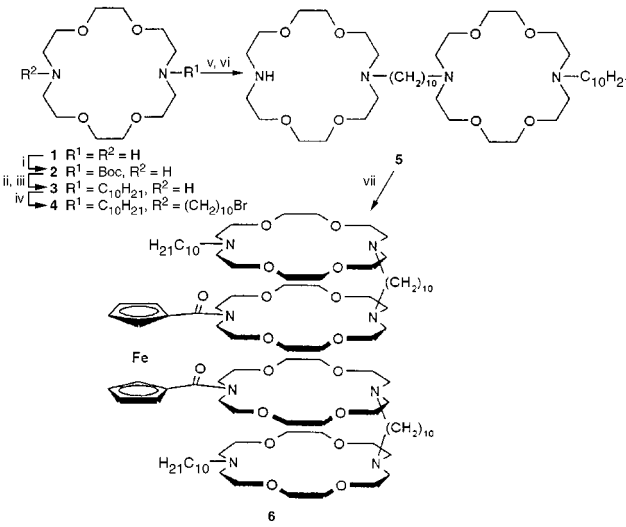

Scheme 1 *Reagents and conditions*: i, Boc_2O, 1,4-dioxane, 44%; ii, $Br(CH_2)_9CH_3$, Na_2CO_3, KI, PrCN, 80%; iii, TFA, CH_2Cl_2, 94%; iv, $Br(CH_2)_{10}Br$, Na_2CO_3, KI, PrCN, 56%; v, **2**, Na_2CO_3, KI, PrCN, 67%; vi, TFA, CH_2Cl_2, 94%; vii, 1,1′-bis(chlorocarbonyl)ferrocene, Et_3N, toluene, 58%.

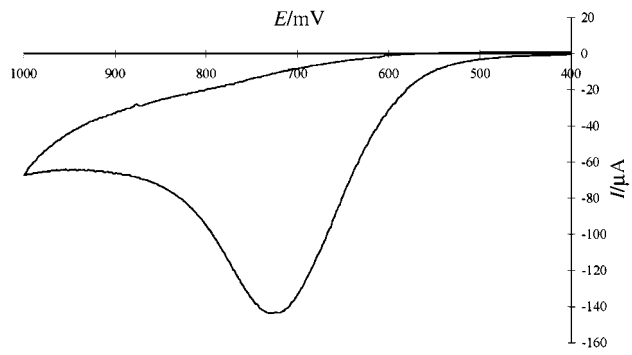

Fig. 1 Anodic voltammetric response of **6** (5×10^{-3} M in MeCN/0.2 M Bu_4NClO_4); working electrode: glassy carbon; counter electrode: Pt wire; reference electrode: Ag/AgCl; scan rate: 50 mV s^{-1}.

Table 1 Electrochemical data for metal complexes formed from ligand **6**

	Metal[a]			
	Na^+		Ca^{2+}	
Ratio metal : **6**	E_A[b]/mV	ΔE/mV	E_a[b]/mV	ΔE/mV
free **6**	727	—	727	—
1 : 1	—[c]	—[c]	755	28
2 : 1	758	31	792	65
3 : 1	782	55	867	140
4 : 1	775	48	874	147
10 : 1	757	30	884	157

[a] Triflate salts. [b] Determined in MeCN containing 0.2 M Bu_4NClO_4 as the supporting electrolyte. Solutions of **6** were 5×10^{-3} M and potentials were determined with reference to an Ag/AgCl, working electrode: glassy carbon; scan rate: 50 mV s^{-1} E_A represents the anodic voltammetric response. [c] Not recorded.

amide carbonyls, thus *reducing* the 'through bond' electron withdrawal from the ferrocene centre. With Ca^{2+}, however, the shift continued to be anodic throughout the concentration range, which may be due to the stronger coordination of the amide functions with the higher charge density Ca^{2+} ion. It should also be noted that addition of excess cations regenerated, at least in part, the reversibility of the CV wave.

An 'inside-out' patch excised from cells derived from Hamster brain§ was exposed to a solution of the synthetic channel and then tested for K^+ transport with potentials ranging from +60 to −60 mV across the membrane. The results against a control are shown in Fig. 2. Analysis of the data shows clear evidence of ion transport *promoted* by the artificial channel at both negative and positive pipette potentials. In addition, changing the potential across the patch from −60 to +60 mV results in a reduction of the transmembrane current (*i.e.* rectification) as the inside of the cell changes from negative to positive potential. For example, at −80 mV the average single channel current amplitude was −4.0 pA (equivalent to a conductance of 50 pS) whereas at +80 mV the same average current was +2.4 mA (30 pS). The results suggest the incorporation of an artificial channel with a degree of voltage control over cation transport. It is conceivable, however, that **6** is in some way activating endogenous channels within the biological membrane and hence lipid bilayer experiments are in progress to check this possibility. The details of this work will be published at a later stage but for now we report that **6**, together with several analogues, has shown similar channel activity in lipid bilayers to that reported by Gokel for non-redox-active artificial channels.[7,16,17] Thus the results obtained with the biological membrane may be viewed with more confidence as an example of an *artificial* channel with a degree of redox control over cation transport, one step nearer to the natural system.

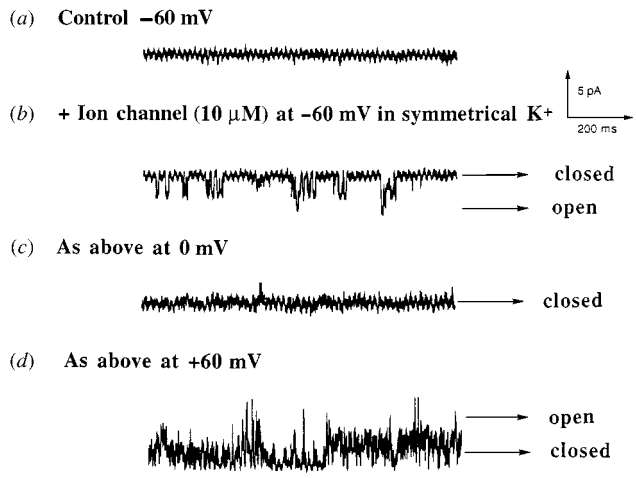

Fig. 2 Recordings of K^+ transport across an 'inside-out' patch when exposed to a solution of **6** (at 10 μM) and with a potential difference across the channel varying from −60 to +60 mV.

We are indebted to the EPSRC for a ROPA Award (to G. K.) and to the NIH for grants to A. C. H (nos. NS 26496 and NS 01641). Thanks are also due to Dr K. Welham (ULIRS, School of Pharmacy, Brunswick Sq., London WC1 1AX) for high-resolution mass spectra and to Jane Hawkes and John Cobb King's College and ULIRS for NMR spectra.

Notes and references

† The analogous cobalticenium hexafluorophosphate channel (to be reported later) gave well-behaved, fully reversible electrochemistry.
‡ Similar results were obtained using a Pt working electrode except that the current response was much lower for the same concentration.
§ Hypothalamic neurons were acutely dissociated from coronal hampster (5–15 day old) brain slices and superfused with a solution containing NaCl (140 mM) , KCl (2.5 mM), $CaCl_2$ (3 mM), glucose (3 mM) and HEPES (pH 7.4, 10 mM). Channel currents were recorded from inside-out patches using standard techniques. Fire-polished, borosilicate glass pipetttes were fabricated with a two-stage pull and filled with a solution containing: KCl (125 mM) , NaCl (10 mM), $CaCl_2$ (3 mM), glucose (3 mM) and HEPES (pH 7.4, 10 mM) which typically had resistances of 5–10 MΩ. After excision, the patches were held at indicated pipette potentials and the cell bathing solution was replaced with the above pipette solution. The artificial channel solution (in DMSO) was dissolved in the bathing solution (usually at 10 μM) and introduced to the patch at equivalent flow rates to the control. All currents were acquired using an Axoclamp 200A interfaced to a computer running pClamp6 software (Axon Instr.). Data were fitted at 1 kHz with a low-pass 8-pole Bessel filter, sampled at 4 kHz and analysed using pClamp6.

1 W. D. Stein, *Channels, Carriers and Pumps*, Academic Press, New York, 1990.
2 G. W. Gokel and O. Murillo, *Acc. Chem. Res.*, 1996, **29**, 425.
3 A. Nakano, Q. Xie, J. Mallen, L. Echegoyen and G. W. Gokel, *J. Am. Chem. Soc.*, 1990, **112**, 1287; O. Murillo, S. Watanabe, A. Nakano and G. W. Gokel, *J. Am. Chem. Soc.*, 1995, **117**, 7665.
4 O. Murillo, I. Suzuki, E. Abel and G. W. Gokel, *J. Am. Chem. Soc.*, 1996, **118**, 7628.
5 O. Murillo, E. Abel, G. E. M. McGuire and G. W. Gokel, *Chem. Commun.*, 1997, 2147.
6 F. Riddell and M. Hayer, *Biochem. Biophys. Acta*, 1985, **817**, 313; D. Buster, J. Hinton, F. Milltree and D. Shungu, *Biophys. J.*, 1988, **53**, 145.
7 E. Abel, E. S. Meadows, I. Suzuki, T. Jin and G. W. Gokel, *Chem. Commun.*, 1997, 1145.
8 P. Schmitt, P. D. Beer, M. G. B. Drew and P. Sheen, *Angew. Chem., Int. Ed. Engl.*, 1997, **36**, 1840.
9 P. J. Cragg, M. C. Allen and J. W. Steed, *Chem. Commun.*, 1999, 553.
10 D. A. Dougherty and H. A. Lester, *Angew. Chem., Int. Ed.*, 1998, **37**, 2329.
11 N. Voyer and M. Robitaille, *J. Am. Chem. Soc.*, 1995, **117**, 6599.
12 K. Ho, C. Nichols, G. Lederer, J. Lytton, P. M. Vassilev, M. V. Kanazirska and S. C. Herbert, *Nature*, 1993, **362**, 31; Y. Kubo, T. J. Baldwin, Y. N. Jan and L. Y. Jan, *Nature*, 1993, **362**, 127.
13 J. D. Schmitt, M. S. P. Sansom, I. D. Kerr, G. G. Lunt and R. Eisenthal, *Biochemistry*, 1997, **36**, 1115.
14 All compounds gave NMR data consistent with the proposed structures. *Selected data* for **2**: [HRMS-FAB, $(M + H)^+$] calc. for $C_{17}H_{35}N_2O_6$: 363.2495; found 363.2505. For **3**: [HRMS-FAB, $(M + H)^+$] calc. for $C_{22}H_{46}N_2O_4$: 403.3500; found 403.3536. For **4**: [HRMS-FAB, $(M + Na)^+$] calc. for $C_{32}H_{65}BrN_2O_4Na$: 643.4025; found 643.4010: For **5**. [HRMS-FAB, $(M + Na)^+$] calc. for $C_{44}H_{89}N_4O_8Na$: 824.6578; found 824.6548: For **6**. [HRMS-FAB, $(M + Na)^+$] calc. for $C_{100}H_{186}FeN_8O_{18}Na$: 1866.3132; Found 1866.3040.
15 C. D. Hall and S. Y, F. Chu, *J. Organomet. Chem.*, 1995, **498**, 221.
16 G. E. M. Maguire, E. S. Meadows, C. L. Murray and G. W. Gokel, *Tetrahedron Lett.*, 1997, **38**, 6339.
17 C. L. Murray, E. S. Meadows, O. Murillo and G. W. Gokel, *J. Am. Chem. Soc.*, 1997, **119**, 7887.

Communication 9/04069B

A highly active solid superacid catalyst for *n*-butane isomerization: persulfate modified Al_2O_3–ZrO_2

Y. D. Xia, W. M. Hua, Y. Tang and Z. Gao*

Department of Chemistry, Fudan University, Shanghai 200433, P.R. China

Received (in Cambridge, UK) 15th June 1999, Accepted 23rd August 1999

A new solid superacid catalyst of persulfate modified Al_2O_3–ZrO_2 has been prepared for the first time; it displays extraordinarily high catalytic activity and stability for the isomerization of *n*-butane.

In recent years, sulfated zirconia superacids have attracted increasing attention because they can give high activity at low temperature for *n*-butane isomerization, which has recently become a very important reaction in the petrochemical industry owing to growing environmental constraints and requirements for high-octane-number gasoline.[1–3] However, a rapid deactivation of this catalyst has often been observed at high temperature. In order to improve the lifetime of SO_4^{2-}/ZrO_2 catalysts for *n*-butane isomerization, the presence of hydrogen and/or addition of a small amount of Pt or Ni have been suggested.[4,5] Although Fe- and Mn-promoted sulfated zirconia are *ca.* three orders of magnitude more active than SO_4^{2-}/ZrO_2 for *n*-butane isomerization at low temperature,[6] they are deactivated quickly at 250 °C in the presence of hydrogen or at 60 °C in the presence of nitrogen.[7,8] We found that sulfated oxides of Cr–Zr, Fe–Cr–Zr and Fe–V–Zr were 2–3 times more active than sulfated Fe–Mn–Zr for *n*-butane isomerization, but these transition metal-doped sulfated zirconias also deactivated rapidly in the presence of hydrogen at high temperature.[8,9] In our previous results,[10,11] the addition of Al to sulfated zirconia significantly enhanced the activity and stability of the catalyst for *n*-butane isomerization at 250 °C in the presence of H_2. Persulfate modified zirconia is more active than sulfated zirconia for the isomerization of *n*-butane. The main problem in this research area is the durability of the catalyst during isomerization of *n*-butane. Here, we report a new solid superacid catalyst that is more active and stable for *n*-butane isomerization than any sulfated zirconia-based catalysts yet reported.

The new catalyst was prepared as follows: aqueous ammonia was added dropwise to a mixed solution of $ZrOCl_2{\cdot}8H_2O$ and $Al(NO_3)_3{\cdot}9H_2O$ until pH = 9–10. After washing the mixed hydroxide and drying at 383 K overnight it was immersed in 0.5 M ammonium persulfate solution for 30 min. The persulfated $Al(OH)_3$–$Zr(OH)_4$ was then filtered off, dried at 383 K overnight and calcined at 923 K in static air for 3 h. The new catalyst, a white solid, had a surface area of 80.8 $m^2\ g^{-1}$ and contained 3.0 mol% Al_2O_3 and 3.5 wt% sulfate. Sulfated zirconia was made for comparison in the same manner by immersing dried $Zr(OH)_4$ in 0.5 M sulfuric acid, followed by calcination at 923 K in static air for 3 h. The sulfated zirconia, also a white solid, had a surface area of 113.0 $m^2\ g^{-1}$ and contained 4.0 wt% sulfate. *n*-Butane isomerization on the catalysts was carried out at 523 K in a fixed-bed continuous flow reactor under ambient pressure with WHSV = 0.3 h^{-1} and an H_2 : butane molar ratio of 10 : 1. Before testing, each catalyst was pretreated *in situ* in dry air at 723 K for 3 h. The products were analyzed with an on-line gas chromatograph equipped with a flame ionization detector.

The major reaction product of *n*-butane isomerization at 523 K is isobutane and by-products are propane and isopentane. The selectivity to isobutane for the SO_4^{2-}/ZrO_2 and $S_2O_8^{2-}/Al_2O_3$–ZrO_2 catalysts is > 95%. Table 1 shows the variation of the conversion of *n*-butane at 523 K with time on stream for both catalysts. During the initial 1 h of reaction both catalysts are rapidly deactivated. After being on stream for 2 h the conversions of both catalysts then drop more slowly. The $S_2O_8^{2-}/Al_2O_3$–ZrO_2 catalyst reaches a steady state for *n*-butane isomerization after 2 h on stream (although it deactivates more rapidly than SO_4^{2-}/ZrO_2 during the initial 1 h of reaction), indicating that it is more stable than SO_4^{2-}/ZrO_2 for the reaction of *n*-butane isomerization. Both the initial and steady state activities of the $S_2O_8^{2-}/Al_2O_3$–ZrO_2 catalyst are much higher than those of SO_4^{2-}/ZrO_2. As compared with SO_4^{2-}/ZrO_2, $S_2O_8^{2-}/Al_2O_3$–ZrO_2 is 2.1 times more active after being on stream for 6 h.

The stability of the $S_2O_8^{2-}/Al_2O_3$–ZrO_2 catalyst has been investigated by running the reaction at 523 K continuously for 200 h. As illustrated in Fig. 1, the initial conversion on $S_2O_8^{2-}/Al_2O_3$–ZrO_2 is 51.8%, dropping to 37.8% after 2 h, and then remaining constant at *ca.* 37.4% up to 200 h without further observable deactivation. In other words, *n*-butane isomerization proceeds steadily on $S_2O_8^{2-}/Al_2O_3$–ZrO_2 at a level of 72% of its equilibrium conversion. In view of its high isomerization activity and stablity, $S_2O_8^{2-}/Al_2O_3$–ZrO_2 can be regarded as an excellent candidate for a commercial-scale *n*-butane isomerization catalyst.

After running on stream for 6 h, the amount of coke deposited on the $S_2O_8^{2-}/Al_2O_3$–ZrO_2 catalyst is 1.0 wt%, which is

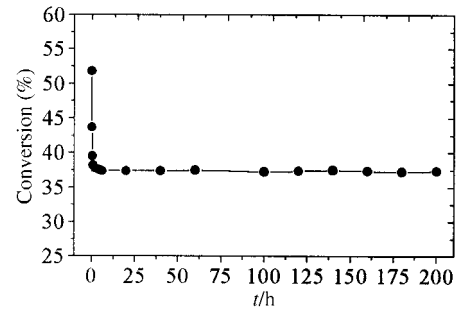

Fig. 1 Long-term test of $S_2O_8^{2-}/Al_2O_3$–ZrO_2 catalyst for *n*-butane isomerization at 523 K.

Table 1 Activities of solid superacid catalysts for *n*-butane isomerization at 523 K

	Conversion (%)							
Catalyst	2 min	10 min	60 min	120 min	180 min	240 min	300 min	360 min
SO_4^{2-}/ZrO_2	27.7	25.2	23.5	21.6	20.4	19.3	18.1	17.5
$S_2O_8^{2-}/Al_2O_3$–ZrO_2	51.8	43.7	38.2	37.8	37.7	37.7	37.4	37.3

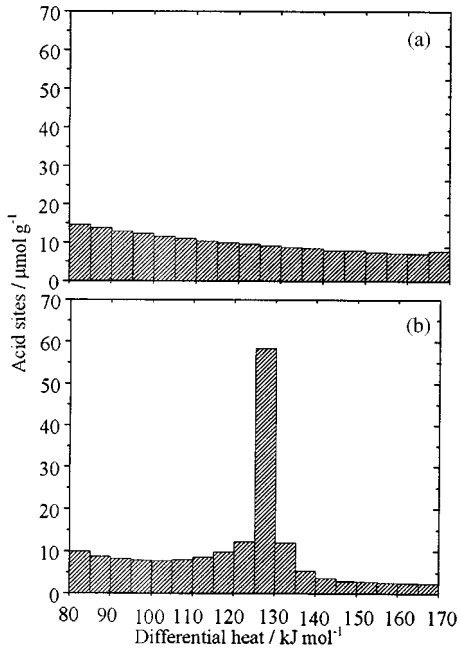

Fig. 2 Histograms of acid strength distributions for (a) SO_4^{2-}/ZrO_2 and (b) $S_2O_8^{2-}/Al_2O_3–ZrO_2$ catalysts.

slightly less than that on SO_4^{2-}/ZrO_2 (1.3 wt%). Furthermore, the amount of coke deposited on $S_2O_8^{2-}/Al_2O_3–ZrO_2$ remained almost unchanged from 6 to 200 h, showing that the initial drop in activity during 0–2 h is probably caused by catalyst coking; after this time coking and deactivation slowed down. Both catalysts can recover their activities completely after treatment in air at 723 K and can be used repeatedly, further demonstrating that the fast deactivation of the catalysts during the initial period of the reaction is mainly caused by coking.

Microcalorimetric measurements of NH_3 adsorption on SO_4^{2-}/ZrO_2 and $S_2O_8^{2-}/Al_2O_3–ZrO_2$ catalysts were conducted. The differential heat of adsorption (*i.e.* heat generated after microadsorption on the adsorption system which has already reached equilibrium) decreases with increasing NH_3 coverage, indicating a distribution of acid site strength in both catalysts. Fig. 2 shows histograms of the distribution of acid site strengths. The strengths of the acid sites on SO_4^{2-}/ZrO_2 are more evenly distributed than for $S_2O_8^{2-}/Al_2O_3–ZrO_2$. Although the total amount of acid sites with a differential adsorption heat above 80 kJ mol^{-1} for $S_2O_8^{2-}/Al_2O_3–ZrO_2$ (174.2 μmol g^{-1}) is nearly the same as that for SO_4^{2-}/ZrO_2 (178.2 μmol g^{-1}), the former posseses 2.9 times more acid sites with a differential heat between 125 and 140 kJ mol^{-1}, which have been reported in an earlier study[12] as being the effective

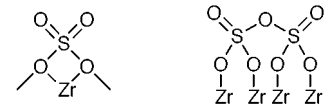

Fig. 3 Structure of active sites **I** and **II**.

active sites for *n*-butane isomerization. Hence, the abundance of sites with intermediate acid strengths on $S_2O_8^{2-}/Al_2O_3–ZrO_2$ is the main reason for its remarkable activity and stability for the *n*-butane isomerization reaction. Our recent study[11] has shown that the characteristic stretching frequency of covalent S=O bonds for persulfate modified zirconia is at 1398 cm^{-1}, which is different from that for SO_4^{2-}/ZrO_2 at 1388 cm^{-1}; we postulate that $S_2O_7^{2-}$ is responsible for this stretching frequency in agreement with earlier studies.[13,14] On the persulfate modified oxide superacid, the main structure of the active sites is **II** (Fig. 3), whereas active site **I** predominates on the sulfated oxide superacid. The difference in the structure of the active sites for each of the catalysts is probably another reason why the catalytic activity and stability of $S_2O_8^{2-}/Al_2O_3–ZrO_2$ for the isomerization of *n*-butane are much higher than those of SO_4^{2-}/ZrO_2.

Notes and references

1 B. H. Davis, R. A. Keogh and R. Srinivasan, *Catal. Today*, 1994, **20**, 219.
2 A. Corma, *Chem. Rev.*, 1995, **95**, 559.
3 X. Song and A Sayari, *Catal. Rev.-Sci. Eng.*, 1996, **38**, 329.
4 F. Garin, D. Andriamasinoro, A. Abdulsamad and J. Sommer, *J. Catal.*, 1991, **131**, 199.
5 M. A. Coelho, D. E. Resasco, E. C. Sikabwe and R. L. White, *Catal. Lett.*, 1995, **32**, 253.
6 C. Y. Hsu, C. R. Heimbuch, C. T. Armes and B. C. Gates, *J. Chem. Soc., Chem. Commun.*, 1992, 1645.
7 V. Adeeva, J. W. de Haan, J. Janchen, G. D. Lei, V. Schunemann, L. J. M. van de Ven, W. M. H. Sachtler and R. A. van Santen, *J. Catal.*, 1995, **151**, 364.
8 C. X. Miao and Z. Gao, *Chem. J. Chin. Univ.*, 1997, **18**, 424.
9 C. X. Miao, W. M. Hua, J. M. Chen and Z. Gao, *Catal. Lett.*, 1996, **37**, 187.
10 Z. Gao, Y. D. Xia, W. M. Hua and C. X. Miao, *Top. Catal.*, 1998, **6**, 101.
11 Y. D. Xia, W. M. Hua and Z. Gao, *Acta Chim. Sinica*, in press.
12 K. B. Fogash, G. Yaluris, M. R. Gonzalez, P. Ouraipryvan, D. A. Ward, E. I. Ko and J. A. Dumesic, *Catal. Lett.*, 1995, **32**, 241.
13 M. Bensitel, O. Saur, J. C. Lavalley and B. A. Morrow, *Mater. Chem. Phys.*, 1988, **19**, 147.
14 C. Morterra, G. Cerato, C. Emanuel and V. Bolis, *J. Catal.*, 1993, **142**, 349.

Communication 9/04783B

Highly active Pd^{II} cyclometallated imine catalyst for the Suzuki reaction

Haim Weissman and David Milstein*

Department of Organic Chemistry, The Weizmann Institute of Science, 76100 Rehovot, Israel.
E-mail: comilst@weizmann.weizmann.ac.il

Received (in Cambridge, UK) 2nd August 1999, Accepted 19th August 1999

The cyclopalladated, phosphine-free imine complex 1 is an excellent catalyst for the Suzuki cross-coupling, leading to more than 10^5 turnovers with non-activated aryl bromides; the catalyst is air and thermally stable.

The Suzuki palladium-catalyzed cross-coupling reaction of organoboron compounds with organic halides or related electrophiles [eqn. (1)] represents a useful synthetic method for carbon–carbon bond formation and has attracted much current

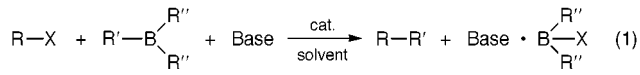

interest.[1] Usually palladium phosphine complexes are utilized as catalysts and the reactions are conducted under inert atmosphere. Palladium–carbene complexes and other phosphine-free catalysts have been recently utilized.[2] Very efficient catalysis of the Suzuki reaction using palladium complexes incorporating cyclometallated phosphine and phosphite complexes have recently been reported.[3]

We have reported on highly active PCP-type[4] and cyclometallated imine[5] catalysts for the Heck reaction. The phosphine-free imine complexes lead to more than a million turnovers in some cases. Furthermore, the catalysts are very thermally and air stable and can be recovered after catalysis. We now find that the palladium imine catalyst **1**† is among the best known for the Suzuki reaction. It catalyzes the coupling of aryl bromides with phenylboronic acid in extremely high efficiency [eqn. (2)].

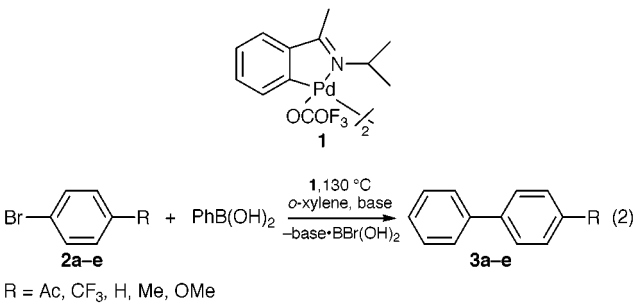

The general procedure for the coupling reaction is as follows: to a solution containing 2.5×10^{-5} mmol of catalyst **1** were added 5 mmol of 4-BrC_6H_4R (1:200000 catalyst:substrate ratio), 7.5 mmol of $PhB(OH)_2$ and 10 mmol of K_2CO_3. The mixture was heated to 130 °C with stirring in 13 ml of *o*-xylene (distilled from Na/benzophenone) under air or N_2 atmosphere. The reaction was usually over after 2 h. The reaction mixture was sampled and analyzed by GC and GC-MS techniques. Typical results are presented in Table 1.

Our catalytic system is one of the most active, especially with respect to the non-activated aryl bromides **2a**–**c**. Increasing the amount of phenylboronic acid (from 1.5 to 2 equiv. relative to the bromide) had a beneficial effect on the yield. Similar results were obtained when a nitrogen atmosphere was used. The reaction is not very sensitive to the solvent used, as similar results were obtained in dioxane.‡

In order to gain insight into the mechanism of the reaction, a competitive reaction with the five aryl bromides **2a**–**e** was performed under pseudo-first order conditions with respect to $PhB(OH)_2$. A solution containing 2.5×10^{-5} mmol of catalyst **1**, 5 mmol of each of the bromides **2a**–**e**, 0.75 mmol of $PhB(OH)_2$ and 1 mmol of K_2CO_3 was heated at 130 °C with stirring in 13 ml of *o*-xylene under air. The concentrations of the various coupling products were determined by GC. The resulting Hammett plot is exhibited in Fig. 1.

The use of σ_P^- constants results in a better fit than σ_P constants, indicating some conjugation of π-electron density with the *para* substituent in the transition state. The correlation yields a value of $\rho \approx 1$. While this electronic effect is not surprising, since electron withdrawing substituents are expected to accelerate the Ar–Br oxidative addition step, the ρ value is too low to fit a rate-determining nucleophilic aromatic substitution. For example, a ρ value of 5.2 was obtained for oxidative addition of aryl chlorides to electron rich Pd^0 complexes.[6] This indicates a subsequent rate-determining step with different electronic requirements, such as the transmetallation step. It is noteworthy that a similar value of $\rho = 1.34$ was obtained for the Heck reaction of aryl iodides involving PCP–Pd^{II} catalysts, which is unlikely to proceed by the traditional Pd^0/Pd^{II} mechanism.

Table 1 Suzuki coupling catalyzed by the imine complex **1** according to eqn. (2)

ArBr[a]	Catalyst/substrate ratio	Base (mmol)	$PhB(OH)_2$ (mmol)	Atmosphere	Yield (%)	TON (10^3)	*t*/h[b]
4-BrC_6H_4OMe	5×10^{-6}	K_2CO_3 (10)	7.5	N_2	51	102	16
	5×10^{-6}	K_2CO_3 (10)	7.5	air	57	114	16
	5×10^{-6}	K_2CO_3 (11.5)	10	air	60	120	3
	5×10^{-6}	K_3CO_4 (10)	7.5	air	68	136	22
4-BrC_6H_4Me[c]	5×10^{-6}	K_2CO_3 (10)	7.5	N_2	78	156	16
	5×10^{-6}	K_2CO_3 (10)	7.5	air	82	160	16
PhBr	5×10^{-6}	K_2CO_3 (10)	7.5	N_2	66	132	2
	5×10^{-6}	K_2CO_3 (11.5)	10	air	90	180	3
4-BrC_6H_4Ac	1×10^{-6}	K_2CO_3 (10)	7.5	air	59	590	16
	1×10^{-6}	K_2CO_3 (11.5)	10	air	84	840	16
4-$BrC_6H_4CF_3$	5×10^{-6}	K_2CO_3 (10)	7.5	N_2	93	186	16
	5×10^{-6}	K_2CO_3 (10)	7.5	air	90	180	14.5

[a] Amounts: ArBr (5 mmol) *o*-xylene (13 ml). Reaction temperature: 130 °C. [b] This is the time after which the reaction was analyzed. It might have been over at an earlier stage. [c] The same catalytic activity was observed in dioxane as a solvent.

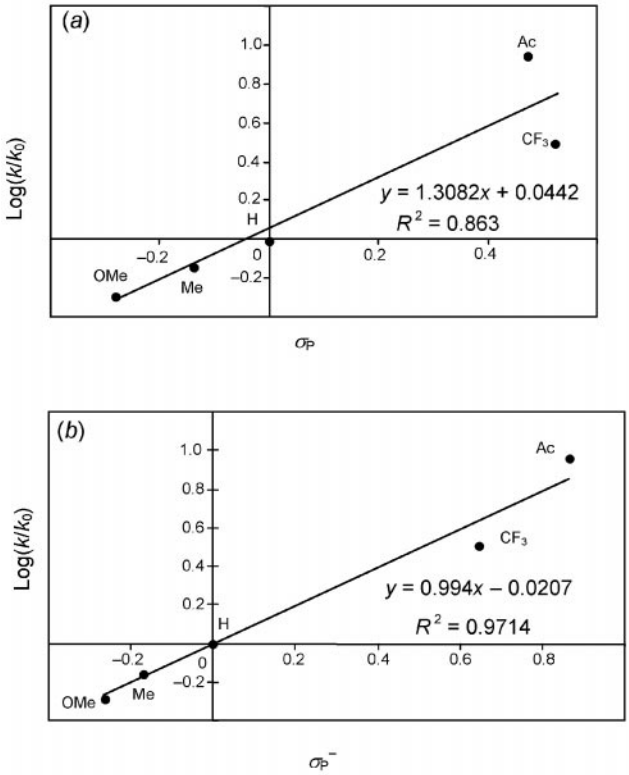

Fig. 1 Hammett correlation of the competitive reaction of aryl bromides with $PhB(OH)_2$ using (*a*) σ_P constants and (*b*) σ_P^- constants at 130 °C in *o*-oxylene.

In summary, the phosphine-free cyclopalladated imine complex **1** shows very high catalytic activity and yields in the Suzuki cross-coupling reaction of aryl bromides with phenylboronic acid. The system exhibits unprecedented turnovers with non-activated aryl bromides. The catalyst system is very thermally and air stable. Further investigations aimed at clarification of the scope and mechanism of this reaction are currently in progress.

This work was supported by the Israel Science Foundation, Jerusalem, Israel, by the Ministry of Science, Jerusalem, Israel, and the MINERVA Foundation, Munich, Germany. D. M. is the holder of the Israel Matz Professorial Chair of Organic Chemistry.

Notes and references

† X-Ray structure and NMR characterization have been reported in ref. 5.

‡ The reaction is sensitive to impurities in the solvent. Use of *o*-xylene not distilled from sodium may result in significantly lower efficiency.

1 Reviews and very recent references: N. Miyaura and A. Suzuki, *Chem. Rev.*, 1995, **95**, 2457; A. Suzuki, *Metal-catalyzed Cross-coupling Reactions*, ed. F. Diederich and P. J. Stang, Wiley-VCH, Weinheim, 1998, ch. 2, p. 49; A. Suzuki, *J. Organomet. Chem.*, 1999, **576**, 147; G. C. Fu and A. F. Littke, *Angew. Chem., Int. Ed*., 1998, **37**, 3387; J. P. Wolfe and S. L. Buchwald, *Angew. Chem., Int. Ed*., 1999, **38**, 2413.

2 W. A. Herrmann, C. P. Reisinger and M. Spiegler, *J. Organomet. Chem.*, 1998, **557**, 93; C. M. Zhang, J. K. Huang, M. L. Trudell and S. P. Nolan, *J. Org. Chem.*, 1999, **64**, 3804; D. S. McGuinness, K. J. Cavell, B. W. Skelton and A. H. White, *Organometallics*, 1999, **18**, 1596; T. I. Wallow and B. M. Novak, *J. Org. Chem*., 1994, **59**, 5034; M. Morenomanas, F. Pajuelo and R. Pleixats, *J. Org. Chem*., 1995, **60**, 2396; M. T. Reetz, R. Breinbauer and K. Wanninger, *Tetrahedron Lett*., 1996, **37**, 4499; N. A. Bumagin and V. V. Byakov, *Tetrahedron*, 1997, **53**, 14 437; D. Badone, M. Baroni, R. Cardamone, A. Ielmini and U. Guzzi, *J. Org. Chem*., 1997, **62**, 7170; C. G. Blettner, W. A. Konig, W. Stenzel and T. Schotten, *J. Org. Chem*., 1999, **64**, 3885.

3 M. Beller, H. Fischer, W. A. Herrmann, K. Öfele and C. Brossmer, *Angew. Chem., Int. Ed. Engl*., 1995, **34**, 1848; D. A. Albisson, R. B. Bedford, S. E. Lawrence and P. N. Scully, *Chem. Commun.*, 1998, 2095; W. A. Herrmann and V. P. W. Böhm, *J. Organomet. Chem.*, 1999, **572**, 141.

4 M. Ohff, A. Ohff, M. E. van der Boom and D. Milstein, *J. Am. Chem. Soc*., 1997, **119**, 11 687.

5 M. Ohff, A. Ohff and D. Milstein, Israel Patent Appl. 121346 (filed on 20.07.1997); M. Ohff, A. Ohff and D. Milstein, *Chem. Commun*., 1999, 357.

6 M. Portnoy and D. Milstein, *Organometallics*, 1993, **12**, 1665.

Communication 9/06246G

An unprecedented 3D coordination network composed of two intersecting helices

Owen R. Evans, Zhiyong Wang and Wenbin Lin*

Department of Chemistry, Brandeis University, Waltham, MA 02454, USA. E-mail: wlin@brandeis.edu

Received (in Columbia, MO, USA) 22nd June 1999, Accepted 9th August 1999

A hydro(solvo)thermal reaction between $Zn(ClO_4)_2·6H_2O$ and *Z*-3-(4-cyanostyryl)pyridine affords an unprecedented chiral 3D coordination polymer $Zn\{Z$-[4-2-(3-pyridyl)ethenyl]benzoate$\}_2·0.5H_2O$ with two intersecting six-fold helices, which shows a modest SHG activity owing to the essentially non-conjugate nature of the bridging ligand.

Chiral coordination networks are of great interest because of their potential utility in second-order nonlinear optical (NLO) applications,[1] chiral separations, and asymmetric catalysis.[2] Among many chiral structural motifs,[3] helices are of particular interest owing to their structural similarity to nucleic acids.[4] The chirality of such complexes has also shown potential in asymmetric catalysis.[2] We recently demonstrated the construction of acentric and chiral square grids using bifunctional *trans*-pyridylethenylbenzoate linking ligands.[1] In contrast, we believe that steric interactions in *cis*-pyridylethenylbenzoate will cause the pyridyl and phenyl group to significantly deviate from coplanarity. Such 'skewing' of coordination sites in the *cis*-pyridylethenylbenzoate should favor the formation of a helical structure. Herein we wish to report the synthesis and characterization of an unprecedented chiral 3D network resulting from the crosslinking of two distinct helices, $Zn\{Z$-[4-2-(3-pyridyl)ethenyl]benzoate$\}_2·0.5H_2O$, **1**.

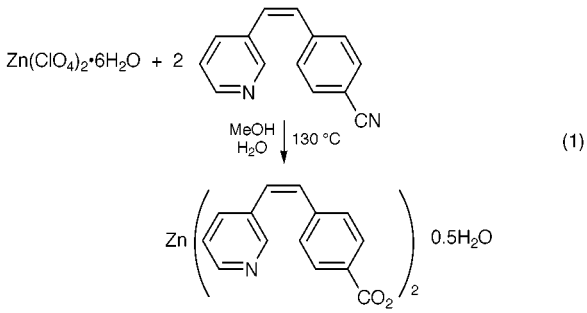

Compound **1** was obtained in 60.5% yield by treating $Zn(ClO_4)_2·6H_2O$ and *Z*-3-(4-cyanostyryl)pyridine under hydro(solvo)thermal conditions [eqn. (1)].[5,6]† The IR spectrum of **1** shows two strong symmetric C=O stretches at 1361 and 1400 cm^{-1}, suggesting both monodentate and bidentate coordination of the carboxylate groups.[7] The formulation of **1** is supported by elemental analysis and thermogravimetric analysis results.[8]

A single crystal X-ray diffraction study of **1**‡ reveals an infinite 3D coordination polymer consisting of two distinct crosslinked helices. Compound **1** crystallizes in the chiral space group $P3_2$. The basic building block of **1** contains two crystallographically nonequivalent Zn atoms, four *Z*-[4-2-(3-pyridyl)ethenyl]benzoate (*Z*-L) ligands, and one solvated water molecule (Fig. 1).[9] The four *Z*-L ligands adopt two drastically different confirmations: the *Z*-L^1 and *Z*-L^2 ligands are similar with a dihedral angle of 47.2 and 4.75° between the phenyl and pyridyl rings, while the dihedral angles for the *Z*-L^3 and *Z*-L^4 ligands are 70.3 and 70.1°. The Zn1 center adopts a *cis*-octahedral configuration by coordinating to the carboxylate groups of *Z*-L^3 and *Z*-L^4 in a semichelating fashion and to the pyridyl nitrogen atoms of *Z*-L^1 and *Z*-L^2. In contrast, the Zn2 center adopts a tetrahedral geometry by coordinating to the carboxylate groups of *Z*-L^1 and *Z*-L^2 in a monodentate fashion and to the pyridyl nitrogen atoms of *Z*-L^3 and *Z*-L^4.

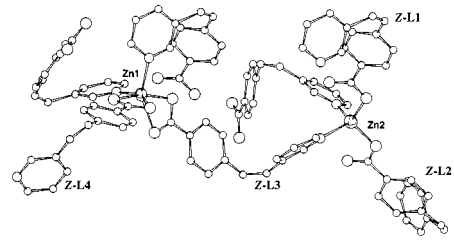

Fig. 1 Coordination geometry in **1** of Zn1 and Zn2 centers. The ellipsoids represent zinc centers, while the circles with increasing sizes represent C, N and O, respectively. Zn1–O distances: 2.084(4), 2.086(5), 2.319(5), and 2.335(5) Å; Zn2–O distances: 1.954(4) and 1.956(4) Å. The Zn–N distances range from 2.03 to 2.08 Å.

The Zn1 and Zn2 centers are bridged by *Z*-L^3 and *Z*-L^4 to form an infinite sixfold helix parallel to the *c* axis (the Zn–Zn separations are 12.15 and 12.16 Å, respectively). The helices directed by the *Z*-L^3 and *Z*-L^4 are of the right-handed screw type and will be referred to as the primary helix (Fig. 2). The primary helix has a helical period of 44.18 Å, and each helical repeat contains three Zn1 and three Zn2 centers.

Conformationally similar *Z*-L^1 and *Z*-L^2 ligands serve to link Zn1 centers of a primary helix to Zn2 centers of adjacent primary helices. Each primary helix is covalently linked to six

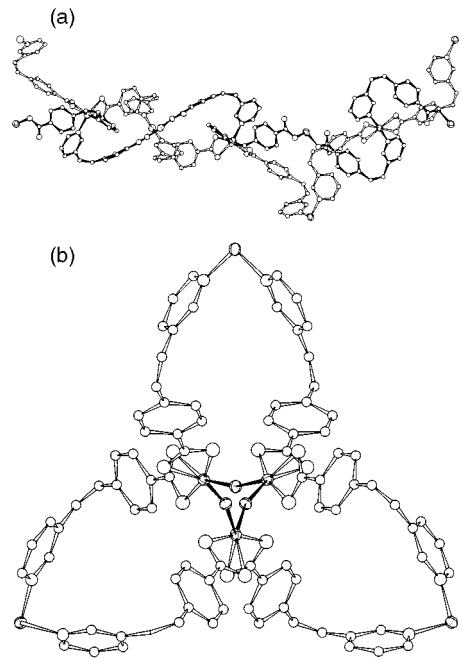

Fig. 2 A view of the cross-link between a primary helix and a secondary helix in **1** as shown down (a) the (111) face and (b) the *c* axis. The open bonds represent the primary helix,while the filled bonds represent the secondary helix. For clarity, the *Z*-L^1 and *Z*-L^2 ligands have been omitted in (b).

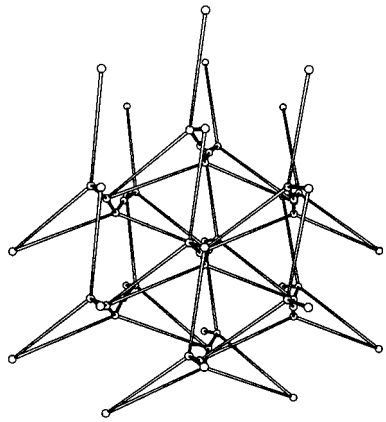

Fig. 3 A perspective view of **1** slightly away from the *c* axis showing the 3D network resulting from the crosslinking of primary helices with secondary helices. Only Zn atoms are shown. The primary helices are represented as open bonds, while the secondary helices are represented as filled bonds.

neighboring primary helices. The Zn–Zn separations (7.47 and 7.49 Å) along the *Z*-L[1] and *Z*-L[2] bridges are significantly shorter than those along the *Z*-L[3] and *Z*-L[4] bridges. More interestingly, the connectivity propagated by *Z*-L[1] and *Z*-L[2] results in the formation of a secondary sixfold helix parallel to the *c* axis [Fig. 2(b)]. The secondary helix is of the left-handed screw type and crosslinks the primary helices to afford an infinite 3D network (Fig. 3).

Many discrete helical structures[10] and infinite helical coordination polymers[11] have been synthesized over the past decade. In some of these helical structures, neighboring helices are connected to each other *via* crosslinking to form 3D networks.[12] However, the structure of **1** is unprecedented in that the 'crosslinks' (the secondary helices) in **1** also display a helical-type structure. Both Zn1 and Zn2 centers in **1** are rendered chiral *via* coordination to the carboxylate and pyridyl functionalities of the bridging ligands. Linking of chiral repeats units into a non-interpenetrated network has thus ensured the bulk chirality of **1**. Preliminary Kurtz powder second harmonic generation (SHG) measurements[13] indicated that **1** exhibits an expected modest powder SHG efficiency ($I^{2\omega}$ = 6 *vs.* α-quartz) because of the non-conjugate nature of the *Z*-L ligand. Future work is directed toward the synthesis of efficient NLO materials *via* the incorporation of highly conjugated linking ligands.

We acknowledge NSF (CHE-9727900 and CHE-9875544) and ACS–PRF for financial support. We also thank Dr Scott R. Wilson and the Materials Chemistry Laboratory at University of Illinois at Urbana-Champaign for X-ray data collections.

Notes and references

† *Preparation of* $Zn(C_{14}H_{10}NO_2)_2{\cdot}0.5H_2O$: a heavy walled Pyrex tube containing a mixture of $Zn(ClO_4)_2{\cdot}6H_2O$ (0.045 g, 0.125 mmol) and *Z*-3-(4-cyanostyryl)pyridine (0.052 g, 0.5 mmol) in methanol (0.2 mL) and water (0.05 mL) was frozen and sealed under vacuum, and placed inside an oven at 120 °C. Colorless hexagonal crystals were obtained after 72 h of heating. Yield (0.040 g, 60.5%). Anal. calc. (found) for $C_{28}H_{21}N_2O_{4.5}Zn$: C, 64.3 (64.1); H, 4.05 (4.04); N, 5.36 (5.59%).

‡ *Crystal data* for **1**: trigonal, space group $P3_2$, a = 9.865(1), c = 44.179(2) Å, U = 3723.2(3) Å^3, Z = 6, D_c = 1.40 g cm^{-3}, T = 173 K, Mo-Kα radiation (λ = 0.71073 Å), μ = 10.3 cm^{-1}. Least-squares refinement based on 4589 reflections with $I > 2\sigma(I)$ and 643 parameters led to convergence, with a final value of $R1$ = 0.045, $wR2$ = 0.098, and goodness of fit = 0.82. Flack parameter = −0.033(14). CCDC 182/1378.

1 (*a*) W. Lin, O. R. Evans, R.-G. Xiong, Z. Wang and G. K. Wong, *Angew. Chem., Int. Ed.*, 1999, **38**, 536; (*b*) W. Lin, O. R. Evans, R.-G. Xiong and Z. Wang, *J. Am. Chem. Soc.*, 1998, **120**, 13 272; (*c*) C. Janiak, T. G. Scharmann, P. Albrecht, F. Marlow and R. Macdonald, *J. Am. Chem. Soc.*, 1996, **118**, 6307; (*d*) H. Zhang, X. Wang and B. K. Teo, *J. Am. Chem. Soc.*, 1996, **118**, 11 813.

2 D. A. Evans, K. A. Woerpel and M. J. Scott, *Angew. Chem., Int. Ed. Engl.*, 1992, **31**, 430; H. Yamamoto, N. Murase and K. Maruoka, *J. Org. Chem.*, 1993, **58**, 2938.

3 M. J. Zaworotko, *Chem. Soc. Rev.*, 1994, 283; C. Janiak, *Angew. Chem., Int. Ed. Engl.*, 1997, **36**, 1431; O. M. Yaghi, H. Li, C. Davis, D. Richardson and T. L. Groy, *Acc. Chem. Res.*, 1998, **31**, 474; S. R. Batten and R. Robson, *Angew. Chem., Int. Ed.*, 1998, **37**, 1461.

4 H. Lodich, D. Baltimore, A. Berk, S. L. Zipursky, P. Matsudaira and J. Darnell, *Molecular Cell Biology*, Scientific American Books, New York, 5th edn., 1995.

5 *Z*-3-(4-cyanostyryl)pyridine was prepared in 27% yield by a room-temperature Wittig reaction between (4-cyanobenzyl)triphenylphosphonium bromide and 3-pyridinecarboxaldehyde with NaOH as the base in dichloromethane. The product was purified by silica gel column chromatography [hexane–ethyl acetate (1 : 1)].

6 The slow hydrolysis of a cyanopyridine precursor to the desired pyridinecarboxylate ligand has been shown to be the key for the construction of polymeric coordination networks.[1b] Also see: O. R. Evans, Z. Wang, R.-G. Xiong, B. M. Foxman and W. Lin, *Inorg. Chem.*, 1999, **38**, 2969.

7 R. C. Mehrotra and R. Bohra, *Metal Carboxylates*, Academic Press, New York, 1983.

8 Thermogravimetric analyses indicated a 1.7% weight loss in the range 130–240 °C for **1** (1.7% expected for the loss of one half of water molecule per formula unit).

9 The solvated water molecule (O9) is *ca.* 3.5 Å away from both O1 and O3.

10 J.-M. Lehn, A. Rigault, J. Siegel, J. Harrowfield, B. Chevrier and D. Moras, *Proc. Natl. Acad. Sci. USA*, 1987, **84**, 2565; J.-M. Lehn and A. Rigault, *Angew Chem., Int. Ed. Engl.*, 1988, **27**, 1095; U. Koert, M. M. Harding and J.-M. Lehn, *Nature* (*London*), 1990, **346**, 339.

11 M. W. Hosseini, C. Kaes, C. E. F. Rickard, B. W. Skelton and A. H. White, *Angew. Chem., Int. Ed.*, 1998, **37**, 920; M. J. Zaworotko, C. Seward and K. Biradha, *Angew. Chem., Int. Ed.*, 1999, **38**, 492; G. Ciani, L. Carlucci, D. W. Gudenberg and D. M. Proserpio, *Inorg. Chem.*, 1997, **36**, 3812; L. Carlucci, G. Ciani, D. M. Proserpio and A. Sironi, *Inorg. Chem.*, 1998, **37**, 5941; R. W. Saalfrank, M. Decker, F. Hampel, K. Peters and H. G. Schnering, *Chem. Ber.*, 1997, **130**, 1309; X.-T. Wu, B. Wu, W.-J. Zhang, S.-Y. Yu and X.-T. Wu, *J. Chem. Soc., Dalton Trans.*, 1997, 1795.

12 R. C. Haushalter, J. Zubieta, V. Soghomonian, Q. Chen and C. J. O'Connor, *Science*, 1993, **259**, 1596; R. Robson, B. F. Hoskins and S. R. Batten, *Angew. Chem., Int. Ed. Engl.*, 1997, **36**, 636; M. R. Sundberg, R. Kivekas and J. K. Koskimies, *J. Chem. Soc., Chem. Commun.*, 1991, 526; R. Robson, B. F. Hoskins, H. Hamit, S. R. Batten and B. F. Abrahams, *Chem. Commun.*, 1996, 1313; M. Munakata, L. P. Wu, T. Kuroda-Sowa, M. Maekawa, K. Moriwaki and S. Kitagawa, *Inorg. Chem.*, 1997, **36**, 5416.

13 S. K. Kurtz, *J. Appl. Phys.*, 1968, **39**, 3798.

Communication 9/05009D

Macropolyhedral boron-containing cluster chemistry. The $[SB_{17}H_{19}]^-$ anion: a *nido*-ten-vertex : *arachno*-ten-vertex cluster architecture and the first single-sulfur macropolyhedral thiaborane

Tomáš Jelínek,[ab] Colin A. Kilner,[b] Simon A. Barrett,[b] Mark Thornton-Pett[b] and John D. Kennedy*[b]

[a] *The Institute of Inorganic Chemistry of the Academy of Sciences of the Czech Republic, 25068 Řež-by-Prague, The Czech Republic*

[b] *The School of Chemistry of the University of Leeds, Leeds, UK LS2 9JT. E-mail: J.Kennedy@chemistry.leeds.ac.uk*

Received (in Cambridge, UK) 7th July 1999, Accepted 9th August 1999

Reaction of *syn*-$B_{18}H_{22}$ with metabisulfite gives a good yield of the first single-sulfur macropolyhedral thiaborane, the $[SB_{17}H_{19}]^-$ anion, which exhibits the unusual *arachno–nido* two-borons-in-common cluster fusion mode.

In the development of boron-containing cluster chemistry, the inhibiting cluster-size limit of about twelve to fourteen vertices that is a characteristic of single-cluster chemistry can be exceeded by the intimate fusion of smaller clusters to generate fused-cluster 'macropolyhedral' species. Of the known macropolyhedral species, the thiaboranes constitute very malleable molecular matrices with which to examine and extend the variety of structure available in this macropolyhedral boron-containing cluster chemistry.[1,2] However, all previously reported species have been dithiaboranes, and macropolyhedral monothiaboranes have, surprisingly, previously been lacking. Here we now report the first macropolyhedral monothiaborane, the $[SB_{17}H_{20}]^-$ anion, of *nido*-decaborano-(8′,7′:5,10)-*arachno*-6-thiadecaboranate constitution, obtained in good yield from the reaction of *anti*-$B_{18}H_{22}$ with potassium metabisulfite, $K_2S_2O_5$. Although metabisulfite and sulfite reactions have previously been used for sulfur-atom incorporation into single-cluster heteroboranes,[3] they have not previously been applied to binary boranes or to macropolyhedral species.

Four portions of $K_2S_2O_5$ (4 × 0.5 g, total 2.0 g) were added at 6 h intervals to a stirred solution of *anti*-$B_{18}H_{22}$ (0.2 g, 910 μmol) in a mixture of thf (40 cm^3) and dilute HCl (*ca*. 4 M, 30 cm^3). Stirring was continued for 2 days at ambient temperature, the mixture was filtered from the solid residue, and a solution of $[PPh_4]Cl$ (0.4 g, 1.07 mmol) in H_2O (20 cm^3) added to the filtrate. After evaporation *in vacuo*, the solid residue was extracted with CH_2Cl_2 (2 × 20 cm^3), the extract dried, filtered, and then subjected to column chromatography (silica gel, 2 cm × 20 cm) using CH_2Cl_2 as eluent. The fraction with R_F 0.22 [analytical TLC, silica G on aluminium (silufol, Kavalier, Prague), 100% CH_2Cl_2] was collected, filtered, evaporated and recrystallised from chloroform–hexane to give $[PPh_4][SB_{17}H_{20}]$ (380 mg, 656 μmol, 72%). No other chromatographically mobile products were found in significant amounts. The preparation is reproducible at the 70% level.

This product was characterised by an all-atom single-crystal X-ray diffraction analysis (Fig. 1)† allied with corroborative NMR spectroscopy.‡ The cluster architecture of the $[SB_{17}H_{20}]^-$ anion is seen to derive formally from the fusion of the structure of an [*arachno*-6-$SB_9H_{12}]^-$ anion [4] with a *nido*-$B_{10}H_{14}$ structure, with two boron atoms held in common [schematic connectivity structures **I** and **II**, unlettered vertices are BH(*exo*) units]. In accord with this, the NMR data for the two subclusters trace to the respective shielding patterns of the [*arachno*-6-$SB_9H_{12}]^-$ anion[5] and *nido*-$B_{10}H_{14}$, which have mutually distinct shielding patterns, there being a typical inversion of shielding sequence when otherwise equivalent positions in *nido* and *arachno* ten-vertex clusters are compared.[5] There are only three significant deviations from these shielding parallels: (a) for the *conjuncto* B(10) position the shielding, at $\delta(^{11}B)$ −3.0 differs substantially from either single cluster model, but is nevertheless between the positions observed for the two models (δ +10.2 and −33.8), which is expected; (b) the *nido*-decaboranyl B(8′) and B(10′) resonances at $\delta(^{11}B)$ +12.5 and −8.6, respectively, differentiate considerably from the value of +0.5 for *nido*-$B_{10}H_{14}$ itself; (c) the *nido*-decaboranyl B(5′) position adjacent to the B(10) fusion site is much more highly shielded at δ −27.8 than the equivalent position in *nido*-$B_{10}H_{14}$ itself at δ +0.5. For (b) and (c) it is probably significant here that the *nido*-decaboranyl long 'gunwale' distance, B(5)–B(8′), at 2.032(5) Å, is much longer than the other gunwale distance B(10′)–B(5′) of 1.914(7) Å at the opposite side of this sub-cluster, demonstrating markedly differential bonding induced by the constraints of the fusion to the other, *arachno*, subcluster. In *nido*-$B_{10}H_{14}$ itself this distance is 1.973(5) Å (by neutron diffraction).[6] Mechanist-

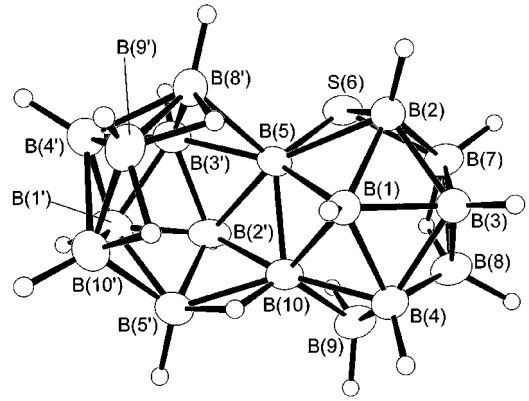

Fig. 1 Crystallographically determined molecular structure of the $[SB_{17}H_{20}]^-$ anion in $[PPh_4][SB_{17}H_{20}]$. Selected interatomic distances (in Å) are as follows: from S(6) to B(2) 1.953(3), B(5) 1.937(4) and B(7) 1.948(4), B(7)–B(8) 1.852(3), B(8)–B(9) 1.882(6), B(9)–B(10) 1.922(6), B(5)–B(10) 1.839(4), B(5)–B(8′) 2.032(5), B(8′)–B(9′) 1.778(5), B(9′)–B(10′) 1.830(7), B(10′)–B(5′) 1.914(7) and B(5′)–B(10) 1.843(5). These dimensions are for one of two independent $[SB_{17}H_{20}]^-$ anions in the unit cell; the dimensions for the other anion are within experimental deviation of these.

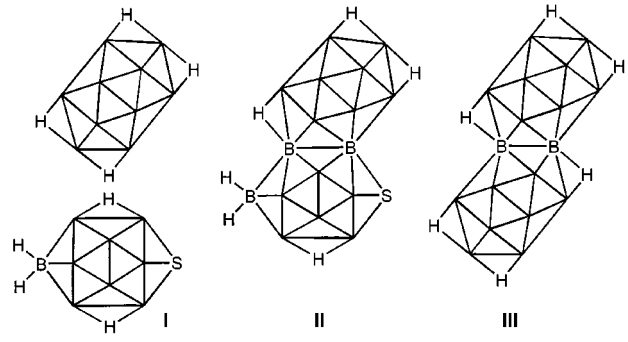

ically the conversion of *anti*-$B_{18}H_{22}$ (schematic **III**) to the $[SB_{17}H_{20}]^-$ anion (schematic **II**) has involved a net reductive replacement of $\{BH + H\}^-$ by $\{S\}^{2-}$, associated with a skeletal rearrangement. With no labelling we cannot speculate as to which of the original boron atoms of the *anti*-$B_{18}H_{22}$ skeleton is lost. In view of the great variety already exhibited by thiaborane macropolyhedral chemistry when sulfur atoms are incorporated in the cluster assemblies,[1,2] and in view of this high yield route from *anti*-$B_{18}H_{22}$, for which a variety of routes have long been known,[7] and which is also currently available commercially, the synthesis of this new $[SB_{17}H_{20}]^-$ species will constitute a very useful starting point for continued explorative investigation in macropolyhedral boron-containing cluster chemistry.

Contribution no. 76 from the Řež-Leeds Anglo–Czech Polyhedral Collaboration (ACPC). We thank the Grant Agency of the Academy of Sciences of the Czech Republic (grant no. A403 2701), the UK EPSRC (grant nos. J/56929, K/05818, L/49505 and M/83360) and the Royal Society (London) for support, and the Royal Society of Chemistry for a Journals Grant for International Authors.

Notes and references

† *X-Ray data*: crystallisation was from dichloromethane–hexane. *Crystal data* for $[PPh_4][SB_{17}H_{20}]$; $C_{24}H_{40}B_{17}PS$: M = 575.36, monoclinic, space group $P2_1/a$, a = 13.7139(2), b = 21.8452(4), c = 22.0843(4) (7) Å, β = 98.3210(11)°, U = 6546.43(19) Å^3, Z = 8, Mo-Kα radiation, λ = 0.71073 Å, μ = 0.166 mm^{-1}, T = 100(2) K, $R1$ = 0.0594 for 9943 observed reflections with $I > 2.0\sigma(I)$ and $wR2$ = 0.1557 for all 12855 unique reflections. Methods and programs were standard;[8] CCDC 182/1367. See http://www.rsc.org/suppdata/cc/1999/1905/ for crystallographic files in .cif format.

‡ *NMR data*: $CDCl_3$ solution of $[PPh_4][SB_{17}H_{20}]$ at 294–300 K, ordered as assignment $\delta(^{11}B)$ [$\delta(^1H)$] $^1J(^{11}B–^1H)$/Hz: BH(1) −38.1 [−0.94] 144; BH(2) *ca.* −10.2 [+3.36] *J* obscured; BH(3) −32.8 [+1.22] 145; BH(4) +0.6 [+2.95] 142; B(5){≡B(7′)} *ca.* −10.2 [*conjuncto* position, no bound H]; BH(7) −11.1 [+2.40] *ca.* 148; BH(8) −42.7 [−0.10] 146 (*exo*) and 37 (bridge); BH(9) *ca.* −8.6 [+2.06 (*exo*) and +1.02 (*endo*)] *J* obscured; B(10) {≡(B(6′)} −3.0 [*conjuncto* position, no bound H]; BH(1′) +10.0 [+3.58] 143; BH(2′) −24.5 [+1.71] 159; BH(3′) −9.3 [+2.07] *J* obscured; BH(4′) −41.6 [−0.03] 152; BH(5′) −27.8 [+1.71] 150 (*exo*) and 29 (bridge); BH(8′) +12.5 [+3.75] 151; BH(9′) −1.3 [+3.06] 165 and BH(10′) *ca.* −8.6 [+1.89] *J* obscured; additional $\delta(^1H)$ values for H(7,8) *ca.* −2.02, H(5′,10) *ca.* −2.02, H(8′,9′) −0.73 and H(9′,10′) −3.36, and for $[PPh_4]^+$ at *ca.* +7.5 to +7.8 (20H, complex multiplet); assignments by [$^{11}B–^{11}B$], [$^1H–^1H$] and $^1H–\{^{11}B\}$ correlation experiments.

1 T. Jelínek, J. D. Kennedy and B. Stíbr, *J. Chem. Soc., Chem. Commun.*, 1994, 1415; T. Jelínek, J. D. Kennedy, B. Stíbr and M. Thornton-Pett, *Angew. Chem., Int. Ed. Engl.*, 1994, **33**, 1599; P. Kaur, J. Holub, N. P. Rath, J. Bould, L. Barton, B. Stíbr and J. D. Kennedy, *Chem. Commun.*, 1996, 273; T. Jelínek, B. Stíbr, J. D. Kennedy and M. Thornton-Pett, in *Advances in Boron Chemistry*, ed. W. Siebert, Royal Society of Chemistry, Cambridge, 1997, pp. 426–429; T. Jelínek, J. D. Kennedy, B. Stíbr and M. Thornton-Pett. *Inorg. Chem. Commun.*, 1998, **1**, 179; T. Jelínek, I. Cisarová, B. Stíbr, J. D. Kennedy and M. Thornton-Pett, *J. Chem. Soc., Dalton Trans*., 1998, 2965.

2 P. Kaur, J. D. Kennedy, M. Thornton-Pett, T. Jelínek and B. Stíbr, *J. Chem. Soc., Dalton Trans.*, 1996, 1775; P. Kaur, M. Thornton-Pett, W. Clegg and J. D. Kennedy, *J. Chem. Soc., Dalton Trans.*, 1996, 4155; P. Kaur, A. Brownless, S. D. Perera, P. A. Cooke, T. Jelínek, J. D. Kennedy, M. Thornton-Pett and B. Stíbr, *J. Organomet. Chem.*, 1998, **557**, 181.

3 J. Plesek, S. Heřmánek and Z. Janousek, *Collect. Czech. Chem. Commun*., 1977, **42**, 785; V. A. Brattsev, S. P. Knyazev, G. N. Danilova and V. I. Stanko, *Zh. Obsch. Khim.*, 1975, **45**, 1393; K. Base, S. Heřmánek and F. Hanousek. *J. Chem. Soc., Chem. Commun.*, 1984, 299.

4 K. Nestor, X. L. R. Fontaine, N. N. Greenwood, J. D. Kennedy and M. Thornton-Pett, *J. Chem. Soc., Dalton Trans.*, 1991, 2657.

5 M. Bown, X. L. R. Fontaine, and J. D. Kennedy, *J. Chem. Soc., Dalton Trans.*, 1988, 1467.

6 A. Tippe and W. C. Hamilton, *Inorg. Chem.*, 1969, **8**, 464.

7 A. R. Pitochelli and M. F. Hawthorne, *J. Am. Chem. Soc.*, 1962, **84**, 3218; J. Dobson, P. C. Keller and R. Schaeffer, *Inorg. Chem.*, 1968, **7**, 399; D. F. Gaines, C. K. Nelson and G. A. Steehler, *J. Am. Chem. Soc.*, 1984, **196**, 7266; G. B. Jacobsen, D. G. Meina, J. H. Morris, C. Thompson, S. J. Andrews, D. Reed, A. J. Welch and D. F. Gaines, *J. Chem. Soc., Dalton Trans.*, 1985, 1645.

8 COLLECT, Data Collection Strategy Program, Nonius, 1999; DENZO-SMN, Z. Otwinowski and W. Minor, Processing of X-ray Diffraction Data Collected in Oscillation Mode, *Methods Enzymol.*, 1997, **276**, 307.

Communication 9/05473A

Modified mesoporous silicate MCM-41 materials: immobilised perruthenate—a new highly active heterogeneous oxidation catalyst for clean organic synthesis using molecular oxygen

Andrew Bleloch,[a] Brian F. G. Johnson,[b] Steven V. Ley,[b] Adam J. Price,[b] Douglas S. Shephard[b] and Andrew W. Thomas[b]

[a] *Cavendish Laboratory, Madingley Road, Cambridge, UK CB3 OHE*
[b] *Department of Chemistry, University of Cambridge, Lensfield Road, Cambridge, UK CB2 1EW. E-mail: svl1000@cam.ac.uk*

Received (in Liverpool, UK) 4th August 1999, Accepted 13th August 1999

A new oxidation catalyst containing perruthenate immobilised within MCM-41 has been prepared and used in the clean oxidation of alcohols to carbonyl compounds with molecular oxygen.

Previously, we[1] and others[2] demonstrated that tetrapropylammonium perruthenate (TPAP)[3] may serve as a convenient catalyst for the oxidation of alcohols to carbonyl derivatives by molecular oxygen. Furthermore, we discovered that when bound to a polystyrene bead the same catalytic species (RuO_4^-–polymer supported perruthenate) provided a cleaner synthetic alternative.[4] However, because of difficulties in the recycling of the PSP reagent (that may be attributed to oxidative degradation of the polystyrene support), we decided to investigate other materials as suitable supports. Here we report that on tethering this same perruthenate catalytic species within the mesoporous solid MCM-41, a remarkably clean and more efficient catalyst is produced.[5]

The mesoporous solid MCM-41 has both internal and external surfaces supporting silanol groups (SiOH) which may be suitably derivatised to immobilise a known catalytically active species (Fig. 1).[6] Treatment of this material with the appropriate amount of Ph_2SiCl_2 (using a proven methodology) effectively caps the external surface inhibiting any further reaction and yielding material **1**.[7] Further treatment of **1** with [3-(trimethoxysilyl)propylamine] yields a material with the internal $Si(CH_2)_3NH_2$ tether. After treatment with HBF_4 to give the tethered primary ammonium system $Si(CH_2)_3NH_3^+$ **2**, the required perruthenate catalyst **3** may be prepared by ion exchange with potassium perruthenate in aqueous solution.

Material **3** has been found to serve as a highly effective and clean catalyst for the oxidation of primary alcohols to aldehydes with a superior performance over that of the previously reported polymer based system (PSP). The oxidations, using our previously published protocol, produced the corresponding aldehydes in less than 3 h using 10 wt% of solid catalyst;[8] significantly, the aldehydes were free of contaminants.

Material **1** was also treated with 3-bromopropyltrichlorosilane to yield material **4** containing a propyl tether with a bromohead group. Substitution with either Me_3N or Et_3N to form the corresponding quaternary ammonium species, followed by ion exchange with potassium perruthenate, afforded the catalytic species **5** and **6** respectively. The black solid **5** was found to be an equally efficient catalyst for the oxidation reactions (Scheme 1) and **6** was found to be a more highly active recoverable and reusable catalyst for the preparation of a wide range of aldehydes (see Table 1). Optimum results were obtained when 10 wt% of the solid catalyst **6**[9] in a solution of the alcohol in toluene was employed. Maximum yields were found on heating the mixture at 80 °C for between 30 min and 3 h, in an oxygen atmosphere. The reactions were faster if a suspension of the catalyst in dry toluene was pre-saturated with oxygen. Alternatively, the reactions may be run in MeCN, CH_2Cl_2 or toluene, but in these cases a reaction time of 12 h was required for completion. Addition of up to 50 wt% of the catalyst led to complete formation of the aldehyde without any over-oxidation to the acid. Recovery and re-use of the catalyst has been investigated (3 mg of the catalyst **6**, and 30 mg of the

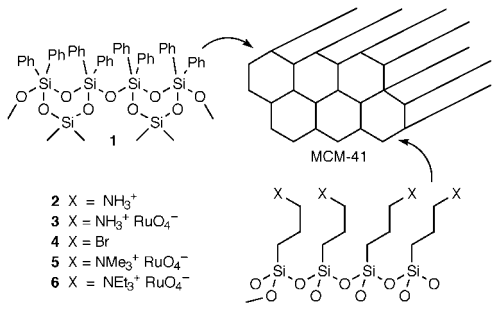

Fig. 1 Catalyst structures.

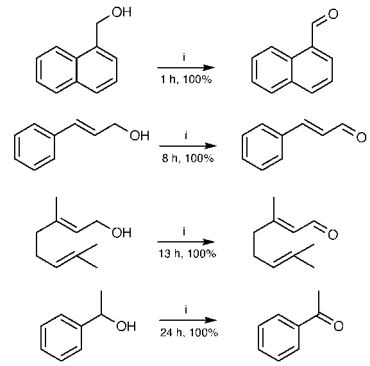

Scheme 1 *Reagents and conditions*: i, O_2, **5** (10 wt%), toluene, 80 °C, for time shown.

Table 1 Oxidation of **7** to **8**, using catalyst **6**

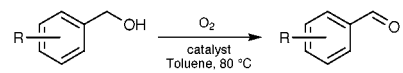

R	Catalyst **6** (wt%)	*t*/h	Yield (%)
H	10	0.5	quant.
4-Cl	10	1.0	quant.
4-OMe	10	2.0	quant.
3-OMe	10	3.0	quant.
2-OMe	10	2.0	quant.
4-NO_2	10	2.0	quant.
2-NO_2	10	3.0	quant.
4-F	10	1.0	quant.
3-CF_3	10	2.0	quant.
4-OBn	10	2.0	quant.

alcohol **7**). In each case, the pure aldehyde product **8** was obtained in quantitative yield, after 1 h, using oxygen in toluene as the oxidant at 80 °C, even after 12 recycle runs.[10] The catalyst **6** was efficiently used for the oxidation of allylic alcohols to the corresponding enals, and acetophenone was obtained from 1-phenylethanol. However, neither cyclohexanol nor cyclohexenol were converted to the corresponding ketones using this method. Finally, catalyst **6** was used in the preparation of aldehyde **9** from alcohol **10** on a 1 g scale, using only 25 mg of the triethylammonium catalyst **6** following the previously mentioned toluene/oxygen protocol (Scheme 2). A quantitative yield of the pure aldehyde **9** was obtained. This aldehyde was used in a ten-step linear synthesis of the potent analgesic natural product epibatidine, which employed only solid supported reagents.[11]

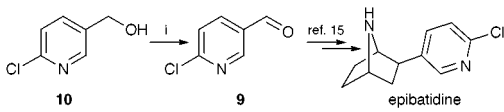

10 **9** epibatidine

Scheme 2 *Reagents and conditions*: i, O_2, **6** (2.5 wt%), toluene, 80 °C, 12 h.

Instead of oxygen, NMO or trimethylamine *N*-oxide (TMAO) may be used as oxidant, and although this protocol was efficient in generating the desired aldehydes in high yield, a noticeable contamination by both ruthenium and an organic impurity was found. These were probably unreduced, involatile NMO or TMAO, and a product formed by β-elimination (Hofmann elimination) of the ammonium species. Only in this experiment was the catalyst found not to be reusable.

Leaching was shown not to take place with **6** under the conditions employed. Thus, oxidation was allowed to proceed to 50% completion, and the solid catalyst was removed by filtration and stored under argon; the filtrate was then heated at 80 °C under an oxygen atmosphere and no further oxidation was observed by HPLC after 12 h. The catalyst was then re-added to the reaction mixture, the reaction was re-established and complete oxidation was observed in less than 1 h under the usual conditions.

In separate experiments designed to help elucidate the catalytically active species we have established that: (i) MCM-41 alone shows no activity; (ii) diphenylsilyl capped MCM-41 treated with potassium perruthenate (lacking the supporting tether) shows little activity and complete leaching; (iii) uncapped MCM-41 treated with potassium perruthenate (lacking the supporting tether) shows little activity and complete leaching; (iv) colloidal RuO_2 absorbed within the MCM-41 mesopores[12] shows no activity. These experiments demonstrate that a perruthenate derived species is responsible for the catalysis and not RuO_2.[13] Scanning transmission electron microscopy (STEM) revealed that coverage of the MCM-41 internal surface was uniform (also the external surface of Carbosil *vide infra*). There was no evidence for the formation of colloidal RuO_2.[14] It is worth noting that X-ray diffraction studies of the catalysts **5** and **6** indicate that long range order in the MCM-41 structure is reduced, whilst STEM showed that there are residual 'domains' of parallel mesopores. An alternative synthetic route was used to reproduce **6** without the loss of long range order by eliminating the water solvated ion exchange. However no superior performance was observed under the same reaction conditions. X-Ray diffraction also revealed that no large inorganic crystallites were formed in the catalyst preparation. We have also demonstrated that an aerogel silica tethered triethylammonium perruthenate species (preparation akin to **6**) is a good oxidation catalyst although significantly longer reaction times are needed (5 h on a 0.1 mmol scale).

In summary, we have developed a new, highly active, recoverable and re-usable heterogeneous catalytic oxidant **6** for the oxidation of alcohols to carbonyl derivatives by molecular oxygen. It may be prepared from the siliceous MCM-41 material following a reliable tethering method and ion exchange with potassium perruthenate. The immobilisation of other reagents using the improved MCM-41 support should allow us to incorporate these new solid supported reagents in our future clean chemistry programmes.[15]

Notes and references

1 R. Lenz and S. V. Ley, *J. Chem. Soc., Perkin Trans. 1*, 1997, 3291.

2 I. E. Mark, P. R. Giles, M. Isukazaki, C. J. Urch and S. M. Brown, *J. Am. Chem. Soc.*, 1997, **119**, 12 661.

3 S. V. Ley, J. Norman, W. P. Griffith and S. P. Marsden, *Synthesis*, 1994, 640.

4 B. Hinzen and S. V. Ley, *J. Chem. Soc., Perkin Trans. 1*, 1997, 1907; B. Hinzen, R. Lenz and S. V. Ley, *Synthesis*, 1998, 977.

5 Several reviews considering various aspects of MCM-41 and other mesoporous materials have appeared: J. Y. Ying, C. P. Mehnert and M. S. Wong, *Angew. Chem., Int Ed.*., 1999, **38**, 56; S. Biz and M. L. Occelli, *Catal. Rev. Sci. Eng*., 1998, **40**, 329; K. Moller and T. Bein, *Chem. Mater*., 1998, **10**, 2950; A. Corma, *Top. Catal.*, 1997, **4**, 249; G. D. Stucky, Q. Huo, A. Firouzi, B. F. Chmelka, S. Schacht, I. G. Voigt-Martin and F. Schuth, in *Progress in Zeolite and Microporous Materials, Studies in Surface Science and Catalysis*, Vol 105, ed. H. Chon, S.-K. Ihm, Y. S. Uh, Elsevier, Amsterdam, 1997, 3; C. J. Brinker, *Curr. Opin Solid State Mater. Sci*., 1996, **1**, 798; N. K. Raman, M. T. Anderson and C. J. Brinker, *Chem. Mater*., 1996, **8**, 1682; D. M. Antonelli and J. Y. Ying, *Curr. Opin. Colloid Interface Sci.*, 1996, **1**, 523; P. Behrens, *Angew. Chem., Int. Ed. Engl*., 1996, **35**, 515; X. S. Zhao, G. Q. Lu and G. J. Millar, *Ind. Eng. Chem. Res.*, 1996, **35**, 2075; A. Sayari, *Chem. Mater*., 1996, **8**, 1840.

6 For different methods of tethering chiral catalysts, see D. E. De Vos, S. De Wildemann, B. F. Sels, P. J. Grobet and P. A. Jacobs, *Angew. Chem., Int. Ed.*, 1999, **38**, 980; B. F. G. Johnson, S. A. Raynor, D. S. Shephard, T. Maschmeyer, J. M. Thomas, G. Sankar, S. Bromley, R. D. Oldroyd, L. Gladden and M. D. Mantle, *Chem. Commun.*, 1999, 1167.

7 D. S. Shephard, W. Zhou, T. Maschmeyer, J. M. Matters, C. L. Roper, S. Parsons, B. F. G. Johnson and M. J. Duer, *Angew. Chem., Int. Ed.*, 1998, **37**, 2719; T. Maschmeyer, R. D. Oldroyd, G. Sankar, J. M. Thomas, I. J. Shannon, J. A. Klepetko, A. F. Masters, J. K. Beattie and C. R. A. Catlow, *Angew. Chem., Int. Ed. Engl.*, 1997, **36**, 1639; J. Liu, X. Feng, G. E. Fryxell, L.-Q. Wang, A. Y. Kim and M. Gong, *Adv. Mater*., 1998, **10**, 161.

8 10 wt% of the solid catalyst **3** corresponds to 0.3 wt% Ru by ICP analysis.

9 10 wt% of the solid catalyst **6** corresponds to 1.1 wt% Ru by ICP analysis.

10 *General procedure* for the oxidation of alcohols: To a solution of the alcohol (30.0 mg) in dry toluene (5 cm^3) was added MCMSP **6** (3.0 mg) and the resulting mixture heated at 80 °C, for 30 min to 3 h in an oxygen atmosphere. After cooling, filtration of the mixture followed by evaporation of the solution afforded the pure aldehyde in quantitative yield (Table 1). The solid catalytic oxidant reagent can be re-used many times (up to 12 times without loss of activity). It can be easily filtered through a polypropylene filter or through a bond elut cartridge and then washed off the surface with toluene. In addition, recovery by centrifugation was also found to be quantitative.

11 J. Habermann, S. V. Ley and J. S. Scott, *J. Chem. Soc., Perkin Trans. 1*, 1999, 1253.

12 D. S. Shephard, G. Sankar, J. M. Thomas, D. Ozkaya, B. F. G. Johnson, R. Raja, R. D. Oldroyd and R. G. Bell, *Chem. Eur. J*., 1998, **4**, 1214.

13 In experiments (i) and (iv), no oxidation was observed after 50 h, in toluene/oxygen at 80 °C, implying that a perruthenate derived species was responsible for the catalysis and not RuO_2. In experiments (i) and (iii), approximately 10 and 70% oxidation, respectively, to the aldehyde was observed after 3 days under the same conditions and complete leaching of potassium perruthenate was observed in both cases. The used solid material from experiments (ii) and (iii) showed no catalytic oxidative activity when reused.

14 D. G. Lee, Z. Wang and W. D. Chandler, *J. Org. Chem.*, 1992, **57**, 3276.

15 B. Hinzen and S. V. Ley, *J. Chem. Soc., Perkin Trans. 1*, 1998, 1; F. Haunert, M. H. Bolli, B. Hinzen and S. V. Ley, *J. Chem. Soc., Perkin Trans. 1*, 1998, 2235; S. V. Ley, M. H. Bolli, B. Hinzen, A.-G. Gervois and B. J. Hall, *J. Chem. Soc., Perkin Trans. 1*, 1998, 2239; M. H. Bolli and S. V. Ley, *J. Chem. Soc., Perkin Trans. 1*, 1998, 2243; J. Habermann, S. V. Ley and J. S. Scott, *J. Chem. Soc., Perkin Trans. 1*, 1998, 3127; M. Caldarelli, J. Habermann and S. V. Ley, *J. Chem. Soc., Perkin Trans. 1*, 1999, 107; S. V. Ley, A. W. Thomas and H. Finch, *J. Chem. Soc., Perkin Trans. 1*, 1999, 669; S. V. Ley, O. Schucht, A. W. Thomas and P. J. Murray, *J. Chem. Soc., Perkin Trans. 1*, 1999, 1251.

Communication 9/06354D

meta- and *para*-Bis[zirconyl(IV)amino]cyclophanes; 1,3- or 1,4-$C_6H_4[\bar{N}(SiMe_3)]_2$ as bridging ligands†

Stephane Daniele, Peter B. Hitchcock and Michael F. Lappert*

The Chemistry Laboratory, University of Sussex, Brighton, UK BN1 9QJ. E-mail: m.f.lappert@sussex.ac.uk

Received (in Basel, Switzerland) 17th May 1999, Accepted 17th July 1999

The structurally characterised *meta*- and *para*-dimetallacyclophanes $[R\bar{N}(C_6H_4)N(R)Zr(NMe_2)_2N(R)(C_6H_4)\bar{N}(R)Zr(NMe_2)_2]$ (R = $SiMe_3$), obtained from $[\{Zr(NMe_2)_3(\mu\text{-}NMe_2)\}_2]$ and $C_6H_4[N(H)R]_2$-1,3 or -1,4 (2 mol), are catalysts (with methylaluminoxane) for the polymerisation of ethylene.

There has been much recent interest in chelating bis(amido) ligands in the context of zirconium(IV) or titanium(IV) chemistry, in part because of their ability to catalyse the polymerisation of olefins. Examples of such catalysts have been $[Zr(LL)(CH_2Ph)_2]$ with methylaluminoxane (MAO) [LL = 2,2′-{N($C_6H_4Bu^t$-*p*)}$_2$-6,6′-Me_2-(C_6H_3)$_2$],[1] $[Ti(L'L')Me_2]$ with $B(C_6F_5)_3$ [L′L′ = N(R)$(CH_2)_3$NR, R = $C_6H_3Me_2$-2,6];[2] for a review, see ref. 3. The *ortho*-*N*,*N*′-bis(silylated)amidobenzene ligands have also been employed as chelating moieties in group 14 metal and also zirconium(IV) complexes, as exemplified by [(Sn{N($SiMe_3$)}$_2C_6H_4$-1,2)$_2$(μ-tmen)][4] and [Zr({N(SiPr^i_3)}$_2C_6H_4$-1,2)$_2$].[5]

We now draw attention to the role of the isomeric *meta*- and *para*-*N*,*N*′-disilylated bis(amido)benzene ligands in zirconium chemistry. Of particular novelty is the discovery that their bonding mode differs from that of the chelating and terminally bonding *ortho* isomer. The *N*,*N*′-bis(trimethylsilyl)-1,3- or -1,4-diamidobenzene ligands behave in a bridging fashion, giving rise to binuclear derivatives such as **1**–**4**. These are either open chain molecules (**1** or **2**) or are macrocycles (**3** or **4**).

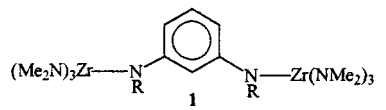

1

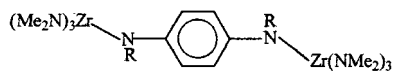

2

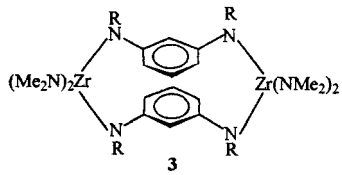

3

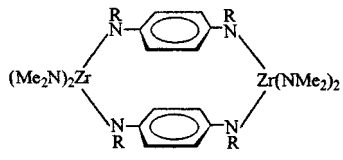

4

An alternative method of generating a binuclear [Cu^{II}] amido-based cyclophane from 1,4-$C_6H_4(NH_2)_2$ has been reported: by cyclocondensation of the latter with ethylenediaminetetraacetic anhydride and successive treatment with Na_2CO_3 and $CuCl_2 \cdot 2H_2O$.[6]

Treatment of $[\{Zr(NMe_2)_3(\mu\text{-}NMe_2)\}_2]$ with 1,3- or 1,4-$C_6H_4[N(H)R]_2$ (R = $SiMe_3$) (2 mol) gave (ii in Scheme 1) yellow crystals of the cyclophane **3** or **4**, respectively, while the intermediates **1** and **2** were isolated (albeit with significant proportions of **3** and **4**) (i in Scheme 1) when equimolar quantities of these reagents were used. The conversion of each acyclic compound **1** or **2** into the macrocycle **3** or **4** was evidently faster than the formation of **1** or **2**, respectively. Complexes **3** or **4** were resistant to further transamination, when an excess of the appropriate diamine was employed.

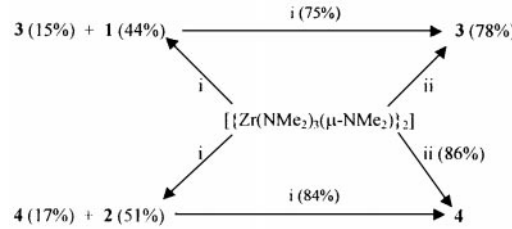

Scheme 1 Synthesis of the crystalline complexes **1**–**4**. *Reagents and conditions*: $C_6H_4[N(H)SiMe_3]_2$-1,3 or -1,4 (i, 1 mol; ii, 2 mol), PhMe, 0 °C, 20 h and then crystallisation from *n*-pentane, 4 °C.

The new, pale yellow (**3** or **4**) or colourless (**1** or **2**), highly air-sensitive, readily aromatic hydrocarbon-soluble, crystalline compounds **1**–**4** gave satisfactory microanalyses (C, H, N), as well as multinuclear NMR spectra.‡ For each complex, the ^{1}H NMR spectra displayed single sets of sharp signals, consistent with the illustrated structures, and for **3** and **4** confirmed (X-ray) for the crystalline complexes.§ A common feature as between **3** and **4** on the one hand and **1** and **2** on the other, was that the aromatic and $SiMe_3$ ^{1}H NMR signals for the former were more shielded while the converse was the case for the NMe_2 signals.

The X-ray molecular structures of complexes **3** and **4** are shown in Figs. 1 (**3**) and 2 (**4**) and selected geometric parameters

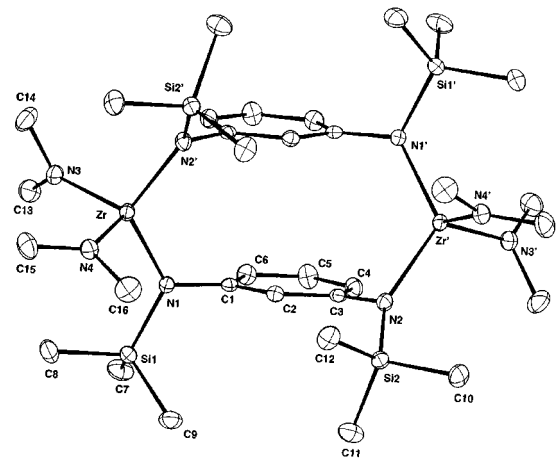

Fig. 1 The molecular structure of **3**.

† No reprints available.

Table 1 Selected geometric parameters for **3** and **4**

Compound	av. Zr–N_{endo}/Å	av. Zr–N_{exo}/Å	*endo*-N–Zr–N′/°	MeN–Zr–N′Me/°	C_{ipso}–N–Zr/°	$\Delta(C_6H_4–C_6H_4)^a$/Å	C_6H_4/C_6H_4 displ.^{b}/Å
3	2.094(2)	2.031(2)	119.32(8)	105.29(10)	122.9(2), 103.7(2)	3.43	0.75
4	2.086(2)	2.026(2)	121.21(8)	102.11(9)	115.31(12), 107.27(12)	3.48	0.15

[a] This refers to the distance between the two C_6 planes. [b] This refers to the lateral displacement of the two C_6 planes.

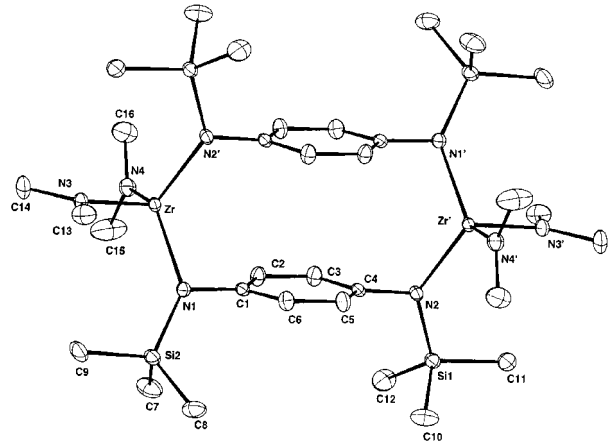

Fig. 2 The molecular structure of **4**.

are compared in Table 1. The aromatic rings are related by a crystallographic twofold axis for **3** and an inversion centre for **4**. They are parallel in both structures, the planes being separated by 3.43 (**3**) or 3.48 (**4**) Å but show a sideways displacement (**3** > **4**). The endocyclic N–Zr–N′ bond angle is somewhat wider in **4** than **3** but the converse is so for the Me_2N–Zr–N′Me_2 angle; while for each, the average endocyclic Zr–N bond length is significantly longer than the exocyclic, but both are unexceptional; for example, the average Zr–N bond lengths are 2.08 Å for [Zr({N(SiPr$^i_3$)}$_2$$C_6H_4$-1,2)$_2$],[5] and 2.06 Å for [Zr{η^5-$C_5H_4C(Me)_2C_9H_6$-η^5}$(NMe_2)_2$].[7] The sum of the angles at each nitrogen atom is close to 360°.

Each of the metallocyclophanes **3** and **4**, in the presence of MAO, was active as a catalyst for the polymerisation of ethylene, and this activity was substantially enhanced if **4** was pretreated with an excess (10 mol) of chlorotrimethylsilane to yield **5**; the polyethylenes had very high average molecular weights.¶ Complex **5** is tentatively formulated as $RN(C_6H_4)N(R)Zr(Cl)_2N(R)(C_6H_4)N(R)ZrCl_2$, an analogue of **4** (having only the terminal amido groups displaced by chloride ligands).

Compounds **1**–**4** are the first binuclear, four-coordinate zirconium(IV) amides and are also unusual in being heteroleptic. The cyclophanes **3** and **4** are of further interest in being macrocycles having both Lewis acid (Zr) and base [N(R) and C_6] sites and having parallel C_6 rings separated by distances close to that (3.35 Å) found in graphite. This ambiphilicity, as well as the catalytic properties of these compounds, are under further investigation as are comparisons of the use of these *meta*- and *para*-*N*,*N*′-bis(trimethylsilyl)bis(amido)benzene ligands in the context of complexes of other metals [for Ge^{II} and Sn^{II}, see refs. 8 and 9].

We thank the EU for the award of a Marie Curie fellowship to S. D. and to Dr M. Kristen and BASF (Ludwigshafen) for other support.

Notes and references

‡ *Selected spectroscopic data*: for **1**: ^{1}H NMR (300.1 MHz, 298 K, $C_6D_5CD_3$) δ 7.04 (t, *J* 7.2 Hz, 1H), 6.58 (d, *J* 7.2 Hz, 2H), 6.25 (s, 1H), 2.84 (s, NMe_2, 36H), 0.23 (s, $SiMe_3$, 18H). ^{13}C{^{1}H} NMR (75.5 MHz, 298 K, $C_6D_5CD_3$) δ 151.3, 132.0, 126.6, 122.9 (C_6H_4), 42.3 (NMe_2), 1.8 ($SiMe_3$). For **2**: ^{1}H NMR (300.1 MHz, 298 K, C_6D_6) δ 6.91 (s, 4H), 2.87 (s, NMe_2, 36H), 0.24 (s, $SiMe_3$, 18H). ^{13}C{^{1}H} NMR (75.5 MHz, 298 K, C_6D_6) δ 142.8, 128.9 (C_6H_4), 41.9 (NMe_2), 1.5 ($SiMe_3$). For **3**: ^{1}H NMR (300.1 MHz, 298 K, $C_6D_5CD_3$) δ 6.68 (t, *J* 7.0 Hz, 1H), 6.28 (d, *J* 7.0 Hz, 2H), 6.08 (s, 1H), 3.05 (s, NMe_2 12H), 0.14 (s, $SiMe_3$, 18H). ^{13}C{^{1}H} NMR (75.5 MHz, 298 K, $C_6D_5CD_3$) δ 150.2, 130.9, 125.6, 121.8 (C_6H_4), 43.4 (NMe_2), 2.3 ($SiMe_3$). For **4**: ^{1}H NMR (300.1 MHz, 298 K, C_6D_6) δ 6.50 (s, 4H), 3.10 (s, NMe_2, 12H), 0.18 (s, $SiMe_3$, 18H). ^{13}C{^{1}H} NMR (75.5 MHz, 298 K, C_6D_6) δ 144.0, 127.9 (C_6H_4), 43.2 (NMe_2), 2.0 ($SiMe_3$).

§ *Crystal data*: for **3**, $C_{32}H_{68}N_8Si_4Zr_2$, M = 859.7, T = 173(2) K, space group *C*2/*c* (no. 15), a = 14.234(2), b = 17.771(4), c = 18.860(4) Å, β = 109.55(2)°, U = 4496(2) Å^3, Z = 4, μ(Mo-Kα) = 0.60 mm^{-1}, specimen 0.40 × 0.30 × 0.30 mm, 4123 reflections collected for 2 < θ < 25°, 3963 independent (R_{int} = 0.0167), R_1 = 0.031 for 3288 reflections with I > 2σ(I), wR_2 = 0.077 for all data. For **4**, $C_{32}H_{68}N_8Si_4Zr_2$, M = 859.7, T = 173(2) K, space group $P\bar{1}$ (no. 2), a = 9.005(4), b = 10.128(8), c = 13.168(9) Å, α = 69.17(6), β = 80.33(4), γ = 78.63(5)°, U = 1094(1) Å^3, Z = 1, μ(Mo-Kα) = 0.62 mm^{-1}, specimen 0.3 × 0.3× 0.3 mm, 6379 reflections collected for 2 < θ < 25°, all independent, R_1 = 0.031 for 5617 reflections with I > 2σ(I), wR_2 = 0.082 for all data. CCDC 182/1351. See http://www.rsc.org/suppdata/cc/1999/1909/ for crystallographic files in .cif format.

¶ *Polymerisation data*: an aliquot (25 cm^3) of a solution (**3** or **4**), or a suspension (**5**) in toluene [6 × 10^{-4} mol l^{-1} catalyst, MAO (3 × 10^{-1} mol) in toluene (1 l)] was pressurised with C_2H_4 (2.4 bar) at 20 °C for 15 min, whereafter the mixture was quenched by addition of methanolic HCl. The polymer was filtered off, washed with successively 1 M aq. HCl, water and MeOH and then dried at 80 °C. The activity corresponded to 0.11 (**3**) [or 0.15 (**4**) or 14.72 (**5**)] × 10^3 g polymer bar^{-1} h^{-1} (mol cat)$^{-1}$. The polymer had high average molecular weight (≈ 2 × 10^6 g mol^{-1}), determined by viscosity determinations; solubility problems excluded the use of traditional GPC experiments.

1 F. G. N. Cloke, T. J. Geldbach, P. B. Hitchcock and J. B. Love, *J. Organomet. Chem.*, 1996, **506**, 343.
2 J. D. Scollard and D. H. McConville, *J. Am. Chem. Soc.*, 1996, **118**, 10 008.
3 G. J. P. Britovsek, V. C. Gibson and D. F. Wass, *Angew. Chem., Int. Ed. Engl.*, 1999, **38**, 428.
4 H. Braunschweig, B. Gehrhus, P. B. Hitchcock and M. F. Lappert, *Z. Anorg. Allg. Chem.*, 1995, **621**, 1922.
5 K. Aoyagi, P. K. Gantzel, K. Kalai and T. D. Tilley, *Organometallics*, 1996, **15**, 923.
6 M. B. Inoue, E. F. Velazquez, F. Medrano, K. L. Ochoa, J. C. Galvez, M. Inoue and Q. Fernando, *Inorg. Chem.*, 1998, **37**, 4070.
7 W. A. Herrmann, M. J. A. Morawietz and T. Priermei, *J. Organomet. Chem.*, 1996, **506**, 351.
8 H. Braunschweig, C. Drost, P. B. Hitchcock, M. F. Lappert and L. J.-M. Pierssens, *Angew. Chem., Int. Ed. Engl.*, 1997, **36**, 261.
9 H. Braunschweig, P. B. Hitchcock, M. F. Lappert and L. J.-M. Pierssens, *Angew. Chem., Int. Ed. Engl.*, 1994, **33**, 1156.

Communication 9/03921J

Hexahomotrioxacalix[3]arene: a scaffold for a C_3-symmetric phosphine ligand that traps a hydrido-rhodium fragment inside a molecular funnel

Cedric B. Dieleman,[a] Dominique Matt,*[a] Ion Neda,[b] Reinhard Schmutzler,[b] Anthony Harriman[c] and Reza Yaftian[d]

[a] *Groupe de Chimie Inorganique Moléculaire, UMR 7513 CNRS, 1 rue Blaise Pascal, F-67008 Strasbourg Cedex, France. E-mail: dmatt@chimie.u-strasbg.fr*
[b] *Institut für Anorganische Chemie und Analytische Chemie der Universität, Postfach 3329, D-38023 Braunschweig, Germany*
[c] *Ecole Européenne de Chimie, Polymères et Matériaux, 1 rue Blaise Pascal, F-67008 Strasbourg Cedex, France*
[d] *Department of Chemistry, University of Zandjan, PO box 313, 45195 Zandjan, Iran*

Received (in Cambridge, UK) 13th July 1999, Accepted 6th August 1999

Stereoselectivity around an H–Rh–CO fragment has been realized by reaction of the hexahomotrioxacalix[3]arene-derived triphosphine 4 with [Rh(acac)(CO)$_2$]; the resultant trigonal bipyramidal complex has the Rh–H bond directed inside the cavity.

Phosphorus-bearing calixarenes have received considerable attention both for their ionophoric receptor properties and their facility for localizing reactive transition metal centres adjacent to the cavity.[1] To date, most studies have been concerned with functionalized calix[4]arenes,[2] while the corresponding hexahomotrioxacalix[3]arenes **1** remain relatively unexplored,

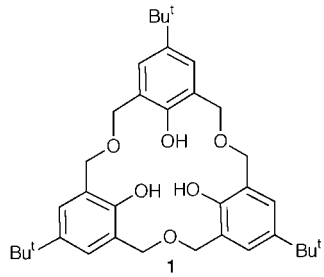

1

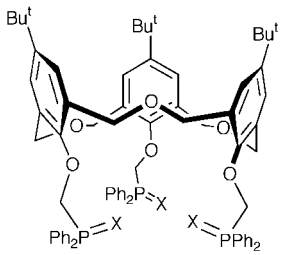

2 X = O
4 X = lone pair

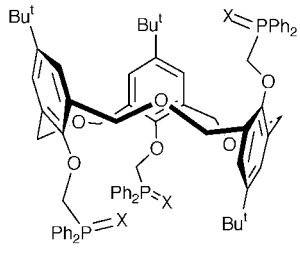

3 X = O
5 X = lone pair

although such receptors have been equipped with P^{III}- or P^{V}-based binding sites.[3,4] The larger macrocyclic unit provided by **1** looks to be particularly appropriate for use as a platform on which to build C_3-symmetrical ligands able to operate as conical receptors.[5–8] We now describe the synthesis and properties of the first triphosphine ligands, and their corresponding oxides, formed by anchoring $CH_2P(O)Ph_2$ groups to the phenolic oxygen atoms of a calix[3] matrix.

Complete phosphorylation was achieved by reacting **1** with NaH and $Ph_2P(O)CH_2OTs$ in toluene at 90 °C for three days. The reaction resulted in formation of a 4:1 mixture of the (non-interconverting) phosphine oxides **2** and **3**.† Separation by column chromatography afforded pure **2** in 72% yield, but the isolated samples of **3** always contained small amounts of **2**. Consistent with a C_3-symmetrical structure, the ^{31}P NMR spectrum of **2** shows a single peak at δ_P 24.9 while the corresponding ^{1}H NMR spectrum displays a unique AB system for the $ArCH_2$ methylene groups. Compound **3** adopts a partial cone conformation as deduced from the presence of two singlets of intensity 2:1 in the ^{31}P NMR spectrum, together with three AB patterns for the $ArCH_2$ groups in the ^{1}H NMR spectrum. The phosphine oxides **2** and **3** could be reduced with $PhSiH_3$ in refluxing toluene, affording the triphosphines **4** and **5**,† respectively, in quantitative yield. The partial cone structure of **5** (Fig. 1) was confirmed by an X-ray diffraction study.‡ It should be emphasised that compounds **2**–**5** are highly soluble in alkanes.

The triphosphorylated calixarene **2** was found to be an active phase-transfer agent for rare-earth picrates (from water to CH_2Cl_2).§ Extraction experiments carried out with seven rare-earth cations (Y, La, Pr, Nd, Sm, Eu and Gd) showed the extraction percentages to be significantly higher than those obtained with conventional phosphine oxides, *e.g.* trioctylphosphine oxide, or the phosphato-calix[4]arenes reported recently by Harrowfield *et al.*[9] Interestingly, the highest selectivity was found for those elements with an ionic radius close to that of praseodymium; similar peak selectivity was observed recently with a *cone*-calix[4]arene substituted by four $CH_2P(O)Ph_2$ phosphine oxide arms tethered at the lower rim.[10] Our findings confirm previous observations showing that phosphorus-based ligands built on calixarenes may display different extraction properties than do their acyclic counterparts.[11]

Ligand **4** looks to be an ideal scaffold for the formation of C_3-symmetrical complexes. Thus, treatment of **4** with [Mo(CO)$_3$-(cycloheptatriene)] in refluxing THF afforded the colourless complex **6**† in high yield (Scheme 1). The carbonyl region of the IR spectrum displays two strong absorption bands showing the presence of an $Mo(CO)_3$ unit with local C_{3v} symmetry.[12] Tridentate *fac*-coordination of the tripod was inferred from the appearance of a singlet at δ_P 25.7 in the ^{31}P NMR spectrum. In **6**, the tripodal arms retain the metal centre beneath the cavity. Likewise, complex **7**,† formed in quantitative yield on reaction of **4** with $[Au(THF)(THT)]PF_6$ (THT = tetrahydrothiophene),

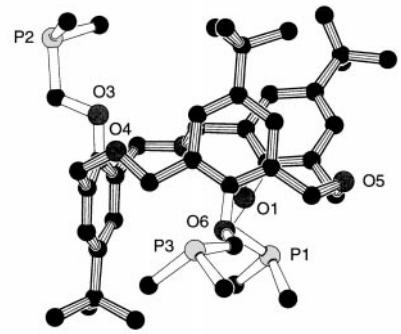

Fig. 1 PLUTON view of triphosphine **5**. For clarity, only the *ipso* carbon atoms of the PPh groups are shown.

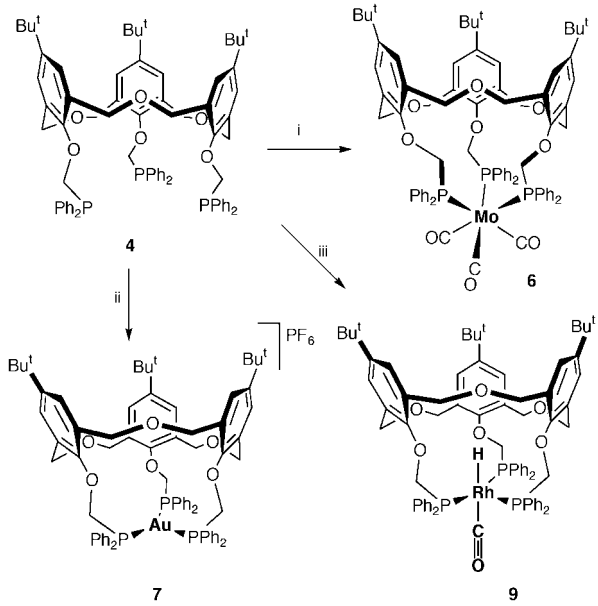

Scheme 1 *Reagents and conditions*: i, [Mo(CO)$_3$(cycloheptatriene)], THF, reflux; ii, [Au(THT)(THF)]PF$_6$, CH_2Cl_2; iii, [Rh(acac)(CO)$_2$], 20 bar H_2/CO, toluene, 70 °C.

positions a metal centre across one entrance of the cone. In this case, the trigonal AuP_3 fragment strapped across the lower rim exaggerates the conical nature of the calix[3] unit. A similar funnel-shaped silver complex **8**† (not drawn) was also obtained quantitatively from reaction with $AgBF_4$. The room temperature NMR data of both these cationic complexes are in full accord with a C_{3v} symmetrical structure. As deduced from a variable temperature NMR study made with **8,** the threefold symmetry of this complex is only virtual and corresponds in fact to an averaged structure. Indeed, the A_3X (X = Ag) pattern observed at 25 °C in the ^{31}P NMR (202.45 MHz) spectrum broadens on decreasing the temperature and eventually changes to an A_2BX system, while maintaining finite AgP coupling constants. The C_s symmetry observed at low temperature probably minimizes the strain within two of the three metallomacrocycles formed by complexation, but the exact structure of the complex is not known. Loss of C_3 symmetry at low temperature has previously been observed in a titanium-capped cone homooxacalix[3]arene, but in this case the structural modification appears to be controlled by a stereodynamic process occurring at the metal centre.[13]

A remarkable feature of triphosphine **4** concerns its ability to trap and orientate a linear H–Rh–CO fragment. Thus, treatment of a toluene solution of **4** and [Rh(acac)(CO)$_2$] with 20 bar of H_2/CO at 70 °C afforded complex **9**† in *quantitative* yield (Scheme 1). The latter species is characterized by a strong carbonyl absorption band at 1977 cm^{-1} while all NMR data are consistent with a threefold symmetry axis. The ^{31}P NMR spectrum, for example, shows a doublet at δ_P 36.4 (J_{RhP} = 153 Hz) due to the phosphorus atoms with the ^{1}H NMR spectrum displaying a quartet at δ_H −9.70 for the hydrido ligand. The small J_{PH} value (14 Hz) is in full agreement with a trigonal bipyramidal geometry. Two-dimensional ROESY (500 MHz) experiments unambiguously revealed that the hydride lies close to the methylenic Ar*CH*$_2$O groups¶ and to the PCH_2 protons. This is a clear indication that the Rh–H bond is directed inside the funnel. This particular orientation of the organometallic fragment is presumably stabilised by weak interactions between the hydride group and the phenolic oxygen atoms that also serve to enlarge the open mouth of the cavity.

As exemplified by complexes **7**–**9**, the tridentate homooxacalix[3]arene **4** facilitates formation of chelate complexes where the phosphine ligands occupy three equatorial sites. This strategy positions a transition metal centre at the bottom of a cone-shaped molecule and, in the case of Rh, leaves an axial coordination site trapped inside the cavity. It is anticipated that the preferential entrapment of Rh–H *vs*. Rh–CO will promote selective insertion reactions with appropriately sized substrates that enter the cavity.

Notes and references

† Satisfactory elemental analyses were obtained for all new compounds. *Selected data* for **2**: δ_H($CDCl_3$) 6.74 (s, 6H, *m*-ArH), 4.61 (d, $^2J_{PH}$ 3, 3H each, PCH_2O), 4.61 and 4.31 (AB q, ^2J 13, 6H each, $ArCH_2$), 1.42 (s, 27H, Bu^t); δ_P(CD_2Cl_2) 24.9. For **3**: δ_H($CDCl_3$) 4.75 and 4.43 (AB q, ^2J 10, 2H each, PCH_2O), 4.56 (s, 2H, PCH_2O), 4.66 and 4.13 (AB q, ^2J 13, 2H each, $ArCH_2$), 4.53 and 4.06 (AB q, ^2J 13, 2H each, $ArCH_2$), 3.95 and 3.79 (AB q, ^2J 13, 2H each, $ArCH_2$), 0.94 and 0.84 (2s, 18H + 9H, Bu^t); δ_P($CDCl_3$) 26.3 and 25.7. For **4**: δ_H($CDCl_3$): 6.89 (s, 6H, *m*-ArH), 4.51 (s, 6H, PCH_2O), 4.51 and 4.47 (AB q, ^2J 4, 6H each, $ArCH_2$), 1.06 (s, 27H, Bu^t); δ_P($CDCl_3$) −20.0. For **5**: δ_H($CDCl_3$) 4.67 and 4.53 (AB q, ^2J 10, 2H each, PCH_2O), 4.62 (s, 2H, PCH_2O), 4.61 and 4.01 (AB q, ^2J 13, 2H each, $ArCH_2$), 4.42 and 4.12 (AB q, ^2J 13, 2H each, $ArCH_2$), 3.85 and 3.74 (AB q, ^2J 13, 2H each, $ArCH_2$), 1.02 and 0.91 (2s, 18H + 9H, Bu^t); δ_P($CDCl_3$) −17.4 and −19.9. For **6**: ν_{max} (KBr)/cm^{-1} 1946s, 1854s (C=O); δ_H(CD_2Cl_2) 6.82 (s, 6H, *m*-ArH), 5.17 (s, 6H, PCH_2O), 4.10 and 3.84 (AB q, ^2J 4, 6H each, $ArCH_2$), 1.08 (s, 27H, Bu^t); δ_P($CDCl_3$) 25.7. For **7**: δ_H($CDCl_3$) 6.75 (s, 6H, *m*-ArH), 5.05 (s, 6H, PCH_2O), 4.47 and 4.25 (AB q, ^2J 4, 6H each, $ArCH_2$), 1.03 (s, 27H, Bu^t); δ_P($CDCl_3$) 29.7. For **8**: δ_H(CD_2Cl_2) 6.95 (s, 6H, *m*-ArH), 5.22 (s, 6H, PCH_2O), 4.50 and 4.02 (AB q, ^2J 4, 6H each, $ArCH_2$), 1.13 (s, 27H, Bu^t); δ_P($CDCl_3$) 6.1 (2d, J_{107AgP} 312, J_{109AgP} 360). For **9**: ν_{max}(KBr)/cm^{-1} 1977s (C=O); δ_H(C_6D_6) 5.15 (s, 6H, PCH_2O), 4.70 (H_A) and 4.12 (H_B) (AB q, ^2J 4, 6H each, $ArCH_2$), 1.13 (s, 27H, Bu^t), −9.70 (q, $^2J_{PH}$ 14, 1H, Rh-H); δ_P(C_6D_6) 33.4 (d, J_{PRh} 153).

‡ *Crystal data* for **5** $C_{154}H_{180}O_{17}P_6$•$3CH_3OH$•H_2O, *M* 2488.98, triclinic, space group $P\bar{1}$, colourless prisms, *a* 13.0120(7), *b* 13.3008(4), *c* 21.468(1) Å, *V* 3687.2(5) Å^3, *Z* 1, D_c 1.12 g cm^{-3}, μ 0.133 mm^{-1}, *F*(000) 1330. Data were collected on a Nonius KappaCCD diffractometer (graphite Mo-Kα radiation, λ = 0.71073 Å) at −100 °C. 27813 reflections collected ($2.5 \leqslant \theta \leqslant 30.5°$), 7778 data with $I > 3\sigma(I)$. The structure was solved using the Nonius (ref. 14) package and refined by full-matrix least-squares with anisotropic thermal parameters for all non-hydrogen atoms except for the phenyl rings attached to P(3), H_2O and two MeOH molecules which were refined isotropically. Some disorder was found for the P(3)Ph_2 group adopting two possible orientations with equal occupancy. In Fig. 1 one of the two possible orientations is shown. Final results: *R*(*F*) 0.091, *wR*(*F*) 0.122, GOF 1.065, 791 parameters, largest difference peak 1.339 e Å^{-3}. CCDC 182/1368. See http://www.rsc.org/suppdata/cc/1999/1911/ for crystallographic data in .cif format.

§ Extraction percentage of rare-earth picrates by **2** (the rare-earths are ranged according to increasing atomic number) : Y, 4.0; La, 42.0; Pr, 43.0; Nd, 42.5; Sm, 38.5; Eu, 33.5; Gd, 31.5. Conditions: $[M(Pic)_3]_{initial}$ = $[Ligand]_{initial}$ 2.5 × 10^{-4} M, *T* 293 K, solvent: CH_2Cl_2. A separate experiment was performed for each metal.

¶ The ArCH_2 protons appear as an AB system, with δ_A 4.70 and δ_B 4.12. Only the signal at δ 4.70 correlates with the hydride.

1 C. Wieser-Jeunesse, D. Matt, M. R. Yaftian, M. Burgard and J. M. Harrowfield, *C. R. Acad. Sci. Ser. II*, 1998, 479.
2 I. S. Antipin, E. K. Kazakova, W. D. Habicher and A. I. Konovalov, *Russ. Chem. Rev.*, 1998, **67**, 905.
3 I. Neda, T. Kaukorat and R. Schmutzler, *Main Group Chem. News*, 1998, **6**, 4.
4 F. J. Parleviet, PhD Thesis, University of Amsterdam, 1998.
5 C. D. Gutsche and L. J. Bauer, *J. Am. Chem. Soc.*, 1985, **107**, 6052.
6 K. Araki, N. Hashimoto, H. Otsuka and S. Shinkai, *J. Org. Chem.*, 1993, **58**, 5958.
7 P. D. Hampton, C. E. Daitch, T. M. Alam and E. A. Pruss, *Inorg. Chem.*, 1997, **36**, 2879.
8 P. J. Cragg, M. C. Allen and J. W. Steed, *Chem. Commun.*, 1999, 553.
9 J. M. Harrowfield, M. Mocerino, B. J. Peachey, B. W. Skelton and A. H. White, *J. Chem. Soc., Dalton Trans.*, 1996, 1687.
10 M. R. Yaftian, M. Burgard, D. Matt, C. B. Dieleman and F. Rastegar, *Solvent Extr. Ion Exch.*, 1997, **15**, 975.
11 F. Hamada, T. Fukugaki, K. Murai, G. W. Orr and J. L. Atwood, *J. Inclusion Phenom. Mol. Recognit. Chem.*, 1991, **10**, 57.
12 P. Stössel, H. A. Mayer, C. Maichle-Mössmer, R. Fawzi and M. Steimann, *Inorg. Chem.*, 1996, **35**, 5860.
13 P. D. Hampton, C. E. Daitch, T. M. Alam, Z. Bencze and M. Rosay, *Inorg. Chem.*, 1994, **33**, 4750.
14 OpenMoleN, *Interactive Structure Solution*, Nonius B.V., Delft, The Netherlands, 1997.

Communication 9/05677G

Diastereoselective Baylis–Hillman reaction of 4-oxoazetidine-2-carbaldehydes: rapid, stereocontrolled and divergent radical synthesis of highly functionalised β-lactams fused to medium rings

Benito Alcaide,* Pedro Almendros and Cristina Aragoncillo

Departamento de Química Orgánica I, Facultad de Ciencias Químicas, Universidad Complutense, 28040-Madrid, Spain. E-mail: alcaideb@eucmax.sim.ucm.es

Received (in Liverpool, UK) 21st June 1999, Accepted 30th July 1999

Baylis–Hillman adducts derived from enantiopure 1-alkenyl- or alkynyl-4-oxoazetidine-2-carbaldehydes are used for the stereoselective and divergent preparation of highly functionalised β-lactams fused to medium rings through novel, chemocontrolled tandem radical addition–cyclization sequences.

The Baylis–Hillman reaction is an emerging carbon–carbon bond forming reaction for the preparation of densely functionalysed products involving an activated alkene, a carbon electrophile and a suitable catalyst (particularly a tertiary amine).[1] On the other hand, synthetic methodologies based on free radical cyclization reactions have experienced an impressive growth and are the focus of extensive studies. This wide research has been fostered by its operational simplicity, its tolerance to substrate functionalization, and the fact that it proceeds usually with high degrees of regio- and stereo-control.[2]

The increased resistance of bacteria to the commonly used β-lactam antibiotics[3] and the ever-growing new applications of these products in fields ranging from enzyme inhibition to the use of azetidin-2-ones as starting materials to develop new synthetic methodologies, has triggered a renewed interest in the construction of new systems having the azetidin-2-one ring as a common feature.[4] Our interest in the use of 4-oxoazetidine-2-carbaldehydes as substrates for intramolecular cyclization processes[5] prompted us to evaluate the combination of the Baylis–Hillman reaction with free-radical methodology as a route to unusual, chiral non-racemic bicyclic β-lactams. We report here novel, simple strategies for the stereoselective and divergent preparation of medium sized ring-fused highly functionalized bicyclic β-lactams **1** and **2** based on chemocontrolled tandem radical addition–cyclization sequences (Scheme 1). The useful and expedient approach described herein presents the opportunity to merge the rapidly expanding fields of Baylis–Hillman reaction and radical chemistry. The problems associated with the formation of medium sized rings are widely appreciated. Even the formation of seven-membered rings in the 7-*exo-trig* mode is likely to be unsuccessful in most cases (at 25 °C, $k_{7\text{-}exo} < 7 \times 10^{-1}\ s^{-1}$). Nevertheless, several authors were able to prepare seven-membered rings by radical cyclization on substrates bearing only a limited degree of freedom, including β-lactam-tethered haloalkenes or alkynes[6,7] and aryl-bridged compounds.[8]

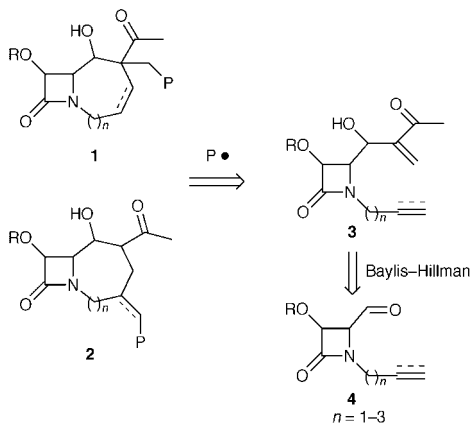

Scheme 1

Baylis–Hillman adducts **3** were easily prepared by DABCO-mediated reaction of enantiopure 4-oxoazetidine-2-carbaldehydes **4** with methyl vinyl ketone in excellent yields and stereoselectivities (Scheme 2). Alkenyl or alkynyl aldehydes **4** were easily prepared as single *cis*-enantiomers from imines of (*R*)-2,3-*O*-isopropylidenepropanal, through Staüdinger reactions with the corresponding acid chlorides in the presence of Et_3N,[9] followed by standard transformations of the acetal moiety.[5] The Baylis–Hillman reaction using protected α-amino aldehydes has been attempted with limited success, due to partial racemisation of the chiral aldehyde by DABCO after prolongate exposure times.[10] We were pleased to find that the Baylis–Hillman reaction proceeds faster than racemization (our typical reaction time ranging from 18 h for **4a** to 72 h for **4b**) using an equimolar amount of DABCO and 10 equiv. of methyl vinyl ketone and performing the experiment in MeCN at low temperature (−20 °C).†

Subjection of any organic molecule to a high enough temperature in the gas phase results in the formation of free radicals. When the molecule contains bonds with dissociation energies from 20 to 40 kcal mol^{-1}, cleavage can be caused in the liquid phase. The dissociation energy of the $PhCH_2$–H bond is 88 kcal mol^{-1}, so the generation of the benzylic radical is an unexpected process *via* heating at usual temperatures.[11] To our

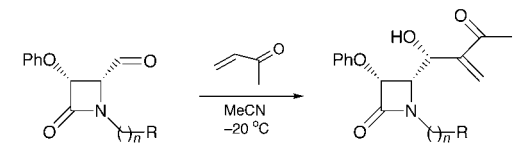

4a *n* = 1, R = vinyl
4b *n* = 1, R = ethynyl
4c *n* = 2, R = ethynyl
4d *n* = 3, R = ethynyl

3a *n* = 1, R = vinyl, de > 97%, 80%
3b *n* = 1, R = ethynyl, de = 92%, 78%
3c *n* = 2, R = ethynyl, de > 97%, 67%
3d *n* = 3, R = ethynyl, de > 97%, 60%

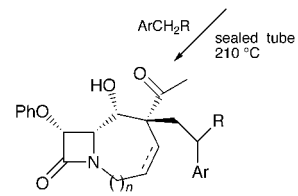

1a *n* = 1, R = H, Ar = Ph, 37%
1b *n* = 1, R = H, Ar = 4-MeC_6H_4, 45%
1c *n* = 1, R = H, Ar = 4-MeC_6H_4, 60%
1d *n* = 1, R = OH, Ar = Ph, 20%
1e *n* = 2, R = H, Ar = 4-MeC_6H_4, 53%

Scheme 2

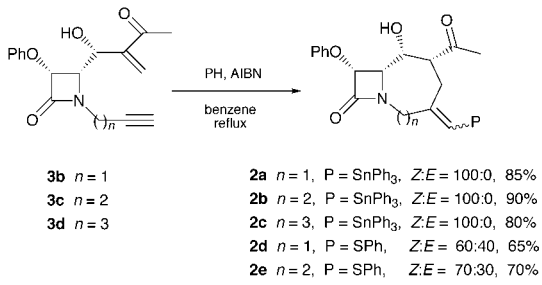

3b $n = 1$
3c $n = 2$
3d $n = 3$

2a $n = 1$, P = $SnPh_3$, $Z:E$ = 100:0, 85%
2b $n = 2$, P = $SnPh_3$, $Z:E$ = 100:0, 90%
2c $n = 3$, P = $SnPh_3$, $Z:E$ = 100:0, 80%
2d $n = 1$, P = SPh, $Z:E$ = 60:40, 65%
2e $n = 2$, P = SPh, $Z:E$ = 70:30, 70%

Scheme 3

surprise, Baylis–Hillman adduct (+)-**3a**, on heating in toluene or *p*-xylene in a sealed tube at 210 °C, formed the bicyclic products **1a**, **b**, which were isolated in modest yields (37–45%).‡ Use of chlorobenzene or anisole as solvents gave unaltered starting material (+)-**3a**. When enyne (+)-**3b** was used instead of diene (+)-**3a** the reaction proceeded in the same manner, giving product (+)-**1c** in good yield (60%). Furthermore, thermal treatment of enyne (+)-**3c** with *p*-xylene gave the bicycle (+)-**1e** in reasonable yield (Scheme 2). Interestingly, the use of benzyl alcohol allowed us to obtain the hemiacetal derivative of compound **1d**. Although this latter compound was isolated in low yield (20%) this is an interesting case because three new chiral centers are generated in a highly stereoselective manner.§ All compounds **1** were obtained as single diastereomers. When a catalytic amount of hydroquinone was added, the reaction rate was considerably reduced and the product yield fell dramatically. This fact confirms that a radical reaction is involved. Also, together with compounds **1**, 1,2-diarylethanes were isolated as byproducts in all cases. These products may be formed by recombination of the initially generated benzylic radicals.

In view of the particular disposition of the 1,5- and 1,6-enyne azetidin-2-ones to undergo 5-*exo* and 6-*exo* tin promoted radical cyclization,[12] we examined the applicability of this methodology to our novel Baylis–Hillman 1,ω-enyne substrates **3b**–**3d** for the synthesis of less common bicyclic β-lactams. This approach in the synthesis of seven-membered or higher sized rings has not been hitherto applied.[13] A dramatic change in the chemoselectivity was observed when the bicyclic β-lactam (+)-**2a** was formed as the exclusive product from (+)-**3b**, in nearly quantitative yield as crude product. The tin-promoted radical reaction was also useful in the conversion of the homologous 1,4-tethered enynes (+)-**3c** and (+)-**3d** into the corresponding bicyclic systems with similar efficiency and selectivity. Compounds **2** were exclusively obtained as *Z*-isomers. In addition, PhSH reacted smoothly with β-lactams (+)-**3b** and (+)-**3c** in the presence of AIBN, in boiling benzene, to give in good yields the corresponding phenylthiovinyl derivatives as mixtures of easily separable *Z* and *E* isomers (Scheme 3). The bicyclic structure (by DEPT, HETCOR, and COSY) and the stereochemistry (by vicinal proton couplings and NOE experiments) of compounds **1** and **2** were established by NMR one- and two-dimensional techniques.

Formation of bicyclic β-lactams **1** and **2** can be explained in terms of a competition between a tandem radical Michael addition–*endo*-cyclization and a tandem radical addition–Michael addition, depending on the electronic nature of the radical promoter (Scheme 4). The more nucleophilic benzylic radical would favour formation of compounds **1**, while the more electrophilic radicals, such as PhS· and Ph_3Sn·, should promote formation of compounds **2**. The high stereoselectivity of the processes can be tentatively interpreted in terms of the allylic strain model of Giese, showing for planar substituents such as Ac good levels of 1,2-stereoinduction on α-substituted β-oxy radicals (types **5** and **6** in Scheme 4).[14]

We would like to thank the DGES (MEC-Spain, grant PB96-0565) for financial support. P. A. thanks the DGES (MEC, Spain) for a 'Contrato de Incorporación'. C. A. thanks the DGI (CEC-Comunidad de Madrid-Spain) for a fellowship.

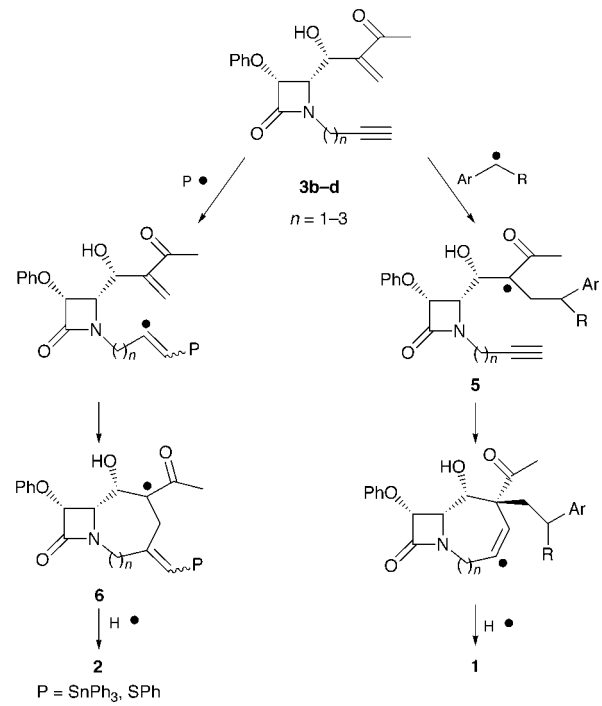

Scheme 4

Notes and references

† When the reaction was performed at room temperature maintaining the molar ratio of reagents (aldehyde:DABCO:methyl vinyl ketone = 1:1:10), partial epimerisation together with some unreacted aldehyde were observed.

‡ *Representative experimental procedure* for thermal promoted tandem radical reaction: A solution of Baylis–Hillman adduct **3** (0.2 mmol) in the corresponding benzylic solvent (10 ml) was heated in a sealed tube at 210 °C for 3 h. The reaction mixture was allowed to cool to room temperature, the solvent was removed under reduced pressure and, after purification by flash chromatography, bicycles **1** were obtained in analytically pure form.

§ All new compounds were fully characterised by spectroscopic methods and microanalysis and/or HRMS.

1 Reviews: E. Ciganek, *Org. React.*, 1997, **51**, 201; D. Basavaiah, P. D. Rao and R. S. Hyma, *Tetrahedron*, 1996, **52**, 8001.
2 For leading references, see: D. P. Curran, N. A. Porter and B. Giese, in *Stereochemistry of Radical Reactions*, VCH Publishers, New York, 1996; D. P. Curran, in *Comprehensive Organic Synthesis*, ed. B. M. Trost, Pergamon, Oxford, 1992, vol 4, ch. 4.2.
3 See, for example: D. Niccolai, L. Tarsi and R. J. Thomas, *Chem. Commun.*, 1997, 2333; V. Hook, *Chem. Br.*, 1997, **33**, 34; J. Davies, *Science*, 1994, **264**, 375.
4 See for example: Symposia-in-Print Number 8, Recent Advances in the Chemistry and Biology of β-Lactams and β-Lactam antibiotics, ed. G. I. Georg, *Bioorg. Med. Chem. Lett.*, 1993, **3**, 2159.
5 B. Alcaide and P. Almendros, *Tetrahedron Lett.*, 1999, **40**, 1015.
6 J. Knight, P. J. Parsons and R. Southgate, *J. Chem. Soc., Chem. Commun.* 1986, 78; J. Knight and P. J. Parsons, *J. Chem. Soc., Perkin Trans. 1* **1987**, 1237.
7 M. D. Bachi, F. Frolow and C. Hoornaert, *J. Org. Chem.*, 1983, **48**, 1841.
8 D. L. Boger and R. Mathvink, *J. Org. Chem.*, 1988, **53**, 3377.
9 G. I. Georg and V. T. Ravikumar, in *The Organic Chemistry of β-Lactams*, ed. G. I. Georg, VCH, Weinheim, 1993, ch. 3, p. 295.
10 S. E. Drewes, A. A. Khan and K. Rowland, *Synth. Commun.*, 1993, **23**, 183.
11 W. B. Motherwell and D. Crich, in *Free Radical Chain Reactions in Organic Synthesis*, Academic Press, London, 1991, ch. 6, pp. 183–185 and references cited therein.
12 B. Alcaide, I. M. Rodríguez-Campos, J. Rodríguez-Lopez and A. Rodríguez-Vincente, *J. Org. Chem.*, 1999, **64**, 5377.
13 The only related example is by Parsons *et al.* and refers to the cyclization of *N*-(2-bromoprop-2-en-1-yl)-4-allylazetidin-2-one to yield a homocarbacephem derivative. See ref. 6.
14 B. Giese, M. Bulliard, J. Dickhaut, R. Halbach, C. Hassler, U. Hoffmann, B. Hinzen and M. Senn, *Synlett*, 1995, 116.

Communication 9/05017E

ChemComm

Dendritic biomimicry: microenvironmental effects on tryptophan fluorescence†

David K. Smith* and Lars Müller

Department of Chemistry, University of York, Heslington, York, UK YO10 5DD. E-mail: dks3@york.ac.uk

Received (in Cambridge, UK) 4th August 1999, Accepted 12th August 1999

Branched tryptophan derivatives were synthesised and their optical properties investigated in a range of solvents: the steady state fluorescent emission from the indole ring sheds light on both the nature of a hydrogen bonding dendritic microenvironment and the optical behaviour of tryptophan residues in biological systems.

Tryptophan is undoubtedly the most important source of emission in proteins.[1] The wavelength of emission has proven to be very sensitive to the environmental conditions, and has consequently been extensively used as a probe of the local environment within a protein.[2] It has recently been proposed that branched macromolecules (dendrimers)[3] can mimic some aspects of protein behaviour,[4] in particular by creating unique microenvironments within their three dimensional superstructures.[5] Simple, well-understood environmental probes have been used in an attempt to yield a better understanding of this effect of dendritic encapsulation.[6] Here we target the synthesis of dendritic tryptophan derivatives containing a single tryptophan unit buried within the branched environment,[7] the emissive properties of which should respond to the environment generated by the branched shell. The results provide new information about the dendritic microenvironment, and have relevance to understanding the emissive properties of tryptophan in the protein environment, an area of intense research activity.[1]

Tryptophan derivatives **G0**, **G1** and **G2** were synthesised using a convergent coupling strategy in which *N-tert*-butoxycarbonyl-protected L-tryptophan was coupled with Bu^tNH_2 or pre-formed dendritic branches of first or second generation respectively.[8] Coupling was achieved using DCC/HOBt in CH_2Cl_2 with Et_3N as base; typical reaction times were 72 h. Products were purified by silica or gel permeation column chromatography as appropriate.†

The steady state fluorescence emission spectra of these new dendritic amino acids were measured in a range of different solvents.‡ It is well-known that environmental polarity is important in controlling the red shift of tryptophan fluorescence.[9] Firstly, compound **G0** was investigated in order to ascertain the effect of solvent on derivatives with this type of functionalisation—the emission wavelengths are provided in Table 1. Dependent on the solvent, fluorescent emission was observed between 321.5 and 343.5 nm. Attempts to correlate the data with Kamlet and Taft's π^* parameter,[10] a measure of polarity which is divorced from specific interactions such as hydrogen bonds, failed. Analysis of the data indicates that hydrogen bond acceptor solvents (THF, EtOAc and MeCN) were more red shifted than would have been expected on the basis of π^* alone, whilst hydrogen bond acceptor and donor solvents (Pr^iOH and MeOH) were shifted yet further to the red. Therefore, the hydrogen bond donor and acceptor ability of the solvent, as well as its polarity, apparently control the emission wavelength.[11] This is in stark contrast to the solvatochromic probe used by Fréchet and co-workers to investigate a dendritic microenvironment,[5a] the emission wavelength of which correlated well with π^* (polarity) alone.

As expected, therefore, the solvent plays key roles in controlling the fluorescence. The major question, however, was whether the dendritic shell would modify this behaviour, generating a unique microenvironment for the tryptophan residue. Consequently, the steady state emissive behaviour of **G1** and **G2** was investigated and compared with that of **G0** (Table 1).

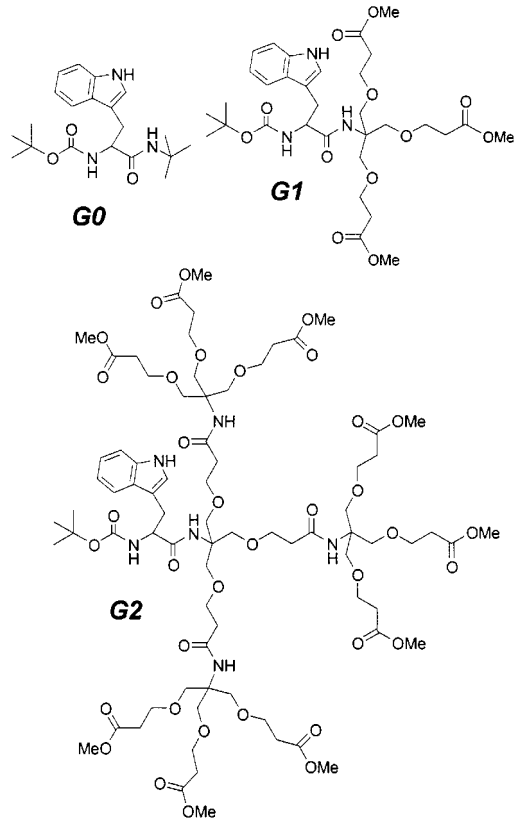

The branched shell did indeed have a dramatic and progressive effect on the emission of the tryptophan residue. Fréchet and co-workers found that, in their system, the effect of the dendritic branching correlated with the solvent polarity

Table 1 Emissive wavelengths for **G0**, **G1** and **G2** measured in a range of solvents. All wavelengths are ±0.5 nm

Solvent	π^{*a}	λ_{max}/nm			Dendritic effect[b]/nm
		G0	**G1**	**G2**	
Non-hydrogen bonding					
Cyclohexane	0.00	321.5	326.5	332	10.5
Benzene	0.59	330	331	333.5	3.5
CH_2Cl_2	0.82	332.5	333.5	335.5	3.0
Hydrogen bond acceptors					
EtOAc	0.55	332	332.5	333.5	1.5
THF	0.58	332.5	333	333	0.5
MeCN	0.75	337.5	337	338	0.5
Hydrogen bond donors and acceptors					
Pr^iOH	0.48	340.5	340	339	−1.5
MeOH	0.60	343.5	343	342.25	−1.25

[a] Kamlet and Taft's polarity parameter (ref. 10). [b] λ_{max}(**G2**) − λ_{max}(**G0**).

† Spectral data for **G0**, **G1** and **G2** are available from the RSC web site, see http://www.rsc.org/suppdata/cc/1999/1915/

parameter π^*, indicating that the effect of the branched shell was to moderate the polarity experienced by the solvatochromic probe. In this case, however, no correlation was observed. Rather, the magnitude of the dendritic effect was primarily dependent on the ability of the solvent to form specific interactions, in particular, hydrogen bonds. Three different types of behaviour were observed:

(i) Non-hydrogen bonding solvents: The most marked effect occurred in primarily non-hydrogen bonding solvents (cyclohexane, benzene, CH_2Cl_2) with the emission wavelength shifting bathochromically on dendritic functionalisation. In cyclohexane, for example, **G0** emitted at 321.5 nm, **G1** at 326.5 nm and **G2** at 332 nm, a remarkable total shift (dendritic effect) of 10.5 nm. This indicates that the branched shell strongly perturbs the local environment of the tryptophan residue.[5,6a] Furthermore, whilst for **G0** there was a large difference in emission wavelength between apolar cyclohexane and more polar CH_2Cl_2 (11 nm), this solvent-generated difference was much smaller for branched analogue **G2** (3.5 nm). In other words, attachment of the branched shell strongly reduces the effect of solvent polarity.

(ii) Hydrogen bond acceptor solvents: In such solvents (EtOAc, THF, MeCN), the dendritic shell had a much smaller effect on the emission wavelength (dendritic effects of between 0.5 and 1.5 nm), even though some of these solvents have polarities comparable to, or lower than, CH_2Cl_2. This provides strong supporting evidence that polarity is not the only important factor in controlling tryptophan fluorescence.

(iii) Hydrogen bond acceptor and donor solvents: In such solvents (MeOH, Pr^{i}OH) the dendritic effect is once again of smaller magnitude, but this time in the opposite direction, with the emission maximum shifted hypsochromically by around 1.5 nm after dendritic functionalisation.

It is therefore clear that the dendritic effect is much smaller in competitive solvents than in non-competitive solvents. This indicates that specific tryptophan solvation effects, such as hydrogen bonding, play a crucial role. It is proposed that, in non-competitive solvents, an intramolecular *hydrogen bond* is formed between the dendritic shell (C=O) and the N–H group of the tryptophan residue at the focal point. Such a hydrogen bond would act as a tether, holding the polar peptidic branched shell in close proximity to the tryptophan subunit, modulating the polarity of its local environment, and hence perturbing its fluorescence spectrum much more strongly.[12] In competitive solvents, the solvent is itself able to interact with the tryptophan residue, and the branched shell consequently has a much smaller effect.

Further evidence for the dendritic creation of a hydrogen bonding interaction in non-competitive solvents is provided by the downfield perturbation of the ^{1}H NMR shift (in $CDCl_3$) of the N–H proton in the indole ring. This resonance shifts from δ 8.10 for **G0** to δ 8.60 for **G1** to δ 9.45 for **G2**.

Such hydrogen bonding microenvironments have been previously postulated as being important in controlling the behaviour of dendritic receptors.[13] This report clearly illustrates the dramatic effect that such hydrogen bond interactions can have inside branched superstructures—in clear analogy with the importance of hydrogen bonds in controlling the structure and behaviour of enzymes.

In summary, dendritically modified tryptophans have been synthesised and their optical properties investigated. A remarkable dendritic effect[5] on emission wavelengths was observed. It is proposed that in non-competitive solvents, there is a *hydrogen bonding microenvironment*[13] for the encapsulated tryptophan residue, leading to enhanced dendritic effects. In addition to providing clear characterisation of this type of dendritic microenvironment, these results emphasise the potential importance of microenvironmental hydrogen bonds in controlling the fluorescence of tryptophan residues in the apolar interior of enzymes. This is significant given the wide use of tryptophan emission as a probe of protein structure.[1] Further work using these, and more deeply encapsulated, dendritic tryptophan derivatives to probe kinetic aspects of fluorescence quenching is planned. Other biologically relevant fragments will also be encapsulated in order to ascertain additional microenvironmental effects on function, and generate new, easily tuneable forms of molecular behaviour.

D. K. S. acknowledges The University of York for financial assistance and the Erasmus programme (L. M).

Notes and references

‡ Emission spectra measured after excitation at 290 nm. [Tryptophan derivative] = 1×10^{-4} M, except from **G1** and **G2** in cyclohexane which exhibited limited solubility, [**G1**] = 5×10^{-5} M, [**G2**] = 2×10^{-5} M.

1 M. R. Eftink, *Methods Biochem. Anal.*, 1991, **35**, 127 and references therein; P. R. Callis, *Methods Enzymol.*, 1997, **278**, 113 and references therein.

2 H. Lami and N. Glasser, *J. Chem. Phys.*, 1986, **84**, 597; Y. Chen and M. D. Barkley, *Biochemistry*, 1998, **37**, 9976 and references therein.

3 For reviews of dendrimer chemistry see: G. R. Newkome, C. N. Moorefield and F. Vögtle, *Dendritic Molecules: Concepts, Syntheses, Perspectives*, VCH, Weinheim, 1996; H.-F. Chow, T. K.-K. Mong, M. F. Nongrum and C.-W. Wan, *Tetrahedron*, 1998, **54**, 8543; O. A. Matthews, A. N. Shipway and J. F. Stoddart, *Prog. Polym. Sci.*, 1998, **23**, 1.

4 D. K. Smith and F. Diederich, *Chem. Eur. J.*, 1998, **4**, 1353 and references therein.

5 For representative examples see: (*a*) C. J. Hawker, K. L. Wooley and J. M. J. Fréchet, *J. Am. Chem. Soc.*, 1993, **115**, 4375; (*b*) S. Mattei, P. Seiler, F. Diederich and V. Gramlich, *Helv. Chim. Acta*, 1995, **78**, 1904; (*c*) P. J. Dandliker, F. Diederich, A. Zingg, J.-P. Gisselbrecht, M. Gross, A. Louati and E. Sanford, *Helv. Chim. Acta*, 1997, **80**, 1773; (*d*) C. B. Gorman, B. L. Parkhurst, W. Y. Su and K.-Y. Chen, *J. Am. Chem. Soc.*, 1997, **119**, 1141; (*e*) C. Devadoss, P. Bharathi and J. S. Moore, *Angew. Chem., Int. Ed. Engl.*, 1997, **36**, 1633.

6 (a) C. M. Cardona and A. E. Kaifer, *J. Am. Chem. Soc.*, 1998, **120**, 4023; (*b*) D. K. Smith, *J. Chem. Soc., Perkin Trans. 2*, 1999, 1563

7 Dendrimers functionalised with peripheral tryptophan units have been reported: G. R. Newkome, X. Lin and C. D. Weis, *Tetrahedron: Asymmetry*, 1991, **2**, 957.

8 G. R. Newkome and X. Lin, *Macromolecules*, 1991, **24**, 1443; J.-F. Nierengarten, T. Habicher, R. Kessinger, F. Cardullo, F. Diederich, V. Gramlich, J.-P. Gisselbrecht, C. Boudon and M. Gross, *Helv. Chim. Acta*, 1997, **80**, 2238.

9 P. R. Callis and B. K. Burgess, *J. Phys. Chem. B*, 1997, **101**, 9429.

10 M. J. Kamlet, J.-L. Abboud, M. H. Abraham and R. W. Taft, *J. Org. Chem.*, 1983, **48**, 2877; C. Reichardt, *Solvents and Solvent Effects in Organic Chemistry*, 2nd edn., VCH, Weinheim, 1990.

11 This was recently shown to be the case for the solvatochromism of β-naphthol: K. M. Solntsev, D. Huppert and N. Agmon, *J. Phys. Chem. A*, 1998, **102**, 9599.

12 The structural importance of hydrogen bond interactions in dendrimers has been stressed previously for a simple amide-amine type dendrimer: A. W. Bosman, M. J. Bruining, H. Kooijman, A. L. Spek, R. A. J. Janssen and E. W. Meijer, *J. Am. Chem. Soc.*, 1998, **120**, 8547.

13 J. P. Collman, L. Fu, A. Zingg and F. Diederich, *Chem. Commun.*, 1997, 193; D. K. Smith and F. Diederich, *Chem. Commun.*, 1998, 2501; D. K. Smith, A. Zingg and F. Diederich, *Helv. Chim. Acta*, 1999, **82**, 1225.

Communication 9/06367F

Typeset and printed by Black Bear Press Limited, Cambridge, England

ChemComm
FEATURE ARTICLE

Liquid-phase chemistry: recent advances in soluble polymer-supported catalysts, reagents and synthesis

Paul Wentworth Jr. and Kim D. Janda*

Department of Chemistry, The Scripps Research Institute and the Skaggs Institute for Chemical Biology, 10550 N. Torrey Pines Road, La Jolla CA92037, USA. E-mail: kdjanda@scripps.edu

Received (in Cambridge, UK) 11th March 1999, Accepted 20th April 1999

Chemistry on soluble polymer-matrices, termed liquid-phase organic synthesis, is emerging as a viable alternative or adjunct to the classical solid-phase approach across the broad spectrum of polymer-supported organic chemistry. This review details the significant advances in liquid-phase synthetic methodologies, reagents, catalysts and supports that have appeared from 1997 to the present.

Introduction

Cross-linked polymer supports are now ubiquitous throughout the fields of combinatorial chemistry, organic synthesis and catalysis.[1,2] However, emerging problems associated with the heterogeneous nature of the ensuing chemistry and with 'on-bead' spectroscopic characterisation[3] has meant that soluble polymers are being developed as alternative matrices for combinatorial library production[4] and organic synthesis.[5,6] Synthetic approaches that utilise soluble polymers, termed 'liquid-phase' chemistry, couple the advantages of homogeneous solution chemistry (high reactivity, lack of diffusion phenomena and ease of analysis) with those of solid phase methods (use of excess reagents and easy isolation and purification of products). Separation of the functionalized matrix is achieved by either solvent or heat precipitation, membrane filtration or size-exclusion chromatography.

Poly(alkene oxide)s such as poly(ethylene glycol) (PEG) are amongst the most studied soluble polymers for organic synthesis,[7,8] with polyethylene oligomers[9] and poly(styrene)s[10,11] also receiving considerable attention. The wide applicability of PEG is directly linked to its broad solubility profile: soluble in DMF, dichloromethane, toluene, acetonitrile, water and methanol, but insoluble in diethyl ether, *tert*-butyl methyl ether, isopropyl alcohol[12] and cold ethanol.

In liquid-phase chemistry, where a soluble polymer is being iteratively derivatized either terminally or on side-chain residues, a balance has to be reached between loading capacity (substitution per gram of polymer) and the solubility profile of the resulting polymer derivative. As the molecular weight of the matrix is lowered, the end-groups have a proportionally greater effect on the physical properties of the polymer derivative, which can result in non-quantitative precipitation and low polymer recoveries. PEG of molecular weight 3000 to 5000 is typically utilised in liquid-phase strategies. The polymer chains can be terminated with either two hydroxy groups (dihydroxy-PEG) or with one hydroxy group and one methyl ether (monomethoxy-PEG). Lower molecular weight PEG matrices give a correspondingly higher loading per gram of support and if dihydroxy-terminated PEG is chosen the loading is double that of a monomethoxy-PEG of the same molecular weight. Throughout this review *vide infra*, the balance of loading and polymer recovery is discussed with optimal conditions being described for a number of cases.

Soluble polymer-supported synthesis

Targeted synthesis

The utility of combinatorial chemistry within drug discovery is ultimately linked to the ability to rapidly construct complex molecules on polymer supports. With this in mind, a polymer-supported approach to the prostaglandin core was seen as an important benchmark in the progress of this chemistry. Chen and Janda have successfully utilised Noyori's[13] three component coupling strategy, in a 'liquid-phase' format, for the synthesis of PGE_2 methyl ester[10] **1a** and $PGF_{2\alpha}$[11] **1b** (Scheme 1).

The synthetic strategy hinged upon the choice of a soluble polymer support that could withstand extreme reaction and workup conditions. While PEG is ostensibly the polymer of choice for most facets of liquid-phase chemistry, its use in this case was contraindicated for two reasons: insolubility in THF at low temperatures and its solubility in water which precluded aqueous extraction/removal of organometallic byproducts. A non-crosslinked copolymer of styrene and chloromethylstyrene (3 mol%), previously used for peptide synthesis,[14] was prepared (0.3 mmol g^{-1} loading) and incorporated as the polymer matrix. This copolymer is soluble in THF, dichloromethane and ethyl acetate even at low temperatures, but is insoluble in methanol and water so that purification can involve both aqueous extraction and precipitation techniques.

The synthetic approach to PGE_2 methyl ester **1a** involved an initial attachment of the cyclopentanoid alcohol **2** to the soluble co-polymer *via* Ellman's tetrahydropyran linker.[15] The vinyl-

Paul Wentworth Jr. obtained both his BSc (Hons) in Chemistry and Pharmacology (1991) and PhD in Organic Chemistry (1994) from the University of Sheffield, the latter under the supervision of Professor G. Michael Blackburn. In 1994 he began postdoctoral studies involving antibody-catalysis, enzyme inhibition and combinatorial chemistry, with Professor Kim. D. Janda at The Scripps Research Institute. Since 1997, as an Assistant Professor in the Department of Chemistry at Scripps, he has pursued research into combinatorial and polymer-supported chemistry and programmable biocatalysis.

Kim D. Janda obtained his PhD in Organic Chemistry (1984) from the University of Arizona. He joined the Scripps Institute in 1985 as a postdoctoral fellow and in 1987 was promoted to the faculty, where he is currently the Ely Callaway Jr. Professor of Chemistry. His research interests include catalytic antibodies, polymer-supported methodologies, combinatorial chemistry, immunopharmacotherapy, and enzyme inhibition. He is the recipient of an Alfred P. Sloan fellowship (1993–1995), and an Arthur C. Cope Scholar award (1998). He is a co-founder of two companies: Combichem Inc. and Drug Abuse Sciences.

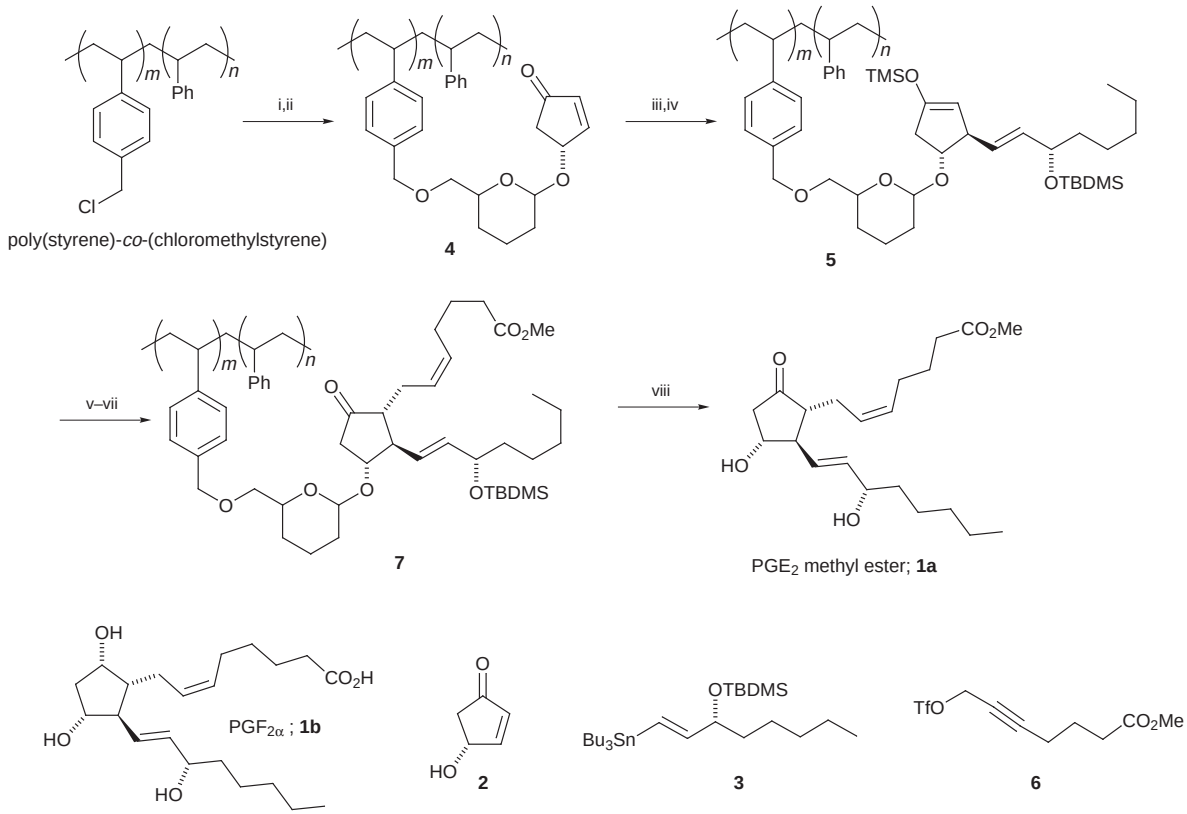

Scheme 1 *Reagents and conditions*: i, 6-(hydroxymethyl)-3,4-dihydro-2*H*-pyran (3 equiv.), NaH (3.3 equiv.), DMA, room temp., 24 h; ii, **2** (3.0 equiv.), PPTS (0.5 equiv.), CH_2Cl_2, 40 °C, 16 h; iii, **3** (4.2 equiv.), $Li_2CuCNMe_2$ (3.9 equiv.), THF, −78 °C, 15 min; iv, TMSCl (15 equiv.), −78 °C, 30 min; Et_3N (30 equiv.), 0 °C, 15 min; v, MeLi (3 equiv.), THF, −23 °C, 30 min; vi, **6** (6 equiv.), −78 °C, 10 min, then −23 °C, 30 min; vii, H_2, 5% Pd–$BaSO_4$, quinoline, benzene–cyclohexane (1 : 1), room temp., 48 h; viii, 48% aq. HF–THF (3 : 20, v/v), 45 °C, 6 h.

stannane ω-chain **3** was then added to **4** in the presence of $Li_2CuCNMe_2$ in THF at −78 °C. Following reaction of the intermediary enolate with TMSCl, the stable polymer-bound silyl enol ether **5** was isolated. The α-chain was then incorporated, as its respective triflate **6**, by trapping of the intermediate enolate formed following addition of MeLi to **5** in THF (−23 °C). Following partial reduction of the α-chain alkyne, the polymer-bound *Z* alkene **7** was cleaved from the support, with accompanying deprotection of the silyl ether protecting group to give **1a** in an overall yield of 37% for the eight step route. The main features to note are that the polymer recovery mass balance was > 97% and only one polymer-bound species was detected by routine NMR analysis, for each step of the synthesis.

Versatile and practical methodology for the construction of oligosaccharides of high structural complexity and in a combinatorial fashion is of tremendous interest. Solid-phase synthesis of oligosaccharides has improved dramatically over the past several years but can still suffer from problems such as decreased glycosylation rates, incomplete coupling and lowered stereoselectivities.[16] Building on an initial report by Krepinsky,[17] Dreef-Tromp and co-workers[18] utilised monomethoxy-PEG as a soluble polymer-support for their synthetic approach to heparan sulfate-like oligomers **8a**–**g**.

The PEG-supported acceptors **9** and **10** were prepared by an initial esterification of the free primary hydroxy group of the dissacharides **11** and **12** with succinic anhydride, followed by attachment to monomethoxy-PEG *via* esterification of the terminal carboxy group (Scheme 2). Subsequent glycosylations of the PEG-supported iduronic acids **9** and **10** were performed in an iterative three step cycle involving deprotection of the levulinoyl group, TMSOTf assisted coupling with disaccharide glycosyl donors as their respective trichloroacetimidates, and capping of the unreacted 4-hydroxy groups.

Optimisation studies led to excellent coupling efficiencies (> 95%) being achieved and the anomeric control (complete α-substitution) was comparable to that observed with the classical solution-phase approach. The PEG polymer support facilitated the synthetic strategy by allowing an excess of reagents to be used while ensuring that intermediates along the route could be purified by simple precipitation with high polymer recovery (> 95%). Furthermore, the extent of glycosylation could be followed routinely by ^{1}H NMR of the PEG-bound derivatives.

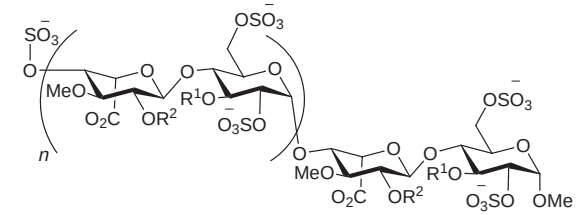

8a *n* = 2; $R^1 = SO_3^-$; R^2 = Me
8b *n* = 4; $R^1 = SO_3^-$; R^2 = Me
8c *n* = 5; $R^1 = SO_3^-$; R^2 = Me
8d *n* = 2; R^1 = Me; $R^2 = SO_3^-$
8e *n* = 3; R^1 = Me; $R^2 = SO_3^-$
8f *n* = 4; R^1 = Me; $R^2 = SO_3^-$
8g *n* = 5; R^1 = Me; $R^2 = SO_3^-$

Enzyme-assisted strategies for the synthesis of oligosaccharides is recognised as a promising alternative to chemical synthesis because of high regio- and stereo-selective reactions without the need for protecting groups. An efficient methodology for the construction of carbohydrates, including oligosaccharide and sphingoglycolipids, has been developed by Nishimura and Yamada.[19,20] They synthesised a vinylic oligosaccharide monomer **13** which, when treated with acrylamide under radical polymerisation conditions, formed a water-soluble copolymer **14** (Scheme 3). This water-soluble conjugate (**14**), was then used as a primer for a regioselective sialylation reaction catalysed by rat liver βGal1→3/4GlcNAc α-2,3-sialyltransferase, in the presence of CMP-NeuAc,[21] to generate the soluble polymer-supported trisaccharide **15** in quantitative yield.

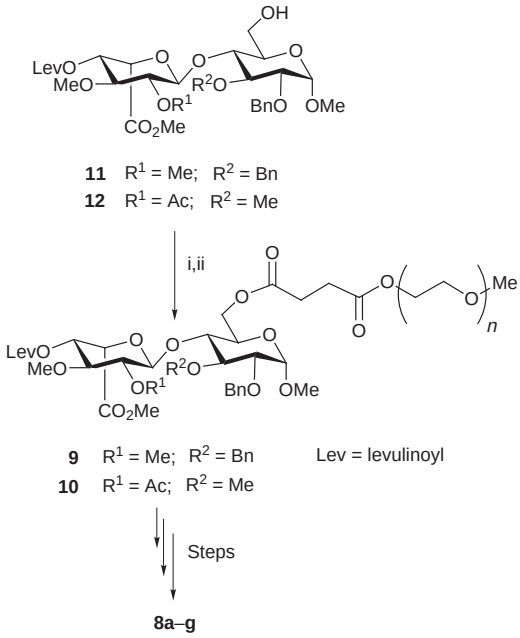

Scheme 2 *Reagents and conditions*: i, succinic anhydride, DMAP, pyridine; ii, MeO-PEG-OH, 1-(3-dimethyaminopropyl)-3-ethylcarbodiimide hydrochloride (EDC), DMAP, CH_2Cl_2.

Purification of **15** from the enzyme and excess sugar building block by gel-filtration chromatography was facilitated by the presence of the poly(acrylamide) support. Subsequent treatment of **15** with leech ceramide glycanase in the presence of an excess of ceramide as an acceptor generated the transglycosidated product GM3 (**16**) in 61% yield. Thus this polymer-supported enzyme approach afforded the glycolipid GM3 in 56% yield from the readily available precursor/monomer **13**, a remarkable improvement in both the ease of synthesis and overall yield when compared to that of chemical synthesis.[22]

Synthetic methodology

C–C Bond formation. In addition to the extended synthetic strategies *vide supra*, exploration into chemical methodology on soluble supports continues to make significant advances. The development of efficient methods of forming carbon–carbon bonds is an important objective for any polymer-supported methodology. The reactions of stabilised carbanions with carbon centred electrophiles is one of the most common approaches in this area and Lamaty and co-workers[23] have exploited this methodology on PEG. Alkylation of the imine **17** was achieved with a range of electrophiles (RX) with K_2CO_3 as a base (Scheme 4). In the solution phase, a quaternary

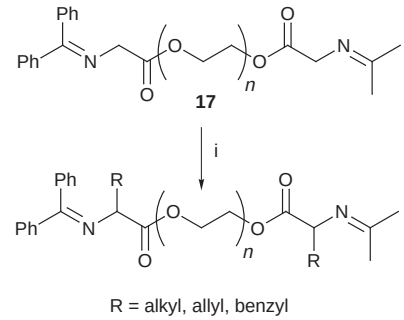

Scheme 4 *Reagents and conditions*: i, RX (2 equiv.), K_2CO_3 (4 equiv.), MeCN, reflux, 14 h (54–75%).

ammonium salt is required as a phase-transfer catalyst (PTC) to ensure complete alkylation. Interestingly the PEG support acted as a sufficiently powerful PTC under the conditions of the reaction that no ammonium salt was required. Dihydroxy-PEG_{2000} was utilised as the matrix of choice in this system which resulted in high loading capacities (1.0 mmol g^{-1}). However the authors note that the precipitation and recovery of the matrix after each reaction step was difficult and sometimes low yielding.

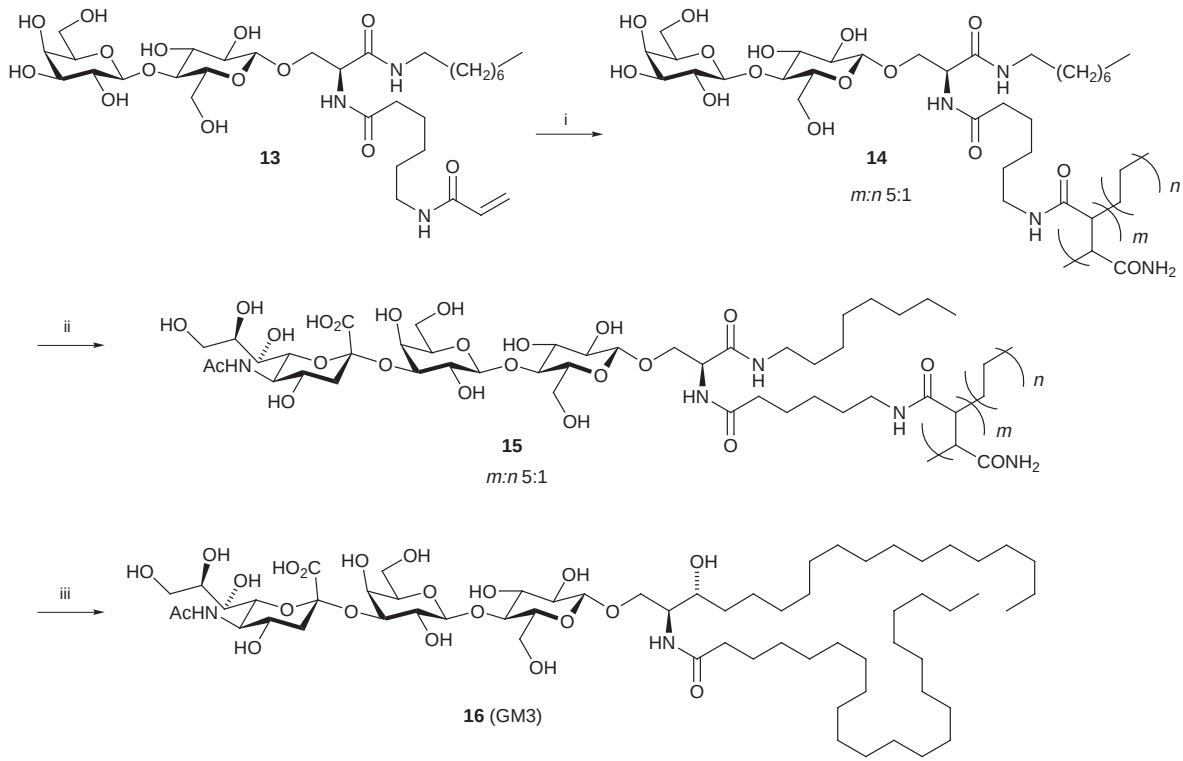

Scheme 3 *Reagents and conditions*: i, acrylamide (4.0 equiv.), *N,N,N'N'*- TMEDA (0.4 equiv.), ammonium peroxodisulfate (APS), 50 °C, 2 d (92%); ii, CMP-NeuAc (1.2 equiv.), α-2,3-sialyltransferase (0.3 unit), bovine serum albumin, $MnCl_2$, calf intestinal alkaline phosphate (20 unit), sodium cacodylate buffer (50 mM, pH 7.49), 37 °C, 3 d (> 99%); iii, ceramide (4 85 equiv.), ceramide glycanase (0.01 unit), Triton CF-54 (1 drop), sodium citrate buffer (50 mM, pH 6.0), 37 °C, 17 h (61%).

The biaryl subunit is an important pharmacophore in a variety of biologically active compounds. Blettner and co-workers[24] utilised the first example of a Suzuki cross-coupling reaction on PEG, in a parallel array format, to generate libraries of substituted biaryls (Scheme 5). They studied a range of

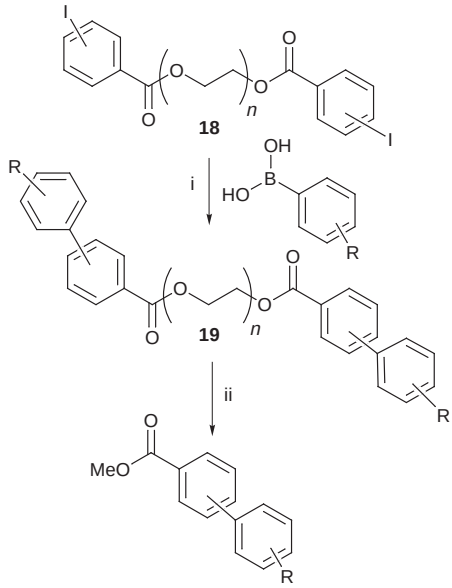

Scheme 5 *Reagents and conditions*: i, arylboronic acid (2 equiv.), $Pd(PPh_3)_4$ (0.05 equiv.), aq. Ma_2CO_3 (2 M; 2.5 equiv.), DMF, 110 °C, sealed tube, 10 h; ii, Et_3N–MeOH (1 : 4), 85 °C, sealed tube, 2 d.

molecular weight PEGs and found that dihydroxy PEG_{6000} (0.33 mmol g^{-1}) and monomethoxy PEG_{5000} (0.2 mmol g^{-1}) supported aryl iodides **18** and biaryls **19** could be purified by precipitation, but that dihydroxy PEG_{4000} (0.5 mmol g^{-1}) derivatives had to be purified by parallel flash column filtration. Polymer recovery by precipitation ranged from 90–98%, whereas due to the polydispersity of PEG, recovery by column filtration was only variable (52–74 %).

Heterocycle formation. There is considerable precedence describing solution-phase dipolar cycloaddition reactions with alkenes and alkynes for the synthesis of aromatic and non-aromatic five-membered ring heterocycles.[25] Several examples of solid-phase cycloaddition reactions have also been reported.[26] Recently, the first example of a liquid-phase 1,3-dipolar cycloaddition reaction was reported (Scheme 6).[27]

The PEG-supported alkyne **20** underwent smooth cycloaddition with a range of carbohydrate-derived primary azides **21a**–**c** to generate the regioisomeric, polymer-bound triazoles **22a**–**c** in good yields (73–86%).

The search for novel scaffolds on which molecular diversity can be constructed is an ongoing challenge throughout the field of combinatorial chemistry.[28] Janda and co-workers have synthesised a 3-aminoimidazoline-2,4-dione library[29] **23** on a monomethoxy-PEG_{5000} support (Scheme 7). The aminoimidazolinedione core is a rigid five-membered ring heterocycle with two points of diversification. The first diversity element R^1 was introduced as an amino acid isocyanate **24a**, the second as a Boc-aza-amino acid **24b**. The last step in the route involved a smooth cyclization–cleavage reaction, with maintenance of the stereochemical integrity of C-5, which furnished the scaffold **23** free in solution.

Pyrazolidine-3,5-diones **25a** are a class of heterocyclic compounds with four potential sites for diversification (Scheme 8). They are used for the treatment of arthritis but gastric irritation can limit their therapeutic application.[30] Therefore analogues are being sought that maintain the therapeutic profile but possess reduced side-effects. Janda and co-workers[12] have developed a liquid-phase approach to the synthesis of the

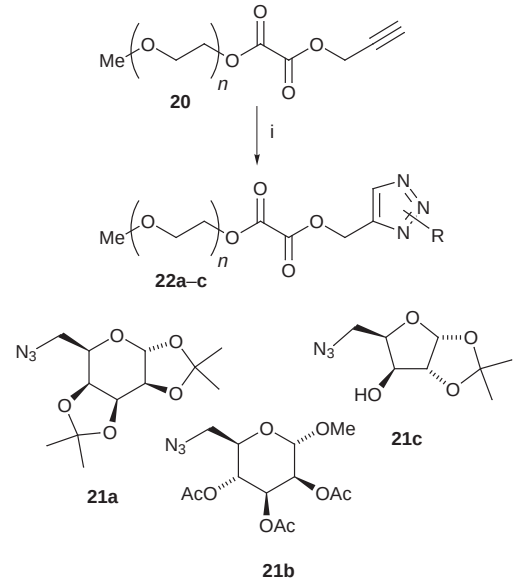

Scheme 6 *Reagents and conditions*: i, RN_3 (**21a**–**c**) (2 equiv.), toluene, reflux, 12 h.

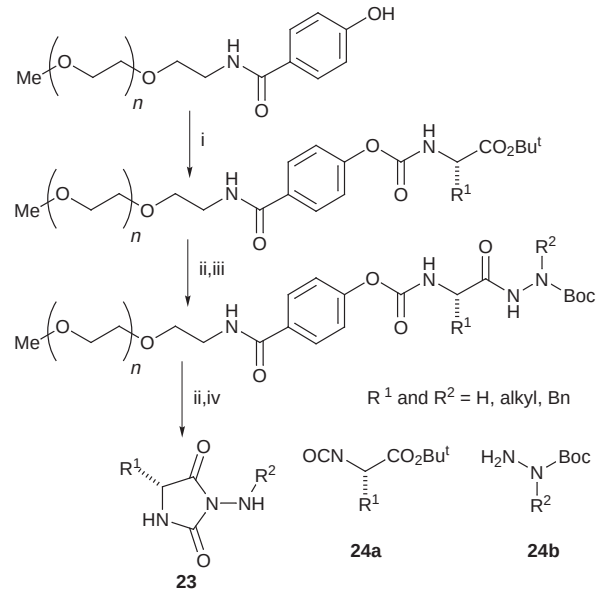

Scheme 7 *Reagents and conditions*: i, **24a**, Et_3N; ii, TFA, CH_2Cl_2; iii, **24b**, DCC; iv, dilution, Pr^i_2NEt (1.1 equiv.).

pyrazolidine-3,5-dione **25b** which involves an initial preparation of malonate **26** which is attached to PEG *via* Janda's ethyl phenyl sulfide traceless linker.[31,32] The malonate **26** was alkylated and de-esterified under standard conditions to give the polymer-supported diacid **27**. Ring closure to form the heterocyclic core was followed by oxidation of the sulfide linker and cleavage of sulfone **28** with Na–Hg amalgam to give *rac*-**25b** in excellent overall yield (61% for six steps).

Soluble polymer-supported reagents and catalysts

Combinatorial library construction has to date occurred almost exclusively on solid polymer supports. However, to reduce the effort involved in transferring solution-phase chemical methodology onto polymers, a notable shift towards solution-phase chemical library generation is occurring. However, to facilitate rapid library generation and purification, a whole new generation of functional polymer reagents and catalysts are being developed.[33–35]

An important application of soluble polymer-supports has been the use of PEG-supported hydroquinidine cinchona

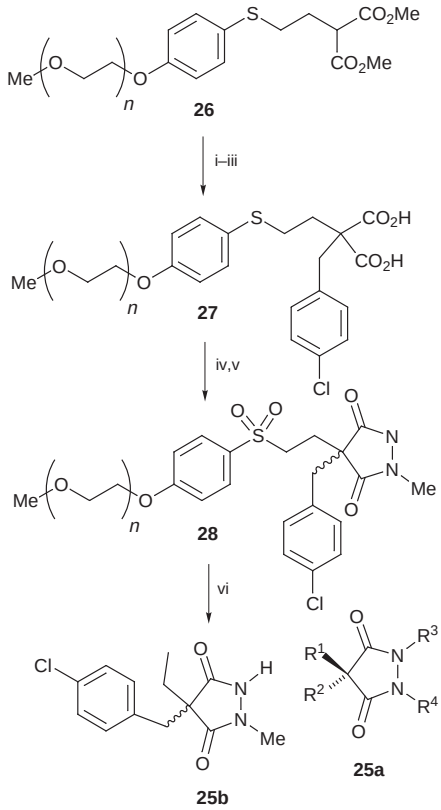

Scheme 8 *Reagents and conditions*: i, 4-chlorobenzyl chloride, Cs_2CO_3, DMF, room temp., 17 h; ii, NaOH, H_2O, room temp., 5 h; iii, Amberlite® IR-120 (plus), room temp., 1 h (94% from **26**); iv, methylhydrazine, benzotriazol-1-yloxytrispyrrolidinophosphonium (PyBOP), Pr^i_2NEt, DMF, room temp., 43 h (98%); v, $KHSO_5$, H_2O, room temp., 3 h (90%); vi, 5% Na–Hg, Na_2HPO_4, MeOH–DMF (1 : 8), room temp., 18 h, (74%).

alkaloid ligands **29** in the Sharpless asymmetric dihydroxylation reaction of olefins.[36,37] Following their seminal reports in this area, Han and Janda[38] have studied the dihydroxylation of *trans*-cinnamic acid on different polymer-supports: Merrifield and Wang resins, Tentagel and PEG. Various reaction parameters were modified: the amount of ligand/metal and reaction time. Under all conditions, the liquid-phase PEG support provided the best results and compared favourably with the dihydroxylation of a solution-bound cinnamic acid derivative. Bolm and Gerlach[39] have further improved the liquid-phase asymmetric dihydroxylation reaction, by utilising cinchona alkaloid–pyridazine–PEG conjugates **30** as ligands. This new strategy led to shortened reaction times, good yields and improved enantioselectivities (up to 99% ee).

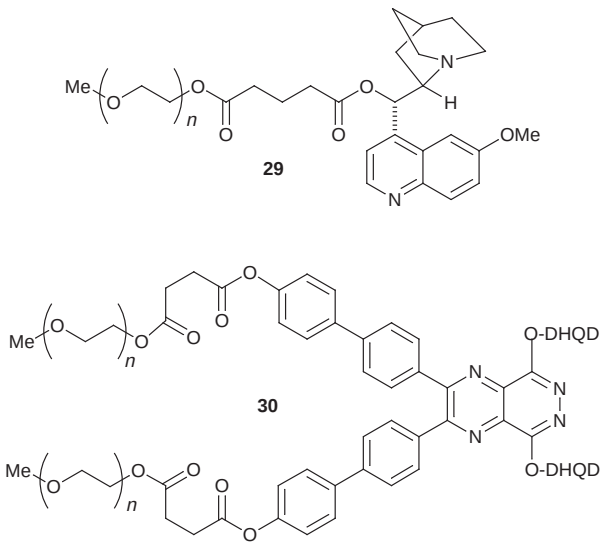

A soluble polymer-supported scandium catalyst, poly(allylscandium triflylamide) ditriflate **31** was used for three-component condensation reactions between aldehydes, amines and silylated nucleophiles, to generate β-amino ketones, β-

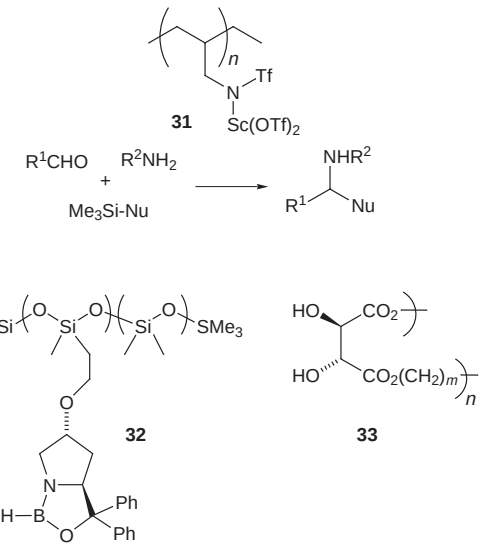

amino esters and α-amino nitriles in excellent yields.[40] The polymer-supported catalyst was recovered by precipitation in hexanes, and could be reused without loss in activity. The scandium catalyst **31** also catalysed aldimine selective reactions in the presence of aldehydes.[41] In the presence of **31**, aldimines reacted almost exclusively with silyl enolates without forming adducts with aldehydes, a common side-reaction using the more conventional $Sc(OTf)_3$ catalyst. The authors attributed this unique chemoselectivity to the stability of the aldimine–polymer–supported catalyst complex.

The recovery and reuse of polymer-supported catalysts is one of the major benefits associated with this strategy, especially when dealing with chiral catalysts which can be tremendously expensive to prepare. The commercially available copolymer of methylhydrosiloxane and dimethylsiloxane was utilised as a soluble support for Corey's chiral oxazaborolidine.[42] The reduction of a family of prochiral ketones was catalysed by polymer-adduct **32** with > 98% ee, comparable to the solution-phase oxazaborolidine counterpart. The polymer-supported catalyst, in contrast to most of the cases discussed *vide supra* is not a solid, and so was removed from the reaction mixture by size-exclusion filtration, rather than by precipitation. The strategy is compatible with automation and could see ultimate application in a continuous flow reactor system.

The linear poly(tartrate ester) **33** has been successfully applied in a liquid-phase variant of the enantioselective Sharpless epoxidation reaction.[43] The active polymer species was prepared by treating L-(+)-tartaric acid with a variety of diols under standard polycondensation conditions. However, the observed enantioselectivity for the epoxidation of *trans*-hex-2-en-1-ol was moderate (up to 79% ee), the solution-phase reaction with L-(+)-dimethyltartrate gave 98% ee showing that there exists some scope for improvement.

A number of examples of liquid-phase reagents have appeared recently. Janda and co-workers[44] synthesised a PEG-functionalized triarylphosphine **34** and showed that it is a more reactive reducing agent in the Staudinger and Mitsunobu etherification reactions than a Merrifield resin-bound counterpart. A number of PEG-matrices were studied and dihydroxy-PEG_{3400} (0.58 mmol g^{-1}) was found to be the lowest molecular weight matrix that consistently afforded excellent polymer phosphine recovery (> 97%) following precipitation from diethyl ether.

A monomethoxy-PEG-supported scialic acid glycosyl donor **35** has been utilised in a liquid-phase glycosylation reaction

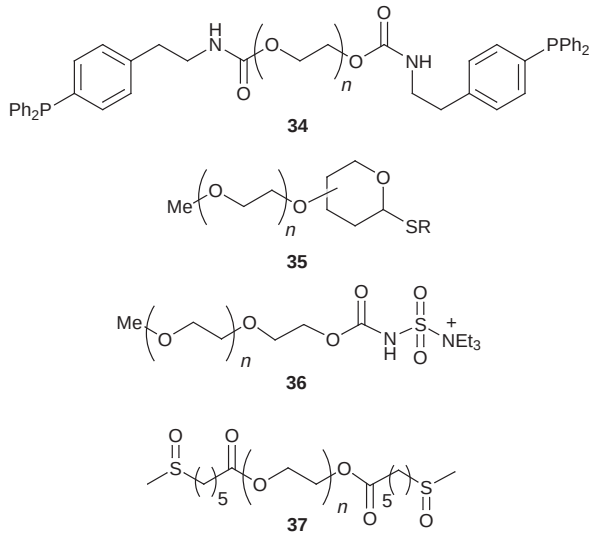

with galactose analogues to give α-linked disaccharides.[45] A PEG-supported variant of the Burgess reagent **36** has been developed for application in a soluble polymer-supported approach to the cyclodehydration of β-hydroxyamides and thioamides.[46] Interestingly, the PEG-supported reagent was found to be much more stable than the solution-phase counterpart and had an extended shelf-life. Vederas and co-workers[47] have synthesised a PEG-supported sulfoxide **37** as a recyclable and odourless alternative for the Swern oxidation. The sulfoxide facilitated the oxidation of a range of alcohols in yields comparable to that of DMSO in solution. The reagent was also recyclable as the spent polymer could be smoothly and quantitatively oxidised back to **37** by treatment with sodium metaperiodate.

In a soluble-polymer strategy analogous to resin-capture,[48] Hori and Janda[49] facilitated the purification of a solution-phase library of β-amino alcohols with a monomethoxy-PEG_{5000}-supported dialkyl borane reagent **38** (Fig. 1). Simple addition of

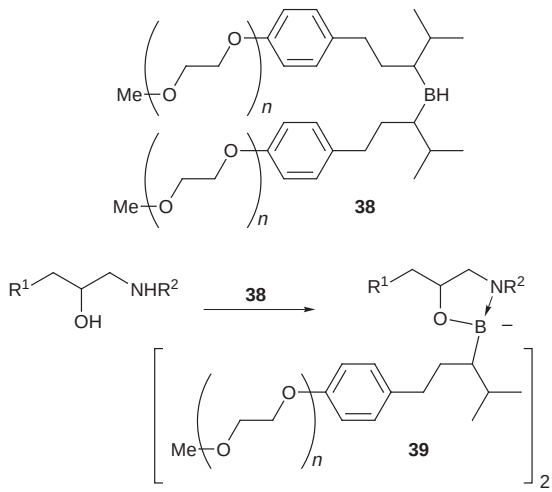

Fig. 1 Liquid-phase 'fishing-out' strategy: PEG-supported dialkylborane **38** facilitates the purification of β-amino alcohols by removal from crude reaction mixtures as polymer-supported 1,2-oxazaborolidines **39**.

38 to a crude reaction mixture containing the required product, followed by precipitation into diethyl ether, gave the polymer-supported 1,3,2-oxazaborolidine **39** from which the amino alcohol was released by acid treatment. By using this 'fishing-out' strategy amino alcohols were isolated greater than 95% pure.

Development of new soluble polymer supports

In comparison with the plethora of supports commercially available for solid-phase synthesis, there is a relative dearth of soluble polymers available to satisfy the increasing demands of liquid-phase chemistry. This reality has lead a number of groups to focus on the development of new supports possessing unique properties within the liquid-phase arena.

By incorporating a sequential normal/living free radical polymerisation strategy with bifunctional initiator **40**[50] and the styryl and vinyl monomers **41a**–**e**, Janda and co-workers[51] have generated linear block copolymer libraries (Fig. 2).

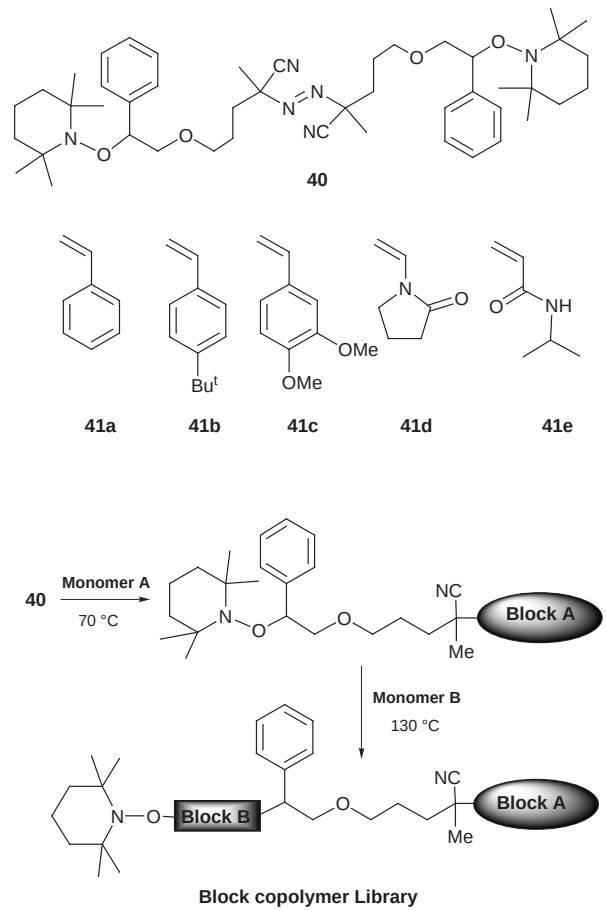

Fig. 2 Bifunctional initiator **40** and monomers **41a**–**e** utilised in a parallel format for block copolymer library generation.

The solubility profile of each library member was then determined in a broad range of organic solvents and water. A copolymer of 4-*tert*-butylstyrene and 3,4-dimethoxystyrene **42** was found to have a solubility profile complementary to that of PEG: soluble in THF and diethyl ether, but insoluble in methanol and water, and was studied as a potential new matrix for liquid-phase chemistry (Scheme 9). The nitrile moieties, located between the two polymer chains, could be smoothly reduced with either $LiAlH_4$ or by catalytic reduction, to generate amino groups as loci for chemical derivatization.

The resulting amino groups of **43** possessed comparable reactivity to that of cyclohexylamine in solution as determined by an imine forming reaction. Derivatization of the amine groups of **43** with a diphosphine ligand **44** gave the polymer-supported chiral diphosphine **45**. The extent of derivatization and oxidation state of the phosphine ligands was routinely monitored by ^1H and ^{31}P NMR spectroscopy. Exchange of $[Rh(cod)Cl]_2$ with the diposphine **45** generated a polymer-supported rhodium(I) species which catalysed the homogeneous enantioselective hydrogenation of dehydroamino acid **46**. The observed ee, stereochemical preference, and kinetics of formation of amino acid **47**, determined by ^1H NMR spectroscopy,

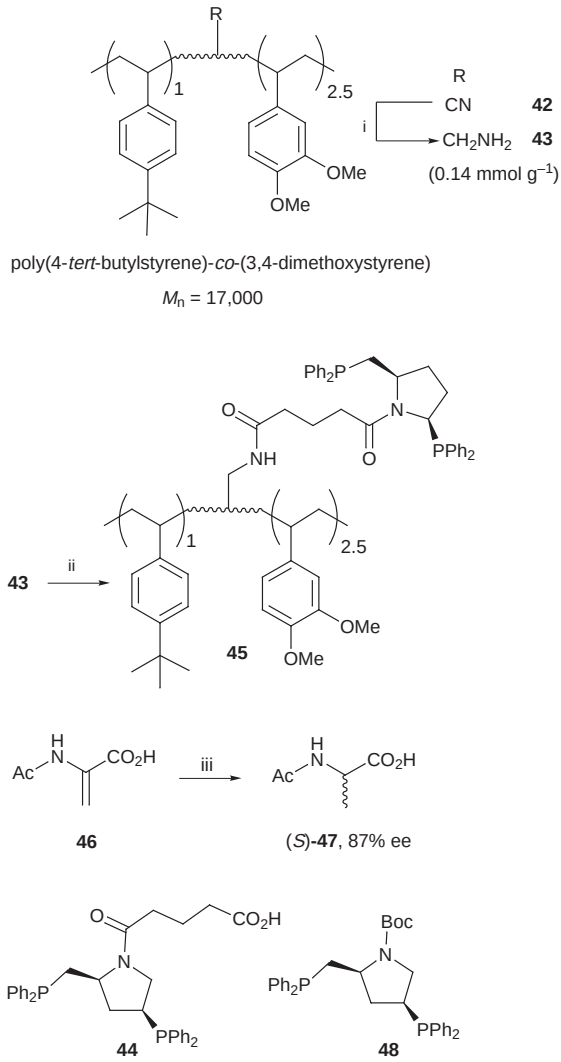

Scheme 9 *Reagents and conditions*: i, $LiAlH_4$ (76 equiv.), THF, reflux, 2 h (quant.); ii, **44** (4 equiv.), DMAP (6 equiv.), EDC (8 equiv.), THF, room temp., 4 h (quant.); iii, **45** (0.04 equiv.), $[Rh(cod)Cl]_2$ (0.02 equiv.), THF, room temp., 4 h, then **46** (1.0 equiv.), H_2 (20 psi), THF, 2 d.

were comparable to that observed with the solution-phase ligand **48**. Isolation of (*S*)-**47** was facilitated in the liquid-phase strategy as the polymer-supported catalyst was removed by simple precipitation into methanol while the solution-phase reaction required silica gel chromatography.

The block copolymer library approach shows how rapidly new linear supports can be assimilated using combinatorial chemistry methods. The only disappointing feature is the low loading capacity of the new materials (*ca.* 0.15 mmol g^{-1}), a result of the uncontrolled nature of the radical polymerisation process. However, the authors note that by increasing the initiator to monomer ratio the polymer chain length will be reduced and so the loading can be improved.

Bergbreiter and co-workers[52] have generated a number of co- and ter-polymers of *N*-isopropylacrylamides **49a–e** which are soluble in water below their lower critical solution temperature (LCST), but precipitate quantitatively at temperatures above their LCST. Thus they can be used as matrices for so-called 'smart' reagents and catalysts.

A concern when generating polymer-supported species where the functional groups are not substituted at the termini, but rather on side-chains along the polymer backbone, is that the reactivity and accessibility of these groups may not be the same as if the reaction were performed in solution. However the rate of catalytic reduction of the nitroarene groups of the poly(*N*-isopropylacrylamide) PNIPAM derivative **49d** below its LCST was equivalent to that of a solution-phase reduction of

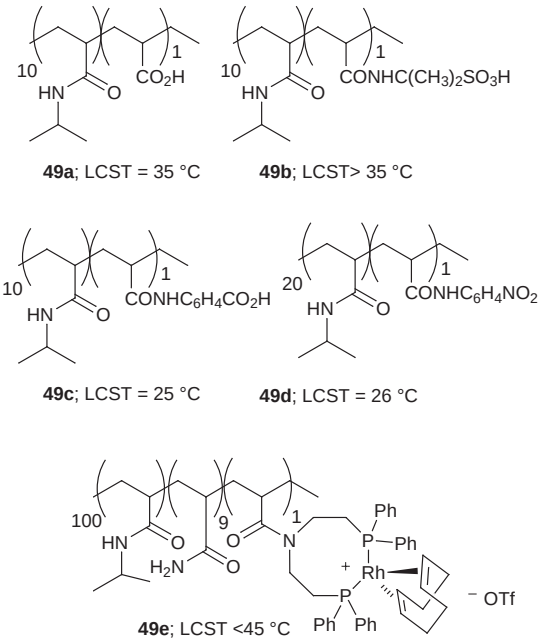

3-acetamidonitrobenzene. The reduction of **49d** effectively ceased on heating above its LCST, showing the 'smart' nature of these polymers as substrate supports. Several PNIPAM-bound rhodium(I) catalysts were prepared including the cationic phosphine-ligated catalyst **49e**. Interestingly the rate of hydrogenation of allyl alcohol catalysed by **49e** was found to be considerably lower than that of a non-polymer bound catalyst, this was found to be caused by hydrogen bonding of the PNIPAM side-chain residues to the cationic rhodium centre. However, replacing the cationic rhodium(I) centre of **49e** with a neutral rhodium(I) core nullified this effect and the soluble-polymer supported approach was as effective as its solution-phase variant.

As discussed *vide supra* the successful use of liquid-phase supports has always been a compromise between loading and solubility profile. By comparison with solid-phase approaches this can appear to be a drawback, as a relatively large weight of polymeric material has to be utilised for a small return of product at the end. However, Cozzi and co-workers[53] have linked dendrimer chemistry to that of PEG chemistry and produced new soluble PEG-supports with expanded functional group capacity. A dihydroxy-PEG_{4600} core (0.43 mmol g^{-1}) was functionalized as a *m*-dicarboxyphenyl derivative which, following standard transformations, yielded a tetrahydroxyaryl-PEG_{4600} **50** with a loading capacity of 0.86 mmol g^{-1} (Scheme 10). This high-loading PEG-derivative was then utilised in a synthetic scheme to generate β-lactam **51**, all of the intermediates being purified by precipitation into diethyl ether with excellent polymer recovery. This shows that the solubility profile of the PEG_{4600} core has not been compromised by the higher terminal substitution. The second generation dendrimer **52** (loading of 1.73 mmol g^{-1}) was also prepared, although its solubility characteristics and utility in synthesis has yet to be demonstrated.

The past two years have seen an explosion in the utility of soluble polymers as supports in combinatorial and organic chemistry. Their unique properties which facilitate purification and easy analysis are making them increasingly useful to academics and industrialists alike and the increasing scope and removal of associated limitations of these matrices can only serve to increase their incorporation into the broad field of polymer-supported chemistry.

Acknowledgements

Financial support for our work in this area was supplied by the NIH and the Skaggs Institute for Chemical Biology.

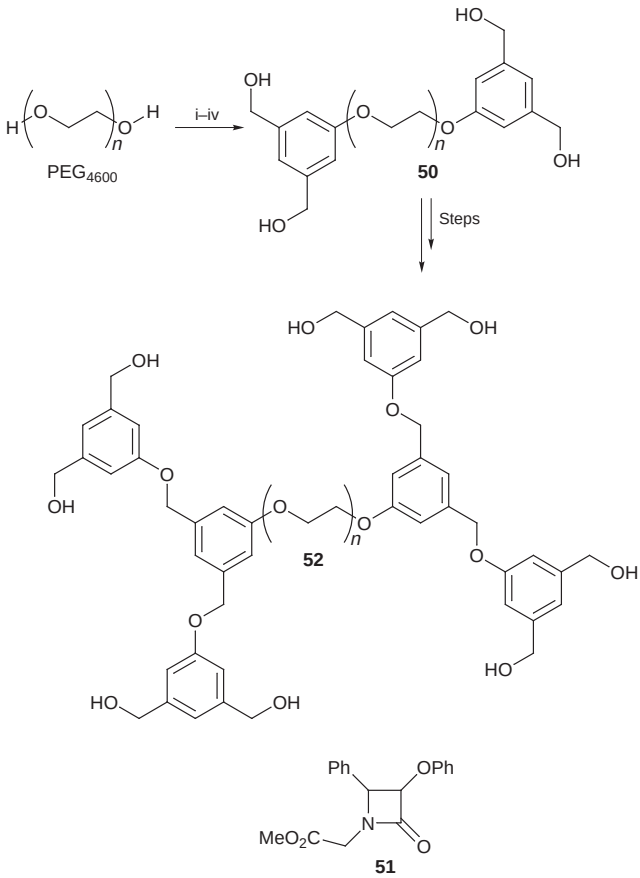

Scheme 10 *Reagents and conditions*: i, MsCl; ii, dimethyl 5-hydroxyisophthalate (3 equiv.), Cs_2CO_3 (3 equiv.), DMF, 50 °C, 15 h (95%); iii, aq. KOH (2 M), room temp., 15 h (70 %); iv, DIBAL-H (10 equiv.), toluene, reflux, 15 h (60%).

Notes and references

1 J. S. Fruchtel and G. Jung, *Angew. Chem., Int. Ed. Engl.*, 1996, **35**, 17.
2 L. A. Thompson and J. A. Ellman, *Chem. Rev.*, 1996, **96**, 555.
3 B. Yan, *Acc. Chem. Res.*, 1998, **31**, 621.
4 H. Han, M. M. Wolfe, S. Brenner, and K. D. Janda, *Proc. Natl. Acad. Sci. U.S.A.*, 1995, **92**, 6419.
5 D. J. Gravert and K. D. Janda, *Chem. Rev.*, 1997, **97**, 489.
6 K. E. Geckeler, *Adv. Polym. Sci.*, 1995, **121**, 31.
7 M. Mutter, H. Hagenmaier and E. Bayer, *Angew. Chem., Int. Ed. Engl.*, 1971, **10**, 811.
8 E. Bayer and M. Mutter, *Nature*, 1972, **237**, 512.
9 D. E. Bergbreiter, *ACS Symp. Ser.*, 1986, **308**, 17.
10 S. Chen and K. D. Janda, *J. Am. Chem. Soc.*, 1997, **119**, 8724.
11 S. Chen and K. D. Janda, *Tetrahedron Lett.*, 1998, **39**, 3943.
12 X.-Y. Zhao, W. A. Metz, F. Sieber, and K. D. Janda, *Tetrahedron Lett.*, 1998, **39**, 8433.
13 R. Noyori and M. Suzuki, *Angew. Chem., Int. Ed. Engl.*, 1984, **23**, 847.
14 M. Narita, *Bull. Chem. Soc. Jpn.*, 1978, **51**, 1477.
15 J. A. Ellman and L. A. Thompson, *Tetrahedron Lett.*, 1994, **35**, 9333.
16 J. J. Krepinsky, in *Modern Methods of Carbohydrate Synthesis*, ed. S. H. Khan and R. A. O'Neill, Harwood Academic Publishers, 1996.
17 S. P. Douglas, D. M. Withfield and J. J. Krepinsky, *J. Am. Chem. Soc.*, 1991, **113**, 5095.
18 C. M. Dreef-Tromp, H. A. M. Willems, P. Westerduin, P. van Veelen and C. A. A. van Boeckel, *Bioorg. Med. Chem. Lett.*, 1997, **7**, 1175.
19 S.-I. Nishimura and K. Yamada, *J. Am. Chem. Soc.*, 1997, **119**, 10 555.
20 K. Yamada, E. Fujita and S.-I. Nishimura, *Carbohydr. Res.*, 1998, **305**, 443.
21 S. Sabesan and J. C. Paulson, *J. Am. Chem. Soc.*, 1986, **108**, 2068.
22 Y. Ito and J. C. Paulson, *J. Am. Chem. Soc.*, 1993, **115**, 1603.
23 B. Sauvagnat, F. Lamaty, R. Lazaro and J. Martinez, *Tetrahedron Lett.*, 1998, **39**, 821.
24 C. G. Blettner, W. A. Koenig, W. Stenzel and T. Scotten, *Synlett*, 1998, 295.
25 A. Padwa, *1,3-Dipolar Cycloaddition Chemistry*, John Wiley & Sons, New York, 1984.
26 J.-F. Cheng and A. M. M. Mjalli, *Tetrahedron Lett.*, 1998, **39**, 939.
27 M. Moore and P. Norris, *Tetrahedron Lett.*, 1998, **39**, 7027.
28 E. M. Gordon, R. W. Barrett, W. J. Dower, S. P. A. Fodor and M. A. Gallop, *J. Med. Chem.*, 1994, **37**, 1385.
29 J. Yoon, C.-W. Cho, H. Han and K. D. Janda, *Chem. Commun.*, 1998, 2703.
30 D. Lednicer and L. A. Mitschner, in *The Organic Chemistry of Drug Synthesis*, Wiley, New York, 1977.
31 X.-Y. Zhao and K. D. Janda, *Tetrahedron Lett.*, 1997, **38**, 5437.
32 X.-Y. Zhao and K. D. Janda, *Bioorg. Med. Chem. Lett.*, 1998, **8**, 2439.
33 P. Wentworth Jr. and K. D. Janda, *Curr. Opin. Biotechnol.*, 1998, **9**, 109.
34 S. J. Shuttleworth, S. M. Allin and P. K. Sharma, *Synthesis*, 1997, 1217.
35 R. J. Booth and J. C. Hodges, *Acc. Chem. Res.*, 1999, **32**, 18.
36 H. Han and K. D. Janda, *J. Am. Chem. Soc.*, 1996, **118**, 7632.
37 H. Han and K. D. Janda, *Tetrahedron Lett.*, 1997, **38**, 1527.
38 H. Han and K. D. Janda, *Angew. Chem., Int. Ed. Engl.*, 1997, **36**, 1731.
39 C. Bolm and A. Gerlach, *Angew. Chem., Int. Ed. Engl.*, 1997, **36**, 741.
40 S. Kobayashi, S. Nagayama and T. Busujima, *Tetrahedron Lett.*, 1996, **37**, 9221.
41 S. Kobayashi and S. Nagayama, *Synlett*, 1997, 653.
42 M. Felder, G. Giffels and C. Wandrey, *Tetrahedron: Asymmetry*, 1997, **8**, 1975.
43 L. Canali and D. C. Sherrington, *Chem. Commun.*, 1997, 123.
44 P. Wentworth Jr., A. M. Vandersteen and K. D. Janda, *Chem. Commun.*, 1997, 759.
45 L. O. Kononov, Y. Ito and T. Ogawa, *Tetrahedron Lett.*, 1997, **38**, 1599.
46 P. Wipf and S. Venkatraman, *Tetrahedron Lett.*, 1996, **37**, 4659.
47 J. h. Harris, Y. Liu, S. Chai, M. D. Andrews and J. C. Vederas, *J. Org. Chem.*, 1998, **63**, 2407.
48 T. A. Keating and R. W. Armstrong, *J. Am. Chem. Soc.*, 1996, **118**, 2574.
49 M. Hori and K. D. Janda, *J. Org. Chem.*, 1998, **63**, 889.
50 D. J. Gravert and K. D. Janda, *Tetrahedron Lett.*, 1998, **39**, 1513.
51 D. J. Gravert, A. Datta, P. Wentworth Jr. and K. D. Janda, *J. Am. Chem. Soc.*, 1998, **120**, 9481.
52 D. E. Bergbreiter, B. L. Case, Y.-S. Liu and J. W. Caraway, *Macromolecules*, 1998, **31**, 6053.
53 M. Benaglia, R. Annunziata, M. Cinquini, F. Cozzi, and R. Stefano, *J. Org. Chem.*, 1998, **63**, 8628.

Paper 9/01955C

Preparation of an organophilic palladium montmorillonite catalyst in a micellar system

Zoltán Király,*[a] Bernadett Veisz,[a] Ágnes Mastalir,[b] Zsolt Rázga[c] and Imre Dékány[a]

[a] *Department of Colloid Chemistry, University of Szeged, Aradi Vt. 1, H-6720 Szeged, Hungary. E-mail: zkiraly@chem.u-szeged.hu*
[b] *Department of Organic Chemistry, University of Szeged, Dóm tér 8, H-6720 Szeged, Hungary*
[c] *Laboratory for Electron Microscopy, University of Szeged, Kossuth L. sgt. 40, H-6725 Szeged, Hungary*

Received (in Oxford, UK) 30th June 1999, Accepted 23rd August 1999

The cation-exchange reaction between sodium montmorillonite and tetradecyltrimethylammonium bromide serving as a stabilizing agent in a palladium hydrosol led to the formation of alkylammonium montmorillonite with simultaneous immobilization of the palladium nanoparticles in the organoclay host; the Pd-organoclay proved to be catalytically active in olefin hydrogenation in the liquid phase.

The incorporation of Pd^{2+} ions, Pd(II) complexes or metallic Pd particles between the silicate layers of montmorillonite permits liquid-phase hydrogenation reactions with improved catalytic activity and specificity as compared with those involving supported Pd catalysts prepared by conventional impregnation routes, or with Pd(II) catalysts used in homogeneous solution. Pd(II) acetate and Pd(II) chloride have earlier been anchored to internal surface sites of montmorillonite *via* bipyridyl, diphenylphosphine and other linkages to produce interlamellar functionalized montmorillonite Pd(II) catalysts.[1,2] Reaction of ion-exchanging Na^+-montmorillonite with $[Pd(NCMe)_4]^{2+}$ and subsequent reduction of the Pd^{2+} in methanol afforded highly-dispersed metallic Pd particles in the clay galleries.[3] Ethanol is both a solvent and a reducing agent for Pd(II) acetate.[4] The preferential adsorption of ethanol from dilute hydrocarbon solutions in the interlamellar spaces of alkylammonium montmorillonite[5,6] and alumina-pillared montmorillonite[7] provided a suitable environment for *in situ* reduction of the Pd(II) acetate precursor in the interlamellar spaces of the clay host. The present work describes a new pathway for the production of organophilic Pd-montmorillonite (Pd-M) with a good control over the size of the Pd nanoparticles and the Pd content of the clay. The method involves the synthesis of a monodispersed Pd hydrosol with subsequent deposition of the Pd particles onto the clay lamellae.

The preparation of the Pd hydrosol and a systematic study relating to the control over the Pd particle size were performed under the following experimental conditions. 25–200 μL of Pd(II) acetylacetonate [$Pd(acac)_2$] solution (0.5–3 w/v% in $CHCl_3$) were added to 10 mL of tetradecyltrimethylammonium bromide (C_{14}TAB) surfactant solution [5–50 times the critical micelle concentration (cmc = 3.9 mM at 298 K in water)]. An excess of NH_2NH_2 solution (55 w/w% in water) was then introduced into the micellar system, which was left under vigorous stirring overnight to produce ultrafine Pd particles stabilized by the cationic surfactant.

The preparation of Pd-M and a systematic study concerning the control over the Pd content of the Pd-organoclay included the following experimental conditions. 50–200 mL of Pd hydrosol (stabilized with C_{14}TAB, 5–50 times the cmc) were added to 100–500 mL Na^+-montmorillonite suspension (0.1–2 w/w% in water) and the system was mixed vigorously overnight. The surfactant molecules rendered the clay surface hydrophobic, in parallel with the adsorption of the Pd particles on the silicate surface. The Pd-M material was purified by several centrifugation/redispersion cycles in ethanol and finally dried in the oven.

The proposed mechanism for the successive formation of the Pd hydrosol and the Pd-organoclay is outlined in Fig. 1. Whereas water is a poor solvent, $CHCl_3$ is a good solvent for $Pd(acac)_2$. The apparent solubility of $CHCl_3$ in water increases considerably if a sufficient quantity of C_{14}TAB surfactant is present in the aqueous phase (c > cmc). This solubilization effect allows the preparation of an aqueous colloidal solution of $Pd(acac)_2$ previously dissolved in $CHCl_3$. The UV-VIS spectra (UVIKON 930 spectrophotometer) of $Pd(acac)_2$ indicated a shift in the absorbance maximum in the micellar solution (340 nm) as compared with that in pure $CHCl_3$ solvent (327 nm). This observation may be attributed to the change in the microenvironment of $Pd(acac)_2$ upon solubilization, or to the formation of an adduct between the surfactant and the palladium salt.[8] In either case, the addition of an aqueous NH_2NH_2 solution to the $Pd(acac)_2$–$CHCl_3$–C_{14}TAB–water micellar system resulted in the formation of nanoscale Pd particles, partly sterically and partly electrostatically stabilized by the cationic surfactant molecules adsorbed on the surface of the particles (Fig. 1). The size distribution of the Pd particles in the hydrosol was determined by using a Philips C-10 transmission electron microscope (TEM) at 100 kV, assisted by the UTHSCSA Image Tool program. The present preparation method yielded spherical, monodispersed particles with a good control of size in the range 1.5–6 nm. We found that the particle size in the Pd hydrosol decreases with a decrease of the $Pd(acac)_2$ concentration and, in particular, with an increase of the C_{14}TAB concentration.

The formation of Pd-M was readily achieved by mixing the hydrosol with a dilute montmorillonite suspension. Reaction of the ion-exchanging Na^+-montmorillonite with the stabilizing (and in part with free) cationic surfactant molecules resulted in the formation of organophilic alkylammonium montmorillonite with the simultaneous release and subsequent deposition of the Pd nanoparticles onto the surface of the silicate layers (Fig. 1).

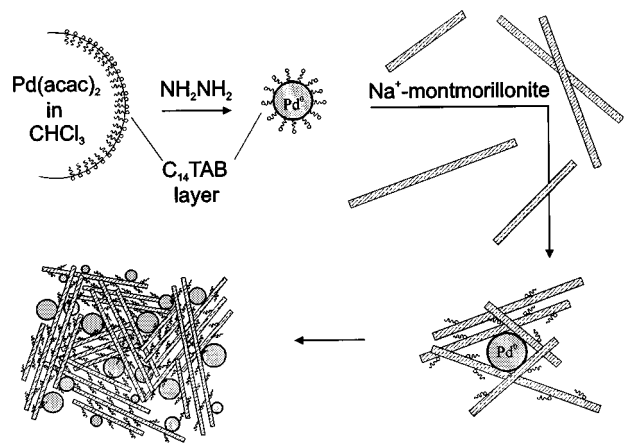

Fig. 1 Schematic illustration of the proposed mechanism for the successive formation of Pd hydrosol and Pd-organoclay in a micellar system.

Table 1 Characterization of organophilic Pd-montmorillonite catalysts

Catalyst code number	d(TEM)/nm	Pd (w/w%) (UV–VIS)	Pd (w/w%) (ICP–AES)	$10^{-3}r_i$[a] (styrene)	$10^{-3}r_i$[a] (hex-1-ene)	$10^{-3}r_i$[a] (cyclohexene)
Pd-M1	2.42	0.09	0.11	275.1	101.8	9.5
Pd-M2	3.25	1.15	1.32	34.8	26.5	5.8
Pd-M3	5.21	1.68	1.90	1.8	1.1	0.8

[a] Initial rate of hydrogenation, r_i [mL H_2 (g Pd min)$^{-1}$], in toluene.

TEM images indicated that the particles are more or less uniformly distributed on the external surface sites. The Pd contents of the Pd-M samples were determined indirectly by measuring the absorbance of the supernatant at 600 nm[9] during adsorptive removal of the Pd colloids by montmorillonite. Further, the Pd content was measured directly by inductively coupled plasma atomic emission spectroscopy at 229.7 nm[7] (ICP-AES, Jobin Yvon 24). It was established that the Pd content of the organoclay increases with decreasing solid to liquid ratio and, in particular, with decreasing surfactant concentration. X-Ray diffraction measurements on dry Pd-M samples were made with a Philips 1820 diffractometer (40 kV, 35 mA, Cu-Kα radiation) in the diffraction angle range 2θ = 1–10°. Each material gave a broad d_{001} reflection, with an interlayer spacing substantially smaller than the mean diameter of the Pd particles as determined by TEM. This finding is consistent with a disordered deposition of layer packets encapsulating the Pd particles (Fig. 1). A regular pattern of intercalation of the Pd species between the layers is unlikely.

Pd-M can be dispersed in organic solvents (ethanol, benzene, acetone, *etc*.) that are generally used in contact catalytic hydrogenation reactions in the liquid phase. Three Pd-M samples were selected for catalytic test reactions (Table 1). Toluene was used as the reaction medium: this solvent readily wets and swells the organoclay and provides access to the Pd particles for the reactant molecules. The rates of styrene, hex-1-ene and cyclohexene hydrogenation were recorded by using an automated vibration reactor at atmospheric pressure at 303 K. Typically, the reaction vessel contained 1 mL of toluene, 0.1 mL of substrate and a calculated amount of catalyst loaded with 25 μg of Pd. A Hewlett Packard GC–MS apparatus (HP 5890; HP 5970) was used for product analysis. Close correlations were found between the catalytic activity and the position of the C=C double bond of the substrate, and the catalytic activity and the degree of dispersion of the Pd particles (Table 1). For a given substrate, the initial rate of hydrogenation, r_i, increases appreciably with decreasing particle size. For a given Pd-M catalyst, r_i increases in the sequence styrene > hex-1-ene > cyclohexene. The C=C bond in conjugation with the aromatic ring displays the highest affinity toward the uptake of hydrogen, and the reactivity is higher for the terminal olefin than for the internal one. GC–MS analysis at intermediate stages indicated that the consecutive (isomerization plus hydrogenation) reactions hex-1-ene→(*trans*- and *cis*-hex-2-ene)→*n*-hexane are superimposed on the hydrogenation reaction hex-1-ene→*n*-hexane. While the simultaneous hydrogenation and isomerization of hex-1-ene were found to be fast processes, as was the hydrogenation of styrene, the rate of conversion to *n*-hexane was moderated by the appearance of the hex-2-ene isomers and the kinetic curve resembled that of cyclohexene (internal olefin).

It is anticipated that the basic principles of the present preparation method can be applied to other systems where the metallic particles are stabilized by ionic surfactants and the solid support is an oppositely charged ion exchanger. For example, if transition metal particles (M) stabilized by anionic surfactants are mixed with positively charged layered double hydroxides (LDH), organophilic M-LDH will be formed, which can be used in contact catalytic reactions in organic solvents. Experimental work on this system is currently being undertaken.

Z. K. and Á. M. gratefully acknowledge the financial support of the Hungarian Scientific Foundation through grants OTKA T025002 and T026430.

Notes and references

1 K. Ravikumar, B. M. Choudary and Zafir Jamil, *J. Chem. Soc., Chem. Commun.*, 1986, 130.
2 B. M. Choudary, G. V. M. Sharma and P. Barathi, *Angew. Chem., Int. Ed. Engl.*, 1989, **28**, 465.
3 M. Crocker, J. G. Buglass and R. H. M. Herold, *Chem. Mater.*, 1993, **5**, 105.
4 K. Esumi, T. Itakura and K. Torigoe, *Colloids Surf.*, 1994, **82**, 111.
5 Z. Király, I. Dékány, Á. Mastalir and M. Bartók, *J. Catal.*, 1996, **161**, 401.
6 Á. Mastalir, F. Notheisz, Z. Király, M. Bartók and I. Dékány, *Stud. Surf. Sci. Catal.*, 1997, **108**, 477.
7 A. Szücs, Z. Király, F. Berger and I. Dékány, *Colloids Surf.*, 1998, **139**, 109.
8 N. Arul Dhas and A. Gedanken, *J. Mater. Chem.*, 1998, **8**, 445.
9 D. N. Furlong, A. Launikonis, H. F. Sasse and J. V. Sanders, *J. Chem. Soc., Faraday Trans. 1*, 1984, **80**, 571.

Communication 9/05321B

Facile α-deprotonation–electrophilic substitution of quinuclidine and DABCO

Satinder V. Kessar,* Paramjit Singh, Kamal N. Singh and Sandeep K. Singh

Department of Chemistry, Panjab University, Chandigarh-160014, India. E-mail: svkessar@panjabuniv.chd.nic.in

Received (in Cambridge, UK) 2nd July 1999, Accepted 30th July 1999

Deprotonation of BF_3 complexes of quinuclidine or DABCO by Schlosser base and subsequent reaction with electrophiles affords α-substituted products in moderate to good yields.

A number of drugs and molecules acting as chiral catalysts have a quinuclidine (**1**) framework with an appendage at a carbon atom α to the bridgehead nitrogen.[1] We envisaged a direct access to such compounds from the basic system *via* a Lewis acid promoted amine deprotonation procedure,[2] even though removal of a secondary α-proton from a piperidine ring is often problematic.[3] In the event, strong BF_3 activation in conjunction with the use of a superbase (Bu^sLi/Bu^tOK) proved to be effective for deprotonation of **1** (Scheme 1).[4,5] Subsequent reaction with electrophiles proceeded smoothly to afford a variety of products **4** in moderate to good yields (Table 1).† Barton's *N*-oxide approach is the only other route available for similar elaboration of the quinuclidine framework.[6] Our method

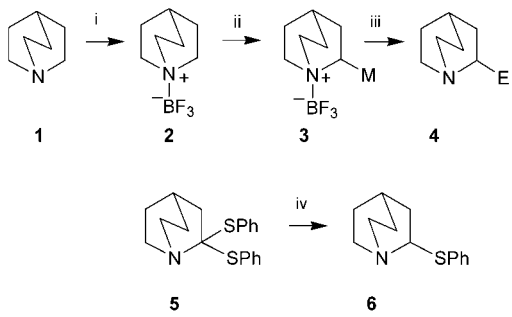

Scheme 1 *Reagents and conditions:* i, $BF_3.Et_2O$ (1.1 equiv.), 0 °C, 0.25 h, THF; ii, Bu^sLi/Bu^tOK (2.2 equiv.). −78 °C, 2 h; iii, electrophile (2.2 equiv.), −78 °C, 30 min, 30 min, −30 °C, then HCl (10%); iv, lithium naphthalenide, THF, −78 °C AcOH.

Table 1 Reaction of deprotonated BF_3-complexed bridgehead amines

Entry	Amine	Electrophile	Product	Yield (%)[a]
1	**1**	BnBr	**4a** E = Bn	34
2	**1**	BzOEt	**4b** E = Bz	74
3	**1**	$(p\text{-}MeOC_6H_4)_2C{=}O$	**4c** E = $C(OH)(p\text{-}MeOC_6H_4)_2$	68
4	**1**	PhCH=O	**4d** E = CH(OH)Ph	
			threo[b]	72
			erythro	< 6[c]
5	**1**	1-Naphthaldehyde	**4e** E = CH(OH)-1-naphthyl	
			threo	41
			erythro	15
6	**1**	2-Naphthaldehyde	**4f** E = CH(OH)-2-naphthyl	
			threo	40
			erythro	24
7	**1**	PhSSPh	**5**	52
			6	4
8	**7**	BzOEt	**8a** E = Bz	51
9	**7**	$Ph_2C{=}O$	**8b** E = $C(OH)Ph_2$	72
10	**7**	1-Naphthaldehyde	**8c** E = CH(OH)-1-naphthyl	
			threo	36
			erythro	40

[a] Yields are for pure products isolated after chromatography or crystallisation. [b] Ref. 7. [c] Could not be obtained in pure form.

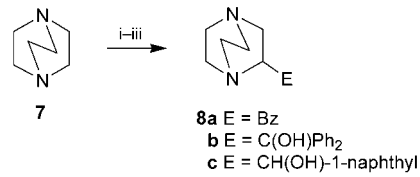

Scheme 2 *Reagents and conditions:* i–iii as in Scheme 1.

avoids separate *N*-oxide formation–deoxygenation steps and the overall yields for the two procedures are comparable.

The Lewis acid activation method was also explored to obtain a quinuclidine with an α-attached sulfur atom, which with its various oxidation states can provide novel bidentate ligands. On reaction of **1** with diphenyl disulfide under standard conditions the disubstituted compound **5** was obtained as the major product (52%). However, it could be cleanly reduced to the desired monosubstituted compound **6** with lithium naphthalenide in THF.[8] Finally, this methodology was extended to α-deprotonation–electrophilic substitution of DABCO (**7**) (Scheme 2).‡ This readily available diazabicyclooctane has also been used extensively to modify organic reactions.[9] However, few reports of the synthesis and use of DABCO analogs of natural and synthetic quinuclidine compounds have appeared in the literature and their potential, as ligands and drugs, has remained largely unexplored.[10]

Notes and references

† All compounds were characterised by ^1H NMR and ^{13}C NMR spectroscopy and mass spectrometry. Mps of known compounds corresponded with literature values. *Selected data* for **4f** (*threo*): mp 104–105 °C (hexane); $\delta_H(CDCl_3$, 300 MHz) 1.13–1.33 (m, 2H), 1.38–1.55 (m, 4H) (C-3H, C-5H, C-7H), 1.75 (br s, 1H, C-4H), 2.73–2.89 (m, 2H), 2.93–2.99 (m, 2H), 3.05–3.15 (m, 1H) (C-2H, C-6H, C-8H), 4.52–4.55 (d, *J* 9.7, 1H, C-9H), 7.43–7.49 (m, 2H, ArH), 7.54–7.57 (d, *J* 8.6, 1H, ArH), 7.81–7.84 (m, 4H, ArH); $\delta_C(CDCl_3)$ 21.5 (CH), 25.8 (CH_2), 26.8 (CH_2), 29.4 (CH_2), 41.4 (CH_2), 49.6 (CH_2), 62.6 (CH), 74.7 (CH), 125.0 (CH), 125.7 (CH), 125.9 (CH), 126.5 (CH), 127.7 (CH), 127.9 (CH), 128.0 (CH and Cq), 133.2 (Cq), 138.7 (Cq); *m*/*z* 268 (M^+ + 1, 11.9%), 267 (M^+, 54.7), 250 (11.2), 158 (12.0), 141 (14.4), 129 (28.9), 111 (57.2), 82 (100) (Calc. for $C_{18}H_{21}NO$, 267.1623. Found 267.1628). For **6**: mp 65–66 °C (hexane); $\delta_H(CDCl_3$, 300 MHz) 1.25 (br s, 1H), 1.31–1.38 (m, 1H), 1.51–1.54 (m, 3H), 1.82 (br s, 1H), 2.02–2.10 (m, 1H) (C-3H, C-4H, C-5H, C-7H), 2.69–2.78 (m, 1H), 2.99–3.11 (m, 2H), 3.49–3.59 (m, 1H) (C-6H, C-8H), 4.50–4.56 (t, *J* 8.6, 1H, C-2H), 7.14–7.17 (d, *J* 7.1, 1H, ArH), 7.22–7.27 (t, *J* 7 Hz, 2H, ArH), 7.41–7.44 (d, *J* 7.4, 2H, ArH); $\delta_C(CDCl_3)$ 22.7 (CH), 25.5 (CH_2), 26.8 (CH_2), 34.5 (CH_2), 40.8 (CH_2), 48.6 (CH_2), 65.8 (CH), 126.0 (CH), 128.7 (2CH), 129.2 (2CH), 136.9 (Cq); *m*/*z* 220 (M^+ + 1, 14.8%), 219 (M^+, 100), 218 (17.9), 186 (30.7), 142 (31.5), 110 (80.0), 98 (79.0), 82 (25.8) (Calc. for $C_{13}H_{17}NS$, 219.1081. Found 219.1083).

‡ *Conditions* for α-deprotonation–electrophile reaction of DABCO: To a solution of Bu^tOK (2.2 mmol) and Bu^sLi (2.2 mmol) in THF (6 ml) at −78 °C was added slowly *via* a cannula a solution of DABCO–BF_3 complex (1.0 mmol) in THF (4 ml) under a nitrogen atmosphere. After stirring for 2 h, a solution of the electrophile (2.2 mmol) in THF (2 ml) was added dropwise. The temperature was maintained at −78 °C for 30 min and then allowed to rise to −30 °C over a period of 30 min. The reaction mixture was quenched with 10% HCl (5 ml) and worked up.

1 R. Verpoorte, J. Shripsema and T. van der Leer, *The Alkaloids*, ed. A. Brossi, Academic Press, New York, 1988, vol. 34, p 332; M. S. Ashwood, A. W. Gibson, P. G. Houghton, G. R. Humphrey, D. C.

Roberts and S. H. B. Wright, *J. Chem. Soc., Perkin. Trans. 1*, 1995, 641; K. B. Sharpless, W. Amberg, Y. L. Bennani, G. A. Crispino, J. Hartung, K.-S. Jeong, H.-L. Kwong, K. Morikawa, Z.-M. Wang, D. Xu and X.-L. Zhang, *J. Org. Chem.*, 1992, **57**, 2768; K. E. Simons, A. Ibbotson, P. Johnston, H. Plum and P. B. Wells, *J. Catal.*, 1994, **150**, 321; M. J. O'Donnell, *Catalytic Asymmetric Synthesis*, ed. I. Ojima, VCH, Weinheim, 1993, p. 389.

2 S. V. Kessar, P. Singh, R. Vohra, N. P. Kaur and K. N. Singh, *J. Chem. Soc., Chem. Commun.*, 1991, 568; S. V. Kessar, P. Singh, K. N. Singh and M. Dutt, *J. Chem. Soc., Chem. Commun.*, 1991, 570; S. V. Kessar and P. Singh, *Chem. Rev.*, 1997, **97**, 721.

3 R. E. Gawley and K. Rein, *Comprehensive Organic Synthesis*, ed. B. M. Trost and I. Fleming, Pergamon, New York, 1991, vol. 1, p 459 and vol. 3, p. 65.

4 M. Schlosser and J. Hartmann, *Angew. Chem., Int. Ed. Engl.*, 1973, **12**, 508; W. Bauer and L. Lochmann, *J. Am. Chem. Soc.*, 1992, **114**, 7482; P. Caubere, *Chem. Rev.*, 1993, **93**, 2317.

5 Attempted deprotonation with alkyllithiums was unsuccessful and use of 2 equiv. of Schlosser base seems necessary. BH_3 activation is ineffective in this case although it is very useful for removal of more acidic α-protons. M. R. Ebden, N. S. Simpkins and D. N. A. Fox, *Tetrahedron Lett.*, 1995, **36**, 8697; E. Vedejs and J. T. Kendall, *J. Am. Chem. Soc.*, 1997, **119**, 6941.

6 D. H. R. Barton, R. Beugelmans and R. N. Young, *Nouv. J. Chim.*, 1978, **2**, 363. For $TiCl_3$ reduction modification of this procedure see: K. B. Sharpless, H. C. Kolb and P. G. Andersson, *J. Am. Chem. Soc.*, 1994, **116**, 1278.

7 The *threo* and *erythro* configurations were assigned on the basis of coupling constants between C-2 and C-9 methine protons in the NMR spectrum. T. Kametani, H. Matsumoto, Y. Satoh, H. Nemoto and K. Fukumoto, *J. Chem. Soc., Perkin Trans. 1*, 1977, 376.

8 T. Cohen, W. M. Daniewski and R. B. Weisenfeld, *Tetrahedron Lett.*, 1978, 4665.

9 K. B. Sharpless and R. Oi, *Tetrahedron Lett.*, 1991, **32**, 4853.

10 K. Soai, A. Oshio and H. Yoneyama, *Tetrahedron: Asymmetry*, 1992, **3**, 359.

Communication 9/05359J

ChemComm

Origin of diastereoselectivity in the addition of allylsilane to chiral acyclic mixed acetals

Kavita Manju and Sanjay Trehan*

Department of Chemistry, Panjab University, Chandigarh-160 014, India. E-mail: strehan@panjabuniv.chd.nic.in

Received (in Cambridge, UK) 9th June 1999, Accepted 12th August 1999

Addition of allylsilane to chiral acyclic mixed acetals has been found to proceed *via* an S_N1 mechanism and a model has been proposed to explain the observed diastereoselectivity.

Over the last couple of decades great strides have been made in the Lewis acid catalysed reaction of chiral acetals with silyl nucleophiles. Chiral cyclic acetals have been studied in detail and the mechanism as well as the diastereofacial selectivity of their reaction is now well-established.[1] Despite the fact that chiral mixed acyclic acetals prepared *in situ* give homoallylic ethers in high diastereoselectivity,[2] an understanding of the origin of the diastereoselectivity is lacking. In order to comprehend the origin of the diastereoselectivity one needs to first establish the mechanism (S_N1 or S_N2) because there is support for both type of mechanisms in the literature.†[3] If the reaction proceeds *via* an S_N2 mechanism, then the origin of the diastereoselectivity should lie in the diastereoselective formation of a silyl acetal intermediate which would undergo allylation in a stereospecific manner (Scheme 1). In such a case the diastereomeric ratio of the silyl acetal (**3a**:**3b**) and homoallylic ether (**4a**:**4b**) should be the same. Alternatively, if the reaction proceeds *via* an S_N1 mechanism, a common oxocarbenium ion **5** will be formed from both the silyl acetal intermediates. The diastereoselectivity in this case will be determined by the extent of 1,3-induction[4] and will be independent of the ratio of the silyl acetals (**3a**:**3b**) (Scheme 1). Houk has proposed a theoretical model for the nucleophilic addition on this type of oxocarbenium ion by invoking a weak 1,3-allylic interaction and has shown reaction occurring from the most stable conformation **5′** giving **4b** as the major product.[5] Herein, we report our results which establish the mechanism and the diastereoselectivity of this reaction.

Chiral ester **6** prepared from (*R*)-1-phenethyl alcohol and hydrocinnamic acid was treated with 1 equiv. of DIBAL-H and the intermediate was treated with TMSOTf and pyridine[6] to give acetal **7a**/**7b** as a mixture of diastereomers in the ratio of 54:46 (Scheme 2).‡ This mixture of acetals was treated with 0.1 equiv. of TMSOTf and 1.5 equiv. of allyltrimethylsilane in toluene at −78 °C to give homoallylic ether **8a**/**8b** in 79% yield. The diastereomeric ratio was found to be 82:18 from its ^{1}H NMR, which was vastly different from its precursor acetals. Identical diastereoselectivity was also obtained when hydrocinnamaldehyde was treated with the trimethylsilyl ether of (*R*)-1-phenethyl alcohol and allyltrimethylsilane in the presence of TMSOTf in toluene at −78 °C. These two experiments suggests an S_N1 mechanism whether the mixed acetal is prepared *in situ* or is isolated before allylation.

The configuration of the newly created chiral centre was established to be *S* from the optical rotation of the corresponding homoallylic alcohol **9a**/**9b** {$[\alpha]_D$ −12.6 (*c* 1, $CHCl_3$); lit.[7] +16.9 (*c* 1, $CHCl_3$) for the *R* isomer with 80% ee} obtained by treatment of **8a**/**8b** with iodotrimethylsilane.[8] Thus the major diastereomer formed is (*S*,*R*)-**8a**, just as reported in earlier work,[2] and not (*R*,*R*)-**8b** as as identified mistakenly by Houk as the major product obtained by Mukaiyama[2b] and Seebach[2c] while applying his model.[5] Since the Houk model is not applicable to the system under investigation an alternate model is desirable. The reaction of the oxocarbenium ion intermediate is expected to be exothermic in nature, therefore in the absence of any polar group in the chiral centre, the ground state conformation of the oxocarbenium ion should be important in determining the diastereoselectivity.[9] In order to establish the importance of steric or stereoelectronic effects on the conformational preferences of the oxocarbenium ion intermediate leading to the product, various silyl ethers with R groups of increasing steric bulk were synthesised and used in the allylation reaction.[10] The results are summarised in Table 1. The configuration of the products was assigned as done earlier except when silyl ethers with isopropyl groups were used, because they could not be prepared in reasonable optical purity. In these cases the configuration was established by correlation of their ^{1}H NMR with that of **8**.

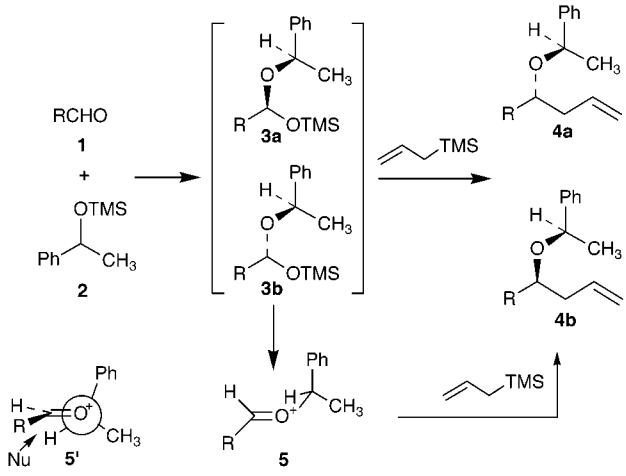

Scheme 1

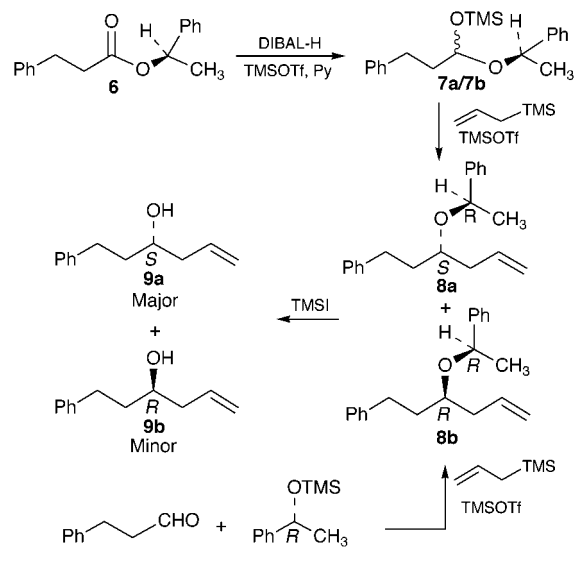

Scheme 2

Table 1 Reaction of hydrocinnamaldehyde with various silyl ethers and allylsilane[ab]

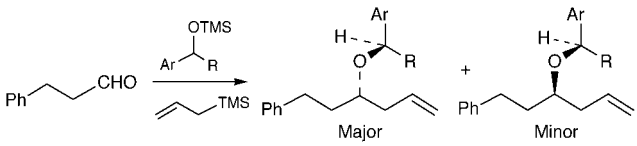

Entry	Ar	R	Diastereomer ratio[c]	Yield (%)
1	Ph	Me	82:18 (4.5:1)	89
2	Ph	Et	85:15 (5.7:1)	82
3	Ph	Pr^i	86:14 (6.1:1)[d]	85
4	*o*-Tolyl	Me	88:12 (7.3:1)	82
5	*o*-Tolyl	Et	93:07 (13.3:1)	88
6	*o*-Tolyl	Pr^i	91:09 (10.1:1)[d]	80

[a] All reactions were carried out in toluene at −78 °C under nitrogen atmosphere. [b] Enantiomeric excess of silyl ethers used in entries 1, 2, 4 and 5 were 94, 89, 90 and 81% respectively (ref. 11) and (±)-silyl ethers were used in entries 3 and 6. [c] Diastereomeric ratio was determined *via* ^{1}H NMR. [d] Configuration was established by correlation of ^{1}H NMR with that of **8**.

If steric effects were important, then one would expect a decrease in diastereoselectivity with a decrease in the steric difference between the medium and large groups. However, the opposite trend was observed and generally diastereoselectivity increased as the size of the alkyl group increased in the two series studied (Table 1, entries 1–3 and 4–6). This suggests that stereoelectronic effects stabilise certain select conformations of the oxocarbenium ion leading to the product. In the absence of any electrostatic effects,[12] the important stereoelectronic interactions between the three groups of the chiral centre and the C=O bond which can restrict the conformational mobility of the chiral centre are σ*–π* and π–π* (hyperconjugation).[13,14] However, conformation **10** obtained using the σ*–π* interaction[10] is similar to Houk's model[5] and therefore does not appear to be important. Therefore hyperconjugation between the substituents of the chiral centre and the oxocarbenium ion appears to be the predominant stereoelectronic interaction.

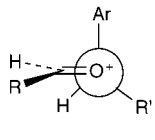

10

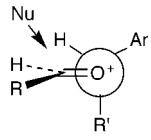

11a

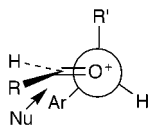

11b

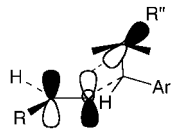

12

We suggest that the reaction proceeds through a conformation where the alkyl group occupies the *anti* position. In conformations **11a** and **11b** besides normal α–β C–C hyperconjugative stabilisation of the oxocarbenium ion there is an additional stabilisation due to bonding between the β–γ substituents, as depicted in **12**.[14c] This stabilisation is greater for a C–C bond than for a C–H bond.[14c] Therefore ethyl or isopropyl groups should stabilise conformations **11a** and **11b** more than a methyl group over other conformations. This additional stabilisation is missing for bonding between the chiral carbon and aryl groups or hydrogen.§¶‖

We conclude that C–C hyperconjugative stabilisation of the oxocarbenium ion restricts the conformation of the chiral centre to **11a** and **11b** leading to major and minor diastereomers. The observed diastereoselectivity is due to the differential interaction of the nucleophile with the hydrogen in **11a** and the aryl groups in **11b**. Accordingly higher diastereoselectivity is observed for the *o*-tolyl series.

We thank CSIR for financial support. K. M. also thanks U. G. C. for senior research fellowship.

Notes and references

† Mukaiyama has proposed an S_N2 mechanism for the allylation of chiral mixed acyclic acetals [ref. 2(*b*)].

‡ No attempt was made to assign the configuration of the newly generated acetal chiral centre in the major and minor isomer.

§ Since C(sp^3)–C(sp^2) is a stronger bond therefore C(sp^3)–C(sp^2) hyperconjugation may not be as important as C(sp^3)–C(sp^3) hyperconjugation.

¶ The silyl ether of 1-deutero-1-phenylethyl alcohol gave product in an 86:14 ratio (compare Table 1, entry 1). The increase in diastereoselectivity indicates that the C–H or C–D bond stabilises the oxocabenium ion by inductive effects and not by hyperconjugation (ref. 15).

‖ Linderman has also invoked hyperconjugative stabilisation of the oxocarbenium ion intermediate by R_3Si in diastereoselective Mukaiyama-type aldol reactions of silyl-substituted mixed acyclic acetals (ref. 16). We thank one of the referees for bringing this reference to our notice.

1 S. E. Denmark and N. G. Almstead, *J. Am. Chem. Soc.*, 1991, **113**, 8089; R. Silverman, C. Edington, J. D. Elliott and W. S. Johnson, *J. Org. Chem.*, 1987, **52**, 180; K. Maruoka and H. Yamamoto, *Angew. Chem., Int. Ed. Engl.*, 1985, **24**, 668; P. A. Bartlett, W. S. Johnson and J. D. Elliott, *J. Am. Chem. Soc.*, 1983, **105**, 2088; J. M. McNamara and Y. Kishi, *J. Am. Chem. Soc.*, 1982, **104**, 7371.

2 (*a*) A. Mekhalfia and I. E. Markó, *Tetrahedron Lett.*, 1991, **32**, 4779; (*b*) T. Mukaiyama, M. Ohshima and N. Miyoshi, *Chem. Lett.*, 1987, 1121; (*c*) R. Imwinkelreid and D. Seebach, *Angew. Chem., Int. Ed. Engl.*, 1985, **24**, 765.

3 D. Sames, Y. Liu, L. DeYoung and R. Polt, *J. Org. Chem.*, 1995, **60**, 2153; T. Sammakia and R. S. Smith, *J. Am. Chem. Soc.*, 1994, **116**, 7915; I. Mori, K. Ishihara, L. A. Flippin, K. Nozaki, H. Yamamoto, P. A. Bartlett and C. H. Heathcock, *J. Org. Chem.* 1990, **55**, 6107; S. E. Denmark and T. M. Willson, *J. Am. Chem. Soc.*, 1989, **111**, 3475; I. Mori, P. A. Bartlett and C. H. Heathcock, *J. Am. Chem. Soc.*, 1987, **109**, 7199.

4 R. W. Hoffmann, *Chem. Rev.*, 1989, **89**, 1841.

5 J. L. Broeker, R. W. Hoffmann and K. N. Houk, *J. Am. Chem. Soc.*, 1991, **113**, 5006.

6 S. Kiyooka, M. Shirouchi and Y. Kaneko, *Tetrahedron Lett.*, 1993, **34**, 1491.

7 N. Minowa and T. Mukaiyama, *Bull. Chem. Soc. Jpn.*, 1987, **60**, 3697

8 M. E. Jung and M. A. Lyster, *J. Org. Chem.*, 1977, **42**, 3761.

9 G. Frenking, K. F. Köhler and M. T. Reetz, *Tetrahedron*, 1991, **47**, 9005.

10 E. P. Lodge and C. H. Heathcock, *J. Am. Chem. Soc.*, 1987, **109**, 3353.

11 E. J. Corey, R. K. Bakshi and S. Shibata, *J. Am. Chem. Soc.*, 1987, **109**, 5551; H. Takahashi, T. Kawakita, M. Ohno, M. Yoshioka and S. Kobayashi, *Tetrahedron*, 1992, **48**, 5691.

12 S. S. Wong and M. N Paddon-Row, *J. Chem. Soc., Chem. Commun.*, 1991, 327. Also see ref. 11.

13 N. T. Anh and O. Eisenstein, *Nouv. J. Chim.*, 1977, **1**, 62.

14 (*a*) S. Berger, B. W. K. Diehl and H. Künzer, *Chem. Ber.*, 1987, **120**, 1059; (*b*) W. J. Hehre and L. Salem, *J. Chem. Soc., Chem. Commun.* 1973, 754; (*c*) L. Radom, J. A. Pople and P. v. R. Schleyer, *J. Am. Chem. Soc.*, 1972, **94**, 5935.

15 W. M. Schubert, R. B. Murphy and J. Robins, *J. Org. Chem.*, 1970, **35**, 951; V. J. Shiner Jr. and J. S. Humphrey Jr., *J. Am. Chem. Soc.*, 1963, **85**, 2416.

16 R. J. Linderman and T. V. Anklekar, *J. Org. Chem.*, 1992, **57**, 5078.

Communication 9/04608I

The effect of an anionic starburst dendrimer on the crystallization of $CaCO_3$ in aqueous solution

Kensuke Naka,*[a] Yasuyuki Tanaka,[a] Yoshiki Chujo*[a] and Yoshikatsu Ito[b]

[a] *Department of Polymer Chemistry, Graduate School of Engineering, Kyoto University, Yoshida, Sakyo-ku, Kyoto, 606-8501, Japan. E-mail: ken@chujo.synchem.kyoto-u.ac.jp*

[a] *Department of Synthetic Chemistry and Biological Chemistry, Graduate School of Engineering, Kyoto University, Yoshida, Sakyo-ku, Kyoto, 606-8501, Japan*

Received (in Cambridge, UK) 12th July 1999, Accepted 25th August 1999

Crystallization of $CaCO_3$ in the presence of poly(amidoamine) (PAMAM) dendrimer containing carboxylate groups at the external surface resulted in the formation of spherical vaterite crystals whereas rhombohedral calcite crystals were formed in the absence of additive.

In nature, biological organisms produce polymer–inorganic hybrids which have superior mechanical properties as compared to synthetic hybrids.[1] Small amounts of acidic-rich proteins play a major role in forming such hybrids by influencing mineral crystal nucleation and growth.[2] On the basis of specific interactions, 'matrix' proteins or other macromolecules affect crystal morphology by inhibiting the growth of particular crystal faces. The processes and materials that control such crystal growth are of great interest in the field of material chemistry, in particular in the construction of composite materials analogous to those produced by nature. Crystallization of inorganics in the presence of various synthetic polymers has been investigated as a model of biomineralization. Synthetic anionic polypeptide analogues and anionic non-peptide polymers have also been found to be potent inhibitors or habit modifiers of inorganic crystallization.[3–5] Studies of inorganic crystallization in the presence of soluble polymers, modeled on biogenic proteins, have shown that the selectivity for certain crystal faces appears to be highly dependent on the secondary structure of the macromolecules. For example, poly-L-aspartate, with a predominantly β-sheet conformation, produces more argonite than poly-L-glutamate, which has a random conformation.[3]

Poly(amidoamine) (PAMAM) dendrimers with carboxylate groups at the external surface, denoted half-generation or G = *n*.5 dendrimers have been proposed as mimics of anionic micelles or proteins.[6] The starburst structures are disklike shapes in the early generations, whereas the surface branch cell becomes substantially more rigid and the structures are spherical for later generations.[7] Owing to their unique and well defined secondary structures, anionic starburst dendrimers should be good candidates for studying inorganic crystallization. Although the interaction of the negative surface of the dendrimers with metal ions has been extensively examined,[8] the effect of dendrimers on inorganic crystallization in aqueous solution has not been reported. Here we studied crystallization of $CaCO_3$ in the presence of anionic PAMAM dendrimers and found that the anionic starburst dendrimer was a habit modifier which affected the crystal morphology upon crystallization. We used calcium carbonate ($CaCO_3$) as the inorganic phase, since its crystals are easily characterized, and since the morphology of $CaCO_3$ has been shown to be subject to control in biomineralization processes.[9]

The precipitation of $CaCO_3$ in the presence and the absence of the PAMAM dendrimer (G = 1.5) was carried out under the same conditions as used by Cölfen *et al.*[10] to prevent heterogeneous nucleation at the glass walls.† $CaCO_3$ crystal formation occurring after addition of the reactants was readily

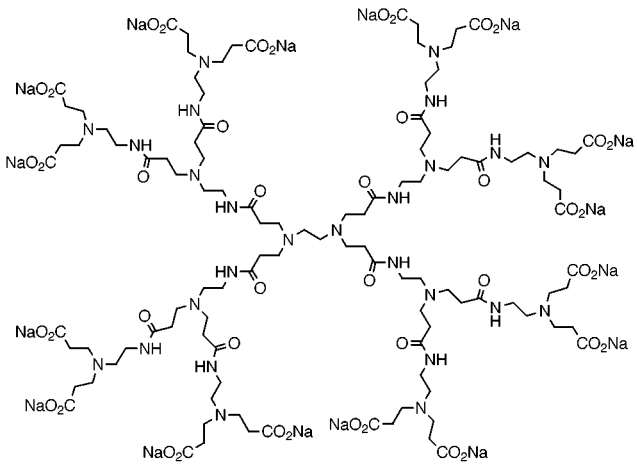

PAMAM dendrimer (G = 1.5)

observed from a sudden increase in the turbidity of the solution. This solution was then kept at 25 °C under N_2 for 4 days with gentle stirring. Owing to the complexation of the dendrimer with calcium ions, the saturated concentration of calcium ions in the presence of PAMAM dendrimer (G = 1.5) was 1.3 times higher than that in the absence of the additive. The crystalline $CaCO_3$ was washed with water to remove contaminating dendrimers that were not involved in the crystals. The yields of the crystalline products in the absence and presence of the dendrimer were 51 and 61%, respectively. The dendrimer content in the crystalline $CaCO_3$ was 33 wt% as determined by elemental analysis. These results indicate that the anionic dendrimer was bound to the crystalline $CaCO_3$.

The precipitation of $CaCO_3$ in the presence of the Na salt of poly(acrylic acid) (PAA) (M_n = 5100) was also carried out under the same conditions as above. The concentration of calcium ions in the presence of the Na salt of PAA was twice that in the absence of the additive before a sudden increase in the turbidity of the solution was observed. In the presence of the Na salt of PAA, the formation of crystalline $CaCO_3$ was prevented and amorphous $CaCO_3$ was collected after incubation at 25 °C under N_2 for 4 days. This indicates that PAA acts as an inhibitor for crystal formation.[11]

The crystal phase of $CaCO_3$ obtained in the presence of the PAMAM dendrimer was characterized by FTIR analysis.[12] Bands at 877 and 746 cm^{-1} indicated the formation of vaterite while bands at 874 and 712 cm^{-1} characteristic of calcite were scarcely observable.

By contrast, according to IR spectroscopy, the crystal phase of $CaCO_3$ obtained in the absence of dendrimer was calcite. The IR spectrum of $CaCO_3$ obtained in the presence of the Na salt of PAA suggested an amorphous character. Crystal phases $CaCO_3$ were further confirmed by XRD; in the presence of dendrimer,

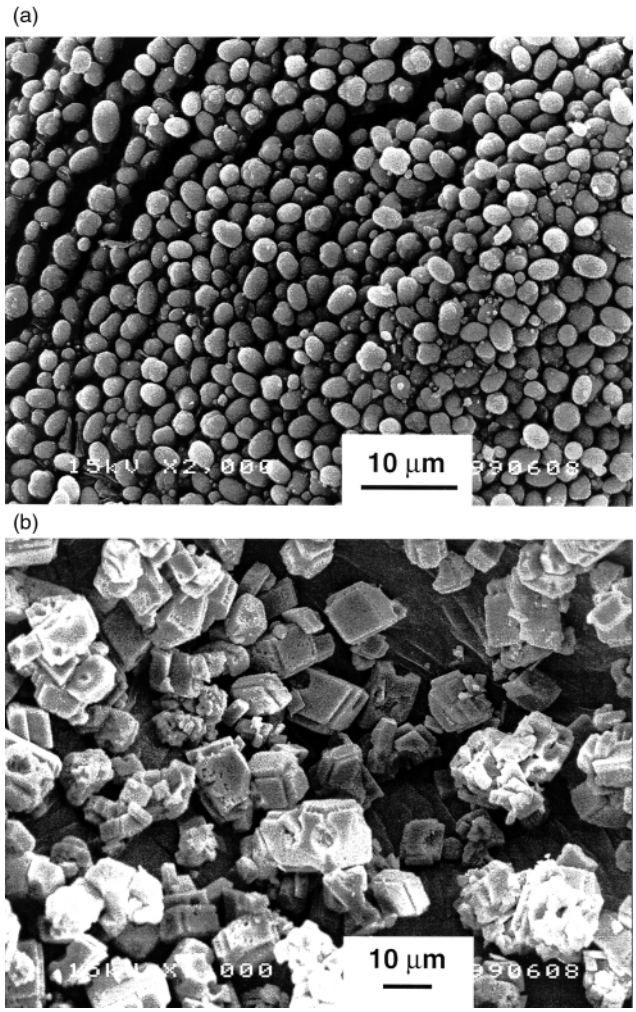

Fig. 1 Scanning electron micrographs of calcium carbonate in the presence (a) and the absence (b) of PAMAM dendrimer (G = 1.5).

the precipitate consisted entirely of vaterite (> 99%) while in the absence of dendrimer, the reflections were characteristic for calcite.

SEM observations showed that the vaterite particles were spherical [Fig. 1(a)] with an average particle diameter of 1–2 μm. SEM also showed that calcite crystals obtained in the absence of the polymer were rhombohedral [Fig. 1(b)]. Vaterite transforms readily and irreversibly into thermodynamically more stable forms when in contact with water and complete phase transformation into the thermodynamically stable calcite form occurs within 80 h and usually much faster under the conditions described above.[10] It is well known that vaterite transforms into the stable calcite form *via* a solvent-mediated process.[13] Stable spherical vaterite crystals have already been reported in the presence of various divalent cations,[14] a surfactant [bis(2-ethylhexyl)sodium sulfonate (AOT)],[15] and double-hydrophilic block copolymers.[10] We speculate that the vaterite surface is stabilized by the carboxylate-terminated dendrimer in aqueous solution to prevent phase transformation. If the Ca–O bonds to a polymer ligand are easily dissociated by water, then the polymer is thought not to be occluded in the $CaCO_3$ crystal, and solvent-mediated vaterite–calcite transformation would occur. Strong Ca–O bonds are thus required to alter the obtained polymorph of $CaCO_3$.‡ In the presence of the PAMAM dendrimer, further washing of the vaterite crystal with water did not change the crystal morphology. Although a template mechanism involving dendrimers appears to be of a complex nature since simultaneous $CaCO_3$ nucleation and interaction with the polymer is expected, the complexation properties of PAMAM dendrimers may be a major factor in the mineralization of calcium ions.

In conclusion, we present the first example of crystallization of $CaCO_3$ in the presence of an anionic starburst dendrimer. Whereas a linear poly(carboxylic acid), PAA, acts as an inhibitor for crystal formation, the dendrimer was a habit modifier and affected the crystal morphology upon $CaCO_3$ crystallization. The complexes of anionic starburst dendrimers with calcium ions are considerably stronger for higher generations than for lower generations. Investigations are now underway on crystallization of $CaCO_3$ in the presence of anionic starburst dendrimers of even higher generations.

Notes and references

† PAMAM dendrimer (G = 1.5) (16 surface carboxylate groups) was purchased from Aldrich. $CaCO_3$ crystallization was carried out as follows. A solution of 1.56×10^{-1} mmol of the dendrimer (corresponding to 2.50 mmol of $-CO_2Na$) in 300 ml distilled water was adjusted to pH 8.5 with NH_3 (aq). Then 0.5 M $CaCl_2$ aqueous solution (adjusted to pH 8.5) and 0.5 M $(NH_4)_2CO_3$ aqueous solution (adjusted to pH 10.2) were injected *via* syringe into the reaction mixture at 25 °C under N_2 with stirring. After a sudden increase in the turbidity of the solution, this solution was then kept at 25 °C under N_2 for 4 days with gentle stirring. $CaCO_3$ crystallization in the absence of the dendrimer was carried out using a 300 ml aqueous solution containing 2.50 mmol of NaCl instead of the dendrimer solution.
‡ Stoichiometric exchanges of alkali-metal ions with divalent cations such as Ca^{2+} have been reported for anionic PAMAM dendrimers.[6]

1 I. A. Aksay, M. Trau, S. Manne, I. Honma, N. Yao, L. Zhou, P. Fenter, P. M. Eisenberger and S. M. Gruner, *Science*, 1996, **273**, 892.
2 L. Addadi and S. Weiner, *Proc. Natl. Acad. Sci. USA*, 1985, **82**, 4110.
3 Y. Levi, S. Albeck, A. Brack, S. Weiner and L. Addadi, *Chem. Eur. J.*, 1998, **4**, 389.
4 N. Ueyama, T. Hosoi, Y. Yamada, M. Doi, T. Okamura and A. Nakamura, *Macromolecules*, 1998, **31**, 7119.
5 L. A. Gower and D. A. Tirrell, *J. Cryst. Growth*, 1998, **191**, 153.
6 D. A. Tomalia, A. M. Naylor and W. A. Goddard III, *Angew. Chem., Int. Ed. Engl.*, 1990, **29**, 138.
7 M. Francesca and D. A. Tomalia, *J. Am. Chem. Soc.*, 1994, **116**, 661.
8 L. Balogh and D. A. Tomalia, *J. Am. Chem. Soc.*, 1998, **120**, 7355.
9 S. Mann, *Nature*, 1988, **332**, 119.
10 H. Cölfen and M. Antonietti, *Langmuir*, 1998, **14**, 582; M. Sedlák, M. Antonietti and H. Cölfen, *Macromol. Chem. Phys.*, 1998, **199**, 247.
11 A. P. Hudson, F. E. Woodward and G. T. McGrew, *J. Am. Oil. Chem. Soc.*, 1988, **65**, 1353; D. Verdoes, D. Kashichiev and G. M. van Rosmalen, *J. Cryst. Growth*, 1992, **118**, 401.
12 G. Xu, N. Yao, I. A. Aksay and J. T. Groves, *J. Am. Chem. Soc.*, 1998, **120**, 11977.
13 A. Lopezmacipe, J. Gomezmorales and R. Rodriguezclemente, *J. Cryst. Growth*, 1996, **166**, 1015.
14 L. Brecevic, *J. Chem. Soc., Faraday Trans.*, 1996, **92**, 1017.
15 A. Lopezmacipe, *J. Cryst. Growth*, 1996, **166**, 1015.

Communication 9/05618A

An $Al_{12}R_8^-$ cluster as an intermediate on the way from aluminium(I) compounds to aluminium metal†

Andreas Purath, Ralf Köppe and Hansgeorg Schnöckel*

Institut für Anorganische Chemie, Universität Karlsruhe (TH), Engesserstr. Geb. 30.45, D-76128 Karlsruhe, Germany. E-mail: hg@achpc9.chemie.uni-karlsruhe.de

Received (in Basel, Switzerland) 26th May 1999, Accepted 19th August 1999

A new Al_{12} cluster resembling a small section of the aluminium lattice has been prepared by the reaction of AlCl solution with $LiN(SiMe_3)_2$.

Metastable aluminium monohalide solutions generated *via* condensation of high temperature AlX molecules[1] have proved to be potential precursors for the synthesis of aluminium atom clusters. Besides Al_4Cp_4*[2] as the first example, recently an Al_{77} cluster[3] was prepared which is the largest metal atom cluster characterised by X-ray structure determination to date. In order to understand the formation of the Al_{77} cluster that may be viewed as one of the final steps in the reaction pathway to the bulk metal, we attempted to isolate smaller intermediates. Very recently we were able to characterise an $Al_7R_6^-$ species with a unique D_{3d} structure containing a 'naked' Al atom 'sandwiched' by two Al_3R_3 ring systems.[4] Here we report the cluster anion $Al_{12}R_8^-$ [R = $N(SiMe_3)_2$] which may be the next step on the way to the Al_{77} cluster.

Black crystals of $Li(OEt_2)_3^+[Al_{12}\{N(SiMe_3)_2\}_8]^-$ **1** were formed after heating an $LiN(SiMe_3)_2$–AlCl solution (toluene–diethyl ether) to *ca.* 60 °C and subsequently storing at room temperature for 10 days (Scheme 1)‡.

$$29\ AlCl + 26\ LiN(SiMe_3)_2 \longrightarrow 24\ LiCl + 2\ Li^+[Al_{12}\{N(SiMe_3)_2\}_8] + 5\ [Al\{N(SiMe_3)_2\}_2]Cl$$

1

Scheme 1

In comparison to the Al_{12} cluster, the Al_7 cluster [4] is formed by the same reaction under milder conditions (24 h at 20 °C and several weeks at −25 °C).

The structural result of the X-ray structure determination of **1** is shown in Fig. 1.§ The structure of the $Al_{12}[N(SiMe_3)_2]_8^-$ anion is similar to that of a neutral $In_{12}R_8$ cluster compound (R = $SiBu^t_3$) published recently by Wiberg *et al.*[5] The EPR spectrum of a solid sample of **1** confirmed the radical character of the anion. Like the In_{12} cluster, the anion of **1** can be regarded as a section of the metal lattice as indicated in Fig. 2.

In order to understand the formation of the negatively charged Al_{12} cluster in contrast to the neutral In_{12} molecule preliminary DFT calculations[6] were performed for the species $In_{12}H_8$, $In_{12}H_8^-$, $Al_{12}H_8$ and $Al_{12}H_8^-$. The bonding situation for the In_{12} and Al_{12} cluster compounds is comparable in the following sense: addition of a single electron mostly influences the two apical Al3–Al5 bonds. This is evident by inspection of Table 1 which lists the calculated Al–Al distances of the model compounds $Al_{12}H_8$ and $Al_{12}H_8^-$. The discrepancies with respect to the observed distances in **1** disappear if NH_2 ligands are applied in place of H, *e.g.* for $Al_{12}(NH_2)_8^-$.[7] However, to obtain a complete insight into the electronic structure, extensive calculations including incorporation of $N(SiMe_3)_2$ ligands and without any symmetry restrictions have to be performed.

Calculations for the In_{12} compounds revealed similar trends and the $In_{12}R_8^-$ anion should be also a stable species. However,

† Dedicated to Professor Nils Wiberg on the occasion of his 65th birthday.

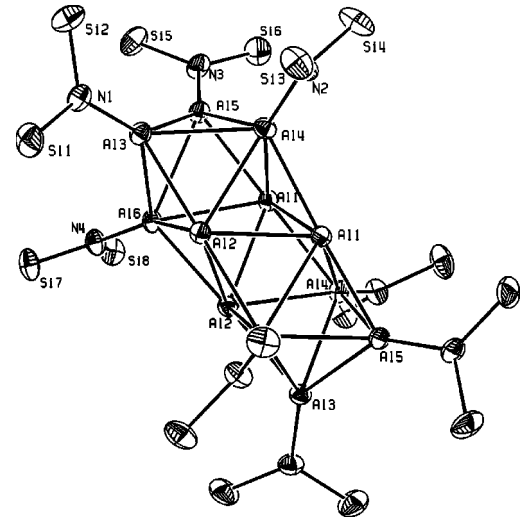

Fig. 1 Molecular structure of **1** (50% probability thermal ellipsoids; methyl groups are omitted for clarity). Selected distances (pm): Al–Al (see Table 1), Al–N 184.8 (av.), N–Si 174.4 (av.).

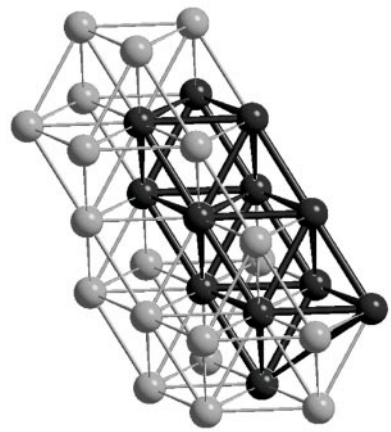

Fig. 2 Section of the aluminium metal lattice (ccp); an Al_{12} unit is accentuated.

Table 1 Selected Al–Al bond lengths for $Al_{12}[N(SiMe_3)_2]_8^-$ **1** (experimentally determined) as well as $Al_{12}(NH_2)_8^-$ (S_4), $Al_{12}H_8^-$ (D_{2d}) and $Al_{12}H_8$ (D_{2d}) (calculated)

d/pm	$Al_{12}[N(SiMe_3)_2]_8^-$	$Al_{12}(NH_2)_8^-$	$Al_{12}H_8^-$	$Al_{12}H_8$
Al1–Al5	259.8	259.4	254.3	251.4
Al2–Al6′	268.2	266.1	270.0	272.4
Al3–Al5	254.2	253.3	263.5	278.3
Al3–Al6	279.9	275.2	269.2	267.9
Al1–Al1′	263.0	273.3	271.6	270.2
Al1-Al4'	278.8	273.9	277.3	279.9

the higher electron affinity of Al^+ relative to In^+ may be the reason for its higher tendency to achieve a lower oxidation state (between 1 and 0): the average oxidation state of the Al atoms in $Al_{12}R_8^-$ is +0.58 while a value of +0.66 is found for In in $In_{12}R_8$.

20 triangular faces are present in **1** as also found in the well known Al_{12} species $Al_{12}R_{12}^{2-}$ (R = Bu^i) with icosahedral symmetry.[8] Such a related *closo* $Al_{12}R_{12}^{2-}$ anion may be one of the primary intermediates during the formation of **1**. If 2 R^- groups are removed from such an intermediate, an $Al_{12}R_{10}$ species will be formed which is similar to the distorted icosahedral $Al_{12}(AlBr_2)_{10}$ that we have published recently.[9]

$$Al_{12}R_{12}^{2-} \xrightarrow{-2R^-} Al_{12}R_{10} \xrightarrow{+2e^-,\,-2R^-} Al_{12}R_8 \xrightarrow{+e^-} Al_{12}R_8^-$$

Scheme 2

Further reduction to $Al_{12}R_{10}^{2-}$ and dissociation of two additional R^- ligands would lead to an $Al_{12}R_8$ molecule or the corresponding anion observed here. Since similar cluster compounds are obtained for In and Al, the proposed mechanism may represent the general pathway during reduction processes leading to the bulk metal. Therefore, intermediates similar to **1** can also be expected for other metals. However, the size of the metal atoms must be compatible with the size of the ligands, *i.e.* the large supersilyl ($SiBu^t_3$) ligands are suitable for protecting the large In_{12} cluster whereas the smaller $N(SiMe_2)_2$ groups match the smaller Al_{12} cluster.

Owing to the radical character of **1**, further physical measurements are underway in order to obtain more detailed information about the electronic structure of this Al_{12} cluster compound which is an example of a metal atom cluster in the sense first stated by Cotton;[10] *i.e.* an assembly of metal atoms which are essentially connected by direct bonds. The presence of metal–metal bonds has been a primary reason for the increasing interest in metal cluster chemistry over the last two decades. However, while most ligand stabilised clusters published so far do not fulfil the original criterion of Cotton, **1** is a archetypal metal atom cluster since four or six Al atoms are directly bonded to each Al atom. Furthermore, in **1** the number of ligands is smaller than the number of metal atoms and no bridging ligands are present. In our opinion these latter two criteria should be fulfilled in order to regard a compound as a genuine metal atom cluster.

We acknowledge the financial support of the Deutsche Forschungsgemeinschaft and the Fonds der Chemischen Industrie. We also thank Bernd Pilawa for recording EPR spectra.

Notes and references

‡ *General considerations*: all experiments were carried out under dry argon in a glovebox (Mbraun MB 150-GI) or under dry nitrogen using standard Schlenk techniques. Solvents were dried over potassium and degassed prior to use. EPR spectra were recorded on a BRUKER ESP 300 E.

Synthesis: 8.6 ml cold (−78 °C) AlCl solution (0.29 M, toluene–Et_2O) (2.5 mmol) was added dropwise to 500 mg (3.0 mmol) solid $LiN(SiMe_3)_2$. The reaction mixture was then heated quickly to 60 °C and stored for 2 h at this temperature. Subsequently, the dark brown solution was separated from solid LiCl. Storing at room temp. gave black crystals of **1** after 10 days. Yield in crystalline form: 11 mg (0.006 mmol) 28%; EPR (solid) $g_\perp$ = 2.015 ($\Delta B_{1/2}$ = 38.9 G), $g_\parallel$ = 2.23 (weak).

§ *Crystal data*: $C_{60}H_{152}Al_{12}LiN_8O_3Si_{16}$ **1**, M = 1836.2, monoclinic, space group $P2/n$, Z = 2, a = 20.893(2), b = 13.0123(10), c = 21.455(2) Å, β = 98.134(11)°, V = 5774.5(9) Å^3, μ(Mo-Kα) = 0.30 mm^{-1}, T = 213(1) K, 31005 reflections collected/10283 (R_{int} = 0.0600) independent/6348 with $I > 2\sigma(I)$. The structure was solved by direct methods and refined by full-matrix least squares on F^2 to final values of $R1[F > 4\sigma(F)]$ = 0.0553 and $wR2$ = 16.83 (all data). The diethyl ether molecules co-ordinated to the Li atom are strongly disordered. In treatment of this disorder we disregarded occupancies for hydrogen atoms. CCDC 182/1389. See http://www.rsc.org/suppdata/cc/1999/1933/ for crystallographic files in .cif format.

1 C. Dohmeier, D. Loos and H. Schnöckel, *Angew. Chem.*, 1996, **108,** 141; *Angew. Chem., Int. Ed. Engl.*, 1996, **35**, 129

2 C. Dohmeier, R. Robel, M. Tacke and H. Schnöckel, *Angew. Chem.*, 1991, **103**, 594; *Angew. Chem., Int. Ed. Engl.*, 1991, **30**, 564

3 A. Ecker, E. Weckert and H. Schnöckel, *Nature*, 1997, **387**, 379

4 A. Purath, R. Köppe and H. Schnöckel, *Angew. Chem., Int. Ed.*, in press.

5 N. Wiberg, T. Blank, H. Nöth and W. Ponikwar, *Angew. Chem.*, 1999, **111**, 887; *Angew. Chem., Int. Ed.*, 1999, **38**, 839.

6 *Ab initio* calculations have been performed using: (a) Turbomole: O. Treutler and R. Ahlrichs, *J. Chem. Phys.*, 1995, **102**, 346; (b) Functional BP86: A. D. Becke, *Phys. Rev. A*, 1998, **38**, 3098; J. P. Perdew, *Phys. Rev. B*, 1996, **33**, 8822; (c) RIDFT: K. Eichhorn, O. Treutler, H. Öhm, M. Häser and R. Ahlrichs, *Chem. Phys. Lett.*, 1995, **242**, 652; K. Eichkorn, F. Weigend, O. Treutler and R. Ahlrichs, *Theor. Chem. Acc.*, 1997, **97**, 119

7 For the radical anion $Al_{12}(NH_2)_8^-$ most of the calculated Al–Al distances are very close to those of **1**. A complete accordance with the experimentally determined structural data can not be expected since the NH_2 ligand is different from the $N(SiMe_3)_2$ group for the following reasons. (a) The N atom in the NH_2 group is pyramidally coordinated whereas a planar surrounding is observed for the $N(SiMe_3)_2$ groups. (b) The orientation of the NR_2 groups towards the Al_{12} core should be different for both amide groups for steric reasons and therefore a different interaction of the lone pair of the N atom with the Al_{12} core can be expected. In order to save computing time a symmetry restriction (S_4) was applied for the $Al_{12}(NH_2)_8$ species. The electron affinity for the process $Al_{12}(NH_2)_8 \rightarrow Al_{12}(NH_2)_8^-$ has been calculated to be exothermic by −145 kJ mol^{-1}.

8 W. Hiller, K.-W. Klinkhammer, W. Uhl and J. Wagner, *Angew. Chem.*, 1991, **103**, 182; *Angew. Chem., Int. Ed. Engl.*, 1991, **30**, 179

9 C. Klemp, R. Köppe, E. Wecker and H. Schnöckel, *Angew. Chem.*, 1999, **111**, 1852; *Angew. Chem., Int. Ed.*, 1999, **38**, 1740

10 F. A. Cotton, *Quart. Rev. Chem. Soc.*, 1966, 389

Communication 9/04247D

Synthesis and structure of a thiolate-bridged nickel–iron complex: towards a mimic of the active site of NiFe-hydrogenase

Sian C. Davies, David J. Evans,* David L. Hughes, Steven Longhurst and J. Roger Sanders

Department of Biological Chemistry, John Innes Centre, Norwich Research Park, Colney, Norwich, UK NR4 7UH. E-mail: dave.evans@bbsrc.ac.uk

Received (in Cambridge, UK) 2nd July 1999, Accepted 24th August 1999

The reaction, under carbon monoxide, of $[Fe(NS_3)(CO)]^-$ [NS_3 = $N(CH_2CH_2S)_3^{3-}$] with $[NiCl_2(dppe)]$ gives the structurally characterised dinuclear thiolate-bridged complex $[\{Fe(NS_3)(CO)_2\text{-}S,S'\}NiCl(dppe)]$, which has structural features similar to those of the active site of NiFe-hydrogenase.

Hydrogenases catalyse the reversible reduction of protons to dihydrogen. The NiFe-hydrogenase from *Desulfovibrio gigas*, as aerobically isolated in the inactive form, has been characterised recently by X-ray crystallography.[1,2] This indicates that the active site is most likely a dinuclear thiolate-bridged nickel–iron complex in which the nickel atom is coordinated by four cysteinate-sulfur atoms, two of which bridge to a six-coordinate iron atom. In the aerobically isolated crystals there is an additional bridging feature, probably oxo or hydroxo, which is unlikely to be present in the active form of the enzyme.[2,3] The other ligands to iron, as shown by crystallography and spectroscopy,[2] are, unusually for biology, two cyanides and one carbon monoxide. There are no examples in the chemical literature of synthetic analogues with bis(thiolate-bridged) nickel to iron with carbon monoxide bound to the iron atom, although $[\{NiL\text{-}S\}Fe(CO)_4]$ [H_2L = *N*,*N*′-bis(ethanethiol)-1,5-diazacyclooctane][4] and $[\{NiL'\text{-}S,S'\}Fe(NO)_2]$ (H_2L' = *N*,*N*′-diethyl-3,7-diazanonane-1,9-dithiolate)[5] have one or other of these features. In this work we have employed the complex $[Fe(NS_3)(CO)]^-$[6] as a chelate ligand to nickel to prepare a bis(thiolate-bridged) nickel–iron complex which has both of these structural features and has similarities to the active site of NiFe-hydrogenase.

The reaction, under a CO atmosphere, of $[NiCl_2(dppe)]$ with $[NEt_4][Fe(NS_3)(CO)]$ gives the dinuclear complex $[\{Fe(NS_3)(CO)_2\text{-}S,S'\}NiCl(dppe)]$ **1**,† the structure of which is shown in Fig. 1.‡ The iron atom is octahedrally coordinated, with two of the thiolate ligand arms also bridging to the nickel atom. The Ni is five-coordinate in a square pyramidal pattern in which the Ni atom is displaced 0.307(2) Å from the base plane towards the chloride ligand in the apical site. The normals to the S_3C 'equatorial' plane about the Fe atom and the P_2S_2 base plane about the Ni atom are inclined at 19.4(1)°. The NS_3 ligand arrangement is different from those reported previously[6,7] in trigonal bipyramidal complexes of iron and vanadium, where there is approximate threefold symmetry in the ligand. Here, the three thiolate sulfur atoms are arranged meridionally about the Fe and the pair of mutually *trans* thiolate arms of the ligand are essentially mirror images (with opposite S–C–C–N torsion angles). The carbonyl ligands are opposite the amino nitrogen atom and one of the bridging sulfur atoms.

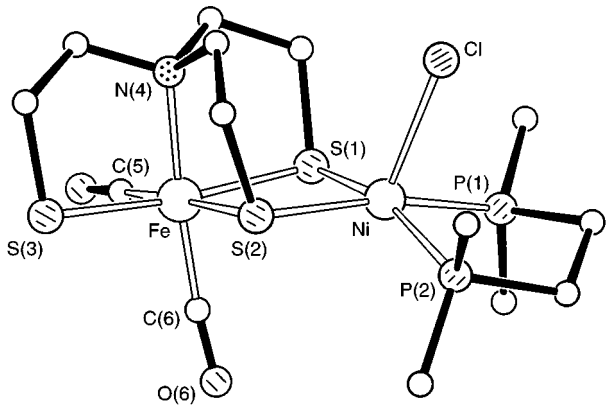

Fig. 1 A molecule of $[\{Fe(NS_3)(CO)_2\text{-}S,S'\}NiCl(dppe)]$ **1** showing the principal atoms. The phenyl groups of the dppe ligand have been omitted for clarity. Selected distances (Å) and angles (°): Fe–S(1) 2.281(3), Fe–S(2) 2.331(3), Fe–S(3) 2.306(3), Fe–N(4) 2.031(8), Fe–C(5) 1.783(12), Fe–C(6) 1.741(10), Ni···Fe 3.308(2), Ni–S(1) 2.247(3), Ni–S(2) 2.255(3), Ni–P(1) 2.164(3), Ni–P(2) 2.196(3), Ni–Cl 2.508(3); S(1)–Fe–S(2) 85.2(1), S(1)–Ni–S(2) 87.8(1), Fe–S(1)–Ni 93.9(1), Fe–S(2)–Ni 92.3(1).

Complex **1** is a good structural analogue of the proposed active site of NiFe-hydrogenase, Fig 2. The core of **1** is dinuclear with nickel bound to iron by a bis(thiolate-bridge) and the iron atom binds two carbon monoxides. The Ni···Fe distance of 3.308 Å is similar to those found for other thiolate-bridged nickel complexes (2.80–3.76 Å[4,5,8–10]) but is longer than the Ni···Fe distance, 2.9 Å, in the as isolated, inactive NiFe-hydrogenase.[1,2] However, recent theoretical calculations predict that in the active states of the enzyme the Ni···Fe distance is > 2.9 Å.[3]

The C–O stretching frequencies in the IR spectrum of **1** are at 1944 and 2000 cm^{-1}. The 1944 cm^{-1} feature is assigned to the axial CO and appears at a similar position to the axial CO stretch in the trinuclear complexes $[M\{Fe(NS_3)(CO)\text{-}S,S'\}_2]$ [M = Fe (1937 cm^{-1});[6] Co (1937 cm^{-1});[11] Ni (1934 cm^{-1})[11]] and to the CO band (1947 cm^{-1}) for the inactive form of *D. gigas* NiFe-hydrogenase.[2] Mössbauer parameters at 77 K (rel. natural Fe at 298 K) are: isomer shift (IS) 0.07 mm s^{-1} and quadrupole splitting (QS) 0.56 mm s^{-1}, consistent with octahedral low-spin iron(II). When the synthesis is performed under dinitrogen or argon, rather than CO, a complex **2**, probably a mono-CO complex, is formed with a carbonyl stretch at 1903 cm^{-1} and Mössbauer parameters of IS 0.23 mm s^{-1} and QS 0.40 mm s^{-1}. When an acetonitrile solution of **2** is stirred under a CO atmosphere it is converted to the dicarbonyl complex **1**.

The potential catalytic properties of the complex **1** will be investigated in the future.

We thank the Biotechnology and Biological Sciences Research Council for funding and The John Innes Foundation for a Studentship (S. L.). Professor R. L. Richards, John Innes Centre, is thanked for valued discussions.

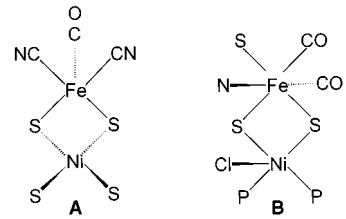

Fig. 2 A schematic comparison of the proposed enzyme active site (**A**) and the core of complex **1** (**B**).

Notes and references

† Under an atmosphere of carbon monoxide, to a stirred suspension of [$NiCl_2$(dppe)] (0.79 g , 1.5 mmol) in MeCN (100 cm^3) was added a solution of [NEt_4][Fe(NS_3)(CO)] in MeCN (20 cm^3). Dissolution was complete after 30 min. On standing overnight a dark brown, crystalline product was obtained, which was collected by filtration, washed with diethyl ether and dried (0.99 g, 83%). Found: C, 50.8; H, 4.3; N, 2.2; Fe, 6.2; Ni, 7.5. $C_{34}H_{36}ClFeNNiO_2P_2S_3$ requires: C, 51.1; H, 4.5; N, 1.8; Fe, 7.0; Ni, 7.4%. λ_{max}/nm (ε/dm^3 mol^{-1} cm^{-1}) (CH_2Cl_2) 325 (18831), 494 (2614).

‡ *Crystal data:* $C_{34}H_{36}ClFeNNiO_2P_2S_3$, M = 798.8, triclinic, space group $P\bar{1}$ (no. 2), a = 11.5630(11), b = 12.068(2), c = 12.348(2) Å, α = 91.563(13), β = 91.289(10), γ = 92.839(10)°, V = 1719.9(4) Å^3. Z = 2, D_c = 1.54 g cm^{-3}, F(000) = 824, T = 293 K, μ(Mo-Kα) = 1.36 mm^{-1}, λ(Mo-Kα) = 0.71069 Å. 4782 Unique reflections were measured to θ_{max} 23° (2254 with $I > 2\sigma_I$). Structure determined by direct methods in SHELXS,[12] refined with all data, on F^2, in SHELXL[13] to wR_2 = 0.151; for the 'observed' data, R_1 = 0.058.

CCDC 182/1390. See http://www.rsc.org/suppdata/cc/1999/1935/ for crystallographic files in .cif format

1 A. Volbeda, M.-H. Charon, C. Piras, E. C. Hatchikian, M. Frey and J. C. Fontecilla-Camps, *Nature*, 1995, **373**, 580.

2 A. Volbeda, E. Garcin, C. Piras, A. L. de Lacey, V. M. Fernandez, E. C. Hatchikian, M. Frey and J. C. Fontecilla-Camps, *J. Am. Chem. Soc.*, 1996, **118**, 12 989.

3 S. Niu, L. M. Thomson and M. B. Hall, *J. Am. Chem. Soc.*, 1999, **121**, 4000; L. De Gioia, P. Fantucci, B. Guigliarelli and P. Bertrand, *Inorg. Chem.*, 1999, **38**, 2658; P. Amara, A. Volbeda, J. C. Fontecilla-Camps and M. J. Field, *J. Am. Chem. Soc.*, 1999, **121**, 4468.

4 C.-H. Lai, J. H. Reibenspies and M. Y. Darensbourg, *Angew. Chem., Int. Ed. Engl.*, 1996, **35**, 2390.

5 F. Osterloh, W. Saak, D. Haase and S. Pohl, *Chem. Commun.*, 1997, 979.

6 S. C. Davies, D. L. Hughes, R. L. Richards and J. R. Sanders, *Chem. Commun.*, 1998, 2699.

7 S. C. Davies, D. L. Hughes, Z. Janas, L. Jerzykiewicz, R. L. Richards, J. R. Sanders and P. Sobota, *Chem. Commun.*, 1997, 1261.

8 F. Osterloh, W. Saak, D. Haase and S. Pohl, *Chem. Commun.*, 1996, 777.

9 G. J. Colpas, R. O. Day and M. J. Maroney, *Inorg. Chem.*, 1992, **31**, 5053.

10 D. K. Mills, Y. M. Hsiao, P. J. Farmer, E. V. Atnip, J. H. Reibenspies and M. Y. Darensbourg, *J. Am. Chem. Soc.*, 1991, **113**, 421.

11 D. J. Evans, S. Longhurst, R. L. Richards and J. R. Sanders, unpublished work.

12 G. M. Sheldrick, *Acta Crystallogr., Sect. A*, 1990, **46**, 467.

13 G. M. Sheldrick, SHELXL, Program for crystal structure refinement, University of Göttingen, Germany, 1993.

Communication 9/05353K

Au-colloid–'molecular square' superstructures: novel electrochemical sensing interfaces

Michal Lahav, Rachel Gabai, Andrew N. Shipway and Itamar Willner*

Institute of Chemistry, The Hebrew University of Jerusalem, Jerusalem 91904, Israel. E-mail: willnea@vms.huji.ac.il

Received (in Cambridge, UK) 28th April 1999, Revised manuscript received 3rd August 1999, Accepted 19th August 1999

New sensing interfaces have been constructed by the non-covalent crosslinking of 12 nm Au colloids with 'molecular square' transition-metal complexes.

The development of methodologies that take advantage of supramolecular, microenvironmental or quantum effects in order to assemble highly ordered structures displaying sensoric, electronic or photoelectrochemical activites is being extensively studied.[1] Colloidal nanoparticles have been used for the organization of complex assemblies such as patterned surfaces,[2] 'strings'[3] and, in particular, multilayer architectures.[4] These nanoparticles may be passive structural elements, or may contribute to the functionality of the assembly with electronic, optical or catalytic properties.[5] We have recently reported[6] on layered superstructures of citrate-coated Au nanoparticles (12 ± 1 nm) that are crosslinked by oligocationic bipyridinium-containing receptor molecules. These assemblies are stabilized by electrostatic interactions between the negatively charged nanoparticles and the positively charged crosslinkers,[7] and exhibit three-dimensional conductivity, allowing the electrochemical sensing of a series of π-donor substrates.

Recently, a new class of water-soluble transition-metal complexes with cyclophane-like structures was developed[8] by Fujita and Stang. This series of 'molecular square' compounds, consisting of bipyridine units linked by metal ions (*e.g.* Pd^{2+} or Pt^{2+}) was examined as a general methodology for the preparation of new molecular cavities for host–guest interactions.[9] A series of square Re(I) complexes was employed for the sensing of anions by following the enhanced luminescence of the complex upon the encapsulation of an analyte.[10] Complexation results in a change of the intramolecular electron transfer quenching energetics. These molecular square complexes bear positive charges and so were anticipated to crosslink Au nanoparticles to yield novel superstructure architectures. Here, we wish to report on the organization, characterization and sensing properties of Au nanoparticle layered superstructures crosslinked by 'square-type' metal complexes.

Superstructures of Au nanoparticles were constructed on indium-doped tin oxide (ITO) conductive glass, as outlined in Scheme 1. The cleaned surface was first functionalized with 3-aminopropyltriethoxysilane to give a positively charged amine surface, which was treated with a citrate-stabilized Au colloid (12 ± 1 nm).[11] The resulting Au-colloid layer was then treated with the 'Pd-square' $[(en)Pd(4,4'\text{-bipy})]_4(NO_3)_8$ (**1**)[8a] or the 'Cd-square' $[Cd(4,4'\text{-bipy})]_4(NO_3)_8$ (**2**) to give a first receptor layer. By stepwise treatments of the superstructure with the Au-nanoparticle solution and the crosslinking component, interfaces of a controllable number of layers were generated. The resulting crosslinked Au–nanoparticle superstructures are very stable as a consequence of multi-site ion pairing, and the particles can only be removed from the ITO surface by physical scratching. The structures of the Au arrays were probed by three methods: Fig. 1(a) shows the absorbance spectrum of the array upon the stepwise assembly of layers. While the typical plasmon absorbance associated with gold nanoparticles (λ = 518 nm) is present, the growth of layers results in the appearance of an additional absorbance band at λ *ca.* 650 nm, similar to the absorbance changes experienced by an Au-colloid solution upon the formation of large (of the order of 1 μm) aggregates, and is attributed to interparticle plasmon coupling.[12] Fig. 1(b) shows cyclic voltammograms of the Au-nanoparticle surfaces in assemblies containing 1–5 layers of **1**-crosslinked Au nanoparticles. The Au surface area of the assembly increases almost linearly with the growth of the number of layers. From the diameter of the particles (12 ± 1 nm) the surface area of a single particle can be obtained, and by coulometric analysis of the Au reduction wave, the Au particle density is estimated to be 0.2×10^{11} particles $\times$ cm^{-2} per layer. The formation of the assembly of **1** and **2** and the nanoparticles is supported by XPS measurements. For a five-layer assembly, the Au : Pd ratio is *ca.* 30 : 1. This ratio is very similar to that observed for a three-layer assembly. Since the formation of the array is evident from the increase of the plasmon absorbance and cyclic voltammogram of the array, these results indicate

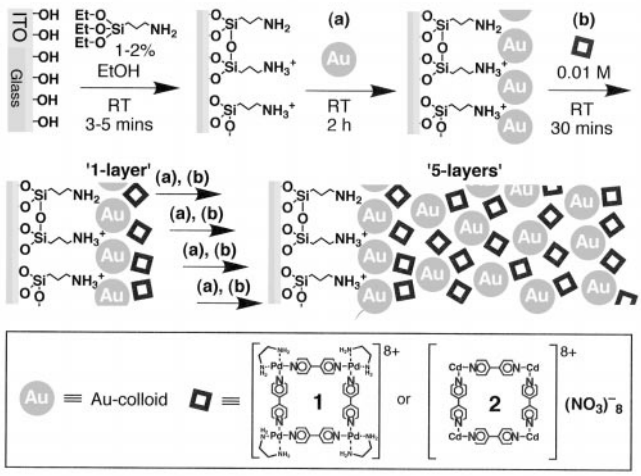

Scheme 1 The stepwise assembly of the three-dimensional array of the Palladium–bipyridine 'square' and Au nanoparticles on a conductive ITO support.

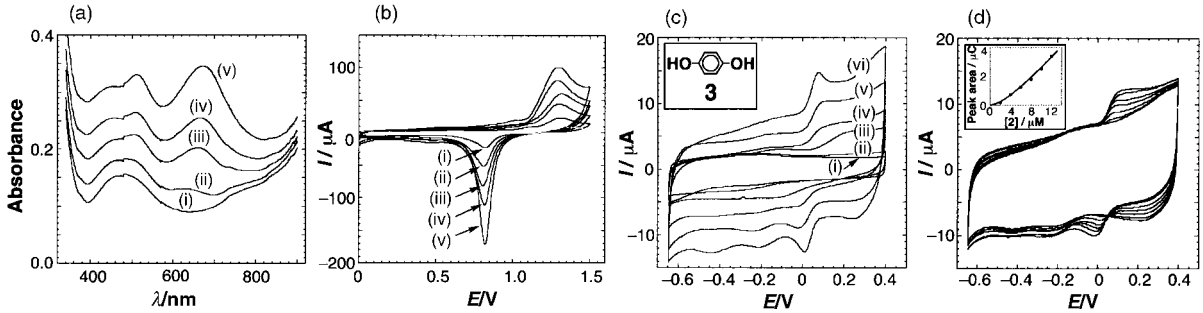

Fig. 1 (a) Absorbance spectra of the **1**–Au-colloid superstructure: (i) one Au layer, (ii) two Au layers, (iii) three Au layers, (iv) four Au layers and (v) five Au layers. (b) Cyclic voltammograms of the layered **1**-crosslinked Au-colloid assemblies corresponding to the electrochemical oxidation and reduction of the particle surface. (i)–(v) Correspond to 1–5 layers of Au particles. Experiments were carried out in 1.0 M H_2SO_4, scan rate 50 mV s^{-1}. (c) Cyclic voltammograms of the **1**-crosslinked Au-colloid arrays in the presence of hydroquinone **3** (1×10 M^{-5}). (i) ITO electrode modified only with a layer of Au colloid (ii)–(vi) 1–5 Au nanoparticle layers. All data were recorded under argon in 0.1 M phosphate buffer solution, pH = 7.2, scan rate 100 mV s^{-1}. (d) Cyclic voltammograms of a layered **1**–Au-nanoparticle array (five layers) in 0.1 M phosphate buffer (pH = 7.2) containing *p*-hydroquinone at concentrations of 0.2×10^{-6}, 0.4×10^{-6}, 0.6×10^{-6}, 0.8×10^{-6}, 1.0×10^{-6} and 1.2×10^{-6} M. Inset: Calibration curve corresponding to the electrochemical sensing of **3**. Data for (c) and (d) were recorded under argon, scan rate 100 mV s^{-1}.

that the analysis reflects the composition of the top layer of the assembly. As XPS measurements reveal a small Si signal, corresponding to the substrate surface, we estimate that *ca.* 15% of the surface is made up of unmodified domains. For the Cd^{2+}-square **2**–Au nanoparticle superstructure, the Au : Cd ratio was found to be *ca.* 100 : 1.

The crosslinker $[(en)Pd(4,4'\text{-bipy})]_4^{8+}$ **1** acts as a π-acceptor receptor for the complexation of π-donor substrates such as dialkoxybenzene derivatives.[13] Fig. 1(*c*) shows cyclic voltammograms of ITO electrodes modified with various numbers of Au-particle and **1** layers in the presence of *p*-hydroquinone **3** at a bulk concentration of 1×10^{-5} M. At this concentration no electrochemical response for **3** is observed at the electrode modified by a single Au-nanoparticle layer. Similarly, interaction of **3** (1×10^{-5} M) with an *N*,*N*′-diaminoethyl-4,4′-bipyridinium crosslinked Au-particle array (five layers)[4b] does not yield any noticeable electrochemical response. These observations indicate that neither the increased surface area of the electrode nor non-specific interactions of **3** with the polycationic–Au-nanoparticle assembly are the origin for the electrical response of **3**. Fig. 1(c) shows that the electrical response of **3** is enhanced as the number of layers is increased. Binding of **3** to the receptor units increases its local concentration at the electrode surface, and allows its electrochemical sensing by the three-dimensional conductive Au array. A further aspect to note is the decrease in the peak-to-peak separation of the redox wave of **3** as the number of layers is increased. This suggests improved interfacial electron transfer kinetics as the particle density of the assembly increases, presumably owing to enhanced conductivity.

Fig. 1(d) shows the electrical response of a five-layer Au-nanoparticle superstructure in the presence of different concentrations of **3**. Fig. 1(d) (inset) shows the derived calibration curve, corresponding to the coulometric assay of the electrochemical responses of **3** at different bulk concentrations. After electrochemical sensing of **3**, the analyte can be washed off by immersion of the electrode in a buffer solution, regenerating the sensing interface.

In conclusion, we have applied polycationic metal complexes as crosslinking 'molecular squares' for assembling three-dimensional conductive arrays of Au nanoparticles. The resulting superstructures act as functional interfaces for the concentration of π-donor analytes enabling their electrochemical sensing.

This research is supported by the Israel Science Foundation founded by The Israel Academy of Sciences and Humanities. We thank Dr Hagai Cohen for the XPS measurements. A. N. S. acknowledges a postdoctoral fellowship from the Royal Society (London, UK).

Notes and references

1 J. J. Hickman, D. Ofer, P. E. Laibinis, G. M. Whitesides and M. S. Wrighton, *Science*, 1991, **252**, 688; K. D. Schierbaum, T. Weiss, E. U. Thorden van Zelzen, J. F. G. Engbersen, D. N. Reinhoudt and W. Göpel, *Science*, 1994, **265**, 1413; T. Parpaleix, J.-M. Laval, M. Majda and C. Bourdillon, *Anal. Chem.*, 1992, **64**, 641; A. Doron, M. Portnoy, M. Lion-Dagan, E. Katz and I. Willner, *J. Am. Chem. Soc.*, 1996, **118**, 8937; E. Katz, V. Heleg-Shabtai, I. Willner, H. K. Rau and W. Haehnel, *Angew. Chem., Int. Ed. Engl.*, 1998, **37**, 3253; M. T. Stauffer, J. A. Grosko, K. Z. Ismail and S. G. Weber, *J. Chem. Soc., Chem. Commun.*, 1995, 1695; A. Doron, M. Portnoy, M. Lion-Dagan, E. Katz and I. Willner, *J. Am. Chem. Soc.*, 1996, **118**, 8937; A. Doron, E. Katz, G. Tao and I. Willner, *Langmuir*, 1997, **13**, 1783.

2 T. Vossmeyer, E. DeIonno and J. R. Heath, *Angew. Chem., Int. Ed. Engl.*, 1997, **36**, 1080; F. Burnmeiste, C. Schaefle, B. Keilhofer, C. Bechinger, J. Boneberg and P. Leiderer, *Adv. Mater.*, 1998, **10**, 495.

3 S. M. Marinakos, L. L. Brousseau III, A. Jones and D. L. Feldheim, *Chem. Mater.*, 1998, **10**, 1214.

4 (*a*) T. Vossmeyer, E. DeIonno and J. R. Heath, *Angew. Chem., Int. Ed. Engl.*, 1997, **36**, 1080; (*b*) R. Blonder, L. Sheeney and I. Willner, *Chem. Commun.*, 1998, 1393; (*c*) J. Schmitt, G. Decher, W. J. Dressick, S. L. Brandow, R. E. Geer, R. Shashidhar and J. M. Calvert, *Adv. Mater.*, 1997, **9**, 61; (*d*) M. D. Musick, C. D. Keating, M. H. Keefe and M. J. Natan, *Chem. Mater.*, 1997, **9**, 1499; (*e*) M. Lahav, T. Gabriel, A. N. Shipway and I. Willner, *J. Am. Chem. Soc.*, 1999, **121**, 258.

5 *Simple Charge Tunneling Coulomb Blockade Phenomena in Nanostructures*, ed. H. Grabar and M. H. Devoret, NATO ASI Series B294, Plenum, New York, 1992; P. Mulvaney, *Langmuir*, 1996, **12**, 788; *Clusters and Colloids*, ed. G. Schmid, VCH, New York, 1994; H. Fendler and F. C. Meldrum, *Adv. Mater.*, 1995, **7**, 607; L. N. Lewis, *Chem. Rev.*, 1993, **93**, 2693.

6 A. N. Shipway, M. Lahav, R. Blonder and I. Willner, *Chem. Mater.*, 1999, **11**, 13; M. Lahav, A. N. Shipway and I. Willner, *J. Chem. Soc., Perkin Trans. 2*, 1999, 1925; M. Lahav, A. N. Shipway, I. Willner, M. B. Nielsen and J. F. Stoddart, submitted.

7 For other examples of electrostatically stabilized colloid arrays, see: R. Iler, *J. Colloid Interface Sci.*, 1966, **21**, 569; J. Schmitt, G. Decher, W. J. Dressick, S. L. Brandow, R. E. Geer, R. Shashidhar and J. M. Calvert, *Adv. Mater.*, 1997, **9**, 61.

8 (*a*) M. Fujita, J. Yazaki and K. Ogura, *J. Am. Chem. Soc.*, 1990, **112**, 5645; (*b*) P. J. Stang, D. H. Cao, S. Saite and A. M. Arif, *J. Am. Chem. Soc.*, 1995, **117**, 6273.

9 P. J. Stang, *Chem. Eur. J.*, 1998, **4**, 19; M. Fujita and K. Ogura, *Bull. Chem. Soc. Jpn.*, 1996, **69**, 1471; M. Fujita, J. Yazaki and K. Ogura, *Chem. Lett.*, 1991, 1031; P. J. Stang and B. Olenyuk, *Acc. Chem. Res.*, 1997, **30**, 502.

10 R. V. Slone, D. I. Yoon, R. M. Calhoun and J. T. Hupp, *J. Am. Chem. Soc.*, 1995, **117**, 11 813; R. V. Slone, K. D. Benkstein, S. Bélanger, J. T. Hupp, I. A. Guzei and A. L. Rheingold, *Coord. Chem. Rev.*, 1998, **171**, 221.

11 J. Turkevich, P. C. Stevenson and J. Hiller, *Discuss. Faraday Soc.*, 1951, **11**, 55; A. Doron, E. Katz and I. Willner, *Langmuir*, 1995, **11**, 1313; M. Fujita, Y. J. Kwon, S. Washizu and K. Ogura, *J. Am. Chem. Soc.*, 1994, **116**, 1151.

12 M. Quinto and U. Kreibig, *Surf. Sci.*, 1986, **172**, 557; C. P. Collier, R. J. Saykally, J. J. Shiang, S. E. Henrichs and J. R. Heath, *Science*, 1997, **277**, 1978.

13 M. Fujita, J. Yazaki and K. Ogura, *Tetrahedron Lett.*, 1991, **32**, 5589.

Communication 9/06310B

Efficient photocatalytic decomposition of water with the novel layered tantalate $RbNdTa_2O_7$

Masato Machida,* Jun-ichi Yabunaka and Tsuyoshi Kijima

Department of Applied Chemistry, Faculty of Engineering, Miyazaki University, 1-1 Gakuen Kibanadai Nishi, Miyazaki 889-2192, Japan. E-mail: machida@material.chem.miyazaki-u.ac.jp

Received (in Cambridge, UK) 30th June 1999, Accepted 23rd August 1999

Under UV irradiation, $RbNdTa_2O_7$, the first example of an active photocatalyst containing partially occupied 4f levels, demonstrated efficient evolution of stoichiometric H_2/O_2 mixtures from pure water even in the absence of loaded metal catalysts.

A variety of mixed metal oxides containing TiO_6, NbO_6 or TaO_6 octahedral units have been extensively studied as photocatalysts. Representative catalysts reported so far include $SrTiO_3$[1,2] $Na_2Ti_6O_{13}$,[3] $BaTi_4O_9$,[4] $K_2Ti_4O_9$,[5] $K_4Nb_6O_{17}$,[6] $K_2La_2Ti_3O_{10}$[7] and $K_3Ta_3Si_2O_{13}$,[8] which show potential activities for the decomposition of pure water. We have especially noted the use of layered materials because of the possibility of modifying the chemical composition as well as microstructure by means of ion-exchange or intercalation, which is useful for designing photocatalysts based on semiconducting metal oxide sheets.[9] The present work has been directed towards the synthesis of novel layered perovskite tantalates $RbLnTa_2O_7$ (Ln = La, Pr, Nd or Sm), and evaluation of their photochemical activity for the decomposition of pure water. We report here the highly efficient evolution of stoichiometric H_2/O_2 mixtures over $RbNdTa_2O_7$ even in the absence of sacrificial agents and loaded metal catalysts.

The $RbLnTa_2O_7$ samples with various lanthanoids were prepared according to the procedure reported by Toda and Sato[10] for $RbLaTa_2O_7$. Calculated amounts of powdered carbonates or oxides (Rb_2CO_3, Ln_2O_3, Pr_6O_{11}, CeO_2 and Ta_2O_5, Rare Metallic Co. Ltd., Japan) were mixed together and calcined at 1100 °C for 10 h in air. The crystal structure of the products were identified by use of a powder X-ray diffractometer (XRD, Shimadzu XD-D1) equipped with Cu-Kα radiation (30 kV, 20 mA). Diffuse reflectance spectra were recorded with a UV–VIS spectrometer (Jasco V-550). Photocatalytic H_2 evolution from water was conducted in an inner irradiation quartz cell, which was connected to a closed circulation system. The powder sample of the tantalate (0.2 g) was suspended in distilled water (200 cm^3) in the cell by use of a magnetic stirrer. The reaction mixture was deaerated by evacuation and then flushed with Ar gas (20 kPa). The reaction was carried out by irradiating the mixture with light from a 400 W high-pressure Hg lamp. Gas evolved during irradiation was analyzed by an on-line gas chromatograph (Hitachi, TCD, Ar carrier, MS-5A and Porapak-Q columns). Evolution of H_2 and O_2 only was detected.

X-Ray diffraction patterns of the La sample (Ln = La) consisted of single phase of layered perovskite, $RbLaTa_2O_7$, and all the reflections were indexed based on a tetragonal lattice (*P*4/*mmm*, a = 0.3885 nm, c = 1.112 nm) as reported previously.[10] Similar patterns were also obtained for Ln = Pr, Nd and Sm, and were free from reflections due to the starting materials or other impurities. By contrast, the systems containing Ln = Ce, Eu, or heavier lanthanoids consisted of mixtures of other lanthanoid tantalates, such as $EuTaO_4$ and $TbTa_3O_9$, and unreacted oxides. For Ln = Ce, the reduction of Ce^{4+} to Ce^{3+} required to compensate the charge neutrality in $RbCeTa_2O_7$ did not take place during calcination in air, while the product in the other systems appear to be dependent on the ionic radius of Ln^{3+}. It is well known that the structural stability of perovskite-type oxides (ABO_3) can be easily estimated by calculating the tolerance factor defined as $t = (r_A + r_O)/\sqrt{2}(r_B + r_O)$, where r_A, r_B and r_O are the radii of the respective ions, *i.e.*, t would be unity for an ideal cubic structure.[11] In the present system, the value of t decreases from 0.920 for Ln = La with decreasing ionic radii of Ln^{3+} and no layered perovskite was produced at $t < 0.90$ (Ln = Ce, Eu and heavier lanthoids). Therefore, the geometrical arrangement of the perovskite unit (Ln–Ta–O) governs the structural stability even in a layered structure.

Fig. 1 shows the UV–VIS diffuse reflectance spectrum of $RbLnTa_2O_7$. The La sample showed a clear absorption edge at *ca.* 300 nm and the corresponding band gap energy was *ca.* 3.8 eV, quite close to that of Ta_2O_5. This can be explained by the reported band structure of the perovskite tantalate, where oxygen 2p and Ta s and p orbitals form the valence band and a high-lying antibonding band, respectively, whereas 5d states of the Ta occupy the wide intermediate gap.[12] Therefore, the band gap is likely to occur between the top of the oxygen 2p band and the bottom of the Ta 5d(t_{2g}) band. The position of the absorption edge was more or less red-shifted in the other three samples (Ln = Pr, Nd and Sm). Besides the band gap transition, these samples showed several sharp absorptions in the visible region (> 350 nm). As indicated in Fig. 1, the positions of these absorptions are in accord with the internal 4f transitions observed in corresponding Ln(III) complexes, which give rise to narrow absorption bands quite unlike band gap transitions.[13] The localized 4f levels in the present tantalate systems are

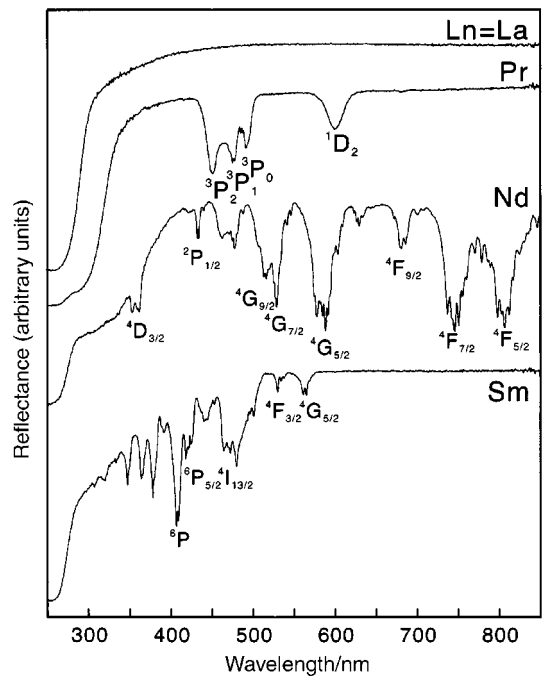

Fig. 1 UV-VIS diffuse reflectance spectra of $RbLnTa_2O_7$. Symbols for each absorptions show the excited states of isolated Ln 4f. The ground states are: La, $^1S_0$; Pr, $^3H_4$; Nd, $^4I_{9/2}$; Sm, $^6H_{5/2}$.

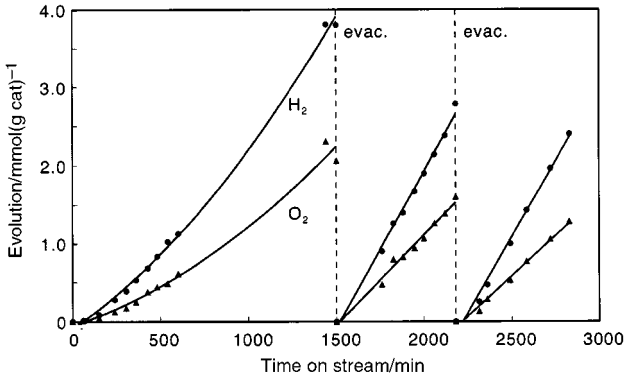

Fig. 2 Gas evolution from distilled water over $RbNdTa_2O_7$ under irradiation of UV light from 400 W high-pressure Hg lamp. Catalyst, 0.2 g, H_2O, 200 cm^3. The rate of gas evolution over $RbLnTa_2O_7$ is summarized in Table 1.

Table 1 Rates of gas evolution over $RbLnTa_2O_7$

	Evolution rate/ μmol h^{-1} (g cat)$^{-1}$	
Catalyst	H_2	O_2
$RbLaTa_2O_7$	6.0	2.8
$RbPrTa_2O_7$	4.2	Trace
$RbNdTa_2O_7$	234.8	126.4
$RbSmTa_2O_7$	53.2	28.7
0.1wt% Pt/P25	< 3	0

considered to lie within the band gap. However, it should be noted that several absorptions overlapping the onset of the absorption edge in the Nd and Sm systems are not ascribable to internal transitions. In particular, a much broader absorption in the range 300–400 nm suggests possible charge-transfer transitions between Ln 4f and other bands.

The four as-prepared layered tantalates were applied to the photocatalytic decomposition of pure water in the absence of sacrificial agents. Fig. 2 shows the time course of gas evolution over $RbNdTa_2O_7$ while rate data of all the tantalate samples are given in Table 1. The $RbLnTa_2O_7$ samples, with the exception of the Ln = Pr case, gave stoichiometric evolution of H_2 and O_2. Interestingly, the rate of gas evolution was found to be strongly dependent on Ln^{3+} and was at a maximum for the Nd system. In this case, the rate of H_2 and O_2 evolution in the first run increased initially with progress of the reaction, but then became constant at 234.8 and 126.4 μmol h^{-1} (g cat.)$^{-1}$, respectively, after 10 h. A plausible reason for the upwardly deviating gas evolution in the initial stage is CO_2 adsorption onto the as-prepared samples, since structural change of the tantalate was unobservable by XRD. After evacuating the system, almost the same rate was reproduced in the second and third runs. The total amount of H_2 and O_2 evolved during these runs reached 6.32 and 3.25 mol (mol cat.)$^{-1}$, respectively, suggesting that the reaction proceeded stoichiometrically and catalytically. A Degussa P25 catalyst loaded with 0.1wt% Pt as well as Ta_2O_5 were also applied to the reaction as reference samples; only H_2 was evolved over these catalysts at the rate of < 3 μmol h^{-1} (g cat.)$^{-1}$, two orders of magnitude less than that for $RbNdTa_2O_7$. The prominent feature of the Nd system is the efficient formation of stoichiometric H_2/O_2 mixtures even without loading of metal catalysts such as Pt, Ni, and Cu. This is in complete contrast to conventional photocatalysts, such as TiO_2, which require the assistance of such metal catalysts to bring about water splitting. Reported photocatalysts that can decompose pure water in the absence of metal catalysts are $K_4Nb_6O_{17}$,[6] $K_2La_2Ti_3O_{10}$,[7] $K_3T_3Si_2O_{13}$[8] and ZrO_2.[14] However, the rate of H_2/O_2 evolution over $RbNdTa_2O_7$ is much higher compared to these reported catalysts. Furthermore, a most promising advantage of the present layered tantalates is the wide variety of possible structural modifications that can be made by means of ion exchange, intercalation and/or pillaring. In particular, the preparation of pillared layered structures capable of creating nanocomposites between different metal oxides in porous framework is expected to be a useful strategy for the development of excellent photocatalysts, which cannot be achieved for other semiconducting oxide systems.

The reason for the high photocatalytic activity for $RbNdTa_2O_7$ is not clear at this stage. To our knowledge, however, $RbNdTa_2O_7$ is the first example of a photocatalyst containing partially occupied 4f levels. It should be noted that the sequence of the activity, Nd > Sm ≫ La ≈ Pr (Fig. 2), is well reflected by the different shape of absorption edge (Fig. 1) which is possibly influenced by charge-transfer transitions. This is considered to largely be a consequence of the partially occupied Ln 4f levels, which form localized states within the band gap of the Ta–O sublattice. This may imply that excitation of Ln 4f electrons plays a key role in the photocatalysis of the present layered perovskite tantalates.

The one of the authors (M. M.) thanks Tokuyama Science Foundation for financial support.

Notes and references

1 J. Lehn, J. Sauvage, R. Ziessel and L. Halaire, *Isr. J. Chem.*, 1982, **22**, 168.
2 K. Domen, S. Naito, T. Ohnishi and K. Tamaru, *Chem. Phys. Lett.*, 1982, **92**, 433.
3 Y. Inoue, T. Kubokawa and K. Sato, *J. Chem. Soc., Chem. Commun.*, 1990, 1298.
4 Y. Inoue, T. Niiyama, Y. Asai and Y. Sato, *J. Chem. Soc., Chem. Commun.*, 1992, 579.
5 S. Uchida, Y. Yamamoto, Y. Fujishiro, A. Watanabe, O. Ito and T. Sato, *J. Chem. Soc., Dalton Trans.*, **93**, 1997, 3229.
6 A. Kudo, A. Tanaka, K. Domen, K. Maruya, K. Aika and T. Ohnishi, *J. Catal.*, 1988, **111**, 67.
7 T. Takata, K. Shinohara, A. Tanaka, M. Hara, J. N. Kondo and K. Domen, *J. Photochem. Photobiol. A: Chem.*, 1997, **106**, 45.
8 A. Kudo and H. Kato, *Chem. Lett.*, 1997, 867.
9 M. Machida, J. Yabunaka, H. Taniguchi and T. Kijima, in *Preparation of Catalysts VII*, ed. B. Delmon, P. A. Jacobs, R. Maggi, J. A. Martens, P. Grange and G. Poncelet, Elsevier, Amsterdam, 1998, p. 951.
10 K. Toda and M. Sato, *J. Mater. Chem.*, 1996, **6**, 1067.
11 M. Goldshmidt, *Skr. Nor. Videnk.-Akad. Kl. 1:Mat.-Naturvidensk. Kl.*, 1926, **8**.
12 R. J. H.Voorhoeve, in *Advanced Materials in Catalysis*, ed. J. J. Burton and R. L. Garten, Academic Press, New York, 1977, p. 129.
13 J. L. Ryan and C. K. Jørgensen, *J. Phys. Chem.*, 1966, **70**, 2845.
14 K. Sayama and H. Arakawa, *J. Phys. Chem.*, 1993, **97**, 531.

Communication 9/05246A

Structural consequences of hydroxamate and tropolonate binding to iron porphyrins

Lin Cheng,[a] Masood A. Khan,[a] Douglas R. Powell,[b] Richard W. Taylor[a] and George B. Richter-Addo*[a]

[a] *Department of Chemistry and Biochemistry, University of Oklahoma, 620 Parrington Oval, Norman, OK 73019, USA. E-mail: grichteraddo@ou.edu*

[b] *X-ray Structural Laboratory, Department of Chemistry, University of Wisconsin, 1101 University Avenue, Madison, WI 53706, USA*

Received (in Bloomington, IN, USA) 7th July 1999, Accepted 13th August 1999

The solid-state structures of iron porphyrin hydroxamate complexes reveal an unusual monodentate η¹-O binding mode; the bidentate η²-O,O binding of the tropolonate anion results in an apical displacement of iron of 0.80 Å from the 24-atom mean porphyrin plane.

Hydroxamic acids are ubiquitous in biology.[1] Hydroxamate groups are present in a large number of siderophores, and the hydroxamic acid functional group is a constituent of certain antibiotics, antifungal agents, tumor inhibitors, and even some food additives.[1,2] The troponoid functional group is present in a number of alkaloids and antibiotics.[3] The tropolone group has been used as a model for the antimitotics colchicine (Col) and trimethylcolchicine (Tmca), and it has been shown that some Ru and Pt complexes of Col and Tmca exhibit antitumor activity comparable to that of cisplatin.[4] The coordination chemistry of hydroxamic acids and their derivatives has been reviewed,[1,5] and the hydroxamate functional group behaves as a typical chelating (bidentate, η²) ligand towards metals in their complexes. Hydroxamic acids can be viewed as valence isoelectronic analogs of NONOates (diazeniumdiolates),[6] in which the C–H(X) group has been replaced with the valence isoelectronic N atom.

We recently reported that the Cupferron anion ($Ph[N_2O_2]^-$, an NONOate) binds in a bidentate mode to iron(III) porphyrins.[7] Surprisingly, there have been very few reports on the interactions of hydroxamic acids (or hydroxamates) with synthetic metalloporphyrins[8] or natural heme biomolecules,[9] and there has been no report on the interaction of tropolone with metalloporphyrins. Thus, we sought to determine the nature of binding of typically bidentate hydroxamates (with non-equivalent O-donor atoms, NO *vs*. CO) and the tropolonate anion (with equivalent O-donor atoms) with the metal center in metalloporphyrins. The ligands were selected to include an acyclic hydroxamic acid where the O-donor atoms could exist in *cis* or *trans* conformations, a cyclic hydroxamic acid with the O-donor atoms locked in the *cis* conformation, and tropolone where the O-donor atoms are locked in the *cis* form. We are now pleased to report our preliminary results on (i) the unambiguous determination of an unusual η¹ interaction of hydroxamates with iron(III) porphyrins, and (ii) the remarkable structural consequence of η² binding of the tropolone anion with an iron(III) porphyrin.

Benzohydroxamic acid (4 equiv.) was reacted with $[Fe(oep)]_2(\mu\text{-}O)$ (0.050 g, 0.042 mmol) in toluene at 70 °C for 1.5 h. Upon cooling, black microcrystals precipitated which were collected by filtration and dried to give [Fe(oep)(ONHCOPh)]·HONHCOPh (**1**·HONHCOPh) in 52% isolated yield.†‡ The molecular structure of **1**·HONHCOPh [Fig. 1(a)] reveals an unusual η¹-O binding mode for this acyclic hydroxamate ligand, which displays moderate hydrogen-bonding[10] [N(5A)–O(2C) 2.750(5) Å, O(1A)–O(1C) 2.673(5) Å] to a second hydroxamic acid molecule.§ The average Fe–N(por) bond length is 2.052 Å and is in the range typical of five-coordinate iron(III) high-spin porphyrins,[11] and the Fe atom is pulled out by 0.48 Å from the 24-atom porphyrin plane. Unexpectedly, the reaction of a stirred suspension of [Fe(tpivpp)Cl] in THF (in the presence of a small amount of pyridine) with a 1:1 mixture of excess benzohydroxamic acid and NaH at room temperature for 1.5 h results, after crystallization in air, in the formation of the previously reported $[Fe(tpivpp)(NO_2)(py)]$ in 25% isolated yield which we identified by X-ray crystallography. This known compound was previously obtained from the reaction of $[Fe(tpivpp)(NO_2)_2]^-$ with pyridine.[12] The net formation of $[Fe(tpivpp)(NO_2)(py)]$

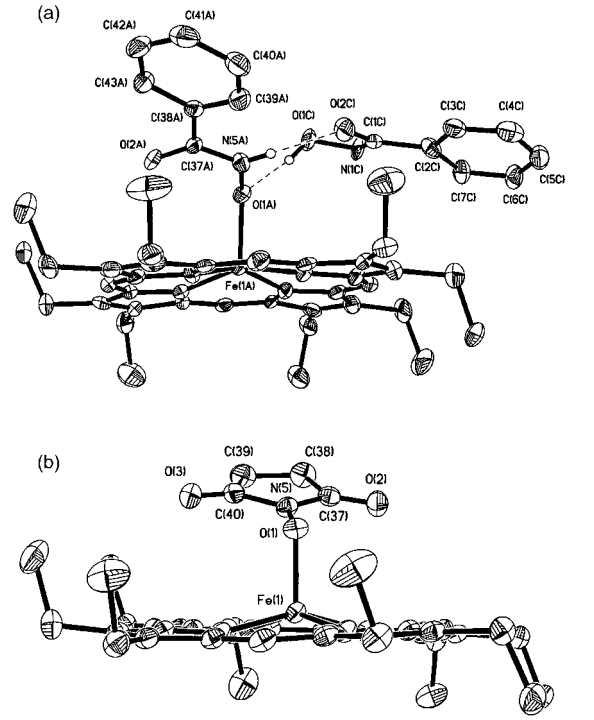

Fig. 1 (a) Molecular structure of one of the two independent molecules of **1**·HONHCOPh. Hydrogen atoms have been omitted for clarity. Selected bond distances (Å) and angles (°) (the data for the second independent molecule are shown in square brackets): Fe(1A)–N(por) 2.049(4)–2.057(4) [2.043(4)–2.056(4)], Fe(1A)–O(1A) 1.927(4) [1.923(3)], O(1A)–N(5A) 1.377(5) [1.363(5)], N(5A)–C(37A) 1.341(6) [1.333(6)], C(37A)–O(2A) 1.235(6) [1.237(6)], O(1C)–O(1A) 2.673(5) [2.876(5)], O(2C)–N(5A) 2.750(5) [2.739(6)], O(1C)–N(1C) 1.402(5) [1.389(5)], N(1C)–C(1C) 1.309(6) [1.321(7)], C(1C)–O(2C) 1.251(6) [1.242(6)]; Fe(1A)–O(1A)–N(5A) 111.0(3) [108.3(3)], O(1A)–N(5A)–C(37A) 118.8(4) [121.3(5)]. (b) Molecular structure of **2**. Hydrogen atoms have been omitted for clarity. Selected bond distances (Å) and angles (°): Fe(1)–N(por) 2.055(2)–2.065(2), Fe(1)–O(1) 1.9163(14), O(1)–N(5) 1.367(2); Fe(1)–O(1)–N(5) 115.32(11).

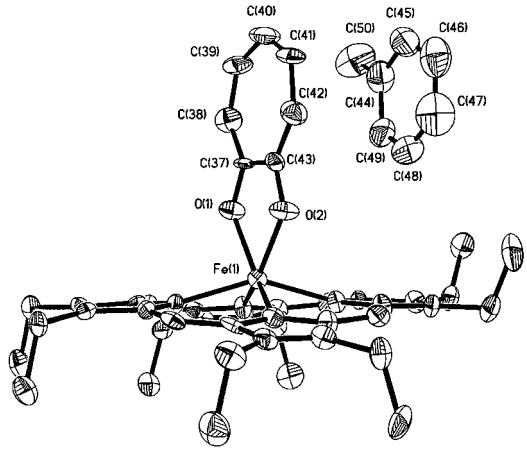

Fig. 2 Molecular structure of **3**·C_6H_5Me. Hydrogen atoms have been omitted for clarity. Selected bond distances (Å) and angles (°): Fe–N(por) 2.088(7)–2.161(9), Fe(1)–O(1) 2.064(6), Fe(1)–O(2) 2.067(6), O(1)–C(37) 1.256(9), O(2)–C(43) 1.261(11), C(37)–C(43) 1.486(12), C(39)–C(40) 1.37(2), C(40)–C(41) 1.39(2); Fe(1)–O(1)–C(37) 120.5(6), O(1)–C(37)–C(43) 113.2(8), C(37)–C(43)–O(2) 112.3(8), C(43)–O(2)–Fe(1) 120.7(6).

from benzohydroxamic acid is remarkable and, to the best of our knowledge, is the first report of a hydroxamate effectively donating its 'NO' group to a metal center.¶

The related reaction of *N*-hydroxysuccinimide $HONC_4H_4O_2$ (4 equiv.) with $[Fe(oep)]_2(\mu\text{-}O)$ (0.060 g, 0.050 mmol) in hot toluene gave, after work-up, $[Fe(oep)(\eta^1\text{-}ONC_4H_4O_2)]$ **2** in 78% isolated yield.†‖ The molecular structure is shown in Fig. 1(b), and the η^1-O binding mode of the hydroxamate ligand is also revealed, this time with no additional hydrogen-bonding interactions that stabilize this binding mode. The carbonyl O atoms do not interact with the metal center, with (carbonyl)O-to-Fe distances of 3.85 Å [O(3)] and 3.79 Å [O(2)]. The Fe atom is apically displaced by 0.44 Å from the 24-atom porphyrin plane towards the axial ligand.

We then employed tropolone in these reactions in order to obtain an η^2-O,O binding mode of the axial ligand. The reaction of tropolone with $[Fe(oep)]_2(\mu\text{-}O)$ in hot toluene gave, after work-up, dark purple microcrystals of $[Fe(oep)(\eta^2\text{-}OC_7H_5\text{-}O)]$·toluene (**3**·$C_6H_5Me$) in 86% isolated yield.†** The molecular structure of **3**·C_6H_5Me is shown in Fig. 2. The most noticeable features of the structure are (i) the tropolonate ligand is bound to the iron center in a bidentate mode, with essentially equivalent Fe–O distances and an O–Fe–O bite angle of 73.1(2)°,†† (ii) the tropolone plane is nearly coincident with a (por)N–Fe–N(por) plane containing diagonal porphyrin nitrogens, (iii) the toluene molecule is coplanar with the tropolone ligand and is in close proximity (*ca.* 3.5 Å) to it, and most importantly (iv) the Fe atom is apically displaced by 0.80 Å from the 24-atom plane** of the porphyrin towards the tropolone ligand! To the best of our knowledge, this is the *largest* reported mean displacement of an Fe atom from a porphyrin plane. In comparison, related displacements of 0.69, 0.60 and 0.61 Å have been observed for $[Fe\{t(p\text{-}OMe)pp\}\{\eta^2\text{-}ONN(Ph)O\}]$,[7] $[Fe(tpp)(\eta^2\text{-}O_2NO)]$,[15] and $[Fe(tpivpp)(\eta^2\text{-}O_2NO)]$,[16] respectively.

The research results discussed in this publication were made possible by the OCAST award for project number HN97-088 from the Oklahoma Center for the Advancement of Science and Technology (USA). M. A. K. and D. R. P. thank the National Science Foundation (CHE-9310384 and CHE-9310428) and the respective universities for funds for the purchase of the X-ray instrumentation. We thank Dr Scheidt for providing us with a preprint of ref. 11 prior to publication.

Notes and references

† All three compounds give satisfactory elemental analyses (±0.4%) for C, H and N: tpivpp = picket fence porphyrinato dianion. Crystal data were collected on Bruker (Siemens) P4 diffractometers with Mo-Kα radiation (λ = 0.71073 Å). The structures were solved using the SHELXTL system and refined by full-matrix least squares on F^2 using all reflections. The X-ray structural study of **1**·HONHCOPh was performed at the University of Wisconsin using a SMART/CCD system, and the studies for **2**·C_6H_5Me and **3**·C_6H_5Me were performed at the University of Oklahoma.

‡ *Data for* **1**·HONHCOPh: IR (KBr, cm^{-1}): ν_{CO} = 1632s br; also 2965m, 2929w, 2870w, 1575s, 1515w, 1469s, 1451s, 1373m, 1312m, 1269m, 1216w, 1147s, 1111w, 1056m, 1016s, 982m, 958s, 916w, 894m, 841m, 795w, 748w, 731w, 697s, 677w. UV–VIS [λ/nm (ε/mM^{-1} cm^{-1}), 1.10×10^{-5} M in benzene]: 351(40), 394(74), 488(8). *Crystal data*: $C_{50}H_{57}FeN_6O_4$, M = 861.87, monoclinic, $P2_1/c$, a = 26.165(5), b = 14.2716(18), c = 24.375(4) Å, β = 99.390(2)°, V = 8980(3) $Å^3$, Z = 8, D_c = 1.275 g cm^{-3}, T = 138(2) K. Final $R1$ = 0.0746 (GOF = 0.956) for 7645 'observed' reflections with $I > 2\sigma(I)$. The structure contains two independent molecules which have similar geometry [Fig. 1(a)]. CCDC 182/1388.

§ The related $[Fe\{t(p\text{-}Me)pp\}(L)]$ (L = benzohydroxamate, Cupferrate) complexes were proposed on the basis of IR spectroscopy to contain monodentate axial ligands[5] although we have shown by X-ray crystallography that the [Fe(por)(Cupferrate)] [por = tpp, t(*p*-OMe)pp] complexes display bidentate η^2-O,O coordination of the axial cupferrate ligands.[7]

¶ The acid-catalyzed hydrolysis of hydroxamic acids to give hydroxylamines and the parent carboxylic acids has been reviewed.[13]

‖ *Data for* **2**: IR (KBr, cm^{-1}): ν_{CO} = 1703s; also 2964s, 2933s, 2871m, 1469m, 1456m, 1436w, 1373m, 1315w, 1268m, 1212s, 1147m, 1110w, 1055m, 1015m, 982w, 958s, 916w, 840m, 748w, 729m, 698w, 656w, 475w. UV–VIS [λ/nm (ε/mM^{-1} cm^{-1}), 1.02×10^{-5} M in benzene]: 372(74), 397(92), 500(10), 525(10), 620(7). *Crystal data*: $C_{40}H_{48}FeN_5O_3\cdot C_6H_5CH_3$, M = 794.82, triclinic, $P\bar{1}$, a = 13.2595(10), b = 13.2893(11), c = 13.9116(11) Å, α = 74.034(6), β = 69.406(5), γ = 65.593°, V = 2065.3(3) $Å^3$, Z = 2, D_c = 1.278 g cm^{-3}, T = 173(2) K. Final $R1$ = 0.0461 (GOF = 1.045) for 5742 'observed' reflections with $I > 2\sigma(I)$. The structure contains a disordered toluene solvent molecule. CCDC 182/1388.

** *Data for* **3**·C_6H_5Me: IR (KBr, cm^{-1}): ν_{CO} 1591s; also 2965s, 2929m, 2871m, 1520s, 1495w, 1469m, 1437s, 1406m, 1366s, 1314w, 1268m, 1226s, 1218m, 1143m, 1110m, 1055s, 1013s, 980m, 954s, 914m, 877m, 842m, 748m, 738m, 729s, 714w, 695s, 543m. UV–VIS [λ/nm (ε/mM^{-1} cm^{-1}), 1.01×10^{-5} M in benzene]: 332(42), 393(76), 556(12). *Crystal data*: $C_{50}H_{57}FeN_4O_2$, M = 801.85, monoclinic, $P2_1$, a = 10.409(3), b = 14.473(3), c = 14.803(3) Å, β = 109.16(2)°, V = 2106.6(8) $Å^3$, Z = 2, D_c = 1.264 g cm^{-3}, T = 173(2) K. Final $R1$ = 0.0706 (GOF = 1.093) for 3546 'observed' reflections with $I > 2\sigma(I)$. The esds for the displacements of the 24 individual C and N atoms from the calculated least-squares plane lie in the range 0.006–0.009 Å, with the Fe atom displaced 0.802(2) Å from this plane. CCDC 182/1388.

†† The D_3 symmetric $[Fe(tropolonate)_3]$ complex exhibits a related O–Fe–O bite angle of 77.8°.[14]

1 B. Kurzak, H. Kozlowski and E. Farkas, *Coord. Chem. Rev.*, 1992, **114**, 169.
2 M. J. Miller, *Chem. Rev.*, 1989, **89**, 1563 and references therein.
3 G. Fischer, *Adv. Heterocycl. Chem.*, 1996, **66**, 285.
4 J. B. Helms, L. Huang, R. Price, B. P. Sullivan and B. A. Sullivan, *Inorg. Chem.*, 1995, **34**, 5335.
5 R. C. Mehrotra, in *Comprehensive Coordination Chemistry*, ed. G. Wilkinson, Pergamon Press, Oxford, 1987, vol. 2, ch. 15.9.
6 L. K. Keefer, R. W. Nims, K. M. Davies and D. A. Wink, *Methods Enzymol.*, 1996, **268**, 281.
7 G.-B. Yi, M. A. Khan and G. B. Richter-Addo, *Inorg. Chem.*, 1995, **34**, 5703; G. B. Richter-Addo, *Acc. Chem. Res.*, 1999, **32**, 529.
8 C. D. Shaffer and D. K. Straub, *Inorg. Chim. Acta*, 1989, **158**, 167.
9 G. Smulevich, A. Feis, C. Indiani, M. Becucci and M. P. Marzocchi, *J. Biol. Inorg. Chem.*, 1999, **4**, 39 and references therein.
10 G. A. Jeffrey, *An Introduction to Hydrogen Bonding*, ed. D. G. Truhlar, Oxford University Press, New York, 1997, Table 2.1, p. 12.
11 W. R. Scheidt, in *The Porphyrin Handbook*, ed. K. M. Kadish, K. M. Smith and R. Guilard, Academic Press, New York, 1999, ch. 16, Tables 5–8, in press.
12 H. Nasri, Y. Wang, B. H. Huynh, F. A. Walker and W. R. Scheidt, *Inorg. Chem.*, 1991, **30**, 1483.
13 K. K. Ghosh, *Indian J. Chem., Sect. B*, 1997, **36**, 1089.
14 T. A. Hamor and D. J. Watkin, *Chem. Commun.*, 1969, 440.
15 M. A. Phillippi, N. Baenziger and H. M. Goff, *Inorg. Chem.*, 1981, **20**, 3904.
16 O. Q. Munro and W. R. Scheidt, *Inorg. Chem.*, 1998, **37**, 2308.

Communication 9/05485E

Iridium(III) bis-terpyridine complexes displaying long-lived pH sensitive luminescence

Matteo Licini and J. A. Gareth Williams*

Department of Chemistry, University of Durham, South Road, Durham, UK DH1 3LE.
E-mail: J.A.G.Williams@durham.ac.uk

Received (in Cambridge, UK) 30th July 1999, Accepted 27th August 1999

A bis-terpyridine complex of iridium(III) incorporating a pendent pyridyl group displays long-lived emission at pH 7 in air-equilibrated aqueous solution, but both the lifetime and intensity are reduced by a factor of > 8 upon protonation of the pyridyl nitrogen; structurally similar complexes with pendent phenolic groups are only weakly emissive and their ground-state absorption spectra show a new, low-energy band (λ = 468 nm) upon deprotonation.

Molecular luminescent sensors that are able to signal the presence of molecules or ions in aqueous solution are of current interest because of their application to the analysis of biological or environmental samples.[1] Luminescent metal complexes are under investigation for such applications owing in part to the long-lived emission which some of them display, allowing discrimination from the shorter-lived background fluorescence often present in such samples.[2] Although systems based on certain lanthanide(III) ions show promise,[2,3] there are few complexes of transition metal ions with suitably long luminescence lifetimes under ambient conditions. The photophysical properties of polypyridyl ruthenium(II) complexes continue to attract a great deal of attention; sensors for pH incorporating a $Ru(bpy)_3^{2+}$ reporter have been described[4] and a study of a range of derivatives of $Ru(bpy)_3^{2+}$ bearing pyridyl and phenolic substituents has revealed pH-sensitive MLCT emission.[5] Similarly, a bis-terpyridine ruthenium(II) complex incorporating a pendent terpyridyl group displayed enhanced luminescence upon protonation, the lifetime increasing from 4 to 80 ns.[6] Short lifetimes of this magnitude are typical and seriously limit the utility of such ruthenium complexes in applications where longer lifetimes are desirable.

Recent work on bis-terpyridine complexes of iridium(III), such as **1**, has highlighted the very different photophysical properties compared to the Ru(II) analogues.[7,8] Intense ligand-centred emission has been observed in solution (τ > 1 μs under ambient conditions). We have now prepared complexes **2**–**5** in which the terpyridine ligands bear pendent protonatable (pyridyl) or deprotonatable (phenolic) groups. The ligands used here, 4′-tolyl-2,2′:6′,2″-terpyridine (ttpy), 4′-(4-pyridyl)-2,2′:6′,2″-terpyridine (qtpy) and 4′-(4-hydroxyphenyl)-2,2′:6′,2″-terpyridine (tpy-OH), were prepared using established methods.[9a–c] Complexes **3** and **5** were prepared *via* the intermediacy of (ttpy)$IrCl_3$, itself obtained by reaction of $IrCl_3 \cdot 3H_2O$ with 1 equiv. of ttpy in refluxing ethanol. Subsequent reaction with 1 equiv. of tpy-OH or qtpy in ethylene glycol at 200 °C for 1 h led to **3** and **5** respectively after chromatographic separation on silica. The symmetric complex **4** was prepared by a related route involving reaction of (qtpy)$IrCl_3$ with qtpy, whilst complex **2** could be obtained by the direct reaction of $IrCl_3 \cdot 3H_2O$ with 2 equiv. of tpy-OH in refluxing ethylene glycol.†

The ground-state absorption spectra of all four complexes in aqueous solution at pH 6 (NO_3^- salts) showed strong absorption bands (ε 10^4–10^5 dm^3 mol^{-1} cm^{-1}) in the region 250–400 nm. In the case of the pyridyl-appended complexes **4** and **5**, which are pale yellow, no significant change in the absorption spectrum was observed upon protonation. This is consistent with predominantly ligand-centred transitions (as proposed tentatively for the parent complex **1**[8]), rather than MLCT transitions: the latter would be expected to show a significant red-shift upon protonation, as the π-acceptor ability of the ligand is enhanced [*e.g.* for the Ru(II) and Fe(II) analogues of **4**, a red-shift of the MLCT absorption of 14 and 25 nm, respectively, has been reported upon protonation[10]]. On the other hand, the phenolic-substituted complexes **2** and **3**, also pale yellow at pH 6, became deep orange upon increasing the pH to 10 and a new, well defined band appeared in the absorption spectrum centred at 468 nm (Fig. 1). A somewhat similar colour change was seen for the free ligand itself but, in this case, arises from the tailing of a band centred below 400 nm into the visible region. The appearance of the long-wavelength band in the present instance must reflect the efficacy of the tripositive iridium centre in promoting delocalisation of the negative charge of the phenolate over the entire ligand framework, imparting some quinone character to the ligand and an associated ligand-centred transition of low energy.[11] From the change in absorbance as a function of pH, the ground-state

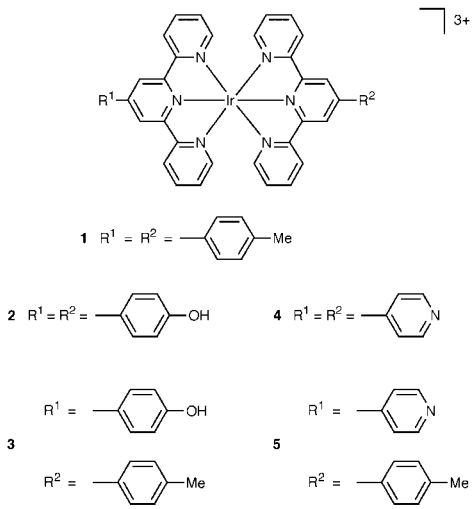

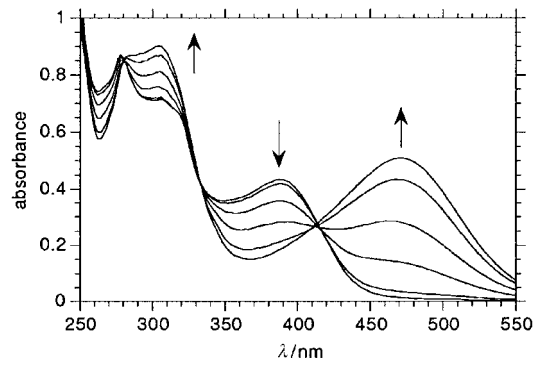

Fig. 1 Room temperature absorption spectra of complex **2** in aqueous solution at pH 5.3, 6.7, 7.6, 8.3, 9.0, 10.1. The arrows indicate the changes in the spectrum which occur as the pH is increased (addition of KOH).

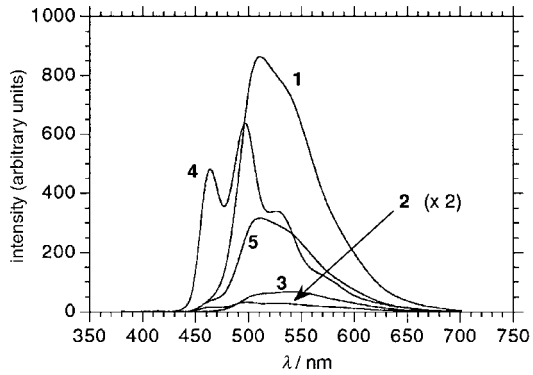

Fig. 2 Room temperature luminescence spectra of air-equilibrated, isoabsorbant aqueous solutions of **1**–**5** at pH 6.0, λ_{ex} = 364 nm.

pK_a of the complex was found to be 8.1. This is considerably more acidic than phenol itself (pK_a 10.0), which is a further indication of the stabilisation of the negative charge which may occur in the complex.

Room temperature luminescence spectra of air-equilibrated aqueous solutions of the complexes are shown in Fig. 2. Whereas the well resolved bands and emission maxima of complex **4** (and, to a somewhat lesser extent, **2**) resemble those of the unsubstituted bis-terpyridine complex, $Ir(terpy)_2^{3+}$,[7,8] the spectra of complexes **3** and **5** are more similar to the tolyl-substituted complex **1**. The sensitive dependence of the emission profile on the presence of 4′-substituents has been noted previously and discussed in terms of a greater delocalisation of the LC excited state over the 4′-aryl substituents.[8] Thus, it appears that the tolyl group must be more effective in this role than either the phenol or pyridyl substituents, or that the dihedral angle between the tolyl and terpy fragments in the excited state is more favourable for such delocalisation than for the other ligands. The phenol-appended complex **2** was only weakly emissive and found to be completely quenched upon deprotonation of the phenol. For the mixed ligand complex **3**, the emission was considerably more intense and only modestly reduced (by a factor of 1.6) over the pH range 6–10; the residual emission at high pH in this complex is thus likely to be due to the tolyl-terpyridine ligand only.

The effect of protonation on the luminescence of complex **5** is striking. Although no significant change in the spectral profile of **5** was observed (again supporting the assignment of the transitions as predominantly ligand-centred), the intensity of the emission was reduced by *ca.* 8-fold on lowering the pH from 7 to 2 (Fig. 3). Significantly, the lifetime was also reduced by a comparable factor, from 4.7 μs at pH 7 to 0.48 μs at pH 2 (caption to Fig. 3). It is well established that the mixing of d–π* charge transfer excited states into emissive π–π* ligand-centred states can promote deactivation and thereby shorten the observed lifetimes.[7] Protonation of complex **5** will lower the energy of the MLCT excited states, as noted above, leading to increased mixing with the emissive LC state and hence to the shorter lifetimes and reduced intensities which are observed. The pK_a of the excited state was found to be 4.1, significantly lower than the value of 5.25 for pyridine itself. This may be ascribed in part to electrostatic effects: protonation of the pendent pyridine increases the overall charge from +3 to +4, and also to the presence of the electron-withdrawing metal–terpyridyl unit on the 4-position of the pendent pyridine, which will serve to reduce the basicity of the uncoordinated nitrogen. Complex **4** also showed a reduction in lifetime and intensity over the same pH range, but by a smaller factor (τ = 1.1 μs at pH 7, τ = 0.34 μs at pH 2, in air-equilibrated aqueous solution).

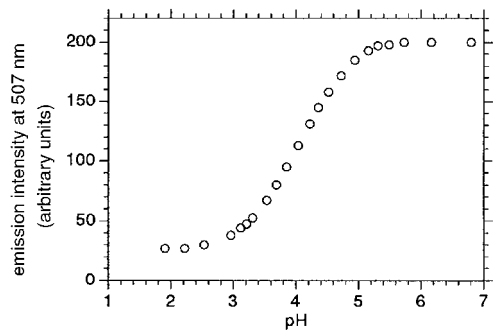

Fig. 3 Effect of pH on the emission intensity of complex **5** (monitored at 507 nm) in air-equilibrated aqueous solution, λ_{ex} = 360 nm. At the pH extremes, monoexponential decay of emission was observed and the following lifetimes were obtained: pH 6.2, τ = 4.7 μs; pH 2.0, τ = 0.48 μs. The corresponding values in degassed solution were 11.1 and 0.60 μs, respectively.

In summary, the iridium complexes described, especially complex **5**, constitute potential new sensory systems for pH, where changes in lifetime as well as intensity may be used to characterise the pH dependence, and which may be amenable to time-resolved detection methods.

We thank Dr A. Beeby for assistance with time-resolved spectroscopy and Drs L. Flamigni, F. Barigelletti, J.-P. Collin and J.-P. Sauvage, with whom the foundatory work for these studies was carried out.[8] Financial support from the University of Durham is gratefully acknowledged.

Notes and references

† The identity and purity of the complexes were confirmed by high-resolution NMR spectroscopy and electrospray ionisation mass spectrometry. *Selected spectroscopic data*: complex **4**: ^{1}H NMR (300 MHz, D_2O, NO_3^- salt): δ 9.50 (4H, s, H$^{3'}$), 9.21 (4H, d, ^3J 6.3 Hz, H^m), 8.97 (4H, d, ^3J 8.4 Hz, H^3), 8.64 (4H, d, ^3J 6.3 Hz, H^o), 8.42 (4H, dd, ^3J 8.4, 7.8 Hz, H^4), 8.02 (4H, d, ^3J 5.4 Hz, H^6), 7.71 (4H, dd, ^3J 7.8, 5.4 Hz, H^5); (H^o and H^m denote protons *ortho* and *meta* to the nitrogen of the pendent pyridine). ESMS (+) (PF_6^- salt): *m/z* 479 $[M^{3+} + PF_6^-]^{2+}$, 407 $[M^{3+} + e^-]^{2+}$, 271 $[M]^{3+}$, where M denotes cation **4**, mass 813. Interpretation of the NMR data of the mixed ligand complexes **3** and **5** was facilitated by the spectra of **1**, **2** and **4**, and was fully consistent with the structures shown.

1 A. P. de Silva, H. Q. N. Gunaratne, T. Gunnlaugsson, A. J. M. Huxley, C. P. McCoy, J. T. Rademacher and T. R. Rice, *Chem. Rev.*, 1997, **97**, 1515; *Fluorescent Chemosensors of Ion and Molecule Recognition*, ed. A. W. Czarnik, American Chemical Society, Washington DC, 1993.
2 E. F. G. Dickson, A. Pollak and E. P. Diamandis, *J. Photochem. Photobiol. B*, 1995, **27**, 3; D. Parker and J. A. G. Williams, *J. Chem. Soc., Dalton Trans.*, 1996, 3613.
3 A. P. de Silva, H. Q. N. Gunaratne and T. E. Rice, *Angew. Chem., Int. Ed. Engl.*, 1996, **35**, 2116; D. Parker, P. K. Senanayake and J. A. G. Williams, *J. Chem. Soc., Perkin Trans. 2*, 1998, 2129.
4 R. Grigg, J. M. Holmes, S. K. Jones and W. D. J. A. Norbert, *J. Chem. Soc., Chem. Commun.*, 1994, 185.
5 A. M. W. Cargill Thompson, M. C. C. Smailes, J. C. Jeffery and M. D. Ward, *J. Chem. Soc., Dalton Trans.*, 1997, 737.
6 F. Barigelletti, L. Flamigni, M. Guardigli, J.-P. Sauvage, J.-P. Collin and A. Sour, *Chem. Commun.*, 1996, 1329.
7 N. P. Ayala, C. M. Flynn, Jr., L. Sacksteder, J. N. Demas and B. A. DeGraff, *J. Am. Chem. Soc.*, 1990, **112**, 3837.
8 J.-P. Collin, I. M. Dixon, J.-P. Sauvage, J. A. G. Williams, F. Barigelletti and L. Flamigni, *J. Am. Chem. Soc.*, 1999, **121**, 5009.
9 (*a*) J.-P. Collin, S. Guillerez, J.-P. Sauvage, F. Barigelletti, L. de Cola, L. Flamigni and V. Balzani, *Inorg. Chem.*, 1991, **30**, 4230; (*b*) L. Persaud and G. Barbiero, *Can. J. Chem.*, 1991, **69**, 315; (*c*) W. Spahni and G. Calzaferri, *Helv. Chim. Acta*, 1984, **67**, 450.
10 E. C. Constable and A. M. W. Cargill Thompson, *J. Chem. Soc., Dalton Trans.*, 1994, 1409.
11 Ward and coworkers have reported on the appearance of a similar band (albeit at higher energy) accompanying the deprotonation of a phenol-appended ruthenium trisbipyridine complex,[5] which only appeared when the substitution pattern was such as to provide a direct pathway of conjugation from the phenol-OH to a metal-coordinated nitrogen, as is also possible in the terpyridyl ligand described here. The lower energy of the band in the present instance probably reflects the higher positive charge on Ir(III) compared to Ru(II).

Communication 9/06203C

ChemComm

New supramolecular packing motifs: π-stacked rods encased in triply-helical hydrogen bonded amide strands

Matthew P. Lightfoot, Francis S. Mair,* Robin G. Pritchard and John E. Warren

Department of Chemistry, UMIST, PO Box 88, Manchester UKM60 1QD. E-mail: frank.mair@umist.ac.uk

Received (in Cambridge, UK) 30th June 1999, Accepted 18th August 1999

The structure of *N,N′,N″*-tris(2-methoxyethyl)benzene-1,3,5-tricarboxamide consists of aryl rings self-assembled using a novel conjunction of organizational motifs into a π-stack surrounded by a triple helical network of hydrogen bonds, in a manner suggestive of a new mode of organization for some columnar liquid crystals.

Central to the goal of crystal engineering is the discovery of molecular building blocks that can assemble in a pre-determined fashion to generate structural components[1] such as sheets,[2] ribbons,[3] tubes[4] and rods.[5] Often the hydrogen bond is used as a method of linking self-complementary molecules into such supramolecular components,[6] just as it is often used by Nature in defining protein structure. During the course of studies directed at the characterisation of alternative linking units, such as alkali metals, we synthesised† the triamide *N,N′,N″*-tris(2-methoxyethyl)benzene-1,3,5-tricarboxamide **1**. Here we report its remarkable crystal structure,‡ composed of infinite π-stacked rods supported by a triple helical network of hydrogen bonds (**1**$_n$).

The only similar structure in the literature was reported by Hamilton and co-workers in 1995.[7] A cyclohexyl unit was used as the scaffold for three amide functions, all of which pointed in the same direction, approximately perpendicular to the average plane of the ring, so as to generate a perfectly self-complementary building unit held by three C=O–HN hydrogen bonds. The mode of its self-organization is depicted in **2**.

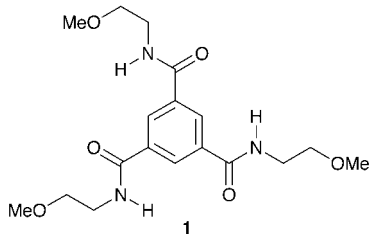

1

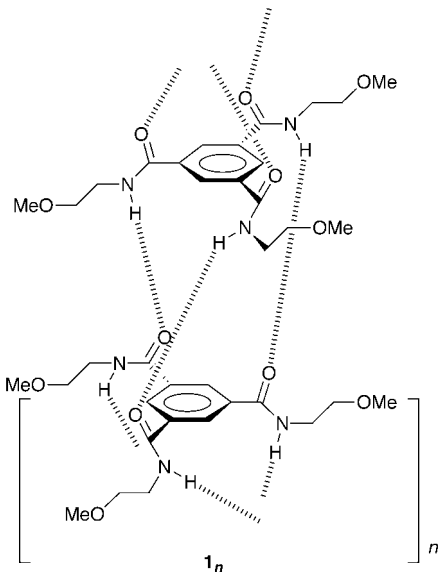

1$_n$

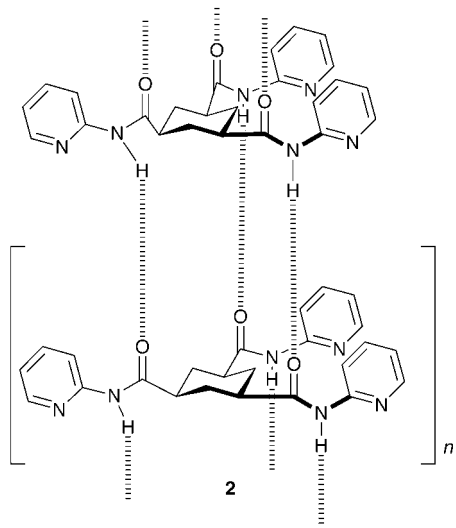

2

Our supramolecular rod **1** differs from **2** in two important and related respects: the use of an aromatic central scaffold, as opposed to a saturated cyclohexyl ring, and the disposition of the three amide bonds, which are partially tilted in **1** and perpendicular to the ring in **2**.

The central aromatic framework in **1** allows for a further self-assembly mechanism, additional to the three hydrogen bonds, through π-stacking. There is one molecule of **1** in the asymmetric unit (Fig. 1). The stack is generated by the crystallographic 2_1 screw axis leading to an inter-ring plane separation of $b/2$, as prescribed by the $P2_1$ space group.‡ The inter-ring centroid distance is therefore 3.62 Å. This is compatible with computed distances in the π-facial arrangement of the gas-phase benzene dimer (3.60 Å),[8] and, inter-

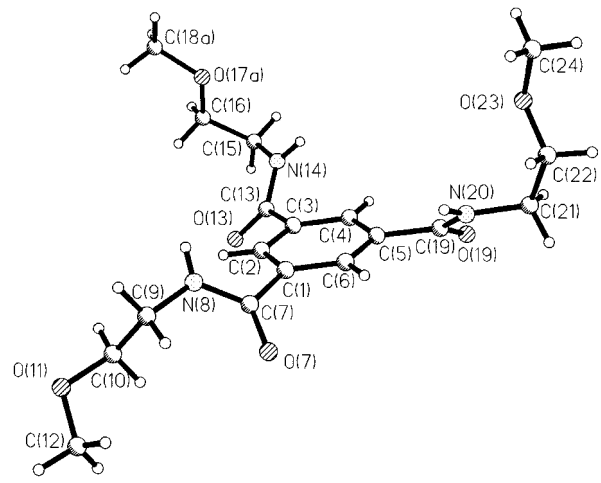

Fig. 1 Molecular structure of **1**. Minor contributor to two-fold disorder in one sidearm is omitted for clarity.

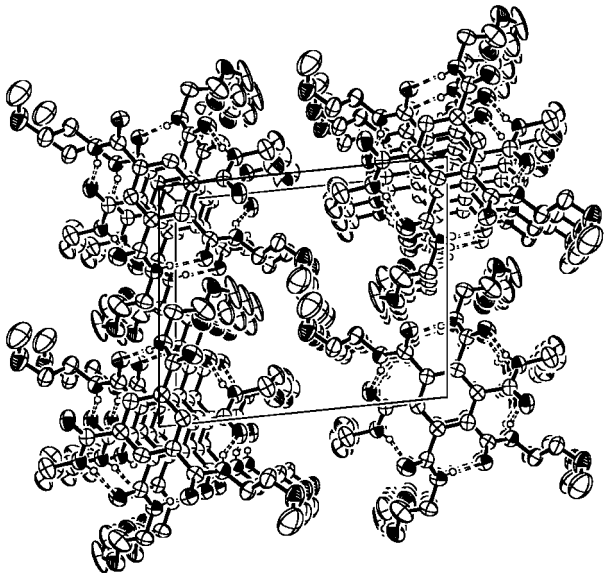

Fig. 2 Packing diagram of **1**, viewed along the *b*-axis. Non-amide hydrogen atoms and minor contributor to side-arm disorder omitted for clarity.

estingly, is similar to distances inferred from sharp peaks seen in X-ray diffraction patterns of discotic liquid crystalline phases based on aromatic cores.[9]

One such mesophase is composed of molecular cores similar to **1**, but extended using intramolecularly hydrogen bonded bipyridine units.[10] Others are more similar still, being identical to **1** but for longer alkyl chains on each amide function. Thermotropic mesophases are formed by such triamides with pentyl to octadecyl groups.[11] Furthermore, highly viscoelastic phases were formed by these species in organic solvents.[12] The methyl variant was crystallised as a model compound: in *N*,*N*′*N*″-trimethylbenzene-1,3,5-tricarboxamide, only a single amide is involved in the third dimension, the other two amides (approximately coplanar with the aryl ring) being involved in generating sheet morphology.[12] The slightly longer alkyl groups of **1** appear to make this mode of organization less favourable. The columnar structure exhibited by **1** may offer a better clue as to the nature of the novel mesophases[11] and lyotropism[12] observed. However, the particular type of primitive rectangular column packing exhibited by **1** (Fig. 2) has not previously been characterised in studies of columnar liquid crystals.[9]

Aromatic amides prefer coplanarity of the carbonyl with the aryl for conjugative reasons, as exemplified in the almost totally planar *N*,*N*′,*N*″-tris(6-methyl-2-pyridyl)benzene-1,3,5-tricarboxamide.[13] In **2** the amides are virtually perpendicular to the ring,[7] while in **1** the conflict between the demands of conjugation and the demands of intermolecular hydrogen bonding result in partial tilting, so that in place of the three vertical strands in **2**, a triple helical network of hydrogen bonds, as shown in Fig. 3, arises. These pack in the polar $P2_1$ space group with parallel alignment, such that spontaneous generation and resolution of supramolecular chirality has occurred from achiral solutions of **1**. The mean planes of the three amide units make angles of 36.8, 42.4 and 45.5° with the aryl mean plane. All therefore point their dipoles at approximately 60° from the column axis, and are helically wrapped around that axis with a pitch of 21.7 Å. The O–N distances are 2.94, 2.95, and 3.01 Å, in the normal range for amide N(H)–O interactions.

Our attempts to probe the structural effect of replacement of the amide hydrogen with alkali metals continue.

We thank the EPSRC for supporting this research and the referees for their useful comments.

Notes and references

† *Experimental data* for **1**: Methoxyethylamine (18.35 ml, 0.21 mol) was added to a solution of benzene-1,3,5-tricarbonyl trichloride (18.79 g, 0.07 mol) and Et_3N (29.59 ml, 0.21 mol) in Et_2O (350 ml) at 0 ºC. The solution was stirred at room temperature for 20 h. The resultant yellow powder was filtered and dissolved in $CHCl_3$ and then washed with 2 M HCl (aq.) (2 × 50 ml). Solvent removal and recrystallisation from hot EtOH produced colourless needles in a yield of 56%. A second crop of crystals was obtained giving a combined yield of 78%. Satisfactory C, H and N analyses were obtained.

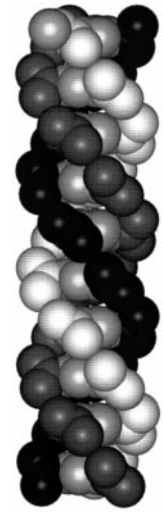

Fig. 3 Diagram of **1** showing triple-helical hydrogen bonding network. Each O, C, N(H)–O helical strand is a different shade of grey. Hydrogen atoms and methoxyalkyl side-arms omitted for clarity.

‡ *Crystal data* for **1**: $C_{18}H_{25}N_3O_6$, M = 379.41, monoclinic, space group $P2_1$, a = 10.776(3), b = 7.241(3), c = 13.028(3) Å, β = 95.84(3)º, U = 1011.4(6) Å^3, Z = 2, D_c = 1.246 Mg m^{-3}, μ = 0.094 mm^{-1}, (Mo-Kα, λ = 0.71069 Å), F(000) = 404, T = 393 K. Rigaku AFC6S diffractometer, crystal size 0.2 × 0.3 × 0.2 mm, θmax 25.02º, 1944 reflections measured, 1944 unique. Final $R_w = [\Sigma w(F_o^2 - F_c^2)^2/\Sigma(wF_o^2)^2]^{1/2}$ = 0.1629 for all data, conventional R = 0.0636 for 1337 observed reflections. Data was of insufficient quality to determine absolute configuration. Disorder on one side chain was modelled to occupancies of 78:22%. Only the major contributor is shown. CCDC 182/1381. See http://www.rsc.org/suppdata/cc/1999/1945/ for crystallographic data in .cif format.

1 G. R. Desiraju, *Chem. Commun.*, 1997, 1475; G. R. Desiraju, *Angew. Chem., Int. Ed. Engl.*, 1995, **34**, 2311; C. B. Aakeröy, *Acta Crystallogr., Sect. B.*, 1997, **53**, 569; D. Braga and F. Grepioni, *Coord. Chem. Rev.*, 1999, **183**, 19.

2 X. Zhao, Y.-L. Change, F. W. Fowler and J. W. Lauher, *J. Am. Chem. Soc.*, 1990, **112**, 6627; F. Garcia-Tellado, S. J. Geib, S. Goswami and A. D. Hamilton, *J. Am. Chem. Soc.*, 1991, **113**, 9265; M. J. Krische, J.-M. Lehn, N. Kyritsakas and J. Fischer, *Helv. Chim. Acta*, 1998, **81**, 1909; J. J. Wolff, F. Gredel, T. Oeser, H. Irngartinger and H. Pritzkow, *Chem. Eur. J.*, 1999, **5**, 29.

3 J.-M. Lehn, M. Maskal, A. DeCian and J. Fischer, *J. Chem. Soc., Perkin Trans. 2*, 1992, 461; M. W. Hosseini, R. Ruppert, P. Schaeffer, A. DeCian, N. Kyritskas and J. Fischer, *Chem. Commun.*, 1994, 2135; R. Macías, N. P. Rath and L. Barton, *J. Organomet. Chem.*, 1999, **581**, 39, J. C. MacDonald and G. M. Whitesides, *Chem. Rev.*, 1994, **94**, 2383.

4 M. R. Ghadini, J. R. Granja, R. A. Milligan, D. E. McRee and N. Khazanovich, *Nature*, 1993, **366**, 324.

5 I. S. Choi, X. Li, E. E. Simanek, R. Akaba and G. M. Whitesides, *Chem. Mater.*, 1999, **11**, 684.

6 S. Subramanian and M. J. Zaworotko, *Coord. Chem. Rev.*, 1994, **137**, 357.

7 E. Fan, J. Yang, S. J. Geib, T. C. Stoner, M. D. Hopkins and A. D. Hamilton, *J. Chem. Soc., Chem. Commun*., 1995, 1251.

8 P. Hobza, H. L. Selze and E. W. Schlag, *J. Am. Chem. Soc.*, 1994, **116**, 3500.

9 S. Chandrasekhar and G. S. Ranganath, *Rep. Prog. Phys*., 1990, **53**, 57.

10 A. R. A. Palmans, J. A. J. M. Vekemans, H. Fischer, R. A. Hikmet and E. W. Meijer, *Chem. Eur. J.*, 1997, **3**, 300.

11 Y. Matsanuga, N. Miyajima, Y. Nakayasu, S. Saki and M. Yonega, *Bull. Chem. Soc. Jpn.*, 1988, **61**, 207.

12 K. Hanabusa, C. Koto, M. Kimura, H. Shirai and A. Kakehi, *Chem. Lett.*, 1997, 429.

13 B. König, O. Möller, P. Bubenitschek and P. G. Jones, *J. Org. Chem.*, 1995, **60**, 4291.

Communication 9/05245C

Progress towards viridin: synthesis of the pentacyclic furanosteroid ring system *via o*-benzoquinonoid cycloadditions

Fabio E. S. Souza[a] and Russell Rodrigo*[b]

[a] *Department of Chemistry, University of Waterloo, Waterloo, Ontario, Canada N2L 3G1*
[b] *Department of Chemistry, Wilfrid Laurier University, Waterloo, Ontario, Canada N2L 3C5. E-mail: rrodrigo@wlu.ca*

Received (in Corvallis, OR, USA) 8th July 1999, Accepted 17th August 1999

The pentacyclic ring system of viridin is synthesised in nine steps from 4-methylguaicol by means of successive cycloadditions involving *o*-benzoquinonoid intermediates generated *in situ*.

The viridin family of pentacyclic furanosteroidal antibiotics[1] isolated from various species of fungi possess several unusual structural features. Viridin **1** contains an aromatic ring C, a

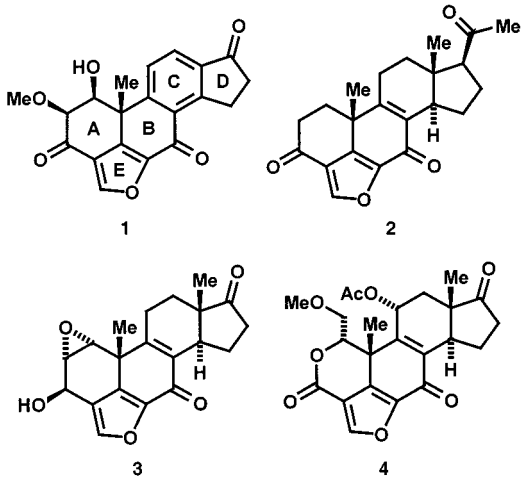

highly oxygenated ring A and a furan ring in a 'triterpenoid' location, betraying its biogenetic origins from lanosterol. Virone **2**, wortmannolone **3**[2] and wortmannin **4**[3] have an additional 'angular' methyl group at C-13 and *trans* C/D ring fusion. Viridin has powerful species specific anti-fungal activity, and wortmannin has attracted some attention as an anti-inflammatory agent and, more recently, as a potent inhibitor of phosphatidylinositol 3-kinase in neutrophils of the guinea pig.[4]

Apart from a long and low yielding conversion[5] of hydrocortisone to wortmannin no synthesis of any of these compounds has been achieved, but two other studies in this area have been reported.[6] Our recent explorations in the use of *o*-benzoquinonoid intermediates for natural product synthesis had led to the preparation[7] of the pentacyclic system **5** of viridin from benzindanone **6** and penta-2,4-dienol in one step (Scheme 1). However, we were unable to selectively reduce the C-10 thiol ester of **5** to the desired methyl group and even worse, an attempt at prior installation of the methyl group as in the model

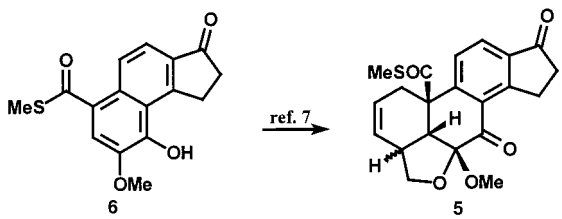

Scheme 1

substrate 2-methoxy-4-methylnaphthol resulted in failure of the intramolecular Diels–Alder (IMDA) reaction with the pentadienol under the usual oxidative conditions. We now report that the problems associated with the incorporation of the C-10 methyl group have been overcome and the first synthesis of the desired pentacycle **7** has been achieved in nine steps from 4-methylguaicol **8**.

The acid **9** was conveniently prepared on a multi-gram scale from **8** by Kolbe–Schmitt carboxylation[8,9] followed by BBr_3 demethylation (72% overall). This methylcatechol containing the carbon skeleton of ring B will serve as a linchpin for the attachment of rings CD and AE in two separate annulations employing novel *o*-benzoquinonoid protocols recently developed in our laboratory. When treated with an excess of 1-nitrohepta-4,6-diene[10] in the presence of bis(trifluoroacetoxy)iodobenzene (BTIB) it underwent a sequence of reactions (oxidation to the *o*-quinone, regiospecific Diels–Alder cycloaddition, decarboxylation of the β-keto acid adduct and rearomatisation) to provide the dihydronaphthalene **10** in 86% yield. This remarkable 'one-pot' process, in which the evanescent carboxy group of **9** plays a key role,[11] is the equivalent of a regiospecific cycloaddition of the 5,6-benzyne derived from 4-methylcatechol. Methylation of **10** with Me_3OBF_4 is both selective and quantitative. The methyl ether **11** was acetylated and subjected to the intramolecular nitrile oxide cycloaddition[12] by treatment with *p*-chlorophenyl isocyanate and Et_3N to produce the isoxazoline **13** after hydrolytic work-up with aqueous base. Catalytic hydrogenolysis (10% Pd/C, boric acid) then generated the benzindanone **14**, representing the BCD rings of viridin, as a single diastereomer[13] (52% overall, Scheme 2).

Rings A and E were now attached to the benzene ring of **14** by our *o*-benzoquinone monoketal procedure.[7] Treatment of **14** with BTIB in the presence of excess penta-2,4-dienol produced the monoketal **15** which reacted *in situ* by both possible IMDA pathways to produce a 1:1 mixture of two inseparable *endo*-adducts, pentacycles **16** and **17** (path A, quinonoid double bond as dienophile), and bridged adduct **18** (path B, quinonoid ring as diene). The assignments of relative stereochemistry to **16** and **17** are based on our previous experience[7,14] with the IMDA reactions of *o*-quinone monoketals, and the *endo* stereochemistry of the adducts is confirmed by the fact that both lose MeOH very readily to form the dienone unit of ring B. *Exo* adducts of this type do not eliminate MeOH.[14] The stereochemical issue with **18** was decided on the assumption that one face of **15** is more crowded than the other because of the *cis* CD ring fusion of this compound; the reaction is therefore presumed to occur at the less congested face of the diene unit of **15**. We are endeavouring to confirm this assignment by an X-ray crystal structure. Bridged adduct **18** was easily separated from the mixture of two diastereomeric pentacycles and when subjected to the Cope rearrangement in refluxing tetrachloroethane provided the target **7** in 65% yield. The diastereomers **16** and **17** when treated with TsOH in benzene with exposure to air provided the same compound (**7**) by dehydration and spontaneous aromatisation of ring C.

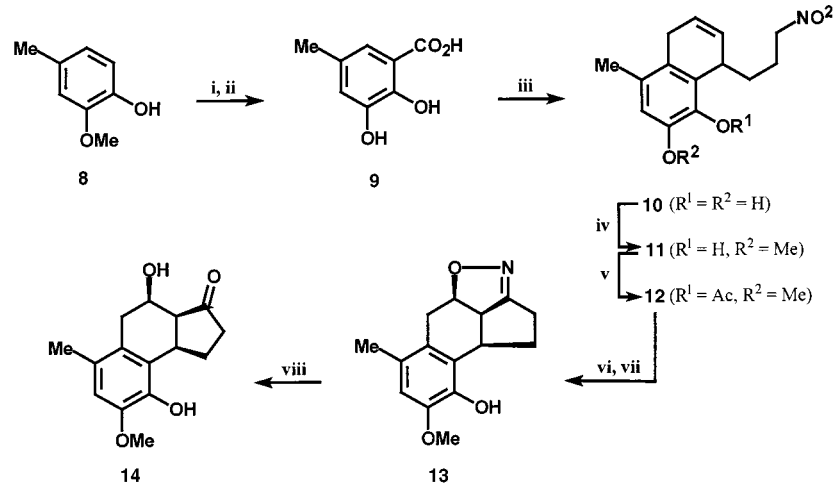

Scheme 2 *Reagents and conditions:* i, K_2CO_3, CO_2 (800 psi), 200 °C, 4 h; ii, BBr_3, CH_2Cl_2, −78 °C to room temp. (72%, two steps); iii, 1-nitrohepta-4,6-diene (5 equiv.), BTIB, THF (86%); iv, K_2CO_3, Me_3OBF_4, CH_2Cl_2 (100%); v, Ac_2O, pyridine; vi, *p*-ClC_6H_4NCO, Et_3N, C_6H_6, room temp., 36 h; vii, NaOH, H_2O–THF (84%, three steps); viii, H_2, Pd/C, H_3BO_3, MeOH–THF–H_2O (100%).

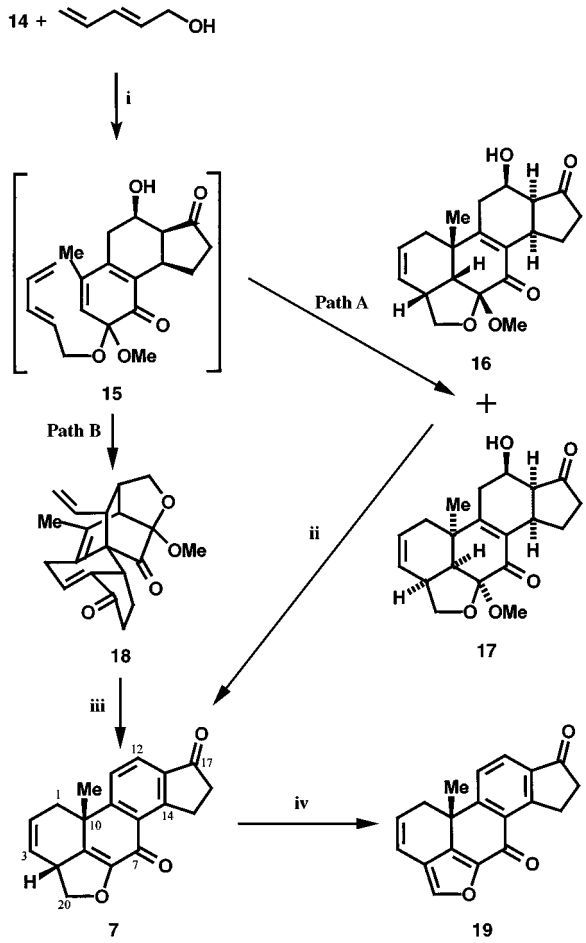

Scheme 3 *Reactions and conditions:* i, BTIB, THF (path A: 33%, path B: 31%); ii, TsOH, C_6H_6, 45 °C, 4 h (50%); iii, $Cl_2CHCHCl_2$, reflux, 48 h (65%); iv, *p*-chloranil, xylenes, reflux, 36 h (60%).

The nine-step sequence described above is not only the first synthesis of the ring system of viridin, but it also makes **7** available in sufficient quantity (19% overall, Scheme 3) to enable a comprehensive investigation for installation of the oxygen substituents in ring A, by derivatisation of the C_2–C_3 alkene, to be undertaken. Dehydrogenation of the dihydrofuran is facile and can be effected at any convenient stage; in fact, the conversion **7** → **19** has already been achieved in 60% yield. The benzindanone **14** offers possibilities for modification into the C/D non-aromatic analogues (*e.g.* **2**, **3** and **4**). Many obvious problems remain before any of these antibiotics can be synthesised, but we regard this short and flexible route to the pentacyclic system[15] as an important first step on the way to members of the viridin family.

We thank the Natural Sciences and Engineering Research Council of Canada for support of this work.

Notes and references

1 For a recent review, see J. R. Hanson, *Nat. Prod. Rep.*, 1995, **12**, 381.
2 M. M. Blight and J. F. Grove, *J. Chem. Soc., Perkin Trans. 1*, 1986, 1317.
3 T. J. Pecher, H-P. Weber and S. Kis, *J. Chem. Soc., Chem. Commun.*, 1972, 1061.
4 T. Okada, L. Sakuma, Y. Fukui, O. Hazeki and M. Ui, *J. Biol. Chem.* 1994, **269**, 3563.
5 S. Sato, M. Nakada and M. Shibasaki, *Tetrahedron Lett.*, 1996, **37**, 6141.
6 S. Honzawa, T. Mizutani and M. Shibasaki, *Tetrahedron Lett.*, 1999, **40**, 311; C. A. Broka and B. Ruhland, *J. Org. Chem.*, 1992, **57**, 4888.
7 R. Carlini, K. Higgs, C. Older, S. Randhawa and R. Rodrigo, *J. Org. Chem.*, 1997, **62**, 2330.
8 O. Baine, G. F. Adamson, J. W. Barton, J. L. Fitch, D. R. Swayampati and H. Jeskey, *J. Org. Chem.*, 1954, **19**, 510. We thank Warren Wallace for laboratory assistance with the preparation of **9**.
9 The acid **9** had been previously prepared by the $CuSO_4$ catalysed reaction of 3-bromo-5-methylsalicyclic acid with NaOH: D. D. Weller and E. P. Stirchak, *J. Org. Chem.*, 1983, **48**, 4873. We were unable to obtain good yields of **9** by this method in spite of several attempts.
10 Prepared from 1-iodohepta-4,6-diene and silver nitrite in 68% yield; see E. Vedejs, T. H. Eberlein and R. G. Wilde, *J. Org. Chem.*, 1988, **53**, 2220 for the synthesis of the iodide.
11 R. Carlini, C-L. Fang, D. Herrington, K. Higgs, R. Rodrigo and N. Taylor, *Aust. J. Chem.*, 1997, **50**, 271.
12 A.P. Kozikowski and C-S. Li, *J. Org. Chem.*, 1987, **52**, 3541 and pertinent references therein.
13 D. P. Curran, *J. Am. Chem. Soc.*, 1983, **105**, 5826.
14 R. Carlini, K. Higgs, R. Rodrigo and N. Taylor, *Chem. Commun.*, 1998, 65.
15 *Selected data* for **7:** δ_H(500 MHz, $CDCl_3$) 1.51 (s, Me), 2.18 (dd, *J* 17.8, 3.1, H-1α), 2.67 (m, H-15), 2.74 (dd, *J* 17.8, 2.3, H-1β), 3.67 (m, H-16), 4.00 (app dt, *J* 10.3, 2.6, H-4), 4.06 (dd, *J* 10.7, 8.1, H-20α), 4.87 (dd, *J* 9.8, 8.1, H-20β), 5.74 (app s, H-2, H-3), 7.55 (d, *J* 8.1, H-11), 7.89 (d, *J* 8.1, H-12). Full details will be published later.

Communication 9/05731E

Seeds obtained from a hydrated polymorph permit crystallisation of an elusive anhydrous organometallic zwitterion

Dario Braga,*[a] Gianna Cojazzi,[b] Lucia Maini,[a] Marco Polito[a] and Fabrizia Grepioni*[c]

[a] *Dipartimento di Chimica G. Ciamician, Università di Bologna, Via Selmi 2, 40126 Bologna, Italy. E-mail: dbraga@ciam.unibo.it; URL: http://catullo.ciam.unibo.it*

[b] *Centro CNR per la Fisica delle Macromolecole c/o Dipartimento di Chimica G. Ciamician, Università di Bologna, Via Selmi 2, 40126 Bologna, Italy*

[c] *Dipartimento di Chimica, Università di Sassari, Via Vienna 2, 07100 Sassari, Italy. E-mail: grepioni@ssmain.uniss.it*

Received (in Basel, Switzerland) 21st June 1999, Accepted 15th August 1999

Single crystals of the anhydrous polymorphic modification of the organometallic zwitterion [$Co^{III}(\eta^5$-$C_5H_4CO_2H)(\eta^5$-$C_5H_4CO_2)$] can only be obtained by seeding the solution with *seeds* prepared after stepwise dehydration and consequent phase transition at 506 K of the hydrated material [$Co^{III}(\eta^5$-$C_5H_4CO_2H)(\eta^5$-$C_5H_4CO_2)]\cdot 3H_2O$.

The control of crystallisation processes is of great interest both in crystal engineering,[1] where molecular materials with predefined organisation of the component molecules or ions are sought, and in the study of polymorphism,[2] where different polymorphs of the same substance may show different physical properties.

Here we report that single crystals of the elusive anhydrous polymorphic modification of the neutral zwitterion [$Co^{III}(\eta^5$-$C_5H_4CO_2H)(\eta^5$-$C_5H_4CO_2)$], **ZW**, can be obtained by *seeding* the starting solution† with 'seeds' prepared by stepwise dehydration and subsequent phase transition of the hydrated species [$Co^{III}(\eta^5$-$C_5H_4CO_2H)(\eta^5$-$C_5H_4CO_2)]\cdot 3H_2O$, **ZW**$\cdot 3H_2O$. This hydrate is the only product of the crystallisation from a aqueous solution of [$Co^{III}(\eta^5$-$C_5H_4CO_2H)(\eta^5$-$C_5H_4CO_2)$] obtained from the organometallic cationic diacid $[Co^{III}(\eta^5$-$C_5H_4CO_2H)_2]^+$.[3] Both **ZW** and **ZW**$\cdot 3H_2O$ have been structurally characterised by single crystal‡ and powder diffraction while the conversion of the initial product **ZW**$\cdot 3H_2O$ into anhydrous **ZW** has been monitored by thermogravimetry.

The most relevant features of **ZW**$\cdot 3H_2O$ and **ZW** can be summarised as follows.

(i) In contrast to the related dicarboxylic acid [$Fe^{II}(\eta^5$-$C_5H_4CO_2H)_2$] and the parent cation $[Co^{III}(\eta^5$-$C_5CO_2H)_2]^+$,[4] in crystalline **ZW**$\cdot 3H_2O$ there are no O–H···O hydrogen bonds between the $-CO_2H$/–COO groups, while C–H···$O_{(CO_2/CO_2H)}$ hydrogen bonded 'dimers' (D) are formed as shown in Fig. 1(a).

(ii) The dimeric units are linked in chains *via* a further, almost symmetric, bifurcated C–H···$O_{(CO_2/CO_2H)}$ hydrogen bond (C) between two adjacent C–H groups of a cyclopentadienyl ring and one O-atom lone-pair resulting in the formation of 'pipelines' through the crystal.

(iii) The pipelines are occupied by three water molecules per formula unit [Fig. 1(b)]. Two molecules are linked *via* O–H···O hydrogen bonds to the $-CO_2$/$-CO_2H$ groups on the walls of the channels and provide links between zwitterion stacks, whilst the central molecule interacts solely with the neighbouring water molecules.

(iv) Thermogravimetric analysis (TGA)§ shows that **ZW**$\cdot 3H_2O$ releases one water molecule at 378 K (Fig. 2). Powder diffraction‡ shows that the crystal structure remains almost unchanged. This first dehydration is reversible and the crystal is rehydrated in *ca.* 24 h at room temperature in the air. The remaining two water molecules are lost together at *ca.* 506 K. The second loss of water is immediately followed by a phase transition to a different crystalline form as revealed by powder diffraction.

(v) Most remarkably, crystallisation from an *aqueous* solution of the powder obtained from TGA at 506 K in the presence of *seeds* (a small portion of the *same* powder) leads to formation of single crystals of the species **ZW**. The structure of **ZW** is based on a one-dimensional network of O–H···O bonded zwitterion molecules (Fig. 3). Comparison of the calculated and

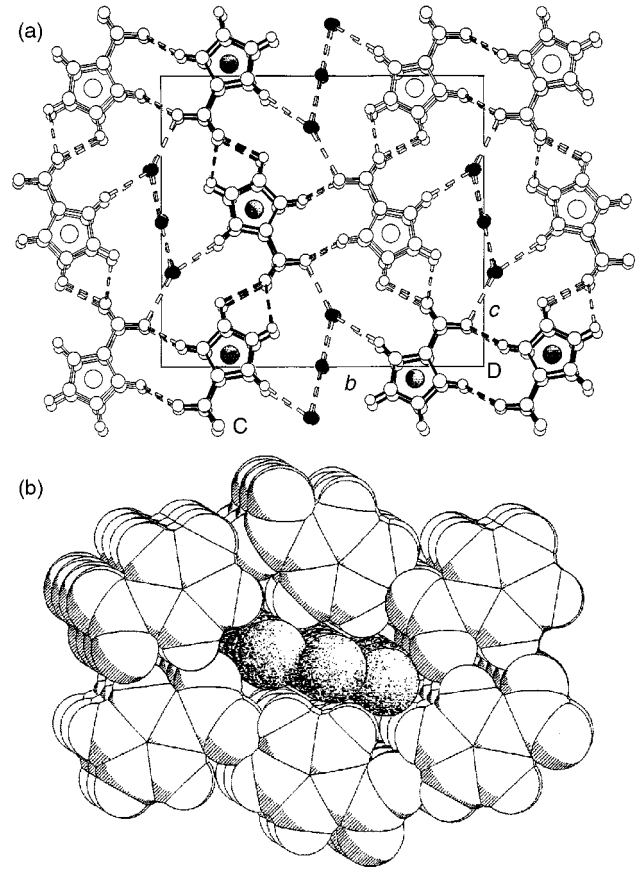

Fig. 1 (a) The zwitterions [$Co^{III}(\eta^5$-$C_5H_4CO_2H)(\eta^5$-$C_5H_4CO_2)$] pile up along the *a*-axis with the $-CO_2(H)$ groups pointing inward along the channels and forming O–H···O hydrogen bonds with two rows of water molecules. The organometallic units interact solely by means of C–H···O hydrogen bonds. Note how the 'dimers' (motif D) are linked in chains *via* bifurcated C–H···O hydrogen bonds; filled atom spheres represent the water oxygens. (*b*) Space filling representation of the channel in [$Co^{III}(\eta^5$-$C_5H_4CO_2H)(\eta^5$-$C_5H_4CO_2)]\cdot 3H_2O$, **ZW**$\cdot 3H_2O$, showing the three water molecules (dotted shading) occupying the channel. Relevant O···O distances (Å) are $O_{CO_2/CO_2H}\cdots O_{water}$ 2.758, 2780; $O_{water}\cdots O_{water}$ 2.823, 2838(2) Å.

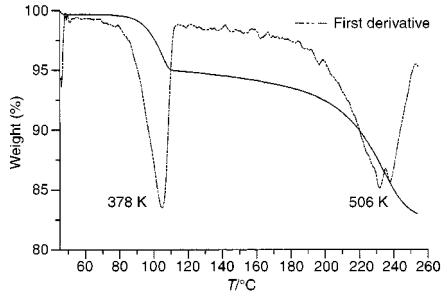

Fig. 2 TGA plot of the dehydration process. Note how the first water molecule is lost at 378 K, while the other two water molecules are released at 506 K. This second loss of water is followed by a phase transition.

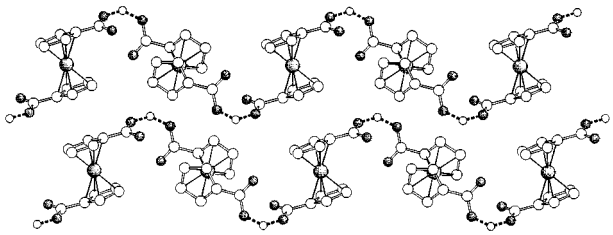

Fig. 3 Chains of O–H···O bonded zwitterions [$Co^{III}(\eta^5$-$C_5H_4CO_2H)(\eta^5$-$C_5H_4CO_2)$] in the anhydrous crystalline phase **ZW** crystallised *via* seeding of the solution obtained from the dehydrated powder; O···O 2.456(2) Å.

measured powder spectra of **ZW** confirms that the powder obtained at 506 K and the single crystals precipitated at room temperature after seeding possess the same structure. Importantly, crystallisation of the original solution mentioned in point (i), in the presence of seeds of **ZW**, also leads to isolation of the anhydrous crystalline material **ZW**, while, in the *absence* of seeds, the hydrated species **ZW**·$3H_2O$ is obtained.

Crystalline **ZW**·$3H_2O$ can be seen as a pseudo-polymorphic modification of **ZW**. The anhydrous form appears to be thermodynamically less stable and can only be obtained by dehydration of **ZW**·$3H_2O$ or *via* seeding of the solution, *i.e.* very likely under kinetic control.

It is worth stressing that the C–H···O bonds between zwitterions and the O–H···O bonds between zwitterion and water molecules along the walls of the channels are sufficient to keep the crystal together up to *ca.* 500 K. To the best of our knowledge, **ZW**·$3H_2O$ is the first case of an organometallic nanoporous material[5] with channels formed *via* C–H···O hydrogen bonds, with two structural water molecules acting as O–H···O bridges along the channels. Potential applications of nanoporous compounds are in catalysis, molecular sieves, molecule storage, ion exchange and solid sensors.[6]

The characterisation of **ZW** shows, *inter alia*, that single crystals of elusive polymorphic modifications can be obtained by controlling the crystallisation process *via* seeding, a crystallisation technique exploited also in organometallic solid state chemistry.[7] Clearly, the possibility of obtaining microcrystalline seeds by *non-solution* techniques (*dehydration* but also *grinding*[8]) is fascinating and opens up potentially useful alternative routes for the engineering of molecular materials.

We thank MURST (project Supramolecular Devices) and the University of Bologna (project Innovative Materials) for financial support.

Notes and references

† The starting material, **ZW**·$3H_2O$, is obtained from an aqueous solution of the salt {[$Co^{III}(\eta^5$-$C_5H_4CO_2H)(\eta^5$-$C_5H_4CO_2)$]·[$Co^{III}(\eta^5$-$C_5H_4CO_2H)_2$]}$^+$-[PF_6]$^-$ (0.3 mmol, 0.209 g, 20 ml water) after extraction of [$Co^{III}(\eta^5$-$C_5H_4CO_2H)_2$]$^+$[PF_6]$^-$ with nitromethane (70 ml in total).[3] Evaporation of the aqueous solution yielded yellow, sword-like, crystals of **ZW**·$3H_2O$ (0.099 g). Correspondence between the structure determined by single-crystal X-ray diffraction (see below) and the bulk material was confirmed by powder diffraction measurements.

‡ *Crystal data*: **ZW**·$3H_2O$: monoclinic, space group $P2_1/n$, a = 6.707(3), b = 14.997(4), c = 13.453(4) Å, β = 99.84(1)°, Z = 4, V = 1333(8) Å^3, μ = 1.316 mm^{-1}, θ range 3–25°, T = 223(2) K, 2230 independent reflections, $R1$ [$I > 2\sigma(I)$] 0.0851, wR^2 (all data, F^2) 0.2467.

ZW: monoclinic, space group $C2/c$, a = 7.403(2), b = 10.964(8), c = 12.293(3) Å, β = 94.30(3)°, Z = 4, V = 995.0(8) Å^3, μ = 1.722 mm^{-1}, θ range 3–25°, T = 273(2) K, 863 independent reflections, $R1$ [$I > 2\sigma(I)$] 0.0362, wR^2 (all data, F^2) 0.0996. The SHELXL97[9a] package was used for structure solution and refinement based on F^2. SCHAKAL97[9b] was used for all graphical representations. Diffraction data on **ZW**·$3H_2O$ have been collected on three different crystal specimens to investigate the small disorder affecting the inner O-atom occupying the centre of the channel (site occupancies between 0.80 and 1.00). CCDC 182/1386. See http://www.rsc.org/suppdata/cc/1999/1949/ for crystallographic files in .cif format. Powder diffractograms of **ZW**·$3H_2O$ calculated on the basis of the single crystal structure, measured at room temperature, measured after the first dehydration at 378 K, and measured after phase transition upon complete removal of the three water molecules, and a comparison between this latter diffractogram and the calculated spectrum of **ZW** are available as supplementary material upon request to the authors.

§ TGA was carried out on a Perkin-Elmer TGA-7 instrument in open Al pans under N_2 atmosphere. The loss in weight at the two temperatures (see Fig. 2) corresponds to one and two water molecules per **ZW** molar unit, respectively.

1 See, for example: G. R. Desiraju, *Crystal Engineering: The Design of Organic Solids*, Elsevier, Amsterdam, 1989; *Crystal Engineering: from Molecules and Crystals to Materials*, ed. D. Braga, F. Grepioni and A. G. Orpen, Kluwer Academic Publishers, Dordrecht, 1999, in press.
2 D. Dunitz and J. Bernstein, *Acc. Chem. Res.*, 1995, **28**, 193; J. Bernstein, R. J. Davey and J.-O. Henck, *Angew. Chem., Int. Ed.*, 1999, in press.
3 D. Braga, L. Maini, M. Polito and F. Grepioni, *Organometallics*, 1999, **18**, 2577.
4 F. Takusagawa and T. F. Koetzle, *Acta Crystallogr., Sect. B*, 1979, **35**, 2888; D. Braga, L. Maini and F. Grepioni, *Angew. Chem., Int. Ed.*, 1998, **37**, 2240.
5 See, for example: R. Robson and S. R. Batten, *Angew. Chem., Int. Ed.*, 1998, **37**, 1460; M. E. Davis, *Chem. Eur. J.*, 1997, **3**, 1745; R. Bishop, *Chem. Soc. Rev.*, 1996, 311.
6 See, for example: V. A. Russell, C. C. Evans, W. Li and M. D. Ward, *Science*, 1997, **276**, 575; I. W. C. E. Arends, R. A. Sheldon, M. Wallau and U. Schuchard, *Angew. Chem., Int. Ed. Engl.*, 1997, **36**, 1144; C. L. Bowes and G. A. Ozin, *Adv. Mater.*, 1996, **8**, 13.
7 P. Seiler and J. D. Dunitz, *Acta Crystallogr., Sect. B*, 1982, **38**, 1741; J. D. Dunitz, *Acta Crystallogr., Sect. B*, 1995, **51**, 619.
8 D. Braga, L. Maini and F. Grepioni, *Chem. Commun.*, 1999, 937.
9 (*a*) G. M. Sheldrick SHELXL97, Program for Crystal Structure Determination, University of Göttingen, Göttingen, Germany, 1997; (*b*) E. Keller, SCHAKAL97, Graphical Representation of Molecular Models, University of Freiburg, Germany, 1997.

Communication 9/04951G

Metal–radical approach to high spin molecules: a pentanuclear μ-cyano $Cr^{III}Ni^{II}$(radical)$_2$ complex with a low-lying $S = 9$ ground state

Arnaud Marvilliers,[a] Yu Pei,[a] Joan Cano Boquera,[a] Kira E. Vostrikova,[b] Carley Paulsen,[c] Eric Rivière,[a] Jean-Paul Audière[a] and Talal Mallah*[a]

[a] *Laboratoire de Chimie Inorganique, UMR CNRS 8613, Université Paris-Sud, 91405 Orsay, France. E-mail: mallah@icmo.u-psud.fr*
[b] *Inorganic Chemistry Institute, Lavrentieva Av., 630090 Novosibirsk, Russia*
[c] *Centre de Recherche sur les Très Basses Températures, CNRS, 25, av. des Martyrs, F-38054 Grenoble, France*

Received (in Oxford, UK) 15th June 1999, Accepted 26th August 1999

Reacting hexacyanochromate(III) with a mononuclear Ni(II) complex chelated by two bidentate organic radicals leads to a pentanuclear complex with three different kinds of paramagnetic species interacting ferromagnetically and stabilising a high spin $S = 9$ ground state.

The metal–radical approach has been successful to design one of the first one-dimensional ferrimagnetic chains that order ferromagnetically at low temperature; nitronyl nitroxyde organic radicals have been used as bis-monodentate ligands for Mn(hfac)$_2$ to do so.[1] Using the same approach, it was possible to stabilise a hexanuclear ring containing six *cis*-Mn(hfac)$_2$ entities connected by the phenyl nitronyl nitroxide radical and leading to a ground state $S = 12$.[2] Recently, Rey and coworkers reported the preparation of a bidimensionnal honeycomb like network that orders ferromagnetically at $T_C = 1.4$ K by using the bis-bidentate imidazolato nitronyl nitroxide radical as a bridging ligand for Mn(II) metal ions.[3] Inoue and Iwamura prepared another honeycomb network using a triradical molecule to connect Mn(hfac)$_2$ complexes.[4] The first extended system containing three different paramagnnetic species was reported by Kahn and coworkers.[5]

On the other hand, one of us has developed a step-by-step approach using $[Cr(CN)_6]^{3-}$ as a template to assemble mononuclear Ni(II) and Mn(II) complexes bearing pentadentate ligands as blocking chelates. Two high spin molecules, $Cr^{III}Ni^{II}_6$ and $Cr^{III}Mn^{II}_6$, possessing spin ground states $S = 15/2$ and 27/2, respectively, were thus designed.[6,7]

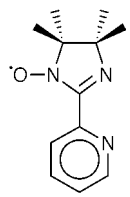

IM2-py

By combining these two approaches, we have designed a polynuclear molecule using a new mononuclear Ni(II) complex bearing two pyridine imino nitroxide bidentate ligands IM2-py [IM2-py = 2-(2-pyridyl)-4,4,5,5-tetramethyl-4,5-dihydro-1H-imidazolyl-1-oxy][8] acting simultanesouly (i) as bulky chelates to preclude the formation of an extended network and (ii) as an extra shell of paramagnetic species to enhance the value of the spin ground state. The nature of the different components [Cr(CN)$_6$, Ni(II), IM2-py] has been chosen to realise ferromagnetic interaction between the paramagnetic species in order to stabilise the highest spin state as the ground state.

A solution of the free radical IM2-Py (2×10^{-3} mol) in 30 ml of acetonitrile was added dropwise to 20 ml of acetonitrile containing [Ni(H$_2$O)$_6$](ClO$_4$)$_2$ (1×10^{-3} mol). A precipitate appeared immediately which was filtered off, washed with acetonitrile and dried under vacuum.† Elemental analysis indicated the formula [Ni(IM2-py)$_2$(H$_2$O)$_2$](ClO$_4$)$_2$.‡ The second step consisted in reacting [NBu$_4$]$_3$[Cr(CN)$_6$] with the Ni(II) complex in water to give a bright red precipitate immediately. The best yield was obtained for a Ni : Cr stoichiometric ratio of 3 : 2. Elemental analysis§ and thermogravimetric analysis fit well with the presence of two Cr(CN)$_6$ for three Ni(IM2-py)$_2$ and seven water molecules which corresponds to the formula [Cr(CN)$_6$]$_2$[Ni(IM2-py)$_2$]$_3$·7H$_2$O. The IR spectrum of the new species presents all the features expected for the organic radical as well as two bands at 2160 and 2128 cm^{-1} corresponding to the elongation asymmetric vibrations of bridged[6] and non-bridged cyanides, respectively. The new compound is soluble in most common solvents but is insoluble in water as expected for a neutral species. Unfortunately, crystals suitable for X-rays analysis were not obtained. However, the UV–VIS spectrum (MeOH, $c = 3 \times 10^{-2}$ mol l^{-1}) presents a band assigned to the $^3T_{2g} \leftarrow {}^3A_{2g}$ transition of the Ni(II) chromophores ($E = 11\,363$ cm^{-1}, $\varepsilon = 35.9$ l mol^{-1} cm^{-1}) which is shifted to higher energy in comparison to that of the mononuclear [Ni(IM2-py)$_2$(H$_2$O)$_2$]$^{2+}$ complex ($E = 10\,416$ cm^{-1}, $\varepsilon = 45$ l mol^{-1} cm^{-1}). Since the nitrogen end of the cyanide induces a stronger crystal field than water,[12] we deduce that the observed solubility is not due to some decomposition of an extended network in solution but to the fact that the compound is composed of soluble discrete polynuclear species retaining the same structure (presence of bridging cyanides) in solution as found in the solid state. The structure proposed is that of a pentanuclear complex where three *cis*-Ni(IM2-py)$_2$ molecules act as bridges for two Cr(CN)$_6^{3-}$ entities as depicted in Fig. 1. This structure¶ is actually based on that of the pentanuclear complex [Fe(CN)$_6$]$_2$[Ni(bpm)$_2$]$_3$·7H$_2$O [bpm = bis(1-pyrazolyl)methane] described recently by Murray and coworkers.[13]

In order to check our assumption on the structure and to investigate the nature of the ground state, we carried out

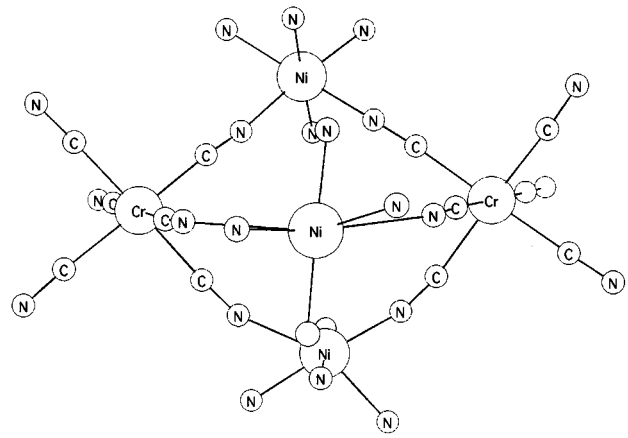

Fig. 1 Proposed model for the structure of the pentanuclear complex. Only the first coordination sphere of the nickel atoms is represented.

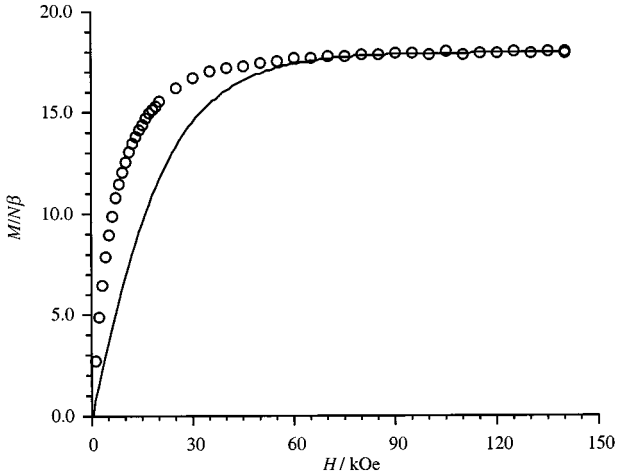

Fig. 2 *M vs.* H plot at T = 2.2 K (○) experimental, (——) sum of the calculated Brillouin functions for two S = 3/2 (Cr^{III}, g_{Cr} = 1.98), three S = 1 (Ni^{II}, g_{Ni} = 2.07) and six S = 1/2 (radical, g_{Rad} = 2.00).

magnetisation measurements on a powdered sample. The magnetisation *vs.* field plot (Fig. 2) (T = 2.2 K, H = 0–140 kOe) shows that the value at saturation (18.1 μ_B) corresponds to the expected value for ferromagnetic interaction between Cr(III) and Ni(II) on the one hand and between Ni(II) and the organic radicals on the other. Susceptibility *vs.* temperature measurements were carried with an applied field H = 2 kOe in the temperature range 300–30 K and at H = 30 Oe below 30 K to avoid saturation. On cooling, $\chi_M T$ increases and reaches a maximum at T = 6.5 K, then decreases (Fig. 3). The $\chi_M T$ value at the maximum (42 $cm^3\ mol^{-1}$ K) is very close to that expected for an S = 9 ground state (45 $cm^3\ mol^{-1}$ K for an average g value of 2) which corresponds to the parallel alignment of the local spins of the eleven paramagnetic species. In order to extract the exchange coupling parameters from the experimental data, a home-made routine was used to perform a calculation‖ of $\chi_M T$ as a function of temperature for different values of J_{CrNi} and J_{NiRad} by setting the local g values to g_{Cr} = 1.98, g_{Ni} = 2.07 and g_{Rad} = 2.00. The calculated curves for J_{NiRad} = 150 K (105 cm^{-1}) and J_{CrNi} = 9, 11, 13, 15 and 17 K are shown in the inset of Fig. 3. The best agreement between the experimental and the calculated data is obtained, in the temperature range 300–8 K, for J_{CrNi} = 13 K (9 cm^{-1}) and J_{NiRad} = 150 K (105 cm^{-1}). It is possible at this level to introduce a parameter θ that takes into account the decrease of $\chi_M T$ at low temperature as due to antiferromagnetic intermolecular interactions,** a very good agreement is obtained with θ = −0.45 K (Fig. 3). The sign and the values of the exchange coupling parameters are in the same range as have already been found for $CrNi_6$ (J_{CrNi} = 15 cm^{-1})[6] and $Ni(hfac)_2(IM2\text{-}py)$ (J_{NiRad} = 128 cm^{-1}).[9]

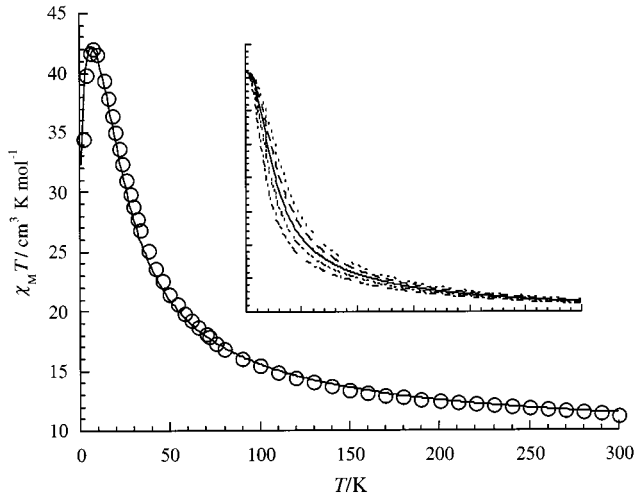

Fig. 3 $\chi_M T$ *vs.* T plot (○) experimental, (——) calculated for J_{CrNi} = 150 K and J_{NiRad} = 13 K. Inset: calculated $\chi_M T$ *vs.* T curves.

We are currently working on this combined strategy to design new high-spin molecules using bidentate organic radicals not only as a peripheral paramagnetic shell but also as bridging ligands.

This work has been supported by the European Marie Curie Research Training Grant, proposal Nr ERB4001GT965355.

Notes and references

† **CAUTION**: perchlorate salts should be used in small quantities and handled with care; explosion may occur.

‡ Anal. Found (calc.) for $C_{24}H_{36}N_6Cl_2O_{12}Ni$: C, 39.80(39.48); H, 5.02(4.97); N, 11.62(11.51); Cl, 9.85(9.71); Ni, 7.80(8.03)%. The IM2-py radical is assumed to act as a bidentate ligand *via* its two nitrogen atoms as has already been observed for $Ni(hfac)_2(IM2\text{-}py)$[9] and $Cu(hfac)_2(IM2\text{-}py)$.[10] This is reasonable since the imino nitrogen atom is a much better Lewis base than the oxygen atom of the nitroxide group. The preferred isomer of this complex is *cis* because steric hindrance between the bulky ligands preclude their presence in the same plane as is the case for $Ni(bipy)_2Cl_2$.[11]

§ Anal. Found (calc.) for $C_{84}H_{110}N_{30}O_{13}Ni_3Cr_2$: C, 49.85(49.74); H, 5.32(5.46); N = 20.86(20.71); Ni, 8.57(8.68); Cr, 4.97(5.12)%.

¶ Corey–Pauling–Koltun (CPK) molecular models were used to demonstrate the absence of any steric hindrance between the ligands' methyl groups in the proposed structure.

‖ The quantity $\chi_M T$ is related to the fluctuation of the magnetisation M, which is calculated from the energy eigenvalues and spin eigenfunctions. The eigensystem solution has been achieved by diagonalising the energy matrix. For our compound the number of microstates is given by $(2S_{Cr} + 1)^2 \times (2S_{NI} + 1)^3 \times (2S_{Rad} + 1)^6$ = 27 648. However, the matrices are built from the spin function basis in the M_S sub-spaces, where M_S is the z-component of the spin quantum number S. In this case, the size of the largest matrix that must be diagonalised which corresponds to the M_S = 0 subspace is 4390 × 4390.

** ac Susceptibility measurements which were performed down to 100 mK show the absence of long-range magnetic order, a behaviour different from the ferromagnetic order found for Murray's pentanuclear complex $[Fe(CN)_6]_2[Ni(bpm)_2]_3 \cdot 7H_2O$. The decrease of $\chi_M T$ may be due to a zero-field splitting effect and not to intermolecular antiferromagnetic interacion. Unfortunately, zero-field splitting could not be included owing to prohibitive calculation times.

1 A. Caneschi, D. Gatteschi, J.-P. Renard, P. Rey and R. Sessoli, *J. Am. Chem. Soc.*, 1989, **111**, 785; M. A. Caneschi, D. Gatteschi, J.-P. Renard, P. Rey and R. Sessoli, *Inorg. Chem.*, 1989, **28**, 3914; A. Caneschi, D. Gatteschi, P. Rey and R. Sessoli, *Inorg. Chem.*, 1988, **27**, 1756; A. Caneschi, D. Gatteschi, P. Rey and R. Sessoli, *Acc. Chem. Res.*, 1989, **22**, 392.

2 A. Caneschi, D. Gatteschi, J. Laugier, P. Rey, R. Sessoli and C. Zanchini, *J. Am. Chem. Soc.*, 1988, **110**, 2795.

3 K. Fegy, D. Luneau, T. Ohm, C. Paulsen and P. Rey, *Angew. Chem., Int. Ed.*, 1998, **37**, 1270.

4 K. Inoue and H. Iwamura, *J. Am. Chem. Soc.*, 1994, **116**, 3173.

5 H. O. Stumpf, L. Ouahab, Y. Pei, D. Grandjean and O. Kahn, *Science*, 1993, **261**, 447; H. O. Stumpf, L. Ouahab, Y. Pei, P. Bergerat and O. Kahn, *J. Am. Chem. Soc.*, 1994, **116**, 3866.

6 T. Mallah, C. Auberger, M. Verdaguer and P. Veillet, *J. Chem. Soc., Chem. Commun.*, 1995, 61.

7 A. Sculler, T. Mallah, A. Nivorozkhin, J.-L. Tholence, M. Verdaguer and P. Veillet, *New J. Chem.*, 1996, **20**, 1.

8 J. N. Helbert, P. W. Kopf, E. H. Poindexter and B. E. Wagner, *J. Chem. Soc., Dalton Trans.*, 1975, 998.

9 P. Rey, D. Luneau and A. Cogne, in *Magnetic Molecular Materials*, ed. D. Gatteschi, O. Kahn, J. S. Miller and F. Palacio, Kluwer, Dordrecht/Boston/London, NATO series 198, 1990, p. 203.

10 D. Luneau, P. Rey, J. Laugier, P. Fries, A. Caneschi, D. Gatteschi and R. Sessoli, *J. Am. Chem. Soc.*, 1991, **113**, 1245.

11 C. M. Harris and E. D. McKenzie, *J. Inorg. Nucl. Chem.*, 1967, **29**, 1047; H. Ojima and K. Nonoyama, *Z. Anorg. Allg. Chem.*, 1977, **429**, 282.

12 D. F. Shriver, S. H. Shriver and S. E. Anderson, *Inorg. Chem.*, 1965, **5**, 725.

13 K. V. Langenberg, S. R. Batten, K. J. Berry, D. C. R. Hockless, B. Moubaraki and K. S. Murray, *Inorg. Chem.*, 1997, **36**, 5006; Murray mentioned in this paper that the same structure is obtained when $Ni(bpm)_2$ is replaced by $Ni(bipy)_2$.

Communication 9/05736F

An unusual [4 + 4 + 4] bishelical complex, $Cu_3(H_2L)(L)\cdot 2H_2O$ [H_4L' = *N,N′*-bis(3-hydroxysalicylidene)-1,4-diaminobutane]: synthesis and crystal structure

Jesús Sanmartín,[a] Manuel R. Bermejo,[a] Ana M. García-Deibe,[a] Oscar Piro[b] and Eduardo E. Castellano[c]

[a] *Dpto. de Química Inorgánica, Facultade de Quimica, Campus Sur, Universidade de Santiago de Compostela, E-15706 Santiago de Compostela, Galicia, Spain. E-mail: qimb45@uscmail.usc.es*
[b] *Dpto. de Física, Facultad de Ciencias Exactas, Universidad de La Plata, C. C. 67-1900 La Plata, Argentina*
[c] *Instituto de Física de São Carlos, Universidade de São Paulo, C.P. 369, 13560-970, São Carlos, SP, Brazil*

Received (in Basel, Switzerland) 25th June 1999, Accepted 2nd August 1999

An electrochemical cell [$Cu_{(+)}$|MeCN + H_4L|$Pt_{(-)}$] (H_4L = title ligand), yielded powdery $[Cu_2(L)(H_2O)]_n$ and crystalline $Cu_3(H_2L)(L)\cdot 2H_2O$; the crystal structure of the latter shows an unusual helicate with an isosceles triangle core assembled by two μ-phenoxo bridges [Cu···Cu 3.413(3) and 3.858(3) Å], in which tetracoordinated Cu ions are in tetrahedrally distorted square planar environments.

The coordinating ability of compartmental ligands has been the subject of research owing to the interesting optical, magnetic and structural properties of polynuclear complexes.[1,2] Furthermore, there is much interest in the development of new polydentate ligands that can organise supermolecules upon complexation to two or more metal ions.[3]

We have recently reported some mono- and bi-nuclear Cu(II) complexes with asymmetrical Schiff bases.[4] This work has been extended to the direct electrochemical synthesis of polynuclear Cu(II) complexes with the title ligand, H_4L (prepared by condensation of 2,3-dihydroxybenzaldehyde and 1,4-diaminobutane in a 2:1 molar ratio) as a simple and efficient procedure to obtain them.

The electrochemical method [in this case summarised as: $Cu_{(+)}$|MeCN + H_4L|$Pt_{(-)}$] has been widely used by us.[5,6] An MeCN solution of H_4L (0.20 g) was electrolysed (V = 6.8 V) for a given time (3.25 h) according to the reaction $Cu_{(s)} + H_4L \rightarrow Cu(H_2L) + H_{2(g)}$. Anodic copper dissolved in the reaction mixture (0.066 g), whilst hydrogen evolved at the Pt cathode. An insoluble product was isolated which was analytically and spectroscopically identified† as $Cu_2(L)(H_2O)$ **1** (yield: 58%). The resulting solution was slowly evaporated and small crystals, suitable for X-ray diffraction studies,‡ were identified as $Cu_3(H_2L)(L)\cdot 2H_2O$, **2**·$2H_2O$ (yield 25%).

A single-crystal diffraction analysis of **2**·$2H_2O$ revealed an asymmetric unit containing half a molecule, with the central Cu(2) ion lying on a twofold axis. The neutral trinuclear complex is formed by two molecules of the coordinated ligand, one tetraanionic, L^{4-}, the other dianionic, H_2L^{2-}, and two water molecules linked by hydrogen bonds to the outer phenolic atoms of H_2L^{2-}, O(11) and O(11A). The molecular structure along with the atomic numbering scheme for the asymmetric unit is shown in Fig. 1. All atoms generated by the symmetry operation related to the twofold axis ($-x$, y, 0.5 $-$ z) have been labelled with an A.

The three Cu(II) ions are held together by two μ-phenoxo bridges, through O(20) and O(20A) of L^{4-}. The Cu(2)···Cu(1) distances, 3.413(3) Å, are similar to those found for other trinuclear copper complex which also contain alkoxo bridges between the central and terminal Cu(II) ions, but here they show a more planar geometry.[7] The longer Cu(1)···Cu(1A) distance, 3.858(3) Å, seems to be imposed by the spatial arrangement of both ligands and the three metal centres form an isosceles triangle arrangement.

These Cu···Cu separations are similar to those found for some copper(II) proteins such as oxyhaemocyanin from *Plimulus polyphemus*[8] (3.6 Å) which contain N-donor atoms and oxo-bridges. Furthermore, the trinuclear site of oxidised ascorbate oxidase from green zucchini[9,10] is also approximately isosceles triangular; two such sites are present with intermetallic distances in the range 3.66–3.90 Å.

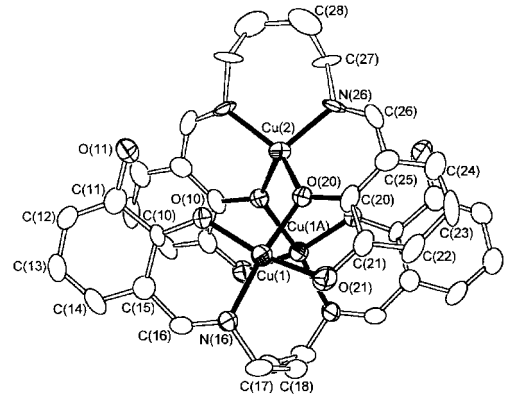

Fig. 1 ORTEP plot for **2**, showing the numbering scheme of the asymmetric unit. H-atoms and disordered atoms have been omitted for clarity. Significant distances (Å): Cu(1)–O(10) 1.872(8), Cu(1)–O(21) 1.900(8), Cu(1)–N(16) 1.950(10), Cu(1)–O(20) 1.976(8), Cu(2)–O(20) 1.905(9). Angles (°) around Cu(1) 84.0(4)–161.2(4), around Cu(2) 94.4(5)–139.0(4).

The central Cu(2) ion lies within the N_2O_2 inner compartment of L^{4-}. This donor set is usually quasi-planar in homo- and hetero-binuclear complexes containing very related ligands, but with a $(CH_2)_2$ or $(CH_2)_3$ chain. [11,12] However, in the present case with a $(CH_2)_4$ chain it is very severe tetrahedrally distorted. The longer $(CH_2)_4$ is more flexible and allows the ligand to twist and so achieve additional coordination to Cu(1) and Cu(1A) by means of both outer O_2 donor sets [O(20) and O(20A), acting as μ-phenoxo bridges], instead of a more typical binucleating fashion ($N_2O_2 + O_4$) for this type of ligand. Thus, L^{4-} is clearly behaving as a helicand with three metal-binding domains ($O_2 + N_2O_2 + O_2$). The helical arrangement is shown schematically in Fig. 2.

The absence of spacers other than the $(CH_2)_4$ between these donor sets, and the pronounced twist observed probably causes uncertainty in the atomic positions of the methylene chain. This may result in the observed disorder of its atoms, which are found in two different positions [C(27) and C(27′); C(28) and C(28′); with *ca.* 60 and 40% occupation factors, respectively]. In spite of this unusual ligand behaviour, the inner N_2O_2 compartment of L^{4-} still retains a suitable environment to effectively coordinate a copper(II) ion with usual bond lengths, but not in an ideally planar arrangement.

As Cu(1) and Cu(1A) do not satisfy their co-ordination numbers with co-ordination only to L^{4-}, the other ligand unit H_2L^{2-} must complete these. This ligand is bisbidentate and binucleating, by use of the double NO donor set of its inner

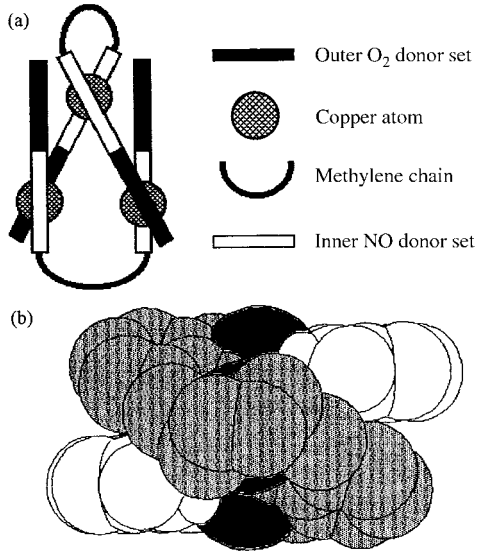

Fig. 2 (a) A scheme showing the helical arrangement for **2** and (b) a space-filling model of **2**, showing the helicand behaviour of L^{4-} (grey) and H_2L^{2-} (white) surrounding the three metal centes (black).

compartment. Thus, the NO_3 environment of Cu(1) and Cu(1A) is achieved through the O-atoms of L^{4-} [O(20) and O(21)], and the inner O(10) and N(16) atoms of H_2L^{2-} complete the coordination sphere leading to a slightly distorted square-planar coordination environment. The distortion appears to be caused by the steric hindrance between both ligand units and the twist of L^{4-} (Fig. 2). The other two potential donor oxygen atoms, O(11) and O(11A), remain protonated and are uncoordinated, but are linked by hydrogen interactions to solvated water molecules.

The bisbidentate bonding fashion observed for H_2L^{2-} (ON + NO), has been previously reported for other acyclic imines with similar[13] (but not helicand) and different donor atom sets (N_2 + N_2 but helicand).[3] However, H_2L^{2-} is not as twisted as L^{4-}, and adopts a nearly 'stepped-like' conformation, so that the two aromatic ring planes are almost parallel and fairly well separated. Overall, an unusual [4 + 4 + 4] bishelical arrangement is formed by three metal centres and two ligand units (Fig. 2).

This complex differs from usual bishelical structures, in which both helixes are similar or virtually so and the metal environments are seldom planar but more usually tetra- or octahedral.[3] Probably, the reasons for such an unusual arrangement can be found in the type of ligand used. It was previously reported that related ligands containing $(CH_2)_2$ and $(CH_2)_3$ chains could coordinate in both compartments (N_2O_2 + O_4) to Cu(II) ions.[11] The behaviour in the present system can be regarded as potentially compartmental, binucleating and leading to essentially square-planar coordination. L^{4-} acts as a trinucleating (O_2 + N_2O_2 + O_2) ligand while H_2L^{2-} is binucleating (ON + NO). Thus, the more flexible $(CH_2)_4$ chain ligand can coordinate two (NO + NO) and even three (O_2 + N_2O_2 + O_2) metal centres. Each moiety of L^{4-} is binucleating (O_2 + ON) but the flexible $(CH_2)_4$ chain allows the ligand to fold and so contain a metal centre in its inner compartment, in what can even be considered as O_2 + ON + NO + O_2 ligating behaviour.

Thus, both ligand units with their repeated metal-binding domains and a very flexible $(CH_2)_4$ chain spacer, lead to a bishelical arrangement. Perhaps, since there is no spacer between the inner NO and the outer O_2 donor sets of each moiety, both units cannot behave in the same way, as there would be a high steric hindrance between them (Fig. 2).

The assembling behaviour of this potentially N_2O_4 donor Schiff base is also unusual, as the majority of molecular threads giving rise to helicates incorporate at least one pyridine-type nitrogen donor.[3] The L^4 unit is unusual in that O-atoms predominantly coordinate and despite the presence of a long spacer it is bound to three close metal centres.

Although both ligand units show diverse behaviour, all the Cu–N and Cu–O distances are very similar in both cases, *ca.* 1.95 and 1.90 Å, respectively, which are within the usual range for copper ions coordinated to Schiff bases. Only the Cu(1)–O(20) distance [1.976(8) Å] is slightly longer than those usually found in the literature.[14] This is probably because O(20) is acting as a μ-bridge between Cu(2) and Cu(1).

Further studies are in progress; for example, magnetic data show a significant dependence with structure. EPR data for **2**·$2H_2O$ indicate a strucural change at *ca.* 100 K, probably related to the $(CH_2)_4$ moiety and its disorder.

We would like to thank Xunta de Galicia (Spain) for financial support (XUGA 20901B97).

Notes and references

† Elemental analysis. Found (calc.): for **1**: C, 45.4(46.0); H, 3.4(3.8); N, 6.5(6.0), O, 17.5(17.1%); for **2**·$2H_2O$: C, 49.8(49.3); H, 3.9(4.4); N, 6.3(6.4); O, 17.9(18.2%).

‡ *Crystal data* for **2**·$2H_2O$: $C_{36}H_{38}Cu_3N_4O_{10}$, M_r = 877.32, monoclinic, space group *C*2/*c* (no. 15), a = 17.098(7), b = 13.871(6), c = 15.366(7) Å, β = 110.0630(6)°, Z = 4, U = 3423(3) Å^3, T = 293 K, μ(Mo-Kα) = 1.914 mm^{-1}; 3146 reflections measured, 3021 reflections unique (R_{int} = 0.1634), $R1$ = 0.0611, $wR2$ = 0.1386; for all data $R1$ = 0.2972, $wR2$ = 0.2269. The structure was solved by standard direct methods and refined against F^2 by least squares.[15] All non-hydrogen atoms of the complex were readily located and refined anisotropically, except disordered atoms C(27′) and C(28′), which were treated isotropically. For H-atoms a riding model was employed, except for those bound to O-atoms, which were directly identified on Fourier maps, and given isotropic displacement parameters of 0.1 Å^2. Data were corrected for Lorentz and polarisation effects, and at a later stage in the refinement, an analytical absorption correction was applied. CCDC 182/1359. See http://www.rsc.org/suppdata/cc/1999/1953/ for crystallographic files in .cif format.

1 K. D. Karlin and J. Zubieta, *Copper Coordination Chemistry and Biochemistry. Biochemical and Inorganic Perspectives*, Adenine, Guilderland, NY, 1983.
2 P. A. Vigato, S. Tamburini and D. E. Fenton, *Coord. Chem. Rev.*, 1990, **106**, 25.
3 E. C. Constable, in *Comprehensive Supramolecular Chemistry*, ed. J. L. Arwood, J. E. D. Davies, D. D. McNicol, F. Vögtle, J. P. Sauvage and M. W. Hosseini, Pergamon, Oxford, 1996, p. 213.
4 J.-P. Costes, F. Dahan, M. I. Fernández-Garciá, M. B. Fernández-Fernández, A. M. García-Deibe and J. Sanmartin, *Inorg. Chim. Acta*, 1998, **274**, 73.
5 J. Sanmartín, M. R. Bermejo, J. A. García-Vázquez, J. Romero, A. Sousa, A. Brodbeck, A. Castiñeiras, W. Hiller and J. Strähle, *Z. Naturforsch., Teil B*, 1993, **48**, 431.
6 M. R. Bermejo, M. Fondo, A. M. González, O. L. Hoyos, A. Sousa, C. A. McAuliffe, W. Hussein, R. G. Pritchard and V. M. Novotorsev, *J. Chem. Soc., Dalton Trans.*, 1999, 2211.
7 P. V. Bernhardt and P. C. Sharpe, *J. Chem. Soc., Dalton Trans.*, 1998, 1087.
8 K. A. Magnus, H. Ton-That and J. E. Carpenter, *Bioinorganic Chemisty of Copper*, Chapman & Hall, New York, 1993.
9 A. Messerschmidt, R. Ladenstein, R. Huber, M. Bolognesi, L. Aviliano, R. Petruzzelli, A. Rossi and A. Finazzi-Agró, *J. Mol. Biol.*, 1992, **224**, 179.
10 A. Messerschmidt, A. Rossi, R. Ladenstein, R. Huber, M. Bolognesi, G. Gatti, A. Marchesini, R. Petruzelli and A. Finazzo-Agró, *J. Mol. Biol.*, 1989, **206**, 513.
11 P. Guerriero, S. Tamburini, P. A. Vigato, U. Russo and C. Benelli, *Inorg. Chim. Acta*, 1993, **213**, 279.
12 U. Casellato, P. Guerriero, S. Tamburini, S. Sitran and P. A. Vigato, *J. Chem. Soc., Dalton Trans.*, 1991, 2145.
13 M. Watkinson, M. Fondo, M. R. Bermejo, A. Sousa, C. A. McAuliffe, R. G. Pritchard, N. Jaiboon, N. Aurangzeb and M. Naeem, *J. Chem. Soc., Dalton Trans.*, 1999, 31.
14 R. H. Holm and M. J. O'Connor, *Prog. Inorg. Chem.*, 1971, **14**, 241.
15 SHELX97: Programs for Crystal Structure Analysis (Release 97-2). G. M. Sheldrick, Institüt für Anorganische Chemie der Universität, Tammanstrasse 4, D-3400 Göttingen, Germany, 1998.

Communication 9/05133C

ChemComm

Simple silica-particle template synthesis of mesoporous carbons

Sangjin Han and Taeghwan Hyeon*

School of Chemical Engineering and Institute of Chemical Processes, Seoul National University, Seoul 151-742, Korea. E-mail: thyeon@plaza.snu.ac.kr

Received (in Cambridge, UK) 20th July 1999, Accepted 27th August 1999

A simple preparative method for mesoporous carbons with high pore volumes using surfactant stabilized silica particles as templates is reported.

The synthesis of mesoporous M41S silica materials by Mobil researchers has stimulated explosive research on the preparation of inorganic porous materials through template approaches.[1] A large variety of mesoporous inorganic materials have been prepared using various types of organic templates including surfactant self-assemblies and block copolymers.[2] Uniform sized polymer latex spheres and emulsions have also been utilized to produce mesoporous inorganic materials with larger pores of >10 nm.[3]

Porous carbons have been extensively used as adsorbents in many separation and purification processes.[4] These porous carbons are generally microporous and the production of mesoporous carbons is extremely important for their applications in the separation and adsorption of bulky organic materials. Inorganic templates have been used to tune the pore size of carbon materials.[5] Recently, we have developed a new synthetic method to generate porous carbon materials with pores of >50 nm using commercial silica sol as a template.[6] Here, we report the fabrication of mesoporous carbon with narrow pore size distribution and high pore volume through surfactant stabilized silica particles as templates.

In previous work, we simply added carbon precursor, resorcinol and formaldehyde (RF) into Ludox HS-40 silica sol solution.[6] The resulting RF–silica composite was carbonized and etched with HF solution to obtain carbon materials with pores ranging in size from 10 to 60 nm [Fig. 1(a), dashed line]. The average particle size of HS-40 silica sol was reported to be 12 nm, and obviously the aggregates of silica particles are acting as templates. In order to obtain a more uniform pore size distribution, isolated silica particles stabilized by surfactant were applied as templates. The overall synthetic procedure is shown in Scheme 1. In a typical synthesis, 5 g of cetyltrimethylammonium bromide (CTAB) was added to 100 mL of an aqueous Ludox HS-40 silica sol solution (40 wt% silica with average particle size of 12 nm), and the mixture was stirred for 20 min at 50 °C, resulting in a muddy slurry. The stabilized silica particles were then collected by filtration under vacuum, and washed with double-distilled water to remove un-adsorbed surfactant. Resorcinol–formaldehyde gel (RF gel) was used as a carbon precursor.[7] A solution of 1 resorcinol: 2 formaldehyde: 0.014 Na_2CO_3 (catalyst): 5.62 H_2O with pH 7.3 was added dropwise under mild suction to be infiltrated into the CTAB-stabilized silica particles. The resulting yellow RF–silica composite was aged at 85 °C for three days to obtain a red RF gel–silica composite. The composite was carbonized at 850 °C for 3 h under nitrogen to yield a silica–carbon composite. To remove the silica template, the carbon–silica composite was stirred in 48 wt% aqueous HF solution for 12 h. The BET surface area was found to be 1512 $m^2\ g^{-1}$. The N_2 adsorption isotherm shown in the inset of Fig. 1(a) (continuous line) exhibited type IV behavior (hysteresis at high relative pressure), indicating the presence of mesopores. The BJH (Barrett–Joyner–Halenda) cumulative pore volume (corresponding to pores >2 nm) was extremely high (3.6 $cm^3\ g^{-1}$). The pore size distribution of the carbon material was narrow with an average pore size of 12 nm along with a shoulder around 15 nm [continuous line in Fig. 1(a)]. The overall pore size distribution is similar to the reported particle size distribution of Ludox HS-

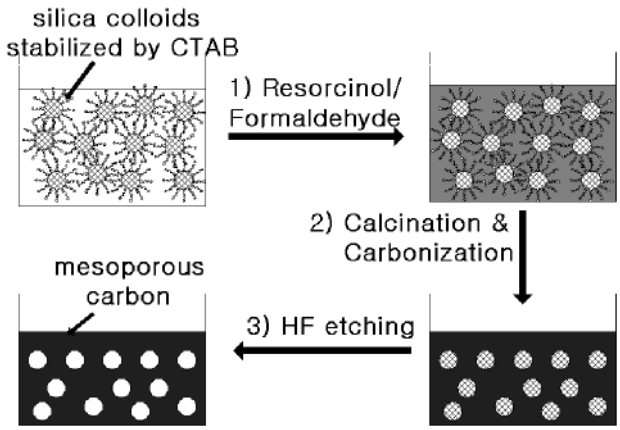

Scheme 1 Synthetic strategy for uniform mesoporous carbons. 1) gelation of resorcinol and formaldehyde (RF) in the presence of CTAB-stabilized silica particles; 2) carbonization of RF gel–silica composite at 850 °C to obtain carbon–silica composite; HF etching of silica templates to obtain mesoporous carbons.

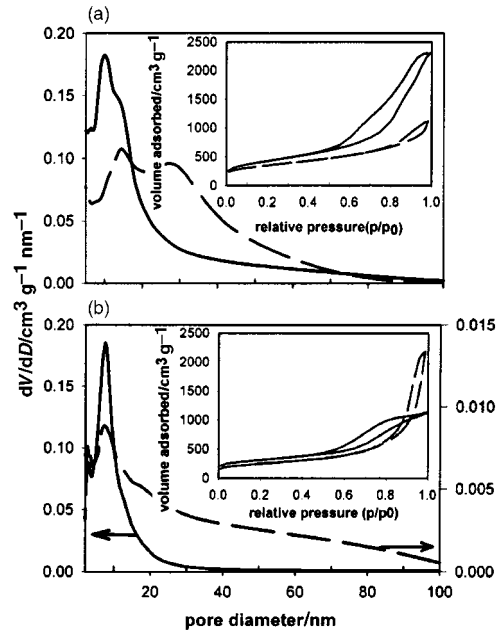

Fig. 1 The pore size distributions calculated from the adsorption branch of the nitrogen isotherm by the BJH method and the corresponding N_2 adsorption and desorption isotherms (insets) of mesoporous carbons. (a) (—) carbon prepared with CTAB-stabilized Ludox HS-40 silica sols as template and (----) carbon prepared with Ludox HS-40 silica sol aggregates as template. (b) (—) carbon prepared with CTAB-stabilized Ludox SM-30 silica sols as template and (----) carbon prepared with Ludox SM-30 silica sol aggregates as template. The isotherms were collected at 77 K on a Micrometrics ASAP2000 Gas Adsorption Analyzer after the carbon materials were degassed at 200 °C at 10 μTorr for 5 h.

30 silica sol (30 wt% silica).[8] By contrast, a carbon xerogel derived from the sol–gel polymerization of resorcinol–formaldehyde (RF) at pH 8 without silica templates was nearly nonporous. These results clearly demonstrate that the stabilized silica particles are acting as a true template for the formation of mesopores.

We have also produced carbon material using CTAB-stabilized Ludox SM-30 silica (30 wt% of silica with average particle size of 8 nm) particles as templates. The resulting carbon material revealed a very narrow pore size distribution centered at 8 nm [Fig. 1(b), continuous line]. The pore volume of the carbon material was high (1.69 $cm^3\ g^{-1}$) and the BET surface area of the material was found to be 1089 $m^2\ g^{-1}$. Carbon materials produced through SM-30 silica sol without a surfactant stabilization exhibited a relatively broad pore size distribution ranging from 8 to 100 nm [Fig. 1(b), dashed line]. Our present results demonstrate that uniform mesoporous carbons with pore size around 10 nm and very high pore volume can be easily fabricated by using surfactant-stabilized silica sol particles as templates.

We are grateful to the Korea Science and Engineering Foundation (Basic Research Program #98-05-02-03-01-3) for financial support.

Notes and references

1 C. T. Kresege, M. E. Leonowicz, W. J. Roth, J. C. Vartuli and J. S. Beck, *Nature*, 1992, **359**, 710.
2 S. A. Bagashaw and T. J. Pinnavaia, *Angew. Chem., Int. Ed. Engl.*, 1996, **35**, 1102; P. Yang, D. Zhao, D. I. Maroglese, B. F. Chmelka and G. D. Stucky, *Nature*, 1999, **396**, 152; J. Y. Ying, C. P. Mehnert and M. S. Wong, *Angew. Chem., Int. Ed.*, 1999, **38**, 57.
3 A. Imhof and D. J. Pine, *Nature*, 1997, **389**, 948; T. Holland, C. F. Blandford and A. Stein, *Science*, 1998, **281**, 538; J. E. G. J. Wijnhoven and W. L. Vos, *Science*, 1998, **281**, 802.
4 F. Rodriguez-Reinoso, in *Introduction to Carbon Technology*, ed. H. Marsh, E. A. Heintz and F. Rodriguez-Reinoso, Universidad de Alicante, Secretariado de Publications, Alicante, 1997, p. 35.
5 G. Che, B. B. Lakshmi, E. R. Fisher and C. R. Martin, *Nature*, 1998, **393**, 346; A. A. Zakhidov, R. H. Baughman, Z. Iqbal, C. Cui, I. Khayrullin, S. O. Dantas, J. Marti and V. G. Ralchenko, *Science*, 1998, **282**, 897.
6 S. Han and T. Hyeon, *Carbon*, 1999, **37**, 1645.
7 R. W. Pekala, *J. Mater. Sci.*, 1989, **24**, 3221.
8 J. C. Giddings, S. K. Ratanathanawongs, B. N. Barman, M. H. Moon, G. Liu, B. T. Tjelta and M. E. Hansen, in *The Colloid Chemistry of Silica*, ed. H. E. Bergna, American Chemical Society, Washington, DC, 1996, p. 309.

Communication 9/05848F

ChemComm

Synthesis of the porphyrin-fused porphyrin, [2]porphyracene

Ken-ichi Sugiura,* Takuya Matsumoto, Satoshi Ohkouchi, Yasuhisa Naitoh, Tomoji Kawai, Yoshio Takai, Kantaro Ushiroda and Yoshiteru Sakata*

The Institute of Scientific and Industrial Research (ISIR), Osaka University, 8-1 Mihogaoka, Ibaraki, Japan. E-mail: sakata@sanken.osaka-u.ac.jp

Received (in Cambridge, UK) 27th July 1999, Accepted 24th August 1999

A novel porphyrin-fused porphyrin is formed by an oligomerization reaction of a (porphyrinato)nickel complex with $TeCl_4$; the isolated compound, [2]porphyracene, was characterized by spectroscopic methods and direct observation using scanning tunnelling microscopy; the excitation energy value of 13460 cm^{-1} (743 nm) is the lowest value reported for porphyrin dimers.

Porphyrins hold a unique position among organic compounds since they have a small HOMO–LUMO gap and can incorporate almost all types of metal ions in the central cavity.[1] Reflecting these characteristics, porphyrins are present not only in various biological systems, but are applied in many advanced materials. Recently much efforts has been focused on the expansion, contraction, isomerization and modification of the porphyrin chromophore to lead to more elaborated functions.[2–7]

In the course of our synthetic study on chalcogen substituted porphyrins for advanced materials,[8] we serendipitously discovered a novel reaction between [5,15-bis(3,5-di-*tert*-butylphenyl)porphyrinato]nickel **2** with tellurium(IV) tetrachloride ($TeCl_4$) to give a highly conjugated porphyrin-fused porphyrin. Here we report the new expanded porphyrin **1a**, denoted [2]porphyracene (porphyrin + acene; the number [2] implies the number of porphyrin nuclei) since this condensation manner is an acene type.

To prepare **3** which has a $TeCl_3$ group at a *meso*-position, the reaction of **2** with 1 equiv. of $TeCl_4$ in dry CH_2Cl_2 at room temperature[9] was carried out. The obtained reaction mixture was analyzed by matrix assisted laser desorption ionization time-of-flight (MALDI-TOF) mass spectrometry and was found to give a series of peaks from M^+ = 1483 up to 6000 with equal mass spacings of *ca.* 744. This indicates clearly, contrary to the initial expectation, the formation of oligomeric products of **2**, from the dimer to the octamer. Separation of the dimer fraction from higher oligomers was successfully achieved using gel permeation liquid chromatography. The dimer fraction was further separated into three components **A**, **B** and **C** having M^+ = 1483, 1716 and 1949, respectively, using silica-gel flash chromatography. In a typical reaction, 48.3 mg of **1** and 8.8 mg of $TeCl_4$ gave 15.0 mg of **A**, 1.0 mg of **B**, 0.7 mg of **C**, and 20.0 mg of higher oligomers. The ^{1}H NMR spectrum of the main product **A** is different from those of porphyrin dimers directly connected at *meso–meso* or *meso*-β positions.[6] On the basis of detailed ^{1}H NMR analysis including truncated driven differential nuclear Overhauser effect measurements and MALDI-TOF mass spectra, the structure of **A** was assigned to be **1a** (Fig. 1) where the two porphyrin rings are fused at β- and *meso*-positions. The structures of **B** and **C** were assigned to be **1b** and **1c**, respectively, in a similar manner.

To confirm the structural assignment, we performed a direct observation of **1a** using scanning tunnelling microscopy (STM) (Fig. 2).† The STM image of **1a** adsorbed on a Cu(100) surface shows four lobes arranged in a parallelogram which are attributable to 3,5-di-*tert*-butylphenyl groups which are STM active substituents.[10] The size of the parallelogram is 13 × 9 Å which is consistent with the molecular size of **1a** estimated by a preliminary molecular geometry calculation [15.5 × 8.8 Å; Fig. 2(c)].

Aromatic protons of **1a** (H^b, H^c, H^d, H^e, H^f and H^{meso}) were upfield shifted by 0.18–0.67 ppm compared with the corre-

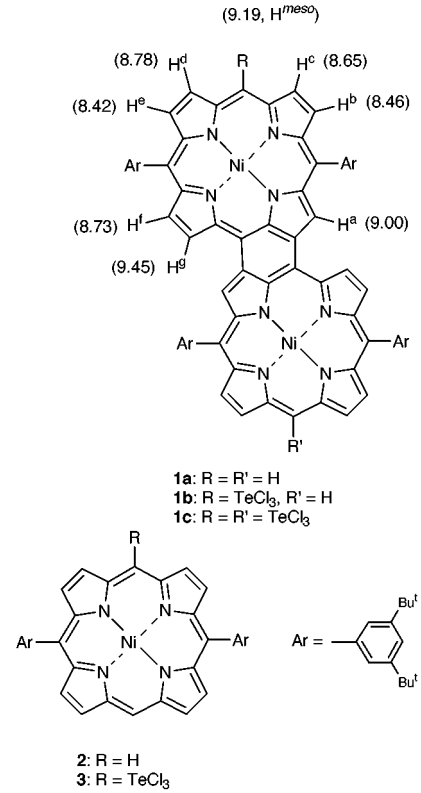

Fig. 1 Compounds **1**–**3** along with ^{1}H NMR assignments for **1a**.

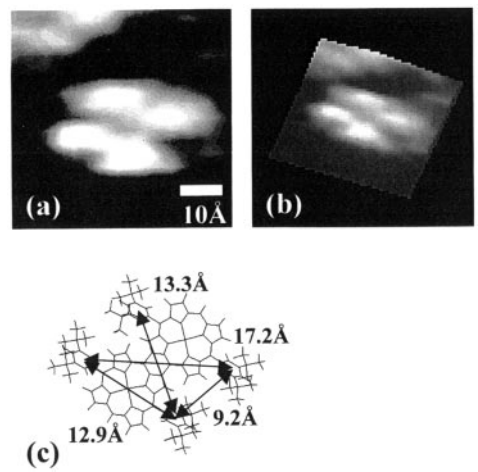

Fig. 2 STM image of **1a**: (a) top view, (b) perspective view, (c) molecular geometry of **1a**. The image shows a four-lobed pattern in a parallelogram arangement. The observed size of the parallelogram is 13 × 9 Å.

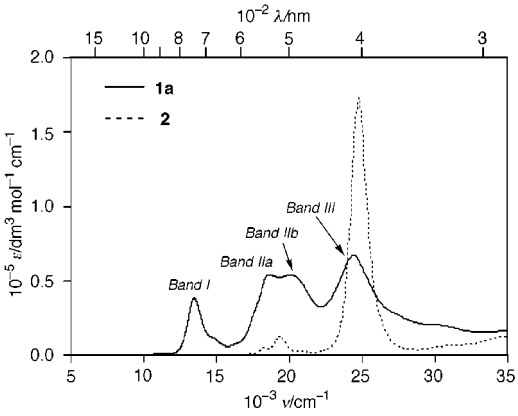

Fig. 3 Absorption spectra of [2]porphyracene **1a** (solid line) and **2** (dotted line) in $CHCl_3$.

sponding protons of **2** indicating the electron donating nature of the fused porphyrin ring. On the other hand, aromatic protons H^a and H^g showed downfield shifts of 0.09 and 0.34 ppm, respectively, owing to the ring current effect of the adjacent macrocycle and the compression effect from the sterically crowded protons.

The electronic spectra of **1a** and **2** are shown in Fig. 3. The spectrum of **1a** is essentially composed of three bands, band I, Q-band-like bands IIa and IIb and Soret-band-like band III. Reflecting the highly conjugated structure, band I appeared at 13460 cm^{-1} (743 nm) *i.e.* at a much longer wavelength than those of a porphyrin dimer connected by an acetylene linkage reported by Therien and coworkers (λ_{max} 14640 cm^{-1}; 683 nm)[2] or fused dimers reported by Crossley and Burn (λ_{max} 14180 cm^{-1}; 705 nm)[4] and by Smith and coworkers (λ_{max} 15340 cm^{-1}; 652 nm).[5] The other absorption bands of **1a**, bands IIa, IIb and III, were at quite similar wavelengths to those of **2**, although the intensity of band III was decreased and those of bands IIa and IIb were increased. These phenomena suggest a lowering of the symmetry and new π-electronic system for [2]porphyracene.

Considering that reported oxidative oligomerization of porphyrins take place at *meso–meso* and/or *meso*-β positions to form a single connection,[6] it is unprecedented that the present edge-fused oligomerization reaction of the nickel porphyrin complex takes place to give a double connection. Since the corresponding free base of **2** did not give oligomeric products, increased reactivity of the nickel porphyrin **2** at its β-positions may be responsible for the reaction.[6e] As shown in Scheme 1, the dimerization reaction of **2** probably takes place through a cyclic intermediate **4**,[11] which has not, so far, been detected. The final detelluration reaction is similar to that of bis(aryl)tellurium dichloride to give aryl coupling products.[9] The isolation of **1b** and **1c** suggests that these are the intermediates of [4]porphyracene and higher oligomers.

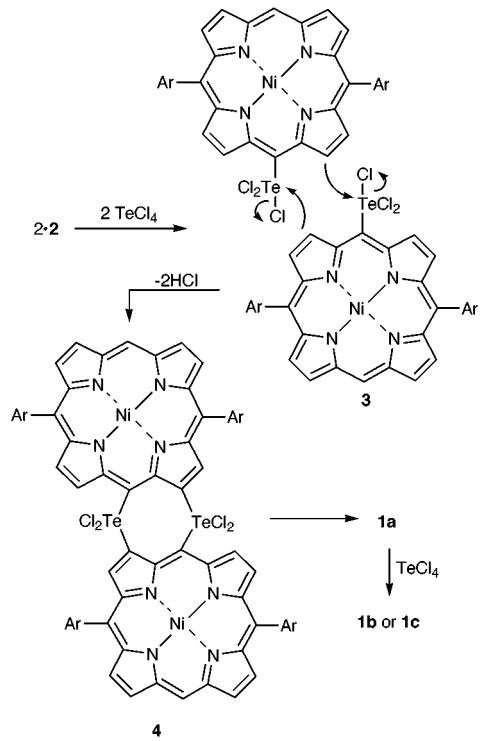

Scheme 1 A proposed reaction mechanism for dimerization.

In conclusion, a novel and highly conjugated [2]porphyracene has been isolated. In addition to the expanded π-system of the porphyrin, [2]porphyracene has two central cavities for homo- or hetero-metallation. These characteristics will allow us to use porphyracene for the preparation of advanced materials. We are currently investigating detailed properties of [*n*]porphyracenes including characterization of higher oligomers.

This work was supported in part by a Grant-in-Aid for Scientific Research on Priority Area (#11136222 "Metal-assembled Complexes" to K-i.S and #10146103 "Creation of Characteristic Delocalized Electronic Systems" to Y. S.) from the Ministry of Education, Science, Sports and Culture, Japan. We appreciate the technical assistance provided by the Materials Analysis Center of ISIR, Osaka University.

Notes and references

† The STM image was observed with a home-made ultrahigh vacuum apparatus. An atomically clean single crystal Cu(100) surface was used as the substrate onto which **1a** was sublimed. Details of STM experiments will be published elsewhere.

1 *Porphyrins and Metalloporphyrin*, ed. K. M. Smith, Elsevier, Amsterdam, 1975; *The Porphyrins*, ed. D. Dolphin, Academic Press, New York, 1978, vol. 8.
2 V. S.-Y. Lin, S. G. DiMagno and M. J. Therien, *Science*, 1994, **264**, 1105; V. S.-Y. Lin and M. J. Therien, *Chem. Eur. J.*, 1995, **1**, 645.
3 J. L. Sessler and S. J. Weghorn, *Expanded, Contracted & Isomeric Porphyrins*, ed. J. E. Baldwin, F. R. S. Magnus and P. D. Magnus, Pergamon, New York, 1997.
4 M. J. Crossley and P. L. Burn, *J. Chem. Soc., Chem. Commun.*, 1987, 39.
5 L. Jaquinod, O. Siri, R. G. Khoury and K. M. Smith, *Chem. Commun.*, 1998, 1261.
6 (*a*) K. Susumu, T. Shimidzu, K. Tanaka and H. Segawa, *Tetrahedron Lett.*, 1996, **37**, 8399; (*b*) A. Osuka and H. Shimizu, *Angew. Chem., Int. Ed. Engl.*, 1997, **36**, 135; (*c*) R. G. Khoury, L. Jaquinod and K. M. Smith, *Chem. Commun.*, 1997, 1057; (*d*) T. Ogawa, Y. Nishimoto, N. Yoshida, N. Ono and A. Osuka, *Chem. Commun.*, 1998, 337; (*e*) T. Ogawa, Y. Nishimoto, N. Yoshida, N. Ono and A. Osuka, *Angew. Chem., Int. Ed.*, 1999, **38**, 176.
7 T. D. Lash, S. T. Chaney and D. T. Richter, *J. Org. Chem.*, 1998, **63**, 9076.
8 K.-i. Sugiura, M. R. Kumar, T. K. Chandrashekar and Y. Sakata, *Chem. Lett.*, 1997, 291; K.-i. Sugiura, K. Ushiroda, T. Tanaka, M. Sawada and Y. Sakata, *Chem. Lett.*, 1997, 927.
9 The reductive aryl coupling reaction of bis(aryl)tellurium dichloride is well established: J. Bergman, *Tetrahedron*, 1972, **28**, 3323; J. Bergman, R. Carlsson and B. Sjöberg, in *Organic Synthesis*, ed. W. E. Noland, Wiley, New York, 1988, coll. vol. VI, pp. 468–471.
10 T. Takami, J. K. Gimzewski, R. R. Schlittler, T. Jung, Ch. Gerber, K. Sugiura and Y. Sakata, *Abstracts of Papers, 50th National Meeting of the Japanese Physical Society*, Kanagawa, Japanese Physical Society, Tokyo, 1995, Abstract 28p-PSB-29; T. A. Jung, R. R. Schlittler, J. K. Gimzewski, H. Tang and C. Joachim, *Science*, 1996, **271**, 181; T. A. Jung, R. R. Schlittler and J. K. Gimzewski, *Nature*, 1997, **386**, 696; J. K. Gimzewski and C. Joachim, *Science*, 1999, **283**, 1683.
11 In the iodination reaction of 5,15-diphenylporphyrin, the second substitution reaction occurs at the β-position: R. W. Boyle, C. K. Johnson and D. Dolphin, *J. Chem. Soc., Chem. Commun.*, 1995, 527; A. Nakano, H. Shimidzu and A. Osuka, *Tetrahedron Lett.*, 1998, **39**, 9489.

Communication 9/06073A

ChemComm

Fixation and spontaneous dehydrogenation of methanol on a triruthenium–iridium framework: synthesis and structure of the cluster anion $[HRu_3Ir(CO)_{12}(OMe)]^-$

Susanne Haak,† Antonia Neels, Helen Stœckli-Evans, Georg Süss-Fink* and Christophe M. Thomas

Institut de Chimie, Université de Neuchâtel, Avenue de Bellevaux 51, CH-2000 Neuchâtel, Switzerland.
E-Mail: GEORG.SUESS-FINK@ICH.UNINE.CH

Received (in Basel, Switzerland) 7th July 1999, Accepted 19th August 1999

The anionic mixed-metal cluster $[Ru_3Ir(CO)_{13}]^-$ 1, found to be catalytically active in the carbonylation of methanol, reacts with methanol at 70 °C to give, with O–H activation of the substrate, the cluster anion $[HRu_3Ir(CO)_{12}(OMe)]^-$ 2, which upon prolonged reaction loses formaldehyde to give the cluster anion $[H_2Ru_3Ir(CO)_{12}]^-$ 3; both anions 2 and 3 crystallise together as the double-salt $[N(PPh_3)_2]_2[HRu_3Ir(CO)_{12}(OMe)][H_2Ru_3Ir(CO)_{12}]$ the single-crystal X-ray structure analysis of which reveals a butterfly Ru_3Ir skeleton for 2 and a tetrahedral Ru_3Ir skeleton for 3.

Mixed-metal clusters have received steadily increasing attention over the last three decades owing to their inherent catalytic potential.[1] The presence of different metals in the same complex may have synergistic effects in the catalytic activity.[2] Recently we reported a series of Ru_3Ir and Os_3Ir mixed-metal clusters which show reasonable catalytic activity in the carbonylation of methanol to give acetic acid.[3,4] The cluster anions $[Ru_3Ir(CO)_{13}]^-$ **1** and $[Os_3Ir(CO)_{13}]^-$ **4**, used as catalyst precursors in this process, are however unstable under the reaction conditions, which has been confirmed by the isolation of the fragmentation products $Ir_4(CO)_{12}$ and $[N(PPh_3)_2][M(CO)_3I_3]$ (M = Ru, Os).[4] In this context we were interested in the behaviour of these anionic clusters towards reagents participating in the catalytic process, especially in the reaction with methanol.

The anion $[Ru_3Ir(CO)_{13}]^-$ **1** (as its $[N(PPh_3)_2]^+$ salt) reacts with methanol at 70 °C within 2 h to give the anionic cluster $[HRu_3Ir(CO)_{12}(OMe)]^-$ **2** [eqn. (1)], as indicated by a colour change of the solution from red to orange. The formation of **2** involves O–H activation of the methanol molecule, which is split into μ-H and μ-OMe ligands, replacing a carbonyl group of the starting compound. Anion **2** can be isolated as the $[N(PPh_3)_2]^+$ salt by extraction with diethyl ether after evaporation of the reaction solution to dryness, washing of the residue with hexane–dichloromethane (5:1) and recrystallisation from ethanol–pentane (1:3) at −18 °C.‡

$$\underset{\mathbf{1}}{[Ru_3Ir(CO)_{13}]^-} + MeOH \rightarrow \underset{\mathbf{2}}{[HRu_3Ir(CO)_{12}(OMe)]^-} + CO \quad (1)$$

Upon prolonged reaction (48 h) in methanol, especially at higher temperature (90 °C), anion **2** is transformed into the anion $[H_2Ru_3Ir(CO)_{12}]^-$ **3** with liberation of formaldehyde [eqn. (2)]. The formation of formaldehyde is evidenced by the ^1H NMR spectrum of the reaction mixture, which shows the signal for HCHO at δ 9.75 as well as a signal at δ 5.31 attributed to the formaldehyde trimer trioxane (by comparison with an authentic sample).

$$\underset{\mathbf{2}}{[HRu_3Ir(CO)_{12}(OMe)]^-} \rightarrow \underset{\mathbf{3}}{[H_2Ru_3Ir(CO)_{12}]^-} + HCHO \quad (2)$$

If the thermal reaction of **1** with methanol at 90 °C is stopped half-way (after 12 h), both anions **2** and **3** are present in the solution, and the double-salt $[N(PPh_3)_2]_2[HRu_3Ir(CO)_{12}(OMe)][H_2Ru_3Ir(CO)_{12}]$ can be isolated by crystallisation of the reaction residues from a 4:1 mixture of diethyl ether and hexane.

A suitable crystal§ of this double-salt revealed the molecular structure of both anions **2** and **3** (Fig. 1 and 2), disordered over the same position. Three of the four metal positions are occupied by metal atoms of both anions **2** and **3**, whereas one ruthenium atom splits into Ru(1) for anion **2** and Ru(1a) for anion **3**, the refinement of the occupancy factors giving a 1:1 ratio. In contrast to anion **2**, anion **3** is already known,[3] its structure in the double-salt being very similar to that we found in the salt $[N(PPh_3)_2][H_2Ru_3Ir(CO)_{12}]$.[3]

In anion **2**, the dihedral angle Ru(1)–Ir(1)–Ru(3)–Ru(2), that is to say the spreading of the wing tips is relatively small (82.9°) compared to those in other chalcogen- or halogen-bridged clusters, such as $HRu_3Co(CO)_{12}(\mu\text{-}SMe_2)$ (96.1°)[5] or $HRu_3Ir(CO)_{12}(\mu\text{-}Cl)$ (89.3°).[6] A similar dihedral angle as in **2** has been observed in the hydroxy-bridged osmium cluster cation $[H_4Os_4(CO)_{12}(\mu\text{-}OH)]^+$ (82.3°).[7] As a result of the small dihedral angle, the distance between the wing tip metal atoms Ru(1) and Ru(2) is only 3.3536(2) Å. The hydride-bridged edge Ru(1)–Ru(3), at 3.095(5) Å, is significantly longer than all the other metal–metal bonds. The wing tips are bridged asymmetrically by the methoxy group, the Ru–O bond distances being 2.02(2) and 2.16 (2) Å, respectively. This is well in line with the bond lengths found in other methoxy-bridged clusters, such as $HOs_3Pt_2(CO)_{10}(\mu_5\text{-}C)(\mu\text{-}OMe)(PCy_3)_2$[8] or $Os_3(CO)_{10}(\mu$-

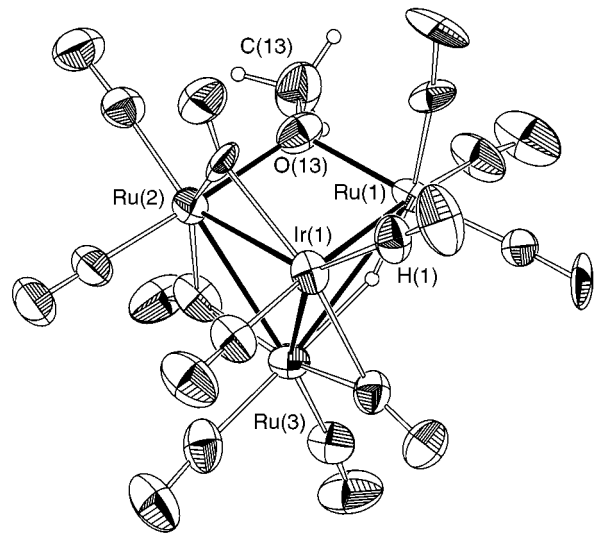

Fig. 1 Molecular structure of $[HRu_3Ir(CO)_{12}(OMe)]^-$ **2** showing the atom numbering scheme. Selected bond distances (Å) and angles (°): Ir(1)–Ru(1) 2.854(2), Ir(1)–Ru(2) 2.758(1), Ir(1)–Ru(3) 2.737(1), Ru(1)–Ru(3) 3.095(5), Ru(2)–Ru(3) 2.797(1), Ru(1)–H(1) 1.47(1), Ru(3)–H(1) 1.77(1), Ru(1)–O(13) 2.02(2), Ru(2)–O(13) 2.16(2), O(13)–C(13) 1.39(3), Ru(1)–O(13)–C(13) 119.3(16), Ru(2)–O(13)–C(13) 125.7(16).

† Present address: Department of Chemistry, University of Sheffield, Sheffield, UK S3 7HF.

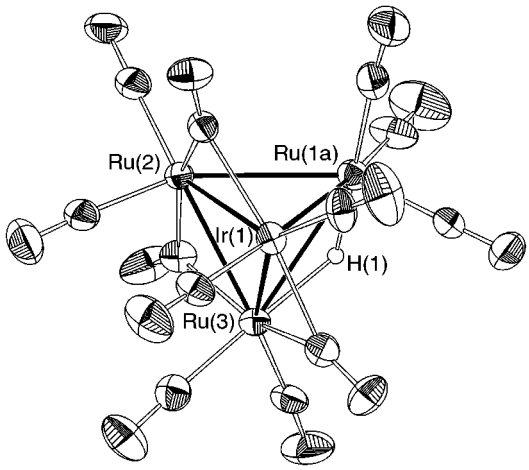

Fig. 2 Molecular structure of $[H_2Ru_3Ir(CO)_{12}]^-$ **3** showing the atom numbering scheme. Selected bond distances (Å): Ir(1)–Ru(1A) 2.689(6), Ru(1A)–Ru(2) 2.878(4), Ru(1A)–Ru(3) 2.866(6), Ru(3)–H(1) 1.77(1), Ru(1A)–H(1) 1.37(1). The second hydride ligand spanning Ru(1A)–Ru(2), only having an occupancy factor of 50%, could not be located in the double-salt, but was found in $[N(PPh_3)_2][H_2Ru_3Ir(CO)_{12}]$.[3]

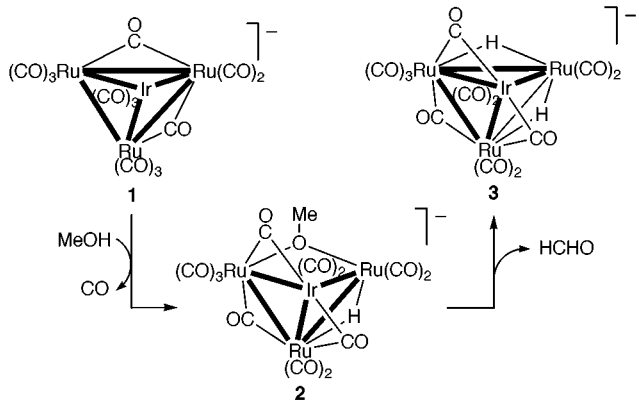

Scheme 1

$OMe)_2$.[9] The methyl group sticks out of the Ru(1)–Ru(2)–O(13) plane with an angle of 13.7°, in accordance with observations for $Os_3(CO)_{10}(\mu\text{-}OMe)_2$.[9] Anion **2** is consistent with the effective atomic number rule which requires an electron count of 62 valence electrons for butterfly clusters.

The reaction sequence involving the cluster anions **1**, **2** and **3** and the oxidation of methanol to formaldehyde is very interesting (Scheme 1). Anion **1** contains a closed tetrahedral Ru_3Ir metal framework, which is opened by the reaction with methanol to give anion **2** containing a butterfly Ru_3Ir skeleton, the wing tips of which are bridged by the methoxy ligand. The elimination of formaldehyde in going from **2** to **3** implies the reclosing of the butterfly Ru_3Ir skeleton to a closed metal tetrahedron.

We are grateful to the BASF AG (Germany) for financial support of this work. We also thank the Johnson Matthey Technology Centre (United Kingdom) for a generous loan of ruthenium trichloride hydrate.

Notes and references

‡ *Analytical and spectroscopic data*: for $[N(PPh_3)_2][HRu_3Ir(CO)_{12}(OMe)]$. Analysis. Found: C, 41.97; H, 2.65; N, 1.00. Calc. for $C_{49}H_{34}IrNO_{13}P_3Ru_3$: C, 41.97; H, 2.44; N, 1.00%. IR(thf): 2071vw, 2035w, 2016s, 2006s, 1968vs, 1817m, 1805m cm^{-1}. ^1H NMR (200 MHz, 294 K, $CDCl_3$): δ −14.28 (s, 1H), 2.94 (s, 3H), 7.39–7.70 (m, 30H).

For $[N(PPh_3)_2][H_2Ru_3Ir(CO)_{12}]$. Analysis. Found: C, 41.93; H, 2.17; N, 1.08. Calc. for $C_{48}H_{32}IrNO_{12}Ru_3$: C, 42.02; H, 2.35; N, 1.02%. IR(thf): 2074w, 2038s, 2005vs, 1968m, 1952m, 1819w, 1805w cm^{-1}. ^1H NMR (200 MHz, 294 K, $CDCl_3$): δ −20.64 (s, 2H), 7.40–7.70 (m, 30H).

§ *Crystallographic data* for $[N(PPh_3)_2]_2[HRu_3Ir(CO)_{12}(OMe)][H_2Ru_3Ir(CO)_{12}]$, $C_{117}H_{66}N_2Ir_2O_{25}P_4Ru_6$, M = 1387.18, monoclinic, space group $P2_1/c$, a = 14.966(1), b = 19.743(1), c = 17.07781) Å, β = 98.541(10)°, V = 4989.8(7) $Å^3$, Z = 2, D_c = 1.846 g cm^{-3}, μ(Mo-Kα) = 3.675 mm^{-1}, 38776 reflections measured ($2\theta_{max}$ = 52.08°), 5302 observed data [$I > 2\sigma(I)$] used in the refinement, $R1$ = 0.0588, $wR2$ = 0.1501 ($R1$ = 0.1042, $wR2$ = 0.1674 for all data). Intensity data were collected at 293(2) K on a Stoe Imaging Plate Diffractometer system (IPDS) equipped with a one-circle goniometer using Mo-Kα graphite-monochromated radiation (λ = 0.71073 Å). 200 exposures (3 min per exposure) were obtained at an image plate distance of 70 mm with $0 < \varphi < 200°$ with the crystal oscillating through 1° in φ. The structure was solved by direct methods (SHELXS-97[10]) and refined using weighted full-matrix least squares on F^2 (SHELXL-97[11]). A high disorder was found in the double-salt resulting in refined occupancies of 0.5 for Ru(1), Ru(1a) and the corresponding CO ligands. The methoxy group which is coordinated to Ru(1) and Ru(2) also has an occupancy of 0.5. Despite an empirical absorption correction being applied using DIFABS[12] (T_{min} = 0.168, T_{max} = 0.640), a large peak of electron density near one of the ruthenium atoms remained, which may be due to the disorder.

CCDC 182/1387. See http://www.rsc.org/suppdata/cc/1999/1959/ for crystallographic files in .cif format.

1 P. Braunstein and J. Rose, in *Comprehensive Organometallic Chemistry 2*, ed. E. W. Abel, F. G. A. Stone and G. Wilkinson, Elsevier, Oxford, 1995, vol. 10, p. 351.
2 E. Rosenberg and R. M. Laine, in *Catalysis by Di- and Polynuclear Metal Complexes*, ed. R. D. Adams and F. A. Cotton, Wiley–VCH, New York, 1998, p. 1; G. Süss-Fink and M. Jahncke, in *Catalysis by Di- and Polynuclear Metal Complexes*, ed. R. D. Adams and F. A. Cotton, Wiley–VCH, New York, 1998, p. 167.
3 G. Süss-Fink, S. Haak, V. Ferrand and H. Stœckli-Evans, *J. Chem. Soc., Dalton Trans.*, 1997, 3861.
4 G. Süss-Fink, S. Haak, V. Ferrand and H. Stœckli-Evans, *J. Mol. Catal. A*, 1999, **143**, 163.
5 S. Rossi, J. Pursianen and T. A. Pakkanen, *Organometallics*, 1991, **10**, 1390.
6 A. U. Härkönen, M. Ahlgrèn, T. A. Pakkanen and J. Pursianen, *J. Organomet. Chem.*, 1996, **519**, 205.
7 B. F. G. Johnson, J. Lewis, P. R. Raithby and C. Zuccaro, *J. Chem. Soc., Dalton Trans.*, 1980, 716.
8 L. J. Farrugia, A. D. Miles and F. G. A. Stone, *J. Chem. Soc., Dalton Trans.*, 1985, 2437.
9 V. F. Allen, R. Mason and P. B. Hitchcock, *J. Organomet. Chem.*, 1977, **140**, 297.
10 G. M. Sheldrick, *Acta Crystallogr., Sect. A*, 1990, **46**, 467.
11 G. M. Sheldrick, SHELXL-97, University of Göttingen, Germany, 1997.
12 N. Walker and D. Stuart, *Acta Crystallogr., Sect. A*, 1990, **46**, 158.

Communication 9/05487A

ChemComm

From porphyrin sponges to porphyrin sieves: a unique crystalline lattice of aquazinc tetra(4-carboxyphenyl)porphyrin with nanosized channels

Yael Diskin-Posner and Israel Goldberg*

School of Chemistry, Sackler Faculty of Exact Sciences, Tel-Aviv University, 69978 Ramat-Aviv, Tel-Aviv, Israel. E-mail: goldberg@post.tau.ac.il

Received (in Cambridge, UK) 27th July 1999, Accepted 25th August 1999

A unique supramolecular solid assembly with very wide channels has been formulated with aquazinc tetra(4-carboxyphenyl)porphyrin building blocks; the open porphyrin lattice is sustained by characteristic stacking interactions and multiple hydrogen bonding, it comprises only about 39% of the crystal volume, and preserves its crystallinity up to about 360 K.

A remarkable effort has been directed in recent years towards the design, by noncovalent *supramolecular* synthesis, of new molecular solids with structural and functional similarity to the inorganic zeolites.[1,2] We have also launched an extensive research program in this area, utilizing porphyrin metallomacrocycles as building blocks. The latter readily form expansible clathrates with guest components of versatile size and shape, in which the architecture of the porphyrin lattice is, however, strongly conserved.[3] Indeed, the vast majority of these structures consist of offset-stacked porphyrin layers with an average interlayer distance of 4.5 Å, the layered arrangement of the roughly flat porphyrin species representing a fundamental property of the porphyrin–porphyrin interaction.[3–5] We anticipated that the transformation from materials with variable interporphyrin voids ('sponges') to materials with fixed-size tubular cavities ('sieves') can be achieved by incorporation of a suitable molecular recognition algorithm in the porphyrin building blocks.[4] Here we report on a novel porphyrin-sieve type structure with rather large channels, the crystal lattice of which consists of a single component, aquazinc tetra(4-carboxyphenyl)porphyrin (aqua-ZnTCPP), and occupies only 39% of the crystal volume. The architecture of this structure is determined entirely by interporphyrin hydrogen bonding and stacking interactions, without resorting to external auxiliaries. The only other known example of a porphyrin-based lattice with wide open channels consists of heterogeneous assemblies of porphyrins *via* transition metal bridges.[2] The interiors of the channels in both crystals are partly filled with a small number of disordered molecules of nitrobenzene, which acts as a template.

We have shown previously that molecules of ZnTCPP may self-assemble through self-complementary hydrogen bonding in different ways to yield hollow network architectures.[4d,e] This includes formation of two-dimensional arrays with large interporphyrin voids (16 × 21 Å)† through $(CO_2H)_2$ hydrogen bonding between the terminal carboxylic functions of adjacent porphyrins.[4d] However, the latter were found to mutually interlock into one another to fill the interporphyrin voids, as commonly observed for other systems with large intermolecular spacing.[6] More recently, two-dimensional patterns with considerably smaller cavities (8.5 × 11.0 Å)† have also been constructed, by utilizing potassium or sodium 18-crown-6 as template.[4e] These networks do not interpenetrate as the interporphyrin voids are conveniently accommodated by the macrocyclic template.

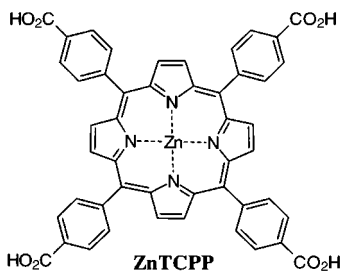

ZnTCPP

From the above observations it has become clear that in order to prevent interpenetration in the former case and to yield network structures with larger pores, it is essential to use sizeable solubilizing and templating agents with a low tendency to interact with the ZnTCPP lattice. After numerous trials, the following experimental procedure based on slow diffusion gave successful results. First, tetra(4-aminophenyl)porphyrin was dissolved in nitrobenzene, and this solution was placed at the bottom of a glass tube. This porphyrin derivative bears four amino groups which on one hand represent non-complementary binding sites for self-assembly, and on the other hand are weaker proton donors than the carboxylic function (and therefore have little chance to interact with the ZnTCPP). A second layer of ethylene glycol was placed above this solution. Then, a third layer of ZnTCPP dissolved in MeOH was placed on top. In such a manner, the ZnTCPP was allowed to diffuse slowly from the MeOH phase into the bottom layer. At saturation after several days, a phase separation occurred at the bottom solution yielding tiny needle-shaped crystals of ZnTCPP and an amorphous solid containing the tetraaminoporphyrin. The presence of the tetraaminoporphyrin in the bottom solution is essential in order to drive the ZnTCPP into the nitrobenzene layer (ZnTCPP is otherwise insoluble in nitrobenzene) and thus facilitate its self-organization *via* $(CO_2H)_2$ hydrogen bonding [Fig. 1(*a*)] around the nitrobenzene template (see below).

Fig. 1 illustrates the fascinating porphyrin sieve structure which characterizes the emerged crystals.‡ It consists of open very efficiently hydrogen-bonded networks of aqua-ZnTCPP, which stack in an offset manner along the normal direction. Four porphyrin units and eight hydrogen bonds [at OH···O distances of 2.611(4) Å] encircle any given pore within the network. The perpendicular distance between adjacent layers is 4.68 Å. The porphyrin core is slightly inclined (by 18°) with respect to plane of the network, as a result of which the van der Waals width of the open channel propagating through the crystal at its narrowest point is reduced from 16 Å[4d,e] to about 15 Å. In spite of the fact that the aqua-ZnTCPP lattice occupies only about 39% (after accounting for the van der Waals radii of all the atoms including hydrogens) of the crystal volume,[7] the presence of neither tetraaminoporphyrin nor of other species in the interporphyrin channels could be identified from the diffraction data. NMR experiments do indicate however that the crystals contain nitrobenzene solvent with an approximate 1 : 4 porphyrin : solvent ratio (which slowly reduces with time).§ The randomly distributed residual electron density peaks found in the channels did not exceed 0.85 e $Å^{-3}$, suggesting only partial occupancy of the channels (the very loose crystal packing is reflected also in relatively large atomic thermal displacement parameters) and a significant disorder of the solvent molecules even at 115 K. Nevertheless, the structure refinement based on

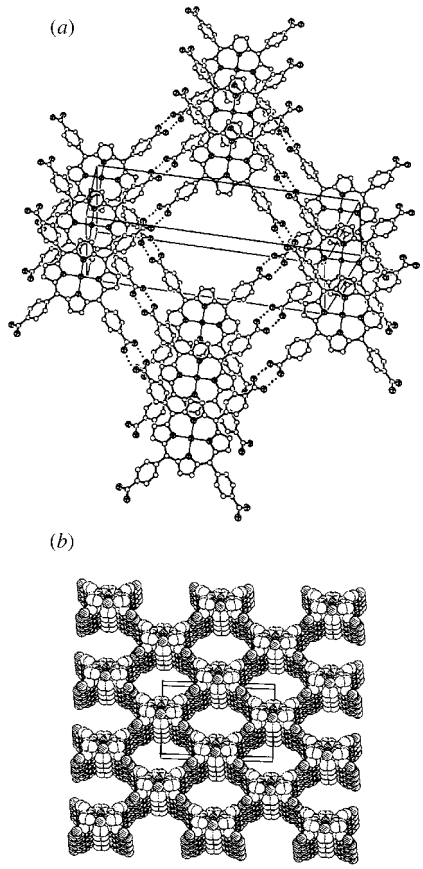

Fig. 1 (*a*) Ortep illustration of the crystal lattice, projected approximately on the plane of the porphyrin layers, showing their offset-stacked organization (the axial water bound to zinc is omitted for clarity). (*b*) Space-filling (CPK) representation of the open structure, viewed approximately down the channels which propagate along the *c*-axis of the crystal lattice. It shows best the space proportions between porphyrin lattice and the 1.5 nm wide open channels (the latter being partly occupied by disordered nitrobenzene solvent).

the ZnTCPP lattice alone converged at a relatively low (for such 'hollow' systems) *R*1 value of 13.9%. These surprising observations led us to conduct independent full-set measurements on three different crystals, but all provided identical results. Crystals of this material do deteriorate slowly when left in an open air, but are quite stable when covered with a very thin layer of light oil. Their structure and morphology does not change upon heating or cooling (apart from natural thermal expansion or contraction) within the temperature range of 115–360 K, as indicated by repeated measurements of the crystal data on the same crystal at various temperatures in this range. Despite the solvent disorder, the experimental data monitored by a CCD detector were sensitive enough to allow at this stage the location of all the hydrogen atoms on the porphyrin framework in difference Fourier maps. As the contribution of the disordered solvent to the diffraction pattern could not be rigorously included in the crystallographic calculations, it was subtracted in the next stage by the Squeeze/Bypass procedure.[8] The resulting refinement of the aqua-ZnTCPP lattice converged with reasonable precision at a considerably lower *R*1 value of 7.1%, without affecting to any significant extent the porphyrin structure. The combination of the above findings confirm with a high degree of certainty the correctness of this unique structure.

This study demonstrates that hydrogen bonding interactions combined with dominant molecular shape features (van Waals forces) can be very effective in formulations of nanoporous materials from porphyrin building blocks which recognize each other through multiple molecular recognition sites, in the presence of a suitable template. The enthalpies of such interactions when considered alone are relatively small, 20–33 kJ mol^{-1} for hydrogen bonds in the carboxylic acid dimers,[9] and $\leq$46 kJ mol^{-1} for π–π stacking between two partially overlapping zinc porphyrin moieties.[5] However, their cooperative effect (each ZnTCPP is involved in eight hydrogen bonds and is sandwiched between two adjacent porphyrins) approaches the strength of a covalent bond, and appears to be adequate to stabilize the observed molecular sieve structure even with only partial occupation of the 1.5 nm wide channels by solvent. Thus, although the porphyrin lattice occupies only 39% of the crystal volume, it forms an ordered and relatively stable solid. The preset study, along with the previous observations,[4d,e] also shows the ability of the ZnTCPP system to self-assemble into different supramolecular architectures (pseudo-polymorphism), and emphasizes the significance of the templating agent in inducing the preferred organization.

This research was supported in part by the Israel Science Foundation founded by the Israel Academy of Sciences. The assistance of Dr A. Rudi with the NMR measurements is gratefully acknowledged.

Notes and references

† Dimensions of interporphyrin voids refer throughout this paper to distances between van der Waals surfaces of the porphyrin framework.

‡ *Crystal data* for aqua-ZnTCPP: $C_{48}H_{28}N_4O_8Zn{\cdot}H_2O{\cdot}\ 4(C_6H_5NO_2)$,§ M_r = 1364.6, monoclinic, space group *C*2/*m*, a = 19.622(1), b = 29.649(1), c = 7.513(1) Å, β = 99.24(1)°, V = 4314.2(6) Å^3, Z = 2, ρc. = 1.050 g cm^{-3}, μ(MoKα) = 0.34 mm^{-1}, T = 115 K, 6103 measured reflections (one hemisphere), 3629 unique reflections, R_{int} = 0.039. The diffraction data of the poorly diffracting crystals were collected on a KappaCCD diffractometer system, using Mo-Kα (λ = 0.7107 Å) radiation and 0.5° ϕ and ω scans. Final R1 = 0.139 for 2329 reflections with $F > 4\sigma(F)$, R1 = 0.194, wR2 = 0.381 and GoF = 1.379 for all 3629 data. All hydrogen atoms of the porphyrin framework were located on difference Fourier maps; their positions were slightly adjusted to conform to standard bond lengths and angles. The porphyrin complex (with five-coordinate zinc ion) is located on, and disordered about, the inversion center. Only very diffused residual electron density was observed in the channel voids. It corresponds to a highly disordered nitrobenzene solvent, the structure of which could not thus be modeled. After subtraction of the disordered and diffused solvent contribution to the diffraction pattern (see text) (ref. 7, 8), final R1 = 0.071 for 2096 reflections with $F > 4\sigma(F)$, R1 = 0.112, wR2 = 0.198 and GoF = 0.985 for all 3629 data. CCDC 182/1391. See http://www.rsc.org/suppdata/cc/1999/1961/ for crystallograpic data in .cif format.

§ Content of the disordered solvent species in the analysed crystals was assessed by ^{1}H NMR (DMSO, 500MHz): δ 8.80 (8H, s, β-pyrrole of ZnTCPP), 8.25 (8H, d, nitrophenol), 7.85 (4H, t, nitrophenol), 7.70 (8H, t, nitrophenol).

1 P. Brunet, M. Simard and J. D. Wuest, *J. Am. Chem. Soc.*, 1997, **119**, 2737; M. J. Zaworotko, *Nature*, 1997, **386**, 220; H. J. Choi, T. S. Lee and M. P. Suh, *Angew. Chem., Int. Ed.*, 1999, **38**, 1405.

2 B. F. Abrahams, B. F. Hoskins, D. M. Michail and R. Robson, *Nature*, 1994, **369**, 727; S. R. Batten and R. Robson, *Angew. Chem., Int. Ed.*, 1998, **37**, 1460.

3 M. P. Byrn, C. J. Curtis, Y. Hsiou, S. I. Khan, P. A. Sawin, S. K. Tendick, A. Terzis and C. E. Strouse, *J. Am. Chem. Soc.*, 1993, **115**, 9480; M. P. Byrn, C. J. Curtis, I. Goldberg, Y. Hsiou, S. I. Khan, P. A. Sawin, S. K. Tendick and C. E. Strouse, *J. Am. Chem. Soc.*, 1991, **113**, 6549.

4 (*a*) R. Krishna Kumar, S. Balasubramanian and I. Goldberg, *Chem. Commun.*, 1998, 1435; (*b*) R. Krishna Kumar, S. Balasubramanian and I. Goldberg, *Inorg. Chem.*, 1998, **37**, 541; (*c*) R. Krishna Kumar and I. Goldberg, *Angew. Chem., Int. Ed.*, 1998, **37**, 3027; (*d*) P. Dastidar, Z. Stein, I. Goldberg and C. E. Strouse, *Supramol. Chem.*, 1996, **7**, 257; (*e*) Y. Diskin-Posner, R. Krishna Kumar and I. Goldberg, *New J. Chem.*, 1999, **23**, 885.

5 C. A. Hunter, M. N. Meah and J. K. M. Sanders, *J. Am. Chem. Soc.*, 1990, **112**, 5773; C. A. Hunter and J. K. M. Sanders, *J. Am. Chem. Soc.*, 1990, **112**, 5525.

6 F. H. Herbstein, M. Kapon and G. M. Reisner, *Proc. R. Soc. London, Ser. A*, 1981, **376**, 301; O. Ermer, *J. Am. Chem. Soc.*, 1988, **110**, 3747.

7 As calculated by PLATON, A. L. Spek: *Acta Crystallogr., Sect. A*, 1990, **46**, C34.

8 P. Van der Sluis and A. L. Spek, *Acta Crystallogr., Sect. A*, 1990, **46**, 194.

9 G. A. Jeffrey, *An Introduction to Hydrogen Bonding*, Oxford University Press, New York, 1997, p. 56; G. M. Whitesides, E. E. Simanek, J. P. Matias, C. T. Seto, D. N. Chin, M. Mammen and D. M. Gordon, *Acc. Chem. Res.*, 1995, **32**, 37.

Communication 9/06085E

Allylsilylation and stannylation of 1,2-diketones using bifunctional allylsilane–allylstannane reagents *via* photoinduced electron transfer reaction

Akio Takuwa,* Hiroyuki Saito and Yutaka Nishigaichi

Department of Material Science, Faculty of Science and Engineering, Shimane University, Matsue 690-8504, Japan. E-mail: takuwa@riko.shimane-u.ac.jp

Received (in Cambridge, UK) 16th August 1999, Accepted 31st August 1999

Bifunctional allylsilane–allylstannane and allylstannane–allylstannane reagents react photochemically with 1,2-diketones to give α-ketohomoallyl alcohols having an allylsilane moiety and α-ketohomoally alcohols having an allylstannane moiety respectively in excellent yields, and the remaining allylstannane moiety further reacts effectively with another diketone in the presence of $Mg(ClO_4)_2$ to afford a bis-α-ketohomoallyl alcohol.

The addition of allylsilane[1] and allylstannane[2] with various carbonyl compounds has been widely used as one of the most useful procedures for C–C bond formation. The process generally requires promoters such as Lewis acids which activate the electrophilic function of carbonyl compounds towards nucleophilic attack by the allylmetal reagents.[1–3] On the other hand, light-promoted addition *via* photoinduced electron transfer (PET) from allylstannane[4] and allylsilane[5] to the photoexcited carbonyl compounds has recently attracted considerable interest from both synthetic and mechanistic viewpoints. In these photoadditions, allylstannanes are good electron donors compared with the corresponding allylsilanes. For example, we found that the reaction of allylstannanes with benzophenones gave homoallylic alcohols *via* PET,[4] whereas allylsilanes behaved as an ordinary alkene to produce oxetanes and hydrogen abstraction products[6] without PET reaction. This observation prompted us to examine the photoadditon reactions of bifuntional allylsilane–allylstannane reagent **1** and allylstannane–allylstannane reagent **2** with 1,2-diketones. We expected that the differences in the reactivity of allylstannane and allylsilane would permit their differentiation in the bifunctional reagents under photochemical conditions.

Irradiation (> 400 nm) of the absorption band of benzil **3a** (0.02 mol dm^{-3}) in a N_2-purged MeCN–benzene (5 : 1 v/v) solution containing 3-tributylstannyl-2-[(trimethylsilyl)methyl-]propene[7] **1** (0.03 mmol dm^{-3}) for 3 h at ambient temperature (Scheme 1) afforded an α-ketohomoallyl alcohol having an allylsilane moiety (**4a**). The 1 : 1 adduct **4a** was isolated in 90% yield by preparative TLC (silica gel, hexane–Et_2O, 4 : 1 v/v) and the structure was determined from its spectral properties and elemental analysis.† The allylsilane unit in the product **4a** does not react further with benzil even under prolonged irradiation or even under irradiation in the presence of $Mg(ClO_4)_2$ (*vide infra*).

The bifunctional allylsilane–allylstannane reagent **1** also reacted photochemically with other diketones **3** to produce the corresponding α-ketohomoallyl alcohols containing allylsilane moieties in moderate to good yields (Table 1, entries 1–4).

On the other hand, the light promoted reaction of **3** with 3-triphenylstannyl-2-[(triphenylstannyl)methyl]propene[8] **2** afforded two types of addition products, an α-ketohomoallyl alcohol with an allylstannane moiety **5** (1 : 1 adduct) and a bis-α-ketohomoallyl alcohol **6** (1 : 2 adduct), depending on the ratio of

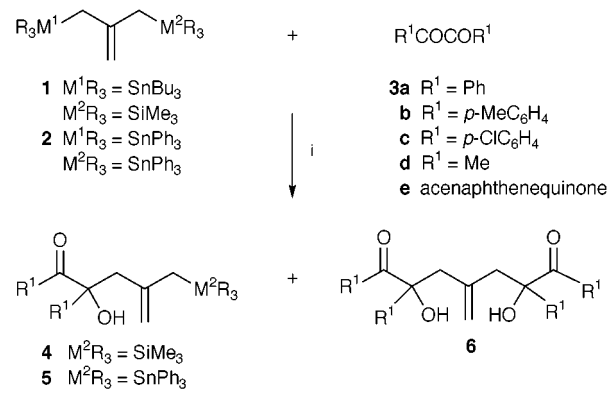

Scheme 1 *Reagents and conditions*: i, *hν* (> 400 nm), MeCN–benzene (4 : 1, v/v).

Table 1 Photoaddition reaction of the bifunctional allylmetal reagents with diketones

Entry	Allylmetal	Diketone	Ratio **1** (or **2**) : **3**	*t*/h	Products	(% yield)[a]
1	**1**	**3a**	1.5 : 1	3	**4a** (90)[b]	**6a** (0)
2	**1**	**3b**	1.5 : 1	3	**4b** (92)[b]	**6b** (0)
3	**1**	**3c**	1.5 : 1	3	**4c** (78)[b]	**6c** (0)
4	**1**	**3d**	1.5 : 1	3	**4d** (57)	**6d** (0)
5	**2**	**3a**	1.5 : 1	3	**5a** (96)	**6a** (0)
6	**2**	**3a**	1.5 : 1	3[c]	**5a** (86)	**6a** (8)
7	**2**	**3a**	0.5 : 1	12	**5a** (25)	**6a** (56)[d]
8	**2**	**3a**	0.5 : 1	3[c]	**5a** (4)	**6a** (90)[d]
9	**2**	**3b**	1.5 : 1	3	**5b** (98)	**6b** (0)
10	**2**	**3b**	0.5 : 1	12	**5b** (14)	**6b** (67)[d]
11	**2**	**3c**	1.5 : 1	3	**5c** (98)	**6c** (0)
12	**2**	**3c**	0.5 : 1	12	**5c** (17)	**6c** (71)[d]
13	**2**	**3c**	0.5 : 1	3[c]	**5c** (< 1)	**6c** (91)[d]
14	**2**	**3e**	1.5 : 1	3	**5e** (61)	**6e** (0)

[a] Isolated yields. [b] A small amount of butylated product, 1,2-diaryl-2-hydroxyhexan-1-one, was also produced. [c] Irradiation was carried out in the presence of 5 equiv. of $Mg(ClO_4)_2$. [d] Diastereomer ratio was 1 : 1.

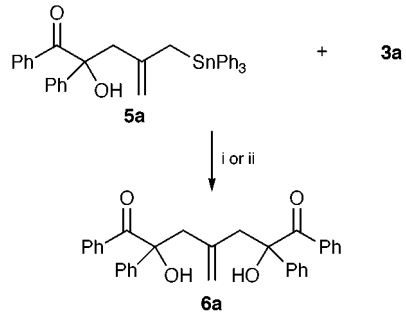

Scheme 2 *Reagents and conditions*: i, *hν* (> 400 nm), MeCN-benzene (4 : 1, v/v); ii, *hν* (> 400 nm), $Mg(ClO_4)_2$, MeCN-benzene (4 : 1, v/v).

the bifunctional reagent **2** to the 1,2-diketones (Table 1). Thus irradiation of benzil in the presence of a 1.5-fold molar excess of the reagent **2** for 3 h produced the 1 : 1 adduct **5a** in very high yield (96%),‡ while irradiation in the presence of 0.5 equiv. of **2** gave both **5a** and 1 : 2 adduct **6a**, where the ratio of **5a** : **6a** gradually decreased with increasing irradiation time; these two adducts were isolated respectively in 25 and 56% yield after irradiation for 12 h (entry 7). These results show that the addition reactions proceed stepwise. Other diketones **3** also gave the 1 : 1 adduct **5** and/or the 1 : 2 adduct **6** in good yields, depending on the ratio of the substrates and the reagent as shown in Table 1.

The present allylsilylation and stannylation may be initiated by PET from the bifunctional reagents to the photoexcited diketones to generate the organometalic radical cation (**1**$^{\bullet+}$ or **2**$^{\bullet+}$)-ketyl radical anion (**3**$^{\bullet-}$) pair. The selective cleavage of the Sn–C(allyl) bond of the radical cation **1**$^{\bullet+}$ produces β-[(trimethylsilyl)methyl]allyl radical because of the Si–C bond being stronger than the Sn-C bond.[9] The resulting allyl radical couples with **3**$^{\bullet-}$ to give allylsilylated product **4**. In the case of the reaction using allylstannane–allylstannane reagent **2**, the β-[(triphenylstannyl)methyl]allyl radical formed by the fragmentation of **2**$^{\bullet+}$ couples with the ketyl radical **3**$^{\bullet-}$ to yield the allylstannylated product **5**.

Next we examined the subsequent addition step from 1 : 1 adduct **5** to 1 : 2 adduct **6**. Irradiation of an MeCN–benzene solution containing benzil (0.01 mmol dm^{-3}) and isolated **5a** (0.01 mmol dm^{-3}) for 3 h gave the 1 : 2 adduct **6a** in 55% yield (Scheme 2).

Interestingly, when the irradiation was carried out in the presence of 5 equiv. of $Mg(ClO4)_2$ under otherwise identical conditions, the yield of **6a** increased to 90%. These results suggest that the second addition reaction also proceeds *via* PET and Mg^{2+} accelerates the PET reaction, probably due to the higher reducing ability of the Mg^{2+}–benzil complex compared to that of uncomplexed benzil.[10] Therefore, the photochemical reaction of the bifunctional reagent **2** with 1,2-diketones in the presence of $Mg(ClO_4)_2$ was examined. The 1 : 2 adduct **6** was obtained in very high yield (> 90%) from the reaction with 0.5 equiv. of **2** in the presence of $Mg(ClO_4)_2$ (entries 8 and 13). Even in the reaction of benzil with an excess amount of **2** a small amount (8%) of **6** was also produced in the presence of the metal salt (entry 6). These results show that the first step of the PET reaction is faster than the second one and that Mg^{2+} should catalyze the present PET reaction.

In conclusion, the light-promoted addition reaction of bifunctional allylmetal reagents to 1,2-diketones yielded α-ketohomoallyl alcohols bearing allylsilane or allylstannane groups in high yields *via* single electron transfer reaction. These products are unlikely to be obtained from well known Lewis acid-promoted reactions, as they have both nucleophilic (allylmetal group) and electrophilic (carbonyl) functions in the same molecule which are sensitive to Lewis acids.[11] In addition, bis-α-ketohomoallyl alcohols were effectively produced by stepwise photoinduced electron transfer reaction between allylstannane–allylstannane reagent and 1,2-diketones. More detailed studies on the bifunctional reagents under photochemical conditions and the intramolecular cyclization reaction of the resulting α-ketohomoallyl alcohols are in progress in our laboratory.

This work was supported by a Grand-in-aid for Scientific Research (No 11640535) from the Ministry of Education, Science, Sports and Culture, Japan.

Notes and references

† *Selected data for* **4a** : needles, mp 77–79 °C; $\delta_H(CDCl_3$, 270 MHz) −0.02 [s, $Si(CH_3)_3$, 9H], 1.16 (d, *J* 13.2, C*H*HSiMe_3, 1H), 1.39 (d, *J* 13.2, CH*H*SiMe_3, 1H), 2.86 (d, *J* 13.4 , C*H*H, 1H), 3.18 (d, *J* 13.4, CH*H*, 1H), 4.08 (s, OH, 1H), 4.56 (s, C*H*H=, 1H), 4.72 (s, CH*H*=, 1H) and 7.26-7.86 (m, Ar*H*, 10H); ν_{max}(KBr)/cm^{-1} 3487, 1679, 1249, 1234 and 842; *m*/*z* 233 [(M − PhCO)$^+$], 105 (PhCO$^+$) and 73 (Me_3Si^+).

‡ *Selected data for* **5a**: prisms, mp 110–111 °C; $\delta_H(CDCl_3$, 270 MHz) 2.19 (d, *J* 11.0, C*H*HSnPh_3, 1H), 2.30 (d, *J* 11.0, CH*H*SnPh_3, 1H), 2.77 (d, *J* 13.7, C*H*H, 1H), 3.02 (d, *J* 13.7, CH*H*, 1H), 4.10 (s, OH, 1H), 4.47 (s, C*H*H=, 1H), 4.87 (s, CH*H*=, 1H) and 7.21–7.74 (m, Ar*H*, 25H); ν_{max}(KBr)/cm^{-1} 3515, 3059, 1671, 1428, 1239, 1073, 729 and 701.

1 I. Fleming, J. Dunogues and R. Smithers, *Org. React.*, 1989, **37**, 57.
2 Y. Yamamoto and N. Asao, *Chem. Rev.*, 1993, **93**, 2207.
3 Y. Nishigaichi, A. Takuwa, Y. Naruta and K. Maruyama, *Tetrahedron*, 1993, **49**, 7395.
4 A. Takuwa, H. Tagawa, H. Iwamoto, O. Soga and K. Maruyama, *Chem. Lett.*, 1987, 1091; A. Takuwa, Y. Nishigaichi, T. Yamaoka and K. Iihama, *J. Chem. Soc., Chem. Commun.*, 1991, 1359; A. Takuwa, Y. Nishigaichi, S. Ebara and H. Iwamoto, *Chem. Commun.*, 1998, 1789.
5 S. Fukuzumi and T. Okamoto, *J. Am. Chem. Soc.*, 1994, **116**, 5503.
6 A. Takuwa, N. Fujii, H. Tagawa and H. Iwamoto, *Bull. Chem. Soc. Jpn.*, 1986, **59**, 2959.
7 D. L. J. Clive, C. C. Paul and Z. Wang, *J. Org. Chem.*, 1997, **62**, 7028.
8 S. Chandrasekhar, S. Latour, J. D. Wuest and B. Zacharie, *J. Org. Chem.*, 1983, **48**, 3810.
9 E. Butcher, C. J. Rhodes, M. Standing, R. S. Davidson and R. Bowser, *J. Chem. Soc., Perkin Trans. 2*, 1992, 1469.
10 S. Fukuzumi, *Bull. Chem. Soc. Jpn.*, 1997, **70**, 1.
11 G. E. Keck and A. Palani, *Tetrahedron Lett.*, 1993, **34**, 3223; G. Majetich, H. Nishidie and Y. Zhang, *J. Chem. Soc., Perkin Trans. 1*, 1995, 453.

Communication 9/06620I

Temperature compensation in the oscillatory hydrogen peroxide–thiosulfate–sulfite flow system

Gyula Rábai*[a] and Ichiro Hanazaki*[b]

[a] *Institute of Physical Chemistry, Kossuth Lajos University, H-4010 Debrecen, Hungary. E-mail: rabaigy@tigris.klte.hu*

[b] *Department of Chemistry, Faculty of Sciences, Hiroshima University, Kagamiyama, Higashi-Hiroshima 739-8526, Japan*

Received (in Cambridge, UK) 13th August 1999, Accepted 23rd August 1999

A simple controlling mechanism assuming reasonable activation energies for the reaction steps is used to simulate temperature compensation of the period length of the large amplitude sustained pH oscillations observed experimentally in a H_2O_2–$S_2O_3^{2-}$–SO_3^{2-}–H^+ aqueous flow reaction system under optimized conditions.

The period length of the rhythm in many biological clocks is largely unaffected by temperature changes which occur in a certain physiological range.[1–3] This behavior is called temperature compensation, and it is very important for the correct timing of numerous periodic processes (for example, light and dark periods in photoperiodic responses) that whould be, by and large, independent of environmental factors such as, for example, temperature. Such behavior is in contrast to that observed in chemical oscillators where an increase in temperature leads generally to a significant increase in the frequency,[4–6] since all the composite reactions accelerate as expected from the Van't Hoff's rule. An old unanswered question is whether temperature compensation is confined to circadian and ultradian rhythms, or whether homogeneous chemical oscillators may be able to act similarly.[7]

According to recent theoretical considerations, temperature compensation can be obtained in simple oscillator models, such as the Brusselator,[7] the Oregonator,[8] or the Goodwin model.[9] The theory states that temperature compensation in a reaction kinetic network requires an appropriate balance in activation energy-weighted rate constant sensitivities between opposing processes. In order to find experimental evidence for the theory, we have studied the temperature sensitivity of several pH oscillators[10] and found that a recently designed H_2O_2–$S_2O_3^{2-}$–SO_3^{2-}–H^+ system[11] exhibited temperature compensation under certain conditions.

In our experiments, we used a water-jacketed cylindrical-shaped glass vessel with a liquid volume of 12.5 ml as a continuous-flow stirred tank reactor (CSTR). The CSTR was equipped with a Horiba electrode to measure the pH and the temperature inside the reactor. The time–pH data were collected by a computer through a pH meter and an A/D converter with a sampling rate of 1 Hz. A 1.0 cm long Teflon-covered stirrer bar was used to ensure uniform mixing. Two input solutions were prepared daily: one contained 0.0270 M H_2O_2, the other contained all the remaining components, such as 0.010 M $Na_2S_2O_3$, 0.0040 M Na_2SO_3 and 5.0×10^{-4} M H_2SO_4, together. The input solutions were kept from air to avoid any effect of O_2 and CO_2. The reactor was fed with these solutions by means of an EYELA peristaltic pump. The mixing ratio was 1.0 : 1.0, so the input concentrations in the combined feed were half of those in the input solutions.

Our first task was to determine the temperature range where regular pH oscillations were exhibited. Shown in Fig. 1 is a state diagram spanned in the normalized flow rate (k_0)–T plane. The range of oscillations is rather narrow at low k_0 values. It is shifted to the higher temperatures and widens significantly as k_0 increases. At $k_0 = 4.0 \times 10^{-3}$ s^{-1} the range is as wide as 10 °C.

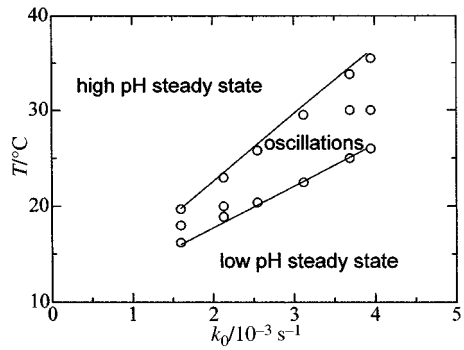

Fig. 1 Measured state diagram in the k_0–T plane. Input concentrations: $[H_2O_2]_0 = 0.0135$, $[S_2O_3^{2-}]_0 = 0.0050$, $[SO_3^{2-}]_0 = 0.0020$, $[H^+]_0 = 5.0 \times 10^{-4}$ M. k_0 is the reciprocal residence time in the CSTR.

Above and below the oscillatory region a high pH steady state (pH 8–9) and a low pH steady state (pH 4–5.5) exist, respectively. Inside the oscillatory region, the amplitudes were found to decrease gradually with increasing temperature as the upper border was approached. Transition to the low pH steady state with decreasing temperature was sharp. The system behavior became chaotic at low flow rates.[11] Here we attempted to avoid such behavior so we kept the flow rate relatively high.

Secondly, we studied the period length of the sustained oscillations as a function of temperature in the disclosed range. An average period length was calculated in minutes for each temperature on the basis of a long run containing at least 20 periods. Reproducibility of the period length was within 6%. As shown in Fig. 2, period length turned out to be remarkably constant throughout the temperature range of oscillations at a fixed flow rate and input concentrations. Some significant deviation from the average period was measured along the borders of the oscillatory region. The pH amplitude and the waveform were altered by temperature changes. The most striking effect was that the high pH stage of a period appeared

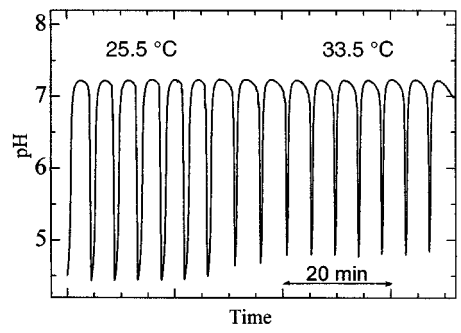

Fig. 2 Measured temperature compensation. Average period lengths at 25.5 and 33.5 °C are 4.45 and 4.41 min, respectively. Input concentratons as in Fig. 1, $k_0 = 3.60 \times 10^{-3}$ s^{-1}.

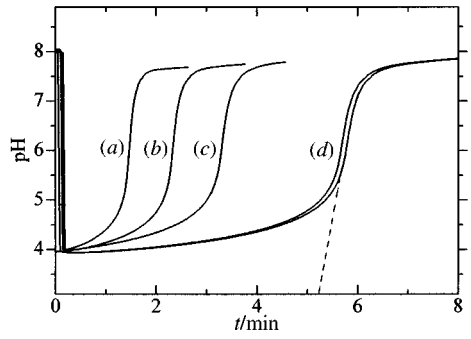

Fig. 3 Measured time–pH traces at (*a*) 36.0, (*b*) 30.0 (*c*) 26.0 and (*d*) 20.0 °C in a closed system. Double curve (*d*) shows the reproducibility. Initial concentrations: $[H_2O_2]_0$ = 0.0135, $[S_2O_3^{2-}]_0$ = 0.0050, $[H^+]_0$ = 5.0 × 10^{-4}, $[SO_3^{2-}]_0$ = 0.0020 M. Dashed line shows how the induction time was determined for the estimation of an apparent activation energy.

to be longer, and the low pH stage become shorter, with increasing temperature. As a result the average period length remained constant (Fig. 2). At k_0 = 3.90 × 10^{-3} s^{-1}, we measured the following average periods at different temperatures: 3.52 min (26.0 °C), 3.54 min (28.6 °C), 3.63 min (31.7 °C), and 3.40 min (35.8 °C). We can conclude that in the range 26.0–35.8 °C, complete temperature compensation has been achieved. Similar behavior was measured in the case of other fixed k_0 values inside the oscillatory region, but the period length decreased with increasing flow rate. On the other hand, however, it is surprising that the dynamical behavior exhibited extreme temperature sensitivity under other experimental conditions. For example, at $[H_2O_2)_0$ = 0.0070, $[S_2O_3^{2-}]_0$ = 0.0050, $[SO_3^{2-}]_0$ = 0.020, $[H^+]_0$ = 0.0010 M, and k_0 = 5.56 × 10^{-4} s^{-1} an interesting period doubling route from large amplitude regular oscillations through alternating small and large amplitudes (P2) to chaos could be observed as the temperature gradually changed from 25.0 through 24.0 to 22.0 °C, respectively.

We studied the effect of temperature on the kinetics in a closed reactor where no oscillations take place. Typical pH–time curves are presented in Fig. 3 where a sudden drop followed by an S-shaped increase in the pH is seen. An apparent activation energy, characteristic of the overall reaction rate, E_a = 67.0 kJ mol^{-1} could be determined by extrapolating the steepest section of the increasing part of the pH–time curves to the time axis and plotting the logarithm of the reciprocal intercept against 1/*T*. Such a value of E_a suggests a usual temperature dependence indicating that the temperature compensation of the oscillatory frequency found in the CSTR does not result from an unusually small temperature sensitivity of the system. A special control mechanism must instead be responsible for the behavior.

We carried out numerical simulations on the basis of the mechanism[11] shown in Scheme 1 to see whether it could be responsible for the temperature compensation. Mass action kinetics laws for steps (1)–(7) were taken into account. Two sets of estimated rate constant values were assigned for 26 and 36 °C (Table 1) and were used to simulate oscillations with a semi-implicit Runge Kutta method. Activation energies of the composite reactions were chosen to fall into a chemically reasonable range (25–92 kJ mol). The calculated periods are

$H_2O_2 + S_2O_3^{2-} \rightleftharpoons HOS_2O_3^- + OH^-$ (1/−1)
$H_2O_2 + HOS_2O_3^- \rightarrow 2HSO_3^- + H^+$ (2)
$S_2O_3^{2-} + S_2O_3 \rightarrow S_4O_6^{2-}$ (3)
$H_2O \rightleftharpoons H^+ + OH^-$ (4/−4)
$H_2O_2 + HSO_3^- \rightarrow SO_4^{2-} + H_2O + H^+$ (5)
$H_2O_2 + HSO_3^- + H^+ \rightarrow SO_4^{2-} + H_2O + 2H^+$ (5′)
$HSO_3^- \rightleftharpoons H^+ + SO_3^{2-}$ (6/−6)
$HOS_2O_3^- + H^+ \rightleftharpoons S_2O_3 + H_2O$ (7/−7)

Scheme 1

Table 1 Estimated activation energies and rate constants for 26 and 36 °C

Step	E_i/kJ mol^{-1}	k_i^{26}	k_i^{36}	Units
(1)	56.8	0.030	0.063	M^{-1} s^{-1}
(−1)	36.0	5.0 × 10^3	8.0 × 10^3	M^{-1} s^{-1}
(2)	92.2	0.015	0.05	M^{-1} s^{-1}
(3)	61.2	9.0	20.0	M^{-1} s^{-1}
(4)	31.0	8 × 10^{-4}	1.2 × 10^{-3}	k_4 $[H_2O]$ M s^{-1}
(−4)	31.0	8 × 10^{10}	1.2 × 10^{11}	M^{-1} s^{-1}
(5)	31.0	8.0	12.0	M^{-1} s^{-1}
(5′)	34.2	1.6 × 10^7	2.5 × 10^7	M^{-2} s^{-1}
(6)	75.1	3.0 × 10^3	8.0 × 10^3	s^{-1}
(−6)	25.8	5.0 × 10^{10}	7.0 × 10^{10}	M^{-1} s^{-1}
(7)	25.8	1.5 × 10^3	2.1 × 10^3	M^{-1} s^{-1}
(−7)	67.1	0.025	0.060	s^{-1}

almost the same for both sets of rate constants. Calculated oscillations at °C are preceded by an hour long induction period. Calculations were carried out with k_0 = 3.9 × 10^{-3} s^{-1}. Both the calculated amplitudes and waveforms resemble their experimental counterparts. Low and high pH steady states could also be reproduced with simulations.

Differences in activation energies of the composite reactions seem to be important for temperature compensation by this mechanism. The length of the neutral region (pH *ca.* 7) of a period is determined by the time required for the consumption of SO_3^{2-}. since SO_3^{2-} is produced in steps (2) (92.2 kJ mol^{-1} and (6) (75.1 kJ mol^{-1}) with high activation energies and consumed in steps (−6) (25.8 kJ mol^{-1}), (5) (31.0 kJ mol^{-1}) and (5′) (34.2 kJ mol^{-1}) with low activation energies, its production rate increases more rapidly with temperature than its consumption rate, causing an increase in its average lifetime. As a result, the length of the neutral stage increases with temperature. At the same time, the length of the low pH stage decreases with increasing temperature, as expected from the curves in Fig. 3. The two opposite changes compensate each other under certain conditions leading to constant periods at different temperatures.

In conclusion, a simple chemical system is presented which exhibits temperature compensation in its oscillatory frequency in a CSTR. We found that a mechanism proposed earlier[11] can account for such behavior. We suspect that temperature compensation may be found in other pH oscillators with similar mechanism. It remains to be seen whether pH oscillators with such behavior can provide any reasonable guide to the control mechanism of biological clocks. However, the reversibility of some composite processes may be a common feature of chemical and biological temperature compensation.

Financial support was obtained from the Hungarian Science Foundation (OTKA 25076) and from the Japan Society for Promotion of Science.

Notes and references

1 C. S. Pittendrigh and P. C. Caldarola, *Proc. Natl. Acad. Sci. U.S.A.*, 1973, **70**, 2697.
2 I. Balzer and R. Hardeland, *Int. J. Biometeorol.*, 1988, **32**, 231.
3 L. N. Edmunds, *Cellular and Molecular Bases of Biological Clocks*, Springer-Verlag, New York, 1988.
4 E. Koros, *Nature*, 1974, **251**, 703.
5 G. Nagy, E. Koros, N. Oftedal, K. Tjelflaat and P. Ruoff, *Chem. Phys. Lett.*, 1996, **250**, 255.
6 E. Kumpinsky and I. R. Epstein, *J. Phys. Chem.*, 1985, **89**, 688.
7 P. Ruoff, *J. Interdiscip. Cycle Res.*, 1992, **23**, 92.
8 P. Ruoff, *Physica D*, 1995, **84**, 204.
9 P. Ruoff and L. Rensing, *J. Theor. Biol.*, 1996, **179**, 275.
10 Gy. Rábai, M. Orbán and I. R. Epstein, *Acc. Chem. Res.*, 1990, **23**, 258.
11 Gy. Rábai and I. Hanazaki, *J. Phys. Chem.*, 1999, **103**, 7268.

Communication 9/06598I

ChemComm

Direct synthesis of AlSBA mesoporous molecular sieves: characterization and catalytic activities

Yinghong Yue,[a] Antoine Gédéon,[a] Jean-Luc Bonardet,[a] Nick Melosh,[b] Jean-Baptiste D'Espinose[a] and Jacques Fraissard[a]

[a] *Laboratoire, S.I.E.N, CNRS-ESA 7069, Université P. et M. Curie, Case Courrier 196. 4 place Jussieu, 75252 Paris Cedex 05, France. E-mail: ag@ccr.jussieu.fr*

[b] *Department of Chemical Engineering, UCSB, Santa Barbara, California 93106, USA*

Received (in Cambridge, UK) 24th June 1999, Accepted 31st August 1999

Aluminium-incorporated SBA mesoporous materials have been obtained for the first time by direct synthesis; the resulting materials retain the hexagonal order and physical properties of purely siliceous SBA-15 and present higher catalytic activities in the cumene cracking reaction than AlMCM-41 materials.

Mesoporous molecular sieves, MCM-41, have attracted much interest because of their potential application in reactions or separations involving bulky molecules.[1,2] The synthesis and catalytic applications of AlMCM-41 have been reported by various authors.[3–8] The crucial problem is that AlMCM-41 has poor hydrothermal stability, either in steam or in hot water.[7,9] This becomes a serious limitation to the application of these new materials. Recently, Zhao *et al.*[10] reported the synthesis of a novel mesoporous silica denoted SBA-15 using an organic copolymer to organize the structure of a polymerizing silica precursor template. This material has a more regular structure and thicker walls than MCM-41, resulting in much higher stability. The aluminium-containing SBA-15 was also obtained by post-synthesis.[11,12] Here, we report a direct synthesis of aluminium-incorporated SBA mesoporous molecular sieves using a triblock copolymer as template. The physical properties and catalytic activities of the resulting materials were also studied.

The aluminium-containing SBA mesoporous solid was prepared as follows: 9 mL of tetraethyl orthosilicate (TEOS) and a calculated amount of aluminium tri-*tert*-butoxide, to obtain a given Si/Al ratio (10 or 20), were added to 10 mL of aqueous HCl at pH 1.5. This solution was stirred for > 3 h and then added to a second solution containing 4 g triblock poly(ethylene oxide)–poly(propylene oxide)–poly(ethylene oxide) ($EO_{20}PO_{70}EO_{20}$, Aldrich) in 150 mL of aqueous HCl at pH 1.5 at 313 K. The mixture was stirred for another 1 h and allowed to react at 313 or 373 K for 48 h. The solid obtained was filtered off, dried at 373 K, and finally calcined in air flow (9 L h^{-1}) at a heating rate of 24 K h^{-1} up to 823 K and then maintained at this temperature for 4 h. The sample of SBA-15 was prepared according to the literature.[10] The samples studied are denoted AlSBAX(T_s) where X and T_s represent the Si/Al ratio and the synthesis temperature, respectively.

Table 1 gives the preparation conditions and textural properties of the resulting aluminium-incorporated mesoporous molecular sieves, together with the data of SBA-15 for comparison. The textural properties of AlSBA are similar to those of SBA-15. Fig. 1 shows the N_2 adsorption–desorption isotherm and pore size distribution of the AlSBA10(373) sample. The isotherm shows a clear H1-type hysteresis loop at high relative pressure, suggesting that AlSBA has very regular mesoporous channels despite their large pore size, which was also proved by its narrow gaussian pore size distribution. The BET surface areas and mesopore volumes of AlSBA determined by nitrogen adsorption–desorption at 77 K are in the range 689–1022 m^2 g^{-1} and 0.63–1.53 cm^3 g^{-1}, respectively. The calculated pore diameters by the BJH method are in the range of 3.6–7.4 nm, depending on the preparation temperature (T_s).

Table 1 Preparation and properties of AlSBA samples

Sample	Si/Al (in gel)	T_s/K	Synthesis pH	S_{BET}/ m^2 g^{-1}	Pore diameter/ nm	V_p/cm^3 g^{-1}
AlSBA10(373)	10	373	1.5	1004	7.4	1.53
AlSBA20(373)	20	373	1.5	1022	7.4	1.40
AlSBA10(313)	10	313	1.5	689	4.0	0.64
AlSBA20(313)	20	313	1.5	788	3.6	0.63
SBA-15(373)	—	373	< 0	901	6.5	1.20
SBA-15(313)	—	313	< 0	762	4.4	0.67

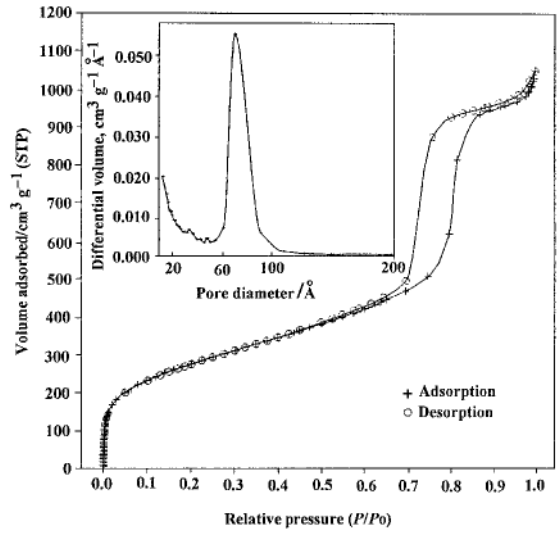

Fig. 1 N_2 adsorption–desorption isotherms of AlSBA10(373) at 77 K. The insert shows the BJH pore size distribution calculated from the desorption branch of the isotherm.

Transmission electron microscopy images show well ordered hexagonal arrays of 1D mesoporous channels and confirm that the AlSBA samples have a 2D *P6mm* hexagonal structure as does SBA-15.[11] Fig. 2 shows the TEM images of the AlSBA10(373) sample. The distance between two consecutive centres of hexagonal pores estimated from the TEM image is *ca.* 10 nm. The average thickness of the wall is *ca.* 3 nm, which is much larger than for MCM-41, and the pore diameter is around 7 nm, in agreement with the N_2 adsorption measurements.

Fig. 3(a) shows the ^{27}Al MAS NMR spectrum of the AlSBA10(373) sample. It exhibits signals at δ 52 from four-coordinate Al, at δ 38 from five-coordinate Al and at δ 0 from six-coordinate Al. This proves that a large amount of aluminium is incorporated in the framework of this sample, though some non-framework aluminium is still present. Such non-framework

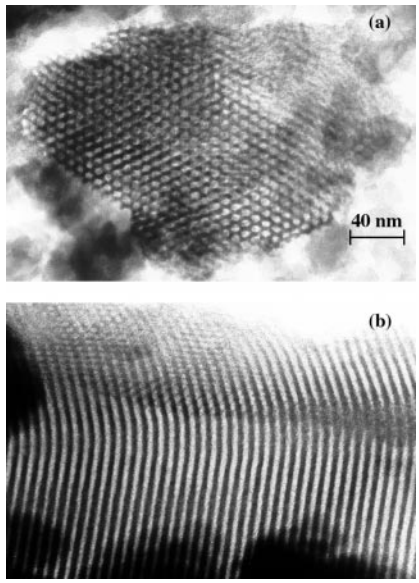

Fig. 2 TEM images of AlSBA10(373): (a) in the direction of the pore axis and (b) in the direction perpendicular to the pore axis.

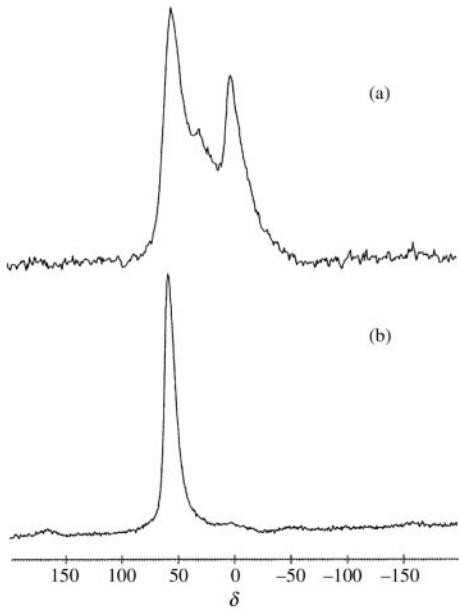

Fig. 3 ^{27}Al MAS NMR spectra of the AlSBA10(373) sample before (a) and after NH_4Cl washing (b).

aluminium was eliminated by washing the solid in NH_4Cl solution [Fig. 3(b)].

The stability of AlSBA samples following various treatments was also studied. XRD patterns of the AlSBA10(373) sample after calcination at 1073 K, steaming at 823 K and treatment in solution at different pH (Fig. 4) exhibit one very intense line and two weak lines, which are similar to those of the parent sample, indicating that the hexagonal structure of the AlSBA was not affected by these treatments. Compared with the same treatments on Al-MCM-41,[9] it can be concluded that the stabilities of AlSBA samples are much higher.

The catalytic activities of AlSBA samples towards the cumene cracking reaction have been investigated. The reaction was performed in a continuous-flow fixed-bed microreactor system with helium (25 mL min^{-1}) as carrier gas. The catalyst load for the tests was 100 mg and was preheated at 573 K for 3 h before reaction. A stream of cumene vapor in helium (25 mL min^{-1}) was generated using a saturator at room temperature. The steady state activities are given in Table 2. All samples have considerable activity in spite of their different textural properties, and the catalytic activity depends strongly on the Si/Al ratio. The activity towards cumene cracking of AlSBA

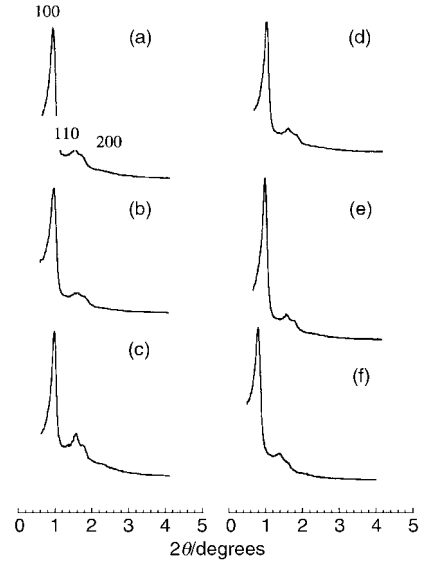

Fig. 4 XRD patterns of the initial AlSBA10(373) sample (a) and after a variety of treatments: (b) calcination at 1073 K; (c) steaming at 823 K; (d) in pH = 2 solution; (e) in pH = 7 solution and (f) in pH = 11 solution.

Table 2 Activities for cumene cracking reaction

	Conversion (%)		
Catalyst	473 K	523 K	573 K
AlSBA10(373)	12.6	43.2	87.0
AlSBA20(373)	2.5	17.1	56.0
AlSBA10(313)	12.8	34.8	86.5
AlSBA20(313)	9.4	27.7	75.8
SBA-15(373)	0	0	0
AlPSMCM5 (Si/Al = 5)[13]	—	—	50.0

molecular sieves is much higher than that of AlMCM-41[13] or AlSBA-15 prepared by post synthesis.[12] The only products of the cracking are benzene and propene, indicating that the active sites of this kind of material are of the Brönsted type. Currently we are performing two dimensional ^{27}Al solid state NMR (HETCOR) experiments to identify and establish the framework location of aluminium in these solids. Ammonia chemisorption and temperature-programmed desorption (TPD) and ^{1}H NMR at 4 K are being used to quantify the strength of the acidic sites.

Notes and references

1 C. T. Kresge, M. E. Leonowicz, W. J. Roth, J. C. Vartuli and J. S. Beck, *Nature*, 1992, **359**, 710.
2 J. S. Beck, J. C. Vartuli, W. J. Roth, M. E. Leonowicz, C. T. Kresge, K. D. Schmitt, C. T.-W. Chu, D. H. Olson, E. W. Sheppard, S. B. McCullen, J. B. Higgins and J. L. Schlenker, *J. Am. Chem. Soc.*, 1992, **114**, 10 834.
3 R. Schmidt, D. Akporiaye, M. Stocker and O. H. Ellestad, *J. Chem. Soc., Chem. Commun.*, 1994, 1493.
4 Z. H. Luan, C. F. Cheng, W. Z. Zhou and J. Klinowski, *J. Phys. Chem.*, 1995, **99**, 1018.
5 K. R. Kloetstra, H. W. Zandbergen and H. van Bekkum, *Catal. Lett.*, 1995, **33**, 157.
6 R. B. Borade and A. Clearfield, *Catal. Lett.*, 1995, **31**, 267.
7 J. M. Kim, J. H. Kwak, S. Jun and R. Ryoo, *J. Phys. Chem.*, 1995, **99**, 16 742.
8 Y. Sun, Y. H. Yue and Z. Gao, *Appl. Catal.*, 1997, **161**, 105.
9 D. Trong On, S. M. J. Zaidi and S. Kaliaguine, *Microporous Mesoporous Mater.*, 1998, **22**, 211.
10 D. Zhao, J. Feng, Q. Huo, N. Melossh, G. H. Fredrickson, B. F. Chmelka and G. D. Stucky, *Science*, 1998, **279**, 548.
11 Z. Luan, M. Hartmann, D. Zhao, W. Zhou and L. Kevan, *Chem. Mater.*, 1999, **11**, 1621.
12 M. Cheng, Z. Wang, K. Sakurai, F. Kumata, T. Saito, T. Komatsu and T. Yashima, *Chem. Lett.*, 1999, **2**, 131.
13 R. Mokaya and W. Jones, *Chem. Commun.*, 1997, 2185.

Communication 9/04467A

CdS/CdSe core/sheath nanostructures obtained from CdS nanowires

Yi Xie,*[ab] Ping Yan,[b] Jun Lu,[c] Yitai Qian[a] and Shuyuan Zhang[a]

[a] *Structure Research Laboratory, University of Science and Technology of China, Hefei, Anhui 230026, P.R. China. E-mail: yxie@ustc.edu.cn*
[b] *Department of Chemistry, University of Science and Technology of China, Hefei, Anhui 230026, P.R. China*
[c] *Department of Chemical Physics, University of Science and Technology of China, Hefei, Anhui 230026, P.R. China*

Received (in Cambridge, UK) 13th July 1999, Accepted 3rd September 1999

CdS/CdSe core/sheath nanowires with diameters of 7.7/0.75 nm were prepared by treating CdS nanowires with selenium in tributylphosphine (TBP) at 100 °C for 24 h and were characterized by X-ray powder diffraction, transmission electron microscopy, high resolution TEM, UV–VIS absorption spectra, photoluminescence spectra and X-ray photoelectron spectroscopy.

Nanowires are of both fundamental and technological interest especially in the field of conductance quantization[1] and nanodevices.[2] Hybrid one-dimensional structures in axial or radial directions are essential to realize nanodevices. To date, both axial heterojunctions[3] and radial core/sheath structures[4] have been reported. Recently, routes to zero-dimensional core/shell II–VI semiconductors have been rapidly developed: core/shell semiconductors of CdS/$Cd(OH)_2$,[5] CdSe/ZnS,[6,7] CdSe/ZnSe,[8,9] CdS/HgS/CdS[10] and CdSe/CdS[11–13] are examples. These systems normally show decreased fluorescence lifetimes, higher stability and electronic accessibility in comparison with organic capped derivatives and are, in some cases, superior to existing fluorophores when applied as biological labels.[14] However, to our knowledge, core/sheath nanowires of II–VI semiconductors have not, as yet, been reported.

We have succeeded in preparing quantum confined CdS nanowires (4×200 nm)[15] using cadmium dithiocarbamate as a precursor,[16] and it is possible to prepare CdS/CdSe core/sheath nanowires by treatment of CdS nanowires. Since phosphine chalcogenides such as TBPSe,[12] Et_3PTe[17a] and TOPSe[18] have been widely used as chalcogen sources in the synthesis of II–VI nanocrystals we attempted to grow a CdSe sheath with Se in TBP. Here the reaction is described as a substitution-type process [eqn. (1)] considering the substantial difference between the solubility products of CdS ($K_{sp} = 1.4 \times 10^{-19}$) and CdSe ($K_{sp} = 1.4 \times 10^{-35}$). The detailed mechanism may involve chemical transportation of selenium by TBP [eqn. (2)] similarly to that of Te by R_3P.[17]

$$\mathrm{CdS + Se} \xrightarrow{\text{TBP, 100 °C, 12 h}} \mathrm{CdSe + S} \quad (1)$$

$$\mathrm{TBP + Se} \rightleftharpoons \mathrm{TBPSe} \quad (2)$$

The CdS nanowires were synthesized by using a modification of our previous method:[15] cadmium diethyldithiocarbamate $[Cd(Et_2NCS_2)_2]_2$ (1 g) was dissolved in ethylenediamine (en) (30 ml) and heated in a Teflon-lined autoclave at 80 °C for 12 h, then the yellow CdS nanowires were filtered off and washed with ethanol. After being dried in vacuum at room temperature for 2 h, CdS nanowires (0.576 g, 4 mmol) and selenium (0.016 g, 0.2 mmol) were ultrasonically dispersed in 20 ml TBP, transferred to a Teflon-lined autoclave, kept at 100 °C for 24 h, and then cooled to room temperature naturally. The product was filtered off, washed with ethanol, and dried in vacuum at room temperature for 2 h.

The black selenium powder disappeared and the yellow CdS nanowires turned red, the characteristic color of CdSe. X-Ray photoelectron spectroscopy (XPS)† was used to measure the composition of the core/sheath nanowires, the signal was fitted by Gaussians according to the literature[12] and gave a S/Se ratio of 93 : 7, consistent with the molar ratio of reactants added.

Fig. 1 shows the X-ray powder diffraction (XRD)‡ patterns for CdS and CdS/CdSe core/sheath nanowires, respectively. The (002) peak is much stronger and narrower than the other peaks for both nanowires, indicating that both were elongated along the *c*-axis and the shape was well preserved in the conversion reaction. According to the Scherrer formula, the average diameter is 6.5 nm for the CdS nanowires and 8.0 nm for the CdS/CdSe core/sheath nanowires. The reflection peaks of the core/sheath nanowires shifted only little from those characteristic of pure CdS to CdSe. The X-ray data may be consistent with both a core/shell structure[12] and a solid solution, so transmission electron microscopy (TEM) and high resolution TEM was carried out to confirm the former structure.

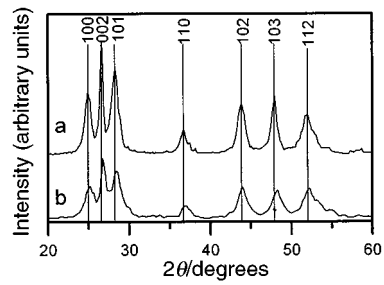

Fig. 1 XRD patterns of (a) CdS/CdSe core/sheath nanowires and (b) CdS nanowires.

TEM§ images of CdS and CdS/CdSe samples both show monodispersed wire-like shapes [Fig. 2(a) and (b)]. The average diameter is 6.7 nm for CdS nanowires and 8.5 nm for the core/sheath nanowires, which are consistent with the diameters estimated by the Scherrer formula. The retention of morphology unambiguously indicates a successful CdSe sheath growth since the likelihood for separately formed CdSe nanocrystals to be wire-like is very low. Further evidence for the core/sheath structure is from image contrast observations: CdS/CdSe core/sheath nanowires show much more contrast than the CdS nanowires owing to the stronger electron scattering power of selenium.

The size of the CdS/CdSe core/sheath nanowires is so small that only high resolution TEM (HRTEM) images give direct evidence of their formation. Fig. 2(c) and 2(d) show typical HRTEM¶ images for CdS and CdS/CdSe core/sheath nanowires respectively. The core/sheath nanowires consist of a 0.75 nm sheath and a 7.7 nm core, which is only a little larger than CdS only nanowires (6.9 nm) and in good agreement with the size estimated by the Scherrer formula. The sheath is thicker than expected from the Se to S ratio (7:93), one explanation is that the sheath is a compositionally graded interface between pure CdS and pure CdSe.

The UV–VIS absorption spectra of the CdS nanowires and CdS/CdSe core/sheath nanowires dispersed in water are shown in Fig. 3(a) and (b), respectively. There is little difference in the profile of the two spectra and an absorption peak at 472 nm is

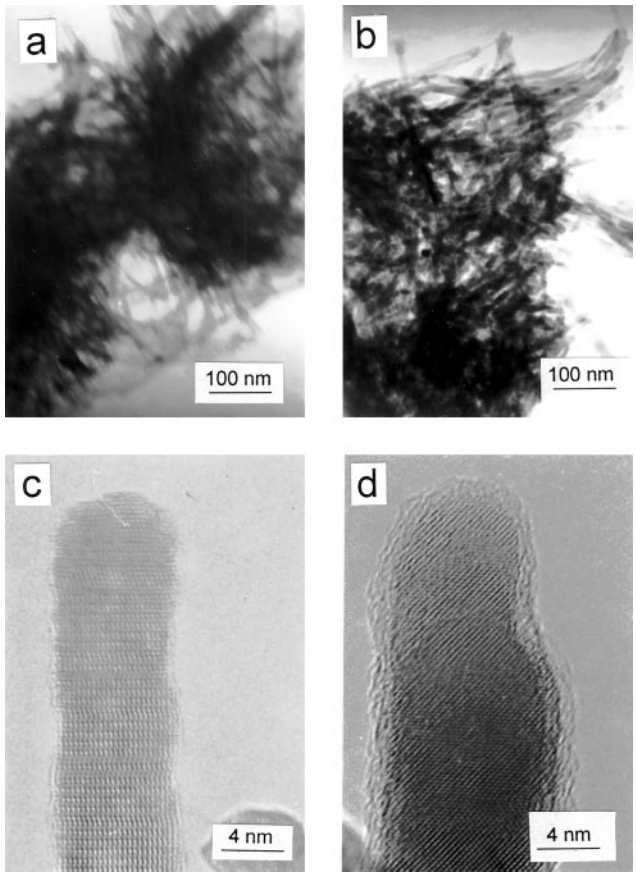

Fig. 2 TEM images of (a) CdS nanowires and (b) CdS/CdSe core/sheath nanowires along with HRTEM images of (c) CdS nanowires and (d) CdS/CdSe core/sheath nanowires.

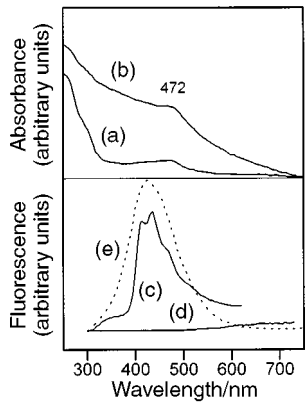

Fig. 3 Absorption spectra of (a) CdS nanowires and (b) CdS/CdSe core/sheath nanowires along with fluorescence emission spectra (excited at 250 nm) of (c) CdS nanowires, (d) CdS/CdSe core/sheath nanowires and (e) CdS/CdSe core/sheath nanowires dispersed in 1 M $CdSO_4$ solution.

common to both. This is consistent with a report that the major component of a core/shell particle dominates the absorption spectra.[9] By contrast, the photoluminescence (PL) spectra for the CdS-only and CdS/CdSe core/sheath nanowires are totally different [Fig. 3(c) and (d)] with the sheath completely quenching the fluorescence of CdS nanowires as found in the CdS/CdSe core/shell system.[11] When excess cadmium cations ($CdSO_4$) were added to a dispersion of the CdS/CdSe nanowires in water, the fluorescence was restored to virtually the previous level [Fig. 3(e)]. Accumulation of Cd^{2+} at the surface may destroy sites where radiationless recombination of charge carriers can occur.[5]

In summary, CdS/CdSe core/sheath nanowires with diameters of 7.7/0.75 nm were prepared from CdS nanowires and this method may be modified to prepare other core/sheath nanowires.

Financial support from the Chinese National Foundation of Natural Science Research through the Outstanding Youth Fund and Huo Yingdong Foundation for Young Teachers are gratefully acknowledged.

Notes and references

† XPS were recorded on an ESCALab MKII instrument with Mg-Kα radiation as the exciting source.
‡ XRD patterns were obtained on a Japan Rigaku D/Max γA rotation anode X-ray diffractometer with Ni-filtered Cu-Kα radiation (λ = 1.54178 Å).
§ TEM measurements were made on a Hitachi H-800 transmission electron microscope with an accelerating voltage of 200 kV.
¶ High-resolution electron microscopy (HREM) images of the as-prepared nanowires were taken on a JEOL-2010 transmission electron microscope.

1 M. Bockrath, D. H. Cobden, J. Lu, A. G. Rinzler, R. E. Smalley, L. Balents and P. L. McEuen, *Nature*, 1999, **397**, 598.
2 P. G. Collins, A. Zettl, H. Bando, A. Thess and R. E. Smalley, *Science*, 1997, **278**, 100.
3 J. Hu, M. Ouyang, P. Yang and C. M. Lieber, *Nature*, 1999, **399**, 48.
4 Y. Zhang, K. Suenaga, C. Colliex and S. Iijima, *Science*, 1998, **281**, 973; K. Suenaga, C. Colliex, N. Demoncy, A. Loiseau, H. Pascard and F. Willaime, *Science*, 1997, **278**, 653; C. N. R. Rao, R. Sen, B. C. Satishkumar and A. Govindaraj, *Chem. Commun.*, 1998, 1525; G. M. Meng, L. D. Zhang, C. M. Mo, S. Y. Zhang, Y. Qin, S. P. Feng and H. J. Li, *J. Mater. Res.*, 1998, **13**, 2533; A. M. Morales and C. M. Lieber, *Science*, 1998, **279**, 208.
5 L. Spanhel, M. Haase, H. Weller and A. Henglein, *J. Am. Chem. Soc.*, 1987, **109**, 5649.
6 M. A. Hines and P. Guyot-Siommest, *J. Phys. Chem.*, 1996, **100**, 468.
7 A. R. Kortan, R. Huli, R. L. Opila, M. G. Bawendi, M. L. Steigerwald, P. J. Carroll and L. E. Brus, *J. Am. Chem. Soc.*, 1990, **112**, 1327; B. O. Dabbousi, J. Rodriguez-Viejo, F. V. Mikulec, J. R. Heine, H. Mattoussi, R. Ober, K. F. Jensen and M. G. Bawendi, *J. Phys. Chem. B*, 1997, **101**, 9463.
8 M. Danek, K. F. Jensen, C. B. Murray and M. G. Bawendi, *Chem. Mater.*, 1996, **8**, 172.
9 C. F. Hoener, K. A. Allan, A. J. Bard, A. Campion, M. A. Fox, T. E. Mallouk, S. E. Webber and J. M. White, *J. Phys. Chem.*, 1992, **96**, 3812.
10 A. Mews, A. Eychmüller, M. Giersig, D. Schooss and H. Weller, *J. Phys. Chem.*, 1994, **98**, 934; A. Mews, A. V. Kadavanich, U. Banin and A. P. Alivisatos, *Phys. Rev. B: Condens. Matter*, 1996, **53**, 13 242.
11 Y. Tian, T. Newton, N. A. Kotov, D. M. Guldi and J. H. Fendler, *J. Phys. Chem.*, 1996, **100**, 8927.
12 X. Peng, M. C. Schlamp, A. V. Kadavanich and A. P. Alivisatos, *J. Am. Chem. Soc.*, 1997, **119**, 7019.
13 N. Revaprasadu, M. A. Malik, P. O'Brien and G. Wakefield, *Chem. Commun.*, 1999, 1573.
14 M. Bruchez Jr., M. Moronne, P. Gin, S. Weiss and A. P. Alivisatos, *Science*, 1998, **281**, 2013; W. C. W. Chan and S. Nie, *Science*, 1998, **281**, 2016.
15 P. Yan, Y. Xie, Y. Qian and X. Liu, *Chem. Commun.*, 1999, 1293.
16 T. Trindade, P. O'Brien and X. Zhang, *Chem. Mater.* 1997, **9**, 523.
17 M. L. Steigerwald and C. R. Sprinkle, *Organometallics*, 1988, **7**, 245; R. A. Zingaro, B. H. Stevens and K. Irgolic, *J. Organomet. Chem.*, 1965, **4**, 320.
18 C. B. Murray, D. J. Norris and M. G. Bawendi, *J. Am. Chem. Soc.*, 1993, **115**, 8706.

Communication 9/05669F

ChemComm

Crystal structure of $[Me_3Sb–SbMe_2]_2[(MeSbBr_3)_2]$, a trimethylstibine adduct of the dimethylstibenium ion or a stibinostibonium salt?

Henrik Althaus, Hans J. Breunig* and Enno Lork

University of Bremen, FB 02, PO Box 334440, D28334 Bremen, Germany. E-mail: breunig@chemie.uni-bremen.de

Received (in Basel, Switzerland) 19th July 1999, Accepted 30th August 1999

Scrambling reactions of dimethylantimony bromide in absence of solvent give the ionic complex $[Me_3Sb–SbMe_2]_2$-$[(MeSbBr_3)_2]$, with cations consisting of pyramidal Me_3Sb bound to bent Me_2Sb units through short (282 pm) Sb–Sb bonds and dimeric anions adopting the geometry of edge sharing tetragonal pyramids where methyl groups are in apical *trans* positions.

In contrast to the rich chemistry of phosphenium cations[1] very little is known of stibenium cations, R_2Sb^+ or of Lewis acid base adducts of the type $[B{\rightarrow}SbR_2]^+$. The diphenylstibenium cation, Ph_2Sb^+ was reported as a product of the electrochemical oxidation of $Ph_2Sb–SbPh_2$ in tetrahydrofuran (thf).[2] Pioneering work in the field of adducts was done by Summers and Sisler and others,[3–6] who studied reactions of trialkyls of phosphorus, arsenic or antimony with organohalo-phosphines, -arsines, or -stibines and reported the formation of 'arsinophosphonium salts' and related compounds of the type $[R_3EER_2]X$ (E = P, As, Sb; X = Cl, Br, I). These ionic species were characterized by measurement of their conductance in nitromethane. Recently an X-ray crystal structure analysis of an adduct was carried out on the ionic complex $[Me_2Sb–SbMe_2–SbMe_2][Me_2SbBr_2]$ obtained by reaction of Me_2SbBr with $Me_2Sb–SbMe_2$.[7] The chemical properties of the cation of this complex correspond to an adduct of tetramethyldistibine coordinated on the dimethylstibenium ion, Me_2Sb^+, the latter being formed together with $Me_2SbBr_2^-$ by transfer of Br^- from one Me_2SbBr molecule to another. However neither the distibine nor the dimethylstibenium unit could be distinguished in the crystal structure. The geometrical data of the cation correspond instead to the stibonium ion, $[R_2R'_2Sb]^+$ (R = Me, R′ = Me_2Sb).[7]

We have now investigated reactions with transfer of bromide between Me_2SbBr and $MeSbBr_2$ in presence of Me_3Sb as donor and report here the formation and the X-ray crystal structure determination of a novel ionic complex $[Me_3Sb–SbMe_2]_2$-$[(MeSbBr_3)_2]$ **1**. The cation of **1** is a trimethylstibine adduct of the dimethylstibenium ion and with view on isolobal relations between Me_2Sb^+ and CH_2 or Me_3Sb and Me_3P it can be considered as an analogue of phosphorus ylides. The alternative description as stibonium ion $[R_3R'Sb]^+$ (R = Me, R′ = Me_2Sb) is useful to underline the close relation with $[R_2R'_2Sb]^+$[7] and $[R_4Sb]^+$[8] in a family of stibonium ions, where now only the members $[RR'_3Sb]^+$ and $[R'_4Sb]^+$ are still unknown. Also the relation between **1** and tetramethyldistibine is intriguing. In fact, **1** might also be envisaged as a quaternization product of $Me_2SbSbMe_2$, which is not accessible by other methods. In contrast to tetraalkyldiphosphines which are easily quaternized by reactions with methylating agents such as methyl iodide, the analogous reactions of diarsines or distibines lead to fission of the (weaker) As–As or Sb–Sb bonds.[14] The anion of **1** is a dimer of methyltribromoantimonate(III). It is a novel example of a known type of 'ate' complexes of antimony(III). Several related aryl compounds[9–12] and one alkyl derivative[13] have been reported.

Crystals of **1** were grown in 80% yield in an attempt to crystallize dimethylantimony bromide by cooling the melt to −28 °C for several weeks. The formation of **1** can be explained by stepwise reactions according to eqn. (1) and (2). First the irreversible formation of the components Me_3Sb and $MeSbBr_2$ according to eqn. (1) may occur, which is a known reaction.[14] The following possible steps are summarized in eqn. (2). They include the transfer of bromide from Me_2SbBr to $MeSbBr_2$ and the coordination of Me_3Sb on the cation. The dimethylantimony bromide used as starting material should be of very high purity. It is best prepared by the reaction of tetramethyldistibine with bromine.[14]

$$2\ Me_2SbBr \longrightarrow Me_3Sb + MeSbBr_2 \quad (1)$$

$$2\ Me_2SbBr + 2\ Me_3Sb + 2\ MeSbBr_2 \rightleftharpoons \underset{\mathbf{1}}{[Me_3Sb\text{-}SbMe_2]_2[MeSbBr_3]_2} \quad (2)$$

In contrast to other organometallic compounds with Sb–Sb bonds such as the yellow or red distibines or cyclostibines, crystals of **1** are colourless. They are slightly soluble in non-polar organic solvents. ^1H NMR spectra in C_6D_6 show however that on dissolution the components Me_2SbBr, Me_3Sb and $MeSbBr_2$ are formed in the reverse of reaction (2). Later Me_3SbBr_2 and reduced methylantimony species are formed irreversibly.[15]

The crystal structure of **1** was determined by single crystal X-ray structure analysis. The structure of the cation is shown in Fig. 1. Fig. 2 shows the arrangement and the interactions between the ions. The cation consists of a pyramidal trimethylantimony unit bonded to a bent dimethylantimony unit through an antimony–antimony bond. The Sb–Sb bond length of **1** [282.05(12) pm] lies in the normal range of Sb–Sb single bond lengths as found in $Me_2Sb–SbMe_2$ [283.8(1)],[16] $(PhSb)_6$ [283.6–283.9(1)],[17] $[Me_2Sb–SbMe_2–SbMe_2][Me_2SbBr_2]$ [282.03(4)],[7] $Me_3Sb–Sb(Me)I_2$ [285.9(1)][18] and $Me_3Sb–SbI_3\cdot$thf [284.3(1) pm].[19] The C–Sb bond lengths to the onium centre of **1** [Sb(2)–C 210.6(11)–212.1(11)] are shorter than in the Me_2Sb group [Sb(1)–C 214.9(10), 216.5(12)] but longer than in $[Me_4Sb]I$ [Sb–C 204.3(2), 207.0(1) pm].[20] The C–Sb–C bond angles in the Me_3Sb unit in **1** are wide [103.1(5)–104.4(5)°] compared to uncoordinated Me_3Sb (94, 98°)[21] or the angles in solid $Me_2Sb–SbMe_2$ [C–Sb–C

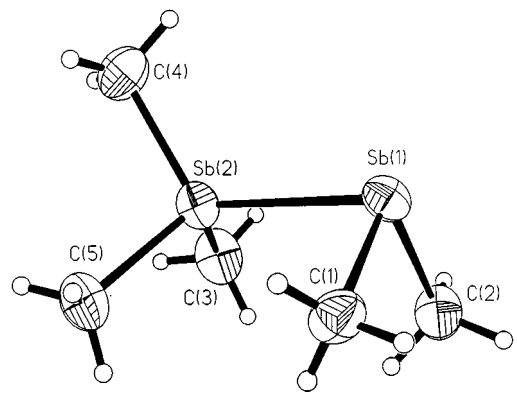

Fig. 1 The molecular structure of the cation $[Me_3Sb–SbMe_2]^+$ of **1**. Distances (pm) and angles (°): Sb(1)–Sb(2) 282.05(12), Sb(1)–C 214.9(10), 216.5(12), Sb(2)–C 210.6(11)–211.1(12); C(1)–Sb(1)–Sb(2) 91.0(4), C(2)–Sb(1)–Sb(2) 91.3(3), C(1)–Sb(1)–C(2) 94.3(5), C–Sb(2)–C 103.7(6), 103.1(5), 104.4(5), C(2)–Sb(1)–Sb(2)–C(3) 23.09(1), C(1)–Sb(1)–Sb(2)–C(5) 0.82(1).

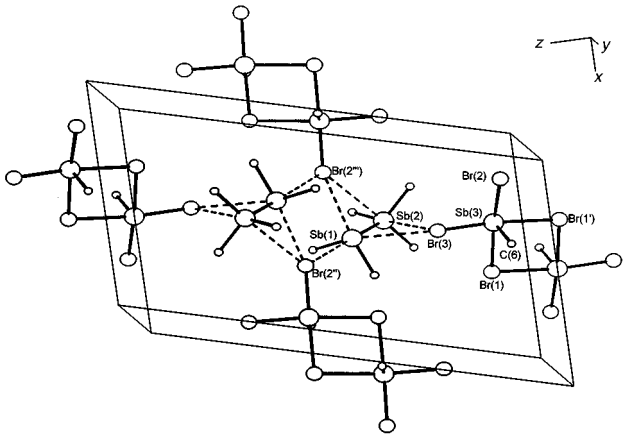

Fig. 2 Crystal structure of **1** with intermolecular interactions. Distances (pm) and angle (°): Sb(3)–C(6) 212.1(11), Sb(3)–Br(3) 263.24(16), Sb(3)–Br(2) 273.04(13), Sb(3)–Br(1) 289.17(13), Sb(3)–Br(1′) 302.72(16); Sb(1)···Br(2″) 354.3(21), Sb(1)···Br(2‴) 373.2(9), Sb(1)···Br(3) 383.0(23), Sb(2)···Br(2‴) 384.2(28), Sb(2)···Br(3) 391.2(4); Sb(2)–Sb(1)···Br(2″) 170.92(1).

88.6(5)–100.7(5)°, C–Sb–Sb [94.3(4)–94.4(4)°][16] but they lie in the range of C–Sb–C angles of the other complexes of Me_3Sb, *cf.* $Me_3Sb{\rightarrow}SbI_2Me$ [C–Sb–C, 101.3(3)–106.1(4)],[18] $Me_3Sb{-}SbI_3{\cdot}thf$ [102.9(5)–105.6(5)].[19] The widening of the angles on complexation may indicate a transition from the p^3 configuration of the free Me_3Sb to the sp^3 hybridisation in the adducts. The bond angles around the antimony atom of the Me_2Sb unit lie between 91.0(4) and 94.3(5)° corresponding to the p^3 configuration. In terms of the VSEPR model the angles at Sb(1) would reflect the stereochemical activity of the lone pair at antimony.

The loss of colour going from $Me_2Sb{-}SbMe_2$ (yellow melt and solution, red crystals) to $Me_3Sb{-}SbMe_2^+$ may result from the different orbitals forming the antimony–antimony bonds of the respective species.

The almost rectangular angles of $Me_2Sb{-}SbMe_2$ suggest that the Sb–Sb bond is formed by overlap of two 5p orbitals. In contrast, in the case of **1** the overlap of a sp^3 orbital at the four-coordinate antimony atom and a p-orbital at the three-coordinate Sb should be more effective resulting in the stabilization of the HOMO, a Sb–Sb σ-orbital and an increase in energy of the LUMO, a Sb–Sb σ*-orbital. HOMO–LUMO transitions lie in the visible region in the case of $Me_2SbSbMe_2$ but shift to the UV region of the spectra for **1**. The structure of the anions is composed of two tetragonal pyramids around the antimony atoms sharing an edge of the square base. The methyl groups are in apical positions, *trans* to each other. This type of structure is usual for organo halogeno antimonates.[9–13] It is also of interest to consider the interactions between the cation and the anion of **1**. There are three interionic Sb···Br contacts with distances shorter than the sum of van der Waals radii of Sb and Br (410 pm). The closest intermolecular contact [354.3(21) pm] exists between Sb(1) of the dimethylantimony unit and Br(2‴), one of the terminal bromine atoms of the anion. The Sb–Sb···Br angle is close to linearity. It is easy to assume that a prolongation of the dative Sb–Sb bond and a shortening of the Sb(1)···Br(2‴), contact leads to Me_2SbBr, the starting material.

Br(2‴) and Br(3) are in bridging positions above the Sb–Sb bond with contact distances of 373.2(9), 384.2(28) pm and 383.0(23); 391.2(4) pm, respectively. It is very likely that this interaction not only stabilizes the cation but also controls the unusual ecliptic conformation of the cation.

Notes and references

† *Crystal data* for $C_{12}H_{36}Br_6Sb_6$ **1**: M = 1390.35, monoclinic, a = 1189.4(2), b = 771.1(2), c = 1906.7(5) pm, β = 107.06(2), V = 1671.8(7) Å^3, T = 173(2) K, space group $P2_1/n$, Z = 2, μ(Mo-K) = 11.949 mm^{-1}, 4409 reflections measured, 3408 unique (R_{int} = 0.0354) which were used in all calculations. The final $wR(F^2)$ was 0.1391. The crystal was attached with Kel-F-oil to a glass fiber and cooled under a nitrogen stream to 173 K. After L_p and absorption correction (ψ-scans) the structure was solved by direct methods. CCDC 182/1398. See http://www.rsc.org/suppdata/cc/1999/1971/ for crystallographic files in .cif format.

1 M. Sanchez, M.-R. Mazières, L. Lamandé and R. Wolf, in *Multiple Bond and Low Coordination in Phosphorus Chemistry*, ed. M. Regitz and O. J. Scherer, Georg Thieme Verlag, Stuttgart, New York, 1990.
2 Y. Mourad, Y. Mugnier, H. J. Breunig and M. Ates, *J. Organomet. Chem.*, 1990, **388**, C9.
3 J. C. Summers and H. H. Sisler, *Inorg. Chem.*, 1970, **9**, 863.
4 J. M. F. Braddock and G. E. Coates, *J. Chem. Soc.*, 1961, 3208.
5 W. Seidel, *Z. Anorg. Allg. Chem.*, 1964, **330**, 141.
6 G. E. Coates and J. G. Livingstone, *Chem. Ind.* (*London*), 1958, 1366.
7 H. J. Breunig, M. Denker and E. Lork, *Angew. Chem.*, 1996, **108**, 1081; *Angew. Chem., Int. Ed. Engl.*, 1996, **35**, 1005.
8 H. J. Breunig, K. H. Ebert, S. Gülec, M. Dräger, D. B. Sowerby, M. J. Begley and U. Behrens, *J. Organomet. Chem.*, 1992, **427**, 39.
9 M. Hall and D. B. Sowerby, *J. Organomet. Chem.*, 1988, **347**, 59.
10 H. Preut, F. Huber and G. Alonzo, *Acta Crystallogr., Sect. C*, 1987, **43**, 46.
11 H. J. Breunig, K. H. Ebert, J. Probst, Y. Mourad and Y. Mugnier, *J. Organomet. Chem.*, 1996, **514**, 149.
12 H. J. Breunig, M. Denker and E. Lork, *Z. Anorg. Allg. Chem.*, 1999, **625**, 117.
13 A. Silvestru, H. J. Breunig, K. H. Ebert and R. Kaller, *J. Organomet. Chem.*, 1995, **501**, 117.
14 H. J. Breunig and H. Jawad, *J. Organomet. Chem.*, 1983, **243**, 417.
15 H. J. Breunig and W. Kanig, *Phosphorus Sulfur*, 1982, **12**, 149.
16 O. Mundt, H. Riffel, G. Becker and A. Simon, *Z. Naturforsch., Teil B*, 1984, **39**, 317.
17 H. J. Breunig, K. Häberle, M. Dräger and T. Severengiz, *Angew. Chem.*, 1985, **97**, 62; *Angew. Chem., Int. Ed. Engl.*, 1985, **24**, 72.
18 H. J. Breunig, M. Denker and K. H. Ebert, *J. Chem. Soc., Chem. Commun.*, 1994, 875.
19 M. Denker, H. J. Breunig, R. E. Schulz and E. Lork, *Z. Anorg. Allg. Chem.*, 1998, **624**, 81.
20 H. J. Breunig, K. H. Ebert, S. Gülec, M. Dräger, D. B. Sowerby, M. J. Begley and U. Behrens, *J. Organomet. Chem.*, 1992, **427**, 39.
21 M. Wieber, *Sb Organoantimony Compounds*, Part 1, *Gmelin Handbook of Inorganic Chemistry*, Springer Verlag, Berlin, 1981, p. 11.

Communication 9/05837K

The origin of the second relaxation process in the $[Mn_{12}O_{12}(O_2CR)_{16}(H_2O)_4]$ single-molecule magnets: 'Jahn–Teller isomerism' in the $[Mn_{12}O_{12}]$ core

Ziming Sun,[a] Daniel Ruiz,[a] Neil R. Dilley,[b] Mönica Soler,[c] Joan Ribas,[d] Kirsten Folting,[c] M. Brian Maple,[b] George Christou*[c] and David N. Hendrickson*[a]

[a] *Department of Chemistry-0358, University of California at San Diego, La Jolla, CA 92093-0358, USA. E-mail: dhendrickson@ucsd.edu*
[b] *Department of Physics, University of California at San Diego, La Jolla, CA 92093-0358, USA*
[c] *Department of Chemistry and Molecular Structure Center, Indiana University, Bloomington, IN 47405-7102, USA. E-mail: christou@indiana.edu*
[d] *Department of Chemistry, University of Barcelona, 08028-Barcelona, Spain*

Received (in Bloomington, IN, USA) 6th August 1999, Accepted 27th August 1999

The origin of the second, faster relaxation process in Mn_{12} molecules has been identified as a different relative orientation of the Jahn–Teller elongation axes of the Mn^{III} ions, which we have termed 'Jahn–Teller isomerism'.

Single-molecule magnets are of great current interest because they represent nanoscale magnetic particles of a sharply defined size that offer, amongst other things, the potential of access to the ultimate high-density information storage devices.[1–3] They also provide excellent examples of species exhibiting quantum tunnelling of magnetization.[4–6] Out-of-phase ac magnetic susceptibility signals (χ_M'') and magnetization hysteresis loops are characteristic of SMMs, whose properties result from a large spin (S) ground state and negative magnetic anisotropy. The first SMM reported was $[Mn_{12}O_{12}(O_2CMe)_{16}(H_2O)_4]$ **1**; ($8Mn^{III}$, $4Mn^{IV}$), with S = 10 and a zero-field splitting parameter (D) of -0.5 cm^{-1}, and Friedman *et al.*[4] subsequently reported steps on its magnetization hysteresis plots indicative of quantum tunnelling. Since then, variation of the $[Mn_{12}O_{12}(O_2CR)_{16}(H_2O)_4]$ carboxylate group and/or solvent molecules of crystallization have been shown to have significant effects on the hysteresis plots and the quantum tunnelling behaviour.[2,7,8]

An interesting observation is the presence often of two different χ_M'' signals for a given complex, which we have assigned as due to two polymorphs in the sample with slightly different environments about the Mn_{12} molecules.[7,8] For $[Mn_{12}O_{12}(O_2CC_6H_4Me\text{-}4)_{16}(H_2O)_4]$ **2**, the **2**·$HO_2CC_6H_4Me$-4 (space group $C2/c$) and **2**·$3H_2O$ ($I2/a$) forms have χ_M'' peaks in the 2–4 and 4–7 K ranges, respectively.[8] The *precise* molecular origin of the differing magnetic behaviour has not been clear, however, but we herein report this as due to the existence of isomeric forms of the $[Mn_{12}O_{12}]$ core involving different relative orientations of Mn^{III} Jahn–Teller distortion axes. We have termed this new effect 'Jahn–Teller isomerism'.

The complexes $[Mn_{12}O_{12}(O_2CCH_2Bu^t)_{16}(H_2O)_4]$ **3** and $[Mn_{12}O_{12}(O_2CC_6H_4F\text{-}2)_{16}(H_2O)_4]$ **4** were prepared as described elsewhere.[7a] The χ_M'' *vs.* T behaviour of **4** (Fig. 1) shows that it is a mixture of the 'low-temperature' (LT) and 'high-temperature' (HT) species in an approximate 12 : 1 ratio, with peaks in the 2–3 and 4–6 K ranges, respectively. Complex **3** shows an essentially identical plot.[8b] The structure of **3**·CH_2Cl_2·CH_3NO_2† appears typical of this class of molecule but closer examination [Fig. 2(a)] reveals that one Mn^{III} Jahn–Teller (JT) elongation axis is abnormally oriented, equatorially rather than axially. As a result, the JT axis contains an oxide ion, O(18), a situation which is highly unusual; JT elongation axes usually orient as to avoid the strong Mn^{III}–O^{2-} bonds, normally the shortest bonds about the metal. The usually observed JT orientations are as in the HT molecule **2**·$3H_2O$ [Fig. 2(b)] *i.e.* all axial. In contrast, close examination of the structure of **2**·$HO_2CC_6H_4Me$-4 shows that this LT form of **2** also has an abnormally oriented JT axis, whereas **1** and other Mn_{12} species with HT χ_M'' peaks show the normal JT orientation. Thus, we conclude that the abnormal orientation of a Mn^{III} JT axis is the

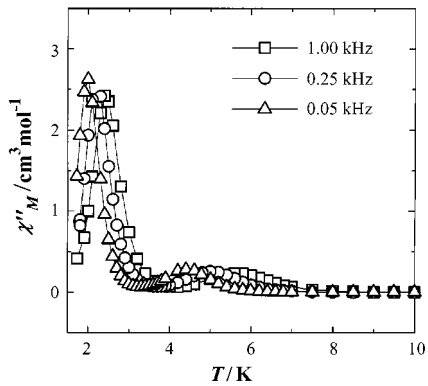

Fig. 1 Plot of the out-of-phase (χ_M'') *vs.* T behaviour of **4** at the indicated ac oscillation frequencies.

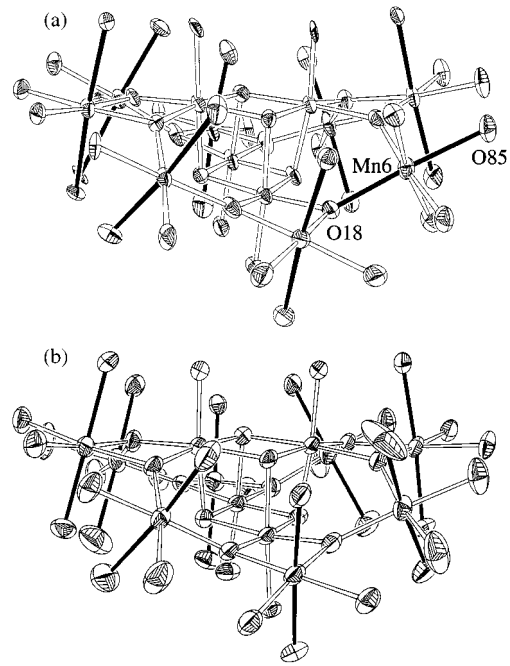

Fig. 2 The core of complex **3** emphasizing the abnormal Jahn–Teller orientation (a), and the core of **2**·$3H_2O$ showing the normal orientation (b). For **3**: Mn(6)–O(18) 2.073(7) Å, Mn(6)–O(85) 2.160(8) Å, other bonds to Mn(6) 1.873(8)–1.969(8) Å, other Mn^{III}–O^{2-} bonds 1.845(7)–1.919(7) Å.

origin of the LT χ_M'' peak.‡ This will alter the orientation of the singly occupied d_{z^2} orbital, and the influence on the relaxation rate could thus be due to a change in (i) the ground state *S* value, (ii) the separations to low-lying excited states, (iii) the molecular *D* value, or (iv) a combination of these. Further work is in progress to address this point.

The different temperatures for the LT and HT χ_M'' peaks correspond to faster and slower relaxation rates, respectively. The two separate processes were quantified for complex **4** by using the ac χ_M'' *vs. T* data to obtain Arrhenius plots; additional data on the LT process were obtained at 1.05 and 1.10 K using a Faraday magnetometer with a ^{3}He dilution refrigerator. The plots and obtained parameters are shown in Fig. 3. The HT process has an activation energy (*U*) of 65.2 K, similar to that of **1** (60–64 K),[1b,9] whereas the LT form has a much smaller *U* of 31.9 K. Similar Arrhenius data were found for complex **3**.

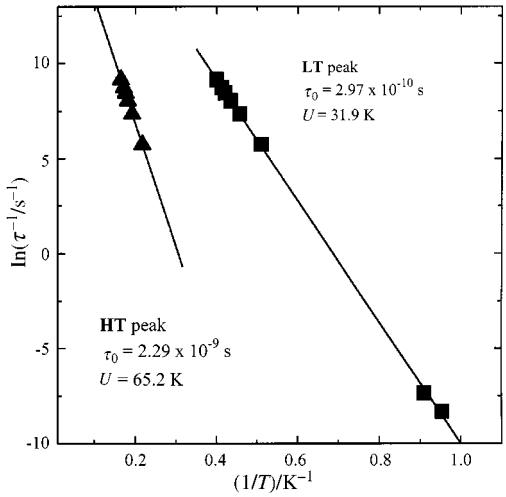

Fig. 3 Plots of the natural logarithm of the magnetization relaxation rates *vs.* 1/*T* for complex **4**: *U* is the activation energy and τ_o is the pre-exponential of the Arrhenius equation.

In summary, the LT χ_M'' *vs. T* responses of some Mn_{12} species are a result of their containing an abnormally oriented JT axis. This represents a type of isomerism not seen before and which can be defined as two or more non-equivalent forms differing in the relative orientation of one (or more) JT axes. We offer the term 'Jahn–Teller isomerism' for this new effect.

The work was supported by the National Science Foundation.

Notes and references

† *Crystal data* for **3**·CH_2Cl_2·CH_3NO_2: $C_{98}H_{189}Cl_2Mn_{12}NO_{50}$, M = 2911.71, triclinic, $P\bar{1}$, a = 16.422(2), b = 27.434(3), c = 15.814(2) Å, α = 101.78(1), β = 101.79(1), γ = 76.90(1)°, Z = 2, U = 6699 Å^3, μ(Mo-Kα) = 11.630 mm^{-1}, D_c = 1.44 g cm^{-3}, T = −174 °C. The structure was solved by direct methods (SHELXTL) and refined (on *F*) using 10 081 reflections with $F > 2.33\sigma(F)$ to $R(R_w)$ values of 0.0725 (0.0563). CCDC 182/1395. See http: //www.rsc.org/suppdata/cc/1999/1973/ for crystallographic files in .cif format.

‡ Fresh samples of **3**·CH_2Cl_2·CH_3NO_2 show essentially only the LT peak. With time at room temperature, solvent molecules of crystallization are slowly lost (confirmed by elemental analysis), and the LT/HT ratio decreases. Thus, the LT form is the structurally characterised form and the relative amount of HT form increases with solvent loss. Full details will be reported in the full paper.

1 (*a*) R. Sessoli, H.-L. Tsai, A. R. Schake, S. Wang, J. B. Vincent, K. Folting, D. Gatteschi, G. Christou and D. N. Hendrickson, *J. Am. Chem. Soc.*, 1993, **115**, 1804; (*b*) R. Sessoli, D. Gatteschi, A. Caneschi and M. A. Novak, *Nature*, 1993, **365**, 141.

2 G. Aromi, S. M. J. Aubin, M. A. Bolcar, G. Christou, H. J. Eppley, K. Folting, D. N. Hendrickson, J. C. Huffman, R. C. Squire, H.-L. Tsai, S. Wang and M. W. Wemple, *Polyhedron*, 1998, **17**, 3005.

3 S. M. J. Aubin, N. R. Dilley, L. Pardi, J. Drzystek, M. W. Wemple, L.-C. Brunel, M. B. Maple, G. Christou and D. N. Hendrickson, *J. Am. Chem. Soc.*, 1998, **120**, 4991.

4 J. R. Friedman, M. P. Sarachik, J. Tejada, J. Maciejewski, R. Ziolo, *J. Appl. Phys.*, 1996, **79**, 6031; J. R. Friedman, M. P. Sarachik, J. Tejada and R. Ziolo, *Phys. Rev. Lett.*, 1996, **76**, 3830.

5 L. Thomas, F. Lionti, R. Ballou, D. Gatteschi, R. Sessoli and B. Barbara, *Nature*, 1996, **383**, 145.

6 J. Tejada, R. Ziolo and X. X. Zhang, *Chem. Mater.*, 1996, **8**, 1784.

7 (*a*) H. J. Eppley, H.-L. Tsai, N. de Vries, K. Folting, G. Christou and D. N. Hendrickson, *J. Am. Chem. Soc.*, 1995, **117**, 301; (*b*) D. Ruiz, Z. Sun, B. Albela, K. Folting, J. Ribas, G. Christou and D. N. Hendrickson, *Angew. Chem. Int. Ed.*, 1998, **37**, 300.

8 (*a*) S. M. J. Aubin, Z. Sun, I. A. Guzei, A. L. Rheingold, G. Christou and D. N. Hendrickson, *Chem. Commun.*, 1997, 2239; (*b*) Z. Sun, D. Ruiz, E. Rumberger, C. D. Incarvito, K. Folting, A. L. Rheingold, G. Christou and D. N. Hendrickson, *Inorg. Chem.*, 1998, **37**, 4758.

9 M. A. Novak and R. Sessoli, in *Quantum Tunneling of Magnetization-QTM '94*, ed. L. Gunther and B. Barbara, Kluwer, Dordrecht, 1995, pp. 171–188; M. A. Novak, R. Sessoli, A. Caneschi and D. Gatteschi, *J. Magn. Magn. Mater.*, 1995, **146**, 211.

Communication 9/06451F

ChemComm

An amidine-functionalized cobalt(III) cage complex: synthesis, structure and properties

Patricia M. Angus,*[ab] Alan M. Sargeson*[ab] and Anthony C. Willis*[a]

[a] *Research School of Chemistry, Australian National University, Canberra ACT 0200 Australia. E-mail: sargeson@rsc.anu.edu.au*

[b] *Department of Chemistry, Faculty of Science, Australian National University, Canberra ACT 0200, Australia*

Received (in Cambridge, UK) 5th August 1999, Accepted 31st August 1999

The template synthesis, structure and properties of an unusual tricyclic amidine-functionalized triaza-trithia cobalt(III) cage complex are described.

Functionalized cages have been prepared previously by condensing the templates $[Co(sen)]^{3+}$ [sen = 4,4′,4″-ethylidynetris(3-azabutan-1-amine)] and $[Co(ten)]^{3+}$ [ten = 4,4′,4″-ethylidynetris(3-thiabutan-1-amine)] with methanal and a carbon acid containing either an aldehyde, a ketone or an ester functional group. In the first two instances, condensation between the functional group and a coordinated amine resulted in the formation of a cage complex with an imine incorporated in the ligand framework whereas an amide-functionalized cage resulted when an ester was used.[1–3] Malononitrile (pK_a = 11)[4] is used here as a bifunctional carbon acid to form amidine-functionalized cobalt(III) cage complexes with three nitrogen and three sulfur donor atoms, the first example of a cage complex incorporating that functional group. The condensation of a coordinated amine with a pendant nitrile to form a coordinated amidine has not previously been applied to cage synthesis. These functionalized cage complexes are important because variations in functional groups and substituents, as well as in donor atoms, modulate substantially the physical properties of these complexes.[2,6,7]

Two red cage complexes were isolated by ion-exchange chromatography from the reaction of $[Co(ten)]Cl(ClO_4)_2$[2,8] and malononitrile in aqueous methanal at pH 10.† The first red species was assigned as an N_3S_3 amidine cage with an amide group as an apical substituent {$[Co(Me,H_2NCO\text{-}7\text{-amino}\ N_3S_3sar\text{-}6\text{-ene})]^{3+}$} (Scheme 1, **2**) using ^1H and ^{13}C NMR spectra recorded in DMSO-d_6 and microanalytical data; the same molecule was then prepared using 2-cyanoacetamide instead of malononitrile as the carbon acid.[9] The ^{13}C NMR spectrum of the second species showed that it contained two sp^2 functional groups (δ 162, 164), one of which might have been an amidine but the other could not be identified with certainty. Its surprising structure was revealed by an X-ray crystallographic analysis of the perchlorate salt and is shown in Fig. 1.‡ The ^1H and ^{13}C NMR spectra and the microanalysis of the whole fraction were consistent with this structure.§

The X-ray analysis established that the cobalt(III) ion was fully encapsulated in a pseudo-octahedral environment and that an amidine functional group was incorporated into the cage framework. The conformation of the strand containing the amidine functional group was *ob* while that of the other strands was characteristically *lel*.[10] The carbon–nitrogen bond lengths in the amidine group {C(2)–N(1) 1.915, C(2)–N(5) 1.318 Å} are comparable with those reported for other secondary amidines chelated to cobalt(III) and so is the cobalt(III)–amidine nitrogen bond length (1.915 Å).[5] An unusual feature of this cage is the structure of the cap. The amidine and amide functional groups have been cross-linked with a methylene group to form a near-planar diazine heterocycle fused to the cap as a subsidiary feature which is surprisingly stable to hydrolysis.

A mechanism for the formation of the cage complex is described in Scheme 1. The initial product (not detected) has to be an amidine cage with a nitrile substituent at the apex (Scheme 1, **3**). Clearly the nitrile group undergoes rapid intermolecular hydrolysis to give the amidine cage complex with an apical amide substituent (Scheme 1, **2**). This degree of activation of a remote functional group towards intermolecular attack is unusual. In amide cage complexes of cobalt(III), in which the cage ligand is deprotonated and bonded at the amide nitrogen, nitrile substituents are inert.[3] Similarly in monodentate cobalt(III) complexes of ligands containing a remote nitrile group and coordinated through nitrile, amide or amidine groups, no intermolecular hydrolysis of the remote functional group has been observed under basic conditions.[11] Here, the facile hydrolysis of the apical nitrile group reflects the attachment of this section of the neutral cage ligand to cobalt(III) through *three* chelate rings, thus maximizing its activation by the metal ion.

In the final stage of the synthesis methanal has added to the *exo*-nitrogen of the amidine in aqueous base and the resulting

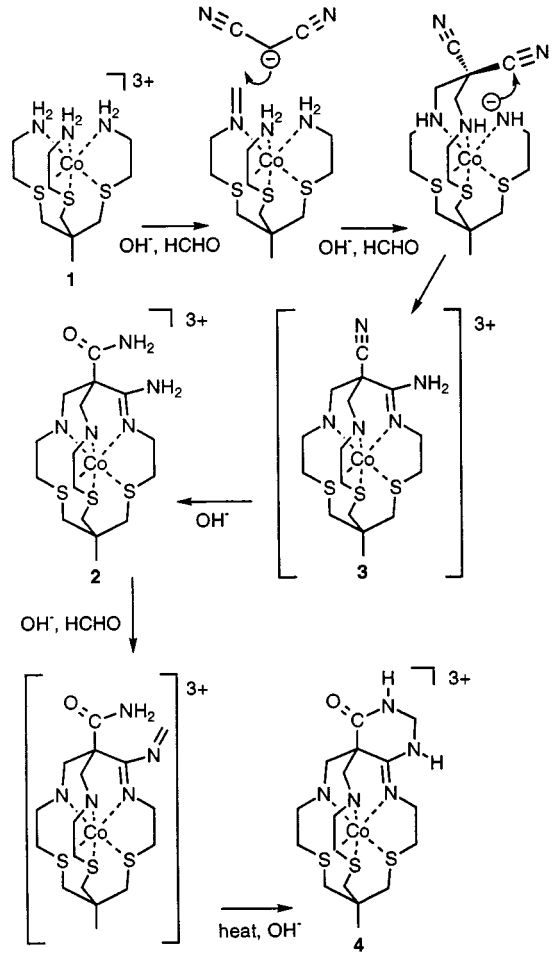

Scheme 1

imine is attacked by the neighbouring deprotonated amide so that the groups were cross-linked to complete the heterocyclic ring. Aldehydes readily and reversibly add to amidines,[12] and this was doubtless facilitated in the present case by the increased acidity of the amidine coordinated to cobalt(III).[5] Such cross-linking between nitrogenous functional groups is a well known reaction when proteins and peptides are treated with aqueous methanal and a variety of functional groups may be connected in this way.[13] The heterocyclic cage was also synthesized directly from the amide-substituted amidine cage (**2**) and aqueous methanal but only at 60 °C or higher. At ambient temperature only a dimeric species was detected, formed by intramolecular cross-linking between two amidine functional groups. In the original synthesis the heat necessary for intramolecular cross-linking was produced by polymerization of malononitrile in aqueous base, a rapid, exothermic reaction which occurred in parallel with cage formation.

In the electronic spectrum of the heterocyclic amidine cage complex, bands arising from the d–d transitions were found at 496 and 363 (shoulder) nm (ε = 720 and 815 dm^3 mol^{-1} cm^{-1}, respectively). These were intermediate in energy and intensity between those of triamine and amide-functionalized N_3S_3 cage complexes.[2,7b] The UV region of the spectrum contained two intense bands at 288 and 210 nm (ε = 140 00 and 20 000 dm^3 mol^{-1} cm^{-1}, respectively). These are attributed to S→Co charge transfer bands. These low-spin Co$^{III/II}$ molecules should display rapid electron transfer characteristics and the chemistry in general points to useful paths for tying other functional groups and sensors to the cage complex.

This work was supported by the Australian Research Council. We thank the Microanalytical Section of the Research School of Chemistry (ANU) for the analyses.

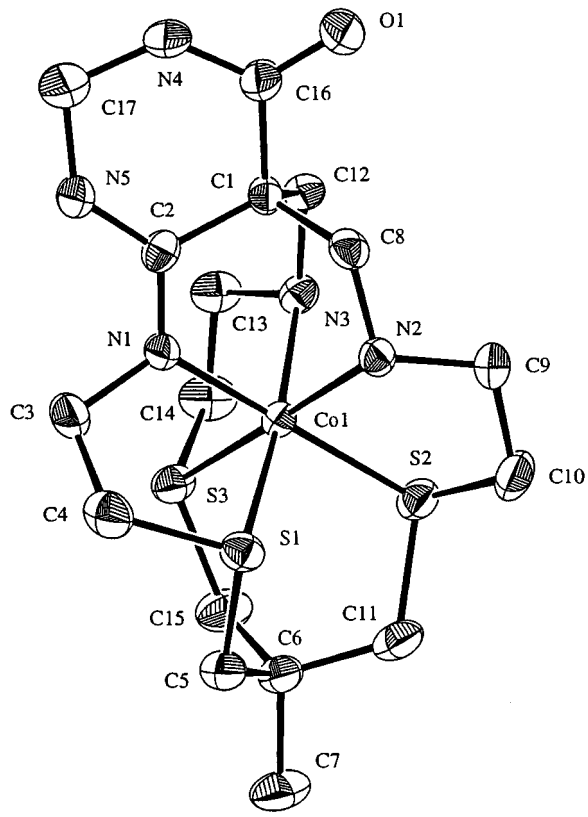

Fig. 1 ORTEP plot of the tricyclic amidine-functionalized N_3S_3 cage complex cation (the hydrogens attached to carbon and nitrogen atoms have been omitted for clarity).

Notes and references

† [Co(ten)]Cl(ClO$_4$)$_2$ (1.0 g) and malononitrile (5 mL) were dissolved in aqueous methanal (38%, 30 mL) in a 750 mL beaker in a fumehood and gradually treated with Na_2CO_3 (0.5 g). There was considerable effervescence and the solution became quite hot. After 30 min the reaction was quenched with acetic acid to pH 5 and water (200 mL) was added. The mixture was extracted with chloroform to remove excess polymeric material, then the aqueous phase was filtered and absorbed on Dowex 50W-X2 cation exchange resin. The column was washed with water then eluted with 2 M HCl which removed some Co^{II} species, ten·3HCl and some non-encapsulated by-products. Elution with 3 M HCl removed a large tripositive red band which was evaporated to dryness, dissolved in water (300 mL) and chromatographed on SP-Sepahadex cation exchange resin. The column was eluted with 0.1 M K_2SO_4 solution which separated trace amounts of the addition products then two red bands which were collected and desalted separately by chromatography on Dowex and elution with 3 M HCl followed by rotary evaporation. The first complex was recrystallized as the chloride–tetrachlorozincate salt {7-amino-8-carboxamide-1-methyl-3,13,16-trithia-6,10,19-triazabicyclo[6.6.6]icosa-6-enecobalt(III) chloride-tetrachlorozincate hydrate}, 0.22 g, 17% yield {^{1}H NMR (δ, DMSO-d^6): 1.30 (3H), CH_3; 2.50–4.05, complex methylene envelope; 7.35, 7.51, amine NH; 7.66, 7.83, amide NH_2; 8.12, 8,64, amidine NH_2}. The second complex (Scheme 1, **4**) was crystallized from aqueous sodium perchlorate solution with ethanol (0.20 g, 14% yield). **CAUTION**: perchlorate salts are potentially explosive and should only be handled in small quantities.

‡ *Crystal data*: $CoC_{17}H_{33}N_5O_{14}S_3Cl_3$; M = 792.95, monoclinic, space group $P2_1/c$ (no. 14), a = 12.931(2), b = 10.404(2), c = 21.463(4) Å, β = 99.65(1)°, U = 2846.6(8) Å^3, T = 23 ± 1 °C, Z = 4, μ(Mo-Kα) = 11.81 cm^{-1}, 7086 reflections measured (Philips PW1100/20 diffractometer), 6908 unique (R_{int} = 0.018) and 4290 > 3σ. The final R was 0.042. One of the anions is disordered. CCDC 182/1392. See http://www.rsc.org/suppdata/cc/1999/1975/ for crystallographic files in .cif format.

§ ^{1}H NMR spectrum (δ, DMSO-d_6): 1.28 (3H, CH_3), 2.9–3.85 (complex methylene envelope), 4.66 (m, NCH_2N), 7.44 (1H), 7.58 (1H) (amine NH), 9.22 (1H), 9.53 (1H), (amide and amidine NH). ^{13}C NMR spectrum (δ, DMSO-d_6): 28.8 (CH_3), 35.9, 37.3, 38.2, 38.4, 42.1 (2C) (CH_2S), 41.8 ($C_{q(S)}$); 50.1, 51.5, 51.6, 51.7, 52.5, 52.9, 53.2 (CH_2N, $C_{q(N)}$); 162.3, 164.1 (HNC=N, O=CNH).

1 A. Höhn, R. J. Geue and A. M. Sargeson, *J. Chem. Soc., Chem. Commun.*, 1990, 1473.
2 P. Lay, J. Lydon, A. W.-H. Mau, P. Osvath, A. M. Sargeson and W. H. F. Sasse, *Aust. J. Chem.*, 1993, **46**, 641.
3 R. J. Geue, W. R. Petri, A. M. Sargeson and M. R. Snow, *Aust. J. Chem.*, 1992, **45**, 1681.
4 R. G. Pearson and R. L. Dillon, *J. Am. Chem. Soc.*, 1953, **75**, 2439.
5 D. A. Buckingham, C. R. Clarke, B. M. Foxman, G. J. Gainsford, A. M. Sargeson, M. Wein and A. Zanella, *Inorg. Chem.*, 1982, **21**, 1986; L. Roecker, J. D. Lydon, A. C. Willis, A. M. Sargeson and E. Deutsch, *Aust. J. Chem.*, 1989, **42**, 339; J. Springborg, R. J. Geue, A. M. Sargeson, D. Taylor and M. R. Snow, *J. Chem. Soc., Chem. Commun.*, 1978, 647.
6 A. M. Bond, G. A. Lawrance, P. A. Lay and A. M. Sargeson, *Inorg. Chem.*, 1983, **22**, 2010.
7 (*a*) L. R. Gahan, G. A. Lawrance and A. M. Sargeson, *Inorg. Chem.*, 1984, **23**, 4369; (*b*) P. Osvath, A. M. Sargeson, B. W. Skelton and A. H. White, *J. Chem. Soc., Chem. Commun.*, 1991, 389; (*c*) R. Bhula, A. P. Arnold, G. J. Gainsford and W. G. Jackson, *Chem. Commun.*, 1996, 143.
8 L. R. Gahan, T. W. Hambley, A. M. Sargeson and M. R. Snow, *Inorg. Chem.*, 1982, **21**, 2699.
9 P. M. Angus and A. M. Sargeson, manuscript in preparation.
10 For an explanation of the *lel* and *ob* terminology, see: *Inorg. Chem.*, 1970, **9**, 1.
11 R. J. Balahura and W. L. Purcell, *Inorg. Chem.*, 1979, **18**, 937 and references therein; P. M. Angus and W. G. Jackson, *Inorg. Chem.*, 1996, **35**, 7196.
12 R. L. Shriner and F. W. Neumann, *Chem. Rev.*, 1944, 351.
13 H. Fraenkel-Conrat and H. S. Olcott, *J. Am. Chem. Soc.*, 1948, **70**, 2673 and references therein.

Communication 9/06389G

Strong ferromagnetic coupling in the K_2NiF_4-structured oxide $La_{0.8}Sr_{1.2}Mn_{0.6}Rh_{0.4}O_4$

P. D. Battle,* J. C. Burley, E. J. Cussen, G. C. Hardy, M. A. Hayward, L. D. Noailles and M. J. Rosseinsky*

Inorganic Chemistry Laboratory, Department of Chemistry, University of Oxford, South Parks Road, Oxford, UK OX1 3QR. E-mail: peter.battle@chem.ox.ac.uk; matthew.rosseinsky@chem.ox.ac.uk

Received (in Oxford, UK) 9th August 1999, Accepted 3rd September 1999

Substitution of diamagnetic Rh^{III} into the antiferromagnet $LaSrMnO_4$ produces the first example of a K_2NiF_4 ($n = 1$ Ruddlesden–Popper) oxide with strong ferromagnetic interactions—in 50 kG at 5 K the magnetisation of $La_{0.8}Sr_{1.2}Mn_{0.6}Rh_{0.4}O_4$ is close to saturation at 2.50 μ_B per Mn cation; the bulk magnetisation stems from the alignment by the magnetic field of ferromagnetic (Mn/Rh)O_2 sheets which are not magnetically ordered along [001] in zero applied field.

There has been a resurgence of interest in ferromagnetic oxides owing to the strong coupling between spin ordering and charge transport found in the $La_{1-x}Sr_xMnO_3$ perovskites which display colossal magnetoresistance (MR).[1] This suppression of the zero-field resistance in an applied field can be as large as $100\Delta\rho/\rho(H = 0) = 99.9\%$ in fields of over 50 kG, but achieving significant MR in the low fields required for information storage applications has proved a difficult barrier for the current generation of materials. Increasing attention[2] is now being paid to the intrinsically layered $n = 2$ members of the Ruddlesden–Popper (RP) $A_{n+1}B_nO_{3n+1}$ series, for example $La_{1.8}Sr_{1.2}Mn_2O_7$,[3] which display MR in fields as low as 3 kG owing to the small barrier to the field aligning the magnetisation between the perovskite blocks in the layer stacking sequence. Ferromagnetism has not yet been demonstrated in the two-dimensional $Sr_{1+x}La_{1-x}MnO_4$ $n = 1$ member of the RP series, with the Sr_2MnO_4[4] and $LaSrMnO_4$ end-members being antiferromagnets while the $Mn^{III/IV}$ solid solutions are spin glasses.[5] Here, we demonstrate that substitution of formally diamagnetic Rh^{III} into $Sr_{1.2}La_{0.8}MnO_4$ produces a material with short-range spin ordering in zero field which achieves a moment of 2.50 μ_B per manganese in a 50 kG field.

Preliminary investigation of the Sr–La–Rh–Mn–O phase field at the $n = 1$ RP composition under air and N_2 atmospheres indicated that our initial target composition $LaSrMn_{0.6}Rh_{0.4}O_4$ was strongly polyphasic, with $La_2O_3/La(OH)_3$ impurities showing that a higher Sr/La ratio, and thus metal oxidation state, was required for phase purity. This is consistent with the reported failure to prepare $SrLaRhO_4$[6] in contrast with $Sr_{1.2}La_{0.8}RhO_4$. $Sr_{1.2}La_{0.8}Mn_{0.6}Rh_{0.4}O_4$ was therefore prepared by reaction of Rh_2O_3, MnO_2, $SrCO_3$ and La_2O_3 at 1000, 1200 and 1250 °C for 24 h each, followed by 4 further days at 1250 °C, all firings being performed in air. This produced a material of 99.5% $n = 1$ RP phase with $a = 3.88761(6)$, $c = 12.5176(2)$ Å. The only impurity visible to X-ray powder diffraction is 0.5% by mass La_2O_3, a diamagnetic material which will not interfere with magnetic measurements.

Magnetisation *vs.* temperature measurements† made in an applied field of 100 G suggest (Fig. 1) complex magnetism with the possibility of magnetic long range order. Hysteresis is apparent between the ZFC and FC data below an anomaly in M/H at 180 K, and below 35 K both the ZFC and FC magnetisations rise sharply, with the ZFC showing a maximum at 13.5 K. Data collected in a field of 1000 G showed similar features although the ZFC magnetisation continued to rise down to 5 K. The $M(H)$ magnetisation isotherm at 5 K (Fig. 2) indicates strong ferromagnetic coupling, with a moment approaching saturation at 2.50 μ_B per Mn at 5 K; the magnetisation remains a non-linear function of field to temperatures in excess of 100 K although saturation is clearly not reached in 50 kG. Neutron powder diffraction data† (D2B, ILL) are consistent with the idea of a phase exhibiting strong ferromagnetic coupling but without the long-range magnetic order suggested by the magnetometry experiments. Rietveld-refinement[7] of data collected at both 290 and 1.7 K proceeded smoothly (at 290 K, $R_{wpr} = 5.35\%$, $\chi^2 = 2.4$; at 1.7 K, $R_{wpr} = 5.14\%$, $\chi^2 = 1.6$) within a model which considered only nuclear scattering from the $La_{0.8}Sr_{1.2}Mn_{0.6}Rh_{0.4}O_4$ composition, thus

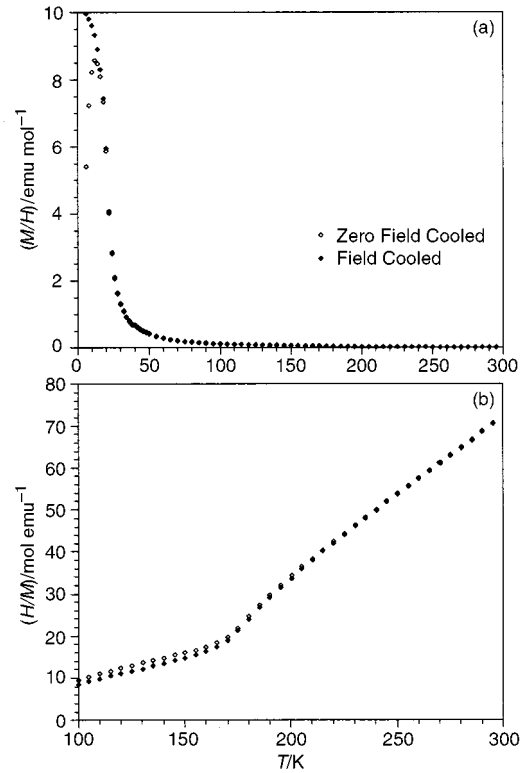

Fig. 1 (a) Molar magnetic susceptibility (M/H) and (b) inverse susceptibility (H/M) of $Sr_{1.2}La_{0.8}Mn_{0.6}Rh_{0.4}O_4$ measured in a field of 100 G: field cooled (FC) and zero-field cooled (ZFC) data are shown as filled and empty symbols, respectively.

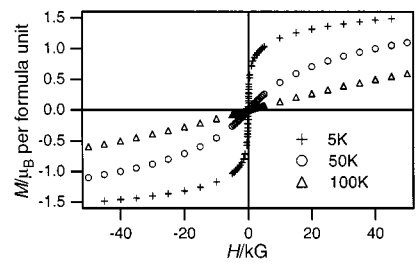

Fig. 2 Magnetisation per formula unit as a function of field and temperature for FC $Sr_{1.2}La_{0.8}Mn_{0.6}Rh_{0.4}O_4$. At 5 K, $H_{M=0} = 72 \pm 5$ G, $M_{H=0} = 0.15 \pm 0.02$ μ_B.

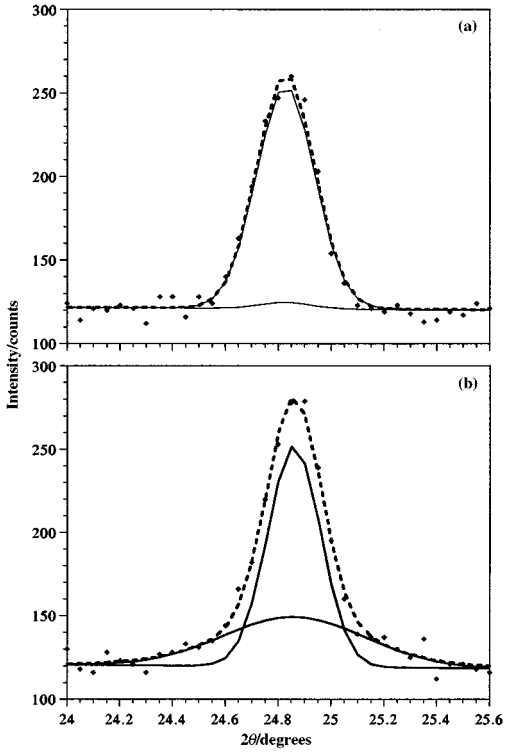

Fig. 3 Neutron powder diffraction measurements on $Sr_{1.2}La_{0.8}Mn_{0.6}Rh_{0.4}O_4$ at (*a*) 290 K and (*b*) 1.7 K, showing the two component fit (solid lines) to the 101 reflection: the extra broad diffuse scattering observed at 1.7 K is suggestive of magnetic short range ordering within the 2D layers.

conclusively demonstrating the absence of magnetic long-range order. Close inspection of the low-angle 002 and 101 reflections (which are sensitive to magnetic scattering owing to the angular dependence of the form factor) shows that the latter (Fig. 3), but not the former, develops weak but well defined broad, extra scattering at low temperature. The profile of the 101 reflection at 290 K can be fitted by two pseudo-Voigt functions in the ratio 0.966 : 0.034; the principal peak has a negligible Lorentzian component. At 1.7 K the ratio is 0.584 : 0.416; the stronger component is again essentially Gaussian but the weaker, broader component has a significant Lorentzian contribution. The growth in the latter component of the 101, but not the 002, is consistent with ferromagnetic correlations developing within but not between the two-dimensional $(Mn/Rh)O_2$ sheets.

The oxidation state of the Rh substituent at the electronically active B site is not directly defined by our measurements, but consideration of the established oxide chemistries of Mn and Rh leads to the assumption that Rh is present solely as Rh^{III} (low spin t_{2g}^6), resulting in a mean Mn oxidation state of + 3.33. The measured value of the magnetisation as it approaches saturation is a significant but reduced fraction of that (3.66 μ_B per Mn) to be expected from a fully aligned array of Mn cations in this oxidation state; the cause of the difference has yet to be determined. The presence of a transition at 180 K restricts the temperature range which can be analysed using the Curie–Weiss law and the enforced proximity to a phase transition will limit the validity and accuracy of the value of 5.54 μ_B per Mn derived for the effective magnetic moment in 100 G by fitting in the range $250 \leq T/K \leq 300$; comparisons with calculated values are therefore nonsensical. The ferromagnetic Weiss constant of +106 K is however consistent with the lower temperature magnetisation and neutron scattering measurements.

Substitution of diamagnetic low-spin Rh^{III} has a surprising effect on the magnetism of manganates having the K_2NiF_4 structure. Although the presence of both Mn^{III} and Mn^{IV} allows ferromagnetic double and super exchange, and the same oxidation state (3.33) produces ferromagnetism in the $n = \infty$ Mn-only perovskites,[8] in the pure 2D manganate series, oxidation of the antiferromagnet $La_{1-x}Sr_{1+x}MnO_4$ beyond the +3.2 oxidation state results in the suppression of antiferromagnetic ordering but not in the onset of ferromagnetism:[9] $La_{0.7}Sr_{1.3}MnO_4$ is a canonical spin-glass showing the classical FC/ZFC magnetisation divergence. The substitution of Rh on the B sites clearly enhances ferromagnetic Mn–Mn coupling in $Sr_{1.2}La_{0.8}Mn_{0.6}Rh_{0.4}O_4$, at least within the $(Mn/Rh)O_2$ layers perpendicular to [001]. One interpretation of the currently available data is that each individual $(Mn/Rh)O_2$ sheet develops a spontaneous magnetisation when 2D magnetic ordering occurs at 180 K, with the resultant magnetic moments being aligned by an applied field; saturation is approached in 50 kG at 5 K, and 100 G has a significant effect below 35 K. However, the magnetic consequences of ferromagnetic $n = \infty$ intergrowths in RP phases are well known[10] and further measurements are necessary before firm conclusions can be drawn. Increasing the Mn concentration further above the 2D square site percolation limit of 0.5 and optimisation of the mean metal oxidation state are important future improvements on this new recipe for generating ferromagnetic interactions in 2D manganates.

We acknowledge funding from the UK EPSRC.

Notes and references

† X-Ray powder diffraction data were recorded using a Siemens D5000 diffractometer with Cu-Kα_1 radiation. Magnetisation measurements were made with a Quantum Design MPMS5 SQUID magnetometer on samples contained within gelatin capsules. Neutron powder diffraction data were recorded at λ = 1.59 Å on the D2B powder diffractometer with the sample contained in a vanadium can in an ILL 'Orange' cryostat at both 1.7 and 290 K. Space group *I*4/*mmm*, Sr/La on 0,0,*z*, Mn/Rh on 0,0,0, O1 on 0,0,*z*, O2 on 1/2,0,0. At 290 K, a = 3.88763(7), c = 12.5184(3) Å, $z_{Sr/La}$ = 0.35862(7), z_{O1} = 0.16501(9); Mn/Rh–O 2.066(1) Å ×2, 1.94381(4) Å ×4. At 1.7 K, a = 3.88303(7), c = 12.4814(3) Å, $z_{Sr/La}$ = 0.35885(6), z_{O1} = 0.16462(9); Mn/Rh–O 2.058(1) Å ×2, 1.94151(3) Å ×4.

1 A. P. Ramirez, *J. Phys.: Condens. Matter*, 1997, **9**, 8171.
2 P. D. Battle and M. J. Rosseinsky, *Curr. Opin. in Solid State Mater. Sci.*, 1999, **4**, 163.
3 Y. Moritomo, A. Asamitsu, H. Kuwahara and Y. Tokura, *Nature*, 1996, **380**, 141.
4 J. C. Bouloux, J. L. Soubeyroux, G. le-Flem and P. Hagenmuller, *J. Solid State Chem.*, 1981, **38**, 34.
5 Y. Moritomo, Y. Tomioka, A. Asamitsu and Y. Tokura, *Phys Rev. B: Condens. Matter*, 1995, **51**, 3297.
6 T. Shimura, M. Itoh, Y. Inaguma and T. Nakamura, *Phys. Rev. B: Condens. Matter*, 1994, **49**, 5591.
7 H. M. Rietveld, *J. Appl. Crystallogr.*, 1969, **2**, 65.
8 G. H. Jonker and J. H. vanSanten, *Physica*, 1950, **16**, 337.
9 R. A. Mohan-Ram, P. Ganguly and C. N. R. Rao, *J. Solid State Chem.*, 1987, **70**, 82.
10 S. D. Bader, R. M. Osgood, D. J. Miller, J. F. Mitchell and J. S. Jiang, *J. Appl. Phys.*, 1998, **83**, 6385.

Communication 9/06543A

An improved vinylalumination procedure replacing HMPA with NMO for the hydroalumination of α-acetylenic esters and ketones

P. Veeraraghavan Ramachandran,* M. Venkat Ram Reddy and Michael T. Rudd

H. C. Brown and R. B. Wetherill Laboratories of Chemistry, Purdue University, West Lafayette, Indiana 47907-1393, USA. E-mail: chandran@purdue.edu

Received (in Corvallis, OR, USA) 15th July 1999, Accepted 20th August 1999

Replacing carcinogenic HMPA with NMO, a higher yielding, enviornmentally benign procedure for the vinylalumination of carbonyl compounds with [α-(ethoxycarbonyl)-vinyl]diisobutylaluminium and its β-methyl or -phenyl analogs, as well as [α-(acetyl)vinyl]diisobutylaluminium has been developed.

Vinylalumination,[1] a carbon–carbon bond forming reaction of vinylaluminium derivatives with electrophiles, provides Morita–Baylis–Hillman[2] type products without the reaction's limitations. For example, (i) the electrophiles are not limited to reactive carbonyls and imines, (ii) the reaction times are considerably shorter, and (iii) β-substitution of the vinyl moiety is readily accommodated.

Although known for over a decade, the lack of extensive utilization of this potentially useful reaction may be due to the presence of a carcinogenic material, HMPA,[3] as the complexing agent with DIBAL-H for the hydroalumination of propiolates. Several possible replacements for HMPA, such as 1,3-dimethyl-3,4,5,6-tetrahydro-2(1*H*)-pyrimidone (DMPU),[4a] 1,3-dimethylimidazolidin-2-one (DMEU or DMI),[4b] and quinuclidine *N*-oxide (QNO)[4c] have been reported in the literature. Since DMPU and DMI might undergo reduction with DIBAL-H and QNO is not economical, we studied a series of other amine oxides as complexing agents. Although mixtures of DIBAL-H and aromatic amine oxides, such as pyridine and picoline *N*-oxides, did not provide the required hydroalumination product, aliphatic trialkylamine oxides, such as trimethylamine *N*-oxide and NMO, were found to be suitable complexing agents for the hydroalumination of propargylic esters and ketones. Our study with the relatively inexpensive NMO revealed it to be an excellent HMPA alternative for vinylaluminations, improving the reaction conditions and providing superior yields of the products. We also noticed that Lewis acid catalysis[1d] and low reaction temperatures[1d] are not essential for reactions with the β-methyl and -phenyl substituted reagents.

The addition of DIBAL-H to a suspension of NMO in THF provided a clear solution. The reaction of ethyl propiolate **1a** in THF with 1.5 equiv. DIBAL-H–NMO in hexanes at 0 °C provided the [α-(ethoxycarbonyl)vinyl]diisobutylaluminium **2a**. Benzaldehyde **4** (1.2 equiv.) was added to this reagent at 0 °C and warmed to room temperature. The reaction was complete within 4 h. Hydrolysis using 1.0 *M* HCl, followed by chromatography, provided 96% yield of the product **5a** (Scheme 1). Earlier procedures employing HMPA utilized 2 equiv. of the aldehyde.[1] We observed that the hydrolysis was much more facile when compared to the reactions using HMPA.[1] The reaction provided high yields of the products with all of the aldehydes, *viz.* butyraldehyde **6**, isobutyraldehyde **8**, pivalaldehyde **10** and fluoral **12**.

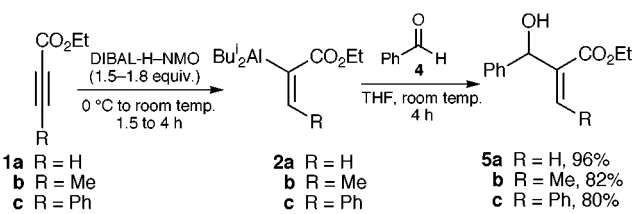

Scheme 1

The corresponding β-substituted vinylaluminium reagent, [α-(ethoxycarbonyl)-β-methylvinyl]diisobutylaluminium **2b**, reacted with **4** smoothly to provide ethyl (*Z*)-1-hydroxy-1-phenylbut-2-enoate **5b** in 82% yield (Scheme 1). The β-phenylvinyldiisobutylaluminium reagent **2c** yielded 80% of the corresponding *Z* product **5c**. The stereochemistry of the alkenes (^{1}H NMR) is exclusively *Z*.[1e] In contrast to the earlier reported procedure involving HMPA,[1d] neither of these reactions require Lewis acid catalysis or low temperatures (−78 °C).

The reaction of acetophenone **14** with **2a** was sluggish. We worked up the reaction after 2 d and obtained only 12% yield of the product **15a** along with 25% of recovered **14** and a mixture of unidentified products. Addition of 10% of a Lewis acid, such as $BF_3{\cdot}Et_2O$, provided a small amount of the product with most of the ketone recovered. Upon the addition of 1 equiv. of $BF_3{\cdot}Et_2O$, the reaction was complete within 4 h, and work up provided a 74% yield of **15a** (Table 1, entry 12). Butan-2-one **16** reacted similarly, in the presence of 1 equiv. of $BF_3{\cdot}Et_2O$, providing the product in 75% yield (Table 1, entry 15). Reagents **2b** and **2c** gave similar results with these ketones.

An activated ketone, such as 2,2,2-trifluoroacetophenone **18**, reacted similar to an aldehyde, without Lewis acid, and the product **19a** was obtained in 95% yield (Table 1, entry 18). We then examined the reaction of **2a** with ethyl pyruvate **20**, and obtained the corresponding product alcohol in 95% yield (Table 1, entry 19).

The procedure was then extended to α-acetylvinyldiisobutylaluminium **3a**, prepared *via* the hydroalumination of but-3-yn-2-one with DIBAL-H–NMO complex (Scheme 2). A 23–31% yield of products from benzaldehyde and butyraldehyde for a reaction of **3a** prepared with DIBAL-H–HMPA was reported by Tsuda.[1a] Replacement of HMPA with NMO provided a 36% yield of **22a**. However, utilization of 2 equiv. of the reagent improved the yield to 95% (Scheme 2). We used these modified conditions for the reaction of the same series of aldehydes (**4**, **6**, **8**, **10**, **12**) with **3a** and the products were obtained in 72–95% yield. However, ketones did not react with **3a**. All of the results are summarized in Table 1.

In conclusion, we have described a significantly improved procedure for the vinylalumination of a variety of carbonyl compounds with [α-(ethoxycarbonyl)vinyl]- and (α-acetylvinyl)diisobutylaluminium. Replacement of carcinogenic HMPA with readily available NMO in the hydroalumination step makes this procedure environmentally benign. The work up is simpler and the yields of the products are considerably higher in most cases. We have also shown that Lewis acid catalysis and low reaction temperatures are not essential for reactions with

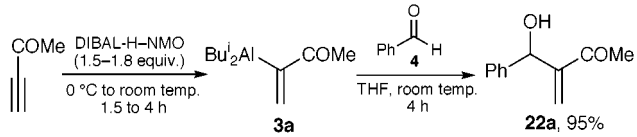

Scheme 2

Table 1 Vinylalumination of aldehydes and ketones[a]

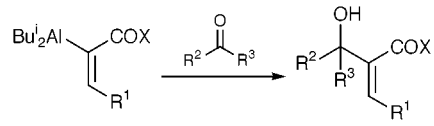

	Reagent			R^2COR^3			Product	
Entry	No.	R^1	X	No.	R^2	R^3	No.	Yield[b] (%)
1	**2a**	H	OEt	**4**	Ph	H	**5a**	96 (83)[a]
2	**2b**	Me	OEt	**4**	Ph	H	**5b**	82 (58)[d]
3	**2c**	Ph	OEt	**4**	Ph	H	**5c**	80 (61)[d]
4	**2a**	H	OEt	**6**	Pr	H	**7a**	90
5	**2b**	Me	OEt	**6**	Pr	H	**7b**	90
6	**2c**	Ph	OEt	**6**	Pr	H	**7c**	75
7	**2a**	H	OEt	**8**	Pr^i	H	**9a**	88
8	**2a**	H	OEt	**10**	Bu^t	H	**11a**	72
9	**2a**	H	OEt	**12**	CF_3	H	**13a**	80
10	**2b**	Me	OEt	**12**	CF_3	H	**13b**	70
11	**2c**	Ph	OEt	**12**	CF_3	H	**13c**	75
12	**2a**	H	OEt	**14**[e]	Ph	Me	**15a**	74
13	**2b**	Me	OEt	**14**[e]	Ph	Me	**15b**	72
14	**2c**	Ph	OEt	**14**[e]	Ph	Me	**15c**	70
15	**2a**	H	OEt	**16**[e]	Et	Me	**17a**	75
16	**2b**	Me	OEt	**16**[e]	Et	Me	**17b**	80
17	**2c**	Ph	OEt	**16**[e]	Et	Me	**17c**	70
18	**2a**	H	OEt	**18**	Ph	CF_3	**19a**	95 (70)[f]
19	**2a**	H	OEt	**20**	Me	CO_2Et	**21a**	95 (65)[g]
20	**3a**	H	Me	**4**[h]	Ph	H	**22a**	95
21	**3a**	H	Me	**6**[h]	Pr	H	**23a**	72
22	**3a**	H	Me	**8**[h]	Pr^i	H	**24a**	80
23	**3a**	H	Me	**10**[h]	Bu^t	H	**25a**	80
24	**3a**	H	Me	**12**[h]	CF_3	H	**26a**	84

[a] The reactions were carried out in THF at room temperature with 1.2 equiv. of the carbonylcompound. [b] All of the yields are of isolated, purified products. Values in parenthesis are from a reaction with the reagent made using DIBAL-H–HMPA. [c] Ref. 1(*a*). [d] Ref. 1(*d*). [e] 1 equiv. of BF_3•Et_2O was added. [f] Ref. 1(*e*). [g] Ref. 1(*f*). [h] 2 equiv. of reagent was essential for complete reaction.

the β-methyl and -phenyl substituted reagents. Further explorations and a study of the mechansim of this reaction are in progress.

Financial assistance from the Purdue Borane Research Fund is gratefully acknowledged.

Notes and references

1 (*a*) T. Tsuda, T. Yoshida and T. Saegusa, *J. Org. Chem.*, 1988, **53**, 1037; (*b*) Y. Génisson, C. Massardier, I. Gautier-Luneau and A. E. Greene, *J. Chem. Soc., Perkin Trans. 1*, 1996, 2869; (*c*) L. H. Zu and E. P. Kundig, *Helv. Chim. Acta*, 1994, **77**, 1480; (*d*) G. Li, H. X. Wei and S. Willis, *Tetrahedron Lett.*, 1998, **39**, 4607; (*e*) P. V. Ramachandran, M. V. R. Reddy, M. T. Rudd and J. R. de Alaniz, *Tetrahedron Lett.*, 1998, **39**, 8791; (*f*) P. V. Ramachandran, M. V. R. Reddy and M. T. Rudd, *Tetrahedron Lett.*, 1999, **40**, 627.

2 For the most recent review of the Morita–Baylis–Hillman reaction, see: E. Ciganek, *Org. React.*, 1997, **51**, 201.

3 J. F. Schmutz, *Chem. Eng. News*, 1978, **56 (3)**, 39; H. Spencer, *Chem. Ind.*, 1979, 728.

4 (*a*) T. Mukhopadhyay and D. Seebach, *Helv. Chim. Acta*, 1982, **65**, 385; (*b*) E. Juaristi, P. Murer and D. Seebach, *Synthesis*, 1993, 1243; (*c*) I. A. O'Neil, J. Y. Q. Lai and D. Wynn, *Chem. Commun.*, 1999, 56.

Communication 9/05836B

ChemComm

Isolation and characterization of the tetralithium salt of [5]radialene tetraanion stabilized by silyl groups

Tsukasa Matsuo, Hidetoshi Fure and Akira Sekiguchi*

Department of Chemistry, University of Tsukuba, Tsukuba, Ibaraki, 305–8571, Japan.
E-mail: sekiguch@staff.chem.tsukuba.ac.jp

Received (in Cambridge, UK) 2nd August 1999, Accepted 31st August 1999

Persilyl-substituted [5]radialene 3 was reacted with lithium metal in THF to yield dark red crystals of the tetralithium salt of tetraanion 4 with a novel ten-center, fourteen π-electron system stabilized by silyl groups.

Polyanions with extended π-electron systems have attracted considerable interest owing to their unique structures and electronic properties.[1,2] However, polyanions of polycyclic hydrocarbons have only rarely been observed and they are one of the most attractive synthetic targets. Corannulene **1** having a

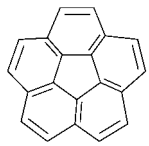

1

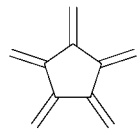

2

twenty π-electron system has a doubly-degenerate, low-lying LUMO that can accept up to four electrons to form corannulene tetraanion.[3] Scott *et al.* reported on the interesting dimer structure of the tetralithium salt of corannulene tetraanion and its derivatives in solution.[4] [5]Radialene **2** with a cross-conjugated ten π-electron system possesses a central unit of corannulene. However, to the best of our knowledge, there have been no studies on the anion species of [5]radialene derivatives. Herein, we report the first successful isolation, characterization and molecular structure of the tetralithium salt of the [5]radialene tetraanion derivative with a novel ten-center, fourteen π-electron system stabilized by silyl groups.

Reduction of **3**[5] with excess lithium metal in dry, oxygen free THF at room temperature led to the formation of a dark red solution of the tetraanion of **3** (Scheme 1). Crystallization from hexane afforded air- and moisture-sensitive dark red crystals of the tetralithium salt **4**.†

The molecular structure of **4** was determined by X-ray diffraction, as shown in Fig. 1.‡ The tetralithium salt (**4**) is monomeric and forms contact ion pairs (CIPs) in the crystals. One THF molecule is coordinated to each lithium ion. All four lithium ions are bonded to four quaternary carbon atoms of the [5]radialene π-skeleton as well as to the oxygen atoms of THF. Li1 and Li2 are located above and below the adjacent seven-membered rings (denoted **A** for the C1–C5–C10–Si7–CH_2-Si8-C6 ring and **B** for the C1–C2–C7–Si2–CH_2–Si1–C6 ring, respectively), whereas Li3 is located below the isolated seven-membered ring (denoted **C** for the C4–C3–C8–Si4–CH_2-Si5-C9 ring). The remaining Li4 is situated above one of the two

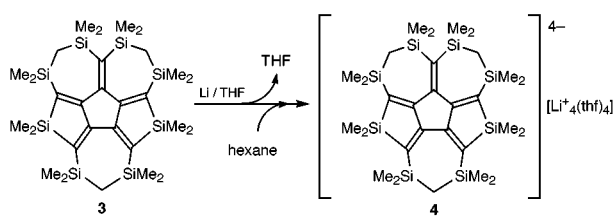

3 4

Scheme 1

silacyclopentadiene rings (denoted **D** for the C2–C3–C8–Si3–C7 ring and **E** for the C5–C4–C9–Si6–C10 ring, respectively). The distances between lithium and carbon atoms range from 2.10(1) to 2.44(2) Å (av. 2.23 Å). The two seven-membered rings **A** and **B** have highly twisted conformations about the C1–C6 bond, whereas the other seven-membered ring **C** and the two five-membered rings **D** and **E** are almost coplanar.

A comparison of the structural parameters of neutral molecule **3**[5] and tetraanion **4** is quite interesting. The ten carbon atoms (C1–C10) which constitute the π-electron system of the skeleton of **4** are almost coplanar as a consequence of the delocalization of the negative charge. The C1–C6 distance in **4** [1.523(8) Å] is considerably elongated by 0.148 Å relative to that of **3** [1.375(4) Å]. The C3–C8 and C4–C9 distances in **4** are also elongated by 0.143 and 0.066 Å, compared with those of **3** [1.363(4) Å]. The C2-C7 and C5-C10 distances in **4** are also stretched by 0.059 and 0.044 Å, relative to those of **3** [1.362(4) and 1.363(4) Å]. By contrast, the C3–C4 distance in **4** [1.377(8) Å] is remarkably shortened by 0.106 Å with respect to that of **3** [1.483(4) Å]. The C1–C2 and C1–C5 distances in **4** are shortened by 0.056 and 0.044 Å compared with those in **3** [1.506(4) and 1.485(4) Å]. These structural features are reflected by the LUMO and next LUMO of **3** (Fig. 2).[6] That is, in the LUMO of **3**, the exocyclic bonds are all antibonding, whereas the endocyclic bonds are all bonding. In the next LUMO of **3**, the exocyclic bonds, and C2–C3 and C4–C5 bonds are antibonding, while the C1–C2, C1–C5 and C3–C4 bonds are bonding.

The central five-membered ring (C1–C2–C3–C4–C5) of **4** has an almost planar structure, as determined by the sum of the bond angles (539.9°). However, this five-membered ring does not form an equilateral pentagon, as observed in the dilithium salt of hexasilylfulvene dianion with a six-center, eight π-

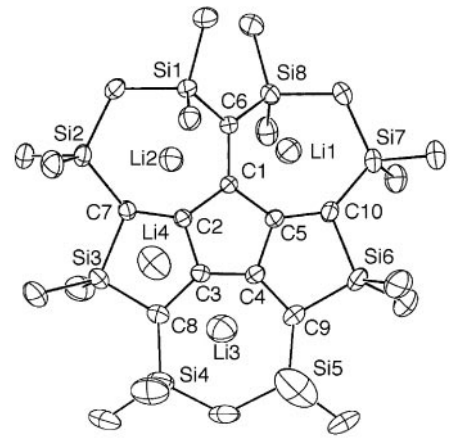

Fig. 1 Structure of **4** (THF and hydrogen atoms are omitted for the clarity). Selected bond distances (Å) are: C1–C2 1.450(7), C1–C5 1.441(8), C1–C6 1.523(8), C2–C3 1.484(8), C2–C7 1.421(8), C3–C4 1.377(8), C3–C8 1.506(8), C4–C5 1.526(8), C4–C9 1.429(8), C5–C10 1.407(8), C6–Si1 1.824(6), C6–Si8 1.815(6), C7–Si2 1.830(6), C7–Si3 1.898(6), C8–Si3 1.823(7), C8–Si4 1.798(7), C9–Si5 1.812(7), C9–Si6 1.829(7), C10–Si6 1.876(6), C10–Si7 1.841(6).

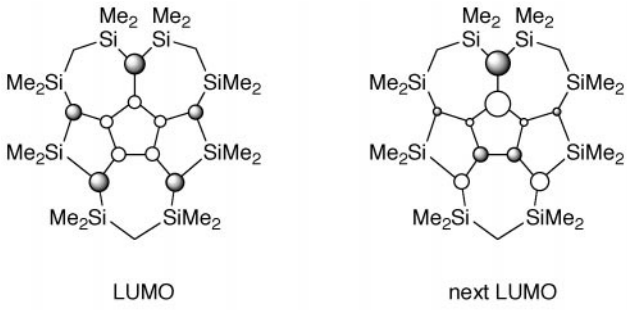

Fig. 2 Schematic representation of LUMO and next LUMO of **3** calculated by PM3.

electron system,[7] and the tetralithium salt of octasilyltrimethylenecyclopentene tetraanion with an eight-center, twelve π-electron system.[2] This suggests that the [5]radialene tetraanion **4** has no aromatic character resulting from the cyclopentadienide ion. The bond lengths of the Si–C (quaternary carbons) bonds of **4** (av. 1.835 Å) are shorter than those of **3** (av. 1.873 Å) due to delocalization of the negative charge onto the silicon centers by pπ–σ* conjugation.

The NMR data of **4** in toluene-d_8 indicate formation of highly symmetric CIPs with C_2 groups symmetry, the C1–C6 bond being a two-fold axis. The four methyls of two $SiMe_2$ groups and the two hydrogen atoms of CH_2 for rings **A** and **B** are magnetically nonequivalent, due to the fixed five- and seven-membered rings. On the other hand, the two hydrogen atoms of CH_2 for ring **C** are magnetically equivalent. Thus, the ^{1}H NMR spectrum of **4** in toluene-d_8 reveals the presence of eight signals for the methyl groups, two doublets for the ring **A** and **B** methylene groups with a geminal coupling constant of 13.2 Hz, and one singlet for the ring **C** methylene group. In the ^{29}Si NMR spectrum, four signals are observed at δ −20.1, −16.7, −15.0, and 18.5, which are shifted to higher field in comparison to those of **3** (δ −12.0, −10.0, −8.4 and 30.9). The ^{13}C NMR spectrum shows six signals for quaternary carbon atoms at δ 15.1, 40.8, 81.0, 93.1, 131.8 and 178.9. The signal appearing at δ 15.1 is assignable to the C6 carbon atom, which is considerably up-field shifted relative to that of **3** (δ 164.7) by $\Delta\delta$ −149.6 ppm. The other exocyclic carbons (C7, C8, C9 and C10) are also shifted to higher field by the four electron reduction (δ 40.8 and 81.0 for **4**; δ 163.2 and 172.0 for **3**). Apparently, the negative charge is largely delocalized over the five exocyclic carbon atoms in the π-skeleton of **4** and is stabilized by the eight silyl groups. Interestingly, the ^{6}Li NMR spectrum of **4** displays only one signal at δ −0.18. This indicates that the four Li^+ ions of **4** are not fixed to the π-skeleton, but are fluxional; the four Li^+ ions are migrating over the π-skeleton of [5]radialene on the NMR time scale.[8]

This work was supported by a Grant-in-Aid for Scientific Research (Nos. 09239101, 10304051, 1113321, 11166209) from the Ministry of Education, Science and Culture of Japan, and TARA (Tsukuba Advanced Research Alliance) fund.

Notes and references

† The crystals of **3** (21 mg, 0.033 mmol) and lithium metal (30 mg, 4.3 mmol) were placed in a reaction tube with a magnetic stirrer. After degassing the tube, dry oxygen-free THF (0.8 ml) was introduced by vacuum transfer and stirred at room temperature to give a dark red solution of **4** within 1 h. After the solvent was removed *in vacuo*, degassed hexane was introduced by vacuum transfer. After the lithium metal had been removed from the tube, the solution was cooled to afford dark red crystals of **4** quantitatively; δ_H(300 MHz, C_7D_8) −0.15 (d, *J* 13.2, 2H, CH_2), −0.11 (s, 6H, CH_3), 0.14 (s, 2H, CH_2), 0.28 (s, 6H, CH_3), 0.30 (s, 6H, CH_3), 0.33 (s, 6H, CH_3), 0.35 (s, 6H, CH_3), 0.36 (s, 6H, CH_3), 0.49 (s, 6H, CH_3), 0.54 (d, *J* 13.2, 2H, CH_2), 0.62 (s, 6H, CH_3), 1.35 (br s, 16H, THF), 3.52 (br s, 16H, THF); δ_C(75.5 MHz, C_7D_8) 2.8 (CH_3), 5.6 (CH_3), 6.0 (CH_3), 6.6 (CH_3), 7.0 (CH_3), 7.3 (CH_3), 7.5 (CH_3), 7.7 (CH_3), 15.1 (C), 15.9 (CH_2), 16.5 (CH_2), 25.4 (THF), 40.8 (C), 66.6 (THF), 81.0 (C), 93.1 (C), 131.8 (C), 178.9 (C); δ_{Si}(59.6 MHz, C_7D_8) −20.1, −16.7, −15.0, 18.5; δ_{Li}(44.2 MHz, C_7D_8) −0.18.

‡ *Crystal data* for **4**: $C_{45}H_{86}Li_4O_4Si_8$, *M* = 943.63, monoclinic, *a* = 48.328(3), *b* = 13.470(1), *c* = 21.676(1) Å, β 115.003(3)°, *V* = 12788(1) Å^3, *T* = 180 K, space group *C*2/*c*, *Z* = 8, ρ_{calc} = 0.981 g cm^{-3}. Diffraction data were collected on a MacScience DIP2030K Image Plate Diffractometer employing graphite-monochromatized Mo–Kα radiation (λ = 0.71070 Å). The final *R* factor was 0.0775 (R_w = 0.2358) for 6138 reflections with $I > 3\sigma(I)$. Single crystals of **4** were obtained by crystallization from hexane, mounted in a glass capillary tube and transferred to the cold gas stream of the diffractometer. The structure was solved by the direct method and refined by the full-matrix least-squares method using SHELXL-97 program. Some of the carbon atoms of the THF molecules have elongated thermal ellipsoids due to disorder. CCDC 182/1394. See http://www.rsc.org/suppdata/cc/1999/1981/ for crystallographic data in .cif format.

1 For reviews, see: K. Müllen, *Chem. Rev.*, 1984, **84**, 603; M. Rabinovitz, *Top. Curr. Chem.*, 1988, **14**, 99; A.-M. Sapse and P. v. R. Schleyer, *Lithium Chemistry: A Theoretical and Experimental Overview*, Wiley, New York, 1995.

2 For recent papers, see: H. Bock, K. Gharagozloo-Hubmann, C. Näther, N. Nagel and Z. Havlas, *Angew. Chem., Int. Ed. Engl.*, 1996, **35**, 631; A. Sekiguchi, T. Matsuo and C. Kabuto, *Angew. Chem., Int. Ed. Engl.*, 1997, **36**, 2462; A. Sekiguchi, T. Matsuo and R. Akaba, *Bull. Chem. Soc. Jpn.*, 1998, **71**, 41; H. Bock, Z. Havlas, D. Hess and C. Näther, *Angew. Chem., Int. Ed.*, 1998, **37**, 502.

3 A. Ayalon, M. Rabinovitz, P.-C. Cheng and L. T. Scott, *Angew. Chem., Int. Ed. Engl.*, 1992, **31**, 1636.

4 A. Ayalon, A. Sygula, P.-C. Cheng, M. Rabinovitz, P. W. Rabideau and L. T. Scott, *Science*, 1994, **265**, 1065; M. Baumgarten, L. Gherghel, M. Wagner, A. Weitz, M. Rabinovitz, P.-C. Cheng and L. T. Scott, *J. Am. Chem. Soc.*, 1995, **117**, 6254.

5 Persilylated [5]radialene **3** was obtained by the intramolecular reaction of hexadecamethyl-3,6,8,11,14,16,19,21–octasilacycloicosa-1,4,9,12,17-pentayne with an excess of [$Mn(CO)_3(C_5H_4Me)$] by irradiation (λ > 300 nm) in refluxing THF, see: T. Matsuo, H. Fure and A. Sekiguchi, *Chem. Lett.*, 1998, 1101.

6 PM3 calculation was performed with geometry optimization. The geometry of **3** by X-ray diffraction was successfully reproduced by PM3 calculation.

7 T. Matsuo, A. Sekiguchi, M. Ichinohe, K. Ebata and H. Sakurai, *Organometallics*, 1998, **17**, 3143; T. Matsuo, A. Sekiguchi and H. Sakurai, *Bull. Chem. Soc. Jpn.*, 1999, **72**, 1115.

8 As the temperature was lowered, the ^{6}Li NMR signal broadened and eventually yielded two very sharp signals at δ −0.55 and 0.08 with the same intensity at 187 K. This can be explained by assuming that the two Li^+ ions (Li1 and Li2) are fixed to the seven-membered rings (**A** and **B**), whereas the other two Li^+ ions (Li3 and Li4) are still fluxional over two five-membered rings (**D** and **E**) and one seven-membered ring (**C**). Since the latter three rings are almost coplanar, the fluxional behavior of the two Li^+ ions (Li3 and Li4) is not hindered even at 187 K. The possibility of producing a solvent-separated ion pair (SSIP) in toluene-d_8 is unlikely. The ^{6}Li NMR in THF-d_8 gave broad and complex signals.

Communication 9/06253J

Enantioselective electrocatalytic oxidation of racemic amines using a chiral 1-azaspiro[5.5]undecane *N*-oxyl radical

Yoshitomo Kashiwagi,*[a] Futoshi Kurashima,[a] Chikara Kikuchi,[a] Jun-ichi Anzai,[a] Tetsuo Osa[a] and James M. Bobbitt[b]

[a] *Graduate School of Pharmaceutical Sciences, Tohoku University, Aramaki, Aoba-ku, Sendai 980-8578, Japan. E-mail: kashi@mail.pharm.tohoku.ac.jp*

[b] *Department of Chemistry, University of Connecticut, Storrs, Connecticut 06269-3060, USA*

Received (in Cambridge, UK) 21st July 1999, Accepted 23rd August 1999

A preparative electrocatalytic oxidation of racemic amines, which contain a chiral centre α to the amino group, on (6*S*, 7*R*, 10*R*)-4-acetylamino-2,2,7-trimethyl-10-isopropyl-1-azaspiro[5.5]undecane *N*-oxyl yielded mixtures of carbonyl compounds (54.3–66.1%) and amines (33.9–45.7%) after 5 h of electrolysis, in which the current efficiency, turnover number, enantiopurity of the remaining (*R*)-isomers and *S* values were 90.7–94.8%, 21.7–26.5, 62–78% and 4.7–5.8, respectively.

Optically active amines are some of the most important chiral intermediates in organic synthesis. They have been prepared by many methods, including optical resolution of their racemates, usually by preferential crystallization.[1] Several enantioselective chemical oxidations for optical resolution of the racemates using chiral aminoxyl radicals have been reported, but these works were mainly carried out with secondary alcohols as the racemate.[2–4] On the other hand, 2,2,6,6-tetramethylpiperidin-1-yloxyl is known to be an effective redox mediator for the electrooxidation of amines to nitriles and carbonyl compounds.[5–7] Here we report the first efficient, enantioselective electrocatalytic oxidation of a number of racemic amines using (6*S*, 7*R*, 10*R*)-4-acetylamino-2,2,7-trimethyl-10-isopropyl-1-azaspiro[5.5]undecane *N*-oxyl **1**[3] as a chiral 1-azaspiro-[5.5]undecane *N*-oxyl radical.

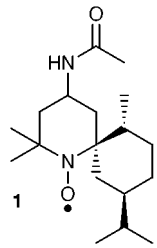

The cyclic voltammetry† of **1** was carried out in a MeCN solution containing 0.1 M $NaClO_4$ as supporting electrolyte. Fig. 1 shows the cyclic voltammogram (CV) of **1**, in which a reversible redox couple was observed. This redox couple corresponds to one-electron oxidation of the oxoammonium ion. Similar electrochemical behavior has been reported by Bobbitt *et al.*[3] The redox potential and peak split between the anodic and cathodic peak potentials were +0.62 V (*vs.* Ag/AgCl) and 70 mV, respectively. These values are comparable to those for TEMPO derivatives.[8] In addition, the diffusion coefficient of **1** was estimated to be 1.3×10^{-5} cm^2 s^{-1} based on a plot of the peak current *vs.* the square root of scan rate in the cyclic voltammetry.[9] These observations suggest a possible use of **1** as catalyst in the electrocatalytic oxidation of amines.

The enantioselective oxidation of a chiral amine on **1** was investigated using (*R*)-(+)- and (*S*)-(−)-1-phenylethylamine [(*R*)-PEA and (*S*)-PEA] as substrates. The CVs of 0.1 M (*R*)-PEA and (*S*)-PEA in the presence of 0.8 M 2,6-lutidine as deprotonating agent are shown in Fig. 1. The anodic peak current for (*S*)-PEA was significantly enhanced in comparison with the blank voltammogram (**1** itself) and a small cathodic peak was observed on the reverse scan, showing that (*S*)-PEA was efficiently oxidized electrocatalytically. In contrast to the CV for (*S*)-PEA, the anodic peak current for (*R*)-PEA increased only slightly. These results clearly show that the electrocatalytic oxidation of (*S*)-PEA on **1** occurred in preference to that of (*R*)-PEA.

Preparative potential-controlled electrolysis was performed on a graphite felt electrode (Nippon Kynol Inc., $5 \times 5 \times 5$ mm) in MeCN–H_2O (4:1) solution, using an 'H type divided cell separated by a cationic exchange membrane (Nafion 117). The anolyte contained 0.05 mmol of **1**, 1 mmol of substrate, 0.5 mmol of tetralin as a chromatographic standard, 4 mmol of 2,6-lutidine and 0.5 mmol of $NaClO_4$ in a total volume of 5 ml. The catholyte was 5 ml of MeCN–H_2O (4:1) solution containing 0.5 mmol of $NaClO_4$. The electrolysis was carried out at +0.8 V *vs.* Ag/AgCl under an argon atmosphere. During electrolysis, aliquots of anolyte were analyzed occasionally by HPLC.‡ The consumption of racemic 1-phenylethylamine and formation of acetophenone are plotted against electrolysis time in Fig. 2. 1-Phenylethylamine was probably oxidized to the corresponding imine, the expected oxidation intermediate, which can be easily hydrolyzed to acetophenone; imine was not actually detected. After 5 h of electrolysis, the (*R*)- and (*S*)-forms of 1-phenylethylamine were oxidized to acetophenone in 45.9 and 92.4% yield, respectively. The current efficiency and turnover number (given by ratio of mole of product ×2/mol of **1**) were 91.5% and 26.2, respectively, at 5 h of electrolysis. The remaining (*R*)-PEA and (*S*)-PEA equalled 56.1 and 7.6%, respectively. Thus, the ee of the unreacted amine was 78%. The efficiency of the resolution is characterized by the selectivity factor, *S* (= k_s/k_R).[9] The *S* value of this reaction was 5.3.

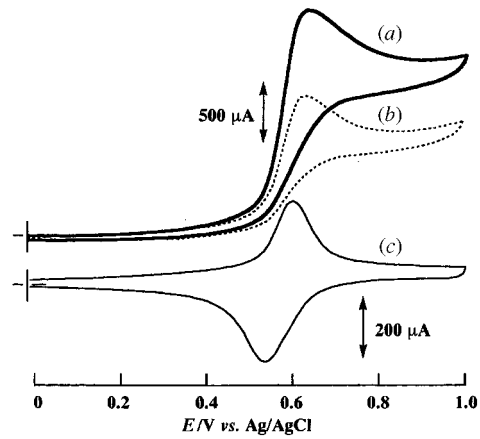

Fig. 1 Cyclic voltammograms of 0.01 M **1** in 0.1 M $NaClO_4$/MeCN at the scan rate of 50 mV s^{-1}: (*a*) in the presence of 0.1 M (*S*)-PEA and 0.2 M 2,6-lutidine, (*b*) in the presence of 0.1 M (*R*)-PEA and 0.2 M 2,6-lutidine, and (*c*) blank.

Table 1 Electrocatalytic oxidation of racemic secondary amines by **1**

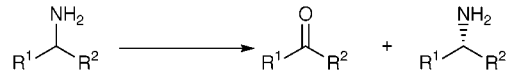

R^1	R^2	Amine	Charge/C	Efficiency[a] (%)	Ee (%)	Conversion (%)	*S*	TON[b]
Ph	Me	R	137.9	91.5	78	65.4	5.3	26.2
p-Tol	Me	R	134.6	94.8	75	66.1	4.7	26.5
1-Naphthyl	Me	R	115.5	90.7	62	54.3	5.8	21.7
2-Naphthyl	Me	R	124.8	92.3	66	59.7	4.9	23.9
$PhMeCHCH_2$	H	—	192.4	96.1	0	95.8	0	38.3

[a] Current efficiency. [b] Turnover number.

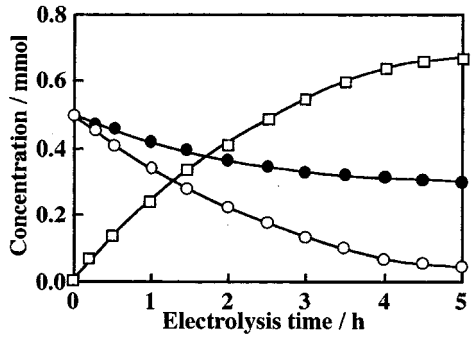

Fig. 2 Macroelectrolysis of racemic PEA by **1** in the presence of 2,6-lutidine: (●) (*R*)-PEA, (○) (*S*)-PEA and (□) acetophenone.

The results from the enantioselective oxidation reactions of a variety of racemic amines are shown in Table 1. In the electrocatalytic oxidation of the racemic amines such as 1-(1-naphthyl)ethylamine, 1-(2-naphthyl)ethylamine and 1-(*p*-tolyl)ethylamine, which contain a chiral centre α to the amino group, the (*S*)-isomers were oxidized in preference to the (*R*)-isomers. After 5 h of electrolysis, the racemic amines were oxidized to the corresponding ketones in 90.7–94.8% current efficiency, 54.3–66.1% yield and 100% selectivity. The turnover numbers based on **1** are larger than 21. The enantiopurity of the remaining (*R*)-isomers and *S* values were 62–78% and 4.7–5.8, respectively. On the contrary, the electrooxidation of 2-phenylpropylamine, which has a chiral centre β to the amino group, was not enantioselective. After 5 h of electrolysis, it was oxidized to the corresponding aldehyde in 96.1% current efficiency, 95.8% yield and 100% selectivity. The turnover numbers based on **1** is 38.3. These facts mean that an α-hydrogen in a chiral centre adjacent to the amino group is necessary to attain an enantioselective oxidation in the present system. The enantioselective oxidation with **1** is applicable to the optical resolution of racemic secondary amines.

This work was supported in part by Grants-in-Aid for Scientific Research on Priority Areas (No. 11119208: 'Innovative Synthetic Reactions') and for Encouragement Research (No. 10771266) from the Ministry of Education, Science, Sports and Culture of Japan.

Notes and references

† A glassy carbon disk electrode (3 mm diameter) and a platinum wire were employed as working electrode and counter electrode, respectively. The anode potentials were referred to Ag/AgCl (saturated AgCl and Me_2EtNCl in MeCN). Cyclic potential sweeps were generated by a Hokuto Denko Model HABF-501 potentiostat/galvanostat. Cyclic voltammograms were recorded on a Graphtec Model WX1200 X-Y recorder. All electrochemical measurements were carried out at room temperature (*ca.* 20 °C).

‡ The HPLC analysis was carried out using Daisel CHIRALCELL-OD column (46 mm $\phi \times 250$ mm). The column temperature was kept constant at 40 °C. The analytes were eluted by Pr^iOH–*n*-hexane (2:33) at 0.7 ml min^{-1} flow rate, and detected by UV absorption at 254 nm.

1 H. Nohira, M. Kai, M. Nohira, J. Nishikawa, T. Hoshiko and K. Saigo, *Chem. Lett.*, 1981, 951.
2 C. Berti and M. J. Perkins, *Angew. Chem., Int. Ed. Engl.*, 1979, **18**, 864.
3 Z. Ma, G. Huang and J. M. Bobbitt, *J. Org. Chem.*, 1993, **58**, 4837.
4 S. D. Rychnovsky, T. L. McLernon and H. Rajapakse, *J. Org. Chem.*, 1996, **61**, 1194.
5 M. F. Semmelhack and C. R. Schmid, *J. Am. Chem. Soc.*,1983, **105**, 6732.
6 F. MacCorquodale, J. A. Crayston, J. C. Walton and D. J. Worsfold, *Tetrahedron Lett.*, 1990, **31**, 771.
7 Y. Kashiwagi, F. Kurashima, C. Kikuchi, J. Anzai, T. Osa and J. M. Bobbitt, *J. Chin. Chem. Soc.*, 1998, **45**, 135.
8 J. M. Bobbitt and M. C. L. Flores, *Heterocycles*, 1988, **27**, 509.
9 A. J. Bard and L. R. Faulkner, *Electrochemical Methods*, Wiley, New York, 1980, p. 215.
10 $S = \ln[(1 - C)(1 - ee)]/\ln[(1 - C)(1 + ee)]$, where ee is the fractional enantiomeric excess and *C* is the conversion. For a discussion of kinetic resolutions see: H. B. Kagan and J. C. Fiaund, *Top. Stereochem.*, 1988, **18**, 249.

Communication 9/05894J

Integrated synthesis of conduritols A–F using a single chiral building block

Masatoshi Honzumi, Kou Hiroya, Takahiko Taniguchi and Kunio Ogasawara*

Pharmaceutical Institute, Tohoku University, Aobayama, Sendai 980-8578, Japan.
E-mail: konol@mail.cc.tohoku.ac.jp

Received (in Cambridge, UK) 7th July 1999, Accepted 31st August 1999

Six possible diastereomers of conduritols have been synthesized diastereoselectively in an integrated manner starting from a single chiral precursor, which served as a synthetic equivalent of chiral *cis*-1,4-dihydroxycyclohexa-2,5-diene.

Although only two conduritols, A **1** and F **6**, occur in Nature, four other possible diastereomers, conduritols B **2**, C **3**, D **4** and E **5**, are known[1]. Since they are useful for the preparation of

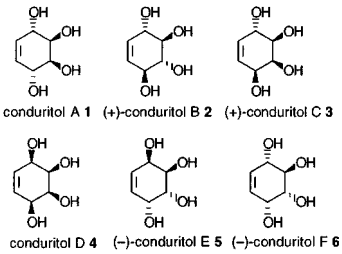

physiologically active cyclitols and their derivatives, a considerable number of syntheses have been reported to date.[2] The majority of syntheses, however, are limited to preparation of particular members of conduritols and there has been no precedent which is capable of producing all six conduritols diastereoselectively from a single precursor in an integrated manner. As we have developed an efficient preparation[3] of the tricyclic monoacetate **7** serving as a synthetic equivalent of chiral *cis*-1,4-dihydroxycyclohexa-2,5-diene in both enantiomeric forms by lipase-mediated asymmetric desymmetrization of a *meso* precursor, we examined diastereocontrolled preparation of all six conduritols on the basis of inherent steric and chemical functionalities comprised in this chiral building block.[4] We report herein the first integrated synthesis of conduritols A–F **1**–**6** starting from the single chiral compound (+)-**7** using a methoxymethyl (MOM) ether as the common protecting group.

The acetate[3] **7** was first transformed into the bromo ether **8** in three steps[2e] to discriminate one of two olefin functionalities and to block the secondary hydroxy functionality in the molecule. On acid-catalyzed removal of the MOM protecting group, followed by the Mitsunobu reaction,[5], **8** afforded the *exo*-benzoate **9**, mp 135–136 °C, $[\alpha]_D^{28}$ −260.1 (*c* 1.02, $CHCl_3$), whose dihydroxylation occurred from the convex face to furnish the *exo-cis*-diol **10**, $[\alpha]_D^{30}$ −66.6 (*c* 0.96, $CHCl_3$), diastereoselectively. On the other hand, **8** was transformed into the single *trans*-diol **12**, $[\alpha]_D^{26}$ −60.5 (*c* 1.18, $CHCl_3$), through the *exo*-epoxide **11**, mp 93–94 °C, $[\alpha]_D^{28}$ +0.9 (*c* 1.02, $CHCl_3$), on sequential MOM deprotection, benzoylation, convex face selective epoxidation and acid treatments. In the latter conversion, the epoxide **11** was cleaved diastereo- and regioselectively by the participation[6] of the benzoate functionality in the presence of a Lewis acid to give a mixture of two regioisomeric benzoates, which, however, converged on the single isomer **12** on stirring with TsOH in CH_2Cl_2 (Scheme 1).

Utilizing the *cis*-diol **10**, (+)-conduritol C **3** was first prepared. On alkaline methanolysis followed by MOM protection, **10** gave the tri-MOM ether **13**, $[\alpha]_D^{29}$ −101.4 (*c* 1.05, $CHCl_3$), whose bromo ether linkage was reductively cleaved with zinc in the presence of acetic acid[2e] to regenerate the olefin and the hydroxy functionalities to give rise to the tricyclic alcohol **14**, $[\alpha]_D^{31}$ +14.4 (*c* 1.02, $CHCl_3$). Thermolysis of **14** was carried out at this stage in refluxing Ph_2O in the presence of $NaHCO_3$[7] to give the cyclohexenol **15**, $[\alpha]_D^{28}$ +123.5 (*c* 0.54, $CHCl_3$), by retro-Diels–Alder reaction. When the carbonate was absent, the yield of **15** was diminished considerably. Stirring **15** with saturated methanolic HCl at room temperature[8] induced smooth MOM deprotection to give (+)-conduritol C **3**, mp 129–130 °C, $[\alpha]_D^{30}$ +209.1 (*c* 0.62, H_2O) [lit.,[2f] mp 128–129 °C, $[\alpha]_D^{20}$ +215 (*c* 2.01, H_2O)]. As shown below, under these acid-catalyzed conditions, the MOM protecting group of the other conduritols was neatly removed to afford the corresponding conduritols after removal of low volatiles under reduced pressure followed by washing the residue with an appropriate solvent (Scheme 2).

The *trans*-diol **12** was served as the precursor for the synthesis of three conduritols, (+)-B **2**, (−)-E **5** and (−)-F **6**. Thus, **12** was first transformed into the tri-MOM ether **16**, $[\alpha]_D^{30}$ −78.0 (*c* 1.15, $CHCl_3$), by sequential debenzoylation and MOM protection. Reductive cleavage of **16**, followed by thermolysis of the resulting **17**, $[\alpha]_D^{31}$ −80.8 (*c* 0.94, $CHCl_3$), afforded the cyclohexenol **18**, $[\alpha]_D^{27}$ +55.5 (*c* 0.79, $CHCl_3$), which gave (−)-conduritol F **6**, mp 129–130 °C, $[\alpha]_D^{28}$ −70.2 (*c* 0.15, MeOH) [lit.[2g] for (+)-enantiomer: mp 128–130 °C, $[\alpha]_D^{23}$ +75.1 (*c* 0.33, MeOH)], on MOM deprotection. The alcohol **18**, on the other hand, was first treated with 4-nitrobenzoic acid[9] under Mitsunobu conditions[5] to give the epimeric alcohol **19**, $[\alpha]_D^{30}$ −106.6 (*c* 1.07, $CHCl_3$), after alkaline methanolysis, which on MOM-deprotection, afforded (−)-conduritol E **5**, mp 191–192 °C, $[\alpha]_D^{29}$ −330.3 (*c* 0.18, H_2O) [lit.[2g] for (+)-enantiomer: mp 192–194 °C, $[\alpha]_D^{30}$ +327 (*c* 0.22, H_2O)].

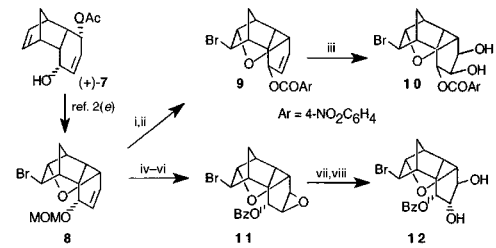

Scheme 1 *Reagents and conditions*: i, conc. HCl–MeOH–THF (91%); ii, 4-$NO_2C_6H_4CO_2H$, DIAD, PPh_3, THF (86%); iii, OsO_4 (cat.), NMO, aq. THF (97%); iv, conc. HCl–MeOH–THF (91%);. v, BzCl, pyridine, DMAP (cat.), CH_2Cl_2 (99%); vi, MCPBA, CH_2Cl_2 (91%); vii, $BF_3{\cdot}OEt_2$, toluene (100%); viii, TsOH (cat.), CH_2Cl_2, room temp., 3 d (76%).

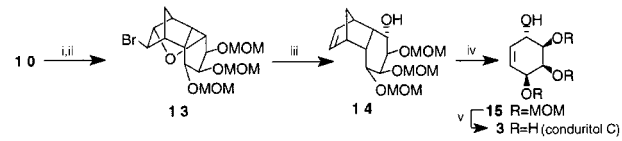

Scheme 2 *Reagents and conditions*: i, NaOMe, MeOH; ii, MOMCl, Pr^i_2NEt, CH_2Cl_2 (89%); iii, Zn, AcOH, MeOH (85%); iv, $NaHCO_3$, Ph_2O, reflux, 30 min (84%); v, sat. HCl–MeOH (93%).

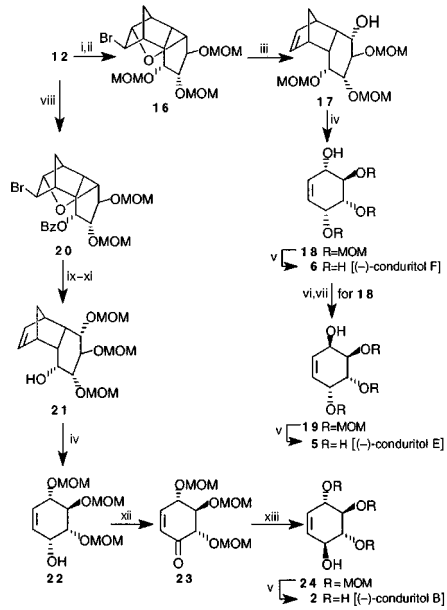

Scheme 3 *Reagents and conditions*: i, NaOMe, MeOH; ii, MOM-Cl, Pr^i_2NEt, $(CH_2Cl)_2$ (92%); iii, Zn, AcOH, MeOH (91%); iv, $NaHCO_3$, Ph_2O, reflux, 30 min (77% for **18**; 96% for **22**); v, sat. HCl–MeOH (100% for **2**, **5**, **6**); vi, 4-$NO_2C_6H_4CO_2H$, DIAD, PPh_3, THF (74%); vii, K_2CO_3, MeOH (94%); viii, MOMCl, Pr^i_2NEt, CH_2Cl_2 (97%); ix, Zn, AcOH, MeOH (99%); x, MOMCl, Pr^i_2NEt, CH_2Cl_2 (82%); xi, K_2CO_3, MeOH (94%); xii, PCC, CH_2Cl_2 (94%); xiii, $NaBH_4$–$CeCl_3$ (93%).

On the other hand, the *trans*-diol **12** was first transformed into the di-MOM ether **20**, $[\alpha]_D^{30}$ −73.6 (*c* 1.01, $CHCl_3$), which was further transformed into the tricyclic alcohol **21**, $[\alpha]_D^{31}$ −8.0 (*c* 1.04, $CHCl_3$), by sequential reductive cleavage, MOM protection and debenzoylation. Themolysis of **21** afforded the cyclohexenol **22**, $[\alpha]_D^{28}$ +24.5 (*c* 1.01, $CHCl_3$), which was epimerized to **24**, $[\alpha]_D^{29}$ +142.1 (*c* 1.03, $CHCl_3$), *via* the cyclohexenone **23**, $[\alpha]_D^{30}$ +41.4 (*c* 1.05, $CHCl_3$), by oxidation followed by diastereoselective 1,2-reduction in the presence of cerium(III) chloride.[10] Compound **24** afforded (+)-conduritol B **2**, mp 174–175 °C, $[\alpha]_D^{28}$ +153.5 (*c* 0.31, MeOH) [lit.[2c] mp 174–175 °C, $[\alpha]_D^{20}$ −179 (*c* 1.2, MeOH)], on MOM deprotection (Scheme 3).

Although enantiocontrol is not required for the construction of the two remaining conduritols, A **1** and D **4**, having *meso* structures, the same intermediate **8** was used as the starting material to demonstrate the potential of our building block. Thus, **8** was first transformed into the tri-MOM ether **25**, $[\alpha]_D^{26}$ −33.0 (*c* 1.01, $CHCl_3$), which was then converted to the cyclohexenol **27**, $[\alpha]_D^{25}$ −8.7 (*c* 1.11, $CHCl_3$), by sequential MOM protection, reductive cleavage and thermolysis. Compound **27** afforded conduritol A **1**, mp 141–142 °C (lit.,[2a] mp 140–141 °C), on MOM deprotection.

Compound **8**, on the other hand, was first transformed into the dibenzyl ether **28**, mp 91–92 °C, $[\alpha]_D^{29}$ −63.1 (*c* 1.32, $CHCl_3$), which, on sequential reductive cleavage and thermolysis, gave the cyclohexenol **29**, $[\alpha]_D^{27}$ +12.8 (*c* 1.05, $CHCl_3$). On sequential diastereoselective dihydroxylation, MOM protection, debenzylation and thiocarbonylation, **29** furnished the *meso* cyclohexane **30**. Refluxing **30** with trimethyl phosphite[11,12] allowed smooth dethiocarbodioxylation to give the cyclohexene **31** which afforded conduritol D **4**[2b] on MOM deprotection (Scheme 4).

In conclusion, the present synthesis provides the first integrated route to all possible conduritol diastereomers with complete diastereocontrol starting from a single chiral building block by using MOM ether as the common protecting group.

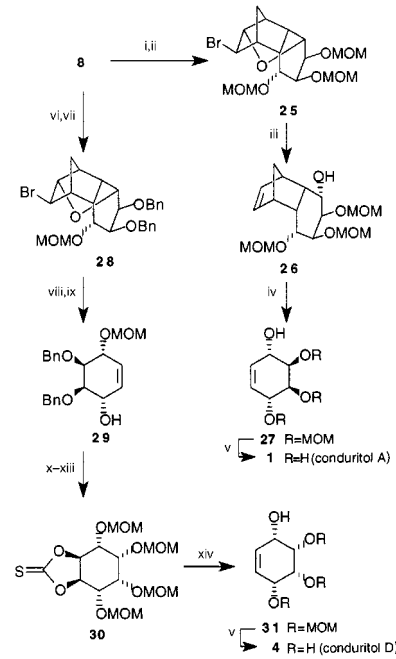

Scheme 4 *Reagents and conditions*: i, OsO_4 (cat.), NMO, aq. THF (97%); ii, MOMCl, Pr^i_2NEt, CH_2Cl_2 (95%); iii, Zn, AcOH, MeOH (91%); iv, $NaHCO_3$, Ph_2O, reflux, 30 min (93%) (90% for **29**); v, sat. HCl–MeOH (100% for **1** and **4**); vi, OsO_4 (cat.), NMO, aq. THF (97%); vii, BnBr, NaH, reflux, 30 min, Bu_4NI, THF (97%); viii, Zn, AcOH, MeOH (98%); ix, $NaHCO_3$, Ph_2O, (90%); x, OsO_4 (cat.), NMO, aq. THF; xi, MOMCl, Pr^i_2NEt, CH_2Cl_2 (96%); xii, H_2, $Pd(OH)_2$, MeOH (93%); xiii, $Im_2C{=}S$, toluene (94%); xiv, $(MeO)_3P$, reflux (97%).

Notes and references

† Satisfactory analytical (combustion and/or high resolution mass) and spectroscopic (IR, ^1H and ^{13}C NMR, MS) data were obtained for isolable new compounds.

1 Pertinent reviews, see: M. Balci, Y. Sütbeyaz and H. Seçen, *Tetrahedron*, 1990, **46**, 3715; P. Vogel, D. Fattori, F. Gasparini and C. Le Drian, *Synlett*, 1990, 173; H. A. J. Carless, *Tetrahedron: Asymmetry*, 1992, **3**, 795; M. Balci, *Pure Appl. Chem*., 1997, **69**, 97.

2 Some recent examples, see: (*a*) Y. Sütbeyaz, H. Seçen and M. Balci, *J. Chem. Soc., Chem. Commun*., 1988, 1330 (A); (*b*) H. A. J. Carless and O.Z. Oak, *Tetrahedron Lett.*, 1989, **30**, 1719 (A and D); (*c*) C. Le Drian, J. P. Vionnet and P. Vogel, *Helv. Chim. Acta*, 1990, **73**, 161 (B and F); (*d*) B. M. Trost and E. J. Hembre, *Tetrahedron Lett.*, 1999, **40**, 219 (B); (*e*) S. Takano, M. Moriya, Y. Higashi and K. Ogasawara, *J. Chem. Soc., Chem. Commun*., 1993, 177 (C); (*f*) H. Yoshizaki and J.-E. Bäckvall, *J. Org. Chem*., 1998, **63**, 9339 (C); (*g*) T. Yoshimitsu and K. Ogasawara, *Synlett*, 1995, 257 (E and F).

3 S. Takano, Y. Higashi, T. Kamikubo, M. Moriya and K. Ogasawara, *Synthesis*, 1993, 948; H. Konno and K. Ogasawara, *Synthesis*, 1999, 1135.

4 K. Ogasawara, *Pure Appl. Chem.*, 1994, **66**, 2119: K. Ogasawara, *J. Synth. Org. Chem. Jpn.*, in the press.

5 O. Mitsunobu, *Synthesis*, 1981, 1.

6 M. Prystas, H. Gustafsson and F. Sorm, *Collect. Czech. Chem. Commun.*, 1971, **36**, 1487.

7 T. Kamikubo and K. Ogasawara, *J. Chem. Soc., Chem. Commun.*, 1995, 1951.

8 T. Kamikubo and K. Ogasawara, *Chem. Lett.*, 1996, 987.

9 S. F. Martin and J. A. Dodge, *Tetrahedron Lett.*, 1991, **32**, 3017.

10 A. L. Gemal and J. L. Luche, *J. Am. Chem. Soc.*, 1981, **103**, 5454.

11 E. J. Corey and R. A. E. Winter, *J. Am. Chem. Soc.*, 1963, **85**, 2677.

12 T. L. Nagabhushan, *Can. J. Chem.*, 1970, **48**, 383.

Communication 9/05462F

ChemComm

Synthesis of soluble combinatorial libraries of crown ether-ester analogues *via* the cyclodepolymerisation of linear polyesters

Pathavuth Monvisade, Philip Hodge* and Clare L. Ruddick

Department of Chemistry, University of Manchester, Oxford Road, Manchester, UK M13 9PL. E-mail: philip.hodge@man.ac.uk

Received (in Cambridge, UK) 14th July 1999, Accepted 23rd August 1999

Cyclodepolymerisation of functional linear polyesters gives macrocycles which, on equilibration *via* transesterification, give soluble combinatorial libraries of crown ether-ester analogues, one consisting of 30 different 18- or 27-membered rings and another consisting of 29 different 24- or 36-membered rings.

Combinatorial chemistry has great potential to assist in solving a wide variety of chemical problems.[1,2] Most frequently to date it has involved the synthesis of combinatorial libraries on insoluble polymer supports and the target molecules have been peptides[3] or potential pharmaceuticals.[4] There are, however, other synthetic approaches and other targets of interest, for example, the synthesis of libraries in solution[5] and the synthesis of libraries to assist in the optimisation of recognition properties.[6]

Cyclic oligomers can often be prepared efficiently by the cyclodepolymerisation (CDP) of condensation polymers.[7,8] CDP involves treating a dilute solution, typically *ca.* 2% w/v, of an appropriate polymer with a catalyst that brings about the cleavage and reformation of the polymer linkages. At low concentrations the formation of cyclics is much more likely than the formation of chains. Thus, treating linear polyesters in dilute solution with a transesterification catalyst affords cyclic oligoesters in excellent yields.[7] Crown ethers are an important class of compounds, many of which can recognise cations, and we now report that CDP can be used to synthesise soluble libraries of crown ether-ester analogues made up of 18-membered and 27-membered rings containing all the combinations of the moieties in cyclics **1**–**4** and of 24- and 36-membered rings made up of all the combinations of the moieties in cyclics **13** and **14**. Although in the 18-membered ring family the binding of cations is expected to be achieved mainly *via* the ether, thioether or *tertiary* amine moieties,[9] as the rings become larger binding may also be achieved through the ester carbonyl groups. The natural ionophore valinomycin, for example, a depsipeptide which has a 36-membered ring, binds K^+ with high selectivity using the carbonyl groups of six ester linkages.[10]

Polymers **5**–**8** were synthesised by standard procedures from the appropriate dimethyl ester, ethylene glycol, and a catalytic amount of titanium isopropoxide (Scheme 1). The yields and the molecular weight data of the products are summarised in the Table. Treatment of 2% w/v solutions of each individual polymer in chlorobenzene with 2 mol% of di-*n*-butyltin oxide at 183 °C brought about CDP and the formation of the expected series of cyclic oligomers.[11] Although the reactions were substantially complete in 24 h, they were nevertheless carried out for 7 days to ensure that equilibrium was reached. It is evident from the results, summarised in Table 1, that the cyclic fractions from polymers **5**–**8**, generally isolated by passing the crude product down a short column of alumina, consisted of 61–80% of the 18-membered ring dimers (**1**–**4**; $n = 2$), and 14–18% of the 27-membered ring trimers (**1**–**4**; $n = 3$). Larger cyclic oligomers were also present[11] but only the dimers and trimers were considered to be present in sufficient amounts to be useful in the present project. It is clear that none of the functionalities involved caused the formation of, say, a particular cyclic trimer to be much more heavily favoured than any other. Thus, the various motifs present were expected to 'mix' well in combinatorial experiments.

When an equimolar mixture of the cyclics from each of the three polymers **5**, **6** and **8**, as a 2% w/v solution in chlorobenzene, was treated with 3 mol% of di-*n*-butyltin oxide

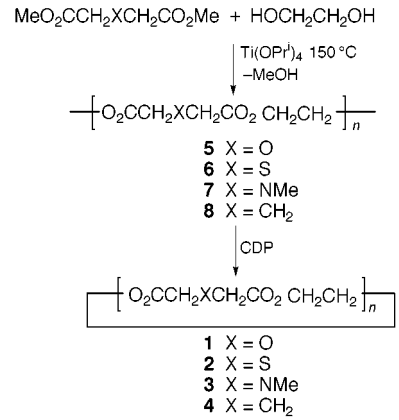

Scheme 1

Table 1 Properties of polymers and the composition of the CDP products

Starting polymer	Yield (%)	$\overline{M}_n$[a]	$\overline{M}_w$[a]	Yield of cyclic oligomers (%)	Composition of CDP product (%)[b]		
					Cyclic dimer	Cyclic trimer	Other cyclics
5	92	1 500	2 300	53	74	17	9
6	56	3 000	4 300	70	66	18	16
7	54	19 200	28 700	69	80	14	6
8	74	14 300	25 400	94	61	17	22
11	81	1 700	2 200	71	51	21	14
12	83	2 900	4 300	61	48	19	31

[a] By GPC relative to polystyrene standards. [b] By GPC on a column specifically designed to analyse oligomers. The materials unaccounted for were either linear oligomers or polymer.

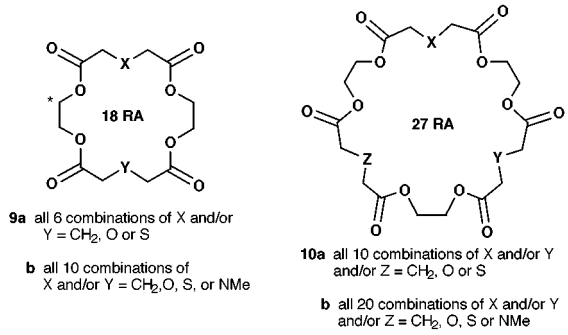

9a all 6 combinations of X and/or Y = CH_2, O or S

b all 10 combinations of X and/or Y = CH_2,O, S, or NMe

10a all 10 combinations of X and/or Y and/or Z = CH_2, O or S

b all 20 combinations of X and/or Y and/or Z = CH_2, O, S or NMe

at 183 °C for 7 days, equilibration was achieved through transesterification and the product contained all the six expected combinations of the cyclic 'dimers' **9a** (75% by weight by GPC analysis) and all the ten expected combinations of the cyclic 'trimers' **10a** (15% by weight). Similar mixtures could be prepared directly by mixing the polymers **5**, **6** and **8** and subjecting them to CDP. The positive-ion chemical ionisation mass spectrum of the equilibrated products showed major signals for every expected combination. The relative sizes of the signals in mass spectra do not accurately reflect the proportions of the various species present, but by ^{13}C NMR spectroscopy it was shown that the amounts of all the cyclic 'dimers' were the same within a factor of 2, the most useful signal being that asterisked in **9**. The position of this signal is sensitive to the type of groups at both X and Y. This region of the ^{13}C NMR spectrum is shown in Fig. 1. There is no reason to doubt that the cyclic 'trimers' **10a** were also all present in comparable amounts. A mixture of the four polymers **5**–**8** was equilibrated similarly. The positive-ion chemical ionization mass spectrum of the product showed significant signals for all 10 combinations of 'dimers' **9b** and all 20 combinations of 'trimers' **10b**.

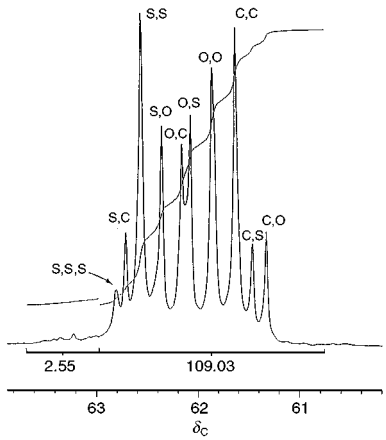

Fig. 1 Part of the ^{13}C NMR spectrum of the mixture obtained by equilibrating cyclic oligomers **1**, **2**, and **4**. The part of the spectrum shown is due to the asterisked carbon atoms in **9**. Assignments were made on the basis of studies of the NMR spectra of the pure cyclic dimers and combinatorial mixtures prepared from just two types of cyclic oligomers.

Polymers **11** and **12** were similarly prepared, characterised and subjected to CDP (Scheme 2, Table 1). In these cases the proportions of the cyclic dimers (24-membered rings) and trimers (36-membered rings) were *ca.* 2.:1 by weight. Equilibration of the cyclics from the two polymers gave solutions containing, as judged by positive-ion chemical ionisation and MALDI-TOF mass spectrometry, libraries of all nine combinations of the 24-membered rings (**15**) and all 20 combinations of the 36-membered rings (**16**). In this system the total number of possible combinations is enhanced because there is a choice in both the diacid and diol segments of the macrocycles, and, in some 'trimers', a choice in the sequence of the segments which results in isomer formation.

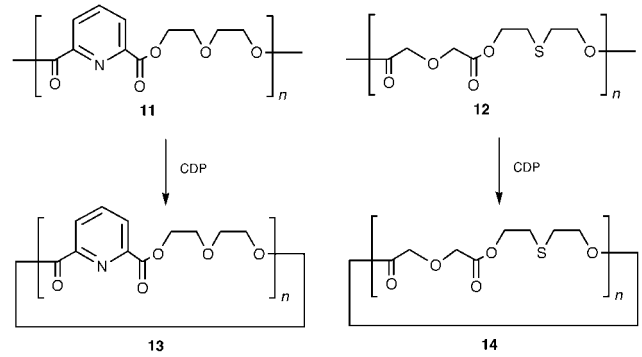

Scheme 2

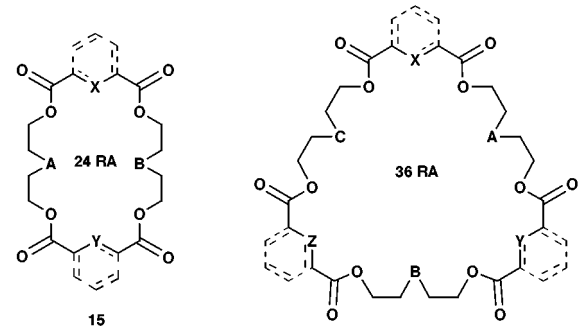

All 9 combinations of X and/or Y = O or pyridine and A and/or B = O or S

All 20 combinations of X and/or Y and/or Z = O or pyridine and A and/or B and/or C = O or S

Research related to the above has been carried out by Sanders' group.[12–14] They have prepared macrocyclic esters directly from monomers and equilibrated *pairs* of families of the macrocycles. In their work most of the building blocks were rigid,[12–14] and, unlike in the present study, not all pairs of rings 'mixed' well.[13] Successful mixing could, however, be achieved by including ephedrine derivatives, which are relatively flexible, in the equilibrating system.[14]

Having shown that libraries of cyclic recognition systems can be prepared *via* CDP of polyesters, work is currently in hand to prepare other types of soluble libraries by CDP and to develop methods for screening the various soluble libraries.

We thank the Thai Government for a PhD Studentship for P. M. and the EPSRC ROPA Scheme for financial support.

Notes and references

1 *Combinatorial Chemistry, Synthesis and Application*, ed. S. R. Wilson and A. W. Czarnik, Wiley, New York, 1997.
2 *Combinatorial Peptide and Non-peptide Libraries*, ed. G. Jung, VCH, Weinheim, 1996.
3 G. Lowe, *Chem. Soc. Rev.*, 1996, **25**, 309.
4 N. K. Terrett, *Tetrahedron*, 1995, **51**, 8135.
5 E. A. Wintner and J. Rebek, in ref. 1, ch. 5, pp. 95–117.
6 K. Lewandowski, P. Murer, F. Svec and J. M. J. Fréchet, *Chem. Commun.*, 1998, 2237.
7 B. R. Wood, J. A. Semlyen and P. Hodge, *Polymer*, 1997, **38**, 2287.
8 A. Ben-Haida, I. Baxter, H. M. Colquhoun, P. Hodge, F. H. Kohnke and D. J. Williams, *Chem. Commun.*, 1997, 1533.
9 R. M. Izatt, K. Pawlak, J. S. Bradshaw and R. L. Bruening, *Chem. Rev.*, 1991, **91**, 1721.
10 M. Dobler, in *Comprehensive Supramolecular Chemistry*, ed. J. L. Atwood, J. E. D. Davies, D. D. MacNicol and F. Vogtle, Pergamon, Oxford, 1992, vol. 1, ch. 5, pp. 267–313.
11 H. Jacobson and W. H. Stockmayer, *J. Chem. Phys.*, 1950, **18**, 1600.
12 P. A. Brady, R. P. Bonar-Law, S. J. Rowan, C. J. Suckling and J. K. M. Sanders, *Chem. Commun.*, 1996, 319.
13 S. J. Rowan and J. K. M. Sanders, *J. Org. Chem.*, 1998, **63**, 1536.
14 S. J. Rowan, P. S. Lukeman, D. J. Reynolds and J. K. M. Sanders, *New J. Chem.*, 1998, 1015.

Communication 9/05685H

ChemComm

Concerning kinetic resolution by the Sharpless asymmetric dihydroxylation reaction

Hamish S. Christie, David P. G. Hamon* and Kellie L. Tuck

Chemistry Department, University of Adelaide, S.A. 5005, Australia. E-mail: dhamon@chemistry.adelaide.edu.au

Received (in Cambridge, UK) 6th August 1999, Accepted 31st August 1999

The transition state for the product-determining step in the Sharpless asymmetric dihydroxlation reaction is not product-like, and effective kinetic resolution can occur when one face of a chiral alkene is hindered.

Sharpless asymmetric dihydroxlation (AD)[1] and asymmetric epoxidation (AE)[2] reactions have proved to be very effective means whereby asymmetry can be introduced into molecules starting from prochiral alkenes and allylic alcohols respectively. The AE reaction has also proved useful for effecting kinetic resolution of chiral allylic alcohols. However, with only a few exceptions, the AD reaction has not been effective for carrying out kinetic resolutions and the reasons for this are not well understood.[1]

It is known[3] that the AD reaction of 1-phenylcyclohexene proceeds with high asymmetric induction. Therefore, reaction of these reagents with 1-phenyl-4-*tert*-butylcyclohexene **1** would also be expected to proceed with high asymmetric induction but two diastereomeric products should result. For instance with AD-mix-β the enantioenriched diastereomers **2** and **3** should form (Scheme 1). If these molecules exist predominantly in the expected chair conformers, the diastereomer **2** has the phenyl group in an equatorial position whereas the phenyl group in the other diastereomer **3** has an axial orientation. The diastereomer **3** will be several kJ mol^{-1} higher in energy than the diastereomer **2**.[4] Therefore, if the transition state (TS) for the product-determining step in the AD reaction is product-like, there would be a considerable difference in the rate of formation of these two diastereomers, and an effective kinetic resolution should be possible.

The AD reaction on the alkene **1** was performed following Sharpless's recommended procedure[5] for tri-substituted alkenes (AD-mix-β, $MsNH_2$, Bu^tOH–H_2O, 0 °C). Equal quantities of the diols **2** and **3**,[6] eluting in that order, were obtained, in 84% yield after 'flash' silica gel chromatography. The enantiomeric purity of each diol was determined by the use of NMR chiral shift reagent experiments. The diol **2** from the AD reaction had > 99% ee[7] and the diol **3** had > 95% ee.[8] The racemic diols were obtained using the Sharpless method with quinuclidine as ligand to give the racemic diols in a ratio of ~ 4.5 : 1.

The kinetic resolution was also studied under the normal conditions for the AD reaction and the relative rates for the enantiomers (*E*) were determined following a literature procedure[9] which is related to the relationship derived by Kagan.[10] The percentage conversion of the racemic substrate was followed by NMR spectroscopy. The remaining alkene was separated from the diols **2** and **3**. The ee of the remaining alkene **1** was determined by conversion, using the achiral dihydroxylation reaction, into the same diols **2** and **3**. The enantiopurity of the major diol was then determined as already described. In two separate experiments, conducted at 0 °C, the reactions were stopped at 15 and 94% conversion respectively. The ee for the remaining alkene, for the former reaction, was determined as ~ 4% and, for the latter, as ~ 86%. This computes to an *E* of ~ 2 in each case. This value of *E* is too small for effective kinetic resolution. Clearly the TS of the product-determining step is not product-like.

It can be reasoned that, if the product-determining step in the AD reaction is reactant-like and if the alkene is highly enantiofacially directing, then a kinetic resolution should be effective when there is considerable difference in the ease of approach to the two faces of a chiral alkene.[11] Such an effect has been demonstrated[12] recently for one molecule, which displays axial chirality. Recently we completed[13] an asymmetric synthesis of grandisol in which the key step is the kinetic resolution of the primary allylic alcohol **4** by a Sharpless AE reaction. The

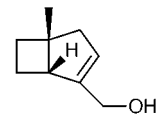

4

key feature in that resolution is that the molecule presents both an open convex face and a more-hindered, concave face to the reagents. The reaction proceeds to give products of attack on one face only, the convex face. This system appeared suitable to pursue the study of the kinetic resolution by the AD reaction. Indeed, the alkene **5** appears ideal for this study. Control of product formation in the Sharpless AD reaction should be determined mainly by the enantiofacial selectivity of the styrene moiety. The concave face of this molecule is hindered, so there should be a considerable difference in the rate of reaction of the enantiomers of this molecule and kinetic resolution should be effective.

Reaction of the bicycloketone **6**[14] with PhMgBr and Et_2O at 0 °C gave, in 88% yield, a single racemic alcohol, mp 56–58 °C, presumed to be the diastereomer **7** (Scheme 2). Dehydration of this alcohol (CH_2Cl_2, Et_3N, MsCl, 0 °C) gave as an oil the alkene **5** (81%).[15] A kinetic resolution of this substrate was examined in two separate experiments with 26 and 50% oxidant respectively. However, because the alkene **5** is somewhat unstable, in each case the ees for both the diol (presumed to be enantiomer **8**, based on the application of Sharpless' mnemonic) and the recovered alkene **5** were determined, after separation, in the following way. The diol **8** was converted to the mono Mosher ester derivative [(+)-MTPA, CH_2Cl_2, DCC, DMAP] and the ee determined.[16] The alkene was converted to the same diol (presumed to be mainly **9**) by the achiral dihydroxylation

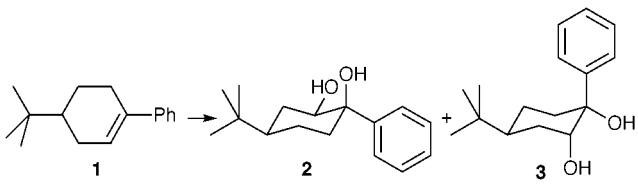

1 **2** **3**

Scheme 1

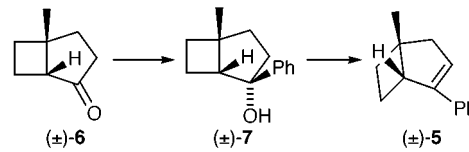

(±)-**6** (±)-**7** (±)-**5**

Scheme 2

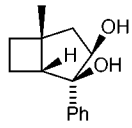

8

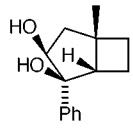

9

reaction (quinuclidine ligand) and this diol was converted to the mono Mosher ester derivative from which the ee was obtained. The ees for the diols in the two reactions were 88 and 80%, and for the alkenes they were 52 and 80%, respectively. The enantiomeric ratios for these two reactions calculate to E = 26 and 21, respectively (the same within experimental error), which translates to an effective kinetic resolution (> 95% ee at 60% conversion).

In conclusion, we find that the reaction of 1-phenyl-4-*tert*-butylcyclohexene with AD-mix-β gives the two diastereomers **2** and **3** in very high enantiopurity. However, the rate difference between formation of the two enantiomers is only small ($E \sim 2$) and kinetic resolution is ineffective. We also find that the reaction of the alkene **5** with AD-mix-β gives an effective kinetic resolution ($E > 20$) and only one diastereomeric diol is formed. These results are consistent with an early, rather than a late, transition state for the product-determining step in the Sharpless AD reaction.

Notes and references

1 M. S. VanNieuwenhze and K. B. Sharpless, *J. Am. Chem. Soc.*, 1993, **115**, 7864; H. V. Kolb, M. S. VanNieuwenhze and K. B. Sharpless, *Chem. Rev.*, 1994, **94**, 2483 and references therein.

2 R. A. Johnson and K. B. Sharpless, *Catalytic Asymmetric Synthesis*, ed. I. Ojima, VCH, New York, 1993, pp. 103–158.

3 S. B. King and K. B. Sharpless, *Tetrahedron Lett.*, 1994, **35**, 5611.

4 A value of 15.9 kJ mol^{-1} was obtained by calculation. Gaussian 94 (revision C), Gaussian, Inc., Pittsburgh, PA., 1995.

5 K. B. Sharpless, W. Amberg. Y. L. Bennani, G. A. Crispino, J. Hartung, K.-S. Jeong, H.-L. Kwong, K. Morikawa, Z.-M. Wang, D. Xu and X.-L. Zhang, *J. Org. Chem.*, 1992, **57**, 2768.

6 Diols **2** and **3** show C*H*OH resonances at δ 4.02 (dd, J 11, 4 Hz) and 4.38 (m, width at half height < 10 Hz), respectively, in the ^{1}H NMR (after D_2O exchange). These diols have been prepared before in racemic form, see G. Berti, B. Macchia and F. Macchia, *Tetrahedron*, 1968, **24**, 1755.

7 Chiral shift reagent [Eu(hfc)$_3$] in 15% C_6D_6–CCl_4. The Bu^t protons' resonance due to the minor enantiomer was not visible by proton NMR, but the ^{13}CH satellite of the Bu^t protons' resonance of the major isomer was. Addition of 1% of the racemate gave a discernible peak for the minor enantiomer.

8 Chiral shift reagent [Eu(tfc)$_3$] in 15% C_6D_6–CCl_4. Addition of 5% of the racemate was required before a discernible peak for the Bu^t protons' resonance of the minor enantiomer could be detected.

9 V. S. Martin, S. S. Woodard, T. Katsuki, Y. Yamada, M. Ikeda and K. B. Sharpless, *J. Am. Chem. Soc.*, 1981, **103**, 6237.

10 G. Balavoine, A. Moradpour and H. B. Kagan, *J. Am. Chem. Soc.*, 1974, **96**, 5152.

11 Initially we synthesised (3*RS*,6*RS*)-3-*tert*-butyl-1,6-diphenylcyclohexene but it did not appear to undergo the AD reaction. This synthesis will be reported in the full paper.

12 J. M. Gardiner, M. Nørret and I. H. Sadler, *Chem. Commun.*, 1996, 2709.

13 D. P. G. Hamon and K. L. Tuck, submitted for publication.

14 R. L. Cargill, J. R. Dalton, G. H. Morton and W. E. Caldwell, *Org. Synth.*, 1984, **62**, 118.

15 The radical inhibitor, 2,6-di-*tert*-butyl-*p*-cresol, was added during the work-up procedure, otherwise much lower yields of this alkene were obtained.

16 In the ^{1}H NMR spectrum, methoxy resonances at δ 3.37 and 3.53 for the diastereomers produced from the racemic diol showed separation at the base-line.

Communication 9/06423K

ChemComm

Asymmetric transformation (deracemisation) of an atropisomeric bisheterocyclic amine†

Michael P. Coogan,*[a] David E. Hibbs[b]‡ and Emma Smart[a]

[a] *Department of Chemistry, University of Durham, Science Laboratories, South Road, Durham, UK DH1 3LE. E-mail: m.p.coogan@durham.ac.uk*

[b] *Department of Chemistry, University of Wales, Cardiff, Park Place, Cardiff, UK CF1 3TB*

Received (in Liverpool, UK) 21st June 1999, Accepted 11th August 1999

Heating (±)-6,8,14,17-tetrahydro-7*H*-[1,2,5]triazepino[3,2-*b*:7,1-*b*′]diquinazoline-14,17-dione 1 with (+)-CSA gives (−)-1 with >90% ee *via* a crystallisation-induced asymmetric transformation, the first non-racemic example of a C_2 symmetric bisheterocycle which is atropisomeric by virtue of retarded rotation around an N–N bond.

The efficacy of substituted 1,1′-binaphthyls as ligands for metals in catalytic asymmetric reactions has prompted interest in other aspects of atropisomerism: recently hindered aryl amides[2a] and novel binaphthyl ligands and analogues[2b] have been the focus of interest. One system which displays hindered rotation due largely to an electronic rather than steric barrier is the N–N bond of peracylhydrazines.[3] Atkinson *et al.*[4] have shown that the N–N bond in 3-diacylaminoquinazolin-4-ones is a chiral axis when the acyl groups are different and, by analogy, N–N linked biquinazolinones would be expected to display atropisomerism (axial chirality). However, although a range of 3,3′-biquinazoline-4,4′-diones have been prepared,[5] the issue of chirality was not addressed. A stereostable chiral axis in such compounds could lead to the design of novel ligands for metals in catalytic asymmetric reactions. Having verified the presence of chirality it was hoped that, rather than resolution of enantiomers, a deracemisation reaction (asymmetric transformation, AT)[1] could be developed. Vedejs and co-workers have obtained diastereomerically pure materials by AT at the stereogenic but stereolabile heteroatoms of chiral organoboron[6a] and organophosphorus[6b] compounds. Notably, Vedejs and Donde[6b] achieved crystallisation-induced AT at a stereogenic phosphorus utilising an alkoxycarbonylphosphine to both introduce a chiral auxiliary, and lower the barrier to inversion, allowing racemisation at around the melting point (Scheme 1). In the work described here a high barrier to rotation (racemisation) coexists with high crystallinity, and the electronic nature of the barrier is exploited, allowing it to be moderated *via* protonation.

2,2′-Bis(bromomethyl)-3,3′-biquinazoline-4,4′-dione **2** was prepared in two steps from **3**[5] in 58% yield *via* the unstable bisbromoacetate **4** (Scheme 2). The bromomethylene protons of **2** are observed as an AB system [δ 4.43, 4.32 (J 12.0 Hz)] indicating chirality (slow rotation around the N–N bond on the NMR time scale). VT NMR showed line broadening above 60 °C, however even at 135 °C free rotation was not observed around the N–N bond (non-coalescence) which indicates a *minimum* barrier to rotation in the order of 85 kJ mol^{-1}.

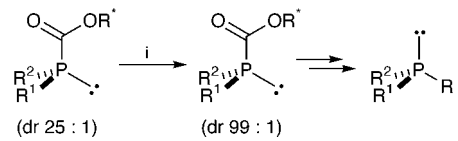

Scheme 1 *Conditions*: i, crystalline state, 50 °C, 22 h.

† See ref. 1.

‡ Corresponding author for crystallography.

Treatment of a solution of **2** in THF with aqueous NH_3 gave 6,8,14,17-tetrahydro-7*H*-[1,2,5]triazepino[3,2-*b*:7,1-*b*′]diquinazoline-14,17-dione **1** [*m/z* 331 (100%)]§ in 74% yield; none of the anticipated diamine **5** was detected. In amine **1** the diastereotopic protons in each methylene unit [δ 4.00, 3.93 (J 13.2 Hz)] confirmed that rotation around the N–N bond was slow on the NMR time scale; again in VT NMR experiments coalescence was not observed at 135 °C, indicating a minimum barrier to rotation of 85 kJ mol^{-1}. No separation of ^{1}H NMR signals was observed in the presence of acetylmandelic acid[7] or tartaric acid. However, in the presence of 2 equiv. of (+)-CSA, two sets of AB pattens were observed [δ 4.89, 4.75, 4.70 and 4.68 (J 14.4 Hz for all signals)] equating to the two diastereoisomeric salts. To investigate possible AT, a sample of **1** and 2 equiv. of (+)-CSA was suspended in toluene and heated at reflux for 16 h, then evaporated and analysed by ^{1}H NMR. Astonishingly, only one set of diastereotopic protons was observed (δ 4.89, 4.70), along with decomposition products. Base washing gave **1** identical with authentic material which on treatment with CSA displayed only one set of methylene signals, implying that the sample was essentially a single enantiomer. To ascertain whether this phenomenon was due to selective decomposition or AT, optimisation experiments were undertaken in various solvents at a range of temperatures and concentrations. Optimum conditions were heating **1** at reflux with benzene containing (+)-CSA (2 equiv.) for 40 h, which gave an apparent diastereoisomer ratio of >10:1 (judged by NMR) with negligible decomposition. The recovered **1** after base washing accounted for 82% of the starting material, which is incompatible with a selective decomposition of one enantiomer, and had specific rotation $[\alpha]_D$ −643 (c 0.1, CH_2Cl_2) (Scheme 3), raised by a single recrystallisation to −688 (c 0.011, CH_2Cl_2), at which point (+)-CSA as an NMR shift

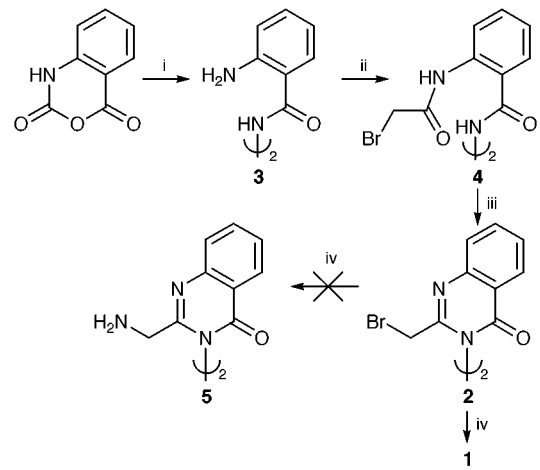

Scheme 2 *Reagents and conditions*: i, $H_2NNH_2{\cdot}H_2O$ (0.5 equiv.), EtOH, reflux, 16 h, 84%; ii, $BrCH_2COBr$, Et_3N, DMF, 0 °C; iii, TsOH (10 mol%), PhMe, reflux (Dean and Stark), 58% for 2 steps; iv, 35% aq. NH_3 (100 equiv.), THF, 74%.

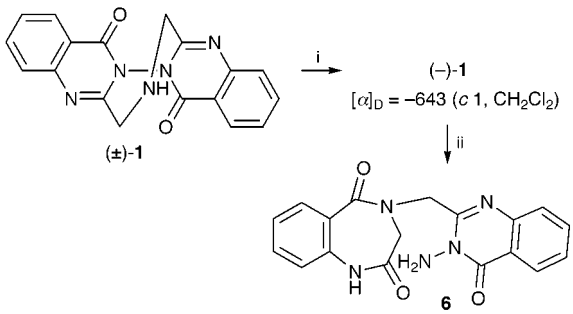

Scheme 3 *Reagents and conditions*: i, (+)-CSA (2 equiv.), PhH (3.8 ml mol^{-1}), reflux, 40 h; ii, HBr, EtOH–H_2O or $CoSO_4$, EtOH–H_2O.

reagent indicated that the material was enantiopure (> 98% ee).

The use of a paucity of a 'poor' solvent is essential; a *solution* of **1** with 2 equiv. of CSA (1,2-dichloroethane) at 83 °C (*vs.* 80 °C for benzene) for 40 h gave only the racemic material and, on prolonged heating (72 h), decomposition. Two samples of **1** (0.1 mmol) plus 2 equiv. of CSA heated at reflux for 16 h in 10 ml (entirely dissolved) and 1 ml (two phase) of benzene gave diastereoisomer ratios 1 : 1 and 3 : 1, respectively. The use of higher temperatures was detrimental: 2 h at 135 °C led to complete decomposition. These data are indicative of a crystallisation induced AT [see ref. 1(*c*) for a full explanation of the principles involved] rather than the formation of a thermodynamically favourable salt. The racemisation process would appear to be acid catalysed: a solution of (−)-**1** and CSA showed appreciable racemisation (diastereoisomer ratio 4 : 1) after 1 week at room temperature, whereas a solution of the free base showed minimal racemisation after 14 days, and the rate of racemisation of **1** even at 110 °C was slow ($t_{1/2}$ > 24 h at 110 °C). The crystalline material retained its original ee during the same period. It is unlikely that protonation of the secondary amine will assist rotation around the N–N bond, thus it is proposed that protonation of the quinazolinone 1-(imine) nitrogens (hence the requirement for CSA, a strong acid) and the resultant amidinium ion resonance to N-3 reduces the barrier to rotation around the N–N bond. Attempts to grow crystals containing heavy atoms suitable for the determination of absolute configuration with HBr or aqueous $CoSO_4$ led not to the respective salt/complex but to the rearranged hydrolysis product **6** (Scheme 3) as determined by single crystal diffraction.¶ This facile hydrolysis is atypical of biquinazolinones.

We thank Dr Alan Kenwright, Ian McKeag and Catherine Heffernan for VT NMR studies and Dr P. G. Steel for helpful discussions and the generous donation of materials.

Notes and references

§ All new compounds were fully characterised. *Selected data* for **1**: mp 218.2–220.6 °C (decomp.) (EtOH); δ_H(300 MHz, $CDCl_3$) 8.38 (2H, dd, *J* 8.1, 1.2, 2 × H6), 7.91 (2H, ddd, *J* 8.1, 7.2, 1.5, 2 × H7), 7.81 (2H, dd, *J* 7.5, 1.5, 2 × H9), 7.63 (2H, ddd, *J* 8.1, 7.5, 1.2, 2 × H8), 4.08, 4.02 (4H, 2 × d, *J* 13.5, 2,2′-CH_2), 2.01 (br, NH). For **2**: mp 228.6 °C (EtOAc); δ_H(300 MHz, $CDCl_3$) 8.31 (2H, ddd, *J* 8.1, 1.5, 0.6, 2 × H6), 7.93 (4H, m, 2 × H7 + H8), 7.60 (2H, ddd, *J* 6.9, 1.5, 1.2, 2 × H9), 4.43 (2H, d, *J* 12.0, 2 × H2′), 4.32 (H, d, *J* 12.0, 2 × H2″).

¶ *Crystal data* for **6**: $C_{18}H_{15}N_5O_3$, *M* = 349.35, triclinic, Space group $P\bar{1}$, μ = 0.101 mm^{-1}, *R*1 = 0.2872, *wR*2 = 0.1412, *a* = 4.684(4), *b* = 13.470(5), *c* = 13.786(6) Å, α = 73.144(10), β = 78.90(2), γ = 88.302(10)°, *V* = 816.6(8) $Å^3$, *T* = 293(2) K, *Z* = 2, reflections collected/unique 2307/2201 [*R*(int) = 0.0696]. CCDC 182/1375. See http://www.rsc.org/suppdata/cc/1999/1991/ for crystallographic data in .cif format.

1 (*a*) Asymmetric Transformation refers to 'an asymmetric transformation of the second knd', R. Kuhn, *Chem. Ber.*, 1932, **65**, 49; (*b*) For a recent review of controlled racemisation and asymmetric transformation, see E. J. Ebbers, G. J. A. Ariaans, J. P. M. Houbiers, A. Bruggink and B. Zwannenburg, *Tetrahedron*, 1997, **53**, 9417; (*c*) For a recent paper on asymmetric transformation, the introduction of which sets out the principles and correct terminology, see N. A. Hassan, E. Bayer and J. C. Jochims, *J. Chem. Soc., Perkin Trans. 1*, 1998, 3747; (*d*) For rare cases of the application of asymmetric transformation to chiral allenes, see M. Node, K. Nishide, J. Fujiwara and S. Ichihashi, *Chem. Commun.*, 1998, 2363; Y. Naruse, H. Watanabe, Y. Ishiyama and T. Yoshida, *J. Org. Chem.*, 1997, **62**, 3862.

2 (*a*) See J. Clayden, *Angew. Chem., Int. Ed. Engl.*, 1997, **36**, 949 and references therein; (*b*) See *e.g.* S. Vyskocil, M. Smrcina and P. Kocovsky, *Tetrahedron Lett.*, 1998, **39**, 9289; G. Chelucci, A. Bacchi, D. Fabbri, A. Saba and F. Ulgheri, *Tetrahedron Lett.*, 1998, **40**, 553.

3 S. M. Verma and R. Prasad, *J. Org. Chem.*, 1973, **38**, 1004.

4 R. S. Atkinson, E. Barker, P. J. Edwards and G. A. Thompson, *J. Chem. Soc., Perkin Trans. 1*, 1996, 1047; R. S. Atkinson, E. Barker, C. J. Price and D. R. Russell, *J. Chem. Soc., Chem. Commun.*, 1994, 1159.

5 P. S. N. Reddy and A. K. Bhavani, *Indian J. Chem., Sect. B*, 1992, **31**, 740.

6 (*a*) E. Vedejs, S. C. Fields, R. Hayashi, S. R. Hitchcock, D. R. Powell and M. R. Schrimpf, *J. Am. Chem. Soc.*, 1999, **121**, 2460; (*b*) E. Vedejs and Y. Donde, *J. Am. Chem. Soc.*, 1997, **119**, 9293.

7 S. C. Benson, P. Cai, M. Colon, M. A. Haiza, M. Tokles and J. K. Snyder, *J. Org. Chem.*, 1988, **53**, 5335.

Communication 9/05018C

ChemComm

Chromium bis(phosphoranimine) complexes; bridging chromium carbenes with no CO or Cp supporting ligands†

Aparna Kasani, Robert McDonald and Ronald G. Cavell*

Department of Chemistry, University of Alberta, Edmonton, Alberta, Canada T6G 2G2.
E-mail: Ron.Cavell@ualberta.ca

Received (in Bloomington, IN, USA) 29th June 1999, Accepted 27th August 1999

Novel dimeric and tetrametallic Cr(II) bridging carbene complexes supported by bis(phosphinimine) ligands are described.

Many carbene complexes have been synthesized since the first report by Fischer;[1] these extremely useful compounds have found widespread applications in organic synthesis and catalysis.[2–5] Chromium carbene chemistry is dominated by low-valent derivatives stabilized in general by carbonyl ligands.[6] High valent chromium carbene derivatives are rare[7–9] in contrast to the heavier group 6 metals, molybdenum and tungsten, which provide numerous examples of carbonyl-free carbene complexes.[3,4,10] Only three carbonyl-free chromium carbene complexes have been structurally characterized[11–13] although several attempts to make such chromium systems have been reported.[13–15] Here, we describe the synthesis and structure of a novel dimeric and tetrametallic carbene bridged chromium complexes obtained by a new route; the preliminary dilithiation of bis(iminophosphorano)methane[16,17] followed by the simple metathetical reaction of this salt with a metal halide. Using this and related routes we have recently prepared Ti and Zr carbene complexes.[18,19] The Cr complex described herein represents the first example of a bridging chromium carbene which is devoid of the usual carbonyl or cyclopentadienyl supporting ligands and it also represents the first example of a chromium carbene complex which contains two phosphorus substituents on the carbene carbon atom. In addition the partially substituted tetrachromium complex was also isolated and characterized.

Chromium dichloride (as the THF adduct) reacted with $Li_2\{C(Ph_2P{=}NSiMe_3)_2\}$ **1**[16,17] with elimination of 2 moles of LiCl to give $[Cr\{\mu_2\text{-}C(Ph_2P{=}NSiMe_3)_2\text{-}\kappa^4C,C',N,N'\}]_2$ **2**‡ as a paramagnetic, red, air-sensitive crystalline solid (Scheme 1). A small quantity of a green complex was also isolated from the 1:1 reaction which proved to be the partially substituted tetranuclear complex $[Cr_2(\mu\text{-}Cl)_2\{\mu_2\text{-}C(Ph_2P{=}NSiMe_3)_2\text{-}\kappa^4C,C',N,N'\}(LiCl)(THF)_2]_2$ **3**. The latter was prepared in good yield by the reaction of 0.5 molar equivalent of the ligand with the metal precursor.§ The room temperature magnetic moments for **2** and **3**, respectively, were 2.76 μ_B (for the dimer) and 6.28 μ_B (for the tetrachromium unit). The magnetic moments of **2** and **3** are too low to account for the total number of unpaired electrons for Cr(II) which suggests interaction between the metals. The Cr–Cr bond distances in **2** and **3** however are not indicative of strong metal–metal interactions.[20]

The molecular structure of $[Cr\{\mu_2\text{-}C(Ph_2P{=}NSiMe_3)_2\text{-}\kappa^4C,C',N,N'\}]_2$ **2**¶ (Fig. 1)[21] shows the complex to be a dimer with two independent molecules in the asymmetric unit. The basic framework of **2** consists a central square plane of two chromium atoms bridged by two carbene centers to form a planar Cr_2C_2 four membered, ring. The ligand backbone forms four fused, four-membered rings which are assembled from the bridging carbene carbon, the metal, the phosphorus and the imine nitrogen atoms. These four Cr, N, P, C rings arrange themselves above and below the central Cr_2C_2 plane to create a saddle-like structure in which the geometry around each Cr is approximately tetrahedral. Each of the iminophosphorane nitrogen units coordinate to the metal so that the ligand adopts a $\mu_2\text{-}\kappa^4$ coordination. The two planar four-membered metallocyclic rings in **2** which are subtended around a specific carbene center [Cr(1), N(1), P(1), C(1) and Cr(2), N(2), P(2), C(1)] and [Cr(1), N(3), P(3), C(2) and N(4), P(4), C(2), Cr(2)] make respective dihedral angles of 46.8(1) and 44.8(2)°. The two different molecules in **2** have slightly different Cr–Cr distances averaging 2.573(2) Å.

The molecular structure of the tetranuclear chromium complex $[Cr_2(\mu\text{-}Cl)_2\{\mu_2\text{-}C(Ph_2P{=}SiMe_3)_2\text{-}\kappa^4C,C',N,N'\}(LiCl)(THF)_2]_2$ **3** has been determined and substantiates the arrangement shown in Scheme 1 but is not illustrated here (see electronic supplementary information). This complex also contains carbene centers bridging two chromium atoms [Cr(1), Cr(2)] but in this case there are two types of Cr centers. One type forms a central Cr_2Cl_2 unit with a chlorine bridged Cr–Cr

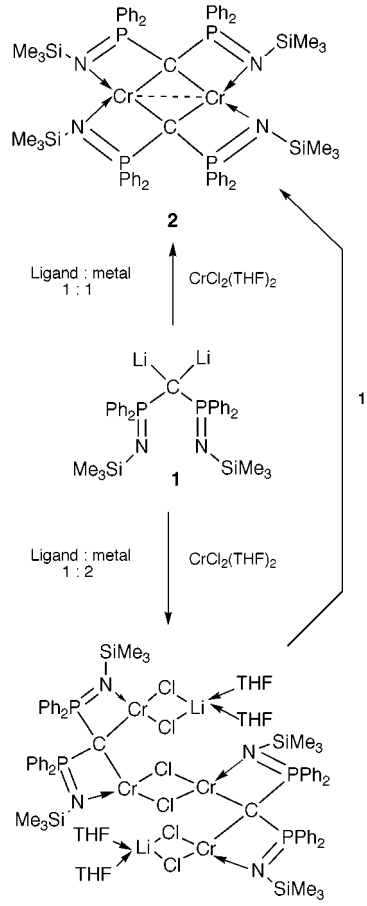

Scheme 1

† Electronic supplementary information (ESI) available: crystal structure of **3**, metrical parameters and crystal data. See http://www.rsc.org/suppdata/cc/1999/1993

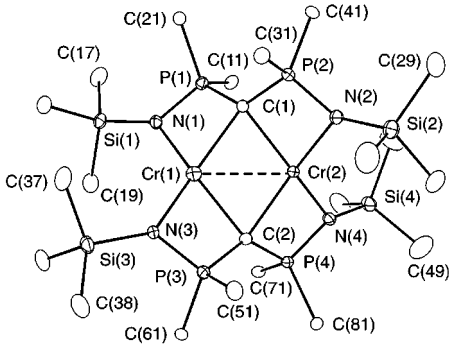

Fig. 1 An ORTEP[21] view of one of the crystallographically independent molecules of **2** showing the atom labelling scheme. The hydrogen atoms and phenyl carbon atoms except for *ipso*-C have been removed for clarity and the remaining atoms are represented by Gaussian ellipsoids at the 20% probability level. Selected interatomic distances (Å) and angles (°) for molecule A: Cr(1)–C(1) 2.148(5), Cr(2)–C(1) 2.137(5), Cr(1)–C(2) 2.150(5), Cr(2)–C(2) 2.128(5), Cr(1)–N(1) 2.103(5), Cr(1)–N(3) 2.093(5), Cr(2)–N(2) 2.091(4), Cr(2)–N(4) 2.081(4), Cr(1)–Cr(2) 2.569(1), N(1)–P(1) 1.605(5), P(1)–C(1) 1.702(6), P(2)–C(1) 1.724(6), P(2)–N(2) 1.603(5); Cr(1)–C(1)–Cr(2) 73.7(2), N(1)–Cr(1)–C(1) 76.2(2), N(2)–Cr(2)–C(1) 77.0(2), C(1)–Cr(1)–C(2) 105.7(2), P(1)–C(1)–P(2) 132.0(3), N(1)–P(1)–C(1) 105.0(3).

distance of 3.508(1) Å. Each of these Cr atoms is then also bound to a bridging carbene unit connecting it to another chromium and the distance between these carbon bridged Cr atoms is 2.9425(8) Å. The second type of Cr atom is connected to a solvated Li center *via* two chloride bridges. Imine nitrogens complete the roughly tetrahedral coordination about the Cr. There are two four-membered rings subtended from each carbene center and the dihedral angle between these two planar four-membered rings is 60.97(9)°. Both Cr–Cr distances in **3** are longer than those in **2**. The Cr–Cr distances in **2** fall in between the alkyl bridging distances in $[\{Cp^*Cr(\mu Me)\}_2(\mu\text{-}CH_2)]$ [2.394(1) Å)][12] and $[Cp^*Cr(\mu\text{-}CHSiMe_3)]_2$ [2.687(4) Å].[11] The Cr–C distances in **2** [2.137(5) Å] and in **3** [2.170(3) Å] are slightly longer than those in the aforementioned Cr(III) alkylidene complexes, 2.042(8)[12] and 2.013(12) Å[11] respectively. As expected for neutral amine coordination, the Cr–N distances in **2** and **3** are longer than observed for Cr-amide complexes.[22]

The bond distances within the bicyclic framework of both **2** and **3** are also considerably altered relative to corresponding values in free bisiminophosphoranomethane ligands;[23,24] the P=N bond distances are slightly elongated and the endocyclic P–C bond distances are significantly shorter but the exocyclic P–C bond distances are not affected. These factors suggest that there is a delocalization of π-electron density within each of the two four membered rings. The P–C–P bond angles [av. 131.7(3)° in **2** and 131.4(2) in **3**)] are significantly expanded compared to the corresponding values in $MeCH\{Ph_2P{=}N(C_6H_4Me\text{-}p)\}_2$ [112.39(19)°][23] as well as in $H_2C\{Cy_2P{=}NSiMe_3\}_2$ [117.41(12)°].[24]

Thus we have prepared and structurally characterized a novel dimeric and tetranuclear chromium carbene complexes **2** and **3** wherein the bridging carbene is supported by phosphinimines**.** Access to such complexes is straightforward given the availability of the new dilithium salt. Reactivity studies of these new carbene complexes are presently being pursued.

We thank the Natural Sciences and Engineering Research Council of Canada, NOVA Chemicals Ltd. and the University of Alberta for financial support.

Notes and references

‡ *Preparation of* **2**: all experimental manipulations were performed under rigorously anaerobic conditions using Schlenk techniques or an argon-filled glovebox. The dilithium salt $Li_2C(Ph_2P{=}NSiMe_3)_2$ **1**,[16] (0.32 g, 0.56 mmol) was added to a stirred suspension of $CrCl_2(THF)_2$ (0.15 g, 0.56 mmol) in THF (10 ml) at room temp. The reaction mixture turned green and then red. The mixture was stirred at room temp. for 2 days. The solvent was then evaporated and the residue was extracted with 8 ml of diethyl ether and filtered to remove LiCl. The diethyl ether solution was reduced to one-half volume, and the red crystalline product, which deposited at room temp. over a period of two days, was filtered off and dried under vacuum. Yield: 0.19 g, 55.6%, μ_{eff} = 2.76 μ_B.

§ *Preparation of* **3**: anaerobic techniques were used. To a stirred suspension of $CrCl_2(THF)_2$ (0.20 g, 0.75 mmol) in THF (10 ml), the dilithium salt $Li_2C(Ph_2P{=}NSiMe_3)_2$ **1**,[16] (0.21 g, 0.37 mmol) was added at room temp. The reaction mixture turned green and was stirred at room temp. for 1 day. The solvent was then evaporated and the residue was extracted with 15 ml of diethyl ether and filtered to remove LiCl. The diethyl ether solution was reduced to one-half volume 1 ml of THF was added, and the solution cooled at −15 °C for 3 days to give a green crystalline product which was filtered off and dried under vacuum. Yield: 0.21 g, 61.1%. μ_{eff} = 6.28 μ_B.

¶ *Crystal data* for **2**: monoclinic, $P2_1/n$ (a non-standard setting of $P2_1/c$, no. 14), a = 22.1588(9), b = 26.7524(12), c = 23.2798(11) Å, β = 96.410(1)°, V = 13714.0(11) Å^3, Z = 4, μ = 0.522 mm^{-1}. The structure was solved by direct methods and refined by full-matrix least squares procedures: R_1 = 0.0774 and 0.1512, (wR_2 = 0.2099 and 0.2480) for 12700 reflections with $F_o^2 \geqslant 2\sigma(F_o^2)$ and all data, respectively. CCDC 182/1397.

1 E. O. Fischer and A. Maasböl, *Angew. Chem., Int. Ed. Engl.* 1964, **3**, 580.
2 See for example: W. D. Wulff, *Organometallics*, 1998, **17**, 3116; K. H. Dötz, H. Fischer, P. Hofmann, F. R. Kreissl, U. Schubert and K. Weiss, *Transition Metal Carbene Complexes*, Verlag Chemie, Weinheim, 1983; M. P. Doyle and D. C. Forbes, *Chem. Rev.*, 1998, **98**, 911; P. J. Brothers and W. R. Roper, *Chem. Rev.*, 1988, **88**, 1293; C. F. Bernasconi, *Chem. Soc. Rev.*, 1997, **26**, 299; K. J. Ivin, *Olefin Metathesis*, Academic Press, London, 1983; K. H. Theopold, *Eur. J. Inorg. Chem.*, 1998, 15.
3 J. Feldman and R. R. Schrock, *Prog. Inorg. Chem.*, 1991, **39**, 1.
4 R. R. Schrock, *Acc. Chem. Res.*, 1990, **23**, 158.
5 K. H. Dötz and P. Tomuschat, *Chem. Soc. Rev.*, 1999, **28**, 187.
6 M. J. Winter, ch 3, *Hexacarbonyls and Carbonyl Complexes of Carbon σ-Bonded Ligands of Chromium, Molybdenum and Tungsten*, in *Comprehensive Organometallic Chemistry II*, ed. E. W. Abel, F. G. A. Stone and G. Wilkinson, Pergamon, Oxford, 1995, vol. 5, pp. 155–214.
7 A. C. Filippou, D. Wössner, B. Lungwitz and G. Kociok-Köhn, *Angew. Chem., Int. Ed. Engl.*, 1996, **35**, 876.
8 M. P. Coles, V. C. Gibson, W. Clegg, M. R. J. Elsegood and P. A. Porrelli, *Chem. Commun.*, 1996, 1963.
9 J. Sundermeyer, K. Weber and H. Pritzkow, *Angew. Chem., Int. Ed. Engl.*, 1993, **32**, 731.
10 S. Woodward and M. J. Winter, ch. 5, *Organometallic Complexes of Chromium, Molybdenum and Tungsten without Carbonyl Ligands*, in *Comprehensive Organometallic Chemistry II*, ed. E. W. Abel, F. G. A. Stone and G. Wilkinson, Pergamon, Oxford, 1995, vol. 5; pp. 281–329.
11 R. A. Heintz, S. Leelasubcharoen, L. M. Liable-Sands, A. L. Rheingold and K. H. Theopold, *Organometallics*, 1998, **17**, 5477.
12 S. K. Noh, R. A. Heintz, C. Janiak, S. C. Sendlinger and K. H. Theopold, *Angew. Chem.*, 1990, **102**, 805; *Angew. Chem., Int. Ed. Engl.*, 1990, **29**, 775.
13 S. Hao, J.-I. Song, P. Berno and S. Gambarotta, *Organometallics*, 1994, **13**, 1326.
14 G. Bhandari, Y. Kim, J. M. McFarland, A. L. Rheingold and K. H. Theopold, *Organometallics*, 1995, **14**, 738.
15 J. L. Hubbard and W. K. McVicar, *J. Am. Chem. Soc.*, 1986, **108**, 6422.
16 A. Kasani, R. P. Kamalesh Babu, R. McDonald and R. G. Cavell, *Angew. Chem., Int. Ed.*, 1999, **38**, 1483.
17 C. M. Ong and D. W. Stephan, *J. Am. Chem. Soc.*, 1999, **121**, 2939.
18 R. G. Cavell, R. P. Kamalesh Babu, A. Kasani and R. McDonald, *J. Am. Chem. Soc.*, 1999, **121**, 5805.
19 R. P. Kamalesh Babu, R. McDonald and R. G. Cavell, *Organometallics*, 1999, **18**, in press.
20 F. A. Cotton and R. A. Walton, *Multiple Bonds Between Metal Atoms*, John Wiley and Sons, New York, 1982, p. 466.
21 C. K. Johnson, ORTEP, Report ORNL No. 5138, Oak Ridge National Laboratory, Oak Ridge, TN, 1976.
22 K. B. P. Ruppa, K. Feghali, I. Kovacs, K. Aparna, S. Gambarotta, G. P. A. Yap and C. Bensimon, *J. Chem. Soc., Dalton Trans.*, 1998, 1595.
23 M. W. Avis, C. J. Elsevier, N. Veldman, H. Kooijman and A. L. Spek, *Inorg. Chem.*, 1996, **35**, 1518.
24 R. P. Kamalesh Babu, R. McDonald, R. G. Cavell, X-ray structure of $CH_2\{PCy_2{=}NSiMe_3\}_2$, University of Alberta Structure Determination Laboratory, Report RGC 9802.

Communication 9/05241K

ChemComm

$[NBnMe_3]_2[Fe_2Cu_4(SePr^i)_8Cl_2]$ and $[NBnMe_3]_2[Fe_3Cu(SePr^i)_6Cl_3]$, novel heterometallic chalcogenolate complexes with dodecahedral and octahedral selenium cages

Jörg Lackmann, Ralf Hauptmann, Stefan Weißgräber and Gerald Henkel*

Gerhard-Mercator-Universität Duisburg, Lotharstr.1, Institut für Synthesechemie, D-47048 Duisburg, Germany. E-mail: biohenkel@uni-duisburg.de

Received (in Basel, Switzerland) 25th June 1999, Accepted 17th August 1999

$[Fe_2Cu_4(SePr^i)_8Cl_2]^{2-}$, an unprecedented hexanuclear mixed iron–copper–selenolate cage complex containing a dodecahedral selenium framework and $[Fe_3Cu(SePr^i)_6Cl_3]^{2-}$, a related tetranuclear complex anion with an octahedral selenium arrangement, are described.

The chemistry of transition-metal chalcogenolate complexes continues to attract widespread attention owing to their role as synthetic analogues for the active sites of various metalloproteins such as alcohol dehydrogenase, ferredoxins, blue copper proteins or nitrogenases.[1,2] In a broader context, they display a large variety of stoichiometries and structures which have no parallels in other species. In contrast to the large number of homometallic bi- and poly-nuclear chalcogenolate complexes known so far, complexes containing different kinds of metal atoms are comparatively rare. They include $[Au_3Cu_3(SCH_2CH_2S)_4]^{2-}$,[3] $[Au_4Cu_2(SCH_2CH_2S)_4]^{2-}$,[3] $[Au_2Ag_2(SCH_2CH_2S)_4]^{2-}$,[3] $[Cu_6In_3(SEt)_{16}]^-$,[4] $[Eu_2M_2(SPh)_8(py)_6]$ (M = Cd, Hg),[5] $[Eu_2Zn_2(SPh)_8(thf)_6]$,[5] $[CuIn(ER)_4(PPh_3)_2]$ (E = S, Se)[6] and $[(PPh_3)_2Cu_2M(EC_6H_4Me)_6]$.[7,8] (M = Mo, W; E = S, Se)

Recently, we synthesized novel heterometallic thiolate complexes by reacting homometallic thiolate precursors with simple copper halides. The octanuclear complex anion $[Mn_4Cu_4S(SPr^i)_{12}]^{2-}$[9] is accessible by reaction of $[Mn_2(SPr^i)_6]^{2-}$[10] with CuCl. The mixed sulfide–thiolate compound contains a central Cu_4Mn_4 metal cube defined by interpenetrating copper and manganese tetrahedra which is stabilised by an interstitial sulfide ion and edge-bridging thiolate groups. In the case of $[Fe_3Cu(SPr^i)_6Cl_3]^{2-}$,[11] $[Fe_2(SPr^i)_6]^{2-}$ was used as the thiolate precursor. The mixed iron–copper complex has a truncated adamantane-type structure which can be derived from the structure of the parent homometallic complex of the general formula $[Fe_4(SR)_6X_4]^{2-}$ (X = Cl, Br, I, ER)[12] by replacement of a $\{FeX\}^+$ unit by Cu^+. Following this methodical approach, the chemistry of selenolate precursors under similar reaction conditions has also been investigated. In this paper, the complex anions $[Fe_3Cu(SePr^i)_6Cl_3]^{2-}$ **2** and $[Fe_2Cu_4(SePr^i)_8Cl_2]^{2-}$ **4** are described, which represent the first structurally characterized selenolate complexes containing different transition metals ions.

Both complex anions are formed in the reaction of $[NBnMe_3]_2[Fe_2(SePr^i)_6]$ with $FeCl_2$ and CuCl in acetonitrile simultaneously and were isolated as their corresponding $[NBnMe_3]^+$ salts **1** and **3** in form of light brown (**1**) or red (**3**) solids.† The structures of **1** and **3** were determined by X-ray crystallography.‡

Crystals of **1** are composed of isolated complex anions **2** and $[NBnMe_3]^+$ counter cations. They are isotypic with the corresponding sulfur derivative $[NBnMe_3]_2[Fe_3Cu(SPr^i)_6Cl_3]$ whose structural properties have already been discussed.[11] The structure of **2** is depicted in Fig. 1.

The Fe_3Cu framework of **2** is a trigonal pyramid with edges completely bridged by selenolate groups. The iron and three selenium atoms, Se(4), Se(5) and Se(6), define a compressed trigonal prism with homoatomic triangular and heteroatomic prismatic faces. The copper atom does not reside exactly within the triangular selenium face, but is shifted by 0.067 Å towards the Fe atoms (mean Cu–Fe 3.351 Å). The mean Fe–Fe and Se–Se distances within the Fe_3Se_3 prism are 4.051 and 4.066 Å, respectively, whereas the Fe–Se distances are much smaller (mean value 2.471 Å).

The complete set of selenium atoms are arranged in a distorted octahedral fashion. With edge lengths of 4.322 Å the triangle Se(1)–Se(2)–Se(3) is significantly larger than the opposite one [Se(4)–Se(5)–Se(6), mean edge length 4.066 Å]. The first triangle is neither capped by a $\{FeCl\}^+$ unit nor centered by Cu^+. The triangles Se(1)–Se(3)–Se(4), Se(1)–Se(2)–Se(5) and Se(2)–Se(3)–Se(6) are capped by $\{FeCl\}^+$ units, achieving an idealised C_3 symmetry of **2**. Each iron atom has a distorted pseudo-tetrahedral $FeSe_3Cl$ coordination with selenium atoms in metal bridging positions and a terminal chloride ligand. The average Fe–Se distance of 2.471 Å is very close to the value of 2.463 Å found in $[Fe_2(SePr^i)_6]^{2-}$.[13]

The complete anionic entity **2** can also be considered as being composed of the complex anion $[Fe_3(SePr^i)_6Cl_3]^{3-}$ and a Cu^+ cation which is probably needed to stabilise the structure.

Trigonal-planar $CuSe_3$ as well as pseudo-tetrahedral $FeSe_3Cl$ coordination sites related to those observed in **2** are also characteristic constituents of the hexanuclear complex anion **4** (Fig. 2).

In contrast to **2** which contains an octahedral selenium framework, the selenium atoms in **4** define a triangulated dodecahedron. This dodecahedron [Fig. 3(a)] is composed of two interpenetrating tetrahedra, a compressed one consisting of Se(1), Se(4), Se(7) and Se(8) (atom type A) and an elongated one consisting of Se(2), Se(3), Se(5) and Se(6) (atom type B). The Cu atoms occupy one of the two tetrahedral sets of four triangular faces of the dodecahedron which are defined by one B and two A type selenium atoms. One half of the four triangular faces defined by one A and two B type selenium atoms are capped by $\{FeCl\}^+$ units.

From another point of view, the Cu atoms bridge the four short edges of the compressed tetrahedral substructure defined

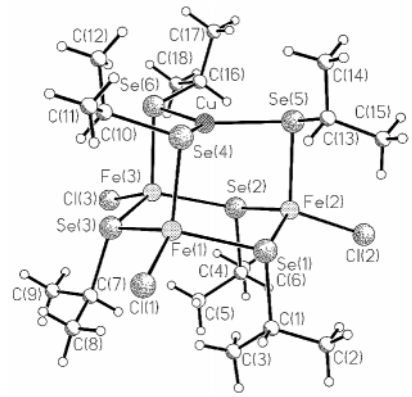

Fig. 1 $[Fe_3Cu(SePr^i)_6Cl_3]^{2-}$: molecular structure with atomic labels.

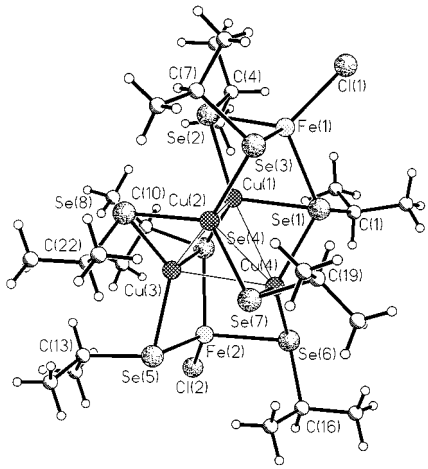

Fig. 2 $[Fe_2Cu_4(SePr^i)_8Cl_2]^{2-}$: molecular structure with atomic labels.

by the four A type selenium atoms and form an additional bond each to a B type selenium atom of the elongated tetrahedral substructure.

The Cu–Cu distances range from 2.656(6) to 2.988(8) Å, whereas the Fe(1)–Cu(1) and Fe(2)–Cu(2) distances are 2.748(7) and 2.853(8) Å, respectively. The mean Fe–Se distance is 2.469 Å. This value is very close to the values of 2.471 Å found in **2** and 2.463 Å found in $[Fe_2(SePr^i)_6]^{2-}$.[13]

The remarkable condensation principle observed here, for the first time, leads to two novel μ_3-selenolate bridges which connect two different metal types (Cu_2Fe). In addition, four heterometallic μ-selenolate bridges (CuFe) are also present. The two Cl^- ions are non-bridging in nature and expand the ligand spheres of the Fe atoms towards slightly distorted $FeSe_3Cl$ tetrahedra.

The complex anion **4** can formally be expanded by introducing two further $\{FeCl\}^+$ groups capping the remaining two triangular faces defined by one A and two B type selenium atoms [Se(2), Se(3), Se(8) and Se(5), Se(6), Se(7)]. The structure of the corresponding hypothetical electroneutral $[Fe_4Cu_4(SePr^i)_8Cl_4]$ molecule is shown in Fig. 3(b) (the additional $\{FeCl\}^+$ groups are drawn with open bonds). This complex contains two $\{Fe_2(\mu\text{-}SePr^i)_2(SePr^i)_2Cl_2\}$ subunits whose structural properties are very similar to those observed in the binuclear complexes of general formula $[Fe_2(\mu\text{-}SR)_2(SR)_4]^{2-}$ (R = Me, Et, Pr^i, *c*-C_6H_{11}, Bu^t).[14] These subunits are linked with the central Cu_4 tetrahedron *via* selenolate bridges. Further expansion of the metal–selenium cage by adding Cu^+ ions or $\{FeCl\}^+$ subunits to the metal-free triangular faces of the selenium dodecahedron defined by one A and two B type atoms is not possible owing to strong repulsions.

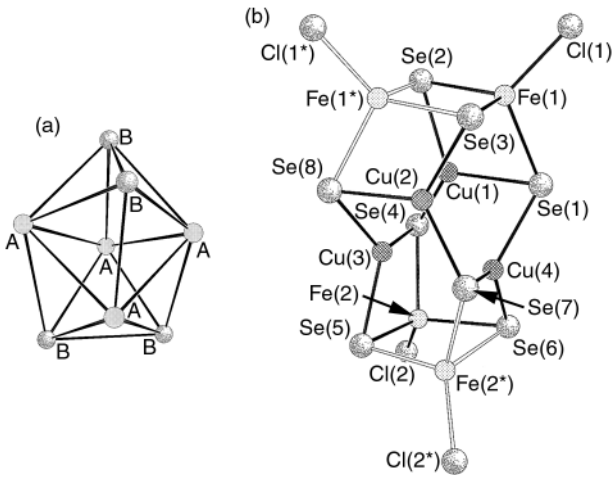

Fig. 3 (a) The triangulated Se_8 dodecahedron of $[Fe_2Cu_4(SePr^i)_8Cl_2]^{2-}$ showing the tetrahedral substructures defined by A and B type selenium atoms. (b) Structure of the hypothetical complex $[Fe_4Cu_4(SePr^i)_8Cl_4]$ (alkyl groups omitted, additional atoms marked with asterisk).

In summary, we have prepared and structurally characterised the first mixed-metal iron–copper–selenolate complexes containing octahedral (**2**) and novel triangulated dodecahedral (**4**) selenium frameworks.

Financial support from the Deutsche Forschungsgemeinschaft (DFG), from the Bundesminister für Bildung, Wissenschaft und Forschung (BMBF) and from the Fonds der Chemischen Industrie is gratefully acknowledged.

Notes and references

To a solution of $[NBnMe_3]_2[Fe_2(SePr^i)_6]$ (2.86 g, 2.5 mmol) in MeCN (40 ml) was added 0.32 g of $FeCl_2$ (2.5 mmol) followed by addition of 0.25 g of CuCl (2.5 mmol) under stirring. The solution changed from black–brown to orange–brown, the suspension was stirred for 24 h, and the black residue was filtered off. The filtrate was reduced in volume (*ca.* 20 ml). Dark red platelets of **1** and light brown columns of **2** were obtained in a 9:1 molar ratio after diffusion of *ca.* 20 ml of diethyl ether into the solution.

‡ *Crystal data*. Siemens P4RA four circle diffractometer, rotating anode generator, Mo-Kα radiation (λ = 0.71073 Å), graphite monochromator, scintillation counter, T = 150 K, empirical absorption correction; direct methods, full-matrix least-squares refinement, non-hydrogen atoms anisotropic unless otherwise stated, H atoms at idealised positions, one common isotropic temperature factor for H within each organic residue, one extinction parameter, one scaling factor.

1: $C_{38}H_{74}N_2Cl_3Fe_3CuSe_6$, M = 1144.45, monoclinic, a = 10.890(3), b = 12.191(3), c = 41.782(9) Å, β = 96.39(2)°, V = 5512.52 Å^3, space group $P2_1/n$, Z = 4, D_c = 1.651 g cm^{-3}, μ(Mo-Kα) = 5.29 mm^{-1}, transmission range 0.981–0.688, $2\theta_{max}$ = 48°, ω scan, crystal dimensions *ca*. 0.52 × 0.21 × 0.13 mm, 8558 unique reflections, $R(F)$ = 0.0662 for 4798 reflections with $I > 2\sigma(I)$, $wR(F^2)$ = 0.1837 for all data, 488 variables.

2: $C_{44}H_{88}N_2Cl_2Fe_2Cu_4Se_8$, M = 1713.60, monoclinic, a = 14.832(2), b = 16.450(3), c = 26.524(4) Å, β = 105.29(1), V = 6242.43 Å^3, space group Cc, Z = 4, D_c = 1.823 g cm^{-3}, μ(Mo-Kα) = 6.57 mm^{-1}, transmission range 0.997–0.484, $2\theta_{max}$ = 54°, ω scan, crystal dimensions *ca*. 0.45 × 0.21 × 0.11 mm, 4815 unique reflections, $R(F)$ = 0.0714 for 3187 reflections with $I > 2\sigma(I)$, $wR(F^2)$ = 0.188 for all data, 372 variables; isopropyl groups and counter cations isotropic, one common C–C distance within the isopropyl groups [1.475(7) Å], one common N–C distance within the counter cations [1.491(7) Å], phenyl groups with idealised geometries.

CCDC 182/1384. See http://www.rsc.org/suppdata/cc/1999/1995/ for crystallographic files in .cif format.

1 I. G. Dance, *Polyhedron*, 1986, **5**, 1037; P. J. Blower and J. R. Dilworth, *Coord. Chem. Rev.*, 1987, **76**, 121; B. Krebs and G. Henkel, *Angew. Chem.*, 1991, **103**, 785; *Angew. Chem., Int. Ed. Engl.*, 1991, **30**, 769; I. Dance and K. Fisher, *Prog. Inorg. Chem.*, 1994, **41**, 637.
2 B. Krebs and G. Henkel, *Rings, Clusters and Polymers of Main Group and Transition Elements*, ed. H. Roesky, Elsevier, Amsterdam, 1989, p. 439.
3 G. Henkel, B. Krebs, P. Betz, H. Fietz and K. Saatkamp, *Angew. Chem.*, 1988, **100**, 1373; *Angew. Chem., Int. Ed. Engl.*, 1988, **27**, 1326.
4 W. Hirpo, S. Dhingra and M. G. Kanatzidis, *J. Chem. Soc., Chem. Commun.*, 1992, 557.
5 M. Brewer, J. Lee and J. G. Brennan, *Inorg. Chem.*, **1995**, 34, 5919.
6 W. Hirpo, S. Dhingra, A. C. Sutorik and M. G. Kanatzidis, *J. Am. Chem. Soc.*, 1993, **115**, 1597.
7 P. M. Boorman, H. B. Kraatz, M. Parvez and T. Ziegler, *J. Chem. Soc., Dalton Trans.*, 1993, 433.
8 J. M. Ball, P. M. Boorman, J. F. Fait and T. Ziegler, *J. Chem. Soc., Chem. Commun.*, 1989, 722.
9 H.-O. Stephan, M. G. Kanatzidis and G. Henkel, *Angew. Chem.*, 1996, **108**, 2257; *Angew. Chem., Int. Ed. Engl.*, 1996, **35**, 2135.
10 H.-O. Stephan and G. Henkel, *Polyhedron*, 1996, **15**, 501.
11 H.-O. Stephan, G. Henkel and M. G. Kanatzidis, *J. Chem. Soc., Chem. Commun.*, 1997, 67.
12 D. Coucouvanis, M. Kanatzidis, E. Simhon and N. C. Baenziger, *J. Am. Chem. Soc.*, 1982, **104**, 1874.
13 R. Hauptmann, J. Lackmann, C. Chen and G. Henkel, *Acta Crystallogr., Sect. C*, 1999, **55**, 1084.
14 K. S. Hagen and R. H. Holm, *Inorg. Chem.*, 1984, **23**, 418; R. Hauptmann, J. Lackmann and G. Henkel, *Z. Kristallogr.*, 1999, 214, 132; R. Hauptmann, J. Lackmann and G. Henkel, *Z. Kristallogr.*, 1999, 214, 137.

Communication 9/05134A

A direct access to layered zirconium-phosphonate materials from dialkylphosphonates

Paul-Alain Jaffrès,[a] Vincent Caignaert[b] and Didier Villemin*[a]

[a] *LCMT, UMR CNRS 6507, Ecole Nationale Supérieure d'Ingénieur de Caen, Université de Caen, ISMRA, 6Bd du Maréchal Juin, F-14050 Caen, France. E-mail: didier.villemin@ismra.fr*

[b] *CRISMAT, UMR CNRS 6508, Ecole Nationale Supérieure d'Ingénieur de Caen, Université de Caen, ISMRA, 6Bd du Maréchal Juin, F-14050 Caen, France*

Received (in Cambridge, UK) 2nd July 1999, Accepted 3rd September 1999

Reaction of dialkylphosphonates with zirconium salts in acidic aqueous media provides a facile route to crystalline hybrid zirconium phosphonate materials.

Since the first synthesis of a layered zirconium phosphonate,[1] many other layered materials involving different metals [M(IV) or M(II)] have been synthesised. Some of these materials may have practical applications as supported catalysts,[2] protonic conductors[3] and molecular sieves.[4] These materials which possess a well ordered structure, are synthesised by reaction of a phosphonic acid with a metal(IV) or a metal(II) source in water or sometimes with an organic co-solvent. In order to increase the crystallinity of these materials, the addition of a mineralising agent (HF) or the use of hydrothermal conditions[5] can be employed.

Phosphonic acids, which form the necessary precursor to synthesise metal phosphonate materials, are generally obtained by reaction of a phosphonate with either a hydrogen halide (HCl, HBr) in aqueous medium or by using the method of McKenna *et al.*[6] These phosphonates are easily obtained by the Arbusov reaction[7] or by a palladium or nickel assisted phosphonation when aromatic phosphonates are required.[8] It is worth noting that, unlike dialkylphosphonates, the purification of phosphonic acids can not be readily achieved using chromatographic or distillation methods. Owing to their strong polarity and the formation of strong intermolecular hydrogen bonds.

With the aim of avoiding the prior synthesis of phosphonic acids, we report here an easy method to synthesise hybrid metal phosphonate materials by using phosphonates instead of phosphonic acids as precursors.

In a preliminary result (entry 1, Table 1) zirconium bis(methylphosphonate) **5** was obtained in quantitative yield from the reaction of dimethyl methylphosphonate **1** with zirconyl chloride **4** in an acidic aqueous solution (9 M HCl) under reflux for 24 h . This first result indicates that methyl phosphonic acid, which is progressively produced *in situ* by hydrolysis of phosphonate **1**, reacts immediately with zirconyl chloride **4** to yield **5** in quantitative yield.† Analyses of material **5** (microanalyses, XRD powder diffraction pattern, IR), as synthesised from phosphonate **1** or from phosphonic acid **2** (Alberti's method) are identical.‡ It is interesting that the microanalysis of material **5** does not show any increase in carbon content that might come from the phosphonate function. This observation indicates that the hybrid material does not contain any product resulting from monohydrolysis of phosphonate **1**.

Taking into account this interesting result, the influence of experimental conditions on crystallinity of **5** has been studied. Powder XRD patterns and surface area data (BET) were used to obtain information about the degree of crystallinity of the materials. In particular, BET analysis is an interesting indicator of the crystallinity and granulometry of resulting materials. In a previous study, concerning zirconium bis(methylphosphonate) **5**, a direct relationship between the crystallinity and specific area was demonstrated (greater crystallinity leads to a smaller surface area).[9]

The use of HBr (entry 2, Table 1) instead of HCl (entry 1) affords after refluxing for 24 h, a poorly crystalline sample of material **5** (S_{BET} = 378.1 m^2 g^{-1}). This observation may be explained by the well known difference in the affinity of chloride and bromide ions for Zr(IV) (Cl > Br).[10] Furthermore, bromide is a better nucleophile than chloride and this property enhances the kinetics of the hydrolysis of phosphonate to phosphonic acid. Both factors, *i.e.* the greater affinity of HCl towards Zr and the slower hydrolysis of phosphonate by use of HCl, contribute to a decrease in the rate of reaction between phosphonic acid and Zr(IV), leading to more crystalline hybrid materials.

In order to compare the influence of the substrate (phosphonate or phosphonic acid), on the crystallinity of the resulting material, **5** was synthesised from both precursors dimethyl methylphosphonate **1** (entry 1) and methylphosphonic acid **2** (entry 3) under identical experimental conditions. The materials obtained from both experiments exhibit the same characteristics (IR, microanalyses) with the exception of their specific area. The use of phosphonate **1** leads to a slightly more crystalline material (S_{BET} = 96.6 m^2 g^{-1}) compared to the material obtained from the corresponding phosphonic acid **2** (S_{BET} = 119.0 m^2 g^{-1}).

Using diethyl methylphosphonate **3** (entry 4) in a 24 h reflux experiment leads to a sample of **5** that is less crystalline compared to that prepared using dimethyl methylphosphonate **1** (entry 1). From these results it appears that dimethylphosphonate is the best choice when short refluxing times are required.

Table 1 Reaction of phosphonates **1**–**3** or phosphonic acid **2** with zirconyl chloride **4** leading to compound **5**

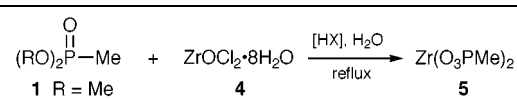

Entry	Substrate	[HX]/M	*t*/h	Mole ratio **1**, **2** or **3**/Zr	S_{BET} (**5**)/m^2 g^{-1}
1	**1**	9[a]	24	3	96.6
2	**1**	9[b]	24	3	378.1
3	**2**	9[a]	24	3	119.0
4	**3**	9[a]	24	3	249.2
5	**1**	12.2[a]	24	3	86.0
6	**1**	12.2[a]	24	1.66	38.4
7	**2**	12.2[a]	24	1.66	26.0
8	**1**	12.2[a]	112	1.66	27.6
9	**1**	9[a]	112	1.66	28.8
10	**1**	3[a]	112	1.66	62.3
11	**1**	0[c]	112	1.66	203.4

[a] HCl. [b] HBr. [c] Water was used as solvent.

Since it is often the aim to synthesise hybrid materials possessing functionalised pendant organic groups (chiral molecules[11] or ligands), it is worth considering the effect of using an excess of metal salt, in order to avoid the loss of costly organic substrate. By using an excess of zirconyl chloride we observed that the phosphonate/Zr ratio has a great influence on the crystallinity of the resulting material. Indeed, a slight excess of zirconyl chloride (1.2 equiv.) yields a more crystalline sample of material **5** (entry 6, S_{BET} = 38.4 $m^2\ g^{-1}$) when compared to the use of an excess of phosphonate (entry 5, S_{BET} = 86.0 $m^2\ g^{-1}$). By using the same excess of zirconyl chloride, it appears that the use of phosphonic acid leads to a material **5** with a slightly better crystallinity (entry 7, S_{BET} = 26.0 $m^2\ g^{-1}$) compared to the use of dimethyl methylphosphonate **1** (entry 6, S_{BET} = 38.4 $m^2\ g^{-1}$).

Finally the effect of HCl concentration upon the crystallinity of **5** was investigated. When **5** was synthesised by using a high concentration of HCl (> 9 M) the same surface areas (S_{BET} = 28 $m^2\ g^{-1}$) were obtained (entry 8 and 9) while the use of a 3 M HCl solution (entry 10) yields a less crystalline material (S_{BET} = 62 $m^2\ g^{-1}$). In absence of acid (entry 11) the same material **5** was isolated in quantitative yield and characterised by IR, microanalysis and XRD powder pattern. However, BET analysis (203.4 $m^2\ g^{-1}$) indicated a poorly crystalline material. Despite the pH of the solution in this experiment being clearly acidic (pH = 1) owing to zirconyl chloride, the concentration of HCl was low (0.3 M) compared to experiments carried out in 9 M HCl. The synthesis of hybrid materials using a very low concentration of HCl could be useful when precursors are sensitive to strong acidic solutions such as when ether or cyano functions are used.

Fig. 1 shows some powder X-ray diffractograms for materials **5**, which corroborate the results obtained by BET measurement.

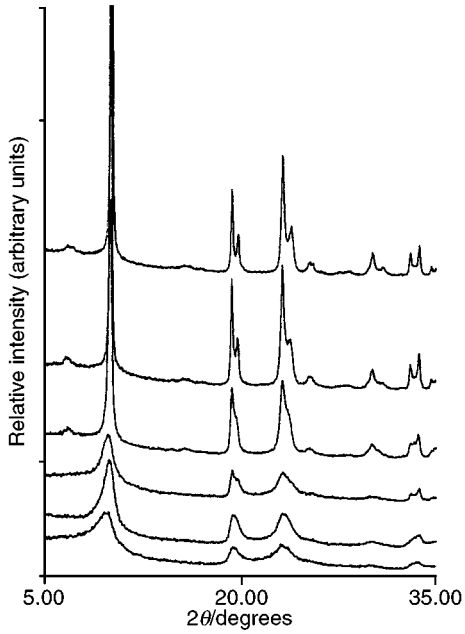

Fig. 1 Powder X-Ray diffractograms for material **5** corresponding to experiments detailed in Table 1: (a) entry 5, (b) entry 13, (c) entry 6, (d) entry 7, (e) entry 11, (f) entry 8. Corresponding BET surface areas ($m^2\ g^{-1}$: (a) 249.2, (b) 203.4, (c) 86.0, (d) 38.4, (e) 28.8, (f) 26.0.

This new method is compatible with the use of other phosphonates. Materials **6** and **7** (Table 2) prepared by this method are identical to those prepared previously by other synthetic routes. In the case of compound **7**, a pillared structure was obtained. In addition, novel materials **8**–**10**, have been synthesised by using this method and were fully characterised.

The access to new zirconium phosphonate materials shows the advantage of using a phosphonate directly rather than a phosphonic acid. Thus the number of steps to produce the necessary organic substrate is reduced and its purification can be more easily accomplished. Furthermore, very slight differences, in terms of crystallinity, have been observed between this new method and that using phosphonic acid. It has also been demonstrated that this new method is suitable for the use of different phosphonates and diphosphonates to give either layered or pillared structures.

Table 2 Synthesis of layered zirconium phosphonates **6**–**10**

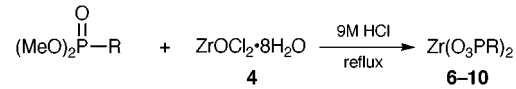

Entry	R	Product	Interlayer distance/Å
1	CH_2CO_2H[a]	**6**[a]	11.1 (Lit.[12] 11.1)
2[c]	$CH_2C_6H_4CH_2$	**7**[d]	10.9 (Lit.[13] 10.8)
3	CH_2Ph	**8**[b]	15.8
4	Et	**9**[b]	10.8
5	CCl_3	**10**[b]	11.5

[a] Ethyl dimethylphosphonoacetate was used as substrate but hydrolysis of the ester function leads to carboxylic functionalities in the interlayer space. [b] n = 2. [c] Dimethyl α,α′-*p*-xylenediphosphonate was used and a pillared structure was obtained. [d] n = 1.

We would like to thank Monique Duyme (UMR-CNRS 6506) for BET measurements.

Notes and references

† *Example of preparation of compound* **5** (*entry 9, Table 1*): a solution of dimethyl methylphosphonate (3.72 g, 30 mmol) and zirconyl chloride (5.80 g, 18 mmol) in aqueous 9 M HCl solution (120 ml) was refluxed for 112 h. The solid was recovered by filtration, washed with distilled water (200 ml) and acetone (50 ml), dried at 40 °C for 18 h and at 200 °C for 24 h.

‡ *Selected microanalyses for compound* **5**: Anal. calc. for $Zr(O_3PCH_3)_2$: C, 8.60; H, 2.17; P, 22.18. Found (entry 3, Table 1) : C, 8.32; H, 2.27; P, 20.15; Found (entry 1, Table 1): C, 8.37; H, 2.54; P, 22.03%.

1 G. Alberti, U. Costantino, S. Allulli and N. Tomassini, *J. Inorg. Nucl. Chem.*, 1978, **40**, 1113.
2 D. Villemin, P.-A. Jaffrès, B. Nechab and F. Courivaud, *Tetrahedron Lett.*, 1997, **38**, 6581; D. Deniaud, B. Schollorn, D. Mansuy, J. Rouxel, P. Battioni and B. Bujoli, *Chem. Mater.*, 1995, **7**, 995; M. G. Clerici, G. Alberti, M. Malentacchi, G. Bellussi, A. Prevedello and C. Corno, *Eur. Pat. Appl.*, EP 386 845, 1990 (*Chem. Abstr.*, 1991, **114**, 165078s); M. B. Dines, P. M. DiGiacomo and K. P. Callahan, *US Pat.*, 4 384 981, 1981 (*Chem. Abstr.*, 1983, **99**, 121445b).
3 G. Alberti, M. Casciola, U. Costantino, A. Peraio and E. Montoneri, *Solid State Ionics*, 1992, **50**, 315.
4 A. Clearfield, *NATO Asi. Ser., Ser. C*, 1993, 159 (*Chem. Abstr.*, 1994, **120**, 207190d).
5 K. Maeda, Y. Kiyozumi and F. Mizukami, *Angew. Chem., Int. Ed. Engl.*, 1994, **33**, 2335.
6 C. E. McKenna, M. T. Higa, N. H. Cheung and M. C. McKenna, *Tetrahedron Lett.*, 1977, 155.
7 R. Engel, *Synthesis of Carbon–Phosphorus Bonds*, CRC Press, Boca Raton, FL, 1987, p. 21.
8 T. Hirao, T. Masunaga, N. Yamada, Y. Ohshiro and T. Agawa, *Bull. Chem. Soc. Jpn.*, 1982, **55**, 909; P. Tavs, *Chem. Ber.*, 1970, **103**, 2428.
9 M. B. Dines and P. C. Griffith, *J. Phys. Chem.*, 1982, **86**, 571.
10 R. G. Pearson, *Hard and Soft Acids and Bases*, Dowden, Huchinson and Ross, Inc., 1973, p. 183.
11 P.-A. Jaffrès, N. Bar and D. Villemin, *J. Chem. Soc., Perkin Trans. 1*, 1998, 2083.
12 M. B. Dines and P. M. DiGiacomo, *Inorg. Chem.*, 1981, **20**, 92.
13 M. B. Dines, P. M. Digiacomo, K. P. Callahan, P. C. Griffith, R. H. Lane and R. E. Cooksey, *ACS Symp. Ser.*, 1982, **192**, 223.

Communication 9/05354I

Synthesis and reaction of 1,4-acetal-bridged 2,3,5,6-tetramethylidene-bicyclo[2.2.0]hexane: the first Diels–Alder route to Dewar benzenes

Masakazu Ohkita, Takanori Suzuki and Takashi Tsuji*

Division of Chemistry, Graduate School of Science, Hokkaido University, Sapporo 060-0810, Japan. E-mail: tsuji@sci.hokudai.ac.jp

Received (in Cambridge, UK) 2nd August 1999, Accepted 3rd September 1999

The 1,4-acetal-bridged derivative of hitherto unknown 2,3,5,6-tetramethylidenebicyclo[2.2.0]hexane, which produces the Dewar benzene skeleton through two successive Diels–Alder reactions with dienophiles, has been synthesized in four steps from dimethyl acetylenedicarboxylate and 1,4-dichlorobut-2-ene.

In the course of our studies on the chemistry of highly strained cyclophanes generated from the corresponding Dewar derivatives,[1] we were interested in developing a new general method for the preparation of Dewar benzenes,[2] especially a versatile one that is applicable to the synthesis of Dewar isomers of polyacenes.[3] An intriguing possibility is the application of hitherto unknown 2,3,5,6-tetramethylidenebicyclo[2.2.0]hexane skeleton **2**[4] because its two successive Diels–Alder reactions with dienophiles formally produce a Dewar benzene structure and subsequent dehydrogenation of the two six-membered rings thus formed would give the corresponding 9,10-Dewar anthracene skeleton. We designed a 1,4-acetal-bridged derivative **1** to prevent an undesired aromatization of the Dewar benzene product under the thermal cycloaddition conditions. Here we report an efficient synthesis of **1** and its Diels–Alder reaction with dienophiles, which represents the first preparation of a Dewar benzene structure by a Diels–Alder reaction.

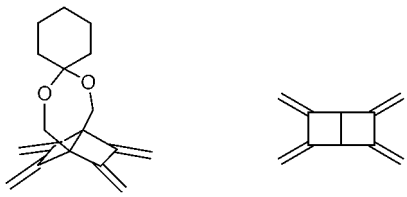

1 **2**

The synthesis of **1** is simple and straightforward (Scheme 1).† Thus, irradiation of dimethyl acetylenedicarboxylate (DMAD) in 1,4-dichlorobut-2-ene with a high-pressure mercury lamp at 12 °C afforded a mixture of bicyclo[2.2.0]hexane derivatives **3** in 32% yield. $LiAlH_4$ reduction of the esters **3** followed by treatment of the resultant diols with 1,1-dimethoxycyclohexane under the influence of a catalytic amount of TsOH provided cyclohexylidene acetal **4** in 48% yield. Quadruple dehydrochlorination of **4** with *t*-BuOK in the presence of 18-crown-6 at room temperature afforded desired **1** in 78% yield as a colorless oil. Compound **1** is prone to polymerization, as has been observed in other bisdiene systems,[5] but shows adequate stability to allow its chromatographic purification and spectroscopic characterization.‡

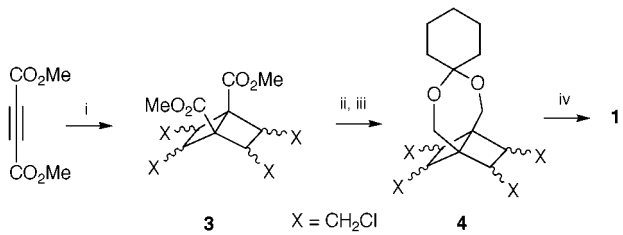

3 X = CH_2Cl **4**

Scheme 1 *Reagents and conditions*: i, *hν*, 1,4-dichlorobut-2-ene, 12 °C, 32%; ii, $LiAlH_4$, Et_2O, 90%; iii, 1,1-dimethoxycyclohexane, TsOH, benzene, 40%; iv, *t*-BuOK, 18-crown-6, THF, room temp., 78%.

Reaction of **1** with DMAD proceeded smoothly in benzene at 65 °C to afford 1:2 adduct **5** in 65% yield. The structure of **5** was confirmed by X-ray structural analysis (Fig. 1), which clearly indicates a Dewar benzene structure along with nearly flat cyclohexa-1,4-diene rings and a seven-membered acetal ring adopting a twist conformation in the solid state.§ Dehydrogenation of **5** to 9,10-Dewar anthracene derivative **6** was accomplished (87% yield) with activated MnO_2 in benzene at room temperature. Reaction of **1** with *N*-phenylmaleimide (65 °C,

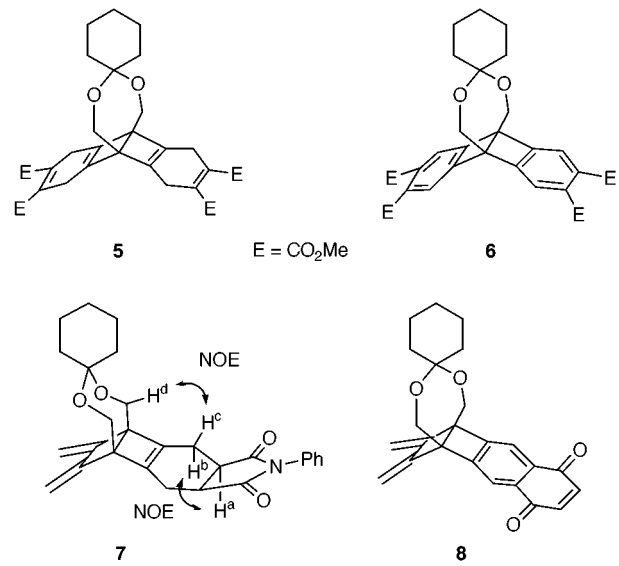

5 E = CO_2Me **6**

7 **8**

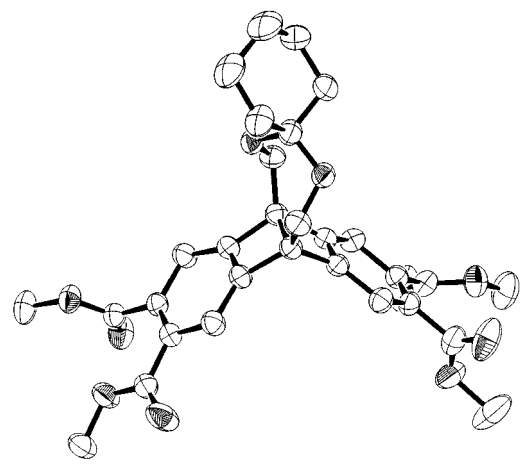

Fig. 1 Molecular structure of **5**. Hydrogen atoms are omitted for clarity.

4 h) gave **7** in 75% yield as a major product, whose stereochemistry was determined by examining the NOESY spectrum; H^c which is *trans* to H^a exhibits a NOE with H^d. The formation of **7** may be most reasonably explained by the *exo*-orientation approach of the dienophile from the *endo*-face of **1**. Reaction of **1** with benzo-1,4-quinone (65 °C, 44 h) followed by successive treatment of the adduct with DDQ in acetonitrile and activated MnO_2 in benzene afforded **8**, a possible precursor for cyclic polyacenequinone derivatives, in 55% yield.

In summary, we have successfully developed a novel Diels–Alder route to Dewar benzenes as well as Dewar polyacenes by introducing **1** as a new bisdiene molecule. Further elaboration and an application of the present method to the syntheses of novel cyclophanes as well as polyacenes are the subjects of our ongoing study.

This work was supported in part by a Grant-in-Aid for Scientific Research (No. 09640620) from the Ministry of Education, Science, Sports, and Culture of Japan. We thank Professor Tamotsu Inabe (Hokkaido University) for the use of X-ray analytical facilities.

Notes and references

† All new compounds were characterized spectroscopically.

‡ *Selected data* for **1**: δ_H (400 MHz, $CDCl_3$) 1.40 (m, 2 H), 1.49 (m, 4 H), 1.69 (m, 4 H), 4.02 (s, 4 H), 4.89 (s, 4 H), 5.28 (s, 4 H); δ_C (100 MHz, $CDCl_3$) 22.79, 25.71, 33.27, 60.99, 62.14, 103.62, 104.10, 150.46; ν(neat)/cm^{-1} 2932, 2860, 1100, 882; λ_{max} (hexane)/nm (ε/dm^3 mol^{-1} cm^{-1}) 231 (7800), 238 (16700), 255 (sh, 6900); *m/z* 270 (M^+, 0.5), 172 (100).

§ *Crystal data* for **5**: $C_{30}H_{34}O_{10}$, M = 554.59, colorless crystals (0.2 × 0.2 × 0.2 mm), monoclinic, space group $P2_1/n$, a = 7.814(2), b = 20.404(2), c = 17.643(2) Å, β = 101.77(1)°, V = 2753.8(6) $Å^3$, D_c = 1.338 g cm^{-3}, Z = 4, Mo-Kα radiation (λ = 0.71069 Å), T = 296 K, μ = 1.00 cm^{-1}, F(000) = 1176. A total of 6494 unique reflections were collected, of which 3903 observed reflections [$I > 3\sigma(I)$] were used in the structure solution (direct methods) and refinement (full-matrix least-squares) to give final R = 0.041 and R_w = 0.037. CCDC 182/1399. See http://www.rsc.org/suppdata/cc/1999/1999/ for crystallographic data in .cif format.

1 T. Tsuji, in *Advances in Strained and Interesting Organic Molecules*, ed. B. Halton, JAI Press, Greenwich, CT, 1999, vol. 7, p. 103 and refs. therein.

2 A. Greenberg and J. F. Liebman, *Strained Organic Molecules*, Academic Press, New York, 1978; F. Bickelhaupt and W. H. de Wolf, *Recl. Trav. Chim. Pays-Bas*, 1988, **107**, 459; F. Bickelhaupt and W. H. de Wolf, in *Advances in Strained and Interesting Organic Molecules*, ed. B. Halton, JAI Press, Greenwich, CT, 1993, vol. 3, p. 185; Y. Tobe, *Top. Curr. Chem.*, 1994, **172**, 1; V. V. Kane, W. H. de Wolf and F. Bickelhaupt, *Tetrahedron*, 1994, **50**, 4575.

3 R. N. McDonald, D. G. Fvickey and G. M. Muschik, *J. Org. Chem.*, 1972, **37**, 1704; N. C. Yang, R. V. Carr, J. K. Mcvey and S. A. Rice, *J. Am. Chem. Soc.*, 1974, **96**, 2297; W. Pritschins and W. Grimme, *Tetrahedron Lett.*, 1982, **23**, 1151.

4 Generation of compound **2** from 1,2,4,5-tetramethylidenebenzene has been discussed, see: J. H. Reynolds, J. A. Berson, K. K. Kumashiro, J. C. Duchamp, K. W. Zilm, A. Rubello and P. Vogel, *J. Am. Chem. Soc.*, 1992, **114**, 763; J. H. Reynolds, J. A. Berson, J. C. Scaiano and A. B. Berinstain, *J. Am. Chem. Soc.*, 1992, **114**, 5866; R. Liu, X. Zhou and J. F. Hinton, *J. Am. Chem. Soc.*, 1992, **114**, 6925.

5 P. Vogel and A. Florey, *Helv. Chim. Acta*, 1974, **57**, 200; O. Pilet and P. Vogel, *Helv. Chim. Acta*, 1981, **64**, 2563; R. J. Graham and L. A. Paquette, *J. Org. Chem.*, 1995, **60**, 5770.

Communication 9/06239D

ChemComm

Selective adsorption of oligonucleotides on switchable self-assembled monolayers

Börje Sellergren,*[a] Frank Auer[a] and Thomas Arnebrant[b]

[a] *Department of Inorganic Chemistry and Analytical Chemistry, Johannes Gutenberg University, Mainz, Duesbergweg 10-14, 55099 Mainz, Germany. E-mail: borje@ak-unger.chemie.uni-mainz.de*
[b] *Institute for Surface Chemistry, Royal Institute of Technology, Stockholm, Sweden*

Received (in Cambridge, UK) 28th June 1999, Accepted 31st August 1999

Short oligonucleotides adsorb rapidly and selectively on pH-switchable self-assembled layers of bisbenzamidines on modified gold substrates.

Today's methods of gene analysis require rapid detection of specific DNA or RNA base sequences present in small amounts in complex mixtures.[1] These commonly make use of pre-synthesized probe oligonucleotides or oligonucleotide analogues[2] capable of hybridizing specifically to the sequence of interest.[3] Different techniques for detection of the hybridization reaction are available. These can rely on either the use of labeled probes,[3] *e.g.* radioactive, fluorescent and chemiluminescent, or the use of unlabeled probes where the probe usually is covalently bound to a surface and the hybridization reaction is detected microgravimetrically,[2,4] optically[5,6] or electrochemically.[7] The chemical modification of the probe required in these techniques may cause problems such as *e.g.* slow or nonspecific hybridization reactions and, in the case of sensors, may prevent their reuse.

Techniques for reversible attachment of the probe to the surface would be attractive in this regard. We report here a system for base-selective and reversible adsorption of nucleic acids to a surface reflected in layer thickness changes that can be detected optically.

The system is based on α,ω-bis(4-amidinophenoxy)alkanes **1**

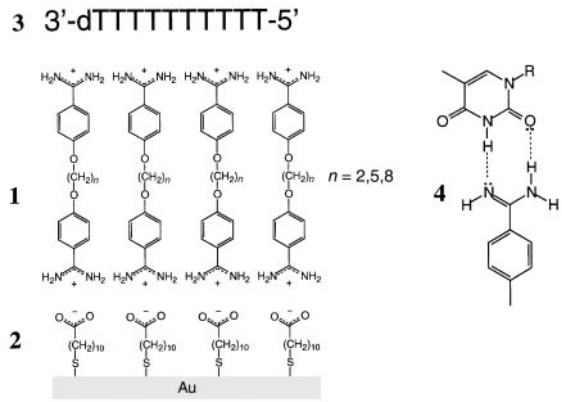

that we previously showed form stable ordered pH-switchable layers on gold or modified gold substrates.[8,9] In view of the DNA binding properties of the bisbenzamidines[10,11] we decided to investigate whether the amidine layers exhibit selectivity for oligonucleotides enriched in one particular base or whether the system can be used to detect DNA hybridization. First we compared the adsorption of a 10-mer of deoxythymidylic acid (T10) **3** using three bisbenzamidines with different alkyl chain lengths (Table 1). The bisbenzamidines gave rapid increases in layer thickness where, for the longer amidines, the final thickness approached the molecular length corresponding to an extended conformation of the amphiphile.[9] A marked increase in the layer thickness was thereafter produced upon addition of the oligonucleotide. The change in thickness increased with the molecular length of the bisbenzamidine. It is known that bisbenzamidines interact with and may precipitate nucleic acids,[12] suggesting that the film formation is related to the different solubilities of the amidine–nucleic acid pairs. However, no visible precipitation was observed in the experiments and the changes in film thickness observed with SiO_2 surfaces under otherwise identical conditions were negligible. This was also the case when performing the experiment on the bare MUA SAM, leaving out the amidine. A preadsorbed amidine layer is thus necessary for the additional DNA layer buildup.

It is seen in Fig. 1 that the bands characteristic for the amidines are present in the IR absorption spectra of the SAM modified with **1** (n = 5). The position and intensities of the bands corresponding to N–H and O–H stretching vibrations (at *ca*. 3159 and 3355 cm^{-1}) show that the amidine groups are involved in hydrogen bonding, presumably with the SAM carboxylic acid head groups.[9] A comparison of the intensities of the bands corresponding to the C–H out-of-plane bending vibration (840 cm^{-1}, weak) and the ring C=C stretching vibration (1611 cm^{-1}, strong) further shows that this amidine prefers an orientation with the phenyl groups oriented nearly perpendicular to the surface.[9] After adsorption of the oligonucleotide additional bands appeared. The main change was the appearance of bands assigned to the phosphate groups at 1000–1270 cm^{-1}, the increase in intensity and broadening of the band corresponding to the N–H and O–H stretching to lower frequencies and the reduced intensity of the ring C=C stretching vibration parallel to an increase in intensity of the C–H out-of-plane vibration. These observations indicate further extensive hydrogen bonding in the adsorbed DNA layer as well as a

Table 1 Layer thicknesses upon consecutive addition of bisbenzamidines and a 10-mer DNA oligonucleotide to a self-assembled monolayer (SAM) of mercaptoundecanoic acid (MUA) on gold[a]

	Layer thickness/Å			
DNA oligo-nucleotide[b]	**1** (n = 5)		**1** (n = 8)	
	amidine[c]	DNA[d]	amidine[c]	DNA[d]
T10[e]	13 ± 1	14 ± 2	23 ± 1	33 ± 3
C10	12 ± 0	2 ± 1	24 ± 2	3 ± 3
G10	14 ± 1	11 ± 1	24 ± 3	2 ± 1
A10	14 ± 1	1 ± 1	25 ± 5	12 ± 1

[a] The substrates were then immersed in a quartz ellipsometric cuvette containing 5 ml sodium borate buffer (0.01 M, pH 8.7, prepared from boric acid) thermostatted to 25 °C and equipped with a small magnetic stirrer and a pH electrode. Adsorption of compounds were then monitored *in situ* by null ellipsometry (ref. 8,9) assuming a film refractive index of 1.45. The reported values were determined when the change in the polariser angle had levelled off. After one experiment the surfaces were restored by adjusting the pH to 2–3 with 0.1 M HCl followed by rinsing with water. [b] 10-mer DNA oligonucleotides of deoxythymidylic acid (T10), deoxycytidylic acid (C10), deoxyguanylic acid (G10) and deoxyadenylic acid (A10). [c] Increase in layer thickness *ca*. 200 s after addition of **1** (n = 5) or **1** (n = 8) (100 μl of a 2.5 mM stock solution). [d] Increase in layer thickness 200–300 s after addition of the oligonucleotide (5 μl of a 0.5 mg ml^{-1} stock solution) to the solution described in note *c*. The spread of the thickness values from duplicate runs has been indicated. [e] Using **1** (n = 2) the layer thickness of **1** was 11 ±1 Å and of T10 was 5 ±1 Å.

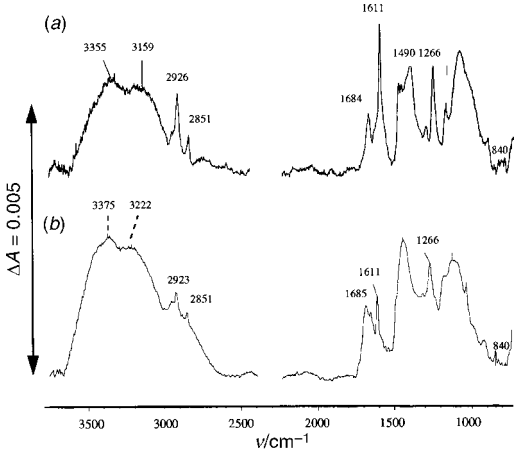

Fig. 1 Baseline corrected IR reflection absorption spectra of SAMs of MUA modified with (*a*) **1** (*n* = 5) and (*b*) **1** (*n* = 5) and a 15-mer random sequence DNA oligonucleotide.

change in the average tilt angle of the phenyl groups, the latter effect possibly due to adsorption of additional randomly ordered amidine molecules or an induced disorder of the SAM.

Table 1 shows the estimated final layer thicknesses upon addition of **1** (*n* = 5) or **1** (*n* = 8) in a first step and a 10-mer oligonucleotide in a second step. A striking difference in DNA base selectivity is seen when comparing the two amidines. Compound **1** (*n* = 5) binds preferentially T10 and G10 whereas **1** (*n* = 8) shows affinity for T10 and A10. Thus exchanging **1** (*n* = 5) with **1** (*n* = 8) in the second layer changes the base preference from G10 to A10. It should be noted that Brønsted basic head groups in close-packed monolayers, due to electrostatic effects, may be significantly less basic than the corresponding base in solution.[13,14] At the pH of the experiment, a proportion of the amidine groups may thus be uncharged. These groups may offer complementary binding sites for thymine resulting in the binding motif **4** similar to the one proposed to occur in a Langmuir–Blodgett film of guanidine and thymine functionalized amphiphiles at the air water interface,[15] or between thymine and amidine in complexes between ds-DNA and bisbenzamidines.[10]

In order to investigate whether the consecutive addition protocol could be used to detect DNA hybridizations, we used a 10-mer probe[4] with a sequence complementary to the *Eco*R1 binding site of single stranded M13 phage DNAs (7249 base pairs). In order to test the selectivity, four 10-mer oligonucleotides with a varying number of mismatches were used. As seen in Fig. 2 the adsorption of the probe sequence (DNA 1) gave an

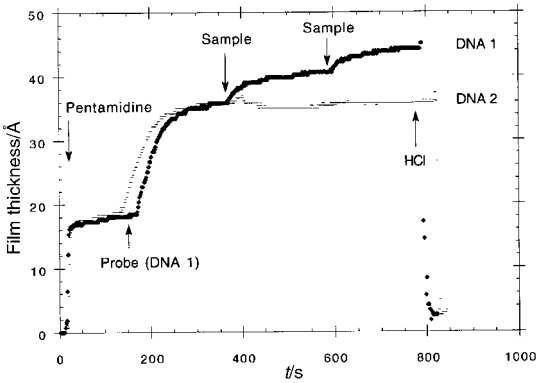

Fig. 2 Film thickness, estimated by *in situ* ellipsometry, *versus* time after the consecutive addition of **1** (*n* = 5), a 10-mer DNA probe (5 μl of a 0.5 mg ml^{-1} stock solution) and a sample oligonucleotide (2 × 5 μl of a 0.5 mg ml^{-1} stock solution) to a SAM of MUA on gold, as described in Table 1. The following DNA sequences were used with the number of antiparallel mismatches given in parantheses. Probe sequence: DNA 1: 3′-dTGCTTAAGGG-5′ (4); sample sequences: DNA 2: 3′-dCCCTTAAGCA-5′ (0); DNA 3: 3′-dCCCTGAAGCA-5′ (1); DNA 4: 3′-dAGCCGTACCC-5′ (7). The changes in layer thickness caused by the sample oligonucleotides were as follows: DNA 1: +9 Å; DNA 2: 0 Å; DNA 3: +3 Å; DNA 4: +9 Å. The spread of the thickness values from duplicate runs was less than 2 Å.

increase in film thickness of *ca.* 17 Å. Subsequent additions of the probe, as sample sequence, resulted in an additional 9 Å increase in film thickness. Adding instead a fully complementary sample sequence (DNA 2) resulted in no change or a slight decrease in layer thickness. A more pronounced decrease in the layer thickness was observed when adding a larger amount of DNA 2. Thus adding five times more DNA 2 resulted in a decrease in layer thickness of about 5 Å. The larger the number of mismatches, the larger the increase in film thickness caused by the sample sequence.

Additional control experiments were performed. The probe layer thickness depended on the sequences of the probe. For instance whereas sequences 1 and 4 (in Fig. 2) gave an increase in thickness of about 16 Å, sequences 2 and 3 resulted in an increase of about 10 Å. However, in the hybridization test, probe sequences giving similar thicknesses responded in accordance with the number of mismatches in the chain. Thus when adding sequence 1 to a surface saturated with DNA 2, 3 or 4, an additional increase in thickness of 1, 5 and 7 Å respectively was observed. Finally, regardless of the order of addition of the oligonucleotides the same end thickness was observed. This indicates a reversible adsorption process with a rapid exchange of adsorbates. As in the case of the adsorption of homo-oligonucleotides the molecular basis for the observed thickness changes remains obscure. The behaviour contrasts with what is commonly observed in hybridzation reactions using probes covalently bound to the surface.[2,4,6] In these cases, hybridization results in an increase in layer thickness. It is likely that rigid rod like double stranded DNA adsorbs more weakly or in a more compact conformation to the surface than more flexible single stranded DNA. The latter may more easily adjust its conformation to maximize the attractive interactions with the surface amidine groups.

The above results show that self-assembled monolayers of bisbenzamidines can be used for base selective binding of nucleic acids. Our future studies will show whether the system can be extended to polynucleotides and complex PCR products. Alternatively the protocol may be useful in studies of drug–DNA or protein–DNA interactions.

Financial support from the Deutsche Forschungsgemeinschaft (grant number SE 777/2-2), the Deutsche Akademische Austauschdienst (DAAD) and the Swedish Institute (SI) and materials support from Interactiva GmbH (Ulm, Germany) and Rhône-Poulenc Rohrer (Helsingborg, Sweden) is gratefully acknowledged.

Notes and references

1 K. J. Skogerboe, *Anal. Chem.*, 1995, **67**, 449R.
2 J. Wang, E. Palecek, P. E. Nielsen, G. Rivas, X. Cai, H. Shiraishi, N. Dontha, D. Luo and P. A. Farias, *J. Am. Chem. Soc.*, 1996, **118**, 7667.
3 B. D. Hames and S. J. Higgins, *Gene Probes I*, ed. B. D. Hames and S. J. Higgins, IRL Press, New York, 1995.
4 Y. Okahata, Y. Matsunobu, K. Ijiro, M. Mukae, A. Murakami and K. Makino, *J. Am. Chem. Soc.*, 1992, **114**, 8299.
5 J. J. Storhoff, R. Elghanian, R. C. Mucic, C. A. Mirkin and R. L. Letsinger, *J. Am. Chem. Soc.*, 1998, **120**, 1959.
6 P. Nilsson, B. Persson, M. Uhlen and P. A. Nygren, *Anal. Biochem.*, 1995, **224**, 400.
7 S. Mikkelsen, *Electroanalysis*, 1996, **8**, 15.
8 B. Sellergren, A. Swietlow, T. Arnebrant and K. Unger, *Anal. Chem.*, 1996, **68**, 402.
9 F. Auer, D. W. Schubert, M. Stamm, T. Arnebrant, A. Swietlow, M. Zizlsperger and B. Sellergren, *Chem. Eur. J.*, 1999, **5**, 1150.
10 M. Cory, R. R. Tidwell and T. A. Fairley, *J. Med. Chem.*, 1992, **35**, 431.
11 P. A. Greenidge, T. C. Jenkins and S. Neidle, *Mol. Pharmacol.*,1993, **43**, 982.
12 D. R. Makulu and T. P. Waalkes, *J. Natl. Cancer. Inst.*, 1975, 305.
13 T. R. Lee, R. I. Carey, H. A. Biebuyck and G. M. Whitesides, *Langmuir*, 1994, **10**, 741.
14 M. Bryant and R. M. Crooks, *Langmuir*, 1993, **9**, 385.
15 D. Y. Sasaki, K. Kurihara and T. Kunitake, *J. Am. Chem. Soc.*, 1992, **114**, 10 994.

Communication 9/05193G

ChemComm

Copper(II), in the parts per million range, modulates photochemical and photosensitizing properties of tolmetin *via* electron transfer with a triplet carbanion

S. Sortino,*[ab] J. C. Scaiano,[b] G. De Guidi[a] and L. L. Costanzo[a]

[a] *Dipartimento di Scienze Chimiche, Università di Catania, Viale Andrea Doria 8 I-95125 Catania, Italy. E-mail: ssortino@dipchi.unict.it*

[b] *Department of Chemistry, University of Ottawa, 10 Marie Curie, Ottawa, Ontario, Canada K1N 6N5*

Received (in Cambridge, UK) 4th August 1999, Accepted 31st August 1999

Copper(II), at very low levels of concentration, modulates the distribution of tolmetin stable photoproducts as well as inhibits the DNA cleavage photoinduced by the drug, *via* a highly efficient electron transfer process with the main transient species generated in the tolmetin photolysis.

Tolmetin, 2-[5-(*p*-toluoyl)-1-methylpyrrol-2-yl]acetic acid (TM), is a non-steroidal anti-inflammatory drug (NSAID) and is known to induce toxic effects on biosubstrates which can be associated with light exposure.[1–3] Like other NSAIDs,[4,5] a photodecarboxylation reaction is believed to be responsible for the TM photoinduced damage.[3] In light of this, the problem of finding suitable bio-compatible devices which may control drug photodegradation and, as a consequence, exert a photoprotective action towards the photoinduced damage, is receiving growing attention. Our previous work pointed out that the use of metal ions at very low concentrations may represent a valid tool in inhibiting toxic effects photoinduced by drugs,[6–9] as well as a potential strategy for modulating the photochemical pathways involved in drug photodegradation. Furthemore, patents concerning copper(II) compounds with antioxidant activity have been registered.[10–12] Despite encouraging experimental results, the role played by the metal ions in this field is still unclear and complex. On the basis of these considerations we proposed to elucidate the role of copper(II) in the photochemistry of TM and on its photosensitizing activity towards DNA by combining steady-state and time-resolved techniques. Recent studies on the transient photochemistry of this drug have pointed out that TM photodecarboxylation is triggered by a short-lived excited triplet state involving a triplet carbanion as the key intermediate in the photodecomposition.[13,14] Stable photoproduct **1** is formed. A minor pathway, consisting of a photoionization process followed by fast decarboxylation and formation of a dimeric species such as stable photoproduct **2**, was also noticed (Scheme 1).

The results of the HPLC analysis of a nitrogen saturated, irradiated TM solution at pH 7.4 led to the photoproduct distribution shown in Fig. 1. As shown, addition of copper(II) in the micromolar range does not influence the photodegradation efficiency of the starting compound but provokes remarkable changes in the distribution of the two photoproducts. It can be seen that the reduction of the photoproduct **1** is accompanied by a corresponding increase in the amount of photoproduct **2**.

Since the photodegradation quantum yield is unaffected by the metal ion, the behavior observed accounts for the reaction between copper(II) and the transient intermediates formed in the TM photolysis. Inasmuch as the increase of the percentage of the photoproduct **2** has to involve an increase in the pyrrolyl radical concentration, we can hypothesize that an electron transfer from the triplet carbanion to copper(II), leading to the formation of the pyrrolyl radical and copper(I), may explain the observed behavior. This hypothesis is confirmed by monitoring

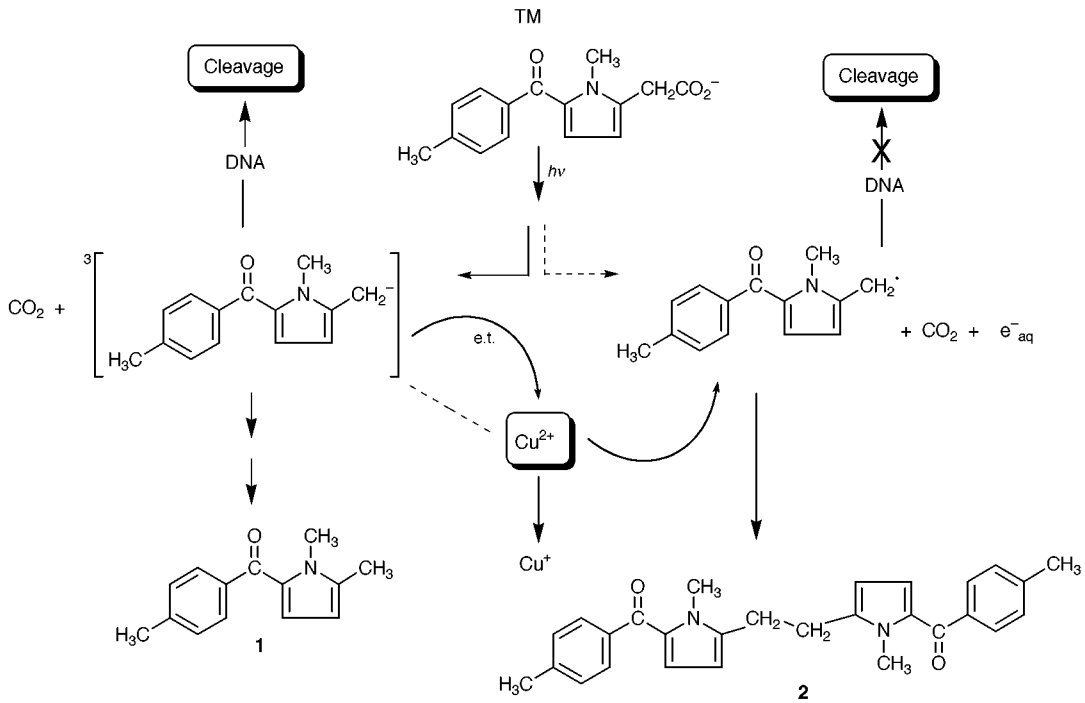

Scheme 1

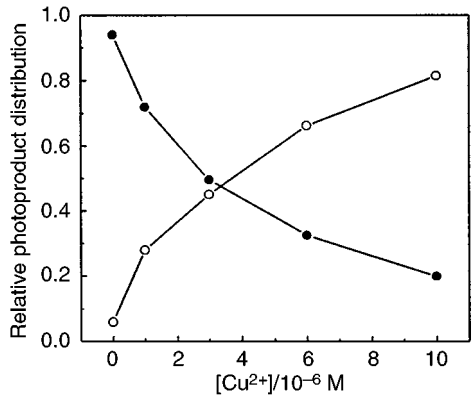

Fig. 1 Relative distribution of TM photoproducts at various copper(II) concentrations: (●) **1** and (○) **2**.

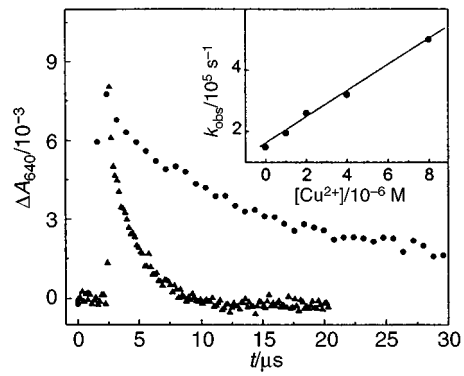

Fig. 2 Kinetic decay of the TM triplet carbanion (●) in the absence and (▲) in the presence of Cu^{2+} (7×10^{-6} M). Inset: plot for the quenching of the triplet carbanion by Cu^{2+}.

the triplet carbanion decay at 640 nm using nanosecond laser flash photolysis techniques. As showed in Fig. 2, this transient species is quenched by addition of copper(II) and a bimolecular quenching constant of $4.5–10^{10}$ M^{-1} s^{-1} (inset in Fig. 2) is obtained.

This value is higher than the diffusion-controlled rate and indicates a strong electrostatic interaction between the two reactants, due to their opposite charges.

These data are in good agreement to those obtained from steady state experiments. Indeed, the fraction of carbanion quenched by a certain concentration of copper(II) fits well both the percentage decrease of the photoproduct **1** and the increase of the photoproduct **2**. Further confirmation that the quenching mechanism occurs through an electron transfer reaction is provided by the high amount of copper(I) detected after TM irradiation in N_2O saturated solution.† Addition of sodium bathocuproinedisulfonate (BCDS) under N_2O atmosphere turns the irradiated solution red, which shows the characteristic absorption of the copper(I)–BCDS complex at 484 nm.[15]

Low concentrations of copper(II) were also used in DNA photocleavage experiments. As shown in Table 1, the metal ion inhibits markedly the amount of DNA damage photoinduced by TM.

Since the main transient intermediate produced in these experimental conditions is always the triplet carbanion, we believe that an electron transfer between this species and DNA nucleobases can trigger the photoinduced damage. The hypothesis is supported by formation of reduction products of DNA nucleobases observed in experiments performed using single nucleosides. These results can be rationalized on the basis of the influence of the metal ion on the TM photoproduct distribution. Due to the intermolecular electron transfer with cupric ions, the active DNA photocleaver triplet carbanion is converted into a pyrrolyl radical. Given its chemical structure, this species is highly stable, is inefficient for abstraction of hydrogen from the DNA backbone, and the only method of decay is a self-reaction to generate the photoproduct **2**.

Table 1 TM photoinduced DNA cleavage in anaerobic conditions in the presence of different amounts of Cu^{2+}

Cleavage (%)	$[Cu^{2+}]/10^{-7}$ M
67 ± 7	0.0
55 ± 6	1.0
42 ± 5	5.0
30 ± 4	10.0

The overall results, summarized in Scheme 1, provide a clear example in which an oligoelement such as copper(II) interacts efficiently at very low concentration with the intermediate of a photochemical reaction. This process modulates remarkably the distribution of the stable photoproducts and inhibits considerably DNA drug photoinduced damage by turning a species very highly reactive towards the biosubstrate into an unreactive one.

Financial support from MURST (cofinanziamento di programmi di ricerca di rilevante interesse nazionale) and the Natural Sciences and Engineering Research Council of Canada are acknowledged. Critical reading of the manuscript by Professor G. Condorelli is also gratefully acknowledged.

Notes and references

† N_2O was used as an electron scavenger in order to avoid formation of copper(I) by direct capture of the hydrated electron photoejected by TM.

1 B. A. Vandijk, P. B. Rico, A. Hoitsma and V. A. Kunst, *Transfusion*, 1989, **29**, 638.
2 J. E. Squires, P. D. Mintz and S. Clark, *Transfusion*, 1985, **25**, 410.
3 S. Giuffrida, G. De Guidi, S. Sortino, R. Chillemi, L. L. Costanzo and G. Condorelli, *J. Photochem. Photobiol. B: Biol.*, 1995, **29**, 125.
4 F. Boscà and M. A. Miranda, *J. Photochem. Photobiol. B: Biol.*, 1998, **43**, 1.
5 G. De Guidi, S. Giuffrida, P. Miano and G. Condorelli, in *Modern Topics in Photochemistry and Photobiology*, ed. F. Vargas, Trivandium, India, 1997, pp. 65–67.
6 L. L. Costanzo, G. De Guidi, S. Giuffrida, S. Sortino and G. Condorelli, *J. Inorg. Biochem.*, 1995, **59**, 1.
7 S. Giuffrida, G. De Guidi, P. Miano, S. Sortino, G. Condorelli and L. L. Costanzo, *J. Inorg. Biochem.*, 1996, **63**, 253.
8 G. De Guidi, S. Giuffrida, G. Condorelli, L. L. Costanzo, P. Miano and S. Sortino, *Photochem. Photobiol.*, 1996, **63**, 455.
9 R. P. Bonomo, E. Conte, G. De Guidi, G. Maccarrone, E. Rizzarelli and G. Vecchio, *J. Chem. Soc., Dalton Trans.*, 1996, 4351.
10 L. R. Pickard, *Br. Pat. Appl.*, 1987, GB. 2, 213.060.
11 U. Weser and R. Miesel, *German Pat. Appl.*, 1990, P3912642.
12 U. Weser, H. J. Hartmann and R. Miesel, *German Pat. Appl.*, 1991, P3920826.5.
13 S. Sortino and J. C. Scaiano, *Photochem. Photobiol.*, 1999, **69**, 167.
14 S. Sortino, J. C. Scaiano, G. De Guidi and S. Monti, *Photochem. Photobiol.*, in the press.
15 W. Baoxing, S. Fayi and D. Shaojun, *J. Electroanal. Chem.*, 1993, **43**, 356.

Communication 9/06349H

ChemComm

Functional analysis of phenylalanine 365 in hopene synthase, a conserved amino acid in the families of squalene and oxidosqualene cyclases†

Tsutomu Hoshino* and Tsutomu Sato

Department of Applied Biological Chemistry, Faculty of Agriculture, and Graduate School of Science and Technology, Niigata University, Ikarashi, Niigata 950-2181, Japan. E-mail: hoshitsu@agr.niigata-u.ac.jp

Received (in Cambridge, UK) 9th July 1999, Accepted 3rd September 1999

Two bicyclic products were accumulated by the mutant F365A, showing the amino acid residue is located close to the transient C-8 carbocation intermediate in the active site cavity; the mutants of F365Y and F365W significantly accelerated the cyclization reaction at low temperatures.

The cyclization of squalene **1** into the pentacyclic triterpene hopene **2**, mediated by the prokaryotic squalene-hopene cyclase (SHC), is one of the most sophisticated biochemical reactions (Scheme 1).[1] Oxidosqualene also undergoes the polyolefin cyclization by eukaryotic cyclases, in a similar manner to **1**.[1] Recent investigations on the molecular biology of the two cyclases[2] and on the substrate analogues[1,3] have encouraged mechanistic studies on the polycyclization reactions. The acyclic molecule **1** is believed to be folded into an all pre-chair conformation inside the enzyme cavity,[1] but the involvement of a ring expansion process has recently been disclosed with respect to the D-ring formation.[4a,b] Such a ring expansion reaction also occurs in C-ring formation by lanosterol synthase.[4c,d] An X-ray crystal structure of the SHC from *Alicyclobacillus acidocaldarius* has been reported and a reaction mechanism proposed.[5] However, site-directed mutagenesis experiments are required to verify the catalytic functions of the residues of the presumed active center. To date, only a few essential components of these active sites have been demonstrated by point mutation experiments.[4b,6] The polycyclization cascade has been proposed to proceed by the stabilization of discrete carbocation intermediates *via* cation–π interaction with aromatic amino acid residues of the cyclases,[7] but no kinetic evidence has been reported. In a series of point mutation experiments conducted by us, Phe365, which is conserved among all the known prokaryotic SHCs and eukaryotic cyclases,[2,5,6c] has been identified as having a stabilizing function for the transient C-8 carbocation intermediate. We show here kinetic data of the mutated SHCs of F365Y and F365W.

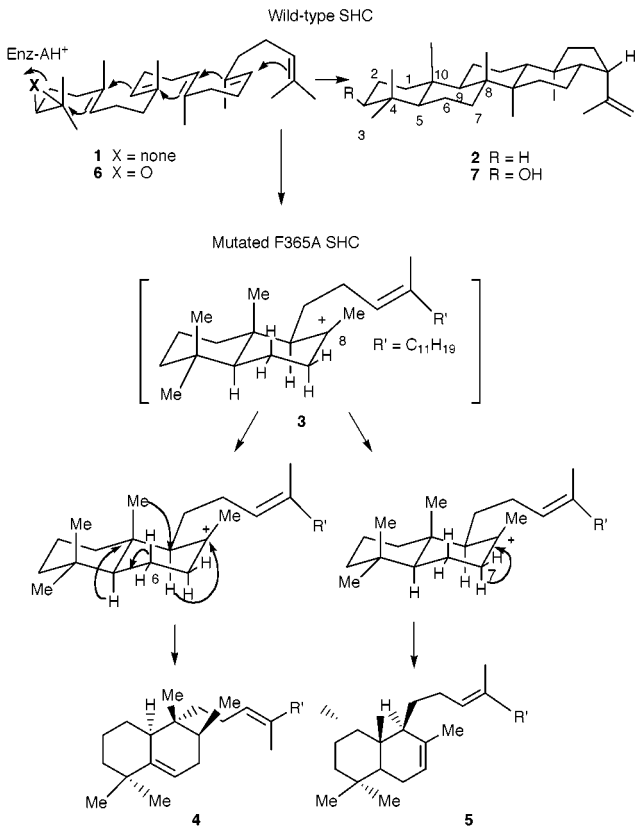

Scheme 1

Cell-free homogenates of the *E. coli* clone encoding the mutated F365A SHC, prepared from 8 L culture, were incubated with **1** (105 mg) at pH 6.0 and 55 °C for 16 h. The GC analysis showed the presence of two major products (**4** and **5**), a little of **2** and recovered **1** in the reaction mixture. Separation on a SiO_2 column using hexane as an eluent afforded **4** (27.8 mg), **5** (25.1 mg), **2** (3.0 mg) and **1** (32.4 mg). Analyses of the 2D NMR spectra revealed that the structures of **4** and **5** had a 6/6-fused bicyclic skeleton.[8] Formation of **4** and **5** suggested that the sequential cyclization reactions are quenched at the bicyclic stage of the putative intermediate **3**. A series of 1,2-shifts of hydrides and a methyl group in an antiparallel fashion could trigger the deprotonation at C-6 to produce **4**, while a deprotonation at C-7 could give rise to **5** (Scheme 1). These findings indicate that the F365 residue is critical to the completion of the polycyclization and that the π-electron of this side chain may stabilize the transient C-8 carbocation. There were no detectable amounts of mono- or tri-cyclic products, further suggesting that the F365 residue is close to the C-8 cation in the enzyme cavity, but not near the mono- and tricyclic intermediary carbocations, which is consistent with the recent suggestion inferred from X-ray analysis.[5]

To validate the proposed role of the cation–π interaction, the mutants F365Y and F365W were constructed based on the idea that the higher electron density of the π–electrons, the faster cyclization reaction. Fig. 1 depicts the specific activities of these mutants against incubation temperatures. The mutant F365Y completed the polycyclization to the final product **2** without any intermediate being observed, differing from F365A, and exhibited a remarkable increase in the reaction rate at low temperatures (10–50 °C); the F365Y produced **2** even at a temperature as low as 10 °C, a temperature at which the wild-type SHC has no significant activity. The activation energy (E_{act}), estimated from the Arrhenius plots,[9] was greatly reduced; *e.g.* 37.0 kJ mol^{-1} for the F365Y compared with 50.1 kJ mol^{-1} for the wild-type. The higher electron density of the tyrosine residue apparently gives rise to a faster cyclization reaction. The K_m values of the wild-type and F365Y were determined from the Lineweaver–Burk plots to be 16.9 ± 0.6 (30–60 °C) and 502 ± 12 μM (10–50 °C), respectively, suggesting that the substrate affinity for F365Y was greatly decreased. An unusual profile was found between activities and temperatures (Fig. 1). Three

† Spectroscopic data for **4** and **5**, Arrhenius plots for **1** and **6** and CD spectra for the relevant SHCs are available from the RSC web site, see http://www.rsc.org/suppdata/cc/1999/2005/

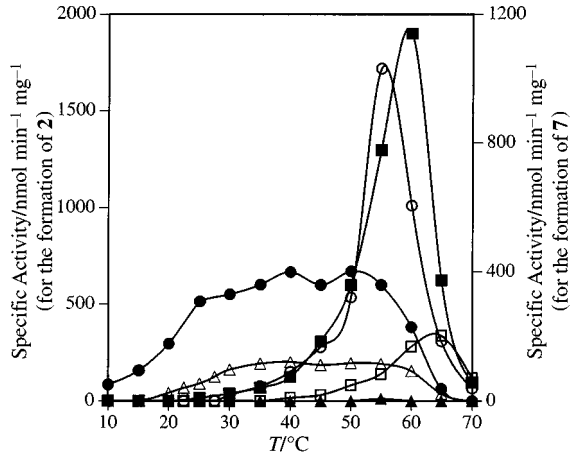

Fig. 1 Specific activities for the formations of **2** (closed symbols) and **7** (open symbols) against incubation temperatures are given for the wild-type SHC (■, □), the mutants of F365Y(●, ○) and F365W (▲, △). One mg of **1** or **6** was incubated with 5 μg of the homogeneously purified SHCs for 60 min at pH 6.0.

distinctive phases were observed: at 10–25°C, the activities were increased; at 30–50 °C, a steady state was reached; at 55–70 °C, the activities decreased due to irreversible thermal denaturation.[10] The enzyme activity of the F365W was negligible (Fig. 1) despite the higher electron density of the indole ring, which may result from the significantly decreased binding of **1** to the catalytic site. The CD spectra of the three mutants were superimposable on that of the wild-type. However, significant local change may be indeed likely and this may have no visible effect on the overall CD spectra.

(3*S*)-2,3-Oxidosqualene **6** also undergoes the cyclization by SHC to form 3β-hydroxyhopene **7**.[3b,6c,11] Compound **6** was incubated as another enzymic test to obtain further evidence for the cation–π interaction. F365Y had a remarkably enhanced activity, 5-fold higher than the wild-type, and showed a bell-shaped curve (Fig. 1).[10] As expected, F365W also had higher activity than the wild-type at temperatures below 50 °C, but exhibited an unusual profile analogous to that of **1** with the F365Y.[10] No intermediate products were detected in the reaction mixtures of **6** by either F365Y and F365W, whereas the 3-hydroxy derivatives corresponding to bicyclic intermediates were accumulated by the F365A without completion of the polycyclization, further supporting the idea that the residue at 365 must be an aromatic amino acid. The values of E_{act}[9] with **6** were 53.6, 49.9 and 42.8 kJ mol^{-1}, respectively, for the wild-type, the F365Y and the F365W mutants, which is in good agreement with the cation–π interaction concept. The enhanced K_m values for these mutants were also observed with **6**; the K_m of the F365W was largest.[11]

The faster cyclization reactions at lower temperatures with the Tyr and the Trp mutants suggest that the cation–π interaction is likely to occur for the squalene cyclization cascade. The bulky aromatic substituents make the active site region less compact. A somewhat loosely packed protein structure may be more flexible at low temperatures leading to high catalytic activity, as is found for psychrophilic enzymes.[12a] More detailed studies are required to gain greater insight into the kinetics of these mutants.[10]

The previously unknown **4** and the known products **5** (γ-polypodatetraene),[13] which have a 6/6-fused bicyclic skeleton, were produced by the site-directed mutant of F365A due to the lack of π-electrons, suggesting that the major function of Phe365 would be assigned for stabilization of the C-8 carbocation intermediate possibly *via* a cation–π interaction.

Notes and references

1 I. Abe, M. Rohmer and G. D. Prestwich, *Chem. Rev.*, 1993, **93**, 2189.
2 E. J. Corey, H. Cheng, C. H. Baker, S. P. T. Matsuda, D. Li and X. Song, *J. Am. Chem. Soc.*, 1997, **119**, 1289.
3 (*a*) T. Hoshino and T. Kondo, *Chem. Commun.*, 1999, 731; (*b*) B. Robustell, I. Abe and G. D. Prestwich, *Tetrahedron Lett.*, 1998, **39**, 957.
4 (*a*) C. Pale-Grosdemange, C. Feil, M. Rohmer and K. Poralla, *Angew. Chem., Int. Ed.*, 1998, **37**, 2237; (*b*) T. Sato, T. Abe and T. Hoshino, *Chem. Commun.*, 1998, 2617; (*c*) E. J. Corey and H. Cheng, *Tetrahedron Lett.*, 1996, **37**, 2709; (*d*) T. Hoshino and Y. Sakai, *Chem. Commun.*, 1998, 1591.
5 K. U. Wendt, K. Poralla and G. E. Schulz, *Science*, 1997, **277**, 1811; K. U. Wendt, A. Lenhart and G. E. Schulz, *J. Mol. Biol*. 1999, **286**, 175.
6 (*a*) C. Feil, R. Sussmuth, G. Jung and K. Poralla, *Eur. J. Biochem.*, 1996, **242**, 51; (*b*) T. Sato,Y. Kanai and T. Hoshino, *Biosci. Biotechnol. Biochem.*, 1998, **62**, 407; (*c*) T. Sato and T. Hoshino, *Biosci. Biotechnol. Biochem.*, 1999, **63**, 1171.
7 D. A. Dougherty, *Science*, 1996, **271**, 163.
8 Analyses of NMR data (H-H COSY 45, HOHAHA, NOESY, DEPT, HMQC and HMBC) unequivocally supported the structures proposed for **4** and **5**.
9 The temperatures for the Arrhenius plots for **1** were in the range of 30–60 and 10–25 °C for the wild-type and for the F365Y, respectively, while in the case of **6** they were 40–60, 30–50 and 20–30 °C, respectively, for the wild-type, the F365Y and the F365W.
10 Our working hypothesis for the interpretation of this unusual behaviour is as follows. Reversible denaturation[12b] may gradually occur from 30 to 50 °C, and the denaturation may be attributable to the more enhanced susceptibility of the mutants to the exothermic high energy, which is released by the cyclization reaction,[5] because the geometrical change occurred at the active site region (significantly increased K_m). As for the F365Y, temperature dependency for the reaction is different between **1** and **6**. This may be closely related to the increased degree of K_m, leading to the unusual profile for **1** (K_m = 502 μM, more sensitive to higher temperatures), but to a bell-shape for **6** (K_m = 182 μM, less sensitive). If the denaturation could not occur, the k_{cat} of **1** may have been significantly increased at 30–50 °C. This idea may also be true for the case of **6** by the F365W (K_m = 357 μM).[11] The denaturation process was confirmed to be reversible; the F365Y was exposed at 40 °C for 60 min and then incubated with **1** at 20 °C, but showed the same activity as that without such treatment. To validate our hypothesis, further evidence is required.
11 Kinetic data for the reactions of **6**, measured at 40 °C and for 60 min, are as follows: k_{cat} 1.4, 12.2 and 17.2 min^{-1}, and K_m 0.72, 181.8 and 357.2 μM, respectively, for the wild-type, F365Y and F365W. The more bulky the substituents, the larger the values of K_m. The k_{cat}s and K_ms of the wild-type for the reactions of **1** and **6** at 60 °C are as follows: 288.5 min^{-1} and 16.7 μM for **1**; 23.6 min^{-1} and 0.84 μM for **6**.[6c]
12 (*a*) P. W. Hochachka and G. N. Somero, in *Biochemical Adaptation*, Princeton University Press, 1984; (*b*) K. Hiromi, Y. Takasaki and S. Ono, *Bull. Chem. Soc. Jpn.*, 1963, **36**, 563; W. B. Neely, *J. Am. Chem. Soc.*, 1959, **81**, 4416.
13 K. Shiojima, Y. Arai, K. Masuda, T. Kamada and H. Ageta, *Tetrahedron Lett.*, 1983, **24**, 5733.

Communication 9/05559B

ChemComm

Hydrogen bonding and cooperativity effects on the assembly of alkyl- and perfluoroalkyl-sulfonyl naphthols: F···F non-bonded interactions†

Janusz Kowalik,* Donald VanDerveer, Caroline Clower and Laren M. Tolbert

School of Chemistry and Biochemistry, Georgia Institute of Technology, Atlanta, GA 30332-0400, USA. E-mail: janusz.kowalik@chemistry.gatech.edu.

Received (in Corvallis, OR, USA) 16th July 1999, Accepted 24th August 1999

Important differences in the crystal packing of 6-perfluorohexylsulfonyl-2-naphthol (1F) including π–π stacking aromatic interactions and F···F non-bonded contacts, in contrast to its nonfluorinated analog (1), appear to translate into differences between their photophysical properties both in the solid state and in solution.

Photoacid generators produce acids upon irradiation. They are important in the field of polymeric photosensitive systems, as initiators for polymerizations,[1] for crosslinking of oligomers and polymers,[2] for polymer degradation,[3], and for conversion of acid-sensitive functional groups attached to the polymers.[4]. Especially important technological applications involve manufacturing of photoresists and UV curing materials.[5] A drawback to common (ionic) photoacid generators is that once incorporated, they usually remain within the polymeric structure, degrading the long-term stability of the polymers.

A less widely explored approach lies with generators that produce acids only for the duration of the photochemical event, thus allowing for a better control of the ensuing chemistry. Our interest in photoacids stems from the observation that hydroxy aromatics, weakly acidic in the ground state, become strong acids upon photoexcitation.[6] We have established that naphthol derivatives strategically substituted with electron-withdrawing substituents yield significantly stronger acids ('enhanced photoacids') in the excited state.[7] The electron withdrawing efficiency of substituents[8] seems to have a similar effect on the ionization in the excited state, rendering systems substituted with functionalities of large positive Hammett constant (σ_p) values better photoacids (proton donors).

Since the σ_p value for the pentafluoroethylsulphonyl group is 1.08,[9] *versus* 0.66[10] for the cyano functionality, we synthesized and tested the 6-perfluorohexylsulfonyl-2-naphthol (**1F**), and its nonfluorinated analog (**1**) for comparison. Scheme 1 illustrates our synthetic approach.

The 6-(isobutoxycarbonyloxy)naphthalene-2-sulfonyl chloride, a starting material for both reaction avenues leading to **1** and **1F**, was obtained in a two-step process involving masking of the hydroxy group in 6-hydroxynaphthalene-2-sulfonic acid by allowing it to react with isobutyl chloroformate under Schotten–Baumann conditions,[11] followed by a reaction with $POCl_3$.[12] Reduction of the acid chloride with zinc metal yielded the corresponding zinc salt of the sulfinic acid, which was alkylated without isolation of the sulfinic acid with *n*-hexyl bromide, using a modified procedure of Mal.[13] The hydroxy group protection in the obtained sulfone was then removed by hydrolysis with LiOH in THF–water to yield **1**. Since heteroatom alkylations with perfluoroalkyl iodides proceed *via* a radical-ion chain mechanism,[14] an alternative procedure was developed for the synthesis of **1F**. Reduction of the sulfonyl chloride with PPh_3[15] yielded the corresponding thiol, which then reacted smoothly with perfluorohexyl iodide to provide the aryl perfluorohexyl thioether. Oxidation with MCPBA and subsequent deprotection of the hydroxy functionality led to sulfone **1F**.

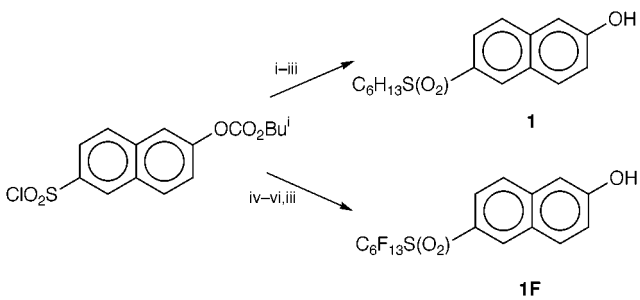

Scheme 1 *Reagents and conditions*: i, Zn, NaOH, H_2O–dioxane; ii, $C_6H_{13}Br$, DBU, DMF; iii, LiOH, 50% H_2O–THF; iv, PPh_3, PhH; v, NaOEt, $C_6F_{13}I$, DMF; vi, MCPBA, EtOAc, reflux.

† Atomic numbering schemes and stereoviews for **1** and **1F** are available from the RSC web site, See http://www.rsc.org/suppdata/cc/1999/2007/

Preliminary studies of the emission spectroscopy of **1** and **1F** in aqueous–organic solutions showed considerable differences in the relative intensities of the fluorescence.[16] Emission of the perfluoroalkyl analog was quenched by 40 × in MeOH (Fig. 1).

Similar effects were observed qualitatively in the solid state, using 366 nm radiation from a hand-held laboratory UV-VIS lamp to produce a bright fluorescence of the nonfluorinated sulfone, in contrast with a very low intensity fluorescence of the perfluoroalkyl analog. It was shown, that intermolecular π–π interactions effectively quenched the solid state fluorescence, the degree of fluorescence quenching can be used as an indicator of intermolecular π–π interactions.[17]

Recent reports from Tung's laboratory indicate that perfluoroalkyl esters of naphthalenecarboxylic acid form aggregates of unknown structure in aqueous organic solvents, leading to formation of excimers upon excitation, and chemical dimerizations as a consequence.[18] Hydrophobic attraction as well as other forces, such as hydrogen bonding,[19] are powerful

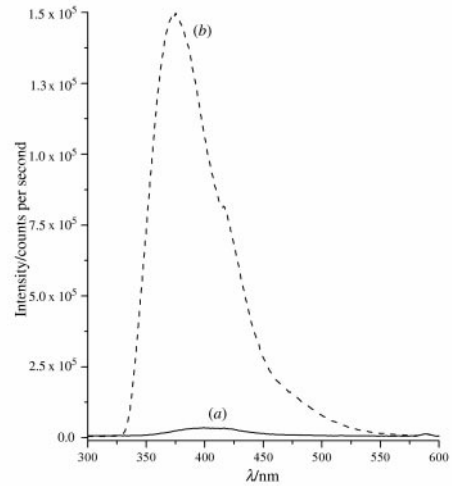

Fig. 1 Emission spectra of (*a*) **1F** and (*b*) **1** in MeOH. Concentration = 4×10^{-5} M, λ_{ex} = 295 nm.

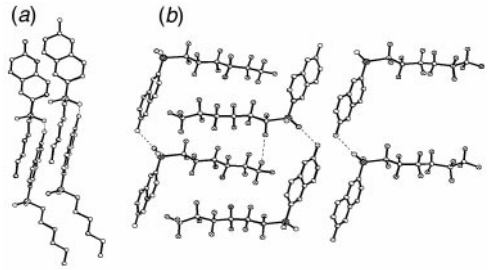

Fig. 2 Packing diagram of (*a*) **1** and (*b*) **1F**. For clarity, hydrogen atoms are omitted. The hydrogen bonds and F···F non-bonded interactions are specified by dotted lines.

tools in forming supramolecular assemblies both in solution and in the solid state. Molecular recognition leading to aggregation and nucleation may as a result become productive in generating crystals.[20] Although the dynamics of these systems remains complex, one might assume that the forces that play a role in molecular recognition in self-organized systems in solution would be reflected in the crystal. Following this assumption we determined the crystal and molecular structures of **1**‡ and **1F**§ (see Fig. 2).

X-Ray analysis reveals that both **1** and **1F** crystallize in monoclinic unit cells, containing four molecules of **1**, and eight molecules of **1F**. The common motif present in both structures is an infinite, intermolecular, linear network of hydrogen bonds OH···OS(O)–. It passes through the crystals in the direction of the *b* axis, making the molecular arrangement supramolecular in nature. Distances are typically 2.78 Å.[21] The differences in the crystal packing are substantial. In the case of **1F** there is a distinct segregation of the well-ordered perfluoroalkane chains from the aromatic rings. The perfluorohexyl chains are nearly parallel. There is a pronounced proximity between the fluorine atom attached to the α carbon (*vs.* sulfonyl group) and the terminal CF_3 group of the next molecule. The distance between the corresponding fluorine atoms is 2.85 Å, which positions them within the range of a non-bonded interaction (van der Waals radius for fluorine is 1.47 Å).[22] We believe that the strong electron withdrawing character of the sulfonyl moiety renders the α fluorine atoms more positive than the terminal ones, effecting a dipolar interaction. This interaction along with the electrostatic repulsion between the π-electrons of the aromatic rings and the fluorine atoms,[23] substantially contribute to the crystal architecture of **1F**. The naphthol rings in **1F** partially overlap in layers 3.52 Å apart. This value relates well with 3.5 Å (interplanar distance in graphite)[24] and is still smaller than 3.81 Å, where the electronic interaction between the aromatic chromophores was found to exist.[25] The attractive π–π interaction is believed to be another element stabilizing the crystal structure of **1F**. By contrast, the planes of the aromatic rings that are positioned parallel to each other in the crystal of **1** are separated by 7.7 Å and are interdigitated with the alkyl chains. There is no interactive proximity between the hexyl chains, and the aromatic chromophores are removed beyond the limit of electron interactions between them.

In summary, three cooperative attractive interactions present in **1F** produce a crystal lattice where a strong chromophore interaction seems to effectively deactivate fluorescence in the solid state. In contrast, the more intense fluorescence of the non-fluorinated analog is attributed to the absence of that interaction. We therefore conclude that similar behavior in solution supports the notion that extensive aggregation of **1F** in MeOH and in water–organic solvent systems is caused by the same attractive interactions as those present in the solid state.

Support of this research from the NSF, grant no. CHE 9727157, is gratefully acknowledged.

Notes and references

‡ *Crystal data* for **1**: $C_{16}H_{20}O_3S$, M = 292.38, monoclinic, a = 5.6190(2), b = 15.8672(6), c = 17.1890(7) Å, β = 96.581(2)°, U = 1522.4(1) Å^3 , T = 173 K, space group Cc (No. 9), Z = 4, μ(Mo-K) = 0.217 mm^{-1}, 4774 reflections measured, 2387 unique (R_{int} = 0.049) which were used in all calculations. The final $wR(F^2)$ was 0.1335 (all data). Single crystals of **1** were recrystallised from Pr^{i}OH, mounted on a glass fiber with stopcock grease and placed in the cold gas stream of the diffractometer. The structure was solved using direct methods and refined by full-matrix least-squares on F^2.

§ *Crystal data* for **1F**: $C_{16}H_7F_{13}O_3S$, M = 526.28, monoclinic, a = 33.291(1), b = 9.9469(2), c = 11.4174(3) Å, β = 99.187(1)°, U = 3732.3 (2) Å^3, T = 173 K, space group $P2_1/c$ (No. 14), Z = 8, μ(Mo-K) = 0.32 mm^{-1}, 18775 reflections measured, 6536 unique (R_{int} = 0.086), which were used in all calculations. The final $wR(F^2)$ was 0.284 (all data). The **1F** was recrystallised from Pr^{i}OH, mounted on a glass fiber using stopcock grease and placed in the cold gas stream of the diffractometer. The structure was solved using direct methods and refined by full-matrix least-squares on F^2. CCDC 182/1393. See http://www.rsc.org/suppdata/cc/1999/2007/ for crystallographic data in .cif format.

1 Y. Wei, W. Wang, J. M. Yeh, B. Wang, D. C. Yang and J. K. Murray, *Adv. Mater*., 1994, **6**, 372.
2 J. M. Harvard, M. Yoshida, D. Pasini, N. Vladimirov, J. M. J. Frechet, D.R. Medeiros, K. Patterson, S. Yamada, C. G. Willson and J. D. Byers, *J. Polym. Sci., Part A: Polym. Chem.*, 1999, **37**, 1225; H. S. Yu, T. Yamashita and K. Horie, *Macromolecules*, 1996, **29**, 1144; K. H. Chae, I. J. Park and M. H. Choi, *Bull. Korean Chem. Soc.*, 1993, **14**, 614.
3 S. G. Moon, K. Naitoh and T. Yamaoka, *Chem. Mater*., 1993, **5**, 1315.
4 S. T. Kim, J. B. Kim, C. M. Chung and K. D. Ahn, *J. Appl. Polym. Sci.*, 1997, **66**, 2507; J. P. Chen, J. P. Gao and Z. Y. Wang, *J. Polym. Sci., Part A: Polym. Chem.*, 1997, **35**, 9; H. K. Kim and C. K. Ober, *Polym. Bull.*, 1992, **28**, 33.
5 For a recent review see: M. Shirai and M. Tsunooka, *Bull. Chem. Soc. Jpn*., 1998, **71**, 2483 and references cited therein.
6 L. G. Arnaut and S. J. Formosinho, *J. Photochem. Photobiol. A*: *Chem.*, 1993, **75**, 1; L. G. Arnaut and S. J. Formosinho, *J. Photochem. Photobiol. A*: *Chem.*, 1993, **75**, 21.
7 K. M. Solntsev, D. Huppert, L. M. Tolbert and N. Agmon, *J. Am. Chem. Soc.*, 1998, **120**, 7981; E. Pines, D. Pines, T. Barak, B.-Z. Magnes, L. M. Tolbert and J. E. Haubrich, *Ber. Bunsenges. Phys. Chem.*, 1998, **102**, 511; D. Huppert, L. M. Tolbert and S. Linares-Samaniego, *J. Phys. Chem.*, 1997, **101**, 4602; I. Carmeli, D. Huppert, L. M. Tolbert and J. E. Huppert, *Chem. Phys. Lett.*, 1996, **260**, 109.
8 K. Hansch, A. Leo and R. W. Taft, *Chem. Rev.*, 1991, **91**, 165.
9 N. V. Kondratenko, V. I. Popov, A. A. Kolomeitsev, E. P. Saenko, V. V. Prezhdo, A. E. Lutskii and L. M. Yagupol'skii, *Zh. Org. Khim.*, 1980, **16**, 1049.
10 D. H. McDaniel. and H. C. Brown, *J. Org. Chem*., 1958, **23**, 420
11 P. Karrer and P. Leiser, *Helv. Chim. Acta*, 1944, **27**, 678.
12 S. Fujita, *Synthesis*, 1981, 423.
13 G. Biswas and D. Mal, *J. Chem. Res. (S)*, 1988, 308.
14 V. N. Boiko and G. M. Shchupak, *J. Fluorine Chem*., 1994, **69**, 207.
15 S. Oae and H. Togo, *Bull. Chem. Soc. Jpn*., 1983, **56**, 3802.
16 J. Kowalik, C. Clower and L. M. Tolbert, to be published.
17 K. Shirai, M. Matsuoka and K. Fukunishi, *Dyes Pigm.*, 1999, **42**, 95.
18 C.-H. Tung and H.-F. Ji, *J. Phys. Chem.*, 1995, **99**, 8311; C.-H. Tung and H.-F. Ji, *J. Chem. Soc., Faraday Trans.*, 1995, **91**, 2761.
19 M. C. Calama, R. Hulst, R. Fokkens, N. M. M. Nibbering, P. Timmerman and D. N. Reinhoudt, *Chem. Commun*., 1998, 1021; K. A. Jolliffe, M. C. Calama, R. Fokkens, N. M. M. Nibbering, P. Timmerman and D. N. Reinhoudt, *Angew. Chem., Int. Ed.*, 1998, **37**, 1247; C. J. Kepert, D. Hesek, P. D. Beer and M. J. Rosseinsky, *Angew. Chem., Int. Ed.*, 1998, **37**, 3158; M. Mascal, J. Hansen, P. S. Fallon, A. J. Blake, B. R. Heywood, M. H. Moore and J. P. Turkenburg, *Eur. Chem. J*., 1999, **5**, 381.
20 A. Gavezzotti and G. Filippini, *Chem. Commun.*, 1998, 287; A. Gavezzotti, *Eur. Chem. J*., 1999, **5**, 567.
21 W. C. Hamilton and J. A. Ibers, *Hydrogen Bonding in Solids*, W. A. Benjamin, New York, Amsterdam, 1968, p.16.
22 A. Bondi, *J. Phys. Chem.*, 1964, **68**, 441.
23 N. Hayashi, T. Mori and K. Matsumoto, *Chem. Commun.*, 1998, 1905.
24 G. Pimentel and R. Spratley, *Chemical Bonding Clarified Through Quantum Mechanics*, Holden-Day, San Francisco, California, 1969, p. 256.
25 H. Langhals, T. Potrawa, H. Nöth and G. Linti, *Angew. Chem., Int. Ed. Engl.*, 1989, **28**, 478.

Communication 9/05940G

The first [2,3]-sigmatropic rearrangement of allylic nitro compounds

Estelle Dumez, Jean Rodriguez and Jean-Pierre Dulcère

RéSo, Réactivité en Synthèse organique, UMR 6516, Faculté des Sciences et Techniques de St Jéróme, Boîte D12, Av. Esc. Normandie-Niemen, F-13397, Marseille Cedex 20, France. E-mail: jean-pierre.dulcere@reso.u-3mrs.fr

Received (in Cambridge, UK) 19th July 1999, Accepted 23rd August 1999

Allylic nitro compounds 1a–d undergo [2,3]-sigmatropic rearrangement in refluxing 1,2,4-trichlorobenzene, to afford rearranged alcohols 3a–d and carbonyl compounds 4a–d; the heating, under the same conditions, of a mixture of nitroalkenes 7a–c, propargyl alcohols or amine 8 and Bu^{t}OK promotes a one-pot formation of allylic alcohols 3a–c.

The influence of zwitterionic moities such as sulfoxides or amine oxides at the 3-position of hexa-1,5-dienes has been investigated and some interesting results showed that acceleration of either [3,3]- or [2,3]- sigmatropic rearrangement could be observed.[1a] Unlike for these substituents, it has been shown that allylic nitro compounds do not participate in [2,3]-sigmatropic rearrangements under thermolysis at 110 °C in toluene.[1b]

We have recently described the facile preparation of allylic nitro compounds **1a**–**d** by Bu^{t}OK-promoted oxa- and aza-Michael addition–intramolecular carbocyclization of prop-2-ynyl alcohols or amines with α,β-disubstituted nitroalkenes.[2]

Here we report on our initial investigations of the first thermal conversion of these valuable substrates into allylic alcohols and the corresponding α,β-unsaturated carbonyl derivatives.

Heating a solution of nitro olefines **1a**–**d** in trichlorobenzene at 214 °C induces a rapid [2,3]-rearrangement providing nitrite intermediates which undergo homolytic fission of the O–NO bond. Subsequent disproportionation of the resulting alkoxyl radical thus derived gives rise to alcohols **3** (12–15%) and carbonyl compounds **4**[3] (13–18%) according to a well-known process[4] (Scheme 1).

The transient formation of alkyl nitrites was established by the isolation of **2a**† (10%) along with **3a** (13%) and **4a** (7%). A selective suprafacial [2,3]-sigmatropic rearrangement leading to **2d** accounts for the stereochemistry of **3d**.‡ Indeed, the homolytic fission does not alter the configuration of the functional carbon center.

Because of their higher degree of unsaturation, we also decided to study under the same reaction conditions the behaviour of easily accessible allenyl nitro compound **1e**.[5] Interestingly, **1e** under thermolysis at 214 °C undergoes [2,3]-sigmatropic rearrangement and cleanly affords keto oxime **5**§ (23%), along with trace amounts of acetyl dihydrofuran **6** (Scheme 2).

Extensive studies[6] of either thermally or photochemically induced transformations of alkyl nitrites resulted in the observation that only photochemically generated 'activated' alkoxyl radical intermediates could lead to oximes by hydrogen-atom transfer reactions. Indeed, although thermally induced transformations afford carbonyl derivatives according to either disproportionation or acid catalysis, vapour-phase pyrolysis of nitrites with apropriate structures follows identical pathways and leads to identical products than photolysis.

Thus, formation of oxime **5**, which formally results from incorporation of nitric oxide after homolytic scission, could be explained by a [1,3]-sigmatropic rearrangement of the vinyl nitrite unit in **A**. Although isolated in small amounts, the formation of acetyl dihydrofuran **6** could support the occurrence of an early homolytic fission stage.

In order to increase the efficiency of the overall process, we adapted our procedure previously developed for the preparation of allylic nitro compounds[2] through a domino reaction initiated by Michael addition of propargylic alcohols or amine **8** to nitroalkenes. We therefore discovered that exchanging THF for refluxing trichlorobenzene resulted in a one-pot formation of rearranged alcohols (8–13%), directly from nitroalkenes **7a**–**c** and propargylic alcohols or amine **8**. Interestingly, the formation of the corresponding aldehydes could not be detected under the reaction conditions, probably due to the rapid consumption of the nitrite intermediate in the presence of a strong base such as Bu^{t}OK¶ (Scheme 3).

Similarly, the one-pot conversion of nitroalkene **7c** in the presence of chlorobutynol **9** and Bu^{t}OK afforded keto oxime **5** in 10% yield (Scheme 4).

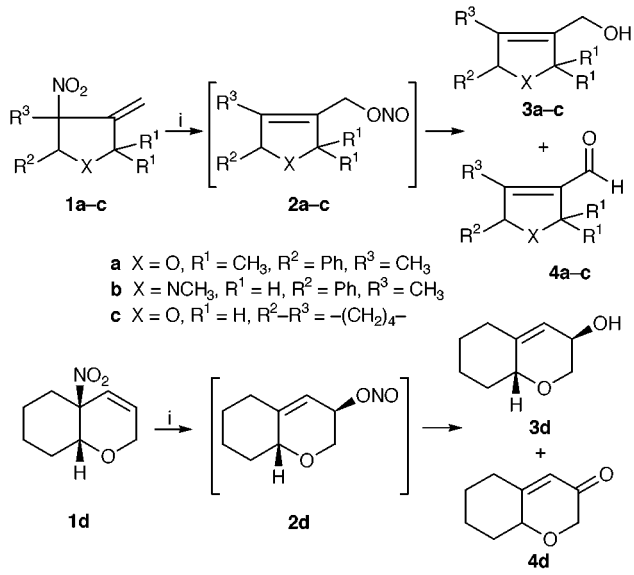

Scheme 1 *Reagents and conditions*: i, 1,2,4-trichlorobenzene, 214 °C, 20–45 min (25–30%).

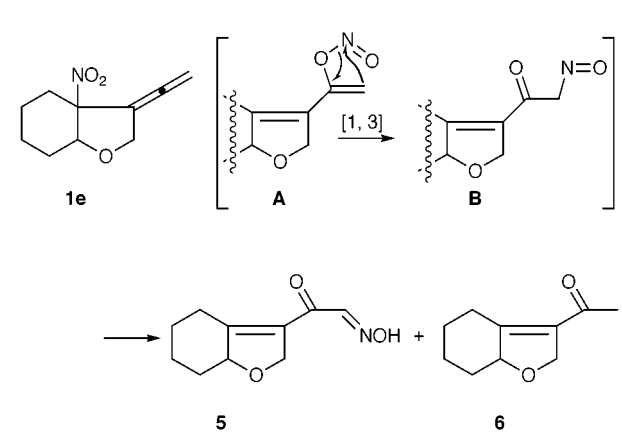

Scheme 2 *Reagents and conditions*: i, 1,2,4-trichlorobenzene, 214 °C, 5 min (**5**: 23%, **6**: trace).

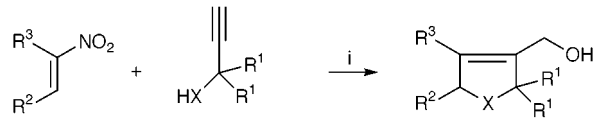

7a–c **8** **3a–c**

Scheme 3 *Reagents and conditions*: i, **8** (X = NMe, O) (1.5 equiv.), 1,2,4-trichlorobenzene, Bu^{t}OK (1.2 equiv.), room temp., 5 min, then 214 °C, 45 min (8–13%).

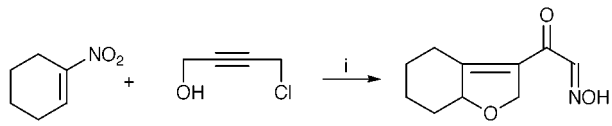

7c **9** **5**

Scheme 4 *Reagents and conditions*: i, **9** (1.5 equiv.), 1,2,4-trichlorobenzene, Bu^{t}OK (1.2 equiv.), room temp., 5 min, then 214 °C, 2 min (10%).

In conclusion, the Bu^{t}OK/thermally induced one-pot reaction of nitroalkenes with alkynyl alcohols constitutes a new four-step domino reaction which involves [2,3]-sigmatropic rearrangement of allyl and allenyl nitro compounds and provides a new route to elaborated 2,5-dihydro-furans or -pyrroles.

We are grateful to Dr S. Zard (Ecole Polytechnique, Palaiseau), for useful suggestions.

Notes and references

† *Selected data* for **2a**: δ_H(400 MHz, $CDCl_3$) 1.19 (s, 3H), 1.47 (s, 3H), 1.61 (s, br, 3H), 4.97 (d, *J* 13.6, 1H), 5.02 (d, *J* 13.6, 1H), 5.59 (s, 1H), 7.26–7.39 (m, 5H); δ_C(100 MHz, $CDCl_3$) 10.8, 27.0, 27.8, 70.5, 88.1, 89.0, 127.5, 128.7, 129.9, 129.4, 139.2, 140.0.

‡ *Selected data* for **3d**: δ_H(400 MHz, $CDCl_3$) 1.35 (m, 2H), 1.75 (m, 3H), 1.95 (m, 2H), 2.23 (ddt, *J* 13.9, 4.4, 2.2, 1H), 3.34 (dd, *J* 11, 6.9, 1H), 3.91 (br t, *J* 5.1, 1H), 3.95 (dd, *J* 11, 4.7, 1H), 4.18 (br s, 1H), 5.53 (br d, *J* 1.8, 1H); δ_H(400 MHz, C_6D_6) 1.23–1.05 (m, 2H), 1.54–1.31 (m, 3H), 1.72 (m, 1H), 2.02 (m, 2H), 3.27 (dd, *J* 10.6, 7.7, 1H), 3.75 (m, 1H), 3.92 (dd, *J* 10.6, 5.1, 1H), 4.10 (m, 1H), 5.41 (br d, *J* 1.6, 1H); δ_C(100 MHz, $CDCl_3$) 24.5, 27.3, 33.2, 33.5, 63.6, 68.3, 75.2, 120.4, 143.3; stereochemistry has been assigned by NOESY correlation (in C_6D_6).

§ *Selected data* for **5**: *m/z* (12 eV) 195.1 (1.5%), 179.1 (11.4), 178.1 (100), 150.1 (52.1), 123.1 (14.9); ν/cm^{-1} 3691, 3559, 3156, 2983, 1817, 1795, 1711, 1650, 1610, 1470, 1382, 1097; δ_H(400 MHz, $CDCl_3$) 1.18–1.46 (m, 5H), 1.99 (m, 1H), 2.25 (m, 1H), 3.57 (dm, *J* 14.5, 1H), 4.65 (m, 1H), 5.07 (dt, *J* 12, 3.5, 1H), 5.17 (ddd, *J* 12.0, 5.3, 1.8, 1H), 7.62 (s, 1H), 9.79 (br s, 1H); δ_C(100 MHz, $CDCl_3$) 23.1, 26.4, 26.9, 35.4, 75.9, 86.4, 126.4, 150.8, 157.9, 185.8.

¶ Alkyl nitrites have been shown to undergo nitrosyl transfer to alcohols (ref. 7) or amines (ref. 8) either in acidic or basic conditions (ref. 9).

1 (*a*) I. E. Marko, in *Comprehensive Organic Synthesis*, ed. B. M. Trost, Pergamon, New York, 1991, vol. 3, p. 913; R. Brückner, in *Comprehensive Organic Synthesis*, ed. B. M. Trost, Pergamon, New York, 1991, vol. 6, p. 873; (*b*) J. R. Hwu and D. A. Anderson, *J. Chem. Soc., Perkin Trans. 1*, 1991, 3199; S.-C. Tsay, H. V. Patel and J. R. Hwu, *Synlett*, 1998, 939.

2 E. Dumez, J. Rodriguez and J.-P. Dulcère, *Chem. Commun.*, 1997, 1831.

3 For related Lewis acid promoted selective preparation of alcohols and carbonyl compounds with alkyl nitrites, see: C. Pérez, S. Pérez, M. A. Zavala, R. M. Pérez and F. O. Guadarrama, *Synth. Commun.*, 1998, **28**, 3011.

4 D. R. H, Barton, J. M. Beaton, L. E. Geller and M. Pechet, *J. Am. Chem. Soc.*, 1961, **83**, 4076.

5 J.-P. Dulcère and E. Dumez, *Chem. Commun.*, 1997, 971.

6 A. L. Nussbaum and C. H. Robinson, *Tetrahedron*, 1962, **17**, 35; D. H. R. Barton, G. C. Ramsay and D. Wege, *J. Chem. Soc.* (*C*), 1967, 1915.

7 J. H. Bayless, F. D. Mendicino and L. Friedman, *J. Am. Chem. Soc.*, 1965, **87**, 5790; S. Oae, N. Asai and K. Fujimori, *J. Chem. Soc., Perkin Trans. 2*, 1978, 1124.

8 A. D. Allen and G. R. Schonbaum, *Can. J. Chem.*, 1961, **39**, 940.

9 M. J. Crookes and D. L. H. Williams, *J. Chem. Soc., Perkin Trans. 2*, 1989, 1319.

Communication 9/05828A

Exploitation of a novel 'on–off' photoinduced electron-transfer (PET) sensor against conventional 'off–on' PET sensors†

Hideomi Kijima,[a] Masayuki Takeuchi,[a] Andrew Robertson,[a] Seiji Shinkai,*[a] Christopher Cooper[b] and Tony D. James[b]

[a] *Department of Chemistry and Biochemistry, Graduate School of Engineering, Kyushu University, Fukuoka 812-8581, Japan. E-mail: seijitcm@mbox.nc.kyushu-u.ac.jp*
[b] *School of Chemistry, University of Birmingham, Edgbaston, Birmingham, UK B15 2TT*

Received (in Cambridge, UK) 23rd August 1999, Accepted 3rd September 1999

A novel PET sensor for sugar sensing which changes its fluorescence intensity in an 'on–off' manner was designed from (tetraphenylporphyrinato)tin(IV)

The concept of photoinduced electron-transfer (PET) sensors has been exploited by de Silva, Czarnik and others for spectroscopic sensing of metal ions and ionic, organic compounds.[1,2] It was later shown that this concept can be successfully applied to spectroscopic sensing of neutral molecules: for example, in a 2-aminomethylphenylboronic acid skeleton the Lewis acidity of the boronic acid group is markedly intensified upon complexation with saccharides, which eventually suppresses the fluorescence quenching efficiency of the amino group.[3–5] A typical example is compound **1** in which the

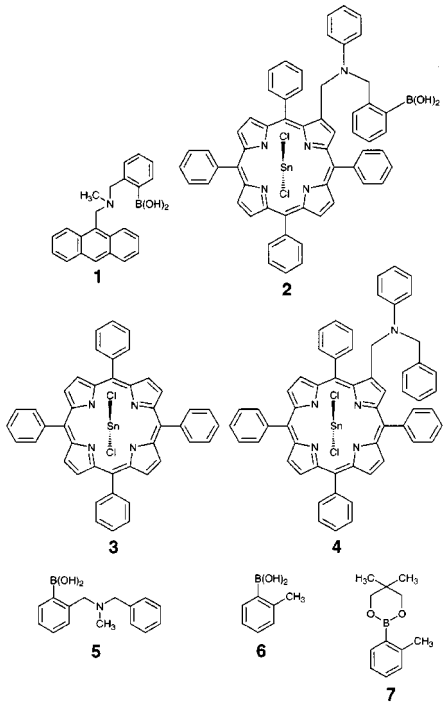

relative fluorescence intensity increases upon complexation with saccharides.[3] This is a typical '*off–on–type*' PET sensor. It occurred to us that judging from the various requirements for the quantitative analyses of saccharides, a reversed '*on–off–type*' PET sensor would be also useful for spectroscopic sensing. With these objectives in mind we synthesized compound **2** bearing a (tetraphenylporphyrinato)tin(IV) moiety as a fluorescent site[6] and a 2-aminomethylphenylboronic acid group as a saccharide-binding site. Computer simulations[7] suggested that, upon binding to the boronic acid moiety, the ligands are

† Electronic supplementary information (ESI) available: colour version of Fig. 1. See http://www.rsc.org/suppdata/cc/1999/2011/

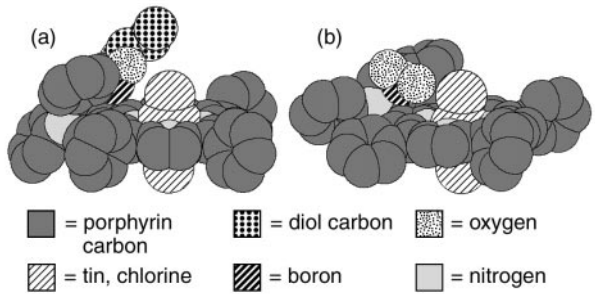

Fig. 1 Minimum energy structures for (a) butane-1,2-diol complexed **2** (b) free **2**: butane-1,2-diol; hydrogens have been omitted for clarity. The B–N distance in (a) is 4.6 Å and in (b) is 3.06 Å. This distance in the free porphyrin can be reduced to allow B–N interaction by thermal motions but steric buffeting between the ligand and the porphyrin prevents this from occurring upon complexation of the diol. Colour version available at http://www.rsc.org/suppdata/cc/1999/2011/

suspended over the plane of the porphyrin where the boron and nitrogen atoms are too far apart to interact (Fig. 1). In the case of the free receptor, however, the boron and tertiary nitrogen can come close enough to interact, including an '*exo*' interaction within the cleft of the adjacent *meso* phenyl rings. Hence, if diol complexation reduces the B–N interaction, **2** should act as a novel 'on–off–type' PET sensor. Compounds **3** and **4**[5] were used as reference compounds related to **2**.

Compounds **2** and **4** were synthesized according to Scheme 1 and identified by ^{1}H NMR and mass (SIMS) spectral evidence and elemental analyses. Initially, we carried out spectroscopic measurements in an aqueous system (25 °C, water : MeOH, 1 : 1 v/v). As expected the fluorescence intensity (I) decreased with increasing saccharide concentrations (pH 10.0 [**2**] = 2.0×10^{-7} mol dm^{-3}, λ_{ex} 417 nm, λ_{em} 605 nm; *e.g.*, I/I_0 = 0.92 and 0.78 at [D-fructose] = 1.0×10^{-3} and 1.0×10^{-2} mol dm^{-3}). We noticed, however, that the fluorescence is sensitive to slight changes in pH and buffer concentration because of axial ligand (Cl^-) substitution.‡ To avoid the complexity arising from axial ligand substitution, the fluorescence measurements were carried out in dichloromethane (but not in aqueous solution) to clarify the mechanism for the fluorescence decrease.

Fig. 2(a) shows the fluorescence spectra of **2**, **3** and **4** in the absence of saccharides: the excitation wavelength is 431 nm near the Soret band. Since the absorbance of these three compounds is similar to each other at this wavelength, one can directly compare their fluorescence intensities. It can be seen from Fig. 2(a) that the fluorescence intensity of **4** (at 605 nm) is only 10.8% of that of **3**, indicating that the intramolecular amino group in **4** efficiently quenches the fluorescence of the (tetraphenylporphinato)tin(IV) moiety. In **2**, on the other hand, the fluorescence intensity was reduced to 31.6% of that of **3**. This implies that the partial B–N interaction does exist but the amino group still retains the fluorescence quenching ability.

Fig. 2(b) shows the fluorescence spectra of **2** in the presence of an excess of a variety of diols; as expected from the original

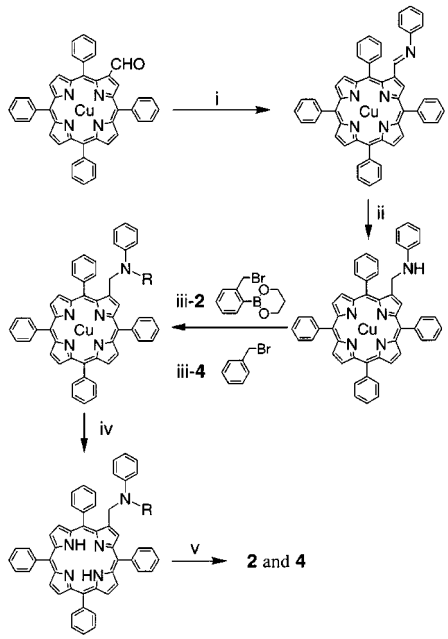

Scheme 1 *Reagents and conditions* [yields]: i, aniline, benzene, reflux [89%]; ii, $NaBH_3CN$, THF, r.t. [58%]; iii, K_2CO_3, THF, reflux [iii **2**; 29%, iii **4**; 50%]; iv, HCl(g), $CHCl_3$, r.t. [iv **2**; 69%, iv **4**; 80%]; v, $SnCl_2$, DMF, 120 °C [**2**; 68%, **4**; 70%].

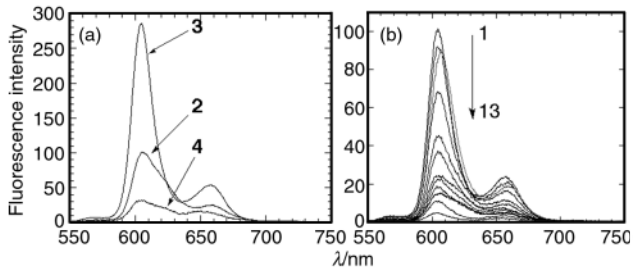

Fig. 2 (a) Fluorescence spectra of **2**, **3** and **4** (2.00×10^{-7} mol dm^{-3}) at 25 °C in CH_2Cl_2: excitation at 431 nm. (b) Fluorescence spectra of **2** (2.00×10^{-7} mol dm^{-3}) in the presence of various diols and saccharides (3.00×10^{-3} mol dm^{-3}) at 25 °C in dichloromethane: excitation 424 nm: 1, none; 2, pinacol; 3, dimethyl L-tartarate; 4, pentane-2,4-diol; 5, *cis*-cyclohexane-1,2-diol; 6, 1,2-diphenylethane-1,2-diol; 7, 2,2-dimethylpropane-1,3-diol; 8, (2*R*,3*R*)-butane-2,3-diol; 9, catechol; 10, butane-1,2-diol; 11, butane-1,3-diol; 12, 1,2,5,6-*O*-bis(isopropylidene)-D-mannitol; 13, (*R*)-1-phenylethane-1,2-diol.

molecular design, complexation with diols decreased the fluorescence intensity of **2**. As a general trend, sterically bulky diols such as (*R*)-1-phenylethane-1,2-diol and 1,2,5,6-*O*-bis(isopropylidene)-D-mannitol and diols with a high affinity for the boronic acid group such as butane-1,2-diol and butane-1,3-diol (frequently used as a protecting group for the boronic acid group) reduced the fluorescent intensity to a large extent. The fluorescence spectra of **3** and **4** were scarcely changed by the addition of these diols, indicating that the spectral change is due to the boronic acid–diol interaction. From plots of the fluorescence intensity *vs.* [diol] for selected diols, the association constants (K_{ass}) were estimated: $K_{ass} = 1.9 \times 10^4$ dm^3 mol^{-1} for 2,2-dimethylpropane-1,3-diol (DMPD), 2.6×10^2 dm^3 mol^{-1} for cyclohexane-1,2-diol, 5.0×10^3 dm^3 mol^{-1} for pentane-2,4-diol and 1.0×10^5 dm^3 mol^{-1} for catechol.

To obtain further insights into the fluorescence decrease induced by the addition of diols we measured ^1H and ^{11}B NMR spectra. In ^1H NMR spectroscopy (600 MHz, $CDCl_3$, 25 °C) DMPD gave a singlet peak at δ 2.16 for the OH protons. When an equimolar amount of **2** (5.0×10^{-3} mol dm^{-3}) was added, this peak nearly disappeared. This change indicates that DMPD forms a six-membered cyclic boronate ester with **2**. It is known that complexation of **5** in aqueous solutions causes an upfield shift of the boron signal of *ca.* 12.0 ppm.[8] In ^{11}B NMR spectroscopy [192 MHz, $CDCl_3$, 25 °C, external standard $B(OMe)_3$] we confirmed that the boron peak for **7** appears at a chemical shift higher by 2.4 ppm than that for **6**. These results indicate that the up-field shift is induced by both the B–N interaction and diol complexation. Compound **2** gave a singlet peak at δ 13.0 but upon addition of an equimolar amount of DMPD (2.5×10^{-2} mol dm^{-2}) a new strong peak appeared at δ 9.0. The shift width is only 4.0 ppm which is sufficiently rationalized by simple complexation with DMPD. We believe, therefore, that even though DMPD is bound to the boronic acid moiety in **2**, the B–N interaction is not specifically intensified as in the case of the previous 'off–on–type' PET sensors. To the best of our knowledge, this is the first example of an 'on–off–type' PET sensor for sugar sensing.[9]

The present study has demonstrated that a novel 'on–off–type' PET sensor can be designed by skilful utilization of steric crowding. Hence, it is now possible to choose either 'on–off–type' or 'off–on–type' PET sensors according to the experimental requirements. This indicates the high potential and versatility of combining the B–N interaction with the PET systems.

Notes and references

‡ Supporting information is available on request.

1 A. P. De Silva, H. Q. N. Gunarathe and C. P. McCoy, *Chem. Commun.*, 1996, 2399; A. P. De Silva, H. Q. N. Gunarathe, C. McVeigh, G. E. M. Maguine, P. R. S. Maxwell and E. Q'Hanlon, *Chem. Commun.*, 1996, 2191; A. P. De Silva, H. Q. N. Gunaratne, T. Gunnlaugsson, C. P. McCoy, P. R. S. Maxwell, J. T. Rademacher and T. E. Rice, *Pure Appl. Chem.*, 1996, **68**, 1443; A. P. De Silva, H. Q. N. Gunaratne, T. Gunnlaugsson, A. J. M. Huxley, C. P. McCoy, J. T. Rademacher and T. E. Rice, *Chem. Rev.*, 1997, **97**, 1515.

2 A. W. Czarnik, *Acc. Chem. Res.*, 1994, **27**, 302; A. W. Czarnik, *Fluorescent Chemosensors for Ion and Molecular Recognition*, ACS Books, Washington, DC, 1993.

3 T. D. James, K. R. A. S. Sandanayake and S. Shinkai, *J. Chem. Soc., Chem. Commun.*, 1994, 477; T. D. James, K. R. A. S. Sandanayake and S. Shinkai, *Angew. Chem., Int. Ed. Engl.*, 1994, **33**, 2207; T. D. James, K. R. A. S. Sandanayake, R. Iguchi and S. Shinkai, *J. Am. Chem. Soc.*, 1995, **117**, 8982; T. D. James, P. Linnane and S. Shinkai, *Chem. Commun.*, 1996, 281; T. D. James, H. Shinmori, M. Takeuchi and S. Shinkai, *Chem. Commun.*, 1996, 705; T. D. James, H. Shinmori and S. Shinkai, *Chem. Commun.*, 1997, 71.

4 For comprehensive reviews, see: T. D. James, K. R. A. S. Sandanayake and S. Shinkai, *Supramol. Chem.*, 1995, **6**, 141; K. R. A. S. Sandanayake, T. D. James and S. Shinkai, *Pure Appl. Chem.*, 1996, **68**, 281; S. Shinkai and M. Takeuchi, *Trends Anal. Chem.*, 1996, **15**, 188; T. D. James, K. R. A. S. Sandanayake and S. Shinkai, *Angew. Chem., Int. Ed. Engl.*, 1996, **35**, 1910.

5 More recently, Cooper and James reported a PET chemosensor with an anthracene fluorophore appending an *o*-aminomethylphenyl boronic acid group and a crown ether group which selectively binds glucosamine: C. R. Cooper and T. D. James, *Chem. Commun.*, 1997, 1419.

6 It is known that the amino group is capable of quenching the fluorescence of the (tetraphenylporphinato)tin(IV) moiety: R. Grigg and W. D. J. A. Norkert, *J. Chem. Soc., Chem. Commun.*, 1992, 1298.

7 Computer simulations were performed using CDiscover as implemented by Insight II ver. 98.0 on a Silicon Graphics Octane workstation. Conformations were explored with molecular dynamics simulations using the ESFF forcefield at 500 K for 40 ps with subsequent minimisation of low energy conformations.

8 C. R. Cooper, N. Spencer and T. D. James, *Chem. Commun.*, 1998, 1365.

9 An alternative mechanism was briefly considered after mass spectrometry consistently demonstrated the loss of one chloride ligand during measurements. Although this phenomenon could result simply from losing chloride to achieve a positive charge, we also considered the possibility of displacement of chloride by a boron-attached oxygen to yield a B–O–Sn self-complexed macrocycle. IR and NMR experiments produced no evidence for this interaction, however, and it was therefore discarded.

Communication 9/06825B

Photo-induced metastable linkage isomers of ruthenium nitrosyl porphyrins

Dmitry V. Fomitchev,*[a] Philip Coppens,*[a] Tianshu Li,[b] Kimberly A. Bagley,[b] Li Chen[c] and George B. Richter-Addo*[c]

[a] *Department of Chemistry, State University of New York at Buffalo, Buffalo, New York 14260-3000, USA. E-mail: coppens@acsu.buffalo.edu*
[b] *Department of Chemistry, State University College of New York at Buffalo, Buffalo, New York, 14222, USA*
[c] *Department of Chemistry and Biochemistry, University of Oklahoma, 620 Parrington Oval, Norman, Oklahoma, 73019, USA*

Received (in Bloomington, IN, USA) 30th June 1999, Accepted 28th August 1999

IR spectroscopic results, combined with earlier crystallographic and spectroscopic evidence on Fe and Ru nitrosyl complexes, indicate that metastable η^1-O and η^2-NO linkage isomers are formed on low-temperature irradiation of the nitrosyl metalloporphyrins (OEP)Ru(NO)L (L = O-i-C_5H_{11}, SCH_2CF_3); the new compounds are stable at low temperature, but revert to the ground state on warming.

Nitric oxide (NO) plays a crucial role in several biologically important processes such as intercellular signal transduction, blood pressure regulation, and cytotoxic activity of immune systems.[1] NO is synthesized *in vivo* by the enzyme NO synthase, which contains a (por)Fe(SR) heme active site.[2] NO is now known to be produced by several heme-containing denitrifying enzymes.[3] One of the major biological functions of NO is to bind to the metal center of heme-containing soluble guanylyl cyclase, resulting in activation of the enzyme.[4] NO is also known to bind to other heme-containing biomolecules such as cytochrome P450, Hb, Mb, cytochrome *c* oxidase, and heme-containing nitrite reductases.[5]

The photochemistry of nitrosyl metalloporphyrins and -hemes reveal photodenitrosylation (A) and recombination (B) processes [eqn. (1)][6–8] that are probably governed by factors

$$\text{(por)M(NO)} \underset{\text{B}}{\overset{\text{A}}{\rightleftharpoons}} \text{(por)M} + \text{NO} \qquad (1)$$

that include metal oxidation state and the identity and orientation of the *trans* (proximal) ligand. Distal pocket residues also play a role in the geminate recombination of NO in heme proteins.[10] The results of kinetic studies of photochemically induced loss and recombination of NO with hemoproteins[9,10] and metalloporphyrins[11,12] suggest that recombination is a fast and multistage process at room temperature. Clearly, the mechanisms of NO approach, release and subsequent binding to heme and heme models require further investigation.

Until recently, established or proposed descriptions of NO binding to the metal center in heme or heme models have been restricted to N-binding of the NO group to the metal in either linear or bent forms. We have reported novel X-ray crystal structures of coordination and organometallic compounds with photoinduced O-bound (η^1-O) and side-on (η^2-NO) bound nitrosyl groups.[13–15]

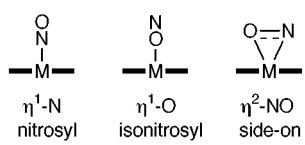

These compounds were of the {MNO}^{6} and {MNO}^{10} formulations.[16] We were thus interested in determining if such linkage isomers could exist for group 8 {MNO}^{6} nitrosyl metalloporphyrins of the form (por)M(NO)X with X *trans* to NO. Here, we report the first spectroscopic detection of η^1-O and η^2-NO linkage isomers of nitrosyl metalloporphyrins.

Irradiation of (OEP)Ru(NO)L [L=O-i-C_5H_{11} **1**,† SCH_2CF_3 **2**;†[17] KBr pellets; 330 < λ < 460 nm; Xe lamp][18] at 20 K for 15 min results in IR spectral changes that are attributed to the formation of metastable states possessing η^1-O and η^2-NO linkage isomers (Table 1). For example, irradiation of the alkoxide compound **1** (υ_{NO} 1791 cm^{-1}) results in a reduction of intensity of the original υ_{NO} band, and the appearance of new bands at 1645 and 1497 cm^{-1}. Difference spectra from the samples before and after 15 min of photolysis are shown in Fig. 1(a). Upon ^{15}N labeling, these 1791 and 1645 cm^{-1} bands are downshifted by 36 cm^{-1} (expected shift of 34 cm^{-1} based on simple two-body model), whereas the 1497 cm^{-1} band is downshifted by 17 cm^{-1}. Similar results are observed during photolysis of the thiolate compound **2** [Fig. 1(b) and Table 1].

The following observations support the assignment of the new bands as being due to photoinduced η^1-O and η^2-NO linkage isomers at 20 K, respectively.

(i) Photolysis does not produce free NO which has an absorption band at 1880 cm^{-1}.[19]

(ii) The intensities of the parent nitrosyl bands were restored after the photolysis had ceased and the samples were warmed to room temperature and cooled back to 20 K. Thus, the light-induced reaction is thermally reversible, indicating the formation of a metastable species. For compound **1**, the new band at 1645 cm^{-1} can be seen only below 160 K, while the second new band at 1497 cm^{-1} can be generated only below 80 K. For compound **2**, the new bands are generated simultaneously upon irradiation at temperatures below 60 K. In all cases the photo-induced bands persist for at least several hours if the initial temperature is maintained.

(iii) Both new bands are subject to the ^{15}N-isotope shift, and thus associated with υ_{NO} (Table 1). Thus, the isotope shifts of the η^1-O υ_{NO} bands are 36 and 27 cm^{-1} for photoexcited **1** and **2**, respectively. The isotope shifts of the η^2-NO υ_{NO} bands are 17 and 19 cm^{-1}. Similar υ_{NO} downshifts of 19 and 14 cm^{-1} upon ^{15}N labeling were recently reported for Cr(η^2-NO)[20] and V(η^2-NO),[21] respectively, generated in an Ar matrix .

Table 1 Wavenumbers (cm^{-1}) and shifts of IR absorption bands of nitrosyl and light-induced isomers with iso- and side-on bound nitrosyl of complexes **1** and **2**

	υ(RuN–O)	υ(RuO–N)	υ[Ru(η^2-NO)]
(OEP)Ru(NO)(O-i-C_5H_{11})			
^{14}N	1791	1645 (−146)	1497 (−294)
^{15}N	1755	1609 (−146)	1480 (−275)
$\upsilon(^{14}N) - \upsilon(^{15}N)$	36	36	17
(OEP)Ru(NO)(SCH_2CF_3)			
^{14}N	1788	1660 (−128)	1546 (−242)
^{15}N	1753	1633 (−120)	1527 (−226)
$\upsilon(^{14}N) - \upsilon(^{15}N)$	35	27	19

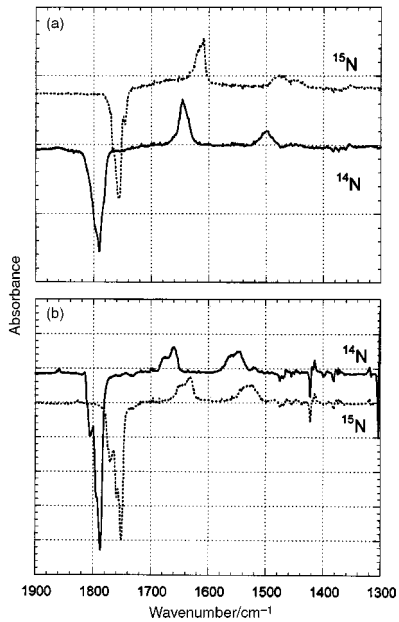

Fig. 1 Difference spectra (spectrum after irradiation minus spectrum prior to irradiation for 15 min) for the ^{14}N and ^{15}N labeled compounds (a) (OEP)Ru(NO)(O-i-C_5H_{11}) and (b) (OEP)Ru(NO)(SCH_2CF_3). The bimodal structure of some of the shifted bands is attributed to crystalline disorder and two possible orientations of the NO group. Conversion percentages are estimated as 1 and 1.5% for (a) and (b), respectively.

(iv) The observed decreases in υ_{NO} upon conversion from nitrosyl to isonitrosyl (η^1-O) and to side-on (η^2-NO) bound nitrosyl (Table 1) are very similar to those recorded for other excited Fe, Ru, Os and Ni nitrosyl complexes.[14,15,22–27] DFT calculations on the nitrosyl linkage isomers in $Na_2[Fe(CN)_5(NO)]\cdot 2H_2O$[28] predict related downshifts of υ_{NO} by 108 and 320 cm^{-1} for the η^1-O and η^2-NO isomers, respectively.

(v) Downshifts in a number of porphyrin skeletal modes (in the region 1600–900 cm^{-1})[31,32] by 3–5 cm^{-1} upon photolysis are also consistent with the data available for six-coordinate Fe(II) porphyrins which indicate that the reduction of π-acid character of the axial ligand causes downshifts of the skeletal absorption bands.[33]

Finally, we report that we have observed similar linkage isomers in two other complexes (OEP)Ru(NO)(Cl) **3** and [(OEP)Ru(NO)(py)]$^+$ **4**, thus expanding the range of compounds to include those having O-, S-, halide- and N-donors *trans* to NO.

In summary, we conclude that the low-temperature IR spectroscopic evidence presented here indicates that η^1-O and η^2-NO linkage isomers are achievable metastable states in nitrosyl metalloporphyrins.

Support of this work by the National Science Foundation (CHE9615586, P. C.; CHE9625065, G. B. R.-A.; MCB9723828, K. A. B.), the National Institutes of Health (R29GM53586, G. B. R.-A.), and the Petroleum Research Fund administered by the American Chemical Society (PRF28664AC3, P. C.) is gratefully acknowledged.

Notes and references

† OEP = octaethylporphyrinato dianion. (OEP)Ru(NO)(O-i-C_5H_{11}) was obtained from the reaction of (OEP)Ru(CO) with isoamyl nitrite. The ^{15}NO labeled analog was prepared using ^{15}N−labeled isoamyl nitrite. *Crystallographic data* for **1**: dark−red monoclinic crystals, space group *Pn*, a = 8.329(2), b = 10.627(2), c = 22.533(5) Å, β = 91.90(2)°, V = 1993.4 Å^3, Z = 2, T = 298 K, μ = 0.568 mm^{-1}, R_1 = 0.070, wR_2 = 0.187, GOF = 1.0.

(OEP)Ru(NO)(SCH_2CF_3) was prepared as previously described, and its purity checked by IR and ^{1}H NMR spectroscopy.[17] The ^{15}NO labeled analogue was prepared in 79% yield by reacting (OEP)Ru(CO) with $^{15}NOBF_4$ and then $KSCH_2CF_3$. *Crystallographic data* for **2**: dark-violet monoclinic crystals, space group *Pn*, a = 8.418(2), b = 10.485(2), c = 22.236(4), β = 91.80(3)°, V = 1961.6 Å^3, Z = 2, T = 298 K, μ = 0.641 mm, R_1 = 0.062, wR_2 = 0.138, GOF = 1.1. CCDC 182/1396.

1 *Nitric Oxide: Biochemistry, Molecular Biology, and Therapeutic Implications*, ed. L. Ignarro and F. Murad, *Advances in Pharmacology*, Academic Press, San Diego, 1995, vol. 34; *Nitric Oxide: Principles and Applications*, ed. J. Lancaster, Academic Press, San Diego, 1996; *Nitric Oxide*, ed. L. Packer, *Methods in Enzymology*, Academic Press, San Diego, 1996, vol. 268, 269; 1999, vol. 301.
2 M. A. Marletta, *Cell*, 1994, **78**, 927.
3 T. C. Hollocher, in *Nitric Oxide: Principles and Applications*, ed. J. Lancaster, Academic Press, San Diego, 1996, pp. 289–344; P. A. Williams, V. Fülop, E. F. Garman, N. F. W. Saunders, S. J. Ferguson and J. Hajdu, *Nature*, 1997, **389**, 406; T. C. Hollocher and J. B. Hibbs, Jr., in *Methods in Nitric Oxide Research*, ed. M. Feelisch and J. S. Stamler, John Wiley and Sons, New York, 1996, pp. 119–146.
4 Y. Zhao, C. Hoganson, G. T. Babcock and M. A. Marletta, *Biochemistry*, 1998, **37**, 12 458 and references therein.
5 L. Cheng and G. B. Richter-Addo, in *Porphyrin Handbook*, ed. R. Guillard, K. Smith and K. M. Kadish, Academic Press, San Diego, in press.
6 E. A. Morlino and M. A. J. Rodgers, *Prog. React. Kinet.*, 1998, **23**, 91; P. C. Ford, J. Bourassa, K. Miranda, B. Lee, I. Lorkovic, S. Boggs, S. Kudo and L. Laverman, *Coord. Chem. Rev.*, 1998, **171**, 185.
7 M. Hoshino, K. Ozawa, H. Seki and P. C. Ford, *J. Am. Chem. Soc.*, 1993, **115**, 9568.
8 A. F. Duprat, T. G. Traylor, G.-Z. Wu, M. Coletta, V. S. Sharma, K. N. Walda and D. Magde, *Biochemistry*, 1995, **34**, 2634.
9 K. N. Walda, X. Y. Liu, V. S. Sharma and D. Magde, *Biochemistry*, 1994, **33**, 2198.
10 M. L. Carlson, R. Regan, R. Elber, H. Li and G. N. Phillips, J. S. Olson and Q. H. Gibson, *Biochemistry*, 1994, **33**, 10 597; J. S. Olson and G. N. Phillips, *J. Biol. Chem.*, 1996, **271**, 17 593.
11 I. S. Zavarine, A. D. Kini, B. H. Morimoto and C. P. Kubiak, *J. Phys. Chem. B*, 1998, **102**, 7287.
12 E. A. Morlino and M. A. Rodgers, *J. Am. Chem. Soc.*, 1996, **118**, 11 798.
13 P. Coppens, D. V. Fomitchev, M. D. Carducci and K. Culp, *J. Chem. Soc., Dalton Trans.*, 1998, 865.
14 D. V. Fomitchev, T. R. Furlani and P. Coppens, *Inorg. Chem.*, 1998, **37**, 1519.
15 M. D. Carducci, M. R. Pressprich and P. Coppens, *J. Am. Chem. Soc.*, 1997, **119**, 2669.
16 J. H. Enemark and R. D. Feltham, *Coord. Chem. Rev.*, 1974, **13**, 339.
17 G.-B. Yi, M. A. Khan and G. B. Richter-Addo, *Inorg. Chem.*, 1996, **35**, 3453.
18 The experimental set-up allows simultaneous IR data collection and photolysis of a sample maintained at cryogenic temperature: K. A. Bagley, E. C. Duin, W. Roseboom, S. P. J. Albracht and W. H. Woodruff, *Biochemistry*, 1995, **34**, 5527.
19 K. Nakamoto, *Infrared and Raman Spectra of Inorganic and Coordination Compounds, Part B*, John Wiley and Sons, New York, 1997, p. 149.
20 M. Zhou and L. Andrews, *J. Phys. Chem. A*, 1998, **102**, 7452.
21 M. Zhou and L. Andrews, *J. Phys. Chem. A*, 1999, **103**, 478.
22 J. A. Güida, O. E. Piro, P. S. Schaiquevich and P. J. Aymonino, *Solid State Commun.*, 1997, **101**, 471.
23 Th. Woike, H. Zollner, W. Krasser and S. Haussühl, *Solid State Commun.*, 1990, **73**, 149.
24 Th. Woike and S. Haussühl, *Solid State Commun.*, 1993, **86**, 333.
25 D. V. Fomitchev and P. Coppens, *Inorg. Chem.*, 1996, **35**, 7021.
26 J. A. Güida, O. E. Piro and P. J. Aymonino, *Inorg. Chem.*, 1995, **34**, 4113.
27 O. Crichton and A. J. Rest, *J. Chem. Soc., Dalton. Trans.*, 1977, 986.
28 B. Delley, J. Schefer and Th. Woike, *J. Chem. Phys.*, 1997, **107**, 10 067.
29 M. F. Sisemore, M. Selke, J. N. Burstyn and J. S. Valentine, *Inorg. Chem.*, 1997, **36**, 979, and references therein; R. B. VanAtta, C. E. Strouse, L. K. Hanson and J. S. Valentine, *J. Am. Chem. Soc.*, 1987, **109**, 1425; C.-H. Yang, S. J. Dzugan and V. L. Goedken, *J. Chem. Soc., Chem. Commun.*, 1985, 1425.
30 L. M. Proniewicz, I. R. Paeng and K. Nakamoto, *J. Am. Chem. Soc.*, 1991, **113**, 3294.
31 X. Y. Li, R. S. Czernuszewicz, J. R. Kincaid, P. Stein and T. G. Spiro, *J. Phys. Chem.*, 1990, **94**, 47; C. Piffat, D. Melamed and T. G. Spiro, *J. Phys. Chem.*, 1993, **97**, 7441.
32 T. Kitagawa and Y. Ozaki, *Struct. Bonding* (*Berline*), 1987, **64**, 71.
33 T. G. Spiro, in *Iron Porphyrins*, ed. A. B. P. Lever and H. B. Gray, Addison-Wesley, MA, 1983, vol. 2, pp. 91–152.

Communication 9/05285B

ChemComm

A periodic density functional study of BEDT–TTF salts†

S. A. French,* P. Day and C. R. A. Catlow

The Royal Institution of Great Britain, 21 Albemarle Street, London, UK W1X 4BS. E-mail: sam@ri.ac.uk

Received (in Oxford, UK) 20th August 1999, Accepted 31st August 1999

We report the first *ab initio* computational study of the structural and electronic properties of BEDT–TTF charge transfer salts, which have wide ranging physical properties which are derived primarily from the packing of the donor-radical cations. The calculations accurately reproduce the observed crystal structure of the material and provide new information on the electronic structure of the (BEDT-TTF)[$FeBr_4$] salt.

BEDT–TTF [bis(ethylenedithio)tetrathiafulvalene] or 'ET', first synthesised by Mizuno *et al.*[1] has been extensively studied as it is the organic component of a family of superconducting molecular charge transfer salts. An important structural feature of these systems, based on the donor molecule ET, is the separation of the organic cations and the inorganic anion into alternating layers and stacks. As a consequence, there are many lattice packings of ET, which lead to insulating, semiconducting, metallic and superconducting phases. These physical properties result primarily from the packing of the donor-radical cations in the crystal structure. The orientation and distance between the cations has a critical influence on the electronic behaviour. The sulfur–sulfur interaction is the major influence on the intermolecular interactions owing to the larger size of these heteroatoms. However, the exact mechanistic process by which superconduction occurs below T_c, is unknown.

To investigate the structure and electronic properties of these molecular charge transfer salts we have used density functional theory (DFT); periodic boundary conditions were employed and the calculations were performed using the DMol[3] code,[2] with the local density (LD) exchange and correlation functionals of Perdew and Wang.[3] DMol[3] uses numerical basis sets where the basis functions are given as values on an atomic centred spherical polar mesh. Calculations were performed using the double numeric + polarisation (DNP) basis set. Previously it has only been possible to perform single point calculations but with the increase in computer power we can now perform a full geometry optimisation within the constraint of the observed cell dimensions on (ET)$FeBr_4$.[4] These calculations thus represent a considerable advance in the level of theory applied to these systems, and they include a detailed treatment of steric and crystal field effect; they are, however computationally expensive. We note that previous studies have used much simpler levels of theory such as extended Huckel theory[5–7] or have simply considered the isolated organic cation.[8, 9]

First let us consider the calculated structure. From Fig. 1 and Table 1 it is clear that there is excellent agreement between calculated and experimental structures. There are minor deviations in the hydrogen positions but this is consistent with the crystallographic data[4] which shows hydrogen having the largest thermal ellipsoids. Analyses of the bond lengths in Table 1 show excellent agreement with the experimental values.

Turning now to the electronic structure of the salts, we recall that the mechanism of superconductivity is unknown but clearly charge transfer is vital. The Mulliken population analysis allows examination of the charge distribution on each constituent atom; the combined value for the ET molecule is 0.784 of an electron clearly showing that charge transfer has occurred. By analysing

† Electronic supplementary information (ESI) available: colour versions of the Figures. See http://www.rsc.org/suppdata/cc/1999/2015/

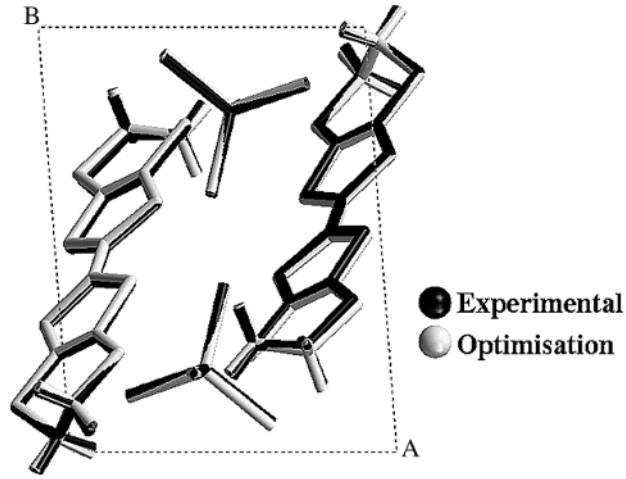

Fig. 1 Superposition of experimental (crystal structure) and calculated structure of (ET)$FeBr_4$.

the spin distribution we find that the calculated spin for the anion, 4.935 electrons is very close to the expected value of 5/2 electron pairs per high spin d^5 Fe^{3+}. As expected, the description of the spin on the anion shows that there is covalent bonding between iron and bromine as the spin density indicates 0.31 electrons donated from iron to each bromine. Of interest is the spin distribution over the ET molecule. The single spin left upon ET after charge transfer implies an unpaired spin on both ET molecules in the unit cell. The Mulliken population analysis shows no spin on the ET cation which suggests that a covalent bond is formed between ET molecules of opposite spin. The bonding interaction is within the combined van der Waals radius of sulfur at *ca.* 3.5 Å.

In the superconducting phases of ET salts, the formation of stacks leads to holes being present at an intermolecular distance of *ca.* 3.6 Å which has led to the hypothesis that the intermolecular sulfur–sulfur interactions are an important component of the interstack transfer integrals and hence the electronic band structure. (ET)$FeBr_4$ has been experimentally categorised as an insulator, owing to the formation of dimers. The calculated band gap of −0.265 eV agrees with the experimental observation. Analysis of the highest occupied

Table 1 Comparison of experimental (crystal structure) and calculated bond lengths (Å) for (ET)$FeBr_4$.

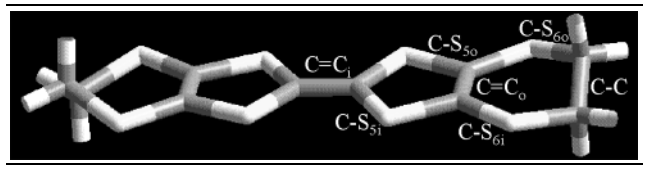

	Exptl.	Calc.		Exptl.	Calc.
Fe–Br	2.337	2.327	$C–S_{6i}$	1.741	1.741
$C=C_i$	1.383	1.383	$C–S_{60}$	1.818	1.810
$C=C_o$	1.371	1.388	C–C	1.497	1.448
$C–S_{5i}$	1.733	1.723	C–H	1.105	0.95
$C–S_{5o}$	1.742	1.730			

molecular orbital (HOMO) of (ET)$FeBr_4$ agrees with previous experimental studies[10–12] and calculations using extended Huckel theory (EHT) and tight binding schemes,[5–7] that the orbital is situated on the ET molecules and in particular on sulfur. For (ET)$FeBr_4$ there are clearly no pathways for the hopping of conduction electrons owing to the barrier of the anions.

Our calculations show that, using DFT methods, it is possible to model accurately the structures and electronic properties of these important materials and it is clear that QM calculations provide a tool for further insight into the electronic properties both of the constituent molecules and their salts.

We are grateful to EPSRC for financial support. We would like to thank MSI for the provision of all the software used and partial support of the project.

Notes and references

1 M. Mizuno, A. Gariot and M. Cava, *J. Chem. Soc., Chem. Commun.*, 1978, 18.
2 Cerius[2] 3.5, *Molecular Simulations*, San Diego, 1997.
3 J. P. Perdew and Y. Wang, *Phys. Rev. B: Condens. Matter*, 1992, **45**, 13 244.
4 T. Mallah, C. Hollis, S. Bott, M. Kurmoo, P. Day, M. Allan and R. H. Friend, *J. Chem. Soc., Dalton. Trans.*, 1990, 859.
5 T. Mori, A. Kobayashi, Y. Sasaki, H. Kobayashi, G. Saito and H. Inokuchi, *Bull. Chem. Soc. Jpn.*, 1984, **57**, 627.
6 C. E. Campos, P. S. Sandhu, J. S. Brooks and T. Ziman, *Phys. Rev. B: Condens. Matter*, 1996, **53**, 12 725.
7 J. Shumway, S. Chattopadhyay and S. Satpathy, *Phys. Rev. B: Condens. Matter*, 1996, **53**, 6677.
8 J. C. R. Faulhaber, D. Y. K. Ko and P. R. Briddon, *Synth. Met.*, 1993, **60**, 227.
9 E. Demiralp and W. A. Goddard, *J. Phys. Chem.*, 1994, **98**, 9781.
10 G. Bar, S. N. Magonov, W. Liang and M. H. Whangbo, *Synth. Met.*, 1995, **72**, 189.
11 A. Sekiyama, T. Susaki, A. Fujimori, T. Sasaki, N. Toyota, T. Kondo, G. Saito, M. Tsunekawa, T. Iwasaki, T. Muro, T. Matsushita, S. Suga, H. Ishii and T. Miyahara, *Phys. Rev. B: Condens. Matter*, 1997, **56**, 9082.
12 M. Yoshimura, H. Shigekawa, H. Nejoh, G. Saito, Y. Saito and A. Kawazu, *Phys. Rev. B: Condens. Matter*, 1991, **43**, 13 590.

Communication 9/06841D

Typeset and printed by Black Bear Press Limited, Cambridge, England

Strigol-type germination stimulants: the C-2′ configuration problem

Peter Welzel,* Susanne Röhrig and Zenka Milkova

Institut für Organische Chemie der Universität Leipzig, Talstr. 35, D-04103 Leipzig, Germany. E-mail: welzel@organik.orgchem.uni-leipzig.de

Received (in Cambridge, UK) 24th February 1999, Accepted 23rd June 1999

Germination of root parasites of the Scrophulariaceae and the Orobanchaceae is known to be induced by chemicals which are released from the roots of their host plants. An important class of germination stimulants are the strigolactones. Reviewed are (i) the connection of the configuration at C-2′ of the strigolactones and their seed germination potencies, (ii) methods for configurational assignment at C-2′, and (iii) stereocontrol at C-2′ in the synthesis of strigolactones.

Introduction

Root parasitic flowering plants of the genera *Striga*, *Alectra* (Scrophulariaceae) and *Orobanche* (Orobanchaceae) and their respective host plants use a very interesting system of chemical communication. It has long been known that germination of the seeds of the parasites is stimulated by compounds exuded from the roots of their host plant into the soil. Well-known stimulants are strigol (**1**) and its acetate (isolated from *Striga* hosts[1] and from cotton, *Gossypium hirsutum*,[2] a non-host), as well as sorgolactone (**2**, isolated from the root exudates of *Sorghum vulgare*,[3] a host for *Striga*). Recently, orobanchol, an isomer of strigol, has been isolated by Yokota *et al.* from root exudates of the host, *Trifolium pratense*. It is assumed that the secondary hydroxy group in orobanchol is attached to C-4.[4] Finally, from the root exudates of *Vigna unguiculata*[5] (host for *Striga* and *Alectra*) a compound, alectrol, has been isolated. A structure has been proposed for this compound that has recently been rejected.[6]

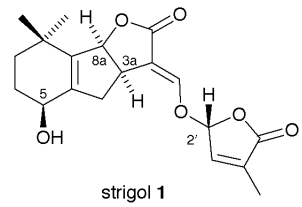

strigol **1**

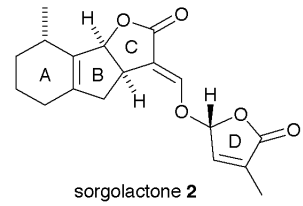

sorgolactone **2**

It has been claimed that the true stimulants are in fact hydroquinones of type **3** (dihydrosorgoleone).[7] This suggestion will not be further discussed here. The present review will rather restrict itself to the problem of the strigol-type stimulants (also called strigolactones).

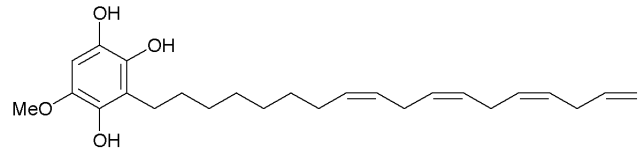

dihydrosorgoleone **3**

Structure–activity relationships

The exchange of chemical information indicated above raises basic questions, such as: (i) which structural features of the stimulants are essential to elicit a high seed germination potency; (ii) how is the chemical signal released from the host recognized by the seed; and (iii) how does the primary chemical signal initiate the biochemical processes that are involved in germination?

Whereas over the years an appreciable knowledge on the structure–activity relationships has accumulated (mainly driven by the desire to use this system for a novel approach of parasitic weed control), questions (ii) and (iii) are largely unanswered. Even the results of structure–activity investigations are not clear-cut. They indicate that very specific interactions exist between the stimulants and the binding site(s) at the seeds. However, it has been demonstrated that the interactions are species–dependent and may vary from test to test. Structure–activity relationships obtained from different test systems should, thus, be compared only with great care. The problem has been reviewed and discussed in detail by Zwanenburg and co-workers who also recommended a standard bioassay.[8]

In addition, the configuration at the various stereogenic centres of the stimulants is of great importance with respect to seed germination activity. Much of the older work was performed with mixtures of stereoisomers and is, thus, of

Peter Welzel recieved his PhD from the University of Bonn (with R. Tschesche). After a postdoctoral fellowship with D.H.R. Barton at Imperial College in London he returned to Bonn to work for his habilitation. In 1973 he was appointed Professor at the Ruhr University in Bochum. In 1993 he moved to the University of Leipzig where his is Professor of Organic Chemistry.

Susanne Röhrig received her Diploma from the Ruhr University in Bochum in 1994, and her PhD, entitled 'C-2′-stereoselective synthesis of strigol-type compounds', from the University of Leipzig (with Peter Welzel) in 1997. She is currently a Postdoctoral Fellow in the group of Professor Peter Seeberger at the Massachusetts Institute of Technology.

Zenka Milkova received her MSc from the University of Burgas, Bulgaria, in 1968, and her PhD from the University of Sofia, Bulgaria, in 1976. In 1976 she became a Research Fellow at the Institute of Organic Chemistry, Bulgarian Academy of Sciences (Sofia), where in 1990 she was made an Associate Professor. During this time, she spent two periods (1981–1982 and 1987–1988) as a Research Fellow in the group of Peter Welzel at the Ruhr University in Bochum. Between 1991 and 1992 she worked for Janssen at the Facultes Universitaires Notre-Dame de la Paix (Namur, Belgium). Since 1999 she has been Reader for Organic Chemistry at the University 'Neophit Rilski' (Blagoevgrad, Bulgaria).

limited value. As such, only results from single stereoisomers will be considered.

The first study with pure strigol isomers was published by Hauck and Schildknecht who found that strigol (**1**) was active (half-maximum germination) for *Striga asiatica*, *Orobanche aegyptiaca* at concentrations of 6×10^{-11} and 7×10^{-10} mol l^{-1}, respectively. The non-natural *ent*-strigol had to be 500 and 300 times more concentrated to be as active. For *Alectra vogelii*, however, *ent*-strigol was 20 times more active than the natural isomer.[9]

The Hauck study was complemented by work of Bergmann *et al.* showing that, in addition to the absolute configuration, the configuration at C-2′ is of major importance, at least as far as *Orobanche crenata* is involved (see Table 1).[10]

Table 1 Activity of strigol analogues in *O. crenata* seed germination bioassays: $c_{½}$ = concentration of half maximal stimulation of germination (ref. 10)

Compound	Configuration at C-2′	$c_{½}$/mol l^{-1}	$c_{½}$ (relative)
Strigol (**1**)	*R*	$8.5\ 10^{-8}$	1.0
ent-Strigol	*S*	$3.4\ 10^{-6}$	40.0
2′-*epi*-Strigol	*S*	$2.3\ 10^{-6}$	27.1
ent-2′-*epi*-strigol	*R*	$1.0\ 10^{-6}$	11.8
rac-GR24 (**4**)	*RS*	$3.4\ 10^{-7}$	
rac-2′-*epi*-GR24	*SR*	$3.4\ 10^{-6}$	

The largest collection of experimental results comes from Binne Zwanenburgś laboratory. Homogeneous stereoisomers in the GR7 (**5**),[11] GR24 (**4**),[12] demethylsorgolactone (**6**),[13] sorgolactone (**2**)[14] and Nijmegen 1 (**7**)[15] series have been

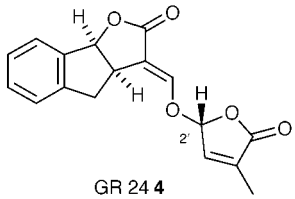

GR 24 **4**

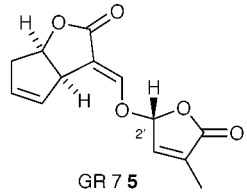

GR 7 **5**

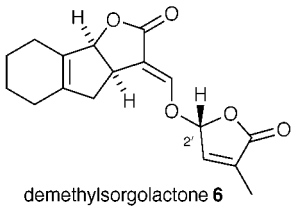

demethylsorgolactone **6**

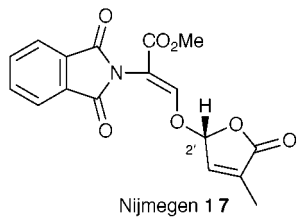

Nijmegen 1 **7**

prepared. Tables 2 and 3 summarize the structure-activity results for GR7 and GR24. Similar results have been obtained for the other series.

Zwanenburg has stressed that in each experiment a reference compound should be used in order to get reliable results.[8] In most cases a mixture of GR 24 stereoisomers has been employed to serve this purpose. Using a mixture may be tolerated as long as one can be sure that only GR 24 itself (configuration as shown in formula **4**) is biologically active (as was found to be the case for *Striga hermonthica* and *Orobanche crenata*, see Table 3). It was also observed by the Nijmegen group that at higher concentrations differences between various stereoisomers are hidden because all of them are active. Zwanenburg solved this problem by defining a 'sensitive concentration' in each set of experiments in which differences for the stereoisomers are clearly visible (see Tables 2 and 3). Of course, the best solution for this problem is to determine an accurate dosage–activity curve in each case and extract an ED_{50} value (*cf.* the Hauck[9] and Bergmann[10] work described above).

From the results summarized here it follows that single stereoisomers differ greatly in their stimulating activities (under the proper conditions) which appears to permit the conclusion that germination stimulants are highly selectively recognized at the surface of the parasitic seeds. In almost all cases studied so far the correct configuration at C-2′ is of major importance.

Table 2 Germination percentages after exposure to solutions of GR7 (ref. 11)

Species	Compound	Configuration at C-2′	Germination (%) 1 mg l^{-1}	Germination (%) 0.01 mg l^{-1}
S. hermonthica	GR7 (5)	*R*	52.2 + 5.2	30.0 ± 4.1
S. hermonthica	2′*epi*-GR7	*S*	37.4 ± 4.9	—
S. hermonthica	*ent*-GR7	*S*	16.0 ± 5.2	—
S. hermonthica	*ent*-2′-*epi*-GR7	*R*	52.5 ± 4.4	—
S. hermonthica	GR24 (**4**)	[a]	61.3 ± 5.2	68.2 ± 4.9
O. crenata	GR7 (**5**)	*R*	76.6 ± 2.4	22.6 ± 2.4
O. crenata	2′-*epi*-GR7	S	26.0 ± 3.0	—
O. crenata	*ent*-GR7	*S*	3.1 ± 1.2	—
O. crenata	*ent*-2′-*epi*-GR7	*R*	76.4 ± 3.2	—
O. crenata	GR24 (**4**)	[a]	78.4 ± 3.7	13.3 ± 2.9

[a] Mixture of four stereoisomers.

The C-2′ stereochemical problem

Synthesis of strigol-type compounds is interesting for several reasons: (i) to understand the structure–activity relationships of this fascinating chemical communication system; (ii) to set the chemical basis for studying the biochemistry of the recognition and germination processes, respectively and (iii) to develop a novel method for parasitic weed control. Parasitic weeds of the genera *Striga*, *Orobanche* and *Alectra* cause severe damage to gramineous and leguminous crops in the Mediterranean and tropical areas of Africa and the eastern hemisphere. It is known that inducing germination in the absence of the host plant results in starvation of the seedlings after a short time. Thus, introducing a stimulant into the soil to induce germination of the parasitic weeds before planting the desired crop would represent a very selective method for parasitic weed control.[16]

Table 3 Germination percentages after exposure to solutions of GR24 (ref. 12)

Species	Compound	Configuration at C-2′	Germination (%) 1 mg l^{-1}	Germination (%) 0.01 mg l^{-1}
S. hermonthica	GR24 (**4**)	*R*	56.2 ± 4.6	32.5 ± 4.5
S. hermonthica	2′-*epi*-GR24	*S*	40.8 ± 2.5	—
S. hermonthica	*ent*-GR24	*S*	4.0 ± 0.6	—
S. hermonthica	*ent*-2′-*epi*-GR24	*R*	54.2 ± 2.6	—
O. crenata	GR24 (**4**)	*R*	48.9±1.3	38.5 ± 0.4[a]
O. crenata	2′-*epi*-GR24	*S*	24.5 ± 1.1	17.2 ± 1.5[a]
O. crenata	*ent*-GR24	*S*	—	—[a]
O. crenata	*ent*-2′-*epi*-GR24	*R*	12.3 ± 0.6	4.1 ± 0.9[a]

[a] At 0.05 mg l^{-1}

Some of the synthetic analogues have as high a germinating activity as strigol. It is clear now that in each series of compounds only one of the stereoisomers is highly active. For many reasons it is, thus, desirable to use this one active isomer in pure form in the different research and application areas mentioned above.

For the synthesis of stereohomogeneous strigol-type compounds four approaches have been employed. (i) Synthesis of a racemic ABC fragment *rac*-**8** (often in truncated form), subsequent formylation (*rac*-**8** → *rac*-**9**) and coupling to the racemic and stereolabile bromo (or chloro) lactone *rac*-**10** to yield the two racemic 2′-epimers *rac*-**11** and *rac*-**12** (Scheme 1). The final products had then to be resolved by a suitable method.[9,17]

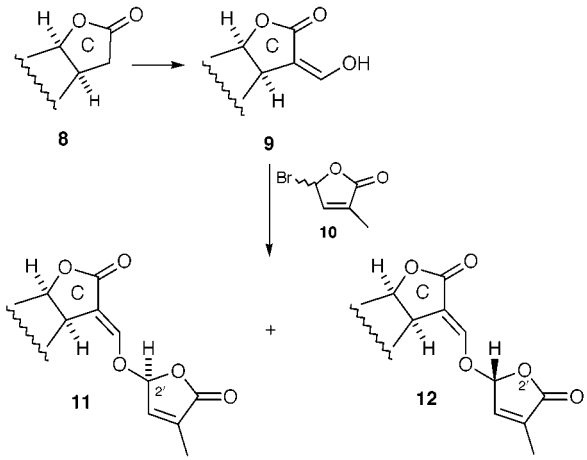

Scheme 1

(ii) Synthesis of the enantiomerically pure ABC fragment **8**, formylation and coupling to racemic **10** to yield **11** and **12** as single stereoisomers.[11,12,18–20]

(iii) Synthesis of the ABC fragment in racemic form and coupling after formylation to a homochiral equivalent **14** of the halo butenolide **10** to yield one pair of stereoisomers (if **14** has appropriate stereodirecting properties) from which the desired compound **16a** is released, accompanied by a second stereoisomer **16b** (Scheme 2). In this approach the configuration at C-2′ is known in the final products.[12–15,21,22]

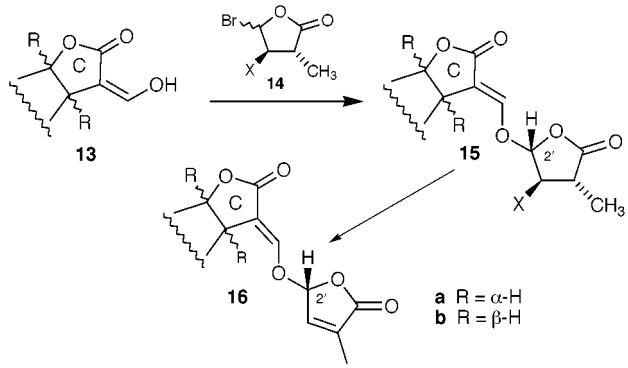

Scheme 2

(iv) Synthesis of the ABC fragment as a single enantiomer, formylation, coupling to **14**, and release of **16a** as a single stereoisomer with known configuration at all stereogenic centres.[22,23]

Routes (i) and (ii) may be called classical since all of the older syntheses were performed along these lines.[24] Clearly, after separation of the C-2′ epimers (in most cases easily achieved), the configuration at C-2' had to be determined. Configurational assignment at C-2′ is, however, hampered by the fact that obviously in all known examples the ^{1}H and ^{13}C NMR spectra of strigol-type C-2′ epimers are identical.[25]

In the following paragraphs methods are summarized which can be applied to determine the C-2′configuration. Then synthetic approaches will be reviewed that allow stereocontrol at C-2′. Such methods [routes (iii) and (iv), *vide supra*] have been developed only very recently.

Methods for configurational assignment at C-2′ of strigolactones

X-Ray analysis

For a long time X-ray analysis was the only means by which the configuration, especially that at C-2′, of strigol-type compounds could be established. X-Ray structures are now available of strigol (**1**),[17,26] its 5-epimer **20**,[25] 5-deoxystrigol,[27] of sorgolactone (**2**),[28] of analogues GR 7 (**5**),[29] GR 24 (**4**),[30] GR 28 (**17**)[25] and of compound Nijmegen 1 (**7**).[15]

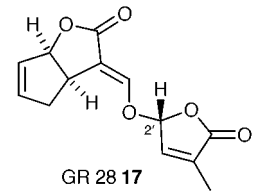

Chemical correlation

With many reference compounds of known relative configuration now available (by X-ray analysis), configurational assignment at C-2′ by chemical correlation methods becomes feasable. Yet, this approach has been used very rarely. The C-2′ configuration of the 5-epimer of strigol (**20**) has been assigned by correlation. Thus, *rac*-**20** was converted to *rac*-**18** using the Mitsunobu procedure and the product was shown to be identical with a sample obtained from *rac*-strigol (**1**) by acetylation (Scheme 3). This correlation was secured by dichromate oxidation of both *rac*-**1** and *rac*-**20**, which furnished the same ketone *rac*-**19**. Analogously, the 2′-epimer of *rac*-**20** was correlated with the 2′-epimer of *rac*-strigol.[25]

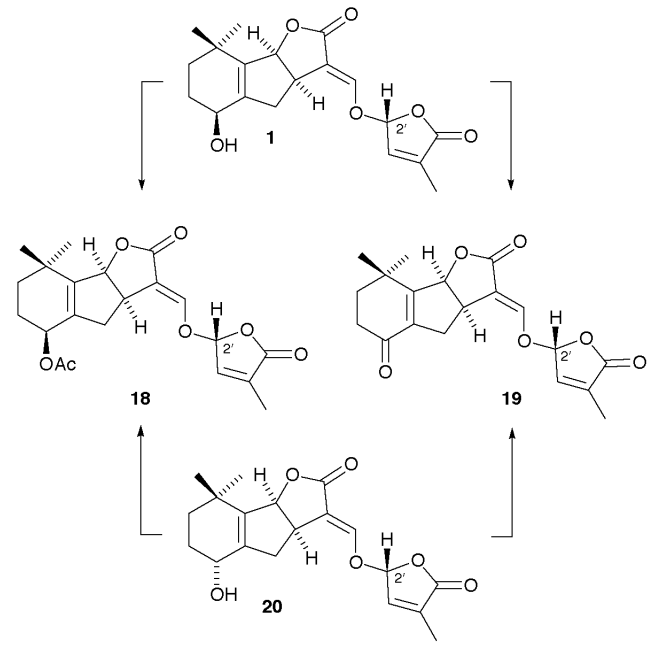

Scheme 3

Circular dichroism

The relative and absolute configuration of sorgolactone (**2**) has tentatively been assigned on the basis of the similar CD spectra

of **2** and strigol (**1**).[3] The configuration of strigol is known from X-ray studies.[17,26] The configurational assignment of sorgolactone was recently confirmed by synthesis.[28,31] Fig. 1 displays

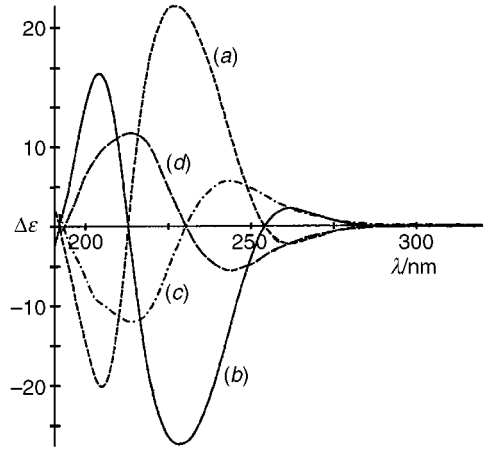

Fig. 1 CD spectra of (*a*) **1**, (*b*) *ent*-**1**, (*c*) 2′-*epi*-**1** and (*d*) *ent*-2′-*epi*-**1**.

the CD spectra of strigol (**1**), its 2′-epimer, and their enantiomers. The CD curves are, of course, sum curves of the different chromophores present in **1** and its stereoisomers. Frischmuth *et al.*[25] studied the CD spectra of **21** and *ent*-**21**, as well as of

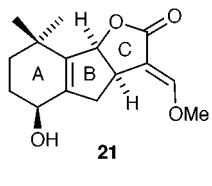

21

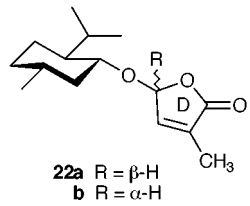

22a R = β-H
b R = α-H

Feringa's compounds **22a** and *ent*-**22a**[32] which are reference compounds for the ABC and D parts, respectively, of the strigol isomers. It was found that the CD spectra of the strigol isomers can reasonably well be constructed from the CD spectra of the appropriate ABC and D models, indicating that (to a first approximation) there is no electronic interaction between the two chromophoric systems and, in addition, that the conformations of the 2′-epimers are similar. Thus, the configuration at C-2′ of a pair of C-2′ epimers can be obtained from their CD difference spectrum in which the contribution of the ABC chromophor is cancelled out and twice the CD of the ring D chromophore remains.[33]

A comparison of the CD spectra of **21** and *ent*-**21** with those of **22a** and *ent*-**22a** revealed that the CD band around 250 nm of **22a**/**22b** extends to a longer wavelength than that of **21a** and *ent*-**21**. This means that in the region of about 270 nm of strigolactones only the contribution of the ring D chromophor determines the spectra. Therefore, in strigolactones the configuration at C-2′ can directly be correlated with the sign of the CD around 270 nm. 2′*R* compounds have a negative CD around 270 nm whereas the CD of 2′*S* compounds is positive at this wavelength. This rule has proven its value in several series of strigolactones, in particular in the GR 28,[22] demethylsorgolactone[13] and sorgolactone series.[14]

Stereoselective synthesis

More effective than any of the procedures summarized above are, of course, synthetic methods that allow installation of the correct configuration at C-2′ predictably. This will be the topic of the following paragraph.

Synthetic approaches that allow control of the C-2′ configuration of strigol-type compounds

A general introduction to the problem has been given by Frischmuth *et al.*[34] We shall review here only sequences that lead to stereohomogeneous strigolactones. In addition only sequences will be summarized leading to compounds that contain the methyl group in unit D since it has been found that this methyl group is essential for the bioactivity.[8]

The Michael addition–nucleophilic substitution–elimination approach[22,35]

Following Feringa's work, from *rac*-**23** and (−)-menthol the two diastereoisomers **22a** and **22b** were prepared and separated by crystallization at low temperatures.[32] On addition of thiophenol in the presence of triethylamine **22a** formed adducts **24** and **25** with the phenylthio group *trans* to the menthyloxy substituent (Scheme 4). Similar reactions were performed with

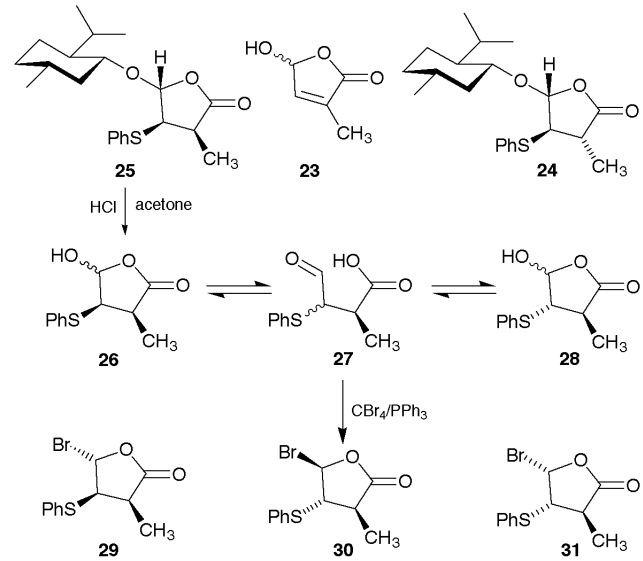

Scheme 4

22b. The phenylthio group was introduced with the aim of stereodirecting the coupling of the butenolide moiety to the ABC part of strigolactones. On acid-catalyzed removal of the auxiliary menthyl group from **25** a mixture of compounds was formed which contained more components than expected. When the hydrolysis products of **26** were treated with CBr_4 and PPh_3 three bromo derivatives were obtained which could be separated and shown by careful spectral analysis to have structures **29**–**31**. The formation of **30** and **31** can be explained assuming the hemiacetal hydrolysis products of **25** to be in equilibrium with the ring-opened aldehyde, the α-position of which is, of course, stereolabile.

Coupling of **31**, *ent*-**31** (obtained analogously) and **29** was performed with racemic **32** and with homochiral **32** and its enantiomer (accessible *via* resolution[22,35] and the elegant Pd-mediated enantioselective syntheses of cyclopent-2-en-1-ylacetic acid that have been developed in the laboratories of Trost[36] and Helmchen[37]) using silver carbonate and silver silicate, respectively, as promotors (Scheme 5). The conditions resemble the classical Königs–Knorr glycosylation with the phenylthio substituent as the stereodirecting neighbouring group. Silver silicate turned out to be a more suitable promotor. The results indicate that the phenylthio substituent does indeed force the nucleophilic attack at C-2′ to the opposite face of the ring. The sequence Michael addition–nucleophilic substitution–elimination is, thus, appropriate to control the configuration at C-2′ of strigolactones and to prepare **17**, **34** and *ent*-**34** [on routes (iii) and (iv), *vide supra*]. The problematic point is the stereolability

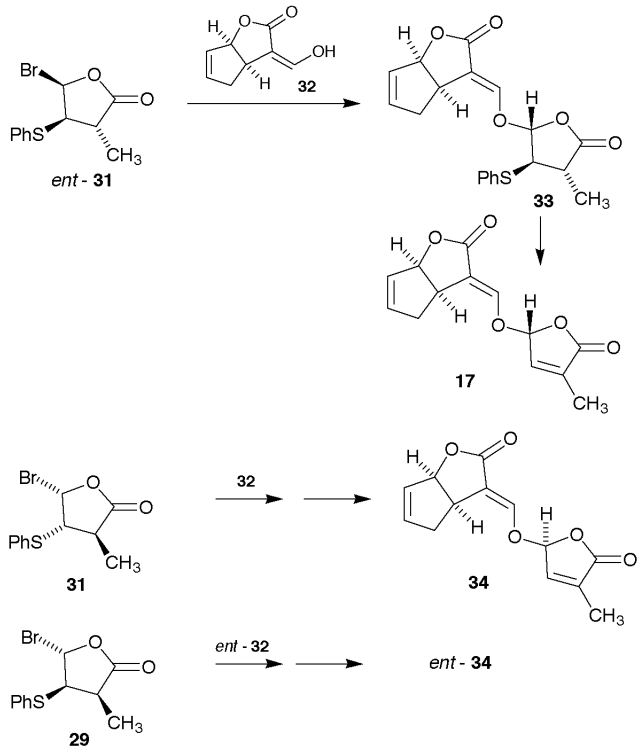

Scheme 5

of **27**, which makes the method unsuitable for practical applications.

The Zwanenburg approach[38]

Stereocontrol at C-2′ has been achieved by Zwanenburg by a sequence involving a Diels–Alder and a retro-Diels–Alder reaction. Compounds **37b** and *ent*-**37b** in which the *endo* face is sterically blocked have been used as synthetic equivalents of **14**. Diels–Alder reaction of cyclopentadiene with citraconic anhydride (Scheme 6), followed by $Li(OBu^t)_3AlH$ reduction of *rac*-

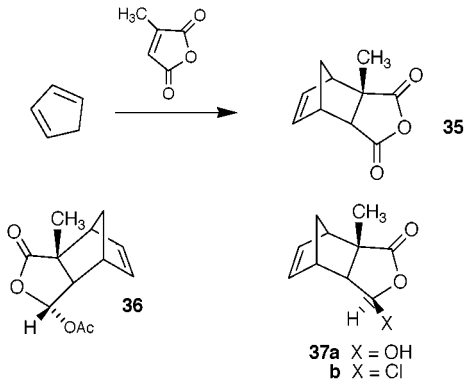

Scheme 6

35 provided *rac*-**37a** which was resolved either classically *via* the (+)- and (−)-menthyl acetals[21] or by making use of an enzymic kinetic resolution yielding *endo*-acetate **36** and the *exo*-alcohol **37a**, both in enantioenriched form.[39] Compounds **37a** and **36** were converted to chlorides **37** and *ent*-**37b**, respectively.

Coupling of **37b** to *rac*-**38** provided a 1 : 1 mixture of **39** (R = β-H) and **39** (R = α-H) (Scheme 7). Cycloreversion then led to diastereoisomers **5** and **40** with known configuration at C-2′. The enantiomers of **5** and **40** were prepared accordingly, making use of *ent*-**37b**.[21]

In a completely analogous fashion the follwing compounds were synthesized GR24 (**4**), its 2′-epimer, and their enantiomers;[12] demethylsorgolactone (**6**), the 2′-epimer and their

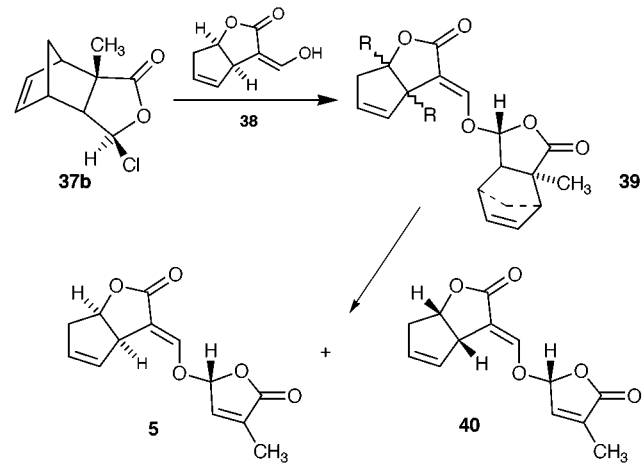

Scheme 7

enantiomers;[13] the sorgolactone stereoisomers **41a**–**d** and their enantiomers;[14] Nijmegen 1 and its enantiomer (**7**).[15]

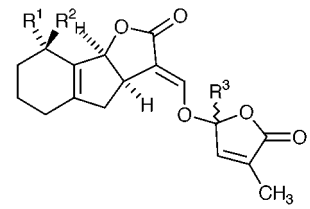

41a R^1 = Me, R^2 = H, R^3 = β-H
b R^1 = Me, R^2 = H, R^3 = α-H
c R^1 = H, R^2 = Me, R^3 = β-H
d R^1 = H, R^2 = Me, R^3 = α-H

The Zwanenburg method, which has proven its merits, involves a resolution step. The advantage of the procedure when excuted as described until now [route (iii) *vide supra*] is that all stereoisomers of a given stimulant are available, a fact that is useful in the context of structure–activity work.

Use of the Winterfeldt template[23,40]

A highly selective route has been developed in Leipzig, which also involves the cycloaddition–cycloreversion strategy but replaces the resolution step, characteristic of the Zwanenburg approach, by an enantioselective synthesis. More specifically, the Winterfeldt diene **42**[41] which is available from the Hajos–Wiechert ketone was employed in the Diels–Alder reaction. Cycloaddition of **42** with citraconic anhydride to yield *endo*-adduct requires high-pressure conditions.[42] Reduction of the adduct with $Li(OBu^t)_3AlH$ furnished **43** as the main product. The coupling of **44** to the other half of the strigolactones posed problems and only the sequence **43** + **44** → **45** was successful (Scheme 8). On flash vacuum pyrolysis (500 °C, 10^{-6} bar), retro-Diels–Alder cleavage occurred and provided strigolactone *ent*-**34** as a single stereoisomer.

The synthesis of *ent*-**34** represents an example of route (iv) (*vide supra*). The important chiral materials used in the synthesis, Winterfeldtś template and **44** (obtained from Helmchenś iodo lactone[37]) are available *via* enantioselective reactions under the control of chiral catalysts.

Epilogue

It appears that many of the problems involved in the chemistry of strigol-type compounds have been solved in the past few years. One may wish to see application of these results in investigations aimed at understanding the mode of action of the strigolactones.

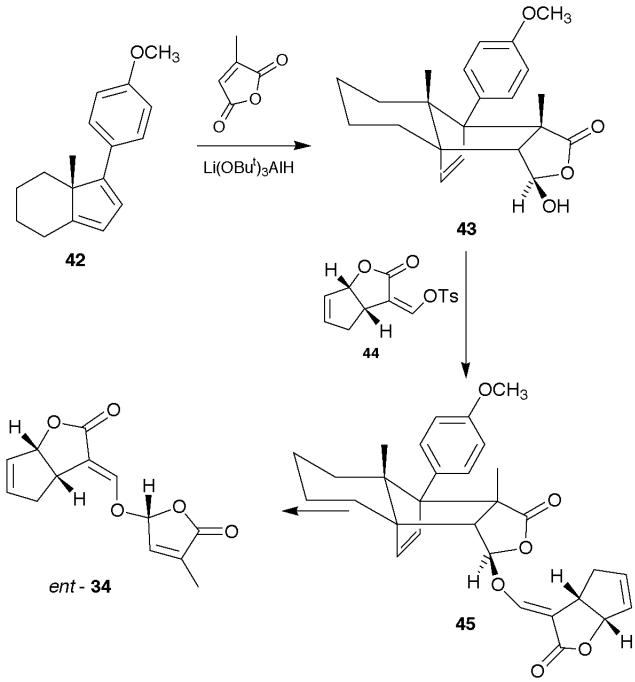

Scheme 8

Acknowledgements

It is a great pleasure to thank all colleagues who contributed to the work of our group. Their names are found in the references. We thank Professor B. Zwanenburg for the data in Table 3. Special thanks go to Professor G. Helmchen (Heidelberg) who generously provided us with the iodolactone of optically active cyclopentenylacetic acid, the precursor of **44**. We also wish to thank the Minister für Wissenschaft und Forschung des Landes Nordrhein Westfalen und the Minister für Wissenschaft und Kunst des Freistaats Sachsen (PhD fellowships), the Deutsche Forschungsgemeinschaft, and the Fonds der Chemischen Industrie for generous financial support.

References

1 B. A. Siame, Y. Weerasuriya, K. Wood, G. Ejeta and L. G. Butler, *J. Agric. Food Chem.*, 1993, **41**, 1486.
2 C. E. Cook, L. P. Whichward, B. Turner, M. E. Wall and G. H. Egley, *Science*, 1966, **154**, 1189; C. E. Cook, L. P. Whichard, M. E. Wall, G. H. Egley, P. Coggon, P. A. Luhan and A. T. McPhail, *J. Am. Chem. Soc.*, 1972, **94**, 6198.
3 C. Hauck, S. Müller and H. Schildknecht, *J. Plant Physiol.*, 1992, **139**, 474.
4 K. Mori, J. Matsui, T. Yokota, H. Sakai, M. Bando and Y. Takeuchi, *Tetrahedron Lett.*, 1999, **40**, 943.
5 S. Müller, C. Hauck and H. Schildknecht, *J. Plant Growth Regul.*, 1992, **11**, 77.
6 K. Mori, J. Matsui, M. Bando, M. Kido and Y. Takeuchi, *Tetrahedron Lett.*, 1998, **39**, 6023.
7 G. D. Fate and D. G. Lynn, *J. Am. Chem. Soc.*, 1996, **118**, 11369, and references therein.
8 E. M. Mangnus, P. L. A. Stommen and B. Zwanenburg, *J. Plant Growth Regul.*, 1992, **11**, 91.
9 C. Hauck and H. Schildknecht, *J. Plant Physiol.*, 1990, **136**, 126.
10 C. Bergmann, K. Wegmann, K. Frischmuth, E. Samson, A. Kranz, D. Weigelt, P. Koll and P. Welzel, *J.Plant Physiol.*, 1993, **142**, 338.
11 E. M. Mangnus and B. Zwanenburg, *J. Agric. Food Chem.*, 1992, **40**, 697.
12 J. W. J. F. Thuring, G. H. L. Nefkens and B. Zwanenburg, *J. Agric. Food Chem.*, 1997, **45**, 2278.
13 J. W. J. F. Thuring, N. W. J. T. Heinsman, R. W. A. W. M. Jacobs, G. H. L. Nefkens and B. Zwanenburg, *J. Agric. Food Chem.*, 1997, **45**, 507.
14 Y. Sugimoto, S. C. M. Wigchert, J. W. J. F. Thuring and B. Zwanenburg, *J. Org. Chem.*, 1998, **63**, 1259.
15 G. H. L. Nefkens, J. W. J. F. Thuring, M. F. M. Beenakkers and B. Zwanenburg, *J. Agric. Food Chem.*, 1997, **45**, 2273.
16 A. W. Johnson, *Chem. Brit.*, 1980, **16**, 82.
17 D. W. Brooks, H. S. Bevinakatti and D. R. Powell, *J. Org. Chem.*, 1985, **50**, 3779.
18 J. B. Heather, R. S. D. Mittal and C. J. Sih, *J. Am. Chem. Soc.*, 1976, *98*, 3661.
19 U. Berlage, J. Schmidt, Z. Milkova and P. Welzel, *Tetrahedron Lett.*, 1987, **28**, 3095, see also T. Staroske, M. Käsler and P. Welzel, *Chirality*, 1997, **9**, 463; J. Schröer and P. Welzel, *Tetrahedron*, 1994, **50**, 6839.
20 E. Samson, K. Frischmuth, U. Berlage, U. Heinz, K. Hobert and P. Welzel, *Tetrahedron*, 1991, **47**, 1411.
21 J. W. J. F. Thuring, G. H. L. Nefkens, R. Schaafstra and B. Zwanenburg, *Tetrahedron*, 1995, **51**, 5047.
22 S. Röhrig, L. Hennig, M. Findeisen, P. Welzel, K. Frischmuth, A. Marx, T. Petrowitsch, P. Koll, D. Müller, H. Mayer-Figge and W. S. Sheldrick, *Tetrahedron*, 1998, **54**, 3413.
23 S. Röhrig, L. Hennig, M. Findeisen, P. Welzel and D. Müller, *Tetrahedron*, 1998, **54**, 3439.
24 For leading references, see U. Berlage, J. Schmidt, U. Peters and P. Welzel, *Tetrahedron Lett.*, 1987, **28**, 3091.
25 K. Frischmuth, U. Wagner, E. Samson, D. Weigelt, P. Koll, H. Meuer, W. S. Sheldrick and P. Welzel, *Tetrahedron: Asymmetry*, 1993, **4**, 351.
26 P. Coggon, P. A. Luhan and A. T. McPhail, *J. Chem. Soc., Perkin Trans. 2*, 1973, 465.
27 K. Frischmuth, E. Samson, A. Kranz, P. Welzel, H. Meuer and W. S. Sheldrick, *Tetrahedron*, 1991, **47**, 9793.
28 K. Mori, J. Matsui, M. Bando, M. Kido and Y. Takeuchi, *Tetrahedron Lett.*, 1997, **38**, 2507
29 W. P. Bosman, J. M. M. Smits, P. T. Beurskens, E. M. Mangnus and B. Zwanenburg, *J. Crystallogr. Spectrosc. Res.*, 1992, **22**, 503.
30 W. P. Bosman, J. M. M. Smits, P. T. Beurkens, E. M. Mangnus, R. J. Dommerhelt, R. L. P. De Jong and B. Zwanenburg, *J. Crystallogr. Spectrosc. Res.*, 1992, **22**, 625; F. G. Moers, J. M. M. Smits, P. T. Beurskens and B. Zwanenburg, *J. Chem. Crystallogr.*, 1995, **25**, 429
31 Y. Sugimoto, S. C. M. Wigchert, J. W. J. F. Thuring and B. Zwanenburg, *Tetrahedron Lett.*, 1997, **38**, 2321.
32 Review: B. L. Feringa, B. de Lange, J. F. G. A. Jansen, J. C. de Jong, M. Lubben, W. Faber and E. P. Schudde, *Pure Appl. Chem.*, 1992, **64**, 1865.
33 For further work on the CD spectra of this class of compound, cf. J. K. Gawronski, A. van Oeveren, H. van der Deen, C. W. Leung and B. Feringa, *J. Org. Chem.*, 1996, **61**, 1513.
34 K. Frischmuth, D. Müller and P. Welzel, *Tetrahedron*, 1998, **54**, 3401.
35 K. Frischmuth, A. Marx, T. Petrowitsch, U. Wagner, K. Koerner, S. Zimmermann, H. Meuer, W. S. Sheldrick and P. Welzel, *Tetrahedron Lett.*, 1994, **28**, 4973.
36 B. M. Trost and R. C. Bunt, *J. Am. Chem. Soc.*, 1994, **116**, 4089.
37 P. Sennhenn, B. Gabler and G. Helmchen, *Tetrahedron Lett.*, 1994, **35**, 8595.
38 For a short review, see B. Zwanenburg and J. W. J. F. Thuring, *Pure Appl. Chem.*, 1997, **69**, 651
39 J. W. J. F. Thuring, G. H. L. Nefkens, M. A. Wegman, A. J. H. Klunder and B. Zwanenburg, *J. Org. Chem.*, 1996, **61**, 6931.
40 S. Röhrig, L. Hennig, M. Findeisen, P. Welzel and D. Müller, *Tetrahedron Lett.*, 1997, **31**, 5489.
41 E. Winterfeldt, *Chem. Rev.*, 1993, **93**, 827; C. Borm, D. Meibom and E. Winterfeldt, *Chem. Commun.*, 1996, 887
42 E. Winterfeldt and V. Wray, *Chem. Ber.*, 1992, **125**, 2159.

Paper 9/01530B

ChemComm

A metallo-supramolecular double-helix containing a major and a minor groove

Michael J. Hannon,* Claire L. Painting and Nathaniel W. Alcock

Department of Chemistry, University of Warwick, Gibbet Hill Road, Coventry, UK CV4 7AL.
E-mail: m.j.hannon@warwick.ac.uk

Received (in Basel, Switzerland) 19th July 1999, Accepted 8th September 1999

Control of the microarchitecture in a metallo-supramolecular double-helical array results from inter-strand edge–face π-stacking interactions which pull the ligand strands together thereby creating two distinct helical grooves (major and minor).

Double-helical molecular architectures retain a unique fascination because life itself is encoded within double-helical DNA arrays. The assembly of synthetic double-helical architectures through metallo-supramolecular design has been an area of intense activity and the construction principles necessary to assemble a double-helix are now fairly well established.[1] However challenges in defining the precise topography or conformation of the helical superstructure remain. To this end, we have recently illustrated how careful selection of the spacer group used to separate the metal-binding domains can be used to control the directionality of ligand strands within a helix.[2] We wish now to report a system, based on our inexpensive and readily-prepared imine ligands,[2,3] in which π-stacking interactions between the spacer groups control the microarchitecture of the helix and give rise to a double-helix containing major and minor grooves reminiscent of B-DNA.

The two distinct grooves in B-DNA arise from the positions through which the sugar–phosphate backbones are connected to the purine and pyrimidine bases; the two strands are not arranged along the vector of the cohesive forces (hydrogen bonds) which hold the helix together but both displaced to one side. This contrasts with the situation found in most synthetic metallo-helicates. The metal binding units usually form an integral part of the ligand backbone.[1] The inherent coordination preferences of the metal ions used in the assembly process (most commonly octahedral or tetrahedral) position these binding units (and hence the ligand strands) symmetrically on opposite sides of the helix. This leads to two equivalent grooves. Achieving distinct grooves within metallo-helicate architectures of this type would therefore appear to require ligand strands that are predisposed to associate on one side of the helical axis.

We have recently described triple-helical complexes formed from the reaction of ligand L[1] with octahedral metal ions.[3] In these triple-helical architectures, inter-strand face–edge π-stacking interactions (aromatic C–H···π)[4] are observed between the phenylene rings of the diarylmethane spacer-groups. Such secondary inter-strand interactions might provide a suitable tool for controlling the spatial orientation of ligand strands in a double-helicate superstructure and we have therefore examined the effect of interacting ligands of this type with tetrahedral metal ions.

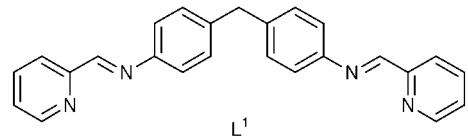

L[1]

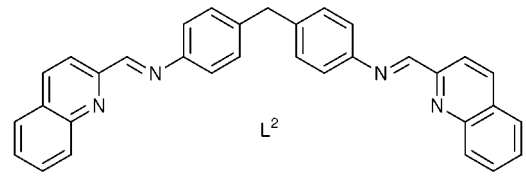

L[2]

Ligand L[2] is prepared in 93% yield by mixing ethanolic solutions containing 2 equivalents of 2-quinolinecarbaldehyde and 1 equivalent of 4,4′-methylenedianiline. Reaction of L[2] with silver(I) acetate in methanol yields a pale-yellow solution from which a yellow solid is obtained on treatment with $[NH_4][PF_6]$.[5] Mass spectrometry (FAB and ESI) is consistent with the formation of a dimeric species of formula $[Ag_2(L^1)_2][PF_6]_2$. Recrystallisation of the compound from acetonitrile by benzene diffusion afforded X-ray quality crystals and we have determined the X-ray crystal structure to examine the molecular conformation.[6]

The structure reveals a dimeric $[Ag_2(L^2)_2]^{2+}$ cation (Fig. 1). Each silver(I) centre occupies a four-coordinate pseudo-

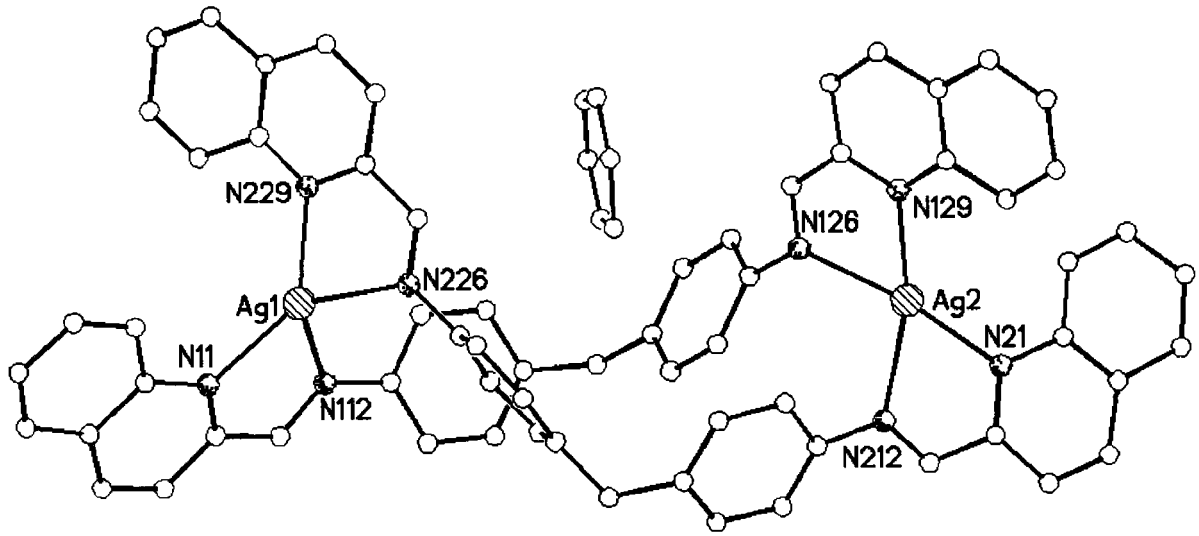

Fig. 1 View of the cation $[Ag_2(L^2)_2]^{2+}$.

tetrahedral environment bound to two pyridylimine units, one from each ligand. The two ligands wrap around the metal–metal axis giving rise to a double-helical structure, both enantiomers of which are observed. The phenyl rings of the diarylmethane spacer, which separates the metal binding units, are face–edge π-stacked[4] with those on the adjacent ligand strand (centroid–centroid: 5.1 and 5.2Å). To achieve this the two ligand strands are pulled together on one side of the helical axis and this leads inevitably to the presence of two distinct grooves (major and minor). The solid state structure reveals a benzene solvent molecule located in the larger (major) groove, however no specific interactions (face–face or face–edge π–π) are identifiable between this benzene and the walls of the groove.

While the solid state structure reveals this sophisticated helical microarchitecture, the solution behaviour is more complicated.[5] Electrospray mass spectrometry reveals the presence only of dinuclear $\{M_2L_2\}$ species. There are two possible basic configurations for such a species. The two ligand strands may either wrap around the metal–metal axis (*rac*-isomer) giving rise to a double-helix or one may pass above the metal–metal axis while the other passes beneath (*meso*-isomer) giving a non-helical metallo-cyclophane.[2,7] The room temperature ^{1}H NMR spectrum of an acetonitrile solution of the silver(I) complex reveals a single set of proton resonances. However on cooling (233 K, 400 MHz) the resonances broaden, indicating some form of fluxional behaviour. The spectrum in dichloromethane solution is broadened at room temperature, and at low temperature (193 K, 400 MHz) reveals two discrete solution species. The (non-diastereotopic) CH_2 protons permit assignment of these species. For the *rac*- (helical) isomer the protons are equivalent and a single resonance is observed while in the *meso*-isomer the structure of the metallo-macrocycle renders them inequivalent and two doublets result. The equilibrium between these species is temperature dependent with the percentage of helical isomer present increasing with decreasing temperature, indicating that this isomer is favoured enthalpically.[8] Two phenyl resonances are observed for the helix; four would be expected in a frozen-out π-stacked configuration. In view of the weak nature of π-stacking interactions it is perhaps unsurprising that this is not observed and it is unclear whether in solution the helical isomer does contain two distinct grooves or whether it has relaxed into a more conventional double-helicate structure with equivalent grooves. The absence of significant upfield shifts for either of the phenyl resonances might support the latter.

We have shown that secondary interactions between the spacer units may be used to control the superstructure of a helical array in the solid state. We are currently extending our studies to examine further routes for controlling the precise microarchitecture of supramolecular arrays.

We are grateful to the Nuffield Foundation (Awards to newly appointed science lecturers, M. J. H.) and the EPSRC (C. L. P.) for support, the EPSRC and Siemens Analytical Instruments for grants in support of the diffractometer and the Swansea National Mass Spectrometry Centre for recording the mass spectra.

Notes and references

1 J.-M. Lehn, *Supramolecular Chemistry—Concepts and Perspectives*, VCH, Weinheim, 1995; D. Philp and J. F. Stoddart, *Angew. Chem., Int. Ed. Engl.*, 1996, **35**, 1155; E. C. Constable, *Prog. Inorg. Chem.*, 1994, **42**, 67; G. Baum, E. C. Constable, D. Fenske, C. E. Housecroft and T. Kulke, *Chem. Eur. J.*, 1999, **5**, 1862; C. Piguet, G. Bernardinelli and G. Hopfgartner, *Chem. Rev.*, 1997, **97**, 2005; R. W. Saalfrank and I. Bernt, *Curr. Opin. Solid State Mater. Sci.*, 1998, **3**, 407; A. F. Williams, *Pure Appl. Chem.*, 1996, **68**, 1285; J. S. Fleming, K. L. V. Mann, S. M. Couchman, J. C. Jeffery, J. A. McCleverty and M. D. Ward, *J. Chem. Soc., Dalton Trans.*, 1998, 2047; M. Albrecht and R. Frohlich, *J. Am. Chem. Soc.*, 1997, **119**, 1656 and references therein.

2 M. J. Hannon, S. Bunce, A. J. Clarke and N. W. Alcock, *Angew. Chem., Int. Ed.*, 1998, **38**, 1277

3 M. J. Hannon, C. L. Painting, A. Jackson, J. Hamblin and W. Errington, *Chem. Commun.*, 1997, 1807.

4 For examples of such interactions, see E.-I. Kim, S. Paliwal and C. S. Wilcox, *J. Am. Chem. Soc.*, 1998, **120**, 11 192; Y. Umezawa, S. Tsuboyama, K. Honda, J. Uzawa and M. Nishio, *Bull. Chem. Soc. Jpn.*, 1998, **71**, 1207; M. Nishio, Y. Umezawa, M. Hirota and Y. Takeuchi, *Tetrahedron*, 1995, **51**, 8665; C. A. Hunter, *Chem. Soc. Rev.*, 1994, **23**, 101 and references therein.

5 *Selected data* for $[Ag_2(L^2)_2][PF_6]_2$: MS (FAB): *m*/*z* 585 $\{Ag(L^2)\}$, 1061 $\{Ag(L^2)_2\}$, 1168 $\{Ag_2(L^2)_2\}$, 1313 $\{Ag_2(L^2)_2(PF_6)\}$. MS (ESI): *m*/*z* 584 $\{Ag_2(L^2)_2\}^{2+}$, 1313 $\{Ag_2(L^2)_2(PF_6)\}^+$ (Found: C, 52.7; H, 3.3; N, 7.5. Calc. for $Ag_2C_{66}H_{48}N_8P_2F_{12}\cdot 2H_2O$: C, 53.0; H, 3.5; N, 7.5%). ^{1}H NMR (CD_3CN, 250 MHz, 298 K): δ 9.31 (2H, s, H^i), 8.78 (2H, d, *J* 8.1 Hz, $H^{3/4}$), 8.18 (2H, d, *J* 8.1 Hz, $H^{3/4}$), 8.13 (2H, d, *J* 8.0 Hz, $H^{5/8}$), 8.00 (2H, d, *J* 8.1 Hz, $H^{5/8}$), 7.70 (4H, m, $H^{6,7}$), 7.51 (4H, d, *J* 8.4 Hz, Ph), 7.23 (4H, d, *J* 8.4 Hz, Ph), 3.89 (2H, s, CH_2).
^{1}H NMR (CD_2Cl_2, 400 MHz, 183 K): δ 9.30 (3H, d, *J* 6.4 Hz, H^i *rac*), 9.24 (2H, d, *J* 6.9 Hz, H^i *meso*), 8.72 (5H, m, $H^{3/4}$ *rac* + *meso*), 8.14 (5H, m, $H^{3/4}$ *rac* + *meso*), 8.06 (5H, m, $H^{5/8}$ *rac* + *meso*), 7.94 (2H, d, *J* 8.0 Hz, $H^{5/8}$ *meso*), 7.90 (3H, d, *J* 8.0 Hz, $H^{5/8}$ *rac*), 7.65 (10H, m, $H^{6,7}$ *rac* + *meso*), 7.55 (3H, d, *J* 8.4 Hz, Ph *rac*), 7.43 (2H, d, *J* 8.4 Hz, Ph *meso*), 7.29 (3H, d, *J* 8.4 Hz, Ph *rac*), 7.13 (2H, d, *J* 8.4 Hz, Ph *meso*), 3.80 (3H, s, CH_2 *rac*), 3.86 (1H, d, *J* 9.8 Hz, CH_2 *meso*), 3.75 (1H, d, *J* 9.8 Hz, CH_2 *meso*).

6 *Crystal data* for $C_{45.5}H_{36.75}AgF_6N_{4.25}P$: M = 895.88, triclinic, space group $P\bar{1}$, a = 13.351(3), b = 15.931(3), c = 20.478(3) Å , α = 86.741(5), β = 83.700(5), γ = 73.329(5)°, U = 4145.8(14) Å^3 (by least squares refinement on 5622 reflection positions), Z = 4, μ(Mo-Kα) = 0.589 mm^{-1}, 16667 reflections measured on a Bruker AXS SMART system, 10674 unique (R_{int} = 0.0539). T = 180(2) K. Absorption correction by Ψ-scans; minimum and maximum transmission factors: 0.73; 0.93. The lattice contains three fully occupied (as shown by test refinement) but highly mobile benzene molecules and one acetonitrile molecule (50% occupancy). Goodness-of-fit was 0.997, $R1$[for 5837 reflections with $I > 2\sigma(I)$] = 0.0744, $wR2$ = 0.2093. Refinement used SHELXTL (G. M. Sheldrick, 1997). CCDC 182/1403. See http://www.rsc.org/suppdata/cc/1999/2023/ for crystallographic files in .cif format.

7 Such *meso*- and *rac*-systems have also been observed by other workers. See, for example: A. Bilyk, M. M. Harding, P. Turner and T. W. Hambley, *J. Chem. Soc., Dalton Trans.*, 1994, 2783; C. O. Dietrich-Buchecker, J. F. Nierengarten, J. P. Sauvage, N. Armaroli, V. Balzani and L. DeCola, *J. Am. Chem. Soc.*, 1993, **115**, 11 237.

8 The temperature range over which the resonances of the two isomers are distinct is insufficient for accurate determination of thermodynamic parameters. Simple modelling reveals that the box conformation cannot accommodate inter-strand π-stacking interactions. If maintained in solution, the face–edge π-stacking interactions may contribute to the enthalpic preference for the helix and the concomitant restrictions on the free rotation of the phenyl rings in the helix might contribute to the entropic preference for the *meso*-isomer.

Communication 9/05795A

ChemComm

Gemini surfactants: studying micellisation by ^1H and ^{19}F NMR spectroscopy

Ivan Huc* and Reiko Oda

Institut Européen de Chimie et Biologie, ENSCPB Av. Pey Berland, BP 108, 33402 Talence Cedex, France.
E-mail: ivan.huc@iecb-polytechnique.u-bordeaux.fr

Received (in Liverpool, UK) 27th July 1999, Accepted 1st September 1999

For some cationic Gemini surfactants, exchange between the bulk solution and micelles or other aggregates occurs slowly on the NMR timescale; thus NMR spectroscopy provides an efficient tool for studying micelle formation and mixing of various surfactants.

Among the various aggregates amphiphilic molecules form in water, micelles are by far the most common and the most thoroughly studied.[1] The critical micelle (aggregation) concentration (c.m.c.), or the threshold concentration above which monomers co-operatively assemble into micelles (or other aggregates), can be determined by surface tension measurements or conductimetry.[1] Above the c.m.c. rapid exchange occurs between amphiphiles in the bulk and in the micelles (Fig. 1). For single chain surfactants, characteristic times for this exchange are generally of the order of 1 ns to 1 ms and fast techniques such as ultrasonic absorption are required for their measurements.[2,3] Slower techniques such as NMR show averaged signals for the surfactant molecules in their various states.[4] Both c.m.c. values and exchange rates between surfactants in the bulk and in the micelles depend critically on the size of hydrophobic groups in the surfactants. In most cases, simple laws can be expressed between these physical parameters and the number of CH_2 groups in the hydrophobic part of the surfactants.[2,5,6]

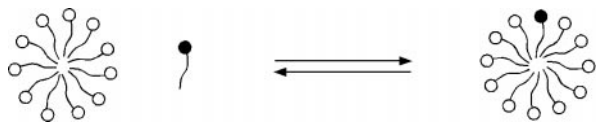

Fig. 1 Schematic representation of surfactant exchange between micelles and bulk phase.

Dimeric (Gemini) or oligomeric surfactants, which consist of two or more conventional surfactant units linked at their polar head groups by a spacer, are attracting a lot of attention in the area of surfactant research because of the many unusual properties that they feature.[7,8] A direct consequence of the presence of two hydrophobic tails in dimeric surfactants is a sharp and uniform decrease in the c.m.c. values, which are 1 to 2 orders of magnitude lower than that of their monomeric counterparts.[7] For the same reason, slower exchange between dimeric surfactants in the bulk and in the aggregates could be anticipated. We now report on such unusually slow exchange and the consequent occurrence of separate ^1H and ^{19}F NMR signals for surfactants in the bulk and in micelles.

The surfactants studied here belong to the series of *n*-2-*m* bis-quaternary ammonium bromides whose structures are shown below.[9] Hydrocarbon, fluorocarbon as well as hybrid hydrocarbon–fluorocarbon[10] surfactants were tested.

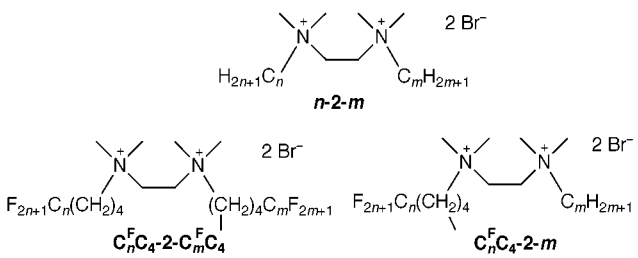

Thus, the ^1H NMR spectrum of 14-2-14 in D_2O below its c.m.c. shows one set of sharp signals corresponding to the monomer in the bulk (Fig. 2c). Above the c.m.c. the lines broaden and a second set of signals appears, corresponding to the micelles (Fig. 2a and 2b). The intensity of the micelle signals increases linearly with the surfactant concentration, whilst the intensity of the monomer signals levels off above the c.m.c. The protons belonging to the polar head are deshielded up to 0.2 ppm in the micelles, and are very distinct from the monomer signals. This downfield shift is likely to be the result of the proximity between the cations in the micelles. For the protons belonging to the alkyl chains, chemical shifts are not so different and the various signals partly overlap.

The c.m.c. value can be estimated by integrating the monomer signals and comparing these with an internal standard, or more accurately determined by diluting the sample beyond the disappearance of the micelle signals and plotting the signal intensities as a function of concentration. For 14-2-14, the value measured upon dilution in D_2O (0.12 mM) matches well that obtained using conductimetry in H_2O (0.16 mM). The slight discrepancy may be attributed to expectable differences between H_2O and D_2O.

Line-shape analysis of the broadened signals gives the lifetimes of monomeric and aggregated species at various concentrations, and the characteristic time of exchange τ.[11]† For 14-2-14, τ (0.1 s) is orders of magnitude longer than for single chain surfactants.[3] In a series of *n*-2-*m* surfactants, τ increases with $n + m$. The chain length difference $n - m$ does not considerably affect the exchange, and similar spectra are obtained for 18-2-8 and 16-2-10 ($n + m = 26$), or for 18-2-10, 16-2-12 and 14-2-14 ($n + m = 28$). The borderline between fast and slow exchange on the NMR timescale at 25 °C lies between $n + m = 24$ and $n + m = 26$. As shown in Fig. 2d, two sets of

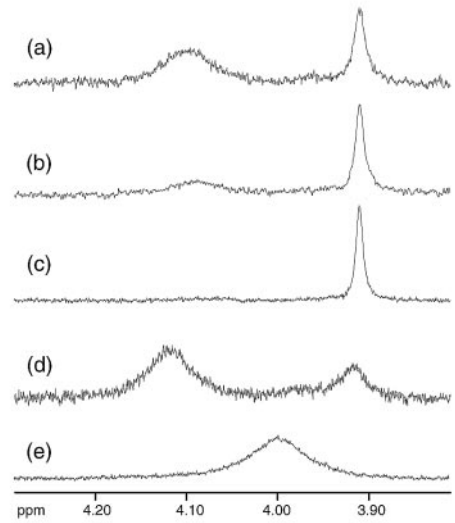

Fig. 2 Part of the 400 MHz ^1H NMR spectra of dimeric surfactants at various concentrations in D_2O (25 °C). The signals observed are those of the $N^+CH_2CH_2N^+$ protons for molecules in the bulk phase (3.92 ppm) and in the micelles (4.03–4.13 ppm). (a) [14-2-14] = 0.25 mM; (b) [14-2-14] = 0.167 mM; (c) [14-2-14] = 0.125 mM; (d) [18-2-8] = 0.5 mM; (e) [12-2-12] = 1.25 mM.

signals are present for 18-2-8 above its c.m.c. (0.3 mM). These signals are broader than those of 14-2-14, indicating faster exchange (τ = 0.04 s). Coalescence occurs for 12-2-12 (c.m.c. = 0.95 mM), and a single broad signal representing a weighted average of monomers and aggregated surfactants is seen (Fig. 2e). For all these dissymetric surfactants, the aggregates formed over a large range of concentration above the c.m.c. have been shown to be micelles.[9] In the case of 14-2-14, slopes of conductivity *versus* concentration suggests that micelles are also formed above the c.m.c., at least over a short concentration range. Bilayers were observed at 5 mM.[9]

Such slow exchange on the NMR timescale between monomeric and aggregated amphiphiles has been reported once for a neutral fluorinated surfactant, forming hydrogen bonds in an aggregated state.[12] These authors recognised the presence of large aggregates (not micelles), and suggested that this may be of importance in the large values of the measured lifetimes.[12] Lipids are much more hydrophobic than usual detergents and also exchange slowly between monomeric and vesicular states.[2,13] However, their critical aggregation concentrations are in the nanomolar range and below,[13] and are too small for NMR investigations. To the best of our knowledge our observations, using micelle-forming hydrocarbon cationic amphiphiles for which no forces other than the hydrophobic effect stabilise the aggregates, are unprecendented.

^{19}F and ^{1}H NMR spectra of the fluorocarbon Gemini surfactant $C_8^FC_4$-2-$C_8^FC_4$ and the hybrid hydrocarbon–fluorocarbon surfactant $C_8^FC_4$-2-12 also show distinct signals for monomers and aggregated surfactants (Fig. 3a).[10] The c.m.c. values deduced from dilution experiments or integration against a CF_3CH_2OH internal standard are 0.03 and 0.2 mM respectively, compared to 0.028 and 0.2 mM measured by conductimetry. For the hybrid surfactant $C_8^FC_4$-2-12, conductimetry and cryo-TEM observations confirm that the aggregates formed are micelles.[10] For the fluorocarbon surfactant $C_8^FC_4$-2-$C_8^FC_4$, vesicles seem to form even at such low concentrations, and the c.m.c. is probably a critical vesicular concentration.[10] The high sensitivity to the environment of fluorine chemical shifts results in large differences between the signals in the bulk and in the aggregates (up to 2.2 ppm for the terminal -CF_3 group). The ^{19}F nuclei located in the hydrophobic part of the molecules are shielded in the micelles and their signals shift upfield, whereas signals of the ^{1}H nuclei close to the polar heads shift downfield.

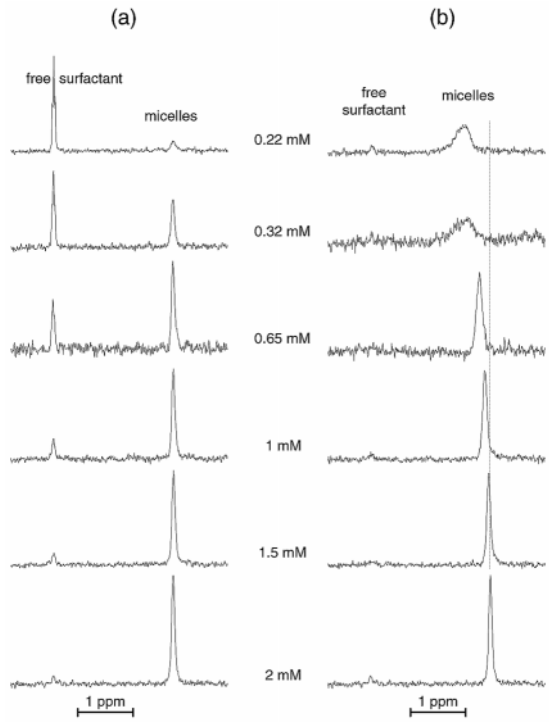

Fig. 3 Part of the 400 MHz ^{19}F NMR spectra of $C_8^FC_4$-2-12 as a function of concentration in 9 : 1 H_2O–D_2O (25 °C). The region covers the signals of the terminal -CF_3 groups in the bulk and in micelles. (a) no additives; (b) in the presence of 12-2-12 at constant total concentration, [$C_8^FC_4$-2-12] + [12-2-12] = 2 mM. The c.m.c. of 12-2-12 is 0.95 mM.

Slow exchange renders NMR studies of co-micellisation of various surfactants very tractable. The example of $C_8^FC_4$-2-12 and 12-12-12 shown in Fig. 3b represents a good illustration. When $C_8^FC_4$-2-12 and 12-2-12 are mixed in different proportions, it can clearly be seen that the hybrid fluorocarbon–hydrocarbon surfactant exists predominantly in the micellar state at concentrations close to, and even below, its c.m.c. At such low concentrations, $C_8^FC_4$-2-12 molecules remain in micelles consisting for the most part of 12-2-12 molecules. The co-micellisation can be traced by following the ^{19}F chemical shifts of $C_8^FC_4$-2-12 (Fig. 3b). As the mixed micelles become richer in 12-2-12, the fluorocarbon chains are less shielded than with pure $C_8^FC_4$-2-12, and the signals assigned to the micelles shift downfield. The concomitant broadening of these signals may result from the distribution of micelle composition, and not from faster exchange with 12-2-12 rich micelles. A ^{1}H NMR spectrum of these mixed micelles presents the original pattern of an aggregate with which one surfactant exchanges slowly, and the other rapidly. A more thorough investigation of the exchange rates for these surfactants is now in progress.

This work was supported by the Centre National de la Recherche Scientifique and the Institut Européen de Chimie et Biologie. We thank E. J. Dufourc for assistance with NMR measurements.

Notes and references

† Determination of the characteristic time of exchange τ may be performed using 1D polarisation transfer or 2D exchange spectroscopy. An estimate can be very simply obtained from lineshape analysis of a sample at a concentration twice the c.m.c. At this concentration the lifetimes of monomeric and aggregated species are both equal to τ, whose value is then given by $1/\tau = \pi\Delta\Delta\nu$, where $\Delta\Delta\nu$ is the linewidth difference between the monomer signal at twice the c.m.c. (broadened by the exchange) and below the c.m.c. (no exchange), as obtained from a least-square analysis of the spectra. The τ values can be measured as long as separate signals are observed, which requires $1/\tau < |\nu_m - \nu_a|$, where ν_m and ν_a are the monomer and the aggregate signal frequencies.

1 C. Tanford, in *The Hydrophobic Effect: Formation of Micelles and Biological Membranes*, Wiley-Interscience, New York, 1973.
2 J. Israelachvili, in *Intermolecular & Surface Forces*, 2nd edn., Academic Press, San Diego, 1991, p. 375.
3 M. Frindi, B. Michel, H. Levy and R. Zana, *Langmuir*, 1994, **10**, 1140 and refs. therein.
4 N. Muller, *J. Phys. Chem.*, 1972, **76**, 3017.
5 M. Frindi, B. Michels and R. Zana, *J. Phys. Chem.*, 1991, **95**, 4832.
6 R. Zana, *J. Colloid Interface Sci.*, 1980, **78**, 330.
7 See M. J. Rosen and D. J. Tracy, *J. Surfactants Detergents*, 1998, **1**, 547.
8 For selected examples, see R. Zana and Y. Talmon, *Nature*, 1993, **362**, 228; F. M. Menger and C. A. Littau, *J. Am. Chem. Soc.*, 1993, **115**, 10 083; N. A. J. M. Sommerdijk, M. H. L. Lambermon, M. C. Feiters, R. J. M. Nolte and B. Zwanenburg, *Chem. Commun.*, 1997, 1423; K. Jennings, I. Marshall, H. Birrell, A. Edwards, N. Haskins, O. Sodermann, A. J. Kirby and P. Camilleri, *Chem. Commun.*, 1998, 1951; R. Oda, I. Huc, M. Schmutz, S. J. Candau and F. C. MacKintosh, *Nature*, 1999, **399**, 566.
9 R. Oda, I. Huc and S. J. Candau, *Chem. Commun.*, 1997, 2105; R. Oda, I. Huc, J.-C. Homo, B. Heinrich, M. Schmutz and S. J. Candau, *Langmuir*, 1999, **15**, 2384.
10 A full account of the synthesis and aggregation behaviour of these new fluorinated compounds is in preparation.
11 J. I. Kaplan and G. Fraenkel, in *NMR of Chemically Exchanging Systems*, Academic Press, New York, 1980.
12 B. M. Fung, D. L. Mamrosh, E. A. O'Rear, C. B. Frech and J. Afzal, *J. Phys. Chem.*, 1988, **92**, 4405; W. Guo, T. A. Brown and B. M. Fung, *J. Phys. Chem.*, 1991, **95**, 1829.
13 D. Marsh, in *CRC Handbook of Lipid Bilayers*, CRC Press, Boca Raton, 1990.

Communication 9/06141J

ChemComm

Developing osmium(II) tris(2,2′-bipyridyl) derivatives as reagents for luminogenic assays

Abdelkrim El-ghayoury, Anthony Harriman* and Raymond Ziessel*

Laboratoire de Chimie, d'Electronique et Photonique Moléculaires, Ecole Européenne de Chimie, Polymères et Matériaux, Université Louis Pasteur, 25 rue Becquerel, F-67087 Strasbourg Cedex 02, France.
E-mail: ziessel@chimie.u-strasbg.fr

Received (in Cambridge, UK) 23rd July 1999, Accepted 8th September 1999

The combined effects of an ethynylene substituent and reversible energy transfer to an appended anthracene unit provide access to luminophoric osmium(II) tris(2,2′-bipyridyl) derivatives of unusually long triplet lifetime and whose improved optical properties might provide new analytical opportunities.

Derivatives of ruthenium(II) polypyridine complexes are being used for an ever-increasing number of luminogenic assays, especially for biological systems.[1] An attractive feature of these chromophores concerns the relatively long-lived phosphorescence observed for certain complexes at room temperature in deoxygenated solution. Indeed, several strategies are available by which to both prolong the emission lifetime[2,3] and shift the emission maximum to longer wavelength.[4,5] The corresponding osmium(II) polypyridine complexes,[6] which possess attractive absorption and emission spectral profiles, have been largely ignored as regards analytical applications because of their relatively short emission lifetimes. We now describe a simple approach to extend the triplet lifetime of osmium(II) tris(2,2′-bipyridyl) derivatives and, at the same time, push the emission maximum to lower energy.

This strategy requires access to luminescent 'Os(bpy)' (bpy = 2,2′-bipyridine) derivatives functionalized with two key elements. The first requirement involves direct substitution of an alkyne group on the bpy ring. This ensures selective charge injection from the metal centre to the alkyne-bearing bpy ligand under illumination and, because of extended electron delocalization, lowers the triplet energy.[7] The second requirement is to attach a chromophore at the opposite end of the alkyne that can transfer triplet energy reversibly to the 'Os(bpy)' unit.[2,3,8] This demands careful balancing of the triplet energies of the two units and we have found that anthracene is a useful energy shuttle for such systems. In order to obtain the required triplet energy, however, it was necessary to attach ethynylene groups at both the 9- and 10-positions of the anthracene subunit but this has the advantage of providing access to mono- and bi-nuclear 'Os(bpy)'-based systems and to mixed-metal complexes. Several such compounds were synthesized† and their photophysical properties examined in deoxygenated acetonitrile at 20 °C. For brevity, we describe only the properties of **OBA**. We note that, although triplet energy transfer between 'Os(bpy)' derivatives and anthracene has been reported,[9,10] neither reversible energy transfer nor prolongation of the triplet lifetime has been considered before.

The absorption spectrum recorded for **OBA** shows intense transitions between 400 and 520 nm due to the anthracene-based ditopic ligand (Fig. 1). These π,π* transitions overlap the weaker metal-to-ligand, charge-transfer (MLCT) bands associated with the 'Os(bpy)' unit but the corresponding spin-forbidden MLCT transitions can be seen as a tail stretching towards 800 nm. This latter band allows excitation into the 'Os(bpy)' chromophore at wavelengths where few other species absorb and where light scattering from biological materials is less significant. Fluorescence from the ditopic ligand is completely quenched when the terminal 'Os(bpy)' unit is in

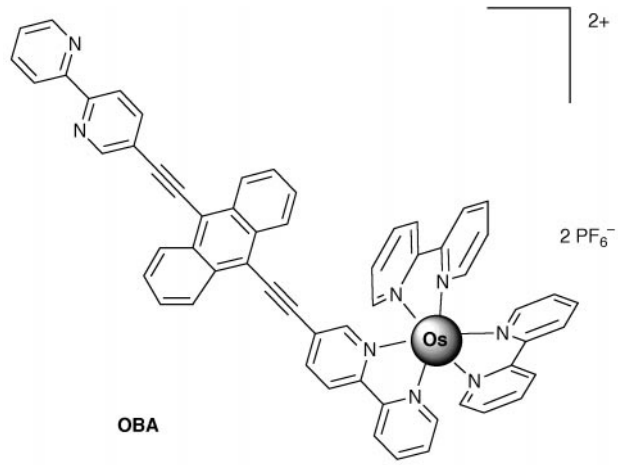

place, owing to rapid intramolecular electronic energy transfer. As such, the ditopic ligand acts as a light harvester for the lowest-energy triplet state localized on the 'Os(bpy)' unit.

Luminescence from **OBA** is observed at 20 °C (Fig. 1), the maximum being around 800 nm, that can be assigned to emission from the 'Os(bpy)' terminal. This emission, for which the quantum yield (Φ_L) is 0.0012, decays *via* exponential kinetics corresponding to a triplet lifetime (τ_T) of 415 ± 15 ns. The triplet energy (E_T) calculated by fitting[9] the emission spectrum is 13150 cm^{-1}. These values can be compared with those measured for the parent $[Os(bpy)_3]^{2+}$ complex (Φ_L = 0.0046; τ_T = 60 ns; E_T = 14640 cm^{-1}) showing that, despite its lower triplet energy, **OBA** possesses much the longer-lived triplet state.

The differential triplet absorption spectrum recorded for **OBA** after excitation with a 15 ns laser pulse at 600 nm (Fig. 2)

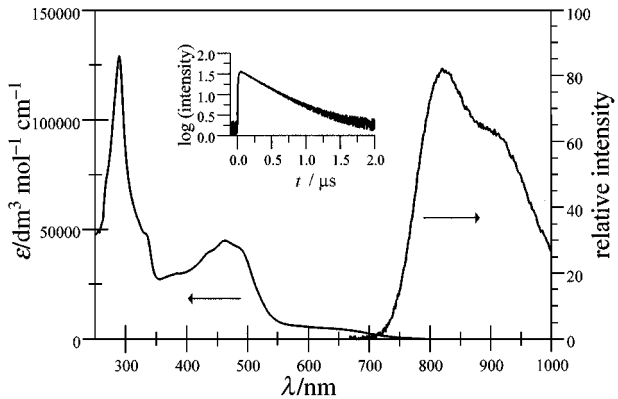

Fig. 1 Absorption and corrected emission spectra recorded for **OBA** in deoxygenated acetonitrile at 20 °C. The emission spectral profile is independent of excitation wavelength while the corrected excitation spectrum matches well with the absorption spectrum. The insert shows the time-resolved emission profile recorded at 850 nm after excitation with a 15 ns laser pulse at 600 nm.

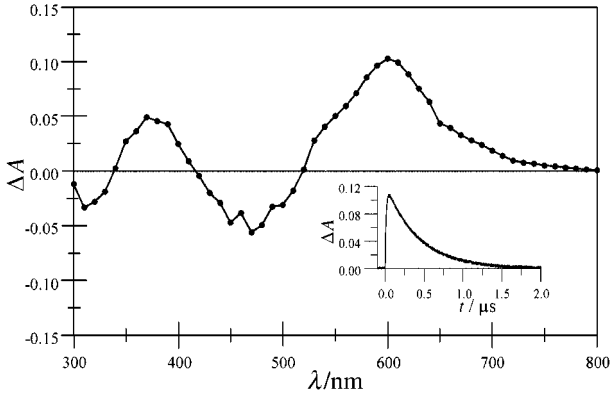

Fig. 2 Differential triplet absorption spectrum recorded for **OBA** in deoxygenated acetonitrile after excitation with a 15 ns laser pulse at 600 nm. The insert shows the decay profile recorded at 600 nm.

is very similar to that measured for the ditopic ligand, although the latter does not phosphoresce in deoxygenated acetonitrile at 20 °C. The absorption signal decays *via* exponential kinetics, at all wavelengths, with an average triplet lifetime of 420 ± 20 ns. Identical spectra and decay kinetics are observed following laser excitation at 355, 450, 600 or 650 nm. The simplest explanation[2,3] for these observations is that the triplet states localised on the 'Os(bpy)' fragment and on the anthracene-based ditopic ligand are in thermal equilibrium at 20 °C. The two triplets decay with a common lifetime of 420 ± 20 ns to restore the ground state. Consistent with this hypothesis is the observation that the triplet energy of the ditopic ligand, established from phosphorescence spectra recorded in micellar media,[11] is 12400 cm^{-1}. Thus, the triplet energy gap is 750 cm^{-1}, with the anthracene-like triplet lying at lower energy, while the equilibrium constant (K) can be estimated as being *ca* 40. This latter value implies that the fraction (α) of 'Os(bpy)' triplets in the equilibrium distribution is only 2.5%. This residual 'Os(bpy)' triplet is highly luminescent, however, since the observed Φ_L is *ca*. 25% that of the parent complex where the triplet yield is quantitative. The 'Os(bpy)' fragment in **OBA**, in fact, is roughly 10-fold more emissive than the parent complex when due allowance is made for the relative concentrations. This increase arises from the longer triplet lifetime (*cf*. 420 *vs*. 60 ns) and longer radiative lifetime (*cf*. 18 *vs*. 13 μs) provided by the improved optical properties.

The rate constant for decay of the equilibrated triplets ($k_D = 1/\tau_T$) can be expressed[2] in terms of the individual rate constants associated with deactivation of triplets localised on the ditopic ligand (k_A) and on the 'Os(bpy)' fragment (k_O).

$$k_D = \alpha k_O + (1 - \alpha)k_A,\ K = (1 - \alpha)/\alpha$$

Since k_A ($= 1.4 \times 10^5\ s^{-1}$) is known from measurements made for the ditopic ligand and $\alpha = 0.025$, it follows that $k_O \approx 9 \times 10^7\ s^{-1}$. This seems a reasonable value for an ethynylated 'Os(bpy)' derivative, where triplet lifetimes tend to range between 10 and 60 ns.[7] As such, reversible triplet energy transfer between the subunits stabilizes the 'Os(bpy)' triplet by a factor ($S = k_O\tau_T$) of *ca*. 38-fold.

Direct excitation into the 'Os(bpy)' chromophore with a sub-ps laser pulse at 600 nm indicates that the equilibrium mixture of triplets is established with a first-order rate constant of $3.0 \times 10^{10}\ s^{-1}$. Allowing for $K = 40$, we can estimate rate constants for triplet energy transfer from 'Os(bpy)' to the anthracene-like triplet ($k_F = 2.9 \times 10^{10}\ s^{-1}$) and for the corresponding reverse process ($k_R = 7.3 \times 10^8\ s^{-1}$). Both reactions are exceptionally fast, especially the reverse step which is strongly endergonic, because of the superb electronic conductivity of the alkyne connector.[12]

Illumination of **OBA** in O_2-saturated acetonitrile generates singlet molecular oxygen, as monitored by its characteristic time-resolved luminescence behaviour. The lifetime of the so generated singlet molecular oxygen ($\tau_D = 75 \pm 5$ μs) remained independent of the concentration of **OBA** while protracted steady-state illumination with an argon ion laser emitting at 514 nm did not damage the chromophore. Clearly, the ethynylene groups stabilize the anthracene unit against oxygenation.[10,13]

In summary, we describe a strategy for designing 'Os(bpy)'-based luminophores possessing improved optical properties and an unusually long-lived triplet state. There are, of course, other ways to prolong the triplet lifetime; *e.g.* freezing the solution or raising the triplet energy.[6] Such approaches do not produce valuable luminogenic reagents. In contrast, combining the special electronic properties[3,7,8,12] (*e.g.* directionality, conductivity, delocalisation) of the alkyne with reversible triplet energy transfer to an anthracene-like subunit provides a useful reagent of exceptional thermal and photostability. It is important to emphasise the complementarity of the system in that each of the three units is essential. Thus, the 'Os(bpy)' fragment provides a long-wavelength absorption profile and the necessary luminescent centre. The alkynylene connector offers structural integrity and an excellent conduit for intramolecular electron exchange whereas the anthracene unit prolongs the triplet lifetime of the emitting species.

We thank Johnson-Mathey PLC for their very generous loan of precious metal salts. Some of the laser spectroscopic studies were made at the Free Radical Research Facility at the Paterson Institute for Cancer Research, Manchester, UK. We thank the EU for providing financial support for the FRRF and to cover travel costs.

Notes and references

† Synthetic details will be reported elsewhere. All new compounds gave satisfactory elemental analyses and were authenticated by ^1H and ^{13}C NMR, FTIR and MS.

1 A. Harriman, *Photochemistry*, RSC Specialist Periodical Report, Cambridge, 1999, vol. 30, ch. 1.
2 W. E. Ford and M. A. J. Rodgers, *J. Phys. Chem*., 1991, **96**, 2917.
3 A. Harriman, M. Hissler, A. Khatyr and R. Ziessel, *Chem. Commun*., 1999, 735.
4 G. F. Strouse, J. R. Schoonover, R. Duesing, S. Boyde, W. E. Jones Jr. and T. J. Meyer, *Inorg. Chem*., 1995, **34**, 473.
5 M. J. Cook, A. P. Lewis, G. S. G. McAuliffe, V. Skarda, A. J. Thompson, J. L. Glasper and D. J. Robbins, *J. Chem. Soc., Perkin Trans. 2*, 1984, 1293.
6 S. Boyde, G. F. Strouse, W. E. Jones Jr. and T. J. Meyer, *J. Am. Chem. Soc*., 1989, **111**, 7448.
7 V. Grosshenny, A. Harriman, F. M. Romero and R. Ziessel, *J. Phys. Chem*., 1996, **100**, 1491.
8 M. Hissler, A. Harriman, A. Khatyr and R. Ziessel, *Chem. Eur. J*., 1999, in press.
9 Z. Murtaza, A. P. Zipp, L. A. Worl, D. K. Graff, W. E. Jones Jr., W. D. Bates and T. J. Meyer, *J. Am. Chem. Soc*., 1991, **113**, 5113.
10 P. Belser, R. Dux, M. Book, L. De Cola and V. Balzani, *Angew. Chem., Int. Ed. Engl*., 1995, **34**, 595.
11 M. Skrilec and L. J. Cline Love, *Anal. Chem*., 1980, **52**, 1559.
12 V. Grosshenny, A. Harriman and R. Ziessel, *Angew. Chem., Int. Ed. Engl*., 1995, **34**, 2705.
13 C. Weinheimer, Y. Choi, T. Caldwell, P. Gresham and J. Olmsted III, *J. Photochem. Photobiol. A: Chem.*, 1994, **78**, 119.

Communication 9/05979B

ChemComm

New rhodium-catalyzed amination reactions†‡

Harald Trauthwein,[a] Annegret Tillack[b] and Matthias Beller*[b]

[a] *Aventis Research and Technologies, Industriepark Höchst, 65926 Frankfurt, Germany*
[b] *Institut für Organische Katalyseforschung an der Universität Rostock e.V., Buchbinderstr. 5-6, 18055 Rostock, Germany. E-mail: matthias.beller@ifok.uni-rostock.de*

Received (in Basel, Switzerland) 17th May 1999, Accepted 1st September 1999

New transition metal-catalyzed reactions of norbornadiene with secondary amines are reported.

The development of efficient protocols for the construction of carbon–nitrogen bonds is of interest owing to the fundamental importance of amines as natural products, pharmacological agents, fine chemicals, and dyes.[1] Regarding the various possibilities to form C–N bonds, the catalytic hydroamination of olefins is the most atom economic process.[1]

In addition, a wide variety of olefins and amines are both inexpensive and readily available starting materials. Hence, considerable efforts have been undertaken to develop metal-catalyzed hydroamination processes.[2] Among the first transition metal catalysts for hydroamination were Rh salts, *e.g.* $RhCl_3$ introduced by Du Pont.[3] Although a number of Rh complexes catalyze the reaction of ethylene with secondary amines with yields of up to 70%, other olefins do not react. Interestingly, Brunet *et al.*[4] demonstrated later, that $[Rh(PEt_3)_2Cl]_2$ catalyzes both the oxidative amination and the hydroamination of styrene with aniline. Recently, we became interested in catalytic hydroaminations. Our approach to this problem was based on the use of cationic Rh complexes in order to enhance the reactivity of the resulting catalysts. Indeed, a mixture of $[Rh(cod)_2]^+BF_4^-$/2 PPh_3 catalyzes the reaction of aromatic olefins with secondary amines.[5] Surprisingly, no hydroamination takes place, but a rare example of intramolecular oxidative amination is observed to yield *N*-(2-arylethenyl)amines and arylethane in good yields. Here, we describe the first extensions of this methodology to aliphatic olefins, especially norbornadiene (nbd).

The addition of nucleophiles H–X to nbd yields, in general, tricyclic pseudo-1,4-addition products (Scheme 1). This reaction is catalyzed by both acids and Pd complexes.[6]

Adaptation of our previously reported procedure for the oxidative amination of styrene with morpholine to nbd yields, under standard conditions (2.5 mol% $[Rh(cod)_2]^+BF_4^-$, 5 mol% PPh_3, THF reflux), three new amination products **3a**, **4a** and **5a** in 25, 33 and 31% yield, respectively[7] (Scheme 2, Table 1). Furthermore, small amounts (< 3%) of hydrodimerization **6** and hydrooligomerization products were observed. The structure of **3a** and **4a** was unambiguously proved by ^1H and ^{13}C NMR spectroscopy and MS, *e.g.* the ^{13}C NMR spectrum of **3a** exhibit one quaternary, two different secondary and two tertiary carbon centers of the nortricyclene group and two signals of the morpholino ring, while the ^{13}C NMR spectrum of **4a** exhibits one quaternary, four different tertiary and two secondary carbon centers of the nortricyclene group and four signals of the two morpholino rings. **5a** has been identified by GC–MS. Interestingly, **4a** is obtained as a pure diastereomer, where the two morpholino rings point away from each other.

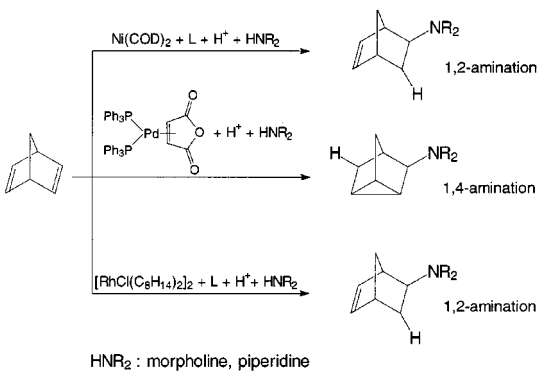

Scheme 1 Known addition of amines to nbd.

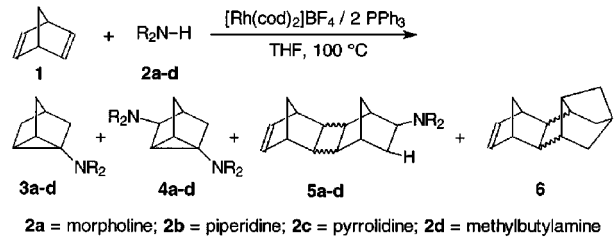

Scheme 2 Rh-catalyzed reaction of morpholine with nbd.

Table 1 Reaction of morpholine with norbornadiene

Entry	Catalyst (mol%)	Solvent	Olefin: amine	Yield **3a**[a] (%)	Yield **4a**[a] (%)
1	2.5	THF	4:1	25	33
2	5	THF	4:1	43	14
3	10	THF	4:1	47	5
4	2.5	THF	10:1	7	46
5	2.5	THF	1:2	32	7
6	2.5	Toluene	4:1	3	88

[a] The yield (referred to amine) was determined by GC using an internal standard.

Concerning **3a** and **4a** it is noteworthy that, unlike in previously published amination procedures of nbd, at least one amine is bound directly to one of the C atoms of the cyclopropyl ring. This structural motif can only be explained by a *pseudo*-1,3-addition mode to nbd.[8] To the best of our knowledge *pseudo*-1,3-additions of nucleophiles H–Nu (Nu = NR_2, OR, SR, *etc.*) to nbd have not been reported previously.

Next, we modified the reaction conditions in order to improve the selectivity of the amination reaction. In a series of reactions carried out on 5 mmol scale the amount of catalyst, reaction temperature, solvent and olefin to amine ratio was varied. Reactions employing a larger amount of catalyst (5, 10 mol%) gave significantly higher yields of **3a** (up to 47%) while the yield of the diaminated product **4a** is decreased to only 5%. Use of a ten-fold excess of norbornadiene to morpholine resulted in a drastic decrease of **3a** (7%), but **4a** is obtained in 46%. Consistently at lower amine to olefin ratio the yield of **4a** is

† Dedicated to Professor Dirk Walther on the occasion of his 60th birthday.
‡ Considered as Part 7 of the series Anti-Markovnikov-reactions; for part 6 see M. Beller, H. Trauthwein, M. Eichberger, C. Breindl and T. E. Müller, *Eur. J. Inorg. Chem.*, 1999, 1121.

increased. The use of toluene at higher reaction temperature appeared to be especially suitable for the formation of the diaminated product **4a** (88%).

Analogous to morpholine we reacted other secondary amines and aniline with nbd in the presence of 5 mol% $[Rh(cod)_2]^+BF_4^-$ and 10 mol% PPh_3 in THF in a glass pressure tube at 100 °C (Table 2). While aniline gave only non-aminated dimerization products of nbd, all secondary amines gave a total yield of amination products of 84–99%.

Table 2 Reaction of norbornadiene with amines[a]

Entry	Amine	Yield amines[b] (%)	Yield **3**[c] (%)	Yield **4** (%)
1	Morpholine **2a**	91	43	14[c]
2	Piperidine **2b**	99	52	17[d]
3	Pyrrolidine **2c**	84	52	10[d]
4	*n*-Butylmethylamine **2d**	90	46	13[d]

[a] Ratio of nbd:amine = 4:1, 5 mol% $[Rh(cod)_2]BF_4/2PPh_3$ relative to amine, 20 h reflux in THF. [b] Overall yield of amination products (**3** + **4** + **5**). [c] The yield (referred to amine) was determined by GC using an internal standard. [d] The yield (referred to amine) was determined by GC by percentage area.

The major product under these conditions were the mono-amination products **3b**–**d**. However, in all cases significant amounts of 2,5-bis(*N*-amino)tricyclo[2.2.1.$0^{2,6}$]heptane **4b**–**d** and aminated nbd dimers were formed.

Here, we describe the first example of the catalytic *pseudo*-1,3-addition of nucleophiles (amines) to nbd. In general, amination of nbd with amines proceeds in high yield but with only moderate selectivity. Although the reaction has not been fully optimized, yields of 2-(*N*-morpholino)tricyclo-[2.2.1.$0^{2,6}$]heptane **3a** of *ca.* 50% were obtained in THF at 100 °C. On the other hand a high yield (88%) of 2,5-bis(*N*-morpholino)tricyclo[2.2.1.$0^{2,6}$]heptane **4a** was obtained in toluene at 140 °C. While little mechanistic work has been conducted on the new amination reaction at this time, we propose that the reaction occurs by a catalytic cycle shown in Scheme 3.

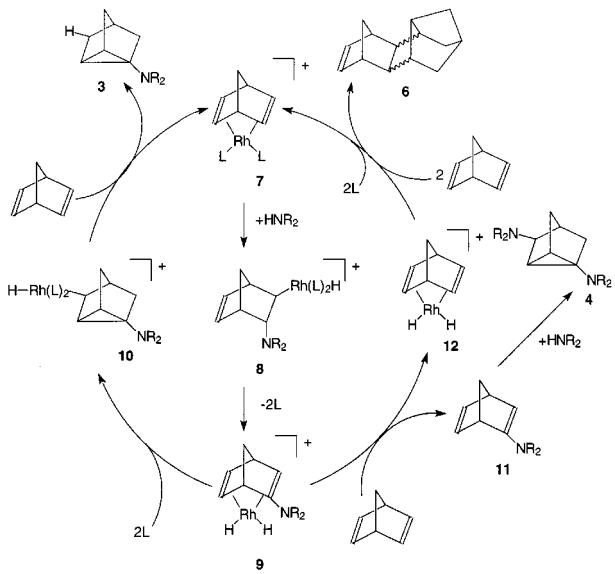

Scheme 3 Proposed mechanism for the Rh-catalyzed amination of nbd.

Olefin exchange of cyclooctadiene by nbd will give the corresponding nbd complex **7**. Here, the double bonds are activated for a nucleophilic attack of the amine leading to **8**. Alternatively, **8** may be formed by insertion of the olefin into the Rh–N bond of a hydridoamidorhodium species. Although this mechanism seems unlikely owing to the stereochemistry required for the following β-hydride elimination, it has been shown that cationic Rh complexes are able to activate N–H bonds under similar conditions.

β-Hydride elimination would form the Rh–dihydride complex with a chelating enamine ligand **9**. Stepwise hydrogen transfer with concurrent double bond shift would give the Rh alkyl complex **10**. Subsequently, reductive elimination yields **3**. On the other hand ligand exchange of the enamine with nbd would yield **11** and **12**. It is known in the literature[9] that **11** reacts with amines to give **4**. While it is easy to explain the improved yield of **4** with increased olefin to amine ratio owing to the increased ligand exchange with nbd, we do not understand the influence of the catalyst concentration. In addition it is obvious that higher reaction temperatures (140 °C, toluene) favor the ligand exchange, hence yielding **4** predominantly. The occurrence of the hydrodimerization product **6** confirms the existence of Rh–hydride species.

Regarding the synthetic value of this new method, it is important to note that a number of aliphatic polycyclic amines such as amantadine, memantine, venritidine, carmantadine, oxphaman and amantocillin are interesting pharmacologically active compounds.[10] New analogs may be prepared by our method.

In conclusion, we have developed a new type of Rh-catalyzed amination. Here, nbd is aminated in an unusual *pseudo*-1,3-addition mode. Both mono- as well as di-aminated products are accessible as major products.

This work is supported by the Deutsche Forschungsgemeinschaft (BE 1931/3-1).

Notes and references

1 For leading reviews of hydroamination, see: M. Beller and T. Müller, *Chem. Rev.*, 1998, **98**, 675; D. M. Roundhill, *Chem. Rev.* 1992, **92**, 1; J.-J. Brunet, D. Neibecker and F. Niedercorn, *J. Mol. Catal.*, 1989, **49**, 235.

2 Recent examples: R. Dorta, P. Egli, F. Zürcher and A. Togni, *J. Am. Chem. Soc.*, 1997, **119**, 10 857; J.-J. Brunet, *Gazz. Chim. Ital.*, 1997, **127**, 111; V. M. Arrenodo, S. Tian, F. E. McDonald and T. J. Marks, *J. Am. Chem. Soc.*, 1999, **121**, 3633.

3 D. R. Coulson, *Tetrahedron Lett.*, 1971, **12**, 429.

4 J.-J. Brunet, D. Neibecker and K. Philippot, *J. Chem. Soc., Chem. Commun.*, 1992, 1215; *Tetrahedron Lett.*, 1993, **34**, 3877; J.-J. Brunet, G. Commenges, D. Neibecker and K. Philippot, *J. Organomet. Chem.*, 1994, **469**, 221.

5 M. Beller, M. Eichberger and H. Trauthwein, *Angew. Chem., Int. Ed. Engl.*, 1997, **36**, 2225; M. Beller, M. Eichberger and H. Trauthwein, *Catalysis of Organic Reactions*, ed. F. Herkes, Marcel Dekker, New York, 1998; M. Beller, H. Trauthwein, M. Eichberger, J. Herwig, T. E. Müller and O. Thiel, *Eur. J. Chem.*, 1999, **5**, 1306; M. Beller, H. Trauthwein, M. Eichberger, C. Breindl, T. E. Müller and A. Zapf, *J. Organomet. Chem.*, 1998, **566**, 277; M. Beller, H. Trauthwein, M. Eichberger, C. Breindl and T. E. Müller, *Eur. J. Inorg. Chem.*, 1999, 1121.

6 L. Schmerling, J. P. Luvisi and R. W. Welak, *J. Am. Chem. Soc.*, 1956, **78**, 2819; J. Kiji, S. Nishimura, S. Yoshikawa, E. Sasakawa and J. Furukawa, *Bull. Chem. Soc. Jpn.*, 1974, **47**, 2523.

7 *General procedure:* 89.3 mg $[Rh(cod)_2]BF_4$ (0.22 mmol) and 115.4 mg PPh_3 (0.44 mmol) were mixed in 10 ml THF. Subsequently, 0.38 ml morpholine (4.40 mmol) and 1.92 ml nbd (17.6 mmol) were added at room temp. The reaction was heated to reflux for 20 h before being cooled to room temp. After removal of the solvent *in vacuo*, the residue was dissolved in 20 ml CH_2Cl_2 and extracted three times with 5% HCl. NaOH was added to the combined aqueous phases until a pH of 9 was reached. The aqueous phase was then extracted three times with CH_2Cl_2. The combined organic layers were dried over $MgSO_4$ and the solvent was distilled off. The products were obtained after column chromatography ($CHCl_3$–MeOH = 30:1). Isolated yields: **3a**: 32% (252 mg); **3b**: 40% (312 mg); **3c**: 37% (266 mg); **3d**: 34% (268 mg); **4c**: 4% (23 mg).

8 We term this reaction of amines with norbornadiene a pseudo-1,3-addition in agreement with literature for 1,4-addition reactions.

9 A. G. Cook, M. L. Absi and V. K. Bowden, *J. Org. Chem.*, 1995, **60**, 3169.

10 G. D. Diana and F. Pancic, *Angew. Chem.*, 1976, **88**, 458; E. X. Albuquerque, A. T. Eldefrawi, M. E. Eldefrawi, N. A. Mansour and M.-C. Tsai, *Science*, 1978, **199**, 788; Negwer, *Organic-chemical Drugs and their Synonyms*, Fachinformationszentrum Chemie, Berlin.

Communication 9/03920A

Templating mesoporous silicates on surfactant ruthenium complexes: a direct approach to heterogeneous catalysts

Helen B. Jervis,[a] Maria E. Raimondi,[b] Robert Raja,[d] Thomas Maschmeyer,*[c] John M. Seddon*[b] and Duncan W. Bruce*[a]

[a] *School of Chemistry, University of Exeter, Stocker Road, Exeter, UK EX4 4QD. E-mail: d.bruce@exeter.ac.uk*
[b] *Department of Chemistry, Imperial College of Science, Technology and Medicine, South Kensington, London, UK SW7 2AZ*
[c] *Laboratory of Applied Organic Chemistry and Catalysis, TU Delft, Julianalaan 136, 2628 BL Delft, The Netherlands*
[d] *Davy Faraday Research Laboratory, The Royal Institution of Great Britain, 21 Albemarle Street, London, UK W1X BS*

Received (in Cambridge, UK) 27th July 1999, Accepted 8th September 1999

Mesoporous silicas have been obtained by the true liquid crystal templating (TLCT) method, using a surfactant Ru^{II} complex as the template; on calcination, ruthenium-containing particles are deposited into the pores; the materials show high catalytic selectivity for the hydrogenation of hex-1-ene.

Since the discovery of the utility of surfactants as templates for mesoporous solids by Mobil,[1] there has been an explosion of interest in these mainly siliceous solids, particularly as pore sizes from, for example, 20–100 Å are now routinely available. For much of the time since these initial developments, the situation has been rather unsatisfactory as there was little pre-emptive control which could be employed to direct the structure of the materials to be synthesised. Thus, while a given set of conditions could reproducibly lead to a given material with given dimensions, some of the structural parameters (pore size, wall thickness, degree of crystallinity) of the solid were largely unpredictable prior to the first experiment. The exact mechanism of the templating attracted much speculation and debate. This was partly due to the fact that the surfactant was present above the critical micelle concentration (cmc), but at concentrations below those necessary for mesophase formation. More recently, this situation changed rather dramatically with the development of the true liquid crystal templating (TLCT) synthesis by Attard *et al.*[2] In this approach, a lyotropic liquid crystal phase was first formed and templating took place around the pre-formed mesophase in a sol–gel hydrolysis of tetramethoxysilane (TMOS). In forming these solids, both neutral and cationic surfactants could be employed. The various approaches to liquid crystal templating have been reviewed recently.[3]

Because of the pore sizes available in mesoporous solids, one of the great attractions is the possibility to carry out reactions therein, using molecules which would not have been able to get inside the pores of microporous materials. This reactivity can take a number of forms. First, it is possible simply to use the acidity of the mesopore surface to facilitate reactions. This is particularly attractive when doping aluminium into the silica, so as to generate Brønsted acid sites. On these sites, ion exchange can take place and the acidity or basicity of the material can be controlled. It is also possible to introduce molecular catalytic species, which may be tethered to the mesopore, to carry out reactions in confined environments. Another avenue for catalytic functionalisation is the deposition of metal particles within the pores and to use the materials as heterogeneous catalysts.[4] In the latter two approaches, it is necessary to pre-form the mesoporous solid and then to introduce the catalyst, or as has recently been shown, to introduce an extra metal-based species during gel formation.[5] What we describe here is the production of a mesoporous solid containing deposited metal particles in one step from the surfactant, exploiting the dual functionality of the surfactant ruthenium complex as, both, structure directing and catalytic site generation agent.

Some of us have been interested in the synthesis and mesomorphism of surfactant metal complexes,[6] and in particular the study of the lyotropic mesomorphism of surfactant derivatives of tris(bipyridine)ruthenium(II) (Fig. 1).[7] As part of this work, we were interested to see whether these complexes could be used to template mesoporous silicates, and in particular whether the TLCT approach could be adopted. To this end, we employed the dinonadecyl-substituted complex **1**, which we know to form a hexagonal H_1 phase in water at elevated temperatures.

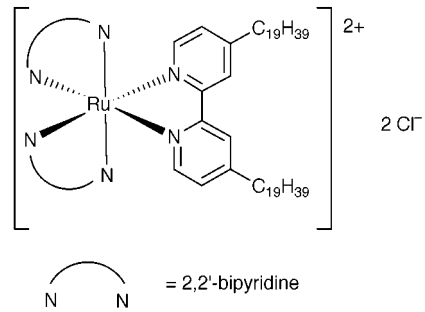

Fig. 1 Structure of the ruthenium complex used for templating.

Thus, a 50 wt% mixture of **1** in water acidified to pH 2 with H_2SO_4 was prepared and maintained at 60 °C, and was shown by polarised optical microscopy to have a non-geometric texture typical of the hexagonal H_1 phase at this temperature. A small amount of methanol was added to the mesophase preparation, in order to aid mixing of the reagents, and was removed under a dynamic vacuum immediately after addition of the TMOS. Hydrolysis of the TMOS starts immediately and the methanol so produced was removed under gentle, dynamic vacuum as it was generated. After 2 h, the gel formation was complete and a strongly red-coloured gel remained, coloured due to the ruthenium complex contained therein. Interestingly, this gel still retains the texture of the hexagonal H_1 phase when viewed in the polarising microscope. The gel was then calcined in air at 600 °C for 6 h leading to a blackened silicate which we calculate to have 6 wt% Ru.

Investigation of this mesoporous silicate by transmission electron microscopy shows a material which retains the hexagonal symmetry of the mesophase on which it was templated and which contains relatively evenly distributed particles of RuO_2 (Fig. 2). Evaluation of the surface area by N_2 adsorption isotherm measurements gave a type IV absorption–desorption isotherm, confirming that the material is mesoporous and led to values in the range 870–980 $m^2\ g^{-1}$ being established

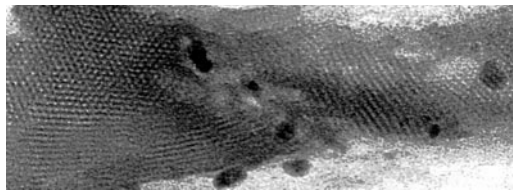

Fig. 2 TEM of the as-obtained silicate (×240 000).

for the BET surface area (depending on the sample). The same measurements also showed a very narrow pore size dispersity (half peak height values of 20–40 Å). In addition, evaluation of the surface-area-to-bulk ratio suggested rather high surface area particles with a CO dispersion of 15%. This compares with a value of 7.5% for MCM-41 impregnated with ruthenium nitrosyl nitrate [$Ru(NO)(NO_3)_3$] which was then converted to RuO_2.[8]

The materials were then tested as catalysts in the hydrogenation of hex-1-ene without prior reduction in hydrogen as a simple model system.[9] Thus, at 373 K and under 22 bar of H_2, hexene was hydrogenated *only* to *n*-hexane[10] at a turnover frequency of 877 mol hexane(mol Ru h)$^{-1}$. This exceeds turnover rates for hydrogenation on AgRu nanoparticles on MCM41 [690 mol hexane(mol metal h)$^{-1}$] under the same conditions,[11] although in its unoptimised state, it falls short of the rates[12] obtained for CuRu nanoparticles on the same support [1560 mol hexane(mol metal h)$^{-1}$].[4]

H. B. J., M. E. R. and T. M. thank the EPSRC and the EU for support. Generous loans of ruthenium salts and access to data from Johnson Matthey are gratefully acknowledged.

Notes and references

1 C. T. Kresge, M. E. Leonowicz, W. J. Roth, J. C. Vartuli and J. S. Beck, *Nature*, 1992, **359**, 710.
2 G. S. Attard, J. C. Glyde and C. G. Göltner, *Nature*, 1995, **378**, 366.
3 M. Raimondi and J. M. Seddon, *Liq. Cryst.*, 1999, **26**, 305.
4 See, for example: D. S. Shephard, T. Maschmeyer, G. Sankar, J. M. Thomas, D. Ozkaya, B. F. G. Johnson, R. Raja, R. D. Oldroyd and R. G. Bell, *Chem. Eur, J.*, 1998, **4**, 1214.
5 M. E. Raimondi, L. Marchese, E. Gianotti, T. Maschmeyer, J. M. Seddon and S. Coluccia, *Chem. Commun.*, 1999, 87.
6 D. W. Bruce, D. A. Dunmur, P. M. Maitlis, J. M. Watkins and G. J. T. Tiddy, *Liq. Cryst.*, 1992, **11**, 127; D. W Bruce, I. R. Denby, G. J. T. Tiddy and J. M Watkins, *J Mater. Chem.*, 1993, **3**, 911; J. D. Holbrey, D. W. Bruce and G. J. T. Tiddy *J. Chem. Soc., Dalton Trans.*, 1995, 1769.
7 D. W. Bruce, J. D. Holbrey, A. R. Tajbakhsh and G. J. T. Tiddy, *J. Mater. Chem.*, 1993, **3**, 905.
8 We thank Johnson Matthey for letting us have sight of these results.
9 The catalytic reactions were performed in a PEEK-lined high pressure reactor (Cambridge Reactor Design) equipped with a stirrer and liquid sampling valve (for withdrawing samples under pressure to evaluate kinetics). In a typical reaction the autoclave was charged with *ca.* 50 g of hex-1-ene and the activated catalyst (*ca.* 20 mg, heated in vacuum at 463 K for 4 h) was directly introduced into the reactor without exposing it to air. The reactor was then pressurised with H_2 to 20 bar and heated to 373 K. Samples were periodically withdrawn without perturbing the pressure in the reactor and analysed by GC using 1,2-dichlorobenzene as the internal standard; a typical mass-balance showed minimal sample loss.
10 Apart from *n*-hexane, isomerised products, namely *cis*-and *trans*-hex-2-ene and small amounts *trans*-hex-3-ene were obtained when Cu_4Ru_{12}, Ag_4Ru_{12} or Pd_6Ru_6 were employed as catalysts for the hydrogenation of hex-1-ene (see ref. 4). There is no detectable thermocracking.
11 D. S. Shephard, T. Maschmeyer, B. F. G. Johnson, J. M. Thomas, G. Sankar, D. Ozkaya, W. Zhou and R. D. Oldroyd, *Angew. Chem., Int. Ed Engl.*, 1997, **36**, 2242.
12 The catalytic performance of the Ag_4Ru_{12} and Cu_4Ru_{12} catalysts was also evaluated under identical conditions, hence meaningful comparisons of TOF may be made.

Communication 9/06087A

Columnar mesophases from tetrahedral copper(I) cores and Schiff-base derived polycatenar ligands

Laurent Douce,[a] Abdelkrim El-ghayoury,[a] Antoine Skoulios[b] and Raymond Ziessel*[a]

[a] *Laboratoire de Chimie, d'Electronique et de Photonique Moléculaires, Ecole Européenne de Chimie, Polymères et Matériaux, Université Louis Pasteur, ESA 7008 au CNRS, 25 rue Becquerel, F-67087 Strasbourg Cedex 2, France. E-mail: ziessel@chimie.u-strasbg.fr*

[b] *Groupe de Matériaux Organiques, IPCMS, UMR 7504 au CNRS, 23 rue du Loess, F-67037 Strasbourg Cedex , France*

Received (in Basel, Switzerland) 26th May 1999, Accepted 1st September 1999

In the presence of copper(I), certain di- and tri-topic ligands derived from reaction of substituted anilines with 2-pyridinecarbaldehyde or 2,6-pyridinedicarbaldehyde form a new type of polycatenar metallomesogen around the tetrahedral metallic centre.

Metal complexes derived from Schiff-bases are known to form a large variety of molecular architectures, ranging from macrocyclic helicates to infinite coordination polymers.[1,2] In particular, 2-iminopyridines, readily formed *via* reversible reaction between an (achiral or chiral) amine and an appropriate aldehyde, are attractive building blocks for assembling intricate supramolecular species[3] and active polymerization catalysts.[4,5] These ligands can display unusual binding behaviour towards certain cations, leading to the formation of highly stable metallohelicates.[6] The main advantage of such ligands, however, relates to the availability of a free imino site that can be functionalized with a wide variety of appendages. Indeed, the structural attributes provided by 2-iminopyridines look highly promising for the assembly of metallomesogens by attaching flexible paraffinic tails and subsequent rigidification of the head-group by complexation with copper(I) cations. It is worth noting that silver complexes constructed from polycatenar scaffoldings and which exhibit columnar liquid-crystalline mesophases have previously been studied.[7]

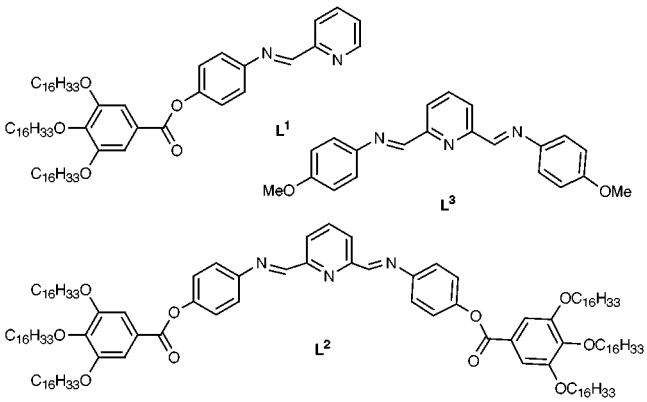

Ligands L^1 and L^2 were prepared in 99 and 86% isolated yield, respectively by refluxing 2-formylpyridine or 2,6-diformylpyridine and the corresponding aniline[8] in ethanol containing a trace amount of acetic acid. Each ligand has a well defined melting point at 58 °C (L^1) on 56 °C (L^2). Ligand L^3, which serves as a reference compound, was synthesized by a similar route and has a melting point of 159 °C.

Reaction of either ligand in dichloromethane with 0.5 equiv. of $[Cu(MeCN)_4]BF_4$ leads to immediate formation of a deep-red colouration indicative of complexation of copper(I) to four nitrogen donor ligands[9] {λ_{max} = 505, 500 (sh) and 500 (sh) nm with ε = 5100, 2600 and 3000 dm^3 mol^{-1} cm^{-1}, respectively for $[Cu(L)^n)_2]BF_4$ (n = 1–3) **1**–**3**}. Mass spectrometry is consistent with the isolated products being monomeric without contamination from polynuclear structures. These products, therefore, may be assigned the general formula $[Cu(L^n)_2]BF_4$.† A schematic representation of the complexes and a computer generated CPK model of one of the structures is shown in Fig. 1.

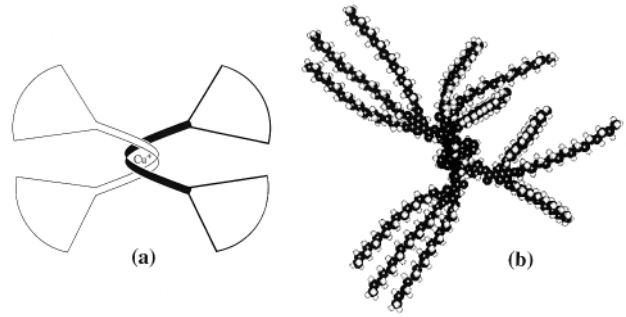

Fig. 1(a) Idealized pictoral representation of complex **2** representing the disk-shape and (b) CPK energy-minimised conformation.

Direct involment of the terminal imino groups in the coordination sphere was confirmed by solid-state and solution-phase FTIR studies and by both ^{1}H and ^{13}C NMR spectroscopy. The NMR studies also indicate that the two ligands bound to Cu(I) are equivalent while the relatively broad signals belonging to the aromatic protons, together with a broad imine signal (for complexes **1** and **2**) are attributed to a fast exchange process between coordinated and free imino N atoms. Similar internal flexibility has been observed previously for related macrocyclic[10] and terpyridine[11] based copper(I) complexes. Solid state FTIR studies of complex **2** reveal the presence of two imino stretching vibrations; one lying close to that of the free ligand ($\nu_{C=N}$ 1626 cm^{-1}) and the second occurring at lower frequency ($\nu_{C=N}$ = 1588 cm^{-1}) owing to coordination to the metal centre. X-Ray crystallography made for a single crystal of complex **3** indicates that two L^3 ligands are wrapped around a single copper cation, each ligand being coordinated *via* a pyridine-imine fragment, while the pendant imino arm is directed away from the metal centre in a *trans* configuration (Fig. 2).‡

It is noteworthy that, despite the *cis* arrangment of the coordinated py-CH=N- fragment and the *trans* conformation of the uncoordinated imino subunit, the overall ligand adopts an almost planar structure. The four-coordinate copper(I) cation shows Cu–N(py) and Cu–N(imine) distances of *ca* 2.085 and 2.021 Å, respectively with chelate bite angles of 81.6 and 81.1°. The uncoordinated imino fragment lies *ca.* 4.706 Å from the cation. There is obvious distortion around the metallic centre that might explain why the molecule stacks into columns, favouring a liquid-crystalline phase (*vide infra*), a situation which is also clearly observed in the CPK energy-minimised conformation [Fig. 1(*b*)].

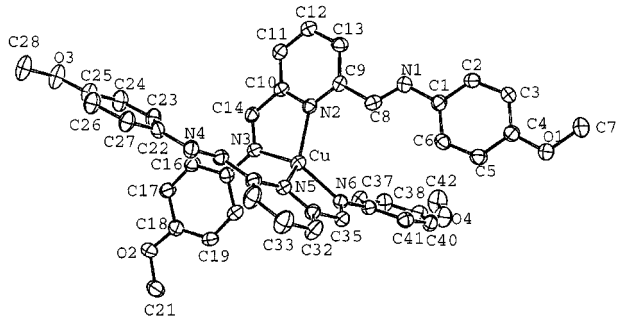

Fig. 2 ORTEP view of complex **3** showing 50% probability thermal ellipsoids. The hydrogen atoms are omitted for clarity.

Although non-mesomorphic themselves, ligands L^1 and L^2 produce thermotropic liquid-crystalline complexes when co-ordinated to copper(I), as demonstrated by differential scanning calorimetry (DSC) and polarizing optical microscopy (POM). The DSC thermograms of **2**, recorded from 20 to 130 °C, contain two sharp peaks, each of which indicates a reversible first-order phase transition. The peak at 49 °C (ΔH = 149.2 kJ mol^{-1}) corresponds to melting of the crystal into a liquid-crystalline phase whereas the peak at 117 °C (ΔH = 3.1 kJ mol^{-1}) can be attributed to clearing of the liquid crystal into an isotropic melt (values are given for the third cycle). The high stability of complex **2** was demonstrated by the absence of significant perturbation of the DSC patterns following several heating–cooling cycles. The optical textures observed for **2** during slow cooling from the isotropic melt are typical of a columnar phase (with pseudo focal-conic textures). This birefringent texture is maintained at room temperature. In contrast, complex **1** melts into the liquid crystal phase at 48 °C (ΔH = 84.6 kJ mol^{-1}) and has a clearing point at 75 °C (ΔH = 10.3 kJ mol^{-1}), but only on the first heating stage. It appears, therefore, that complex **1** is thermally unstable, a feature not entirely unexpected in view of the lack of substituents at the 6-position.

The columnar structure of the liquid crystal phases of **1** and **2** was confirmed by X-ray diffraction studies. It is seen that the rigid aromatic units that comprise the core of the pseudo-tetrahedral copper(I) complexes are superposed on top of one another and embedded in a disordered matrix provided by the molten alkyl chains. These columns are packed laterally into a two-dimensional hexagonal unit cell having parameters of 60 and 47 Å for **1** and **2**, respectively as measured at 60 °C from the small-angle reflection. The larger value found for **1** suggests that a 'phosmidic-type' of columnar mesophase is formed (where several individual molecules aggregate to form a disk), whereas for **2** the individual molecules stack one on top of the other to form columns as in conventional discoid liquid crystalline material.

Liquid crystals obtained from purely organic molecules comprising a tetrahedral carbon atom substituted with four semi-rigid subunits bearing flexible terminal alkyl chains have been reported.[12] However, complexes **1** and **2** are, to the best of our knowledge, the first examples of metallomesogens built around a single tetrahedral metal cation. Many unsuccessful attempts to engineer such metallomesogens have been attempted in the past.[13,14] As such, these materials differ markedly from the liquid-crystalline metallohelicate built around a central binuclear copper(I) helicate.[15] It should be stressed that the 2-iminopyridine moiety is readily amenable for systematic investigation of how the length and number of appended alkyl chains influence the liquid-crystalline properties, especially melting temperature, and to establish the structural and thermodynamic factors that assembles the aromatic cores into columns. Such information, which is critical for a proper theoretical description of metallomesogens, is not yet available for any liquid-crystalline material. We are well aware that the polycatenar ligand L^2 is an attractive substrate for reaction with metal cations that favour octahedral coordination geometries.

We thank Professor Anthony Harriman for his critical review of the manuscript and for the energy-mimimised structure and Dr. Benoît Heinrich (IPCMS) for fruitful and helpful discussions.

Notes and references

† Full synthetic details will be given elsewhere. All new compounds were authenticated by NMR, FTIR, MS and elemental analyses (required values in parentheses). *Selected data*: **L¹**: $\delta_{C=N}$ 8.64 ($CDCl_3$); $\nu_{C=N}$ 1626 cm^{-1} (KBr pellet, FAB$^+$ *m/z* 1023.3 [M + H]$^+$, C, 78.59 (78.62), H, 10.62 (10.83), N, 2.57 (2.74%). **L²**: $\delta_{C=N}$ 8.72 ($CDCl_3$), $\nu_{C=N}$ 1626 cm^{-1} (KBr pellet); FAB$^+$ *m/z* 1967.3 [M + H]$^+$, C, 78.43 (78.72), H, 10.53 (11.01), N, 1.99 (2.13%). **1**: 92% yield; $\delta_{C=N}$ 9.18 ($CDCl_3$); $\nu_{C=N}$ 1589 cm^{-1} (KBr pellet); FAB$^+$ *m/z* 2109.2 [M-BF_4]$^+$, C, 72.98 (73.24), H, 9.73 (10.09), N, 2.23 (2.55%). **2**: 98% yield; $\delta_{C=N}$ 8.79 ($CDCl_3$); $\nu_{C=N}$, 1626, 1588 cm^{-1} (KBr pellet); FAB$^+$ *m/z* 3996.8 [M −BF_4]$^+$, C, 75.12 (75.50); H, 10.21 (10.61); N, 1.53 (2.05%, calculated with one water molecule).

‡ *Crystal data* for **3**: $C_{42}H_{38}N_6O_4Cu{\bullet}2BF_4{\bullet}H_2O{\bullet}CH_2Cl_2$, *M* = 1785.26, triclinic, space group $P\bar{1}$, red crystals, *a* = 12.6180(7), *b* = 13.075(1), *c* = 13.783(1) Å, α = 84.437(9), β = 80.643(9), γ = 70.631(9), *V* = 2114.4 Å^3, *Z* = 1, μ = 0.645 mm^{-1}. Data were collected on a Kappa CCD diffractometer (graphite Mo-Kα radiation, λ = 0.71073 Å) at −100 °C. 15930 reflections collected ($2.5 \leq 2\theta \leq 26.36°$), 4186 data with $I > 3\sigma(I)$. The structure was solved using the Nonius OpenMoleN[16] package and refined by full-matrix least squares with anisotropic thermal parameters for all non-hydrogen atoms except for the solvent molecules (the latter are disordered). Final results: $R(F)$ = 0.079, $wR(F)$ = 0.105, GOF = 1.189, 542 parameters. CCDC 182/1402.

1 S. Brooker, R. J. Kelly and P. Plieger, *Chem. Commun*., 1998, 1079.
2 P. K. Bowyer, K. A. Porter, A. D. Rae, A. C. Willis and S. B. Wild, *Chem. Commun*., 1998, 1153.
3 M. J. Hannon, C. L. Painting, A. Jackson, J. Hamblin and W. Errington, *Chem. Commun*., 1997, 1807.
4 D. M. Haddleton, D. J. Duncalf, D. Kukulj, A. M. Heming, A. J. Shooter and A. J. Clark, *J. Mater. Chem.*, 1998, **8**, 1525.
5 G. J. P. Britovsek, V. C. Gibson, B. S. Kimberley, P. J. Maddox, S. J. Mctavish, G. A. Solan, A. J. P. White and D. J. Williams, *Chem. Commun*., 1998, 849.
6 R. Ziessel, A. Harriman, J. Suffert, M.-T. Youinou, A. De Cian and J. Fischer, *Angew. Chem., Int. Ed. Engl.* 1997, **36**, 2509.
7 B. Donnio and D. W. Bruce, *J. Mater. Chem.*, 1998, **8**, 1993; *New J. Chem.*, 1999, 275.
8 H.-T. Nguyen, C. Destrade and J. Malthête, *Adv. Mater*., 1997, **9**, 375.
9 A. Juris and R. Ziessel, *Inorg. Chim. Acta*, 1994, **225**, 251.
10 R. Ziessel and M.-T. Youinou, *Angew. Chem., Int. Ed. Engl*., 1993, **32**, 877.
11 A. El-ghayoury, A. Harriman, A. De Cian, J. Fischer and R. Ziessel, *J. Am. Chem. Soc*., 1998, **120**, 9973.
12 J. Malthête, *New J. Chem.*, 1996, **20**, 925.
13 A. Pegenau, T. Hegmann, C. Tschierske and S. Diele, *Chem. Eur. J*., 1999, **5**, 1643.
14 B. Donnio and D. W. Bruce, *Struct. Bonding* (*Berlin*), 1999, **95**, 193.
15 A. El-ghayoury, L. Douce, A. Skoulios and R. Ziessel, *Angew. Chem., Int. Ed.*, 1998, **37**, 2205.
16 OpenMoleN, Interactive Structure Solution, Nonius B. V., Delft, The Netherlands, 1997.

Communication 9/04245H

ChemComm

Convergent synthesis of the IJKLM ring fragment of ciguatoxin CTX3C

Tohru Oishi, Yoko Nagumo, Mitsuru Shoji, Jean-Yves Le Brazidec, Hisatoshi Uehara and Masahiro Hirama*

Department of Chemistry, Graduate School of Science, Tohoku University, and CREST, Japan Science and Technology Corporation (JST), Sendai 980-8578, Japan. E-mail: hirama@ykbsc.chem.tohoku.ac.jp

Received (in Cambridge, UK) 23rd August 1999, Accepted 7th September 1999

The IJKLM ring fragment of CTX3C, an important member of the ciguatoxin family, was synthesized *via* ring-closing metathesis using the Tebbe reagent and an improved method of reductive hydroxy ketone cyclization.

Ciguatoxin (CTX1B, **1**) and its congeners, CTX3C (**2**) and **3**, are the causative toxins of ciguatera seafood poisoning prevalent in the tropics and subtropics.[1] Although numerous synthetic studies have been reported because of the striking structure and biological activity of these compounds, efficient synthetic methods are still needed for total synthesis. During the course of our synthetic studies directed toward **1**,[2] we recently succeeded in synthesizing the ABCDE ring framework of **1** based on alkylation and ring-closing metathesis (RCM).[3] We describe herein a convergent synthesis of the IJKLM ring fragment of **2**.

Two synthetic routes were envisaged as outlined in Scheme 1. Tebbe reagent mediated transformation[4] of ester **8** (or **9**) into cyclic enol ethers **6** (or **7**), followed by hydroboration–oxidation and reductive hydroxy ketone cyclization protocol[5] provides the IJKLM ring system.

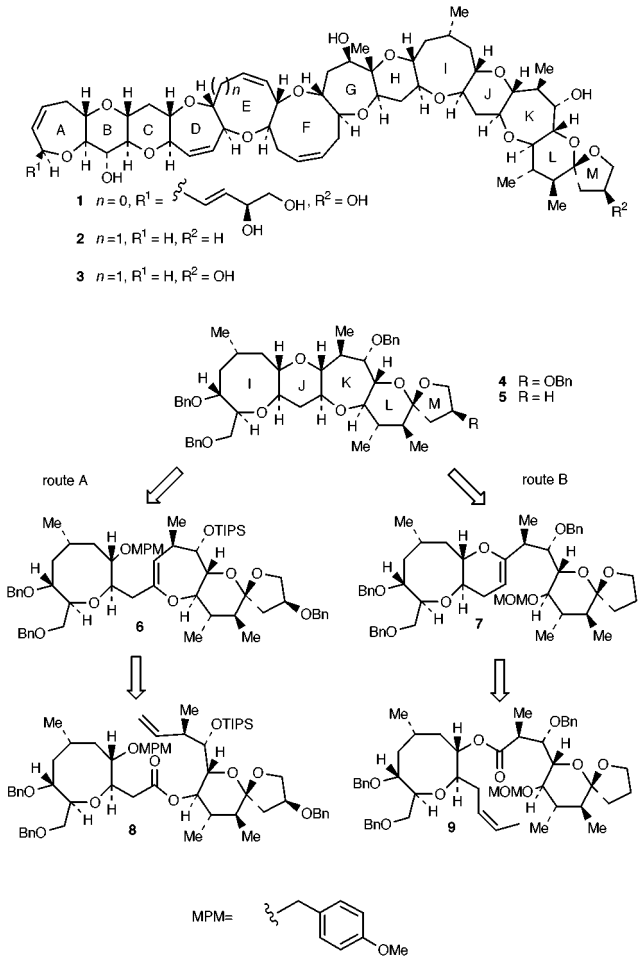

Scheme 1

Precursors of the esters **8** and **9** were synthesized as shown in Scheme 2. Carboxylic acid **11** and alcohol **12** were prepared from the I ring moiety **10**[6,7] by the standard procedures. Synthesis of the carboxylic acid **19** corresponding to the LM ring moiety of **2** was initiated with **13**.[8] Hydroboration of **13** using BBN and treatment of the resulting alcohol with CSA gave spiroacetal **14** in 92% yield. Conventional protecting group transformation of **14** yielded alcohol **16**. Dess–Martin periodinane oxidation of **16** followed by asymmetric crotylation using (*R*,*R*,*Z*)-crotylboronate **17**[9] furnished **18** as a single stereoisomer. Protection of the hydroxy group of **18** as a benzyl ether and oxidative cleavage of the double bond gave **19** in 95% yield. Alcohol **20** corresponding to the LM ring moiety of **1** and **3** was synthesized in an analogous manner starting from **15**.[8]

Synthesis of the IJKLM ring fragment was first attempted *via* route A (Scheme 3). Condensation of **11** with **20** using DCC gave **8** in 54% yield, which was treated with the Tebbe reagent in THF at 60 °C. However, olefination of the carbonyl group of **8** did not proceed, and only the initial material **8** was recovered even after 6 h.

The alternative route B was then examined. Coupling of **12** with **19** gave **9** in 74% yield. In contrast to **8**, treatment of **9** with

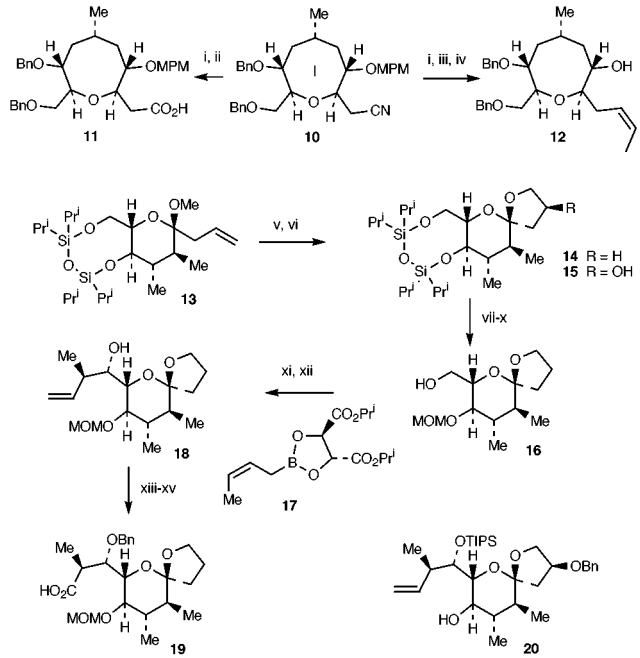

Scheme 2 *Reagents and conditions*: i, DIBAL-H, CH_2Cl_2, −78 °C; ii, $NaClO_2$, NaH_2PO_4, 2-methylbut-2-ene, Bu^tOH, H_2O, 41% (2 steps); iii, $Ph_3P^+EtBr^-$, BuLi, THF, −78 °C to room temp., 48% (*Z*:*E* = 4:1, 21% recovery of aldehyde); iv, DDQ, CH_2Cl_2, H_2O, 0 °C, 89%; v, BBN, THF then NaOH, H_2O_2, 88%; vi, CSA, CH_2Cl_2, 92%; vii, TBAF, THF; viii, Bu^tCOCl, Et_3N, CH_2Cl_2, 0 °C to room temp.; ix, MOMCl, Pr^i_2EtN, CH_2Cl_2, 0 to 35 °C; x, $LiAlH_4$, Et_2O, 0 °C to room temp., 76% (4 steps); xi, Dess–Martin periodinane, CH_2Cl_2: xii, **17**, toluene, MS4A, −78 to −60 °C, then $NaBH_4$, −60 to 0 °C, 45% (2 steps, 70% based on recovery of **16**); xiii, NaH, BnBr, THF, DMF, 89%; xiv, OsO_4, NMO, Bu^tOH, H_2O, then $NaIO_4$, pH 7 buffer; xv, $NaClO_2$, NaH_2PO_4, 2-methylbut-2-ene, Bu^tOH, H_2O, 95% (2 steps).

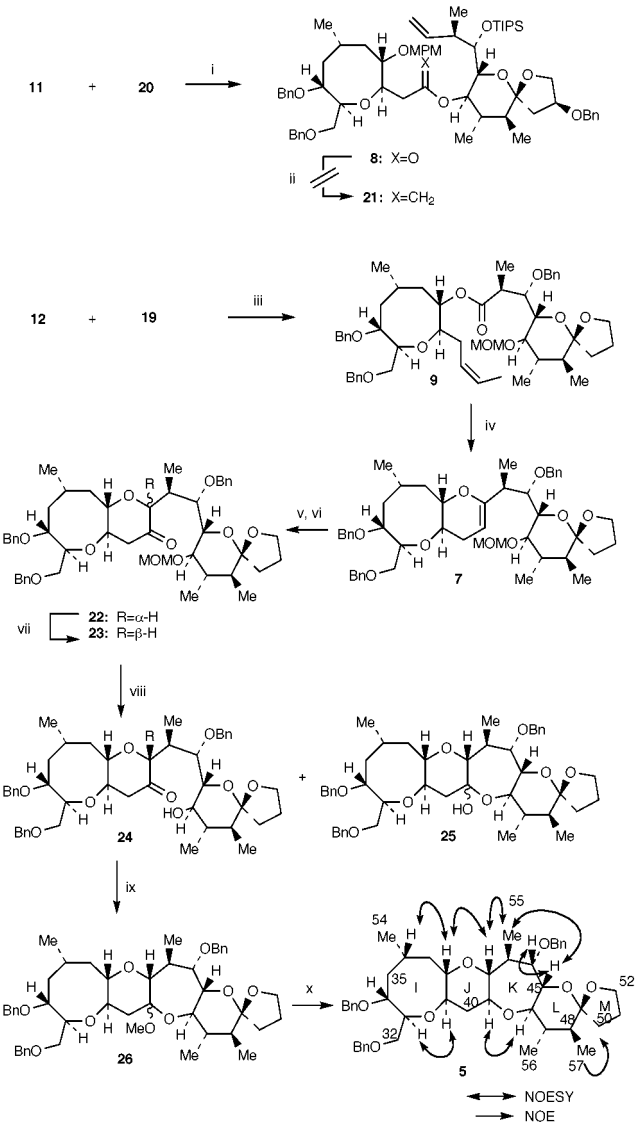

Scheme 3 *Reagents and conditions*: i, DCC, DMAP, CSA, CH_2Cl_2, 35 °C, 54% (38% recovery of **20**); ii, Tebbe reagent, THF, 60 °C, 95% recovery of **8**; iii, DCC, DMAP, CSA, CH_2Cl_2, 35 °C, 74%; iv, Tebbe reagent, THF, 60 °C, 63%; v, BH_3, THF, 0 °C then NaOH, H_2O_2, 0 °C, 73%; vi, Dess–Martin periodinane, CH_2Cl_2, 100%; vii DBU, CH_2Cl_2, room temp., 1 h; viii, TMSBr, CH_2Cl_2, −78 to −50 °C, **24**: 30%, **25**: 30%; ix, $CH(OMe)_3$, CSA, benzene, 70 to 80 °C, 50%; x, Et_3SiH, $BF_3{\cdot}OEt_2$, CH_2Cl_2, −73 to 0 °C, 71%.

the Tebbe reagent at 60 °C resulted in the formation of cyclic enol ether **7** in 63% yield *via* methylenation and subsequent RCM.[4] Hydroboration of **7** followed by Dess–Martin periodinane oxidation gave a separable 3:1 mixture of **22** and **23** in 73% yield. The undesired isomer **22** was effectively converted to a 1:1 mixture of **22** and **23** by treatment with DBU in CH_2Cl_2 at room temperature. Removal of the MOM group of **23** with TMSBr gave keto alcohol **24** (30%) and hemiacetal **25** (30%). Direct treatment of the mixture of **24** and **25** with Et_3SiH–TMSOTf[5] gave no products due to reductive hydroxy ketone cyclization. However, reduction of the corresponding methyl acetal[3] **26**, which was prepared from the mixture of **24** and **25**, proceeded stereoselectively using $BF_3{\cdot}OEt_2$ (1.0 equiv.) and Et_3SiH in excess to afford the IJKLM ring fragment **5** in 71% yield without affecting the spiroacetal LM ring moiety.[10] The stereochemistry of **5** was unambiguously determined by ^1H NMR analysis (NOESY and NOE experiments).[11]

In conclusion, we have established a highly convergent route to the IJKLM ring fragment of CTX3C *via* the Tebbe reagent mediated ring-closing metathesis and an improved hydroxy ketone cyclization. Further studies directed toward total synthesis of ciguatoxins are currently in progress in our laboratory.

Fellowships to Y. N. and J.-Y. L. B. from the Japanese Society for the Promotion of Science are gratefully acknowledged.

Notes and references

1 M. Murata, A. M. Legrand, Y. Ishibashi, M. Fukui and T. Yasumoto, *J. Am. Chem. Soc.*, 1990, **112**, 4380; M. Satake, M. Murata and T. Yasumoto, *Tetrahedron Lett.*, 1993, **34**, 1975; M. Satake, A. Morohashi, H. Oguri, T. Oishi, M. Hirama, N. Harada and T. Yasumoto, *J. Am. Chem. Soc.*, 1997, **119**, 11 325; M. Satake, M. Fukui, A. M. Legrand, P. Cruchet and T. Yasumoto, *Tetrahedron Lett.*, 1998, **39**, 1197.

2 T. Suzuki, O. Sato, M. Hirama, Y. Yamamoto, M. Murata, T. Yasumoto and N. Harada, *Tetrahedron Lett.*, 1991, **32**, 4505; H. Oguri, S. Hishiyama, T. Oishi and M. Hirama, *Synlett*, 1995, 1252; H. Oguri, S. Hishiyama, O. Sato, T. Oishi, M. Hirama, M. Murata, T. Yasumoto and N. Harada, *Tetrahedron*, 1997, **53**, 3057; T. Oishi, Y. Nagumo and M. Hirama, *Synlett*, 1997, 980; T. Oishi, Y. Nagumo and M. Hirama, *Chem. Commun.*, 1998, 1041; H. Oguri, S.-Y. Sasaki, T. Oishi and M. Hirama, *Tetrahedron Lett.*, 1999, **40**, 5405; H. Oguri, S.-I. Tanaka, S. Hishiyama, T. Oishi, M. Hirama, T. Tumuraya, Y. Tomioka and M. Mizugaki, *Synthesis*, in the press. For recent synthetic studies of other groups, see: T. Oka and A. Murai, *Tetrahedron*, 1998, **54**, 1; T. Oka, K. Fujiwara and A. Murai, *Tetrahedron*, 1998, **54**, 21; M. Inoue, M. Sasaki and K. Tachibana, *Angew. Chem., Int. Ed.*, 1998, **37**, 965; M. Sasaki, T. Noguchi and K. Tachibana, *Tetrahedron Lett.*, 1999, **40**, 1337; S. Hosokawa and M. Isobe, *J. Org. Chem.*, 1999, **64**, 37; R. Saeeng and M. Isobe, *Tetrahedron Lett.*, 1999, **40**, 1911.

3 K. Maeda, T. Oishi, H. Oguri and M. Hirama, *Chem. Commun.*, 1999, 1063.

4 K. C. Nicolaou, M. H. D. Postema and C. F. Claiborne, *J. Am. Chem. Soc.*, 1996, **118**, 1565; K. C. Nicolaou, M. H. D. Postema, E. W. Yue and A. Nadin, *J. Am. Chem. Soc.*, 1996, **118**, 10 335; J. S. Clark and J. G. Kettle, *Tetrahedron Lett.*, 1997, **38**, 123; J. S. Clark and J. G. Kettle, *Tetrahedron Lett.*, 1997, **38**, 127; J. D. Rainier and S. P. Allwein, *J. Org. Chem.*, 1998, **63**, 5310; J. S. Clark and J. G. Kettle, *Tetrahedron*, 1999, **55**, 8231.

5 K. C. Nicolaou, C.-K. Hwang and D. A. Nugiel, *J. Am. Chem. Soc.*, 1989, **111**, 4136; K. C. Nicolaou, K. R. Reddy, G. Skokotas, F. Sato, X.-Y. Xiao and C.-K. Hwang, *J. Am. Chem. Soc.*, 1993, **115**, 3558; K. C. Nicolaou, C.-K. Hwang, M. E. Duggan, D. A. Nugiel, Y. Abe, K. B. Reddy, S. A. DeFrees, D. R. Reddy, R. A. Awartani, S. R. Conley, F. P. J. T. Rutjes and E. A. Theodorakis, *J. Am. Chem. Soc.*, 1995, **117**, 10 227; E. Alvarez, R. Pérez, M. Rico, R. M. Rodríguez and J. D. Martín, *J. Org. Chem.*, 1996, **61**, 3003.

6 T. Oishi, M. Shoji, K. Maeda, N. Kumahara and M. Hirama, *Synlett*, 1996, 1165; T. Oishi, K. Maeda and M. Hirama, *Chem. Commun.*, 1997, 1289; T. Oishi, M. Maruyama, M. Shoji, K. Maeda, N. Kumahara, S.-I. Tanaka and M. Hirama, *Tetrahedron*, 1999, **55**, 7471.

7 The concise route to **10** *via* RCM has been recently developed: T. Oishi, M. Kosaka and M. Hirama, unpublished results.

8 T. Oishi, M. Shoji, N. Kumahara and M. Hirama, *Chem. Lett.*, 1997, 845.

9 W. R. Roush, K. Ando, D. B. Powers, A. D. Palkowitz and R. L. Halterman, *J. Am. Chem. Soc.*, 1990, **112**, 6339.

10 Excess amount of $BF_3{\cdot}OEt_2$ caused reductive opening of the spiroacetal.

11 *Selected data* for **5**: δ_H (600 MHz, $CDCl_3$) 0.89 (3H, d, *J* 6.3, Me57), 1.02 (3H, d, *J* 6.0, Me56), 1.08 (3H, d, *J* 7.1, Me54), 1.11 (3H, d, *J* 7.7, Me55), 1.41 (1H, br q, *J* 11.7, H40$_{ax}$), 1.50–1.57 (2H, m, H48, H47), 1.63 (1H, br dt, *J* 14.2, 10.2, H37), 1.68 (1H, br ddd, *J* 15.2, 9.5, 6.4, H35), 1.73–1.81 (2H, m, H51, H50), 1.83–1.88 (1H, m, H37), 1.90–1.98 (4H, m, H50, H36, H35, H51), 2.15 (1H, qdd, *J* 7.7, 4.6, 3.5, H43), 2.40 (1H, br dt, *J* 12.0, 4.8, H40$_{eq}$), 2.87 (1H, dd, *J* 9.3, 4.6, H42), 3.06 (1H, br td, *J* 9.6, 3.0, H38), 3.23 (1H, ddd, *J* 11.3, 9.0, 4.4, H39), 3.35 (1H, t, *J* 9.5, H46), 3.41 (1H, br td, *J* 9.2, 2.8, H34), 3.43 (1H, br dd, *J* 3.5, 1.0, H44), 3.44 (1H, dd, *J* 10.0, 6.5, H32), 3.60 (1H, br ddd, *J* 9.3, 6.5, 2.1, H33), 3.64 (1H, dd, *J* 9.5, 1.0, H45), 3.68 (1H, dd, *J* 10.0, 2.1, H32), 3.75 (1H, br q, *J* 7.5, H52), 3.82 (1H, ddd, *J* 11.2, 9.3, 5.0, H41), 3.87 (1H, br td, *J* 7.8, 4.5, H52), 4.32 (1H, d, *J* 11.1, CH_2Ph), 4.55 (2H, s, CH_2Ph), 4.58 (1H, d, *J* 11.1, CH_2Ph), 4.63 (1H, d, *J* 12.2, CH_2Ph), 4.68 (1H, d, *J* 12.2, CH_2Ph), 7.20–7.40 (15H, m, Ph); MALDI-TOF MS calc. for $C_{46}H_{60}O_8Na$ ($M+Na^+$) 763.4186, found 763.4151.

Communication 9/06834A

ChemComm

A novel pyridine-templated open framework gallophosphate

David S. Wragg, Ivor Bull, Gary B. Hix and Russell E. Morris*

School of Chemistry, University of St. Andrews, St. Andrews, Fife, Scotland, UK KY16 9ST.
E-mail: rem1@st-and.ac.uk

Received (in Oxford, UK) 9th August 1999, Accepted 10th September 1999

A new type of gallium phosphate open framework material has been prepared from solvothermal synthesis and its structure solved using microcrystal X-ray diffraction at a synchrotron source.

The rational design of open framework materials is an established goal of materials science.[1] The potential uses for rationally designed molecular sieves are many, but of particular interest are the applications of such materials as shape selective catalysts for fine chemical synthesis. Within this area the study of gallium phosphates has provided a wide range of interesting new open framework structures, including Cloverite,[2] which has the largest pore size of any microporous material. The work of Férey has illustrated particularly well the structural richness of the gallophosphate system.[3]

The most common methods of preparing open framework materials use templating and the cross-linking of layered materials. Templating involves the use of an organic molecule to organise the inorganic framework into an open structure, while cross-linked materials consist of layers that are joined together so as to produce voids and cavities in the interlayer region. This paper reports the synthesis of a new open framework gallium phosphate material which contains features of both of these types of structures; layers of open zeolite-like structure linked to form a completely novel type of open framework architecture with interconnecting eight membered ring channels. The new material is templated by pyridine.

In the course of a systematic study of the effects of various conditions on the product of a solvothermal gallium phosphate synthesis in which pyridine serves as both solvent and template, a novel type of open framework gallium phosphate structure has been prepared. The new material, pyridine-GaPO-1 [formula: $Ga_6(PO_4)_6F_2{\cdot}2C_5H_6N{\cdot}H_2O$], was prepared by a solvothermal synthesis with pyridine (99%, Fischer) as the solvent and hydrofluoric acid (70% solution in pyridine) as a source of fluoride ions. Phosphoric acid (0.2 g, 85% weight aqueous solution, Aldrich) was diluted with a small amount (2 ml) of distilled water in a plastic beaker and to this pyridine (0.8 ml) was added with vigorous stirring. Ground gallium sulfate (0.5 g, 99.8%, Aldrich) was then added, followed by hydrofluoric acid (*ca.* 0.02 ml) giving an approximate molar oxide ratio of Ga_2O_3: P_2O_5: F: 8 pyridine: 8 H_2O. The mixture (pH 5) was stirred at room temperature for 20 min, transferred to a Teflon-lined stainless steel autoclave and heated at 180 °C for 72 h. The product, a crop of tiny colourless crystals, was recovered by suction filtration, washed with distilled water and acetone and dried at room temperature.

The crystal size (max. 20 × 20 × 8 μm) proved too small for single crystal data collection on a conventional laboratory four circle diffractometer, so data were collected using a Bruker AXS SMART CCD area-detector at the high-flux microcrystal diffraction facility (station 9.8) of the SRS at Daresbury using a wavelength of 0.6849 Å.†

The structure can be thought of as consisting of two parts. The first is a zeolite-related layer made up of $Ga_2P_2O_8$ single four-rings (S4Rs). These S4Rs are linked together to form a layer that contains eight-ring windows. When viewed parallel to the (11$\bar{1}$) direction (Fig. 1), the structure closely resembles that of the zeolite ABW,[4] which is comprised of eight-rings linked by four-rings. This topology has also been observed for a number of other zeolites and zeolite analogues.[5] All of the gallium and phosphorus atoms in layered regions of the structure are tetrahedrally coordinated to four oxygen atoms, and the gallium and phosphorus atoms alternate. These zeolite-like layers are linked into a three-dimensional structure by cross-linking units consisting of a dimeric unit of octahedrally coordinated gallium atoms. The two gallium-centred polyhedra share the two fluorine atoms that make one edge of the octahedra to give a unit with the formula $Ga_2F_2O_8$. The overall structure consists of a three-dimensional framework with interconnecting eight-ring channels (Fig. 2) formed by the linking of the layers, producing pores that run parallel to the plane of the layers, and by the zeolitic nature of the layers themselves, which stack on top of each other to form channels perpendicular to the plane of the layers (Fig. 3). The $Ga_2F_2O_8$ unit causes half of the eight-ring channels to be distorted to an almost circular shape, while the others maintain the oval form normally observed in gallium phosphates. The dimeric $Ga_2F_2O_8$

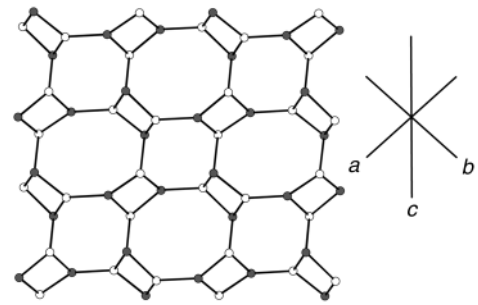

Fig. 1 A view of the zeolite-like layers parallel to the (11$\bar{1}$) direction illustrating the system of eight-rings connected by four-rings. The gallium and phosphorus atoms are shown as open and shaded spheres, respectively. The oxygen atoms would then be placed near the centres of the lines joining the Ga and P atoms.

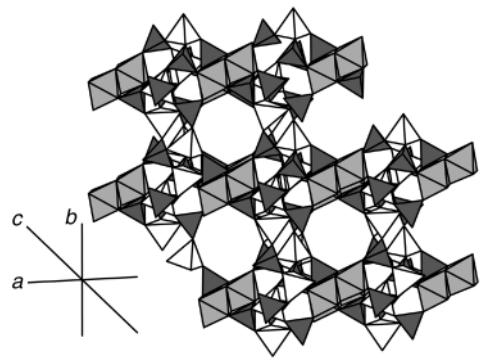

Fig. 2 Polyhedral view of the inorganic framework parallel to the (11$\bar{1}$) direction showing the linking of the layers by the $Ga_2F_2O_8$ dimer and the channels produced that run parallel to this direction. The layers run vertically up the diagram. Template molecules are not shown. The shaded and unshaded tetrahedra are PO_4 and GaO_4, respectively, and the $Ga_2F_2O_8$ unit is shown as lightly shaded edge sharing octahedra.

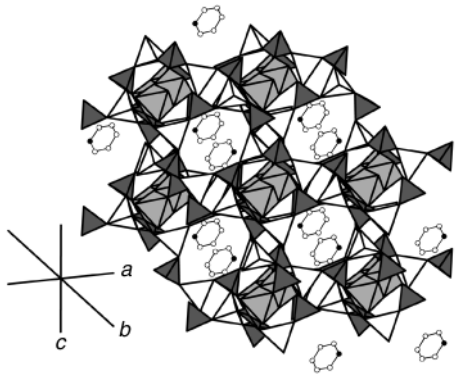

Fig. 3 Polyhedral view parallel to the $(11\bar{1})$ direction showing the eight-ring channels produced by the stacking of the zeolite layers. Also shown is the position of the pyridine template molecules inside these channels. The shaded and unshaded tetrahedra are PO_4 and GaO_4 respectively, and the $Ga_2F_2O_8$ unit is shown as lightly shaded edge sharing octahedra. The nitrogen atoms are shown as shaded spheres and the carbons as unshaded spheres.

unit found linking the layers has not been observed previously in this type of material but the linking of layers into a 3D structure is similar to that observed in the previously reported cyclam-GaPO material,[6] in which an octahedral gallium–cyclam complex joins layers of double four-ring units.

The pyridine template is protonated and hydrogen bonded to a solvent water molecule, which is disordered over two crystallographic sites. The strong binding of this water molecule is illustrated by thermogravimetric analysis, which shows a mass loss corresponding to the loss of water at around 250 °C (observed 1.2%; calculated 1.5%). A second mass loss corresponding to loss of pyridine occurs between 330 and 360 °C (observed 13.0%; calculated 13.3%). The material loses crystallinity at this temperature.

The authors would like to thank Dr David Taylor and Dr Simon Teat of the SRS for their help in the X-ray data collection and the EPSRC for funding. R. E. M. would like to thank the Royal Society for provision of a Personal Research Fellowship.

Notes and references

† *Crystal data* for $Ga_6(PO_4)_6F_2{\cdot}2C_5H_6N{\cdot}H_2O$: M = 1204.38, triclinic, space group $P\bar{1}$ (no. 2), a = 11.391(4), b = 12.414(3), c = 12.846(4) Å, α = 71.04(3), β = 68.39(2), γ = 66.88(2)°, U = 1518.3(8) Å^3, T = 150 K, D_c = 2.630 g cm^{-3}, Z = 2, μ(Mo-Kα) = 5.682 mm^{-1}, 7704 reflections measured, 7319 observed (R_{int} = 0.029) which were used in all calculations. The final $wR(F^2_{all\ data})$ was 0.1288 and $R(F_{all\ data})$ was 0.0481. The crystal structure was solved using direct methods and refined by full-matrix least squares on F^2. Corrections were made for synchrotron beam intensity decay as part of the standard inter-frame scaling procedures.

CCDC 182/1407. See http://www.rsc.org/suppdata/cc/1999/2037/ for crystallographic files in .cif format.

1 R. E. Morris and S. J. Weigel, *Chem. Soc. Rev*., 1997, **26**, 309; M. E. Davis and R. F. Lobo, *Chem. Mater*., 1992, **4**, 756.
2 M. Estermann, L. B. McCusker, Ch. Baerlocher, A. Merrouche and H. Kessler, *Nature*, 1991, **352**, 320.
3 G. Férey, *J. Fluorine Chem*., 1995, **72**, 187; G. Férey, *C.R. Acad. Sci. Ser. C.*, 1998, **1**, 1.
4 R. M. Barrer and E. A. D. White, *J. Chem. Soc*., 1951, 1267.
5 W. M. Meier, D. H. Olson and Ch. Baerlocher, *Atlas of Zeolite Structural Types*, Elsevier, New York, 4th edn., 1996.
6 D. S. Wragg, G. B. Hix and R. E. Morris, *J. Am. Chem. Soc*., 1998, **120**, 6822.

Communication 9/06544J

An unpaired electron incarcerated within an icosahedral borane cage: synthesis and crystal structure of the blue, air-stable {[*closo*-$B_{12}(CH_3)_{12}$]·}$^-$ radical

Toralf Peymann, Carolyn B. Knobler and M. Frederick Hawthorne*

Department of Chemistry and Biochemistry, University of California, Los Angeles, Los Angeles, CA 90095–1569, USA. E-mail: mfh@chem.ucla.edu

Received (in Bloomington, IN, USA) 5th July 1999, Accepted 2nd September 1999

Oxidation of the permethylated icosahedral borane [*closo*-$B_{12}(CH_3)_{12}$]$^{2-}$ 1, by ceric(IV) ammonium nitrate in acetonitrile affords the blue, air-stable paramagnetic anion {[*closo*-$B_{12}(CH_3)_{12}$]·}$^-$ 2, which has been characterized, among other means, by X-ray crystallography.

Radicals differ significantly in reactivity as their persistence largely depends upon the unpaired electron's chemical and physical environment.[1] A major effect that stabilizes paramagnetic species is steric crowding. A radical center surrounded by bulky groups is more persistent than similar species without this protection. Recently, we reported the synthesis of the camouflaged permethylated *closo*-borane [*closo*-$B_{12}(CH_3)_{12}$]$^{2-}$ **1**.[2] Here, we describe paramagnetic {[*closo*-$B_{12}(CH_3)_{12}$]·}$^-$ **2**, obtained from **1** by one-electron oxidation with ceric(IV) ammonium nitrate (CAN) in acetonitrile. In species **2** the unpaired electron is trapped within the hydrocarbon sheath of the permethylated borane cage. Hence, this deep blue radical-anion is surprisingly stable with respect to reaction with oxygen. The anion **2** was characterized by high-resolution fast atom bombardment mass spectrometry (HR-FAB-MS), electron paramagnetic resonance (EPR), UV–VIS spectroscopy, and cyclic voltammetry. Furthermore, the crystal structure of [Ph_3P=N=PPh_3]**2** (PPN**2**), was determined by single crystal X-ray diffraction.

Following CAN oxidation of [NBu^n_4]$_2$**1** (TBA)$_2$**1**, in acetonitrile, the anion **2** was isolated as a PPN salt in 66% yield.† Reduction of **2** with $NaBH_4$ in ethanol regenerated **1** in good yield (Scheme 1).

A solid sample of PPN**2** exhibits an EPR signal with g = 2.0076. The UV–VIS spectrum (Fig. 1) of the blue salt [NEt_4]**2** (TEA**2**) in acetonitrile displays absorption in the visible region.

Cyclic voltammetry (100 mM NEt_4PF_6, Ag/AgCl, MeCN) of **2** reveals a reversible wave with $E_{1/2}$ = 0.44 V for the one-electron process **2** + e$^-$ → **1**. The reduction potential of **2** matches the corresponding oxidation potential previously determined for **1**.[2] The X-ray crystal structure‡ (Fig. 2) confirms that **2** is a permethylated monoanionic *closo*-borane.

In the solid state, the anionic cluster of PPN**2** is less distorted from icosahedral symmetry than the dianionic species **1** studied as a [$(2\text{-}C_5H_4N)_2CH_2$]$^{2+}$ salt [B–B bond lengths: **2** 178.5(8)–180.5(7) pm, **1** 174(1)–181(1) pm, B–C bond lengths: **2** 159.8(9)–161.3(8) pm; **1** 159(1)–170(1) pm].[2] The maximum across-cage methyl carbon separations average 668 pm for the dianionic species **1**,[2] compared to 663 pm for the monoanion **2**. The greater distortion of **1** may be explained by the charge-transfer interaction of the dipositive [$(2\text{-}C_5H_4N)_2CH_2$]$^{2+}$ counter ion and the dianion **1**. This interaction is suggested by the unique color of the blood-red [$(2\text{-}C_5H_4N)CH_2$]**1** salt.[2]

Paramagnetic persubstituted polyhedral *closo*-boranes such as {[*closo*-B_6X_6]·}$^-$ **3**,[3] {[*closo*-B_9X_9]·}$^-$ **4**[4] (X = Cl, Br, I) and [*closo*-$CB_{11}Me_{12}$]· **5**,[5] have been reported previously. As in the synthesis of **2**, these species were obtained *via* metal-ion oxidation of the corresponding reduced borane clusters. In each case, solutions of these paramagnetic species are moderately stable, but decolorize after prolonged contact with air.

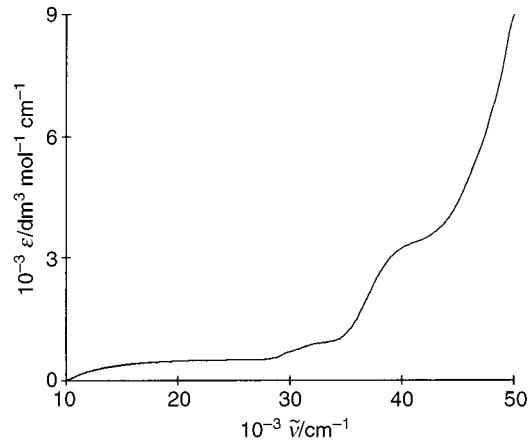

Fig. 1 UV–VIS absorption spectrum of TEA**2** in acetonitrile.

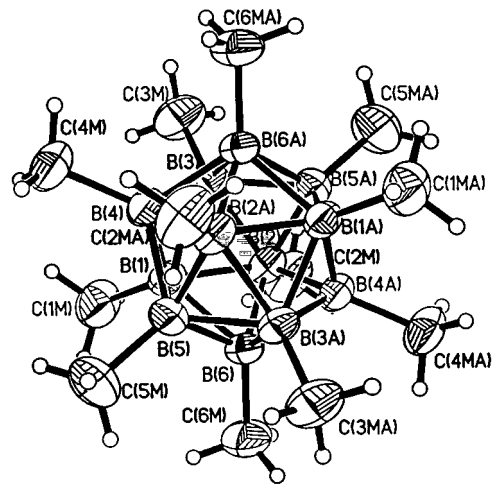

Fig. 2 ORTEP diagram of {[*closo*-$B_{12}(CH_3)_{12}$]·}$^-$ **2**. The ellipsoids represent a 30% probability level. Selected bond lengths (pm): B–B 178.5(8)–180.5(7), B–C 159.8(9)–161.3(8). Atoms X(*n*) and X(*n*A) are symmetry-related by an inversion center.

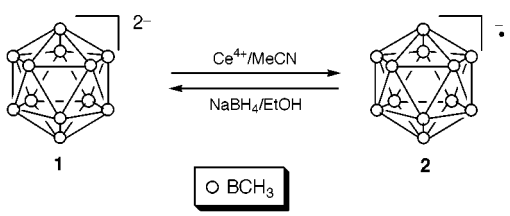

Scheme 1 Chemical interconversion of {[*closo*-$B_{12}(CH_3)_{12}$]·}$^-$ **2** and [*closo*-$B_{12}(CH_3)_{12}$]$^{2-}$ **1**.

The species **2** presents unique possibilities inherent in the concept of camouflaged polyhedral boranes.[7] Here, the persubstitution stabilizes an unusual oxidation state that has not been obtained from the 'naked' parent species [*closo*-$B_{12}H_{12}]^{2-}$ **7**. Upon electrochemical oxidation ($E_{1/2}$ = 1.43 V *vs* SCE), the dianion **7** instead dimerizes [eqn. (1)] by an undetermined mechanism with loss of one *exo* H-atom and dimerization of B_{12}-cages to form the B–H–B bridge of $[B_{24}H_{23}]^{3-}$.[8]

$$2\ [closo\text{-}B_{12}H_{12}]^{2-} \rightarrow [B_{24}H_{23}]^{3-} + H^{+} + 2e^{-} \quad (1)$$

The latter species is structurally related to [a^2-$B_{20}H_{19}]^{3-}$.[9] This reaction pathway is not available for the permethylated radical **1**.

In conclusion, we have presented the synthesis and characterization of {[*closo*-$B_{12}(CH_3)_{12}]^{\bullet}\}^{-}$ **2**, a surprisingly air-stable paramagnetic *closo*-borane. The unique persistence of **2** provided by the steric encumberance of the twelve methyl substituents suggests that **2** might find use in applications requiring a paramagnetic weakly coordinating anion.[10]

We thank Mike Diehl for the EPR measurement. This work was supported by the U.S. Department of Energy (DE-FG02-95ER61975).

Notes and references

‡ *Synthetic procedure for* PPN**2**: A sample of $(TBA)_2$**1** (0.23 g, 0.29 mmol) was dissolved in acetonitrile (5 ml) and an acetonitrile solution (5 ml) of ceric(IV) ammonium nitrate (0.16 g, 0.29 mmol) was added. The reaction mixture, which immediately turned deep blue, was stirred for 5 min and then added to 50 ml of water. The precipitate was separated by filtration, dissolved in ethanol (10 ml), and again filtered. To the filtrate, PPNCl (1.70 g, 2.90 mmol) dissolved in ethanol (10 ml) was added. Upon cooling overnight near 0 °C, the dark blue PPN**2** (0.16 g, 0.19 mmol, 66% yield) separated by crystallization.

Negative HR-FAB-MS: found: *m*/*z* 310.4022; calc. 310.4014.

‡ *Crystal data* for PPN**2** $C_{48}H_{66}B_{12}NP_2$, M = 878.04, monoclinic, a = 3466(3), b = 934.2(8), c = 1869(2) pm, U = 5.120(7) nm^3, T = 298 K, space group $C2/c$, Z = 4, μ(Mo-Kα) = 1.2 cm^{-1}, 4900 unique reflections measured, 2489 reflections were considered observed [$I > 2\sigma(I)$] and all data were used in all calculations. The final R factor ($R = \Sigma||F_o|-|F_c||/\Sigma|F_o|$) was 0.066 (for 2489 independent reflections). The structure was solved using statistical methods and refined by full-matrix least squares on F^2. CCDC 182/1405. See http://www.rsc.org/suppdata/cc/1999/2039/ for crystallographic files in .cif format.

1 D. Griller and K. U. Ingold, *Acc. Chem. Res.*, 1976, **9**, 13.
2 T. Peymann, C. B. Knobler and M. F. Hawthorne, *J. Am. Chem. Soc.*, 1999, **121**, 5601.
3 A. Heinrich, H.-L. Keller and W. Preetz, *Z. Naturforsch., Teil B*, 1990, **45**, 184.
4 E. H. Wong and R. M. Kabbani, *Inorg. Chem.*, 1980, **19**, 451.
5 B. T. King, B. C. Noll, A. J. McKinley and J. Michl, *J. Am. Chem. Soc.*, 1996, **118**, 10 902.
6 J. E. Huheey, E. A. Keiter and R. L. Keiter, *Inorganic Chemistry*, Harper Collins College Publishers, New York, 4th edn., 1993, p. 798.
7 W. Jiang, C. B. Knobler and M. F. Hawthorne, *Angew. Chem., Int. Ed. Engl.*, 1995, **34**, 1332; T. Peymann, A. Herzog, C. B. Knobler and M. F. Hawthorne, *Angew. Chem., Int. Ed.*, 1999, **38**, 1062.
8 R. J. Wiersema and R. L. Middaugh, *Inorg. Chem.*, 1969, **8**, 2074.
9 R. A. Watson-Clark, C. B. Knobler and M. F. Hawthorne, *Inorg. Chem.*, 1996, **35**, 2963.
10 S. H. Strauss, *Chem. Rev.*, 1993, **93**, 927.

Communication 9/05406E

ChemComm

A novel single source precursor route to self capping CdS quantum dots

Mike Lazell and Paul O'Brien*†

Department of Chemistry, Imperial College of Science, Technology and Medicine, London, UK SW7 2AY. E-mail: p.obrien@ic.ac.uk

Received (in Cambridge, UK) 29th July 1999, Accepted 8th September 1999

The synthesis of CdS nanocrystals has been carried out from the thermolysis in a dynamic vacuum, between 150 and 300 °C, of the novel asymmetric cadmium dithiocarbamate [Cd{$S_2CNMe(C_{18}H_{37})$}$_2$]; the particles 'self cap' during preparation; different size nanocrystals were synthesised, at different temperatures, and there was a change in phase from cubic to hexagonal CdS at a decomposition temperature of 300 °C.

Nanocrystalline semiconductors have electronic properties intermediate between those of molecular entities and macrocrystalline solids and are at present the subject of intense research.[1–6] Nanometric semiconductor particles exhibit novel properties owing to the large number of surface atoms (and resultant states) and/or the three-dimensional confinement of electrons. Altering the size of the particle alters the degree of confinement of the electrons, and affects the electronic structure of the solid, in particular 'band edges', which are tunable with particle size. Nanoparticles of semiconductors have many potential applications and demonstration devices including light-emitting diodes,[7,8] photocatalysts[9,10] and electrochemical cells[1,6,11] have been reported.

We are interested in developing novel routes to these materials and have previously reported the use of single source precursors to prepare several II–VI chalcogenides.[12–14] These nanocrystals are organically capped with tri-*n*-octylphosphine oxide (TOPO). Other capping groups such as 4-ethylpyridine have also been used to solubilise nanocrystals, for example, InP.[15] We have also recently reported the use of trioctylphosphine sulfide as an air/moisture stable sulfiding precursor[16] for cadmium or zinc sulfide. However, to date there has only been one paper[17] describing the synthesis of nanocrystals in a process in which the particle is capped by a ligand transferred from the precursor; as a single parent molecule is involved, we term this process 'self-capping'. Finely divided silver has been prepared from the salts of fatty acids by a bulk pyrolysis. Here we report the first synthesis of self-capped CdS nanocrystals *via* thermolysis at 150–300 °C, in a dynamic vacuum, of the novel asymmetric cadmium dithiocarbamate, [Cd{$S_2CNMe(C_{18}H_{37})$}$_2$].

The cadmium dithiocarbamate precursor, [Cd{$S_2CNMe(C_{18}H_{37})$}$_2$] was prepared from the amine $HNMe(C_{18}H_{37})$, using a method described elsewhere.[14] The precursor was thermolysed *in vacuo* at temperatures ranging between 150 and 300 °C‡. The resulting solid was readily redispersed in pyridine. The absorption edges of the nanoparticles were calculated using the direct band gap method. The onset of absorption for all the samples showed a clear blue shift: 150 °C, *ca.* 430 nm (2.88 eV), 200 °C, 449 nm (2.76 eV), 250 °C, 465 nm (2.66 eV) as compared to that of bulk CdS, 515 nm (2.41 eV) [Fig. 1(*a*)]. The CdS samples all showed Stokes shifts in their photoluminescence spectra [Fig. 1(*b*)]. However, the observed Stokes shift decreases as the particle size increases: 150 °C, absorption maxima, A_{max}, at 454 nm (2.73 eV) (λ_{exc} = 370 nm) a Stokes shift, (SS), of 0.15 eV; 200 °C, A_{max} = 472 nm (2.63 eV) (λ_{exc} = 400 nm), SS = 0.13 eV; 250 °C, A_{max} = 482 nm (2.57 eV) (λ_{exc} = 390 nm), SS = 0.09 eV. This trend in the shifts of the absorption maxima in the PL spectra is as expected.

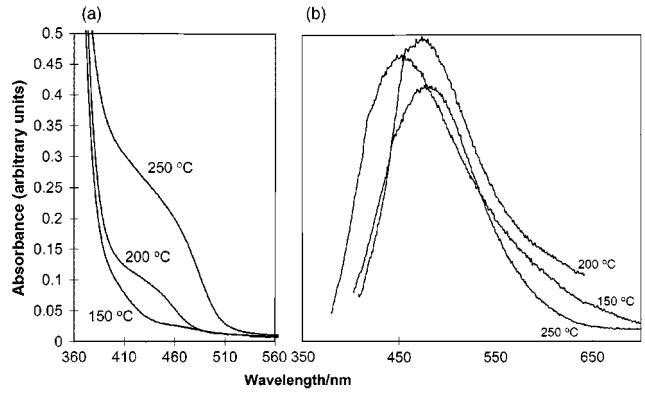

Fig. 1 (a) UV and (b) PL spectra for CdS samples.

XRD of the powdered samples showed an interesting feature in the as-prepared CdS nanoparticles (Fig. 2). The CdS samples prepared at temperatures of 150–250 °C could be indexed to the standard patterns of the cubic phase.§ The largest particles of CdS from the thermolysis at 300 °C, were clearly of the hexagonal phase. There is no evidence that there is a mixing of phases as described by Bawendi *et al.* for CdSe nanocrystals prepared from inverse micelles.[18] The broadening of the peaks in the XRD patterns for all samples is typical of nanoparticles.

The nanoparticles were analysed by IR spectroscopy to establish the nature of the capping group. The capping agent of the nanocrystals could presumably be HNR′R″ or $S_2CNR'R''$. The IR showed no stretches associated with a C–N bond from the CdS nanocrystal samples (a typical C–N bond stretch was seen in the precursor sample). This suggests that the CdS nanocrystals are capped by $HNMe(C_{18}H_{37})$. ^1H and ^{13}C NMR spectroscopy show resonances associated with the amine. This taken with the IR data, is good evidence that the capping group is $HNMe(C_{18}H_{37})$. X-Ray photoelectron spectroscopy was used to analyse the CdS samples prepared at 200 and 300 °C. The analysis shows the presence of Cd, S, N and C. The ratio of C

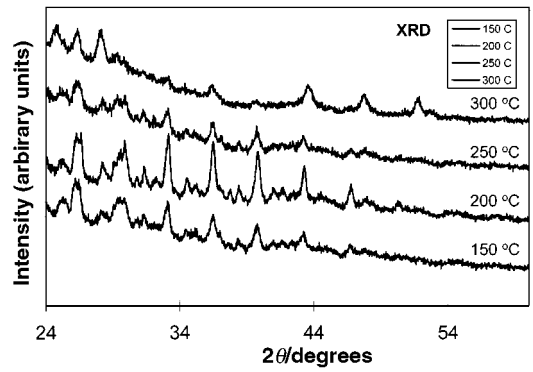

Fig. 2 XRD patterns for the as-prepared CdS samples.

† Present address: The Manchester Materials Science Centre and The Chemistry Department, The University of Manchester, Oxford Road, Manchester, UK M13 9PL.

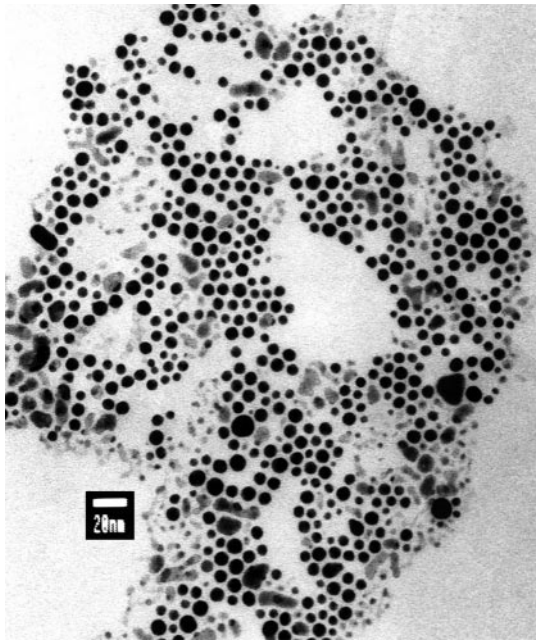

Fig. 3 TEM image of CdS nanoparticles prepared at 150 °C.

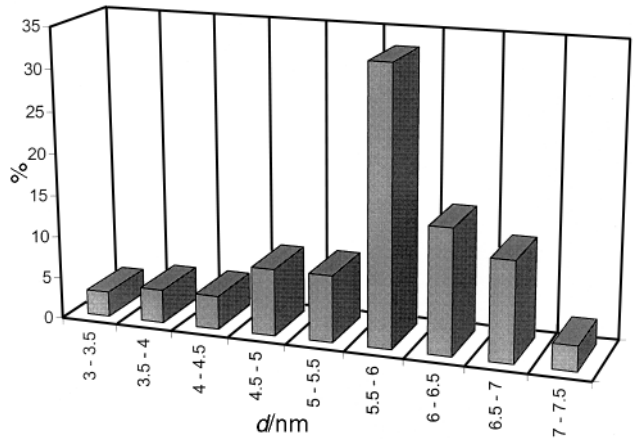

Fig. 4 Size distribution of CdS nanoparticles.

to Cd in the 200 °C sample was significantly higher than in the sample prepared at 300 °C. This observation suggests that there is less capping agent on the sample prepared at 300 °C than that prepared at 200 °C. Hence, the CdS samples prepared at 150–250 °C are very soluble in pyridine while the sample prepared at 300 °C is only partially soluble. TEM images (Fig. 3) show quantum dots of CdS synthesised at 150 °C, which are not agglomerated. The size distribution of the dots is shown in Fig. 4. The dots are predominately of size 5.5–6 nm. The dots synthesised at 250 °C appear to have a halo-like tail structure. This could be the capping group emanating from the CdS nanoparticle. The estimated diameters of the dots are between 5 and 7 nm (Table 1); as calculated using the Scherrer equation and the direct band gap method from the onset of absorption in the UV spectra. These values compare well with those obtained from the TEM images.

Table 1 UV and PL data and calculated diameters of particles using the direct bandgap method (onset of absorption from UV spectra) and the Scherrer equation (XRD data).

Sample[a]	Onset of abs./eV	Abs. max./eV	Av. size/nm (Calc. from UV)	Calc. size/nm (Scherrer eqn.)
150	2.88	2.73	4.5	5
200	2.76	2.63	5	5.5
250	2.66	2.57	6	6

[a] Preparation temperature/°C.

In conclusion, good quality, self capped CdS nanoparticles have been synthesised from the vapour phase thermolysis of the novel cadmium dithiocarbamate, $[Cd\{S_2CNMe(C_{18}H_{37})\}_2]$. The CdS nanoparticles are cubic in nature when prepared at 150–250 °C and hexagonal at 300 °C. The CdS samples were characterised by UV–VIS, IR, PL, XRD, XPS, NMR and TEM. Studies into other metal sulfide precursors are ongoing.

This work has been funded by an EPSRC grant to P. O. B. We would like to thank Mr Keith Pell (QMW) for TEM, Mr Jin-Ho Park (IC) for XRD and Dr Karol Senkiw (IC) for XPS. P. O. B is the Sumitomo/STS Professor of Materials Chemistry at IC and from 1/9/99 Professor of Inorganic Materials at The Manchester Materials Science Centre and The Chemistry Department, Manchester University.

Notes and references

‡ Into a quartz vessel was put *ca.* 0.5 g of $[Cd\{S_2CNMe(C_{18}H_{37})\}_2]$. The decomposition apparatus was then put into a carbolite tube furnace. The apparatus was opened to a dynamic vacuum, *ca.* 0.01 mm Hg, there was also a liquid nitrogen trap to condense any volatiles from the thermolysis. The decomposition apparatus was heated at a range of temperatures, 150–300 °C, for 1 h (timed from temperature stabilisation). The vessel was allowed to cool and the contents, varying from off-white-yellow (150 °C) to dark orange (300 °C), were removed.

§ Optical measurements of the nanoparticles were carried out on a Philips PU 8710 spectrophotometer. The sample solutions were placed in silica cuvettes (path length = 1 cm). The samples were in pyridine solutions and pyridine was used as the reference. IR spectra were carried out using a Matteson Polaris FT-IR spectrometer with Nujol mulls. ^1H and ^{13}C solution NMR spectra were recorded on a Bruker AM 500 or a DRX 400 in $CDCl_3$. XRD patterns were measured using a Siemens D500 series automated powder diffractometer using Cu-Kα radiation at 40 kV/40 mA with a secondary graphite crystal monochromator. Samples were supported on glass slides (5 cm^2). PL measurements were obtained using a Spex FluoroMax instrument with a xenon lamp (150 W) and a 152 P photomultiplier tube as a detector. Silica cuvettes of 1 cm path length were used. Solutions were made using pyridine. A JOEL 2000 FX MK1 electron microscope operating at 200 kV with an Oxford Instruments AN 10000 EDS analyser was used for the conventional TEM micrographs. The samples for TEM were prepared by placing a drop of a dilute solution of sample in toluene on a copper grid (400 mesh, Agar). The excess solvent was wicked away with a paper tip and the sample allowed to dry completely at room temperature. The XPS measurements were performed in the ultra-high vacuum chamber (base pressure 10^{-8} Pa) of a VG ESCALAB-Mk II (VG Scientific) using Al-Kα excitation (analyser pass energy of 50 eV). The energy scale was calibrated using C 1s (at 284.4 eV) as a reference.

1 D. Dounghong, J. Ramsden and M. Grätzel, *J. Am. Chem. Soc*., 1982, **104**, 2977.
2 R. Rossetti, J. L. Ellison, J. M. Gibson and L. E. Brus, *J. Chem. Phys*., 1984, **80**, 4464.
3 A. Henglein, *Chem. Rev*., 1989, **89**, 1861.
4 M. L. Steigerwald and L. E. Brus, *Acc. Chem. Res*., 1990, **23**, 183.
5 Y. Wang and N. Herron, *J. Phys. Chem*., 1991, **95**, 525.
6 H. Weller, *Adv. Mater*., 1993, **5**, 88.
7 B. O. Dabbousi, M. G. Bawendi, O. Onitsuka and M. F. Rubner, *Appl. Phys. Lett*., 1995, **66**, 1316.
8 V. L. Colvin, M. C. Schlamp and A. P. Alivisatos, *Nature*, 1994, **370**, 354.
9 F. Hakimi, M. G. Bawendi, R. Tumminelli and J. R. Haavisto, *US Pat.*, 5260957, 1993.
10 C. K. Grätzel and M. Grätzel, *J. Am. Chem. Soc*., 1979, **101**, 7741.
11 A. Hagfeldt and M. Grätzel, *Chem. Rev*., 1995, **95**, 49.
12 T. Trindade, P. O'Brien and Xiao-mei Zhang, *Chem. Mater*., 1997, **9**, 523.
13 M. Green and P. O'Brien, *Adv. Mater. Opt. Electron*., 1997, **7**, 277.
14 B. Ludolph, M. A. Malik, P. O'Brien and N. Revaprasadu, *Chem. Commun*., 1998, 1849 and references therein.
15 M. Green and P. O'Brien, *Chem. Commun*., 1998, 2459.
16 M. Lazell and P. O'Brien, *J. Mater. Chem*., 1997, **7**, 1381.
17 K. Abe, T. Hanada, Y. Yoshida, N. Tanigaki, H. Takiguchi, H. Nagasawa, M. Nakamoto, T. Yamaguchi and K. Yase, *Thin Solid Films*, 1998, **329**, 524.
18 M. G. Bawendi, A. R. Kortan, M. L. Steigerwald and L. E. Brus, *J. Chem Phys*., 1989, **11**, 7282.

Communication 9/06160F

Reactive intermediates from carbonylation of ruthenium(I) carbonyl carboxylates. Isolation, molecular structures and chemical properties of dinuclear unbridged ruthenium carbonyl trifluoroacetates

Tiziana Funaioli,*[a] Fabio Marchetti[b] and Giuseppe Fachinetti*[a]

[a] *Dipartimento di Chimica e Chimica Industriale, Università di Pisa, via Risorgimento 35, I-56126 Pisa, Italy. E-mail: funfac@dcci.unipi.it*

[b] *Dipartimento di Ingegneria Chimica, dei Materialti, delle Materie Prime e Metallurgia, Università degli Studi di Roma 'La Sapienza', via del Castro Laurenziano 7, I-00195 Roma, Italy*

Received (in Basel, Switzerland) 19th July 1999, Accepted 29th August 1999

Carboxylato-bridged Ru(I) carbonyl complexes are activated by CO towards both disproportionation and reaction with dihydrogen, through the intermediacy of the unbridged metal–metal bonded valence isomers $(OC)_5RuRu(CO)_3(OCOCR_3)_2$ and $[Ru(CO)_4(OCOCR_3)]_2$.

Catalysis chemistry involving carboxylato-bridged Ru(I) carbonyl complexes of formula $Ru_2(\mu\text{-}\eta^2\text{-}O_2CR)_2(CO)_6$ includes the acid-cocatalyzed water gas shift reaction[1] (WGSR) and the related Reppe olefin carbonylation,[2] CO hydrogenation[3] and syngas homologation of aliphatic carboxylic acids.[4] Furthermore, in the presence of tertiary phosphines, carboxylato-bridged Ru(I) carbonyl complexes are used as catalytic precursors for the addition of carboxylic acids to alkynes,[5] the hydrogenation of carboxylic acids[6] and esters,[7] and the hydroformylation of alkenes.[8] Concerning the nature of the species promoting the activation of simple molecules and organic substrates in these catalytic processes, the present study highlights the unsaturation of $Ru_2(\mu\text{-}\eta^2\text{-}O_2CR)_2(CO)_6$ complexes, vacant coordination sites being generated by the rearrangement of the bridging carboxylato ligands. Thus, $Ru_2(\mu\text{-}\eta^2\text{-}O_2CCF_3)_2(CO)_6$ **1** was found to reversibly add two CO ligands yielding hitherto unknown dinuclear unbridged ruthenium carbonyl carboxylates. The rate of CO uptake is markedly affected by the medium: in toluene, forcing conditions (150 °C, P_{CO} = 120 atm) are required to convert **1** to a nearly equimolar mixture of $(OC)_5RuRu(CO)_3(OCOCF_3)_2$ **2** [ν_{CO} (Nujol mull) 2173m, 2116s, 2102m, 2075s, 2053m and 2023m cm^{-1}] and $[Ru(CO)_4(OCOCF_3)]_2$ **3** [ν_{CO} (Nujol mull) 2133s, 2093vs, 2077s and 2051s cm^{-1}]† [eqn. (1)].

$$\underset{\mathbf{1}}{2\ Ru_2(\mu\text{-}\eta^2\text{-}O_2CCF_3)_2(CO)_6} + 4\ CO \rightleftharpoons \underset{\mathbf{2}}{(OC)_5RuRu(CO)_3(OCOCF_3)_2} + \underset{\mathbf{3}}{[Ru(CO)_4(OCOCF_3)]_2} \quad (1)$$

Remarkably, with trifluoroacetic acid as solvent, reaction (1) is an equilibrium at room temperature. Presumably, hydrogen bonding between bridging carboxylato ligands and solvent molecules assists the conversion of the bridging carboxylato ligand to its monodentate arrangement. Gas volumetric measurements and IR analysis show that **1**, **2** and **3** are present in a 1 : 2.5 : 4 molar ratio in a 0.046 M trifluoroacetic acid solution of **1** under CO at atmospheric pressure.

The molecular structures‡ of **2** and **3** are shown in Fig. 1 and 2, respectively. Binuclear Ru carbonyl complexes without bridging ligands are rare, only anionic $[Ru(CO)_4]_2^{2-}$ [9] and neutral $[Ru(CO)_4(GaCl_2\cdot THF)]_2$[10] and $[Ru(CO)_4(SnMe_3)]_2$[11] being structurally characterized. Compounds **2** and **3** show Ru–Ru distances of 2.836 and 2.853 Å, respectively, indicating a strong metal–metal bond, as compared to the dinuclear compound $[Fe(CO)_4(CO_2CMe_3)_2]_2$,[12] with an Fe–Fe distance of 2.840 Å.

Compound **2**, in which the $Ru(CO)_5$ moiety acts as a donor ligand towards the Ru(II) 16-electron centre, is stable both in the solid state and in diethyl ether solution and constitutes the first structurally characterized adduct of the $Ru(CO)_5$ donor unit. Such an interaction stabilizes $Ru(CO)_5$ towards decarbonylation; however, upon adding an equimolar amount of CF_3CO_2Cs to a 0.02 M THF solution of **2**, free $Ru(CO)_5$ is immediately released into solution where it slowly converts to $Ru_3(CO)_{12}$. According to eqn. (2), the eighteen-electron complex $Ru(CO)_5$ is substituted by the trifluoroacetato ligand yielding the anionic Ru(II) carbonyl complex **4** which was identified spectroscopically [ν_{CO} (THF) 2142m, 2089s, 2072s cm^{-1}].[1]

On these grounds, we conclude that exposure of a solution containing carboxylato-bridged Ru(I) carbonyl complexes to CO can result in equilibrium (1) and then in an irreversible

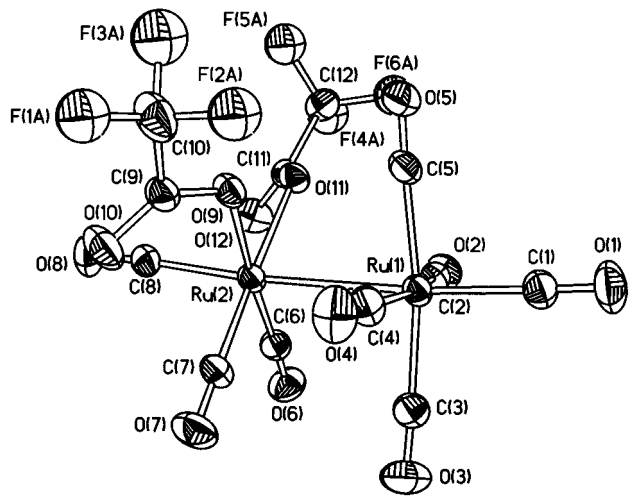

Fig. 1 The molecular structure of **2**. The molecule possesses an approximate mirror plane, although this is not an operation of the space group. Only the most populated positions of the disorderd CF_3 groups have been represented. The ellipsoids are at 30% probability. Selected bond lengths (Å) and angles (°): Ru(1)–C(4) 1.964(9), Ru(1)–C(3) 1.964(9), Ru(1)–C(2) 1.966(8), Ru(1)–C(5) 1.991(9), Ru(1)–C(1) 2.016(8), Ru(1)–Ru(2) 2.8526(8), Ru(2)–C(6) 1.875(8), Ru(2)–C(7) 1.891(8), Ru(2)–C(8) 1.969(8), Ru(2)–O(11) 2.109(5), Ru(2)–O(9) 2.118(5); C(4)–Ru(1)–C(3) 89.6(4), C(4)–Ru(1)–C(2) 166.4(3), C(3)–Ru(1)–C(2) 89.4(3), C(4)–Ru(1)–C(5) 89.9(3), C(3)–Ru(1)–C(5) 171.2(3), C(2)–Ru(1)–C(5) 89.0(3), C(4)–Ru(1)–C(1) 96.7(3), C(3)–Ru(1)–C(1) 95.5(3), C(2)–Ru(1)–C(1) 96.9(3), C(5)–Ru(1)–C(1) 93.3(3), C(4)–Ru(1)–Ru(2) 83.4(2), C(3)–Ru(1)–Ru(2) 89.3(2), C(2)–Ru(1)–Ru(2) 83.1(2), C(5)–Ru(1)–Ru(2) 81.9(2), C(1)–Ru(1)–Ru(2) 175.2(3), C(6)–Ru(2)–C(7) 89.3(3), C(6)–Ru(2)–C(8) 90.4(3), C(7)–Ru(2)–C(8) 93.2(3), C(6)–Ru(2)–O(11) 94.2(3), C(7)–Ru(2)–O(11) 174.8(3), C(8)–Ru(2)–O(11) 90.7(3), C(6)–Ru(2)–O(9) 176.4(3), C(7)–Ru(2)–O(9) 93.2(3), C(8)–Ru(2)–O(9) 92.0(3), O(11)–Ru(2)–O(9) 83.18(19), C(6)–Ru(2)–Ru(1) 91.0(2), C(7)–Ru(2)–Ru(1) 91.5(2), C(8)–Ru(2)–Ru(1) 175.1(2), O(11)–Ru(2)–Ru(1) 84.58(13), O(9)–Ru(2)–Ru(1) 86.35(14).

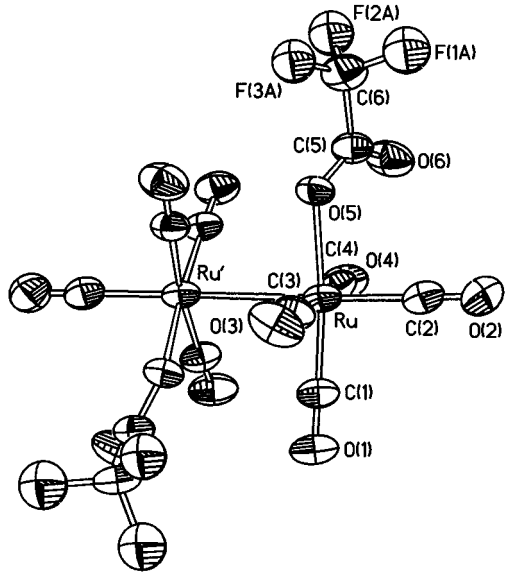

Fig. 2 The molecular structure of **3**. The molecule possesses a twofold axis of symmetry. Only the most populated positions of the disordered CF_3 groups have been represented. The ellipsoids are at 30% probability. Selected bond lengths (Å) and angles (°): Ru–C(1) 1.885(11), Ru–C(4) 1.946(12), Ru–C(3) 1.947(11), Ru–C(2) 1.982(16), Ru–O(5) 2.104(6), Ru–Ru′ 2.836(2); C(1)–Ru–C(4) 89.3(5), C(1)–Ru–C(3) 89.7(4), C(4)–Ru–C(3) 174.1(5), C(1)–Ru–C(2) 94.7(5), C(4)–Ru–C(2) 92.8(5), C(3)–Ru–C(2) 93.1(5), C(1)–Ru–O(5) 173.7(4), C(4)–Ru–O(5) 93.6(4), C(3)–Ru–O(5) 86.8(3), C(2)–Ru–O(5) 90.6(4), C(1)–Ru–Ru′ 87.5(4), C(4)–Ru–Ru′ 88.7(4), C(3)–Ru–Ru′ 85.4(4), C(2)–Ru–Ru′ 177.3(4), O(5)–Ru–Ru′ 87.1(2). ′ = $-x + 1/2, -y + 3/2, z$.

$$\underset{\mathbf{2}}{(OC)_5RuRu(CO)_3(OCOCF_3)_2} + CF_3CO_2^- \rightleftharpoons Ru(CO)_5 + \underset{\mathbf{4}}{[fac\text{-}Ru(CO)_3(OCOCF_3)_3]^-} \quad (2)$$

disproportionation [eqn. (2)], in the presence of the free carboxylato ligand.

We showed that the disproportionation of **1** constitutes the key step of some catalytic processes such as CF_3CO_2H-cocatalyzed WGSR[1] and the related Reppe olefin carbonylations.[2] It now appears that the reaction is a consequence of the carbonylation of **1** giving the reactive adduct **2**. Presumably, this conclusion is general and applies also to carboxylato-bridged Ru(I) carbonyl complexes other than **1**: for instance, $Ru_2(\mu\text{-}\eta^2O_2CMe)_2(CO)_6$, which is indefinitely stable in an acetato-acetic acid solution, was found to absorb CO and to disproportionate at room temperature and atmospheric pressure.

Finally, the present findings can help to elucidate the dihydrogen activation promoted by carboxylato-bridged Ru(I) carbonyl complexes, a step common to several catalytic processes involving ruthenium. Both in toluene and in trifloroacetic acid, **1** fails to react with dihydrogen even under harsh conditions. However, two distinct reaction pathways are encountered under 120 atm of H_2–CO (v/v = 1 : 1), as a function of the solvent: in toluene at 130 °C, $Ru(CO)_5$ and trifluoroacetic acid are quantitatively formed within 1 h while in trifluoroacetic acid catalytic hydrogenation of the solvent to 2,2,2-trifluoroethanol occurs. While the catalytic reaction, which has few precedents in homogeneous catalysis,[13] is under investigation, it is evident that dihydrogen activation by **1** requires CO. An interpretation for this could be given by considering the nature of **2** and **3**, namely the species present under CO. A radical pathway initiated by Ru–Ru bond fission in **3**[14] or, alternatively a H_2 heterolytic splitting promoted by the Ru(II) centre of **2** can then be envisaged. In this connection, the chemistry of these ruthenium(II) containing species is reminiscent of the dihydrogen activation processes promoted by cobalt carbonyl species, which have been reported in earlier studies from these laboratories.[15] It thus appears that the formation of rather weak metal–metal bonds is required.

The authors thank the Ministero dell'Università e della Ricerca Scientifica e Tecnologica (MURST), Programmi di Ricerca Scientifica di Rilevante Interesse Nazionale, Cofinanziamento 1998–9, for financial support, Professor F. Calderazzo for helpful discussions, Mr F. Del Cima for skillful technical assistance and Chimet SpA for a gift of ruthenium.

Notes and references

† Compound **1** (0.8 g, 1.38 mmol) was suspended in 50 ml of toluene in a glass ampoule which was placed in a stainless-steel autoclave, pressurized with CO up to 120 atm and heated to 150 °C in a thermostatted oil bath. After slow cooling and gas venting, the glass ampoule was found to contain pale yellow crystals of two different shapes, while only traces of carbonyl complexes where detected by IR spectroscopy in the liquid phase. The air stable crystals were selected according to their shape. The X-ray single-crystal study showed $(OC)_5RuRu(CO)_3(OCOCF_3)_2$ **2** to constitute the stick-shaped crystals and $[Ru(CO)_4(OCOCF_3)]_2$ **3** to form prismatic shaped crystals. The diffractometric measurements were carried out with a Siemens P4 diffractometer using Mo-Kα radiation, λ = 0.71073 Å. The intensity data were corrected for Lorentz and polarisation effects and for absorption by using a ψ-scan method.[16] Calculations were carried out with the SHELX97[17] program. In both studies, the disordered CF_3 groups were refined as distributed with fixed geometry in two limiting positions. At the end of both refinements residual peaks and holes of *ca.* ±1 e Å^{-3} were present in the CF_3 regions of the difference Fourier maps.

‡ *Crystal data*: **2**, colourless crystals, $C_{12}F_6O_{12}Ru_2$; M = 652.3, T = 293(2) K, a = 8.151(1), b = 15.740(1), c = 15.857(1) Å, β = 95.46(1)°, monoclinic $P2_1/c$ (no. 14), U = 2025.2(3) Å^3; Z = 4; μ = 1.603 mm^{-1}; crystal size = 0.35 × 0.18 × 0.09 mm. 3565 independent reflections were collected (R_{int} = 0.0184). Final reliability factors for 273 parameters: R_1 = 0.0481 calculated for 2826 reflections with $I > 2\sigma(I)$, wR_2 = 0.1140 calculated for all 3565 reflections in the refinement; GOF = 1.018. $R_1 = \Sigma \mid |F_0| - |F_c| \mid / \Sigma |F_0|$; $wR_2 = \{\Sigma[w(F_o^2 - F_c^2)^2]/\Sigma[w(F_0^2)^2]\}^{\frac{1}{2}}$, GOF = $[\Sigma[w(F_o^2 - F_c^2)^2]/(N - P)]^{\frac{1}{2}}$, where N, P are the numbers of observations and parameters, respectively.

3, light yellow crystals, $C_{12}F_6O_{12}Ru_2$; M = 652.3, T = 293(2) K, a = 9.020(1), b = 12.716(2), c = 17.748(2) Å, orthorhombic *Pccn* (no. 56), U = 2035.7(5) Å^3; Z = 4; μ = 1.595 mm^{-1}; crystal size = 0.28 × 0.21 × 0.13 mm. 1595 independent reflections were collected (R_{int} = 0.0208). Final reliability factors for 137 parameters: R_1 = 0.0536 calculated for 964 reflections with $I > 2\sigma(I)$, wR_2 = 0.1557 calculated for all 1595 reflections in the refinement; GOF = 1.028. CCDC 182/1401. See http://www.rsc.org/suppdata/cc/1999/2043/ for crystallographic files in .cif format.

1 G. Fachinelli, T. Funaioli, L. Lecci and F. Marchetti, *Inorg. Chem.*, 1996, **35**, 7217.
2 T. Funaioli, C. Cavazza, F. Marchetti and G. Fachinetti, *Inorg. Chem.*, 1999, **38**, 3361.
3 B. D. Dombek, *J. Am. Chem. Soc.*, 1980, **102**, 6855.
4 J. F. Knifton, *J. Mol. Catal.*, 1981, **11**, 91.
5 M. Rotem and Y. Shvo, *J. Organomet. Chem.*, 1993, **448**, 189.
6 U. Mattcoli, G. Menchi, M. Bianchi, P. Frediani and F. Piacenti, *Gazz. Chim. Ital.*, 1985, **115**, 603.
7 U. Matteoli, G. Menchi, M. Bianchi and F. Piacenti, *J. Mol. Catal.*, 1991, **64**, 257.
8 J. Jenck, P. Kalck, F. Pinelli, M. Siani and A. Thorez., *J. Chem. Soc., Chem. Commun.*, 1988, 1428; P. Kalck, M. Siani, J. Jenck, R. Perylle and Y. Peres, *J. Mol. Catal.*, 1991, **67**, 19.
9 L.-Y. Hsu, N. Bhattacharyya and S. G. Shore, *Organometallics*, 1985, **4**, 1483.
10 G. N. Harakas and B. R. Whittlesey, *Inorg. Chem.*, 1997, **36**, 2704.
11 J. A. K. Howard, S. C. Kellett and P. Woodward, *J. Chem. Soc., Dalton Trans.*, 1975, 2332.
12 D. Luart, M. Sellin, P. Laurent, J.-Y. Salaün, R. Pichon, L. Toupet and H. des Abbayes, *Organometallics*, 1995, **14**, 4989.
13 D.-H. He, N. Wakasa and T. Fuchikami, *Tetrahedron Lett.*, 1995, **36**, 1059.
14 P. Frediani, M. Bianchi, A. Salvini and F. Piacenti, *J. Chem. Soc., Dalton Trans.*, 1990, 3663.
15 G. Fachinetti, G. Fochi, T. Funaioli and P. F. Zanazzi, *Angew. Chem., Int. Ed. Engl.*, 1987, **26**, 680; G. Fachinetti, T. Funaioli and M. Marcucci, *J. Organomet. Chem.*, 1988, **353**. 393.
16 A. C. T. North, D. C. Phillips and F. S. Mathews, *Acta Crystallogr., Sect. A*, 1968, **24**, 351.
17 G. M. Sheldrick, SHELX-97, An Integrated System for Solving, Refining and Displaying Crystal Structures from Diffraction Data, University of Göttingen, Germany, 1997.

Communication 9/05798F

Synthesis, structural characterisation and luminescence studies of the first alkynyl stabilised platinum–cadmium complexes

J. P. H. Charmant,[a] L. R. Falvello,[b] J. Forniés,*[b] J. Gómez,[ac] E. Lalinde,*[c] M. T. Moreno,[c] A. G. Orpen[a] and A. Rueda[b]

[a] *School of Chemistry, University of Bristol, Bristol, UK BS8 1TS*
[b] *Departamento de Química Inorgánica, Instituto de Ciencia de Materiales de Aragón, Universidad de Zaragoza-Consejo Superior de Investigaciones Científicas, 50009 Zaragoza, Spain. E-mail: forniesj@posta.unizar.es*
[c] *Departamento de Química, Universidad de La Rioja, 26001, Logroño, Spain*

Received (in Cambridge, UK) 5th August 1999, Accepted 10th September 1999

The simple 1:2 adduct $(NBu_4)_2[\{Pt(\mu\text{-}\kappa C^{\alpha}:\eta^2\text{-}C{\equiv}CPh)_4\}(CdCl_2)_2]$ 2 containing unusual η^2-alkyne Cd interactions, as well as the unexpected tetranuclear dimer $(NBu_4)_2[\{Pt(\mu\text{-}\kappa C^{\alpha}C^{\alpha}\text{-}C{\equiv}CPh)_4\}_2(CdCl_2)_2]$ 1 stabilised by alkynyl bridging ligands and platinum–cadmium bonding interactions, have been characterised by X-ray crystallography and their luminescence properties have been also investigated.

Although cadmium organometallics have long been used in organic synthesis,[1] there have been relatively few studies on the species themselves.[2] In particular, alkynyl cadmium complexes are limited to the polymeric derivatives $[Cd(C{\equiv}CR)_2]_n$, (R = H,[3a] Ph,[3a,b] C_6H_{13}[3b]) and to the recently reported mononuclear complex $[Cd(C{\equiv}CPh)_2(tmen)]$,[3c] which is the only example of a structurally characterised cadmium alkynyl complex. Heteropolynuclear organocadmium species with Cd(II) in different environments and with nuclearity ranges from two to seven (or even larger, *i.e.* 9 or 13), have been reported,[1,2] but, up to now, complexes of this type involving alkynyl ligands are unknown.

In the last few years we have shown that anionic homoleptic alkynylplatinate(II) species are suitable precursors for the synthesis of remarkable trinuclear species $[\{Pt(\mu\text{-}\kappa C^{\alpha}:\eta^2\text{-}C{\equiv}CR)_4(ML_n)_2\}]^{x-}$ displaying very unusual η^2-alkyne–M bonding interactions [ML_n = $Pd(\eta^3\text{–}C_3H_5)$,[4a] x = 0; HgX_2,[4b] $CoCl_2$,[4c] x = 2). By using a similar synthetic approach we have now been able to prepare the first examples of organometallic mixed-metal platinum–cadmium compounds.[5] Here, we report the syntheses, X-ray crystal structures and luminescence properties of a trinuclear complex $(NBu_4)_2[\{Pt(\mu\text{-}\kappa C^{\alpha}:\eta^2\text{-}C{\equiv}CPh)_4\}(CdCl_2)_2]$ **2**, stabilised by unusual η^2-alkynyl–Cd interactions, along with the unexpected tetranuclear cluster $(NBu_4)_2[\{Pt(\mu\text{-}\kappa C^{\alpha}C^{\alpha}\text{-}C{\equiv}CPh)_4\}(CdCl)]_2$ **1** containing four Pt(II)–Cd(II) interactions and with alkynyl bridging ligands displaying a rather unusual $\mu\text{-}\kappa C^{\alpha}C^{\alpha}$ bonding mode.

The complex $(NBu_4)_2[Pt(C{\equiv}CPh)_4]$[6] was treated in acetone at room temperature with $CdCl_2{\cdot}2.5H_2O$ (1:2 molar ratio) with the aim of preparing 1:2 adducts analogous to the trinuclear PtM_2 (M = Hg,[4b] Co[4c]) derivatives mentioned above. However, after 50 min of stirring a microcrystalline yellow solid (**1**, 30% yield) was obtained by partial evaporation of the solvent and cooling.† Complex **1** was identified by a single-crystal X-ray diffraction study as the unexpected tetranuclear compound $(NBu_4)_2[\{Pt(\mu\text{-}\kappa C^{\alpha}C^{\alpha}\text{-}C{\equiv}CPh)_4\}_2(CdCl)_2]$ (see below). In addition, evaporation of the filtrate to dryness and treatment with isopropyl alcohol gave the desired trinuclear adduct $(NBu_4)_2[\{Pt(\mu\text{-}\kappa C^{\alpha}:\eta^2\text{-}C{\equiv}CPh)_4\}(CdCl_2)_2]$ **2** as a white solid (45% yield). As might be expected, if the reaction is carried out under similar conditions, but with a 1:1 molar ratio, only the 1:1 Pt/Cd complex **1** is obtained, in high yield (82%).

X-Ray structure analyses of both compounds have been carried out (Fig. 1 and 2). As can be seen, while the anion in **2**‡

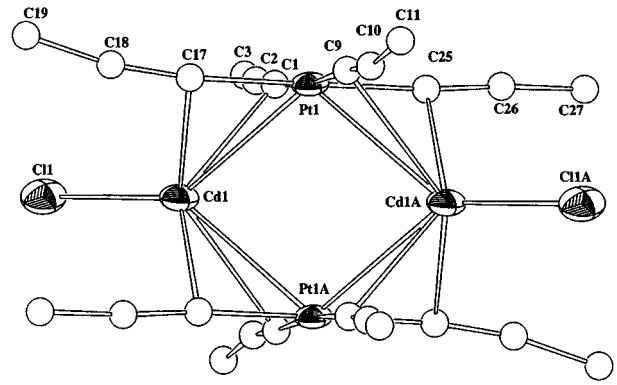

Fig. 1 Structure of the anion $[\{Pt(\mu\text{-}\kappa C^{\alpha}C^{\alpha}\text{-}C{\equiv}CPh)_4\}_2(CdCl)_2]^{2-}$ in complex **1**. Selected interatomic distances (Å) and angles (°): Pt–C(1) 2.013(5), Pt–C(9) 2.014(5), Pt–Cd 2.960(1), Cd–C(1) 2.463(4), Cd–C(9) 2.604(5), C(1)–C(2) 1.210(7), C(9)–C(10) 1.208(7); C(2)–C(1)–Pt(1) 178.7(5), C(10)–C(9)–Pt(1) 174.3(5), C(1)–C(2)–C(3) 172.6(5), C(9)–C(10)–C(11) 172.9(6).

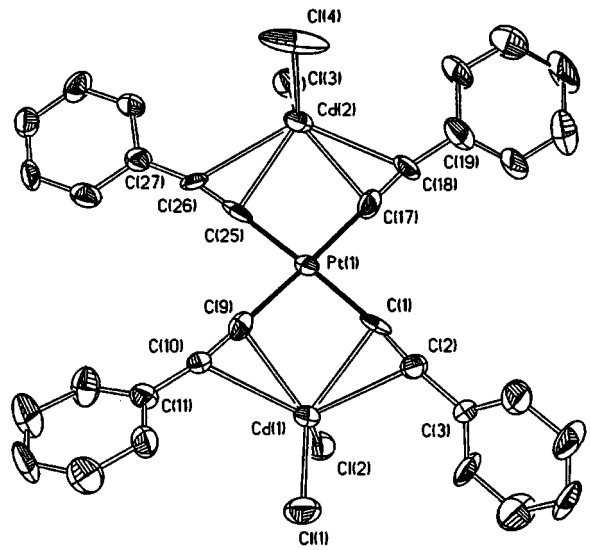

Fig. 2 Structure of the anion $[\{Pt(\mu\text{-}\kappa C^{\alpha}:\eta^2\text{-}C{\equiv}CPh)_4\}(CdCl_2)_2]^{2-}$ in complex **2** (phenyl groups have been omitted for clarity). Selected interatomic distances (Å) and angles (°): Pt(1)–C(1) 1.989(13), Pt(1)–C(9) 2.012(13), Pt(1)–C(17) 2.003(13), Pt(1)–C(25) 1.996(15), Cd(1)–C(1) 2.459(11), Cd(1)–C(9) 2.403(11), Cd(1)–C(2) 2.576(12), Cd(1)–C(10) 2.670(11), Cd(2)–C(17) 2.423(12), Cd(2)–C(25) 2.428(11), Cd(2)–C(18) 2.598(14), Cd(2)–C(26) 2.657(12); C(2)–C(1)–Pt(1) 173.1(10), C(10)–C(9)–Pt(1) 178.3(10), C(18)–C(17)–Pt(1) 176.8(12), C(26)–C(25)–Pt(1) 176.9(10), C(1)–C(2)–C(3) 173.4(13), C(9)–C(10)–C(11) 169.7(12), C(17)–C(18)–C(19) 168.5(14), C(25)–C(26)–C(27) 167.3(13).

is the expected 1 : 2 bis(η^2-alkyne) adduct, the centrosymmetric tetranuclear anion of **1**‡ is formed by two eclipsed 'Pt(C≡PCh)$_4$' units which are connected by two CdCl fragments. In **2**, the two chlorine atoms and the midpoints of the respective *cis* η^2-alkyne fragments form a pseudo-tetrahedral coordination environment about each cadmium, with the $CdCl_2$ fragments almost perpendicular to the coordination plane of the platinum atom (97.4 and 91.1°). On the other hand, in **1** the cadmium atoms are in a rather complicated environment formed by a chlorine atom, four C_α atoms of four alkynyl entities and two Pt–Cd bonds.

The Cd–Cl distances are very similar in the two complexes [2.435(2) **1**, 2.393(4)–2.427(3) Å **2**] and are comparable to other Cd–Cl distances.[2e] It is worth noting that although in both anions the alkynyl ligands remain σ-bonded to the platinum centre their interactions with the cadmium centres are very different in the two complexes. Thus, in **2**, each cadmium is η^2-bonded to two *cis* alkynyl functions, which have the common bonding mode μ-κC$^\alpha$:η^2(σ–π). The Cd atoms are displaced from the Pt(II) coordination plane [1.0878 Å Cd(1) and 0.4405 Å Cd(2)], generating non-planar PtC_4Cd cores. The Pt–Cd distances [Pt(1)–Cd(1) 3.2063(10) Å and Pt(1)–Cd(2) 3.3117(10) Å] are close to the sum of van der Waals radii (3.4 Å)[7] suggesting that only very weak interactions, if any, are present. In contrast, in the tetranuclear anion of **1**, the cadmium atoms are bonded only to the C_α carbon atoms of four alkynyl functions (two associated with each Pt atom), which display the less usual μ-κC$^\alpha$C$^\alpha$(σ-Pt, σ-Cd) bonding mode. The interactions of the C_β atoms with Cd centres can be considered negligible. The very short Pt–Cd distance, close to the sum of the Pauling covalent radii,[8] and the Pt–C_α–Cd bond angles, somewhat smaller than 90° [range 78.59(16)–82.15(16)°], support the possibility of direct bonding interactions between Pt(II) and Cd(II). The donor properties of a d^8 ML$_n$ complex, particularly enhanced in anionic platinate complexes, are now well documented.[9,10] Presumably, in this complex the four Pt···Cd bonding interactions are responsible for the structure and stability of this tetranuclear anionic cluster. However, the particular preference for the final rhombic planar Pt_2Cd_2 metal core [Cd–Pt–Cd 104.49(3)°; Pt–Cd–Pt 75.51(3)°] with the chlorine atoms also contained in the same plane is not clear at the moment. Probably, the driving force in the formation of **1** could be rationalised as an equilibrium between Pt···Cd, Cd···alkynyl and Cd···Cl bonding interactions.

The different bonding mode of the alkynyl ligand in both complexes is particularly reflected in the ν(C≡C) absorption, which in **1** is shifted to slightly higher frequency (2095 cm^{-1}) than in the starting material [$(NBu_4)_2$[Pt(C≡CPh)$_4$][6] 2075 cm^{-1}] and in **2** is shifted to a lower frequency (2066 cm^{-1}).

The presence of metal–metal interactions in **1** is also suggested by preliminary studies of the optical properties of both complexes, which are strongly emissive in frozen solutions ($CHCl_3$) and in the solid state at room temperature. Complex **2** displays a structured emission (maxima at *ca.* 432 and 471 nm; λ_{max}^{exc} = 335 nm, Stokes shift 6703 cm^{-1}) with a vibrational spacing of 2095 cm^{-1} characteristic of ν(C≡C), which is somewhat similar to that of the precursor $(NBu_4)_2$[Pt(C≡CPh)$_4$] (vibronic structural band at *ca.* 447 nm). Thus, the presence of two $CdCl_2$ units η_2 attached to the acetylenic entities does not induce a significant change in this emission, which on the basis of previous spectroscopic work with alkynyl compounds is attributed to a $\pi^*/p_z \rightarrow d_{z^2}$ transition (MLCT).[11] In contrast, complex **1** exhibits an asymmetric emission (with a low energy tail) centred at λ_{max}^{exc} *ca.* 495 nm (20202 cm^{-1}, hwhm of 1873 cm^{-1}). The absence of vibronic progression in the emission profile and the observed red-shift of both the emission and excitation maxima (λ_{max}^{exc} 433 nm) suggest a significant contribution of the Pt–Cd interactions to the orbitals (probably HOMO) involved in the optical transition. On the basis of previous results,[12] we tentatively attribute this emission to the transition π^*(C≡CPh) → CC (Pt_2Cd_2) (cluster centred to ligand charge transfer), mixed with a metal–metal (Pt–Cd) based charge transfer. Further investigation of the reactivity of other alkynyl platinum complexes towards different cadmium substrates and studies (including molecular orbital calculations) of their properties are currently in progress.

We thank the Dirección General de Enseñanza Superior (Spain, Projects PB95-0003C02-01 02 and PB95-0792) and the University of La Rioja (Project API-99/B17 and a grant to J. G.) for financial support.

Notes and references

† Experimental details and spectroscopic data (including emission and excitation spectra of **1** and **2**) available as supplementary material upon request to the authors.

‡ *Crystallographic data*: **1**·2CH_2Cl_2, $C_{49}H_{58}CdCl_3NPt$, M = 1074.80, monoclinic, space group $C2/m$, a = 20.490(5), b = 16.330(7), c = 16.311(4) Å, β = 120.013(16)°, V = 4726(3) Å^3, Z = 4, λ(Mo-Kα) = 0.71073 Å, μ(Mo-Kα) = 3.609 mm^{-1}, 5560 independent reflections measured at 173 K, 4560 data with $I > 2\sigma(I)$, 364 parameters. Final R indices: R_1 = 0.0383, wR_2 = 0.1074 (0.0485 and 0.1116 for all data). One of the phenyl rings was found to be disordered with common *ipso*-C(11) and *para*-C(14) positions. The disorder was modelled with fixed 50% site occupancy for the disordered *meta* and *para* carbons.

2·0.6H_2O: empirical formula, $C_{64}H_{92}Cd_2Cl_4N_2Pt$·0.6$H_2O$, M = 1461.60, monoclinic, space group $I2/a$, a = 40.625(6), b = 20.3820(10), c = 25.482(4) Å, β = 106.540(10)°, V = 20227(5) Å^3, Z = 12, λ (Mo-Kα) = 0.71073 Å, μ (Mo-Kα) = 2.981 mm^{-1}, 17819 independent reflections measured at 150 K, 10355 data with $I > 2\sigma(I)$, 1024 parameters. Final R indices R_1 = 0.0745, wR_2 = 0.1882. The crystallographic assymetric unit contains 1.5 molecules of compound **2**, the core of the two molecules are essentially identical. The discussion of the structure refers to the molecule on a general position. The geometric parameters for the molecule residing on a centre of symmetry can be found in the supplementary material. CCDC 182/1408. See http://www.rsc.org/suppdata/cc/1999/2045/ for crystallographic files in .cif format.

1 (*a*) P. Knochel, *Comprehensive Organometallic Chemistry II*, ed. E. W. Abel, F. G. A. Stone and G. Wilkinson, Elsevier, Amsterdam, 1995, vol. 11, pp. 183–190; (*b*) J. Cason and F. S. Prout, *Org. Synth. III*, 1995, 601; (*c*) J. Boersma, *Comprehensive Organometallic Chemistry*, ed. G. Wilkinson, F. G. A. Stone and E. W. Abel, Pergamon Press, Oxford, 1982, vol. 2, p. 858.

2 (*a*) Ref. 1(*c*), pp. 852–862; (*b*) *Organometallic Compouds of Zinc, Cadmium and Mercury*, ed. J. L. Wardell, Chapman and Hall, London, 1985; (*c*) P. O'Brien, ref. 1(*a*), vol. 3, pp. 196–206; (*d*) G. Parkin, *Encyclopedia of Inorganic Chemistry*, ed. R. B. King, Wiley, Chichester, 1994, vol. 1, pp. 469–477; (*e*) C. E. Holloway and M. Melník, *J. Organomet. Chem.*, 1996, **522**, 167 and references therein.

3 (*a*) R. Nast and C. Richers, *Z. Anorg. Allg. Chem.*, 1963, **319**, 320; (*b*) E. A. Jeffery and T. Mole, *J. Organomet. Chem.*, 1968, **11**, 393; (*c*) D. Barr, A. J. Edwards, P. R. Raithby, M.-A. Rennie, K. Verhorevoort and D. S. Wright, *J. Chem. Soc., Chem. Commun.*, 1994, 1627.

4 (*a*) J. R. Berenguer, J. Forniés, E. Lalinde and F. Martínez, *Organometallics*, 1996, **15**, 4537; (*b*) J. R. Berenguer, J. Forniés, E. Lalinde, A. Martín and M. T. Moreno, *J. Chem. Soc., Dalton Trans.*, 1994, 3343; (*c*) I. Ara, J. R. Berenguer, J. Forniés and E. Lalinde, *Inorg. Chim. Acta*, 1997, **264**, 199.

5 Only a few Pt,Cd compounds have been reported: M. N. Bochkarev, G. A. Razuvaev, L. P. Mairova, N. P. Makarenko, V. I. Sokolov, V. V. Bashilov and O. A. Rentov, *J. Organomet. Chem.*, 1977, **131**, 399; F. Bonati and H. C. Clark, *Can. J. Chem.*, 1979, **57**, 483; C. Pettinari, F. Marchetti, A. Cingolani, S. I. Troyanov and A. Drozdov, *J. Chem. Soc., Dalton Trans.*, 1998, 3335.

6 P. Espinet, J. Forniés, F. Martínez, M. Tomaś, E. Lalinde, M. T. Moreno, A. Ruiz and A. J. Welch, *J. Chem. Soc., Dalton Trans.*, 1990, 791.

7 J. E. Huheey, E. A. Keiter and R. L. Keiter, *Inorganic Chemistry*, Harper Collins College Publishers, New York, 4th edn., 1993, p. 292.

8 J. G. Stark and H. G. Wallace, *Chemistry Data Book*, John Murray, London, 1976 (1.48 + 1.39 = 2.87 Å).

9 L. R. Falvello, J. Forniés, A. Martín, R. Navarro, V. Sicilia and P. Villarroya, *Inorg. Chem.*, 1997, **36**, 6166 and references therein.

10 G. Aullón and S. Alvarez, *Inorg. Chem.*, 1996, **35**, 3137 and references therein.

11 L. Sacksteder, E. Baralt, B. A. DeGraff, C. M. Lukehart and J. N. Demas, *Inorg. Chem.*, 1991, **30**, 2468.

12 I. Ara, J. Forniés, J. Gómez, E. Lalinde, R. I. Merino and M. T. Moreno, *Inorg. Chem. Commun.*, 1999, **2**, 62; (*b*) J. P. H. Charmant, J. Forniés, J. Gómez, E. Lalinde, R. I. Merino, M. T. Moreno and A. G. Orpen, *Organometallics*, 1999, **18**, 3353.

Communication 9/06394C

A double step synthesis of mesoporous micrometric spherical MSU-X silica particles

Cédric Boissière, Arie van der Lee, Abdeslam El Mansouri, André Larbot and Eric Prouzet*

Laboratoire des Matériaux et Procédés Membranaires, (CNRS UMR 5635) E.N.S.C.M, 8 rue de l'Ecole Normale, F-34280 Montpellier Cedex 5, France. E-mail:prouzet@cit.enscm.fr

Received (in Oxford, UK) 10th August 1999, Accepted 9th September 1999

Spherical particles of mesoporous MSU-X silica in the micrometric size range have been obtained through a new double step process that led to an easy and highly reproducible synthesis pathway giving micelle templated structures with a large surface area and narrow pore size distribution

Micelle templated structures (MTS), like the mesoporous alumino-silicates M41S (MCM-41, MCM-48) are synthesized through an assembly mechanism between long chain quaternary ammonium compounds and inorganic species. They exhibit desirable properties such as high surface area (*ca.* 1000 $m^2\ g^{-1}$) and narrow pore size distribution in the range 20–100 Å.[1,2] Since their discovery, many groups have succeeded in expanding this new field to other ionic surfactants.[3] The possibility of using non-ionic surfactants such as those based on polyethylene oxide and block-copolymers was also demonstrated,[4–9] which led to a whole family of mesoporous silicas such as MSU-V,[10] MSU-G[11] and MSU-*X* (*X* = 1–4), where *X* refers to the non-ionic surfactant molecules that can be either alkyl PEO, alkyl–aryl PEO, polypropylene oxide PEO block copolymers or ethoxylated derivatives of sorbitan fatty esters (Tween™).[4] Although some reactions proceed in acidic or basic media,[12] syntheses of MSU-X materials were generally reported to occur at neutral pH even though syntheses using non-ionic block copolymers under highly acidic conditions (SBA-type materials) were also successfully explored.[8,13]

Whatever the nature of the template, among possible applications such as catalysts, grafting supports, or filtration materials, the use of MTS for chromatography applications has been claimed for years. However, this latter application requires the ability to synthesize homogeneous batches of spherical particles with a mean diameter of at least 5 μm.[14] Even if such particles have been observed once in a pH-dependent synthesis of MCM-41 particles,[15] until now the only specific syntheses have been of sub-μm particles of MCM-41 or MCM-48 materials[16–18] or 2 μm HMS particles.[19] Here, we describe the synthesis of MSU-X silica with perfectly controlled size and shape that would be suitable for liquid phase chromatography applications.

Our synthesis is based on a sodium fluoride aided hydrolysis of tetraethoxysilane dissolved in a dilute solution of non-ionic polyethylene oxide-based surfactants.[6,20] Depending on the initial mixing conditions, a milky mixture is usually obtained that settles to give a colorless microemulsion if conditions are carefully chosen. The final product contains aggregates of small particles (*ca.* 300 nm) with a 3D worm-hole porous structure.[21] We modified this synthesis process by an apparently slight but actually drastic change in the preparation. The main feature of this new approach lies in the capability to discriminate the assembly step from the hydrolysis step. To this purpose we added an intermediate step that utilises a mild acidic medium (pH *ca.* 2–4) in which, prior to the reaction, a stable colorless microemulsion containing all reactants is obtained. Hence, whatever the initial homogeneity of the surfactant–TEOS mixture, the homogeneity at the molecular level is always attained before the reaction starts. Moreover, one can use a TEOS/surfactant molar ratio of up to 25 or a swelling agent such as 1,3,5-trimethylbenzene and still obtain a stable colorless microemulsion, without any reaction. Hence, this approach does not proceed from previously reported systems such as for the synthesis of SBA materials that use block copolymers[8,13] or the synthesis of modified MSU-X materials through an acid $[N^0(N^+)X^-I^-]$ pathway[12] because these syntheses used acid as the hydrolysis catalyst whereas we use it only as an emulsion breaker (actually, a slight hydrolysis is observed but only after several days). As previously reported, the actual catalyst of the hydrolysis still remains sodium fluoride.[6]

In a typical synthesis, TEOS (Aldrich Chemicals) was dispersed in a 0.02 M solution of Tergitol 15S12 ($CH_3(CH_2)_{14}(EO)_{12}$, Union Carbide Chemicals) up to a molar ratio TEOS/surf. = 8. A milky emulsion was obtained, but the addition of 0.25 M hydrochloric acid (final pH between 2.0 and 4.0) destroys this emulsion within minutes, giving a perfectly colorless microemulsion composed of 6–7 nm monodisperse particles containing both surfactant and TEOS, as observed by dynamic light scattering experiments.[22] The solution was left to stand for 18 h and the hydrolysis of TEOS was induced by the addition of a small amount of sodium fluoride [NaF/TEOS = 1–4 (mol%)]. The reaction begins after *ca.* 1 h and although it is almost totally complete after 6 h, the mixture was allowed to stand for 3 days at 35 °C. A white powder was obtained with a yield close to 100% which was filtered off, dried and calcined at 620 °C for 6 h after a 6 h step at 200 °C (heating rate of 3 °C min^{-1}). This new process was successfully applied to the whole family of nonionic surfactants and block-copolymers of MSU-*x* (*x* = 1–4) materials and preparation of large batches was also successful.

The X-ray pattern (Fig. 1) exhibits a single narrow peak assigned to the pore center to center correlation length, characteristic of a worm-hole structure of the porous framework of MSU compounds.[4,6] Transmission electron microscopy (not shown here) reveals that the whole material is made of such a porous framework and that there is no amorphous component. As shown in Fig. 2, the nitrogen adsorption–desorption

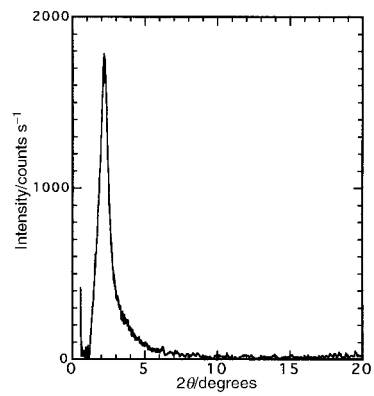

Fig. 1 X-Ray patterns of calcined MSU-1 silica obtained with Tergitol 15S12 and a NaF/TEOS ratio of 4 mol%. The pattern was recorded with a Bruker D5000 diffractometer in Bragg–Brentano reflection geometry. Cu-$L_{3,2}$ radiation was employed that was monochromatized by a graphite single crystal in the diffracted beam.

isotherm is typical of a well defined porous framework without any textural porosity, but the pore size is very dependent on the amount of fluoride. Keeping other parameters constant, the sample synthesized with a 1 mol% NaF/TEOS ratio exhibited a surface area of 910 m^2 g^{-1} and a pore diameter of 24Å (according to the Broekhoff and de Boer model[23]) whereas the sample synthesized with a NaF/TEOS ratio of 4 mol% gave a material with a pore diameter of 35 Å (surface area 1053 m^2 g^{-1}). Along with the higher crystallinity of the calcined material, the ability to increase the pore size by 10 Å by simply changing the amount of fluoride is one of the new features of this synthesis, which makes it different from previous reaction pathways.[4,6,12] This cannot be assigned to a salt effect since adding large amounts of NaCl does not affect the pore size.

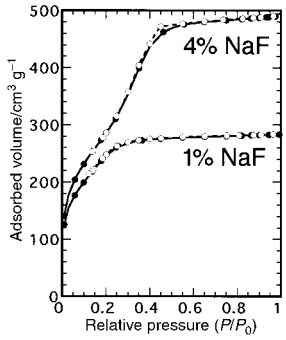

Fig. 2 Nitrogen adsorption (●) and desorption (○) isotherms of MSU-1 silica synthesized with Tergitol 15S12 and different NaF/TEOS molar ratios. Nitrogen adsorption isotherms were measured at 77 K on a micromeretics 2010 Sorptometer using standard continuous procedures and samples degassed at 150 °C for 15 h.

Since the reaction begins in a homogeneous medium, the final shape and size of particles will depend on the respective kinetics of the nucleation and aggregation processes. This competition depends on the quantity of nucleation seeds, and hence upon the NaF/TEOS ratio and on the concentration of the reagents. At low concentrations ([Tergitol 15S12] = 0.02 M), the aggregation process leads to spherical particles as shown by SEM (Fig. 3). The low rate of nucleation (NaF/TEOS = 1–2 mol%) allows the particles to grow up to the micrometer range and the homogeneity of the starting mixture leads to a quite narrow size distribution. Indeed, the mean size of the spherical particles displayed in Fig. 3(A) is 7 μm. A particle size analysis shows that while 98% of the powder volume is comprised of particles < 10 μm, 83% lie in the 3–8 μm size range. However, since the synthesis was not optimized for the preparation of isolated single particles, some of them that grew too closely together are stuck by grain boundaries that appeared during the particle growth.

The key of this reaction is the ability to separate the assembly step from the condensation step. This approach defines not only an improvement of previously reported syntheses of MSU-X materials, but also a different concept, which is particularly illustrated by the different behavior of some synthesis parameters such as sodium fluoride content. Similarly, syntheses using ethoxylated sorbitan molecules (Tween surfactants), which lead to nanometric particles when synthesized by the usual process,[7] also gives micrometric spherical particles when this new process is applied [Fig. 3(B)]. This makes this synthesis a new example of the versatility of the non-ionic route for the synthesis of MTS materials. Both the simple synthetic pathway along with the possibility to control all steps of the reaction, and the well defined morphology and nanostructure of the resulting powders make them suitable for future liquid phase chromatography applications that are currently being investigated.

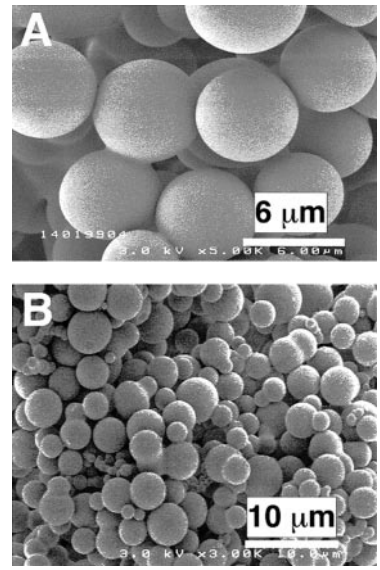

Fig. 3 SEM photograph of (A) calcined MSU-1 silica obtained with Tergitol 15S12, a molar ratio TEOS/surfactant = 8 and NaF/TEOS = 1 mol% and (B) calcined MSU-4 silica obtained with Tween 20, a molar ratio TEOS/surfactant = 4 and NaF/TEOS = 2 mol%. Spherical micrometric particles can be obtained with both surfactants but the mean size depends on various synthesis parameters, especially the TEOS/surfactant and NaF/TEOS ratios. SEM micrographs were obtained on a Hitachi S-5400 FEG microscope.

Notes and references

1 C. T. Kresge, M. E. Leonowicz, W. J. Roth, J. C. Vartuli and J. S. Beck, *Nature*, 1992, **359**, 710.
2 J. S. Beck, J. C. Vartuli, W. J. Roth, M. E. Leonowicz, C. T. Kresge, K. D. Schmitt, C. T.-W. Chu, D. H. Olson, E. W. Sheppard, S. B. McCullen, J. B. Higgins and J. L. Schlenker, *J. Am. Chem. Soc.*, 1992, **114**, 10 834.
3 Q. Huo, D. I. Margolese, U. Ciesla, D. G. Demuth, P. Feng, T. E. Gier, P. Sieger, A. Firouzi, B. F. Chmelka, F. Schüth and G. D. Stucky, *Chem. Mater.*, 1994, **6**, 1176.
4 S. A. Bagshaw, E. Prouzet and T. J. Pinnavaia, *Science*, 1995, **269**, 1242.
5 S. A. Bagshaw and T. J. Pinnavaia, *Angew. Chem., Int. Ed. Engl.* 1996, **35**, 1102.
6 E. Prouzet and T. J. Pinnavaia, *Angew. Chem., Int. Ed. Engl.* 1997, **36**, 516.
7 E. Prouzet, F. Cot, G. Nabias, A. Larbot, P. J. Kooyman and T. J. Pinnavaia, *Chem. Mater.*, 1999, **11**, 1498.
8 D. Zhao, J. Feng, Q. Huo, N. Melosh, G. H. Fredrickson, B. F. Chmelka and G. D. Stucky, *Science*, 1998, **279**, 548.
9 G. S. Attard, J. C. Glyde and C. G. Göltner, *Nature*, 1995, **378**, 366.
10 P. Tanev and T. J. Pinnavaia, *Science*, 1996, **271**, 1267.
11 S.-S. Kim, W. Zhang and T. J. Pinnavaia, *Science*, 1998, **282**, 1302.
12 S. A. Bagshaw, T. Kemmitt and N. B. Milestone, *Microporous Mesoporous Mater.*, 1998, **22**, 419.
13 D. Zhao, Q. Huo, J. Feng, B. F. Chmelka and G. D. Stucky, *J. Am. Chem. Soc.*, 1998, **120**, 6024.
14 R. Rosset, M. Caude and A. Jardy, *Manuel Pratique de Chromatographie en Phase Liquide*, Masson, Paris, 1996.
15 H. Yang, G. Vovk, N. Coombs, I. Sokolov and G. A. Ozin, *J. Mater. Chem.*, 1998, **8**, 743.
16 M. Grün, I. Lauer and K. K. Unger, *Adv. Mater.*, 1997, **9**, 254.
17 M. Grün, K. K. Unger, A. Matsumoto and K. Tsutsumi, *Microporous Mesoporous Mater.*, 1999, **27**, 207.
18 K. Schumacher, M. Grün and K. K. Unger, *Microporous Mesoporous Mater.*, 1999, **27**, 201.
19 G. Büchel, M. Grün, K. K. Unger, A. Matsumoto and K. Tsutsumi, *Supramol. Sci.*, 1998, **5**, 253.
20 A. C. Voegtlin, F. Ruch, J. L. Guth, J. Patarin and L. Huve, *Microporous Mater.*, 1997, **9**, 97.
21 F. Cot, P. J. Kooyman, A. Larbot and E. Prouzet, in *Mesoporous Molecular Sieves 1998*, ed. L. Bonneviot, F. Beland, C. Danumah, S. Giasson and S. Kaliaguine, Elsiever Science, Amsterdam, Lausanne, New York, Oxford, Shannon, Singapore, Tokyo, 1998, vol. 117.
22 C. Boissière, A. Larbot and E. Prouzet, unpublished work.
23 J. C. P. Broekhoff and J. H. de Boer, *J. Catal.*, 1968, **10**, 377.

Communication 9/06509A

An unusual matrix of stereocomplementarity in the hydroxylation of monohydroxy fatty acids catalysed by cytochrome P_{450} from *Bacillus megaterium* with potential application in biotransformations

Farjad Ahmed,[ac] Eiman H. Al-Mutairi,[d] Kathryn L. Avery,[ac] Paul M. Cullis,[ac] William U. Primrose,[bc] Gordon C. K. Roberts[bc] and Christine L. Willis[d]

[a] *Department of Chemistry, University of Leicester, Leicester, UK LEI 7RH. E-mail: pmc@le.ac.uk*
[b] *Department of Biochemistry, University of Leicester, Leicester, UK LEI 7RH*
[c] *Centre for Mechanisms of Human Toxicity, University of Leicester, Leicester, UK LEI 7RH*
[d] *School of Chemistry, University of Bristol, Cantock's Close, Bristol, UK BS8 1TS*

Received (in Liverpool, UK) 20th July 1999, Accepted 6th September 1999

Cytochrome P_{450} from *Bacillus megaterium* catalyses the diastereoselective hydroxylations of 13-hydroxymyristic acid, to predominantly *erythro*-12,13-dihydroxymyristic acid, and of 12-hydroxymyristic acid to give predominantly *threo*-12,13-dihydroxymyristic acid, in reactions that are stereocomplementary and with considerable potential application in biotransformations.

During the past decade, purified enzymes have been widely used to effect transformations of value in synthetic chemistry.[1] In addition to the familiar and widely exploited hydrolases and reductases, there remains a considerable range of potentially interesting and challenging enzyme-catalysed chemical transformations, mostly notably the functionalisation of unactivated positions, to be exploited in this context. We report here the results of our studies on the stereoselectivity and regioselectivity shown by cytochrome P_{450} from *Bacillus megaterium* in the hydroxylation of hydroxy fatty acids, and note a quite remarkable matrix of stereoselective complementarity.

Cytochromes P_{450} form a diverse superfamily of enzymes capable of inserting an atom of oxygen into a dazzling range of substrates, *e.g.* fatty acids, prostaglandins, steroids, polycyclic aromatics.[2] In contrast to the mammalian cytochromes P_{450} which are membrane-bound proteins, cytochromes P_{450} from bacterial sources have proved more tractable for study at the molecular level by virtue of being soluble proteins. The most extensively studied of the bacterial enzyme systems is cytochrome $P_{450\,CAM}$ from *Pseudomonas* which catalyses the hydroxylation of camphor to the 5-*exo*-hydroxycamphor.[3] This system is a typical three component system requiring a cytochrome P_{450} reductase, an iron–sulfur electron transfer protein and the cytochrome P_{450} hydroxylase protein, and exhibits a comparatively tight substrate specificity. Both of these features detract from its use in biotransformations although a number of mutant proteins of broader specificity have recently been reported. In contrast, the class 2 cytochrome P_{450} from *Bacillus megaterium* requires only a single redox component and this forms part of the multifunctional protein that incorporates both the flavoprotein NADPH reductase domain and the heme-containing P_{450} domain.[4] The enzyme has been overexpressed[5] and an X-ray crystal structure of the P_{450} domain has been determined.[6] Cytochrome $P_{450\text{-}BM3}$ catalyses the hydroxylation of a range of fatty acids to give mono- and dihydroxylated fatty acids. Capdevila *et al.* have reported the selective oxidation of arachidonic acid,[7] and our own preliminary observations suggest that the range of potential alternative substrates accepted by the enzyme may be quite large, including steroids, coumarins and sulfides.[8] To determine its potential utility in carrying out useful biotransformations we have explored the regio- and stereo-selectivity in the $P_{450\text{-}BM3}$ catalysed oxidation of hydroxylated fatty acids.

Wild-type cytochrome $P_{450\text{-}BM3}$ is known to catalyse the monohydroxylation of fatty acids such as myristic and palmitic acids at the ω-1, ω-2 and ω-3 positions, and also to give rise to lesser amounts of dihydroxylated products.[4a] The production of these dihydroxylated products clearly arises from a 'second round' of hydroxylation of the first formed monohydroxy fatty acids. The monohydroxy fatty acids are evidently poorer substrates for cytochrome $P_{450\text{-}BM3}$ (Table 1) such that the amount of dihydroxylation product observed will depend on the extent of reaction and the reaction conditions. Although there has been a considerable amount of work reported on the regioselectivity of monohydroxylation of fatty acids by cytochrome $P_{450\text{-}BM3}$,[4a] hitherto there have been no studies on the stereochemical courses of these processes. Furthermore, there has been little reported on the hydroxylation of functionalised fatty acids. In this study we have exploited the enantiomers of 12-hydroxy- **1** and (*R*)-13-hydroxy-myristic acid **2**.

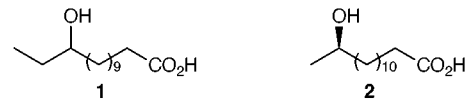

The route for the enantioselective synthesis of 12-hydroxymyristic acid is shown in Scheme 1. The enzyme-catalysed reduction of 2-oxobutanoic acid with either lactate dehydrogenase from *Bacillus stearothermophilus* (*BS*-LDH)[9] or hydroxyisocaproate dehydrogenase from *Lactobacillus bulgaricus* subsp. *delbruckeii* (*LB*-hicDH),[10] gave, after esterification, methyl 2-hydroxybutanoate (*S*)-**3** and (*R*)-**3** respectively. A straightforward series of reactions led to the conversion of the hydroxy ester **3** to the C_6-aldehyde **4** which, on reaction with the C_8-ylide, led to formation of predominantly the *Z*-alkene **5**. Finally deprotection of the alcohol and reduction of the double bond gave either (*S*)- or (*R*)-12-hydroxymyristic acid **1**. (*R*)-13-Hydroxymyristic acid **2** was prepared by a similar route from ethyl (*R*)-3-hydroxybutanoate.

In order to identify the products from the cytochrome P_{450}-catalysed oxidation of **1** and **2**, authentic samples of *erythro*- and *threo*-12,13-dihydroxymyristic acids **6** and **7** were required. Treatment of acetaldehyde with the ylide derived from the C_{12}-salt **8** gave a 9:1 mixture of *Z*:*E* alkenes **9** and **10** (Scheme 2).

Table 1

Substrate	K_M/μM	k_{cat}[a]/min^{-1}
Myristate	8	3127
(13*R*)-Hydroxymyristate	33	139
(12*R*)-Hydroxymyristate	32	119
(12*S*)-Hydroxymyristate	11	72

[a] k_{cat} values are based upon monitoring of NADPH turnover, and with the exception of myristate, where the coupling efficiency is known to be very high, have not been corrected for uncoupled peroxidase for oxidase activity. The values for hydroxymyristic acid are therefore upper estimates.

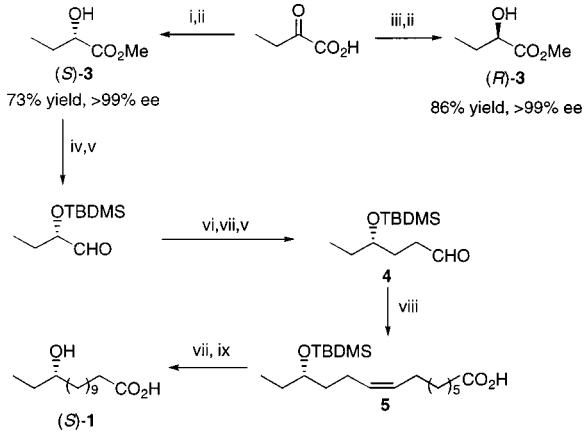

Scheme 1 *Reagents and conditions*: i, *BS*-LDH, NADH, FDH, HCO_2Na; ii, CH_2N_2; iii, *LB*-hicDH, NADH, FDH, HCO_2Na; iv, TBDMSOTf, pyridine; v, DIBAL-H, toluene, −78 °C; vi, Ph_3PCHCO_2Et, CH_3CN; vii, H_2, Pd on $CaCO_3$; vii, $Ph_3P^+CH(CH_2)_6CO_2H$ Br^-, NaH, DMSO; xi, TBAF, THF.

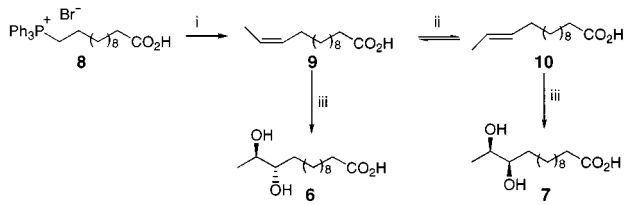

Scheme 2 *Reagents*: i, Bu^tOK, CH_3CHO; ii, I_2; iii, OsO_4 (cat), NMO.

Dihydroxylation of **9** using catalytic osmium tetroxide in the presence of *N*-methylmorpholine *N*-oxide (NMO) gave the *erythro*-diol **6**. Isomerisation of the double bond with iodine followed by dihydroxylation gave predominantly the *threo*-diol **7**.

Incubation of either enantiomer of 12-hydroxymyristic acid **1** or (*R*)-13-hydroxymyristic acid **2** with cytochrome $P_{450\text{-}BM3}$ together with an NADPH-regenerating system[11] (NADP, glucose-6-phosphate, $MgCl_2$ and glucose-6-phosphate dehydrogenase) both gave 12,13-dihydroxymyristic acid as a major product (yields from 13*R*: 85%; 12*R*: 79%; 12*S*: 64% based on total products identified by GC).[12] Using the authentic samples obtained above we have shown that hydroxylation of (*R*)-12-hydroxymyristic acid catalysed by cytochrome $P_{450\text{-}BM3}$ not only occurred regioselectivity but also stereoselectivity at ω-1 giving predominantly the *threo*-12,13-dihydroxymyristic acid [(12*S*,13*S*)-12,13-dihydroxymyristic acid, 80%; (12*S*,13*R*)-12,13-dihydroxymyristic acid 20%] (Scheme 3). Similarly (*S*)-12-hydroxymyristic acid was regioselectivity and stereoselectively hydroxylated at the ω-1 position to give predominantly the enantiomeric *threo*-12,13-dihydroxymyristic acid diastereoisomer [(12*R*,13*R*)-12,13-dihydroxymyristic acid, 80%; (12*R*,13*S*)-12,13-dihydroxymyristic acid 20%]. In contrast to

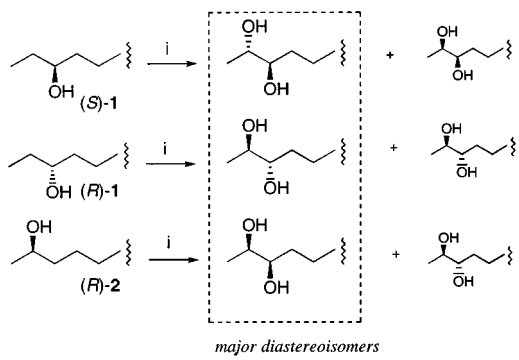

Scheme 3 *Reagents and conditions*: i, $P_{450\ BM3}$, NADP, glucose-6-phosphate, $MgCl_2$, glucose-6-phosphate dehyrogenase, phosphate buffer (0.1 M, pH 8.0).

this, starting from the (*R*)-13-hydroxymyristic acid, cytochrome $P_{450\text{-}BM3}$ catalyses the second hydroxylation at the ω-2 position stereoselectivity to give predominantly the *erythro*-12,13-dihydroxymyrisitic acid [(12*S*,13*R*)-12,13-dihydroxymyristic acid, 85%; (12*R*,13*R*)-12,13-dihydroxymyristic acid 15%] (Scheme 3). Clearly, in all three cases the preference is for oxygen insertion into the C–H of the methylene group *adjacent* to the hydroxymethylene moiety, rather than into the C–H of the hydroxymethylene goups itself, which would lead to the corresponding ketone. This would be consistent with a mechanism that does not involve a hydrogen abstraction since placement of the radical centre on the carbon atom bearing the hydroxy group would have been expected to be energetically preferred.

The observation of stereoselective hyroxylation of even flexible long chain hydroxy fatty acids catalysed $P_{450\text{-}BM3}$ has demonstrated an interesting, stereocomplementary matrix of biotransformations. The one major drawback that can be envisaged is the requirement for NADPH, however we have already addressed this by developing two systems in which the reducing equivalents are provided directly from an electrode thus allowing the oxidation to be driven electrochemically.[13] We have also demonstrated that $P_{450\text{-}BM3}$ is not restricted to long chain fatty acids and will tolerate a wide range of functionality in the chain. This system holds great potential for further exploitation in synthetic chemistry.

Notes and references

1 C. H. Wong, G. J. Shen, R. L. Pederson, Y. F. Wang and W. J. Hennen, *Methods Enzymol.*, 1991, **202**, 591.

2 *Cytochrome P450: Structure Mechanism and Biochemistry*, ed. P. R. Ortiz de Montellano, 2nd edn., Plenum Press, New York, 1995.

3 T. L. Poulos, B. C. Finzel and A. J. Howard, *J. Mol. Biol.*, 1987, **195**, 687.

4 (*a*) Y. Miura and A. J. Fulco, *Biochem. Biophys. Acta*, 1975, **388**, 305; (*b*) L. O. Narhi and A. J. Fulco, *J. Biol. Chem.*, 1986, **261**, 7160.

5 J. S. Miles, A. W. Munro, B. N. Rospendowski, W. E. Smith, J. McKnight and A. J. Thompson, *Biochem. J.* 1992, **288**, 503.

6 K. G. Ravichandran, S. S. Boddupalli, C. A. Hasemann, J. A. Peterson and J. Deisenhofer, *Science*, 1993, **261**, 731; H. Li and T. L. Poulos, *Nat. Struct. Biol.*, 1997, **4**, 140.

7 J. H. Capdevila, S. Wei, C. Helvig, J. R. Flack, Y. Belosludtsev, G. Truan, S. E. Graham-Lorence and J. A. Peterson, *J. Biol. Chem.*, 1996, **271**, 22663.

8 F. Ahmed, A. Celik, P. M. Cullis, W. U. Primrose and G. C. K. Roberts, unpublished results.

9 Full details of the synthetic route will be published later. For previous biotransformations to give hydroxy acids, see D. Bur, M. A. Luyten, H. Wynn, L. P. Provencher, J. B. Jones, M. Gold, J. D. Friesen, A. R. Clarke and J. J. Holbrook, *Can. J. Chem.*, 1989, **69**, 1065; B. L. Hirschbein and G. M. Whitesides, *J. Am. Chem. Soc.*, 1982, **104**, 4458; M.-J. Kim and J. Y. Kim. *J. Chem. Soc., Chem. Commun.*, 1991, 326.

10 N. Bernard, K. Johnsen, J. L. Gelpi, J. A. Alvarez, T. Ferain, D. Garmyn, P. Hols, A. Cortes, A. R. Clarke, J. J. Holbrook and J. Delcour, *Eur. J. Biochem.*, 1997, **244**, 213.

11 C. H. Wong and G. M. Whitesides, *J. Am. Chem. Soc.*, 1981, **103**, 4890.

12 Enzymatic oxidation of fatty acids was performed by mixing cytochrome P_{450} (30 μM), substrate (10 mM) and a NADPH-regenerating system (comprising 10 mM NADP, 10 mM glucose-6-phosphate, 10 mM $MgCl_2$ and 1 unit glucose-6-phosphate dehydrogenase) in phosphate buffer (15 ml, 0.1 M, pH 8.0). After incubation for 1 h, the reactions were stopped by addition of 10 mL of 1 M HCl and the products extracted with ethyl acetate (2 × 15 mL). GC-EIMS analysis (70 eV) of the corresponding methyl ester was carried out on a Kratos Concept mass spectrometer (Kratos Instruments. Inc) equipped with a direct capillary interface to a Shimadzu 14A GC with electron impact ionisation using a HP35 capillary GC column (30 m × 0.25 μM HP35, Hewlett Packard). Chromatography of the sample was performed at a linear flow rate of helium gas of 68 cm s^{-1} and, after 2 min at 180 °C, the temperature was raised to 270 °C (at a rate 8 °C min^{-1}) and then held at 270 °C.

13 F. Ahmed, A. P. Abbott, W. U. Primrose, P. M. Cullis and G. C. K. Roberts, unpublished work, 1999, patent applied for.

Communication 9/05974A

ChemComm

Influence of a dimetal ion binding ferrocene ligand on the samarium diiodide promoted pinacol coupling reaction

Torben Birk Christensen, Ditte Riber, Kim Daasbjerg and Troels Skrydstrup*

Department of Chemistry, University of Aarhus, Langelandsgade 140, 8000 Aarhus C, Denmark. E-mail: ts@kemi.aau.dk

Received (in Liverpool, UK) 25th May 1999, Accepted 1st September 1999

Substantial yield increases have been noted in the use of a di-SmI_2 binding ligand for the pinacol coupling of alkyl aldehydes compared to 1:1 complexes of SmI_2 and tetraglyme. High diastereoselectivities of *ca.* 10:1 are also observed for α-substituted alkyl aldehydes in favour of the (±)-isomers.

Samarium diiodide is an important one-electron reducing agent which has been employed in a multitude of organic synthetic transformations.[1] When pertinent, these reactions are generally associated with high levels of stereochemical control. One exception is the intermolecular pinacol coupling reaction of carbonyl compounds[2] to access vicinal diol systems. With aryl ketones or aldehydes, these reactions have been reported to be high yielding,[3,4] but are also characterised by low diastereoselectivities (±:*meso, ca.* 1.3:1), the exception being when certain metal complexes of aryl aldehydes are used.[5] Only a few examples of alkyl aldehydes have been studied so far where similar ±:*meso* ratios were noted.[3] In our efforts to improve the diastereoselectivities of the SmI_2 promoted pinacol coupling of aryl and alkyl aldehydes, we have recently reported on the beneficial effects the addition of tetraglyme derivatives to the one electron reducing agent may have prior to the coupling step.[6]

We have been interested in synthesising ligands which can bind two divalent samarium ions with the purpose of investigating their influence on the diastereoselectivities and yields in the SmI_2-induced pinacol coupling (Scheme 1). Here we show that the use of one such example may significantly increase yields of the vicinal diols obtained from branched alkyl aldehydes, while still retaining the high ±-selectivity.

As a dimetal ion complexing agent, we prepared the bis-tetraglyme derivative **1** possessing a metallocene unit as the connector (Scheme 1). This ligand was chosen primarily because of the affinity of tetraglyme for divalent samarium ions,[6,7] while rotational freedom of the cyclopentadienyl rings around the iron core[8] allows radical or anionic intermediates of the pinacol coupling to easily find suitable conformations between the two lanthanide metal centers. The ability of ferrocene to absorb in the visible light region also simplifies the isolation of this ligand type upon chromatographic separation of the products.

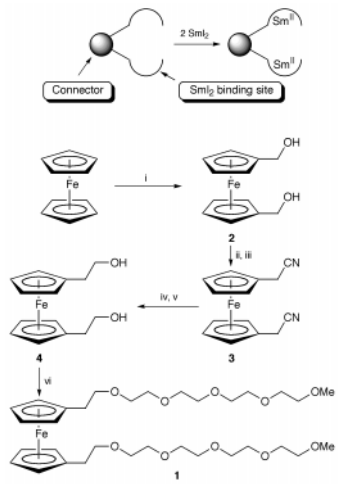

Scheme 1 *Reagents and conditions:* i, 2.1 equiv. BuLi, 2.1 equiv. TMEDA, then $(CH_2O)_n$, 54%; ii, PCl_3, THF–Pyr; iii, KCN, H_2O–THF, 52% (2 steps); iv, NaOH, EtOH, 89%; v, $LiAlH_4$, THF, 77%; vi, 3.0 equiv. NaH, DMF, then 3.5 equiv. $MeO(CH_2CH_2O)_4Ts$, 86%.

The synthesis of the ferrocene ligand **1** is depicted in Scheme 1, adapting procedures previously developed by Frejd[9] and Moritani.[10] Formation of bis(hydroxymethyl)ferrocene **2** was easily achieved by direct lithiation of ferrocene with 2 equiv. of BuLi followed by addition of paraformaldehyde. The dichloride obtained by treating **2** with PCl_3 was immediately converted to the dicyanide **3**. Basic hydrolysis and reduction then gave the crystalline diol **4** (mp 43–44 °C). Introduction of the complete side chains was achieved by alkylation of **4** with the tosylate of tetraethylene glycol monomethyl ether affording **1** as an orange–brown coloured oil in 86% yield.

Addition of a 0.1 M THF solution of SmI_2 to 0.5 equiv. of ligand **1** at 20 °C leads to darkening of the solution with eventual precipitation of a black solid. An immediate reaction was noted upon subjecting this mixture to benzaldehyde affording a *ca.* 5:1 diastereoselectivity in favour of the *meso*-isomer (Table 1, entry 1). Augmenting the ligand to divalent samarium ratio to 1:1 had no effect on either the *meso*:± selectivity nor the yields (entry 2). Whereas no notable improvement in the diastereoselectivity of the diol product is noted with ligand **1** compared with a similar reaction using 1 equiv. of tetraglyme (entry 3), these results do suggest that **1** binds two metal ions.†

Noteworthy are the effects observed in the pinacol coupling of alkyl aldehydes. The tetraglyme–SmI_2 complex converts cyclohexanecarbaldehyde to a 10:1 mixture of ±:*meso* isomers albeit in low yield (29%) after 24 h at 20 °C (entry 4). Under similar conditions with **1**–2SmI_2, this yield was remarkably increased to 81% (entry 5) while still maintaining the high diastereoselectivity, making this method competitive with other metal reducing systems.[2] On the other hand, premixing SmI_2 to 1 equiv. of ligand **1** prior to the addition of cyclohexanecarbaldehyde maintains the high diastereoselectivity but lowers the yield of the reaction to 38% (entry 6), a result which resembles that of the tetraglyme–SmI_2 complex. The same trend was noted with tetrahydrobenzaldehyde, where a 24% increase in the pinacol coupling yield was noted with a ±:*meso* selectivity of 11:1 (entries 7 and 8) when ligand **1** was employed instead of tetraglyme.

In the SmI_2 induced dimerisation of isobutyraldehyde, the reaction is less clean affording a modest yield of the diol (entry 9, 44%) with a diastereoselectivity of 1.9:1. Whereas, this yield is even lower with tetraglyme (entry 10), the use of the **1**–2SmI_2 complex retains the 44% yield while increasing the selectivity to 10:1 (entry 11).

The Tischenko-type side reactions are problematic with linear aldehydes such as *n*-octanal, but again an increase in the yield of the coupled product is observed when using ligand **1** (entries 12 and 13). Interestingly, in this case the diastereo-

Table 1 Effect of a dimetal ion binding ligand on the SmI_2 promoted pinacol coupling.[a]

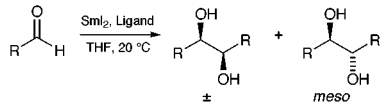

Entry	Aldehyde	Ligand (equiv.)[b]	Yield (%)[c]	Diastereosel (±:*meso*)
1	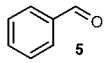 **5**	1 (0.5)	89	1:5.0
2	**5**	1 (1.0)	92	1:5.5
3	**5**	Tetraglyme (1.0)	83	1:5.9[d]
4	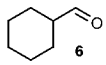 **6**	Tetraglyme (1.0)	29	10:1
5	**6**	1 (0.5)	81	10:1
6	**6**	1 (1.0)	38	13:1
7	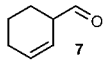 **7**	Tetraglyme (1.0)	53	14:1[e]
8	**7**	1 (0.5)	77	11:1[e]
9	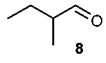 **8**	None	44	1.9:1
10	**8**	Tetraglyme (1.0)	24	10:1
11	**8**	1 (0.5)	44	10:1
12	$CH_3(CH_2)_6CHO$ **9**	Tetraglyme (1.0)	45	3.0:1
13	**9**	1 (0.5)	68	2.2:1
14	 **10**	None	79	8.5:1
15	**10**	Tetraglyme (1.0)	0	—
16	**10**	1 (0.5)	0	—

[a] Conditions: complexed or uncomplexed SmI_2 (0.1 M, 1.5 equiv.), aldehyde (1 equiv.), THF, 20 °C. [b] Based on the number of equivalents of SmI_2 added. [c] Based on isolated, chromatographically pure material. [d] Taken from ref. 6. [e] Determined after catalytic hydrogenation (Pd/C, H_2) of the diastereomeric mixture of diols.

selectivity is low suggesting that substitution at the α-position of the alkyl aldehyde is necessary for obtaining the high ±:*meso* ratio when using the polyethyleneglycol complexing agents. Increasing the steric bulkiness, as exemplified with pivalaldehyde, surprisingly led to no pinacol coupling with either tetraglyme or **1** (entries 15 and 16). Nevertheless, without these ligands SmI_2 promoted this dimerisation with an 8.5:1 selectivity (entry 14). The steric bulkiness of the aldehyde was sufficient to induce a high diastereoselectivity. These results again support the notion that uncomplexed SmI_2 is not available in solution when the one electron reducing agent is added to 0.5 equiv. of ligand **1**.

The combined findings suggest the formation of a complex between two samarium(II) metal ions and **1** as illustrated in Scheme 2. Coordination of the two aldehyde units to each of the two oxophilic metallic centers may then take place. The slow reactivity of alkyl aldehydes also suggests that there is only a low concentration of a ketyl radical species in solution. The close proximity of the carbon radical center to the other aldehyde, which possesses a low-lying LUMO due to its coordination to SmI_2, could lead to a radical addition step with concomitant reduction of the resulting alkoxyl radical by SmI_2.[6] A two electron reduction of the aldehyde to dianion **11**, which eventually couples to a second aldehyde, is a possible alternative mechanism because ligand **1** improves significantly the yields of these pinacol coupling reactions compared to that of tetraglyme, and although little effect is seen on the diastereoselectivities, these preliminary observations tend to support the radical addition mechanism where the entropy contribution is less important owing to the pseudo-intramolecular nature of this reaction.

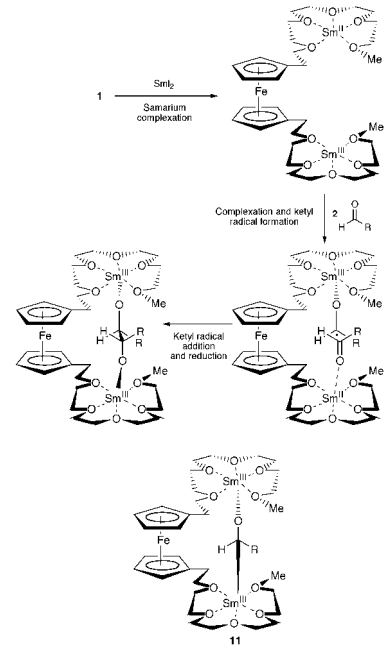

Scheme 2

In conclusion, we have shown that dimetal binding ligands can have a substantial effect on the SmI_2 induced pinacol coupling of alkyl aldehydes compared to that of tetraglyme. Efforts are underway to increase the utility of such ligands. The introduction of either planar chirality in the connector or asymmetric carbon centers in the tetraglyme units may also lead to the development of an asymmetric version of the pinacol coupling reaction with alkyl aldehydes.

We thank the University of Aarhus and the Danish National Science Foundation for generous financial support.

Notes and references

† Preliminary investigations of this complex by cyclic voltametry imply that the metallocene center does not influence the oxidation potential of SmI_2 (ref. 6 and 11).

1 For recent reviews on the application of SmI_2 in organic synthesis: A. Krief and A.-M. Laval, *Chem. Rev.*, 1999, **99**, 745; G. A. Molander and C. R. Harris, *Chem. Rev.*, 1996, **96**, 307; G. A. Molander and C. R. Harris, *Tetrahedron*, 1998, **54**, 3321; T. Skrydstrup, *Angew. Chem., Int. Ed. Engl.*, 1997, **36**, 345.

2 For several recent reviews on the pinacol coupling, see: T. Wirth, *Angew. Chem., Int. Ed. Engl.*, 1996, **35**, 61; R. G. Dushin, in *Comprehensive Organometallic Chemistry II*, ed. L.S. Hegedus, Pergamon, Oxford, 1995, vol. 12, p. 1071; A. Fürstner, *Angew. Chem., Int. Ed. Engl.*, 1993, **32**, 164. See also: A. Gansäuer and D. Bauer, *Eur. J. Org. Chem.*, 1998, 2673; Y. Yamamoto, R. Hattori and K. Itoh, *Chem. Commun.*, 1999, 825 and references therein.

3 J. Souppe, L. Danon, J. L. Namy and H. B. Kagan, *J. Organomet. Chem.*, 1983, **250**, 227; T. Honda and M. Katoh, *Chem. Commun.*, 1997, 369; R. Nomura, T. Matsuno and T. Endo, *J. Am. Chem. Soc.*, 1996, **118**, 11 666; N. Miyoshi, S. Takeuchi and Y. Ohgo, *Chem. Lett.*, 1993, 2129.

4 One exception is the SmI_2–HMPA induced pinacol coupling of benzaldehyde: J.-S. Shiue, C.-C. Lin and J.-M. Fang, *Tetrahedron Lett.*, 1993, **34**, 335.

5 N. Taniguchi, N. Kaneta and M. Uemura, *Tetrahedron*, 1998, **54**, 12 775.

6 H. L. Pedersen, T. B. Christensen, R. J. Enemærke, K. Daasbjerg and T. Skrydstrup, *Eur. J. Org. Chem.*, 1999, 565.

7 T. Imamoto, T. Hatajima, N. Takiyama, T. Takeyama, Y. Kamiya and T. Yoshizawa, *J. Chem. Soc., Perkin Trans. 1*, 1991, 3127.

8 G. W. Gokel, J. C. Medina and C. Li, *Synlett*, 1991, 677.

9 A.-S. Carlström and T. Frejd, *J. Org. Chem.*, 1990, **55**, 4175.

10 A. Sonoda and I. Moritani, *J. Organomet. Chem.*, 1971, **26**, 133.

11 R. J. Enemærke, K. Daasbjerg and T. Skrydstrup, *Chem. Commun.*, 1999, 343.

Communication 9/04278D

Isotypical *N*,*N*-dialkylcarbamato lanthanide complexes covering a range of 11 atomic numbers: direct experimental assessment of the lanthanide contraction in trivalent molecular compounds

Ulrich Abram,[a] Daniela Belli Dell'Amico,[b] Fausto Calderazzo,*[b] Cinzia Della Porta,[b] Ulli Englert,[c] Fabio Marchetti[d] and Alessandra Merigo[b]

[a] *Forschungszentrum Rossendorf, Institute of Radiochemistry, c/o Dresden University of Technology, Institute of Analytical Chemistry, 01062 Dresden, Germany*
[b] *Dipartimento di Chimica e Chimica Industriale, Università di Pisa, via Risorgimento 35, 56126 Pisa, Italy. E-mail: facal@dcci.unipi.it*
[c] *Institut für Anorganische Chemie der RWTH, Professor-Pirlet-Strasse 1, D-52074 Aachen, Germany*
[d] *Dipartimento di Ingegneria Chimica, dei Materiali, delle Materie Prime e Metallurgia, Università «La Sapienza» di Roma, via del Castro Laurenziano, 7, Box 15 Roma 62, I-00185 Roma, Italy*

Received (in Basel, Switzerland) 15th June 1999, Accepted 7th September 1999

The *N*,*N*-diisopropylcarbamato complexes of lanthanides(III) from neodymium (*Z* = 60) to ytterbium (*Z* = 70) were found to be isotypical, with Ln–O distances decreasing steadily with increasing *Z*, the lanthanide contraction in this series of molecular complexes being provisionally assigned to an increasing bond strength with increasing atomic number of the central metal atom.

The well known lanthanide contraction was originally recognized[1a] on the basis of X-ray diffractometric data on the ionic oxides and fluorides of the trivalent cations and estimated to correspond to about a 15% decrease of the radii on going from cerium to lutetium,[1] a correction[1b,c] being required for the decreasing coordination numbers (CN) along the series. In fact, no isotypical coordination compounds of lanthanides are known, for halide or oxide ligands, to cover the whole series; normally, changes of both space group and CN are encountered, on going from the first part to the second one[1d,e] of the series.

Coordination chemistry of lanthanides (Ln) is a subject of increasing interest,[2] the focus of the current studies being on uncharged complexes of Ln(III),[3] in view of their role in biochemistry[3a] and in carbon–carbon and carbon–nitrogen bond forming reactions,[3b–r] mainly catalyzed by organometallic derivatives [4] of these elements. A better understanding of these systems should originate from the synthesis of isotypical (*i.e.* with constant CN and geometry) and *neutral* compounds and by the determination of their interatomic parameters through diffraction methods.

We now report the preparation of some isotypical *N*,*N*-dialkylcarbamato complexes of the lanthanides. Although *N*,*N*-dialkylcarbamato complexes of transition d elements are well established,[5] such lanthanide derivatives are still in their infancy, mainly due to synthetic difficulties.[6]

The synthesis of the new *N*,*N*-diisopropylcarbamato derivatives of La, Nd, Eu, Gd and Ho, of the same general formula, has now been achieved by using the ether complexes $LnCl_3(ether)_x$ (ether = THF or Et_2O),[7] as starting materials [eqn. (1)]. Yields

$$4\ LnCl_3(ether)_x + 12\ CO_2 + 24\ NHPr^i_2 \longrightarrow Ln_4(O_2CNPr^i_2)_{12} + 12\ [NH_2Pr^i_2]Cl + 4x\ ether \quad (1)$$

(Ln = La, f^0; Nd, f^3; Eu, f^6; Gd, f^7; Ho, f^{10}; Er, f^{11})

of recrystallized product are generally moderate (20%) to satisfactory (50%).

The new isopropyl derivatives of Nd(III), Eu(III), Gd(III) and Ho(III) were found to be moderately soluble in hydrocarbons; these compounds are isotypical with one another and with the already known Yb(III) analogue.[6]

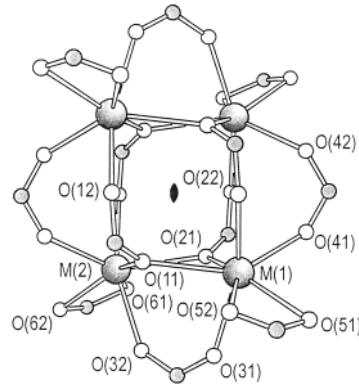

Fig. 1 Molecular structure of the lanthanide derivatives $M_4(O_2CNPr^i_2)_{12}$; M = Nd (*Z* = 60), Gd (*Z* = 64), Ho (*Z* = 67), Yb (*Z* = 70). The heptacoordinated metal atoms are shown with their oxygen donor atoms.

Complete crystal data were collected for the Nd (*Z* = 60), Gd (*Z* = 64), and Ho (*Z* = 67) derivatives,† to be compared with the already available information for the isostructural Yb species (*Z* = 70).[6] In these tetranuclear compounds, the heptacoordinate lanthanide is surrounded by terminal bidentate, bridging bidentate and bridging tridentate diisopropylcarbamato groups. The molecular core of the tetranuclear derivatives is schematically shown in Fig. 1.

The Ln–O average bond distances of the new *N*,*N*-diisopropylcarbamato complexes can be factorized as a function of the type of bonding (Table 1, Fig. 2). The Ln–O bond distance contracts along our series with increasing *Z*; more precisely, by assuming that the lanthanide-coordinated oxygen has the same radius of 1.21 Å as that of bicoordinated oxygen,[1c] the lanthanide contraction, averaged over the four different types of ligands (Table 1) is *ca.* 8% over the eight *Z* values from Nd to

Table 1 Average Ln–O bond distances (Å) in tetranuclear *N*,*N*-diisopropylcarbamato complexes of lanthanides, for different coordination modes. The quadratic dispersion from the average values is given in parentheses.

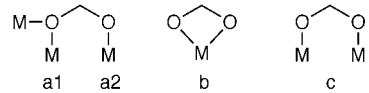

	Nd	Gd	Ho	Yb
a1	2.48(1)	2.40(2)	2.37(2)	2.34(5)
a2	2.33(1)	2.27(1)	2.24(1)	2.25(4)
b	2.42(1)	2.36(2)	2.33(2)	2.28(3)
c	2.35(2)	2.29(1)	2.26(1)	2.21(3)

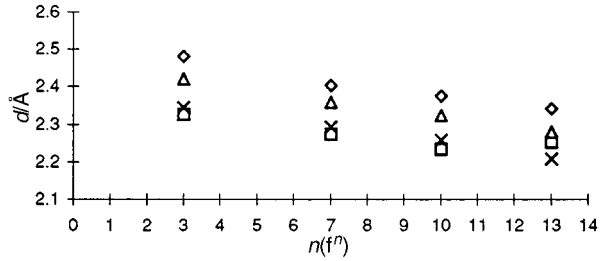

Fig. 2 Lanthanide(III)–oxygen bond distances (Å) *vs.* f^n electronic configuration in the tetranuclear *N,N*-diisopropylcarbamato complexes $M_4(O_2CNPr^i_2)_{12}$; M = Nd (Z = 60), Gd (Z = 64), Ho (Z = 67), and Yb (Z = 70). The ordinate axis shows the average Ln–O bond distances (Å): (◇) type a1, (□) type a2, (△) type b, (×) type c (from top to bottom, see Table 1). The anomalous behavior of the a2 distance for Yb is presumably due to the lower accuracy of the crystal data.[6]

Ho, Yb being excluded because of the lower accuracy of the older structural determination. This result can be linearly extrapolated to the 15 Z series from La to Lu giving a 14% average contraction over the whole series. This is substantially in agreement with the earlier findings for the predominantly ionic oxides.[1c]

An examination of the crystallographic literature[9] has disclosed a few other series of isotypical molecular compounds of lanthanides, namely, (η^6-arene)aryloxides, $Ln(OC_6H_3Pr^i\text{-}2,6)_3(THF)_2$ and THF adducts of tris(cyclopentadienyl), $Ln(\eta^5\text{-}C_5H_5)_3(THF)$, the expected decreasing trend of Ln–O interatomic distances being similarly observed.

A plausible interpretation of the present data is that the bond lanthanides form with oxygen-containing ligands becomes steadily stronger along the series. This suggests that relatively weaker bonds in the oxidation state +III should be found, for lanthanides, at the beginning of the series. This finding may be significant in connection with the catalytic phenomena observed[3e,h,k,n,o–r] with lanthanides.

Work is in progress collecting further accurate crystallographic data on other compounds of this lanthanide series.

The authors wish to thank the Ministero dell'Università e della Ricerca Scientifica e Tecnologica (MURST), Programmi di Ricerca Scientifica di Rilevante Interesse Nazionale, Cofinanziamento MURST 1998-9, the Consiglio Nazionale delle Ricerche (CNR, Roma), the Deutsche Akademischer Austauschdienst (Vigoni Programme) for financial support and Professor Joachim Strähle, Universität Tübingen, for continuous support and interest and for helpful discussions. A generous gift of lanthanide oxides by Rhône-Poulenc Recherches is gratefully acknowledged.

Notes and references

† Complete crystal data were collected for the Nd (Z = 60), Gd (Z = 64), and Ho (Z = 67) derivatives, $Ln_4(O_2CNPr^i_2)_{12}$. The measurements were carried out with a CAD4 and a Siemens P4 diffractometers equipped with Mo-$K\alpha$ radiation (λ = 0.71073 Å). All compounds were monoclinic, space group $C2/c$ (no.15). The intensity data were corrected for Lorentz and polarisation effects by means of the suitable programs.[8] For the Nd and Ho samples, the solvent molecule (octane and heptane, respectively) was found to be slightly disordered; for Gd, the solvent was not localised. Some degree of disorder was occasionally present in the diisopropyl groups. At the end of refinement, residual peaks and holes of *ca.* ± 1 e Å^{-3} were present in the zones of disordered groups or the metal in the difference Fourier maps.

$Nd_4(O_2CNPr^i_2)_{12}\cdot 2C_8H_{18}$: violet crystals, $C_{100}H_{204}Nd_4N_{12}O_{24}$, M = 2535.7, T = 253(2) K, a = 28.97(1), b = 20.064(8), c = 23.549(9) Å, β = 107.44(4)°, U = 13060(9) Å^3, Z = 4; μ = 1.63 mm^{-1}; crystal size = 0.2 × 0.2 × 0.3 mm. Independent reflections 7909. Final reliability factors for 611 parameters: R_1 = 0.067 for 3686 reflections with $I > 2\sigma(I)$, wR_2 = 0.179 for all 7418 reflections in the refinement; GOF = 0.941.

$Gd_4(O_2CNPr^i_2)_{12}\cdot 2C_7H_{16}$: colourless crystals, $C_{98}H_{200}Gd_4N_{12}O_{24}$, M = 2559.7, T = 203(2) K, a = 29.041(8), b = 19.676(2), c = 23.170(8) Å, β = 107.52(1)°, U = 12625(6) Å^3, Z = 4, μ = 2.14 mm^{-1}, crystal size = 0.35 × 0.3 × 0.1 mm. Independent reflections 11367, R_{int} = 0.0257. Final reliability factors for 559 parameters without restraints: R_1 = 0.0489, wR_2 = 0.1209 for 6713 reflections with $I > 2\sigma(I)$; GOF = 1.056.

$Ho_4(O_2CNPr^i_2)_{12}\cdot 2C_7H_{16}$: light yellow crystals, $C_{98}H_{200}Ho_4N_{12}O_{24}$, M = 2590.4, T = 293(2) K, a = 29.130(2), b = 19.844(2), c = 23.131(1) Å, β = 107.24(1)°, U = 12770(2) Å^3, Z = 4; μ = 2.51 mm^{-1}; crystal size = 0.82 × 0.48 × 0.35 mm. 8868 independent reflections. Final reliability factors for 467 parameters: R_1 = 0.039 calculated for 6711 reflections with $I > 2\sigma(I)$, wR_2 = 0.110 for all 8868 reflections in the refinement; GOF = 1.041.

$Eu_4(O_2CNPr^i_2)_{12}\cdot 2C_7H_{16}$: pink crystals, $C_{98}H_{200}Eu_4N_{12}O_{24}$, M = 2538.5, T = 203(2) K, a = 29.074(5), b = 19.699(5), c = 23.211(4) Å, β = 107.65(2)°, U = 12668(4) Å^3, Z = 4. The intensity data of the Eu derivative were not collected.[8] CCDC 182/1404. See http://www.rsc.org/suppdata/cc/1999/2053/ for crystallographic files in .cif format

1 (*a*) D. H. Templeton and C. H. Dauben, *J. Am. Chem. Soc.*, 1954, **76**, 5237; (*b*) R. D. Shannon and C. T. Prewitt, *Acta Crystallogr., Sect. B*, 1969, **25**, 925; (c) R. D. Shannon, *Acta Crystallogr., Sect. A*, 1976, **32**, 751; (*d*) A. F. Wells, *Structural Inorganic Chemistry*, Clarendon Press, Oxford, 5th edn., 1984, p. 421; (*e*) D. H. Templeton and G. F. Carter, *J. Phys. Chem.*, 1954, **58**, 940.

2 F. A. Hart, in *Comprehensive Coordination Chemistry*, ed. G. Wilkinson, R. D. Gillard and J. A. McCleverty, Pergamon Press, Oxford, 1987, vol. 3, p. 1059.

3 (*a*) A. L. Feig, W. G. Scott and O. C. Uhlenbeck, *Science*, 1998, **279**, 81; (*b*) P. L. Watson, *J. Am. Chem. Soc.*, 1982, **104**, 337; (*c*) P. L. Watson and D. C. Roe, *ibid.*, 1982, **104**, 6471; (*d*) H. Mauermann, P. N. Swepston and T. J. Marks, *Organometallics*, 1985, **4**, 200; (*e*) G. Jeske, H. Lauke, H. Mauermann, P. N. Swepston, H. Schumann and T. J. Marks, *J. Am. Chem. Soc.*, 1985, **107**, 8091; (*f*) P. L. Watson and G. W. Parshall, *Acc. Chem. Res.*, 1985, **18**, 51; (*g*) G. Jeske, L. E. Schock, P. N. Swepston, H. Schumann and T. J. Marks, *J. Am. Chem. Soc.*, 1985, **107**, 8103; (*h*) G. Jeske, H. Lauke, H. Mauermann, H. Schumann and T. J. Marks, *J. Am. Chem. Soc.*, 1985, **107**, 8111; (*i*) M. R. Gagné and T. J. Marks, *J. Am. Chem. Soc.*, 1989, **111**, 4108; (*j*) G. A. Molander and J. O. Hoberg, *J. Org. Chem.*, 1992, **57**, 3266; (*k*) M. R. Gagné, C. L. Stern and T. J. Marks, *J. Am. Chem. Soc.*, 1992, **114**, 275; (*l*) M. A. Giardello, V. P. Conticello, L. Brard, M. Sabat, A. L. Rheingold, C. L. Stern and T. J. Marks, *J. Am. Chem. Soc.*, 1994, **116**, 10212; (*m*) M. A. Giardello, V. P. Conticello, L. Brard, M. R. Gagné and T. J. Marks, *ibid*, 1994, **116**, 10241; (*n*) Y. Li and T. J. Marks, *Organometallics*, 1996, **15**, 3770; (*o*) C. Qian, Y. Ge, D. Deng, Y. Gu and C. Zhang, *J. Organomet. Chem.*, 1988, **344**, 175; (*p*) S. Zhiquan, O. Jun, W. Fusong, H. Zhenya, Y. Fusheng and Q. Baogong, *J. Polym. Sci.: Polym. Chem. Ed.*, 1980, **18**, 3345; (*q*) Z. Shen, *Inorg. Chim. Acta*, 1987, **140**, 7; (*r*) P. Biagini, G. Lugli, L. Abis and R. Millini, *New J. Chem.*, 1995, **19**, 713.

4 F. T. Edelmann, *Comprehensive Organometallic Chemistry*, ed. E. W. Abel, F. G. A. Stone and G. Wilkinson, Volume Editor, M. F. Lappert, Pergamon Press, Oxford, 2nd edn., 1995, vol. 4, p.11.

5 L. Abis, D. Belli Dell' Amico, C. Busetto, F. Calderazzo, R. Caminiti, C. Ciofi, F. Garbassi and G. Masciarelli, *J. Mater. Chem.*, 1998, **8**, 751; L. Abis, D. Belli Dell' Amico, C. Busetto, F. Calderazzo, R. Caminiti, F. Garbassi and A. Tomei, *J. Mater. Chem.*, 1998, **8**, 2855.

6 D. Belli Dell'Amico, F. Calderazzo, F. Marchetti and G. Perego, *J. Chem. Soc., Dalton Trans.*, 1983, 483.

7 D. Belli Dell'Amico, F. Calderazzo, C. della Porta, A. Merigo, P. Biagini, G. Lugli and T. Wagner, *Inorg. Chim. Acta*, 1995, **240**, 1.

8 G. M. Sheldrick, SHELXS86, A FORTRAN program for the solution of X-ray structures, University of Göttingen, 1986; G. M. Sheldrick, SHELXL93, A FORTRAN program for the refinement of X-ray structures, University of Göttingen, 1993; DIFABS absorption correction: N. Walker and D. Stuart, *Acta Crystallogr., Sect. A*, 1983, **39**, 158; PSI: A. C. T. North, D. C. Phillips and F. S. Mathews, *Acta Crystallogr., Sect. A*, 1968, **24**, 351.

9 The structural data were found in the CCDC database ("CCDC, The Cambridge Crystallographic Data Centre", F. H. Allen, S. Bellard, M. D. Brice, B. A. Cartwright, A. Doubleday, H. Higgs, T. Hummelink, B. G. Hummelink-Peters, O. Kennard, W. D. S. Motherwell, J. R. Rodgers and D. G. Watson, *Acta Crystallogr., Sect. B*, 1979, **35**, 2331). A list of relevant references can be provided on request.

Communication 9/04792A

ChemComm

New quadrupolar fluorophores with high two-photon excited fluorescence

Lionel Ventelon,[a] Laurent Moreaux,[b] Jerome Mertz[b] and Mireille Blanchard-Desce*[a]

[a] *Département de Chimie, Ecole Normale Supérieure (UMR 8640), 24, rue Lhomond, 75231 Paris Cedex 05, France. E-mail: mbdesce@junie.ens.fr*

[b] *Laboratoire de Physiologie, Neurobiologie et Diversité Cellulaire (UMR 7637), Ecole Supérieure de Physique et Chimie Industrielle, 10, rue Vauquelin, 75231 Paris Cedex 5, France*

Received (in Cambridge, UK) 30th July 1999, Accepted 8th September 1999

New quadrupolar fluorophores that exhibit enhanced two-photon excited fluorescence were designed according to a molecular engineering approach based on push-push and pull-pull elongated molecules built from a rigid conjugated core (either dihydrophenanthrene or dithienothiophene).

Molecular two-photon absorption (TPA)[1] has found many applications over recent years, including optical power limitation,[2] three-dimensional optical data storage,[3] microfabrication,[4] up-conversion,[5] *etc*. Applications that specifically require excited state fluorescence include two-photon excited fluorescence (TPEF) microscopy,[6] which has gained widespread popularity in the biology community owing to its ability to image at an increased penetration depth in tissue with reduced photodamage. Key ingredients for efficient molecular TPEF are a large two-photon absorption cross section σ_2, and a high fluorescence quantum yield Φ. In most cases, TPEF microscopy applications have relied on molecules originally designed for one-photon fluorescence.[7] It has become increasingly clear, however, that molecules specifically engineered for TPEF may significantly outperform these more conventional molecules.[8] To this end, we have designed, synthesised and characterised new quadrupolar molecules which exhibit enhanced TPEF.

It has been recently observed[8a] that symmetrical phenylene–vinylene oligomers bearing electron-releasing (or electron-withdrawing) groups can display very large σ_2, seemingly correlated to a symmetrical quadrupolar charge redistribution occurring between the edges and the centre of the molecule. Following some of these observations, our goal was to achieve significant two-photon absorption while maintaining high fluorescence quantum yields by the symmetrical grafting of two semi-rigid conjugated rods bearing either donor or acceptor terminal substituents onto a rigid conjugated central building block. The central conjugated block is designed to allow electronic conjugation and high fluorescence yield, and may assist quadrupolar charge redistribution. The dihydrophenanthrene (DHP) and dithienothiophene (DTT) systems, which permit electronic delocalisation and possess decreased rotational degree of freedoms (due to the fused rings in the case of DTT and to the presence of the bis(methylene) bridge in the case of DHP), appeared to be appropriate central moieties. Styrene moieties were selected as conjugated rods.

Based on the above strategy, we have prepared molecules **1**-**4** that possess an extended conjugated system[9] (approximately 22–24 Å long) and either donor (push-push molecules **1**, **3**) or acceptor (pull-pull molecules **2**, **4**) terminal groups (Scheme 1). Molecules derived from DHP can be prepared *via* a double Wittig condensation from symmetrical bisfunctional reagents derived from DHP. Wittig reaction under liquid-liquid[10] or solid-liquid phase transfer conditions[11] of 2.1 equiv. of phosphonium salt **W1**[12] with bisaldehyde **A**[13] afforded push-push molecule **1** in 60% yield after purification by column chromatography on silica gel. Conversely, pull-pull molecule **2** was prepared in 90% yield by reaction of bisphosphonium **W2** with 2 equiv. of commercially available aldehyde **B** , followed by acidic deprotection. The key reagent **W2** was obtained from DHP according to a two step procedure in 50% overall yield.

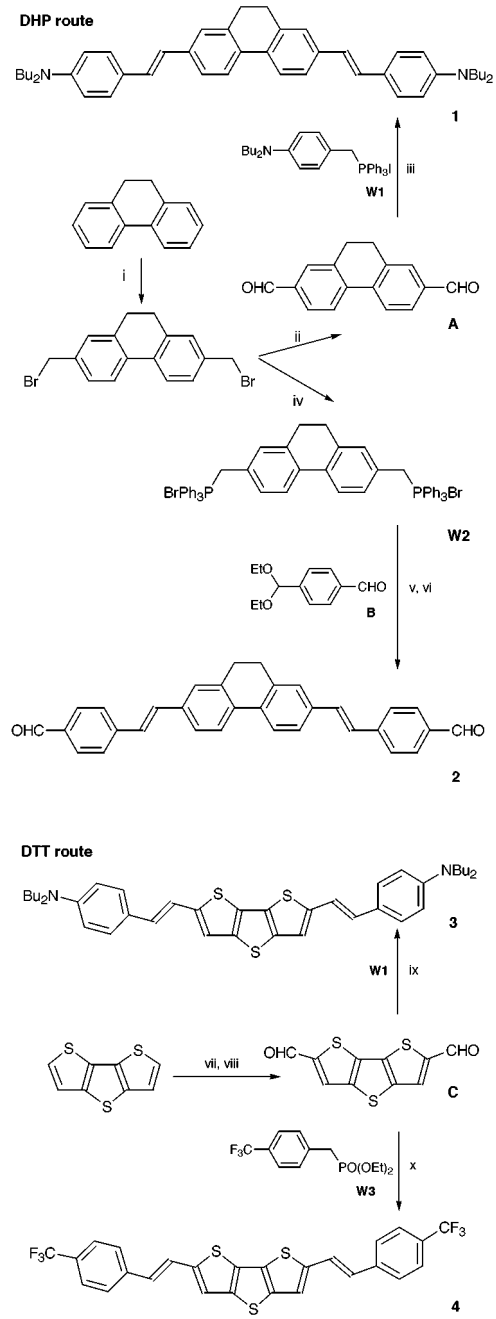

Scheme 1 *Reagents and conditions :* i, $(CH_2O)_3$, HBr, H_3PO_4, 24 h, 90 °C; ii, $NaHCO_3$, DMSO, 4 h, 115 °C; iii, **W1** (2.1 equiv.), CH_2Cl_2, 50% NaOH, 5 h, room temp.; iv, $P(Ph)_3$ (2 equiv.), CH_2Cl_2, 24 h, room temp.; v, **B** (2 equiv.) CH_2Cl_2, 50% NaOH, 24 h, room temp.; vi, 10% HCl, THF, 1 h, room temp.; vii, BuLi, THF, −78 °C; viii, DMF, −78 °C; ix, **W1** (2.1 equiv.), $KOBu^t$, CH_2Cl_2, 5 h, room temp.; x, **W3** (2.2 equiv.), NaH, THF, 24 h, room temp.

Table 1 One and two-photon absorption and fluorescence properties of fluorophores **1**-**4**. The experimental uncertainty is estimated to be ±15% for TPEF measurements and ±5% for fluorescence quantum yield determinations.

	λ_{max}(abs)/nm	λ_{max}(em)/nm	Φ	λ_{max}(TPA)/nm	$\sigma_2\Phi/10^{-50}$ cm^4 s photon^{-1}	$\sigma_2/10^{-50}$ cm^4 s photon^{-1}
1	421	540	0.77	765	930	1200
2	397	513	0.83	< 730	> 260 [a]	> 320
3	465	582	0.63	795	340	530
4	424	510	0.44	< 730	> 80[a]	> 180

[a] $\sigma_2\Phi$ values measured at 730 nm, the TPA maximum being blue-shifted in the case of fluorophores **2** and **4**.

The same methodology was implemented for the synthesis of molecules **3** and **4** derived from DTT which were prepared in 80–90% yield by reacting bisaldehyde **C**[14] under solid-liquid phase transfer conditions[11] with 2.2 equiv. of either phosphonium salt **W1** or phosphonate **W3**. Molecules **1**–**4** were isolated as pure all-*E* compounds after crystallisation as established by NMR, elemental analyses and/or high resolution mass spectrometry.

The two-photon excitation cross sections were determined by comparing the TPEF of molecules **1**-**4** to that of fluorescein using a mode-locked Ti : sapphire laser operating between 730 and 970 nm and delivering linearly-polarised ~80 fs pulses at 80 MHz. This experimental protocol is described in detail by Xu and Webb[7] and provides the TPEF cross section $\sigma_2\Phi$. The corresponding σ_2 values can then be derived by determining the fluorescence quantum yield Φ from fluorescence measurements.

The experimental data are collected in Table 1. We conclude from these data that fluorophores **1**-**4** indeed combine very large two-photon absorption cross-sections and high fluorescence quantum yields. In particular fluorophores **1** and **3** display σ_2 values more than two orders of magnitude larger than *p*-bis[*o*-methylstyryl]benzene,[7] a shorter generic molecule that lacks donor or acceptor end groups. This demonstrates the importance of the donor (or acceptor) end groups and of the length and electronic function of the central moiety, both of which govern quadrupolar charge redistribution. We note that fluorophores **1** and **3** exhibit very large TPEF cross sections over a wide spectral range (Fig. 1) spanning the visible red to the near IR (700–970 nm). This spectral window is particularly advantageous for imaging in biological tissues.[15] Both fluorophores **1** and **3** have a TPEF cross section about an order of magnitude larger than conventional fluorophores such as fluorescein or rhodamine. Push-push fluorophores **1** and **3** appear to lead to larger TPA cross-sections than corresponding pull-pull derivatives **2** and **4**, concomitant with a red-shift of both one-photon absorption and TPA maxima. Fluorophores **2** and **4** which maintain large TPA cross-sections and display excellent transparency in a wide range of the visible region are promising candidates for optical power limitation applications.

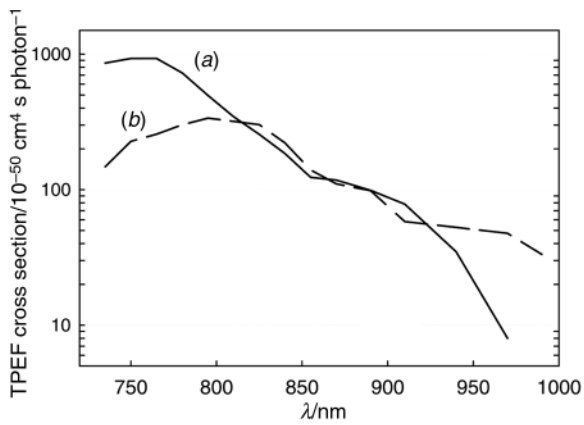

Fig. 1 TPEF excitation spectra of fluorophores (*a*) **1** and (*b*) **3** dissolved in DMSO (10^{-4} M).

In summary, we have demonstrated a successful strategy for the design of fluorophores that combines very large two-photon absorption cross sections and high fluorescence quantum yields. This opens interesting prospects for several applications, particularly in the fields of two-photon microscopy and optical power limitation.

We thank the Délégation Générale pour l'Armement (DGA) for a fellowship to L.V. and the CNRS for a fellowship (BDI) to L.M.. We also acknowledge the Institut Curie for financial support.

Notes and references

1 M. Göppert-Mayer, *Ann. Phys. (Leipzig)*, 1931, **9**, 273; W. L. Petitcolas, *Annu. Rev. Phys. Chem.*, 1967, **18**, 233.
2 G. S. He, G. C. Xu, P. N. Prasad, B. A. Reinhardt, J. C. Bhatt and A. G. Dillard, *Opt. Lett.*, 1995, **20**, 435; J. E. Ehrlich, X. L. Wu, I.-Y. S. Lee, Z.-Y. Hu, H. Röckel, S. R. Marder and J. W. Perry, *Opt. Lett*., 1997, **22**, 1843.
3 D. A. Parthenopoulos and P. M. Rentzepis, *Science*, 1989, 245, **843**; J. H. Strickler and W. W. Webb, *Opt. Lett*., 1991, **16**, 1780.
4 B. H. Cumpston, S. P. Ananthavel, S. Barlow, D. L. Dyer, J. E. Ehrlich, L. L. Erskine, A. A. Heikal, S. M. Kuebler, I.-Y.S. Lee, D. McCord-Maughon, J. Qin, H. Röckel, M. Rumi, X.-L. Wu, S. R. Marder and J. W. Perry, *Nature*, 1999, **398**, 51.
5 A. Mukherjee, *Appl. Phys. Lett.*, 1993, **62**, 3423; J. D. Bhawalkar, G. S. He, C.-K. Park, C. F. Zhao, G. Ruland and P. N. Prasad, *Opt. Commun.*, 1996, **124**, 33.
6 W. Denk, J. H. Strickler and W. W. Webb, *Science*, 1990, **248**, 73.
7 C. Xu and W. W. Webb, *J. Opt. Soc. Am. B*, 1996, **13,** 481.
8 (*a*) M. Albota, D. Beljonne, J.-L. Brédas, J. E. Ehrlich, J.-Y. Fu, A. A. Haeikal, S. E. Hess, T. Kogej, M. D. Levin, S. R. Marder, D. McCord-Maughon, J. W. Perry, H. Röckel, M. Rumi, G. Subramaniam, W. W. Webb, X.-L. Wu and C. Xu, *Science*, 1998, **281**, 1653; (*b*) B. A. Reinhardt, L. L. Brott, S. J. Clarson, A. G. Dillard, J. C. Bhatt, R. Kannan, L. Yuan, G. S. He and P. N. Prasad, *Chem. Mater*., 1998, **10**, 1863.
9 Increasing the extent of quadruplar charge redistribution is expected to lead to an increase of σ_2.
10 M. Blanchard-Desce, I. Ledoux, J.-M. Lehn, J. Malthête and J. Zyss, *J. Chem. Soc., Chem Commun.*, 1988, 737.
11 V. Alain, S. Rédoglia, M. Blanchard-Desce, S. Lebus, K. Lukaszuk, R. Wortmann, U. Gubler, C. Bosshard and P. Günter, *Chem. Phys.*, 1999, **245**, 51.
12 M. Blanchard-Desce, C. Runser, A. Fort, M. Barzoukas, J.-M. Lehn, V. Bloy and V. Alain, *Chem. Phys*., 1995, **199**, 253.
13 A. Helms, D. Heiler and G. McLendon, *J. Am. Chem. Soc.*, 1992, **114**, 6227.
14 O.-K. Kim, A. Fort, M. Barzoukas, M. Blanchard-Desce and J.-M. Lehn, *J. Mater. Chem.*, 1999, **9**, 2227.
15 C. Xu, W. Zipfel, J. B. Shear, R. M. Williams and W. W. Webb, *Proc. Natl. Acad. Sci., U.S.A.*, 1996, **93**, 10763.

Communication 9/06182G

Hemispherical synthesis of dendritic poly(L-lysine) combining sixteen free-base porphyrins and sixteen zinc porphyrins

Naoki Maruo,[a] Motonori Uchiyama,[a] Tamaki Kato,[a] Toru Arai,[a] Hideo Akisada[b] and Norikazu Nishino*[a]

[a] *Department of Applied Chemistry, Faculty of Engineering, Kyushu Institute of Technology, Kitakyushu 804-8550, Japan. E-mail: nishino@che.kyutech.ac.jp*

[b] *Department of Environmental Chemistry, Faculty of Engineering, Kyushu Kyoritsu University, Kitakyushu 807-8585, Japan*

Received (in Cambridge, UK) 10th August 1999, Accepted 7th September 1999

Dendritic poly(L-lysine) combining sixteen free-base porphyrins and sixteen zinc porphyrins hemispherically at the fifth generation was successfully synthesised and showed intramolecular fluorescence energy transfer in DMF.

Before Tomalia proposed the 'dendrimer', a new type of macromolecule,[1] Aharoni *et al*. had described the synthesis and properties of dendritic poly(L-lysine)s up to tenth generation.[2] Unlike the original concept of the dendrimer described Tomalia, the amino groups of L-lysine are not of course symmetrical. However, the chirality of L-lysine is advantageous in the design of functional dendrimers. In addition, the L-lysine residue is useful in combining a special functional group in large numbers at the desired generation. At the fifth generation, there are thirty two side chain amino groups where functional group-carrying L-lysines can be combined. More advantageously, peptide synthetic chemistry can be conveniently applied for design and synthesis of functionalized dendritic poly(L-lysine) by incorporation of photochemically interesting groups such as porphyrin rings.

Porphyrin rings have been formed into clusters using dendritic approaches by several research groups.[3] The most recent clusters involve nine porphyrin rings with designed metallation. However, we hoped to utilise a totally different type of design and synthesis of macromolecules combining a large number of porphyrin rings in any appropriate arrangement. We introduced a number of porphyrin rings (eight, sixteen or thirty-two) into a dendritic poly(L-lysine) in almost the same stratum.[4] The porphyrins showed extremely strong split circular dichroism (CD) ($[\theta]_{428} - [\theta]_{407} = 2.0 \times 10^6$ deg cm^2 dmol^{-1}) under certain conditions (toluene–DMF = 9:1, v/v), while they were silent in DMF. In the present study, we attempted to introduce a crowd of free-base porphyrins and a crowd of zinc porphyrins in separate hemispheres of dendritic poly(L-lysine) (Fig. 1).

The Boc and Fmoc[5] chemistries were alternately applied to build the desired **1** by hemispherical synthesis (Fig. 2). The synthesis was started by the condensation of N^{α},N^{ε}-di-*tert*-butoxycarbonyl-L-lysine [Boc-L-Lys(Boc)-OH] and hexamethylenediamine with benzotriazol-1-yloxytris(dimethylamino)-phosphonium hexafluorophosphate (BOP) and 1-hydroxybenzotriazole (HOBt). The resulting half-amine [Boc-L-Lys(Boc)-NH$(CH_2)_6$NH$_2$] was condensed with N^{α},N^{ε}-difluoren-9-ylmethoxycarbonyl-L-lysine [Fmoc-L-Lys(Fmoc)-OH]. TFA was used to remove the Boc group (0 °C, 1 h), then the Boc hemisphere was expanded by a second condensation with 2 equiv. of Boc-L-Lys(Boc)-OH. The Fmoc protection was removed with 20% piperidine in DMF, then the Fmoc hemisphere was expanded by a second condensation with 2 equiv. of Fmoc-L-Lys(Fmoc)-OH. Thus, Boc and Fmoc chemistries were repeated alternately up to the fourth generation. The condensation reaction proceeded quantitatively (room temperature, 1 h). The completion of the condensation was confirmed at each step by a Kaiser test.[6] At the fifth generation, sixteen Boc-L-Lys(Por(2H))-OH moieties were introduced to the Boc hemisphere of the dendritic poly(L-lysine) intermediate. Expansion of Boc hemisphere to the seventh generation was carried out to bury the free-base porphyrins appropriately in a stratum of the dendritic poly(L-lysine).[4] Subsequently, another half side was condensed with sixteen Fmoc-L-Lys(Por(Zn))-OH moieties with the aid of *O*-(7-azabenzotriazol-1-yl)-1,1,3,3-tetramethyluronium hexafluorophosphate (HATU) and 1-hydroxy-7-azabenzotriazole (HOAt). The hemispherical elongation was repeated to give **1**, whose surface is completely covered by seventh generation of Boc-L-Lys(Boc) groups.

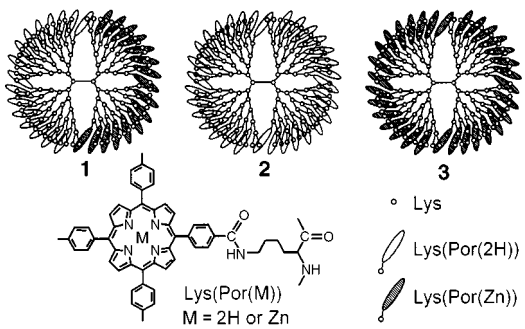

Fig. 1 Dendritic poly(L-lysine)s combining sixteen free-base porphyrins and sixteen zinc porphyrins separately (**1**), thirty-two free-base porphyrins (**2**) and thirty-two zinc porphyrins (**3**) at the fifth generation and covered by an additional two generations. The end-protecting group is *tert*-butoxycarbonyl.

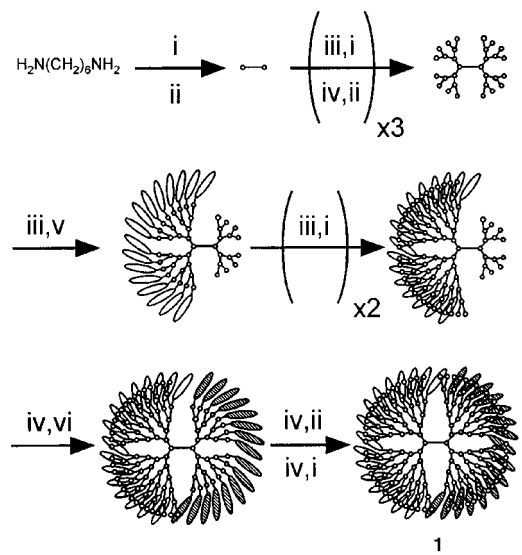

Fig. 2 Synthetic route for dendritic poly(L-lysine) combining hemispherically separated free-base and zinc porphyrins. *Reagents and conditions*: i, Boc-L-Lys(Boc)-OH, BOP, HOBt; ii, Fmoc-L-Lys(Fmoc)-OH, BOP, HOBt; iii, TFA; iv, 20% piperidine in DMF; v, Boc-L-Lys(Por(2H))-OH, BOP, HOBt; vi, Fmoc-L-Lys(Por(Zn))-OH, HATU, HOAt.

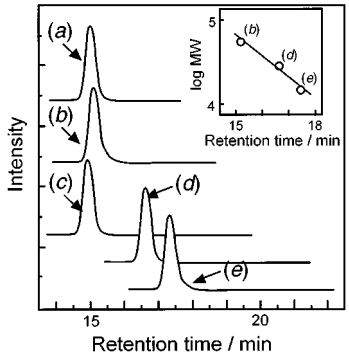

Fig. 3 Analytical size-exclusion chromatograms of dendrimers **1** (*a*), **2** (*b*) and **3** (*c*) and two smaller size homologues (*d*), (*e*) of **2** in DMF. The molecular weights are 56 047, 55 033, 57 061, 27 446 and 13 653 respectively.

Species **1** was purified using a Sephadex LH-60 column (1.8 × 70 cm, DMF) and analyzed by size exclusion chromatography [TSKgel G3000H_{XL} (7.8 × 300 mm) column, with DMF, 2 ng of sample, detected by absorption at 420 nm]. Species **1** was eluted at 14.97 min, the retention time being very close to that (15.16 min) of dendritic poly(L-lysine) combining thirty-two free-base porphyrins (**2**), which was synthesized as previously reported elsewhere.[4] The dendritic poly(L-lysine) with thirty-two zinc porphyrins (**3**) was prepared from **2** and $Zn(OAc)_2$ in CH_2Cl_2–MeOH (3:1, v/v). The formation of **3** was monitored by the disappearance of the Qx(0,0) band of **2** at 650 nm in the absorption spectrum within 3 h. Species **3** showed a single peak at 14.81 min in the size exclusion chromatograph.

The retention times of **1**, **2** and **3** were compared with smaller dendritic poly(L-lysine)s combining eight and sixteen free-base porphyrins[4] at the third and fourth generations, respectively. As shown in the inset of Fig. 3, there is a linear relation between the retention times (17.41, 16.74 and 15.16 min) and the logarithms of the molecular weights (13 653, 27 446 and 55 033) of the dendritic poly(L-lysine)s combining eight, sixteen and thirty-two free-base porphyrins.

Three types of dendritic poly(L-lysine) with thirty-two porphyrins, hemispherically separated free-base and zinc porphyrins (**1**), all free-base porphyrins (**2**) and all zinc porphyrins (**3**), were further characterized by UV-VIS absorption, CD and fluorescence spectra measurements. The absorption spectra in DMF of **2** and **3** were similar to the monomeric free-base and zinc porphyrins respectively. The dendrimer with hemispherically mixed porphyrins (**1**) showed slight deviation (data not shown) from the 1:1 additive spectrum of those of free-base and zinc porphyrins (**2** and **3**). The CD spectra of dendrimers in DMF showed no Cotton effect at the Soret band, whether the porphyrins were free-base or metallated. After addition of toluene (toluene–DMF = 9:1, v/v), **2** with only free-base porphyrins showed an intense split CD ($[\theta]_{428} - [\theta]_{407} = 2.0 \times 10^6$ deg cm^2 dmol^{-1}) for the Soret band as previously observed.[4] However, **1** showed a much weaker CD ($[\theta]_{438} - [\theta]_{421} = 1.8 \times 10^5$ deg cm^2 dmol^{-1}) under the same conditions, while **3** with all zinc porphyrins showed a weak CD ($[\theta]_{440} - [\theta]_{427} = 1.1 \times 10^5$ deg cm^2 dmol^{-1}). The chiral arrangement of free-base porphyrins induced by nonpolar solvent was obviously affected by the crowd of zinc porphyrins.

The fluorescence spectra of the dendrimers are shown in Fig. 4. The dendrimers **2** and **3** in DMF gave typical fluorescence emission upon excitation at 560 nm.[7] A mixed solution of **2** and **3** gave an almost additive spectrum corresponding to both porphyrins. The hemispherical dendrimer **1** gave a fluorescence spectrum in which emission at 610 nm from the zinc porphyrin was significantly quenched. By calculation, about 43% of the

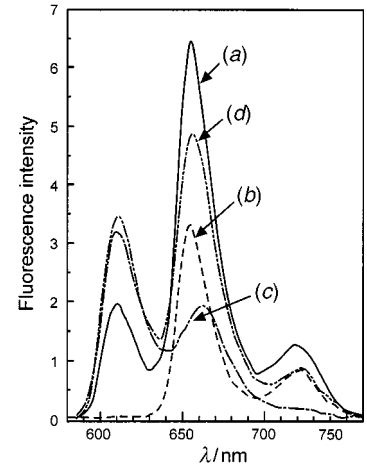

Fig. 4 Fluorescence spectra of dendritic poly(L-lysine)s combining (*a*) hemispherical free-base and zinc porphyrins (**1**, 5.8 μM), (*b*), all free-base porphyrins (**2**, 2.9 μM), (*c*) all zinc porphyrins (**3**, 2.9 μM) and (*d*) a mixture of **2** and **3** (2.9 μM, respectively) in DMF. Excitation at 560 nm.

fluorescence energy of the excited zinc porphyrins was transferred to the free-base porphyrins on the other hemisphere. This fact suggests that about seven of the sixteen porphyrins in each hemisphere might locate on the boundary of said hemisphere, resulting in close contact. The efficiency of the energy migration was slightly increased to 46% by the addition of toluene (toluene–DMF = 9:1, v/v), suggesting that the energy transfer occurs mainly at the hemispherical boundaries and with almost no relation to the mobility of the chromophores.

In conclusion, we have succeeded in the synthesis of dendritic poly(L-lysine) combining separate crowds of free-base and zinc porphyrins, and preliminarily observed fluorescence energy transfer from zinc porphyrins to free-base porphyrins probably due to close contact at the boundaries of the hemispheres. We will further study light harvesting[8] by porphyrin systems arranged in a stratum of the dendrimer. Although they are too primitive to model the antenna chlorophyll membrane proteins revealed recently,[9] it should be possible to mimic the effect of accumulation of porphyrin rings in the compact zone.

Notes and references

1 D. A. Tomalia, H. Baker, J. Dewald, M. Hall, G. Kallos, S. Martin, J. Roeck, J. Ryder and P. Smith, *Polym. J.*, 1985, **17**, 117.
2 S. M. Aharoni, C. R. Crosby III and E. K. Walsh, *Macromolecules*, 1982, **15**, 1093.
3 D. L. Officer, A. K. Burrell and D. C. W. Reid, *Chem. Commun.*, 1996, 1657; C. C. Mak, N. Bampos and J. K. M. Sanders, *Angew. Chem., Int. Ed.*, 1998, **37**, 3020; A. Nakano, A. Osuka, I. Yamazaki, T. Yamazaki and Y. Nishimura, *Angew. Chem., Int. Ed.*, 1998, **37**, 3023; T. Norsten and N. Branda, *Chem. Commun.*, 1998, 1257; S. L. Darling, C. C. Mak, N. Bampos, N. Feeder, S. J. Teat and J. K. M. Sanders, *New J. Chem.*, 1999, **23**, 359.
4 N. Maruo and N. Nishino, *Kobunshi Ronbunshu*, 1997, **54**, 731.
5 J. Meienhofer, *Biopolymers*, 1981, **20**, 1761; G. B. Fields and R. L. Noble, *Int. J. Peptide Protein Res.*, 1990, **35**, 161.
6 E. Kaiser, R. L. Colescott, C. D. Bossinger and P. I. Cook, *Anal. Biochem.*, 1970, **34**, 595.
7 N. Nishino, R. W. Wagner and J. S. Lindsey, *J. Org. Chem.*, 1996, **61**, 7534.
8 D-L. Jiang and T. Aida, *Nature*, 1997, **388**, 454.
9 G. McDermott, S. M. Prince, A. A. Freer, A. M. Hawthornthwaite-Lawless, M. Z. Papiz, R. J. Cogdell and N. W. Isaacs, *Nature*, 1995, **374**, 517.

Communication 9/06501F

Bonded *peri*-interactions govern the rate of racemisation of atropisomeric 8-substituted 1-naphthamides†

Jonathan Clayden,* Catherine McCarthy and Madeleine Helliwell‡

Department of Chemistry, University of Manchester, Oxford Road, Manchester, UK M13 9PL. E-mail: j.p.clayden@man.ac.uk

Received (in Liverpool, UK) 3rd August 1999, Accepted 10th September 1999

8-Substituted tertiary 1-naphthamides are chiral, atropisomeric compounds at room temperature, and the rate at which they racemise (by rotation about the Ar–CO bond) depends principally on the extent to which the 8-substituent undergoes incipient nucleophilic addition to the amide carbonyl group, as indicated by X-ray crystallography.

Substituents at the 1- and 8-positions of a *peri*-disubstituted naphthalene lie too close for comfort. Strain is the driving force behind their reactions, and anything that relieves strain is enormously favoured over anything that makes it worse.[1,2] Strain governs the shape of 1,8-disubstituted naphthalenes too: the rings are frequently severely distorted, with the 1- and 8-substituents bending away from one another both in the plane of the ring and perpendicular to it.[3]

Our interest in hindered naphthalenes began with the discovery that 2-substituted tertiary naphthamides **1**, which are axially chiral by virtue of restricted rotation about the Ar–CO axis,[4] undergo highly stereoselective reactions: reagent approach is governed by differentiation of the two faces of the naphthalene ring by the steric and electronic properties of the amide group.[5] Here we show that an 8-substituent can provide a barrier to Ar–CO bond rotation sufficiently large that 8-substituted-1-naphthamides **2** can be configurationally stable chiral compounds even without a bulky 2-substituent. Moreover, we demonstrate that the role of the 8-substituent in hindering rotation is not a steric but an electronic one, depending on the degree of bonded interaction between the 8-substituent and the amide group. [6]

In order to study the rate of racemisation of 8-substituted 1-naphthamides we made four 8-substituted amides **2b**–**e** and, from them, three 2,8-disubstitued amides **4b**–**d**. For crystallographic comparison we also made the *N*,*N*-dimethylamide **3a**.[7] Each of the six compounds **2b**–**d** and **4b**–**d** was resolved by

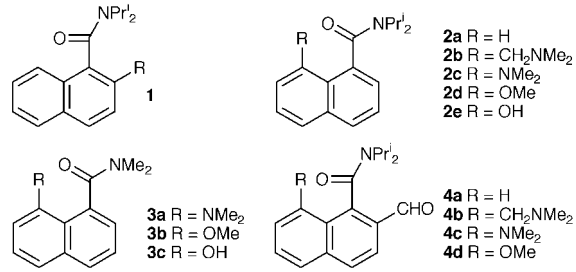

HPLC on a chiral stationary phase (Whelk-O1 from Regis or Chiralpak-AD from Daicel),[4,8–11] and the separated enantiomers were allowed to racemise in 5–20% EtOH or Pr^{i}OH in hexane at the temperatures shown in Table 1. The change in ee with time was followed by HPLC and in each case showed a simple first order decay—the rate constant for enantiomerisation, *k*, is given in Table 1. $\Delta G^{\ddagger}$ for this process, which represents the barrier to Ar–CO bond rotation, was calculated using the Eyring equation and is also shown in Table 1, along with an estimated half-life for racemisation of each compound at 20 °C, assuming the invariance of $\Delta G^{\ddagger}$ with temperature.[4]

Clearly, 8-substituted 1-naphthamides are atropisomeric: they have a half life at 20 °C greater than 1000 s[12] even in the absence of a 2-substituent, and the most effective 8-substituent, the OMe group, raises the barrier to rotation about the Ar–CO bond by over 30 kJ mol^{-1} (compare entries 1 and 4; 9 and 12)—an OMe group in the 2-position has a similar effect.[4] Despite their greater steric size,[13] the CH_2NMe_2 and NMe_2 substituents have less significant effects in both the 8- and 2,8-disubstituted naphthamides: an 8-CH_2NMe_2 substituent

† A colour version of Fig. 1 is available from the RSC web site, see http://www.rsc.org/suppdata/cc/1999/2059/

‡ Author to whom crystallography enquiries should be addressed.

Table 1 Correlating kinetic and crystallographic measurements

Entry	Compound	*T*/°C	k[a]/10^{-5} s^{-1}	$\Delta G^{\ddagger}$[b]/kJ mol^{-1}	$t_{1/2}$[c] (20 °C)	Lenth/Å			Angle (°)							
						d	δC	δN	θ_1	θ_2	θ_3	θ_4	α	β	γ	δ
1[d]	**2a**	—	—	74.5[e]	1 s	—	—	—	—	—	—	—	—	—	—	—
						2.90	0.034	0.000	113.8	124.2	121.6	118.8	87.7	104.7	81.4	83.8
2[d,f]	**2b**	2	2.6 ± 0.5	91.3	16 min	2.89	0.032	0.009	113.3	124.6	121.0	118.8	90.0	102.7	81.0	84.8
3	**2c**	50	19.5 ± 1.8	102.2	27 h	2.76	0.051	0.017	114.0	125.4	118.5	121.2	96.7	98.6	80.5	90.4
4	**2d**	55	4.3 ± 0.4	108.0	12 days	2.62	0.049	0.028	116.0	124.2	114.8	124.2	97.0	98.6	79.8	95.4
						2.83	0.076	0.030	115.3	123.7	116.9	121.2	97.9	95.8	81.4	93.4
5[f]	**2e**	—	—	—	—	2.67	0.083	0.051	116.0	123.2	116.7	122.8	101.6	92.6	80.7	93.3
6[g]	**3a**	—	—	96.9	3 h	2.70	0.055	0.060	115.5	124.7	117.0	122.9	98.7	96.5	81.3	91.4
7[h]	**3b**	—	—	—	—	2.60	0.039	0.113	115.1	124.0	114.4	122.7	103.3	90.0	80.8	96.4
8[h]	**3c**	—	—	—	—	2.62	0.051	0.070	116.2	123.6	116.5	122.7	97.0	97.8	81.2	94.2
9[d]	**4a**	2	4.2 ± 0.1	90.2	12 min	—	—	—	—	—	—	—	—	—	—	—
10[d]	**4b**	50	4.4 ± 0.2	106.2	6 days	—	—	—	—	—	—	—	—	—	—	—
11	**4c**	50	0.39 ± 0.05	112.7	80 days	—	—	—	—	—	—	—	—	—	—	—
12	**4d**	60	< 0.05	> 122	> 10 years	—	—	—	—	—	—	—	—	—	—	—

[a] Rate of enantiomerisation (1/2 × rate of racemisation). [b] Barrier to enantiomerisation. [c] Estimated half-life for racemisation at 20 °C. [d] Kinetic data from ref. 4. [e] Determined by variable temperature NMR. [f] Two molecules in unit cell, crystallographic data given for both. [g] Kinetic data from ref. 9. [h] Crystallographic data from ref. 3.

raises the barrier to rotation about Ar–CO by only about half as much as a comparably sized 2-substituent.[4] There is evidently a non-steric effect at work in the 8-substituted naphthamides,[14] and in order to clarify the nature of that effect we determined the X-ray crystal structures of **2b**–**e** and **3a**. These are shown in Fig. 1.§

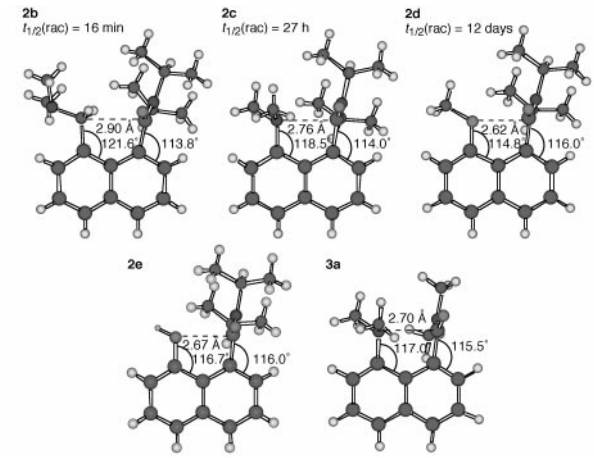

Fig. 1 X-Ray crystal structures. $t_{1/2}$(rac) = half-life for racemisation in solution at 20 °C.

The X-ray structures show that, far from repelling one another, the R and carbonyl groups of **2**, **3** and **4** are drawn together when R = NMe_2 or OMe: only **2b**, with R = CH_2NMe_2, has θ_4 (see Fig. 2) < 120°. Dunitz[3] has shown that pairs of *peri* substituents, one an electrophilic carbonyl group and the other a nucleophilic heteroatom, can exhibit bonding interactions, and we believe this is what we are observing here.

Increasing bonding between R and C=O should lead to several effects, illustrated in Fig. 2. R should bend in towards C=O (θ_4 and δ increase as θ_3 decreases), while the distance *d* between R and the carbonyl carbon atom should decrease as the bond begins to form. The C=O group should adjust its alignment relative to R to let R approach at the 'Burgi–Dunitz angle'[15] of 107° (α should move from 90° towards 107°). The arrangement of atoms around the carbonyl group should move away from trigonal planar towards tetrahedral (δC measures the displacement of the carbonyl carbon atom from the plane of its neighbours), and for the amides the amide nitrogen atom should begin to pyramidalise as it loses conjugation with C=O, the lone pair developing *anti* to the incoming nucleophile (δN measures the displacement of this nitrogen atom from the plane of its neighbours). These values were measured from the crystal structures, and are shown in Table 1. Also included for comparison are the data for the known[3] structures **3b** and **3c**.

The consistent changes in all measured values from entry 2 through entry 3 to entry 4, and from entry 5 to entry 6, makes it clear that the degree of *peri*-bonding increases as R changes from CH_2NMe_2 to NMe_2 to OMe. This is also the order of increasing barrier to Ar–CO bond rotation, and we deduce that this barrier to rotation is controlled not primarily by a repulsive, steric interaction with R but by an attractive bonding interaction. The stereogenic axis of **2** has moved some way towards being a stereogenic centre with a much higher barrier to thermal inversion. The same trend is evident in the barriers to enantiomerisation of **4**.

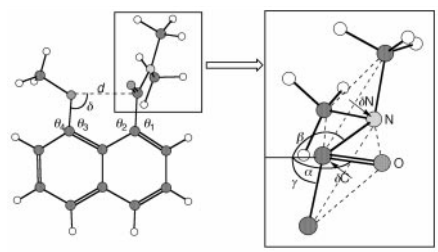

Fig. 2 Geometry of the crystal structures: key measurements. δC and δN are the deviation of each atom from the plane of its neighbours.

The degree of *peri*-bonding also increases to some extent as the amide changes from NPr^i_2 to NMe_2. The last effect is presumably steric in origin, and it is more significant with R = NMe_2 (compare entries 3 and 6) than with R = OMe (compare entries 4 and 7). This may explain why, surprisingly, R = OMe seems to be a acting as a better nucleophile than R = NMe_2: NMe_2 is simply bigger and so cannot get as close to the amide—especially an *N*,*N*-diisopropylamide.

We conclude from these observations that 8-substituted 1-naphthamides can be atropisomeric even in the absence of a 2-substituent, and that the principal factor controlling their rate of racemisation is the electronic nature of the 8-substituent and its ability to form a partial bond to the amide carbonyl group. Given their potential as chiral reagents, ligands or auxiliaries,[16] we expect 8-alkoxy or 8-amino substituents to be an important feature of thermally stable chiral atropisomeric amides.

We are grateful to the EPSRC and Zeneca Pharmaceuticals for an Industrial CASE award (to C. McC.), and to Dr John Cumming and Professor Garry Procter for helpful discussions.

Notes and references

§ *Crystal data* for **2b**: $C_{20}H_{28}N_2O$, M = 312.45, triclinic, $P\bar{1}$, μ = 4.95 cm^{-1}, R = 0.074, R_W = 0.055, a = 11.245(2), b = 16.635(2), c = 10.714(2) Å, α = 96.95(1), β = 101.14(2), γ = 73.22(1)°, V = 1878.0(6) $Å^3$, T = 23.0 °C, Z = 4, 8399 reflections, 7668 unique, R_{int} 0.038. For **2c**: $C_{29}H_{26}N_2O$, M = 298.43, orthorhombic, *Pbcn*, μ = 5.26 cm^{-1}, R = 0.053, R_W = 0.046, a = 15.514(6), b = 15.239(2), c = 15.305(3) Å, α = 96.95(1), β = 101.14(2), γ = 73.22(1)°, V = 3618(1) $Å^3$, T = 23.0 °C, Z = 8, 4041 reflections. For **2d**: $C_{28}H_{23}NO_2$, M = 285.39, monoclinic, $P2_1/n$, μ = 5.86 cm^{-1}, R = 0.048, R_W = 0.033, a = 7.956(1), b = 14.530(1), c = 14.392(2) Å, β = 97.53(1)°, V = 1649.3(4) $Å^3$, T = 23.0 °C, Z = 4, 3731 reflections, 3494 unique, R_{int} 0.022. For **2e**: $C_{27}H_{21}NO_2$, M = 271.36, monoclinic, $P2_1/c$, μ = 5.59 cm^{-1}, R = 0.065, R_W = 0.040, a = 10.790(3), b = 25.204(4), c = 11.938(2) Å, β = 104.56(2)°, V = 3142(1) $Å^3$, T = 23.0 °C, Z = 8, 6753 reflections, 6392 unique, R_{int} = 0.026. For **3a**: $C_{25}H_{28}N_2O$, M = 242.32, monoclinic, $P2_1/c$, μ = 5.44 cm^{-1}, R = 0.056, R_W = 0.050, a = 8.753(2), b = 13.781(2), c = 12.168(1) Å, β = 107.865(10)°, V = 1397.0(3) $Å^3$, T = 23.0 °C, Z = 4, 3079 reflections, 2911 unique, R_{int} 0.021. CCDC 182/1412. See http://www.rsc.org.suppdata/cc/1999/2059 for crystallographic data in .cif format.

1 A. J. Kirby and J. M. Percy, *Tetrahedron*, 1988, **44**, 6903.
2 A. J. Kirby and J. M. Percy, *Tetrahedron*, 1988, **44**, 6911.
3 W. B. Schweizer, G. Procter, M. Kaftory and J. D. Dunitz, *Helv. Chim. Acta*, 1978, **61**, 2783.
4 A. Ahmed, R. A. Bragg, J. Clayden, L. W. Lai, C. McCarthy, J. H. Pink, N. Westlund and S. A. Yasin, *Tetrahedron*, 1998, **54**, 13277.
5 J. Clayden, *Synlett*, 1998, 810.
6 The compounds were made by the methods of refs. 1–3. For further details, see J. Clayden, C. S. Frampton, C. McCarthy and N. Westlund, *Tetrahedron*, in press. See also A. J. Birch, M. Salahud-Din and D. C. C. Smith, *J. Chem. Soc. (C)*, 1966, 523; C. Kiefl and A. Mannschreck, *Synthesis*, 1995, 1033.
7 Mannschreck (ref. 9) has determined the barrier to Ar–CO bond rotation of amide **3a** by variable temperature HPLC techniques.
8 M. A. Cuyegkeng and A. Mannschreck, *Chem. Ber.*, 1987, **120**, 803.
9 A. Mannschreck, H. Zinner and N. Pustet, *Chimia*, 1989, **43**, 165.
10 W. H. Pirkle, C. J. Welch and A. J. Zych, *J. Chromatogr.*, 1993, **648**, 101.
11 F. Gasparrini, D. Misiti, M. Pierini and C. Villani, *Tetrahedron: Asymmetry*, 1997, **8**, 2069.
12 M. Oki, *Top. Stereochem.*, 1983, **14**, 1.
13 E. L. Eliel and S. H. Wilen, *Stereochemistry of Organic Compounds*, Wiley, New York, 1994.
14 For another example of electronic control over the rate of bond rotation in *peri*-substituted naphthamides, see F. Cozzi, M. Cinquini, R. Annuziata and J. S. Siegel, *J. Am. Chem. Soc.*, 1993, **115**, 5330.
15 H. B. Bürgi, J. D. Dunitz, J. M. Lehn and G. Wipf, *Tetrahedron*, 1974, **30**, 1563.
16 J. Clayden, *Angew. Chem., Int. Ed. Engl.*, 1997, **35**, 949.

Communication 9/06398F

ChemComm

Two-step synthesis of homochiral monoaminals of tricarbonylphthalaldehydechromium complex

Françoise Rose-Munch,[a] Vanessa Gagliardini,[a] Anne Perrotey,[a] Jean-Philippe Tranchier,[a] Eric Rose,*[a] Pierre Mangeney,[b] Alexandre Alexakis,[b] Tonis Kanger[b] and Jacqueline Vaissermann[c]

[a] *Laboratoire de Synthèse Organique et Organométallique, UMR 7611, Université Pierre et Marie Curie, 4 place Jussieu, 75252Paris Cedex 05, France. E-mail: rose@ccr.jussieu.fr*
[b] *Laboratoire de Chimie des Organoéléments, UMR 7611, Université Pierre et Marie Curie, 4 place Jussieu, 75252Paris Cedex 05, France*
[c] *Laboratoire de Chimie Inorganique et Matériaux Moléculaires, ESA 7071, Université Pierre et Marie Curie, 4 place Jussieu, 75252Paris Cedex 05, France*

Received (in Liverpool, UK) 20th July 1999, Accepted 6th September 1999

Tricarbonylphthalaldehydechromium complex can be prepared using a 'one pot' procedure starting from tricarbonylbenzenechromium: the protection of one aldehyde function by chiral diamines leads to the formation of two diastereoisomers of the monoaminal of the phthlaldehyde complexes, efficient precursors of enantiopure *ortho*-substituted alkenyl arene complexes.

Tricarbonyl(η^6-arene)chromium complexes have been considered as important intermediates in organic synthesis.[1] Since unsymmetrically 1,2- or 1,3-substituted complexes have planar chirality, recent research in this field has been focused on the development of efficient routes to optically active complexes.[2–6]

We have shown that chiral diamines having a C_2 axis of symmetry can be considered as an efficient tool for the asymmetric formation of aminals of *o*-substituted tricarbonyl(benzaldehyde)chromium complexes.[3a,7] The ease of handling such aminal complexes prompted us to use them in the preparation of enantiopure monoaminals of tricarbonylphthaldehydechromium complexes, which could be used as precursors of homochiral *o*-substituted styrene complexes for example.[4,8,9]

We now present results which demonstrate that chiral diamines may be used for the preparation of homochiral *o*-substituted styrene complexes from tricarbonylphthaldehydechromium complex **3**. This new synthon has several attractive features, among which the most interesting is the possibility of differentiating the two aldehyde functionalties, thus breaking the plane of symmetry and introducing asymmetry. Compound **3** is easily and efficiently synthesised in a 'one-pot' procedure, by a new methodology, starting from a simple complex: tricarbonylbenzenechromium **7**.

Our first attempts to prepare synthon **3** were as follows: benzaldehyde ethane-1,2-diyl acetal **1** treated with BuLi (4 equiv.) at −78 °C and then with DMF was converted into the monoacetal of phthlaldehyde **2** in 49% yield. Hydrolysis of the acetal did not occur in good yield, as decomplexation of the tricarbonylchromium function became the dominant mode of reaction.[10b] Indeed complex **3** was obtained only in 22 and 19% using either H_2SO_4[3b,c,10] or HCO_2H[11] (Scheme 1). It was also possible to obtain complex **3** by treating tricarbonylbenzaldehydechromium complex **4** with the diamine $MeNHCH_2CH_2NMe_2$ **5** and BuLi.[12] Indeed the amino alcoholate intermediate **6** can be *ortho*-lithiated in order to react with DMF, giving complex **3** in 35% yield only (Scheme 1). Thus, we examined the possibility of obtaining complex **3** directly from tricarbonylbenzenechromium complex **7**, in a one-pot procedure, using the amide $Me_2NCH_2CH_2NMeCHO$ **8**. Complex **7** at −78 °C was treated with BuLi (1.2 equiv.). The formamide **8** (1 equiv.) was added and stirred for 30 min at −30 °C. BuLi (3 equiv.) and DMF (3 equiv.) were then added sequentially. Hydrolysis of the reaction mixture with 0.1 M HCl gave a red solution, which was chromatographed on a silica gel column. Benzaldehyde complex **4** was the first product eluted with a 3:2 mixture of Et_2O–light petroleum (15% after recrystallisation). The second product, the phthaldaldehydechromium complex **3**, eluted with a 7:3 mixture of Et_2O–light petroleum and was obtained in 41% yield after recrystallisation as red crystals (Scheme 1).

Among the various ways to desymmetrise **3**, we focussed on the selective formation of the chiral monoaminal. Condensation of (*R*,*R*)-1,2-bis(*N*-methylamino)cyclohexanediamine **9a**[2] with complex **3** gave two diastereoisomers **10**† in 76% yield which were easily separated by silica gel chromatography (44 and 32% yield) (Scheme 2). After separation, the diastereomeric composition of each stereoisomer was checked by ^{1}H NMR[3a] which showed one singlet for the aminalic proton H7 at δ 4.81 and 4.23. Alternatively, condensation of (*R*,*R*)-1,2-bis(*N*-methylamino)-1,2-diphenylethane[7,8] **9b** with phthalaldehyde **3** at room temperature for 30 min gave two diastereoisomers **11**, inseparable by silica gel chromatography, in the ratio 56:44 in 78% yield. Fortunately, their separation could be achieved by precipitation of one diastereomer **11a** (whose aminalic proton resonated at low field: δ 5.53), which gave suitable crystals for an X-ray analysis, and thus allowed assignment of the aminalic proton chemical shift of this diastereomer by ^{1}H NMR. The ORTEP view, shown in Fig.1, indicated a (1*S*,2*R*) configuration.‡ It is worth noting that the conformation of the $Cr(CO)_3$ tripod is almost staggered with respect to the carbons of the arene ring and that unexpectedly the aldehyde function is not in the plane of the arene ring. Indeed we observed a 12° angle between the carbon–oxygen double bond and the plane of the ring in the direction opposite to the organometallic moiety.

Once synthon **3** was desymmetrised, the free aldehyde functionality of monoaminals **10** and **11** may be reacted with various reagents. As an illustration of this concept, we describe

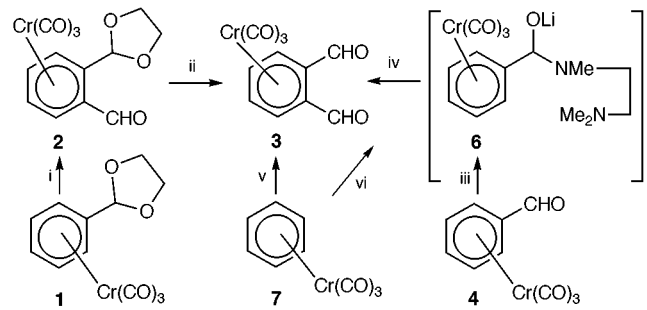

Scheme 1 *Reagents and conditions:* i, BuLi, DMF, THF, 49%; ii, H_2SO_4, 22% or HCO_2H, 19%; iii, BuLi, $NMe_2CH_2CH_2NHMe$ **5**, THF; iv, BuLi, DMF, THF, 35% from **4**; v, BuLi, $Me_2NCH_2CH_2NMeCHO$ **8**, THF, then BuLi, DMF, then 0.1 M HCl, 41% (and **4**, 15%); vi, BuLi, $Me_2NCH_2CH_2N$-MeCHO **8**, THF.

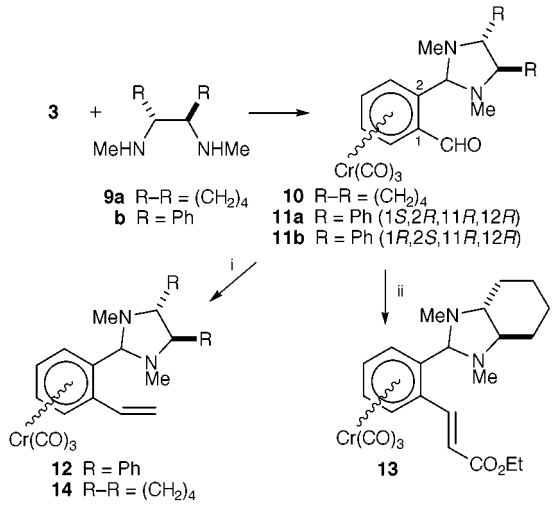

Scheme 2 *Reagents and conditions:* i, separation of the diastereoisomers, then $MePPh_3Br$, $NaNH_2$, Et_2O, 16% for **12a**, 28% for **12b**; ii, separation of the diastereoisomers, then $[P(O)(OEt)_2]NaCHCO_2Et$, room temp., 87% for **13a**, 85% for **13b**.

here the olefination of the free aldehyde, to obtain optically pure *o*-substituted styrene complexes. Treating the diastereoisomers **10a** or **10b** with $MePPh_3Br$ and $NaNH_2$ in dry Et_2O gave the styrene derivatives **12a** in 16% yield or **12b** in 28% yield. Complexes **11a** and **11b** also reacted with $MePPh_3Br$ and $NaNH_2$ to afford the optically pure styrene derivatives **14a** and **14b** (in 23 and 18% yield) which can be separated by column chromatography. More interestingly, reaction of complex **10a** with the carbanion of the phosphonate $[P(O)(OEt)_2]NaCHCO_2Et$ occured smoothly giving complex **13a**† as orange crystals in 87% yield. The same reaction with diastereoisomer **10b** gave complex **13b**† in 85% yield.

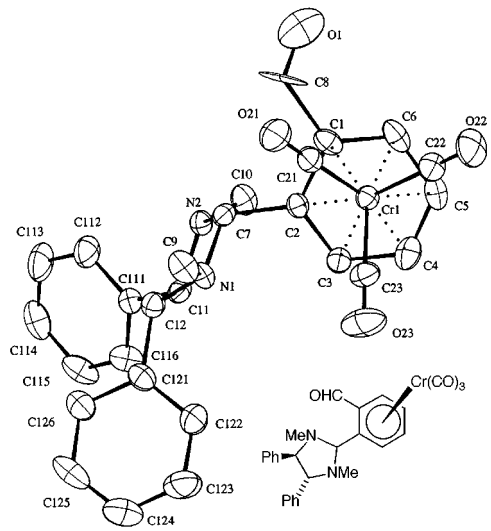

Fig. 1 ORTEP view of the molecular structure of complex **11a**. Selected interatomic distances (Å): Cr(1)–C(1) 2.180(7); Cr(1)–C(2)2.220(6); Cr(1)–C(3) 2.196(6); Cr(1)–C(4) 2.199(7); Cr(1)–C(5) 2.199(7); Cr(1)–C(6) 2.191(7).

In conclusion, these preliminary results open up, *via* a 'one-pot' procedure from benzenechromium complex, a ready access to phthalaldehydechromium complex. It is worth noting that this represents a *facile bifunctionnalisation of benzene* which can lead to chiral *ortho*-disubstituted arenechromium complexes. It can be used for the synthesis of enantiomerically pure styrenechromium complexes substituted at the *ortho* position by potentially versatile aminal groups. The scope of the applications of these new homochiral complexes is currently being investigated in our laboratory.

Notes and references

† *Typical procedure* for **10**: A mixture of complex **3** (0.1 g, 0.37 mmol), diamine **9a** (63 mg, 0.45 mmol) and molecular sieves in dry Et_2O (25 ml) was stirred for 25 min at room temperature under N_2. The solution turned orange. After silica gel chromatography, the first diastereoisomer was eluted with Et_2O–NEt_3–cyclohexane (70 : 0.01 : 30) and obtained in 44% yield (64 mg). The second diastereoisomer was eluted with Et_2O–0.01% NEt_3 and obtained in 32% yield (46 mg). *Selected data* for **10b**: δ_H(400 MHz, $CDCl_3$) 1.13–1.37 (m, 4H), 1.84–2.1 (m, 4H), 2.37 (s, 3H), 2.49 (s, 3H), 2.58 (m, 2H), 4.23 (s, 1H, H7), 5.49 (m, 2H, H4, H5), 5.58 (m, 1H, H6), 5.62 (m, 1H, H3), 10.3 (s, 1H); $[\alpha]_D^{20}$ −98 ($CHCl_3$, *c* 0.08). For **13b**: δ_H 1.23–1.19 (m, 4H), 131 (t, *J* 7, 3H), 1.78–1.82 (m, 4H), 2.27 (s, 3H), 2.28 (m, 2H), 2.56 (s, 3H), 4.30 (q, *J* 7, 2H), 5.21 (d, *J* 6, 1H, H6), 4.39 (s, 1H, H7), 5.30 (d, *J* 6, 1H, H6), 5.36 (m, 1H, H5), 5.47 (m, 1H, H4), 6.03 (d, *J* 6, 1H, H3), 6.22 (d, *J* 15, 1H), 7.87 (d, *J* 15, 1H); $[\alpha]_D^{20}$ +340 ($CHCl_3$, *c* 0.01). All novel complexes (**10**–**14**) were characterised by microanalyses, NMR and IR spectra and low resolution MS.

‡ *Crystal data* for **11a**: $C_{27}H_{24}N_2O_4Cr$, M = 492.5, orthorhombic, space group $P2_12_12_1$, a = 7.333(2), b = 14.455(3), c = 22.976(4) Å, D_C = 1.34 g cm^{-3} , Z = 4, 0.20 × 0.20 × 0.64 mm, μ = 4.91 cm^{-1}, 1466 data collected at room temperature on a Nonius CAD4 diffractometer. Absorption correction using DIFABS was applied (T_{min} = 0.92, T_{max} = 1). Anomalous dispersion terms and correction of secondary extinction were applied. The structure was solved by standard Patterson–Fourier techniques and refined by least-squares analysis using anisotropic thermal parameters for all non-hydrogen atoms. H atoms were located on a difference Fourier map and introduced in the refinement as fixed contributors with an overall isotropic thermal parameter. 1771 reflections, with $I > 3\sigma(I)$, were used to solve and refine the structure to R = 0.042 and R_w = 0.048 (unit weights), 309 least-squares parameters. The programs used were CRYSTALS and CAMERON. The shape of the anisotropic displacement ellipsoid for C8 suggests some disorder. Unfortunately, attempts to deal with this disorder failed. CCDC 182/1409. See http://www.rsc.org/suppdata/cc/1999/2061 for crystallographic data in .cif format.

1 F. Rose-Munch and E. Rose, *Curr. Org. Chem.*, 1999, **3**, 493; F. Rose-Munch, V. Gagliardini, C. Renard and E. Rose, *Coord. Chem. Rev.*, 1998**, 178**–**180**, 249; M. F. Semmelhack, in *Comprehensive Organometallic Chemistry II*, ed. E. W. Abel, F. G. A. Stone and G. Wilkinson, Pergamon, Oxford, 1995, vol. 12, p. 979.

2 See for example: B. Schnell, G. Bernardinelli and E. P. Kündig, *Synlett*, 1999, **3**, 348; E. P. Kündig, D. Armurrio, G. Anderson, D. Beruben, K. Khan, A. Ripa and L. Ronggang, *Pure Appl. Chem.*, 1997, **69**, 543; A. Solladié-Cavallo, G. Solladié and E. Tsamo, *J. Org. Chem.*, 1979, **44**, 4189; G. Jaouen and A. Meyer, *J. Am. Chem. Soc.*, 1975, **97**, 4667.

3 (*a*) A. Alexakis, P. Mangeney, I. Marek, F. Rose-Munch, E. Rose and A. Semra, *J. Am. Chem. Soc.*, 1992, **114**, 8288; (*b*) Y. Kondo, J. R. Green and J. Ho, *J. Org. Chem.*, 1993, **58**, 6182; (*c*) S. G. Davies and C. L. Goodfellow, *J. Chem. Soc., Perkin Trans. 1*, 1990, 393.

4 M. Uemura, A. Daimon and Y.Hayashi, *J. Chem. Soc., Chem. Commun.*, 1995, 1943.

5 A. Quattropani, G. Bernardinelli and E. P. Kündig, *Helv. Chim. Acta*, 1999, **82**, 90.

6 S. Top, G. Jaouen, J. Gillois, C. Baldoli and S. Maiorana, *J. Chem. Soc., Chem. Commun.*, 1988, 284; B. Malézieux, G. Jaouen, J. Salatin, J. A. S. Howell, M. G. Palin, P. McArdle and M. O'Gara, *Tetrahedron: Asymmetry*, 1995, **3**, 375; K. Nakamura, K. Ishihara, A. Ohno, A. Uemura, H. Nishimura and Y. Hayashi, *Tetrahedron Lett.*, 1990, **31**, 3603.

7 A. Alexakis, T. Kanger, P. Mangeney, F. Rose-Munch, A. Perrotey and E. Rose, *Tetrahedron: Asymmetry*, 1995, **6**, 47 and 2135.

8 S. G. Davies, O. M. L. Furtado, D. Hepworth and T. Loveridge, *Synlettt*, 1995, 69.

9 P. W. N. Christian, R. Gil, K. Muniz-Fernandez, S. E. Thomas and A. T. Nierzchleyski, *J. Chem. Soc., Chem. Commun.*, 1994, 1569.

10 (*a*) A. Perrotey, D. Thesis, Paris, 1996; (*b*) The same sequence (**1**⟶⟶**3**) was applied by E. P. Kündig and H. Ratni in 65% yield with a different hydrolysing system: private communication.

11 A. Gorgues, *Bull. Soc. Chim. Fr.*, 1974, 529.

12 D. L. Commins and J. D. Brown, *J. Org. Chem.*, 1984, **49**, 1078; the asymmetric version was developed earlier: see ref. 7(*b*) and R. A. Ewin, A. M. Macleod, D.A. Price, N.S. Simpkins and A.P.Watt, *J. Chem. Soc., Perkin Trans. 1*, 1997, 401.

Communication 9/06043J

ChemComm

Acid/base-catalyzed ester hydrolysis in near-critical water

Heather P. Lesutis, Roger Gläser, Charles L. Liotta and Charles A. Eckert*

Schools of Chemical Engineering and Chemistry and Biochemistry and Specialty Separations Center, Georgia Institute of Technology, Atlanta, GA 30332-0100, USA. E-mail: cae@che.gatech.edu

Received (in Corvallis, OR, USA) 2nd August 1999, Accepted 1st September 1999

Hydrolyses of substituted benzoic acid esters in near-critical water (250–300 ºC) show autocatalytic kinetic behavior and surprisingly give the same rate constant regardless of substituent, suggesting that an acid-catalyzed mechanism predominates under our reaction conditions.

Liquid water in the near-critical region (250–300 °C) is a unique, environmentally benign solvent which affords opportunities for pollution minimization in a wide variety of commercially important chemical processes.[1–3] As the temperature is raised, the hydrogen bonding in water diminishes.[4,5] Both the relative permittivity and the density decrease,[6] giving near-critical water properties similar to those of typical polar organic solvents. While near-critical water can still solubilize salts, it can also dissolve organic compounds.[7]

In addition, the ionization constant of water increases by three orders of magnitude in going from ambient to near-critical conditions,[8] making it a strong source of both hydronium and hydroxide ions. These ions can act as catalysts in acid- or base-catalyzed conversions, respectively.[1,9] Because the protons and hydroxide ions derived from the auto-ionization of hot water do not require neutralization, formation of unwanted salt by-products can be reduced or eliminated in many processes. Further, the ease of separation of products from water by cooling to ambient conditions makes it an economically viable replacement for less environmentally benign solvents.

Because near-critical water is such a promising solvent for a wide variety of processes, we sought a more thorough understanding of chemical reactions and mechanisms in this medium. We chose to study the hydrolysis of several simple benzoic acid esters as a model system (Scheme 1) to elucidate mechanistic pathways followed in near-critical water. It has previously been shown that the main products formed from the hydrolyses of di-*n*-butyl phthalate[10] and ethyl acetate[11] in near-critical water are the corresponding acids and alcohols. The formation of thermolysis products, such as alkenes and carbon oxides, is considerably slower in near-critical water than when performed neat.

Several 3.0 ml titanium reactors were loaded with benzoate ester and an excess of water (Aldrich, HPLC grade), where the excess of water makes the back reaction negligible. Reactors were placed in a heating block at 250 °C, and pairs of reactors were removed and quenched at various reaction times. Reactor contents were diluted in acetone and analyzed using GC-FID and GC-MS.

Data measuring conversion *vs.* time yielded S-shaped curves (Fig. 1), suggesting an autocatalytic mechanism. Because benzoic acid is one of the products, autocatalysis suggests the

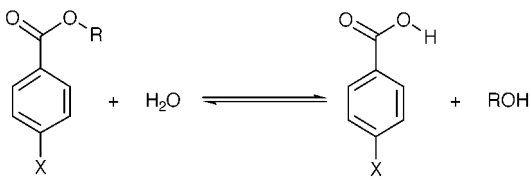

Scheme 1

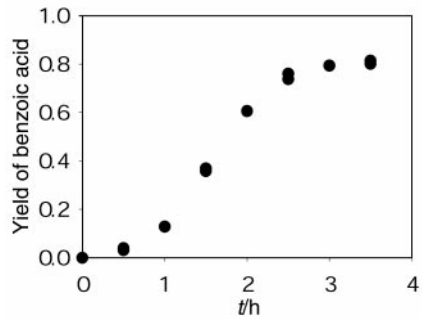

Fig. 1 Fractional conversion of *n*-propyl benzoate *vs.* time.

reaction is acid-catalyzed. The $A_{AC}2$ mechanism for acid-catalyzed hydrolysis of esters yields a rate equation of the form shown in eqn. (1),

$$\frac{dx}{dt} = k[\text{ester}][H_2O][H^+] \quad (1)$$

where $k = k_2 K_1$;[12] k_2 is the rate constant for the addition of water to the protonated ester, and K_1 is the equilibrium constant for the protonation of the ester (Scheme 2). The second step is rate-determining, and its product equilibrates rapidly to benzoic acid and the alcohol. The concentration of protons is determined from the dissociation constant of water and that of benzoic acid at 250 °C. The dissociation constant of benzoic acid under our conditions is 3.7×10^{-6} M,[13,14] and the Hammett reaction constant ρ for this dissociation increases by only 2% from 25 to 250 °C.[15] We calculated values for the dissociation constants of *p*-chlorobenzoic acid and *p*-trifluoromethylbenzoic acid at 250 °C and integrated numerically to ascertain k for each reaction. Table 1 reports these rate constants as products of k_2 and K_1*, where K_1* is the equilibrium constant for protonation of the nonsubstituted ester. For the acidity of the substituted benzoic acids, we assumed that the effect of substituents on the equilibrium constant for acid dissociation is the same as that for protonation of the ester.

Rates of hydrolysis of isobutyl benzoate were also measured at 260 and 300 °C. Utilizing dissociation constants of benzoic acid at these temperatures,[13,15] the activation energy was

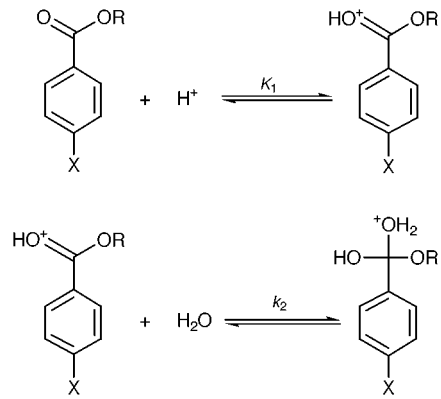

Scheme 2

Table 1 Rate constants at 250 °C for the hydrolysis of benzoate esters, where K_1* is the equilibrium constant for the protonation of nonsubstituted ester

R	X	k_2K_1*/l² mol^{-2} h^{-1}
Me	H	26.9 ± 2.5
Et	H	25.7 ± 0.9
Pr	H	10.4 ± 0.5
Bu	H	17.1 ± 0.6
Bu^i	H	6.7 ± 0.3
Bu^i	Cl	7.4 ± 0.6
Bu^i	CF_3	7.0 ± 0.5

calculated to be 101 ± 13 kJ mol^{-1}, indicating that mass transfer limitations were negligible. Similar activation energies were obtained for the acid-catalyzed hydrolysis of substituted benzoic acid esters in low temperature aqueous solvents with a stoichiometric addition of acid.[16]

As expected, longer alkyl chains on the esters yield slower hydrolyses, and the branched butyl benzoate hydrolyzes more slowly than the linear butyl benzoate. As the carbonyl carbon becomes more sterically hindered, nucleophilic attack by water becomes more difficult, resulting in a slower hydrolysis.

Hydrolyses of substituted isobutyl benzoates provide further evidence that an acid-catalyzed mechanism predominates under near-critical conditions. It is clear from Table 1 that substituents have very little effect on rates of hydrolysis of benzoic acid esters under these conditions. Because of competing effects in the first two steps of the $A_{AC}2$ mechanism (Scheme 2), substituents exhibit a negligible effect on the rate constants. This negligible substituent effect is a well-documented characteristic of ester hydrolysis *via* an acid-catalyzed mechanism in aqueous solvents at lower temperature.[17] Hammett plots of acid-catalyzed ester hydrolyses have ρ = 0, compared to ρ = 2.4 for base-catalyzed hydrolyses of esters.[17] In addition to the reactions reported in Table 1, the hydrolysis of isobutyl *p*-hydroxybenzoate was also attempted, but the hydroxy group is strongly electron donating (σ = −0.38), and the ester decarboxylated.

In summary, benzoate esters can be cleaved to benzoic acid and the corresponding alcohol in near-critical water without the addition of any acid or base catalyst. Preliminary investigations indicate that the pathway for acid-catalyzed hydrolysis according to an $A_{AC}2$ mechanism is dominant. First, the S-shaped conversion *vs*. time curve is consistent with autocatalysis. The acidity of near-critical water seems sufficient to initiate hydrolysis of the benzoate and formation of the autocatalytic species benzoic acid. Also, the addition of electron-withdrawing substituents does not affect reaction rate, as predicted by the proposed acid-catalyzed mechanism and demonstrated for many acid-catalyzed hydrolyses in the literature. Thus, despite the fact that near-critical water is quite different from water under ambient conditions, hydrolyses in it follow the mechanistic pathway commonly observed at lower temperatures.

We would like to thank Kris Griffith for synthesizing the substituted benzoic acid esters and Greg Ladzinske for help collecting data.

Notes and references

1 A. R. Katritzky, S. M. Allin and M. Siskin, *Acc. Chem. Res.*, 1996, **29**, 399.
2 J. An, L. Bagnell, T. Cablewski, C.R. Strauss and R.W. Trainor, *J. Org. Chem.*, 1997, **62**, 2505.
3 L. J. Seacock, Jr., D. C. Elliot, E. G. Baker and R. S. Butner, *Ind. Eng. Chem. Res.*, 1993, **32**, 1535.
4 Y. Guissani and B. Guillot, *J. Chem. Phys.*, 1993, **98**, 8221.
5 E. T. Ryan, T. Xiang, K. P. Johnston and M. A. Fox, *J. Phys. Chem. A*, 1997, **101**, 1827.
6 R. W. Shaw, T. B. Brill, A. A. Clifford, C. A. Eckert and E. U. Franck, *Chem. Eng. News*, 1991, **69**, 26.
7 B. Kuhlmann, E. M. Arnett and M. Siskin, *J. Org. Chem.*, 1994, **59**, 3098.
8 W. L. Marshall and E. U. Franck, *J. Phys. Chem. Ref. Data*, 1981, **10**, 295.
9 K. Chandler, F. Deng, A. K. Dillow, C. L. Liotta and C. A. Eckert, *Ind. Eng. Chem. Res.*, 1997, **36**, 5175.
10 J. M. L. Penninger, *Fuel*, 1988, **67**, 490.
11 P. Krammer, S. Mittelstädt and H. Vogel, *Chem. Eng. Technol.*, 1999, **22**, 126.
12 T. H. Lowry and K. S. Richardson, *Mechanism and Theory in Organic Chemistry*, Harper and Row, New York, NY, 1987, pp. 717–723.
13 A. J. Read, *J. Solution Chem.*, 1981, **10**, 437.
14 R. M. Kettler, D. J. Wesolowski and D. A. Palmer, *J. Solution Chem.*, 1995, **24**, 385.
15 E. L. Shock, *Am. J. Sci.*, 1995, **295**, 496.
16 E. W. Timm and C. N. Hinshelwood, *J. Chem. Soc.*, 1938, 862.
17 H. H. Jaffe, *Chem. Rev.*, 1953, **53**, 191.

Communication 9/06401J

ChemComm

Glycosidase-catalysed synthesis of α-galactosyl epitopes important in xenotransplantation and toxin binding using the α-galactosidase from *Penicillium multicolor*

Suddham Singh, Michaela Scigelova and David H. G. Crout*

Department of Chemistry, University of Warwick, Coventry, UK CV4 7AL. E-mail: msrky@csv.warwick.ac.uk

Received (in Cambridge, UK) 26th July 1999, Accepted 2nd September 1999

The α-galactosidase from *Penicillium multicolor* catalyses highly regioselective galactosyl transfer on to mono- and disaccharide acceptors that have a non-reducing terminal galactose unit to give products containing the α-D-Gal*p*-(1→3)-D-Gal*p* epitope found on pig tissue and which is responsible for the hyperacute rejection response in xenotransplantation of pig organs into man.

The α-D-Gal*p*-(1→3)-β-α-Gal*p* moiety of glycoconjugates has been found to be of considerable biological importance. It has attracted attention mainly because of its significance in the development of the xenotransplantation of animal organs into human patients,[1] a development driven on the one hand by the success of organ transplantation in the latter part of the twentieth century and on the other by an acute shortage of donor organs. Current research is directed towards the use of pig organs in humans (discordant xenotransplantation), as the pig is considered the best organ donor given the constraints imposed by the popular opposition to the use of organs from primates. The major problem with pig-to-man xenotransplantation is the extremely rapid human antibody-mediated hyperacute rejection that occurs following transplantation into human patients. The antigenic epitopes responsible for this hyperacute rejection response contain the α-D-Gal*p*-(1→3)-β-D-Gal*p* terminus and have been identified as α-D-Gal*p*-(1→3)-β-D-Gal*p*-R, α-D-Gal*p*-(1→3)-β-D-Gal*p*-(1→4)-β-D-Glc*p*-R, α-D-Gal*p*-(1→3)-β-D-Gal*p*-(1→4)-β-D-GlcNAc*p*-R and α-D-Gal*p*-(1→3)-β-D-Gal*p*-(1→4)-β-D-GlcNAc*p*-(1→3)-β-D-Gal*p*-(1→4)-β-D-Glc*p*-R, known collectively as 'α-Gal' epitopes.[2] These epitopes specifically bind to human anti-α-Gal antibodies during xenotransplantation.[3] They are found on tissues of almost all mammals except man and old world primates. Antibodies against the α-Gal epitope expressed in man comprise approximately 1% of circulating immunoglobulin G.[4] Recent investigations have shown that human anti-Gal antibodies can bind to, and be neutralised by, α-Gal-related oligosaccharides.[5] An α-D-Gal*p*-(1→3)-β-D-Gal*p*-(1→4)-β-D-GlcNAc*p* trisaccharide, representing the natural α-Gal epitope, is capable of neutralising anti-Gal antibodies at low concentrations.[6] A further reason for interest in the α-Gal epitope is that it has been identified as a receptor for the toxin from *Clostridium difficile*, a micro-organism that is a major cause of antibiotic-associated diarrhoea and the causative agent of a serious condition, pseudomembranous colitis, in the elderly following antibiotic therapy.[7]

The possibility of utilising the adhesion of bacteria and viruses to specific carbohydrates has become an attractive goal in attempts to find alternatives to antibiotic therapy. Developments in this area have taken place against a background of increasing concern about the development of antibiotic resistance in important species of pathogenic bacteria.[8] An immobilised version of the *C. difficile* toxin receptor is in development for the treatment of *C. difficile*-associated diarrhoea.[9]

The use of α-Gal oligosaccharides for clinical applications would require large amounts of α-Gal oligosaccharides. Conventional synthesis of carbohydrates, although well developed over the last decade, requires multiple protection and deprotection steps.[10] Consequently, enzymatic synthesis is an attractive alternative for the synthesis of oligosaccharides.[11] Enzymatic syntheses of α-Gal oligosaccharides have been reported.[12] However, the α-galactosyl transferase method requires the use of a complex donor and is limited by the availability of the appropriate enzymes.[12*a*] The use of glycosidases has been reported but these have been limited by rather low yields and by the production of mixtures.[12*b–d*]

Here we report simple, regiospecific, glycosidase-catalysed syntheses of α-D-Gal*p*-(1→3)-β-D-Gal*p*-OMe and α-D-Gal*p*-(1→3)-α-D-Gal*p*-OMe disaccharides and α-D-Gal*p*-(1→3)-β-D-Gal*p*-(1→4)-D-Glc*p* and α-D-Gal*p*-(1→3)-β-D-Gal*p*-(1→4)-D-GlcNA*cp* trisaccharides catalysed by an α-galactosidase from *Penicillium multicolor* discovered during a major screening programme for synthetically useful glycosidases.[13] The great advantage of this enzyme is that it is highly specific for α-(1→3) transfer and thus represents a considerable improvement over existing methods for the synthesis of α-Gal oligosaccharides.

Transfer of an α-galactosyl unit from *p*-nitrophenyl α-D-galactopyranoside **1** on to methyl β-D-galactopyranoside **2** using an α-galactosidase from *Penicillium multicolor* gave only one disaccharide α-D-Gal*p*-(1→3)-β-D-Gal*p*-OMe **3** in 43% yield [Scheme 1(*a*)]. Similarly, transfer of an α-galactosyl unit from donor **1** on to methyl α-D-galactopyranoside **4** gave the disaccharide α-D-Gal*p*-(1→3)-α-D-Gal*p*-OMe **5** in 46% yield [Scheme 1(*b*)]. These results suggest that by changing the conformation at the anomeric position in the acceptors **2** and **4** the regioselectivity of the transfer was not affected. This indicates that 'anomeric control', in which regioselectivity is influenced by the anomeric configuration in the glycosyl acceptor, does not operate in this system.[14] In both cases the product obtained was a (1→3)-linked disaccharide.

Transfer of the α-galactosyl unit from donor **1** on to lactose **6** gave again the (1→3)-linked product α-D-Gal*p*-(1→3)-β-D-Gal*p*-(1→4)-D-Glc*p* **7** in 25% yield [Scheme 1(*c*)]. Similarly transfer of α-galactosyl unit from the donor **1** on to lactosamine **8** gave the trisaccharide α-D-Gal*p*-(1→3)-β-D-Gal*p*-(1→4)-D-GlcNA*cp* **9** in 32% yield [Scheme 1(*d*)].

In all these reactions the conversion (donor) was 40–50%. This was not taken into account in calculating yields. The incomplete consumption of donor indicated product inhibition. If this could be overcome, even higher yields should be obtainable. We found that the released *p*-nitrophenol inhibited the enzyme and showed that this inhibition could be largely overcome by operating in less concentrated solutions. Thus by decreasing the overall concentration of donor **1** (from 0.34 to 0.17 M) and the acceptor **8** (from 1.3 to 0.65 M), 90% conversion was achieved and the isolated yield of the trisaccharide **9** increased from 32% to 48%.

The α-galactosidase used in these experiments was isolated from Lactase P from *Penicillium multicolor* (KI Chemicals, Japan). The proteins from a crude extract were precipitated by EtOH (50% v/v) and separated by DEAE-Sepharose [equilibrated with potassium phosphate buffer (10 mM, pH 6.5) and eluted with a linear gradient of NaCl (0–0.8 M)] followed by

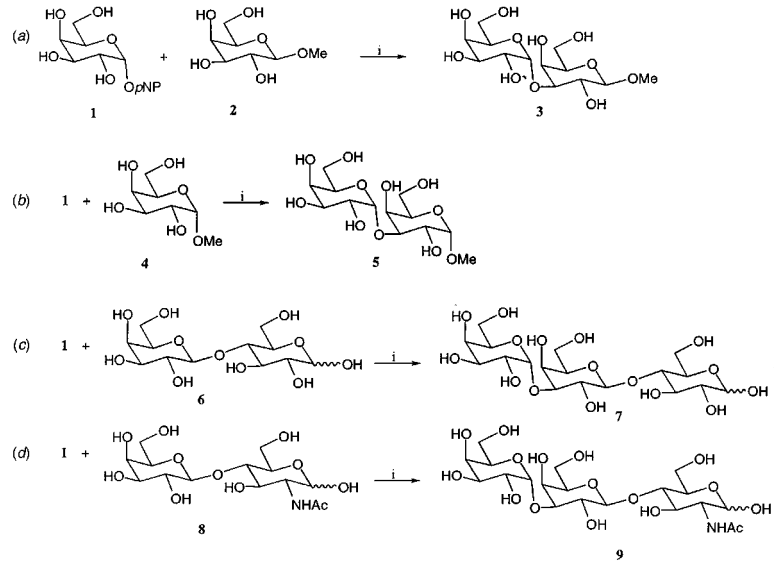

Scheme 1 *Conditions*: i, α-Galactosidase from *Penicillium multicolor; p*NP = *p*-nitrophenyl.

chromatography on ceramic hydroxyapatite [equilibrated with potassium phosphate buffer (5 mM, pH 6.5) and eluted with a linear gradient (5–400 mM) of potassium phosphate buffer (pH 6.5)]. Active fractions were concentrated using a Centriprep (Amicon) membrane with a 30 kDa cut-off to give a preparation [6.4 U cm^{-3}, 150 U (mg protein)$^{-1}$] free of β-galactosidase activity.

The method described here provides a remarkably simple one-step enzymatic synthesis of α-galactosyl epitopes and can be scaled up for clinical applications. Given the potential demand for α-Gal di- and tri-saccharides, the method described here offers an inexpensive and economical route to these compounds.

In a typical experiment *p*-nitrophenyl α-D-galactopyranoside **1** (0.1 g, 0.332 mmol) and *N*-acetyllactosamine **8** (0.5 g, 1.305 mmol) in citrate–phosphate buffer (0.05 M, 2 ml, pH 4.0) were incubated with the α-galactosidase from *Penicillium multicolor* (0.15 cm^3, 0.96 U) at 30 °C for 6 h. The reaction was stopped by heating in a boiling water bath for 5 min. Examination of the crude product by HPLC indicated that a single trisaccharide was formed. The product mixture was purified by carbon–Celite chromatography[15] to give trisaccharide **9** in 48% yield. The product was confirmed to be a single isomer by ^{1}H and ^{13}C NMR.

We thank the Biotechnology and Biological Sciences Research Council (UK) for financial support and Dr K. Ajisaka for providing the Lactase P.

Notes and references

1 J. L. Platt, *Nature*, 1998, 392, Suppl. 11.
2 R. P. Rother and S. P. Squinto, *Cell*, 1996, **86**, 185.
3 D. K. C. Cooper, E. Koren and R. Oriol, *Immunol. Rev*., 1994, **141**, 31.
4 U. Galili, B. A. Macher, J. Buehler and H. B. Shohet, *J. Exp. Med*., 1985, **162**, 573.
5 P. M. Simon, F. A. Neethling, S. Taniguchi, P. L. Goode, D. Zopf, W. W. Hancock and D. K. C. Cooper, *Transplantation*, 1998, **65**, 346; T. Cairns, J. Lee, L. Goldberg, T. Cook, P. Simpson, D. Spackman, A. Palmer and D. Taube, *Transplantation*, 1995, **60**, 1202; F. A. Neethling, E. Koren, Y. Ye, S. V. Richards, M. Kujundzic, R. Oriol and D. K. C. Cooper, *Transplantation*, 1994, **57**, 959.
6 U. Galili and K. L. Matta, *Transplantation*, 1996, **62**, 256.
7 G. F. Clark, H. C. Krivan, T. D. Wilkins and D. F. Smith, *Arch. Biochem. Biophys*., 1987, **257**, 217.
8 *Towards Anti-Adhesion Therapy for Microbial Diseases*, ed. I. Kahane and I. Ofek, Plenum Press, New York and London, 1996; U. J. Nilsson, L. D. Heerze, Y. C. Liu, G. D. Armstrong, M. M. Palcic and O. Hindsgaul, *Bioconjugate Chem*., 1997, **8**, 466.
9 L. D. Heerze, M. A. Kelm, J. A. Talbot and G. D. Armstrong, *J. Infect. Dis*., 1994, **169**, 1291.
10 G.-J. Boons, *Tetrahedron*, 1996, **52**, 1095.
11 D. H. G. Crout and G. Vic, *Curr. Opin. Chem. Biol*., 1998, **2**, 98.
12 (*a*) J. Fang, J. Li, X. Chen, Y. Zhang, J. Wang, Z. Guo, W. Zhang, L. Yu, K. Brew and P. G. Wang, *J. Am. Chem. Soc*., 1998, **120**, 6635; (*b*) K. G. I. Nilsson, *Tetrahedron Lett*., 1997, **38**, 133; (*c*) G. Vic, C. H. Tran, M. Scigelova and D. H. G. Crout, *Chem. Commun*., 1997, 169; (*d*) I. Matsuo, H. Fujimoto, M. Isomura and K. Ajisaka, *Bioorg. Med. Chem. Lett*., 1997, **7**, 255.
13 M. Scigelova, S. Singh and D. H. G. Crout, *J. Mol. Catal. B: Enzym*., 1999, **6**, 483.
14 D. H. G. Crout, O. W. Howarth, S. Singh, B. E. P. Swoboda, P. Critchley and W. T. Gibson, *J. Chem. Soc., Chem. Commun*., 1991, 1550; S. Singh, M. Scigelova, P. Critchley and D. H. G. Crout, *Carbohydr. Re*s., 1997, **305**, 363.
15 W. W. Binkley, *Adv. Carbohydr. Chem*., 1955, **10**, 55.

Communication 9/06020K

Fine-tuning of pore size of MCM-41 by adjusting the initial pH of the synthesis mixture

Anjie Wang*[a] and Toshiaki Kabe[b]

[a] *Laboratory of Comprehensive Utilization of Carbonaceous Resources, Dalian University of Technology, 158 Zhongshan Road, Dalian 116012, P.R. China. E-mail: hykyb@mail.dlptt.ln.cn*

[b] *Department of Applied Chemistry, Faculty of Technology, Tokyo University of Agriculture and Technology, 2-24-16 Nakacho, Koganei, Tokyo 184, Japan*

Received (in Cambridge, UK) 3rd August 1999, Accepted 8th September 1999

The pore size of MCM-41 can be finely tuned from 38.3 to 52.7 Å with a narrow distribution by carefully adjusting the initial pH of the synthesis mixture from 11.5 to 10.0.

MCM-41, with well-defined mesopores and extremely high surface area, has been the focus of much research interest since its discovery by the researchers at the Mobil Research and Development Corporation in 1992.[1] The precise tuning of its pore size is among the many favorable properties of MCM-41. Recently, many synthesis techniques, aiming at enlarging the pore size with narrow distribution, have been developed.[2] Some approaches use surfactants with different chain lengths or binary templating agents to expand the pore size.[1–3] Other routes use high temperatures in synthesis or postsynthesis treatment.[4–6]

It is well known that MCM-41 is typically characterized by an X-ray reflection in the vicinity of $2\theta = 2°$. However, the mesoporous materials synthesized by different researchers were not exactly the same under similar synthesis conditions (temperature, mixture composition, *etc.*),[1,7] unlike the case of microporous zeolite synthesis in which the characteristic X-ray reflections are well known. In our recent study, it was shown that the difference in the d_{100} spacing stems from the initial pH of the synthesis mixture, and we found that the pore sizes of the synthesized materials can be adjusted in a relatively wide range (> 14 Å) with a narrow pore distribution by varying the initial pH of the synthesis mixture.

The general procedure for synthesizing MCM-41 is as follows: 5.2 g of sodium silicate hydrate from Kigida Chemical Co. Ltd. (Japan) was dissolved in 25 ml of deionized water. The pH of the solution was adjusted to the desired value by adding 4 M H_2SO_4 to obtain a silica gel. A precision pH paper (Macherey-Nagel, Germay) was used to determine the pH of the gel. After vigorously stirring for 30 min at ambient temperature, an aqueous solution of CTAB (cetyltrimethylammonium bromide) was added into the gel to produce the synthesis mixture (typical composition: SiO_2•0.5Na_2O• 0.24CTAB•60H_2O). The mixture was allowed to stir at ambient temperature for 1 h, then placed in a static stainless steel autoclave kept at different temperatures for various time periods. After cooling to ambient temperature, the resulting solid material was recovered by filtration, washed with water and dried at 353 K for 4 h. The as-synthesized materials were calcined at 823 K for 6 h.

The X-ray diffraction patterns were recorded on a Rigaku RAD-2X diffractometer using nickel-filtered Cu-Kα radiation at 35 kV and 20 mA. Nitrogen adsorption measurements were performed using a Coulter SA 3100 adsorption analyzer which reports adsorption isotherm and BET specific surface area and pore volume automatically. Before the adsorption analysis the samples were outgased for 4 h at 573 K. The primary mesopore size w_d is determined by using eqn. (1), the distance between pore centers a_0 is calculated using eqn. (2), and the pore wall thickness b_d is given by eqn. (3).[8]

$$w_d = 1.213 d_{100} \sqrt{\frac{2.2V_p}{1 + 2.2V_p}} \quad (1)$$

$$a_0 = 2d_{100}/\sqrt{3} \quad (2)$$

$$b_d = a_0 - w_d \quad (3)$$

The X-ray diffraction patterns of samples synthesized at different pH are shown in Fig. 1. It can be seen that all the samples prepared at pH 10.0–12.0 show strong reflections at *ca.* $2\theta = 2°$, indicating that the mesostructures are well developed. Moreover, the interplanar spacing d_{100} changes between 38.4 and 53.8 Å when the initial pH of the synthesis mixture varies from 11.5 to 10.0. The material prepared at pH 12.0 seems to be a lamellar mesophase, showing no distinct X-ray diffraction peaks after calcination. And no X-ray reflections were determined for the samples prepared at pH < 10.0 and pH > 12.0.

The synthesis conditions and characteristic parameters of the obtained mesoporous materials are summarized in Table 1. It is indicated that the mesostructures prepared at pH 10.0–11.5 are well developed with high surface area and large pore volume. When the initial pH of the synthesis mixture changes from 11.5 to 10.0, the pore size of the product varies from 38.3 to 52.7 Å and the pore wall thickness increases from 6.0 to 9.4 Å. The mesophase obtained at pH 12.0 has relatively low surface area and small pore volume, indicating that the structure may collapse after calcination.

The effects of CTAB/silica ratio and synthesis temperature on the pore size were also investigated. As shown in Table 2, the

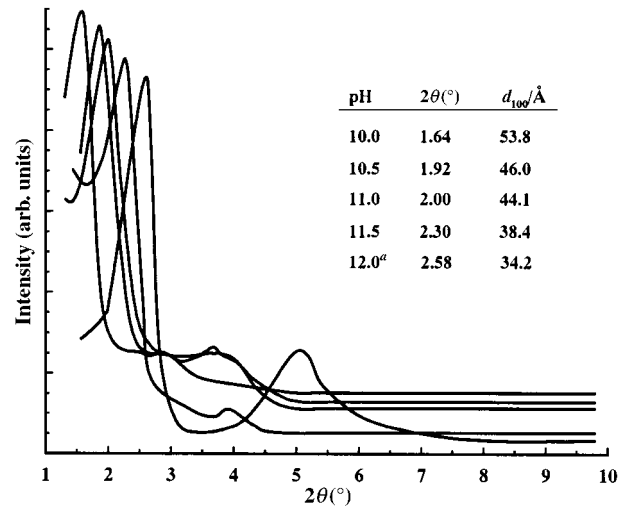

Fig. 1 X-Ray diffraction patterns of the mesoporous materials synthesized at pH 10.0–12.0. [a] As-synthesized material which showed no reflections after calcination at 823 K for 6 h.

Table 1 Synthesis conditions and structural parameters of MCM-41 prepared at different pH using the same mixture composition

T/K	t/h	pH	d_{100} spacing/Å	S_{BET}/ m^2 g^{-1}	V_p/ cm^3 g^{-1}	w_d/Å	a_0/Å	b_d/Å
403	36	10.0	53.8	833	0.85	52.7	62.1	9.4
403	12	10.5	46.0	1046	1.00	46.3	53.1	6.8
403	12	11.0	44.1	1022	1.05	44.7	50.9	6.2
403	11	11.5	38.4	1261	0.95	38.3	44.3	6.0
403	36	12.0	34.2[a]	421	0.49	—	—	—

[a] The as-synthesized sample, which showed no X-ray diffraction reflection after calcination at 823 K for 6 h.

Table 2 Preparation of MCM-41 at different CTAB/SiO_2 molar ratios and temperatures

T/ K	t/h	pH	CTAB/SiO_2 ratio	d_{100} spacing/Å
403	12	11.0	0.24	44.1
403	12	11.0	0.18	43.7
403	12	11.0	0.12	43.3
373	72	11.0	0.24	42.0

mesostructure characterized by the d_{100} spacing undergoes little change when varying the CTAB/silica ratio from 0.12 to 0.24 at pH 11.0. The synthesis temperature greatly affects the polymerization rate of the silica wall, but has little influence on the pore size of MCM-41, when elevated from 373 to 403 K.

Since the variation of pH only changes the OH^- concentration in the mixture, we propose that the pH of the synthesis mixture may affect the mesopore size by altering the charge matching pattern in the mixture. According to the model proposed by Huo and co-workers,[9] there are two basic pathways, one *via* direct self-assembly of a cationic inorganic species (I^+) and an anionic surfactant (S^-), and the other mediated by counterions of opposite charge. Our results seem to suggest that the synthesis of MCM-41 by our approach may take the mediated pathway, with OH^- working as the counterion. Because the mesopores are hexagon-shaped due to the Si–O bond conformation, while the micelles of the surfactant are theoretically spherical to minimize surface tension, the pores and the micelles do not match geometrically. We propose that the I^- anions and S^+ cations may be mediated by a layer of aqueous solution of inorganic ions (*i.e.* OH^-) which balance the charges. At lower pH, the thickness of the counterion layer may increase to keep the total OH^- constant in order to balance the charge, resulting in the enlargement of the pore size of the product. pH variation may also change the electrostatic charge distribution in the mixture, affecting the interactions of head groups in the micelle and resulting in the expansion of the micelle.[10]

The results reported here provide a convenient way of finely tuning the pore size of mesoporous MCM-41, which is promising in pore engineering and 'molecular sieving' with adjustable pore size, and may find wide application in shape-selective catalysis in fine chemicals, bio-separation and adsorption.

The authors thank Associate Professor A. Ishihara, Dr W. Qian, Mr J. Lee and Mr H. Shirai for their kind help, and thank the Chinese and Japanese governments for financial support in carrying out the Cultural Exchange Program.

Notes and references

1 J. S. Beck, J. C. Vartuli, W. J. Roth, M. E. Leonowicz, C. T. Kresge, K. D. Schmitt, C.T-W. Chu, D. H. Olson, E. W. Sheppard, S. B. McCullen, J. B. Higgins and J. L. Schlenker, *J. Am. Chem. Soc.*, 1992, **114**, 10834.
2 A. Sayari, Y. Yang, M. Kruk, and M. Jaroniec, *J. Phys. Chem. B*, 1999, **103**, 3651.
3 Q. Huo, D. I. Margolese and G. D. Stucky, *Chem. Mater.*, 1996, **8**, 1147.
4 C. Cheng, W. Zhou, D. H. Park, J. Klinowski, M. Hargreaves, and L. F. Gladden, *J. Chem. Soc., Faraday Trans.*, 1997, **93**, 359.
5 M. Kruk, M. Jaroniec and A. Sayari, *J. Phys. Chem. B*, 1999, **103**, 4590.
6 A. Corma, Q. Kan, M. T. Navarro, J. Pérez-Pariente and F. Rey, *Chem. Mater.*, 1997, **9**, 2123.
7 X. Chen, L. Huang and Q. Li, *J. Phys. Chem. B*, 1997, **101**, 8460.
8 M. Kruk, M. Jaroniec and A. Sayari, *Langmuir*, 1997, **13**, 6267.
9 Q. Huo, D. I. Margolese, U. Ciesla, P. Feng, T. E. Gier, P. Sieger, R. Leon, P. M. Petroff, F. Schüth and G. D. Stucky, *Nature*, 1994, **368**, 317.
10 A. Monnier, F. Schüth, Q. Huo, D. Kumar, D. Margolese, R. S. Maxwell, G. D. Stucky, M. Krishnamurty, P. Petroff, A. Firouzi, M. Janicke and B. F. Chmelka, *Science*, 1993, **261**, 1299.

Communication 9/06275K

A large enhancement in the binding affinity of artificial hosts by Os^{VI} chelation

Kyu-Sung Jeong,* Jung Wha Lee, Tae-Yoon Park and Sung-Youn Chang

Department of Chemistry, Yonsei University, Seoul 120-749, Korea. E-mail: ksjeong@alchemy.yonsei.ac.kr

Received (in Cambridge, UK) 2nd August 1999, Accepted 8th Septmber 1999

Mononuclear Os^{VI}-chelated macrocycles, self-assembled from OsO_4, 2,3-dimethylbut-2-ene and bispyridyl ligands, bind diamides much more strongly than the Os^{VI}-free ligands ($\Delta\Delta G$ = −14.6 kJ mol^{-1}).

Self-assembly by weak noncovalent interactions has recently attracted a great deal of attention in the area of host–guest and supramolecular chemistry. The strategy has been effectively used to synthesise artificial receptors in which two or more subunits are spontaneously coordinated to a metal ion to generate a binding cavity complementary to the targeted substrates.[1] On the other hand, metal ion chelation to one part of a flexible host may result in the structural reorganisation of another binding site, leading to allosteric behaviour in the binding events.[2–5] Here, we have prepared three bispyridyl ligands **1a**–**c** that spontaneously self-assemble into the corresponding macrocyclic complexes **2a**–**c** in the presence of alkene and OsO_4,[6,7] and compared the binding affinities of **1a**–**c** and **2a**–**c** toward diamide guests.

As shown in Scheme 1, the bispyridyl ligands **1a**–**c** were prepared by dropwise addition of diamines **4a**–**c** followed by aminolutidine **5** to a solution of pyridine-2,6-dicarbonyl dichloride **5** in CH_2Cl_2. The yields were 10–18% after repeated chromatography. The neutral macrocyclic complexes **2a**–**c** were spontaneously assembled within a few minutes by addition of OsO_4 (~1 equiv., 0.1 M in toluene) to a 1:1 molar mixture of the ligands **1a**–**c** and 2,3-dimethylbut-2-ene in a $CHCl_3$ at room temperature. After concentration, the residues were thoroughly washed with Et_2O to afford the Os^{VI}-complexes **2a**–**c** as brown solids (66–88% yield).

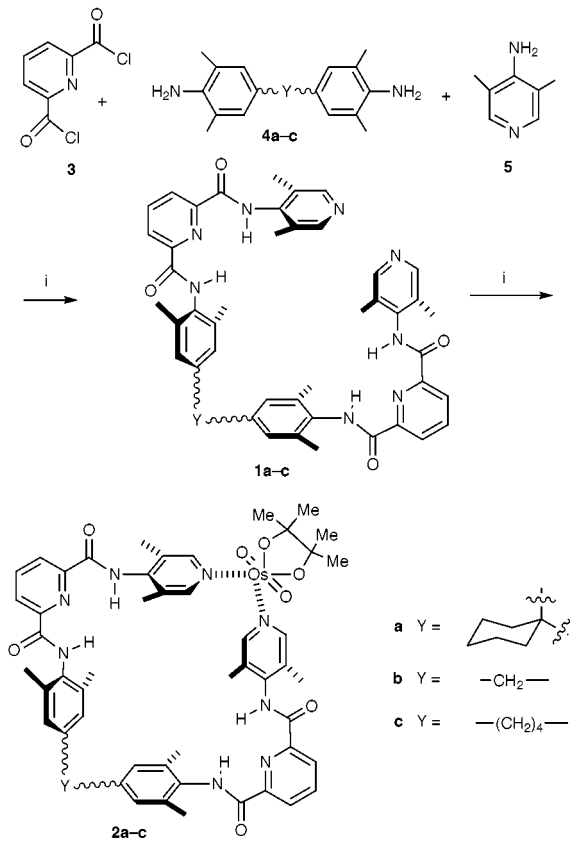

Scheme 1 *Reagents and conditions*: i, $EtNPr^i_2$, 0 °C to room temp.; ii, 2,3-dimethylbut-2-ene, OsO_4.

Elemental analysis of the products agreed well with 1:1:1 molar composition of OsO_4, 2,3-dimethylbut-2-ene and the ligand. Their IR spectra show a strong, characteristic band near 830 cm^{-1} diagnostic of the *trans* O=Os=O moiety of the octahedral dioxoosmium^{VI} complexes.[8] In the ^{1}H NMR spectra, the lutidyl C–H resonances of **2a**–**c** were shifted downfield (~0.28 ppm) relative to those for ligands **1a**–**c**, as expected upon coordination of the nitrogen to the Os^{VI} ester. The ^{1}H NMR spectra remain constant over a wide range of concentrations (0.25–10 mM) and temperatures (−40 to 40 °C) in $CDCl_3$, indicating that no aggregation or dissociation occurs under these conditions. ^{1}H NMR integration also confirmed a 1:1 molar ratio of the ligand and 2,3-dimethylbut-2-ene. The FAB-MS analyses strongly support the formation of mononuclear complexes **2a**–**c**. For example, the mass spectrum of **2a** shows the molecular ion [MH$^+$] peak at 1169.4 (intensity 1.8%, 1168.4 calc. for $C_{56}H_{64}N_8O_8{}^{192}Os$), [M − O]$^+$ at 1152.4 (intensity 3.3%), and [M − $(O_2C_2(CH_3)_4)$]$^+$ at 1052.4 (intensity 2.4%). The observed isotopic distribution patterns of all these peaks are consistent with those calculated for the mononuclear macrocycle **2a**. The complexes **2b** and **2c** also show the same FAB-MS spectral behaviour as seen for complex **2a**.

The binding properties of hosts **1a**–**c** and **2a**–**c** with diamide guests **6** and **7** were revealed in $CDCl_3$ by ^{1}H NMR titration

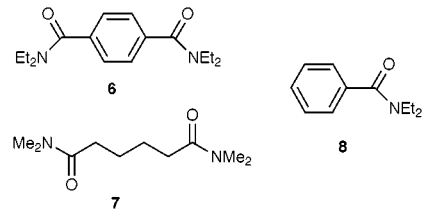

experiments, performed by adding the guest solution (5–10 mM) to the host stock solution (1–2 mM, 500 μl) in small potions. The time-averaged signals for the free and bound species were observed due to a fast exchange on the NMR time–scale. The association constants (K_a/M^{-1}) were calculated by non-linear least-squares fitting[9] of the titration data, which corresponded well to the expression for a 1:1 binding isotherm. All the hosts contain two different NH protons, and both N–H signals of the hosts were significantly downfield shifted ($\Delta\delta \geq$ 1 ppm) when guests **6** and **7** were added, indicating significant hydrogen bond formation. As a representative example, the two NH signals in the Os^{VI} complex **2a** were shifted downfield from δ 8.83 and 9.22 to δ 9.80 and 10.62, respectively, upon complexation with terephthalamide **6**. The titration curves, plotting either NH chemical shift change *vs.* equivalents of guest, gave essentially identical association constants within experimental error (<5%), indicating that both NHs are involved in a single binding mode.

As seen in Table 1, the association constants between Os-free ligands **1a**–**c** and guests **6** and **7** decrease in the order **1a** > **1b** > **1c**. This is expected because **1a** contains conformationally the most rigid linker, while **1c** possesses the most flexible

Table 1 Association constants (K_a/M^{-1}) of ligands **1a–c** and Os complexes **2a–c** with diamide guests **6** and **7** in $CDCl_3$ at 25 ± 1 °C

Guest	Ligand	K_a/M^{-1} [a]	Os complex	K_a/M^{-1} [a]	$\Delta\Delta G°$/ kJ mol^{-1} [b]
6	**1a**	2800	**2a**	1.7×10^4	−4.5
6	**1b**	580	**2b**	1.9×10^4	−8.6
6	**1c**	80	**2c**	2.9×10^4	−14.6
7	**1a**	210	**2a**	1.6×10^4	−10.7
7	**1b**	95	**2b**	2.9×10^4	−14.2
7	**1c**	30	**2c**	6.1×10^3	−13.2

[a] Titrations were duplicated and errors in K_a are within 10% for $K_a < 1 \times 10^4$ M^{-1} and within 30% for $K_a > 1 \times 10^4$ M^{-1}. [b] $\Delta\Delta G° = \Delta G°$(Os complex) − $\Delta G°$(ligand).

linker. More important a trend in the association constants is that Os complexes **2a–c** bind the guests **6** and **7** much more strongly than the corresponding Os-free ligands **1a–c**. The difference in the binding energy is up to $\Delta\Delta G° = -14.6$ kJ mol^{-1}, depending on the linker group; the more flexible the linker is, the greater the difference observed. The large enhancements of the association constants in the Os^{VI} complexes are possibly attributed to the following two factors. One is the conformational preorganization of the hosts **2a–c** as a consequence of Os^{VI} chelation, which greatly reduces the conformational entropy loss upon association of the host and guest. Another contributing factor may be the increased hydrogen-bonding donor ability of the lutidyl N–H protons as a result of Os^{VI} chelation to the terminal nitrogens.

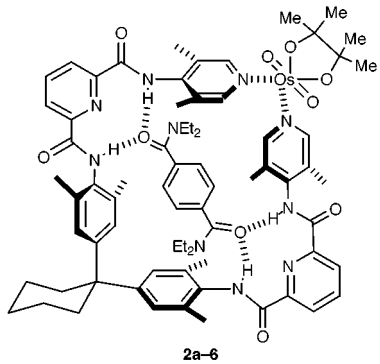

2a–6

The ligand **1a** and its Os^{VI} complex **2a** strongly bind diamide guest **6**, while they bind only slightly the monoamide analogue, *N*,*N*-diethylbenzamide **8** ($K_a \leq 15$ M^{-1} in $CDCl_3$, observed $\Delta\delta_{max} \leq 0.15$ ppm). The Job plots[10] showed a 1:1 stoichiometry between the host **1a** or **2a** and the diamide guest **6**. These observations clearly indicate that two hydrogen-bonding sites in the hosts must simultaneously participate in the complexation, as shown in the proposed structure of the complex **2a**·**6**. Additional evidence for the complex structure was obtained from ^{1}H NMR spectroscopy (Fig. 1). When **2a** and **6** are mixed in a 1:1 molar ratio, the NH signals of the host **2a** are largely downfield shifted ($\Delta\delta \geq 1$ ppm), and more importantly, the aryl C–H signal of the guest **6** is significantly upfield shifted ($\Delta\delta \sim 1.5$ ppm). The latter strongly suggests that the guest **6** is located inside the cavity surrounded by the host aryl walls,

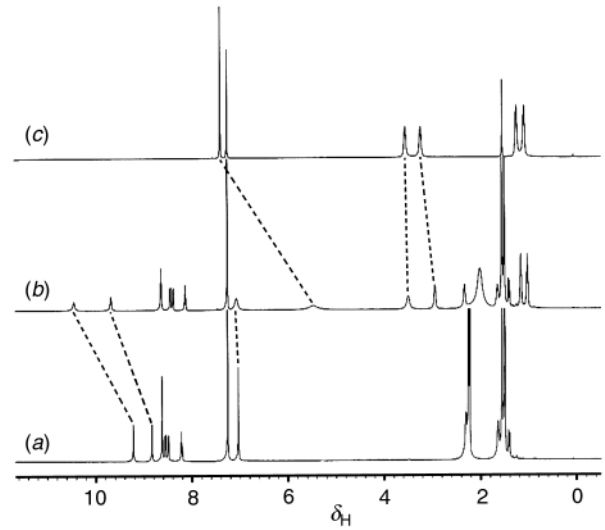

Fig. 1 ^{1}H NMR spectra of (*a*) host **2a** (3 mM), (*b*) host **2a** (3 mM) + guest **6** (3 mM), and (*c*) guest **6** (3 mM) in $CDCl_3$ at 25 °C.

which induce an anisotropic shielding environment in the ^{1}H NMR spectrum.

In conclusion, we have shown the self-assembly of cleft-like bispyridyl hosts into the corresponding macrocycles by Os^{VI} ester chelation, which significantly increases the binding affinity toward guests. Further studies are underway to develop optically active hosts for the chiral recognition of peptide derivatives.

This work was financially supported in part by Yonsei University and the Korea Science and Engineering Foundation (96-0501-04-01-03).

Notes and references

1 For reviews, see: B. Linton and A. D. Hamilton, *Chem. Rev*., 1997, **97**, 1669; M. Fujita, *Chem. Soc. Rev*., 1998, 417; P. J. Stang, *Chem. Eur. J.*, 1998, **4**, 19; D. L. Caulder and K. N. Raymond, *J. Chem. Soc., Dalton Trans.*, 1999, 1185; also, see for self-assembling receptors *via* hydrogen bonds: J. Rebek, Jr., *Acc. Chem. Res.*, 1999, **32**, 278.
2 H.-J. Schneider and D. Ruf, *Angew. Chem., Int. Ed. Engl*., 1990, **29**, 1159.
3 Y. Kobuke and Y. Satoh, *J. Am. Chem. Soc.*, 1992, **114**, 789.
4 M. Inouye, T. Konishi and K. Isagawa, *J. Am. Chem. Soc.*, 1993, **115**, 8091.
5 M. Yamamoto, M. Takeuchi and S. Shinkai, *Tetrahedron Lett.*, 1998, **39**, 1189.
6 For the preparation of binuclear macrocyclic boxes using this self-assembling motif, see: K.-S. Jeong, Y. L. Cho, J. U. Song, H.-Y. Chang and M.-G. Choi, *J. Am. Chem. Soc.*, 1998, **120**, 10983.
7 For covalently-bonded macrocycles with amide groups, see: C. A. Hunter and L. D. Sarson, *Angew. Chem., Int. Ed. Engl*., 1994, **33**, 2313.
8 M. Schröder, *Chem. Rev*., 1980, **80**, 187.
9 R. S. Macomber, *J. Chem. Educ.*, 1992, **69**, 375.
10 K. A. Connors, *Binding Constants*, Wiley, New York, 1987, p. 24.

Communication 9/06252A

ChemComm

Synthesis and unusual properties of the first 2,3,7,8,12,13,17,18-octabromo-5,10,15,20-tetraalkylporphyrin

Nora Y. Nelson,[a] Craig J. Medforth,*[a] Daniel J. Nurco,[a] Song-Ling Jia,[b] John A. Shelnutt[b] and Kevin M. Smith*[a]

[a] *Department of Chemistry, University of California, Davis, California 95616, USA. E-mail: medforth@indigo.ucdavis.edu*

[b] *Nanomolecular Materials and Interfaces Department, Sandia National Laboratories, Albuquerque, New Mexico 787185-1349, USA*

Received (in Corvallis, OR, USA) 3rd June 1999, Accepted 7th September 1999

The new perhalogenated porphyrin 2,3,7,8,12,13,17,18-octabromo-5,10,15,20-tetrakis(trifluoromethyl)porphinato-nickel(II) exhibits several striking features, including an extremely ruffled macrocycle with a very short Ni–N distance, an unusually red-shifted optical spectrum, and, surprisingly, hindered rotation of the *meso*-trifluoromethyl substituents ($\Delta G^{\ddagger}_{278}$ = 47 kJ mol^{-1}).

During the last decade a number of highly nonplanar dodeca-substituted porphyrins have been synthesized, including dodecaarylporphyrins (*e.g.* **1**), dodecaalkylporphyrins (*e.g.* **2**), octaalkyltetraphenylporphyrins (*e.g.* **3**), tetraaryloctahaloporphyrins (*e.g.* **4**), octaethyltetranitroporphyrin (**5**), and systems with substituents fused to the pyrrole rings (*e.g.* **6**).[1] Detailed studies of these compounds have provided a much greater understanding of the effects of nonplanar distortions on the properties of porphyrins, and have also led to speculation about possible functional roles for the nonplanar deformations seen for some tetrapyrroles in biological systems.[1] Two classes of dodecasubstituted porphyrin which have so far proved elusive are the tetraalkyloctahaloporphyrins (**7**) and octaalkyltetrahaloporphyrins (**8**); the non-availability of these compounds can be related to undesirable side-reactions (*e.g.* benzylic substitution and bromodealkyation) which occur during the bromination of tetraalkyl- and octaalkyl-porphyrins.[2] Here we report the first synthesis of a tetraalkyloctahaloporphyrin, **9** (M = Ni), and describe some of the unusual features of this compound.

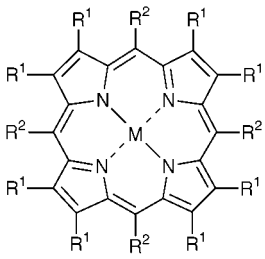

1 $R^1 = R^2 = Ph$
3 $R^1 = Et$, $R^2 = Ph$
4 $R^1 = Br$, $R^2 = Ph$
5 $R^1 = Et$, $R^2 = NO_2$
7 R^1 = halogen, R^2 = alkyl
8 R^1 = alkyl, R^2 = halogen
9 $R^1 = Br$, $R^2 = CF_3$
10 $R^1 = H$, $R^2 = CF_3$
11 $R^1 = H$, $R^2 = Bu^t$
12 $R^1 = Br$, $R^2 = C_6F_5$
13 $R^1 = H$, $R^2 = Ph$
14 $R^1 = H$, $R^2 = C_6F_5$

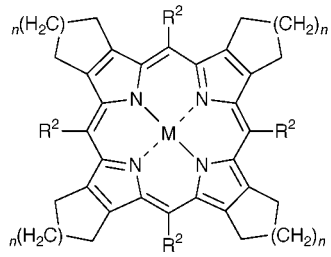

2 $R^2 = (CH_2)_4CH_3$, $n = 1$
6 $R^2 = Ph$, $n = 2$ or 3

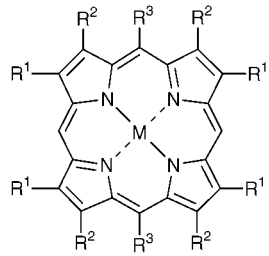

15 R^1 = Me, R^2 = Et, R^3 = alkyl

In an attempt to avoid the side-reactions seen during the bromination reactions of tetraalkyl- and octaalkyl-porphyrins, we investigated bromination of the tetra(perfluoroalkyl)porphyrin **10** (M = Ni). The precursor porphyrin **10** (M = 2H) was prepared using a literature procedure.[3] Refluxing **10** (M = 2H) with $Ni(acac)_2$ in toluene gave **10** (M = Ni) which was more suitable for use in the bromination reactions. Bromination of **10** (M = Ni) proved difficult but was eventually achieved by refluxing a solution of the porphyrin in $CHCl_3$ containing a large excess of Br_2 for 10 days under argon. The perhalogenated porphyrin **9** (M = Ni) was then isolated in 88% yield after column chromatography (silica gel/cyclohexane) and recrystallization (from CH_2Cl_2 with slow diffusion of MeOH). Porphyrin **9** (M = Ni) gave satisfactory mass spectral analysis (M^+ 1269.27; calc. for $C_{24}N_4Br_8F_{12}Ni$ 1269.27) and microanalysis (found C, 23.54; H, 0.00; N, 4.43; calc. C, 23.79; H, 0.00; N, 4.62%), and was further characterized by X-ray crystallography and visible and NMR spectroscopy as described below.

The crystal structure of **9** (M = Ni)† (Fig. 1) revealed a very ruffled macrocycle in which the *meso* positions were displaced alternately up or down by an average of 1.06 Å with respect to the least-squares plane of the porphyrin ring. The average out-of-plane displacement for all of the porphyrin atoms with respect to the least-squares plane of the porphyrin macrocycle was 0.50 Å. By these measures **9** (M = Ni) is the most ruffled porphyrin ever reported; the largest ruffling distortion previously observed was for **11** (M = Zn), where the corresponding displacements were only 0.90 and 0.44 Å.[4] The conformation seen for **9** (M = Ni) can be contrasted with the saddle conformation seen for the perhalogenated tetraarylporphyrin **12** (M = Ni),[5] where the *meso* carbons are in the least-squares plane of the porphyrin macrocycle and the pyrrole rings are tilted alternately up or down. The strongly ruffled structure of **9** (M = Ni) is accompanied by an extremely short Ni–N distance of only 1.88 Å. This can be compared to Ni–N distances of 1.90 Å in the very saddle-distorted porphyrin **12** (M = Ni)[5] and 1.96 Å in planar (triclinic A) NiOEP.[6] The significant shortening of the Ni–N distance seen for **9** (M = Ni) is consistent with the

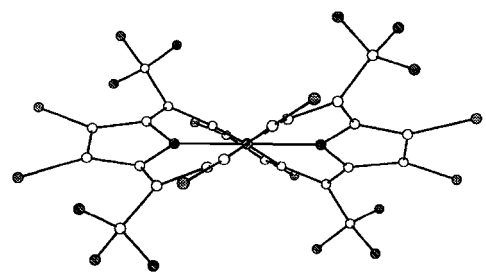

Fig. 1 Crystal structure of porphyrin **9** (M = Ni).

larger degree of core contraction expected for ruffling *versus* other types of nonplanar distortion.[7] Molecular modelling studies using a previously published force-field[7–9] demonstrated that the conformations seen in the crystal structures of **9** (M = Ni) and **12** (M = Ni) were the minimum energy structures for these porphyrins, and that the different Ni–N distances in the two compounds could be accurately reproduced.

Porphyrin **9** (M = Ni) possesses some unusual spectroscopic characteristics. Nonplanarity is known to cause a red-shift in the optical spectra of porphyrins due to a greater destabilization of the HOMO compared with the LUMO,[1] and the optical spectrum of **9** (M = Ni) [λ/nm (ε/dm^3 mol^{-1} cm^{-1}) 444 (77 000), 636 (8100) and 690 (24 000)] is indeed red-shifted compared to the spectrum of **10** (M = Ni) [408 (120 000), 550 (7700) and 590 (25 000)]. However, the red-shift of the $Q_{(0,0)}$ band upon addition of eight β bromo substituents to **10** (M = Ni) (2450 cm^{-1}) is substantially larger than that seen upon addition of eight β bromo substituents to **13** (M = Ni) (1050 cm^{-1}) or **14** (M = Ni) (1250 cm^{-1}) which yields saddle-distorted macrocycles. This suggests that the porphyrin π-system may be more sensitive to ruffle *versus* saddle distortions of the macrocycle. Additional support for this idea comes from the fact that other properties related to the porphyrin π-system (*e.g.* the frequencies of Raman marker lines[10] and the magnitude of the porphyrin ring current effect[11]) are also affected more by ruffle than by saddle distortions.

The 283 MHz ^{19}F NMR spectrum of **9** (M = Ni) in CD_2Cl_2 at ambient temperature displayed an unusually broad signal at δ −39 (referenced to internal CF_2Cl_2 at δ −8.0)[12] for the *meso* trifluoromethyl substituents. Heating the complex resulted in a sharp singlet at δ −39.0, whereas cooling produced two signals at δ −34.7 (d, 2F, $J_{F\text{-}F}$ = 114 Hz) and −47.8 (t, 1F, $J_{F\text{-}F}$ = 114 Hz). The activation energy ($\Delta G^{\ddagger}$) for the observed dynamic process was calculated to be 47 kJ mol^{-1} at the coalescence temperature of 278 K. In contrast, the unbrominated precursor **10** (M = Ni) gave a single sharp CF_3 signal at all of the temperatures studied. The non-equivalence of the trifluoromethyl fluorines in **9** (M = Ni) indicates that rotation of the CF_3 groups is slow on the NMR timescale at low temperatures. Hindered CF_3 rotation is a rare phenomenon but has been observed in some very sterically crowded compounds. For example, the activation energy for CF_3 rotation in CF_3CCl_2I is 36 kJ mol^{-1} at 201 K,[13] with the coupling constant between the fluorines being 101 Hz in the slow exchange spectrum. The unusually slow rotation of the CF_3 groups in **9** (M = Ni) provides evidence of a very high degree of steric crowding in this compound.

In earlier NMR studies of nonplanar porphyrins, dynamic processes in **1** (M = 4H),[14] **2** (M = Ni)[14] and **15** (M = 2H or Zn)[15] were initially attributed to macrocyclic inversion but subsequently reassigned as substituent rotation.[16–18] In an attempt to avoid any confusion about the nature of the dynamic process in **9** (M = Ni), we used molecular mechanics calculations[8,9] to estimate the energies of the two possible CF_3 rotation pathways (CF_3 rotation about a ruffled porphyrin core *versus* CF_3 rotation during inversion of the porphyrin macrocycle). The barrier for rotation of the CF_3 groups in the ruffled structure was calculated to be 34 kJ mol^{-1}. The lowest energy inversion–rotation barrier (103 kJ mol^{-1}) was found between the ruffled structure (designated αβαβ) and a structure which had three CF_3 groups on the same side of the porphyrin plane (designated αααβ). On the basis of these calculated energies it seems probable that the process being observed for **9** (M = Ni) is rotation of the CF_3 groups in the ruffled structure.

Porphyrin **9**, with a novel combination of a strongly ruffled macrocycle and very electron-withdrawing substituents, clearly has many unusual features even when compared with other very nonplanar dodecasubstituted porphyrins. It will be interesting to investigate this porphyrin further and perhaps to examine how **9** compares with tetraaryloctahaloporphyrins in terms of catalyzing the oxygenation reactions of unactivated alkanes.[19]

This work was supported by grants from the National Institutes of Health (HL 22252) and the National Science Foundation (CHE-96-23117). Sandia is a multiprogram laboratory operated by Sandia Corporation, a Lockheed-Martin company, for the United States Department of Energy under Contract DE-ACO4-94AL85000.

Notes and references

† Crystals were grown by the slow diffusion of cyclohexane into a CH_2Cl_2 solution of **9** (M = Ni) ($C_{24}N_4Br_8F_{12}Ni$). The selected crystal (0.06 × 0.06 × 0.04 mm) had an orthorhombic unit cell, space group *Pnma*, cell dimensions a = 8.1106(7), b = 23.587(2), c = 15.5831(14) Å, V = 2981.2(5) Å^3, Z = 4 (FW = 1270.27). Data were collected in ω scan mode to 2θmax = 63° (29685 total reflections measured) on a Bruker SMART 1000 diffractometer with graphite monochromated radiation from a ceramic sealed tube source [λ(Mo-Kα) = 0.71073 Å]. The crystal was cooled to 93(2) K during data collection with an anhydrous N_2 stream supplied from a CryoIndustries low temperature apparatus. The structure was solved by direct methods (SHELXS-97) and refined (based on F^2 using all data) by full matrix least-squares methods with 232 parameters (SHELXL-97). Of 3511 unique reflections used in the refinement ($2\theta_{max}$ = 55°), 1937 were observed [$I > 2\sigma(I)$]. An empirical absorption correction (SADABS) (ref. 20) was applied [T_{min} = 0.546, T_{max} = 0.657, ρ_{calc} = 2.83 g cm^{-3}, μ = 11.47 mm^{-1}]. Final R factors were $R1$ = 0.042 (observed data) and $wR2$ = 0.077 (all data). CCDC 182/1413.

1 J. A. Shelnutt, X.-Z. Song, J.-G. Ma, S.-L. Jia, W. Jentzen and C. J. Medforth, *Chem. Soc. Rev.*, 1998, **27**, 31 and references cited.
2 N. Y. Nelson, C. J. Medforth, R. G. Khoury, D. J. Nurco and K. M. Smith, *Chem. Commun.*, 1998, 1687 and references cited.
3 S. G. DiMagno and R. A. Williams, *J. Org. Chem.*, 1994, **59**, 6943.
4 M. O. Senge, T. Ema and K. M. Smith, *J. Chem. Soc., Chem. Commun.*, 1995, 733.
5 D. Mandon, P. Ochsenbein, J. Fischer, R. Weiss, K. Jayaraj, R. N. Austin, A. Gold, P. S. White, O. Brigaud, P. Battioni and D. Mansuy, *Inorg. Chem.*, 1992, **31**, 2044.
6 D. L. Cullen and E. F. Meyer, *J. Am. Chem. Soc.*, **1974**, *96*, 2095.
7 X.-Z. Song, L. Jaquinod, W. Jentzen, D. J. Nurco, S.-L. Jia, R. G. Khoury, J.-G. Ma, C. J. Medforth, K. M. Smith and J. A. Shelnutt, *Inorg. Chem.*, 1998, **37**, 2009.
8 J. A. Shelnutt, C. J. Medforth, M. D. Berber, K. M. Barkigia and K. M. Smith, *J. Am. Chem. Soc.*, 1991, **113**, 4077.
9 X.-Z. Song, W. Jentzen, S.-L. Jia, L. Jaquinod, D. J. Nurco, C. J. Medforth, K. M. Smith and J. A. Shelnutt, *J. Am. Chem. Soc.*, 1996, **118**, 12975.
10 R. Franco, J.-G. Ma, Y. Lu, G. C. Ferreira and J. A. Shelnutt, *Biochemistry*, 1999, in press.
11 C. J. Medforth, C. M. Muzzi, K. M. Shea, K. M. Smith, R. J. Abraham, S. Jia and J. A. Shelnutt, *J. Chem. Soc., Perkin Trans. 2*, 1997, 839.
12 R. K. Harris and B. E. Mann, *NMR and the Periodic Table*, Academic Press, 1978.
13 F. J. Weigert and W. Mahler, *J. Am. Chem. Soc.*, 1972, **94**, 5314.
14 C. J. Medforth, M. O. Senge, K. M. Smith, L. D. Sparks and J. A. Shelnutt, *J. Am. Chem. Soc.*, 1992, **114**, 9859.
15 K. Maruyama, T. Nagata and A. Osuka, *J. Phys. Org. Chem.*, 1988, **1**, 63.
16 C. J. Medforth, M. O. Senge, T. P. Forsyth, J. D. Hobbs, J. A. Shelnutt and K. M. Smith, *Inorg. Chem.*, 1994, **33**, 3865.
17 M. O. Senge, C. J. Medforth, T. P. Forsyth, D. A. Lee, M. M. Olmstead, W. Jentzen, R. K. Pandey, J. A. Shelnutt and K. M. Smith, *Inorg. Chem.*, 1997, **36**, 1149.
18 C. M. Muzzi, C. J. Medforth, L. Voss, M. Cancilla, C. Lebrilla, J.-G. Ma, J. A. Shelnutt and K. M. Smith, *Tetrahedron Lett.*, 1999, 6159.
19 J. E. Lyons, P. E. Ellis and H. K. Myers, *J. Catal.*, 1995, **155**, 59.
20 SADABS, An empirical absorption program written by G. M. Sheldrick and based upon the method of R. H. Blessing, *Acta Crystallogr., Sect. A*, 1995, **51**, 33.

Communication 9/04532E

ChemComm

High-affinity nucleic acid recognition using 'LNA' (locked nucleic acid, β-D-*ribo* configured LNA), '*xylo*-LNA' (β-D-*xylo* configured LNA) or 'α-L-LNA' (α-L-*ribo* configured LNA)

Vivek K. Rajwanshi, Anders E. Håkansson, Ravindra Kumar and Jesper Wengel*

Center for Synthetic Bioorganic Chemistry, Department of Chemistry, University of Copenhagen, Universitetsparken 5, DK-2100 Copenhagen, Denmark. E-mail:wengel@kiku.dk

Received (in Cambridge, UK) 18th August 1999, Accepted 8th September 1999

Remarkably strong binding affinities towards complementary single stranded DNA and RNA were obtained for 10- and 14-mer LNAs (locked nucleic acids) containing diastereoisomeric β-D-*ribo*, β-D-*xylo* or α-L-ribo configured LNA thymine monomers; a possible relevance of these results in relation to nucleic acid evolution is discussed.

As recently summarized, Eschenmoser and co-workers have intensively studied the basic chemical properties of a number of potential natural nucleic acid alternatives containing various hexopyranosyl or pentopyranosyl monomeric units.[1] Many of these alternatives have displayed efficient and strong Watson–Crick base-paring, indicating that this property has not been a decisive driving force during the evolution of RNA (ribofuranosyl nucleic acids),[1b] at least not with respect to the carbohydrate part of RNA. The possibilities exist that RNA was selected for synthetic reasons favouring the formation of RNA, or for functional reasons inherent in the β-D-ribofuranosyl structure of RNA. In the latter scenario it is conceivable that the RNA structure resulted from selection and optimization among irregular nucleic acids consisting of mixtures of, *e.g.* different pentofuranosyl and/or pentopyranosyl monomeric nucleotide units. Although several pentofuranosyl configurational isomers of RNA have been synthesized, *e.g.* the β-L-ribofuranosyl[2] and β-D-arabinofuranosyl[3] isomers, their binding affinities, especially in stereoirregular oligonucletides, have not been much studied.

We and others have recently reported unprecedented thermal affinities of duplexes involving the oligonucleotide analogue 'LNA'[4] (locked nucleic acid, $\mathbf{T^L}$, β-D-*ribo* isomer, Fig. 1).† The furanose ring of LNA, being part of a dioxabicyclo[2.2.1]heptane skeleton, is efficiently locked in a C3'-*endo* (N-type) conformation. We have initiated a program focusing on the synthesis and properties of conformationally locked configurational isomers of LNA. Very recently, we have published the syntheses of the first two diastereoisomeric forms of LNA, namely '*xylo*-LNA' ($\mathbf{xT^L}$, β-D-*xylo* isomer,† Fig. 1) containing one or more 2'-*O*,4'-*C*-methylene-β-D-xylofuranosyl nucleotide monomer(s), and 'α-L-LNA' ($^{\alpha L}\mathbf{T^L}$, α-L-*ribo* isomer,† Fig. 1) containing one or more 2'-*O*,4'-*C*-methylene-α-L-ribofuranosyl nucleotide monomer(s).[5]

The LNA oligomers **5** and **7**–**9** (Table 1) were synthesized on an automated DNA synthesizer by use of the phosphoramidite approach[6] using conditions (pyridine hydrochloride; 10 min coupling time; > 98% step-wise coupling yields) optimized earlier for synthesis of *xylo*-LNA and α-L-LNA.[5] Importantly, the use of polystyrene supports, loaded with the 3'-end penultimate thymidine monomer, allowed synthesis of the (almost)‡ fully modified *xylo*-LNA **7** and α-L-LNA **8**. The oligomers **5** and **7**–**9** were synthesized in the DMT-*ON* mode and, after cleavage from the solid support, purified using disposable reversed phase chromatography cartridges (Cruachem) yielding products with > 80% purity as judged from capillary gel electrophoresis. The compositions of LNAs **5**, **7** and **9** were verified by MALDI-MS analysis.§

In Table 1, hybridization data for 10- and 14-mer thymine LNA derivatives are shown. Sharp and monophasic transitions were obtained in all experiments (except with *xylo*-LNA **5**) towards complementary DNA (dA_{14}) or complementary RNA (rA_{14}). Control experiments without complementary strands showed no indication of the formation of well-defined and stable homocomplexes (no cooperative self-melting). The results obtained for references **1** and **2** and for the different LNA derivatives **3**, **4** and **6** have been reported earlier.[4a,5] Especially noteworthy is the unprecedented binding affinity of the fully modified parent LNA **6**[4a] and the apparent and significant

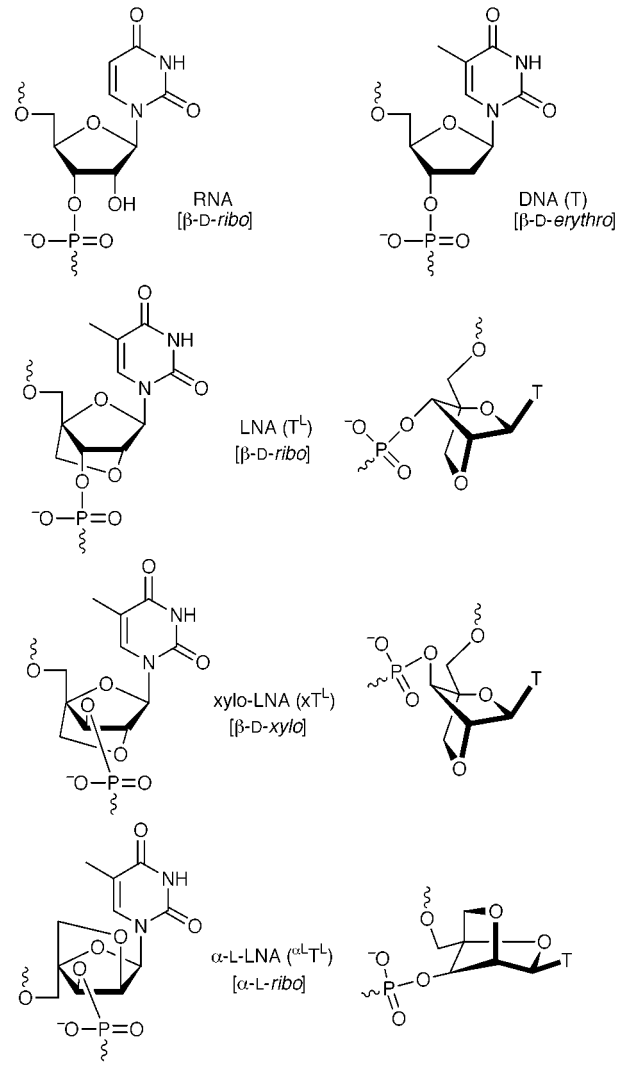

Fig. 1 Structure of the monomeric nucleotide units of RNA, DNA (T), LNA ($\mathbf{T^L}$), *xylo*-LNA ($\mathbf{xT^L}$) and α-L-LNA ($^{\alpha L}\mathbf{T^L}$); the configurations are shown in the square brackets; thymine derivatives are shown except in the case of RNA (uracil derivative shown). Also indicated are the locked furanose conformations of the three differently configured LNA monomers as obtained from molecular modelling ($\mathbf{T^L}$: C3'-*endo* conformation; $\mathbf{xT^L}$: C3'-*endo* conformation: $^{\alpha L}\mathbf{T^L}$: C3'-*exo* conformation).

affinity enhancing properties of LNA monomers as well as α-L-LNA monomers when incorporated into otherwise unmodified DNA strands (LNA **3**[4a] and α-L-LNA **4**;[5] ΔT_m = +5.0 and +4.5 °C towards complementary RNA, respectively; ΔT_m = increase in T_m value per modification; T_m = melting temperature, see text below Table 1).

A detrimental effect caused by the introduction of *xylo*-LNA monomers (*xylo*-LNA **5**) on the thermal stability can be seen from Table 1, confirming earlier obtained results for a singly substituted *xylo*-LNA.[5] In contrast, the fully-modified *xylo*-LNA **7** displayed very strong binding affinity towards DNA and RNA (ΔT_m = +3.1 and +4.3 °C, respectively). Likewise, remarkable thermal affinities were obtained for the fully-modified α-L-LNA **8** (ΔT_m = +4.8 °C towards DNA and +5.3 °C towards RNA). Modeling studies on α-L-LNA monomer $^{\alpha L}\mathbf{T}^{L}$ and LNA monomer $\mathbf{T}^{L}$ indicate a three-dimensional proximity of the thymine moieties and of the 5'- and 3'-oxygen atoms. This apparent structural similarity, despite the inverted configurations at the 2'-, 3'- and 4'-carbon atoms, offers an explanation of the observed very strong binding of the 14-mer 'stereoirregular LNA' **9** (containing four consecutive $\mathbf{T}^{L}$ monomers and four consecutive $^{\alpha L}\mathbf{T}^{L}$ monomers) towards both DNA and RNA (ΔT_m = +4.0 and +4.4 °C, respectively).

The results presented herein demonstrate that conformational restriction of fully modified diastereoisomeric LNA derivatives with β-D-*xylo* and α-L-*ribo* configurations (*xylo*-LNA **7** and α-L-LNA **8**) leads to high-affinity recognition of complementary DNA and RNA.¶ Thus, whereas LNA[4] is the nucleic acid analogue synthesized so far displaying the strongest binding affinity towards complementary DNA and RNA, the T_m values obtained herein likewise rank *xylo*-LNA and α-L-LNA, together with *e.g.* 2'-fluoro N3'-P5' phosphoramidates[7] and hexitol nucleic acids,[8] among the strongest DNA and RNA binders known. This is an important point with respect to the possibility of using LNA derivatives as antisense oligonucleotides or diagnostic probes.

Interestingly, whereas Eschenmoser and co-workers have found efficient cross-pairing between the diastereoisomeric conformationally restricted *pentopyranosyl* family of nucleic acid analogues but no pairing of these towards RNA,[1] the three differently configured *pentofuranosyl* LNAs discussed herein are able to very efficiently bind to RNA (itself a pentofuranosyl system). These results, in combination with the RNA-binding reported for β-D-arabinofuranosyl nucleic acids,[3f] suggest that constitution (rather than configuration) could have been a decisive factor in an early-stage combinatorial chemical evolution of the nucleic acid structure. It can be imagined that eventual optimization based on functional aspects, *e.g.* base-pairing strength or potential for stereoregular non-enzymatic replication, caused by differences in configuration and thus conformational equilibria between the various pentofuranosyl (or pentopyranosyl) diastereoisomers, could have favoured the current β-D-ribofuranosyl structure of the nucleic acids.

We are continuing our examination of the LNA family of molecules. A fourth LNA diastereoisomer ('α-L-*xylo*-LNA') is currently being synthesized which, together with the three diastereoisomers discussed herein and an enantiomeric RNA target, will allow us to study the properties of all eight possible LNA stereoisomers (in stereoregular or stereoirregular oligomers).‖

The Danish Natural Science Research Council, The Danish Technical Research Council and Exiqon A/S are thanked for financial support. Dr Carl Erik Olsen is thanked for recording MALDI-MS spectra, and Ms Britta M. Dahl is thanked for synthesis of the LNAs.

Table 1 Hybridization data for diastereosiomeric LNAs and reference strands

	Sequence	dA_{14} complement		rA_{14} complement	
		T_m/°C[a]	ΔT_m/°C[b]	T_m/°C[a]	ΔT_m/°C[b]
1[c]	T_{14}	36/32[d]	Ref.[e]	32/28[d]	Ref.[e]
2[c]	T_{10}	24/20[d]	Ref.[e]	18	Ref.[e]
3[c]	$T_5(\mathbf{T}^{L})_4T_5$	42	+1.5	52	+5.0
4[f]	$T_5(^{\alpha L}\mathbf{T}^{L})_4T_5$	36	+1.0	46	+4.5
5	$T_5(\mathbf{xT}^{L})_4T_5$	n.t.[g]		n.t.[g]	
6[c]	5'-$(\mathbf{T}^{L})_9$T	80	+6.2[h]	71	+5.9[h]
7	5'-$(\mathbf{xT}^{L})_9$T	48	+3.1	57	+4.3
8	5'-$(^{\alpha L}\mathbf{T}^{L})_9$T	63	+4.8	66	+5.3
9	5'-$T_3(\mathbf{T}^{L})_4(^{\alpha L}\mathbf{T}^{L})_4T_3$	64	+4.0[i]	63	+4.4[i]

[a] Melting temperatures (T_m values) obtained from the maxima of the first derivatives of the melting curves (A_{260} *vs.* temperature) recorded in medium salt buffer (10 mM $NaHPO_4$, 100 mM NaCl, 0.1 mM EDTA, pH 7.0) using 1.5 mM concentrations of the two complementary strands assuming identical extinction coefficients for all thymine nucleotides [ref. 4(*b*)]. [b] The change in T_m value per modification (ΔT_m) compared with the T_m value for the reference of similar length. [c] Ref. 4(*a*). [d] The T_m values obtained for the reference strands varied from one experimental series to another [ref. 4(*a*), 5]. [e] Reference duplex. [f] Ref. 5. [g] No transition was observed above 20 °C. [h] In the original publication [ref. 4(*a*)], these ΔT_m values were erroneously calculated as +4.9 and +4.3 °C. [i] These ΔT_m values are calculated average values for the different LNA monomers incorporated.

Notes and references

† We have defined LNA as an oligonucleotide containing one or more 2'-*O*,4'-*C*-methylene-β-D-ribofuranosyl nucleotide monomer(s). The natural β-D-ribo configuration is generally assigned to LNA (and LNA monomers) as the positioning of the 1-nitrogen and 2'-, 3'- and 5'-oxygen atoms are equivalent to the one found in RNA. Strictly following carbohydrate nomenclature, however, the configuration of LNA nucleosides depends on the priorities between the two 4'-*C*-substituents (β-D-*ribo* or α-L-*lyxo* configuration in the case of parent LNA). Analogously, all *xylo*-LNA derivatives and all α-L-LNA derivatives are considered as having β-D-*xylo* and α-L-*ribo* configuration, respectively.

‡ For synthetic ease, the LNAs **6**-**8** were synthesized on commercially available T-supports. However, these LNAs are described herein as 'fully modified'.

§ MALDI-MS ($[M-H]^-$; found/calc.): **5** (4305.4/4307.8); **7** (3229.8/3231.1); **9** (4421.4/4419.8).

¶ The generality (base-pairing selectivity, mixed sequence contexts, strand orientations *etc*.) of the hybridization of diastereoisomeric forms of LNA has yet to be proven as has already been done for the parent LNA (ref. 4).

‖ The indirect evaluation of the RNA binding affinity of the remaining four LNA stereoisomers will be undertaken in a collaborative project with Dr Stefan Pitsch (Institute of Organic Chemistry, ETH, Zürich), involving the use of enantiomeric RNA. It should be noted that the formation of LNA derivatives of *arabino* and *lyxo* configuration† is precluded because of the inherent *syn*-positioning of the 2'-oxygen and 4'-carbon atoms.

1 (*a*) M. Beier, F. Reck, T. Wagner, R. Krishnamurthy and A. Eschenmoser, *Science*, 1999, **283**, 699; (*b*) A. Eschenmoser, *Science*, 1999, **284**, 2118.

2 G. W. Ashley, *J. Am. Chem. Soc.*, 1992, **114**, 9731; S. Pitsch, *Helv. Chim. Acta*, 1997, **80**, 2286.

3 (*a*) M. J. Damha, N. Usman and K. K. Ogilvie, *Can. J. Chem.*, 1989, **67**, 831; (*b*) J. M. L. Pieters, E. de Vroom, G. A. van der Marel, J. H. van Boom, T. M. G. Koning, R. Kaptein and C. Altona, *Biochemistry*, 1990, **29**, 788; (*c*) M. Resmini and W. Pfleiderer, *Bioorg. Med. Chem. Lett.*, 1994, **4**, 1909; (*d*) P. A. Giannaris and M. Damha, *Can. J. Chem.*, 1994, **72**, 909; (*e*) T. Mikita and G. P. Beardsley, *Biochemistry*, 1994, **33**, 9195; (*f*) M. J. Damha, C. J. Wilds, A. Noronha, I. Brukner, G. Borkow, D. Arion and M. A. Parniak, *J. Am. Chem. Soc.*, 1998, **120**, 12976.

4 (*a*) S. K. Singh, P. Nielsen, A. A. Koshkin and J. Wengel, *Chem. Commun.*, 1998, 455; (*b*) A. A. Koshkin, S. K. Singh, P. Nielsen, V. K. Rajwanshi, R. Kumar, M. Meldgaard, C. E. Olsen and J. Wengel, *Tetrahedron*, 1998, **54**, 3607; (*c*) S. K. Singh and J. Wengel, *Chem. Commun.*, 1998, 1247; (*d*) A. A. Koshkin, P. Nielsen, M. Meldgaard, V. K. Rajwanshi, S. K. Singh and J. Wengel, *J. Am. Chem. Soc.*, 1998, **120**, 13252; (*e*) S. Obika, D. Nanbu, Y. Hari, J. Andoh, K. Morio, T. Doi and T. Imanishi, *Tetrahedron Lett.*, 1998, **39**, 5401; (*f*) J. Wengel, *Acc. Chem. Res.*, 1999, **32**, 301.

5 V. K. Rajwanshi, A. E. Håkansson, B. M. Dahl and J. Wengel, *Chem. Commun.*, 1999, 1395.

6 M. H. Caruthers, *Acc. Chem. Res.*, 1991, **24**, 278.

7 D. G. Schultz and S. M. Gryaznov, *Nucleic Acids Res.*, 1996, **24**, 2966.

8 C. Hendrix, H. Rosemeyer, I. Verheggen, F. Seela, A. Van Aerschot and P. Herdewijn, *Chem. Eur. J.*, 1997, **3**, 110; C. Hendrix, H. Rosemeyer, B. De Bouvere, A. Van Aerschot, F. Seela and P. Herdewijn, *Chem. Eur. J.*, 1997, **3**, 1513.

Communication 9/06713B

Polymer supported cobalt carbonyl complexes as novel traceless alkyne linkers for solid-phase synthesis

Alex C. Comely,*[a] Susan E. Gibson (née Thomas)[a] and Neil J. Hales[b]

[a] *Department of Chemistry, King's College London, Strand, London, UK WC2R 2LS. E-mail: susan.gibson@kcl.ac.uk*
[b] *AstraZeneca, Mereside, Alderley Park, Macclesfield, UK SK10 4TG*

Received (in Liverpool, UK) 22nd July 1999, Accepted 1st September 1999

The immobilisation of functionalised alkynes onto 'polymer-bound triphenylphosphine', their chemical manipulation and subsequent release has been demonstrated for the first time, thus illustrating that cobalt carbonyl complexes can be used as 'traceless' π-alkyne linkers.

Solid-phase synthesis continues to excite ever-greater interest,[1] particularly as a means to facilitate the elaboration of compound libraries *via* combinatorial chemistry.[2] Of especial importance to this technology is the linker, the structural motif which joins the substrate under chemical manipulation to the polymeric support. A legacy of solid-phase peptide synthesis is the release of compounds bearing carboxylic acid or amide functionality derived from an ester linkage. While appropriate for some target molecules, this has rather limited appeal in a more general synthetic sequence. Efforts to address this problem have stimulated the evolution of 'traceless' linkers,[3] those which leave minimal vestige of the solid support upon release of the product. A good example is the tethering of compounds containing an aromatic ring by means of an aryl–silicon bond.[4] The linker is cleaved to reveal only a hydrogen atom at the former aromatic linkage site.

In this respect, transition metals offer a very alluring solution: the temporary and reversible immobilisation of an unsaturated substrate *via* π-interactions to the molecular scaffold dispenses with the functional group transformation necessarily required by a covalent system. In recent months this concept was illustrated for the first time with the immobilisation of arenes through a chromium carbonyl linker.[5] Liberation of the product by oxidative decomplexation returns the aromatic ring unchanged.

Surprisingly, there currently exists no method for the release of an alkyne from a polymeric support.[6] A system which allows the addition and later release of this functionality, without a compromise to its integrity, would thus represent a valuable extension to linker technology. The chemistry of cobalt carbonyl alkyne complexes is well established in the solution phase and has been applied to great effect in organic synthesis:[7] alkyne protection,[7a] the Nicholas reaction[7b] and Pauson–Khand cyclisations,[7c] for example, are amply documented. Given the ease of formation and tolerance to diverse reaction conditions of these complexes, it appeared to us that cobalt carbonyl species offered considerable potential as alkyne linkers for solid-phase synthesis.

Our initial investigations involved the reaction of 'polymer-bound triphenylphosphine'† with $Co_2(CO)_8$ in THF at room temperature to generate a cobalt carbonyl resin, a support to which alkynes could be added directly (Scheme 1). The purple, stable resin was characterised on the basis of its IR and ^{31}P NMR spectra: strong absorptions ascribed to ionic **1** were accompanied by weaker peaks indicating a minor presence of the monophosphine-substituted complex **2**.[8] Heating of this resin at 60 °C in 1,4-dioxane cleanly converted it into a second form, assigned the structure of the neutral bisphosphine **3** on the basis of its IR and ^{31}P NMR spectra.[9]

The alkyne complexation of a phosphine-substituted cobalt carbonyl complex, $[(Bu_3P)Co(CO)_3]_2$, has been reported.[10] In view of the elevated temperature required, the simultaneous conversion of (**1** + **2**) into **3** *and* complexation of an alkyne becomes a feasible transformation (Scheme 2). Treatment of the resin bearing complexes **1** and **2** with hex-5-yn-1-ol in 1,4-dioxane at 70 °C generated the purple resin-bound alkyne complexes **4**, presumably *via* the intermediary carbonyl complex **3**. Comparison of overlapping sets of IR absorptions with literature data,[11] and data from samples of $Ph_3P(OC)_2CoCo(CO)_3$(hex-5-yn-1-ol) and $[Ph_3P(OC)_2Co]_2$(hex-5-yn-1-ol) prepared ourselves, indicates the presence of both mono- and bisphosphine substituted alkyne complexes, **4a** and **4b**, and that the latter is the major component.‡ The ^{31}P NMR spectrum of **4a**/**4b** supports alkyne complexation (with a 20% phosphorus site occupancy).

Acetylation of resin **4** to afford **5** using acetic anhydride–NEt_3 is supported by an additional acetate absorption at 1734 cm^{-1}. Decomplexation was achieved by aerial oxidation in CH_2Cl_2 under white light for 72 h. Filtration and washing of the brown polymeric residue delivered hex-5-yn-1-yl acetate as the sole product in 70 ± 20% yield from **4**.

A second approach with the same overall objective involved the reaction of 'polymer-bound triphenylphosphine' with a preformed alkyne complex (indirect loading) (Scheme 2). Designed to permit comparison between the two routes, hex-5-yn-1-ol was complexed with $Co_2(CO)_8$ to give **6**, a deep red oil (85%). Loading onto the polymer was effected in THF at 50 °C to afford **4**§ possessing similar IR characteristics to the resin prepared by the direct method. A comparison of the strengths of bands attributed to the mono- and bisphosphine derivatives[11] identifies the former as the major component *via* this route.‡ ^{31}P NMR spectroscopy is extremely valuable here.¶ A well-resolved resonance integrates to an 80% complexation of phosphorus sites (the benign phosphine oxide, polymer-$P(O)Ph_2$, occupying the remaining 20%) and a loading of 0.94 ± 0.02 mmol[hexynol] g^{-1}. Acetylation proceeded as before: that the metal carbonyl stretches and the ^{31}P NMR spectrum undergo no change demonstrates the stability of this linker to these conditions. Hex-5-yn-1-yl acetate (12 mg, 60 ± 10% from **4**) was recovered from the resin following acetylation of resin **4** (150 mg) and decomplexation over 72 h.

Each loading technique has its own advantage: overall yields *via* indirect loading are significantly higher than those obtained from direct loading. The latter, however, obviates pre-formation of a cobalt alkyne complex and thus offers convenience: once

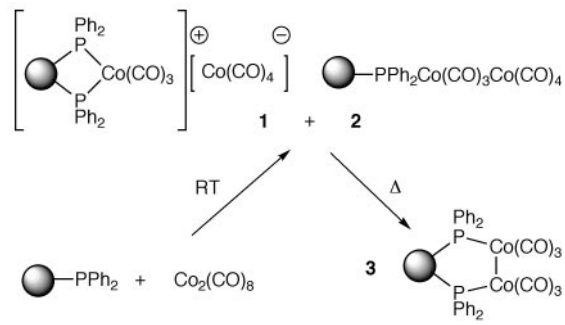

Scheme 1

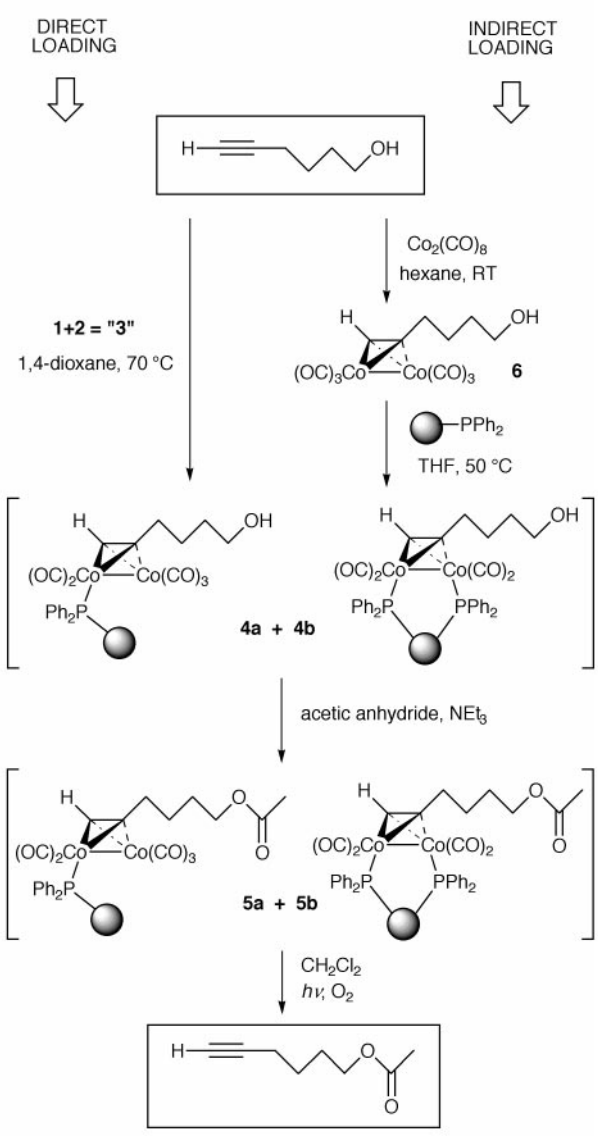

Scheme 2

prepared, the resin-linker complex (**1** + **2**) can be stored and used as required.

Finally, in preliminary experiments to explore the versatility of this linker, alcohol **4** (prepared by direct loading) was oxidised in the presence of SO_3·py-activated DMSO and NEt_3[12] to afford the aldehyde complex **7** (Scheme 3), displaying a diagnostic aldehyde stretch at 1723 cm^{-1}. Significantly, all other data (IR and ^{31}P NMR) of resin **7** are unchanged from those of **4**, thus demonstrating the linker's stability to these oxidising conditions. Hex-5-yn-1-al was isolated in 17 ± 5% yield after decomplexation as before (the low yield here is attributed to the volatility of the aldehyde).

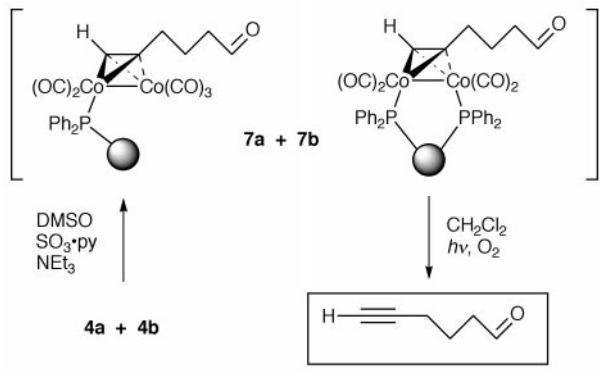

Scheme 3

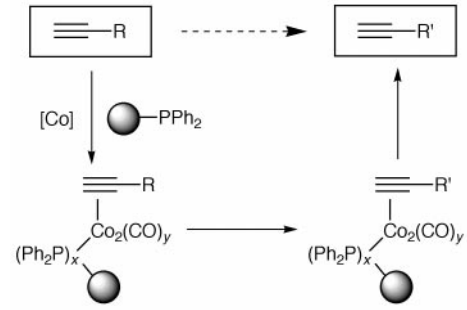

Scheme 4

In conclusion, we have demonstrated for the first time the utility of cobalt carbonyl complexes as linkers for the 'traceless' immobilisation and subsequent release of alkyne substrates (Scheme 4). The linker is stable to certain widely-used reaction conditions and the work described herein is applicable to various combinatorial methods.

The authors thank Jon Cobb for invaluable NMR assistance and AstraZeneca for a studentship (ACC).

Footnotes and references

† 'Polymer-bound triphenylphosphine' (commercially available from Fluka, ~1.6 mmol P g^{-1}) describes a diphenylphosphino polystyrene polymer crosslinked with 2% divinylbenzene.

‡ Details of estimates used in this study are as follows: **4a**:**4b** ratios were estimated from IR intensities (3:7 and 6:4 for direct and indirect routes respectively). Solution calibration studies verify this estimate. Solid phase ^{31}P NMR spectra can be accurately integrated but show no resolution of mono- and bisphosphine derivatives. The error margins for yield and loading calculations are estimated as follows: IR spectra, 5%; ^{31}P NMR spectra, direct method, 10%; ^{31}P NMR spectra, indirect method 5%.

§ The experimental procedure for indirect formation of **4** is as follows: polymer-bound triphenylphosphine (1 g, ~1.6 mmol P) was suspended in oxygen-free anhydrous THF (10 cm^3) and allowed to swell for 30 min under nitrogen agitation. A solution of hexacarbonyl(hex-5-yn-1-ol)dicobalt(0) complex (1.2 g, 3.2 mmol) in anhydrous THF (5 cm^3) was added and the black suspension was heated to 50 °C for 4 h. After cooling, the resin beads were filtered, washed with alternate aliquots of THF and Et_2O until the filtrate became colourless, and dried *in vacuo* to afford deep purple beads of **4** (1.46 g, 80% P site occupancy, 0.94 ± 0.02 mmol[hexynol] g^{-1}).

¶ Polymer samples for ^{31}P NMR were swollen in THF and scanned with a D_2O capillary lock at 145.7 MHz for 2 h. Different phosphine species are readily distinguished: polymer-PPh_2-[Co], δ_P = 50–80; polymer-P(O)Ph_2, δ_P = 28.8; polymer-PPh_2, δ_P = −6.3.

1 A. R. Brown, P. H. H. Hermkens, H. C. J. Ottenheijm and D. C. Rees, *Synlett*, 1998, 817.
2 F. Balkenhohl, C. von dem Bussche-Hünnefeld, A. Lansky and C. Zechel, *Angew. Chem., Int. Ed. Engl.*, 1996, **35**, 2288.
3 P. H. H. Hermkens, H. C. J. Ottenheijm and D. C. Rees, Tetrahedron Report No. 418, *Tetrahedron*, 1997, **53**, 5643.
4 M. J. Plunkett and J. A. Ellman, *J. Org. Chem.*, 1997, **62**, 2885.
5 S. E. Gibson (née Thomas), N. J. Hales and M. A. Peplow, *Tetrahedron Lett.*, 1999, **40**, 1417.
6 Alkynes have been immobilised *via* Michael addition but are liberated as enones, N. W. Hird, K. Irie and K. Nagai, *Tetrahedron Lett.*, 1997, **38**, 7111; or ketones, N. W. Hird, M. Crawshaw, K. Irie and K. Nagai, *Tetrahedron Lett.*, 1997, **38**, 7115; and the cyclocondensation of acetylenic ketones with a resin-bound thiouronium salt has generated pyrimidine heterocycles, D. Obrecht, C. Abrecht, A. Grieder and J. M. Villalgordo, *Helv. Chim. Acta.*, 1997, **80**, 65.
7 (*a*) K. M. Nicholas and R. Pettit, *Tetrahedron Lett.*, 1971, 3475; (*b*) T. Nakamura, T. Matsui, K. Tanino and I. Kawajima, *J. Org. Chem.*, 1997, **62**, 3032; (*c*) for a recent review of the asymmetric reaction: O. Geis and H. G. Schmaltz, *Angew. Chem., Int. Ed.*, 1998, **37**, 911.
8 R. A. Dubois, P. E. Garrou, K. D. Lavin and H. R. Allcock, *Organometallics*, 1986, **5**, 460.
9 C. De-An and C. U. Pittman Jr., *J. Mol. Catal.*, 1983, **21**, 405.
10 A. J. Poe, *J. Organomet. Chem.*, 1975, **94**, 235.
11 For a representative monophosphine derivative see: G. Váradi, A. Vizi-Orosz, S. Vastag and G. Pályi, *J. Organomet. Chem.*, 1976, **108**, 225; and for a bisphosphine derivative see, M. F. D'Agostino, C. S. Frampton and M. J. McGlinchey, *Organometallics*, 1990, **9**, 2972.
12 A. M. Fivush and T. M. Willson, *Tetrahedron Lett.*, 1997, **38**, 7151.

Communication 9/06048K

Ditopic ligands for the simultaneous solvent extraction of cations and anions

David J. White,*[a] Norman Laing,[a] Hamish Miller,[a] Simon Parsons,[a] Simon Coles[b] and Peter A. Tasker*[a]

[a] *Department of Chemistry, The University of Edinburgh, Joseph Black Building, Kings Buildings, West Mains Rd., Edinburgh, UK EH9 3JJ. E-mail: P.A.Tasker@ed.ac.uk*

[b] *EPSRC National Crystallography Service, Department of Chemistry, University of Southampton, Southampton, UK SO17 1BJ*

Received (in Basel, Switzerland) 9th August 1999, Accepted 13th September 1999

Incorporation of a dianionic binding site for transition metal cations and a dicationic binding site for anions into a lipophilic molecule has produced a ligand with a high efficacy for the solvent extraction of a transition metal salt [$M^{2+}X^{2-}$].

Most man-made processes to separate transition metal ions from aqueous solutions depend on ion exchange processes, in which the desired metal cation M^{n+} replaces a different metal cation (often Na^+) or protons from an anionic group in a complexing agent.[1] Such complexing agents are deployed on solid supports in processes using ion exchange resins, or in a water immiscible liquid in solvent extraction. Although toxic or detrimental metal ions may be sequestered in this way, true purification of the aqueous stream is not achieved because (i) the number of ions present in solution is, at best, unchanged and is often increased; (ii) in the case of proton exchange the pH of the stream may be significantly lowered; and (iii) the anions remain in solution. The harmful effects of anionic species such as phosphate and sulfate have led to control of environmental discharge levels for these species.

These considerations, combined with the need for novel separation technologies to process leach solutions in primary metal recovery, have led us to investigate a new class of extractant which simultaneously sequesters both a transition metal cation and its attendant anion in a ditopic system with the features illustated in Scheme 1.

There are few examples of ligands which simultaneously bind cations and anions and the majority of these address alkali or alkali earth metal or ammonium salts.[2] A recent example invovles the extraction of technetium as the $[NH_4][TcO_4]$ ion pair.[3] Our prototype for a new class of ditopic ligand (Scheme 2) has a ligand framework similar to the uranyl salen anion receptors of Reinhoudt and coworkers,[4] but is designed to provide separate dianionic and dicationic binding sites which are derived from the zwitterionic form of the ligand created by transferring the phenolic protons to the nitrogen atoms of the pendant morpholine groups (Schemes 1 and 3). These features provide for efficient stripping to recycle the extractant and for

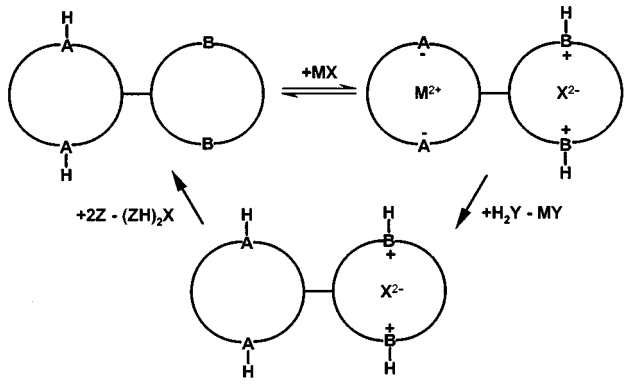

Scheme 1 Schematic representation of ditopic ligands for metal salts with diacid/dibasic sites to enable the hydrometallurgical unit operations of concentration and separation.

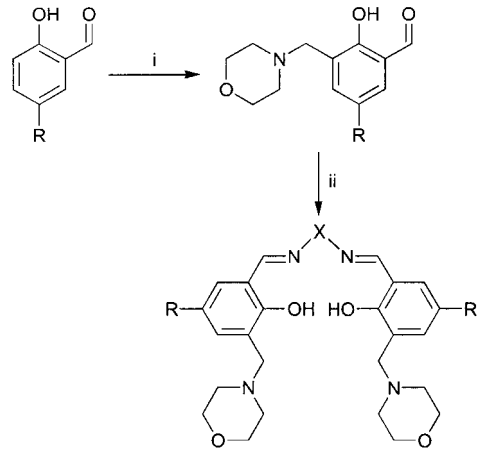

Scheme 2 i, 4-Ethoxyethylmorpholine, MeCN, N_2, reflux 66 h; ii, diamine, Et_2O–EtOH (1 : 1), room temp. 12 h. R = Me, Bu^t or nonyl (mixed isomer); X = CH_2CH_2 or $CH_2CH_2CH_2$, H_2NXNH_2 = (±)-*trans*-cyclohexane-1,2-diamine or benzene-1,2-diamine. Ligands referred to here are **1**: R = Bu^t, X = CH_2CH_2, **2**: R = nonyl, H_2NXNH_2 = (±)-*trans*-cyclohexane-1,2-diamine.

the possibility of separately recovering the metal and anion components in articles of commerce. These new ligands, exemplified by **1** and **2** (Scheme 2), can be readily prepared in a four-step convergent synthesis from a substituted salicylaldehyde, paraformaldehyde, morpholine and a diamine of choice.†

When a chloroform solution of the lipophilic ligand **2** (0.01 M) is contacted with aqueous $CuSO_4$ (1 M) at pH 3.8 a dark brown colour develops rapidly. Analysis of the organic phase by ICP-AES for copper and sulfur indicates close to 100% loading of $CuSO_4$. Some of the possible modes of binding of divalent transition metals and their attendant anions have been defined

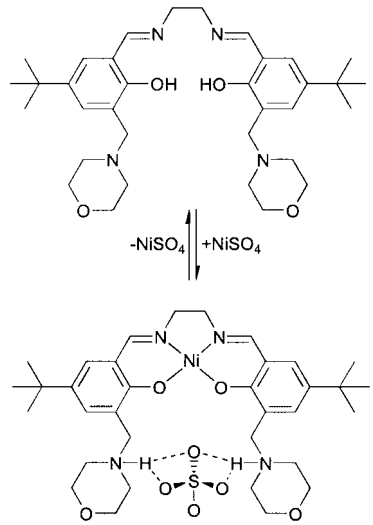

Scheme 3 Sequestration of $NiSO_4$.

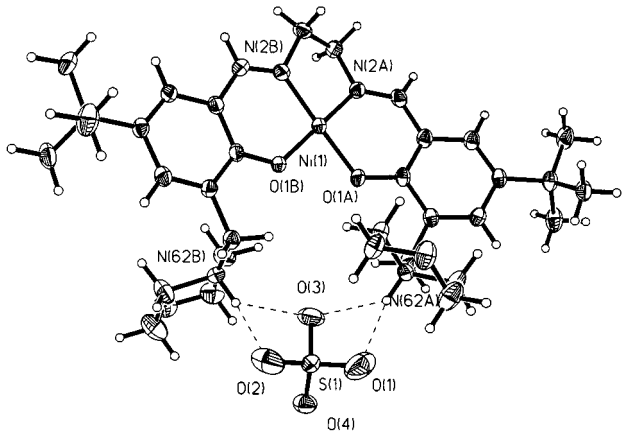

Fig. 1 Molecular structure of [Ni(**1**)SO_4]. Selected bond lengths (Å) and angles (°): Ni(1)–N(2A) 1.846(2), Ni(1)–N(2B) 1.858(2), Ni(1)–O(1A) 1.848(2), Ni(1)–O(1B) 1.854(2); O(1A)–Ni(1)–N(2A) 93.67(8), O(1B)–Ni(1)–N(2B) 94.51(8).

by X-ray structure determinations of nickel(II) complexes of ligand **1** which were readily crystallised from methanol. Reaction of **1** with $NiSO_4·7H_2O$ in methanol (Scheme 3) yields an orange precipitate with a FAB mass spectrum and microanalysis data consistent with the formulaion of the product as [Ni(**1**)SO_4]·$6H_2O$.[5]

An X-ray crystal structure‡ shows (Fig. 1) that the Ni^{2+} cation is coordinated in the planar $N_2O_2^{2-}$ cavity of the salen moiety with bond distances and angles typical of such coordination environments.[6] The coordination of the Ni^{2+} ion has two important effects on the structure of the ligand. The two protons liberated from the phenols of the metal binding site have been transferred to the nitrogen atoms of the pendant morpholine groups and the ligand has been organised to bring the two morpholine groups into close proximity[7] to produce a dicationic binding site for the sulfate anion. This represents an example of cooperativity[8] in which binding of the metal cation directly enhances binding of the anion. The sulfate dianion is bound by both electrostatic interactions and two separate bifurcated hydrogen bonds, one to each quaternary amine (Table 1).

Table 1 Hydrogen bonded distances (Å) and angles (°) around the sulfate anion in [Ni(**1**)SO_4]

	N···O	N–H···O	H···O
O1···H62A–N62A	2.870(4)	166.2	1.958
O2···H62B–N62B	2.923(3)	154.1	2.322
O3···H62A–N62A	2.993(4)	128.8	2.058
O3···H62B–N62B	2.915(4)	132.1	2.209

Note: the N–H distances were fixed at 0.91 Å. H-bonds were assigned using the Platon program[15] to interactions of the oxygen and nitrogen atoms that were < 3.12 Å.

The prototype extractants exemplified by **1** have useful features for developing working systems[9] for the recovery of metal salts from process streams, acid mine drainage streams or effluents. The disposition of both the salicylaldimine units and the pendant amine functions can be separately varied in attempts to 'tune' selectivity for particular combinations of metal cation and attendant anions. The aldimine functionality is resistant to hydrolysis[10] when used in solvent extraction processes, even when contacted with relatively strong acidic media providing the options for efficient stripping protocols as otulined in Scheme 1. These and the possibility of immobilising the extractants on solid supports are the subject of current work.

We thank Mr J. Millar and Mr W. Kerr for obtaining NMR spectra, Mr A. Taylor and Mr H. MacKenzie for mass spectra and Ms L. Eades for elemental analysis. We gratefully acknowledge the EPSRC for a ROPA award (GRM/33303) and Avecia plc for funding.

Notes and references

† *Experimental procedures:* the starting 2-hydroxy-5-alkylbenzaldehydes were prepared by the method of Levin and coworkers[11] and 4-ethoxymethyl morpholine and hydroxy-3-(morpholin-4-ylmethyl)benzaldehydes by the methods described by Fenton and coworkers.[12]

Example syntheses: **1**: 2-hydroxy-3-(morpholin-4-ylmethyl)-5-*tert*-butylbenzaldehyde (6 g, 21.7 mmol) was dissolved in diethyl ether (60 ml) and added to a solution of ethane-1,2-diamine (0.636 g, 10.6 mmol) in ethanol (60 ml). The resulting yellow solution was stirred overnight then concentrated *in vacuo* to give a yellow oil which on trituration in hexane at −78 °C gave a waxy yellow solid. This was washed with hexane (15 ml) and diethyl ether (15 ml) and dried *in vacuo* (5.8 g, 95%); mp 155–158 °C (Found: C, 70.60; H, 9.06; N, 9.67. Calc. for $C_{34}H_{50}N_4O_4$: C, 70.56; H, 8.71; N, 9.68%). MS (FAB, thioglycerol) *m/z*, 579 (MH^+ 62%).

[Ni(**1**)SO_4]: **1** (0.50 g, 86 mmol) was dissolved in hot methanol (30 ml) and added to a hot solution of $NiSO_4·7H_2O$ (0.245 g, 0.86 mmol) in methanol (20 ml), instantly producing a dark orange colour. On standing the product precipitated as a deep red solid (0.59 g, 93.6%). Recrystallisation from MeOH–H_2O (3 : 1) gave a red microcrystalline material formulated as [Ni(**1**)SO_4]·$6H_2O$; mp 235–240 °C (Found: C, 48.86; H, 7.37; N, 6.53. Calc. for $C_{34}H_{62}N_4NiO_{14}S$: C, 48.53; H, 7.43; N, 6.66%). MS (FAB, thioglycerol) *m/z* 733 [(LNiSO_4)H^+ 10.1%]. Crystals suitable for X-ray diffraction were obtained by evaporation of a saturated methanol solution of the complex.

‡ *Crystal data*: [Ni(**1**)SO_4]·3.75MeOH: The structure was solved by Patterson methods (DIRDIF)[13] and refined against F^2 (SHELXL-97).[14] $C_{37.75}H_{65}N_4NiO_{11.75}S$, M = 518.14, monoclinic, space group $P2/c$, a = 18.9754(4), b = 12.8666(3), c = 19.7197(4) Å, β = 118.571(1)°, U = 4228.2(2), Z = 4, D_c = 1.332 g cm^{-3}, T = 150(2) K, μ(Mo-Kα) = 0.571 mm^{-1}, wR_2 = 0.1457 (8643 independent reflections), R = 0.0502 [$F > 4\sigma(F)$]. The MeOH solvate (2.701 e/cell) was treated in the manner described by van der Sluis and Spek.[15] CCDC 182/1414. See http://www.rsc.org/suppdata/cc/1999/2077/ for crystallographic files in .cif format.

1 D. S. Flett, *Hydrometallurgy*, 1992, **30**, 327.
2 M. T. Reetz, in *Comprehensive Supramolecular Chemistry*, ed. J. L. Atwood, J. E. D. Davies, D. D. MacNicol and F. Vogle, Elsevier Press, Oxford, 1996.
3 P. D. Beer, P. K. Hopkins and J. D. McKinney, *Chem. Commun.*, 1999, 1253.
4 D. M. Rudkevich, W. P. R. V. Stauthamer, W. Verboom, J. J. F. Engbersen, S. Harkema and D. N. Reinhoudt, *J. Am. Chem. Soc.*, 1992, **114**, 9671.
5 When **1** was treated with nickel(II) acetate in methanol the neutral complex [Ni(**1** − 2H)] was formed which has been characterised crystallographically. The ability to isolate neutral complexes containing *either* a metal salt, *e.g.* [Ni(**1**)SO_4] *or* the metal cation alone *e.g.* [Ni(**1** − 2H)] is a special feature of these ditopic ligands and depends on the pH of solution or the basicity of the conjugate anion. Complete details will be reported in a full paper.
6 A survey of the CCDC reveals 66 square planar Ni(II) salen complexes. Ni–N and Ni–O distances average 1.86 and 1.85 Å, repectively: D. A. Fletcher, R. F. McMeeking and D. J. Parkin, *J. Chem. Inf. Comput. Sci.*, 1996, **36**, 746.
7 A preliminary X-ray structure of the free ligand shows that in the solid state the torsion around the ethylene linker group places the chelating units in a *trans* configuration and it is therefore not predisposed for complexation. During the course of this work the structure of a related ligand was published and also shows the *trans* configuration. S. Shanmura Sundara Raj, R. Thirumugan, G. Shanmugan, Hoong-Kun Fung, J. Manomani and M. Kandaswamy, *Acta Crystallogr., Sect C*, 1999, **55**, 94.
8 J.-M. Lehn, *Angew. Chem., Int. Ed. Engl.*, 1988, **27**, 89.
9 P. A. Tasker and D. J. White, *Br. Pat.*, BP 9907485.8, 1999.
10 J. Szymanowski, in *Hydroxyoximes and Copper Hydrometallurgy*, CRC Press, Boca Raton, FL, 1993, p. 62.
11 R. Aldred, R. Johnston, D. Levin and J. Neilan, *J. Chem. Soc., Perkin Trans. 1*, 1994, 1823.
12 H. Adams, N. A. Bailey, D. E. Fenton and G. Papageorgiou, *J. Chem. Soc., Dalton Trans.*, 1995, 1883.
13 P. T. Beurskens, G. Beurskens, W. P. Bosman, R. D. Gelder, S. Garcia-Granda, R. O. Gould, R. Israël and J. M. M. Smits, DIRDIF-96, University of Nijmegen, The Netherlands, 1996.
14 G. M. Sheldrick, SHELXL-97, University of Göttingen, Germany, 1997.
15 P. van der Sluis and A. L. Spek, *Acta Crystallogr., Sect. A*, 1990, **46**, 194.

Communication 9/06490G

ChemComm

A highly diastereoselective [2,3]-sigmatropic N,O rearrangement

Steven D. Bull,[a] Stephen G. Davies,*[a] Simon Jones,[a] Jacqueline V. A. Ouzman,[a] Anne J. Price[a] and David J. Watkin[b]

[a] *The Dyson Perrins Laboratory, University of Oxford, South Parks Road, Oxford, UK OX1 3QY. E-mail: steve.davies@chemistry.ox.ac.uk.*
[b] *Chemical Crystallography Laboratory, University of Oxford, 9 Parks Road, Oxford, UK, OX1 3PD*

Received (in Liverpool, UK) 20th July 1999, Accepted 15th September 1999

Lithium (*E*)-*N*-benzyl-*O*-(4-methoxy-4-phenylbut-2-enyl)-hydroxylamide undergoes a highly diastereoselective rearrangement *via* a chelated transition state, to afford after reduction, *syn*-3-benzylamino-4-methoxy-4-phenylbut-1-ene as a single diastereoisomer.

Intramolecular sigmatropic rearrangements have found widespread use in synthetic organic chemistry, primarily due to the high selectivities observed in these transformations.[1] We have recently reported on a novel intramolecular [2,3]-rearrangement of *N*-benzyl-*O*-allylic hydroxylamines **1** to afford *N*-benzyl-*N*-hydroxyallylamines **2**, which may be reduced to the corresponding *N*-benzyl-*N*-allylamines **3** in good yield (Scheme 1).[2] The transition state of this N,O rearrangement may be compared with that of the [2,3]-Wittig rearrangement;[3] deprotonation of **1** affords a lithium amide which rearranges through an envelope like transition state.

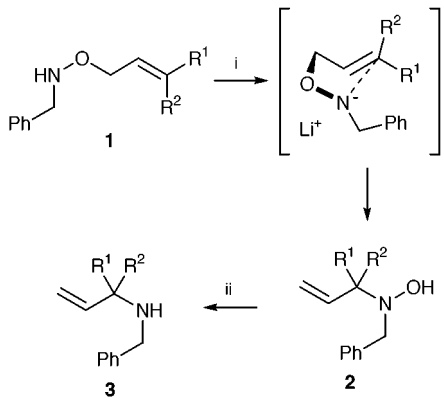

Scheme 1 *Reagents and conditions*: i BuLi, THF; ii, Zn, aq. HCl.

Previous investigations into the synthetic utility of the [2,3]-Wittig rearrangement[4] have revealed that allylic ethers with stereogenic centres bearing a heteroatom substituent adjacent to the migration terminus have the capacity to undergo diastereoselective rearrangement.[5] For example, deprotonation of allylic ether **4** with BuLi in THF at −78 °C affords the rearranged product **5**, containing two new stereogenic centres, in 66% de (Scheme 2)[6]. Facial selectivity in this case is controlled *via* a transition state where the carbanion attacks antiperiplanar to the heteroatom *via* a conformation which directs the allylic hydrogen on the original stereogenic centre to the 'inside' site.

This type of stereoelectronic effect might also operate to control facial selectivity during the [2,3]-N,O rearrangement of the lithium anion of (*E*)-*N*-benzyl-*O*-(4-methoxy-4-phenylbut-2-enyl)hydroxylamine **6**, however in contrast to the Wittig rearrangement, in this case the possibility of chelation control is also present. If N,O rearrangement of the lithium anion of **6** proceeds *via* a transition state where facial selectivity is determined by stereoelectronic effects, then the *anti*-diastereoisomer **7** will be formed (Scheme 3), while a rearrangement pathway which proceeds *via* a chelated transition state would result in the *syn*-diastereoisomer **8** (Scheme 4).

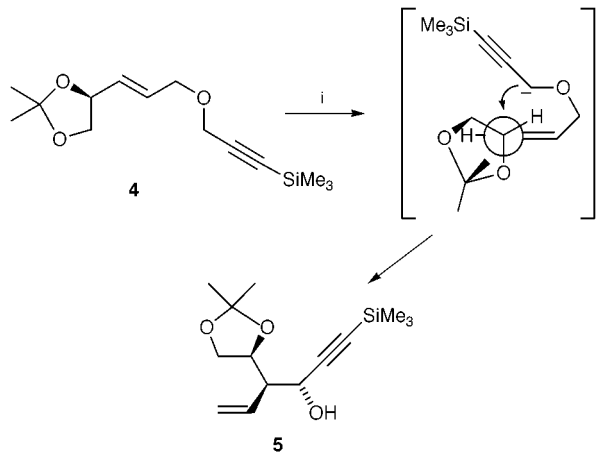

Scheme 2 *Reagents and conditions*: i, BuLi, THF, −78 °C.

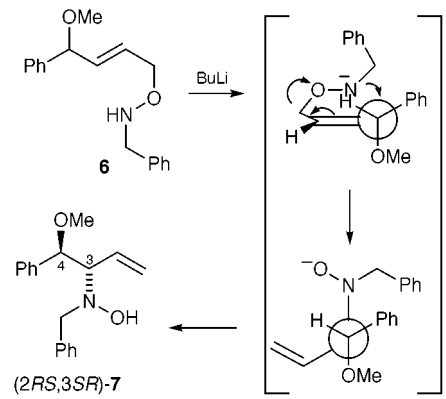

Scheme 3

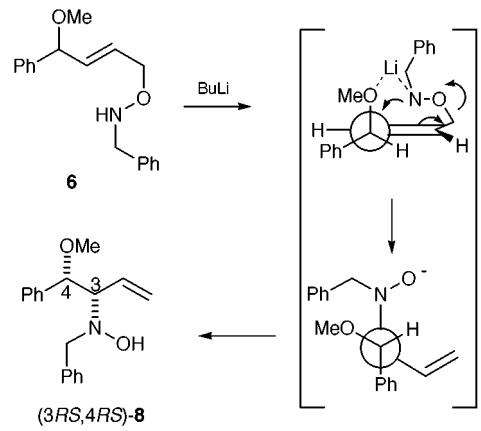

Scheme 4

Thus (*E*)-*N*-benzyl-*O*-(4-methoxy-4-phenylbut-2-enyl)hydroxylamine **6** was prepared from racemic methyl *O*-methylmandelate **9** *via* our previously described synthetic protocol for this class of hydroxylamine.[2] Methyl *O*-methylmandelate **9** was reduced with DIBAL-H in toluene at −78 °C and the resulting aldehyde treated *in situ* with ethoxycarbonylmethylene(triphenyl)phosphorane to afford the α,β-unsaturated ester **10** in an unoptimised 53% yield. Reduction of ester **10** with DIBAL-H in toluene gave allylic alcohol **11** in 80% yield, which was treated with NBS in the presence of PPh_3 to afford an unstable allylic bromide **12**. Subsequently, the crude reaction product of the bromination reaction was treated with the potassium anion of *syn*-benzaldehyde oxime to afford oxime **13** in an overall 45% yield from allylic alcohol **11**. Reduction of oxime **13** with pyridine·borane/HCl gave the desired rearrangement substrate (±)-(*E*)-*N*-benzyl-*O*-(4-methoxy-4-phenylbut-2-enyl)hydroxylamine **6** in 57% yield (Scheme 5).

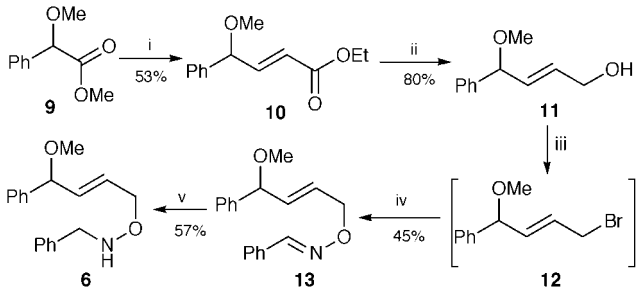

Scheme 5 *Reagents and conditions*: i, DIBAL-H, toluene, −78 °C, then $Ph_3P{=}CHCO_2Et$; ii, DIBAL-H, toluene, −78 °C; iii, NBS, PPh_3, CH_2Cl_2; iv, PhCH=NOK, THF; v, pyridine·BH_3, EtOH, HCl.

Treatment of hydroxylamine **6** with 1.1 equiv. of BuLi in THF at −78 °C, followed by warming to room temperature over 1 h resulted in complete [2,3]-rearrangement to afford a single diastereoisomer of 3-benzyl(hydroxy)amino-4-methoxy-4-phenylbut-1-ene **8** in 94% conversion as determined by ^{1}H NMR spectroscopic analysis of the crude reaction mixture. Subsequent reduction of the unstable *N*-hydroxy compound **8** to *syn*-3-benzylamino-4-methoxy-4-phenylbut-1-ene **14** with zinc in aqueous hydrochloric acid was achieved in 63% isolated yield (Scheme 6).†

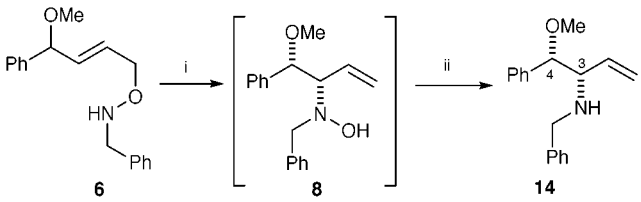

Scheme 6 *Reagents and conditions*: i BuLi, THF, −78 to 25 °C; ii, Zn, aq. HCl.

X-Ray crystallographic analysis of the crystalline HCl salt of *syn*-3-benzylamino-4-phenylbut-1-ene **14** clearly revealed that [2,3]-rearrangement of **6** had occurred to afford *syn*-**8** where the relative stereochemistry of the two newly formed stereogenic centres was (3*RS*,4*RS*) (*vide infra*) (Fig. 1).‡

The *syn*-selectivity of diastereoisomer **14** found during rearrangement of **6** is clearly in accord with the chelation control transition state model described in Scheme 4, rather than the stereoelectronic model described in Scheme 3.

In conclusion, (*E*)-*N*-benzyl-*O*-(4-methoxy-4-phenylbut-2-enyl)hydroxylamine **6** undergoes a highly diastereoselective rearrangement to afford, after reduction, *syn*-3-benzylamino-4-methoxy-4-phenylbut-1-ene **14** containing two new stereogenic centres with complete diastereoselectivity *via* a chelated transition state.

Notes and references

† *Selected data* for **14**: mp 41–43 °C; δ_H (400 MHz, $CDCl_3$) 3.21 (3H, s, OCH_3), 3.31 (1H, t, *J* 8.2, $CHCH{=}CH_2$), 3.62 (1H, d, *J* 13.2, $NHCH_2$), 3.87 (1H, d, *J* 13.2, $NHCH_2$), 4.07 (1H, d, *J* 8.2, MeOC*H*), 4.93 (1H, d, *J* 17.2, $CH{=}CH_2$), 5.03 (1H, d, *J* 10.4, $CH{=}CH_2$), 5.48–5.56 (1H, m, $CH{=}CH_2$), 7.23–7.35 (10H, m, ArC*H*); δ_C(100 MHz, $CDCl_3$) 51.2 ($NHCH_2Ph$), 56.8 (OCH_3), 66.9 ($NHCHCH{=}CH_2$), 86.6 (PhCHOMe), 118.6 ($CH{=}CH_2$), 126.7, 127.8, 127.9, 128.0, 128.1, 128.3 (10 × ArCH), 136.7 ($CH{=}CH_2$), 138.9 (*ipso*-ArC), 140.5 (*ipso*-ArC); *m/z* (APCI+) 323 (13%), 269 (12), 268 (100, MH^+), 237 (13), 236 (82, $M^+ - OMe$) (HRMS: calc. for $C_{18}H_{21}NO$, 268.1701; Found, 268.1706).

‡ *Crystal data* for **14**·HCl·H_2O: $C_{18}H_{24}ClNO_2$, *M* = 321.84, monoclinic, space group *P*1 2_1/n 1, *a* = 6.403(1), *b* = 27.046(1), *c* = 10.252(1) Å, β = 97.85(2)°, *V* = 1758.8 Å^3, *T* = 180 K, *Z* = 4, D_c = 1.21 g cm^{-3}, *T* = 180 K, μ(Mo-*K*α) = 0.22 mm^{-1}, 3109 independent reflections were measured, of which 2050 were used, *R* = 0.11, R_W = 0.16. Rint = 0.08. The sample was one of many pieces cut from clear plate-like crystals. Although the cut samples remained clear, the diffraction patterns showed that they were always severely damaged by shearing parallel to the large face during the cutting. The final sample was obtained by repeatedly shaving very thin slices away from the edges of the original large crystal. The best obtainable diffraction pattern did not represent a simple single crystalline sample. Data extraction from the 90 images (180 degrees) collected on a Nonius DIP2000 diffractometer were complicated by the presence of more than one reciprocal lattice. Reflections from the strongest lattice were used as the basis for the structure analysis, but were inevitably contaminated by data from the weaker lattice. We could not determine a valid twin law relating the two lattices—the sample was probably polycrystalline. The weakest data showed the greatest discrepancy between F_o and F_c, presumably because the accidental overlap of a strong component of the minor lattice on a weak component of the strong lattice had a more damaging effect than the inverse. Data with $I < 6\,\sigma(I)$ were therefore excluded from the refinement. The value of '6' is subjective, but was chosen by looking at the residual distribution so as to preserve as many 'fair' reflections as possible, and at the same time reject as many 'suspect' reflections as possible. Only one of the water hydrogen atoms could be located. CCDC 182/1415. See http://www.rsc.org/suppdata/cc/1999/2079/ for crystallographic data in .cif format.

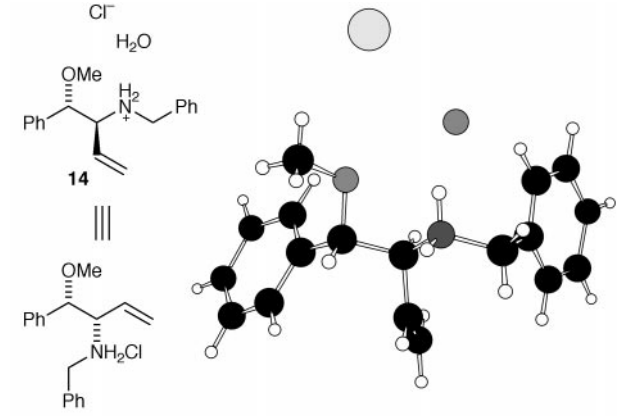

Fig. 1 X-Ray crystal structure of the hydrated HCl salt of *syn*-(3*RS*,4*RS*)-**14**.

1 S. M. Roberts, in *Comprehensive Functional Group Transformations*, ed. A. R. Katritzky, O. Meth-Cohn and C.W. Rees, Pergamon, Oxford, 1995, vol. 1, p. 404.
2 S. G. Davies, S. Jones, M. A. Sanz, F. C. Teixeira and J. F. Fox, *Chem. Commun.*, 1998, 2235.
3 Y. D. Wu, K. N. Houk and J. A. Marshall, *J. Org. Chem.*, 1990, **55**, 1421.
4 For examples of the synthetic utility of the [2,3]-Wittig rearrangement, see T. Nakai and K. Mikami, *Chem. Rev.*, 1986, **86**, 885; 'The Wittig Rearrangement' in *C-C σ Bond Formation*, ed. G. Pattenden, vol. 3 of *Comprehensive Organic Synthesis* ed. B. M. Trost and I. Fleming, Pergamon, Oxford, 1990, p. 975.
5 K. Mikami and T. Nakai, *Synthesis*, 1991, 594; R. Brückner and H. Priepke, *Angew. Chem.*, 1988, **27**, 278; H. Priepke and R. Brückner, *Chem. Ber.*, 1990, **123**, 153.
6 R. Brückner, *Chem. Ber.*, 1989, **122**, 193; E. Nakai and T. Nakai, *Tetrahedron Lett.*, 1988, **29**, 4587.
7 For an example where the diastereoselectivity observed for a [2,3]-Wittig rearrangement has been rationalised *via* a chelated transition state, see S. W. Scheuplein, A. Kusche, R. Brückner and K. Harms, *Chem. Ber.*, 1990, **123**, 917.

Communication 9/05981D

ChemComm

Sol–gel process: temperature effect on textural properties of a monophasic hybrid material

Geneviève Cerveau, Robert J. P. Corriu* and Eric Framery

Laboratoire de Chimie Moléculaire et Organisation du solide, UMR 5637, Université Montpellier II, cc 007, Place E. Bataillon, 34095 Montpellier Cedex 5, France. E-mail: cmos@crit.univ-montp2.fr

Received (in Cambridge, UK) 26th July 1999, Accepted 21st September 1999

Monophasic hybrid materials with controlled porosity are obtained by varying the temperature, without change of the polycondensation at silicon atoms, confirming the kinetic control of formation of the solids.

The sol–gel processes which correspond to an inorganic polycondensation offer very wide possibilities since they allow the synthesis of materials from the molecular scale as illustrated in Scheme 1.[1] Hybrid organic–inorganic materials are one of the most attractive targets achievable by this chemistry.[2–8] Using the sol–gel route, it is possible to introduce a large variety of organic moieties into inorganic matrices, so leading to the possibility to tailor physico-chemical properties.[2] However, textural control of the solids obtained by the sol–gel route is difficult. For instance, it is known that the aging and drying of gels influence the textural properties for both silica and hybrid solids.[1,3] Furthermore, it has been observed that textural parameters (specific surface area, porosity, *etc*.) drastically change with the experimental conditions,[9–12] and some correlation with kinetic measurements in the first steps of the process have been performed.[1,13] These solids are considered as unstable[1] and reproducibility is often difficult to obtain from literature data since all the experimental details are of importance and are not always precisely reported. However, while *all* experiments are reproducible when a precise analytical procedure is *strictly* followed[9–12] predictability of the obtained product is not yet possible. We have shown previously that organic-inorganic materials are kinetically controlled solids with the properties of the solids being highly dependent on the chemical parameters such as nature and concentration of the catalyst,[9,10] nature of the solvent,[11] concentration of the precursor,[9] nature of the leaving group[11] and nature of the organic unit.[9,12] Here, we report the drastic influence of temperature which is a very important physical parameter for kinetic studies.

Adequate predictability will be attained when the parameters which control all the different steps of the sol–gel type synthesis are known (precursor → oligomers → polymers → colloids → sol → gel). The results presented here suggest that the polycondensation at silicon does not control the textural properties of the resulting solids.

The hydrolytic polycondensation of the molecular precursor 1,4-$C_6H_4[Si(OMe)_3]_2$ **1** (Scheme 1) has been studied in THF using tetrabutylammonium fluoride (TBAF) as catalyst at the −20, 3, 20 and 55 °C.† The entire experiment (addition of the reagents, gelation, aging) was performed at the given temperature. NMR and BET measurements were from the same sample.

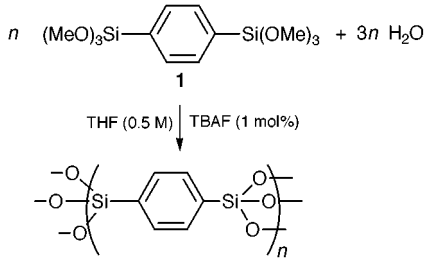

Scheme 1

Considering the identification of the solids at the 'molecular level', ^{13}C and ^{29}Si CP MAS NMR spectra showed that no SiC bonds had been cleaved during reaction.[14,15] The ^{13}C CP MAS spectra showed the presence of the unmodified organic fragment along with some residual methoxy groups. For all solids the ^{29}Si CP MAS NMR spectra exhibited only T^1 [C–Si(OR)$_2$(OSi)], T^2 [C–Si(OR)(OSi)$_2$] and T^3 [C–Si(OSi)$_3$] substructures with no signal in the ranges δ −90 to −110 being observed. While CP MAS spectroscopy is not quantitative, it has been shown[12,16] that single pulse experiments (SPE) do not reveal any significant variation in relative peak intensities from CP MAS spectra if hydrogen atoms are absent in the direct vicinity of the studied nucleus. For the hybrid materials studied here, quantitative reliable ^{29}Si SPE MAS NMR spectra of gels obtained from **1** have been collected and compared to the ^{29}Si CP MAS NMR spectra.[12] The SPE MAS and CP MAS percentages found for the different T^x units were found to be similar. The percentages of the different substructures determined by deconvolution of CP MAS spectra (Table 1) gives a good estimation of the degree of polycondensation of the silsesquioxane network. We observe that the temperature of the hydrolysis–polycondensation reaction has no influence on the polycondensation around silicon, the relative contributions of the T^x units being very similar whatever the temperature.

Table 1 ^{29}Si CP MAS NMR data for xerogels obtained from **1**

Xerogel	*T*/°C	Site population[a] (%)			Level of condensation (%)
		T^1	T^2	T^3	
1a	−20	18	49	33	71
1b	+3	19	53	28	69
1c	+20	16	64	20	67
1d	+55	18	42	40	74

[a] Obtained by deconvolution of ^{29}Si CP MAS NMR spectra.

By contrast, specific surface areas and porosities of the xerogels appeared to be very sensitive to temperature. They were determined by 35-point adsorption–desorption isotherm plot measurements[17] and evaluated using the BET equation.[18] The determination of the porous volume by the BJH method[19,20] and evaluation of the microporous volume by the analysis of the *t*-plot diagram were performed in each case. The values of specific surface areas were very high whatever the temperature being in the range 900–1300 m^2 g^{-1}. The main influence of the temperature was observed in the porosity of the gels. The shape of the curves of the adsorption–desorption isotherms depended strongly on the temperature (Fig. 1). At low temperature [−20 °C (**1a**) and 3 °C(**1b**)], the isotherms were of type I [Fig. 1(a) and (b)] indicating a largely microporous solid with a low mesoporous contribution, though vestiges of hysteresis loops characteristic of capillary filling of mesopores were evident. The microporous volume represented 40–55% of total porous volume. The mesopores did not exhibit a narrow pore size

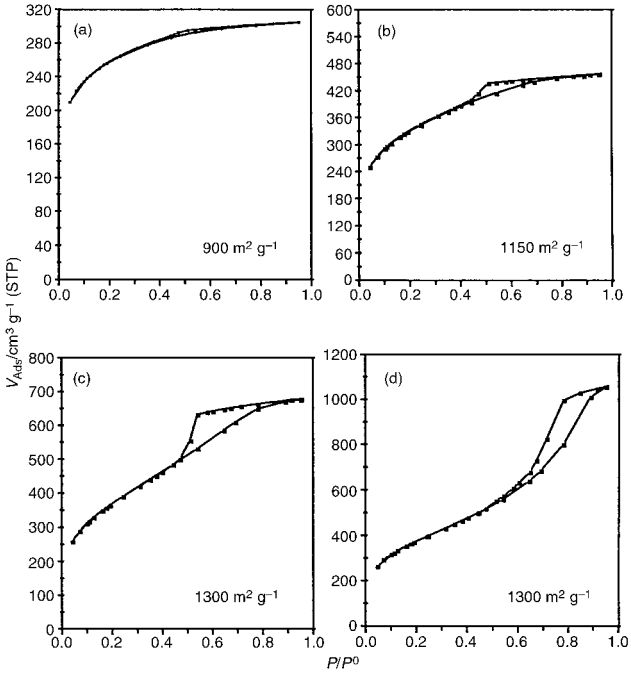

Fig. 1 N_2 adsorption–desorption isotherms of xerogels at −20 (a), 3 (b), 20 (c) and 55 °C (d).

distribution (20–120 Å). When the temperature was raised to +20 °C (**1c**), the isotherm became characteristic of type IV [Fig. 1(c)]. The microporous volume was 10% and the mesopore size lay in the range 20–120 Å. At +55 °C (**1d**), only 5% of micropores were present and mesopores showed a narrow pore size distribution (55–70 Å) characteristic of isotherms of type IV [Fig. 1(d)]. The results presented here thus show the drastic influence of temperature on the texture of the xerogels variation of which allows control of the porosity of the materials. At low temperatures, solids were mainly microporous whereas at higher temperature mesoporous solids with narrow pore size distribution were obtained.

In summary, this work confirms that hybrid materials obtained by hydrolytic polycondensation are under kinetic control. The temperature appears to be a fundamental parameter which allows the control of the textural properties of the solids. However, the drastic change observed in the porosity is not correlated with any change in the degree of polycondensation at silicon which remains insensitive to the temperature. This fact suggests that textural properties such as porosity are not controlled by the process of polycondensation at silicon.

Notes and references

† *Experimental procedure*: the preparation of gels was carried out according to the following general procedure. The precursor **1** was analytically pure (Anal. Calc. for $C_{12}H_{22}O_6Si_2$: C, 45.26; H, 6.96; Si, 17.64. Found: C, 44.88; H, 6.91; Si, 17.41%). The preparation of xerogel **1a** is given as an example. To 2.86 g (9 mmol) of **1** in 9 ml of dry (distilled over Na) THF (3 μmol H_2O/ml measured by the Karl Fisher method) was added at −20 °C a solution in 8.40 ml of dry THF of 90 μl (90 μmol) of TBAF (in THF, $[F^-]$ = 1 mol l^{-1} as measured by electrochemistry[21]) and 486 μl (27 mmol) of H_2O. The mixture was kept at −20 °C and after 90 min a monolithic gel had formed. After further aging for 6 days at −20 °C, the solid was collected, ground and washed twice with ethanol, acetone and diethyl ether. The resulting solid was dried at 120 °C *in vacuo* for 3 h yielding 1.70 g of a white powder **1a**. CP MAS NMR: ^{13}C, δ 133.6 (aromatic C), 50.7 (residual OMe); ^{29}Si, δ −62.0 (T^1), −69.5 (T^2), −78.0 (T^3).

1 C. J. Brinker and G. W. Scherer, *Sol–Gel Science*, Academic Press, London, 1990; L. L. Hench and J. K. West, *Chem. Rev.*, 1990, **90**, 33.
2 R. J. P. Corriu, *Polyhedron*, 1998, **17**, 925; G. Cerveau and R. J. P. Corriu, *Coord. Chem. Rev.*, 1998, **180** (**2**), 1051 and references therein.
3 D. A. Loy and K. J. Shea, *Chem. Rev.*, 1995, **95**, 1431 and references therein.
4 P. Judeinstein and C. Sanchez, *J. Mater. Chem.*, 1996, **6**, 511; B. Lebeau, S. Brasselet, J. Zyss and C. Sanchez, *Chem. Mater.*, 1997, **9**, 1012.
5 U. Schübert, N. Hüsing and A. Lorenz, *Chem. Mater.*, 1995, **7**, 2010.
6 R. J. P. Corriu, J. J. E. Moreau, P. Thépot and M. Wong Chi Man, *Chem. Mater.*, 1992, **4**, 1217; G. Cerveau, R. J. P. Corriu and N. Costa, *J. Non-Cryst. Solids*, 1993, **163**, 226; G. Cerveau, R. J. P. Corriu and C. Lepeytre, *J. Mater. Chem.*, 1995, **5**, 793; *Chem. Mater.*, 1997, **9**, 2561; J-P. Bezombes, C. Chuit, R. J. P. Corriu and C. Reyé, *J. Mater. Chem.*, 1998, **8**, 1749; C. Chuit, R. J. P. Corriu, G. Dubois and C. Reyé, *Chem. Commun.*, 1999, 723.
7 S. T. Hobson and K. J. Shea, *Chem. Mater.*, 1997, **9**, 616.
8 S. W. Carr, M. Motevalli, D. Li Ou and A. C. Sullivan, *J. Mater. Chem.*, 1997, **7**, 865.
9 G. Cerveau, R. J. P. Corriu and C. Fischmeister-Lepeytre, *J. Mater. Chem.*, 1999, **9**, 1149.
10 G. Cerveau, R. J. P. Corriu and E. Framery, *Polyhedron*, 1999, in press.
11 G. Cerveau, R. J. P. Corriu and C. Lepeytre, *J. Organomet. Chem.*, 1997, **548**, 99.
12 G. Cerveau, R. J. P. Corriu, C. Lepeytre and P. H. Mutin, *J. Mater. Chem.*, 1998, **8**, 2707.
13 J. C. Pouxviel and J-P. Boilot, *J. Non-Cryst. Solids*, 1987, **84**, 374; J. C. Pouxviel, J.-P. Boilot, J. C. Beloeil and J-Y. Lallemand, *J. Non-Cryst. Solids*, 1987, **89**, 345; F. Devreux, J-P. Boilot and F. Chaput, *Phys. Rev. A: Gen. Phys.*, 1990, **41**, 6901; J. Sanchez, S. E. Rankin and A. V. McCormick, *Ind. Eng. Chem. Res.*, 1996, **37**, 117; S. E. Rankin, C. W. Macosko and A. V. McCormick, *Chem. Mater.*, 1998, **10**, 2037.
14 M. Mägi, E. Lippmaa, A. Samoson, G. Engelhardt and A. R. Grimmer, *J. Phys. Chem.*, 1984, **88**, 1518.
15 H. Marsmann, *^{29}Si NMR Spectroscopic Results*, ed. P. Diehl, E. Fluck and R. Kosfeld, Springer Verlag, Berlin, 1981.
16 H. W. Oviatt, K. J. Shea and J. H. Small, *Chem. Mater.*, 1993, **5**, 943.
17 S. J. Gregg and S. W. Sing, *Adsorption, Surface Area and Porosity*, Academic Press, London, 1982.
18 S. Brunauer, P. H. Emmet and E. Teller, *J. Am. Chem. Soc.*, 1938, **60**, 309.
19 S. Brunauer, L. S. Deming, W. S. Deming and E. Teller, *J. Am. Chem. Soc.*, 1940, **62**, 1723.
20 E. Barett, L. Joyner and P. Halenda, *J. Am. Chem. Soc.*, 1951, **73**, 373.
21 D. A. Skoog, D. M. West and F. J. Holler, *Fundamentals of Analytical Chemistry*, Sanndersq College Publishing, International Edition, New York, 1992, p. 873.

Communication 9/06033B

ChemComm

Synthesis and characterisation of an octupolar polymer and new molecular octupoles with off-resonant third order optical nonlinearities

Frédéric Chérioux,*[a] Hervé Maillotte,[b] Pierre Audebert[a]† and Joseph Zyss[c]

[a] *Laboratoire de Chimie et Electrochimie Moléculaire, UFR Sciences et Techniques, 16 route de Gray, F-25030 Besancon cedex, France. E-mail: frederic.cherioux@univ-fcomte.fr*

[b] *Laboratoire d'Optique P.M. Duffieux, Unité Mixte de Recherche CNRS/Université de Franche-Comté no 6603, Institut des Microtechniques de Franche-Comté, UFR Sciences et Techniques, 16 route de Gray, F-25030 Besancon cedex, France.*

[c] *Laboratoire de Photonique Quantique et Moléculaire, Unité Mixte de Recherche CNRS no 8537, Ecole Normale Supérieure, 61 Avenue du Président Wilson, F-94235 Cachan cedex, France*

Received (in Cambridge, UK) 21st July 1999, Accepted 10th September 1999

The first synthesis and Z-scan measurements of an octupolar polymer with off-resonant third order nonlinear optical properties are discussed; two other new molecular thiophene-based octupoles with similar nonlinearities are also reported.

In the quest for materials suitable for electro-optical and all-optical devices,[1] the last decade has witnessed considerable interest in the quadratic nonlinear optical (NLO) properties of organic or organometallic octupolar molecules.[2] Such octupolar compounds with multi-directional charge-transfer transitions enlarge the scope of molecular engineering for nonlinear optics,[3] previously restricted to dipolar compounds with single-directional charge-transfer transitions. Improving the NLO efficiency/transparency (or figure-of-merit) trade-off stands out among the important goals of this approach. Indeed, the particular symmetry of octupoles may lead to a better transparency and improved stability compared with classical dipoles,[2] although the question has not been completely elucidated as yet.[4] Besides, all-optical poling, which does not require a permanent dipole, has been shown to allow for noncentrosymmetric statistical macroscopic orientation.[2]

In all-optical applications based on the optical Kerr effect, it is also of paramount importance to improve the figures-of-merit[5] (recalled below) of cubic NLO materials because high nonlinear refractive indices in dipolar organics are generally obtained *via* resonant enhancement, at the expense of large linear or nonlinear absorption losses. However, only a small number of studies have reported cubic NLO properties of octupolar compounds. Large nonlinear refractive indices have been effectively measured in only two recent works, one dealing with organic octupolar molecules[6] and the second with organometallic octupolar complexes.[7] But in both cases, resonant enhancement of the nonlinear refractive index occurred, resulting from, respectively, three- or two-photon dispersion effects associated with absorption losses.

Moreover, to the best of our knowledge, no synthesis of octupolar polymers having NLO properties has so far been reported in the literature in spite of their potential interest towards further material and device investigations.

We report here the first efficient synthesis of an octupolar polymer {poly[2,4,6-tris(5′-(5-allylthio-2,2′-bithienyl-5-yl)-1,3,5-triazine]} as well as two new molecular octupoles [2,4,6-tris(5′-alkylthio-2,2′-bithienyl-5-yl)-1,3,5-triazine] which exhibit large non-resonant nonlinear refractive indices. The synthesis, UV-visible spectroscopy and Z-scan measurements of these three compounds are presented and their figures-of-merit are also discussed.

† Present Address: PPSM-Département de Chimie, Unité Mixte de Recherche CNRS n°8531, Ecole Normale Supérieure, 61 Avenue du Président Wilson, F-94235 CACHAN cedex, France.

We chose 5-*n*-butylthio-2,2′-bithiophene **1a** and 5-allylthio-2,2′-bithiophene **1b** as precursors in view of the two following assets: (i) the *n*-butyl chain of **1a** helps to increase the solubility of final molecule **2a**, and (ii) the allylthio function of **1b** can be easily homopolymerised using AIBN as a radical initiator.[8]

These two precursors **1a**,**b** were synthesised following Hill *et al.*[9] All products were purified by column chromatography with light petroleum–CH_2Cl_2 (1 : 1) as eluent. According to our earlier method,[10] octupoles **2a**,**b** were synthesised *via* a triple aromatic nucleophilic substitution of 3 equiv. of 5′-alkylthio-2,2′-bithienyl-5-yllithium salt on cyanuric chloride (see Scheme 1). Such reactions are efficient, with yields as high as 90%. The trisubstituted products **2a**,**b**‡ were only isolated because such reactions are activated by the mesomer attractive power of the three nitrogen atoms of cyanuric chloride. This electronic property stabilises the intermediate species of the aromatic nucleophile substitution. Octupoles **2** display D_{3h} symmetry. These molecules are completely planar in the absence of steric hindrance around the 1,3,5-triazine centre. Such symmetry has been confirmed by *ab initio* and semi-empirical computations as well as by electrochemical characterisation in the case of similar octupolar molecules.[11]

The new polymer **3** was synthesised in quantitative yield by radical homopolymerisation of octupolar monomer **2b** with AIBN as radical precursor (see Scheme 2). In order to obtain the pure polymer only, the reaction was continued until monomer **2b** was no longer detectable by thin layer chromatography. The crude polymer was then precipitated in Et_2O to obtain pure polymer **3**‡ as an orange–yellow powder. The octupolar character of monomer **2b** is retained during its homopolymerisation because the monomer is based on a very rigid sp^2 skeleton. All products **2** and **3** are very soluble in toluene at concentrations close to 0.1 mol l^{-1}. Also, THF is a good solvent. The polymer was analysed by SEC (THF solution, evaluation by comparison with a polystyrene standard) giving M_n = 1970 g mol^{-1}, M_w = 4800 g mol^{-1} and polydispersity =

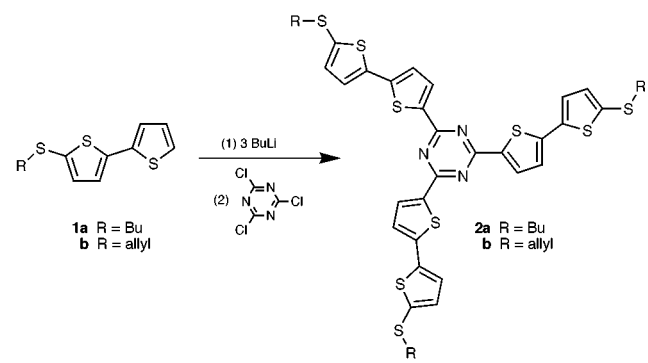

Scheme 1

2.43. Therefore, from SEC analysis, polymer **3** can be considered as an oligomer (3–6 monomers).

UV-visible spectra in toluene exhibit a single narrow linear absorption band of 30 nm width, centred at 380 and 376 nm for octupoles **2** and polymer **3**, respectively.

Z-scan measurements were performed in the picosecond range using a sensitive single-shot multi-channel method.[12] With this method, it was possible to perform closed- and open-aperture Z-scans for the same incident pulse to allow simultaneous measurements of the nonlinear refractive index and the nonlinear absorption.[13] Linearly polarised 50 ps TEM_{00} pulses at 1064 nm were delivered by a mode-locked Nd:YAG laser at a repetition rate of 10 Hz. The confocal parameter in our experimental setup was $Z = 23.5$ mm. All compounds were tested in solution (concentration 0.12 mol l^{-1}) in toluene with a 2 mm thick quartz cell. Under our experimental conditions, the nonlinear refraction of the solvent alone was beneath the baseline noise of our apparatus. The nonlinear samples were measured with an incident energy of $E = 37$ μJ and a linear transmittance[14] $S = 0.62$ for n_2 measurements (closed-aperture Z-scan) and $S = 1$ for β measurements (open-aperture Z-scan). The nonlinear refractive indices n_2 and the two-photon absorption coefficients β for all compounds were measured according to the procedure described by Sheik-Bahae *et al.*[14] The experimental data were calibrated using the standard CS_2 reference ($n_{2(CS2)} = 3.5 \times 10^{-18}$ m^2 W^{-1}).

For all three compounds, the measured relative nonlinear index $n_2/n_{2(CS2)}$ was 0.6. None of the octupoles **2** and polymer **3** exhibited detectable two-photon absorption at 1064 nm. This is in accordance with the position of the linear absorption peak wavelengths, giving a two-photon absorption band around 760 nm, far from the exciting wavelength. Hence, octupoles **2** and polymer **3** in solution have an off-resonant nonlinear refractive index close to that of pure CS_2. The expected extrapolated values n_2 for the solutes are close to the best off-resonance nonlinear refractive index data reported for single crystal polydiacetylene toluene-*p*-sulfonate (PTS)[15] ($n_2 = 2.2 \times 10^{-16}$ m^2 W^{-1} @ $\lambda = 1600$ nm). However, one should keep in mind that the extrapolation from solution to the solid state is not straightforward. Nonlinear refraction and absorption measurements on thin solid films of the new polymer **3** are currently being performed so as to investigate this critical issue.

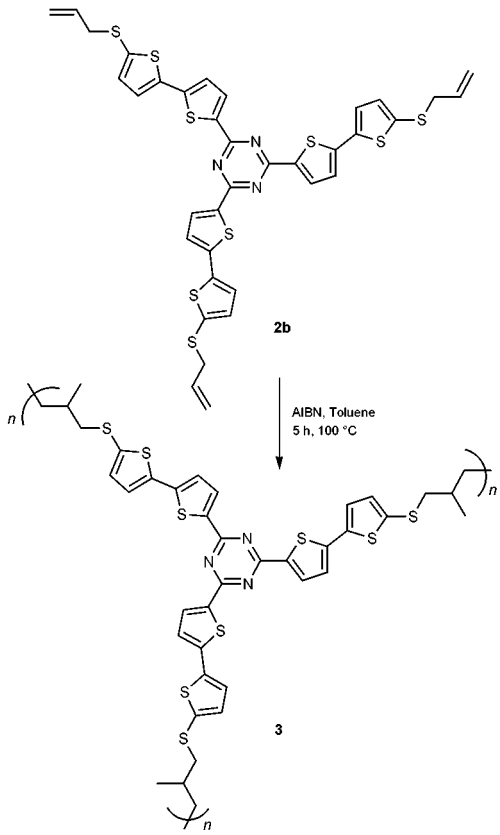

Scheme 2

Stegeman *et al.*[5] defined two figures-of-merit, $W = n_2 I/\alpha\lambda$ and $T = \lambda\beta/n_2$, to assess the suitability of a cubic NLO material for realistic all-optical applications based on the optical Kerr effect. The two criteria, $W >> 1$ or $T << 1$, must be satisfied whether the nonlinearity and the losses in the material are dominated by linear or two-photon absorption, respectively. As no linear (α) or two-photon (β) absorption has been detected in our measurements, we have introduced the limit sensitivities ($\alpha_{min} < 0.05$ m^{-1} and $\beta_{min} < 2 \times 10^{-12}$ m W^{-1}) of our experimental setup. For compounds **2** and **3**, this yields $W > 2200$ and $T < 1$ as an estimation of the lower and upper limits of the figures-of-merit *W* and *T*, respectively. All three materials in solution exhibit very good figures-of-merit. Moreover, the photostability of the polymer in solution has been found to be very satisfactory up to energies per pulse of 120 μJ, *i.e.* intensities up to 18 GW cm^{-2}, corresponding to the damage threshold of the quartz cell.

In conclusion, we have reported the synthesis of the first octupolar polymer and two new octupolar thiophene-based molecules, which exhibit off-resonant third order NLO properties. Due to the absence of detectable linear and nonlinear absorption at 1064 nm, the figures-of-merit are good. Moreover, no modification with respect to the nature of the substituant has been detected on the nonlinear refractive index and on the linear and two-photon absorption properties.

The authors thank Dr A. J. Attias (DMSC, ONERA, France) for his help with the polymer characterisation by SEC.

Notes and references

‡ HRMS analysis of **2a**: $M^{+\cdot} = 837$. **2b**: $M^{+\cdot} = 789$. All NMR data are in agreement with the three proposed structures.

1 D. S. Chemla and J. Zyss, *Nonlinear Optical Properties of Organic Molecules and Crystals*, Academic Press, New York, 1987; H. S. Nalwa and S. Myata, *Nonlinear Optics of Organic Molecules and Polymers*, CRC Press, Boca Raton, 1997.

2 J. Zyss, *Nonlinear Opt.*, 1991, **1**, 3; J. Zyss, *J. Chem. Phys.*, 1993, **98**, 6583; J. Zyss and I. Ledoux, *Chem. Rev.*, 1994, **94**, 77; M. Joffre, D. Yarron, R. Silbey and J. Zyss, *J. Chem. Phys.*, 1992, **97**, 5607; J. Zyss and S. Brasselet, *Opt. Lett.*, 1997, **22**, 1464; S. Brasselet and J. Zyss, *J. Opt. Soc. Am. B*, 1998, **15**, 257.

3 C. Dhenault, I. Ledoux, I. D. W. Samuel, J. Zyss, M. Bourgault and H. LeBozec, *Nature*, 1995, **374**, 339; J. Zyss, S. Brasselet, V. R. Thalladi and G. R. Desiraju, *J. Chem. Phys.*, 1998, **109**, 658; T. Verbiest, K. Clays, C. Samyn, J. Wolff, D. Reinhoudt and A. Persoons, *J. Am. Chem. Soc.*, 1994, **116**, 9320.

4 S. Stadler, R. Dietrich, G. Bourhill and C. Bräuchle, *Opt. Lett.*, 1996, **21**, 251.

5 G. I. Stegeman, in *Nonlinear Optics of Organic Molecules and Polymers*, ed. H. S. Nalwa and S. Myata, CRC Press, Boca Raton, 1997, pp.799–812.

6 D. R. Greve, S. B. Schougaard, T. Geisler, J. C. Petersen and T. Bjornholm, *Adv. Mater.*, 1997, **9**, 1113.

7 A. M. McDonagh, M. G. Humphrey, M. Samoc, B. Luther-Davies, S. Houbrechts, T. Wada, H. Sasabe and A. Persoons, *J. Am. Chem. Soc.*, 1999, **121**, 1405.

8 H. F. Marks, *Encyclopaedia of Polymer Science and Technology*, Wiley, New York, 1964, vol. 1, p. 750.

9 M. G. Hill, J. F. Penneau, B. Zinger, K. R. Mann and L. L. Miller, *Chem. Mater.*, 1992, **4**, 1106.

10 F. Chérioux, L. Guyard and P. Audebert, *Chem. Commun.*, 1998, 2225.

11 F. Chérioux, P. Audebert and P. Hapiot, *Chem. Mater.*, 1998, **10**, 1984.

12 A. Marcano, O. H. Maillotte, D. Gindre and D. Métin, *Opt. Lett.*,1996, **21**, 101; F. E. Hernandez, A. Marcano and O. H. Maillotte, *Opt. Commun.*, 1997, **134**, 529.

13 F. Chérioux, P. Audebert, H. Maillotte, L. Grossard, F. E. Hernandez and A. Lacourt, *Chem. Mater.*, 1997, **9**, 2921.

14 M. Sheik-Bahae, A. A. Said, T. Wei, D. J. Hagan and E. W. Van Stryland, *IEEE J. Quantum Electron.*, 1990, **26**, 760.

15 B. W. Lawrence, M. Cha, J. U. Kang, W. Torruellas, G. Stegeman, G. Baker, J. Meth and S. Etemad, *Electron. Lett.*, 1994, **30**, 5.

Communication 9/05899K

'Sticky' gold colloids through protection–deprotection and their use in complex metal–organic–inorganic architectures†

Marcus Bartz, Nicole Weber, Jörg Küther, Ram Seshadri‡ and Wolfgang Tremel*

Institut für Anorganische und Analytische Chemie, Johannes Gutenberg-Universität Mainz, Duesbergweg 10-14, D-55099 Mainz, Germany. E-mail: tremel.wolfgang@t-online.de

Received (in Oxford, UK) 17th August 1999, Accepted 1st September 1999

Exposing bare gold colloids to long-chain dithiols results in their precipitation owing to cross-linking of the thiol groups with gold surfaces; here, we demonstrate that through the use of a dithiol that has one of the thiol groups protected, we can, through attachment followed by deprotection, prepare gold colloids with exposed thiol; the uses of such 'sticky' colloids in creating complex architectures is demonstrated by using them to template the growth of PbS particles.

The notion that gold colloids in the nanometre range provide surfaces on which thiol self-assembly can be achieved has been employed by us for a variety of new functionalizations. Using suitable thiols, we have, for example, attached polymerization catalysts on colloid surfaces.[1] The use of thiol monolayer surfaces on gold in templating the crystallization of inorganic minerals such as calcium carbonate[2,3] has been extended by us to the use of thiol-coated colloids as crystallization nuclei.[4,5] This has opened a new dimension of surface-templated crystallizations since a dispersed, spherical colloid offers a very different geometry from a large, planar surface.

In coating gold colloids with thiols in solution, there are a few points that need to be examined. The first is that the thiol should protect the colloid and keep it in solution. The second is that the surface functionality of the thiol (the ω group on the long chain) should be compatible with the use to which the colloids are put. For example, in a previous work, we used long chain glycol-based thiols to take colloids into aqueous solution but the surfaces so formed on the colloids inhibit the crystallization of calcium carbonate.[5] We have been interested in coating dithiols on gold colloids since particles so coated would offer an SH functionality on the surface (the ω group) that would be compatible with inorganic sulfides. However, if dithiols are added to a gold colloid sol, immediate precipitation results owing to the cross-linking of the thiols with the colloid surfaces.[6]

The strategy that we present here borrows from peptide chemistry and uses a protection group for the thiol functionality.[7] We have prepared half-protected dithiols **1** with $n = 6$,

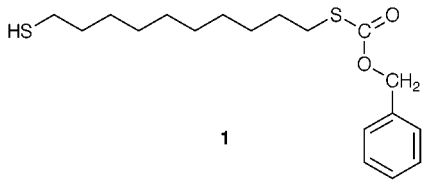

1

10 and 12.§ The self-assembly of these thiols on flat gold surfaces and the possibility to deprotect the ω thiol functionality with aq. NH_3 has been established using surface plasmon resonance spectroscopy (SPS), as has the propensity of the deprotected surface to stick gold colloids. The thiols have been assembled on gold colloids¶ in a toluene solution. The colloids are precipitated by and washed with methanol followed by redissolving them in CH_2Cl_2 where the protecting group is removed with aq. NH_3. These 'sticky' colloids are then dissolved in THF and PbS‖ is deposited around them. The templated growth of PbS particles on SAM surfaces has been studied extensively by Meldrum *et al.*[8]

Fig. 1 displays the SP spectra** of a clean gold surface and the surface after various steps of thiol self-assembly, deprotection, exposure to colloids, *etc.* as explained in the figure caption and associated scheme. These establish the possibility to deprotect the surface as well as to subsequently stick gold colloids on it. Fig. 2 displays SE micrographs of PbS particles grown from THF solutions in the absence (a) and in the presence of dithiol-coated gold colloids (b,c). The thiol group in Fig. 2(b) is still protected so the significant modification in the morphology of the particles and their spherical shape, suggests that the particles are grown around the colloids with unprotected thiol groups in (c). At the present time, we are unable to establish whether it is a single colloidal particle that nucleates the growth of a PbS shell or a cluster of particles. We have determined that it is not the thiol alone that results in the morphologies displayed in (c) (through the inhibition of certain surfaces for example) so the colloid does play a critical role. Attempts to understand the nature of the architecture through the preparation of smaller shells and the use of TE microscopy are under way.

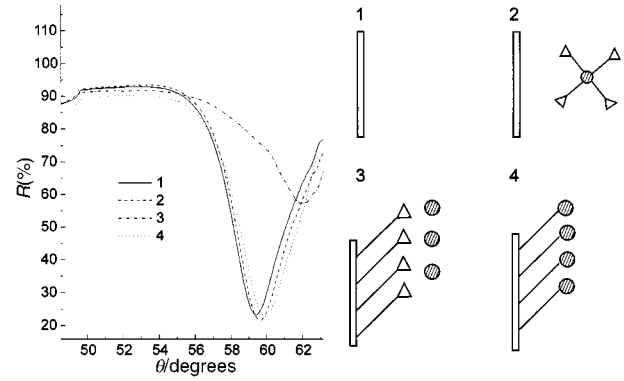

Fig. 1 Surface plasmon spectra of a clean gold surface (1), a clean gold surface exposed to protected gold colloids (2), a gold surface modified with the half protected decanedithiol and exposed to bare gold colloids (3) and a gold surface after deprotection of the dithiol and exposure to bare gold colloids (4). The schemes on the right correspond to the different SP spectra with rods indicating the thiol, spheres the gold colloids, and triangles the protecting groups.

PbS is a semiconductor and the thiol layer is insulating. We recognize links between the structures of MOSFETs (Metal oxide semiconductor based field effect transistors) and of the metal colloid, thiol, PbS architectures presented here. The materials that are the subject of the present work could perhaps be referred to as 'MOSFETs in a test tube'.

We thank Professor W. Knoll (Max-Planck-Institut für Polymerforschung Mainz) for help and encouragement and Dr F. C. Meldrum for preliminary TEM studies. Degussa AG is thanked for a generous gift of chemicals. R. S. would like to acknowledge the RSC for a Journals Grant.

† Dedicated to Professor Felsche on the occasion of his 60th birthday.

‡ Present address: Solid State & Chemistry Unit, Institute of Science, Bangalore 560 012, India.

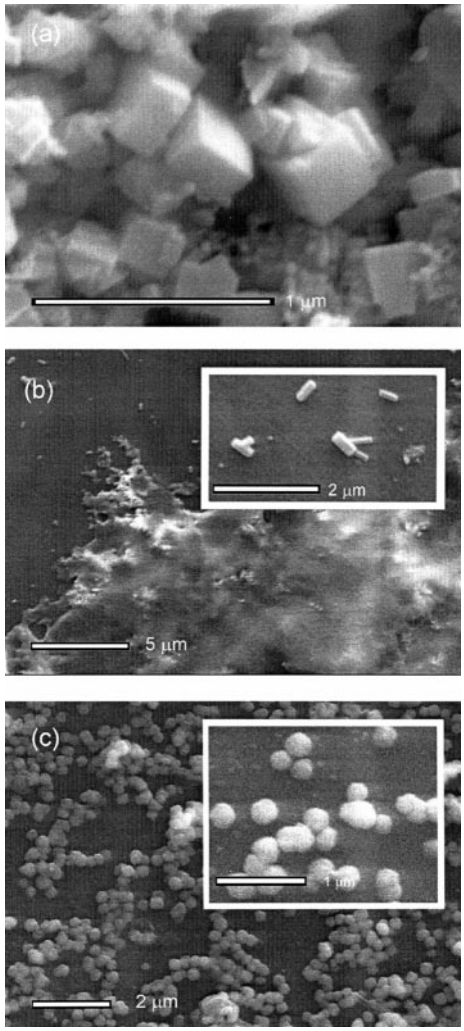

Fig. 2 Scanning electron micrographs of the products obtained after crystallization of PbS. (a) Crystallization in the absence of gold colloids. The crystals so formed correspond to the cubic system of lead sulfide; (b) image of products crystallizing in the presence of protected gold colloids; (c) round particles found after crystallization of PbS in the presence of unprotected gold colloids.

Notes and references

§ The dithols were prepared from 1,*n*-dibromo alkanes using the Bunte Salt method.[1,9] The protection of one of the thiol groups using the benzoyloxocarbonyl group was achieved using a procedure of Scott and Harrison after modification.[10] Briefly, to the dithiol (5 g) in acetone (50 ml) with 2 M NaOH in water (60 ml), benzoyloxycarbonyl chloride (2.8 g) in acetone (20 ml) and 2 M NaOH (40 ml) in water were added simultaneously dropwise, over 30 min while cooling with ice. After stirring overnight at room temp. the acetone was removed and the residue was worked up with diethyl ether. The organic layer was separated and chromatographed on silica to separate **1** from the unprotected and diprotected compounds.

¶ Gold colloids were prepared in toluene following the method of Brust *et al.*[11] Deprotection could be carried out with aq. NH_3 (40 ml) in CH_2Cl_2 (40 ml), stirring overnight. The deprotected colloids in the organic layer were collected after removing the solvent and dissolved in THF for the crystallization experiments.

‖ Crystallization of PbS was carried out using an aqueous solution (3 mmol) of $PbNO_3$ (3 ml) in THF (100 ml) and deprotected gold colloids (0.1 g) were added. After glass slides were placed at the bottom of the vessel it was exposed to an H_2S-atmosphere in a desiccator for 24 h. The solvent was removed and the glass slides were dried at room temperature. The material collected on the slides were studied by X-ray diffraction (Siemens D5000, transmission, Cu-Kα_1 radiation) to confirm the NaCl structure of PbS and by SE microscopy (Zeiss DSM 962).

** SPS measurements were performed in the Kretschmann configuration.[12] Optical coupling was achieved with a LASFN9 prism (n = 1.85 at λ = 632.8 nm) and index matching fluid (n = 1.70) between the prism and the BK270 glass slides. The plasmon was excited with p-polarized radiation using a He–Ne laser (632.8 nm, 5 mW). The glass slides were cleaned with aq. NH_3–H_2O_2–water (1:1:7) for 10 min at 80 °C and coated with gold using a Balzers BAE250 vacuum coating unit under a pressure of $< 5 \times 10^{-6}$ hPa, typically depositing 48 nm of gold after first depositing 2 nm of Cr. The slides were exposed to the organic thiol solution (10 mmol) for 24 h.

1 M. Bartz, J. Küther, R. Seshadri and W. Tremel, *Angew. Chem.*, 1998, **110**, 2646; *Angew. Chem., Int. Ed.*, 1998, **37**, 2466.
2 J. Küther, R. Sheshadri, W. Knoll and W. Tremel, *J. Mater. Chem.*, 1998, **8**, 641.
3 J. Küther, G. Nelles, R. Seshadri, M. Schaub, H.-J. Butt and W. Tremel, *Chem. Eur. J.*, 1998, **4**, 1834.
4 J. Küther, R. Seshadri and W. Tremel, *Angew. Chem.*, 1998, **110**, 3196; *Angew. Chem., Int. Ed.*, 1998, **37**, 3044; J. Küther, R. Seshadri, G. Nelles, W. Assenmancher, H.-J. Butt, W. Mader and W. Tremel, *Chem. Mater.*, 1999, **11**, 1317.
5 M. Bartz, J. Küther, G. Nelles, N. Weber, R. Seshadri and W. Tremel, *J. Mater. Chem.*, 1999, **9**, 1121.
6 M. Brust, D. Bethell, D. J. Schiffrin and C. J. Kiely, *Adv. Mater.*, 1995, **7**, 795.
7 T. W. Greene, *Protective Groups in Organic Synthesis*, John Wiley & Sons, New York, 1981.
8 F. C. Meldrum, J. Flath and W. Knoll, *Langmuir*, 1997, **13**, 2033; F. C. Meldrum, J. Flath and W. Knoll, *J. Mater. Chem.*, 1999, **10**, 711.
9 H. Distler, *Angew. Chem.*, 1967, **11**, 520; H. Wolf, PhD Thesis, Universität Mainz, 1995.
10 P. W. Scott and I. T. Harrison, *J. Org. Chem.*, 1981, **46**, 1914.
11 M. Brust, M. Walker, D. Bethell, J. Schiffrin and R. Whyman, *J. Chem. Soc., Chem. Commun.*, 1994, 801.
12 E. Kretschmann, *Z. Phys*, 1971, **241**, 313.

Communication 9/06715I

Hyperbranched chiral catalysts for the asymmetric reduction of ketones with borane

Carsten Bolm,* Nadine Derrien and Andreas Seger

Institut für Organische Chemie, RWTH Aachen, Professor-Pirlet-Strasse 1, D-52074 Aachen, Germany. E-mail: carsten.bolm@oc.rwth-aachen.de

Received (in Liverpool, UK) 28th July 1999, Accepted 6th September 1999

Optically active dendritic amino alcohols catalyse the enantioselective borane reduction of ketones with good yields and high enantiomeric excesses.

Dendrimers represent a new class of polymeric compounds which are distinguished from traditional polymers by their unusual fractal-like architecture.[1] Due to their unique characteristic features they appear attractive for applications in the fields of biology and materials sciences as well as for use in homogeneous catalysis.[2,3] For enantioselective catalysis chiral dendrimers[4] are required; as yet, however, very few dendritic chiral catalysts have been described.[5–11] In a recent study we reported on the synthesis of chiral dendrimer-bound pyridyl alcohols and their application in the asymmetric addition of diethylzinc to benzaldehyde.[11] Various generations of these hyperbranched chiral catalysts (hccs) were tested, and gratifyingly, no significant loss of catalyst activity and enantioselectivity was observed, when compared to catalysis with the parent pyridyl alcohol. Thus, even in reactions with higher hcc generations the resulting secondary alcohols were obtained in satisfying yields, having ees of up to 86%. Considering possible applications of dendritic chiral catalysts in continuously operated membrane reactors,[3e,12] we also envisioned other strategies for the synthesis of optically active alcohols. Here, we report the first use of dendritic catalysts for the enantioselective borane reduction of prochiral ketones leading to the desired products with up to 96% ee.

Readily available building block (*S*)-**1** was chosen as a chiral unit, since high catalytic efficiency and convenient applicability of various compounds containing **1** had been elegantly demonstrated by Itsuno *et al.*[13,14] In addition, results of catalyses with polymer-supported **1** under homogeneous[12a] and heterogeneous[14] conditions could serve as reference points. Chiral dendrimers (*S*)-**2** to (*S*)-**5** were synthesised in good yields by the convergent-growth approach introduced by Hawker and Fréchet[15] using (*S*)-2-amino-3-(*p*-hydroxyphenyl)-1,1-diphenylpropan-1-ol (**1b**) and appropriate polyether wedges derived from 3,5-dihydroxybenzyl alcohol or 4,4-bis(4′-hydroxyphenyl)pentanol, respectively.[16]

The asymmetric borane reductions[17] were studied under the following conditions: 10 mol% of dendritic amino alcohol (*S*)-**2** to (*S*)-**5**, BH_3•SMe_2 as reductant, THF as solvent, at room temperature. Various prochiral substrates were used, and the results are summarised in Table 1.

In general, excellent ketone conversion was achieved, and the corresponding optically active alcohols were obtained in good yields (> 75%). The enantioselectivities were high (81–96% ee), and reductions of alkyl aryl ketones led to the predominant formation of the (*R*)-configured products. Compared to the parent systems containing **1**, all hccs performed well. For example, even with stoichiometric amounts of **1a** only 87% ee had been achieved in the reduction of acetophenone.[13] Here, with 10 mol% of catalyst (*S*)-**4**, (*R*)-1-phenylethanol was obtained with 91% ee. Among all hccs evaluated in this reaction (Table 1, entries 1–4), (*S*)-**4** was the best catalyst in terms of yield and ee. Presumably, the higher rigidity of the dendritic backbone in **2** and **3** and the increased steric crowding in the

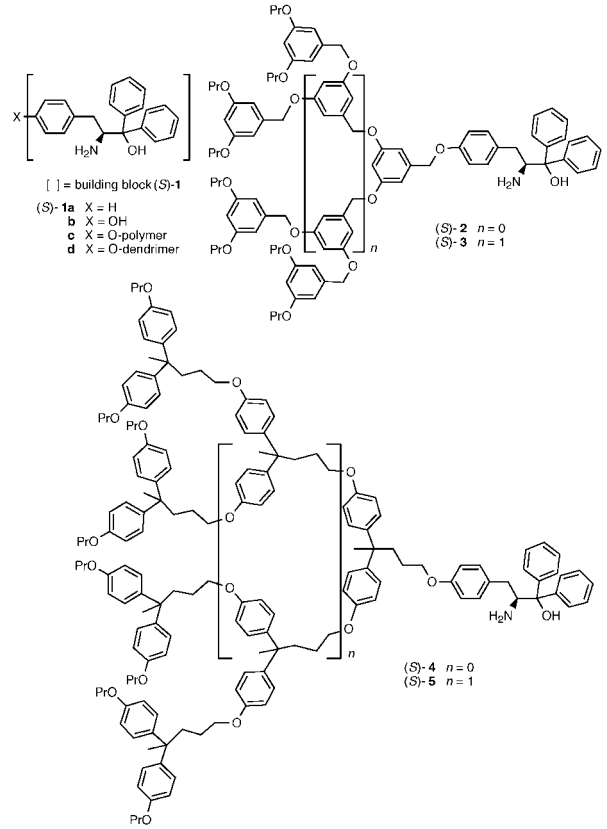

Table 1 Enantioselective borane reduction of various ketones using hccs **2–5**

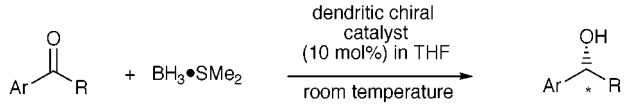

Entry	Ketone	Dendritic amino alcohol	Yield (%)[a]	Alcohol ee (%)[b]	Abs. config.[c]
1	PhC(O)Me	**2**	80	89	(*R*)
2	PhC(O)Me	**3**	78	88	(*R*)
3	PhC(O)Me	**4**	80	91	(*R*)
4	PhC(O)Me	**5**	79	89	(*R*)
5	PhC(O)Et	**2**	82	84	(*R*)
6	PhC(O)Et	**3**	80	82	(*R*)
7	Tetralone	**4**	80	86	(*R*)
8	Tetralone	**5**	78	81	(*R*)
9	$PhC(O)CH_2OTBDPS$	**4**	76	91	(*S*)
10	$PhC(O)CH_2OTBDPS$	**5**	75	91	(*S*)
11	$PhC(O)CH_2Cl$	**4**	82	96	(*S*)
12	$PhC(O)CH_2Cl$	**5**	80	94	(*S*)

[a] After column chromatography. [b] Determined by HPLC using a chiral stationary phase. [c] Determined by comparison of optical rotations with literature values.

higher-generation catalyst **5** led to product formation with slightly reduced enantioselectivity.

The highest ee values were found in reductions of α-chloroacetophenone giving the corresponding alcohol with up to 96% ee (Table 1, entries 11 and 12). These results are particularly important because α-(chloromethyl)benzyl alcohol is a valuable precursor for the synthesis of phenyloxirane.[18]

The potential of these new dendritic catalysts which operate homogeneously is also highlighted by the fact that under heterogeneous conditions with polymeric **1c** significantly lower enantioselectivities were achieved (*cf.* acetophenone: 76% ee; propiophenone: 79% ee; α-chloroacetophenone: 84% ee).[14,19]

In summary, we have demonstrated the feasibility of performing highly enantioselective borane reductions of prochiral ketones using dendritic catalysts (hccs), and we are currently investigating their possible applications in continuously operating reactor systems.[20,21]

We are grateful to the Bundesministerium für Forschung und Technologie (BMFT) and the Fonds der Chemischen Industrie for financial support of this work. We thank the Degussa-Hüls for the generous donation of chemicals.

Notes and references

1 For a selection of general reviews, see: H.-F. Chow, T. K.-K. Mong, M. F. Nongrum and C.-W. Wan, *Tetrahedron*, 1998, **54**, 8543; G. R. Newkome, C. N. Moorefield and F. Vögtle, *Dendritic Molecules: Concepts, Syntheses, Perspectives*, VCH, Weinheim, 1996; D. A. Tomalia, A. M. Naylor and W. A. Goddard III, *Angew. Chem.*, 1990, **102**, 119; *Angew. Chem., Int. Ed. Engl.*, 1990, **29**, 138; D. A. Tomalia and H. D. Durst, *Top. Curr. Chem.*, 1993, **165**, 193; J. Issberner, R. Moors and F. Vögtle, *Angew. Chem.*, 1994, **106**, 2507; *Angew. Chem., Int. Ed. Engl.*, 1994, **33**, 2413; V. Balzani, S. Campagna, G. Denti, A. Juris, S. Serroni and M. Venturi, *Acc. Chem. Res.*, 1998, **31**, 26; N. Ardoin and D. Astruc, *Bull. Soc. Chim. Fr.*, 1995, **132**, 875; F. Zeng and S. C. Zimmerman, *Chem. Rev*., 1997, **97**, 1681; 'Dendrimers', *Top. Curr. Chem.*, 1998, **197**; M. Fischer und F. Vögtle, *Angew. Chem*., 1999, **111**, 935; *Angew. Chem., Int. Ed*., 1999, **38**, 884 and refs. therein.

2 J. W. J. Knapen, A. W. van der Made, J. C. de Wilde, P. W. N. M. van Leeuwen, P. Wijkens, D. M. Grove and G. van Koten, *Nature*, 1994, **372**, 659.

3 For later examples of *achiral* dendritic catalysts, see: (*a*) C. C. Mak and H.-F. Chow, *Macromolecules*, 1997, **30**, 1228; (*b*) H.-F. Chow and C. C. Mak, *J. Org. Chem*., 1997, **62**, 5116; (*c*) M. T. Reetz, G. Lohmer and R. Schwickardi, *Angew. Chem*., 1997, **109**, 1559; *Angew. Chem., Int. Ed. Engl*., 1997, **36**, 1526; (*d*) I. Morao and F. P. Cossío, *Tetrahedron Lett*., 1997, **38**, 6461; (*e*) N. J. Hovestad, E. B. Eggeling, H. J. Heidbüschel, J. T. B. H. Jastrzebski, U. Kragl, W. Keim, D. Vogt and G. van Koten, *Angew. Chem*., 1999, **111**, 1559; *Angew. Chem., Int. Ed.*, 1999, **38**, 1655.

4 For a review on chirality in dendritic architectures, see: H. W. I. Peerlings and E. W. Meijer, *Chem. Eur. J.*, 1997, **3**, 1563.

5 H. Brunner, *J. Organomet. Chem*., 1995, **500**, 39; H. Brunner and S. Altmann, *Chem. Ber*., 1994, **127**, 2285; H. Brunner and J. Fürst, *Tetrahedron*, 1994, **50**, 4303; H. Brunner and G. Net, *Synthesis*, 1995, 423.

6 M. S. T. H. Sanders-Hovens, J. F. G. A. Jansen, J. A. J. M. Vekemans and E. W. Meijer, *Polym. Mater. Sci. Eng*., 1995, **73**, 338.

7 D. Seebach, R. E. Marti and T. Hintermann, *Helv. Chim. Acta*, 1996, **79**, 1710; P. B. Rheiner, H. Sellner and D. Seebach, *Helv. Chim Acta*, 1997, **80**, 2027; P. B. Rheiner and D. Seebach, *Polym. Mater. Sci. Eng*., 1997, **77**, 130.

8 T. Suzuki, Y. Hirokawa, K. Ohtake, T. Shibata and K. Soai, *Tetrahedron: Asymmetry*, 1997, **8**, 4033.

9 S. Yamago, M. Furukawa, A. Azuma and J.-I. Yoshida, *Tetrahedron Lett*., 1998, **39**, 3783.

10 C. Köllner, B. Pugin and A. Togni, *J. Am. Chem. Soc*., 1998, **120**, 10 274.

11 C. Bolm, N. Derrien and A. Seger, *Synlett*, 1996, 387.

12 (*a*) G. Giffels, J. Beliczey, M. Felder and U. Kragl, *Tetrahedron: Asymmetry*, 1998, **9**, 691; (*b*) J. Beliczey, G. Giffels, U. Kragl and C. Wandrey, *Tetrahedron: Asymmetry*, 1997, **8**, 1529; (*c*) M. Felder, G. Giffels and C. Wandrey, *Tetrahedron: Asymmetry* 1997, **8**, 1975; (*d*) U. Kragl and C. Dreisbach, *Angew. Chem*., 1996, **108**, 684; *Angew. Chem., Int. Ed. Engl.*, 1996, **35**, 642; (*e*) U. Kragl, C. Dreisbach and C. Wandrey, *Applied Homogeneous Catalysis with Organometallic Compounds*, ed. B. Cornils and W. A. Herrmann, VCH, Weinheim, 1996, p. 832.

13 S. Itsuno, M. Nakano, K. Miyazaki, H. Masuda, K. Ito, A. Hirao and S. Nakahama, *J. Chem. Soc., Perkin Trans. 1*, 1985, 2039.

14 S. Itsuno, M. Nakano, K. Ito, A. Hirao, M. Owa, N. Kanda and S. Nakahama, *J. Chem. Soc., Perkin Trans. 1*, 1985, 2615; S. Itsuno, K. Ito, T. Maruyama, N. Kanda, A. Hirao and S. Nakahama, *Bull. Chem. Soc. Jpn.*, 1986, **59**, 3329; S. Itsuno, Y. Sakurai, K. Ito, A. Hirao and S. Nakahama, *Polymer*, 1987, **28**, 1005; S. Itsuno, Y. Sakurai, K. Ito, T. Maruyama, S. Nakahama and J. M. J. Fréchet, *J. Org. Chem*., 1990, **55**, 304.

15 C. J. Hawker and J. M. J. Fréchet, *J. Am. Chem. Soc*., 1990, **112**, 7638; C. Hawker and J. M. J. Fréchet, *J. Chem. Soc., Chem. Commun*., 1990, 1010.

16 Details of the syntheses will be published elsewhere. See also: N. Derrien, dissertation, RWTH Aachen 1998.

17 Reviews: E. J. Corey and C. J. Helal, *Angew. Chem.*, 1998, **110**, 2092; *Angew. Chem. Int. Ed.*, 1998, **37**, 1986; S. Wallbaum and J. Martens, *Tetrahedron: Asymmetry*, 1992, **3**, 1475; V. K. Singh, *Synthesis*, 1992, 605.

18 E. J. Corey, S. Shibata and R. K. Bakshi, *J. Org. Chem*., 1988, **53**, 2861.

19 Soluble polymers containing **1** give comparable results; see ref. 12(*a*).

20 C. Bolm, *Selective Reactions of Metal-Activated Molecules*, ed. H. Werner and P. Schreier, Vieweg, Braunschweig, 1998, p. 5.

21 For a recent study on the use of dendritic palladium catalysts in a membrane reactor, see N. Brinkmann, D. Giebel, G. Lohmer, M. T. Reetz and U. Kragl, *J. Catal.*, 1999, **183**, 163.

Communication 9/06258K

ChemComm

Use of photoinduced energy-transfer to probe solvent-dependent conformational changes in a flexible Ru/Os dinuclear complex

Nicholas C. Fletcher,[a] Michael D. Ward,*[a] Susana Encinas,*[b] Nicola Armaroli,[b] Lucia Flamigni[b] and Francesco Barigelletti*[b]

[a] *School of Chemistry, University of Bristol, Cantock's Close, Bristol, UK BS8 1TS. E-mail: mike.ward@bristol.ac.uk*
[b] *Istituto FRAE–CNR, Via P. Gobetti 101, 40129 Bologna, Italy. E-mail: franz@frae.bo.cnr.it*

Received (in Basel, Switzerland) 18th August 1999, Accepted 13th September 1999

Solvent-dependent conformational changes of a poly(oxoethylene) bridge linking $[Ru(bipy)_3]^{2+}$ and $[Os(bipy)_3]^{2+}$ units can be probed by measuring the extent of Ru→Os photoinduced energy transfer.

Photoinduced energy-transfer between Ru(II) and Os(II) polypyridine units across nanometric bridging ligands has been extensively studied recently,[1–5] largely because of the relevance of such complexes to potential applications such as light energy collection and conversion[5] and luminescence-based sensors and switches.[6–8] In such complexes the bridging ligand is of fundamental importance. It can be either geometrically rigid or flexible, so that the distance between the photoactive partners may be fixed or may vary; and it may contain electronically conducting or insulating units. In some cases, some units of the bridge can also interact with the environment, so that modulation or switching of the Ru→EOs energy transfer process can be observed.[2]

We describe here a Ru(II)/Os(II) dyad in which the two metal components are separated by a flexible poly(oxoethylene) chain derived from penta(ethylene glycol).† In these complexes the

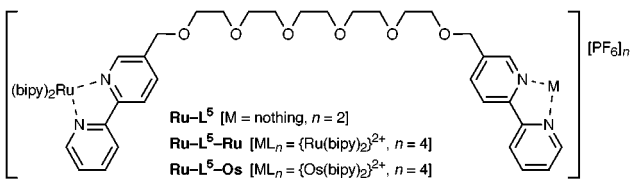

conformation of the poly(oxoethylene) chain is expected to be solvent dependent, based on the known properties of poly(ethylene glycol)[9] and various simple model compounds,[10] and this in turn is expected to lead to controllable variation of the metal–metal separation, d_{MM}. In this study, by using steady-state and time-resolved luminescence measurements, we show that for **Ru-L^5-Os** the Ru→Os energy transfer can indeed be influenced by the solvent and we ascribe this effect to differences in the conformation of the poly(oxoethylene) chain.[11]‡

Table 1 lists some spectroscopic and photophysical properties for the mononuclear model complex **Ru-L^5**, and the heterodinuclear complex **Ru-L^5-Os**, as obtained in neat MeOH (protic) and CH_2Cl_2 (aprotic) solvents. Fig. 1 compares the luminescence spectra obtained by exciting samples of **Ru-L^5-Os** in mixed MeOH–CH_2Cl_2 solvent of varying proportions. The excitation wavelength was 450 nm so that both the Ru and Os-based chromophores were excited, approximately in a 1:0.8 ratio, (Table 1). The luminescence spectra of **Ru-L^5-Os** (Fig. 1) feature two band maxima, occurring in the ranges 600–606 and 710–715 nm. The relative intensities of these are consistent with the occurrence of partial quenching (*ca.* 90%) of the Ru unit, owing to Ru→Os energy transfer (ΔG *ca.* −0.3 eV). Thus, the band at *ca.* 600 nm is due to a residual Ru-based emission, and the band at *ca.* 710 nm is Os-based, with a luminescence intensity which includes contributions from both direct excitation and Ru→Os sensitisation. It will be seen that as the solvent polarity decreases (from MeOH to CH_2Cl_2), the Ru-based emission relatively decreases in intensity with respect to the Os-based emission, consistent with improved Ru→Os energy transfer arising from a shorter metal–metal separation.

This was confirmed by analysis of the time-resolved luminescence decay of **Ru-L^5-Os**, which was measured in the same mixed-solvent system at the wavelengths of the two emission band maxima. At 600 nm a single (Ru-based) exponential decay was found; at 710 nm the Os-based decay took place according to a dual exponential law, with a rise time and a decay time. We found that in each case the Ru-based decay time (obtained at 600 nm) corresponds to the Os-based rise time (observed at 710 nm), consistent with the occurrence of Ru→Os energy transfer. Also, on the basis of $k_{en} = 1/\tau_q - 1/\tau$ we can obtain the Ru→Os energy transfer rate constant as a function of solvent composition (τ is the lifetime of the reference complex, **Ru-L^5**). The results are shown graphically

Table 1 Spectroscopic and photophysical data[a]

	Absorption		Emission[b]		
	λ_{max}/nm (10^{-3} ε/dm^3 mol^{-1} cm^{-1})		λ_{max}/nm	10^2 Φ	τ/ns
MeOH					
Ru-L^5	287 (90.0)	450 (13.4)	604	1.6	240
Ru-L^5-Ru	287 (147)	450 (27.6)	606	1.5	210
Ru-L^5-Os	289 (145)	450 (24.6)	606,[c] 715[d]		18.8,[c] 32[d]
CH_2Cl_2					
Ru-L^5	287 (97.0)	453 (14.4)	598	3.3	410
Ru-L^5-Ru	288 (145)	452 (27.6)	600	3.5	405
Ru-L^5-Os	289 (150)	452 (26.6)	600,[c] 710[d]		5.8,[c] 65[d]

[a] Room temperature, in the indicated air-equilibrated solvents. Sample concentrations were 2×10^{-5} M. [b] Excitation wavelength 450 nm. The emission maxima (±2 nm) are from uncorrected spectra. Quantum yield values (±20%) are from corrected spectra. Lifetimes are accurate to ±8%. [c] Ru-based luminescence. [d] Os-based luminescence.

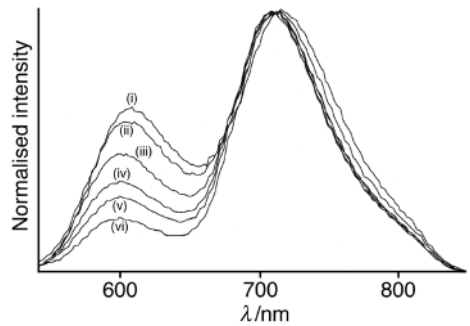

Fig. 1 Normalised luminescence spectra of **Ru-L^5-Os** in mixed MeOH–CH_2Cl_2 solvents (spectroscopic grade) of proportions (MeOH–CH_2Cl_2): (i) 100:0; (ii) 80:20; (iii) 60:40, (iv) 40:60; (v) 20:80; (vi) 0:100. The solutions were isoabsorptive at the excitation wavelength (450 nm) and the spectra are normalised to the Os-based emission.

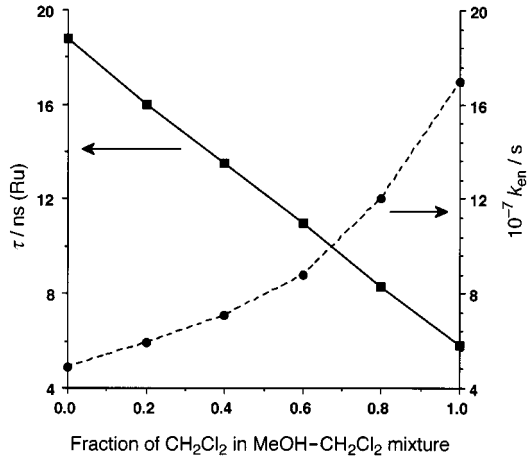

Fig. 2 Photophysical behaviour of **Ru-L^5-Os** in mixed MeOH–CH_2Cl_2 solvents, showing the steady decrease of Ru-based emission lifetime (squares, solid line) and the concomitant increase in Ru→EOs energy-transfer rate constant (circles, dashed line) as solvent polarity decreases.

in Fig. 2. It is clear that improved quenching of the Ru emission as the solvent polarity decreases is accompanied by improved Ru→Os energy transfer. The extent of quenching for the Ru-based emission in **Ru-L^5-Os** is therefore solvent dependent, being maximised in neat CH_2Cl_2. As a control experiment, a 1:1 mixture of **Ru-L^5** and $[Os(bipy)_3]^{2+}$ (each 2×10^{-5} M) resulted in no detectable quenching of the Ru-based luminescence, confirming that intermolecular effects are not significant, as would be expected at these low concentrations.

Two possible mechanisms, exchange and dipole–dipole, can be invoked to account for Ru→EOs energy transfer.[12] It is well documented that through-bond, two-electron exchange is likely to be involved for cases where the bridging ligand is highly unsaturated,[1,2,4] because the energetically accessible HOMO and LUMO orbitals of the bridge provide a pathway linking the appropriate metal orbitals.[13] In contrast, saturated units behave like insulators towards electronic communication because the HOMO–LUMO energy separation is large. EHMO calculations on the poly(oxoethylene) chain [taken as $Me(OCH_2CH_2)_5OMe$] indicate that its HOMO–LUMO energy gap (32 eV) is comparable to that of the corresponding hydrocarbon chain [taken as $Me(CH_2)_{16}Me$] (41 eV),[14] so the amount of the intermetal electronic communication mediated by the bridging ligand L^5 is expected to be negligible. On this basis, we ascribe the occurrence of energy transfer in **Ru-L^5-Os** to the dipole–dipole (Förster) mechanism, [eqn. (1)].[12]

$$k_{en}^{F} = \frac{8.8\times10^{-25}K^2\Phi}{d_{MM}{}^6 n^4 \tau} J^F \qquad (1)$$

where Φ and τ are the luminescence quantum yield and lifetime, respectively, of the energy donor (**Ru-L^5**); J^F is the integral overlap between the luminescence spectrum of the donor (Ru chromophore) and the absorption spectrum of the acceptor (Os chromophore), K^2 is a geometric factor (taken as 2/3), and n is the refractive index of the solvent. From eqn. (1) and by using the pertinent spectroscopic (Table 1) and calculated parameters ($J^F = 4.7 \times 10^{-14}$ cm^6 mol^{-1} in both solvents), we conclude that $d_{MM} = 15$ and 12 Å in neat MeOH and CH_2Cl_2, respectively. These values may be compared with the calculated[14] end-to-end distance of 22 Å for the fully extended ligand L^5.

This solvent-dependence of the bridging ligand conformation is exactly consistent with the known behaviour of both poly(ethylene glycol)[9] and simple model compounds such as dimethoxyethane.[10] In these molecules the conformation about the central C–C bond of the OCH_2CH_2O unit is predominantly *trans* in a low-polarity medium, but predominantly *gauche* in a high-polarity medium. The *gauche* conformation, which results in a higher dipole moment for the poly(oxoethylene)chain, is also associated with a more expanded structure for the chain—in exact agreement with our observations.

In conclusion, with **Ru-L^5-Os** we have used Ru→EOs energy transfer as a diagnostic tool for probing solvent-specific conformational properties of a flexible bridging ligand. This is an appealing way of providing quantitative information on the conformations of soluble polymers, an area of considerable importance.[9] Work is also in progress to probe the use of metal cations to control the conformation of the bridging ligand and hence the metal–metal interaction.[15]

We thank the European Community for a post-doctoral fellowship (S.E., contract no. 980226) and for a COST award (COST-D11-0004/98), and the EPSRC (UK) for a post-doctoral fellowship (N.C.F.).

Notes and references

† *Preparations*: L^5: penta(ethylene glycol) (0.310 g, 1.26 mmol) in dry THF (100 ml) was treated with NaH (60% dispersion in mineral oil; 0.40 g, 10.0 mmol) and stirred at room temp. for 40 min. When effervescence ceased, 5-bromomethyl-2,2′-bipyridine (1.30 g, 5.20 mmol) was added, and the mixture was refluxed for 24 h. After removal of the solvent the brown residue was chromatographed on silica, eluting with 10% methanol in CH_2Cl_2, to give the product (the second major fraction off the column) as a clear oil after removal of the solvent. Yield 0.704 g, 97%.

$[Ru(bipy)_2(L^5)][PF_6]_2$ **Ru-L^5**: reaction of L^5 (327 mg, 57 μmol) and $[Ru(bpy)_2Cl_2]\cdot 2H_2O$ (240 mg, 0.46 mmol) in EtOH at reflux for 3 h afforded an orange–red solution. Chromatography on Sephadex-SP25, eluting with 0.3 M aqueous NaCl, afforded a red band from which **Ru-L^5** precipitated on addition of NH_4PF_6: yield, 0.262 g (35%). Also isolated was the dinuclear complex $[\{Ru(bipy)_2\}_2(L^5)][PF_6]_4$ **Ru-L^5-Ru** (eluted with 0.5 M aqueous NaCl); yield, 0.088 g (9%).

$[(bipy)_2Ru(L^5)Os(bipy)_2][PF_6]_4$ **Ru-L^5-Os**: A mixture of **Ru-L^5** (74.6 mg, 0.58 mmol) and $[Os(bpy)_2Cl_2]$ (60 mg, 98 μmol) were heated together at 120 °C for 24 h in ethylene glycol (10 ml). The reaction mixture was cooled, added to water (100 ml) and introduced onto Sephadex SP25, and the primary green band eluted with 0.55 M aqueous sodium chloride solution. The product was precipitated with NH_4PF_6 and collected on Celite. The nearly pure compound was further purified by chromatography on Sephadex-LH20 eluting with acetone–methanol (1:1) to give pure **Ru-L^5-Os**: yield; 84.3 mg (70%). Satisfactory ^{1}H NMR and mass spectroscopic data, and elemental analyses, have been obtained for all new compounds.

‡ The solvent-dependent conformation of a polypeptide chain has been exploited to modulate photoinduced electron-transfer between covalently linked $[Ru(bipy)_3]^{2+}$ (donor) and fullerene (acceptor) units: see ref. 11.

1 V. Balzani, A. Juris, M. Venturi, S. Campagna and S. Serroni, *Chem. Rev.*, 1996, **96**, 759 and references therein.
2 A. Harriman and R. Ziessel, *Chem.Commun.*, 1996, 1707; L. De Cola and P. Belser, *Coord. Chem. Rev.*, 1998, **177**, 301 and references therein.
3 N. Armaroli, F. Barigelletti, G. Calogero, L. Flamigni, C. M. White and M. D. Ward, *Chem. Commun.*, 1997, 2181.
4 F. Barigelletti, L. Flamigni, J.-P. Collin and J.-P. Sauvage, *Chem. Commun.*, 1997, 333.
5 C. A. Bignozzi, J. N. Schoonover and F. Scandola, *Prog. Inorg. Chem.*, 1997, **44**, 1.
6 *Transition Metals in Supramolecular Chemistry*, eds. L. Fabbrizzi and A. Poggi, Kluwer, Dordrecht, 1994.
7 A. P. de Silva, H. Q. N. Gunaratne, T. Gunnlaugsson, A. J. M. Huxley, C. P. McCoy, J. Rademacher and T. E. Rice, *Chem. Rev.*, 1997, **97**, 1515.
8 R. E. Holmlin, R. T. Tong and J. K. Barton, *J. Am. Chem. Soc.*,1998, **120**, 9724.
9 M. Björling, G. Karlström and P. Linse, *J. Phys. Chem.*, 1991, **95**, 6706 and references therein.
10 M. Andersson and G. Karlström, *J. Phys. Chem.*, 1985, **89**, 4957.
11 A. Polese, S. Mondini, A. Bianco, C. Toniolo, G. Scorrano, D. M. Guldi and M. Maggini, *J. Am. Chem. Soc.*, 1999, **121**, 3446.
12 Th. Förster, *Discuss. Faraday Soc.*, 1959, **27**, 7; D. L. Dexter, *J. Chem. Phys.*, 1953, **21**, 836.
13 W. B. Davies, W. A. Svec, M. A. Ratner and M. R. Wasielewski, *Nature*, 1998, **396**, 60.
14 Molecular modelling was performed using the AM1 and EHMO programs from the CS ChemDraw 4.0 package.
15 D. Monti, M. Venanzi, G. Mancini, F. Marotti, L. La Monica and T. Boschi, *Eur. J. Org. Chem.*, 1999, 1901.

Communication 9/06737J

Synthesis and structure of η^5-bonded pyrrolyl complexes of calcium and strontium

Herbert Schumann,* Jochen Gottfriedsen and Jörg Demtschuk

Institut für Anorganische und Analytische Chemie der Technischen Universität Berlin, Straße des 17. Juni 135, D-10623 Berlin, Germany. E-mail: schumann@chem.tu-berlin.de

Calcium and strontium diiodide react with 2,5-di-*tert*-butylpyrrolylsodium in THF yielding [M(pyr*)$_2$(THF)] (M = Ca, Sr; pyr* = NC$_4$H$_2$Bu$^t_2$-2,5) for which NMR spectra and the X-ray structures confirm the η^5-bonding character of the ligands.

2,5-Di-*tert*-butylpyrrolyl (pyr*) complexes of some main group elements (Pb, Sn), transition metals (Ti, Fe, Co), and lanthanides (Nd, Sm, Tm, Yb, Lu) are already known.[1,2] In all these complexes, the pyr* ligand coordinates to the metal atom in an η^5-π-bonding fashion. The two bulky *tert*-butyl substituents at the 2,5-carbon atoms of the pyr* ring prevent a σ-donor coordination of the pyrrolyl nitrogen atom to the corresponding metal. Another coordination mode of the pyr* ligand was established for a binuclear zinc complex in which a pyr* ligand is bridging the two metal centers by forming a σ-N donor bond to one zinc atom and coordinating the other zinc atom by the 3,4-carbon atoms of the pyr* ring in an η^2-fashion.[3] Whereas a series of homoleptic alkyl-substituted cyclopentadienyl complexes of alkaline earth metals have been synthesized in recent years,[4] corresponding pyrrolyl (synonymous with azacyclopentadienyl) complexes of these metals have not been described until now. For this reason, we started to examine the coordination behaviour of pyr* towards alkaline earth metals and report here, the results we obtained for calcium and strontium.

The reaction of 2,5-di-*tert*-butylpyrrolylsodium with calcium diiodide or strontium diiodide (2:1 mole ratio, Scheme 1) in THF at room temperature afforded the mono-THF adducts of bis(2,5-di-*tert*-butylpyrrolyl)calcium and bis(2,5-di-*tert*-butylpyrrolyl)strontium [M(pyr*)$_2$(THF)] [M = Ca (**1**), Sr (**2**)], which were isolated in yields of 50% by crystallization from *n*-hexane at −20 °C. The colorless crystals of **1** melt at 113 °C, whereas those of **2** decompose at 200 °C, but sublime at 179 °C/0.5 mbar without decomposition. Both compounds are soluble in polar and non-polar solvents such as THF, diethyl ether, toluene, benzene, or *n*-hexane.

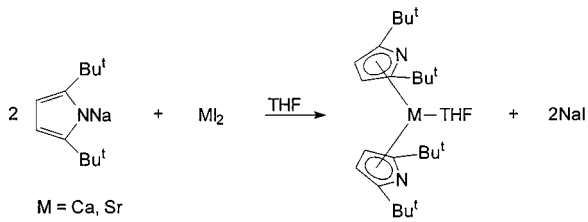

Scheme 1 Synthesis of the pyrrolyl complexes

In the NMR spectra of **1** and **2**, recorded in benzene-d$_6$, the ^{1}H/^{13}C resonances of the 3,4-CH groups of the pyr* ring show shifts of δ 6.34/105.2 for **1** and δ 6.30/104.5 for **2**. Since in the solution spectra of [Li(pyr*)(THF)$_2$][3] (the solid state structure establishes Li–N$_{pyr*}$ σ-bonds) and [Na(pyr*)][2b] (no solid state structure determined) the corresponding signals appear at δ 5.61/96.8 and δ 5.59/100.13, respectively, the low field shifts of the CH resonances of **1** and **2** are indicative of π-bonded pyr* ligands.

The single crystal X-ray structure analyses of **1** and **2** show monomers with a bent sandwich structure, thus unequivocally confirming the π-bonding nature of the pyr* ligands. Except for the different ionic radii of calcium and strontium, the two complexes are isostructural. Each structure shows two independent molecules, A and B, and each unit cell contains four molecules A, eight molecules B, and four disordered hexane (solvent) molecules. A and B differ only slightly in bond distances and angles. Molecules A possess a twofold rotation axis. In each of the four molecules **1**A,B (Fig. 1) and **2**A,B, the metal atom is seven-coordinated by two η^5-π-bonded pyr*

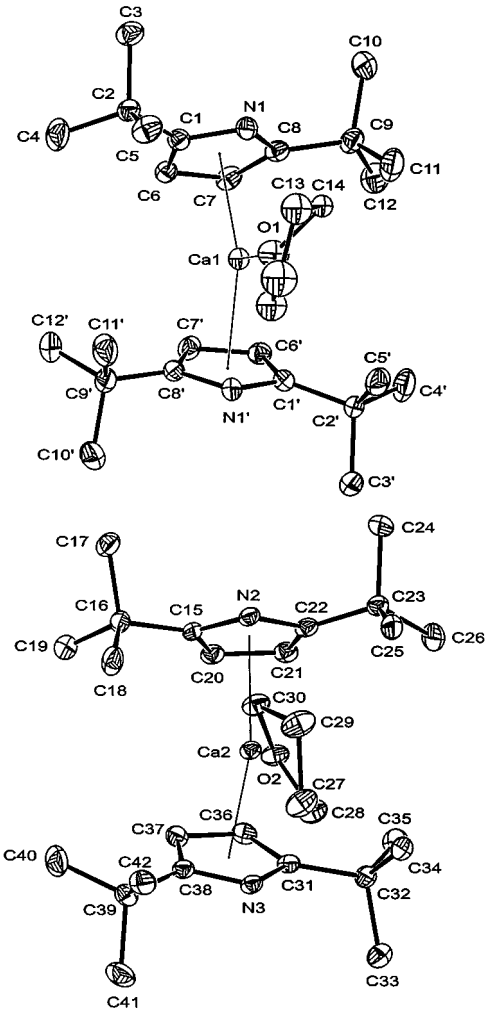

Fig. 1 ORTEP plot of the structure and numbering scheme of **1**, with 30% probability thermal ellipsoids. For clarity, all hydrogens are omitted. Selected bond lengths (Å) and angles (°) with estimated standard deviations of **1** and {**2**}: M–Cg 2.376(16)(A)/2.381(2)(B)/2.381(2)(B) {2.520(1)(A)/2.530(5)(B)/2.530(10)(B)}, M–O 2.373(4)(A)/2.389(3)(B) {2.538(6)(A)/2.533(4)(B)}; Cg–M–Cg 127.4(3)(A)/127.74(7)(B) {122.0(2)(A)/124.0(3)(B)}.

ligands and one THF molecule in a pseudo-trigonal planar arrangement. The pyr* rings are planar within limits of error with the 2,5-*tert*-butyl substituents placed above these planes away from the metal center. The pyr* ring planes form interplanar angles of 47.67 and 45.55° in **1**A and **1**B or 51.11 and 47.77° in **2**A and **2**B, with the ring nitrogen atoms situated at the 'open' side. The Cg–M–Cg angles (Cg defines the centroid of the pyr* ring) of 127° for **1**A,B or 122 and 124° for **2**A and **2**B are smaller than the $Cp_{centroid}$–M–$Cp_{centroid}$ angles in comparable cyclopentadienyl complexes, *e.g.* in $\{M[C_5H_3(SiMe_3)_2\text{-}1,3]_2(THF)\}$[5] [135° (M = Ca), 134° (M = Sr)], whereas the average M–Cg distances of 2.38 Å (**1**A,B) and 2.525 Å (*2*A,B) are in good agreement with the M–$Cp_{centroid}$ distances estimated for the above mentioned cyclopentadienyl complex [2.397 Å (M = Ca), 2.551 Å (M = Sr)]. The ring slippage towards the nitrogen atom of 0.126 Å (**1**A), 0.172 and 0.178 Å (**1**B), 0.178 Å (**2**A), and 0.214 and 0.207 Å (**2**B) indicates a certain tendency of the pyr* ligand towards an η^3-bonding mode. The third ligand, the O-coordinated THF is disordered in molecules A. The hexane solvent molecules do not have any contacts to the molecules of **1** and **2**.

We are grateful to the Fonds der Chemischen Industrie and the Deutsche Forschungsgemeinschaft for financial support.

Notes and references

† *Syntheses*: the reactions were carried out in an atmosphere of purified argon (Schlenk techniques) using dry, oxygen-free solvents. 2,5-Di-*tert*-butylpyrrole[6] and 2,5-di-*tert*-butylpyrrolylsodium[2b] were prepared according to published procedures.

1: To a suspension of 0.9 g (3.06 mmol) CaI_2 in 50 ml THF 1.23 g (6.12 mmol) of $Na[NC_4H_2Bu^t_2\text{-}2,5]$ were added in portions. After stirring the mixture for 12 h at 25 °C, the THF was removed *in vacuo* (10^{-2} mbar) followed by the addition of 80 ml hexane to the remaining solid. The clear solution was decanted from undissolved NaI and concentrated to a volume of 20 ml. Crystallization at −20 °C yielded 0.68 g (47.4%) of colorless **1**. Mp: 113 °C. ^{1}H NMR (benzene-d_6, 200 MHz): δ 6.34 (s, 4H, H-3,4), 3.83 (m, 4H, THF) 1.36 (s, 36H, Bu^t), 1.18 (m, 4H, THF). $^{13}C\{^1H\}$ NMR (benzene-d_6, 50.32 MHz): δ 153.51 (C-2,5), 105.19 (C-3,4), 70.64 (THF), 33.84 (CCH_3), 31.33 (CCH_3), 25.12 (THF). MS (EI, 60 °C, ^{40}Ca): *m*/*z* (%) 396 (8) $[M-THF]^+$, 218 (4) $[Ca(pyr^*)]^+$, 179 (21) $[(pyr^*)H]^+$, 164 (100) $[(pyr^*)H-Me]^+$.

2: This complex was synthesized in analogy to **1**, from 0.85 g (2.49 mmol) of SrI_2 and 1.0 g (5.0 mmol) of $Na[NC_4H_2Bu^t_2\text{-}2,5]$ in 50 ml THF. Crystallization from hexane (15 ml) at −20 °C yielded 0.65 g (50.6%) of colorless **2**. Subl: 179 °C (0.5 mbar); decomp. 200 °C. ^{1}H NMR (benzene-d_6, 200 MHz): δ 6.30 (s, 4H, H-3,4), 3.59 (m, 4H, THF) 1.38 (s, 36H, Bu^t), 1.14 (m, 4H, THF). $^{13}C\{^1H\}$ NMR (benzene-d_6, 50.32 MHz): δ 153.05 (C-2,5), 104.51 (C-3,4), 69.60 (THF), 33.70 (CCH_3), 31.31 (CCH_3), 24.97 (THF). MS (EI, 220 °C, ^{88}Sr): *m*/*z* (%) 444 (1) $[M-THF]^+$, 266 (6) $[Sr(pyr^*)]^+$, 179 (22) $[(pyr^*)H^+]$, 164 (100) $[(pyr^*)H-Me]^+$.

‡ *Crystal data* for $C_{42}H_{72}Ca_{1.5}N_3O_{1.5}(C_6H_{14})_{0.5}$ **1** and $C_{42}H_{72}Sr_{1.5}N_3O_{1.5}(C_6H_{14})_{0.5}$ **2** (corresponding data for **2** in square brackets): M = 746.26 [813.54] monoclinic [monoclinic], a = 36.43(2) [36.693(4)], b = 14.843(3) [14.866(5)], c = 18.053(3) [18.172(10)] Å, β = 108.45(3) [108.61(3)]°, U = 9259(6) [9395(6)] Å, T = 163(2) [163(2)] K, space group *C*2/*c* (no. 15) [*C*2/*c*(no. 15)], Z = 8 [8], μ = 0.225 [1.743] mm^{-1}, 7523 [7541] reflections measured, 7115 [7262] unique reflections (R_{int} = 0.0460 [0.0519]) used in all calculations. Final $wR(F^2)$ 0.1009 [0.1227] (all data) and 0.0730 [0.0594] [$I > 2\sigma(I)$]. An Enraf-Nonius CAD4 diffractometer with monochromated Mo-Kα radiation was used (λ = 0.71069 Å). The structures were solved using direct methods. Data were corrected for Lorenz, polarization and absorption effects.

CCDC 182/1411. See http://www.rsc.org/suppdata/cc/1999/2091/ for crystallographic files in .cif format.

1 M. Köckerling, S. Stubenrauch, D. Bläser and R. Boese, *J. Chem. Soc., Chem. Commun*., 1991, 1368; N. Kuhn, K. Jendal, R. Boese and D. Bläser, *Chem. Ber*., 1991, **124**, 89; N. Kuhn, G. Henkel and S. Stubenrauch, *Angew. Chem*., 1992, **104**, 766; N. Kuhn, G. Henkel and S. Stubenrauch, *J. Chem. Soc., Chem. Commun*., 1992, 760; M. Köckerling, S. Stubenrauch, R. Boese and D. Bläser, *J. Organomet. Chem*., 1992, **440**, 289.

2 (*a*) H. Schumann, J. Winterfeld, H. Hemling and N. Kuhn, *Chem. Ber*., 1993, **126**, 2657; (*b*) H. Schumann, E. C. E. Rosenthal, J. Winterfeld and Gabriele Kociok-Köhn, *J. Organomet. Chem*., 1995, **495**, C12; (*c*) H. Schumann, E. C. E. Rosenthal, J. Winterfeld, R. Weimann and J. Demtschuk, *J. Organomet. Chem*., 1996, **507**, 287.

3 M. Westerhausen, M. Wieneke, H. Nöth, T. Seifert, A. Pfitzner, W. Schwarz, O. Schwarz and J. Weidlein, *Eur. J. Inorg. Chem*., 1998, 1175.

4 M. L. Hays and T. P. Hanusa, *Adv. Organomet. Chem*., 1996, **40**, 117; (b) P. Jutzi and N. Burford, *Metallocenes*, ed. A. Togni and R. L. Halterman, Wiley–VCH, New York, 1998, p. 28.

5 L. M. Engelhardt, P. C. Junk, C. L. Raston and A. H. White, *J. Chem. Soc., Chem. Commun*., 1988, 1500; P. Jutzi, W. Leffers, G. Müller and B. Huber, *Chem. Ber*., 1989, **122**, 879.

6 R. Ramasseul and A. Rassat, *Chem. Commun*., 1965, 453.

Communication 9/06654C

Unusual desulfurization of a nickel dithiolene by bis(2-diphenylphosphinophenyl)phenylphosphine (tp) to produce Ni(tp)(R_4btimdt) [R_4btimdt = 5,5′-bis(1,3-dialkyl-4-imidazolidine-2-thione-4-thiolate], the first complex of this class of ligands

Francesco Bigoli,[a] Paola Deplano,*[b] Maria Laura Mercuri,[b] Maria Angela Pellinghelli,[a] Gloria Pintus[b] and Emanuele F. Trogu[b]

[a] *Dipartimento di Chimica Generale ed Inorganica, Chimica Analitica, Chimica Fisica, Università degli Studi di Parma, Centro di Studio per la Strutturistica Diffrattometrica del CNR, Area delle Scienze 17A, I-43100 Parma, Italy*

[b] *Dipartimento di Chimica e Tecnologie Inorganiche e Metallorganiche, Università di Cagliari, Cittadella di Monserrato, S. P. Monserrato-Sestu, I-09131 Monserrato, Cagliari, Italy. E-mail: deplano@vaxca1.unica.it*

Received (in Cambridge, UK) 5th August 1999, Accepted 7th September 1999

A novel desulfurization reaction induced on the title nickel dithiolenes by a tripodal phosphine producing the first complex of the S,S-dianionic title ligand, which belongs to a novel family of redox active heterocycles, and the fully oxidised trimeric form of this ligand are described.

The interest in the [Ni(R_2timdt)$_2$] complexes **1** (R_2timdt is the −1 charged 1,3-dialkyl-imidazolidine-2,4,5-trithione)[1,2] and related derivatives,[3] is related both to their possible application as near-IR dyes,[4] and for their chemistry. In fact they are promising candidates in neodymium lasers (which operate at 1064 nm) technology, since they show low-energy electronic absorption,[4] typical of this class of complexes, at *ca.* 1000 nm with remarkably high absorption coefficients coupled with a high thermal and photochemical stability. Moreover these complexes show a rich and peculiar chemistry, being the source of a variety of unusual products including mixed-valence complexes[2] and new sulfur-rich donors which have not been obtained, as yet, by other routes.[3]

As a further example of a peculiar behaviour of this class of nickel dithiolenes, we report here, the results obtained by reacting **1** with mono- and poly-functional phosphines. While with mono- (PPh_3) or bi-functional [dppe = 1,2-bis(diphenylphosphino)ethane] phosphines the reagents are recovered unchanged, the reaction of **1** with a tri-functional phosphine [tp = bis(2-diphenylphosphinophenyl)phenylphosphine] unexpectedly produces [Ni(tp)(R_4btimdt)] (R = Bu, **2**) [R_4btimdt = 5,5′-bis(1,3-dialkyl-4-imidazolidine-2-thione-4-thiolate] according to Scheme 1.[5]

The molecular structure of [Ni(tp)(Bu_4btimdt)] **2**,[6] is shown in Fig. 1 with the corresponding atom-labelling scheme. The nickel ion is coordinated in a trigonal bipyramidal geometry with the three P atoms of the tp ligand lying on a face of the bipyramid. The chelation of tp produces the formation of two pentaatomic rings showing an 'envelope' conformation. The newly formed ligand Bu_4btimdt acts as a bidentate ligand being coordinated to the metal through the two thiolato sulfur atoms, in such a way that a heptaatomic ring including the metal is formed.

Complex **2** contains the first example of the S,S dinegative chelating ligand Bu_4btimdt, generated *in situ* by elimination of one of the two vicinal sulfur atoms on each ligand coordinated

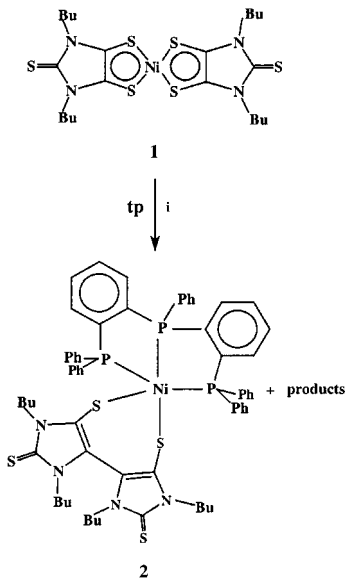

Scheme 1 i, tp in excess, THF, reflux in N_2, 24 h.

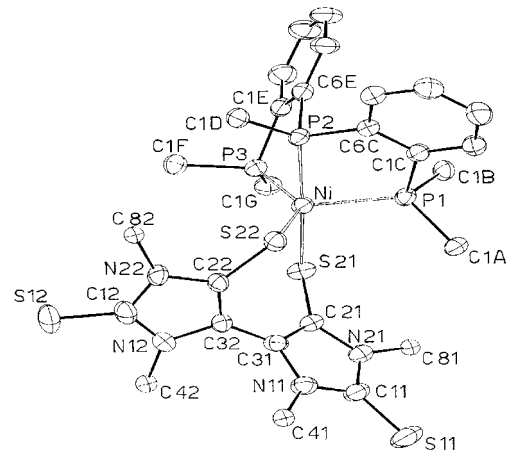

Fig. 1 Molecular structure of [Ni(tp)(Bu_4btimdt)] **2** (Bu and Ph groups omitted for clarity). Selected bond distances (Å) and angles(°): Ni–S(21) 2.270(3), Ni–S(22) 2.342(3), Ni–P(1) 2.296(3), Ni–P(2) 2.171(3), Ni–P(3) 2.203(3), S(11)–C(11) 1.686(8), S(21)–C(21) 1.710(7), S(12)–C(12) 1.698(9), S(22)–C(22) 1.745(10); S(21)–Ni–S(22) 100.5(1), S(21)–Ni–P(1) 97.6(1), S(21)–Ni–P(2) 170.0(1), S(21)–Ni–P(3) 85.9(1), S(22)–Ni–P(1) 103.5(1), S(22)–Ni–P(2) 88.4(1), S(22)–Ni–P(3) 136.5(1), P(1)–Ni–P(2) 84.7(1), P(1)–Ni–P(3) 118.4 (1), P(2)–Ni–P(3) 84.4(1).

to the metal in the nickel dithiolene with concomitant C–C coupling between the two imidazole rings.

A dianion, H_2X^{2-}, belonging to the same class of Bu_4btimdt^{2-} has been obtained *via* an unusual method by reacting elemental sulfur with 1-methylimidazole.[7] This anion was isolated in the solid state as the salt $(PPh_4)_2H_2X$ structurally characterized, and proposed as a new ligand of special interest owing to its multi-electron redox properties. However, to the best of our knowledge, its coordination chemistry is still unexplored. Also a neutral compound obtained from oxidation of this ligand has been isolated but not characterized.

These ligands are related to the class of 4,5,6,7-tetrathiocino[1,2-*b*:3,4-*b*′]diimidazolyl-1,3,8,10-tetraalkane-2,9-dithiones **3**[8] which exhibit promising anticancer properties now under testing *in vivo* by National Cancer Institute of Bethesda (USA).

By reacting **3** with an alcoholate, the R_4btimdt anion is formed in solution and can be isolated in the complex [Ni(dppe)(R_4btimdt)], when [Ni(dppe)Cl_2] is added to the reaction mixture, buffered with ammonium acetate. When non-coordinated, the anion is oxygen sensitive and attempts to isolate it as a salt gave a mixture from which the new macrocycle **4** was isolated in low yield. Macrocycle **4** is prepared more conveniently (40% yield) by buffering with ammonium acetate and oxidizing the reaction mixture with O_2 or H_2O_2.[9] **4** can be considered as a trimer of R_4btimdt where the monomeric units are linked together through disulfide bridges.

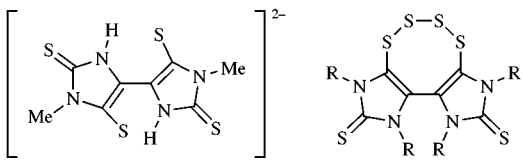

H_2X^{2-} **3**

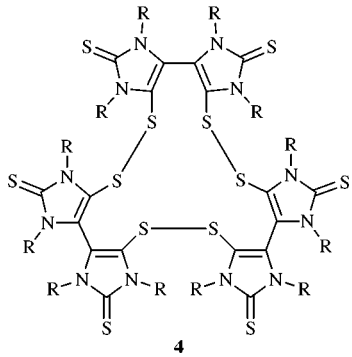

4

Crystals suitable for structural characterization were obtained for **4**·2EtOH (R = Et). Its molecular structure,[6] is shown in Fig. 2 with the corresponding atom-labelling scheme. The molecule has a twofold axis. The structural data are similar to those previously observed by us in thione derivatives with similar moieties.[2,8] Interactions of the type S···C and C···C[3.46(1)–3.79(3) Å] determine the packing so that the eighteen-membered rings of the molecules give rise to channels, parallel to *c*, which contain the guest solvent molecules.

In conclusion a novel desulfurization reaction with concomitant C–C coupling between two imidazoline rings, not reported previously, has been described. This reaction represents a promising template synthesis to prepare, starting from nickel dithiolenes, new chelating S,S-dianionic ligands, which are not easily attained by other routes.

This work was supported by Ministero dell'Università e della Ricerca Scientifica (MURST 40%, Chimica dei Materiali).

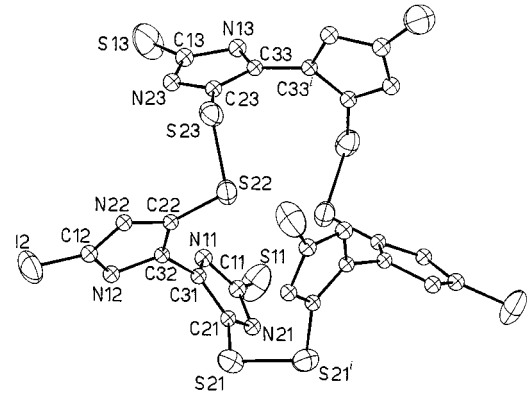

Fig. 2 Molecular structure of **4** (Et groups and sovent molecules omitted for clarity). Selected bond distances (Å) and angles(°): S(21)–S(21^i) 2.087(4), S(22)–S(23) 2.074(3), S(11)–C(11) 1.657(7), S(12)–C(12) 1.666(7), S(13)–C(13) 1.676(8), S(21)–C(21) 1.740(7), S(22)–C(22) 1.725(7), S(23)–C(23) 1.750(8); C(21)-S(21)– S(21^i) 106.8(3), C(22)–S(22)–S(23) 107.1(2), C(23)–S(22)–S(23) 107.9(3). [^{i}: $-y$, $-x$, 3/2 − z].

Notes and references

1 F. Bigoli, P. Deplano, F. A. Devillanova, V. Lippolis, P. J. Lukes, M. L. Mercuri, M. A. Pellinghelli and E. F. Trogu, *J. Chem. Soc., Chem. Commun*., 1995, 371.

2 F. Bigoli, P. Deplano, F. A. Devillanova, J. R. Ferraro, V. Lippolis, P. J. Lukes, M. L. Mercuri, M. A. Pellinghelli, E. F. Trogu and J. M. Williams, *Inorg. Chem.*, 1997, **36**, 1218.

3 F. Bigoli, P. Deplano, M. L. Mercuri, M. A. Pellinghelli, G. Pintus, E. F. Trogu, G. Zonnedda, H. H. Wang and J. M. Williams, *Inorg. Chim. Acta*, 1998, **273**, 175.

4 U. T. Mueller-Westerhoff, B. Vance and D. I. Yoon, *Tetrahedron*, 1991, **47**, 909.

5 *Preparation of* **2**: [Ni(Bu_2timdt)$_2$] (50 mg) and an excess of tp bis (2-diphenylphosphinophenyl)phenylphosphine[10] (200 mg) (1:4 molar ratio) were mixed and refluxed in THF (50 mL), under N_2 for 24 h. The solution turned from olive-green to purple. The solvent was removed *in vacuo* and by repeated fractional crystallization from MeCN–Et_2O of the crude product, a complete separation of **2** from the excess of the less solubie tp was achieved. Well shaped pure red–brown crystals (70 mg, 72% yield), were obtained.

6 *Crystal data for compound* **2**: $C_{64}H_{69}N_4NiP_3S_4$, M = 1174.09, triclinic, $P\bar{1}$, a = 11.057(4), b = 12.973(6), c = 23.023(9) Å, α = 78.69(2), β = 75.88(2), γ = 69.89(2)°, V = 2984(2) Å^3, Z = 2, μ = 28.66 cm^{-1}, T = 293(2) K, 11299 reflections measured, 11299 unique data. For 4879 observed reflections with [$I > 2\sigma(I)$] and 606 parameters the final R_1 = 0.0882 [wR_2 = 0.3283(all data)]. For compound **4**: $C_{46}H_{72}N_{12}O_2S_{12}$, M = 1209.88, tetragonal, $P4_32_12$, a = 12.915(6), c = 36.122(5) Å, V = 6025(4) Å^3, Z = 4, μ = 44.15 cm^{-1}, T = 293(2) K, 6328 reflections measured, 5724 unique data (R_{int} = 0.0495), Flack abs. structure parameter = 0.04(5). For 4184 observed data with [$I > 2\sigma(I)$] and 260 parameters the final R_1 = 0.0817 [wR_2 = 0.2932(all data)]. Data were collected from an Enraf-Nonius CAD4 diffractometer (Cu-Kα radiation, λ = 1.54184 Å). In the final refinement rigid-body constraints for all butyl groups in **2** and for solvent molecules in **4**, occupancy factor of 0.55 and 0.45 for the atoms of the two images of the disordered ethyl group in **4**. CCDC 182/1406.

7 S. Al-Ahmad, B. Boje, J. Magull, T. B. Rauchfuss and Y. Zheng, *J. Am. Chem. Soc.*, 1995, **117**, 1145.

8 F. Bigoli, P. Deplano, M. L. Mercuri, M. A. Pellinghelli, A. Sabatini, E. F. Trogu and A. Vacca, *Can. J. Chem.*, 1995, **73**, 380 and references therein.

9 *Preparation of* **4**: Compound **3** (R = Et) (0.50 g) and Na (1.0 g) in dry methanol were stirred overnight under nitrogen. The obtained clear yellow solution was buffered with an excess of ammonium acetate. Air was bubbled over a period of 1 h and an orange–yellow solid precipitated. The crude product contained white–yellowish crystals of sulfur which were removed by washing with CS_2, in which the desired product is less soluble. The product was recrystallized from CH_2Cl_2–EtOH to give pure orange–red crystals (0.17 g, 40% yield).

10 B. Chiswell and L. M. Venanzi, *J. Chem. Soc. A*, 1966, 417.

Communication 9/06392G

ChemComm

Novel concise synthesis of 2-substituted 3,4-dihydro-2*H*-1,4-benzoxazines by ring opening of glycidols under solid-liquid phase transfer catalysis conditions†

Domenico Albanese,* Dario Landini and Michele Penso

Dipartimento di Chimica Organica e Industriale dell'Università e Centro CNR, via Golgi 19, I-20133 Milano, Italia. E-mail: domenico@iumchz.chimorg.unimi.it

Received (in Liverpool, UK) 2nd August 1999, Accepted 17th September 1999

The ring opening of glycidols with *N*-(2-fluorophenyl)toluene-*p*-sulfonamide under SL-PTC conditions, followed by ring closure with Bu^{t}OK, provides a novel high yielding synthesis of 2-substituted 3,4-dihydro-2*H*-1,4-benzoxazines.

3,4-Dihydro-2*H*-1,4-benzoxazine derivatives have received considerable attention due to their wide range of biological and therapeutic properties.[1] The 1,4-benzoxazine skeleton is usually built up by cyclocondensation of *o*-aminophenols with various dibromo derivatives[2] or α-halogeno acyl bromides.[3] Recently 2-vinyl-1,4-benzoxazines have also been prepared with ees up to 79% by reaction of (*Z*)-1,4-diacetoxybut-2-ene with *N*-protected *o*-aminophenols in the presence of a palladium catalyst associated with phospine ligands.[4,5]

Following an alternative approach we devised a novel synthesis of 2-substituted 3,4-dihydro-2*H*-1,4-benzoxazines through formation of the C–N bond by ring opening of glycidols with a suitable nitrogen nucleophile. The benzoxazine synthesis could be completed through nucleophilic aromatic substitution of a good leaving group incorporated in the incoming nucleophile. We report herein our preliminary results in this area which reveals that the new approach enables the efficient synthesis of non-racemic chiral 2-substituted benzoxazines.

In previous papers we reported on the ring opening of epoxides with nitrogen nucleophiles under solid/liquid phase transfer catalysis (SL-PTC) conditions affording corresponding β-hydroxyamides in good to excellent yields.[6,7] On the basis of these results and due to the good nucleofugality of fluoride anion in aromatic nucleophilic substitution, *N*-(2-fluorophenyl)toluene-*p*-sulfonamide **1** was chosen as the nitrogen nucleophile incorporating the aromatic moiety of benzoxazine and the leaving group.

Thus, the ring opening was performed by stirring at 90 °C a heterogeneous mixture of 1,2-epoxy-3-phenoxypropane **2a**, sulfonamide **1** (1.1 equiv.), anhydrous K_2CO_3 (0.1 equiv.), $BnEt_3NCl$ (0.1 equiv.) and dioxane, affording *N*-(2-fluorophenyl)-*N*-(2-hydroxy-3-phenoxypropyl)toluene-*p*-sulfonamide **3a** in 95% yield after 17 h (Scheme 1). The optimisation of reaction conditions (Table 1) led us to discover that the best results were obtained without solvent, giving 94% of **3a** after 1 h. The PTC agent is essential in order to give high yields in short reaction times since 56 h were necessary to generate 86% of **3a** in the absence of $BnEt_3NCl$.

Table 1 Synthesis of β-hydroxysulfonamide **3**[a]

Entry	Epoxide	Dioxane/M	*t*/h	Yield (%)[b]
1	**2a**	2.5	17	95
2	**2a**	10	3	85
3	**2a**	—	1	94
4	**2a**	—	56	86[c]
5	(*S*)-**2b**	—	2	90

[a] All reactions carried out using 1.1 equiv. of sulfonamide **1**, 0.1 equiv. of $BnEt_3NCl$ and 0.1 equiv. of anhydrous K_2CO_3. [b] Isolated yield. [c] Without $BnEt_3NCl$.

† Experimental and spectral data for **3a**,**b**, **4a**,**b** and **5a**,**b** are available from the RSC web site, see http://www.rsc.org/suppdata/cc/1999/2095/

The ring opening takes place in a completely regioselective fashion, affording β-hydroxysulfonamides derived from the nucleophilic attack on the less substituted carbon atom of the oxirane ring. In accordance with the observed regiochemistry, non-racemic chiral glycidols generate enantiopure β-hydroxysulfonamides, as revealed in the case of (2*S*)-[(benzyloxy)methyl]oxirane (*S*)-**2b** which generates (2*R*)-*N*-(2-fluorophenyl)-*N*-(2-hydroxy-3-benzyloxypropyl)toluene-*p*-sulfonamide-(*R*)-**3b** in 90% yield after 2 h.‡

With a viable route to β-hydroxysulfonamides **3** in hand, it remained to perform the ring closing step to demonstrate the utility of this strategy. The 1,4-benzoxazine ring can be formed by intramolecular nucleophilic substitution (S_Ni Ar) of fluoride anion promoted by a suitable base. In particular the base should selectively generate the alkoxide anion without direct substitution of fluoride. Only isolated examples of S_Ni Ar of fluoride anion by thiolate[8] or phenolate anion[9] have been reported along with a single example of bromide substitution by phenolate.[10] The task was achieved with a cheap non-nucleophilic strong base such as Bu^{t}OK. In fact *N*-tosyl-2-phenoxymethyl-

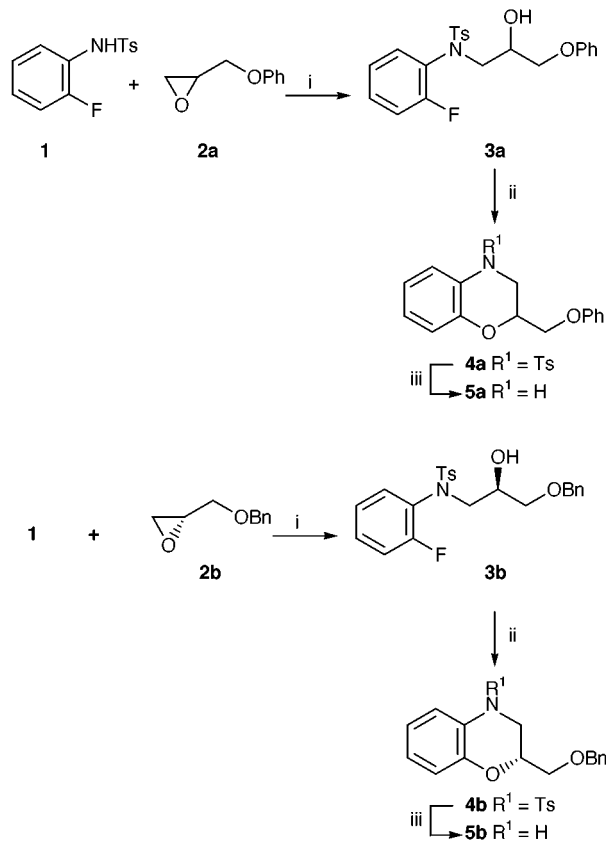

Scheme 1 *Reagents and conditions*: i, K_2CO_3–$BnEt_3NCl$, 90 °C; ii, Bu^{t}OK, THF, reflux; iii, Na, naphthalene, DME, −78 °C.

1,4-benzoxazine **4a** was isolated in 85% yield when reacted with Bu^{t}OK in THF for 30 min at reflux. Moreover the yield could be increased up to 92% by portionwise addition of Bu^{t}OK. Similarly (*R*)-**3b** was converted into the corresponding 1,4-benzoxazine (*R*)-**4b** in 86% yield after 1 h.

It is likely that the ring closure proceeds through a pure S_Ni Ar mechanism due to the activation exerted by the *p*-tolylsulfonyl group even though an $S_{RN}1$ or benzyne pathway cannot at the moment be ruled out.

In order to probe the scope and limitations of the process, *N*-(2-chlorophenyl)-*N*-(2-hydroxy-3-phenoxypropyl)toluene-*p*-sulfonamide **7** was prepared in 94% yield by ring opening of **2a** with *N*-(2-chlorophenyl)toluene-*p*-sulfonamide **6** as previously described. However **7** did not generate the corresponding benzoxazine when treated with Bu^{t}OK.

Removal of the *N*-tosyl group with Na/naphthalene[11] gave the unprotected 1,4-benzoxazines **5a,** (*R*)-**5b** in 77–84% yield. Conversion of (*R*)-**5b** into the corresponding Mosher amide confirmed that the ring closure occurs without racemisation.§

In view of the availability of a wide variety of enantiopure epoxides[12] this method provides a straightforward and new approach towards the synthesis of chiral 2-substituted 3,4-dihydro-2*H*-1,4-benzoxazines since the stereocenter of the epoxide is not affected during the ring opening and the next cyclisation occurs without racemisation.

Financial support from CNR and MURST (National Project 'Stereoselezione in Sintesi Organica, Metodologie e Applicazioni') is acknowledged.

Notes and references

‡ ^{19}F NMR analysis of the Mosher's ester (ref. 13) prepared from (*R*)-**3b** and (*R*)-α-methoxy-α-(trifluoromethyl)phenylacetyl chloride showed a single signal for the aromatic fluorine at δ −118.607, whereas the diastereomeric esters obtained from racemic **3b** showed two separated signals at δ −118.319 and −118.607.

§ ^{1}H NMR analysis of the Mosher's amide prepared from (*R*)-**5b** and (*R*)-α-methoxy-α-(trifluoromethyl)phenylacetyl chloride showed a single signal for the methoxy group at δ 3.82m, whereas the diastereomeric amides obtained from racemic **5b** showed two separated signals at δ 3.76 and 3.82.

1 D. W. Combs, M. S. Rampulla, S. C. Bell, D. H. Klaubert, A. J. Tobia, R. Falotico, B. Haertlein, C. Lakah-Weiss and J. B. Moor, *J. Med. Chem.*, 1990, **33**, 380; E. T. D'Ambra, G. K. Estep, R. M. Bell, A. M. Eissenstat, A. K. Josef, J. S. Ward, A. D. Haycock, R. E. Baizman, M. F. Casiano, C. N. Beblin, M. S. Chippari, D. J. Greo, K. R. Kullnig and T. G. Daley, *J. Med. Chem.*, 1992, **35**, 124; M. Largeron, H. Dupuy and M. B. Fleury, *Tetrahedron*, 1995, **51**, 4953.

2 T. Kuroita, M. Sakamori and T. Kawakita, *Chem. Pharm. Bull.*, 1996, **44**, 756.

3 Y. Matsumoto, R. Tsuzuki, A. Matsuhisa, K. Takayama, T. Yoden, W. Uchida, M. Asano, S. Fujita, I. Yanagisawa and T. Fujikura, *Chem. Pharm. Bull.*, 1966, **44**, 103.

4 A. Yamazaki, I. Achiwa and K. Achiwa, *Tetrahedron: Asymmetry*, 1996, **7**, 403.

5 P. Lhoste, M. Massacret and D. Sinou, *Bull. Soc. Chim. Fr.*, 1997, **134**, 343.

6 D. Albanese, D. Landini and M. Penso, *Tetrahedron*, 1997, **53**, 4787.

7 D. Albanese, D. Landini, M. Penso and S. Petricci, *Tetrahedron*, 1999, **55**, 6387.

8 G. Campiani, A. Garofalo, I. Fiorini, M. Botta, V. Nacci, A. Tafi, A. Chiarini, R. Budriesi, G. Bruni and M. Romeo, *J. Med. Chem.*, 1995, **38**, 4393.

9 S. Carrington, A. H. Fairlamb and I. S. Blagbrough, *Chem. Commun.*, 1998, 2335.

10 G. E. Bonvicino, L. H. Yogodzinski and R. A. Hardy Jr., *J. Org. Chem.*, 1962, **27**, 4272.

11 J. J. Folmer, C. Acero, D. L. Thai and H. Rapoport *J. Org. Chem.*, 1998, **63**, 8170.

12 E. N. Jacobsen, *Comprehensive Organometallic Chemistry II*, ed. E.W. Abel, F. G. A. Stone, G. Wilkinson and L. H. Hegedus, Pergamon, Oxford, 1995, vol. 12, ch.11.1; R. A. Johnson and K. B. Sharpless, *Catalytic Asymmetric Synthesis*, ed. I. Ojima, VCH, New York, 1993, ch. 4.1.

13 J. A. Dale, D. L. Dull and H. S. Mosher, *J. Org. Chem.*, 1969, **34**, 2453.

Communication 9/06260B

Photophysical studies on the photochromism of *trans*-10b,10c-dimethyldihydropyrene

R. Scott Murphy, Yongsheng Chen, Timothy R. Ward, Reginald H. Mitchell* and Cornelia Bohne*

Department of Chemistry, University of Victoria, PO Box 3065, Victoria, B.C., Canada, V8W 3V6. E-mail: bohne@uvic.ca

Received (in Corvallis, OR, USA) 8th July 1999, Accepted 7th September 1999

Photophysical studies on the photochromism of *trans*-10b,10c-dimethyldihydropyrene showed that several transients, including the triplet excited state of the cyclophanediene, were observed.

Dimethyldihydropyrene derivatives and their isomeric cyclophanes can be interconverted photochemically. Once the less stable isomer is formed photochemically it reverts back to the more stable form in a thermal reaction.[1] In the case of *trans*-10b,10c-dimethyldihydropyrene (DMDHP, Scheme 1), the cyclophanediene (CPD) is the less stable isomer by 3 kcal mol^{-1}.[2]

Photochromic molecules have considerable potential as optical switches.[3–5] Dimethyldihydropyrene derivatives are photochromic and have been synthetized with sophisticated multiple switching sites.[6,7] However, photophysical studies have mostly been limited to irradiation with broadband light sources. Although theoretical studies have discussed the possible intermediates involved in the isomerization reaction,[2,8] experimentally no studies have been reported on the detection of reactive intermediates. The latter is the subject of this report.

DMDHP was synthesized as previously described.[9] Its absorption spectrum extends up to 650 nm,[10] and when excited (PTI QM-2 fluorimeter) at 470 nm its fluorescence centered at 640 nm was observed. The energy for the S_1 state is 44 kcal mol^{-1},[11] and its geometry is similar to that of the ground state since no wavelength shift was observed between the emission maximum and the absorption maximum at the longest wavelength. The CPD absorption is shifted to the blue because this molecule is less conjugated than DMDHP and the S_1 energy is higher than 80 kcal mol^{-1}.

Laser flash photolysis[12] was employed to obtain the transient spectra for DMDHP. A flow cell was used to ensure that a fresh solution was irradiated for each laser pulse. Irradiation of DMDHP at 355 nm led to a bleaching at wavelengths longer than 300 nm and the detection of transients in the 250–320 nm region (Fig. 1). No transient signals were detected between 550 and 650 nm. Upon excitation, DMDHP is transformed into transients with higher molar absorptivities in the UV region of the spectrum and loss of absorption in the visible region. For delays longer than 70 ns the transient spectrum had a maximum at 280 nm (transient **I**) and an isosbestic point was observed at 310 nm (inset Fig. 1). The latter suggests that at long delays only DMDHP and **I** were present. At very short delays (< 50 ns) a transient at 310 nm was detected (transient **II**). The transient kinetics showed a short- and a long-lived component (Fig. 2). The lifetimes for these components were the same for the decay at 280–290 nm and the growth at 340 nm, indicating that **I** and

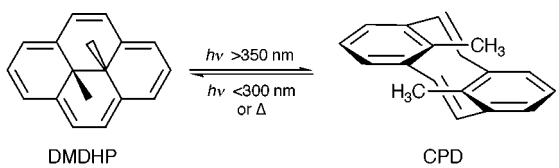

Scheme 1

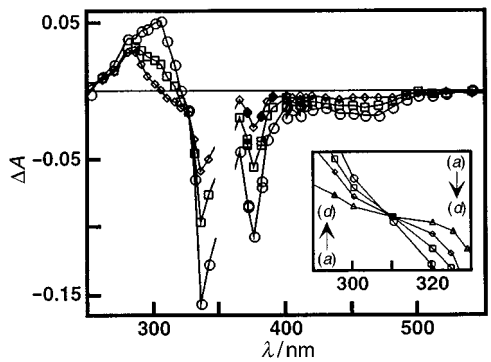

Fig. 1 Transient absorption spectra of DMDHP in cyclohexane at short delays after the laser pulse: (○) 10, (□) 50 and (◇) 70 ns. The inset shows the absorption region close to the isosbestic point at long delays: (*a*) 1, (*b*) 5, (*c*) 10 and (*d*) 15 μs.

II reformed DMDHP. Transient **I** did not decay back to the baseline [inset (*a*) in Fig. 2] and the bleaching at 340 nm did not completely recover (≤ 2 ms). This 'permanent' absorption change was assigned to the formation of CPD. The lifetime of **I** was longer than 5 μs and was very dependent on the presence of trace amounts of oxygen. The lifetime for **II** was shorter than the time-resolution of our system (< 12 ns) and the time-profile observed was that of the laser pulse (Fig. 2).

CPD, obtained by irradiating DMDHP in MeCN at −40 °C above 550 nm, was excited at 266 nm and −35 °C.[13] At 280 nm bleaching was observed indicating that some CPD reacted. In contrast, at 340 and 470 nm a positive absorption appears suggesting that CPD was isomerized into DMDHP. These results show that the transient phenomena being observed are due to the photochromism of DMDHP.

Quenching studies were performed to obtain information about the chemical nature of **I**. Oxygen readily reacts with **I** [(3.3 ± 0.6) 10^9 M^{-1} s^{-1}]. Quenchers with different triplet energies (E_T) were employed to check if **I** is a triplet excited

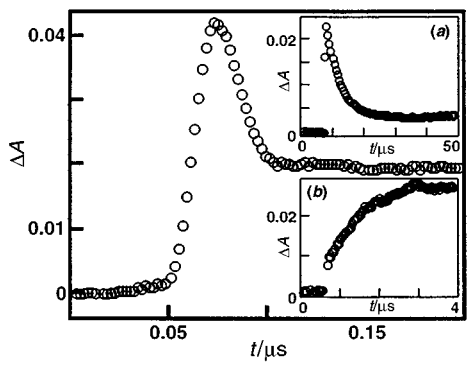

Fig. 2 Kinetic traces for the decay of transient **II** monitored at 290 nm (short time scale). Inset (*a*) shows the decay of transient **I** at 280 nm on a long time scale. Inset (*b*) shows the growth for triplet β-carotene (20 μM) when DMDHP is irradiated.

state. Cyclohexa-1,3-diene (E_T = 52 kcal mol^{-1})[14] or ferrocene (E_T = 38 kcal mol^{-1})[15] did not shorten the lifetime of **I**. However, β-carotene (E_T = 21 kcal mol^{-1})[14] quenched **I**. The triplet β-carotene was observed as a growth at 520 nm [Fig. 2, inset *(b)*] and the quenching rate constant was estimated to be *ca.* 10^{10} M^{-1} s^{-1}. These results show that **I** is a triplet state with an energy between 21 and 38 kcal mol^{-1}.

The quantum yield for the DMDHP to CPD photoisomerization ($\phi_{DMDHP\rightarrow CPD}$) was estimated from the magnitude of the'permanent' bleaching ($\tau \geq 2$ ms) at 470 nm using benzophenone [(ϕ_{isc} = 1, $\varepsilon(BP)_{530}$ = 7220 M^{-1} cm^{-1}][14] as a standard. Samples in cyclohexane containing benzophenone or DMDHP with matched absorptions at the laser excitation wavelength were excited at different laser energies and the values of ΔA at 530 nm for benzophenone and the bleaching at 470 nm for DMDHP were measured. These values are related by eqn. (1) [$\varepsilon(DMDHP)_{470}$ = 8200 ± 600 M^{-1} cm^{-1}, from *A vs.* [DMDHP] plots].

$$|\Delta A(\text{DMDHP})| = \frac{\varepsilon(\text{DMDHP})_{470}\,\phi_{\text{DMDHP}\rightarrow\text{CPD}}}{\varepsilon(\text{BP})_{530}\,\phi_{isc}}\Delta A(\text{BP}) \quad (1)$$

The recovered value for $\phi_{DMDHP\rightarrow CPD}$ (0.03 ± 0.01, three determinations) agrees well with the reported value (0.02).[1]

Based on the quenching by β-carotene and the absorption maximum at 280 nm, we assign **I** to the excited triplet state of CPD. The absorption at 280 nm indicates that, compared to DMDHP, a considerable amount of conjugation was lost, suggesting that the transannular bond was broken. Twisting of the bonds without breaking the transannular bond will not lead to a significant loss of conjugation. For this reason transient **I** cannot be the triplet excited state of DMDHP. The triplet CPD has a biradical character. In this respect, **I** is similar to the triplets of photoenols and xylylenes where these excited states are the biradicals of the corresponding ground state molecules.[16–18] The decay of **I** is probably determined by the rate of intersystem crossing to the singlet biradical which will rapidly form DMDHP or CPD.

The energy for **I** has been bracketed between 22 and 38 kcal mol^{-1} which overlaps with the energy for the transition state for the thermal reversion of CPD to DMDHP (Fig. 3). The triplet and singlet biradical reaction surfaces are likely to be close to the ground state surface and the reaction can proceed diabatically to the ground state surface once intersystem crossing to the singlet biradical occurs. In contrast, the reactivity from the excited singlet DMDHP could occur through a concerted or biradical mechanism. Although the formation of CPD was previously attributed to the reaction of the excited singlet DMDHP[1] it cannot be excluded that some CPD is formed from an excited triplet state with a low quantum yield.

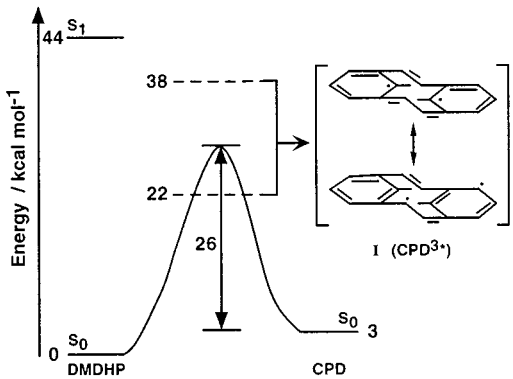

Fig. 3 Diagram representing the thermal conversion between DMDHP and CPD and some of the excited states of these isomers (only two resonance structures for **I** are shown).

Transient **II** cannot be definitely assigned because of its short lifetime. Its spectrum shows a maximum at 310 nm indicating that the DMDHP conjugation has been lost and **II** cannot be the excited singlet or triplet state of DMDHP. In addition, **II** is not the excited singlet state of CPD, since this state is not accessible on energetic grounds from the S_1 of DMDHP. One possibility, which is still speculative, is that **II** corresponds to the singlet biradical of CPD. Since the lifetime for **II** is shorter than the lifetime for triplet CPD, **II** can only be detected at short delays when formed from the excited singlet of DMDHP.

In conclusion, we report for the first time the transients formed in the irradiation of DMDHP. Detailed future studies on the photophysics of DMDHP derivatives will establish the importance of these transients when designing switches with high photoisomerization quantum yields.

C. B. and R. H. M. thank the Natural Sciences and Engineering Council of Canada (NSERC) for the support of their research programs. R. S. M. and T. R. W thank the University of Victoria and NSERC for postgraduate scholarships. The authors thank L. Netter for software development.

Notes and references

1 H. R. Blattmann and W. Schmidt, *Tetrahedron*, 1970, **26**, 5885.
2 W. Schmidt, *Helv. Chim. Acta*, 1971, **54**, 862.
3 S. L. Gilat, S. H. Kawai and J. M. Lehn, *Chem. Eur. J.*, 1995, **1**, 275.
4 M. Irie, *Pure Appl. Chem.*, 1996, **68**, 1367.
5 F. Pina, M. Maestri and V. Balzani, *Chem. Commun.*, 1999, 107.
6 R. H. Mitchell, *Eur. J. Org. Chem.*, in press.
7 R. H. Mitchell, T. R. Ward, P. W. Wang and P. W. Dibble, *J. Am. Chem. Soc.*, 1999, **121**, 2601.
8 W. Schmidt, *Tetrahedron Lett.*, 1972, **7**, 581.
9 R. H. Mitchell and V. Boekelheide, *J. Am. Chem. Soc.*, 1974, **96**, 1547.
10 V. Boekelheide and J. B. Phillips, *J. Am. Chem. Soc.*, 1967, **89**, 1695.
11 H. R. Blattmann, V. Boekelheide, E. Heilbronner and J. P. Weber, *Helv. Chim. Acta*, 1967, **50**, 68.
12 Y. Liao and C. Bohne, *J. Phys. Chem.*, 1996, **100**, 734.
13 J. N. Moorthy, S. L. Monahan, R. B. Sunoj, J. Chandrasekhar and C. Bohne, *J. Am. Chem. Soc.*, 1999, **121**, 3093.
14 S. L. Murov, I. Carmichael and G. L. Hug, *Handbook of Photochemistry*, 2nd, revised and expanded edn., Marcel Dekker, New York, 1993, p. 420.
15 A. Farmilo and F. Wilkinson, *Chem. Phys. Lett.*, 1975, **34**, 575.
16 J. C. Scaiano, *Chem. Phys. Lett.*, 1980, **73**, 319.
17 C. V. Kumar, S. K. Chattopadhyay and P. K. Das, *J. Am. Chem. Soc.*, 1983, **105**, 5143.
18 V. Wintgens, F. J. C. Netto Ferreira, H. L. Casal and J. C. Scaiano, *J. Am. Chem. Soc.*, 1990, **112**, 2363.

Communication 9/05725K

Construction of tetracyclic ring systems by $Co_2(CO)_8$-catalyzed tandem [2 + 2 + 1]/[2 + 2 + 2] cycloaddition reaction of diynes: a simple one-pot reaction†

Soon Hyeok Hong,[a] Jong Wook Kim,[a] Dai Seung Choi,[a] Young Keun Chung*[a] and Sueg-Geun Lee[b]

[a] *Department of Chemistry and Center for Molecular Catalysis, College of Natural Sciences, Seoul National University, Seoul 151-742, Korea. E-mail: ykchung@plaza.snu.ac.kr*

[b] *Korea Research Institute of Chemical Technology, PO Box 9, Daedeogdanji, Daejeon, Korea*

Received (in Cambridge, UK) 21st July 1999, Accepted 10th September 1999

The $Co_2(CO)_8$-catalyzed tandem [2 + 2 + 1]/[2 + 2 + 2] cycloaddition reaction of terminal diynes under CO produces an unnatural novel tetracyclic compound.

Transition metal-catalyzed cycloaddition reactions of unsaturated substrates have provided many prominent methods for the construction of complex cyclic compounds.[1] Among them, the [2 + 2 + 1] cycloaddition provides a powerful tool for the assembly of five-membered ring containing polycyclic natural products. In particular, the Pauson–Khand [2 + 2 + 1] cycloaddition has attracted much attention for the preparation of a variety of cyclopentenone systems.[2] However, cyclopentadienones[3] have played no role in five-membered ring construction due to their high reactivity in Diels–Alder reactions, even though some cyclopentadienone derivatives are known. Transition metal-mediated [2 + 2 + 1] cycloaddition of two alkynes with CO can be a good way to generate and stabilize cyclopentadienones. However, the application of this method to organic synthesis has been hampered[4] by low yields, and the requirement for the presence of specific substituents, and the necessity of a demetalation step, even though $Fe(CO)_5$ or $CpCo(CO)_2$ have successfully been employed in some intramolecular carbonylative cycloaddition reactions.[5,6] All the reported reactions are stoichiometric. In the studying the Pauson–Khand reaction,[7] we became interested in the cycloaddition reaction of hepta-1,6-diynes employing $Co_2(CO)_8$ as catalyst because no successful examples of catalytic [2 + 2 + 1] cycloaddition reactions of α,ω-diynes had been reported.

Here we report a facile construction of unnatural novel tetracyclic compounds by the $Co_2(CO)_8$-catalyzed tandem [2 + 2 + 1]/[2 + 2 + 2] cycloaddition reactions of diynes under CO.

Reaction of diethyl dipropargylmalonate **1** in CH_2Cl_2 in the presence of 2.5 mol% $Co_2(CO)_8$ at 100 °C for 2 days under 20 atm of CO gave a tandem [2 + 2 + 1]/[2 + 2 + 2] cycloaddition reaction to produce the tetracyclic enone derivative **2** in 85% yield as the sole product (Scheme 1 and Table 1).†

The structure of **2** was established by ^1H and ^{13}C NMR spectroscopic investigations (COSY, long range COSY, DEPT, HETCOR, long range HETCOR, phase sensitive NOESY, and 2D-INADEQUATE),‡ mass spectrometry and elemental analysis. No isomerized products were observed. The reaction involves the formation of four carbon–carbon bonds. Although this multibond formation reaction seems to be complex, it is simple and provides a unique pathway to a tetracyclic framework. The reaction of a 4,4-*gem*-disubstituted 1,6-diyne **3**, under the same reaction conditions, gave a tetracyclic enone derivative **4** in 78% yield. The present reaction can be extended to the use of an oxygen-containing ether. Subjecting the oxygen-containing substrate **5** to the same reaction conditions provided the oxatetracyclic enone derivative **6** in 35% yield. The nitrogen containing substrate **7** produced azatetracyclic enone derivative **8** in 89% yield. All the terminal diynes except dipropargyl ether gave high yields. For the mono-substituted

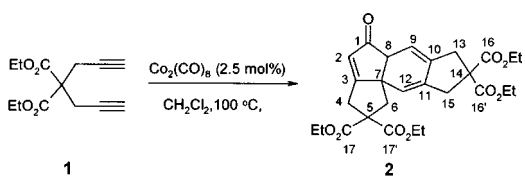

Scheme 1

† Synthetic and spectroscopic details for **2**, **4**, **6**, **8**, **10** and **13** are available from the RSC web site, see http://www.rsc.org/suppdata/cc/1999/2099/

Table 1 Cycloaddition reactions of diynes [a]

Diyne	Cycloadduct	Yield (%)[b]
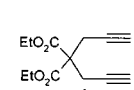	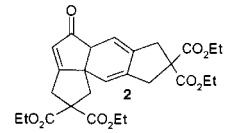	85%
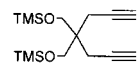	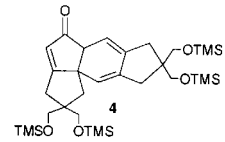	78%
	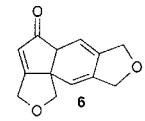	35%
	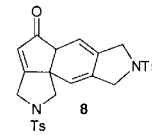	89%
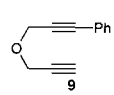	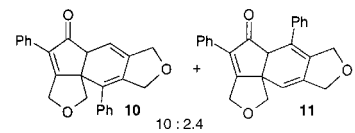	80%
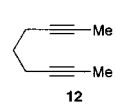	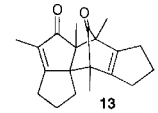	19%
	—	NR
	—	NR

[a] $Co_2(CO)_8$ (2.5 mol%) CO (20 atm), 100 °C, CH_2Cl_2. [b] Isolated yields.

1,6-diyne **9**, a 10 : 2.4 mixture of two regioisomers (**10** and **11**) was obtained in 80% yield. For the disubstituted 1,6-diyne **12**, a [4 + 2] cycloaddition between [2 + 2 + 1] cycloadducts gave **13** in 19% yield with concomitant formation of unidentified polymeric materials. The steric effect of substituents at the external terminus of the diyne substrates is an important factor for the second [2 + 2 + 2] cycloaddition to proceed. Substrates (**14** and **15**) bearing substituents at the external termini of the alkyne and substrates having tethers lengthened or shortened by one carbon did not afford the corresponding tetracyclic compounds.

The following observations may provide some clues to help understand the catalytic reaction. Treatment of **1** with $Co_2(CO)_8$ in the presence of cyclopentenone afforded **16**[8] (Scheme 2). Cyclopentenone was not involved in the cycloaddition reaction. Resubjecting **16** to the original cyclization conditions ($Co_2(CO)_8$, CH_2Cl_2, 20 atm CO, 100 °C, 2 days) gave no corresponding cycloaddition product (Scheme 3).

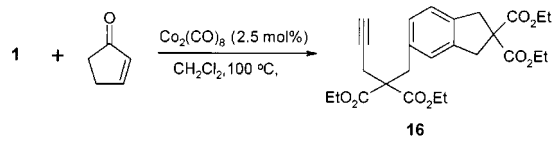

Scheme 2

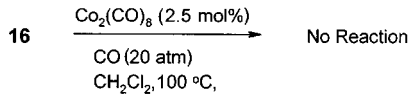

Scheme 3

Thus, the [2 + 2 + 2] cycloaddition reaction between diyne substrates does not occur before the [2 + 2 + 1] cycloaddition between CO and a substrate. We presume that initially a [2 + 2 + 1] cycloaddition between diyne and carbon monoxide catalyzed by $Co_2(CO)_8$ gives the corresponding bicyclic cyclopentadienone, and a subsequent [2 + 2 + 2] cycloaddition reaction between the bicyclic cyclopentadienone and diyne catalyzed by $Co_2(CO)_8$ leads to the tetracyclic cyclopentenone. We cannot rule out the possibility of alkene insertion to give a cobaltacycloheptadiene intermediate and reductive elimination of the tetracyclic cyclopentenone.

In summary, the reaction described herein demonstrates a novel one-step entry to unprecedented tetracyclic enone systems from acyclic starting substrates. The starting materials are readily prepared, and the resulting fused tetracycles have an unnatural framework which is difficult to prepare using conventional methods.

We acknowledge the Korea Science and Engineering Foundation (KOSEF) (96-0501-03-01-3), the Ministry of Education (1998-015-D00165), and the KOSEF through the Center for Molecular Catalysis for financial support.

Notes and references

‡ *Selected data* for **2**: $\delta_H(CDCl_3)$ 5.94 (d, *J* 2.2, H^2), 5.78 (dddd, *J* 5.6, 2.2, 2.0, 1.9, H^9), 5.34 (ddd, *J* 2.3, 2.0, 1.9, H^{12}), 4.23 (q, *J* 7.0, CH_2CH_3, 2H), 4.15–4.08 (m, CH_2CH_3, 6H), 3.56 (dd, *J* 17.2, 2.2, H^4), 3.17 (d, *J* 17.2, H^4), 3.04 (ddd, *J* 5.6, 2.2, 2.0, H^8), 3.01 (ddd, *J* 16.7, 2.0, 2.0, H^{13}), 2.87 (ddd, *J* 16.7, 2.2, 2.2, H^{13}), 2.85 (dd, *J* 16.6, 2.0, H^{15}), 2.82 (dd, *J* 16.6, 2.3, H^{15}), 2.55 (d, *J* 14.1, H^6), 2.15 (d, *J* 16.6, H^6), 1.23 (t, *J* 7.0, CH_3, 3H), 1.19 (t, *J* 7.1, CH_3, 3 H), 1.18 (t, *J* 7.0, CH_3, 3H), 1.15 (t, *J* 7.1, CH_3, 3H); $\delta_C(CDCl_3)$ 210.05, 186.07, 171.40, 170.90, 170.85, 170.71, 135.78, 134.33, 125.56, 119.30, 115.76, 62.12, 62.04, 61.47, 61.42, 59.12, 58.56, 56.39, 54.81, 47.06, 38.51, 38.20, 34.64, 13.83, 13.79, 13.78, 13.78, $\nu_{max}(Et_2O)$/cm^{-1} 1737.2, 1718.0 (CO) [HRMS: calc. 500.2046 (M^+), obs. 500.2043].

1 Review articles: M. Lautens, W. Klute and W. Tam, *Chem. Rev.*, 1996, **96**, 49; I. Ojima, M. Tzamarioudaki, Z. Li and R. J. Donovan, *Chem. Rev.*, 1996, **96**, 635; H.-W. Frühauf, *Chem. Rev.*, 1997, **97**, 523; C. P. Dell, *J. Chem. Soc., Perkin Trans. 1*, 1998, 3873.

2 P. L. Pauson, *Tetrahedron*, 1985, **41**, 5855; N. E. Schore, *Chem. Rev.*, 1988, **88**, 1081; N. E. Schore, *Org. React.*, 1991, **40**, 1; N. E. Schore in *Comprehensive Organic Synthesis*, ed. B. M. Trost, I. Fleming, Pergamon, Oxford, 1991, vol. 5, pp. 1037; N. E. Schore, in *Comprehensive Organometallic Chemistry II*, ed. E. W. Abel, F. G. A. Stone and G. Wilkinson, Pergamon Press, Oxford, 1995, vol. 12, pp. 703–739; N. Jeong, in *Transition Metals for Organic Synthesis*, ed. M. Beller and C. Bolm, Wiley-VCH, Weinheim, 1998, vol. 1, pp. 560–577.

3 M. A. Ogliaruso, M. G. Romanelli and E. I. Becker, *Chem. Rev.*. 1965, **65**, 261; E. W. Garbisch, Jr. and R. F. Sprecher, *J. Am. Chem. Soc.*, 1969, **91**, 6785.

4 L. S. Liebeskind and A. Bombrun, *J. Am. Chem. Soc.*, 1991, **113**, 8736; S. U. Tumer, J. W. Herndon and L. A. J. McMullen, *J. Am. Chem. Soc.*, 1992, **114**, 8394; J. W. Herndon and P. P. Patel, *Tetrahedron Lett.*, 1997, **38**, 59.

5 U. Krüerke, C. Hoogzand and W. Hübel, *Chem. Ber.*, 1961, **94**, 2817; J. L. Boston, D. W. A. Sharp and G. Wilkinson, *J. Chem. Soc.*, 1962, 3488; D. Fornals, M. A. Pericàs, F. Serratosa, J. Vinaixa, M. Font-Altaba, and X. Solans, *J. Chem. Soc., Perkin Trans. 1*, 1987, 2749; D. J. Sikora and M. D. Rausch, *J. Organomet. Chem.*, 1984, **276**, 21; E. Müller, R. Thomas, M. Sauerbier, E. Langer and D. Streichfuss, *Tetrahedron Lett.*, 1971, 521.

6 A. J. Pearson, R. J. Shively and R. A. Dubbert, *Organometallics*, 1992, **11**, 4096; A. J. Pearson and R. J. Shively, Jr., *Organometallics*, 1994, **13**, 578; A. J. Pearson and A. Perosa, *Organometallics*, 1994, **13**, 5178; H.-J. Knolker, J. Heber and C. H. Mahler, *Synlett*, 1992, 1002.

7 N. Jeong, Y. K. Chung, B. Y. Lee, S. H. Lee and S.-E. Yoo, *Synlett*, 1991, 204; Y. K. Chung, B. Y. Lee, N. Jeong, M. Hudecek and P. L. Pauson, *Organometallics*, 1993, **12**, 220; N. Jeong, S. Hwang, Y. Lee and Y. K. Chung, *J. Am. Chem. Soc.*, 1994, **116**, 3159; N. Y. Lee and Y. K. Chung, *Tetrahedron Lett.*, 1996, **37**, 3145; J. W. Kim and Y. K. Chung, *Synthesis*, 1998, 142.

8 S.-i. Ikeda, H. Watanabe and Y. Sato, *J. Org. Chem.*, 1998, **63**, 7026.

Communication 9/05888E

ChemComm

Zinc-mediated domino elimination–alkylation of methyl 5-iodopentofuranosides: an easy route to unsaturated carbohydrates for transition metal-catalyzed carbocyclizations

Lene Hyldtoft, Carina Storm Poulsen and Robert Madsen*

Department of Organic Chemistry, Technical University of Denmark, DK-2800 Lyngby, Denmark. E-mail: okrm@pop.dtu.dk

Received (in Cambridge, UK) 27th August 1999, Accepted 16th September 1999

5-Iodopentofuranosides are converted with zinc and allyl/propargyl bromide into dienes/enynes which are further used in carbohydrate annulation reactions.

Domino reactions are becoming a very attractive tool for enhancing synthetic efficiency by allowing several bond-forming transformations to be carried out in a single synthetic operation.[1] Such a strategy could be particularly important in the area of carbohydrate chemistry: because carbohydrates are densely functionalized, synthetic applications are often hampered by the need for many reaction steps, usually for manipulation of different protecting groups. In particular, the conversion of carbohydrates into carbocycles is a major task and has been the subject of intense study due to the biological significance of the products.[2] Herein, we report a zinc-mediated domino elimination–alkylation of methyl 5-deoxy-5-iodopentofuranosides to prepare carbohydrate-derived dienes and enynes. These are important substrates for transition metal-catalyzed carbocyclizations,[3] and we demonstrate the use of the obtained dienes in the ring-closing metathesis reaction.[4,5]

Zinc-mediated reductive elimination of ω-iodoglycosides is a valuable reaction for introducing a terminal double bond in carbohydrates,[6] but the instability of the liberated aldehyde can be a problem leading to side reactions and decomposition. We reasoned that the aldehyde could be trapped *in situ* by a Barbier-type alkylation[7] (Table 1). Zinc would then serve a dual purpose by promoting both the reductive elimination and reacting with an alkyl halide to perform the Barbier reaction. Hereby, a C–C double bond, a C–C single bond and a new stereocenter would be generated in the same pot.

Allyl and propargyl bromide were selected as the alkyl halides. Initial experiments were carried out on isopropylidene ribofuranoside **1**.[8] When **1** was reacted with allyl bromide and zinc, the desired diene was obtained in quantitative yield as a 4:1 diastereomeric mixture (entry 1, Table 1). Switching to propargyl bromide gave rise to the corresponding enyne, but now in an improved 9:1 diastereomeric ratio (entry 2). Notably, no isomerization from alkyne to allene was observed under these conditions. In general, for these sequential transformations to go to completion, 3 equiv. of allyl bromide was needed while the reaction with propargyl bromide required 5 equiv. Allyl bromide was added at the beginning of the reaction while propargyl bromide was added during the course of the reaction to minimize the formation of Wurtz coupling products. The reactions were carried out under sonication in aq. THF.[7] The THF:H_2O ratio influenced the rate, but had little effect on the diastereoselectivity. Addition of more H_2O generally enhanced the rate of the overall transformation.

These conditions were then applied to substrates **2**–**5** (Table 1). Interestingly, the reaction of unprotected ribofuranoside **2** with allyl bromide now gave the opposite diastereomer as the major product as compared to isopropylidene-protected **1** (entries 1 and 3). However, the reaction of **2** with propargyl bromide failed to give any of the desired enyne. The reason for this is not clear, but is probably associated with the unprotected hydroxy groups. As a result, the remaining furanosides were

Table 1 Domino elimination–alkylation of methyl 5-iodofuranosides[a]

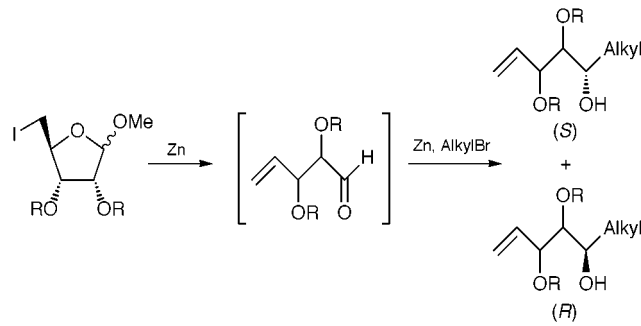

Entry	Furanoside	Alkyl Br	Yield (%) (*S*:*R*)[b]
1	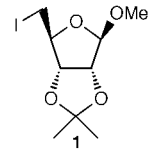 **1**		quant. (4 :1)[c]
2		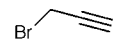	73 (9 : 1)
3	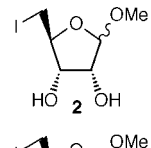 **2**		quant. (3 : 7)
4		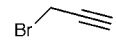	0
5	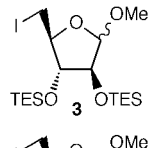 **3**		82 (3 : 7)[c]
6		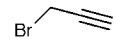	56 (3 : 7)
7	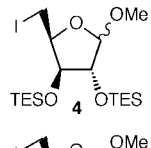 **4**		89 (3 : 1)
8		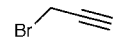	61 (7 : 3)
9	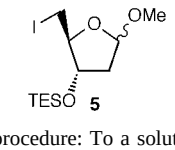 **5**		94 (5 : 6)[c]
10		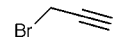	64 (2 : 3)

[a] General procedure: To a solution of the iodofuranoside (1.6 mmol) and allyl bromide (0.4 ml) in THF–H_2O (4:1, 10 ml) was added zinc (1 g, pre-activated with aq. HCl). The mixture was sonicated at 40 °C for 4 h under Ar atmosphere, filtered through Celite, and worked up by extraction with CH_2Cl_2 or stirring with ion-exchange resin followed by flash chromatography. [b] The stereochemistry of the enynes from the propargylations was assigned after hydrogenation to the corresponding dienes with Lindlar catalyst. In entry 10 the stereochemistry of the major enyne isomer was determined after conversion into its known MEM-protected derivative (ref. 9). Hydrogenation with Lindlar catalyst subsequently showed that the major diene isomer in entry 9 had the same absolute stereochemistry. [c] Protecting group removed in the work-up by acidic ion-exchange resin.

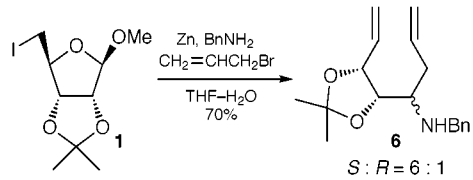

Scheme 1

protected as triethylsilyl (TES) ethers **3**–**5**. The reaction of these in the presence of allyl/propargyl bromide proceeded smoothly to give the dienes/enynes in good to excellent yields (entries 5–10). Unfortunately, the 2-deoxyribose substrate **5** gave a poor diastereoselectivity in the alkylation. For the protected furanosides **1**, **3** and **4**, on the other hand, the selectivity for addition to the intermediate aldehyde generally followed the Felkin–Anh model.[10]

The intermediate aldehyde can potentially be intercepted with an amine prior to the alkylation (Scheme 1). The alkylation would then take place on the formed imine resulting in the introduction of an amino group. In fact, treatment of **1** with zinc, benzylamine and allyl bromide succeeded in giving the amino diene product **6** in both good yield and diastereoselectivity. To prevent significant allylation of the intermediate aldehyde, it was important to add allyl bromide slowly during the course of the reaction.

Dienes and enynes are useful in transition metal-catalyzed carbocyclizations.[3] Hydroxylated enynes have previously been used in palladium-catalyzed coupling of the A-ring in vitamin D derivatives[9,11] and in cobalt-mediated Pauson–Khand reactions.[12] Hydroxylated dienes are useful for carbocyclization by ring-closing olefin metathesis. We have carried out the metathesis reaction on the major dienes from the allylations by the use of 5–10% Grubbs catalyst $[RuCl_2(CHPh)\{PCy_3\}_2]$[13] in CH_2Cl_2 (Table 2). These reactions also allow the stereochemical outcome of the allylations to be determined. The unprotected dienes in entries 1–4 all gave the desired cyclohexenes **7**–**10** in near quantitative yields. When the ammonium salt of diene **6** (Scheme 1) was subjected to Grubbs catalyst, significant decomposition took place and only a moderate yield of the cyclohexene could be obtained. However, when **6** was N-acetylated the ring-closing metathesis reaction went smoothly to give **11** in very high yield (entry 5, Table 2).

Table 2 Ring-closing olefin metathesis of the major diene products from the allylations

Entry	Diene	Cyclohexene	Yield (%)
1	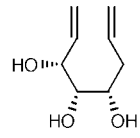	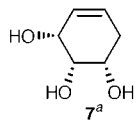 **7**[a]	96
2	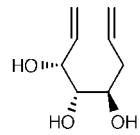	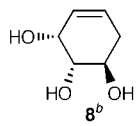 **8**[b]	95
3	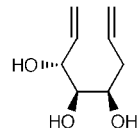	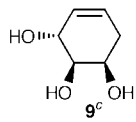 **9**[c]	97
4	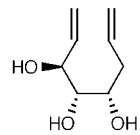	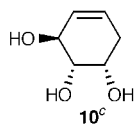 **10**[c]	95
5	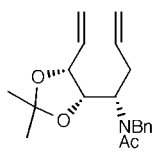	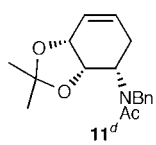 **11**[d]	94

[a] Ref. 14, [b] Ref. 15. [c] Ref. 16. [d] Ref. 17.

In conclusion, we have developed a zinc-mediated elimination–alkylation of 5-iodopentofuranosides which permits 'one-pot' formation of several bonds and a stereocenter in a controlled manner. The obtained dienes and enynes are valuable in carbohydrate annulation by transition metal catalysis, and we have processed the dienes in the ring-closing metathesis reaction. Hereby, a range of complex carbocyclic structures are easily available as chiral building blocks from cheap sugar starting materials by two consecutive organometallic transformations.

We thank the Danish Natural Science Research Council for financial support.

Notes and references

1 L. F. Tietze, *Chem. Rev.*, 1996, **96**, 115; L. F. Tietze and U. Beifuss, *Angew. Chem., Int. Ed. Engl.*, 1993, **32**, 131.
2 D. I. Dalko and P. Sinaÿ, *Angew. Chem., Int. Ed.*, 1999, **38**, 773; R. J. Ferrier and S. Middleton, *Chem. Rev.*, 1993, **93**, 2779.
3 I. Ojima, M. Tzamarioudaki, Z. Li and R. J. Donovan, *Chem. Rev.*, 1996, **96**, 635.
4 For recent reviews, see: U. K. Pandit, H. S. Overkleeft, B. C. Borer and H. Bieräugel, *Eur. J. Org. Chem.*, 1999, 959; D. L. Wright, *Curr. Org. Chem.*, 1999, **3**, 211; A. Fürstner, *Top. Organomet. Chem.*, 1998, **1**, 37.
5 For recent applications of ring-closing olefin metathesis in carbohydrate chemistry, see: P. Kapferer, F. Sarabia and A. Vasella, *Helv. Chim. Acta*, 1999, **82**, 645; H. Ovaa, J. D. C. Codée, B. Lastdrager, H. S. Overkleeft, G. A. van der Marel and J. H. van Boom, *Tetrahedron Lett.*, 1999, **40**, 5063; A. Kornienko and M. d'Alarcao, *Tetrahedron: Asymmetry*, 1999, **10**, 827; O. Sellier, P. Van de Weghe, D. Le Nouen, C. Strehler and J. Eustache, *Tetrahedron Lett.*, 1999, **40**, 853.
6 B. Bernet and A. Vasella, *Helv. Chim. Acta*, 1979, **62**, 1990, 2400, 2411; M. Nakane, C. R. Hutchinson and H. Gollman, *Tetrahedron Lett.*, 1980, **21**, 1213; A. Fürstner, D. Jumbam, J. Teslic and H. Weidmann, *J. Org. Chem.*, 1991, **56**, 2213.
7 J.-L. Luche, L. A. Sarandeses, in *Organozinc Reagents—A Practical Approach*, ed. P. Knochel and P. Jones, OUP, Oxford, 1999, p. 307.
8 L. M. Lerner, *Carbohydr. Res.*, 1977, **53**, 177.
9 R. M. Moriarty, J. Kim and H. Brumer III, *Tetrahedron Lett.*, 1995, **36**, 51.
10 M. Chérest, H. Felkin and N. Prudent, *Tetrahedron Lett.*, 1968, 2199; N. T. Anh, *Top. Curr. Chem.*, 1980, **88**, 145.
11 B. M. Trost, J. Dumas and M. Villa, *J. Am. Chem. Soc.*, 1992, **114**, 9836; R. M. Moriarty and H. Brumer III, *Tetrahedron Lett.*, 1995, **36**, 9265.
12 C. Mukai, J. S. Kim, M. Uchiyama and M. Hanaoka, *Tetrahedron Lett.*, 1998, **39**, 7909.
13 P. Schwab, R. H. Grubbs and J. W. Ziller, *J. Am. Chem. Soc.*, 1996, **118**, 100.
14 Structure confirmed by acetylation to the known triacetate: J. Bange, A. F. Haughan, J. R. Knight and J. Sweeney, *J. Chem. Soc., Perkin Trans. 1*, 1998, 1039.
15 T. Hudlicky, H. Luna, H. F. Olivo, C. Andersen, T. Nugent and J. D. Price, *J. Chem. Soc., Perkin Trans. 1*, 1991, 2907.
16 The structure of enantiomeric **9** and **10** was determined by OsO_4 catalyzed dihydroxylation to the same symmetrical quercitol, (1β,2β,3α,4β,5β)-pentahydroxycyclohexane: S. J. Angyal and L. Odier, *Carbohydr. Res.*, 1982, **100**, 43.
17 Structure assigned after hydrogenation of the double bond and ^1H NMR analysis of the resulting cyclohexane.

Communication 9/06953D

ChemComm

A liquid-crystalline hexa-adduct of [60]fullerene

Thierry Chuard,[a] Robert Deschenaux,*[a] Andreas Hirsch*[b] and Hubert Schönberger[b]

[a] *Institut de Chimie, Université de Neuchâtel, Av. de Bellevaux 51, 2000 Neuchâtel, Switzerland. E-mail: robert.deschenaux@ich.unine.ch*

[b] *Institut für Organische Chemie, Universität Erlangen-Nürnberg, Henkestrasse 42, 91054 Erlangen, Germany. E-mail: hirsch@organik.uni-erlangen.de*

Received (in Oxford, UK) 24th June 1999, Accepted 16th August 1999

A hexa-adduct of [60]fullerene was synthesized by addition of a mesomorphic twin cyanobiphenyl malonate derivative to C_{60}; whereas the malonate derivative gave a monotropic nematic phase, the fullerene hexa-adduct showed an enantiotropic smectic A phase.

The recent discovery of [60]fullerene-containing thermotropic liquid crystals[1] is of interest considering the current activity devoted to the search of fullerene-based new materials.[2] The unique magnetic, optical and redox properties of [60]fullerene (C_{60}) and its derivatives motivated these studies.[3]

The above liquid-crystalline mono-adduct C_{60} derivatives[1] were prepared by functionalizing the C_{60} core with a mesomorphic malonate framework containing cholesterol as a mesomorphic promoter. These materials showed smectic A phases.

[60]Fullerene offers multiple possibilities for the design of functionalized derivatives.[4] To further explore the capability of C_{60} to give rise to mesomorphic structures, we focussed on hexa-adducts. Observation of liquid-crystalline properties from such an addition pattern would be of interest to rationalize and better understand the *structure–liquid-crystalline properties* relationship for this new family of liquid crystals.

We describe herein the synthesis, characterization and thermal behavior of the fullerene hexa-adduct **1**, which represents a novel example of a mesomorphic C_{60} derivative, and of the fullerene mono-adduct **2**. Compounds **1**† and **2**† were

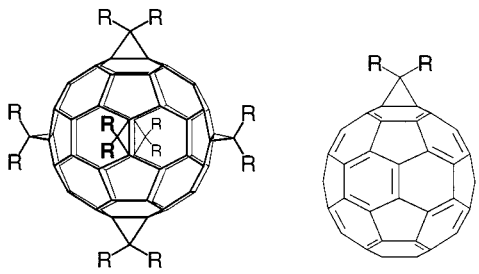

1

2

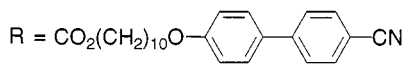

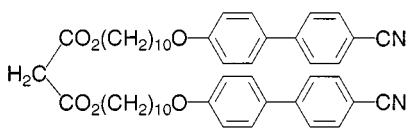

3

prepared by addition of the malonate derivative **3**† to C_{60} in 9 and 43% yield, respectively. The thermal properties of **3** are also reported. The liquid-crystalline phases‡ and thermal properties§ of **1**–**3** were investigated by differential scanning calorimetry (DSC, rate: 10 °C min^{-1} under N_2) and polarized optical microscopy (POM).

Malonate derivative **3** gave a monotropic nematic phase (I → N: 87 °C, ΔH = 2.7 kJ mol^{-1}; N → Cr: 57 °C, ΔH = 50 kJ mol^{-1}; peak transitions)¶ which was identified by POM from the observation of typical *schlieren* and homeotropic textures.

Mono-adduct **2** was found to be non-mesomorphic. The only event which was observed was melting of the sample into the isotropic fluid (Cr → I: 114 °C, ΔH = 31 kJ mol^{-1}; peak transition; first heating run).

Hexa-adduct **1** gave interesting results. By DSC, an endotherm was detected at 133 °C (ΔH = 42 kJ mol^{-1}, *i.e.* 3.5 kJ mol^{-1} per cyanobiphenyl group; onset transition) during the first heating run. Reversibility of this transition was observed during the cooling scan. The formation of a liquid-crystalline phase was observed by POM between about 80 and 133 °C. Slow cooling of the sample from the isotropic fluid revealed the formation of focal-conic and homeotropic textures typical of the smectic A phase (Fig. 1). The transition recorded by DSC at 133 °C corresponded to the clearing point. The fact that no melting point was detected by DSC is, most likely, a consequence of the amorphous character of **1** in the solid state (**1** was recovered by evaporation of the solvents after preparative HPLC†); no glass transition was observed by DSC.

The bulky C_{60} unit acts as a spacer separating the molecules from each other: for mono-adduct **2**, the intermolecular interactions are too weak to generate mesomorphism. The influence of C_{60} can be thwarted by using malonate derivatives possessing a higher liquid-crystalline character than that of **3**, as we have already demonstrated.[1]

The liquid-crystalline behavior of **1** emphasizes the role played by C_{60} in the case of hexa-addition: assembling twelve cyanobiphenyl units around a focal point generates the required structural anisotropy and intermolecular interactions for mesomorphism to occur. It is noteworthy that polyaddition can be used for the preparation of fullerene-containing thermotropic liquid crystals from addends with low liquid-crystalline tendencies. Observation of a smectic A phase for **1** indicates that the cyanobiphenyl units are not oriented radially around the C_{60} but

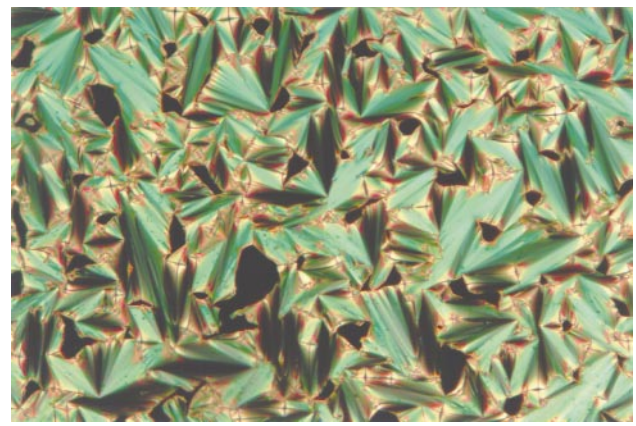

Fig. 1 Thermal optical micrograph of the focal-conic fan texture displayed by **1** in the smectic A phase upon cooling the sample (0.01 °C min^{-1}) from the isotropic liquid to 129 °C.

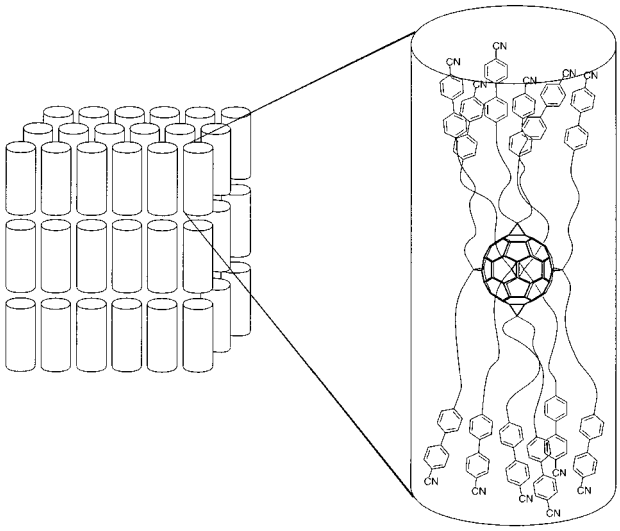

Fig. 2 Proposed model for the organization of **1** within the smectic A phase.

form a cylinder-like structure with the mesogenic fragments oriented upward and downward. Such a structure favors the formation of layers (Fig. 2) as reported for liquid-crystalline dendrimers[5] and siloxysilane derivatives[6] which are analogous to **1**, *i.e.* a central core is functionalized by a large number of mesogenic groups.

The liquid-crystalline properties obtained from the hexa-adduct described above and mono-adducts we recently reported[1] prove that C_{60} can be employed in designing a great variety of mesomorphic materials.

R. D. acknowledges the Swiss National Science Foundation for financial support.

Notes and references

† Experimental procedure for **3**: prepared from 4′-cyano-4-hydroxybiphenyl, 10-bromodecan-1-ol and malonyl chloride analogously to the synthesis of bis{10-{4-[(cholest-5-en-3β-yloxy)carbonyl]phenoxy}decyl} propanedioate [ref. 1(*a*)]; δ_H(400 MHz, $CDCl_3$) 7.68 (d, 4H, arom.), 7.63 (d, 4H, arom.), 7.52 (d, 4H, arom.), 6.98 (d, 4H, arom.), 4.14 (t, 4H, CO_2CH_2), 4.00 (t, 4H, OCH_2), 3.37 (s, 2H, $O_2CCH_2CO_2$), 1.84–1.77 (m, 4H, aliph.), 1.68–1.61 (m, 4 H, aliph.), 1.51–1.43 (m, 4H, aliph.), 1.37–1.25 (m, 20H, aliph.); δ_C(100 MHz, $CDCl_3$) 166.68, 159.76, 145.22, 132.52, 131.21, 128.28, 127.02, 119.07, 115.04, 110.01, 68.11, 65.61, 41.66, 29.44, 29.39, 29.32, 29.18, 29.15, 28.43, 26.00, 25.74. (Anal. calc. for $C_{49}H_{58}N_2O_6$ (771.01): C, 76.33; H, 7.58; N, 3.63. Found: C, 76.17; H, 7.79; N, 3.61%.

For **1**: Under nitrogen, 9,10-dimethylanthracene (116 mg, 0.562 mmol) was added to a solution of C_{60} (40.5 mg, 0.0562 mmol) in PhMe (60 ml, HPLC grade). The solution was stirred for 2 h. Then **3** (433.6 mg, 0.562 mmol), CBr_4 (186.1 mg, 0.562 mmol) and DBU (171 mg, 1.125 mmol) were added. The mixture was stirred for 3 weeks protected from light and evaporated to dryness. The crude mixture was purified by flash-chromatography on silica gel 60 (0.04–0.063 nm, Merck); elution with hexane (to remove 9,10-dimethylanthracene) and then with PhMe–EtOAc 96 : 4 gave **1** ($R_f \cong 0.25$, PhMe–EtOAc 96 : 4, Riedel-de Haen TLC-Sheets 60 F254) which was detected by mass spectrometry (see below). Further purification of the recovered sample by preparative HPLC (diameter of the column: 2 cm, elution rate: 15 ml min^{-1}) on Nucleosil (5μ) (first: PhMe–EtOAc 95.5 : 4.5, 9.1 min; second: PhMe–EtOAc 97 : 3, 26.3 min) gave pure **1** (26.8 mg, 9%) as a pale yellow solid. δ_H(400 MHz, $CDCl_3$) 7.66 (d, 24 H, arom.), 7.60 (d, 24H, arom.), 7.49 (d, 24H, arom.), 6.95 (d, 24H, arom.), 4.23 (t, 24H, CO_2CH_2), 3.96 (t, 24H, OCH_2), 1.80–1.73 (m, 24H, aliph.), 1.71–1.64 (m, 24H, aliph.), 1.45–1.37 (m, 24H, aliph.), 1.36–1.23 (m, 120H, aliph.); δ_C(100 MHz, $CDCl_3$) 163.84, 159.74, 145.79, 145.13, 141.13, 132.52, 131.24, 128.77, 126.99, 119.00, 115.02, 110.09, 69.13, 68.10, 66.95, 45.45, 29.52, 29.48, 29.41, 29.24, 28.42, 26.06, 25.83; *m/z* (FAB-MS, NBA), 5334 (M^+).

For **2**: To a solution of C_{60} (193 mg, 0.268 mmol) and **3** (201 mg, 0.261 mmol) in dry PhMe (100 ml), were added CBr_4 (93 mg, 0.280 mmol) and then, dropwise, DBU (78 mg, 0.512 mmol). The reaction mixture was stirred at room temperature for 18 h under light protection and concentrated. Purification of the residue by column chromatography (silica gel, 0.070–0.200 mm, SDS; eluent: PhMe) and crystallization (PhMe–EtOAc, overnight at room temperature and then for one day at 8 °C) gave pure **2** (163 mg, 43%). δ_H(400 MHz, $CDCl_3$) 7.68 (d, 4H, arom.), 7.63 (d, 4 H, arom.), 7.51 (d, 4 H, arom.), 6.97 (d, 4 H, arom.), 4.50 (t, 4H, CO_2CH_2), 3.99 (t, 4H, OCH_2), 1.88–1.76 (m, 8H, aliph.), 1.48–1.29 (m, 24H, aliph.) Anal. calc. for $C_{109}H_{56}N_2O_6$ (1489.65): C, 87.89; H, 3.79; N, 1.88. Found: C, 87.89; H, 3.99; N, 1.84%.

‡ Cr = crystal state, I = isotropic liquid, N = nematic phase.

§ For instrumentation, see: R. Deschenaux, F. Turpin and D. Guillon, *Macromolecules*, 1997, **30**, 3759.

¶ Two crystalline forms, which melted at 85 and 96 °C (onset transitions), were observed by POM. Those crystals with the higher melting point, initially present as traces, grew slowly upon annealing the sample at 88 °C.

1 (*a*) T. Chuard and R. Deschenaux, *Helv. Chim. Acta*, 1996, **79**, 736; (*b*) R. Deschenaux, M. Even and D. Guillon, *Chem. Commun.*, 1998, 537; (*c*) B. Dardel, R. Deschenaux, M. Even and E. Serrano, *Macromolecules*, 1999, **32**, 5193.

2 M. Prato, *J. Mater. Chem.*, 1997, **7,** 1097.

3 C. Boudon, J.-P. Gisselbrecht, M. Gross, L. Isaacs, H. L. Anderson, R. Faust and F. Diederich, *Helv. Chim. Acta*, 1995, **78**, 1334; C. S. Foote, *Top. Curr. Chem.*, 1994, **169**, 347; P.-M. Allemand, K. C. Khemani, A. Koch, F. Wudl, K. Holczer, S. Donovan, G. Gruner and J. D. Thompson, *Science*, 1991, **253**, 301; P. W. Stephens, D. Cox, J. W. Lauher, L. Mihaly, J. B. Wiley, P.-M. Allemand, A. Hirsch, K. Holczer, Q. Li, J. D. Thompson and F. Wudl, *Nature*, 1992, **355**, 331.

4 F. Djojo and A. Hirsch, *Chem. Eur. J.*, 1998, **4**, 344.

5 M. W. P. L. Baars, S. H. M. Söntjens, H. M. Fischer, H. W. I. Peerlings and E. W. Meijer, *Chem. Eur. J.*, 1998, **4**, 2456; J. Barbera, M. Marcos and J. L. Serrano, *Chem. Eur. J.*, 1999, **5**, 1834; I. M. Saez and J. W. Goodby, *Liq. Cryst.*, 1999, **26**, 1101.

6 J. W. Goodby, G. H. Mehl, I. M. Saez, R. P. Tuffin, G. Mackenzie, R. Auzély-Velty, T. Benvegnu and D. Plusquellec, *Chem. Commun.*, 1998, 2057; G. H. Mehl and J. W. Goodby, *Chem. Commun.*, 1999, 13.

Communication 9/05058B

A chemiluminescent catalytic antibody†

James D. Stevenson, Anja Dietel and Neil R. Thomas*

School of Chemistry, University of Nottingham, University Park, Nottingham, UK NG7 2RD. E-mail: neil.thomas@nottingham.ac.uk

Received (in Cambridge, UK) 12th August 1999, Accepted 9th September 1999

A monoclonal antibody elicited against a phosphonate transition state analogue was shown to initiate chemiluminescence from luminogenic spiro[adamantane-2,3′-(1,2-dioxetane)] substrates by selectively cleaving a benzoate ester triggering group.

Serendipity has played a large part in the identification of many of the catalytic antibodies reported in the literature to date.[1] Typically, 5–50 monoclonal antibodies selected on the basis of their affinity for a transition-state analogue as judged by Enzyme-Linked ImmunoSorbent Assay (ELISA)[2] have been produced in sufficient quantity to screen for catalytic activity. Such an approach has led to the identification of, at best, a handful of catalysts. Given that the humoral response generates at least 10^8 unique antibody binding sites, only a tiny fraction are examined for their catalytic activity. The probability of identifying the most efficient antibody catalyst for any given reaction from the library available using this approach is therefore very low, as screening for catalysis only occurs at a late stage. As a result it is currently difficult to optimise either the design of the antigen to elicit antibodies for a specific reaction, or the immunisation and immortalisation protocol (*in vivo* or *in vitro*, hybridoma or bacteriophage display) used in their creation. In order to overcome this limitation we present here an example of the use of a chemiluminescent reporter assay in the identification of an antibody catalyst.[3] Chemiluminescent assays benefit from low background interference and are finding increasing use in the analytical laboratory. The assay system described here offers the opportunity for catalytic activity to be detected at an early stage in antibody production when only small quantities of antibody are available, and hence should allow large libraries of antibodies or other materials to be screened for hydrolytic activities.

Recently, a number of papers have appeared which use either *screening* or *selection* methods for the identification of new catalysts: the complementation of auxotrophic bacteria,[4] the use of fluorogenic substrates,[5] immobilised mechanism based inhibitors,[6] catELISA,[7] proximity coupling,[8] or pH indicators.[9] Compared to many of these approaches the highly sensitive chemiluminescent assay system based around a spiroadamantyl-substituted dioxetane substrate offers a simple one-step approach for which automated equipment is already commercially available.

Thermally stable spiroadamantyl-substituted dioxetanes, which undergo enzyme triggered chemiluminescence, have been developed for use in chemiluminescent reporter assays.[10] These luminogenic substrates undergo Chemically Initiated Electron-Exchange Luminescence (CIEEL) following cleavage of a triggering group which can be tailored to the desired enzyme activity. The dioxetanes offer the advantages of an efficient chemiluminescent reaction (ϕ_{CL} = 10^{-3}–10^{-6} in aqueous solution) which has both a long half-life and low background interference. To determine the utility of CIEEL for identifying new catalytic activities we chose the simple example

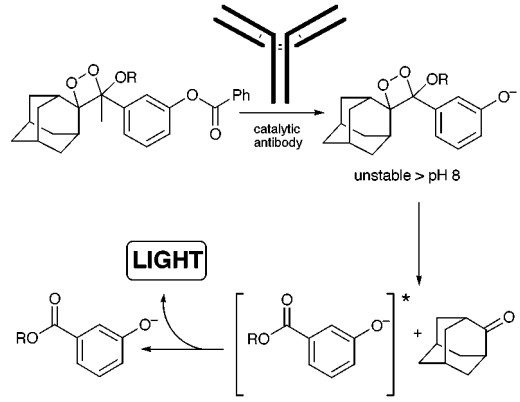

Scheme 1

of ester hydrolysis (Scheme 1), and designed a transition-state analogue (hapten **1**)† based around a phosphonate core accordingly. In order to direct most of the antibody–antigen recognition towards the phosphonate portion of the transition-state analogue, the reactive and potentially immunogenic adamantyl dioxetane moiety was omitted from hapten **1**. The position of the linker arm in the hapten for attachment to an appropriate carrier protein was chosen to orientate the dioxetane group away from the antigen binding site. This ensures that the excited ester generated following dioxetane decomposition will be released quickly from the antigen binding site, minimising the possibility of quenching of the excited state through molecular collision with the antibody, rather than through light emission.

Hapten **1** was conjugated to both Bovine Serum Albumin (BSA) and Keyhole Limpet Hemocyanin (KLH) *via* its *N*-hydroxysuccinimide ester, using standard carbodiimide chemistry.[11] The degree of conjugation to the relevant carrier protein was established using the trinitrobenzenesulfonic acid (TNBS) assay.[12]

Three Balb/c mice were hyperimmunised with the KLH conjugate (4 × 100 μg per mouse) over a period of 15 weeks, and hybridomas were generated from the spleens of these mice by fusion with P3X63Ag8 myeloma cells using standard protocols.[13] Twenty-six hybridomas producing antibodies specific for hapten **1** were identified by ELISA, and 10 of these were selected for cloning.

Substrate **2** was synthesised by modifying a route previously described.[14] Introduction of the benzoate triggering group could

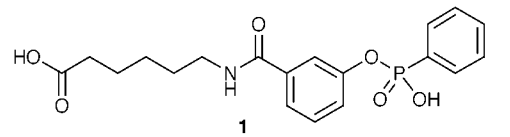

1

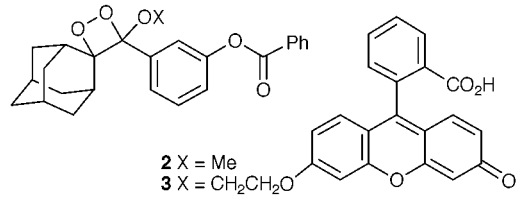

† Experimental details for the preparation and characterisation of hapten **1** and substrates **2** and **3,** and the monoclonal antibodies together with kinetic data are provided as electronic supplementary information. See http://www.rsc.org/suppdata/cc/1999/2105/

only be accomplished on the methyl enol ether intermediate, and not on the 3-hydroxyaryl spiroadamantyl dioxetane itself. The conditions for the chemiluminescent assay were as follows: the antibody (2 μM final concentration) was taken up in 190 μl of Tris HCl (50 mM, pH 9.0) in individual microtitre plate wells and was preincubated at 30 °C. The dioxetane **2** in MeCN (10 μl) (at the appropriate stock concentration to give a final substrate concentration of 1–100 μM in the incubation) was then added, and the light generated over a period of 2 h was measured using a Dynex MLX Microtitre® plate luminometer. The chemiluminescent decomposition of **2** occurs in a reasonable quantum yield ($\phi_{CL} = 1.4 \times 10^{-5}$), however, this was significantly improved by addition of fluorescein (2 mM) to the incubation medium ($\phi_{CL} = 1.0 \times 10^{-4}$). A further improvement in signal was obtained by covalently tethering the fluorescein to the dioxetane substrate **3** ($\phi_{CL} = 1.1 \times 10^{-3}$).[10] This increases the quantum yield from 0.0012% for the phenolate generated from **2** to 0.39% for the phenolate from **3** due to the efficient intramolecular energy transfer to the fluorescer. In turn this extends the lower detection limit for dioxetane decomposition from 10^{-13} moles for **2** to 10^{-16} moles for **3**. The synthetic route for the preparation of substrate **3** is described in the supporting material.† The increase in sensitivity it provides is clearly seen in Fig. 1, which also demonstrates that the antibodies are capable of at least five substrate turnovers per antigen-binding site.

Of the eight monoclonal antibodies which survived to this stage, antibody 7F11 was identified as an active catalyst and produced a chemiluminescent signal which was well above background levels with both dioxetane substrates. Larger quantities of this antibody were produced for detailed kinetic studies. The antibody-catalysed hydrolysis obeyed saturation kinetics with $k_{cat} = 0.020\ s^{-1}$, $K_m = 2.5$ μM for substrate **2** and $k_{cat} = 0.0028\ s^{-1}$, $K_m = 3.1$ μM for substrate **3** respectively. The lower k_{cat} value for substrate **3** can be explained by an increased amount of non-productive binding of this substrate (the reaction is inhibited by fluorescein which bears some structural resemblance to the hapten). No light was detected in the absence of the antibody, or in the presence of non-catalytic mAb's with either substrate. Therefore, assuming an upper limit for k_{uncat} of $1 \times 10^{-8}\ s^{-1}$ based on the detection limit of the chemiluminescent assay, the rate enhancement (k_{cat}/k_{uncat}) observed is 2.0×10^6 for substrate **2**, and 2.8×10^5 for substrate **3**, respectively. This suggests that 7F11 is one of the most efficient antibodies at catalysing benzoate hydrolysis that has yet been obtained,[1] although it is still several orders of magnitude slower than comparable esterases. The antibody is inhibited competitively by hapten **1** with Dixon analysis of the kinetic data affording a K_i value of 97 nM.† This result demonstrates that the catalysis is due to an antibody, rather than a contaminating enzyme. We are currently producing a single-chain antigen-binding fragment of 7F11 to further confirm this fact.

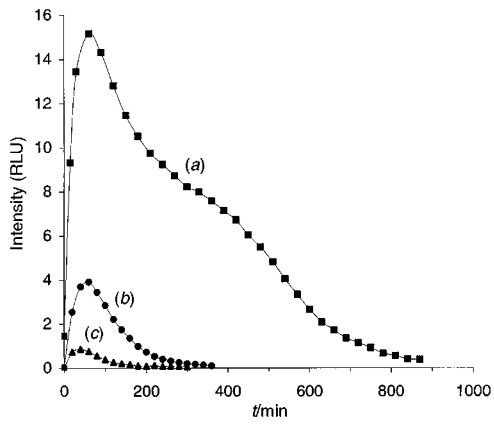

Fig. 1 Total light emission for 20 μM dioxetane (**2** or **3**) in 200 μl of 50 mM Tris buffer at pH 9.0, 37 °C in the presence of antibody 7F11 (2 μM): (*a*) **3**, (*b*) **2** + fluorescein (2 mM) and (*c*) **2**.

In conclusion we have shown that it is possible to identify antibody catalysts using a chemiluminescent substrate system. The absolute sensitivity of the assay using substrate **3** is sufficient for detection of catalysts in hybridoma supernatants or phage-displayed antibody libraries[5] and these are currently being screened. Modification of the spiroadamantyl dioxetane to allow screening of other hydrolytic activities, and for 'remote' release is currently underway. The use of the chemiluminescent catalytic antibody in a chemiluminescent imaging system is being investigated as a possible replacement for enzyme–secondary antibody conjugates, or for enzyme–antibody/protein A fusion proteins as required by ELISA.[15] These self-marking antibodies could be useful in a wide range of immunochemical assays including microtitre plate immunoassays, immunoblotting and immunohistochemistry.

This research was supported by a Royal Society Fellowship to N. R. T., an EPSRC studentship to J. D. S. and funding from the University of Nottingham. Drs Michael Price, Graeme Denton and Barbara Gunn are acknowledged for their assistance in the creation of monoclonal antibodies, and Dr Nigel Kenward for useful discussions.

Notes and references

1 Reviews: D. R. Liu and P. G. Schultz, *Angew. Chem., Int. Ed.,* 1999, **38**, 36; J.-L. Reymond, *Top. Curr. Chem.,* 1999, **200**, 59; G. M. Blackburn, A. Datta, H. Denham and P. Wentworth, *Adv. Phys. Org. Chem.,* 1998, **31**, 249; N. R. Thomas, *Nat. Prod. Rep.,* 1996, **13**, 479.

2 J. R. Crowther, *ELISA Theory & Practice*, Humana Press, Totowa, New Jersey, 1995.

3 A synthesis for an alternative hapten and proposed antibody chemiluminescence reaction was reported during the course of this work: M. Sawa, Y. Imaeda, J. Hiratake, R. Fujii, R. Umeshita, M. Watanabe, H. Kondo and J. Oda, *Bioorg. Med. Chem. Lett.,* 1998, **8**, 647. However the generation of an antibody catalyst by these workers has yet to be reported. A catalytic antibody for the luminol-peroxidase reaction has also been reported: L. J. Kricka and X. Ji, *Biolumin. Chemilum.: Proc. Int. Symp. 7th 1993,*1993, 518. The authors were not able to demonstrate unequivocally that this activity, which was short-lived, was not due to a contaminating enzyme, or purely a hydrophobic effect.

4 J. A. Smiley and S. J. Benkovic, *Proc. Natl. Acad. Sci. U.S.A.,* 1994, **91**, 8319.

5 N. Bensel, N. Bahr, M. T. Reymond, C. Schenkels and J.-L. Reymond, *Helv. Chim. Acta,* 1999, **82**, 44

6 B. Avalle, S. Vanwetswinkel and J. Fastrez, *Bioog. Med. Chem. Lett.,* 1997, **7**, 479; C. F. Barbas, A. Heine, G. F. Zhong, T. Hoffman, S. Gramatikova, R. Bjornestedt, B. List, J. Anderson, E. A. Stura, I. A. Wilson and R. A. Lerner, *Science*, 1997, **278**, 2085.

7 F. Taran, P. Y. Renard, C. Creminon, A. Valleix, Y. Frobert, P. Pradelles, J. Grassi and C. Mioskowski, *Tetrahedron Lett.,* 1999, **40**, 1887, 1891; G. Macbeath and D. Hilvert, *J. Am. Chem. Soc.,* 1994, **116**, 6106; D. S. Tawfik, B. S. Green, R. Chap, M. Sela and Z. Eshhar, *Proc. Natl. Acad. Sci. U.S.A.,* 1993, **90**, 373.

8 J.-L. Jestin, P. Kristensen and G.Winter, *Angew. Chem., Int. Ed.,* 1999, **38**, 1196; H. Pedersen, S. Hölder, D. P. Sutherlin, U. Schwitter, D. S. King and P. G. Schultz, *Proc. Natl. Acad. Sci. U.S.A.,* 1998, **95**, 10 523.

9 L. E. Janes, A. C. Lowendahl and R. J. Kazlauskas, *Chem. Eur. J.,* 1998, **4**, 2324.

10 A. P. Schaap, R. S. Handley and B. P. Giri, *Tetrahedron Lett.,* 1987, **28**, 935; S. Beck and H. Köster, *Anal. Chem.,* 1990, **62,** 2258; A. P. Schaap and H. Akhavan-Tafti, US Patent (U.S.P. WO90/07511) 1990**;** W. Adam, I. Bronstein, A. V. Tromfimov and R. F. Vasilev, *J. Am. Chem. Soc.,* 1999, **121**, 958.

11 G. T. Hermanson, *Bioconjugate Techniques*, AP, San Diego, 1996, p. 169.

12 R. B. Saishidhar, A. K. Capoor and D. Ramana, *J. Immunol. Methods,* 1994, **167**, 121. An average hapten density of 24 copies of **1** per BSA was found, whilst 49% of the free lysines in the polymeric KLH had been derivatised.

13 E. Harlow and D. Lane, *Antibodies: A Laboratory Manual*, Cold Spring Harbor, New York, 1988.

14 R. Curci, L. Lopez, L. Troisi, S. M. K. Rashid and A. P. Schaap, *Tetrahedron Lett*., 1987, **28**, 5319.

15 R. E. Kontermann, P. Martineau, C. E. Cummings, A. Karpas, D. Allen, E. Derbyshire and G. Winter, *Immunotechnology*, 1997, **3**, 137.

Communication 9/06566K

ChemComm

A novel and highly regioselective Cr-mediated route to functionalised quinone boronic ester derivatives

Mark W. Davies,[a] Christopher N. Johnson[b] and Joseph P. A. Harrity*[a]

[a] *Department of Chemistry, University of Sheffield, Brook Hill, Sheffield, UK S3 7HF. E-mail: j.harrity@sheffield.ac.uk*

[b] *Discovery Chemistry Europe, SmithKline Beecham, New Frontiers Science Park, Harlow, Essex, UK CM19 5AW*

Received (in Liverpool, UK) 10th August 1999, Accepted 13th September 1999

A novel and highly regioselective route to quinone boronic ester derivatives has been developed using a Fischer carbene mediated benzannulation process.

Arylboronic acids and esters represent one of the most heavily utilised classes of synthetic intermediates of recent times.[1] These compounds are typically prepared using alkyllithium or Grignard reagents and a suitable boronic ester or halide. More recently, palladium catalysed coupling of aryl halides with alkoxydiboron[2] or alkoxyborane[3] reagents has provided a mild alternative for conducting this transformation. In an effort to develop an efficient method for the preparation of complex aryl boronic esters, we envisaged a conceptually novel approach to these compounds by the employment of a Dötz annulation reaction[4] of Fischer carbene complexes[5] with alkynylboronates.[6] As illustrated in Scheme 1, this approach would provide a direct technique for the assembly of highly functionalised boronic ester derivatives from simple starting materials. We were mindful that disubstituted alkynes generally undergo insertion with low levels of regioselectivity[7] and therefore our initial goal was to investigate whether arylboronic esters could be prepared in this manner with useful levels of regiocontrol.

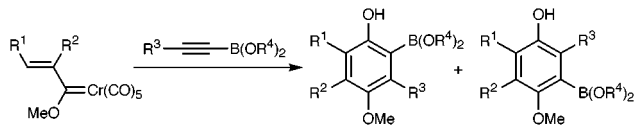

Scheme 1

As shown in Scheme 2, we were pleased to find that complex **1** reacted smoothly with pinacol ester **2** to provide arylboronate **3** in excellent yield, and remarkably, as a single regioisomer. Notably, a minor quantity of deboronated cyclisation product **4** was also produced but was easily separated from **3** by chromatography. The origin of the generation of **4** has not been unambiguously established although it likely arises from protodeboronation of **2** followed by annulation of the terminal alkyne.[8] The regiochemistry of boronate ester **3** was elucidated by X-ray crystallography and shows that the boronate unit is inserted adjacent to the methoxy unit.[9] We also examined the

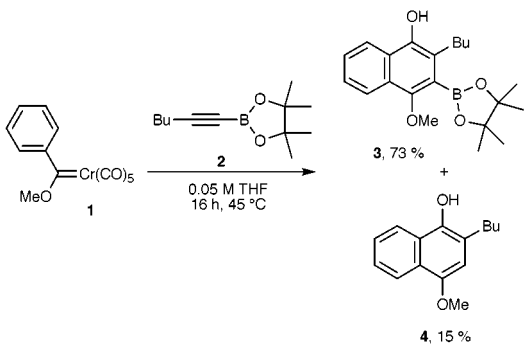

Scheme 2

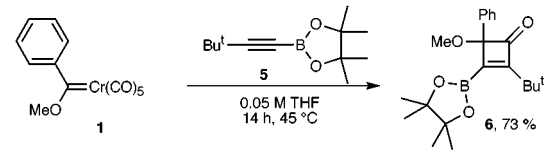

Scheme 3

scope of the cyclisation process with respect to sterically hindered alkynylboronates (Scheme 3). The employment of *tert*-butyl substituted boronate **5** led only to the formation of cyclobutenone **6**. This result is in accord with Yamashita's observations that bulky electron deficient alkynes provide cyclobutenone products at the expense of benzannulated compounds.[10] Nonetheless, again a single regioisomer was observed and the product displayed an analogous insertion pattern to that outlined in Scheme 2.[9]

Having developed the technique to access hydroquinone boronic esters we turned our attention to conversion of these compounds to the corresponding quinones. As outlined in Scheme 4, hydroquinone **3** was oxidised smoothly to **7** in good yield with cerium ammonium nitrate in only 30 min at room temperature. *Significantly, these quinones represent a novel class of boronic esters and are a potentially valuable source of a range of quinone containing medicinally important agents.*[11] Whilst a thorough investigation of the functionalisation of the carbon–boron bond must await future studies, we have found that **7** is readily further oxidised to hydroxyquinone **8** through treatment with basic H_2O_2 for 20–30 min.

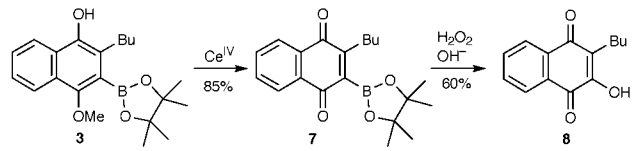

Scheme 4

In general, direct oxidation of the crude reaction mixture after benzannulation provided a simple and routine method for the isolation of quinone boronic ester compounds (Scheme 5). We briefly investigated the scope of this technique with respect to alkynylboronates and Fischer carbene complexes, as shown in Table 1.

Initial screening showed the reaction to be efficient in both polar and non-polar solvents. However, THF gave consistently higher yields of boronate esters. We attempted to promote the reaction by the employment of dry state conditions (Table 1, entry 3).[12] Unfortunately, adsorption onto silica gel served only

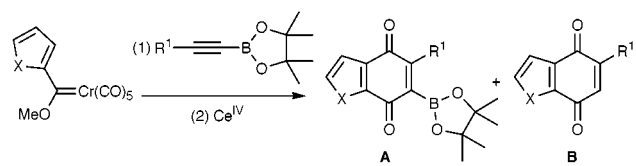

Scheme 5

Table 1 Benzannulation reaction of alkynylboronates and Fischer carbene complexes (see Scheme 5)

Entry	X	R^1	Conditions[a]	Product **A**	Yield (%)	Product **B**	Yield (%)
1	CH=CH **1**	Bu **2**	THF, 45 °C	**7**	66	**9**	6
2	CH=CH **1**	Bu **2**	Hexane, 45 °C	**7**	62	**9**	35
3	CH=CH **1**	Bu **2**	SiO_2, 45 °C	**7**	0	**9**	84
4	O **10**	Bu **2**	THF, 65 °C	**11**	47	**12**	30
5	CH=CH **1**	Ph **13**	THF, 45 °C	**14**	57	**15**	12
6	O **10**	Ph **13**	THF, 65 °C	16	35	**17**	42

[a] Reaction conditions: (1) 0.05 M solution of complex and 3 equiv. of alkyne heated for 14–16 h under inert atmosphere. (2) Crude reaction mixture dissolved in Et_2O and stirred for 0.5 h with 0.5 M Ce^{IV} in 0.1 M aq. HNO_3.

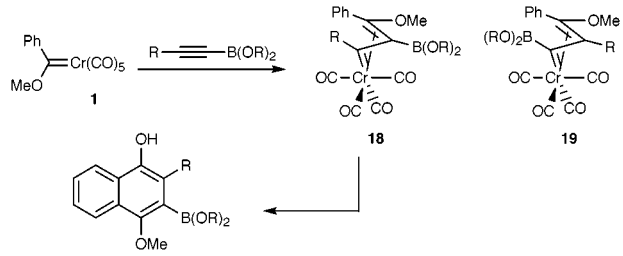

Scheme 6

to provide quinone **9**, albeit in high yield. The reaction was found to be readily extended to furan complex **10**, although higher temperatures and longer reaction times were generally required for complete conversion and resulted in the recovery of larger quantities of deboronated products (entries 4 and 6, Table 1). Nonetheless, these quinones were again isolated as single regioisomers.[13]

The origin of the high preference of insertion of the boronate group in the more hindered position adjacent to the MeO group is not clear at this time, however we are currently investigating three possible rationales. The insertion may simply be sterically controlled and therefore follows traditional insertion patterns where the boronate unit acts as the sterically less demanding group.[14] Alternatively, Hofmann has proposed that η^3-vinylcarbene complex intermediates are responsible for controlling regiochemical insertion patterns.[15] Therefore, **19** may be energetically disfavoured due to the positioning of the electron withdrawing boronate unit adjacent to the electrophilic carbene carbon atom (Scheme 6). Finally, a model proposed by Wulff to explain the contrasteric insertion of alkynylstannanes in the benzannulation process may be invoked whereby the regiochemistry is controlled by a Lewis acid/base interaction [CO→B(OR)$_2$] in the metallohexatriene intermediate **18**, thus directing regiochemical insertion.[16]

In conclusion, this study provides a rapid and efficient approach to a novel class of hydroquinone and quinone boronate esters.[17] Additionally, the boron unit is incorporated into these structures in a reliable and predictable fashion, and with excellent selectivity. Studies on the origin of regioselectivity are currently underway as are the employment of these intermediates in transition metal catalysed C–C coupling reactions.

The authors are grateful to the EPSRC for a studentship (M. W. D.) and to SmithKline Beecham for generous financial support. We also wish to thank Dr S.L. Heath and Mr H. Adams for assistance with X-ray data.

Notes and references

1 For a review see: A. Suzuki, *Pure Appl. Chem.*, 1994, **66**, 213.
2 T. Ishiyama, M. Murata and N. Miyaura, *J. Org. Chem.*, 1995, **60**, 7508.
3 M. Murata, S. Watanabe and Y. Masuda, *J. Org. Chem.*, 1997, **62**, 6458.
4 For a recent review see: K. H. Dötz and P. Tomuschat, *Chem. Soc. Rev.*, 1999, **28**, 187.
5 For an overview on the synthesis of Fischer carbene complexes see: E. O. Fischer, C. G. Kreiter, H. J. Kollmeier, J. Muller and R. D. Fischer, *J. Organomet. Chem.*, 1971, **28**, 237.
6 For the synthesis of alkynylboronates, see: H. C. Brown, N. G. Bhat and M. Srebnik, *Tetrahedron Lett.*, 1988, **29**, 2631.
7 W. D. Wulff, P. C. Tang and J. S. McCallum, *J. Am. Chem. Soc.*, 1981, **103**, 7677; K .H. Dötz, J. Muhlemeier, U. Schubert and O. Orama, *J. Organomet. Chem.*, 1983, **247**, 187; W. D. Wulff, K. S. Chan and P. C. Tang, *J. Org. Chem.*, 1984, **49**, 2293.
8 Alkynylboronates are readily hydrolysed to the parent alkyne in the presence of protic reagents, (ref. 6), it is therefore plausible that the phenolic benzannulated product mediates alkyne protodeboronation. Indeed, hex-1-yne was recovered in the volatile material isolated from the reaction mixture in Table1, entry 1.
9 *Crystal data* for **3**: $C_{21}H_{29}BO_4$, M = 356.25, triclinic, a = 9.4916(6), b = 11.1685(8), c = 18.9638(13) Å, α = 90.1890(10), β = 91.2770(10), γ = 92.5080(10)°, U = 2007.9(2) Å^3, Z = 4, D_c = 1.179 g cm^{-3}, space group $P\bar{1}$ (no. 2), T = 150 K, Mo-Kα radiation (λ = 0.71073 Å), μ(Mo-Kα) = 0.079 mm^{-1}, F(000) = 768. Data were collected in the range 1.83 < θ < 28.36°, 5420 independent reflections (R_{int} = 0.0549), final R = 0.0778, with allowance for the thermal anisotropy of all non-hydrogen atoms. For **6**: $C_{21}H_{29}BO_4$, M = 356.25, monoclinic, a = 8.845(2), b = 19.493(5), c = 12.055(3) Å, β = 103.804(6)°, U = 2018.5(10) Å^3, Z = 4, D_c = 1.172 g cm^{-3}, space group $P2_1/n$ (a non-standard setting of $P2_1/c$, no. 14), T = 150 K, Mo-Kα radiation (λ = 0.71073 Å), μ(Mo-Kα) = 0.079 mm^{-1}, F(000) = 768. Data were collected in the range 2.03 < θ < 28.31°, 1895 independent reflections (R_{in} = 0.0932), final R = 0.0618, with allowance for the thermal anisotropy of all non-hydrogen atoms. CCDC 182/1418.
10 A. Yamashita and A. Toy, *Tetrahedron Lett.*, 1986, **27**, 3471.
11 For example see: *Anthracycline and Anthracenedione - Based Anticancer Agents*, in *Bioactive Molecules*, ed. J. W. Lown, Elsevier, Oxford, 1988, vol. 6.
12 J. P. A. Harrity, W. J. Kerr and D. Middlemiss, *Tetrahedron Lett.*, 1993, **34**, 2995.
13 The rigorous establishment of compounds **11** and **16** is ongoing but at present is assumed to follow the same insertion patterns as outlined in Scheme 4.
14 The *A* value of the alkynyl substituent can often serve as a useful guide to predicting regioselectivity (ref. 10). In this context, studies are underway to determine the *A* value of a range of boronic ester moieties and will be the subject of a future disclosure.
15 P. Hofmann, M. Hämmerle and G. Unfried, *New J. Chem.*, 1991, **15**, 769.
16 S. Chamberlin, M. L. Waters and W. D. Wulff, *J. Am. Chem. Soc.*, 1994, **116**, 3113.
17 Typical experimental procedure as exemplified by benzannulation of complex **1** and alkyne **2** (Scheme 2): to a solution of **1** (102 mg, 0.327 mmol) in THF (6.4 ml) was added alkyne **2** (204 mg, 0.980 mmol) *via* syringe under nitrogen. The reaction mixture was stirred at 45 °C for 14 h and concentrated by rotary evaporation. Purification of the resulting residue by silica gel chromatography provided hydroquinone **4** (ref. 18) (11 mg, 15%) and boronate ester **3** (85 mg, 73%) which could be crystallised from hexanes to provide an amber solid, mp 116–116.5 °C.; δ_H (250 MHz, $CDCl_3$)0.96 (3H, t, J 7.3, CH_3CH$_2$), 1.42 (12H, s, CH_3), 1.47–1.72 (4H, m, CH$_2$CH_2CH$_3$), 2.73 (2H, app t, J 7.9, C=CCH_2), 3.91 (3H, s, CH_3O), 4.93 (1H, br s, O*H*), 7.39–7.53 (2H, m, Ar-*H*) 7.95–8.03 (1H, m, Ar-*H*), 8.05–8.13 (1H, m, Ar-*H*); δ_C (62.9 MHz, $CDCl_3$) 14.1, 24.7, 24.9, 30.2, 33.0, 63.5, 84.0, 121.6, 122.0, 124.3, 125.2, 125.9, 126.6, 144.4, 153.9; ν_{max}/cm^{-1} 3445 (br), 2991 (m), 2977 (m), 1662 (m), 1142 (s) (calc. for $C_{21}H_{29}BO_4$: C, 70.80; H, 8.20. Found: C, 70.67; H, 8.36%).
18 ^{13}C and ^{1}H spectra of **4** were identical to an authentic sample prepared from hex-1-yne: A. Yamashita, S. Ayako, R. G. Schaub, M. K. Bach, G. J. White and A. Toy, *J. Med. Chem.*, 1990, **33**, 775.

Communication 9/06643H

Catalysis of aldehyde imination by hydrogen bonding with a simple organic disulfonamide receptor

Konstantinos Kavallieratos† and Robert H. Crabtree*

Sterling Chemistry Laboratory, Department of Chemistry, Yale University, PO Box 208107, New Haven, CT 06520-8107, USA. E-mail: robert.crabtree@yale.edu

Received (in Columbia, MO, USA) 9th July 1999, Accepted 15th September 1999

The disulfonamide receptor 1 catalyzes imine formation from aldehyde and amine, apparently by binding the transition state for the rate-determining nucleophilic attack of amine on the aldehyde.

Catalysis by abiotic receptors[1] is a rapidly developing field in supramolecular chemistry, and systems have been developed that mimic enzyme properties by binding preferentially the transition state over the ground (reactant) state.[2] Most compounds developed for that purpose are macrocycles.[3] Molecular clefts with appropriately convergent recognition sites can give unexpectedly strong binding for anionic substrates[4] and some elegant examples of open clefts catalyzing reactions involving anionic transition states *via* hydrogen bonding have been reported.[5] The increased skeleton flexibility in open clefts *vs.* macrocycles can be favorable for catalysis if the open-chain receptor accommodates better the changes along the reaction coordinate.[1b] In other examples, interaction of the anionic intermediate with a metal center[6] rather than with a hydrogen bond donor group is responsible for catalysis. Some of the reported cases[6b–f] involve imine formation catalysis.

Receptor **1** seemed a good choice as an imine formation

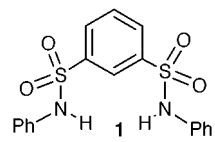

1

catalyst because it is known[4b] to bind strongly to halide ions as well as acetate [*e.g.* $K_a(M^{-1}) = 2.1 \times 10^4$ for the 1:1 complex with OAc^-]. The reaction of an aldehyde with an amine to give an imine was chosen as the catalytic reaction because the rate determining[7] nucleophilic attack of amine has a R(Nu)HC–O^- transition state that should be bound more tightly than the starting aldehyde. The imine product, having only one lone pair, is not expected to be optimally bound by the receptor, so catalyst poisoning by the imine product should be avoided. We now find that the easily available[4b] disulfonamide **1** catalyzes the reaction of eqn. (1) at −20 °C in CD_2Cl_2 with anhydrous $MgSO_4$ present to remove water (Bn = benzyl).

$$p\text{-}MeC_6H_4CHO + BnNH_2 \rightarrow p\text{-}MeC_6H_4CH{=}NBn + H_2O \quad (1)$$

Initial rate experiments, carried out under pseudo-first order conditions[8] show that **1** (8 mol% *vs.* RCHO) is an effective catalyst for the reaction, causing a 6.1-fold acceleration of imine formation (Figs. 1 and 2) as measured by ^{1}H NMR resonance integrations. The initial rate of imine formation was increased by a factor of 6.1 in the presence of catalyst as compared to the control which did not contain **1**. Eqn. (1) is subject to general acid catalysis, and the most appropriate control is *o*-chlorophenol because it has a pK_a (8.49) most comparable with the disulfonamide **1** (p$K_a \approx 8.05$).[9] As shown in Fig. 1(*c*), even 100 mol% of *o*-chlorophenol only shows a small rate acceleration *versus* 8 mol% of **1** [Fig. 1(*a*)]. 100 mol% of phenol [pK_a = 9.89, Fig. 1(*e*)] gave almost no acceleration. Only much stronger acids, such as *p*-nitrophenol [pK_a = 7.15, Fig. 1(*b*)], gave substantial acceleration.

By analogy with the known[4] mode of association of anions with the receptor, a favorable two point hydrogen bonding interaction of the two convergent sulfonamide groups with the anionic oxygen of the transition state for eqn. (1) (see **2**) may be responsible for catalysis.

The known[4b] binding properties of **1** with oxyanions allow an estimate of the association constant (K_a) for the transition state **2**. For acetate, the observed K_a of 2.1×10^{-4} M^{-1} corresponds to a ΔG of binding of −24.2 kJ mol^{-1}. By transition state theory, often used to predict rate enhancements,[10] the rate acceleration is related to the ratio of the binding constant of the receptor with the transition state *versus* the binding constant with the substrate. We were not able to accurately determine the binding constant with the substrate owing to exchange of the

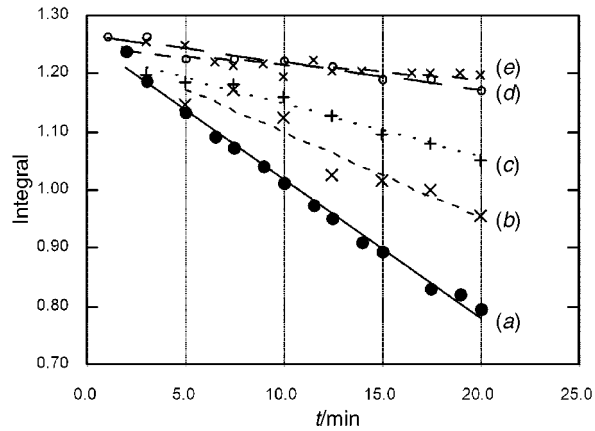

Fig. 1 Initial rate data (change in CHO integral at δ 9.94): (*a*) 8 mol% **1**; (*b*) 8 mol% *p*-nitrophenol, (*c*) 100 mol% *o*-chlorophenol, (*d*) no additive, (*e*) 100 mol% phenol.

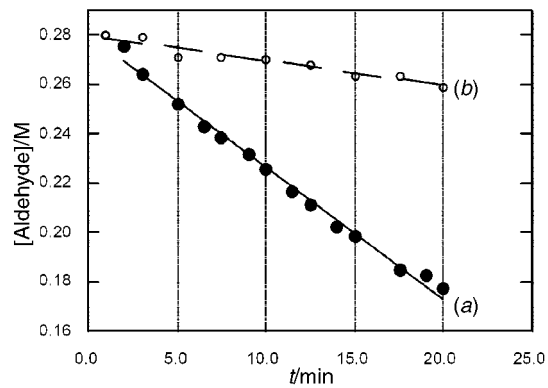

Fig. 2 The decrease of the aldehyde concentration with time (derived from the ^{1}H NMR integral of the aldehyde proton) under pseudo first-order conditions showing (*a*) the catalytic effect of the receptor *versus* (*b*) the uncatalyzed rate.

† Present address: ORNL, Bldg. 4500S, MS-6119, PO Box 2008, Oak Ridge, TN 37831-6119, USA.

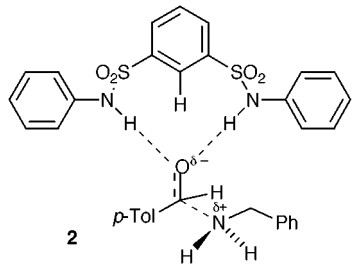

2

N–H sulfonamide resonance with trace protic impurity and the chemical shift change for the C–H aromatic resonance being too small to allow accurate titration monitoring. From literature data,[5a] association constants in CH_2Cl_2 for hydrogen bond receptors having two convergent hydrogen bond donor groups with neutral carbonyl substrates are in the range of 1 to 2×10^3 M^{-1}. Assuming that the transition state is bound to the receptor approximately as well as acetate (2×10^4 M^{-1}) an acceleration factor of 10–20 is predicted, a value comparable with the experimental value of 6.1.

Molecular cleft receptors, even very simple ones like **1**, can be catalytically active for reactions such as eqn. (1), where the transition state for the slow step is thought to be bound more strongly than starting materials or products. As a cleft rather than a macrocycle, this receptor is expected to bind the substrate carbonyl group without significantly blocking access of the nucleophile to the carbonyl.

We thank the US National Science Foundation for funding, and Professor David J. Austin for valuable suggestions.

Notes and references

1 (*a*) A. D. Hamilton, *Frontiers in Bioorganic Chemistry*, H. Dugas ed., Springer, Berlin, 1991, vol. 2. p. 117; (*b*) D. A. Bell and E. V. Anslyn, *Hydrogen-Bonding Receptors: Open-Chain Catalytic Systems*, in *Comprehensive Supramolecular Chemistry*, ed. F. Vögtle, Pergamon, New York, 1996, vol. 2 ch. 14 pp. 439–475; (*c*) M. C. Feiters, *Supramolecular Catalysis*, ed. D. N. Reinhoudt, Pergamon, New York, 1996, vol. 10, ch. 11, pp. 267–360; (*d*) R. Breslow, *Acc. Chem. Res.*, 1995, **28**, 146; (*e*) A. J. Kirby, *Angew. Chem., Int. Ed. Engl.*, 1996, **35**, 707; (*f*) Y. Murakami, J. Kikuchi, Y. Hisaeda and O. Hayashida, *Chem. Rev.* 1996, **96**, 721.

2 B. Zhang and R. Breslow, *J. Am. Chem. Soc.*, 1997, **119**, 1676; M. W. Hosseini, J.-M. Lehn, K. C. Jones, K. E. Plute, K. Bowman-Mertes and M. P. Mertes, *J. Am. Chem. Soc.*, 1989, **111**, 6330; H. Fenniri, C. Dellaire, D. P. Funeriu and J.-M. Lehn, *J. Chem. Soc., Perkin Trans. 2*, 1997, 2073.

3 B. Dietrich, P. Viout and J.-M. Lehn, *Macrocyclic Compounds Chemistry. Aspects of Organic and Inorganic Supramolecular Chemistry*, VCH, Weinheim, 1992; F. Vögtle and E. Weber, *Host Guest Complex Chemistry, Macrocycles: Synthesis, Structure, Applications*, Springer, Berlin, 1985.

4 (*a*) K. Kavallieratos, S. R. de Gala, D. J. Austin and R. H. Crabtree, *J. Am. Chem. Soc.*, 1997, **119**, 2325; (b) K. Kavallieratos, C. M. Bertao and R. H. Crabtree, *J. Org. Chem.*, 1999, **64**, 1675.

5 (*a*) E. Fan, C. Vicent and A. D. Hamilton, *New J. Chem.*, 1997, **21**, 81; (*b*) J. Rebek, Jr., B. Askew, P. Ballester and A. Costero, *J. Am. Chem. Soc.*, 1988, **110**, 923; (*c*) J. Rebek, Jr., B. Askew, D. Killoran, D. Nemeth and F.-T. Lin, *J. Am. Chem. Soc.*, 1987, **109**, 2426; (*d*) P. Tecilla, S.-K. Chang and A. D. Hamilton, *J. Am. Chem. Soc.*, 1990, **112**, 9586; (*e*) V. Jubian, R. P. Dixon and A. D. Hamilton, *J. Am. Chem. Soc.*, 1992, **114**, 1120; (*f*) J. Smith, K. Ariga and E. V. Anslyn, *J. Am. Chem. Soc.*, 1993, **115**, 362; (*g*) J. Wolfe, D. Nemeth, A. Costero and J. Rebek, Jr., *J. Am. Chem. Soc.*, 1988, **110**, 983; (*h*) T. Motomura, K. Inoue, K. Kobayashi and Y. Aoyama, *Tetrahedron Lett.*, 1991, 4757.

6 (*a*) V. van Axel-Castelli, A. Dalla Cort, L. Mandolini and D. N. Reinhoudt, *J. Am. Chem. Soc.*, 1998, **120**, 12 688; (*b*) G. L. Eichhorn and J. C. Bailer, *J. Am. Chem. Soc.*, 1953, **75**, 2905; (*c*) G. L. Eichhorn and I. M. Trachtenberg, *J. Am. Chem. Soc.*, 1954, **76**, 1954; (*d*) A. R. Boate and D. R. Eaton, *Inorg. Chim. Acta*, 1982, **61**, 25; (*e*) A. R. Boate and D. R. Eaton, *Can. J. Chem.*, 1976, **54**, 3895; (*f*) A. R. Boate and D. R. Eaton, *Can. J. Chem.*, 1977, **55**, 2432.

7 E. S. Gould, *Mechanism and Structure in Organic Chemistry*, Holt, Reinhart and Winston, N.Y., 1959, p. 543.

8 With excess amine, observing the disappearance of the *p*-Me and CHO resonances of the aldehyde and the appearance of the *p*-Me and CH_2 resonances of the imine. In a typical experiment, a 5 mm NMR tube containing *p*-tolualdehyde (0.025 ml, 0.21 mmol) and anhydrous $MgSO_4$ (5.2 mg, 0.043 mmol) in 0.750 ml of CD_2Cl_2 was introduced into the probe and left at −20 °C to equilibrate. Receptor **1** (6.3 mg, 0.016 mmol) was added and the spectrum recorded, then $BnNH_2$ (0.250 ml, 2.3 mmol) was added and the aldehyde resonances (δ 9.94, 2.45) and the imine resonances (δ 4.80, 2.41) were monitored. Plotting the integration values *vs*. time for the first 20 min and linear fitting of the straight line gave the initial rates.

9 F. A. Cotton and P. F. Stokely, *J. Am. Chem. Soc.*, 1970, **92**, 294; G. Dauphin and A. Kergomard, *Bull. Soc. Chim. Fr.*, 1961, **3**, 486.

10 S. J. Benkovic, A. D. Napper and R. A. Lerner, *Proc. Natl. Acad. Sci. U.S.A.*, 1988, **85**, 5355.

Communication 9/05838I

ChemComm

Water and hydrogen atom elimination from ionised *n*-propanol: extraordinarily large kinetic isotope effects

Richard D. Bowen,*[a] Simon J Mandeville,[a] Moschoula A. Trikoupis[b] and Johan K Terlouw[b]

[a] *Chemical and Forensic Sciences, University of Bradford, Bradford, West Yorkshire, UK, BD7 1DP. E-mail: r.d.bowen@bradford.ac.uk*

[b] *Department of Chemistry, McMaster University, Hamilton, Ontario L8S 4M1, Canada*

Received (in Cambridge, UK) 24th August 1999, Accepted 16th September 1999

Hydrogen atom loss from ionised *n*-propanol occurs specifically from the α-carbon atom and is subject to a kinetic isotope effect of approximately 500 : 1; somewhat smaller, though still very large, isotope effects are manifested in water loss, which is initiated by an essentially site-specific 1,4-hydrogen transfer.

The properties and reactions of ions in the absence of solvent may be conveniently studied by mass spectrometry. Low-energy (metastable) ions almost always dissociate from the ground electronic state with internal energies in the transition states that are comparable to those found in classical solution experiments.[1,2] Perhaps the most compelling evidence indicating the importance of relative critical energies[3] in influencing the relative rates of competing reactions of metastable ions is the frequent intervention of kinetic isotope effects, some of which are large, especially for small species.[4,5]

Direct bond cleavages, which are probably the simplest of all elementary chemical reactions, are ubiquitous in the dissociation of radical cations.[6] Isotope effects often contain information on bond cleavages and several detailed studies have shown that alkyl radical elimination by seemingly simple cleavages may be more complicated than expected.[7–11] The related process of hydrogen atom loss occurs less frequently,[6] and may involve some unique features.

Metastable ionised *n*-propanol **1**$^{+\cdot}$, dissociates by two routes, each of which has been shown to proceed with extremely high site selectivity.[12] The dominant reaction, loss of water, takes place after a unidirectional 1,4-hydrogen transfer from the γ-carbon atom to the oxygen atom to give the distonic[13] ion,[14] ·$CH_2CH_2CH_2OH_2^+$, **1δ**, which then expels water to form ionised cyclopropane, **2**$^{+\cdot}$. About 2% of **1**$^{+\cdot}$ dissociates by eliminating a hydrogen atom to give protonated propionaldehyde **3** (Scheme 1). Labelling evidence[12] provides indirect evidence that one of the α-hydrogen atoms is specifically lost, but expulsion of deuterium (D·) rather than protium (H·) has not yet been detected. Thus, it has been shown that both $CH_3CH_2CH_2OH^{+\cdot}$ and $CH_3CD_2CH_2OH^{+\cdot}$ eliminate predominantly H_2O and a minor proportion of H·. On the other hand, $CD_3CH_2CH_2OH^{+\cdot}$ loses HOD and H· in comparable quantities. Moreover, $CH_3CH_2CD_2OH^{+\cdot}$ expels essentially only H_2O (but no H· or D·), whereas $CH_3CH_2CHDOH^{+\cdot}$ loses mainly H_2O, a little H·, but no D·.

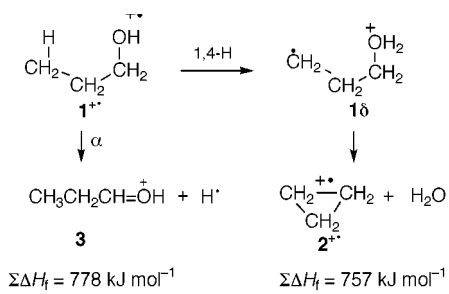

Scheme 1

These data indicate that both the 1,4-hydrogen transfer which initiates water loss and cleavage of the carbon–hydrogen bond resulting in hydrogen atom elimination are influenced by very large isotope effects. Although a lower limit of 30 : 1 for the isotope effect for hydrogen atom loss was set,[12] an accurate value could not be determined because $CH_3CH_2CHDOH^{+\cdot}$ does not lose D· at a measurable rate. However, the overall isotope effect on water loss was estimated to be *ca.* 44 : 1 from the difference in the ratios of hydrogen atom and water lost from $CH_3CH_2CH_2OH^{+\cdot}$ and $CD_3CH_2CH_2OH^{+\cdot}$. The total enthalpy of formation (778 kJ mol^{-1}) of the products of hydrogen atom loss, which appears to involve little or no reverse critical energy[15] even though it entails a large isotope effect, is only slightly higher than that (757 kJ mol^{-1}) of the products of water expulsion.[12] Moreover, the energy of the transition state for the 1,4-hydrogen transfer must lie above 757 kJ mol^{-1} because this step is rate-limiting and subject to an isotope effect. Consequently, the competition between water and hydrogen atom loss is strongly influenced by relatively small differences in the energetics of these reactions.

In order to obtain a better estimate of the ^{2}H isotope effect on hydrogen atom loss and to determine whether this process also shows a ^{13}C isotope effect, a wider range of labelled analogues of **1**$^{+\cdot}$ has been investigated (Table 1). In general, where these data overlap with those previously reported,[12] the agreement is good, although there are some minor variations that may be attributed to instrumental parameters. Hydrogen atom loss competes slightly more effectively with water loss and the kinetic energy releases are marginally larger in the new data. Three significant deductions may be made from the new data.

Table 1 Reactions of metastable ionised *n*-propanol and labelled analogues

	Neutral species lost							
	H_2O		HOD[a]		H·		D·	
Initial structure	*R*[b]	*T*[c]	*R*[b]	*T*[c]	*R*[b]	*T*[c]	*R*[a]	*T*[c]
$CH_3CH_2CH_2OH^{+\cdot}$	97.4	1.4			2.6	8.3		
$CH_3CH_2CHDOH^{+\cdot}$	93.6	1.6			6.4	10.0	< 0.05	
$CH_3CH_2CD_2OH^{+\cdot}$	100	1.7					< 0.01	
$CH_3CD_2CH_2OH^{+\cdot}$	89.9	1.2	[d]		10.1	10.3		
$CD_3CH_2CH_2OH^{+\cdot}$	[d]		41.0	1.9	59.0	12.4		
$CH_2DCH_2CH_2OH^{+\cdot}$	77.8	2.0	7.5	2.2	2.8	12.3		
$CD_3CH_2CHDOH^{+\cdot}$	[d]		49.4	1.7	30.5	8.8	0.1	[e]
$CH_3CH_2{}^{13}CH_2OH^{+\cdot}$	92.4	1.5			7.6	4.3		
$CD_3CH_2{}^{13}CH_2OH^{+\cdot}$			42.4	1.6	57.6	7.7		

[a] None of these metastable ionised labelled propanols loses D_2O. [b] *R* = Relative abundances normalised to a total of 100 units and measured by metastable peak heights on the VG Analytical ZAB-R mass spectrometer (ref. 20). [c] *T* = Kinetic energy release (in kJ mol^{-1}), estimated from the width at half-height of the appropriate metastable peak with no correction for the width of the main beam. Values are quoted to one decimal place to aviod introducing rounding errors. [d] Extremely weak peaks were detected, but these signals are attributable to water loss from the ^{13}C satellite signal of the $[M–H]^+$ peak. [e] Peak too weak to permit accurate measurements.

First, the value of *ca*. 54:1 obtained for the overall isotope effect on water loss is quite similar to that (*ca*. 44:1) reported previously[12] from considering the suppression of HOD loss relative to H· elimination from $CD_3CH_2CH_2OH^{+\cdot}$ compared to the behaviour of $CH_3CH_2CH_2OH^{+\cdot}$. However, the loss of H_2O and HOD in the ratio of *ca*. 10:1 from $CH_2DCH_2CH_2OH^{+\cdot}$ corresponds to a much smaller primary isotope effect of only *ca*. 5:1 for the initial hydrogen transfer step. This value is a lower limit and would be approximately doubled if account were taken of the overlapping loss of H_2O and HOD in similar quantities from the ^{13}C satellite signal of the oxonium ion, $CH_2DCH_2CH{=}OH^+$, formed by hydrogen atom loss from $CH_2DCH_2CH_2OH^{+\cdot}$. The discrepancy between the extremely large overall isotope effect and the much less pronounced, although still substantial, primary isotope effect probably indicates that a significant secondary isotope effect operates in this system. Thus, the rate of D transfer from the CD_3 group of $CD_3CH_2CH_2OH^{+\cdot}$ is reduced by both a primary isotope effect (because a C–D bond is being broken) and a secondary isotope effect (because a CD_2 group in which the hybridisation at carbon changes from sp^3 to sp^2 is left at the migration origin). In contrast, the rate of D transfer from the CH_2D group of $CH_2DCH_2CH_2OH^{+\cdot}$ is reduced by the same primary isotope effect (because a C–D bond is being broken), but the secondary isotope effect does not operate (because a CH_2 group is at the migration origin). Although secondary isotope effects usually are smaller than primary isotope effects, there are clear examples of systems in which secondary effects are comparable in magnitude to primary effects.[16] Water loss from $\mathbf{1}^{+\cdot}$ appears to be another example of this behaviour.

Secondly, a better estimate for the isotope effect on hydrogen atom loss may be obtained by considering the behaviour of $CD_3CH_2CHDOH^{+\cdot}$ because the dominant water loss reaction is slowed by the isotope effects influencing the initial D transfer, thus permitting H· (and, to a very limited extent, D·) loss to compete. Even so, the signal for D· loss is barely detectable and is only *ca*. 0.2% of that for H· elimination. This enormous isotope effect of *ca*. 500:1 is probably the largest so far detected in the dissociation of any ion containing four heavy atoms. This estimate is a lower limit for the primary isotope effect since any secondary isotope effect would favour D· loss.

Thirdly, the small but reproducible increase in the ratio of HOD to H· loss from $CD_3CH_2CH_2OH^{+\cdot}$ (0.70:1) and $CD_3CH_2{}^{13}CH_2OH^{+\cdot}$ (0.74:1) gives a value of *ca*. 1.06:1 for the overall ^{13}C isotope effect on hydrogen atom loss. This value is increased to *ca*. 1.2 if peak areas rather than heights are used to estimate the relative abundances of the competing processes. Although ^{13}C isotope effects are by their nature much smaller than ^2H isotope effects and this particular ^{13}C isotope effect is quite large, it is surprisingly small in view of the enormous ^2H isotope effect of *ca*. 500:1. Furthermore, the behaviour of $CH_3CH_2{}^{13}CH_2OH^{+\cdot}$, for which the ratio of H_2O loss relative to H· elimination (12:1) is reduced compared to that (37:1) for $CH_3CH_2CH_2OH^{+\cdot}$, seems to suggest that water loss is somehow affected by a ^{13}C isotope effect (*ca*. 3.1:1 from peak heights or *ca*. 2.1:1 from peak areas). Any such ^{13}C isotope effect on water loss would offset that on hydrogen atom elimination and give values of *ca*. 3.2:1 (peak heights) or 2.6:1 (peak areas) for the true ^{13}C isotope effect on hydrogen atom loss. This value is exceptionally large and is in keeping with the enormous ^2H isotope effect of *ca*. 500:1.

The unanticipated conclusion that water loss is affected by a ^{13}C isotope effect is supported by a similar reduction in the ratio of H· loss relative to H_2O elimination (15:1) for $CH_3CH_2CHDOH^{+\cdot}$, compared to that found for $CH_3CH_2CH_2OH^{+\cdot}$, thus suggesting that a secondary ^2H isotope effect of *ca*. 2.6:(peak heights) or *ca*. 2.5:1 (peak areas) also discriminates against water loss. Recent high-level molecular orbital calculations on ionised ethanol reveal that the C–C bond is unusually long.[17] Geometry optimisations at the MP2(FC)6-311G** level[18] of theory using the GAUSSIAN 94 suite of programs[19] indicate that the C(1)–C(2) bond is similarly elongated (to 1.738 Å) in the lowest energy structure of $\mathbf{1}^{+\cdot}$. In contrast, the corresponding bond in $\mathbf{1\delta}$ is not appreciably elongated (1.515 Å) and is very similar in length to the C(2)–C(3) bond (1.501 Å). The peculiar geometry of the minimum energy form of $\mathbf{1}^{+\cdot}$ may provide a key to explain the unusual features of water and hydrogen atom loss. This structure is inappropriate for water elimination (the methyl and hydroxy groups are held well apart, thus preventing the initial hydrogen transfer) and hydrogen atom elimination (the wrong bond is stretched and further elongation would lead to ethyl radical loss by α-cleavage). In order to facilitate either water or hydrogen atom elimination, quite considerable changes to the C(1)–C(2) bond length would be necessary, thus accounting for the large isotope effects on both reactions.

Regardless of their precise origin, the sheer magnitude of these isotope effects, particularly that for hydrogen atom loss, reveals that α-cleavage and hydrogen transfers are sometimes complex processes worthy of further investigation.

Financial support from the British Mass Spectrometry Society, the Fred Elison Travel Fund and the Natural Sciences and Engineering Research Council of Canada (NSERC) is gratefully acknowledged.

References

1 R. G. Cooks, J. H. Beynon, R. M. Caprioli and G. R. Lester, *Metastable Ions*, Elsevier, Amsterdam, 1973.
2 For reviews, see: D. H. Williams, *Acc. Chem. Res.*, 1977, **10**, 280; R. D. Bowen, D. H. Williams and H. Schwarz, *Angew. Chem., Int. Ed. Engl.*, 1979, **18**, 451; R. D. Bowen and D. H. Williams, in *Rearrangements in Ground and Excited States*, ed. P. DeMayo, Academic Press, New York, 1980, vol. 1, ch. 2.
3 The expression 'critical energy' corresponds conceptually to the term 'activation energy', A. Maccoll, *Org. Mass Spectrom.*, 1980, **15**, 225.
4 For examples of extremely large isotope effects in very small hydrocarbon ions, see: C. Lifshitz and L. Sternberg, *Int. J. Mass Spectrom. Ion Phys.*, 1969, **2**, 303; U. Lohle and Ch. Ottinger, *J. Chem. Phys.*, 1969, **51**, 3097; M. L. Vestal and J. H. Futrell, *J. Chem. Phys.*, 1970, **52**, 978; L. P. Hills, M. L. Vestal and J. H. Futrell, *J. Chem. Phys.*, 1971, **54**, 3834.
5 For a review of the mechanistic significance of extreme isotope effects, see: A. Thibblin and P. Ahlberg, *Chem. Soc. Rev.*, 1989, **18**, 209.
6 F. W. McLafferty and F. Turecek, *Interpretation of Mass Spectra*, 4th edn., University Science Books, Mill Valley, California, 1993.
7 J. J. Zwinselmann, N. M. M. Nibbering, N. E. Middlemiss, J. H. Vajda and A. G. Harrison, *Int. J. Mass Spectrom. Ion Phys.*, 1981, **38**, 163.
8 T. Weiske and H. Schwarz, *Chem. Ber.*, 1983, **116**, 323; T. Weiske, H. Halim and H. Schwarz, *Chem. Ber.*, 1985, **118**, 495; T. Weiske and H. Schwarz, *Tetrahedron*, 1986, **42**, 6245.
9 S. Hammerum and P. J. Derrick, *J. Chem. Soc., Chem Commun.*, 1985, 996.
10 S. Ingemann, S. Hammerum and P. J. Derrick, *J. Am. Chem. Soc.*, 1988, **110**, 3869; S. Ingemann, S. Hammerum, P. J. Derrick, R, H. Fokkens and N. M. M. Nibbering, *Org. Mass Spectrom.*, 1989, **24**, 885; S. Ingemann, E. Kluft, N. M. M. Nibbering, C. E. Alison, P. J. Derrick, and S. Hammerum, *Org. Mass Spectrom.*, 1991, **26**, 875.
11 R. D. Bowen and A. D. Wright, *J. Chem. Soc., Chem. Commun.*, 1991, 1055; 1992, 96; A. D. Wright and R. D. Bowen, *Can. J. Chem.*, 1993, **71**, 1073.
12 R. D. Bowen, A. W. Colburn and P. J. Derrick, *J. Am. Chem. Soc.*, 1990, **113**, 1132 and references therein.
13 B. F. Yates, W. J. Bouma and L. Radom, *J. Am. Chem. Soc.*, 1984, **106**, 5805.
14 For a review, see: S. Hammerum, *Mass Spectrom. Rev.*, 1988, **7**, 123.
15 F. Lossing, *J. Am. Chem. Soc.*, 1977, **99**, 7256.
16 R. D. Bowen and P. J. Derrick, *J. Chem. Soc., Perkin Trans. 2*, 1992, 1041.
17 J. W. Gauld and L. Radom, *Chem. Phys. Lett.*, 1997, **275**, 28.
18 W. J. Hehre, L. Radom, P. v. R. Schleyer and J. A. Pople, *An Initio Molecular Orbital Theory*, Wiley, New York, 1986.
19 J. B. Foresman and A. Firsch, *Exploring Chemistry with Electronic Structure Methods*, Gaussian Inc., Pittsburgh, PA, 1996, ch. 7.
20 H. F. van Garderen, P. J. A. Ruttink, P. C. Burgers, G. A. McGibbon and J. K. Terlouw, *Int. J. Mass Spectrom. Ion Processes*, 1992, **121**, 159.

Communication 9/06881C

Photochemistry of 2-azido-4,6-dichloro-*s*-triazine: matrix isolation of a strained cyclic carbodiimide containing four nitrogen atoms in a seven-membered ring

Götz Bucher,*[a] Fred Siegler[b] and J. Jens Wolff*[b]

[a] *Lehrstuhl für Organische Chemie der Ruhr-Universität Bochum, Universitätsstr. 150, D-44801 Bochum, Germany. E-mail: goetz.bucher@orch.ruhr-uni-bochum.de*

[b] *Organisch-Chemisches Institut der Ruprecht-Karls-Universität Heidelberg, Im Neuenheimer Feld 270, D-69120 Heidelberg, Germany*

Received (in Cambridge, UK) 23rd July 1999, Accepted 17th September 1999

2-Azido-4,6-dichloro-*s*-triazine 1, matrix-isolated in Ar at 10 K, yields triplet nitrene 2 and the strained cyclic carbodiimide 3 upon photolysis.

The photochemistry of phenyl azides has been a controversial topic for a long time.[1,2] The generally accepted pathway includes primary formation of an open-shell singlet nitrene[3,4] followed by intersystem crossing (ISC) to the ground-state triplet nitrene and/or cycloaddition to a neighbouring C=C double bond in the arene system. The efficiency of the latter reaction depends on factors such as temperature and substitution. It yields didehydroazepines *via* intermediary azirines.[5] Heteroaromatic aryl azides have also been studied in some detail.[6] For instance, 2-pyridylnitrene **4**, generated from 2-azidopyridine or the isomeric tetrazolopyridine, yields didehydro-1,3-diazepine **5** (a cyclic carbodiimide) upon photolysis

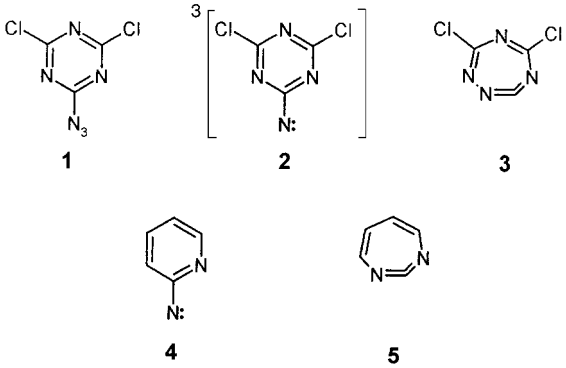

1 **2** **3** **4** **5**

in an Ar matrix.[7] A variety of heteroaromatic aryl nitrenes could be characterized by EPR,[8] and in some instances also by IR spectroscopy.[6]

The products isolated following thermolysis[9] or photolysis[10] of azido-*s*-triazines in solution exclusively arise from reactions of the triplet or singlet nitrenes. Thus, thermolysis of 2-azido-4,6-dimethoxy-1,3,5-triazine **6** in cyclohexane yielded the C–H insertion product **7** and the aminotriazine **8**.[9] The formation of **8** is likely due to a reaction of the ground-state triplet nitrene, while **7** is probably formed through the S_1 state of the nitrene. Surprisingly, no products ascribable to reactions of a didehydrotetrazepine (*e.g.* **9**) have been reported. Their absence could be due to a lack of stability, or it could reflect an increased barrier for cycloaddition towards a nitrogen atom. Here we present our recent results on the photolysis of matrix-isolated 2-azido-4,6-dichloro-*s*-triazine **1** which are different from the ones described for **6**.

The matrix isolation set-up used in these experiments has been described elsewhere.[11] Argon was chosen as the matrix material. During deposition, the cold window (KBr or sapphire) was kept at 30 K, otherwise the temperature of the matrix was held at 10 K. Azide **1**[12] was sublimed at 10 °C/10^{-6} mbar. In experiments using UV–VIS detection, it was photolysed by the

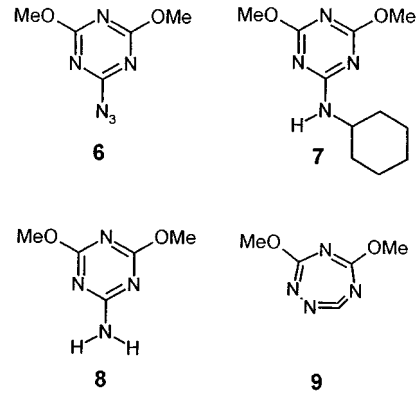

6 **7** **8** **9**

output of a 75 W Xe arc lamp coupled to a monochromator. The irradiation wavelength selected was 320 nm. In the case of IR detection, the output of a mercury low-pressure lamp (λ = 254 nm) was used. Brief irradiation (8 min) under these conditions led to the disappearance of the IR bands of **1** and to the formation of new bands at $\tilde{\nu}$ = 1951.2, 1550.0, 1467.6, 1446.4, 1254.5, 1246.8, 1110.2 and 1050.0 cm^{-1} along with some weaker bands below 900 cm^{-1} and around 2100 cm^{-1}. Upon extended irradiation with λ = 254 nm, these bands disappeared again, while the new absorptions at $\tilde{\nu}$ = 2271.2, 2214.2, 2112.9 and 2094.4 cm^{-1} were indicative of nitrile and possibly isonitrile and/or cumulene functionalities in the final product mixture.[13] Long-wavelength irradiation (λ > 420 nm) of the primary photoproducts led to a decrease in intensity of some bands ($\tilde{\nu}$ = 1467.6, 1446.4, 1254.5, 1246.8, 848.7, 787.9 and 580 0 cm^{-1}), while the intensity of other bands ($\tilde{\nu}$ = 1951.2, 1550.0, 1110.2, 1050.0 and 814.4 cm^{-1}) increased. Thus, the experimental findings are consistent with two compounds (these can be interconverted by long-wavelength photolysis) being predominantly formed during the initial stages of photolysis, which yield other, presumably ring-opened products, upon extension of 254 nm photolysis. In the UV–VIS, the product primarily formed showed absorption maxima at λ = 330 and 356 nm and a broad band between 380 and 490 nm with vibrational fine structure. Irradiation into this band (λ > 420 nm, Hg high pressure lamp with cut-off filter) led to the disappearance of the primary photoproduct and to the formation of a secondary photoproduct with λ_{max} = 328 and 352 nm (Fig. 1). Consistent with the results obtained using IR spectroscopy, this secondary photochemistry proved to be at least partially reversible. Photolysis of the product mixture thus obtained using λ = 320 nm again led to the formation of the spectrum with λ_{max} = 330, 356 and 380–490 nm, albeit with slightly reduced intensity. A likely explanation for this behaviour is formation of secondary (ring-opened) photoproducts, which do not show pronounced long-wavelength absorptions.

The vibrational spectra of triplet nitrene **2** and dehydrotetrazepine **3** were calculated using density functional theory (B3LYP with a 6-31G* basis, unscaled).[14] The comparison with

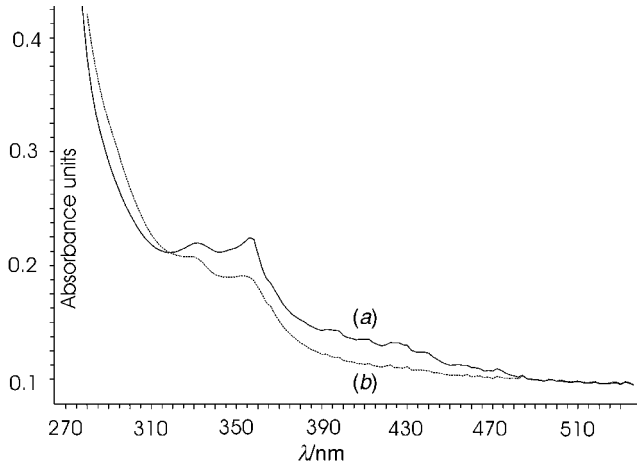

Fig. 1 (*a*) UV–VIS spectrum obtained after photolysis (3 h, λ = 320 nm) of **1** in Ar, 10 K. (*b*) UV–VIS spectrum obtained by photolyzing the same sample subsequently with λ = 475–620 nm, 2 h.

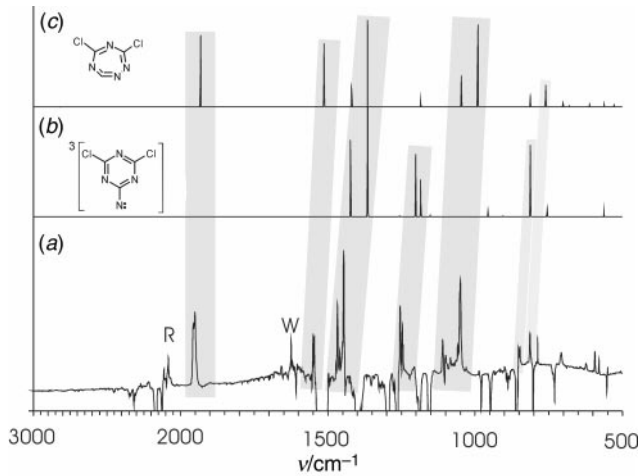

Fig. 2 (*a*) Difference IR spectrum obtained by subtracting the spectrum of **1** (Ar, 10 K) from the spectrum obtained after 8 min photolysis (λ = 254 nm). The bands pointing downward belong to **1**. Bands pointing upward are assigned to **2** and **3**, with the exception of the bands labelled W (water) and R (ring-opened secondary photoproduct). (*b*) Calculated IR spectrum (UB3LYP 6-31G*) of triplet nitrene **2**. (*c*) Calculated IR spectrum of **3** (B3LYP 6-31G*). The correlation with the experimental spectrum is highlighted by grey shading. The intensity of the band at $\tilde{\nu}$ = 1446.4 cm^{-1} is *ca.* 0.2 absorbance units.

the experimental data shows **2** and **3** to be indeed formed as primary products (Fig. 2).[15] This assignment is also consistent with the UV–VIS data, as the characteristics of the product initially formed upon photolysis at 320 nm (λ_{max} = 330 and 356 nm, broad band between 380 and 490 nm) are in line with the expected behavior of a triplet nitrene.[2]

The UV–VIS-spectrum attributed to **3** (λ_{max} = 328 and 352 nm) is very similar to a spectrum obtained by Yamada *et al.*[16] in a glassy EPA matrix at 77 K that was assigned to arise from triplet 4,6-dimethoxy-*s*-triazinyl nitrene. It thus appears likely that the product observed by them has to be reassigned to didehydrotetrazepine **9** or to its trapping products.[17]

The observation of didehydrotetrazepine **3** upon photolysis of azide **1** in an argon matrix could indicate that tetrazepines may actually be formed in the solution photochemistry of triazinyl azides. Experiments directed towards the isolation of derivatives of these heterocycles therefore may prove useful and are in progress.

G. B. thanks W. Sander for supporting this work. J. J. W. acknowledges financial support by the VW Stiftung and the Deutsche Forschungsgemeinschaft (Heisenberg stipend for J. J. W., Graduiertenkolleg stipend for F. S.).

Notes and references

1 M. S. Platz, *Acc. Chem. Res*., 1995, **28**, 487.
2 G. B. Schuster and M. S. Platz, *Advances in Photochemistry*, Wiley, New York, 1992, vol. 17, p. 69.
3 N. P. Gritsan, T. Yuzawa and M. S. Platz, *J. Am. Chem. Soc*., 1997, **119**, 5059.
4 R. Born, C. Burda, P. Senn and J. Wirz, *J. Am. Chem. Soc*., 1997, **119**, 5061.
5 W. L. Karney and W. T. Borden, *J. Am. Chem. Soc*., 1997, **119**, 1378.
6 R. A. Evans, M. W. Wong and C. Wentrup, *J. Am. Chem. Soc.*, 1996, **118**, 4009.
7 C. Wentrup, C. Thétaz, E. Tagliaferri, H. J. Lindner, B. Klitschke, H.-W. Winter and H. P. Reisenauer, *Angew. Chem., Int. Ed. Engl*., 1980, **19**, 566.
8 M. Kuzaj, H. Lüerssen and C. Wentrup, *Angew. Chem., Int. Ed. Engl.*, 1986, **25**, 480.
9 R. Kayama, S. Hasunuma, S. Sekiguchi and K. Matsui, *Bull. Chem. Soc. Jpn*., 1974, **47**, 2825.
10 R. Kayama, H. Shizuka, S. Sekiguchi and K. Matsui, *Bull. Chem. Soc. Jpn*., 1975, **48**, 3309.
11 W. Sander, *J. Org. Chem.*, 1989, **54**, 333.
12 *Synthesis* of **1**: The preparation given before (C. V. Hart, *J. Am. Chem. Soc*., 1928, **50**, 1928) gave only mixtures of products that could not be separated by crystallization, and the melting point stated to be 85 °C is most likely incorrect. The following method was successful: To a solution of cyanuric chloride (3.000 g, 16.27 mmol) in acetone (20 ml) in a small separation funnel, a solution of NaN_3 (1.000 g, 15.38 mmol) in water (10 ml) was added and the mixture shaken for 5 min. The organic phase was then separated and allowed to evaporate at room temperature. The crystals were chromatographed (silica gel, CH_2Cl_2–light petroleum = 1:1) to give pure **1** (1.13 g, 5.92 mmol, 36%) as a colorless powder, mp 59.5–61 °C; δ_H(300 MHz, $CDCl_3$) no signal; δ_C(75.5 MHz, $CDCl_3$) 171.39, 172.60; *m/z* (FAB) 190.99 (100, M + H$^+$); $\tilde{\nu}_{max}$/cm^{-1} (Ar, 10 K) 2168.9 (s), 1531.0 (vs), 1512.0 (vs), 1396.8 (s), 1295.8 (s), 1268.0 (s), 1187.6 (m), 1159.9 (m), 947.9 (w), 857.2 (m), 803.8 (w), 730.5 (vw).
13 The characterization of these final products is in progress; results will be published at a later time.
14 GAUSSIAN 98 software was used in the calculations.
15 *Selected data* for **2**: $\tilde{\nu}_{max}$/cm^{-1} (Ar, 10 K) 1467.6 (s), 1446.4 (vs), 1254.5 (s), 1246.8 (m), 852.9 (w), 848.7 (w), 787.9 (m), 580.0 (w). For **3**: $\tilde{\nu}_{max}$/cm^{-1} (Ar, 10 K) 1957.0 (vs), 1951.2 (vs), 1550.0 (m), 1546.2 (m), 1110.2 (m), 1050.0 (vs), 814.4. An N=C=N stretching band at $\tilde{\nu}$ = 1957.0 cm^{-1} for **3** is in the range expected for such a compound. For comparison, simple open-chain *N*-dialkylamino substituted carbodiimides absorb at ν = 2090 cm^{-1} (ref. 18). The decrease in frequency in **3** reflects the decrease in bond energy induced by strain. A similar trend has been observed in the case of other cyclic carbodiimides (ref. 6).
16 H. Yamada, H. Shizuka and K. Matsui, *J. Org. Chem.*, 1975, **40**, 1351.
17 There is a complete lack of absorption beyond λ = 420 nm in the spectra given by Yamada *et al.* However, a broad band would be expected for a triplet nitrene. In an EPA matrix, trapping of the didehydrotetrazepine by EtOH has to be considered.
18 W. S. Wadsworth, Jr. and W. D. Emmons, *J. Org. Chem*., 1964, **29**, 2816.

Communication 9/05971G

Studies on enzymatic hydrolysis of thymidin-3′-yl thymidin-5′-yl phosphorofluoridates and the corresponding phosphorothiofluoridates

Konrad Misiura,[a] Martin Bollmark,[b] Jacek Stawinski[b] and Wojciech J. Stec*[a]

[a] *Department of Bioorganic Chemistry, Centre of Molecular and Macromolecular Studies PAS, 90-363 Lodz, Poland. E-mail: wjstec@bio.cbmm.lodz.pl*

[b] *Department of Organic Chemistry, Arrhenius Laboratory, Stockholm University, S-10691 Stockholm, Sweden*

Received (in Liverpool, UK) 13th August 1999, Accepted 8th September 1999

***Spleen* or *snake venom* nuclease-assisted cleavage of P–F bonds in nucleotides bearing a phosphorofluoridate moiety occurs at negatively charged phosphates only.**

Catalytic promiscuity of enzymes has attracted the attention of researchers studying the problem of a common binding site and common mechanistic features in catalysis involving substrates bearing functional groups different from those naturally cleaved by these enzymes.[1] Since such studies may shed light on the evolutionary diversification of enzymes, each example of 'unusual' activity of enzymes requires meticulous scrutiny.

In this respect, the cleavage of the P–O bond in dinucleoside 3′,5′-phosphorofluoridates ($N_{PF}N'$) by *spleen* phosphodiesterase (*spleen* PDE) and *snake venom* phosphodiesterase (*sv* PDE), as reported recently in several papers by Dabkowski *et al.*,[2] attracted our attention. Both enzymes are known as phosphodiester hydrolases that cleave oligonucleotides with natural 3′-5′-phosphodiester linkages to produce the corresponding nucleoside 3′- or 5′-phosphates.[3] These enzymes are known to require the presence of a negative charge at the cleavable phosphate moiety[4] and can also accept as substrate various charged oligonucleoside phosphate analogues. For example, dinucleoside 3′,5′-phosphorothioates ($N_{PS}N'$)[5] are recognised by *snake venom* phosphodiesterase albeit the rate of cleavage of the diastereomers differs significantly. This observed stereodifferentiation has been used for determination of absolute configuration of $N_{PS}N'$[6] and related compounds, *e.g.* ATPαS[7] and thymidine 5′-phosphorothiofluoridate,[8] and also as a practical method of preparing single diastereomers of $N_{PS}N'$ by selective degradation of a pool of chemically synthesised oligonucleoside phosphorothioates[9] In contrast to these, uncharged dinucleotide analogues, *e.g.* dinucleoside alkyl phosphates and dinucleoside methylphosphonates, are not substrates for *sv* and *spleen* PDE, most likely due to the lack of a negative charge at the cleavage site.[10]

In light of the above, the results of Dabkowski *et al.*[2] have to be viewed with caution, although a speculation that the strongly polarised P–F bond could mimic the P–O$^-$ bond cannot be rejected *a priori*. However, the reported data[2] (*viz.* presence of thymidine, thymidine 5′-phosphorofluoridate and unreacted $T_{PF}T$, after 3 h exposure to *sv* PDE in enzymatic buffer solution) seemed to be at odds with the hydrolytic instability of $N_{PF}N'$ in buffered media[11] and the fact that nucleoside 5′-phosphorofluoridate monoesters are known to be good substrates for *sv* PDE yielding nucleoside 5′-phosphates as products.[12] These factors prompted us to reinvestigate the problem of the susceptibility of uncharged nucleotide analogues containing the P–F bond towards *snake venom* and *spleen* phosphodiesterases, and as model compounds for our studies we chose a dinucleoside 3′,5′-phosphorofluoridate and the corresponding phosphorothiofluoridate.

Dithymidine 3′,5′-phosphorofluoridate **1** (mixture of two diastereomers, *ca.* 1:1 ratio) was obtained by two independent methods[11,13] and isolated by means of silica gel chromatography.† The reference compounds, thymidine 3′-phosphorofluoridate **2** and thymidine 5′-phosphorofluoridate **3** were obtained either in DBU-assisted reactions of protected thymidine 3′- or 5′-(2-oxo-3-oxa-1-thia-2-phosphaspiro[4.5]decane)s[14] with triethylamine trishydrofluoride,‡ or independently, in reactions of pyridine solutions of suitably protected thymidine hydrogen 3′- or 5′-phosphonate with trimethylsilyl chloride, followed by treatment with iodine and triethylamine trishydrofluoride.[15]

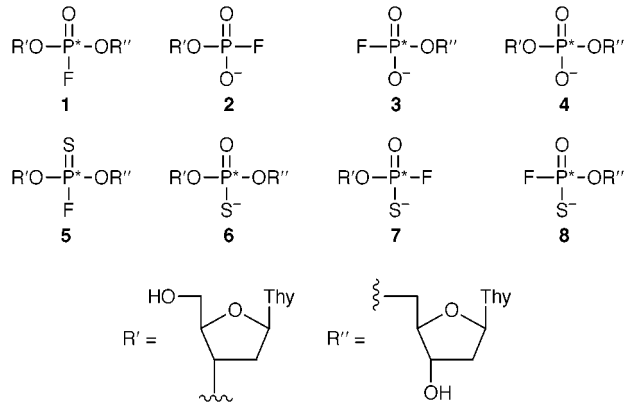

The hydrolytic stability of phosphorofluoridate **1** was checked in various buffer solutions using an RP-HPLC assay.§ It was found that compound **1** (0.1 mM) dissolved in 0.05 M acetate buffer (pH 5.0) (*spleen* PDE buffer) at 37 °C was quantitatively hydrolysed within 5 min providing dithymidine 3′,5′-phosphate **4**. The same results were obtained using 0.1 M Tris-HCl (pH 8.0) containing 20 mM $MgCl_2$ (*sv* PDE buffer) as medium. Incubations performed in a presence of *spleen* PDE¶ (0.15 U ml^{-1}) and *sv* PDE¶ (0.005 U ml^{-1}), using the same buffer systems as for the blank experiments, in both instances resulted in formation of phosphodiester **4** only (5 min, no starting material present) without detectable amounts of phosphorofluoridate **2** and **3**, respectively (RP-HPLC analysis using genuine samples of **2**, **3** and **4**). Prolonged incubation times (20, 40 and 60 min) led to a gradual hydrolysis of the initially formed phosphodiester **4** to produce thymidine and thymidine 3′- or 5′-phosphate, respectively. In separate experiments we found that rates of enzymatic hydrolysis (*sv* and *spleen* PDE) of pure phosphodiester **4** and that produced *in situ* from phosphorofluoridate **1** were identical, indicating that fluoride anion neither accelerated nor inhibited the activity of these phosphodiesterases.

We also confirmed earlier observations by Wittmann[12] and others[12] that products of a putative enzymatic hydrolysis of phosphorofluoridate **1** claimed by Dabkowski *et al.*,[2] *viz.* compounds **2** or **3**, are substrates for phosphodiesterases. We found that phosphorofluoridate **2** was hydrolysed by *spleen* PDE slower than phosphodiester **4**, and thus if **1** were a substrate for this enzyme (cleavage of the P–O bond), transient formation of **2** would be anticipated. In the instance of *sv* PDE, we could not exclude a remote possibility that phosphorofluoridate diester **1** underwent slow enzymatic hydrolysis with

P–O bond cleavage to produce thymidine 5′-phosphorofluoridate **3**, since the latter was found to be a better substrate for the enzyme than phosphodiester **4**.

A diastereomeric mixture of dithymidine 3′,5′-phosphorothiofluoridate **5** (ratio *ca.* 1:1)[8,13] was also examined as a potential substrate for *spleen* and *snake venom* phosphodiesterases. Compound **5**‖ was found to be significantly more hydrolytically stable than its oxo congener **1** in the buffer solutions used (*vide supra*) and required *ca.* 1 h at 37 °C for complete hydrolysis to produce dithymidine 3′,5′-phosphorothioate **6**. Attempted enzymatic hydrolysis of **5** was performed using a 10× higher concentration of *spleen* and *sv* PDE than those used in experiments with phosphorofluoridate **1**. It was found that during incubations of **5** with *spleen* and *sv* PDE no trace of products resulting from P–O bond cleavage, *i.e.* thymidine 3′-*O*-phosphorothiofluoridate **7**[8,15] or 5′-phosphorothiofluoridate **8**,[8,15] respectively, could be detected (RP-HPLC assay). After 1 h, the only product present was phosphorothioate diester **6** (diastereomeric ratio *ca.* 1:1) that upon prolonged enzymatic incubation (samples analysed after 2, 4 and 8 h) yielded gradually thymidine and thymidine 3′- or 5′-phosphorothioate, respectively, as the sole products. For the reactions performed in the presence of *sv* PDE, as expected, a stereoselective digestion of (R_P)-**6** was observed.[6] Since in our earlier studies[8] we demonstrated that (R_P)-phosphorothiofluoridate **8** is a good substrate for *sv* PDE one should expect the accumulation of (S_P)-phosphorothiofluoridate **8** in the reaction mixture, if an enzymatic cleavage of the P–O bond in **5** produced both diastereomers of **8**.

In conclusion, the presented results on enzymatic hydrolysis of dithymidine 3′,5′-phosphorofluoridate **1** and dithymidine 3′,5′-phosphorothiofluoridate **5** by *spleen* and *snake venom* phosphodiesterases indicate that these compounds first undergo chemical hydrolysis to dinucleotides **4** and **5**, respectively, which are subsequently hydrolysed enzymatically to the corresponding nucleoside and nucleotide derivatives. The released fluoride anion under the reaction conditions did not inhibit the nucleolytic activity of the investigated enzymes.

These studies support the earlier findings that *sv* and *spleen* PDE accept as substrates negatively ionised phosphate derivatives and thus the enzymatic hydrolysis of phosphorofluoridate diesters by these enzymes reported by Dabkowski *et al.*[2] could not be confirmed.

Work presented here was financially assisted by the State Committee for Scientific Research (KBN), grant no. 4 PO5F 006 17 (to W. J. S), the Swedish Natural Science Research Council, and the Swedish Foundation for Strategic Research.

Notes and references

† *Selected data* for **1**: δ_P(CD_3OD, 121 MHz) − 9.5 and −10.1 ($^1J_{PF}$ 971, 980); δ_F(CD_3OD, 282 MHz) −80.6 and −81.2 ($^1J_{FP}$ 973, 984); δ_H (CD_3OD, 300 MHz) 6.27 (2H, m, H-1′, two anomeric protons), 5.24 (2H, m, H-3′).

‡ *Syntheses and selected data* for **2** and **3**: 5′-*O*-dimethoxytritylthymidine 3′-*O*-(2-oxo-3-oxa-1-thia-2-phosphaspiro[4.5]decane) (ref. 14) was dissolved in dry MeCN. To this solution a 1 M solution of triethylamine trishydrofluoride in dry THF (1 equiv.) and DBU (2 equiv.) were added. After 15 min the reaction mixture was concentrated and redissolved in 80% AcOH and left for 1 h. Crude **2** was purified by DEAE-Sephadex chromatography using 0.05 to 0.5 M $Et_3NH^+HCO_3^-$ buffer (pH 7.5) as an eluent. Compound **2** was obtained in 65% yield: δ_P(D_2O, 81 MHz) −5.60 ($^1J_{PF}$ 932); δ_F(D_2O, 188 MHz) −80.7 ($^1J_{PF}$ 932); *m/z* (−FAB) 323.1 (M − H). Synthesis of **3** was performed in the same way starting from 3′-*O*-methoxyacetylthymidine 5′-*O*-(2-oxo-3-oxa-1-thia-2-phosphaspiro[4.5]-decane) and using conc. ammonia for deprotection (yield, 20%): δ_P(D_2O, 81 MHz) −6.29 ($^1J_{PF}$ 933); δ_F(D_2O, 188 MHz) −77.7 ($^1J_{PF}$ 934); *m/z* (−FAB) 323.1 (M − H).

§ Conditions for HPLC analysis: Econosphere C18 column; buffer A, 0.1 M NH_4OAc; buffer B, 0.04 M NH_4OAc in 80% MeCN; gradient up to 60% buffer B in 15 min; flow 1 ml min^{-1}.

¶ *Spleen* and *sv* PDE were from Sigma (P-6897 and P-6877, respectively).

‖ *Selected data* for **5**: δ_P(CD_3OD, 121 MHz) 61.9 and 61.2 ($^1J_{PF}$ 1071, 1082); δ_F(CD_3OD, 282 MHz) −44.9 and −45.0 ($^1J_{F\text{-}P}$ 1072, 1084); δ_H(CD_3OD, 300 MHz) 6.27 (2H, m, H-1′, two anomeric protons), 5.31 (2H, m, H-3′).

1 J. O'Brien and D. Herschlag, *Chem. Biol.*, 1999, **6**, 91.
2 W. Dabkowski, F. Cramer and J. Michalski, *J. Chem. Soc., Perkin Trans.* 1, 1992, 1447; W. Dabkowski, J. Michalski, J. Wasiak and F. Cramer , *J. Chem. Soc., Perkin Trans. 1*, 1994, 817; W. Dabkowski, J. Michalski and F. Cramer, in *Methods in Molecular Biology, Vol. 20: Protocols for Oligonucleotides and Analogs*, ed. S. Agrawal, Humana Press, Totowa, NJ, 1993, pp. 245–260.
3 *Enzymatic Handbook*, ed. D. Schomburg and M. Salzmann, Springer, Berlin, 1991.
4 A. Gerlt, in *The Enzymes, Vol. 20*, ed. D. S. Sigman, Academic Press, New York, 1992, pp. 95–139; J. A. Gerlt, in *Nucleases, 2nd Edn.*, ed. S. M. Linn, R. S. Lloyd and R. J. Roberts, Cold Spring Harbor Laboratory Press, 1993, pp. 1–34.
5 F. Eckstein, *Ann. Rev. Biochem.*, 1985, **54** , 367.
6 M. J. Burgers, F. Eckstein and D. H. Hunneman, *J. Biol. Chem.*, 1979, **254**, 7476; F. R. Bryant and S. J. Benkovic, *Biochemistry*, 1979, **18**, 2825.
7 M. J. Burgers and F. Eckstein, *J. Biol. Chem.*, 1979, **254**, 6889.
8 K. Misiura, D. Szymanowicz and W. J. Stec, *Collect. Czech. Chem. Commun.*, 1996, **61**, S101; K. Misiura, D. Szymanowicz and W. J. Stec, *Chem. Commun.*, 1998, 515.
9 H. Almer, J. Stawinski and R. Strömberg, *J. Chem. Soc., Chem. Commun.*, 1994, 1459; H. Almer, J. Stawinski and R. Strömberg, *Nucleic Acids Res.*, 1996, **24**, 3811.
10 P. S. Miller, J. C. Barret and P. O. P. Ts'o, *Biochemistry*, 1974, **13**, 4887; P. Guga, M. Koziolkiewicz, A. Okruszek, B. Uznanski and W. J. Stec, *Nucleosides Nucleotides*, 1987, **6**, 111.
11 K. Misiura, D. Pietrasiak and W. J. Stec, *J. Chem. Soc., Chem. Commun.*, 1995, 613.
12 R. Wittmann, *Chem. Ber.*, 1963, **96**, 771; Q. W. Nichol, A. Numura and A. Hampton, *Biochemistry*, 1967, **8**, 1008; Z. Kucerova and J. Skoda, *Biochim. Biophys. Acta*, 1971, **247**, 194.
13 M. Bollmark and J. Stawinski, *Chem. Commun.*, 1997, 991.
14 W. J. Stec, B. Karwowski, M. Boczkowska, P. Guga, M. Koziolkiewicz, M. Sochacki, M. W. Wieczorek and J. Blaszczyk, *J. Am. Chem. Soc.*, 1998, **120**, 7156.
15 M. Bollmark and J. Stawinski, *Tetrahedron Lett.*, 1996, **32**, 5739.

Communication 9/06659D

ChemComm

Palladium- and copper-catalyzed cross-coupling and carbonylative cross-coupling of organotellurium compounds with organostannanes

Suk-Ku Kang,* Sang-Woo Lee and Hyung-Chul Ryu

Department of Chemistry, Sungkyunkwan University, Natural Science Campus, Suwon 440-746, Korea. E-mail: skkang@chem.skku.ac.kr

Received (in Cambridge, UK) 28th July 1999, Accepted 13th September 1999

The palladium- and copper-catalyzed cross-coupling of diaryl- or divinyl tellurium dichlorides with organostannanes has been achieved in the presence of $PdCl_2$ (10 mol%) or CuI (10 mol%) with Cs_2CO_3 (2 equiv.) in MeCN in good to moderate yields; alternatively, the palladium- and copper-catalyzed carbonylative cross-coupling of organotellurium dichlorides with organostannanes was readily accomplished under atmospheric pressure of CO in good to moderate yields.

The palladium-catalyzed cross-coupling of organostannanes with an organic electrophile (*i.e.* halides and triflates), known as the Stille reaction,[1] has become an extremely powerful tool for the construction of carbon–carbon bonds. As alternatives to organic electrophiles, hypervalent iodonium salts[2] and the main group metal lead[3] have been employed in the cross-coupling with organostannaes. Recently Uemura *et al.* reported[4] the palladium-catalyzed carbonylation[4a] and homocoupling[4b] of vinyltellurides as well as the Heck type reaction[4c] of vinyltellurides. However the cross-coupling of aryl- or vinyltellurium dichlorides with organostannanes is not known. We assumed that the use of tellurium as one of the 6A group metals would expand the scope of the cross-coupling reaction. Here we report the palladium- and copper-catalyzed cross-coupling and carbonylative cross-coupling of diaryl- and divinyl-tellurium dichlorides[5] with organostannanes.

The results of Pd- and Cu-catalyzed cross-coupling and carbonylative cross-coupling of diaryl- or divinyl-tellurium dichlorides in MeCN at room temperature are summarized in Scheme 1 and Table 1. The palladium-catalyzed coupling of diphenyltellurium dichloride **1a** with 2-furyltributylstannane **2b** was carried out to find the optimum conditions. Of the catalysts tested [$PdCl_2$, $Pd(PPh_3)_4$, $Pd_2(dba)_3{\cdot}CHCl_3$, $PdCl_2(PPh_3)_2$], $PdCl_2$ was the best choice. Among the bases used, Cs_2CO_3 was more suitable than K_2CO_3, Na_2CO_3 and NaOMe. As solvent MeCN was the most preferable. In our hands, the cross-coupling of $PhTeCl_3$, *p*-$MeOC_6H_4TeCl_3$ and (*E*)-$PhCH{=}CHTeCl_3$ with 2-furylstannane gave the cross-coupling products in rather low yields. Diphenyltellurium dichloride **1a** reacted with 2-furyltributylstannane **2b** in the presence of $PdCl_2$ (10 mol%) and Cs_2CO_3 (2 equiv.) in MeCN at room temperature for 3 h to afford 2-phenylfuran (**3a**)[6] in 89% isolated yield. Under the same conditions but with CuI (10 mol%) as catalyst at 70 °C the reaction gave **3a** in 72% yield (method B in entry 1, Table 1). We tested various copper catalysts to discover a palladium-free Stille protocol, and the cross-coupling of the organostannane **2b** with **1a** was achieved at 70 °C. Of the catalysts used, CuI (10 mol%) was the most preferable among CuI, CuBr, and $Cu(OAc)_2$. As base, Cs_2CO_3 was more suitable than K_2CO_3, Na_2CO_3 and NaOMe. The solvent MeCN was the best choice, presumably because of the solubility of organotellurium compounds. The reaction of di(*p*-methoxyphenyl)tellurium dichloride **1b** with **2b** in the presence of $PdCl_2$ at room temperature and CuI at 70 °C proceeded to give 2-(*p*-methoxyphenyl)furan **3b**[7] in 89 and 68% yields, respectively (methods A and B in entry 2). This coupling method was also applied to alkenyl-substituted stannane **2d**. The reaction of **1b** with β-(*E*)-styrylstannane **2d** gave the substituted stilbene **3d**[8] (entry 4). When di[β-(*Z*)-styryl]tellurium dichloride **1c** was treated with 2-furylstannane **2b**, 2-β-(*Z*)-styryl substituted furan **3e** was readily obtained in 70 and 56% yields, respectively (methods A and B in entry 5). The (*Z*)-stereochemistry of **3e** was confirmed by the coupling constant J = 12.1 Hz for the vinylic protons.

We then extended this reaction to carbonylative cross-coupling with organostannanes (Scheme 2). The diphenyltellurium dichloride **1a** was successfully coupled with 2-furyltributylstannane **2b** under atmospheric pressure of CO under palladium or copper catalysis to furnish 2-benzoylfuran **4a**[9] in 84 and 63% isolated yields (methods A and B in entry 7).

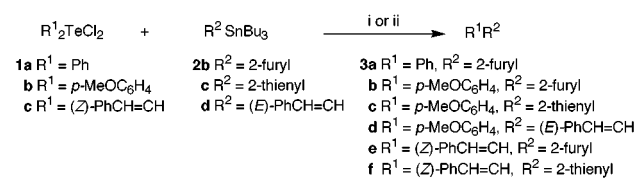

Scheme 1 *Reagents and conditions:* i (method A), $PdCl_2$ (10 mol%), MeCN, Cs_2CO_3 (2 equiv.), room temp., 3 h; ii (method B), CuI (10 mol%), MeCN, Cs_2CO_3 (2 equiv.), 70 °C, 7 h.

Table 1 Pd- and Cu-catalyzed cross-coupling and carbonylative cross-coupling of organotellurium dichloride with organostannanes

Entry	Organotellurium compounds	Organostannanes	Reaction conditions[a]	Products	Isolated yields (%)
Cross-coupling					
1	**1a**	**2b**	A	**3a**	89
			B		72
2	**1b**	**2b**	A	**3b**	89
			B		68
3	**1b**	**2c**	A	**3c**	88
			B		65
4	**1b**	**2d**	A	**3d**	81
5	**1c**	**2b**	A	**3e**	70
			B		56
6	**1c**	**2c**	A	**3f**	76
			B		61
Carbonylative cross-coupling					
7	**1a**	**2b**	A	**4a**	84
			B		63
8	**1a**	**2c**	A	**4b**	85
			B		65
9	**1a**	**2f**	A	**4c**	82
10	**1b**	**2a**	A	**4d**	83
11	**1b**	**2c**	A	**4e**	83
			B		70
12	**1b**	**2e**	A	**4f**	90
13	**1c**	**2b**	A	**4g**	70
			B		52

[a] A: $PdCl_2$ (10 mol%), Cs_2CO_3 (2 equiv.), room temp. B: CuI (10 mol%), Cs_2CO_3 (2 equiv.), 70 °C. Carbonylative cross-coupling carried out under atmospheric pressure of CO.

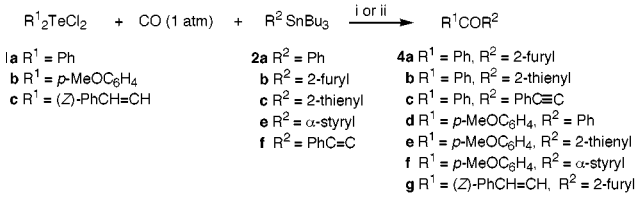

Scheme 2 *Reagents and conditions:* i (method A), $PdCl_2$ (10 mol%), MeCN, Cs_2CO_3 (2 equiv.), room temp., 3 h; ii (method B), CuI (10 mol%), MeCN, Cs_2CO_3 (2 equiv.), 70 °C, 7 h.

Treatment of **1a** with 2-thienyltributylstannane **2c** under the same conditions afforded 2-benzoylthiophene **4b**[10] in 85% yield (entry 8). This carbonylative coupling was also applied to alkynyltributylstannane **2f** to provide alkynyl-substituted ketone **4c** (entry 9).[11] For the di(*p*-methoxyphenyl)tellurium dichloride **1b**, phenyltributylstannane **2a** and 2-thienyltributylstannane **2c** were smoothly coupled to give ketones **4d**[11] and **4e**,[11] respectively, in 83% yield (entries 10 and 11). When the tellurium dichloride **1b** was treated with α-styryltributylstannane **2e**, unexpectedly the carbonylative cross-coupled product **4f**[12] was obtained as the sole product in 90% yield without any *cine*-substitution[13] product (entry 12). Finally, di[β-(*Z*)-styryl]tellurium dichloride **1c** was successfully coupled with **2b** under CO to afford β-(*Z*)-styryl-substituted ketone **4g**[14] in 70 and 52% yields, respectively (methods A and B in entry 13).

In considering a plausible mechanism for the cross-coupling it is presumed that oxidative addition of organotellurium compounds with Pd^0 or Cu^I gives $R^1PdTeR^2Cl_2$ or $R^1CuTeR^2Cl_2$, which is subjected to transmetallation with stannanes followed by reductive elimination to afford the cross-coupled products.

In summary, the palladium- and copper-catalyzed cross-coupling and carbonylative cross-coupling of diorganotellurium dichlorides with organostannanes were achieved under mild conditions in good to moderate yields.

Generous financial support for the Center for Molecular Design and Synthesis (CMDS) and KOSEF (99-0501-02-01-3) is gratefully acknowledged.

Notes and references

1 J. K. Stille, *Angew. Chem., Int. Ed. Engl.*, 1986, **25**, 508; T. N. Mitchell, *Synthesis*, 1992, 803; V. Farina, *Pure Appl. Chem*., 1996, **68**, 73.

2 R. M. Moriarty and W. R. Epa, *Tetrahedron Lett.*, 1992, **33,** 4095; R. J. Hinkle, G. T. Poulter and P. T. Stang, *J. Am. Chem. Soc.*, 1993, **115**, 11 626; S.-K. Kang, H.-W. Lee, J.-S. Kim and S.-C. Choi, *Tetrahedron Lett.*, 1996, **37**, 3723; S. K. Kang, H.-W. Lee, S.-B. Jang, T.-H. Kim and J.-S. Kim, *Synth. Commun.*, 1996, **26**, 4311.

3 S.-K. Kang H.-C. Ryu and S.-C. Choi, *Chem. Commun.*, 1998, 1317.

4 (*a*) K. Ohe, H. Takahashi, S. Uemura and N. Sugita, *J. Org. Chem.*, 1987, **52**, 4859; (*b*) Y. Nishibayashi, C.-S. Cho, K. Ohe and S. Uemura, *J. Organomet. Chem.*, 1996, **526**, 335; (*c*) Y. Nishibayashi, C.-S. Cho, K. Ohe and S. Uemura, *J. Organomet. Chem.*, 1996, **507**, 197.

5 N. Petragnani, in *Tellurium in Organic Synthesis*, Academic Press, 1994 and references therein. General procedure as follows. Diphenyltellurium dichloride (**1a**): $TeCl_4$ (40 mmol) and PhHgCl (80 mmol) were heated under reflux in anhydrous dioxane (100 ml) for 2 h. The solution is cooled to 10 °C and the $HgCl_2$ dioxane precipitate filtered off and washed with cold dioxane (15 ml). The filtrate was poured with stirring into 1% ice-cold HCl (400 ml). The dichlorides precipitate as crystalline solids and were recrystallized from benzene–light petroleum (bp 30–60 °C. Di[β-(*Z*)-styryl]tellurium dichloride (**1c)**: $NaBH_4$ (9 mmol) was added in small portions to a stirred suspension of Te (3 mmol) in EtOH (15 ml), and THF (5 ml) was added to the hot mixture, which was then refluxed. After 15 min the mixture turned dark violet and the reflux was continued until all the Te had disappeared. The heat source was removed and the phenylacetylene (7.8 mmol) added. When the color changed to yellow, the mixture was cooled at room temperature, diluted with EtOAc (50 ml) and washed first with saturated aqueous NH_4Cl (3 × 30 ml) and then with brine (3 × 30 ml). The organic phase was separated, dried ($MgSO_4$) and evaporated in a rotary evaporator. The residue dissolved in a small amount of $CHCl_3$ was treated dropwise, while cooling (ice bath) and stirring, with a solution of an equimolar amount of SO_2Cl_2 in the same solvent. By addition of a large excess of light petroleum (bp 30–60 °C) the dihalide precipitates as a crystalline solid.

6 A. Pelter, M. Rowlands and G. Clements, *Synthesis*, 1987, 51.

7 S.-K. Kang, J.-S. Kim and S.-C. Choi, *J. Org. Chem.*, 1997, **62**, 4208.

8 S.-K. Kang, T.-G. Baik and S.-Y. Song, *Synlett*, 1999, **3**, 327.

9 G. Zadel and E. Breitmaier, *Angew. Chem., Int. Ed. Engl.*, 1992, **23**, 1070.

10 S.-K. Kang, K.-H. Lim, P.-S. Ho, S.-K. Yoon and H.-J. Son, *Synth. Commun.*, 1998, **28**, 1481.

11 S.-K. Kang, P.-S. Ho, S.-K. Yoon, J.-C. Lee and K.-J. Lee, *Synthesis*, 1998, 823.

12 *Selected data* for **4f**: δ_H(400 MHz, $CDCl_3$) 7.91 (dd, 2 H, *J* 4.0, 2.0), 6.91 (dd, 2 H, *J* 4.0, 2.0), 4.92 (d, 1 H, *J* 2.8), 4.67 (d, 1 H, *J* 2.8), 3.92 (q, 2 H, *J* 7.1), 3.86 (s, 3 H), 1.40 (t, 3 H, *J* 7.1); *m/z* 235 (M^+), 234 (M), 162 (34%), 135 (100), 107 (10), 92 (19), 77 (27) (HRMS: calc. for $C_{13}H_{14}O_4$: 234.0887, found: 234.0889).

13. K. Kikukwa, H. Uemura and T. Matsuda, *J. Organomet. Chem*., 1986, **311**, c44; G. Stork and R. C. A. Isaacs, *J. Am. Chem. Soc*., 1990, **112**, 7399; C. A. Busacca, J. Swestock, R. E. Johnson, T. R. Bailey, L. Musza and C. A. Rodger, *J. Org. Chem*., 1994, **59**, 7553; V. Farina and M. A. Hossian, *Tetrahedron Lett*., 1996, **37**, 6997; S.-H. Chen, *Tetrahedron Lett*., 1997, **38**, 4741.

14 *Selected data* for **4a**: δ_H(500 MHz, $CDCl_3$) 6.49 (m, 1 H), 6.85 (d, 1 H, *J* 12.1), 6.99 (d, 1 H, *J* 12.1), 7.29 (m, 1 H), 7.32 (m, 3 H), 7.50 (m, 3 H); ν_{max}(KBr)/cm^{-1} 3132, 2340, 1660, 1620, 1572, 1465; *m/z* 198 (M^+), 197 (M, 100%), 141 (31), 103 (25).

Communication 9/06127D

Chiral recognition of amino acids by electrospray ionisation mass spectrometry/mass spectrometry

Zhong-Ping Yao,[a] Terence S. M. Wan,*[b] Ka-Ping Kwong[a] and Chun-Tao Che*[ac]

[a] *Department of Chemistry, Hong Kong University of Science & Technology, Clear Water Bay, Hong Kong. E-mail: chctche@ust.hk*
[b] *Racing Laboratory, Hong Kong Jockey Club, Shatin Racecourse, Hong Kong*
[c] *School of Chinese Medicine, The Chinese University of Hong Kong, Shatin, Hong Kong*

Received (in Cambridge, UK) 28th July 1999, Accepted 10th September 1999

Chiral recognition of 19 common amino acids is achieved by investigating the collision-induced dissociation spectra of protonated trimers formed by electrospray ionisation of amino acids in the presence of one of the following chiral selectors: L- and D-*N*-*tert*-butoxycarbonylphenylalanine (BPhe), L- and D-*N*-*tert*-butoxycarbonylproline (BPro) and L- and D-*N*-*tert*-butoxycarbonyl-*O*-benzylserine (BBSer).

Chiral recognition is an important topic in chemistry and biochemistry. A number of approaches[1] have been used for the chiral recognition of organic compounds, including polarimetry, circular dichroism, nuclear magnetic resonance, chromatography and capillary electrophoresis. Attentions has also been paid to the use of mass spectrometry[2,3]due to the many advantages of the technique, *e.g.* high sensitivity, short analysis time, ability to analyse mixtures by tandem mass spectrometry (MS/MS) or in combination with chromatography, and the ability to study the intrinsic properties of the chiral effect by isolating the interacting molecules in the gaseous phase.

Since the first observation of chiral effects in mass spectrometry by Fales and Wright,[4] about 50 papers have been published in this field.[3] In most of the studies, enantiomers were allowed to ionise in the presence of chiral selectors, and chiral recognition was observed by comparing the relative extent of the formation (MS) or fragmentation (MS/MS) of the diastereomeric complex ions. While chemical ionisation (CI)[5–8] was the main ionisation mode used in the early development of chiral mass spectrometry, significant results have been reported by applying the fast atom bombardment (FAB) mode.[9–14] A number of data evaluation methods are also available for the analysis, such as the relative peak intensity method (*i.e.* the internal standard method),[9] the deuterium-labelled method,[10] the stability constant method,[11] and the two-internal-standards method.[12] In spite of these efforts, only limited success has been achieved; so far, not even a single class of chiral compounds can be systematically recognised by mass spectrometry. In general, problems encountered in the systematic recognition of a class of chiral compounds include the limited recognition ability of chiral selectors and the poor reproducibility of mass spectra, as well as the requirement of high concentration or high volatility for the association between enantiomers and chiral selectors.

We now report the first systematic study of chiral recognition of 19 amino acids by comparing the relative extent of fragmentation (MS/MS signal intensities) of the diastereomeric protonated trimers formed by the amino acids and chiral selectors. Three new chiral selectors, namely, L- and D-*N*-*tert*-butoxycarbonylphenylalanine (BPhe), L- and D-*N*-*tert*-butoxycarbonylproline (BPro) and L- and D-*N*-*tert*-butoxycarbonyl-*O*-benzylserine (BBSer), were used in the present study. Electrospray ionisation (ESI)[15] was applied to provide complex ions of the amino acids and chiral selectors; a typical mass spectrum of the amino acid/chiral selector mixture is depicted in Fig. 1. Thus, the amino acid (X) combines with chiral selector (Y) to form protonated dimer XYH^+, protonated trimer XY_2H^+, protonated tetramer XY_3H^+ *etc*. The protonated trimers (XY_2H^+) were subsequently chosen for investigation because of their high intensities and large chiral discrimination toward most amino acids. The XY_2H^+ complex ion was fragmented by collision-induced dissociation (MS/MS) to form protonated dimers XYH^+ (Fig. 2). All amino acids were studied in four combinations with the chiral selectors, *i.e.* LD and DL (heterochiral) and LL and DD (homochiral), and the chiral recognition ratio *R* was defined according to eqn. (1).[14]

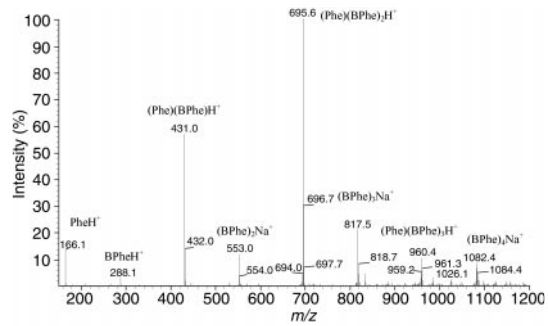

Fig. 1 ESI spectrum of a mixture of Phe (1 mM) and BPhe (1 mM). Major cluster ions are indicated. Conditions for ESI: heated capillary 50 °C, sheath gas 60 psi, spray voltage 4 kV, syringe pump 10 μL min^{-1}. Samples were run on a Finnigan LCQ mass spectrometer.

$$R = \frac{([XYH^+]/[XY_2H^+\})_{\text{hetero}}}{([XYH^+]/[XY_2H^+])_{\text{homo}}} = \frac{([XYH^+]/[XY_2H^+])_{\text{LD}} + ([XYH^+]/[XY_2H^+])_{\text{DL}}}{([XYH^+]/[XY_2H^+])_{\text{LL}} + ([XYH^+]/[XY_2H^+])_{\text{DD}}} \quad (1)$$

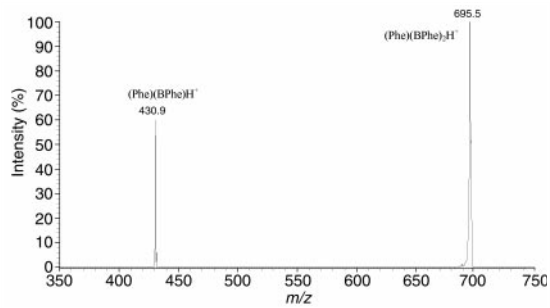

Fig. 2 MS/MS spectrum of protonated trimer from Phe and BPhe. Collision energy was 8%, isolation width 18 u, mass range 350–750 u.

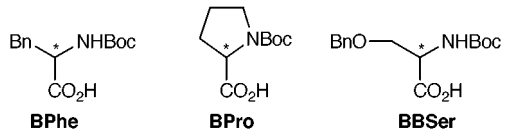

Table 1 Chiral discrimination of BPhe, BPro and BBSer toward amino acids as observed in the MS/MS spectra of the protonated trimers[a]

	BPhe			BPro			BBSer					
Amino acids	*R*	SD_R[b]	SD_R/R (%)	*R*	SD_R[b]	SD_R/R (%)	*R*	SD_R[b]	SD_R/R (%)	Suitable chiral selectors[c]		
Ala	1.044	0.006	0.59	1.074	0.006	0.56	1.143	0.012	1.05			BBSer
Arg[d]	1.416	0.007	0.49	2.027	0.015	0.74	0.640	0.005	0.73	BPhe,	BPro,	BBSer
Asn	0.938	0.003	0.34	1.163	0.004	0.34	0.992	0.011	1.06		BPro	
Asp	0.810	0.005	0.57	1.102	0.007	0.64	1.061	0.006	0.57	BPhe,	BPro	
Cys	1.054	0.006	0.55	1.122	0.005	0.45	1.262	0.009	0.71		BPro,	BBSer
Gln	1.905	0.013	0.66	2.042	0.009	0.44	2.953	0.039	1.32	BPhe,	BPro,	BBSer
Glu	0.855	0.003	0.32	1.752	0.010	0.57	0.615	0.006	0.99	BPhe,	BPro,	BBSer
His	1.738	0.008	0.45	2.107	0.015	0.71	4.316	0.027	0.63	BPhe,	BPro,	BBSer
Ile	1.025	0.007	0.68	1.060	0.006	0.57	1.572	0.012	0.76			BBSer
Leu	1.021	0.005	0.45	0.989	0.008	0.85	1.493	0.012	0.80			BBSer
Lys	0.840	0.005	0.57	0.945	0.004	0.45	0.378	0.004	1.03	BPhe,		BBSer
Met	1.152	0.005	0.45	1.470	0.017	1.16	1.277	0.010	0.78	BPhe,	BPro,	BBSer
Phe	0.812	0.004	0.46	1.096	0.004	0.36	0.928	0.008	0.83	BPhe	BPro[e]	
Pro	2.002	0.014	0.70	2.340	0.021	0.90	0.734	0.007	0.91	BPhe,	BPro,	BBSer
Ser	1.012	0.004	0.39	1.313	0.007	0.53	0.992	0.010	1.02		BPro	
Thr	1.158	0.006	0.52	1.166	0.005	0.43	1.078	0.009	0.83	BPhe,	BPro	
Trp	0.566	0.003	0.55	1.934	0.009	0.47	0.494	0.007	1.42	BPhe,	BPro,	BBSer
Tyr	0.894	0.006	0.62	1.137	0.006	0.53	0.963	0.010	0.99	BPhe,	BPro	
Val	1.046	0.009	0.83	1.050	0.008	0.76	1.527	0.014	0.92			BBSer

[a] All enantiomerically pure L- and D-BPhe, BPro, BBSer and amino acids were purchased from Sigma and used without further purification. [b] Standard deviation for *R*. [c] $R > 1.1$ or $R < 0.9$. [d] Protonated trimers in low intensities, thus the MS/MS spectra of protonated dimers were measured instead. [e] Should also be suitable.

The results (Table 1) indicated that the maximum relative standard deviation for the chiral recognition ratio *R* is 1.42%. Therefore at the 99% (or better) probability level, any chiral recognition ratio falling outside the range of 1.000 ± 0.081 *(i.e.* $1.000 \pm 9.92 \times 1.42\%/3^{0.5}$) would indicate a significant discrimination of chirality. In other words, chiral discrimination could be recognised by an *R* value larger than 1.1 or smaller than 0.9. On this basis, our data clearly show that each amino acid could be discriminated by at least one chiral selector, suggesting a successful chiral recognition of all 19 amino acids by mass spectrometry using BPhe, BPro and/or BBSer as chiral selectors.

In summary, we have developed a mass spectrometric method to recognise the chirality of common amino acids. The results indicate that ESI-MS/MS is a promising approach for chiral recognition. This method can provide abundant complex ions even when the samples are at low concentrations or bear large/labile groups. The continuous introduction of sample mixtures *via* a syringe pump and the averaging of MS/MS spectra ensure a high precision of the results. ESI-MS/MS can be used to study the chirality of compounds in a mixture, and it only requires minimal sample preparation.

This work was financially supported by an RGC Competitive Earmarked Research Grant (HKUST 598/95P) and a Royal Society of Chemistry Research Fund Grant. The LCQ instrument used in this study was provided by the Biotechnology Research Institute of HKUST.

Notes and references

1 P. Schreier, A. Bernreuther and M. Huffer, *Analysis of Chiral Organic Molecules: methodology and application*, Walter de Gruyter, Berlin, 1995.

2 F. J. Winkler and J. S. Splitter, in *Application of Mass Spectrometry to Organic Stereochemistry*, ed. J. S. Splitter and F. Turecek, VCH, New York, 1994, ch. 16, pp. 365–370.

3 M. Sawada, *Mass Spectrom. Rev.*, 1997, **16**, 73.

4 H. M. Fales and G. J. Wright, *J. Am. Chem. Soc.*, 1977, **99**, 2339.

5 S. M. Hua, Y. Z. Chen, L. F. Jiang and S. M. Xue, *Org. Mass Spectrom.*, 1986, **21**, 7.

6 Y. Z. Chen, H. Li, H. J. Yang, S. M. Hua, H. Q. Li, F. Z. Zhao and N. Y. Chen, *Org. Mass Spectrom.*, 1988, **23**, 821.

7 J. Martens, S. Lubben and W. Schwarting, *Z. Naturforsch., Teil B*, 1991, **46**, 320.

8 J. C. Tabet, *Tetrahedron*, 1987, **43**, 3413.

9 M. Sawada, Y. Okumura, M. Shizuma, Y. Takai, Y. Hidaka, H. Yamada, T. Tanaka, T. Kaneda, K. Hirose, S. Misumi and S. Takahashi, *J. Am. Chem. Soc.*, 1993, **115**, 7381.

10 M. Sawada, Y. Takai, H. Yamada, S. Hirayama, T. Kaneda, T. Tanaka, K. Kamada, T. Mizooku, S. Takeuchi, K. Ueno, K. Hirose, Y. Tobe and K. Naemura, *J. Am. Chem. Soc.*, 1995, **117**, 7726.

11 G. Pocsfalvi, M. Liptak, P. Huszthy, J. S. Bradshaw, R. M. Izatt and K. Vekey, *Anal. Chem.*, 1996, **68**, 792.

12 A. Dobo, M. Liptak, P. Huszthy and K. Vekey, *Rapid Commun. Mass Spectrom.*, 1997, **11**, 889.

13 G. Smith, and J. A. Leary, *J. Am. Chem. Soc.*, 1996, **118**, 3293.

14 K. Vekey and G. Czira, *Anal. Chem.*, 1997, 69, 1700.

15 Solutions of D- and L-amino acids and D- and L-BPro (2 mM) were prepared in 50% MeOH containing 1% AcOH. Solutions of D- and L-BPhe and D- and L-BBSer (2 mM) were prepared in MeOH. The solutions of amino acid and chiral selector were mixed in a 1:1 ratio prior to mass spectrometric analysis. Mass spectrometry was carried out in a Finnigan LCQ instrument (San Jose, CA, USA) fitted with an ESI ion source. Conditions for ESI were: heated capillary 50 °C, sheath gas 60 psi, spray voltage 4 kV, syringe pump 10 μL min^{-1}. The LCQ was operated with the Automatic Gain Control (AGC) mode. The AGC target values were: Full MS—5e + 007, MS^n—2e + 007. The default maximum injection time was 500 ms with 5 micro scans. Helium was introduced and maintained a pressure of 1 mtorr for improving the trapping efficiency of the ion trap and for use as the collision gas during the MS/MS process. Typical MS/MS conditions were: relative collision energy 8%, isolation width 18 u and mass range 300–850 u when BBSer was used as the chiral selector; relative collision energy 6.5%, isolation width 15 u and mass range 250–700 u for BPro; and relative collision energy 8%, isolation width 18 u and mass range 300–800 u for BPhe.

Communication 9/06131B

Dual p- and n-type doping in an acid sensitive alternating bi(ethylenedioxythiophene) and pyridine polymer

David J. Irvin, C. J. DuBois, Jr. and John R. Reynolds*

Department of Chemistry, Center for Macromolecular Science and Engineering, University of Florida, Gainesville, FL 32611, USA. E-mail: reynolds@chem.ufl.edu

Received (in Columbia, MO, USA) 7th June 1999, Accepted 9th August 1999

Poly[2,5-bis(3,4-ethylenedioxy-2-thienyl)pyridine] exhibits multi-color electrochromism *via* easily accesible p- and n-type doping, and can be switched between a pale blue reduced state, a red neutral state, and a blue–purple oxidized state.

The ability to easily access both p- and n-type redox states in conducting and electroactive polymers may lead to useful materials.[1] While it is well-known that conjugated hydrocarbon polymers can be both p- and n-type doped, only recently has this been made possible in an electrochemically deposited film.[2] It has been shown by de Leeuw[3] that nitrogen-containing poly(heterocycles) induce stability in n-doped systems. One such example is poly(pyridine), which has a reduction potential of −2.1 V.† Other examples include poly(quinoline-2,6-diyl) which reversibly n-dopes at −1.8 V, along with poly(1,5-naphthyridine)[3] and poly(4,4′-dialkyl-2,2′-bithiazole-5,5′-diyl)s.[4] Relatively electron rich polyheterocycles are typically used in oxidative electropolymerization due to their propensity to form highly electroactive materials. While their p-doping characteristics are well-documented and can be outstanding, few systems show useful n-doping.[5–9] In many instances where a reduction is observed, the process is either irreversible and leads to rapid degradation of electroactivity, or leads to pinned anions and not true n-doping.[6]

We have undertaken a study of polyheterocycles containing alternating electron donor (D) and acceptor (A) units prepared *via* efficiently oxidatively polymerizable D–A–D monomers. Judicious choice of D and A units allows control of the energies of the π-system's effective HOMO and LUMO levels, which determine the polymer's oxidative (p-doping) and reductive (n-doping) properties, respectively. Thus, it has been shown that the electronic band gap of the polymer can be reduced significantly.[10] In addition, by using repeat units that are sensitive to the chemical environment, polymers that can provide an optical or electrical response upon exposure to species in electrolyte solutions can be used as sensor materials.

In designing an electroactive polymer that has three accessible charge states (oxidized, neutral, and reduced), while simultaneously being responsive to the pH of the bathing electrolyte solution, we prepared poly[2,5-bis(3,4-ethylenedioxy-2-thienyl)pyridine] [poly(BEDOT-Py)], which is efficiently synthesized *via* the corresponding D–A–D monomer. We have previously shown that 3,4-ethylenedioxythiophene is extremely effective as the oxidatively polymerizable moiety for the synthesis of poly(BEDOT-arylene)s that are highly electroactive and provide structurally controlled electrochromic properties.[11,12] It has been shown that while separate films of poly[2,5-bis(2-thienyl)pyridine] (PBTh-Py) can be p- or n-type doped, an electrochemical memory effect precludes both states from being accessed in a single film.[13] In addition to its propensity to stabilize reduced systems, the pyridine central unit is sufficiently basic to yield distinct spectroscopic shifts in an acidic medium and may be useful as a pH sensitive switching material.

BEDOT-Py was synthesized using a Negishi-type aryl cross coupling reaction (93% yield). Electropolymerization/film formation of poly(BEDOT-Py) was carried out using either repeated scan or constant potential methods from 10 mM BEDOT-Py and 0.1 M Bu_4NClO_4 in MeCN–CH_2Cl_2 (1:1) or 7.5 mM BEDOT-Py and 0.1 M Bu_4NClO_4 in MeCN. The monomer oxidizes at a bare Pt electrode with a peak ($E_{p,m}$) at 0.65 V. The redox processes for poly(BEDOT-Py) include broad oxidation and reduction (to the neutral form) peaks centered at 0.55 and 0.37 V, respectively, resulting in an $E_{1/2}$ of 0.49 V. While the monomer's $E_{p,m}$ is comparable to BEDOT-benzene (0.61 V), the resultant poly(BEDOT-Py) exhibits a higher $E_{1/2}$ by >250 mV when compared to poly(BEDOT-benzene).[11] This confirms the dominance of the terminal EDOT during polymerization, while the electron-accepting pyridine has a strong effect on the polymer's redox properties.

To study the optical properties and combined p- and n-doping electrochemistry, poly(BEDOT-Py) was deposited potentiostatically from a 7.5 mM MeCN solution since CH_2Cl_2 is not stable to the reduction potentials used during the experiment. Fig. 1 shows a combination of the separate and stable oxidative and reductive cyclic voltammetric scans for a film deposited onto a Pt button electrode. This method allowed isolation of the two processes while experiments conducted by repeatedly cycling

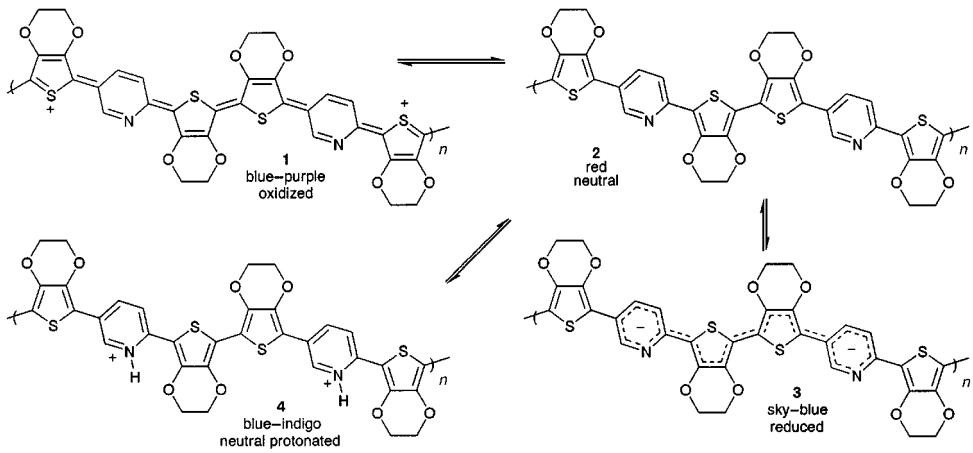

Scheme 1

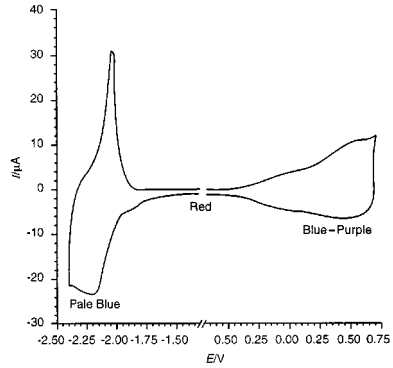

Fig. 1 Oxidative and reductive cyclic voltammetric scan of poly(BEDOT-Py) on a Pt button in 0.1 M TBAP in MeCN; scan rate = 100 mV s^{-1}.

between p- and n-doped states led to the formation of pre-peaks that increased in intensity with each subsequent scan. These pre-peaks, which may be due to trapped charge carriers,[6] can be misinterpreted as redox doping peaks if separate oxidation and reduction experiments are not performed.

The band gap of neutral poly(BEDOT-Py) is estimated to be 1.9 eV from the onset of the π–π* transition, with λ_{max} = 478 nm. It was observed that, with increasing film thickness, the absorbance does not change significantly at energies below 1.9 eV, indicating a well-reduced polymer with little or no trapped charges.

The observance of reduction peaks in the cyclic voltammogram is not proof on n-doping. It has been shown that reduction of polybithiophene does not lead to n-doping, and this process has been attributed to the formation of pinned anionic states.[6] Our group has observed similar results in cyanovinylene-linked poly(biheterocycles).[14] To establish the definitive formation of charge carriers and the ability to access both the p- and n-type states in a single film, spectroelectrochemistry was carried out on poly(BEDOT-Py) through both the oxidative and reductive processes. It should be noted that the latter experiment requires rigorous exclusion of oxygen and water due to the reactivity of the reductively doped state. Fig. 2(*a*) shows the spectroelectrochemical series for p-doping from 0.0 to +1.0 V, while Fig. 2(*b*) shows the series for n-doping from 0.0 to −1.8 V. When the polymer is held between −1.5 and +0.2 V the neutral film is a deep red in color. This optical state is quite similar to polythiophene and its alkyl substituted analogs, and, as expected, the band gap lies between the values observed for poly(3,4-ethylenedioxythiophene) (PEDOT) and polypyridine. Stepwise oxidation [Fig. 2(*a*)] leads to the typical evolution of the spectra for p-doping with peaks at *ca.* 1 and 1.75 eV as bipolaronic charge carriers are formed. The oxidized form is a deep blue–purple in color, again analogous to the polythiophene parent.

Comparison of the results shown in Fig. 2(*a*) and 2(*b*) bring out the unique spectroscopic nature of this polymer upon reduction. The similarity of the results, loss of intensity of the interband transition with concurrent evolution of peaks at 1 and 1.75 eV, are proof of the facile n-doping of this polymer and the fact that both the p- and n-doped states can be attained in the same film. Interestingly, the relative intensity of these two

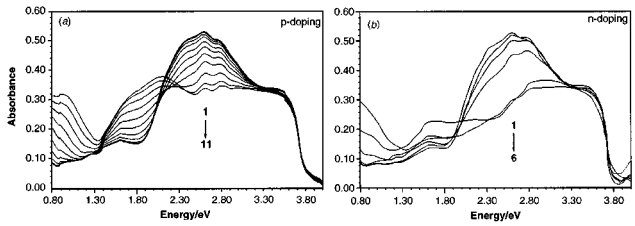

Fig. 2 Spectroelectrochemical series for p- and n-type doping of poly(BEDOT-Py): (*a*) p-doping at (1) 0.0, (2) 0.1, (3) 0.2, (4) 0.3, (5) 0.4, (6) 0.5, (7) 0.6, (8) 0.7, (9) 0.8, (10) 0.9 and (11) 1.0 V; (*b*) n-doping at (1) 0.0, (2) −1.4, (3) −1.5, (4) −1.6, (5) −1.7 and (6) −1.8 V.

peaks is different in the two forms. While they are similar in intensity in the p-doped form, the NIR peak is dominant in the n-doped form. This has a profound effect on the electrochromic properties as the n-doped form is sky-blue in color and more highly transmissive to visible light. Note the high degree of light transmission between 1.5 (825 nm) and 2.5 eV (500 nm) corresponding to a major fraction of the visible spectrum. This is similar to the optical properties observed for the p-doped PEDOT family of polymers.

A unique property of poly(BEDOT-Py) is that it contains sites that can be quaternized. A series of UV–VIS–NIR spectra were obtained for the neutral film as a function of pH upon exposure to an aqueous citric acid buffer and 0.1 M HCl. There is little change in λ_{max} as the pH is reduced to 2, upon which there is a sharp 70 nm red-shift through pH 1 as the band gap is lowered to 1.5 eV. The neutral film changes from red to indigo–blue with exposure to acid, and the resulting band gap is close to that observed for the PEDOT family of polymers. It is interesting to note that protonation of the film occurs at a much higher acidity than for pyridine. This observation is supported in the literature in which a set of thiophene- and furan-substituted pyridines show a marked decrease in basicity relative to pyridine and can be attributed to an electron-withdrawing inductive effect of the 2-EDOT rings.[15] The films can be reversibly switched between the protonated and neutral state by exposure to 1 M HCl followed by rinsing with deionized water.

The unique chemical and electrochemical properties of poly(BEDOT-Py) are outlined in Scheme 1. The as-made blue–purple p-doped state **1** can be converted to the red neutral form **2** upon reduction. The neutral form can be reversibly reoxidized back to **1**, reduced to the sky-blue n-doped state **3**, or protonated to yield blue–indigo polycationic, electrochemically neutral state **4**. Studies are underway to further elucidate the redox properties of polycationic polymer **4** (both protonated and alkylated), and gain a deeper understanding of the n-doped form **3**.

This work was supported by grants from the AFOSR (F49620-96-1-0067), the NSF (CHE 96-29854), and the NAWC, China Lake CA. We appreciate the donation of EDOT from the AG Bayer corporation.

Notes and references

† All potentials given *vs.* Ag/Ag^+.

1 For reviews in this field, see *Handbook of Conducting Polymers*, 2nd edn., ed. T. A. Skotheim, R. L. Elsenbaumer and J. R. Reynolds, Marcel Dekker, New York, 1998.
2 J. Debad and A. J. Bard, *J. Am. Chem. Soc.*, 1998, **120**, 2476.
3 D. M. De Leeuw, M. M. J. Simenon, A. R. Brown and R. E. F. Einerhand, *Synth. Met.*, 1997, **87**, 53.
4 M. D. Curtis, H. Cheng and J. I. Nanos, *Macromolecules*, 1998, **31**, 205.
5 J. P. Ferraris, C. Henderson, D. Torres and D. Meeker, *Synth. Met.*, 1995, **72**, 147.
6 G. Zotti, G. Schiavon and S. Zecchin, *Synth. Met.*, 1995, **72**, 275.
7 T. Kanbara, Y. Miyazaki and T. Yamamoto, *J. Polym. Sci., Polym. Chem. Ed.*, 1995, **33**, 999.
8 T. Yamamoto, K. Sugiyama, T. Kushida, T. Inoue and T. Kanbara, *J. Am. Chem. Soc.*, 1996, **118**, 3930.
9 T. Yamamoto, H. Suganuma, T. Maruyama, T. Inoue, Y. Muramatsu, M. Arai, D. Komarudin, N. Ooba, S. Tomaru, S. Sasaki and K. Kubota, *Chem. Mater.*, 1997, **9**, 1217.
10 J. Roncali, *Chem. Rev.*, 1997, **97**, 173.
11 G. A. Sotzing, J. R. Reynolds and P. J. Steel, *Chem. Mater.*, 1996, **8**, 882.
12 J. A. Irvin and J. R. Reynolds, *Polymer*, 1998, **39**, 2339.
13 I. H. Jenkins, U. Salzner and P. G. Pickup, *Chem. Mater.*, 1996, **8**, 2444.
14 G. A. Sotzing, C. A. Thomas, J. R. Reynolds and P. J. Steel, *Macromolecules*, 1998, **31**, 3750.
15 R. A. Jones and P. U. Civcir, *Tetrahedron*, 1997, **53**, 11 529.

Communication 9/04584H

Reduction of *N*-arylporphyrins to *N*-arylphlorins: opposite stereochemical courses as a function of the reducing agent

Romain Ruppert, Christophe Jeandon, Anna Sgambati and Henry J. Callot*

Faculté de Chimie, 1 rue Blaise Pascal, 67008 Strasbourg Cedex, France. E-mail: callot@chimie.u-strasbg.fr

Received (in Cambridge, UK) 13th July 1999, Accepted 17th September 1999

Electrochemical or $Na_2S_2O_4$ reduction of *N*-arylporphyrins gives stable phlorins epimeric to those obtained by tosylhydrazine or $NaBH_4$ reduction.

Phlorins are non-aromatic tetrapyrrolic macrocyclic isomers of chlorins. In these dihydroporphyrins the two additional hydrogens are located at the *meso* and N positions. The first stable phlorin was isolated by R. B. Woodward[1] during the synthesis of chlorophyll *a*. Factors favouring the formation of phlorins by chemical or electrochemical reduction or by nucleophilic addition to porphyrins are steric strain,[1,2] complexation with high valent metal ions,[3] and electrophilicity of the macrocycle.[4]

We found[5–7] that the reduction of *N*-arylporphyrins **1** with tosylhydrazine or $NaBH_4$ gave *N*-arylphlorins **2** (*N*,*meso*-dihydroporphyrins; *anti* isomer) instead of the expected *N*-arylchlorins (β,β-dihydroporphyrins). It was proposed that in this case the driving force of the reaction, as well as the explanation for the stability of the products, was the rotation experienced by the *N*-substituted pyrrole resulting in a significant decrease of the steric strain.

Recently,[8] a phlorin derived from heme *c* was proposed as an intermediate in the catalytic cycle of hydroxylamine oxidoreductase (HAO). This phlorin is a heme *c* group arylated at C-5 by a tyrosine moiety. The position of the aryl group above the plane in the intermediate strongly suggested an C-5 sp^3 carbon and thus a phlorin. Here we describe the preparation and structural characterization of new phlorins whose out-of-plane *meso*-aryl groups bear a resemblance to such intermediates.

We found that reduction of *N*-arylprophyrins **1** with aged $NaBH_4$ gave a mixture of the expected phlorin and a very similar product, at least where the UV-visible data were concerned. This product proved to be rather unstable under chromatographic conditions, but NMR data suggested an epimeric structure. In order to assign a structure to this new phlorin and to find conditions suitable for its preparation in acceptable yields, we tested a new set of reducing agents. Borane·THF was not satisfactory, giving mixtures of phlorins and dihydrophlorins *etc.*, but cathodic reduction, sodium dithionite and dihydropyridine **4** (Hantzsch ester) all gave quantitatively phlorins (Scheme 1).

Electrochemical reduction of *N*-aryl-*meso*-tetraphenylporphyrin **1** was performed in an electrolysis cell fitted with three compartments separated by glass frits (Hg cathode, Pt counter electrode, SCE reference electrode). The experiments were conducted on a 25 to 50 μmol scale in a protic electrolyte (THF–MeOH, 2:1; 0.25 M LiCl). The reduction of the porphyrin and the concomitant reduction of the protons led to an increase of the electrolyte basicity during electrolysis. Therefore, the working potential (−0.8 to −1.2 V *vs.* SCE) was continuously adjusted during the electrolysis in order to keep the current density approximatively constant (5 mA cm^{-2}). The progress of the reaction was followed by TLC and showed that only one reduction product was formed. A very simple work-up procedure (addition of CH_2Cl_2, washing with water and crystallisation of the crude product from CH_2Cl_2–MeOH) afforded the pure phlorins **3a** or **3b** as green crystals (60% isolated yield.) Phlorins **3a** and **3b** were found to be stable as solids and stable enough in solution to grow crystals (see below), but reverted to the starting *N*-arylporphyrins **1a** and **1b** rapidly when chromatographed.

Compounds **3a** and **3b** showed phlorin UV-visible spectra [**3a**: λ_{max} 422 nm (ε = 34000) and 685 (29700)]. The NMR spectra of **3a** and **3b** revealed the loss of aromaticity suffered by the porphyrin ring: the pyrrolic protons are located between *ca.* δ 6.5 and 7, the *meso* proton of **3b** was found at δ 6.87, a value 2.53 ppm downfield from that of the *meso* proton of **2b** (δ 4.34). Of particular interest are the signals of the *N*-anisyl group protons of **3b**: the aromatic protons appear at δ 5.78, 5.96, 6.13 and 6.29, strongly suggesting a face-to-face (*syn*) arrangement of this group and the *meso*-phenyl attached to the reduced bridge (the *N*-phenyl analog **3a** showed a broadening of the *N*-phenyl signals, possibly due to restricted rotation). In the epimeric phlorin **2b** (*anti*), the anisyl protons are located between δ 6.4 and 6.8.

Single crystals of *syn*-phlorin **3a** could be obtained by slow diffusion of MeOH in a solution of **3a** in $CHCl_3$. The structure could be solved† and is shown in Fig. 1. The close face-to-face arrangement of the phenyl rings was confirmed, and is illustrated by the very short distance (3.14 Å) between the closest C atoms. The rotation of the *N*-phenyl pyrrole is shown by its angles with the remaining pyrrole units: AC = 106°; AB

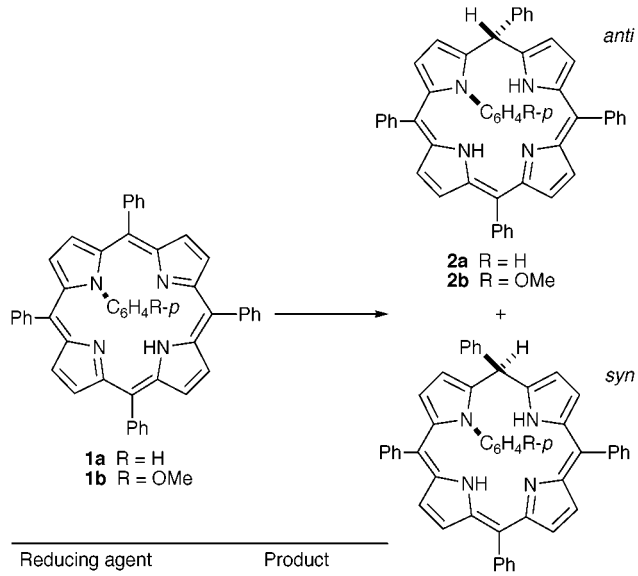

Reducing agent	Product
$TsNHNH_2$	**2**
$NaBH_4$	**2**
cathodic reduction (Hg)	**3**
$Na_2S_2O_4$	**3**
4	**2** + **3** (1:2)

Scheme 1

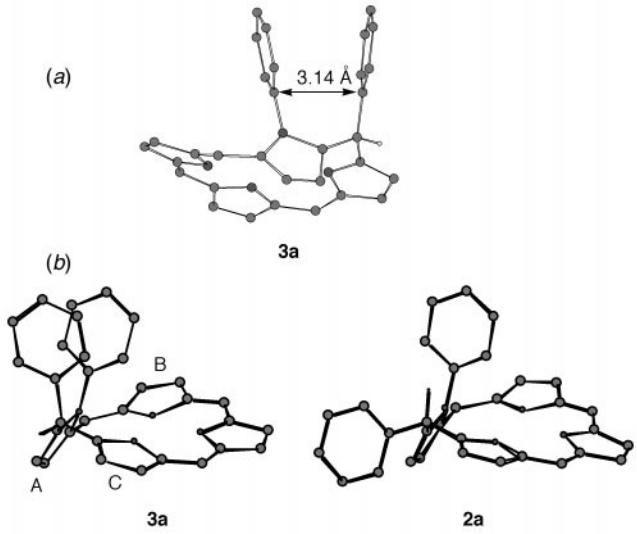

Fig. 1 (*a*) Side-view of phlorin **3a**, showing the face-to-face arrangement of the *meso*-and *N*-phenyl groups, and (*b*) comparison of phlorin **3a** with the epimeric **2a** (for the sake of clarity, three *meso*-phenyl groups and all of the hydrogen atoms except the *meso*-H are omitted).

= 130°. This last value is very similar to that found in *N*-*o*-tolyl-*meso*-tetraphenylporphyrin,[9] showing that all the deformation of the macrocycle occurred across the reduced bridge.

The use of an excess of sodium dithionite as a reducing agent in a biphasic system (water–CH_2Cl_2, 1:1) containing NMe_4Cl gave phlorins **3** from porphyrins **1** in 70% isolated yield. However, reduction of **1b** by Hantzsch ester **4** (6 equiv. in refluxing PhCl; microwave oven, 0.5 h), although quantitative, gave a mixture of both *syn* and *anti* phlorins **2b** and **3b** (1:2 ratio), Approximately 2.5 equiv. of **4** were consumed.

These results suggest two mechanistically different routes from *N*-arylporphyrins **1** to the corresponding phlorins.[10] Under electron transfer conditions (cathodic reduction, sodium dithionite) a radical anion was formed and the *meso*-bridge specifically protonated on the face opposite to the *N*-substituent. Further reduction of the radical and protonation gave **3**. Reducing agents like $NaBH_4$ or Hantzsch ester **4** are hydride donors and transferred this hydride irreversibly to the porphyrin. Tosylhydrazine reduction, although involving intermediates, might similarly begin with a nucleophilic attack of the *meso*-bridge. In these cases, steric hindrance to the approach of the reagent may govern the isomeric ratio, with the most hindered hydride donor, **4**, having difficulty approaching from the same side of the *N*-aryl group as $NaBH_4$ or tosylhydrazine, and giving *syn* **3** as the major component.

We thank the 'Service Commun de Rayons X' (A. Decian and N. Kyritsakas) for solving the structure, and A. Roth for help.

Notes and references

† *Crystal data* for **8**: $C_{50}H_{36}N_4$, M = 692.87, monoclinic, space group $P\,1\,2_1/n\,1$; a = 17.662(2), b = 11.6074(7), c = 20.335(2) Å, β = 112.669(4)°, V = 3846(1) Å^3, Z = 4, D_c = 1.20 g cm^{-3}. A total of 29669 ± h ± k + l reflections was collected on a green crystal of dimensions 0.20 × 0.15 × 0.08 mm^3, using a KappaCCD diffractometer, graphite monochromated Mo-Kα, 2.5 < θ < 27.57, T = 294 K. 4462 unique reflections having I > 3 $\sigma(I)$ were used to determine and refine the structure. Final results: R = 0.072, Rw = 0.093, GOF = 1.524, largest peak in final difference = 1.619 e Å^{-3}. CCDC 182/1417. See http//www.rsc.org/suppdata/cc/1999/2123/ for crystallographic data in .cif format.

1 R. B. Woodward, *Angew. Chem.*, 1960, **72**, 651.
2 H. H. Inhoffen, P. Jäger, R. Mählhop and C.-D. Mengler, *Liebigs Ann.*, 1967, **704**, 188; T. Ema, M. O. Senge, N. Y. Nelson, H. Ogoshi and K. M. Smith, *Angew. Chem., Int. Ed. Engl.*, 1994, **33**, 1879.
3 H. Sugimoto, *J. Chem. Soc., Dalton Trans.*, 1982, 1169; H. Segawa, R. Azumi and T. Shimidzu, *J. Am. Chem. Soc.*, 1992, **114**, 7564.
4 J. Setsune, T. Ikeda, T. Iida and T. Kitao, *J. Am. Chem. Soc.*, 1988, **110**, 6572; J. Setsune, Y. Ishimaru and T. Kitao, *Chem. Lett.*, 1990, 1351; J. Setsune, H. Yamaji and T. Kitao, *Tetrahedron Lett.*, 1990, **31**, 5057; J. Setsune, K. Wada and H. Higashino, *Chem. Lett.*, 1994, 213.
5 B. Krattinger and H. J. Callot, *Chem. Commun.*, 1996, 1341.
6 B. Krattinger and H. J. Callot, *Tetrahedron Lett.*, 1996, **37**, 7699.
7 B. Krattinger and H. J. Callot, *Eur. J. Org. Chem.*, 1999, 1857.
8 D. M. Arciero and A. B. Hooper, *Biochem. Soc. Trans.*, 1998, **26**, 385; D. M. Arciero, M. Hendrich, T. Iverson, D. Rees and A. B. Hooper. ACS National Meeting, Anaheim, March 21–25, 1999, abstr. INOR 333; see also: D. M. Arciero, A. B. Hooper, M. Cai and R. Timkovich, *Biochemistry*, 1993, **32**, 9371.
9 S. Aizawa, Y. Tsuda, K. Hatano and S. Funahashi, *Inorg. Chem.*, 1993, **32**, 1119.
10 A mechanistic dichotomy was also observed during the reductive demetallation of silver and copper porphyrins: J. A. Cowan and J. K. M. Sanders, *Tetrahedron Lett.*, 1986, **27**, 1201.

Communication 9/05676I

ChemComm

Unprecedented and novel hetero [6+3] cycloadditions of fulvene: a facile synthesis of the 11-oxasteroid framework

Bor-Cherng Hong,* Hsu-I Sun and Zhong-Yi Chen

Department of Chemistry, National Chung Cheng University, Chia-Yi, 621, Taiwan, R. O. C.
E-mail: chebch@ccunix.ccu.edu.tw

Received (in Cambridge, UK) 24th August 1999, Accepted 9th September 1999

In contrast to the Diels–Alder reaction of fulvenes and benzoquinone, 6-dimethylaminofulvene reacts with benzoquinones to give the hetero [6+3] cycloaddition adduct, constituting an efficient and novel route to cyclopenta[*c*]-chromenes including 11-oxasteroids.

Fulvene and its derivatives have received a great deal of attention over the years.[1] Cycloadditions of fulvenes (*e.g.* [4+3],[2] [2+2],[3] [4+2],[4] [2+4],[5] [6+4],[6] [6+2][7]) provide general and powerful approaches to various polycyclic systems and natural products. We recently reported a new type of reaction: the [6+3] cycloaddition of fulvenes[8] for the facile synthesis of indane derivatives.[9] In conjunction with our continuing efforts in fulvene chemistry,[10] we have developed a novel hetero [6+3] cycloaddition of 6-dimethylaminofulvene[11] to benzoquinone that provides a series of cyclopenta[*c*]chromene derivatives. The latter constitute the basic skelton of biologically active 11-oxasteroids.

Fulvenes usually react with benzoquinones to give the [4+2] cycloaddition adducts (Scheme 1).[12] In contrast, we have found that reaction of the 6-dimethylaminofulvene **1** and benzoquinone results in the formation of the oxatricyclic product **2** (Scheme 2).[13] Syntheses of the cyclopenta[*c*]pyrans and cyclopenta[*c*]chromene have received a lot of attention.[14] To the best of our knowledge, this is the first example of the synthesis of the 3-oxa-bicyclo[4.3.0]nonane system *via* the [6+3] approach. Reaction of 6-dimethylaminofulvene and benzoquinone in benzene at 25 °C for 20 min provided the cyclopenta[*c*]chromene **2** in 65% yield as the only isolable adduct (entry 1, Table 1). The structure of **2** was assigned based on IR, ^{1}H and ^{13}C NMR, COSY, DEPT, HMQC, HMBC, MS and HRMS analyses.† This striking difference in the chemoselectivity of fulvene **1** *vs*. regular fulvenes may be attributed to an increase in the electron density of the 6-dimethylaminofulvene π-system. The formation of **2** may be rationalized *via* the following stepwise mechanism, shown in Scheme 2. Initial addition of **1** to benzoquinone generates the zwitterionic intermediate **3**, and tautomerization followed by loss of dimethylamine (path **A**) gives the hetero [6+3] product **2**. On the other hand, the direct cyclization of the hydroquinone intermediate (path **B**) is prohibited since it would lead to a highly strained and unstable product **4**. The reason why the pentalene product **5** does not form is not clear. This may be due to the HSAB principle, namely that *O*-alkylation (hard base) of the iminium salt (hard acid) is favored over the *C*-alkylation (soft base).

A series of homologous benzoquinones were also reacted with **1** to give the corresponding cyclic products **6**–**14** (entries 2–10, Table 1). Reaction of **1** with 1,4-naphthoquinone affords the adduct **13** (Table 1, entry 9), which constitutes the basic skeleton of the 11-oxasteroids. The synthesis and physiological activity of heterosteroids have received a lot of attention over the years.[15] In light of the physiological significance of the 11-oxoadrenocortical hormones, heterosteroids in which the methylene group at position 11 is replaced by a heteroatom are of special interest (Scheme 3).[16] For example, 11-oxaprogesterone **15** shows little progestational activity, but had significantly enhenced ovulation inhibitory activity. In addition, 11-oxaestradiol **16** shows extremely low estrogenic (uterotropic) activity but possesses antifertility activity.[17] The ratio of antifertility activity to estrogenic activity is *ca.* 10 times larger than estradiol. Many other 11-oxasteroids with antiandrogenic, corticoid and antiinflammatory activities have been reported.[18] However, the syntheses of oxasteroids reported so far are based on tedious transformation of available steroids (10–22 steps),[19] a serious bottleneck for the biological testing of 11-oxasteroids. Hydrogenation of **13** for 1 and 6 h affords **17** and **18**, respectively. As illustrated by the entries of Table 1, the combination of [6+3] cycloaddition followed by hydrogenation allows a rapid and efficient entry into the terahydropyran ring systems as well.

In summary, the hetero [6+3] cycloaddition provides a remarkably efficient route to the 3-oxabicyclo[4.3.0]nonane system. This method also establishes the experimental framework for a conceptually new approach to 11-oxasteroids. Further investigation of the scope of this hetero [6+3] cycloaddition as well as the application of this methodology to

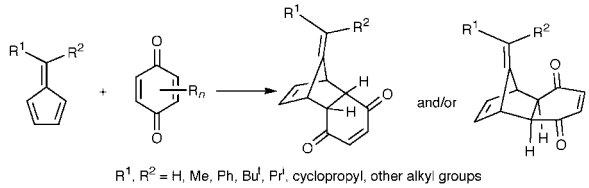

Scheme 1

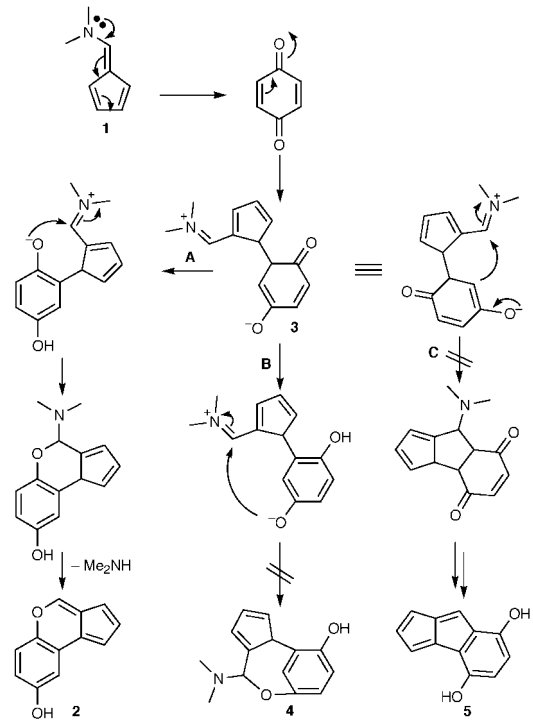

Scheme 2

Table 1 Hetero [6+3] cycladdition of benzoquinones to fulvene

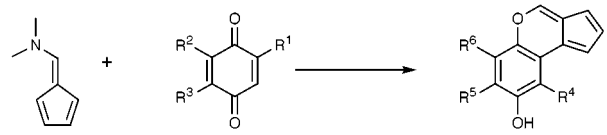

Entry	Benzoquinone R¹	R²	R³	Product	R⁴	R⁵	R⁶	Yield (%)[a]
1	H	H	H	**2**	H	H	H	65[b]
2	Me	H	H	**6a**	H	H	Me	82
				6b	H	Me	H	(2.1 : 1)
3	Me	H	Me	**7**	Me	H	Me	77
4	Me	Me	H	**8**	Me	Me	H	77
5	Cl	H	H	**9a**	H	Cl	H	86
				9b	H	H	Cl	(2.2 : 1 : 3.8)
				9c	Cl	H	H	
6	Cl	H	Cl	**10**	Cl	H	Cl	85
7	Cl	Cl	H	**11**	Cl	Cl	H	80
8	Br	H	Br	**12**	Br	H	Br	79
9	H	–CH=CHCH=CH–		**13**	H	–CH=CHCH=CH–		75
10	H	–CH=CHC(OH)=CH–		**14**	H	–CH=C(OH)CH=CH–		82

[a] Isolated yield based on starting fulvene. [b] Some of the products decomposed during the purification or after few hours at ambient temperature. However, protection of the alcohol as a benzoate (Et_3N, cat. DMAP, BzCl) in one pot before work up gave the stable benzoate of **2** in better yield (75%).

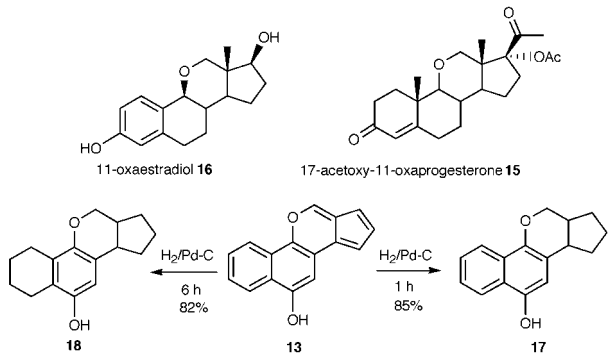

Scheme 3

the synthesis of various oxasteroids for biological studies are currently underway in our laboratories.

This research was supported by the National Science Council (NSC 88-2113-M-194-013) and National Chung Cheng University. The authors also thanks to Dr Sepehr Sarshar for valuable discussions.

Notes and references

† All new compounds gave satisfactory spectral and analytical data. Typical experimental procedure: To a solution of 6-dimethylaminofulvene **1** (ref. 20) (242.2 mg, 2 mmol) in dry benzene (3 ml) was added a solution of benzoquinone (259.2 mg, 2.4 mmol) in dry benzene (3 ml). The suspension was vigorously stirred for 20 min at 25 °C. The solution was concentrated *in vacuo* and the residue was purified by flash column chromatography with 8% EtOAc–hexane (R_f = 0.30 in 10% EtOAc–hexane) to give **2** as a yellow solid (239.2 mg, 65% yield). ν_{max}(neat)/cm^{-1} 3300–3000, 2930, 1627, 1470, 1359, 1194, 1092, 816, 738; δ_H(DMSO-d_6, 400 MHz) 6.77–6.78 (dd, *J* 4.5, 0.8, 1 H), 6.85–6.88 (m, 2 H), 7.00–7.02 (dd, *J* 4.6, 2.5, 1 H), 7.32–7.33 (d, *J* 2.8, 1 H), 7.50-7.52 (d, *J* 9, 1 H), 8.64 (s, 1 H); δ_C(DMSO-d_6, 100 MHz) 106.85 (CH), 110.81 (CH), 113.11 (CH), 115.43 (CH), 119.22 (CH), 121.25 (C), 123.29 (C), 123.64 (C), 131.96 (CH), 141.37 (C), 147.54 (CH), 154.91 (C); *m/z* 184 (M^+, 100), 155 (13), 128 (17), 127 (14), 92 (17), 77 (10), 63 (15), 51 (21) [calc. for $C_{12}H_8O_2$ (M^+): 184.0524; found 184.0521].

1 For a recent review on fulvene chemistry, see: M. Neuenschwander, in *The Chemistry of Double-Bonded Functional Groups*, ed. S. Patai, Wiley, Chichester, 1989, vol. 2, p. 1131.
2 D. I. Rawson, B. K. Carpenter and H. R. Hoffmann, *J. Am. Chem. Soc.*, 1979, **101**, 1786; R. Noyori, Y. Hayakawa, H. Takaya, S. Murai, R. Kobayashi and N. Sonoda, *J. Am. Chem. Soc.*, 1978, **100**, 1759.
3 K. Imafuku and K. Arai, *Synthesis*, 1989, 501; L. A. Paquette, J. A. Colapret and D. R. Andrews, *J. Org. Chem.*, 1985, **50**, 201.
4 M. Harre, P. Raddatz, R. Walenta and E. Winterfeldt, *Angew. Chem., Int. Ed. Engl.*, 1982, **21**, 480; R. Gleiter and O. Borzyk, *Angew. Chem., Int. Ed. Engl.*, 1995, **34**, 1001.
5 Y. Himeda, H. Yamataka, I. Ueda and M. Hatanaka, *J. Org. Chem.*, 1997, **62**, 6529; V. Nair, A. G. Nair, K. V. Radhakrishnan, M. V. Nadakumar and N. P. Rath, *Synlett*, 1997, 767.
6 Y. N. Gupta, M. J. Doa and K. N. Houk, *J. Am. Chem. Soc.*, 1982, **104**, 7336; Z.-I. Yoshida, M. Shibata, E. Ogino and T. Sugimoto, *Angew. Chem., Int. Ed. Engl.*, 1985, **24**, 60.
7 M. Suda and K. Hafner, *Tetrahedron Lett.*, 1977, 2453; T. C. Wu and K. N. Houk, *J. Am. Chem. Soc.*, 1985, **107**, 5308.
8 B.-C. Hong, S.-S. Sun and Y.-C. Tsai, *J. Org. Chem.*, 1997, **62**, 7717.
9 For a recent review in the synthesis of indan systems, see: B.-C. Hong and S. Sarshar, *Org. Prep. Proced. Int.*, 1999, **31**, 1.
10 For previous papers in this series, see: B.-C. Hong, Z.-Y, Chen and E. S. Kumar, *J. Chem. Soc., Perkin Trans. 1*, 1999, 1135; B.-C. Hong and J.-H. Hong, *Tetrahedron Lett.*, 1997, **38**, 255; B.-C. Hong and S.-S. Sun, *Chem. Commun.*, 1996, 937.
11 For the other types of reactions of 6-aminofulvene, see: D. Mukherjee, L. C. Dunn and K. N. Houk, *J. Am. Chem. Soc.*, 1979, **101**, 251; T. Ishizu, M. Mori and K. Kanematsu, *J. Org. Chem.*, 1981, **46**, 526.
12 A. G. Griesbeck, K. Peters, E.-M. Peters and H. G. Schnering, *Angew. Chem., Int. Ed. Engl.*, 1990, **29**, 803; G. Mehta, S. H. K. Reddy and S. Padma, *Tetrahedron*, 1991, **47**, 7821.
13 This skeleton is present in many natural products, see: F. A. Davis and B.-C. Chen, *J. Org. Chem.*, 1993, **58**, 1751; A. Arnoldi, A. Bassoli, G. Borgonovo and L. Merlini, *J. Chem. Soc., Perkin Trans. 1*, 1995, 2447.
14 These skeletons occur widely in many natural products, see: K. Shimano, Y. Ge, K. Sakaguchi and S. Isoe, *Tetrahedron Lett.*, 1996, **37**, 2253; J.-L. Brayer, J.-P. Alazard and C. Thal, *Chem. Commun.*, 1983, 257; K. C. Joshi, P. Singh, S. Taneja, P. J. Cox, R. A. Howie and R. H. Thomson, *Tetrahedron*, 1983, **38**, 2703.
15 R. C. Rastogi, M. N. R. Chowdhury and C. R. Engel, *Steroids*, 1973, **21**, 147.
16 H. Suginome, S. Yamada and J. B. Wang, *J. Org. Chem.*, 1990, **55**, 2170; K. Hildebrandt, T. Debaerdemaeker and W. Friedrichsen, *Tetrahedron Lett.*, 1988, **29**, 2045.
17 C. R. Engel, I. H. Ibrahim, D. Mukherjee, R. Szöghy and V. S. Salvi, *Heterocycles*, 1989, **28**, 905.
18 S. Takegawa, N. Koizumi, M. Mieda and K. Shibata, *Chem. Pharm. Bull.*, 1996, **44**, 746; A. Planas, N. Sala and J.-J. Bonet, *Helv. Chim. Acta*, 1989, **72**, 725; H. Suginome and J. B. Wang, *Bull. Chem. Soc. Jpn.*, 1989, **62**, 193.
19 C. R. Engel, S. Salvi and M. N. R. Chowdhury, *Steroids*, 1975, **25**, 781.
20 For the preparation of 6-dimethylaminofulvene, see: K. Hafner, K. H. Vopel, G. Ploss and C. Konig, *Liebigs. Ann. Chem.*, 1963, **661**, 52.

Communication 9/06877E

Photochemically generated nitrilium phosphane-ylid tungsten complexes and their reactivity towards alkyne and nitrile derivatives

Rainer Streubel,* Hendrik Wilkens and Peter G. Jones

Institut für Anorganische und Analytische Chemie der Technischen Universität Braunschweig, Postfach 3329, D-38106 Braunschweig, Germany. E-mail: r.streubel@tu-bs.de

Received (in Basel, Switzerland) 14th July 1999, Accepted 6th September 1999

The photochemically generated nitrilium phosphane-ylid tungsten complex 2 reacts with different activated alkynes, dimethyl acetylenedicarboxylate (DMAD) (i) and ethyl acetylenecarboxylate (ii), and nitriles, ethyl cyanoformate (ECF) (iii) and 1-piperidinonitrile (iv), giving [3+2] cycloaddition products such as the 2*H*-1,2-azaphosphole complexes 3 (i) and 4 (ii), the 2*H*-1,4,2-diazaphosphole complex 5 (iii) and the 2*H*-1,3,2-diazaphosphole complex 7 in good to excellent yields, the latter complexes, 4–7, being formed regioselectively; the structure of the first ester-functionalized 2*H*-1,4,2-diazaphosphole complex 5 was established by X-ray analysis.

Nitrile ylides **II**, which are useful reactive intermediates in synthetic chemistry, can be generated by thermally[1] or photochemically[2] induced ring opening of 2*H*-azirenes **I** or by *N*-terminal 1,1-addition of singlet carbenes **III** to nitriles[3] (Scheme 1). So far, nitrilium phosphane-ylid complexes **V** have been transiently formed only by thermal ring opening of 2*H*-azaphosphirene complexes **IV**[4] or by *N*-terminal 1,1-addition of singlet type terminal phosphanediyl complexes **VI** to nitriles:[5] we have termed the latter process C,N,P-1,3-dipole transylidation. Although the yields are sometimes unsatisfactory, thermally induced ring opening of 2*H*-azaphosphirene complexes provides access to, *e.g.*, 2*H*-1,2-azaphosphole,[4] 2*H*-1,4,2-diazaphosphole[6] and 2*H*-1,3,2-diazaphosphole complexes.[6] In order to broaden the synthetic applicability of 2*H*-azaphosphirene complexes in synthetic chemistry, we have now started to investigate their photochemistry in the presence of activated alkynes and nitriles as trapping reagents; the first results are reported here.

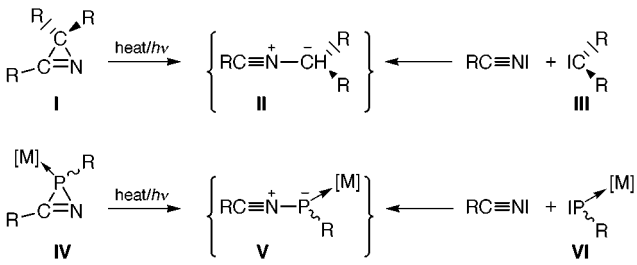

Scheme 1 Synthetic routes to nitrile ylides and nitrilium phosphane-ylid complexes ([M] = metal complex fragment, R denotes ubiquitous organic substituents).

Photochemical ring opening of the 2*H*-azaphosphirene complex **1**[7] in pentane–benzonitrile (50–100 : 1) at −50 °C in the presence of 2 equiv. of dimethyl acetylenedicarboxylate (DMAD) (i), ethyl acetylenecarboxylate (ii), ethyl cyanoformate (ECF) (iii) and 1-piperidinonitrile (iv) furnished the [3+2] cycloaddition products in good to excellent yields (80–95 %), which are significantly higher than those obtained by thermal reactions. Reactions (i) and (ii) yielded 2*H*-1,2-azaphosphole complexes **3**[4] and **4**, and (iii) and (iv) the 2*H*-1,4,2-diazaphosphole complex **5** and the 2*H*-1,3,2-diazaphosphole complex **7**.[6] Of note is the very high regioselectivity of reactions (ii) and (iii) and also that of (iv); in the latter case the regioisomer **7** provides support for the assumption of a transylidation process, giving complex **6** and a subsequent [3+2] cycloaddition of this reactive intermediate to benzonitrile. It is also remarkable that satisfying results were obtained only if pentane–benzonitrile mixtures were employed as solvent for these low-temperature photochemical reactions (Scheme 2).

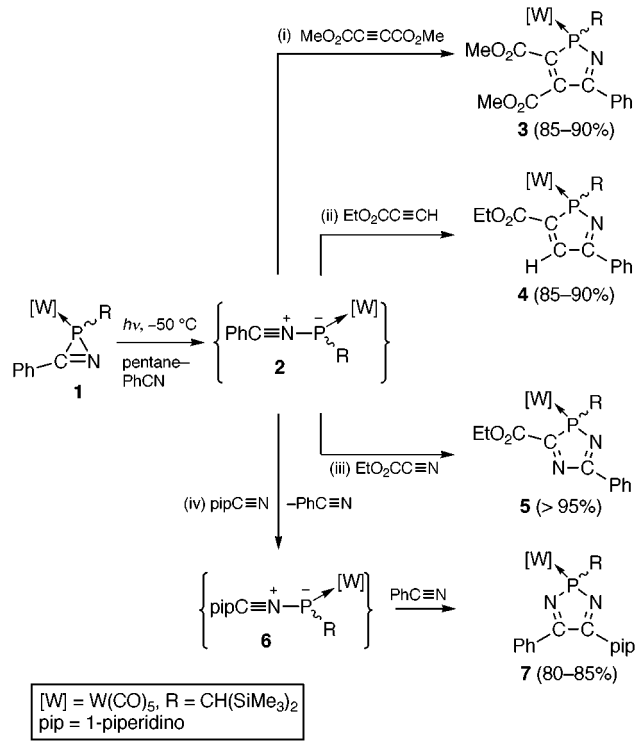

Scheme 2 *Reagents and conditions*: (i), (ii) a solution of 0.14 mmol of **1,** 80 mL *n*-pentane, 0.5 mL benzonitrile and 0.5 mmol alkyne was irradiated at −50 °C for 1.5 h (low-pressure Hg-lamp, Heraeus TQ150); evaporation of the solvent yielded complexes **3** and **4** as orange to red oils, which, in the case of complex **4**, yielded **4** as an orange solid (mp 61 °C, decomp.) after work-up by column chromatography at low temperature and crystallization from pentane; (iii) a solution of 0.28 mmol of **1**, 80 mL *n*-pentane, 0.5 mL benzonitrile and 16 mmol ethyl cyanoformate was irradiated at −50 °C for 2 h, work-up by column chromatography at low temperature and crystallization from pentane afforded **5** as red crystals (mp 67 °C, decomp.); (iv) a solution of 0.14 mmol of **1**, 80 mL *n*-pentane, 0.5 mL benzonitrile and 0.5 mmol 1-piperidinonitrile was irradiated at −50 °C for 1 h; evaporation of the solvent yielded **7** as a yellow oil.

Apart from the known complexes **3** and **7**, the composition of complex **4** and the ester-functionalized 2*H*-1,4,2-diazaphosphole complex **5** were confirmed by elemental analyses and mass spectrometry† and the structural formulation is based on the characteristic NMR spectral data† in solution. Furthermore, the ring constitution of complex **5** was confirmed by X-ray structure analysis‡ (Fig. 1).

The phosphorus nuclei of **4** and **5** display resonances at δ 94.4 and 122.4, which are in the expected range of such heterocycle complexes, with phosphorus–tungsten coupling constants

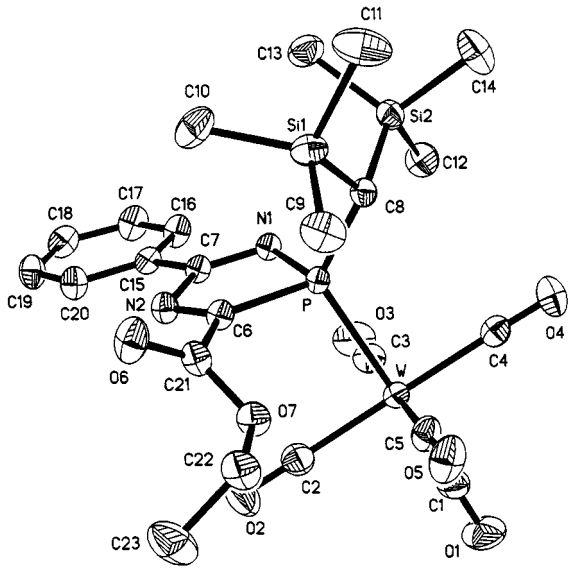

Fig. 1 Molecular structure of complex **5** in the crystal. Radii are arbitrary. Selected bond lengths (Å) and angles (°): P–W 2.5039(5), N1–P 1.7007(16), P–C6 1.8678(19), C6–N2 1.284(2), N2–C7 1.438(2), C7–N1 1.287(2), P–C8 1.8221(19); N1–P–C6 89.05(8), P–C6–N2 110.61(13), N2–C7–N1 119.60(16), C7–N1–P 110.08(13), W–P–C8 121.98(6).

|*J*(W,P)| of 227.2 and 233.6 Hz, respectively. The assignment of the resonances to the carbon atoms of the heterocyclic system in complexes **4** and **5** is unambiguous, if the carbon atoms are bonded either to phosphorus or to hydrogen leading in the first case to significantly greater magnitudes of |*J*(P,C)| (in general) and/or to characteristic spectra if DEPT experiments were performed. The carbon atom resonances of the heterocycle in complex **4** appear at δ 138.0 (C^3), 162.4 (C^4) and 170.5 (C^5) with phosphorus–carbon coupling constants |*J*(P,C)| of 23.5, 9.0 and 9.6 Hz, respectively. The ^{1}H resonance at δ 8.41 with a 32.7 Hz coupling to phosphorus is also structurally important; it is significantly low-field shifted compared to 4-substituted constitutional isomers, which have resonances at δ *ca*. 7.5.[8] As in the 3,5-diphenyl-substituted 2*H*-1,4,2-diazaphosphole tungsten complex **8**,[6] the ester-functionalized complex **5** displays a typical phosphorus resonance (**5**: δ 122.4, |*J*(W,P)| 233.6 Hz; **8**: δ 110.6, |*J*(W,P)| 227.8 Hz[6]). The ester group effectively increases not only the coupling constant |*J*(W,P)|, but also |*J*(P,C)|, which was observed in the ^{13}C NMR spectra of complex **5** for the C^3- and C^5-resonances (**5**: δ 195.6, |*J*(P,C)| 29.8 Hz and 167.2, |*J*(P,C)| 7.0 Hz; **8**: δ 198.5, |*J*(P,C)| 22.3 Hz and 169.5, |*J*(P,C)| 5.1 Hz[6]).

The five-membered ring system of the 2*H*-1,4,2-diazaphosphole complex **5** is almost planar and the phenyl group subtends an interplanar angle to the five-membered ring of 4.2°, thus enabling an efficient π–π electron interaction of the two rings. The N–C distances, N1–C7 1.287(2) and N2–C6 1.284(2) Å, are in the typical range of nitrogen–carbon double bonds;[9] the latter is somewhat shorter than the value of 1.302(9) Å in complex **8**.[6] The coordination spheres of the phosphorus atoms in **5** and **8** are both distorted tetrahedral, displaying identical $\Sigma°P_{PR_3}$ values [310.9° (**5**) and 311° (**8**)], identical N1–P–C6 angles [89.05(8)° (**5**) and 90.2(3)° (**8**)[6]] and only slightly different W–P–C8 angles [121.98(6)° (**5**) and 119.6(3)° (**8**)[6]], but different phosphorus–tungsten distances of 2.5039(5) Å (**5**) and 2.532(2) Å (**8**).[6] Together with the other distances and angles, this shows a predominant electronic effect of the ester group on these structural parameters.

We are currently investigating the reactivity of photochemically generated nitrilium phosphane-ylid complexes towards other π-systems.

This work was supported by the Fonds der Chemischen Industrie and by the Deutsche Forschungsgemeinschaft; the Figure was prepared by Mr F. Ruthe.

Notes and references

† Satisfactory elemental analyses were obtained for complexes **4** and **5**. NMR data were recorded in $CDCl_3$ solution at 50.3 MHz (^{13}C) and 81.0 (^{31}P), using $SiMe_4$ and 85% H_3PO_4 as standard references; *J*/Hz. Selected spectroscopic data: **4**: ^{13}C NMR: δ 19.1 (d, $^1J_{PC}$ 4.4, P*C*H), 138.0 (d, $^{(2+3)}J_{PC}$ 23.5, P–*C*=C), 162.4 (d, $^{(2+3)}J_{PC}$ 9.0, P–C=*C*), 163.8 (d, $^3J_{PC}$ 17.2, *C*O_2Et), 170.5 (d, $^{(2+3)}J_{PC}$ 9.6, P–N=*C*), 196.3 (d, $^2J_{PC}$ 6.4, *cis*-CO), 198.4 (d, $^2J_{PC}$ 21.0, *trans*-CO); *m/z* (EI) 715 (M^+, 10). **5**: ^{13}C NMR: δ 21.9 (d, $^1J_{PC}$ 3.8, P*C*H), 167.2 (d, $^{(2+3)}J_{PC}$ 7.0, P–N=*C*), 163.3 (d, $^3J_{PC}$ 28.2, *C*O_2Et), 195.6 (d, $^{(1+4)}J_{PC}$ 29.8, P–*C*=N), 196.3 (d, $^2J_{PC}$ 6.2, *cis*-CO), 198.6 (d, $^2J_{PC}$ 23.1, *trans*-CO); *m/z* (EI) 716 (M^+, 32).

‡ *Crystal data* for **5**: $C_{23}H_{29}N_2O_7PSi_2W$; M = 716.48, triclinic, space group group $P\bar{1}$, a = 10.5466(10), b = 10.7010(11), c = 13.8717(14) Å, α = 79.915(3), β = 82.215(3), γ = 75.406(3)°, U = 1484.8(3) Å^3, Z = 2, D_c = 1.603 Mg m^{-3}, μ = 4.065 mm^{-1}, F(000) = 708, 7327 independent reflections to 2θ max. 56°, T = 143 K, S = 1.019, $R[F, > 4\sigma(F)]$ = 0.0186, $wR(F^2)$ = 0.0438, 25 restraints and 332 parameters, highest peak 1.142 and deepest hole −0.539 e Å^{-3}.

The X-ray data set was collected with monochromated Mo-Kα radiation (λ = 0.71073 Å) on a Bruker SMART 1000 CCD area detector. Absorption correction based on multiple scans. The structure was solved by the Patterson method and refined anisotropically by full-matrix least squares on F^2.[10] H atoms were included using a riding model (except methyl groups: refined as rigid groups). CCDC 182/1410. See http://www.rsc.org/suppdata/cc/1999/2127/ for crystallographic files in .cif format.

1 P. K. Claus, in *Houben Weyl, Methoden Org. Chem*., 1990, vol. E14b(1), p 1.
2 A. Padwa, *Acc. Chem. Res.*, 1976, **9**, 371.
3 A. Padwa and S. F. Hornbuckle, *Chem. Rev.*, 1991, **91**, 263.
4 R. Streubel, H. Wilkens, A. Ostrowski, C. Neumann, F. Ruthe and P. G. Jones, *Angew. Chem., Int. Ed. Engl*., 1997, **36**, 1492.
5 H. Wilkens, J. Jeske, P. G. Jones and R. Streubel, *Chem. Commun.*, 1998, 1529.
6 H. Wilkens, F. Ruthe, P. G. Jones and R. Streubel, *Chem. Eur. J.*, 1998, **4**, 1542.
7 R. Streubel, A. Ostrowski, S. Priemer, U. Rohde, J. Jeske and P. G. Jones, *Eur. J. Inorg. Chem.*, 1998, 257.
8 R. Streubel and H. Wilkens, unpublished work.
9 F. H. Allen, O. Kennard, D. G. Watson, L. Brammer, A. G. Orpen and R. Taylor, *J. Chem. Soc., Perkin Trans. 2*, 1987, S1.
10 G. M. Sheldrick, SHELXL-97, program for crystal structure refinement, University of Göttingen, 1997.

Communication 9/05752H

ChemComm

Membrane transport of neurotransmitter acetylcholine and related compounds across a phospholipid bilayer by a calix[6]arene ester

Takashi Jin

Section of Intelligent Materials and Device, Research Institute for Electronic Science, Hokkaido University, Sapporo, 060-0812, Japan. E-mail: jin@imd.es.hokudai.ac.jp

Received (in Cambridge, UK) 24th August 1999, Accepted 20th September 1999

A calix[6]arene ester 2 acts as a carrier for neurotransmitters such as acetylcholine, carbachol and choline in a phospholipid bilayer membrane.

Artificial acetylcholine receptors have been of great interest for the development of acetylcholine detection techniques[1,2] and for the understanding of biological recognition[3] of acetylcholine (ACh). Several macrocyclic compounds[1–6] have been reported as artificial acetylcholine receptors which recognize the quaternary ammonium moiety of acetylcholine. Recently, it was reported that sulfonated calix[4]- and calix[6]-arenes have binding abilities toward acetylcholine and related choline derivatives in water.[2,6] To the best of our knowledge, however, there has been no report of membrane transport of acetylcholine mediated by synthetic ionophores for the detection and separation of acetylcholine. We now report that a calix[6]arene ester **2** can act as a selective acetylcholine carrier in a phospholipid bilayer membrane.

Calixarene esters are known to have selective ion complexing abilities, and also have ion transporting abilities toward alkali-metal ions.[7–10] For example, calix[4]-, calix[5]- and calix[6]-arene esters act as selective Na^+ ,[7–10] K^+ [10] and Cs^+ carriers[7,10] in bilayer membranes as well as in bulky liquid membranes. Although much information has been accumulated on the metal ion transport properties of calixarene esters, molecular ion transport properties of the calixarenes are known to a lesser extent.[11] Here we have focused our attention on the use of calixarene esters as quaternary ammonium ion carriers, and examined their membrane transport abilities for neurotransmitters such as acetylcholine, carbachol (carbamylcholine) and choline in a phospholipid bilayer system.

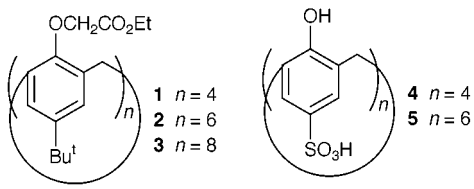

Five calixarene derivatives **1**–**5** were tested for their neurotransmitter transport abilities. Compounds **1**–**3** were prepared according to the literature method.[7] The sulfonated calixarenes **4** and **5** were purchased from Acros Organics. Membrane transport of neurotransmitters by calixarene derivatives across planar phospholipid bilayers was investigated by a voltage clamp method.[10,12] Planar phospholipid bilayers[12,13] (soybean phospholipids) were prepared at an aperture (diameter, 0.2 mm) in a Teflon film (thickness, 12.5 μm) which separated two Teflon chambers† (*cis* and *trans* chamber; volume, 1.7 ml). Calixarenes were added as 100 μM DMSO solutions to the *cis* chamber after the formation of the bilayers.

Fig. 1(*a*) shows the generation of membrane currents upon the addition of calix[6]arene ester **2** to the *cis* chamber, where both chambers were filled with 100 mM acetylcholine chloride solutions (pH 7.2, 25 mM HEPES-TRIS buffer). Membrane currents resulting from the transport of acetylcholine cations (ACh^+) were measured at an external voltage at 100 mV. In the absence of **2**, membrane conductance was *ca*. 200 GΩ: the control level of the membrane current was 0.5 pA at 100 mV. When a microliter aliquot (20 μl) of the DMSO solution of **2** was added to the chamber, the membrane conductance immediately increased. A control experiment was performed where only neat DMSO was added to the *cis* chamber. The addition of 200 μl of DMSO did not change the membrane conductance. To confirm the transport of ACh^+ across the phospholipid bilayer, the membrane conductance was measured under LiCl (100 mM)/LiCl (100 mM) ionic conditions. The addition of **2** (20 μl) to the chamber filled with the LiCl solution did not lead to the generation of membrane current, suggesting that the membrane current observed in Fig. 1(*a*) is due to the transport of ACh^+ cations, not the transport of Cl^- anions. Fig. 1(*b*) shows the concentration dependence of calix[*n*]arene esters *versus* the membrane currents. With increasing concentration of **2**, the membrane currents significantly increased. In contrast, the addition of **1** and **3** did not increase the membrane conductance for concentrations of calixarenes up to 10 μM. Furthermore, we tested water-soluble sulfonated calix[4]- and calix[6]-arene, which are known to form 1:1 acetylcholine complexes[6] in water. The addition (100 μl) of these calixarenes, however, did not increase the membrane conductance. Except for **2**, we could not detect ion transport for acetylcholine in the bilayer membrane.

The evidence for the complexation of acetylcholine with **2** was confirmed by the ^1H NMR measurements in $CDCl_3$. Fig. 2 shows the changes in ^1H NMR spectrum of acetylcholine in the

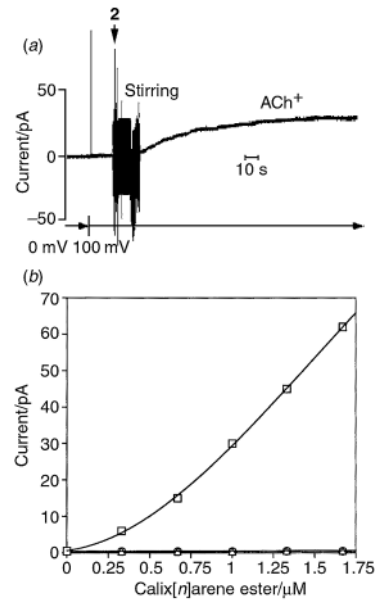

Fig. 1 (*a*) Generation of membrane currents (ACh^+) at 100 mV upon the addition of 20 μl of **2** (100 μM DMSO solution); (*b*) the membrane currents (ACh^+) *versus* the concentration of calix[*n*]arene ester in the *cis* chamber: (○) **1**, (□) **2** and (△) **3**.

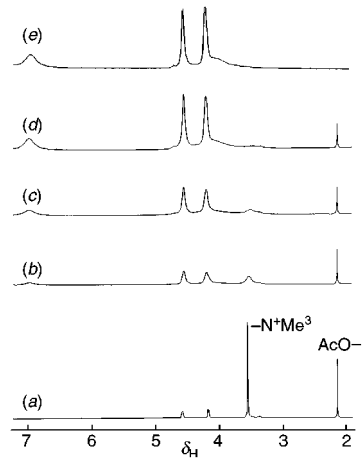

Fig. 2 Changes in ^{1}H NMR spectra ($CDCl_3$) of acetylcholine in the presence of **2**: [**2**]/[ACh] = (*a*) 0, (*b*) 0.5, (*c*) 1 and (*d*) 2, [ACh] = 14 mM. For comparison, the ^{1}H NMR spectrum of **2** is shown in (*e*).

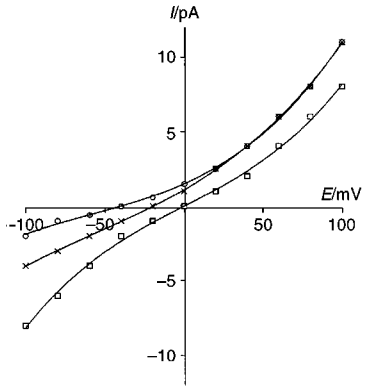

Fig. 3 The current–voltage (*I-E*) curves for different ionic conditions (pH = 7.2, 25 mM HEPES–TRIS buffer). All measurements were carried out at 25 °C. (□) ACh^+(*cis*)/ACh^+(*trans*), (×) $Carbachol^+/ACh^+$ and (○) $Choline^+/ACh^+$.

presence of **2**. Upon addition of **2**, the N^+Me_3 protons (δ 3.54) in acetylcholine moved to lower field ($\Delta\delta$ −0.06 ppm at [**2**]/[ACh] = 2) and the signal became very broad upon increasing the ratio of [**2**]/[ACh]. On the other hand, the chemical shift of the CH_3CO protons in acetylcholine was not affected by the addition of **2**: the line broadening of the CH_3CO singnal was much less than that of the N^+ Me_3 signal. The shift of the N^+ Me_3 protons to lower magnetic field suggests that the binding site of acetylcholine toward **2** is the quaternary ammonium moiety, not the acetyl moiety.[2] The line broadening of both the N^+Me_3 and CH_3CO protons in the presence of **2** may be explained by a fast exchange between the complexed and free acetylcholines on the NMR time scale: the resolved signals resulting from the two acetylcholine species were not observed at [**2**]/[ACh] < 1.

To evaluate the transport selectivity of **2** for acetylcholine and related compounds (carbachol and choline), we examined current–voltage (*I-E*) relations. Fig. 3 shows the *I-E* curves for three sets of ionic conditions (100 mM Cl^- salts). In the case of ACh^+/ACh^+ ionic conditions, a non-linear *I-E* curve which did not obey Ohm's law was obtained. This voltage-dependent *I-E* curve suggests that the transport of acetylcholine proceeds *via* a carrier mechanism.[14,15] In fact, a similar voltage-dependent *I-E* curve for a ACh^+/ACh^+ system has also been observed in the case of calix[*n*]arene ester-mediated carrier transport of alkali-metal ions across phospholipid bilayer membranes.[8,10] To determine ion permeability ratios, we exchanged the acetylcholine solution in the *cis* chamber with other neurotransmitter solutions and then measured *I-E* curves. It should be noted that in the X^+ (*cis*)/ACh^+ (*trans*) ionic conditions, positive currents of *ca*. 2 pA were generated at 0 V. This implies that acetylcholine cations are transported by **2** from the *trans* to the *cis* chamber in the absence of external voltages. From the *I-E* curves in the X^+/ACh^+ ionic conditions, the reversal potentials were determined as follows: −18 mV for $Carbachol^+/ACh^+$ and −42 mV for $Choline^+/ACh^+$. According to the Goldman–Hodgkin–Katz equation,[15] the reversal potentials ($\Delta\phi$) in XCl (*cis*)/YCl (*trans*) systems is related to the ion permeability (*P*), as shown in eqn. (1), where *R* and *F* express the gas constant and

$$\Delta\phi = \frac{RT}{F}\ln\frac{P_X[X]_{cis} + P_{Cl}[Cl]_{trans}}{P_Y[X]_{trans} + P_{Cl}[Cl]_{cis}} \quad (1)$$

the Faraday constant, respectively. Since **2** does not transport choline anions across the bilayer membranes (P_{Cl} = 0), the cation permeability ratio (P_X/P_Y) can be easily calculated as follows: 0.48 for $P_{Carbachol^+}/P_{ACh^+}$ and 0.18 for $P_{Choline^+}/P_{ACh^+}$. The permeability of acetylcholine across the planar bilayer membrane is larger than that of carbachol and choline by a factor of 2.1 and 5.6, respectively. This result shows that the calix[6]arene ester **2** acts as a selective acetylcholine carrier in a phospholipid bilayer membrane. The lower transport selectivity of choline and carbachol toward **2** may be due to the higher hydrophilicities of those compounds, which depress the stability of the complex in the water–lipid interface.

In conclusion, we have demonstrated that a calix[6]arene ester **2** can transport neurotransmitters, especially acetylcholine, across a phospholipid bilayer. For the other calix[4]- and calix[8]-arene esters (**1** and **3**) and sulfonated calixarenes (**4** and **5**), we could not determine the neurotransmitter transport activity in the bilayer membrane. To the best of our knowledge, this is the first report of an artificial acetylcholine carrier which is active in a phospholipid bilayer membrane. We believe that the calix[6]arene ester **2** has potential for use as an acetylcholine carrier in biological membrane systems.

We thank Mr E. Yamada for the measurement of ^{1}H NMR spectra.

Notes and references

† The side to which the compounds were added was defined as the '*cis*' chamber and the opposite side was the '*trans*' chamber. The external voltage was fed to the *trans* chamber *via* an Ag/AgCl electrode and the *cis* chamber was grounded *via* an Ag/AgCl electrode.

1 M. Inoue, K. Hashimoto and K. Isagawa, *J. Am. Chem. Soc.*, 1994, **116**, 5517.
2 K. Nak Koh, K. Araki, A. Ikeda, H. Ohtsuka and S. Shinkai, *J. Am. Chem. Soc.*, 1996, **118**, 755.
3 D. A. Dougherty and D. A. Stauffer, *Science*, 1990, **250**, 1558.
4 R. Méric, J.-P. Vigneron and J.-M. Lehn, *J. Chem. Soc., Chem. Commun.*, 1993, 129.
5 L. Garel, B. Lozach, J.-P. Dutasta and A. Collet, *J. Am. Chem. Soc.*, 1993, **115**, 11 652.
6 J.-M. Lehn, R. Meric, J.-P. Vigneron, M. Cesario, J. Guilhem, C. Pascard, Z. Asfari and J. Vicens, *Supramol. Chem.*, 1995, **5**, 97.
7 F. Arnaud-Neu, E. M. Collins, M. Deasy, G. Ferguson, S. J. Harris, B. Kaitner, A. J. Lough, M. A. McKervey, E. Marques, B. L. Ruhl, M. J. Schwing-Weil and E. M. Seward, *J. Am. Chem. Soc.*, 1989, **111**, 8681.
8 T. Jin, M. Kinjo, T. Koyama, Y. Kobayashi and H. Hirata, *Langmuir*, 1996, **12**, 2684.
9 N. Kimizuka, T. Wakiyama, A. Yanagi, S. Shinkai and T. Kunitake, *Bull. Chem. Soc. Jpn.*, 1996, **69**, 3681.
10 T. Jin, M. Kinjo, Y. Kobayashi and H. Hirata, *J. Chem. Soc., Faraday Trans.*, 1998, **94**, 3135.
11 S.-K. Chang, H.-S. Hwang, H. Son, J. Youk and Y. S. Kang, *J. Chem. Soc., Chem. Commun.*, 1991, 217.
12 W. Hanke and W.-R. Schlue, *Planar Lipid Bilayers*, Academic Press, San Diego, 1993.
13 M. Montal and P. Mueller, *Proc. Natl. Acad. Sci. U.S.A.*, 1972, **69**, 3561.
14 M. Inabayashi, S. Miyauchi, N. Kamo and T. Jin, *Biochemistry*, 1995, **34**, 3455 and references therein.
15 *Membrane Transport*, ed. S. L. Bonting and J. J. H. H. M. de Pont, Elsevier, New York, 1981.

Paper 9/06874K

ChemComm
FEATURE ARTICLE

Thiazolylketoses: a new class of versatile intermediates for glycoside synthesis

Alessandro Dondoni* and Alberto Marra

Dipartimento di Chimica, Laboratorio di Chimica Organica, Università di Ferrara, Via Borsari 46, 44100 Ferrara, Italy. E-mail: adn@dns.unife.it

Received (in Cambridge, UK) 11th May 1999, Accepted 13th July 1999

An account is provided on the very recent work carried out in the authors' laboratory dealing with the preparation of thiazolylketose acetates and their use as effective glycosyl donors in reactions with oxygen, carbon, nitrogen and phosphorus nucleophiles. These reagents are formed by addition of 2-lithiothiazole to sugar lactones followed by acetylation of the resulting thiazolylketoses. Coupling reactions, promoted by TMSOTf in CH_2Cl_2, are described with primary and secondary sugar alcohols, trimethylsilyl azide, triethyl phosphite and various *C*-nucleophiles. Suitable transformations of the resulting glycosides are carried out owing to the ready conversion of the thiazole ring into the formyl group followed by reduction to alcohol and/or oxidation to carboxylic acid. Thus, anomeric glycosyl amino acids, ketosyl and ulosonyl disaccharides and phosphonates have been prepared. Special applications include the synthesis of *O*-glycosyl calix[4]arene derivatives (calixsugars) and a cyclic ketotrisaccharide. The triethylsilane reduction of thiazolylketose acetates leads to thiazolyl *C*-glycosides that once subjected to the thiazole-to-formyl conversion afford formyl *C*-glycosides. These anomeric sugar aldehydes are convenient starting reagents for the synthesis of various *C*-glycosides and *C*-glycoconjugates, such as (1→6)-disaccharides and oligosaccharides, glycosyl aminoacids (glycine, serine, asparagine), and a galactocerebroside. Formyl *C*-glycosides participate in the azomethine ylide 1,3-dipolar cycloaddition reaction to C_{60} fullerene to give sugar fullerenes. The cover illustration shows some products of these reactions and a view of Palazzo dei Diamanti (Palace of Diamonds), a beautiful and unique building in the architectural context of Ferrara, constructed in the first half of 1500. The façade of the Palace is decorated with more than eight thousand five-hundred diamond shaped small blocks of marble.

Alessandro Dondoni has been Professor of Organic Chemistry at the University of Ferrara since 1975. His research interests include the design of new reagents and the development of stereoselective synthetic methods. Recent work has been focussed on the preparation of natural product-like compounds, particularly small peptide and glycoconjugate analogues. He started a new program on glycosylated calixarenes and calixarene-containing polymers. In 1999 he obtained the Avogadro–Minakata Lectureship Award of the Chemical Society of Japan and the Ziegler–Natta Lectureship Award of the German Chemical Society. In the same year he was awarded the Lincei National Academy prize in Chemistry sponsored by the Italian Minister of Cultural Heritage and Activities.

Alberto Marra graduated in Pharmaceutical Sciences from the University of Pisa in 1985 and obtained his PhD in Organic Chemistry from the University Paris VI in 1989 under the supervision of Professor P. Sinaÿ. He spent one more year in Paris at the Ecole Normale Supérieure as Associated Researcher of the French National Research Council. He was postdoctoral Research Associate at the University of Zurich with Professor A. Vasella (1991) and then moved to the University of Ferrara where he joined the group of Professor A. Dondoni. He was appointed to a lectureship in Organic Chemistry at the Faculty of Engineering from 1992 to 1998 and was promoted to the position of Associate Professor in 1998 at the same University. As in his early activities, his present research interest centres on carbohydrate chemistry. Recent work also deals with the synthesis and properties of calixarene derivatives.

Introduction

Carbohydrates, mainly in the form of oligosaccharides and glycoconjugates (glycoproteins and glycolipids), have been recognized in relatively recent years to play a vital role in fundamental biological functions such as cell-to-cell recognition and cell-to-external agents interactions.[1] These processes are manifested in living organisms by various phenomena, some of which are beneficial, such as fertilization and immune defence, some others are detrimental such as inflammation, viral and bacterial infections, cancer metastasis.[2] Problems still exist in determining the exact function at the molecular level of carbohydrate moieties in a given glycoconjugate. To explore these properties, glycobiology, the science dealing with the nature and role of carbohydrates in biological events,[1] is posing a pressing need for access to usable quantities of natural oligosaccharides and glycoconjugates in homogeneous and pure form. However the isolation and purification of these materials from natural sources are quite difficult and when possible provide the products in very low yields. The same need exists for unnatural analogues of oligosaccharides and glycoconjugates that may be used in structure–activity relationship (SAR) and drug development studies. Thus, organic synthesis constantly reinforced and rejuvenated by the design of new reagents and the invention of new methods[3] is providing a great contribution to the solution of these problems. Remarkable progress has been made in recent years in the field of natural oligosaccharide synthesis[4] both in solution and the solid phase as well as glycopeptide[5] and glycolipid synthesis.[6] To this end some monosaccharide building blocks have been conveniently exploited, among which glycals[7] and 1,6-anhydro sugars[8] have proved their importance. Nevertheless, innovations are still required in this area. On the other hand, the synthesis of carbon-linked sugars, *e.g.* disaccharide[9] and a few oligosaccharide[10] isosteres, has been reported in relatively recent years while the methods employed lack generality. The same situation exists for the synthesis of carbon-linked glycosyl amino acids[11] that may serve as building blocks for the preparation of modified glycopeptides. Hence substantial development of existing methods and invention of new approaches are needed in this area as well.

We report in this account on the preparation and use of a new class of sugar building blocks, namely thiazolylketoses, which

activated as *O*-acetyl derivatives **1** serve as efficient glycosyl donors toward various oxygen, carbon, nitrogen and phosphorous nucleophiles (Scheme 1). The thiazole ring of the resulting

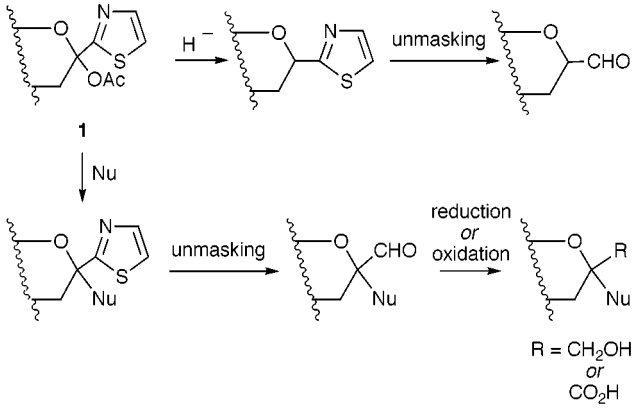

Scheme 1

coupling products is readily transformed into the formyl group that in turn is oxidized to carboxylic acid or reduced to alcohol. A special transformation of acetates **1** consists in their reduction and thiazole-to-formyl conversion, so called *unmasking*, to give formyl *C*-glycosides, a class of valuable intermediates for the synthesis of various and more complex *C*-glycosides.

Preparation of thiazolylketose acetates

Given the well documented service of thiazole as a formyl group equivalent in numerous synthetic methods,[12] the idea that was behind this programme was to install the thiazole ring at the anomeric carbon of sugars and take advantage of the above synthetic equivalence to reach synthetic targets otherwise difficult or impossible to access. While other manipulatable groups, such as cyano,[13] 2-furyl,[14] 1,3-dithianyl,[15] and alkynyl,[16] have been installed at the anomeric carbon of sugars and in some cases transformed into the formyl or carboxylate group, they can hardly compete with thiazole for combining high stability and ready conversion into the corresponding masked functionality under conditions which are tolerated by other protective groups and do not affect the configuration of stereocenters of the molecule. The thiazole-to-formyl protocol consists of a three-reaction sequence (*N*-methylation, reduction, metal-assisted hydrolysis), each step taking place under almost neutral and non-oxidative conditions.[12]

After several unsuccessful approaches of direct glycosylation of thiazole at C-2, the addition of 2-metallated thiazoles to sugar lactones turned out to be the method of choice in our programme.[17] It was not of secondary importance that both reagents can be easily prepared starting from inexpensive, commercially available materials and therefore the reactions can be carried out on a multigram scale. Typically, the reaction of 2,3,4,6-tetra-*O*-benzyl-D-galactonolactone **2a** with 2-lithiothiazole **3**, generated *in situ* from 2-bromothiazole and BuLi at −78 °C in Et_2O, followed by quenching with an aqueous pH 7 buffer produced the thiazolylketose α-**5a** that was isolated in 78% yield by chromatography (Scheme 2). Treatment of this ketose with Ac_2O–Et_3N at room temperature afforded the corresponding *O*-acetate α-**1a** in essentially quantitative yield (method A). On the other hand, quenching the crude reaction mixture at low temperature with Ac_2O, the ketose acetate anomer β-**1a** was obtained in 68% yield (method B). Thus, it appeared that the acetylation at low temperature allows the efficient trapping of the β-ketose **4a**, the product of kinetic selectivity arising from the addition of **3** to the less hindered face of the lactone **2a**. Evidently, the conversion of the β-ketose **4a** into the more stable α-anomer **5a** must occur quite rapidly at room temperature, being very likely controlled by the electronic effect of the ring oxygen (anomeric effect).

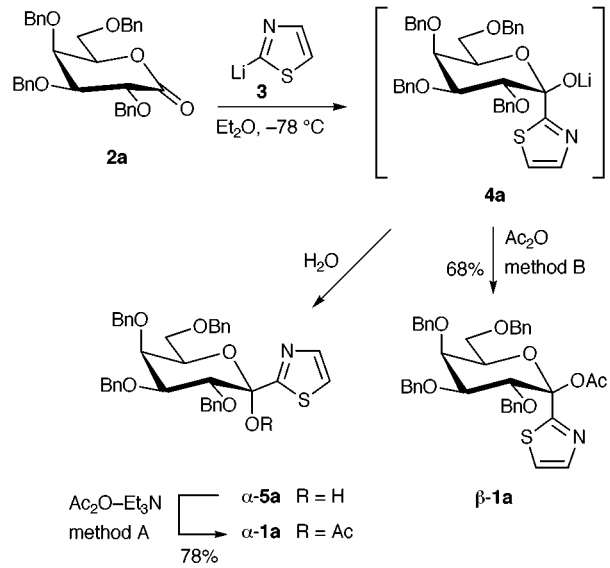

Scheme 2

The above reaction scheme was expanded to various pyrano- as well as furano-lactones. In all cases the addition of **3** to the chosen lactone proceeded smoothly to give the thiazolylketose **5** in the hemiketalic form with only occasionally the presence of the open-chain isomer. The corresponding thiazolylketose acetates **1b**–**g** were prepared as either α- or β-anomers depending on the quenching method A or B (Fig. 1). The yields

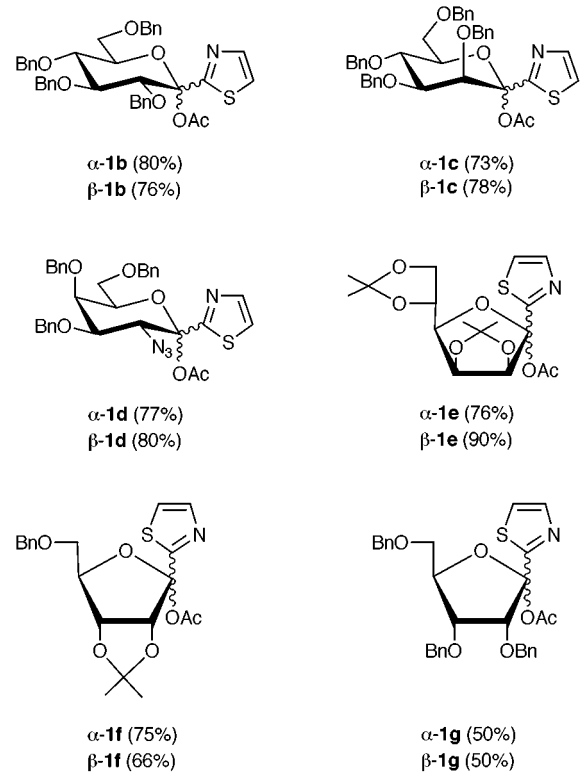

Fig. 1

of isolated products were consistently close to those quoted in Scheme 2. Noteworthy among the compounds prepared is the 2-azidogalactose derivative **1d** since this compound can be the precursor of galactosamine derivatives of biological relevance.[18]

Instead of 2-lithiothiazole **3** generated *in situ* at low temperature, 2-trimethylsilylthiazole (2-TST) **6** can be employed as a stable thiazol-2-yl carbanion equivalent in addition reactions to sugar lactones (Scheme 3). We observed that **6** in the presence of equimolar tris(dimethylamino)sulfonium di-

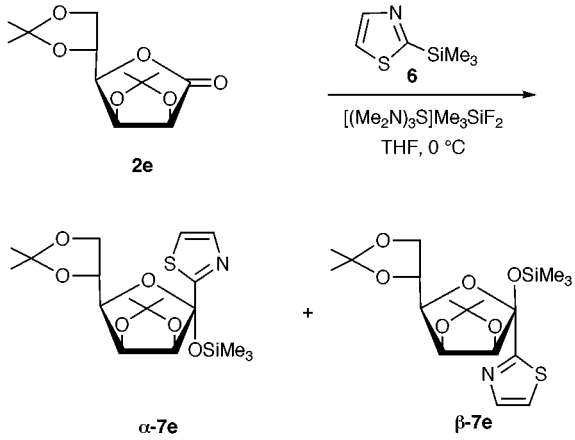

Scheme 3

fluorotrimethylsilicate (TASF) reacts readily with the D-mannonofuranolactone diacetonide **2e** to give the trimethylsilyl thiazolylketoside **7e** as a mixture of α- and β-anomers in 4.5 : 1 ratio and 92% overall yield.[19] Thus, unlike the spontaneous reactions of 2-TST **6** with other carbon electrophiles (aldehydes, ketones, acyl chlorides),[12] this reaction requires the activation of **6** by a fluoride ion releasing promoter. Although the silylated thiazolylketose **7e** can eventually be converted into the acetate **1e** by desilylation and acetylation, the method does not appear to offer substantial advantages over that employing 2-lithiothiazole **3** since it requires more steps and the use of TASF, an expensive and difficult to handle reagent. In fact, other fluoride ion releasing promoters (Bu_4NF, CsF) proved to be much less efficient in this reaction since the thiazolylketose **5e** was recovered in *ca*. 10% yield together with unreacted **2e**.

Why activation of thiazolylketoses as *O*-acetates?

Rather soon at the outset of this research we realized that the thiazolylketose **5a** and the other analogues could hardly be used as glycosyl donors. Efficient ketosyl donors, such as those bearing an electron-rich substituent at the anomeric centre, are known to be very reactive under Lewis acid catalysis at low temperature. For example glycosidation[20] and anomeric deoxygenation[14f,h] of furylketoses occur rapidly under these conditions. On the other hand we failed to reduce various pyrano- and furano-ketoses **5** either under radical or polar conditions.[17] Very likely the electron-poor character of the thiazole ring and interaction with the catalyst through the basic nitrogen atom cause the unsuccessful reactions. Thus, the activation of thiazolylketoses **5** by conversion of the hydroxy group into a better leaving group appeared to be a prerequisite for the use of these compounds as glycosyl donors. The conversion into *O*-acetates **1** turned out to be a winning move since these compounds are easy and inexpensive to prepare, are stable to storage, and nevertheless sufficiently reactive under polar glycosylation conditions. Finally, although their reactions occur at room temperature, the stereoselectivity ranged from good to excellent levels based on high yield of isolated products. Some reactions are illustrated below in support to these anticipated results.

N-Glycosidation and formal synthesis of (+)-hydantocidin

The first test on the ability of thiazolylketose acetates **1** to serve as glycosyl donors (Scheme 1) was carried out with trimethylsilyl azide ($TMSN_3$) as nitrogen nucleophile.[21] Equally important for synthetic purposes, was proving the compatibility of various functional group manipulations, particularly the cleavage of the thiazole ring adjacent to the quite reactive azido group. The synthesis of the peculiar α-azido aldehyde **8** sharing its central carbon atom with the D-ribofuranose ring constituted an interesting target in the above context. The importance of **8** relies on its being an advanced intermediate[22] for the synthesis of the herbicide and plant growth regulator (+)-hydantocidin, a natural product produced by fermentation processes[23] (Scheme 4).

Scheme 4

Either α- or β-anomer of thiazolyl-D-ribofuranose acetate **1f** proved to be an excellent glycosyl donor toward $TMSN_3$ upon activation by trimethylsilyl triflate (TMSOTf) in CH_2Cl_2 at room temperature.[21] In both cases, the reaction afforded the same mixture of α- and β-azido glycosides **9** in 1 : 3 ratio and 84% overall yield (Scheme 5). After separation and identification of the major stereoisomer β-**9**, the conversion to the azido aldehyde **8** was carried out with satisfactory yield (57%) by suitable adjustments of the standard thiazole-to-aldehyde procedure to avoid cycloaddition side-reactions between the *N*-methylthiazolium ring, an intermediate of the unmasking protocol, and the adjacent azido group acting as a 1,3-dipolar partner. The conversion of **8** into the anomeric spirohydantoin of D-ribose featured by (+)-hydantocidin was reported earlier by Mio and co-workers.[22]

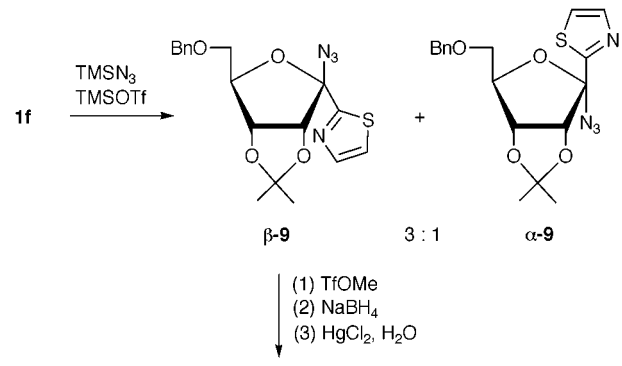

Scheme 5

A better evaluation of the scope of the *N*-glycosidation reaction was obtained starting from the D-galactoketopyranose acetate **1a** and the D-mannoketofuranose acetate **1e**. The *N*-glycosidation of these compounds with $TMSN_3$ under the above conditions occurred with high α-selectivity to give exclusively the anomeric azido sugars **10** and **11** in gratifying 88 and 84% isolated yields (Scheme 6). This stereochemical outcome is that expected on the basis of a glycosidation reaction scheme proceeding through a sugar oxycarbenium ion intermediate undergoing a sterically controlled nucleophilic addition (Fig. 2). Evidently, this stereochemical control was much weaker in the case of the D-riboketofuranose **1f** due to the intrinsic configuration of this sugar and consequently the azide **9** was formed as a mixture of α- and β-anomers (Scheme 5). Taking advantage of the modified conditions of the thiazole-to-formyl protocol developed for the conversion of **9** to **8**, compounds **10** and **11** were transformed into the azido aldehydes **12** and **13** without any problem. At this stage, a further elaboration was carried out as a confirmation of the synthetic value of the thiazole sugars **1**. Crude aldehydes **12** and **13** were oxidized to the azido esters **14** and **15** that in turn were transformed into the sugar aminoesters

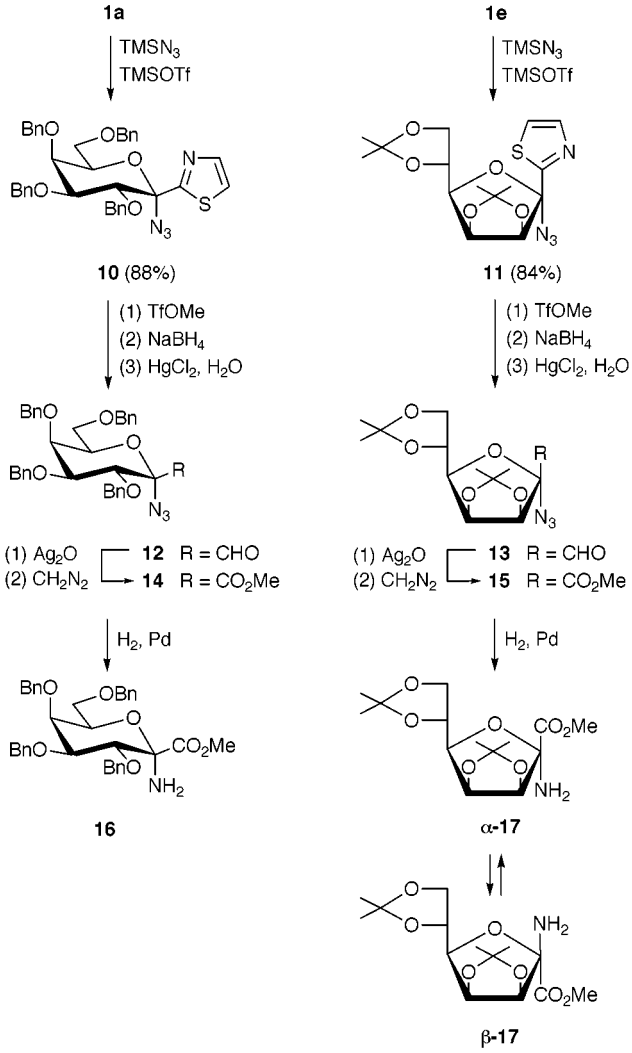

Scheme 6

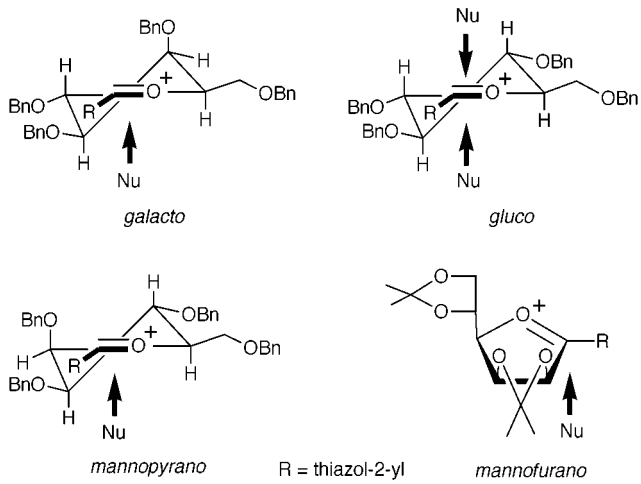

Fig. 2

16 and **17** by selective reduction of the azido group by Pd-catalyzed hydrogenation. Compounds **16** and **17** are representative of a new class of unnatural glycosyl amino acids which can be considered as anomeric sugar glycines wherein the central carbon atom of the amino acid coincides with C-1 of the sugar moiety.

P-Glycosidation by Arbuzov-type reaction

Triethyl phosphite was the model phosphorus nucleophile employed in this study. It underwent α-selective glycosylation reaction by various thiazolylketose acetates **1** in an Arbuzov-type coupling reaction carried out in CH_2Cl_2 at room temperature[24] to give exclusively glycosyl phosphonates **18** as α-D-anomers in high isolated yields (Table 1). As an exception, the

Table 1 *P*-Glycosidation of thiazolyketose acetates **1** with $P(OEt)_3$ (TMSOTf, CH_2Cl_2, room temperature)

Acetate **1**	Phosphonate **18**	Phosphonates **19** and **20**
1a	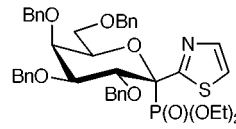 **18a** (84%)	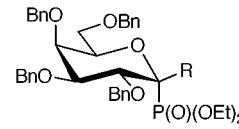 **19a** R = CH_2OH (61%) **20a** R = CO_2Me (62%)
1b	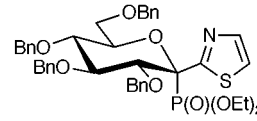 **α-18b** (52%)	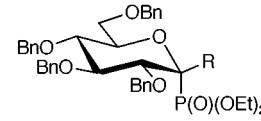 **α-19b** R = CH_2OH (58%) **α-20b** R = CO_2Me (62%)
1b	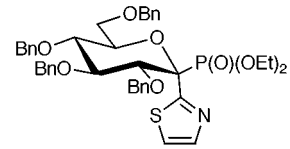 **β-18b** (35%)	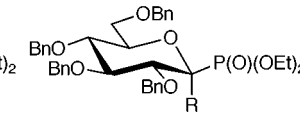 **β-19b** R = CH_2OH (56%) **β-20b** R = CO_2Me (59%)
1c	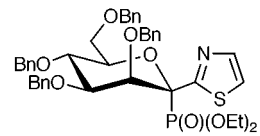 **18c** (88%)	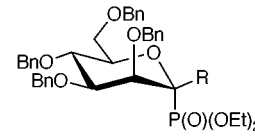 **19c** R = CH_2OH (50%) **20c** R = CO_2Me (51%)
1d	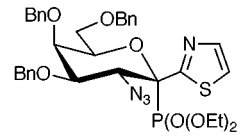 **18d** (78%)	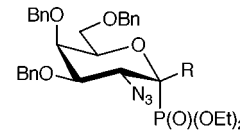 **19d** R = CH_2OH (57%) **20d** R = CO_2Me (59%)
1e	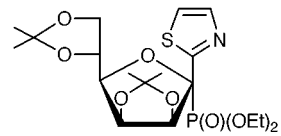 **18e** (93%)	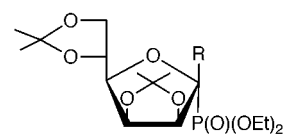 **19e** R = CH_2OH (56%) **20e** R = CO_2Me (54%)

gluco derivative **18b** although isolated in excellent yield was composed of a mixture of α- and β-anomers in 3:2 ratio. Thus, also in this case the stereochemistry of the glycosidation reaction appears to be controlled by steric factors emerging in the sugar oxycarbenium ion intermediate. The lack of selectivity of the D-glucoketopyranose acetate **1b** is not surprising in view of the small steric difference around the two diastereotopic faces of the corresponding oxycarbenium ion (Fig. 2).

There is current interest in the synthesis of glycosylphosphonate analogues[25] of aldose 1-phosphates, the biological glycosyl donors,[26] because the unnatural *P*-glycosides can act as

inhibitors of carbohydrate processing enzymes and therefore can serve as lead structures in drug discovery against carbohydrate-based metabolic disorders.[2b] Having easy access to thiazolylglycosylphosphonates **18** we were in a position to prepare isopolar glycosylphosphonate analogues of ketose and ulosonic acid 2-phosphates. Accordingly, phosphonates **18a**–**e** were converted into the corresponding aldehydes by the standard thiazole-to-formyl protocol[27] and each product was both reduced to the alcohol **19** (ketosylphosphonate) and oxidized to carboxylic acid **20** (ulosonylphosphonate) (Table 1). Finally, in order to demonstrate a viable route to fully deprotected phosphonic acids, the alcohol and acid protective groups of phosphonates **19a** and **20a** were removed to give the free ketosyl and ulosonyl phosphonic acids **21a** and **22a**, respectively (Scheme 7). It is worth mentioning that the assignment of the anomeric configuration of phosphonates of the *mannopyrano* and *mannofurano* series was carried out by hitherto unreported heteronuclear NOE experiments consisting of the irradiation of the phosphorus nucleus instead of the adjacent protons.[24] In closing this section, it has to be pointed out that phosphonates **19** and **20** represent two new classes of *P*-glycosides. A single example of a ketosylphosphonate was previously reported, *i.e.* the isopolar monophosphonate analogue of β-D-fructose 2,6-bisphosphate prepared in the Vasella laboratory some years ago.[28]

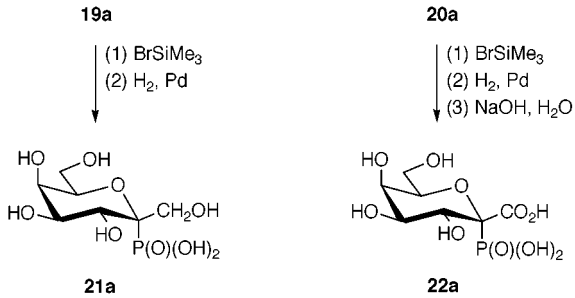

Scheme 7

C-Glycosidation and synthesis of a *C*-ketodisaccharide

A positive response on the synthetic utility of thiazolylketose acetates **1** as glycosyl donors came also from their reactions with carbon nucleophiles. The multigram scale coupling of **1a** with trimethylsilyl cyanide (TMSCN), furan and allyltrimethylsilane under the usual mild conditions (TMSOTf, CH_2Cl_2, room temperature) afforded exclusively the corresponding α-D-linked *C*-glycosides **23a**–**c** in good yields (Scheme 8).[29] The allyl derivative **23c** was obtained upon desilylation (Bu_4NF) of the initially formed thiazolium salt **24**. Intuitively, this compound should be formed *via* intramolecular alkylation of the thiazole ring by the anomeric propyl cation intermediate generated in the first step of the *C*-glycosylation reaction. As a further demonstration of the key service of thiazole, the heterocycle of compounds **23a**–**c** was transformed into the formyl group and the resulting crude aldehydes were reduced to give the *C*-ketosides **25a**–**c** (Scheme 9).

Unlike alkyl and aryl *C*-aldosides,[30] *C*-ketosides have been described in only a few instances.[16g,31] The problem of the control of the stereochemistry at the anomeric centre becomes even more difficult in these cases. With the allyl *C*-thiazolylgalactoside **23c** in hand, we sought a rapid entry to the β-D-(1→6)-*C*-ketodisaccharide **30** (Scheme 10), *i.e.* the galactose counterpart of the *C*-Glu-β-D-(1→6)-Glu recently prepared in the Schmidt laboratory starting from the protected D-gluconolactone.[32] Thus, in three successive steps the double bond of the allyl chain of **23c** was hydroxylated, the diol protected as an acetonide, and the thiazole ring transformed into the formyl

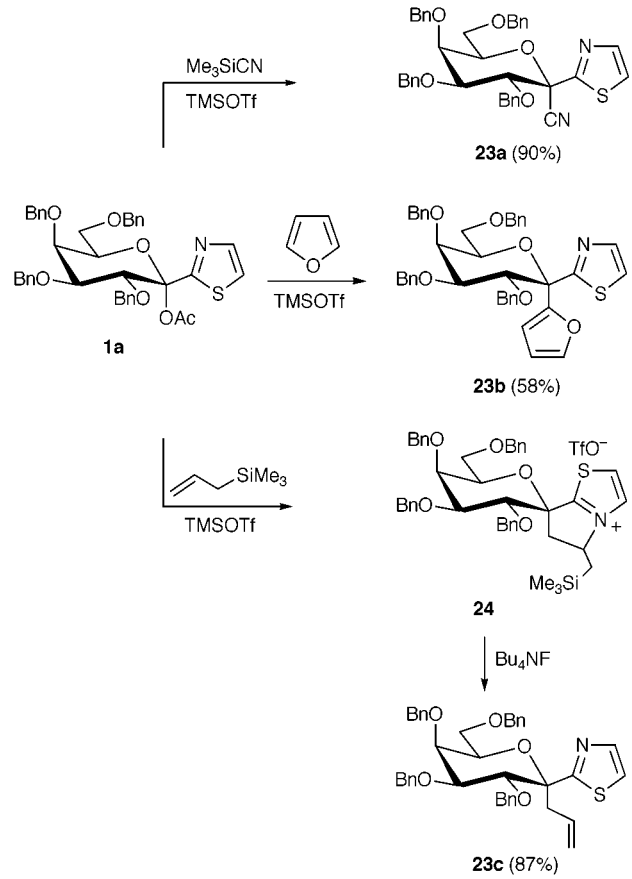

Scheme 8

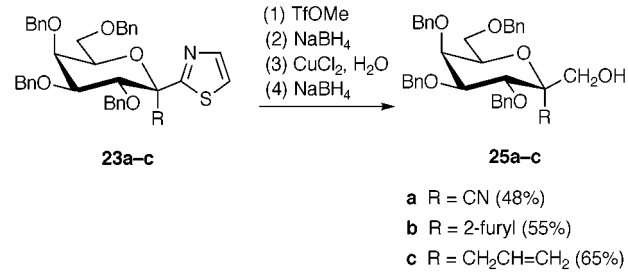

Scheme 9

group. Then the olefination of the aldosulose **27** with the ylide generated from the phosphonium salt **28** gave the olefin **29** as a single *Z*-isomer although in rather low yield (24%). Nevertheless this compound was transformed into the deprotected target product **30** by reduction of the double bond and removal of all hydroxy protective groups.[29] It has been suggested[32] that *C*-ketodisaccharides like **30** can be employed for the synthesis of inhibitors of carbohydrate processing enzymes.

O-Glycosidation with sugar alcohols

At this stage the challenge lay in demonstrating that ketose acetates **1** were suitable glycosyl donors toward more complex nucleophiles such as primary and secondary sugar alcohols. While the *O*-glycosidation of aldoses is routine owing to the numerous efficient methods developed in the last two decades or so,[4] the same reaction with ketoses has been much less exploited. Recent methods have been described involving the use of a phosphite activated fructofuranose[33] and variously activated ketopyranoses.[34] Danishefsky in early syntheses of ulosonic acids[20a] employed furylketoses as glycosyl donors since the furan ring is an electron-rich heterocycle that favours

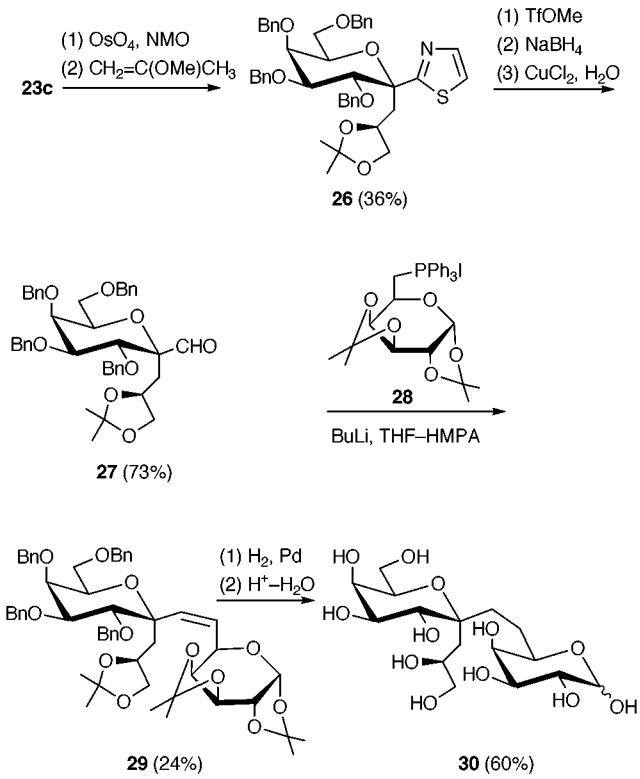

Scheme 10

the glycosidation reaction and at the same time serves as a masked carboxylate group. Thus it was quite rewarding to find that despite the electron-poor character of thiazole, either α- or β-anomers of the *galactopyrano*, *glucopyrano* and *mannofuranno* thiazolylketose acetates **1a**, **1b**, and **1e** reacted under the usual conditions (TMSOTf, CH_2Cl_2, room temperature) with methyl 2,3,4-tri-*O*-benzyl- and 2,3,6-tri-*O*-benzyl-α-D-glucopyranoside acceptors **31** and **32** to give the corresponding thiazolylketodisaccharides **33a**-**37e** in fairly good isolated yields[20b] (Table 2). The α-D selectivity was the rule for the reactions of **1a** and **1e**, whereas the gluco derivative **1b** gave α- and β-D-linked disaccharides **35b** in nearly equal amounts. It was proved that the use of the participating solvent acetonitrile does not affect the above stereochemical outcome. These results are in agreement with the transition state models outlined in Fig. 2. The glycosidation of **1e** with the primary sugar alcohol **31** was compared with the reaction of other mannoketofuranosyl donors with the same alcohol (Scheme 11). As expected, the inactivated furylketose **38** reacted more readily than **1e** to give at low temperature the ketodisaccharide **39** in satisfactory yield. On the other hand the glycosidations of the methylketose acetate **40** and methylulosonate acetate **41** were less efficient as judged from the lower yield of isolated ketosyl disaccharide **42** and the almost complete lack of formation of the ulosonyl disaccharide **43.** The role of thiazole on the reactivity of thiazolylketose acetates **1** as glycosyl donors is open to conjecture. It was suggested[20b] that the heterocyclic ring exerts an anchimeric effect as shown in **A** that assists the acetoxy group removal induced by the Lewis acid E and therefore favours the formation of the oxycarbenium ion intermediate **B** (Scheme 12).

It appeared important in the above context to demonstrate the convenient use of thiazolylketoses for the preparation of disaccharides that are otherwise difficult to access. Compound **43** as well as ulosonyl disaccharides in general represent one of those categories of compounds. Thus, the thiazolyl ketodisaccharide **37e** was subjected to the usual thiazole-to-formyl deblocking protocol and the resulting crude aldosulose **44** was both reduced to the ketose **45** and oxidized to the ulosonate **43** in good overall yields (Scheme 13). The same procedure was applied to the other disaccharides of Table 2 to afford similar results.

Table 2 *O*-Glycosidation of thiazolyketose acetates **1** with sugar alcohols **31** and **32** (TMSOTf, CH_2Cl_2, room temperature)

Acetate **1**	Alcohol **31** or **32**	Ketodisaccharides **33**–**37**
1a	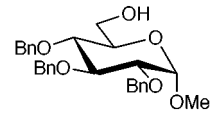 **31**	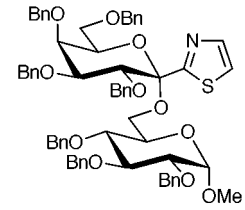 **33a** (73%)
1a	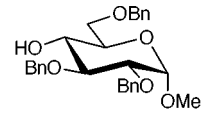 **32**	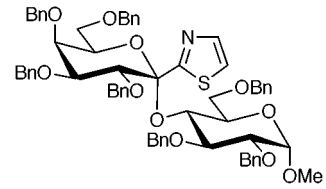 **34a** (60%)
1b	**31**	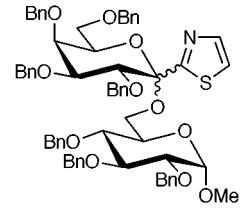 **α-35b** (38%) **β-35b** (25%)
1e	**31**	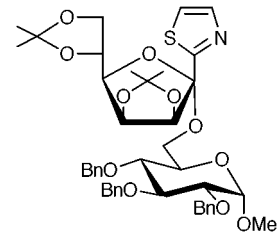 **36e** (70%)
1e	**32**	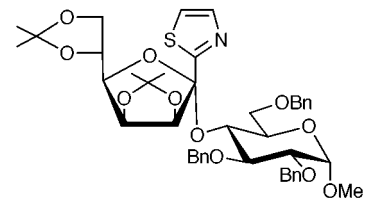 **37e** (62%)

In closing this section a short comment is worth notice with regard to the use of the furyl instead of the thiazolyl group in this synthetic methodology. For example the readily available furylketodisaccharide **39** shown in Scheme 11 is in principle a precursor of the ulosonyl disaccharide **43** *via* the oxidative cleavage of the furan ring to carboxylic acid.[35] In a similar way other ulosonyl disaccharides should be accessible starting from the furyl analogues of compounds **33a**–**37e** of Table 2. However, the strong oxidizing reagents, such as RuO_4 or O_3, that are employed for the unmasking of the carboxylate function from the furan ring impose some caution on the use of this approach since harsh oxidative conditions are likely to be incompatible with various functional and protective groups such as the benzyl group.[36]

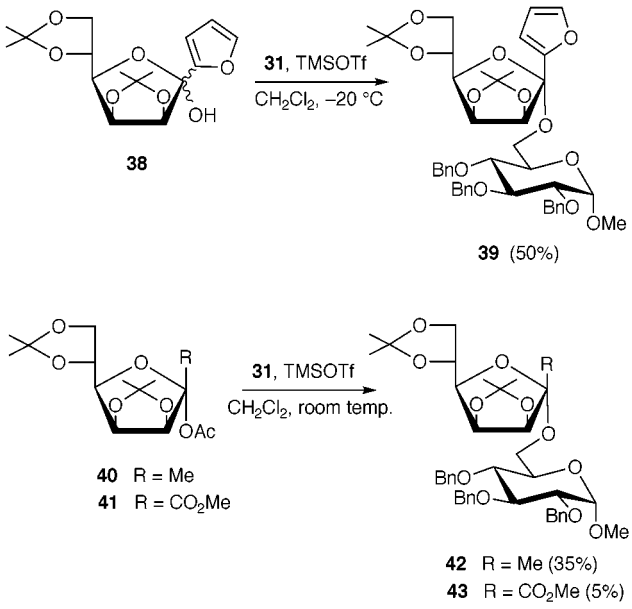

Scheme 11

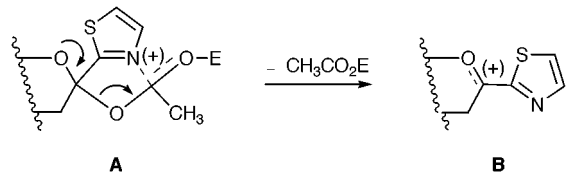

Scheme 12

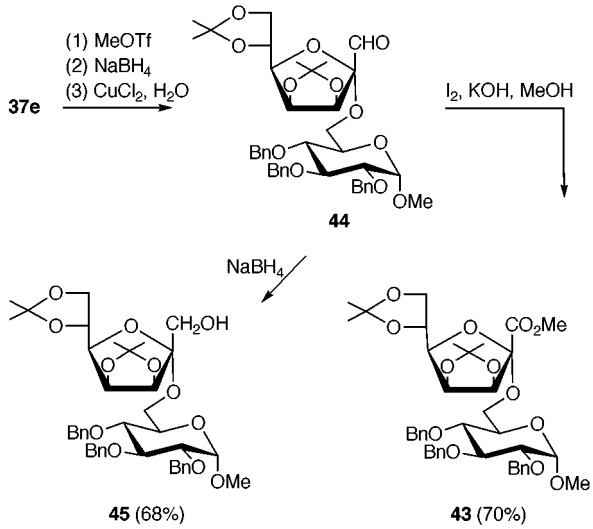

Scheme 13

O-Glycosidation with calix[4]arene alcohols

The rather special glycosylation of primary alcohols attached to one rim of the quite popular macrocyclic phenol-formaldehyde oligomers called calixarenes,[37] belongs to a research programme in our laboratory aiming at the construction of well organized chiral polar domains anchored to a rigid scaffold.[38] The idea behind this project is to use these potentially water soluble systems, named calixsugars, as selective receptors of chiral highly polar organic molecules. Applications in biological systems can also be foreseen as multivalent ligands and inhibitors.[39] Initial work was centred on the *O*-glycosylation of calix[4]arene derived diols and tetrols with aldoses.[38a,b] Then, the coupling of these polyols with thiazolylketose acetates **1** provided the opportunity of a multiple installation of ketosyl and ulosonyl groups.[40] A complete reaction sequence is illustrated in Scheme 14. The reaction of the D-*galacto*

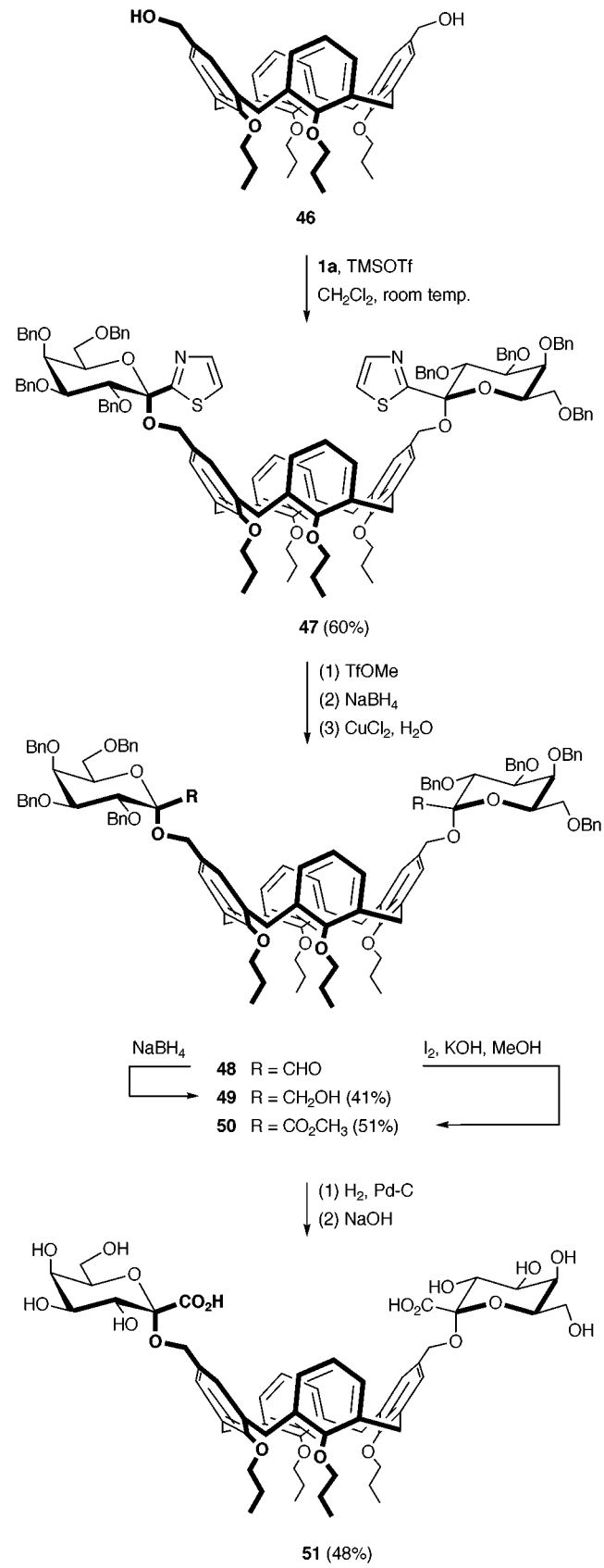

Scheme 14

derivative **1a** with the symmetrical calixarene diol **46** under the usual TMSOTf promoted conditions (CH_2Cl_2, room temperature) afforded the bis-*O*-ketosyl calixarene derivative **47** in good isolated yield. It was firmly established by NMR analysis

that both ketosyl moieties were linked with an α-D (axial) orientation and that the calixarene system retained the cone conformation as in the initial compound **46**. Application of the reaction conditions illustrated in Scheme 13 for the elaboration of **37e** transformed the product **47** into the dialdehyde **48**, which in turn was either reduced to the diol **49** or oxidized to the diester **50**. Finally debenzylation and saponification of **50** afforded the protective group free calixsugar **51** featuring two heptulosonic acid moieties at the upper rim. Compound **51** represents the first member of a class of calixsugars bearing charged functional groups at C-1 of the sugar moieties.

Iterative *O*-glycosidation and synthesis of a cyclic ketotrisaccharide

Having demonstrated the feasibility of the ketodisaccharide synthesis under the thiazolylketose paradigm, we wondered whether the method could be extended to the synthesis of higher oligomers by iterative glycosylation and thiazole cleavage. The orthogonally activated thiazolylketose phosphite **53**, obtained from the thiazolylketose **5a**, and the pentenyl hydroxymethylketoside **52** were used in the stepwise assembly of 2→1-ketoside units to give linear and cyclic D-*galacto*-2-heptulopyranose oligomers[41] (Scheme 15). The first chain-elongation cycle

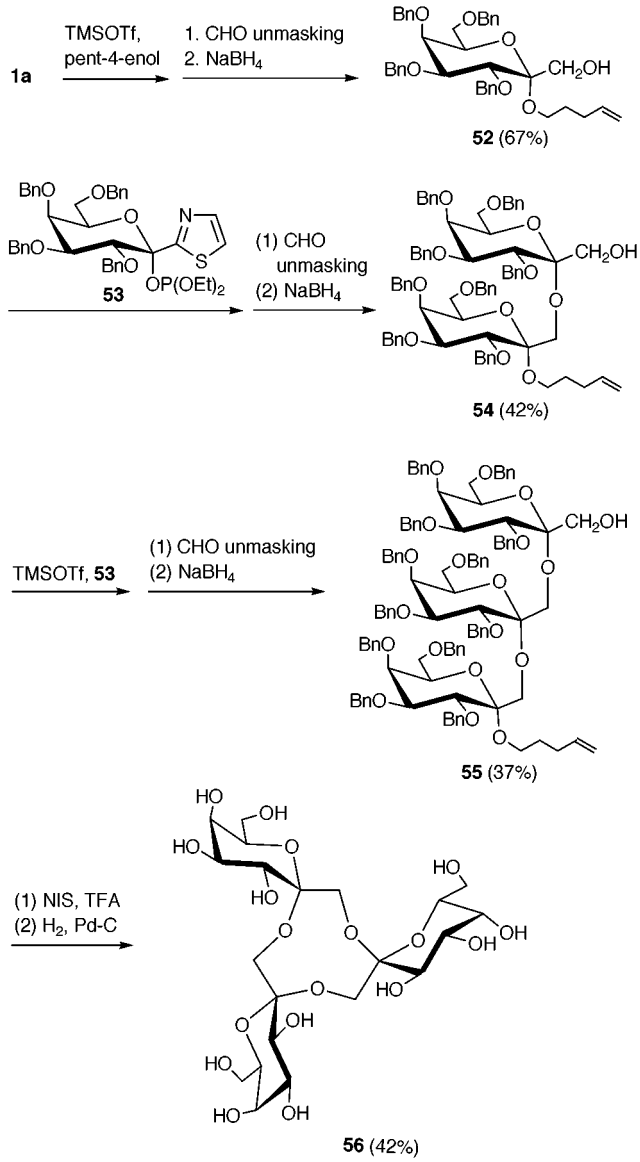

Scheme 15

consisted of the TMSOTf promoted coupling between **53** acting as the glycosyl donor and **52** acting as the acceptor followed by the aldehyde liberation from thiazole and reduction to alcohol. This reaction sequence afforded the ketodisaccharide **54** that in turn was used as the acceptor in a second cycle to give the ketotrisaccharide **55** in satisfactory overall yields. Although there were no apparent indications that we reached the limit of the application of the linear iterative process, the intramolecular cyclization in **55** was demonstrated to occur readily under the Fraser-Reid glycosylation conditions using *N*-iodosuccinimide and trifluoromethanesulfonic acid as promoters.[42] Exhaustive debenzylation of the resulting product afforded the hydroxy group free and water soluble cyclic (α,α,α)-D-ketotrisaccharide **56**. There are no precedents for natural or synthetic cyclic oligosaccharides[4c] similar to compound **56** featuring pyranose units arranged in a spiro fashion around a crown ether skeleton. Related products are the so-called cyclofructins, namely cyclic oligosaccharides constituted by (2→1)-linked fructofuranose units, which are obtained by enzymatic degradation of inulin.[43] Compound **56** can be considered a special type of carbohydrate-based crown ether, *i.e.* a 1,4,7-trioxacyclononane carrying three pyranose rings whose anomeric carbon atoms are part of the methylene bridges. Also from this perspective, no examples can be found in the literature.[44] As a crown-ether, perbenzylated **56** exhibited a remarkable complexing ability in organic solvents toward various ions including calcium and magnesium.

Reduction of thiazolylketose acetates

While the removal of the hydroxy group of the ketose α-**5a** was unsuccessful under various conditions,[17] the corresponding acetates α-**1a** and β-**1a** were readily reduced upon treatment with excess triethylsilane in the presence of TMSOTf as described in the above glycosidation reactions (Scheme 16).

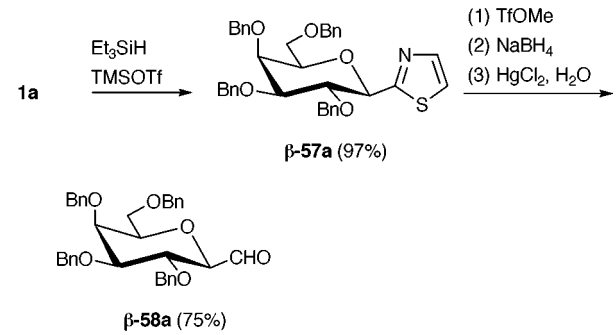

Scheme 16

Under optimized conditions the reaction afforded the β-linked thiazolyl *C*-glycoside β-**57a** in very good isolated yield (97%). This compound was transformed into the corresponding aldehyde β-**58a** that constituted the final target of the whole procedure. The same reaction sequence was employed for the preparation of various α- and β-D-linked formyl *C*-glycosides **58** (Fig. 3) starting from the ketose acetates **1** shown in Fig. 1. Most acetates **1** (*galactopyrano*, *mannopyrano*, *mannofurano*) were reduced with very high levels of diastereoselectivity to give essentially the β-anomer *C*-glycoside **57** according to the transition state models shown in Fig. 2. Thus, in all these cases only the β-linked aldehydes **58c**–**e** were obtained. As expected, the reduction of glucopyranosylketose acetate α-**1b** or β-**1b** was unselective as it afforded a mixture of α- and β-linked *C*-thiazolyl glycosides in a 1:1 ratio. In this case, both α- and β-formyl *C*-glucopyranosides **58b** were prepared. However in a more recent work[45] we observed that the SmI_2 promoted deoxygenation of ketose acetates **1** occurs with opposite diastereoselectivity to that obtained by the use of Et_3SiH–TMSOTf. A remarkable example is the reduction of the *mannofurano* derivative α-**1e** in which the inversion of selectivity is almost complete[9a] (Scheme 17). Therefore both α- and β-linked aldehydes **58e** were prepared with good efficiency

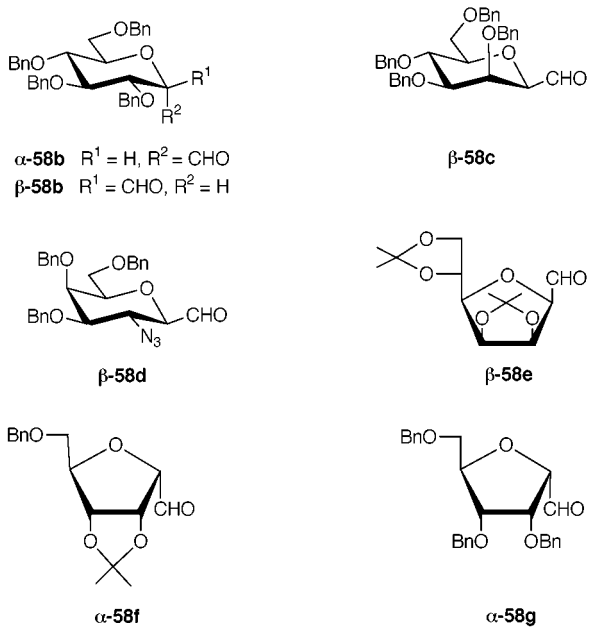

Fig. 3

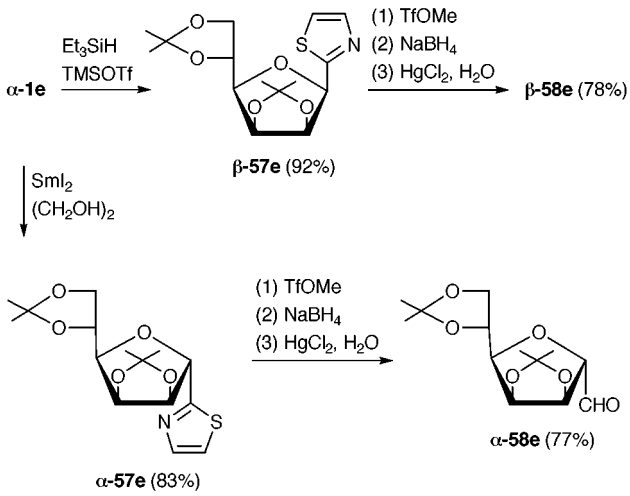

Scheme 17

starting from the same thiazolylketose acetate α-**1e**. Unfortunately the tunable stereoselective reduction was much less efficient with other acetates **1**.

Since the installation of the formyl group at the anomeric carbon of carbohydrates is far from being a trivial problem, other synthetic methods have been reported which use various formyl group equivalents.[10a,15,16e,16j,46] However the application of these methods has often been limited to the synthesis of one or two compounds. On the other hand the efficiency and wide scope of the above thiazole-based method is substantiated by the preparation of a variety of glycopyranosyl and glycofuranosyl aldehydes **58**. The service of the thiazole ring as a formyl group equivalent appeared to have been especially highlighted in this synthetic methodology!

Synthetic applications of formyl *C*-glycosides

The highly reactive formyl group of sugar aldehydes **58** makes these compounds attractive building blocks in synthetic endeavours to more complex *C*-glycosides. The axial (α-D) or equatorial (β-D) orientation of this substituent already *in situ* on the sugar moiety overcomes the problem associated with the control of the stereochemistry of the *C*-glycosidation reaction. The programme was inaugurated with the synthesis of *C*-glycosyl α-amino acids[20c] by application of a nitrone based aminohomologation technique of aldehydes developed in our group.[12,47] The method is succinctly illustrated in Scheme 18 wherein the key step is the addition of 2-lithiothiazole **3** to the

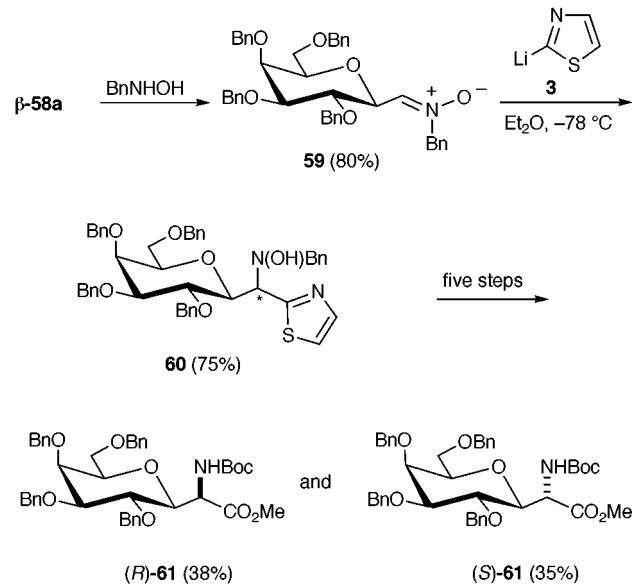

Scheme 18

nitrone **59** generated from the aldehyde β-**58a**. This reaction afforded the *N*-benzyl hydroxylamine **60** in satisfactory yield (75%) but as a mixture of epimers in *ca*. 3:1 ratio. Suitable elaboration of **60** including reductive *N*-dehydroxylation by $TiCl_3$ and transformation of the thiazole ring into the carboxylate group, afforded the (*R*)- and (*S*)-epimer α-amino ester **61** (*C*-glycosyl glycines) that were individually isolated and characterized (38 and 35%, respectively).[20c]

The above synthesis of *C*-glycosyl α-amino acids suffered from poor stereochemical control in the construction of the glycinyl group. The same problem did not exist in a more recent approach to a class of *C*-glycosyl amino acids featuring a three-carbon atom tether.[11] In this method the masked α-amino acid moiety is already present in the form of an oxazolidine ring in the silyl enol ether **62** employed as a reagent in the coupling reaction with the aldehyde β-**58a** (Scheme 19). The resulting

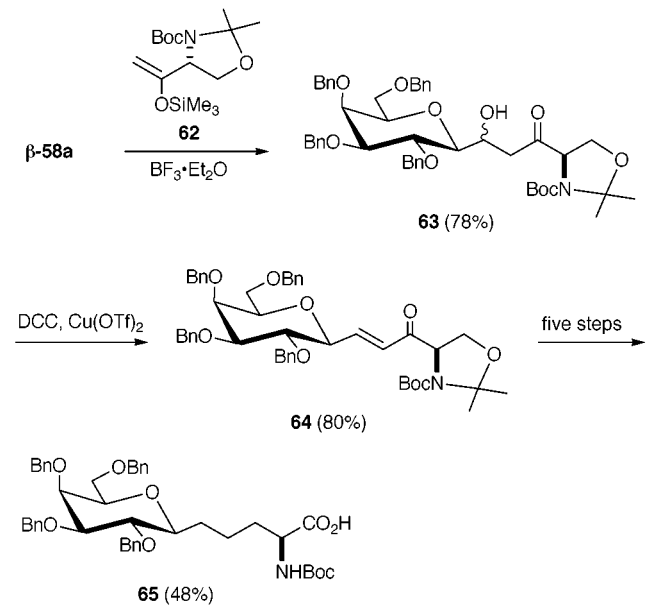

Scheme 19

aldol **63** was isolated as a mixture of diastereomers in good overall yield and transformed into the sugar amino acid **65**

through a series of reactions involving the stepwise removal of the two oxygen atoms from the carbon chain and the oxidative cleavage of the oxazolidine ring. The same reaction sequence was employed for the preparation of the *gluco* and *manno* analogues of **65**. These amino acids represent a class of hitherto unreported carbon-linked isosteres of *N*-glycosyl asparagines wherein the amidic group has been replaced by an ethylene group. In a related programme were also prepared α- and β-linked galactose and glucose serine methylene isosteres by coupling of silyl enol ether **62** with the corresponding glycosyl trichloroacetimidates.[11] Despite considerable efforts, the yield of this glycosidation reaction could not be increased to values higher than 22–32% of isolated product. A complementary approach to this class of *C*-glycosyl amino acid was demonstrated[48] by the synthesis of the galactose derivative **70** (Scheme 20) whose relevance as a precursor to biologically active

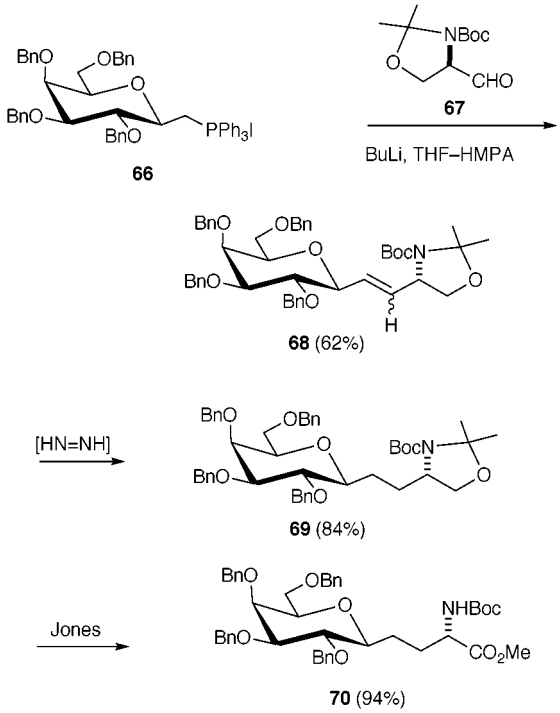

Scheme 20

compounds was earlier demonstrated by Bednarski.[49] In our synthesis the aldehyde β-**58a** was transformed into the phosphonium iodide **66** and the ylide generated from the latter was coupled with the quite popular amino aldehyde **67**.[50] From the resulting alkene the conversion to the amino acid **70** was straightforward by reduction of the double bond with *in situ* generated diimide and one-step cleavage of the oxazolidine ring with Jones' reagent.

As an extension of the chemistry described above we have considered[51] the synthesis of the carbon-linked galactose cerebroside **74** featuring a carbon–carbon bond between the carbohydrate and the ceramide moieties (Scheme 21). In natural

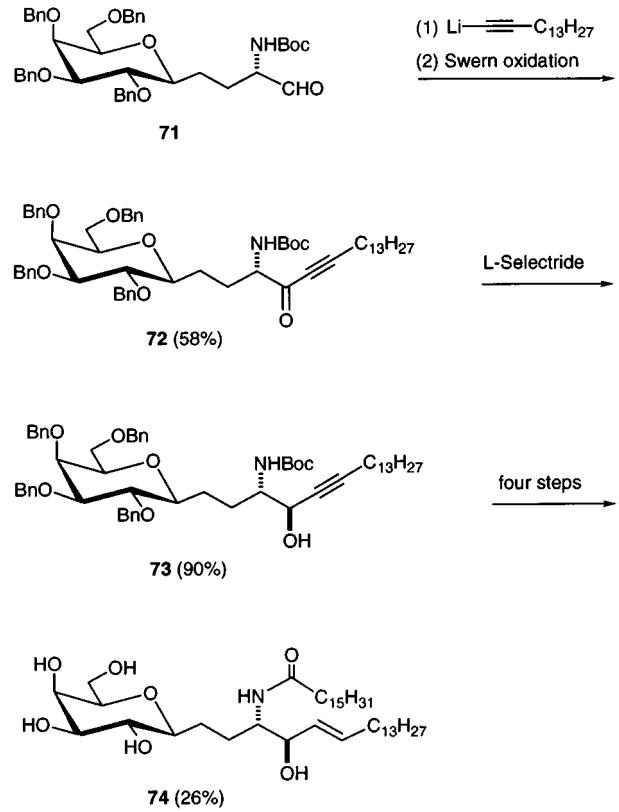

Scheme 21

compounds these molecular fragments are connected by an oxygen atom. Taking advantage of the satisfactory entry to compound **69** shown in Scheme 20, a rapid assembly of the remaining parts directed to the synthesis of **74** was easily envisaged. By a suitable elaboration of the oxazolidine ring, compound **69** was transformed into the α-amino aldehyde **71** to which pentadec-1-ynyllithium was added and the resulting crude mixture of diastereomeric amino alcohols was oxidized to the ketone **72**. Highly stereoselective reduction of this compound with L-selectride (dr 95%) afforded the amino alcohol **73** showing the correct *anti* relationship between the amino and hydroxy groups as in natural sphingosines. The synthesis of **74** was completed by reduction of the triple bond and replacement of the *N*-Boc with the long chain stearoyl group.

As a further development of this programme, we envisaged the reaction of formyl *C*-glycosides **58** with carbohydrate

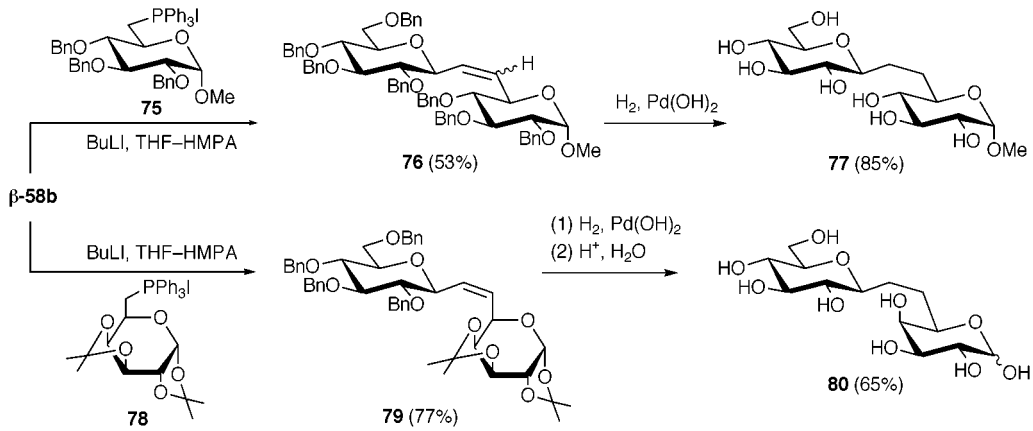

Scheme 22

derivatives bearing a suitable functional group to give carbon-linked disaccharides.[9a] We selected the coupling of **58** with glycopyranose 6-phosphoranes directed to the synthesis of (1→6)-*C*-disaccharides, genuine isosteres of natural products as pointed out by Sinaÿ in the early eighties.[52] The method is illustrated in Scheme 22 showing as an example the synthesis of methyl β-D-*C*-gentiobioside **77** (*C*-Glcβ1,6Glc). A two step reaction sequence constituted by the Wittig olefination of β-**58b** with the ylide generated from the glucopyranose phosphonium salt **75** and the concomitant reduction and debenzylation of the alkene **76** leads to the *C*-disaccharide **77** in a simple and efficient manner.[9a] In a similar way was carried out the synthesis of the *gluco*-to-*galacto*-linked isomer **80** (*C*-Glcβ1,6Gal) with only a minor change that was required for the removal of the isopropylidene protective group. The versatility of this approach was demonstrated in the synthesis of various (1→6)-*C*-disaccharides with both α- and β-linkages (Table 3).

Table 3 Selected (1,6)-*C*-disaccharides prepared form formyl *C*-glycosides **58** by the olefination-reduction sequence

Aldehyde **58**	Phosphonium salt **75** or **78**	*C*-Disaccharides **81**–**85**
β-**58a**	**75**	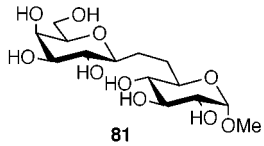 **81**
β-**58a**	**78**	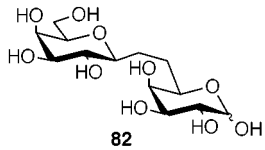 **82**
β-**58c**	**78**	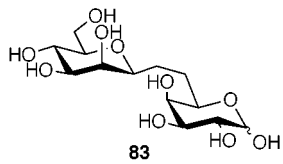 **83**
β-**58d**	**75**	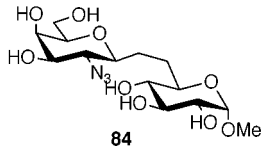 **84**
β-**58g**	**78**	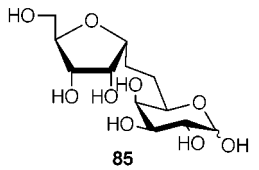 **85**

It was in dealing with this issue that we sought the application of iterative olefination for the assembly of more extensive carbon-linked (1→6)-oligosaccharide chains. In a first approach[10e] the chain growing was initiated by coupling the readily available dialdose **87** with the ylide generated from the phosphonium salt **86** (Scheme 23). The orthogonal protection of the hydroxy groups in the resulting sugar alkene **88** allowed a rapid generation of the aldehyde **89** by desilylation and oxidation of the primary alcohol. This olefination cycle was reiterated twice. Unfortunately the yield of isolated alkene that was rather good in the first cycle (**88**, 70%) dropped substantially in the second (**90**, 36%) and third cycle (**92**, 11%) due to the partial consumption of aldehydes **89** and **91** by 1,2-elimination of BnOH. Nevertheless compounds **88**, **90** and **92** were transformed in the corresponding carbon-linked di-, tri- and tetra-saccharides by desilylation, debenzylation and reduction of the double bonds.

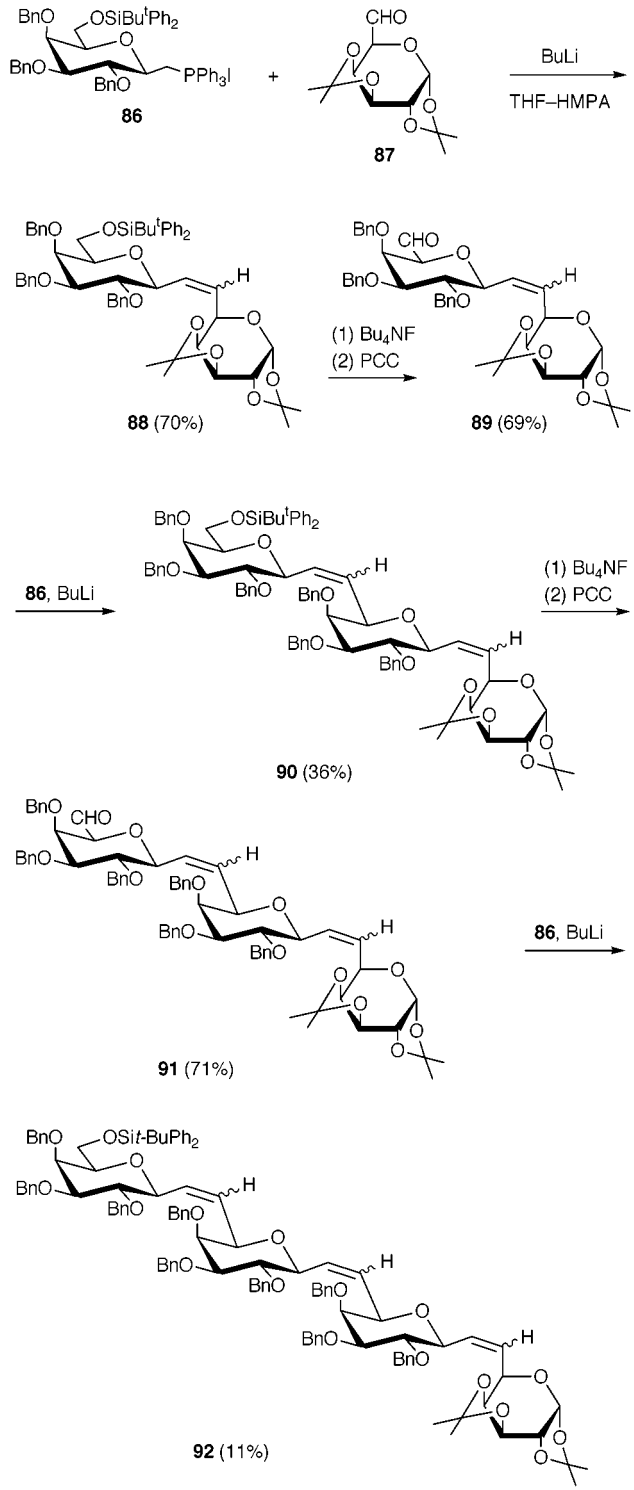

Scheme 23

In closing this section, the use of formyl *C*-glycosides in sugar-fullerene synthesis deserves a short description. Among the multitude of fullerene derivatives that have been prepared in recent years,[53] fullerenes bearing one or more carbohydrate moieties have been reported only in two instances.[54] The interest for glycosylated fullerene derivatives stems from the hope of changing the physicochemical properties of fullerene and improve solubility and biocompatibility. We have installed sugar moieties derived from aldehydes **58** on C_{60} by the Prato azomethine ylide method.[55] In particular, heating a mixture of C_{60} fullerene, *N*-methylglycine (sarcosine), and the aldehyde β-**58a** in refluxing toluene resulted in the formation of a rather

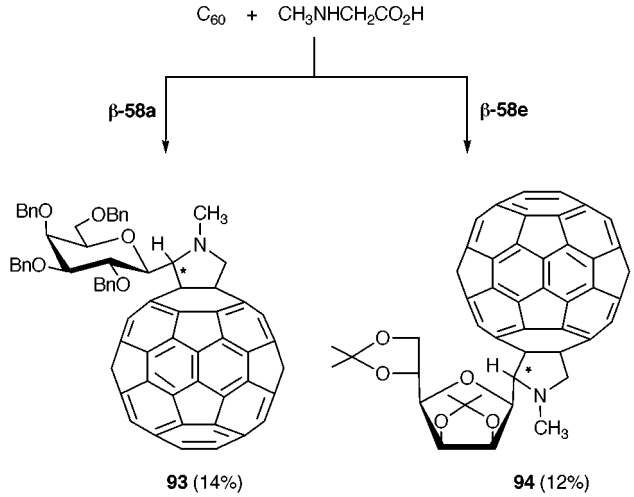

Scheme 24

complex mixture of 1,3-dipolar cycloadducts (Scheme 24). The monoadduct **93** was formed as a 2:1 mixture of diastereomers which were separated and characterized. Similar results were obtained by the use of the aldehyde β-**58e**.

Conclusion

The results that have been presented in this account demonstrate that thiazolylketoses constitute an emerging class of valuable intermediates for carbohydrate synthesis. Once suitably activated by conversion of the anomeric hydroxy group into a good leaving group, they become excellent ketosyl donors. This role appears quite wide in scope as proved by the different types of glycosyl acceptors employed as well as their structural variations. To complete the picture, there is the remarkable contribution of the thiazole ring, which serves as a precursor to various very important functionalities (CHO, CH_2OH, CO_2H), and allows the preparation of various classes of ketosides, some of which are very difficult to access, such as ulosonyl ketosides. The conversion of thiazolylketoses into formyl *C*-glycosides represents a special evolution channel of this chemistry into new synthetic methods for *C*-glycoside synthesis. The synthesis of some important targets (*C*-glycosyl amino acids, *C*-cerebrosides, *C*-oligosaccharides) has been illustrated in this report but further improvements and developments of the methods employed are still required. The extension of these methods to solid-phase techniques should have priority in future research programmes. Other objectives can be also delineated. For example, a formyl *C*-glycoside and compounds derived from it have recently been employed in the Ugi and Passerini multicomponent reactions as an access to glycoconjugate libraries.[56] Thus the combinatorial synthesis in other multicomponent systems, for instance the Biginelli reaction,[57] offers another wide field of application of formyl *C*-glycosides.

Acknowledgement

It is a pleasure to address special thanks to Marie-Christine Scherrmann (Université Paris XI, Orsay), who initiated and developed a great deal of this research during her time in our laboratory as a post-doctoral research associate. We are also grateful to all who contributed to this programme and whose names appear in the references. This work has been supported by various agencies, including the Ministero dell' Università e della Ricerca Scientifica e Tecnologica (MURST COFIN 98), Ministero degli Affari Esteri, Consiglio Nazionale delle Ricerche, Ministère des Affaires Etrangères-Programme Lavoisier (France), the European Community (Erasmus and TMR programmes), Association pour la Recherche contre le Cancer (France), CAPV (Spain) and the United States Research Office.

References

1 Reviews: A. Varki, *Glycobiology*, 1993, **3**, 97; A. Kobata, *Acc. Chem. Res.*, 1993, **26**, 319; Y. C. Lee and R. T. Lee, *Acc. Chem. Res.* 1995, **28**, 321; R. A. Dwek, *Chem. Rev.*, 1996, **96**, 683; R. U. Lemieux, *Acc. Chem. Res.*, 1996, **29**, 373.

2 (*a*) K.-A. Karlsson, *Molecular Mechanism of Microbial Adhesion*, Springer-Verlag, New York, 1988; (*b*) Z. J. Witczack, *Curr. Med. Chem.* 1995, **1**, 392; (*c*) E. F. Hounsell, in *Carbohydrate Chemistry*, ed. G.-J. Boons, Blackie Academic & Professional, London, 1998, pp. 430–447; (d) P. Sears and C.-H. Wong, *Chem. Commun.*, 1998, 1161; (*e*) H. Lis and N. Sharon, *Chem. Rev.*, 1998, **98**, 637.

3 T.-L. Ho, *Tactics of Organic Synthesis*, Wiley, New York, 1994; W. A. Smit, A. F. Bochkov and R. Caple, *Organic Synthesis. The Science behind the Art*, The Royal Society of Chemistry, Cambridge, 1998; *Organic Synthesis Highlights III*, ed. J. Mulzer and H. Waldmann, Wiley-VCH, Weinheim, 1998; *Green Chemistry*, ed. P. T. Anastas and T. C. Williamson, Oxford University Press, Oxford, 1998.

4 Reviews: (*a*) H. Paulsen, *Angew. Chem., Int. Ed. Engl.*, 1982, **21**, 155; (*b*) R. R. Schmidt, *Angew. Chem., Int. Ed. Engl.*, 1986, **25**, 212; (*c*) K. Toshima and K. Tatsuta, *Chem. Rev.*, 1993, **93**, 1503; (*d*) G.-J. Boons, *Tetrahedron* 1996, **52**, 1095; (*e*) G.-J. Boons, *Contemp. Org. Synth.*, 1996, **3**, 173; (*f*) P. H. Seeberger and S. J. Danishefsky, *Acc. Chem. Res.*, 1998, **31**, 685; (*g*) G. Gattuso, S. A. Nepogodiev and J. F. Stoddart, *Chem. Rev.*, 1998, **98**, 1919; (*h*) H. M. I. Osborn and T. H. Khan, *Tetrahedron*, 1999, **55**, 1807. Recent selected articles: (*i*) J. Rademann, A. Geyer and R. R. Schmidt, *Angew. Chem., Int. Ed.*, 1998, **37**, 1241; (*j*) K. C. Nicolau, N. Watanabe, J. Li, J. Pastor and N. Winssinger, *Angew. Chem., Int. Ed.*, 1998, **37**, 1559; (*k*) T. Zhu and G.-J. Boons, *Angew. Chem., Int. Ed.*, 1998, **37**, 1898; (*l*) D. K. Baeschlin, A. R. Chaperon, V. Charbonneau, L. G. Green, S. V. Ley, U. Lücking and E. Walther, *Angew. Chem., Int. Ed.*, 1998, **37**, 3423; (*m*) Z. Zhang, I. R. Ollmann, X.-S. Ye, R. Wischnat, T. Baasov and C.-H. Wong, *J. Am. Chem. Soc.*, 1999, **121**, 734.

5 Reviews: H. Kunz, *Angew. Chem., Int. Ed. Engl.*, 1987, **26**, 294; H. Paulsen, *Angew. Chem., Int. Ed. Engl.*, 1990, **29**, 823; H. Kunz, *Pure Appl. Chem.*, 1993, 65, 1223; M. Meldal and K. Bock, *Glycoconjugate J.*, 1994, **11**, 59; G. Arsequell and G. Valencia, *Tetrahedron: Asymmetry*, 1997, **8**, 2839.

6 A. Hasegawa and M. Kiso, in *Preparative Carbohydrate Chemistry*, ed. S. Hanessian, Marcel Dekker, New York, 1997, pp. 357–379; R. Roy, in *Carbohydrate Chemistry*, ed. G.-J. Boons, Blackie Academic & Professional, London, 1998, pp. 243–321.

7 Recent reviews: B. Fraser-Reid, *Acc. Chem. Res.*, 1996, **29**, 57; S. J. Danishefsky and M. T. Bilodeau, *Angew. Chem., Int. Ed. Engl.*, 1996, **35**, 1380.

8 R. D. Guthrie, in *The Carbohydrates, Chemistry and Biochemistry*, ed. W. Pigman and D. Horton, Academic Press, San Diego, 1972, vol. 1A, pp. 423–478; M. Cerny and J. Stanek, *Adv. Carbohydr. Chem. Biochem.*, 1977, **34**, 23; H. Schiweck, M. Munir, K. M. Rapp, B. Schneider and M. Vogel, in *Carbohydrates as Organic Raw Materials*, ed. F. W. Lichtenthaler, VCH, Weinheim, 1991, pp. 57–94; M. Bols, *Carbohydrate Building Blocks*, Wiley, New York, 1996, pp. 43–48.

9 Selected recent papers: (*a*) A. Dondoni, H. M. Zuurmond and A. Boscarato, *J. Org. Chem.*, 1997, **62**, 8114; (*b*) E. D. Rekaÿ, G. Rubinstenn, J.-M. Mallet and P. Sinaÿ, *Synlett*, 1998, 831; (*c*) O. Jarreton, T. Skrydstrup, J.-F. Espinosa, J. Jiménez-Barbero and J.-M. Beau, *Chem. Eur. J.*, 1999, **5**, 430.

10 *C*-Trisaccharides: (*a*) T. Haneda, P. G. Goekjian, S. H. Kim and Y. Kishi, *J. Org. Chem.*, 1992, **57**, 490; (*b*) A. Wei, A. Haudrechy, C. Audin, H. S. Jun, N. Haudrechy-Bretel and Y. Kishi, *J. Org. Chem.*, 1995, **60**, 2160; (*c*) D. P. Sutherlin and R. W. Armstrong, *J. Am. Chem. Soc.*, 1996, **118**, 9802; (*d*) D. P. Sutherlin and R. W. Armstrong, *J. Org. Chem.*, 1997, **62**, 5267. *C*-Tetrasaccharides: (*e*) A. Dondoni, M. Kleban, H. Zuurmond and A. Marra, *Tetrahedron Lett.*, 1998, **39**, 7991.

11 A. Dondoni, A. Marra and A. Massi, *J. Org. Chem.*, 1999, **64**, 933 and references therein.

12 A. Dondoni, *Synthesis*, 1998, 1681.

13 G. Grynkiewicz and J. N. BeMiller, *Carbohydr. Res.*, 1982, **108**, 229; F. G. De las Heras, A. San Felix and P. Fernández-Resa, *Tetrahedron*, 1983, **39**, 1617; D. B. Tulshian and B. Fraser-Reid, *J. Org. Chem.*, 1984, **49**, 518; R. W. Myers and Y. C. Lee, *Carbohydr. Res.*, 1984, **132**, 61; K. C. Nicolau, R. E. Dolle, A. Chucholowski and J. L. Randall, *J. Chem. Soc., Chem. Commun.*, 1984, 1153; M. Hoffman and R. R. Schmidt, *Liebigs Ann. Chem.*, 1985, 2403; Y. Araki, N. Kobayashi, K. Watanabe and Y. Ishido, *J. Carbohydr. Chem.*, 1985, **4**, 565; G. D. Kini, C. R. Petrie, W. J. Hennen, N. K. Dalley, B. E. Wilson and R. K. Robins,

Carbohydr. Res., 1987, **159**, 81; T. Mukaiyama and S. Kobayashi, *Carbohydr. Res.*, 1987, **171**, 81; M. T. García López, F. G. De las Heras and A. San Félix, *J. Carbohydr. Chem.*, 1987, **6**, 273; K. Tatsuta, J. Hayakawa and Y. Tatsuzawa, *Bull. Chem. Soc. Jpn.*, 1989, **62**, 490; K. N. Drew and P. H. Gross, *J. Org. Chem.*, 1991, **56**, 509.

14 (*a*) G. Grynkiewicz and J. N. BeMiller, *Carbohydr. Res.*, 1982, **108**, C1; (*b*) G. Grynkiewicz and J. N. BeMiller, *Carbohydr. Res.*, 1984, **131**, 273; (*c*) R. R. Schmidt and G. Effenberger, *Liebigs Ann. Chem.*, 1987, 825; (*d*) Y. Ichikawa, M. Isobe, M. Konobe and T. Goto, *Carbohydr. Res.*, 1987, **171**, 193; (*e*) S. J. F. Macdonald, W. B. Huizinga and T. C. McKenzie, *J. Org. Chem.*, 1988, **53**, 3371; (*f*) S. Czernecki and G. Ville, *J. Org. Chem.*, 1989, **54**, 610; (*g*) R. W. Friesen and R. W. Loo, *J. Org. Chem.*, 1991, **56**, 4821; (*h*) A. Dondoni, A. Marra and M.-C. Scherrmann *Tetrahedron Lett.*, 1993, **34**, 7323; (*i*) M. Yokoyama, A. Toyoshima, T. Akiba and H. Togo, *Chem. Lett.*, 1994, 265.

15 M. E. Lasterra Sánchez, V. Michelet, I. Besnier and J. P. Genêt, *Synlett*, 1994, 705.

16 Review: M. Isobe, R. Nishizawa, S. Hosokawa and T. Nishikawa, *Chem. Commun.*, 1998, 2665. See also: (*a*) J. G. Buchanan, A. R. Edgar and M. J. Power, *J. Chem. Soc., Perkin Trans. 1*, 1974, 1943; (*b*) J.-M. Lancelin, P. H. A. Zollo and P. Sinaÿ, *Tetrahedron Lett.*, 1983, **24**, 4833; (*c*) V. Bolitt, C. Mioskowski and J. R. Falck, *Tetrahedron Lett.*, 1989, **30**, 6027; (*d*) A. D. Rycroft, G. Singh and R. H. Wightman, *J. Chem. Soc., Perkin Trans. 1*, 1995, 2667; (*e*) J. Désiré and A. Veyrières, *Carbohydr. Res.*, 1995, **268**, 177; (*f*) M. F. Wong, K. L. Weiss and R. W. Curley, *J. Carbohydr. Chem.*, 1996, **15**, 763; (*g*) K. Tomooka, H. Yamamoto and T. Nakai, *J. Am. Chem. Soc.*, 1996, **118**, 3317; (*h*) M. A. Leeuwenburgh, C. M. Timmers, G. A. van der Marel, J. H. van Boom, J.-M. Mallet and P. Sinaÿ, *Tetrahedron Lett.*, 1997, **38**, 6251; (*i*) S. Hosokawa, B. Kirschbaum and M. Isobe, *Tetrahedron Lett.*, 1998, **39**, 1917; (*j*) T. Lowary, M. Meldal, A. Helmboldt, A. Vasella and K. Bock, *J. Org. Chem.*, 1998, **63**, 9657.

17 A. Dondoni and M.-C. Scherrmann, *J. Org. Chem.*, 1994, **59**, 6404.

18 Galactosamine-based *C*-disaccharides and *C*-glycosyl aminoacids have been recently reported: G. Rubinstenn, J. Esnault, J.-M. Mallet and P. Sinaÿ, *Tetrahedron: Asymmetry*, 1997, **8**, 1327; D. Urban, T. Skrydstrup and J.-M. Beau, *Chem. Commun.*, 1998, 955.

19 A. Dondoni and A. Marra, *Heterocycles*, 1999, **50**, 419.

20 (*a*) S. J. Danishefsky, M. P. DeNinno and S.-H. Chen, *J. Am. Chem. Soc.*, 1988, **110**, 3929; (*b*) A. Dondoni, A. Marra, I. Rojo and M.-C. Scherrmann, *Tetrahedron*, 1996, **52**, 3057; (*c*) A. Dondoni, F. Junquera, F. L. Merchàn, P. Merino, M.-Scherrmann and T. Tejero, *J. Org. Chem.*, 1997, **62**, 5484.

21 A. Dondoni, M.-C. Scherrmann, A. Marra and J.-L. Delépine, *J. Org. Chem.*, 1994, **59**, 7517.

22 S. Mio, Y. Kumagawa and S. Sugai, *Tetrahedron*, 1991, **47**, 2133.

23 M. Nakajima, K. Itoi, Y. Takamatsu, H. Okazaki, T. Kinoshita, M. Shindou, K. Kawakubo, T. Honma, M. Toujigamori and T. Haneishi, *J. Antibiot.*, 1991, **44**, 293; H. Haruyama, T. Takayama, T. Kinoshita, M. Kondo, M. Nakajima and T. Haneishi, *J. Chem. Soc., Perkin Trans. 1*, 1991, 1637.

24 A. Dondoni, S. Daninos, A. Marra and P. Formaglio, *Tetrahedron*, 1998, **54**, 9859.

25 For a review on the isosteric glycosylphosphonates, see: F. Nicotra, in *Carbohydrate Mimics*, ed. Y. Chapleur, Wiley-VCH, Weinheim, 1998, pp. 67–85. Non-isosteric glycosylphosphonates, selected papers: A. Vasella and R. Wyler, *Helv. Chim. Acta*, 1991, **74**, 451; N. J. Barnes, M. A. Probert and R. H. Wightman, *J. Chem. Soc., Perkin Trans. 1*, 1996, 431; M.-J. Rubira, M.-J. Pérez-Pérez, J. Balzarini and M.-J. Camarasa, *Synlett*, 1998, 177; B. Müller, T. J. Martin, C. Schaub and R. R. Schmidt, *Tetrahedron Lett.*, 1998, **39**, 509.

26 S. David, *The Molecular and Supramolecular Chemistry of Carbohydrates. A Chemical Introduction to the Glucosciences*, Oxford University Press, Oxford, 1997, pp. 177–185; P. Collins and R. Ferrier, *Monosaccharides*, Wiley, Chichester, 1995, pp. 46–49; W. Fitz and C.-H. Wong, in *Preparative Carbohydrate Chemistry*, ed. S. Hanessian, Marcel Dekker, New York, 1997, pp. 485–504.

27 A. Dondoni, A. Marra and D. Perrone, *J. Org. Chem.*, 1993, **58**, 275.

28 A. Dessinges and A. Vasella, *Carbohydr. Res.*, 1988, **174**, 47.

29 A. Dondoni, C. Ferrari and A. Marra, to be published.

30 For a recent review, see: Y. Du and R. J. Linhardt, *Tetrahedron*, 1998, **54**, 9913.

31 M. P. Dillon, H. Maag and D. M. Muszynski, *Tetrahedron Lett.*, 1995, **36**, 5469; S. Peukert and B. Giese, *Tetrahedron Lett.*, 1996, **37**, 4365.

32 H. Streicher, A. Geyer and R.R. Schmidt, *Chem. Eur. J.*, 1996, **2**, 502.

33 T. Müller, R. Schneider and R. R. Schmidt, *Tetrahedron Lett.*, 1994, **35**, 7517.

34 B. M. Heskamp, D. Noort, G. A. van der Marel and J. H. van Boom, *Synlett*, 1992, 713; B. M. Heskamp, G. H. Veeneman, G. A. van der Marel, C. A. A. van Boeckel and J. H. van Boom, *Tetrahedron*, 1995, **51**, 5657.

35 G. Schmid, T. Fukuyama, K. Akasaka and Y. Kishi, *J. Am. Chem. Soc.*, 1979, **101**, 259; H. Akita, H. Koshiji, A. Furuichi, K. Horikoshi and T. Oishi, *Chem. Pharm. Bull.*, 1984, **32**, 1242; S. J. Danishefsky, W. H. Pearson and B. E. Segmuller, *J. Am. Chem. Soc.*, 1985, **107**, 1280; T. Mukayama, R. Tsuzuki and J. Kato, *Chem. Lett.*, 1985, 837; M. P. DeNinno, S. J. Danishefsky and G. Schulte, *J. Am. Chem. Soc.*, 1988, **110**, 3925; S. J. Danishefsky and C. J. Maring, *J. Am. Chem. Soc.*, 1989, **111**, 2193.

36 P. Angibeaud, J. Defaye, A. Gadelle and J.-P. Utille, *Synthesis*, 1985, 1123; P. F. Schuda, M. B. Cichowicz and M. R. Heimann, *Tetrahedron Lett.*, 1983, **24**, 3829.

37 C. D. Gutsche, *Calixarenes, Monograph in Supramolecular Chemistry, Vol. 1*, ed. J. F. Stoddart, Royal Society of Chemistry, Cambridge, 1989; *Calixarenes, a Versatile Class of Macrocyclic Compounds*, ed. J. Vicens and V. Böhmer, Kluwer, Dordrecht, 1991; V. Böhmer, *Angew. Chem., Int. Ed. Engl.*, 1995, **34**, 713; M. Takeshita and S. Shinkai, *Bull. Chem. Soc. Jpn.*, 1995, **68**, 1088; P. Lhoták and S. Shinkai, *J. Synth. Org. Chem. Jpn.*, 1995, **53**, 963; D. Diamond and M. A. McKervey, *Chem. Soc. Rev.*, 1996, 15; C. D. Gutsche, *Calixarenes Revisited, Monograph in Supramolecular Chemistry, Vol. 6*, ed. J. F. Stoddart, Royal Society of Chemistry, Cambridge, 1998.

38 (*a*) A. Marra, M.-C. Scherrmann, A. Dondoni, A. Casnati, P. Minari and R. Ungaro, *Angew. Chem., Int. Ed. Engl.*, 1994, **33**, 2479; (*b*) A. Dondoni, A. Marra, M.-C. Scherrmann, A. Casnati, F. Sansone and R. Ungaro, *Chem. Eur. J.*, 1997, **3**, 1774; (*c*) A. Dondoni, M. Kleban and A. Marra, *Tetrahedron Lett.*, 1997, **38**, 7801.

39 M. Mammen, S.-K. Choi and G. M. Whitesides, *Angew. Chem., Int. Ed.*, 1998, **37**, 2754.

40 A. Marra, A. Dondoni and F. Sansone, *J. Org. Chem.*, 1996, **61**, 5155.

41 A. Dondoni, A. Marra and M.-C. Scherrmann, to be published.

42 B. Fraser-Reid and R. Madsen, in *Preparative Carbohydrate Chemistry*, ed. S. Hanessian, Marcel Dekker, New York, 1997, pp. 339–356; R. Madsen and B. Fraser-Reid, in *Modern Methods in Carbohydrate Synthesis*, ed. S. H. Khan and R. A. O'Neill, Harwood, Amsterdam, 1996, pp. 155–170.

43 M. Kawamura, T. Uchiyama, T. Kuramoto, Y. Tamura and K. Mizutani, *Carbohydr. Res.*, 1989, **192**, 83; T. Kida, Y. Inoue, W. Zhang, Y. Nakatsuji and I. Ikeda, *Bull. Chem. Soc. Jpn.*, 1998, **71**, 1201; S. Immel, G. E. Schmitt and F. W. Lichtenthaler, *Carbohydr. Res.*, 1998, **313**, 91.

44 R. Miethchen and V. Fehring, *Liebigs Ann. /Recl.*, 1997, 553.

45 A. Dondoni and A. Marra, to be published.

46 W. R. Kobertz, C. R. Bertozzi and M. D. Bednarski, *Tetrahedron Lett.*, 1992, **33**, 737; C. R. Bertozzi and M. D. Bednarski, *Tetrahedron Lett.*, 1992, **33**, 3109.

47 A. Dondoni and D. Perrone, *Aldrichim. Acta*, 1997, **30**, 35.

48 A. Dondoni, A. Marra and A. Massi, *Tetrahedron*, 1998, **54**, 2827.

49 C. R. Bertozzi, P. D. Hoeprich and M. D. Bednarski, *J. Org. Chem.*, 1992, **57**, 6092; C. R. Bertozzi, D. G. Cook, W. R. Kobertz, F. Gonzales-Scarano and M. D. Bednarski, *J. Am. Chem. Soc.*, 1992, **114**, 10639.

50 P. Garner and J. M. Park, *J. Org. Chem.*, 1987, **52**, 2361. For an improved synthesis of aldehyde **67**, see: A. Dondoni and D. Perrone, *Synthesis*, 1997, 527.

51 A. Dondoni, D. Perrone and E. Turturici, *J. Org. Chem.*, 1999, **64**, 5557.

52 D. Rouzaud and P. Sinaÿ, *J. Chem. Soc., Chem. Commun.*, 1983, 1353.

53 Reviews: A. Hirsch, *Angew. Chem., Int. Ed. Engl.*, 1993, **32**, 1138; N. Martin, L. Sánchez, B. Illescas and I. Pérez, *Chem. Rev.*, 1998, **98**, 2527.

54 P. Uhlmann, E. Harth, A. B. Naughton and A. Vasella, *Helv. Chim. Acta*, 1994, **77**, 2335; A. Yashiro, Y. Nishida, M. Ohno, S. Eguchi and K. Kobayashi, *Tetrahedron Lett.*, 1998, **39**, 9031.

55 M. Prato and M. Maggini, *Acc. Chem. Res.*, 1998, **31**, 519; T. Da Ros and M. Prato, *Chem. Commun.*, 1999, 663.

56 O. Lockhoff, *Angew. Chem., Int. Ed.*, 1998, **37**, 3436.

57 For a review, see: C. O. Kappe, *Tetrahedron*, 1993, **49**, 6937.

Paper 9/03758F

Facile, metal promoted, oxidation of η^4-1,3-diphosphacyclobutadiene by water or methanol: synthesis of [MoCl(CO)(η^4-1,3-$P_2C_2Bu^t_2$)(η^5-L)] (L = C_5H_5, C_5Me_5) and [MoCl(CO){η^3,λ^3,λ^5-$PC_2Bu^t_2PH(OR)$}(η^5-L)] (L = C_5H_5, R = H, Me)

Andrew S. Weller,[a] Christopher D. Andrews,[a] Andrew D. Burrows,[a] Michael Green,*[a] Jason M. Lynam,[a] Mary F. Mahon[a] and Cameron Jones[b]

[a] *Department of Chemistry, University of Bath, Claverton Down, Bath, UK BA2 7AY. E-mail: a.s.weller@bath.ac.uk*
[b] *Department of Chemistry, University of Wales Cardiff, PO Box 912, Park Place, Cardiff, UK CF1 3TB*

Received (in Basel, Switzerland) 29th June 1999, Accepted 13th September 1999

The new complexes [MoCl(CO)(η^4-1,3-$P_2C_2Bu^t_2$)(η^5-L)] (L = C_5H_5 1, C_5Me_5 2) are reported; facile oxidation of 1 with water or methanol affords a rare example of a mixed valence phosphaphosphonietinyl in [MoCl(CO){η^3,λ^3,λ^5-$PC_2Bu^t_2$-PH(OR)}(η^5-C_5H_5)] (R = H, Me), which has also been structurally characterised for R = H.

We have previously reported on studies directed towards the development of the transition metal chemistry of η^2(4e)-bonded phosphaalkynes.[1,2] Mindful of the relationship between phosphaalkynes and their isoelectronic alkyne counterparts we have examined the reactivity of P≡CBu^t towards the molybdenum complexes [MoCl(CO)$_3$L] (L = η^5-C_5H_5 or η^5-C_5Me_5). It has been shown[3,4] that [MoCl(CO)$_3$(η^5-C_5H_5)] reacts thermally with PhC_2Ph to form the four-electron donor diphenylacetylene complex [MoCl(η^2-PhC_2Ph)(CO)(η^5-C_5H_5)]. In the event, however, this study has revealed for the first time that a coordinated 1,3-diphosphacyclobutadiene ligand can undergo a facile and selective reaction with water or methanol to give a mixed valence η^3,λ^3,λ^5-phosphaphosphonietinyl ligand.

Addition of 2.1 equiv. of P≡CBu^t to pentane solutions of [MoCl(CO)$_3$L] (L = η^5-C_5H_5 or η^5-C_5Me_5) and gentle heating (40 °C) for 78 and 24 h respectively, results in the isolation of orange [MoCl(CO)(η^4-1,3-$P_2C_2Bu^t_2$)L] (L = η^5-C_5H_5 **1**, η^5-C_5Me_5 **2**) in moderate and good yield, respectively.

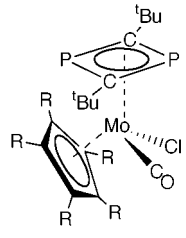

1 R = H
2 R = Me

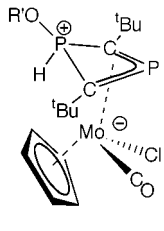

3 R' = H
4 R' = Me

A single crystal X-ray diffraction study performed on **2** confirmed the structure, and this will be reported in full at a later date.[5] The NMR spectra of **1** and **2** are also fully consistent with this description.† Two different environments are observed for each of the phosphorus and carbon atoms in the 1,3-diphosphacyclobutadiene ring and the appended Bu^t groups, as a consequence of the asymmetry introduced by the carbonyl and chloride ligands. This demonstrates that the 1,3-$P_2C_2Bu^t_2$ ligand does not rotate on the NMR timescale at room temperature, an observation that has been precluded previously by the relatively high symmetry of associated metal fragments in other 1,3-diphosphacyclobutadiene complexes.[6,7] However, the 1,3-diphosphacyclobutadiene ligand in **1** does begin to rotate on the NMR timescale at higher temperatures, the onset of coalescence of the Bu^t signals being observed in the ^{1}H NMR spectrum at +60 °C at 400 MHz.

Complex **2** is remarkably stable to the ambient environment, C_6D_6 solutions remaining unchanged (by ^{1}H and ^{31}P{^{1}H} NMR spectroscopy) on exposure to air or water for 2 weeks. In sharp contrast, **1** undergoes reaction with water (slowly with atmospheric, *ca.* 2 days on addition of 10 equiv.) or methanol (7 days) to afford complexes in which one of the coordinated phosphorus atoms has undergone formal oxidative addition of HOR (R = H, Me). The resulting complexes [MoCl(CO){η^3,λ^3,λ^5-PC_2-Bu^t_2PH(OR)}L] (L = η^5-C_5H_5, R = H **3**, or Me **4**), are formed in essentially quantitative yield for **3** and in *ca.* 90% yield for **4** (impurities present are compound **3** and at least two other unidentified compounds). The solid state structure of **3** is shown in Fig. 1.‡

It is apparent that one of the phosphorus atoms is no longer coordinated to the metal [Mo(1)···P(1) 2.8745(13) Å]. Moreover, P(1) is bent away from the plane of the η^3-phosphaallyl group [C(12)–P(2)–C(7)] by 25.12° and also bears a hydroxy group [P(1)–O(1) 1.581(3) Å] and a direct P–H bond. Both the hydroxy and phosphorus bound hydrogens were located in the difference map and refined without constraints. The remaining bond lengths and angles are consistent with the description of **3** as a η^3,λ^3,λ^5-phosphaphosphonietinyl complex, and as such are unremarkable.

From a bonding perspective, **3** can be viewed in terms of the two canonical forms **A** and **B**; one in which there is a formal bond between Mo and P(1) (**A**) or a zwitterionic alternative in which there is no bond between these two atoms (**B**). On the basis of the long Mo–P(1) distance coupled with the fact that in the IR spectrum the carbonyl group stretch is observed at > 60 cm^{-1} to lower frequency compared with **1,** which is consistent with a negative charge on Mo, we suggest that **B** represents the

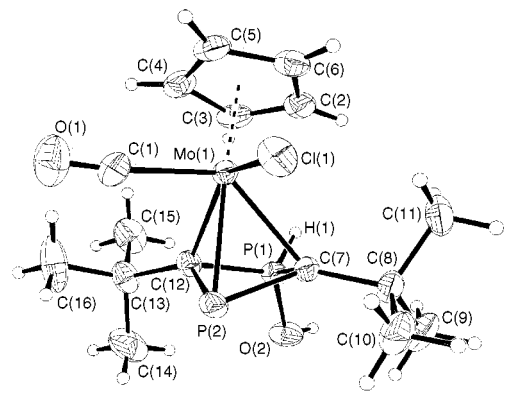

Fig. 1 Crystal structure of one molecule within the asymmetric unit of compound **3** showing the labelling scheme used. Thermal ellipsoids are represented at the 30% probability level. Selected bonds distances (Å): Mo(1)–Cl(1) 2.5468(11), Mo(1)–C(1) 2.036(4), Mo(1)–P(1) 2.8745(13), Mo(1)–P(2) 2.4179(10), P(2)–C(12) 1.848(3), P(2)–C(7) 1.839(3), P(1)–C(12) 1.742(3), P(1)–C(7) 1.742(3), P(1)–O(2) 1.581(3).

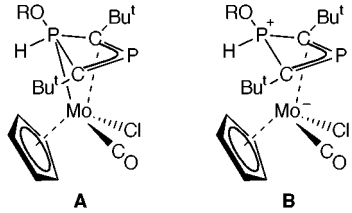

mode of bonding in **3**. In either canonical form P(1) may be considered formally as being phosphorus(V).

The NMR data for **3** and **4** are very similar; for both compounds H(1) is observed as a doublet of doublets in the ^{1}H NMR spectrum, the very large value of one of the couples [J(PH) ≈ 500 Hz] confirming the presence of a direct P–H bond. Although the hydroxy proton in **3** is not observed in the ^{1}H NMR spectrum, presumably owing to fast exchange in solution, in **4** the methoxy group is clearly seen as an integral 3H doublet. In the ^{31}P{^{1}H} NMR spectra of **3** and **4** two different phosphorus environments are observed [**3**: δ(^{31}P) 8.9, −15.8, **4**: δ(^{31}P) 10.6, −16.7], shifted significantly to higher field from those in **1**, with the broader, low field resonance, split on retention of coupling to ^{1}H.

As previously stated, the formulation of compounds **3** and **4** corresponds to the unprecedented selective oxidative [P(III)→P(V)] addition of water or methanol respectively to one of the phosphorus centres present in the 1,3-diphosphacyclobutadiene complex, **1**. Although it has been previously shown that one of the phosphorus lone pairs of a coordinated 1,3-diphosphacyclobutadiene can coordinate onto transition metal Lewis acid fragments,[8] it seems unlikely that the formation of **3** or **4** involves an initial deprotonation of H_2O or MeOH (Scheme 1, pathway **a**,) followed by nucleophilic attack by HO^- or MeO^- on the resulting [1,3-PP(H)C_2]$^+$ ring. More likely is pathway **b** of Scheme 1 since it has been previously reported [9] that in the solid state structure of [Mo(η^5-C_9H_7)(CO)$_2$(η^4-1,3-$P_2C_2Bu^t_2$)][BF_4] the [BF_4]$^-$ anion is bonded to one of the phosphorus centres resulting in the formation of the zwitterionic species [Mo(η^5-C_9H_7)(CO)$_2$(η^3-1,3-$PC_2Bu^t_2PFBF_3$)] **5**. Whereas, in solution, [BF_4]$^-$ rapidly dissociates from **5**, in the case of the formation of **3** and **4**, *trans*-nucleophilic attack by H_2O or MeOH is consummated by addition of H^+ to the phosphorus centre. Additional support for this mechanism comes from the zwitterionic complex [Ru(η^5-C_5H_5)(η^3-1,3-$PC_2Bu^t_2PFCBu^tP$)] **6**, generated from a putative intermediate resulting from [PF_6]$^-$ attack at a coordinated 1,3-diphosphacyclobutadiene ring.[10] There is, of course, a more subtle variation on these two pathways, which depends on hydrogen bonding (Scheme 1) and involves simultaneous protonation and nucleophilic attack. In agreement with these suggestions, involving rate determining breaking of an OH bond, is the observation of a large positive kinetic isotope effect $k_D/k_H \approx 3.6$ [$t_{1/2}$(H_2O) 5.5 h, $t_{1/2}$ (D_2O) 20 h].

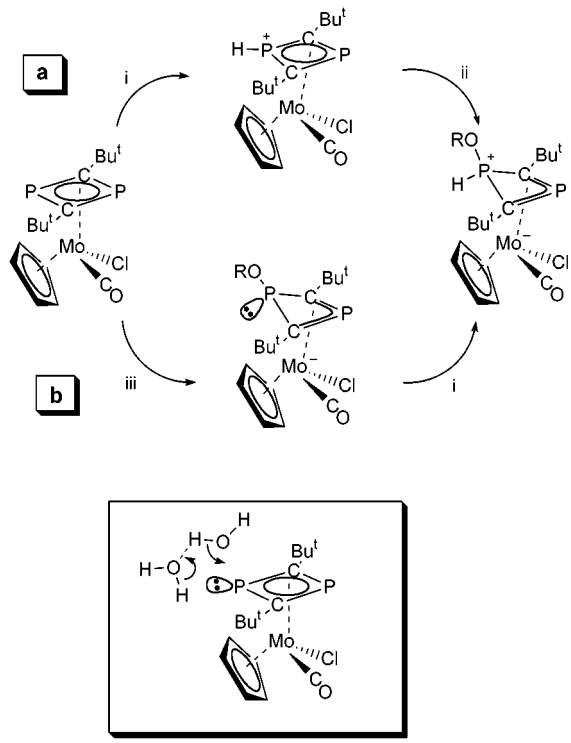

Scheme 1 *i* + [H]$^+$; *ii* + [OR]$^-$ (R = H or Me); *iii* + HOR (R = H or Me), −[H]$^+$.

We have reported here the synthesis of two new readily accessible 1,3-diphosphacyclobutadiene complexes, and for one, facile oxidative addition of water or methanol, a reaction without precedent. The robust nature of **2** combined with the reactivity of **1** presages a wealth of chemistry associated with this system which is currently under investigation.

We thank the EPSRC (J. M. L.) and the University of Bath (C. D. A.) for support.

Notes and references

† *Selected NMR data for the new complexes*: **1**: ^{1}H(CD_2Cl_2) δ 5.66 (s, 5 H, C_5H_5), 0.89 (br, 9 H, Bu^t), 0.69 (br, 9 H, Bu^t). ^{31}P{^{1}H}(CD_2Cl_2) δ 86.9 (s, 1 P), 71.1 (s, 1 P). IR (pentane) 1988 cm^{-1}. **2**: ^{1}H(CD_2Cl_2) δ 1.90 (s, 15 H, C_5Me_5), 0.86 (s, 9 H, Bu^t), 0.82 (s, 9 H, Bu^t). ^{31}P{^{1}H}(CD_2Cl_2) δ 101.7 [d, 1 P, J(PP) 7 Hz], 74.4 (br, 1 P). IR (CH_2Cl_2) 1961 cm^{-1}. **3** ^{1}H [$(CD_3)_2CO$] δ 8.11 [dd, 1 H, P*H*, J(PH) 4, 499 Hz], 5.58 (s, 5 H, C_5H_5), 1.24 (s, 9 H, Bu^t), 1.03 (s, 9 H, Bu^t). ^{31}P [$(CD_3)_2CO$] δ 8.9 [d, 1 P, J(HP) 499 Hz], −15.8 (s, 1 P). IR (KBr) 1921 cm^{-1}. **4**: ^{1}H(C_6D_6) δ 8.00 [dd, 1 H, PH, J(PH) 5, 496 Hz], 5.41 (s, 5 H, C_5H_5), 3.90 [d, 3 H, POMe, J(PH) 12 Hz], 1.00 (s, 9 H, Bu^t), 0.80 (s, 9 H, Bu^t). ^{31}P[$(CD_3)_2CO$] δ 10.6 [d, 1 P, J(HP) 496 Hz], −16.7 (s, 1 P). IR (KBr) 1889 cm^{-1}.

‡ *Crystal data*: **3:** $C_{16}H_{25}ClMoO_2P_2\cdot0.25CH_2Cl_2$, M = 463.92, λ = 0.71069 Å, triclinic, space group $P\bar{1}$ (no. 2), a = 10.067(2), b = 13.036(4), c = 17.169(4) Å, α = 67.90(2), β = 87.66(2), γ = 72.60(1)°, U = 1985.5(9) Å^3, Z = 4, T = 293(2) K, D_c = 1.552 g cm^{-3}, μ = 1.028 mm^{-1}, F(000) = 946; 6974 unique reflections, all data; R_1 = 0.0400 wR_2 = 0.0771 (all data). CCDC 182/1420. See http://www.rsc.org/suppdata/cc/1999/2147/ for crystallographic files in .cif format.

1 G. Brauers, M. Green, C. Jones and J. F. Nixon, *J. Chem. Soc., Chem. Commun.*, 1995, 1125.
2 N. Carr, M. Green, M. F. Mahon, C. Jones and J. F. Nixon, *J. Chem. Soc., Chem. Commun.*, 1995, 2191.
3 J. L. Davidson and D. W. A. Sharp, *J. Chem. Soc., Dalton Trans.*, 1975, 2531.
4 J. L. Davidson, M. Green, F. G. A. Stone and A. J. Welch, *J. Chem. Soc., Dalton Trans.*, 1976, 738.
5 A. S. Weller, C. D. Andrews, A. D. Burrows, M. Green, J. M. Lynam and M. F. Mahon, *unpublished work.*
6 (a) P. Binger, R. Milczarek, R. Mynott, M. Regitz and W. Rösch, *Angew. Chem. Int. Ed. Engl.*, 1986, **25**, 644; (b) F. G. N. Cloke, K. R Flower, P. B. Hitchcock and J. F. Nixon, *J. Chem. Soc., Chem. Commun.*, 1994, 489; (c) P. B. Hitchcock, M. J. Maah and J. F. Nixon, *J. Chem. Soc., Chem. Commun.*, 1986, 737.
7 The complex [Mo(η^4-$P_2C_2Bu^t_2$)$_3$] [ref. 6(*b*)] has static 1,3-diphosphacyclobutadiene rings on the NMR timescale, but is also sterically very crowded.
8 P. B. Hitchcock, M. J. Maah, J. F. Nixon and C. Woodward, *J. Chem. Soc., Chem. Commun.*, 1987, 844; H. F. Dare, J. A. K. Howard, M. U. Pilotti, F. G. A. Stone and J. Szameitat, *J. Chem. Soc., Chem. Commun.*, 1989, 1409.
9 P. B. Hitchcock, M. J. Maah, J. F. Nixon and M. Green, *J. Organomet. Chem.*, 1994, **466**, 153.
10 P. B. Hitchcock, C. Jones, J. F. Nixon, *Angew. Chem. Int. Ed. Engl.* 1994, **33**, 463.

Communication 9/05240B

ChemComm

Mono-amidinate complexes stabilized by a new sterically-hindered amidine†

Joseph A. R. Schmidt and John Arnold*

Department of Chemistry, University of California at Berkeley and Chemical Sciences Division, Lawrence Berkeley National Laboratory, Berkeley, California 94720-1460, USA. E-mail: arnold@socs.berkeley.edu

Received (in Bloomington, IN, USA) 12th July 1999, Accepted 16th September 1999

A novel amidinate ligand incorporating a bulky terphenyl group is used to prepare unusual, low-coordinate lithium and yttrium mono-amidinate complexes.

The search for ancillary ligands capable of facilitating a wide variety of catalytic processes is a challenging problem in inorganic chemistry. Metal complexes incorporating amidinate ligands have been actively studied over the past few years; a broad range of chemistry has appeared and important applications, for example, olefin polymerization, have been described.[1–7] A major goal of work in this area is to prepare ligands that can be easily tuned, sterically and electronically, in order to promote the formation of complexes displaying unusual structures and reactivities.

We now report the synthesis of a novel amidinate ligand incorporating a bulky terphenyl group that exerts steric control in its metal derivatives. The synthesis of an unusual Li salt and examples of Ln mono-amidinates are described. These are noteworthy since bis-amidinates are generally formed in Ln systems,[8,9] a situation that parallels, to some extent, the related cyclopentadienyl chemistry to which amidinates are frequently compared.[1,10]

Previous efforts to prepare bulky amidinates relied on adamantyl or $C_6H_3Pr^i_2$-2,6 substitutions at the N atoms,[11–13] giving rise to ligands that are essentially bulky only in the amidine plane [Fig. 1(a)]. In contrast, we envisaged use of a terphenyl substituent on the amidine carbon atom to provide steric hindrance not only in the plane of the ligand, but also above and below this plane, resulting in a more 'bowl'-shaped environment [Fig. 1(b)]. Terphenyl groups are now well known to support unusual coordination environments,[14–17] the closest analogy to our work being the formation of hindered carboxylate complexes reported recently.[18,19]

The sterically demanding amidine *N*,*N*′-diisopropyl(2,6-dimesityl)benzamidine (Hdimb)[20] was isolated in 94% yield by addition of *N*,*N*′-diisopropylcarbodiimide to 2,6-dimesityl-(lithiobenzene)[21] followed by an aqueous work-up (Scheme 1).

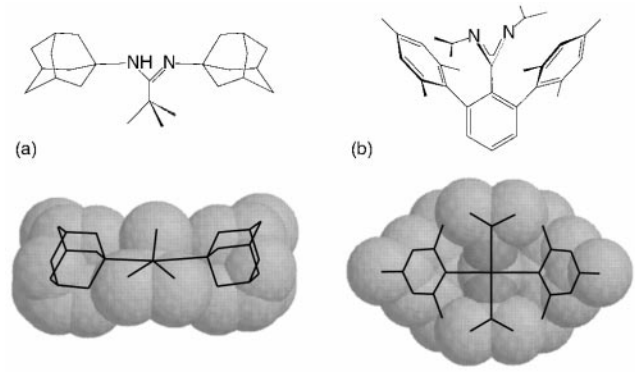

Fig. 1 Side (wire) and top (space-filling) views of (*a*) *N*,*N*′-bis(adamantyl)neopentamidine (ref. 12) and (*b*) *N*,*N*′-diisopropyl(2,6-bismesityl)benzamidine.

† Electronic supplementary information (ESI) available: characterization data.

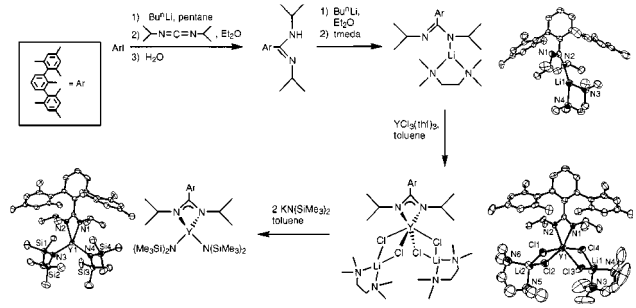

Scheme 1

In contrast to simple non-bulky amidines examined previously, the ^{1}H NMR spectrum of Hdimb is complex at room temp., showing two independent sets of amidine resonances. TOCSY data allowed deconvolution of the ^{1}H NMR resonances into two independent sets of peaks. As shown in Fig. 2, the four Pr^i resonances are differentiated into two pairs: one pair from the imine N and one pair from the amine N. A NOESY spectrum showed chemical exchange between the two Pr^i groups in each pair.[22] We attribute this exchange to interconversion between the *Z*- and *E*-*syn* isomers on the NMR timescale. Recently, Boeré *et al*. reported similar structural effects in bulky *N*,*N*′-bis(2,6-diisopropylphenyl)benzamidines.[13]

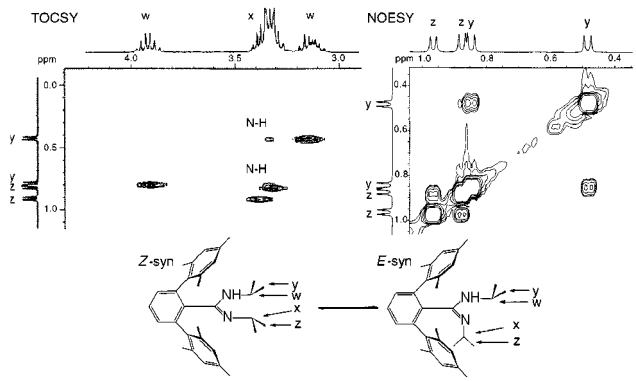

Fig. 2 2D ^{1}H NMR spectra and the indicated equilibrium.

Lithiation of the amidine with Bu^nLi in hexanes, followed by addition of *N*,*N*,*N*′,*N*′-tetramethylethylenediamine (tmeda) gave the Li derivative [(dimb)Li(tmeda)] [20] shown in Scheme 1, which was isolated in 64% yield as colorless crystals from Et_2O. The ^{1}H NMR spectrum shows two different Pr^i resonances, three inequivalent mesityl methyls, and two different mesityl aromatic signals, indicating an unsymmetrical product with C_s symmetry. For comparison, Li salts of simple amidines such as $[PhC(PhN)_2]$Li(tmeda) show spectra consistent with C_{2v} symmetry in solution.[23] The solid-state structure of [(dimb)Li-(tmeda)][24] (Scheme 1) shows that the amidinate is coordinated in a monodentate fashion to the Li which resides in a distorted trigonal planar environment [sum of angles around Li = 358.4(3)°] made up of one amidinate N atom and both tmeda N atoms. Some localization is evident in the N–C–N core, with C(1)–N(1) 1.316(4) Å and C(1)–N(2) 1.337(4) Å. The amidi-

nate N–Li bond [1.942(6) Å] is the shortest observed in a Li amidinate complex and the N–C–N angle is substantially more obtuse [126.5(3)°] than in related species.[25] In contrast, the N(tmeda)–Li bonds [2.115(6) and 2.126(6) Å] are typical.[26] To our knowledge, all reported complexes of the type (amidinate)-Li(tmeda) display four-coordinate Li in solution and in the solid state.[23] We attribute the unusual Li coordination in our compound to steric effects arising from the sterically bulky amidinate ligand.

The Li salt is a useful reagent for the synthesis of metal amidinates. For example, reaction of 1 equiv. of the Li amidinate with $YCl_3(thf)_3$ proceeds as shown in Scheme 1, with the colorless, crystalline product being isolated in moderate yield from Et_2O. The empirical formula, [(dimb)YCl_4Li_2-(tmeda)$_2$],[20] follows straightforwardly from ^{1}H NMR spectroscopy and elemental analysis, and confirmation of the solid-state structure is provided by X-ray diffraction.[27,28] The six-coordinate Y ion resides in a distorted octahedral coordination environment with a single amidinate ligand coordinated in the usual bidentate fashion. Examination of Y–Cl and Y–N bond lengths (av. 2.66 and 2.32 Å, respectively) show no anomalous values, although the N–C–N bond angle in the amidinate (*ca.* 111°) is nearly 5° less obtuse than in related Y compounds.[8,9,29–31] Although mixed amidinate/cyclopentadienyl and amidinate/cyclooctatetraenyl compounds have been previously characterized,[31,32] studies involving Y compounds having exclusively amidinate ligands as ancillary ligands have only resulted in the formation of bis-amidinate compounds,[8,9] making this the first example of a mono-amidinate yttrium halide species.

To test the robustness of the mono-amidinate moiety, (dimb)Y, towards substitution chemistry, [(dimb)YCl_4Li_2-(tmeda)$_2$] was treated with $KN(SiMe_3)_2$ as shown in Scheme 1. The metathesis proceeded smoothly to form [(dimb)Y{N-$(SiMe_3)_2$}$_2$][20] in excellent yield as colorless crystals from pentane. The compound shows a simple ^{1}H NMR spectrum and the solid state structure again features a mono-amidinate complex with the Y now four-coordinate in a distorted tetrahedron.[33] The Y–N(amidinate) bond lengths (av. 2.34 Å) are nearly the same as those observed in the parent compound and the N–C–N bond angle has opened slightly (113°), yet it remains narrower than previously reported related complexes.[8,9,31] The Y–N(amide) bond lengths (av. 2.24 Å) are well within the expected range.[34]

The authors gratefully acknowledge the Department of Defense Science and Engineering Graduate (NDSEG) Fellowship Program for fellowship support (JARS), as well as Dr Corey Liu for insightful discussions regarding the 2D NMR data.

Notes and references

1 J. Barker and M. Kilner, *Coord. Chem. Rev.*, 1994, **133**, 219.
2 J. R. Hagadorn and J. Arnold, *Organometallics*, 1998, **17**, 1355.
3 G. D. Whitener, J. R. Hagadorn and J. Arnold, *J. Chem. Soc., Dalton Trans.*, 1999, 1249.
4 F. A. Cotton, C. A. Murillo and I. Pascual, *Inorg. Chem.*, 1999, **38**, 2182.
5 R. D. Simpson and W. J. Marshall, *Organometallics*, 1997, **16**, 3719.
6 K. Shibayama, S. W. Seidel and B. M. Novak, *Macromolecules*, 1997, **30**, 3159.
7 Y. L. Zhou and D. S. Richeson, *Inorg. Chem.*, 1997, **36**, 501.
8 R. Duchateau, C. T. van Wee, A. Meetsma and J. H. Teuben, *J. Am. Chem. Soc.*, 1993, **115**, 4931.
9 R. Duchateau, C. T. van Wee, A. Meetsma, P. T. van Duijnen and J. H. Teuben, *Organometallics*, 1996, **15**, 2279.
10 F. T. Edelmann, *Coord. Chem. Rev.*, 1994, **137**, 403.
11 M. P. Coles, D. C. Swenson, R. F. Jordan and V. G. Young, *Organometallics*, 1997, **16**, 5183.
12 M. P. Coles, D. C. Swenson, R. F. Jordan and V. G. Young, *Organometallics*, 1998, **17**, 4042.
13 R. T. Boeré, V. Klassen, and G. Wolmershäuser, *J. Chem. Soc., Dalton Trans.*, 1998, 4147.
14 X. M. He, R. A. Bartlett, M. M. Olmstead, K. Ruhlandt-Senge, B. E. Sturgeon and P. P. Power, *Angew. Chem., Int. Ed. Engl.*, 1993, **32**, 717.
15 B. Schiemenz and P. P. Power, *Organometallics*, 1996, **15**, 958.
16 J. R. Su, X.-W. Li, R. C. Crittendon and G. H. Robinson, *J. Am. Chem. Soc.*, 1997, **119**, 5471.
17 B. Twamley, C. D. Sofield, M. M. Olmstead and P. P. Power, *J. Am. Chem. Soc.*, 1999, **121**, 3357.
18 D. Lee and S. J. Lippard, *J. Am. Chem. Soc.*, 1998, **120**, 12153.
19 J. R. Hagadorn, L. Que and W. B. Tolman, *J. Am. Chem. Soc.*, 1998, **120**, 13531.
20 *NMR data* (*J*/Hz): Hdimb (300 MHz) δ (*Z*-syn) 7.180 (t, 1H, *J* 5), 6.967 (d, 2H, *J* 5), 6.864 (s, 4H), 3.439 (s, 1H), 3.420 (spt, 1H, *J* 6), 3.257 (spt, 1H, *J* 6), 2.279 (s, 12H), 2.208 (s, 6H), 0.872 (d, 6H, *J* 6), 0.483 (d, 6H, *J* 6); (*E*-syn) 7.140 (t, 1H, *J* 5), 6.943 (d, 2H, *J* 5), 6.846 (s, 2H), 6.816 (s, 2H), 4.015 (spt, 1H, *J* 6), 3.484 (spt, 1H, *J* 6), 3.464 (s, 1H), 2.172 (s, 6H), 2.162 (s, 6H), 2.143 (s, 6H), 0.962 (d, 6H, *J* 6), 0.845 (d, 6H, *J* 6); [(dimb)Li(tmeda)] (500 MHz) δ 7.244 (t, 1H, *J* 7.5), 7.096 (d, 2H, *J* 7.5), 6.929 (s, 2H), 6.888 (s, 2H), 3.635 (spt, 1H, *J* 6), 2.978 (s, 6H), 2.798 (spt, 1H, *J* 6), 2.377 (s, 4H), 2.237 (s, 6H), 1.533 (s, 12H), 1.452 (s, 4H), 1.193 (d, 6H, *J* 6), 0.851 (d, 6H, *J* 6); [(dimb)YCl_4Li_2(tmeda)$_2$] (500 MHz) δ 7.124 (d, 2H, *J* 9), 7.082 (t, 1H, *J* 9), 7.009 (s, 4H), 3.453 (spt d, 2H, J_{HH} 6, J_{YH} 2.5), 2.514 (s, 12H), 2.233 (s, 6H), 2.107 (s, 24H), 1.750 (s, 8H), 1.119 (d, 12H, *J* 6); [(dimb)Y{$N(SiMe_3)_2$}$_2$] (500 MHz) δ 7.042 (t, 1H, *J* 7.5), 6.832 (d, 2H, *J* 7.5), 6.776 (s, 4H), 3.392 (spt d, 2H, J_{HH} 6, J_{YH} 2.5), 2.209 (s, 6H), 2.091 (s, 12H), 1.028 (d, 12H, *J* 6), 0.273 (s, 36H). Full characterization data are available in the supplementary information (http://www.rsc.org/suppdata/cc/1999/2149/).
21 C.-J. F. Du, H. Hart and K.-K. D. Ng, *J. Org. Chem.*, 1986, **51**, 3162.
22 J. K. M. Sanders and B. K. Hunter, *Modern NMR Spectroscopy: A Guide for Chemists*, Oxford University Press, Oxford, 1993.
23 J. Barker, D. Barr, N. D. R. Barnett, W. Clegg, I. Cragg-Hine, M. G. Davidson, R. P. Davies, S. M. Hodgson, J. A. K. Howard, M. Kilner, C. W. Lehmann, I. Lopez-Solera, R. E. Mulvey, P. R. Raithby and R. Snaith, *J. Chem. Soc., Dalton Trans.*, 1997, 951.
24 *Crystal data* for $C_{37}H_{55}N_4Li$: *M* = 562.81, orthorhombic, *Pbca* (no. 61), *a* = 17.7707(4), *b* = 19.7667(5), *c* = 20.3416(4) Å, *V* = 7145.4(2) Å^3, *T* = 160 K, *Z* = 8, μ(Mo-Kα) = 0.061 mm^{-1}, 34508 reflections measured, 7118 unique (R_{int} = 0.067), final *R* = 0.040, R_w = 0.043, R_{all} = 0.056. CCDC 182/1423.
25 T. Gebauer, K. Dehnicke, H. Goesmann and D. Fenske, *Z. Naturforsch., Teil B*, 1994, **49**, 1444 and references therein.
26 L. M. Engelhardt, W.-P. Leung, C. L. Raston, P. Twiss and A. H. White, *J. Chem. Soc, Dalton Trans.*, 1984, 321.
27 In the crystal structure, both tmeda units exhibit a degree of disorder. The first tmeda unit, refined anisotropically, shows the usual twofold disorder in the ethylene backbone, and only one of the two configurations is shown. The region involving the second tmeda unit was found to be occupied by either one tmeda or two Et_2O units (*ca.* 50% each) in the final crystallographic model and was refined isotropically. The portion of the model with tmeda occupancy is shown here.
28 *Crystal data* for $C_{44}H_{73}Cl_4Li_2N_5OY$: *M* = 932.69, monoclinic, $P2_1/n$ (no. 14), *a* = 10.9930(4), *b* = 16.4195(5), *c* = 29.0041(9) Å, β = 93.891(1)° *V* = 5223.2(3) Å^3, *T* = 158 K, *Z* = 4, μ(Mo-Kα) = 1.356 mm^{-1}, 25212 reflections measured, 9579 unique (R_{int} = 0.077), final *R* = 0.054, R_w = 0.063, R_{all} = 0.137. CCDC 182/1423.
29 Q. Chen, Y. D. Chang and J. Zubieta, *Inorg. Chim. Acta*, 1997, **258**, 257 and references therein.
30 H. Schumann, F. Erbstein, R. Weimann and J. Demtschuk, *J. Organomet. Chem.*, 1997, **536**, 541 and references therein.
31 R. Duchateau, A. Meetsma and J. H. Teuben, *Organometallics*, 1996, **15**, 1656.
32 U. Kilimann and F. T. Edelmann, *J. Organomet. Chem.*, 1994, **469**, C5.
33 *Crystal data* for $C_{43}H_{75}N_4Si_4Y$: *M* = 849.34, orthorhombic, *Pbca* (no. 61), *a* = 18.6326(6), *b* = 21.4487(5), *c* = 24.4451(7) Å, *V* = 9769.4(4) Å^3, *T* = 140 K, *Z* = 8, μ(Mo-Kα) = 1.325 mm^{-1}, 47309 reflections measured, 9772 unique (R_{int} = 0.085), final *R* = 0.030, R_w = 0.031, R_{all} = 0.105. CCDC 182/1423. For all structures see http://www.rsc.org/suppdata/cc/1999/2149/ for crystallographic files in .cif format.
34 H. Schumann, E. C. E. Rosenthal, G. Kociok-Kohn, G. A. Molander and J. Winterfeld, *J. Organomet. Chem.*, 1995, **496**, 233 and references therein.

Communication 9/05620C

Promotion by sulfur of gold catalysts for crotyl alcohol formation from crotonaldehyde hydrogenation

Jillian E. Bailie and Graham J. Hutchings*

Department of Chemistry, Cardiff University, PO Box 912, Cardiff, UK CF10 3TB. E-mail: hutch@cardiff.ac.uk

Received (in Cambridge, UK) 11th August 1999, Accepted 22nd September 1999

Thiophene doping of supported gold catalysts increases the rate of formation of the unsaturated alcohol for the hydrogenation of the α,β-unsaturated aldehyde, crotonaldehyde, providing the first example of the promotion of gold by sulfur.

During the last decade the use of gold as a heterogeneous catalyst has been the subject of renewed interest, with most research being directed at oxidation reactions, particularly the room temperature oxidation of carbon monoxide.[1,2] The activity of such catalysts has been associated with the existence of sites at the gold–support interface where an intimate contact between the small hemispherical gold particles (< 6 nm) and the support exists.[1] Relatively little attention has been given to the development of Au-based hydrogenation catalysts and in addition there have been no studies concerning the role of promoters or additives with gold catalysts. Most previous studies of Au as hydrogenation catalysts involve relatively simple molecules such as CO and CO_2[3–5] and alkadienes,[6] whereas there are only a very limited number of reports of selective hydrogenation of multifunctional organic molecules.[7,8] Molecules such as α,β-unsaturated aldehydes, ketones and esters are difficult to hydrogenate with high selectivity to the corresponding unsaturated alcohols. However, these reactions are of considerable importance in many areas of the chemical industry, often being employed in the manufacture of fine chemicals, pharmaceuticals and fragrances. For example, crotyl alcohol is currently produced using stoichiometric hydrogen donors and an improved catalytic process would be advantageous. Many studies[9–14] of the hydrogenation of α,β-unsaturated aldehydes and ketones have tried to gain fundamental information on selectivity control in these reactions by using different approaches in attempts to design and develop suitable catalysts.

The present work shows that supported Au catalysts, when appropriately prepared, can be highly selective for the formation of unsaturated alcohols, and furthermore, pre-treatment of supported Au catalysts with thiophene can improve the selectivity to crotyl alcohol in the hydrogenation of crotonaldehyde, whilst also maintaining catalytic activity.

ZnO and ZrO_2 supported Au (5 wt% Au^0) were prepared by a co-precipitation technique and Au/SiO_2 was prepared by impregnation.† Reactions were carried out in a continuous flow, fixed-bed, micro-reactor at atmospheric pressure (weight hourly space velocity = 0.7 h^{-1}, H_2 : crotonaldehyde = 14:1) using on-line GC analysis. The catalysts (200 mg) were reduced *in situ* in a flow of hydrogen at 250 °C for 1 h. Crotonaldehyde was fed into the system by means of a calibrated syringe pump into a flow of hydrogen. Modification of the catalyst was achieved *via* direct injection of 0.5 μl thiophene into a flow of hydrogen with the catalyst at 250 °C after reduction.

The results obtained for the hydrogenation of crotonaldehyde at 250 °C over unmodified and thiophene-treated samples are given in Table 1. After an initial stabilisation period, both Au/ZnO and Au/ZrO_2 catalysts display similar activities while the Au/ZnO is more selective for C=O bond hydrogenation to give crotyl alcohol. Both Au/ZnO and Au/ZrO_2 when modified by sulfur, after initial stabilisation, give much higher rates of synthesis of crotyl alcohol when compared to the undoped catalyst (Fig. 1). It is also observed that the rate of butanal formation is maintained when Au/ZnO is modified by sulfur and is slightly decreased for the reaction over sulfur modified Au/ZrO_2. However, when sulfur modification of silica supported Au is examined, it is observed that sulfur effectively decreases the rate of hydrogenation as would usually be expected. This indicates that the nature of the oxide support is of importance to observe this rate enhancement. It is suggested from these observations that sites present on the surface of ZnO and ZrO_2 supported catalysts are very different in nature to those available at the surface of Au/SiO_2. Examination of the Au particle size for the catalysts has been carried out using both X-ray line broadening and transmission electron microscopy. For catalysts prepared by co-precipitation, the Au particles are typically 2–4 nm in size. However, the catalysts prepared by impregnation exhibit much larger particle sizes (typically > 150 nm). It is this difference in particle size which we consider to be important and the high catalytic activity and selectivity of Au catalysts is associated with small Au particles.

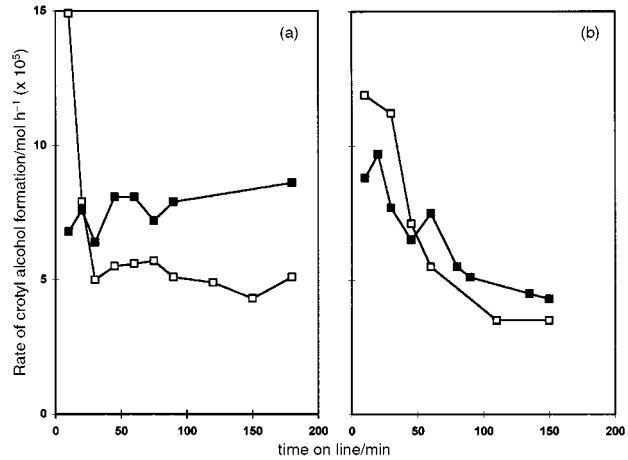

Fig. 1 Effect of thiophene addition on the rate of crotyl alcohol formation (mol $h^{-1} \times 10^5$) over (a) Au/ZnO and (b) Au/ZrO_2: (□) Unmodified, (■) Thiophene treated.

An Au/ZnO catalyst was also prepared by impregnation and subjected to the same reduction and reaction treatments as the Au/ZnO catalysts prepared by co-precipitation. The catalyst prepared by impregnation was found to be inactive in the hydrogenation of crotonaldehyde, emphasising that the method of preparation of Au/ZnO is crucial for this reaction system.

For Au/ZnO it was observed that increasing the temperature of reduction from 250 to 400 °C resulted in a progressive increase in selectivity to crotyl alcohol (reaching a maximum of 82% for Au/ZnO reduced at 400 °C) without major loss of activity. This selectivity is much higher than previous literature data for this reaction.[11–14]

Initial characterisation of these systems by *in situ* FTIR studies of CO adsorption have been performed.‡ CO adsorption on reduced, unmodified, Au/ZnO prepared by co-precipitation produced a band at 2035 cm^{-1} at low CO coverages which shifted to 2045 cm^{-1} as the amount of CO adsorbed was increased. This band has been tentatively assigned to CO

Table 1 Crotonaldehyde hydrogenation at 250 °C over unmodified and thiophene-treated 5 wt% Au catalysts

			Selectivity (%)[a]					
Catalyst	*t*/min	Conv. (%)	B-AL	C-OL	B-OL	2EH	2E2H	Others
Au/ZnO	10	41.4	43.8	29.7	10.7	4.6	2.1	9.1
	30	8.7	37.8	47.8	—	—	0.9	13.5
	60	8.9	35.1	51.7	—	—	—	13.2
	180	7.8	34.1	54.1	—	—	1.1	10.7
S-Au/ZnO	10	27.9	44.5	20.0	15.8	1.5	1.6	16.6
	30	9.3	32.3	56.6	—	—	—	11.1
	60	11.1	29.6	60.6	—	—	—	8.8
	180	10.9	26.8	65.4	—	—	—	7.8
Au/ZrO_2	10	30.4	45.1	32.5	13.7	2.7	—	5.9
	30	18.2	38.8	50.9	5.1	—	—	5.2
	60	12.0	49.1	38.2	5.9	—	—	6.9
	150	9.2	54.5	32.1	7.1	—	—	6.3
$S\text{-}Au/ZrO_2$	10	21.3	42.3	34.3	13.3	7.8	—	2.3
	30	14.2	37.9	44.6	7.2	8	—	2.3
	60	12.2	40.8	50.8	5.9	—	—	2.5
	150	7.5	44.5	47.8	4.8	—	—	2.9
Au/SiO_2	10	11.2	96.2	—	—	—	—	3.8
	30	23.2	97.7	—	—	—	—	2.3
	60	21.9	97.9	—	—	—	—	2.1
	180	21.6	97.8	—	—	—	—	2.2
$S\text{-}Au/SiO_2$	10	8.6	98.2	—	—	—	—	1.8
	40	11.9	98.6	—	—	—	—	1.4
	60	13.3	98.5	—	—	—	—	1.5
	180	14.6	98.4	—	—	—	—	1.6

[a] B-AL = butanal, C-OL = crotyl alcohol, B-OL = butan-1-ol, 2EH = 2-ethylhexanal, 2E2H = 2-ethylhex-2-enal, Others = butane and trace C_3 molecules. S-prefix indicates thiophene modified sample.

adsorbed on Au defect sites or isolated Au atoms in the support matrix. Preadsorption of thiophene at 250 °C caused this band to shift to higher wavenumbers by 15 cm^{-1} and a shift of similar magnitude to higher wavenumbers was again observed as the CO coverage increased. This shift, which we consider to be electronic in nature, provides evidence for the direct modification of the Au surface by thiophene or products of thiophene adsorption.

One possible explanation of the superior catalytic performance of the Au/ZnO and Au/ZrO_2 catalysts, compared to the Au/SiO_2 system, can be based on the work of Haruta,[1,2] concerning CO oxidation, that when Au catalysts are prepared by co-precipitation the support can provide interfacial sites adjacent to hemispherical Au particles that are involved in the activation of reactants, either alone or in association with nearby Au sites. In this case, the presence of sites at the Au-support interface on Au/ZnO and Au/ZrO_2 surfaces could be responsible for the preferential activation of the carbonyl function to hydrogenation. Obviously, such interfacial sites would not then be present on the Au/SiO_2 since no crotyl alcohol was detected. This could be due to the presence of larger, less strongly bonded particles which are more spherical in shape as is often observed with Au catalysts prepared by impregnation. The effect of thiophene may therefore be to electronically modify these interface sites in such a way as to improve activation of the carbonyl group or alternatively to create new active sites by the modification of non-interfacial sites.

We consider these results are the first observation of a promotional effect of sulfur for a Au catalyst. It is clear that the observed promotion is dependent on the nature of the preparation method and the oxide support. We have made no attempt to optimise the rate enhancement and it can be expected that further improvements can be observed by appropriate modification of the experimental conditions and catalyst design. We thank the EPSRC and Synetix for financial support. We also acknowledge C. H. Rochester, J. A. Anderson and H. A. Abdullah of Dundee University for *in situ* FTIR studies.

Notes and references

† Au/ZnO and Au/ZrO_2 were prepared by mixing solutions of $Zn(NO_3)_2{\cdot}H_2O$ or $Zr(O)(NO_3)_2{\cdot}xH_2O$ with $HAuCl_4$ solution, which all contained calculated amounts of Zn, Zr and Au salts required to give a 5 wt% loading of Au^0 on ZnO or ZrO_2. The mixed solutions were heated to 80 °C and 1 M Na_2CO_3 solution was added with continual stirring until a pH of *ca.* 9 was reached. The precipitate was then aged for 20 min prior to vacuum filtration, washing with approximately 1 l of hot deionised H_2O and drying overnight at 110 °C. The samples were then calcined at 400 °C for 4 h in static air. The Au/SiO_2 catalyst was prepared by adding the required amount of silica (Cab-O-sil M5) to a solution containing a calculated amount of $HAuCl_4$ to give a 5 wt% loading of Au^0. The mixture was allowed to evaporate to dryness at 80 °C (approximately 5 hours) with continual stirring after which the residual cake was dried overnight at 110 °C and calcined at 300 °C for 4 h in static air.

‡ A catalyst disc was mounted in a glass IR cell linked to a vacuum line and reduced *in situ* in a flow of hydrogen at 250 °C for 1 h. The sample was then cooled to room temperature and exposed to increasing pressures of CO and FTIR spectra were recorded after each addition of CO. For modified samples, a low level (< 1 mm Hg) of thiophene was admitted to the sample at 250 °C immediately after reduction. The sample was then cooled to room temperature and CO adsorption was performed and monitored by FTIR spectroscopy as before.

1 M. Haruta, *Catal. Today*, 1997, **36**, 153.
2 M. Haruta, *Catal. Surveys Jpn.*, 1997, **1**, 61.
3 H. Sakuri and M. Haruta, *Appl. Catal.*, 1995, **127**, 93.
4 H. Sakuri, S. Tsubota and M. Haruta, *Appl. Catal.*, 1993, **102**, 125.
5 M. Shibata, N. Kawata, T. Matsumoto and H. M. Kimura, *Chem. Lett.*, 1985, 1605.
6 D. A. Buchannan and G. Webb, *J. Chem. Soc., Faraday Trans 2*, 1978, **70**, 134.
7 M. Shibata, N. Kawata, T. Matsumoto and H. M. Kimura, *J. Chem. Soc., Chem. Commun.*, 1988, 154.
8 M. Shibata, N. Kawata, T. Matsumoto and H. M. Kimura, *Japan–France Seminar on Catalysis with Metal Compounds*, Tokyo, 1987, p. 98.
9 G. J. Hutchings, F. King, I. P. Okoye, M. B. Padley and C. H. Rochester, *J. Catal.*, 1994, **148**, 453.
10 G. J. Hutchings, F. King, I. P. Okoye, M. B. Padley and C. H. Rochester, *J. Catal.*, 1994, **148**, 464.
11 P. Claus, *Top. Catal.*, 1998, **5**, 51.
12 V. Ponec, *Appl. Catal.*, 1997, **149**, 27.
13 R. L. Augustine, *Catal. Today*, 1997, **37**, 419.
14 M. A. Vannice and B. Sen, *J. Catal.*, 1989, **115**, 65.

Communication 9/06538E

ChemComm

Base-catalyzed cleavage and homologation of polyhedral oligosilsesquioxanes

Frank J. Feher,* Raquel Terroba and Joseph W. Ziller

Department of Chemistry, University of California, Irvine, CA 92697-2025, USA. E-mail: fjfeher@uci.edu

Received (in Bloomington, IN, USA) 5th August 1999, Accepted 9th September 1999

Readily available $Cy_6Si_6O_9$ 2 (Cy = c-C_6H_{11}) reacts with aqueous NEt_4OH in THF to afford *endo*-C_{2h}-$Cy_6Si_6O_7(OH)_4$ 3a, which upon further hydrolysis produces $CySi(OH)_3$ fragments capable of reacting with 3a to produce *endo*-C_3-$Cy_7Si_7O_9(OH)_3$ 1b; the reaction of 2 with aqueous NEt_4OH in the presence of (vinyl)$Si(OMe)_3$ affords *endo*-C_s-Cy_6(vinyl)$Si_7O_9(OH)_3$ 1c *via* trapping of 3a with monosilanes derived from (vinyl)$Si(OMe)_3$.

Polyhedral oligosilsesquioxanes (POSS) are an interesting class of three-dimensional Si/O clusters derived from the hydrolytic condensation of trifunctional organosilicon monomers (*i.e.* $RSiX_3$).[1–3] Since their discovery in 1946,[4] many stoichiometrically well defined POSS frameworks have been reported, including a wide variety of fully condensed $[RSiO_{3/2}]_n$ frameworks with synthetically useful functional groups.[5–14] Until very recently, the reaction chemistry of fully condensed POSS frameworks was limited mainly to organic transformations of the group attached to silicon. Clean reactions involving the selective cleavage of framework Si–O bonds were virtually unknown.[15] This situation has changed dramatically over the past three years,[16–20] and it is now possible to effect the selective cleavage of one or more Si–O–Si linkages by reacting $R_6Si_6O_9$ and $R_8Si_8O_{12}$ frameworks with strong acids (*e.g.* $HBF_4{\cdot}OEt_2$–BF_3 or triflic acid). Still, there are enormous incentives for developing practical methods for synthesizing incompletely condensed POSS frameworks, particularly trisilanols such as **1a**.

Here we report a number of unprecedented reactions involving $R_6Si_6O_9$ frameworks, including the base-catalyzed homologation of $Cy_6Si_6O_9$ **2** to $Cy_6(R)Si_7O_9(OH)_3$, where R = Cy **1b** or vinyl **1c**. The implications of these results for both the continued development of POSS-based hybrid inorganic–organic polymers and the use of silsesquioxanes as ligands for transition-metal catalysts are discussed.

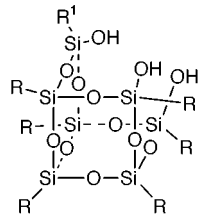

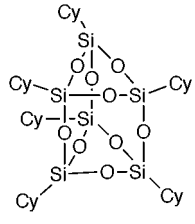

2

1a R = alkyl R^1 = functionalized organic
b R = R^1 = Cy = c-C_6H_{11}
c R = Cy R^1 = vinyl

The reaction of **2**[21–23] with aqueous NEt_4OH in THF occurs rapidly over a period of several hours at room temperature. The first product to appear is a C_{2h}-symmetric tetrasilanol derived from cleavage of both Si_3O_3 rings. This product was assigned as **3a** on the basis of multinuclear NMR spectroscopy and electrospray mass spectrometry data.† Of particular spectroscopic relevance was the ^{29}Si NMR spectrum ($CDCl_3$), which exhibited two resonances at δ −59.4 and −68.8 with relative integrated intensities of 4:2. These resonances, as well as the resonances observed in both the ^{1}H and ^{13}C NMR spectra for this compound, were strikingly similar to those observed for known tetrasilanol **3b**,[24] suggesting that hydrolysis of both Si_3O_3 rings occurred with complete retention of stereochemistry at Si.

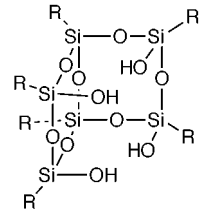

3a R = Cy
b c-C_7H_{13}

Tetrasilanol **3a** can be isolated as a white microcrystalline solid in 63% yield after 1 h at 25 °C. If the reaction is allowed to continue for several hours, ^{29}Si NMR resonances for **3a** are gradually replaced by the characteristic resonances for trisilanol **1b**,[22] which can be isolated in 30–40% yield after the resonances for **3a** disappear.

The base-catalyzed decomposition of **3a** by NEt_4OH in wet THF is not surprising. However, the formation of trisilanol **1b** in good yield is quite remarkable considering that the only Si-containing species present at the start of the reaction contains six Si atoms. This observation suggested the mechanism illustrated in Scheme 1, and it prompted us to examine the reaction of **2** with NEt_4OH in the presence of silane monomers capable of producing reactive $RSi(OH)_3$ fragments faster than the decomposition of **3a**. The results from these experiments confirm our mechanistic hypothesis, and they provide a potentially general route to trisilanols with six cyclohexyl groups and one unique pendant group. For example, the reaction of **2** with aqueous NEt_4OH in the presence of (vinyl)$Si(OMe)_3$ affords trisilanol **1c** in excellent isolated yield.‡ Similar results are observed when aqueous NEt_4OH is added to a solution of **2** and either $[H_2C{=}CH(CH_2)_6Si(OMe)_3$ or *p*-$ClCH_2C_6H_4Si(OMe)_3$.

The structure of **1c** can be unambiguously assigned on the basis of multinuclear NMR spectroscopy data: (i) both the ^{13}C and ^{29}Si NMR data are consistent with a C_s-symmetric

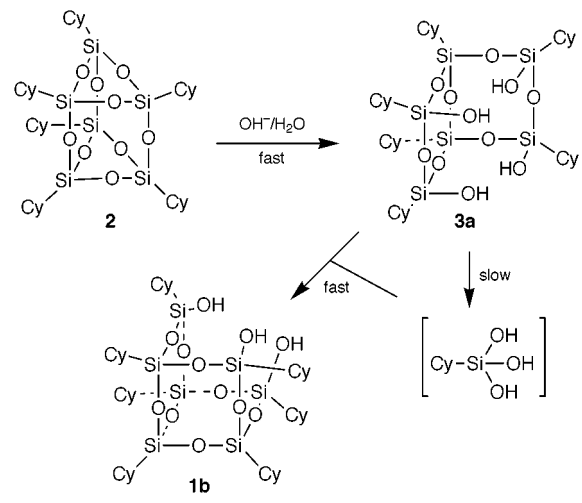

Scheme 1

$Si_7O_9(OH)_3$ framework; (ii) the ^{29}Si NMR spectrum exhibits one downfield resonance characteristic of two CySi(OH) groups in Si_4O_4 rings (δ −60.0 *cf.* δ −68.7 for $Cy_8Si_8O_{12}$) and one upfield resonance assignable to a single (vinyl)Si(OH) group in a Si_4O_4 ring [δ −71.9 *cf.* δ −80.1 for $(vinyl)_8Si_8O_{12}$]; (iii) the ^1H NMR spectrum exhibits resonances for six Cy groups and one vinyl group, as well as a single time-averaged OH resonance at δ 7.01 for the three mutually hydrogen-bonded SiOH groups. ^1H resonances at δ 6–7 for SiOH groups are characteristic of incompletely-condensed silsesquioxanes with three or more mutually hydrogen-bonded Si–OH groups.[22,24–27] It would be difficult to rationalize this feature without structure **1c**. Our assignment of **1c** is also supported by electrospray mass spectrometry data and a preliminary single crystal X-ray diffraction study, which is good enough to establish that **1c** adopts the same hydrogen-bonded dimeric structure observed for other crystallographically characterized $R_7Si_7O_9(OH)_3$ compounds,[20,22] but not good enough to locate all of the carbon atoms on the disordered organic groups.§

We have only begun to explore the scope and generality of these reactions, but it is already clear that base-catalyzed homologation of $R_6Si_6O_9$ will find many applications. From the standpoint of developing new routes to POSS-based hybrid inorganic–organic polymers,[8,28,29] our results with Cy-substituted frameworks provide access to many new synthons for preparing well defined POSS monomers. In fact, our homologation methodology represents an important advance in silsesquioxane chemistry, if it can be generalized to synthesize heteroleptic trisilanols from other $R_6Si_6O_9$ frameworks[30]—especially silylated spherosilicates.[9,31–34] [*e.g.* $(TMSO)_6Si_6O_9$][9,35] For applications such as catalytic epoxidation of olefins by $Cy_7Si_7O_9TiX$ (X = NR_2, OR, Cp),[36,37] the ability to produce trisilanol ligands with reactive pendant groups provides an attractive method for immobilizing the catalyst.[38] We are currently exploring these possibilities and will provide a full account of our work in due course.

These studies were supported by Hybrid Plastics (Fountain Valley, CA) under an Advanced Technologies Program grant from the National Institute of Standards and Technology and the National Science Foundation.

Notes and references

† *Preparation of* **3a**: a solution of $Cy_6Si_6O_9$ (200 mg, 0.24 mmol) and 35% aqueous NEt_4OH (0.1 mL, 0.25 mmol) in THF (2.5 mL) was stirred at 25 °C for 1 h then neutralized with dilute aqueous HCl. Evaporation of the volatiles, dissolution in Et_2O, drying over $MgSO_4$, and concentration afforded **3a** as a white microcrystalline solid in 63% yield (135 mg). $^{29}Si\{^1H\}$ NMR (99.3 MHz, $CDCl_3$, 25 °C) δ −59.4, −68.8 (s, 4:2). ^1H NMR (500 MHz, $CDCl_3$, 25 °C) δ 7.02 (br s, 4 H, OH), 1.78 (vbr m, 30H), 1.28 (vbr m, 30H), 0.81 (vbr m, 6H). $^{13}C\{^1H\}$ NMR (125.8 MHz, $CDCl_3$, 25 °C) δ 27.55, 27.47, 26.86, 26.62 (CH_2); 23.68, 23.16 (4:2, SiCH). MS (ESI, 100% MeOH): *m/z* 846 ($[M + H]^+$, 48%), 869 ($[M + Na]^+$, 95%), 885 ($[M + K]^+$, 100%). Anal. Calc. (found) for $C_{36}H_{70}O_{11}Si_6$: C, 51.02 (51.00); H, 8.33 (8.23)%.

‡ *Preparation of* **1c**: a solution of 35% aqueous NEt_4OH (0.2 mL, 0.50 mmol) was added to a solution of $Cy_6Si_6O_9$ (409 mg, 0.49 mmol) and $(vinyl)Si(OMe)_3$ (0.08 mL, 0.48 mmol) in THF (5 mL). The solution was stirred for 75 min then worked up as described above to afford **1c** as a white microcrystalline solid. The crude product, which is obtained in practically quantitative yield, is > 90% pure by NMR spectroscopy. Colorless crystals were obtained in 23% yield after one recrystallization from toluene–acetonitrile. $^{29}Si\{^1H\}$ NMR (99.3 MHz, $CDCl_3$, 25 °C) δ −60.0 (s, 2 Si, Cy–Si–OH), −68.1 (s, 1 Si), −69.0 (s, 2 Si), −69.6 (s, 1 Si), −71.9 [s, 1 Si, (vinyl)Si–OH]. ^1H NMR (500 MHz, $CDCl_3$, 25 °C) δ 7.01 (br s, 3 H, OH), 5.90 (m, 3 H, –CH=CH_2), 1.75, 1.26, 0.78 (m, 66 H, C_6H_{11}). $^{13}C\{^1H\}$ NMR (125.8 MHz, C_6D_6, 25 °C) δ 135.36 (s, =CH_2), 130.80 (s, –CH=), 27.51, 27.45, 26.81, 26.66, 26.58, 26.54, 26.48 (s, CH_2); 23.81, 23.53, 23.35, 23.09 (s, CH). MS (ESI, 100% MeOH): *m/z* 917 ($[M + H]^+$, 75%), 939 ($[M + Na]^+$, 100%). Anal. Calc. (found) for $C_{38}H_{72}O_{12}Si_7$ C, 49.74 (49.44); H, 7.91 (7.70)%.

§ Trisilanol **1c** crystallizes as well formed but very poorly diffracting crystals from toluene–acetonitrile. *Crystal data* for **1c**: $C_{38}H_{72}O_{12}Si_7$, M = 917.59, orthorhombic, space group *Cmca*, a = 19.179(2), b = 23.530(2), c = 22.519(2) Å, V = 10162.5(18) Å^3, T = 158 K, Z = 8, D_c = 1.199 M g m^{-3}, μ = 0.239 mm^{-1}, $F(000)$ = 3952, λ = 0.71073 Å, crystal dimensions: 0.47 × 0.43 × 0.40 mm, 3.28 ⩽ 2θ ⩽ 56.6°; of the 32677 collected reflections, 6378 are independent and only 1392 (22%) had $I > 2.0\sigma(I)$.

1 M. G. Voronkov and V. Lavrent'ev, *Top. Curr. Chem.*, 1982, **102**, 199.
2 R. H. Baney, M. Itoh, A. Sakakibara and T. Suzuki, *Chem. Rev.*, 1995, **95**, 1409.
3 P. G. Harrison, *J. Organomet. Chem.*, 1997, **542**, 141.
4 D. W. Scott, *J. Am. Chem. Soc.*, 1946, **68**, 356.
5 F. J. Feher and T. A. Budzichowski, *J. Organomet. Chem.*, 1989, **379**, 33.
6 F. J. Feher, D. Soulivong, A. G. Eklund and K. D. Wyndham, *Chem. Commun.*, 1997, 1185.
7 F. J. Feher, K. D. Wyndham, D. Soulivong and F. Nguyen, *J. Chem. Soc., Dalton Trans.*, 1999, 1491.
8 J. J. Schwab and J. D. Lichtenhan, *Appl. Organomet. Chem.*, 1998, **12**, 707.
9 R. Weidner, N. Zeller, B. Deubzer and V. Frey, *US Pat*. 5 047 492, 1991.
10 U. Dittmar, B. J. Hendan, U. Flörke and H. C. Marsmann, *J. Organomet. Chem.*, 1995, **489**, 185.
11 C. Zhang and R. M. Laine, *J. Organomet. Chem.*, 1996, **521**, 199.
12 T. E. Gentle and A. R. Bassindale, *J. Inorg. Organomet. Pol.*, 1995, **5**, 281.
13 S. E. Yucks and K. A. Carrado, *Inorg. Chem.*, 1996, **35**, 261.
14 J. V. Crivello and R. Malik, *J. Polym. Sci., Part A: Polym. Chem.*, 1997, **35**, 407.
15 E. Rikowski and H. C. Marsmann, *Polyhedron*, 1997, **16**, 3357.
16 F. J. Feher, D. Soulivong and G. T. Lewis, *J. Am. Chem. Soc.*, 1997, **119**, 11 323.
17 F. J. Feher, D. Soulivong and A. E. Eklund, *Chem. Commun.*, 1998, 399.
18 F. J. Feher, J. J. Schwab, D. M. Tellers and A. Burstein, *Main Group Chem.*, 1998, **2**, 169.
19 F. J. Feher, F. Nguyen, D. Soulivong and J. W. Ziller, *Chem. Commun.*, 1999, 1705.
20 F. J. Feher, R. Terroba and J. W. Ziller, *Chem. Commun.*, submitted.
21 J. F. Brown and L. H. Vogt, *J. Am. Chem. Soc.*, 1965, **87**, 4313.
22 F. J. Feher, D. A. Newman and J. F. Walzer, *J. Am. Chem. Soc.*, 1989, **111**, 1741.
23 H. Behbehani, B. J. Brisdon, M. F. Mahon and K. C. Molloy, *J. Organomet. Chem.*, 1994, **469**, 19.
24 F. J. Feher, T. A. Budzichowski, R. L. Blanski, K. J. Weller and J. W. Ziller, *Organometallics*, 1991, **10**, 2526.
25 F. J. Feher, J. J. Schwab, D. M. Tellers and A. Burstein, *Main Group Chem.*, 1997, **2**, 169.
26 T. W. Hambley, T. Maschmeyer and A. F. Masters, *Appl. Organomet. Chem.*, 1992, **6**, 253.
27 M. Unno, K. Takada and H. Matsumoto, *Chem. Lett.*, 1998, 489.
28 E. G. Shocky, A. G. Bolf, P. F. Jones, J. J. Schwab, K. P. Chaffee, T. S. Haddad and J. D. Lichtenhan, *Appl. Organomet. Chem.*, 1999, **13**, 311.
29 J. D. Lichtenhan, *Silsesquioxane-Based Polymers* in *Polymeric Materials Encyclopedia*, ed. J. C. Salamone, CRC Press, Inc., New York, 1996, Volume 10, pp. 7768–7778.
30 A. R. Bassindale, T. E. Gentle, J. Hardy, I. MacKinnon, M. Maesano, P. Taylor, A. Watt and Y. Yang, *12th Int. Symp. Organosilicon Chem., Sendai, Japan*, May 1999.
31 P. A. Agaskar, *Inorg. Chem.*, 1990, **29**, 1603.
32 D. Hoebbel, I. Pitsch, T. Reiher, W. Hiller, H. Jancke and D. Muller, *Z. Anorg. Allg. Chem.*, 1989, **576**, 160.
33 I. Hasegawa, *Trends Organomet. Chem.*, 1994, **1**, 131.
34 I. Hasegawa, M. Ishida and S. Motojima, *Synth. React. Inorg. Met.-Org. Chem.*, 1994, **24**, 1099.
35 P. G. Harrison, R. Kannengiesser and C. J. Hall, *Main Group Met. Chem.*, 1997, **20**, 137.
36 M. Crocker, R. H. M. Herold and A. G. Orpen, *Chem. Commun.*, 1997, 2411.
37 H. C. L. Abbenhuis, S. Krijnen and R. A. van Santen, *Chem. Commun.*, 1997, 331.
38 S. Krijnen, H. C. L. Abbenhuis, R. W. J. M. Hanssen, J. H. C. van Hoof and R. A. van Santen, *Angew. Chem., Int. Ed.*, 1998, **37**, 356.

Communication 9/06397H

ChemComm

Diastereoisomerism and inter-metallic electronic communication: synthesis and structural analysis of a fully conjugated macrocyclic exo-ditopic ligand bearing two 2,2′-bipyridine units and of its binuclear osmium diastereoisomers

Jean-Jacques Lagref,[a] Mir Wais Hosseini,*[a] Jean-Marc Planeix,[a] André De Cian[b] and Jean Fischer[b]

[a] *Laboratoire de Chimie de Coordination Organique, Université Louis Pasteur, UMR CNRS 7512, F-67000 Strasbourg, France. E-mail: hosseini@chimie.u-strasbg.fr*

[b] *Laboratoire de Cristallochimie et Chimie Structurale, Université Louis Pasteur, UMR CNRS 7512, F-67000 Strasbourg, France*

Received (in Basel, Switzerland) 16th August 1999, Accepted 16th September 1999

The synthesis of a new macrocyclic exo-ditopic ligand bearing two, 2,2′-bipyridine units interconnected at the 4 and 4′ positions by two –CH=CH– spacers was achieved, and its Os(II) homobinuclear diastereomeric complexes were prepared, separated and characterised in the solid state by X-ray diffraction on single crystals; the two stereoisomers showed almost identical electrochemical and UV–VIS characteristics and rather weak metal–metal interactions.

Inter-metallic electronic communication in di- or poly-nuclear transition metal complexes is currently under active investigation.[1] Often, this challenging problem is further complicated by stereoisomerism which occurs when metals with octahedral coordination geometry and chelating ligands are used.[2] The role of diastereoisomerism on the physical properties of metal complexes has recently been elegantly discussed.[3] The combination of Ru(II) and/or Os(II) and bipyridine containing ligands has been shown to exhibit interesting photochemical and electrochemical properties. In order to study intramolecular short- and long-range electron or energy transfer, a variety of homo- and hetero-bincuclear complexes bearing oligopyridine ligands have been prepared.[3,4]

We believed that compound **1** might be of interest for studying both inter-metallic communication between metal centers through conjugation and the effect of diastereoisomerism on such a process. The design of **1** was based on two 2,2′-bipyridine units doubly interconnected at the 4 and 4′ positions by two π systems (CH=CH). The choice of 4 and 4′ positions for interconnecting the two chelate moieties was based on electronic and geometric reasons. For some time now, we have been involved in the design and synthesis of exo-bis-bidentate ligands based on two 2,2′-bipyridine units interconnected at the 4 and 4′ positions by two alkyl[5] as well as two silyl[6] spacers.

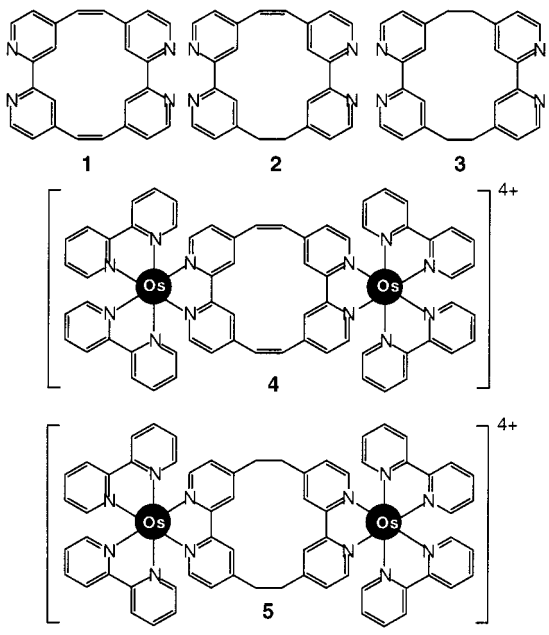

Here, we report the first synthesis and solid state structural analysis of compound **1** and of its binuclear Os(II) diastereoisomeric complexes **4** as well as the redox behavior of separated and structurally characterised *rac*-**4** (Δ,Δ;Λ,Λ) and *meso*-**4** (Δ,Λ) diastereoisomers.

The synthesis of ligand **1** was based on the dehydrogenation of the previously reported compound **3**.[5a] Thus, treatment of **3** with 2.5 equiv. of DDQ[7] in bromobenzene at 132 °C for 20 h, afforded a mixture of the starting material **3** (20%), the partially oxidized compound **2** (10–15%) and the desired compound **1** (30% isolated yield). Attempts to increase the yield by changing the reaction conditions such as the DDQ/**3** ratio, temperature or reaction time failed. Owing to the rather close R_f values for compounds **1**–**3**, the separation had to be performed carefully and was achieved by column chromatography (Al_2O_3, AcOEt–$CHCl_3$–EtOH = 60:39:1). The pure compound **1** was further recrystallised from CH_2Cl_2–hexane. In addition to NMR spectroscopy, compound **1** was also characterised by X-ray diffraction on single crystals.

Using the ligand **1**, the synthesis of binuclear Os(II) diastereomeric complexes **4** with PF_6^- as the counter anion was achieved in 62% yield upon refluxing a mixture of **1** and $Os(2,2'\text{-bipy})_2Cl_2$ in butanol–water (2:1) for 24 h under an argon atmosphere. The dark green solid thus obtained after evaporation was then dissolved in water, and upon addition of KPF_6 and heating at 40 °C for 3 min, the binuclear Os(II) complexes **4** were recovered by filtration as a 4:6 mixture of *meso*- and *rac*-**4** stereoisomers. Diastereoisomeric separation of *rac*- and *meso*-**4** was achieved by column chromatography (Sephadex SP C25, 0.1 M sodium *O*,*O*′-dibenzoyl-L-tartrate in H_2O) following reported procedures.[8] Single crystals of both stereoisomers were obtained after two weeks by the slow diffusion of benzene into a nitromethane solution containing the complex at 6–8 °C. For comparison purposes, homobinuclear Os(II) diastereomeric complexes **5** using the ligand **3** were also prepared and separated.

In the solid state, the structure of *meso*-**4** was studied by X-ray diffraction on a single crystal† (Fig. 1). In addition to *meso*-**4**, $4PF_6^-$, $2C_6H_6$, $2MeNO_2$ and $2H_2O$ molecules were present in the solid state. In marked contrast with the free ligand **3**, both bipy units in the complex adopt a *cisoid* conformation with NCCN dihedral angles of −2 and 4° allowing, as expected, the chelation of Os(II) cations. The macrocycle is not planar but rather adopts a bent conformation with CCCC dihedral angles around the ethylene spacers of 3.9 and 7.6°. For both Os(II) centers, the coordination sphere is composed of six nitrogen atoms amongst which four are belonging to the two auxiliary bipy units, and the remaining two are part of the macrocyclic ligand **1**. The coordination geometry around each Os(II) was

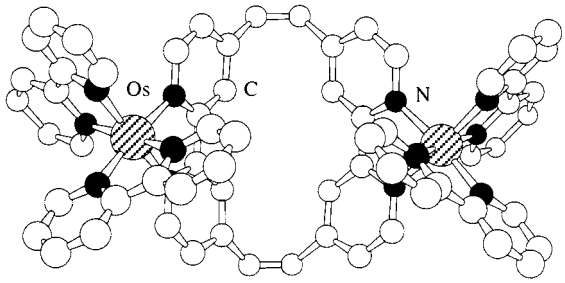

Fig. 1 X-Ray crystal structure of the *meso*-**4** Os(II) binuclear complex obtained with ligand **1**. For the sake of clarity, anions, solvent molecules and H atoms are not represented (for distances and angles see text).

almost octahedral with an average Os–N distance of *ca.* 2.05 Å. The two Os(II) centres are separated by a distance of 9.368 Å.

The structure of *rac*-**4** was also studied by X-ray diffraction on a single crystal† (Fig. 2). In this case, in addition to *rac*-**4**, $4PF_6^-$, C_6H_6 and $2MeNO_2$ molecules were found to be present in the crystal. As before, both bipy units in the complex adopt a *cisoid* conformation with NCCN dihedral angles of −9.4 allowing the coordination of Os(II) cations in the chelate mode. The macrocycle is again not planar but adopts a bent shape with a CCCC dihedral angle around the ethylene spacers of 4.7°. Again, both Os(II) centers are coordinated to six nitrogen atoms with an average Os–N distance of *ca.* 2.05 Å and in almost octahedral geometry. Interestingly, the two Os(II) centers are separated by a distance of 8.177 Å.

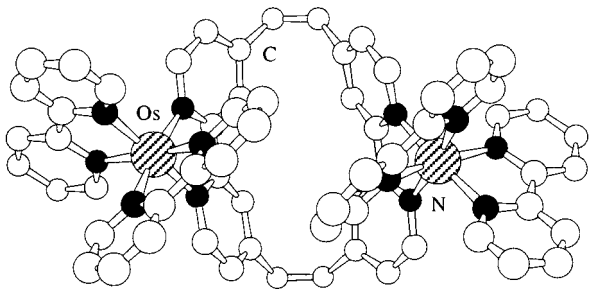

Fig. 2 X-Ray structure of the *rac*-**4** Os(II) binuclear complex obtained with ligand **1**. For the sake of clarity, anions, solvent molecules and H atoms are not represented (for distances and angles see text).

The electrochemical behaviour of *meso*-**4**, *rac*-**4** and **5** as a mixture of stereoisomers was studied by cyclic voltametry (CV) at 1 mM concentration under argon (MeCN, 25 °C, 0.1 M NBu_4PF_6, Pt disk, ferrocene as internal reference, potential values are given with respect to SCE). Although the Os–Os distances for the *meso*-**4** (9.368 Å) and the *rac*-**4** (8.177 Å) stereoisomers are substantially different, for both complexes, only one reversible di-electronic oxidative wave at 0.84 and 0.87 V were observed, respectively. For **5** also a single wave was observed at 0.83 V. Attempts to separate the observed waves into two mono-electronic components using differential pulsed voltametry were unsuccessful. Interestingly, the ΔE_p values of 90 and 88 mV observed for *meso*- and *rac*-**4**, respectively, were significantly higher than the ΔE_p of 70 mV obtained for **5** or the expected value of 59 mV for a reversible process. This observation indicates a weak but nevertheless existing electronic communication between the two Os(II) centers. The rather weak nature of the communication may be rationalised on the basis of structural information obtained in the solid state. Indeed, because of the strength imposed by the rather short spacers that leads to the bent conformation of the macrocyclic portion of ligand **1** in the complexes **4**, the conjugation between the two bipyridine units through the ethylene bridges may be significantly weakened.

In conclusion, using the conjugated macrocyclic exo-ligand **1** based on the interconnection of two 2,2′-bipyridine units by two ethylene spacers at the 4 and 4′ positions, two diastereoisomeric binuclear Os(II) complexes **4** were synthesised, separated and structurally characterised in the crystalline phase. Both *meso*- and *rac*-**4** isomers showed identical electrochemical characteristics and rather weak metal–metal interactions. The photochemical behaviour of both **4** and **5** as well as their heterobinuclear Ru(II)Os(II) complexes are under current investigation. The formation of coordination networks using compound **1** is also currently under study.

We thank the CNRS and the Institut Universitaire de France (IUF) for financial support.

Notes and references

† *meso*-**4** (brown crystals, 173 K): $C_{64}H_{48}N_{12}Os_2{\cdot}4PF_6{\cdot}2C_6H_6{\cdot}2CH_3NO_2{\cdot}2H_2O$, M = 2259.78, triclinic, space group $P\bar{1}$, a = 15.9680(4), b = 15.8640(9), c = 20.9420(7) Å, α = 80.74(3), β = 67.57(3), γ = 77.10(2), U = 4762.9(5) Å^3, Z = 2, D_c = 1.58 g cm^{-3}, Mo-Kα radiation, KappaCCD, μ = 2.834 mm^{-1}, 13822 data with $I > 3\sigma(I)$, R = 0.061, R_w = 0.076.

rac-**4** (brown crystals, 173 K): $C_{64}H_{48}N_{12}Os_2{\cdot}4PF_6{\cdot}C_6H_6{\cdot}2CH_3NO_2$, M = 2145.63, orthorhombic, space group *Pbcn*, a = 26.3232(7), b = 13.9495(2), c = 21.4335(7) Å, U = 7870.3(6) Å^3, Z = 4, D_c = 1.81 g cm^{-3}, Mo-Kα radiation, KappaCCD, μ = 3.423 mm^{-1}, 7843 data with $I > 3\sigma(I)$, R = 0.031, R_w = 0.053. CCDC 182/1419.

1 V. Balzani, A. Juris, M. Venturi, S. Campagna and S. Serroni, *Chem. Rev.*, 1996, **96**, 759.
2 U. Knof and A. von Zelewski, *Angew. Chem., Int. Ed.*, 1999, **38**, 302.
3 F. R. Keene, *Coord. Chem. Rev.*, 1997, **166**, 121.
4 K. Wärnmark, P. N. W. Baxter and J.-M. Lehn, *Chem. Commun.*, 1998, 993; R. Ziessel, M. Hissler, A. El-ghayoury and A. Harriman, *Coord. Chem. Rev.*, 1998, **178**–**180**, 1251; S. Campagna, S. Serroni, S. Bodige and F. M. MacDonnell, *Inorg. Chem.*, 1999, **38**, 692.
5 (*a*) C. Kaes, M. W. Hosseini, R. Ruppert, A. De Cian and J. Fischer, *J. Chem. Soc., Chem. Commun.*, 1995, 1445; (*b*) C. Kaes, M. W. Hosseini, A. De Cian and J. Fischer, *Tetrahedron Lett.*, 1997, **38**, 3901; (*c*) C. Kaes, M. W. Hosseini, A. De Cian and J. Fischer, *Tetrahedron Lett.*, 1997, **38**, 4389; C. Kaes, M. W. Hosseini, C. E. F. Rickard, B. W. Skelton and A. H. White, *Angew. Chem., Int. Ed.*, 1998, **37**, 920.
6 C. Kaes, M. W. Hosseini, R. Ruppert, A. De Cian and J. Fischer, *Tetrahedron Lett.*, 1994, **35**, 7233; C. Kaes, M. W. Hosseini, A. De Cian and J. Fischer, *Chem. Commun.*, 1997, 2290.
7 D. Walker and J. D. Hiebert, *J. Chem. Soc.*, 1966, 153.
8 T. J. Rutherford, O. Van Gijte, A. Kirsch-De Mesmaeker and F. R. Keene, *Inorg. Chem.*, 1997, **36**, 4465.

Communication 9/06651I

ChemComm

The first observation of a muonium–carbonyl adduct with a negative muon coupling constant

Christopher J. Rhodes,*[a] Ivan D. Reid[b] and Roderick M. Macrae[c]

[a] *School of Pharmacy and Chemistry, Liverpool John Moores University, Byrom St., Liverpool, UK L3 3AF. E-mail: PACCRHOD@livjm.ac.uk*
[b] *Muon Spectroscopy Group, Paul Scherrer Institut, CH-3057 Villigen, Switzerland*
[c] *The Institute of Physical and Chemical Research (RIKEN), 2-1 Hirosawa, Wako, Saitama 351-01, Japan*

Received (in Cambridge, UK) 12th July 1999, Accepted 16th September 1999

Muonium atom addition to cyclopent-4-ene-1,3-dione I leads to the adduct radical II; in contrast with all other muonium adducts of carbonyl (C=O) compounds so far studied, in which the isotropic muon coupling is of positive sign, the temperature dependence of the muon coupling in II reveals that its sign is negative; this may be explained as a consequence of the electronic 'push–pull' interaction within the MuO–C–C=C–C=O system, which reduces the out-of-plane vibrational amplitude of the muon by increasing the MuO–C/MuO=C partial π-bond character.

There have been a number of studies[1–12] made of free radicals formed by addition of the light hydrogen isotope, muonium (a hydrogen atom with a positive muon as its nucleus) to compounds containing a single carbonyl (C=O) group, which include aldehydes, ketones, esters and amides. All these radicals possess the common structural feature of a muonium atom which is bound close to the radical plane (C$^{\bullet}$–O–Mu), but which can make vibronic (out-of-plane) excursions from it: the observed coupling is now a compromise between two contributions; one providing negative spin density in the muonium 1s orbital, arising from spin polarisation of the O–Mu bond by spin density at the oxygen atom, and the second, which is a positive transfer of spin density to the muon, as the out-of-plane vibration permits a degree of overlap with the spin bearing formal carbon $2p_z$ orbital. This may be expressed by, $A(\mathrm{Mu}) = B_0 + B_1 \cdot f(T)$, with B_0 being of negative sign.

In consequence, the muon couplings measured in carbonyl adducts are all small (which contrasts the large, positive, values normally found in carbon centred radicals[13,14]), and in all examples so far investigated are of positive sign, as deduced from the fact that the couplings all increase with increasing temperature,[1,2] and so the positive term $B_1 \cdot f(T)$ is dominant.

Recently,[1] we reported a theoretical study of the muonium adduct of a 1,2-dicarbonyl compound (biacetyl, MeCOCOMe), which aimed to explain its extremely small experimental coupling of 1.9 MHz (at 294 K), but were unable to decide entirely between the possible effects (i) and (ii) mentioned below, and now appeal to experimental evidence. To this end, we have measured the temperature dependence of the isotropic muon coupling (Table 1) which is positive, and therefore shows[1,2] that the sign of the coupling is also positive; so although the two contributions are now almost equal, the transfer of positive spin density still wins, but the very low value of the coupling means that the muon is more closely confined to the radical plane than in all cases of radicals derived from a *single* carbonyl group. The presence of the second C=O group, therefore, has a profound effect on the electronic structure of the radical. There are two possible reasons for this: (i) the adduct has adopted an s-*cis* geometry, with an intramolecular hydrogen (Mu) bond between the two oxygen atoms (**III**); (ii) the s-*trans* conformation of the parent biacetyl molecule is preserved, but the electronic 'push–pull' character of the Mu–O–C–C=O system confines the muon by increasing the O–C/O=C π-bond character of the Mu–O–C unit (it is this which determines the potential barrier to the out-of-plane excursion of the bound muon[1,2]).

Table 1 Temperature dependences of the muon coupling in the adduct radicals formed from cyclopent-4-ene-1,3-dione **I**[a] and biacetyl[b]

Coupling[a]/ MHz	*T*/K	Coupling[b]/ MHz	*T*/K
5.42	242	1.64	284
4.68	255	1.90	294
4.16	265	2.06	297
3.40	275	2.29	303
2.83	285	4.45	323
2.26	299	5.65	335
1.81	303		
1.58	308		

In order to examine the influence of a potential 'through-bond', π-electronic effect, in the absence of intramolecular hydrogen bonding, we chose a dicarbonyl substrate, cyclopent-4-ene-1,3-dione **I**, in which the carbonyl groups are in communication *via* a C=C bond, but are fixed mutually *trans* by the bridging methylene group, so that intramolecular H(Mu)-bonding is impossible.

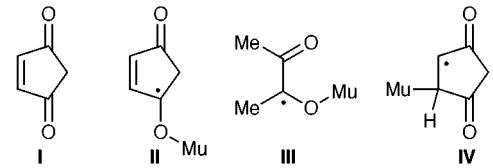

Two radicals were detected using the transverse-field muon spin rotation (TF-MuSR) method[13,15] (Fig. 1): the desired carbonyl adduct **II**, for which the coupling measured as a function of temperature is shown in Table 1, and the C=C adduct **IV** with a coupling of 384 MHz measured at 299 K; the relative yields are 0.35 (C=O) and 0.65 (C=C).

It is quite clear that the coupling decreases in absolute magnitude as the temperature increases—the first example of such behaviour for a muonium/carbonyl adduct. Since the out-of-plane vibrational amplitude of the muon increases on heating, and so the interaction with positive spin density must also increase, the overall muon hyperfine coupling constant must be of *negative* sign (the term B_0 being dominant), becoming more positive at the higher temperature. This means that the O=C π-bond character of the Mu–O–C group can be significantly enhanced by the electronic effect alone, and so an intramolecular hydrogen bond is not required to explain the unexpectedly small coupling either in this or in the biacetyl/muonium adduct; indeed, the effect is greatest in the present example, probably owing to its more extensive conjugation.

This electronic system, which is unusual for a free radical, is now the subject of calculations at various levels of theory in an effort to probe their relative application in the elucidation of

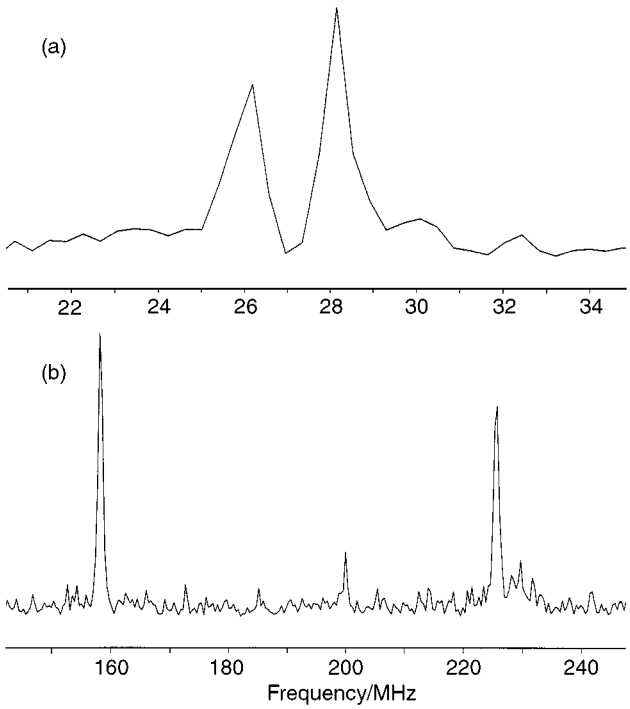

Fig. 1 Transverse-field MuSR spectrum of radicals formed by muonium atom addition to **I** at 299 K, the low-frequency region (a) corresponding to **II** while that (b) at much higher frequencies corresponds to **IV**.

detailed electronic and vibrational effects in organic free radicals.

We thank the Leverhulme Trust, RIKEN and the Paul Scherrer Institut for grants in support of this work.

Notes and references

1 R. M. Macrae, C. J. Rhodes, K. Nishiyama and K. Nagamine, *Chem. Phys. Lett.*, 1996, **259**, 103.
2 C. J. Rhodes and M. C. R. Symons, *Magn. Reson. Chem.*, 1996, **34**, 631.
3 D. Buttar, R. M. Macrae, B. C. Webster and E. Roduner, *J. Chem. Soc. Faraday Trans.*, 1990, **86**, 220.
4 R. M. Macrae, B. C. Webster and E. Roduner, *Muon Studies in Solid State Physics*, IOP Short Meetings no. 22, 1988, p. 95.
5 A. Hill, S. F. J. Cox, R. de Renzi, C. Bucci, A. Vecli and M. C. R. Symons, *Hyperfine Interact.*, 1984, **17**–**19**, 815.
6 S. F. J. Cox, D. A. Geeson, C. J. Rhodes, E. Roduner, C. A. Scott and M. C. R. Symons, *Hyperfine Interact.*, 1986, **32**, 763.
7 K. Venkateswaran, R. F. Kiefl, M. V. Barnabas, J. M. Stadlbauer, B. W. Ng, Z. Wu and D. C. Walker, *Chem. Phys. Lett.*, 1988, **145**, 289.
8 M. Heming, E. Roduner, B. D. Patterson, W. Odermatt, J. Schneider, H. Baumeler, H. Keller and I. M. Savic, *Chem. Phys. Lett.*, 1986, **128**, 100.
9 D. Buttar, R. M. Macrae, B. C. Webster and E. Roduner, *Hyperfine Interact.*, 1990, **65**, 927.
10 G. M. Aston, J. A. Stride, U. A. Jayasooria and I. D. Reid, *Hyperfine Interact.*, 1997, **106**, 157.
11 C. J. Rhodes, C. S. Hinds and I. D. Reid, *J. Chem. Soc., Faraday Trans.*, 1996, **92**, 4265.
12 C. J. Rhodes, I. D. Reid and R. A. Jackson, *Hyperfine Interact.*, 1997, **106**, 193.
13 D. C. Walker, *Muon and Muonium Chemistry*, Cambridge University Press, Cambridge, 1983.
14 There is but one example of a carbon centred radical with a negative muon coupling, $Me_3SiCHMu\cdot$, which arises from the unique α-position of the muon which, therefore, receives spin density from spin-polarisation of the C–Mu bond; B. Addison-Jones, P. W. Percival, J.-C. Brodovitch and F. Ji, *Hyperfine Interact.*, 1997, **106**, 143.
15 E. Roduner, *The positive muon as a probe in free radical chemistry. Potential and limitations of the μSR techniques*, Lecture notes in chemistry, vol. 49. Heidelberg, Springer, 1988.

Communication 9/05636J

ChemComm

The structural characterisation of $Ph_3PSe(Ph)I$. The first charge transfer (CT) complex of a tertiary phosphine containing a pseudohalogen

Philip D. Boyle, Stephen M. Godfrey,* Charles A. McAuliffe, Robin G. Pritchard and Joanne M. Sheffield

Department of Chemistry, University of Manchester Institute of Science and Technology, Manchester M60 1QD. E-mail: stephen.m.godfrey@umist.ac.uk

Received (in Basel, Switzerland) 26th July 1999, Accepted 6th September 1999

The reaction of 2 mol equivalents of triphenylphosphine with diphenyldiselenyldiiodine ($Ph_2Se_2I_2$) produces the charge transfer (CT) complex $Ph_3PSe(Ph)I$ in quantitative yield; this compound represents the first report of a CT complex of a tertiary phosphine that contains a pseudohalogen.

The ability of organic molecules that contain a group 15 or 16 donor atom to form charge transfer (CT) complexes with dihalogens or interhalogens has long been recognised,[1] however, it is only relatively recently that such complexes have been crystallographically characterised. The structural identification of these materials has now proved to be a topical area with several research groups currently involved in investigating a variety of these materials that have shown remarkable diversity in their solid-state structure. Thus, the dihalogen adducts of tertiary phosphines,[2–6] arsines,[7] stibines,[8] tertiary phosphine sulfides,[9–11] selenides,[12,13] diorgano sulfides[14] and selenides[15,16] and selenoamides[17,18] have all received considerable study. In addition, very recently the CT complexes of cyclic thioethers with I_2 and IBr have been extensively studied by Schröder and coworkers.[19–21] Generally speaking, adducts of diiodine or IX (X = Br, Cl) are CT compounds which contain an approximately linear E–I–X arrangement (E = P, As, S, Se) whereas adducts of the lighter dihalogens usually produce an X–E–X arrangement with the E atom in trigonal bipyramidal, disphenoidal see-saw or T-shaped geometry depending on the E atom and the organic substituents, although some exceptions to this rule have been identified. Despite the ongoing interest in these dihalogen adducts, very little is known regarding the pseudohalogen adducts of these donor molecules, despite the fact that the solid-state structures of such systems are likely to be quite different to the dihalogen analogues owing to electronic and especially steric factors. We have recently reported[22] that reaction of R_3P with XCN results in the formation of ionic compounds $[R_3PCN]X$ [R = 2,4,6-$(MeO)_3C_6H_2$, 2,6-$(MeO)_2C_6H_3$, $NCCH_2CH_2$, C_6H_{11} or $PhCH_2$; X = Br or I] which display no cation–anion interaction regardless of the nature of R or X. In order to establish the identity of a CT complex of a tertiary phosphine adduct containing both halide and pseudohalide moieties, we have turned our attention to the reaction of 2 mol equivalents of triphenylphosphine with diphenyldiselenyl diiodide. The very interesting structure of $Ph_2Se_2I_2$, itself a CT adduct, has been described by du Mont and coworkers[23] and consists of a dimeric centrosymmetric moiety containing short [2.775(1) Å] and long [3.588(1) Å] iodine–iodine distances. $Ph_2Se_2I_2$ was reacted with 2 mol equivalents of Ph_3P in dichloromethane according to eqn. (1).

$$2\,Ph_3P + Ph_2Se_2I_2 \xrightarrow[N_2(g),\ \text{room temp.}]{ca.\ 1\ d,\ CH_2Cl_2} Ph_3PSe(Ph)I \qquad (1)$$

Triphenylphosphine reacts very rapidly with $Ph_2Se_2I_2$, this being evident from the dramatic colour change in the reaction vessel (from the deep burgundy of $Ph_2Se_2I_2$ to bright yellow upon addition of Ph_3P). Nevertheless, the reaction mixture was allowed to stir for *ca.* 1 d to ensure reaction completion. The resultant compound, $Ph_3PSe(Ph)I$, was isolated in quantitative yield. Recrystallisation of this bright yellow powder from dichloromethane–diethyl ether solution (*ca.* 1:1) produced a large quantity of well formed crystals, one of which was selected for analysis by single crystal X-ray diffraction. The crystal structure of $Ph_3PSe(Ph)I{\cdot}CH_2Cl_2$ is illustrated in Fig. 1 (the dichloromethane solvate molecule is omitted for clarity). This compound is clearly shown to adopt a CT structure analogous to triphenylphosphine diiodine, $Ph_3P–I–I$. The *d*(Se–I) in $Ph_3PSe(Ph)I$, 3.2564(5) Å, lies well within the van der Waals' radius for the iodine and selenium atoms (4.1 Å) and is similar to *d*(I–I) in Ph_3PI_2, 3.142(2) Å,[2] and significantly shorter than *d*(I–I) in $PhMe_2PI_2$, 3.408(2) Å.[24] There are no non-bonded long-range contacts between $Ph_3PSe(Ph)I$ and the dichloromethane solvate molecule (which shows no sign of disorder) or between $Ph_3PSe(Ph)I$ and an adjacent molecule.

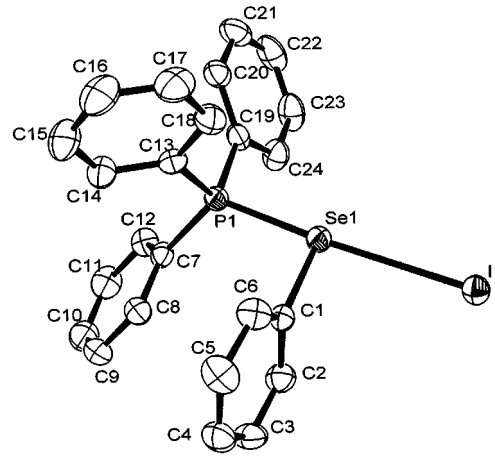

Fig. 1 Perspective view of the molecular structure of $Ph_3PSe(Ph)I$. Selected bond lengths (Å) and angles (°): Se(1)–I(1) 3.2564(5), Se(1)–P(1) 2.2585(9), Se(1)–C(1) 1.921(3), C(1)–Se(1)–P(1) 93.59(9), P(1)–Se(1)–I(1) 176.09(5), C(1)–Se(1)–I(1), 88.84(5).

There is great similarity between Ph_3PI_2 and $Ph_3PSe(Ph)I$ in the $^{31}P\{^1H\}$ NMR spectra of the two materials. We have previously reported that $Ph_3PI–I$ ionises in $CDCl_3$ to produce the ionic $[Ph_3PI]I$ (δ 44). Remarkably, the $^{31}P\{^1H\}$ NMR spectrum of $Ph_3PSe(Ph)I$ in CD_2Cl_2 shows a single peak at δ 44 *i.e.* identical to that observed for $[Ph_3PI]I$. No phosphorus–selenium coupling constant was obtained from this spectrum; however, $^1J(^{13}C–^{31}P)$ = 111 Hz. This preliminary NMR data would seem to suggest, therefore, that either (a) $[Ph_3PI]^+$ and $Ph_3PSe(Ph)I$ are electronically very similar, or (b) in solution $Ph_3PSe(Ph)I$ exists as $[Ph_3PI][SePh]$. The absence of P–Se coupling seems to suggest that the latter option is correct; our investigations into the structure of $Ph_3PSe(Ph)I$ in solution are continuing and will be discussed in detail in a full report of this work. The solid-state CT nature of $Ph_3PSe(Ph)I$ is confirmed by the geometry at the selenium centre which is T-shaped [P(1)–Se(1)–C(1) 93.59(5)°, P(1)–Se(1)–I(1) 176.09(5)°, C(1)–Se(1)–I(1) 88.84(5)°] and not bent, as would be expected for an ionic compound. The *d*(P–Se) of 2.2585(9) Å lies within the range

expected for a P–Se single bond and is very similar to the *d*(P–Se) we have previously observed for T-shaped dibromine adducts of tertiary phosphine selenides [*e.g.* *d*(P–Se) for $(Me_2N)_3PSeBr_2$ = 2.262(2) Å].[13] No compound of formula $R_3PSe(R)X$ has previously been reported. However, the related ionic compound $[Ph_3PSeMe][ClO_4]$ has been described by Jones and Thöne[25] and exhibits a P–Se–C bond angle of 97°, closer to that expected for bent geometry at the selenium centre. As previously stated, $Ph_3PSe(Ph)I$ represents the first reported CT complex of a tertiary phosphine which contains a pseudohalogen and we are currently investigating whether this compound is able to oxidise crude metal powders analogous to our previous studies concerning R_3PI_2. Our results will form the basis of a forthcoming paper.

We would like to thank the EPSRC for a research studentship to P. D. B.

Notes and references

† *Crystal data* for $C_{25}H_{22}Cl_2IPSe$: M = 630.16, triclinic, space group $P\bar{1}$ (no. 2), a = 9.2713(11), b = 10.329(3), c = 13.245(2) Å, α = 91.77(2), β = 93.31(1), γ = 95.35(1)°, U = 1259.9(4) Å^3, T = 203 K, Z = 2, μ(Mo-Kα) = 30.01 cm^{-1}, 4714 reflections measured, 4411 unique (R_{int} = 0.0108) which were all used in calculations. The final $wR(F^2)$ was 0.0543 (all data). Single crystals of $Ph_3PSe(Ph)I$ were recrystallised from diethyl ether–dichloromethane solution (1 : 1) at *ca.* 50 °C. On cooling to RT a large crop of yellow crystals appeared after *ca.* 3 d. A chosen crystal was mounted in inert oil and transferred to the cold N_2 gas stream of the diffractometer. The structure was solved using direct methods and refined by full-matrix least squares on F^2.

CCDC 182/1400. See http://www.rsc.org/suppdata/cc/1999/2159/ for crystallographic files in .cif format.

1 F. A. Cotton and G. Wilkinson, *Advanced Inorganic Chemistry*, Wiley Interscience, New York, 5th edn., 1990, ch. 14, p. 549.
2 N. Bricklebank, S. M. Godfrey, C. A. McAuliffe, R. G. Pritchard and P. J. Kobryn, *J. Chem. Soc., Dalton Trans.*, 1993, 101.
3 W. W. du Mont, M. Bätcher, S. Pohl and W. Saak, *Angew. Chem., Int. Ed. Engl.*, 1987, **26**, 912.
4 S. M. Godfrey, C. A. McAuliffe, I. Mushtaq, R. G. Pritchard and J. M. Sheffield, *J. Chem. Soc., Dalton Trans.*, 1998, 3815.
5 S. M. Godfrey, C. A. McAuliffe, R. G. Pritchard, J. M. Sheffield and G. M. Thompson, *J. Chem. Soc., Dalton Trans.*, 1997, 4823.
6 F. Ruthe, W. W. du Mont and P. G. Jones, *Chem. Commun.*, 1997, 1947.
7 N. Bricklebank, S. M. Godfrey, H. P. Lane, C. A. McAuliffe, R. G. Pritchard and J. M. Moreno, *J. Chem. Soc., Dalton Trans.*, 1995, 3873.
8 N. Bricklebank, S. M. Godfrey, H. P. Lane, C. A. McAuliffe and R. G. Pritchard, *J. Chem. Soc., Dalton Trans.*, 1994, 1694.
9 D. C. Apperley, N. Bricklebank, S. L. Burns, D. E. Hibbs, M. B. Hursthouse and K. M. Abdul Malik, *J. Chem. Soc., Dalton Trans.*, 1998, 1289.
10 W. I. Cross, S. M. Godfrey, S. L. Jackson, C. A. McAuliffe and R. G. Pritchard, *J. Chem. Soc., Dalton Trans.*, 1999, 2225.
11 M. Arca, F. A. Devillanova, A. Garau, F. Isaia, V. Lippolis, G. Verani and F. Demartin, *Z. Anorg. Allg. Chem.*, 1998, **624**, 745.
12 S. M. Godfrey, S. L. Jackson, C. A. McAuliffe and R. G. Pritchard, *J. Chem. Soc., Dalton Trans.*, 1996, 4499.
13 S. M. Godfrey, S. L. Jackson, C. A. McAuliffe and R. G. Pritchard, *J. Chem. Soc., Dalton Trans.*, 1998, 4201.
14 B. Regelmann, K. W. Klinkhammer and A. Schmidt, *Z. Anorg. Allg. Chem.*, 1997, **623**, 1633.
15 S. M. Godfrey, C. A. McAuliffe, R. G. Pritchard and S. Sarwar, *J. Chem. Soc., Dalton Trans.*, 1997, 1031.
16 S. M. Godfrey, C. A. McAuliffe, R. G. Pritchard and S. Sarwar, *J. Chem. Soc., Dalton Trans.*, 1997, 3504.
17 F. Bigoli, A. M. Pellinghelli, P. Deplano, F. A. Devillanova, V. Lippolis, M. L. Mecuri and E. F. Trogu, *Gazz. Chim. Ital.*, 1994, **124**, 445.
18 F. Cristiani, F. Demartin, F. A. Devillanova, F. Isaia, V. Lippolis and G. Verani, *Inorg. Chem.*, 1994, **33**, 6315.
19 A. J. Blake, F. Cristiani, F. A. Devillanova, A. Garau, L. M. Gilby, R. O. Gould, F. Isaia, V. Lippolis, S. Parsons, C. Radek and M. Schröder, *J. Chem. Soc., Dalton Trans.*, 1997, 1337.
20 A. J. Blake, F. Cristiani, F. A. Devillanova, A. Garau, L. M. Gilby, R. O. Gould, F. Isaia, V. Lippolis, S. Parsons, C. Radek and M. Schröder, *J. Chem. Soc., Dalton Trans.*, 1998, 2037.
21 A. J. Blake, F. Cristiani, F. A. Devillanova, A. Garau, F. Isaia, V. Lippolis, S. Parsons and M. Schröder, *J. Chem. Soc., Dalton Trans.*, 1999, 525.
22 S. M. Godfrey, C. A. McAuliffe, R. G. Pritchard and J. M. Sheffield, *J. Chem. Soc., Dalton Trans.*, 1998, 1919.
23 S. Kubiniok, W. W. du Mont, S. Pohl and W. Saak, *Angew. Chem., Int. Ed. Engl.*, 1987, **27**, 431.
24 N. Bricklebank, S. M. Godfrey, H. P. Lane, C. A. McAuliffe, R. G. Pritchard and J. M. Moreno, *J. Chem. Soc., Dalton Trans.*, 1995, 2421.
25 P. G. Jones and C. Thöne, *Z. Kristallogr.*, 1994, **209**, 78.

Communication 9/06039A

Resonance Raman evidence for the interconversion between an $[Fe^{III}–\eta^1\text{-}OOH]^{2+}$ and $[Fe^{III}–\eta^2\text{-}O_2]^+$ species and mechanistic implications thereof

Raymond Y. N. Ho,[a] Gerard Roelfes,[b] Roel Hermant,[c] Ronald Hage,[c] Ben L. Feringa*[b] and Lawrence Que, Jr.*[a]

[a] *Department of Chemistry and Center for Metals in Biocatalysis, University of Minnesota, Minnesota 55455, United States of America. E-mail: que@chem.umn.edu*

[b] *Department of Organic and Molecular Inorganic Chemistry, University of Groningen, Nijenborgh 4, 9747 AG Groningen, The Netherlands. E-mail: feringa@chem.rug.nl*

[c] *Unilever Research Laboratory, Olivier van Noortlaan 120, 3133 AT Vlaardingen, The Netherlands.*

Received (in Bloomington, IN, USA) 8th July 1999, Accepted 21st September 1999

The deprotonation of $[Fe^{III}(N4Py)(\eta^1\text{-}OOH)]^{2+}$ 1 gives $[Fe^{III}(N4Py)(\eta^2\text{-}OO)]^+$ 2, as unequivocally demonstrated by resonance Raman spectroscopy, and leads to the loss of alkane hydroxylation activity by 1.

Iron–peroxo species have been established or postulated in the chemistry of dioxygen activation at mononuclear iron centres in biology.[1,2] For example, activated BLM,† the form of the antitumor drug bleomycin responsible for its DNA cleavage activity,[3,4] is formulated as a low spin $Fe^{III}–\eta^1$-OOH species.[5] Similarly, an $Fe^{III}–\eta^1$-OOH moiety is strongly implicated in the mechanism of cytochrome P450 and considered the key intermediate immediately prior to the cleavage of the O–O bond to generate the high valent iron–oxo oxidant.[6] Both $Fe^{III}–\eta^1$-OOH species are proposed to derive from the one-electron reduction of oxy adducts ($[Fe–O_2]^{2+}$) and subsequent protonation, possibly *via* an $[Fe^{III}–\eta^2\text{-}O_2]^+$ species. Such $[Fe^{III}–\eta^2\text{-}O_2]^+$ species are also postulated to be the source of nucleophilic peroxides that are implicated in substrate oxidations by heme enzymes such as aromatase[7] and heme oxygenase.[8] A related $[Fe^{III}–\eta^2\text{-}O_2]^+$ species has been suggested to account for the *cis*-dihydroxylation chemistry of the Rieske dioxygenases.[9] Significant effort has been devoted in the characterisation of small molecule analogues of such peroxo intermediates. Two high spin $[Fe^{III}–\eta^2\text{-}O_2]^+$ species, namely $[Fe^{III}(EDTA)(O_2{}^{2-})]$[10,11] and $[Fe(porphyrin)O_2]^-$,[12] have been identified, while the first examples of synthetic $Fe^{III}–\eta^1$-OOH species have just appeared in the last few years.[13–15] We have sought to establish a precedent for the interconversion between an $[Fe^{III}OOH]^{2+}$ species and its deprotonated form $[Fe^{III}O_2]^+$, implicit in the mechanisms of bleomycin and cytochrome P450. Such an equilibrium was recently reported for Fe^{III}(N-R-trispicen) complexes (R = Me, Et, Bn),[16] but no Raman data was provided to establish the binding mode of the $[Fe^{III}O_2]^+$ species. Here, we provide unequivocal Raman evidence for the η^2-peroxo binding in the $[Fe^{III}(N4Py)O_2]^+$ species, obtained from the deprotonation of the $[Fe^{III}(N4Py)(\eta^1\text{-}OOH)]^{2+}$ species. In addition we show for the first time that protonation of the $[Fe^{III}O_2]^+$ species is essential for alkane oxidation.

The purple $[Fe^{III}(N4Py)(OOH)]^{2+}$ complex **1** (λ_{max} 547 nm, ε_M 1300 dm^3 mol^{-1} cm^{-1}) is generated at −20 °C by addition of 5 equiv. H_2O_2 to a methanolic solution of $[Fe^{III}$(N-4Py)(OMe)$]^{2+}$, obtained by pretreating $[Fe^{II}(N4Py)(MeCN)]^{2+}$ with 5 equiv. H_2O_2 at room temperature.[15] Upon addition of 5 equiv. NH_3 (aq) at −45 °C, the purple chromophore converts to a blue species **2** (Scheme 1) with an absorption maximum at 685 nm (ε_M 520 dm^3 mol^{-1} cm^{-1}). Addition of perchloric acid reverses this colour change and quantitatively regenerates the original purple solution. The conversion of **1** to **2** can also be monitored by EPR spectroscopy. Addition of base converts the characteristic low-spin Fe^{III} EPR spectrum of **1** with *g* values at 2.3, 2.1 and 1.9 to one with an intense isotropic signal at g = 4.3, which is typical of a mononuclear rhombic high-spin Fe^{III} center (E/D = 1/3). In the case of the Fe^{III}(N-R-trispicen) complexes, the addition of base to the Fe^{III}–OOH species converts them to high-spin Fe^{III} complexes with more axial EPR spectra ($E/D \approx 0.08$).[16]

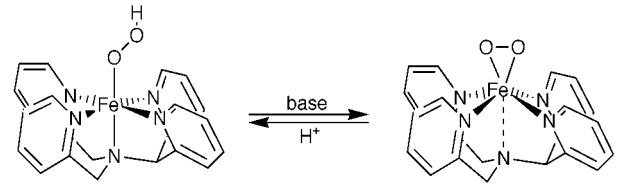

1 2

Scheme 1 Proposed structures for **1** and **2**.

Electrospray ionisation mass spectrometry provides the elemental composition of **2**. As reported earlier, the ESMS of **1** shows a prominent feature at *m*/*z* 555, whose mass and isotope distribution pattern unequivocally assigns this ion as {[Fe(N-4Py)(OOH)]ClO_4}$^+$.[13a] The ESMS of **2**, on the other hand, exhibits a prominent feature at *m*/*z* 455, a value which corresponds to the loss of $HClO_4$, relative to that of **1**. The isotope distribution pattern associated with this feature matches well with that calculated for, $[Fe(N4Py)(OO)]^+$, thus supporting the notion that **2** is the conjugate base of **1**.

Resonance Raman spectroscopy provides further insight into this transformation. Excitation into the peroxo-to-iron(III) charge transfer band of **1** generates a Raman spectrum with features at 632 and 790 cm^{-1} [Fig. 1(*a*)].‡ The latter is unequivocally assigned to ν(O–O) by its ^{18}O shift of −46 cm^{-1}, while the former is associated with a coupled Fe–OOH mode.[14] These features are considered the Raman signature for a low spin Fe(III)–OOH species. Conversion to **2** results in a significantly different Raman spectrum with prominent peaks at 495 and 827 cm^{-1} [Fig. 1(b)].§ The use of $H_2{}^{18}O_2$ shifts the two features to 478 ($\Delta\nu$ = −17) and 781 ($\Delta\nu$ = −46) cm^{-1}, respectively [Fig. 1(c)], which are fully consistent with their assignments as ν(Fe–O_2) ($\Delta\nu_{calc}$ −18 cm^{-1}, based on Hooke's Law for diatomic harmonic oscillators) and ν(O–O) ($\Delta\nu_{calc}$ −47 cm^{-1}), respectively. Consistent with these assignments, the introduction of ^{54}Fe in **2** does not affect the 827 cm^{-1} vibration but upshifts the 495 cm^{-1} feature by 3 cm^{-1} ($\Delta\nu_{calc}$ +3 cm^{-1}) [Fig. 1(d)]. Furthermore, unlike for **1**,[14] the use of $^2H_2O_2$ does not affect the Raman spectrum of **2**. Thus the Raman spectra support the notion that **2** is an $[Fe^{III}–O_2]^+$ complex.

Strong evidence for the η^2-peroxo binding mode has been obtained from the Raman spectrum of **2** with H_2O_2 containing 61% ^{18}O (Fig. 2).¶ Although the various isotopic components of

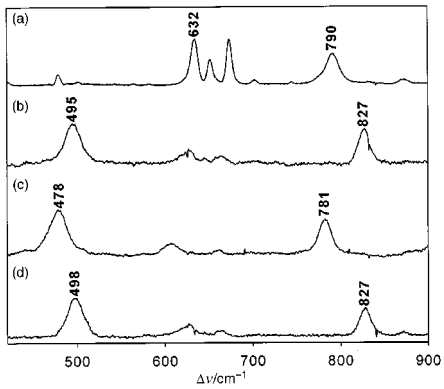

Fig. 1 Resonance Raman spectra of **1** and **2**. (a) **1** generated by the addition of 5 equiv. H_2O_2 to a methanolic solution of $[Fe^{III}(N4Py)(OMe)]^{2+}$ (10 mM) at −35 °C. (b) **2** generated by the addition of 5 equiv. NH_3(aq) to the solution of **1** at −35 °C. (c) Same as (b), except $H_2{}^{18}O_2$ was used. (d) Same as (b) except that the ^{54}Fe complex was used. All spectra were obtained with a backscattering geometry on liquid-N_2 frozen samples using 568.2 nm laser excitation at 20 mW power at the sample. The Raman frequencies were referenced to indene.

the ν(Fe-O_2) feature centred at 486 cm^{-1} are unresolved, three peaks associated with the ν(O–O) feature are readily discerned at 781, 802 and 826 cm^{-1} and can be fitted with peaks having approximately equal linewidths. The fact that the peak arising from the $^{16}O^{18}O$ isotopomer has a linewidth equal to those of $^{16}O^{16}O$ and $^{18}O^{18}O$ isotopomers strongly implies an η^2-peroxo binding mode, as found for $[Fe^{III}(EDTA)(\eta^2\text{-}O_2)]$[10,11] and suggested for $[Fe^{III}(N\text{-}R\text{-}trispicen)(O_2)]^+$.[16] At this point, we do not have enough information to determine whether the iron centre in **2** becomes seven-coordinate, as illustrated in Scheme 1, or remains six-co-ordinate by a decrease in the denticity of the N4Py ligand. The latter may come about by detachment of one of the pendant pyridines or, by breaking the already weak tertiary amine bond as the η^2-peroxo ligand pulls the iron centre further out of the plane defined by the four pyridine ligands to achieve a coordination geometry similar to that found in the structure of $[Mn(TPP)(\eta^2\text{-}O_2)]^-$.[17]

With the peroxo binding mode of **2** established, we now compare the relative abilities of **1** and **2** to oxidise substrates. We have previously found that $[Fe^{II}(N4Py)(MeCN)]^{2+}$ can catalyse the hydroxylation of cyclohexane with H_2O_2 in acetone *via* intermediate **1**.[13a] With 5 equiv. H_2O_2, we observe 1.6 and 0.4 turnovers of cyclohexanol and cyclohexanone, respectively. In CD_3OD the number of turnovers is lower, 0.8 and 0.4 turnovers, respectively, owing to a competing oxidation of the solvent to $D_2C{=}O$ (1.4 turnovers). When 5 equiv. NH_3 (aq) is added prior to or after the formation of **1** in CD_3OD, no oxidation of cyclohexane is observed. These results suggest that, whereas **1** is capable of activating the O–O bond to oxidise alkanes, **2** is unreactive towards such substrates, resembling the inertness of other $[Fe^{III}(\eta^2\text{-}O_2)]$ species.[11,18] Our demonstration of an $[Fe^{III}(\eta^1\text{-}OOH)]$/$[Fe^{III}(\eta^2\text{-}OO^-)]$ interconversion allows us to support unequivocally the hypothesis that protonation of the peroxo species activates it for participation in the oxygen activation mechanisms by iron enzymes.[6,11]

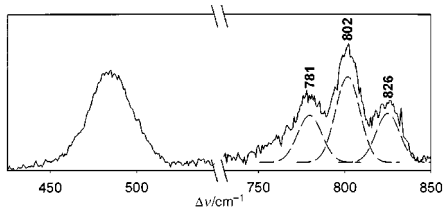

Fig. 2 Raman spectrum of **2** generated with a statistical mixture of H_2O_2 isotopomers (61% ^{18}O). The dashed lines represent the curve fit of the features associated with the ν(O–O) peaks. The curve was fitted with three peaks with the $^{18}O^{18}O$ feature constrained to a frequency of 781 cm^{-1} and a linewidth of 16 cm^{-1} as found for $[Fe(N4Py)(^{18}O_2)]^+$. The fitted data gave the other two peaks at 802 and 826 cm^{-1} with linewidths of 16.3 and 15.9 cm^{-1}, respectively. The latter matched well the properties of the ν(O–O) feature in $[Fe(N4Py)(^{16}O_2)]^+$.

We acknowledge C. M. Jeronimus-Stratingh and A. P. Bruins for advice and assistance with mass spectrometric measurements and financial support from Unilever (Vlaardingen, The Netherlands) and the National Institutes of Health (Grant GM-33162).

Notes and references

† Abbreviations used: BLM = bleomycin; N4Py = *N*-[bis(2-pyridyl)methyl]-*N*,*N*-bis(2-pyridylmethyl)amine; N-R-trispicen = *N*-alkyl-*N*,*N*′,*N*′-tris(2-pyridylmethyl)ethane-1,2-diamine.

‡ Resonance Raman spectra were collected on an Acton AM-506 spectrometer (2400-groove grating) using Kaiser Optical holographic super-notch filters with a Princeton Instruments liquid N_2-cooled (LN-1100PB) CCD detector with 4 or 2 cm^{-1} spectral resolution. Spectra were obtained by back-scattering geometry on liquid N_2 frozen samples using 568.2 nm laser excitation from a Spectra Physics 2030-15 argon ion laser and a 375B CW dye (Rhodamine 6G). Raman frequencies were referenced to indene.

§ Aside from the features at 495 and 827 cm^{-1}, weaker features at 625 , 645, 664 cm^{-1} are also observed and are sensitive to ^{18}O labeling. However the intensities of these features vary relative to the intensities of the 495 and 827 cm^{-1} features with different samples, suggesting that these minor features are not associated with **2**. We have ruled out the possibility that these minor features are associated with **1** since the features at 626, 648, and 668 cm^{-1} are slightly shifted from those of **1** and a corresponding 790 cm^{-1} feature is not observed. The assignment of these features is currently under investigation.

¶ $H_2{}^{18}O_2$ (90% ^{18}O-enriched, 2% solution in $H_2{}^{16}O$) was obtained from ICON Services Inc. The statistical mixture of H_2O_2 (61% ^{18}O) was prepared by the reduction of O_2 (statistical mixture with 61% ^{18}O from ICON Services Inc.) according to a literature procedure (A. J. Sitter and J. Terner, *J. Labelled Compd. Radiopharm.*, 1984, **22**, 461).

1 M. Sono, M. P. Roach, E. D. Coulter and J. H. Dawson, *Chem. Rev.*, 1996, **96**, 2841.
2 L. Que, Jr. and R. Y. N. Ho, *Chem. Rev.*, 1996, **96**, 2607.
3 S. A. Kane and S. M. Hecht, *Prog. Nucl. Acid Res. Mol. Biol.*, 1994, **49**, 313.
4 J. Stubbe and J. W. Kozarich, *Chem. Rev.*, 1987, **87**, 1107.
5 J. W. Sam, X.-J. Tang and J. Peisach, *J. Am. Chem. Soc.*, 1994, **116**, 5250.
6 D. L. Harris and G. H. Loew, *J. Am. Chem. Soc.*, 1998, **120**, 8941.
7 M. J. Coon, A. D. N. Vaz and L. L. Bestervelt, *FASEB J.*, 1996, **10**, 428.
8 P. R. Ortiz de Montellano, *Acc. Chem. Res.*, 1998, **31**, 543.
9 D. Ballou and C. Batie, in *Oxidases and Related Redox Systems*, ed. T. E. King, H. S. Mason and M. Morrison, Alan R. Liss, New York, 1988, p. 211.
10 S. Ahmad, J. D. McCallum, A. K. Shiemke, E. H. Appelman, T. M. Loehr and J. Sanders-Loehr, *Inorg. Chem.*, 1988, **27**, 2230.
11 F. Neese and E. I. Solomon, *J. Am. Chem. Soc.*, 1998, **120**, 12 829.
12 E. McCandlish, A. R. Miksztal, M. Nappa, A. G. Sprenger, J. S. Valentine, J. D. Stong and T. G. Spiro, *J. Am. Chem. Soc.*, 1980, **102**, 4268.
13 (*a*) M. Lubben, A. Meetsma, E. C. Wilkinson, B. Feringa and L. Que, Jr., *Angew. Chem., Int. Ed. Engl.*, 1995, **34**, 1512; (*b*) I. Bernal, I. M. Jensen, K. B. Jensen, C. J. McKenzie, H. Toftlund and J. P. Tuchagues, *J. Chem. Soc., Dalton Trans.*, 1995, **22**, 3667; (*c*) C. Kim, K. Chen, J. Kim and L. Que, Jr., *J. Am. Chem. Soc.*, 1997, **119**, 5964; (*d*) M. E. de Vries, R. M. La Crois, G. Roelfes, H. Kooijman, A. L. Spek, R. Hage and B. L. Feringa, *Chem. Commun.*, 1997, 1549.
14 R. Y. N. Ho, G. Roelfes, B. L. Feringa and L. Que, Jr., *J. Am. Chem. Soc.*, 1999, **121**, 264.
15 G. Roelfes, M. Lubben, K. Chen, R. Y. N. Ho, A. Meetsma, S. Genseberger, R. M. Hermant, R. Hage, S. K. Mandal, V. G. Young, Jr., Y. Zang, H. Kooijman, A. L. Spek, L. Que, Jr. and B. L. Feringa, *Inorg. Chem.*, 1999, **38**, 1929.
16 A. J. Simaan, F. Banse, P. Mialane, A. Boussac, S. Un, T. Kargar-Grisel, G. Bouchoux and J.-J. Girerd, *Eur. J. Inorg. Chem.*, 1999, 993; K. B. Jensen, C. J. McKenzie, L. P. Nielsen, J. Z. Pedersen and H. M. Svendsen, *Chem. Commun.*, 1999, 1313.
17 R. B. VanAtta, C. E. Strouse, L. K. Hanson and J. S. Valentine, *J. Am. Chem. Soc.*, 1987, **109**, 1425.
18 M. Selke and J. S. Valentine, *J. Am. Chem. Soc.*, 1998, **120**, 2652.

Communication 9/05535E

Influence of short- and long-range factors in the Brønsted acidity of MCM-22 zeolite

German Sastre, Vicente Fornes, and Avelino Corma*

Instituto de Tecnologia Quimica U.P.V.-C.S.I.C. Universidad Politecnica de Valencia. Av. Los Naranjos s/n, 46022 Valencia, Spain. E-mail: acorma@itq.upv.es

Received (in Cambridge, UK) 27th July 1999, Accepted 24th September 1999

The acidity of the Brønsted sites of MCM-22 zeolite is calculated by atomistic simulation techniques and the effects of long- and short-range contributions in acidity are analysed; the two IR bands detected experimentally are reproduced in the calculations.

Since their introduction in fluid catalytic cracking, zeolites have been widely used as solid acid catalysts in a growing number of industrial chemical processes such as reforming, isomerisation, hydrocracking, oligomerisation, and others. Much attention has been devoted to the acid function in zeolites, and in particular Brønsted acidity has been characterised mainly by IR and NMR spectroscopies, as well as by computational chemistry methods.

The first simulations of Brønsted acidity in zeolites, employed the cluster model and the quantum chemistry methodology. Clusters of the size of the disiloxane molecule with a Si atom substituted by a trivalent atom T^{III}, mainly Al, and a proton bound to the oxygen atom in the $SiOT^{III}$ bridge are able to give reasonable OH stretching frequencies compared to IR experiments.[1] Among other results from quantum chemistry studies, a linear correlation was found between OH stretching frequency and SiO(H)Al angle,[2] and this has been used to explain acidity differences between different zeolites or between different acid centres in a given zeolite. The question whether the long range factors—not accounted by the cluster model—do influence the acidity and to what extent, has led to calculations both with larger clusters and with periodic boundary conditions. The latter, require a considerable amount of computational resources, and thus less demanding methodologies to treat periodic solids such as those based on force fields are a reasonable alternative.

In spite of their lower accuracy, owing to the interactions neglected or averaged, force field methods have been successfully used to characterise different properties of zeolites such as cell parameters, geometry, framework stability, Al distribution, and Brønsted acidity.[3] This methodology allows us to assess the short- and long-range contributions to acidity, and this makes it possible to span the number of calculations necessary to explore the different locations of the acid centres in a zeolite. It is the aim of this work to carry out a characterisation of the Brønsted acidity of the MCM-22 zeolite, and compare the results with IR data.

The calculations have been performed using the GULP code,[4] employing the Ewald method for summation of the long-range Coulombic interactions, and direct summation of the short-range interactions with a cutoff distance of 12 Å. The RFO technique was used as the cell minimisation scheme with a convergence criterion of a gradient norm below 0.001 eV $Å^{-1}$. An empirical shell model forcefield[5] (denoted empirical ff), and an *ab initio* shell model forcefield d[6] (denoted *ab initio ff*), have been used throughout. Electric fields, and OH stretching frequencies have been calculated with the GULP code. OH frequencies have been corrected for the empirical forcefield by substracting an anharmonicity constant of 150 cm^{-1},[7], and for the *ab initio* forcefield by multiplying by a factor of 0.90.[8].

The hexagonal *P*6/*mmm* structure of pure silica MCM-22[9] has been used as a starting point and then has been minimised without symmetry constraints. Then, a single Al atom has been introduced in the unit cell to create a Brønsted site and the resulting cell has been again minimised. The Al atom has been introduced in all the eight different T positions of the MCM-22 structure (Fig. 1), and the proton has been placed in all the four non-equivalent oxygen atoms linked to the corresponding Al in each case. Only the protons located on SiOSi angles of 180º have been excluded, which correspond to the Si(1)–O–Si(1), and the Si(4)–O–Si(5) sites (Fig. 1). 29 different possibilities were considered, and this comes from the possible locations of a proton on each of the four oxygens linked to eight different T sites (32 possibilities), from which the T(1)–O–T(1), T(4)–O–T(5) and T(5)–O–T(4) linkages have been subtracted. We distinguish between T(x)–T(y) and T(y) – T(x) ($1 \leqslant x,y \leqslant 8$) because in the first case the Al is on T(x), whereas in the second case the Al is on T(y).

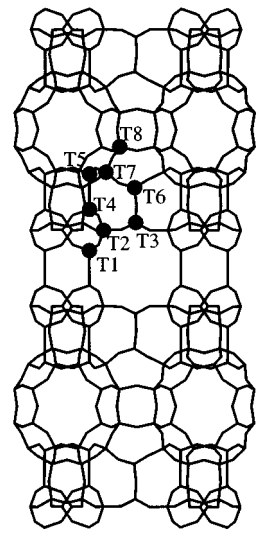

Fig. 1 Structure of MCM-22 showing the eight different T sites. Two independent void systems are present: a sinusoidal 10 MR, and a system of large (12 MR in size) cavities interconnected by short 10 MR conduits.

We have calculated the stretching OH frequency, ν(OH), for all the cases and the results are shown in Fig. 2, where they are plotted against the modulus of the electric field at the proton site, $|E_H|$. Two conclusions are drawn from this plot. First, the calculated values of ν(OH) (with the empirical ff) cover a wide range of 3530–3640 cm^{-1} (Fig. 2), and they can be grouped in two bands: one around 3550 cm^{-1}, and the other around 3610 cm^{-1}. This result can be compared with experimental measurements of ν(OH) by IR spectroscopy performed on calcined MCM-22 of Si/Al ≈ 15, where two bands appear at 3575 and 3620 cm^{-1}.[10] Similarly, bands at 3550 and 3650 cm^{-1}appear when using the *ab initio* forcefield (Fig. 2). The agreement with experiment is very reasonable, with the advantage that the simulations give a more detailed information about the origin of each OH frequency. The protons of MCM-22 can vibrate into four different environments: 'unaccessible' (for those which can not be reached by sorbate molecules), 'cross' (in the

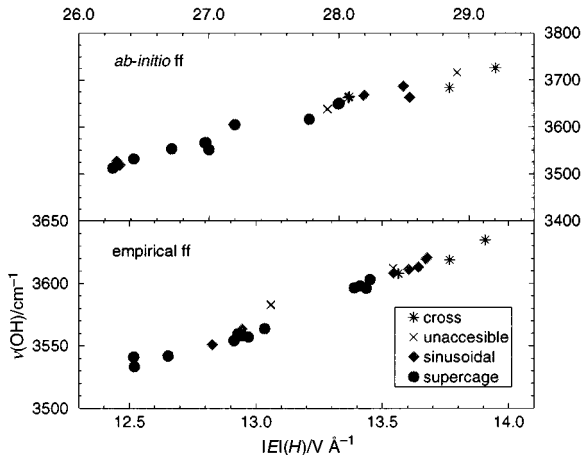

Fig, 2 Correlation between the modulus of the electric field at the proton ($|E_H|$) and the calculated OH stretching frequency, ν(O–H) in the Brønsted sites of MCM-22. The location of the protons is indicated in the figure, showing no relation between environment and OH frequency. Two forcefields have been used as described in the text.

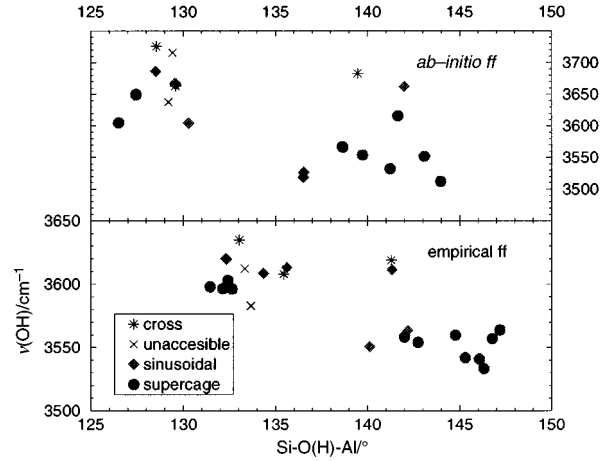

Fig, 3 Relation between the Si–O(H)–Al angle and the calculated OH stretching frequency, ν(OH) in the Brønsted sites of MCM-22. The location of the protons is indicated in the figure, showing no relation between environment and Si–O(H)–Al angle. The lack of correlation between Si–O(H)–Al angle and ν(OH) shows that the long-range factors (as well as the short-range) are important to determine the acidity. Two forcefields have been used as described in the text.

intersection between supercages), 'sinusoidal' (in the 10 MR sinusoidal system), and 'supercage' (inside the 12 MR supercage). Fig. 2 shows that some Brønsted sites located in the supercage belong to the low frequency band whereas others in the supercage belong to the high frequency band, and the same can be said about sites located in the sinusoidal system. A relation between cavity size and OH stretching frequency has not been found, in agreement with previous results.[11] The second conclusion we draw refers to the relationship between ν(OH) and the modulus of the electric field at the proton site, $|E_H|$, which is a straight line regardless of the forcefield employed (Fig. 2), thus showing the direct correlation between the two properties. This shows the influence of the long range factors on acidity, as the electric field is caused by all the atoms of the zeolite framework.

In order to further explore the role of the short- and long-range factors in the Brønsted acidity we have plotted the OH stretching frequency against the Si–O(H)–Al angle, the latter being a geometric property that has been related to acidity as noted above. The results in Fig. 3 show a much poorer correlation than in the previous case. We find cases for which increasing angles give increasing frequencies and also cases with the opposite behaviour. Although the points are scattered (Fig. 3), a somewhat loose correlation shows decreasing OH frequencies as the Si–O(H)–Al angles increase, as noted in the literature.[2] The present calculations show that short range factors such as Si–O(H)–Al angles are not sufficient to fully explain the Brønsted acidity, and that a better correlation is found with a long range property, the modulus of the electric field at the proton site.

We thank the Spanish CICYT (project MAT-97-1016-C02-01) for financial support.

Notes and references

1 J. Sauer, *J. Mol. Catal.*, 1989, **54**, 312.
2 H. V. Brand, L. A. Curtiss and L. E. Iton, *J. Phys. Chem.*, 1992, **96**, 7725; A. Redondo and P. J. Hay, *J. Phys. Chem.*, 1993, **97**, 11 754; Y. Jeanvoine, J. G. Angyan, G. Kresse and J. Hafner, *J. Phys. Chem. B*, 1998, **102**, 5573.
3 *Modelling of Structure and Reactivity in Zeolites*, ed. C. R. A. Catlow, Academic Press, London, 1992.
4 J. D. Gale, *J. Chem. Soc., Faraday Trans.*, 1997, **93**, 629.
5 R. A. Jackson and C. R. A. Catlow, *Mol. Simul.*, 1988, **1**, 207; K.-P. Schröder, J. Sauer, M. Leslie, C. R. A. Catlow and J. M. Thomas, *Chem. Phys. Lett.*, 1992, **188**, 320.
6 K.-P. Schröder and J. Sauer, *J. Phys. Chem.*, 1996, **100**, 11 043.
7 N. H. Henson, A. K. Cheetham and J. D. Gale, *Chem. Mater.*, 1996, **8**, 664.
8 M. Sierka and J. Sauer, *Faraday Discuss.*, 1997, **106**, 41.
9 M. A. Camblor, A. Corma, M. J. Diaz-Cabañas and C. Baerlocher, *J. Phys. Chem. B*, 1998, **102**, 44.
10 A. Corma, C. Corell, V. Fornes, W. Kolodziejski and J. Perez-Pariente, *Zeolites*, 1995, **15**, 576.
11 G. Sastre and D.W. Lewis, *J. Chem. Soc., Faraday Trans.*, 1998, **94**, 3049.

Communication 9/06053G

Chemistry in interphases. The solid-phase synthesis of well defined rhodium and iridium phosphine complexes†

Joachim Büchele and Hermann A. Mayer*

Institut für Anorganische Chemie der Universität Tübingen, Auf der Morgenstelle 18, 72076 Tübingen, Germany. E-mail: hermann.mayer@uni-tuebingen.de

Received (in Cambridge, UK) 5th August 1999, Accepted 27th September 1999

After polyethylene glycol functionalized metal complexes were supported by the sol–gel technique the organometallic protection group was eliminated in a combined photochemical/oxidative procedure and the immobilized non-coordinated ligand was treated with organometallic fragments to give new supported well defined rhodium and iridium complexes.

Transition metal catalysts anchored onto insoluble supports are of great interest since they are useful in industrial scale processes.[1–3] They allow easy purification as well as catalyst recycling and therefore play an important role with respect to ecological and economic aspects.[4,5] The main draw backs of catalysts which are bound to the surface of pre-formed supports are leaching of the active metal centre and reduced reactivity and selectivity compared to their homogeneous counterparts.[6] The simultaneous co-condensation of various types of alkoxysilanes with functionalized metal complexes under sol–gel process conditions lead to highly cross-linked polymers as stationary phases. If these stationary phases are penetrated by a mobile phase (solvent, reactant) particular regions exist in which the reactive centres become highly mobile.[6,7] Such interphases display reduced leaching and high reactivity and selectivity.[6] The synthesis of stationary phases is challenging as hydrolysable functional groups have to be attached to transition metal complex fragments. In addition the precursor complexes of the catalytically active species also have to withstand the sol–gel conditions which are considered as mild in terms of temperature but the chemical conditions (solvent, pH) are often not in favour of the reactive centre. Here, we present our preliminary findings on the support of well defined transition metal complexes using the $Mo(CO)_3$ fragment as the protecting group.[8]

The synthesis of the polyethylene glycol functionalized molybdenum complex **1** was carried out as described earlier.[9] The average chain length *x* was adjusted to 5–10, 50, 145 and 285, respectively. The properties of the PEG-functionalized molybdenum complexes **1** vary from amorphous powders with high decomposition points (x = 5–10) to waxy materials with low melting points (x = 145, 285). The solubility changes from CH_2Cl_2, acetone to THF and water with increasing chain length and the swelling abilities increase in the same order. The hydroxylic end groups of the homologous polymers of **1** react with $Cl(CH_2)_3Si(OEt)_3$ under Williamson ether synthesis conditions to the corresponding tris[(triethoxy)silyl] functionalized complexes **2**.‡ Simultaneous co-condensation of **2** with various amounts (y = 0, 6, 30 equivalents) of tetraethoxysilane (TEOS) allows generation of organic–inorganic hybrid polymers with different properties. When y is small (y = 0, 6) the PEG-functions dominate the character of the material (*vide supra*). Increasing the amount of TEOS (y = 30) leads to materials which are more like silica.§ As the polyethylene glycol spacers already offer a high flexibility, TEOS was used as co-condensing agent to achieve a high cross-linking of the polymer. To remove the $Mo(CO)_3$ protecting group from **3**, a suspension of the polymer in THF was irradiated with UV light in the presence of N_2O. After activation of the metal carbonyl bond with UV light the oxygen transferring agent N_2O is able to selectively oxidise the $Mo(CO)_3$ fragment to MoO_3 and generate **4** quantitatively.[8]¶ This was shown by a shift of the ^{31}P resonance to higher field (δ 29) in the ^{31}P CP MAS spectrum of **4** and confirmed by the absence of the ν(CO) absorptions due to the $Mo(CO)_3$ fragment in the IR spectrum. After conversion of MoO_3 into MoO_4^- with K_2CO_3 the molybdate was extracted by washing procedures. While a number of functionalized phosphine monomers were accessible in this manner in homogeneous solution[8] a partial oxidation of the supported phosphine ligand **4** is observed in the interphase. This was attributed to the high oxophilicity of the polyethylene glycol groups and is prevented by adding reducing agents like PBu^n_3 to the suspension. The quantitative replacement of the carbonyl fragment demonstrates the easy accessibility of the metal complex in the polymer material by small molecules like N_2O. When the supported tripodal phosphine ligand **4** is treated with Vaska's complex no reaction is observed. Obviously the $Ir(PPh_3)_2(CO)Cl$ complex is too large to enter the interphase and react with the tripodal phosphine. The dimers $[M(cod)Cl]_2$ (M = Rh, Ir) are readily split by **4** in the presence of $NaBPh_4$ to form the new anchored rhodium and iridium complexes **5,6**.‖ The characteristic ^{31}P NMR signals are shifted to δ 38.4 and −7, respectively.

All materials were characterised by multinuclear solid-state NMR spectroscopy. The ^{29}Si CP MAS NMR spectra confirm the presence of a polysiloxane network built up with different T (δ −56.0 to −66.3, T^1–T^3) and Q (δ −91.0 to −109.9, Q^2–Q^4) species. The ^{31}P CP MAS NMR spectra of the polymers **3**–**6** display single unique resonances characteristic for the complexes and ligand, respectively. The spectra are comparable

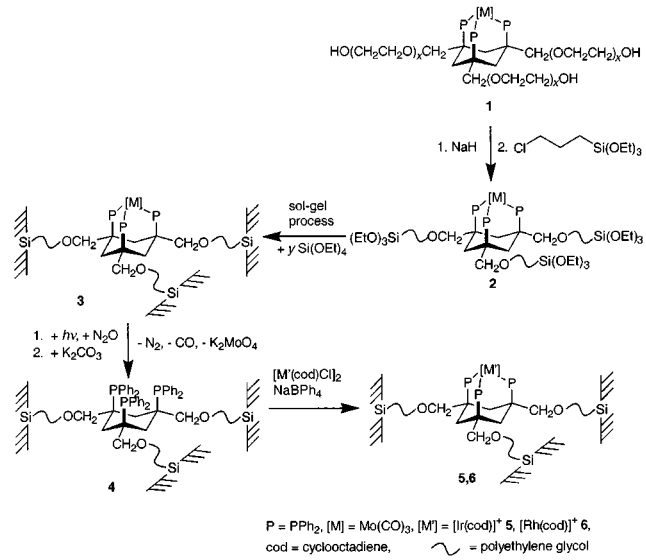

Scheme 1

† Dedicated to Professor Reinhard Schmutzler on the occasion of his 65th birthday.

with the corresponding monomer complexes in solution. This confirms the integrity of the reactive centres in the polymers and establishes that the method described above allows the support of well defined transition metal complexes. Interestingly the linewidth of the ^{31}P resonances strongly depend on the spacer lengths as well as the amount of co-condensate used and shows large differences between the ligand **4** and the complexes **3**, **5** and **6**, respectively. It was found that the flexibility of the supported complexes increases when the degree of polymerisation of the PEG spacer is expanded from 50 to 145. If the degree of polymerisation is enlarged to 285 the mobility is reduced which is caused by a stronger interaction among the polyethylene glycol chains. The strong increase of the linewidth from the ligand **4** to the complexes **5** and **6** is interpreted in terms of the larger chemical shift dispersion in metal complexes. This is caused by the hindered rotation of the phenyl groups of the sterically crowded transition metal complexes in the solid state.

The Deutsche Forschungsgemeinschaft and the Fonds der Chemischen Industrie are greatly acknowledged for financial support.

Notes and references

‡ *Standard procedure for* **2**: after a suspension of **1** (258 mg, 0.249 mmol) and NaH (54 mg, 2.241 mmol) in 70 ml of THF was stirred for 2 h at 80 °C, 357 μl (1.494 mmol) of $Cl(CH_2)_3Si(OEt)_3$ were added dropwise at room temp. and stirred for 20 h at 60 °C. The reaction mixture was allowed to cool to room temp. and was neutralised and separated from precipitated salts by passing the suspension over a column of dry NH_4Cl (3 cm). The solvent was removed *in vacuo* and the oily residue treated with 30 ml of *n*-pentane. The yellow precipitate was separated and washed with *n*-pentane three times and dried *in vacuo*, Yield: 288 mg (70.0%). IR (KBr, cm^{-1}): 1938, 1849 ν(CO). $^{31}P\{^1H\}$ NMR ($CDCl_3$): δ 46.7. ^1H NMR (acetone-d_6): δ 0.54–0.60 (m, $SiCH_2$), 1.17 (t, $^3J_{HH}$ 7.2 Hz, OCH_2CH_3), 1.55–1.75 (m, $SiCH_2CH_2$), 1.77–1.93 (m, $CH H_e$), 2.44–2.79 (m, $CH H_a$), 3.30–3.62 (m, OCH_2-$CH_2OCH_2CH_2$), 3.75 (q, $^3J_{HH}$ 7.2 Hz, OCH_2CH_3), 7.05–7.39 (m, C_6H_5). $^{13}C\{^1H\}$ NMR ($CDCl_3$): δ 7.1 (s, $SiCH_2$), 17.5 (s, OCH_2CH_3), 23.3 (s, $SiCH_2CH_2$), 30.3 (m, CH_2), 39.3 (br s, CP), 57.3 (s, OCH_2CH_3), 67.4–76.7 (m, $OCH_2CH_2OCH_2CH_2$), 127.5 (s, *m*-C_6H_5), 128.9 (s, *p*-C_6H_5), 136.3 (m, *ipso*-, *o*-C_6H_5).

§ *Standard procedure for* **3**: compound **2** (182 mg, 0.11 mmol), TEOS and H_2O were homogenised for 30 min at room temp. with a minimum amount of ethanol (0.5 ml). After one drop of $SnBu^n_2(OAc)_2$ was added, the reaction mixture was warmed to 60 °C for 4 h and dried for another 4 h at 60 °C. The inhomogeneous gel particles were stirred in *n*-hexane (3 times for 3 h in 50 ml) and after drying *in vacuo* (1 h) washed with ethanol, acetone and *n*-hexane (each 3 × 10 ml) and again dried *in vacuo*. IR (KBr, cm^{-1}): 1936, 1846 ν(CO). ^{31}P CP MAS NMR: δ 45.0 (s). ^{29}Si CP MAS NMR (Si-substructure): δ −59.7 (T^2), −67.2 (T^3), −92.1 (Q^2), −100.8 (Q^3), −109.2 (Q^4).

¶ *Standard procedure for* **4**: a suspension of **3** in 50 ml acetone placed in a double-walled Duran Schlenk tube was degassed and 5 ml of PBu^n_3 added under N_2O atmosphere. The vigorously stirred suspension was cooled to 10 °C and N_2O was added (1.3–1.5 bar). The reaction mixture was irradiated for 30 min with the UV-light of a TQ 150W (Original Hanau) high-pressure mercury lamp, which was located 5 cm from the Schlenk tube. After complete conversion of the educt (monitored by ^{31}P CP MAS NMR spectroscopy) the red solution was filtered off and the yellow powder was washed twice with 5 ml of an aqueous solution of K_2CO_3 (0.05 M) and three times each with 10 ml of acetone and *n*-pentane. The material was dried *in vacuo*. ^{31}P CP MAS NMR: δ 29.8 (s).

‖ *Standard procedure for* **5** *and* **6**: to 227 mg (0.035 mmol) of **4** suspended in 35 ml of CH_2Cl_2 were added 21.9 mg (0.035 mmol) of $[Ir(cod)Cl]_2$. The yellow suspension was stirred for 30 min and 24 mg (0.07 mmol) of $NaBPh_4$ in 4 ml of CH_2Cl_2 was added to the reaction mixture. After stirring for 20 h the product was separated from the solution, washed with acetone and *n*-hexane (each 3 × 5 ml) and dried *in vacuo*. IR (KBr, cm^{-1}): 1415 ν(C=C). ^{31}P CP MAS NMR: δ 7.3 (br s). Material **6** was prepared according to the same procedure except that the suspension of **4** was added to the solution of $[Rh(cod)Cl]_2$ in CH_2Cl_2. IR (KBr, cm^{-1}): 1462 ν(C=C). ^{31}P CP MAS NMR: δ 38.4 (br s).

1 P. Panster and S. Wieland, in *Applied Homogeneous Catalysis with Organometallic Compounds*, ed. B. Cornils and W. A. Herrmann, VCH, Weinheim, 1966, vol. 2, p. 605.
2 F. R. Hartley, *Supported Metal Complexes*, Reidel, Dordrecht, 1985.
3 J. Blum, D. Avnir and H. Schumann, *CHEMTECH.*, 1999, 32.
4 O. Kröcher, R. A. Köppel and A. Baiker, *Chem. Commun.*, 1996, 1497.
5 U. Schuber, *New J. Chem.*, 1994, **18**, 1049.
6 E. Lindner, T. Schneller, F. Auer and H. A. Mayer, *Angew. Chem., Int. Ed.*, 1999, **38**, 2154.
7 E. Lindner, M. Kemmler, T. Schneller and H. A. Mayer, *Inorg. Chem.*, 1995, **34**, 5489.
8 P. Stößel, H. A. Mayer, C. Maichle-Mössmer, R. Fawzi and M. Steimann, *Inorg. Chem.*, 1996, **35**, 5860.
9 P. Stößel, H. A. Mayer and F. Auer, *Eur. J. Inorg. Chem.*, 1998, 37.

Communication 9/06390K

Pt^{II} coordination to guanine-N7: enhancement of the stability of the Watson–Crick base pair with cytosine

Roland K. O. Sigel and Bernhard Lippert*

Fachbereich Chemie, Universität Dortmund, D-44221 Dortmund, Germany. E-mail: Lippert@pop.uni-dortmund.de

Received (in Cambridge, UK) 1st April 1999, Revised manuscript received 19th August 1999, Accepted 27th September 1999

Concentration-dependent ^{1}H NMR shift experiments in $(CD_3)_2SO$ reveal that Pt^{II}-coordination to N7 of guanine enhances the stability of the Watson–Crick pair with cytosine.

Metal ions are indispensable for charge compensation of negatively charged nucleic acid strands, thereby relieving mutual repulsion.[1] On the other hand, in cases of high affinity to donor atoms of the heterocyclic nucleobases, metal ions can lead to a concentration-dependent destabilisation of double-stranded DNA.[2] Different reasons can be responsible for these findings, *e.g.* blocking of hydrogen bonding sites, loss of electronic complementarity, or steric distortion. In recent years theoretical calculations have addressed the question how metal ion coordination to the periphery of a base pair or a base triple influences the strength of the nucleobase associate.[3–6] In some cases, polarisation effects of the metal ion have been proposed to lead to an enforcement of hydrogen bridges (*e.g.* GC-pair, GGC-triplet), whereas in other cases the hydrogen bonds apparently are not affected (*e.g.* AAT-triplet).[3a] To the best of our knowledge, it has not been examined until now, if such an influence also occurs in solution, and definitely no relevant studies have been conducted with respect to N7-platination of guanine. Predictions are difficult to make: on the one hand, N7-metalation acidifies the N1 proton[7]—a feature expected to lead to a strengthening of the hydrogen bond to cytosine-N3—on the other hand the simultaneous reduction of the basicity of O6 should reduce the acceptor property of this atom towards the amino proton of cytosine, thereby weakening the base pair with cytosine. As demonstrated by X-ray crystallography, Watson–Crick base pairing is, in principle, also possible with N7-platinated guanine,[8,9] as further confirmed by solution studies with DNA fragments containing intrastrand-G,G adducts.[10,11] However, no conclusions concerning the thermodynamic strength of such base pairs can be drawn from these observations. Our own solution studies in $(CD_3)_2SO$ with the model nucleobase 9-ethylguanine (Hegua) and 1-methylcytosine (Hmcyt), as well as with the three Pt^{II} complexes **1**–**3**[12–14] (Scheme 1) now definitely prove that N7 platination of Hegua enhances the stability of the Watson–Crick base pair with Hmcyt.

We have determined the association constant of the Watson–Crick base pair Hegua–Hmcyt by evaluating the concentration-dependent change of the chemical shift of the NH protons which are involved in base pair formation through hydrogen bonding.† The obtained value of $K = 6.9 \pm 1.3$ dm^3 mol^{-1} is in good agreement with data from the literature for guanosine/cytidine in the same solvent.[15] The corresponding values for the Watson–Crick base pairs of Hmcyt with the Pt^{II} complexes **1**, **2** and **3** are $K = 13.2 \pm 2.0$, $K = 22 \pm 10$ and $K = 16.3 \pm 4.0$ dm^3 mol^{-1} (all errors correspond to twice the standard deviation). As an example, the chemical shift of the NH protons is shown as a function of the concentration of the two partners Hmcyt and **2** (Fig. 1) together with a stackplot of the aromatic part of the ^{1}H NMR spectra at four different concentrations of the same components. All the other ^{1}H NMR resonances are practically concentration-independent in the presence of the corresponding partner, showing that no other interactions between the nucleobases (*e.g.* stacking) are present in $(CD_3)_2SO$ solution and that also the change in ionic strengths during the dilution experiment has no effect on the chemical shifts. It should be

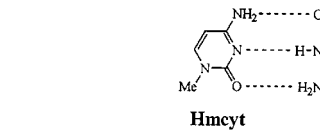

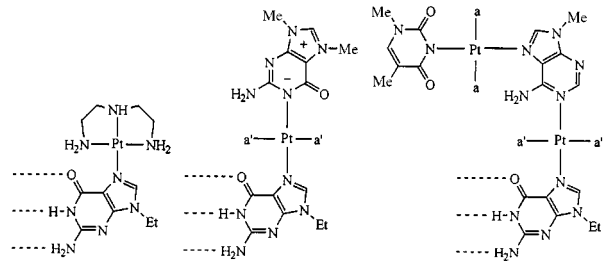

Scheme 1

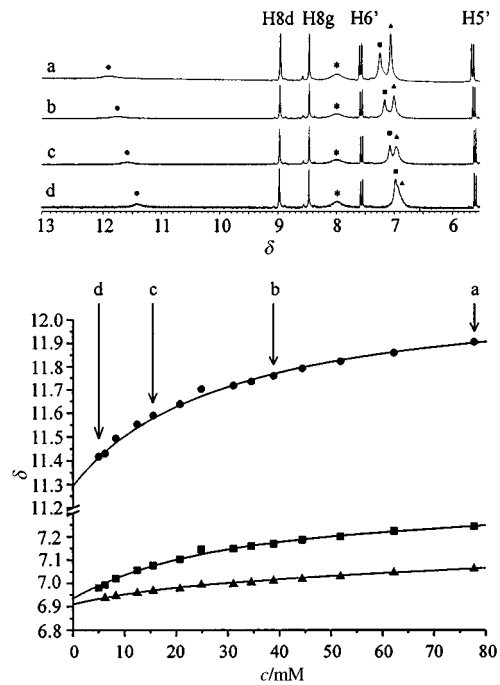

Fig. 1 Stackplot of the aromatic ^{1}H NMR spectra of a 1 : 1 mixture of **2** and Hmcyt in $(CD_3)_2SO$ at various concentrations (77.72, 38.86, 15.54, 4.97 mM, from top); the NH protons of the Hegua and Hmcyt moieties show a dependence in concentration whereas all other resonances [including NH_2 of the 7,9-dimethylguanine (*)] are unaffected (top part). In the bottom part the concentration dependency of the chemical shifts of the NH protons of 9-ethylguanine (N1H, ●; NH_2, ■) and 1-methylcytosine (NH_2, ▲) of the same system are shown. The arrows indicate those concentrations of the mixture of which the spectra are shown at the top.

noted that diluting a solution of the single compounds does not result in a change in chemical shift. The distinctly stronger influence on the N1H resonance of Hegua as compared to the two NH_2 resonances ($\Delta\delta \approx 2:1$), is in accord with the view that only one of the two amino protons takes part in base pairing, yet that there is signal averaging owing to fast rotation of the exocyclic amino group. Similar arguments apply to the NH_2 resonance of Hmcyt.

The ^{1}H NMR data for **1**–**3** prove that Pt^{II} coordination at the N7 position of 9-ethylguanine significantly enhances the stability of the Watson–Crick base pair with 1-methylcytosine in $(CD_3)_2SO$. Considering the proven similarity of nucleotides and their corresponding model nucleobases with respect to platinum binding properties, we propose that our observations are true for nucleotides as well. We note that although stability constants for Watson–Crick pairs have been determined, without exception, in non-physiological solvents such as Me_2SO or $CHCl_3$, they still reflect the different stabilities of G, C and A, T pairs in double stranded DNA. This fact further corroborates our claim.

The question whether an enhancement in base pair stability translates into a thermal stabilisation of DNA depends, however, on additional factors, such as conformational changes upon Pt^{II} coordination, DNA sequence, or ionic strength of the medium,[16] in which the melting behaviour of platinated DNA is measured. Thus the observed lowering of the melting point T_m of DNA containing bifunctional *cis*-$(NH_3)_2Pt(G,G)$ adducts is probably largely due to DNA distortion and loss of stacking, which overrules any gain in base pair stability between platinated G and C in the complementary strand brought about by the heavy metal. The accessibility of solvent (H_2O) to bases in a kinked DNA structure and the resulting competition with H_2O for H bonding sites at the bases might also contribute to this situation. The reported[17] increase in T_m of DNA at low levels of monofunctional (dien)Pt^{II} binding (base : Pt < 0.01) and at low ionic strength (10 mM $NaClO_4$) is in line with a stabilisation of GC pairs as described now, though it should also be noted that at higher platination levels conformational distortion of DNA leads again to a drop in T_m.[16,17]

The authors wish to thank the following institutions for support of this work: Deutsche Forschungsgemeinschaft (DFG), Fonds der Chemischen Industrie (FCI), and the Swiss National Science Foundation and the Swiss Federal Office for Education and Science (TMR fellowship to R. K. O. S.; No. 83EU-046320).

Notes and references

† An equimolar mixture of Hegua, **1**, **2** or **3** and Hmcyt in $(CD_3)_2SO$ was stepwise diluted in the concentration range of *ca.* 80–10 mM and at each concentration a ^{1}H NMR spectrum was recorded. The concentration-dependent chemical shifts of the NH protons involved in Watson–Crick base pairing were fitted with a non-linear least-squares program after Newton–Gauss, similar to a procedure described in ref. 18. Three independent dilution experiments were measured and evaluated; fitting the chemical shifts of each of the three NH protons, three association constants were obtained for each experiment, from which the weighted mean K^* was calculated. From these three values of K^*, the final association constant K was calculated, corresponding to the weighted mean of these three values. All errors correspond to twice the standard deviation. For the system **1**–Hmcyt, the resonances of the NH_2 groups of the guanine ligand and 1-mcyt coincide, so that only two data sets could be evaluated.

$(CD_3)_2SO$ was dried over 4 Å molecular sieves for at least one week before use. The residual water concentration was *ca.* 10 mM. It should be noted that there is an inverse relationship between the water content and K: the higher the concentration of the residual water, the lower the K value. The same is true for non-platinated guanine, but here the influence of the water concentration is less pronounced.

^{1}H NMR spectra were recorded on a Bruker AC200 (200.13 MHz) instrument at 20 °C. The quintet of $(CD_3)(CHD_2)SO$ was used as internal reference (δ 2.5025 relative to TMS).

1 W. Saenger, *Principles of Nucleic Acid Structure*, Springer, New York, 1984.
2 G. L. Eichhorn and Y. A. Shin, *J. Am. Chem. Soc.*, 1968, **90**, 7323.
3 J. Sponer, M. Sabat, J. V. Burda, A. M. Doody, J. Leszczynski and P. Hobza, *J. Biomol. Struct. Dyn.*, 1998, **16**, 139; J. Sponer, J. V. Burda, M. Sabat, J. Leszczynski and P. Hobza, *J. Phys. Chem. A*, 1998, **102**, 5951; J. V. Burda, J. Sponer, J. Leszczynski and P. Hobza, *J. Phys. Chem. B*, 1997, **101**, 9670; J. Sponer, J. V. Burda, P. Mejzlik, J. Leszczynski and P. Hobza, *J. Biomol. Struct. Dyn.*, 1997, **14**, 613.
4 E. H. S. Anwander, M. M. Probst and B. M. Rode, *Biopolymers*, 1990, **29**, 757.
5 S. R. Gadre, S. S. Pundlik, A. C. Limaye and A. P. Rendell, *Chem. Commun.*, 1998, 573.
6 V. N. Potaman and V. N. Soyfer, *J. Biomol. Struct. Dyn.*, 1998, **16**, 145; V. N. Potaman and V. N. Soyfer, *J. Biomol. Struct. Dyn.*, 1994, **11**, 1035.
7 G. Schröder, B. Lippert, M. Sabat, C. J. L. Lock, R. Faggiani, B. Song and H. Sigel, *J. Chem. Soc., Dalton Trans.*, 1995, 3767.
8 H.-K. Choi, S. K.-S. Huang and R. Bau, *Biochem. Biophys. Res. Commun.*, 1988, **156**, 1125; I. Dieter-Wurm, M. Sabat and B. Lippert, *J. Am. Chem. Soc.*, 1992, **114**, 357.
9 P. M. Takahara, C. A. Frederick and S. J. Lippard, *J. Am. Chem. Soc.*, 1996, **118**, 12309.
10 D. Yang, S. S. G. E. van Boom, J. Reedijk, J. H. van Boom and A. H.-J. Wang, *Biochemistry*, 1995, **34**, 12912 and references therein.
11 F. Herman, J. Kozelka, V. Stoven, E. Guittet, J.-P. Girault, T. Huynh-Dinh, J. Igolen, J.-Y. Lallemand and J.-C. Chottard, *Eur. J. Biochem.*, 1990, **194**, 119.
12 G. Frommer, H. Schöllhorn, U. Thewalt and B. Lippert, *Inorg. Chem.*, 1990, **29**, 1417.
13 R. K. O. Sigel, M. Sabat, E. Freisinger, A. Mower and B. Lippert, *Inorg. Chem.*, 1999, **38**, 1481.
14 Synthesis of the 1-methylthymine containing complex **3** (ClO_4^- salt) is in analogy to the corresponding 1-methyluracil compound: R. K. O. Sigel, S. M. Thompson, E. Freisinger and B. Lippert, *Chem. Commun.*, 1999, 19.
15 R. Newmark and C. R. Cantor, *J. Am. Chem. Soc.*, 1968, **90**, 5010.
16 R. Zaludova, V. Kleinwächter and V. Brabec, *Biophys. Chem.*, 1996, **60**, 135; V. Brabec, J. Reedijk and M. Leng, *Biochemistry*, 1992, **31**, 12397.
17 J. P. Macquet, J. L. Butour and N. P. Johnson, in *Platinum, Gold, and Other Metal Chemotherapeutic Agents*, ed. S. J. Lippard, American Chemical Society, Washington, DC, 1983, p. 75.
18 H. Sigel, K. H. Scheller, V. M. Rheinberger and B. E. Fischer, *J. Chem. Soc., Dalton Trans.*, 1980, 1022.

Communication 9/02650I

ChemComm

Synthesis and structural analysis of mercaptothiacalix[4]arene

Photon Rao,[a] Mir Wais Hosseini,*[a] André De Cian[b] and Jean Fischer[b]

[a] *Laboratoire de Chimie de Coordination Organique, Université Louis Pasteur, (CNRS UMR 7512), F-67000 Strasbourg, France. E-mail: hosseini@chimie.u-strasbg.fr*
[b] *Laboratoire de Cristallochimie et Chimie Structurale, Université Louis Pasteur, (CNRS UMR 7512), F-67000 Strasbourg, France*

Received (in Basel, Switzerland) 27th July 1999, Accepted 13th September 1999

The synthesis of *p-tert*-butyltetramercaptotetrathiacalix[4]arene 1 bearing eight sulfur atoms was achieved in high overall yield (80%); the synthetic strategy used was based on the synthesis of *p-tert*-butyltetrathiacalix[4]arene 2, treatment of the latter with *N,N*-dimethylthiacarbamoyl chloride under mild conditions, thermal transposition of the *O*-thiacarbamoyl into the *S*-thiacarbamoyl derivatives in quantitative yield and deprotection of the sulfur centres by treatment with hydrazine hydrate; the conformation of compound 1 was investigated in the solid state by X-ray diffraction on a single crystal, which revealed that compound 1 adopts the 1,3-alternate conformation.

Calixarenes, and in particular, calix[4]arene derivatives are among the most used macrocyclic frameworks.[1] The increasing interest in calixarenes is due to the almost endless structural as well as functional possibilities that such backbones allow to explore. Indeed, one may not only elaborate new compounds by modifying the upper and/or the lower rim of the calix unit, but one may also replace the methylene junction between the aromatic moieties by other elements or groups. Recently, the synthesis[2] and the structural analysis[3] of thiacalix[4]arenes, which are a new class of calix[4]arene derivatives, based on the substitution of the CH_2 groups linking the aromatic rings by sulfur atoms was reported.[4] Furthermore, the partial as well as complete oxidation of the thioether junctions into sulfoxide[5] and sulfone[6] respectively was achieved. For the parent calix[4]arene derivatives, the binding of metal cations[1] and main group elements such as silicon[7] takes place at the lower rim through the OH groups. For the thiacalixarene derivatives, it has been demonstrated that upon replacement of the methylene groups by sulfur atoms, the number of coordination sites increases leading thus to a large diversity in the coordination properties.[8] For sulfur containing calixarenes, the synthesis of di[9]- and tetra[10,11]-mercapto calix[4]arenes, in which two and four OH groups were replaced by two and four SH groups, respectively, as well as their ability to bind mercury cation was reported. More recently, other examples of dimercapto calix[4]arene derivatives bearing two long alkyl chains was achieved and their ability to extract selectively Hg^{2+} cations from water into $CHCl_3$ was demonstrated.[12] We believe that ligand **1**, which is based on the thiacalixarene framework and bears four SH groups, may be of great interest for both its coordination features and as a backbone for the elaboration of other ligands.

Here we report the first synthesis and the solid state X-ray structure of tetramercaptotetrathiacalix[4]arene **1**.

The synthesis of **1** was first attempted by treatment of *p-tert*-butylthiophenol by S_8 under the same conditions as those used for the preparation of thiacalixarene **2**.[2] Unfortunately, no condensation reaction could be detected using these conditions. The synthesis of **1** was then based on the preparation of the tetrathiacalixarene **2**[2] and subsequent transformation of all four OH groups into SH functionalities. The key step in the strategy used was the thermal Newman–Kwart rearrangement of the $OCSNMe_2$ groups into $SCONMe_2$,[9–11,13,14] followed by the generation of the SH groups. In a first attempt, compound **2** was treated with *N,N*-dimethylthiacarbamoyl chloride ($ClCSNMe_2$) in diglyme at 180 °C[10] and in the presence of NaH as base. Unfortunately, the condensation generated a variety of di- and tri-substituted derivatives. No tetra substituted conformer could be isolated from the ensuing complicated mixture. However, dithiacarbamate compounds **3** (10%) and **4** (10%) and trithiacarbamate compounds **5** (10%), **6** (10%) and **7** (8%) were isolated and structurally characterised either by 2-D NMR or by X-ray diffraction on single crystals in the case of **4**–**6**. In order to generate the tetra-substituted derivatives, one could, as previously reported for tetramercaptocalix[4]arene,[10] treat further the di- or tri-substituted compounds above by $ClCSNMe_2$; instead, the formation of the tetra-substituted compounds was investigated under other basic and solvent conditions. It was found that the treatment of **2** with $ClCSNMe_2$ in refluxing acetone in the presence of K_2CO_3 afforded two tetra-substituted compounds **8** (12%) and **9** (80%). Whereas the structure of **8** was elucidated in the solid state by X-ray diffraction on a single crystal, the conformation of compound **9** was studied by 2-D NMR methods.

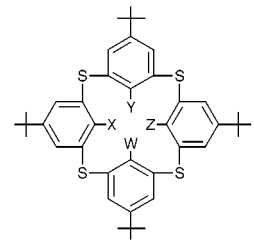

1 X = Y = Z = W = SH
2 X = Y = Z = W = OH
3 or **4** X = Z = OH, Y = W = $OCSNMe_2$
5, **6** or **7** X = OH, Y = Z = W = $OCSNMe_2$
8 or **9** X = Y = Z = W = $OCSNMe_2$
10 or **11** X = Y = Z = W = $SCONMe_2$

Based on the observation mentioned above, in order to study the role of alkali metal cations M^+ present in M_2CO_3 (M = Li, Na, K and Cs) on the yield of formation of the tetra-substituted compounds, a systematic investigation was undertaken. Whereas for Li^+ cation, 30% of the disubstituted compound **4** and 5% of the trisubstituted conformer **6** were obtained, in the presence of Na^+, 30% of **4** and 3% of **7** were isolated. For Cs^+ as for K^+, 12% of **8** and 80% of **9** were obtained. The effect of alkali metal cations on the alkylation of **2** has been previously investigated.[15] In marked contrast with *p-tert*-butylcalix[4]arene for which under the same conditions no tetra substituted derivative could be obtained, for tetrathiacalixarene **2**, the tetra-substituted conformers were formed in 92% yield under rather mild conditions.

Since for the final compound **1**, the SH groups may freely pass though the annulus of the calix, we believed that it was not necessary to separate the 1,2-alternate **8** and the 1,3-alternate **9** conformers. Thermal rearrangement was thus performed in quantitative yield on the purified mixture of the two conformers **8** and **9** at 300 °C *in vacuo*. As expected, two transposed

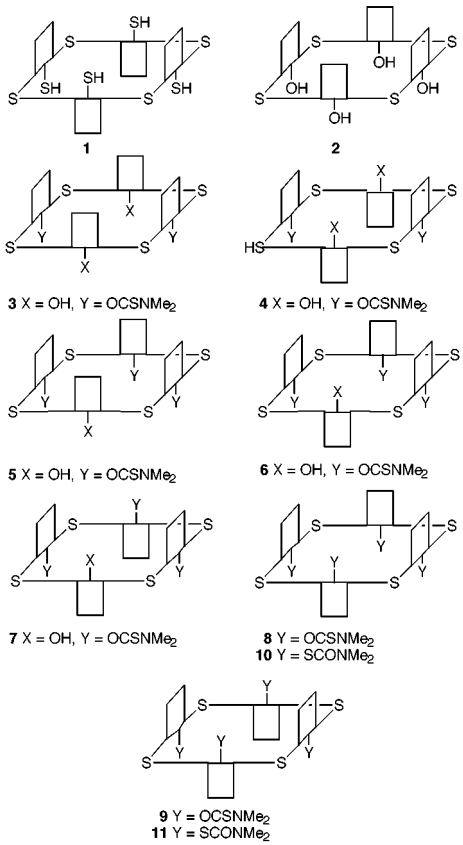

conformers **10** and **11** were obtained. The final deprotection of the sulfur groups leading to the desired compound **1** was first attempted under reductive conditions using $LiAlH_4$ in either refluxing THF for 2 h, and at room temperature for 3 h. In both cases, 50 and 75% of an undesired compound in which three out of four $SCONMe_2$ units were transformed into SH groups was obtained. Refluxing the mixture in THF for a longer period of time resulted in the decomposition of the mixture of conformers. Finally, the desired compound **1** could be obtained in 90% yield upon treatment of the mixture of **10** and **11** by hydrazine hydrate at 100 °C for 18 h. It is worth noting that starting from **2**, the overall yield for the synthesis of **1** was 80%.

In $CDCl_3$ solution at 25 °C, the ^1H NMR spectrum of **1** was extremely simple and comprised a singlet (δ 7.84) corresponding to the aromatic protons and two other singlets at δ 1.25 and 4.72 corresponding to the *tert*-butyl and SH groups, respectively. Owing to the absence of the methylene groups, using only NMR observations, the differentiation between the cone and 1,3-alternate conformers is not feasible. However, the solid state conformation of **1** could be studied by X-ray diffraction on a single crystal (Fig. 1).† In marked contrast with the parent compound **2** which adopts the cone conformation in the crystalline phase,[3] compound **1** adopts the 1,3-alternate conformation in the crystalline phase. The aromatic rings located on the same face of the ligand are almost parallel. The average C–S and C–SH distances are 1.78 and 1.76 Å, respectively.

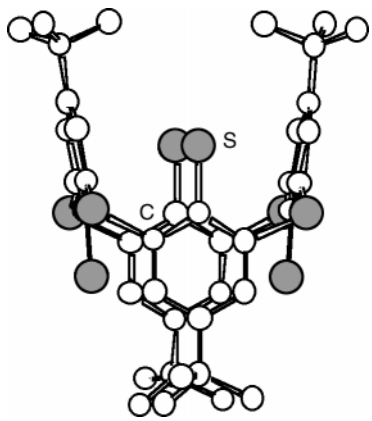

Fig. 1 : X-Ray analysis of *p-tert*-butyltetramercaptotetrathiacalix[4]arene **1**. For the sake of clarity, H atoms and solvent molecules are not represented (for distances see text).

In conclusion, a fast and efficient synthesis of compound **1** was achieved. In the solid state, it was shown that **1** adopts the 1,3-alternate conformation. The complexation ability of **1** towards transition metal cations is currently under investigation.

We thank the CNRS and the Institut Universitaire de France (IUF) for financial support. P. R. thanks the French Embassy in New Delhi for a scholarship.

Notes and references

† *Crystallographic data* for **1** (colourless crystals, 173 K), $C_{121}H_{139}Cl_2OS_{24}$, M = 2449.90, triclinic, space group $P\bar{1}$, a = 14.9058(4), b = 18.8600(4), c = 24.5600(7) Å, α = 84.044(2), β = 80.888(2), γ = 78.386(2)°, U = 6659.2(4) Å^3, Z = 2, D_c = 1.22 g cm^{-3}, Mo-Kα graphite kappaCCD, μ = 0.470 mm^{-1}, 12582 data with $I > 3\sigma(I)$, R = 0.077, R_w = 0.096. The disordered *tert*-butyl groups were refined isotropically over two sites with 50% occupancy. CCDC 182/1421. See http://www.rsc.org/suppdata/cc/1999/2169/ for crystallographic files in .cif format.

1 C. D. Gutsche, *Calixarenes Revisited, Monographs in Supramolecular Chemistry*, no. 1, ed. J. F. Stoddart, RSC, Cambridge, 1998.
2 H. Kumagai, M. Hasegawa, S. Miyanari, Y. Sugawa, Y. Sato, T. Hori, S. Ueda, H. Kamiyama and S. Miyano, *Tetrahedron Lett.*, 1997, **38**, 3971; T. Sone, Y. Ohba, K. Moriya, H. Kumada and K. Ito, *Tetrahedron Lett*, 1997, **38**, 10 689.
3 H. Akdas, L. Bringel, E. Graf, M. W. Hosseini, G. Mislin, J. Pansanel, A. De Cian and J. Fischer, *Tetrahedron Lett.*, 1998, **39**, 2311.
4 M. W. Hosseini, *Calixarene Molecules for Separation*, ed. G. J. Lumetta, ACS, Washington, DC, 1999, in press.
5 G. Mislin, E. Graf, M. W. Hosseini, A. De Cian and J. Fischer, *Chem. Commun.*, 1998, 1345.
6 G. Mislin, E. Graf, M. W. Hosseini, A. De Cian and J. Fischer, *Tetrahedron Lett.*, 1999, **40**, 1129.
7 X. Delaigue, M. W. Hosseini, A. De Cian, J. Fischer, E. Leize, S. Kieffer and A. Van Dorsselaer, *Tetrahedron Lett.*, 1993, **34**, 3285; F. Hajek, E. Graf and M. W. Hosseini, *Tetrahedron Lett.*, 1996, **37**, 1409; F. Hajek, M. W. Hosseini, E. Graf, A. De Cian and J. Fischer, *Angew. Chem., Int. Ed. Engl.*, 1997, **36**, 1760.
8 G. Mislin, E. Graf, M. W. Hosseini, A. Bilyk, A. K. Hall, J. McB. Harrowfield, B. W. Skelton and A. H. White, *Chem. Commun.*, 1999, 373.
9 X. Delaigue, M. W. Hosseini, N. Kyritsakas, A. De Cian and J. Fischer, *J. Chem. Soc., Chem. Commun.*, 1995, 609.
10 C. G. Gibbs and C. D. Gutsche, *J. Am. Chem. Soc.*, 1993, **115**, 5338; C. G. Gibbs, P. K. Sujeeth, J. S. Rogers, G. G. Stanley, M. Krawiec, W. H. Watson and C. D. Gutsche, *J. Org. Chem.*, 1995, **60**, 8394.
11 X. Delaigue, J. McB. Harrowfield, M. W. Hosseini, A. De Cian, J. Fischer and N. Kyritsakas, *J. Chem. Soc., Chem. Commun.*, 1994, 1579.
12 P. Rao, M. W. Hosseini, A. De Cian and J. Fischer, *Eur. J. Inorg. Chem.*, 1999, submitted.
13 X. Delaigue and M. W. Hosseini, *Tetrahedron Lett.*, 1993, **34**, 8111.
14 M. S. Newman and H. A. Karnes, *J. Org. Chem.*, 1966, **31**, 3980; Y. Ting, W. Verboom, L. G. Groenen, J.-D. van Loon and D. N. Reinhoudt, *J. Chem. Soc., Chem.Commun.*, 1990, 1432.
15 N. Iki, F. Narumi, T. Fujimoto, N. Morohashi and S. Miyano, *J. Chem. Soc., Perkin Trans. 2*, 1998, 2745; H. Akdas, G. Mislin, E. Graf, M. W. Hosseini, A. De Cian and J. Fischer, *Tetrahedron Lett.*, 1999, **40**, 2113.

Communication 9/06058H

ChemComm

Vinyl esters as ethylene equivalents in the Khand annulation reaction

William J. Kerr,* Mark McLaughlin, Peter L. Pauson and Sarah M. Robertson

Department of Pure and Applied Chemistry, University of Strathclyde, 295 Cathedral Street, Glasgow, Scotland, UK G1 1XL. E-mail: cbas69@strath.ac.uk

Received (in Liverpool, UK) 13th August 1999, Accepted 6th September 1999

A preparatively convenient and mild method for modified Khand cycloadditions is described; vinyl esters are employed as the olefinic reaction partner to provide cyclopentenone products more normally obtained with ethylene.

The simple one step cobalt carbonyl mediated annulation of an alkyne, an alkene, and carbon monoxide to form substituted cyclopentenones (the Khand reaction)[1] has emerged as one of the most widely used organometal-based transformations in organic synthesis. Indeed, in recent years the development of modified techniques for promoting this reaction has led to its increased utilisation in a wide variety of synthetic endeavours.[1,2] In particular, the application of amine *N*-oxide promoters has allowed the annulations to be performed under mild reaction conditions to deliver highly improved product yields.[3] More specifically, studies in our own laboratory have led to *N*-oxide techniques which allow the application to both asymmetric cyclisation strategies[4] and to the establishment of markedly improved procedures for use with gaseous alkenes such as ethylene.[2h,5] Here we report the discovery of a novel use of non-gaseous ethylene equivalents in the Khand cyclisation.

With a view to gaining access to (poly)oxygenated cyclopentenones and, more especially, with the advent of the mild amine *N*-oxide strategies, we envisaged that it would be possible to employ relatively sensitive vinyl esters as olefinic substrates. Since the phenylethyne–cobalt complex **1** was known[6,7] to give mixtures of 4- and 5-ethoxy-1-phenylcyclopent-2-en-1-one in poor yield when treated with ethyl vinyl ether under the generally less effective traditional reaction conditions, this complex was utilised in our initial experiments with vinyl acetate **2**. To our surprise, under the *N*-oxide conditions shown in Scheme 1 the only organic product isolated was the monosubstituted 2-phenylcyclopent-2-en-1-one **3**, lacking the anticipated acetate functional unit. Despite the moderate 53% yield, we recognised that this result had considerable potential as the basis for the development of a procedure which would employ what could be considered as a non-gaseous ethylene equivalent in Khand cycloadditions. To this end, we sought to optimise this modified Khand process by varying the reaction promoter, the vinyl ester, and the general reaction conditions.

In the reaction shown in Scheme 1, the ketone **3** had been obtained using trimethylamine *N*-oxide dihydrate at 45 °C. On the other hand, by employing the alternative mild oxidant, *N*-methylmorpholine *N*-oxide monohydrate (NMO·H_2O),[3a] we found that the same class of transformation could be promoted at room temperature. In turn, this *N*-oxide was adopted for use in comparative experiments. As can be seen from Table 1, in reactions with complex **1**, a range of vinyl esters (**2**, **4**–**6**) all successfully afforded the cyclopentenone **3**. Additionally, use of vinyl bromide **7** also led to the formation of the same enone product.†

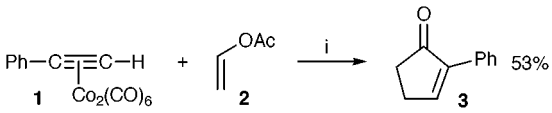

Scheme 1 *Reagents and conditions*: i, Me_3N^+–O^-·$2H_2O$ (9 equiv.), toluene–MeOH (10:1), 45 °C.

Table 1 Modified Khand reactions of vinyl substrates with phenylethyne complex **1**[a]

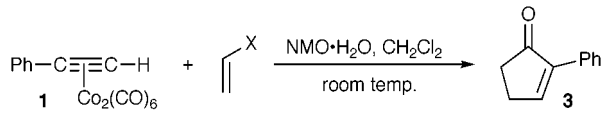

	X	Yield of **3** (%)
2	AcO	52
4	CF_3CO_2	50
5	BzO	58
6	Bu^tCO_2	31
7	Br	54

[a] 9–10 equiv. of NMO·H_2O employed.

Based on the results shown in Table 1, vinyl benzoate **5** was selected for further optimisation. Subsequently, it was established that slow (syringe pump) addition of the *N*-oxide promoter (NMO·H_2O) over a 3 h period led to an excellent 80% yield of **3** at room temperature.‡ Indeed, the enhanced efficiency of this modified Khand process now compares favourably with the optimum yields achieved when using ethylene gas with Me_3N^+–O^-·$2H_2O$ and complex **1**; ethylene reaction at 40 °C and 25–30 atm provides a 71% yield of **3** whilst reaction at room temperature and 1 atm proceeds in 55% yield.[2h,5b]

Having developed the slow addition procedure, these conditions were applied to a range of alkyne complexes (Table 2).§ Overall, we have found that the efficiency of the new vinyl benzoate technique is at least comparable with the optimum ethylene methods and, in most instances (where a comparison can be made), significant enhancement in the yield of cyclopentenone can be realised. A particularly vivid example of the improved efficacy of the ethylene equivalent method is provided when THP-protected propargyl alcohol is utilised as the alkyne substrate; using vinyl benzoate with NMO·H_2O at

Table 2 Modified Khand reactions of vinyl benzoate **5** with alkynes[a]

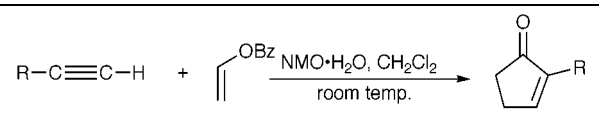

R	Product	Yield (%)
Ph	**3**	80
n-C_5H_{11}	**8**	77
Me_3SiCH_2	**9**	45
$THPOCH_2$	**10**	87
$THPO(CH_2)_2$	**11**	80
$HO(CH_2)_2$	**12**	61
$HOCH_2$	**13**	33

[a] Typically the alkyne $Co_2(CO)_6$ complex and excess vinyl benzoate (as co-solvent)¶ are stirred as NMO·H_2O (8–10 equiv.) is added over 0.5–3 h as a solution in CH_2Cl_2 before stirring is continued at room temp.

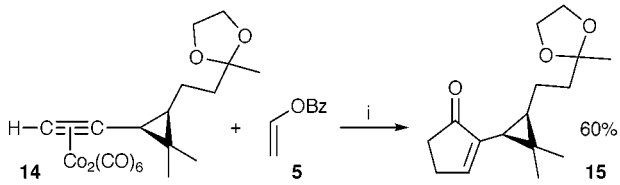

Scheme 2 *Reagents and conditions*: i, NMO·$2H_2O$ (10 equiv.), CH_2Cl_2, 2 h addition, room temp.

room temperature an excellent 87% yield of cyclopentenone **10** is achieved, whereas the maximum yield obtained under the optimum ethylene conditions was only 33%.[2h,5b]‖

As a final example, and to show the utility of the modified methods in natural product synthesis, we chose to employ alkyne complex **14**. In our previously reported total synthesis of (+)-taylorione,[2h,5a] the key step in our sequence towards this target had been the Khand reaction of **14** with ethylene. When reacted with vinyl benzoate under the conditions described here (Scheme 2), complex **14** gave cyclopentenone **15** in a 60% yield.** This result constitutes an improvement in the carefully optimised yield of 41% obtained for the same transformation with ethylene under ambient conditions. On the other hand, it is not equal to the best autoclave yield of 81% achieved with $Me_3N^+–O^-·2H_2O$ at 40 °C and 25 atm. Nonetheless, it is worth noting that, in the instances where higher yields are achievable using gaseous alkenes, autoclave facilities and conditions of elevated temperature and pressure are required. In contrast, the ethylene equivalent procedures disclosed here show how cheap, readily available and easily handled vinyl esters can be employed under ambient conditions to provide cyclopentenone products in yields which are at least competitive with and, more usually, improved over those of the equivalent optimised ethylene process.

In the developed modified Khand process it is clear that the isolated cyclopentenones are the products of reduction. In this respect, the C–O cleavage and subsequent replacement of the ester oxygen with H must involve a low oxidation state cobalt species, as this would be expected, under the reaction conditions, to be the only available reducing agent. Additionally, the reaction only proceeds to give the reduced products under inert (N_2) atmospheres. However, when using vinyl acetate **2** with complex **1** in air only a very low yield (7%) of the 5-acetoxycyclopentenone is obtained. We believe that the required hydrogen atom to complete the reduction process is supplied from water (*e.g.* from the hydrated *N*-oxide). This theory was supported when the reaction of **1** and **2**, promoted by anhydrous NMO, was performed in the presence of excess D_2O and exclusively yielded 5-deuterio-2-phenylcyclopent-2-en-1-one. Such regioselective incorporation of deuterium also implies that the reductive cleavage occurs after the coupling of the alkyne and alkene.

In summary, we have developed a novel method by which vinyl esters can be utilised as non-gaseous ethylene equivalents in the Khand annulation. The mild conditions and simple techniques employed provide significant advantages, both in terms of practical convenience and, in the majority of cases explored, reaction yield, over the corresponding gaseous alkene procedures.

We gratefully acknowledge financial support from the Carnegie Trust for a postgraduate scholarship (M. M.) and Pfizer Central Research, Sandwich, for generous funding of our research endeavours. We also thank the EPSRC Mass Spectrometry Service, University of Wales, Swansea, for analyses.

Notes and references

† Under more traditional conditions of elevated temperature with no *N*-oxide promoters, in reaction with complex **1**, vinyl bromide had been shown to give the product of reductive debromination, cyclopentenone **3**, in the low yield of 19% (ref. 8).

‡ Performing the NMO slow addition experiments for the reaction of complex **1** with vinyl benzoate **5** at a range of higher or lower temperatures (from −70 to 40 °C) led to less efficient cyclisations and lower yields of **3**.

§ All compounds exhibited satisfactory analytical and spectral data.

¶ Excess vinyl benzoate is readily recoverable on completion of the reaction.

‖ Using thermal conditions with no promoter, THP-protected propargyl alcohol completely failed to yield any cyclopentenone products when reacted with ethylene (ref. 9).

** This result provides the ketal protected form of the recently reported (+)-nortaylorione (ref. 10) and constitutes a formal total synthesis of this natural product, which has been prepared from **15** by our novel PPh_3/CBr_4 ketal deprotection method [ref. 2(*h*), 5(*a*), 11].

1 For reviews see: O. Geis and H.-G. Schmalz, *Angew. Chem., Int. Ed.*, 1998, **37**, 911; N. E. Schore, *Org. React.*, 1991, **40**, 1; N. E. Schore, in *Comprehensive Organic Synthesis*, ed. B. M. Trost and I. Fleming, Pergamon, Oxford, 1991, vol. 5, p. 1037.

2 (*a*) J. Cassayre and S. Z. Zard, *J. Am. Chem. Soc.*, 1999, **121**, 6072; (*b*) M. Ishizaki, K. Iwahara, K. Kyoumura and O. Hoshino, *Synlett*, 1999, 587; (*c*) M. M. Bruendl, S. G. Van Ornum, T.-M. Chan and J. M. Cook, *Tetrahedron Lett.*, 1999, **40**, 1113; (*d*) R. B. Grossman, *Tetrahedron*, 1999, **55**, 919; (*e*) H. Corlay, E. Fouquet, E. Magnier and W. B. Motherwell, *Chem. Commun.*, 1999, 183; (*f*) L. M. Harwood and L. S. A. Tejera, *Chem. Commun.*, 1997, 1627; (*g*) T. F. Jamison, S. Shambayati, W. E. Crowe and S. L. Schreiber, *J. Am. Chem. Soc.*, 1997, **119**, 4353; (*h*) J. G. Donkervoort, A. R. Gordon, C. Johnstone, W. J. Kerr and U. Lange, *Tetrahedron*, 1996, **52**, 7391 and references cited therein.

3 (*a*) S. Shambayati, W. E. Crowe and S. L. Schreiber, *Tetrahedron Lett.*, 1990, **31**, 5289; (*b*) N. Jeong, Y. K. Chung, B. Y. Lee, S. H. Lee and S.-E. Yoo, *Synlett*, 1991, 204; (*c*) Y. K. Chung, B. Y. Lee, N. Jeong, M. Hudecek and P. L. Pauson, *Organometallics*, 1993, **12**, 220; (*d*) M. E. Krafft, I. L. Scott, R. H. Romero, S. Feibelmann and C. E. Van Pelt, *J. Am. Chem. Soc.*, 1993, **115**, 7199.

4 W. J. Kerr, G. G. Kirk and D. Middlemiss, *Synlett*, 1995, 1085; A. M. Hay, W. J. Kerr, G. G. Kirk and D. Middlemiss, *Organometallics*, 1995, **14**, 4986; W. J. Kerr, G. G. Kirk and D. Middlemiss, *J. Organomet. Chem.*, 1996, **519**, 93.

5 (*a*) C. Johnstone, W. J. Kerr and U. Lange, *Chem. Commun.*, 1995, 457; (*b*) A. R. Gordon, C. Johnstone and W. J. Kerr, *Synlett*, 1995, 1083.

6 M. C. Croudace and N. E. Schore, *J. Org. Chem.*, 1981, **46**, 5357.

7 D. C. Billington, W. J. Kerr, P. L. Pauson and C. F. Farnocchi, *J. Organomet. Chem.*, 1988, **356**, 213; C. F. Farnocchi, W. J. Kerr, M. McLaughlin, A. S. Nicol, P. L. Pauson and S. M. Robertson, unpublished observations.

8 I. U. Khand and P. L. Pauson, *J. Chem. Res.*, 1977, (S) 9; (M) 168.

9 H. J. Jaffer, PhD Thesis, University of Strathclyde, 1982.

10 C. M. de Oliveira, V. L. Ferracini, M. A. Foglio, A. de Meijere and A. J. Marsaioli, *Tetrahedron: Asymmetry*, 1997, **8**, 1833.

11 C. Johnstone, W. J. Kerr and J. S. Scott, *Chem. Commun.*, 1996, 341.

Communication 9/06660H

ChemComm

Electrocatalysis of neurotransmitter catecholamines by 2,4,6-triphenylpyrylium ion immobilized inside zeolite Y supercages

A. Doménech,*[a] M. T. Doménech-Carbo,[b] H. García[c] and María S. Galletero[c]

[a] *Departament of Analytical Chemistry, University of Valencia, Dr. Moliner, 50, 46100 Burjasot, Valencia, Spain. E-mail: tdomenec@crbc.upv.es*

[b] *Departament of Conservation of Cultural Heritage, Polytechnical University of Valencia, Camino de Vera s/n. 46022 Valencia, Spain*

[c] *Institute of Chemical Technology CSIC-UPV, Polytechnical University of Valencia, Camino de Vera s/n. 46022 Valencia, Spain*

Received (in Cambridge, UK) 22nd July 1999, Accepted 23rd September 1999

2,4,6-Triphenylpyrylium ions entrapped inside the supercages of Y zeolite exert a remarkable catalytic effect toward the electrochemical oxidation of dopamine and norepinephrine (neurotrasmitter catecholamines) in neutral aqueous media.

Encapsulation of organic species inside the rigid matrix of microporous zeolites has proved to be a general methodology to control the molecular properties of the incorporated guest.[1] Zeolites are a large family of crystalline aluminosilicates whose structure defines strictly uniform channels and cavities of molecular dimensions (micropores). It is in these internal voids where a guest can be accommodated provided that its molecular size is smaller than the void dimensions. In particular, the structure of zeolite Y is formed by an array of spherical cavities (1.4 nm diameter) that are tetrahedrally interconnected through four smaller apertures (0.74 nm diameter).

We have already reported that the bulky 2,4,6-triphenylpyrylium ion (TP^+, ≈ 1.3 nm) can be prepared inside the zeolite Y supercages through a 'ship-in-a-bottle' synthesis that relies on the diffusion of much smaller synthetic precursors.[2] After the encapsulation, TP^+ remains mechanically immobilized inside the zeolite Y supercages, but it still can interact with smaller molecules through the cavity windows.

Recently one of us has shown that while the BF_4^- salt of TP^+ in water undergoes a rapid hydrolytic ring opening, when TP^+ is encapsulated within the restricted space provided by the supercages of zeolite, the host framework protects it from the nucleophilic attack of water.[3] As a result, TP^+ within Y zeolite (TPY) is completely persistent in water. This opens the opportunity for new applications of TP^+ in aqueous media, as reported herein on the catalytic effect of TPY on the electrochemical oxidation of catecholamines in aqueous solution.

The electrochemistry of pyrylium ions in solution is well understood. TP^+ undergoes one-electron reduction in protic solvents.[4] Controlled potential electrolysis produces the corresponding dipyran which in turn can be reoxidized back to TP^+. In aprotic solvents, reduction of pyrylium ions leads to the corresponding bipyranylidene together with pyrane.[5] In this case, the transient reduction wave is controlled kinetically by the irreversible dimerization of the radicals formed after the initial electron transfer.[6] Bipyranylidene and pyrane are produced by the reversible reduction of the dimer.[7] We have found that upon encapsulation in the internal voids of zeolites, owing to the impossibility to form dimers, pyrylium ions display an apparently more simple electrochemistry consisting on the quasi-reversible reduction to TP. Compartmentalization of TP^+ inside the zeolite Y impedes its diffusion and eventually that of the corresponding TP pyranyl radicals, and therefore radical coupling is inhibited.

Preliminary experiments on the electrochemistry of TP^+ incorporated within zeolite Y confirmed the inhibition of dimerization processes. Paraloid B72† and Elvacite 2044,‡ were used to obtain polymer film electrodes containing TPY as modifiers. As can be seen in Fig. 1, polymer film electrodes (PFEs) modified by zeolite Y containing TP^+, TPY-MEs, exhibit a well defined reduction process. As can be seen in Fig. 2, cyclic voltammograms show a one-electron couple at an equilibrium potential of −0.28 V *vs.* SCE in acetonitrile. The peak potential separation is about 150 mV suggesting that the electrochemical process is kinetically reversible. The morphology of voltammograms is practically identical upon immersion of the modified electrode in neutral aqueous solutions, denoting that hydrolytic ring opening is inhibited by encapsulation. The voltammetric response is enhanced on increasing the contact time of the electrode into the solution and remains stable upon repetitive cycling of the potential scan. The absence of additional peaks in repetitive cyclic voltammetry denotes that no parallel chemical reactions occur. Identical results were obtained at working electrodes with self-supported finely ground zeolite pressed onto the surface of the bare electrode. Although the internal *versus* external nature of the electrochemical response involved in zeolite-modified electrodes remains controversial,[8,9] it appears that the observed electrochemistry is essentially attributable to the population of TP^+ located at the boundary region of zeolite grains.[10,11]

The reduction process involves the incorporation of charge-balancing positive ions from the supporting electrolyte to the zeolite boundary sites and can be represented by eqn. (1).

$$TP^+_{(zeolite)} + M^+_{(sol)} + e^- = TP^\bullet_{(zeolite)} + M^+_{(zeolite)} \quad (1)$$

Encapsulation of pyrylium ions inside zeolite Y and the resulting stability in aqueous solutions has enabled us to test this material as an electrocatalyst for the oxidation of the neuro-

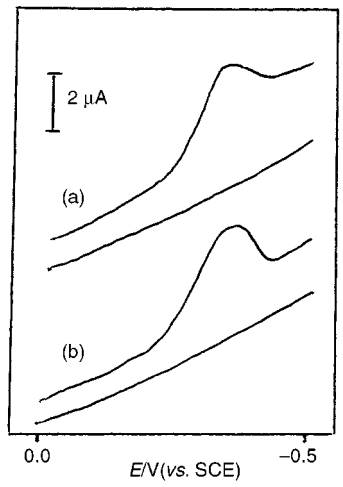

Fig. 1 Cathodic differential pulse voltammograms, including the base line, for TPY modified electrodes: (a) in MeCN (0.10 M NEt_4ClO_4) and (b) in water (0.15 M $NaClO_4$). v = 2 mV s^{-1} ΔU = 100 mV.

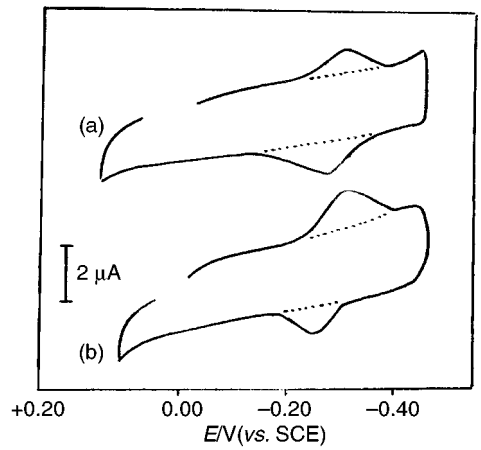

Fig. 2 Cyclic voltammograms, including the base line (dotted line), for TPY-MEs: (a) in MeCN (0.10 M NEt_4ClO_4) and (b) in water (0.15 M $NaClO_4$). v = 100 mV s^{-1}.

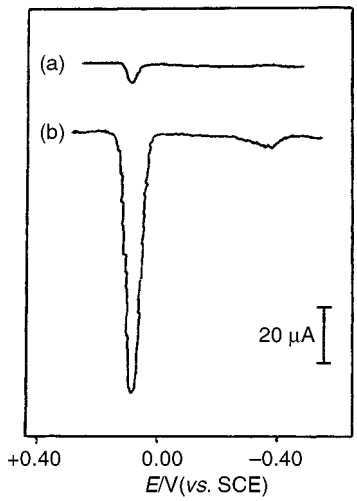

Fig. 3 Anodic DPVs for different electrodes immersed into a 1.0×10^{-4} M solution of dopamine in aqueous phosphate buffer, pH = 7.05: (a) glassy carbon electrode and (b) TPY-ME. v = 8 mV s^{-1}. ΔU = 100 mV.

transmitter catecholamines, dopamine and norepinephrine. These compounds play an essential role in neurochemistry. Since the loss of neurotransmitter-containing neurons may result in some serious diseases such as Parkinsonism,[12] the determination of such compounds in real biological systems is an obvious target in neurochemical studies.[13]

Dopamine and norepinephrine have a common dihydroxyphenethylamine moiety that is responsible for their observed electrochemistry. These species exhibit a well defined electrochemical oxidation at *ca.* +0.2 V *vs.* SCE in neutral aqueous media. The electrochemical oxidation process leads to the corresponding *o*-quinone which can be intracycled and again oxidized.[14] This electrode process has been previously used for analytical purposes by using unmodified[15] and modified electrodes.[16]

At zeolite-modified electrodes lacking encapsulated TP^+, Y-MEs, the oxidation peak of dopamine or norepinephrine is almost identical to that recorded at the basal glassy carbon electrode. In contrast, using TPY-MEs, the peak current is about 10–20 times enhanced with respect the peak obtained at the basal glassy carbon electrode. As an example, the catalytic effect of TPY on the electrochemical oxidation of dopamine is shown in Fig. 3. On scanning the potential in the anodic direction, an oxidation peak appears at −0.25 V, that corresponds to the oxidation of TP to TP^+ in the electrochemically accessible sites of the zeolite. A second prominent anodic peak is observed at *ca.* +0.20 V corresponding to the enhanced dopamine oxidation. Similar results were obtained for norepinephrine solutions. In both cases, the electrocatalytic effect was not observed at modified electrodes containing pristine Y zeolite lacking encapsulated pyrylium groups, indicating that the electrocatalytic effect must be attributed to the fraction of pyrylium ions located at the boundary sites of the zeolite particles. The electrocatalytic current increases on lowering the potential scan rate and increasing the contact time of the modified electrode with the solution prior to the electrochemical runs. All these data indicate that the net electrocatalytic effect depends on the net amount of diffusive transfer into the zeolite particles.

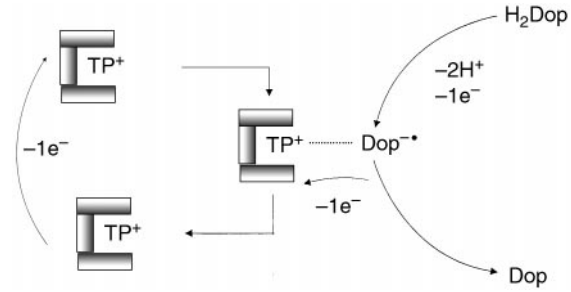

Scheme 1

The measured peak currents for dopamine and norepinephrine oxidations produced linear calibration graphs for 1×10^{-6} to 1×10^{-4} M concentrations of catecholamine. The sensitivity for dopamine oxidation using differential pulse voltammetry (12 A cm^{-2} M^{-1}) is similar to that for norepinephrine oxidation (10 A cm^{-2} M^{-1}), enabling the use of TPY-MEs as electrochemical sensors.

The oxidation process of dopamine and norepinephrine involves two consecutive one-electron transfer processes coupled with deprotonation reactions. The electrocatalytic effect is likely to be caused by the stabilization of the catecholamine anion radical intermediates resulting from the first electron transfer process upon adduct formation with surface-confined pyrylium, with a subsequent electron-transfer that yields the *o*-quinone and surface-confined TP, as depicted in Scheme 1.

The observation of this novel electrocatalytic effect using pyrylium ion incorporated stabilized into zeolites realizes the new opportunities that the stabilization of organic species by encapsulation inside the rigid framework of microporous materials can offer, such as for the development of new electrochemical sensors with light selectivity and increased sensitivity.

Notes and references

† Ethyl methacrylate (70%)–methyl acrylate (30%) co-polymer (P[EMA/MA]).

‡ *n*-butyl methacrylate homopolymer (PnBMA).

1 J. C. Scaiano and H. García, *Acc. Chem. Res.*, in press.
2 A. Corma, V. Fornés, H. García, M. A. Miranda, J. Primo and M. J. Sabater, *J. Am. Chem. Soc.*, 1994, **116**, 2276.
3 A. Sunjuán, M. Alvaro, G. Aguirre, H. García and H. Scaiano, *J. Am. Chem. Soc.*, 1998, **120**, 7351.
4 P. Zuman and C. L. Perrin, *Organic Polarography*, Interscience, New York, 1969, p. 283.
5 C. Amatore, A. Jutand, F. Pflüger, C. Jallabert, H. Strezelecka and M. Weber, *Tetrahedron Lett.*, 1989, **30**, 1383.
6 C. Amatore, A. Jutand and F. Pflüger, *J. Electroanal. Chem.*, 1987, **218**, 361.
7 C. Amatore, M. Azzabi, P. Calas, A. Jutand, C. Lefrou and Y. Rollin, *J. Electroanal. Chem.*, 1990, **288**, 45.
8 F. Bedioui, J. Devynck and K. J. Balkus Jr., *J. Phys. Chem.*, 1996, **100**, 8607.
9 D. R. Rolison, C. A. Bessel, M. D. Baker, C. Senaratne and J. Zhang, *J. Phys. Chem.*, 1996, **100**, 8610.
10 N. J. Turro and M. García-Garibay, in *Photochemistry in Organized Media*, ed. V. Ramamurthy, VCH, New York, 1991, pp. 1–38.
11 C. A. Bessel and D. R. Rolison, *J. Phys. Chem. B*, 1997, **101**, 1148.
12 R. M. Wightman, L. J. Lay and A. C. Michael, *Anal. Chem.*, 1988, **60**, 769A.
13 R. D. O'Neill, *Analyst*, 1994, **119**, 767.
14 J. L. Ponchon, R. Cespuglio, F. Gonon, M. Jouvet and J.-F. Pujol, *Anal. Chem.*, 1979, **51**, 1483.
15 G. N. Kamau, W. S. Willis and J. F. Rusling, *Anal. Chem.*, 1985, **57**, 545.
16 A. Ciszewski and G. Milczarek, *Anal. Chem.*, 1999, **71**, 1055 and references therein.

Communication 9/05929F

Low metal loading Ru-MCM-41 stereocontrolled hydrogenation of prostaglandin intermediates

S. Coman,[a] M. Florea,[a] F. Cocu,[a] V. I. Pârvulescu,*[a] P. A. Jacobs,[b] C. Danumah[c] and S. Kaliaguine[c]

[a] *University of Bucharest, Department of Chemical Technology and Catalysis, B-dul Regina Elisabeta 4-12, Bucharest 70346, Romania. E-mail: V_PARVULESCU@chim.upb.ro*

[b] *KU Leuven, Department Interphase Chemistry, Centrum Surface Chemistry and Catalysis, 92 Kardinaal, Mericierlaan, B-3001 Leuven, Belgium*

[c] *Universite Laval, Departement de Genie Chimique, Ste Foy, QC, Canada G1K 7P4. E-mail: Kaliagui@gch.ulaval.ca*

Received (in Oxford, UK) 31st August 1999, Accepted 23rd September 1999

Low metal loading Ru-MCM-41 (0.134 and 0.667 wt% Ru) have been prepared by adsorption of ruthenocene from a diethyl ether solution, calcination and reduction under flowing hydrogen at 350 °C; the physical characteristion by a combination of several techniques has shown that Ru is homogeneously distributed inside the MCM pores, and that it is only partially reduced; these catalysts exhibit a very high diastereoselectivity in hydrogenation of an F prostaglandin intermediate leading only to the 11*S*,15*R* diastereomer.

Diastereoselective hydrogenation is generally considered to occur on high loading noble metal catalysts (min. 5 wt%) in the absence of any chiral modifiers.[1,2] Some beneficial effects of the latter[3] or of some chiral auxiliaries have even been reported.[4,5] In all these cases the diastereoselectivity is related to some specific features of the metallic species or to the choice of an adequate reaction solvent. Otherwise the reaction product is a racemic blend. In most cases the diastereomeric excess (de) is low. Diastereoselective hydrogenation of α,β-unsaturated carbonyl compounds such as prostaglandin intermediates (Scheme 1) raises some additional problems because the interesting compounds are the allylic alcohols and from the thermodynamic point of view it is easier to hydrogenate the C=C double bound than the carbonylic one. Some shape selectivity effects have already been reported in the case of cinnamaldehyde hydrogenation[6] but it is still not clear if, for high metal loading and microporous supports, the effect of some adjacent Lewis sites, which are well known to exert a positive influence in this reaction, is not responsible for the observed results.

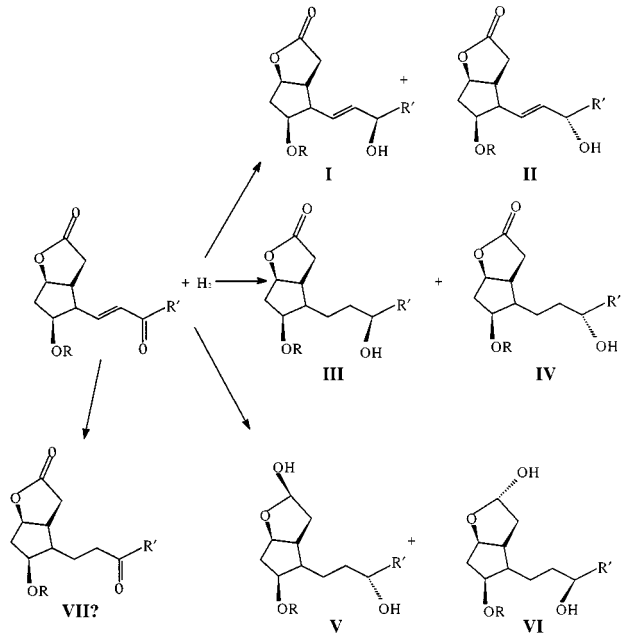

Scheme 1 Possible routes in hydrogenation of the F prostaglandin intermediate.

Here, we report a first example of the positive influence exerted by the mesoporous texture in the diastereoselective hydrogenation of a F prostaglandin intermediate on Ru-MCM-41 catalysts with very low Ru content using hydrogen as the reducing agent. Hydrogenation of the 15-carbonylic bond with generation of the chiral allylic structure is of special interest for these molecules because of its pharmaceutical applications.

The MCM-41 silica catalyst support was synthesised using sodium silicate (Aldrich) as the source of silicon and hexadecyltrimethylammonium bromide as the template. The synthesis was conducted at 70 °C and pH 11 for 7 days. The MCM-41 material was then filtered off, washed, dried and calcined at 550 °C for 12 h. The calcined material had a BET surface area of 1127 $m^2\ g^{-1}$ and a BJH pore diameter of 27 Å.

The catalysts used in the present study were prepared by adsorption of ruthenocene from a diethyl ether solution. After Ru deposition the catalysts were dried and calcined for 6 h at 550 °C, after raising the temperature at 1 °C min^{-1}. The reduction of these catalysts was performed under flowing hydrogen for 3 h at 350 °C with a heating rate of 1 °C min^{-1}. The Ru loading was determined using ICP-AES. Catalysts containing 0.134 and 0.667 wt% Ru were respectively obtained. The catalysts were characterised using surface area measurements by standard N_2 adsorption at 77 K, H_2-TPR, Mossbauer spectroscopy, H_2-chemisorption and XRD. The parameters determined using the above measurements are reported in Table 1.

Hydrogenation of the substrate was carried out in a stainless steel stirred autoclave under 2–8 atm hydrogen pressure at 20 °C using a solution of prostaglandine intermediate in anhydrous

Table 1 Characteristics of the Ru-MCM-41 catalysts

	MCM-41 Catalyst	
Property	0.13 wt% Ru	0.67 wt% Ru
BET surface area/$m^2\ g^{-1}$	807	739
BJH pore diameter/nm	2.6	2.6
Ru $3p_{3/2}$/eV	462.7	462.2
Ru/Si (XPS)	3.4×10^{-3}	5.3×10^{-3}
Ru/Si (ICP-AES)	2.8×10^{-3}	10.4×10^{-3}
Reduction degree (%)	16.6	39.5
Ru^0/Ru^{IV},[a] (%)	17.2	41.3
Adsorbed $H_2/cm^3\ g^{-1}$	0.0601	0.2202
Dispersion[b] (%)	20.8	14.8
d_{Ru}[b]/nm	6.5	9.1

[a] Determined from Mossbauer spectroscopy. [b] Determined from H_2 chemisorption.

methanol, ethanol or isopropyl alcohol. Analysis of the reaction products was carried out by HPLC using a Nucleosil 5C18 column as well as by ^{13}C and ^{1}H NMR. The diastereoselective excess (de) was defined using eqn. (1):

$$de = \{[(15R) - (15S)]/[(15R) + (15S)]\} \times 100 \quad (1)$$

We defined 15*R* and 15*S* as the allylic chiral products from the reaction scheme.

Data presented in Table 1 show that at such low loadings, Ru is only partially reduced. The same conclusion was reached from the H_2-TPR measurements. In addition these determinations indicated only one reduction peak thus suggesting the presence of only one reducible Ru species. The good concordance beween the XPS and the analytical Ru/Si ratios suggests that Ru is homogeneously distributed inside the mesopores. However, H_2-chemisorption results indicate that even at such a low concentration Ru has a tendency to agglomeration. XRD indicates however (no diffraction peak of Ru or of a Ru compound), that these particles are rather small which is again in good concordance with chemisorption data.

The activity of the Ru-MCM-41 catalysts was found to increase with Ru content (Fig. 1). For each catalyst, increasing the pressure resulted in an increase of both the conversion and the selectivity to allylic alcohol. For the catalyst containing 0.13 wt% Ru the conversion increases by 15 times, and for that with 0.67 wt% Ru by 5 times, when the pressure is increased from 2 to 8 atm. At an Ru loading of 0.67 wt% a conversion of near 100% was reached. In all cases the formation of the allylic alcohol occurs with a total de in the 11*S*,15*R* form (product **II** in Scheme 1). Other studies using high Ru loading on zeolite Y,[6] showed that when the reaction occurs on the external surface of the catalysts, and in the absence of any chiral modifiers, only the racemic blend was obtained. Under these conditions an increase of the pressure led to a decrease of the selectivity to allylic alcohol.

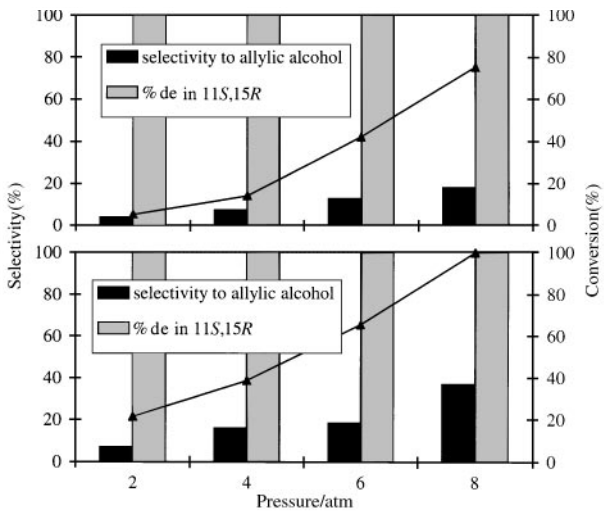

Fig. 1 Variation of the conversion, selectivity to allylic alcohol and de *vs.* pressure (a) 0.13 wt% Ru-MCM-41, (b) 0.67 wt% Ru-MCM-41; solvent methanol, room temp., 2h).

The variation of the same parameters as a function of the solvent (Fig. 2) shows that the solvent affects the total conversion and the selectivity to allylic alcohol. The best conversions were obtained using methanol and the best selectivities to allylic alcohol with isopropyl alcohol. The de was 100% in the 11*S*,15*R* form irrespective of the solvent nature.

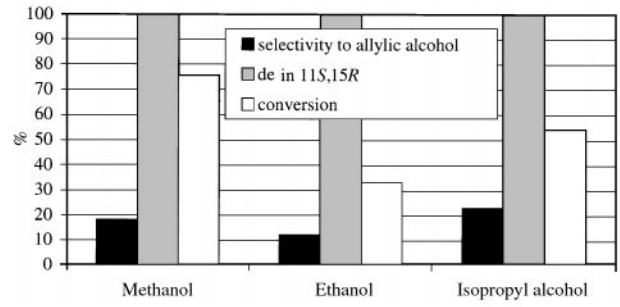

Fig. 2 Variation of the conversion, selectivity to allylic alcohol and de with solvent (0.67 wt% Ru-MCM-41, room temp. 2 h).

To explain these data one should accept that all the reaction parameters, namely the conversion, the selectivity to allylic alcohol and the diastereoselectivity are determined by the access of the prostaglandin intermediate to the MCM pores. The kinetic diameter of this molecule is rather high, and its penetration in the pores is diffusionally controlled. Ru is well distributed inside of these and even if it exhibits a tendency to agglomeration, the metal patches are smaller than those generally reported to have activity in such reactions. A deeper penetration of the reactant molecule leads to an increased number of molecules involved in a direct CO···Ru interaction. Under these conditions, because of the relatively small Ru size, the hydrogenation of the C=C double bond becomes less favoured and the selectivity to allylic alcohol increases. Other effects such as pore hindrance could be expected. The MCM-41 support is a pure silica, and therefore no Lewis acid sites are expected. The complete diastereoselective hydrogenation is very probably the consequence of the steric hindrance described below. As mentioned above the 11-OH group is in the *S* conformation. Owing to this conformation, an extended hydrogen bond interaction *via* the hydrogen of the alcohol group is possible. Because of this, hydrogen will attack the CO bond on the other side of the F prostaglandin intermediate molecule leading to the 15*R* isomer (compound **II** in Scheme 1). A cooperative contribution between the solvent and the pore hindrance is also sustained by the observed differences in conversion and selectivity in various solvents.

In conclusion, this data shows that the diastereoselective hydrogenation of large enones such as the F prostaglandin intermediate can be improved by using pore size controlled mesoporous materials as support for the ruthenium. It is also shown that in such a surrounding these reactions could also be carried out at very low metal loading, namely < 1 wt%, which is rather unusual for such large molecules.

Notes and references

1 G. C. Andrews, T. C. Crawford and B. E. Bradley, *J. Org. Chem.*, 1981, **46**, 2976.
2 A. G. M. Barrett and F. Damiani, *J. Org. Chem.*, 1999, **64**, 1410.
3 F. Cocu, S. Coman, C. Tanase, D. Macovei and V. I. Pârvulescu, *Stud. Surf. Sci. Catal.*, 1997, **108**, 207.
4 T. Munegumi, T. Maruyama, M. Takasaki and K. Harada, *Bull. Chem. Soc. Jpn.*, 1990, **63**, 1832.
5 V. S. Ranade, G. Consiglio and R. Prins, *Catal. Lett.*, 1999, **58**, 71.
6 D. G. Blackmond, R. Oukaci, B. Blanc and P. Gallezot, *J. Catal.*, 1991, **131**, 401.
7 A. Dobre, M. Florea and V. I. Pârvulescu, to be submitted.

Communication 9/07119I

ChemComm

Synthesis of a new mesoporous carbon and its application to electrochemical double-layer capacitors

Jinwoo Lee,[a] Songhun Yoon,[a] Taeghwan Hyeon,*[a] Seung M. Oh[a] and Ki Bum Kim[b]

[a] *School of Chemical Engineering, Seoul National University, Seoul 151-742, Korea. E-mail: thyeon@plaza.snu.ac.kr*
[b] *School of Materials Science and Engineering, Seoul National University, Seoul 151-742, Korea*

Received (in Cambridge, UK) 24th August 1999, Accepted 1st October 1999

A mesoporous carbon with regular three-dimensionally interconnected 2 nm pore arrays using AlMCM-48 as a template has been synthesised; the mesoporous carbon exhibited excellent performance as an electrochemical double layer capacitor.

The development of mesoporous silica materials by Mobil Oil researchers in 1992 stimulated explosive research on the preparation of porous materials through template approaches.[1] Various types of organic templates including surfactant self-assemblies, block copolymers and polymer lattices have been utilized to synthesize such mesoporous inorganic materials.[2] Recently many types of nanostructured carbons have been produced through templating approaches.[3] Electrochemical double-layer capacitors (EDLCs) find new promising applications as pulse power sources for digital communication devices and electric vehicles.[4] The popularity of these devices is derived from their higher energy density relative to conventional capacitors and their longer cycle life and higher power density relative to batteries. Here, we report the first synthesis of a mesoporous carbon material with regular three-dimensionally interconnected pore channels. We also present preliminary results on the EDLC performance of the mesoporous carbon. In our approach, a mesoporous MCM-48 aluminosilicate with three-dimensional channel structure has been utilized as a template. Mesoporous silica MCM-48 was prepared by the reported method.[1] Aluminium was implanted onto MCM-48 to generate strong acid catalytic sites for the polymerization of phenol and formaldehyde. Phenol and formaldehyde were incorporated into the pores of aluminium-implanted MCM-48 (AlMCM-48) by heating for 12 h at 90 °C under reduced pressure. The polymerization of phenol and formaldehyde to obtain the phenol resin inside AlMCM-48 was carried out by heating the mixture under a nitrogen atmosphere at 125 °C for 5 h.[5] The resulting AlMCM-48–phenol resin composite was heated under an N_2 flow at a heating rate of 5 °C min^{-1} to 700 °C and held there for 7 h to carbonize phenol resin inside the MCM-48 channels. The dissolution of MCM-48 frameworks using 48% aqueous hydrofluoric acid (HF) generated mesoporous carbon, designated SNU-1 (Seoul National University).

The ordered mesoporous structure of SNU-1 was investigated by X-ray diffraction (XRD), transmission electron microscopy (TEM) and gas adsorption measurements. XRD patterns were obtained at various times during the course of the synthesis. Fig. 1(a) shows the characteristic pattern of the AlMCM-48 template with a *d* spacing value of 3.37 nm.[6] To our surprise, intense peaks at $2\theta = 1.6$ and 2.7° from the long-range ordering of mesopores is clearly shown in the XRD pattern of SNU-1 carbon [Fig. 1(b)]. This result revealed that the carbon networks formed inside the mesopores of AlMCM-48 are strong enough to survive even after the removal of the aluminosilicate framework by HF etching. Elemental analysis (EA) revealed a high C/H molar ratio of 9.3 and < 1 mol% aluminosilicate residue in the SNU-1 carbon material (EA result: 93.24% C, 0.84% H, 0.09% N, 2.56% O). TEM studies of mesoporous SNU-1 carbon showed a regular array of 2 nm diameter holes separated by 2 nm thick carbon walls (Fig. 2). The specific surface area of SNU-1 was found to be 1257 m^2 g^{-1} from

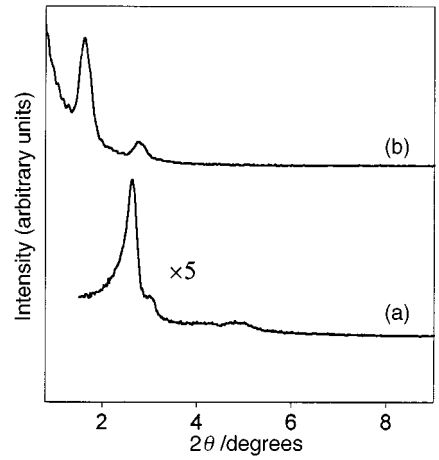

Fig. 1 X-Ray diffraction (XRD) patterns of AlMCM-48 template (a) and mesoporous SNU-1 carbon (b). Trace (a) was obtained with a Rigaku D/Max-3C diffractometer equipped with a rotating anode and Cu-Kα radiation ($\lambda = 0.15418$ nm) and trace (b) was acquired on a Bruker GADDS small-angle X-ray scattering diffractometer with a general area detector.

nitrogen BET adsorption measurements. This is comparable to values reported for other mesoporous inorganic materials. Nitrogen adsorption–desorption curves showed hysteresis at high relative pressure characteristic of mesopores. The pore size distribution data calculated from the adsorption branch of the nitrogen isotherm by the BJH (Barrett–Joyner–Halenda) method showed that pores are uniform with an average pore size of 2.3 nm (Fig. 3).

The EDLC performance of SNU-1 was compared to the most popularly applied activated carbon, MSC-25. Fig. 4 shows the cyclic voltammograms of two carbon electrodes that were obtained in organic electrolyte (1 M NEt_4BF_4 in propylene carbonate). An immediately apparent feature is that SNU-1 shows a more ideal capacitor behavior than MSC-25 with a steeper current change at the switching potentials (0.0 and 3.0 V), resulting in a more rectangular-shaped (mirror-imaged) *i*–*V* curve. An important characteristic of electrical energy storage in a capacitor is that energy is retrievable in discharge over the same potential range as that required to store the energy on charging, otherwise the energy storage is limited. The slow changes at the switching potentials in the cyclic voltammogram (CV) of MSC-25 electrode stem from the slow re-organization

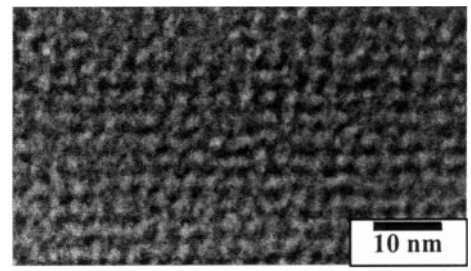

Fig. 2 Transmission electron micrograph (TEM) of mesoporous SNU-1 carbon. The image was obtained with a Phillips CM-20 instrument.

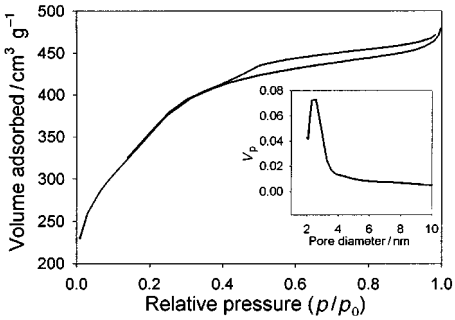

Fig. 3 N_2 adsorption and desorption isotherms of mesoporous SNU-1 carbon. (Inset) The corresponding pore size distribution curve calculated from the adsorption branch of the nitrogen isotherm by the BJH method. V_p is the incremental pore volume. The isotherms were collected at 77 K on a Micrometrics ASAP2010 Gas Adsorption Analyzer after the carbon material was degassed at 250 °C at 30 μTorr for 5 h.

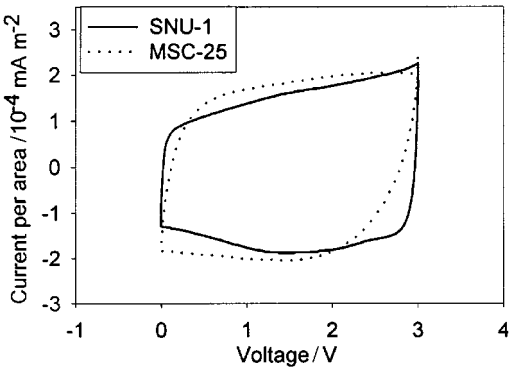

Fig. 4 Cyclic voltammograms of SNU-1 and MSC-25 activated carbon in organic electrolyte (1 M NEt_4BF_4 in propylene carbonate). A two-electrode system consisting of working and counter electrodes was used. These two electrodes were fabricated with equal amounts of the carbon materials. CV measurements were made in the potential range 0–3 V with a scan rate of 5 mV s^{-1}.

of the double layer owing to slow ionic motions in micropores. The steep changes in the CV of the SNU-1 electrode in turn reflect the dominance of regular interconnected mesopores among electrochemically usable pores.

When cyclic voltammetry of SNU-1 carbon was performed in an aqueous electrolyte solution (2 M H_2SO_4), a similar rectangular-shaped pattern was obtained. Rectangular-shaped cyclic voltammograms over a wide range of scan rates is the ultimate goal in EDLC. This behavior is very important for practical applications. First, a higher energy density is expected, because the usable potential range is wide. Second, a higher power density is expected as the critical scan rate is increased. SNU-1 carbon is much closer to this behavior than MSC-25. When cyclic voltammograms were recorded for these two carbons in an aqueous electrolyte solution by varying the scan rate from 5 to 50 mV s^{-1}, SNU-1 carbon retained a rectangular shape up to a scan rate of 20 mV s^{-1}. By contrast, MSC-25 carbon showed a deformed cyclic voltammogram at a scan rate of 10 mV s^{-1} and a completely collapsed one at a scan rate of 20 mV s^{-1}.

We are grateful to the Korea Science and Engineering Foundation (Basic Research Program #98-05-02-03-01-3) for financial support.

Notes and references

1 C. T. Kresege, M. E. Leonowicz, W. J. Roth, J. C. Vartuli and J. S. Beck, *Nature*, 1992, **359**, 710; J. S. Beck, J. C. Vartuli, W. J. Roth, M. E. Leonowicz, C. T. Kresge, K. D. Schmitt. C. T.-W. Chu, D. H. Olson, E. W. Shepard, S. B. McCullen, J. B. Higgins and J. L. Schlenker, *J. Am. Chem. Soc.*, 1992, **114**, 10 834.

2 S. A. Bagashaw and T. J. Pinnavaia, *Angew. Chem., Int. Ed. Engl.*, 1996, **35**, 1102; P. Yang, D. Zhao, D. I. Maroglese, B. F. Chmelka and G. D. Stucky, *Nature*, 1999, **396**, 152; D. Zhao, J. Feng, Q. Huo, N. Melosh, G. H. Fredrickson, B. F. Chmelka and G. D. Stucky, *Science*,1998, **279**, 548; J. Y. Ying, C. P. Mehnert and M. S. Wong, *Angew. Chem., Int. Ed.*, 1999, **38**, 57; T. Holland, C. F. Blandford and A. Stein, *Science*, 1998, **281**, 538.

3 S. Subramoney, *Adv. Mater.*, 1998, **10**, 1157; G. Che, B. B. Lakshimi, E. R. Fisher and C. R. Martin, *Nature*, 1998, **393**, 347; A. A. Zakhidov, R. H. Baughman, Z. Iqbal, C. Cui, I. Khayrullin, S. O. Dantas, J. Marti and V. G. Ralchenko, *Science*, 1998, **282**, 897.

4 *Proceedings of The Symposium on Electrochemical Capacitors*, ed. F. M. Delnick and M. Tomkiewicz, The Electrochemical Society, Pennington, NJ, 1996.

5 S. A. Johnson, E. S. Brigham, P. J. Olliver and T. E. Mallouk, *Chem. Mater.*, 1997, **9**, 2448.

6 M. W. Anderson, *Zeolites*, 1997, **19**, 220.

Communication 9/06872D

Synthesis and characterization of polyolefin–silicate nanocomposites: a catalyst intercalation and *in situ* polymerization approach†

Jeffrey S. Bergman,[a] Hua Chen,[b] Emmanuel P. Giannelis,[b] Malcolm G. Thomas[c] and Geoffrey W. Coates*[a]

[a] *Department of Chemistry and Chemical Biology, Baker Laboratory, Cornell University, Ithaca, NY 14853, USA. E-mail: gc39@cornell.edu*
[b] *Department of Materials Science and Engineering, Cornell University, Ithaca, NY 14853, USA*
[c] *Cornell Center for Materials Research, Clark Hall, Cornell University, Ithaca, NY 14853, USA*

Received (in Columbia, MO, USA) 7th July 1999, Accepted 27th September 1999

An organically modified fluorohectorite intercalated by a well-defined cationic palladium complex forms an exfoliated polyolefin–silicate nanocomposite material when exposed to olefinic monomer.

Polymer nanocomposites are a class of hybrid materials composed of an organic polymer matrix that is imbedded with inorganic particles which have at least one dimension in the nanometer size range.[1] At this scale, they can strongly impact the macroscopic properties of the polymer even though the materials typically contain only a few weight percent of the inorganic modifier. Dramatically improved properties such as higher heat distortion temperatures, enhanced flame resistance, increased modulus, better barrier properties, decreased thermal expansion coefficient, and altered electronic and optical properties have been discovered.[1–3] Due to the synergistic effects that result from adding a small amount of an inexpensive silicate, the synthesis and characterization of polymer nanocomposites has been intensely investigated in the last decade.[4] The majority of these studies have employed layered, anionic phyllosilicates as the inorganic component due to their high aspect ratio and ease of ionic modification. However, a simple physical mixture of the polymer and an intact, multilayered silicate does not typically yield improved properties. It is imperative that the polymer separates the individual silicate sheets, either in an intercalated morphology (silicate registry is retained) or preferably in a delaminated (or exfoliated) structure that is microscopically isotropic.

Despite the prime importance of polyethylene and polypropylene in a diverse array of applications, the synthesis of polyolefin–silicate nanocomposites remains a scientific challenge. Polymer nanocomposites can be synthesized by three primary strategies. The first is the melt intercalation of a polymer into an organically modified silicate.[5] Although this strategy works well with polar polymers such as polysiloxanes, polyethers and polystyrene,[1] polypropylene nanocomposites have only been formed using maleic anhydride modified polypropylene oligomers,[6] and ammonium-modified silicates are only partially intercalated by polyethylene.[7] The second strategy is the *in situ* formation of a layered silicate in an aqueous polymer solution.[8] Even though the development of this promising technique is just in its infancy, it will likely be limited to polymers that are soluble in water. A third strategy that is receiving increasing attention involves a silicate that is intercalated by an initiator or catalyst,[9] and, upon introduction of a monomer an intercalated or exfoliated polymer nanocomposite is formed (Scheme 1). This approach can eliminate both entropic and enthalpic barriers associated with intercalating polar silicates with nonpolar polymers, and has been used to synthesize a range of polymer nanocomposites. Concerning polyolefins, O'Hare and coworkers have reported the intercalation of synthetic layered silicates with a cationic Ziegler–Natta catalyst after protecting the internal surfaces with methylaluminoxane.[10,11] Addition of propylene produced polypropylene oligomers, however the post-polymerization structure of the silicate–polymer mixture was not reported.[10] It must be noted that the silicate galleries often contain protic impurities and polar functional groups; therefore only a select group of initiators and catalysts can be employed in unprotected silicate galleries. Although the vast majority of olefin polymerization catalysts are highly sensitive to Lewis bases and water, Brookhart and coworkers have reported a remarkable class of late-transition metal olefin polymerization catalysts that are particularly stable under these conditions.[12,13] In this paper we report the synthesis of polyolefin nanocomposites by employing these robust catalysts using an *in situ*, 'ship-in-the-bottle' polymerization approach.

We chose to investigate Brookhart's single component palladium-based complex {**1**; [{2,6-$Pr^i_2C_6H_3N$=C(Me)C(Me)=$NC_6H_3Pr^i_2$-2.6}$Pd(CH_2)_3CO_2Me$][$B(C_6H_3(CF_3)_2$-3,5)$_4$]}[13] and the well-studied synthetic silicate fluorohectorite (**2**)[14] as the polymerization catalyst and inorganic component of our composite, respectively. Lithium cations occupy the galleries of synthetic fluorohectorite; initial attempts to intercalate **2** with **1** failed, as evidenced by an immutable powder X-ray diffraction (XRD) pattern. Therefore we turned to an organically modified fluorohectorite (C_{14}N-**2**) that had 1-tetradecylammonium cations in the place of the interlayer lithium cations.[14] Suspension of C_{14}N-**2** in a toluene solution of **1**† yielded an orange–brown powder (Pd-**2**) that was visually

† Electronic supplementary information (ESI) available: Scanning transmission microscope (STEM) bright-field image of Pd-2. See http://www.rsc.org/suppdata/cc/1999/2179/

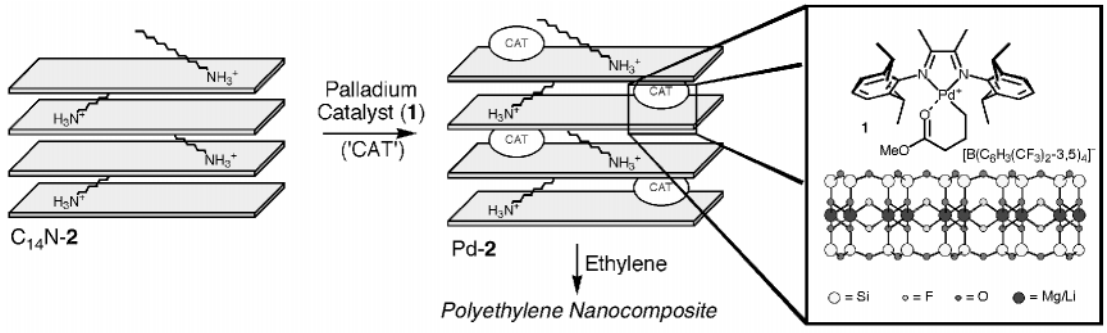

Scheme 1

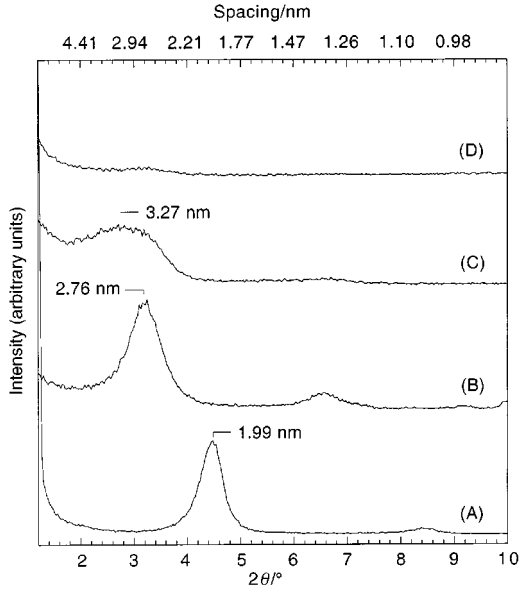

Fig. 1 Plot of powder X-ray diffraction intensity *versus* scattering angle: (A) 1-tetradecylammonium modified fluorohectorite (C_{14}N-**2**); (B) C_{14}N-**2** after intercalation by **1** (Pd-**2**); (C) Pd-**2** after exposure to ethylene for 135 min; (D) Pd-**2** after exposure to ethylene for 24 h.

different from the white, pristine C_{14}N-**2**. This reaction is irreversible, as **1** cannot be extracted from Pd-**2** with excess toluene. Powder XRD of Pd-**2** revealed a structural change of the silicate, as an increase in the basal spacing of C_{14}N-**2** from 1.99 to 2.76 nm was measured. Molecular modeling shows that an interlayer spacing of at least 2.1 nm is necessary for **1** to exist in the interlayer galleries; therefore the new spacing of 2.76 nm can easily accommodate the palladium complex. However, on the basis on these results, it was not clear whether this reaction was a cation exchange process, in which ammonium ions were exchanged for the cation of **1**, or whether the entire ionic palladium complex entered the silicate without ammonium discharge. Analysis of the material remaining in solution after intercalation using ^{1}H NMR spectroscopy revealed the absence of shifts due to the aliphatic ammonium cation, and the ratio of signal intensities assigned to the cation and anion of unintercalated **1** remained unchanged. These results clearly demonstrate that both the cation and anion of **1** enter the ammonium-modified silicate, and the ammonium cation remains in the silicate as well. The driving force for this reaction is not currently known.

To investigate the polymerization activity of Pd-**2**, the dry solid was exposed to ethylene gas.‡ Over a two hour period, we observed monomer consumption and a dramatic increase in the size of the silicate–catalyst composite. After 12 h, the Pd-**2** material was unrecognizable; in the place of a small amount of orange, Pd-**2** powder was a large mass of colorless, rubbery polymer. Based on the elemental analysis of Pd-**2** and the assumption that all intercalated palladium species produced polyethylene, the turnover frequency [TOF = mol ethylene/(mol Pd h)] of the catalyst in Pd-**2** is 162 h^{-1}. Consistent with the results of Brookhart, the polymer produced is highly branched. Analysis of the toluene-extracted polyethylene by gel-permeation chromatography revealed high molecular weight polymer (M_n = 159 000; M_w = 262 000 *versus* polystyrene standards).[13] To establish the arrangement of the silicate sheets in the polymer matrix, the polyethylene composite formed after 24 h was examined by powder XRD. The complete absence of diffraction peaks strongly suggests the formation of an exfoliated polymer nanocomposite. Under the same conditions addition of propylene gas to Pd-**2** also produces a polypropylene–silicate nanocomposite, however at a much slower rate (TOF = 5.6 h^{-1}).

To further confirm that silicate delamintion occurs during ethylene polymerization, we monitored the progress of the reaction using XRD. Shown in Fig. 1 are the XRD data as a function of reaction time. At t = 0, the mean repeat distance of the silicate sheets is 2.76 nm. After exposure of Pd-**2** for 135 minutes the interlayer spacing increases to 3.27 nm. The significant increase in peak width is due to the loss of crystallinity of the silicate. Finally, at 24 h the XRD revealed the absence of significant diffraction, consistent with dispersion. Since XRD only provides informative data at spacings less than 5 nm, we employed scanning transmission electron microscopy (STEM) to provide structural information at larger layer spacings (longer reaction times). By terminating the reaction at 12 h, we were able to identify layer spacings in the 5–8 nm range, well outside the range that we could achieve by XRD. A bright-field STEM image of the nanocomposite is available as supplementary data (http://www.rsc/org/suppdata/cc/1999/2179). It shows overlaid stacks of the silicate layers (dark area), where the polymer-intercalated layers remain predominantly coplanar at this stage of the reaction.

In conclusion, we report the first synthesis and characterization of polyolefin nanocomposite materials using an *in situ* polymerization approach. In the initial stages of the reaction polymer-intercalated silicates are formed; at later stages of the reaction the XRD data are consistent with silicate exfoliation. Efforts to extend this strategy for the synthesis of nanocomposite materials using isotactic polypropylene and linear polyethylene as the continuous phase are currently underway.

We gratefully acknowledge the Cornell Center for Materials Research (an NSF-funded MRSEC, DMR-9632275) and its facilities for support of this research. We thank Professor M. Brookhart for helpful discussions. G.W.C. gratefully acknowledges a Camille and Henry Dreyfus New Faculty Award, an Alfred P. Sloan Research Fellowship, an NSF Career Award, as well as Dupont and 3M for support of this research.

Notes and references

† Fluorohectorite (**2**) employed in these experiments had a cation exchange capacity of 1.5 mmol Li^+ g^{-1} ($Li_{1.12}[Mg_{4.88}Li_{1.12}]Si_8O_{20}F_4$). The initial interlayer spacing is 1.20 nm. The catalyst-intercalated fluorohectorite was synthesized by adding 50 ml of dry toluene to 95 mg of C_{14}N-**2**[14] and 155 mg of **1**, and stirring for 12 h at 22 °C. The suspension was filtered off, washed with toluene, and dried *in vacuo* to give 174 mg of Pd-**2**. Based on the increase in weight of C_{14}N-**2**, the composition of Pd-**2** is calculated to be $(\mathbf{1})_{0.55}\{H(CH_2)_{14}NH_3\}_{1.12}[Mg_{4.88}Li_{1.12}]Si_8O_{20}F_4$. Based on the interplanar spacing of Pd-**2** (27.6 Å) and an estimated volume of **1** (1750 Å^3), the composition of Pd-**2** is calculated (neglecting the contribution of surface-bound **1**) to be $(\mathbf{1})_{0.4}\{H(CH_2)_{14}NH_3\}_{1.12}[Mg_{4.88}Li_{1.12}]Si_8O_{20}F_4$. Elemental analysis of Pd-**2** corresponds to $(\mathbf{1})_{0.7}\{H(CH_2)_{14}NH_3\}_{1.12}[Mg_{4.88}Li_{1.12}]Si_8O_{20}F_4$: calc. (found): C, 36.38 (36.47); H, 3.92 (4.15); N, 1.75 (1.58%). Therefore, the composition of Pd-**2** can only be estimated at the current time.

‡ Ethylene gas (80 psi) was reacted with solid Pd-**2** (129 mg) at 22 °C for 12 h, yielding 3.50 g of a rubbery, white solid.

1 E. P. Giannelis, *Adv. Mater.*, 1996, **8**, 29.
2 Z. Wang and T. J. Pinnavaia, *Chem. Mater.*, 1998, **10**, 3769.
3 Y. Kojima, A. Usuki, M. Kawasumi, A. Okada, Y. Fukushima, T. Kurauchi and O. Kamigaito, *J. Mater. Res.*, 1993, **8**, 1185.
4 R. Dagani, *Chem. Eng. News*, 1999, **77**(**23**), 25.
5 R. A. Vaia, K. D. Jandt, E. J. Kramer and E. P. Giannelis, *Chem. Mater.*, 1996, **8**, 2628.
6 M. Kawasumi, N. Hasegawa, M. Kato, A. Usuki and A. Okada, *Macromolecules*, 1997, **30**, 6333.
7 H. G. Jeon, H. T. Jung, S. W. Lee and S. D. Hudson, *Polym. Bull.*, 1998, **41**, 107.
8 K. A. Carrado and L. Xu, *Chem. Mater.*, 1998, **10**, 1440.
9 M. W. Weimer, H. Chen, E. P. Giannelis and D. Y. Sogah, *J. Am. Chem. Soc.*, 1999, **121**, 1615.
10 J. Tudor, L. Willington, D. O'Hare and B. Royan, *Chem. Commun.*, 1996, 2031.
11 J. Tudor and D. O'Hare, *Chem. Commun.*, 1997, 603.
12 L. K. Johnson, C. M. Killian and M. Brookhart, *J. Am. Chem. Soc.*, 1995, **117**, 6414.
13 L. K. Johnson, S. M. Mecking and M. Brookhart, *J. Am. Chem. Soc.*, 1996, **118**, 267.
14 R. A. Vaia, R. K. Teukolsky and E. P. Giannelis, *Chem. Mater.*, 1994, **6**, 1017.

Communication 9/05540A

Change of electron-transfer path-selectivity in a triad by F^--coordination at a boronate-ester bridge

Hideo Shiratori,[a] Takeshi Ohno,[b] Koichi Nozaki[b] and Atsuhiro Osuka*[a]

[a] *Department of Chemistry, Graduate School of Science, Kyoto University, Kyoto 606-8502, Japan. E-mail: osuka@kuchem.kyoto-u.ac.jp*

[b] *Department of Chemistry, Graduate School of Science, Osaka University, Toyonaka, 560-8531, Japan*

Received (in Cambridge, UK) 10th August 1999, Accepted 28th September 1999

In a triad comprising of a zinc porphyrin donor (ZP) appended to a naphthalene-1,8:4,5-tetracarboxylic diimide (NI) and a pyromellitic diimide (PI) through a boronate ester and an acetal bridge, respectively, F^--coordination at the boronate bridge induced clear switching of the electron-transfer path from ^{1}ZP* → NI to ^{1}ZP* → PI.

Electron-transfer (ET) path-selectivity is one of the key issues in understanding the mechanism of primary charge separation in photosynthetic reaction centers (RCs).[1] In spite of the highly C_2 symmetric structure, only the L-branch is ET active in RC. This ET path-selectivity is strongly guided by the surrounding proteins in which electron carriers of the RC are embedded and it seems difficult to realize ET flow along the M-branch even in RCs of a variety of site-directed mutants.[2] Control of ET path-selectivity such that an unfavorable ET path can be made preferential over a favorable one without a drop in rate by external input will be quite useful not only for construction of artificial ET molecular devices but also in understanding the factors which govern biological ET reactions. In order to realize this control, the external input must trigger two effects, *i.e.* to *block* a *favorable* ET path and simultaneously to *accelerate* an *unfavorable* ET path. Here, we demonstrate that this ET path control is indeed possible in triad **1** comprising of a zinc porphyrin donor (ZP) appended to a naphthalene-1,8:4,5-tetracarboxylic diimide (NI) and a pyromellitic diimide (PI), through a boronate ester and an acetal bridge, respectively (Scheme 1). Important structural features are as follows; (1) the two bridges are similar in length,[3] (2) NI is a stronger electron acceptor than PI by 0.3 V,[4] and (3) intramolecular ET from ^{1}ZP* to NI across a boronate bridge can be suppressed upon F^--coordination.[5]

In benzene, the fluorescence intensities of **1**, **2** and **3** relative to that of **4** were 0.45, 0.44 and 0.89, respectively. This fluorescence quenching suggests intramolecular charge separation (CS) between ^{1}ZP* and NI or PI which has been confirmed by picosecond-time resolved transient absorption spectra (Fig. 1).[6] Absorption peaks due to the radical anion were observed at 475, 610 and 790 nm (NI^-) for **2**, and at 721 nm (PI^-) for **3**, providing clear evidence for formation of NI^-–ZP^+ and ZP^+–PI^-,[4] respectively. The transient absorption studies revealed that excitation of ZP with 532 nm laser pulses in **2** and **3** yielded NI^-–ZP^+ with τ_{CSN} = 0.52 ns and ZP^+–PI^- with τ_{CSP} = 1.1 ns, respectively.[7] Lifetimes of these ion pairs were both longer than 6 ns. Upon similar laser excitation of ZP in **1**, the absorbance due to ^{1}ZP* around 460 nm decayed with τ = 0.46 ns, and the transient absorption spectrum at 3 ns delay time is practically the same as that of **2** except for a small band at 721 nm due to PI^-, indicating that CS between ^{1}ZP* and NI is dominant in **1**. Comparison of decay time constants of ^{1}ZP* in **1**–**3** led to the conclusion that excitation of ZP in **1** leads to formation of NI^-–ZP^+ and ZP^+–PI^- in a ratio of 11:1 (Scheme 2).

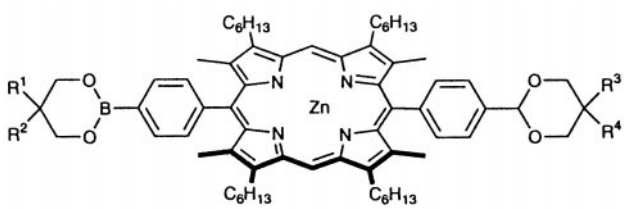

1 ; R^1=NI, R^3=PI, R^2=R^4=H
2 ; R^1=NI, R^2=H, R^3=R^4=Me
3 ; R^1=R^2=Me, R^3=PI, R^4=H
4 ; R^1=R^2=R^3=R^4=Me

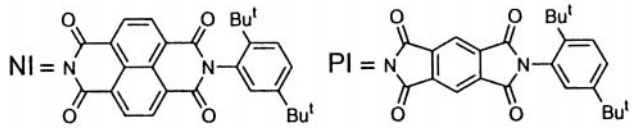

Scheme 1 Structures model **1** and reference molecules **2**–**4**.

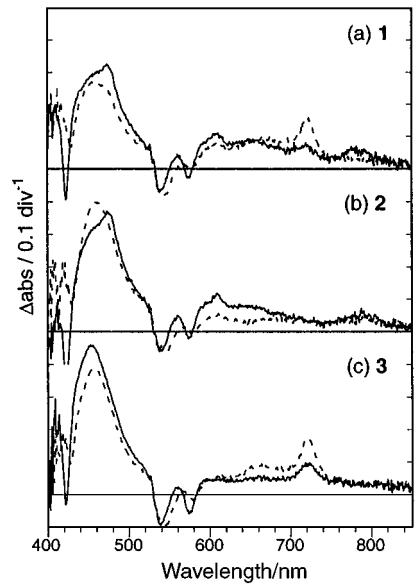

Fig. 1 Transient absorption spectra of (a) **1**, (b) **2** and (c) **3** in benzene at 3 ns; (——) no TBAF; (·····) in the presence of 1.2 equiv. TBAF.

In the presence of 1.2 equiv. of tetra-*n*-butylammonium fluoride (TBAF), relative fluorescence intensities of **1**, **2** and **3** to **4** were 0.65, 0.98 and 0.72, respectively. The transient absorption spectra of **2** [Fig. 1(b), dotted line] are practically the same as those of **4** (not shown) from 20 ps to 6 ns delay times, featuring no CS but simple intersystem crossing of ^{1}ZP* → ^{3}ZP* with τ = 1.5 ns. Thus CS between ^{1}ZP* and NI in **2** is completely suppressed in a F^--coordinated form as reported previously.[5] This CS suppression may be explained in terms of decreased electronic coupling between ^{1}ZP* and NI across a F^--coordinated boronate bridge possibly due to the high energy LUMO of the bridge in comparison to that in a neutral bridge.[8] Considering the similar CS suppression in **1**, its fluorescence quenching should be ascribed to CS between ^{1}ZP* and PI. This

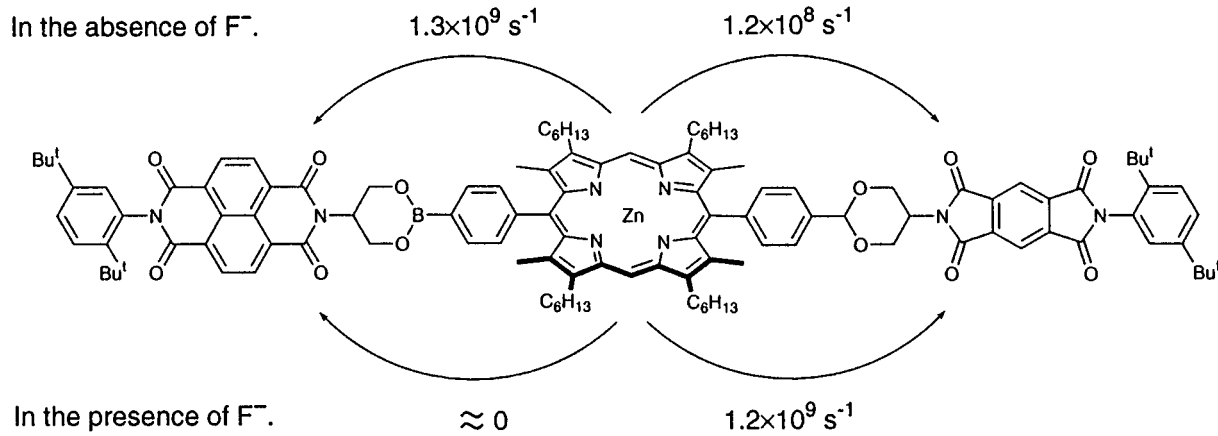

Scheme 2 ET-path selectivity of **1** in the absence and presence of F^-.

has been confirmed by the transient absorption spectrum [Fig. 1(a), dotted line], which shows the appearance of a 721 nm absorption peak, thus indicating CS between ^{1}ZP* and PI instead of NI. Here it is interesting to note that the F^--coordination not only blocks ET to NI but also accelerates ET to PI significantly. On the basis of the analysis of the time profile of the rise at 721 nm, the CS rate constant in F^--coordinated **1** has been determined to be 1.2×10^9 s^{-1}, which is *ca.* 10 times larger compared to that occurring in neutral **1**. Similar acceleration of CS between ^{1}ZP* and PI was also observed in F^--coordinated **3** ($k_{CS} = 6.5 \times 10^8$ s^{-1}). The acceleration of CS between ^{1}ZP* and PI upon F^--coordination on the boronate bridge can be explained on the basis of Coulomb interaction between the negative charge on the F^--coordinated boron atom and the ion-pair ZP^+–PI^-. In nonpolar solvents like benzene, the tetracoordinated boronate exists as a tight ion pair. However, it is reasonable to consider that electrostatic attraction between the negative charge at the tetracoordinated boronate and the positive charge at the ZP^+ must be most influential among other electrostatic interactions in the system and thus the F^--coordination eventually leads to a decrease in the energy level of ZP^+–PI^-, thereby enhancing CS reaction between ^{1}ZP* and PI.

Switching of ET path-selectivity of **1** upon F^--coordination is summarized in Scheme 2, where the ET to NI is suppressed mainly by the electronic factor and the ET to PI is accelerated mainly by the nuclear factor. The boronate-bridged acceptor–donor–acceptor architectures will be useful, since they provide a convenient and efficient way to control the ET path selectivity in a predictable manner as such that ET over the boronate-bridge will be suppressed and ET in the opposite direction from the boronate bridge will be accelerated.

This work was partly supported by Grant-in-Aids for Scientific Research from the Ministry of Education, Science, Sports, and Culture of Japan, and by CREST (Core Research for Evolutional Science and Technology) of Japan Science and Technology Corporation (JST).

Notes and references

1 J. Deisenhofer and J. R. Norris, *The Photosynthetic Reaction Center*, Academic Press, New York, 1993; N. Woodbury and J. P. Allen, in *Anoxygenic Photosynthetic Bacteria*, ed. R. E. Blankenship, M. T. Madigan and C. E. Bauer, Kluwer Academic Publishers, Dordrecht, 1995.

2 C.-K. Chan, L. X.-Q. Chen, T. J. DiMagno, S. L. Nance, M. Schiffer and J. R. Norris, *Chem. Phys. Lett.*, 1991, **176**, 366; B. A. Heller, D. Holten and C. Kirmaier, *Science*, 1995, **269**, 940.

3 The center-to-center distances are estimated by MM2 calculations (Chem3D ver.4, AM1); 17.2 Å for ZP–NI and 16.8 Å for ZP–PI.

4 A. Osuka, R. Zhang, K. Maruyama, T. Ohno and K. Nozaki, *Bull. Chem. Soc. Jpn.*, 1993, **66**, 3773. The one-electron redox potentials have been measured in DMF by cyclic voltammetry: E_{ox}(ZP) = 0.22 V, E_{red}(NI) = −0.94 V and E_{red}(PI) = −1.24 V *vs.* ferrocence–ferrocenium ion.

5 H. Shiratori, T. Ohno, K. Nozaki, I. Yamazaki, Y. Nishimura and A. Osuka, *Chem. Commun.*, 1998, 1539.

6 Picosecond time-resolved transient absorption spectra were measured on Ar-bubbled 8×10^{-5} M benzene solutions by using mode-locked Nd^{3+}:YAG laser system (Continuum PY-1C-10, fwhm: 17 ps) with second harmonic output at 532 nm for excitation: A. Yoshimura, K. Nozaki, N. Ikeda and T. Ohno, *J. Phys. Chem.*, 1996, **100**, 1630.

7 CS rate constants k_{CS} were calculated according to the equation; $k_{CS} = \tau^{-1} - \tau_0^{-1}$, where τ and τ_0 are the lifetimes of ^{1}ZP* in **1**–**3** and **4**, respectively.

8 H. M. McConell, *J. Chem. Phys.*, 1961, **35**, 508; S. Lasson, *J. Am. Chem. Soc.*, 1981, **103**, 4034; M. N. Paddon-Row, *Acc. Chem. Res.*, 1997, **27**, 18 and references therein.

Communication 9/06497D

ChemComm

Rapid syntheses of difluorinated polyols using a cleavable carbamate

Andrew S. Balnaves,[a] Michael J. Palmer[b] and Jonathan M. Percy*[a]

[a] *School of Chemistry, University of Birmingham, Edgbaston, Birmingham, UK B15 2TT. E-mail: jmpercy@chemistry.bham.ac.uk*
[b] *Pfizer Central Research, Sandwich, UK CT13 9NJ*

Received (in Cambridge, UK) 6th September 1999, Accepted 28th September 1999

Trifluoroethyl *N*-[2-(*tert*-butyldiphenylsilyloxy)ethyl]-*N*-isopropylcarbamate undergoes smooth dehydrofluorination–metallation followed by $BF_3{\cdot}OEt_2$ mediated addition to aldehydes to afford a range of allylic alcohols; aldol reaction with a second aldehyde, then reduction, affords products which can be deprotected to afford difluorinated polyols.

We have been developing metallated difluoro-enol carbamates[1] derived from trifluoroethanol as versatile building blocks[2] for the synthesis of selectively fluorinated polyfunctional molecules. To date, we have concentrated on *N*,*N*-diethylcarbamates which, while synthetically versatile[3,4] and inexpensive to synthesise, are chemically robust. The latter property represents an apparent impediment to carbamate cleavage and hydroxy group unmasking so recently, we made use of the cleavable carbamate described by Derwing and Hoppe,[5] synthesising **1** by a standard route (Scheme 1). Dehydrofluorination–metallation to **2a** proceeded smoothly under our published conditions[6] and allylic alcohols **3a**–**c** were synthesised in moderate to good yield using $BF_3{\cdot}OEt_2$ to attenuate the transacylation reaction.[7] Acceptable yields of **3d** and **3e** (46 and 71% respectively) could only be secured by transmetallating **2a** to **2b** using $MgBr{\cdot}OEt_2$ prepared freshly according to the method of Harwood *et al*.,[8] and raising the reaction temperature to −30 °C before the addition of the Lewis acid and electrophile. Next, we explored the aldol chemistry and confirmed that our published conditions transferred smoothly; adducts **4a**–**e** were duly prepared (Scheme 2) in moderate to good yields by treatment of the allylic alcohols with BuLi at low temperature and allowing the enolate solution to warm to −10 °C before the addition of the aldehyde electrophile. Stereoselectivities were low as expected but the *syn* and *anti* diastereoisomers could be separated by careful column chromatography.†

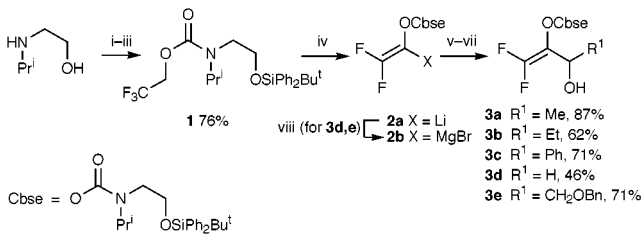

Scheme 1 *Reagents and conditions*: i, Bu^tPh_2SiCl (1.1 equiv.), DMAP (0.5 equiv.), CH_2Cl_2, reflux, 12 h; ii, diphosgene (0.5 equiv.), Et_3N (1.5 equiv.), CH_2Cl_2, 0 °C, then room temp., 16 h; iii, CF_3CH_2ONa, THF, reflux, 16 h; iv, LDA, THF (2.0 equiv.), –78 °C; v, R^1CHO; vi, $BF_3{\bullet}OEt_2$, then warm to 0 °C; vii, NH_4Cl (aq.); viii, $MgBr_2{\bullet}OEt_2$.

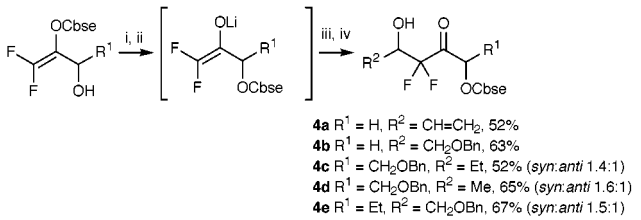

Scheme 2 *Reagents and conditions*: i, BuLi, THF, –78 °C; ii, warm to –10 °C; iii, R^2CHO; iv, NH_4Cl (aq.).

To make further progress in the direction of polyol targets, reduction of **4c** was attempted under the stereoselective conditions described by Kuroboshi and Ishihara,[9] but very sluggish reactions ensued (Scheme 3). We had hoped that the reductions would proceed smoothly, and that the β-hydroxy group would provide control over the stereochemical course of the reduction, overriding any asymmetric induction exerted by the adjacent (α) stereogenic centre. Under the *syn*-selective conditions (DIBAL-H, $ZnCl_2$, TMEDA), both the yield of **5a** and **5b** (31% combined) and stereoselectivity (1.8:1 *syn*:*anti*)‡ were low from *syn*-**4c** and the conversion was poor (37% recovered **4c** after 6 h), a consequence presumably of the bulk of the carbamoyloxy group. The *anti*-selective Meerwein–Pondorf–Verley reduction [$Al(OPr^i)_3$, PhH] conditions were more successful affording a higher (66% combined) yield of **5a** and **5b**. However, whereas the published procedure achieves the reduction smoothly overnight at room temperature, we failed to observe any reaction until the mixture had stirred for 4 days. We then turned our attention to the less stereochemically complex **4b**; both stereoselective reductions failed completely, so to take compound through to the diol stage, we performed a simple $NaBH_4$ reduction and isolated a 2:1 mixture of *syn*- and *anti*-diols **6a** and **6b** in 78% yield (Scheme 4).§ Attempts to cleave the carbamate protection then ensued. We modified the published conditions and found that dilute HF in aqueous MeCN effected a satisfactory desilylation, allowing triols **7a** and **7b** to be isolated in 84% yield. Exposure to KOH (1 equiv.) in MeOH at room temperature allowed the isolation of **8a** and **8b** in a disappointing 20% yield. However, removing the MeOH *in vacuo* then taking the residue up in EtOAc followed by an extractive work up yielded separable triols **8a** and **8b** (78%),

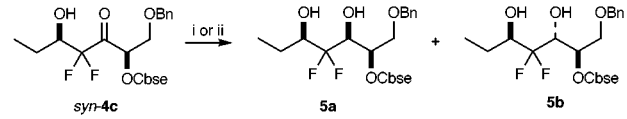

Scheme 3 *Reagents and conditions*: i, DIBAL-H, $ZnCl_2{\bullet}$TMEDA, THF, –78 °C; ii, $Al(OPr^i)_3$, PhH, room temp., 4 days.

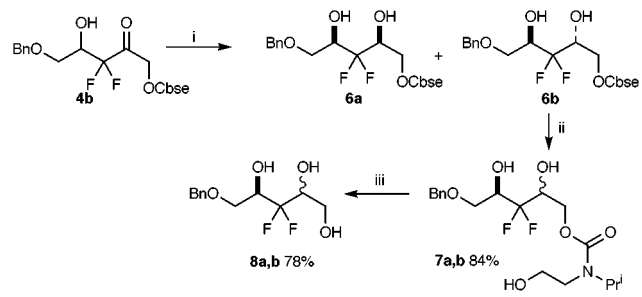

Scheme 4 *Reagents and conditions*: i, $NaBH_4$, MeOH, 0 °C; ii, 48% HF (aq.)–MeCN (1:9), room temp.; iii, KOH (1.0 equiv.), MeOH, room temp.

proving that the Hoppe carbamate can be deployed successfully in our dehydrofluorination–metallation and aldol chemistry *and* that protecting group removal can be achieved under mild conditions. Clearly, there exists considerable scope for the improvement of functional group manipulation chemistry: studies describing our efforts to develop stereoselective reduction chemistry and optimise deprotection will be described elsewhere.

The authors wish to thank the Engineering and Physical Sciences Research Council of Great Britain and Pfizer Central Research for a CASE Award (to A. S. B.).

Notes and references

† Diastereoisomer ratios were assigned on the basis of ^{19}F NMR chemical shifts as described in ref. 6.

‡ This assignment assumes the same sense of stereoselection as that described in ref. 9.

§ The two diastereoisomers have radically different ^{19}F NMR spectra; one isomer appears as a well-separated AB system split further by $^{3}J_{H\text{-}F}$ couplings whereas the other appears as a broad unresolved signal. We have tentatively assigned these spectra to the 1,3-*syn* and 1,3-*anti* diastereoisomers **6a** and **6b** respectively on the basis that the fluorine atoms in the former are decidedly heterotopic. In the latter, the *pseudo*-C_2 symmetry confers a degree of homotopicity upon the fluorine atoms, hence the appearance of the signal observed. Obviously, definitive proof of this assignment is being sought currently.

1 J. A. Howarth, W. M. Owton, J. M. Percy and M. H. Rock, *Tetrahedron*, 1995, **51**, 10 289.
2 J. M. Percy, *Top. Curr. Chem.*, 1997, **193**, 131. For recent related chemistry of difluorinated enolates and enols, see I. Fleming, R. S. Roberts and S. C. Smith, *J. Chem. Soc., Perkin Trans. 1*, 1998, 1215; T. Brigaud, P. Doussot and C. Portella, *J. Chem. Soc., Chem. Commun.*, 1994, 2117; T. Brigaud, O. Lefebvre, R. Plantierroyon and C. Portella, *Tetrahedron Lett.*, 1996, **37**, 6115; O. Lefebvre,T. Brigaud and C. Portella, *Tetrahedron*, 1998, **54**, 5939; Y. Kodama, H. Yamane, M. Okumura, M. Shiro and T. Taguchi, *Tetrahedron*, 1995, **51**, 12217; K. Uneyama, K. Maeda, T. Kato and T. Katagiri, *Tetrahedron Lett.*, 1998, **39**, 3741; O. Lefebvre, T. Brigaud and C. Portella, *Tetrahedron*, 1999, **55**, 7233.
3 M. Tsukazaki and V. Snieckus, *Tetrahedron Lett.*, 1993, **34**, 411.
4 J. Lee, M. Tsukazaki and V. Snieckus, *Tetrahedron Lett.*, 1993, **34**, 415.
5 C. Derwing and D. Hoppe, *Synthesis*, 1996, 149.
6 A. S. Balnaves, T. Gelbrich, M. B. Hursthouse, M. E. Light, M. J. Palmer and J. M. Percy, *J. Chem. Soc., Perkin Trans. 1*, 1999, 2525.
7 The non-fluorinated system derived from acetaldehyde enolate proceeds from alkoxide to enolate unhindered by the presence of Lewis acids; see S. Sengupta and V. Snieckus, *J. Org. Chem.*, 1990, **55**, 5680.
8 L. M. Harwood, A. C. Manage, S. Robin, S. F. G. Hopes, D. J. Watkin and C. E. Williams, *Synlett*, 1993, 777.
9 M. Kuroboshi and T. Ishihara, *Bull. Chem. Soc. Jpn.*, 1990, **63**, 1185.
10 M. Schlosser, T. Jenny and Y. Guggisberg, *Synlett*, 1990, 704.

Communication 9/07174A

ChemComm

Efficient Rh^{II} binaphthol phosphate catalysts for enantioselective intramolecular tandem carbonyl ylide formation–cycloaddition of α-diazo-β-keto esters

David M. Hodgson*[a] Paul A. Stupple[a] and Craig Johnstone[b]

[a] *Dyson Perrins Laboratory, Department of Chemistry, University of Oxford, South Parks Road, Oxford, UK OX1 3QY. E-mail: david.hodgson@chem.ox.ac.uk*

[b] *AstraZeneca, Mereside, Alderly Park, Macclesfield, Cheshire, UK SK10 4TG*

Received (in Liverpool, UK) 19th August 1999, Accepted 17th September 1999

Catalytic enantioselective tandem carbonyl ylide formation–cycloadditions of α-diazo-β-keto ester 1 using 0.5 mol% dirhodium tetrakis(1,1′-binaphthyl-2,2′-diyl phosphate) catalysts 7–9 and 14 to give the cycloadduct 3 in good yields and up to 90% ee are described.

There are currently few methods to achieve catalytic enantioselective 1,3-dipolar cycloadditions, despite the potential utility of such asymmetric transformations.[1] In 1997 we reported the first observations of catalytic enantioselective tandem carbonyl ylide formation–cycloaddition (up to 53% ee) using unsaturated α-diazo-β-keto esters.[2] For example, reaction of α-diazo-β-keto ester **1** using 1 mol% Rh_2(*S*-DOSP)$_4$ **2** in hexane at room temperature gave cycloadduct (+)-**3**† in 93% yield and 52% ee (Scheme 1).[3]

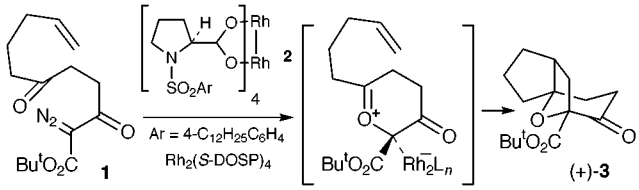

Scheme 1

More recently, research groups led by Doyle,[4] Ibata[5] and Hashimoto[6] have reported conceptually related (but intermolecular) asymmetric carbonyl ylide cycloadditions. The asymmetric induction in these cycloadditions was low (< 30% ee), aside from the work by Hashimoto using α-diazo ketones with DMAD as the dipolarophile, where ees up to 92% were reported (Scheme 2, R^1 = H, R^2 = Ph, absolute sense of asymmetric induction not determined).

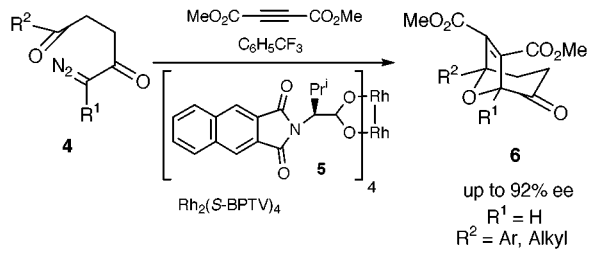

Scheme 2

Although we have screened a number of chiral rhodium carboxylate catalysts with α-diazo-β-keto ester **1**,[7] none have delivered asymmetric induction levels close to those observed with Rh_2(*S*-DOSP)$_4$ **2**. Also, applying the optimised catalyst–solvent combination for intermolecular cycloaddition of α-diazo ketones with DMAD reported by Hashimoto[6] [Rh_2(*S*-BPTV)$_4$ **5**, $PhCF_3$, *cf*. Scheme 2] to α-diazo-β-keto ester **1** at 25 °C resulted in only essentially racemic cycloadduct **3** (90% yield, 1% ee). Furthermore, cycloadduct **6** (R^1 = CO_2Et, R^2 = Me) was obtained in only 33% ee under the same conditions in the reaction of α-diazo-β-keto ester **4** (R^1 = CO_2Et, R^2 = Me) with DMAD [α-diazo ketone **4** (R^1 = H, R^2 = Me) gave cycloadduct in 80% ee].[6] These latter results indicate that ee is rather sensitive to variation in the electronic structure of the dipole. A variety of chiral, non-racemic dirhodium carboxylates and carboxamidates have been extensively examined as asymmetric catalysts in a number of diazocarbonyl transformations.[4] However, in seeking to develop more efficient catalysts for asymmetric carbonyl ylide formation–cycloaddition, we were attracted to the isolated reports in 1992 by Pirrung[8] and McKervey[9] concerning 1,1′-binaphthyl-2,2′-diyl phosphate (BNP) catalysts Rh_2(*S*-BNP)$_4$ (*ent*-**7**) and Rh_2(*R*-BNP)$_2$(O_3CH)$_2$·5H_2O respectively for diazocarbonyl decomposition. C–H insertion and cyclopropanation were among the asymmetric processes investigated (up to 60% ee). Here we communicate our preliminary studies on such catalysts which lead to improved enantioselectivities in tandem carbonyl ylide formation–cycloaddition of α-diazo-β-keto esters.

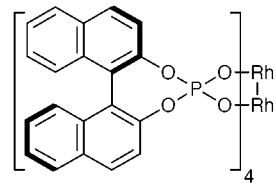

Rh_2(*R*-BNP)$_4$ **7**

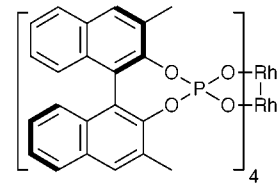

Rh_2(*R*-DMBNP)$_4$ **8**

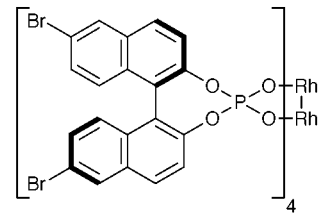

Rh_2(*R*-DBBNP)$_4$ **9**

Initial investigation of Pirrung's structurally well-defined catalyst Rh_2(*R*-BNP)$_4$ **7** with α-diazo-β-keto ester **1** in hexane at 25 °C gave an immediate improvement in ee of the cycloadduct (+)-**3** (64% ee, Table 1, entry 1) compared with Rh_2(*S*-DOSP)$_4$ **2** (52% ee), even though Rh_2(*R*-BNP)$_4$ **7** was only partially soluble in hexane at 25 °C. Interestingly, asymmetric induction was maintained in CH_2Cl_2 at 25 °C (65% ee, entry 2); this compares with 8% ee previously obtained using Rh_2(*S*-DOSP)$_4$ **2** in CH_2Cl_2.[2] Whilst Rh_2(*R*-BNP)$_4$ **7** remained soluble in CH_2Cl_2 at 0 °C, no improvement in ee was observed (64%, entry 3). The results with Rh_2(*R*-BNP)$_4$ **7** prompted a study of the effects of structural variation of the binaphthyl core on enantioselectivity.

Substitution at the 3,3′-positions was first examined using Rh_2(*R*-DMBNP)$_4$ **8**, which was prepared (79%) by an analo-

Table 1 Effect of catalyst on the yields and enantioselectivities of formation of cycloadduct **3** from α-diazo-β-keto ester **1**

Entry	Catalyst	Solvent	*T*/°C	Yield of **3** (%)	Ee of **3** (%)[a]
1	**7**	hexane	25	65	64
2	**7**	CH_2Cl_2	25	83	65
3	**7**	CH_2Cl_2	0	55	64
4	**8**	CH_2Cl_2	25	50	7
5	**9**	hexane	25	34	66
6	**9**	CH_2Cl_2	25	67	58
7	**9**	CH_2Cl_2	0	36	61
8	**14**	CH_2Cl_2	25	80	68
9	**14**	hexane	25	76	81
10	**14**	hexane	0	81	88 (89)
11	**14**	hexane	−15	66	90 (90)

[a] Ees were determined on the methyl ester [obtained from **3** by hydrolysis–esterification (TFA, CH_2Cl_2, then MeOH, TsOH)] by ^{1}H NMR analysis of the split methoxy signal using Pr(hfc)$_3$. Ees in parentheses were determined on the benzyl oxime ether (*O*-benzylhydroxylamine hydrochloride, NaOAc, MeOH) of the methyl ester by HPLC analysis (Daicel Chiralpak AD, 10% EtOH–hexane) of the major geometric isomer.

gous procedure[8] to Rh_2(*R*-BNP)$_4$ from $Rh_2(OAc)_4$ by ligand exchange using the known 3,3′-dimethyl-1,1′-binaphthyl-2,2′-diyl hydrogen phosphate.[10] However, reaction of Rh_2(*R*-DMBNP)$_4$ **8** with α-diazo-β-keto ester **1** led to no cycloadduct in hexane and a low ee (7%) of (+)-**3** in CH_2Cl_2 (Table 1, entry 4), possibly due to steric congestion at the axial binding sites on the dirhodium core, which (in CH_2Cl_2) might also facilitate catalyst release to give the free ylide for cycloaddition. Substitution at the 6,6′-positions has been a successful tactic to alter asymmetric induction with binaphthyl-based catalysts.[11] Rh_2(*R*-DBBNP)$_4$ **9**, available from 6,6′-dibromo-1,1′-binaphthyl-2,2′-diyl hydrogen phosphate,[12] induced similar ees to Rh_2(*R*-BNP)$_4$ **7** (entries 5–7). With the primary aim of investigating a more hydrocarbon-soluble catalyst, Rh_2(*R*-DDBNP)$_4$ was synthesised according to Scheme 3.

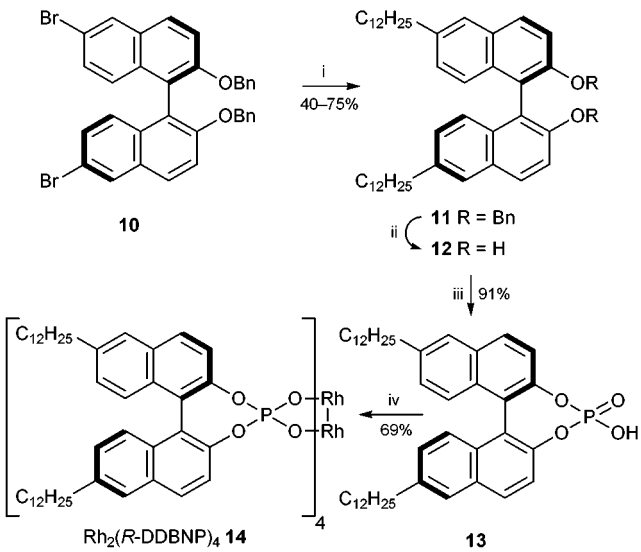

Scheme 3 *Reagents and conditions*: i, $C_{12}H_{25}MgBr$, $Ph_2P(CH_2)_3PPh_2$–$NiCl_2$ (1 mol%), Et_2O, reflux, 48 h; ii, TMSCl, NaI, MeCN, $PhCH_3$, 40 °C, 2 h (89%); iii, $POCl_3$, Py, 25 °C, 1 h, then H_2O, $NaHCO_3$; iv, $Rh_2(OAc)_4$, PhCl, reflux, 5 h.

The known bisether **10**[13] was cross-coupled[14] with commercially available dodecylmagnesium bromide (40–75%, Scheme 3). Deprotection of the resultant didodecyl bisether **11** using TMSI[15] gave diol **12** (89%). Formation of the acid **13** (91%) from the diol **12** under standard conditions followed by ligand exchange[16] gave Rh_2(*R*-DDBNP)$_4$ **14** (69%).‡ Although only a slight rise in the ee of (+)-**3** was noted with Rh_2(*R*-DDBNP)$_4$ **14** in CH_2Cl_2 (Table 1, entry 8) compared with Rh_2(*R*-BNP)$_4$ **7** at 25 °C, the new catalyst was significantly more effective in hexane (81% ee, entry 9). Moreover, catalyst solubility and activity were maintained in hexane at 0 °C and asymmetic induction rose to give the cycloadduct (+)-**3** in 81% yield and 89% ee (entry 10). A similar ee (90%) was observed on conducting the reaction at −15 °C (entry 11) whereas reaction at −30 °C was very slow and gave a complex product mixture from which no cycloadduct was isolable.

Our results indicate that dirhodium tetrakis(1,1′-binaphthyl-2,2′-diyl phosphate) catalysts can be superior to the more commonly utilised carboxylates and carboxamidates in asymmetric transformations of diazocarbonyl compounds and deserve to be more fully investigated.

We thank Zeneca (now AstraZeneca) for support of this work, St. Hugh's College for a Jubilee Scholarship (to P. A. S.), the EPSRC National Mass Spectrometry Service Centre for mass spectra and Dr D. J. Watkin (Chemical Crystallography Laboratory, University of Oxford) and J. Ouzman for assistance with the X-ray structure analysis. We are also grateful to Professor M. C. Pirrung (Duke University) for an initial test sample of Rh_2(*S*-BNP)$_4$ and Dr I. Nash (AstraZeneca) for useful discussions.

Notes and references

† The absolute configuration of the predominant cycloadduct enantiomer (+)-**3** formed using α-diazo-β-keto ester **1** and Rh_2(*S*-DOSP)$_4$ **2** is as shown in Scheme 1 and was determined by crystallographic analysis following hydrolysis using TFA, esterification with (1*S*)-*endo*-(−)-borneol, oxime formation using $HONH_2$ with the major diastereomer and finally reaction with 3,5-dinitrobenzoyl chloride. *Crystal data* for (+)-**3**: $C_{28}H_{33}N_3O_9$, M = 555.58, orthorhombic, a = 6.415(2), b = 19.871(5), c = 21.298(8) Å, U = 2714.8 Å^3, T = 190 K, space group $P2_12_12_1$ (no. 19), Z = 4, μ(Cu-K) = 0.81 mm^{-1}; R_w = 0.040 (3133 independent reflections), R = 0.046 [$I > 3\sigma(I)$]. CCDC 182/1422. See http://www.rsc.org/suppdata/cc/1999/2185/ for crystallographic data in .cif format.

‡ *Selected data* for **14**: $[\alpha]_D^{25}$+60.9 (c 0.03 in $CHCl_3$); δ_H(400 MHz; $CDCl_3$; $CHCl_3$) 0.89 (24H, t, J 6.7), 1.21–1.34 (144H, m), 1.68–1.71 (16H, m), 2.75 (16H, t, J 7.5), 7.18 (8H, d, J 8.7), 7.43 (8H, d, J 8.7), 7.56 (8H, d, J 8.9), 7.65 (8H, s) and 7.77 (8H, d, J 8.9); δ_C(100 MHz; $CDCl_3$; $CDCl_3$) 14.1 (Me), 22.7, 29.4, 29.5, 29.6, 29.6, 29.7, 31.2, 31.9, 35.8 (11 × CH_2), 121.2 (CH), 121.6 (quat.), 126.7 (CH), 127.1 (CH), 128.0 (CH), 130.4 (CH), 130.7 (quat.), 132.0 (quat.), 139.9 (quat.) and 147.2 (quat.).

1 K. V. Gothelf and K. A. Jørgensen, *Chem. Rev.*, 1998, **98**, 863; A. Padwa and M. D. Weingarten, *Chem. Rev.*, 1996, **96**, 223.
2 D. M. Hodgson, P. A. Stupple and C. Johnstone, *Tetrahedron Lett.*, 1997, **38**, 6471.
3 A carboxamidate catalyst gave racemic cycloadduct, see ref. 2.
4 M. P. Doyle and D. C. Forbes, *Chem. Rev.*, 1998, **98**, 911.
5 H. Suga, H. Ishida and T. Ibata, *Tetrahedron Lett.*, 1998, **39**, 3165.
6 S. Kitagaki, M. Anada, O. Kataoka, K. Matsuno, C. Umeda, N. Watanabe and S. Hashimoto, *J. Am. Chem. Soc.*, 1999, **121**, 1417.
7 P. A. Stupple, unpublished results.
8 M. C. Pirrung and J. Zhang, *Tetrahedron Lett.*, 1992, **33**, 5987.
9 N. McCarthy, M. A. McKervey, T. Ye, M. McCann, E. Murphy and M. P. Doyle, *Tetrahedron Lett.*, 1992, **33**, 5983.
10 D. J. Cram, R. C. Helgeson, S. C. Peacock, L. J. Kaplan, L. A. Domeier, P. Moreau, K. Koga, J. M. Mayer, Y. Chao, M. G. Siegel, D. H. Hoffman and G. D. Y. Sogah, *J. Org. Chem.*, 1978, **43**, 1930.
11 H. Sasai, T. Tokunaga, S. Watanabe, T. Suzuki, N. Itoh and M. Shibasaki, *J. Org. Chem.*, 1995, **60**, 7388; M. Terada, Y. Motoyama and K. Mikami, *Tetrahedron Lett.*, 1994, **35**, 6693.
12 *U.S. Pat.*, 3 848 030, 1974 (*Chem. Abstr.*, 1973, **78**, 43129b).
13 T. Hamada, T. Fukuda, H. Imanishi and T. Katsuki, *Tetrahedron*, 1996, **52**, 515.
14 B. J. Brisdon, R. England, K. Reza and M. Sainsbury, *Tetrahedron*, 1993, **49**, 1103.
15 G. A. Olah, S. Narang, B. G. B. Gupta and R. Malhotra, *J. Org. Chem.*, 1979, **44**, 1247.
16 H. J. Callot and F. Metz, *Tetrahedron*, 1985, **41**, 4495.

Communication 9/06787F

Abatement of N_2O in the selective catalytic reduction of NO_x on platinum zeolite catalysts upon promotion with vanadium

Yvonne Traa, Beate Burger and Jens Weitkamp*

Institute of Chemical Technology I, University of Stuttgart, 70550 Stuttgart, Germany. E-mail: jens.weitkamp@po.uni-stuttgart.de

Received (in Cambridge, UK) 27th August 1999, Accepted 29th September 1999

The selectivity to N_2O during the selective catalytic reduction of NO_x on platinum-containing zeolite catalysts is reduced by incorporation of vanadium into the catalyst.

The selective catalytic reduction of nitrogen oxides by hydrocarbons is a promising process for the purification of exhaust gases from diesel-powered engines. Since the average temperature of diesel exhaust gases is well below 300 °C,[1] platinum-containing catalysts have proven to be efficient for this process owing to their low lightoff temperature. Another important advantage of platinum-containing catalysts is that they are comparatively insensitive to water in the exhaust gas.[2] However, a major drawback of these catalysts is that large portions of the nitrogen oxides are converted to nitrous oxide rather than to nitrogen. Nitrous oxide is highly undesirable, since it is a strong greenhouse gas and contributes to stratospheric ozone destruction.

In the past, several attempts were undertaken to overcome the N_2O problem with platinum-containing catalysts: Doumeki *et al.* reported that the selectivity to N_2 can be enhanced by using organoplatinum complexes such as $PtMe(OSiPh_3)(cod)$ instead of inorganic complexes as precursors for the preparation of Pt/SiO_2 or Pt/Al_2O_3 catalysts.[3] However, the N_2O selectivity remained as high as 65%. Wunsch *et al.* found that, upon adding CeO_2 to a Pt/ZSM-5 catalyst ($m_{CeO_2}/m_{Pt} \approx 4$), the maximum NO_x conversion increased from 48 to 59% without a change in temperature, whereas the selectivity to N_2O decreased from 62 to 54%.[4] More favourable results were reported by Seker and Gulari who observed an N_2O selectivity of only 17% on a Pt/alumina catalyst not prepared by the usual impregnation procedure but by a sol–gel process.[5] These results seem to be very promising, but further tests on the long-term and hydrothermal stability of the catalyst have yet to come. A totally different approach was followed by Burch and Ottery by changing the reductant: On a Pt/Al_2O_3 catalyst, no detectable amount of N_2O was formed with toluene as reducing agent at any temperature.[6] However, with this method one would be bound to toluene as reductant which is not a constituent of the exhaust gas stream.

We followed still another approach: in order to tune the activity and selectivity of platinum-containing catalysts we used a second metal as promoter. As depicted in Fig. 1, the selectivity to N_2O (S_{N_2O}) on platinum- and/or vanadium-containing H-ZSM-35 zeolites decreases considerably with increasing vanadium content of the catalyst. By contrast, the maximal NO_x conversion ($X_{NO_x,max}$) at T_{max} on Pt-V/H-ZSM-35 samples is similar to that on catalysts containing platinum only (Table 1). However, with increasing vanadium content of the samples, the temperature at the maximal NO_x conversion shifts to higher values. An explanation for this effect could be that the platinum is diluted by vanadium and, thus, the platinum clusters are smaller, facilitating effective NO_x reduction only at higher temperatures.

On catalysts containing platinum *and* vanadium, oscillations of the NO_x concentration with large amplitudes ($\Delta X_{NO_x,max}$[8]) tend to occur [Fig. 2(a), *cf.* ref. 9]. Owing to these oscillations, a precise determination of the selectivity to N_2O (*cf.* Fig. 1)

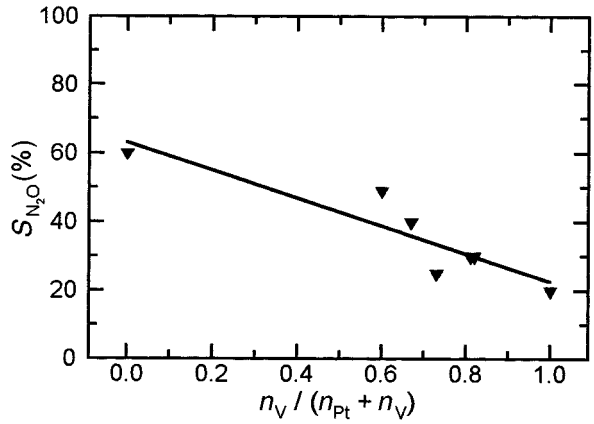

Fig. 1 Average selectivity to N_2O in the selective catalytic reduction of NO_x with propene as a function of the molar ratio $n_V/(n_{Pt} + n_V)$ of platinum- and/or vanadium-containing H-ZSM-35 zeolites.[7]

Table 1 Catalytic results on platinum- and/or vanadium-containing H-ZSM-35 samples

Catalyst	$X_{NO_x,max}$ (%)	$\Delta X_{NO_x,max}$ (%)	T_{max}/°C
1.0V/H-ZSM-35[a]	41	—	303
2.6Pt–3.1V/H-ZSM-35	81	19	215
0.9Pt–1.0V/H-ZSM-35	89	32	205
3.0Pt–2.2V/H-ZSM-35	82	21	212
1.9Pt–1.0V/H-ZSM-35	90	26	196
2.6Pt–1.0V/H-ZSM-35	97	40	177
2.7Pt/H–ZSM-35	85	—	165

[a] The numbers before the metals indicate the metal content in wt% in the dry catalyst.

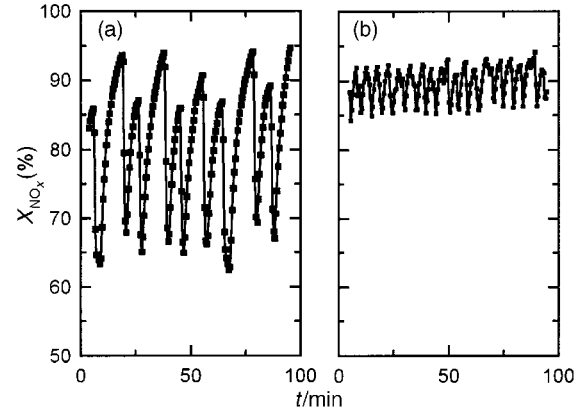

Fig. 2 NO_x conversion on (a) 0.2 g 2.6Pt–1.0V/H-ZSM-35, T_{cat} = 183 °C and (b) 0.2 g 2.6Pt–1.0V/H-ZSM-35 diluted with 0.7 g quartz, $T_{cat.}$ = 190 °C.

turns out to be difficult, because the N_2 concentration fluctuates considerably. Obviously, reaction, adsorption and desorption take place simultaneously and cannot be separated more properly, since the N_2O and N_2 concentrations change independently. First attempts to reduce the amplitude of the oscillations by diluting the catalyst with quartz sand are promising: for a mechanical mixture of the catalyst with quartz, the amplitude of the oscillations is strongly decreased, whereas the average NO_x conversion is even increased from 81 to 90% [Fig. 2(b)].

These observations prompted us to look in some detail into previously proposed reaction mechanisms. Burch *et al.* proposed that, on platinum, NO molecules are adsorbed in addition to N and O atoms resulting from NO dissociation.[10] The formation of N_2 can then be accounted for by recombination of two adsorbed N atoms, while the formation of N_2O is best interpreted in terms of the reaction of an adsorbed NO molecule with an N atom. We speculate that, in our system, most platinum atoms have vanadium atoms as next nearest neighbours. Owing to the higher affinity of vanadium for oxygen, the dissociation of NO could then be promoted resulting in a lower NO concentration on the surface and, hence, a lower selectivity to N_2O.

In conclusion, vanadium as a promoter is able to reduce considerably the selectivity to N_2O during the selective catalytic reduction of nitrogen oxides on platinum-containing zeolite catalysts. If the oscillations occurring on Pt–V/H-zeolites do not affect activity in real car exhausts or if the amplitudes can be strongly reduced by coating the catalyst onto monoliths in much the same way as this can be achieved by dilution with quartz, a major obstacle for the use of platinum catalysts in diesel exhaust gases could be overcome.

The authors gratefully acknowledge financial support by Deutsche Forschungsgemeinschaft, Fonds der Chemischen Industrie and Max Buchner-Forschungsstiftung.

Notes and references

1 P. Zelenka, W. Cartellieri and P. Herzog, *Appl. Catal. B*, 1996, **10**, 3.
2 H. K. Shin, H. Hirabayashi, H. Yahiro, M. Watanabe and M. Iwamoto, *Catal. Today*, 1995, **26**, 13.
3 R. Doumeki, M. Hatano, H. Kinoshita, E. Yamashita, M. Hirano, A. Fukuoka and S. Komiya, *Chem. Lett.*, 1999, 515.
4 R. Wunsch, G. Gund, W. Weisweiler, B. Krutzsch, K. E. Haak, G. Wenninger and F. Wirbeleit, *SAE Trans., Sect. 4*, No. 962 044, 1996, 1892.
5 E. Seker and E. Gulari, *J. Catal.*, 1998, **179**, 339.
6 R. Burch and D. Ottery, *Appl. Catal. B*, 1996, **9**, L19.
7 The catalytic experiments were performed in a flow-type apparatus with a fixed-bed reactor at atmospheric pressure. The gaseous components of the model exhaust gas were premixed and afterwards saturated with water vapour at 45 °C. Typically, the feed contained *ca.* 0.02 vol% NO_x, 0.06 vol% C_3H_6, 0.03 vol% CO, 4 vol% CO_2, 9 vol% O_2 and 10 vol% H_2O in He at a flow rate of 150 cm^3 min^{-1}. Tests with water concentrations of 6.6 and 3.3 vol% revealed that the influence of water on the average NO_x conversion is small. The mass of the hydrated catalyst amounted to 200 mg. The product stream was analysed for NO_x with a chemiluminescence detector; all other components were analysed by capillary gas chromatography.
8 Amplitude of the oscillations as difference between maximum and minimum NO_x conversion.
9 Y. Traa, M. Breuninger, B. Burger and J. Weitkamp, *Angew. Chem. Int. Ed. Engl.*, 1997, **36**, 2113.
10 R. Burch, P. J. Millington and A. P. Walker, *Appl. Catal. B*, 1994, **4**, 65.

Communication 9/06961E

The radical anion of acepentalene

Armin de Meijere,[a] Fabian Gerson,[b] Peter R. Schreiner,[a] Pascal Merstetter[b] and Franz-Manfred Schüngel[a]

[a] *Institut für Organische Chemie der Georg-August Universität, Tammannstr. 2, D-37077 Göttingen, Germany. E-mail: pschrei@gwdg.de*

[b] *Institut für Physikalische Chemie der Universität Basel, Klingelbergstr. 80, CH-4056 Basel, Switzerland. E-mail: gerson@ubaclu.unibas.ch*

Received (in Cambridge, UK) 27th August 1999, Accepted 14th September 1999

In the radical anion ($\mathbf{1}^{\bullet-}$) of acepentalene, generated by photooxidation of the corresponding dianion ($\mathbf{1}^{2-}$), the spin population appears to be evenly distributed over the nine-membered perimeter due to a rapid interconversion between two bowl-shaped C_s forms and a relatively low lying planar C_{2v} transition structure (TS).

Although the acepentalene dianion moiety $\mathbf{1}^{2-}$ in the recently isolated acepentalenediide **1**–Li_2[1,2] is non-planar, it must be considered as aromatic undergoing a rapid bowl-to-bowl inversion, according to NMR data. While the parent compound, neutral acepentalene **1**, which thus far was experimentally characterized only by mass spectrometry, is antiaromatic, based on computed data,[3,4] the corresponding radical anion, $\mathbf{1}^{\bullet-}$, should lie 'in between'. The aromatic nature of open-shell species, in general, is an experimentally unanswered question which was addressed in a computational investigation just recently.[5] In this context, we report on the generation and combined experimental as well as computational characterization of $\mathbf{1}^{\bullet-}$.

The title species was generated by photooxidation of $\mathbf{1}^{2-}$ to $\mathbf{1}^{\bullet-}$.[6,7] Following this procedure, a 10^{-3} M solution of **1**–Li_2 in anhydrous THF was sealed under argon in an EPR cell and UV-irradiated *in situ* at 250 K. The resulting spectrum (Fig. 1; g = 2.0022 ± 0.0002) exhibits a septet arising from six equivalent protons spaced by $|a_H|$ = 0.215±0.005 mT. The spectrum did not markedly change in the 200–270 K temperature range. The hyperfine components were very broad, having a peak-to-peak distance of 0.1 mT. The half-life of the observed paramagnetic species was about 10 min at 250 K, as deduced from the decay of the EPR signals.

Undoubtedly, the six-proton septet originates from the radical anion $\mathbf{1}^{\bullet-}$ formed by loss of an electron from $\mathbf{1}^{2-}$. The equivalence of the protons and the lack of a marked temperature dependence indicate that any dynamic process must be rapid on the hyperfine time-scale (10^7 s^{-1}). In addition to the bowl-to-bowl inversion, $\mathbf{1}^{\bullet-}$ should be subject to an interconversion between two Jahn–Teller structures. The large width of the hyperfine components is in line with such an effect,[8,9] although some broadening may also be caused by an unresolved hyperfine splitting from the ^7Li nucleus of the Li^+ counterions present abundantly in the solution. In contrast to the closed-shell diamagnetic dianion $\mathbf{1}^{2-}$, the radical anion $\mathbf{1}^{\bullet-}$ should have a degenerate singly occupied orbital (*e* or *e*") if it pertains C_{3v} or D_{3h} symmetry. Simple Hückel molecular orbital (HMO) models for structures with these symmetries would lead to a description in which the unpaired electron density is distributed evenly over the nine-membered π-perimeter, so that the spin distribution in $\mathbf{1}^{\bullet-}$ should be similar to that of the hitherto unknown nonatetraenyl radical. Each of the nine peripheral π-centers in $\mathbf{1}^{\bullet-}$ is thus expected to bear 1/9th of the total spin population which, using the proportionality factor Q = −2.2 to −2.6 mT for cyclic radical anions, yields the coupling constant a_H = −0.24 to −0.29 mT. The finding that the observed value $|a_H|$ is smaller may be due to the bowl-shaped geometry of $\mathbf{1}^{\bullet-}$. Deviations of the π-system from planarity are known to decrease the $|a_H|$ value of the proton attached to a π-center because they provide positive contributions to the negative coupling constant of such a proton.[10,11] On the other hand, the symmetry of $\mathbf{1}^{\bullet-}$ may be lower owing to Jahn–Teller distortion, modifying the coupling constant.

To elucidate this point further, we utilized computational methods to characterize the structure of $\mathbf{1}^{\bullet-}$ and to determine the barrier for ring inversion. As done before,[3] gradient-corrected density functional theory (Becke–3–Lee–Yang–Parr, B3LYP),[12–14] in conjunction with the 6-31G* basis set[15] as implemented in the GAUSSIAN 94 program suite,[16] was used for geometry optimizations (B3LYP/6-31G*); stationary points were characterized by analytical vibrational frequency computations which were also used to correct for zero-point vibrational energies (ZPVE) and thermal effects. As spin contamination (expressed in the spin operator expectation value of Slater determinants, $< S^2 >$) may pose a problem for open-shell species, single-point energies on these geometries were evaluated at two higher levels of theory, namely at B3LYP/6-311+G**[17,18] and MP4SDQ/cc-pVDZ.[19]

Computations in C_{3v} or D_{3h} symmetry result in electronically unstable (symmetry breaking) or higher-order stationary structures, *i.e.* $\mathbf{1}^{\bullet-}$ undergoes Jahn–Teller distortion to a lower, non-degenerate symmetry (C_s, Fig. 2). The bowl–inversion transi-

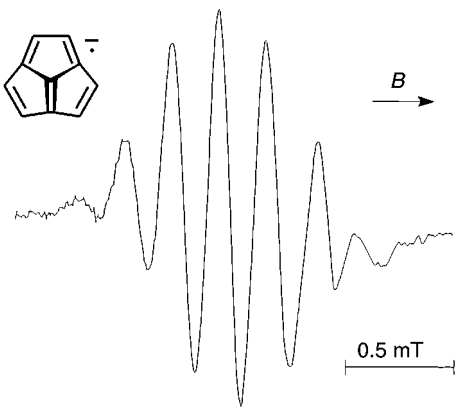

Fig. 1 EPR spectrum of the radical anion $\mathbf{1}^{\bullet-}$ in THF; counterion Li^+, T = 250 K.

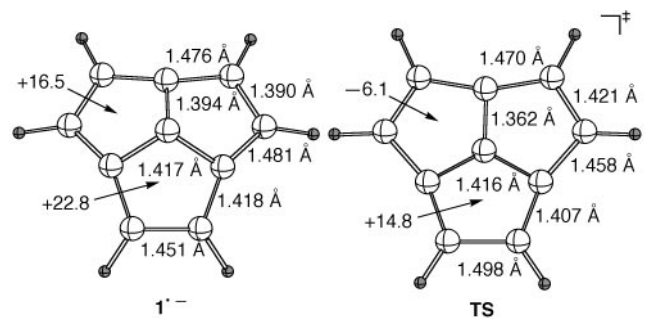

Fig. 2 B3LYP/6-31G* optimized structures of $\mathbf{1}^{\bullet-}$ (C_s) and the **TS** (C_{2v}) for the bowl-to-bowl inversion. Ring centers: NICS values (see text).

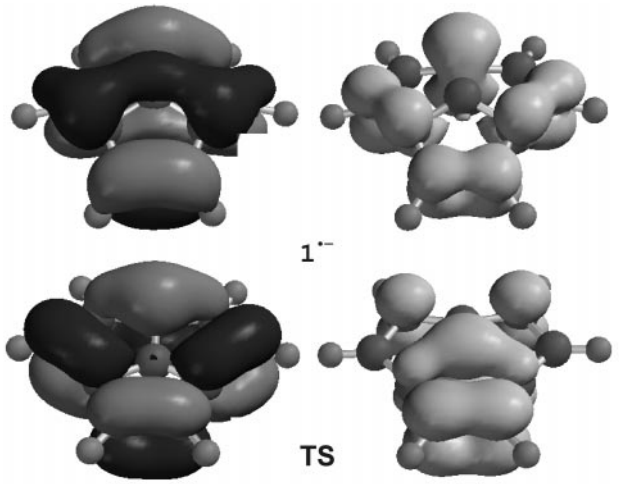

Fig. 3 SOMO (left) and spin populations (right) of the acepentalene radical anion (top) and its transition structure for bowl-to-bowl inversion (bottom).

tion structure, **TS**, is, as expected, planar (C_{2v}) and is associated with a relatively low barrier: $\Delta G^{\ddagger}_{298}$ = 6.9 and 6.1 kcal mol^{-1} at B3LYP/6-311+G** ($< S^2 >$ = 0.76) and MP4SDQ/cc-pVDZ ($< S^2 >$ = 1.13), respectively. This is in accord with a rapid exchange of the two bowl-shaped **1**$^{\bullet-}$ minima on the EPR time scale so that the corresponding spectrum shows only a time-averaged structure. Hence, the hyperfine coupling constants reflect the electron spin distribution of **1**$^{\bullet-}$ *and* the **TS**, which are complementary due to symmetry (Fig. 3, right). By analogy, the highest singly occupied molecular orbitals (SOMOs) for these two structures are similarly shaped (Fig. 3, left), so that the overall spin and electron distribution averaged over both structures indeed appears to be rather symmetrical, in agreement with the observed EPR spectrum.

The inversion barrier for **1**$^{\bullet-}$ is low and comparable to that of **1** and **1**$^{2-}$: $\Delta H^{\ddagger}$ = 5.4 and 7.1 kcal mol^{-1} at B3LYP/6-311+G*//B3LYP/6-31G* + ZPVE, respectively.[3] The inherent strain energy in the **TS** apparently is overcome by a significant aromatic character of the five-membered rings in the **TS** as assessed by computing the nucleus-independent chemical shifts (NICS computed in the geometric ring centers; NICS is a probe for aromaticity: negative values correspond to aromatic, positive to antiaromatic character) [20] which are much smaller in the **TS** than in **1**$^{\bullet-}$ (Fig. 2). While **1**$^{\bullet-}$ clearly has antiaromatic cyclopentadienyl moieties, the **TS** consists of two aromatic and one antiaromatic ring. The same arguments hold true for **1** which is, at least in its bowl-shaped singlet state, highly antiaromatic (the ground state is a triplet).

This work was supported by the Deutsche Forschungsgemeinschaft (Fellowship to P. R. S.), the Fonds der Chemischen Industrie, and the companies BASF, Bayer, Chemetall, Degussa and Hüls (gifts of chemicals).

Notes and references

1 R. Haag, F.-M. Schüngel, B. Ohlhorst, T. Lendvai, H. Butenschön, T. Clark, M. Noltemeyer, T. Haumann, R. Boese and A. de Meijere, *Chem. Eur. J.*, 1998, **4**, 7.
2 R. Haag, R. Fleischer, D. Stalke and A. de Meijere, *Angew. Chem.*, 1995, **107**, 1642; *Angew. Chem., Int. Ed. Engl.*, 1995, **34**, 1492.
3 T. K. Zywietz, H. Jiao, P. v. R. Schleyer and A. de Meijere, *J. Org. Chem.*, 1998, **63**, 3417.
4 R. Haag, D. Schröder, T. Zywietz, H. Jiao, H. Schwarz, P. v. R. Schleyer and A. de Meijere, *Angew. Chem.*, 1996, **108**, 1413; *Angew. Chem., Int. Ed. Engl.* 1996, **35**, 1317.
5 V. Gogonea, P. v. R. Schleyer and P. R. Schreiner, *Angew. Chem.*, 1998, **110**, 2045; *Angew. Chem., Int. Ed. Engl.*, 1998, **37**, 1945.
6 D. Wilhelm, J. L. Courtneidge and A. G. Davies, *J. Chem. Soc., Chem. Commun.*, 1984, 810.
7 W. Huber, *Tetrahedron Lett.*, 1985, **26**, 181.
8 W. D. Hobey and A. D. McLachlan, *J. Chem. Phys.*, 1960, **33**, 1695.
9 H. M. McConnell and A. D. McLachlan, *J. Chem. Phys.*, 1961, **34**, 1.
10 F. Gerson, K. Müllen and E. Vogel, *Helv. Chim. Acta*, 1971, **54**, 2731.
11 F. Gerson, K. Müllen and E. Vogel, *J. Am. Chem. Soc.*, 1972, **94**, 2924.
12 C. Lee, W. Yang and R. G. Parr, *Phys. Rev. B*, 1988, **37**, 785.
13 A. D. Becke, *Phys. Rev. A*, 1988, **38**, 3098.
14 A. D. Becke, *J. Chem. Phys.*, 1993, **98**, 1372.
15 P. C. Hariharan and J. A. Pople, *Theor. Chim. Acta*, 1973, **28**, 213.
16 M. J. Frisch, G. W. Trucks, H. B. Schlegel, P. M. W. Gill, B. G. Johnson, M. A. Robb, J. R. Cheeseman, T. Keith, G. A. Petersson, J. A. Montgomery, K. Raghavachari, M. A. Al-Laham, V. G. Zakrzewski, J. V. Ortiz, J. B. Foresman, J. Cioslowski, B. B. Stefanov, A. Nanayakkara, M. Challacombe, C. Y. Peng, P. Y. Ayala, W. Chen, M. W. Wong, J. L. Andres, E. S. Replogle, R. Gomperts, R. L. Martin, D. J. Fox, J. S. Binkley, D. J. Defrees, J. Baker, J. P. Stewart, M. Head-Gordon, C. Gonzalez and J. A. Pople, GAUSSIAN 94, Rev. C3, Pittsburgh PA, 1995.
17 T. Clark, J. Chandrasekhar, G. W. Spitznagel and P. v. R. Schleyer, *J. Comput. Chem.*, 1983, **4**, 294.
18 G. W. Spitznagel, T. Clark, J. Chandrasekhar and P. v. R. Schleyer, *J. Comput. Chem.*, 1982, **3**, 363.
19 T. H. Dunning Jr., in *Basis Sets: Correlation-Consistent*, ed. P. v. R. Schleyer, N. L. Allinger, T. Clark, J. Gasteiger, P. A. Kollman, H. F. Schaefer III and P. R. Schreiner, Wiley, Chichester, 1998, pp. 88–115.
20 P. v. R. Schleyer, C. Maerker, A. Dransfeld, H. Jiao, and N. J. R. van Eikema Hommes, *J. Am. Chem. Soc.*, 1996, **118**, 6317.

Communication 9/06972K

Chemoselective allylation of aldimine with allyltriethylgermane by the combined use of BF_3•OEt_2 and AcOH

Takahiko Akiyama,* Junko Iwai, Yuji Onuma and Hirotaka Kagoshima

Department of Chemistry, Faculty of Science, Gakushuin University, 1-5-1, Mejiro, Toshima-ku, Tokyo 171, Japan. E-mail: takahiko.akiyama@gakushuin.ac.jp

Received (in Cambridge, UK) 17th September 1999, Accepted 28th September 1999

Allyltriethylgermane reacts with aldimines in preference to aldehydes by means of BF_3•OEt_2 and AcOH to afford homoallylic amines in high yields; three component syntheses of homoallytic amines starting from aldehyde, aniline and allylgermane were successfully achieved.

Lewis acid promoted nucleophilic addition of allylic organometallics to imines constitutes an important reaction for the preparation of homoallylic amines.[1] Although numerous kinds of activator of aldimines have been reported, the addition toward aldimines has been less extensively explored due to its inherent lower reactivity in comparison with that toward aldehydes.[2] Recently, several groups have developed imine selective activators.[3] For instance, Yamamoto and co-workers reported Pd^{II} catalyzed chemoselective allylation of aldimines with allylstannanes.[4] Kobayashi and co-workers found that lanthanide or scandium triflate[5] mediated allylation reactions proceeded smoothly toward aldimines in preference to aldehydes.[6] BF_3•OEt_2 catalyzed chemoselective allylation of aldimines, generated from aldehydes and carbamates[7] or sulfonamides,[8] with allylsilane has been realized. We have also reported that $Sc(OTf)_3$ catalyzed allylation with allylgermane took place highly chemoselectively toward aldimines in preference to aldehydes.[9]

We have recently shown that Brønsted acids activate imines chemoselectively in the presence of aldehydes in aqueous media.[10] Thus, upon reaction of aldimines and silyl enolates in the presence of a catalytic amount of HBF_4, Mannich-type reactions proceeded smoothly in aqueous media to afford β-amino carbonyl compounds in high yields. Three component syntheses of β-amino carbonyl compounds starting from aldehydes and anilines have been also successfully achieved. Furthermore, the Brønsted acid catalyzed Mannich-type reaction proceeded smoothly in water without organic solvent in the presence of surfactants such as SDS.[11]

We report herein that aldimines underwent allylation with allylgermane highly chemoselectively in preference to aldehydes by the combined use of BF_3•OEt_2 and AcOH and that three-component syntheses utilizing aldehydes, amines and allylgermanes furnished homoallylic amines in high yields.

In the first place, the chemoselectivity of the allylation with allylgermane was studied and the results are shown in Table 1. On reaction of an equimolar amount of benzaldehyde and *N*-benzylideneaniline in the presence of allyltriethylgermane (1.5 equiv.) and BF_3•OEt_2 (1.0 equiv.) in MeCN at room temperature, allylation proceeded towards aldehyde to afford a homoallylic alcohol **1a** in a good yield accompanied by a homoallylic amine **2a**. Interestingly, addition of a proton source changed the reaction course dramatically and the aldimine underwent allylation exclusively. As an additive, AcOH gave the best result. It is noted that the present allylation did not proceed at all with the aldimine derived from benzaldehyde and benzylamine. The presence of the *N*-aryl group is mandatory.

After screening the reaction conditions, use of 1.0 equiv. of BF_3•OEt_2 and 0.5 equiv. of AcOH gave the best results.[12,13] It is noted that allylation did not proceed at all with AcOH alone without BF_3•OEt_2. Results for the chemoselective allylation with several aromatic aldimines are shown in Table 2. Allylation of the aldimines proceeded smoothly and showed high chemoselectively in preference to the aldehyde.

Since aldimines are not always stable, it would be synthetically quite useful if the allylation of imines could be achieved *via* reaction with aldimines generated *in situ* from aldehydes and amines. The three component synthesis of homoallylic amines starting from aldehyde, amine and allylgermane took place smoothly in the presence of BF_3•OEt_2 (0.5 equiv.), AcOH (1.0 equiv.) and MS 3A in MeCN to afford homoallylic amines in high yields; the results are shown in Table 3. Not only aldimines derived from aromatic aldehydes but also those derived from aliphatic and α-keto aldehydes worked reasonably well to afford the corresponding homoallylic amines in high yields.

Finally, the chemoselectivity of Si, Ge and Sn reagents was studied. In the presence of equimolar amounts of aldimine and aldehyde, allylic metals were treated with BF_3•OEt_2 (0.5 equiv.) and AcOH (1.0 equiv.) and the results are shown in Table 4. The reaction with allylsilane was sluggish and the corresponding adduct was obtained in a low yield. Although the reactivity of

Table 1 Effect of the additive

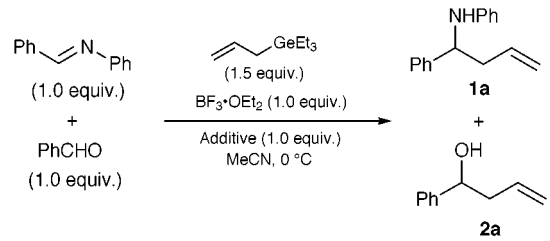

Entry	Additive	Yield of **1a** (%)	Yield of **2a** (%)
1	None	42	88
2	H_2O	72	< 1
3	MeOH	79	< 1
4	AcOH	86	7
5	BzOH	75	< 1

Table 2 Results of the allylation

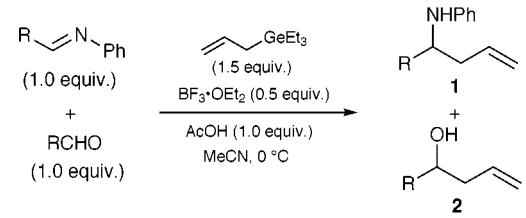

Entry	R	Yield of **1** (%)	Yield of **2** (%)
1	Ph	90	< 1
2	p-$NO_2C_6H_4$	87	6
3	p-ClC_6H_4	86	< 1
4	p-$CH_3C_6H_4$	75	7
5	p-$MeOC_6H_4$	72	< 1

Table 3 Results of the three-component allylation

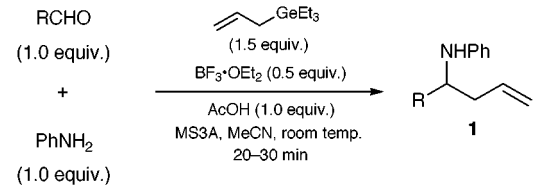

Entry	R	Yield of **1** (%)
1	Ph	81
2	p-$NO_2C_6H_4$	87
3	p-ClC_6H_4	83
4	c-C_6H_{11}	80
5	Bu^t	80
6	PhCO[a]	88

[a] PhCOCHO•H_2O was employed.

Table 4 Reactivity of 14-group allylic organometallics

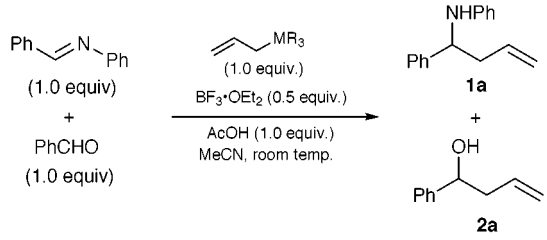

Entry	MR_3	Yield of **1a** (%)	Yield of **2a** (%)
1	$SiMe_3$	19	< 1
2	$GeEt_3$	79	< 1
3	$SnBu_3$	82	9

allylstannane turned out to be higher than that of allylgermane, allylgermane showed the highest chemoselectivity toward aldimines.

In summary, we have found a simple method for the selective allylation of aldimines. Salient features are (i) environmentally benign organogermanium reagents are employed, (ii) the combination of a conventional Lewis acid and a Brønsted acid is found to be an effective activator of aldimines, and (iii) addition of a small amount of protic acid to BF_3•OEt_2 alters the reactivity dramatically.

Partial financial support from the Ministry of Education, Science and Culture of Japan (Grant-in-Aid for Scientific Research) and the Takeda Award in Synthetic Organic Chemistry, Japan, is gratefully acknowledged.

Notes and references

1 E. F. Kleinman and R. A. Volkmann, in *Comprehensive Organic Synthesis*, ed. B. M. Trost and I. Fleming, Pergamon, Oxford, 1991, vol. 2, p. 975; Y. Yamamoto and N. Asao, *Chem. Rev.*, 1993, **93**, 2207.
2 R. A. Volkmann, in *Comprehensive Organic Synthesis*, ed. B. M. Trost and I. Fleming, Pergamon, Oxford, 1991, vol. 1, p. 355; R. Bloch, *Chem. Rev.*, 1998, **98**, 1407.
3 Although Grieco and co-workers reported three allylations of aldimines generated *in situ* from aldehyde, only formaldehyde was employed. See: S. D. Larsen, P. A. Grieco and W. F. Fobare, *J. Am. Chem. Soc.*, 1986, **108**, 3512; P. A. Grieco and A. Bahsas, *J. Org. Chem.*, 1987, **52**, 1378.
4 H. Nakamura, N. Asao and Y. Yamamoto, *J. Chem. Soc., Chem. Commun.*, 1995, 1273; H. Nakamura, H. Iwama and Y. Yamamoto, *J. Am. Chem. Soc.*, 1996, **118**, 6641.
5 S. Kobayashi, *Synlett*, 1994, 689; S. Kobayashi, *Eur. J. Org. Chem.*, 1999, 15.
6 S. Kobayashi and S. Nagayama, *J. Org. Chem.*, 1997, **62**, 232; S. Kobayashi and S. Nagayama, *J. Am. Chem. Soc.*, 1997, **119**, 10 049.
7 S. J. Veenstra and P. Schmid, *Tetrahedron Lett.*, 1997, **38**, 997.
8 Y. Masuyama, J. Tosa and Y. Kurusu, *Chem. Commun.*, 1999, 1075.
9 T. Akiyama and J. Iwai, *Synlett*, 1998, 273.
10 T. Akiyama, J. Takaya and H. Kagoshima, *Synlett*, 1999, 1045; T. Akiyama, J. Takaya and H. Kagoshima, *Chem. Lett.*, 1999, 947.
11 T. Akiyama, J. Takaya and H. Kagoshima, *Synlett*, 1999, 1426.
12 Use of commercially available BF_3•2AcOH gave comparable results.
13 Brønsted acid, generated from BF_3•OEt_2 and 0.5 equiv. of AcOH, may be the active species. For examples of the intramolecular allylation of imines with allylstannanes wherein protic acids have been employed, see: I. Kadota, J.-Y. Park and Y. Yamamoto, *Chem. Commun.*, 1996, 841; J.-Y. Park, I. Kadota and Y. Yamamoto, *J. Org. Chem.*, 1999, **64**, 4901.

Communication 9/07538K

Synthetic studies directed towards the potent cytotoxic natural product ottelione A: stereoselective construction of the complete framework

Goverdhan Mehta* and D. Srinivasa Reddy

Department of Organic Chemistry, Indian Institute of Science, Bangalore, 560 012, India.
E-mail: diroff@admin.iisc.ernet.in

Received (in Cambridge, UK) 8th August 1999, Accepted 29th September 1999

A stereoselective strategy for the rapid acquisition of the complete framework (dideoxyottelione A) of the promising cytotoxic agent ottelione A, with four contiguous stereogenic centres on a hydrindane skeleton and a sensitive 4-methylenecyclohex-2-enone functionality, from the readily available Diels–Alder adduct of 1,2,3,4-tetrachloro-5,5-dimethoxycyclopentadiene and norbornadiene, is delineated.

Towards the end of 1998, the isolation and structure determination of two novel, diastereomeric 4-methylenecyclohex-2-enone moiety-bearing natural products, otteliones A and B, from the fresh water plant *Ottelia alismoides* that grows partially under water, was reported.[1] While ottelione B was assigned structure **1**, even the most incisive analyses of the

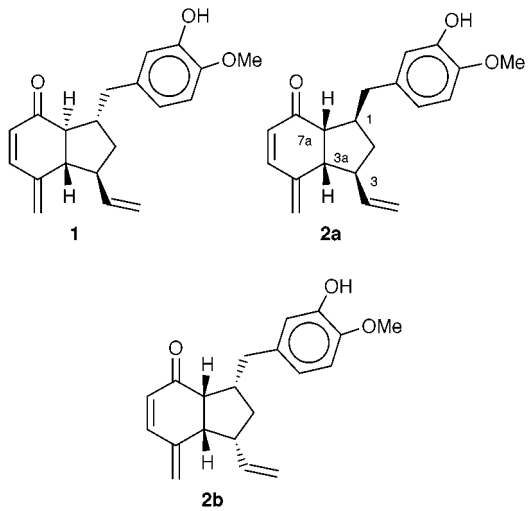

NMR data and modelling did not permit unambiguous assignment to ottelione A. For ottelione A, structures **2a** and **2b** were considered and on the basis of available data **2a** was very much favoured without fully ruling out **2b**.[1] Ottelione A was also found to be identical with the compound reported earlier in the patent literature by Leboul and Provost at Rhone-Poulenc Rorer.[2] Our interest in otteliones A and B was aroused by the observation of remarkable antitumor and antileukemia activity exhibited by them.[1–3] It was shown that **1** and **2** inhibit tubulin polymerisation into microtubules in a manner reminiscent of colchicine, vincristine and vinblastine. When subjected to *in vitro* screening against a panel of *ca*. 60 human tumor cell lines at NCI, both **1** and **2** showed remarkable cytotoxicity against most of the cell lines at nM–pM concentrations.[1] Such a promising biological activity profile, the unusual bicyclic structure with four stereogenic centres, the presence of a sensitive 4-methylenecyclohex-2-enone moiety[4] and the uncertainty associated with the structure assigned to ottelione A **2** prompted us to explore synthetic approaches towards this novel molecule. Herein, we describe a stereoselective and flexible approach, targeted towards the favoured formulation **2a** for

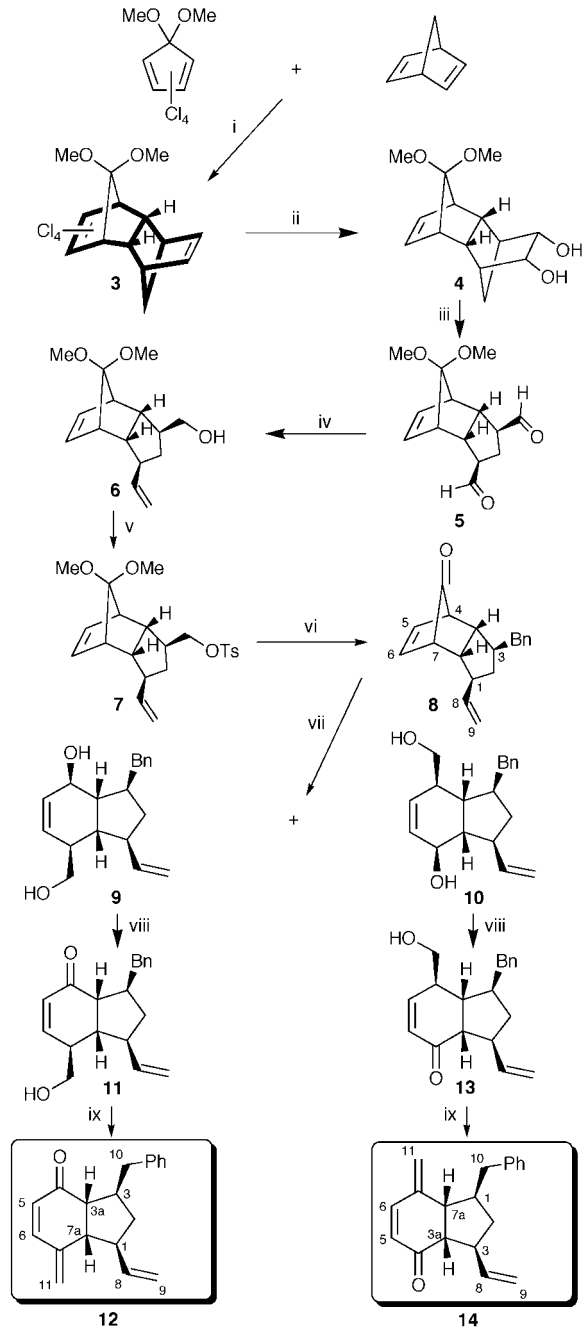

Scheme 1 *Reagents and conditions*: i, reflux, 14 h, 93%; ii, OsO_4, NMO, 24 h, 90%, then Na/NH_3, THF, EtOH, 15 min, 65%; iii, $NaIO_4$, aq. THF, 30 min, 85%; iv, $MePPh_3Br$, Bu^tOK, THF, 10 min, then $NaBH_4$, MeOH, 15 min, 42% for two steps; v, TsCl, Py, 4 h, 95%; vi, PhMgBr, CuBr, 30 min, 62%, then Amberlyst-15, acetone, 2 h, 95%; vii, 30% H_2O_2–NaOH, MeOH, 12 h, then $LiAlH_4$, THF, 2 h, 50–60% for two steps; viii, PDC, EtOAc, cat. AcOH, 2 h, 75%; ix, MsCl, DMAP, CH_2Cl_2, 4 h, then DBU, CH_2Cl_2, 45 min, 90% for two steps.

ottelione A, which has resulted in the acquisition of the complete framework of ottelione A and set the stage for the synthesis of the natural product.

The key element of our projected synthesis of ottelione A **2a** was the identification of the stereochemically well-defined tricyclic compound **3**,[5] readily available through inverse electron demand Diels–Alder reaction between 1,2,3,4-tetrachloro-5,5-dimethoxycyclopentadiene and norbornadiene, as a propitious starting point (Scheme 1). In **3**, the bicyclic hydrindane framework as well as all the four stereogenic centres present in ottelione A are firmly imbedded (see bold lines in **3**) and the main task was to disengage the requisite framework from **3**, preserving the stereochemical features, and sequentially generate the complex and extensive functionalization pattern present in the target molecule **2a**.

Regioselective OsO_4-mediated dihydroxylation of the unsubstituted norbornene double bond in **3**[5] and reductive dehalogenation furnished the *cis*-diol **4**.[6] Periodate cleavage led to the dialdehyde **5** which was directly subjected to controlled mono-Wittig olefination and the remaining aldehyde functionality was reduced to furnish **6**. Tosylation of the hydroxy group in **6** to **7** and Cu^{I} mediated cross-coupling reaction with PhMgBr and acetal deprotection readily led to **8**[6] with the correct stereochemical disposition at all the four stereogenic centres (*cf*. 1, 3, 3a and 7a positions in **2a**)[1] and the desired two substituents on the five-membered ring. The hydrindane framework from the key compound **8** was extracted through Baeyer–Villiger oxidation to two regioisomeric lactones (55:45) and LAH reduction to furnish the diols **9** and **10**, respectively. PDC oxidation of **9** and **10** led to the enones **11**[6] and **13**,[6] respectively, and extensive high field 2D NMR studies on these enones established their structural identity.[6] The sensitive 4-methylenecyclohex-2-enone moiety from **11** was generated quite uneventfully through conversion of the primary hydroxy group to the mesylate and DBU mediated elimination to yield dideoxyottelione A **12**[6] (Scheme 1). The ^{1}H and ^{13}C NMR data for **12** exhibited remarkable similarity to that of the natural product **2a**, as the only difference between them is the presence of the aromatic substitution in the latter. In a similar manner, enone **13** was transformed to **14**,[6] a regioisomer of the natural series in which the benzyl and vinyl moieties are interchanged.

In short, we have outlined a simple and flexible strategy, emanating from abundantly available starting materials, towards a promising cytotoxic natural product ottelione A **2a**. Our approach can be readily adapted to the synthesis of **2a** itself through minor tactical modifications and is inherently well-suited to delivering a variety of analogues for biological evaluation. Efforts along these lines are underway and will be reported shortly.

We thank JNCASR for financial support and the SIF facility at I.I.Sc. for the high field NMR data. One of us (D. S. R.) thanks UGC for a research fellowship.

Notes and references

1 S-E. N. Ayyad, A. S. Judd, W. T. Shier and T. R. Hoye, *J. Org. Chem*., 1998, **63**, 8102.

2 J. Leboul and J. Prevost, French Patent WO96/00205, 1996 (*Chem. Abstr*., 1996, **124**, 242296).

3 H. Li, H. Li, X. Qu, C. Zhao Y. Shi, L. Guo and Z. Yuan, *Zhongguo Zhongyao Zazhi (Chin. J. Chin. Mat. Med.)*, 1995, **20**, 115, 128.

4 D. F. Murray, M. W. Baum and M. Jones, Jr, *J. Org. Chem*., 1986, **51**, 1; M. E. Jung and H. L. Rayle, *Synth. Commun*., 1994, **24**, 197; H. Wild, *J. Org. Chem*., 1994, **59**, 2748.

5 K. Mackenzie, *J. Chem. Soc*., 1960, 473; R. K. McCulloch, A. R. Rye and D. Wege, *Aust. J. Chem*., 1974, **27**, 1929.

6 All compounds were fully characterized on the basis of their spectral and analytical data. *Selected data* for **8**: δ_H(300 MHz, $CDCl_3$): 7.31–7.13 (m, 5H), 6.42 (dd, 1H, *J* 6.9, 3.6), 6.28 (dd, 1H, *J* 6.9, 3.6), 5.80 (ddd, 1H, *J* 17.7, 10.2, 7.2), 5.02–4.92 (m, 2H), 2.96 (m, 1H), 2.81 (dd, 1H, *J* 13.2, 6.0), 2.58 (dd, 1H, *J* 13.2, 8.4), 2.47–2.27 (m, 3H), 2.04–1.95 (m, 1H), 1.80–1.63 (m, 2H), 1.27–1.16 (m, 1H); δ_C(75 MHz, $CDCl_3$) 203.2, 141.1, 141.0, 132.9, 132.4, 128.6 (2C), 128.4 (2C), 126.0, 113.8, 51.2, 50.4, 47.1, 47.0. 46.3, 44.7, 41.1, 40.1; *m*/*z* (70 eV, EI) 264 (M^+). For **12**: δ_H (500 MHz, $CDCl_3$) 7.36–7.18 (m, 5H, arom), 6.97 (d, 1H, *J* 10, H_6), 5.93 (d, 1H, *J* 10, H_5), 5.67 (ddd, 1H, *J* 17.2, 10.2, 8.2, H_8), 5.39 (s, 1H, H_{11}), 5.25 (s, 1H, H_{11}), 5.02 (d, 1H, *J* 10.2, H_9), 4.90 (d, 1H, *J* 17.1, H_9), 3.02 (d of quintet, 1H, *J* 8, 3.4, H_3), 2.94 (dd, 1H, *J* 15, 7.2, H_{10}), 2.78 (dd, 1H, *J* 10.8, 8.5, H_{7a}), 2.70 (dd, 1H, *J* 13.6, 8.7, H_{10}), 2.62 (dd, 1H, *J* 8.2, 3.5, H_{3a}), 2.30–2.23 (m, 1H, H_1), 2.03–1.97 (m, 1H, H_2), 1.25 (ddd, 1H, *J* 13.1, 10.5, 7.5, H_2); δ_C(75 MHz, $CDCl_3$) 199.7 (C quat.), 145.6 (CH), 140.5 (2C, C quat.), 140.4 (CH), 129.0 (2C, CH), 128.3 (2C, CH), 126.4 (CH), 126.0 (CH), 121.6 (CH_2), 115.9 (CH_2), 53.7 (CH), 50.1 (CH), 48.7 (CH), 42.5 (CH_2), 41.2 (CH), 37.5 (CH_2); *m*/*z* (70 eV, EI) 264 (M^+). For **14**: δ_H(500 MHz, $CDCl_3$) 7.26–7.10 (m, 5H, arom), 7.01 (d, 1H, *J* 10, H_6), 5.92 (d, 1H, *J* 10, H_5), 5.87 (ddd, 1H, *J* 17.2, 10, 7, H_8), 5.44 (s, 1H, H_{11}), 5.35 (s, 1H, H_{11}), 5.04 (d, 1H, *J* 17.2, H_9), 4.97 (d, 1H, *J* 10, H_9), 3.18–3.10 (m, 1H, H_3), 2.98 (dd, 1H, *J* 13.4, 4.1, H_{10}), 2.78 (t, 1H, *J* 8.3, H_{7a}), 2.70 (dd, 1H, *J* 7.9, 4, H_{3a}), 2.34 (dd, 1H, *J* 13.3, 10.3, H_{10}), 2.05–1.90 (m, 2H, H_1, H_2), 1.22 (ddd, 1H, *J* 13.1, 9.5, 7.5, H_2); δ_C(75 MHz, $CDCl_3$) 199.5 (C quat.), 145.6 (CH), 142.2 (CH), 141.8 (C quat.), 140.6 (C quat.), 128.7 (2C, CH), 128.3 (2C, CH), 126.5 (CH), 126.0 (CH), 121.4 (CH_2), 113.3 (CH_2), 55.1 (CH), 49.3 (CH), 46.3 (CH), 43.7 (CH), 40.5 (CH_2), 37.1 (CH_2); *m*/*z* (70 eV, EI) 264 (M^+).

Communication 9/07273J

Synthesis and identification of two halogenated bipyrroles present in seabird eggs

Gordon W. Gribble,*[a] and David H. Blank[a] and Jerry P. Jasinski[b]

[a] *Department of Chemistry, Dartmouth College, Hanover, NH 03755-3564, USA. E-mail: grib@dartmouth.edu*
[b] *Department of Chemistry, Keene State College, Keene, NH 03435-2001, USA*

Received (in Corvallis, OR, USA) 13th August 1999, Accepted 22nd September 1999

Two of the four halogenated bipyrroles recently discovered in seabird eggs and eagle liver samples have been identified by synthesis as 1,1′-dimethyl-3,3′,4,4′,5,5′-hexabromo-2,2′-bipyrrole 1 and 5,5′-dichloro-1,1′-dimethyl-3,3′,4,4′-tetrabromo-2,2′-bipyrrole 2, and the structure of the latter compound, which is the major component in the mixture, is further confirmed by X-ray crystallography.

Although more than 3200 naturally occurring organohalogen compounds are now known to exist,[1] most of these are produced by marine organisms, bacteria, fungi and terrestrial plants. Very few have been found in higher animals. The recent report[2] of the presence of several novel halogenated bipyrroles in the eggs of Pacific and Atlantic Ocean seabirds (albatross, puffin, gull, petrel, auklet) and in bald eagle liver samples dramatically reveals that natural organohalogen compounds are more pervasive in the environment than previously believed.

Although sufficient material was not available for full characterization of these compounds, low- and high-resolution mass spectrometry tentatively identified the four major groups of compounds, $C_{10}H_6N_2Br_4Cl_2$, $C_{10}H_6N_2Br_6$, $C_{10}H_6N_2Br_5Cl$ and $C_{10}H_6N_2Br_3Cl_3$, as hexahalogenated 1,1′-dimethyl-2,2′-bipyrroles.[2] We now describe the synthesis and identification of two congeners in this mixture as 1,1′-dimethyl-3,3′,4,4′,5,5′-hexabromo-2,2′-bipyrrole **1** and 5,5′-dichloro-1,1′-dimethyl-3,3′,4,4′-tetrabromo-2,2′-bipyrrole **2**, and establish their probable identity with the two major compounds found in seabird eggs. Bipyrrole **2** appears to be the major seabird compound and is present, for example, in bald eagle liver at a concentration up to 140 ppb.

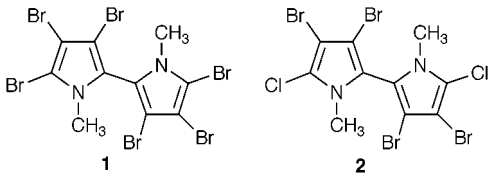

We began with the premise that the compound with molecular formula $C_{10}H_6N_2Br_6$ would have structure **1** and that, given the propensity of pyrroles to undergo electrophilic substitution at C-2, compound $C_{10}H_6N_2Br_4Cl_2$ most likely would have structure **2**. This proved to be correct. Our syntheses of **1** and **2** are shown in Scheme 1.

The known[3] 1,1′-dimethyl-2,2′-bipyrrole **4**, which is readily available from 1-methylpyrrole **3**, was treated with excess NBS to give **1**† in 79% yield. Regioselective halogen–lithium exchange to give the presumed more stable 5,5′-dilithio intermediate followed by chlorination with 2 equiv. of hexachloroethane[4] gave **2**† in 80% yield. The structures of **1** and **2** are fully established by spectral and analytical data, and the X-ray crystallographic molecular structure of **2**‡ is shown in Fig. 1. Compound **2** was also prepared by treating **4** with NCS to give **5**‡ (97% yield). Reaction of **5** with excess NBS afforded **2** in 76% yield, identical with the material prepared from **1**. A one pot reaction of **4** first with NCS and then NBS was less successful and led to a mixture.[5] Interestingly, this mixture closely matched by GC-MS the natural product mixture from the seabirds that contains several other halogenated bipyrroles of formulas $C_{10}H_6N_2Br_4Cl_2$, $C_{10}H_6N_2Br_5Cl$ and $C_{10}H_6N_2Br_3Cl_3$, perhaps implicating a somewhat random biological halogenation sequence involving first chlorination with chloroperoxidase and then bromination with bromoperoxidase.[1] In any event, based on a data set of retention times derived from a series of chromatograms, compounds **1** and **2** are the probable compounds found in the seabirds.[6]

The presumed dietary origin of these halogenated bipyrroles is unknown, although it is relevant that 3,3',4,4',5,5'-hexabromo-2,2'-bipyrrole has been isolated from the marine bacterium *Chromobacterium* sp. along with 2,3,4,5-tetrabromopyrrole.[7] Furthermore, several polybrominated 1-methylpyrroles and polychlorinated pyrroles are produced naturally.[1] Compound **2** and the other as yet unidentified mixed

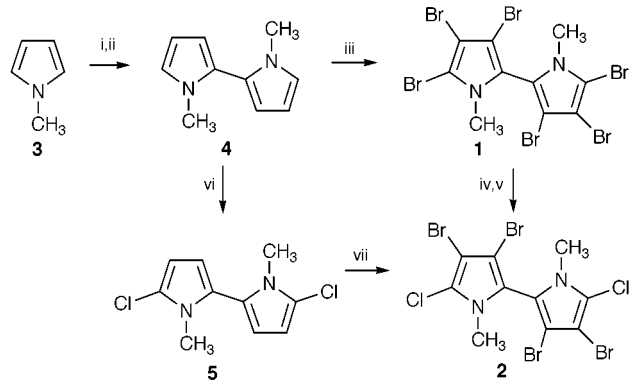

Scheme 1 *Reagents and conditions*: i, BuLi; ii, $NiCl_2$ (55% for 2 steps); iii, NBS (7 equiv.), −78 °C to room temp. (79%); iv, BuLi; v, Cl_3CCCl_3, −78 °C to room temp. (80% for 2 steps); vi, NCS (2 equiv.), −78 °C to room temp. (97%); vii, NBS (5 equiv.), −78 °C to room temp. (76%).

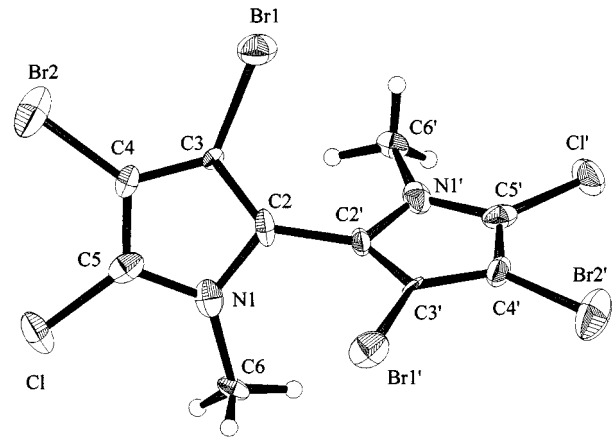

Fig. 1 ORTEP view of the molecular structure of **2.** Thermal ellipsoids are drawn at the 30% probability level. The dihedral angles between the pyrrole ring planes are 67 and 106°.

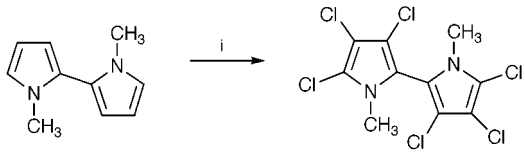

4 6

Scheme 2 *Reagents and conditions*: i, NCS (7 equiv.), −78 °C to room temp. (91%).

bromochlorobipyrroles represent the first examples of naturally occurring pyrroles containing both chlorine and bromine.[8]

We have also synthesized the hexachloro analogue **6**† by treating **4** with excess NCS (Scheme 2). The use of sulfuryl chloride in chlorinations of **4** to give either **5** or **6** was less successful.

The obvious relationship of these polyhalogenated bipyrroles to polychlorinated biphenyls (PCBs) leads one to wonder if the former natural compounds will have similar toxicity profiles to the anthropogenic PCBs. One further wonders if some of the earlier reports of anthropogenic chlorinated compounds in seabirds, fish, and marine mammals were in reality describing, at least in part, naturally occurring organohalogen compounds.

We thank the donors of the Petroleum Research Fund administered by the American Chemical Society for partial support of this project, Dr Ross Norstrom and Sheryl Tittlemier for their assistance and interest on this project, Jennifer Taylor and Sarah Lievens for technical assistance, and Drs Jonathan Sessler and Philip Gale for some unpublished carbon-13 NMR spectral data on bromopyrroles for comparison purposes.

Notes and references

† *Selected data* for **1**: mp 247–248 °C; δ_H(300 MHz, $CDCl_3$) 3.50 (s, 6 H); δ_C($CDCl_3$) 122.5, 107.0, 103.6, 101.5 and 35.7; *m*/*z* (M^+) 628, 630, 632, 634, 636, 638, 640 (1:6:15:20:15:6:1); (M^+ − Br) 550, 552, 554, 556, 558, 560 (1:5:10:10:5:1); (M^+ − $Br)_2$ 472, 474, 476, 478, 480 (1:4:6:4:1) (Calc. for $C_{10}H_6N_2Br_6$: C, 18.96; H, 0.95; N, 4.42; Br, 75.67. Found: C, 19.19; H, 0.93; N, 4.42; Br, 75.44%). For **2**: mp 221 °C (decomp.); δ_H(500 MHz, $CDCl_3$) 3.46 (s, 6 H); δ_C($CDCl_3$) 121.0, 119.6, 103.6, 98.1 and 34.3; *m*/*z* (M^+) 544, 424, 384, 192, 139 (Calc. for $C_{10}H_6N_2Br_4Cl_2$: C, 22.05; H, 1.11; N, 5.14; Cl, 13.02; Br, 58.68. Found: C, 23.06; H, 1.18; N, 5.21; Cl, 12.80; Br, 57.72%). For **4**: oil; δ_H(300 MHz, $CDCl_3$) 3.60 (s, 3 H), 6.27 (m, 4 H) and 6.80 (m, 2 H); δ_C($CDCl_3$) 125.4, 122.9, 110.8, 107.6 and 34.7; *m*/*z* (M^+) 160, 159, 145, 132, 118. 117. For **5**: oil which solidified slowly; δ_H(500 MHz, DMSO-d_6) 3.36 (s, 6 H), 6.18 (m, 4 H); δ_C(DMSO-d_6) 125.2, 117.3, 111.6, 107.1 and 32.6; *m*/*z* (M^+) 228, 213, 193, 178, 152; (M^+) 228, 230, 232 (5:3:1); (M^+ − CH_3 213, 215, 217 (5:3:1); (M^+ − Cl) 193, 195 (3:1); (M^+ − CH_3 − Cl) 178, 180 (3:1); (M^+ − CH_3 − N − CCl) 152, 154 (3:1). For **6**: mp 209 °C (decomp.); δ_H(300 MHz, $CDCl_3$) 3.46 (s, 6 H); δ_C($CDCl_3$) 116.8, 116.7, 113.8, 108.7 and 33.1; *m*/*z* (M^+) 364, 366, 368, 370, 372 (3:5:4:2:1) (Calc. for $C_{10}H_6N_2Cl_6$: C, 32.74; H, 1.65; N, 7.64; Cl, 57.98. Found: C, 32.85, H, 1.67; N, 7.61; Cl, 57.83%).

‡ *Crystal data* for **2**: The compound crystallized from acetone as cloudy white prismatic crystals in the orthorhombic system *Pbcn* (#60). Unit cell dimensions are as follows: a = 12.438(6), b = 8.753(6), c = 13.696(3) Å, V = 1491(1) $Å^3$, Z = 4. The crystal data were collected on an AFC6S diffractometer, Mo-Kα radiation, at 296 K. Total data collected = 1460 and 310 with $I > 4\sigma(I)$. Full-matrix least-squares refinement based on F^2 of 82 parameters has an agreement value, $R1$, of 0.047 and a weighted R ($wR2$) of 0.248. The error of fit is 0.92 and the maximum residual density is 0.73 e $Å^3$. CCDC 182/1425.

1 G. W. Gribble, *Prog. Chem. Org. Nat. Prod.*, 1996, **68**, 1; G.W. Gribble, *Acc. Chem. Res.*, 1998, **31**, 141; G.W. Gribble, *Chem. Soc. Rev.*, 1999, **28**, 335.
2 S. A. Tittlemier, M. Simon, W. M. Jarman, J. E. Elliott and R. J. Norstrom, *Environ. Sci. Technol.*, 1999, **33**, 26.
3. T. Kauffmann and H. Lexy, *Chem. Ber.*, 1981, **114**, 3674.
4 J. Bergman and L. Venemalm, *J. Org. Chem.*, 1992, **57**, 2495.
5 H. M. Gilow and D. E. Burton, *J. Org. Chem.*, 1981, **46**, 2221, report that pyrrole chlorination with NCS is less selective than is bromination with NBS.
6 S. A. Tittlemier and R. J. Norstrom, personal communication, whom we thank for making these comparisons.
7 R. J. Andersen, M. S. Wolfe and D. J. Faulkner, *Mar. Biol.*, 1974, **27**, 281.
8 The bromochloro pyrrolomycins F_1, F_{2a}, F_{2b}, F_3 are 'forced metabolites' and are not considered to be natural products: N. Ezaki, M. Koyama, Y. Kodama, T. Shomura, K. Tashiro, T. Tsuruoka, S. Inouye and S. Sakai, *J. Antibiot.*, 1983, **36**, 1431. Similarly, bromonitrins A–C, which also contain chlorine and bromine, are only produced when bromide is added to the culture medium and are not considered natural: M. Ajisaka, K. Kariyone, K. Jomon, H. Yazawa and K. Arima, *Agric. Biol. Chem.*, 1969, **33**, 294.

Communication 9/06655A

ChemComm

The first enantiocontrolled synthesis of naturally occurring polyoxygenated cyclohexenylmethanol dibenzoates (–)-zeylenol, (–)-uvarigranol G, (–)-tonkinenin A and (+)-pipoxide

Kou Hiroya and Kunio Ogasawara*

Pharmaceutical Institute, Tohoku University, Aobayama, Sendai 980-8578, Japan.
E-mail: konol@mail.cc.tohoku.ac.jp

Received (in Cambridge, UK) 12th July 1999, Accepted 22nd September 1999

The first enanticontrolled synthesis of five naturally occurring polyoxygenated cyclohexenylmethanol dibenzoates has been achieved to confirm three [(–)-zeylenol, (–)-uvarigranol G, (+)-pipoxide], revise one [(–)-tonkinenin A] and disprove one [(–)-epizeylenol] of the proposed structures.

The isolation has been reported[1] of five polyoxygenated cyclohexenylmethanol dibenzoates, (–)-zeylenol[2,3] **1**, (–)-epizeylenol[2,4] **2**, (–)-uvarigranol G[5] **3**, (–)-tonkinenin A[6] **4** and (+)-pipoxide[2,7] **5**, from plants of the genus *Uvaria* which are

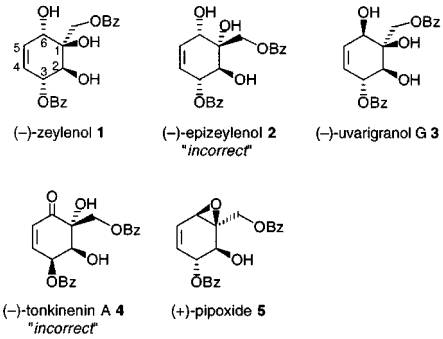

widely distributed across Asia, Africa, and Australia and are used in Chinese traditional medicine to treat digestive disorders. Although the structures of two, **1** and **5**, have been determined unambiguously on the basis of chemical correlation[8] and the racemic synthesis of the latter as well as X-ray analysis[7] of the racemate, the structures of the other three were proposed only on the basis of spectroscopic measurements. Since the diastereo- and enantio-controlled synthesis of these natural products has so far not been reported, we were interested in the construction of these natural products utilizing the chiral cyclohexanoid building block[9] **7** prepared from the *meso*-enediol **6** by either a catalytic[10] or an enzymatic[11] asymmetric desymmetrization procedure. We report here our study leading to the first diastereo- and enantio-controlled synthesis of all of these five compounds which concluded the validity of the proposed structures of three, (–)-zeylenol **1**, (–)-uvarigranol G **3** and (+)-pipoxide **5**, and the invalidity of two, (–)-epizeylenol **2** and (–)-tonkinenin A **4**. The present work has determined the structure of (–)-tonkinenin A not as **4** but as **19**, unambiguously, although the structure of (–)-epizeylenol still remains to be ascertained.

Besides diastereo- and enantio-controlled introduction of their oxygen functionalities, one difficulty which had to be resolved in the construction of these polyoxygenated molecules was regioselective introduction of two benzoyl groups on appropriate oxygen functionalities. To this end, we first transformed the (+)-siloxy ketone[10,11] **7** into the β-hydroxyketo ester† **8**, mp 110 °C, $[\alpha]_D^{29}$ +60.1 (*c* 0.95, $CHCl_3$), by sequential α-methoxycarbonylation and convex-face selective α-hydroxylation as we have carried out in the synthesis of its enantiomer (Scheme 1).[12] Reduction of **8** with $NaBH_4$ occurred diastereoselectively from the convex-face to give the single *trans*-1,2-diol **9**. To block the cyclopentene olefin, **9** was exposed to NBS to give the bromo ether **10**, $[\alpha]_D^{29}$ −22.6 (*c* 2.65, $CHCl_3$). Dehydration of **10**, followed by reduction of the resulting α,β-unsaturated ester **11**, mp 155–156 °C, $[\alpha]_D^{29}$ −8.4 (*c* 1.45, $CHCl_3$), gave the primary alcohol **12** which, on desilylation, afforded the diol **13** having an appropriate structure for dibenzoylation and diastereoselective dihydroxylation. Thus, **13** was benzoylated to give the dibenzoate **14**, mp 134–135 °C, $[\alpha]_D^{28}$ −36.1 (*c* 1.31, $CHCl_3$), whose dihydroxylation using a catalytic amount of OsO_4 and NMO occurred stereoselectively from the convex-face to give the single diol **15**. At this stage, the cyclopentene olefin was regenerated by treating the bromo ether

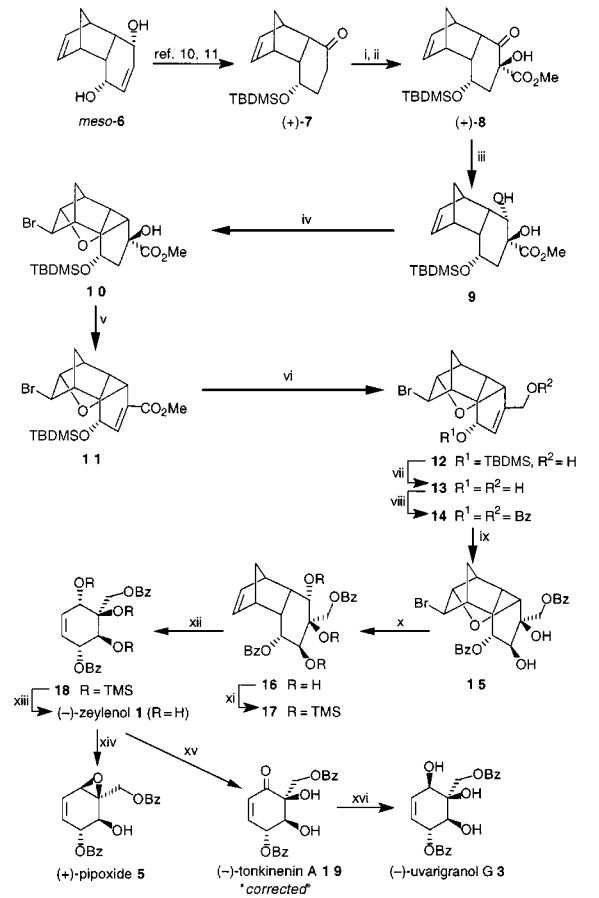

Scheme 1 *Reagents and conditions*: i, NaH, $(MeO)_2CO$, THF, room temp. (89%); ii, O_2, KF, $(EtO)_3P$, DMSO, ~30 °C (82%); iii, $NaBH_4$, MeOH–THF, −15 °C; iv, NBS, CH_2Cl_2, −15 °C (96%, 2 steps); v, $POCl_3$, pyridine, 50 °C (84%); vi, DIBAL-H, toluene, −78 °C; vii, Bu_4NF, THF, room temp. viii, BzCl, pyridine, DMAP (cat.) (97%, 3 steps); ix, OsO_4 (cat.), NMO, aq. THF, room temp. x, Zn, NH_4Cl, aq. THF, reflux (96%, 2 steps); xi, TMSCN, DMF, 80 °C; xii, Ph_2O, reflux, 15 min; xiii, HF; MeCN (83%, 3 steps); xiv, DEAD, PPh_3, THF (62%); xv, MnO_2, CH_2Cl_2–AcOEt (5:1) (100%); xvi, $NaBH_4/CeCl_3 \cdot 7H_2O$, MeOH, −70 °C (100%).

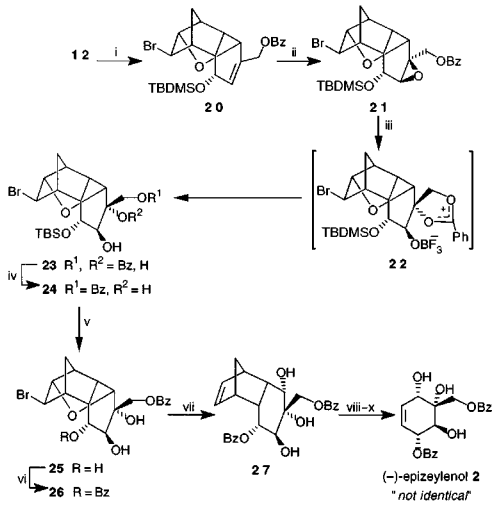

Scheme 2 *Reagents and conditions*: i, BzCl, pyridine, DMAP (cat.) (90%); ii, *M*CPBA, CH_2Cl_2, room temp. (91%); iii, $BF_3{\cdot}OEt_2$, toluene, –20 °C; iv, TsOH, $CHCl_3$, ~30 °C; v, HF, MeCN, THF, ~30 °C (83%, 3 steps); vi, BzCl (1 equiv.), pyridine, DMAP (cat.) (52%); vii, Zn, NH_4Cl, aq. THF, reflux (77%); viii, TMSCN, DMF, 80 °C; ix, Ph_2O, reflux, 25 min; x, HF, MeCN, ~30 °C (76%, 3 steps).

15 with zinc in aqueous THF containing NH_4Cl to give the triol **16**, mp 166–168 °C, $[\alpha]_D^{29}$ −55.4 (*c* 0.66, $CHCl_3$), having four contiguous oxygen functionalities on the cyclohexane moiety.

Having introduced the requisite functionalities, the triol **16** was pertrimethylsilylated using TMSCl[13] in DMF to give the silyl ether **17** which was heated in refluxing Ph_2O for 15 min to give (–)-zeylenol **1**, mp 129–130 °C, $[\alpha]_D^{23}$ −140.5 (*c* 1.02, $CHCl_3$) [lit.,[3] mp 144–145 °C, $[\alpha]_D^{25}$ −116.3 (*c* 0.915, $CHCl_3$)], after desilylation of the crude product.

(+)-Pipoxide **5** was obtained from (–)-zeylenol **1** under Mitsunobu conditions.[14] Thus, on treatment with DEAD and PPh_3 in THF, **1** afforded (+)-pipoxide **5**, mp 129 °C, $[\alpha]_D^{28}$ +55.2 (*c* 0.78, $CHCl_3$) [lit.,[7] mp 152 °C, $[\alpha]_D^{23}$ +53 (*c* 0.02, $CHCl_3$)], stereoselectively.

In order to obtain (–)-uvarigranol G **3**, which was proposed as the C-6 epimer of (–)-zeylenol **1**, we attempted its synthesis from **1** by sequential allylic oxidation and stereoselective reduction. Thus, we first treated **1** with MnO_2 in a mixture of CH_2Cl_2 and EtOAc to give the enone **19**. To our surprise, the physical and spectroscopic data of the enone **19**, mp 158–160 °C, $[\alpha]_D^{27}$ −26.0 (*c* 0.89, MeOH), obtained quantitatively, were found to be identical with those of (–)-tonkinenin A, mp 158–159 °C,[6] $[\alpha]_D^{24}$ −21.6 (*c* 1.71, MeOH),[6] which was proposed as **4**.[6] Thus, we were able to accomplish the first synthesis of this natural product unexpectedly and have revised its structure as **19**. As expected, reduction of **19** with $NaBH_4$/$CeCl_3$[15] allowed diastereoselective reduction of the enone carbonyl to give (–)-uvarigranol G **3**, mp 62–64 °C, $[\alpha]_D^{29}$ −45.8 (*c* 0.73, $CHCl_3$) [lit.,[5]: mp 67–69 °C, $[\alpha]_D^{16}$ −44 (*c* 0.08, $CHCl_3$)].

To obtain (–)-epizeylenol **2**, which was proposed as the C-1 epimer of (–)-zeylenol **1**, the primary alcohol **12** was benzoylated to give **20**, which was converted into the epoxide **21**, diastereoselectively, from the convex-face (Scheme 2). On exposure to $BF_3{\cdot}OEt_2$[16] in toluene, **21** afforded a mixture of the secondary and the primary monobenzoates **23** and **24** after hydrolytic work-up, presumably through the 1,3-dioxolenium intermediate **22**. The mixture without separation was then stirred in $CHCl_3$ containing TsOH to converge to the single primary monobenzoate **24**, which was desilylated to give the triol **25**, mp 208–209, $[\alpha]_D^{30}$ –70.3 (*c* 0.92, THF). Benzoylation of **25** using 1 equiv. of BzCl allowed regioselective monoacylation at the desired position to give the single dibenzoate **26**, mp 254–256 °C, $[\alpha]_D^{31}$ −94.4 (*c* 0.59, THF), along with a minor amount of the separable regioisomer. The observed preferential generation of **26** may be due to the steric hindrance of the primary benzoate functionality, which shields the *exo*-hydroxy functionality considerably. The bromo ether linkage of **26** was then cleaved reductively to yield the triol **27**, mp 169–170 °C, $[\alpha]_D^{28}$ –64.5 (*c* 0.54, $CHCl_3$). As above, on sequential per-*O*-silylation, thermolysis and desilylation, **27** afforded the cyclohexene dibenzoate having the structure **2** which was proposed as (–)-epizeylenol, mp 154–155 °C, $[\alpha]_D^{27}$ −139.1 (*c* 0.22, $CHCl_3$), but its physical and spectroscopic data were not identical with those reported for the natural product, mp 206–207 °C.[4] It was also confirmed that the secondary benzoyl functionality of **2** was not rearranged during these transformation reactions as it afforded the corresponding 6-keto derivative, mp 230–232 °C, $[\alpha]_D^{29}$ −220.5 (*c* 0.12, $CHCl_3$). Thus, the proposed structures of (−)-epizeylenol **2** and (−)-tonkinenin A **4** were both found to be erroneous.

We thank the Takeda Science Foundation for financial support.

Notes and references

† Satisfactory analytical (combustion and/or high resolution mass) and spectroscopic (IR, ^1H and ^{13}C NMR, MS) data was obtained for isolable new compounds.

1 A pertinent review, see: V. S. Parmar, O. D. Tyagi, A. Malhotra, S. K. Singh, K. S. Bisht and R. Jain, *Nat. Prod. Rep*., 1994, **15**, 219.
2 C. Thebtaranonth and Y. Thebtaranonth, *Acc. Chem. Res*., 1986, **19**, 84.
3 S. D. Jolad, J. J. Hoffmann, K. H. Schram, J. R. Cole, M. S. Tempesta and R. B. Bates, *J. Org. Chem*., 1981, **46**, 4267.
4 S. D. Jolad, J. J. Hoffmann, J. R. Cole, M. S. Tempesta and R. B. Bates, *Phytochemistry*, 1984, **23**, 935.
5 X.-P. Pan, R.-Y. Chen and D.-Q. Yu, *Phytochemistry*, 1998, **47**, 1063.
6 W.-M, Zhao, G.-W. Qin, R.-Z. Yang, T.-Y. Jiang. W.-X. Li, L. Scott and J. K. Snyder, *Tetrahedron*, 1996, **52**, 12 373.
7 G. W. Holbert, B. Ganem, D. V. Engen, J. Clardy, L. Borsub, K. Chantrapromma, C. Sadavongvivad and Y. Thebtaranonth, *Tetrahedron Lett.*, 1979, 715.
8 G. R. Schulte and B. Ganem, *Tetrahedron Lett.*, 1982, **23**, 4299.
9 K. Ogasawara, *Pure Appl. Chem*., 1994, **66**, 2119.
10 K. Hiroya, Y. Kurihara and K. Ogasawara, *Angew. Chem., Int. Ed. Engl*., 1995, **34**, 2287.
11 H. Konno and K. Ogasawara, *Synthesis*, 1999, 1135.
12 K. Hiroya and K. Ogasawara, *Chem. Commun*., 1998, 2033.
13 K. Mai and G. Patil, *J. Org. Chem*., 1986, **51**, 3545.
14 O. Mitsunobu, *Synthesis*, 1981, 1; D. L. Hughes, *Org. React*., 1992, **42**, 335; D. L. Hughes, *Org. Prep. Proced. Int*., 1996, **28**, 127.
15 A. L. Gemal and J. L. Luche, *J. Am. Chem. Soc*., 1981, **103**, 5454.
16 M. Prystas. H. Gustafsson and F. Sorm, *Collect. Czech. Chem. Commun*., 1971, **36**, 1487.

Communication 9/05631I

Mannich functionalization of $C_{59}N$

Frank Hauke and Andreas Hirsch*

Institut für Organische Chemie, Henkestrasse 42, D-91054 Erlangen, Germany.
E-mail: hirsch@organik.uni-erlangen.de

Received (in Liverpool, UK) 17th August 1999, Accepted 13th September 1999

The thermal treatment of the heterofullerene dimer $(C_{59}N)_2$ with ketones and aldehydes in the presence of TsOH and air leads to Mannich-type functionalized heterofullerenes $RC_{59}N$.

We have shown recently[1] that arylated heterofullerenes $ArC_{59}N$ are easily accessible in yields up to 90% by the treatment of $(C_{59}N)_2$ **1**[2–5] with an electron-rich aromatic in the presence of TsOH and air. The proposed mechanism of this reaction involves an electrophilic aromatic substitution by $C_{59}N^+$, which is presumed to be formed *via* homolysis of the dimer, followed by oxidation of the $C_{59}N$ radical. The oxidation is a critical step, since running the reaction under an argon atmosphere did not yield arylated products. Here we report on the facile formation of the Mannich bases $RC_{59}N$ [R = CH(R′)COR″], obtained by the analogous treatment of **1** using enolizable aldehydes, ketones and 1,3-diketones as nucleophiles.

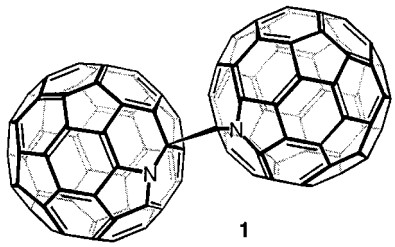

1

Mannich bases **2** and **3** were obtained in almost quantitative yield by the treatment of **1** in 1,2-dichlorobenzene with 20 equiv. of acetone or acetophenone and 40 equiv. of TsOH at 150 °C in a constant stream of air (Scheme 1). After 15 min the conversion was completed. The isolation of the products was achieved by flash chromatography on silica gel using toluene as mobile phase, where **2** and **3** elute as the least polar olive green coloured fraction.

The complete structural characterization of **2** and **3** was carried out by ^{1}H NMR, ^{13}C NMR, UV–VIS and FT-IR spectroscopy as well as by mass spectrometry.† The ^{1}H NMR spectrum of **2**, for example, shows singlets for the methylene and the methyl groups at δ 4.91 and 2.79. The ^{13}C NMR spectrum clearly proves C_s symmetry, showing the 30 expected fullerene resonances in the sp^2 region between δ 155 and 123. The methylene group and the methyl group resonate at δ 53.84 and 30.90, respectively. The signal at δ 78.37 is due to the resonance of the sp^3 C-atom of the fullerene skeleton. The carbonyl C-atom resonates at δ 201.80. Except for the resonances of the addends the ^{13}C NMR spectrum of **3** is qualitatively the same. The UV–VIS spectra of the olive green solutions of **2** and **3**, with the most intensive absorptions located at 257, 320, 445, 589 and 724 nm, display the typical fingerprint for this type of heterofullerene derivatives.[1–5] The FT-IR spectra of **2** and **3** show the typical characteristics of fullerene derivatives (monoadducts), especially the absorptions in the fingerprint region between 480 and 590 cm^{-1}, with the strongest peak at about 524 cm^{-1}. The absorptions at 1729 (**2**) and 1692 cm^{-1} (**3**) are due to the C=O vibrations. EI mass spectrometry shows the M^+ peak of each compound together with a strong fragmentation peak at *m/z* 722 for $C_{59}N^+$.

The treatment of **1** with aldehydes like propanal and decanal under the same experimental conditions led also to complete conversion and the formation of the Mannich bases **4** and **5** respectively (Scheme 2). However, in these cases the aldol condensation products **6** and **7** are formed simultaneously. The amount of condensation products **6** and **7** increases with increasing reaction time, indicating that the condensation step proceeds with the initially formed heterofullerene derivatives **4** and **5**. Aldehydes **4**–**6** were completely characterized by ^{1}H NMR, ^{13}C NMR, UV–VIS and FT-IR spectroscopy as well as by mass spectrometry and exhibit very similar properties to ketones **2** and **3**. The *trans* configuration at the C=C double bonds in **6** and **7** was determined by NOE NMR spectroscopy.

The corresponding reactions of **1** with 1,3-diketones afforded the functionalized azafullerene derivatives **8** and **9** (Scheme 3) which were completely characterized. The fact that the addition proceeded exclusively at the terminal instead of the central C-atoms of the 1,3-diketones is presumably due to steric hindrance. The tautomerization within **8** is comparatively fast on the NMR timescale because only one set of signals for the protons of the addend are found. In the ^{1}H NMR spectrum of **9**, however, two sets of signals for the two corresponding tautomers are found, indicating a much slower process. This is also demonstrated by the fact that the two individual signals for the protons of the hydrogen bridges at δ 15.91 and 15.82 are much sharper than those of **8**. In the reaction mixture obtained from the treatment of **1** with heptane-3,5-dione, in addition to **9** another component **10**, with a simpler ^{1}H NMR spectrum showing one set of signals for magnetically equivalent methyl,

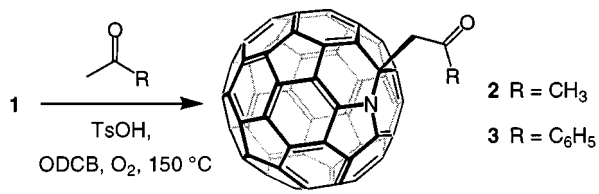

Scheme 1

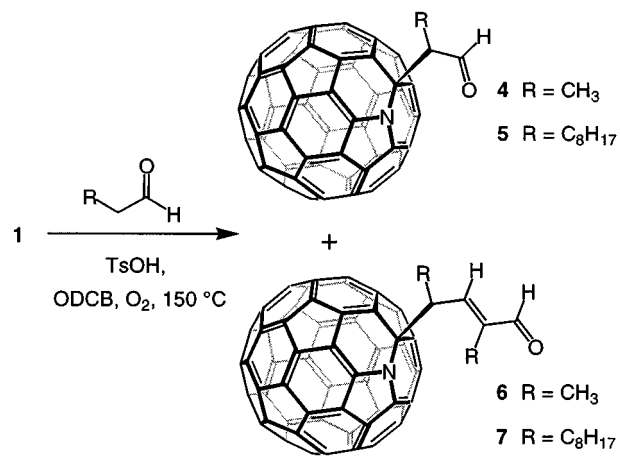

Scheme 2

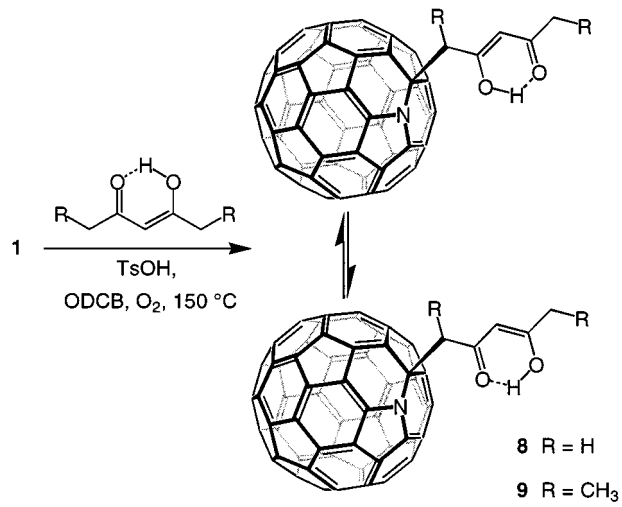

Scheme 3

methine, enol and olefinic protons, could be detected. The spectroscopic data of **10** are consistent with a bisadduct formed as a side product.

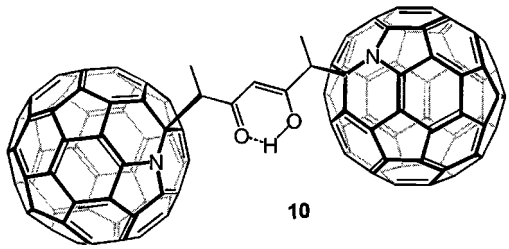

The findings of this contribution support the formation of $C_{59}N^+$ from the dimer **1** after thermolysis and oxidation of the radical $C_{59}N$ (Scheme 4). In the arylations reported previously[1] $C_{59}N^+$ serves as electrophile for the attack of electron-rich aromatics. In the present cases it reacts here with enolizable ketones and aldehydes to afford Mannich bases involving a heterofullerene sphere (Scheme 4). This new derivatization method of $C_{59}N$ opens up a facile access to a broad variety of new functionalized heterofullerenes.

We thank the DFG for financial support.

Notes and references

† *Selected data* for **2**: ν(KBr)/cm^{-1} 2920, 2850, 1729, 1582, 1550, 1509, 1459, 1437, 1422, 1387, 1358, 1317, 1291, 1237, 1185, 1166, 1145, 1118, 1092, 779, 765, 745, 730, 721, 613, 579, 568, 554, 524, 499 and 482; λ_{max}(CH_2Cl_2)/nm 257, 320, 445, 589 and 724; δ_H(400 MHz, CS_2–20% $CDCl_3$) 4.91 (s, 2H) and 2.79 (s, 3H); δ_C(100.5 MHz, CS_2–20% $CDCl_3$) 201.80 (C=O, 1C), 154.94 (2C), 148.31 (2C), 147.37 (2C), 147.11 (2C), 146.90 (4C), 146.38 (2C), 146.31 (2C), 146.02 (2C), 145.75 (2C), 145.50 (2C), 144.90 (2C), 144.74 (2C), 144.14 (4C), 143.79 (2C), 142.89 (2C), 142.54 (2C), 141.88 (2C), 141.56 (2C), 141.22 (2C), 141.01 (2C), 140.83 (2C), 140.78 (2C), 139.43 (2C), 137.41 (2C), 137.35 (2C), 127.26 (2C), 124.63 (2C), 78.37 (1C), 53.84 (CH_2, 1C) and 30.90 (CH_3, 1C); *m/z* (EI) 772 (M^+) and 722 ($C_{59}N^+$). For **3**: ν(KBr)/cm^{-1} 3054, 2950, 2851, 1692, 1594, 1579, 1550, 1446, 1422, 1393, 1344, 1317, 1290, 1215, 1197, 1175, 1092, 1045, 987, 769, 746, 732, 721, 703, 685, 644, 577, 568, 524, 504, 481, 470 and 429; λ_{max}(CH_2Cl_2)/nm 257, 320, 445, 589 and 724; δ_H(400 MHz, CS_2–20% $CDCl_3$) 8.40 (m, 2H), 7.74 (m, 1H), 7.67 (m, 2H) and 5.45 (s, 2H); δ_C(100.5 MHz, CS_2–20% $CDCl_3$) 193.80 (C=O, 1C), 155.02 (2C), 148.57 (2C), 147.57 (1C), 147.36 (2C), 147.10 (2C), 146.93 (2C), 146.87 (2C), 146.34 (2C), 146.26 (2C), 145.97 (2C), 145.73 (2C), 145.55 (1C), 145.44 (2C), 144.85 (2C), 144.71 (2C), 144.09 (4C), 143.77 (2C), 142.85 (2C), 142.54 (2C), 141.83 (2C), 141.53 (2C), 141.18 (2C), 141.03 (2C), 140.80 (2C), 140.75 (2C), 139.39 (2C), 137.42 (2C), 136.58 (2C), 134.93 (i-Ar, 1C), 133.50 (p-Ar, 1C), 128.76 (Ar, 2C), 128.23 (Ar, 1C), 124.78 (2C), 78.59 (1C) and 49.45 (CH_2, 1C); *m/z* (EI) 841 (M^+) and 722 ($C_{59}N^+$). Mannich bases **4**–**6**, **8** and **9** were also completely characterized and exhibit comparable spectroscopic properties. In particular, the UV–VIS spectra of all compounds are virtually identical and the resonances of the C-atoms of the fullerene core in the ^{13}C NMR spectra are very similar.

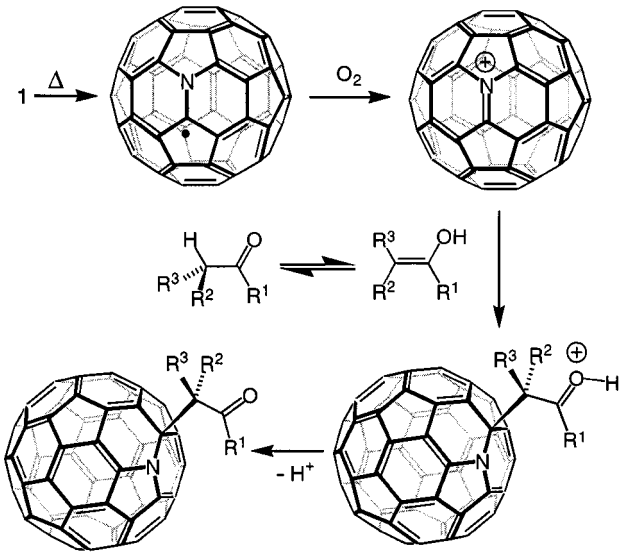

Scheme 4

1 B. Nuber and A. Hirsch, *Chem. Commun.*, 1998, 406.
2 J. C. Hummelen, B. Knight, J. Pavlovich, R. Gonzalez and F. Wudl, *Science*, 1995, **269**, 1554.
3 B. Nuber and A. Hirsch, *Chem. Commun.*, 1996, 1421.
4 J. C. Hummelen, C. Bellavia-Lund and F. Wudl, *Top. Curr. Chem.*, 1999, **199**, 93.
5 A. Hirsch and B. Nuber, *Acc. Chem. Res.*, 1999, in press.

Communication 9/06711F

ChemComm

Encapsulation of polysilane into shell cross-linked micelles

Takanobu Sanji, Yuriko Nakatsuka, Fuminobu Kitayama and Hideki Sakurai*

Department of lndustrial Chemistry, Faculty of Science and Technology, Science University of Tokyo, 2641 Yamazaki Noda, Chiba 278-8510, Japan. E-mail: sakurai@ci.noda.sut.ac.jp

Received (in Oxford, UK) 9th August 1999, Accepted 29th September 1999

The cross-linking reaction of the poly(methacrylic acid) block of poly(1,1-dimethyl-2,2-dihexyldisilene)-*b*-poly(methacrylic acid) with 1,10-diaza-4,7-dioxadecane and 1-ethyl-3-(3-dimethylaminopropyl)carbodiimide hydrochloride afforded the first shell cross-linked micelles of polysilane.

Very recently, a vesicle of an amphiphilic multi-block copolymer with poly(phenylmethylsilane) has been reported.[1] We also reported preparation and formation of micelles of an amphiphilic diblock copolymer, poly(1,1 -dimethyl-2,2-dihexyldisilene)-*b*-poly(2-hydroxyethyl methacrylate).[2]

In this area of the chemistry, the formation and properties of shell cross-linked micelles (SCMs) have been investigated actively in recent years.[3,4] The macromolecular architectures of SCMs are nanometer-sized, with amphiphilic core-shell spheres that are prepared by the self-assembly of amphiphilic block copolymers into polymer micelles, followed by cross-linking of the side chains along the block composing the shell of the polymer micelles. Here, polysilane-based shell cross-linked micelles are reported for the first time.

Poly(1,1-dimethyl-2,2-dihexyldisilene)-*b*-poly(methacrylic acid) **1** (PMHS-*b*-PMAA) was prepared by the sequential anionic polymerization of masked disilenes[5] and trimethylsilyl methacrylate, followed by hydrolysis of the trimethylsilyl protecting group (Scheme 1).† The copolymer, insoluble in $CHCl_3$, was converted to methyl-esterified copolymer by the reaction with CH_2N_2 and the molecular weight was estimated by size exclusion chromatography with $CHCl_3$ as eluent (M_n = 2.8 × 10^4, M_w/M_n = 1.07, calibrated with polystyrene standards). Then the molecular weight of **1** was estimated to be $M_n = 2.4 \times 10^4$. The ^{1}H NMR data of **1** in D_2O gave the relative proportion of PMHS to PMAA and the chemical formula of the copolymer was estimated as $(PMHS)_{12}(PMAA)_{240}$. NMR analysis might underestimate the proportion of polymerization of the polysilane block, because the region of the polysilane blocks on the block polymer has a colloidal nature.

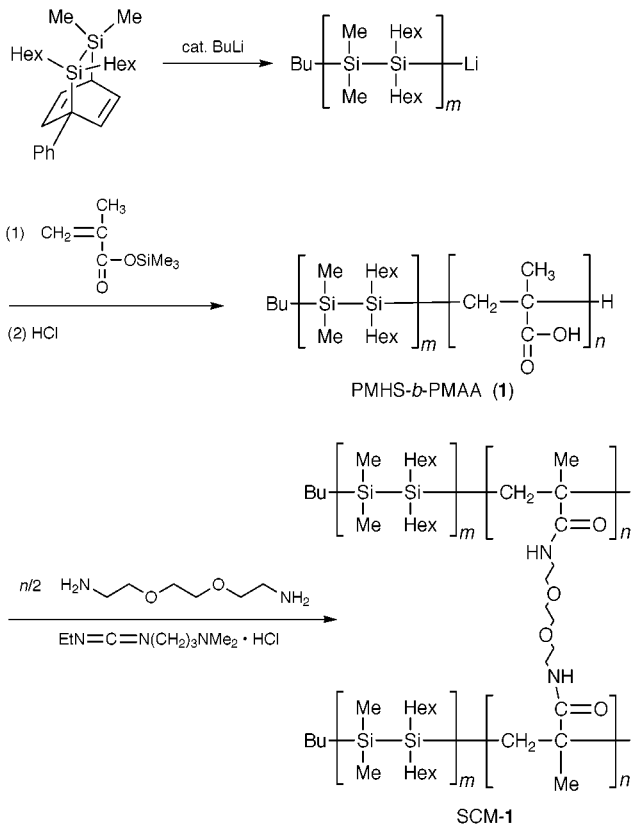

Scheme 1

PMHS-*b*-PMAA **1**, which is soluble in water, is expected to self-assemble in water to form polymer aggregates. In fact, dynamic light scattering (DLS) studies indicated the formation of near-monodisperse micelle, with an intensity-averaged micelle diameter of 170 nm in water (0.2 g l^{-1}, 25 °C). Since the calculated length of the stretched copolymer is about 60 nm with an assumption of all *trans* conformation, the micelle may be swollen to some extent. At this stage, the possibility that **1** forms vesicles instead of micelles cannot be excluded, but the formation of spherical SCMs (*vide infra*) supports the formation of micelles. The critical micelle concentration (CMC) was found for **1** to be 8.1 × 10^{-9} mol l^{-1} as studied by the fluorescence probe method with 8-anilinonaphthalene-l-sulfonic acid (ANS) in water. The hydrophobic PMHS block should exist as the core with the hydrophilic PMAA block as the shell, since the PMHS shows UV absorption at λ_{max} 330 nm, similar to the case of PMHS-*b*-poly(2-hydroxyethyl methacrylate).[2]

Since **1** has a reactive methacrylic acid block, the shell cross-linking reaction of the polymer micelles was examined. A solution of the polymer micelles was prepared in water at a concentration high enough to allow the formation of micelles. The shell cross-linking of the carboxylic acid on the poly(methacrylic acid) block of **1** was achieved by the reaction with 1,10-diaza-4,7-dioxadecane and 1-ethyl-3-(3-dimethylaminopropyl)carbodiimide hydrochloride to the solution.[6]‡ After the cross-linking reaction, ^{1}H NMR signals of the cross linked block copolymer could not be detected in D_2O solution because of very long relaxation times due to its colloidal nature, despite the apparent solubility. Although an amount of cross-linking reagent equivalent to the methacrylic acid units was used, the proportion of the cross-linked methacrylic acid units on the block copolymer to the uncross-linked was *ca.* 50% as estimated by ^{1}H NMR in D_2O–THF-d_8. However, it is difficult to estimate the ratio of the cross-linking accurately. Upon addition of an excess of THF-d_8 to the solution, however, signals of the PMHS core part became observable, indicating that the PMHS block was solvated under these conditions. Interestingly, DLS studies indicated that SCM-**1** in THF was monodispersed, the intensity-averaged diameter of the particles being 230 nm. The (uncross-linked) block copolymer **1** in THF does not form particles. This fact indicates clearly the formation of SCM-**1**. These significant changes in particle size must result from the solvation of the PMHS blocks under these conditions.

Further studies supported the formation of SCMs. In the solid state CP-MAS ^{29}Si NMR of SCM-**1**, two signals were observed at δ_{Si} −27.6 and −35.7, assignable to dihexylsilylene and

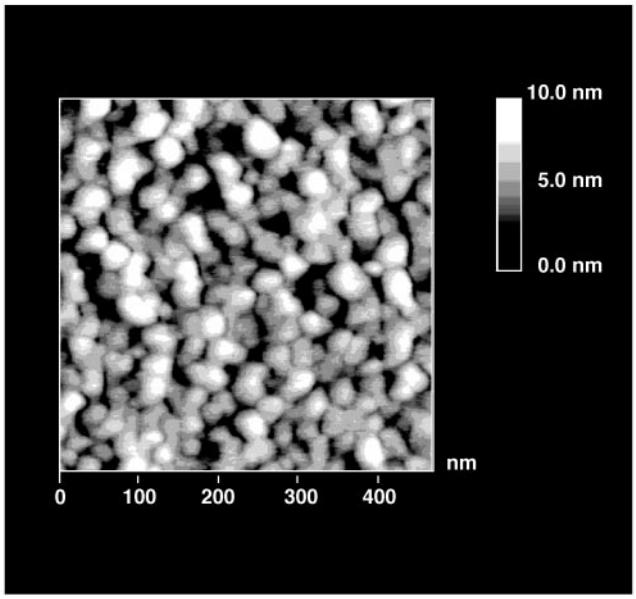

Fig. 1 AFM image of SCM-**1** film of Pyrex glass plate.

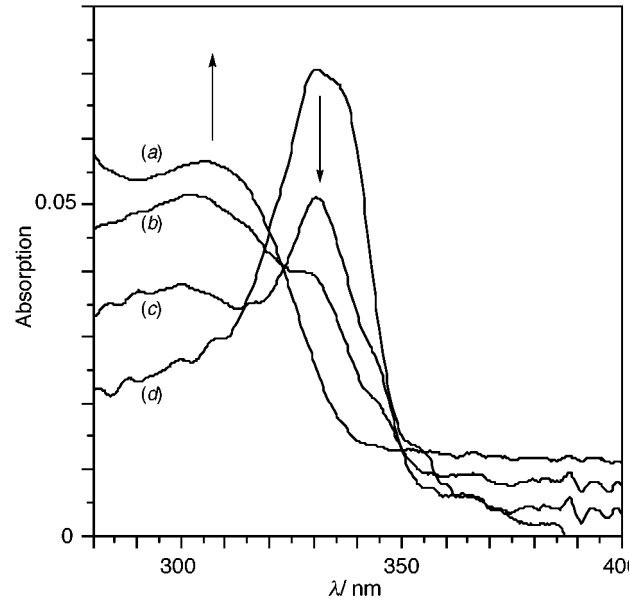

Fig. 2 UV absorption of SCM-**1** in H_2O: (*a*) 0, (*b*) 10, (*c*) 20 and (*d*) 100% H_2O.

dimethylsilylene units, respectively. The IR spectrum of SCM-**1** shows absorption bands for both the carboxylic acid and the amide groups at 1710, 1631 and 1569 cm^{-1}, although that of **1** shows only the absorption band for the carboxylic acid at 1702 cm^{-1}. The DLS studies indicated the intensity-averaged diameter of the particles to be 160 nm with monodispersed spheres, which agreed very closely with the size of the original micelles composed of the block copolymer **1**.

An atomic force microscopy (AFM) image of SCM-**1** provided information on the size and shape of the shell cross-linked spheres.[7] Samples for AFM measurement were prepared by placing a drop of SCM-**1** solution in water (0.045 mg ml^{-1}) on the surface of a Pyrex glass plate and allowing it to dry in air. Fig. 1 shows the AFM image of SCM-**1** film on a Pyrex glass plate operating in the contact mode. Spherical particles of *ca.* 25 nm diameter in the dry state are clearly observed. Under the conditions, the cross-linked corona will eventually shrink onto the glassy PMHS core as the film dries. The measured radius of the dry sphere may fit the molecular length of **1**.

It is worthwhile to examine the electronic properties of the polysilanes encapsulated as the core and protected by the cross-linked hydrophilic corona, since polysilanes exhibit unique electronic spectra depending upon their conformation, which is sensitive to the environment around the chain.[8] SCM-**1** shows an absorption maximum at 333 nm, which is almost identical to those observed both in the solid state and in micelle **1**, where the PMHS block takes the *trans* conformation.[9] This indicates that the PMHS blocks form the unsolvated micelle core, with the cross-linked PMMA forming the solvated corona. In a water–THF mixed solvent, however, the absorption maximum of SCM-**1** undergoes an abrupt shift from 333 to 305 nm (Fig. 2). In THF, SCM-**1** shows an absorption maximum at 305 nm, indicating that the PMHS block takes a random-coil conformation. The (uncross-linked) block copolymer **1** in THF also shows absorption maximum at 305 nm.

We thank Dr Satomi Ohnishi of the National Institute of Materials and Chemical Research for AFM measurements. This work was supported by a Grant-in-Aid from the Ministry of Education (New Polymers and Nano-Organized Systems) and the Japan Society for the Promotion of Science (Research for the Future Program).

Notes and references

† A hexane solution of BuLi (0.72 mmol) was added to 1-phenyl-7,7-dihexyl-8,8-dimethyl-7,8-disilabicyclo[2.2.2]octa-2,5-diene (masked disilene, 2.0 g, 4.9 mmol) and THF (20 ml) at −78 °C. The mixture was stirred for 20 min after removal of the cooling bath. After complete polymerization of the masked disilenes, trimethylsilyl methacrylate (0.77 g, 4.9 mmol) was added to the reaction mixture at −78 °C. The mixture was stirring for 2 h at −78 °C and then a few drops of 1.5 M HCl solution were added to the mixture. After removal of the solvent, fractional precipitation followed by drying *in vacuo* gave water-soluble polymer **1** as a white powder (270 mg, 15.2%). *Spectral data* for **1**: δ_H(D_2O, 300 MHz) 0.08 (br s), 0.87–1.26 (br), 1.78 (br s); δ_C(D_2O, 75.5 MHz) 17.2, 45.4, 49.2, 184.5; ν_{max}(KBr)/cm^{-1} 1702 (COOH).

‡ Synthesis of SCM-**1**: to an aqueous solution of PMHS-*b*-PMAA (100 mg in 22 ml H_2O, 4.5 mg ml^{-1}), 1,10-diaza-4,7-dioxadecane (0.18 mg, 0.21 mmol) and 1-ethyl-3-(3-dimethylaminopropyl)carbodiimide hydrochloride (0.23 mg, 1.20 mmol) were added at room temperature. The amount of the cross-linking reagents corresponds to 100% of the total amount of methacrylic acid units. The mixture was stirred for 1 h at room temperature and then transferred to a dialysis bag followed by dialysis against distilled water for 2 days. After drying *in vacuo*, a solid sample of SCM-**1** was obtained (90 mg, 90%). *Selected data* for SCM-**1**: δ_H(D_2O–THF-d_8, 300 MHz) 0.4–0.5 (br s, $SiMe_2$), 1.15–1.68 (br, $SiHex_2$, CH_3), 2.08 (br s, CH_2C); δ_C(D_2O–THF-d_8, 75.5 MHz) 18.6, 44.8, 54.3, 166, 177; δ_{Si}(Solid-state CP-MAS) −35.7, −27.6; ν_{max}(KBr)/cm^{-1} 3600–2500 (OH), 1710 (COOH), 1631, 1569 (NHC=O).

1 S. J. Holder, R. C.Hiorns, N. A. J. M. Sommerdijik, S. J. Williams, R. G. Jones and R. J. M. Nolte, *Chem. Commun.*, 1998, 1445; N. A. J. M. Sommerdijik, S. J. Holder, R. C.Hiorns, R. G. Jones, and R. J. M. Nolte, *Polym. Mater. Sci. Eng.*, 1999, **80**, 29.
2 T. Sanji, F. Kitayama and H. Sakurai, *Macromolecules*, 1999, **32**, 5718.
3 K. B. Thurmond II, T. Kowalewski and K. L. Wooley, *J. Am. Chem. Soc.*, 1996, **118**, 7239; K. B. Thurmond II, T. Kowalewski and K. L. Wooley, *J. Am. Chem. Soc.*, 1997, **119**, 6656; H. Huang, T. Kowalewski, E. E. Remsen, R. Gertzmann and K. L. Wooley, *J. Am. Chem. Soc.*, 1997, **119**, 11 653; K. L. Wooley, *Chem. Eur. J.*, 1997, **3**, 1397.
4 V. Bütün, N. C. Billingham and S. P. Armes, *J. Am. Chem. Soc.*, 1998, **120**, 12 135.
5 K. Sakamoto, K. Obata, H. Hirata, M. Nakajima and H. Sakurai, *J. Am. Chem. Soc.*, 1989, **111**, 7641.
6 G. G. Moore, T. A. Foglia and T. J. McGhan, *J. Org. Chem.*, 1979, **44**, 2425.
7 L. Zhang and A. Eizenberg, *Science*, 1995, **268**, 1728; L. Zhang and A. Eizenberg, *J. Am. Chem. Soc.*, 1996, **118**, 3168; K. Yu and A. Eizenberg, *Macromolecules*, 1996, **29**, 6359; Y. Yu and A. Eizenberg, *J. Am. Chem Soc.*, 1997, **119**, 8383.
8 P. Trefonas 111, J. R. Damewood, Jr., R. West and R. D. Miller, *Organometallics*, 1985, **4**, 1318; L. H. Harrah and J. M. Zeigler, *J. Polym. Sci., Polym. Lett. Ed.*, 1985, **23**, 209.
9 K. Sakamoto, M. Yoshida and H. Sakurai, *Macromolecules*, 1990, **23**, 4494; K. Sakamoto, M. Yoshida and H. Sakurai, *Macromolecules*, 1994, **27**, 881.

Communication 9/06545H

A new bifunctional ligand: $C_5Me_4SiMe_2OSiMe_2O^{2-}$. Synthesis, properties and crystal structure of the first Yb(II) half-sandwich complex with a heterobidentate cyclopentadienyl ligand, $[\{(\eta^5\text{-}C_5Me_4)SiMe_2OSiMe_2(\eta^1\text{-}O)\}Yb(thf)]_2$

Alexander A. Trifonov,[a] Evgenii N. Kirillov,[a] Axel Fischer,[b] Frank T. Edelmann[b] and Mikhail N. Bochkarev*[a]

[a] *G. A. Razuvaev Institute of Organometallic Chemistry of Russian Academy of Sciences, Tropinina str. 49, 603600, Nizhny Novgorod, Russia. E-mail: mboch@imoc.sinn.ru*

[b] *Otto-von-Guericke-Universität Magdeburg, Universitätsplatz 2, D-39106 Magdeburg, Germany*

Received (in Basel, Switzerland) 18th August 1999, Accepted 3rd October 1999

The synthesis and crystal structure of the Yb(II) half-sandwich complex $[\{(\eta^5\text{-}C_5Me_4)SiMe_2OSiMe_2(\eta^1\text{-}O)\}Yb(thf)]_2$ containing the new linked tetramethylcyclopentadienyl-silanolate ligand $C_5Me_4SiMe_2OSiMe_2O^{2-}$ are reported.

Lanthanide compounds coordinated by bidentate cyclopentadienyl ligands with different coordination mode capacities are of essential fundamental interest from the point of view of their structure, stability and chemical properties. Various cyclopentadienyl ligands bearing in the side chain a Lewis base group such as an ether,[1,2c] amine,[1c,2] or phosphine[3] have been successfully employed in organolanthanide chemistry and derived complexes have attracted considerable interest in recent years. Examples of substituted cyclopentadienyl ligands with a pendant functional group able to form σ Ln–X (X = oxygen,[4] nitrogen[5]) bonds and to realize constrained geometry complexes are not numerous and are limited mainly to the trivalent Sc, Y and Lu derivatives of the linked cyclopentadienyl-amido class.[5a–e] To the best of our knowledge, half-sandwich *divalent* lanthanide analogues have not yet been reported.

Complexes with heterobifunctional cyclopentadienyl ligands are very intriguing and promising because of their use as effective and stereoselective catalysts in various reactions. The complex $[\{(\eta^5\text{-}C_5Me_4)SiMe_2(\eta^1\text{-}NCMe_3)\}(PMe_3)Sc(\mu_2\text{-}H)]_2$ has been shown to exhibit catalytic activity in α-olefin polymerization[5b] while the 'ate'-complexes $Li[Ln\{(\eta^5\text{-}C_5R_4)SiMe_2(\eta^1\text{-}NCH_2CH_2X)\}_2]$ (Ln = Y, Lu; $C_5R_4 = C_5Me_4$, $C_5H_3Bu^t$; X = OMe, NMe_2) readily initiate ring-opening polymerization of ε-caprolactones.[5d]

The present research was aimed towards the preparation of a new functionalized cyclopentadienyl ligand with a pendant hydroxy group suitable for coordination to a divalent lanthanide ion and to the synthesis of the corresponding Yb(II) derivative. Related ligands with pendant O or N functional groups are of great importance in organotransition metal chemistry.[6] Up to now, linked cyclopentadienyl-silanol ligands have not been described. 1,1,3,3-Tetramethyl-3-tetramethylcyclopentadienyl-disiloxane-1-ol was synthesized in two steps (Scheme 1).

$$C_5Me_4HLi \xrightarrow{i} \underset{\mathbf{1}}{C_5Me_4HMe_2SiOSiMe_2Cl} \xrightarrow{ii} \underset{\mathbf{2}}{C_5Me_4HMe_2SiOSiMe_2OH}$$

Scheme 1 *Reagents and conditions*: i, $ClMe_2SiOSiMe_2Cl$, molar ratio $C_5Me_4HLi:ClMe_2SiOSiMe_2Cl$ = 1:5, thf, 18 h room temp.; ii, H_2O, py, thf, 4 h, room temp.

In the first step (Scheme 1, step i)† a five-fold excess of $ClMe_2SiOSiMe_2Cl$ was used to avoid possible formation of $C_5Me_4HMe_2SiOSiMe_2C_5Me_4H$. Hydrolysis of **1** was carried out in thf in the presence of pyridine and afforded **2** in 68% yield, which was purified by flash chromatography on silica gel. Compound **2**‡ gave a satisfactory microanalysis and ^1H NMR spectrum. An HPLC analysis confirmed its purity.

For the synthesis of the targeted ytterbium(II) complex the reaction of protolytic substitution of naphthalene in highly reactive $(C_{10}H_8)Yb(thf)_2$ **3**[7] by the new ligand was used. Similar reactions have been previously shown to be a convenient synthetic route to various Yb(II) and Yb(III) derivatives.[8] Interaction of $(C_{10}H_8)Yb(thf)_2$ with $C_5Me_4HSiMe_2OSiMe_2OH$ readily occurs in thf at room temperature, affording H_2, $C_{10}H_8$ and $[\{(\eta^5\text{-}C_5Me_4)SiMe_2OSiMe_2(\eta^1\text{-}O)\}Yb(thf)]_2$ **4** (Scheme 2) which was obtained as ruby red crystals after recrystallization from thf–hexane in 57% yield.§ Surprisingly no oxidation with formation of Yb^{3+} species takes place during the course of the reaction despite the presence of siloxide functional groups.

$$(C_{10}H_8)Yb(thf)_2 + C_5Me_4HMe_2SiOSiMe_2OH \xrightarrow{-H_2,\ -C_{10}H_8} \underset{\mathbf{4}}{[\{(\eta^5\text{-}C_5Me_4)SiMe_2OSiMe_2(\eta^1\text{-}O)\}Yb(thf)]_2}$$

Scheme 2

Compound **4** is highly sensitive to oxygen and moisture, soluble in thf and DME, sparingly soluble in toluene and diethyl ether and insoluble in aliphatic hydrocarbons. Magnetic measurement and NMR studies have shown **4** to be diamagnetic, corresponding to the Yb^{2+} oxidation state. Compound **4** has been characterized by microanalysis, IR and ^1H NMR spectroscopy as well as by an X-ray diffraction study (Fig. 1).¶ The dimeric complex possesses inversion symmetry imposing the central four membered ring Yb–O2–Yba–O2a to be planar. The endocyclic ytterbium oxygen distances are slightly different [Yb–O2 227.4(2), Yb–O2a 231.9(2) pm] and somewhat shorter than the exocyclic one [Yb–O3 238.1(1) pm). The tetra-

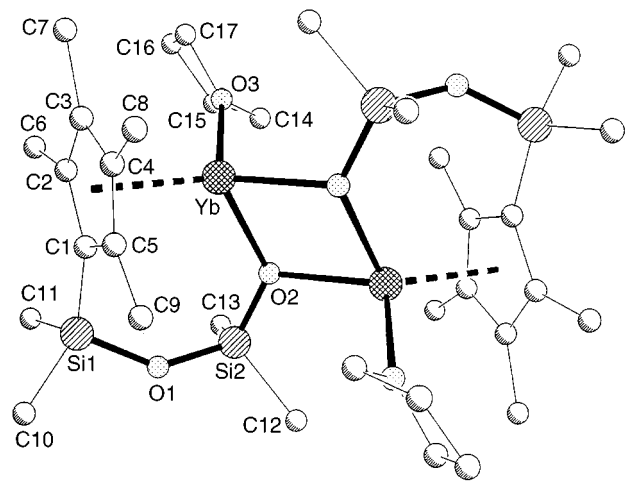

Fig. 1

methylcyclopentadienyl ligand is essentially planar with an ytterbium–centroid distance of 241 pm. The thf molecule displays an envelope conformation with O3 52.5 pm out of the plane defined by C14, C15, C16 and C17. The mean deviation from this best plane is 5.2 pm. The silicon oxygen bond lengths vary from 161.2(2) pm (Si2–O2, the ytterbium briding oxygen) to 164.7(2) pm (Si1–O1).

In an initial reactivity study it was found that **4** does not catalyze propylene polymerization at 20 °C and atmospheric pressure.

We thank the Russian Fund of Basic Research for financial support of this work (RFBR Grants No. 99-03-32905 and 93-03-04131).

Notes and references

† *Synthesis* of **1**: to the solution of 5.04 g (24.85 mmol) of $ClSiMe_2OSiMe_2Cl$ in 20 ml of thf solid C_5Me_4HLi (0.637 g, 4.97 mmol) was added under stirring at −30 °C. The reaction mixture was stirred for 2 h, warmed to room temp. and left overnight. The volatiles were removed under reduced pressure (20 mm Hg), the residue was washed with hexane and the extract was filtered to separate the product from LiCl. Hexane was evaporated under reduced pressure and the resulting yellow oil was distilled under vacuum (106–108 °C/4 mm Hg) yielding 1.26 g (88%) of **1**. Anal. Calc. for $C_{13}H_{25}ClOSi_2$: C, 54.07; H, 8.65; Cl, 12.27. Found: C, 54.36; H, 8.18; Cl, 12.73%. ^{1}H NMR ($CDCl_3$): δ 0.04–0.08 (m, 12H, $SiMe_2$), 1.94 (s, 6H, C_5Me_4H), 2.00 (s, 6H, C_5Me_4H), 2.98 (m, 1H, C_5Me_4H).

‡ *Synthesis* of **2**: to a solution of **1** (1.26 g, 4.36 mmol) and 0.35 ml (0.345 g, 4.36 mmol) of pyridine(py) in 15 ml of thf, 0.078 ml (4.36 mmol) of H_2O were added dropwise at 0 °C and the reaction mixture warmed to room temp. and stirred for 4 h. A white precipitate was separated by filtration; thf was evaporated in vacuum and the resulting pale-yellow oil purified by flash chromatography on silica gel 60 (cyclohexane–ethylacetate, 20 : 1) yielding 0.79 g (68%) of **2**. Anal. Calc. for $C_{13}H_{26}O_2Si_2$: C, 57.76; H, 9.61; Si, 20.78. Found: C, 57.30; H, 9.57; Si, 20.34%. ^{1}H NMR ($CDCl_3$): δ 0.04–0.08 (m, 12H, $SiMe_2$), 1.90 (br s, 1H, OH), 1.92 (s, 6H, $C_5\mathit{Me}_4H$), 2.00 (s, 6H, $C_5\mathit{Me}_4H$), 2.98 (m, 1H, $C_5Me_4\mathit{H}$).

§ *Synthesis* of **4**: to a suspension of 0.62 g (1.39 mmol) of **3** in 25 ml of thf a solution of 0.38 g (1.40 mmol) of **2** in 10 ml of thf was added slowly under vigorous stirring. The reaction mixture turned reddish-brown, the residue of **3** slowly dissolved and H_2 evolved. After 16 h the solution was filtered, thf was evaporated under vacuum and the resulting brown residue was heated (1 h, 50 °C) to separate by sublimation the naphthalene by-product (0.16 g, 93%). The resulting brown solid was recrystallized from thf–hexane to afford 0.41 g (57%) of **4** as ruby red crystals. Anal. Calc. for $C_{17}H_{32}O_3Si_2Yb$: C, 39.77; H, 6.23; Yb, 33.69. Found: C, 39.55; H, 6.11; Yb, 33.98%. IR (Nujol, KBr, cm^{-1}): 460, 610, 680, 740, 800, 830, 890, 950, 1025, 1035, 1050, 1075, 1150, 1260, 1325. ^{1}H NMR (d^8-thf): δ 0.04 (s, 6H, $SiMe_2$), 0.21 (s, 6H, $SiMe_2$), 1.84 (s, 6H, C_5Me_4), 1.93 (s, 6H, C_5Me_4).

¶ *Crystal data*: the measurement on **4** was performed at −100 °C using a Siemens SMART CCD system with Mo-Kα X-radiation (λ = 0.71073 Å) and a graphite monochromator. A selected crystal of **4** was coated with mineral oil, mounted on a glass fibre and transferred to the cold nitrogen stream (Siemens LT-2 attachment). A full hemisphere of the reciprocal space was scanned by ω in three sets of frames of 0.3°. As an absorption correction the SADABS routine was applied.

4: $C_{34}H_{64}O_6Si_4Yb_2$, M = 1027.29, orthorhombic, space group *Pbca*, a = 14.6684(10), b = 16.4898(2), c = 17.3574(2) Å, U = 4198.39(8) Å^3, Z = 4, D_c = 1.625 Mg m^{-3}, F(000) = 2048, μ(Mo-Kα) = 4.579 mm^{-1}, max/min transmission 1.00/0.69, ruby red prism 0.56 × 0.52 × 0.32 mm. A total of 26491 reflections were collected, over a range $2.2 < \theta < 28.3°$, of which 5197 were independent (R_{int} = 0.023). The structure was solved by direct methods.[9] Refinement was by full-matrix least squares on F^2 and converged to $R1$ = 0.0194 (conventional) and $wR2$ = 0.0461 (all data), with goodness of fit = 1.091, 216 parameters, weighting scheme $[\sigma^2(F_o^2) + 0.0181P)^2 + 4.3441P]$, where $P = (F_o^2 + 2F_c^2)/3$. CCDC 182/1430.

1 (*a*) B. Wang, D. Deng and C. Qian, *New J. Chem.*, 1995, **19**, 15; (*b*) D. Deng, X. Zeng, C. Qian, J. Sun, A. Dormond, D. Baudry and M. Visseaux, *J. Chem. Soc., Dalton Trans.*, 1994, 1665; (*c*) W. A. Hermann, R. Anwander, F. C. Munk and W. Scherer, *Chem. Ber.*, 1993, **126**, 331; (*d*) D. A. Laske, R. Duchateau, J. H. Teuben and A. L. Spek, *J. Organomet. Chem.*, 1993, **426**, 149; (*e*) A. A. Trifonov, P. Van de Weghe, J. Collin, A. Domingos and I. Santos, *J. Organomet. Chem.*, 1997, **527**, 225; (*f*) H. Schumann, F. Erbstein, K. Hermann, J. Demtschuk and R. Weimann, *J. Organomet. Chem.*, 1998, **526**, 255.

2 (*a*) P. Jutzi, J. Dahlhaus and M. O. Kristen, *J. Organomet. Chem.*, 1993, **450**, C1; (*b*) G. Paolucci, R. D'Ippolito, C. Ye, C. Qian, J. Gräper and D. R. Fischer, *J. Organomet. Chem.*, 1994, **471**, 97; (*c*) J. R. Van den Hende, P. B. Hitchcock, M. F. Lappert and T. A. Nile, *J. Organomet. Chem.*, 1994, **474**, 79; (*d*) G. A. Molander, H. Schumann, E. C. Rosenthal and J. Demtschuk, *Organometallics*, 1996, **15**, 3817.

3 H. H. Karsch, V. Graf, M. Riesky and E. Witt, *Eur. J. Inorg. Chem.*, 1998, 1403.

4 A. A. Trifonov, F. Ferri and J. Collin, *J. Organomet. Chem.*, in press.

5 (*a*) P. J. Shapiro, E. Bunel, W. P. Schaefer and J. E. Bercaw, *Organometallics*, 1990, **9**, 867; (*b*) P. J. Shapiro, W. P. Cotter, W. P. Schaefer, J. A. Labinger and J. E. Bercaw, *J. Am. Chem. Soc.*, 1994, **116**, 4623; (*c*) Y. Mu, W. E. Piers, D. C. MacQuarrie, M. J. Zaworotko and V. G. Young, *Organometallics*, 1996, **15**, 2720; (*d*) K. C. Hultzsch, T. P. Spaniol and J. Okuda, *Organometallics*, 1997, **16**, 4845; (*e*) K. C. Hultzsch, T. P. Spaniol and J. Okuda, *Organometallics*, 1998, **17**, 485.

6 Y.-X. Chen and T. J. Marks, *Organometallics*, 1997, **16**, 3649; P. J. Sinnema, L. Van der Veen, A. L. Spek, N. Veldman and J. H. Teuben, *Organometallics*, 1997, **16**, 4245; F. Amor, T. P. Spaniol and J. Okuda, *Organometallics*, 1997, **16**, 4765; A. L. McKnight, M. A. Masood, R. M. Waymouth and D. A. Strauss, *Organometallics*, 1997, **16**, 2879; Y.-X. Chen, P.-F. Fu, C. L. Stern and T. J. Marks, *Organometallics*, 1997, **16**, 5958; E. C. G. Gielens, J. Y. Tiesnitsch, B. Hessen and J. H. Teuben, *Organometallics*, 1998, **17**, 1652; L. Schwink, P. Knochel, T. Eberle and J. Okuda, *Organometallics*, 1998, **17**, 7; A. K. Hughes, A. Meetsma and J. H. Teuben, *Organometallics*, 1993, **12**, 1936; G. Lanza, I. L. Fragalá and T. J. Marks, *J. Am. Chem. Soc.*, 1998, **120**, 8257; J. Okuda, S. Verch, T. P. Spaniol and R. Stürmer, *Chem. Ber.*, 1996, **129**, 1429.

7 M. N. Bochkarev, I. M. Penyagina, L. N. Zakharov, Yu. F. Rad'kov, E. A. Fedorova, S. Ya. Khorshev and Yu. T. Struchkov, *J. Organomet. Chem.*, 1989, **378**, 363; M. N. Bochkarev, I. L. Fedushkin, V. K. Cherkasov, V. I. Nevodchikov, H. Schumann and F. H. Görlitz, *Inorg. Chim. Acta*, 1992, **201**, 69; M. N. Bochkarev, V. V. Khramenkov, Yu. F. Rad'kov, L. N. Zakharov and Yu. T. Struchkov, *J. Organomet. Chem.*, 1991, **421**, 29.

8 M. N. Bochkarev, A. A. Trifonov, E. A. Fedorova, N. S. Emelyanova, T. A. Basalgina, G. S. Kalinina and G. A. Razuvaev, *J. Organomet. Chem.*, 1989, **372**, 217.

9 G. M. Sheldrick, SHELXTL, Structure Determination Software Programs, Version 5.03 (PC), Siemens Analytical X-Ray Instruments, Madison, WI, 1995.

Communication 9/06741H

ChemComm

Intracluster transmetalation of cuprates with stannanes

Cristina Mateo, Diego J. Cárdenas, Belén Martín-Matute and Antonio M. Echavarren*

Departamento de Química Orgánica, Universidad Autónoma de Madrid, Cantoblanco, 28049 Madrid, Spain. E-mail: anton.echavarren@uam.es

Received (in Liverpool, UK) 5th August 1999, Accepted 13th September 1999

Alkylarylcuprates with intramolecularly tethered stannanes undergo an intracluster Cu^{I}/Sn^{IV} transmetalation to yield arylstannanes.

Transmetalation of diorganocuprates with alkenyltrialkylstannanes allows for the selective synthesis of mixed organocuprates with concomitant formation of stable tetraalkylstannanes [eqn. (1)].[1] This method has been successfully extended to the

$$R^1SnR^2_3 + R^3{}_2CuLi \longrightarrow R^1R^3CuLi + R^3SnR^2_3 \qquad (1)$$

preparation of allyl cuprates.[2] However, despite the synthetic importance of this reaction[1–3] little is known about its mechanism.

We have been able to isolate the Pd/Sn and Pd/Si transmetalation steps of the Stille and Hiyama coupling reactions, respectively, by performing the reaction intramolecularly in a system which was unable to reductively eliminate because of the instability of the resulting organic product [eqn. (2)].[4] We

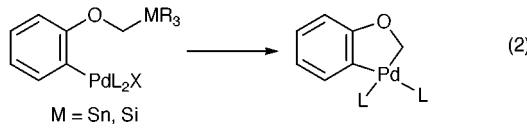

(2)

decided to use a similar approach to study the Cu/Sn transmetalation.

Recently, Sakamoto demonstrated that mixed arylmethylcuprates can be obtained from iodobenzenes by iodine–copper exchange reaction with [$LiCuMe_2$·LiCN] (**1a**).[5,6] Therefore, we chose to study the reactivity of arylcuprates **3**, synthesised by reaction of aryl iodide **2** with **1** (Scheme 1 and Table 1). Upon warming of the solution of **3a**[7] from −78 to 23 °C, arylstannane **4a** was cleanly formed in high yield by an apparent intramolecular Cu/Sn transmetalation.[8,9]† A similar reaction was observed with cuprates **3b**–**d** formed *in situ* from aryl iodide **2** by reaction with the corresponding homocuprates **1b**–**d**, although yields were lower due to the slower iodine/copper exchange reaction as compared with that of **1a**. Stannane **4a** was also obtained by reaction of **2** with [$LiCuMe_2$·LiI], although the reaction was not so clean. Reaction of **2** with either MeLi or BuLi (2 equiv. each) failed to give any of the rearranged products **4a** or **4b**, instead yielding **5** after hydrolysis.

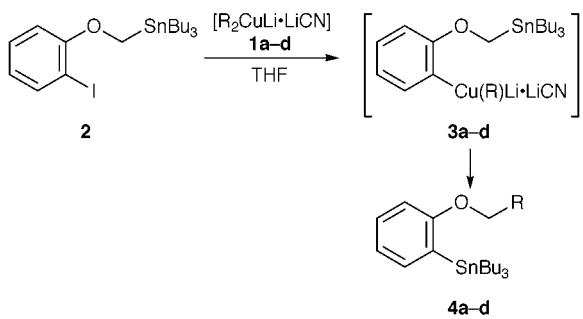

Scheme 1

Table 1 Reaction of stannane **2** with cuprates **1a**–**d**

1 (equiv.)	R	Product	Isolated yield (%)
1a (1.1)	Me	**4a**	96
1a (2.0)	Me	**4a**	38
1b (1.6)	Bu	**4b**	40
1b (2.0)	Bu	**4b**	50
1c (1.5)	Bu^t	**4c**	37
1c (2.0)	Bu^t	**4c**	26
1d (1.2)	Ph	**4d**	43

Arylstannanes **4** presumably arise by Cu/Sn transmetalation, followed by reaction of the resulting cuprate with RI formed in the first iodine/copper exchange process. Although a direct intramolecular process on **3** appears to be forbidden due to endocyclic restriction,[10] the following experiment also excludes a simple intermolecular pathway. Thus, treatment of a mixture of stannane **5** and iodobenzene with **1a** failed to give any of ethers **6a**,**b** and phenyltributylstannane.[11] Similarly, no Cu^{I}/Sn^{IV} exchange was observed between **5** and [$LiCuPh_2$·LiCN] (**1d**).

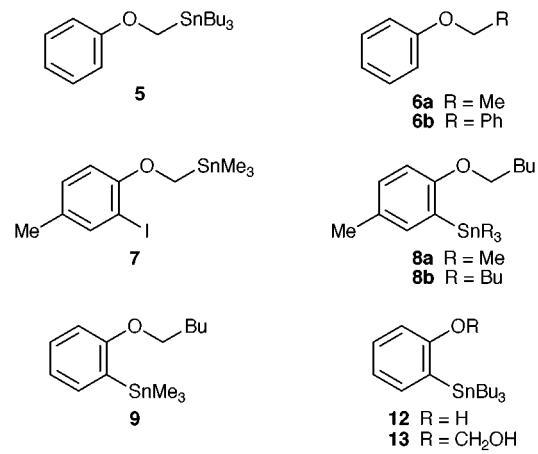

On the other hand, treatment of a 1:1 mixture of **2** and **7** with [Bu_2CuLi·LiCN] led to a mixture of the four possible products **4b**, **8a**, **8b** and **9**.[12] Although apparently puzzling, this crossover experiment can be readily explained if the usual dimeric structure of the cuprates is taken into account (Scheme 2).[13] Thus, reaction of cuprates **1** with the aryl iodides would furnish

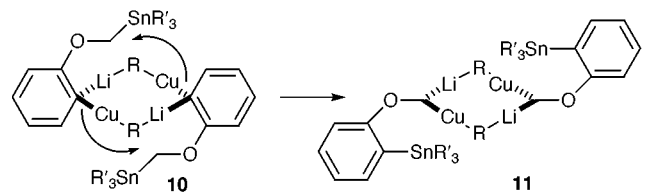

Scheme 2

dimer alkylarylcuprates **10**,[14] which could suffer a selective intracluster transmetalation to afford mixed cuprate **11**. Evidence for the formation of species **11** was obtained by the isolation of stannane **12**[15] in the reactions of **1b** with **2**, presumably as a result of the hydrolysis of hemiketal **13** resulting from the oxidation of cuprate **11** (R = R′ = Bu) by oxygen. Final coupling of cuprates **11** with RI (R = Me, Bu, Bu^t, Ph) formed in the first iodine/copper exchange reaction accounts for the formation of products **4a–d** (Scheme 1).

Thus the present study demonstrates that transmetalation of stannanes with cuprates can proceed in an intracluster manner. This is also the first example of transmetalation of alkylstannanes with organocuprates. Similar transformations could be conceived with organostannanes bonded to the lithium atoms of cuprate dimers through the appropriate directing groups.

We are grateful to the DGES (Project PB97-0002-C2-02) for support of this research and to the MEC for a predoctoral fellowship to B. M.-M.

Notes and references

† *Preparation* of **4a**: MeLi (1.6 M solution in hexanes, 0.93 ml, 1.49 mmol) was added into a suspension of CuCN (66 mg, 0.74 mmol) in THF (4 ml) at −78 °C. After stirring at −78 °C for 3 h, the light yellow solution was treated with a solution of **2** (350 mg, 0.67 mmol) in THF (5 ml). The resulting mixture was allowed to reach 23 °C over 17 h. A saturated NH_4Cl–NH_3 buffered solution (pH = 8, 50 ml) and Et_2O (100 ml) were then added. After the usual extractive workup and chromatography (SiO_2, hexanes) **4a** was obtained as a colorless oil (264 mg, 96%); δ_H($CDCl_3$, 200 MHz) 7.37 (dd, *J* 6.6, 1H), 7.32–7.24 (m, 1H), 6.94 (br t, *J* 7.1, 1H), 6.78 (br d, *J* 8.1, 1H), 3.99 (q, *J* 6.9, 2H), 1.65–1.12 (m, 15H), 1.08–0.99 (m, 6H), 0.92–0.84 (m, 9H); δ_C($CDCl_3$, 75 MHz) 163.09, 136.99 [^2J(^{13}C–Sn) 23], 130.24, 129.60, 120.7 [^1J(^{13}C–Sn) 40], 109.35 [^2J(^{13}C–Sn) 21], 62.92, 29.20 [^3J(^{13}C–Sn) 19], 27.42 [^2J(^{13}C–Sn) 58], 14.92, 13.70, 9.83 [^1J(^{13}C–^{119}Sn) 333.3, ^1J(^{13}C–^{117}Sn) 332.6]; *m/z* (EI) 411 (M^+), 355 (100%) (Calc. for $C_{20}H_{36}OSn$: C, 58.42; H, 8.82. Found: 58.45; H, 9.15%).

1 J. R. Behling, K. A. Babiak, J. S. Ng, A. L. Campbell, R. Moretti, M. Koerner and B. H. Lipshutz, *J. Am. Chem. Soc.*, 1988, **110**, 2641. This method has been successfully extended for the preparation of allyl cuprates.

2 B. H. Lipshutz, R. Crow, S. H. Dimock, E. L. Ellsworth, R. A. J. Smith and J. R. Behling, *J. Am. Chem. Soc.*, 1990, **112**, 4063.

3 M. Benecie and K. Khuong-Huu, *Synlett*, 1992, 266.

4 D. J. Cárdenas, C. Mateo and A. M. Echavarren, *Angew. Chem., Int. Ed. Engl.*, 1994, **33**, 2445; C. Mateo, D. J. Cárdenas, C. Fernández-Rivas and A. M. Echavarren, *Chem. Eur. J.*, 1996, **2**, 1596; C. Mateo, C. Fernández-Rivas, A. M. Echavarren and D. J. Cárdenas, *Organometallics*, 1997, **16**, 1997; C. Mateo, C. Fernández-Rivas, D. J. Cárdenas and A. M. Echavarren, *Organometallics*, 1998, **17**, 3661.

5 Y. Kondo, T. Matsudaira, J. Sato, N. Murata and T. Sakamoto, *Angew. Chem., Int. Ed. Engl.*, 1996, **35**, 736.

6 For the structure of organocuprates generated from CuCN: N. Krause, *Angew. Chem., Int. Ed.*, 1999, **38**, 79.

7 Formation of an arylcuprate intermediate was demonstrated by the formation of *o*-allylphenol by treatment *o*-iodophenol allyl ether with **1a** (73% yield). For a similar rearrangement: J. Barluenga, R. Sanz and F. J. Fañanás, *Tetrahedron Lett.*, 1997, **38**, 6103.

8 Best results were obtained with 1.1–1.5 equiv. of cuprate **1a**. The use of larger amounts led to lower yields of **4a**, presumably as a result of the early quenching of MeI by the excess **1a** (ref. 5).

9 The mixed cuprates could not be prepared by the direct Sn/Cu exchange from the *o*-substituted arylstannanes, probably due to steric hindrance. Thus, no reaction was observed in the reaction of **1a** or **1b** with 2-(tri-*n*-butylstannylmethoxy)phenyltri-*n*-butylstannane, while the reaction between phenyltri-*n*-butylstannane and **1b** yields tetra-*n*-butylstanne (74% isolated yield).

10 P. Beak, *Acc. Chem. Res.*, 1992, **25**, 215; M. L. Kurtzweil, D. Loo and P. Beak, *J. Am. Chem. Soc.*, 1993, **115**, 421

11 The only new stannane was methyltributylstannane, resulting from the selective transmetalation of **5** with [LiCuMePh·LiCN]. A similar reaction with [$LiCuBu_2$·LiCN] afforded Bu_4Sn.

12 Determined by ^{1}H NMR and GC-EI-MS analysis.

13 G. van Koten, S. L. James and J. T. B. H. Jastrzebski, *Comprehensive Organometallic Chemistry II*, Pergamon, Oxford, 1995, vol. 3, ch. 2.

14 Coordination of the ethers to the lithium atoms is omitted for clarity in Scheme 2. The arrows in **10** only indicate the group connectivity in the rearranged product **11**.

15 Variable amounts of **12** and phenol, the product of protodestannylation of **12**, were obtained when oxygen was present before the aqueous workup.

Communication 9/06399D

A new approach towards the synthesis of sp³ 1,1-diiodoalkanes

Lionel Aufauvre,[a] Paul Knochel[b] and Ilan Marek[a]*

[a] *Department of Chemistry and Institute of Catalysis Science and Technology, Technion-Israel Institute of Technology, Technion City, Haifa 32 000, Israel. E-mail: chilanm@tx.technion.ac.il*

[b] *Institute fur Organische Chemie der Ludwig-Maximilians-Universitat Munchen Butenandstr.5-13, D-81377 Munchen, Germany*

Received (in Cambridge, UK) 10th September 1999, Accepted 24th September 1999

An easy and straightforward method for the synthesis of *gem*-diiodo derivatives is reported.

Carbenoids **1**, in which a single carbon atom carries both a metal atom and a leaving group, are valuable reactive molecules and have been used extensively in organic synthesis.[1] They are generally prepared from *gem*-dihaloalkanes by metal–halogen exchange and more specifically from 1,1-diiodoalkanes **2** since they are far more reactive than the corresponding other halogens; in some cases iodides are the only reactive halides[2] [eqn. (1)].

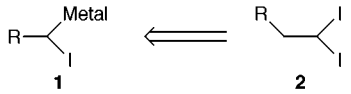

(1)

Unfortunately, they are also more difficult to prepare because of this high C–I bond reactivity. Indeed, few methods have been reported for their preparation[3] and to date, the more versatile approach is based on the alkylation of the diiodomethyllithium or diiodomethylsodium with reactive electrophiles.[4] The major drawback of this strategy is that these reactants are unstable at temperatures above −95 °C, which preclude their preparation on a large scale. So, in the course of our studies on the synthesis and reactivity of carbenoids,[5] we needed a more general approach for the preparation of 1,1-diiodoalkanes allowing access to a large variety of carbon skeletons on multigram scales. For this purpose, we have investigated the iodolysis of 1,1-bis(diisobutylalumino)alkanes,[6] which are readily accessible *via* double hydroalumination of alk-1-ynes.[7] As expected the deuterolysis of 1,1-bis(diisobutylalumino)hexane gave us 1,1-dideuterohexane in good chemical yield (which proved the presence of the 1,1-bisanion) but the addition of 2 equiv. of I_2 gave only the 1-iodohexane, as described in Scheme 1.

In order to obtain *gem*-diiodohexane, it was necessary to add more than 6 equiv. of I_2 since each isobutyl group on the aluminium atom reacts faster than the carbenoid **3**. To overcome this large excess of iodine, we thought to use a hydroaluminating reagent with nontransferable alkyl groups, such as dichloroaluminium hydride[8] ($HAlCl_2$). This is easily obtained by mixing $AlCl_3$ with $LiAlH_4$[9] as described in eqn. (2).

The LiCl formed during the preparation of $HAlCl_2$ is not troublesome for the following step and no separation was required. The double hydroalumination of various alkynes with

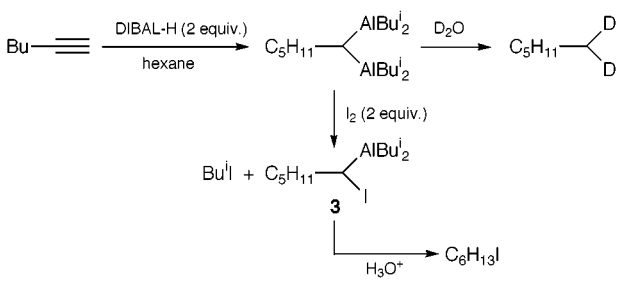

Scheme 1

$$3\ AlCl_3 + LiAlH_4 \xrightarrow{Et_2O} 4\ AlCl_2H + LiCl \qquad (2)$$

$HAlCl_2$ occurs in very high yields (> 95%) even on a large scale (except entry 3, Table 1). Moreover, the addition of 2 equiv. of I_2 at 0 °C leads now to the formation of 1,1-diiodoalkane derivatives as described in Scheme 2 and in Table 1.

The results reported in Table 1 fulfil our expectations. In the experiments described in the entries 1, 2 and 6 the yields in 1,1-diiodoalkanes are good.

Table 1 Synthesis of 1,1-diiodoalkanes

Entries	R	Compounds	Yield (%)[a]
1	Hexyl	**4**	81
2	Octyl	**5**	75
3	Bu^t	**6**	52
4	Ph	**7**	50
5	$PhCH_2$	**8**	46
6	$PhCH_2CH_2$	**9**	75

[a] Isolated yields after hydrolysis.

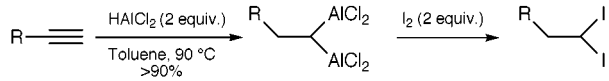

Scheme 2

For the double hydroalumination of *tert*-butylacetylene (entry 3) the yield is lower since it was difficult to obtain in good yield the corresponding 1,1-bis(dichloroalumino)-3,3-dimethylbutane (the starting material is very volatile). The presence of an electon-withdrawing substituent on the triple bond, as in phenylacetylene (entry 4), increases the acidity of the acetylenic hydrogen and hence leads to increased metalation during the double hydroalumination. Thus, the reaction of phenylacetylene with 2 equiv. of $HAlCl_2$ in toluene gives the expected product but a possible metalation of the triple bond could impair the yield of the bis-alane (entry 4). In a similar way, when the reaction is performed on 3-phenylprop-1-yne (entry 5), the presence of acidic benzylic and propargylic hydrogens decrease the yield. Moreover, the hydrolysis of the reaction mixture is also a crucial step and needs to be done at 0 °C. Indeed, after iodinolysis, 2 equiv. of the strong Lewis acid $IAlCl_2$ are present in the reaction and can affect the chemical yield (see experimental procedure[10]).

In conclusion, we have elaborated a new and straightforward approach for the one-pot synthesis of sp³ 1,1-diiodoalkanes in good yield *via* the synthesis of 1,1-bis(dichloroalumino)alkanes. Low temperature is not required (90 °C for the bismetallic synthesis and 0 °C for the reaction with I_2) and the method has been applied to large scale preparations.

I. M. is Holder of the Lawrence G. Horowitz Career Development Chair, is a Ygal Alon fellow and Evelyn and Salman Grand Academic Lectureship-USA. This research was supported by a grant from the German-Israeli Foundation for Scientific Research and Development (I-535-083.05/97) and by

the fund for the promotion of research at the Technion. The authors thank the Scientific Department of the French Embassy in Israel.

Notes and references

1 V. Schulze and R. W. Hoffmann, *Chem. Eur. J.*, 1999, 5.
2 J. Villieras, C. Bacquet and J. F. Normant, *Bull. Soc. Chim. Fr.*, 1975, 1797.
3 A. G. Martinez, A. H. Fernandez, R. M. Alvarez, J. O. Barcina, C. G. Gomez and L. R. Subramanian, *Synthesis*, 1993, 1063; D. H. R. Barton, G. Bashiardes and J.-L. Fourrey, *Tetrahedron*, 1988, **44**, 147; A. G. Martinez, A. H. Fernandez, R. Malvarez, A. G. Fraile, J. B. Calderon, J. O. Barcina, M. Hanack and L. R. Subramanian, *Synthesis*, 1986, 1076; F. Chemla, I. Marek and J. F. Normant, *Synlett*, 1993, 665.
4 P. Charreau, M. Julia and J. N. Verpeaux, *Bull. Soc. Chim. Fr.*, 1990, **127**, 275.
5 A. Rao Sidduri, M. J. Rozema and P. Knochel, *J. Org. Chem.*, 1993, **58**, 2694.
6 I. Marek and J. F. Normant, *Chem. Rev.*, 1996, **96**, 3241.
7 A. M. Piotrowski, D. B. Malpass, M. P. Boleslawski and J. J. Eisch, *J. Org. Chem.*, 1988, **53**, 2829.
8 G. Wilke and H. Muller, *Justus Liebigs Ann. Chem.*, 1960, **629**, 222; J. J. Eisch, H. Gopal and S. G. Rhee, *J. Org. Chem.*, 1975, **40**, 2064.
9 The $LiAlH_4$ was used as an ethereal solution which was titrated either by the iodometric method (H. Felkin, *Bull. Soc. Chim. Fr.*, 1951, **18**, 347) or with salicylaldehyde phenylhydrazone as indicator (B. E. Love and E. G. Jones, *J. Org. Chem.*, 1999, **64**, 3755).
10 *Experimental procedure*: To a suspension of $AlCl_3$ (0.66 g, 4.95 mmol, 1.65 equiv.) in 3 ml of pentane and 7.5 ml of Et_2O was added an ethereal solution of $LiAlH_4$ (1.09 M, 1.51 ml, 1.65 mmol, 0.55 equiv.) at room temperature. After stirring for 5 min, the solvents were removed at room temperature under vacuum (20 mmHg) through $CaCl_2$ to give a white suspension of LiCl and $HAlCl_2$ (6.6 mmol, 2.2 equiv.). 6 ml of toluene was then added, followed by dec-1-yne (0.415 g, 3 mmol, 1 equiv.). The reaction mixture was heated at 90 °C for 3 h to give the 1,1-bis(di-chloroalumino)decane. After cooling to 0 °C, 20 ml of THF was added and a solution of I_2 (1.675 g, 6.6 mmol, 2.2 equiv.) in 20 ml of cold THF was then added. The reaction mixture was allowed to warm to room temperature and stirred for 15 min. The reaction mixture was then transferred into a cold solution (0 °C) of aqueous HCl (1 M, 100 ml). After stirring for 5 min, the aqueous layer was extracted with Et_2O, the collected organic phases were washed with aq.$Na_2S_2O_3$ and saturated brine, and then dried over $MgSO_4$. After filtration and evaporation of the solvents, the residue was chromatographed on silica gel.

Communication 9/07355H

Ferromagnetic ordering in the perovskite $La_{1.5}Sr_{0.5}RhMnO_6$

B. Bakowski,[a] P. D. Battle,*[a] E. J. Cussen,[a] L. D. Noailles,[a] M. J. Rosseinsky,*[a] A. I. Coldea[b] and J. Singleton[b]

[a] *Inorganic Chemistry Laboratory, Department of Chemistry, University of Oxford, South Parks Road, Oxford, UK OX1 3QR. E-mail: peter.battle@chem.ox.ac.uk; matthew.rosseinsky@chem.ox.ac.uk*

[b] *Clarendon Laboratory, Department of Physics, University of Oxford, Parks Road, Oxford, UK OX1 3PU*

Received (in Oxford, UK) 10th September 1999, Accepted 5th October 1999

The non-metallic, magnetically-dilute, cation-disordered perovskite $La_{1.5}Sr_{0.5}RhMnO_6$ is shown to be a soft ferromagnet with T_C = 105 K with an ordered magnetic moment of 3.56(8) μ_B per Mn.

There has been a resurgence of interest in ferromagnetic oxides due to the strong coupling between spin ordering and charge transport found in the $La_{1-x}Sr_xMnO_3$ perovskites, which display colossal magnetoresistance (MR).[1] The Mn(III) perovskite $LaMnO_3$ is an antiferromagnetic insulator below 143 K, but the partial oxidation to Mn(IV) which occurs when Sr^{2+} is substituted for La^{3+} changes the electronic properties markedly. At low temperatures, $La_{1-x}Sr_xMnO_3$ is a ferromagnetic insulator for $0.1 \leqslant x \leqslant 0.15$ and a ferromagnetic metal for $0.15 \leqslant x \leqslant 0.6$.[2] The temperature of the transition to the magnetically ordered phase is a function of x, but for $x \geqslant 0.15$ it is coincident with the metal–insulator transition, and the highest MR effects are seen around this point. The suppression of the zero-field resistance in an applied field can be as large as 100 $\Delta\rho/\rho(H = 0)$ = 99.9% in fields of over 50 kG, but achieving significant MR in the low fields required for information storage applications has proved a difficult barrier for the current generation of materials. The present lack of understanding of the MR effect in perovskites has hindered attempts to overcome this barrier; although it is agreed that double exchange is an important factor, it is also recognised that it is not the only factor.[3] A number of strategies have been adopted in order to enhance our understanding of the electronic properties relevant to MR in oxides, with particular emphasis on the magnetic behaviour of mixed-valence manganates. We demonstrate here that ferromagnetism is retained in $La_{1.5}Sr_{0.5}RhMnO_6$, a non-metallic perovskite with a 50% diluted Mn sublattice where the mean oxidation state is $Mn^{3.5+}$.

Preliminary investigation of the $La_{2-x}Sr_xRhMnO_6$ system in air showed that a sample with the nominal composition La_2MnRhO_6 was polyphasic, with La_2O_3/$La(OH)_3$ impurities being apparent in diffraction patterns. However, we were able to prepare monophasic perovskite samples in the system $La_{2-x}Sr_xRhMnO_6$ for x = 0.2, 0.5 and 0.6, that is by increasing the mean oxidation state of the transition metal; the composition $La_{1.5}Sr_{0.5}RhMnO_6$ will be the focus of this communication. Samples were prepared by the reaction of pre-dried La_2O_3, $SrCO_3$, MnO_2 and Rh_2O_3 for 24 h at 800 °C, followed by 48 h at 1000 and 1200 °C and ending with 96 h at 1400 °C. The products were quenched in liquid nitrogen after the final heating to ensure the formation of a highly crystalline, homogeneous product. The X-ray diffraction patterns of samples prepared in this way showed only the peaks expected from a $GdFeO_3$ - like pseudo-cubic perovskite.[4]

Magnetisation *versus* temperature measurements† made in an applied field of 100 G suggested that all three compositions order ferromagnetically, with T_C = 95, 105 and 105 K for x = 0.2, 0.5 and 0.6 respectively. The data collected on the composition x = 0.5 are shown in Fig. 1; Curie–Weiss behaviour is not observed within the measured temperature range, and hysteresis is apparent between the ZFC and FC data below T_C. The $M(H)$ magnetisation isotherm at 5 K is characteristic of a soft ferromagnet, with a saturation magnetisation of 3.9(1) μ_B per Mn being achieved in 10 kG at 5 K. Neutron powder diffraction data† (D2B, ILL) collected on the x = 0.5 composition prove that this sample exhibits long range ferromagnetic ordering at low temperature. Rietveld[5] refinement of data collected at 290 K proceeded smoothly (R_{wpr} = 4.97%, χ^2 = 1.96) within a model which considered only nuclear scattering; there was no evidence of Mn/Rh cation ordering over the six-coordinate sites. Successful analysis (R_{wpr} = 5.30 %, χ^2 = 2.0) of the data collected at 1.7 K required the inclusion of an ordered magnetic moment of 3.56(8) μ_B on the Mn cations; the atomic moments align along the [010] axis. Four-probe dc conductivity measurements showed (Fig. 2) that the compound is non-metallic, albeit with a varying activation energy, both above and below the Curie temperature.

The oxidation states of the different cations which occupy the electronically active B site are not directly defined by our measurements, but consideration of the established oxide chemistries of Mn and Rh leads to the assumption that Rh is present solely as Rh^{III} (low spin t_{2g}^6), resulting in a mean Mn

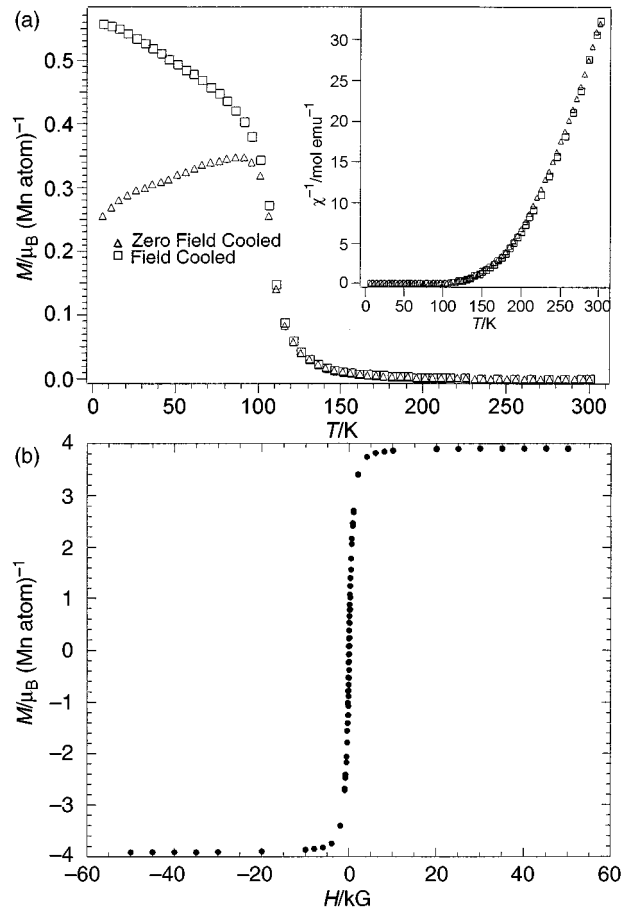

Fig. 1 (a) Temperature dependence of magnetisation and (inset) inverse molar susceptibility of $La_{1.5}Sr_{0.5}RhMnO_6$, measured in a field of 100 G. (b) Magnetisation as a function of field at 5 K for $La_{1.5}Sr_{0.5}RhMnO_6$.

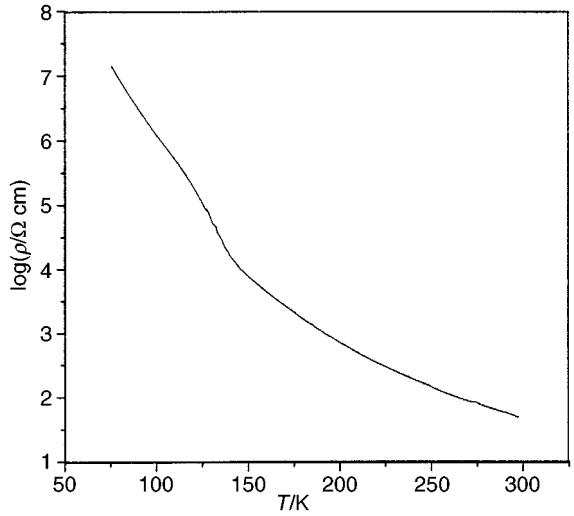

Fig. 2 Temperature dependence of the electrical resistivity of $La_{1.5}Sr_{0.5}RhMnO_6$.

oxidation state of +3.5 in $La_{1.5}Sr_{0.5}RhMnO_6$. This is the same oxidation state that occurs in $La_{0.5}Sr_{0.5}MnO_3$, a ferromagnetic, metallic composition with $T_C \approx 350$ K. Although the ferromagnetism of the Rh-free sample has been ascribed to double exchange, the non-metallic nature of the $x = 0.5$ composition rules out the conventional form of that mechanism in $La_{1.5}Sr_{0.5}RhMnO_6$. Our results suggest that ferromagnetic superexchange interactions dominate the magnetic coupling in the 1:1 random array of localised-electron Mn^{3+} and Mn^{4+} cations, and that they are strong enough to produce long-range magnetic order at 105 K, even with 50% dilution by a diamagnetic cation. The magnitude of the ordered magnetic moment determined by neutron diffraction is as large as can be expected for a mean oxidation state of $Mn^{3.5+}$. The Goodenough–Kanomori rules[6] would then suggest that ferromagnetic σ superexchange between Mn^{3+} and Mn^{4+} cations is a very strong effect in this compound, and that it outweighs the antiferromagnetic interactions between pairs of like ions. However, this argument ignores the effect that local atomic displacements will have on the sign of the magnetic exchange constants. Although our neutron diffraction data indicate that the six-coordinate environment of the disordered transition metal species is an essentially regular octahedron, this is a description of the average site, and the temperature-dependence of the anisotropic thermal parameters indicates that static disorder is present, most noticably on the O(1) sublattice. We must therefore guard against over-simplification of the problem.

The behaviour of $La_{1.5}Sr_{0.5}RhMnO_6$ contrasts sharply with that of another magnetically-dilute, mixed-valence perovskite, $Sr_2FeTiO_{5.81}$, which shows spin-glass behaviour at low temperatures.[7] In this and other related materials, the absence of ordering in the cation distribution has been held responsible for the lack of long-range magnetic order. It is therefore reasonable to postulate that in the present case, Mn^{3+}/Mn^{4+} ordering does occur, but over a distance scale too short to be detected in a neutron diffraction experiment. This should be investigated using the appropriate experimental techniques. An alternative explanation to that based on superexchange could lie in the relatively extensive nature of the Rh 4d orbitals, which might allow significant Mn–Rh–Mn coupling, leading to the partial delocalisation of an e_g electron and hence ferromagnetic coupling. This model effectively removes the distinction between Mn^{3+} and Mn^{4+} oxidation states and invokes double exchange over a limited volume. Although we are not yet able to elucidate in detail the cause of ferromagnetism in $La_{1.5}Sr_{0.5}RhMnO_6$, it is a significant observation to be considered when discussing the relative importance of double exchange and superexchange in oxides which show colossal MR.

We acknowledge funding from the UK EPSRC.

Notes and references

† X-Ray powder diffraction data were recorded using a Siemens D5000 diffractometer with Cu-Kα_1 radiation. Magnetisation measurements were made with a Quantum Design MPMS5 SQUID magnetometer on samples contained within gelatin capsules. Electrical resistivity measurements were made on a sintered pellet using graphite-paste contacts and a current of $\leqslant$ 10 μA. Neutron powder diffraction data were recorded at $\lambda = 1.59$ Å on the powder diffractometer D2B with the sample contained within a vanadium can in an ILL 'Orange' cryostat at both 1.7 and 290 K. Space group *Pbnm*, Sr/La on *x*,*y*,1/4, Mn/Rh on 1/2,0,0, O1 on *x*,*y*,1/4, O2 on *x*,*y*,*z*. At 290 K, $a = 5.5544(1)$, $b = 5.5216(1)$, $c = 7.8258(2)$ Å, $x_{Sr/La} = -0.0051(4)$, $y_{Sr/La} = 0.0286(3)$, $x_{O(1)} = 0.0703(5)$, $y_{O(1)} = 0.4914(4)$, $x_{O(2)} = -0.2831(3)$, $y_{O(2)} = 0.2819(3)$, $z_{O(2)} = 0.0363(2)$; Mn/Rh–O(1) = 1.9956(5) × 2, Mn/Rh–O(2) = 1.989(2) × 2, 2.001(2) Å × 2. At 1.7 K, $a = 5.54476(9)$, $b = 5.5191(1)$, $c = 7.8161(2)$ Å

1 A. P. Ramirez, *J. Phys.: Condens. Matter*, 1997, **9**, 8171.
2 A. Urushibara, Y. Moritomo, T. Arima, A. Asamitsu, G. Kido and Y. Tokura, *Phys. Rev. B*, 1995, **51**, 14 103.
3 A. J. Millis, P. B. Littlewood and B. I. Shraiman, *Phys. Rev. Lett.*, 1995, **74**, 5144.
4 S. Geller, *J. Chem. Phys.*, 1956, **24**, 1236.
5 H. M. Rietveld, *J. Appl. Crystallogr.*, 1969, **2**, 65.
6 J. B. Goodenough, *Magnetism and the Chemical Bond*. Wiley, New York, 1963.
7 T. C. Gibb, P. D. Battle, S. K. Bollen and R. J. Whitehead, *J. Mater. Chem.*, 1992, **2**, 111.

Communication 9/07531C

ChemComm

Palladium catalysed cross-coupling of (fluoroarene)tricarbonylchromium(0) complexes

David A. Widdowson* and René Wilhelm

Department of Chemistry, Imperial College of Science Technology and Medicine, London, UK SW7 2AY. E-mail: d.widdowson@ic.ac.uk

Received (in Liverpool, UK) 2nd August 1999, Accepted 29th September 1999

Fluoroarenetricarbonylchromium(0) complexes were found to undergo Suzuki reactions with arylboronic acids to form biaryltricarbonylchromium(0) complexes in the presence of trimethylphosphine/palladium dibenzylideneacetone and caesium carbonate or caesium fluoride.

The Suzuki reaction is one of the most widely used and successful processes for the synthesis of biaryls and styrenes.[1] Although aryl iodides and bromides are the most commonly used halide partners in the reaction, in some remarkable recent developments, aryl chlorides, hitherto regarded as inert to palladium coupling, have been shown to be effective participants provided that an electron-withdrawing group on the aryl ring[2] (including an η^6-tricarbonylchromium group[3]) or a basic phosphine ligand for palladium[4–9] is present. In the latter case, it has been shown that tricyclohexylphosphine and tri-*tert*-butylphosphine ligands on the palladium catalyst are particularly effective, even with electron rich aryl chlorides.[4] We have previously demonstrated the unique synthetic potential of monofluoroarene complexes in the synthesis of polyfunctionalised aromatics[10,11] and given the ease and efficiency with which chloroarenetricarbonylchromium complexes undergo cross-coupling reactions,[3] we were prompted to attempt the Suzuki reaction of the fluoro complexes as a route to highly functionalised biaryls. We now report the first step towards that objective, the palladium catalysed cross-coupling of aryl fluorides.

Using standard conditions for Suzuki coupling,[1] tetrakis(triphenylphosphine)palladium catalyst, fluorobenzenetricarbonylchromium(0) and phenylboronic acid gave the coupled complex but only in trace amounts (Table 1, run 1). When the reaction was repeated with tris(dibenzylidenacetone)dipalladium/tricyclohexylphosphine and caesium fluoride as the base (Fu conditions[4]), no coupled product was detectable (run 2) but tris(dibenzylidenacetone)dipalladium/trimethylphosphine (run 3) did produce the biphenyltricarbonylchromium(0) complex in 52% yield.

Table 1 Suzuki coupling reactions of fluorobenzenetricarbonylchromium(0) and phenylboronic acid

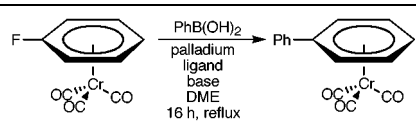

Run	Ligand	Palladium	Base (equiv.)	Yield (%)
1[a]	—	$Pd(PPh_3)_4$	Na_2CO_3 (2.2)	Trace
2	PCy_3	$Pd_2(dba)_3$	CsF (4)	0
3	PMe_3	$Pd_2(dba)_3$	CsF (4)	52
4	—	$Pd_2(dba)_3$	CsF (4)	0
5[b]	PMe_3	$Pd_2(dba)_3$	—	0
6	PMe_3	$Pd_2(dba)_3$	Cs_2CO_3 (2.2)	61
7	PMe_3	—	Cs_2CO_3 (2.2)	0

[a] Toluene as solvent. [b] 4-Methoxyphenylboronic acid replaced phenylboronic acid.

The participation of a fluoroarene, albeit as its tricarbonylchromium complex, in a palladium catalysed cross coupling is unprecedented[12] and required careful evaluation. Control experiments covering the more obvious factors were carried out and the results are summarised in Table 1. Firstly, the ready displacement of fluoride in these complexes by other nucleophiles,[13–16] particularly higher halides, which could then undergo cross-coupling, required that the system be free of any source of such nucleophiles. Thus no solvent/additive which might release higher halide was used and initially, high purity (99.9%) caesium fluoride was used as the base. In principle fluoride should be catalytic but attempts to demonstrate this failed.

The ineffectiveness of tricyclohexylphosphine as ligand (run 3) could be a consequence of steric hindrance between the bulky tricarbonylchromium unit and the bulky phosphine, and the smaller trimethylphosphine was used in all subsequent experiments. In the absence of any phosphine, the coupling failed (run 4). Reaction without a base (run 5) also failed but the use of caesium carbonate (run 6) increased the yield to 61%. A reaction in the presence of base and phosphine but without palladium (run 7) gave no coupling. The presence of unchanged starting material from this reaction removed the possibility that a borate anion was displacing the fluoride group from the complex and that the resultant arylborate was the active cross coupling partner. This result also demonstrated the unreactivity of neutral phosphine to the fluoro complex, but to reinforce this conclusion a reaction between trimethylphosphine and fluorobenzene complex under cross-coupling conditions was attempted. The complex was recovered unchanged in 98% yield. This precludes a process of phosphonium salt formation and participation of this in cross-coupling[17,18] as the reaction sequence.

These experiments provide strong evidence for direct participation of the fluorobenzene complex in the coupling process with the implication of an unprecedented oxidative addition of the C–F bond to the palladium(0) intermediate.[19] Whether this is a concerted insertion [Scheme 1, path (a)] or an addition–elimination sequence [Scheme 1, path (b)] *via* an *exo*-addition[20] of palladium to form **1** followed by fluoride loss to produce **2** cannot be determined at this point. The insertion product could be active in the catalytic cycle in either neutral (**3**) or cationic (**2**) form.[12]

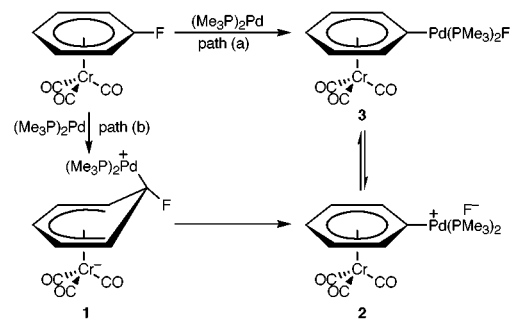

Scheme 1

Table 2 Suzuki coupling reactions of η^6-(fluorobenzene)tricarbonylchromium(0)

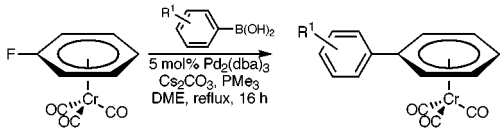

Run	R^1	Yields (%)
1	H	61
2	4-MeO	87
3	2-MeO	78
4	4-Me	81
5	2-Me	79
6	4-Br	0[a]

[a] An intractable oligomeric/polymeric material containing no chromium(0) was produced.

With suitable conditions established, the fluorobenzenechromium complex was coupled with a series of electron-rich arylboronic acids (Table 2).[21] Both moderately hindered (runs 3, 5) and unhindered boronic acids (runs 1, 2, 4) gave good yields. The polymerisation of 4-bromophenylboronic acid under the reaction conditions can be attributed to the greater reactivity of the C–Br bond over the C–F bond.

To further investigate the scope of this process, the more electron-rich 4-methoxyfluorobenzenetricarbonylchromium complex was studied.[21] The yields (Table 3), with both the moderately hindered and the unhindered boronic acids, were comparable to those of the parent complex despite the expected reduction in reactivity of the alkoxy analogue.

Table 3 Suzuki coupling reactions of η^6-(4-fluoromethoxybenzene)-tricarbonylchromium(0)

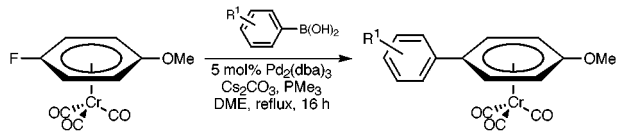

Run	R^1	Yield (%)
1	H	76
2	2-Me	77
3	4-Me	74

These results clearly raise intriguing mechanistic questions, which we continue to address. The couplings demonstrate the versatility of the arenetricarbonylchromium(0) complexes and add further possibilities to the exploitation of their already widely established role in synthesis.

Notes and references

1 A. Suzuki, in *Metal-catalyzed Cross-coupling Reactions*, ed. F. Diederich and P. J. Stang, Wiley-VCH, Weinheim, 1998, p. 49.
2 K.-i. Gouda, E. Hagiwara, Y. Hatanaka and T. Hiyama, *J. Org. Chem.*, 1996, **61**, 7232.
3 W. J. Scott, *J. Chem. Soc., Chem. Commun.*, 1987, 1755.
4 A. F. Littke and G. C. Fu, *Angew. Chem., Int. Ed.*, 1998, **37**, 3387.
5 D. W. Old, J. P. Wolfe and S. L. Buchwald, *J. Am. Chem. Soc.*, 1998, **120**, 9722.
6 F. Firooznia, C. Gude, K. Chan and Y. Satoh, *Tetrahedron Lett.*, 1998, **39**, 3985.
7 C. Zhang, J. Huang, M. L. Trudell and S. P. Nolan, *J. Org. Chem.*, 1999, **64**, 3804.
8 A. F. Little and G. C. Fu, *Angew. Chem., Int. Ed.*, 1999, **38**, 2413.
10 J. P. Gilday and D. A. Widdowson, *J. Chem. Soc., Chem. Commun.*, 1986, 1235.
11 J. P. Gilday and D. A. Widdowson, *Tetrahedron Lett.*, 1986, **27**, 5525.
12 E.-I. Negishi and F. Liu, in *Metal-catalyzed Cross-coupling Reactions*, ed. F. Diederich and P. J. Stang, Wiley-VCH, Weinheim, 1998, p. 1.
13 K. Kirschke, J. Deutsch and H. J. Niclas, *Phosphorus Sulfur Silicon Relat. Elem.*, 1996, **117**, 293.
14 F. Rose-Munch, E. Rose, A. Semra, L. Mignon, J. Garcia-Oricain and C. Knobler, *J. Organomet. Chem.*, 1989, **363**, 297.
15 M. F. Semmelhack, G. Hilt and J. H. Colley, *Tetrahedron Lett.*, 1998, **39**, 7683.
16 V. V. Litvak, P. P. Kun and V. D. Shteingarts, *Zh. Org. Khim.*, 1984, **20**, 753.
17 F. E. Goodson, T. I. Wallow and B. M. Novak, *J. Am. Chem. Soc.*, 1997, **119**, 12 441.
18 M. Sakamoto, I. Shimizu and A. Yamamoto, *Chem. Lett.*, 1995, 1101.
19 H. Yang, H. Gao and R. J. Angelici, *Organometallics*, 1999, **18**, 2285.
20 M. F. Semmelhack, G. R. Clark, J. L. Garcia, J. J. Harrison, Y. Thebtaranonth, W. Wulff and A. Yamashita, *Tetrahedron*, 1981, **37**, 3957.

21 *Typical procedure*: A solution of η^6-(fluorobenzene)tricarbonylchromium(0) (0.300 g, 1.29 mmol), 4-methoxyphenylboronic acid (0.392 g, 2.58 mmol), caesium carbonate (0.925 g, 2.84 mmol), $Pd_2(dba)_3$ (5 mol%, 0.060 g, 0.06 mmol) and PMe_3 (20 mol%, 0.26 ml, 1 M solution in toluene) in deoxygenated DME (9 ml) was stirred under reflux for 16 h. Et_2O (50 ml) was added and the solution was washed with 10% aq. NaOH (15 ml), water (15 ml) and brine (15 ml) and dried over $MgSO_4$. Concentration *in vacuo* followed by column chromatography (eluent: 5% Et_2O–hexane) gave η^6-(4′-methoxybiphenyl)tricarbonylchromium(0) as a yellow crystalline solid (0.360 g, 87%), mp 58–61 °C (Found: C, 59.99; H, 3.69. $C_{16}H_{12}CrO_4$ requires C, 60.01; H, 3.78%); ν_{max}(KBr)/cm^{-1} 2986w, 2838w, 1977s, 1961s, 1887s, 1868s, 1609m, 1508m, 1454m, 1279m, 1249m, 1176m, 1020m, 840m, 819m, 661m, 629s, 535m; δ_H(270 MHz; $CDCl_3$) 7.43 (2H, d, *J* 8.9), 6.93 (2H, d, *J* 8.9), 5.64 (2H, dd, *J* 6.7, 1.0), 5.49 (2H, t, *J* 6.4), 5.28 (1H, tt, *J* 6.2, 1.0), 3.83 (3H, s); δ_C(68 MHz) 233.0, 160.4, 128.6, 128.3, 114.3, 111.2, 93.2, 91.6, 90.9, 55.4; *m/z* (EI) 320 (M^+, 43%), 264 (39), 236 (93), 221 (11), 205 (5), 184 (9), 169 (4), 52 (100) (Observed: M^+ 320.0141; $C_{16}H_{12}CrO_4$ requires 320.0130).

Communication 9/06256D

A highly enantioselective addition reaction of a chiral allylsilane to an activated *N*-acylisoquinolinium ion

Ryohei Yamaguchi,* Masato Tanaka, Tomohiko Matsuda and Ken-ichi Fujita

Faculty of Integrated Human Studies and Graduate School of Human and Environmental Studies, Kyoto University, Yoshida Kyoto 606-8501, Japan. E-mail: yama@kagaku.h.kyoto-u.ac.jp

Received (in Cambridge, UK) 31st August 1999, Accepted 16th September 1999

The addition reactions of a chiral allylsilane to activated *N*-acylisoquinolinium ions proceeded in a highly enantioselective manner (more than 90%) to afford homochiral 1-allyl-1,2-dihydroisoquinolines in good yields.

Considerable efforts have been made for the stereoselective introduction of carbon substituents into isoquinoline systems.[1] Although many diastereo- and enantio-selective methods have been available for the stereoselective addition of carbon nucleophiles to 3,4-dihydroquinolines systems (cyclic imines and imine *N*-oxides),[2,3] few reactions have been reported for stereoselective additions to isoquinoline itself and all of them have exploited the diastereoselective additions of achiral organometallic reagents to isoquinolines with chiral auxiliaries in the activating groups.[4] The enantioselective addition reaction of a chiral organometallic reagent to achiral isoquinoline has not been reported. We have recently reported that quinolines and isoquinolines are activated by $ClCO_2Ph$ and AgOTf such that these *N*-acylated aza-aromatic ions can readily react with allylsilanes and alkynylsilanes to afford allylated and alkynylated products chemo- and regio-selectively in good yields.[5] We disclose here the fact that the addition reaction of a chiral allylsilane to the activated *N*-acylisoquinolinium ion proceeded in a highly enantioselective manner to give homochiral 1-allyl-1,2-dihydroisoquinoline. To the best of our knowledge, this is the first example of the addition reaction of a chiral organometallic reagent to an achiral nitrogen heteroaromatic ion with high enantioselectivity.

Isoquinoline **1a** was activated by treatment with $ClCO_2Ph$ (1.2 equiv.) and a catalytic amount of AgOTf (0.1 equiv.) in MeCN, and then a chiral allylsilane, (*R*)-3-phenyl-3-trimethylsilylpropene **2**[6] (81% ee determined by a chiral GLC analysis), was added to the mixture under ice-cooling. The reaction mixture was stirred at room temperature for 24 h to yield a single 1-allylated 1,2-dihydroisoquinoline adduct **3a** in 54% yield (Scheme 1).† The ^{1}H NMR coupling constant (J = 16 Hz) of the olefinic protons indicates that the stereochemistry of the allylic double bond was *E*. These results suggest that the present allylic silicon substitution reactions proceed in an *anti* S_E2' manner (*vide infra*). Since **3a** could not be separated by chiral HPLC. **3a** was hydrogenated to give tetrahydroisoquinoline derivative **4**, the ee of which was determined to be 77% by chiral HPLC analysis. Thus, it is apparent that the chirality transfer of the present reaction is as high as 95%. Similarly, the reactions of functionalized isoquinolines with (*R*)-**2** proceeded in good yields with a high degree of enantioselectivity (more than 90%) as well. The results are summarized in Table 1.

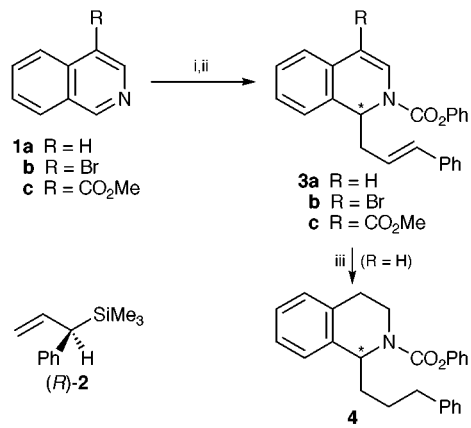

Scheme 1 *Reagents and conditions*: i, $ClCO_2Ph$ (1.2 equiv.), AgOTf (0.1 equiv.), MeCN; ii, (*R*)-**2** (1.0 equiv.), room temp., 24 h; iii, H_2, Pd-C, MeOH. Spectral data for **3b**,**c**, **4**, **6** and **7** are available from the RSC web site, see http://www.rsc.org/suppdata/cc/1999/2213/

Table 1 Enantioselective additions of (*R*)-**2** to activated *N*-acylisoquinolinium ions

Entry	**1**	R	Yield of **3** (%)[a]	Ee of **2** (%)[b]	Ee of **3** (%)	Enantioselectivity (%)
1	**a**	H	54	81	77[c]	95
2	**b**	Br	86	83	78[d]	94
3	**c**	CO_2Me	78	83	77[d]	93

[a] Isolated yield. [b] Determined by a chiral GLC (Chiral-DEX CB) analysis. [c] Determined by a chiral HPLC (SUMICHIRAL OA-2000) analysis of the hydrogenated product **4**. [d] Determined by a chiral HPLC (CHIROSE C1) analysis.

In contrast with the above results, the similar reaction of 3,4-dihydroisoquinoline **5** with (*R*)-**2** showed a moderate degree of enantioselectivity (Scheme 2). The results are summarized in Table 2. Thus, 76% enantioselectivity was obtained in the reaction even at −15 °C. These results could indicate that the planarity of *N*-acyliminium salts is critical to obtain a high degree of the enantioselectivity (*vide infra*).

The absolute configuration of **4** was determined as follows (Scheme 3): **4** (55% ee) was deprotected[7] to give 1-(3-phenylpropyl)-1,2,3,4-tetrahydroisoquinoline **7**, the optical rotation of

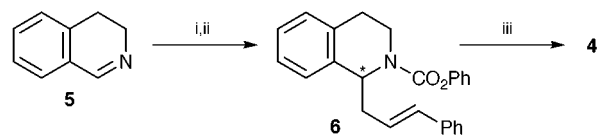

Scheme 2 *Reagents and conditions*: i, $ClCO_2Ph$ (1.2 equiv.), additive (0.1 equiv.), MeCN; ii, (*R*)-**2** (1.0 equiv.), 24 h; iii, H_2, Pd-C, MeOH.

Table 2 Enantioselective additions of (*R*)-**2** (81% ee) to *N*-acyl-3,4-dihydroisoquinolinium ion

Entry	Additive	*T*/°C	Yield of **6** (%)[a]	Ee of **4** (%)[b]	Enantioselectivity (%)
1	AgOTf	0	83	59	73
2	$AgClO_4$	0	67	61	75
3	AgOTf	−15	53	62	76

[a] Isolated yield. [b] Determined by a chiral HPLC (SUMICHIRAL OA-2000) analysis.

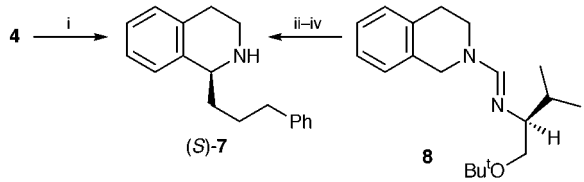

Scheme 3 *Reagents and conditions*: i, KOH, Pr^iOH–H_2O, reflux, 3 d; ii, LDA, THF, −78 °C; iii, $PhCH_2CH_2CH_2Br$, −90 °C; iv, NH_2NH_2, AcOH, EtOH.

which was determined to be levorotatory ($[\alpha]_D^{20}$ −28). Since authentic (*S*)-**7** was prepared from **8** according to Meyers' procedures[8] and the optical rotation of (*S*)-**7** is levorotatory ($[\alpha]_D^{20}$ −43), the absolute configuration of **4** should be *S*. Thus, it is apparent that the reactions of isoquinolines with (*R*)-**2** afford (*S*)-1-[(*E*)-3-phenylprop-2-enyl]-1,2-dihydroisoquinolines in a highly enantioselective manner.

It has been generally proposed[9] that the electophilic addition reactions of chiral, acyclic allylsilanes take place in an *anti*-S_E2' manner to form the allylic *E* double bond. Thus, it is highly probable that the present addition reactions proceed through a highly selective *anti*-S_E2' mode. It has also been suggested that two transition models, *i.e.* antiperiplanar and synclinal, are possible in non-chelation transition states. In the present reactions of isoquinolinium ions with (*R*)-**2**, the antiperiplanar *anti*-S_E2' transition state **A** is expected to produce the (*S*)-adduct, while the synclinal *anti*-S_E2' transition state **B** would produce the (*R*)-adduct. Since the (*S*)-adduct is obtained as mentioned above, it is evident that the reactions proceed through the antiperiplanar *anti*-S_E2' transition state **A** (Fig. 1).

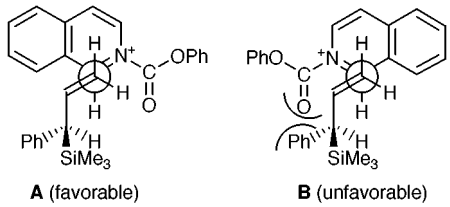

Fig. 1 Possible transition states of the enantioselective *anti*-S_E2' addition reactions of (*R*)-**2** to *N*-acylisoquinolinium ions.

The recent X-ray crystal analysis of an *N*-acylisoquinolinium ion proves that the aromatic rings are coplanar with the carbonyl groups.[10] This conformation is also preferred for maximum overlap of the C=N and C=O bonds, which could make the isoquinolinium ions more electrophilic. Thus, the synclinal *anti*-S_E2' transition state **B** should be unfavorable because of steric repulsion between the carbonyl and the phenyl groups.

In summary, we have demonstrated the highly enantioselective addition reactions of a chiral allylsilane to achiral isoquinolinium ions. A high degree of enantioselectivity (more than 90%) can be obtained in these reactions even at room temperature. Further studies on the reactions of other nitrogen aromatics as well as applications to alkaloids synthesis are underway.

This work was supported by the Ministry of Education, Sciences, Sports and Culture of Japan (No. 10650832).

Notes and references

† *Typical procedure*: To a solution of **1** (1.0 mmol) in MeCN (3.0 ml) was added $ClCO_2Ph$ (0.15 ml, 1.2 mmol, 1.2 equiv.) and AgOTf (0.10 mmol, 0.10 equiv.) at 0 °C. The reaction mixture was stirred for 30 min at 0 °C. Then, to the reaction mixture was added **2** (1.0 mmol, 1.0 equiv.) at 0 °C. The reaction mixture was warmed to room temperature and stirred for 24 h. Et_2O (5.0 ml), aqueous $NaHCO_3$ (3.0 ml) and aqueous Na_2CO_3 (3.0 ml) were added, and the organic layer was separated. The aqueous layer was extracted with Et_2O (5 × 5.0 ml). The combined organic layer was washed with brine and dried over Na_2SO_4. After evaporation of the solvent, the residue was purified by flash column chromatography (eluent: hexane–EtOAc) to give the product. The yields and ees are shown in Table 1. All new compounds gave satisfactory analytical and spectral data. *Selected data* for (*S*)-**3a**: mp 117–119 °C; $[\alpha]_D^{25}$ +266 (*c* 0.075, $CHCl_3$) (77% ee); ν_{max}(KBr)/cm^{-1} 1722, 1633, 1215, 756; δ_H(500 MHz, $CDCl_3$, 55 °C, TMS, a mixture of rotamers) 7.12–7.37 (m, 13H), 7.07 (d, *J* 7, 1H), 7.00 (d, *J* 8.0, 1H), 6.39 (d, *J* 16, 1H), 6.24 (dt, *J* 16, 8, 1H), 6.08, 5.99 (d, *J* 7, 1H), 5.57–5.65 (br m, 1H), 2.58–2.82 (m, 2H); δ_C(125.7 MHz, $CDCl_3$, 55 °C, TMS, a mixture of rotamers) 151.1, 150.9 (C), 137.6, 137.3 (C), 133.5 133.0 (CH), 132.4 (C), 130.4, 130.0 (C), 129.2 (CH), 128.5 (CH), 127.9, 127.8 (CH), 127.3, 127.1 (CH), 127.1, 127.0 (CH), 126.4, 126.3 (CH), 126.3 (CH), 125.8, 125.5 (CH), 125.3, 125.1 (CH), 124.9 (CH), 124.2 (CH), 121.5 (CH), 110.1, 109.5 (CH), 56.9, 55.9 (CH), 39.5, 39.4 (CH_2) (calc. for $C_{25}H_{21}NO_2$: C, 81.72; H, 5.76. Found: C, 81.92; H, 5.86%).

1 For a recent review, see: M. D. Rozwadosky, *Heterocycles*, 1994, **39**, 903.
2 K. T. Wanner and I. Praschak, *Heterocycles*, 1989, **29**, 29; R. P. Polniaszek and L. W. Dillard, *Tetrahedron Lett.*, 1990, **31**, 797; B. Hatano, Y. Haraguchi, S. Kozima and R. Yamaguchi, *Chem. Lett.*, 1995, 1003; H. Suzuki, S. Aoyagi and C. Kibayashi, *Tetrahedron Lett.*, 1995, **37**, 6709,
3 S. G. Pyne and B. Dikic, *J. Org. Chem.*, 1990, **55**, 1932; S. Murahashi, J. Sun and T. Tsuda, *Tetrahedron Lett.*, 1993, **34**, 2645; Y. Ukaji, T. Hatanaka, A. Ahmed and K. Inamoto, *Chem. Lett.*, 1993, 1313; M. Nakamura, A. Hirai and E. Nakamura, *J. Am. Chem. Soc.*, 1996, **118**, 8489; Y. Ukaji, Y. Shimizu, Y. Kenmoku, A. Ahmed and K. Inamoto, *Chem. Lett.*, 1997, 59.
4 D. L. Comins and M. M. Badawi, *Heterocycles*, 1991, **32**, 1869; G. B. Richter-Addo, D. A. Knight, M. A. Dewey, A. M. Arif and J. A. Gladysz, *J. Am. Chem. Soc.*, 1993, **115**, 11 863; D. Barbier, C. Marazano, C. Riche, B. C. Das and P. Potier, *J. Org. Chem.*, 1998, **63**, 1767.
5 R. Yamaguchi, B. Hatano, T. Nakayasu and S. Kozima, *Tetrahedron Lett.*, 1997, **38**, 403; R. Yamaguchi, Y. Omoto, M. Miyake and K. Fujita, *Chem. Lett.*, 1998, 547.
6 T. Hayashi, M. Konishi, Y. Okamoto, K. Kabeta and M. Kumada, *J. Org. Chem.*, 1986, **51**, 3772 and references cited therein.
7 D. L. Comins and A. Dehgani, *J. Org. Chem.*, 1995, **60**, 794.
8 A. I. Meyers, D. A. Dickman and M. Boes, *Tetrahedron*, 1987, **43**, 5095; A. I. Meyers, M. Boes and D. A. Dickman, *Org. Synth.*, 1988, **67**, 60.
9 For recent reviews, see: Y. Yamamoto and N. Asao, *Chem. Rev.*, 1993, **93**, 2207; C. E. Masse and J. S. Panek, *Chem. Rev.*, 1995, **95**, 1293.
10 J. A. King Jr. and G. L. Bryant Jr., *J. Org. Chem.*, 1992, **57**, 5136.

Communication 9/06999B

ChemComm

Synthesis of glycosyl boranes and glycosyl borinates†

Andrea Vasella,* Wolfgang Wenger and Thennati Rajamannar

Laboratorium für Organische Chemie, ETH-Zentrum, Universitätstrasse 16, CH–8092 Zürich, Switzerland. E-mail: vasella@sugar.org.chem.ethz.ch

Received (in Liverpool, UK) 5th August 1999, Accepted 17th September 1999

Insertion of glycosylidene carbenes into a B–C bond of BEt_3 leads to unstable glycosyl boranes, while insertion into a B–C bond of borinic esters yields stable anomeric glycosyl borinates.

Insertion of glycosylidene carbenes, generated by thermolysis or photolysis of glycosylidene diazirines, into HX bonds leads to *O*-, *C*- and *N*-glycosides,[1] glycosyl phosphines[2] and glycosyl stannanes.[3] We speculated that reaction of a borane with the carbene **2** would lead to a zwitterion such as **3**; migration of a B-substituent—as proposed for the reaction of methoxycarbene with trialkylboranes[4]—should lead to the as yet unknown glycosyl boranes (Scheme 1).

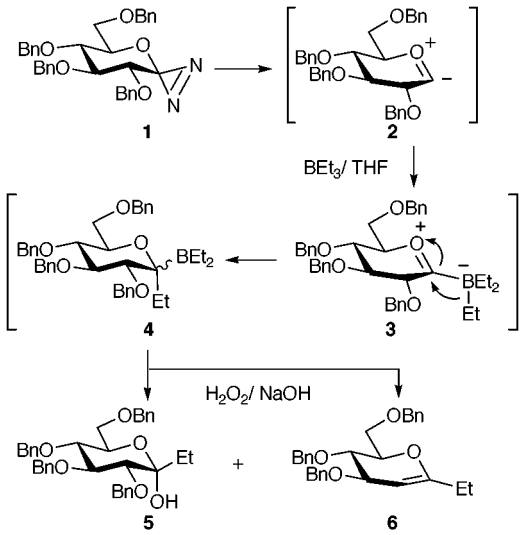

Scheme 1

Thermolysis of the diazirine **1**[5] in degassed THF in the presence of 1.5 equiv. of BEt_3 at 25 °C, followed by treatment with excess 30% alkaline H_2O_2 and aqueous work-up, yielded 55% of hemiacetal **5** and 13% of the *C*-ethylglucal **6**. These products suggest the intermediate formation of anomeric glycosyl boranes **4**. Treatment with alkaline H_2O_2 leads either (depending on the borane configuration?) to oxidation[6] and (after anomerisation?) to the hemiacetal **5**, or to elimination of the C(1) boron substituent and the vicinal benzyloxy group.[7] *trans*-Elimination is suggested by the observation (^{13}C NMR) that **6** is only formed after additon of alkaline H_2O_2. Thermolysis of the diazirine **1** in the presence of 1.5 equiv. of BEt_3 in oxygen-containing THF yielded 25% of the borinic acid **7** after rapid chromatography (Scheme 2). The borinic acid **7** was rapidly converted into the hemiacetal **5** (isolated in *ca.* 75%) by exposure to air, storage in oxygen–containing $CDCl_3$, or treatment with alkaline H_2O_2. The ^{11}B NMR of air-stable mixtures of **7** and 2 equiv. of PPh_3 shows a broad signal at δ 56.5, typical for dialkyl borinic acids.[8] The ^1H NMR shows a broad singlet of an exchangeable H at δ 8.16, corresponding to B–OH, two doublets of quintets at δ 1.8 and 1.6 (2 H), a triplet at δ 0.9 (3 H) for the *C*-ethyl and a multiplet at δ 1.0–0.9 (5 H) of the *B*–Et group. The ^{13}C NMR signal for the boron substituted anomeric carbon is missing, as expected.[9]

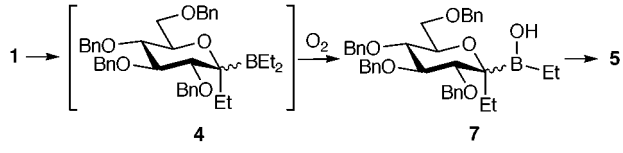

Scheme 2

The intermediate formation of a glycosyl borane was further evidenced by treating the product of thermolysis of **1** and BEt_3 in degassed THF with excess TFA, followed by aqueous work-up (Scheme 3). The resulting cyclic borinic ester **8**, isolated in 45%, showed a ^{11}B signal at δ 51, typical for *O*-alkyl borinates.[10]

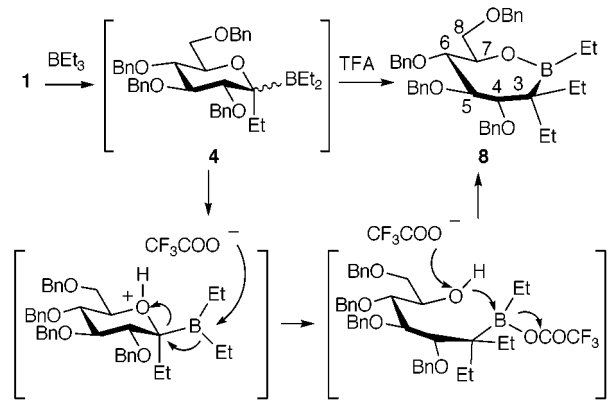

Scheme 3

The ^1H NMR spectrum of **8** shows signals for a $BC(Et)_2$ moiety and a multiplet at δ 0.9–0.7 for a BEt group. H–C(7) is strongly shifted downfield due to the R_2BO substituent [H–C(5) in **6** at δ 4.02, H–C(7) in **8** at δ 4.77].

The formation of **8** is rationalised by protonation of the ring oxygen of **4**, nucleophilic attack of trifluoroacetate at boron, 1,2-migration of an ethyl substituent with concomitant ring-opening, and nucleophilic attack of HO–C(7) at boron. Treatment of **8** with alkaline H_2O_2 in THF leads to the diol **9** (37%) and the alkene **10** (39%) (Scheme 4).

To prepare glycosyl borinates, we exposed the diazirine **1** to the exceptionally stable borinates **11**–**12**[11] derived from 10-bora-9-oxabicyclo[3.3.2]decane (Scheme 5). This led to

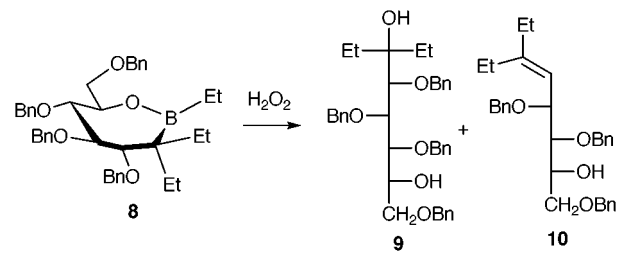

Scheme 4

† Glycosylidene Carbenes Part 28. For Part 27, see ref. 1(*b*).

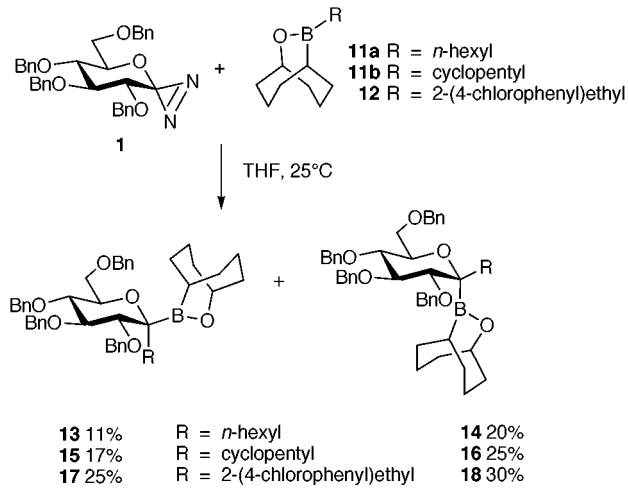

Scheme 5

diastereoisomeric mixtures **13**/**14** (31%; 35:65), **15**/**16** (42%; 40:60) and **17**/**18** (55%; 45:55) that were isolated by flash chromatography. The isomers **15**/**16** and **17**/**18** were separated by HPLC. The glycosyl borinates **13**–**18** were characterized by FAB-MS, ^{11}B NMR, ^{1}H NMR, ^{13}C NMR and IR spectroscopy. They were stable at −10 °C for several weeks and not affected by air.

The configuration of **17** and **18** was deduced from NOE experiments (Fig. 1), with **17** showing NOEs between H–C(2) and H–C(5), H–C(2) and H–C(7), and H–C(1′) and H–C(4), indicating an axial orientation of the anomeric alkyl group. In contradistinction, a small NOE between H–C(1′) and H–C(5) and the lack of other NOEs > 1% for **18** indicate an equatorial orientation of the anomeric alkyl group.

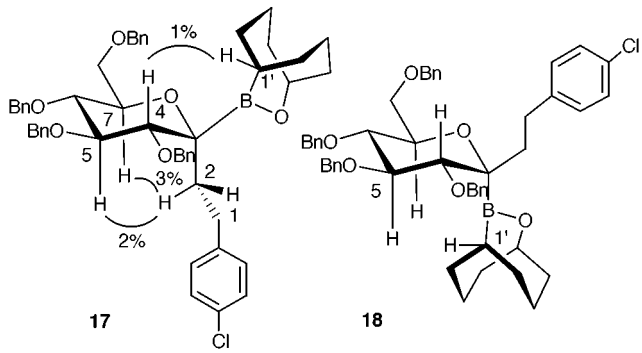

Fig. 1

We thank the Swiss National Science Foundation and F Hoffmann-La Roche, Basel, for generous financial support.

Notes and references

‡ *Synthesis* of **17** and **18**: at 25 °C, a solution of **12** (R,R′ = H, 4-ClC_6H_4, 116 mg, 0.42 mmol) in abs. THF (3 ml) was treated portionwise with a cooled (dry ice, *ca.* −60 °C) solution of **1** (77 mg, 0.14 mmol) in dry CH_2Cl_2 (0.8 ml) within 140 min, stirred for 2 h at 25 °C until complete disappearance of **1**. Evaporation at 20 °C and flash chromatography (hexane–AcOEt–CH_2Cl_2 18:1:1) gave **17**/**18** (61 mg, 55%, 45:55), which were separated by preparative HPLC (hexane–AcOEt 12:1; 9 ml min^{-1}). *Selected data* for **17**: R_f (hexane–AcOEt–CH_2Cl_2 4:1:1) 0.36; $[\alpha]_D^{25}$ +51.4 (*c* 1.16, CH_2Cl_2); ν_{max}(CH_2Cl_2)/cm^{-1} 3032*w*, 2927*m*, 2963*m*, 1604*w*, 1493*m*, 1453*m*, 1420*m*, 1364*m*, 1092*s*, 1027*s*; δ_H(300 MHz, $CDCl_3$) 7.62–7.11 (*m*, 20 arom. H), 4.87 (*d*, *J* 10.6, PhC*H*), 4.85 (*d*, *J* 10.9, PhC*H*), 4.83 (*d*, *J* 10.9, PhC*H*), 4.77 (*d*, *J* 10.9, PhC*H*), 4.71 (*d*, *J* 12.1, PhC*H*), 4.70–4.66 (*m*, BOCH), 4.68 (*d*, *J* 10.9, PhC*H*), 4.66 (*d*, *J* 10.9, PhC*H*), 4.64 (*d*, *J* 12.1, PhC*H*), 3.91 [*t*, *J* 8.7, H–C(5)], 3.74 [*dd*, *J* 11.2, 4.0, H–C(8)], 3.73 [*dd*, *J* 11.2, 1.9, H′–C(8)], 3.68 [*d*, *J* 9.0, irrad. at 3.91 → *d*, *J* ≈ 4, H–C(4)], 3.67–3.63 [*m*, H–C(7)], 3.58 [*t*, *J* 8.4, irrad. at 3.91 → *dd*, *J* ≈ 9, 3, H–C(6)], 2.65–2.56 [*m*, 2 H–C(1)], 2.37–2.27 [*m*, irrad. at 2.6 → *d*, *J* ≈ 10, H–C(2)], 2.22–2.18 (*m*, BCH), 2.01–1.91 [*m*, irrad. at 2.6 → *d*, *J* ≈ 10, H′–C(2)], 2.01–1.46 (*m*, 12 H); δ_C(75 MHz, $CDCl_3$, assignment based on ^{1}H/^{13}C COSY) 142.03 (*s*), 139.00 (2*s*), 138.69, 138.29, 131.12 (3*s*), 129.79–127.12 (several *d*), 84.42 [*d*, C(5)], 81.57 [*d*, C(4)], 79.53 [*d*, C(6)], 75.60, 75.13, 74.73 (3*t*, 3 PhCH_2), 74.19 (*d*, BOCH), 73.51 (*t*, PhCH_2), 72.24 [*d*, C(7)], 69.99 [*t*, C(8)], 32.41 (*t*), 30.63 (*t*), 30.19 [*t*, C(1)], 28.91 [*t*, C(2)], 27.54 (*t*), 25.63 (*t*), 22.89 (*t*), 21.91 (*t*), 21.30 (small br *d*, HCB), signal of C(3) hidden by noise; δ_B(160 MHz, $CDCl_3$) 52.02 (br *s*); *m*/*z* (FAB) 821 (< 1%, [*M* + Na]$^+$), 799 (< 1, [*M* + H]$^+$), 599 (38), 553 (43, [*M* − $BnOBOC_8H_{14}$ + H]$^+$), 447 (44), 181 (100). For **18**: R_f (hexane–AcOEt–CH_2Cl_2 10:1:1) 0.32; $[\alpha]_D^{25}$ +12.0 (*c* 0.65, CH_2Cl_2); ν_{max}(CH_2Cl_2/cm^{-1} 3032*w*, 2927*m*, 1492*m*, 1453*m*, 1418*w*, 1364*m*, 1093*s*, 1027*m*, 1015*m*; δ_H(300 MHz, $CDCl_3$) 7.38–6.99 (*m*, 20 arom. H), 4.98 (*d*, *J* 11.8, PhC*H*), 4.85 (*d*, *J* 10.9, PhC*H*), 4.84 (*s*, PhCH_2), 4.70 (*d*, *J* 11.8, PhC*H*), 4.71–4.67 (*m*, HCOB), 4.68 (*d*, *J* 12.1, PhC*H*), 4.62 (*d*, *J* 10.9, PhC*H*), 4.60 (*d*, *J* 12.1, PhC*H*), 3.96 [*dt*, *J* ≈ 9.6, 4.0, H–C(7)], 3.78–3.70 [*m*, H–C(5), 2 H–C(8)], 3.60 [*t*, *J* 9.6, irrad. at 3.96 → *d*, *J* ≈ 9, H–C(6)], 3.50 [*d*, *J* 9.4, H–C(4)], 2.74–2.67 [*m*, 2 H–C(1)], 2.25–2.21 (*m*, BCH), 2.05–1.95 [*m*, irrad. at 2.70 → *d*, *J* ≈ 12, H–C(2)], 1.99–1.26 (*m*, 13 H); δ_C(75 MHz, $CDCl_3$, assignment based on ^{1}H/^{13}C COSY) 141.75 (*s*), 139.26 (2*s*), 138.2, 137.8, 133.6 (3*s*), 129.9–127.14 (several *d*), 85.93 [*d*, C(5)], 84.90 [*d*, C(3)], 79.54 [*d*, C(6)], 76.00 [*d*, C(7)], 75.37, 75.09, 74.80 (3*t*, 3 PhCH_2); 74.06 (*d*, BOCH), 73.22 (*t*, PhCH_2), 69.93 [*t*, C(8)], 37.14 [*t*, C(2)], 31.82 (*t*), 30.91 (*t*), 29.33 [*t*, C(1)], 26.79 (*t*), 25.77 (*t*), 23.38 (small br *d*, BCH), 22.48 (*t*), 21.92 (*t*), signal of C(3) hidden by noise; δ_B(160 MHz, $CDCl_3$) 53.8 (br *s*); *m*/*z* (FAB) 821 (< 1%, [*M* + Na]$^+$), 799 (< 1, [*M* + H]$^+$), 553 (43, [*M* − $BnOBOC_8H_{14}$ + H]$^+$), 461 (28), 401 (41), 325 (60), 281 (87), 181 (100).

1 (*a*) A. Vasella, *Glycosylidene Carbenes*, in *Bioorganic Chemistry*, *Vol. 3, Carbohydrates*, ed. S. Hecht, OUP, New York, 1999, p. 56 and references therein; (*b*) M. Weber, A. Vasella, M. Textor and N. D. Spencer, *Helv. Chim. Acta*, 1998, **81**, 1359; (*c*) K. Briner and A. Vasella, *Helv. Chim. Acta*, 1992, **75**, 621; (*d*) P. Uhlmann and A. Vasella, *Helv. Chim. Acta*, 1992, **75**, 1979; (*e*) A. Vasella and C. A. A. Waldraff, *Helv. Chim. Acta*, 1991, **74**, 585; (*f*) A. Vasella, P. Dhar and C. Witzig, *Helv. Chim. Acta*, 1993, **76**, 1767; (*g*) T. Rajamannar and A. Vasella, unpublished results on the synthesis of *N*-glycosylsulfonamides.
2 A. Vasella, G. Baudin and L. Panza, *J. Heteroatom Chem.*, 1991, **2**, 151.
3 P. Uhlmann, D. Nanz, E. Bozo and A. Vasella, *Helv. Chim. Acta*, 1994, **77**, 1430.
4 A. Suzuki, S. Nozawa, N. Miyaura and M. Itoh, *Tetrahedron Lett.*, 1969, 2955.
5 K. Briner and A. Vasella, *Helv. Chim. Acta*, 1989, **72**, 1371.
6 G. Zweifel and H. C. Brown, *Org. React.*, 1963, **13**, 1.
7 D. J. Pasto and S. R. Snyder, *J. Org. Chem.*, 1966, **31**, 2777; D. S. Matteson and M. L. Peterson, *J. Org. Chem.*, 1987, **52**, 5116.
8 H. Nöth and B. Wrackmeyer, *NMR: Basic Principles and Progress*, 1978, vol. 14, p. 140.
9 B. Wrackmeyer, *Prog. Nucl. Magn. Reson. Spectrosc.*, 1979, **12**, 227.
10 H. Nöth and B. Wrackmeyer, *NMR: Basic Principles and Progress*, 1978, vol. 14, p. 138.
11 J. A. Soderquist and M. R. Najafi, *J. Org. Chem.*, 1986, **51**, 1330.

Communication 9/06400A

Ferromagnetic order in a μ-cyano Cr^{III}–Mn^{II} assembly with an unusual branched architecture

Arnaud Marvilliers,[a] Simon Parsons,[b] Eric Rivière,[a] Jean-Paul Audière[a] and Talal Mallah*[a]

[a] *Laboratoire de Chimie Inorganique, UMR CNRS 8613, Université Paris-Sud, 91405 Orsay, France. E-mail: mallah@icmo.u-psud.fr*

[b] *Department of Chemistry, The University of Edinburgh, West Mains Road, Edinburgh, UK EH9 3JJ*

Received (in Cambridge, UK) 25th June 1999, Accepted 30th September 1999

Reacting hexacyanochromate(III) with a mononuclear Mn(II) complex chelated by a tetradentate ligand that leaves two coordination sites available in *cis* position leads to a new molecular ferromagnet (T_C = 17 K) with an unusual architecture.

Cyanide-bridged systems are generally obtained by reacting a hexacyanometalate with a mononuclear assembler complex where some of the coordination sites may be blocked by a chelating ligand. In the absence of such ligands or when the ligand is bidentate, three-dimensional cubic networks are obtained.[1,2] On the other hand, when the chelating ligands block more than two coordination sites around the assembler complex, different structures become accessible.[3–5] For example, when $Ni(tren)^{2+}$ [tren = tris(2-aminoethyl)amine is a tetradendate ligand that leaves two available coordination sites on Ni^{II} in *cis* position] is reacted with $[Fe(CN)_6]^{3-}$, a non-cubic three-dimensional compound that orders ferrimagnetically (T_C = 8 K) is obtained.[4] Using $Ni(bpm)_2^{2+}$ [bpm = bis(1-pyrazolyl)methane] instead of $Ni(tren)^{2+}$ affords a discrete pentanuclear complex $[Fe(CN)_6]_2[Ni(bpm)_2]_3\cdot H_2O$.[5] Magnetic ordering at T_C = 23 K is observed owing to intermolecular ferromagnetic interaction. The formation of a discrete μ-cyanide species in the latter and not in the former compound is probably due to the steric hindrance of the bidentate ligand bpm. We have shown as well that such a pentanuclear species is obtained with $Ni(IM2\text{-}py)_2^{2+}$ (IM2-py = 2-(2-pyridyl)-4,4,5,5-tetramethyl-4,5-dihydro-1*H*-imidazolyl-1-oxy] where IM2-py is a bidentate ligand as bulky as bpm or bipy.[6]

Here we report on the structure and the preliminary magnetic properties of a new μ-cyano Cr^{III}–Mn^{II} polymeric compound obtained from the reaction of $Mn^{II}(bispicen)Cl_2$ and hexacyanochromate(III). $Mn^{II}(bispicen)Cl_2$ [bispicen = *N*,*N*′-bis(2-pyridylmethyl)-1,2-ethanediamine] was chosen because bispicen chelates the metal ion leaving the two chloride atoms in *cis*-position.[7] We reasoned that (i) this *cis* arrangement should be retained in the final compound where the two chloride atoms may be substituted by two nitrogen atoms of two $Cr(CN)_6$ units. and (ii) because the size of the manganese complex which is intermediate between that of $Ni(tren)^{2+}$ and $Ni(bpm)_2^{2+}$ [or $Ni(bipy)_2^{2+}$], a compound with a different dimension† should be obtained.

Yellow plates were obtained using the gel technique.[8], X-ray crystallography‡ reveals the formation of a one-dimensional neutral 3/2 : Mn/Cr polymer of formula $[Cr(CN)_6]_2[Mn(bispicen)]_3\cdot 6H_2O\cdot 0.5EtOH$ **1**. The asymmetric unit contains three crystallographically independent manganese and two crystallographically independent chromium ions [Fig. 1(a)]. The body of the one-dimensional assembly (along the *b* crystallographic axis) is made of Cr_2Mn_2 units sharing Cr(1) vertices; each chromium vertex is linked through one apical cyanide to a Mn(bispicen) complex which is itself connected to a terminal molecule of $Cr(CN)_6$. The pendant Mn(3)Cr(2) units are placed alternately below and above the body of the polymer. All the Mn^{II} complexes are surrounded by two $Cr(CN)_6$ entities in *cis* position as expected from the nature of the chelating ligand. The surroundings of the Mn^{II} metal ions is that of a distorted octahedron (see Fig.1 caption). The Mn–N–C angles, where NC is a bridging cyanide, vary from 161.5° to 177.7° for Mn(1) and Mn(2). The highest deviation from 180° is found for the Mn(3)–N(13)–C(13) angle (147.1°). Fig. 1(b) shows a H-bond network along the *a* axis involving four water molecules linking amine nitrogen atoms belonging to a pendant and to an in-body Mn

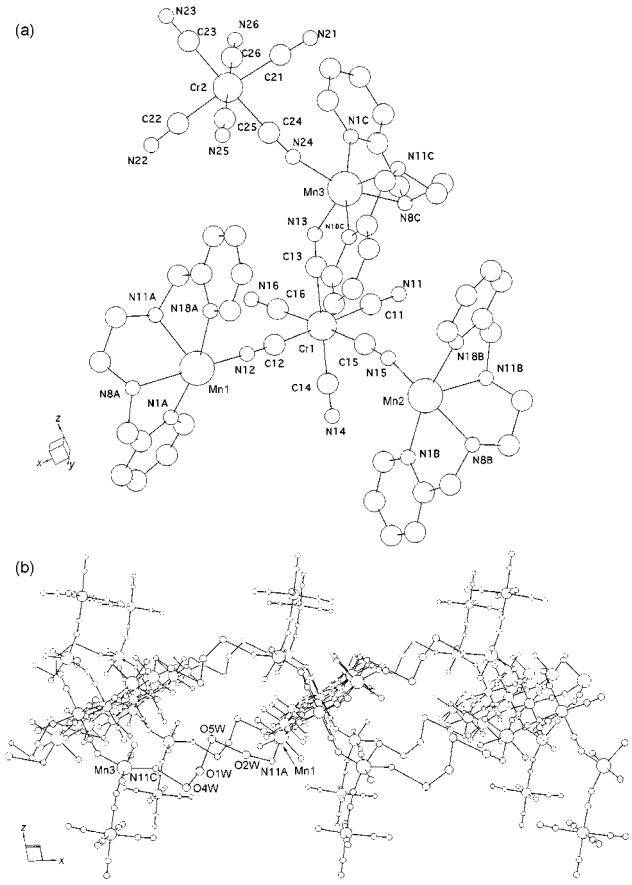

Fig. 1 (a) View of the asymmetric unit with atoms numbering. Selected bond distances and angles: Mn(1)–N(12) 2.162(6), Mn(1)–N(11) 2.173(6), Mn(1)–N(8A) 2.273(5), Mn(1)–N(1A) 2.282(5), Mn(1)–N(11A) 2.291(5), Mn(1)–N(18A) 2.315(5), Mn(2)–N(15) 2.180(6), Mn(2)–N(16) 2.182(6), Mn(2)–N(8B) 2.270(6), Mn(2)–N(1B) 2.276(6), Mn(2)–N(11B) 2.286(5), Mn(2)–N(18B) 2.288(6), Mn(3)–N(24) 2.137(6), Mn(3)–N(13) 2.174(6), Mn(3)–N(11C) 2.249(7), Mn(3)–N(18C) 2.268(6), Mn(3)–N(1C) 2.298(7), Mn(3)–N(8C) 2.330(7), Cr(1)–C(14) 2.045(7), Cr(1)–C(11) 2.055(7), Cr(1)–C(12) 2.055(7), Cr(1)–C(13) 2.056(7), Cr(1)–C(16) 2.068(7), Cr(1)–C(15) 2.078(7), Mn(1)–N(12)–C(12) 177.7(6); Mn(1)–N(11)–C(11) 163.6(5), Mn(2)–N(15)–C(15) 167.3(5), Mn(2)–N(16)–C(16) 161.5(5), Mn(3)–N(13)–C(13) 147.1(6), Mn(3)–N(24)–C(24) = 168.1(6). (b) View along the *b* axis showing the H-bond connections along the *a* axis between the amine nitrogen atoms of pendant and in-body Mn(bispicen) complexes belonging to two different polymers.

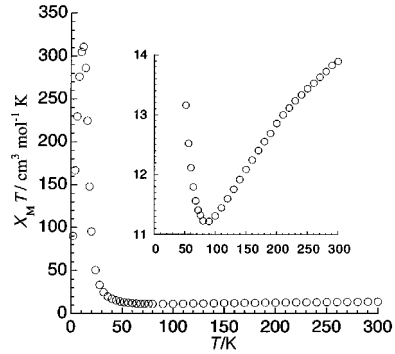

Fig. 2 $\chi_M T$ = f(T) plot performed at H = 1 kOe, the inset shows the decrease of $\chi_M T$ on cooling to T = 84 K.

complex of two different polymers. The other two water and the ethanol molecules do not participate in the extended two-dimensional network. No connection is observed along the *c* direction where the shortest metal–metal distance (11.08 Å) is between two pendant chromium ions of two neighbouring polymers.

Mixing two aqueous solutions of $[NBu^n_4]_3[Cr(CN)_6]$ and Mn(bispicen)Cl_2 in a 2:3 stoichiometric ratio leads to the immediate precipitation of a yellow powder. The IR spectrum of the powder was found to be identical to that of a collection of single crystals obtained by the gel technique. In the 2000–2200 cm^{-1} region, two bands centred at 2151 and 2130 cm^{-1} are present corresponding to bridging and non-bridging cyanides, respectively. TG analysis reveals a mass loss corresponding to six water molecules per unit formula.§

Magnetic studies were carried out on a powdered sample using a SQUID magnetometer. Fig. 2 shows the $\chi_M T$ = f(T) plot performed in an applied field of 1 kOe. On cooling from room temp., $\chi_M T$ (13.9 cm^3 mol^{-1} K) decreases, reaches a minimum at T = 84 K (insert of Fig. 2) then increases abruptly below T = 30 K and reaches a maximum value of 311 cm^3 mol^{-1} K at 11 K. The decrease of $\chi_M T$ on cooling indicates that the exchange interaction between Cr^{III} and Mn^{II} through the cyanide bridge is antiferromagnetic as has already been observed.[11] The abrupt increase of $\chi_M T$ at low temperature and the high value measured at 11 K may be due to a three-dimensional ordering leading to a molecular ferromagnet; the decrease below T = 12 K would in this case be due to the saturation of the susceptibility. In order to confirm this, magnetisation *vs.* field studies were performed at T = 2 K ; the curve shows that saturation is attained (Fig. 3) when a very small field of 400 Oe is applied. This is the signature of the occurrence of a magnetic ordering within the compound. The magnetisation value at H = 55 (8.9 μ_B) confirms the antiferromagnetic interaction between adjacent metal ions. Field cooled magnetisation curve obtained with an applied field of 30 Oe are in line with the presence of a magnetic ordering below a critical tempertaure T_C = 17 K (Fig. 3 insert).¶ The

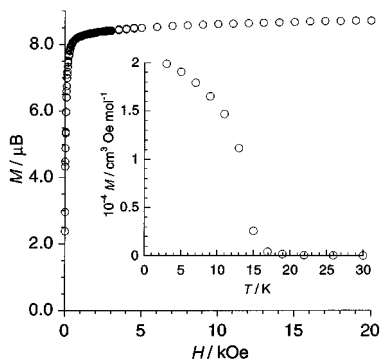

Fig. 3 M = f(H) magnetisation curve at T = 2 K, inset: M = f(T) at H = 30 Oe.

origin of the behaviour is not clear yet. The H-bond network may be responsible of a ferromagnetic interaction between the polymers along the *a* axis. However, since no connections are present in the third direction, only dipolar interactions along the *c* axis can account for the three-dimensional magnetic order.

Magnetic studies on dehydrated samples and on oriented single crystals should bring insights on the origin of three-dimensional order and on the absence of coercive field and remnant magnetisation (curves not presented here) for powders below T_C.

This work was supported by the Franco–British joint program Alliance No. 96175 from the French Foreign Ministry and the British Council.

Notes and references

† We restrict the word dimension here to μ-cyanide bridges, *i.e.* a three-dimensional compound structurally is one where μ-cyanide bridges spread in the three directions of space while a compound containing discrete cyanide-bridged species is zero-dimensional.

‡ *Crystal data* for **1**: $C_{55}H_{63}Cr_2Mn_3N_{24}O_{6.5}$, M = 1433.11, monoclinic, space group $P2_1/n$ a = 17.5085(10), b = 15.5670(10), c = 26.4406(17) Å, U = 7128.6(8) Å^3, β = 94.4330(10), T = 150 K, Z = 4, 31415 reflections measured, of which 10185 were unique (R_{int} = 0.1055). The structure was solved by direct methods (SIR92)[9] and refined with SHELXL-97.[10] The final conventional R-factor [based on F and 10185 data with $F > 4\sigma(F)$] was 0.0793. CCDC 182/1428.

§ Elemental analysis of a powder sample fits well with the proposed formula $Cr(CN)_6]_2[Mn(bispicen)]_3 \cdot 6H_2O$ which does not contain ethanol. Found (calc.) for $C_{54}H_{60}N_{24}O_6Mn_3Cr_2$: C, 45.98 (46.02); H, 4.30 (4.26); N, 23.83 (23.84); Mn, 11.39 (11.69); Cr, 7.25 (7.38)%. Only water is used as solvent when preparing the powder while the crystals are obtained using a gel containing a small amount of ethanol. Since, the crystallographic studies reveal that ethanol does not participate to an extended H-bond network, its absence should not have an influence on the magnetic properties (see below).

¶ Field-cooled magnetisation measurements (H = 30 Oe) were performed on a few single crystals embedded in the gel; below 17 K an abrupt increase confirms that the crystals order magnetically at the same temperature as the powder.

1 V. Gadet, T. Mallah, I. Castro and M. Verdaguer, *J. Am. Chem. Soc.*, 1992, **114**, 9213; T. Mallah, S. Thiébaut, M. Verdaguer and P. Veillet, *Science*,1993, **262**, 1554; W. R. Entley and G. S. Girolami, *Science*, 1995, **268**, 397; S. Ferlay, T. Mallah, R. Ouahès, P. Veillet and M. Verdaguer, *Nature*, 1995, **378**, 701; S. Ferlay, T. Mallah, R. Ouahès, P. Veillet and M. Verdaguer, *Inorg. Chem.*, 1999, **38**, 229.

2 M. Ohba, N. Usaki, N. Fukita and H. Okawa, *Angew. Chem., Int. Ed.*, 1999, **38**, 1795; T. Mallah, A. Marvilliers and E. Rivière, *Philos. Trans. R. Soc.* (*London*) A, 1999, **357**, in press.

3 G. O. Morpugo, V. Mosini, P. Porta, G. Dessy and V. Fares, *J. Chem. Soc., Dalton Trans.*, 1981, 111; M. Ohba, N. Maruono, H. Okawa, T. Enoki and J.-M. Latour, *J. Am. Chem. Soc.*, 1994, **116**, 11 566; H. Miyasaka, N. Matsumoto, N. Re, E. Gallo and C. Floriani, *Inorg. Chem.*, 1997, **36**, 670; S. Ferlay, T. Mallah, J. Vaissermann, F. Bartolomé, P. Veillet and M. Verdaguer, *Chem. Commun.*, 1996, 2481; E. Colacio, J. M. Dominguez-Vera, M. Ghazi, R. Kivekäs, F. Lloret, J. M. Moreno and H. Stoeckli-Evans, *Chem.Commun.*, 1999, 987.

4 S. El Fallah, E. Rentshler, A. Caneshi, R. Sessoli and D. Gatteschi, *Angew. Chem., Int. Ed. Engl.*, 1996, **35**, 1947.

5 K. Van Langenberg, S. R. Batten, K. J. Berry, D. C. R. Hockless, B. Moubaraki and K. S. Murray, *Inorg. Chem.*, 1997, **36**, 5006.

6 A. Marvilliers, Y. Pei, J. Cano Boquera, K. E. Vostrikova, C. Paulsen, E. Rivière, J.-P. Audière and T. Mallah, *Chem. Commun.*, 1999, 1951.

7 H. Toflund, E. Pedersen and S. Yde-Andersen, *Acta Chem. Scand. Ser. A*, 1984, **38**, 693.

8 S. Descurtins, H. W. Schmalle, P. Schneuwly, J. Ensling and P. Gütlich, *J. Am. Chem. Soc.*, 1994, **116**, 9521.

9 A. Altomare, G. Cascarano, Giacovazzo and A. Guagliardi, *J. Appl. Crystallogr.*, 1993, **26**, 343.

10 G. M. Sheldrick, Institüt für Angorganische Chemie der Universität, Tammanstrasse 4, D-3400 Göttingen, Germany, 1998.

11 A. Sciuller, T. Mallah, A. Nivorozkhin, J.-L. Tholence, M. Verdaguer and P. Veillet, *New. J. Chem.*, 1996, **20**, 1.

Communication 9/05191K

Synthesis and structures of two new 12-member ring crown-shaped oxovanadium borophosphates

Yongnan Zhao,† Guangshan Zhu, Wang Liu, Yongcun Zou and Wenqin Pang*

Key Laboratory of Inorganic Synthesis and Preparative Chemistry, Department of Chemistry, Jilin University, Changchun, 130023, China. E-mail: zhaoyn@263.net

Received (in Cambridge, UK) 17th August 1999, Accepted 5th October 1999

Two new oxovanadium borophosphates have been hydrothermally synthesized; they are structural analogues and are both constructed by $[(VO)_{12}\{O_3POB(O)_2OPO_3\}_6]^{18-}$ 12-member ring clusters with NH_4^+ and K^+ cations encapsulated in the rings, respectively; an extended network of hydrogen bonds between anions, cations and crystal water molecules link the structures in three dimensions.

Template synthesis of novel compounds utilizing intrinsic host–guest relationships has opened up a new field for chemists to create microporous, host or cluster structures and has resulted in numerous novel metal phosphates with open frameworks.[1–5] The current interest in vanadium phosphates derives from their notable catalytic properties and structural diversity. Vanadium can bind to oxygen in a variety of valences to form tetrahedra, square pyramids, octahedra or large aggregates by condensation of polyhedra through shared oxygen atoms. Template controlled linking of these units has led to a large number of oxovanadium phosphates with open framework structures.[6] Notably the successful synthesis of $[NH_2Me_2]K_4[V_{10}O_{10}(H_2O)_2(OH)_4(PO_4)]\cdot 4H_2O$ demonstrates that inorganic species can also mimic biologically relevant structures.[7] The three-dimensional frameworks $[HN(CH_2CH_2)_3NH]K_{1.35}[V_5O_9(PO_4)_2]\cdot xH_2O$ and $Cs_3[V_5O_9(PO_4)_2]\cdot xH_2O$ provide the largest cavities of open-framework structures known up to now.[8]

While metal phosphates have been expansively exploited, few reports on the synthesis of metal borophosphates have appeared. The introduction of boron into the framework has been proved to generate novel motifs and unique structures and several microporous aluminoborates have been prepared.[9] Recently the synthesis and structures of several new vanadium borate clusters were reported[10] stimulating chemists to incorporate boron into further inorganic systems. $CoB_2P_3O_{12}(OH)\cdot C_2H_{10}N_2$ was reported as the first microporous metal phosphate.[11] The synthetic $M^IM^{II}(H_2O)_2(BP_2O_8)$ (M^I = Na, K; M^{II} = Mg, Fe, Co, Ni, Zn),[12] $M^{II}[BPO_5]$ (M^{II} = Ca, Sr), $Ba[BP_3O_{12}]$,[13] $Zn[BO_3PO_4]$,[14] $CoBP_3O_{14}$,[15] $Ln_7O_6(BO_3)(PO_4)_2$ (Ln = La, Nd, Gd, Dy)[16] and two mineral phases $Mg_3B_2P_2O_8$,[17] $MnBPO_4(OH)_6$[18] are also examples of borophosphates. Recently Zubieta *et al.* reported the synthesis and structures of VOBOPO-1, a three-dimensional oxovanadium borophosphate $[H_3NCH_2CH_2NH_3]_2(VO)_5(H_2O)\{O_3POB(O)_2OPO_3\}_2]\cdot 1.5H_2O$[19] and VOBOPO-2, the first oxometalate borophosphate molecular cluster, $(H_3NCH_2CH_2NH_3)_2[Na(VO)_{10}\{HO_3POB(O)_2OPO_3H\}_5]\cdot 22.5H_2O$.[20] More recently, a borophosphate anion $[N_2C_6H_{14}]_2VO(PO_3OH)_4(B_3O_3OH)\cdot H_2O$ containing a single vanadium atom was reported.[21] Nevertheless metal borophosphates are still relatively undeveloped. Herein we report the synthesis and structures of two 12-member ring oxovanadium borophosphates, denoted VBP-J1 and VBP-J2 (J = Jilin University), templated by triethylenetetraamine.

Compounds VBP-J1 and VBP-J2 were hydrothermally synthesized using H_3BO_3 (99.5%), H_3PO_4 (85 wt%), NH_4VO_3 (99%), V_2O_5 (99%), KCl (99.5%) and triethylenetetraamine (> 95%) as the starting materials. Typical synthesis of VBP-J1 was performed as follows: 1.0 g H_3BO_3, 3.4 g H_3PO_4 and 1.9 g NH_4VO_3 were first dispersed into 20 ml water under vigorous stirring. Then 1.6 g of triethylenetetraamine were added. The final mixture was sealed in a 40 ml Teflon-lined stainless steel autoclave and heated at 180 °C for two days under autogenous pressure. In the synthesis of VBP-J2, NH_4VO_3 was replaced by 0.75 g V_2O_5 and 2 g KCl. The blue rhombic crystals obtained in both cases were filtered off, washed with water and dried at room temperature. The products were characterized by powder X-ray diffraction, IR, TG, chemical analysis (elemental ratio 2V : 2P : B) and single crystal determinations. Single crystals of VBP-JI (0.15 × 0.10 × 0.05 mm) and VBP-J2 (0.18 × 0.15 × 0.06 mm) were selected for structure analysis.‡

VBP-J1 and VBP-J2 are both constructed by 12-member ring $[(VO)_{12}\{O_3POB(O)_2OPO_3\}_6]^{18-}$ clusters which are charge compensated by protonated triethylenetetraamine. An extended network of hydrogen bonds between anions, cations and crystal water molecules link the structures in three dimensions.

The asymmetric unit of VBP-J1 and VBP-J2 both contain six vanadium atoms, six phosphorus atoms and three boron atoms (Fig. 1). The vanadium atoms are all coordinated by five oxygen atoms to form square pyramids with one short vanadyl (V=O) bond [1.593(5)–1.615(5) Å]. The neighboring two vanadium atoms form an edge-sharing binuclear unit, which shows an *anti*-configuration of the vanadyl groups with respect to the $\{V_2O_2\}$ bridging group. Each binuclear unit is linked to four PO_4 groups by four oxygen atoms. Bond valence calculations give a bond valence for vanadium atoms of 4.[22]

The six phosphorus atoms are each coordinated by four oxygen atoms. The P–O distances range from 1.486(6) to 1.576(6) Å and the O–P–O angles lie between 106.4(3) and 113.0(3)°. In each PO_4 tetrahedron, two oxygen atoms are shared with the VO_5 square pyramid and one oxygen atom is shared with the BO_4 tetrahedron. The remaining oxygen atom is unshared and pendant. Each of the boron atoms is coordinated by four oxygen atoms with B–O distances in the range 1.430(9)–1.505(9) Å. The BO_4 group shares two oxygen atoms with the neighboring two PO_4 tetrahedra and forms a dense $\{O_3POB(O)_2OPO_3\}^{7-}$ borophosphate unit. Similar $\{O_3POB(O)_2OPO_3\}^{7-}$ trimers have been found in VOBOPO-1, VOBPO-2 and $[N_2C_6H_{14}]_2VO(PO_3OH)_4(B_3O_3OH)\cdot H_2O$.[19–21] The $\{BO_4\}$ group contributes a μ_3-bridging oxygen to each of two neighboring binuclear $\{V_2O_{10}\}$ moieties. In this fashion each $\{O_3POB(O)_2OPO_3\}^{7-}$ exhibits three-point attachment to each of two binuclear $\{V_2O_5\}$ sites. The linking of six $\{V_2O_{10}\}$ moieties and six borophosphate ligands produces the 12-member ring structure with NH_4^+ or K^+ cations encapsulated in the rings (Fig. 2). In VBP-J1, the NH_4^+ cation is linked to the six *endo* oxygen atoms of the vanadyl by hydrogen bonds. In VBP-J2, the K^+ cation is six-coordinated by the six *endo* oxygen atoms of the vanadyl groups.

The ring diameters are 5.856(O8A–O8B) × 5.411(O35A–O35B) × 5.560(O22A–O22B) Å and 5.415(O24–O24A) × 5.415(O10–O10A) × 5.235(O36–O36A) Å for VBP-J1 and VBP-J2, respectively. Differences may be accounted for by the difference of the ion diameter between NH_4^+ (1.66 Å) and K^+ (1.44 Å).

In conclusion, two new oxovanadium borophosphates have been hydrothermally synthesized. They are structural analogues and have a similar motif to VOBOPO-1 and VOBOPO-2.[19,20]

† Present address Institute of Physics & Center for Condensed Matter Physics, Chinese Academy of Science, Beijing 100080, China.

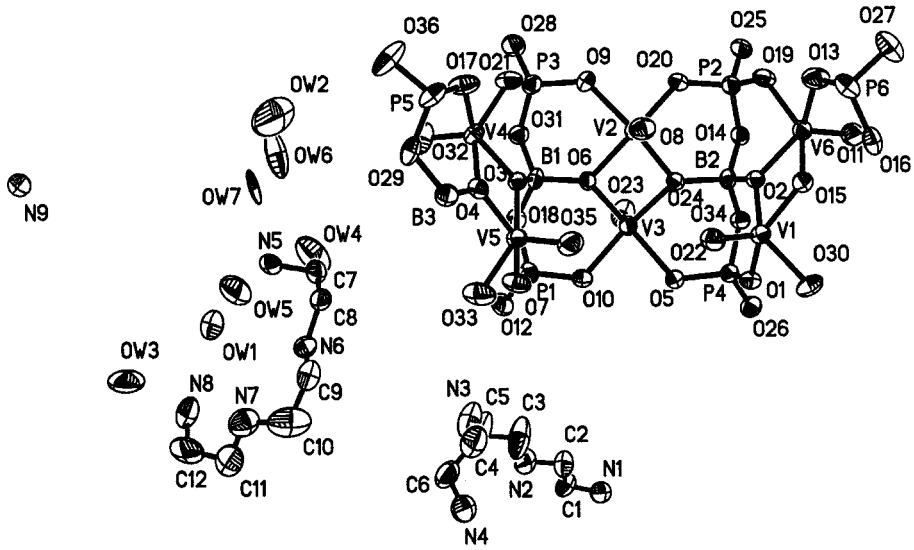

Fig. 1 The asymmetric unit of VBP-J1.

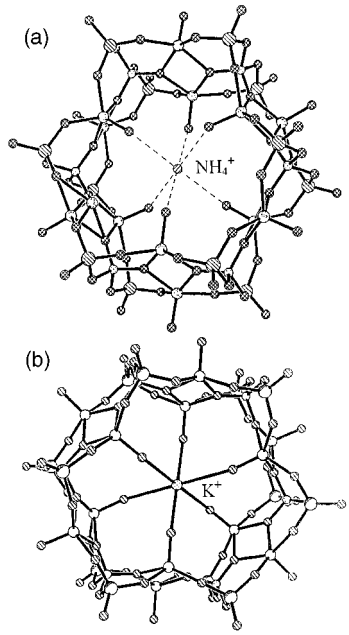

Fig. 2 The 12-member ring clusters of (a) VBP-J1 with NH_4^+ encapsulated in the center and (b) VBP-J2 with K^+ encapsulated in the center.

This successful synthesis leads to the possibility to synthesize larger rings using larger cations than NH_4^+ and K^+. Furthermore the various vanadium oxygen polyhedra with numerous linkage forms of the vanadium oxygen polyhedra, boron oxygen polyhedra and PO_4 tetrahedra are expected to lead to a variety of oxovanadium borophosphates.

The authors are grateful for the financial support of the National Science Foundation of China and the Key Laboratory of Inorganic Synthesis and Preparative Chemistry of Jilin University.

Notes and references

‡ *Crystal data*: VBP-J1: $C_{24}H_{120}B_6N_{17}O_{86}P_{12}V_{12}$, M = 3071.15, orthorhombic, *Pbca*, a = 21.454(11), b = 16.315(6), c = 29.651(12) Å, V = 10378(8) Å^3, Z = 4, D_c = 1.966 g cm^{-3}, T = 293(2) K, λ = 0.7103 Å, μ = 1.343 mm^{-1}; final R_1 = 0.0586, R_w = 0.1708.

VBP-J2: $C_{28}H_{128}B_6KN_{20}O_{84}P_{12}V_{12}$, M = 3076.38, orthorhombic, *Pbca*, a = 21.537(2), b = 16.2667(13), c = 29.717(4) Å, V = 10410.8(18) Å^3, Z = 4, D_c = 2.027 g cm^{-3}, T = 293(2) K, λ = 0.7103 Å, μ = 1.381 mm^{-1}; final R_1 = 0.0576, R_w = 0.1540.

CCDC 182/1429. See http://www.rsc.org/suppdata/cc/1999/2219/ for crystallographic files in .cif format.

1 J. Yu, K. Sugiyama, K. Hiraga, N. Togaashi, O. Terasaki, Y. Tanaka, S. Nakata, S. Qiu and R. Xu, *Chem. Mater.*, 1998, **10**, 3636 and references therein.
2 J. Yu, K. Sugiyama, S. Zheng, S. Qiu, J. Chen, R. Xu, Y. Sakamoto, O. Terasaki, K. Hiraga, M. Light, M. B. Hursthouse and J. M. Thomas, *Chem. Mater.*, 1998, **10**, 1208 and references therein.
3 M. Cchindller, W. Joswig and W. H. Baur, *J. Solid State Chem.*, 1997, **134**, 286 and references therein.
4 K. H. Lii, Y. F. Huang, V. Zima, C. Y. Huang, H. M. Lin, Y. C. Jiang, F. L. Liao and S. L. Wang, *Chem. Mater.*, 1998, **10**, 2609 and references therein.
5 H. H. Y. Sung, J. Yu and I. D. Williams, *J. Solid State Chem.*, 1998, **140**, 46 and references therein.
6 Y. Lu, R. C. Haushalter and J. Zubieta, *Inorg. Chim. Acta*, 1998, **268**, 257 and references therein.
7 V. Soghmonian, Q. Chen, R. C. Haushalter, J. Zubieta and C. J. O'Connor, *Science*, 1993, **259**, 1569.
8 M. Isaque Khan, L. M. Meyer, R. C. Haushalter, A. L. Schweitzer, J. Zubieta and J. L. Dye, *Chem. Mater.*, 1996, **8**, 43.
9 J. Yu, R. Xu, Q. Kan, Y. Xu and B. Xu, *J. Mater. Chem.*, 1993, **3**, 77 and references therein.
10 C. J. Warren, R. C. Haushalter, D. J. Rose and J. Zubieta, *Inorg. Chim. Acta*, 1998, **282**, 123 and references therein, J. T. Rijssenbeek, D. J. Rose, R. C. Haushalter and J. Zubieta, *Angew. Chem., Int. Ed. Engl.*, 1997, **36**, 1008; T. Yamase, M. Suzuki and K. Ohtaka, *J. Chem. Soc., Dalton Trans.*, 1997, 2463; C. J. Warren, D. J. Rose, R. C. Haushalter and J. Zubieta, *Inorg. Chem.*, 1998, **37**, 1140.
11 S. C. Sevov, *Angew. Chem., Int. Ed. Engl.*, 1996, **35**, 2630.
12 R. Kniep, H. G. Will, I. Boy and C. Rohr, *Angew. Chem., Int. Ed. Engl.*, 1997, **36**, 1013.
13 R. Kniep, G. Gozel, B. Eisenman, C. Rohr, M. Asbrand and M. Kizilyalli, *Angew. Chem., Int. Ed. Engl.*, 1994, **33**, 749.
14 K. Bluhm and C. H. Park, *Z. Naturforsch, Teil B*, 1997, **52**, 102.
15 R. P. Bontchev and S. C. Sovov, *Inorg. Chem.*, 1996, **35**, 6910.
16 Y. Shi, J. Liang, H. Zhang, W. Zhuang and G. Rao, *J. Solid State Chem.*, 1997, **129**, 45.
17 P. F. S. Grysta, G. H. Swihart, R. Dimitrievich and M. B. Hossain, *Am. Mineral*, 1991, **76**, 1400.
18 P. B. Moore and S. Ghose, *Am. Mineral*, 1971, **56**, 1527.
19 C. J. Warren, R. C. Haushalter, D. J. Rose and J. Zubieta, *Chem. Mater.*, 1997, **9**, 2649.
20 C. J. Warren, R. C. Haushalter, D. J. Rose and J. Zubieta, *Inorg. Chem. Commun.*, 1998, **1**, 4.
21 R. P. Bontchev, J. Do and A. J. Jacobson, *Inorg. Chem.*, 1999, **38**, 2231.
22 I. D. Brown and D. Altermatt, *Acta Crystallogr., Sect. B*, 1985, **41**, 244.

Communication 9/06668C

Chemically functionalised exfoliated graphite: a new bulk modified, renewable surface electrode

P. Ramesh and S. Sampath*

Department of Inorganic and Physical Chemistry, Indian Institute of Science, Bangalore 560 012, India. E-mail: sampath@ipc.iisc.ernet.in

Received (in Cambridge, UK) 2nd July 1999, Accepted 20th September 1999

Graphite particles are exfoliated and chemically functionalised to covalently attach electroactive molecules and subsequently pressed in the form of a pellet, without the use of a binder, to yield a bulk modified, renewable surface electrode material.

Research on the development and chemical modification of new electrode materials leading to improved catalytic and electroanalytical properties has received considerable attention in the last two decades.[1–14] Murray[1] has pioneered the area of chemically modified electrodes that includes modification of a variety of surfaces such as metals, metal oxides and to some extent carbon. Bulk modification of the material would lead to re-useable electrodes. Presently, the most popular bulk modified electrode is based on carbon paste. However, fouling and contamination of the surface and leaching of the modifier during operation pose significant hurdles in the long-term use of this material. Additionally, use of silicon oil as a binder leads to the deterioration of the material with time. Hence, it is pertinent to have covalently modified, renewable surface electrode materials based on inert binders that do not deteriorate with time. There have been a few attempts based on graphite–epoxy[12] and sol–gel silicate[9–11,13] matrices in this direction. It is very desirable to have the electrodes fabricated without any binder to have an unlimited storage and cycle life. Herein, we report, for the first time, the chemical functionalisation of exfoliated graphite particles and its use as a bulk modified, surface renewable electrode material. The electrodes are in the form of pressed pellets prepared without any binder.

Exfoliated graphite (EG) is an expanded graphite with low density and high temperature resistance.[14] The exfoliation of graphite is a process in which graphite expands by up to hundreds of times along the *c*-axis resulting in a puffed-up material. The compression of the EG results in a material of high lubricity and flexibility. The advantage of compression is that a high density porous substrate is formed with a surface area that is relatively high compared with other graphitic adsorbents.[15] Some of the demonstrated applications of this material include high temperature gaskets, seals, packings, thermal insulators, conductive resin composites, lubricant, catalyst supports and adsorption substrates.[14,16–18] Very few reports deal with the use of this material in electrochemical studies.[19–21]

Natural graphite of particle size 300–400 μm (Stratmin Graphite, USA) were soaked in a mixture of conc. H_2SO_4–HNO_3 (3:1, v/v) for 24 h. The material was then exfoliated by giving a thermal shock at 800 °C in air. The EG particles were treated with a mixture of conc. H_2SO_4–HNO_3 at *ca.* 100 °C for 4 h and the acid was later filtered off. The excess acid present on the material was neutralised with an alkali and the powder was subsequently washed with dilute HCl and excess distilled water. This oxidative pretreatment introduces and increases the number of oxygen containing functional groups on the EG surface. These functional groups thus introduced on to the graphite particles were reduced using $NaBH_4$ in methanol. The resulting –CH_2OH and –OH groups were attached to AQ or Fc using anthraquinone carboxylic acid or ferrocene acetic acid and *N*,*N*′-dicyclohexylcarbodiimide as a coupling agent. Soxhlet extraction with methanol for a prolonged period was carried out to make certain that the material does not contain any physisorbed reactants.

The graphite particles were chemically characterized at every stage by XRD, IR, XPS, elemental analysis and the morphology was followed by SEM. Electrochemistry was carried out using pellets pressed without the use of any binder. Fig. 1 shows the cyclic voltammograms obtained with anthraquinone modified EG electrode. The peak potentials are well defined and the value of ΔE_p ($E_p^c - E_p^a$) varies with the scan rate. The control voltammogram using EG electrode without the electroactive component does not show any redox activity as expected (Fig. 1, inset). The redox peak currents vary linearly with the scan rate showing that the redox species is bound to the surface of the electrode (Fig. 2). However, there is a tendency for the peak currents to saturate at higher scan rates (above 120 mV s^{-1}) which may be due to the proton transport limitation to the bound electroactive species. Additional experiments in buffers of different pH also confirm this. The formal redox potential varies with the solution pH and the slope of the linear plot corresponds to 59 mV $decade^{-1}$ thus confirming that the process involves $2e^-$ and $2H^+$ as expected. The surface coverage was measured by integrating the area under the peak and was found to be 1.2 $\times 10^{-9}$ mol cm^{-2}. This value, however, is only a representative figure since the real surface area is different (owing to roughness created by the emery sheet) from the geometric area used for the calculation. The surface roughness is found to play a major role in the functionalisation and in turn the electroactivity of the modified material. Modified electrodes with smooth surfaces do not give rise to any peaks while an increase in surface roughness leads to better definition of the peaks. The cyclic voltammograms in Fig. 1 has roughness created using a 400 grit SiC paper. The SEM image (Fig. 3) shows the rough surface used in the present study. It is clear that roughening the surface results in an increase in the ratio of edge to basal planes. This points to the fact that the edge planes of the graphite are

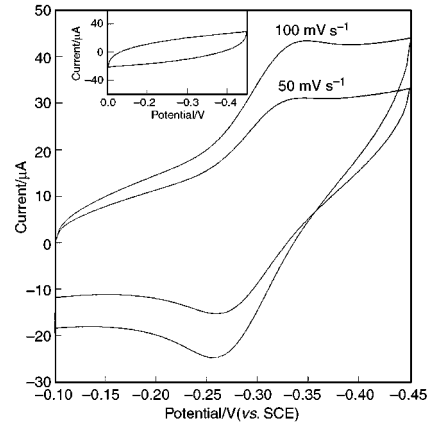

Fig. 1 Cyclic voltammograms of AQ modified EG electrode in acetate buffer, pH 3.5, at two different scan rates. The geometric area of the electrode is 0.08 cm^2. Inset: control cyclic voltammogram of the EG electrode prepared without AQ at a scan rate of 50 mV s^{-1}. Other conditions are as above.

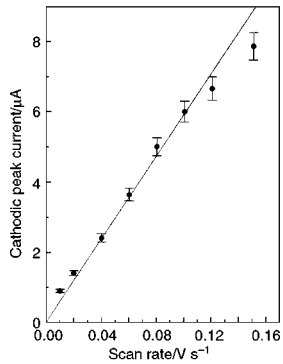

Fig. 2 Plot of reduction peak current *vs.* scan rate for AQ modified electrode in phosphate buffer, pH 7.

those that are functionalised with the redox moiety and are hence electrochemically active.

The bulk modification of the EG leads to reproducible electrochemical data. Mechanical polishing of the electrode exposes a new surface and different surfaces give rise to cyclic voltammograms that are very similar. The standard deviation in the peak currents for four successive polishings was < 5%. The fact that the quinone is chemically attached to the matrix and not physically adsorbed was confirmed by the following: non-modified EG particles were intentionally adsorbed with anthraquinone carboxylic acid and the resulting modified material was subjected to electrochemical measurements. Cyclic voltammograms show that the reduction of the adsorbed quinone occurs at −0.385 V while the chemically bonded quinone is reduced at −0.325 V at a scan rate of 10 mV s^{-1}. The difference in reduction peak potentials is expected to be due to combined effects of physical adsorption and the presence of $–CO_2H$ group for the physisorbed material compared to the chemically functionalised EG. Second, the change in the reduction peak potentials with scan rate is much larger for the physisorbed quinone (120 mV for a change from 10 to 100 mV s^{-1}) than the chemically bound (30 mV for the same range) moiety. This reveals that the electrochemical reduction kinetics and the reversibility of the physisorbed quinone is sluggish compared to the chemically bound AQ. Third, quinones are known to get physically adsorbed on to the basal as well as edge planes and hence the voltammograms on the smooth surfaces (basal planes) are expected to show electrochemical activity.[22] Indeed, this is observed with the physisorbed quinone modified electrode. The chemically functionalised EG material did not show any activity on smooth surfaces and this again confirms the modification on the edge plane surfaces as revealed by the cyclic voltammograms.

The chemical modification is also confirmed by IR measurements. The IR spectrum of the unmodified graphite particles show the presence of phenolic and alcoholic –OH groups on the surface as confirmed by the XPS C 1s spectrum. Treatment with a conc. H_2SO_4–HNO_3 mixture is expected to result in the formation of graphite oxide in addition to other oxygen containing functional groups.[23] Experiments using various techniques have established that graphite oxide contains different amounts of tertiary C–OH groups, ether C–O–C groups, > C=O < double bonds as well as enol and ketone

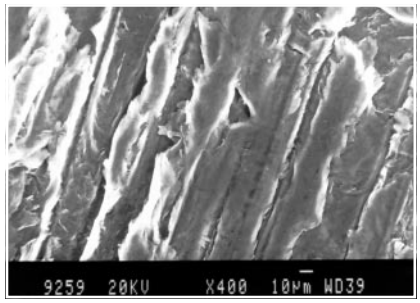

Fig. 3 SEM image of a rough EG electrode. Roughness created using 400 grit SiC paper.

groups.[24] On $NaBH_4$ treatment, the functional groups that are formed on the EG particles, are reduced to –OH and $–CH_2OH$ groups. Subsequent attachment of AQ or Fc through the –OH and $–CH_2OH$ groups on the graphite would result in linkages of the type –COC(=O)AQ/Fc. Hence, the IR of the modified surface is expected to contain carbonyl functionalities from the quinone and the other ester type functionalities as described above. Indeed, the IR spectrum of the modified surface reveals the presence of these functional groups at *ca.* 1700 cm^{-1} for carbonyl and at *ca.* 1200 cm^{-1} for the CC(=O)–O stretch; the reduction in frequency for the latter is due to the conjugation of the phenyl ring. The modification is also confirmed by X-ray photoelectron spectroscopic studies. The deconvoluted C 1s spectrum of EG indicates the presence of graphitic, phenolic and carboxylic functional groups in the ratio of 77 : 4.4 : 18.7 while the AQ modified EG is found to contain graphitic, phenolic, carboxylic and, in addition, carbonyl functional groups in the ratio of 70.7 : 7.5 : 11.1 : 11.8. The presence of *ca.* 12% of carbonyl groups is a clear indication of the modification of EG by AQ. The ferrocene modified EG electrode shows a similar behaviour.

The exfoliated material is easy to prepare and is amenable to chemical modification. As demonstrated here, the electrode can be fabricated without the use of any binder, which is very advantageous. The electron transfer rate, however, increases with increasing number of edge sites. Detailed comparative studies on exfoliated graphite, modified exfoliated graphite, carbon paste and glassy carbon will be reported in due course.

We wish to acknowledge the financial support (start-up funds for S. S.) of the IISc, Bangalore and the DST, New Delhi.

Notes and references

1 R. W. Murray, *Chemically Modified Electrodes in Electroanalytical Chemistry, A Series of Advances*, ed. A. J. Bard, Marcel Dekker, Inc., New York, USA, 1984, vol. 13.
2 J. Wang, A. Brennsteiner and A. P. Sylwester, *Anal. Chem.*, 1990, **62**, 1102.
3 P. R. Moses, L. Wier and R. W. Murray, *Anal. Chem.*, 1975, **47**, 1882.
4 R. M. Ianniello, H. J. Wieck and A. M. Yacynych, *Anal. Chem.*, 1983, **55**, 2067.
5 F. Meier, D. M. Giolando and J. R. Kirchhoff, *Chem. Commun.*, 1996, 2553.
6 J. E. Anderson, J. B. Montgomery and R. Yee, *Anal. Chem.*, 1991, **63**, 653.
7 B. E. Firth, L. L. Miller, M. Mitani, T. Rogers, J. Lennox and R. W. Murray, *J. Am. Chem. Soc.*, 1976, **98**, 8271.
8 B. E. Firth and L. L. Miller, *J. Am. Chem. Soc.*, 1976, **98**, 8272.
9 M. Tsionsky, G. Gun, V. Glezer and O. Lev, *Anal. Chem.*, 1994, **66**, 1747.
10 M. Tsionsky and O. Lev, *Anal. Chem.*, 1995, **67**, 2409.
11 G. Gun, M. Tsionsky and O. Lev, *Mater. Res. Symp. Proc.*, 1994, **346**, 1011.
12 J. Wang and K. Varughese, *Anal. Chem.*, 1990, **62**, 318.
13 A. Walcarius, *Electroanalysis*, 1998, **10**, 1217.
14 D. D. L. Chung, *J. Mater. Sci.*, 1987, **22**, 4190.
15 E. P. Gilbert, P. A. Reynolds and J. W. White, *J. Chem.Soc., Faraday Trans.*, 1998, **94**, 1861.
16 S. J. Gregg and K. S. W. Singh, in *Adsorption, Surface Area and Porosity*, Academic, London, 1982, p. 41.
17 C. Bockel, J. P. Coulomb and N. Dupont-Pavlovsky, *Surf. Sci.*, 1982, **116**, 369.
18 K.Ramanathan, D. Avnir, A. Modestov and O. Lev, *Chem. Mater.*, 1997, **9**, 2533.
19 C. A. Frysz and D. D. L. Chung, *Carbon*, 1997, **35**, 858.
20 Kao Corp., *Jpn. Kokai Tokkyo Koho*, JP 59 78 204, 1984; *Chem. Abstr.*, 1984, **101**, 131358z.
21 K. Fukuda, K. Kikuya, K. Isono and M. Yoshio, *J. Power Sources*, 1997, **69**, 165.
22 A. P. Brown and F. C. Anson, *Anal. Chem.*, 1977, **49**, 1589.
23 J. Zawadzki, *Infrared Spectroscopy in Surface Chemistry of Carbons*, in *Chemistry and Physics of Carbon*, ed. P. A. Thrower, Marcel Dekker, Inc., New York, USA, 1989, vol. 21, p. 207.
24 H. He, T. Riedl, A. Lerf and J. Klinowski, *J. Phys. Chem.*, 1996, **100**, 19954.

Communication 9/05355G

Synthesis and characterisation of *N*-(3-dihydroxyborylphenyl)-5-mercaptopentanamide: a novel self-assembling vicinal diol receptor

Karl D. Pavey,[a] Cedric J. Olliff,*[b] the late Jim Baker[b] and Frank Paul[a]

[a] *Novel Methods Group, CASS, SmithKline Beecham Pharmaceuticals, NFSP (North), Third Avenue, Harlow, Essex, UK CM19 5AW*

[b] *Department of Pharmacy and Biomolecular Science, Cockcroft Building, University of Brighton, Lewes Road, Brighton, East Sussex, UK BN2 4GJ. E-mail: cj01@brighton.ac.uk*

Received (in Oxford, UK) 9th August 1999, Accepted 27th September 1999

A novel self-assembling vicinal diol receptor, *N*-(3-dihydroxyborylphenyl)-5-mercaptopentanamide, has been synthesised *via* a three step procedure, characterised by NMR, mass spectoscopy and FTIR spectroscopy and shown to be functionally active by contact angle analysis, surface plasmon resonance and QCM.

The recent explosion in biosensor technology has led to the need for a greater variety of surface bound receptor systems. Thiol monolayer self-assembly is a technique of growing importance in many fields, particularly for the protection[1] or modification[2] of surfaces and the production of functionalised layers in sensor systems.[3–5]. The chemistry is versatile and robust, with a variety of headgroups attached to long-chain, thiol-terminated backbones. It has been suggested that the development of this technology may be hampered by a lack of new receptor systems.[6] Introduction of novel headgroup chemistry would continue to expand the uses of this technology. Here we report the synthesis of a new self-assembling vicinal diol receptor, based upon a thiol-modified boronic acid.

The interactions of sugars has been of interest to many with an increase in the use of boronic acids as receptors, however much of the work has taken place in free solution[7] or at air–water interfaces.[8] Boronic acids have long been known to interact with heavily hydroxylated species such as glycerol.[9] The semi-specific attachment point for vicinal diol groups, based upon the orientation of two adjacent hydroxy groups within a molecule, is covered in an excellent review by James *et al.*[10] Many saccharides contain hydroxy groups in the correct orientation and form stable cyclic esters when brought into contact with boronic acids.[11] Phenylboronic acids are known to form five-membered rings with *cis*-1,2-diol groups and less stable six-membered rings with the *trans*-isomer.[7] The synthesis of a self-assembling molecular layer capable of binding a wide variety of diol-containing moieties may open a route to producing a range of more specific multi-layer sensors.

Reaction of 3-aminophenylboronic acid **1** with 6-bromopentanoyl chloride in ethanolic solution (Scheme 1) yielded 3-(5-bromopentanoylamino)phenylboronic acid **2**. Further reaction with thiourea in methanolic solution over four days gave thioamidine **3**, which when treated with base prior to acidification was reduced to *N*-(3-dihydroxyborylphenyl)-5-mercaptopentanamide **4**.

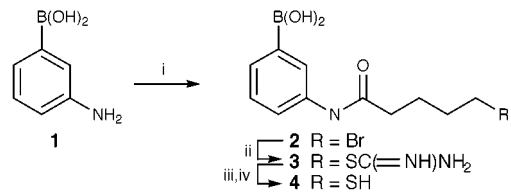

Scheme 1 *Reagents and conditions*: i, 6-bromopentanoyl chloride, $NaHCO_3$, H_2O–EtOH, 25 °C, 2 h, stirred; ii, thiourea, MeOH, 25 °C, 4 days, stirred under N_2; iii, NaOH, MeOH, 25 °C, 4 days, stirred under N_2; iv, HCl.

Analysis of **4** by ^{1}H NMR† spectroscopy showed that > 85% of the sample was the desired thiol boronic acid. A small amount of the 3-aminophenylboronic acid starting material was also present. Further characterisation by LC-MS‡ and FTIR§ analysis gave molecular weight and structural information supporting the NMR data (Table 1).

Table 1 FTIR data for **4**

Position/cm^{-1}	Transmittance (%)	Assignment
3322	4.20	B–OH
2934	41.7	CH_2
2361	79.0	CH_3 (Possible S–H)
1663	3.20	*meta* substituted aromatic
1538	5.70	CH_2–NH
1344	5.80	C–N

The self-assembly characteristics of **4** were investigated by several techniques. Time resolved, sessile drop contact angle measurements of 2 μl water droplets were recorded on 38 nm gold films evaporated onto polished microscope slides. Initial contact angles for water droplets of 64 ± 3° (N = 6) were noted. Upon exposure to a 1 mM ethanolic solution of **4** in a clean environment, the contact angle was observed to decrease with time to 37 ± 2° (N = 6) after 2.5 h (Fig. 1). This is indicative of the rapid self-assembly mechanisms observed in simple long chain thiols on gold surfaces[12] and strongly suggested that surface modification had taken place *via* the widely accepted thiol–gold self-adsorption route,[13] the boronic acid headgroups rendering the surface more hydrophilic.

Characterisation of the self-assembly in real time using a Kretschmann configuration surface plasmon resonance (SPR) instrument, also employing 38 nm gold films as the SPR substrate, gave a 0.31º dual rate increase in SPR angle upon a 2.5 h exposure, at a concentration of the compound in ethanolic solution equal to that used for the contact angle measurements.

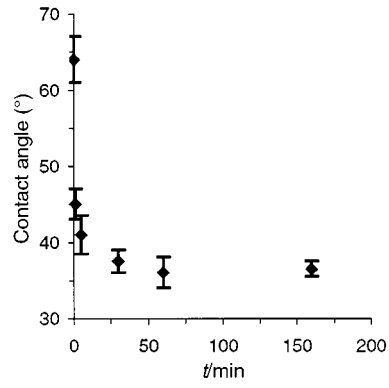

Fig. 1 Plot of sessile drop, water contact angle *vs.* time of immersion for a 38 nm gold coated microscope slide treated with a 1 mM ethanolic solution of **4** (droplet size 2 μl, T = 25 °C, N = 6 ± standard deviation).

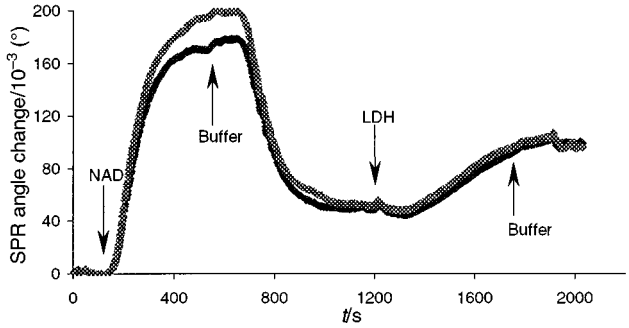

Fig. 2 SPR angle change for the binding of NAD (1 mg m^{-1}) to a gold substrate previously treated with **4** followed by lactate dehydrogenase (1×10^{-6} M) (flow rate = 4 μl min^{-1}, T = 30 °C, pH 7.2 Sorensons PBS).

Increases in SPR angle equate to material attachment to the substrate surface. Non-linear regression using a four parameter, double exponential rise relationship to the SPR data gave R = 0.99 and rate constants, $K1 = 1.1 \times 10^{-3}$ s^{-1} and $K2 = 6.91 \times 10^{-3}$ s^{-1}.The value of the measured $K1$ is of the order found by Debono *et al.*,[14] (4.3×10^{-3} s^{-1}) with SPR for the adsorption of dodecanethiol from ethanolic solution at an equal concentration. These results follow the distinct two step adsorption process found by DeBono *et al.*[14] and Bain *et al.*[12] The results show a very fast initial step lasting a few minutes giving rise to an 80–90% monolayer coverage, followed by a slower step lasting between minutes and hours depending upon the structure of the thiol, in which time the monolayer reorganises and completes its formation.

A similar two stage adsorption profile was observed upon the exposure of a 10 MHz lapped quartz crystal, thickness shear mode sensor with gold electrodes to a 1 mM ethanolic solution of the compound. A total frequency decrease of 126 Hz was recorded over an 8 h period for a single electrode in contact with the solution. The increased time required for the adsorption process to reach equilibrium is thought to be due to surface roughness; 2–3 μm troughs are found in the lapped crystal surface compared to the sub-micron polished surface used for SPR analysis.

Surface functionality of the adsorbed boronic acid SAM was further confirmed by contact angle and SPR experiments. Gold coated slides, previously exposed to the monolayer forming solution, with contact angles measuring 37 ± 2° (N = 6), were placed in a 1 mg ml^{-1} solution of nicotinamide adenine dinucleotide (NAD) in Sorenson's buffer, pH 7.2. Following a 15 min incubation at 30 °C the slides were removed, washed with further buffer, dried and the water contact angle measured as described previously. A further decrease in angle was recorded [27 ± 1.0° (N = 6)], suggesting that binding of the NAD to the surface may have occurred.

Real time analysis of NAD binding (Fig. 2) was carried out using SPR. NAD (1 mg ml^{-1}) in a buffer stream was passed over a boronic acid treated gold slide (4 μl s^{-1}). A residual SPR angle increase of 40 ± 2 millidegrees, (N = 3) verified that NAD had bound to the boronic acid layer. A similar profile was observed for lactose and maltose with SPR angle increases of 32 ± 3 (N = 3) and 24 ± 2° (N = 3) respectively. No residual change in SPR angle was observed when untreated gold surfaces were similarly challenged.

After treatment of the SPR slides with NAD, injections of lactate dehydrogenase (1×10^{-6}M, LDH), followed by a buffer wash were made. Fig. 2 shows strong binding to the NAD treated slides, with a residual SPR angle increase of 47 ± 3° (N = 3) and very little evidence of desorption. No overall change in SPR angle was observed for injection of LDH if the NAD was not present. This would support the binding of NAD *via* its diol groups to the surface, leaving the binding regions, at the adenine and nicotinamide units, available for LDH and a range of other dehydrogenases.[15]

In summary, this report describes a novel self-assembling boronic acid derivative with the potential to specifically interact with vicinal diol groups found within a range of nucleotides, saccharides, antibiotics and other systems. It has been shown that with a clean environment, formation of a correctly orientated layer on the surface is achieved and that vicinal diol containing species attach strongly only to the modified surface. Further, enzyme–cofactor binding has been demonstrated as part of a multilayer system, potentially opening new avenues for enzyme studies, *via* a relatively simple attachment route, applicable to a range of novel analysis tools such as SPR and QCM.

The authors wish to dedicate this paper to the memory of Dr Jim Baker who passed away prior to submission. We thank the EPSRC and SmithKline Beecham for financial support under the CASE award scheme, Award #G77.

Notes and references

† *Selected data* for **4**: δ_H[250 MHz, $CDCl_3$–DMSO-d_6 (1:1)]1.3 (CH_3CO_2H), 2.1, 2.3, 2.5 (CH_2), 3.0 (H_2O), 2.6, 3.4 (CH_2S), 7.1, 7.4, 7.6 (dd, C*H* aromatic), 9.0 (N*H*), 9.1 (CH_3CO_2H).

‡ LC/MS (Finnigan LCQ) yielded a single species of *m/z* (H^+) 254.300 at a retention time of 15.61 min comparable to the calculated mass of 254.101 ($C_{11}H_{16}BNO_3S$).

§ FTIR analysis on a Perkin-Elmer 1720 spectrophotometer, resolution 4 cm^{-1}, 20 scans.

1 L. Deng, M. Mrksich and G. Whitesides, *J. Am. Chem. Soc.*, 1996, **118**, 5136.
2 A. Ulman, *Chem. Rev.*, 1996, **96**, 1533 and references cited therin.
3 N. Nakashima and T. Taguchi, *Colloids Surf.*, 1995, **103**, 159.
4 K. T. Kinnear and H. G. Monbouquette, in *Biosensor and chemical sensor technology*, ACS, Washington, 1995, p. 82.
5 S. Storri, T. Santoni, M. Minunni and M. Mascini, *Biosens. Bioelectron.*, 1998, **13**, 347.
6 J. A. Riggs, R. K. Litchfield and B. D. Smith, *J. Org. Chem.*, 1996, **61**, 1148.
7 T. James, K. R. A. Samankumara Sansanayake and S. Shinkai, *Nature*, 1995, **374**, 345.
8 S. Shinkai, K. Tsukagoshi, Y. Ishikawa and T. Kunitake, *J. Chem. Soc., Chem. Commun.*, 1991, **15**, 1039.
9 L. Vignon, *Compt. Rend.*, 1874, **78**, 148.
10 T. D. James, K. R. A. Samankumara Sansanayake and S. Shinkai, *Angew. Chem., Int. Ed. Engl.*, 1996, **35**, 1910.
11 T. Kuivila, *J. Org. Chem.*, 1954, **19**, 780.
12 C. D. Bain, E. B. Troughton, T. Y. Tao, J. Evall, G. M. Whitesides and R. G. Nuzzo, *J. Am. Chem. Soc.*, 1989, **111**, 321.
13 A. L. Plant, M. Brigham-Burke, E. C. Petrella and D. J. O'Shannessy, *Anal. Biochem.*, 1995, **226**, 342.
14 R. F. Debono, G. D. Loucks, D. D. Manna and U. J. Krull, *Can. J. Chem.*, 1996, **74**, 677.
15 L. Stryer, *Biochemistry*, 4th edn., W. H. Freeman, New York, 1995, p. 498.

Communication 9/06542C

ChemComm

A novel chlorotris(triphenylphosphine)rhodium(I) mediated intramolecular C–C bond forming reaction

P. John Biju and G. S. R. Subba Rao*

Department of Organic Chemistry, Indian Institute of Science, Bangalore 560 012, India.
E-mail: gsrs@orgchem.iisc.ernet.in

Received (in Cambridge, UK) 25th August 1999, Accepted 5th October 1999

A novel Wilkinson's catalyst-mediated carbon–carbon bond forming reaction is described which is exemplified by the synthesis of the polycyclic compounds 14 and 18 from the keto aldehydes 13 and 17.

Transition metal mediated reactions leading to the formation or rupture of the C–H and C–C bonds of organic substrates constitute an area of research of wide importance.[1] In particular those involving C–H activation and decarbonylation of the CO(H) moiety of aldehydes are of considerable interest.[2] Chlorotris(triphenylphosphine)rhodium (I) (Wilkinson's catalyst) is a versatile catalyst for reactions such as hydrogenations,[3] hydrosilylations,[4] hydroformylations,[5] hydroborations,[6] isomerisations,[7] oxidations[8] and cross coupling reactions.[9] The stoichiometric homogeneous decarbonylation of aldehydes using Wilkinson's catalyst is a very useful synthetic transformation. It has been proved beyond doubt that decarbonylation of aldehydes by Wilkinson's catalyst proceeds *via* a stepwise mechanism[10] through an acyl rhodium hydride intermediate **1** and the alkyl rhodium hydride intermediate **2**.

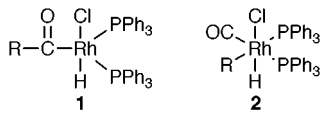

1 **2**

The potential utility of the acyl rhodium hydride intermediate **1** in a variety of reactions, such as hydroacylations (addition to olefins) and the synthesis of organocarbonyl complexes,[11] is currently being intensely studied. We anticipated that the acyl-rhodium hydride intermediate **3** might undergo an intramolecular C–C bond formation (Scheme 1) with suitable substrates having weakly acidic C–H bonds (*e.g.* $CO–CH_2$ or similar systems) *via* an intramolecular hydride migration from the substrate to the Rh metal and the migration of the CO–Rh bond to generate the corresponding 1,3-diketone **4**. We report herein for the first time Wilkinson's catalyst mediated intramolecular carbon–carbon bond formation in the synthesis of polycyclic ring systems.

The synthesis of the requisite substrate, the keto aldehyde **13**, is shown in Scheme 2. Alkylation of the known[12] ketone **6** with LDA/MeI afforded exclusively the ketone **7**, which upon treatment with LDA and 1,4-dibromo-2-methylbut-2-ene afforded the product **8** in good yield. Treatment of **8** with a catalytic amount of perchloric acid (70%) in CH_2Cl_2 furnished the hydroxy enone **9**, which was converted into the tricyclic hydroxy olefin **10** through 5-*exo-trig* allyl radical cyclization[13] *via* treatment with Bu_3SnH. Isomerisation of the olefin **10** was carried out with TsOH in refluxing benzene to afford the hydroxy ketone **11**. $NaBH_4$ borohydride reduction of **11** furnished the 1,2-diol **12**, which was cleaved with periodic acid to the keto aldehyde **13** in quantitative yield.†

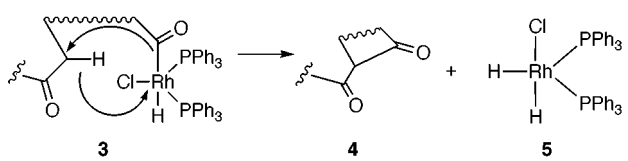

3 **4** **5**

Scheme 1

Treatment of the keto aldehyde **13** with a stoichiometric amount of chlorotris(triphenylphosphine)rhodium(I) in PhCN at 160 °C for 1.5 h afforded the expected 1,3-diketone **14** in 75% yield, whose structure was deduced from its spectral characteristics.† The formation of **14** can be only explained through the acyl rhodium hydride complex **16** of the keto aldehyde **13** (Scheme 3) through the intramolecular hydride transfer mechanism (Scheme 1). An alternative mechanism‡ involving a rhodium(I) catalyzed reversible aldol condensation, followed by the dehydrogenation of the resulting ketol leading to the formation of the product **14**, cannot be ruled out at this stage. This methodology constitutes, the first synthesis of a novel

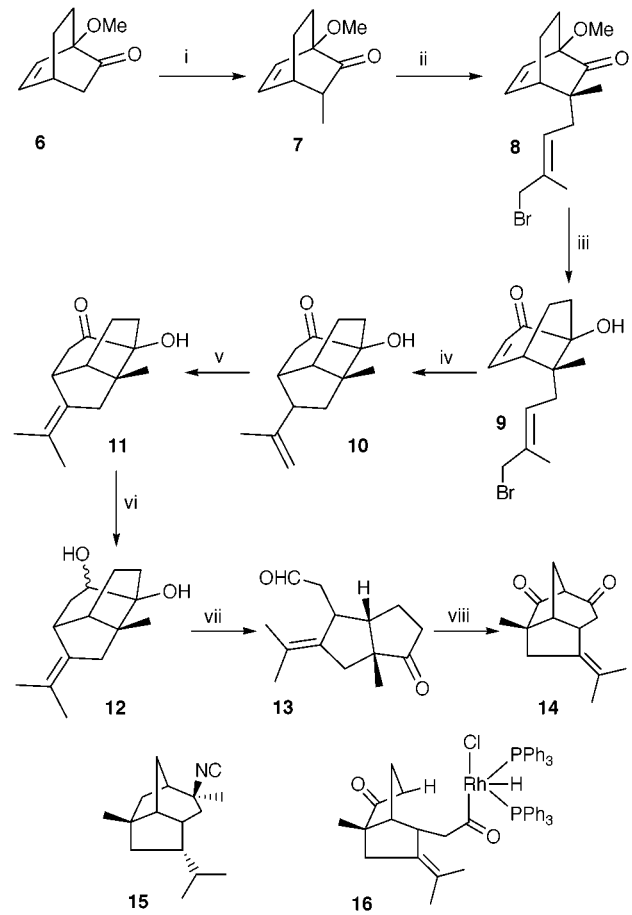

Scheme 2 *Reagents and conditions*: i, LDA, THF, MeI, −78 °C (89%); ii, LDA, THF, HMPA, 1,4-dibromo-2-methylbut-2-ene, −78 °C (76%); iii, $HClO_4$ (cat), CH_2Cl_2, 0.5 h, (76%); iv, Bu_3SnH, AIBN, C_6H_6, reflux, 6 h (80%); v, TsOH, C_6H_6, reflux, 45 min (89%); vi, $NaBH_4$, MeOH, 0 °C (94%); vii, HIO_4, EtOH–H_2O (4:1) (100%); viii, Wilkinson's Catalyst (1 equiv.), PhCN, reflux, 1.5 h (75%).

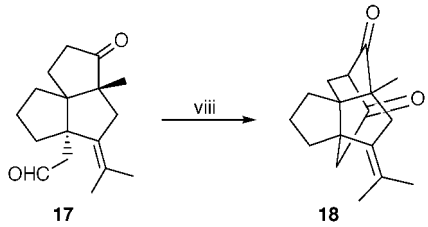

Scheme 3

tricyclo[5.2.1.0^{4,8}]decane derivative, the norallopupukeanane-2,10-dione **14**, and can be used for the synthesis of the natural product 2-isocyanoallopupukeanane[14] **15**. Thus Wilkinson's catalyst can be used in catalytic amounts since the rhodium dihydride species **5** easily eliminates one molecule of hydrogen under the reaction conditions leading to the active catalyst species, the chlorobis(triphenylphosphine)rhodium(I) complex, which is recycled.

Similarly the angular triquinic keto aldehyde[15] **17** is transformed into the tetracyclic 1,3-diketone **18** by treatment with Wilkinson's catalyst under the same conditions in 72% yield.† This reaction is a novel and elegant methodology for the construction of complex polycyclic 1,3-diketones from the corresponding keto aldehydes. In both the examples the anticipated decarbonylation of the aldehyde group did not occur. The scope and limitations of this reaction in the synthesis of cyclic systems is currently under investigation.

Notes and references

† *Selected data* for **13**: ν_{max}/cm^{-1} 2930, 2720, 1730 and 1705; δ_H(300 MHz, $CDCl_3$) 1.16 (3H, s, Me), 1.65 (3H, s, Me), 1.66 (3H, s, Me), 1.70–2.50 (7H, m), 2.56 (1H, dd *J* 6.6, 15.0, C*H*CO), 2.86 (1H, d *J* 15.6, allylic), 3.11–3.19 (1H, m, H_2), 9.80 (1H, s, C*H*O); δ_C(75 MHz, $CDCl_3$) 20.6 (CH_3), 21.5 (CH_3), 22.0 (CH_3), 22.3 (CH_2), 36.1 (CH_2), 38.1 (CH_2), 39.1 (CH), 42.2 (CH_2), 47.4 (CH), 55.2 (C), 125.5 (C), 134.7 (C), 205.6 (CH) and 212.4 (C); *m/z* 220 (M^+, 46.5%), 202 (25), 192 (68), 177 (54), 149 (52), 133 (100), 119 (73), 105 (65) and 91 (70). For **14**: ν_{max}/cm^{-1}2950, 1740 and 1710; δ_H(300 MHz, $CDCl_3$) 1.15 (3H, s, Me), 1.48 (3H, s, Me), 1.55 (3H, s, Me), 2.13–2.33 (4H, m), 2.55 (1H, d, *J* 17.4, H_6), 2.72–2.78 (2H, m, H_6, H_3), 3.29–3.90 (2H, m, H_1, H_4); δ_C(75 MHz, $CDCl_3$) 20.8 (CH_3), 21.2 (CH_3), 21.4 (CH_3), 25.9 (CH_2), 38.5 (CH), 41.1 (CH_2), 42.9 (CH_2), 47.7 (CH), 55.9 (C), 66.4 (CH), 126.2 (C), 136.4 (C), 202.9 (C) and 214.8 (C); *m/z* 218 (M^+, 19%), 190 (28), 135 (29), 121 (55), 120 (100), 105 (25) and 55 (34). For **17**: ν_{max}/cm^{-1} 2910, 2700, 1735 and 1710; δ_H(300 MHz, $CDCl_3$) 1.18 (3H, s, Me), 1.65 (3H, s, Me), 1.72 (3H, s, Me), 1.50–2.30 (11H, m), 2.40 (1H, d *J* 15.3, allylic), 2.80 (1H, d *J* 15.3, allylic), 2.83 (1H, m, C*H*CO), 9.78 (1H, s, C*H*O); *m/z* 260 (M^+, 22%), 244 (54), 232 (55), 217 (29), 189 (60), 173 (62), 161 (100), 147 (66) and 105 (43). For **18**: ν_{max}/cm^{-1} 2960, 1740 and 1700; δ_H(300 MHz, $CDCl_3$) 1.11 (3H, s, Me), 1.52 (3H, s, Me), 1.66 (3H, s, Me), 1.70–1.85 (3H, m), 1.90–2.26 (5H, m), 2.26 (1H, d, *J* 12.9), 2.60 (1H, d, *J* 16.8, allylic), 2.63 (1H, d, *J* 16.8, C*H*CO), 2.93 (1H, d, *J* 16.8, allylic), 3.3 (1H, d, *J* 4.2, bridgehead *H*); δ_C(75, $CDCl_3$) 17.4 (CH_3), 20.7 (CH_3), 22.6 (CH_3), 26.2 (CH_2), 31.6 (CH_2), 32.7 (CH_2), 41.2 (CH_2), 44.4 (CH_2), 49.4 (CH_2), 54.2 (C), 55.6 (C), 62.6 (C), 65.7 (CH), 125.8 (C), 139.3 (C), 202.6 (C) and 214.5 (C); *m/z* 258 (M^+, 14%), 230 (16), 215 (5), 160 (100), 145 (23), 131 (8) and 105 (8).

‡ We thank the referee for this suggestion

1 A. D. Ryabov, *Chem. Rev.*, 1990, **90**, 403; B. A. Arndsten, R. G. Bergman, T. A. Mobley and T. H. Peterson, *Acc. Chem. Res.*, 1995, **28**, 154; B. M. Trost, *Angew. Chem., Int. Ed. Engl.*, 1995, **34**, 259.

2 F. Abu-Hasanayan, M. E. Goldman and A. S. Goldman, *J. Am. Chem. Soc.*, 1992, **114**, 2520; G. Dyker, *Angew. Chem., Int. Ed.*, 1999, **38**, 1698; B. Rybtchinski and D. Milstein, *Angew. Chem., Int. Ed.*, 1999, **38**, 870.

3 A. J. Birch and K. A. M. Walker, *J. Chem. Soc. C*, 1966, 1894; P.-E. Sum and L. Weiler, *Can. J. Chem.*, 1978, **56**, 2700.

4 J. L. Speier, *Adv. Organomet. Chem.*, 1979, **17**, 407; I. Ojima, in *The Chemistry of Organic Silicon Compounds*. ed. S. Patai and Z. Rappoport, Wiley, New York, 1989, vol. **2**, p. 1479.

5 R. L. Pruett, *Adv. Organomet. Chem.*, 1979, **17**, 1; F. H. Jardine, *Polyhedron*, 1982, **1**, 569.

6 K. Burgess, W. A. van der Donk, S. A. Westcott, T. B. Marder, R. T. Baker and J. C. Calabrese, *J. Am. Chem. Soc.*, 1992, **114**, 9350.

7 F. N. Jones and R. V. Lindsey, *J. Org. Chem.*, 1968, **33**, 3838; A. J. Birch and G. S. R. Subba Rao, *Tetrahedron Lett.*, 1968, 3797.

8 H. Bonnemann, W. Nunez and D. M. M. Robe, *Helv. Chim. Acta*, 1983, **66**, 177; P. A. Harland and P. Hodge, *Synthesis*, 1983, 419; A. J. Birch and G. S. R. Subba Rao, *Tetrahedron Lett.*, 1968, 2817.

9 R. Grigg, P. Stevenson and T. Worakun, *J. Chem. Soc., Chem. Commun.*, 1984, 1073; R. C. Larock, K. Narayanan and S. S. Hershberger, *J. Org. Chem.*, 1983, **48**, 4377.

10 K. Ohno and J. Tsuji, *J. Am. Chem. Soc.*, 1968, **90**, 99; M. C. Baird, C. J. Nyman and G. Wilkinson, *J. Chem. Soc. A*, 1968, 348.

11. K. Sakai, J. Ide, O. Oda and N. Nakamura, *Tetrahedron Lett.*, 1972, 1287; K. Sakai, Y. Ishiguro, K. Funakoshi, K. Uneo and H. Suemune, *Tetrahedron Lett.*, 1984, **25**, 961; R. W. Barnhart, D. A. McMorran and B. Bosnich, *Chem. Commun.*, 1997, 589; J. W. Suggs, *J. Am. Chem. Soc.*, 1978, **100**, 640.

12 D. A. Evans, W. L. Scott and L. K. Truesdale, *Tetrahedron Lett.*, 1972, 121.

13 K. Kaliappan and G. S. R. Subba Rao, *J. Chem. Soc., Perkin Trans. 1*, 1997, 3393; K. Kaliappan and G. S. R. Subba Rao, *Chem. Commun.*, 1996, 2331.

14 N. Fusetani, H. J. Wolstenholme and S. Matsunga, *Tetrahedron Lett.*, 1991, 7291.

15 The compound **17** was prepared from the known ketone 7-methoxy-tricyclo[5.2.2.0^{1,5}]undec-8-one (ref. 16), by using the same reaction sequence as for the synthesis of the compound **13**; P. J. Biju, PhD thesis, Indian Institute of Science, 1999.

16 H. K. Hariprakasha and G. S. R. Subba Rao, *Tetrahedron Lett.*, 1997, 38, 5343.

Communication 9/06904F

Porphodimethene–porphyrinogen relationship: the generation of unprecedented forms of porphyrinogen†

Lucia Bonomo,[a] Euro Solari,[a] Rosario Scopelliti,[a] Mario Latronico[b] and Carlo Floriani*[a]

[a] *Institut de Chimie Minérale et Analytique, BCH, Université de Lausanne, CH-1015 Lausanne, Switzerland. E-mail: carlo.floriani@icma.unil.ch*

[b] *Dipartimento di Ingegneria e Fisica dell'Ambiente, Università della Basilicata, I-85100 Potenza, Italy*

Received (in Cambridge, UK) 23rd August 1999, Accepted 17th September 1999

The electrophilic reactivity of the porphodimethene skeleton towards nucleophiles led the establishment of a synthetic methodology to unprecedented forms of porphyrinogen containing the vinylidene substituents as well as other functionalities in the *meso*-positions

The intermediacy of porphodimethenes[1,2] in the oxidation of porphyrinogen to porphyrin is well accepted. Work on the chemistry of the porphodimethene skeleton[3] has suffered, however, for a long time from the absence of a real synthetic methodology, which is now available[4] for exploring its reactivity. Porphodimethenes are the target molecules of this report, since they allow one to enter the field of unprecedented forms of porphyrinogen. The latter compounds have been obtained studying the reactivity of lithium and nickel hexaethylporphodimethenes (5,15-diethyl-*meso*-tetraethylporphyrin) towards nucleophiles. The synthetic sequences are displayed in Schemes 1 and 2.

Complex **1**[4] underwent a stepwise deprotonation by $LiNMe_2$ to the monovinylidene porphomethene complex **2**,[5] containing a trianionic tetrapyrrolic derivative, which undergoes further deprotonation to the bisvinylidene porphyrinogen Ni derivative **3**. Both complexes **2** and **3** can be protonated back to the starting material by employing PyHCl.

The stepwise deprotonation of **1** to **3** requires the preliminary attack of a nucleophile, *i.e.* $[NMe_2]^-$, at the mono-substituted *meso*-position of **1**. Such a pathway is supported by the reactivity of **1** with nucleophiles other than $[NMe_2]^-$, namely LiBu, $LiHBEt_3$ and $LiCH_2CN$, and by the reactions in Scheme 2, leading to *meso*-functionalized octaalkylporphyrinogens.[6] Compounds **2** and **3** have been fully characterized including the X-ray analysis of **3**. The ^1H NMR of **3** revealed the presence of an equimolar mixture of the two possible isomers with two quartets and two doublets of equal intensity for the vinylidene groups and eight doublets for the β-protons to the pyrroles. This spectroscopic analysis has been confirmed with an X-ray structure revealing a statistical distribution of the Me and H groups around the vinylidene carbon, although not in the same ratio observed in solution. We should draw attention to the structural similarity of **3** with the 5,15-dioxoporphyrinogen.[7]

The structure of the anionic moiety of **3** is displayed in Fig. 1, with a selection of the structural parameters which support the proposed bonding scheme.‡ The presence of two *meso*-sp^3 carbons gives rise to a saddle shape conformation of the porphyrinogen with nickel 0.011(3) Å above the N_4 plane. A relevant structural feature is the two short Ni–H contacts [Ni1···H15A and Ni1···H15A′ 2.92 Å (prime denotes a symmetry operation $-x, y, -z + 1/2$)] with two *meso*-ethyl groups from the same face of the N_4 coordination plane.

Complex **3** contains a novel form of porphyrinogen, which may have considerable synthetic potential and may be available either from the demetalation or the transmetalation of **3**. We

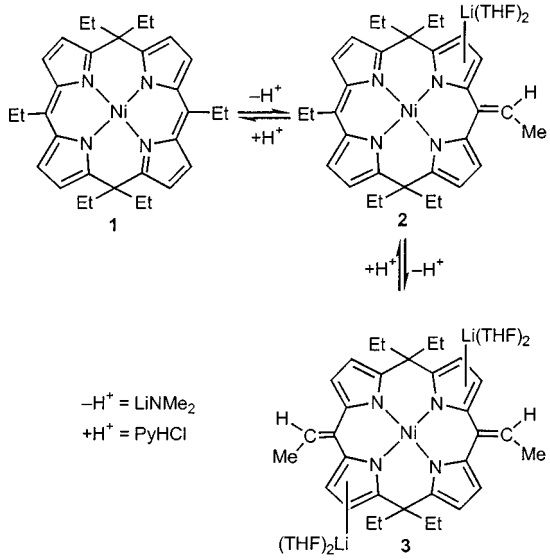

Scheme 1

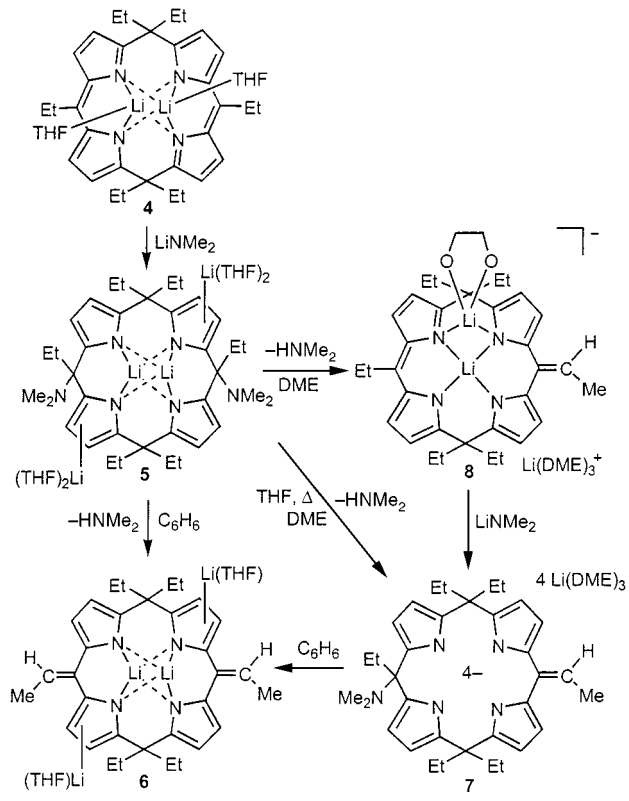

Scheme 2

† Syntheses of complexes **2**, **3**, **5**, **6**, **7** and **8**, and complete ORTEP drawings of **3** and **7**, are available from the RSC web site, see http://www.rsc.org/suppdata/cc/1999/2227/

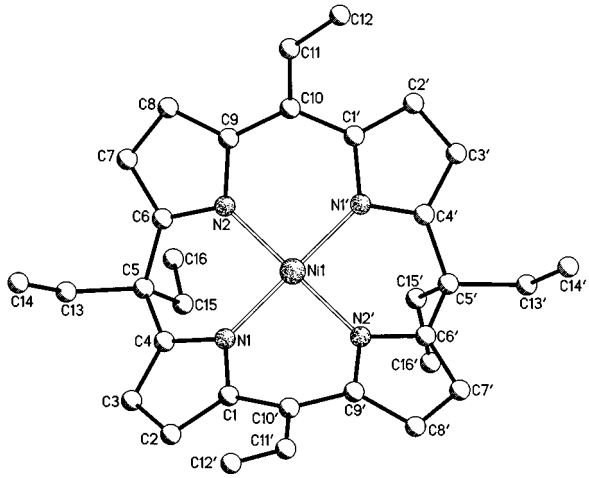

Fig. 1 A plot of the dianion of **3** [hydrogen atoms, $Li(DME)_3^+$ cations and disorder have been omitted for clairty]. Selected bond distances (Å): Nil–N_{av} 1.887(4) C10–C11 1.32(1). Prime indicates the following symmetry operation: $-x, y, \frac{1}{2}-z$.

found, however, a better access to the bisvinylidene porphyrinogen tetraanion bonded to Ni^{II} in **3** from the direct deprotonation of the *meso*-hexaethylporphodimethene dilithium derivative **4**[4] (see Scheme 2).

In addition, such a reaction shed light on the deprotonation mechanism of the porphodimethene skeleton as a function of the metal and the reaction solvent. The addition of $LiNMe_2$ to **4**, regardless of the solvent (THF, DME or benzene), led to the formation of the bisdimethylamino porphyrinogen **5**, which upon heating underwent $HNMe_2$ elimination to give different porphyrinogen derivatives according to the solvent, namely to **6** in benzene, **7** in THF, and **8** in DME. Scheme 2 displays also the relationship between **6**, **7** and (preliminarily) **8**.[5] Compounds in Scheme 2 have all been isolated and characterized. The X-ray structure is reported only for **7**. Those two structures, along with that of **3**, give the complete picture of the vinylidene porphyrinogen derivatives. The structure of the ion pair form of **7** is shown in Fig. 2 with some structural parameters which support the proposed bonding scheme.‡ In the absence of a transition metal ion, the porphyrinogen skeleton does not display any well-defined conformation and **7** occurs either in the ion-separated or in the ion-pair form[8] (Fig. 2). Lithium cations show different geometry: Li1 has a quasi-square planar

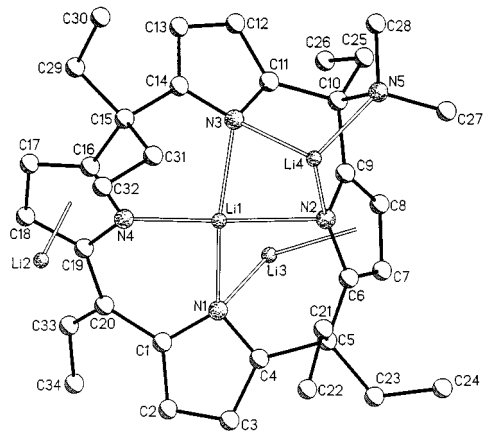

Fig. 2 A view of compound **7** (hydrogen atoms, DME and disorder have been omitted for clarity). Selected bond distances (Å): Li1–N1 2.050(6), Li1–N2 2.206(6), Li1–N3 2.136(6), Li1–N4 1.984(6), Li2–η^5(Pyr) 1.904(6), Li3–η^5(Pyr) 2.183(6), Li3–N1 2.110(7), Li4–N2 2.057(6), Li4–N3 2.070(6), Li4–N5 2.123(6), C30–C33 1.347(5), C10–N5 1.543(4). η^5(Pyr) indicates the centroid.

arrangement [out-of-plane of 0.160(5) Å from the N_4 core], Li2 is η^5-linked to one pyrrolyl moiety, Li3 links one nitrogen atom (N1) and is also η^5-bonded to one pyrrole, while Li4 lies in between two pyrroles and is bonded to the nitrogen of the NMe_2 group. Each lithium cation (except Li1) competes its coordination sphere with DME.

The procedures reported here should be applicable to the synthesis of novel forms of porphyrinogen and functionalization of the *meso*-positions using the reactivity of the porphodimethene skeleton towards nucleophiles, in the case of both the transition metal and the lithium derivatives. Furthermore, the lithiated forms are of direct use for the synthesis of a variety of transition metal derivatives.

Notes and references

‡ *Crystal data* for **3**: $C_{32}H_{36}N_4Ni\cdot2(C_{12}H_{30}LiO_6)$, M = 1089.96, monoclinic, space group $C2/c$, a = 12.269(3), b = 19.417(4), c = 26.192(5) Å, β = 103.49(3)°, V = 6067(2) Å^3, Z = 4, D_c = 1.193 g cm^{-3}, $F(000)$ = 2360, λ (Mo-Kα) = 0.71070 Å, μ = 0.379 mm^{-1}; crystal dimensions 0.18 × 0.15 × 0.10. For 2120 observed reflections [$I > 2\sigma(I)$] and 351 parameters, the conventional R is 0.0689 ($wR2$ = 0.2153 for 3664 independent reflections). For **7**: $C_{46}H_{73}Li_4N_5O_6$, M = 819.85, monoclinic, space group $P2_1/n$, a = 11.755(2), b = 20.644(4), c = 19.117(4) Å, β = 95.22(3)°, V = 4619.9(16) Å^3, Z = 4, D_c = 1.179 g cm^{-3}, $F(000)$ = 1776, λ (Mo-Kα) = 0.71070 Å, μ = 0.076 mm^{-1}; crystal dimensions 0.17 × 0.15 × 0.13. For 4735 observed reflections [$I > 2\sigma(I)$] and 561 parameters, the conventional R is 0.0789 ($wR2$ = 0.2481 for 7078 independent reflections). For both compounds the diffraction data were collected on a mar345 Imaging Plate at 143 K. The structures were solved with direct methods and refined using the full-matrix least-squares on F^2 with all non-H atoms anisotropically defined. CCDC 182/1416. See http://www.rsc.org/suppdata/cc/1999/2227/ for crystallographic data in .cif format.

1 D. Mauzerall and S. Granick, *J. Biol. Chem.*, 1958, **232**, 1141; R. B. Woodward, *Angew. Chem.*, 1960, **72**, 651; A. Treibs and H. Häberle, *Justus Liebigs Ann. Chem.*, 1968, **718**, 183; D. Dolphin, *J. Heterocycl. Chem.*, 1970, **7**, 275.

2 *The Porphyrins, Vol. I*, ed. D. Dolphin, Academic Press, New York, 1978, ch. 3; *The Porphyrins, Vol. II*, ed. D. Dolphin, Academic Press, New York, 1978, ch. 1 and 2; F.-P. Montforts, B. Gerlach and F. Höper, *Chem. Rev.*, 1994, **94**, 327.

3 A. Botulinski, J. W. Buchler and M. Wicholas, *Inorg. Chem.*, 1987, **26**, 1540; J. W. Buchler and L. Puppe, *Justus Liebigs Ann. Chem.*, 1970, **740**, 142; J. W. Buchler, K. L. Lay, P. D. Smith, W. R. Scheidt, G. A. Ruppzecht and J. E. Kenny, *J. Organomet. Chem.*, 1976, **110**, 109; J. W. Buchler, C. Dreher, K. L. Lay, Y. J. A. Lee and W. R. Scheidt, *Inorg. Chem.*, 1983, **22**, 888; J. W. Buchler, K. L. Lay, Y. J. A. Lee and W. R. Scheidt, *Angew. Chem., Int. Ed. Engl.*, 1982, **21**, 432; P. N. Dwyer, J. W. Buchler and W. R. Scheidt, *J. Am. Chem. Soc.*, 1974, **96**, 2789; D. Mauzerall, *J. Am. Chem. Soc.*, 1962, **84**, 2437; M. W. Renner and J. W. Buchler, *J. Phys. Chem.*, 1995, **99**, 8045; P. N. Dwyer, L. Puppe, J. W. Buchler and W. R. Scheidt, *Inorg. Chem.*, 1975, **14**, 1782; A. Botulinski, J. W. Buchler, Y. J. A. Lee and W. R. Scheidt, *Inorg. Chem.*, 1988, **27**, 927; A. Botulinski, J. W. Buchler, B. Tonn and M. Wicholas, *Inorg. Chem.*, 1985, **24**, 3239.

4 J.-M. Benech, L. Bonomo, E. Solari, R. Scopelliti and C. Floriani, *Angew. Chem., Int. Ed.*, 1999, **38**, 1957.

5 L. Bonomo, E. Solari, R. Scopelliti, M. Latronico and C. Floriani, unpublished results.

6 C. Floriani, *Pure Appl. Chem.*, 1996, **68**, 1 and references therein; C. Floriani, *Chem. Commun.*, 1996, 1257 (Feature Article) and references therein.

7 H. H. Inhoffen, J. H. Fuhrhop and F. von der Haar, *Justus Liebigs Ann. Chem.*, 1966, **700**, 92; H. Fischer and A. Treibs, *Justus Liebigs Ann. Chem.*, 1927, **451**, 209.

8 C. Floriani, E. Solari, G. Solari, A. Chiesi-Villa and C. Rizzoli, *Angew. Chem., Int. Ed.*, 1998, **37**, 2245 and references therein; L. Bonomo, O. Dandin, E. Solari, C. Floriani and R. Scopelliti, *Angew. Chem., Int. Ed.*, 1999, **38**, 913 and references therein; S. De Angelis, E. Solari, C. Floriani, A. Chiesi-Villa and C. Rizzoli, *J. Am. Chem. Soc.*, 1994, **116**, 5691; S. De Angelis, E. Solari, C. Floriani, A. Chiesi-Villa and C. Rizzoli, *J. Am. Chem. Soc.*, 1994, **116**, 5702.

Communication 9/06817A

A self-assembled monolayer of a fluorescent guest for the screening of host molecules

Simon Flink, Frank C. J. M. van Veggel* and David N. Reinhoudt*

Department of Supramolecular Chemistry and Technology, and MESA+ Research Institute, University of Twente, PO Box 217, 7500 AE Enschede, The Netherlands. E-mail: d.n.reinhoudt@ct.utwente.nl

Received (in Cambridge, UK) 12th August 1999, Accepted 29th September 1999

The polarity-dependent fluorescence of self-assembled monolayers of dansyl adsorbates on glass enables monitoring of its specific interactions with β-cyclodextrin.

Host–guest interactions are intensively studied phenomena in supramolecular chemistry.[1] The synthesis and functionalization of host molecules has led to a large variety of compounds with high affinities and selectivities for guests, varying from metal ions to (bio)organic molecules. Recent developments in combinatorial chemistry allow the preparation of synthetic receptor libraries.[2] The large number of host molecules that is generated in this way requires analytical techniques which enable the fast selection of suitable hosts for a specific guest. Self-assembled monolayers (SAMs) offer the possibility to immobilize guest derivatives on a variety of substrates, and monitor their interactions with compounds in the contacting solution. So far, several groups have used electrochemically active SAMs of ferrocene for the binding of macrocyclic hosts from aqueous solutions.[3] The complexation of the ferrocene headgroup resulted in a shift of its redox potential, which can be detected by cyclic voltammetry. Fluorescent self-assembled monolayers have rarely been used to monitor host–guest interactions. Hieftje *et al.* used a monolayer of fluorescently labeled single-stranded DNA to monitor interactions with proteins by fluorescence anisotropy.[4] Myles *et al.* reported the detection of barbituric acid derivatives by a self-assembled monolayer of fluorescent receptors on gold.[5] Here we describe the selective binding of β-cyclodextrin to self-assembled dansyl monolayers on quartz and oxidized silicon wafers, detected by fluorescence spectroscopy.

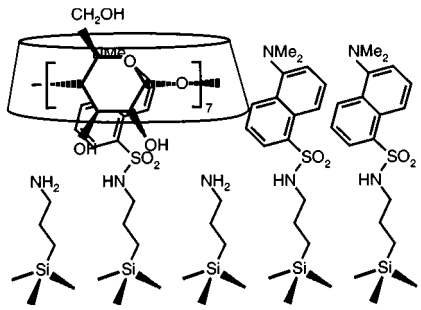

Self-assembled monolayers of dansyl adsorbates were prepared in a two-step procedure. First, a monolayer of 3-aminopropyltriethoxysilane was attached to the substrate.[6] This layer was converted into the desired dansyl SAM by reaction with dansyl chloride.[7] Ellipsometric measurements showed that the initially formed propylamine layer had a thickness of 6.7 ± 0.4 Å, which is close to the estimated length of the molecule (7.5 Å based on CPK models).[8] After reaction with dansyl chloride the layer thickness increased by 5.3 Å to a value of 12.0 ± 0.4 Å. Since the length of a dansyl group is 8.4 Å, the observed increase of only 5.3 Å was attributed to a relatively loose packing of the fluorescent groups. From these numbers a surface coverage of approximately 60% of the most densely packed monolayer was calculated. Wettability studies showed advancing contact angles with water of 67 ± 1 and 58 ± 1° for the 3-aminopropyltriethoxysilane SAM and the dansyl monolayer, respectively.[9] The hysteresis between advancing and receding contact angle for both surfaces was 30 to 35°, which indicates that monolayers were formed with a high degree of disorder. UV-VIS absorbance of the monolayer showed a strong absorption at 220 nm with a shoulder at 250 nm, and a third weak absorption at 330 nm (see Fig. 1).[10] Both position and relative intensity of these peaks are in good agreement with a spectrum of dansylamide taken in MeCN. The absorption at 220 nm was used to estimate the surface density of dansyl groups (ρ) from the Beer–Lambert law ($\rho = A\varepsilon^{-1}$), using the experimentally determined absorption coefficient of dansylamide in MeCN (ε_{220} = 38900 M^{-1} cm^{-1}). The resulting density of 0.93 dansyl groups per 100 Å^2 indicates that only 25% of the amino groups had reacted with dansyl chloride.[11] Based on a CPK model, the adsorbate would cover an area of approximately 52 Å^2. This results in a surface coverage of 50%, which is in reasonable agreement with the 60% surface coverage calculated from the ellipsometric thickness.

Fluorescence measurements of the dansyl SAM in air showed the characteristic broad emission centered at 480 nm.[12] Exposure of the monolayer to water resulted in a shift of the emission maximum to 510 nm. Hence, the well-known polarity dependence of the emission maximum of 1-(dimethylamino)-naphthalene-5-sulfonate[13] was maintained upon its immobilization in a monolayer. Apparently, the packing density was not enough to prevent water from solvating the dansyl groups.

Titration of the layer with aliquots of a concentrated aqueous solution of β-cyclodextrin resulted in an increase of the monolayer fluorescence, accompanied by a shift of the fluorescence maximum from 510 nm (pure water) to 480 nm (11.3 mM of β-cyclodextrin), as shown in Fig. 2. This indicates that the host molecules are bound to the layer, which results in an effective shielding of the dansyl groups from the aqueous environment.[14] The dansyl SAM showed no significant changes of the position or the intensity of the emission maximum in

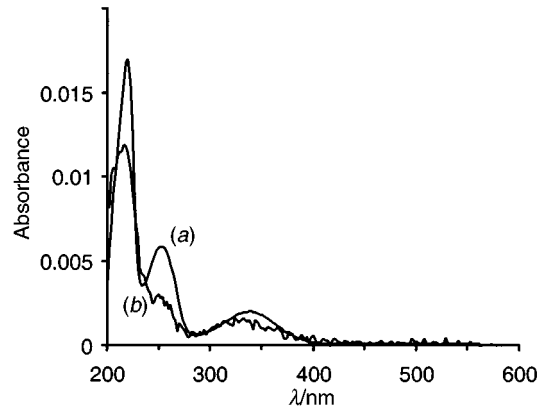

Fig. 1 UV–VIS absorption spectra of (*a*) 44 μM dansylamide in MeCN (shown absorbance was divided by a factor of 100) and (*b*) two dansyl monolayers (one on each side of the quartz slide).

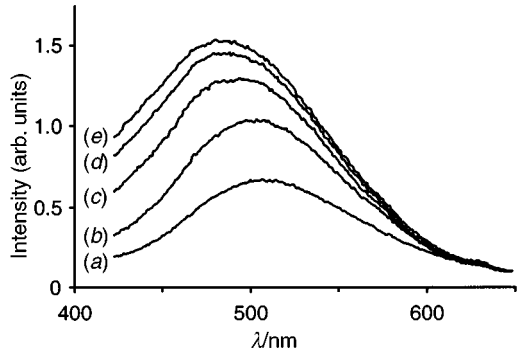

Fig. 2 Emission spectra of a dansyl monolayer (excitation at 350 nm) at different concentrations of β-cyclodextrin in the contacting aqueous solution: (*a*) 0, (*b*) 2.4, (*c*) 5.3, (*d*) 8.8 and (*e*) 11.3 mM.

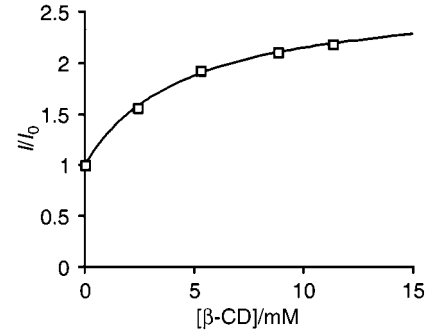

Fig. 3 Relative fluorescence intensity at 505 nm in dependence of the β-cyclodextrin concentration. The solid line shows eqn. (2) with an association constant of K = 221 M^{-1} and k_{compl}/k_{dans} = 2.67.

titration experiments with solutions of α- and γ-cyclodextrin. Hence, the observed changes of the emission spectra were the result of molecular recognition rather than aspecific binding of cyclic oligosaccharides to the dansyl monolayer. Moreover, the addition of aliquots of a competitive guest (50 mM cyclohexanol) to the 10 mM β-cyclodextrin solution resulted in decomplexation from the dansyl layer and changed the wavelength of the emission maximum and its intensity to the values observed in pure water. Due to the covalent binding of the dansyl group to the propylamine monolayer, we exclude the possibility of the complexation of one dansyl group by two β-cyclodextrin molecules as was reported by Dunbar *et al.* for solution experiments.[15] Consequently, the observed phenomena are attributed to the 1 to 1 complexation of the immobilized dansyl guests by β-cyclodextrin hosts.

To provide enough space for every dansyl group to bind a β-cyclodextrin molecule, the average area per dansyl group should be 180 Å^2, which would result in a layer thickness well below the determined 12 Å. This means that not every dansyl is capable of forming an inclusion complex. The determined surface density of fluorophores would allow 60% of the dansyl groups to be complexed by a cyclodextrin molecule. Consequently, the observed emission spectrum is the sum of the two fluorescent species present at the surface (free dansyl, and the complex of β-cyclodextrin and dansyl). The fluorescence intensity (I) at a given wavelength is therefore given by eqn (1),

$$I = k_{dans}[dans] + k_{compl}[comp] \quad (1)$$

where k_{dans} and k_{compl} represent the proportionality constants that connect the intensities and the surface concentration of the species.[16] Combined with the equation for the association constant (K = [compl]/[dans][β-CD]) this results in eqn. (2),

$$\frac{I}{I_0} = \frac{1 + (k_{compl}/k_{dans})K[\beta - CD]}{1 + K[\beta - CD]} \quad (2)$$

where I_0 is the emission intensity in the absence of β-cyclodextrin. From the fit of eqn. (2) to the experimental values, an association constant of 221 ± 19 M^{-1} was obtained (see Fig. 3), which is of the same order of magnitude as the reported values of 100–200 M^{-1} for complexes in aqueous solutions.[14]

In summary, self-assembled monolayers of 3-aminopropyltriethoxysilane can be effectively modified by reaction with sulfonyl chlorides. In this way, different functions like dyes can be introduced. Efficient solvation of the surface-bound dansyl groups maintains their polarity dependent emission, which has been used to study the interactions with several hosts in aqueous solutions.

Notes and references

1 *Comprehensive Supramolecular Chemistry*, ed. J. L. Atwood, J. E. D. Davies, D. D. MacNicol and F. Vögtle, Pergamon, Oxford, 1996.
2 P. Timmerman and D. N. Reinhoudt, *Adv. Mater.*, 1999, **11**, 71; W. C. Still, *Acc. Chem. Res.*, 1996, **29**, 155.
3 R. C. Sabapathy, S. Bhattachatyya, W. E. Cleland, Jr. and C. L. Hussey, *Langmuir*, 1998, **14**, 3797; H. Ju and D. Leech, *Langmuir*, 1998, **14**, 300; L. Zhang, L. A. Godinez, T. Lu, G. W. Gokel and A. E. Kaifer, *Angew. Chem., Int. Ed. Engl.*, 1995, **34**, 235.
4 R. A. Potyrailo, R. C. Conrad, A. D. Ellington and G. M. Hieftje, *Anal. Chem.*, 1998, **70**, 3419.
5 K. Motesharei and D. C. Myles, *J. Am. Chem. Soc.*, 1998, **120**, 7328.
6 D. G. Kurth and T. Bein, *Langmuir*, 1993, **9**, 2965.
7 Modification of the 3-aminopropyltriethoxysilane SAMs was achieved by reaction with 10 mg dansyl chloride and 0.1 ml triethylamine in 25 ml of dry MeCN for 16 h in a glovebox. After the reaction the substrates were extensively rinsed with MeCN, EtOH and $CHCl_3$.
8 Ellipsometry was performed on a Plasmos Ellipsometer (λ = 633 nm) assuming a refractive index of 1.46 for the monolayer and the underlying oxide. The thickness of the silicon oxide layer was measured separately on an unmodified part of the same wafer and subtracted from the total layer thickness determined for the monolayer covered silicon substrate.
9 Experimental details of the contact angle measurements are described in S. Flink, B. A. Boukamp, A. van den Berg, F. C. J. M. van Veggel and D. N. Reinhoudt, *J. Am. Chem. Soc.*, 1998, **120**, 4652.
10 Absorption measurements were performed on a Hewlett Packard 8452A Diode Array Spectrophotometer. The quartz slides were coated with a SAM on each side of the substrate, so that the presented absorption spectra are due to two monolayers. An unmodified quartz slide was used as a blank.
11 For self−assembled propylamine monolayers a surface density of 3.9 amino groups per 100 Å^2 was determined by J. H. Moon, J. H. Kim, K. Kim, T.-H. Kang, B. Kim, C.-H. Kim, J. H. Hahn and J. W. Park, *Langmuir*, 1997, **13**, 4305.
12 Fluorescence emission and excitation spectra were measured with a SLM Instruments SPF-500C spectrofluorometer. The presented emission spectra were recorded after excitation at 350 nm with excitation and emission bandwidths of 7.5 nm.
13 F. Grieser, P. Thistlethwaite, R. Urquhart and L. K. Patterson, *J. Phys. Chem.*, 1987, **91**, 5286.
14 T. Kinoshita, F. Iinuma and A. Tsuji, *Chem. Pharm. Bull.*, 1974, **22**, 2413.
15 R. A. Dunbar and F. V. Bright, *Supramol. Chem.*, 1994, **3**, 93.
16 K. A. Connors, *Binding Constants*, Wiley, New York, 1987.

Communication 9/06563F

ChemComm

Isothiocyanatoporphyrins, useful intermediates for the conjugation of porphyrins with biomolecules and solid supports

Oliver J. Clarke and Ross W. Boyle*

Department of Biological Sciences, University of Essex, Wivenhoe Park, Colchester, Essex, UK CO4 3SQ. E-mail: rossb@essex.ac.uk

Received (in Liverpool, UK) 3rd August 1999, Accepted 23rd September 1999

***meso*-Phenylporphyrins bearing a single isothiocyanate group react efficiently under ambient conditions with primary amino groups on proteins and polystyrene resins.**

Porphyrins are molecules of great interest due to the wide range of potential applications associated with them, these include photochemotherapy,[1] oxidation catalysis,[2] optoelectronics[3] and fluorescence imaging.[4] In order to customise porphyrins for uses such as these it is often necessary to attach the core macrocycle to either biological targeting agents, such as proteins, or solid supports. The conjugation of porphyrins with these species is often complicated by solvent incompatibilities and/or the forcing conditions commonly required to react substituents on the porphyrin periphery. We have recently become interested in developing mild methods for the conjugation of porphyrins and report here a facile method for generating a single isothiocyanate group on a porphyrin and the reaction of these species with amines in solution, on polypeptides and on polystyrene resins.

Previous attempts have been made to conjugate porphyrinoid structures with a variety of biologically active macromolecules including lipoproteins,[5] monoclonal antibodies[6] and serum albumin.[7] Many of these complexes rely on non-covalent linkages which, while more easily formed, are inherently less stable than covalent conjugates. Immunoconjugates[8] have been produced *via* non-covalent interaction of a porphyrin hapten at specific binding sites present on the surface of antibodies. Such porphyrin immunoconjugates have been used to confer specificity to photochemotheraputic techniques but the preparation and stability of the conjugate is heavily dependent on conditions such as solvent, pH and temperature. Clearly a covalently bound porphyrin antibody conjugate would be more flexible in terms of the physical and chemical conditions it could be exposed to. The majority of attempts to covalently conjugate porphyrin molecules with polypeptides have relied on carbodiimide mediated coupling to protein amino residues, *via* carboxy functionality on the macrocycle. These reactions are however slow and require the *in situ* generation of a reactive intermediate, which can lead to extensive loss of porphyrin as the *N*-acyl urea derivative.

Isothiocyanates are commonly used for the attachment of fluorescent probes to sensitive biological substrates under very mild conditions with no by-products,[9] however the use of this type of functionality in porphyrin chemistry has, strangely, not been developed. Collman[10] recently reported the use of porphyrin isocyanates as molecular building blocks for the construction of capped and strapped porphyrins. The high reactivity of isocyanates makes them useful synthetic tools, but their use is complicated by rapid hydrolysis of the NCO group upon exposure to moisture. Currently this synthesis involves reaction of amino porphyrins with highly toxic phosgene or triphosgene under inert atmosphere conditions. Isothiocyanates in contrast are slightly less reactive, but considerably more stable, their hydrolysis being much slower under aqueous conditions. Here we present a convenient method for synthesising porphyrin isothiocyanates and demonstrate their use in porphyrin conjugation with amino bearing substrates.

Acid hydrolysis of mono acetamido porphyrins, synthesised according to Adler *et al.*[11] and Boyle *et al.*,[12] yielded the corresponding mono amino derivatives. Subsequent treatment with 1,1′-thiocarbonyldi-2,2′-pyridone (TDP)[13] in CH_2Cl_2 at room temperature (Scheme 1) gave, quantitatively, the respective monoisothiocyanato porphyrins after 30 to 40 min. The by-product, 2-hydroxypyridine, was easily removed during an aqueous work up. The resulting monoisothiocyanato porphyrins are relatively stable to air and can be handled without the need for inert atmosphere conditions. In order to test the reactivity of these compounds a number of reactions were performed under standard conditions, in solution, using a variety of amines; these results are summarised in Table 1.

It can be seen from these results that the isothiocyanate functionality reacts cleanly and in good to excellent yield with most amines. Primary aliphatic amines were found to react fastest with times typically in the region of 30 min. Aromatic and secondary amines react more slowly and the combination of these structural features in the same molecule (*e.g.* diphenylamine) resulted in no detectable product being formed, even after 10 days. *N*-Terminal amino residues of phenylalanine, leucine and valine were also found to react cleanly. All the resulting thioureidyl porphyrin derivatives showed good stability, including those formed from amino acids. We believed that this was important with regard to the use of monoisothiocyanato porphyrins for bioconjugation with polypeptides.

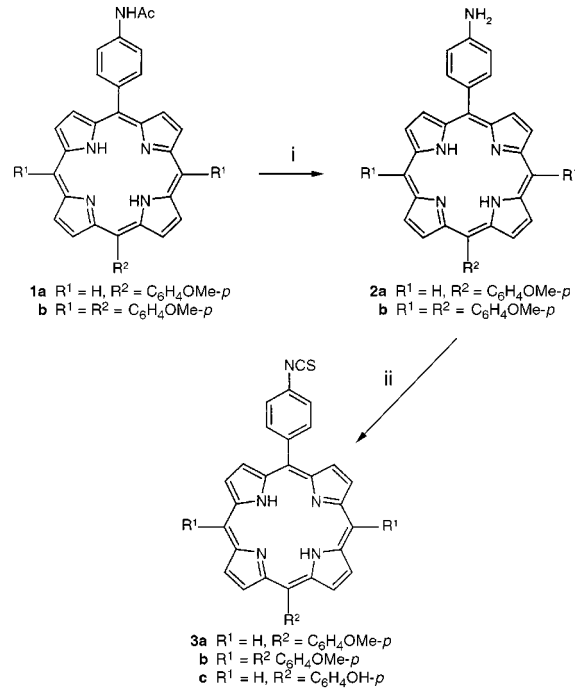

Scheme 1 *Reagents and conditions*: i, 6 M HCl, 100 °C, 3 h, 10% Et_3N–CH_2Cl_2, aqueous workup; ii, 1,1′-thiocarbonyldi-2,2′-pyridone (2 equiv.), CH_2Cl_2, 25 °C, 0.5–1 h, aqueous workup. Porphyrins **1a** to **3c** characterised by ^1H and ^{13}C NMR, MS and UV-VIS spectroscopy.

Table 1 Reactions of monoisothiocyanato porphyrin **3a** with selected amines and amino acids

Entry	Substrate	*t*/h	Yield[a] (%)
1	Allylamine	1	85
2	Benzylamine	2	89
3	Butylamine	0.5	95
4	Cyclohexylamine	1	92
5	L-Phe-OMe-HCl	17	95
6	L-Leu-OMe-HCl	30	91
7	L-Val-OMe-HCl	17	92

[a] Isolated thiourea derivatives characterised by ^{1}H and ^{13}C NMR, MS and UV–VIS.

Table 2 Reactions of monoisothiocyanato porphyrin **3b** with selected amines and amino acids

Entry	Substrate	*t*/h	Yield[a] (%)
1	Allylamine	1	95
2	Aniline	120	65
3	Benzylamine	2	70
4	Butylamine	0.5	98
5	Cyclohexylamine	1	87
6	Isopropylamine	0.5	93
7	Propargylamine	2	64
8	Dibenzylamine	3	78
9	Dicyclohexylamine	2	94
10	Diethylamine	1	92
11	Diphenylamine	240	0[b]
12	L-Phe-OMe-HCl	21	89
13	L-Leu-OMe-HCl	36	94
14	L-Val-OMe-HCl	24	94

[a] Isolated thiourea derivatives characterised by ^{1}H and ^{13}C NMR, MS and UV–VIS. [b] No detectable reaction.

Encouraged by these results we set out to explore the potential of monoisothiocyanato porphyrins for bioconjugation and attachment to polystyrene resins.[14] Bovine and human serum albumin (BSA and HSA) are well-characterised proteins which have been used in drug delivery[15] and for raising antibodies by haptenisation of small molecules. We therefore selected BSA as a model protein to study the potential of monoisothiocyanato porphyrins for bioconjugation. Model reactions on amines with monoisothiocyanato porphyrins had previously been performed in organic solvents; in order to facilitate conjugation with proteins under aqueous conditions, a 5,15-diphenylporphyrin was synthesised bearing a more hydrophilic hydroxy group on one phenyl ring and an isothiocyanate group on the opposing phenyl ring[12] (Scheme 1, **3c**).

In a typical experiment a stock solution of 5-(4-hydroxyphenyl)-15-(4-isothiocyanatophenyl)porphyrin **3c** in anhydrous DMSO (10 mg ml^{-1}) was prepared. 100 μl of the stock solution was added to a gently stirred solution of BSA (10 mg) in carbonate buffer (1 ml, pH 9.2). The reaction was protected from light, and agitated at room temperature for 17 h. Purification of the conjugate was achieved using gel filtration (Sephadex G-25) eluting with carbonate buffer at pH 8.9. The porphyrin–BSA conjugate was contained in the first fluorescent band eluted from the column, and was characterised by SDS-PAGE. Once the gel had been run to completion (200 mA, 45 min) the unstained gel plates were illuminated with a UV lamp revealing a red fluorescent band which, on subsequent staining with silver nitrate, corresponded with BSA at 66 kD in the protein reference ladder.

The UV–VIS spectrum of the red fluorescent material at 66 kD exhibited both the characteristic Soret and Q bands of the porphyrin and an absorption peak at 284 nm corresponding to BSA. The same material showed strong porphyrin fluorescence at 620 nm. Standard spectroscopic methods[16] were used to determine the labelling ratio of the porphyrin–BSA conjugate, which was found to be 1 : 1.

Finally, monoisothiocyanato porphyrin was reacted with Rink amide resin (Novabiochem). Pre-swelling of the resin in CH_2Cl_2 followed by Fmoc deprotection of the amino group in 20% piperidine–DMF, then washing with MeOH, CH_2Cl_2, DMF and water yielded the free amino Rink resin. Monoisothiocyanato porphyrin (3 equiv.) was then mixed with the resin (1 equiv.) in CH_2Cl_2 and agitated for 17 h at 25 °C in the dark. The loading value for monoisothiocyanato porphyrin on the Rink resin was calculated at 0.718 mmol g^{-1}, representing a loading efficiency of 94.1%. Treatment with 1% TFA–CH_2Cl_2 solution for 17 h resulted in quantitative cleavage of porphyrin from the resin as the thiourea derivative. Interestingly, cleavage conditions for Rink amide resin usually require at least 50% TFA solutions.[17]

O. J. C. thanks the University of Essex for a studentship. The authors thank the Wellcome Trust (052724) for financial support and the EPSRC mass spectrometry service, Swansea for analyses.

Notes and references

1 R. Bonnett, *Rev. Contemp. Pharmacother*., 1999, **10**, 1.
2 R. A. Sheldon, *Metalloporphyrins in Catalytic Oxidations*, Marcel Dekker, New York, 1994, p 1.
3 P. Seta, E. Bienvenue, A. L. Moore, T. A. Moore and D. Gust, *Electrochim. Acta*, 1989, **34**, 1723.
4 E. Reddi, A. Segalla, G. Jori, P. K. Kerrigan, P. A. Liddell, A. L. Moore, T. A. Moore and D. Gust, *Br. J. Cancer*, 1994, **69**, 40.
5 M. R. Hamblin and E. L. Newman, *J. Photochem. Photobiol. B: Biol.*, 1994, **26**, 147.
6 L. R. Milgrom and F. O'Neill, *Tetrahedron*, 1995, **51**, 2137.
7 G. R. Parr and R. F. Pasternack, *Bioinorg. Chem.*, 1977, **7**, 277
8 A. Harada, K. Okamoto and M. Kamachi, *Chem. Lett.*, 1991, **6**, 953.
9 G. T. Hermanson, *Bioconjugate Techniques*, Academic Press, London, 1996, p. 303.
10 J. P. Collman, Z. Wang and A. Straumanis, *J. Org. Chem.*, 1998, **63**, 2424.
11 A. D. Adler, F. R. Longo and W. Shergalis, *J. Am. Chem. Soc.*, 1964, **86**, 3145.
12 O. J. Clarke and R. W. Boyle, *Tetrahedron Lett*., 1998, **39**, 7167
13 S. Kim and Y. Yang, *J. Org. Chem.*, 1986, **13**, 2613.
14 J. R. Linsey-Smith, *Metalloporphyrins in Catalytic Oxidations*, Marcel Dekker, New York, 1994, p. 325.
15 A. H. Mukhopadhyay, G. Chaudhuri, S. K. Arora, S. Sehga and S. K. Basu, *Science*, 1989, **244**, 705; A. H. Mukhopadhyay, B. Mukhopadhyay, R. K. Srivastava and S. K. Basu, *Biochem. J*., 1992, **284**, 237; A. H. Mukhopadhyay and B. Mukhopadhyay and S. K. Basu, *Biochem. Pharmacol.*, 1993, **46**, 919.
16 G. T. Hermanson, *Bioconjugate Techniques*, Academic Press, London, 1996, p. 304.
17 B. A. Bunin, *The Combinatorial Index*, Academic Press, San Diego, p. 38.

Communication 9/06298J

ChemComm

An enantioselective synthesis of heteroaromatic *N*-tosyl α-amino acids

Mogens Johannsen*

Department of Organic Chemistry, Technical University of Denmark, Building 201, DK-2800 Lyngby, Denmark. E-mail: okmj@pop.dtu.dk

Received (in Liverpool, UK) 18th August 1999, Accepted 22nd September 1999

A new synthesis of optically active β-indolyl and pyrrolyl *N*-tosyl α-amino acids has been developed which uses readily available starting materials and proceeds with a high degree of enantioselection, giving the α-amino acids with up to 96% enantiomeric purity in 89% yield using 1–5 mol% of a chiral copper(I)–Tol-BINAP catalyst.

Within the last few years new catalysts have emerged for the classical and industrially very important Friedel–Crafts acylation of aromatics.[1] However, the addition of unsaturated compounds such as aldehydes and imines, which would lead to new and interesting compounds with stereogenic centers, has received only scant attention. Moreover, as far as the author is aware, the catalytic asymmetric version of such an addition has only one precedent the addition of ethyl pyruvate to 1-naphthol promoted by a chiral zirconium complex gave the addition product in 56% yield and with 84% ee.[2]

Recently considerable progress has been achieved with the long-standing problem of catalytic enantioselective addition of nucleophiles to imines.[3] This prompted us to investigate the enantioselective addition of a variety of aromatic compounds to imines. We now report our findings using a complex of copper(I) salts and Tol-BINAP[4] (the Lectka system)[3a] to catalyse the enantioselective addition of *N*-tosylimino esters of ethyl glyoxylate to electron-rich aromatics such as indole and pyrrole (Scheme 1).[5]

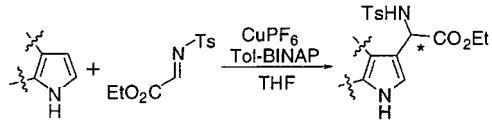

Scheme 1

Using as substrate furan we were able to isolate 15% of the desired aromatic addition product with 38% ee after 2 days at room temperature. This made us focus on the pyrrole and indole systems as these are known to be more active than furan in aromatic electrophilic substitution.[6] To our delight the reaction between indole **1a** and the imine **2** in THF was complete within a few hours, giving the 3-substitution product **3a** in almost quantitative yield and with 87% ee (Table 1, entry 1).[7] Running the reactions at lower temperatures (−20 and −78 °C) increased the enantioselectivity to 91 and 96% ee, respectively (entry 2, 3).[8] A simple recrystallisation gave the enantiopure *N*-protected α-amino acid **3a**.[9,10] Running the same reaction in CH_2Cl_2 gave a more sluggish conversion with more by-products and a lower enantioselection than in THF (entry 4). Finally, the amount of catalyst was reduced to 1 mol% almost without any change in yield or enantioselectivity [> 99% ee, 71% yield (recryst.)] (entry 5).

To test the scope of the reaction a variety of 5-substituted indole derivatives were screened.[11] As evident from Table 2 all the addition reactions give the 3-substituted indole derived amino acids.[12] The addition to the electron-rich methoxy-substituted substrate works particularly well, giving the product in 89% yield and more than 97% ee [> 99% ee, 73% yield (recryst)] (entry 2). The indole substrates with the electron-withdrawing substituents **1c,d** also react in a very enantioselective fashion, but a slightly higher reaction temperature was required in order to complete the reactions (entry 3,4). The 5-brominated indole reacts as the other indoles exclusively at the 3-position giving the addition product in 75% yield and with 88% ee [> 98 % ee, 55% yield (recryst.)] (entry 5).[13] The bromo product offers an interesting opportunity to test a variety C–C coupling reactions to give other enantiomerically pure 5-substituted indole alkaloids.[14]

Table 1 Enantioselective addition of imino ester **2** to indole **1a**

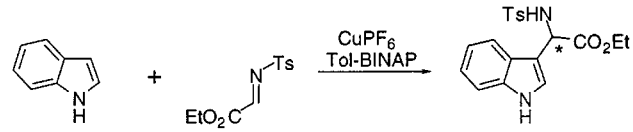

1a **2** **3a**

Entry	Catalyst/ mol%	Solvent	*T*/°C	Yield[a] (%)	Ee[bc] (%)
1	5	THF	room temp.	98	87
2	5	THF	−20	90	91
3	5	THF	−78	89	96
4	5	CH_2Cl_2	−78 to −10	57	78
5	1	THF	−78	89 (71)	94 (> 99)

[a] Yield after recrystallisation in parentheses. [b] Ee after recrystallisation in parentheses. [c] Ee determined by HPLC on a DAICEL OD-H or OJ column.

After having established the generality of the indole additions, focus was turned to the pyrrole systems. Two representative derivatives were chosen as model substrates, *viz.* *N*-methylpyrrole and 2-acetylpyrrole. The catalysed (5 mol% cat.) addition to *N*-methylpyrrole gives according to ^{1}H NMR approxiamtely a 1:1 mixture of the 2- and 3-substituted products **5** and **6**. After flash chromatographic separation, the two regioisomers were obtained in a total yield of 89%, the enantioselectivity being 84 and 56%, respectively. One recrystallisation of the 2-substituted product gave the enantiopure amino acid **6** [27% yield (recryst.)] (Scheme 2).

Table 2 Enantioselective addition of imino ester **2** to 5-substituted indoles **1a–e**

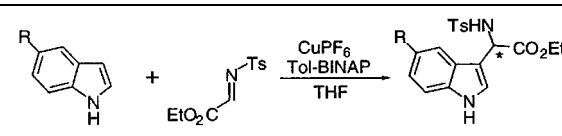

1a–e **2** **3a–e**

Entry	Catalyst/ mol%	R	*T*/°C	Yield[a] (%)	Ee[b] (%)
1	1	**1a** H	−78	89 (71)	96 (> 99)[c]
2	5	**1b** OMe	−78	89 (73)	97 (> 99)[c]
3	5	**1c** NO_2	−78 to −10	71	78
4	5	**1d** CO_2Me	−40	67 (52)	94 (> 98)[d]
5	5	**1e** Br	−10	75 (55)	88 (> 98)[d]

[a] Yield after recrystallisation in parentheses. [b] Ee after recrystallisation in parentheses. [c] Ee determined by HPLC on a DAICEL OD-H or OJ column. [d] Ee determined by ^{1}H NMR using a lanthanide shift reagent (ref. 13).

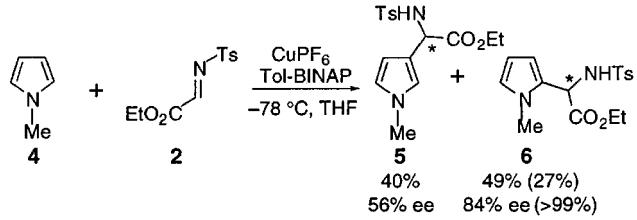

Scheme 2

In contrast to the *N*-methylated pyrrole **4**, the deactivated 2-acetylpyrrole **7** reacts primarily at the 4-position. The addition product was isolated in 76% yield, with a surprisingly high ee of 94% [> 99% ee, 33% yield (recryst.)] when compared to **5** (Scheme 3).

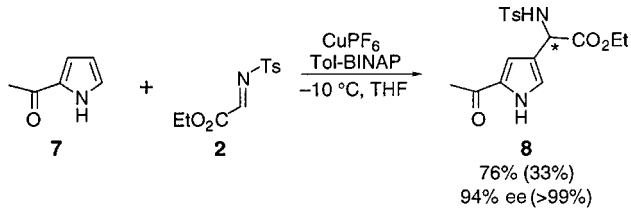

Scheme 3

Finally, it should be mentioned that the catalysed addition of **2** to pyrrole gives the *N*-addition product as the main product. It is the only case where we have observed this kind of amino acetal product during our investigation.

At present not much is known about the mechanism of the reaction. Earlier studies by Lectka *et al.* have shown the capability of the system to effect highly enantioselective imino aldol reactions.[3a,b] On the other hand we have found that the Mannich reaction of 1-morpholinocyclohex-1-ene with the tosyl imine **2** was very fast (< 1 min, −78 °C) giving the anticipated imino aldol product after hydrolysis. However, the enantiomeric excess was very low (< 10% ee). The fact that the enamine moiety of the substrates is a part of a heteroaromatic system is therefore crucial for the effectiveness of this new addition reaction. The present reaction should therefore most adequately be considered as an aromatic electrophilic substitution rather than a Mannich reaction.

In summary a novel synthesis of useful optically pure heteroaromatic α-amino acids has been developed. The procedure allows for the simple preparation of an array of electronically different indole α-amino acids. These might be used in the synthesis of natural products and pharmacologically interesting compounds as well as new chiral ligands for asymmetric catalysis. The presence of the different 5-substituents permits the systematic testing of the influence of electronics on the activity of the new indole derivatives. Simple pyrrole systems also worked well as substrates, giving access to new optically pure heteroaromatic α-amino acids.

Leo Pharmaceutical Products, the Technical University of Denmark and the Danish Ministry of Education are gratefully acknowledged for funding.

Notes and references

1 G. A. Olah, O. Farooq, S. M. F. Farnia and J. A. Olah, *J. Am. Chem. Soc.*, 1988, **110**, 2560; S. Repichet, C. Le Roux, J. Dubac and J.-R. Desmurs, *Eur. J. Org. Chem.*, 1998, **1**, 2743; S. Kobayashi and S. Nagayama, *J. Am. Chem. Soc.*, 1998, **120**, 4554; S. Kobayashi, *Eur. J. Org. Chem.*, 1999, **2**, 15.

2 G. Erker and A. A. H. van der Zeijden, *Angew. Chem.*, 1990, **102**, 543; *Angew. Chem., Int. Ed. Engl.*, 1990, **29**, 512.

3 For the catalytic asymmetric aza-aldol addition: (*a*) D. Ferraris, B. Young, T. Dudding and T. Lectka, *J. Am. Chem. Soc.*, 1998, **120**, 4548; (*b*) D. Ferraris, B. Young, C. Cox, W. J. Drury III, T. Dudding and T. Lectka, *J. Org. Chem.*, 1998, **63**, 6090; (*c*) E. Hagiwara, A. Fujii and M. Sodeoka, *J. Am. Chem. Soc.*, 1998, **120**, 2774; (*d*) S. Kobayashi, S. Komiyama and H. Ishitani, *Angew. Chem.*, 1998, **110**, 1026; *Angew. Chem., Int. Ed.*, 1998, **37**, 979; the aza-ene reaction: (*e*) S. Yao, X. Fang and K. A. Jørgensen, *Chem. Commun.*, 1998, 2547; (*f*) W. J. Drury III, D. Ferraris, C. Cox, B. Young and T. Lectka, *J. Am. Chem. Soc.*, 1998, **120**, 11 006; the aza-Diels–Alder reaction: (*g*) S. Yao, M. Johannsen, R. G. Hazell and K. A. Jørgensen, *Angew Chem.*, 1998, **110**, 3318; *Angew. Chem., Int. Ed.*, 1998, **37**, 3121; the allylation reaction: (*h*) X. Fang, M. Johannsen, S. Yao, N. Gathergood, R. G. Hazell and K. A. Jørgensen, submitted for publication; (*i*) H. Nakamura, K. Nakamura and Y. Yamamoto, *J. Am. Chem. Soc.*, 1998, **120**, 4242; the aza-Strecker synthesis: (*j*) H. Ishitani, S. Komiyama and S. Kobayashi, *Angew. Chem.*, 1998, **110**, 3369; *Angew. Chem., Int. Ed.*, 1998, **37**, 3186; (*k*) M. S. Sigman and E. N. Jacobsen, *J. Am. Chem. Soc.*, 1998, **120**, 5315; (*l*) M. S. Sigman and E. N. Jacobsen, *J. Am. Chem. Soc.*, 1998, **120**, 4901.

4 (*R*)-Tol-BINAP is the abbreviation for the commercial ligand (*R*)-(+)-2,2′-bis(di-*p*-tolylphosphino)-1,1′-binaphthyl.

5 The optically pure heteroaromatic α-amino acids obtained this way are to the best of our knowledge all new compounds which are not easily accesible by any other synthetic route. They all give ^{1}H and ^{13}C NMR spectra in accordance with the assigned structures. It should be mentioned that a derivative of **3a** has previously been prepard *via* an enzymatic resolution (ref. 12). For some excellent reviews on the synthesis of α-amino acids, see: R. M. Williams, *Aldrichim. Acta*, 1992, **25**, 11; R. M. Williams, *Synthesis of Optically Active α-Amino Acids*, Pergamon, New York, 1989; R. O. Duthaler, *Tetrahedron*, 1994, **50**, 1539.

6 For an introduction to heterocyclic chemistry, see *e.g.*: J. A. Joule, K. Mills and G. F. Smith, *Heterocyclic Chemistry*, Stanley Thornes, Cheltenham, 1998.

7 For some recent examples of achiral additions of imines to indoles, see *e.g.*: H. Heaney, G. Papageorgiou and R. F. Wilkins, *Chem. Commun.*, 1988, 1161; H. Heaney, G. Papageorgiou and R. F. Wilkins, *Tetrahedron*, 1997, **53**, 2941; H.-C. Zhang, K. K. Brumfield, L. Jaroskova and B. E. Maryanoff, *Tetrahedron Lett.*, 1998, **39**, 4449.

8 *A representative experimental proceudre:* Synthesis of (1*H*-indol-3-yl)tosylaminoacetic acid ethyl ester **3a**. To a flame dried Schlenk tube was added $CuPF_6(MeCN)_4$ (ref. 15) (7.5 mg, 0.02 mmol) and (*R*)-Tol-BINAP (15 mg, 0.022 mmol) under N_2. The solids were dried on the vacuum line for 1 h before 1.5 ml of dry THF was added *via* syringe. The clear yellow solution was stirred for 1 h before cooling down to −78 °C. Indole **1a** (94 mg 0.80 mmol) and imino ester **2** (ref. 16) (96 mg, 0.40 mmol) dissolved in 0.2 ml dry THF were added and the reaction was stirred overnight. The product was purified by flash column chromatography (30% EtOAc in pentane) giving **3a** as a white solid in 89% yield (93 mg) and 96% ee detected by HLPC using a Chiralcel OD-H column (20% Pr^{i}OH–80% hexane, 0.5 ml min^{-1}); $[\alpha]_D^{rt}$ +102 (*c* 1.0, $CHCl_3$); δ_H (500 MHz, $CDCl_3$) 8.11 (br s, 1H, N*H*), 7.65 (d, 2H, *J* 8.0, Ar), 7.53 (d, 1H, *J* 8.0, Ar), 7.30 (d, 1H, *J* 8.5, Ar), 7.20–7.14 (m, 3H, Ar), 7.10–7.07 (m, 2H, Ar), 5.56 (d, 1H, *J* 8.0, CHN*H*Ts), 5.34 (d, 1H, *J* 8.0, C*H*NHTs), 4.09–3.97 (m, 2H, OCH_2CH_3), 2.36 (s, 3H, $ArCH_3$), 1.12 (t, 3H, *J* 7.0, CH_2CH_3); δ_c (75 MHz, $CDCl_3$) 170.5, 143.2, 137.0, 136.2, 129.2, 127.2, 125.2, 123.4, 122.7, 120.2, 119.1, 111.3, 110.5, 62.0, 53.1, 21.5, 13.9.

9 Several methods exists for the deprotection of similar *N*-tosyl α-amino acids without notable racemisation: T. Shono, Y. Matsumura and T. Kanazawa, *Tetrahedron Lett.*, 1983, **24**, 1259; T. Shono, Y. Matsumura, K. Tsubata, K. Uchida, T. Kanazawa and K. Tsuda, *J. Org. Chem.*, 1984, **49**, 3711; E. Vedejs and S. Lin, *J. Org. Chem.*, 1994, **59**, 1602; See also: T. Kanazawa, T. Hamada, A. Nishida and O. Yonemitsu, *J. Am. Chem. Soc.*, 1986, **108**, 140; T. W. Greene and P. G. M. Wuts, *Protective Groups in Organic Synthesis*, 2nd edn., Wiley-Interscience, New York, 1991, pp. 379–381.

10 For other *N*-protecting groups, see: D. Ferraris, T. Dudding, B. Young, W. J. Drury III and T. Lectka, *J. Org. Chem.*, 1999, **64**, 2168.

11 Many naturally-occurring as well as biologically active indole alkaloids are substituted in the 5-position of the indole system. For some examples see *e.g.*: G. A. Cordell, *Lloydia*, 1974, **37**, 219; K. B. G. Torsell, *Natural Product Chemistry*, 2nd edn., Apotekarsocieteten, Stockholm 1997.

12 Optically pure indolyl glycines have been used in the synthesis of potent antibiotics of the cephalosporin type: L. C. Blaszczak and J. R. Turner, *US Patent*, 4492694, 1985; for the use of racemic indolyl glycine derivtives as antiinflammatorial agents, see *e.g.:* T.-Y. Shen, *US Patent*, 3316260, 1968.

13 The enantiomeric purities of **3d** and **3e** were determined by ^{1}H NMR using a lanthanide shift reagent [Eu(hfc)$_3$]. The ee values after recrystallisation are probably > 99%, but due to the limitations of ^{1}H NMR have been given as > 98%, even though only one enantiomer was detected.

14 M. P. Moyer, J. F. Shiurba and H. Rapoport, *J. Org. Chem.*, 1986, **51**, 1661.

15 G. J. Kubas, *Inorg. Synth.*, 1979, **19**, 90.

16 P. Hamley, A. B. Holmes, A. Kee, T. Ladduwahetty and D. F. Smith, *Synlett*, 1991, 29.

Communication 9/06758B

Typeset and printed by Black Bear Press Limited, Cambridge, England

Recent advances in the preparation of semiconductors as isolated nanometric particles: new routes to quantum dots

Mark Green and Paul O'Brien*†

Department of Chemistry, Imperial College of Science Technology and Medicine, South Kensington, London, UK SW7 2AY. E-mail: p.obrien@ic.ac.uk

Received (in Cambridge, UK) 25th May 1999, Accepted 16th September 1999

Nanoparticles of semiconductor materials have been the subject of intense research in the last five years owing to the novel electronic, catalytical and optical properties observed in such materials. The unusual properties of these so called quantum dots can be attributed to two main factors: the large surface to volume ratio of atoms and the confinement of charge carriers in a 'quantum mechanical box'. Small particles of semiconductors have been prepared by a number of routes, often using colloidal chemistry methods but more recently using organometallic routes. The recent advances have resulted in high quality nanoparticles which have been incorporated into simple devices. In this article we cover some of the key advances in the preparation of nanometric particles of semiconductors. The cover illustration depicts three sizes of TOPO capped CdSe.

Introduction

Isolated quantum dots are a novel form of semiconductor of theoretical interest and with potential to develop as an important class of materials for the electronics industry of the 21st century. The electronic properties of a bulk semiconductor are determined principally by the band gap of the material and its type. Typically, bulk samples of CdS, irrespective of their size once > *ca.* 20 nm, will absorb all electromagnetic radiation with an energy greater than the band gap ($h\nu$ > 2.42 eV); which is classified, in this case, as direct.[1] However, as particles become smaller, their electronic structure changes, eventually the description of the material as containing continuous bands breaks down and there are discrete bonding and antibonding levels in the material.[2] The electronic properties of such small particles are hence more like those of a molecule than an extended solid. The electronic, optical and catalytical properties of such small particles will depend on their size and the material of which they are composed.[3]

For a semiconductor such as CdS, these effects were predicted some years ago to become important in the size range from *ca.* 2 to 10 nm and Brus and coworkers published a number of keynote papers.[4–6] The preparation of stable particles in this size range has presented a considerable challenge to the chemist and such materials have been synthesised from aqueous solutions, adapting the approaches of colloid chemistry, or by the controlled decomposition of organometallic or metal organic compounds. Such small particles have relatively large surface areas and control of their surface chemistry has been important in developing stable forms of these materials and in controlling their properties.

Electronic properties

The 'band gap' of a quantum confined semiconductor is greater than that of the parent bulk material from which it is derived. This is an effect which is a consequence of the confinement of the electron in a three-dimensional 'box' with discrete energy levels rather than in the quasi-continuous band of a bulk material (Fig. 1).[4] The absorption of electromagnetic radiation by quantum dots, of materials such as CdS, is hence relatively easy to appreciate. However, explaining the luminescent

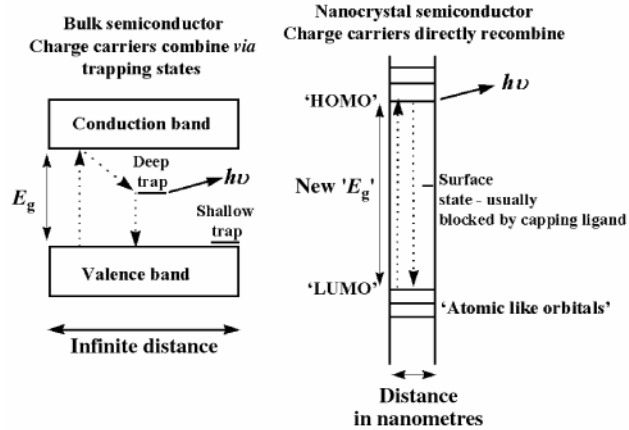

Fig. 1 Spatial electronic state diagram for bulk semiconductor and nanoparticles, after Brus and coworkers.[4]

Dr Mark Green obtained his BSc in chemistry from the Manchester Metropolitan University in 1995. He carried out research for his PhD at Imperial College for Professor Paul O'Brien between 1995 and 1998, studying new routes to nanoparticulate semiconductors. He is currently a post doctoral associate in the O'Brien group looking at nanoparticulate metals and semiconductors.

Professor Paul O'Brien graduated from Liverpool University in 1975, obtained a PhD from the University of Wales, Cardiff in 1978 and was immediately appointed as a lecturer at Chelsea College of Science and Technology. Following the University of London re-structuring, he moved to Queen Mary and Westfield College in 1984 and was promoted to a chair in 1994. In 1995 he moved to Imperial College where he was appointed as a Professor of Inorganic Chemistry and Sumitomo STS Professor of Materials Chemistry (1997–1999) and was Royal Society Amersham fellow (1997–1998). He holds a visiting Professorship at the Georgia Institute of Technology and is also a distinguished scholar at the Molecular Design Institute. In October 1999, he will take up a new position as Professor of Inorganic Materials, a joint appointment between the University of Manchester Chemistry Department and the Manchester Materials Science Centre.

† Current address: Department of Chemistry and the Manchester Materials Science Centre, The University of Manchester, Oxford Road, Manchester, UK M13 9PL.

behaviour of such materials is much more complicated but crucially important in identifying materials of sufficient quality for potential practical application. The ideas that have emerged for explaining such phenomena illustrate an interesting interplay between experiment and theory. Brus explained, on the basis of theoretical considerations and studies of excited state lifetimes, the main features expected in the luminescence spectra of quantum confined semiconductors and successfully anticipated the results of subsequent experiments.[4] Emission from passivated semiconductor quantum dots is often found to be 'band-edge' referring to the direct recombination of charge carriers from the atomic like orbitals (Fig. 1). Charge carriers in bulk semiconductors recombine from deep and shallow traps (crystal and surface defects) giving emission at different wavelengths from the band edge.

An alternative view of such structures, which has some conceptual appeal, is that they may be viewed as 'super atoms'. Electrons within the solids are confined within an approximately spherical particle (the diameter of the quantum dot). The solutions of the Schroedinger equation for this three-dimensional confinement can be viewed for a single electron as resembling a super atom with electronic states which resemble the orbitals of atoms (s, p, d. . .). The transitions observed are analogous to those observed in atomic spectroscopy.[7] Consequently one way to view the current excitement, and interest, in this area of science is that we are put into a position in which we can produce a material which has the electronic properties of a 'tailor-made atom'.

Methods of preparation

Many synthetic methods for nanoparticles have been reported in the literature. Many use methods based on colloid chemistry, decomposition of organometallic compounds or growth in a restricted reaction space. An ideal route should result in pure, monodispersed, crystalline particles which are stable, *i.e.* they have robust surface passivation. Nanoparticles of metals, metal oxides, carbides, borides and nitrides have also been produced and have been reviewed elsewhere.[8–10]

Elemental semiconductors have also been studied. For instance, germanium nanoparticles have been produced by the reaction of $GeCl_4$ and lithium naphthalide in tetrahydrofuran.[11] The quantum dots formed were between 60 and 200 Å in diameter. Laser illumination of a hexane solution resulted in further growth and increased crystallinity. Similarly oxide coated silicon nanoparticles have been produced by the combustion of silane.[12]

Problems with nanoparticles grown by colloidal or restricted growth routes, centre around their air sensitivity and poor crystallinity. Nanoparticles prepared in structured media also have their dimensions dictated by the restricting material. The removal of the matrix or the effect of its removal also needs to be considered when developing strategies for materials of practical importance.

Colloidal routes

The first reported routes to such small particles involved the controlled precipitation of dilute colloidal solutions and the cessation of growth soon after nucleation. The synthesis of highly monodispersed colloids was explained in the 1940's by La Mer *et al.*[13–15] who suggested that if seeds (nuclei) could be made to grow in concert into larger particles, monodispersed sols could be formed. In this early work the particles were typically micrometric. However, if nucleation and growth are properly controlled, particles with dimensions of the order of nanometres can be reproducibly synthesized. Small crystals, which are less stable, dissolve and then re-crystallise on larger more stable crystals; a process known as Ostwald ripening. For such methods to be effective, the quantum dots in question must have low solubility, which can be achieved by the correct choice of solvent, pH, temperature and passivating agent. Highly monodispersed samples are obtained if the processes of nucleation and growth are distinctly separated, *i.e.* fast nucleation and slow growth. The colloidal stability of these crystals has been improved by using solvents with low dielectric constants or by using stabilisers such as a styrene/maleic acid copolymer. Henglein,[16] Brus and coworkers[17,18] and Weller[19] have made significant contributions to this field, especially in studies of CdS.

A typical example involved the reaction between aqueous solutions of $CdSO_4$ and $(NH_4)_2S$. Control of the size of nanocrystalline CdS was achieved by altering nucleation kinetics using pH.[17] Although these methods can be efficient, some important semiconductors cannot easily be synthesised, *e.g.* CdSe, GaAs, InP and InAs. Annealing of amorphous colloidal particles is also a problem as these tend to be low temperature processes producing poorly crystalline material. Such aqueously prepared nanoparticles are not sufficiently stable at higher temperatures for annealing without agglomeration. CdS and ZnS have also been produced from methanolic media without the use of an organic ligand for stabilisation, using the repulsion of the electrostatic double layer to stop agglomeration.[18]

Zn_3P_2 and Cd_3P_2 have both been produced by aqueous methods, by the injection of phosphine gas into a solution of the relevant metal perchlorate.[20,21] The quantum dots obtained were coloured, from white for small Cd_3P_2, to brown for the larger particles. The white particles were reported to have band gaps of up to 4.0 eV. Luminescence was reported to be strong at short wavelength, but little attention was paid to crystal morphology. Murphy and coworkers have produced manganese activated (Mn occupying surface sites) and manganese doped (Mn occupying lattice sites) ZnS dots by aqueous routes, displaying increased quantum yields and orange emissions respectively.[22]

Synthesis in confined matrices

Materials which provide distinct defined cavities have been used to synthesise quantum dots. These well defined zones have been used as nanometre sized reaction chambers. Zeolites,[23] micelles,[24] molecular sieves[25] and polymers[26] have all been used to restrict growth. The matrix may also play a role in determining the final properties of the particle, for example, micelles are labile. CdSe and ZnS nanoparticles have been produced in inverse micelle solutions.[27,28] A microemulsion containing the metal ion was reacted with a silylchalcogenide, resulting in nanoparticles. The surface was then capped by phenyl groups or another semiconductor. The surface composition of the crystals were interesting owing to their ability to react further with other silyl groups owing to the excess Cd^{2+} sites, effectively growing larger and developing a different surface capping.

Growing particles in the internal cavities of zeolites also limits the particle size of materials, usually no larger than 20 nm. CdS has been synthesised in two different zeolites by ion exchange from the sodium cationic form to the cadmium cationic form, followed by exposure to H_2S gas. Depending upon the amount of cadmium utilised, different sized particles were obtained.[23] Cadmium telluride nanoparticles have also been prepared in a sodium or potassium zeolite. Exchange of the metal with cadmium nitrate followed by reduction by hydrogen at 450 °C prepared the zeolite for vapour phase deposition of tellurium, resulting in CdTe clusters. The size of the clusters could be controlled by using either the potassium or sodium resin, which altered pore diameters.[29]

Q-GaP has also been synthesised in the pores of zeolite Y.[30] The vapour transfer of Me_3Ga into a dry Na^+/H^+ exchange zeolite resulted in methane evolution and the formation of

$Me_{3-x}Ga$ sites. Exposure of this to an excess of PH_3 at various temperatures (200–400 °C) resulted in the growth of particles with a size range of 10–12 Å. The nanocrystals formed were analysed by EXAFS and solid state NMR spectroscopy.

Q-PbS was obtained by exchanging Pb^{2+} into ethylene/methacrylic acid copolymer, followed by exposure to H_2S.[26] The size of the particles was again controlled by Pb^{2+} concentration, with sizes ranging from 13 to 125 Å. A similar technique was used to grow in the interlamellar regions of a layered host, $Zr(O_3PCH_2CH_2CO_2H)_2$. Conversion of the host to $M^{II}[Zr(O_3PCH_2CH_2CO_2)_2]$ (M = Pb, Cd, Zn) followed by treatment with H_2E (E = S, Se) resulted in growth of ME nanoparticles.[31]

An organometallic route to polymeric composites of CdSe and ZnSe has been developed by Cole-Hamilton and coworkers.[32–34] The polymer 2-pyridyl-polybutadiene was reacted with a group IIb metal alkyl, to give an adduct. A toluene solution of the polypyridine bound metal alkyl was exposed to H_2Se gas to give a coloured precipitate. The size of the nanoparticles was determined by both the solvent and the reaction temperature (−76 to 60 °C); quantum dots synthesised at lower temperatures were smaller. Hexagonal CdSe was obtained in the size regime 1–6 nm, with the use of light petroleum instead of toluene giving larger particles. The particles were characterised by HRTEM, powder XRD, UV and photo-acoustic spectroscopy (PAS).

Metal–organic routes

A popular method for the preparation of high quality, crystalline, monodispersed nanoparticles was first described by Murray *et al.* in 1993.[35] In this method, a volatile metal alkyl (dimethylcadmium) and a chalcogen source TOPSe (tri-*n*-octylphosphine selenide) were mixed in tri-*n*-octylphosphine (TOP) and injected into hot TOPO (tri-*n*-octylphosphine oxide), a polar coordinating Lewis base solvent. Nucleation of nanoparticulate CdSe was achieved by the sudden introduction of the concentrated reagents resulting in abrupt supersaturation and the formation of nuclei, followed by slower growth and annealing, consistent with an Ostwald ripening process. The nanoparticles were passivated by a monolayer of the solvent ligands and hence could be isolated by solvent/non-solvent interactions. The particles produced by this method were highly monodispersed (±5%, Fig. 2) and crystalline. By varying the

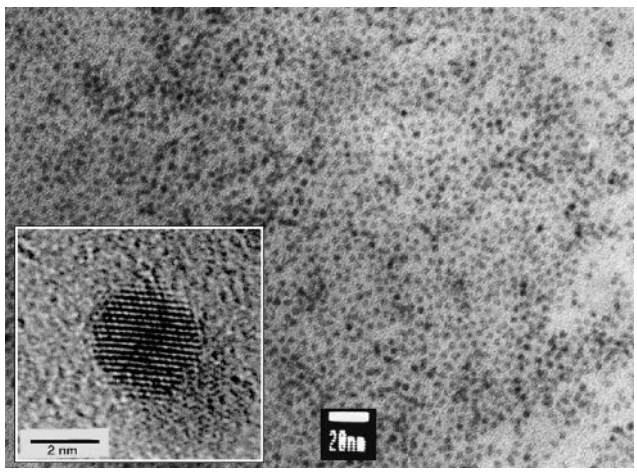

Fig. 2 TEM image of TOPO capped CdSe nanoparticles prepared as described in ref. 38 (scale bar = 20 nm); inset, HRTEM image, scale bar = 2 nm.

temperature of synthesis the diameter can be controlled in the size range 24–230 Å. The organic surface cap can be replaced by other organic groups such as pyridine, 4-picoline, tris(2-ethylhexyl)phosphate, and 4-(trifluoromethyl)thiophenol.[36] Computer modelling of XRD patterns suggests that Q-CdSe prepared at temperatures of up to 300 °C have around one defect per nanocrystal.[35]

Alivisatos and coworkers produced similar quantum dots with fewer crystal defects by using a higher temperature synthesis (350 °C) and tributylphosphine instead of tri-*n*-octylphosphine.[37] Replacing the metal alkyl with an adduct of the metal alkyl produces similar quality quantum dots whilst reducing the risks of using pyrophoric precursors.[38] The physical chemistry of TOPO capped nanoparticles has been thoroughly investigated.[39–41] Emission from TOPO capped II–VI materials is found to be near band edge with quantum yields of *ca.* 10% (Fig. 3).[35]

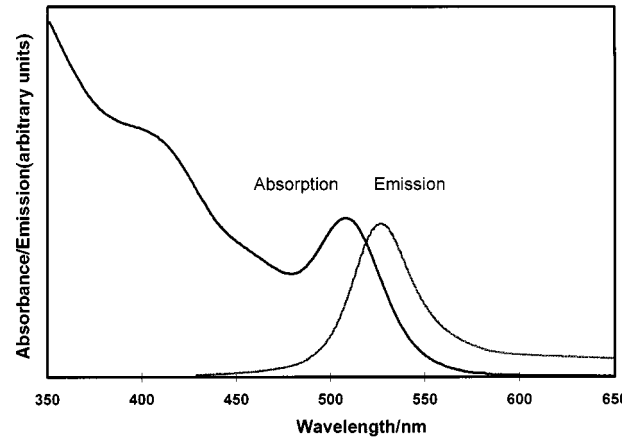

Fig. 3 Electronic and photoluminescence spectra of TOPO capped CdSe nanoparticles prepared as described in ref. 38.

The nanoparticles prepared by this method are of high quality, but the reaction requires harsh/difficult conditions, such as the injection of hazardous metal alkyls at elevated temperatures (*ca.* 350 °C) which is clearly undesirable. One way to avoid such potential problems is the use of a single-molecular precursor in which the metal–chalcogen bond is already in place. Trindade and O'Brien investigated cadmium dithio- and diseleno-carbamate complexes as precursors for the preparation of TOPO capped II–VI materials.[42,43] Thermolysis of the air stable complex $[Cd(S_2CNEt_2)]_2$, in TOPO resulted in high quality nanoparticles of CdS. The thermolysis of the analogous diselenocarbamate complex in TOPO resulted in micrometric particles of selenium. However, compounds of the formula $RCd(E_2CNEt_2)$, (R = neopentyl, Me; E = S, Se) were efficient precursors to CdE nanoparticles on thermolysis in TOPO (reaction scheme shown in Fig. 4). Such compounds eliminate the need for volatile metal alkyls, but are however air-sensitive; air-stable precursors would be preferred. Simple diselenocarbamate complexes of cadmium with unsymmetrical R groups, such as hexyl and methyl $(CdSe_2CNMeHex)_2$, are air stable and are found to be excellent precursors for CdSe.[44] GC–MS studies have suggested the decomposition mechanisms of symmetrical diselenocarbamates, which produce selenium clusters.[45] However, unsymmetrical diselenocarbamates (with alkyl groups longer than hexyl) produce only the metal selenide and organic by-products. Revaprasadu *et al.* have also recently doped nanoparticulate ZnS with Mn, giving emission in the orange region of the visible spectrum rather than the blue.[46]

Hines and Guyot-Sionnest[47] and Revaprasadu *et al.*[48] reported simultaneously the preparation of TOPO capped ZnSe. Hines and Guyot-Sionnest[47] used the same methodology adopted by Bawendi *et al.*,[35] *i.e.* dimethylzinc and tri-*n*-octylphosphine selenide as precursors. However, the use of TOPO/TOP as capping agents failed and a mixture of hexadecylamine and TOPO was used instead. Revaprasadu *et al.*[48] used the single source complex $[EtZn(E_2CNEt_2)]_2$ (E = S, Se) in TOPO to prepare crystalline capped nanoparticles of ZnE. Comparison of Hines' metal alkyl route and the single source route suggests there may be surface differences in the as-

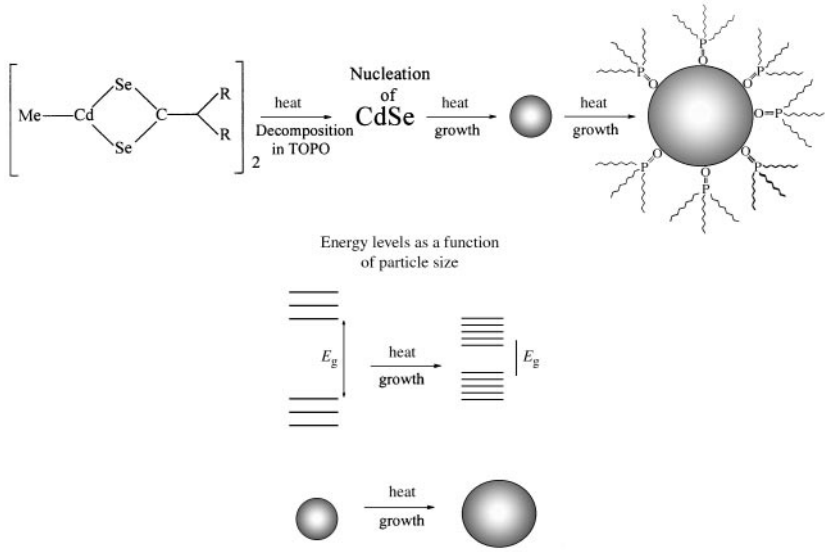

Fig. 4 Theoretical decomposition schematic for the preparation of TOPO capped CdSe using a single source precursor.

prepared materials. Comparisons of CdSe nanoparticles prepared by single source precursors and the metal alkyl by IR spectroscopy again suggest different surface environments which are currently under investigation by our group.

The preparation of lead chalcogenide nanocrystals has also been achieved using various lead dithio- and diseleno-carbamates.[49] Group IV–VI semiconductors are a prime example of materials where precursors such as highly toxic lead alkyls are undesirable. The nanoparticles of lead chalcogenides have a cubic shape inherent in PbS materials (Fig. 5). Nanoparticles of PbE and CdE (E = Se, S) have been linked using bridging ligands such as 2,2′-bipyrimidine.[43]

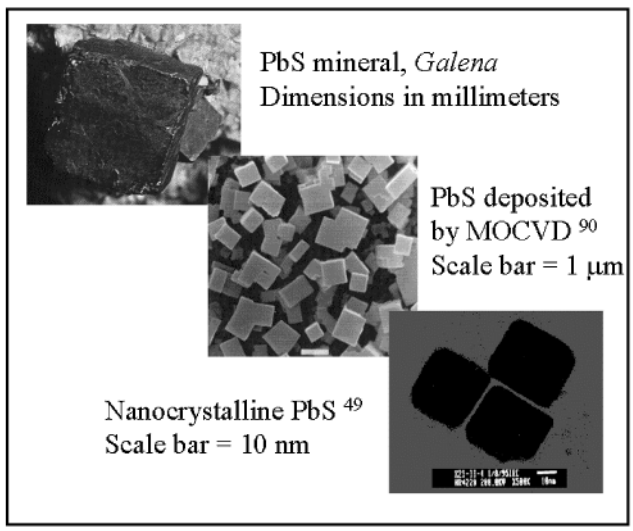

Fig. 5 Photo, SEM and TEM of PbS of various sizes.

Nanoparticles of TOPO capped II–VI materials are found to degrade in the presence of light and oxygen, forming unstable chalcogen oxide species which leave surface defects.[50] One significant recent advance is the preparation of quantum dot–quantum wells, where one nanoparticle is capped by a layer of another semiconductor.[51,52] The surface is then protected and photoluminescence of the core semiconductor is enhanced, with quantum yields of up to 50%. Experiments have also indicated that upon excitation, the hole is confined to the core whilst the electron is delocalised through the entire structure. Precursors for such core–shell structures are generally metal alkyls and bis(trimethylsilyl)sulfide, but core–shell structures of CdSe–CdS have also been grown using single molecular precursors.[53] Thin films of CdSe nanoparticles in a ZnSe matrix, grown by electrospray-organometallic chemical vapour deposition, have also been reported.[54]

The preparation of III–V materials is significantly more difficult to achieve. The increased covalent character results in the routes to crystal formation being hampered by large energetic barriers. There is, therefore, no discrete nucleation step and separation of nucleation and growth is difficult. Precursors for III–V materials, such as $InCl_3$ coordinate to the reaction solvent inhibiting direct reaction between the reagents, which is often suggested as a key step in the nucleation and growth steps.[55] Nozik and coworkers[56] and Alivisatos and coworkers[57] have developed the dehalosilylation reaction as first reported by Wells *et al.*,[58] and Barron and coworkers,[59] to prepare III–V quantum dots capped with TOPO or TOP. In these reactions, $InCl_3$ is complexed to either TOPO or TOP, followed by the injection of $E(SiMe_3)_3$ (E = As, P). Growth and annealing take up to 7 days at *ca.* 265 °C. The size distribution is large (*ca.* 20%) and the final product is contaminated by oxide side products. Photoluminescence from the final material is near to band edge and dependent upon surface oxidation. InP dots are reported not to luminesce until the surface is oxidised, highlighting the importance of the surface state whilst emission from InAs dots is insensitive to oxidation.[57,60] The formation of stable surface species is reported to hinder size fractionation procedures, but is reversible using hydrogen fluoride etching processes.[61]

We have recently developed a single molecular precursor route to InP and GaP using metal diorganophosphides as precursors.[62,63] The compounds $M(PBu^t_2)_3$, (M = Ga, In) are dissolved in 4-ethylpyridine and heated at reflux for up to 7 days. Nanoparticles of *ca.* 8 nm diameter (±20%) could be isolated by solvent/non-solvent interaction and a glass formed upon prolonged evacuation. These single source routes avoid the need for volatile precursors such as silylated pnictides. The use of diorganophosphides has been extended to the preparation of high quality TOPO and 4-ethylpyridine capped Cd_3P_2 using the precursor $[MeCdP(Bu^t)_2]_3$.[64,65] Cadmium phosphide is reported to have a large excitonic diameter (*ca.* 36 nm, *cf.* CdS *ca.* 3 nm) which means the band edge can be shifted over a wide spectral range upon quantum confinement of the charge carriers. Nanometer sized Cd_3P_2 prepared by conventional colloidal chemistry can have band gaps between 0.5 and 4.0 eV. Colloidally prepared Cd_3P_2 is air-sensitive and decomposes upon illumination, whilst TOPO capped Cd_3P_2 appears more resistant to photodegradation. The organic substituent on the diorganophosphide appears to control reactions, changing the

tert-butyl group for a phenyl or cyclohexyl group results in bulk cadmium with an extremely small amount of nanometric material. GC–MS and TGA analysis were used to deduce two competing mechanisms; reductive elimination, which leads to elemental cadmium and β-hydrogen elimination (for $[MeCdP(Bu^t)_2]_3$) resulting in nanoparticles of Cd_3P_2. The mechanisms were found to be temperature dependent, with β-hydrogen elimination predominating at lower (< 150 °C) temperatures giving purer Cd_3P_2.

Zinc phosphide quantum dots have also been prepared by using dimethylzinc and di-*tert*-butylphosphine in either TOPO or 4-ethylpyridine. The nanocrystals are *ca.* 4 nm in diameter, with band gaps shifted up to 3.5 eV depending upon the capping agent and reaction conditions.[66]

TOPO is not the only Lewis base to be utilised in nanocrystal preparation. Nanoparticles of GaP and GaAs have been synthesised by refluxing $GaCl_3$ with either $P(Na/K)_3$ or $As(Na/K)_3$ in toluene/glyme to give crystalline glyme capped quantum dots.[67] The same reaction in aromatic solvents alone again yields nanoparticles which are capped with methanol upon extraction. Nanoparticulate GaP has also been produced through the thermolysis of a single source precursor $[X_2GaP(SiMe_3)_2]_2$ (X = Br, I) and $(Cl_3Ga_2P)_n$ with both decomposing at relatively low temperatures whilst under vacuum to yield crystalline Q-GaP.[68] Q-GaP and Q-GaAs have also been produced by thermolysis of $[H_2GaE(SiMe_3)_2]_3$ (E = P, As) at 450 °C in xylenes, giving nanoparticles *ca.* 5 nm in diameter. The capping agent was not discussed.[69]

The groups of Alivisatos[70] and Nozik[71] used a similar method to Bawendi's[35] to produce GaAs nanoparticles, by refluxing $GaCl_3$ and tris(trimethylsilyl)arsine in quinolene at 240 °C for 3 days. Flame annealing at 450 °C was used to improve crystallinity, but resulted in a slight loss of solubility. Crystalline InAs nanoparticles of size 1–8 nm have been synthesised by the reaction of $In(acac)_3$ with tris(trimethylsilyl)arsine in triglyme at 216 °C for 70 h. Investigations were also carried out into the non-linear optical properties of the resulting materials.[72] The same method was applied successfully to GaAs using $Ga(acac)_3$.[73] These methods are attractive because they present routes that do not use hazardous precursors, *e.g.*, phosphine or arsine.

Nanoparticles of CdSe has been also been synthesised by pyrolysis of the single source precursors $Cd(SePh)_2$ and $[Cd(SePh)_2]_2[Et_2PCH_2CH_2PEt_2]$ in 4-ethylpyridine.[74] Cd_3P_2 has been produced by the methanolysis of $Cd[P(SiPh_3)_2]_2$.[75]

Manipulation of quantum dots

The organisation of quantum dots into ordered structures presents a significant challenge and lends itself to potential industrial applications. Superlattices of TOPO capped CdSe have been prepared by controlled crystallisation in an octane–octanol mixture under reduced pressure.[76] Alivisatos and coworkers have also prepared dimers of TOPO capped CdSe by linking the nanoparticles with *N*-methyl-4-sulfanylbenzamide followed by size selective precipitation.[77] Alivisatos and coworkers have also investigated the effects of mixing organically capped CdSe with the conjugated polymer poly[2-methoxy,5-(2′-ethyl)hexyloxy-*p*-phenylenevinylene] (MEH-PPV).[78] TOPO capped nanoparticles had the surface ligand exchanged for pyridine. The pyridine capped dots were mixed with a solution of polymer and spin coated onto indium tin oxide (ITO) coated glass. Excitation of the polymer resulted in an electron being transferred onto the nanoparticle. This resulted in quenching of polymer luminescence, consistent with charge separation at the polymer/quantum dot interface. The resulting Q-CdSe/MEH-PPV composite luminescence efficiency was found to be 12% when loaded with high concentrations of quantum dots. TEM demonstrated a distinct interconnected network forming at concentrations of *ca.* 90% CdSe. The incorporation of quantum dots into a conducting medium is an essential step towards device fabrication.

The idea of incorporation was further advanced by the removal of surface TOPO and replacement with a polymer back-bone rather than a simple dispersion.[79,80] In this method, nanoparticles of either CdSe or CdSe coated with ZnSe, were prefabricated by the normal method, and added to a solution of copolymer containing phosphine/phosphine oxide norbornene blocks. The addition of $[MTD]_{300}$ and $[NBE\text{-}CH_2O(CH_2)_5P(Oct)_2]_{26}$ (MTD = methyltetracyclododecene, NBE = 5-norbornen-2-yl) resulted in excellent take up of the quantum dots, and led to increased fluorescence, whilst the addition of $[MTD]_{300}$ alone had negligible results. Further addition of the polymer resulted in an increase of 2% in the quantum yield, indicating passivation of the quantum dots by the polymer bound phosphine. TEM experiments showed networks of nanoparticles segregated by phosphine rich domains. An investigation was also undertaken into the potential competition between TOPO and TOP to passivate the surface of the crystals. Further addition of TOPO resulted in a small increase in luminescence, whilst addition of TOP doubled the emission. This suggests TOP binds to the unpassivated selenium sites, whilst TOPO specifically binds to cadmium.

Thin films have also been prepared by spin-coating TOPO capped nanoparticles onto various substrates such as nano-polished monocrystalline semiconductor wafers.[81] Further layers can be added by various methods such as chemical bath (electroless) deposition or MOCVD. Fig. 6 shows a nano-composite prepared by spin coating TOPO capped CdSe onto a GaAs substrate, followed by deposition of a layer of CdS by chemical bath.

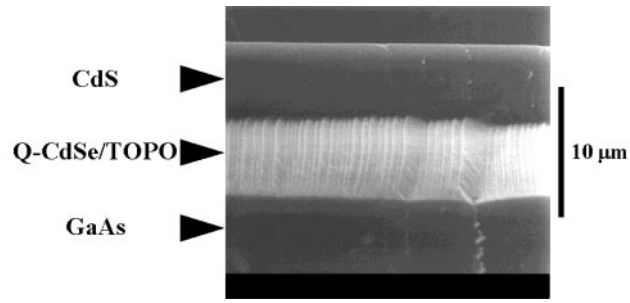

Fig. 6 SEM side profile of a nanocomposite heterostructure. The substrate is nanopolished GaAs. A layer of nanocrystalline CdSe is spin coated on top, followed by a layer of CdS deposited by chemical bath deposition.[81]

Other recent advances of note are the uses of DNA in nanocrystal processing, with possible applications in developing chemical biosensors. Mirkin *et al.* have used thiol capped, non complementary DNA oligonucleotides to assemble 13 nm Au quantum dots into a macroscopic material.[82] In similar work, Alivisatos *et al.* synthesised *ca.* 3 nm Au nanocrystals which were then attached to single strand oligonucleotides, which organised into spatially defined structures on addition of a single complementary DNA strand, due to Watson–Crick interactions.[83]

Applications

Alivisatos and coworkers have produced an electroluminescence device using TOPO capped CdSe nanocrystals with sizes between 3 and 5 nm, and a semiconducting polymer, poly(*p*-phenylene–vinylene) (PPV).[84] The device was fabricated by multiple exposures of a indium tin oxide (ITO) plate or ITO/PPV plate, pre-treated with hexane thiol, to a toluene solution of nanocrystals. For stability, the layer is built up to 1000 Å. Electrical contact is made by silver coated magnesium. The colour of the emission can be controlled by the particle sizes giving red to yellow emissions. At increased voltage, green luminescence from the polymer layer is predominant. This was

then improved upon by fabrication of a LED using CdSe nanocrystals capped with CdS instead of the organic ligand.[85] The device was produced by using the same basic techniques but using a pre-PPV polymer precursor deposited on ITO coated glass. This film was then annealed at 300 °C for 3 h before having CdSe/CdS spin deposited onto the PPV. The use of CdSe/CdS instead of CdSe/TOPO results in an increase in efficiency by a factor of eight and a factor of ten increase in lifetime. This is attributed to the inorganically capped particles being resistant to photo-oxidation.

Electroluminescence has been reported from TOPO capped CdSe when incorporated into thin films of poly(vinylcarbazole) (PVK) and an oxadiazole derivative.[86] The film was then sandwiched between ITO and Al electrodes. The device was tuneable from *ca.* 530 to 650 nm by varying the size of the dots. Low temperature studies (77 K) also indicated that only the nanocrystals luminesced at low voltage, whilst at higher voltages both the dots and the PVK matrix electroluminesce. Electroluminescence efficiency was also found to increase at 77 K.

The anaerobic conditions employed to manufacture TOPO capped quantum dots used in device fabrication have the advantage of avoiding potential doping with oxygen. For this reason, aqueous routes to nanocrystals were often assumed to be unfavourable. However, Gao *et al.* fabricated a device using CdSe nanocrystals synthesised using a Cd salt and H_2Se in aqueous solution with thiolactic acid, at pH 11.[87] The thiolactic acid acted as a capping agent, effectively giving the particle a negatively charged surface, which facilitates adsorption onto the substrate. The size of the particles was controlled by altering the molar ratios between Cd^{2+} and H_2Se, with intense fluorescence obtained by adding an excess of Cd^{2+} shortly after synthesis. Optical glass and ITO coated glass which had been coated with PEI [poly-(ethyleneimine)] to give a positively charged surface, were used as substrates. The next step involved the exposure of the substrate to a solution of the nanoparticles for a defined time giving a monolayer of quantum dots. Positively charged PAH [poly(allylamine hydrochloride)] or a precursor for poly(*p*-phenylene–vinylene) (pre-PPV) were then adsorbed on top. The application of a number of inorganic and organic layers was repeated until 20 double layers had been applied. The CdSe/PPV multilayer film was then obtained by heating the CdSe/pre-PPV at 130 °C *in vacuo* for 11 h. The device was finished by the evaporation of an aluminium electrode on the top layer. The device produced almost white light electroluminescence (500–850 nm) under a forward bias of 3.5–5 V with the positive pole on the ITO electrode. Such a broad emission, similar to that of the CdSe solution, was attributed to deep traps, surface defects and a large size distribution. It is interesting to note that a device incorporating aqueous derived nanocrystals has a broad emission, which may be attributable to doping with oxygen. The device is reported to have a longer lifetime than similar simple organic devices.

Single electron transistors have also been reported in devices in which a single nanoparticle is trapped between two gold electrodes by dithiols.[88] Biological applications are now being explored such as water soluble semiconductor nanoparticle fluorophores used to examine mouse fibroplasts.[89] Other potential uses include amplification of electromagnetic radiation in fibre optic communication systems and non-linear optical effects in the region of absorption edges.

Advances in the preparation of highly luminescent, nearly monodispersed nanocrystals have led to materials which now have the potential for use in optoelectronic applications. The use of oxide nanoparticles in photovoltaic devices is well documented, however, a wide range of other applications are now being investigated. The reproducible preparation and easy manipulation of organically passivated quantum dots offers simple routes to practical devices. The widening of the 'band gap' in a semiconductor quantum dot can be controlled by careful alteration of the particle's dimensions (often referred to as band gap engineering) and has opened up possible new areas of electronic research with a wide range of applications such as tunable diodes and lasers. The degree of control over small particles is exhibited in the preparation of single electron transistors, where the particle can be specifically placed between two electrodes. The preparation and manipulation of semiconductor nanoparticles is an interesting and exciting area of current research.

Acknowledgements

P. O'B. is the Sumitomo/STS Professor of Material Chemistry. We thank the EPSRC for continuing support for the preparation of nanoparticles. M. G. thanks EPSRC and British Telecom for funding postgraduate studies *via* a CASE award.

Notes and references

1 D. R. Lide, *CRC Handbook of Chemistry and Physics*, CRC Press, 73rd student edn., Boca Raton, FL, 1993.
2 M. L. Steigerwald and L. E. Brus, *Acc. Chem. Res.*, 1990, **23**, 183.
3 H. Weller, *Angew. Chem., Int. Ed. Engl.*, 1993, **32**, 41.
4 N. Chestoy, T. D. Harris, R. Hull and L. E. Brus, *J. Phys. Chem.*, 1986, **90**, 3393.
5 L. E. Brus, *J. Phys Chem.*, 1986, **90**, 2555.
6 L. E. Brus, *J. Phys. Chem.*, 1983, **79**, 5566.
7 U. Banin, Y. W. Cao, D. Katz and O. Millo, *Nature*, 1999, **400**, 542.
8 M. Brust, J. Fink, D. Bethel, D. J. Schriffren and C. Kiely, *J. Chem. Soc., Chem. Commun.*, 1995, 1655.
9 J. Tanori and M. P. Pileni, *Adv. Mater.*, 1995, **7**, 862.
10 R. A. Andrievskii, *Russ. Chem. Rev.*, 1994, **63**, 411.
11 A. Kornowski, M. Giersig, M. Vogel, A. Chemseddine and H. Weller, *Adv. Mater.*, 1993, **5**, 634.
12 A. Fojtik and A. Henglein, *Chem. Phys. Lett.*, 1994, **221**, 363.
13 V. K. La Mer and R. H. Dinegar, *J. Am. Chem. Soc.*, 1950, **72**, 4847.
14 T. Johnson and V. K. La Mer, *J. Am. Chem. Soc.*, 1947, **69**, 1184.
15 R. J. Hunter, *Foundations of Colloid Science*, Oxford University Press, 6th edn., Oxford, 1993, vol. 1, pp. 13–17.
16 A. Henglein, *Pure Appl. Phys.*, 1984, **56**, 1215.
17 R. Rossetti, J. L. Ellison, J. M. Gibson and L. Brus, *J. Chem. Phys.*, 1984, **80**, 4464.
18 R. Rossetti, R. Hull and J. M. Gibson, *J. Chem. Phys.*, 1985, **82**, 552.
19 H. Weller, *Adv. Mater.*, 1993, **5** 88.
20 H. Weller, A. Fojtik and A. Henglein, *Chem. Phys. Lett.*, 1985, **117**, 485.
21 M. Haase, H. Weller and A. Henglein, *Ber. Bunsen-Ges. Phys. Chem.*, 1988, **92**, 1103.
22 K. Sookal, B. S. Cullum, S. Michel Angel and C. J. Murphy, *J. Phys. Chem.*, 1996, **100**, 4551.
23 Y. Wang and N. Herron, *J. Phys. Chem.*, 1987, **91**, 257.
24 H. J. Wazke and J. H. Fendler, *J. Phys. Chem.*, 1987, **91**, 854.
25 T. Abe, Y. Tachibana, T. Uematsu and M. Iwamoto, *J. Chem. Soc., Chem. Commun.*, 1995, 1617.
26 Y. Wang, A. Suna, W. Mahler and R. Kasowski, *J. Chem. Phys.*, 1987, **87**, 7315.
27 A. R. Kortan, R. Hull, R. L. Opila, M. G. Bawendi, M. L. Stiegerwald, P. J. Carrol and L. E. Brus, *J. Am. Chem. Soc.*, 1990, **112**, 1327.
28 M. L. Steigerwald, A. P. Alivisatos, J. M. Gibson, T. D. Harris, R. Kortan, A. J. Muller, A. M. Thayer, T. M. Duncan, D. C. Douglas and L. E. Brus, *J. Am. Chem. Soc.*, 1988, **110**, 3046.
29 E. S. Brigham, C. S. Weisbecker, W. E. Rudzinski and T. E. Mallouk, *Chem. Mater.*, 1996, **8**, 2121.
30 J. E. McDougall, H. Eckert, G. D. Stucky, N. Herron, Y. Wang, K. Moller, T. Bein and D. Cox, *J. Am. Chem. Soc.*, 1989, **111**, 8006.
31 G. Cao, L. K. Rabenberg, C. M. Nunn and T. E. Mallouk, *Chem. Mater.*, 1991, **3** 149.
32 S. W. Haggata, X. Li, D. J. Cole-Hamilton and J. R. Fryer, *J. Mater. Chem.*, 1996, **6**, 1771.
33 S. W. Haggata, D. J. Cole-Hamilton and J. R. Fryer, *J. Mater. Chem.*, 1997, **7**, 1969.
34 X. Li, J. R. Fryer and D. J. Cole-Hamilton, *J. Chem. Soc., Chem. Commun.*, 1994, 1715.
35 C. B. Murray, D. J. Norris and M. G. Bawendi, *J. Am. Chem. Soc.*, 1993, **115**, 8706.
36 M. Kuno, J. K. Lee, B. O. Dabbousi, F. V. Mikulec and M. G. Bawendi, *J. Chem. Phys.*, 1997, **106**, 9869.

37 J. E. Bowen-Katari, V. L. Colvin and A. P. Alivisatos, *J. Phys. Chem.*, 1994, **98**, 4109.
38 M. Green and P. O'Brien, *Adv. Mater. Opt. Electron*, 1997, **7**, 277.
39 A. L. Efros, M. Rosen, M. Kuno, M. Nirmal, D. J. Norris and M. Bawendi, *Phys. Rev. B: Condens. Matter*, 1996, **54**, 4843.
40 M. Nirmal, D. J. Norris, M. Kuno, M. G. Bawendi, A. L. Efros and M. Rosen, *Phys. Rev. Lett.*, 1995, **75**, 3728.
41 L. R. Becerra, C. B. Murray, R. G. Griffin and M. G. Bawendi, *J. Chem. Phys.*, 1994, **100**, 3297.
42 T. Trindade and P. O'Brien, *Adv. Mater.*, 1996, **8**, 161.
43 T. Trindade, P. O'Brien and X. Zhang, *Chem. Mater.*, 1997, **9**, 523.
44 B. Ludolph, M. A. Malik, P.O'Brien and N. Revaprasdu, *Chem. Commun.*, 1998, 1849.
45 M. Chunggaze, J. McAleese, P. O'Brien and D. J. Otway, *Chem. Commun.*, 1998, 833.
46 N. Revaprasdu, M. A. Malik and P. O'Brien, *Mater. Res. Soc. Symp. Proc.*, 1999, **536**, 353.
47 M. A. Hines and P. Guyot-Sionnest, *J. Phys. Chem. B*, 1998, **102**, 3655.
48 N. Revaprasadu, M. A. Malik, P. O'Brien, M. M. Zulu and G. Wakefield, *J. Mater. Chem.*, 1998, **8**, 1885.
49 T. Trindade, P. O'Brien, X. Zhang and M. Motevalli, *J. Mater. Chem.*, 1997, **7**, 1011.
50 J. E. Bowen-Katari, V. L. Colvin and A. P. Alivisatos, *J. Phys. Chem.*, 1994, **98**, 4109.
51 X. Peng, M. C. Schlamp, A. V. Kadanavich and A. P. Alivisatos, *J. Am. Chem. Soc.*, 1997, **119**, 7019.
52 B. O. Dabousi, J. Rodriguez-Viejo, F. K. Mikulec, J. R. Heine, H. Matoussi. R. Ober, K. F. Jensen and M. G. Bawendi, *J. Phys. Chem. B*, 1997, **101**, 9463.
53 N. Revaprasadu, M. A. Malik and P. O'Brien, *Chem. Commun.*, 1999, 1573.
54 M. Danek, K. F. Jensen, C. B. Murray and M. G. Bawendi, *J. Cryst. Growth*, 1994, **145**, 714.
55 J. R. Heath and J. J. Shiang, *Chem. Soc. Rev.*, 1998, **27**, 65.
56 O. I. Micic, J. R. Sprague, C. J. Curtis, K. M. Jones, J. L. Machol, A. J. Nozik, H. Giessen, B. Fluegel, G. Mohs and N. Peyghambarian, *J. Phys. Chem.*, 1995, **99**, 7754.
57 A. A. Guzelian, J. E. B. Katari, U. Banin, A. V. Kadavanich, X. Peng, A. P. Alivisatos, K. Hamed, E. Juban, R. H. Wolters, C. C. Arnold and J. R. Heath, *J. Phys. Chem.*, 1996, **100**, 7212.
58 R. L. Wells, C. G. Pitt, A. T. McPhail, A. P. Purdy, S. Shafieezad and H. B. Hallock, *Chem. Mater.*, 1989, **1**, 4.
59 M. D. Healy, P. E. Laibinis, P. Stupik and A. R. Barron, *J. Chem. Soc., Chem. Commun.*, 1989, 359.
60 A. A. Guzelian, U. Banin, A. V. Kadavanich, X. Peng and A. P. Alivisatos, *Appl. Phys. Lett.*, 1996, **69**, 1432.
61 O. I. Micic, K. M. Jones, A. Cahill and A. J. Nozik, *J. Phys. Chem. B*, 1998, **102**, 9791.
62 M. Green and P. O'Brien, *Chem. Commun.*, 1998, 2459.
63 M. Green and P. O'Brien, unpublished work.
64 M. Green and P. O'Brien, *Adv. Mater.*, 1998, **10**, 527.
65 M. Green and P. O'Brien, *J. Mater. Chem.*, 1999, **9**, 243.
66 M. Green and P. O'Brien, unpublished work
67 S. S. Kher and R. L. Well, *Chem. Mater.*, 1994, **6**, 2056.
68 R. L. Wells, M. F. Self, A. T. McPhail, S. R. Aubuchon, R. C. Woudenberg and J. P. Jasinski, *Organometallics*, 1993, **12**, 2832.
69 J. F. Janik, R. L. Wells, V. G. Young, A. L. Rheingold and L. A. Guzei, *J. Am. Chem. Soc.*, 1998, **120**, 532.
70 M. A. Olshavsky, A. N. Goldstein and A. P. Alivisatos, *J. Am. Chem. Soc.*, 1990, **112**, 9438.
71 H. Uchida, C. J. Curtis and A. J. Nozik, *J. Phys. Chem.*, 1991, **95**, 5382.
72 H. Unchida, T. Matsunaga, H. Yoneyama, T. Sakata, H. Mori and T. Sasaki, *Chem. Mater.*, 1993, **5**, 716.
73 H. Uchida, C. J. Curtis, P. V. Kamat, K. M. Jones and A. J. Nozik, *J. Phys. Chem.*, 1992, **62**, 1156.
74 J. G. Brennan, T. Siegrist, P. J. Carrol, S. M. Stuczynski, L. E. Brus and M. L. Steigerwald, *J. Am. Chem. Soc.*, 1989, **111**, 4141.
75 M. A. Matchett, A. M. Viano, N. L. Adolphi, R. D. Stoddard, W. E. Buhro, M. S. Conradi and P. C. Gibson, *Chem. Mater.*, 1992, **4**, 508.
76 C. B. Murray, C. R. Kagan and M. G. Bawendi, *Science*, 1995, **270**, 1335.
77 X. Peng, T. E. Wilson, A. P. Alivisatos and P. G. Schulz, *Angew. Chem., Int. Ed. Engl.*, 1997, **36**, 145.
78 N. C. Greenham, X. Peng and A. P. Alivisatos, *Synth. Met.*, 1997, **84**, 545.
79 D. E. Fogg, L. H. Radzilowski, B. O. Dabbousi, R. R. Schrock, E. L. Thomas and M. G. Bawendi, *Macromolecules*, 1997, **30**, 8433.
80 D. E. Fogg, L. H. Radzilowski, R. Blanski, R. R. Schrock and E. L. Thomas, *Macromolecules*, 1997, **30**, 417.
81 S. Norager and P. O'Brien, unpublished work.
82 C. A. Mirkin, R. L. Letsinger, R. C. Mucic and J. J. Storhoff, *Nature*, 1996, **382**, 607.
83 A. P. Alivisatos, K. P. Johnsson, X. G. Peng, T. E. Wilson, C. J. Loweth M. P. Bruchez and P. G. Schulz, *Nature*, 1996, **382**, 609.
84 V. L. Colvin, M. C. Schlamp and A. P. Alivisatos, *Nature*, 1994, **370**, 354.
85 M. C. Schlamp, X. Peng and A. P. Alivisatos, *J. Appl. Phys.*, 1997, **82**, 5837.
86 B. O. Dabbousi, M. G. Bawendi, O. Onitsuka and M. F. Rubner, *Appl. Phys. Lett.*, 1995, **66**, 1316.
87 M. Gao, B. Richter and S. Kirtein, *Adv. Mater.*, 1997, **9**, 802.
88 D. L. Klein, R. Roth, A. K. L. Lim, A. P. Alivisatos and P. L. McEuen, *Nature*, 1997, **389**, 699.
89 M. Bruchez, M. Moronne, P. Gin, S. Weiss and A. P. Alivisatos, *Science*, 1998, **281**, no. 5385, 2013.
90 T. Trindade and P. O'Brien, *Chem. Vap. Deposit.*, 1997, **3**, 75.

Paper 9/04202D

Methylgallium and methylindium: the first sighting of the simplest organic derivatives of Ga(I) and In(I)

Hans-Jörg Himmel,*[a] Anthony J. Downs,[a] Tim M. Greene[a] and Lester Andrews[b]

[a] *Inorganic Chemistry Laboratory, University of Oxford, South Parks Road, Oxford, UK OX1 3QR. E-mail: tony.downs@chem.ox.ac.uk*

[b] *Department of Chemistry, University of Virginia, Charlottesville, Virginia 22901, USA*

Received (in Basel, Switzerland) 6th September 1999, Accepted 6th October 1999

Gallium or indium atoms are shown to react with methane in solid Ar matrices upon UV photolysis (λ = 200–400 nm) to give initially the methylmetal hydride which undergoes photodissociation on broad-band irradiation (λ = 200–800 nm) to yield the methylmetal(I) compound, CH_3M (M = Ga or In); the products are characterised by their IR spectra afforced by the results of DFT calculations.

Volatile organo or hydrido derivatives of the group 13 metals excite attention particularly by virtue of their use or potential as precursors to the metal or a compound semiconductor.[1,2] Yet the number of such compounds, and especially those with the requisite properties of volatility, thermal stability, *etc*. decreases sharply when aluminium gives way to gallium, and again when gallium gives way to indium.[2,3] The only monomethyl compound of the group 13 metals to be detected previously in the laboratory is CH_3Al, which has been identified in the gas phase by its pure rotational spectrum,[4] by neutralization–reionization mass spectrometry (NRMS),[5] and also in a cooled jet by high-resolution resonance-enhanced multiphoton ionization (REMPI) spectroscopy.[6] Otherwise we are largely dependent on quantum chemical methods[7–10] for whatever knowledge of CH_3Al and CH_3Ga we possess. The incentive for characterising these molecules comes partly from their potential intermediacy in chemical vapour deposition processes starting from trivalent methylmetal compounds[1,2] and partly from the desire to gain a better understanding of the bonding in organometallic compounds of the univalent group 13 metals.

Irradiation of a CH_4-doped Ar matrix containing thermally generated gallium atoms with UV light with λ = 200–400 nm over a period of 10 min resulted in the appearance of new IR absorptions at 1719.7, 752.9, 528.7 and 475.5 cm^{-1}, apparently belonging to a single product **1a** [Fig. 1(b)]. The most intense and distinctive features were those at 1719.7 and 752.9 cm^{-1}. Similar results have been reported earlier,[11,12] the new bands being attributed to the divalent gallium species CH_3GaH formed by insertion of a Ga atom into a C–H bond of methane. Continued irradiation under these conditions produced little further change in the spectrum. By contrast, after photolysis for a further 10 min, with broad-band UV–VIS light (λ = 200–800 nm), the matrix exhibited the IR spectrum depicted in Fig. 1(c). Hence it was apparent that the bands due to **1a** had been totally extinguished, to be replaced by a new family of bands having a common origin in a second product **2a**. These occurred at 2986.9, 1403.9, 1147.9 and 476.2 cm^{-1}, the feature at lowest frequency being the most intense. Extending the period of photolysis gave little further change in the spectrum. The reaction was also followed by monitoring the UV–VIS spectrum of the matrix. Our results are in line with those of Lafleur and Parnis[11] and show that the formation of **1a** occurs at the expense of Ga atoms. The experiments were repeated using either CD_4 or $^{13}CH_4$ as the reagent; the corresponding frequencies for the normal and isotopically enriched versions of **1a** and **2a** are given in Table 1. Experiments carried out for various metal and methane concentrations show that strong signals of **2a** are obtained for conditions that have favoured the generation of **1a** (the greatest yield was achieved using a furnace temperature of 950 ºC and an argon matrix containing 2% CH_4). The obvious inference to be drawn from the IR spectra is that **2a** is the simple methylgallium(I) molecule, CH_3Ga.[13] Previous experiments with GaH_2 and InH_2 have shown that under similar photolysis conditions, cleavage of a Ga–H or In–H bond leads to the formation of the monohydrides, GaH and InH, respectively.[14] DFT calculations[15,16] lead to an

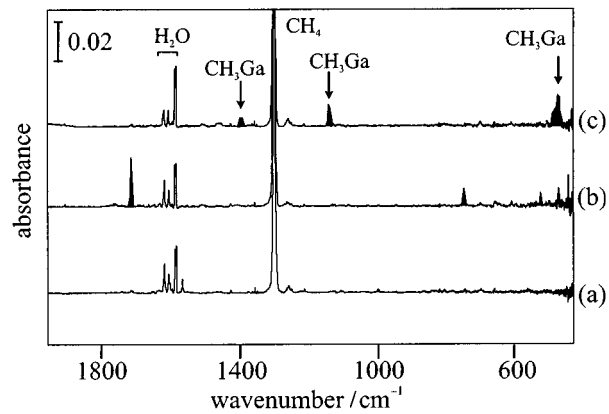

Fig. 1 IR spectra of an Ar matrix containing Ga atoms and CH_4: (a) after deposition; (b) after photolysis with UV light (λ = 200–400 nm) and (c) after broad-band UV-VIS photolysis (λ = 200–800 nm).

Table 1 Observed and calculated frequencies for CH_3Ga

$^{12}CH_3Ga$		$^{13}CH_3Ga$		CD_3Ga			
Obs.	Calc.[a]	Obs.	Calc.[a]	Obs.	Calc.[a]	Assignment	Description of vibrational mode
2986.9	2978.3 (22)	2985.8	2977.3 (23)	2200.4	2138.4 (5)	$\nu_1(a_1)$	$\nu_{sym}(C–H)$
1147.9	1223.2 (21)	1138.8	1215.4 (18)	902.8	948.5 (36)	$\nu_2(a_1)$	$\delta_{sym}(CH_3)$
476.2	472.0 (73)	464.7	459.8 (70)	[b]	432.3 (57)	$\nu_3(a_1)$	ν(Ga-C)
[b]	3049.5 (67)	[b]	3040.7 (67)	[b]	2254.8 (36)	$\nu_4(e)$	$\nu_{asym}(C–H)$
1403.9	1459.6 (33)	1400.1	1457.1 (33)	1025.4	1057.5 (17)	$\nu_5(e)$	$\delta_{asym}(CH_3)$
[b]	498.7 (7)	495.7	494.1 (7)	[b]	373.1 (4)	$\nu_6(e)$	$\rho(CH_3)$

[a] Calculation for singlet $CH_3{}^{69}Ga$. Symmetry C_{3v}: C–H = 1.101 Å, Ga–C = 2.049 Å, H–C–Ga = 111.7° . Intensities (km mol^{-1}) are given in parentheses; r.m.s. deviation of observed from calculated frequencies 3.7%. [b] Too weak to be observed or hiddenby methane absorptions.

Table 2 Observed and calculated frequencies for CH_3In

$^{12}CH_3In$		$^{13}CH_3In$		CD_3In			
Obs.	Calc.[a]	Obs.	Calc.[a]	Obs.	Calc.[a]	Assignment	Description of vibrational mode
2905.2	2989.1 (53)	[b]	2986.3 (54)	[b]	2141.5 (17)	$\nu_1(a_1)$	$\nu_{sym}(C–H)$
1115.3	1220.2 (42)	1107.5	1212.3 (39)	868.1	936.6 (49)	$\nu_2(a_1)$	$\delta_{sym}(CH_3)$
422.1	425.9 (53)	407.7	413.8 (50)	[b]	392.0 (41)	$\nu_3(a_1)$	ν(In–C)
2976.2	3086.5 (78)	[b]	3076.1 (80)	[b]	2279.4 (38)	ν_4(e)	$\nu_{asym}(C–H)$
1424.0	1475.0 (38)	1419.6	1471.6 (38)	[b]	1071.3 (22)	ν_5(e)	$\delta_{asym}(CH_3)$
[b]	533.1 (0.1)	[b]	530.6 (0.1)	[b]	397.7 (0.1)	ν_6(e)	$\rho(CH_3)$

[a] Calculation for singlet $CH_3{}^{115}In$. Symmetry C_{3v}: C–H = 1.103 Å, In–C = 2.226 Å, H–C–In = 111.5°. Intensities (km mol^{-1}) are given in parentheses; r.m.s. deviation of observed from calculated frequencies 5.7%. [b] Too weak to be observed or hidden by methane absorptions.

equilibrium geometry with C_{3v} symmetry for the CH_3Ga molecule. There are therefore six distinct IR-active vibrational fundamentals spanning the representation $3a_1 + 3e$. Our experiments located IR absorptions with relative intensities, frequencies and isotopic shifts in close accord with those predicted here and elsewhere[7,8] by quantum chemical calculations for four of the fundamentals (Table 1). Of the two missing features that due to ν_4 (*e*) was most probably masked by the strong methane absorption, whereas that due to ν_6 (*e*) lacked the intensity to be detected. Quantum mechanical calculations indicate that the excited electron originates in an orbital with a high electron density along the Ga–H axis,[17] so that photodissociation of the Ga–H bond may result. Other possible explanations include the formation of methylgallium from the metal atoms and methyl radicals following decomposition of methylgallium hydride to CH_3· and Ga and H atoms.

Analogous experiments were carried out to follow the reaction of methane with thermally evaporated In. A similar pattern was observed. Thus, irradiation of the matrix at wavelengths between 200 and 400 nm for 10 min led to the appearance of new IR absorptions at 1545.9 and 696 cm^{-1} (Fig. 2). These showed obvious affinities to the IR bands belonging to **1a** and are most plausibly ascribed to the indium analogue **1b**. Subsequent exposure of the matrix to broad-band UV-VIS radiation (λ = 200-800 nm) for 10 min brought about the disappearance of the absorptions due to **1b** with the simultaneous growth of a new set of absorptions at 2976.2, 2905.2, 1424.0, 1115.3 and 422.1 cm^{-1}. The circumstances of the experiment, allied to the spectroscopic resemblance of this second product to **2a**, suggest that it is to be identified with the indium analogue **2b**, CH_3In. The experiments giving rise to the products **1b** and **2b** were repeated using either CD_4 or $^{13}CH_4$ as the reagent, with the results included in Table 2. DFT calculations[15,16] give an optimized geometry resembling closely that of the gallium compound and having the vibrational properties listed in Table 2. In this case our experiments identify five of the six fundamentals, the only absentee being the CH_3 rocking mode, $\rho(CH_3)$, which is anticipated in any case to be unusually weak in IR absorption. Information about the isotopomers CD_3In and $^{13}CH_3In$ is unfortunately rather sparse, partly because we were unable to secure such high concentrations and partly because of the masking effects of other absorptions. Nevertheless, the experimental results approximate closely to the properties computed by DFT methods.

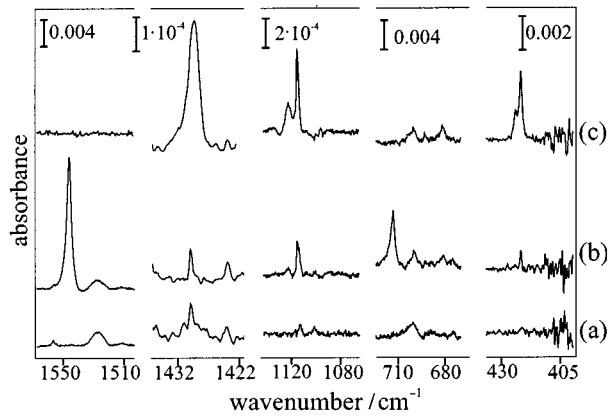

Fig. 2 IR spectra of an Ar matrix containing In atoms and CH_4: (a) after deposition; (b) after photolysis with UV light (λ = 200–400 nm); and (c) after broad-band UV–VIS photolysis (λ = 200–800 nm).

Experiments were also carried out to explore the effects of co-condensing laser-ablated indium atoms with methane and an excess of argon. In this case, IR bands due to both the products **1b** and **2b** were observed upon deposition, presumably as a result of the UV-VIS radiation emanating from the metal target. The subsequent response of the products to further photolysis was as detailed above. These experiments also support our assignments to monometallic species, as it is known[18,19] that laser ablation of solid elements generates predominantly atoms rather than aggregates.

The authors thank (i) the EPSRC for support of this research and for the award of an Advanced Fellowship to T. M. G., and (ii) the Deutsche Forschungsgemeinschaft for the award of a postdoctoral grant to H.-J. H.

Notes and references

1 *E.g.* J. R. Heath and J. J. Shiang, *Chem. Soc. Rev.*, 1998, **27**, 65.
2 *Chemistry of Aluminium, Gallium, Indium and Thallium*, ed. A. J. Downs, Blackie, Glasgow, U.K., 1993.
3 A. J. Downs, *Coord. Chem. Rev.*, 1999, **189**, 59.
4 J. S. Robinson and L. M. Ziurys, *Astrophys. J. Lett.*, 1996, **472**, L131.
5 R. Srinivas, D. Sülzle and H. Schwarz, *J. Am. Chem. Soc.*, 1990, **112**, 8334.
6 D. Clouthier, unpublished results referred to in ref. 7.
7 B. C. Hoffman, C. D. Sherrill and H. F. Schaefer III, *J. Mol. Struct. (THEOCHEM)*, 1996, **370**, 93.
8 B. S. Jursic, *J. Mol. Struct. (THEOCHEM)*, 1998, **428**, 61.
9 D. J. Fox, D. Ray, P. C. Rubesin and H. F. Schaefer III, *J. Chem. Phys.*, 1980, **73**, 3246.
10 S. Q. Jin, Y. Xie and H. F. Schaefer III, *J. Chem. Phys.*, 1991, **95**, 1834.
11 R. D. Lafleur and J. M. Parnis, *J. Phys. Chem.*, 1992, **96**, 2429.
12 Z. L. Xiao, R. H. Hauge and J. L. Margrave, *Inorg. Chem.*, 1993, **32**, 642.
13 IR absorptions attributed to methylgallium were recently observed following the high temperature decomposition of alkylgallium compounds: J. Müller, H. Sternkicker, U. Bergmann and B. Atakan, personal communication.
14 P. Pullumbi, C. Mijoule, L. Manceron and Y. Bouteiller, *Chem. Phys.*, 1994, **185**, 13.
15 DFT calculations employed GAUSSIAN 98 (B3LYP hybrid method, 6-311G* basis set for CH_3Ga and LANL2DZ for CH_3In). No scaling factor was used in the computation of vibrational frequencies.
16 GAUSSIAN 98, Revision A.3: M. J. Frisch *et al.*, Gaussian Inc., Pittsburgh PA, 1998.
17 H.-J. Himmel, T. M. Greene and A. J. Downs, unpublished work.
18 L. Andrews, D. V. Lanzisera and P. Hassanzadeh, *J. Phys. Chem. A*, 1998, **102**, 3259.
19 H. Wang, A. P. Salzberg and B. R. Weiner, *Appl. Phys. Lett.*, 1991, **59**, 935.

Communication 9/07283G

A solid-state phase transition at 41 K involving the cooperative ordering of a fluxional pseudo-Jahn–Teller Cu^{II} system

Michael A. Leech,*[a] Nayan K. Solanki,[b] Malcolm A. Halcrow,[c] Judith A. K. Howard[a] and Slimane Dahaoui[a]

[a] *Department of Chemistry, University of Durham, South Road, Durham, UK DH1 3LE. E-mail: m.a.leech@dur.ac.uk*
[b] *Department of Chemistry, University of Cambridge, Cambridge, UK CB2 1EW*
[c] *School of Chemistry, University of Leeds, Leeds, UK LS2 9IT*

Received (in Cambridge, UK) 24th August 1999, Accepted 7th October 1999

The complex $[Cu\{2,6\text{-di(pyrazol-1-yl)pyridine}\}_2](BF_4)_2$ undergoes a solid-state phase transition at 41 K, involving the cooperative ordering of its planar dynamic pseudo-Jahn–Teller system; this unique phase transition is characterised by single-crystal X-ray diffraction techniques, employing an open-flow helium cryostat.

The structural and electronic consequences of the Jahn–Teller effect in transition metal chemistry continue to be well studied.[1] For Cu^{II} complexes of meridional tris-N-donor ligands, the Jahn–Teller distortion takes the form of an elongated axis, which in the solid state is often dynamically disordered in the molecular *xy* plane (Scheme 1).[2–4]

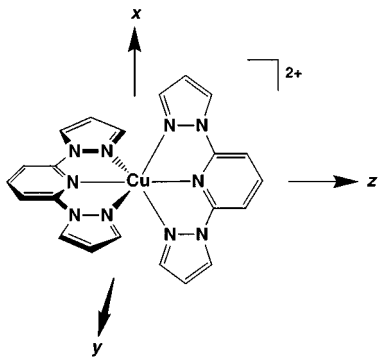

Scheme 1 Molecular axes of $[CuL_2]^{2+}$.

We have recently described one compound that undergoes this behaviour, namely $[CuL_2](BF_4)_2$ [L = 2,6-di(pyrazol-1-yl)pyridine], whose powder EPR spectrum at room temperature exhibits the 'inverse' $g_\perp > g_\parallel > g_e$ pattern typical of a planar dynamic $\{d_{x^2-y^2}\}^1$ Jahn–Teller system.[4] At lower temperatures, this spectrum becomes rhombic as the Jahn–Teller fluxionality is frozen out and the static $g_\parallel > g_\perp > g_e$ spectrum is reached only below 20 K.[4,5] In order to quantify the solid state fluxionality in $[CuL_2](BF_4)_2$,[6] we have undertaken a variable temperature X-ray diffraction study of this compound. We describe herein that it undergoes a unique[1] reversible phase transition at 41 K, involving a complex ordering of the Jahn–Teller axis of elongation in the molecular *xy* plane.

The structure was determined both above (**1**: 50 K) and below (**2**: 31 K) the phase transition. The structure at 50 K reveals one $[CuL_2]^{2+}$ and two $[BF_4]^-$ ions in the asymmetric unit (Fig. 1). One $[BF_4]^-$ ion is disordered over two positions [0.69(3) and 0.31(3) occupied] equivalent to a rotation of approximately 23° about one B–F bond vector. The Cu coordination is distorted slightly from octahedral geometry owing to the conformational requirements of the tridentate ligands. The bond distances within the Cu coordination sphere (Table 1), show short bonds along the molecular *z*-axis, long bonds along the molecular *x*-axis and intermediate length bonds along the molecular *y*-axis. This range reflects the disorder of the Jahn–Teller axis of elongation about the molecular *x*- and *y*-vectors, with the longer

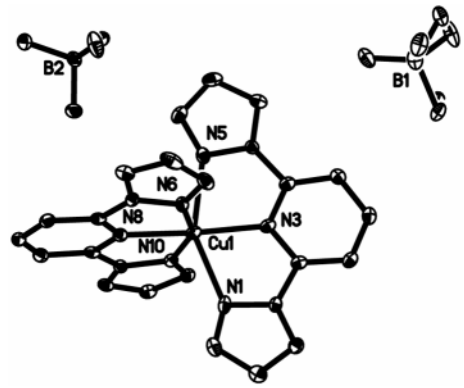

Fig. 1 Crystallographic asymmetric unit at 50 K.

Table 1 Cu–N distances (Å) at 50 and 31 K

		Cu–N distance (Å)		
	50 K	31 K **A**	**B**	**C**
Cu–N6 (*y*-axis)	2.1080(17)	2.058(2)	2.261(2)	2.056(2)
Cu–N10 (*y*-axis)	2.1210(17)	2.076(2)	2.286(2)	2.077(2)
Cu–N5 (*x*-axis)	2.2259(18)	2.282(2)	2.072(2)	2.266(2)
Cu–N1 (*x*-axis)	2.2527(18)	2.290(2)	2.088(2)	2.306(2)
Cu–N3 (*z*-axis)	2.0175(15)	2.028(2)	1.963(2)	2.026(2)
Cu–N8 (*z*-axis)	1.9763(14)	1.967(2)	2.037(2)	1.958(2)

Cu–N bonds along the molecular *x*-axis indicating a larger statistical population in this direction.

On cooling, the crystal undergoes a sharp, reversible phase transition at 41 K accompanied by a tripling of the crystallographic *b* axis. The transition was followed successfully using a CCD diffractometer, by taking a series *hk*0 zone images intermediate to cooling the crystal in −1 K steps. Two such images are shown in Fig. 2, taken at 42 and 40 K. The additional

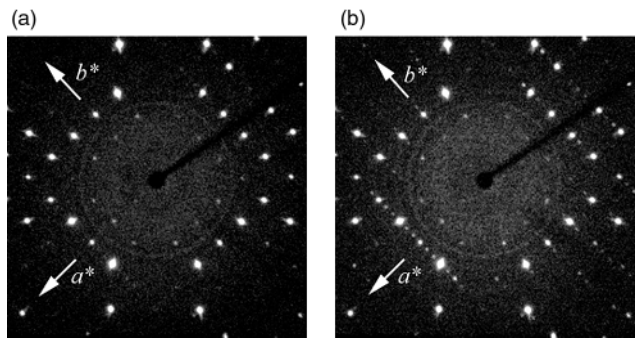

Fig. 2 *hk*0 zone images with the two reciprocal-lattice axes labelled: (a) above the phase change at 42 K and (b) below the phase change at 40 K. The additional reflections in the 40 K image correspond to the tripling of crystallographic *b* axis.

reflections in the 40 K image correspond to the tripling of *b* axis.

The structure at 31 K reveals three $[CuL_2]^{2+}$ and six $[BF_4]^-$ ions in the asymmetric unit (Fig. 3). The Jahn–Teller elongated axis, which is disordered in the molecular *xy* plane above 41 K, is now ordered. The elongated axis of two of the three independent cations (**A** and **C**) are aligned along the molecular *x*-axis, while in the third cation (**B**), it is aligned along the molecular *y*-axis; see Cu–N distances in Table 1. It is interesting to note that the mean Cu–N distances for all three molecules correspond closely to those found in the disordered 50 K structure. This indicates that the population distribution of the elongated axis along the *x* and *y* vectors is similar, both above, and below the phase change. Furthermore, the $[BF_4]^-$ ion, which is disordered above 41 K, is now ordered into three non-equivalent sites, two in one orientation and the third in another. Again, this corresponds to the populations of the two orientations in the disordered structure (0.69 : 0.31). Thus, the ordering of the Jahn–Teller elongated axis in the cation and of the $[BF_4]^-$ ion are intimately linked, suggesting cooperative van der Waals interactions between the two moieties. Cooperative ordering of the Jahn–Teller elongated axis has been seen previously in Tutton salts[7] and copper methoxyacetate.[8] However, these materials possess H-bonded networks, which may act as the mechanism for mediating the cooperative interactions.

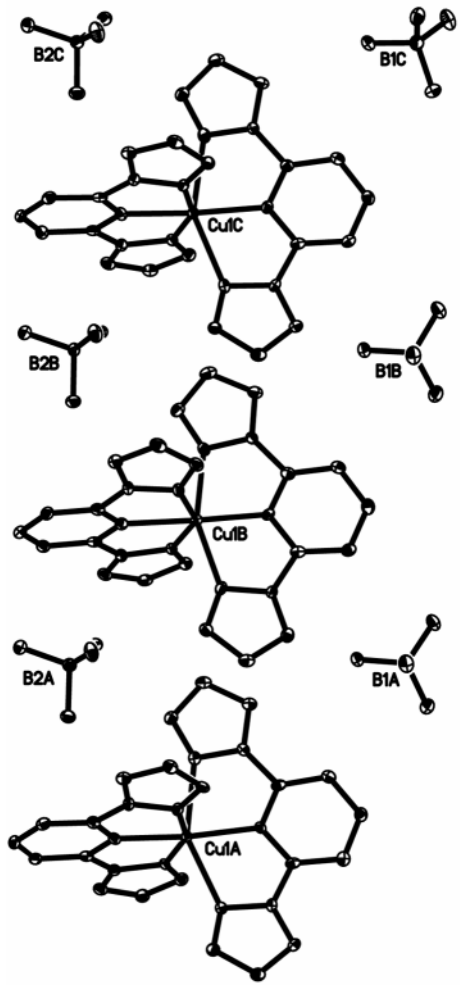

Fig. 3 Crystallographic asymmetric unit at 31 K.

In conclusion, this is the first example of a structurally characterised phase transition, involving the low-temperature ordering of a dynamically disordered Jahn–Teller system. That the mechanism for co-operation between the molecules relies on weak van der Waals interactions alone makes this system unique. Additionally, the reversible phase transition is extremely sharp and shows no hysteresis effects, making this material highly suitable as a temperature standard in the sub-liquid nitrogen temperature range, which has recently become more accessible with the introduction of the open-flow helium cryostat.[9]

The authors would like to thank Dr J. E. Davies (Cambridge) for preliminary studies and the Royal Society (M. A. H.), EPSRC (M. A. L., N. K. S., S. D. and J. A. K. H., Senior Research Fellowship) and ICI R&T Division (N. K. S.) for financial support.

Notes and references

† *Crystal data*: **1**, $C_{22}H_{18}CuN_{10}B_2F_8$, M = 659.62, monoclinic, space group $P2_1$, a = 8.414(1), b = 8.475(1), c = 18.683(2) Å, β = 97.371(2)°, V = 1321.2(2) Å^3, Z = 2, μ = 0.918 mm^{-1} (Mo-Kα, λ = 0.71073 Å), D_c = 1.658 Mg m^{-3}. Selected crystal mounted on nylon fibre using perfluoropolyether oil, cooled slowly to 50(2) K in chilled helium gas flow using Oxford Cryosystems HELIX.[9] 12227 reflections ($2.20 < \theta < 28.01°$) collected on a Bruker SMART-CCD diffractometer (ω-scan, 0.3°/frame) yielding 5261 unique data (R_{int} = 0.0158). The structure was solved by direct methods and refined by full-matrix least squares based on F^2 for all data using SHELXL software. All non-hydrogen atoms were refined with anisotropic displacement parameters, H-atoms were placed geometrically at calculated positions and refined with a riding model. Final $wR(F^2)$ = 0.0593 and $R(F)$ = 0.0232 for all data (417 refined parameters), GOF = 1.047, residuals $\Delta\rho_{min,max}$ = −0.37, 0.38 e Å^{-3}.

2, $C_{22}H_{18}CuN_{10}B_2F_8$, M = 659.62, monoclinic, space group $P2_1$, a = 8.4047(6), b = 25.389(2), c = 18.668(1) Å, β = 97.205(1)°, V = 3952.1(5) Å^3, Z = 6, μ = 0.921 mm^{-1} (Mo-Kα, λ = 0.71073 Å), D_c = 1.663 Mg m^{-3}, T = 31(2) K. Crystal mounting, cooling, data collection, structure solution and refinement methods as for **1**. 23287 reflections ($2.39 < \theta < 27.57°$) collected yielding 9396 unique data (R_{int} = 0.0265) which were used in all calculations. Final $wR(F^2)$ = 0.0738 and $R(F)$ = 0.0303 for all data (1163 refined parameters), GOF = 1.046, residuals $\Delta\rho_{min,max}$ = −0.44, 0.38 e Å^{-3}.

CCDC 182/1436. See http://www.rsc.org/suppdata/cc/1999/2245/ for crystallographic files in .cif format.

1 M. A. Hitchman, *Comments Inorg. Chem.*, 1994, **15**, 197; L. R. Falvello, *J. Chem. Soc., Dalton Trans.*, 1997, 4463.
2 M. Duggan, B. J. Hathaway and J. Mullane, *J. Chem. Soc., Dalton Trans.*, 1980, 690.
3 J.-V. Folgado, W. Henke, R. Allmann, H. Stratemeier, D. Beltrán-Porter, T. Rojo and D. Reinen, *Inorg. Chem.*, 1990, **29**, 2035.
4 N. K. Solanki, E. J. L. McInnes, F. E. Mabbs, S. Radojevic, M. McPartlin, N. Feeder, J. E. Davies and M. A. Halcrow, *Angew. Chem., Int. Ed.*, 1998, **37**, 2221.
5 N. K. Solanki, F. E. Mabbs and M. A. Halcrow, unpublished work.
6 C. J. Simmons, *New J. Chem.*, 1993, **17**, 77.
7 W. Rauw, H. Ashbahs, M. A. Hitchman, S. Lukin, D. Reinen, A. J. Schultz, C. J. Simmons and H. Stratemeier, *Inorg. Chem.*, 1996, **35**, 1902.
8 K. Prout, A. Edwards, V. Mtetwa, J. Murray, J. F. Saunders and F. J. C. Rossotti, *Inorg. Chem.*, 1997, **36**, 2820.
9 A. E. Goeta, L. K. Thompson, C. L. Sheppard, S. S. Tandon, C. W. Lehmann, J. Cosier, C. Webster and J. A. K. Howard. *Acta Crystallogr., Sect. C*, 1999, **55**, 1243.

Communication 9/06876G

Mechanistic aspects of the steam reforming of methanol over a $CuO/ZnO/ZrO_2/Al_2O_3$ catalyst

John P. Breen,* Frederic C. Meunier and Julian R. H. Ross

Centre for Environmental Research, University of Limerick, Limerick, Ireland. E-mail: john.paul.breen@ul.ie

Received (in Cambridge, UK) 5th August 1999, Accepted 11th October 1999

CO is not a primary but is a secondary product of the steam reforming of methanol over a $CuO/ZnO/ZrO_2/Al_2O_3$ catalyst, CO is formed as a secondary product by the reverse WGS reaction only when the methanol has reacted.

The steam reforming of methanol is attracting growing interest as a means of producing hydrogen for use in fuel cells. CO produced in the steam reforming reaction is currently a poison to the promising proton-exchange membrane (PEM) fuel cells and as a result much attention has been focused on the mechanism of CO formation during the reaction. The formation of carbon monoxide as a product and the fact that copper is a good catalyst for the water–gas shift (WGS) reaction[1] has led some workers[2–5] to speculate that a decomposition/WGS reaction sequence is involved [eqn. (1) and (2)]:

$$CH_3OH \rightarrow CO + 2H_2 \quad (1)$$

$$CO + H_2O \rightleftharpoons H_2 + CO_2 \quad (2)$$

$$CH_3OH + H_2O \rightarrow CO_2 + 3H_2 \quad (3)$$

However, Amphlett *et al.*[6,7] have more recently noted that carbon monoxide production is less than that predicted from equilibrium. As a result, they have revised their reaction scheme to one containing parallel reactions, the steam reforming of methanol [eqn. (3)] occurring in parallel to the decomposition of methanol to CO and H_2 [eqn. (1)]; they suggest that adjustment of the CO/CO_2 ratio also occurs as a result of the WGS reaction [eqn. (2)]. Peppley *et al.*[8,9] found that the methanol decomposition reaction is much slower than the steam reforming reaction but argued that it must be included in the overall reaction scheme. Takahashi *et al.*[10] found that methyl formate was formed at low water/methanol ratios and so they incorporated methyl formate into their reaction scheme [eqn. (4)–(6)]:

$$2CH_3OH \rightarrow CH_3OCHO + 2H_2 \quad (4)$$

$$CH_3OCHO + H_2O \rightarrow HCOOH + CH_3OH \quad (5)$$

$$HCOOH \rightarrow CO_2 + H_2 \quad (6)$$

Jiang *et al.*[11,12] carried out a detailed kinetic analysis of the steam reforming reaction and found that the reaction over a $Cu/ZnO/Al_2O_3$ catalyst could also be explained by eqn. (4)–(6), they suggested that the carbon monoxide observed in the product stream is produced *via* the decomposition of methyl formate. Studies of the surface mechanism of the steam reforming reaction have been limited[9] and authors have instead tended to use the large quantity of data published on the methanol synthesis reaction to support their mechanistic surface reaction models.[9,12]

We have previously reported[13] that copper–zirconia containing catalysts are very active for the steam reforming of methanol and that they give good selectivities towards CO_2 production. We have now obtained clear evidence from both kinetic measurements and *in situ* DRIFTS experiments for the formation of CO as a secondary product during the reforming reaction over a $CuO/ZnO/ZrO_2/Al_2O_3$ catalyst and details of the surface species involved in the reaction are given here.

The $CuO/ZnO/ZrO_2/Al_2O_3$ catalyst was prepared by sequential precipitation, the order and method of precipitation having been described elsewhere.[13] The reactants and products of the reaction were analysed by GC equipped with a Porapak Q column. This column gave satisfactory separation of CO and N_2 at a column temperature of 25 °C, the limit of detection for CO was *ca.* 1000 ppm with an accuracy of ±2%. The reaction was carried out in a quartz plug-flow microreactor, the composition of the reactant gases being 28.5% H_2O, 21.5% CH_3OH, with a balance of N_2. Prior to introduction of the reaction mixture, the catalyst was reduced *in situ* in a 5% H_2–N_2 mixture at a temperature of 240 °C for 4 h, ramping to this temperature at a rate of 5 °C min^{-1}. IR measurements were carried out using a Nicolet Magna 550 FTIR fitted with a diffuse reflectance cell and incorporating a high-pressure, high-temperature catalytic chamber.

The effect of contact time on the distribution of reaction products was studied by varying the *W*/*F* ratio while using a constant feed composition at two different temperatures (200 and 300 °C). Fig. 1 shows the methanol conversions and the percentages of hydrogen, carbon dioxide and carbon monoxide in the product stream as a function of the (pseudo-)contact time, *W*/*F* (g min cm^{-3}), at 300 °C. Two equilibrium lines for the carbon dioxide and hydrogen production are also shown as dotted lines; the top line (line '*m*') in each case represents the equilibrium values obtained by excluding carbon monoxide from the calculations whereas the bottom line (line '*n*') shows calculated equilibrium values with the inclusion of carbon monoxide as a product. It must be noted that the equilibrium lines '*m*' and '*n*' correspond to the situation when complete conversion of methanol is assumed; the equilibrium values shown in Fig. 1 are the results of thermodynamic calculations carried out using the HSC Chemistry for Windows software package (Outokumpu Research Oy). This software uses the Gibbs Free Minimisation Method to calculate equilibrium compositions.[14]

At 200 °C, 100% conversion of methanol was not attained and carbon monoxide was not detected in the product stream at any of the pseudo-contact times.

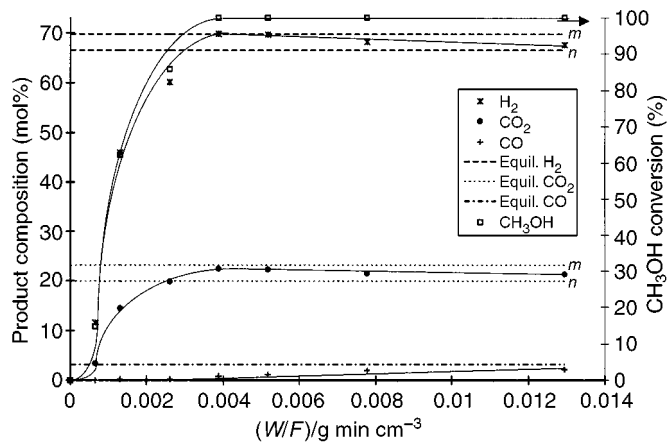

Fig. 1 The influence of *W*/*F* on the product compositions at T = 300 °C over a $CuO/ZnO/ZrO_2/Al_2O_3$ catalyst, m = equilibrium excluding CO from calculations, n = equilibrium including CO in calculations (H_2O/CH_3OH = 1.3, P = 101 kPa).

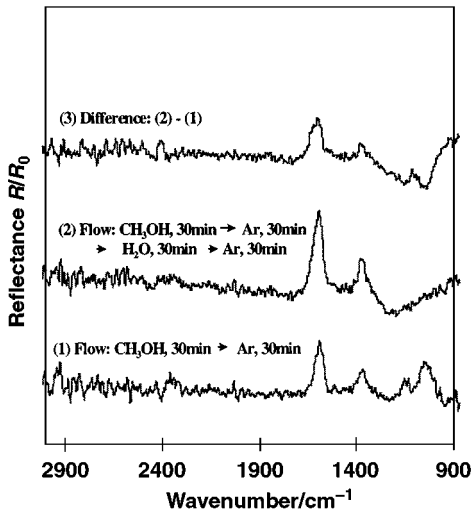

Fig. 2 FTIR spectra of surface species generated by methanol adsorption followed by water adsorption on a $CuO/ZnO/ZrO_2/Al_2O_3$ catalyst at 240 °C.

At 300 °C, the percentages of hydrogen and carbon dioxide produced were higher than those at 200 °C for all values of contact time. Carbon monoxide was not detected at the shorter contact times; however, as the value of *W*/*F* was increased, carbon monoxide was detected and its molar percentage increased steadily with increasing contact time, approaching, but not attaining, the predicted equilibrium value at higher values of *W*/*F*. It is evident from Fig. 1 that carbon monoxide was a secondary product; this effectively rules out the possibility of the occurrence of a mechanism involving methanol decomposition followed by the water–gas shift reaction as proposed by several authors over their catalysts.[2–5].

When 100% methanol conversion was achieved at 300 °C (Fig. 1), the hydrogen and carbon dioxide molar compositions exceeded the equilibrium line '*n*'; at a value of $W/F = 0.00389$ g min cm^{-3}, there was very little carbon monoxide production and the hydrogen and carbon dioxide compositions were very close to the equilibrium values calculated for the steam reforming reaction when carbon monoxide was excluded from the product stream (line '*m*'). At values of $W/F > 0.00389$ g min cm^{-3}, the proportions of hydrogen and carbon dioxide decreased and that of carbon monoxide increased with increasing contact time, approaching equilibrium '*n*' values (a sequence including CO formation) with high contact times. At 100% methanol conversion and a reaction temperature of 300 °C, the carbon dioxide and hydrogen percentages were greater than those predicted by equilibrium (*n*) whereas the carbon monoxide percentages were less than equilibrium predictions by a similar amount at the different values of *W*/*F*.

These results provide evidence of a consecutive reaction scheme in which methanol and water react first to produce carbon dioxide and hydrogen [eqn. (3)] and the carbon dioxide and hydrogen then react *via* the reverse WGS reaction [eqn. (2)] to produce CO. There was no evidence of the occurrence of the methanol decomposition reaction [eqn. (1)].

In order to investigate the nature of the surface species involved in the steam reforming reaction over the $CuO/ZnO/ZrO_2/Al_2O_3$ catalyst, *in situ* IR measurements were carried out. Fig. 2 [spectrum (1)] shows the surface species generated on the surface of the catalyst at 240 °C after passing methanol over the catalyst and then flushing through with Ar. The peaks at 1590 and 1380 cm^{-1} can be attributed to a formate species, the peak at 1150 cm^{-1} to π bonded formaldehyde and the peak centred around 1050 cm^{-1} to a methoxy species.[15] Water was then introduced and the spectrum [Fig. 2, spectrum (2)] taken after the introduction of the water showed that neither the methoxy nor the formaldehyde peaks were evident but that the intensity of the formate peaks had increased. This is illustrated in spectrum (3) of Fig. 2 which shows the difference between spectra (2) and (1). This indicates that the methoxy and/or the formaldehyde species were readily converted to formates by reaction either with gas phase water or more probably with OH groups generated by the dissociative adsorption of water. *In situ* DRIFTS analysis of species during the steam reforming reaction showed that in addition to surface formates, there was an absorption centred at 1033 cm^{-1} which can probably be attributed to gas phase methanol in addition to some adsorbed methoxy species. Gas phase CO_2 (2364 cm^{-1}), was also detected but there was no evidence of either gas phase CO or adsorbed CO species. Formates are known to decompose on $CuO/ZnO/ZrO_2$ aerogels[16] according to eqn. (7) to give either CO and surface OH groups or CO_2 and H_2:

$$OH_{(s)} + CO_{(g)} \leftarrow HCOO^-_{(s)} \rightarrow CO_{2(g)} + 1/2H_{2(g)} \quad (7)$$

The results of the kinetic study, however, showed that CO did not form when methanol was present and that CO_2 and H_2 were the primary products, but that when methanol was fully converted, CO was evident in the gas stream. This points to a mechanism whereby the decomposition of formates to CO is either inhibited in the presence of methanol, or more probably, by the methoxy and/or formaldehyde species formed from the adsorption of methanol on the catalyst. The mechanism of the inhibition of the formation of CO by methanol is the subject of further research.

Notes and references

1 M. V. Twigg, *Catalysis Handbook*, Wolfe Publishing, London, 2nd edn., 1989, p. 283.
2 V. Pour, J. Barton and A. Benda, *Coll. Czech. Chem. Commun.*, 1975, **40**, 2923.
3 J. C. Amphlett, M. J. Evans, R. F. Mann and R. D. Weir, *Can. J. Chem. Eng.*, 1985, **63**, 605.
4 J. Barton and V. Pour, *Coll. Czech. Chem. Commun.*, 1980, **45**, 3402.
5 E. Santacesaria and S. Carra, *Appl. Catal.*, 1983, **5**, 345.
6 J. C. Amphlett, R. F. Mann and B. A. Peppley, in *Proc. 3rd Natural Gas Conversion Symp.*, Sydney, Australia, 7–9 Apr, 1993; *Stud. Surf. Sci. Catal.*, 1994, **81**, 409.
7 J. C. Amphlett, K. A. M. Creber, J. M. Davis, R. F. Mann, B. A. Peppley and D. M. Stokes, in *Proc. 9th World Hydrogen Energy Conf.*, Paris, 1992, p. 1541.
8 B. A. Peppley, J. C. Amphlett, L. M. Kearns and R. F. Mann, *Appl. Catal. A*, 1999, **179**, 21.
9 B. A. Peppley, J. C. Amphlett, L. M. Kearns and R. F. Mann, *Appl. Catal. A*, 1999, **179**, 31.
10 K. Takahashi, N. Takezawa and H. Kobayashi, *Appl. Catal.*, 1982, **2**, 383.
11 C. J. Jiang, D. L. Trimm, M. S. Wainwright and N. W. Cant, *Appl. Catal. A*, 1993, **93**, 245.
12 C. J. Jiang, D. L. Trimm, M. S. Wainwright and N. W. Cant, *Appl. Catal. A*, 1993, **97**, 145.
13 J. P. Breen and J. R. H. Ross, *Catal. Today*, 1999, **51**, 521.
14 W. B. White, S. M. Johnson and G. B. Dantzig, *J. Chem. Phys.*, 1958, **28**, 751.
15 C. Schild, A. Wokaun and A. Baiker, *J. Mol. Catal.*, 1990, **63**, 243.
16 D. Bianchi, T. Chafik, M. Khalfallah and S. J. Teichner, *Appl. Catal. A*, 1995, **123**, 89.

Communication 9/06393E

Stepwise assembly of a polyoxovanadate from mononuclear units in an organic solvent: carboxylate-stabilised fragments in the conversion of $[VOCl_4]^{2-}$ to $[V_{15}O_{36}]^{5-}$

Gail B. Karet,[a] Ziming Sun,[b] William E. Streib,[a] John C. Bollinger,[a] David N. Hendrickson*[b] and George Christou*[a]

[a] *Department of Chemistry and Molecular Structure Center, Indiana University, Bloomington, IN 47405-7102, USA. E-mail: christou@indiana.edu*

[b] *Department of Chemistry-0358, University of California at San Diego, La Jolla, CA 92093-0358, USA. E-mail: dhendrickson@ucsd.edu*

Received (in Bloomington, IN, USA) 6th August 1999, Accepted 30th September 1999

The $[VOCl_4]^{2-}$/AgOAc reaction system in MeCN gives $[V_5O_9Cl(OAc)_4]^{2-}$, $[V_9O_{19}(OAc)_5]^{3-}$ and $[V_{15}O_{36}]^{5-}$ for reagent ratios of 1:2, 1:3 and 1:4, respectively: the V_5 and V_9 cores are fragments of the V_{15} core, suggesting the V_5 and V_9 units are carboxylate-stabilised intermediates in the assembly of the V_{15} polyoxovanadate.

Polyoxometalates represent a venerable and greatly explored area of early transition metal chemistry.[1–4] They are of interest from a variety of viewpoints, including structural aesthetics,[1–4] routes to new materials,[5–7] catalysis[8] and medical applications,[9] to name but a few. These molecular species often possess cage-like structures and in many cases encapsulate a small neutral or charged group.[3,4,10] One such example (amongst many) is the encapsulation of Cl^-, Br^- or CO_3^{2-} 'guests' within the approximately spherical $[V_{15}O_{36}]^{5-}$ polyoxovanadate 'host' cage.[11]

The steps by which a polyoxometallate such as $[V_{15}O_{36}]^{5-}$ assembles and the precise importance of the encapsulated guest to the identity and stability of the host are important to know. Bowl-like polyoxovanadates that can be considered structural fragments of (and putative intermediates to) cage-like structures are rarely encountered but one such example is approximately hemispherical $[V_{12}O_{32}(MeCN)]^{4-}$ containing an MeCN molecule in the concave cavity.[12] In the somewhat related field of fullerene chemistry, the preparation of structural fragments of the fullerene cage, so-called buckybowls, is a very topical area.[13] In this report, we describe the development of methodology that allows possible intermediates in the assembly of the $[V_{15}O_{36}]^{5-}$ cage to be stabilized by carboxylate ligands and identified. This approach has also provided access to the empty $[V_{15}O_{36}]^{5-}$ cage, a host without a guest.

The reaction of $[NEt_4]_2[VOCl_4]$ **1** with 2 equiv. of NaOAc in MeCN under nitrogen, followed by brief exposure to air gives a deep green solution from which can be obtained $[NEt_4]_2[V_5O_9Cl(OAc)_4]\cdot$MeCN **2** ($4V^{IV},V^{V}$) in 20–25% yield: this procedure is analogous to that previously reported for $[NEt_4]_2[V_5O_9Cl(O_2CPh)_4]$.[14] A related reaction using AgOAc in place of NaOAc and omitting the aerial oxidation step also gives **2** in comparable yield. Increase of the $[VOCl_4]^{2-}$:AgOAc reaction ratio to 1:3 gave instead a blue solution which, after *ca.* 50% volume reduction *in vacuo* and filtration, slowly produced dark blue–black crystals of $[NEt_4]_3[V_9O_{19}(OAc)_5]\cdot 2$MeCN **3** ($5V^{IV}$, $4V^{V}$) in 20–30% yield.† Further increase of the reaction ratio to 1:4 gave a purple solution which, after *ca.* 50% volume reduction and filtration, produced dark purple–black crystals of $[NEt_4]_5[V_{15}O_{36}]\cdot 1.28$MeCN **4** ($8V^{IV}$, $7V^{V}$) in 45–50% yield.† The anion of **2** (Fig. 1)‡ has the same $[V_5O_9Cl]^{2+}$ core reported previously[14] for $[V_5O_9Cl(O_2CPh)_4]^{2-}$, with a V_5 square-pyramid (V^{V} at the apex) and O^{2-} and Cl^- ions triply and quadruply bridging the vertical and basal faces, respectively. The novel $[V_9O_{19}]$ core of **3** (Fig. 2) may be considered an extension of the core of **2**, giving an approximately hemispherical bowl that contains an *anti,anti*-bridging AcO^- group. This is reminiscent of $[V_{12}O_{32}(MeCN)]^{4-}$ where a MeCN molecule is held inside a bowl.[12] The other AcO^- groups are like those in **2**, *i.e.* bridging V···V edges of the $[V_xO_y]$ unit and blocking further aggregation. The $[V_{15}O_{36}]^{5-}$ anion of **4** (Fig. 3) is a known polyoxovanadate, but in this case it is empty, previous examples containing an anionic guest ion inside the cage.[11]

Given the similar synthetic procedures to **2**–**4**, it is reasonable to suggest that the $[V_5O_9]$ and $[V_9O_{19}]$ cores of **2** and **3** may be

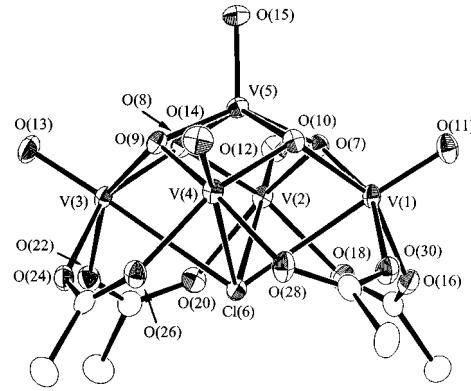

Fig. 1 ORTEP representation with 50% probability ellipsoids of the $[V_5O_9Cl(OAc)_4]^{2-}$ anion of **2**.

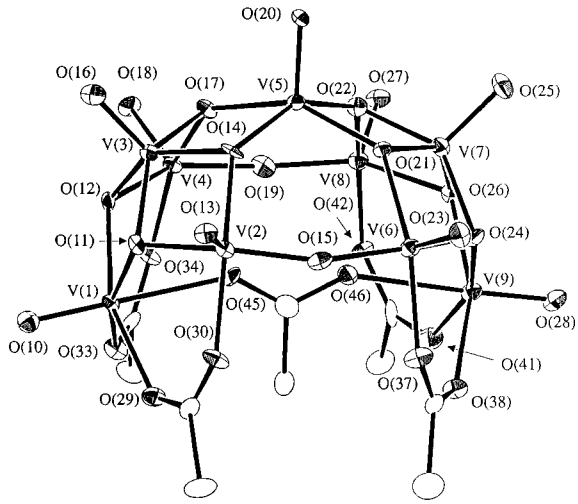

Fig. 2 ORTEP representation with 50% probability ellipsoids of the $[V_9O_{19}(OAc)_5]^{3-}$ anion of **3**.

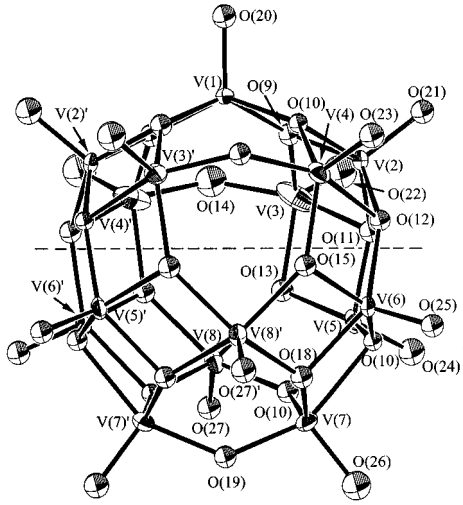

Fig. 3 ORTEP representation with 50% probability ellipsoids of the $[V_{15}O_{36}]^{5-}$ anion of **4**. The $[V_7O_{17}]$ portion of the structure above the dashed line is the same as in the anion of **3** (Fig. 2).

considered carboxylate-stabilised intermediates in the assembly of the $[V_{15}O_{36}]^{5-}$ ion of **4** in MeCN, and that the minimal sequence in its formation is that in eqn. (1). This is supported by

$$[VO]^{2+} \rightarrow [V_5O_9]^{3+} \rightarrow [V_9O_{19}]^{2+} \rightarrow [V_{15}O_{36}]^{5-} \quad (1)$$

the structural relationship between the $[V_9O_{19}]$ core and $[V_{15}O_{36}]^{5-}$ (Fig. 3). A common $[V_7O_{17}]$ unit is seen: in **3**, the O atoms at left and right of this [O(11)/O(12) and O(24)/O(26) of Fig. 2] bind to only two V atoms [V(1) and V(9)], whereas in **4** they bind to four V atoms [V(5), V(5)′, V(6), V(6)′ of Fig. 3] allowing the $[V_{15}O_{36}]$ shell to form. Interestingly, the complete $[V_9O_{19}]$ core of **3** is a fragment of the $[V_{18}O_{42}]$ cage-like polyoxovanadate with T_d symmetry.[4] Note that the acetate O atoms of **2** and **3** occupy sites that would otherwise be occupied by O^{2-} ions giving higher nuclearity products. The AgOAc reagent that causes formation of **2**–**4** from **1** clearly has multiple functions: (i) as a source of AcO^- groups both to stabilise the fragments in **2** and **3** *and* to act as Brønsted bases to facilitate formation of O^{2-} ions from H_2O molecules [O : V ratios are 1 : 1 (**1**), 1.8 : 1 (**2**), 2.1 : 1 (**3**) and 2.4 : 1 (**4**)]; (ii) as a Cl^- abstracting reagent; and (iii) as an oxidizing agent [average V oxidation states are 4+ (**1**), 4.2+ (**2**), 4.44+ (**3**) and 4.47+ (**4**)]. It is thus reasonable that the AgOAc : **1** ratio is so important. Indeed, treatment of redissolved **3** in MeCN with additional AgOAc gives a colour change from blue to purple and subsequent crystallisation of **4**.

The solid-state effective magnetic moment (μ_{eff}) of **3** gradually decreases from 3.62 μ_B at 300 K to 3.15 μ_B at 2.00 K. For **4**, μ_{eff} gradually decreases from 2.86 μ_B at 300 K to 2.67 μ_B at 30.0 K, and then increases slightly to 2.83 μ_B at 3.00 K. Fitting of magnetization data collected in the 0.05–5 T and 2.00–4.00 K ranges gave $S = 3/2$, $g = 1.70$ and $D = 0.00$ cm^{-1} for **3** and $S = 3/2$, $g = 1.62$ and $D = 0.00$ cm^{-1} for **4**. The magnetic properties of $[V_5O_9Cl(O_2CR)_4]^{2-}$ species such as **2** have been previously described.[14] More detailed analysis of the exchange interactions in **3** and **4** will be provided elsewhere.[15]

The formation of **2**–**4** from **1** suggests that stepwise control of the assembly of polyoxometallates may indeed be feasible by suitable choice of solvent and reagents (and their ratios) allowing access to a variety of bowl-like species. Further experimentation along these lines is in progress.

This work was supported by the U.S. Department of Energy.

Notes and references

† Further volume reduction or addition of *e.g.* Et_2O gives significantly greater yields of **3** and **4** but the coloured products are contaminated with white solids. The described procedures avoid this but at the expense of large yields. Dried solids are hygroscopic and analysed satisfactorily (C, H, N).

‡ *Crystal data*: **2**·MeCN: $C_{26}H_{55}ClN_3O_{17}V_5$, M_r = 971.89, monoclinic, space group $C2/c$, a = 16.111(2), b = 14.900(2), c = 33.674(5) Å, β = 91.39(1)°, U = 8081 Å^3, Z = 8, T = 101 K, $R(R_w)$ = 0.0361 (0.0411) using 6432 reflections with $F > 3\sigma(F)$.

3·2MeCN: $C_{38}H_{81}N_5O_{29}V_9$, M_r = 1530.55, triclinic, space group $P\bar{1}$, a = 13.303(1), b = 23.031(1), c = 10.804(1) Å, α = 90.81(1), β = 111.91(1), γ = 94.15(1)°, U = 3060 Å^3, Z = 2, T = 109 K, $R(R_w)$ = 0.0773 (0.0563) using 5037 reflections with $F > 2.33\sigma(F)$. One cation lies on a non-crystallographic mirror plane, disordering its four CH_2 carbon atoms about two well resolved positions.

4·1.28MeCN: $C_{42.56}H_{103.84}N_{6.28}O_{36}V_{15}$, M_r = 2043.92, monoclinic, space group $C2/c$, a = 22.105(3), b = 13.784(2), c = 26.604(4) Å, β = 107.56(1)°, U = 7728 Å^3, Z = 4, T = 101 K, $R(R_w)$ = 0.1111 (0.1125) using 4190 reflections with $I > 2.33\sigma(I)$; the MeCN molecules and three of the cations were badly disordered.

CCDC 182/1440. See http://www.rsc.org/suppdata/cc/1999/2249/ for crystallographic files in .cif format.

1 L. C. W. Baker and D. C. Glick, *Chem. Rev.*, 1998, **98**, 3.
2 Y. P. Jeannin, *Chem. Rev.*, 1998, **98**, 51.
3 M. I. Khan and J. Zubieta, *Prog. Inorg. Chem.*, 1995, **43**, 1.
4 M. T. Pope and A. Muller, *Angew. Chem., Int. Ed. Engl.*, 1991, **30**, 34.
5 E. Coronado and C. J. Gomez-Garcia, *Chem. Rev.*, 1998, **98**, 273.
6 W. G. Klemperer and C. G. Wall, *Chem. Rev.*, 1998, **98**, 297.
7 A. Muller, F. Peters, M. T. Pope and D. Gatteschi, *Chem. Rev.*, 1998, **98**, 239.
8 I. V. Kozhevnikov, *Chem. Rev.*, 1998, **98**, 171; N. Mizuno and M. Misono, *Chem. Rev.*, 1998, **98**, 199.
9 J. T. Rhule, C. L. Hill, D. A. Judd and R. F. Schinazi, *Chem. Rev.*, 1998, **98**, 327.
10 A. Muller, H. Reuter and S. Dillinger, *Angew. Chem., Int. Ed. Engl.*, 1995, **34**, 2328,
11 A. Muller, M. Renk, R. Rohlfing, E. Krickmeyer and J. Doring, *Angew. Chem., Int. Ed. Engl.*, 1990, **29**, 926.
12 V. W. Day, W. G. Klemperer and O. M. Yaghi, *J. Am. Chem. Soc.*, 1989, **111**, 5959.
13 P. W. Rabideau and A. Sygula, *Acc. Chem. Res.*, 1996, **29**, 235.
14 G. B. Karet, Z. Sun, D. D. Heinrich, J. K. McCusker, K. Folting, W. E. Streib, J. C. Huffman, D. N. Hendrickson and G. Christou, *Inorg. Chem.*, 1996, **35**, 6450.
15 G. B. Karet, Z. Sun, D. N. Hendrickson and G. Christou, in preparation.

Communication 9/06448F

ChemComm

Synthesis of racemic brevioxime

Derrick L. J. Clive* and Soleiman Hisaindee

Chemistry Department, University of Alberta, Edmonton, Alberta, Canada T6G 2G2. E-mail: derrick.clive@ualberta.ca

Received (in Corvallis, OR, USA) 10th August 1999, Accepted 24th September 1999

Amine hydrochloride 12 and β-keto thioester 16 were coupled and treated with TFA; the resulting alcohols 18 were oxidized and converted into a mixture of oximes 20, from which the major product, racemic brevioxime 1, was isolated.

We report the synthesis of brevioxime **1** in racemic form. Natural brevioxime, which is optically active, was isolated[1] from the fungus *Penicillium brevicompactum* Dierckx, and is of

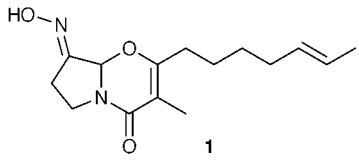

1

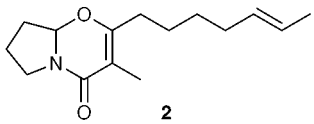

2

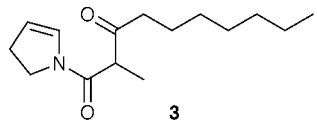

3

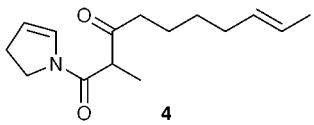

4

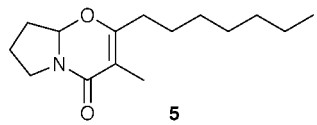

5

potential value as a lead compound in pesticide research because it is an inhibitor of juvenile hormone biosynthesis.[1] The related compounds **2**,[2] **3**[3] and **4**[2] have been obtained from the same fungus. The last two are also inhibitors of juvenile hormone and, while **2** shows insecticidal activity, its primary mode of action does not appear to have been established.

The structure of brevioxime is of an unusual type, and the natural products **1** and **2**, together with the totally synthetic **5**,[3] appear to be the only representatives.†

Our synthetic plan, which was developed after a number of exploratory experiments,‡ was based on the idea that an amide aldehyde of type **6** (Scheme 1) should cyclize[5,7] in the presence of acid, so as to generate the required heterocyclic system directly (**6** → **7** → **8**).

On the basis of the above considerations, we first made the amine hydrochloride **12**. Preparation of this compound was initially troublesome, but we eventually found that it is accessible by the route summarized in Scheme 2. Epoxy acetal **9**, readily available by epoxidation (HOCl, water, < 5 °C; 72%) of acrolein dimethyl acetal,[8] was treated with potassium cyanide (KCN, EtOH–water, room temperature, 24 h; 62%),[9] so as to afford the cyano alcohol **10**, which was protected by silylation (Bu^tMe_2SiCl, Et_3N, CH_2Cl_2, reflux, overnight; 81%). The nitrile function of **10** was then reduced by catalytic hydrogenation in the presence of 6 equiv. of $CHCl_3$ (PtO_2, dry EtOH, $CHCl_3$, 50 psi, 24 h, room temperature; 64–75%);[10] other conditions§ were unsuccessful.

With the amine hydrochloride in hand, the next task was to convert it into a β-keto amide (*cf.* **6**). The preparation of such amides is often best done by treating a β-keto thioester with an amine;[11] in the present case the appropriate β-keto thioester was **16**. We initially made this compound by alkylation of the simple thioester **13**[12] with (*E*)-6-iodohex-2-ene, using the technique of double deprotonation,[13] but the yield was poor (33%). A better route involved acylation[14] of thioester **15**[15] with the imidazolide derived from the known (*E*)oct-6-enoic acid.[16] Under optimum conditions,¶ the required β-keto thioester **16** can be obtained in 64% from acid **14** (Scheme 3).

The amino component and the thioester were coupled by condensation in the presence of silver triflate[11]‖ [**12** + **16** → **17**; Et_3N (2 equiv.), AgOTf (2 equiv.), THF, room temperature, 30 min; 92%]. At this point, exposure to aqueous TFA [50% aq. TFA, $CHCl_3$ (1:2)] brought about the intended series of cyclizations (see Scheme 1), and gave an almost quantitative yield of the desired alcohols **18**, as a 1:1 mixture of diastereoisomers. The chromatographically less polar isomer was easily oxidized by the Dess–Martin reagent (CH_2Cl_2, 2 h, *ca.* 100%), taking the route as far as ketone **19**. The isomeric alcohol was more difficult to oxidize, but it did react with tetrapropylammonium perruthenate (TPAP)[18] [TPAP, NMO, CH_2Cl_2, 4 Å molecular sieves, 2 h; 23%, after correction for recovered starting material (19%)]. Treatment of ketone **19** with hydroxylamine hydrochloride under classical conditions[19] [hydroxylamine hydrochloride (5 equiv.), NaOAc (5.2 equiv.), water, EtOH, 2 h; *ca.* 100%] gave the oximes **20**, with the desired *E*-isomer predominating (4.3:1). This isomer was readily separated by chromatography, so as to afford racemic brevioxime, whose spectroscopic properties (^1H NMR, ^{13}C NMR) were the same as those reported for material isolated from the natural source.

The above route illustrates the utility of the cyclization of an amide nitrogen onto an aldehyde carbonyl for generating certain nitrogen heterocycles. The route is short, if one ignores the simple steps needed to prepare acid **14**, and the approach is convergent, and it should be amenable to the synthesis of analogues.

Acknowledgment is made to the Natural Sciences and Engineering Research Council of Canada and to Merck Frosst for financial support.

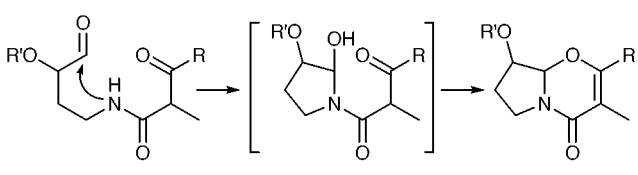

6 **7** **8**

Scheme 1

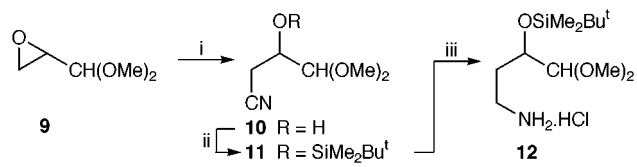

9 **10** R = H; **11** R = $SiMe_2Bu^t$; **12**

Scheme 2 *Reagents and conditions*: i, KCN, EtOH–water, room temp., 24 h, 62%; ii, Bu^tMe_2SiCl, Et_3N, CH_2Cl_2, reflux, overnight, 81%; iii, PtO_2, dry EtOH, $CHCl_3$ (6 equiv.), 50 psi, 24 h, room temp., 64–75%.

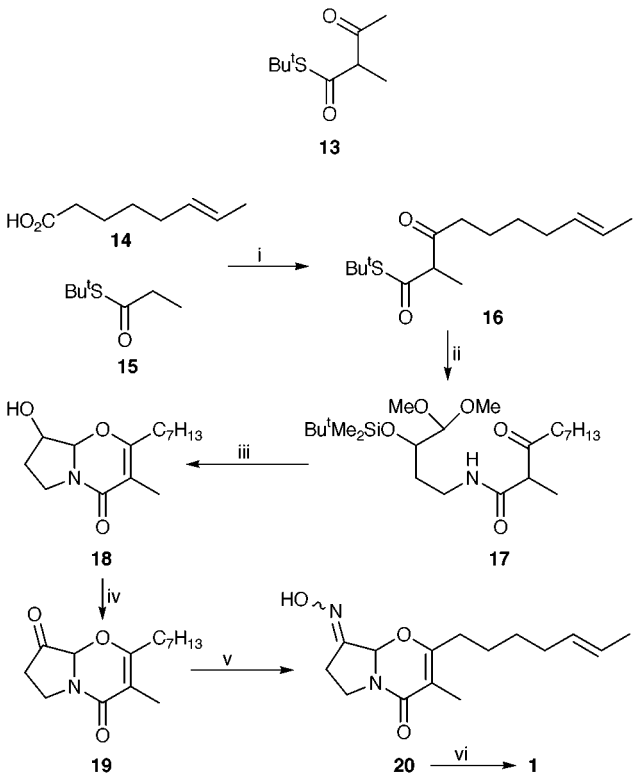

Scheme 3 *Reagents and conditions*: i, see note ¶; ii, amine hydrochloride **12**, Et_3N (2 equiv.), AgOTf (2 equiv.), THF, room temp., 30 min, 92%; iii, 50% aq. TFA, $CHCl_3$ (1 : 2), *ca.* 100%; iv, Dess–Martin reagent, CH_2Cl_2, 2 h, *ca.* 100%; for more polar alcohol, TPAP, NMO, CH_2Cl_2, 4 Å molecular sieves, 2 h, 23%, after correction for recovered alcohol (19%); v, hydroxylamine hydrochloride (5 equiv.), NaOAc (5.2 equiv.), water, EtOH, 2 h, *ca.* 100%; vi, flash chromatography over silica gel.

Notes and references

† However, benzo-fused analogues, such as 1,2,3,3a-tetrahydro-9*H*-pyrrolo[2,1-*b*][1,3]benzoxazin-9-one, are known (see *e.g.* ref. 4), as are substances lacking the 2,3-double bond (see *e.g.* ref. 5).

‡ These were based on *N*-acyl-2-pyrrolines (*cf.* ref. 6).

§ We also tried reduction with $LiAlH_4$ or Pd-C/H_2.

¶ The acid was first converted into its imidazolide (1,1′-carbonyldiimidazole, THF, 0 °C to room temperature, 30 min). The thioester **15** was deprotonated (LDA, THF, −78 °C, 10 min), and the resulting enolate (3 equiv.) was added by cannula to the imidazolide (−78 °C). After 30 min, the cold bath was removed and, after a further 5 min, the mixture was quenched with saturated aqueous ammonium chloride. Instead of the imidazolide, the corresponding derivative of 2,2′-carbonylbis(3,5-dioxo-4-methyl-1,2,4-oxadiazolidine) can be used (*cf.* ref. 17), in which case only 1 equiv. of **15** is required.

‖ We used AgOTf instead of $AgOCOCF_3$ (ref. 11). The AgOTf was added in one portion to a stirred solution of the other components.

1 P. Moya, M. Castillo, E. Primo-Yúfera, F. Couillaud, R. Martínez-Máñez, M.-D. Garcerá, M. A. Miranda, J. Primo and R. Martínez-Pardo, *J. Org. Chem*., 1997, **62**, 8544.
2 Á. Cantín, P. Moya, M.-A. Castillo, J. Primo, M. A. Miranda and E. Primo-Yúfera, *Eur. J. Org. Chem*., 1999, 221.
3 P. Moya, Á. Cantín, M.-A. Castillo, J. Primo, M. A. Miranda, and E. Primo-Yúfera, *J. Org. Chem*., 1998, **63**, 8530.
4 H. Boehme and H. Boeing, *Arch. Pharm. Ber. Dtsch. Pharm. Ges*., 1961, **294**, 556.
5 J. E. Baldwin, C. Hulme, C. J. Schofield and A. J. Edwards, *J. Chem. Soc., Chem. Commun*., 1993, 935.
6 G. A. Kraus and K. Neuenschwander, *J. Org. Chem*., 1981, **46**, 4791.
7 *Cf.* J. A. Robl, *Tetrahedron Lett.*, 1994, **35**, 393; J. E. Baldwin, R. M. Adlington, J. S. Bryans, M. D. Lloyd, T. J. Sewell, C. J. Schofield, H. K. Baggaley and R. Cassels, *J. Chem. Soc., Chem. Commun*., 1992, 877; D. L. J. Clive, D. M. Coltart and Y. Zhou, *J. Org. Chem*., 1999, **64**, 1447.
8 *Cf.* D. I. Weisblat, B. J. Magerlein, D. R. Myers, A. R. Hanze, E. I. Fairburn and S. T. Rolfson, *J. Am. Chem. Soc*., 1953, **75**, 5893.
9 *Cf.* F. Effenberger and V. Null, *Liebigs Ann. Chem*., 1992, 1211.
10 J. A. Secrist, III and M. W. Logue, *J. Org. Chem*., 1972, **37**, 335.
11 S. V. Ley and P. R. Woodward, *Tetrahedron Lett*., 1987, **28**, 3019.
12 J. Sakaki, S. Kobayashi, M. Sato and C. Kaneko, *Chem. Pharm. Bull*., 1990, **38**, 2262.
13 *Cf.* P. M. Booth, C. M. J. Fox and S. V. Ley, *J. Chem. Soc., Perkin Trans. 1*, 1987, 121.
14 *Cf.* B. D. Harris, K. L. Bhat and M. M. Joullié, *Tetrahedron Lett*., 1987, **28**, 2837.
15 I. Patterson and A. N. Hulme, *J. Org. Chem*., 1995, **60**, 3288.
16 M. F. Ansell and S. S. Brown, *J. Chem. Soc*., **1957**, 1788.
17 P. Jouin, J. Poncet, M.-N. Dufour, I. Maugras, A. Pantaloni and B. Castro, *Tetrahedron Lett*., 1988, **29**, 2661.
18 S. V. Ley, J. Norman, W. P. Griffith and S. P. Marsden, *Synthesis*, 1994, 639.
19 B. S. Furniss, A. J. Hannaford, P. W. G. Smith and A. R. Tatchell, *Vogel's Textbook of Practical Organic Chemistry*, 5th edn., Longman, London, 1989, p. 1259.

Communication 9/06579B

An acentric arrangement of *p*-nitroaniline molecules between the layers of kaolinite†

Kazuyuki Kuroda,*[ab] Kouichi Hiraguri,[a] Yoshihiko Komori,[ab] Yoshiyuki Sugahara,[a] Haruyuki Mouri[c] and Yoshiaki Uesu[c]

[a] *Department of Applied Chemistry, Waseda University, Ohkubo-3, Shinjuku-ku, Tokyo 169-8555, Japan. E-mail: kuroda@mn.waseda.ac.jp*
[b] *Kagami Memorial Laboratory for Materials Science and Technology, Waseda University, Nishiwaseda-2, Shinjuku-ku, Tokyo, 165-0051, Japan*
[c] *Department of Physics, Waseda University, Ohkubo-3, Shinjuku-ku, Tokyo, 169-8555, Japan*

Received (in Cambridge, UK) 30th July 1999, Accepted 4th October 1999

***p*-Nitroaniline molecules were intercalated between the layers of kaolinite, and an acentric arrangement of *p*-nitroaniline induced by the asymmteric environment of the interlayer region was accomplished.**

Layered materials have been utilized for immobilizing and organizing functional substances in their interlayer spaces to form supramolecular inorganic–organic hybrid systems.[1–3] The advantage of the use of layered materials is its confinement of guest species in their two-dimensional regions to induce selective orientation. A typical field demanding preferred orientation is nonlinear optics, using organic molecules with hyperpolarizabilities (β) like *p*-nitroaniline (*p*NA), which needs to be oriented noncentrosymmetrically.[4] To achieve an acentric arrangement of *p*NA, various hosts such as cyclodextrins,[5] and microporous and mesoporous molecular sieve hosts[6,7] have been utilized. Layered materials like layered double hydroxides,[8] saponite[9] and $MnPS_3$[10] have also been applied for the arrangement of molecules with hyperpolarizabilities such as *p*NA and stilbazolium ions. However, an outer electrical field[9] or guest-guest interactions[8,10] are needed for alignment of the molecules because the interlayer spaces of the layered materials are sandwiched between identical surfaces of adjacent layers.

Kaolinite has a unique layered structure because the interlayer region is sandwiched between the hydroxy groups of the $AlO_2(OH)_4$ sheets on one side and the oxide arrangements of the silicate sheets on the other[11] [Fig. 1(*a*)], affording an asymmetric nanoenvironment. Guest molecules like DMSO are easily intercalated and aligned in one direction between the layers of kaolinite.[12] Thus, kaolinite is an excellent host material for organizing supramolecular hybrid systems. Here we report the successful formation of a kaolinite–*p*NA intercalation compound and its nonlinear optical properties.

The kaolinite [ideal chemical formula, $Al_2Si_2O_5(OH)_4$] used was KGa1, a highly crystalline Georgia kaolinite obtained from the Source Clays Repository of the Clay Minerals Society (USA).[13] The reactivity of kaolinite for intercalation is very low due to the inherent hydrogen bonding between the layers. Although small polar molecules such as DMSO can be intercalated directly,[14] *p*NA has been reported not to be intercalated into kaolinite.[15] In order to overcome this obstacle, a fine guest displacement method using a kaolinite–methanol intercalation compound as the intermediate was applied (Fig. 1).[16–18] To synthesize a kaolinite-methanol intercalation compound, a kaolinite–*N*-methylformamide (NMF) intercalation compound was prepared and treated repeatedly with methanol eight times to displace NMF completely.[15] The wet kaolinite–methanol intercalation compound (1 g) was stirred in a CH_2Cl_2 solution of *p*NA (0.60 g *p*NA per 20.0 ml CH_2Cl_2) at room temperature for 3 days to form the kaolinite–*p*NA intercalation compound.

The intercalation of *p*NA molecules between the layers of kaolinite was proved by powder X-ray diffraction (Fig. 2). The basal spacing of kaolinite is 0.72 nm and it increased to 1.50 nm in the kaolinite–*p*NA intercalation compound, the value of which was larger than that of the kaolinite–methanol intercalation compound (1.11 nm). The increase of 0.78 nm after intercalation is smaller than the length of the *p*NA molecules (0.90 nm). Considering the amount of *p*NA (24 mass%), which corresponds to $pNA/Al_2Si_2O_5(OH)_4 = 0.6$, the *p*NA molecules are thought to take a monomolecular arrangement, with their molecular axis inclined to the aluminosilicate layers by *ca*. 60° [Fig. 1(*b*)].

In the ^{13}C CP/MAS NMR spectrum of the product, typically four signals due to the aromatic ring carbons of *p*NA were observed at δ 112, 128, 135 and 155,† indicating that the *p*NA molecules were incorporated into the kaolinite. On the other hand, a signal at δ 49 was observed which was assigned to CH_3O, suggesting that a small amount of methanol or methoxy groups attached to the octahedral sheets were present.

The main driving force for the intercalation of *p*NA into kaolinite is thought to be hydrogen bonding between the

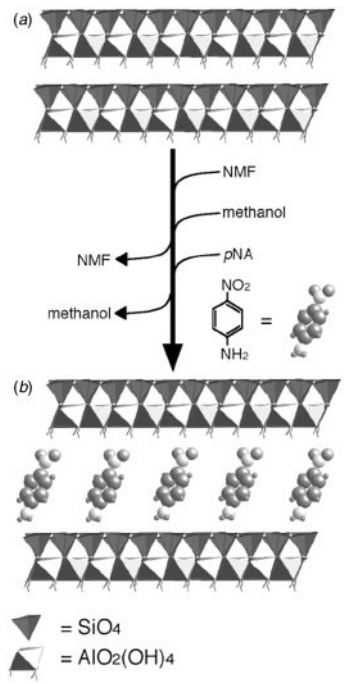

Fig. 1 (*a*) Structure of kaolinite (ref. 11) and (*b*) ideal structure of kaolinite–*p*NA intercalation compound.

† ^{13}C and ^{29}Si CP/MAS NMR and IR spectral data for the kaolinite–*p*NA intercalation compound are available from the RSC web site, see http://www.rsc.org/suppdata/cc/1999/2253/

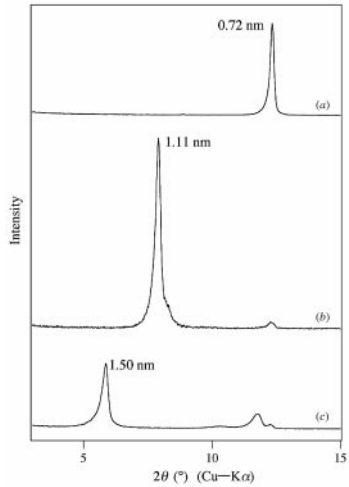

Fig. 2 X-Ray diffraction patterns of (*a*) kaolinite, *(b*) kaolinite–methanol intercalation compound and (*c*) kaolinite–*p*NA intercalation compound.

Table 1 SHG efficiency (referenced to urea) of the samples

Sample	SHG intensity
*p*NA	same level as background
Kaolinite	same level as background
Kaolinite–*p*NA intercalation compound	0.93
Mixture of kaolinite and *p*NA[a]	same level as background
Mixture of kaolinite and *p*NA[b]	0.03–0.05

[a] A physically ground mixture of kaolinite and *p*NA powders. [b] A mixture prepared by dispersing kaolinite with a THF solution of *p*NA.

electrophilic NO_2 groups of *p*NA and the hydroxy groups of kaolinite, which is supported by the intercalation behavior of nitrobenzene and aniline. It was found that nitrobenzene molecules were intercalated between the layers of kaolinite (the basal spacing increased to 1.46 nm) whereas aniline molecules were not.[19] However, the interactions between the NH_2 groups of *p*NA and the silicate sheets of kaolinite presumably contribute to the formation of the kaolinite–*p*NA intercalation compound, because no intercalation reaction took place with *N*,*N*-dimethyl-*p*-nitroaniline.[20]

The interactions between the silicate sheets and the *p*NA molecules were investigated by solid state ^{29}Si NMR spectroscopy.† The Q^3 environments of Si in the tetrahedral silicate sheets of kaolinite showed a signal at around $\delta -91$ with a slight splitting,[21] whereas that of the kaolinite-*p*NA intercalation compound showed the signal shifted to δ −91.5 without splitting. The chemical shift is the same as those observed for kaolinite–alkylamine intercalation compounds (for example, δ −91.5 for an octylamine–kaolinite intercalate) where NH_2 groups interact with the silicate sheets, suggesting that similar interactions are occurring with *p*NA. The IR spectrum of the kaolinite–*p*NA intercalation compound showed that the bands due to $\nu(NH_2)$ at 3494 and 3402 cm^{-1} are shifted to higher wavenumbers than those for *p*NA crystals (3482 and 3361 cm^{-1}).† These findings indicate the presence of weaker hydrogen bondings between NH_2 groups and silicate sheets as compared with those in *p*NA crystals.

The second harmonic generation (SHG) intensities of the materials treated here are shown in Table 1.[22] The kaolinite–*p*NA intercalation compound is SHG active and its intensity is similar to that of urea. No SHG signals were observed for *p*NA crystals, because their second order nonlinear susceptibility is cancelled by their centrosymmetric structure ($P2_1/n$).[23] Almost no signals were observed for kaolinite and a physical mixture of kaolinite with crystalline *p*NA powder where the *p*NA powder was adsorbed only on the outer surface of the kaolinite particles. When *p*NA was dissolved in THF and the solution was mixed with kaolinite to form a mixture where the *p*NA molecules were spread over the outer surface of the mineral, the SHG intensity of the mixture was less than 0.05. Consequently, the observed SHG intensity of the intercalation compound is almost entirely ascribable to *p*NA molecules in the interlayer space of kaolinite; the interactions between the unique interlayer structure of kaolinite and the *p*NA molecules induce the noncentrosymmetric orientation of *p*NA molecules exclusively. Although there are no definitive data on the degree of noncentrosymmetric orientation of the *p*NA molecules, the present results show that kaolinite is an excellent host for immobilizing photofunctional materials in its unique interlayer region. The effect of *p*NA loading on the properties and the preparation of thin films are now under investigation.

The spontaneous arrangement of guest molecules by the interlayer surface structure is a further step towards highly selective catalytic reactions, stereoselective organic synthesis, and the formation of specific molecular assemblies with unusual chemical, photochemical and electrical properties, which will be increasingly important for nanomaterials design for advanced technological applications.

This work was financially supported by a Grant-in-Aid for Scientific Research from the Ministry of Education, Science, Sports and Culture of the Japanese Government. The authors thank Mr Ryoji Takenawa for experimental assistance.

Notes and references

1 *Inorganic Materials*, 2nd edn., ed. D. W. Bruce and D. O'Hare, Wiley, New York, 1996.
2 M. Ogawa and K. Kuroda, *Chem. Rev.*, 1995, **95**, 399.
3 G. Alberti and T. Bein, *Comprehensive Supramolecular Chemistry*, Pergamon, Oxford, 1996, vol. 7.
4 P. N. Prasad and D. J. Williams, *Introduction to Nonlinear Optical Effects in Molecules and Polymers*, Wiley, New York, 1991.
5 S. Tomaru, S. Zembutsu, M. Kawachi and M. Kobayashi, *J. Chem. Soc., Chem. Commun.*, 1984, 1207; D. F. Eaton, *Tetrahedron*, 1987, **43**, 1551.
6 S. D. Cox, T. E. Gier, G. D. Stucky and J. Bierlein, *J. Am. Chem. Soc.*, 1988, **110**, 2986; S. D. Cox, T. E. Gier and G. D. Stucky, *Chem. Mater.*, 1990, **2**, 609; L. Werner, J. Caro, G. Finger and J. Kornatowski, *Zeolites*, 1992, **12**, 658.
7 I. Kinski, H. Gies and F. Marlow, *Zeolites*, 1997, **19**, 375.
8 S. Cooper and P. K. Dutta, *J. Phys. Chem.*, 1990, **94**, 114.
9 M. Ogawa, M. Takahashi and K. Kuroda, *Chem. Mater.*, 1994, **6**, 715.
10 P. G. Lacroix, R. Clément, K. Nakatani, J. Zyss and I. Ledoux, *Science*, 1994, **263**, 658; T. Coradin, R. Clément, P. G. Lacroix and K. Nakatani, *Chem. Mater.*, 1996, **8**, 2153.
11 E. Akiba, H. Hayakawa, S. Hayashi, R. Miyawaki, S. Tomura, Y. Shibasaki, F. Izumi, H. Asano and T. Kamiyama, *Clays Clay Miner.*, 1997, **45**, 781.
12 J. G. Thompson and C. Cuff, *Clays Clay Miner.*, 1985, **33**, 490.
13 S. W. Bailey, *Crystal Structures of Clay Minerals and Their X-Ray Identification: Structure of Layer Silicates*, ed. G. W. Brindley and G. Brown, Mineralogical Society, London, 1980, pp. 1–39.
14 B. K. G. Theng, *The Chemistry of Clay-Organic Reactions*, Adam Hilger, London, 1974, pp. 1–260.
15 J. Tunney and C. Detellier, *Can. J. Chem.*, 1997, **75**, 1766.
16 Y. Komori, Y. Sugahara and K. Kuroda, *J. Mater. Res.*, 1998, **13**, 930.
17 Y. Komori, Y. Sugahara and K. Kuroda, *Chem. Mater.*, 1999, **11**, 3.
18 Y. Komori, Y. Sugahara and K. Kuroda, *Appl. Clay Sci.*, 1999, **15**, 241.
19 Intercalation of nitrobenzene and aniline was performed by stirring wet kaolinite–methanol intercalation compounds in those liquids at room temperature for 3 days.
20 Intercalation reaction was attempted by stirring a wet kaolinite–methanol intercalation compound in a saturated CH_2Cl_2 solution of *N*,*N*-dimethyl-*p*-nitroaniline at room temperature for 3 days.
21 P. F. Barron, R. L. Frost, J. O. Skjemstad and A. J. Koppi, *Nature*, 1983, **302**, 49.
22 The SHG properties were measured with incident light of λ = 1.064 μm from a Nd:YAG laser; the intensity of the transmitted second harmonic wave of λ = 0.532 μm was detected. Samples were ground to pass through a 100 mesh sieve and packed on a glass slide to the thickness of 0.15 mm.
23 K. N. Trueblood, E. Goldish and J. Donohue, *Acta Crystallogr.*, 1961, **14**, 1009.

Communication 9/06206H

ChemComm

Biosynthesis of longianone from *Xylaria longiana*: a metabolite with a biosynthetic relationship to patulin

Rebecca J. M. Goss, Jens Fuchser and David O'Hagan*

Department of Chemistry, Science Laboratories, South Road, Durham, UK DH1 3LE.
E-mail: david.o'hagan@durham.ac.uk

Received (in Cambridge, UK) 9th September 1999, Accepted 1st October 1999

Longianone, a metabolite of *Xylaria longiana*, is an isomer of the well known fungal toxin, patulin; it is demonstrated that longianone is biosynthesised from 6-methylsalicylic acid in a pathway closely related to that found in patulin biosynthesis.

The isolation and structure of the metabolite longianone **1** was recently reported from *Xylaria longiana*.[1] Longianone **1** posesses an intriguing spiro-bicyclic ring structure (1,7-dioxaspiro[4,4]non-2-ene-4,8-dione). It is optically active, however the absolute configuration of the natural product is unknown at present. Structurally, longianone **1** represents a rare parent ring system. The only related bicyclic ring systems are the secosyrins **2** and **3** and their more elaborated co-metabolites, the syringolides **4** and **5**, metabolites of the bacterium *Pseudomonas syringia* pv. *tomato*.[2,3] A biosynthesis has been proposed[3] for the secoserins **4** and **5** which involves the combination of a polyketide chain with a pentose sugar moiety, however this is not based on experimental evidence. Another related ring system is found in the hyperlactones A–C **6** isolated from *Hypericum chinensis*.[4] However, in that case the ester functionality occupies a different site in the ring system and the hyperlactones are clearly terpenoid in origin and have no biosynthetic relationship to longianone **1** or the secosyrins. It is noteworthy that longianone **1** has a structural formula ($C_7H_6O_4$) which is isomeric with the fungal mycotoxin, patulin **7**. Patulin **7** has an intriguing biosynthetic origin derived from oxidative ring opening of the aromatic polyketide metabolite, 6-methylsalicylic acid (6-MSA) **8**[5–8] and the pathway to patulin biosynthesis is illustrated in Scheme 1. The interesting structure of longianone **1** and its constitutional relationship to patulin **7** stimulated us to initiate a biosynthetic investigation of **1** from *X. longiana*.

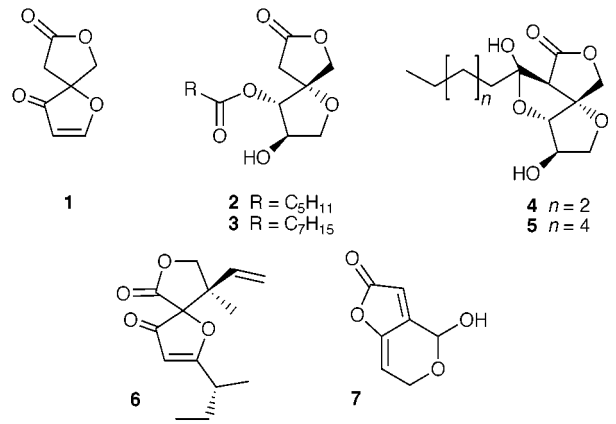

An initial experiment involved feeding [1,2-$^{13}C_2$]acetate to static cultures of *X. longiana*.[1] This resulted in a low (0.4%) but detectable incorporation of isotope into the resultant longianone **1**. ^{13}C NMR analysis revealed reciprocal couplings between C-3/C-4 ($J_{13C\text{-}13C}$ = 55 Hz) and C-5/C-6 ($J_{13C\text{-}13C}$ = 34 Hz) of **1**, indicating the incorporation of two intact acetate units. This was the first indication of a polyketide origin, and the labelling pattern was consistent with the intermediacy of 6-MSA **8** and a similarity to patulin biosynthesis, as illustrated in Scheme 1. In order to reinforce this hypothesis an experiment with [3,5-$^2H_2$]-6-MSA **8a** was conducted. A sample of ethyl 2-hydroxy-6-methylbenzoate was synthesised following an established route,[9] then deuterium was exchanged into the aromatic nucleus by refluxing with DCl, D_2O and MeOD for 24 h and the ester was hydrolysed to [3,5-$^2H_2$]-6-MSA **8a** by refluxing with NaOH. The subsequent feeding experiment resulted in a sample of longianone which was enriched with deuterium (^2H NMR analysis) at C-2 [Fig. 1(*b*)]. There was a minor enrichment at C-3 arising from some exchange into the aromatic precursor **8a** at C-4 during isotope exchange [Fig. 1(*b*)]. *m*-Cresol **9** and *m*-hydroxybenzyl alcohol **10** are established intermediates in patulin biosynthesis[7] and in order to assess if they have a role in longianone biosynthesis they were each prepared enriched with deuterium, and fed in separate experiments to *X. longiana* cultures. An experiment with [2,4,6-$^2H_3$]-*m*-cresol **9a**, prepared

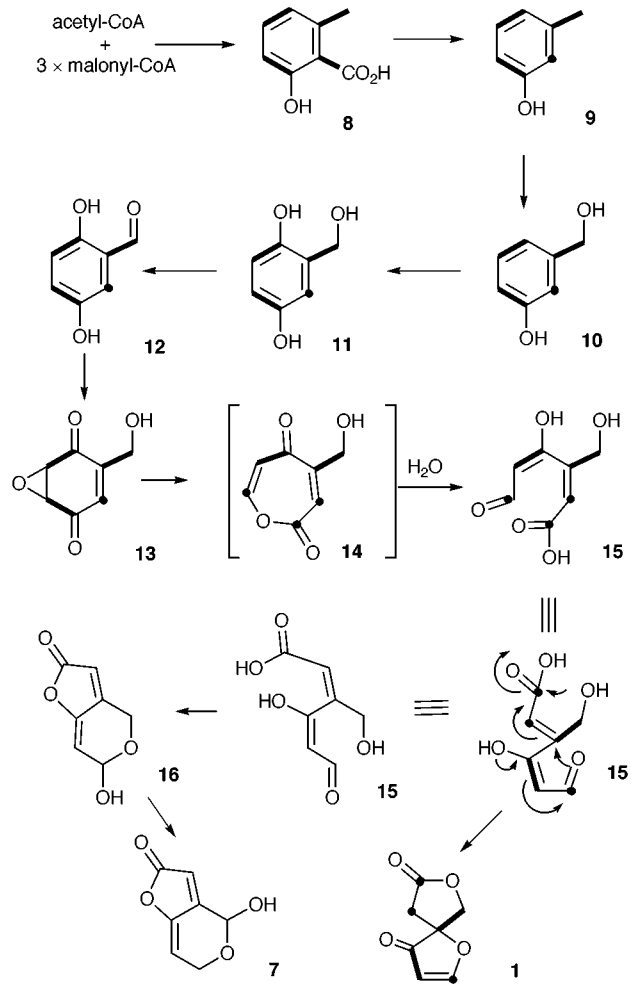

Scheme 1

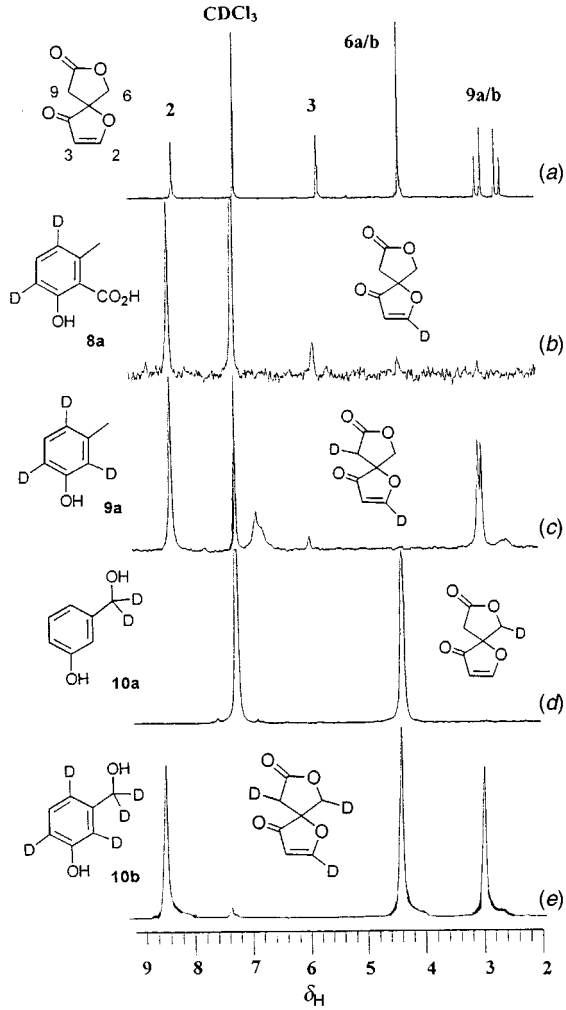

Fig. 1 (*a*) ^{1}H NMR ($CDCl_3$) spectrum and assignment of longianone **1**; (*b*) ^{2}H NMR ($CHCl_3$) spectrum of **1** after feeding **8a**; (*c*) ^{2}H NMR ($CHCl_3$) spectrum of **1** after feeding **9a**; (*d*) ^{2}H NMR ($CHCl_3$) spectrum of **1** after feeding **10a**; (*e*) ^{2}H NMR ($CHCl_3$) spectrum of **1** after feeding **10b**.

by reaction with PBr_3 and D_2O,[10] resulted in deuterium incorporation into **1** at C-2 and C-9 as determined by ^{2}H NMR [Fig. 1(*c*)]. The methylene hydrogens at C-9 are diastereotopic and well resolved by NMR, and the resulting ^{2}H NMR spectrum after feeding **9a** indicated a stereospecific enrichment into C-9, however upon storage (3 months) a slow racemisation was witnessed. Incorporation of 3-hydroxy[α,α-$^2H_2$]benzyl alcohol **10a**, prepared by reducing methyl 3-hydroxybenzoate with $LiAlD_4$, resulted in labelling at C-6 in **1** [Fig. 1(*d*)]. It was not clear from this latter experiment whether both deuterium atoms were processed through to the C-6 methylene group of longianone **1** as these deuterium atoms, which are formally diastereotopic, have nonetheless similar chemical shifts in the resultant ^{2}H and ^{1}H NMR spectra. In order to gain information on this issue a second experiment was carried out using **10b**, which was prepared with deuterium atoms located both at the hydroxymethyl group and at C-2, C-4 and C-6 of the aromatic ring. The resultant ^{2}H NMR spectrum [Fig. 1(*e*)] of longianone **1** showed three clear enrichments at C-2, C-6 and C-9, with *similar intensities*. We have drawn the conclusion therefore that only one deuterium atom from the methylene group of 3-hydroxybenzyl alcohol **10b** became incorporated into the C-6 methylene group of longianone and therefore the hydroxymethyl group is oxidised up to the aldehyde level during the biosynthesis.

The isotopic labelling experiments reveal a common biosynthetic pathway to both longianone **1** and patulin **2** which

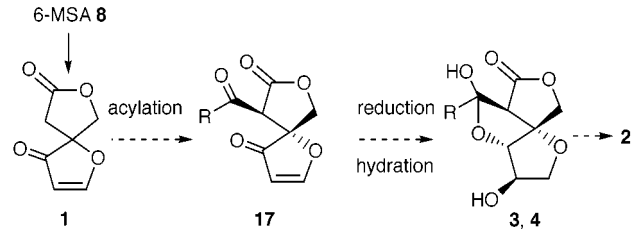

Scheme 2

diverges at a late stage. Both metabolites are derived from 6-MSA **8** and have **9** and **10** as common biosynthetic intermediates. Also oxidation of the hydroxymethyl group to the aldehyde level is revealed as common to both cases and the aromatic ring is cleaved across the same bond. The conversion of gentisaldehyde **12** to phyllostine **13** is a biochemically characterised step[11] in patulin biosynthesis and the intermediacy of neopatulin (also termed isopatulin) has been established from mutant studies,[8] so reasonably the pathway progresses through **14**[12] with hydrolysis to **15**. Different *E/Z* isomers of **15** emerge as the likely branchpoint of the two pathways, with straightforward ester and intramolecular Michael-type cyclisations to generate both rings of longianone. An alternative cyclisation of **15** (ester and hemiacetal formations) generates neopatulin **16** which is a precursor to patulin **7** requiring an oxidation and a reduction. Perhaps longianone **1** is a shunt metabolite of an organism which has lost the capacity to complete patulin **7** biosynthesis.

In view of the above experimental evidence an alternative hypothesis to that recently proposed[2,3] emerges for the biosynthesis of the secosyrins **2** and **3** and the syringolides **4** and **5**. This would involve an origin from a longianone skeleton derived from 6-MSA, followed by acylation α to the lactone to generate intermediate **17**, as illustrated in Scheme 2. Elaborations such as reduction and hydration would generate **4** and **5** and a retro-aldol reaction would generate **2** and **3**. It remains to be determined whether this or the previous proposal[3] is the more valid for the biosynthesis of those metabolites.

We thank Dr Raymond L. Edwards of the University of Bradford for providing a strain of *Xylaria longiana* and Ian McKeag of the University of Durham for ^{2}H NMR analysis. The EU and Isle of Man Education Authority is gratefully acknowledged for a Studentship (R. J. M. G.).

Notes and references

1 R. L. Edwards, D. J. Maitland, C. L. Oliver, M. C. Pacey, L. Shields and A. J. S. Whalley, *J. Chem. Soc., Perkin Trans. 1*, 1999, 715.
2 S. L. Midland, N. T. Keen and J. J. Sims, *J. Org. Chem.*, 1995, **60**, 1118.
3 S. L. Midland, N. T. Keen, J. J. Sims, M. M. Midland, M. M. Stayton, M. J. Smith, E. P. Mazzola, K. J. Graham and J. Clardy, *J. Org. Chem.*, 1993, **58**, 2940.
4 M. Tada, M. Nagai, C. Okumura, J. Osano and T. Matsuzaki, *Chem. Lett.*, 1989, 683.
5 H. Iijima, H. Noguchi, Y. Ebizuka, U. Sankawa and H. Seto, *Chem. Pharm. Bull.*, 1983, **31**, 362.
6 S. W. Tanenbaum and E. W. Bassett, *J. Biol. Chem.*, 1959, **234**, 1861.
7 A. I. Scott and M. Yalpani, *J. Chem. Soc., Chem. Commun.*, 1967, 945.
8 J. Sekiguchi, G. M. Gaucher and Y. Yamada, *Tetrahedron Lett.*, 1979, 41.
9 F. M. Hauser and S. A. Pogany, *Synthesis*, 1980, 814.
10 K. Wähälä, I. Ojanperä, L. Häyri and T. A. Hase, *Synth. Commun.*, 1987, 137.
11 J. Sekiguchi and G. M. Gaucher, *Biochemistry*, 1978, **17**, 1785.
12 M. Bennet, G. B. Gill, G. Pattenden, A. J. Shuker and A. Stapelton, *J. Chem. Soc., Perkin Trans. 1*, 1991, 929.

Communication 9/07311F

First total synthesis of (±)-longianone

Patrick G. Steel*

Department of Chemistry, University of Durham, Science Laboratories, South Road, Durham, UK DH1 3LE. E-mail: p.g.steel@durham.ac.uk

Received (in Cambridge, UK) 9th September 1999, Accepted 1st October 1999

The first total synthesis of (±)-longianone, isolated from *Xyloria longiana*, is reported starting from tetronic acid.

Longianone **1**, recently isolated from the fungal strain *Xyloria longiana* found in various tropical and temperate locations

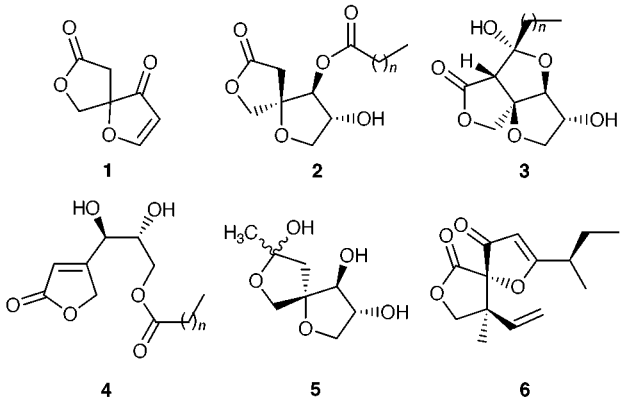

throughout the world, possesses an unusual 1,7-dioxaspiro-[4,4]non-2-ene-4,8-dione skeleton.[1] As such it is the simplest member of a family of structurally related but biosynthetically different natural products containing this spirobicyclic core.[2] These include the bacterial metabolites Secosyrins **2** and the related syringolides **3** and syributins **4** isolated from *Pseudomonas syringae*[3,4] as well as sphydrofuran **5** obtained, much earlier, from a strain of Actinomycetes. Reflecting this unusual skeleton there has been considerable interest in the synthesis of these natural products, resulting in a number of total syntheses.[5–9] A synthesis of a structurally similar natural product, hyperolactone A **6**, which possess an alternative 1,7-dioxaspiro-[4.4]non-2-enedione skeleton, has also been recently communicated.[10] Here we report a highly concise synthesis of (±)-longianone which, in addition to being the first synthesis of this natural product, has potential to provide advanced intermediates for the synthesis of these other natural products.

We envisaged a synthetic route in which the crucial spirocentre could be established by means of an intramolecular radical cyclisation of a suitably functionalised tetronate derivative (Scheme 1).[11] In the ideal situation, the use of an α,β-unsaturated acyl radical precursor **7** (X = O), as pioneered by Pattenden, would generate Longianone in a single operation.[12] Unfortunately, generation of the required acyl selenide was complicated by the instability of several of the proposed intermediates and we turned to a more stepwise route involving cyclisation of a vinyl radical species **7** (X = CHR).

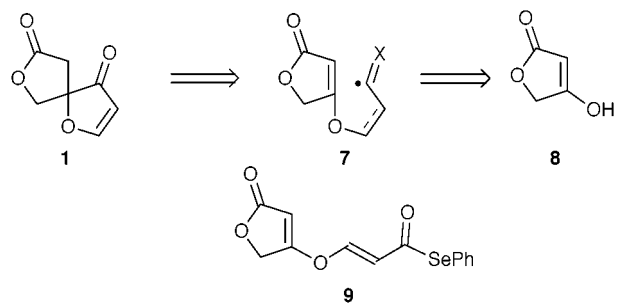

Scheme 1

Condensation of but-3-ynol with tetronic acid **8** was achieved by heating under reflux in a Dean–Stark apparatus using a catalytic amount of TsOH as catalyst (Scheme 2).[13]† Slow addition of Bu_3SnH to a refluxing solution of this vinylogous ester **10** in benzene containing AIBN (10 mol%) afforded a separable 5 : 1 mixture of the desired spirocycle **11** accompanied by the vinyl stannane **12** generated by simple alkyl hydrostannylation.[14] Initial attempts to convert the vinyl stannane to the desired ketone by ozonolysis in CH_2Cl_2 were complicated by preferential formation of the rather unstable aldehyde **15**. This reaction presumably proceeds *via* oxidative cleavage of the carbon–tin bond to give the enol and subsequent tautomerisation. Related conversions of alkyl–tin bonds have been previously reported.[15] This minor difficulty could simply be circumvented by protiodestannylation after separation of the isomeric vinyl stannanes.[16] Subsequent ozonolysis of the resulting alkene **13**, with a reductive work up using dimethyl sulfide, proceeded smoothly to afford the desired bicyclic ketone **14** in good overall yield.

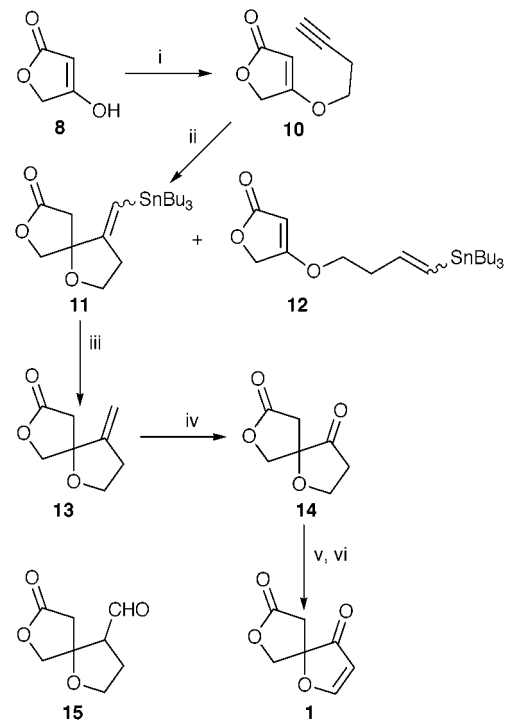

Scheme 2 *Reagents and conditions*: i, but-3-ynol, TsOH, PhH, 18 h, 76%; ii, Bu_3SnH, AlBN (10 mol%), PhH, reflux, 5 h, 71% (**11**:**12** = 5:1); iii, 1 M HCl, CH_2Cl_2, room temp. 1 h, 100%; iv, O_3, CH_2Cl_2, −78 °C, then DMS, −78 °C to room temp., 2 h, 79%; v, PhSeCl, THF, H_2O (cat), 5 days, 38% (+15% **14**); vi, O_3, CH_2Cl_2, −78 °C, then purge N_2 and warm to room temp. 12 h, 44%.

To complete the synthesis we sought a method for the introduction of the α,β-unsaturation which requires selective reaction at the ketone carbonyl group. Initial attempts to generate the silyl enol ether using standard combinations such as LDA/TMSCl or TMSOTf/Et_3N proved unsuccessful. Attempts to directly introduce an α-seleno group through direct reaction of the enolate with PhSeX (X = Cl, SePh) led principally to decomposition of the starting material, presumably *via* β-elimination of the β-alkoxy ketone unit. This conversion was ultimately achieved following an earlier precedent reported by Sharpless involving stirring the ketone and phenylselenenyl chloride in THF containing a trace amount of water.[17] The yellow selenoketone was obtained in moderate yield as a 1 : 1 mixture of diastereoisomers. Attempted oxidation and selenoxide elimination using aqueous oxidants failed to yield any isolable products, presumably due to Michael addition and subsequent ring opening of the lactol ring under the reaction conditions. In the course of his isolation studies Edwards has noted the propensity for the natural product to form the corresponding methanol adduct.[1] These problems could be circumvented by carrying out the oxidation, using ozone as the oxidant, in anhydrous CH_2Cl_2 at −78 °C, followed by warming to room temperature overnight to achieve the elimination. Following simple chromatography, racemic longianone **1**, identical in all respects (TLC, mp, NMR, IR and *m/z*) with an authentic sample,[2] was isolated in 44% yield. All attempts to enhance this process and avoid isolation of the selenide through the use of the corresponding benzeneseleninic anhydride afforded only a trace amount of the desired enone accompanied by significant decomposition.[18]

In conclusion, we report a concise synthesis of (±)-longianone that can also provide access to the structurally related secosyrins and syringolides. Studies in this direction and those towards an enantioselective synthesis are in progress and will be reported in due course.

We thank Professor David O'Hagan for bring this structure to our attention and for providing an authentic sample of longianone, the EPSRC Mass Spectrometry Service at Swansea for accurate mass determinations, Dr A. M. Kenwright and Mr I. H. McKeag for assistance with NMR experiments, and Dr M. Jones for mass spectra.

Notes and references

† All new compounds have satisfactory spectral and analytical data. Yields refer to pure isolated products.

1 R. L. Edwards, D. J. Maitland, C. L. Oliver, M. S. Pacey, L. Shields and A. J. S. Whalley, *J. Chem. Soc., Perkin Trans. 1*, 1999, 715.
2 Although structurally similar it appears that the biosyntheses of these natural products are different. Whereas these other natural products are suggested to be produced through the condensation of a triketide with a pentose unit, longianone is derived from 6-methylsalicyclic acid. See R. J. M. Gross, J. Fuscher and D. O'Hagan, *Chem. Commun.*, 1999, 2255.
3 S. L. Midland, N. T. Keen, J. J. Sims, M. M. Midland, M. M. Stayton, V. Burton, M. J. Smith, E. P. Mazzola, K. J. Graham and J. Clardy, *J. Org. Chem.*, 1993, **58**, 2940.
4 S. L. Midland, N. T. Keen and J. J. Sims, *J. Org. Chem.*, 1995, **60**, 1118.
5 P. Yu, Q. G. Wang, T. Mak and H. Wong, *Tetrahedron*, 1998, **54**, 1783.
6 P. Yu, Y. Yang, Z. Y. Zhang, T. Mak and H. Wong, *J. Org. Chem.*, 1997, **62**, 6359.
7 C. Mukai, S. M. Moharram, S. Azukizawa and M. Hanaoka, *J. Org. Chem.*, 1997, **62**, 8095.
8 M. Carda, E. Castillo, S. Rodriguez, E. Falomir and J. A. Marco, *Tetrahedron Lett.*, 1998, **39**, 8895.
9 H. Yoda, M. Kawauchi, K. Takabe and K. Hosoya, *Heterocycles*, 1997, **45**, 1895 and 1906 and references therein.
10 D. Ichinari, T. Ueki, K. Yoshihara and T. Kinoshita, *Chem. Commun.*, 1997, 1743.
11 Similar radical cyclisations to generate spirocyclic ethers are precedented. See for example, D. S. Middleton, N. S. Simpkins, M. J. Begley and N. K. Terrett, *Tetrahedron*, 1990, **46**, 545.
12 C. J. Hayes and G. Pattenden, *Tetrahedron Lett.*, 1996, **37**, 271.
13 H. Hoffmann, B. Schmidt and S. Wolff, *Tetrahedron*, 1989, **45**, 6113.
14 G. Stork and R. Mook, *J. Am. Chem. Soc.*, 1987, **109**, 2829.
15 R. J. Linderman and M. Jaber, *Tetrahedron Lett.*, 1994, **35**, 5993.
16 The workup of this protiodestannylation is much simplified if the the tin residues are removed by stirring the crude reaction mixture with KF: J. E. Leibner and J. Jacobus, *J. Org. Chem.*, 1979, **44**, 449.
17 K. B. Sharpless, R. F. Lauer and A. Y. Teranishi, *J. Am. Chem. Soc.*, 1973, **95**, 6137.
18 D. H. R. Barton, D. J. Lester and S. V. Ley, *J. Chem. Soc., Perkin Trans. 1*, 1980, 2209.

Communication 9/07313B

Directed *ortho* Metalation and Suzuki–Miyaura cross-coupling connections: regiospecific synthesis of all isomeric chlorodihydroxybiphenyls for microbial degradation studies of PCBs

S. Nerdinger,[a] C. Kendall,[b] R. Marchhart,[a] P. Riebel,[a] M. R. Johnson,[b] C.-F. Yin,[b] L. D. Eltis[c]† and V. Snieckus*[b]

[a] *Guelph-Waterloo Centre for Graduate Work in Chemistry, University of Waterloo, Waterloo, ON, Canada N2L 3G1*
[b] *Department of Chemistry, Queen's University, Kingston, ON, Canada K7L 3N6. E-mail: snieckus@chem.queensu.ca*
[c] *Department of Biochemistry, Université Laval, Québec City, Québec, Canada G1K 7P4*

Received (in Corvallis, OR, USA) 7th September 1999, Accepted 28th September 1999

Monochloro DHBs 1a–d and 2a–c have been regioselectively synthesised in good overall yields by a combination of directed *ortho* metalation and Suzuki–Miyaura cross-coupling.

The aerobic microbial degradation of aromatic compounds such as toluene, naphthalene and biphenyl is an essential link in the global carbon cycle and generally proceeds *via* catechol intermediates involving cleavage by either intradiol or extradiol dioxygenases.[1] For biphenyl, fundamental interest in understanding the respective proposed mechanisms of the extradiol cleavage of catechol by 2,3-dihydroxybiphenyl-1,2-dioxygenases (DHBDs)[2,3] and the subsequent hydrolysis of the ring cleaved product catalysed by 2-hydroxy-6-oxo-6-phenylhexa-2,4-dienoate hydrolase (BphD)[3] (Scheme 1) is intensified by the prospect of exploiting these enzymes in the degradation of environmental pollutants such as polychlorinated biphenyls (PCBs).[4,5] In connection with ongoing studies in this area,[6] we describe the regiospecific synthesis of all six isomeric monochloro-2,3-dihydroxybiphenyls (DHBs) **1b–d** and **2a–c**. The synthetic route takes advantage of combined Directed *ortho* Metalation (D*o*M)[7] and Pd-catalyzed Suzuki–Miyaura cross-coupling[8] reactions, a methodological theme currently evolving in our laboratories.[9] The key conceptual features, depicted for **3–5** (Scheme 2), include new strategies of oxygen-directed metalation group (DMG) use in walk-around-the-ring functionalization (**2a**, **2c**).

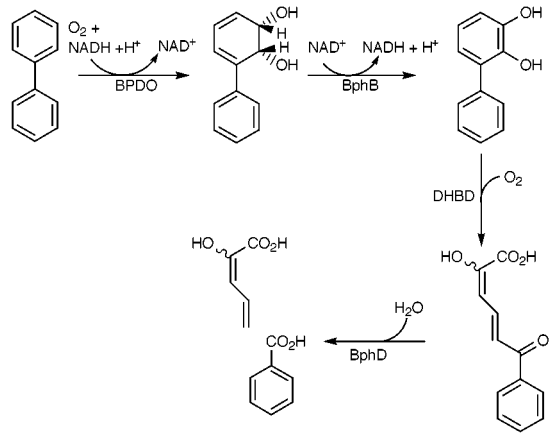

Scheme 1 Enzymes involved in the aerobic microbial degradation of biphenyl and PCBs: BPDO = biphenyl dioxygenase; BphB = 2,3-dihydro-2,3-dihydroxybiphenyl dehydrogenase; DHBD = 2,3-dihyroxybiphenyl dioxygenase; BphD = 2-hydroxy-6-oxo-6-phenylhexa-2,4-dienoate hydrolase.

† Current address: Department of Microbiology and Immunology, University of British Columbia, Vancouver, B.C., Canada V6T 1Z3.

Metalation[7] and a trimethyl borate quench of **6** (Scheme 3) afforded the boronic acid **7** which, in crude form, was subjected to Suzuki–Miyaura cross-coupling with bromobenzene or commercially available isomeric chloroiodobenzenes followed by standard BBr_3 deprotection to furnish biaryls **1a–d** in modest overall yields on a gram scale. A comparable yielding (58%) alternate synthesis (Scheme 4) of parent compound **1a** from 2-MOM biphenyl **8**, prepared (NaH, MOMCl, THF, room temperature) from inexpensive 2-hydroxybiphenyl, proceeded by metalation–boronation–oxidation[10] to introduce an OH^+ synthon to afford **9** followed by hydrolysis.

Intermediate **9** also served for a concise synthesis of 4-chloro-DHB **2a** (Scheme 4). Thus, conversion to the MOM derivative **10** as before followed by a second D*o*M reaction,

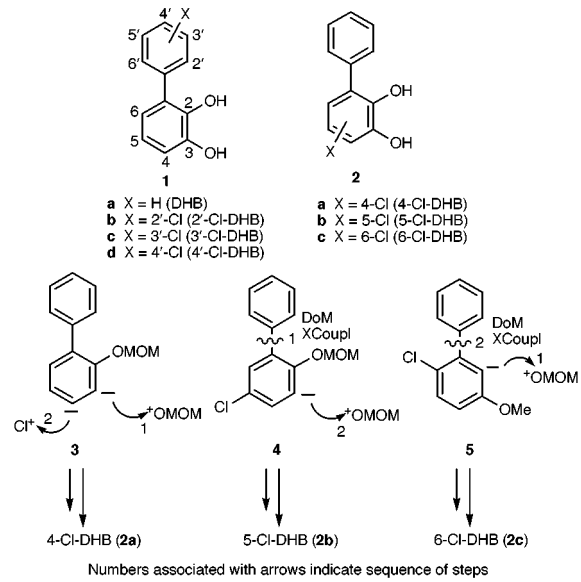

Scheme 2

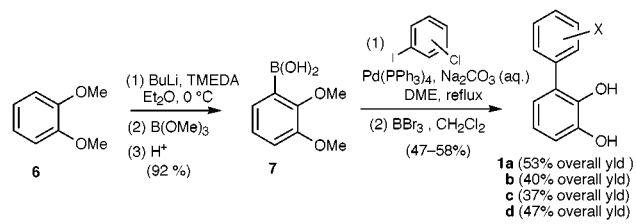

Scheme 3

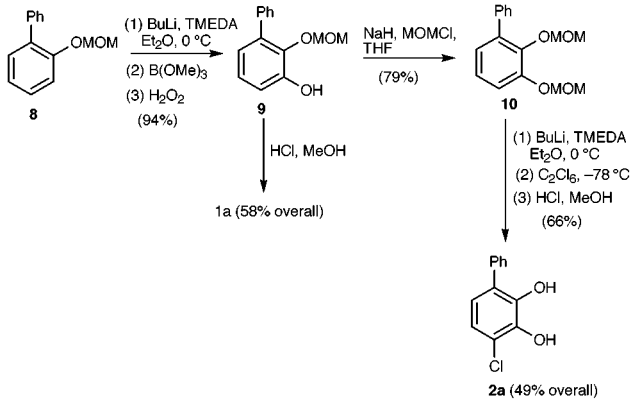

Scheme 4

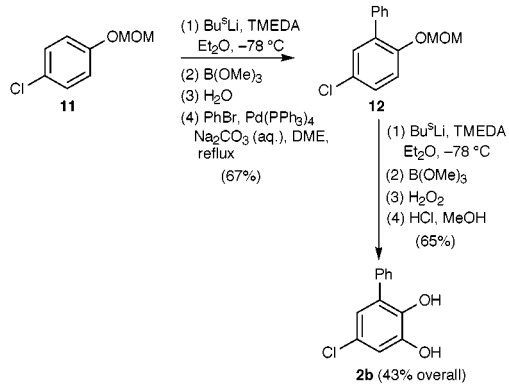

Scheme 5

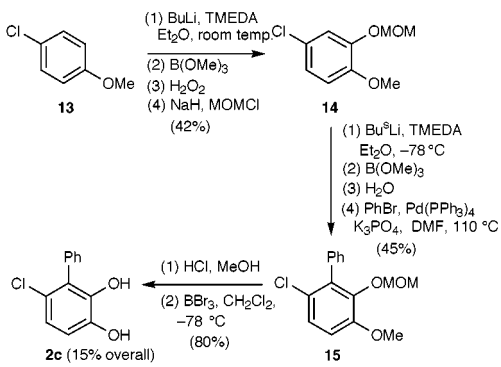

Scheme 6

chlorination with C_2Cl_6, and HCl-mediated deprotection completed the walk-around-the-ring sequence to afford **2a** in good overall yield (49%). The regiospecific construction of 5-chloro-DHB **2b** (Scheme 5) began from the 4-chlorophenol-derived **11** which, upon metalation–boronation-cross-coupling, gave the biphenyl **12**. Adapting the OH^+ synthon introduction as for **8**, followed by hydrolysis, led to **2b** in an acceptable overall yield (43%). The synthesis of 6-chloro-DHB[11] **2c** (Scheme 6) was achieved in a similar fashion, again exploiting the walk-around-the ring sequence. Thus, metalation of **13** followed by boronation–oxidation afforded the intermediate phenol which was converted to the MOM derivative **14**. Subsequent metalation–trimethyl borate quench afforded the 2-boronic acid, which, in crude form, was subjected to Suzuki–Miyaura cross-coupling with bromobenzene to give **15**, followed by hydrolysis and BBr_3 deprotection to afford **2c** (15%). The regiospecificity of all DoM reactions was established by 1D- and 2D-NMR. Final products were obtained in purities > 99% as required for the substrate specificity and inhibition studies of DHBD and BphD.[6]

This work demonstrates the expedient synthesis of all monochloro 2,3-DHBs by the directed *ortho* metalation–Suzuki–Miyaura cross-coupling sequence.[7] The key attribute of DoM, its regioselectivity, is imparted singularly and in an iterative manner (**3**), and leads to single isomer chloro-DHBs in high purity and in gram quantities. The method is being used for the provision of other diverse chloro-DHBs as well as catechols[12] to gain further understanding of the respective catalytic mechanisms of DHBD and BphD.[2,3]‡

We are grateful to NSERC (Strategic grant STP0193182) for generous support of this interdisciplinary study.

Notes and references

‡ All new compounds show analytical and spectral (^1H, ^{13}C NMR, HRMS) data fully consistent with their structures.

1 S. Dagley, in *The Bacteria*, ed. J. R. Sokatch and L. N. Ornston, Academic Press, New York, 1986, pp. 527–555.
2 L. Que and R. Y. N. Ho, *Chem. Rev.*, 1996, **96**, 2607.
3 T. D. H. Bugg and C. J. Winfield, *Nat. Prod. Rep.*, 1998, 513.
4 K. N. Timmis, R. J. Steffan and R. Unterman, *Annu. Rev. Microbiol.*, 1994, **48**, 525.
5 D. D. Focht, *Curr. Opin. Biotechnol.*, 1995, **6**, 341.
6 (*a*) S. Y. K. Seah, G. Terracina, J. T. Bolin, P. Riebel, V. Snieckus and L. D. Eltis, *J. Biol. Chem.*, 1998, **273**, 22943; (*b*) F. H. Vaillancourt, S. Han, P. D. Fortin, J. T. Bolin and L. D. Eltis, *J. Biol. Chem.*, 1998, **273**, 34 887; (*c*) S. Y. K. Seah, G. Labbe, S. Nerdinger, M. R. Johnson, V. Snieckus and L. D. Eltis, submitted for publication.
7 V. Snieckus, *Chem. Rev.*, 1990, **90**, 879.
8 N. Miyaura and A. Suzuki, *Chem. Rev.*, 1995, **95**, 2457; (*b*) A. Suzuki, in *Metal Catalyzed Cross-Coupling Reactions*, ed. F. Diedrich and P. J. Stang, Wiley-VCH, Weinheim, 1998.
9 C. A. Quesnelle, O. B. Familoni and V. Snieckus, *Synlett*, 1994, 349 and references cited therein; V. Snieckus, in *Chemical Synthesis: Gnosis to Prognosis*, ed. C. Chatgilialoglu and V. Snieckus, NATO ASI Series E, 1996, vol. 320, Kluwer, Dordrecht, The Netherlands, p. 191; G. Queguiner, F. Marsais, V. Snieckus and J. Epsztajn, *Adv. Heterocycl. Chem.*, 1991, **52**, 187.
10 A. D. Ainley and F. Challenger, *J. Chem. Soc.*, 1930, 2171.
11 6-Cl-DHB (**2c**) was also prepared as follows: iodination (I_2, $AgOCOCF_3$, $CHCl_3$) of 2,3-dimethoxybiphenyl gave exclusively the 6-iodo isomer which, upon metal–halogen exchange and chlorination (Bu^tLi, THF, −78 °C then C_2Cl_6) followed by deprotection (BBr_3, CH_2Cl_2, −78 °C) furnished **2c** in an overall yield of 29%.
12 3-Et (23% overall), 3-Pr^i (11% overall), 3-Bu^t (28% overall), and 3-Cl species (77% overall) have been prepared by this method (P. Riebel and V. Snieckus, unpublished results and utilized as described elsewhere). [ref. 6(*a*), (*b*)].

Communication 9/07279I

Spontaneous oxidation of a sulfide in zeolite CaY: the unprecedented reaction of a sulfide radical cation with oxygen

Wenhui Zhou and Edward L. Clennan*

Department of Chemistry, University of Wyoming, Laramie, WY 82071, USA. E-mail: clennane@uwyo.edu

Received (in Corvallis, OR, USA) 23rd July 1999, Accepted 24th September 1999

Addition of 1,5-dithiacyclooctane (1,5-DTCO) to CaY resulted in electron transfer formation of the corresponding radical cation, which was characterized by EPR and diffuse reflectance UV–VIS spectrometry and which undergoes an unprecedented reaction with molecular oxygen to give mono- and bis-sulfoxide products.

The spontaneous formation of radical cations in zeolites has been extensively investigated with the realization that electron transfer is pivotal to many processes promoted by these important catalysts.[1] The lifetimes of radical cations are often dramatically extended in the interior of the zeolite allowing spectroscopic characterization, however, these species are not inert[2] and dimerizations,[3] rearrangements,[4] ring contractions,[5] and loss of protons[6,7] have all been observed. We report here the first example of the formation of a 2σ–1σ* radical cation[8] in the interior of CaY and the ability of the zeolite to promote a reaction of this radical cation that is not observed in homogeneous solution.

The substrate chosen for examination was 1,5-dithiacyclooctane (1,5-DTCO). 1,5-DTCO adopts a boat chair conformation in which lone pairs on the two sulfur atoms point in towards one another.[9] Its molecular volume is 193 Å^3 and it can conveniently fit in a 6 × 6 × 6 Å box.[10] Consequently, it can diffuse readily though the 7.4 Å windows into the 13 Å diameter supercages of CaY.

The oxidation of 1,5-DTCO has been extensively examined, and both its radical cation $\mathbf{1}^{+\cdot}$ and dication $\mathbf{1}^{2+}$ have been characterized.[8] The radical cation is conveniently synthesized by one-electron oxidation of 1,5-DTCO or by treatment of the corresponding 1-oxide with acid. The unique stability of $\mathbf{1}^{+\cdot}$ has been attributed to a transannular interaction between the two sulfur atoms to form a three electron bond species. Asmus[11] has described this unique bonding situation as an overlap of the p-orbitals on each sulfur to form a bond consisting of a filled σ and a half-filled σ* orbital. The suggestion, from electrochemical data, that the second oxidation of 1,5-DTCO is 20 mV easier that the first provides a dramatic confirmation of this bonding picture.[12]

Addition of 5 ml of a 0.04 M 1,5-dithiacyclooctane (1,5-DTCO) hexane solution to 0.3 g of a freshly prepared sample of CaY[13] under an argon atmosphere followed by GC monitoring of the hexane revealed a rapid and nearly quantitative (> 96% in all cases) adsorption of the sulfide by the zeolite. Immediate evidence for successful formation of $\mathbf{1}^{+\cdot}$ was provided by the fact that the hexane remained colorless during the absorption process while the zeolite immediately changed color from white to bright yellow.[14] An EPR spectrum of the yellow solid/hexane slurry confirmed this suggestion by exhibiting five lines (g = 2.0123; a_H = 14.50 G) indicative of an unpaired electron on sulfur interacting with four equivalent hydrogens. This EPR and the three line spectra generated by introducing 2,2,8,8-tetradeutero-1,5-dithiacyclooctane into the zeolite (g = 2.0121; a_H = 14.43 G) are nearly identical to those assigned to $\mathbf{1}^{+\cdot}$ by Hirschon and Musker for the solution oxidation of 1,5-DTCO.[15] In addition, the diffuse reflectance UV–VIS spectrum of the yellow zeolite exhibited a λ_{max} at 420 nm identical to that reported for $\mathbf{1}^{+\cdot}$ in MeCN.

The zeolite encapsulated radical cation has a lifetime in excess of 8 h in an argon atmosphere, but the diagnostic yellow color and the EPR signal disappear after approximately 2 h when air is introduced into the reaction mixture. Samples which had been purged with oxygen until the yellow color faded were extracted with THF and the products analyzed by GC or GC/MS. The products were identified by comparison to authentic samples as 1,5-dithiacyclooctane 1,5-dioxide **2** and 1,5-dithiacyclooctane 1-oxide **3**, and were formed in > 90 and < 7% yields, respectively (Scheme 1). This extractive workup procedure resulted in material balances in excess of 80% in all cases, consisting primarily of the products accompanied by only traces of 1,5-DTCO and an unidentified material.

Monitoring of the reaction in air by diffuse reflectance UV-VIS spectrometry (Fig. 1) for more than three half-lives demonstrated that the yellow color (λ_{max} = 420 nm band)

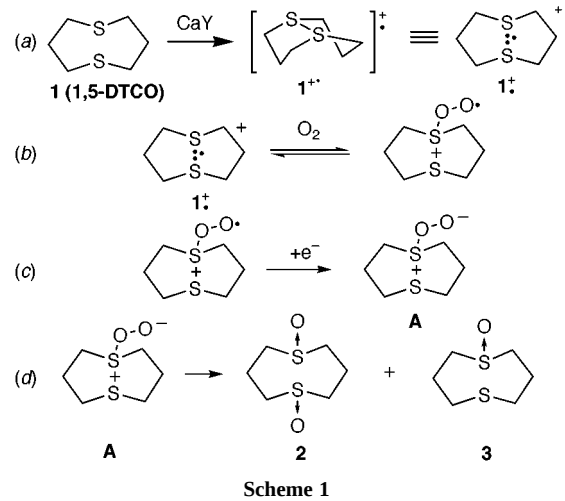

Scheme 1

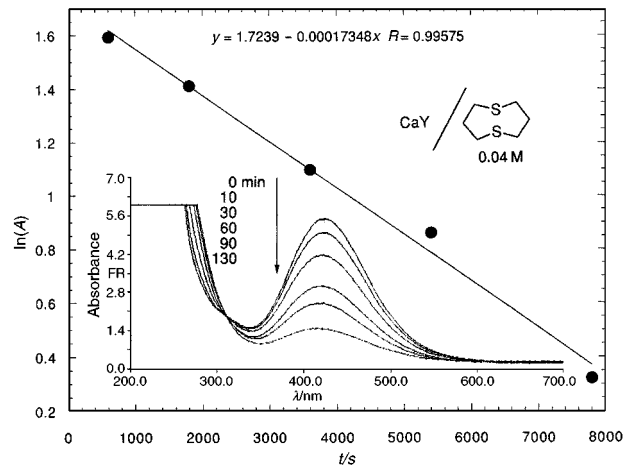

Fig. 1 Plot of the first order decay of the 420 nm band generated by encapsulation of 1,5-DTCO in CaY. Insert: diffuse reflectance UV–VIS spectra of the 1,5-DTCO/CaY sample in the presence of air showing the decrease in the 420 nm band and the isobestic point at 310 nm.

disappears in a strictly first order process. The presence of an isobestic point at 310 nm suggests a simple process, as shown in Scheme 1.

The overall process is initiated by a spontaneous formation of the 2σ–1σ* radical cation. Reported examples of spontaneous formation of sulfur-centered radical cations in the interior of zeolites are rare. Nevertheless, Roth and co-workers[4,5] have reported formation of both diphenyl disulfide and 2-phenyl-1,3-dithiane radical cations in ZSM-5. Electron transfer oxidations of encapsulate substrates [Scheme 1(*a*)] have often been discussed in terms of electron transfer to a Lewis acid or defect site formed during zeolite pretreatment or as an oxidation by absorbed oxygen.[1] The formation of $\mathbf{1}^{+\cdot}$ in CaY is clearly a function of its ease of oxidation. Radical cations were not formed in CaY calcined at 100 or 500 °C upon adsorption of 1,5-dithiacyclononane **4**, 1,4-dithiacycloheptane **5**, 1,3-dithiacyclohexane **6** or 1,4-dithiacyclohexane **7**. All of these bis(sulfides) are more difficult to oxidize than 1,5-DTCO as demonstrated by their oxidation potentials *vs.* Ag/0.01 M $AgNO_3$ in MeCN, shown in Fig. 2.

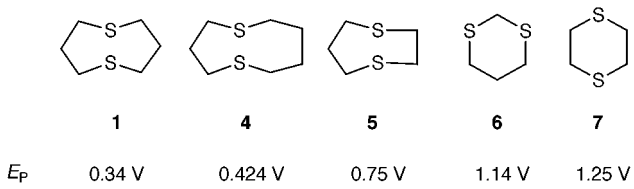

Fig. 2 Oxidation potentials of **1** and **4**–**7**.

The addition of O_2 to $\mathbf{1}^{+\cdot}$ [Scheme 1(*b*)] is unprecedented and is not observed in solution.[16] Asmus has attributed the lack of reactivity of oxygen with 2σ–1σ* sulfur centered radicals to an orbital mismatch between the LUMO on oxygen and the highly energetic antibonding electron in the σ* orbital on sulfur.[11] Consequently, oxidations of sulfur centered radical cations with molecular oxygen have only been accomplished at high O_2 pressures.[17,18] We suggest that the successful oxidation in the interior of the zeolite can be attributed to the proximity of the reducing agent, which traps the oxygen adduct [Scheme 1(*c*)] prior to its reversion to $\mathbf{1}^{+\cdot}$ and O_2. This reduction produces a persulfoxide which is a well established intermediate in the reactions of singlet oxygen with sulfides. The persulfoxide **A** (Scheme 1) has been independently produced by addition of singlet oxygen to 1,5-DTCO in acetone and is known to give predominately the bis(sulfoxide) **2**, identical to the result observed in the interior of the zeolite.[19]

In conclusion, we have demonstrated that CaY is limited in its ability to spontaneously produce sulfur-centered radical cations to easily oxidized sulfides. We further conclude that the reduction potential of the acceptor in CaY is approximately 0.4 V or less *vs.* Ag/0.01 M $AgNO_3$. In addition the minor amount of monosulfoxide **3**, which would be the expected product from reaction of the 1,5-DTCO dication with the residual water in CaY, reveals that the zeolite overwhelmingly functions as a one- rather than as a two-electron oxidizing agent. It is likely that 1,5-DTCO, once oxidized to the radical cation, is restricted in its ability to diffuse to a second oxidizing site to be converted to the dication.

The unprecedented discovery that CaY can promote oxidation at sulfur with only molecular oxygen as an oxidant has far reaching environmental and economic implications. A great need exists for an economical means of selectively oxidizing waste thioethers.[17,18] Further work with other zeolites to extend the generality of this important discovery will be reported in due course.

We thank the National Science Foundation and the donors of the Petroleum Research Fund, administered by the American Chemical Society, for their generous support of this research.

Notes and references

1 V. Ramamurthy, P. Lakshminarasimhan, C. P. Grey and L. J. Johnston, *Chem. Commun.*, 1998, 2411.
2 D. W. Werst, P. Han and A. D. Trifunac, *Radiat. Phys. Chem.*, 1998, **51**, 255.
3 M. Kojima, H. Takeya, Y. Kuriyama and S. Oishi, *Chem. Lett.*, 1997, 997.
4 P. S. Lakkaraju, D. Zhou and H. D. Roth, *J. Chem. Soc., Perkin Trans. 2*, 1998, 1119.
5 H. D. Roth, K. Shen, P. S. Lakkaraju and L. Fernandez, *Chem. Commun.*, 1998, 2447.
6 F. R. Chen and J. J. Fripiat, *J. Phys. Chem.*, 1993, **97**, 5796.
7 P. S. Lakkaraju, D. Zhou and H. D. Roth, *Chem. Commun.*, 1996, 2605.
8 W. K. Musker, *Acc. Chem. Res.*, 1980, **13**, 200.
9 W. N. Setzer, B. R. Coleman, S. R. Wilson and R. S. Glass, *Tetrahedron*, 1981, **37**, 2743.
10 PC Model Serena Software, Bloomington, IN, USA.
11 K.-D. Asmus, in *Sulfur-Centered Reactive Intermediates in Chemistry and Biology*, ed. C. Chatgilialoglu and K.-D. Asmus, Plenum, New York, 1990, vol. 197, pp. 155–172.
12 M. D. Ryan, D. D. Swanson, R. S. Glass and G. S. Wilson, *J. Phys. Chem.*, 1981, **85**, 1069.
13 CaY was prepared by stirring NaY (5 g) at 90 °C for 5 h with 20 ml of a 0.5 M aqueous solution of $CaCl_2$. The ion exchange was repeated three times and the zeolite washed thoroughly with distilled water and dried under vacuum (6×10^{-4} torr) at 100 °C for approximately 24 h prior to use. The occupancy ($<S> \approx 1.5$ molecules of 1,5-DTCO per supercage) was calculated assuming a composition of the unit cell of $Si_{138.7}Al_{53.3}Na_{7.5}Ca_{23.3}O_{384}$ as reported by K. Pitchumani, P. H. Lakshminarasimhan, N. Prevost, D. R. Corbin and V. Ramamurthy, *Chem. Commun.*, 1997, 181.
14 CaY turned yellow instantaneously upon mixing of 1,5-DTCO and the zeolite. Gas chromatographic monitoring of the hexane slurry was conducted approximately 10 min after addition of the 1,5-DTCO to the CaY and revealed >96% absorption had already occurred.
15 A. S. Hirschon, Thesis, University of California Davis, 1979.
16 K. Schäfer, M. Bonifacic, D. Bahnemann and K.-D. Asmus, *J. Phys. Chem.*, 1978, **82**, 2777.
17 D. P. Riley and P. E. Correa, *J. Chem. Soc., Chem. Commun.*, 1986, 1097.
18 D. P. Riley, M. R. Smith and P. E. Correa, *J. Am. Chem. Soc.*, 1988, **110**, 177.
19 E. L. Clennan, D.-X. Wang, K. Yang, D. J. Hodgson and A. R. Oki, *J. Am. Chem. Soc.*, 1992, **114**, 3021.

Communication 9/06052I

ChemComm

Wittig rearrangement of allyl and propargyl furfuryl ethers leading to 2-furylmethanol derivatives

Masayoshi Tsubuki,* Teruyoshi Kamata, Hiroyuki Okita, Mayumi Arai, Atsushi Shigihara and Toshio Honda*

Faculty of Pharmaceutical Sciences, Hoshi University, Ebara 2-4-41, Shinagawa, Tokyo 142-8501, Japan. E-mail: tsubuki@hoshi.ac.jp; honda@hoshi.ac.jp

Received (in Cambridge, UK) 9th September 1999, Accepted 5th October 1999

The first example of the Wittig rearrangement of furfuryl ethers is presented and its application to the preparation of 3-(2-furyl)-3-hydroxy-2-methylpropionates is described.

We have recently shown that the Wittig rearrangement of 3-furylmethyl ethers could proceed to give 2,3- and 1,2-rearrangement products.[1] An advantage of this Wittig rearrangement is that the deprotonation occurred selectively at the allylic position, and either 2,3- or 1,2-rearrangement occurred preferentially depending on the base used. Our interest in defining the scope, limitations and utility of this rearrangement in furylmethyl ethers has directed our attention to Wittig rearrangement of furfuryl ethers. Although the Wittig rearrangement of arylmethyl ethers has been widely studied,[2] there has been no successful report on the rearrangement of a furfuryl ether.[3] Herein, we report the first example of the Wittig rearrangement of allyl and propargyl furfuryl ethers to provide a variety of furyl alcohols, especially 2-furylmethanol derivatives.

The Wittig rearrangement of allyl furfuryl ethers **1a**–**e**†‡ was initially investigated under the conditions[1] described before. Allyl furfuryl ether **1** can theoretically produce both 2,3-rearrangement products **2** and **4** and 1,2-rearrangement products **3** and **5** depending on the position, α and α′, of deprotonation[4] (Scheme 1). The results are summarised in Table 1. Selective deprotonation at the α position was generally effected by Bu^{t}Li in THF at −78 °C, thus providing 2,3-rearrangement products **2a**–**e** as major isomers. In contrast, weaker bases, such as BuLi and Bu^{s}Li, favoured α′ over α deprotonation in the reactions of **1a**–**d**, giving 2,3-rearranged products **5a**–**d** together with 1,2-rearranged products **4a**,**b**. (*Z*)-Crotyl furfuryl ether **1d** afforded *syn* product[5] **2d** with high diastereoselectivity, whereas (*E*)-crotyl ether **1c** yielded *anti* isomer[5] **2c**, albeit in moderate selectivity. It is noteworthy that the (*E*)-crotyl ether **1c** underwent [2,3] Wittig rearrangement furnishing the *anti* isomer **2c** as a major compound, while the corresponding (*E*)-crotyl benzyl ether afforded a mixture in which the *syn* isomer was favoured.[2]

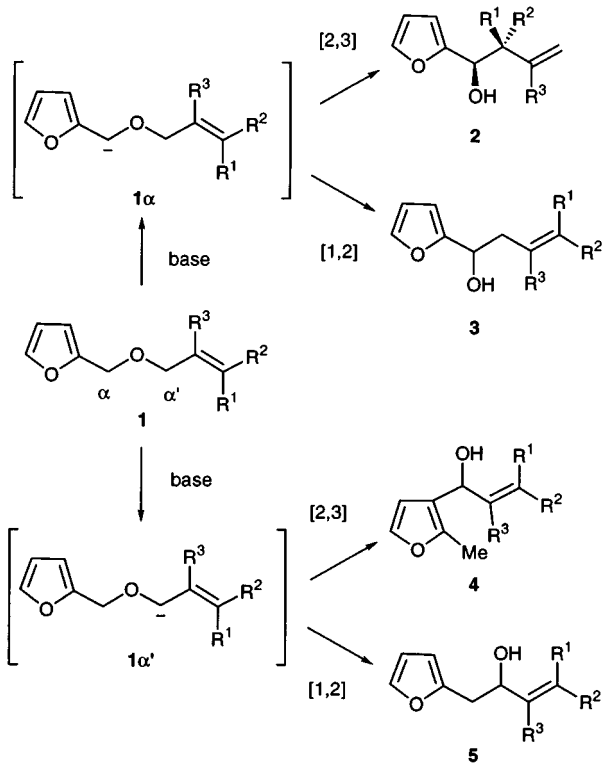

Scheme 1

In order to gain an understanding of the relative thermodynamic stabilities of **1α** and **1α′** anions, we undertook *ab initio* calculations involving full optimisations using the GAUSSIAN 92 quantum mechanical package.§ As one might expect, the calculations suggest that the energy minimums of the **1a**–**e** α anions were favoured by 12.0-28.5 kJ mol^{-1} over the energy minimums of the **1a**–**e** α′ anions at the RHF/6-31+G* level. It became apparent that the energy minimum of the prenyl ether **1e** α anion was predicted to be 9.7 kJ mol^{-1} lower than that of the allyl ether **1a** α anion. These results support the idea that the Wittig rearrangement of allyl furfuryl ethers **1a**–**e** proceeded through deprotonation mainly at the α position, giving 2,3-rearrangement products **2a**–**e**.

Table 2 shows that the diastereoselectivity in the Wittig rearrangement of crotyl ethers **1c**,**d** was influenced by the solvent used. Surprisingly, changing the solvent from THF to Et_2O caused the opposite diastereoselectivity in the reaction of

Table 1 Wittig rearrangement of furfryl ethers **1a**–**e**

Substrate	Base[a]	Yield (%)	Product Distribution[b] (%) 2	3	4	5
1a R^1 = R^2 = R^3 = H	BuLi	53	31[c]		19	50
	Bu^{s}Li	61	30[c]		16	54
	Bu^{t}Li	61	63[c]		17	20
1b R^1 = R^2 = H, R^3 = Me	BuLi	71	23[c]		23	54
	Bu^{s}Li	55	23[c]		15	62
	Bu^{t}Li	69	67[c]		14	19
1c R^1 = R^3 = H, R^2 = Me	BuLi	79	74 (66/34)[d]	—	—	26
	Bu^{s}Li	66	45 (75/25)[d]	—	—	55
	Bu^{t}Li	73	93 (73/27)[d]	—	—	7
1d R^1 = Me, R^2 = R^3 = H	BuLi	59	82 (9/91)[d]	—	—	18
	Bu^{s}Li	70	52 (10/90)[d]	—	—	48
	Bu^{t}Li	64	90 (10/90)[d]	—	—	10
1e R^1 = R^2 = Me, R^3 = H	BuLi	57	82	5	—	13
	Bu^{s}Li	57	56	39	—	5
	Bu^{t}LI	79	91	2	—	7

[a] Reactions were carried out with base in THF at −78 °C. BuLi (10 equiv.) was employed and the reaction was allowed to warm to −20 °C. Bu^{s}Li (3 equiv.) was employed.Bu^{t}Li (5 equiv.) was employed. [b] Determined by 270 MHz NMR analysis of the crude products. [c] [2,3] Rearranged products **2a**,**b** are equal to [1,2] rearranged products **3a**,**b**. [d] In parentheses: the ratio of the *anti* to the *syn* product.

Table 2 Wittig rearrangment of crotyl furfuryl ethers **1c**,**d** with Bu^{t}Li in different solvents at −78 °C

Substrate	Solvent	*syn*:*anti*	Yield (%)
1c	THF[a]	27:73	73
1c	Et_2O	87:13	72[b]
1c	toluene	74:26	69
1c	hexane	78:22	58[b]
1d	THF[a]	90:10	64
1d	Et_2O	94:6	66
1d	toluene	92:8	51
1d	hexane	>99:<1	60[b]

[a] The results from Table 1. [b] Based on the recovery of the starting material.

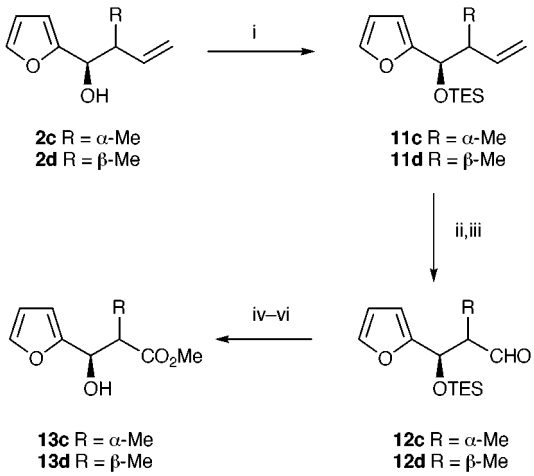

Scheme 2 *Reagents and conditions*: i, TESCl, Pr^i_2EtN, CH_2Cl_2 (87% for **11c**, 89% for **11d**); ii, OsO_4, NMO, acetone–H_2O; iii, $NaIO_4$, CH_2Cl_2–H_2O (2 steps: 54% for **12c**, 47% for **12d**); iv, $NaClO_2$, 2-methylbut-2-ene, NaH_2PO_4, Bu^{t}OH, H_2O; v, MeI, $NaHCO_3$, DMF; vi, TsOH, MeOH (3 steps: 65% for **13c**, 59% for **13d**).

Table 3 Wittig rearrangement of furfuryl propargyl ethers **6a**,**b**

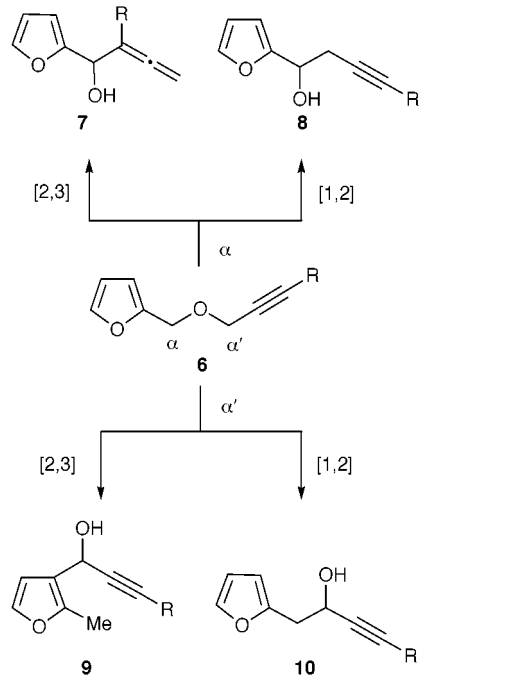

Substrate	Base[a]	Yield (%)	Product Distribution[b] (%) 7	8	9	10
6a R = H	BuLi	73	—	45	6	49
6a R = H	Bu^{s}Li	62	—	65	14	21
6a R = H	Bu^{t}Li	61	—	89	—	11
6b R = Me	BuLi	67	9	—	70	21
6b R = Me	Bu^{s}Li	64	12	—	85	3
6b R = Me	Bu^{t}Li	52	9	—	82	9

[a] Reactions were carried out with base in THF at −78 °C. BuLi (10 equiv.) was employed and the reaction was allowed to warm to −20 °C. Bu^{s}Li (3 equiv.) was employed. Bu^{t}Li (5 equiv.) was employed. [b] Determined by 270 MHz NMR analysis of the crude products.

(*E*)-crotyl ether **1c**. The same trend was observed even in a non-polar solvent. On the other hand, better results were found in Et_2O, toluene and hexane, where 84–98% de was obtained in the reactions of (*Z*)-crotyl ether **1d**. A trace amount of **5c,d** was formed in all cases.

The promising results for the Wittig rearrangement of allyl furfuryl ethers prompted us to examine the rearrangement of propargyl ethers **6a**,**b** (Table 3). For propargyl ether **6a** deprotonation with Bu^{s}Li or Bu^{t}Li proceeded through the dianion at the α and terminal alkyne positions to give 1,2-rearrangement product **8a** preferentially. In contrast, propargyl ether **6b** was deprotonated at the α′ position to produce mainly 2,3-rearrangement product **9b**.

Employing *anti* and *syn* alcohols **2c**,**d** we prepared 3-(2-furyl)-3-hydroxy-2-methylpropionates **13c**,**d**, key intermediates for the synthesis of several natural products.[6] Protection of the hydroxy group in **2c**,**d** as a TES ether afforded **11c**,**d**, which were oxidised to aldehydes **12c**,**d** by dihydroxylation of the alkene followed by glycol cleavage in 47 and 42% yield, respectively. Oxidation of **12c**,**d** with sodium chlorite gave the carboxylic acids, which were esterified and then deprotected with TsOH to furnish propionates **13c**,**d** in 65 and 59% yield, respectively.

In summary, Wittig rearrangement of furfuryl ethers offers a new route for the synthesis of furyl alcohols, especially 2-furylmethanol derivatives.

This work was supported by a Grant-in-Aid for Scientific Reseach (C) from the Ministry of Education, Science, Sports and Culture, Japan.

Notes and references

† Furfuryl ethers **1a**–**e** and **6a**,**b** were prepared by reaction of furfuryl alcohol with the corresponding halides in DMF using 2 equiv. of sodium hydride (ref. 7).

‡ All new compounds exhibited satisfactory elemental analyses and/or HRMS and ^{1}H and ^{13}C NMR and IR spectral data. In general furans with low molecular weight are volatile.

§ MO calculations were performed using the IBM RS/6000 version of the GAUSSIAN 92 suite of programs.

1 M. Tsubuki, H. Okita and T. Honda, *J. Chem. Soc., Chem. Commun.*, 1995, 2135.
2 J. A. Marshall, in *Comprehensive Organic Synthesis*, ed. B. M. Trost and I. Fleming, Pergamon, New York, 1991, vol. 3, p. 975; R. Brückner, in *Comprehensive Organic Synthesis*, ed. B. M. Trost and I. Fleming, Pergamon, New York, 1991, vol. 6, p. 873; T. Nakai and K. Mikami, *Org. React.*, 1994, **46**, 105.
3 Marshall *et al*. have reported a [2,3] Wittig rearrangement of a macrocyclic furan diether, in which the allyl furfuryl ether moiety did not react *via* [2,3] Wittig rearrangement: J. A. Marshall and D. J. Nelson, *Tetrahedron Lett.*, 1988, **29**, 741.
4 pK_a values for 2-methylfuran and MeCH=CH_2 are 43 and 44, respectively. See F. G. Bordwell, *Acc. Chem. Res.*, 1988, **21**, 456.
5 P. G. M. Wuts and G. R. Callen, *Synth. Commun.*, 1986, **16**, 1833; G. Cahiez and P.-Y. Chavant, *Tetrahedron Lett.*, 1989, **30**, 7373.
6 H. Akita, H. Koshiji, A. Furuichi, K. Horikoshi and T. Oishi, *Chem. Pharm. Bull.*, 1984, **32**, 1242; S. F. Martin and D. E. Guinn, *J. Org. Chem.*, 1987, **52**, 5588.
7 J. E. Zanetti, *J. Am. Chem. Soc.*, 1927, **49**, 1061; W. R. Kirner, *J. Am. Chem. Soc.*, 1928, **50**, 1955.

Communication 9/07312D

The *N*-carbamoyl squaramide dimer: a compact, strongly associated H-bonding motif

Anthony P. Davis,*[a] Sylvia M. Draper,[a] Gavin Dunne[a] and Peter Ashton[b]

[a] *Department of Chemistry, Trinity College, Dublin 2, Ireland. E-mail: adavis@tcd.ie*
[b] *School of Chemistry, University of Birmingham, Edgbaston, Birmingham, UK B15 2TT*

Received (in Cambridge, UK) 6th September 1999, Accepted 1st October 1999

_N_-Carbamoyl squaramides 3, readily available from dialkyl squarate 5, form hydrogen-bonded dimers in solution and in non-polar organic solvents; in $CDCl_3$ they show no significant dissociation down to concentrations of ~0.5 mM.

The continuing development of supramolecular self-assembly requires accessible subunits which can be relied upon to associate strongly and predictably through non-covalent interactions. Particular attention has recently been paid to systems capable of forming four intermolecular hydrogen bonds,[1–4] such as the self-complementary 'DDAA' units **1** and **2** studied

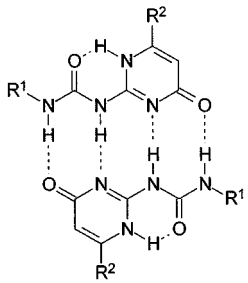

1

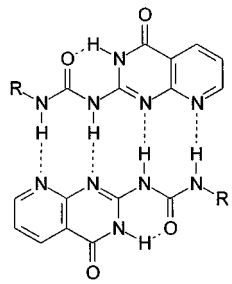

2

by the groups of Meijer[1] and Zimmerman,[2] respectively. These units self-associate essentially completely in solvents such as $CDCl_3$, and are only disrupted by significant quantities of polar solvents such as DMSO.

Herein we report a new homodimer which is related to **1** and **2** but with significant geometric differences. It is nearly as strongly bound, while being exceptionally compact and easy to construct. The new system **3·3** is based on the squaramide unit,

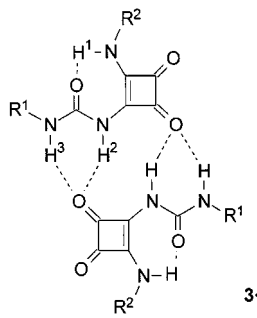

3·3

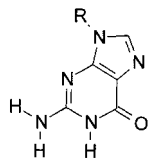

4

previously shown by Ballester, Costa and co-workers to provide a distinctive array of H-bonding sites for molecular recognition.[5,6] Unlike the earlier squaramides, monomer **3** possesses a ureidyl substituent capable in principle of intramolecular hydrogen bonding to the neighbouring NH. The result should be a well-defined, roughly planar structure with an intriguing resemblance to guanine derivatives **4**.

Planning to investigate the interaction of **3** with nucleobases, we synthesized examples **3a** and **3b** from diisopropyl squarate **5** as shown in Scheme 1. Preliminary ^1H NMR binding experiments in $CDCl_3$ gave unexpected results, leading us to suspect that the squaramides self-associated to some degree.

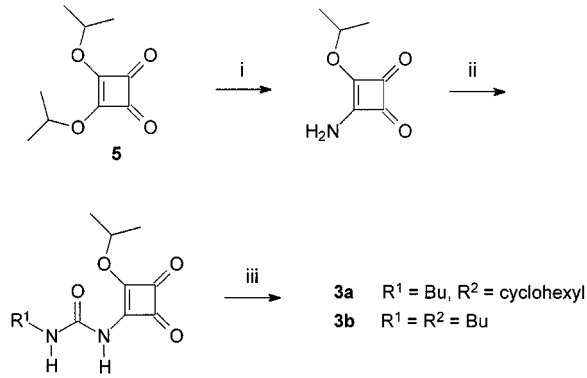

Scheme 1 *Reagents and conditions*: i, NH_3, MeOH–CH_2Cl_2, room temp.; ii, R^1NCO, Et_3N, MeCN, room temp.; iii, R^2NH_2, CH_2Cl_2, room temp.

However, dilution studies in this solvent showed no substantial changes in the spectra of **3a** or **3b** ($\Delta\delta < 0.1$ ppm) over a wide range of concentrations (~25–0.5 mM), suggesting either that association was not taking place or that it was very strong indeed.

Suspecting the latter, we obtained crystals of **3a** from CH_2Cl_2–light petroleum and subjected them to X-ray crystallography.† As shown in Fig. 1, **3a** exists as a centrosymmetric dimer in the crystal, apparently maintained by four NH···O=C hydrogen bonds. The carbamoylsquaramide units are essentially planar, and exhibit the expected intramolecular hydrogen bond.

The hypothesis that **3** dimerises strongly in $CDCl_3$ was tested by NMR studies in the presence of 'competitive' co-solvents. Addition of CD_3CN (up to 40% v/v) to $CDCl_3$ solutions of **3a** resulted in *upfield* movements of all three N*H* signals. For H(1) and H(3) the motions were moderate ($\Delta\delta \sim -0.7$ ppm), while

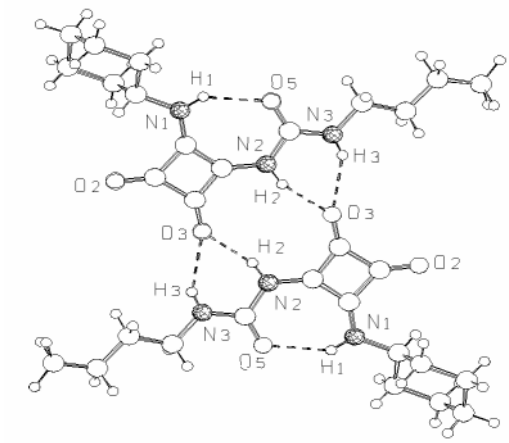

Fig. 1 Crystal structure of **3a** showing the relationship between adjacent H-bonded molecules. Selected distances (Å) and angles (°) are H(1)···O(5) 2.120(2), H(2)···O(3) 1.936(1), H(3)···O(3) 2.204(6), H(1)–N(1) 0.869(6), H(2)–N(2) 0.900(3), H(3)–N(3) 0.832(2); N(1)–H(1)···O(5) 136.65(6), N(2)–H(2)···O(3) 160.96(8), N(3)–H(3)···O(3) 149.03(9), H(2)···O(3)···H(3) 60.81(9).

Table 1 ^{1}H NMR dilution studies for compounds **3** in $CDCl_3$–CD_3CN (95 : 5)[a]

Compound	R^1, R^2	K_d/M^{-1}[b]	$\delta_{dimer} - \delta_{monomer}$ (ppm) H(2)	H(3)
3a	Bu, cyclohexyl	5800 ± 1100	2.32	0.59
3b	Bu, Bu	6100 ± 1300	2.42	[c]
3c	2,6-difluorophenyl, Bu	9800 ± 900	2.99	0.62

[a] Experiments performed at 303 K. Concentrations of **3** were varied between ~25 and ~0.2 mM. [b] Dimerisation constants K_d and error limits (standard deviations) were estimated from the movements of the signal due to H(2) using HOSTEST version 5.0 (ref. 7). [c] Not calculated, due to signal broadening.

for H(2) a substantial $\Delta\delta$ of −2.2 ppm was recorded. In the absence of self-association, downfield motions would have been expected due to the formation of NH···N≡C hydrogen bonds.‡ The observed upfield movements presumably result from the break-up of the aggregate, with the loss or weakening of the stronger NH···O=C hydrogen bonding.

The solvent system $CDCl_3$–CD_3CN (95:5) proved suitable for quantitative ^{1}H NMR dilution studies. Results are summarised in Table 1. In addition to **3a** and **3b**, the difluorophenyl-substituted example **3c** was synthesized (*cf.* Scheme 1) and studied under these conditions.§ In each case the signal due to H(2), which appeared between δ 10.3 and 10.9 at high concentrations, moved upfield upon dilution. The data were consistent with simple 1 : 1 dimerisations, yielding dimerisation constants (K_d) in the range 5×10^3 to 10^4 M^{-1}, and limiting chemical shift differences ($\delta_{dimer} - \delta_{monomer}$) in the range 2.3–3 ppm. The signals due to H(3), starting at δ ~6.5 for **3a**/**b** and δ ~8.1 for **3c**, also moved upfield during the experiments. Their motions were smaller and difficult to follow accurately due to broadening, but generally supported the analyses of H(2). A study of **3a** in $CDCl_3$–$(CD_3)_2SO$ (99 : 1) also suggested dimerisation, but with the lower K_d of ~180 M^{-1}. A re-examination of **3a** in $CDCl_3$ gave data consistent with $K_d \sim 10^6$ M^{-1}, on the assumption that (δ_{dimer}–$\delta_{monomer}$) is likely to be between 3 and 4 ppm in this solvent. The rôle of H(3) in maintaining the dimer was confirmed by a study of *N*-acetylsquaramide **6**, for which a K_d of just 120 M^{-1} was measured in $CDCl_3$–CD_3CN (95 : 5).

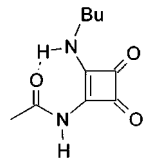

6

The tendency of **3** to dimerise was also revealed in the FAB$^+$ mass spectrum of **3b**. In addition to the monomer at *m/z* 268 (MH^+), there was a significant (~30%) signal for the dimer at *m/z* 535 (M_2H^+). Signals for higher aggregates M_nH^+ (n = 3-5) appeared at <1.5%. Interestingly the addition of AcONa promoted not only the M_nNa^+ signals as expected, but also a series of general formula $[M_n - mH + (m + 1)Na]^+$ ($1 < m < n$). These ions presumably arise from substitution of the relatively acidic H(2) by Na, followed by clustering in various combinations with **3b** itself.

When compared with **1** and **2**, the present system **3**·**3** would seem to be somewhat less strongly associated. For example, K_d values of *ca.* 10^3 M^{-1} are reported for both **1** and **2** in $CDCl_3$–$(CD_3)_2SO$ (95 : 5).[1,2] However, **3**·**3** is more tightly bound than other systems joined by four hydrogen bonds,[3,4] being maintained down to very low concentrations in $CDCl_3$. Given the accessibility, variability and compact size of **3**, this moiety should be capable of playing a distinctive rôle in the design of self-assembling systems.

Financial support for this work was provided by Enterprise Ireland, the Irish Health Research Board and the Wellcome Trust. We are grateful to Professor C. S. Wilcox for access to the HOSTEST binding analysis programme.

Notes and references

† *Crystal data* for **3a**: $C_{15}H_{23}N_3O$, M = 293.36, triclinic, space group $P\bar{1}$, a = 5.9800(4), b = 9.5090(5), c = 14.1543(8) Å, α = 89.694(6), β = 81.471(5), γ = 87.322(5)°, U = 795.10(8) Å^3, Z = 2, D_c = 1.225 g cm^{-3}, T = 293(2) K, μ(Mo-Kα) = 0.086 mm^{-1}, wR_2 = 0.1250 (3009 reflections collected, 2726 unique), R = 0.0510 [$I > 2\sigma(I)$], ENRAF NONIUS CAD4 diffractometer with graphite monochromator, ω-scans, structure solved by automatic direct methods using SHELXS-86 and refined using full-matrix least-squares on F^2 using SHELXL-93 (ref. 8). All the non-hydrogen atoms were refined anisotropically and the hydrogen atoms were located from subsequent difference Fourier maps. CCDC 182/1435. See http://www.rsc.org/suppdata/cc/1999/2265/ for crystallographic data in .cif format.

‡ The N*H* signal for *N*,*N*'-dibutylurea in $CDCl_3$ moves downfield by ~0.13 ppm on addition of 5% CD_3CN.

§ A number of other aryl-substituted *N*-carbamoylsquaramides were prepared but found unsuitable for study, mainly due to solubility problems.

1 R. P. Sijbesma, F. H. Beijer, L. Brunsveld, B. J. B. Folmer, J. H. K. K. Hirschberg, R. F. M. Lange, J. K. L. Lowe and E. W. Meijer, *Science*, 1997, **278**, 1601; F. H. Beijer, R. P. Sijbesma, H. Kooijman, A. L. Spek and E. W. Meijer, *J. Am. Chem. Soc.*, 1998, **120**, 6761.
2 P. S. Corbin and S. C. Zimmerman, *J. Am. Chem. Soc.*, 1998, **120**, 9710.
3 U. Lüning and C. Kühl, *Tetrahedron Lett.*, 1998, **39**, 5735.
4 B. Gong, Y. F. Yan, H. Q. Zeng, E. Skrzypczak-Jankunn, Y. W. Kim, J. Zhu and H. Ickes, *J. Am. Chem. Soc.*, 1999, **121**, 5607.
5 R. Prohens, S. Tomàs, J. Morey, P. M. Deyà, P. Ballester and A. Costa, *Tetrahedron Lett.*, 1998, **39**, 1063.
6 S. Tomàs, R. Prohens, M. Vega, M. C. Rotger, P. M. Deyà, P. Ballester and A. Costa, *J. Org. Chem.*, 1996, **61**, 9394.
7 C. S. Wilcox, in *Frontiers in Supramolecular Chemistry and Photochemistry*, ed. H.-J. Schneider and H. Durr, VCH, Weinheim, 1990, p. 123.
8 G. M. Sheldrick, *Acta Crystallogr., Sect. A*, 1990, **46**, 467; SHELXL-93, University of Gottingen, Germany.

Communication 9/07179B

ChemComm

Synthesis of 3-substituted and 2,3-disubstituted 4-chlorofurans

Ram N. Ram* and I. Charles

Department of Chemistry, Indian Institute of Technology, Delhi, Hauz Khas, New Delhi - 110 016, India.
E-mail: rnram@chemistry.iitd.ernet.in

Received (in Cambridge, UK) 8th September 1999, Accepted 1st October 1999

A simple method for the synthesis of 3-substituted and 2,3-disubstituted 4-chlorofurans is described which involves CuCl/bipy-catalysed regioselective cyclisation of 1-acetoxy-2,2,2-trichloroethyl allyl ethers followed successively by dechloroacetoxylation with Zn dust and tandem dehydrohalogenation–aromatisation with Bu^{t}OK/18-crown-6.

The synthesis of variously substituted furans continues to be of considerable interest[1] due to the presence of the furan nucleus in commercially important pharmaceuticals,[2] flavors[3] and a variety of naturally occurring biologically active compounds.[4] Furans also serve as useful synthetic intermediates for the synthesis of aromatic, alicyclic and acyclic molecules.[5] Since furans undergo electrophilic substitution and lithiation at the 2- and 5-positions, bypassing any of these positions to substitute the 3- and/or 4-positions is not straightforward. Therefore, β-mono-, di- and tri-substituted furans having either or both of the 2- and 5-positions unsubstituted are generally synthesised *via* acyclic routes. If the substituent happens to be a functional group, particularly at the 3- and/or 4-position(s), a variety of furans can be prepared by simple functional group transformations, thus widening the scope of the synthesis. In this respect, bromo and iodo groups have served particularly well by undergoing replacement with alkyl, alkenyl, alkynyl, aryl, heteroaryl, formyl and acyl groups.[5a,6] Since the chloro compounds, in general, are less expensive and more stable, there is considerable current interest in the replacement of the chloro group of aryl and vinyl chlorides with carbon groups.[7] However, there are very few reported methods for the preparation of 3- and/or 4-chlorofurans.[8] Furthermore, these methods have their own limitations with regard to yields,[8a] the nature of the other substituents[8b,e] and the substitution pattern.[8b–e,9] Therefore, herein we disclose a simple, new and broader route to prepare 3-substituted and 2,3-disubstituted 4-chlorofurans, which also complements the few reported methods for 3- and/or 4-chlorofuran synthesis.

Our interest in the chemistry of reactive aldehydes and metal-ion-promoted reactions[10] led us to use a reaction analogous to the reported[11] Cu^I-catalysed cyclisation of β-chloroethyl allyl ethers as the key step for the present synthesis. Thus, chloral hemiacetals, prepared by simply mixing chloral with readily accessible allylic alcohols, after protection as acetates, underwent regioselective cyclisation with CuCl/bipy, as expected, to afford the tetrahydrofurans **1a**–**f**. Dechloroacetoxylation of **1a**–**d** with Zn dust gave the 2,3-dihydrofurans **2a**–**d** as stereoisomeric mixtures in 61–81% overall yields. Dehydrochlorination of **2a**–**d** with KOH/EtOH followed by isomerisation of the crude isofurans with catalytic amounts of conc. H_2SO_4 and purification thereafter by column chromatography (silica gel, *n*-hexane) furnished the 4-chlorofurans **3a**–**d** in 31–65% overall yields (starting from the allyl alcohols). When the dehydrochlorination was performed with Bu^{t}OK/18-crown-6/THF, tandem isomerisation of isofurans was observed, giving the 4-chlorofurans **3a**–**d** in better overall yields (51–74%) (Scheme 1).

During dechloroacetoxylation, reduction of the benzylic chloro group was observed in the case of **1e**–**f**. The 4-chlorofuran **3e** was, however, prepared in 81% overall yield by a simple modification involving preparation of trichloroethyl cinnamyl ether by the reaction of trichloroethanol with cinnamyl bromide, followed by CuCl/bipy cyclisation and dehydrochlorination with DBU (Scheme 2).[12]

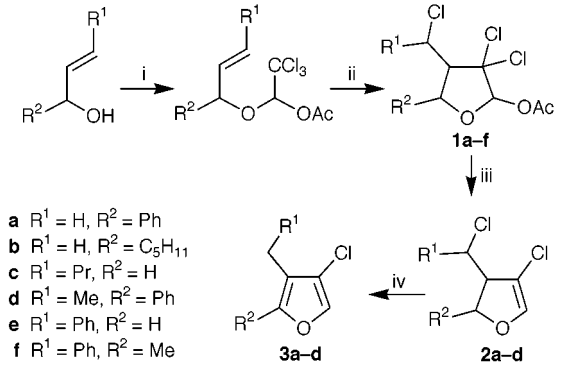

Scheme 1 *Reagents and conditions*: i, CCl_3CHO, 2 h, then Ac_2O, pyridine, DMAP, room temp., overnight; ii, 30 mol% of CuCl/bipy (1:1 mixture), 1,2-dichloroethane, reflux, 2 h; iii, Zn, THF, reflux, 4 h; iv, Bu^{t}OK, 18-crown-6, THF, reflux, 10 h.

These chlorofurans are fairly stable in hydrocarbon solvents but tend to deteriorate in chlorinated or oxygenated solvents. The decomposition is faster when they are stored as neat liquids.

All the compounds have been characterised by IR, NMR and mass spectral studies. The chlorofurans **3** were also characterised by their transformation into the Diels–Alder adducts **4** on reaction with dimethyl acetylenedicarboxylate. In the case of **3a**, the reaction proceeded further to give the phenol **5a** under the reaction conditions used (neat, 100 °C, 10 h). The furan **3b** gave a mixture of the cycloadduct **4b** and the phenol **5b**, which was completely converted into the phenol **5b** on slight warming with $BF_3{\cdot}OEt_2$ (Scheme 3).

An additional advantage of the present method of furan synthesis is that it can be used to prepare 2,3-dihydrofurans as well, which, like furans, are also widely distributed in Nature[13] and are useful synthetic intermediates.[5c,14] This advantage is not

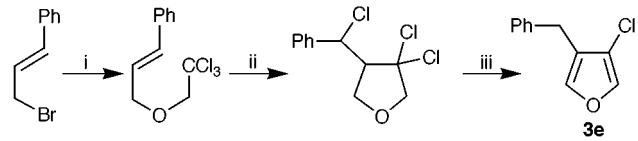

Scheme 2 *Reagents and conditions*: i, CCl_3CH_2OH, K_2CO_3, acetone, reflux, 6 h; ii, 30 mol% of CuCl/bipy (1:1 mixture), 1,2-dichloroethane, reflux, 2.5 h; iii, DBU, benzene, reflux, 3 h.

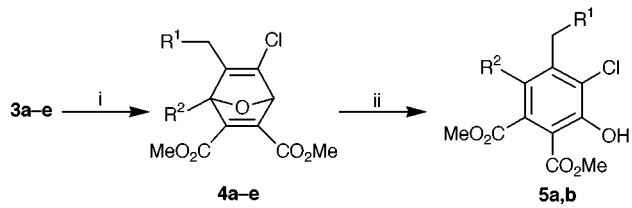

Scheme 3 *Reagents and conditions*: i, DMAD, 100 °C, 10 h; ii, $BF_3{\cdot}OEt_2$, 40–50 °C.

available with the existing methods of β-chlorofuran synthesis. We expect that in the present method of furan synthesis the chloro group might provide a branching point in the synthetic tree at the 2,3-dihydrofuran or furan stage or later during synthetic applications, to give access to a variety of di-, tri- and tetra-substituted furans and other interesting molecules.

Financial assistance by the DST, New Delhi, is gratefully acknowledged.

Notes and references

1 For a general review, see: X. L. Hou, H. Y. Cheung, T. Y. Hon, P. L. Kwan, T. H. Lo, S. Y. Tong and H. N. C. Wong, *Tetrahedron*, 1998, **54**, 1955. For some recent examples, see: J. W. Herndon and H. Wang, *J. Org. Chem*., 1998, **63**, 4564; P. Wipf, L. T. Rahman and S. R. Rector, *J. Org. Chem.*, 1998, **63**, 7132; E. Bures, J. A. Nieman, S. Yu, P. G. Spinazzé, J.-L. J. Bontront, I. R. Hunt, A. Rauk and B. A. Keay, *J. Org. Chem.*, 1997, **62**, 8750; Y. R. Lee, N. S. Kim and B. S. Kim, *Tetrahedron Lett*., 1997, **38**, 5671.

2 K. Nakanishi, *Natural Products Chemistry*, Kodansha, Tokyo, 1974.

3 *The Chemistry of Heterocyclic Flavouring and Aroma Compounds*, ed. G. Vernin, Ellis Horwood, Chichester, 1982.

4 For review, see: P. Bosshard and C. H. Eugster, *Adv. Heterocycl. Chem*., 1966, **7**, 378; F. M. Dean, *Adv. Heterocycl. Chem.*, 1982, **30**, 167; D. M. X. Donnelly and M. J. Meegan, *Comp. Heterocycl. Chem.*, 1984, **4**, 657. For recent examples, see: K.-S. Chen and Y.-C. Wu, *Tetrahedron*, 1999, **55**, 1353; A. Arnone, C. D. Gregorio, G. Nasini and O. V. De Pava, *Tetrahedron*, 1998, **54**, 10199.

5 For review, see: (*a*) B. H. Lipshutz, *Chem. Rev.*, 1986, **86**, 795. For some recent examples, see: (*b*) D. Meng and S. J. Danishefsky, *Angew. Chem., Int. Ed*., 1999, **38**, 1485; (c) R. H. Mitchell, T. R. Ward, Y. Wang and P. W. Dibble, *J. Am. Chem. Soc.*, 1999, **121**, 2601; (*d*) W. E. Noland and B. L. Kedrowski, *J. Org. Chem.*, 1999, **64**, 596; (*e*) J. M. Harris, M. D. Keranen and G. A. O'Doherty, *J. Org. Chem*., 1999, **64**, 2982; (*f*) A. Padwa, M. A. Brodney, B. Liu, K. Satake and T. Wu, *J. Org. Chem.*, 1999, **64**, 3595; (g) A. Frustner and H. Weintritt, *J. Am. Chem. Soc.*, 1998, **120**, 2817; (*h*) M. Kurosu, L. R. Marcin, T. J. Grinsteiner and Y. Kishi, *J. Am. Chem. Soc*., 1998, **120**, 6627.

6 T. Bach and L. Krüger, *Tetrahedron Lett*., 1998, **39**, 1729; M. K. Wong, C. Y. Leung and H. N. C. Wong, *Tetrahedron*, 1997, **53**, 3497; C. Alvarez-Ibarra, M. L. Quiroga and E. Toledano, *Tetrahedron*, 1996, **52**, 4065; S. P. Bew and D. W. Knight, *Chem. Commun*., 1996, 1007; H. J. Reich and R. E. Olson, *J. Org. Chem*., 1987, **52**, 2315; L. N. Pridgen and S. S. Jones, *J. Org. Chem*., 1982, **47**, 1590.

7 C. Zhang, J. Huang, M. L. Trudell and S. P. Nolan, *J. Org. Chem*., 1999, **64**, 3804; B. H. Lipshutz, P. A. Blomgren and S.-K. Kim, *Tetrahedron Lett*., 1999, **40**, 197; X. Bei, T. Crevier, A. S. Guram, B. Jandeleit, T. S. Powers, H. W. Turner, T. Uno and W. H. Weinberg, *Tetrahedron Lett*., 1999, **40**. 3855; B. H. Lipshutz and P. A. Blomgren, *J. Am. Chem. Soc.*, 1999, **121**, 5819; D. W. Old, J. P. Wolfe and S. L. Buchwald, *J. Am. Chem. Soc.*, 1998, **120**, 9722; A. F. Littke and G. C. Fu, *Angew. Chem., Int. Ed*., 1998, **37**, 3387; S. Saito, S. Oh-tani and N. Miyaura, *J. Org. Chem*., 1997, **62**, 8024.

8 (*a*) R. C. Larock and C.-L. Liu, *J. Org. Chem*., 1983, **48**, 2151 (poor yields); (*b*) Y. Tanabe, K.-i. Wakimura, Y. Nishii and Y. Muroya, *Synthesis*, 1996, 388 (2,5-diaryl-3-chlorofurans); (*c*) D. Obrecht, *Helv. Chem. Acta*., 1989, **72**, 447 (2-substituted and 2,5-disubstituted 3-chlorofurans); (*d*) N. D. Ly and M. Schlosser, *Helv. Chem. Acta*., 1977, **60**, 2085 (2-prenyl-3-chlorofuran); (*e*) R. E. Lutz and M. G. Reese, *J. Am. Chem. Soc*., 1959, **81**, 127 (2,5-diaryl-3-chlorofurans).

9 In fact, we could find no report on 3-substituted 4-chlorofurans and only one report on 2,3-disubstituted 4-chlorofurans in which the formation of two 2,3-disubstituted 4-chlorofuran derivatives has been described. These chlorofurans were obtained as a mixture in poor yields, one of which was characterised only by GC-MS [ref. 8(*a*)].

10 L. Singh and R. N. Ram, *J. Org. Chem*., 1994, **59**, 710; R. N. Ram and I. Charles, *Tetrahedron*, 1997, **53**, 7335; R. N. Ram and L. Singh, *Tetrahedron Lett*., 1995, **36**, 5401.

11 J. H. Udding, H. Hiemstra, M. N. A. Van Zanden and W. N. Speckamp, *Tetrahedron Lett*., 1991, **32**, 3123.

12 Although this scheme seems to be more attractive than Scheme 1, both in the number of steps and overall yields, we were not successful in preparing other trichloroethyl ethers by condensing trichloroethanol with secondary allylic halides.

13 P. F. Schuda, *Top. Curr. Chem*., 1980, **91**, 75.

14 T. Saito, M. M. Suzuki, T. C. Akiyama, T. Takeuchi, T. Matsumoto and K. Suzuki, *J. Am. Chem. Soc.*, 1998, **120**, 11 633; S. Wadman, R. Whitby, C. Yeates, P. Kocienski and K. Cooper, *J. Chem. Soc., Chem. Commun*., 1987, 241; A. I. Meyers, C. J. Andres, J. E. Resek, Maureen A. Melaughlin, Charlotte C. Woodall and P. H. Lee, *J. Org. Chem.*, 1996, **61**, 2586; G. Vidari, G. Lanfranchi, P. Sartori and S. Serra, *Tetrahedron: Asymmetry*, 1995, **6**, 2977; H. Kawakami, T. Ebata, K. Okano, K. Matsumoto, K. Koseki and H. Matsushita, Patent; *Chem. Abstr*., 1994, **120**, 107640g.

Communication 9/07270E

A bimodal dithiadiazolyl diradical: crystal structure and magnetic properties of the 2,2′-dimethylbiphenylene bridged derivative

T. M. Barclay,[a] A. W. Cordes,[a] N. A. George,[b] R. C. Haddon,[c] M. E. Itkis[c] and R. T. Oakley*[b]

[a] *Department of Chemistry and Biochemistry, University of Arkansas, Fayetteville, Arkansas 72701, USA*
[b] *Department of Chemistry, University of Waterloo, Waterloo, Ontario, Canada N2L 3G1. E-mail: oakley@sciborg.uwaterloo.ca*
[c] *Departments of Chemistry and Physics and Advanced Carbon Materials Center, University of Kentucky, Lexington, Kentucky 40506, USA*

Received (in Cambridge, UK) 7th September 1999, Accepted 5th October 1999

The two termini of the torsionally strained dithiadiazolyl diradical S_2N_2C–C_6H_3Me–MeC_6H_3–CN_2S_2 3 possess different solid state structural environments; the bulk magnetic susceptibility of 3 is interpreted in terms of the distinct properties of the two radical centres.

The potential applications of 1,2,3,5-dithiadiazolyl (DTDA) radicals in molecular magnets,[1] conductors[2] and thin film devices[3] has led to increasing interest in both the diversity and control of the structural features of these systems.[4] Most monofunctional derivatives associate in the solid state to afford diamagnetic dimers, and suppression of this dimerization hence represents a major experimental challenge. Recently, Rawson and co-workers have reported several radicals that are unassociated[1,5] or only very weakly spin paired.[6] Most significantly, the β-phase of *p*-cyanoperfluorophenyl-DTDA is weakly ferromagnetic below 36 K.[1]

Bifunctional radicals, *e.g.* **1** (R = H, CN, Bu^t)[7,8] and **2**,[3,9] have also been examined, but in the systems studied to date the

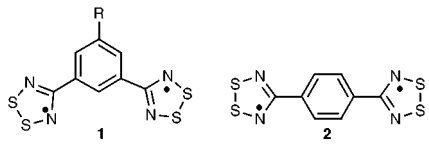

two termini have been crystallographically equivalent, as a result of which the bulk magnetic properties are a function of a single spin centre. In order to explore the relationship between structure and magnetic behavior in DTDA diradicals we have prepared and characterized the 2,2′-dimethylbiphenylene (DMBP) bridged derivative **3** (Scheme 1). We selected this bridge in the hope that torsion about the central C–C bond of DMBP would inhibit both the π-stacked structures found for **1** and the herringbone arrangement exemplified by **2**. Colourless crystals (mp 142–145 °C) of the necessary bis-amidine **4** [$\delta_H(CDCl_3)$ 0.065 (s, *Me*$_3$Si, 54 H), 7.34–7.56 (AA′BB′, 8 H)] were prepared in 65% yield from the dinitrile **5**[10] using standard methodology.[11] Reaction of **4** (3.00 g, 4.3 mmol) with SCl_2 (2.00 g, 19.3 mmol) in 100 ml of MeCN at reflux gave the crude bis(dithiadiazolylium chloride) **6**, which was reduced with Ph_3Sb (2.0 g, 5.7 mmol) to yield **3** (1.36 g, 82%), which was

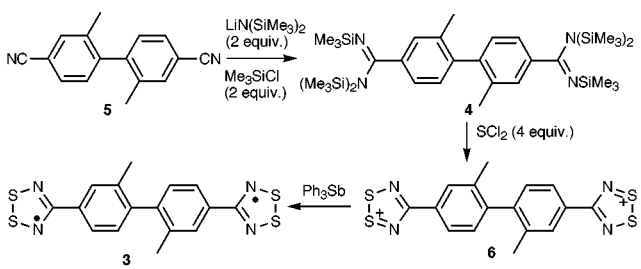

Scheme 1

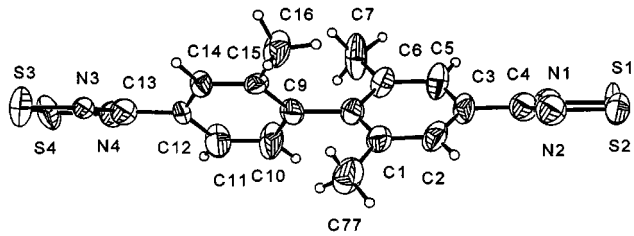

Fig. 1 ORTEP drawing of **3**, illustrating the torsion within the molecule. The C7 (C77) methyl group is disordered.

purified by fractional sublimation at 160–100 °C/10^{-3} torr, affording black reflective nodules, mp 242 °C.†

The molecular structure‡ (Fig. 1) of **3** exhibits a minor disorder in both CN_2S_2 rings, which were refined as rigid groups, and also in one of the methyl groups, which was refined with 50% occupancy of the two (C7/C77) positions. These imperfections aside, the molecule displays the anticipated torsion (74.0°) about the central C–C bond of the DMBP bridge; in biphenyl itself, for example, the two rings are coplanar,[12] but in 2,2′-dimethyl-4,4′-diaminobiphenyl the torsion angle opens to 86°.[13] The crystal packing of **3** (Fig. 2) represents a significant departure from the two classes of solid state motifs represented by **1** and **2**. Moreover the two DTDA radicals within each molecule are located in very different solid state environments. One end (S3/S4) is essentially undimerized, and the arrangement of these DTDA rings resembles an array of footprints running parallel to the *y* direction. At the other end of the molecule the DTDA ring (S1/S2) is dimerized in a *trans*-

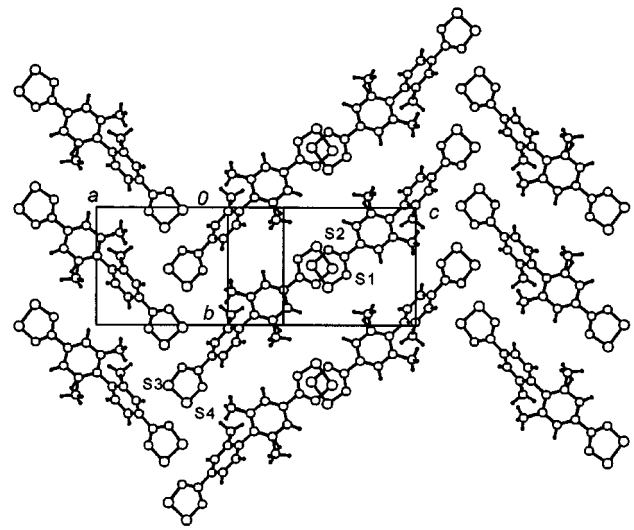

Fig. 2 PLUTO drawing of the layer-like packing in **3**, illustrating the *trans*-cofacial (S1/S2) and undimerized (S3/S4) radical rings. The C7 (C77) methyl group is disordered.

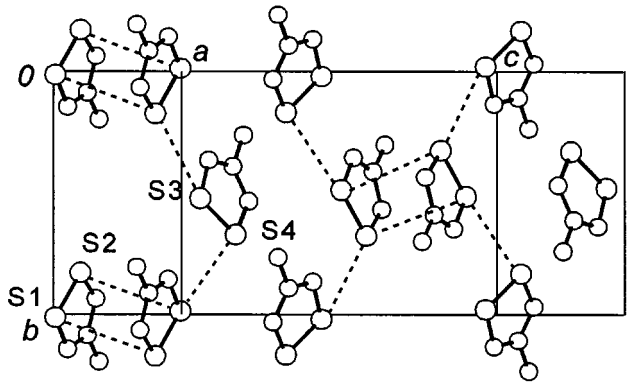

Fig. 3 A single layer of DTDA rings in **3** (DMBP bridges removed), showing close intermolecular contacts.

cofacial manner across an inversion centre to an equivalent radical on a neighbouring molecule. This hitherto unobserved orientation for radical association produces rather long S···S contacts [d(S1···S2′) = 3.68(2) Å], but the separation of the DTDA planes of the dimer is a tight 3.24 Å, easily short enough to effect spin pairing (*vide infra*). We note *en passant* that this mode of dimerization lies near to the proposed transition state for the photochemical isomerization of 1,3,2,4- to 1,2,3,5-DTDAs.[14] Although Fig. 2 suggests the two ends of the molecule are well separated, closer inspection of the packing of the DTDA rings (Fig. 3) reveals two short contacts [d(S1···S4′) = 3.38(2) Å and d(S2···S3′) = 3.38(2) Å]. These dimer/radical bridging interactions may facilitate magnetic exchange between the spins on the S3/S4 rings.

The extent of spin coupling in these two radical environments in **3** has been assessed by magnetic susceptibility measurements over the temperature range 4–400 K. The magnetic behavior (Fig. 4) of the compound can be divided into high (> 200 K), and low (< 200 K) temperature regions, both of which are interpreted in terms of Curie paramagnetism. We associate the low temperature paramagnetism primarily with the undimerized (S3/S4) end of the molecule. On the first scan through this region we find an unpaired spin count of n = 1.11 per molecule. The slight excess paramagnetism over n = 1 may be associated with the high temperature magnetic regime or experimental error. At low temperatures there is a hysteretic phase transition (75–150 K) that quenches some of the molecular spins. The Weiss constant for the ordering transition in all of these states is about −100 K and therefore strongly antiferromagnetic. Thus, at low temperatures, thermal cycling apparently leads to a coupling of some of the radical electrons at this end of the molecule. This may reduce the structural disorder noted above.

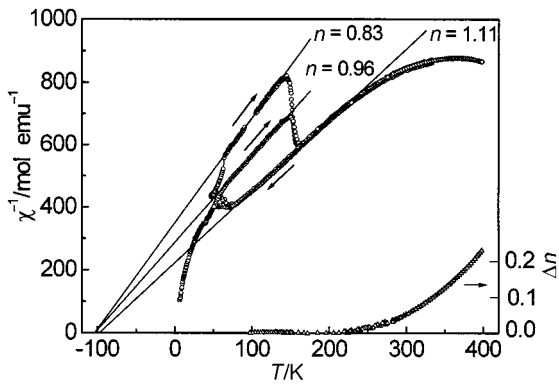

Fig. 4 Plots of $1/\chi$ (χ = magnetic susceptibility) and excess Curie Spins (Δn) of **3** as a function of temperature.

In the high temperature regime the departure from simple n = 1.11 Curie behavior probably arises from the thermal dissociation of the coupled spins at the dimerized (S1/S2) end of the molecule. The excess spins created (Δn) are shown on the right. Similar paramagnetic enhancements at elevated temperatures have been observed in the π-stacked structures of **1**.[7,8]

We thank the Natural Sciences and Engineering Research Council of Canada, the NSF/EPSCoR program (grant number EPS-9452895), the State of Arkansas and the Department of Energy (grant number DE-FG02-97ER45668) for financial support. We also acknowledge the Department of Education for a doctoral fellowship to T. M. B.

Notes and references

† Satisfactory chemical analyses were obtained for compounds **3** and **4**.

‡ *Crystal data* for **3**: Data were collected at 293 K on an Enraf-Nonius automated diffractometer with graphite-monochromated Mo-$K\alpha$ radiation (λ = 0.71073 Å) using θ–2θ scans. The structures were solved by direct methods and refined by full-matrix least-squares analysis which minimized $\Sigma w(\Delta F)^2$. $S_4N_4C_{16}H_{12}$, M = 388.5, monoclinic, space group $P2_1/n$, with a = 11.0371(11), b = 8.489(8), c = 18.854(2) Å, β = 103.299(9)° V = 1719.1(16) Å^3, Z = 4, D_c = 1.50 g cm^{-3}, μ = 0.54 mm^{-1}. 202 Parameters were refined using 1349 unique observed reflections [$I > 1\sigma(I)$] to give R = 0.117 and R_w = 0.142. CCDC 182/1434. See http://www.rsc.org/suppdata/cc/1999/2269/ for crystallographic data in .cif format.

1 A. J. Banister, N. Bricklebank, I. Lavender, J. M. Rawson, C. I. Gregory, B. K. Tanner, W. Clegg, M. R. J. Elsegood and F. Palacio, *Angew. Chem., Int. Ed. Engl.*, 1996, **35**, 2533; G. Antorrena, J. E. Davies, M. Hartley, F. Palacio, J. M. Rawson, J. N. Smith and A. Steiner, *Chem. Commun.*, 1999, 1393.
2 A. W. Cordes, R. C. Haddon and R. T. Oakley, in *The Chemistry of Inorganic Ring Systems*, ed. R. Steudel, Elsevier, Amsterdam, 1992, p. 295; A. W. Cordes, R. C. Haddon and R. T. Oakley, *Adv. Mater.*, 1994, **6**, 798.
3 A. W. Cordes, R. C. Haddon, C. D. MacKinnon, R. T. Oakley, G. W. Patenaude, R. W. Reed, T. Rietveld and K. E. Vajda, *Inorg. Chem.*, 1996, **35**, 7626.
4 A. J. Banister and J. M. Rawson, in *The Chemistry of Inorganic Ring Systems*, ed. R. Steudel, Elsevier, Amsterdam, 1992, p. 323; A. J. Banister and J. M. Rawson, *Adv. Heterocycl. Chem.*, 1995, **62**, 137; T. Torroba, *J. Prakt. Chem.*, 1999, **341**, 99.
5 A. J. Banister, N. Bricklebank, W. Clegg, M. R. J. Elsegood, C. I. Gregory, I. Lavender, J. M. Rawson and B. K. Tanner, *J. Chem. Soc., Chem. Commun.*, 1995, 679.
6 A. J. Banister, A. S. Batsanov, O. G. Dawe, P. L. Herbertson, J. A. K. Howard, S. Lynn, I. May, J. N. B. Smith, J. M. Rawson, T. E. Rogers, B. K. Tanner, G. Antorrena and F. Palacio, *J. Chem. Soc., Dalton. Trans.*, 1997, 2539.
7 M. P. Andrews, A. W. Cordes, D. C. Douglass, R. M. Fleming, S. H. Glarum, R. C. Haddon, P. Marsh, R. T. Oakley, T. T. M. Palstra, L. F. Schneemeyer, G. W. Trucks, R. Tycko, J. V. Waszczak, K. M.Young and N. M. Zimmerman, *J. Am. Chem. Soc.*, 1991, **113**, 3559; A. W. Cordes, R. C. Haddon, R. G. Hicks, D. K. Kennepohl, R. T. Oakley, T. T. M. Palstra, L. F. Schneemeyer, S. R. Scott and J. V. Waszczak, *Chem. Mater.*, 1993, **5**, 820.
8 R. A. Beckman, R. T. Boeré, K. H. Moock and M. Parvez, *Can. J. Chem.*, 1998, **76**, 85.
9 A. W. Cordes, R. C. Haddon, R. T. Oakley, L. F. Schneemeyer, J. Waszczak, K. M. Young and N. M. Zimmerman, *J. Am. Chem. Soc.*, 1991, **113**, 582.
10 H.-W. Schmidt and D. Guo, *Makromol. Chem.*, 1988, **189**, 2029.
11 R. T. Boeré, R. G. Hicks and R. T. Oakley, *Inorg. Synth.*, 1997, **31**, 94.
12 A. Hargreaves and S. H. Rizvi, *Acta Crystallogr.*, 1962, **15**, 365.
13 F. Fowweather, *Acta Crystallogr.*, 1952, **5**, 820.
14 J. Passmore and X. Sun, *Inorg. Chem.*, 1986, **35**, 1313; W. V. F. Brooks, N. Burford, J. Passmore and M. J. Schriver, *J. Chem. Soc., Chem. Commun.*, 1987, 69.

Communication 9/07209H

New insights into the mechanism of methane formation in the protonation of methyl complexes†

Richard A. Henderson* and Kay E. Oglieve

Nitrogen Fixation Laboratory, John Innes Centre, Norwich Research Park, Colney, Norwich, UK NR4 7UH. E-mail: r.a.henderson@ncl.ac.uk

Received (in Cambridge, UK) 1st September 1999, Accepted 7th October 1999

The reaction between $[NiMe\{(Ph_2PCH_2CH_2)_2PPh\}]^+$ and anhydrous HCl (in MeCN) involves initial protonation of nickel to form $[Ni(H)Me\{(Ph_2PCH_2CH_2)_2PPh\}]^{2+}$, but methane is not produced until after additional, direct protonation of the methyl group.

There have been many investigations into the formation of alkanes in the reaction of acid with metal–alkyl complexes,[1–3] and the consensus view is that the mechanism involves either direct protonation of the metal–carbon bond or initial protonation of the metal followed by intramolecular coupling of the hydrido and methyl ligands (Scheme 1).

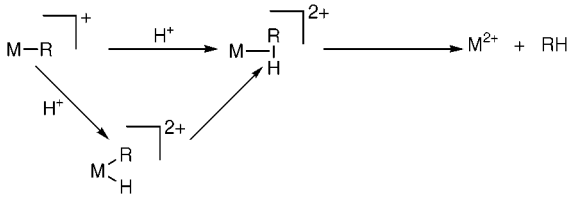

Scheme 1

The kinetics of these reactions are frequently too simple to be diagnostic of one particular mechanism and consequently the detection or isolation of a hydrido species has often been invoked as evidence of the coupling pathway. Here, we describe unprecedented complex kinetics for protonation of an alkyl complex which demonstrates, for the first time, that detection of a hydrido species is an insufficient criteria to define the intimate mechanism of alkane formation. Specifically, we show that initial protonation of $[NiMe(triphos)]^+$ [triphos = $(Ph_2PCH_2CH_2)_2PPh$; eqn. (1)] occurs at nickel to form a hydrido complex, but the formation of methane has to await further direct protonation of the methyl group.

$$[NiMe(triphos)]^+ + HCl \rightarrow [NiCl(triphos)]^+ + MeH \quad (1)$$

The reaction between $[NiMe(triphos)]^+$ and an excess of anhydrous HCl in MeCN occurs in two stages: a rapid, acid-dependent reaction which was studied by stopped-flow spectrophotometry, and the subsequent release of methane which was followed by GLC.

In the reaction between $[NiMe(triphos)]^+$ and HCl alone, the kinetics of the first stage exhibit a first order dependence on the concentration of complex and an apparent first order dependence on the concentration of HCl as described by eqn. (2), and illustrated in Fig. 1.

$$\frac{-d[NiMe(triphos)^+]}{dt} = (3.4 \pm 0.3) \times 10^2 [NiMe(triphos)^+][HCl] \quad (2)$$

The simplicity of these kinetics are consistent with either of the two pathways shown in Scheme 1. However, addition of Cl^-

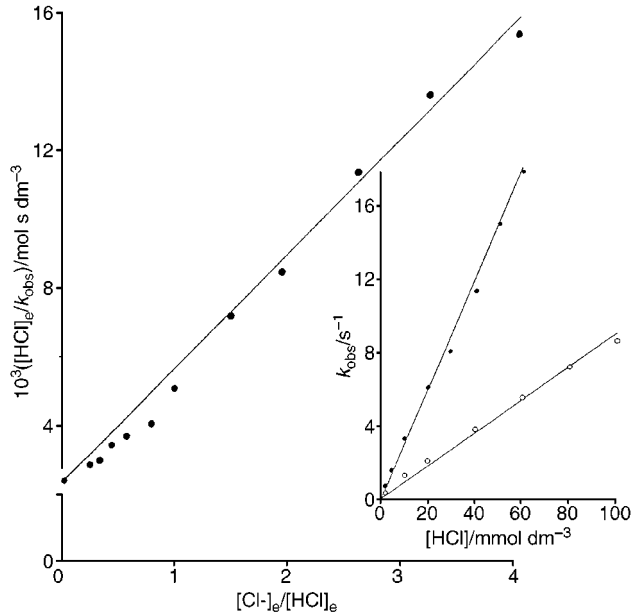

Fig. 1 Dependence of $[HCl]_e/k_{obs}$ on $[Cl^-]_e/[HCl]_e$ for the reaction of $[NiMe(triphos)]^+$ with HCl in the presence of $[NEt_4]Cl$, in MeCN at 25.0 °C. Line drawn is that defined by eqn. (3). [Insert: Dependence of k_{obs} on the concentration of HCl (●) and DCl (○) in the absence of $[NEt_4]Cl$].

reveals a more complicated behaviour (Fig. 1).‡ The *true* rate law is that shown in eqn. (3).

$$\frac{-d[NiMe(triphos)^+]}{dt} = \frac{(3.0 \pm 0.4) \times 10^2 [NiMe(triphos)^+][HCl]_e{}^2/[Cl^-]_e}{1 + (0.78 \pm 0.05)[HCl]_e/[Cl^-]_e} \quad (3)$$

Eqn. (3) demonstrates that two protons bind to the complex prior to methane release. Such kinetics have not been observed before but are in line with the general protonation characteristics of metal sites containing hydrocarbon residues, in which both metal and carbon can be protonated.[4,5]

The mechanism shown in Scheme 2 involves initial, rapid protonation at nickel to form the hydrido species. However, the kinetics dictate that this protonation is insufficient to produce methane. Rather formation of methane has to await additional protonation of the methyl group. Clearly, diprotonation of the

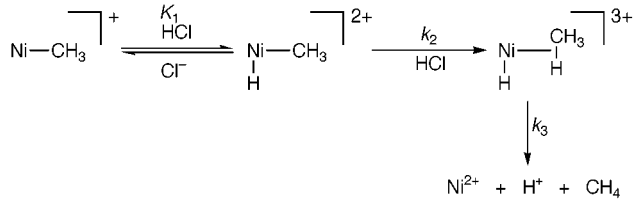

Scheme 2 Mechanism of the formation of methane in the reaction of $[NiMe(triphos)]^+$ with HCl in MeCN.

† Present address: Department of Chemistry, Bedson Building, University of Newcastle, Newcastle upon Tyne, UK NE1 7RU.

nickel is untenable since this would form a formal Ni^{VI} species.

The rate law associated with this mechanism is shown in eqn. (4) and is derived assuming that protonation at nickel is a rapidly established equilibrium, whilst protonation of the carbon is slow and irreversible.

$$\frac{-\mathrm{d}[\mathrm{NiMe(triphos)}^+]}{\mathrm{d}t} = \frac{K_1 k_2 [\mathrm{NiMe(triphos)}^+][\mathrm{HCl}]_e^{\,2}/[\mathrm{Cl}^-]_e}{1 + K_1[\mathrm{HCl}]_e/[\mathrm{Cl}^-]_e} \quad (4)$$

Comparison of eqns. (3) and (4) gives $k_2 = (3.8 \pm 0.4) \times 10^2$ $dm^3\ mol^{-1}\ s^{-1}$ and $K_1 = 0.78 \pm 0.05$. When $[Cl^-]$ is low, eqn. (4) simplifies to eqn. (5), consistent with the experimental observations. Comparison of eqns. (2) and (5) gives $k_2 = (3.4 \pm 0.3) \times 10^2$ $dm^3\ mol^{-1}\ s^{-1}$, in excellent agreement with that derived from eqn. (4).

$$\frac{-\mathrm{d}[\mathrm{NiMe(triphos)}^+]}{\mathrm{d}t} = k_2[\mathrm{NiMe(triphos)}^+][\mathrm{HCl}]_e \quad (5)$$

Consistent with the k_2 step involving rate-limiting protonation of the methyl group, studies with DCl show a primary isotope effect, $(k_2)^H/(k_2)^D = 3.5$ (Fig. 1).

Further evidence that nickel is the most rapidly protonated site comes from ^1H NMR spectroscopy. Our mechanism indicates that the addition of 1 mol equivalent of HCl to a MeCN solution of $[NiMe(triphos)]^+$ will produce an approximately equimolar mixture of the parent complex and $[Ni(H)Me(triphos)]^{2+}$. The ^1H NMR spectrum of such a mixture (Fig. 2)§ shows a multiplet at δ 9.9 (J_{HP} 50 Hz, J_{HP} 430 Hz). We tentatively attribute this low field signal to the hydride ligand in the five-coordinate, formally Ni^{IV} species, $[Ni(H)Me(triphos)]^{2+}$. This multiplet is not present in the ^1H NMR spectra of either $[NiMe(triphos)]^+$ or $[NiCl(triphos)]^+$.

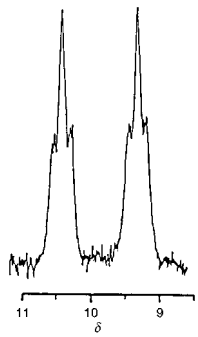

Fig. 2 The multiplet observed in the ^1H NMR spectrum on addition of 1 mol equivalent of HCl to $[NiMe(triphos)]^+$.

Mass spectrometry of the gas formed from the reaction of $[NiMe(triphos)]^+$ and an excess of DCl showed essentially exclusive formation of CH_3D, with little or no other isotopomers. This is also consistent with our mechanism since, once formed, the methane ligand does not undergo proton exchange before it dissociates.

Why does the complex bind two protons when only one is needed for the stoichiometric reaction? Clearly it does not need to. Diprotonation occurs because the nickel is protonated *faster* than the methyl group, and consequently the reaction is *enforced* to operate through the hydrido species. However, intramolecular coupling of the hydride and methyl ligands is *slow* and so methane formation can only occur *after* additional, protonation of the methyl group.

The release of methane (measured by GLC) occurs at a rate which shows a first order dependence on the concentration of complex, but is independent of the concentration of HCl [$k_3 = (4.5 \pm 0.5) \times 10^{-2}$ s^{-1}]. This indicates that, at high concentrations of acid, the putative σ-methane complex is long-lived¶ having a half-life of *ca*. 15 s. Relatively long-lived alkane complexes have been detected previously[6,7] but this kinetic approach has not been adopted before, and potentially is a general method of understanding the factors stabilising such σ-alkane complexes.

The mechanism of methane formation described herein is unexpected, but sufficiently simple that it seems likely that it is not unique to $[NiMe(triphos)]^+$. It is a salutary thought that this pathway has remained unidentified in analogous systems until now because: (i) the detection of hydrido complexes were consistent with the intramolecular coupling pathway (Scheme 1) and (ii) the kinetics of these reactions were not (or could not) be studied in the detailed manner described herein. Just because a hydrido complex is detected in solutions containing acid and a metal alkyl complex does not mean that the hydride is kinetically competent to produce alkane.

We thank BBSRC for supporting this research.

Notes and references

‡ Anhydrous HCl was prepared *in situ* by mixing equimolar amounts of $SiMe_3Cl$ and MeOH in MeCN. The reactions were deliberately performed in MeCN (dried over CaH_2 and distilled immediately prior to use) since solution equilibria (such as pK_a and homoconjugation constants) are known in this solvent.[8] The concentrations of $[HCl^-]_e$ and $[Cl^-]_e$ are those calculated having allowed for the homoconjugation equilibrium, $HCl + Cl^- \rightleftharpoons HCl_2^-$, $K_H = 158.5$ $dm^3\ mol^{-1}$.

§ In these experiments the resonances attributable to the Me groups in $[NiMe(triphos)]^+$ (δ 0.9, unresolved multiplet) and the putative $[Ni(H)Me(triphos)]^{2+}$ are obscured by the peak due to $SiMe_3$ (from the mixture of $SiMe_3Cl$ and CD_3OH used to generate anhydrous HCl). Further evidence that the multiplet at δ 9.9 is attributable to the hydride comes from analogous experiments with DCl where this resonance is missing.

¶ We believe that this is a true measure of the stability of the putative σ-methane complex, rather than an artefact associated with measuring the kinetics of methane transfer from solvent to gas phase, since the rate of the reaction is independent of the concentration of complex used and the speed with which the reaction mixture is agitated.

1 J. K. Kochi, *Organometallic Mechanisms and Catalysis*, Academic Press, New York, 1978, p. 293 and references therein.
2 G. S. Hill, L. M. Rendina and R. J. Puddephatt, *Organometallics*, 1995, **14**, 4966 and references therein.
3 M. W. Holtcamp, J. A. Labinger and J. E. Bercaw, *Inorg. Chim. Acta*, 1997, **265**, 117 and references therein.
4 K. W. Kramarz and J. R. Norton, *Prog. Inorg. Chem.*, 1994, **42**, 1 and references therein.
5 R. A. Henderson, *Angew. Chem., Int. Ed. Engl.*, 1996, **35**, 946 and references therein.
6 X.-Z. Sun, D. C. Grills, S. M. Nikiforov, M. Poliakoff and M. W. George, *J. Am. Chem. Soc.*, 1997, **119**, 7521 and references therein.
7 S. Geftakis and G. E. Ball, *J. Am. Chem. Soc.*, 1998, **120**, 9953 and references therein.
8 K. Izutsu, *Acid–Base Dissociation Constants in Dipolar Aprotic Solvents*, 1990, Blackwell Scientific, Oxford, 1990.

Communication 9/07080J

First synthesis of bis[1,2,3]triazolo[1,5-*b*;5′,1′-*f*][1,3,6]thiadiazepine derivatives by [2+1] condensation of 1,2,3-thiadiazoles with vicinal diamines

Natalya N. Volkova,[a] Evgeniy V. Tarasov,[a] Wim Dehaen*[b] and Vasiliy A. Bakulev*[a]

[a] *Urals State Technical University, 620002 Ekaterinburg, Russia*
[b] *Department of Chemistry, University of Leuven, Celestijnenlaan 200F, B-3001 Heverlee (Leuven), Belgium. E-mail: wim.dehaen@chem.kuleuven.ac.be*

Received (in Cambridge, UK) 16th September 1999, Accepted 8th October 1999

Novel bistriazolo[1,3,6]thiadiazepine derivatives have been prepared by the base-catalyzed condensation of aromatic and aliphatic 1,2-diamines with 5-chloro-1,2,3-thiadiazoles, *via* a multistep process which is thought to involve two Dimroth rearrangements and subsequent loss of hydrogen sulfide by intramolecular nucleophilic substitution.

Seven-membered rings fused with azoles are of special interest as biologically active compounds due to their structural similarity to benzodiazepine tranquilizers and to the aglycon of coformycin nucleoside antibiotics.[1] Despite a large number of papers devoted to various seven-membered heterocycles containing oxygen and nitrogen there are only a few dealing with sulfur containing compounds of this type.[2] We report here a very efficient synthesis of a novel ring system, ditriazolothiadiazepine.

5-Halo-1,2,3-thiadiazoles, when substituted in the 4-position by an electron-withdrawing group, will on reaction with amines undergo a Dimroth rearrangement,[3] and the resulting 5-mercaptotriazoles can react with a second equivalent of thiadiazole to afford 5-(1,2,3-triazol-5-ylsulfanyl)-1,2,3-thiadiazoles.[4] We decided to apply this reaction to 5-chlorothiadiazole ester **1a** and 1,2-phenylenediamine (Scheme 1). We found the outcome of the reaction to be dependant on both reaction time and the presence of Et_3N catalyst. Without catalyst, the only product from the reaction of phenylenediamine and 2 equiv. of **1a** (EtOH, reflux) is the expected [2+1] adduct **4a**. In the presence of 1 equiv. of phenylenediamine, 2 equiv. of **1a** and 3 equiv. of Et_3N, a 2:1 mixture of **4a** and the unexpected bistriazolo[1,5-*b*;5′,1′-*f*][1,3,6]thiadiazepine derivative **5a** was isolated after 3 h reflux in EtOH. Prolonged heating of the reaction mixture gave **5a** as the sole product in 70% yield. Therefore it seemed logical to assume that sulfide **4a** was an intermediate in the formation of **5a**. This fact was confirmed by heating of isolated **4a** with Et_3N in EtOH, which also gave **5a**. The highly symmetrical structure of **5a** was immediately apparent from its ^1H and ^{13}C NMR spectroscopic data.[5]

On the other hand, the 5-chloro-1,2,3-thiadiazole amides **1b**,**c** gave only the sulfides **4b**,**c**, which did not transform to the corresponding fused thiadiazepines **5b**,**c**, even on prolonged heating in the presence of Et_3N. This behaviour is probably the result of the lower reactivity of the thiadiazole 5-carbon of **4b**,**c** towards intramolecular nucleophilic attack. The sulfides **4d**,**e** could be prepared from **2b**,**c** and **1a** in the presence of Et_3N, and cyclized to the unsymmetrically substituted thiadiazepines **5d**,**e**. The compounds **2b**,**c** were prepared from a 2:1 mixture of phenylenediamine and **1b**,**c** in DMF without the addition of Et_3N.

The parent ring system **7** could be prepared by saponification of diester **5a**, followed by the smooth decarboxylation of the diacid **6** by heating the melt at 180 °C. Again, the highly symmetrical structure is apparent from the ^1H and ^{13}C NMR spectroscopic data.[5] The bisamide **5c**, which is not accessible directly from phenylenediamine and **1c**, has been prepared in good yield from **5a** by condensation with excess $MeNH_2$.

The aliphatic 1,2-diaminoethane was reacted with chloroester **1a** (Scheme 2). Again, the outcome of the reaction was dependant on the reaction circumstances. Using the same conditions as above (Et_3N, EtOH, reflux) gave the [4+1] adduct **8** in 60% yield. On the other hand, the reaction of **1a** and ethylenediamine at reflux temperature in $CHCl_3$ gave the bisadduct **9**. Interestingly, **9** rearranged in EtOH with the formation of thiadiazepine **10** when refluxed in the presence of 3 equiv. of Et_3N.

From these results we can conclude that aliphatic amines are more reactive towards the chloroester **1a**. Moreover, the subsequent Dimroth rearrangement of **9** goes faster because the

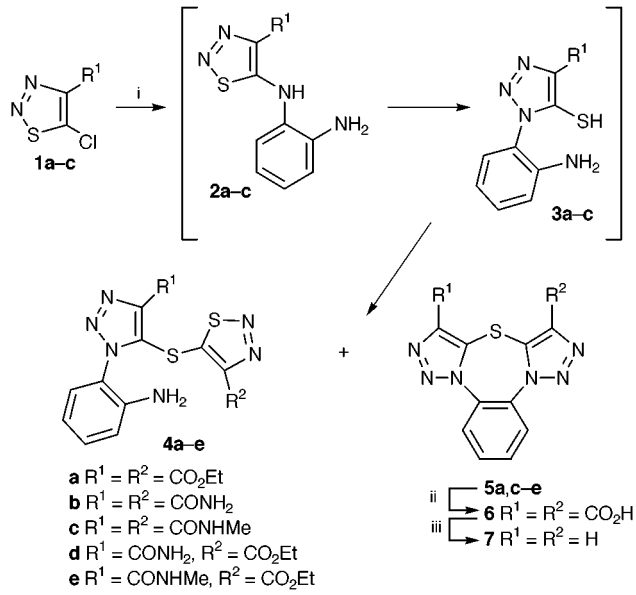

Scheme 1 *Reagents and conditions*: i, Et_3N, EtOH, reflux; ii, NaOH, then HCl; iii, 180 °C.

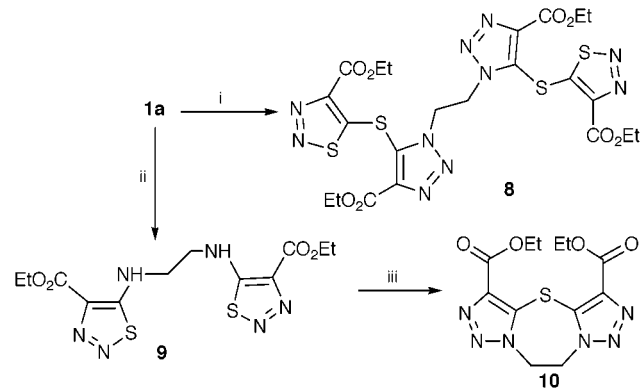

Scheme 2 *Reagents and conditions*: i, EtOH, $H_2NCH_2CH_2NH_2$, reflux; ii, $CHCl_3$, $H_2NCH_2CH_2NH_2$; iii, Et_3N, EtOH, reflux.

resulting *N*-alkyltriazole **11** is more stable than the corresponding *N*-aryltriazole **13**.[6]

We can argue that in both cases, either with aliphatic or aromatic amines, bisthiols of types **11** and **13** are formed, which

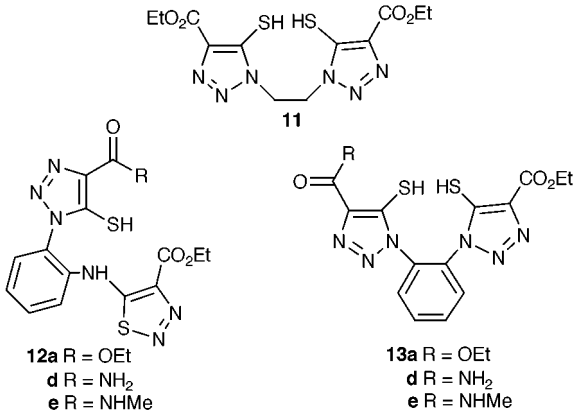

can react *via* an intra- or inter-molecular nucleophilic substitution. For ethylenediamine the bisthiol **11** is formed from **9** by two Dimroth reactions. For aryldiamines the Dimroth reaction of monoadducts **2a**–**c** takes place before the second substitution reaction, with the formation of thiols **3a**–**c**, which are not isolated but immediately react with a second equivalent of 5-chlorothiadiazoles **1a**–**c** to afford **4a**–**c**. Compounds **4d**,**e** are formed in a similar way from **1a** and **2b**,**c**. The 1,2,3-thiadiazole rings of **4a**,**d**,**e** are electron-poor enough to activate for intramolecular amine substitution, and thiols **12a**,**d**,**e** are formed, which undergo fast Dimroth rearrangement to dithiols **13a**,**d**,**e**. Finally, hydrogen sulfide is lost from dithiols **11** or **13a**,**d**,**e** by another intramolecular nucleophilic substitution, yielding thiadiazepines **10** or **5a**,**d**,**e**.

The intramolecular nucleophilic substitution of dithiol **11** is slower because of the more electron-rich and hence less reactive *N*-alkyltriazole, and will only occur if no intermolecular reactions with 5-chlorothiadiazole are possible, *e.g.* on isolated **9**. Otherwise, the [4+1] adduct **8** is obtained. Another, perhaps even more important reason why the intramolecular nucleophilic substitution of **11** is slow can be found in the larger degree of freedom of the flexible ethylene as compared to the rigid 1,2-phenylene group. Indeed, **11** is likely to exist mainly in a conformation with the two heterocyclic thiol groups widely separated.

We thank the University of Leuven, the Ministerie voor Wetenschapsbeleid, the FWO Vlaanderen and the Russian Foundation for Basic Research (Grant 98-03-33044) for financial support.

Notes and references

1 G. I. Birnbaum, J. R. Brisson, S. H. Krawczyk and L. B. Townsend, *J. Am. Chem. Soc*., 1985, **107**, 7635; A. Kamal, B. S. N. Reddy and B. S. P. Reddy, *Bioorg. Med. Chem. Lett*., 1997, **7**, 1825; G. Curotto, D. Donati, G. Finizia and A. Ursini, *Tetrahedron*, 1997, **53**, 7347; E. S. Krichevskii, L. M. Alekseeva, O. S. Anisimova, V. A. Parshin, V. V. Asnina and V. G. Granik, *Khim.-Farm. Zh*., 1997, **31**, 10; T. Watanabe, A. Kakefuda, A. Tanaka, K. Takizawa, S. Hirano, H. Shibata, Y. Yamagiva and I. Yanagisawa, *Chem. Pharm. Bull*., 1998, **46**, 53.

2 D. Hezek and A. Rybar, *Monatsh. Chem*., 1994, **125**, 1273; A. N. Krasovsky, P. M. Kochergin and A. B. Roman, *Khim. Geterotsikl. Soedin*., 1976, **6**, 856.

3 G. L'abbé, *J. Heterocycl. Chem.*, 1984, **21**, 627.

4 Yu. Yu. Morzherin, E. V. Tarasov and V. A. Bakulev, *Khim. Geterotsikl. Soedin*., 1994, **4**, 554; G. L'abbé and E. Vanderstede, *J. Heterocycl. Chem*., 1989, **26**, 1811.

5 *Selected data* for **5a**: mp 164 °C, δ_H($CDCl_3$) 1.48 (6H, t, *J* 7.1, CH_3), 4.51 (4H, q, *J* 7.1, CH_2), 7.79–7.81 (2H, m, CH-arom), 8.08–8.11 (2H, m, CH-arom); δ_C($CDCl_3$) 14.2 (CH_3), 62.1 (CH_2), 126.3 (4,5 CH arom.), 128.2 (1,2-C arom.), 131.4 (3,6 CH arom.), 134.5 (C-5 triazole), 139.7 (C-4 triazole), 159.2 (CO); *m*/*z* 386 ($M^{+\cdot}$, 25), 258 ($M^{+\cdot} - CO_2Et - 2N_2$, 83), 214 ($M^{+\cdot} - 2CO_2Et - N_2$, 71), 186 ($M^{+\cdot} - 2CO_2Et - 2N_2$, 100) (calcd. for $C_{16}H_{16}N_6O_4S$: C, 49.74; H, 3.65; N, 21.75; S, 8.30. Found: C, 49.33; H, 3.99; N, 21.59; Sl 8.32%). For **7**: mp 253 °C; δ_H(DMSO-d_6) 7.87–7.94 (2H, m, CH-arom.), 8.06–8.14 (2H, m, CH-arom.), 8.17 (2H, s, 2CH); δ_C(DMSO-d_6) 126.1 (4,5-CH arom.), 127.8 (C5 triazole), 130.0 (1,2-C arom.), 131.3 (3,6-CH arom.), 135.6 (C4 triazole); *m*/*z* 242 ($M^{+\cdot}$, 61), 186 (M+. − $2N_2$, 100), 102 ($C_7H_4N^+$, 76), 76 ($C_6H_4^{+\cdot}$, 52) (calcd. for $C_{10}H_6N_6S$: C, 49.58; H, 2.50; N, 34.69; S, 8.30. Found: C, 49.68; H, 2.81; N, 34.43; S, 8.32%).

6 G. L'abbé and M. Bruynseels, *J. Chem. Soc., Perkin Trans. 1*, 1990, 1492

Communication 9/07527E

ChemComm

Synthesis, properties and crystal structures of rigid porphyrins fused with bicyclo[2.2.2]octene units

Satoshi Ito,[a] Hidemitsu Uno,[b] Takashi Murashima[a] and Noboru Ono*[a]

[a] *Department of Chemistry, Faculty of Science, Ehime University, Matsuyama 790-8577, Japan. E-mail: onobr@dpc.ehime-u.ac.jp*

[b] *Advanced Instrumentation Center for Chemical Analysis, Ehime University, Matsuyama 790-8577, Japan*

Received (in Cambridge, UK) 14th September 1999, Accepted 5th October 1999

Porphyrins fused with bicyclo[2.2.2]octene frameworks are prepared; the bicyclo[2.2.2] units rigidify the porphyrin ring to maintain planar conformations in solution.

In order to develop new functions and properties of porphyrins, variously substituted porphyrins have been extensively studied. For example, electron withdrawing groups,[1] electron donating groups[2] and sterically hindered groups[3] have been introduced into the porphyrin periphery to control the redox, spectroscopic and catalytic properties of metalloporphyrins. However, porphyrin rings are flexible enough to adopt various distorted conformations such as saddle, wave, ruffle and dome conformations depending the size of periphery substituents and the central metal.[3,4] Furthermore, π–π stacking of porphyrin rings also affects their conformations and electronic properties.[4] Here we report a new type of porphyrin which has a more rigid core than octaethylporphyrin (OEP) and *meso*-tetraphenylporphyrins (TPPS). Our new strategy to control the structure and properties of porphyrins is based on the annelation of porphyrins with bicyclo[2.2.2]octene frameworks, such as **4** and **5** in Scheme 1.† Bicycloannelation of annulenes has been extensively used to control the structure and electronic properties of various aromatic and non-aromatic compounds.[5] Thus, various annulenes fused with bicyclo[5.4.0]octene frameworks give stable oxidized products such as cation radicals and dications.[5] In a similar way, porphyrins fused with bicyclo[2.2.2]octene units are expected to have raised HOMO energies and conformationally rigid structures due to the presence of the fused frameworks.

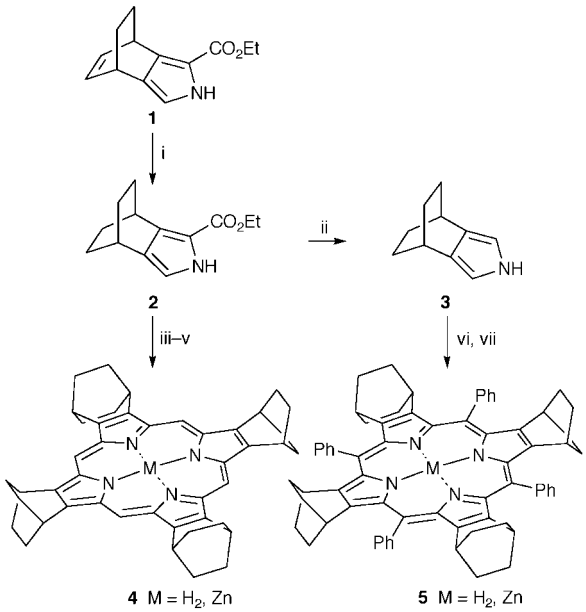

Scheme 1 *Reagents and conditions*: i, H_2, Pd/C, EtOH, room temp., 8 h, 95%; ii,KOH,$HOCH_2CH_2OH$, 160 °C, 2 h, 79%; iii, $LiAlH_4$, THF, 0 °C, 2 h; iv, TsOH, $CHCl_3$, room temp., 12 h; v, *p*-chloranil, room temp., 12 h, 34% (3 steps); vi, PhCHO, $BF_3{\cdot}OEt_2$, $Zn(OAc)_2$, $CHCl_3$, room temp., 12 h; vii, *p*-chloranil, room temp., 3 h, 32% (2 steps).

The key pyrroles **2** and **3** were prepared from **1**[6] by hydrogenation and deethoxycarbonylation. Pyrrole **2** was converted into porphyrin **4** in about 30% yield by reduction with $LiAlH_4$ and the subsequent treatment with acid and oxidation. Porphyrin **5** was prepared by the reaction of **3** with benzaldehyde in the presence of $BF_3{\cdot}OEt_2$ and $Zn(OAc)_2$ and subsequent oxidation.

Theoretical calculations and experimental data on the effects of non-planarity indicate that the HOMO energy should be destabilized with respect to the LUMO energy, resulting in a red shift of the first visible absorption band.[1c] The chemical shifts of NH and the red-shifts of the electronic absorption correlate with deviation from planarity of the porphyrin ring.[3b] So the spectroscopic data of porphyrins **4**, **5** and their Zn complexes were compared with those of other related porphyrins, 2,3,7,8,12,13,17,18-octaethylporphyrin (OEP), 2,3,7,8,12,13,17,18-octamethoxyporphyrin (OMP), 5,10,15,20-tetraphenylporphyrin (TPP) and 2,3,7,8,12,13,17,18-octaethyl-5,10,15,20-tetraphenylporphyrin (OETPP). The electronic absorptions of **4** and Zn-**4** are blue shifted compared to the corresponding OEP and Zn-OEP, and such blue shifts are more enhanced in the Q (0,0) bands. The Q bands of **4** and Zn-**4** are at 610 and 558 nm, respectively, which are considerable blue-shifted compared to those of OEP (622 nm), Zn-OEP (569 nm), OMP (618 nm) and Zn-OMP (573 nm). The Q band of Ni-**4** is at 543 nm, which is also blue shifted compared to Ni-OEP (551 nm). Several factors are operative in the absorption spectra of porphyrins.[1–3] Recent studies show that the shifts of spectra originate from ring conformations and substituent effects.[1a,b] As the substituents of **4** and OEP consist of alkyl groups and have similar electronic properties, ring conformations should be the main factors controlling the blue shifts of **4**. The porphyrin cores are flexible and can adopt various conformations in solution. In fact, NiOEP, NiTPP, CuTPP and other related porphyrins are present as a mixture of both planar and nonplanar conformations in solution.[7] In particular, large deviations from planarity are observed in TTP derivatives.[7] Thus, the blue shifts of **4** and Zn-**4** shows quite clearly that they exist in planar conformations in solution. The ^{1}H NMR chemical shifts also support the planar conformation of **4**. The difference of the chemical shifts between the N-H and *meso*-H resonances of **4**, $\Delta\delta$ = 14.84 ppm, is larger than that of other porphyrins ($\Delta\delta$ of OEP is 13.92 and that of OMP is 14.47 ppm). The planar structure of **4** in solution leads to the large $\Delta\delta$ of **4**.[8]

Conformational distortions of porphyrin rings are enhanced by the introduction of substituents at the *meso* position. The introduction of alkyl, perfluoroalkyl, aryl and nitro groups at the *meso*-positions induces the distortion of porphyrin cores.[1,3] So, **5** and Zn-**5** were prepared, and their properties were compared with those of OETPP and Zn-OETPP. It is well-established that the red shift of absorptions observed for OETPP (686 nm) and Zn-OETPP (637 nm) is due to the non-planar distortions of their rings. On the other hand, the absorption λ_{max} values of **5** (665 nm) and Zn-**5** (551 nm) are not as red-shifted as OETPP and Zn-OETPP, when compared to those of TPP (645 nm) and Zn-TPP (552, 596 nm). The ^{1}H NMR chemical shift of NH in **5** appears

at $\delta -3.10$, whereas those of TPP and OETPP appear at $\delta -2.78$ and -2.0, respectively. These results indicate that **5** and Zn-**5** have planar conformations, while OETPP derivatives adopt nonplanar conformations in solution.

The stereochemistry of the porphyrin macrocycles has been studied extensively by X-ray diffraction. Porphyrin cores are very flexible and most porphyrins adopt nonplanar shapes in the solid state. The shapes are readily changed by periphery substituents, central metals and their axial ligands.[4] For example, Zn-OETPP adopts a saddle conformation,[3a] where a maximum displacement of 1.18 Å (for C_β) from the porphyrin mean plane is observed. The dihedral angles of the phenyl rings with the nitrogen plane are about 45–47°. The structure of Zn-**5**, as shown in Fig. 1,‡ is different from that of Zn-OETPP. The porphyrin ring is fairly planar, exhibiting a mean plane deviation of only 0.06 Å for from the 24 core atoms. The reported mean plane deviation of distorted porphyrins is about 0.3–0.5 Å depending on steric crowding and the size of the central metal.[4] The angles between the phenyl rings and the porphyrin plane of Zn-**5** are 89 and 78°. The structure of Zn-**5** is very close to that of nickel(II) *meso*-tetrakis(2,6-dichlorophenyl)-β-tetranitroporphyrin,[1d] where steric crowding between the phenyl and nitro groups is minmized by adopting a near planar conformation. Nonplanar distortions of OEP and TPP derivatives are derived from ring contraction about the central metal ion or from steric crowding about the porphyrin periphery. On the other hand, steric interactions in porphyrins **4** and **5** shoud be at a minimum in planar or near-planar conformatons, as steric interactions between the bicyclo[2.2.2]octene units are increased by adopting nonplanar conformations. Simple calculations also suggest the planar structure as the most stable conformer for **4** and **5**.

The oxidation potentials were determined by cyclic voltammetry (CV) for Zn-**4** and Zn-**5** in 0.1 M Bu_4NClO_4 in CH_2Cl_2. The CVs of other related porphyrins were also measured under the same conditions. Although the CVs of Zn-**4**, Zn-OEP and Zn-**5** showed two reversible peaks, the highly distorted Zn-OETPP gave only one peak. The first oxidation potentials of Zn-**4** and Zn-**5** were +0.38 and +0.26 V (*vs.* Ag/Ag^+, Fc/Fc^+ = +0.19 V), respectively. They are a little higher than those of Zn-OEP (+0.35 V) and Zn-OETPP (+0.22 V). The second oxidation potential of Zn-**4** (0.74 V) is also a little higher than that of Zn-OEP (+0.68 V). The second oxidation potential of Zn-**5** is 0.43 V, but the CV of Zn-OETPP gives one peak at $E_{1/2}$ = +0.22 V. It is reasonable to assume that the first and second oxidation of Zn-OETPP takes place at this potential. However, further studies are necessary to confirm this conclusion. Although the difference is very small, the HOMO energy levels of Zn-OEP and Zn-OETPP are a little higher than those of Zn-**4** and Zn-**5,** respectively. It is well-established that the distortion of nonplanarity on Zn-OETPP raises the HOMO enegy level.[3,4] The CV data suggest that the HOMO energy of Zn-OEP is also slightly raised by a contribution from nonplanar conformations of Zn-OEP in solution. As the LUMO energy levels are less sensitive to nonplanar distortion compared to the HOMO energy levels,[1] the energy difference between the HOMO and LUMO levels of **4** or Zn-**4** is larger than that of OEP or Zn-OEP. Thus, the absorption spectra of **4** and its metal complexes are blue shifted compared to OEP derivatives. It is noteworthy that the HOMO energy levels of porphyrin derivatives are sensitive to such small deviations from planarity of the porphyrin rings in cases such as OEP in solution. Considering the destabilization effect on the HOMO level of annulenes of the σ–π conjugation of fused bicyclo[2.2.2]octene units, which is general in the other macrocycles,[5] conformational distortions may be major factors in controlling the electronic properties of alkyl substituted porphyrins like **4** and OEP.

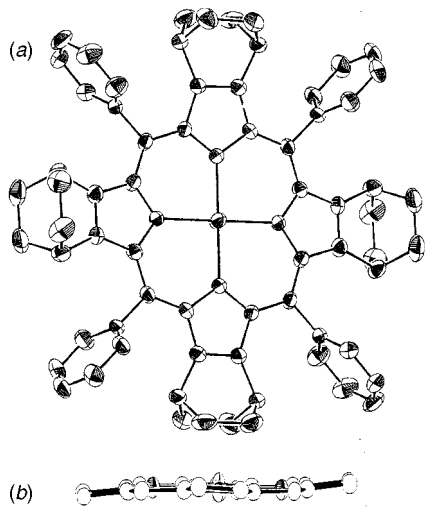

Fig. 1 (*a*) X-Ray crystal structure of Zn-**5**. Hydrogens and solvents are omitted for clarity. Average of bond distance (Å) and angles (°): N–C_α 1.383, Zn–N 2.067, C_α–C_β 1.454, C_β–C_β 1.351, C_α–C_m 1.403, C_m–C_ϕ 1.498; NZnN 90.0, $C_\alpha NC_\alpha$ 107.3, $ZnNC_\alpha$ 126.1, $NC_\alpha C_m$ 125.3, $NC_\alpha C_\beta$ 108.9, $C_\beta C_\alpha C_m$ 125.9, $C_\alpha C_m C_\alpha$ 121.9, $C_\alpha C_\beta C_\beta$ 107.5. (*b*) Edge-on view of Zn-**5** (substituent groups are omitted for clarity).

In conclusion bicyclo[2.2.2]octene frameworks are useful to rigidify porphyrin rings in order to maintain planar conformations in solution. Although planar porphyrins have problems of solubility due to π–π stacking, porphyrins fused with bicyclo[2.2.2]octene units have good solubility in various organic solvents such as CH_2Cl_2, benzene and THF. Thus, porphyrin **4** and its derivatives may be useful as standards for planar porphyrins in solution.

This work was supported by Grants-in aid for Scientific Research from the Ministry of Education, Science, Sports and Culture, Japan (to N.O) and by a Sasakawa Scientific Research Grant from the Japan Science Society (to S.I).

Notes and references

† *Selected data* for **4**: $\delta_H(CDCl_3)$ −4.43 (2H, br s), 1.94–1.98 (16H, m), 2.44–2.48 (16H, m), 4.91 (8H, m), 10.40 (4H, s); $\lambda_{max}(CHCl_3)$/nm (ε/dm^3 mol^{-1} cm^{-1}) 389 (162 000), 492 (15 100), 524 (6200), 558 (6200), 610 (2000). For **5**: $\delta_H(CDCl_3)$ −3.10 (2H, br s), 1.22–1.25 (16H, m), 1.54–1.57 (16H, m), 2.51 (8H, m), 7.70–7.77 (12H, m), 8.25–8.36 (8H, m); $\lambda_{max}(CHCl_3)$/nm (ε/dm^3 mol^{-1} cm^{-1} 434 (222 000), 528 (10 400), 568 (sh), 598 (1900), 665 (3000).

‡ *Crystal data* for Zn-**5**: $C_{68}H_{60}N_4Zn{\cdot}H_2O{\bullet}CHCl_3$, M = 1136.02, monoclinic, space group $P21/c$, a = 9.599 (2), b = 26.053 (7), c = 11.809 (2) Å, β = 104.21 (1)°, U = 2863 (1) Å^3, Z = 2, D_c = 1.318 g cm^{-3}, μ = 0.617 mm-1, Mo-Kα radiation, λ = 0.71073 Å, T = 298 K, 7114 determined 6734 independent, 3158 observed reflections [$I > 2\sigma(I)$], R = 0.080, Rw = 0.054. Non-hydrogen atoms were refined anisotropically except for the chloroform carbon atom. Hydrogen atoms were included but not refined. CCDC 182/1441. See http://www.rsc.org/suppdata/cc/1999/2275/ for crystallographic data in .cif format.

1 (*a*) J. Leroy, A. Bondon, L. Toupet and C. Rolando, *Chem. Eur. J.*, 1997; **3**, 1890; (*b*) S. G. DiMagno, A. K. Wertsching and C. R. Ross, II, *J. Am. Chem. Soc.*, 1995, **117**, 8279; (*c*) P. Ochsenbein, K. Ayougou, D. Mandon, R. Weiss, R. N. Astin, K. Jayaraj, A. Gold, J. Terner and J. Fajer, *Angew. Chem., Int. Ed. Engl.*, 1994, **33**, 348; (*d*) K. Ozette, P. Leduc, M. Palacio, J. F. Bartoli, K. M. Barkigia, J. Fajer, P. Battioni and D. Mansuy, *J. Am. Chem. Soc.*, 1997, **119**, 6442.

2 A. Merz, R. Schropp and J. Rex, *Angew. Chem., Int. Ed. Engl.*, 1993, **32**, 291.

3 (*a*) K. M. Barkigia, M. D. Barber, J. Fajor, C. J. Medforth, M. W. Renner and K. M. Smith, *J. Am. Chem. Soc.*, 1990, **112**, 8851; (*b*) J. Takeda and M. Sato, *Tetrahedron Lett.*, 1994, **35**, 3565.

4 D. J. Nurco, C. J., Medforth, T. P. Forsyth, M. M. Olmstead and K. M. Smith, *J. Am. Chem. Soc.*, 1996, **118**, 10918; T. D. Brennan, W. R. Scheidt and J. A. Schelnutt, *J. Am. Chem. Soc.*, 1988, **110**, 3919.

5 T. Nishinaga, T. Kawamura and K. Komatsu, *Chem. Commun.*, 1998, 2263 and references therein.

6 S. Ito, T. Murashima and N. Ono, *J. Chem. Soc., Perkin Trans. 1*, 1997, 3161.

7 W. Jentzen, E. Unger, X. Z. Song, S. L. Jia, I. T. Tyrk, R. S. Stenner, W. Dreybrodt, W. R. Scheidt and J. A. Shelnutt, *J. Phys. Chem. A*, 1997, **101**, 5789 and references therein.

8 M. S. Somma, C. J. Medforth, N. Y. Nelson, M. M. Olmstead, R. G. Khoury and K. M. Smith, *Chem. Commun.*, 1999, 1221 and references therein.

Communication 9/07460K

Hydrogen storage composites obtained by mechanical grinding of magnesium with graphite carbon

Hayao Imamura,* Yoshirou Takesue, Shinya Tabata, Noriko Shigetomi, Yoshihisa Sakata and Susumu Tsuchiya

Department of Advanced Materials Science and Engineering, Faculty of Engineering, Yamaguchi University, 2-16-1 Tokiwadai, Ube 755-8611 Japan. E-mail: hi-khm@po.cc.yamaguchi-u.ac.jp

Received (in Cambridge, UK) 9th August 1999, Accepted 12th October 1999

Novel hydrogen storage Mg/G composites prepared by mechanical grinding of magnesium (Mg) and graphite carbon (G) with benzene have been found to incorporate new hydrogen-storing sites, other than those due to the magnesium component, and can take up hydrogen reversibly.

Much research effort has been concentrated on the storage of hydrogen in metals, for which magnesium metal and magnesium-containing alloys are considered promising candidate materials.[1] Recently, new carbon materials, *e.g.* carbon nanotubes [2] and graphite nanofibers,[3] have become of interest for possible use in hydrogen storage.

We have proposed the application of composites, prepared by mechanical grinding of magnesium (Mg) and graphite carbon (G) in the presence of organic additives (tetrahydrofuran, cyclohexane or benzene) using a planetary-type ball mill, as novel hydrogen storage materials.[4–7] In the mechanical grinding of magnesium and graphite for Mg/G composite formation, the presence of the organic additives is important in determining the characteristics of the resulting composites. Such organic compounds regulate the solid-phase reaction between magnesium and graphite carbon during grinding, leading to a strong influence on the composite structures and the hydriding–dehydriding properties of the magnesium component. The hydriding activity of these composites is much better than reported previously.[8] In this communication, we report experimental findings that new hydrogen-storing sites, other than those due to the magnesium component in the composites, are formed during grinding in the presence of benzene and that these sites reversibly take up hydrogen.

X-Ray diffraction (XRD) patterns revealed decomposition of the graphite component in the composites with grinding.[4–7] However, there was a great difference in the modes of degradation of the graphite structure between the Mg/G composites ground with and without the organic additives. Raman spectroscopy has proved that upon mechanical grinding, the structural degradation of graphite in the $(Mg/G)_{BN}$† composite predominantly occurs by cleavage along the graphite layers, while the graphite in $(Mg/G)_{none}$† is broken irregularly with no discernible order, leading to rapid amorphization.[7] In marked contrast to the graphite in $(Mg/G)_{none}$, only the cleavage-degraded graphite intimately interacted with finely divided magnesium with charge-transfer as evidenced by XPS, developing a synergism which leads to the enhanced hydrogen-storing properties.[7] These facts reflect differences in hydrogenation behaviour between $(Mg/G)_{BN}$ and $(Mg/G)_{none}$.

For various $(Mg/G)_{BN}$ samples previously exposed to hydrogen at 3 MPa, differential scanning calorimetry (DSC),‡ which was measured at a scanning rate of 5.0 K min^{-1} under a 0.1 MPa hydrogen atmosphere, showed characteristic endothermic peaks (Fig. 1). When pure magnesium powder was used for comparison, DSC indicated that the peak temperature of MgH_2 decomposition was 707 K, close to the results reported by Huot *et al.*[9] The DSC trace of $(Mg/G)_{none}$, ground without any additives, exhibited a broad endothermic peak at 668 K which was similarly assigned to the decomposition of MgH_2. It seems that magnesium particles with cracked irregular surfaces produced by the ball milling technique show improved hydriding–dehydriding kinetics.[10]

The mechanical grinding with benzene led to significant changes in DSC behaviour. A very important characteristic of the DSC traces for $(Mg/G)_{BN}$, prepared at varying grinding times (4–40 h), is that they indicate a series of transformations leading to the formation of composites during grinding. Mechanical grinding of $(Mg/G)_{BN}$ for 4 h led to a DSC peak at about 664 K [Fig. 1(a)]. As only magnesium hydride was identified in the XRD pattern of the sample, this endothermic peak was assigned to decomposition of the hydride. Upon grinding for 10 h or longer, new endothermic peaks, other than that due to the decomposition of MgH_2 appeared. The DSC traces, notably the numbers and temperatures of peaks, changed significantly with grinding. Grinding for 40 h resulted in the loss of all but one peak [Fig. 1(e)]. This was also found to be due to decomposition of MgH_2 by reference to the XRD pattern of the sample. For $(Mg/G)_{BN}$, the endothermic DSC peaks corresponding to decomposition of the magnesium hydride were obviously shifted to lower temperatures as the grinding times were prolonged. To clarify what causes the changes in the DSC traces, temperature programmed desorption (TPD) measurements for the same $(Mg/G)_{BN}$ samples were made *in vacuo* by continuously monitoring desorbed hydrogen *via* quadrupolar

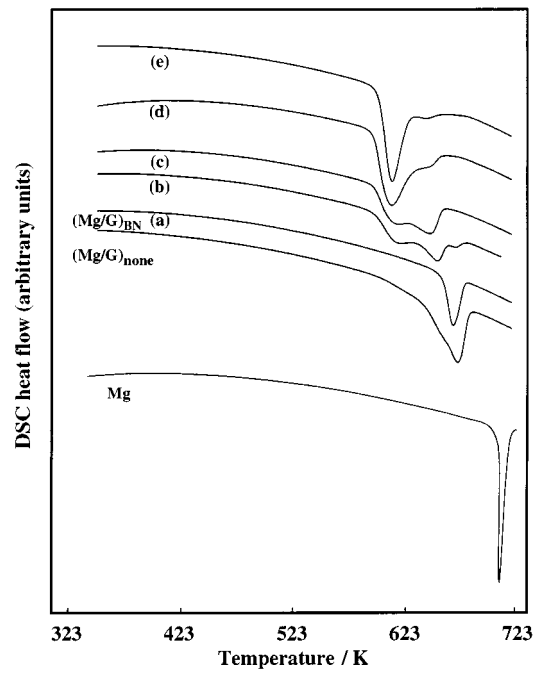

Fig. 1 DSC traces for various $(Mg/G)_{BN}$, $(Mg/G)_{none}$ and Mg samples. The $(Mg/G)_{BN}$ composites were prepared by grinding with benzene (8.0 cm^3) for (a) 4 h, (b) 10 h, (c) 20 h, (d) 30 h and (e) 40 h. $(Mg/G)_{none}$ was prepared by grinding without benzene for 15 h.

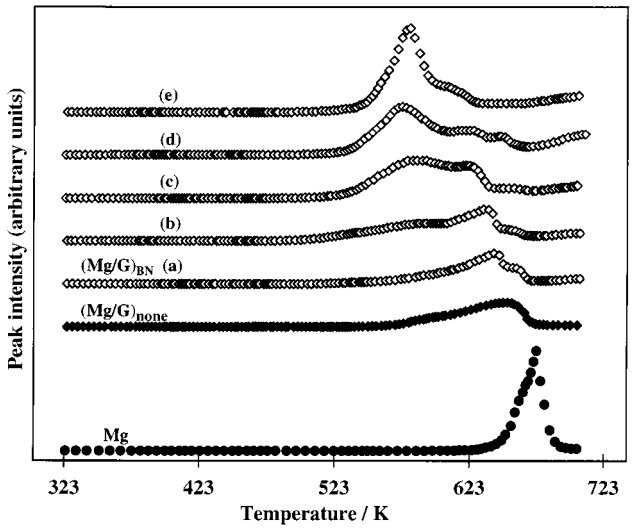

Fig. 2 TPD of various $(Mg/G)_{BN}$, $(Mg/G)_{none}$ and Mg samples. The $(Mg/G)_{BN}$ composites were prepared by grinding with benzene (8.0 cm^3) for (a) 4 h, (b) 10 h, (c) 20 h, (d) 30 h and (e) 40 h. $(Mg/G)_{none}$ was prepared by grinding without benzene for 15 h.

mass spectrometry. As shown in Fig. 2, the TPD results gave a good correspondence with the DSC measurements for each sample; both displayed similar peak shapes and approximately the same number of peaks. This proves that the newly emerged DSC peaks were derived from endothermically desorbed hydrogen. Further confirmation is provided by the fact that the DSC peaks of $(Mg/G)_{BN}$ prepared by grinding for 20 h are essentially reproducible in repeated scans of the same sample when pressurized under 3 MPa of hydrogen, followed by continuous heating from 350 to 700 K under a hydrogen pressure of 0.1 MPa, (Fig. 3).

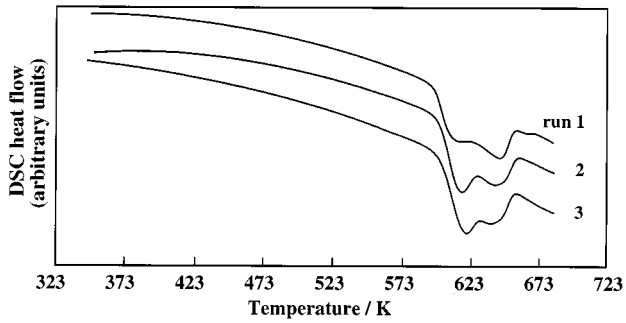

Fig. 3 Repeated DSC measurements (run 1–3) on $(Mg/G)_{BN}$, prepared by grinding with benzene (8.0 cm^3) for 20 h.

Another interesting feature of the hydrogen uptake by $(Mg/G)_{BN}$ is that the DSC traces were significantly dependent upon the pressure of hydrogen to which the sample had been exposed. For $(Mg/G)_{BN}$ ground for 20 h, exposure to hydrogen at pressures up to 0.5 MPa gave a single DSC peak only (Fig. 4), which was assigned to the decomposition of MgH_2. Upon exposure to hydrogen pressure of more than 0.7 MPa, new endothermic peaks other than that due to the decomposition of MgH_2 began to appear and increased with hydrogen pressure applied. These results give evidence that hydrogen storage by sites or phases other than those from the magnesium component simultaneously occurred, in which the pressure dependence of hydrogen uptake was observed. The proportion of additionally stored hydrogen can be roughly estimated from the DSC or TPD peak area; an approximate measurement corresponded to about 50% of the total hydrogen stored by $(Mg/G)_{BN}$ exposed to hydrogen at 3 MPa. The H_2 uptake discovered here is characterized by excellent reversibility and marked pressure dependence. However, there were no changes in the XRD patterns for variations in hydrogen pressure applied; only magnesium hydride was identified in the $(Mg/G)_{BN}$ composite.

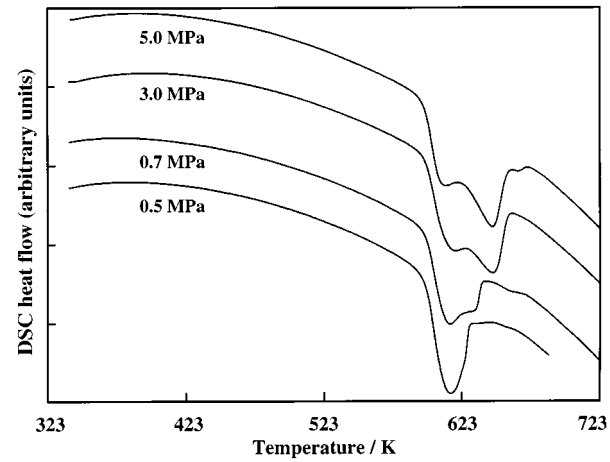

Fig. 4 Influence of hydrogen pressure applied to the sample on the DSC traces of $(Mg/G)_{BN}$, prepared by grinding with benzene (8.0 cm^3) for 20 h.

Exactly which sites in the composites store the additional hydrogen, or the method by which this occurs, is as yet unknown.

Pure graphite itself and graphite subjected to grinding did not take up hydrogen; neither showed any DSC response. $(Mg/G)_{none}$ did not show similar behaviour to that observed for $(Mg/G)_{BN}$. The most effective $(Mg/G)_{BN}$ composites are those in which there are synergic interactions between magnesium and graphite carbon as a result of mechanical grinding with benzene. The formation of Mg/G composites upon such grinding led to not only a drop in the onset temperature of MgH_2 decomposition, but the formation of additional hydrogen-storing sites in $(Mg/G)_{BN}$. However, as shown in Fig. 1(e) and 2(e), prolonged grinding led to detrimental effects on additional hydrogen uptake; the hydrogen-storing sites formed were decomposed. This is probably related to the extent of amorphization of the graphite component by excessive grinding.[7]

This work has been supported in part by a Grant-in-Aid for Scientific Research on Priority Areas (No. 299) from the Ministry of Education, Science, Sports and Culture, Government of Japan.

Notes and references

† Magnesium (99.95%; 100 mesh) and graphite (grade: SP-1) were used as obtained from Rare Metallic Co. Ltd. and Union Carbide Co., respectively. Benzene (BN) was purified by distillation in the presence of sodium wire. The preparation of Mg/G composites was carried out by mechanical grinding using a planetary-type ball mill (High G: BX 254; Kurimoto Ltd.), capable of operating under conditions of 150 G. Magnesium powder (4.2 g) and graphite (1.8 g) were placed in a stainless steel container (160 cm^3; lined with zirconia) with zirconia balls (3 mm in diameter; 238 g) under a dry nitrogen atmosphere. The mixtures were subjected to mechanical grinding with and without benzene (8.0 cm^3) for 4–40 h to yield the Mg/G composites, referred to here as $(Mg/G)_{BN}$ and $(Mg/G)_{none}$, respectively.
‡ DSC measurements were made on a TA Instruments 910S machine with a Thermal Analyst 2200 system.

1 *E.g.* N. Gérard and S. Ono, in, *Hydrogen in Intermetallic Compounds II*, ed. L. Schlapbach Springer, Berlin, 1992, ch. 4, p. 178.
2 P. Chen, X. Wu, J. Lin and K. L. Tan, *Science*, 1999, **285**, 91; C. Dillon, K. M. Jones, T. A. Bekkedahl, H. Kiang, D. S. Bethune and M. J. Heben, *Nature*, 1997, **386**, 377.
3 A. Chambers, C. Park, R. T. A. Baker and N. Rodriguez, *J. Phys. Chem. B*, 1998, **102**, 4253.
4 H. Imamura and N. Sakasai, *J. Alloys Compd.*, 1995, **231**, 810.
5 H. Imamura, N. Sakasai and Kajii, *J. Alloys Compd.*, 1996, **232**, 218.
6 H. Imamura, N. Sakasai and T. Fujinaga, *J. Alloys Compd.*, 1997, **253**–**254**, 34.
7 H. Imamura, Y. Takesue, T. Akimoto and S, Tabata, *J. Alloys Compd.*, 1999, **293**–**295**, 564.
8 M. Miyamoto, *J. Less–Common Met.*, 1983, **89**, 111.
9 J. Huot, E. Akiba and T. Takada, *J. Alloys Compd.*, 1995, **231**, 815.
10 B. Vigeholm, J. Kjoller, B. Larsen and A. S. Pedersen, *J. Less–Common Met.*, 1985, **89**, 135.

Communication 9/06454K

ChemComm

Covalent self-assembly of a dimeric borazaaromatic macrocycle†

Paul J. Comina, Douglas Philp,* Benson M. Kariuki and Kenneth D. M. Harris

School of Chemistry, University of Birmingham, Edgbaston, Birmingham UK B15 2TT. E-mail: dphilp@bham.ac.uk

Received (in Liverpool, UK) 2nd August 1999, Accepted 4th October 1999

Bis(10-hydroxy-10,9-boraza-2-phenanthryl) ether is capable of covalent self-assembly upon dehydration in solution to form the corresponding cyclic dimer.

Self-assembly processes,[1] which allow the construction of large, highly ordered molecular or supramolecular arrays, directly and spontaneously, from simple constituents, are an important and developing[2] area of synthetic chemistry. Strict self-assembly[3] processes require that the pathways leading to the desired product must be completely reversible and that the target assembly should be stable at thermodynamic equilibrium. In addition, all of the information necessary to fabricate the target structure must be encoded within the constituent components of the assembly. Traditionally, these requirements have led to assembly pathways that rely upon non-covalent interactions, such as hydrogen bonding or metal–ligand coordination, to achieve the necessary molecular recognition and organisation. This approach, however, has one major disadvantage—the entropic cost of arranging the required constituents is only compensated for by the enthalpic contributions from relatively weak non-covalent interactions and, therefore, a significant number of these interactions are usually required for self-assembly to be successful. This problem can be overcome by exploiting systems in which the pathway leading to the formation of the target assembly makes use of covalent bonds.[4] The higher enthalpic gain as a result of covalent bond formation more than overcomes the entropic cost of organising[5] the components of the assembling structure and, hence, fewer covalent bonds are required to produce a stable assembly.

Here, we describe the use of a bis(borazaaromatic) in the covalent self-assembly of a dimeric macrocycle and the characterisation of this assembly process by ^{1}H NMR spectroscopy, X-ray diffraction and MALDI-TOF mass spectrometry. In order for covalent self-assembly to be successful, we reasoned that the information required to encode the target assembly must be described by the conformational space[4] accessible to the starting monomer. Hence, we identified the competition between the formation of discrete, cyclic structures and the formation of linear polymers from the same bifunctional monomer as an appropriate starting point for these studies. Accordingly, we designed and prepared the bis(borazaphenanthrene) **1** in five steps from Ph_2O. Compound **1** contains two boraza aromatic units connected by a phenyl ether oxygen atom which allows the two borazaphenanthrene rings to pivot with respect to each other. We have demonstrated[6] that hydroxyborazaaromatics can undergo reversible dehydration in solution to the corresponding anhydrides readily under appropriate conditions. Therefore, several dehydration reactions of **1** can be envisaged (Fig. 1). For example, dehydration may occur to afford a series of linear oligomers of varying chain lengths. In addition, ring closure of the linear oligomers could give rise to cyclic oligomers. In the simplest case, this would give rise to the dimeric anhydride **2** which can potentially exist in two isomeric forms—either face-to-face or helical (Fig. 1).

Compound **1** can be converted readily to the dimeric anhydride **2** in acetone solution, at room temperature, through dehydration by the addition of 4 Å molecular sieves. Conversely, **2** can be readily hydrolysed to give **1** in acetone solution by the addition of an excess (> 10 equiv.) of water. In order to assess the progress of the self-assembly process, a sample of **1** was dissolved in acetone and the evolution of the species present in solution, as a function of time, was monitored by MALDI-TOF mass spectrometry [Fig. 2(*a*)]. Initially, the cyclic dimer **2** and acyclic dimer $\mathbf{A}_2$ [Fig. 2(*a*), t = 0.5 h] are observed in solution. As the dehydration progresses, however, higher molecular weight species, such as the acyclic trimer $\mathbf{A}_3$ and tetramer $\mathbf{A}_4$ can be observed [Fig. 2(*a*), t = 7.5 h], in addition to the desired cyclic dimer **2**. After 4 days, the higher molecular weight species have diminished in concentration and after 12 days, the only oligomeric species present in solution is the cyclic dimer **2**. This behaviour can be rationalised in terms of the kinetic scheme shown in Fig. 2(*b*). The first species formed in the oligomerisation process must be the acyclic dimer $\mathbf{A}_2$. Cyclisation of this species to form the cyclic dimer **2** would be expected to be favourable[7] as it is intramolecular. However, if the effective molarity for this cyclisation[8] is not particularly high then the chain extension pathways, leading from $\mathbf{A}_2$ to $\mathbf{A}_3$ and beyond, will be able to compete to some extent with this cyclisation. This behaviour would explain the emergence of higher oligomers at intermediate time periods. Since the pathways leading to the acyclic oligomers $\mathbf{A}_n$ are reversible, all of the material in the reaction manifold will ultimately be recycled back through $\mathbf{A}_2$ and into the cyclic dimer **2**, which is clearly the thermodynamic product of this process. Hence, once the assembly process is complete, the only oligomeric species present in solution is the cyclic dimer **2**.

Single crystals‡ of **2**, suitable for X-ray diffraction, were grown by slow evaporation of a solution of **2** in acetone and hexane. In this structure, each molecule of **2** is present (Fig. 3) as the helical form§ shown schematically in Fig. 1 and the unit cell contains four pairs of enantiomers. The solid state structure contains channels, aligned parallel to the crystallographic *c* axis, which contain a number of disordered solvent molecules which

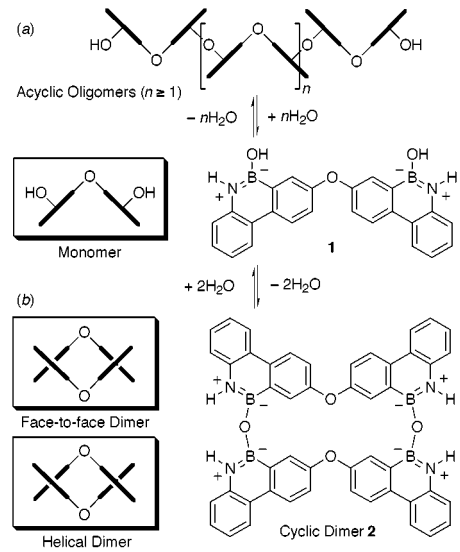

Fig. 1 Compound **1** can be dehydrated to give, for example: (*a*) linear oligomers with a distribution of chain lengths, and (*b*) a discrete cyclic dimer **2** which can adopt either a helical or a face-to-face conformation.

† These compounds have also been referred to as borazaroaromatic species in earlier papers.

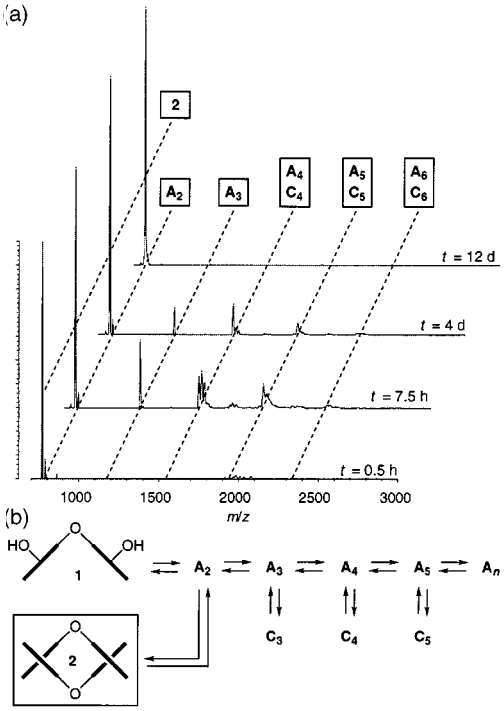

Fig. 2 (*a*) The evolution of the MALDI-TOF mass spectrum of a sample of **1** dissolved in acetone in the presence of 4 Å molecular sieves as a function of time. The elapsed time in this experiment is indicated to the right of each spectrum. (*b*) Proposed kinetic scheme for the equilibration of oligomers of **1**. The acronym $\mathbf{A}_n$ represents acyclic oligomers of **1** containing *n* repeat units and the acronym $\mathbf{C}_n$ represents cyclic oligomers of **1** containing *n* repeat units. Note that, for clarity, all spectra are scaled such that the *m/z* 772 peak, arising from **2**, is the base peak in all spectra. This scaling does not represent the true distribution of species after 0.5 h since the sample contains mostly monomer **1** at this time.

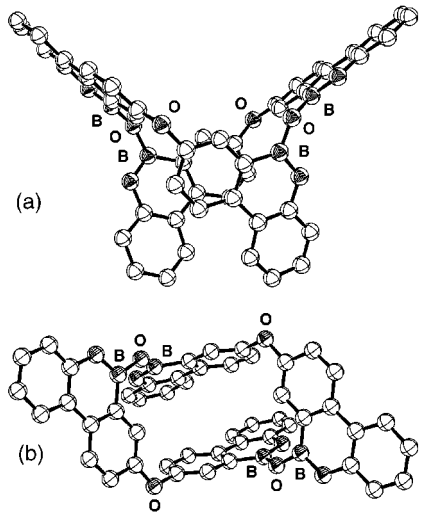

Fig. 3 ORTEP diagrams of the solid state structure of **2** as determined by X-ray diffraction. The molecule is shown in two orientations: (*a*) side view and (*b*) top view. Hydrogen atoms have been omitted for clarity.

are lost rapidly when the crystals are removed from the mother liquor. Examination¶ of these desolvated crystals by MALDI-TOF mass spectroscopy demonstrated that the crystals contained only the cyclic dimer **2**. The desolvated crystals were then heated at 150 °C for 3 h. Further analysis by MALDI-TOF mass spectroscopy demonstrated that, in addition to **1** and **2**, significant quantities of higher molecular weight materials were present. Surprisingly, only oligomers containing an even number of monomer units were observed. Whilst the origin of this selectivity and the mechanism of this process are, as yet, not understood, there are, however, suggestions that this behaviour may be intrinsic to monomer **1** and dimer **2**, and is simply an expression of the natural predispositions[4] of these compounds.

Closer examination of the assembly process in solution [Fig. 2(*a*)] reveals that in the case of the trimer ($\mathbf{A}_3/\mathbf{C}_3$) and pentamer ($\mathbf{A}_5/\mathbf{C}_5$), the acyclic species ($\mathbf{A}_3$ and $\mathbf{A}_5$) are strongly favoured. However, in the case of the tetramer ($\mathbf{A}_4/\mathbf{C}_4$) both the cyclic and acyclic species are formed, with $\mathbf{C}_4$ persisting in solution for a much longer period of time than $\mathbf{A}_4$.

In conclusion, we have demonstrated the utility of bis(boraza aromatic)s as building blocks for strict self-assembly mediated by covalent bond formation. The conformational space accessible to compound **1** successfully encodes for the exclusive formation of the cyclic dimer **2** upon dehydration. Logical extensions of this strategy, which allow the synthesis of more complex self-assembled systems, are currently under investigation in our laboratory.

We thank the Leverhulme Trust (Postdoctoral fellowship for P. J. C.), the EPSRC (Postdoctoral fellowship for B. M. K.) and the BBSRC (Grants 6/B03840 and 6/B04100) for financial support of this work.

Notes and references

‡ *Crystal data* for **2**: $C_{48}H_{32}B_4N_4O_4$ M = 942.29, monoclinic, a = 23.120(5), b = 16.007(3), c = 32.068(8) Å, β = 111.177(4)°, U = 11066(4) Å^3, T = 296 K, space group $I2/a$ (no. 15), Z = 8, μ(Mo-Kα) = 0.1 mm^{-1}, 14279 reflections measured, 5765 unique (R_{int} = 0.174). The final R was 0.1013. The relatively poor R factor for this crystal structure is a consequence of the disordered nature of the solvent situated within the channels described in the text. CCDC 182/1431. See http://www.rsc.org/suppdata/cc/1999/2279/ for crystallographic data in .cif format.

§ In solution, **2** can interconvert between the helical and the face-to-face forms readily.

¶ In order to ensure that the mass spectrum obtained was a good representation of the composition of the heated crystal, samples were dissolved in predried acetone (4 Å molecular sieves), spotted immediately on to the MALDI-TOF target upon which a Co powder matrix had been applied and their mass spectrum recorded on a Kratos Kompact MALDI 3 instrument using 50 shots at a linear laser power of 105.

1 D. Philp and J. F. Stoddart, *Angew. Chem., Int. Ed. Engl.*, 1996, **35**, 1154; D. S. Lawrence, T. Jiang and M. Levett, *Chem. Rev.*, 1995, **95**, 2229; J. S. Lindsey, *New J. Chem.*, 1991, **15**, 153; G. M. Whitesides, J. P. Mathias and C. T. Seto, *Science*, 1991, **254**, 1312.

2 S. V. Kolotuchin and S. C. Zimmerman, *J. Am. Chem. Soc.*, 1998, **120**, 9092; T. Martin, U. Obst and J. Rebek, Jr, *Science*, 1998, **281**, 1842; M. Mammen, E. I. Shakhnovich, J. M. Deutch and G. M. Whitesides, *J. Org. Chem.*, 1998, **63**, 3821; T. B. Norsten, R. McDonald and N. R. Branda, *Chem. Commun.*, 1999, 719; M. Enomoto and T. Aida, *J. Am. Chem. Soc.*, 1999, **121**, 874.

3 Large, complex architectures can be constructed using strict self-assembly. The classical example is the Tobacco Mosaic Virus, see A. Klug, *Angew. Chem., Int. Ed. Engl.*, 1983, **22**, 565.

4 For other elegant examples of covalent self-assembly, see S. J. Rowan, P. A. Brady and J. K. M. Sanders, *Angew. Chem., Int. Ed. Engl.*, 1996, **35**, 2143; P. A. Brady and J. K. M. Sanders, *Chem. Soc. Rev.*, 1997, **26**, 327; S. J. Rowan, D. G. Hamilton, P. A. Brady and J. K. M. Sanders, *J. Am. Chem. Soc.*, 1997, **119**, 2578; S. J. Rowan and J. K. M. Sanders, *J. Org. Chem.*, 1998, **63**, 1536; S. J. Rowan, D. J. Reynolds and J. K. M. Sanders, *J. Org. Chem.*, 1999, **64**, 5804; J. Ipaktschi, R. Hosseinzadeh, P. Schlaf and E. Dreiseidler, *Helv. Chim. Acta*, 1998, **81**, 1821; J. Ipaktschi, R. Hosseinzadeh and P. Schlaf, *Angew. Chem., Int. Ed.*, 1999, **38**, 1658. Sanders uses the term predisposition to describe the encoding of a thermodynamically-favourable oligomeric structure through the conformational properties of the monomer once incorporated into this larger structure. In this language, the conformational space which is open to monomer **1** should predispose, or encode, the formation of a particular oligomer of **1**.

5 An example of this phenomenon, known as nucleation, can be seen in the assembly of oligonucleotides to form double helical structures which is essentially an all-or nothing process once a critical chain length is reached. See D. Pörschke and M. Eigen, *J. Mol. Biol.*, 1971, **62**, 361; M. E. Craig, D. M. Crothers and P. Doty, *J. Mol. Biol.*, 1971, **62**, 383.

6 K. D. M. Harris, B. M. Kariuki, C. Lambropoulos, D. Philp and J. M. A. Robinson, *Tetrahedron*, 1997, **53**, 8599; J. M. A. Robinson, B. M. Kariuki, D. Philp and K. D. M. Harris, *Tetrahedron Lett.*, 1997, **38**, 6281.

7 T. C. Bruice and F. C. Lightstone, *Acc. Chem. Res.*, 1999, **32**, 127.

8 G. Ercolani, *J. Phys. Chem. B*, 1998, **102**, 5699; A. J. Kirby, *Adv. Phys. Org. Chem.*, 1980, **17**, 183.

Communication 9/06257B

Total synthesis of (±)-quinolizidine 207I, an alkaloid from *Mantella baroni*, a Madagascan mantelline frog

Patrick Michel and André Rassat

Département de Chimie, Ecole Normale Supérieure, 75231 Paris Cedex 05, France. E-mail: andre.rassat@ens.fr

Received (in Cambridge, UK) 8th September 1999, Accepted 4th October 1999

The first synthesis of quinolizidine 207I was achieved by a totally stereocontrolled approach starting from a 9-azabicyclo[3.3.1]nonane derivative, thus establishing the exceptional axial stereochemistry of the ethyl group at position 1.

Several alkaloids of the indolizidine **1** and quinolizidine **2** series have been isolated from the skin of certain poisonous frogs and

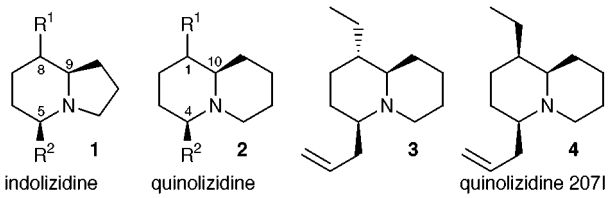

toads.[1] While the structures of the 5,8-disubstituted indolizidines are well-known and have in some cases been confirmed by synthesis,[2] the 1,4-disubstituted quinolizidine are a relatively new class of alkaloids. They have been isolated in minute quantities, and their structure determined mainly on the basis of GC-FTIR and GC-MS: the presence of significant Bohlmann bands[3] in the FTIR spectra shows that the hydrogens at position 4 and 10 are *cis*, but does not provide any information on the relative configuration at position 1, which is only tentative and must be confirmed by synthesis.

One of these alkaloids, quinolizidine 207I, was assigned structure **3** for which a total synthesis was reported in 1997 by Momose and co-workers.[4] However the synthetic material was found to be different from the natural one. Quinolizidine 207I was then reassigned the epimeric structure **4**, the first example of a 1,4-disubstituted quinolizidine with an axial 1-substituent.

We report herein the first synthesis of (±)-**4** (Scheme 1). In this totally stereocontrolled approach, the three asymmetric centres were introduced at an early stage by the use of a *pseudo*-pelletierine derivative **5**. Furthermore, this synthesis is formally enantioselective: because of the C_2 symmetry of the diol precursor of this synthon, it may safely be expected that the enantiomers of this diol as well as all the intermediates obtained in this synthesis will not undergo racemization at any point.

We have recently developed a facile access[5] to this new molecule from cycloocta-1,5-diene by modification of Ganter's approach to related systems.[6] Swern oxidation of **5** followed by a Wittig reaction afforded **6** in 90% yield, as a 1/9 mixture of *Z* and *E* isomers. Although easily separated by column chromatography, this mixture was directly hydrogenated in MeOH with 10% palladium on (wet) charcoal to give the debenzylated amine **7** as a single epimer, of *endo* stereochemistry, as will be proved at the quinolizidine stage. The amine was then protected with BnO_2CCl and the alcohol function liberated with HF to give **9** (82% yield from **6**). In order to open the bicyclic skeleton, this alcohol was oxidised (Swern) and converted to the silyl enol ether **11**. Treatment with O_3 gave the piperidine **12** after reduction and esterification (52% from **9**). Two carbons were added to the alcoholic chain by classical methods, and **13** was obtained (72% from **12**) as a mixture of isomers, after reduction of the methyl ester with Super-Hydride®. After hydrolysis of the dioxolane, hydrogenation with Pd/C removed the carbamate function and at the same time reduced both the double bond and the intermediate imine to yield **14** (69% from **13**). At this stage, the axial stereochemistry of the ethyl side-chain was determined from the coupling constant of the protons at positions 1 and 10, thus establishing the *endo* stereochemistry of this substituent in **7**. Target molecule **4**[7] was then obtained in 25% yield from **14** through two Wittig reactions. The total yield from **5** for this 17-step synthesis is 6.8%.

A sample of this molecule has been analysed at NIH-NIDDK: it had an FTIR spectrum identical in all respects with the natural product and it co-chromatographed with it on the achiral GC column that had produced the best separations in this series.

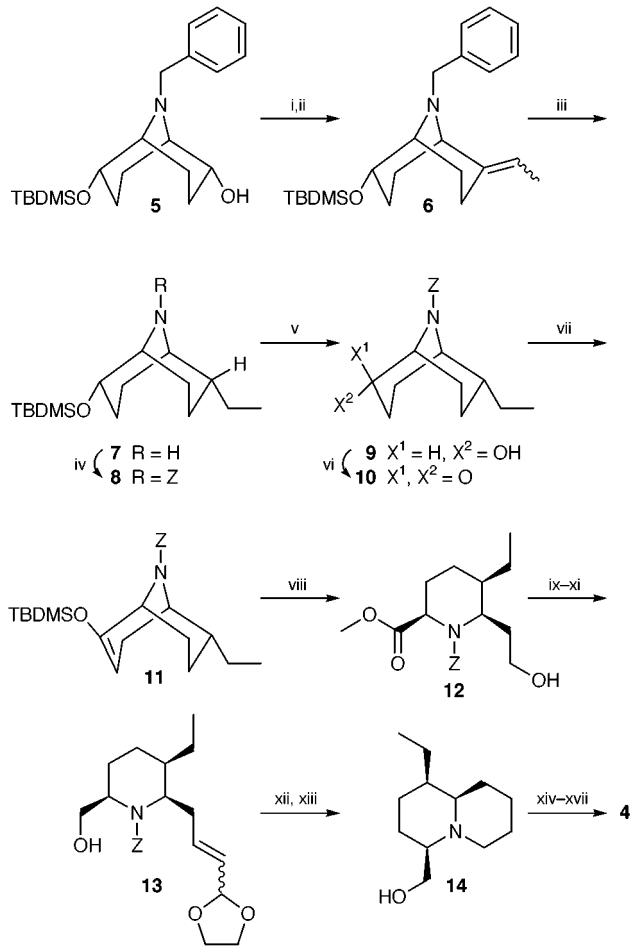

Scheme 1 *Reagents and conditions*: i, Swern oxidation (93%); ii, Ph_3EtPBr, Bu^tOK, THF (98%); iii, H_2, Pd/C 10% (wet), MeOH; iv, ZCl, K_2CO_3, acetone; v, HF 40%, MeCN (82% in 3 septs); vi, Swern oxidation (81%); vii, KH, THF, TBDMSCl (88%); viii, O_3, MeOH–CH_2Cl_2, then $NaBH_4$, then CH_2N_2 (71%); ix, Swern oxidation (81%); x, [$Ph_3PCH_2CH(OCH_2CH_2O)$] Br, Bu^tOK, THF (95%); xi, Super-Hydride®, THF, 0 °C (94%); xii, THF, HCl (1.2 M) (89%); xiii, H_2, Pd/C 10%, MeOH–H_2O (78%); xiv Swern oxidation (75%); xv, ($Ph_3PCH_2OCH_3$)Cl, Bu^tOK, THF (83%); xvi, THF, HCl (4 M); xvii, Ph_3MePBr, Bu^tOK, THF (41% in 2 steps).

Furthermore, the synthetic racemate can be separated on a chiral column, and the natural compound co-chromatographed with one of the synthetic enantiomers.

Because this synthesis is totally stereocontrolled, it establishes the relative configuration of the three epimeric centres: structure **4** can thus definitely be assigned to natural quinolizidine 207I. Since, as said before, this synthesis is formally enantioselective, resolution of an intermediate at an early stage should determine the absolute configuration of the natural product. Work along these lines is in progress.

The strategy used here is general and may provide an easy access not only to other natural (R^1 = Me or Pr) or unnatural quinolizidines **2**, but also to similar natural (R^1 = Me, Et or Pr) or unnatural indolizidines **1**. Syntheses following this approach should make possible a systematic exploration of the unknown pharmacological properties of these two series.

We thank Drs Thomas Spande and John Daly (National Institutes of Health) for providing us with the results of comparisons of our synthetic quinolizidine 207I with the natural alkaloid by GC-FTIR and chiral GC.

Notes and references

1 P. Jain, H. M. Garraffo, H. J. C. Yeh, T. F. Spande, J. W. Daly, N. R. Andriamaharavo and M. Andriantsiferana, *J. Nat. Prod.*, 1996, **59**, 1174; J. W. Daly and T. F. Spande, in *Alkaloids: Chemical and Biological Perspectives, Vol. 4*, ed. S. W. Pelletier, Wiley, New York, 1986, pp. 1–274; J. W. Daly, H. M. Garraffo and T. F. Spande, in *The Alkaloids, Vol. 43*, ed. G. A. Cordell, Academic Press, San Diego, 1993, pp. 185–288; J. W. Daly, in *The Alkaloids, Vol. 50*, ed. G. A. Cordell, Academic Press, New York, 1997, pp. 141–169.

2 A. B. Holmes, A. L. Smith and S. F. Williams, *J. Org. Chem.*, 1991, **56**, 1993; Y. Shisdo and C. J. Kibayashi, *J. Org. Chem.*, 1992, **57**, 2876; R. P. Polniaszek and S. E. Belmont, *J. Org. Chem.*, 1991, **56**, 4868.

3 H. M. Garraffo, L. D. Simon, J. W. Daly, T. F. Spande and T. H. Jones, *Tetrahedron*, 1994, **50**, 11 329.

4 N. Toyooka, K. Tanaka, T. Momose, J. W. Daly and H. M. Garraffo, *Tetrahedron*, 1997, **53**, 9553.

5 P. Michel, PhD Thesis, Université de Paris 6 (France), 1999.

6 R. E. Portmann and C. Ganter, *Helv. Chim. Acta*, 1973, **56**, 1991.

7 *Selected data* for **4**: δ_H(400 MHz, $CDCl_3$) 0.88 (t, *J* 7.5, 3H; CH_3), 1.20–1.83 (m, 14H), 1.85–1.93 (m, 1H, CH), 1.97 (ddd, *J* 11.4, 2.6, 2.6, 1H; CH), 2.12–2.22 (m, 1H; CH), 2.44 (ddddd, *J* 14.2, 6.5, 3.2, 1.6, 1.6, 1H; CH), 3.32–3.38 (m, 1H; CH), 5.02–5.09 (m, 2H; CH_2), 5.85 (dddd, *J* 17.0, 10.3, 7.5, 6.7, 1H; CH); δ_C(100 MHz, $CDCl_3$) 12.45, 18.40, 24.99, 26.20, 26.26, 27.13, 31.01, 38.27, 40.56, 53.00, 64.13, 66.66, 115.88, 136.16.

Communication 9/07261F

First organic–inorganic hybrid materials with controlled porosity incorporating cyclam units

Géraud Dubois,[a] Robert J. P. Corriu,*[a] Catherine Reyé,[a] Stéphane Brandès,[b] Franck Denat[b] and Roger Guilard*[b]

[a] *Laboratoire de Chimie Moléculaire et Organisation du Solide, UMR 5637 CNRS, Université de Montpellier II, Sciences et Techniques du Languedoc, Place E. Bataillon, F-34095 France. E-mail: corriu@crit.univ-montp2.fr*
[b] *Laboratoire d'Ingénierie Moléculaire pour la Séparation et les Applications des Gaz (LIMSAG), UMR 5633, Université de Bourgogne, 6, Boulevard Gabriel, 21100 Dijon, France. E-mail: limsag@u-bourgogne.fr*

Received (in Oxford, UK) 6th September 1999, Accepted 4th October 1999

The sol-gel process has been used to prepare new organic–inorganic hybrid materials with various textures from cyclam derivatives bearing four hydrolysable SiX_3 groups (X = OEt, H) as well as from the corresponding Cu^{II} and Co^{II} complexes of the cyclam derivative (X = OEt).

It is a challenge to prepare materials able to incorporate strongly chelated metal cations which remain chemically accessible. In order to do that, it is necessary to include a good chelating ligand within the solid and to control the texture as well as the structure of the material. Since saturated polyazamacrocycles and especially 1,4,8,11-tetraazacyclotetradecane (cyclam) have long been known for their remarkable binding ability towards transition metal cations,[1,2] we set out to incorporate cyclam units within silica matrices by using the sol-gel process. Indeed the hydrolysis and polycondensation of molecular precursors substituted by more than one hydrolysable groups such as $Si(OR)_3$ allow the preparation of nanostructured hybrid materials.[3–6] This new class of monophasic materials constitutes an expanding area of research in materials science. In this way, the silica matrix is built around the organic moiety during the hydrolytic polycondensation. Silica gel was recently used for the immobilization of polyazacycloalkanes including cyclam, by using a grafting process.[7] However, though this method of attachment of organic groups at the silica surface produced highly effective adsorbents[8,9] and catalysts,[10,11] it presents some drawbacks especially as the loading of the macrocycles is often low (< 0.4 mmol g^{-1}) and is uncontrolled.

Nanocomposite materials incorporating tetraazamacrocycles within silica matrices have been made[12] by the sol-gel process. Here we report the first preparation of monophasic hybrid materials with various textures obtained from isolated cyclam derivatives bearing four hydrolysable SiX_3 groups (X = OEt, H). The hydrolysis of the Cu^{II} and Co^{II} complexes of the cyclam derivative (X = OEt) is also described.

Tetrasilylated cyclam derivative **1** was prepared by reaction of 4 equiv. of 3-iodopropyltriethoxysilane with cyclam under basic conditions;† the corresponding hydrosilylated derivative **2** was obtained by $LiAlH_4$ reduction of **1**.[13] Complexation of Cu^{2+} and Co^{2+} by the tetrasilylated macrocycle **1** was performed in the presence of 1 equiv. of $CuCl_2$ or $CoCl_2$ in THF heated under reflux to afford respectively the complexes **3a** and **3b** in high yield [eqn. (1)]. Sol-gel polycondensation of **1**, **2**, **3a** and **3b** was achieved in the presence of a stoichiometric amount of water (6 equiv.) and under different experimental conditions to yield respectively xerogels **X1a–e**, **X2** and **X3a–b** (Table 1). All the gels were allowed to age for five days at room temperature before being powdered, washed twice with EtOH followed by Et_2O, and finally dried (120 °C at 20 mm Hg for 12 h). It is important to note that after this processing, metal cations were quantitatively retained within the xerogels (measured by elemental analysis and X-ray fluorescence). We had previously observed that 95% of Na^+ and 96% of K^+ was retained within the xerogels obtained by hydrolysis and polycondensation of Na^+ or K^+ complexes of bisilylated dibenzo-18-crown-6.[14] The solid state ^{13}C NMR spectra of the xerogels displayed the

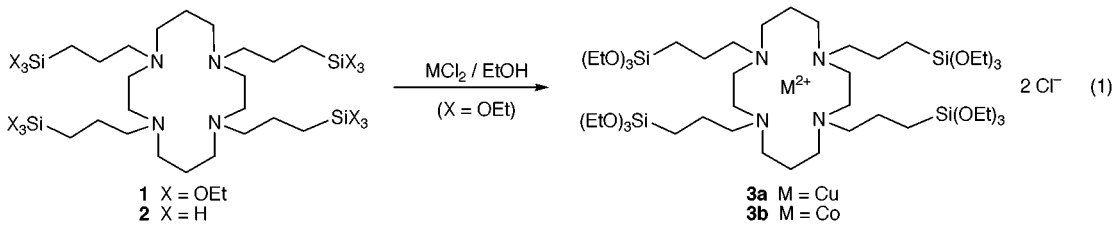

1 X = OEt
2 X = H

3a M = Cu
3b M = Co

Table 1 Hydrolysis and polycondensation of 1 M solution of **1** and **2**, 0.5 M solution of **3a** and 0.25 M solution of **3b** in the presence of a stoichiometric amount of water. BET surface area and mean pore diameters[a] of xerogels

Entry	Precursor	Catalyst	Solvent	*T*/°C	Xerogel	$S_{BET}/m^2\ g^{-1}$	Mean pore diameter/Å
1	**1**	No catalyst	EtOH	24	**X1a**	< 10	—
2	**1**	NH_3[b]	EtOH	22	**X1b**	< 10	—
3	**1**	TBAF (1%)	formamide	22	**X1c**	< 10	—
4	**1**	TBAF (1%)	EtOH	24	**X1d**	370	< 30
5	**1**	TBAF (1%)	EtOH	110[c]	**X1e**	800	20–50
6	**2**	No catalyst	THF	0	**X2**	320	20–60
7	**3a**	TBAF (1%)	THF	22	**X3a**	< 10	—
8	**3b**	TBAF (1%)	THF	26	**X3b**	< 10	—

[a] Calculated by the BJH method. [b] Molar ratio of NH_3/precursor: 158/100. [c] Sealed tube.

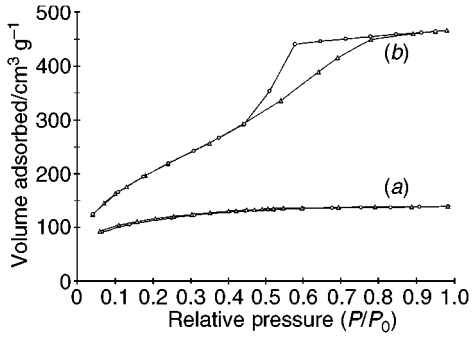

Fig. 1 Sorption isotherms (N_2) for xerogels (*a*) **X1d** and (*b*) **X1e** (Δ = adsorption, ○ = desorption).

signals which characterise the cyclam moieties. Solid state ^{29}Si NMR spectroscopy showed that there was no Si–C bond cleavage during the sol-gel process (absence of any signal corresponding to SiO_4 substructures). All the ^{29}Si NMR spectra display one major resonance centred at δ −65 (substructure T^3 [C–Si(OSi)$_3$]) except for **X1a** and **X1c** which were not well condensed (major substructure T^0 [C-Si(OR)$_3$]). The BET surface areas of the xerogels were determined by N_2 adsorption–desorption measurements and the average pore diameter by the BJH method.[15]

Overall the results reported in Table 1 show that it is possible to obtain materials with various textures by changing the experimental conditions of gelification. The following parameters appear to be of importance.

(1) *Nature of the hydrolysable SiX_3 group* (entries 1 and 6): in the absence of catalyst, the hydrosilane **2** was much more readily hydrolyzed than the corresponding alkoxysilane **1**. Thus, gel formation of **2** took less than 1 min at 0 °C giving rise to the mesoporous xerogel **X2** while that of **1** occurred within 36 h affording the non-porous xerogel **X1a**.

(2) *Nature of the catalyst* (entries 1, 2 and 4): hydrolysis and polycondensation of **1** without catalyst, or in presence of base, yielded respectively the non-porous xerogels **X1a** and **X1b** while hydrolysis of **1** in the presence of 1% TBAF afforded the essentially microporous xerogel **X1d** with a rather large surface area.

(3) *Effect of solvent and of the concentration of the precursor*: all the results reported in Table 1 have been obtained using molar solutions of precursor. We observed that increasing the concentration of the precursor up to 3 M affected neither the specific area nor the pore diameter. In contrast, the nature of the solvent is of importance. Thus, running the hydrolysis in EtOH, THF or CH_2Cl_2 did not change significantly the material, while using formamide as the solvent yielded a material without specific surface area (compare entries 3 and 4).

(4) *Effect of the temperature*: if we compare the results of entries 4 and 5, it is clear that both the surface area and the porosity are strongly dependent on the temperature. The higher the temperature, the larger the surface area and the average pore diameters. The difference between the textures of the xerogels X**1d** and X**1e** appears clearly in Figs. 1 and 2. The adsorption isotherm of **X1d** is typical of a microporous solid [type I of BDDT classification,[15] Fig. 1(*a*)] while that of **X1e** shows a type IV isotherm, characteristic for mesoporous materials [Fig. 1(*b*)]. It is also to be noted that the pore distribution in **X1e** is rather narrow [Fig.2(*b*)], which is not the case for the microporous solid **X1d** [Fig. 2(*a*)]. Another interesting feature of these materials is that they contain up to 1.4 mmol of cyclam per gram of solid (based on nitrogen elemental analyses), which is notably more than the silica gel-supported cyclam.[7]

We have described the preparation of monophasic hybrid materials with various textures from well defined cyclam precursors bearing four hydrolysable SiX_3 groups (X = OEt, H). These materials are fundamentally different from those previously described including cyclam units[7,12] due to the mode of their preparation. We have also shown that the complexation of metal cations by **1** survives the sol-gel process which indicates that, in spite of the high degree of condensation of the network observed in most of the cases, the tetraazamacrocycle is flexible enough to maintain the complexation during the polycondensation. The study of the binding properties of this new class of materials is currently in progress.

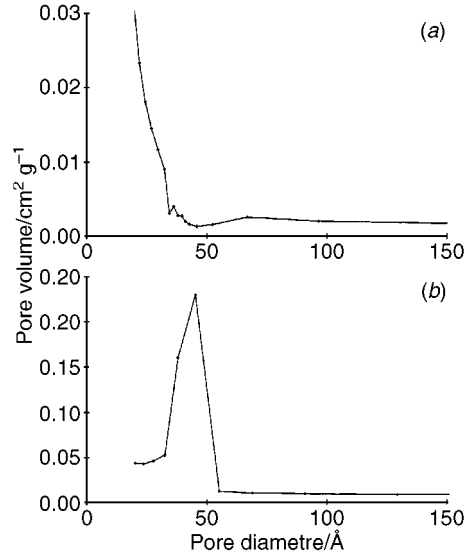

Fig. 2 Pore size distribution curves for (*a*) **X1d** and (*b*) **X1e**.

Notes and references

† *Experimental procedure*: for **1** A mixture of 2 g (10 mmol) of cyclam, 12.41 g (90 mmol) of K_2CO_3 and 13.27 g (40 mmol) of 3-iodopropyltriethoxysilane in 100 ml of MeCN was heated under reflux for 12 h under an argon atmosphere. The solvent was removed *in vacuo* and 100 ml of pentane was added to precipitate the salts. The precipitate was filtered and washed with pentane (2 × 30 ml). Evaporation of pentane gave 9.85 g (9.7 mmol, 97%) of **1** as a colorless oil: δ_H 0.58 (m, 8H, CH_2), 1.23 (t, 36H, CH_3), 1.55 (m, 12H, CH_2), 2.39 (m, 8H, CH_2), 2.51 (m, 8H, CH_2), 2.54 (s, 8H, CH_2), 3.83 (q, 24H, CH_2); δ_C 7.0 (CH_2Si), 17.3 (CH_3), 19.6, 21.9 (CH_2), 49.5, 50.4 (CH_2N), 57.3 (CH_2O), 57.9 (CH_2N); δ_{Si} −44.6. (calc. for $C_{46}H_{104}N_4O_{12}Si_4$. C, 54.33; H, 10.24; N, 5.51. Found: C, 53.90; H, 9.93; N, 5.89%).

1 L. F. Lindoy, *The Chemistry of Macrocyclic Ligand Complexes*, CUP, Cambridge, 1989.
2 P. V. Bernhardt and G. A. Lawrance, *Coord. Chem. Rev.*, 1990, **104**, 297.
3 D. A. Loy and K. J. Shea, *Chem. Rev.*, 1995, **95**, 1431 and references therein.
4 U. Schubert, N. Hüsing and A. Lorenz, *Chem. Mater.*, 1995, **7**, 2010.
5 R. J. P. Corriu and D. Leclercq, *Angew. Chem., Int. Ed. Engl.*, 1996, **35**, 1420 and references therein.
6 G. Cerveau and R. J. P. Corriu, *Coord. Chem. Rev.*, 1998, **178**–**180**, 1051.
7 C. Gros, F. Rabiet, F. Denat, S. Brandès, H. Chollet and R. Guilard, *J. Chem. Soc., Dalton Trans.*, 1996, 1209.
8 L. Mercier and T. J. Pinnavaia, *Adv. Mater.*, 1997, **9**, 500.
9 X. Feng, G. E. Fryxell, L.-Q. Wang, A. Y. Kim, J. Liu and K. M. Kemner, *Science*, 1997, **276**, 923.
10 A. Cauvel, G. Renard and D. Brunel, *J. Org. Chem.*, 1997, **62**, 749.
11 J. H. Clark and D. J. Macquarrie, *Chem. Commun.*, 1998, 853.
12 T. Tsuda and T. Fujiwara, *J. Chem. Soc., Chem. Commun.*, 1992, 1659.
13 R. Corriu, C. Reyé, A. Medhi, G. Dubois, C. Chuit, F. Denat, B. Roux-Fouillet, R. Guilard and G. Lagrange, *Fr. Pat.*, 9800785, 1998.
14 C. Chuit, R. J. P. Corriu, G. Dubois and C. Reyé, *Chem. Commun.*, 1999, 723.
15 S. J. Gregg and K. S. W. Sing, *Adsorption, Surface Area and Porosity*, 2nd edn., Academic Press, New York, 1982.

Communication 9/07217I

ChemComm

A di-iron dithiolate possessing structural elements of the carbonyl/cyanide sub-site of the H-centre of Fe-only hydrogenase

Alban Le Cloirec,[a] Stephen P. Best,[b] Stacey Borg,[b] Sian C. Davies,[a] David J. Evans,[a] David L. Hughes[a] and Christopher J. Pickett*[a]

[a] *Department of Biological Chemistry, John Innes Centre, Norwich Research Park, Norwich, UK NR4 7UH. E-mail: chris.pickett@bbsrc.ac.uk*

[b] *School of Chemistry, University of Melbourne, Parkville, 3052 Victoria, Australia*

Received (in Cambridge, UK) 5th August 1999, Accepted 1st October 1999

The synthesis and characterisation of the first {2Fe2S}-cluster bearing both CO and CN ligands is described; the iron atoms are linked by the bridging 1,3-propanedithiolate unit that has been identified in the crystallographic structure of the {2Fe2S} sub-unit of the H-centre of the all-iron hydrogenase from *Desulfovibrio desulfuricans*.

Two recent X-ray crystallographic structures of Fe-only hydrogenases isolated from *Desulfovibrio desulfuricans*[1] and *Clostridium pasteurianum*[2] show that the H-centre, the active site at which protons are reduced to dihydrogen, is comprised of a conventional {4Fe4S}-cluster linked by a bridging cysteinyl ligand to an extraordinary 'organometallic' di-iron sub-site. The combined structural data, taken together with FTIR data obtained for the Fe-only hydrogenase from *Desulfovibrio vulgaris*,[3] strongly suggest that the sub-site is ligated by terminal CO and CN molecules with the two iron atoms linked by a 1,3-propanedithiolate ligand and bridged by a carbonyl group; the *exo* Fe atom is either coordinatively unsaturated[1] or is ligated with a water molecule[2] [Scheme 1(a)].

We now report the synthesis and characterisation of the first dinuclear iron–sulfur complex with both CO and CN ligation at the iron atoms. Importantly, this dianion also possesses the bridging propanedithiolate structural motif identified in the higher resolution protein X-ray structure.[1]

The known di-iron complex $[(CO)_3FeSCH_2CH_2CH_2S\text{-}Fe(CO)_3]$ **A**[4] reacts with 2 equivalents of NEt_4CN in MeCN at room temperature to give the dianionic salt $[NEt_4]_2[(CO)_2(NC)FeSCH_2CH_2CH_2SFe(CN)(CO)_2]$, $\{[NEt_4]_2\mathbf{B}\}$, essentially quantitatively. $[NEt_4]_2\mathbf{B}$ was isolated as an orange, air-sensitive, crystalline material [Scheme 1(b)].

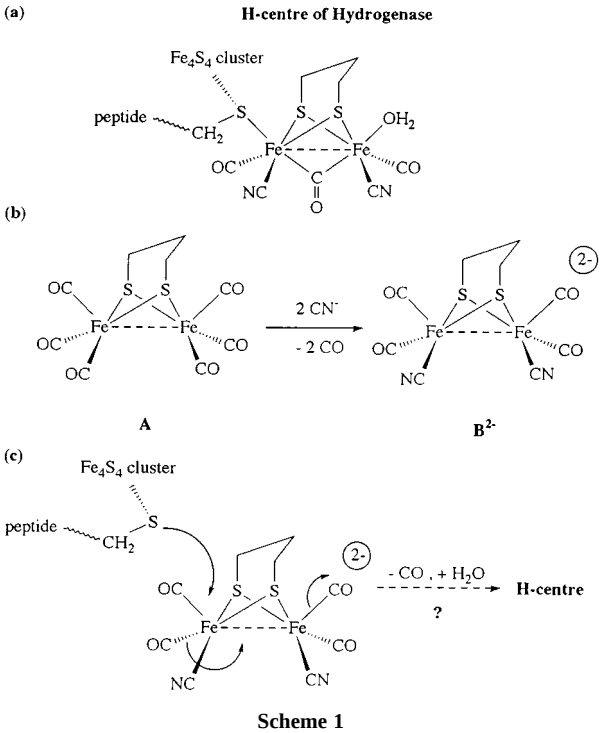

Scheme 1

^1H, $^{13}C\{^1H\}$ NMR and Mössbauer spectroscopy are consistent with the formulation of $[NEt_4]_2\mathbf{B}$ and indicate an arrangement in the dianion with two CO ligands and one CN ligand at each Fe centre. The Mössbauer spectrum displays a well defined doublet with isomer shift and quadrupole splitting parameters similar to those of the parent hexacarbonyl and related molecules with sulfur bridging two metal–metal bonded Fe^I atoms.† FTIR spectra (NEt_4^+ salt, MeCN solution) show ν(CO) 1964s 1922s 1885s and 1871sh cm^{-1} with ν(CN) at 2075m cm^{-1}. The ^{13}CN-labelled salt [18-crown-6·K]$_2$**B** shows $\nu(^{13}CN)$ at 2031 cm^{-1}; the shift in frequency of 44 cm^{-1} from that of the ^{12}CN complex is close to that theoretically expected (43 cm^{-1}). The ν(CO) stretches are not shifted in the labelled complex, this shows that the CN oscillator(s) is not coupled with CO. In addition, the solution FTIR spectrum of the mixed labelled complex shows no additional absorptions which would be indicative of coupling between the two CN ligands.

X-Ray crystallographic analysis of an incomplete, low-angle diffraction data-set confirms the skeletal arrangement of the dianion $\mathbf{B}^{2-}$, *viz.* two iron atoms bridged by the 1,3-propanedithiolate ligand, with dimensions very close to those observed for the sub-unit in the enzyme,[1] and three further ligands (CO/CN) attached to each Fe atom.‡

Normal coordinate analysis, using a Cotton–Kraihanzel force field,[6,7] of the CO IR data shows that the pattern of ν(CO) bands is consistent with the dianion possessing pseudo-C_s symmetry with eclipsed CN ligands as represented in Scheme 1(b).

Given the general robustness of $\{Fe_2S_2(CO)_6\}$ units, it is somewhat surprising that substitution occurs under such mild conditions.[5] The reaction is not confined to **A** but occurs with other dithiolate-bridged di-iron hexacarbonyl clusters, for example, we have synthesised and characterised the bridge-functionalised complex $[NEt_4]_2[(CO)_2(NC)FeSCH_2CH(CH_2OH)SFe(CN)(CO)_2]$, $\{[NEt_4]_2\mathbf{C}\}$ from the corresponding hexacarbonyl precursor.†

Primary (irreversible) reduction of the dianion $\mathbf{B}^{2-}$ occurs at $E_p^{red} = -2.33$ V *vs.* SCE and primary (irreversible) oxidation occurs at $E_p^{ox} = -0.11$ V *vs.* SCE {recorded in MeCN–0.1 M NBu_4BF_4 at vitreous carbon, 100 mV s^{-1}, room temp.}. $\mathbf{B}^{2-}$ is both stable and *very* soluble in water as the $[NEt_4]^+$ salt, although it neither reacts with nor electrocatalyses the reduction of protons in aqueous solution over the pH range 8.4–4.0. Why $\mathbf{B}^{2-}$ does not effect the reduction of protons, whereas the sub-unit of the H-centre does so, is probably linked to the relative electron-richness of the 2Fe2S units. With respect to the synthetic cluster, the enzyme sub-unit has a bridging cysteinyl group formally displacing an electron-withdrawing terminal CO ligand into a bridging mode and also a CO ligand formally replaced by a donor water molecule [Scheme 1(c)]. We thus predict that the enzymic sub-unit would be oxidised at a potential substantially negative of that of $\mathbf{B}^{2-}$ and sufficient to

drive proton reduction at modest pH. That $\mathbf{B}^{2-}$ is both highly water soluble and stable over a wide range of pH suggests that it could be involved in the cellular biosynthesis of the H-centre [Scheme 1(c)].

We thank Elaine Barclay for recording Mössbauer spectra. This work was supported by the BBSRC, the France–UK Alliance Programme, and the Ministère de l'Enseignement Supérieur et de la Recherche.

Note added in proof: We thank Professor J. W. Peters for a pre-print of an X-ray crystallographic study of the CO inhibited form of the Fe hydrogenase from *C. pasteurianum*. This shows CO replaces coordinated H_2O at the distal iron atom of the H-centre 2Fe2S sub-unit *cf.* the inability of $\mathbf{B}^{2-}$ to catalyse proton reduction.

Notes and references

† $[NEt_4]_2\mathbf{B}$: ^{1}H NMR (400 MHz, CD_3CN): δ 1.20 [24H, br, $(CH_3CH_2)_4N^+$], 1.63 (2H, br, $SCH_2CH_2CH_2S$), 1.81 (4H, br, $SCH_2CH_2CH_2S$), 3.17 [16H, br, $(CH_3CH_2)_4N^+$]; ^{13}C{^{1}H} NMR (100 MHz, CD_3CN): δ 7.9 [$(CH_3CH_2)_4N^+$], 23.6 ($SCH_2CH_2CH_2S$), 31.3 ($SCH_2CH_2CH_2S$), 53.2 [$(CH_3CH_2)_4N^+$], 151.2 (CN), 220.6 (CO). Mössbauer spectrum (solid, 77 K, referenced to 25 μm Fe-foil at 298 K): doublet; isomer shift +0.05 mm s^{-1}; quadrupole splitting 1.03 mm s^{-1}. See: *The Organic Chemistry of Iron*, ed. E. A. Koerner von Gustorf, F. W. Grevels and I. Fischler, Academic Press, New York, 1978, vol. 1, pp. 175–211. FTIR (in MeCN): $[18\text{-crown-6}\cdot K]_2\mathbf{B}$: ν(CO) 1871 (sh), 1883s, 1921s, 1963s and ν(CN) 2075m cm^{-1}; ^{13}CN-labelled $[18\text{-crown-6}\cdot K]_2\mathbf{B}$: ν(CO) 1871 (sh), 1883s, 1921s, 1961s and $\nu(^{13}CN)$ 2031m cm^{-1}. FABMS: *m/z* 772 $\{[NEt_4]_3M\}^+$, 586 $\{[NEt_4]_2M - 2CO\}^+$, 530 $\{[NEt_4]_2M - 4CO\}^+$, 457 $\{[NEt_4]MH - 2CO\}^+$, 414 $\{[NEt_4][Fe_2S_2(CN)_2(CO)_2]\}^+$, 413 $\{[NEt_4][Fe_2S(CNH)(CO)_4]\}^+$, 307 $\{[NEt_4]Fe_2S_2H\}^+$, 157 $\{[NEt_4]CNH\}^+$, 130 $[NEt_4]^+$. Microanalysis: $C_{25}H_{46}Fe_2N_4O_4S_2\cdot H_2O$, found (calc.): C, 46.1(45.5); H, 7.95(7.32); N, 8.5(8.5); S, 9.0(9.7); Fe 15.8 (16.7%).

$[NEt_4]_2\mathbf{C}$: ^{1}H NMR (400 MHz, CD_3CN): δ 1.23 [24H, br, $(CH_3CH_2)_4N^+$], 1.55 [1H, dd, ^2J 9, ^3J 6 Hz, $SCHHCH(CH_2OH)S$], 2.22 [2H, m, $SCHHCH(CH_2OH)S$ and $SCH_2CH(CH_2OH)S$], 2.44 (1H, t, ^3J 5.5 Hz, OH), 3.20 [16H, br, $(CH_3CH_2)_4N^+$], 3.36 (1H, dd, ^2J 8.5, ^3J 6.5 Hz, $CHHOH$), 3.47 (1H, dd, ^2J 8.5, ^3J 7 Hz, $CHHOH$); ^{13}C{^{1}H} NMR (100 MHz, CD_3CN): δ 7.7 [$(CH_3CH_2)_4N^+$], 37.0 and 54.3 [$SCH_2CH(CH_2OH)S$], 66.1 (CH_2OH), 53.0 [$(CH_3CH_2)_4N^+$], 66.1 (CH_2OH), 149.2 (CN), 221.4 (CO). Mössbauer spectrum (solid, 77 K, referenced to 25 μm Fe-foil at 298 K): doublet; isomer shift 0.03 mm s^{-1}; quadrupole splitting 1.09 mm s^{-1}. FTIR (in MeCN): ν(CO) 1874 (sh), 1888s, 1924s, 1966s and ν(CN) 2032w and 2076m cm^{-1}. Microanalysis: $C_{25}H_{46}Fe_2N_4O_5S_2\cdot 0.5\ Et_2O$, found (calc.: C, 46.8(46.6); H, 7.47(7.39); N, 8.1(8.1); S, 8.9(9.2); Fe, 15.6(16.1%).

‡ The overall geometry of the anion is well established. The Fe_2(dithiolate) core is well resolved and shows reasonable molecular dimensions, *e.g.* the four Fe–S bonds lie in the range 2.251(17)–2.318(17) Å, mean 2.276(14) Å, and the Fe–Fe distance is 2.528(11) Å. The two S–C bond lengths are 1.87(5) and 1.84(5) Å and the bridging C–C lengths are each 1.60(6) Å. Each iron is five coordinate with a square pyramidal geometry (octahedral coordination completed by a bent Fe–Fe bond[5]).

1 Y. Nicolet, C. Piras, P. Legrand, C. E. Hatchikian and J. C. Fontecilla-Camps, *Structure*, 1999, **7**, 13.
2 J. W. Peters, W. N. Lanzilotta, B. J. Lemon and L. C. Seefeldt, *Science*, 1998, **282**, 1853.
3 A. J. Peirik, M. Hulstein, W. R. Hagen and S. P. J. Albracht, *Eur. J. Biochem.*, 1998, **258**, 572.
4 A. Winter, L. Zsolnai and G. Huttner, *Z. Naturforsch., Teil B*, 1982, **37**, 1430.
5 D. Seyferth, G. B. Womack, M. K. Galagher, M. Cowie, B. W. Hames, J. P. Fackler and A. M. Mazany, *Organometallics*, 1987, **6**, 283 and references therein.
6 F. A. Cotton and G. Wilkinson, *Advanced Inorganic Chemistry*, Wiley, New York, 5th edn., 1988, p. 1036.
7 NCA calculations were performed using the program suite QCMP067 (General Vibrational Analysis System, D. F. McIntosh and M. R. Peterson), Quantum Chemical Program Exchange, Indiana University. Initial values of the CO stretching and interaction force constants were obtained from a previous study of $Fe_2(CO)_6(\mu\text{-}Y)_2$ complexes (G. Bor, *J. Organomet. Chem.*, 1975, **94**, 181).

Communication 9/06391I

Cation-controlled formation of $[\{MCl_4\}_n]^{2n-}$ chains in [4,4′-H_2bipy][MCl_4] (M = Mn, Cd): an alternative to the A_2MCl_4 <100> layer perovskite structure†

Amy L. Gillon,[a] A. Guy Orpen,*[a] Jonathan Starbuck,[a] Xi-Meng Wang,[a] Yolanda Rodríguez-Martín[b] and Catalina Ruiz-Pérez[b]

[a] *School of Chemistry, University of Bristol, Bristol, UK BS8 1TS. E-mail: Guy.Orpen@bristol.ac.uk*
[b] *Departemento de Física Fundamental II, Universidad de La Laguna, 38204 La Laguna, Spain*

Received (in Oxford, UK) 20th September 1999, Accepted 6th October 1999

The *cis*-$MCl_2\cdots HN^+$ chelated hydrogen bond synthon has been exploited in preparation of crystalline [4,4′-H_2bipy][MCl_4] (M = Mn 2 and Cd 3), which shows a one-dimensional substructure of the form $[\{MCl_4\}_n]^{2n-}$ consisting of a kinked chain of doubly edge sharing MCl_6 octahedra. These chains are cross-linked by hydrogen bonding to the [4,4′-H_2bipy]$^{2+}$ ions.

The <100> layer perovskites A_2MX_4 (A = ammonium cation NH_3R^+ or A_2 = $NH_3(CH_2)_nNH_3^{2+}$, *etc.*; M = Cr^{II}, Mn^{II}, Cu^{II}, Cd^{II}, Pb^{II}, *etc.*; X = Cl or other halide) have attracted sustained interest because of their magnetic, electronic and other physical properties and the possibility of tuning both geometry and properties by variation of the organic cation.[1] The hydrogen bond donor properties of the ammonium ions serve to promote the formation of two-dimensional $[\{MCl_4\}_n]^{2n-}$ sheets, whose structure may be formally derived from that of cubic perovskite. We have previously shown that the *cis*-$MCl_2\cdots HN^+$ supramolecular synthon **A** may be used to construct a hydrogen bonded

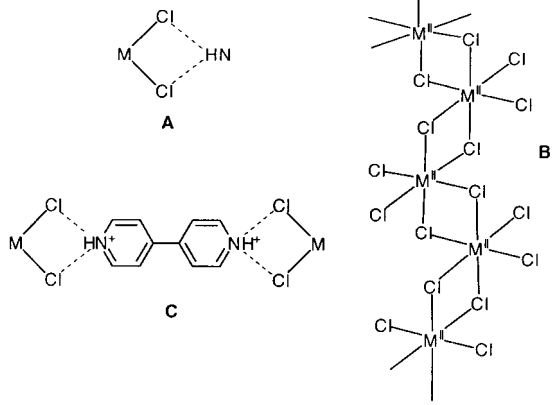

polymeric ribbon structure $\{[4,4'\text{-}H_2bipy][MCl_4]\}_n$ for M = Pt[2] while an hydrogen bonded dimeric ring motif is formed for M = Co.[3] Here, we show that a third family of structures exists of stoichiometry [4,4′-H_2bipy][MCl_4] in which the tetrachlorometallate anions polymerise to form a one-dimensional chain. This form contrasts both with the two other structure types and with the layer perovskite structures seen for primary ammonium salts of the same dianions.

In exploring the range of metals for which [4,4′-H_2bipy]$^{2+}$ salts of $[MCl_4]^{2-}$ ions form the dimeric ring structure we obtained crystals of [4,4′-H_2bipy][MCl_4] (M = Zn **1** and Mn **2**) by routes in which the metal halides were crystallised from aqueous solution in the presence of 4,4′-bipyridinium and chloride ions.‡ The zinc species§ is isostructural (Fig. 1) with its cobalt analogue and shows NH···Cl hydrogen bonds of length 2.30 and 2.63 Å.[3] The manganese species has a quite different structure (Fig. 2) in which the metals are octahedrally coordinated and the $MnCl_6$ octahedra are linked into kinked chains (as in the $ZrCl_4$ structure **B**[4]) which extend along the crystallographic *c* axis. The $[\{MCl_4\}_n]^{2n-}$ chains are linked by NH···Cl hydrogen bonding to [4,4′-H_2bipy]$^{2+}$ into neutral sheets lying parallel to the *ac* plane. In these sheets synthon **A** is used at both ends of the dication (see **C** and Fig. 2). The neutral layers then pack along the *b* axis to form the overall

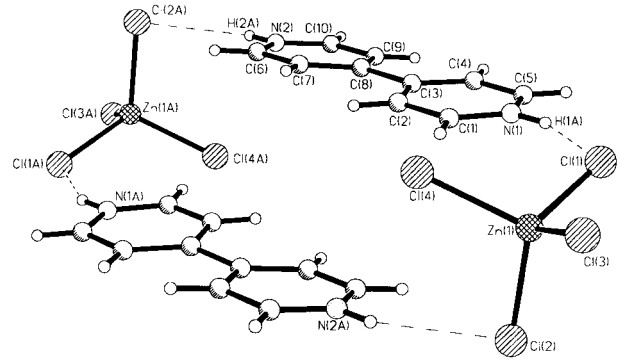

Fig. 1 Structure of the hydrogen bonded dimeric ring in [4,4′-H_2bipy]-[$ZnCl_4$] **1**. The NH···Cl hydrogen bonds are indicated. Important bond lengths (Å): Zn(1)–Cl(1) 2.2934(7), Zn(1)–Cl(2) 2.2977(8), Zn(1)–Cl(3) 2.2526(7), Zn(1)–Cl(4) 2.2546(7).

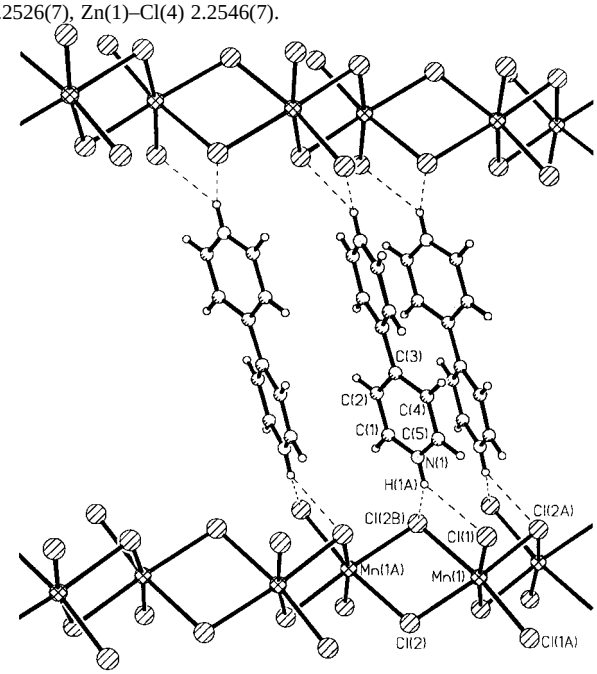

Fig. 2 Structure of a layer of [$MnCl_4$] chains cross-linked by [4,4′-H_2bipy] in crystalline [4,4′-H_2bipy][$MnCl_4$] **2**. The NH···Cl hydrogen bonds are indicated. Important bond lengths (Å): Mn(1)–Cl(1) 2.4904(6) [2.5733(8)], Mn(1)–Cl(2) 2.6294(6) [2.7031(7)], Mn(1)–Cl(2A) 2.5946(7) [2.6672(8)]. Values in square brackets are for the isostructural [4,4′-H_2bipy][$CdCl_4$] **3**.

† Electronic supplementary information (ESI) available: synthesis details for **1**, **2** and **3**. See http://www.rsc.org/suppdata/cc/1999/2287/

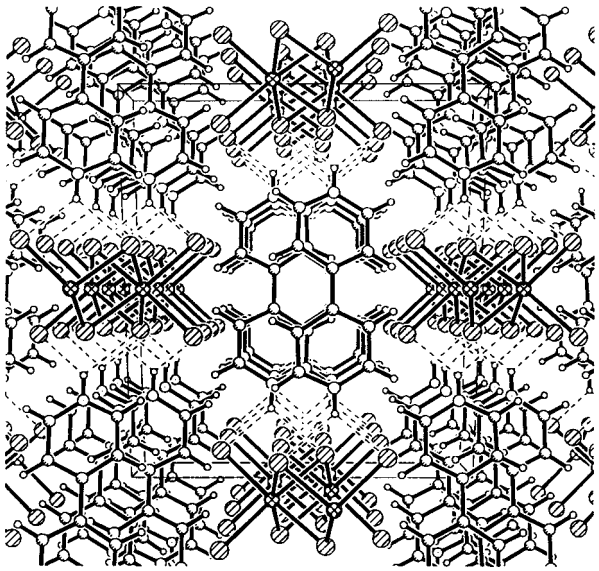

Fig. 3 The crystal structure of [4,4′-H_2bipy][$MnCl_4$] **2** viewed along the *c* axis, parallel to the metal chains. The NH···Cl hydrogen bonds are indicated.

structure (Fig. 3). There is very weak intrachain antiferromagnetic coupling of the paramagnetic Mn^{II} centres with negligible interchain coupling (Mn···Mn distances along the chain are 4.011 Å).¶

Despite the wide variety of cations for which $[MnCl_4]^{2-}$ salts have been structurally characterised, only two structure types have been observed: tetrahedral $[MnCl_4]^{2-}$ units or sheets of corner sharing $\{MnCl_6\}$ octahedra in a <100> layer perovskite structure. As such these $[MnCl_4]^{2-}$ salts are representative of a much larger set of salts of tetrahalometallate dianions of the transition and post-transition metals.[1] For example, of 24 $[CdCl_4]^{2-}$ salts in the Cambridge Structural Database[5] all bar one[6] (which has a chain structure of corner linked trigonal bipyramidal $CdCl_5$ units) also show only isolated tetrahedral (10 examples) or <100> layer perovskite structures (13 examples). In organic–inorganic layer perovskites it is generally thought that the hydrogen bonding capability of the organic (primary ammonium) cations promotes the observed structures. Indeed in general, in these structures each NH_3 makes three strong NH···Cl hydrogen bonds. We reasoned that the different hydrogen bonding capabilities of the [4,4′-H_2bipy]$^{2+}$ cation might provide a general route to the new chain structure type for those metals which are readily able to form octahedral $\{MCl_6\}$ moieties in their +II oxidation state. Given the behaviour of the $[CdCl_4]^{2-}$ salts noted above, cadmium was chosen as a representative example. Treatment of aqueous cadmium chloride with [4,4′-H_2bipy]$^{2+}$ does indeed lead to formation of a salt [4,4′-H_2bipy][$CdCl_4$] **3** in which the new structure type is adopted.‡ Compound **3** is isostructural with its manganese analogue.§ As in **2** synthon **A** is present [NH···Cl 2.54 and 2.60 Å in **3** for Cl(1) and Cl(2), respectively; *cf.* 2.51, 2.58 in **2**] as well as two CH···Cl bonds per chlorine (2.71–2.85 Å in **3**, 2.70–2.85 Å in **2**).

It is noteworthy that the same polymeric $\{MCl_4\}_n$ substructure has been observed in neutral MCl_4 species (*e.g.* $ZrCl_4$)[4] and in monoanionic form (*e.g.* in [Hpy][$SbCl_4$])[7] but not previously in dianionic species. Such chains are a substructure of the familiar $CdCl_2$ structure.[8] Presumably the [4,4′-H_2bipy]$^{2+}$ cation plays a vital role in stabilising the chain structure. As noted above, despite the wide variety of cations employed in salts of $[MCl_4]^{2-}$ (M = Mn or Cd) the new structure type has not previously been observed. The chain structure has as many bridging (four per metal) and terminal (two per metal) chlorines as does the layer perovskite form of the $[\{MCl_4\}_n]^{2n-}$ polymer. However the perovskite structure has nearly linear M–Cl–M bridges (angles typically 160–165°) compared with the much more normal M–Cl–M angles in **2** and **3** [100.29(2) and 99.38(2)°, respectively]. The more open perovskite structure apparently requires greater strain at the μ-Cl site. This strain is presumably compensated by formation of stronger NH···Cl hydrogen bonds (usually six per metal, as in A_2MX_4 structures with A = primary ammonium) than for the chain structure in **2** and **3** where there are just two NH groups per metal. Notably $[Hpy]_2[MnCl_4]$[9] contains tetrahedral manganese centres implying that it is not merely the number of NH hydrogen bond donors that influences the polymerisation of the $MnCl_4$ moieties. The willingness of the metal to be octahedrally coordinated must also be important. Thus the [4,4′-H_2bipy][MCl_4] (M = Co or Zn) salts contain $[MCl_4]$ tetrahedra rather than polymeric anions. Notably the same is true of $[NH_3(CH_2)_nNH_3]^{2+}$ (n = 2, 3) salts of tetrachlorometallate anions: only those cases where M = Zn or Co have tetrahedral dianions. In other cases, *e.g.* M = Cr, Mn, Fe, Ni, Cd or Cu the <100> layer perovskite structure, with octahedral (or distorted octahedral) coordination of the metal, is adopted.

The ability of [4,4′-H_2bipy]$^{2+}$ to control the aggregation of other metal anions, such as metal–oxo species has been noted.[10] In the present case it seems that the hydrogen bonding capability of [4,4′-H_2bipy]$^{2+}$ may provide access to a new faimily of chain polymers of perhalometallate anions which may offer intriguing and potentially useful properties.

Financial support of the Royal Society (a Royal Society China Royal Fellowship to X.-M. W.) and from the Spanish Dirección General de Enseñanza Superior e Investigación Científica through Project PB97-1479-C02-02 is gratefully acknowledged.

Notes and references

‡ *Syntheses* of [4,4′-H_2bipy][MCl_4] (M = Zn **1**, Mn **2** or Cd **3**). Details are available as electronic supplementary information.

§ *Crystal structure analyses* of [4,4′-H_2bipy][MCl_4] **1**–**3**: *Crystal data*: [4,4′-H_2bipy][$ZnCl_4$] **1**: $C_{10}H_{10}Cl_4N_2Zn$, M = 365.37, monoclinic, space group $P2_1/c$ (no. 14), a = 7.6507(12), b = 19.765(4), c = 9.5012(18) Å, β = 108.826(15)°, U = 1359.9(4) Å^3, Z = 4, μ = 2.569 mm^{-1}, T = 173 K, 3112 unique data, $R1$ = 0.026. [4,4′-H_2bipy][$MnCl_4$] **2**: $C_{10}H_{10}Cl_4N_2Mn$, M = 354.94, monoclinic, space group $C2/c$ (no. 15), a = 15.526(2), b = 12.660(3), c = 6.914(2) Å, β = 114.90(2)°, U = 1232.6(5) Å^3, Z = 4, μ = 1.912 mm^{-1}, T = 173 K, 1389 unique data, $R1$ = 0.020. [4,4′-H_2bipy][$CdCl_4$] **3**: $C_{10}H_{10}Cl_4N_2Cd$, M = 412.40, monoclinic, space group $C2/c$ (no. 15), a = 15.612(3), b = 12.746(2), c = 7.0261(12) Å, β = 114.984(3)°, U = 1267.3(4) Å^3, Z = 4, μ = 2.542 mm^{-1}, T = 173, 1448 unique data, $R1$ = 0.025. In **2** and **3** the metal atoms and the cations lie at sites of C_2 symmetry. All hydrogen atoms were located in difference maps and included in idealised positions. X-Ray powder diffraction experiments on bulk samples of **1**, **2** and **3** were consistent with the presence of pure phases with the structures noted above.

CCDC 182/1438. See http://www.rsc.org/suppdata/cc/1999/2287/ for crystallographic files in .cif format.

¶ The magnetic susceptibility of microcrystalline **2** was measured between room temperature and 2 K and shows antiferromagnetic exchange coupling. The molar susceptibility was assumed to be produced by a system of non-interacting linear chains, and the molar susceptibility for these chains calculated according to Fisher's model (M. E. Fisher, *Am. J. Phys.*, 1964, **32**, 343). A satisfactory fit was obtained with Weiss constant θ = −0.024 K, J = −0.1 cm^{-1} and g = 1.99.

1 D. B. Mitzi, *Prog. Inorg. Chem.*, 1999, **48**, 1; P. Day, *J. Chem. Soc., Dalton Trans.*, 1997, 701.
2 G. R. Lewis and A. G. Orpen, *Chem. Commun.*, 1998, 1873.
3 L. J. Barbour, L. R. MacGillivray and J. L. Atwood, *Supramol. Chem.*, 1996, **7**, 167.
4 B. Krebs, *Z. Anorg. Allg. Chem.*, 1970, **378**, 263.
5 F. H. Allen and O. Kennard, *Chem. Des. Automat. News*, 1993, **8**, 1, 31.
6 N. B. Chanh, C. Courseille, R. Duplessix, A. Meresse, M. Couzi and B. Tieke, *Mol. Cryst. Liq. Cryst.*, 1990, **188**, 261.
7 S. K. Porter and R. A. Jacobson, *J. Chem. Soc. A*, 1970, 1356.
8 L. Pauling and J. L. Hoard, *Z. Kristallogr. A*, 1930, **74**, 546.
9 C. Brassy, R. Robert, B. Bachet and R. Chevalier, *Acta Crystallogr., Sect. B*, 1976, **32**, 1371.
10 P. J. Zapf, R. C. Haushalter and J. Zubieta, *Chem. Commun.*, 1997, 321.

Communication 9/07681F

Enantioselective allylic substitution catalyzed by an iridium complex: remarkable effects of the counter cation

Kaoru Fuji,*[a] Naosumi Kinoshita,[a]† Kiyoshi Tanaka[b] and Takeo Kawabata[a]

[a] *Institute for Chemical Research, Kyoto University, Uji, Kyoto 611-0011, Japan. E-mail: fuji@scl.kyoto-v.ac.jp*
[b] *School of Pharmaceutical Sciences, University of Shizuoka, 52-1 Yada, Shizuoka 422-8526, Japan*

Received (in Cambridge, UK) 22nd September 1999, Accepted 4th October 1999

Allylic substitution of a methyl carbonate of cinnamyl alcohol with the anion of dimethyl malonate gave the branched olefin with high enantioselectivity in the presence of (*S*)-1,1′-binaphthyl-2,2′-diyl phenyl phosphite when a combination of lithium and zinc was used as counter cation.

Unlike palladium-catalyzed allylic alkylations, iridium-catalyzed alkylations take place at the more substituted allylic terminus.[1] Recently, asymmetric versions of this reaction have been reported, where chiral phosphinooxazolines[2] or phosphorous amidites[3] were used as ligands. We report here enantioselective allylic substitutions catalyzed by an iridium complex of chiral aryl phosphite (*S*)-**1**.

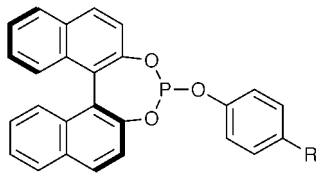

1 R = H
2 R = OMe
3 R = CF_3

We chose **4a** as a standard substrate to avoid ambiguities arising from a chiral centre (Scheme 1), although the ester of an isomeric secondary alcohol, 1-phenylprop-2-en-1-ol, can also be a substrate for the same reaction. It has been reported that the iridium-catalyzed allylic substitution of acetates of secondary alcohols proceeds with 70–80% retention of configuration.[3] Aryl phosphites are known to be efficient ligands for allylic alkylation with soft carbon nucleophiles catalyzed by an iridium complex.[1] Chiral phosphites **1**,[4] **2**[5] and **3**[6] have been used as ligands. Diethylzinc was used as a base because it is known to give a greater ee than other bases in allylic alkylations catalyzed by a palladium–(*R*)-BINAP complex.[7] The results are shown in Table 1. Both electron-releasing and -withdrawing groups on the phenyl rings of the ligands gave lower ees (entries 2 and 3) than the parent phosphite (*S*)-**1** (entry 1). CH_2Cl_2 is the solvent of choice (compare entry 1 with entries 4–6). Allylic methyl carbonate **4b** gave a better yield than the corresponding acetate **4a** in a shorter reaction time (entries 1 and 7).

The effect of the counter cation was investigated using **4b**, and the results are shown in Table 2. A conspicuous feature of these results is that the proportion of (*R*)-**5** to (*S*)-**5** increases as the ionic character of the malonate anion increases (entries 1–3). Thus, (*R*)-**5** was obtained in 36% ee by using Bu^tP_4 base, which is known to generate naked anions.[8,9] Metals, such as lithium and zinc, that strongly coordinate with anion gave (*S*)-**5** as the major enantiomer. The intermediacy of a π-allyl–iridium complex has been suggested for iridium complex-catalyzed allylic alkylation with triphenyl phosphite as ligand.[1] On the other hand, the involvement of a σ-allyl–iridium complex is indicated for the alkylation of secondary allylic acetates.[3] Although there is an apparent divergence of mechanistic considerations, the π-allyl–iridium complex is more likely than the σ-complex when aryl phosphites are used as ligands. The predominant formation of (*S*)-**5** with lithium and/or zinc as the

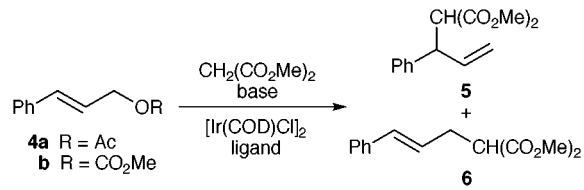

Scheme 1

† Present address: Pharmaceutical Production Department, Tokushima Second Factory, Otsuka Pharmaceutical Co., Ltd., Hiraishi Ebisuno 224-18, Kawauchi-cho, Tokushima 771-0182, Japan.

Table 1 Ir-catalysed allylic alkylation of **4a** and **4b** with dimethyl malonate using $ZnEt_2$ as base[ab]

Entry	Substrate	Ligand	Solvent	Reaction time/h	Combined yield of **5** and **6** (%)	Ratio of **5** : **6** GLC[c]	Ratio of **5** : **6** ^{1}H NMR	Ee of (*S*)-**5**[d](%)
1	**4a**	**1**	CH_2Cl_2	35	58 (64)[e]	92 : 8	—	76
2	**4a**	**2**	CH_2Cl_2	94	57	92 : 8	91 : 9	61
3	**4a**	**3**	CH_2Cl_2	47	62	94 : 6	96 : 4	32
4	**4a**	**1**	toluene	47	57 (58)[e]	82 : 18	81 : 19	67
5	**4a**	**1**	THF	91	40 (49)[e]	84 : 16	85 : 15	20
6	**4a**	**1**	MeCN	48	13 (29)[e]	86 : 14	81 : 19	54
7	**4b**	**1**	CH_2Cl_2	7	88	96 : 4	95 : 5	71
8	**4b**	**1**	THF	68	44 (65)[e]	—	85 : 15	55

[a] General procedure (entry 1): A solution of (*S*)-**1** (81.7 mg, 0.2 mmol), $[Ir(COD)Cl]_2$ (33.6 mg, 0.05 mmol) and cinnamyl acetate (83.1 μl, 0.5 mmol) in dry CH_2Cl_2 (1 ml) was stirred for 45 min under argon. To this solution was added a solution prepared by stirring dimethyl malonate (133 mg, 1.0 mmol) and Et_2Zn (1.0 M in hexane, 1.0 ml) in CH_2Cl_2 (3 ml) under argon for 1 h at room temperature. After stirring for the indicated time, usual extractive work-up with EtOAc followed by preparative TLC (EtOAc–hexane 1 : 6) gave 58 mg of a mixture of **5** and **6**. [b] All reactions were performed at room temperature. [c] Determined by GLC on a Chirasil-DEX CB column at 150 °C. [d] Determined by HPLC on CHIRALCEL OJ-R (MeOH–H_2O = 75 : 25). [e] The number in parenthesis indicates the yield based on the consumed starting material.

counter cation may be explained by the transition state, shown in Fig. 1. The bulky phosphite ligand should be located *trans* to the more-substituted allylic terminus to avoid steric repulsion. Nucleophilic attack *anti* to the phosphite ligand gives (*S*)-**5**. As the anion becomes harder, it favours initial attack at iridium metal, which is harder than the allylic carbon. Intramolecular migration of malonate from iridium to the allylic carbon proceeds to give (*R*)-**5**.

Another feature is that the ee of (*S*)-**5** is remarkably increased to 96% when lithium and zinc are present in the reaction medium (entry 7). It is premature to give a detailed rationalization for this extraordinary increase in ee. However, it is possible that lithium chloride formed *in situ* may play a role.[3] Work is currently underway along these lines.

Table 2 Effect of the counter cation on the allylic alkylation of the carbonate **4b** catalyzed by $[Ir(COD)Cl]_2$–(*S*)-**1** in THF at room temperature[a]

Entry	Base	Reaction time/h	Combined yield of **5**:**6**	Ratio of **5** and **6**[b]	Ee of **5**[c] (%)	Config.
1	Bu^tP_4	24	87	93:7	36	*R*
2	KH	7	90	90:10	18	*R*
3	NaH	24	96	95:5	6	*R*
4	LiH	92	14 (74)[d]	46:54	22	*S*
5	LDA	30	85 (88)[d]	94:6	17	*S*
6	BuLi	30	71 (97)[d]	92:8	24	*S*
7	BuLi/$ZnCl_2$	3	99	93:7	96	*S*

[a] Two equivalents of dimethyl malonate and base were used. [b] Determined by ^1H NMR. [c] Determined by HPLC on a CHIRALCEL OJ-R (MeOH–H_2O = 75:25). [d] The number in parenthesis indicates the yield based on the consumed starting material.

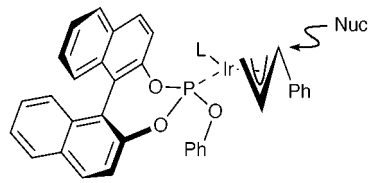

Fig. 1 Transition state structure.

Notes and references

1 R. Takeuchi and M. Kashio, *J. Am. Chem. Soc*., 1998, **120**, 8647; *Angew. Chem., Int. Ed. Engl*., 1997, **36**, 263.
2 J. R. Janssen and G. Helmchen, *Tetrahedron Lett*., 1997, **38**, 8025.
3 B. Bartels and G. Helmchen, *Chem. Commun*., 1999, 741.
4 P. H. Dussault and K. R. Woller, *J. Org. Chem*., 1997, **62**, 1556.
5 M. J. Baker and P. G. Pringle, *J. Chem. Soc., Chem. Commun*., 1991, 1292.
6 Easily prepared by a procedure similar to that for **1**.
7 K. Fuji, N. Kinoshita and K. Tanaka, *Chem. Commun.*, 1999, 1895.
8 R. Schwesinger and H. Schlemper, *Angew. Chem., Int. Ed. Engl*., 1987, **26**, 1167.
9 T. Pietzonka and D. Seebach, *Chem. Ber*., 1991, **124**, 1837.

Communication 9/07680H

ChemComm

Stereoselective radical-tandem reaction of aniline derivatives with (5*R*)-5-menthyloxy-2,5-dihydrofuran-2-one initiated by photochemical induced electron transfer

Samuel Bertrand,[a] Norbert Hoffmann,*[a] Jean-Pierre Pete[a] and Véronique Bulach[b]

[a] *Laboratoire de Réactions Sélectives et Applications, UMR CNRS et Université de Reims Champagne-Ardenne, UFR Sciences, B.P. 1039, F-51687 Reims, Cedex 02, France. E-mail: norbert.hoffmann@univ-reims.fr*

[b] *UMR CNRS No. 7513, Université Louis Pasteur, Laboratoire de Cristallochimie et de Chimie Structurale, Institut Le Bel, 4 rue Blaise Pascal F-67070 Strasbourg, Cedex, France*

Received (in Liverpool, UK) 23rd July 1999, Accepted 5th October 1999

The radical tandem reaction of simple alkyl derivatives of aniline to a chiral furanone can be carried out stereoselectively in high yields; the furanone is also involved as oxidant in a rearomatisation process (formation of by-products) where it can be replaced efficiently by acetone.

Radical reactions have become a valuable tool in preparative organic chemistry,[1] even if control of the stereochemistry involved in these processes is still a challenge in organic synthesis.[2] Radical induced cyclisations and radical-tandem processes are particularly interesting due to the large variety of complex organic molecules available using these methods.[3]

Among radicals having a nucleophilic character which can be considered for addition reactions with electron deficient alkenes, α-aminoalkyl radicals[4] seem very attractive. When prepared directly from tertiary amines, these radicals were reported to add with moderate yields.[5] Similar results were described on the tandem addition of $PhNMe_2$.[6] These reactions become efficient only with functionalised amines especially with α-silylated tertiary amines.[4,7] However, we recently described a very efficient addition of tertiary amines to electron deficient alkenes, using 4,4′-dimethoxybenzophenone or Michler's ketone as sensitizers to produce α-aminoalkyl radicals *via* a photoinduced electron transfer process (PET).[8,9]

We envisaged that an easy and general access to 1,2,3,4-tetrahydroquinoline derivatives might include a multistep process induced by PET. We now report an efficient and stereoselective tandem reaction of *N*,*N*-dialkylanilines with (5*R*)-5-menthyloxy-2,5-dihydrofuran-2-one **1**[10] and the origin of the rearomatisation step involved during the reaction. Owing to their biological activity, these compounds are of great interest.[11]

When a solution of **1** and *N*,*N*-dimethylaniline **2a** in MeCN was irradiated in the presence of 4,4′-bis(*N*,*N*-dimethylamino)-benzophenone **3**, four products were isolated from the reaction mixture (Scheme 1, Table 1, entry 1).† The diastereomers **4a** and **5a** were the expected products from a radical tandem addition of the tertiary aromatic amine to **1**. The configuration of the main product **4a** was also determined by X-ray analysis (Fig. 1).‡ From the structure of **4a**, it could be deduced that the attack of the α-aminoalkyl radical **A** on **1** proceeded mainly *anti* with respect to the menthyloxy substituent.

Table 1 Reaction of different aniline derivatives **2a**–**f** with **1** in the presence of acetone except when indicated

								Yield(%)				
Entry	**2**	R^1	R^2	R^3	R^4	R^5	R^6	**4**	**5**[b]	**6**	**7**	**8**
1[a]	**a**	H	H	H	H	H	H	38	2	—	18	7
2	**a**	H	H	H	H	H	H	74	3	—	—	—
3	**b**	H	H	Me	H	H	H	60	2	—	—	—
4[c]	**c**	H	H	H	Me,H	H	H,Me	21,49	1,3	—	—	—
5	**d**	H	H	H	H	Me	H	78	3	—	—	—
6	**e**	H	H	Me	Me	H	H	64	3	—	—	—
7	**f**	H	H	$-(CH_2)_2-$		H	H	53	3	—	—	—
8	**g**	Me	Me	H	H	H	H	36	—	29	—	—
9	**h**	$-(CH_2)_2-$		H	H	H	H	39	—	32	—	—
10	**i**	$-(CH_2)_3-$		H	H	H	H	48	—	26	—	—

[a] The reaction was been carried out in the absence of acetone. [b] **5** was isolated in the same fraction as **4**. [c] Two regioisomers were formed.

The large amount of byproducts **7** and **8** limited the transformation of **1** into the tricyclic adducts **4a** and **5a**. When the concentration of **1** was diminished (5×10^{-3} mol l^{-1}), the reduction product **7** could be isolated in higher yield (23%), while the formation of **8** could be suppressed. The observation that the reduction products **7** and **8** and products **4a** and **5a** were isolated with similar yields might indicate a coupling of the processes responsible of their formation. Further, formation of **4a** and **5a** needs an oxidation step for rearomatisation. Little information is available on this oxidising step in the absence of oxygen for similar reactions.[12] In order to decrease the amount of reduction products of **1** and to get more information on the formation of the byproducts **7** and **8**, we carried out the reaction with **2a** labeled by deuterium either at the 2, 4 or 6 position of the aromatic ring (**2a′**) or on the methyl groups (**2a″**). From **2a′**, we found that **7′** had incorporated deuterium exclusively in the α-position (degree of deuterium incorporation: 45%). From **2a″**, the deuterium was transferred to the β-position of **7″** (degree of deuterium incorporation: 55%). In both cases deuterium was found in one of the α-positions of **8**. Therefore, the mechanism of the reaction of **1** can be summarised as in Scheme 2. Formation of the α-aminoalkyl radical **A** involves a PET process induced by excited Michler's ketone **3**.[9,13] Addition of **A** to **1** leads to the oxoallyl radical **B** which yields **C** after an intramolecular addition process on the electron rich aromatic ring. The rearomatisation occurs by transfer of a hydrogen atom to **1**. This transfer proceeds in two steps

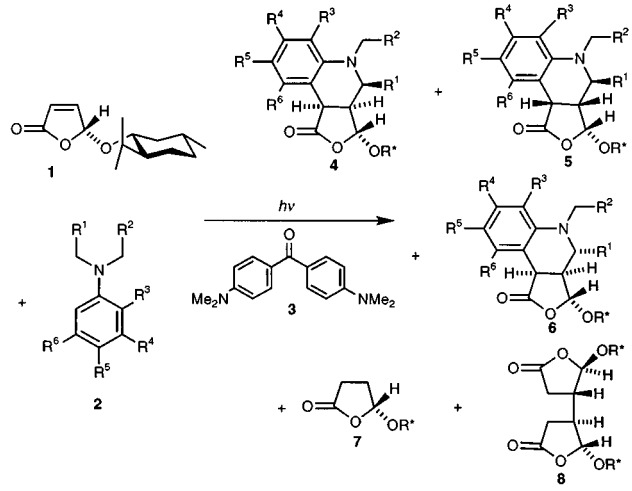

Scheme 1

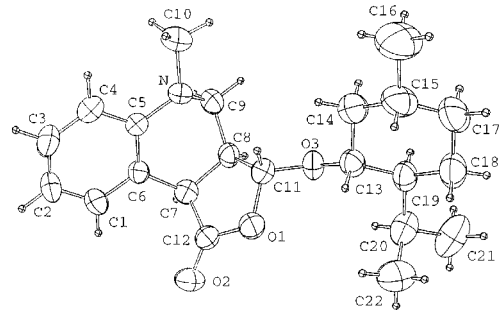

Fig. 1 ORTEP plot of **4a**. Ellipsoids are scaled to enclose 50% of the electronic density. Hydrogen atoms have arbitrary radii.

(Scheme 3). First an electron transfer from **C** to **1** takes place to yield the cationic species **F**. In the second step, a proton is transferred to the radical anion.

When starting from **2a′** deuterated on the aromatic ring, deuterium was transferred to the carbonyl function of **1**. The resulting radical **D** can produce **7′** deuterated at the α-position by tautomerisation and preferred abstraction of hydrogen from an *N*-methyl group of **2a′**.[4] Alternatively, **D** can add to **1** which leads to **8** after hydrogen abstraction from **2a′**. This mechanism also explains the deuteration in the β-position of **7″** and the α-position of **8** when started with **2a″**.

In order to avoid the hydrogen transfer to the substrate **1**, we added a mild oxidant to the reaction mixture (Scheme 2). By addition of acetone in excess, the formation of byproducts **5** and **6** could be completely suppressed and the yield of **4a** and **5a** was doubled (Table 1, entry 2).

Under these optimised reaction conditions, a variety of *N*,*N*-dialkylamino benzenes **2** similarly yielded the corresponding 1,2,3,4-tetrahydroquinolines **4**, **5** and **6** (Scheme 1, Table 1). In the case of the *N*,*N*-dimethylaminobenzenes **2a**–**f**, the facial diastereoselectivity was about 90% (Table 1, entries 1–7). In the reaction of **1** with **2g**–**i**, a total facial selectivity with *anti* approach *vs.* the menthyloxy substituent was observed. However, the configuration of the second chiral center, in the position α to the nitrogen atom, was not efficiently controlled and the products **6g**–**i** were isolated in similar yields (Table 1, entries 8–10).

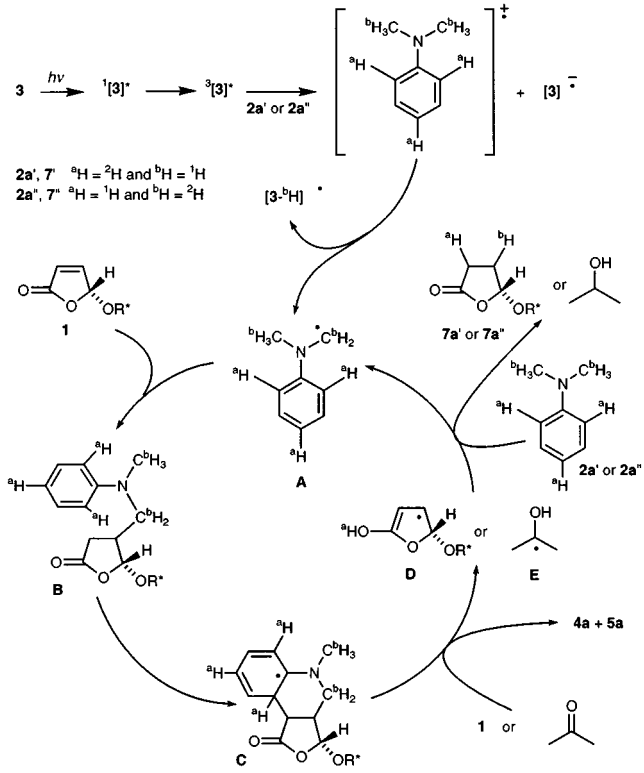

Scheme 2

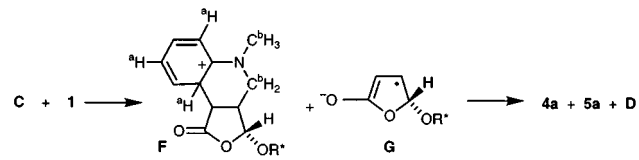

Scheme 3

In conclusion, we have described an efficient and stereoselective addition of tertiary aromatic amines to (5*R*)-(−)-5-menthyloxy-2,5-dihydrofuran-2-one **1** through a radical-tandem process. The reaction, leading to 1,2,3,4-tetrahydroquinoline derivatives **4** involves an oxidative addition on the aromatic ring. When carried out in the presence of acetone, the competitive reduction of **1** was suppressed.

Notes and references

† A Rayonet Photochemical Chamber Reactor equipped with lamps emitting at λ = 350 nm was used as light source. Solutions were degassed with argon prior to the irradiation.

Irradiation of derivatives **2** under optimised conditions (Table 1): A solution of **1** (240 mg, 1 mmol), **2** (20 mmol), **3** (30 mg, 0.1 mmol) and 1 ml acetone in 15 ml MeCN was irradiated for 6 to 7 h. The solvent was evaporated and the residue was subjected to flash chromatography.

‡ *Crystal data* for **4a**: $C_{22}H_{31}NO_3$, M = 357.50, orthorhombic, space group $P2_12_12_1$, a = 8.4839(3), b = 13.709(1), c = 17.887(1) Å, V = 2080.5(4) Å3, Z = 4, ρ_{calc} = 1.14 g cm^{-3}, μ(Mo-Kα) = 0.075 mm^{-1}. Data were collected on a Nonius CAD4-MACH3 diffractometer using Mo-Kα graphite monochromated radiation (λ = 0.71073 Å) at room temperature. Colorless crystal, 0.30 × 0.30 × 0.20 mm^3, 2428 reflections collected, 2.5 < θ < 26.3°. 1459 reflections having $I > 3\sigma(I)$ were used for structure determination and refinement. The structure was solved using direct methods and refined against |*F*|. Hydrogen atoms were introduced as fixed contributors. Absorption corrections from the psi curves of 7 reflections, transmission factors: 0.92/1.00. For all computations the Nonius Open-MoleN package (OpenMoleN, Interactive Structure Solution, Nonius B.V., Delft, The Netherlands 1997) was used. The known configuration of the menthol fragment was therefore used to assign the correct configuration. Final results: $R(F)$ = 0.039, $Rw(F)$ = 0.051, GOF = 1.046, maximum residual electronic density = 0.15 e Å^{-3}. CCDC 182/1432. See http://www.rsc.org/suppdata/cc/1999/2291/ for crystallographic data in .cif format.

1 J. Fossey, D. Lefort and J. Sorba, *Free Radicals in Organic Chemistry*, Wiley, Chichester, 1995.
2 D. P. Curran, N. A. Porter and B. Giese, *Stereochemistry of Radical Reactions*, VCH, Weinheim, 1996.
3 K.-D. Warzecha, X. Xing, M. Demuth, R. Goddard, M. Kessler and C. Krüger, *Helv. Chim. Acta*, 1995, **78**, 2065; S. Bogen, L. Fensterbank and M. Malacria, *J. Org. Chem.*, 1999, **64**, 819 and references cited therein.
4 P. Renaud and L. Giraud, *Synthesis*, 1996, 913.
5 W.H. Urry and O. O. Juveland, *J. Am. Chem. Soc.*, 1958, **80**, 3322; R. C. Cookson, S. M. de B. Costa and J. Hudec, *Chem. Commun.*, 1969, 753; E. Farrant and J. Mann, *J. Chem. Soc., Perkin Trans. 1*, 1997, 1083.
6 (*a*) R. B. Roy and G. A. Swan, *J. Chem. Soc.*, 1969, 1886; S. Murata, K. Teramoto, M. Miura and M. Nomura, *Heterocycles*, 1993, **36**, 2147; S. Araneo, F. Fontana, F. Minisci, F. Recupero and A. Serri, *Tetrahedron Lett.*, 1995, **36**, 4307.
7 Z. Su, P. S. Mariano, D. E. Falvey, U. C. Yoon and S. W. Oh, *J. Am. Chem. Soc.*, 1998, **120**, 10 676.
8 S. Bertrand, C. Glapski, N. Hoffmann and J. P. Pete, *Tetrahedron Lett.*, 1999, **40**, 3169; S. Bertrand, N. Hoffmann and J. P. Pete, *Tetrahedron Lett.*, 1999, **40**, 3173.
9 For photoinduced electron transfer see: J. Mattay, *Synthesis*, 1989, 233; G. J. Kavarnos, *Fundamentals of Photoinduced Electron Transfer*, VCH, New York, 1993.
10 For the synthesis of **1** and its application in organic synthesis see: J. Martel, J. Tessier and J. P. Demoute (Roussel Uclaf), *Eur. Pat Appl.*, 23454, 1981 (*Chem. Abstr.*, 1981, **95**, 24788a); B. L. Feringa, B. de Lange, J. F. G. A. Jansen, J. C. de Jong, M. Lubben, W. Faber and E. P. Schudde, *Pure Appl. Chem.*, 1992, **64**, 1865.
11 A. R. Katritzky, S. Rachwal and B. Rachwal, *Tetrahedron*, 1996, **52**, 15031.
12 X. M. Zhang and P. S. Mariano, *J. Org. Chem.*, 1991, **56**, 1655.

Communication 9/06051K

ChemComm

Polyphenylene dendrimers *via* Diels–Alder reactions: the convergent approach

Uwe-Martin Wiesler and Klaus Müllen*

Max-Planck-Institut für Polymerforschung, Ackermannweg 10, 55128 Mainz, Germany.
E-mail: muellen@mpip-mainz.mpg.de

Received (in Cambridge, UK) 10th September 1999, Accepted 4th October 1999

Polyphenylene dendrimers and dendrons can be obtained using [2 + 4]cycloaddition and Knoevenagel cyclocondensation in a convergent approach.

Due to their outstanding properties, such as molecular shape- and size-persistence and narrow molecular weight distribution, dendrimers are the object of increasing interest.[1] In this context we developed a divergent method to synthesize polyphenylene dendrimers based on the selective Diels–Alder cycloaddition between tetraphenylcyclopentadienones and ethynyls.[2] We are thus able to synthesize dendrimers up to the fourth generation, which exist as shape-persistent nanoparticles.[3]

While the divergent approach builds dendrimers layer-by-layer from a central core to the periphery, the convergent strategy builds the dendrimer in the opposite manner, from the periphery toward the central core. Thus, the dendrimer branches, also called dendrons, are synthesized first and then added to a central core. This approach not only allows the symmetric functionalization of the dendrimer surface as in the divergent approach, but also the controlled functionalization of the dendrimer by adding differently functionalized dendrons to selectively protected cores.[4]

Here, we present a convergent approach for the synthesis of polyphenylene dendrons and dendrimers based on two alternating orthogonal reactions: (i) the Diels–Alder cycloaddition of tetraphenylcyclopentadienones to phenylene-substituted ethynyls, and (ii) the Knoevenagel condensation of benzils with 1,3-diphenylacetones to give cyclopentadienones.

The starting point of the synthesis is 4,4′-diethynylbenzil **1** which contains two ethynylic dienophile units and one ethanedione function which can react in a Knoevenagel condensation (Scheme 1). The starting material **1** is prepared *via* the Sonogashira[5] coupling of triisopropylsilylacetylene and 4,4′-dibromobenzil and subsequent cleavage of the TIPS groups with KF in DMF (70%, yellow crystals).

The two-fold Diels–Alder cycloaddition of an excess of tetraphenylcyclopentadienone **2**, which has to be regarded as a first-generation dendron, to **1** in refluxing xylene leads to the second generation **3** in the form of a benzilic dendron (91%, pale yellow amorphous powder). The Knoevenagel condensation of **3** to the corresponding cyclopentadienone dendron **4** with 1,3-diphenylacetone **5** is achieved in dioxane and in the presence of Bu_4NOH as base. Like **3**, the cyclopentadienone dendron **4** can be easily precipitated in EtOH as a pale red solid in 85% isolated yield.

The next generation benzil **6** is obtained, similar to the second generation, by addition of an excess of dendron **4** to **1** in refluxing xylene. Isolation after precipitation in EtOH affords the benzil **6** as an amorphous yellow powder in 89% yield. Further base-catalyzed condensation of **6** with 1,3-diphenylacetone **5** provides a complex mixture of products, determined by mass spectrometry, consisting of small amounts of third generation cyclopentadienone dendron and further side-products of the polycondensation of **5** with **6**. This can be explained by the high steric hindrance of the polyphenylenic branches of the benzil **6**, which will prefer a conformation where the dendrons (and thus the vicinal carbonyls) are oriented in opposite directions. This arrangement prevents the favourable orientation of the benzilic carbonyls required for the nucleophilic attack of **5** and subsequent formation of the cyclopentadienone ring (see Scheme 1).

The four-fold cycloaddition of an excess of cyclopentadienone dendron **4** to the tetraethynylbiphenyl **7** and the tetrakis(ethynylphenyl)methane **8** in Ph_2O at 200 °C leads to dendrimers **9** and **10**, respectively (see Scheme 2). The products are isolated by precipitation from the reaction mixture using EtOH (89 and 85% isolated yield, respectively). Molecules **9** and **10** correspond to the second generation polyphenylene dendrimer previously made by the divergent method.[6]

Whereas in the synthesis of dendrimer **9** the reactants have to be heated for two days, the reaction time in the case of dendrimer **10** is about one week. The MALDI-TOF mass spectra taken at various stages during the reaction reveal that three ethynyl groups of both cores react rapidly with dendron **4**,

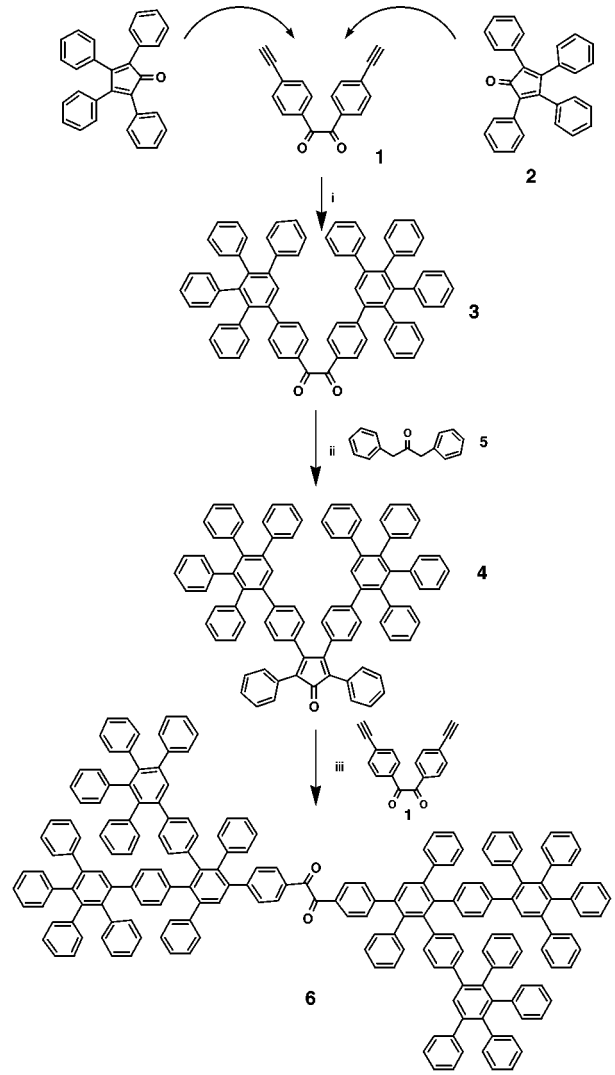

Scheme 1 *Reagents and conditions*: i, xylene, 14 h, 91%; ii, **5**, 1,4-dioxane, Bu_4NOH, 100 °C, 1 h, 85%; iii, **1**, xylene, reflux, 14 h, 89%.

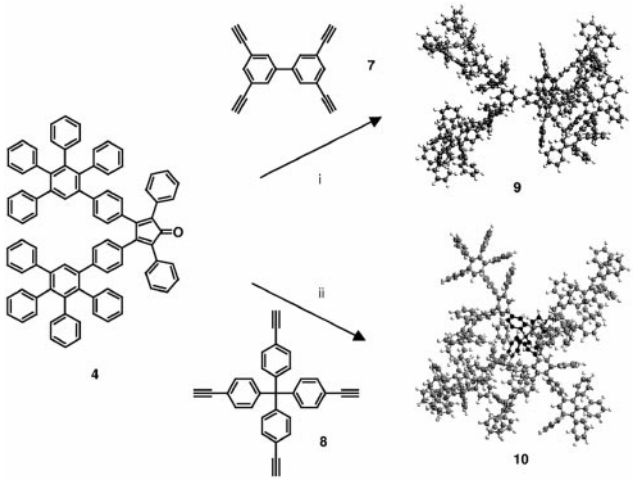

Scheme 2 *Reagents and conditions*: i, **7**, Ph_2O, 200 °C, 2 days, 89%; ii, **8**, Ph_2O, 200 °C, 7 days, 85%.

while the reactivity of the last group depends on the flexibility of the core. In this view the tetraethynylbiphenyl core **7** allows rotation about the phenyl–phenyl bond of the core, so that the fourth ethynyl group can be brought into a favorable position for the sterically demanding cycloaddition of dendron **6**. In contrast the fourth ethynyl groups of the tetrakis(ethynylphenyl)methane core **8** does not have such mobility.

The disparity in reaction times required for obtaining **9** and dendrimer **10** can also be understood examining ball-and-stick models, which are generated using the MM2 (85) force field with the CERIUS 2 program package and applying the Conjugate Gradient 200 algorithm (compare Scheme 2).[7] Whereas dendrimer **9** possesses a dumb-bell like structure, with easily accessible holes close to the phenyl–phenyl bond of the core, the methane center of dendrimer **10** is densely surrounded by phenylene groups which increase the stiffness of the whole molecule and render the core difficult to access.

Neverthless, both the dendrons and the dendrimers are very soluble in organic solvents such as toluene and CH_2Cl_2. Characterization was carried out by field-desorption mass spectrometry for the dendrons with molecular masses up to 2000 g mol^{-1} and matrix-assisted laser desorption ionization time of flight mass spectrometry (MALDI-TOF MS) for the higher molecular mass dendrons and the dendrimers. The purity and monodispersity of the analyzed molecules was confirmed by the perfect agreement between calculated and experimentally determined *m/z* ratios.† A characteristic feature of the synthesized dendrimers **9** and **10** is their high thermal and chemical stability. They decompose under air only at temperatures higher than 550 °C according to thermogravimetric analysis. Their chemical stability is also noteworthy. For example boiling in concentrated HCl or in 30% KOH for seven days fails to produce any decomposition. The dendrimers react only with strong electrophiles, like H_2SO_4, *via* aromatic electrophilic substitution, but without change in the polyphenylene framework. This opens a way to chemically functionalize dendrimers at their surface.

Compared to the divergent approach, the convergent method at first glance yields the same monodisperse products with similarly high yields. However, though the convergent method can be used to synthesize dendrimers only up to the second generation, this method opens the way to dendritic polymers carrying substituents of more than just one kind. In contrast, the divergent approach may be successfully used up to the fourth generation, but it only allows the ordered attachment of one kind of functional group. Both methods have in common the fact that they yield monodiperse polyphenylene dendrimers in high yield.

In conclusion, we can say that: (i) using a convergent approach, polyphenylene dendrons and dendrimers with more than 60 benzene rings can be obtained *via* [2 + 4] cycloadditions and Knoevenagel condensations; (ii) by attachment of the polyphenylene dendrons to different cores, dendrimers with different shapes are obtained; (iii) the dendrimers show high thermal and chemical stability.

Our current investigations involve the convergent synthesis of dendrimers with various substitution patterns as possible carriers in catalysis.

We thank the Foundation of the Chemical Industries (Fonds der Chemischen Industrie) and the Bundesministerium für Bildung und Forschung for financial support.

Notes and references

† *Selected data* for **4**: FD-MS: *m/z* 1145.47, calc. for $C_{89}H_{60}O$: 1145.45; δ_H(500 MHz, $C_2D_2Cl_4$, 393 K) 7.49 (s, 2H), 7.25–7.13 (m, 20H), 6.97 (d, ^3J 8.25, 4H), 6.90–6.72 (m, 30H), 6.67 (d, ^3J 8.25, 4H); δ_C(125 MHz, $C_2D_2Cl_4$, 303 K) 199.0 (C=O), 154.6, 142.5, 142.0, 141.9, 140.9, 140.4, 140.3, 140.1, 140.0, 139.8, 139.4, 131.8, 131.8, 131.7, 131.1, 131.0, 130.5, 130.4, 130.3, 129.7, 129.2, 128.3, 127.9, 127.7, 127.1, 127.0, 126.8, 126.5, 126.0, 125.7, 125.5, 125.2. For **9**: MALD-TOF MS: *m/z* 4720, calc. for $C_{372}H_{250}$: 4720.07; δ_H(500 MHz, $C_2D_2Cl_4$, 393 K) 7.41 (s, 4H), 7.34 (s, 4H), 7.28 (m, 6H), 7.18–6.25 (m, 236H); δ_C(125 MHz, $C_2D_2Cl_4$, 303 K) 199.0 (C=O), 142.3, 142.1, 141.4, 140.8, 140.7, 140.5, 139.5, 139.4, 139.0, 138.7, 138.3, 132.7, 132.0, 131.9, 131.6, 131.3, 130.4, 130.2, 128.9, 128.6, 127.7, 127.2, 127.0, 126.7, 126.3, 125.9, 125.6, 125.4.

1 G. R. Newkome, C. N. Moorefield and F. Vögtle, *Dendritic Molecules*, VCH, Weinheim, 1996; A. W. Bosman, H. M. Janssen and E. W. Meijer, *Chem. Rev.*, 1999, **99**, 1665.
2 F. Morgenroth, E. Reuter and K. Müllen, *Angew. Chem.*, 1997, **109**, 647; *Angew. Chem., Int. Ed. Engl.*, 1997, **36**, 631; F. Morgenroth A. J. Berresheim, M. Wagner and K. Müllen, *Chem. Commun.*, 1998, 1139.
3 F. Morgenroth, C. Kübel and K. Müllen, *J. Mater. Chem.*, 1997, **7**, 1207.
4 C. J. Hawker and J. M. J. Fréchet, *Macromolecules*, 1990, **23**, 4726; K. L. Wooley, C. J. Hawker and J. M. J. Fréchet, *J. Chem. Soc., Perkin Trans. 1*, 1991, 1059; K. L. Wooley, C. J. Hawker and J. M. J. Fréchet, *J. Am. Chem. Soc.*, 1993, **115**, 11 496.
5 S. Takahashi, Y. Kuroyama, K. Sonogashira and N. Hagihara, *Synthesis*, 1980, 627.
6 F. Morgenroth and K. Müllen, *Tetrahedron*, 1997, **53**, 15 349.
7 CERIUS2, Molecular Simulations Inc., Waltham, MA, USA. For more details see ref. 3. Additional data are to be published.

Communication 9/07339F

Dioxygen–copper reactivity at trinuclear centers: formation of hexanuclear and mixed-valent adducts

Kenneth D. Karlin,* Qin-fen Gan and Zoltan Tyeklár

Department of Chemistry, The Johns Hopkins University, Charles & 34th Streets, Baltimore, MD 21218 USA. E-mail: karlin@jhu.edu

Received (in Cambridge, UK) 18th August 1999, Accepted 15th October 1999

New copper(I) complexes $[Cu^{I}_3(mesO^-)]^{2+}$ (3) and $[Cu^{I}_3(mesOH)]^{3+}$ (4) have been generated from a phenol-containing trinucleating ligand, mesOH; reactions with O_2 reflect the unsymmetrical ligand environment, and lead to peroxo and/or hydroperoxo cluster complexes, including those with mixed-valent copper ion centers.

Continuing interest in studies of the reactivity of O_2 with discrete copper(I) complexes is for the most part driven by bioinorganic interests, *i.e.* the occurrence of copper-dioxygen carrier proteins, oxygenases which insert O-atoms into substrates, and oxidases which couple substrate oxidations to copper-mediated O_2-reduction to water or H_2O_2.[1,2] Our own efforts in elucidating fundamental aspects of (ligand)Cu^{I}/O_2 reactivity, and those of others, have focused on mono- or binuclear copper(I) compounds, their kinetics/thermodynamics of reaction,[3] the structures and spectroscopy of O_2-adducts, and substrate reactivity.[2–5] The products most often form *via* a $Cu:O_2$ 2:1 reaction stoichiometry, leading to bridged peroxo [μ-1,2- or μ-$\eta^2:\eta^2$-peroxodicopper(II)], hydroperoxo- or bis-μ-oxo[dicopper(III)] species.[2–5] An exception was described by Stack and co-workers,[6] where a $(L')Cu^{I}:O_2$ 3:1 reaction occurs, producing a mixed-valent cluster, $[Cu_3(\mu\text{-}O)_2(L')_3]^{3+}$ (L′ = *N*,*N*,*N*′,*N*′-tetramethyl-(1*R*,2*R*)-cyclohexanediamine).

Few discrete trinuclear copper(I) complexes exist,[7–9] and still fewer have associated O_2-chemistry.[7,8] Yet, (ligand)-Cu^{I}_3/O_2 chemistry is of considerable interest, since trinuclear copper cores occur in 'blue' multicopper oxidases (*e.g.* ceruloplasmin, ascorbate oxidase, laccase)[1,10] and they are

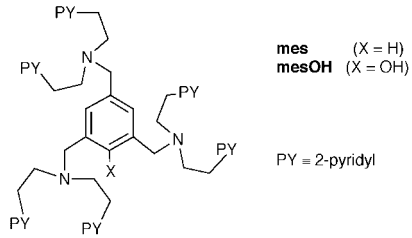

implicated at active sites in the copper-dependent methane monooxygenase.[1,11] It also has been shown in certain systems[12] that three-electron reduction of O_2 (*i.e.* from three Cu(I) ions) is essential for O–O bond reductive cleavage, of relevance in O_2-activation processes. In this report, we describe novel results in (ligand)Cu^{I}_3/O_2 reactivity studies, employing mesOH as an unsymmetrical trinucleating ligand.

Ligand mesOH was obtained following oxygenation of the tricopper(I) complex $[Cu^{I}_3(mes)]^{3+}$ (**1**); the hydroxylation reaction affords a hexanuclear cluster complex $[\{Cu^{II}_3(mesO^-)(OH^-)_2\}_2]^{6+}$ (**2**),[8]† from which mesOH is isolated following copper removal and extraction. By adapting the reactions used to synthesize analogous phenolate-[13] or phenol-containing[14] dinuclear copper(I) compounds, two new trinuclear copper(I) complexes possessing unsymmetrical Cu(I) coordination were prepared (Scheme 1). The bright orange (CH_2Cl_2; λ_{max} 370 nm, ε 16600 M^{-1} cm^{-1}) compound $[Cu^{I}_3(mesO^-)](ClO_4)_2$ (**3**) was prepared by diphenylhydrazine reduction of **2** (as a ClO_4^- salt), in the presence of Et_3N. When this reduction reaction is carried out with **2** (as a BF_4^- salt) in

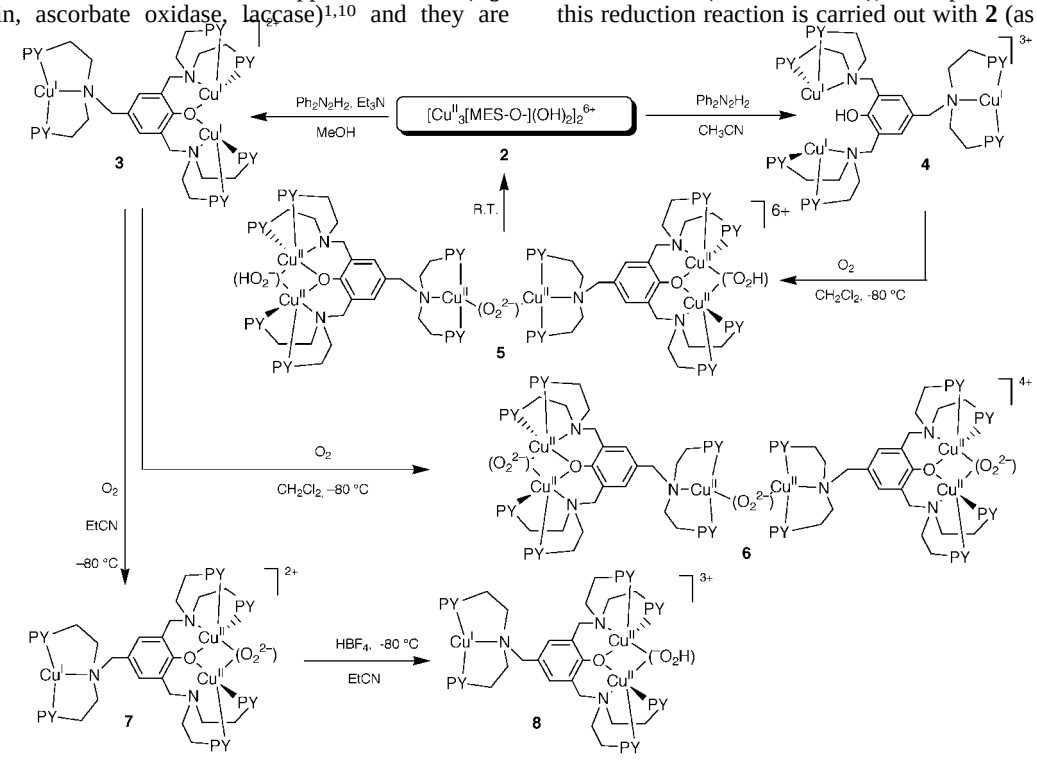

Scheme 1

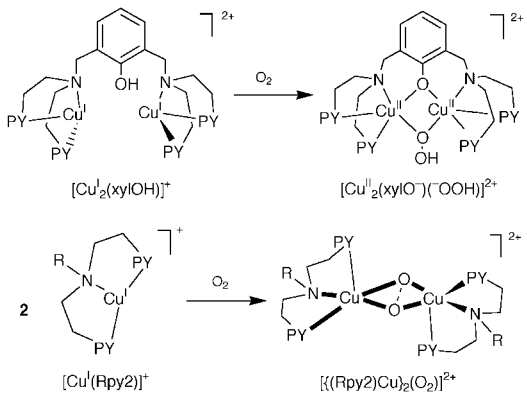

Scheme 2

the absence of base, a yellow compound, $[Cu^{I}_3(mesOH)](BF_4)_3$ (**4**), was isolated.‡ For each of these trinuclear complexes, two of the three copper ions possess features found in dinuclear analogues with phenol or phenoxide groups, $[Cu^{I}_2(xylOH)]^{2+}$ (Scheme 2) and $[Cu^{I}_2(xylO^-)]^+$.[13,14] Consistent with their compound formulations, **3** and **4** are diamagnetic (^1H and ^{13}C NMR spectroscopies).

Reaction of O_2 with **4** in CH_2Cl_2 at −80 °C leads to an intensely green colored solution dominated by strong 368 (ε 14000) and 408 nm (sh, ε 9500 M^{-1} cm^{-1}) charge-transfer (CT) absorptions. The latter band is characteristic of the μ-$^-$OAr/μ-1,1-$^-$OOH dicopper coordination observed for $[Cu^{II}_2(xylO^-)(^-OOH)]^{2+}$ {395 nm (ε 8000 M^{-1} cm^{-1}),[14] while the 368 nm absorption is characteristic of the intense LMCT observed for copper complexes $[\{Cu(Rpy2)\}_2(O_2)]^{2+}$ {λ_{max} 350–365 nm, $\varepsilon \geqslant 12000$ M^{-1} cm^{-1}},[15] with intermolecular μ-η^2:η^2-peroxo-dicopper(II) ligation (Scheme 2).¶ Thus, the oxygenation product of **4** is formulated as a hexanuclear species, $[\{Cu_3(mesO^-)(OOH)\}_2(O_2)]^{6+}$ (**5**), (Scheme 1). Consistent with this formulation, **5** is observed to be EPR silent (frozen CH_2Cl_2) and manometric O_2-uptake measurements (−80 °C, CH_2Cl_2) reveal a reaction stoichiometry of $Cu:O_2$ = 6 : 2.9 (±10%)‖

A related hexanuclear complex **6** also appears to form from O_2-reaction with **3**.‖ This product lacks the the protons available in **4**, thus leading to peroxo species $[\{Cu_3(mesO^-)(O_2)\}_2(O_2)]^{6+}$ (**6**) (Scheme 1) {(CH_2Cl_2, −80°C); λ_{max} 340 (ε 12000), 384 (sh, ε 11000), 482 (ε 6500), 594 nm (sh, ε 2500 M^{-1} cm^{-1})}. This is suggested to possess two peroxo Cu_2-O_2 moieties similar to that observed for $[Cu^{II}_2(xylO^-)(O_2^{2-})]^+$ {385 (ε 2900), 505 (ε 6000), 610 (sh, ε 6500 M^{-1} cm^{-1}},[13] and an intramolecular peroxo species again similar to that in $[\{Cu(Rpy2)\}_2(O_2)]^{2+}$. Accurate manometric O_2-uptake experiments were thwarted by the instability of **6**.

Interestingly, mixed-valent $Cu^{I}Cu^{II}_2$ clusters **7** and **8** were obtained *via* oxygenation of **3** at −80 °C in EtCN as solvent (Scheme 1). The spectrum that develops in the CT region following O_2-reaction with **3** consists of primarily only the 482 and 594 nm (sh) absorptions, again very similar to the spectrum expected for $[Cu^{II}_2(xylO^-)(O_2^{2-})]^{+}$[13] and that found for **6**. The lack of formation of a more intense band in the 340–380 nm regions indicates that the Cu^{I}(Rpy2) moiety in **3** does not react with dioxygen; this is as previously observed for discrete $[Cu^{I}(Rpy2)]^+$ complexes[15] and is explained by the strong nitrile (solvent) coordination, especially at low temperatures. Manometric measurements are also in accord with the formulation of **7**, since $Cu:O_2$ = 3 : 0.95 (±10%) (EtCN, −80 °C). Further confirmation comes from reaction of **7** with excess acid (HBF_4·Et_2O) and workup, which generates hydrogen peroxide in *ca*. 85% of the expected yield (1 H_2O_2 per molecule of **7**), as determined by iodometric titration. A hydroperoxo-containing mixed-valent cluster analogue, **8** (λ_{max} 395 mm), can be generated by addition of one equiv. of H^+ (HBF_4·Et_2O) to **7** (Scheme 1).

In summary, mes-OH as a trinucleating ligand affords novel tricopper(I) complexes **3** or **4**, in which an unsymmetrical ligation for the three copper ions occurs, as observed for the enzymes.[1,10] Based on previously established chemistry for phenoxide (or phenol) dicopper(I) compounds (Scheme 2), we have shown that phenoxide with peroxo- (or hydroperoxo-) dicopper(II) species form upon O_2-reactions with **3** or **4**, and in CH_2Cl_2 as solvent, this leaves the third copper ion to react with O_2 in an intermolecular fashion, affording hexanuclear complexes. In EtCN as solvent, the latter reaction is suppressed, and mixed-valent species form, in which a copper(I) moiety survives oxidation even in the presence of a nearby (hydro)-peroxo-dicopper(II) center. The reasons for this are currently unclear. Evidence for a related hydroperoxo-tricopper [including Cu(I)] entity has been presented by Solomon and co-workers,[1] as an intermediate in the four-electron reduction of O_2 by the enzyme laccase. Further investigations of tricopper(I)/O_2 reactivity patterns are in progress.

Financial support for this research has been made available from the National Institutes of Health, USA (GM28962).

Notes and references

† This product **2** is obtained if ClO_4^- or $CF_3SO_3^-$ are utilized as the counteranion (unpublished results). We previously[8] mistakenly identified **2** as the product formed when using PF_6^-, which is actually a bis-μ-F^- complex, $[\{Cu^{II}_3(mesO^-)(OH^-)(F^-)\}_2]^{6+}$. See also ref. 15(*a*) and S. C. Lee and R. H. Holm, *Inorg. Chem.*, 1993, **32**, 4745.

‡ Satisfactory analytical data (NMR and mass spectral for mesOH; C, H, N combustion analysis for complexes **3** and **4**) have been obtained.

§ A band assignable to the ν(O–H) stretch, expected for **4** in its IR spectrum, was not observed, probably due to interaction of the Ar–OH group with Cu(I) ion(s). The same phenomenon was observed for $[Cu^{I}_2(xylOH)]^{2+}$; for a bis PPh_3 adduct, the expected ν(O–H) stretch was detected.[14]

¶ Some decomposition to a bis-μ-F^- complex may also be occurring, since **4** contains BF_4^-, with fluoride. See footnote † above.

‖ The hexanuclear formaulation is also supported by the existence of the very similar mesO$^-$-containing hexanuclear compound **2** (with X-ray structure). See ref. 8 and footnote †.

1 E. I. Solomon, U. M. Sundaram and T. E. Machonkin, *Chem. Rev.*, 1996, **96**, 2563; J. P. Klinman, *Chem. Rev.*, 1996, **96**, 2541.

2 K. D. Karlin and A. D. Zuberbühler, in *Formation, Structure and Reactivity of Copper Dioxygen Complexes*, ed. J. Reedijk and E. Bouwman, Marcel Dekker, New York, 1999, ch. 14, pp. 469–534; M.-A. Kopf and K. D. Karlin, in *Models of Copper Enzymes and Heme–Copper Oxidases*, ed. B. Meunier, Imperial College Press, London, 2000, ch. 7, p. 309–362, in press.

3 K. D. Karlin, S. Kaderli and A. D. Zuberbühler, *Acc. Chem. Res.*, 1997, **30**, 139.

4 N. Kitajima and Y. Moro-oka, *Chem. Rev.*, 1994, **94**, 737.

5 W. B. Tolman, *Acc. Chem. Res.*, 1997, **30**, 227.

6 A. P. Cole, D. E. Root, P. Mukherjee, E. I. Solomon and T. D. P. Stack, *Science*, 1996, **273**, 1848.

7 Z. Szeverényl, U. Knopp and A. D. Zuberbühler, *Helv. Chim. Acta*, 1982, **65**, 2529; K. Singh, J. R. Long and P. Stavropoulos, *Inorg. Chem.*, 1998, **37**, 1073.

8 K. D. Karlin, Q.-F. Gan, A. Farooq, S. Liu and J. Zubieta, *Inorg. Chem.*, 1990, **29**, 2549.

9 K. D. Karlin, Q.-F. Gan, A. Farooq, S. Liu and J. Zubieta, *Inorg. Chim. Acta*, 1989, **165**, 37; P. Hubberstey and C. E. Russell, *J. Chem. Soc., Chem. Commun.*, 1995, 959; C. Bonnefous, N. Bellec and R. P. Thummel, *Chem. Commun.*, 1999, 1243; C. Walsdorff, S. Park, J. Kim, J. Heo, K.-M. Park, J. Oh and K. Kim, *J. Chem. Soc., Dalton Trans.*, 1999, 923.

10 D. E. Fenton and H. Okawa, *J. Chem. Soc., Dalton Trans.*, 1993, 1349.

11 H.-T. Nguyen, S. J. Elliott, J. H.-K. Yip and S. I. Chan, *J. Biol. Chem.*, 1998, **273**, 7957.

12 K. G. Caulton, G. Davies and E. M. Holt, *Polyhedron*, 1990, **9**, 2319.

13 K. D. Karlin, R. W. Cruse, Y. Gultneh, A. Farooq, J. C. Hayes and J. Zubieta, *J. Am. Chem. Soc.*, 1987, **109**, 2668.

14 K. D. Karlin, P. Ghosh, R. W. Cruse, A. Farooq, Y. Gultneh, R. R. Jacobson, N. J. Blackburn, R. W. Strange and J. Zubieta, *J. Am. Chem. Soc.*, 1988, **110**, 6769.

15 (*a*) I. Sanyal, M. Mahroof-Tahir, S. Nasir, P. Ghosh, B. I. Cohen, Y. Gultneh, R. Cruse, A. Farooq, K. D. Karlin, S. Liu and J. Zubieta, *Inorg. Chem.*, 1992, **31**, 4322; (*b*) H. V. Obias, Y. Lin, N. N. Murthy, E. Pidcock, E. I. Solomon, M. Ralle, N. J. Blackburn, Y.-M. Neuhold, A. D. Zuberbühler and K. D. Karlin, *J. Am. Chem. Soc.*, 1998, **120**, 12 960.

Communication 9/06830I

ChemComm

Towards multianalyte molecule-based sensors: reactivity and photophysical behaviour of hemilabile ligand-containing Ru(II) bipyridyl complexes

Cerrie W. Rogers and Michael O. Wolf*

Department of Chemistry, University of British Columbia, Vancouver, Canada V6T 1Z1. E-mail: mwolf@chem.ubc.ca; fax: 604-822-2847

Received (in Bloomington, IN, USA) 25th August 1999, Accepted 7th October 1999

The concept of using hemilabile ligand-containing complexes as the basis for multianalyte sensors is introduced: the preparation of two such ruthenium complexes (1 and 2) and their reactivity towards a series of donor molecules is reported; differential photoluminescence and absorption responses are observed.

Molecule-based sensors are compounds designed to respond to specific analyte molecules by undergoing changes in readily-monitored physical properties. Ideally, molecule-based sensors should be sensitive to the amount and type of analyte present, while functioning in a reversible fashion. Many different and elegant strategies have been used to detect a variety of analytes, such as metal ions,[1] small anions,[2] gases,[3] biomolecules,[4] and pH.[5]

In this communication, we show how a new class of ruthenium complexes containing hemilabile ligands may be used as the basis for molecule-based sensors. Hemilabile ligands, which contain both substitutionally inert and labile moieties, provide a site for the binding of analytes to a metal center. Importantly, hemilabile ligands have been shown to allow the *reversible* binding of small molecules to metal complexes because of their chelating ability.[6] In a previous study, a rhodium carbonyl complex containing a hemilabile ligand was shown to selectively detect carbon monoxide in a mixture of gases.[3b]

In our approach, multiple analytes may be distinguished *via differences* in the response of a tailor-made complex to different analytes. Two such complexes, $[Ru(bpy)_2(PO)](PF_6)_2$ [PO = 2-(diphenylphosphino)anisole (**1**) and 2-(diphenylphosphino)-phenetole (**2**)], have been prepared and their reactions with a

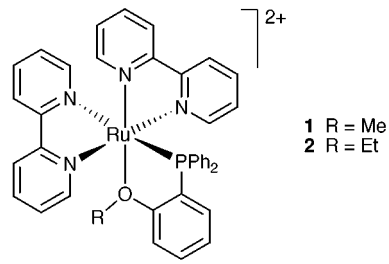

series of analytes examined in solution. In these complexes, the PO ligands are hemilabile because of weak coordination of the ether moiety to the metal, and the bpy groups provide an optical handle. The absorption and emission properties of ruthenium polypyridyl complexes are well-known to be sensitive to the nature of the other ligands on the metal.[7] The bpy ligands also serve to prevent isomerization, a common occurrence with six-coordinate Ru complexes bearing hemilabile ligands.[6]

Complexes **1** and **2** were prepared† by reacting the appropriate PO ligand with 1 equivalent of $[Ru(bpy)_2(Me_2CO)_2](BF_4)_2$. Metathesis to the hexafluorophosphate salts yielded **1** and **2** as yellow powders which are soluble in polar organic solvents and stable for > 10 days in air-saturated solution. The ^{1}H NMR spectrum of **1** obtained at −80 °C (CD_2Cl_2) was unchanged from the spectrum at 25 °C; thus, either the opening-and-closing of the PO ligand does not occur on the NMR timescale, or the opening-and-closing is still fast at −80 °C. Two-dimensional ^{1}H correlation spectroscopy and NOE experiments established that the coordination of the PO ligand in **1** is bidentate.

The reactions of **1** and **2** with a variety of small molecules have been explored. The complexes react rapidly and irreversibly with one equivalent of acetonitrile, resulting in upfield shifts of the methoxy or ethoxy ^{1}H and phosphine ^{3}P NMR resonances of the hemilabile ligand. On the other hand, no reaction occurs with the oxygen donors ether, acetone and methanol.

The complexes **1** and **2** also react with sulfur donors such as ethanethiol, dodecanethiol, dimethyl sulfoxide and dimethyl sulfide. In these cases, the analyte-bound complexes are in equilibrium with the corresponding analyte-free complexes. The equilibrium is conveniently monitored by ^{1}H and ^{31}P NMR since the analyte-bound complexes also show upfield shifts of the methoxy or ethoxy ^{1}H and phosphine ^{31}P NMR resonances of the hemilabile ligand (data for reactions with **1** are shown in Table 1). The reversibility of the reaction of these analytes with **1** and **2** was established by varying the concentration of analyte in solution; this results in the expected changes in the ratios of analyte-bound to analyte-free complex as equilibrium is reestablished.

The equilibrium constant (K) is sensitive to the nature of the analyte and the hemilabile ligand. For example, of the sulfur donors examined, dimethyl sulfide binds with greatest affinity. We also observed differences in analyte affinity between **1** and **2**; for instance, all the sulfur donors bind with higher affinity to **2**. The equilibrium constant for dimethyl sulfide binding to **2** (300 ± 60 M^{-1}) is significantly higher than for binding to **1** (50 ± 10 M^{-1}). These differences suggest that sensor complexes can be designed to react specifically with certain analytes and may be used to distinguish analytes with closely related structures.

Both the analyte-free and analyte-bound complexes are luminescent at 77 K in 2:1 ethanol–acetone. The emission spectrum of **1** contains a band with λ_{max} at 600 nm (Fig. 1A), and the spectrum of **2** is similar; these complexes are both weak red emitters by eye. Addition of CH_3CN to **1** or **2** results in a dramatically more intense, blue-shifted (bright yellow) emission, as shown in Fig. 1B for **1**. Addition of DMSO and

Table 1 Data for **1** and analyte-bound **1**

Analyte	^{1}H NMR $\delta(OCH_3)^a$	^{31}P NMR $\delta(PO)^a$	K/M^{-1} ^{a,b}	λ_{max}/nm (ε/M^{-1} cm^{-1})^c
—	3.71	50.9	—	412 (6900)
CH_3CN	3.14	39.9	—	410 (6900)^d
CH_3CH_2SH	3.23	37.4	7 ± 1	410 (6090)^{d,e}
$CH_3(CH_2)_{11}SH$	3.23	37.4	8 ± 2	410 (6040)^{d,e}
DMSO	2.97^f	37.7^f	0.8 ± 0.1^f	418 (5900)^{d,e}
	3.11^g	29.7^g	0.1 ± 0.02^g	
DMS	2.70	32.8	50 ± 0	410 (6040)^{d,e}

^{a} In CD_2Cl_2; ^{b} > 3 h equilibration time; ^{c} in acetone; ^{d} upon addition of 1000 equiv. of analyte, 5 min equilibration time; ^{e} pseudo-ε intended to show relative intensity of absorption band only; ^{f} major product; ^{g} minor product.

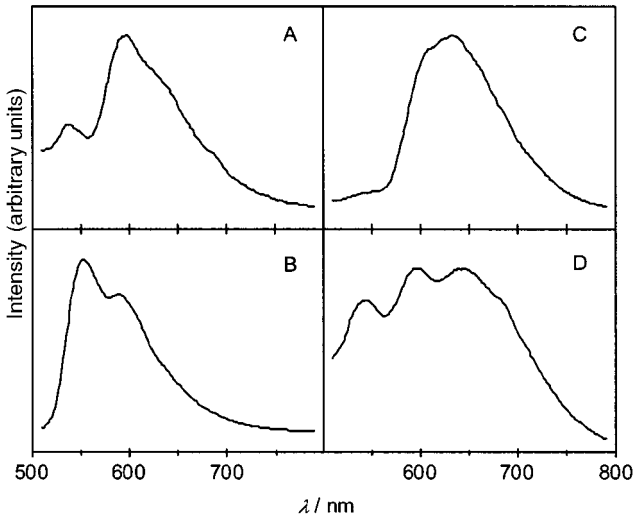

Fig. 1 Emission spectra of complexes at 77 K in 2:1 ethanol–acetone. (A) **1**; (B) **1** with 100 equiv. acetonitrile added; (C) **1** with 100 equiv. DMSO added; (D) **1** with 100 equiv. dodecanethiol added.

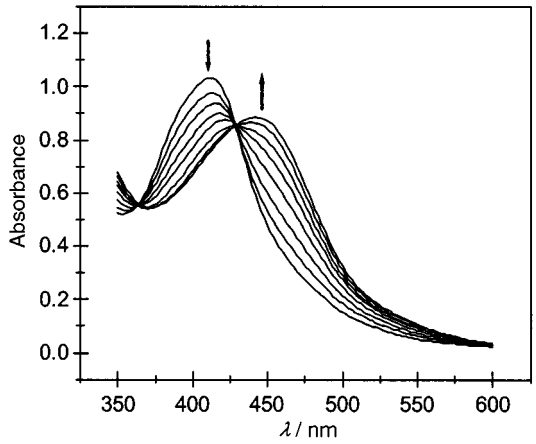

Fig. 2 Visible absorption spectra of **1** in acetone (1.47×10^{-4} M) upon addition of DMSO (0–13 000 equiv.).

dodecanethiol to **1** or **2** also results in shifts in the emission spectra (Fig. 1C and D), but minimal changes in intensity.

Certain analytes also react with **1** and **2** to yield colour changes. For example, of the analytes tested, only DMSO results in a significant colour change with **1** and **2** (Fig. 2 shows this effect for **1**). In this case, the concentration-dependent red shift of the visible absorption spectrum may be used to ascertain the amount of the analyte in solution. It may also be used to distinguish DMSO from related species that do not result in an absorption shift, such as other sulfur donors that produce only very slight colour changes.

These results show that emission characteristics, in combination with absorption, may be used to identify and quantify analytes by reaction with complexes such as **1** and **2**. Selectivity, sensitivity, and room temperature luminescence output are currently being optimized by varying the structures of the hemilabile ligand and ancillary ligand set. Studies are ongoing to incorporate these complexes into thin films to enable the development of solid-state sensors.

We thank the Natural Sciences and Engineering Research Council (NSERC) of Canada for financial support of this work.

Notes and references

† Synthesis of **1** and **2**: one equivalent of the appropriate PO ligand[8] was added to a deaerated acetone solution of $[Ru(bpy)_2(Me_2CO)_2](BF_4)_2$,[9] and the mixture was heated to reflux for 12 h. Filtration and removal of solvent *in vacuo* followed by metathesis to the PF_6 salt afforded **1** or **2** as a yellow powder in 85–90% yield. For **1**: ^{1}H NMR (500 MHz, 25 °C, CD_2Cl_2): δ 8.55 (m, 2H), 8.30 (d, ^3J(H,H) = 5.6 Hz, 2H), 8.13 (m, 2H), 8.01 (d, ^3J(H,H) = 7.7 Hz, 1H), 7.95 (d, ^3J(H,H) = 7.6 Hz, 1H), 7.92–7.36 (m, 15H), 7.33 (dd, ^3J(H,H) = 8.6 Hz, ^4J(H,P) = 4.9 Hz, 1H), 7.24 (m, 1H), 7.17 (m, 1H), 6.97 (m, 2H), 6.39 (m, 2H), 3.71 (s, 3H, CH_3O); ^{31}P{^{1}H} NMR (81.0 MHz, CD_2Cl_2): δ 50.9 (s, PO), −143.8 (septet, ^1J(P,F) = 711 Hz, PF_6). Elemental analysis: calcd. for $C_{39}H_{33}F_{12}N_4OP_3Ru$: C, 47.05; H, 3.34; N, 5.63; found: C, 47.30; H, 3.39; N, 5.70%.

1 J. C. Lockhart, in *Molecular Recognition: Receptors for Cationic Guests*, ed. G. W. Gokel, Pergamon, New York, 1996, vol. 1, p. 605; K. B. Crawford, M. B. Goldfinger and T. M. Swager, *J. Am. Chem. Soc.*, 1998, **120**, 5187; A. P. de Silva, H. Q. N. Gunaratne, T. Gunnlaugsson, A. J. M. Huxley, C. P. McCoy, J. T. Rademacher and T. E. Rice, *Chem. Rev.*, 1997, **97**, 1515.

2 I. H. A. Badr, M. E. Meyerhoff and S. S. M. Hassan, *Anal. Chem.*, 1995, **67**, 2613.

3 (*a*) M. Albrecht, R. A. Gossage, A. L. Spek and G. van Koten, *Chem. Commun.*, 1998, 1003; (*b*) J. I. Dulebohn, S. C. Haefner, K. A. Berlund and K. R. Dunbar, *Chem. Mater.*, 1992, **4**, 506; (*c*) C. A. Mirkin and M. S. Wrighton, *J. Am. Chem. Soc.*, 1990, **112**, 8596; (*d*) W. Y. Xu, K. A. Kneas, J. N. Demas and B. A. DeGraff, *Anal. Chem.*, 1996, **68**, 2605.

4 S. Watanabe, O. Onogawa, Y. Komatsu and K. Yoshida, *J. Am. Chem. Soc.*, 1998, **120**, 229; M. Takeuchi, M. Yamamoto and S. Shinkai, *Chem. Commun.*, 1997, 1731.

5 J. M. Price, W. Y. Xu, J. N. Demas and B. A. DeGraff, *Anal. Chem.*, 1998, **70**, 265; A. P. de Silva, H. Q. N. Gunaratne and T. E. Rice, *Angew. Chem.*, 1996, **108**, 2253; *Angew. Chem., Int. Ed. Engl.*, 1996, **35**, 2116.

6 A. Bader and E. Lindner, *Coord. Chem. Rev.*, 1991, **108**, 27; C. S. Slone, D. A. Weinberger and C. A. Mirkin, *Prog. Inorg. Chem.*, 1999, **48**, 233.

7 D. M. Roundhill, *Photochemistry and Photophysics of Metal Complexes*, Plenum Press, New York, 1994; J. V. Caspar and T. J. Meyer, *Inorg. Chem.*, 1983, **22**, 2444.

8 T. B. Rauchfuss, F. T. Patino and D. M. Roundhill, *Inorg. Chem.*. 1975, **14**, 652; L. Horner and S. Simons, *Phosphorus Sulfur*, 1983, **14**, 189.

9 B. P. Sullivan, D. J. Salmon and T. J. Meyer, *Inorg. Chem.*, 1978, **17**, 3334.

Communication 9/06911I

Inter-anion O–H···O interactions are classical hydrogen bonds

Thomas Steiner

Institut für Chemie – Kristallographie, Freie Universität Berlin, Takustraße 6, D-14195 Berlin, Germany. E-mail: steiner@chemie.fu-berlin.de

Received (in Cambridge, UK) 23rd July 1999, Accepted 4th October 1999

Inter-anion O–H···O interactions have consequences on the covalent bonding of the donor and acceptor moieties that are typical for strong hydrogen bonding; in contrast to published views, they are classified as strong hydrogen bonds, with bond orders of H···O of the magnitude 0.25 valence units.

Of all types of hydrogen bonds, O–H···O is by far the best investigated.[1] At H···O distances larger than about 1.6 Å, hydrogen bonds are primarily electrostatic interactions with only a relatively small charge transfer contribution. With reducing distance, the interaction gradually gains a quasi-covalent nature.[2] The extreme case of the centred hydrogen bond, O···H···O, in which the proton is equally shared between two O-atoms, can be considered as two half covalent bonds.[3] Intermolecular O–H···O hydrogen bonds can be formed between uncharged molecules, but can involve also ions, in particular O–H···O^-, $^+$O–H···O, $^+$O–H···O^-, $^-$O–H···O and $^-$O–H···O^-. Inter-anion hydrogen bonds are frequently observed between ions like HSO_4^-, $H_2PO_4^-$, HPO_4^{2-}, related inorganic anions, and numerous hydrogen carboxylates like hydrogen oxalate, hydrogen fumarate and so on. On the basis of structural and IR spectroscopic data, they are usually considered as strong. An example of a well-studied system is the hydrogen sulfates, which have been extensively investigated by X-ray diffraction and vibrational spectroscopy.[4]

Recently, the usual interpretation of inter-anion O–H···O interactions as hydrogen bonds has been seriously challenged.[5] For the O–H···O interaction in potassium hydrogen oxalate, $K^+[HC_2O_4]^-$, it has been argued that it does not represent a hydrogen bond despite the short O···O distance of 2.52 Å and the linearity of the geometry. As the reason, it is stated that the electrostatic inter-anion repulsion would prevent a stable anion–anion bond. On the basis of *in vacuo* computations on hydrogen oxalate dimers, it is stated that contacts between hydrogen oxalate ions are destabilizing in all geometries, and the geometry found in the crystal is adopted because it is the least destabilizing one. In this view, the O–H···O interaction does not 'link' the ions, but still organises them in space because the anions adopt the 'least destabilizing' mutual arrangement. Because this theoretical paper challenges a large part of the hydrogen bond literature, in particular of the literature on strong hydrogen bonds, a close look at the experimental data is appropriate.

The crystal structure of potassium hydrogen oxalate **1** has been determined by X-ray[6,7] and neutron[8] diffraction. The structure is layered, as shown in Fig. 1(*a*) for the neutron diffraction data. The anions are arranged in infinite chains, and the chains are linked by potassium ions coordinated to the O-atoms. The O–H group of each anion is oriented at a carboxylate O-atom of the next anion in the chain. The published IR absorption spectrum shows the typical features of a strong hydrogen bond (not commented upon in ref. 5).[6] The covalent bonding is quantitatively described by the bond distances given in Fig. 1(*a*). The O–H bond is elongated almost 0.09 Å compared to the typical gas-phase values of monomeric carboxylic acids [0.972(5) Å in formic acid,[9] 0.971(2) Å in acetic acid[10]]. Such a lengthening is inherent to strong hydrogen bonds,[2,3] and is a consequence of weakening of the covalent O–H bond by the bonding H···O interaction. A further indication of the bonding nature of H···O is found in the bond lengths of the carboxylate group. The O–H···O interaction is directed at the O-atom that is *cis* with respect to O–H of the accepting molecule. The corresponding C–O bond is 0.017 Å longer than the C–O bond of the O-atom that does not accept an O–H···O interaction. This means that the acceptor C–O bond is weakened by the O–H···O interaction, as it must be in a strong hydrogen bond.

A second hydrogen oxalate crystal structure has been determined by neutron diffraction, and is very informative here. In dimethylammonium hydrogen oxalate **2**, the anions also form infinite chains linked by short O–H···O interactions [Fig. 1(*b*)].[11] The geometry of the O–H···O contact is very similar to that in **1**, with the covalent O–H bond even being slightly longer, and H···O slightly shorter. Unlike **1**, the interaction is directed at the carboxylate O-atom that is *trans* with respect to O–H of the accepting molecule. Again, the C–O bond of the accepting O-atom is longer than that of the other carboxylate O-atom. The main difference of **1** and **2** is in the interaction pattern of the cations. In a layer of **1**, each K^+ ion coordinates to O-atoms of three anions, two of which are successive in a chain. This could support an argument (implicitly made in ref. 5) that the strong O···K^+···O interaction pulls together the anions within the chains, forcing them to make a short contact that they would otherwise avoid. In **2**, on the other hand, each cation

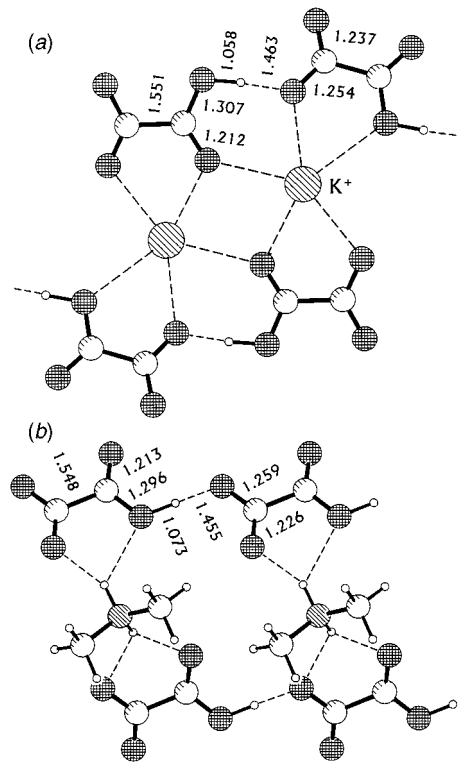

Fig. 1 (*a*) Neutron crystal structure of potassium hydrogen oxalate, determined by Moore and Power (ref. 8). (*b*) Neutron crystal structure of dimethylammonium hydrogen oxalate, determined by Thomas (ref. 11). Distances are given in Å.

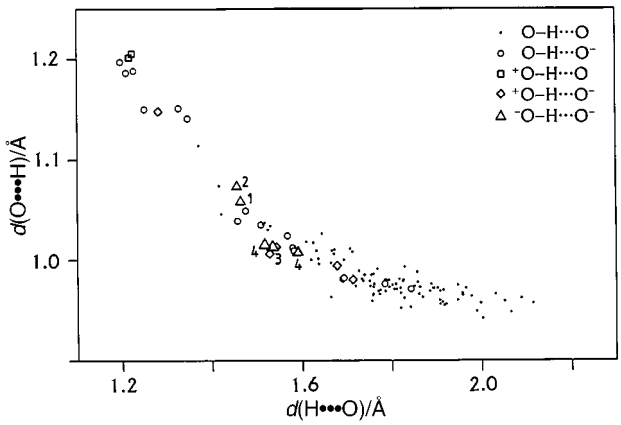

Fig. 2 Lengthening of the covalent O–H bond in O–H···O hydrogen bonds. Scatterplot of data from 125 hydrogen bonds in 66 ordered and error-free neutron crystal structures with $R < 0.06$ (CSD, update 5.16 with 190 307 entries). For the cases $^{+}$O–H···O, $^{+}$O–H···O^{-} and $^{-}$O–H···O^{-}, R values up to 0.09 were allowed. In hydrogen bonds classified as $^{-}$O–H···X, the donor is part of an anion where the negative charge is either delocatized or formally very close to the O–H group. The symbols marked as **1**, **2**, **3** and **4** correspond to the compounds with the same identifiers mentioned in the text.

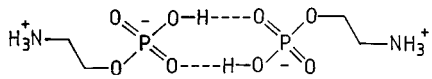

Fig. 3 Structure of 2-aminoethyl phosphate anion dimer.

forms N^{+}–H···O^{-} hydrogen bonds with only two anions, which belong to different chains. There is no anion–cation–anion bridge that could pull the anions together along the chains.

It is of interest to compare the lengthening of the O–H bond in **1** and **2** with the related lengthening in undisputed O–H···O hydrogen bonds of various kinds. Fig. 2 shows the correlation of the O–H and H···O distances in 125 O–H···O interactions found in neutron diffraction crystal structures extracted from the Cambridge Structural Database[12] (details are given in the legend). The overall correlation is as repeatedly published.[2,3,13] It is of importance that the data for different kinds of hydrogen bonds [O–H···O, O–H···O^{-}, $^{+}$O–H···O, $^{+}$O–H···O^{-}] all obey a common function r(O–H) = $f[d$(H···O)]. The data for inter-anion O–H···O interactions, indicated by triangles, *obey this function too*. Four relevant neutron diffraction studies are available: the hydrogen oxalates **1** and **2**, 2-aminoethyl phosphate,[14] **3**, and putrescine diphosphate[15] **4**. The latter two structures are also very interesting. In **3**, the anions form dimers, as shown in Fig. 3, and in **4**, the dihydrogen phosphate ions even form a layer where the anions are connected by interionic O–H···O interactions.

Fig. 2 guides directly to the valence model of the hydrogen bond.[2,3] In this model, O–H and H···O are attributed bond orders or 'valences' s, which depend strictly on the interatomic distances. In hydrogen bonds, the sum of valences at the H-atom is conserved, *i.e.* $s_{O–H} + s_{H···O} = 1.0$. In hydrogen bonds with long H···O, $s_{H···O}$ is small so that $s_{O–H}$ is only slightly reduced from unity, and O–H is only slightly elongated. If H···O is short, however, $s_{H···O}$ becomes large, leading to a large reduction of $s_{O–H}$ and a pronounced elongation of the O–H bond. According to Fig. 2, this is valid for inter-anion O–H···O interactions in the same way as for all other O–H···O hydrogen bonds. For various types of hydrogen bonds X–H···A, the distance dependence of $s_{X–H}$ and $s_{H···A}$ has been parametrized by fitting model functions against structural data (ref. 16 and references therein). Using the most recent parametrization for the case O–H···O,[16] one obtains for the O–H···O interaction in **1** the bond orders $s_{O–H} = 0.73$ and $s_{H···O} = 0.26$. This means that the H-atom is bonded with about ¾ of a valence unit to one O-atom, and with ¼ to the other. The whole interaction O–H···O is, therefore, well inside the quasi-covalent regime of strong hydrogen bonds.[2]

The experimental data discussed above do not indicate any behaviour of inter-anion O–H···O interactions that would fundamentally differ from classical hydrogen bonds. On the contrary, the covalent bonding on the donor as well as on the acceptor sides shows the normal features of strong hydrogen bonding. The effects on the covalent geometries are strong, and indicate that the O–H···O interaction in **1** and related compounds is in the regime of quasi-covalent hydrogen bonds, in which the central hydrogen atom is involved in two bonds of essentially covalent nature.

The author thanks Professor Wolfram Saenger for giving him the opportunity to carry out this study in his laboratory.

Notes and references

1 G. A. Jeffrey and W. Saenger, *Hydrogen Bonding in Biological Structures*, Springer-Verlag, Berlin, 1991; G. A. Jeffrey, *Introduction to Hydrogen Bonding*, Oxford University Press, Oxford, 1997; S. Scheiner, *Hydrogen Bonding. A Theoretical Perspective*, Oxford University Press, Oxford, 1997; G. R. Desiraju and T. Steiner, *The Weak Hydrogen Bond in Structural Chemistry and Biology*, Oxford University Press, Oxford, 1999, pp. 1–28.
2 P. Gilli, V. Bertolasi, V. Ferretti and G. Gilli, *J. Am. Chem. Soc.*, 1994, **116**, 909; V. Bertolasi, P. Gilli, V. Ferretti and G. Gilli, *Chem. Eur. J.*, 1996, **2**, 925.
3 T. Steiner and W. Saenger, *Acta Crystallogr., Sect. B*, 1994, **50**, 348.
4 E. Kemnitz and S. I. Troyanov, *Adv. Mol. Struct. Res.*, 1998, **4**, 79; J. Baran, M. M. Ilczyszyn, M. K. Marchewka and H. Ratajczak, *Spectrosc. Lett.*, 1999, **32**, 83.
5 D. Braga, F. Grepioni and J. J. Novoa, *Chem. Commun.*, 1998, 1959; also see: D. Braga, C. Bazzi, F. Grepioni and J. J. Novoa, *New J. Chem.*, 1999, **23**, 577.
6 B. F. Pedersen, *Acta Chem. Scand.*, 1968, **22**, 2953.
7 H. Einspahr, R. E. Marsh and J. Donohue, *Acta Crystallogr., Sect. B*, 1972, **28**, 2194.
8 F. H. Moore and L. F. Power, *Inorg. Nucl. Chem. Lett.*, 1971, **7**, 873.
9 G. H. Kwei and R. F. Curl, *J. Chem. Phys.*, 1960, **32**, 1592.
10 B. P. van Eijck and E. van Zoeren, *J. Mol. Spectrosc.*, 1985, **111**, 138.
11 J. O. Thomas, *Acta Crystallogr., Sect. B*, 1977, **33**, 2867.
12 F. H. Allen and O. Kennard, *Chem. Des. Autom. News*, 1993, **8**, 1.
13 H. B. Bürgi and J. D. Dunitz, *Acc. Chem. Res.*, 1983, **16**, 153.
14 H.-P. Weber, R. K. McMullan, S. Swaminathan and B. M. Craven, *Acta Crystallogr., Sect. B*, 1984, **40**, 506.
15 F. Takusagawa and T. F. Koetzle, *Acta Crystallogr., Sect. B*, 1979, **35**, 867.
16 T. Steiner, *J. Phys. Chem. A*, 1998, **102**, 7041.

Communication 9/05966K

ChemComm

Mononuclear tris(2-mercapto-1-arylimidazolyl)hydroborato complexes of zinc, [Tm^{Ar}]ZnX: structural evidence that a sulfur rich coordination environment promotes the formation of a tetrahedral alcohol complex in a synthetic analogue of LADH

Clare Kimblin, Brian M. Bridgewater, David G. Churchill and Gerard Parkin*

Department of Chemistry, Columbia University, New York, NY 10027, USA. E-mail: parkin@chem.columbia.edu

Received (in Bloomington, IN, USA) 12th August 1999, Accepted 30th September 1999

The tris(2-mercapto-1-mesitylimidazolyl)borate ligand, [Tm^{Mes}]$^-$, has been used to synthesize {[Tm^{Mes}]Zn-(HOMe)}$^+$, a stable monomeric tetrahedral zinc–methanol complex which resembles the proposed alcohol intermediate in the catalytic cycle of the mechanism of action of liver alcohol dehydrogenase.

The active sites of many zinc enzymes are composed of tetrahedral zinc centers surrounded by a water molecule and a combination of nitrogen, oxygen and sulfur donors derived from amino acid residues of the protein backbone, and may be generally represented as {[$N_xO_yS_z$]Zn^{II}(OH$_2$)}, where $x + y + z = 3$.[1] Although structurally similar, it is evident that the compositions of the {[$N_xO_yS_z$]Zn^{II}(OH$_2$)} active sites are highly varied, ranging from nitrogen rich carbonic anhydrase (CA), {[N$_3$]Zn^{II}(OH$_2$)}, to sulfur rich liver alcohol dehydrogenase (LADH), {[NS$_2$]Zn^{II}(OH$_2$)}.[1] Correspondingly, the chemistry performed by each of these enzymes is distinctly different: for example, CA is a hydrolytic enzyme, whereas LADH is responsible for the oxidation of alcohols.[1] In order to understand why Nature has elected to use different amino acid residues to promote different chemical transformations of zinc enzymes, it is essential to understand how the chemistry of zinc is modified by various donor groups. Here, we describe the syntheses of tetrahedral zinc complexes in a sulfur rich environment of relevance to LADH chemistry,[2] including the structural characterization of an alcohol complex.

Although a large number of [S$_3$] donor ligands are known, many of these are unsuitable for modeling aspects of bioinorganic zinc chemistry since they do not have the ability to inhibit the formation of six-coordinate sandwich complexes. For example, crown thioethers, such as 1,4,7-trithiacyclononane, are insufficiently sterically demanding and do not provide a protective pocket about a metal center that prevents the formation of six-coordinate sandwich complexes.[3] Tripodal thioethers, such as Rabinovich's {MeSi(CH$_2$SMe)$_3$},[4] and Riordan's [RB(CH$_2$SMe)$_3$]$^-$ (R = CH$_2$SMe, Ph, Fc)[5] and [PhB(CH$_2$SR)$_3$]$^-$ (R = Ph,[6] Bu^t [7]) offer much more potential for providing well defined and sterically encumbered coordination sites than their cyclic counterparts. However, of these ligands, only the *tert*-butyl substituted [PhB(CH$_2$SBu^t)$_3$]$^-$ derivative has been reported to be a 'tetrahedral enforcer';[7] thus, a methyl substituent on sulfur does not prevent the formation of six-coordinate compounds, *e.g.* [RB(CH$_2$SMe)$_3$]$_2$Co (R = CH$_2$SMe, Ph).[5a,b]

We are particularly interested in the application of sterically demanding tripodal ligands in which the sulfur atoms are devoid of additional substituents: ligation of this type should more closely resemble that of the negatively charged cysteine thiolates (RS$^-$) at the active site of LADH[1] than would coordination of a thioether (RSR) function. Thus, we considered that modification of Reglinski's tris(mercaptomethylimidazolyl)borate ligand [Tm^{Me}]$^-$,[8] by incorporation of bulky substituents on the imidazolyl rings, could provide a coordination environment that would allow for the isolation of monomeric species of relevance to the mechanism of action of LADH, such as four-coordinate alcohol complexes. Indeed, the aryl substituted ligands [Tm^{Ph}]$^-$ and [Tm^{Mes}]$^-$ are readily obtained by heating LiBH$_4$ with 3 equivalents of 2-mercaptophenylimidazole and 2-mercaptomesitylimidazole,[9] respectively (Scheme 1).

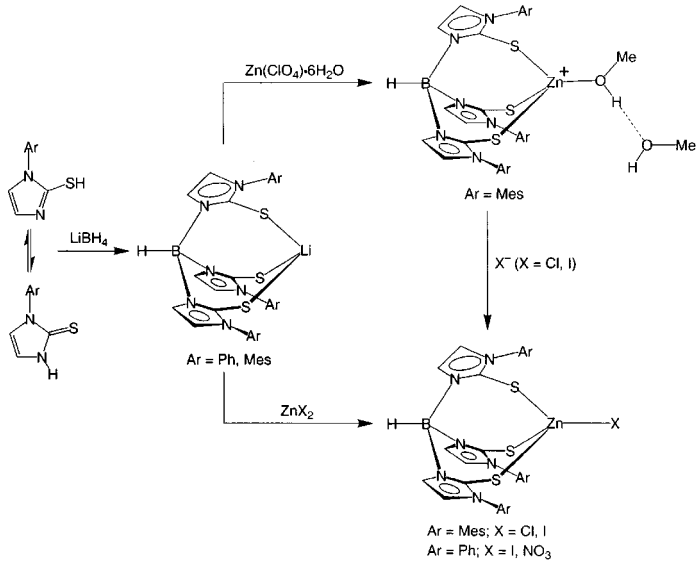

Scheme 1

A critical step in the proposed mechanism of action of LADH involves displacement of water from the active site to give a tetrahedral zinc–alcohol complex, {[NS$_2$]Zn^{II}(HOR)}, as an essential intermediate.[1] Despite their relevance, however, there are no mononuclear tetrahedral zinc complexes of aliphatic alcohols listed in the Cambridge Structural Database,[10] even though there are a substantial number of five- and six-coordinate derivatives.[11] It is, therefore, significant that the cationic alcohol complex {[Tm^{Mes}]Zn(HOMe)}$^+$ may be obtained by reaction of Li[Tm^{Mes}] with Zn(ClO$_4$)$_2$ in methanol (Scheme 1).

The molecular structure of {[Tm^{Mes}]Zn(HOMe)}$^+$ has been determined by X-ray diffraction (Fig. 1), which demonstrates that the [Tm^{Mes}] ligand adopts a propeller configuration.[12] Solution ^{1}H NMR spectroscopic studies indicate that this configuration is also rigid on the NMR time-scale at room temperature. For example, the two *ortho*-methyl groups of each mesityl substituent are chemically inequivalent in the ^{1}H NMR spectrum, thereby indicating that both inversion of the propeller configuration and rotation about the C–N bond are slow on the NMR time-scale.

The zinc coordination geometry in {[Tm^{Mes}]Zn(HOMe)}$^+$ resembles aspects of that in LADH. For example, the Zn–O and average Zn–S bond lengths in {[Tm^{Mes}]Zn(HOMe)}$^+$ {1.993(3) and 2.32[1] Å, respectively} are comparable to those in the

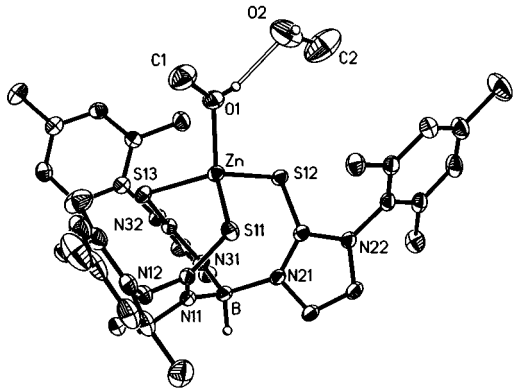

Fig. 1 Molecular structure of $\{[Tm^{Mes}]Zn(HOMe)_2\}^+$ (counter ion omitted for clarity). Selected bond lengths (Å) and angles (°): Zn–O(1) 1.993(3), Zn–S(11) 2.338(1), Zn–S(12) 2.320(1), Zn–S(13) 2.313(1); O(1)–Zn–S(11) 111.37(9), O(1)–Zn–S(12) 105.56(1), O(1)–Zn–S(13) 109.68(9).

$C_6F_5CH_2OH$ adduct of LADH (2.0 and 2.2 Å, respectively).[13] Also noteworthy is the observation that the hydroxy group of the coordinated alcohol of $\{[Tm^{Mes}]Zn(HOMe)\}^+$ participates in a hydrogen bonding interaction with an additional molecule of methanol. This interaction may be viewed as mimicking the hydrogen bond network at the active site of LADH which serves as a relay for proton transfer to the solvent.[13,14] In fact, the hydrogen bonded O···O separation of 2.58 Å between $\{[Tm^{Mes}]Zn(HOMe)\}^+$ and MeOH is effectively identical to that between the zinc bound alcohol at the active site of LADH and Ser–48 (2.6 Å).[13]

The facile isolation of a tetrahedral alcohol complex $\{[Tm^{Mes}]Zn(HOMe)\}^+$ using the tripodal $[S_3]$ tris(mercaptomesitylimidazolyl) ligand is particularly interesting given that the tripodal $[N_3]$ donor tris(imidazolyl)phosphine ligand $[Pim^{Bu^t,Pr^i}]$ yields a zinc hydroxide complex, $\{[Pim^{Bu^t,Pr^i}]ZnOH\}^+$,[15] upon reaction with $Zn(ClO_4)_2$ in methanol. Furthermore, tris(pyrazolyl)hydroborato zinc hydroxide complexes $[Tp^{RR'}]ZnOH$ have also been synthesized using methanol as solvent, in accord with the fact that simple alkoxide derivatives $[Tp^{RR'}]ZnOR$ are extremely sensitive to hydrolysis.[16] In contrast, ^1H NMR spectroscopy and mass spectrometry demonstrate that solutions of $\{[Tm^{Mes}]Zn(HOMe)\}^+$ in methanol are reasonably stable in the presence of water.

The above observations strongly indicate that the sulfur rich coordination environment provided by $[Tm^{Mes}]$ stabilizes alcohol binding to zinc. As such, it suggests that one of the reasons why LADH utilizes a sulfur rich coordination environment is to increase the stability of the required alcohol intermediate with respect to that of an aqua species.[17] In support of this notion, there is only one other structurally characterized complex listed in the Cambridge Structural Database which contains methanol coordinated to a tetrahedral zinc center, and it also possesses a sulfur rich $\{[S_3]Zn(HOMe)\}$ coordination environment; this entity is, however, a portion of a complex polymeric structure, *catena*-$(\mu$-SPh$)[(\mu$-SPh$)_6Zn_4$(MeOH)(SPh)].[18]

Although not readily displaced by water, the methanol ligand in $\{[Tm^{Mes}]Zn(HOMe)\}^+$ is displaced by anions to give neutral $[Tm^{Mes}]ZnX$ derivatives, which may also be obtained by the direct reaction of $Li[Tm^{Mes}]$ with ZnX_2 (Scheme 1). The corresponding $[Tm^{Ph}]ZnX$ (X = I, NO_3) derivatives may be obtained in an analogous manner. The molecular structures of $[Tm^{Mes}]ZnX$ (X = Cl, I) and $[Tm^{Ph}]ZnX$ (X = I, NO_3) have been determined by X-ray diffraction, thereby confirming the monomeric nature of the complexes.[12] It is also worth noting that the nitrate ligand in $[Tm^{Ph}]Zn(ONO_2)$ is coordinated in a unidentate, and not bidentate, manner, thus demonstrating that the $[Tm^{Ph}]^-$ ligand strongly favors tetrahedral coordination in zinc chemistry.

In conclusion, a monomeric tetrahedral zinc–alcohol complex has been obtained using the anionic $[Tm^{Mes}]^-$ sulfur rich donor ligand. The successful isolation of $\{[Tm^{Mes}]Zn(HOMe)\}^+$, and its stability towards water, suggest that sulfur rich coordination sites promote the formation of alcohol adducts. Thus, because such species are essential intermediates in the mechanism of action of LADH, one of the reasons why LADH possesses a sulfur rich active site may be to promote the binding of alcohol to zinc at the active site.

We thank the National Institutes of Health (Grant GM46502) for support of this research.

Notes and references

1 (*a*) B. L. Vallee and D. S. Auld, *Acc. Chem. Res.*, 1993, **26**, 543; (*b*) R. H. Holm, P. Kennepohl and E. I. Solomon, *Chem. Rev.*, 1996, **96**, 2239; (*c*) W. N. Lipscomb and N. Sträter, *Chem. Rev.*, 1996, **96**, 2375; (*d*) E. Kimura, T. Koike and M. Shionoya, *Struct. Bonding* (*Berlin*), 1997, **89**, 1; (*e*) S. Lindskog, *Pharmacol. Ther.*, 1997, **74**, 1; (*f*) K. E. Hightower and C. A. Fierke, *Curr. Opin. Chem. Biol.*, 1999, **3**, 176.

2 For studies modeling aspects of LADH structure and chemistry, see: C. Bergquist and G. Parkin, *Inorg. Chem.*, 1999, **38**, 422; C. Kimblin and G. Parkin, *Inorg. Chem.*, 1996, **35**, 6912; S. C. Shoner, K. J. Humphreys, D. Barnhart and J. A. Kovacs, *Inorg. Chem.*, 1995, **34**, 5933; E. Kimura, M. Shionoya, A. Hoshino, T. Ikeda and Y. Yamada, *J. Am. Chem. Soc.*, 1992, **114**, 10 134; J. F. J. Engbersen, A. Koudijs and H. C. van der Plas, *J. Org. Chem.*, 1990, **55**, 3647; R. M. Kellogg and R. P. Hof, *J. Chem. Soc., Perkin Trans. 1*, 1996, 1651; B. Muller, A. Schneider, M. Tesmer and H. Vahrenkamp, *Inorg. Chem.*, 1999, **38**, 1900.

3 W. N. Setzer, C. A. Ogle, G. S. Wilson and R. S. Glass, *Inorg. Chem.*, 1983, **22**, 266; H. J. Küppers, K. Wieghardt, B. Nuber and J. Weiss, *Z. Anorg. Allg. Chem.*, 1989, **577**, 155.

4 H. W. Yim, L. M. Tran, E. D. Dobbin, D. Rabinovich, L. M. Liable-Sands, C. D. Incarvito, K.-C. Lam and A. L. Rheingold, *Inorg Chem.*, 1999, **38**, 2211.

5 (*a*) C. Ohrenberg, P. H. Ge, P. Schebler, C. G. Riordan, G. P. A. Yap and A. L. Rheingold, *Inorg. Chem.*, 1996, **35**, 749; P. Ge, B. S. Haggerty, A. L. Rheingold and C. G. Riordan, *J. Am. Chem. Soc.*, 1994, **116**, 8406; (*c*) P. J. Schebler, C. G. Riordan, L. Liable-Sands and A. L. Rheingold, *Inorg. Chim. Acta*, 1998, **270**, 543; (*d*) C. Ohrenberg, M. M. Saleem, C. G. Riordan, G. P. A. Yap, A. K. Verma, A. L. Rheingold, *Chem. Commun.*, 1996, 1081.

6 C. Ohrenberg, C. G. Riordan, L. Liable-Sands and A. L. Rheingold, *Coord. Chem. Rev.*, 1998, **174**, 301.

7 P. J. Schebler, C. G. Riordan, I. A. Guzei and A. L. Rheingold, *Inorg. Chem.*, 1998, **37**, 4754.

8 M. Garner, J. Reglinski, I. Cassidy, M. D. Spicer and A. R. Kennedy, *Chem. Commun.*, 1996, 1975; J. Reglinski, M. Garner, I. D. Cassidy, P. A. Slavin, M. D. Spicer and D. R. Armstrong, *J. Chem. Soc., Dalton Trans.*, 1999, 2119.

9 K. Matsuda, I. Yanagisawa and Y. Isomura, *Synth. Commun.*, 1997, **27**, 3565.

10 CSD Version 5.17. 3D Search and Research Using the Cambridge Structural Database, F. H. Allen and O. Kennard, *Chem. Des. Automat. News*, 1993, vol. 8(1), pp. 1 & 31–37.

11 For recent examples, see: T. Brandsch, F.-A. Schell, K. Weis, M. Ruf, B. Müller and H. Vahrenkamp, *Chem. Ber./Recueil*, 1997, **130**, 283 and references therein.

12 $\{[Tm^{Mes}]Zn(HOMe)_2\}(ClO_4)$ is monoclinic, $P2_1/n$, a = 13.5920(11) Å, b = 16.3598(12) Å, c = 20.1484(15) Å, β = 92.037(2)°, V = 4477.4(6) Å^3, T = 233 K, $R1$ = 0.0477, $wR2$ = 0.1036 for 10237 reflections. CCDC 182/1439. See http://www.rsc.org/suppdata/cc/1999/2301/ for crystallographic files in .cif format.

13 S. Ramaswamy, H. Eklund and B. V. Plapp, *Biochemistry*, 1994, **33**, 5230.

14 For studies on Co and Ni complexes which model aspects of hydrogen bonding interactions at the active sites of zinc enzymes, see: C. J. Boxwell and P. H. Walton, *Chem. Commun.*, 1999, 1647; L. Cronin, B. Greener, M. H. Moore and P. H. Walton, *J. Chem. Soc., Dalton Trans.*, 1996, 3337.

15 C. Kimblin, W. E. Allen and G. Parkin, *J. Chem. Soc., Chem. Commun.*, 1995, 1813.

16 See, for example: C. Bergquist and G. Parkin, *Inorg. Chem.*, 1999, **38**, 422; M. Ruf, F. A. Schell, R. Walz and H. Vahrenkamp, *Chem. Ber./Recueil*, 1997, **130**, 101; R. Alsfasser, M. Ruf, S. Trofimenko and H. Vahrenkamp, *Chem. Ber.*, 1993, **126**, 703.

17 In this regard, it has been suggested that the two negative cysteine thiolate residues serve to reduce the tendency to form a zinc hydroxide species and thereby increase the propensity for a coordinated water molecule to be replaced by an alcohol. See ref. 1(*a*).

18 I. G. Dance, *J. Am. Chem. Soc.*, 1980, **102**, 3445.

Communication 9/06561J

ChemComm

A mesoporous ruthenium silica hybrid aerogel with outstanding catalytic properties in the synthesis of *N*,*N*-diethylformamide from CO_2, H_2 and diethylamine

Leo Schmid, Markus Rohr and Alfons Baiker*

Laboratory of Technical Chemistry, Swiss Federal Institute of Technology, ETH Zentrum, CH-8092 Zürich, Switzerland. E-mail: baiker@tech.chem.ethz.ch

Received (in Cambridge, UK) 27th August 1999, Accepted 12th October 1999

A mesoporous ruthenium silica hybrid aerogel containing well dispersed bidentate $RuCl_2[Ph_2P(CH_2)_3PPh_2]_2$ complexes, synthesized using a sol–gel method, affords turnover frequencies up to 18 400 h^{-1} and 100% selectivity from CO_2, H_2 and diethylamine for the formation of *N*,*N*-diethylformamide.

Utilization of carbon dioxide in chemical synthesis has been fostered owing to its abundance, easy handling and non-toxicity.[1] Among several other syntheses the preparation of formic acid derivatives such as methyl formate and *N*,*N*-dimethylformamide have received considerable attention.[2,3] The first successful catalytic syntheses were exclusively based on homogeneous catalysts.[4] The technical potential of this approach is limited by the difficulties in catalyst separation and product recovery steps. This prompted us to search for a heterogeneous catalytic variant of these syntheses.[5–8] In our previous studies the mono- and bi-dentate group VIII metal phosphine complexes were covalently incorporated into microporous silica based xerogels. A considerable improvement in the stability of the active ruthenium complex could be achieved by employing biadentate complexes.[5,8] Although all of these catalysts showed high activity at 100% selectivity to the desired dimethylformamide the intrinsic activity of the free active complexes could not be reached owing to unfavourable microporous structure of the xerogel materials. Here, we report for the first time, the successful synthesis of a mesoporous hybrid aerogel catalyst and compare its catalytic behaviour with the corresponding microporous xerogel. It is shown that the activity of the mesoporous material outperforms the intrinsic activity of the free active ruthenium complex and that of the microporous catalyst by a factor of more than six.

The bidentate ruthenium phosphine complex $RuCl_2(dppp)_2$ **1** [Fig. 1, dppp = $Ph_2P(CH_2)_3PPh_2$] was prepared according to the procedure described in the literature.[9] The synthesis of the corresponding functionalized sol–gel precursor **2** (Fig. 1) and its ligand has also been described in detail.[8]

The hybrid gel catalysts **3a** and **3b** were synthesized from the functionalized precursor **2** by immobilizing this complex within a silica matrix and applying a sol–gel process. To a mixture of 15.22 g (0.10 mol) tetramethylorthosilicate (TMOS) and 7 ml tetrahydrofuran, 1.03 g 65% HNO_3 in 8.81 g H_2O and 27 ml tetrahydrofuran was added dropwise. Subsequently, 0.727 g (5×10^{-4} mol) of **2** in 20 ml tetrahydrofuran was slowly added. After stirring the homogeneous mixture overnight, 4.05 g (0.015 mol) trihexylamine in 15 ml tetrahydrofuran was added dropwise to the solution over 10 min. Within 1 h a solid gel had formed which was aged for 7 days. During this time the tetrahydrofuran which was released from the gel was replaced by ethanol. The gel was dried either by extraction of the solvent with supercritical CO_2 at 22.0 MPa and 41 °C, affording aerogel **3a** or by slow evaporation of the solvent, producing xerogel **3b**. Finally, the gels were washed with acetone and dried in vacuum at 100 °C. All steps, including aging, crushing, washing and drying, were carried out under an argon atmosphere.

^{31}P and ^{29}Si NMR investigations were carried out as described previously.[8] Nitrogen physisorption measurements of the specific surface area and mean pore diameters of the gel catalysts were performed at 77 K using a Micromeritics ASAP 2010 instrument.[6] For catalytic tests a 500 ml stainless steel reactor was used.[7] The products were analyzed by a GC equipped with a TCD and a fused silica capillary column (Supelco SPB-1).

To establish the undestructive incorporation of the active sites, solid state ^{31}P CP MAS NMR measurements for the hybrid gels **3a** and **3b** were compared with liquid ^{31}P NMR investigations of the precursor **2**. The spectra corroborated that no significant change of geometry in the coordination sphere of the phosphorus atoms had taken place. In the spectra of the solid materials, side bands were observed owing to the rotational frequency of the sample during measurements, and the peaks were broader in comparison with liquid ^{31}P NMR results for precursor **2**. Based on earlier EXAFS measurements of immobilized monodentate ruthenium phosphine complexes, which showed that these precursors were incorporated as isolated single entities,[6] it was assumed that cluster formation

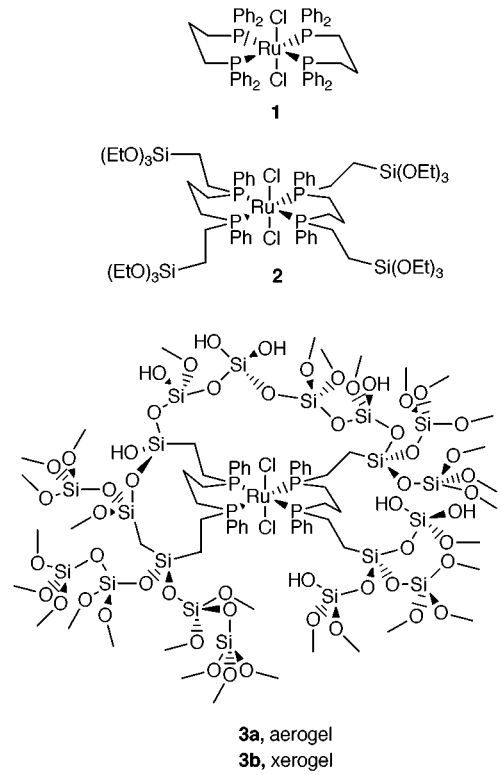

Fig. 1 Ruthenium phosphine complex **1**, which shows good activity and selectivity in the synthesis of formic acid derivatives, is functionalized by silyl ether groups (**2**) and immobilized within a silica matrix affording aerogel **3a** or xerogel **3b**, by different drying procedures.

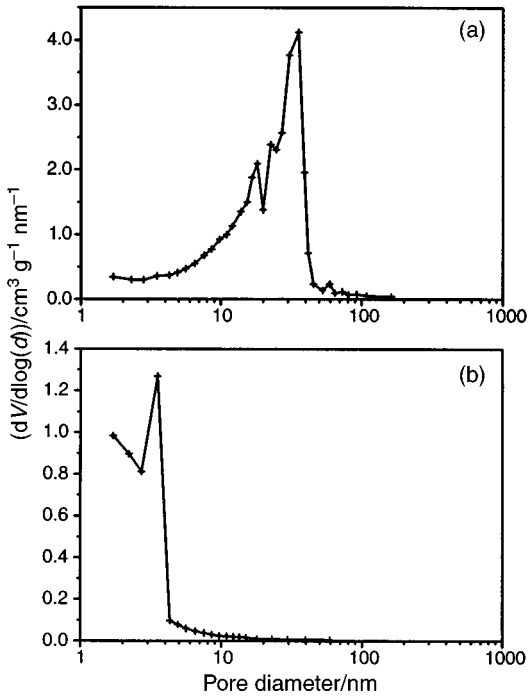

Fig. 2 Pore size distribution of aerogel **3a** (a) and xerogel **3b** (b).

could be excluded also for bidentate complexes. ^{29}Si MAS NMR with single pulse excitation indicated a similar degree of condensation (cross linkage) for aerogel **3a** and xerogel **3b**. Textural properties of the synthesized hybrid gels **3a** and **3b** were investigated by means of nitrogen physisorption and results are shown in Fig. 2. As expected, supercritical drying of the gel applied to **3a** led mainly to mesopores, whereas for xerogel **3b**, dried by thermal evaporation of the solvent, the pore size distribution shifted to much lower values [Fig. 2(b)]. Corresponding t-plots (not shown) indicated a pronounced deviation from linearity for the xerogel between thickness 0.4 to 0.8 nm, which corroborated the presence of micropores.[10] For aerogel **3a**, exhibiting a low amount of micropores, the deviation was much less pronounced. The measured BET surface areas for xerogel **3b** and aerogel **3a** were 1000 and 670 $m^2\ g^{-1}$, respectively. Aerogel **3a** exhibited a nearly four times higher pore volume (1.74 $cm^3\ g^{-1}$) than xerogel **3b** (0.44 $cm^3\ g^{-1}$).

The hybrid gel catalysts **3a** and **3b** were tested in the synthesis of *N*,*N*-diethylformamide from CO_2, H_2 and diethylamine (Scheme 1). A fractional factorial design, including the

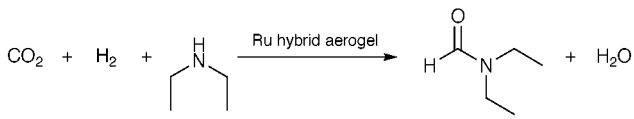

Scheme 1 Synthesis of *N*,*N*-diethylformamide from CO_2 as a C_1-building block with heterogeneous hybrid gels as catalysts.

Table 1 Kinetic data for aerogel **3a** under different reaction conditions. Corresponding results for xerogel **3b** are quoted for comparison

	T/°C	Total pressure/ MPa	Amount of catalyst/ 10^{-7} mol	Turnover frequency/h^{-1}
3a	90	18.0	7.5	4780
3a	110	14.0	2.5	12000
3a	110	18.0	2.5	15300
3a	110	18.0	7.5	18400
3b	110	18.0	7.5	2210

main parameters: temperature, total pressure, amount of catalyst, amount of diethylamine, initial hydrogen pressure, and type of stirrer has been carried out with the aerogel **3a**. The most influential parameters were: amount of catalyst, temperature and total pressure. Some results of the kinetic studies are summarized in Table 1. Note, that depending on the conditions, turnover frequencies up to 18400 h^{-1} were obtained with the mesoporous aerogel **3a**, whereas under the same conditions the microporous xerogel **3b** afforded a value of only 2210 h^{-1}. This improvement is attributed to the favourable textural properties of the aerogel eliminating intraparticle diffusion limitations. In both cases, a selectivity of 100% towards the desired product was found. Surprisingly, the measured turnover frequency, 3130 h^{-1}, for precursor **2** under similar reaction conditions was also significantly lower than that of the aerogel. The reason for this unprecedented increase in activity upon heterogenization is, as yet, not clear. Presumably electronic influences of the silica matrix may play a role. These new aerogels which combine stability with favourable textural properties should also be suitable for the synthesis of higher *N*,*N*-dialkylformamides from CO_2, H_2 and the corresponding dialkylamines.

Financial support by the ETH-Jubiläumsfond and the Bundesamt für Energie is kindly acknowledged.

Notes and references

1 A. Behr, *Angew. Chem., Int. Ed. Engl.*, 1988, **27**, 661.
2 P. G. Jessop, T. Ikariya and R. Noyori, *Chem. Rev.*, 1995, **95**, 259.
3 W. Leitner, *Angew. Chem., Int. Ed. Engl.*, 1995, **34**, 2207.
4 P. G. Jessop, Y. Hsiao, T. Ikariya and R. Noyori, *J. Am. Chem. Soc.*, 1996, **118**, 344.
5 O. Kröcher, R. A. Köppel and A. Baiker, *Chimia*, 1997, **51**, 48.
6 O. Kröcher, R. A. Köppel, M. Fröba and A. Baiker, *J. Catal.*, 1998, **178**, 284.
7 O. Kröcher, R. A. Köppel and A. Baiker, *J. Mol. Catal. A: Chem.*, 1999, **140**, 185.
8 L. Schmid, O. Kröcher, R. A. Köppel and A. Baiker, *Micropor. Mesopor. Mater.*, 1999, in press.
9 R. Mason, D. W. Meek and G. R. Scollary, *Inorg. Chim. Acta*, 1976, **16**, L11.
10 J. C. P. Broekoff, in *Preparation of Heterogeneous Catalysts II, Studies in Surface Science and Catalysis*, ed. B. Delmon, P. Grange, P. Jacobs, and G. Poncelet, Elsevier, Amsterdam, 1979, vol. 3, p. 663.

Communication 9/06956I

ChemComm

Convenient preparation of mononuclear and dinuclear ruthenium hydride complexes for catalytic application

Stefan Busch and Walter Leitner*

Max-Planck-Institut für Kohlenforschung, Kaiser-Wilhelm-Platz 1, 45470 Mülheim an der Ruhr, Germany. E-mail: leitner@mpi-muelheim.mpg.de

Received (in Cambridge, UK) 12th August 1999, Accepted 12th October 1999

A mixture of commercially available [Ru(cod)(η^3-C_4H_7)$_2$] and PCy_3 reacts with H_2 to give [$RuH_2(H_2)_2(PCy_3)_2$] in high yields, whereas [Ru{$Cy_2P(CH_2)_3PCy_2$}(η^3-C_4H_7)$_2$] leads to [{$Cy_2P(CH_2)_3PCy_2$}$RuH(\mu$-H)$_3$Ru(H_2){$Cy_2P(CH_2)_3PCy_2$}] under identical conditions; this new synthetic procedure provides convenient access to this type of ruthenium hydrides for investigation of their potential in catalytic reactions like the Murai-reaction.

The mononuclear ruthenium hydride [$RuH_2(H_2)_2(PCy_3)_2$] **1**[1,2a] and the related binuclear complex [$(PCy_3)_2HRu(\mu$-H)$_3$Ru(H_2)(PCy_3)$_2$] **2**[2] have received considerable attention because of the unique possibility to study η^2-coordinated dihydrogen ligands[3] together with terminal and bridging hydrides in the same coordination sphere. Recent research has demonstrated a remarkable potential of **1** for C–H activation[4] and as a catalyst precursor in C–C bond forming processes, such as olefin metathesis[5] and Murai-type couplings.[6,7]

A major obstacle to a broader investigation of the catalytic properties of **1** and **2** is their time consuming synthesis, involving the highly air sensitive and not readily accessible [Ru(cod)(cot)][8] as a key intermediate. An alternative route to **1** starting from polymeric [$Ru(cod)Cl_2]_n$ was reported recently.[5,9] The generation of complexes $RuH_2L_2(PR_3)_2$ (L = neutral donor ligand) by hydrogenation of [Ru(cod)(η^3-C_4H_7)$_2$)] in the presence of PR_3 and L was described in a patented procedure, but never disclosed in the open literature.[9] None of these methodologies has been applied to the synthesis of derivatives of **1** and **2** bearing chelating bidentate phosphine ligands, which might be of particular interest for catalytic applications.[10]

We now report a very convenient one-step preparation for **1** starting from commercially available [Ru(cod)(η^3-C_4H_7)$_2$)] **3**† (Scheme 1) and the application of the same procedure to the synthesis of derivatives of **2** bearing chelating phosphines (Scheme 2). Preliminary results on the use of **1** in Murai-type coupling reactions are also given.

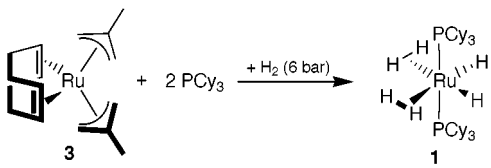

Scheme 1 One-pot synthesis of **1** by hydrogenation of **3** in the presence of PCy_3.

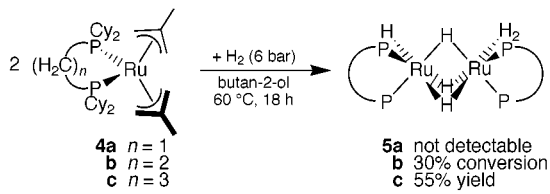

Scheme 2 Hydrogenation of ruthenium bis(allyl) complexes **4a–c** containing chelating phosphine ligands.

For the synthesis of **1** the air stable components **3** and PCy_3 are placed in a thick-walled glass reactor in 1 : 2 stoichiometry. The reactor is evacuated, purged with argon and the solvent is added. The suspension is pressurised with hydrogen (6 bar) and heated for the appropriate reaction time. After cooling to room temperature, the precipitate is collected by cannula filtration, washed twice with small portions of pentane and dried in a hydrogen stream. Under optimised conditions colourless and spectroscopically pure **1** is obtained in almost quantitative yield (Table 1).

Table 1 Optimisation of reaction parameters for the synthesis of **1**[a]

T/°C	Reaction time /h	Yield (%)	Solvent
30	18	47	Pentane
60	18	97	Pentane
60	6	75	Hexane
60	9	85	Butan-2-ol
60	18	93	Butan-2-ol
60	24	83	Butan-2-ol
85	5	74	Butan-2-ol

[a] **3**: 0.375 mmol, PCy_3: 0.75 mmol, solvent: *ca.* 3.5 cm^3.

Applying the same methodology to the mononuclear complex **4c**[11] bearing the chelating dcpp ligand resulted in clean formation of the dinuclear hydride-bridged ruthenium complex **5c**, which was isolated in 55% yield as a bright orange microcrystalline powder (Scheme 2). The structural assignment of **5c** is based on elemental analysis and the excellent agreement of its spectroscopic data with those of **2**.[2]‡

The size of the chelating ring has a strong influence on the reactivity of complexes **4a–c** (Scheme 2): complex **4b** remained

Table 2 Murai-type couplings of sp^2-C–H bonds with ethylene in the presence of **1**[a]

Substrate	*T*/°C	Conversion[b](%)	Products[b]
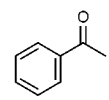	30 50	100 94	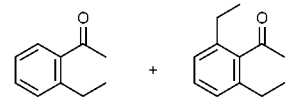 99% 66% 1% 34%
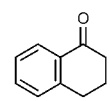	30	22	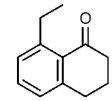
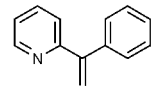	30	86	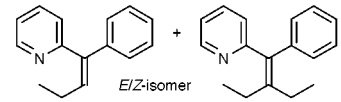 74% *E/Z*-isomer 26%

[a] Substrate: 0.2 mmol, **1**: 0.02 mmol, ethylene: *ca.* 45 mmol (30 bar), solvent: pentane (2.5 cm^3), $V_{Reactor}$:11 cm^3. [b] Determined by GC–MS analysis after 24 h.

largely unreactive and gave low, but clean conversion to **5b** (< 30%).‡ ^{31}P-NMR monitoring of the reaction of **4a** with H_2 indicated also a very slow reaction. Two different phosphorus containing products were formed, but there were no unambiguously detectable signals in the hydride region of the ^{1}H NMR spectrum.

Preliminary results of some Murai-type couplings using **1** as catalyst precursor are summarised in Table 2. In agreement with Chaudret's recent findings, the alkylation of acetophenone with one molecule of ethylene proceeded smoothly in presence of **1** (10 mol%) under mild conditions.[6]§ Appreciable amounts of the dialkylated product were formed at 50 °C. Most notably, coupling of 2-α-styrylpyridine and ethylene occurred readily to give a mixture of mono- and di-alkylated products at 30 °C. This coupling has been previously reported only for rhodium catalysts under much more forcing conditions.[12]

Further evaluation of the new procedure for the synthesis of ruthenium hydrides and detailed investigation of their catalytic behaviour are under way.

Financial support by the Max-Planck-Society and the Deutsche Forschungsgesellschaft is gratefully acknowledged. We thank Dr Tom Baker (Los Alamos National Laboratory) for helpful discussion.

Notes and references

† [Ru(cod)(η^3-C_4H_7)$_2$] was purchased from Fisher Scientific/ACROS Organics and used as received. For synthesis from [Ru(cod)Cl_2]$_n$, see K. S. MacFarlane, S. J. Rettig, Z. Liu and B. R. James, *J. Organomet. Chem*., 1998, **557**, 213.

‡ *Characteristic analytical data for* **5c**: δ_H(C_6D_6, 300 MHz) −11.8 (br), δ_P(C_6D_6, 121 MHz) 67.9. ν_{max}(KBr)/cm^{-1} 2105, 1990, 1552. Found: C, 59.43; H, 9.72; P, 13.03. Calc. for $C_{54}H_{106}P_4Ru_2$: C, 59.97; H, 9.88; P, 11.46%. **5b**: δ_H(C_6D_6, 300 MHz) –11.2, δ_P(C_6D_6, 121 MHz) 114.3.

§ We note that the conversion of acetophenone varied between 50 and 100% in several independent catalytic runs. The reason for this is as yet unclear and is part of our current investigations.

1 B. Chaudret and R. Poilblanc, *Organometallics*, 1985, **4**, 1722.
2 (*a*) T. Arliguie, B. Chaudret, R. H. Morris and A. Sella, *Inorg. Chem*., 1988, **27**, 598; (*b*) B. Chaudret, J. Devillers and R. Poilblanc, *Organometallics*, 1985, **4**, 1727.
3 G. J. Kubas, *Acc. Chem. Res*., 1988, **21**, 120.
4 A. F. Borowski, S. Sabo-Etienne, M. L. Christ, B. Donnadieu and B. Chaudret, *Organometallics*, 1996, **15**, 1427.
5 T. R. Belderain and R. H. Grubbs, *Organometallics*, 1997, **16**, 4001.
6 Y. Guari, S. Sabo-Etienne and B. Chaudret, *J. Am. Chem. Soc*., 1998, **120**, 4228.
7 M. Sonoda, F. Kakiuchi, N. Chatani and S. Murai, *Bull. Chem. Soc. Jpn*., 1997, **70**, 3117.
8 K. Itoh, H. Nagashima, T. Ohshima, N. Oshima and H. Nishiyama, *J. Organomet. Chem.*, 1984, **272**, 179.
9 R. P. Beatty and R. A. Paciello (Du Pont), WO 96/23804, priority date 08/08/1996.
10 W. Leitner, M. Bühl, R. Fornika, C. Six, W. Baumann, E. Dinjus, M. Kaiser, C. Krüger and A. Rufińska, *Organometallics*, 1999, **18**, 1196 and references therein.
11 W. Leitner and C. Six, *Chem. Ber./Recueil*, 1997, **130**, 555; C. Six, B. Gabor, H. Görls, R. Mynott, P. Philipps and W. Leitner, *Organometallics*, 1999, **18**, 3316.
12 Y.-G. Lim, J.-B. Kang and Y. H. Kim, *J. Chem. Soc., Perkin Trans. 1*, 1998, 699.

Communication 9/06580F

The organo-pillared porous magnetic framework $Co_4(SO_4)(OH)_6(H_2NC_2H_4NH_2)_{0.5}\cdot 3H_2O$

Apinpus Rujiwatra,† Cameron J. Kepert‡ and Matthew J. Rosseinsky*†

Inorganic Chemistry Laboratory, Department of Chemistry, University of Oxford, South Parks Road, Oxford, UK OX1 3QR. E-mail: m.j.rosseinsky@liv.ac.uk

Received (in Cambridge, UK) 9th September 1999, Accepted 8th October 1999

The organo-pillared octahedral–tetrahedral (O/T) layer solid $Co_4(SO_4)(OH)_6(H_2NC_2H_4NH_2)_{0.5}\cdot 3H_2O$ is robust to loss of water molecules within the galleries, thermally stable to 300 °C and orders as a metamagnet below 14 K.

Pillared layered solids are an increasingly important class of materials of interest in the areas of sorption, separation and catalysis, as exemplified by the study of layered double hydroxides (positive layer charge),[1] smectite and other classes of clay (negative layer charge)[2] and the metal phosphonates (neutral layers).[3] Here, we report the direct synthesis and structural characterisation by single crystal X-ray diffraction of a novel type of layered hydroxide derived by organic pillaring of the namuwite[4,5]/basic zinc sulfate structure.[6] The multi-component nature of the new solid, its hydration/dehydration behaviour and the straightforward low temperature synthesis all suggest a broad family of such magnetic porous materials should be accessible.

Hydrothermal synthesis is a widely exploited low-temperature route to new solids.[6] Initial attempts to prepare microporous cobalt sulfates with a variety of amine templates at pH of below 7 led to the formation of dense, stable mineral phases such as $Co_3(SO_4)_2(OH)_2\cdot 2H_2O$ which only contain octahedral cobalt.[7] Increasing the pH of the initial synthesis gel from 7.7 to 10.8 led to precipitation of a brown sol (amorphous to X-rays) which on hydrothermal treatment for three days at 180 °C yielded small blue crystals of $Co_4(SO_4)(OH)_6(H_2NC_2H_4NH_2)_{0.5}\cdot 3H_2O$.§ Single crystal X-ray diffraction¶ showed the structure of this phase to arise from the stacking of layers formed by edge-sharing $Co^{II}(OH)_6$ octahedra regularly decorated by tetrahedral Co^{II} sites located above and below the layer at the 1/7 of the octahedral sites which are vacant (Fig. 1). Layer neutrality is completed by sulfate groups projected out from the layer which share one oxygen atom with three neighbouring CoO_6 octahedra and give the layer composition $Co_3^{oct}(SO_4)(OH)_5\cdot Co^{tet}(OH)$.

The coordination at the pseudo-tetrahedral metal site pulled out of the layer consists of three basal hydroxide anions (whose orientation is stabilised by hydrogen bonding to the neighbouring sulfate group) with the apical site occupied by the amine group of the bidentate ethylenediamine ligands. These organic units thus link two adjacent layers covalently *via* the decorating tetrahedral cobalt cations (Fig. 1). The synthesis pH controls whether cobalt is able to adopt this tetrahedral co-ordination.

The void space between the O/T layers separated by the en pillars contains three waters of crystallisation located by hydrogen bonding. The free dimensions of the channels between the pillars are 4.7 × 2.8 Å, occupying 16.5% of the crystal volume. One of the interlayer water molecules is readily lost at ambient temperature as elemental analysis indicates only two water molecules per formula unit. The difference from the composition derived from the low temperature crystallographic study is due to kinetic trapping of this water by the supporting oil at the low measuring temperature. The thermal analysis data in Fig. 2 shows that the remaining interlayer water is lost in two steps at *ca.* 100 and 200 °C to yield $Co_4(SO_4)(OH)_6(H_2NC_2H_4NH_2)_{0.5}\cdot H_2O$ [(b) c = 9.426 Å at 100(2) °C] and the fully dehydrated phase $Co_4(SO_4)(OH)_6(H_2NC_2H_4NH_2)_{0.5}$ [(c) c = 9.339 Å at 200(2) °C], respectively. The retention of the en pillars within the framework up to 200 °C was confirmed by the characteristic vibrational spectrum of the methylene group. Further heating leads to loss of the organic pillars as confirmed by loss of the methylene bending vibrations (Fig. 2, inset) and formation of Co_2O_3 *via* an unidentified crystalline intermediate above 450 °C. Water loss to stage (c) is fully reversible as demonstrated by TGA and *in situ* X-ray powder diffraction measurements of $Co_4(SO_4)(OH)_6(H_2NC_2H_4NH_2)_{0.5}$ on cooling from 200 °C to room temperature in water-saturated gas streams: the c-parameter increases sharply on cooling below 60 °C as water is reabsorbed within the interlayer region (Fig. 2 inset).‖

The *ca.* 1 Å decrease in the c parameter is consistent with a slippage of the layers occurring within the *ab*-plane. The bridging en units, having an N···N distance of 3.1 Å, may facilitate this interlayer compression if there is a tilting of the C–C bond resulting from a 120° rotation about each of the C–N bonds and change in N–C–C–N torsion angle from 60 to 180°.

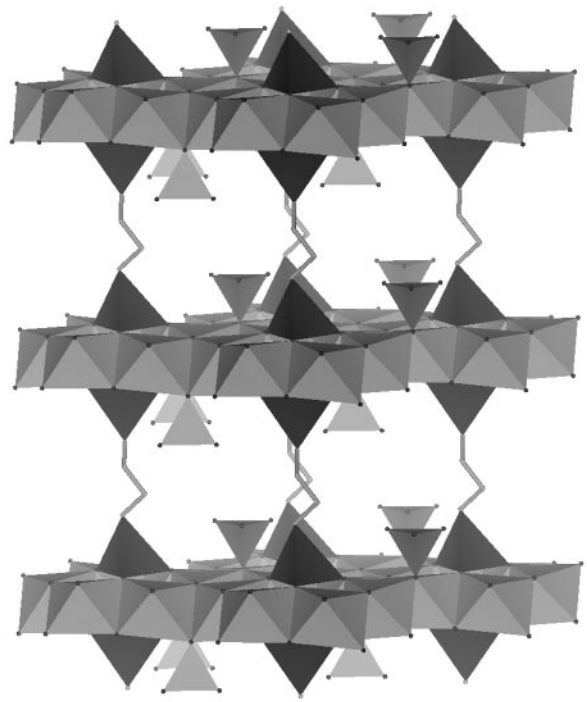

Fig. 1 The octahedral–tetrahedral (O/T) cobalt hydroxide layers of $Co_4(SO_4)(OH)_6(H_2NC_2H_4NH_2)_{0.5}\cdot 3H_2O$ are connected to each other by ethylenediamine pillars through the tetrahedral cobalt ions. The sulfate anions are the light grey tetrahedra decorating the layer. The interlayer water molecules, which can be removed while retaining the structure, are omitted for clarity.

† Present address: Department of Chemistry, University of Liverpool, Liverpool, UK L69 7ZD.

‡ Present address: School of Chemistry, University of Sydney, NSW 2006, Australia.

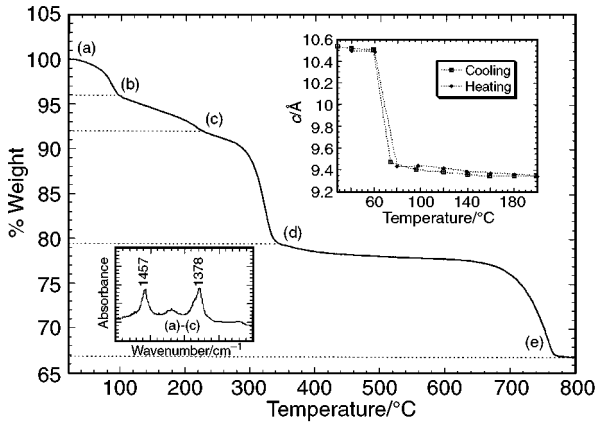

Fig. 2 TGA data under flowing nitrogen for $Co_4(SO_4)(OH)_6(H_2NC_2H_4NH_2)_{0.5}\cdot 2H_2O$ (a), showing loss of the interlayer water to yield the dehydrated pillared phase at (c). Insets show the temperature dependence of the *c*-parameter on heating and cooling in H_2O saturated helium and the IR spectra showing bending and stretching modes of the methylene groups (at 1457, 1378 and 2952, 2891 cm^{-1}).

The loss of 3D ordering with desolvation, as seen by the retention of only the 00l reflections, indicates there is no long range correlation in the direction of the resulting slippages for neighbouring sets of layers.

The magnetic susceptibility obeys the Curie–Weiss law above 190 K with an effective magnetic moment of 4.92(1) μ_B per cobalt, and a Weiss constant of −43(1) K. The downturn in the ZFC magnetisation at 14 K is consistent with antiferromagnetic ordering below this temperature.** Deviation from linearity in $M(H)$ below 190 K indicates the development of short-range order well above this temperature. The magnetisation isotherm at 5 K (Fig. 3) and the corresponding first derivative curve (dM/dH) indicates metamagnetic behaviour with a saturation moment of 1.07 μ_B per Co at 5.0 T and 5 K. Manipulation of the metal sites, pillar and tetrahedral oxyanion

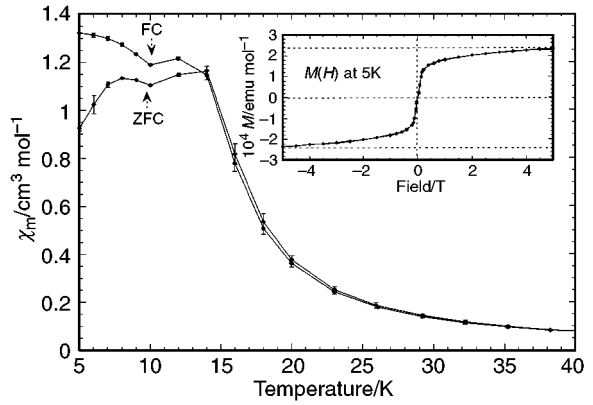

Fig. 3 Temperature dependent molar susceptibility (per mole of cobalt ions: ZFC and FC data collected in an applied field of 100 G). The field dependent magnetisation at 5 K is shown as an inset. The hysteresis at 5 K yields r_m of 336(9) emu mol^{-1} and H_c of 55(1) G.

based on this structure promises enhancement of void volume size, guest sorption and magnetic behaviour in this new class of magnetic porous material.

A. R. thanks the Royal Thai Government for a graduate scholarship, and C. J. K. thanks Christ Church, Oxford for a Junior Research Fellowship.

Notes and references

§ *Experimental*: $Co_4(SO_4)(OH)_6(H_2NC_2H_4NH_2)_{0.5}\cdot 3H_2O$ was synthesised hydrothermally from a mixture of $Co(NO_3)_2\cdot 6H_2O$ (98% Aldrich), H_2SO_4 (98% aq.), ethylenediamine (99% Aldrich) and concentrated aqueous 6 M KOH (pellet, 85+% Aldrich) in a molar ratio 1 : 2 : 0.6 : 5.4 : 100. The initial pH of the mixture was <2 and became about 11 after addition of concentrated $KOH_{(aq)}$, then decreasing gradually to 8 after stirring for 1 h. A dark brown sol was obtained at this stage. The reaction was performed (180 °C, 3 days, autogeneous pressure) in a sealed hydrothermal bomb (22 cm^3 bomb volume and 70% fill factor) fitted with a Teflon liner. Blue plate-like (0.30 × 0.20 × 0.05 mm) crystals mixed with monophasic powder of the same product obtained were washed and rinsed with deionised water and acetone respectively. The elemental analytical formula was $Co_4(SO_4)(OH)_6(H_2NC_2H_4NH_2)_{0.45}\cdot 2.2H_2O$. Found: C, 2.16; H, 2.82; N, 2.52; Co, 47.10; S, 6.41. Calc. C, 2.32; H, 3.11; N, 2.70; Co, 45.51; S, 6.19%.

¶ Diffraction data collection was conducted at 150 K with an Enraf-Nonius DIP2000 diffractometer equipped with fine-focus molybdenum X-ray tube and a graphite monochromator. *Crystal data*: $CH_{16}Co_4NO_{13}S$, M = 517.93, trigonal, space group $P\bar{3}$ (no. 147), a = 8.298(1), c = 10.519(2) Å, U = 627.3(2) $Å^3$, Z = 2, μ(Mo-Kα) = 5.43 mm^{-1} 3396 reflections measured, 875 unique (R_{int} = 0.054) which were used in all calculations. The en pillar and surrounding water molecules are disordered about a threefold axis and were modelled with 1/3-occupation. $R(F)$ = 0.0881 and $R(F^2)$ = 0.2193 for all data. CCDC 182/1437. See http://www.rsc.org/suppdata/cc/1999/2307/ for crystallographic files in .cif format.

‖ Powder diffraction data collection was carried out using a Phillips X-ray diffractometer with Cu-Kα radiation to confirm the purity of the bulk synthesis. High temperature data were collected for 30 ⩽ T/°C ⩽ 400 using a Siemens D5005 X-ray diffractometer with Cu-Kα radiation from a Gobel mirror multilayer monochromator: the sample was under a He or He–H_2O stream within an Anton-Parr HTK1200 high-temperature cell.

** Susceptibility measurements on a monophasic polycrystalline sample were made using a Quantum Design MPMS-SQUID magnetometer with a sample mass of 31.5 mg. Field cooled (FC) and zero-field cooled (ZFC) measurements were performed in applied fields of 100 and 1000 G over the temperature range of 5–300 K.

FTIR data were collected with a Nicolet Magna-IR 560 spectrometer with samples as self-supporting pellets.

Thermogravimetric analysis and differential scanning calorimetry (TGA-DSC) data were collected on a Rheometric Scientific STA 1500 instrument for 20 ⩽ T/°C ⩽ 800 under a nitrogen flow with a heating rate of 2 °C min^{-1}.

1 S. P. Newman and W. Jones, *New J. Chem.*, 1998, **22**, 105.
2 T. J. Pinnavaia, *Science*, 1983, **220**, 365.
3 G. Alberti, U. Costantino, C. Dionigi, S. Murciamascaros and R. Vivani, *Supramol. Chem.* 1995, **6**, 29.
4 L. A. Groat, *Am. Mineral.*, 1996, **81**, 238.
5 R. E. Bevins, S. Turgoose and P. A. Williams, *Mineral. Mag.*, 1982, **46**(338), 51.
6 I. J. Bear, I. E. Grey, I. C. Madsen, I. E. Newnham and L. J. Rogers, *Acta Crystallogr., Sect. B*, 1986, **42**, 32.
7 R. E. Morris and P. A. Wright, *Chem. Ind.* 1998, 256.
8 W. Doubler, *Naturwissenschaften*, 1969, **56**, 327.

Communication 9/07315I

A new route to incompletely-condensed silsesquioxanes: base-mediated cleavage of polyhedral oligosilsesquioxanes

Frank J. Feher,* Raquel Terroba and Joseph W. Ziller

Department of Chemistry, University of California, Irvine, CA 92697-2025, USA. E-mail: fjfeher@uci.edu

Received (in Bloomington, IN, USA) 2nd August 1999, Accepted 7th October 1999

Readily available $R_8Si_8O_{12}$ frameworks react selectively with aqueous Et_4NOH to afford discrete incompletely-condensed silsesquioxanes: reaction of $R_8Si_8O_{12}$ (2a, R = c-C_6H_{11}; 2b, R = Bu^i) with Et_4NOH first produces *endo*-D_2-$R_8Si_8O_{11}(OH)_2$ (3a, R = c-C_6H_{11}; 3b, R = Bu^i), which reacts further with Et_4NOH to produce *endo*-C_2-$R_8Si_8O_{10}(OH)_4$ (5a and 5b) and *endo*-C_3-$R_7Si_7O_9(OH)_3$ (4a, R = c-C_6H_{11}; 4b, R = Bu^i); the reactions of Et_4NOH with $Me_8Si_8O_{12}$ (2c), (c-C_6H_{11})$_7$(H)Si_8O_{12} (2d) and (c-C_6H_{11})$_7$(OH)Si_8O_{12} (2d) also produce the corresponding trisilanols (*i.e. endo*-C_3-$R_7Si_7O_9(OH)_3$ (4a, R = c-C_6H_{11}; 4c, R = Me).

Incompletely condensed polyhedral silsesquioxanes are versatile precursors to a wide range of Si/O and Si/O/M frameworks.[1–7] For many years, the pool of incompletely condensed silsesquioxanes available in synthetically useful quantities was limited to a small number of compounds available *via* hydrolytic condensation of trifunctional silanes possessing relatively bulky organic groups.[8–15] Recently however, our discovery that fully-condensed $[RSiO_{3/2}]_n$ frameworks, such as (c-C_6H_{11})$_6Si_6O_9$ (**1**) and (c-C_6H_{11})$_8Si_8O_{12}$ (**2a**), can be selectively cleaved by strong acids provides access to many useful new incompletely-condensed frameworks.[16–18] In this paper, we report that base catalyzed cleavage of polyhedral silsesquioxanes can be similarly selective. For the first time, cleavage of a single Si–O–Si linkage in $R_8Si_8O_{12}$ can be achieved directly with complete retention of stereochemistry at Si to afford *endo* disilanols with structure **3**. Under more vigorous conditions, cleavage of additional Si–O–Si linkages occurs to produce tetrasilanols with structure **4** and trisilanols with structure **5**.

The reaction of **2a** with aqueous Et_4NOH in THF occurs over a period of several hours at room temperature. The first product to appear in the ^{29}Si NMR spectrum was D_2-symmetric disilanol **3a**, which was identified by its characteristic ^{29}Si NMR resonances at δ −60.4, −67.2, and −69.8 (2:2:4).[16] When the reaction is performed at 25 °C for 1 h with 1.1 molar equivalents of 35% aqueous Et_4NOH, **3a** is obtained as the only reaction product in *ca.* 80% yield (along with 20% of unreacted **2a**). At longer reaction times, resonances for **3a** are gradually replaced by resonances for two additional products. One of these products is C_3-symmetric trisilanol **5a**, which exhibits three resonances at δ −60.1, −67.7, and −69.4 (3:1:3) in the ^{29}Si NMR spectrum.[9] The second product, which exhibits four ^{29}Si resonances at δ −59.3, −61.5, −69.8 and −71.3 (2:2:2:2), as well as prominent peaks at *m/z* 1117.36 $[M + H]^+$ and 1139.37 $[M + Na]^+$ in its electrospray mass spectrum, is most consistent with C_2-symmetric tetrasilanol **4a**. For a typical reaction performed in THF at 25 °C, the ratio of unreacted **2a**:**3a**:**4a**:**5a** was 26:34:17:23 after 9 h and 6:18:26:50 after 15 h. When the reaction was performed in refluxing THF or methyl isobutyl ketone, all of the starting material was consumed within 3 h to produce **5a** in 47% crude yield (23% isolated yield).† The balance of the product mixture exhibited a very broad featureless ^{29}Si NMR spectrum typical of silsesquioxane resins. Samples of **3a** and **5a** prepared by the above procedure were identical in all respects to authentic samples prepared by other means.[9,16]

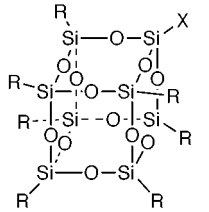

2a R = X = c-C_6H_{11}
b R = X = Bu^i
c R = X = Me
d R = c-C_6H_{11}; X = H
e R = c-C_6H_{11}; X = OH

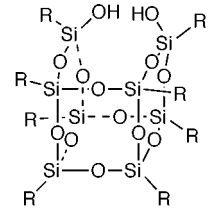

3a R = c-C_6H_{11}
b R = Bu^i
c R = Me

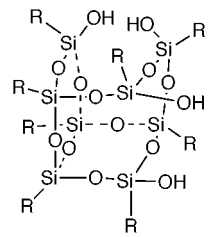

4a R = c-C_6H_{11}
b R = Bu^i

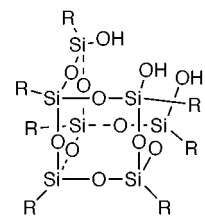

5a R = c-C_6H_{11}
b R = Bu^i
c R = Me

A number of other $R_8Si_8O_{12}$ frameworks react similarly with Et_4NOH. For example, the reactions of **2d** and **2e** with aqueous Et_4NOH (1.1 equiv., THF, reflux, 1 h) both afford **5a** in good (> 50%) yield. These results clearly demonstrate that Si centers possessing H or OH groups are much more readily extracted from the Si_8O_{12} framework than Si centers possessing relatively bulky, electron-rich cyclohexyl groups.

We have only begun to explore the scope and generality of base-mediated silsesquioxane cleavage reactions, but it is already clear that this approach will provide access to a large number of useful new compounds, including many incompletely-condensed frameworks with substituents other than cycloalkyl groups. For example, the reaction of Et_4NOH with (Bu^i)$_8Si_8O_{12}$ (**2b**) appears to produce isobutyl analogs of **3**, **4** and **5**. This reaction is approximately an order of magnitude faster than the reaction of (c-C_6H_{11})$_8Si_8O_{12}$ (**2a**), and it eventually produces a good isolated yield of **5b**,‡ which was identified on the basis of compelling multinuclear NMR data and a single-crystal X-ray diffraction study.§ Similar results are observed with (vinyl)$_8Si_8O_{12}$, (cyclopentyl)$_8Si_8O_{12}$ and $Et_8Si_8O_{12}$. Even $Me_8Si_8O_{12}$ (**2c**), which is notoriously difficult to functionalize because of its very low solubility in organic solvents,[19] reacts with aqueous Et_4NOH to produce an incompletely-condensed framework with spectroscopic features expected for $Me_7Si_7O_9(OH)_3$ (**5c**).¶ The isolated yield is relatively low (< 10%), but the fact that inexpensive and readily available **2c** can be used to produce incompletely-condensed fragments of discrete polyhedral silsesquioxanes has important

implications for many potential applications—particularly the use of polyhedral silsesquioxanes as precursors to hybrid inorganic/organic polymers.[2]

The susceptibility of $R_8Si_8O_{12}$ frameworks to base-catalyzed redistribution and non-selective degradation is well established,[20,21] but the results described above are unprecedented, apparently quite general and of considerable practical importance: it is now possible to prepare synthetically useful quantities of incompletely-condensed silsesquioxanes by selectively removing Si atoms from fully condensed $R_8Si_8O_{12}$ frameworks. Our efforts to expand the scope of this methodology—including our efforts to use spherosilicates as feedstocks—will be reported in due course.

These studies were supported by Hybrid Plastics (Fountain Valley, CA) under an Advanced Technologies Program grant from the National Institute of Standards and Technology, and the National Science Foundation.

Note added in Proof: The reactions of **2a** and **2b** with Et_4NOH have been optimized to produce high isolated yields of disilanols **3a** (77%) and **3b** (98%). Similarly selective cleavage reactions have also been achieved with $R_8Si_8O_{12}$ with R = *c*-C_5H_9 and vinyl.[22]

Notes and references

† Preparation of $Cy_7Si_7O_9(OH)_3$ **(5a)**: A solution of $Cy_8Si_8O_{12}$ (500 mg, 0.46 mmol) and 35% aqueous Et_4NOH (0.2 mL, 0.49 mmol) was refluxed in THF (5 mL) for 4 h then neutralized with dilute aqueous HCl. Evaporation of the volatiles afforded a white solid, which was dissolved in Et_2O and dried over anhydrous $MgSO_4$. Filtration and partial evaporation of the solvent afforded **5a** as a white microcrystalline solid in 23% yield. The product is indistinguishable from authentic **5a** prepared *via* the hydrolytic condensation of $CySiCl_3$.

‡ Preparation of $Bu^i_7Si_7O_9(OH)_3$ (**5b**): A solution of $Bu^i_8Si_8O_{12}$ (400 mg, 0.46 mmol) and 35% aqueous Et_4NOH (0.2 mL, 0.49 mmol) was refluxed in THF (5 mL) for 4 h then neutralized with dilute aqueous HCl. Evaporation of the volatiles afforded a resinous white material, which was dissolved in Et_2O and dried over anhydrous $MgSO_4$. Filtration and evaporation of the solvent afforded crude **5b** as a tacky white solid. Recrystallization from toluene–acetonitrile gave pure **5b** as colorless crystals. Yield 142 mg (39%). Selected characterization data: Anal. Calc. for $C_{28}H_{66}Si_7O_{12}$ (found): C, 42.49 (42.62); H, 8.41 (8.52)%. $^{29}Si\{^1H\}$ NMR (99.3 MHz, C_6D_6, 25 °C) δ −58.5, −66.9, −68.3 (s, 3:1:3); 1H NMR (500 MHz, C_6D_6, 25 °C) δ 7.0 (br s, 3 H, OH), 2.21 (m, 7 H, –CH–), 1.24 (d, J = 6.6 Hz, 18 H, CH_3), 1.21 (d, J = 6.6 Hz, 18 H, CH_3), 1.17 (d, J = 6.6 Hz, 6 H, CH_3), 0.97 (d, J = 7.1 Hz, 6 H, CH_2), 0.95 (d, J = 7.1 Hz, 6 H, CH_2), 0.92 (d, J = 7.0 Hz, 2 H, CH_2), $^{13}C\{^1H\}$ NMR (125.8 MHz, C_6D_6, 25 °C) δ 25.7 (s, CH_3), 25.6 (s, CH_3), 25.5 (s, CH_3), 24.1, 24.05, 24.0 (s, 3:1:3 for CH_2), 23.4, 23.0, 22.6 (s, 3:1:3 for CH). MS (ESI, 100% MeOH): *m/z* 791.16 $[M + H]^+$, 80%); 813.08 $[M + Na]^+$, 100%).

§ Like many polyhedral silsesquioxanes, trisilanol **5b** crystallizes from many solvent systems as well formed but poorly diffracting (even at 158 K) crystals. Attempts to obtain a high quality set of diffraction data were unsuccessful, but a marginal set of data was eventually collected from a large crystal obtained from toluene–acetonitrile. Although the quality of the structure does not warrant a discussion of metrical data, it clearly identifies the trisilanol as *endo*-C_3-[(c-$C_4H_9)_7Si_7O_9(OH)_3$]. Crystal data for **5b** obtained by recrystallization from toluene–acetonitrile: $C_{28}H_{66}O_{12}Si_7$, M = 791.44, monoclinic, space group $P2_1/n$, a = 14.089(3), b = 21.336(5), c = 14.750(3) Å, α = γ = 90°, β = 100.119(4)°, V = 4365.1(17) Å^3, T = 158 K, Z = 4, ρ_{calcd} = 1.204 Mg m^{-3}, μ = 0.268 mm^{-1}, $F(000)$ = 1712, λ = 0.71073 Å, crystal dimensions 0.60 × 0.60 × 0.40 mm, 3.40° ⩽ 2θ ⩽ 57.5°; of the 45556 collected reflections, 10644 are independent, and these were used for the refinement of 424 parameters; R_1 = 0.166, wR_2 = 0.468 with $R_1 = \Sigma||F_o| - |F_c||/\Sigma|F_o|$ and $wR_2 = (\Sigma w(F_o^2 - F_c^2)^2/\Sigma w(F_o^2)^2)^{0.5}$. CCDC 182/1444.

¶ Selected characterization data for **5c**: $^{29}Si\{^1H\}$ NMR (99.3 MHz, C_6D_6, 25 °C) δ −56.8, −64.5, −67.4 (3:1:3); MS (ESI, 100% MeOH) *m/z*: 496.96 ($[M + H]^+$, 100%); 518.86 ($[M + Na]^+$, 75%).

1 P. G. Harrison, *J. Organomet. Chem.*, 1997, **542**, 141.
2 J. J. Schwab and J. D. Lichtenhan, *Appl. Organomet. Chem.*, 1998, **12**, 707.
3 F. J. Feher and T. A. Budzichowski, *Polyhedron*, 1995, **14**, 3239.
4 H. C. L. Abbenhuis, H. W. G. van Herwijnen and R. A. van Santen, *Chem. Commun.*, 1996, 1941.
5 H. C. L. Abbenhuis, S. Krijnen and R. A. van Santen, *Chem. Commun.*, 1997, 331.
6 M. Crocker, R. H. M. Herold and A. G. Orpen, *Chem. Commun.*, 1997, 2411.
7 T. Maschmeyer, M. C. Klunduk, C. M. Martin, D. S. Shepard, J. M. Thomas and B. F. G. Johnson, *Chem. Commun.*, 1997, 1847.
8 J. F. Brown and L. H. Vogt, *J. Am. Chem. Soc.*, 1965, **87**, 4313.
9 F. J. Feher, D. A. Newman and J. F. Walzer, *J. Am. Chem. Soc.*, 1989, **111**, 1741.
10 F. J. Feher, T. A. Budzichowski, R. L. Blanski, K. J. Weller and J. W. Ziller, *Organometallics*, 1991, **10**, 2526.
11 T. W. Hambley, T. Maschmeyer and A. F. Masters, *Appl. Organomet. Chem.*, 1992, **6**, 253.
12 J. F. Brown, *J. Am. Chem. Soc.*, 1965, **87**, 4317.
13 F. J. Feher, J. J. Schwab, D. Soulivong and J. W. Ziller, *Main Group Chem.*, 1997, **2**, 123.
14 M. Unno, K. Takada and H. Matsumoto, *Chem. Lett.*, 1998, 489.
15 O. I. Shchegolikhina, V. A. Igonin, Y. A. Molodtsova and Y. A. Pozdniakova, *J. Organomet. Chem.*, 1998, **562**, 141.
16 F. J. Feher, D. Soulivong and A. E. Eklund, *Chem. Commun.*, 1998, 399.
17 F. J. Feher, D. Soulivong and F. Nguyen, *Chem. Commun.*, 1998, 1279.
18 F. J. Feher, F. Nguyen, D. Soulivong and J. W. Ziller, *Chem. Commun.*, 1999, 1705.
19 L. H. Vogt and J. F. Brown, *Inorg. Chem.*, 1962, **2**, 189.
20 E. Rikowski and H. C. Marsmann, *Polyhedron*, 1997, **16**, 3357.
21 F. J. Feher, K. D. Wyndham, D. Soulivong and F. Nguyen, *J. Chem. Soc., Dalton Trans.*, 1999, 1491.
22 F. J. Feher, R.-Z. Jin, F. Nguyen and K. D. Wyndham, unpublished results.

Communication 9/06242D

ChemComm

Superior amine catalysts for the Baylis–Hillman reaction: the use of DBU and its implications†

Varinder K. Aggarwal* and Andrea Mereu

Department of Chemistry, University of Sheffield, Brook Hill, Sheffield, UK S3 7HF. E-mail: v.aggarwal@sheffield.ac.uk

Received (in Cambridge, UK) 27th September 1999, Accepted 8th October 1999

DBU, which is normally regarded as a hindered and non-nucleophilic base, is in fact the optimum catalyst for the Baylis–Hillman reaction, providing adducts at much faster rates than using DABCO or 3HQD; the scope of the Baylis–Hillman reaction is enhanced using this catalyst and implications of this finding are discussed.

The Baylis–Hillman reaction has great synthetic utility as it converts simple starting materials into densely functionalised products.[1] However, it suffers from low reaction rates (especially for acrylates) and this often limits the range of substrates that are tolerated. Whilst acceleration can be achieved by physical methods this usually requires specialised apparatus. We recently described a chemical method for accelerating the reaction: the use of $La(OTf)_3$ and triethanolamine as cocatalysts, which provided up to 40 fold rate increase over the use of DABCO alone.[2]

Structural variations of the amine catalyst have been probed and DABCO and 3-hydroxyquinuclidine (3-HQD) provide the highest rates. Indeed, if the optimum features of the catalyst are that it should be nucleophilic and unhindered, it is hard to imagine superior ones.[3] Here we describe our study on the nature of the catalyst and the discovery that much higher rates can be achieved with alternative structures.

The rate-determining step of the Baylis–Hillman reaction is the reaction of the aldehyde **4** with the ammonium enolate **3** (Scheme 1).[3] This enolate is formed by conjugate addition of the nucleophilic amine **1** to the Michael acceptor **2** (a reversible process) and therefore to obtain faster rates, higher *concentrations* of the enolate are required. Amines which can shift the equilibrium towards the enolate **3** by stabilising this species should achieve this. We therefore screened a range of amines which all had the potential for the positive charge on nitrogen to be stabilised through conjugation with another heteroatom (Table 1). Of the aromatic heterocyclic catalysts (entries 1, 2) only DMAP gave any Baylis–Hillman adduct,[4] but at a rate only slightly higher than DABCO (Table 2, entries 1, 3). None of the amidine catalysts (entries 4, 5) were stable under the reaction conditions except for DBU **7**, which not only gave a clean reaction but also the fastest rate (Table 1, entry 6; Table 2, entry 6). The substituted guanidine gave a lower yield due to a competing side reaction involving the acrylate (entry 7).

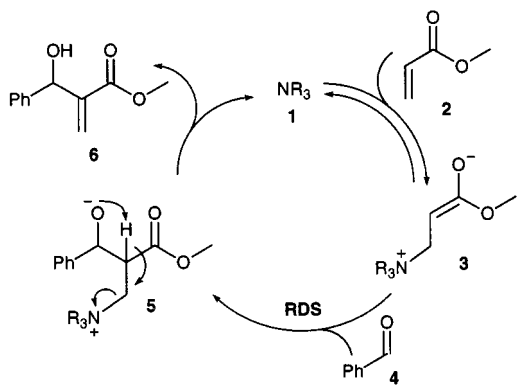

Scheme 1

In comparison with other commonly used catalysts (Table 2), DBU was over an order of magnitude faster than the current best catalyst (3-HQD, entry 4) and superior to the DABCO–$La(OTf)_3$–triethanolamine system that we have developed (entry 2).[2] Even at 10 mol% loading, DBU was superior to both stoichiometric DABCO or 3-HQD (Table 2, entry 5).[5]

We investigated the scope of the DBU-catalysed Baylis–Hillman reaction by reacting benzaldehyde with a range of Michael acceptors (Table 3), and methyl acrylate (Table 4) and cyclohex-2-en-1-one (Table 5) with a range of electrophiles.

Notable examples from Table 3 include a fast reaction with *tert*-butyl acrylate (entry 3; DABCO gives 65% yield after 28 d[6]), and a very rapid reaction with cyclohex-2-en-1-one (entry 5).[7] Methyl vinyl ketone (MVK) is not a suitable substrate with DBU (*vide infra*) but, in any case, is a fast reacting substrate with other catalysts (*e.g.* DABCO).

Notable examples from Table 4 include reaction with 4-anisaldehyde which gave a good yield after just 2 days (entry 5; DABCO gives 90% after 20 d[8]), reaction with the notoriously difficult, hindered and deactivated 2-anisaldehyde (entry 4) and

Table 1 Amine catalysts in the Baylis–Hillman reaction[a]

Entry	Nucleophilic compound	*t*/h	Yield (%)
1	Dimethylaminopyridine	96	87
2	1-Methylimidazole	120	0
3	2-Methyl-2-oxazoline	120	0
4	*N*-Methyl-4,5-dihydroimidazole	1	10[c]
5	DBN	2 min	13[d]
6	DBU	6	89
7	Substituted guanidine[d]	48	30

[a] Reactions conducted on 2 mmol scale using 1:1:1 ratio of benzaldehyde:methyl acrylate:catalyst. [b] Complex mixture of products. [c] A fast reaction occurred but the catalyst decomposed rapidly. [d] 1,3,4,6,7,8-Hexahydro-1-methyl-2*H*-pyrimido[1,2-*a*]pyrimidine.

Table 2 Comparison of DBU with the other catalytic systems[a]

Entry	Catalytic system	Reaction rate[b]	k_{rel}	*t*/h	Yield (%)
1	DABCO	0.016	1	120	91
2	DABCO–$La(OTf)_3$–$N(CH_2CH_2OH)_3$[c]	0.511	31.9	12	83
3	Dimethylaminopyridine	0.038	2.4	96	87
4	3-Hydroxyquinuclidine	0.076	4.8	30	91
5	DBU[d]	0.163	10.2	24	75
6	DBU	0.762	49.5	6	89

[a] Reactions conducted on 2 mmol scale using 1:1:1 ratio of benzaldehyde:methyl acrylate:catalyst. [b] % Product per minute. [c] 1 equiv. of DABCO, 0.05 equiv. $La(OTf)_3$ and 0.5 equiv. $N(CH_2CH_2OH)_3$. [d] 0.1 equiv.

† Experimental and spectroscopic data, and further references, are available from the RSC web site, see http://www.rsc.org/suppdata/cc/1999/2311/

Table 3 Reactions of activated alkenes with benzaldehyde[a]

Entry	Alkenes	*t*/h	Yield (%)
1	Methyl acrylate	6	89
2	Ethyl acrylate	24	80
3	*tert*-Butyl acrylate	72	74[b]
4	Acrylonitrile	3	92
5	Cyclohex-2-en-1-one	0.5	60[c]

[a] Reactions conducted on 2 mmol scale using 1:1:1 ratio of benzaldehyde: alkene : DBU. [b] No side products; 20–25% benzaldehyde and acrylate recovered. [c] No benzaldehyde remained, 30% cyclohex-2-en-1-one recovered.

Table 4 Reactions of carbonyl compounds with methyl acrylate[a]

Entry	Aldehyde	*t*/h	Yield (%)
1	Benzaldehyde	6	89
2	2-Nitrobenzaldehyde	1.5	95
3	4-Nitrobenzaldehyde	1	95
4	2-Anisaldehyde	4	25[b]
5	4-Anisaldehyde	48	62
6	Propionaldehyde	24	17[b]
7	Trimethylacetaldehyde[c]	70	20[b]
8	2,2,2-Trifluoroacetophenone	2	60[d]
9	2,2,2-Trifluoroacetophenone[e]	48	78

[a] Reactions conducted on 2 mmol scale using 1:1:1 ratio of carbonyl compound: acrylate: DBU. [b] Low yield due to decomposition of aldehyde. [c] Reaction performed in presence of 0.05 equiv. $La(OTf)_3$. [d] Product found to be unstable in presence of high concentration of catalyst. [e] 0.1 equiv. DBU used.

Table 5 Reactions of aldehydes with cyclohex-2-en-1-one[a]

Entry	Aldehyde	*t*/h	Yield (%)
1	Benzaldehyde	0.5	60
2	2-Anisaldehyde	50 min	70
3	Cyclohexanecarbaldehyde	7	73
4	Trimethylacetaldehyde[b]	21	75

[a] Reactions conducted on 2 mmol scale using 1:1:1 ratio of aldehyde: cyclohex-2-en-1-one : DBU. [b] 1.2 equiv. cyclohex-2-en-1-one and 0.05% $La(OTf)_3$ used.

for the first time reactions with pivaldehyde (entry 7)[9] and trifluoroacetophenone (entries 8, 9). Pivaldehyde required $La(OTf)_3$ to promote the reaction as no adduct was obtained without it. $La(OTf)_3$ often enhances the rates and gives higher yields of adducts (Table 4, entry 7; Table 5, entry 4) but when used with benzaldehyde a less clean reaction was observed and the additional acceleration was minimal. Aldehydes with enolisable protons gave low yields of Baylis–Hillman adducts because of competing aldol reactions.[10]

Notable examples from Table 5 include high yielding reactions with all the difficult aldehydes (2-anisaldehyde, entry 2; pivaldehyde, entry 4; even the aliphatic enolisable aldehyde cyclohexanecarbaldehyde, entry 3), demonstrating the effectiveness and superiority of this catalyst. Again $La(OTf)_3$ (5 mol%) was required in the reaction with pivaldehyde (entry 4); in its absence 44% yield of adduct was obtained after 4 days. Evidently with faster reacting enones compared to acrylates, enolisable aldehydes are better tolerated.

There is one example of the use of DBU as a catalyst for the Baylis–Hillman reaction although no comment was made on its rate.[11,12] The focus of the paper was on α-alkylation of enones with acrylates as acceptors and it was proposed that DBU acted as a base rather than a nucleophile, with the reaction occurring *via* a diene enolate rather than a β-enolate. This was supported by their observation that reaction between MVK and acetaldehyde only returned starting material. Our observation that

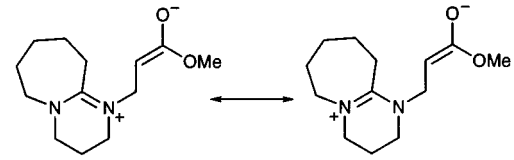

Fig. 1

acrylates work extremely well with DBU as a catalyst indicates that enolisation is *not* a requirement and that the reaction must proceed *via* the β-ammonium enolate derived from DBU and the acrylate. Furthermore we have not been able to reproduce some of their results: when we repeated the reaction between MVK and acetaldehyde we obtained polymeric material instead, no MVK was returned.

We were surprised that DBU worked so well as it is considered to be a non-nucleophilic hindered base; features that are diametrically opposite to what is normally required of amine catalysts for the Baylis–Hillman reaction. DABCO, for example, is one of the best amine catalysts and is an unhindered, nucleophilic base. The incorporation of substituents α to nitrogen result in substantial reduction in rates and this has been ascribed to the lower nucleophilicity of the base due to steric hindrance.[13] In fact, a more likely explanation is that the additional substituent contributes substantial steric hindrance to the β-ammonium enolate intermediate **3** which results in a shift in the equilibrium back to starting materials. In contrast, with DBU the intermediate β-ammonium enolate is stabilised through conjugation (Fig. 1), which increases its equilibrium concentration, and this results in significantly enhanced rates. These studies reveal that to achieve high rates in the Baylis–Hillman reaction the nucleophilicity of the amine is much less important than factors which stabilise the intermediate β-ammonium enolate.

We thank the EPSRC for financial support for this work.

Notes and references

1 For reviews see: D. Basavaiah, P. D. Rao and R. S. Hyma, *Tetrahedron*, 1996, **52**, 8001; E. Ciganek, *Org. React.*, 1997, **51**, 201.
2 V. K. Aggarwal, A. Mereu, G. J. Tarver and R. McCague, *J. Org. Chem.*, 1998, **63**, 7183; V. K. Aggarwal, G. J. Tarver and R. J. McCague, *Chem. Commun.*, 1996, 2713.
3 J. S. Hill and N. S. Isaacs, *J. Phys. Org. Chem.*, 1990, **3**, 285.
4 DMAP has been used as a catalyst for the Baylis–Hillman reaction between cyclohex-2-en-1-one and formaldehyde but no comment was made on its effectiveness or relative rate compared to DABCO. F. Rezgui and M. M. El Gaied, *Tetrahedron Lett.*, 1998, **39**, 5965.
5 At 10 mol% loading of DBU the reaction is somewhat capricious and more reliable results are obtained using a stoichiometric amount of the base. There is a variable amount of catalyst decomposition during the course of the reaction.
6 Y. Fort, M. C. Berthe and P. Caubere, *Tetrahedron*, 1992, **48**, 6371.
7 Cyclopent-2-en-1-one and cyclohept-2-en-1-one were both ineffective.
8 A. Foucaud and F. El Guemmout, *Bull. Chim. Soc. Fr.*, 1989, **3**, 403.
9 Reaction using DABCO reportedly failed. See: M. C. Berthe, P. Caubere and Y. Fort, *Eur. Pat. Appl.*, 1992, EP 465,293 (*Chem. Abstr.*, 1992, **116**, 152605c); *US Pat.*, 1994, 5,332, 836.
10 Low yields of adducts with enolisable aldehydes using DBU as a catalyst have been reported. See: D. Basavaiah and V. V. L. Gowriswari, *Synth. Commun.*, 1987, **17**, 587; P. Auvray, P. Knochel and J. F. Normant, *Tetrahedron*, 1988, **44**, 6095.
11 J. R. Hwu, G. H. Hakimalahi and C. T. Chou, *Tetrahedron Lett.*, 1992, **33**, 6469.
12 The use of DBU in the presence of 2 equiv. of 4-methoxyphenol has also been reported in a patent, although without noting its superior properties. See: K. Oohashi and S. Ido, *Jpn. Kokai Koho JP*, 1993, 05, 17,375 9Cl. C07B41/02 (*Chem. Abstr.*, 1993, **118**, 254552s).
13 R. J. W. Schuurman, A. Vanderlinden, R. P. F. Grimbergen, R. J. M. Nolte and H. W. Scheeren, *Tetrahedron*, 1996, **52**, 8307.

Communication 9/07754E

Molecular braids: quintuple helical hydrogen bonded molecular network†

Wojciech Jaunky,[a] Mir Wais Hosseini,*[a] Jean Marc Planeix,[a] André De Cian,[b] Nathalie Kyritsakas[b] and Jean Fischer[b]

[a] *Laboratoire de Chimie de Coordination Organique, Université Louis Pasteur, (CNRS UMR 7512), F-67000 Strasbourg, France. E-mail: hosseini@chimie.u-strasbg.fr*

[b] *Laboratoire de Cristallochimie et Chimie Structurale, Université Louis Pasteur, (CNRS UMR 7512), F-67000 Strasbourg, France*

Received (in Basel, Switzerland) 18th August 1999, Accepted 13th September 1999

The synthesis of 1, characterized by a calix[4]arene backbone in 1,3-alternate conformation bearing four pyridines acting as hydrogen bond acceptors, was achieved and its solid state structure studied by X-ray diffraction on a single crystal; in the presence of 4,4′-biphenol 6 acting as a dihydrogen bond donor, compound 1 formed infinite single strand helical 1-D molecular networks which upon lateral association were packed in the crystalline phase as quintuple helices.

Molecular networks are formed by molecules possessing complementary interaction sites oriented in a divergent mode. One may tune the dimensionality (1-, 2- or 3-D) and the topology of molecular networks through the interplay between complementary components. Recently, much effort has been invested in obtaining a variety of molecular networks such as inclusion,[1] hydrogen bonded[2] or coordination networks.[3] Concerning 1-D networks, the formation of helical assemblies is a subject of current interest[4,5] and the understanding of lateral interactions between helical 1-D networks remains a challenge. Examples of helical arrangements in a variety of supramolecular assemblies have been reported.[6–8]

Here, we report the synthesis of a new building block **1** characterized by a calix[4]arene backbone in 1,3-alternate conformation and bearing four pyridine groups as hydrogen bond acceptors, as well as the structural analysis of the free ligand and of its helical hydrogen bonded molecular network obtained in the presence of 4,4′-biphenol **6**.

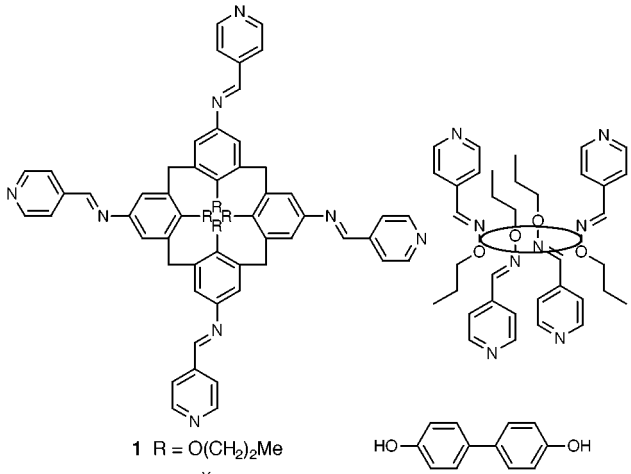

We have been interested in the formation of molecular networks using both H-bonds and electrostatic charge–charge interactions.[9] Molecular units possessing four H-bond acceptor sites occupying the apices of a pseudo-tetrahedron may be used for the formation of helical networks in the presence of H-bond donors possessing two divergently oriented polarised hydrogen atoms. The design of such a tecton may be based on a preorganised moiety such as a calix[4]arene backbone which offers the possibility of anchoring four H-bond acceptors in an alternating mode below and above its main plane. This type of unit is obtained using both the upper- and lower-rims of calix[4]arene. By transforming all four OH into OPr groups, the 1,3-alternate conformation was imposed, whereas by amination of the upper rim, four pyridines as H-bond acceptor groups were introduced through imine junctions. The choice of the imine functionality in *E* configuration connecting pyridines to the calix unit was based on the design of **1** which requires that pyridines should be oriented perpendicularly to the main plane defined by four CH_2 groups of the calix. Using the above mentioned strategy, calix[4]arene derivatives in 1,3-alternate conformation bearing catechol[10] or four nitrile groups[11] have been reported. An analogue of compound **1** with the calix unit in cone conformation was previously prepared.[12]

Dealing with the hydrogen bond donor part, 4,4′-biphenol **6** which possesses two phenolic groups oriented in a divergent mode and thus capable of forming an infinite hydrogen bonded molecular network was chosen.

Starting with **2**,[13] its tetra-alkylation with PrI in refluxing benzene and in the presence of Bu^{t}OK produced the desired compound **3** after crystallisation.[14] The latter, upon *ipso*-

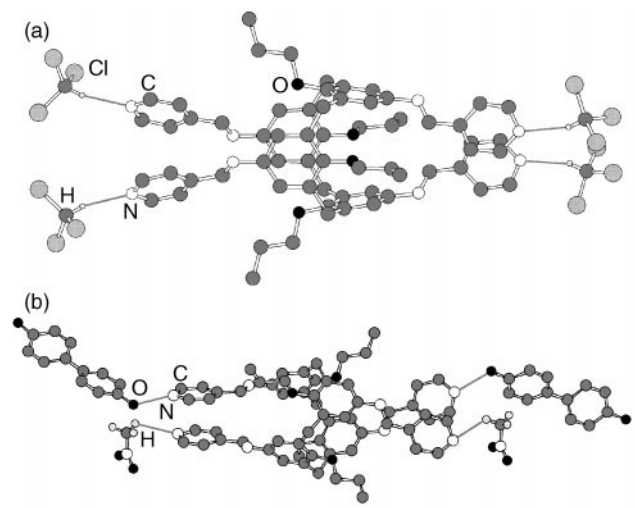

Fig. 1 (a) X-Ray structure of **1**. H atoms except for $CHCl_3$ are omitted for clarity; (b) a portion of the X-ray structure of $(\mathbf{1}\cdot\mathbf{6})_n$ H-bonded network showing the surroundings of **1** and **6**. H atoms except for $MeNO_2$ are omitted for clarity.

† Dedicated to Jean-Marie Lehn on the occasion of his 60th birthday.

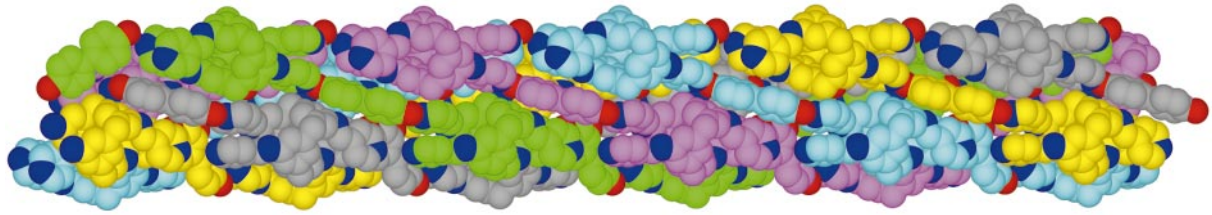

Fig. 2 A portion of the X-ray structure of (**1**·**6**)$_n$ hydrogen bonded network showing the formation of a quintuple helical arrangement comprised of five right handed helical strands represented in different colours for clarity. H atoms, O(CH$_2$)$_2$Me groups and MeNO$_2$ molecules are not shown (for distances and angles see text).

nitration,[14] gave the tetra-nitro compound **4** which was reduced to the amino compound **5** using $SnCl_2$ in EtOH.[10] Finally, treatment of **5** with 4.2 equiv. of 4-pyridylcarbaldehyde in EtOH at 80 °C in the presence of a catalytic amount of AcOH for 12 h afforded compound **1** in 52% yield after crystallisation from $CHCl_3$–MeOH.

The structure of **1** was confirmed by X-ray diffraction on a single-crystal obtained upon cooling from 80 to 25 °C a mixture of $MeNO_2$ (2 ml) and $CHCl_3$ (1 ml) containing compound **1** (2 mg).‡ As expected, compound **1** adopts a slightly pinched 1,3-alternate conformation [Fig. 1(a)]. The imine groups are in *E* configuration with an average C=N distance of 1.256 Å and C–N=C and C–N=C–C dihedral angles of 117.5 and 172.2° and −172.2° respectively. Interestingly all four pyridine units are hydrogen bonded to a $CHCl_3$ molecule with C···N and N···H distances of 3.233 and 2.338 Å respectively and an NHC angle of 156.8° demonstrating the H-bond acceptor feature of the pyridine units.

Upon slow cooling of a $MeNO_2$ (3 ml) solution of **1** (2 mg) and **6** (1.6 mg) from 80 °C to room temp., single crystals were obtained. X-Ray diffraction‡ revealed the formation of a network composed of **1**, **6** and $MeNO_2$ molecules in 1:1:1 ratio. The H-bond acceptor **1** and donor **6** form by mutual bridging a single stranded helical network which crystallises in the non-centric space group $P4_1$ or $P4_3$ [Fig. 1(b)]. The reason for the spontaneous chiral separation remains unclear. The pitch of the helix which extends along the *z* axis is composed of four **1**, four **6** and four $MeNO_2$. For each calix unit, among the four pyridines present, two of them, located on opposite sides of the backbone, participate in the formation of a helical arrangement through strong H-bonds with N···O distances of 2.703 and 2.776 Å. For the remaining two pyridines, each is located in close proximity to one $MeNO_2$ molecule with C···N distances of 3.290 and 3.312 Å. The observed helical structure is derived from the primary structure of ligand **1** which possess a S_4 screw axis. Rather interestingly, probably for best compacting reasons, five helical strands of the same handedness associate laterally in a helical fashion leading to a quintuple helical braid (Fig. 2). The formation of the braided arrangement is probably due to the uncharged nature of **1** and **6** as well as edge-to-face interactions between the pyridine units of **1** and the phenyl groups of **6** which operate in conjunction with van der Waals interactions. Finally, the quintuple helices associate laterally to form the crystal.

In conclusion, using a tetra-H-bond acceptor possessing an S_4 screw axis and a divergently oriented di-H-bond donor, a quintuple helical arrangement was obtained in the crystalline phase. The formation of the supramolecular assembly may be described as the result of molecular organisation at three different levels. The formation of a single stranded H-bonded helical network (first level), the formation of the quintuple helical braided network (second level) and the lateral association of braided networks into the compacted solid (third level). The role of the H-bond donor length and the thickness of H-bond acceptor on the pitch as well as the number of braided strands is currently under investigation.

Notes and references

‡ *Crystallographic data*: for **1** (yellow crystals, 173 K): $C_{64}H_{64}N_8O_4{\cdot}4CHCl_3$, M = 1486.79, tetragonal, space group $I4_1/a$, a = 17.3435(6), b = 17.3435(6), c = 24.104(1) Å, U = 7250.4(9) Å^3, Z = 4, D_c = 1.36 g cm^{-3}, Mo-Kα graphite monochromated radiation, kappaCCD, μ = 0.510 mm^{-1}, 2474 data with $I > 3\sigma(I)$, R = 0.067, R_w = 0.079.

For (**1**·**6**)$_n$ (colourless crystals, 173 K): $C_{64}H_{64}N_8O_4{\cdot}C_{12}H_{10}O_2{\cdot}CH_3NO_2$, M = 1256.53, tetragonal, space group $P4_1$ or $P4_3$, a = 17.208(1), c = 23.775(1) Å, U = 7039(1) Å^3, Z = 4, D_c = 1.19 g cm^{-3}, Mo-Kα graphite monochromated radiation, KappaCCD, μ = 0.078 mm^{-1}. The diffraction power of the crystal was rather poor, only 2057 reflections out of 10545 had $I > 3\sigma(I)$. Therefore, all atoms were kept with isotropic temperature factors and 2724 data with $I > 2\sigma(I)$ were used for refinements. Attempts to determine the absolute configuration using the Friedel's pair method failed. R = 0.099, R_w = 0.120. CCDC 182/1427. See http://www.rsc.org/suppdata/cc/1999/xxxx/ for crystallogrpahic files in .cif format.

1 M. W. Hosseini and A. De Cian, *Chem. Commun.*, 1998, 727.
2 M. C. Etter, *Acc. Chem. Res.*, 1990, **23**, 120; C. B. Aakeröy and K. R. Seddon, *Chem. Soc. Rev.*, 1993, **22**, 397; S. Subramanian and M. J. Zaworotko, *Coord. Chem. Rev.*, 1994, **137**, 357; D. Braga and F. Grepioni, *Acc. Chem. Res.*, 1994, **27**, 51; V. A. Russell and M. D. Ward, *Chem. Mater.*, 1996, **8**, 1654.
3 S. R. Batten and R. Robson, *Angew. Chem., Int. Ed.*, 1998, **37**, 1461.
4 C. Kaes, M. W. Hosseini, C. E. F. Rickard, B. W. Skelton and A. White, *Angew. Chem., Int. Ed.*, 1998, **37**, 920.
5 O. J. Gelling, F. van Bolhuis and B. L. Feringa, *J. Chem. Soc., Chem. Commun.*, 1991, 917; Y. Dai, T. J. Katz and D. A. Nichols, *Angew. Chem., Int. Ed. Engl.*, 1996, **35**, 2109; B. Wu, W.-J. Zhang, S.-Y. Yu and X.-Y. Wu, *Chem. Commun.*, 1997, 1795.
6 J.-M. Lehn, *Supramolecular Chemistry, Concepts and Perspectives*, VCH, Weinheim, 1995; N. Nakashima, S. Asakuma and T. Kunitake, *J. Am. Chem. Soc.*, 1985, **107**, 509; J. H. Georger, A. Singh, R. R. Price, J. M. Schnur, P. Yager and P. E. Schoen, *J. Am. Chem. Soc.*, 1987, **109**, 6169; G. P. Spada, A. Carcuro, F. P. Colonna, A. Garbesi and G. Gottarelli, *Liq. Cryst.*, 1988, **3**, 651; J.-H. Fuhrhop, P. Schnieder, E. Boekema and W. Helfrich, *J. Am. Chem. Soc.*, 1988, **110**, 2861.
7 C. Fouquey, J.-M. Lehn and A. M. Levelut, *Adv. Mater.*, 1990, **5**, 254; S. J. Geib, C. Vicent, E. Fan and A. D. Hamilton, *Angew. Chem., Int. Ed. Engl.*, 1993, **32**, 119; S. Hanessian, A. Gomtsyam, M. Simard and S. Roelens, *J. Am. Chem. Soc.*, 1994, **116**, 4495; K. Tanaka and Y. Kitahara, *Chem. Commun.*, 1998, 1141.
8 E. C. Constable, in *Comprehensive Supramolecular Chemistry*, ed. J. L. Atwood, J. E. D. Davies, D. D. Macnicol and F. Vögtle, Pergamon, 1996, vol. 9 (ed. J.-P. Sauvage and M. W. Hosseini), p. 213; C. Piguet, G. Bernardinelli and G. Hopfgarten, *Chem. Rev.*, 1997, 2005.
9 O. Félix, M. W. Hosseini, A. De Cian and J. Fischer, *Angew. Chem., Int. Ed. Engl.*, 1997, **36**, 102; O. Félix, M. W. Hosseini, A. De Cian and J. Fischer, *New J. Chem.*, 1998, **22**, 1389.
10 G. Mislin, E. Graf and M. W. Hosseini, *Tetrahedron Lett.*, 1996, **37**, 4503.
11 G. Mislin, E. Graf, M. W. Hosseini, A. De Cian, N. Kyritsakas and J. Fischer, *Chem. Commun.*, 1998, 2545.
12 X. Yang, D. McBranch, B. Swanson and D.-Q. Li, *Angew. Chem., Int. Ed. Engl.*, 1996, **35**, 538.
13 C. D. Gutsche and M. Iqbal, *Org. Synth.*, 1989, **68**, 234.
14 W. Verboom, S. Datta, Z. Asfari, S. Harkema and D. N. Reinhoudt, *J. Org. Chem.*, 1992, **57**, 5394.

Communication 9/06728K

Synthesis and structures of a triply-fused incomplete-cubane cluster $[\{(\eta^5\text{-}C_5Me_5)WS_3\}_3Cu_7(MeCN)_9](PF_6)_4$ and a 2D polymer $[(\eta^5\text{-}C_5Me_5)WS_3Cu_3Cl(MeCN)(pz)]PF_6$ (pz = pyrazine)

Jian-Ping Lang, Hiroyuki Kawaguchi and Kazuyuki Tatsumi*

Research Center for Materials Science and Department of Chemistry, Graduate School of Science, Nagoya University, Furo-cho, Chikusa-ku, Nagoya 464-8602, Japan. E-mail: i45100a@nucc.cc.nagoya-u.ac.jp

Received (in Cambridge, UK) 27th July 1999, Accepted 8th October 1999

The reaction of $PPh_4[(\eta^5\text{-}C_5Me_5)WS_3]$ with 3 equiv. of $[Cu(MeCN)_4]PF_6$ in MeCN yielded an unusual high nuclearity W/Cu/S cluster $[\{(\eta^5\text{-}C_5Me_5)WS_3\}_3Cu_7(MeCN)_9](PF_6)_4$ 1, which in turn gave rise to a 2D polymer $[(\eta^5\text{-}C_5Me_5)WS_3Cu_3Cl(MeCN)(pz)]PF_6$ 2 upon treatment with pyrazine in MeCN in the presence of LiCl.

The transition metal-mediated self-assembly of inorganic clusters and extended macromolecular structures is of intense interest to chemists, and a remarkable range of polynuclear structures have emerged.[1–4] Homoleptic acetonitrile complexes $[M(MeCN)_m]^{n+}$ have often been used as convenient precursors for such molecular ensembles of transition metal compounds, since they undergo facile substitution of MeCN and adduct formation with N-donor ligands.[5] On the other hand, we have been interested in construction of new heterometallic sulfide clusters based on the organometallic trisulfide complex anions of group 5 and 6 metals, $[(\eta^5\text{-}C_5Me_5)MS_3]^{2-}$ (M = Nb, Ta)[6,7] and $[(\eta^5\text{-}C_5Me_5)MS_3]^-$ (M = Mo, W).[8,9] As a part of such a study, a series of $(\eta^5\text{-}C_5Me_5)M/M'/S$ clusters, consisting of tungsten and coinage metal atoms (M′), have been synthesized.[10–16] For instance, treatment of $[(\eta^5\text{-}C_5Me_5)WS_3]^-$ with CuNCS, CuBr, CuCl and $[Cu(PPh_3)_2]NO_3$ resulted in the formation of various $(\eta^5\text{-}C_5Me_5)W/Cu/S$ clusters with the nuclearity varying from WCu_3 to W_3Cu_9.[12–16]

In an attempt to expand the scope of the cluster syntheses, we examined the reaction of $PPh_4[(\eta^5\text{-}C_5Me_5)WS_3]$ with $[Cu(MeCN)_4]PF_6$, and isolated a triply-fused incomplete-cubane cluster $[\{(\eta^5\text{-}C_5Me_5)WS_3\}_3Cu_7(MeCN)_9](PF_6)_4$ **1**. Furthermore, we constructed a 2D polymeric structure $[(\eta^5\text{-}C_5Me_5)WS_3Cu_3Cl(MeCN)(pz)]PF_6$ **2** by treating **1** with pyrazine (pz) in the presence of LiCl. We report herein the synthesis and structures of these cluster/polymer compounds.

Compounds **1** and **2** were synthesized by the following procedures. When $[Cu(MeCN)_4]PF_6$ (0.17 g, 0.45 mmol) was added to a red MeCN (20 ml) solution of $PPh_4[(\eta^5\text{-}C_5Me_5)WS_3]$ (0.11 g, 0.15 mmol) under Ar, the solution darkened immediately. After stirring the solution overnight at room temperature, it was concentrated and layered by Et_2O, from which dark red cubic crystals of **1** were obtained in 76% yield. Complex **1** (0.052 g, 0.02 mmol) was then treated with 1 equiv. of LiCl in MeCN for 1 h at room temperature. 1 equiv. of pyrazine was added to the resulting homogenous solution which was stirred for 10 min. Subsequent work-up similar to that used for crystallization of **1** generated dark red plates of **2** in 67% yield. Compounds **1** and **2** are both stable toward oxygen and moisture and soluble in MeCN and DMSO.†

X-Ray analysis of **1**‡ revealed that a discrete cluster complex $[\{(\eta^5\text{-}C_5Me_5)WS_3\}_3Cu_7(MeCN)_9]^{4+}$ is accompanied by four PF_6^- counter anions. Being tetracationic, the cluster is considered as composed of three W(VI) and seven Cu(I) metal ions, and thus no redox process occurred during the cluster forming reaction. As shown in Fig. 1, the tetracationic cluster contains three $(\eta^5\text{-}C_5Me_5)WS_3$ units linked by two copper atoms, Cu(3) and Cu(5), and five more coppers chelate the sulfur ends to form a $W_3Cu_7S_9$ core. While the bridging coppers

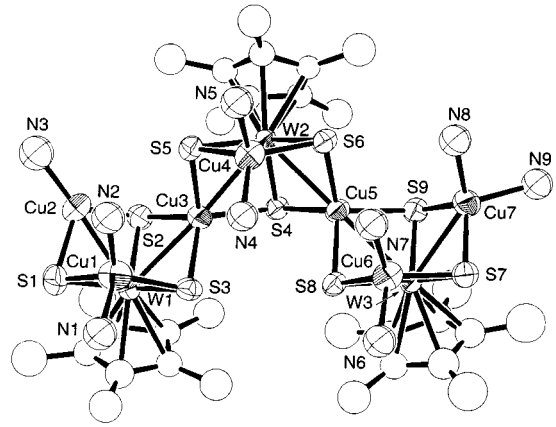

Fig. 1 Structure of the complex tetracation of **1**, with labelling scheme and 50% thermal ellipsoids. The MeCN molecules coordinated at the Cu atoms are represented by the pivotal N atoms only for clarity.

are tetrahedrally surrounded by four sulfurs, a total of nine acetonitrile molecules further coordinate to the latter five coppers to complete their coordination geometries. Alternatively, the core geometry of **1** can be viewed as a corner-shared triply-fused WCu_3S_3 incomplete cubane cluster. Interestingly, the resulting cluster structure is unsymmetric in that Cu(2) coordinates only one acetonitrile while each of the other coppers coordinates two acetonitrile molecules. It is rather surprising that one copper, Cu(2), assumes a trigonal planar coordination geometry with N(MeCN) and two μ_3-S atoms, despite the fact that the cluster was synthesized and recrystallized using MeCN as a solvent. The geometry of each incomplete WS_3Cu_3 cube of **1** is similar to those of the related double incomplete cubane clusters $[PPh_4]_2[(\eta^5\text{-}C_5Me_5)WS_3Cu_3X_3]_2$ (X = Br, Cl), as are the W–(μ_3-S) bond lengths.[12,14] It is noteworthy here that the W–Cu distances of **1** can be classified into three groups; a short W(1)–Cu(2) bond of 2.620(3) Å, long W–Cu(3,5) bonds of 2.759(3)–2.779(3) Å, and the remainder of W–Cu bonds with intermediate distances of 2.695(3)–2.720(4) Å. The observed trend of W–Cu bond lengths correlates with the number of bonding interactions at the Cu centers. The long W–Cu distances occur at Cu atoms, Cu(3) and Cu(5), each of which interacts with four S ligands and two W atoms, while the short W–Cu distance is observed for Cu(2) which interacts with three ligands and one W atom.

Compound **2**‡ has a 2D sheet structure in the crystalline state as shown in Fig. 2, which stacks along the crystallographic *b* axis. Fig. 3 displays the repeating unit of the 2D network and its connectivity. The cluster components, $[(\eta^5\text{-}C_5Me_5)WS_3Cu_3(MeCN)]$, are linked by pyrazine through interactions with Cu(1) and Cu(2′), to form zigzag chains extending along the *a* axis where the orientation of the $[(\eta^5\text{-}C_5Me_5)WS_3Cu_3(MeCN)]$ unit is alternating. The chains are then connected by μ-Cl at Cu(2*) and Cu(3) along the *c* axis. In the pyrazine linkage, two Cu–N bond distances are virtually the same, Cu(1)–N1 1.96(1)

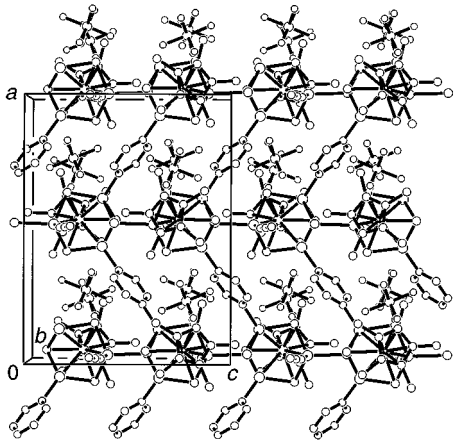

Fig. 2 Extended 2D layer structure of **2** looking down the *b* axis.

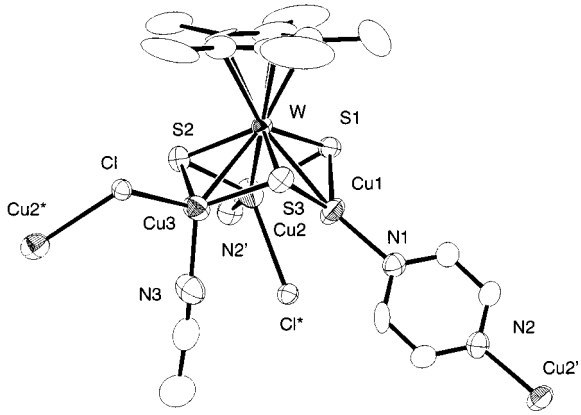

Fig. 3 Structure of a repeating unit of **2** with 50% thermal ellipsoids.

Å *cf.* Cu(2′)–N2 1.99(1) Å, while the μ-Cl bridge occurs in a less symmetric fashion with a Cu(2*)–Cl–Cu(3) angle of 106.8°, and the bonding with Cu(3) is substantially stronger, Cu(2*)–Cl 2.584(4) Å *cf.* Cu(3)–Cl 2.418(4) Å. The resulting 2D network forms a parallelogrammic mesh, and each cavity is filled by a PF_6^- anion. The surfaces of each layer are covered with η^5-C_5Me_5 rings, and the thickness of the layers is estimated to be *ca.* 9.9 Å. The layers are separated by *ca.* 3.5 Å, and no inter-layer bonding interactions were observed. The W(VI) and Cu(I) oxidation states are again retained in **2**, and the geometry of the WS_3Cu_3 incomplete cubane unit resembles closely those of **1** and $[PPh_4]_2[(\eta^5\text{-}C_5Me_5)WS_3Cu_3X_3]_2$.[12,14] Of the three copper atoms, Cu(1) is coordinated by three ligands, N(pz) and two μ_3-S atoms, and the W–Cu(1) distance is relatively short [2.654(2) Å]. On the other hand, Cu(2) and Cu(3) are coordinated by four ligands, N(pz or MeCN), μ-Cl and two μ_3-S atoms, and the W–Cu interactions are slightly weaker [2.673(2) and 2.722(2) Å].

The triply-fused incomplete-cubane $W_3S_9Cu_7$ framework of **1** is broken during the reaction with LiCl and pyrazine, providing a WS_3Cu_3 incomplete-cubane cluster as a building block of the stacked sheet structure of **2**. A key factor of this transformation is coordination of labile MeCN molecules at Cu in **1**. The formation of the intriguing 2D layer structure of **2** suggests that the construction of various types of 2D/3D extended structures will be made possible by reactions of **1** with appropriate hooking ligands such as 4,4′-bipyridine and dicyanoquinodiimine, *etc.*

Notes and references

† Synthetic manipulations were carried out under an argon atmosphere. *Spectroscopic data*: for **1**: IR (KBr, cm^{-1}): ν(C≡N) 2312m, 2279m; ν(P–F) 839vs, 558s; ν(W–S_{br}) 432w, 408m, 410m. UV–VIS (MeCN): λ_{max}/nm (ε/M^{-1} cm^{-1}) 405 (13 000). ^{1}H NMR (DMSO-d_6, 500 MHz), δ 2.18 (s, 45H, η^5-C_5Me_5), 2.08 (s, 27H, MeCN) (Found: C, 21.89; H, 2.71; N, 5.03; S, 10.27. Calc. for $C_{48}H_{72}Cu_7F_{24}N_9P_4S_9W_3$: C, 21.84; H, 2.75; N, 4.78; S, 10.93%). For **2**: IR (KBr, cm^{-1}): ν(C≡N) 2307m, 2287m; ν(P–F) 838vs, 558s; ν(W–S_{br}) 429w, 407m. UV–VIS (MeCN): λ_{max}/nm (ε/M^{-1} cm^{-1}) 421 (4100). ^{1}H NMR (DMSO-d_6, 500 MHz), δ 8.83 (s, 4H pz), 2.17 (s, 15H, η^5-C_5Me_5), 2.07 (s, 3H, MeCN) (Found: C, 21.23; H, 2.48; N, 4.75; S, 10.23. Calc. for $C_{16}H_{22}ClCu_3F_6PS_3W$: C, 21.17; H, 2.45; N, 4.63; S, 10.60%).

‡ *Crystal data* for **1**: $C_{48}H_{72}Cu_7F_{24}N_9P_4S_9W_3$, M = 2639.93, orthorhombic, space group *Pbca*, a = 25.23(1), b = 31.84(1), c = 20.951(8) Å, V = 16835(11) Å^3, Z = 8. Of 8574 reflections collected (Mo-Kα, $2\theta_{max}$ = 45.0°) on a Rigaku AFC7R diffractometer, 5252 [$I > 3.00\sigma(I)$] were observed. The structure was solved by direct methods and expanded using Fourier techniques with the TEXSAN program package. W, Cu, S and P atoms were refined anisotropically while F, N and C atoms were refined isotropically. H atoms were put on the calculated positions without refinement. The R values are $R = \Sigma(|F_o| - |F_c|)/\Sigma|F_o|$ = 0.054 and $R_w = [\Sigma w(|F_o| - |F_c|)^2/\Sigma w|F_o|^2]^{1/2}$ = 0.064. For **2**: $C_{16}H_{22}N_3ClCu_3F_6PS_3W$, M = 907.46, orthorhombic, space group *Pbca*, a = 16.055(3), b = 26.78(1), c = 12.295(5) Å, V = 5285(3) Å^3, Z = 8. Of 5203 reflections collected (Mo-Kα, $2\theta_{max}$ = 50.1°), 2830 [$I > 3.00\sigma(I)$] were observed. The structure was solved by the Patterson method. All nonhydrogen atoms were refined anisotropically, and H positions were idealized. The final R values are R = 0.046 and R_w = 0.050.

CCDC 182/1443. See http://www.rsc.org/suppdata/cc/1999/2315/ for crystallographic files in .cif format.

1 J.-M. Lehn, *Supramolecular Chemistry: Concepts and Perspectives*, VCH, Weinheim, 1995.
2 E. C. Constable, in *Comprehensive Supramolecular Chemistry*, ed. J.-M. Lehn, Pergamon, Oxford, 1996, vol. 9.
3 P. J. Stang and B. Olenyuk, *Acc. Chem. Res.*, 1997, **30**, 502.
4 M. Fujita, F. Ibukuro, H. Hagihara and K. Ogura, *Nature*, 1994, **367**, 720.
5 K. R. Dunber and R. A. Heintz, *Prog. Inorg. Chem.*, 1996, **45**, 283.
6 K. Tatsumi, Y. Inoue, A. Nakamura, R. E. Cramer and W. VanDoorne, *J. Am. Chem. Soc.*, 1989, **111**, 782.
7 K. Tatsumi, H. Kawaguchi, Y. Inoue, A. Nakamura, R. E. Cramer and J. A. Golen, *Angew. Chem., Int. Ed. Engl.*, 1993, **32**, 763.
8 H. Kawaguchi, K. Yamada, J.-P. Lang and K. Tatsumi, *J. Am. Chem. Soc.*, 1997, **119**, 10 343.
9 H. Kawaguchi and K. Tatsumi, *J. Am. Chem. Soc.*, 1995, **117**, 3885.
10 J.-P. Lang, H. Kawaguchi and K. Tatsumi, *Inorg. Chem.*, 1997, **36**, 6447.
11 J.-P. Lang and K. Tatsumi, *Inorg. Chem.*, 1999, **38**, 1364.
12 J.-P. Lang, H. Kawaguchi, S. Ohnishi and K. Tatsumi, *Chem. Commun.*, 1997, 405.
13 J.-P. Lang and K. Tatsumi, *Inorg. Chem.*, 1998, **37**, 160.
14 J.-P. Lang, H. Kawaguchi, S. Ohnishi and K. Tatsumi, *Inorg. Chim. Acta*, 1998, **283**, 136.
15 J.-P. Lang, H. Kawaguchi and K. Tatsumi, *J. Organomet. Chem.*, 1998, **569**, 109.
16 J.-P. Lang and K. Tatsumi, *J. Organomet. Chem.*, 1999, **579**, 332.

Communication 9/06081B

Nitric oxide release from *S*-nitrosoglutathione (GSNO)

Darren R. Noble, Helen R. Swift and D. Lyn H. Williams*

Chemistry Department, University of Durham, South Road, Durham, UK DH1 3LE.
E-mail: d.l.h.williams@durham.ac.uk

Received (in Cambridge, UK) 30th September 1999, Accepted 11th October 1999

In the presence of Cu^{2+} (10^{-5} M) very little NO is generated from GSNO at ~10^{-3} M at pH 7.4, whereas the reaction is quantitative at ~10^{-6} M; this is explicable in terms of the complexation of Cu^{2+} by the product GSSG.

Interest in the biological chemistry of nitric oxide (NO) continues to expand as its range of known biological functions increases. *S*-Nitrosothiols (RSNO) are currently believed to play an important part *in vivo* in the storage and transport of NO.[1] Additionally, RSNO species, particularly *S*-nitrosoglutathione (GSNO), have wide applicability as NO donors.

It has been something of a puzzle that very little NO appears to be generated from GSNO in solution at pH 7.4 when it is at a concentration of ~1×10^{-3} mol dm^{-3}, whereas this nitrosothiol has been, and continues to be, widely used as a NO donor in a variety of experiments, both *in vitro* and *in vivo*. Indeed GSNO has been used for this purpose medicinally.[2] Most of the experiments relating to mechanistic studies of this reaction have followed the disappearance, spectrophotometrically, of the band at ~340 nm, characteristic of all RSNO species. Because of the relatively low extinction coefficients at this wavelength (~10^3 mol dm^{-3} cm^{-1}), suitable concentrations for conventional spectrophotometers are in the range 10^{-3}–10^{-4} mol dm^{-3}. The reaction mechanism has been shown[3] to involve [eqns. (1) and (2)] reaction with Cu^+ generated by reduction of Cu^{2+} by thiolate ion; the former is

$$2Cu^{2+} + 2RS^- = 2Cu^+ + RSSR \quad (1)$$

$$Cu^+ + RSNO = Cu^{2+} + RS^- + NO \quad (2)$$

often present as an impurity at low concentration levels, and the latter is always present at low concentration, because of the slight reversibility of RSNO formation from nitrous acid and a thiol.[4] We,[5] and others,[6] have shown that even at these millimolar concentrations, reaction can, however, be made quantitative by the addition of further amounts of Cu^{2+} or thiolate ion. For example the half-life for effectively quantitative decomposition of GSNO (5×10^{-4} mol dm^{-3}) containing added Cu^{2+} (5×10^{-5} mol dm^{-3}) and glutathione (GSH) (5×10^{-5} mol dm^{-3}) is ~15 min. Addition of the metal ion chelator EDTA stops the reaction completely.

We now report results from the direct measurement of NO produced from GSNO over a range of initial concentrations of GSNO (3×10^{-6} to 4×10^{-4} mol dm^{-3}), all at pH 7.4, and in the presence of added Cu^{2+} (1×10^{-5} mol dm^{-3}). Measurements were made using a commercial NO probe (WPI ISO-NO Mark II), which was calibrated using NO generated from nitrous acid and ascorbate. The results are quite dramatic, and are presented in Fig. 1 as the percentage yield NO as a function of time, generated from the different GSNO concentrations. At the lowest concentrations studied it is clear that the yield of NO is essentially quantitative, whereas as the [GSNO] is increased this yield falls, until at 4×10^{-4} mol dm^{-3} the yield of NO is only ~5%.† The last trace confirms the result (~5% decomposition) obtained spectrophotometrically at this concentration. Again no reaction occurred when EDTA was added. A similar result was obtained without added Cu^{2+}, relying on the impurity Cu^{2+} levels in the water/buffer components, but reaction rates were somewhat less.

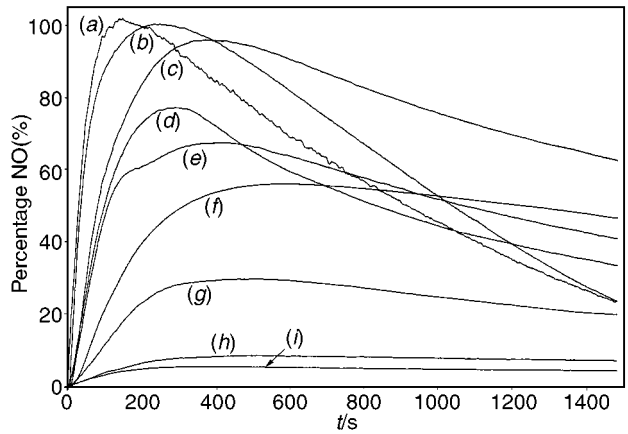

Fig. 1 The percentage NO generated from GSNO in the presence of added Cu^{2+} (1×10^{-5} mol dm^{-3}) as a function of the initial [GSNO]: (*a*) 3.0×10^{-6}, (*b*) 6.2×10^{-6}, (*c*) 1.2×10^{-5}, (*d*) 2.0×10^{-5}, (*e*) 2.3×10^{-5}, (*f*) 3.1×10^{-5}, (*g*) 7.4×10^{-5}, (*h*) 2.2×10^{-4} and (*i*) 3.7×10^{-4} mol dm^{-3}.

An explanation of these unusual results can be obtained if we consider the possibility that the organic product, the oxidised form of glutathione (GSSG), itself complexes the Cu^{2+} ions. Such complexes are well-known,[7] and have been identified spectrally. The suggested structure for the 1:1 complex with GSSG (absorption maxima at 250 and 625 nm) is given as **1**, but at higher [Cu^{2+}] a 2:1 complex has also been isolated and its crystal structure established.[8] The characteristic shoulder at 250 nm could be observed in the final spectrum from GSNO decomposition in our experiments.

To test this idea more directly we carried out the reaction of GSNO (3×10^{-6} mol dm^{-3}) in the presence of increasing amounts of added GSSG in the range 1×10^{-5} to 2×10^{-4} mol dm^{-3}). The results are given in Fig. 2. It is clear that, over this range, the percentage yield of NO decreases progressively from ~90 to ~10%.

Exactly the same pattern (not shown) was found for the reaction studied spectrophotometrically, *i.e.* at higher [GSNO], with added Cu^{2+} and GSH, when again addition of GSSG progressively stopped the reaction at incomplete conversion.

This explains our present set of results. The product GSSG is in effect acting as a metal ion chelator (for Cu^{2+} in this case), preventing reaction from occurring as the copper is removed from solution. It is to be expected that this effect is more marked

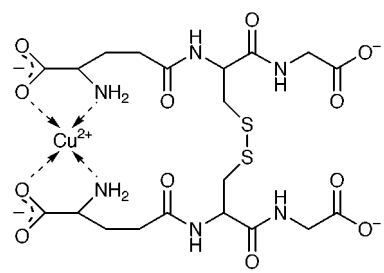

1

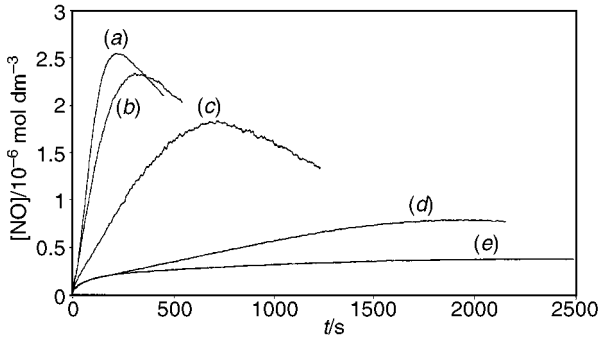

Fig. 2 The percentage NO generated from GSNO (3.1×10^{-6} mol dm^{-3}) in the presence of added Cu^{2+} (1×10^{-5} mol dm^{-3}) as a function of added GSSG: (*a*) 0, (*b*) 1.0×10^{-5}, (*c*) 2.0×10^{-5}, (*d*) 5.0×10^{-5} and (*e*) 2.0×10^{-4} mol dm^{-3}.

at the higher [GSNO], since more GSSG is then generated. Obviously the addition of more Cu^{2+} under these conditions will help promote reaction, as will the addition of GSH, since we propose that thiol/thiolate will be able to generate Cu^{+} from the GSSG–Cu^{2+} complex. We have tested this by addition of GSH to a solution of GSSG–Cu^{2+}, when the low extinction absorbance peak at 625 nm disappeared, and when the specific Cu^{+} chelator neocuproine[9] was added, the characteristic absorbance at 453 nm was immediately formed, corresponding to 82% conversion to Cu^{+}. So added GSH not only generates Cu^{+} from Cu^{2+} to start off the reaction, but also can generate Cu^{+} from the product GSSG–Cu^{2+} complex, allowing reaction to go on to completion. In the absence of added GSH however, when its concentration is very low, the inequality [GSSG] > [GSH] soon applies in the early stages of the reaction, and Cu^{+} cannot be retrieved from the GSSG–Cu^{2+} complex and reaction effectively ceases.

Higher concentrations of added GSH (1×10^{-4} to 1×10^{-3} mol dm^{-3}) inhibit NO formation from GSNO, probably since GSH–Cu^{+} complexes[10] are formed. Much higher thiolate concentrations lead to a totally new reaction where the main nitrogen product is ammonia and not NO.[11]

It has also been suggested[6] that the Cu^{+}-promoted decomposition of GSNO does not involve reoxidation of Cu^{+}, since no complex formation occurred when the specific Cu^{2+} chelator cuprizone was added. We found that Cu^{2+} is complexed more strongly to GSSG than it is to cuprizone, since when Cu^{2+} was added to equal concentrations of cuprizone and GSSG, no cuprizone complex is formed. However, we also find that cuprizone does stop the reaction of *S*-nitroso-*N*-acetylpenicillamine (SNAP), added either at the start or after ~60% reaction. In this case the disulfide does not have an inhibiting effect on the reaction.

We have looked briefly at the decomposition characteristics of *S*-nitrosocysteine (SNC). In contrast to the behaviour of GSNO, SNC decomposes quantitatively to give NO and cystine, even at the higher millimolar concentrations. When we examine the decomposition as a function of initial [SNC], we find that there is no great change, either in the rate of reaction, or in the NO yield over the range 3×10^{-6} to 1×10^{-3} mol dm^{-3}. The absence of the glutamyl residue here does not allow complex formation as in **1**.

It is probable the unreactivity of *S*-nitrosocaptopril at millimolar concentrations arises from the Cu^{2+}-complexing ability of the product disulfide since it contains a similar arrangement of atoms as in the glutamate residue in glutathione. This hypothesis remains to be tested.

A necessary consequence of our present results is that no structure–reactivity conclusions can be drawn from the rate constants (measured over a range of [Cu^{2+}]) of different RSNO structures, *when they have been measured at the millimolar concentration level*. This includes a series of rate constants reported earlier by us.[12] We no longer need to invoke the requirement of bidentate coordination of Cu^{+} with the nitroso group and a free amino group. GSNO and SNC have comparable decomposition reactivities at micromolar concentrations. The apparent greater reactivity of SNC at millimolar concentrations is not due, as previously thought, to the enhanced reactivity of SNC (because of the possibility of strong bidentate coordination of Cu^{+}), but rather due to the much reduced reactivity of GSNO due to the strong chelation of Cu^{2+} by the product GSSG. This effect was also found to be a major factor in the decomposition characteristics of a novel *S*-nitroso sugar derivative.[13]

We thank the EPSRC for a Research Grant which supported this work.

Notes and references

† Ideally the NO traces should level off when reaction is effectively over. The falling away must represent loss of NO either by oxidation or some other reaction.

1 J. S. Stamler, O. Jaraki, J. Osborne, D. I. Simon, J. Keaney, J. Vita, D. Singel, C. R. Valeri and J. Loscalzo, *Proc. Natl. Acad. Sci. U.S.A.*, 1992, **89**, 7674; R. M. Clancy, D. Levartovsky, J. Leszczynska-Piziak, J. Yegudin and S. B. Abramson, *Proc. Natl. Acad. Sci. U.S.A.*, 1994, **91**, 3680.
2 A. de Belder, C. Lees, J. Martin and S. Moncada, *Lancet*, 1995, **345**, 124.
3 A. P. Dicks, H. R. Swift, D. L. H. Williams, A. R. Butler, H. H. Al-Sadoni and B. G. Cox, *J. Chem. Soc., Perkin Trans. 2*, 1996, 481.
4 P. H. Beloso and D. L. H. Williams, *Chem. Commun.*, 1997, 89.
5 D. L. H. Williams, *Chem. Commun.*, 1996, 1085.
6 A. C. F. Gorren, A. Schrammel, K. Schmidt and B. Mayer, *Arch. Biochem. Biophys.*, 1996, **330**, 219.
7 K. Varnagy, I. Sovago and H. Kozlowski, *Inorg. Chim. Acta*, 1988, **151**, 117.
8 K. Miyoshi, Y. Sugiura, K. Ishizu, Y. Iitaka and H. Nakamura, *J. Am. Chem. Soc.*, 1980, **102**, 6130.
9 Y. Yoshida, J. Tsuchiya and E. Niki, *Biochem. Biophys. Acta*, 1994, **1200**, 85.
10 I. G. Dance, *J. Chem. Soc., Chem. Commun.*, 1976, 68; R. Chada, R. Kumar and D. G. Tuck, *J. Chem. Soc., Chem. Commun.*, 1986, 68.
11 S. P. Singh, J. S. Wishnok, M. Keshive, W. Deen and S. R. Tannenbaum, *Proc. Natl. Acad. Sci. U.S.A.*, 1996, **93**, 14 428; A. P. Dicks, E. Li, A. P. Munro, H. R. Swift and D. L. H. Williams, *Can. J. Chem.*, 1998, **76**, 789.
12 S. C. Askew, D. J. Barnett, J. McAninly and D. L. H. Williams, *J. Chem. Soc., Perkin Trans. 2*, 1995, 741.
13 A. P. Munro and D. L. H. Williams, *Can. J. Chem.*, 1999, **77**, 550.

Communication 9/07891F

Porphyrinogen tetraanion functioning as a polymetallic assembler: nickel-*meso*-octaethylporphyrinogen binding four transition metal ions at the periphery

Lucia Bonomo, Euro Solari, Géraldine Martin, Rosario Scopelliti and Carlo Floriani*

Institut de Chimie Minérale et Analytique, BCH, Université de Lausanne, CH-1015 Lausanne, Switzerland. E-mail: carlo.floriani@icma.unil.ch

Received (in Basel, Switzerland) 6th September 1999, Accepted 15th October 1999

Nickel(II)-*meso*-octaethylporphyrinogen dianion behaves as a π-extended ligand binding four M(CO)$_3$ [M = Cr, Mo] fragments at the periphery, so that the porphyrinogen can assemble five metal centers around itself.

The interest in polymetallic frameworks is exponentially increasing in the domain of discovering cooperative metallic properties, *i.e.* magnetic or chemical reactivity, and, in general, in the context of materials science.[1] One of the molecular approaches to extended polymetallic structures is focused on organic fragments which, by displaying a variety of bonding modes, can assemble the maximum number of metal ions around themselves, as shown in the pioneering work by Constable and co-workers.[2] Such an assembly may function as a building block for extended structures. In this context, we should mention the *meso*-octaalkylporphyrinogen tetraanion,

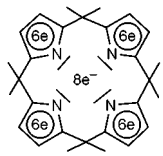

which binds the metal both by the use of the N_4 core and the pyrroles functioning similarly to cyclopentadienyl anions in the periphery.[3–6] A peculiar property of such dimetallic systems is the electron transfer occurring between the ligand and the peripheral metals.[4] The present report deals with the maximum exploitation of the metal binding ability of the porphyrinogen tetraanion making use of its 32 available electrons for binding up to five metal ions.[3e,5]

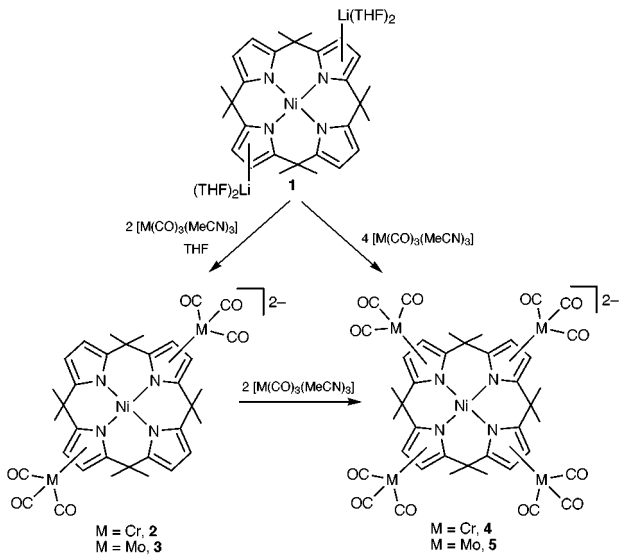

Scheme 1

The synthetic sequence is displayed in Scheme 1. The reaction of the nickel-porphyrinogen dianion **1**[6] with 2 mol $[M(CO)_3(MeCN)_3]$[7] [M = Cr, Mo] led to the dimetallated forms **2** and **3**,† which can be further metallated to **4** and **5**,‡ thus forming polymetallic porphyrinogen complexes (65–80%). Each pyrrole functions as an η^5 binding site in the two step reaction and displaces the three labile acetonitriles from the group VI metals. Although the complexes are displayed in Scheme 1 as anions, they occur as ion-pairs in the solid state with lithium cations binding to the oxygens of the carbonyls.[8] The IR spectra in the solid state are somewhat complicated by

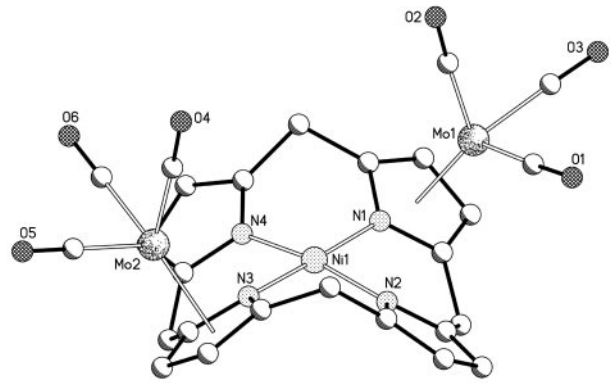

Fig. 1 A plot showing the dianion of compound **3**. Selected bond distances (Å): Ni1–N_{av} 1.877(3), Mo1–η^5(Pyr) 2.087(2), Mo2–η^5(Pyr) 2.091(2), Mo1–C_{av} 1.918(5), Mo2–C_{av} 1.903(6), C–O_{av} 1.177(6), out of plane Ni1–N_4 0.069(2). η^5(Pyr) indicates the centroid.

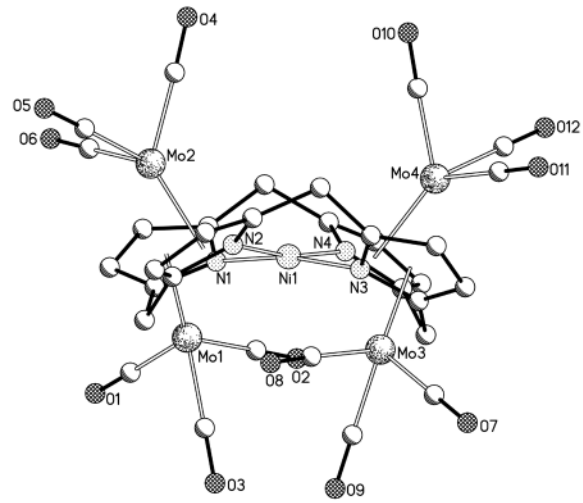

Fig. 2 A plot showing the dianion of compound **5**. Selected bond distances (Å): Ni1–N_{av} 1.874(3), Mo1–η^5(Pyr) 2.079(2), Mo2–η^5(Pyr) 2.086(2), Mo3–η^5(Pyr) 2.084(2), Mo4–η^5(Pyr) 2.087(2), Mo1–C_{av} 1.929(5), Mo2–C_{av} 1.926(5), Mo3–C_{av} 1.921(5), Mo4–C_{av} 1.922(5), C–O_{av} 1.173(6), out of plane Ni1–N_4 0.002(2). η^5(Pyr) indicates the centroid.

the lowering of the local symmetry due to solid state effects and the lithium–oxygen interactions, while in solution all complexes have C–O stretching vibrations according to a C_{3v} symmetry or very close to it. Further characterization has been carried out using ^{1}H NMR and X-ray analysis for both **3** and **5**, the structures being displayed in Figs. 1 and 2, respectively, with some relevant structural parameters provided in the captions.§

The first two $M(CO)_3$ fragments bind η^5 to two *trans*-pyrroles and are arranged *syn* to each other. The porphyrinogen displays a saddle-shape conformation, with the usual trend in the structural parameters. The overall conformation of the ligand does not change significantly moving from **3** to **5**, with the four $M(CO)_3$ fragments η^5-bonded to the four pyrroles. The sequence is up and down, so that two are bonded at the upper face and two at the bottom face. The structural parameters of the Ni-porphyrinogen moiety[6a] are not particularly affected by the presence of the $Mo(CO)_3$ fragments. In both complexes some of the lithium cations are associated with the carbonyl oxygens O1 and O4 in **3**, and O9 in **5**. Complexes **2**–**5** show how the nickel-porphyrinogen complex is a very versatile π-ligand for a variety of M(0) complexes, and how one can proceed from **2**–**5** to build up extended polymetallic structures.

Notes and references

† *Synthesis* of **3**. $[Mo(CO)_3(MeCN)_3]$ (6.10 g, 20.14 mmol) was added to a solution of **1** (9.03 g, 10.07 mmol) in THF (220 cm^3), resulting in a yellow–brown solution which was stirred at room temperature for 24 h. The solvent was evaporated and Et_2O (200 cm^3) was added to the obtained orange oily residue. The mixture was stirred overnight to give a yellow powder which was collected and dried *in vacuo* (9.60 g, 80%). Crystals suitable for X-ray diffraction were grown in Et_2O. (Found: C, 55.05; H, 5.41; N, 4.35. **2**·$Li_2(THF)_3$, $C_{54}H_{72}N_4Li_2Mo_2NiO_9$, requires: C, 54.70; H, 6.12; N, 4.35%). ^{1}H NMR (d_8-THF, 400 MHz, 298 K) δ 6.08 (d, J = 2.93 Hz, 2H, C_4H_2N), 6.01 (d, J = 2.93 Hz, 2H, C_4H_2N), 5.50 (d, J = 2.93 Hz, 2H, C_4H_2N), 5.41 (d, J = 2.93 Hz, 2H, C_4H_2N), 4.98 (dq, J_{gem} = 13.2 Hz, J_{vic} = 7.34 Hz, 2H, CH_2), 3.82 (dq, J_{gem} = 13.6 Hz, J_{vic} = 7.34 Hz, 2H, CH_2), 3.55 (m, 12H, THF), 2.87 (dq, J_{gem} = 12.8 Hz, J_{vic} = 7.34 Hz, 2H, CH_2), 2.72 (dq, J_{gem} = 13.2 Hz, J_{vic} = 7.34 Hz, 2H, CH_2), 2.32 (m, 4H, CH_2), 2.18 (m, 4H, CH_2), 1.46 (m, 18H, THF + CH_3), 1.32 (t, J = 7.34 Hz, 6H, CH_3), 1.20 (t, J = 7.34 Hz, 6H, CH_3), 0.89 (t, J = 7.34 Hz, 6H, CH_3). IR (Nujol, ν_{max}/cm^{-1}) 1916 (s), 1910 (s), 1822 (s), 1789 (s); 1767 (s), 1734 (s). IR (THF, ν_{max}/cm^{-1}) 1914 (sh), 1810 (sh), 1750 (sh). UV/vis(THF) λ_{max}/nm (ε/M^{-1} cm^{-1}) = 230 (34945), 254 (27842), 310 (12981), 444 (702).

‡ *Synthesis* of **5**. $[Mo(CO)_3(MeCN)_3]$ (5.0 g, 16.6 mmol) was added to a solution of **1** (3.72 g, 4.15 mmol) in THF (200 cm^3). The resulting red solution was stirred overnight at room temperature. The solvent was removed under reduced pressure, and the solid collected with Et_2O (150 cm^3). The mother liquor was concentrated, and the violet powder was filtered and dried *in vacuo* (4.24 g, 66%). Crystals suitable for X-ray diffraction were grown in a mixture of DME–benzene. (Found: C, 46.64; H, 5.18; N, 3.24. **3**·$Li_2(THF)_3$, $C_{60}H_{72}N_4Li_2Mo_4NiO_{15}$, requires: C, 46.63; H, 4.69; N, 3.62. ^{1}H NMR: (d_8-THF, 400 MHz, 298 K) δ 5.52 (d, J = 2.93 Hz, 4H, C_4H_2N), 5.27 (d, J = 2.93 Hz, 4H, C_4H_2N), 4.19 (dq, J_{gem} = 13.6 Hz, J_{vic} = 7.34 Hz, 4H, CH_2), 3.58 (m, 12H, THF), 2.78 (dq, J_{gem} = 13.6 Hz, J_{vic} = 7.34 Hz, 4H, CH_2), 1.94 (dq, J_{gem} = 15.2 Hz, J_{vic} = 7.34 Hz, 4H, CH_2), 1.82 (dq, J_{gem} = 15.2 Hz, J_{vic} = 7.34 Hz, 4H, CH_2), 1.74 (m, 12H, THF), 1.11 (t, J = 7.34 Hz, 12H, CH_3), 1.09 (t, J = 7.34 Hz, 12H, CH_3). IR (Nujol, ν_{max}/cm^{-1}) 1919 (sbd), 1825 (sbd), 1746 (sbd). IR (THF, ν_{max}/cm^{-1}) 1917 (sh), 1813 (sh). UV/vis(THF) λ_{max}/nm (ε/M^{-1} cm^{-1}) = 232 (51596), 256 (38660), 308 (17107), 404 (4407).

§ *Crystal data*: for **3**: $C_{62}H_{88}Li_2Mo_2N_4NiO_{11}\cdot C_4H_8O$, M = 1401.94, monoclinic, space group $C2/c$, a = 50.392(4), b = 11.6140(8), c = 23.8148(12) Å, β = 105.537(5)°, V = 13428.3(15) Å^3, Z = 8, D_c = 1.387 g cm^{-3}, F(000) = 5872, λ(Mo-Kα) = 0.71073 Å, μ = 0.707 mm^{-1}, crystal dimensions 0.29 × 0.25 × 0.21. Diffraction data were collected on a KUMA CCD at 143 K. For 9809 observed reflections [$I > 2\sigma(I)$] and 760 parameters, the final R is 0.0536 ($wR2$ = 0.1411 for 11199 independent reflections). For **5**: $C_{60}H_{72}LiMo_4N_4NiO_{15}\cdot Li(C_4H_8O)_4\cdot C_6H_6$, M = 1912.09, monoclinic, space group $P2_1/c$, a = 27.300(6), b = 17.269(2), c = 18.076(2) Å, β = 96.17(2)°, V = 8473(2) Å^3, Z = 4, D_c = 1.499 g cm^{-3}, F(000) = 3936, λ(Mo-Kα) = 0.71070 Å, μ = 0.863 mm^{-1}, crystal dimensions 0.35 × 0.27 × 0.20. Diffraction data were collected on a mar345 Imaging Plate Detector System at 143 K. For 11822 observed reflections [$I > 2\sigma(I)$] and 1010 parameters, the final R is 0.0473 ($wR2$ = 0.1340 for 13785 independent reflections). CCDC 182/1445. See http://www.rsc.org/suppdata/cc/1999/2319/ for crystallographic files in .cif format.

1 *Early Transition Metal Clusters with π-Donor Ligands*, ed. M. H. Chisholm, VCH, New York, 1995; *Advances in Supramolecular Chemistry*, ed. G. W. Gokel, Jai Press, Hampton Hill, England, 1995; F. Vögtle, *Supramolecular Chemistry*, Wiley, New York, 1991; *Transition Metals in Supramolecular Chemistry*, ed. L. Fabbrizzi and A. Poggi, Nato ASI Series, Kluwer, Dordrecht, 1994; E. Tsuchida, *Macromolecular Complexes, Dynamic Interactions and Electronic Processes*, VCH, New York, 1991; *Magnetism, a Supramolecular Function*, ed. O. Kahn, Nato ASI Series, Kluwer, Dordrecht, 1996; *Inorganic Materials*, ed. D. W. Bruce and D. O'Hare, Wiley, New York, 1992.

2 E. C. Constable and C. E. Housecroft, *Chimia*, 1998, **52**, 533; E. C. Constable, *Oligomeric Metal Complexes* in *Electronic Materials: the Oligomer Approach*, ed. K. Müllen and G. Wegner, Wiley–VCH, Weinheim, 1998, p. 273; E. C. Constable, *Chem. Commun.*, 1997, 1073; E. C. Constable, C. E. Housecroft, B. Krattinger, M. Neuburger and M. Zehnder, *Organometallics*, 1999, **18**, 2565.

3 General references are made to: (*a*) C. Floriani, *Pure Appl. Chem.*, 1996, **68**, 1; (*b*) C. Floriani, *Chem. Commun.*, (Feature article), 1996, 1257; (*b*) D. Jacoby, S. Isoz, C. Floriani, A. Chiesi-Villa and C. Rizzoli, *J. Am. Chem. Soc.*, 1995, **117**, 2793; (*c*); 2805; (*d*) C. Floriani, in *Stereoselective Reactions of Metal-Activated Molecules*, ed. H. Werner and J. Sundermeyer, Vieweg, Wiesbaden, 1995, pp. 97–106; (*e*) S. De Angelis, E. Solari, C. Floriani, A. Chiesi-Villa and C. Rizzoli, *Angew. Chem., Int. Ed. Engl.*, 1995, **34**, 1092; (*f*) C. Floriani, E. Solari, G. Solari, A. Chiesi-Villa and C. Rizzoli, *Angew. Chem., Int. Ed.*, 1998, **37**, 2245 and references therein.

4 L. Bonomo, E. Solari, M. Latronico, R. Scopelliti and C. Floriani, *Chem. Eur. J.*, 1999, **5**, 2040.

5 For the relevance of the π-bonding ability of the polypyrrole structure see: M. O. Senge, *Angew. Chem., Int. Ed. Engl.* 1996, **35**, 1923 and references therein. For π-binding between aromatic metalla-porphyrins and a metal see: K. Koczaja Dailey, G. P. A. Yap, A. L. Rheingold and T. B. Rauchfuss, *Angew. Chem., Int. Ed. Engl.*, 1996, **35**, 1833.

6 (*a*) S. De Angelis, E. Solari, C. Floriani, A. Chiesi-Villa and C. Rizzoli, *J. Am. Chem. Soc.*, 1994, **116**, 5691; (*b*) J. Jubb, D. Jacoby, C. Floriani, A. Chiesi-Villa and C. Rizzoli, *Inorg. Chem.*, 1992, **31**, 1306.

7 D. P. Tate, W. R. Knipple and J. M. Augl, *Inorg. Chem.*, 1962, **1**, 433; H. Werner, K. Deckelmann and U. Schönenberger, *Helv. Chim. Acta*, 1970, **53**, 2002.

8 D. F. Shriver and M. J. Sailor, *Acc. Chem. Res.*, 1988, **21**, 374.

Communication 9/07268C

ChemComm
FEATURE ARTICLE

Building molecular wires from the colours of life: conjugated porphyrin oligomers

Harry L. Anderson

Department of Chemistry, University of Oxford, Dyson Perrins Laboratory, South Parks Road, Oxford, UK OX1 3QY. E-mail: harry.anderson@chem.ox.ac.uk

Received (in Cambridge, UK) 25th May 1999, Accepted 13th July 1999

Conjugated porphyrin polymers are giant supramolecular chromophores with extraordinary electrooptical and nonlinear optical properties. Close collaboration between synthetic organic chemists, chemical physicists and theoreticians has yielded new insights into the electronic structure of these remarkable materials. Alkyne-linked oligomers have been most intensively investigated. Several strands of independent work show that the unusual electronic behaviour of these materials can be attributed to strong ground state interporphyrin conjugation, which is amplified in the excited states, and in the oxidised and reduced forms.

Many porphyrin oligomers have been studied as models for natural photosynthetic systems[1] and as enzyme mimics.[2] Most of them are not conjugated; that is to say there is no significant π-overlap between the macrocycles, and their electronic absorption spectra resemble those of their components. Recently several research groups have created conjugated porphyrin oligomers, in which the porphyrin π-systems merge to form giant supramolecular chromophores.[3–14] Conjugated oligomers derived from small heterocycles, such as thiophene, are useful semiconductors,[15] so it is interesting to compare conjugated oligomers derived from larger, more polarisable, aromatic units such as porphyrins. This Feature Article highlights the emerging design principles, and structure–property relationships, for materials of this type, and focuses on interporphyrin conjugation: how to maximise it, how to measure it, and how to use it to make advanced optoelectronic materials.

Harry Anderson is a Lecturer at the Dyson Perrins Laboratory (Organic Chemistry), which is part of the Department of Chemistry at the University of Oxford. He graduated from the University of Oxford in 1987 and did his PhD at the University of Cambridge, with Professor Jeremy Sanders, then spent three years as a Research Fellow, funded by Magdalene College, in Cambridge and one year working with Professor François Diederich at ETH Zürich, before taking up his current post in 1994. His research interests include many aspects of synthetic supramolecular chemistry, with particular emphasis on dyes and conjugated electronic materials.

Porphyrins as building blocks for electronic materials

The word *porphyrin* is derived from the Greek *porphura* meaning purple, and all porphyrins are intensely coloured.[16] The electronic absorption spectrum of a typical porphyrin, such as zinc octaethylporphyrin ZnOEP **1** (Fig. 1) consists of a strong transition to the second excited state ($S_0 \rightarrow S_2$) at about 400 nm (the Soret or B band) and a weak transition to the first excited state ($S_0 \rightarrow S_1$) at about 550 nm (the Q band). Internal conversion from S_2 to S_1 is rapid so fluorescence is only detected from S_1. The B and the Q bands both arise from π–π* transitions and can be explained by considering the four frontier orbitals (the 'Gouterman four orbital model'): two π orbitals (a_{1u} and a_{2u}) and a degenerate pair of π* orbitals (e_{gx} and e_{gy}). The two highest occupied π orbitals happen to have about the same energy. One might imagine that this would lead to two almost coincident absorption bands due to $a_{1u} \rightarrow e_g$ and $a_{2u} \rightarrow e_g$ transitions, but in fact these two transitions mix together by a process known as configurational interaction, resulting in two bands with very different intensities and wavelengths: constructive interference leads to the intense short-wavelength B band, while the weak long-wavelength Q band results from

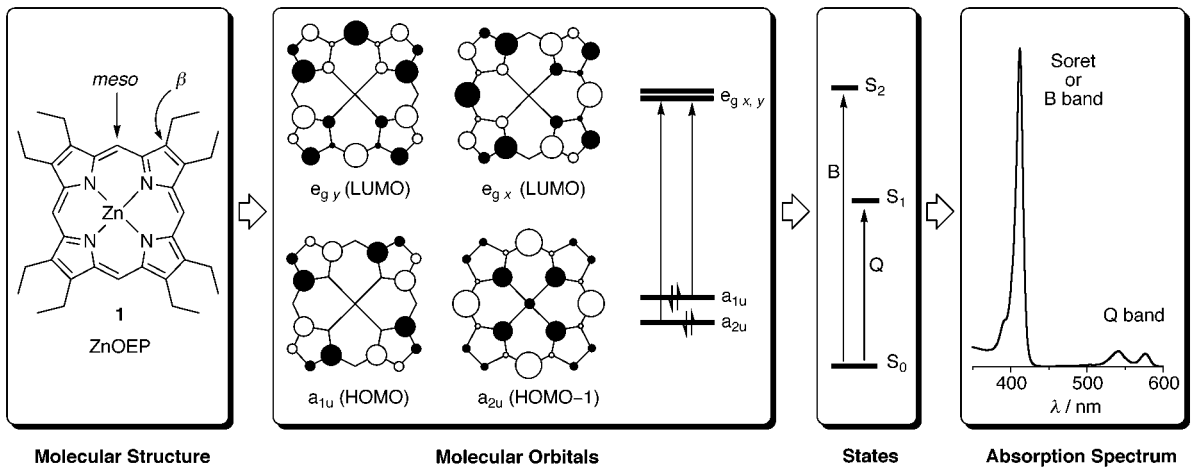

Fig. 1 The four Gouterman molecular orbitals explain the absorption spectra of simple porphyrins, such as **1**.

destructive combinations. The two types of position on the porphyrin periphery are referred to as *meso* and *β*. The a_{1u} orbital has nodes at all four *meso* positions whereas the a_{2u} orbital has high coefficients at these sites (Fig. 1).

Many synthetic porphyrins have *meso*-aryl substituents. These cause only a slight perturbation to the electronic structure, because there is minimal π-overlap between the aryl ring and the porphyrin, due to the large aryl–porphyrin dihedral angles, which result from steric interactions with the *β*-hydrogens. The distribution of aryl–porphyrin dihedral angles for some *ortho*-unsubstituted, *β*-unsubstituted *meso*-aryl porphyrins from the Cambridge Crystallographic Database (CCD)[17] is shown in Fig. 2. The zinc(II), copper(II), nickel(II) and free-base porphyrins have similar distributions of dihedral angles (mean = 73°; standard deviation = 9°). *meso*-Phenylene-linked porphyrin oligomers do not exhibit significant conjugation because of this non-planarity.[1c–f] Directly *meso–meso* bonded porphyrin oligomers are non-conjugated for the same reason.[1f,18] Lindsey and co-workers have investigated a system of *meso–meso* diphenylethyne-linked porphyrin oligomers, which have been called 'molecular photonic wires' because of their efficient inter-porphyrin energy transfer.[1c,d] However, these porphyrin oligomers are not conjugated (so they are not 'molecular wires' in the sense used in this review) because of the *meso*-aryl twist discussed above; their absorption spectra are almost identical to those of the corresponding monomers.[1d] Conjugation was intentionally minimised in the design of these systems to avoid electron-transfer quenching.

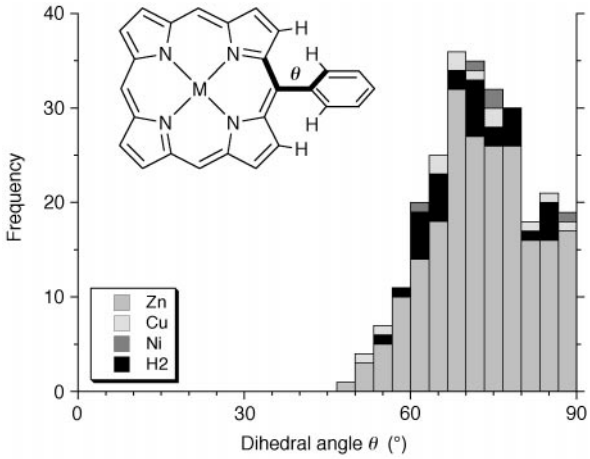

Fig. 2 Distribution of dihedral angles in *meso*-aryl Zn^{II}, Cu^{II}, Ni^{II} and free-base porphyrins, from the CCD, excluding structures with *R* factor > 10% or with disorder (ref. 17).

Types of conjugated porphyrin oligomers and their electronic spectra

The first conjugated porphyrin dimer **2a** was reported by Arnold *et al.* in 1978,[4a] although its unusual properties were not explored until the 1990s, at about the time that Anderson[3a] and Therien[13a–c] reported related *meso*-butadiyne-linked zinc dimers **3** and **5**–**7** respectively. The UV-visible absorption spectra of these dimers all exhibit broadly split B bands and unusually intense red-shifted Q bands, indicating substantial porphyrin–porphyrin conjugation; Fig. 3 compares the absorption spectra of dimer **3** with monomer **4**, which is an ideal model compound because of the identical local porphyrin environment. Polarised spectroscopy[3c] has shown that the more red-shifted components of both the B and Q bands (B_x and Q_x) are polarised down the acetylenic axis of the molecule, whereas the blue-shifted components (B_y and Q_y) are polarised in the perpendicular in-plane direction. Exciton coupling theory would predict some B_x/B_y splitting of this type, but the magnitude of the splitting is far greater than this theory predicts.[3a]

Conjugated porphyrin dimers make challenging subjects for quantum mechanical calculation, even with modern semi-

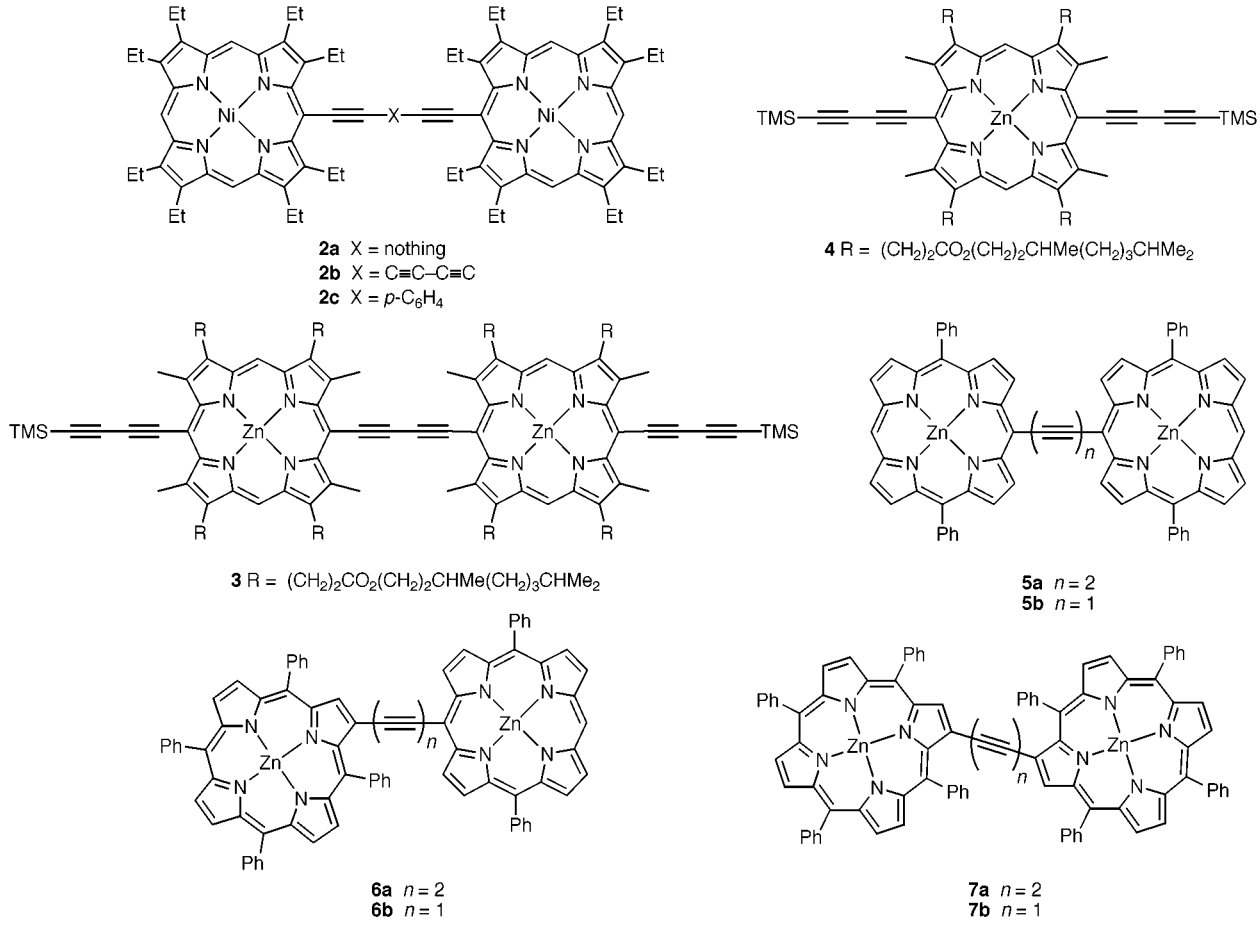

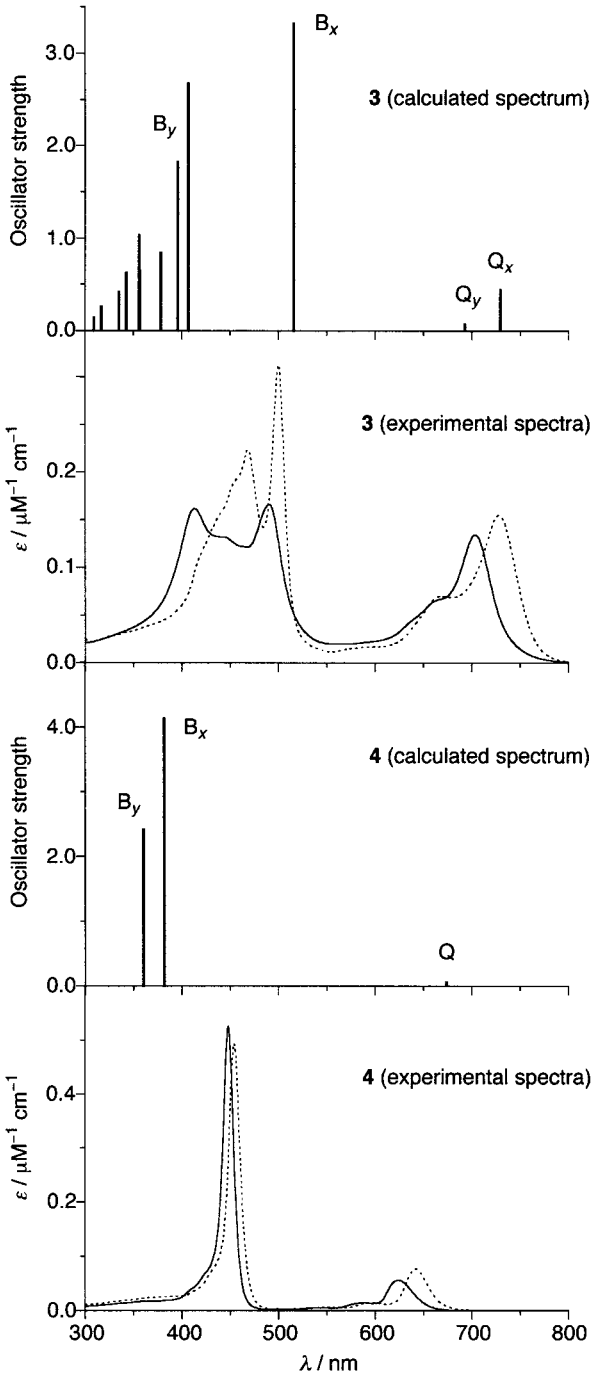

Fig. 3 Experimental and calculated electronic absorption spectra of **3** and **4**. Experimental spectra were recorded in CH_2Cl_2 (plain) and in 1% pyridine–CH_2Cl_2 (dashed) [refs 3(*a*), (*i*)].

empirical techniques. Computational studies have shed light on the electronic absorption spectra of **2**[4e] and **3**.[3i] In both cases the lowest energy transitions were found to be between orbitals delocalised over the entire π-system. Beljonne *et al.* used a combination of the Hartree–Fock Intermediate Neglect of Differential Overlap (INDO) and Single Configurational Interaction (SCI) techniques[3i] to calculate the electronic transitions for **3** and **4** shown in Fig. 3. The dimer **3** was too big for complete geometry optimisation, so its ground state structure was constructed using coordinates from **4**. Satisfactory agreement with the experimental spectra could only be achieved by assuming a reduction in bond length alternation in the central butadiyne in the excited state geometry of **3**, which is evidence of increased conjugation in the excited state. These calculations reproduce the observed B_x/B_y splitting, as well as the red-shift and intensification in the Q_x band.

Beljonne's calculations assumed, for simplicity, that the two porphyrin macrocycles in **3** are coplanar. NMR and UV spectra indicate that a range of dihedral angles are populated when **3** is dissolved and disaggregated, whereas in the bimolecular aggregate $\mathbf{3}_2$ (which is formed in CH_2Cl_2 in the absence of amine ligands) the dimer units tend to lie flat.[3a] The planar aggregated conformation is characterised by a larger B_x/B_y splitting, as illustrated in Fig. 3, which compares the spectra of **3** (in 1% pyridine–CH_2Cl_2) with $\mathbf{3}_2$ (in CH_2Cl_2). The same effect is observed in the supramolecular triple strand array $\mathbf{8{\cdot}9}_2$.

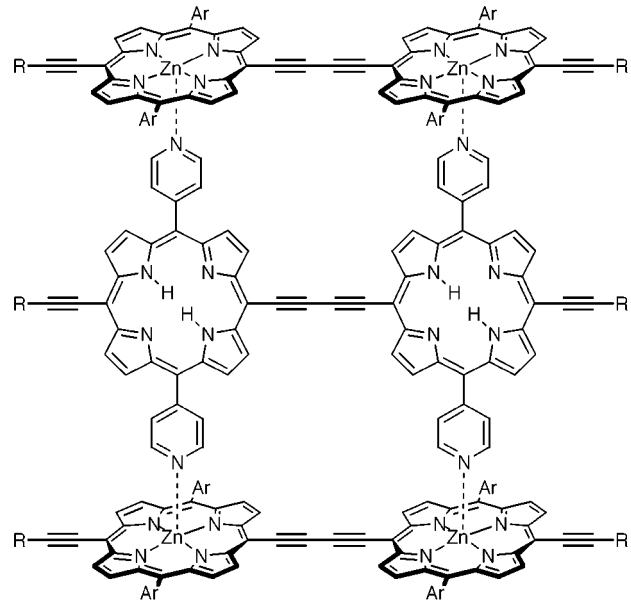

$\mathbf{8{\cdot}9}_2$ R = Si(*n*-$C_{12}H_{13})_3$, Ar = 3,5-$Bu^t_2C_6H_3$

Formation of this assembly tends to hold both dimers **8** and **9** in planar conformations, resulting in increased B_x/B_y splitting and weighting the Q_x band towards longer wavelengths.[3n] Stranger *et al.* have used density functional theory (DFT) to calculate the electronic structure of **2a** as a function of the dihedral angle θ about the butadiyne axis.[4e] Fig. 4(*a*) shows contour plots of the π orbitals ($8b_{1u}$ and $9b_{3g}$) and π* orbitals ($10b_{1u}$ and $10b_{3g}$), which are derived from the a_{2u} and e_{gx} orbitals of the porphyrin monomer unit. The Walsh diagram in Fig. 4(*b*) shows how these molecular orbitals, and the total energy, change with dihedral angle θ. The contours for the $8b_{2g}$, $8a_{1u}$, $6b_{2g}$ and $6a_{1u}$ orbitals are not shown because these are non-delocalised orbitals derived from the e_{gy} and a_{1u} orbitals of the monomer, which have nodes along the butadiyne link. When θ = 90° the molecular orbitals converge to four Gouterman-type orbitals. The gap between the $10b_{1u}$ LUMO and the $9b_{3g}$ HOMO decreases with decreasing θ, as the molecule becomes more conjugated. The calculated potential energy surface is fairly flat for θ = 0–60°, but then rises steeply near the staggered conformation to about 60 kJ mol^{-1} at 90°. This implies that there should be substantial librational freedom, but not free rotation at room temperature. MOPAC calculations[13c] gave a much smaller estimate for the rotational barrier in **5a** (2.5 kJ mol^{-1}).† If these rotational barriers could be determined experimentally, they would give a direct measure of the interporphyrin resonance energy; this has yet to be achieved. The electronic spectra of **2a** indicate that it becomes more planar and more conjugated at lower temperatures. The crystal structure of dimer **9** shows it is completely planar in the solid state.[3m]

Therien and co-workers prepared a short ethyne-linked dimer **5b**, as well as a linear trimer of this type.[13a] Species **5b** has a similar absorption spectrum to **5a**, but with slightly stronger electronic coupling. Ultra-fast pump-probe measurements show that the first excited state of **5a** relaxes to a planar conformation

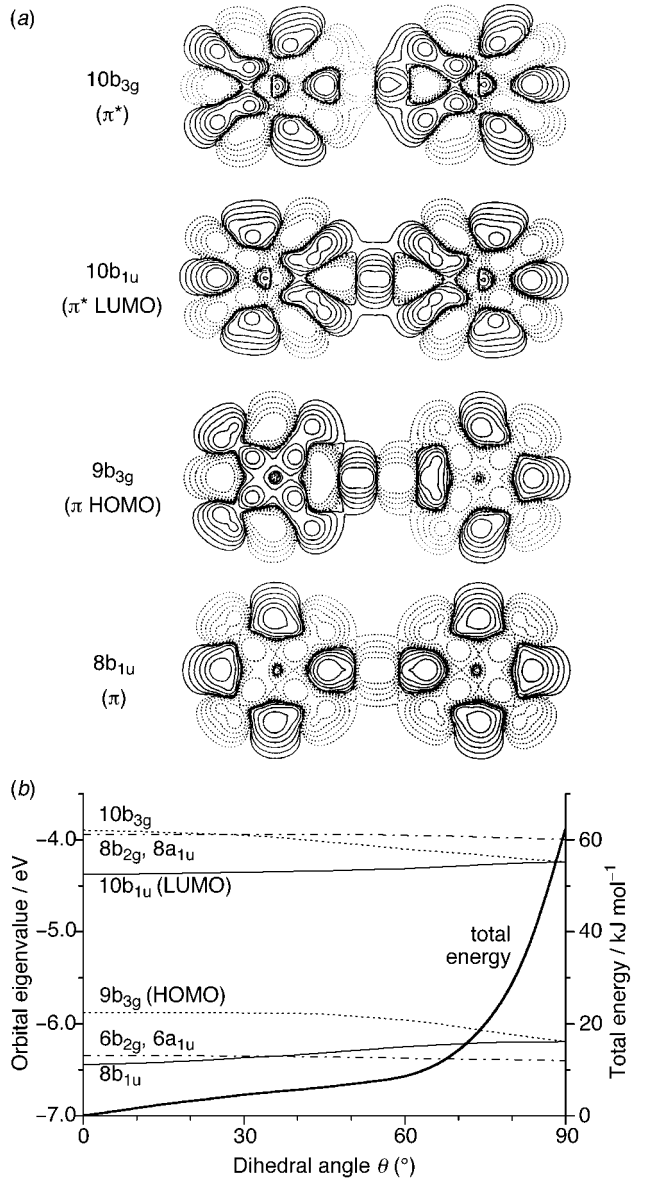

Fig. 4 (*a*) Contour plots for frontier orbitals of **2a** and (*b*) Walsh diagram showing how the energy of these orbitals (and the total energy) vary with the dihedral angle θ about the butadiyne, from DFT calculations (reprinted with permission from ref. 4(*e*); copyright 1996 American Chemical Society).

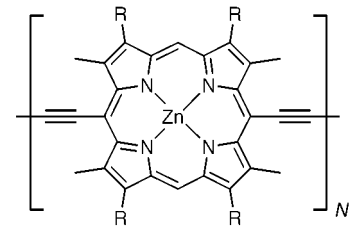

polymer **10** $N \approx 10$–15; end groups unknown

R = $(CH_2)_2CO_2(CH_2)_2CHMe(CH_2)_3CHMe_2$

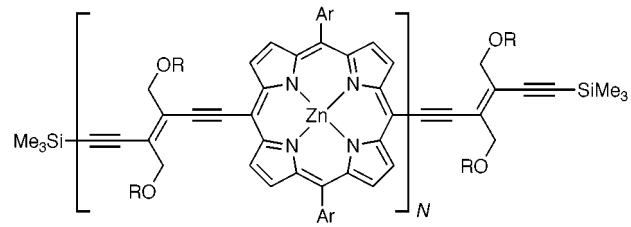

12a $N = 1$
12b $N = 2$
12c $N = 3$

R = $SiBu^tMe_2$, Ar = p-$C_6H_4O(CH_2)_3CO_2Et$

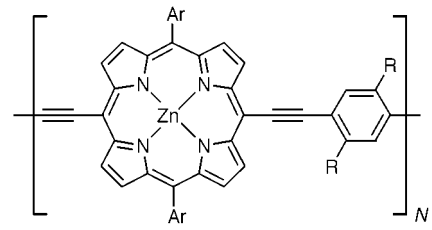

13a R = $OC_{15}H_{31}$ Ar = 2,4,6-$Me_3C_6H_2$

13b R = $CON(C_8H_{17})_2$

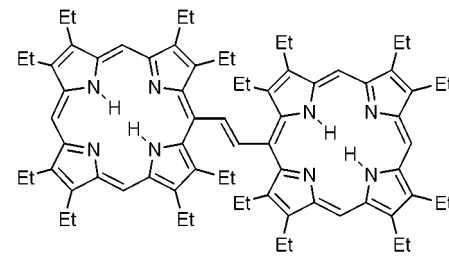

14

on a 30 ps time-scale.[13e] Arnold *et al.* have continued this sequence by studying the octatetrayne-linked dimer **2b**. Doubling the length of the alkyne spacer has a subtle effect on the absorption spectrum, and does not dramatically reduce the interporphyrin electronic coupling.

Comparison of *meso–meso*, *meso–β* and *β–β* linked dimers **5a**–**7a** and **5b**–**7b** shows that *meso-meso* connectivity confers maximum electronic coupling[13c] (*β–β* linked analogues of **2a** demonstrate the same effect[4b,7]). In the ethyne-linked series, poor conjugation in the *meso–β* and *β–β* linked dimers can be attributed to steric clashes, forcing the molecules into orthogonal conformations, whereas in the butadiyne-linked series the effect can only be due to the smaller frontier orbital coefficients at the *β*-positions (Fig. 1).

Examples of higher alkyne-linked conjugated porphyrin oligomers include polymer **10** (with 10–15 macrocycles)[3b] and hexamer **11** (an 83 Å long molecular wire).[3m] These oligomers continue the trends set by the dimers, and exhibit strongly red-shifted and intensified Q bands. For example **10** has a Q absorption band at 873 nm which is more intense than its Soret band (in 1% pyridine–CH_2Cl_2). The whole series of oligomers from monomer to hexamer **11** show a gradual evolution in electronic spectra with increasing chain-length.[3m] Rigid-rod porphyrin oligomers tend to be rather insoluble, but the isodecyl ester side chains of **10** give it excellent solubility, provided an amine is present to ligate the zinc sites. High quality transparent thin films of this polymer are easily prepared from solution (either of pure **10** or as a blend with a transparent polymer matrix). It is remarkable that the absorption spectra of these solid films are sharper than the solution spectra, suggesting that some type of ordered J-aggregate is probably formed. The excellent film forming properties of this conjugated porphyrin polymer have made it suitable for solid state electronic and photophysical investigations. It is a p-type semiconductor and photoconductor.[3d,h,j]

Many conjugated porphyrin dimers have been reported with unsaturated bridges linking alkyne-substituted *meso*-positions, such as **2b**,**c**.[4g] Taylor *et al.* have shown that a 9,10-diethynylanthracene bridge provides even stronger conjugation than a direct butadiyne-link, as judged from the emission spectra;[3l] this can be attributed to stabilisation of the quinoidal/cumulenic resonance canonical by the 9,10-anthrylene unit. The crystal structure of a 1,4-diethynylthiophene bridged dimer has been reported by Arnold *et al.*, and, like **9**, it is planar in the solid state.[4c] Diederich and co-workers have studied a series of (*E*)-

1,2-diethynylethene bridged oligomers **12a**–**c**. The Q band of the dimer **12b** is substantially red-shifted and intensified relative to the monomer **12a**, whereas the spectra of **12b** and **12c** are very similar, indicating that in this series, saturation of the electronic properties is already reached at the dimer.[6] Polymers with 1,4-diethynylarylene bridges **13a**,**b** have been investigated by Jones and co-workers.[8] Although 1,4-diethynylphenylene bridges do not provide optimum conjugation, these polymers are highly conjugated, with intense red-shifted Q bands.

Alkynes seem to provide the ideal way of making conjugated connections between porphyrins. *meso–meso* (*E*)-1,2-Ethene linked dimers also display intriguing conjugation. Chachisvilis *et al.* have shown that dimer **14** exists in solution partly (about 20%) as a conformer with strong conjugation (broad split Soret; Q band at 800–900 nm), although most of the material adopts twisted conformations with very little electronic coupling, and this non-conjugated conformer dominates the absorption spectrum.[12] A trimeric analogue of **14** has been prepared by Higuchi *et al.*,[14] while Vicente and Smith have synthesised hexatriene linked dimers of this type,[11a] but ethene-linked dimers without β-substituents, which should be more conjugated, have yet to be investigated.[13b] Smith's group have also synthesised conjugated planar β-alkene linked chlorophyll dimers.[11b] Officer and co-workers have prepared a β–β butadiene linked dimer, but it does not appear to be significantly conjugated.[10]

Edge-fused structures represent an alternative strategy for ensuring coplanarity and achieving extended π-overlap between porphyrin macrocycles. This approach has been explored by Crossley and co-workers, using 1,4,5,8-tetraazaanthracene bridges as in the tetramer **15**.[5] The interporphyrin electronic coupling in these structures seems to be weaker than in the *meso–meso* alkyne-bridged oligomers discussed above, probably because of the smaller frontier orbital coefficients at the β-positions of a porphyrin, and because the tetraazaanthracene bridge tends to act as an isolated aromatic unit. More strongly coupled analogues include a benzo-bridged dimer reported by Kobayashi *et al.*[9] Smith's group have recently prepared a directly edge-fused trimer **16**[11c] and an amazing benzo-bridged pentamer **17**,[11d] using an ingenious Diels–Alder route. This new synthetic methodology is likely to lead to rapid progress, but so far the electronic coupling in edge-fused oligomers is much less well characterised than that in *meso–meso* alkyne linked compounds.

Electrochemical evidence for conjugation

Conjugation causes splitting in the π and π* levels, reducing the HOMO–LUMO gap. The simplest manifestations of this are a red-shift, and a broadening, in the electronic spectra, as discussed above. The HOMO–LUMO gap can be approximated to the energy of the longest wavelength absorption or emission band. This is referred to as the 'optical gap' E_g. The HOMO–LUMO gap can also be estimated from the difference between the first oxidation and reduction potentials, E_1^{Ox}–E_1^{Red}; the 'electrochemical gap'. Electronic communication in a conjugated porphyrin oligomer also splits the redox potentials. It is widely assumed that the magnitude of this splitting provides a measure of the conjugation, but this may be misleading, as discussed below.

Table 1 summarises the redox characteristics of some conjugated porphyrin dimers, and reference monomers. There is close agreement between optical gaps (E_g in eV) and electrochemical gaps (E_1^{Ox}–E_1^{Red} in V). In general alkyne links reduce the HOMO–LUMO gap by lowering the LUMO (*i.e.* make E_1^{Red} less negative) rather than raising the HOMO (reducing E_1^{Ox}), because alkynes are electron-withdrawing. Comparison of the redox potentials of **2a**–**c** with those of NiOEP, confirms that the C_8 link in **2b** provides about as much conjugation as the C_4 link in **2a**, whereas the $C_2(p\text{-}C_6H_4)C_2$ link in **2c** is relatively insulating.[4h]

Arnold *et al.* have recently reported spectroscopic and electrochemical data on a range of analogues of **2a** with other divalent metals (Co, Cu, Zn, Pd and Pt) in place of Ni.[4k] The metallation state of this dimer has a surprisingly large effect on the porphyrin–porphyrin electronic coupling. The conjugation is greatest in the Ni_2 dimer and weakest in the Zn_2 complex. This accounts for the fact that the spectrum of **2a** resembles that of the $\mathbf{3}_2$ aggregate even when **2a** is not aggregated. Spectroelectrochemical studies have shown that doubly reduced dianions such as $[\mathbf{2a}]^{2-}$ exhibit an extraordinarily intense peak ($\varepsilon > 10^5\ M^{-1}\ cm^{-1}$) in the near-IR at about 1000 nm. Putting two electrons into the $10b_{1u}$ π* orbital (which is bonding with respect to the porphyrin-porphyrin link; see Fig. 4) enhances the interporphyrin electronic coupling and stabilises the $[\mathbf{2a}]^{2-}$ dianion. Thus strong conjugation can *reduce* the splitting between the $[\mathbf{2a}]/[\mathbf{2a}]^-$ and $[\mathbf{2a}]^-/[\mathbf{2a}]^{2-}$ reduction potentials. The same argument accounts for a small splitting in the oxidation potentials, since the $9b_{3g}$ π orbital is anti-bonding with respect to the interporphyrin link. Arnold has developed this idea and used the spectroelectrochemical data on a range of dimers to construct an empirical frontier orbital model for these systems.[4k]

The redox potentials of the (*E*)-1,2-ethene linked dimer **14** indicate that it is strongly conjugated,[4d] with an electrochemical gap of only 1.44 V, whereas its electronic spectra show that only about 20% of the material is in conjugated conformations,[12] as discussed above. This implies that the radical cation and radical anion of this dimer are more conjugated than the neutral molecule. The stabilising effect of conjugation is greater when it results in charge delocalisation, so radical cations and anions tend to adopt more planar conformations than neutral molecules. This effect is illustrated by the crystal structure of the [Cu(TPP•)][$SbCl_6$] radical cation,[19] which exhibits a remarkably small porphyrin–aryl dihedral angle of 41° (compared to the average dihedral angle of 67° for neutral *meso*-phenyl copper porphyrins, Fig. 2).

Nonlinear optics

Just as the stretchiest rubber bands show the greatest deviations from Hooke's law, for a given force, so the most polarisable materials show the greatest optical nonlinearities, for a given electric field. Materials which show large nonlinearities for weak electric fields can be used in all-optical and electro-optical switching devices. The nonlinear relationship between the polarisation *P* and the electric field strength *E* is represented by eqn. (1), where $\chi^{(1)}$ is the bulk linear polarisability, and $\chi^{(2)}$ and $\chi^{(3)}$ are the second and third order nonlinear optical (NLO) susceptibilities (higher terms in E^4 *etc.* are normally ignored).

$$P = \chi^{(1)}E + \chi^{(2)}E^2 + \chi^{(3)}E^3 \quad (1)$$

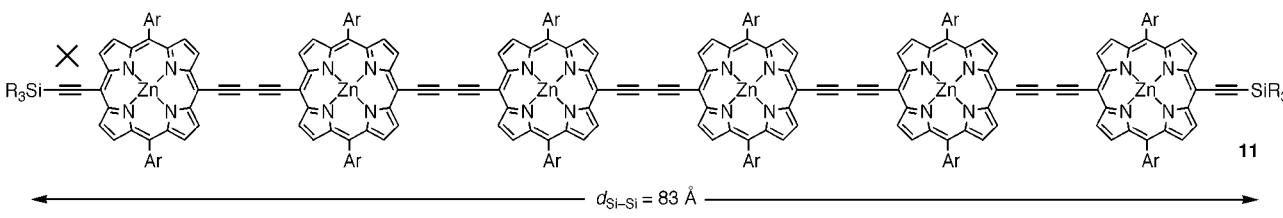

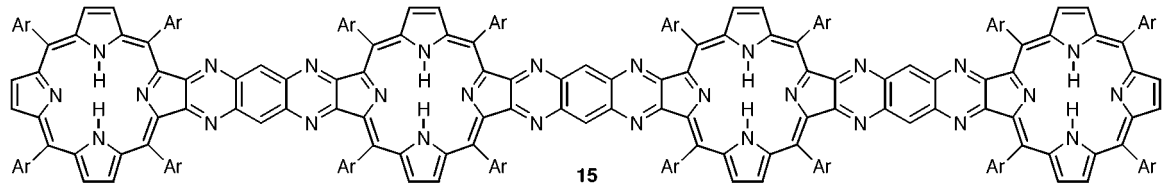

15

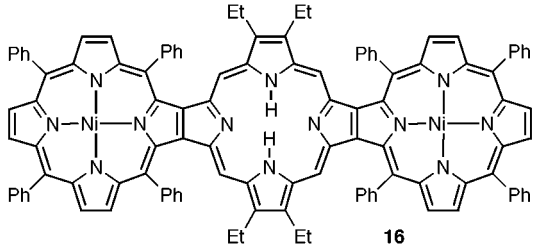

16

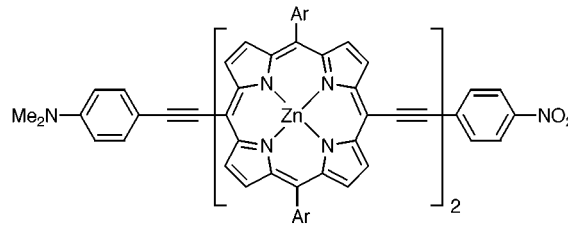

18

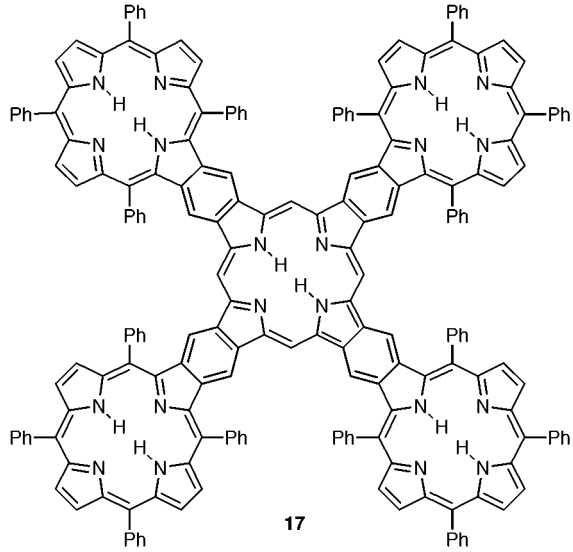

17

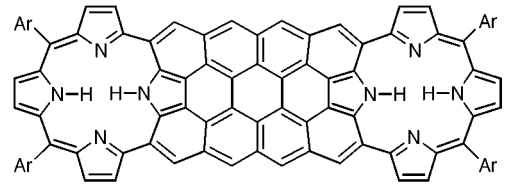

19

Table 1 Redox characteristics of porphyrin dimers and monomers[a]

		E/V *vs.* F_c/F_c^+				
Compound	Linking unit	E_1^{Ox}	E_1^{Red}	E_1^{Ox}–E_1^{Red}/V	E_g/eV	Ref.
NiOEP	—	0.37	−1.87	2.24	2.25	4(*h*)
2a	C_4	0.37, 0.49	−1.56	1.93	2.01	4(*h*)
2b	C_8	0.34, 0.42	−1.47	1.81	2.00	4(*h*)
2c	$C_2(p\text{-}C_6H_4)C_2$	0.36, 0.41	−1.65	2.01	2.08	4(*h*)
12a	—	0.36	−1.50	1.86	1.84	6
12b	$C_2(E\text{-}C_2R_2)C_2$	0.25, 0.45	−1.50	1.75	1.71	6
ZnDPP	—	0.37	−1.63	2.00	2.29	13(*a*)
5b	C_2	0.19, 0.45	−1.59, −1.71	1.78	1.81	13(*a*)
14	$(E)\text{-}C_2H_2$	0.11, 0.21	−1.33	1.44	1.59	4(*d*)

[a] Redox potentials are in V *vs.* Fc/Fc^+; $E_1^{Ox} - E_1^{Red}$ is the electrochemical gap; E_g is the optical solution gap from the longest wavelength absorption; see references for solvents and conditions; NiOEP is the Ni^{II} analogue of **1**; ZnDPP is 5,15-diphenylporphyrin Zn^{II}.

Conjugated porphyrin oligomers have extremely polarisable π-systems, resulting in strong NLO behaviour. Second order behaviour ($\chi^{(2)} \neq 0$; *e.g.* second harmonic generation and the Pockels effect) is only exhibited by non-centrosymmetric structures, which excludes most porphyrin oligomers, although Therien has predicted[13d] that structures such as **18** should have very high $\chi^{(2)}$. Third order behaviour ($\chi^{(3)} \neq 0$; *e.g.* third harmonic generation and the DC Kerr effect) does not require non-centrosymmetry, so is relevant to most of the materials discussed here.

Electroabsorption spectroscopy has shown that polymer **10** has a peak resonant third order NLO response ($|\chi^{(3)}| = 1.0 \times 10^{-15}$ m^2 V^{-2} at 850 nm)‡ which is stronger than those of other conjugated polymers.[3b] This peak response occurs near the wavelength region relevant for telecommunications applications; fibre optic systems commonly operate at 1300 nm. $\chi^{(3)}$ is frequency dependent and in this case it is resonance-enhanced at 850 nm due to Q band absorption. Denning and co-workers have used degenerate four wave mixing (DFWM) to test the NLO behaviour of **10** (both in solution and as a thin film) at 1064 nm, where the absorption is very low.[3o] The off-resonance response at this wavelength ($|\chi^{(3)}| = 3 \times 10^{-17}$ m^2 V^{-2})‡ is stronger than those for most other materials. Fig. 5(*a*) shows the strength of the DFWM signal for a thin film of **10**, as a function of the input light intensity, compared to the background signal. A cubic power dependence is maintained up to a damage threshold of 640 MW cm^{-2}. The DFWM experiment involves irradiating the sample with three laser beams; if the sample has significant $\chi^{(3)}$, these beams interact to create a fourth beam. The time response can be tested by delaying one of the probe beams,

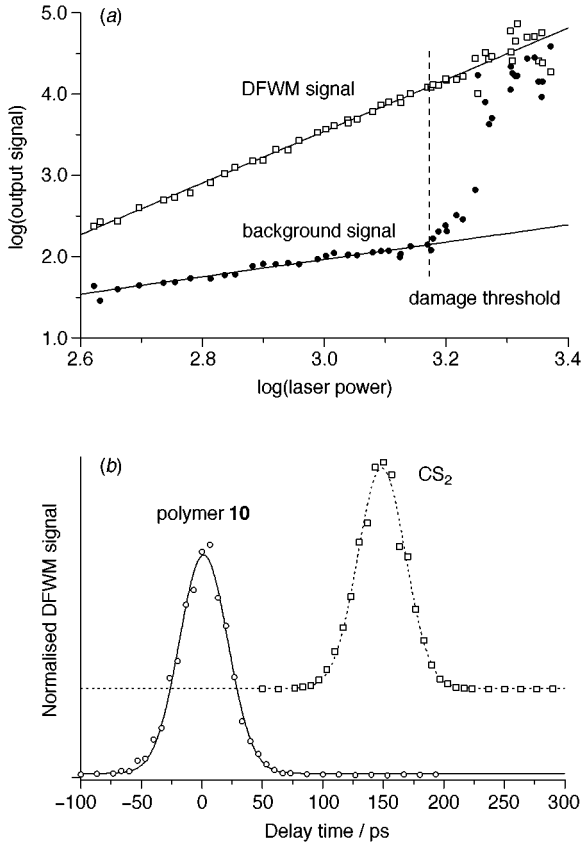

Fig. 5 DFWM measurements on a neat film of polymer **10** at 1064 nm: (*a*) log–log plot of the power dependence of the DFWM and background signals and (*b*) time resolved signals for the polymer film, compared with that for a CS_2 reference (offset for clarity by 150 ps); the smooth curves are fits for a Gaussian function to the data. Both sets of measurements were carried out in the *xyyx* polarisation which minimises non-electronic contributions to the DFWM signal [ref. 3(*o*)].

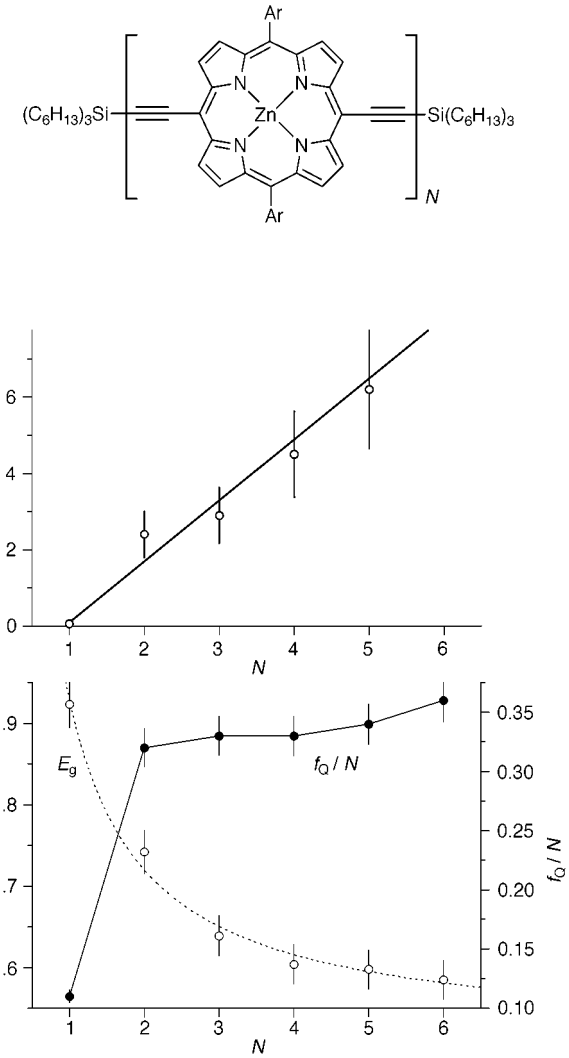

Fig. 6 Variation in (*a*) γ/N and (*b*) *E*g and f_Q/N with the number of macrocycles *N*. All these measurements were made in $CHCl_3$ containing 1% quinuclidine. γ is the magnitude of the *xyyx* tensor from DFWM at 1064 nm. E_g and f_Q are the centre of gravity and oscillator strength of the Q band. The E_g data are fitted to the theoretical curve for $E_g \propto N^{-1}$ [ref. 3(*p*)].

giving results such as those shown in Fig. 5(*b*), for a thin film of **10**, compared with a CS_2 reference. In both cases the response is limited by the pulse width of the laser (45 ps). The decay time of the nonlinearity is much shorter than the excited state lifetime, demonstrating that the mechanism involves a genuine third order electronic polarisation. This type of ultra-fast response is essential for switching applications.

The evolution of the susceptibility per macrocycle, γ/N (the molecular equivalent of $\chi^{(3)}$) with increasing chain length *N* in a series of oligomers of type **12**, has also been investigated using DFWM at 1064 nm.[3p] γ/N increases by almost two orders of magnitude between the monomer and the dimer, then rises linearly from the dimer to the pentamer, with no sign of saturation, as shown in Fig. 6(*a*). Fig. 6(*b*) compares the evolution of the optical band gap E_g and the *Q* band oscillator strength per macrocycle f_Q/N. E_g shows the expected linear dependence on $1/N$, and changes little between the tetramer and the hexamer. f_Q/N rises dramatically on going from the monomer to the dimer, but then hardly changes. γ/N shows a much greater chain length dependence than these classical measures of conjugation. A strong dependence of γ on chain length is also found in other conjugated polymers.[15,20] In non-conjugated *p*-phenylene-linked porphyrin oligomers γ/N is almost independent of the chain length.[18] The polymer **10** has a value of γ/N which is about five times that of the pentamer, consistent with its chain length of $N \approx 10$–15, from small angle neutron scattering. Even in **10**, the optical nonlinearity is about an order of magnitude too low for practical applications. It seems likely that higher molecular weight polymers, and polymers with stronger conjugation, will have stronger NLO behaviour, which will be useful in fabricating ultra-fast switching devices.

Another important type of third order NLO behaviour is optical limiting. When the excited state of a compound absorbs light more strongly than its ground state, the absorption coefficient increases with increasing light intensity. Such materials can limit the transmitted intensity of a light beam, while exhibiting high transmittance at low intensity. They can be used to protect eyes and optical sensors from intense lasers, without significantly obscuring vision. Conjugated porphyrin oligomers such as **3** and **10** show strong nonlinear optical absorption of this type,[3e,k] on a picosecond time-scale, due to photoinduced absorption by long lived triplet states. The molecular design criteria for optical limiting are no better understood than those for maximising $\chi^{(3)}$, but the high oscillator strength and abundance of low energy excited states in these materials are likely to contribute towards both types of third order optical nonlinearity.

Conclusions and outlook

Nonlinear optical applications have been highlighted because they relate directly to conjugation, and because conjugated porphyrin oligomers out-perform all other organic materials in this field. Other applications include biomimetic light harvesting,[13a] molecular-scale electronic components,[5h] and gas sensors.[3g,4f,g,j] All these applications require the porphyrin oligomers to be fabricated into thin films or monolayers, so the

surface chemistry of these compounds is being investigated by several groups.[3f,4f,g,j,5e,g]

Conjugated porphyrin oligomers constitute an active area of research (*ca.* 60 publications in the last 6 years), yet only a few structural types have been explored, and only a few compounds have been subject to detailed photophysical and electrochemical scrutiny. Those structures which have already been investigated in detail have revealed extraordinary electronic and NLO behaviour, resulting mainly from their high polarisability, intense oscillator strength, low HOMO–LUMO gap and abundance of low energy excited states. The strong inter-porphyrin conjugation in the neutral ground states of these oligomers is amplified in their excited states, and in their oxidised and reduced forms. This is a new area of exploration, and it is still easy to design new highly conjugated structures. For example an azo link is almost as sterically unencumbered as an alkyne, and has less bond length alternation. Azo-linked dimers are likely to show strong conjugation, and related structures have been predicted to have strong NLO activity.[21] Hush *et al.* have predicted that *f*-coronene bridged oligomers such as **19** should exhibit phenomenal porphyrin-porphyrin electronic coupling.[5h] The area is full of challenges for both synthetic chemists and theoreticians.

Acknowledgements

The author is indebted to the many people who have worked with him in this area, particularly David Beljonne, Iain Blake, Donal Bradley, Bob Denning, Richard Friend, Steve Kuebler, Guy O'Keefe, Simon Martin, Job Piet, Tim Richardson, Garry Rumbles, Peter Taylor, Jon Thorne, John Warman and Scott Wilson. The author's work in this area has been funded by Magdalene College Cambridge, the EPSRC and the Defence Evaluation and Research Agency (DERA).

Notes and references

† The rotational barrier in 1,2-diphenylethyne is 2.4 kJ mol^{-1} in the ground state and rises to 13–19 kJ mol^{-1} in the first excited state and 24 kJ mol^{-1} in the ground state cation; K. Okuyama, M. C. R. Cockett and K. Kimura, *J. Chem. Phys.*, 1992, **97**, 1649.

‡ Susceptibilities in SI units can be related to esu units using $\chi^{(3)}$ (SI, m^2 V^{-2}) = $(4\pi/9) \times 10^{-8}$ $\chi^{(3)}$ (esu, cm^2 statVolt^{-2}).

1 (*a*) M. R. Wasielewski, *Chem. Rev.*, 1992, **92**, 435; (*b*) A. Harriman and J.-P. Sauvage, *Chem. Soc. Rev.*, 1996, **25**, 41; (*c*) R. W. Wagner, T. E. Johnson and J. S. Lindsey, *J. Am. Chem. Soc.*, 1996, **118**, 11166; (*d*) J. Seth, V. Palaniappan, T. E. Johnson, S. Prathapan, J. S. Lindsey and D. F. Bocian, *J. Am. Chem. Soc.*, 1994, **116**, 10578; (*e*) A. Osuka, N. Tanabe, S. Nakajima and K. Maruyama, *J. Chem. Soc., Perkin Trans. 2*, 1996, 199; (*f*) A. Nakano, A. Osuka, I. Yamazaki, T. Yamazaki and Y. Nishimura, *Angew. Chem., Int. Ed.*, 1998, **37**, 3023.

2 Y. Murakami, J. Kikuchi, Y. Hisaeda and O. Hayashida, *Chem. Rev.*, 1996, **96**, 721; J. K. M. Sanders, *Chem. Eur. J.*, 1998, **4**, 1378.

3 (*a*) H. L. Anderson, *Inorg. Chem.*, 1994, **33**, 972; (*b*) H. L. Anderson, S. J. Martin and D. D. C. Bradley, *Angew. Chem., Int. Ed. Engl.*, 1994, **33**, 655; (*c*) H. L. Anderson, *Adv. Mater.*, 1994, **6**, 834; (*d*) K. Pichler, H. L. Anderson, D. D. C. Bradley, R. H. Friend, P. J. Hamer, M. G. Harrison, C. P. Jarrett, S. J. Martin and J. A. Stephens, *Mol. Cryst. Liq. Cryst.*, 1994, **256**, 415; (*e*) G. E. O'Keefe, G. J. Denton, E. J. Harvey, R. T. Phillips, R. H. Friend and H. L. Anderson, *J. Chem. Phys.*, 1996, **104**, 805; (*f*) M. B. Grieve, T. Richardson, H. L. Anderson and D. D. C. Bradley, *Thin Solid Films*, 1996, **284**, 648; (*g*) V. C. Smith, T. Richardson and H. L. Anderson, *Supramol. Sci.*, 1997, **4**, 503; (*h*) G. E. O'Keefe, J. J. M. Halls, C. A. Walsh, G. J. Denton, R. H. Friend and H. L. Anderson, *Chem. Phys. Lett.*, 1997, **276**, 78; (*i*) D. Beljonne, G. E. O'Keefe, P. J. Hamer, R. H. Friend, H. L. Anderson and J. L. Brédas, *J. Chem. Phys.*, 1997, **106**, 9439; (*j*) J. J. Piet, J. M. Warman and H. L. Anderson, *Chem. Phys. Lett.*, 1997, **266**, 70; (*k*) F. M. Qureshi, S. J. Martin, X. Long, D. D. C. Bradley, F. Z. Henari, W. J. Blau, E. C. Smith, C. H. Wang, A. K. Kar and H. L. Anderson, *Chem. Phys.*, 1998, **231**, 87; (*l*) P. N. Taylor, A. P. Wylie, J. Huuskonen and H. L. Anderson, *Angew. Chem., Int. Ed.*, 1998, **37**, 986; (*m*) P. N. Taylor, J. Huuskonen, G. Rumbles, R. T. Aplin, E. Williams and H. L. Anderson, *Chem. Commun.*, 1998, 909; (*n*) G. S. Wilson and H. L. Anderson, *Chem. Commun.*, 1999, 1539; (*o*) S. M. Kuebler, R. G. Denning and H. L. Anderson, submitted; (*p*) J. R. G. Thorne, S. M. Kuebler, R. G. Denning, I. M. Blake, P. N. Taylor and H. L. Anderson, *Chem. Phys.*, in the press.

4 (*a*) D. P. Arnold, A. W. Johnson and M. Mahendran, *J. Chem. Soc., Perkin Trans. 1*, 1978, 366; (*b*) D. P. Arnold and L. J. Nitschinsk, *Tetrahedron*, 1992, **48**, 8781; (*c*) D. P. Arnold, D. A. James, C. H. L. Kennard and G. Smith, *J. Chem. Soc., Chem. Commun.*, 1994, 2131; (*d*) D. P. Arnold, V. V. Borovkov and G. V. Ponomarev, *Chem. Lett.*, 1996, 485; (*e*) R. Stranger, J. E. McGrady, D. P. Arnold, I. Lane and G. A. Heath, *Inorg. Chem.*, 1996, **35**, 7791; (*f*) D. P. Arnold, D. Manno, G. Micocci, A. Serra, A. Tepore and L. Valli, *Langmuir*, 1997, **13**, 5951; (*g*) D. P. Arnold and D. A. James, *J. Org. Chem.*, 1997, **62**, 3460; (*h*) D. P. Arnold, G. A. Heath and D. A. James, *New J. Chem.*, 1998, 1377; (*i*) D. P. Arnold, D. Manno, G. Micocci, A. Serra, A. Tepore and L. Valli, *Thin Solid Films*, 1998, **327**, 341; (*j*) A. Tepore, A. Serra, D. Manno, L. Valli, G. Micocci and D. P. Arnod, *J. Appl. Phys.*, 1998, **84**, 1416; (*k*) D. P. Arnold, G. A. Heath and D. A. James, *J. Porphyrins Phthalocyanines*, 1999, **3**, 5.

5 (*a*) M. J. Crossley and P. L. Burn, *J. Chem. Soc., Chem. Commun.*, 1987, 39; (*b*) M. J. Crossley and P. L. Burn, *J. Chem. Soc., Chem. Commun.*, 1991, 1569; (*c*) T. X. Lü, J. R. Reimers, M. J. Crossley and N. S. Hush, *J. Phys. Chem.*, 1994, **98**, 11878; (*d*) M. J. Crossley, L. J. Govenlock and J. K. Prashar, *J. Chem. Soc., Chem. Commun.*, 1995, 2379; (*e*) R. Azumi, M. Matsumoto, S. Kuroda, L. G. King and M. J. Crossley, *Langmuir*, 1995, **11**, 4056; (*f*) J. R. Reimers, T. X. Lü, M. J. Crossley and N. S. Hush, *Chem. Phys. Lett.*, 1996, **256**, 353; (*g*) M. J. Crossley and J. K. Prashar, *Tetrahedron Lett.*, 1997, **38**, 6751; (*h*) N. S. Hush, J. R. Reimers, L. E. Hall, L. A. Johnston and M. J. Crossley, *Ann. N.Y. Acad. Sci.*, 1998, **852**, 1.

6 J. Wytko, V. Berl, M. McLaughlin, R. R. Tykwinski, M. Schreiber, F. Diederich, C. Boudon, J.-P. Gisselbrecht and M. Gross, *Helv. Chim. Acta*, 1998, **81**, 1964.

7 J. J. Gosper and M. Ali, *J. Chem. Soc., Chem. Commun.*, 1994, 1707.

8 B. Jiang, S.-W. Yang, D. C. Barbini and W. E. Jones Jr., *Chem. Commun.*, 1998, 213.

9 N. Kobayashi, M. Numao, R. Kondo, S. Nakajima and T. Osa, *Inorg. Chem.*, 1991, **30**, 2241.

10 A. K. Burrell and D. L. Officer, *Synlett*, 1998, 1297; E. E. Bonfantini and D. L. Officer, *Tetrahedron Lett.*, 1993, **34**, 8531.

11 (*a*) M. G. H. Vicente and K. M. Smith, *J. Org. Chem.*, 1991, **56**, 4407; (*b*) L. Jaquinod, M. O. Senge, R. K. Pandey, T. P. Forsyth and K. M. Smith, *Angew. Chem. Int. Ed. Engl.*, 1996, **35**, 1840; (*c*) L. Jaquinod, O. Siri, R. G. Khoury and K. M. Smith, *Chem. Commun.*, 1998, 1261; (*d*) M. G. H. Vicente, M. T. Cancilla, C. B. Lebrilla and K. M. Smith, *Chem. Commun.*, 1998, 2355.

12 M. Chachisvilis, V. S. Chirvony, A. M. Shulga, B. Källebring, S. Larsson and V. Sundström, *J. Phys. Chem.*, 1996, **100**, 13857.

13 (*a*) V. S.-Y. Lin, S. G. DiMagno and M. J. Therien, *Science*, 1994, **264**, 1105; (*b*) M. J. Therien and S. G. DiMagno, *US Pat.* 5 371 199; (*c*) V. S.-Y. Lin and M. J. Therien, *Chem. Eur. J.*, 1995, **1**, 645; (*d*) S. M. LeCours, H.-W. Guan, S. G. DiMagno, C. H. Wang and M. J. Therien, *J. Am. Chem. Soc.*, 1996, **118**, 1497; (*e*) R. Kumble, S. Palese, V. S.-Y. Lin, M. J. Therien and R. M. Hochstrasser, *J. Am. Chem. Soc.*, 1998, **120**, 11489.

14 H. Higuchi, K. Shimizu, J. Ojima, K. Sugiura and Y. Sakata, *Tetrahedron Lett.*, 1995, **36**, 5359.

15 *Electronic Materials: The Oligomer Approach*, ed. K. Mullen and G. Wegner, Wiley-VCH, Chichester, 1998; R. E. Martin and F. Diederich, *Angew. Chem., Int. Ed.*, 1999, **38**, 1350.

16 L. R. Milgrom, *The Colours of Life: An Introduction to the Chemistry of Porphyrins and Related Compounds*, OUP, Oxford, 1997; *The Porphyrins*, ed. D. Dolphin, Academic Press, New York, 1978.

17 D. A. Fletcher, R. F. McMeeking and D. Parkin, *J. Chem. Inf. Comput. Sci.*, 1996, **36**, 746; F. H. Allen and O. Kennard, *Chem. Des. Autom. News*, 1993, **8**, 31.

18 M. Terazima, H. Shimizu and A. Osuka, *J. Appl. Phys.*, 1997, **81**, 2946.

19 B. S. Erler, W. F. Scholz, Y. J. Lee, W. R. Scheidt and C. A. Reed, *J. Am. Chem. Soc.*, 1987, **109**, 2644.

20 R. R. Tykwinski, U. Gubler, R. E. Martin, F. Diederich, C. Bosshard and P. Gunter, *J. Phys. Chem. B*, 1998, **102**, 4451.

21 I. D. L. Albert, T. J. Marks and M. A. Ratner, *Chem. Mater.*, 1998, **10**, 753.

Paper 9/04209A

ChemComm

Kinetic control of stereoselectivity of halide substitution in arene ruthenium pyridyloxazoline complexes; a rare case of net inversion†

Adam J. Davenport, David L. Davies,* John Fawcett, Shaun A. Garratt and David R. Russell

Department of Chemistry, University of Leicester, Leicester, UK LE1 7RH. E-mail: dld3@le.ac.uk

Received (in Cambridge, UK) 30th September 1999, Accepted 19th October 1999

Reaction of [RuCl(Pr^i-pymox)(η^6-mes)]$^+$ 1b [Pr^i-pymox = 4-isopropyl-2-(2-pyridyl)-1,3-oxazoline, mes = 1,3,5-trimethylbenzene] with $AgSbF_6$ then with halide gives [RuX(Pr^i-pymox)(η^6-mes)]$^+$ (X = Cl 1, Br 2, I 3), each as a mixture of diastereomers, the kinetic product being formed preferentially with net inversion of configuration at the metal; the structures of 2a and 2b have been determined by X-ray crystallography.

The stable well defined geometry of half-sandwich complexes makes them useful substrates for the study of the mechanism, particularly the stereochemistry, of substitution reactions at a chiral metal centre.[1] In addition, arene ruthenium complexes are becoming increasingly important in asymmetric catalysis.[2] In order to optimise the enantioselection of such complexes it is important to understand the factors that control diastereoselectivity, the tendency for epimerisation at the metal and the stereochemistry of substitution reactions.

Arene ruthenium(II) complexes have low-spin d^6-configuration and ligand exchange is usually dissociative, as found for anation of $[Ru(H_2O)(bipy)(\eta^6\text{-arene})]^{2+}$.[3] The stereoselectivity of substitution is determined by the stereochemical stability of the five-coordinate intermediate, partial epimerisation at the metal occurs in some cases.[4] In many cases kinetic control of asymmetric induction is hard to prove since the interconversion of the product diastereomers is relatively facile under the reaction conditions, this has lead to erroneous conclusions about stereoselectivity.[5] Nelson and coworkers reported that substitution of some cyclometallated arene ruthenium complexes occurred, in all cases, with preferential retention of configuration, and with very high selectivity in the case of halide exchange.[6]

Coordination of pyridyloxazolines to an '(arene)RuX' fragment can in principle give rise to two isomers (**a** and **b**). Treatment of $[RuCl_2(mes)]_2$ with Pr^i-pymox in refluxing methanol, gave $[RuCl(Pr^i\text{-pymox})(\eta^6\text{-mes})]SbF_6$ as one diastereomer which was shown by X-ray crystallography to have the isopropyl pointing towards the chloride (**1b**) rather than the π-bound ring.[7] Abstraction of chloride with $AgSbF_6$ in acetone–water gives $[Ru(H_2O)(Pr^i\text{-pymox})(\eta^6\text{-mes})][SbF_6]_2$ which reacts with KCl, KBr or NaI in methanol at room temperature to give the halide complexes $[RuX(Pr^i\text{-pymox})(\eta^6\text{-mes})]SbF_6$ (X = Cl **1**, Br **2**, I **3**).†

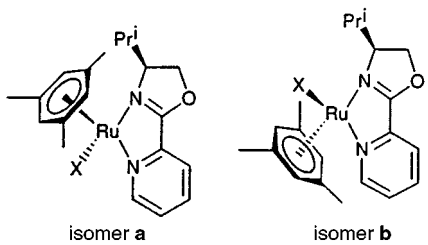

† ^{1}H NMR spectra and satisfactory elemental analyses are available as electronic supplementary information (ESI): See http://www.rsc.org/suppdata/cc/1999/2331/

The ^{1}H NMR spectrum of a crude sample of **2** shows the presence of two diastereomers in an approximate ratio of 75 : 25. Careful recrystallisation allowed separation of the two diastereomers and their structures were determined by X-ray diffraction.‡ Isomer **2b** (Fig. 1) has the isopropyl pointing towards the halide, the same as found previously for the chloride,[7] whilst isomer **2a** (Fig. 2) has the isopropyl pointing towards the π-bound arene. The Ru–N(1), Ru–N(2), distances and the N(1)–Ru–N(2) angle are statistically the same in each isomer and with the chloride **1b**.[7] The Ru–Br bond is slightly longer in isomer **2b**

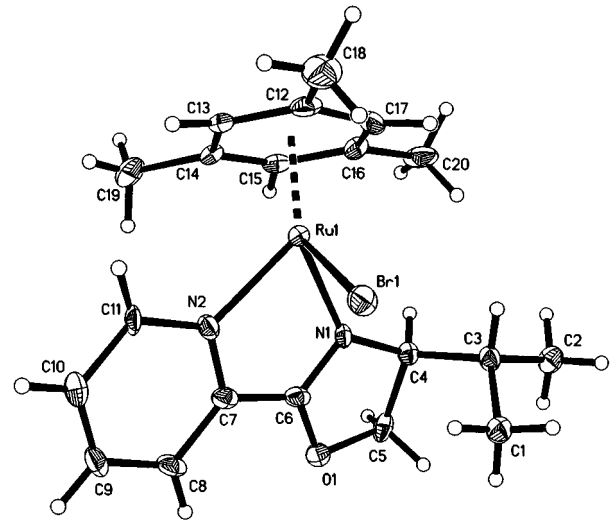

Fig. 1 Molecular structure and atom numbering scheme for the cation of **2b**. Selected bond distances (Å) and angles (°): Ru–N(1) 2.122(11), Ru–N(2) 2.103(10), Ru–Br 2.532(2); N(2)–Ru(1)–N(1) 76.3(4), N(1)–Ru–Br 89.3(3), N(2)–Ru–Br 82.1(3).

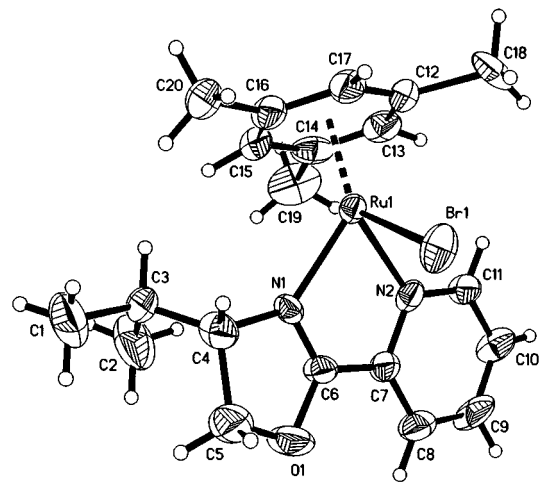

Fig. 2 Molecular structure and atom numbering scheme for the cation of **2a**. Selected bond distances (Å) and angles (°): Ru–N(1) 2.096(10), Ru–N(2) 2.097(13), Ru–Br 2.522(2); N(2)–Ru–N(1) 76.4(5), N(1)–Ru–Br 82.9(3), N(2)–Ru–Br 85.6(4).

than in **2a**. In addition, the N(1)–Ru–Br and N(2)–Ru–Br angles are 89.3(3) and 82.1(3)°, respectively, in **2b**, *i.e.* the oxazoline end of the ligand is inclined slightly away from the bromide to relieve steric congestion between the isopropyl and the bromide; whilst in **2a** the corresponding angles are 82.9(3) and 85.6(4)°, *i.e.* with the pyridine end inclined away from the bromide to minimise steric congestion between the isopropyl and the π-bound arene. The ^{1}H NMR of the crystals showed that **2a** was the major product in the initial mixture.

The chloride (**1**) and iodide (**3**) were formed similarly and the ^{1}H NMR spectra of the crude products show two isomers in a similar 75 : 25 ratio. The ^{1}H NMR spectra, and a crystal structure for **3a**, showed that isomer **a** was preferred in each case. Thus, for **1**, by forming the complex at room temperature we have been able to isolate the kinetic product (**1a**) whilst the preparation in refluxing methanol gave exclusively the thermodynamic isomer (**1b**).[7]

The ^{1}H NMR spectra of crystals of **1a**–**3a** in CD_2Cl_2 showed only the presence of isomer **a**, no trace of isomer **b** was seen even after several days at room temperature. Similarly, the ratios of mixtures of isomers did not change within a few days in CD_2Cl_2 solution. Hence, the configuration at the metal is stable in this solvent. However, in more solvating solvents such as d_4-MeOH or d_6-acetone the isomer ratios were observed to change slowly over a period of days at room temperature or more rapidly at higher temperature, in each case isomer **b** being thermodynamically preferred by at least a ratio of 95 : 5.

Thus, these two-step substitution reactions are unambiguous examples of kinetic control of stereoselectivity with the favoured pathway being a rare case of formal inversion at the metal.[8] We propose the mechanism shown in Scheme 1. Abstraction of halide by Ag^+ provides the aqua/solvent species **4**, epimerisation of which will be much faster than for the halide coordinated species. Species **4a** is expected to react faster since attack of the halide occurs preferentially from the side opposite the oxazoline substituent, *i.e.* the least sterically hindered approach, giving **1a**–**3a** with the isopropyl pointing towards the π-bound arene rather than the halide. The rate of epimerisation of **1**–**3** in methanol is sufficiently slow that it can not account for the amount of isomer **b** formed, *i.e.* the reaction is not forming exclusively isomer **a** followed by epimerisation to isomer **b**. A more precise study of the selectivity, including the effects of different substituents on the oxazoline and the arene and a more detailed kinetic analysis of the reactions will be reported elsewhere.

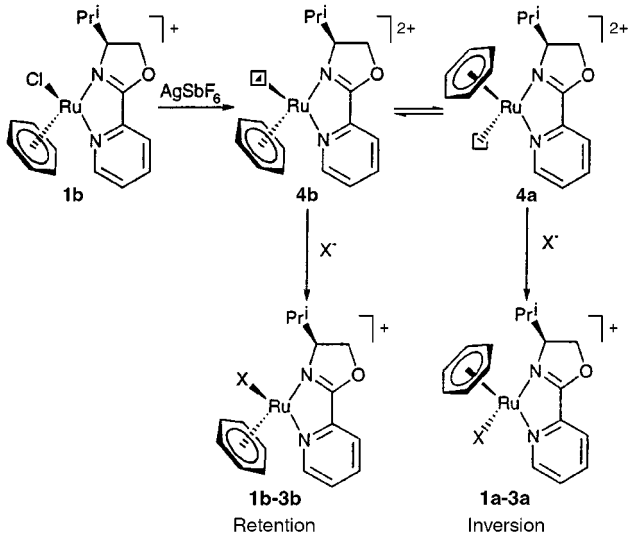

Scheme 1 (i) □ represents a vacant coordination site or a solvent molecule. (ii) Methyl substituents on the arene have been omitted for clarity.

We thank the University of Leicester (S. A. G.) and EPSRC (A. J. D.) for studentships and Johnson Matthey for a loan of $RuCl_3$.

Notes and references

‡ *Crystal data*: for **2b**: $C_{20}H_{26}BrF_6N_2ORuSb$, M = 727.16, orthorhombic, space group $P2_12_12_1$, a = 8.5892(9), b = 9.5732(14), c = 29.369(3) Å, U = 2414.9(5) Å^3, Z = 4, D_c = 2.000 g cm^{-3}, μ = 3.460 mm^{-1}, F(000) = 1408, graphite-monochromated Mo-Kα radiation (λ = 0.71073 Å). Data collected on a Siemens P4 diffractometer at 190 K. 3782 reflections collected with 2.24 < θ < 27.0°, 3570 unique (R_{int} = 0.0429). An analytical absorption correction was applied. The structure was solved by Patterson methods and refined using full-matrix least squares on F^2 (SHELXL96). Anisotropic displacement parameters used for all atoms, hydrogens included in calculated positions (C–H 0.96 Å), with isotropic displacement parameters set to 1.2 U_{eq}(C) or 1.5 U_{eq}(C) for methyl H atoms. Final R_1 = 0.0534, wR_2 (all data) = 0.1364.

For **2a**: $C_{20}H_{26}BrF_6N_2ORuSb$, M = 727.16, orthorhombic, space group $P2_12_12_1$, a = 7.7030(7), b = 12.0995(17), c = 27.223(2) Å, U = 2537.2(5) Å^3, Z = 4, D_c = 1.904 g cm^{-3}, μ = 3.293 mm^{-1}, F(000) = 1408, graphite-monochromated Mo-Kα radiation (λ = 0.71073 Å). Data collected on a Siemens P4 diffractometer at 200 K. 3234 reflections collected with 1.84 < θ < 25.99°, 3152 unique (R_{int} = 0.0238). A ψ-scan absorption correction was applied. The structure was solved by Patterson methods and refined using full-matrix least squares on F^2 (SHELXL96). Anisotropic displacement parameters used for all atoms, hydrogens included in calculated positions (C–H 0.96 Å), with isotropic displacement parameters set to 1.2 U_{eq}(C) or 1.5 U_{eq}(C) for methyl H atoms. Final R_1 = 0.0579, wR_2 (all data) = 0.1804. CCDC 182/1448. See http://www.rsc.org/suppdata/cc/1999/2331/ for crystallographic files in .cif format.

1 V. I. Sokolov, *Chirality and Optical Activity in Organometallic Compounds*, Gordon and Breach Science Publishers, New York, 1990; H. Brunner, *Angew. Chem., Int. Ed.*, 1999, **38**, 1194.
2 R. Noyori and S. Hashiguchi, *Acc. Chem. Res.*, 1997, **30**, 97; K.-J. Haack, S. Hashiguchi, A. Fujii, T. Ikariya and R. Noyori, *Angew. Chem., Int. Ed. Engl.*, 1997, **36**, 285; E. P. Kundig, C. M. Saudan and G. Bernardinelli, *Angew. Chem., Int. Ed.*, 1999, **38**, 1220.
3 L. Dadci, H. Elias, U. Frey, A. Hornig, U. Koelle, A. E. Merbach, H. Paulus and J. S. Schneider, *Inorg. Chem.*, 1995, **34**, 306.
4 H. Brunner, R. Oeschey and B. Nuber, *J. Chem. Soc., Dalton Trans.*, 1996, 1499.
5 H. Brunner, R. Oeschey and B. Nuber, *Inorg. Chem.*, 1995, **34**, 3349.
6 N. Gul and J. H. Nelson, *Organometallics*, 1999, **18**, 709; S. Attar, V. J. Catalano and J. H. Nelson, *Organometallics*, 1996, **15**, 2932; H. D. Hansen, K. Maitra and J. H. Nelson, *Inorg. Chem.*, 1999, **38**, 2150; N. Gul and J. H. Nelson, *Polyhedron*, 1999, **18**, 1835.
7 D. L. Davies, J. Fawcett, S. A. Garratt and D. R. Russell, *Chem. Commun.*, 1997, 1351.
8 F. Morandini, G. Consiglio and V. Lucchini, *Organometallics*, 1985, **4**, 1202.

Communication 9/07873H

ChemComm

Novel peptidomimetic structures: enantioselective synthesis of conformationally constrained lysine, ornithine and alanine analogues from pyroglutamic acid

Rajesh Goswami and Mark G. Moloney*

The Department of Chemistry, Dyson Perrins Laboratory, University of Oxford, South Parks Road, Oxford, UK OX1 3QY. E-mail: mark.moloney@chem.ox.ac.uk

Received (in Liverpool, UK) 3rd August 1999, Accepted 27th September 1999

Conformationally constrained lysine and ornithine analogues, and an L-Ala-L-Ala dipeptide analogue, are available from pyroglutamic acid.

The synthesis of conformationally constrained amino acids is of considerable current interest;[1–4] in addition to their intrinsic interest as ligands for a wide variety of biological receptors, incorporation of these structural elements into peptide chains can be used to generate novel structures of relevance to biological or materials application.[5] Although structurally restricted analogues of a number of amino acids have been described,[6–10] the ω-amino acids have generally only recently begun to attract attention. However, modified lysine chimeras, derived from pyroglutamic acid,[11] and from proline,[9] and a peptidomimetic which includes a conformationally restricted lysine analogue[12] have all recently been reported, as have ornithine[13] and arginine analogues.[14] The synthesis of cyano[15] or indole[16] substituted glutamate analogues has also recently been described.

We have used the readily available lactam **1a** as a template for manipulation to a variety of functionalised pyrrolidinones[17–20] and recently shown its application to the synthesis of conformationally restricted glutamates[21] and aminopyrrolidones.[22] We report here the extension of this versatile approach to the synthesis of several other conformationally restricted amino acids. The well-defined conformation of pyroglutamic acid has been investigated in detail[23] and its application as a template for peptidomimetics previously proposed;[24] the pyrrolidone ring simultaneously restricts τ_1, τ_2 and τ_3 to very limited ranges (from a simple molecular modeling energy minimised structure,[25] these are −144, +23 and −17° respectively) and defines the *cis*-amide bond (Fig. 1).[26]

The lysine chimera was obtained as follows: the enolate of lactam **1a** was treated with $BrCH_2CN$ (Scheme 1), unusually to give exclusively the *endo* adduct **2** in 55% yield;[27] similar alkylations generally proceed under thermodynamic control to give the *exo* product.[19] The *cis* stereochemistry of **2** and **4** was assigned on the basis of NOE data. Reduction of the nitrile function with $NaBH_4$–$CoCl_2$ gave the corresponding amine **3** in 76% yield, and this intermediate was easily converted to the product **4** in a four step (protection, deprotection, oxidation and *in situ* esterification) sequence in 16% overall yield.

The ornithine chimera was obtained from lactam **1b**. Selenenation and elimination to the known enone **5** followed by conjugate addition of the Reformatsky reagent derived from $BrCH_2CN$ gave adduct **6a** in 69% yield as a single diastereomer, as shown by ^{13}C NMR spectroscopic analysis. This strategy has proved to be very successful for manipulation of this position of a pyrrolidone ring.[21] Hydrolysis and decarboxylation using $(Bu_3Sn)_2O$[28] readily afforded the product **6b** in 68% yield, and

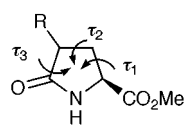

Fig. 1

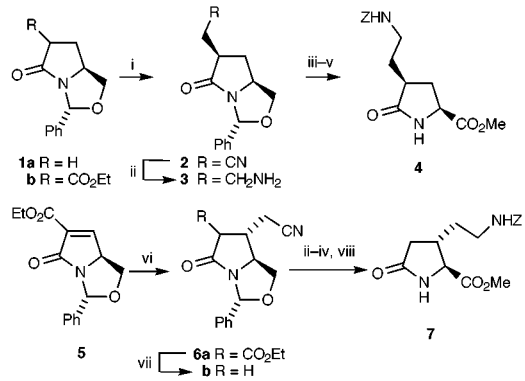

Scheme 1 *Reagents and conditions*: i, LDA, THF, −78 °C then $BrCH_2CN$ (55%); ii, $NaBH_4$, $CoCl_2$, EtOH; iii, ZCl, Et_3N; iv, TFA; v, RuO_2, $NaIO_4$ then CH_2N_2 (34%); vi, Zn, DMPU, $BrCH_2CN$ (69%), room temp.; vii, $(Bu_3Sn)_2O$, toluene, Δ, 16 h (68%); viii, PDC, DMF, then CH_2N_2 (35%).

a similar sequence to that described above gave the product **7** in 14% yield over the four steps. In this case, however, application of RuO_4 in the final oxidation step did not give the desired product, and this step was successful only with PDC/DMF. The *trans* relative stereochemistry of **6a** and **7** was again shown by NOE data.

The presence of an internal amide bond suggested that amination at the C-7 position of **1a** could be used to generate an unusual dipeptide mimetic. Related aminopyrrolidones, aminopiperidones and larger ring heterocycles have recently attracted interest as enzyme inhibitors[29] and peptidomimetic structures.[30–33] Amination of the enolate of lactam **1a** with $(PhO)_2P(O)N_3$ followed by treatment with Boc_2O gave the amino lactam **8** in 50% yield (Scheme 2); surprisingly, the *endo* product, whose stereochemistry was subsequently established, was obtained exclusively. Acidic release of the protecting groups, and reprotection of the C-4 amino function as its benzyloxycarbonyl (Z) derivative, gave the product **9b** in 51% yield over the two steps. Oxidation and esterification in the usual way then gave the product **10**, which was a single stereoisomer at room temperature by NMR analysis, and whose *cis* stereochemistry was shown by NOE spectroscopy. Molecular modeling of the *N*-acetyl analogue **11** of compound **10**[25] demonstrated that two well defined conformations existed, differing by 2.3 kcal mol^{-1} in energy, with the two substituents either pseudodiequatorial or diaxial, and the latter being the more stable; since a 2.7 kcal mol^{-1} energy difference corresponds to a 99:1 ratio of species at equilibrium,[34] the

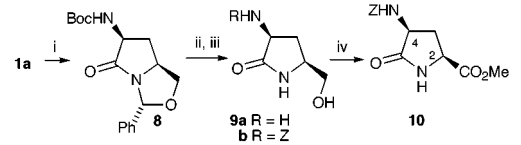

Scheme 2 *Reagents and conditions*: i, LDA, THF, −78 °C, then $(PhO)_2P(O)N_3$, then Boc_2O, −78→O °C (50%) ii, TFA, CH_2Cl_2, room temp., 1 h (quant.); iii, ZCl, DMF–THF, Et_3N, 0 °C, 3 h (51%); iv, PDC, DMF, 40 °C, 12 h, then CH_2N_2 (28%).

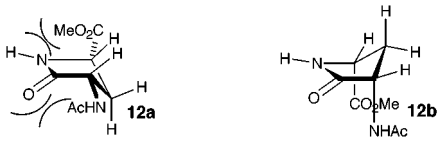

Fig. 2 Conformations of **12a** and **12b**.

minor diequatorial conformer would not be expected to be observable at room temperature by NMR analysis, and ^{1}H NMR VT analysis provided no evidence for the diequatorial conformer even at 223 K. The stability of the diaxial conformer could be attributed to the presence of A-strain[35] between the two substituents and the planar amide system; the importance of torsional strain in five- and six-membered ring heterocycles for the control of stereochemistry has been investigated in detail,[36] although its importance in lactams has only recently been appreciated.[37] Thus, the diaxial conformer minimises the interations of the relatively bulky C(2) and C(4) substituents with the planar amide function (which would occur in the diequatorial conformer **12a**) by placing C(2)-H and C(4)-H in an eclipsing conformation with the lactam system **12b** (Fig. 2). Using the energy minimised structure for **11**, some calculated dihedral angles are given in Table 1; the diaxial conformer most closely resembles a Type VIa (*cis*) β-turn.[38] Thus, this compound could be considered to be a conformationally restricted L-Ala-L-Ala dipeptide analogue, with the central amide bond constrained in the *cis* orientation, and the pyrrolidone ring capable of providing a reverse turn in an attached peptide chain; as such it represents a potential low molecular weight non-hydrophobic turn inducer. A related aminopyrrolidone has also been reported to induce Type II′ β-turn folding in a short peptide, and to exhibit hypoglycaemic activity.[39]

Table 1 Dihedral angles for energy minimised[a] conformations of **11**

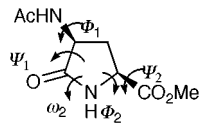

Conformation	Ψ_1 (°)	Φ_2 (°)
Diequatorial	−139	+137
Diaxial	+94	−97

[a] Structures optimised with Chem3D Pro 3.5, available from Cambridge Scientific (MM2 parameters).

In view of the increasing interest in the use of variously modified proline derivatives for subtle conformational control in short peptide sequences,[40–44] the ready synthetic accessibility of enantiopure functionalised pyrrolidones may enable their application as amino acid surrogates particularly where well-defined conformational restriction is required.

We thank The Felix Foundation for funding of a scholarship to R. G., the EPSRC Chemical Database Service at Daresbury[45] and the EPSRC National Mass Spectrometric Service Centre at Swansea.

Notes and references

1 M. D. Fletcher and M. M. Campbell, *Chem. Rev.*, 1998, **98**, 763.
2 A. Dutta, in *Specialist Periodical Reports 'Amino acids, Peptides and Proteins'*, ed. J. S. Davies, Royal Society of Chemistry, Cambridge, 1998, ch. 3.
3 S. Hanessian, G. McNaughton-Smith, H.-G. Lombart and W. D. Lubell, *Tetrahedron*, 1997, **53**, 12789.
4 J. Gante, *Angew. Chem., Int. Ed. Engl.*, 1994, 1699.
5 S. H. Gellman, *Acc. Chem. Res.*, 1998, **31**, 173.
6 S. Hannessian, N. Bernstein, R.-Y. Yang and R. Maguire, *Bioorg. Med. Chem. Lett.*, 1999, **9**, 1437.
7 S. Hannessian and R. Margarita, *Tetrahedron Lett.*, 1998, **39**, 5887.
8 S. Hannessian, R. Margarita, A. Hall and X. Luo, *Tetrahedron Lett.*, 1998, **39**, 5883.
9 Q. Wang, N.A. Sasaki and P. Potier, *Tetrahedron*, 1998, **54**, 15 759.
10 R. Sharma and W. D. Lubell, *J. Org. Chem.*, 1996, **61**, 202.
11 P. J. Murray, *Tetrahedron Lett.*, 1998, **39**, 6721.
12 S. Cappelletti, M. Pegna, A. Zaliani and M. Pinori, *Lett. Pept. Sci.*, 1995, **2**, 161.
13 J. Eustache, A. Grob, C. Lam, O. Sellier and G. Schulz, *Bioorg. Med. Chem. Lett.*, 1998, **8**, 2961.
14 R. Zhang, A. Mamai and J. S. Madalengoitia, *J. Org. Chem.*, 1999, **64**, 547.
15 C. Dugave, J. Cluzeau, A. Menez, M. Gaudry and A. Marquet, *Tetrahedron Lett.*, 1998, **39**, 5775.
16 M. F. Brana, M. Garranzo and J. Perez-Castells, *Tetrahedron Lett.*, 1998, **39**, 6569.
17 J. H. Bailey, D. T. Cherry, K. M. Crapnell, M. G. Moloney, S. B. Shim, M. Bamford and R. B. Lamont, *Tetrahedron*, 1997, **53**, 11 731.
18 M. Bamford, M. Beard, D. T. Cherry and M. G. Moloney, *Tetrahedron: Asymmetry*, 1995, **6**, 337.
19 M. J. Beard, J. H. Bailey, D. T. Cherry, M. G. Moloney, S. B. Shim, K. Statham, M. Bamford and R. B. Lamont, *Tetrahedron*, 1996, **52**, 3719.
20 J. Dyer, S. Keeling and M. G. Moloney, *Tetrahedron Lett.*, 1996, **37**, 4573.
21 J. Dyer, S. Keeling and M. G. Moloney, *Chem. Commun.*, 1998, 461.
22 P. W. H. Chan, I. F. Cottrell and M. G. Moloney, *Tetrahedron Lett.*, 1997, **38**, 5891.
23 P. K. C. Paul, D. J. Osguthorpe and M. M. Campbell, *J. Chem. Soc., Perkin Trans. 1*, 1990, 3363.
24 P. K. C. Paul, P. A. Burney, M. M. Campbell and D. J. Osguthorpe, *Bioorg. Med. Chem. Lett.*, 1992, **2**, 141.
25 Structures optimised with Chem3D Pro 3.5, available from Cambridge Scientific (MM2 Parameters).
26 J. A. Monn, M. J. Valli, R. A. True, D. D. Schoepp, J. D. Leander and D. Lodge, *Bioorg. Med. Chem. Lett.*, 1993, **3**, 95.
27 All new compounds gave satisfactory spectroscopic and/or high resolution mass spectrometric or analytical data.
28 C. J. Salomon, E. G. Mata and O. A. Mascarotti, *J. Org. Chem.*, 1994, **59**, 7259.
29 R. Shankar and A. I. Scott, *Heterocycles*, 1996, **42**, 145.
30 T. Lehmann, D. Michel, M. Glanzel, R. Waibel and P. Gmeiner, *Heterocycles*, 1999, **51**, 1389.
31 A. Nouvet, M. Binard, F. Lamaty, J. Martinez and R. Lazaro, *Tetrahedron*, 1999, **55**, 4685.
32 P. Benovsky, G. A. Stephenson and J. R. Stille, *J. Am. Chem. Soc.*, 1998, **120**, 2493.
33 S. Derrer, N. Feeder, S. J. Teat, J. E. Davies and A. B. Holmes, *Tetrahedron Lett.*, 1998, **39**, 9309.
34 N. Isaacs, *Physical Organic Chemistry*, Longman, London, 1995.
35 R. W. Hoffmann, *Chem. Rev.*, 1989, 1841.
36 D. Seebach, B. Lamatsch, R. Amstutz, A. K. Beck, M. Dobler, M. Egli, R. Fitzi, M. Gautschi, B. Herradon, P. C. Hidber, J. J. Irwin, R. Locher, M. Maestro, T. Maetzke, A. Mourino, E. Pfammatter, D. A. Plattner, C. Schlickli, W. B. Schweizer, P. Seiler, G. Stucky, W. Petter, J. Escalante, E. Juaristi, D. Quintana, C. Miravitlles and E. Molins, *Helv. Chim. Acta*, 1992, **75**, 913.
37 K. Ando, N. S. Green, Y. Li and K. N. Houk, *J. Am. Chem. Soc.*, 1999, **121**, 5334.
38 G. D. Rose, L. M. Gierasch and J. A. Smith, *Adv. Protein Chem.*, 1985, **37**, 1.
39 N. J. Ede, I. D. Rae and M. T. W. Hearn, *Tetrahedron Lett.*, 1990, **31**, 6071.
40 L. Halab and W. D. Lubell, *J. Org. Chem.*, 1999, **64**, 3312.
41 R. Zhang and J. S. Madelengoitia, *J. Org. Chem.*, 1999, **64**, 547.
42 R. Zhang, F. Brownewell and J. S. Madalengoitia, *J. Am. Chem. Soc.*, 1998, **120**, 3894.
43 E. Beausoleil, R. Sharma, S. W. Michnick and W. D. Lubell, *J. Org. Chem.*, 1998, **63**, 6572.
44 P. Dumy, M. Keller, D. E. Ryan, B. Rohwedder, T. Wohr and M. Mutter, *J. Am. Chem. Soc.*, 1997, **119**, 918.
45 D. A. Fletcher, R. F. McMeeking and D. Parkin, *J. Chem. Inf. Comput. Sci.*, 1996, **36**, 746.

Communication 9/06297A

ChemComm

9-Methylgermacrene-B is confirmed as the sex pheromone of the sandfly *Lutzomyia longipalpis* from Lapinha, Brazil, and the absolute stereochemistry defined as *S*

J. Gordon C. Hamilton,[a] Antony M. Hooper,[b] Helen C. Ibbotson,[a] Satoshi Kurosawa,[c] Kenji Mori,[c] Shin-etsu Muto[c] and John A. Pickett*[b]

[a] *School of Life Sciences, University of Keele, Keele, Staffordshire, UK ST5 5BG*
[b] *IACR-Rothamsted, Harpenden, Hertfordshire, UK AL5 2JQ. E-mail: john.pickett@bbsrc.ac.uk*
[c] *Department of Chemistry, Science University of Tokyo, Kagurazaka 1-3, Shinjuku-ku, Tokyo 162-8601, Japan*

Received (in Liverpool, UK) 29th September 1999, Accepted 13th October 1999

The structure of the sex pheromone produced by the male sandfly *Lutzomyia longipalpis*, from the Lapinha Cave (Minas Gerais State) region of Brazil, previously proposed tentatively as the novel homosesquiterpene 9-methylgermacrene-B, is confirmed and the absolute stereochemistry defined as *S* by comparing physical and biological properties of the synthetic enantiomers with the natural product.

The sandfly *Lutzomyia longipalpis* (Lutz and Neiva) (Diptera: Psychodidae) is the vector of the protozoan parasite *Leishmania chagasi* (Cunha and Chagas) (Kinetoplastida: Trypanosomatidae), the causative agent of visceral leishmaniasis in the New World. Male *L. longipalpis* release a sex pheromone, from glands on the tergites of the abdomen,[1] which is highly attractive to females.[2] The sex pheromone gland of *L. longipalpis* from the Lapinha region (Minas Gerais State) in Brazil produces one principal volatile component that is responsible for the attraction of females.[3] It was proposed, mostly on the basis of mass spectrometry on natural material and on products from microchemical reactions, that the pheromone comprised the novel homosesquiterpene 9-methylgermacrene-B **1**.[4] The sex pheromones of other sympatric and allopatric populations of *L. longipalpis* are different;[5] for example, that from the Jacobina region of Brazil (Bahia State) has been confirmed as another novel sesquiterpene, 3-methyl-α-himachalene, with relative stereochemistry defined as 1*RS*,3*RS*,7*RS*.[6] The purpose of this work was to test the proposed structure for the Lapinha *L. longipalpis* sex pheromone by synthesis of 9-methylgermacrene-B and to define the absolute stereochemistry at C-9 by comparison between the natural product and the synthetic enantiomers (*R*)-**1** and (*S*)-**1**.

The overall synthetic approach adopted has recently been developed for sesquiterpene germacrene-B and involves the establishment of the cyclodecadiene ring system by an intramolecular alkylation before finally elaborating the isopropylidene group.[7] Initially, the racemic 9-methylgermacrene-B (**1**) was prepared as in Scheme 1 from geraniol **2**, in order to test the initial structural hypothesis for this pheromone.[4] The NMR data from racemic **1**† were similar to the limited data obtained originally for the natural product.[4] Co-injection on GC‡ (siloxane column) of racemic **1** with the natural product gave one enhanced peak (18.22 min). The mass spectrum of synthetic compound by GC-MS§ was similar to that published for the natural product.[4] Having confirmed the structure of the pheromone as 9-methylgermacrene-B **1**, the enantiomers were then synthesised by the same cyclisation approach but with methyl 3-hydroxy-2-methylpropionate **4** as chiral precursor, *i.e.* (*S*)-**4** to (*R*)-**1** and (*R*)-**4** to (*S*)-**1** as in Scheme 2. The enantiomers of **4** were obtained commercially and (*R*)-**1** was synthesised first, hence some improvements in yield for (*S*)-**1**. The chiral syntheses required introduction of two stereogenic double bonds at **5** and **6** which were both achieved with an *E*/*Z* ratio of >99% by NMR and the final products possessed an ee of >95%. Both (*R*)-**1** and (*S*)-**1** gave NMR and mass spectra essentially the same as for racemic **1**,†§ as expected, and with $[\alpha]_D^{18}$ + 61.4 and $[\alpha]_D^{20}$ −61.3 ($CHCl_3$), respectively. On chiral GC‡, the *R* and *S* isomers of **1** eluted in that order (38.04, 38.20 min) and, when co-injected with racemic **1**, the natural product gave enhancement of the second peak, defining the absolute stereochemistry of the pheromone as (*S*)-9-methylgermacrene-B (*S*)-**1**. It should be noted, as explained previously,[4] that the pheromone is not stable and readily undergoes acid catalysed cyclisation and a Cope rearrangement to the corresponding elemene structure on heating, hence the requirement for cold on-column injection or low injector port temperatures for GC.‡

Bioassays¶ involving attraction of female *L. longipalpis* and conducted in a Y-tube olfactometer resulted in racemic **1** giving 77% attraction compared with 72% (though not statistically significantly different) for an equivalent amount of the natural product. Attraction to (*S*)-**1** was 67% compared with 56% to the (*R*)-**1** isomer. The response to (*S*)-**1** was not significantly different from that of the natural pheromone, whereas the response to the (*R*)-**1** isomer was significantly lower (χ^2 p =

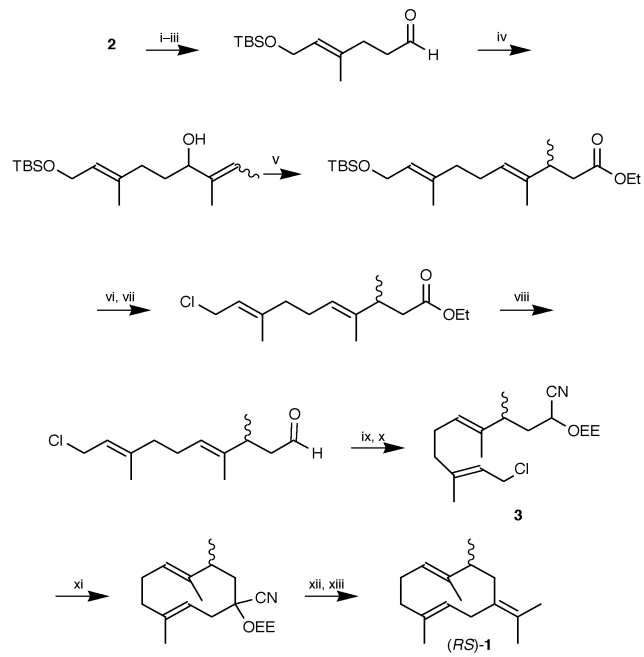

Scheme 1 Yields are for routes to (±)-**1**, and from compound **3** to **1** also are quoted for routes to (*R*)-**1** then (*S*)-**1** in that order. *Reagents and conditions:* i, TBSCl, imidazole, DMF, 96%; ii, MCPBA, $CHCl_3$, 74%; iii, $HIO_4.2H_2O$, Et_2O, THF, 52%; iv, CHMe=CMeMgBr, THF, 55%; v, $CH_3C(OEt)_3$, $C_2H_5CO_2H$, 71% (*E*/*Z*: 98:2); vi, PPTS, MeOH, 87%; vii; Ph_3P, CCl_4; viii, DIBAL-H, CH_2Cl_2; ix, TMSCN, KCN, 18-crown-6, then $BnNMe_3F$, THF, H_2O; x, CH_2=CHOEt, C_6H_6; xi, NaHMDS, THF, 19% (5 steps), 47%, 42%; xii, PPTS, MeOH then aq. NaOH, Et_2O, 18%, 51%, 50%; xiii, Me_2CBr_2, Sm, $CrCl_3$, SmI_2, THF, 56%, 60%, 64%.

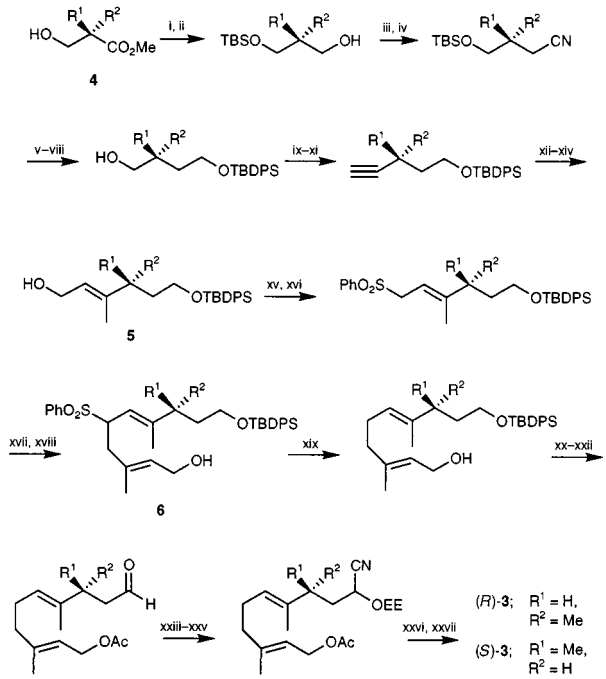

Scheme 2 Yields are quoted for routes to (*R*)-**1** then (*S*)-**1** in that order. *Reagents and conditions:* i, TBSCl, imidazole, DMF, quant., 99%; ii, DIBAL-H, CH_2Cl_2, 85%, 94%; iii, TsCl, Py; iv, NaCN, DMSO, 79%, 84%, 2 steps; v, DIBAL-H, CH_2Cl_2; vi, $NaBH_4$, EtOH, 58%, 65%, 2 steps; vii, TBDPSCl, imidazole, DMF, 89%, 99%; viii, AcOH, THF, H_2O, 84%, 86%; ix, Swern oxidation; x, PPh_3, CBr_4, CH_2Cl_2, 87%, 93%, 2 steps; xi, BuLi, Et_2O, 98%, 98%; xii, Me_3Al, Cp_2ZrCl_2, CH_2Cl_2, H_2O; xiii, BuLi, hexane; xiv, $(CH_2O)_n$, THF, 80%, 80%, 3 steps; xv, PPh_3, CCl_4; xvi, $NaSO_2Ph$, DMF, 76%, 83%, 2 steps; xvii, BuLi, THF, HMPA then (*E*)-$TBSOCH_2C$-$Me{=}CHCH_2Cl$,[8] 78%, 87%; xviii, AcOH, THF, H_2O, 85%, 81%; xix, [$PdCl_2$(dppp)], Super-Hydride, THF, 82%, 81%; xx, Ac_2O, Py, 87%, 95%; xxi, TBAF, THF, 90%, 83%; xxii, Dess–Martin oxidation, 75%, 87%; xxiii, TMSCN, KCN, 18-crown-6; xxiv, $BnMe_3NF$, THF, H_2O; xxv, CH_2=CHOEt, TsOH, C_6H_6, quant., 94%, 3 steps; xxvi, H_2CO_3, MeOH, 87%, 86%; xxvii, LiCl, MsCl, DMF, *s*-collidine, 95%, 90%.

0.009). Thus, while the *S* isomer of **1** is highly active, the *R* isomer is itself also active but does not appear to interfere with the activity of its antipode. This will reduce the need to create highly stereochemically pure (*S*)-**1** for field development of the pheromone in control of these important disease vectors.

The demonstration that the sex pheromone produced by male *L. longipalpis* from the Lapinha region is (*S*)-9-methylgermacrene-B, (*S*)-(*E*,*E*)-7-isopropylidene-4,9,10-trimethylcyclodeca-1(10),4-diene (*S*)-**1**, would suggest that the absolute stereochemistry of that from Jacobina would be (1*S*,3*S*,7*S*)-3-methyl-α-himachalene, since the C-3 methyl is analogous in putative biosynthetic terms to the C-9 methyl of the homogermacrene **1** and the relative stereochemistry has already been established,[6] but this will be reported separately when the hypothesis has been fully tested.

Notes and references

† *Selected NMR data* for (±)-**1**: Spectra were recorded using a JEOL JNM-LA 500 MHz spectrometer. δ_H($CDCl_3$, 500 MHz) 1.04 (3H, d, *J* = 7.0), 1.44 (3H, s), 1.55 (3H, s), 1.68 (3H, s), 1.70 (3H, s), 2.4–1.8 (8H, m), 3.06 (1H, br d, *J* 14.0), 4.39 (1H, br d, *J* 11.0), 4.72 (1H, dd, *J* 12.0, 3.0); δ_C($CDCl_3$, 125 MHz) 11.1, 16.4, 20.4, 20.7, 20.9, 25.3, 34.4, 38.9, 40.7, 46.3, 125.7, 127.0, 128.7, 130.9, 133.7, 140.2.

‡ *GC conditions*: HP-5 (a siloxane) 0.32 mm id × 30 m × 25 μm film thickness, 40 to 150 °C at 5 °C min^{-1}; chiral GC (β-cyclodextrin) 0.25 mm id × 30 m × 25 μm film thickness, 40 to 180 °C at 3 °C min^{-1}.

§ *GC-MS*: 0.32 mm id × 50 m HP-1 (a siloxane × 0.52 μm film thickness, 30 °C on-column injection, then 30 to 200 °C at 5 °C min^{-1}; EI at 70 eV, 250°C (VG-Autospec, Fisons Instruments). *Selected data* for (±)-**1**: *m/z* 121 (100%), 93 (75), 107 (59), 41 (57), 67 (51), 135 (47), 91 (35), 55 (34), 79 (30), 105 (30), 119 (28), 53 (26), 77 (24), 43 (23), 81 (22), 39 (21), 133 (19), 136 (18), 29 (17), 147 (17), 71 (16), 175 (16), 95 (14), 122 (13), 203 (13), 161 (11), 218 (10, M^+).

¶ Virgin female sandflies were removed from larval rearing pots within 10 h after eclosion to ensure that they were unmated. They were provided with a saturated sugar solution on cotton wool and subsequently maintained for 5–6 days in Barraud cages (18 × 18 × 18 cm). Bioassays were conducted in a glass (9 mm internal diameter) Y-tube olfactometer. Zero grade air was passed (2 ml min^{-1}) through two charcoal filters into the test and control arms (10 cm long). The olfactometer was connected to the air supply by Teflon tubing. A filter paper disk (1.5 cm diameter) was inserted into the Teflon tubing at the connection with the olfactometer test and control arms. During bioassays, pheromone extracts or synthetic chemicals in hexane were placed on one of the filter paper disks and hexane in the same quantity as for the test arm was placed on the other filter paper disk. The female sandfly was introduced into the third arm (10 cm long) of the olfactometer and its response observed for 5 min.

1 R. P. Lane, A. Phillips, D. H. Molyneux, G. Procter and R. D. Ward, *Ann. Trop. Med. Parasitol.*, 1985, **79**, 225.
2 I. E. Morton and R. D. Ward, *Med. Vet. Entomol.*, 1989, **3**, 219.
3 J. G. C. Hamilton, M. J. Dougherty and R. D. Ward, *J. Chem. Ecol.*, 1994, **20**, 141; M. J. Dougherty, P. Guerin and R. D. Ward, *Physiol. Entomol.*, 1995, **20**, 23.
4 J. G. C. Hamilton, G. W. Dawson and J. A. Pickett, *J. Chem. Ecol.*, 1996, **22**, 1477.
5 J. G. C. Hamilton and R. D. Ward, *Parassitologia (Rome)*, 1991, **33** (Suppl 1), 283; J. G. C. Hamilton, R. D. Ward, M. J. Dougherty, C. Ponce, E. Ponce, H. Noyes and R. Zeledon, *Ann. Trop. Med. Parasitol.*, 1996, **90**, 533.
6 J. G. C. Hamilton, A. M. Hooper, K. Mori, J. A. Pickett and S. Sano, *Chem. Commun.*, 1999, 355.
7 S. Muto, Y. Nishimura and K. Mori, *Eur. J. Org. Chem.*, in the press.
8 M. Ohsugi and S. Takahashi, *J. Agric. Chem. Soc. Jpn.*, 1973, **47**, 807.

Communication 9/07910F

Immobilization of $Rh(PPh_3)_3Cl$ on phosphinated MCM-41 for catalytic hydrogenation of olefins

Shin-Guang Shyu,* Sheau-Wen Cheng and Der-Lii Tzou

Institute of Chemistry, Academia Sinica, Taipei, Taiwan, ROC. E-mail: sgshyu@chem.sinica.edu.tw

Received (in Cambridge, UK) 7th September 1999, Accepted 13th October 1999

The complex $Rh(PPh_3)_3Cl$ immobilized on MCM-41 modified with $(OEt)_3Si(CH_2)_3PPh_2$ results in a stable hydrogenation catalyst with turnover frequency (TOF) three times higher than that of $Rh(PPh_3)_3Cl$ in the hydrogenation of cyclohexene.

Immobilization of homogeneous catalysis by anchoring the catalyst (usually a metal complex) on a solid support has been studied extensively in the past two decades.[1,2] Recent developments on the mesoporous material MCM-41 provided a new possible candidate for a solid support for immobilization of homogeneous catalysts.[3] MCM-41 has a regular pore diameter of *ca.* 50 Å and a specific surface area $> 700\ m^2\ g^{-1}$.[4] Its large pore size allows passage of large molecules such as organic reactants and metal complexes through the pores to reach to the surface of the channel.[5] In addition, the regular pore size of MCM-41 can provide shape selectivity not provided by silica gel.

Homogeneous catalysts RhR_3Cl (R = Ph, C_8H_{12}) have been successfully immobilized on solid supports through anchoring ligands [*e.g.* $-(CH_2)_nPPh_2$] (n = 1, 2) which are chemically bonded to the surface of the support.[6] For Rh(III) complexes, enhancement of reactivity after immobilization was also reported.[7] By using the same method, $Rh(PPh_3)_3Cl$ was chemically attached on the surface of MCM-41. The resultant catalyst was characterised by various spectroscopic methods, and its catalytic activity evaluated. Herein, we report the preparation, characterisation and catalytic reactivity of this heterogeneous catalyst.

MCM-41 was prepared by hydrothermal reaction of SiO_2 and $Me_3(CH_2)_{15}NMe_3Br$.[8] A powder X-ray pattern indicates that the resultant mesoporous material has a pore diameter of *ca.* 43 Å. MCM-41 was contacted with water for 10 h in order to convert the surface to Si–OH which was further reacted with $(OEt)_3Si(CH_2)_3PPh_2$ to produce a phosphinated MCM-41(MCM-41-P) (Scheme 1).[9] Energy dispersive spectroscopy (EDS) of MCM-41-P clearly indicates that the mesoporous material contains phosphorus.† Solid state ^{31}P NMR of MCM-41-P showed a signal at δ −23.2. This further indicates the ligand has been successfully anchored to the material. The complex $Rh(PPh_3)_3Cl$ was reacted with MCM-41-P in benzene at room temperature overnight (Scheme 2). After filtration, the resultant yellow particles were washed with benzene until the filtrate was colourless. EDS showed that the sample contained Rh.‡ Solid state ^{31}P NMR of the sample showed three signals [Fig. 1(b)]. One of these corresponds to the unreacted anchoring ligand while the other two are assigned to the anchoring ligand and triphenylphosphine ligand coordinated to the Rh complex since they are shifted relative to the ^{31}P signal of $Rh(PPh_3)_3Cl$. However, exact assignments cannot be concluded. These observations indicate that Rh has been successfully immobilized on the mesoporous material.

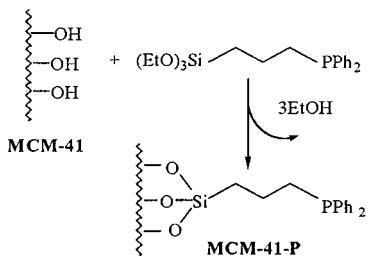

Scheme 1

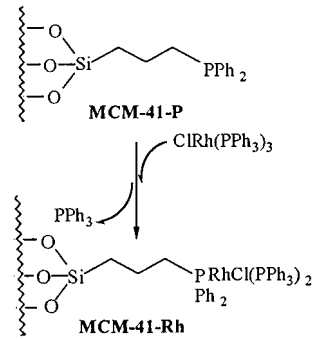

Scheme 2

Catalytic hydrogenation of cyclohexene to cyclohexane was used to test the catalytic activity of the hybrid complex MCM-41-Rh under 150 psi of hydrogen at 75 °C in a Parr reactor. After one cycle, the mixture was filtered and the catalyst was recovered on a filter paper. The filter paper was then cut into small pieces and used as a catalyst in the next cycle of hydrogenation. After fifteen cycles, the catalyst was still active (Fig. 2). The TOF for the first cycle was lower than that of the second cycle. This indicates that it takes some time to activate

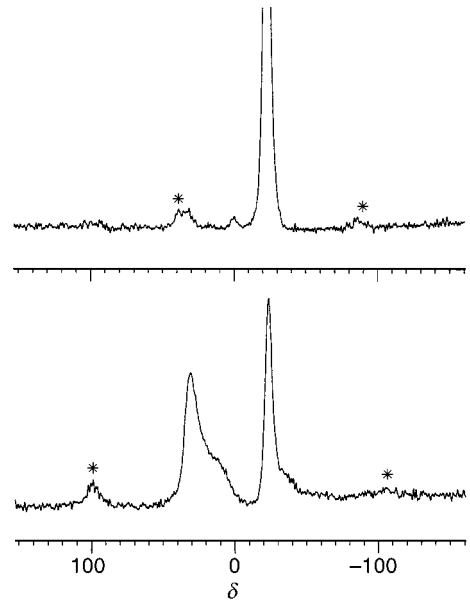

Fig. 1 Solid state ^{31}P NMR spectra of (a) MCM-41-P and (b) MCM-41-Rh. ^{31}P one-pulse experiments were performed on a Bruker AMX 400 spectrometer at a ^{31}P frequency of 161.98 MHz at room temperature. Chemical shifts were referenced to Na_2HPO_4 at 0 ppm. Signals arising from side bands are marked with asterisks.

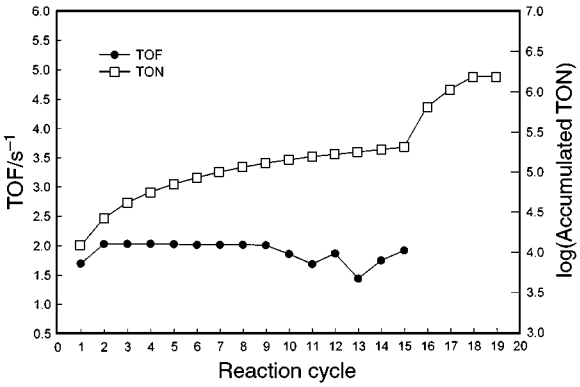

Fig. 2 Turnover frequecy (TOF) and accumulated turnover number (TON) for hydrogenation of cyclohexene by MCM-41-Rh under 150 psi of hydrogen at 75 °C. Product yields were determined by GC. For cycles 1–14, each cycle took 2 h and the solution concentration (cyclohexene in benzene) was 1.6 M. For cycles 15–18, pure cyclohexene was used. The catalyst was prepared by immobilization of 5.01 mg (5.41×10^{-3} mmol) of $Rh(PPh_3)_3Cl$ on 17.1 mg of MCM-41-P.

the catalyst to its best performance level. After the first cycle, the TOF reached *ca.* 2.0 s^{-1} and remained steady up to ten cycles.§ In order to estimate the TON, the hydrogenation of cyclohexene was carried out in pure cyclohexene. The total turnover number was $> 10^6$.¶

In order to evaluate the possibility of leaching,[10] solvent was removed from the reaction solution and benzene (3.0 ml) was added to the reactor to dissolve any possible remaining Rh complex. The UV spectrum of the solution was then recorded. The solution was then filtered through silica gel which can remove any Rh complex and the UV spectrum of the filtrate was run. The difference in absorbance between these two measurements should correspond to absorbance of leached Rh complex. The concentration of leached Rh complex was calculated according to the reported ε value (≈ 6000) at 360 nm of $Rh(PPh_3)_3Cl$.[11] The calculated amount of leached Rh complex is 1.4×10^{-9} mol *i.e. ca.* 0.3% of the Rh complex in the original catalyst.‖

The hydrogenation reaction was also carried out at ambient temperature under 1 atm of hydrogen. The catalyst was prepared by immobilization of 15.5 mg (1.68×10^{-2} mmol) of $Rh(PPh_3)_3Cl$ on 51.0 mg of MCM-41-P. For the first few hours, the catalyst was inactive. This indicates again that some time is required to activate the catalyst. The TOF is *ca.* 150 h^{-1} after subtracting the activation period from the total reaction time.

In order to evaluate the relative activity of MCM-41-Rh, hydrogenation of cyclohexene to cyclohexane with an equivalent amount of $Rh(PPh_3)_3Cl$ was carried out under the same reaction condition (150 psi hydrogen, 75 °C) and theTOF of the reaction was 0.7 s^{-1}. Hence, the TOF of MCM-41-Rh is *ca.* three times that of $Rh(PPh_3)_3Cl$.

The reason for the higher TOF for the hybride catalyst relative to the homogeneous catalyst is not clear. Similar observations were reported when a solid support such as SiO_2 was used for the immobilization of homogeneous catalysts.[7]

We acknowledge support from the China Petroleum Corporation, Academia Sinica and National Science Council.

Notes and references

† P/Si ratio analysis by EDS: 18(1). The ZAF (Z: atomic number effect, A: absorption of X-rays within the specimen, F: fluorescence effect) method was used in the analysis. 30 data points were randomly obtained from each sample.
‡ Rh/Si ratio analysis by EDS: 6.0(7). The ZAF method was used in the analysis. 10 data points were randomly obtained from each sample.
§ Mol substrate reduced (mol catalyst)$^{-1}$ s^{-1}.
¶ Mol substrate reduced (mol catalyst)$^{-1}$.
‖ For the fifth reaction cycle, the absorbance of the solution is 7.32×10^{-3} ($\sigma = 0.84 \times 10^{-3}$). The absorbance of the filtrate is 4.62×10^{-3} ($\sigma = 0.58 \times 10^{-3}$).

1 Y. Iwasawa, in *Tailored Metal Catalysts*, D. Reidel Publishing Company, Dordrecht, Holland, 1986.
2 K. G. Allum, R. D. Hancock, I. V. Howell, R. C. Pitkethly and P. J. Robinson, *J. Organomet. Chem.*, 1975, **87**, 189; K. G. Allum, R. D. Hancock, I. V. Howell, S. McKenzie, R. C. Pitkethly and P. J. Robinson, *J. Organomet. Chem.*, 1975, **87**, 203.
3 C. T. Kresge, M. E. Leonowicz, W. J. Roth, J. C. Vartuli and J. S. Beck, *Nature*, 1992, **359**, 710.
4 J. S. Beck, J. C. Vartuli, W. J. Roth, M. E. Leonowicz, C. T. Kresge, K. D. Schmitt, C. T.-W. Chu, D. H. Olson, E. W. Sheppard, S. B. McCullen, J. B. Higgins and J. L. Schlenker, *J. Am. Chem. Soc.*, 1992, **114**, 10 834.
5 W. Zhou, J. M. Thomas, D. S. Shephard, B. F. G. Johnson, D. Ozkaya, T. Maschmeyer, R. G. Bell and Q. Ge, *Science*, 1998, **280**, 705; T. Maschmeyer, F. Rey, G. Sankar and J. M. Thomas, *Nature*, 1995, **378**, 159; C.-J. Liu, S.-G. Li, W.-Q. Pang and C.-M. Che, *Chem. Commun.*, 1997, 65.
6 R. H. Grubbs and L. C. Kroll, *J. Am. Chem. Soc.*, 1971, **93**, 3062; K. G. Allum, R. D. Hancock, I. V. Howell, T. E. Lester, S. McKenzie, R. C. Pitkethly and P. J. Robinson, *J. Catal.*, 1976, **43**, 331.
7 K. Kochloefl, W. Liebelt and H. Knozinger, *J. Chem. Soc., Chem. Commun.*, 1977, 510.
8 C.-F. Cheng, K. H. Park and J. Klinowski, *J. Chem. Soc., Faraday Trans.*, 1977, **93**, 193.
9 X. Feng, G. E. Frywell, L.-Q. Wang, A. Y. Kim, J. Liu and K. M. Kemner, *Science*, 1997, **276**, 923.
10 K. G. Allum, R. D. Hancock, I. V. Howell, R. C. Pitkethly and P. Robinson, *J. Catal.*, 1976, **43**, 322; C. U. Pittman, Jr., S. K. Wuu and S. E. Jacobson, *J. Catal.*, 1976, **43**, 87.
11 J. A. Osborn, F. H. Jardine, J. F. Young and G. Wilkinson, *J. Chem. Soc. A*, 1966, 1711.

Communication 9/07207A

ChemComm

X-Ray absorption spectroscopic studies of the Cr(IV) 2-ethyl-2-hydroxybutanoato(1−) complex†

Aviva Levina,[a] Garry J. Foran[b] and Peter A. Lay*[a]

[a] *School of Chemistry, University of Sydney, Sydney 2006 NSW, Australia. E-mail: lay_p@chem.usyd.edu.au*
[b] *Australian Nuclear Science and Technology Organisation PMB 1, Menai 2234 NSW, Australia*

Received (in Cambridge, UK) 2nd September 1999, Accepted 19th October 1999

The first X-ray absorption spectrum of the rare Cr(IV) oxidation state has been obtained for the complex with the ehbaH ligand [ehbaH = 2-ethyl-2-hydroxybutanoate(1−)] in frozen aqueous solution (14 K), showing that at pH = 3.5 and in a large excess of the ligand, the predominant form of Cr(IV) is the five-coordinate oxo complex, $[Cr^{IV}O(ehbaH)_2]^0$.

Considerable interest[1,2] has been generated in the aqueous chemistry of Cr(IV) owing to its potential role as an active intermediate in Cr(VI)-induced genotoxicities.[3,4] The structure of a relatively stable Cr(IV)–ehba complex,[5] which has been studied in detail with respect to its reactivity with biomolecules,[6] has been the subject of considerable debate.[7–9] Alternative structures proposed contain either one multiple and four single Cr–O bonds (as in the crystallographically characterised $Na[Cr^{V}O(ehba)_2]$),[10] or six single Cr–O bonds [as in Cr(III)-ehba complexes].[8,9] To differentiate between these possibilities, XAS[5] of the Cr(V/IV/III)–ehba complexes in frozen solutions (14 K) were obtained. To our knowledge, this is the first XAS study of a Cr(IV) complex.

The K-edge XAS was recorded using the Australian National Beamline Facility at the Photon Factory, Tsukuba, Japan.[11] The Cr(IV) solutions were prepared by the addition of 10 mM Cr(VI) to 1.0 M ehba buffer containing 0.10 M As(III) (pH 3.5, 20 °C)[2] and were frozen in liquid N_2 at 50 ± 5 s after mixing, which corresponded to 88 ± 2% of total Cr existing in the Cr(IV) form (measured by UV–VIS spectroscopy).[2,11] The solution of Cr(V) was prepared by dissolving 10 mM of $Na[Cr^{V}O(ehba)_2]$[12] in ehba buffer (1.0 M, pH 3.5, 20 °C). The reaction of 10 mM $Na[Cr^{V}O(ehba)_2]$ with 50 mM of $FeSO_4$ (1.0 M ehba buffer, pH 3.5, *ca.* 1 min at 20 °C) resulted in quantitative formation of a Cr(III)–ehba complex.[13] The solutions of Cr(V) and Cr(III) were stable for at least 15 min at 20 °C (UV–visible spectroscopy) and were frozen in liquid N_2 at *ca.* 2 min after preparation. Photodamage of the samples during the exposure to X-rays was minimized by: (i) using cryogenic conditions (14 K);[14] (ii) moving the beam to a fresh spot on the sample after each set of five scans; and (iii) changing to a fresh sample after 12 h of exposure. The absence of significant photodamage was evident from (i) the absence of observable colour changes in the samples after 12 h of exposure;[15] and (ii) the absence of significant changes in the pre-edge and edge features of the XAS.[11] Averaging, background subtraction and the calculation of theoretical XAFS spectra were performed using the XFIT software package,[16] as described previously,[17] and appropriate constraints and restraints.[11,18] Most of the errors in the determined XAFS bond lengths estimated from the Monte Carlo analysis of the noise in the data[16] did not exceed the conservative systematic error of 0.02 Å.[17] HyperChem software[19] was applied for building the molecular models used to initialise the MS XAFS calculations.

The XANES[5] spectrum of the Cr(IV) complex is compared with those of the Cr(V) and Cr(III) complexes in Fig. 1. In agreement with literature data,[20] the edge energy increases along the series Cr(III) < Cr(IV) < Cr(V). The pre-edge region of the Cr(III)–ehba complex features two weak absorption maxima (symmetry-forbidden 1s → 3d transitions), characteristic for octahedral Cr(III) complexes.[21] By contrast, a more intense pre-edge peak was observed in the XANES of the Cr(IV)–ehba complex, when the edge jump was normalised. This feature gains intensity from a decrease in symmetry from an octahedral geometry and/or an increase in π bonding compared to Cr(III).[21] The pre-edge absorbance for the Cr(IV)–ehba complex is *ca.* three times less intense than that for the Cr(V)–ehba complex (Fig. 1).

The SS fits of the XAFS spectra were used to compare the coordination numbers and the Cr–O bond distances in the first coordination shells of the Cr(V/IV/III)–ehba complexes.[11] Acceptable models are those possessing both low goodness-of-fit values (R < 8%) and physically reasonable values of the threshold energy E_0, the scale factor S_0^2 and the Debye–Waller factors σ_i^2.[11] As expected, the first coordination shell of the Cr(III)–ehba complex was best fitted by the model containing six single Cr–O bonds,[22] and that of the Cr(V)–ehba complex is best fitted by the model containing four single (1.85 Å) and one multiple (1.55 Å) Cr–O bond.[23] Notably, additions of extra [*i.e.* seventh for Cr(III) and sixth for Cr(V)] long (2.2 Å) Cr–X distances to the models significantly improved the R values, but led to unreasonably high σ^2 values.[11] This feature probably reflects the influence of more distant coordination shells.

The best fit for the first coordination shell of the Cr(IV)–ehba complex includes: (i) two Cr–O bonds with lengths (1.89 Å) corresponding to those of the Cr–O(carboxylato) bonds in $Na[Cr^{V}O(ehba)_2]$;[10] (ii) two longer (2.07 and 2.26 Å) Cr–O bonds, assigned to the protonated alkoxo groups of the ligand;[24] and (iii) one short (1.55 Å) Cr–O bond, corresponding to the oxo ligand.[10] As for Cr(V)–ehba, addition of a sixth long (≥2.0 Å) Cr–O bond to the model, though improving the R value slightly, led to unreasonably high σ^2 values.[11] Any models including only single Cr–O bonds (≥1.7 Å), similar to the alternative structure proposed,[8] gave very poor fits.[11] The best model for

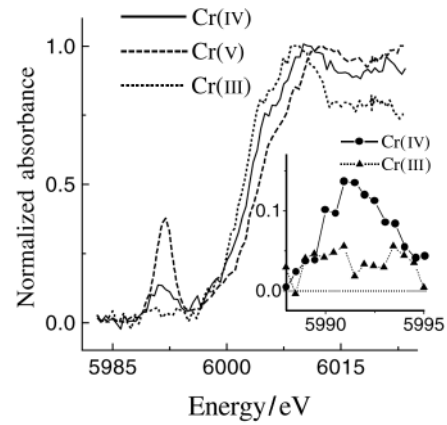

Fig. 1 XANES spectra of frozen (14 K) 10 mM solutions of Cr(V/IV/III)–ehba complexes in 1.0 M ehba buffers, pH 3.5 (average of 20 scans).

† Electronic supplementary information (ESI) available: refer to ref. 11. See http://www.rsc.org/suppdata/cc/1999/2339/

Cr(v)–ehba (*i.e.* with deprotonated alkoxo groups of the ligands) was unsuitable for Cr(IV)–ehba.[11] Thus, comparisons amongst the SS XAFS fits of the first coordination shells for the Cr(V/IV/III)–ehba complexes are consistent with a five-coordinate oxo complex structure **I** for the Cr(IV) complex.

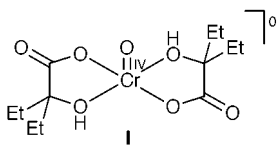

I

When the XAFS of **I** was fitted using MS that included all non-hydrogen atoms[11] a good fit resulted (Fig. 2, R = 18.5%), including significant contributions (⩾10%) of 34 MS paths.[11] In the MS XAFS calculations, bond lengths and angles within the ligands were restrained to be consistent with those within the ehbaH ligand of the crystallographically characterised NH_4-[$V^{IV}O$(ehba)(ehbaH)] complex,[3] but the angles involving the O donors of **I** were allowed to change freely. The refined structure of **I** was of a distorted trigonal-bipyramidal geometry,[11] similar to those of the Cr(V) and V(IV) ehba complexes.[3,10] However, further studies are required to establish the reliability of the bond angles in **I** determined from the MS XAFS calculations. The Cr–O bond lengths determined from the MS analysis (1.56, 1.89, 1.90, 2.06 and 2.24 Å), were the same, within the experimental error, as those determined by SS calculations.

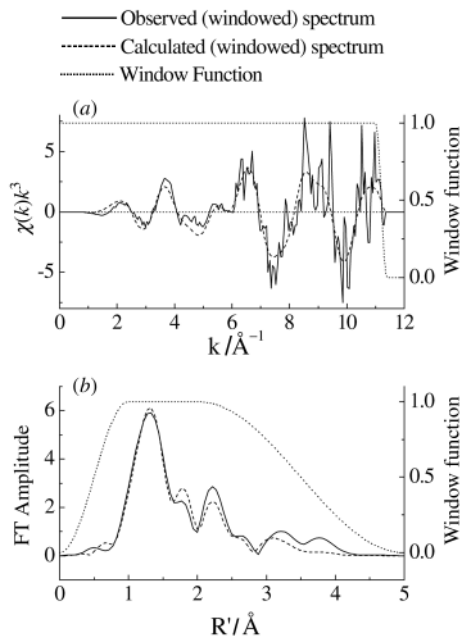

Fig. 2 (a) XAFS spectrum and (b) its Fourier transform for 10 mM **I** (1.0 M ehba buffer, pH 3.5, 14 K, average of 60 scans).

Thus, the SS and MS fitting of the XAFS data, together with the XANES and previous UV–VIS spectroscopic and kinetic studies,[1,2,6] point to **I** as the structure for the Cr(IV) complex under the reaction conditions, while an alternative structure ([$Cr^{IV}(OH)_2$(ehbaH)$_2$])[1,8] is eliminated by the XAFS data.

This work was performed at the Australian National Beamline Facility (ANBF) with support from the Australian Synchrotron Research Program, which is funded by the Commonwealth of Australia under the Major National Research Facilities program. The authors thank Dr James Hester (ANBF) and Mr Colin Weeks (University of Sydney) for assistance with the XAS experiments, Assoc. Professor Trevor Hambley (University of Sydney) for helpful advice on the data analysis and the Australian Research Council for funding.

Notes and references

1 E. S. Gould, *Coord. Chem. Rev*., 1994, **135**/**136**, 651.
2 R. Codd, P. A. Lay and A. Levina, *Inorg. Chem*., 1997, **36**, 5440.
3 G. Barr-David, T. W. Hambley, J. A. Irwin, R. J. Judd, P. A. Lay, B. D. Martin, R. Bramley, N. E. Dixon, P. Hendry, J.-Y. Ji, R. S. U. Baker and A. M. Bonin, *Inorg. Chem*., 1992, **31**, 4906.
4 For recent reviews of the Cr genotoxicity, see: M. Cieślak-Golonka, *Polyhedron*, 1996, **15**, 3667; A. Kortenkamp, M. Casadevall, P. Da Cruz Fresco and R. O. J. Shayer, *NATO ASI Ser., Ser. 2*, 1997, **26**, 15; D. M. Stearns and K. E. Wetterhahn, *NATO ASI Ser., Ser. 2*, 1997, **26**, 55 and references therein.
5 Abbreviations: ehba = 2-ethyl-2-hydroxybutanoate(2−); XAS = X-ray absorption spectra; XANES = X-ray absorption near-edge structure; XAFS = X-ray absorption fine structure; SS = single scattering; and MS = multiple scattering.
6 P. A. Lay and A. Levina, *J. Am. Chem. Soc*., 1998, **120**, 6704; A. Levina, G. Barr-David, R. Codd, P. A. Lay, N. E. Dixon, A. Hammershøi and P. Hendry, *Chem. Res. Toxicol*., 1999, **12**, 371.
7 Quantitative generation of **I** is achieved in dilute aqueous solutions, but its isolation is difficult owing to the decomposition reactions.[1,2]
8 M. C. Ghosh and E. S. Gould, *J. Am. Chem. Soc*., 1993, **115**, 3167.
9 R. N. Bose, B. Fonkeng, G. Barr-David, R. P. Farrell, R. J. Judd, P. A. Lay and D. F. Sangster, *J. Am. Chem. Soc*., 1996, **118**, 7139.
10 R. J. Judd, T. W. Hambley and P. A. Lay, *J. Chem. Soc., Dalton Trans*., 1989, 2205.
11 Electronic supplementary information (ESI) is available (http://www.rsc.org/suppdata/cc/1999/2339/), including: (i) tables showing the parameters of XAS experiments, the conditions, constraints and restraints applied to the XAFS fittings, the results of SS and MS XAFS calculations and the contributions of different scattering paths into the calculated MS XAFS; and (ii) figures showing typical kinetic data of Cr(IV) decomposition; XANES spectra of fresh and exposed Cr(IV) samples, the results of SS XAFS simulations for Cr(V/IV/III)–ehba and the structure of **I** refined by MS XAFS (11 pp.).
12 M. Krumpolc and J. Roček, *J. Am. Chem. Soc*., 1979, **101**, 3206.
13 R. N. Bose and E. S. Gould, *Inorg. Chem.*, 1985, **24**, 2832. The Cr(III) product of the Cr(V) + Fe(II) reaction was identified, on the basis of its UV–VIS spectral and ion-exchange properties, as [$Cr^{III}(OH_2)_2$-(ehbaH)$_2$]$^+$.
14 The use of low temperatures also maximises the MS contributions.
15 The characteristic colours of the complexes are: dark pink for 10 mM Cr(IV); brown–red for 10 mM Cr(V); and green for 10 mM Cr(III).
16 P. J. Ellis and H. C. Freeman, *J. Synchrotron Rad*., 1995, **2**, 190.
17 A. M. Rich, R. S. Armstrong, P. J. Ellis, H. C. Freeman and P. A. Lay, *Inorg. Chem.*, 1998, **37**, 5743.
18 The N_i/p ratio of 1.2 (N_i = number of independent observations; p = number of refined parameters) showed that the restrained MS XAFS calculations[11] were overdetermined and the results are valid (N. Binsted, R. W. Strange and S. S. Hasnain, *Biochemistry*, 1992, **31**, 12 117).
19 *HyperChem*, Version 5.1, Hypercube Inc., Gainesville, FL, 1996.
20 I. Arčon, B. Mitrič and A. Kodre, *J. Am. Ceram. Soc*., 1998, **81**, 222.
21 P. J. Ellis, R. W. Joyner, T. Maschmeyer, A. F. Masters, D. A. Niles and A. K. Smith, *J. Mol. Catal. A: Gen.*, 1996, **111**, 297.
22 The Cr–O bond lengths in the Cr(III)–ehba complex, determined from SS XAFS calculations (1.94 Å),[11] are in agreement with the proposed structure of this complex.[13] The Cr–O bond lengths in [$Cr^{III}(OH_2)_6$]$^{3+}$ (determined from MS XAFS calculations) are 1.97 Å (H. Sakane, A. Muñoz-Páez, S. Díaz-Moreno, J. M. Martínez, R. R. Pappalardo and E. S. Marcos, *J. Am. Chem. Soc.*, 1998, **120**, 10 397).
23 The different Cr–O bond lengths in Na[$Cr^{V}O$(ehba)$_2$] involving the carboxylato and alkoxo moieties (1.90 and 1.80 Å, respectively)[10] are not distinguished by SS XAFS when $k \leqslant 11$ Å^{-1} since the resolution in bond lengths is 0.15 Å.[17] These data are in agreement with the results of SS and MS XAFS calculations for solid Na[$Cr^{V}O$(ehba)$_2$] (T. Maschmeyer, G. Barr-David, P. A. Lay and A. F. Masters, to be submitted).
24 The V–O(alcohol) bond length in NH_4[V^{IV}(ehba)(ehbaH)] is 1.95 Å.[3] The presence of unusually long (> 2 Å) Cr–O bonds in **I** is consistent with the ease of loss of one ehbaH ligand in solution.[1,2]

Communication 9/07113J

Oxidative steam reforming of methanol over CuZnAl(Zr)-oxide catalysts; a new and efficient method for the production of CO-free hydrogen for fuel cells

S. Velu, K. Suzuki* and T. Osaki

Ceramics Technology Department, National Industrial Research Institute of Nagoya, 1-1 Hirate-cho, Kita-ku, Nagoya 462-8510, Japan. E-mail: ksuzuki3@nirin.go.jp

Received (in Cambridge, UK) 31st August 1999, Accepted 15th October 1999

Steam reforming of methanol in the presence of air over CuZnAl(Zr)-oxide catalysts derived from hydrotalcite-like hydroxycarbonate precursors offers CO-free hydrogen suitable for fuel cells with about 100% methanol conversion at around 230 °C.

Hydrogen is forecast to become a major source of energy in the future.[1] Hydrogen fueled vehicles using fuel cells [*e.g.* polymer electrolyte membrane fuel cell (PEMFC)] are under development in an effort to reduce CO_2 emissions which accelerate global warming. In addition, fuel cell-powered vehicles, using hydrogen fuel, do not emit any environmental pollutants, such as NO_x, SO_x and hydrocarbons. For use in fuel cells for mobile applications, hydrogen is typically produced through steam reforming of methanol (SRM) [eqn. (1)] over CuZn-based catalysts.[2] Recently, partial oxidation of methanol (POM) [eqn. (2)] has also been suggested as a route for hydrogen extraction from methanol.[3] Unfortunately, both of these reactions produce considerable amounts of CO (> 100 ppm) as a byproduct. For application in PEMFCs, even traces of CO (> 20 ppm) in the reformed gas deteriorates a Pt electrode and the cell performance is dramatically lowered.[4] Currently, second stage catalytic reactors are being used to remove this CO by the water-gas-shift reaction [eqn. (3)], CO oxidation or methane formation. However, the addition of further steps for fuel gas refinement would lower the total efficiency of the propulsion system. Hence, in order to utilize hydrogen fuel for fuel cells, it is highly desirable to develop a process that can produce hydrogen without CO in the reformed gas.

$$CH_3OH + H_2O \Leftrightarrow 3H_2+CO_2 \quad \Delta H = +49.4 \text{ kJ mol}^{-1} \quad (1)$$

$$CH_3OH + 1/2O_2 \Leftrightarrow 2H_2+CO_2 \quad \Delta H = -192.2 \text{ kJ mol}^{-1} \quad (2)$$

$$CO + H_2O \Leftrightarrow H_2+CO_2 \quad \Delta H = -39.4 \text{ kJ mol}^{-1} \quad (3)$$

In the present study, we have performed the SRM reaction in an oxidizing atmosphere (in the presence of air) over a series of novel CuZnAl(Zr)-oxide catalysts obtained by calcining the CuZnAl(Zr)-hydroxycarbonates containing hydrotalcite (HT)/aurichalcite phases, at 450 °C for 5 h. We demonstrate here for the first time that under the reaction conditions employed, a combined steam reforming–partial oxidation of methanol, termed herein after as "oxidative steam reforming of methanol (OSRM)", reaction takes place to produce CO-free hydrogen with about 100% methanol conversion at 230 °C.

CuZnAl(Zr)-hydroxycarbonate precursors with different Cu:Zn:Al atomic ratios were synthesized by a coprecipitation method at room temperature using a mixture of NaOH and Na_2CO_3 as precipitants.[5] The (Cu+Zn)/Al(Zr) atomic ratio in the starting solution was varied from 2 to 4. The Cu surface areas (S_{Cu}), Cu dispersion (D) and the Cu crystallite sizes (t_{Cu}) were calculated by the TPR-N_2O passivation experiment as described in the literature.[6] Catalytic test reactions were performed in a packed-bed micro-reactor (4 mm i.d.) using 90 mg of the catalyst (particle size 0.30–0.355 mm) in the temperature range 180 to 290 °C at atmospheric pressure. Liquid methanol (for the POM reaction) or premixed water and methanol with a H_2O/CH_3OH molar ratio of 1.3 (for the SRM and OSRM reactions) was fed into the pre-heater at a rate of 1.6 or 2.5 $cm^3\ h^{-1}$ by means of a micro-feeder. Synthetic air (20.2 vol.% O_2 in N_2) at a rate of 10 to 20 $cm^3\ min^{-1}$ and Ar (carrier gas, 43 $cm^3\ min^{-1}$) flows were adjusted by means of a mass flow controller. The reaction products were analyzed on-line using two gas chromatographs equipped with TC detectors and porapak Q and molecular sieve 13 X columns. The performance of the catalyst was evaluated after 25 h of on-stream operation.

The physicochemical properties of the catalysts used in the present study are summarized in Table 1. Initially, a systematic study on the POM reaction was performed over a series of CuZnAl-oxide catalysts without Zr (CZAZ-A through CZAZ-D). Among them, the catalyst CZAZ-C exhibited the best performance. Hence, this catalyst was chosen first to be examined for its catalytic performance in the SRM and OSRM reactions. Fig. 1 compares the catalytic performance of the CZAZ-C catalyst in the POM, SRM and OSRM reactions. As will be noted, the methanol conversion is lowest in the SRM reaction at low temperatures and the conversion rate increases rapidly with increasing reaction temperature. The conversion reaches about 100% at around 290 °C where the selectivity of CO is < 5 mol% (CO concentration ≈ 200 ppm). Interestingly, when air was passed through during the SRM reaction, the conversion approaches 100% at a lower temperature of about 230 °C, without any detectable CO in the reformed gas. Because of the high methanol conversion of about 100%, the H_2 production rate in the OSRM reaction increased by a factor of two compared to that obtained from the SRM or POM reactions. It is of great significance that CO only started forming above 260 °C in the SRM reaction, while it started forming above

Table 1 Physicochemical properties of CuZnAl(Zr)-oxide catalysts

Catalyst	Metal composition of the precursors (atomic ratio)[a]				S_{BET}/ $m^2\ g^{-1}$	H_2 consumption[b]/ mmol g^{-1}	S_{cu}/$m^2\ g^{-1}$	D_{cu} (%)	t_{Cu}/Å
	Cu	Zn	Al	Zr					
CZAZ-A	0.73	0.88	1.00	0.00	56	3.3	203	38.6	26
CZAZ-B	1.02	1.30	1.00	0.00	71	3.6	181	34.3	29
CZAZ-C	1.42	1.71	1.00	0.00	84	6.0	176	33.4	30
CZAZ-D	1.37	1.80	1.00	0.00	108	4.2	227	43.1	23
CZAZ-E	1.40	1.65	0.45	0.55	82	4.7	232	44.0	23
CZAZ-F	1.38	1.72	0.00	1.00	75	4.3	279	52.9	19

[a] Determined by X-ray fluorescence spectroscopy. [b] Hydrogen consumption estimated by the temperature programmed reduction (TPR) experiments.

Table 2 Performance of various CuZnAl(Zr)-oxide catalysts in the oxidative steam reforming of methanol after 25 h of on-stream operation at 230 °C

Catalyst	MeOH conversion		H_2 production rate/		H_2 production rate/CH_3OH	Carbon selectivity (mol%)	
	mol%	Rate/mmol kg^{-1} s^{-1}	mmol kg^{-1} s^{-1}	TOF/10^3 s^{-1}	conversion rate	CO	CO_2
CZAZ-A	37.6	177	378	77	2.1	0.0	100
CZAZ-B	65.4	297	730	166	2.5	0.0	100
CZAZ-C	68.1	348	900	211	2.6	0.0	100
CZAZ-C[a]	100.0	215	542	127	2.5	0.0	100
CZAZ-D	79.6	468	1210	215	2.6	1.2	98.8
CZAZ-E	85.4	630	1626	254	2.6	1.1	98.9
CZAZ-F	90.0	661	1714	295	2.6	0.8	99.2

[a] CH_3OH: 8.8 cm^3 min^{-1}; H_2O: 11.4 cm^3 min^{-1}.

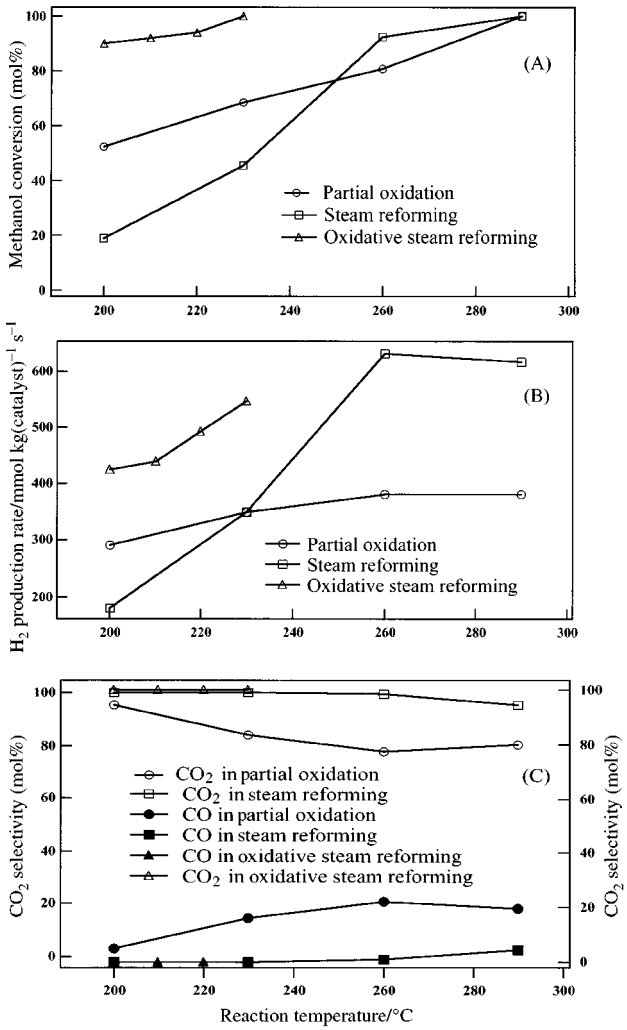

Fig. 1 Effect of temperature on catalytic performance of CZAZ-C catalyst in the partial oxidation, steam reforming, and oxidative steam reforming of methanol; (A) methanol conversion, (B) H_2 production rate, (C) carbon selectivity.

200 °C in the POM reaction. However, in the OSRM reaction, since excess water is present in the feed mixture, the situation is highly favorable for the water-gas-shift reaction [eqn. (3)] to transform CO into CO_2 and H_2.

For the purpose of evaluating the performance of various CuZnAl(Zr)-oxide catalysts in the OSRM reaction, the methanol conversion was reduced by increasing the flow rate of the $CH_3OH + H_2O$ feed mixture to 2.5 cm^3 h^{-1} and the results were collected during 25 h of continuous operation. Table 2 summarizes the catalytic performance of a series of CuZn-Al(Zr)-oxide catalysts in the OSRM reaction. It can be seen that the catalytic activity increases with decreasing Al content in the sample. It is also interesting to note from Table 2 that the best catalytic performance was obtained over the catalyst containing Zr instead of Al (CZAZ-F), indicating that Zr is an effective support for CuZn-based oxide catalysts compared to Al in the OSRM reaction. The undesirable byproduct CO is virtually not produced (or only traces are formed) and catalyst deactivation is insignificant over most of the catalysts (except CZAZ-A). Another interesting feature which will be noticed in Table 2 is that a ratio of H_2 production rate/CH_3OH conversion rate of around 2.5 is obtained over all the catalysts. However in the SRM [eqn. (1)] and POM [eqn. (2)] reactions the H_2 production rate/CH_3OH conversion rate ratios would be 3 and 2, respectively. The value of 2.5 obtained for the OSRM reaction suggests that a combined partial oxidation–steam reforming of methanol is taking place under the present experimental conditions. Hence, the overall reaction can be represented by eqn. (4), which is a combination of eqn. (1) and 2. Eqn. (4) satisfies the H_2 production rate/CH_3OH conversion rate ratio of around 2.5 observed in the present investigation.

$$2CH_3OH + H_2O + 1/2O_2 \Leftrightarrow 5H_2 + 2CO_2 \quad (4)$$

It is clear from the results presented in the present study that the OSRM reaction over these novel CuZnAl(Zr)-oxide catalysts is a very efficient and convenient method for the production of CO-free hydrogen suitable for fuel cells. Besides producing CO-free hydrogen, the OSRM reaction has an additional benefit in that the reaction is exothermic, thereby minimizing energy consumption. A detailed investigation is in progress into the optimization of the catalyst formulations and the reaction operating parameters to further improve the catalytic performance.

Notes and references

1 J. N. Armor, *Appl. Catal., A*, 1999, **176**, 159.
2 J. P. Breen and J. R. H. Ross, *Catal. Today*, 1999, **51**, 521.
3 M. L. Cubeiro and J. L. G. Fierro, *J. Catal*., 1998, **179**, 150.
4 H.-F. Oetjen, V. M. Schmidt, U. Stimming and F. Trila, *J. Electrochem. Soc*., 1996, **143**, 3838.
5 S. Velu, K. Suzuki, M. Okazaki, T. Osaki, S. Tomura and F. Ohashi, *Chem. Mater*., 1999, **11**, 2163.
6 G. C. Bond and S. N. Namijo, *J. Catal*.,1989, **118**, 507.

Communication 9/07047H

$Cs_2Al_2P_2O_9$: an exception to Löwenstein's rule. Synthesis and characterization of a novel layered aluminophosphate containing linear Al–O–Al linkages

Qun Huang and Shiou-Jyh Hwu*

Department of Chemistry and Materials Science and Engineering Program, Clemson University, Clemson, SC 29634-0973, USA. E-mail: shwu@clemson.edu

Received (in Bloomington, IN, USA) 6th September 1999, Accepted 7th October 1999

A caesium aluminophosphate compound synthesized *via* high-temperature, solid-state methods reveals a new composition for a layered AlPO structure; it exhibits a non-Löwensteinian framework which contains linear Al–O–Al linkages in six-rings of alternating Al_2O_7 and PO_4 groups.

In spite of the large number of aluminophosphates known (*ca.* 250 compounds), the only established compositions adopted by layered structures consisting of AlO_4 and PO_4 tetrahedra are $[Al_3P_4O_{16}]^{3-}$, $[AlP_2O_8]^{3-}$, $[Al_2P_3O_{12}H_x]^{(3-x)-}$ (x = 1,2), $[Al(HPO_4)_2(H_2O)_2]^-$, and $[Al_4P_5O_{20}H]^{2-}$.[1] Their frameworks are built up from either 4 × 6, 4 × 8, 4 × 6 × 8, or 4 × 6 × 12 rings. The title compound exhibits a new framework formula, $[Al_2P_2O_9]^{2-}$, which contains an equal number of Al and P atoms. The single crystal structure reveals an unusual feature with respect to the direct Al–O–Al linkages and, in turn, a new type of 4 × 6 aluminophosphate (AlPO) network. All the above mentioned AlPOs, except the current compound, show frameworks avoiding direct Al–O–Al linkages between AlO_4 tetrahedral units; for zeolites (aluminosilicates) this is known as Löwenstein's rule.[2] According to the Löwensteinian structure, each Al is coordinated through oxygen to four Si (or P) and *vice versa* (the 4:0 ordering scheme). Theoretical calculations predict that the formation of Al–O–Al linkages (in the 3:1 ordering scheme, for example) is energetically unfavorable.[3] The experimental findings on compounds prepared by hydrothermal routes, such as the organically templated AlPO synthesis, support this claim.[1] However, calculations based on the lattice energy of an ionic model by Bell, Jackson, and Catlow,[3b] suggest that the energy loss due to the direct linkages could be overcome by thermal energies. This prediction is confirmed by some scattered examples of non-Löwensteinian frameworks prepared by high-temperature methods.[4] Among these exceptions, there are about 45 out of over 2,450 reported aluminosilicates, but only two aluminophosphates. These include sodalite,[4a] a common example for aluminosilicates, as well as metal-containing $MAlPO_5$ (M = Mg, Fe).[4b,c]

Crystals of $Cs_2Al_2P_2O_9$, **1**, were grown by high-temperature, solid-state methods using CsCl flux,[5] and the structure was characterized by single crystal X-ray diffraction methods.[6] As shown in Fig. 1, **1** adopts a layered structure where the aluminophosphate slabs are held together by electropositive Cs^+ cations. The extended AlPO slab consists of alternately arranged Al_2O_7 and PO_4 groups sharing corner oxygen atoms. Each slab adopts a mixed four- and six-ring (4 × 6) network [Fig. 2(a)]. The 4-ring (2Al + 2P) structure is made up from alternating 2 × AlO_4 and 2 × PO_4 groups while the 6-ring (4Al + 2P) is built of 2 × Al_2O_7 and 2 × PO_4 groups. The Al–O–Al linkages [highlighted by solid lines in Fig. 2(a)] exist in the form of Al_2O_7 units in between rows of fused 4-ring units. The latter form a corrugated $Al_2P_2O_4$ chain [Fig. 2(b)], in which the 4-ring units are in a chair configuration.

The aluminium powder may facilitate a chain 'zipping' process *via* oxidation intercalation *en route* to the formation of AlPO slabs.[5] The 4-ring chain shown in [Fig. 2(b)] resembles the so-called precursor structure for extended lattices.[1a] In our study, aluminium powder was employed along with an oxidant, potassium superoxide. This approach is unconventional compared to commonly employed methods using aluminium oxide (or hydroxide) as starting material.[5] For the mechanism, one can imagine the processes of bond breaking *via* dissociation of the Al–O–Al linkages of Al_2O_3, prepared *in situ* in this case,

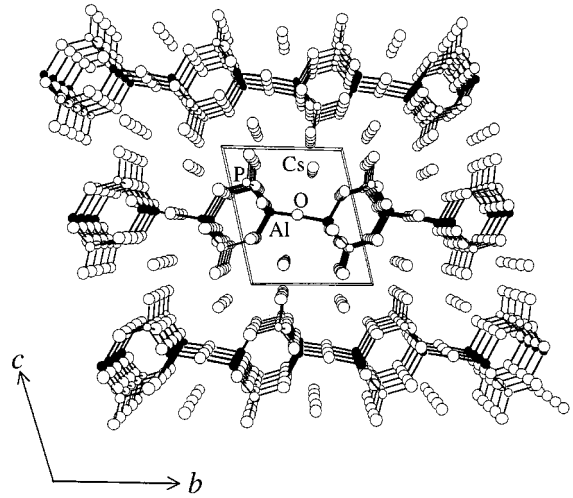

Fig. 1 Projected view showing the layered structure of **1**. The small filled and open circles, as for Fig. 2, represent Al^{3+} and P^{5+} cations, respectively, and the large open circles represent O^{2-} (bonded) and Cs^+ (non-bonded) ions.

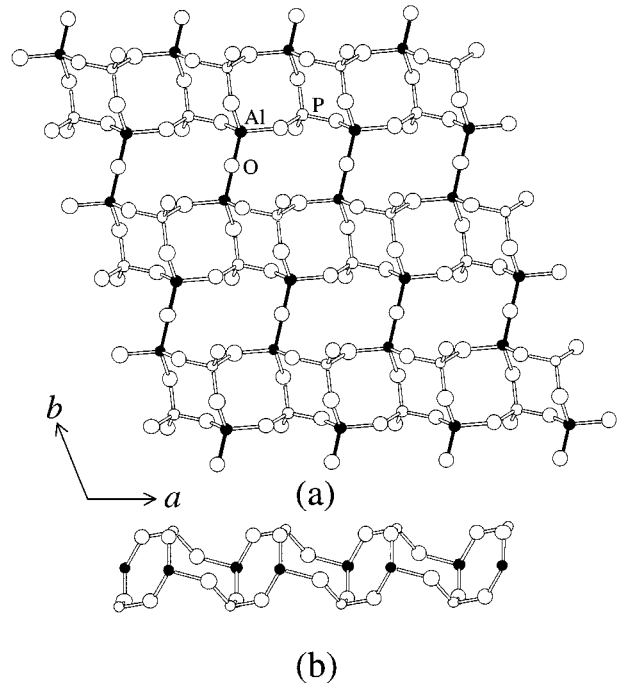

Fig. 2 (a) A partial structure of the $[Al_2P_2O_9]^{2-}$ slab. The linear Al–O–Al linkages are highlighted with thick lines. (b) A side view of fused 4-ring units, see text. The terminal oxygen atoms are omitted for clarity.

followed by bond formation with phosphorus cations through bridging oxygens. While the idea of this reaction pathway is intuitively sound, the framework formation could bypass the formation of Al_2O_3 to undergo simultaneous layer formation *via* oxidative 'zipping' of partially oxidized AlPO chains. Direct heating of a mixture of Al_2O_3 or $Al(OH)_3$, P_2O_5 and CsOH at 800 °C in an open system does not, in fact, yield **1**. Addition of CsCl as a flux results in an as yet unidentified phase, whose PXRD patterns show a close resemblance to those of **1**. Further investigation into the role of aluminium powder is underway.

The title compound reveals a new type of 4 × 6 network and a fascinating framework of interconnected 4-ring chains. Prior to this research, four 4 × 6 network structures were known that adopt the above mentioned $[Al_3P_4O_{16}]^{3-}$ and $[HAl_2P_3O_{12}]^{2-}$ compositions.[1c,7] Fig. 3 presents all the 4 × 6 networks, including the current example, in which only Al^{3+} and P^{5+} cations are shown. The network structures are adopted by, for example, $(NH_3CHMeCH_2NH_3)_3[Al_6P_8O_{32}]\cdot H_2O$ for network type (a), $Co(en)_3[Al_3P_4O_{16}]\cdot 3H_2O$ and *trans*-$Co(dien)_2[Al_3P_4O_{16}]\cdot 3H_2O$ for type (b), $(2\text{-}BuNH_3)_2[HAl_2P_3O_{12}]$ for type (c), $(C_5N_2H_9)_2(NH_4)[Al_3P_4O_{16}]$ for type (d), and **1** for type (e). It should be noted that the major difference among the frameworks consisting of these networks concerns the tetrahedral units. The framework of **1** is comprised of Al_2O_7 units while the others consist of AlO_4 interlinked with PO_4 units only. The networks (a)–(d), therefore, possess the 4 : 0 ordering scheme while network (e) has the 3 : 1 scheme. In addition, the networks (a) and (d) consist of short, (3- and 5-, respectively) edge-shared, four-ring units while (e) contains parallel chains of fused four-rings.

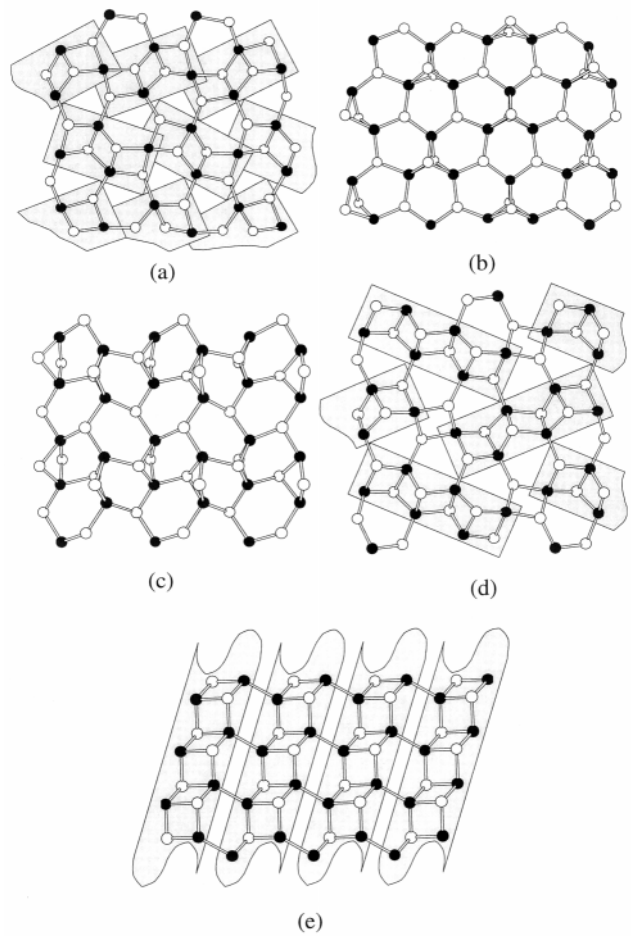

Fig. 3 Five types, (a)–(e), of 4 × 6 Al–P–O frameworks. Aluminum atoms (●) and phosphorus atoms (○) are linked by oxygen bridges (not shown). In (a)–(d), strict alternation of Al and P is observed, whereas in (e), the 3 : 1 ordering scheme is shown. The fused 4-ring units in (a), (d), and (e) are highlighted, see text.

The Al–O–Al linkage in **1** reveals two unusual features; namely, a linear bond angle and a fairly short $Al\text{–}O^b$ (O^b : bridging oxygen in the Al_2O_7 unit) bond. The $Al\text{–}O^b\text{–}Al$ angles are usually nonlinear and are much smaller than 180°. In the frameworks of two previously mentioned non-Löwensteinian compounds, $MgAlPO_5$ and $FeAlPO_5$, for instance, the $Al\text{–}O^b\text{–}Al$ angles are 129.8(2)° and 131.8(2)°, respectively.[4b,c] Also, the $Al\text{–}O^b$ bond in **1**, (1.69 Å) is shorter than the three Al–O^t (O^t : terminal oxygen in the Al_2O_7 unit) bonds, (1.75–1.76 Å). Based on chemical intuition, the linear bond angle and short bridging oxygen to aluminium bond distance suggest possible π character. It would be interesting to look at the thermal behavior of the framework in relation to the $Al\text{–}O^b\text{–}Al$ linkage.

Financial support for this research (DMR-9612148) and access to the single crystal X-ray diffractometer from the National Science Foundation is acknowledged. We thank Professor Myung-Hwan Whangbo for his insightful discussions.

Notes and references

1 (*a*) S. Oliver, A. Kuperman and G. A. Ozin, *Angew. Chem., Int. Ed.*, 1998, **37**, 46; (*b*) L. Vidal, V. Gramlich, J. Patarin and Z. Gabelica, *Chem. Lett.*, 1999, 201; (*c*) J. Yu, J. Li, K. Sugiyama, N. Togashi, O. Terasaki, K. Hiraga, B. Zhou, S. Qiu and R. Xu, *Chem. Mater.*, 1999, **7**, 1727, and references cited therein.

2 W. Löwenstein, *Am. Mineral.*, 1954, **39**, 92.

3 (*a*) R. M. Barrer and J. Klinowski, *Philos. Trans. R. Soc., London A.*, 1977, **285**, 636; (*b*) R. G. Bell, R. A. Jackson and C. R. A. Catlow, *Zeolites*, 1992, **12**, 870; (*c*) C. R. A. Catlow, A. R. George and C. M. Freeman, *Chem. Commun.*, 1996, 1311.

4 (*a*) S. E. Tarling, P. Barnes and J. Klinowski, *Acta Crystallogr., Sect. B*, 1988, **44**, 128; (*b*) K.-F. Hesse and L. Cemic, *Z. Kristallogr.*, 1994, **209**, 346; (*c*) K.-F. Hesse and L. Cemic, *Z. Kristallogr.*, 1994, **209**, 660.

5 0.0540 g of Al (2.0 mmol), 0.1422 g of KO_2 (2.0 mmol), 0.0795 g of CuO (1.0 mmol) and 0.1419 g of P_2O_5 (1.0 mmol) were ground and mixed with the flux CsCl. The charge to flux ratio was 1 : 2 by weight. The reaction was carried out in a carbon-coated quartz ampoule. The mixture was heated up to 500 °C over 24 h, and isothermed for 6 h, followed by heating to 800 °C, and isothermal treatment for an additional 4 d. The reaction was cooled slowly to 500 °C over 72 h, followed by furnace cooling to room temperature. Colorless columnar crystals of **1** (*ca.* 60%), as well as some other unidentified black and white polycrystalline phases (*ca.* 40%), were retrieved from the flux by washing the products with deionized water using suction filtration. EDAX shows no contamination from potassium, chlorine, and copper in this crystalline phase, as the presence of the latter is attributed to CuO used for the synthesis of Cu-containing AlPO. An alternative reaction of $2Al/2KO_2/P_2O_5/4CsCl$ without adding CuO resulted in a slightly lower yield of **1**, *ca.* 50%.

6 *Crystal data* for **1**: $Cs_2Al_2P_2O_9$, M = 525.7, triclinic, space group $P\bar{1}$ (No. 2), a = 4.925(2), b = 7.121(2), c = 8.066(2) Å, α = 96.51(2)°, β = 107.12 (2)°, γ = 108.68(2)°, V = 249.3(1) Å^3, Z = 1, D_c = 3.502 g cm^{-3}, μ(Mo-Kα) = 7.835 mm^{-1}, λ = 0.71073 Å, 3.50° < 2θ < 55.00°. Final R = 0.024, R_w = 0.035, GOF = 1.36 were obtained for all the data and 71 parameters. The final Fourier map had a minimum and maximum of −1.04 and 1.60 eÅ^{-3}, respectively. CCDC 182/1446. See http://www.rsc.org/suppdata/cc/1999/2343/ for crystallographic files in .cif format.

7 $(NH_3CHMeCH_2NH_3)_3[Al_6P_8O_{32}]\cdot H_2O$: I. D. Williams, Q. Gao, J. Chen, L. Y. Nagi, Z. Lin and R. Xu, *Chem. Commun.*, 1996, 1781; $Co(en)_3[Al_3P_4O_{16}]\cdot 3H_2O$: K. Morgan, G. Gainsford and N. Milestone, *J. Chem. Soc., Chem. Commun.*, 1995, 425; *trans*-$Co(dien)_2[Al_3P_4O_{16}]\cdot 3H_2O$: D. A. Bruce, A. P. Wilkinson, M. G. White and J. A. Bertrand, *J. Solid State Chem.*, 1996, **125**, 228; $(2\text{-}BuNH_3^+)_2[HAl_2P_3O_{12}]$: A. M. Chippindale, A. V. Powell, L. M. Bull, R. H. Jones, A. K. Cheetham, J. M. Thomas and R. Xu, *J. Solid State Chem.*, 1992, **96**, 199.

Communication 9/07194F

ChemComm

$Ru(bpy)_3$-based artificial receptors toward a protein surface: selective binding and efficient photoreduction of cytochrome c

Hiroshi Takashima, Seiji Shinkai and Itaru Hamachi*†

Department of Chemistry and Biochemistry, Graduate School of Engineering, Kyushu University, Fukuoka 812-8581, Japan. E-mail: itarutcm@mbox.nc.kyushu-u.ac.jp

Received (in Cambridge, UK) 21st September 1999, Accepted 20th October 1999

The binding properties of a series of $Ru(bpy)_3$ complexes to cytochrome c are described; these compounds act as selective cytochrome c receptors and one derivatie is shown to be a photodriven modulator of the cytochrome c redox state.

Site-specific recognition on a protein surface, including a definite α-helix or β-sheet structure, with an artificial molecule is one of the major goals of recent bioorganic chemistry. A few ligands and receptors have been synthesized to bind proteins by using non-covalent and multi-point forces *via* hydrogen bonding, electrostatic or hydrophobic interactions.[1] However, design of such receptors is generally difficult because protein surfaces are relatively larger than conventional target molecules in host–guest chemistry. We recently demonstrated that lipid bilayer surfaces are promising for domain selective binding of a protein *via* electrostatic interaction.[2] However, more sophisticated interactions are not expected in such a molecular assembly since the spatial juxtaposition of interaction points is not elaborately carried out. Instead we made an attempt to utilize the coordination sphere of ruthenium tris-bipyridine complexes [$Ru(bpy)_3$], asymmetric functionalization of which is effected by simple coordination chemistry.[3] In this communication, we describe the binding properties of a series of $Ru(bpy)_3$ complexes to cytochrome c (Cyt-c) and the efficient electron injection which occurs through photoinduced electron transfer (ET) in their non-covalently linked systems.

The poly-anionic $Ru(bpy)_3$ complexes **1a**–**c** (Scheme 1) were constructed *via* the corresponding Ru bis-bpy complexes as intermediates. The bpy ligand bearing dendritic carboxylate moieties was synthesized according to the modified method in the literature.[4] All compounds were satisfactorily identified by NMR, IR, MALDI-Tof-mass spectroscopy and elemental analysis.‡ The photophysical properties of **1a**–**c** were investigated by absorption and emission spectroscopies, and emission lifetime experiments in a phosphate buffer (pH 7.0). The peak shapes and intensities (ε value at absorption maximum) in the UV-visible spectra of **1a**–**c** are similar to those in the spectrum of the original $Ru(bpy)_3$ complex, except for the 10 nm red-shifted λ_{max} of the MLCT band. This is due to the electron-withdrawing groups at the 4,4′-positions of the bpy ligand. The emission spectra are almost identical to that of the original $Ru(bpy)_3$ complex (λ_{em} 610 nm) upon excitation at the corresponding MLCT band (λ_{em} 615 nm for **1a**, 630 nm for **1b, 1c**). The emission lifetimes of $Ru(bpy)_3$, **1a** and **1b** were determined to be in the range 600–800 ns under anaerobic conditions (ex. 480 nm, em. 610 nm), whereas the lifetime of **1c** is elongated (1500 ns) by the cage effect due to the introduced branching on the three bpy ligands.[5]

The affinity of **1a**–**c** for various proteins was estimated by ultrafiltration binding assays. After incubation of the mixture containing a $Ru(bpy)_3$ derivative (3 μM) and a protein (9 μM) in buffer solution at pH 7.0 (10 mM phosphate) for 1 h, the solution was subjected to ultrafiltration [centricon-10 (Amicon), centrifuge at 7000 rpm, 25 °C]. The protein-bound

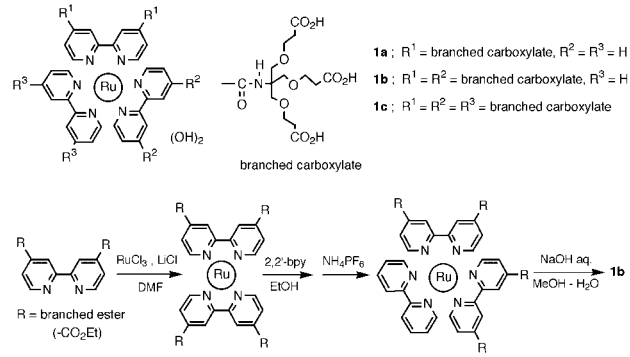

Scheme 1 Structures of $Ru(bpy)_3$-based poly-anionic complexes, **1a**–**c**.

$Ru(bpy)_3$ was not filtered and the fraction of the non-bound $Ru(bpy)_3$ component was determined by monitoring the filtrate spectrophotometrically. The results are summarized in Fig. 1. Obviously, the fraction of protein-bound $Ru(bpy)_3$ increases with an increase in the number of introduced carboxylate groups. Poly-anionic **1c**, bearing 18 carboxylates can bind to the Cyt-c surface 10 times more tightly than the original $Ru(bpy)_3$ complex. The surface of Cyt-c is positively charged at neutral pH, since the isoelectric point (pI) is 10.0.[6a] It is reasonable to assume that the poly-carboxylate clusters of the $Ru(bpy)_3$ complexes can bind to a cationic domain of the Cyt-c surface. Myoglobin (Mb, pI = 7.0), horseradish peroxidase (HRP, pI = 8.0), and cytochrome b_{562} (Cyt-b_{562}, pI = 5.0) were also used as target proteins under the same conditions.[6] The $Ru(bpy)_3$ derivatives pass through the ultrafiltration membrane in these cases, indicating that all Ru complexes examined here exhibit much lower affinities for these proteins, than for Cyt-c. It is clear that the poly-anionic $Ru(bpy)_3$-based complexes **1a**–**c** selectively bind to the Cyt-c surface.

Based on the redox potentials of Cyt-c [0.26 V (Fe^{3+}/Fe^{2+}) *vs.* NHE] and $Ru(bpy)_3$ [−0.86 V ($Ru^{3+}/{}^*Ru^{2+}$) *vs.* NHE], ET from the excited state of $*Ru^{2+}(bpy)_3$ to oxidized Cyt-c is energetically favorable.[3b,7,8] Thus, we studied the photoreduction of Cyt-c by visible light. Upon steady-state photoirradiation [high

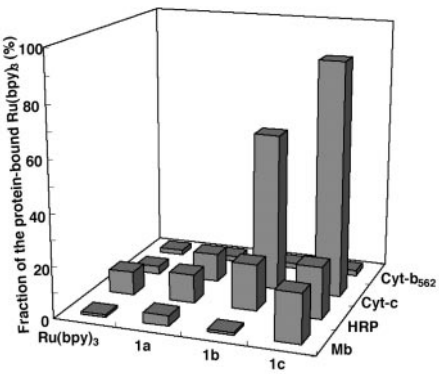

Fig. 1 Summary of the fraction (%) of protein-bound $Ru(bpy)_3$ complexes in solutions of each complex with a protein.

† Visiting professor from the Institute of Molecular Science, Okazaki, Japan.

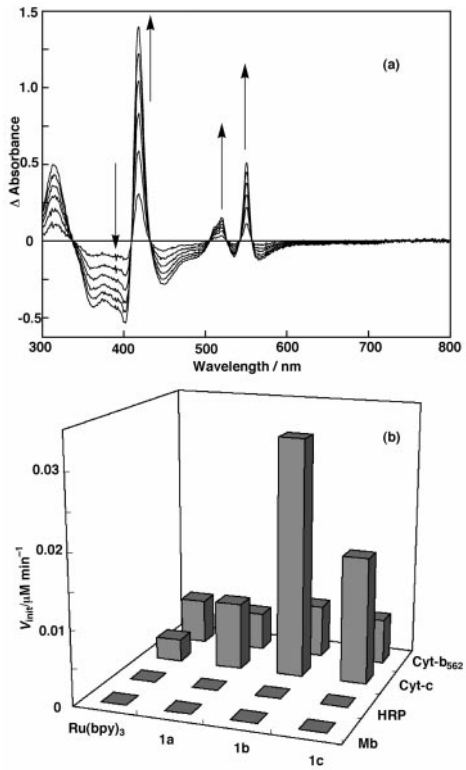

Fig. 2 (a) Time-course changes of the difference absorption spectra upon steady-state photoirradiation. (b) Summary of the initial rates (V_{init}) of photoreduction of various hemoproteins catalyzed by Ru(bpy)$_3$ derivatives.

pressure Hg-lamp (λ > 450 nm)] of a degassed solution consisting of Cyt-c (9 μM), a Ru complex (3 μM) and EDTA (10 mM),[3a,9] absorption bands at 520 and 550 nm attributable to the Q-bands of reduced Cyt-c(II) appeared [Fig. 2(a)]. The initial rates (V_{init}) are summarized in Fig. 2(b). Compared with the original Ru(bpy)$_3$ complex, it is apparent that **1a**–**c** accelerate the photoreduction of Cyt-c. Interestingly, the most effective ET relay was achieved by **1b**, having 12-carboxylates, not by **1c**, having 18-carboxylates. This suggests that not only the number of carboxylate groups, but also the asymmetric spatial orientation around the Ru center are crucial in the net photoreduction efficiency. On the other hand, no acceleration was observed for Mb, HRP and Cyt-b$_{562}$ as substrates of photoreduction, showing good agreement with the results of the binding experiments.

In the present photoreduction system, the Ru complexes should inject electrons into positively charged Cyt-c and simultaneously abstract electrons from negatively charged EDTA. In order to clarify the effect of asymmetric geometry, the ET quenching rates (k_{ET}) of the excited Ru complex by a cationic or anionic quencher were separately investigated by emission lifetime measurement. Since the sacrificial donor EDTA which is used in the photoreduction study has three negative charges at pH 7.0, the $Fe(CN)_6^{3-}$ anion was chosen as the negatively charged quencher.[10] The rate constant, k_{ET}, was calculated by the Stern–Volmer equation and decreases in the order Ru(bpy)$_3$ (k_{ET} = 1.5×10^{10} M^{-1} s^{-1}) > **1a** (4.2×10^9 M^{-1} s^{-1}) > **1b** (2.4×10^8 M^{-1} s^{-1}) > **1c** (8.9×10^7 M^{-1} s^{-1}), showing that ET becomes less efficient with the increasing number of carboxylate residues on the Ru(bpy)$_3$ derivatives.[11] On the other hand, when Cyt-c was used as a cationic quencher, the tight binding of **1c** and **1b** with Cyt-c prevented us from analyzing ET rates as a dynamic quenching mechanism.[12] Instead, pseudo intramolecular ET rates were determined: k_{ET} = 1.9×10^6 s^{-1} for **1c** and 1.8×10^6 s^{-1} for **1b**. In the case of **1a** and Ru(bpy)$_3$, ET rates were estimated from a typical dynamic quenching as follows: 8.3×10^9 M^{-1} s^{-1} for **1a** and 4.1×10^9 M^{-1} s^{-1} for Ru(bpy)$_3$. Thus, at a low concentration of Cyt-c (9 μM), the apparent rate constants are in the order **1c** = **1b** > **1a** > Ru(bpy)$_3$, which is almost opposite to the case with $Fe(CN)_6^{3-}$. These results suggest that the net photoreduction efficiency is controlled by a balance between the accessibility of the Ru complexes to Cyt-c and to sacrificial EDTA.

In conclusion, we have demonstrated that a Ru(bpy)$_3$ derivative **1b** which has an asymmetric charge distribution acts not only as a Cyt-c receptor, but also a photo-driven modulator of the redox state of Cyt-c. The present findings are anticipated to provide access to a combinatorial library of coordination chemistry to generate new Ru(bpy)$_3$-based function modulators which can selectively control protein activity.

Notes and references

‡ *Selected mass spectroscopic and elemental analysis data*: **1a**: MS(MALDI-Tof, CHCA) 1296.36 [M − $(OH)_2$]$^+$; Anal. Calc. for $C_{58}H_{66}N_8O_{22}RuNa_2$: C, 50.59; H, 4.79; N, 8.14. Found C, 50.48; H, 4.45; N, 8.11%. **1b**: MS(MALDI-Tof, CHCA) 2023.89 [M − $(OH)_2$]$^+$; Anal. Calc. for $C_{86}H_{105}N_{10}O_{42}RuNa_5$: C, 47.67; H, 4.67; N, 6.72. Found C, 47.60; H, 4.67; N, 6.72%. **1c**: MS(MALDI-Tof, CHCA) 2750.36 [M − $(OH)_2$]$^+$; Anal. Calc. for $C_{114}H_{152}N_{12}O_{62}RuNa_{17}$: C, 43.13; H, 4.82; N, 5.29. Found C, 43.33; H, 4.46; N, 5.56%.

1 For example, (*a*) H. S. Park, Q. Lin and A. D. Hamilton, *J. Am. Chem. Soc*., 1999, **121**, 8; (*b*) Y. Hamuro, M. C. Calama, H. S. Park and A. D. Hamilton, *Angew. Chem., Int. Ed. Engl*., 1997, **36**, 2680 and references cited therein.

2 I. Hamachi, A. Fujita and T. Kunitake, *J. Am. Chem. Soc.*, 1997, **119**, 9096.

3 (*a*) I. Hamachi, S. Tanaka and S. Shinkai, *J. Am. Chem. Soc.*, 1993, **115**, 10458; (*b*) S. Sakai and T. Sasaki, *J. Am. Chem. Soc*., 1994, **116**, 1587; (*c*) I. Hamachi, S. Tsukiji, S. Shinkai and S. Oishi, *J. Am. Chem. Soc*., 1999, **121**, 5500; (*d*) Y.-Z. Hu, S. Tsukiji, S. Shinkai and I. Hamachi, *Chem. Lett.*, 1999, 517.

4 (*a*) G. R. Newkome, X. Lin and J. K. Young, *Synlett*, 1992, 53; (*b*) J. Issberner, F. Vögtle, L. D. Cola and V. Balzani, *Chem. Eur. J*., 1997, **3**, 706; (*c*) G. R. Newkome, R. Güther, C. N. Moorefield, F. Cardullo, L. Echegoyen, E. Perez-Cordero and H. Luftmann, *Angew. Chem., Int. Ed. Engl*., 1995, **34**, 2023; (*d*) P. J. Dandliker, F. Diederich, M. Gross, C. B. Knober, A. Louati and E. M. Sanford, *Angew. Chem., Int. Ed. Engl*., 1994, **33**, 1739.

5 This value is almost comparable to that of similar compounds, such as dendritic Ru(bpy)$_3$ under anaerobic conditions (1940 ns); see ref. 4(*b*).

6 (*a*) P.-A. Albertsson, S. Sasakawa and H. Walter, *Nature*, 1970, **228**, 1329; (*b*) P. D. Barker, J. L. Butler, P. de Oliveria, H. Allen O. Hill and N. I. Hunt, *Inorg. Chim. Acta*, 1996, **252**, 71.

7 (*a*) P. L. Drake, R. T. Hartson, J. McGinnis and A. G. Sykes, *Inorg. Chem*., 1989, **28**, 1361; (*b*) G. J. Kavarnos and N. J. Turro, *Chem. Rev*., 1986, **86**, 401; (*c*) I. M. Kolthoff and W. J. Tomsicek, *J. Phys. Chem*., 1935, **39**, 945.

8 Although the redox potentials of **1a**–**c** have not been determined thus far, it was reported that the presence of amide groups at the 4 and 4′ positions of bpy positively shifts the redox potential of both $*Ru^{2+}/Ru^{3+}$ and Ru^{2+}/Ru^{3+}. Still, this ET reaction seems favorable, since the potential shift was reported to be within only 0.3–0.4 V; see V. Skarda, M. J. Cook, A. P. Lewis, G. S. G. McAuliffe, A. J. Thomson and D. J. Robbins, *J. Chem. Soc., Perkin Trans. 2*, 1984, 1309. Details are now under way in our laboratory.

9 No obvious effect on the photoreduction was seen in the control experiments; (i) in the absence of Ru(bpy)$_3$ derivatives and (ii) under dark conditions.

10 D. J. Pietrzyk and C. W. Frank, *Analytical Chemistry*, Academic Press, London, 1974, p. 435.

11 The k_{ET} between a Ru(bpy)$_3$, Ru(bpy)$_3$-based dendrimer and anthraquinone-2,6-disulfonate anion (AQ^{2-}) were recently obtained by similar titration experiments of lifetimes, *i.e.* k_{ET} = 1.2×10^{10} M^{-1} s^{-1} for Ru(bpy)$_3$ and k_{ET} = 2.7×10^9 M^{-1} s^{-1} for the Ru(bpy)$_3$-based dendrimer; see F. Vögtle, M. Plevoets, M. Nieger, G. C. Azzellini, A. Credi, L. D. Cola, V. D. Marchis, M. Venturi and V. Balzani, *J. Am. Chem. Soc*., 1999, **121**, 6290.

12 The emission lifetimes of the Ru complexes gradually become shortened by addition of Cyt-c, but the changes for **1b** and **1c** are saturated at low concentrations of Cyt-c.

Communication 9/07642E

A comparison of 1,4-bis(halomethyl)benzenes as monomers for the modified Gilch route to poly[2-methoxy-5-(2′-ethylhexyloxy)-*p*-phenylenevinylene]

Elizabeth M. Sanford,* Angela L. Perkins, Betty Tang, Aimee M. Kubasiak, Jonathan T. Reeves and Kevin W. Paulisse

Department of Chemistry, Hope College, PO Box 9000, Holland, MI 49422-900, USA. E-mail: sanford@hope.edu

Received (in Corvallis, OR USA) 7th September 1999, Accepted 8th October 1999

A comparison of 1,4-bis(bromomethyl)- and 1,4-bis(chloromethyl)-2-(2′-ethylhexyloxy)-5-methoxybenzene as monomers for the modified Gilch route to poly[2-methoxy-5-(2′-ethylhexyloxy)-*p*-phenylenevinylene] was made; the bis(bromomethyl) monomer was found to give substantially higher yields of MEH–PPV with consistently higher molecular weights and narrower polydispersities than the corresponding bis(chloromethyl) monomer.

There is currently renewed interest in poly(*p*-phenylenevinylene) (PPV) and its derivatives due to the potential these polymers have for application in organic light-emitting diodes.[1–3] The two main routes to these polymers, the precursor route and the side chain approach, were developed to address the processability problems of PPV due to low solubility. The precursor approach involves the formation of a soluble precursor polymer that after fabrication can be converted to the final conjugated polymer using solid state thermal or photochemical processes. Both the sulfonium precursor route[4,5] and the halogen precursor route[6,7] have successfully addressed the lack of processibility of insoluble PPV and led to the production of electroluminescent devices from PPV films. The precursor approach, however, has some inherent problems.[2,8,9] The precursor polymers themselves can contain segments where elimination has occurred in 5–50% of polymer. The ill-defined nature of the precursor polymers due to such premature elimination makes their synthesis, storage and subsequent processing difficult. The lack of stability of the sulfonium precursor to PPV has caused problems such as gelation of the precursor polymer and difficulties in processing. Conversion of the precursor polymer to the conjugated form is also expensive and prone to the formation of defects in the resulting polymer due to incomplete elimination and side reactions with the eliminated species. The side chain approach addresses the solubility problems of PPVs by using monomers substituted with solubilizing groups. Ideally, the monomers are then converted directly into the corresponding soluble conjugated polymer that is processible by standard procedures. In 1966 Gilch reported a route to PPVs using the direct polymerization of bis(halomethyl)benzenes in the presence of excess base.[10] Although the polymerization *via* the Gilch route of bis(halomethyl)benzenes substituted with solubilizing groups should lead to soluble PPVs, in practice the preparation of poly[2-methoxy-5-(2′-ethylhexyloxy)-*p*-phenylenevinylene] (MEH-PPV) and poly(2,5-dihexyloxy-*p*-phenylenevinylene) *via* this route led to the gelation and precipitation of the products.[6,11,12] Hsieh *et al.* report that they were able to minimize gelation in the preparation of MEH-PPV by following the procedure of Wudl *et al.*, in which the Bu^{t}OK is added slowly and intermittently.[13,14] The MEH-PPV obtained by Hsieh in this manner, however, could not be filtered through a 0.5–1.0 μm filter indicating microgel formation.[14] Hsieh reports that microgel formation in the production of MEH-PPV has been an under-reported but significant problem in its synthesis. In our laboratory we had indeed encountered a similar problem when exploring a side chain route to MEH-PPV using a modified McMurry reaction of the corresponding dialdehyde. The polymer produced in the reaction appeared to be soluble, but was unfilterable through 0.45 μm filters. Hsieh's report was the first we encountered that addressed the problem of microgel formation in the preparation of MEH-PPV. Hsieh solved this problem in the preparation of MEH-PPV with the development of a modified Gilch route that uses the non-polymerizable additive 4-*tert*-butylbenzyl chloride **3** to control molecular weight and prevent microgel formation.[14] Having 1,4-bis(bromomethyl)-2-(2′-ethylhexyloxy)-5-methoxybenzene **2** in hand, we were curious whether replacing bromine for chlorine would affect polymerization using the modified Gilch route. We found that the polymerization of **2** *via* the modified

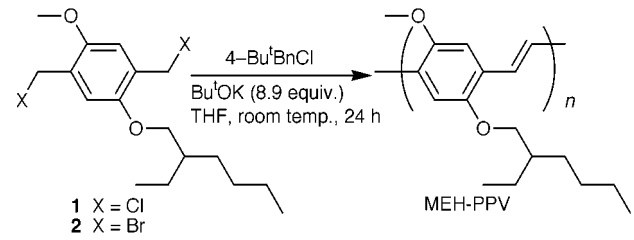

Scheme 1

Table 1 Conditions and results of the polymerization of **1** and **2**

Monomer	[Monomer][a]/ mol l^{-1}	Molar ratio **3**:monomer	M_w[b]/10^{-3}	M_n[b]/10^{-3}	Polydispersity	Yield (%)
1[c]	0.03	0.06	331	66.5	5.0	35
1[c]	0.04	0.06	199	39.1	5.1	39
1[c]	0.06	0.06	164	26.9	6.1	56
1	0.03	0.06	125	16.7	7.5	30
1	0.04	0.06	110	23.8	4.6	46
1	0.06	0.06	99	18.9	5.2	14
2	0.03	0.06	274	84.6	3.2	77
2	0.04	0.06	200	70.3	2.8	79
2	0.06	0.06	146	39.7	3.7	86

[a] 8.9 equiv. of Bu^{t}OK (1.0 mol l^{-1} in THF) was added all at once to an ice-water cooled solution of monomer in THF. [b] Relative to polystyrene in THF. [c] Hsieh *et al*. results for **1** (ref. 14).

Gilch route produced significantly different results than those reported by Hsieh for 1,4-bis(chloromethyl)-2-(2′-ethylhexyloxy)-5-methoxybenzene **1**.†

The polymerizations of both **1** and **2** (Scheme 1) were repeated under the reaction conditions that gave the highest molecular weight and the highest yield of MEH-PPV reported by Hsieh for the modified Gilch route (Table 1).[14] Products were isolated after a single precipitation of the reaction mixtures in methanol. We obtained results similar, but not identical, to those of Hsieh for **1** (Table 1). Overall, our molecular weights were lower, but followed the same trend of decreasing with increasing concentration of **1** in THF. The decrease, however, was less dramatic in our hands. We observed a wider range of polydispersities and obtained yields both slightly better and significantly worse than those reported by Hsieh. All the products were readily soluble in THF, $CHCl_3$ and CH_2Cl_2 and easily filterable through 0.45 μm filters. When 4-*tert*-butylbenzyl chloride was not added to the polymerization of **1**, we did encounter problems in filtering solutions of the polymer through 0.45 μm filters, indicating microgel formation, and obtained extremely low yields. The same procedures were then repeated for **2**. Under all three reaction conditions higher molecular weight material was obtained in significantly higher yield than we observed with **1**, Table 1. The molecular weights that we observed for the polymerization of **2** were similar to those reported by Hsieh for **1** and significantly higher than we observed for **1**. Polydispersities were narrower than those both Hsieh reported and we observed with **1**. Typical data for the elemental analysis of MEH-PPV produced from **2** (C, 77.61; H, 9.23; Br, 0.01%) shows very good agreement with that calculated for $[C_{17}H_{24}O_2]_n$ (C, 78.42; H, 9.29%) and very low bromine content. When no 4-*tert*-butylbenzyl chloride was added to the polymerization of **2**, both the yield and the molecular weight decreased but neither insoluble product nor microgel formation was observed, suggesting that the leaving group helps to prevent microgel formation but does not give as good results as the use of **2** with 4-*tert*-butylbenzyl chloride. ^{1}H NMR, UV, fluorescence and IR spectra of MEH-PPV produced from **1** and **2** are essentially the same and do not vary more than different polymerization runs using **1**. Relative quantum yields, as measured by a ratio of absorbance at 337 nm to integrated fluorescence intensity, did not vary as a function of method of preparation.

In conclusion, the modified Gilch route using the bis(chloromethyl)benzene **1** does indeed give soluble MEH-PPV in poor to moderate yields. Moderate to excellent yields of soluble MEH-PPV were obtained using the bis(bromomethyl)benzene **2**. Both **1** and **2** gave similar products. Elemental analysis data show products from **1** had slightly higher purity (99.5% compared to 99.0%) compared to **2** and had similar halogen content. Products from **2** consistently had higher molecular weights, narrower polydispersities and higher yields than the corresponding reactions with **1** in our hands. We conclude that the bromo monomer **2** gives significantly better yields with consistently higher molecular weights and narrower polydispersities of a comparable quality MEH-PPV than monomer **1** using the modified Gilch route and is recommended when the use of benzyl bromides is convenient.

Acknowledgment is made to the Donors of The Petroleum Research Fund, administered by the American Chemical Society, the Camille and Henry Dreyfus Start-up Grant Program for Undergraduate Institutions, the National Science Foundation under Grant No. CHE-9701800 and the Howard Hughes Medical Institutes Grant to Hope College for funding. We also gratefully acknowledge Dr Stephanie Schaertel, Joseph Gannon and Sarah Smolinski of Grand Valley State University for determining quantum yields of our samples.

Notes and references

† Monomer **2** was prepared from the alkylation of 4-methoxyphenol in the presence of base followed by bromomethylation with paraformaldehyde in HBr and acetic acid (ref. 15) Monomer **1** was prepared by Hsieh in a similar manner (ref. 12). We prepared monomer **1** from **2** using a halogen exchange reaction.

1 P. K. H. Ho, D. S. Thomas, R. H. Friend and N. Tessler, *Science*, 1999, **285**, 233.
2 B. R. Hsieh, *Polym. Mater. Encycl.*, 1996, 6537.
3 J. H. Burroughes, D. D. C. Bradley, A. R. Brown, R. N. Marks, K. MacKay, R. H. Friend, P. L. Burn and A. B. Holmes, *Nature*, 1990, **347**, 539.
4 R. W. Lenz, C. C. Han, J. Stenger Smith and F. E. Karasz, *J. Polym Sci., Part A: Polym. Chem.*, 1998, **26**, 3241.
5 P. M. Lahti, D. A. Modarelli, F. R. Denton III, R. W. Lenz and F. E. Karasz, *J. Am. Chem. Soc.*, 1988, **110**, 7258.
6 W. J. Swatos and B. Gordon III, *Polym. Prepr.* (*Am. Chem. Soc., Div. Polym. Chem.*), 1990, **30**, 505.
7 B. R. Hsieh, H. Antoniadis, D. C. Bland and W. A. Feld, *Adv. Mater.*, 1995, **7**, 36.
8 B. R. Hsieh, V. E. Choong, H. Razafitrimo, Y. L. Gao, H. Antoniadis, D. Roitman and W. A. Feld, *Polym. Prepr.* (*Am. Chem. Soc., Div. Polym. Chem.*), 1996, **75**, 323.
9 B. R. Hsieh, G. E. Johnson, H. Antoniadis, K. M. McCrane and M. Stolka, *US Pat.* 5,558,904, 1996.
10 H. G. Gilch and W. L. Wheelwright, *J. Polym. Sci., Polym. Chem. Ed.*, 1966, **4**, 1337.
11 F. Wudl, P. M. Allemand, G. Srdanov, Z. Ni and D. McBranch, *ACS Symp. Ser.*, 1991, **455**, 683.
12 P. L. Burn, A. Kraft, D. R. Baigent, D. D. C. Bradley, A. R. Brown, R. H. Friend, R. W. Gymer, A. B. Holmes and R. W. Jackson, *J. Am. Chem. Soc.*, 1993, **115**, 10 117.
13 F. Wudl, G. Srdanov, *US Pat.*, 5,189,136, 1993.
14 B. R. Hsieh, Y. Yu, A. C. VanLaeken and H. Lee, *Macromolecules*, 1997, **30**, 8094.
15 M. Gates, *J. Org. Chem.*, 1982, **47**, 578.

Communication 9/07280B

A ruthenium(IV) complex with six sulfur donor atoms

Rabindranath Maiti, Maoyu Shang and A. Graham Lappin*

University of Notre Dame, Department of Chemistry and Biochemistry, 251 Nieuwland Science Hall, Notre Dame, Indiana 46556-5670, USA. E-mail: lappin.1@nd.edu

Received (in Bloomington, IN, USA) 29th June 1999, Accepted 13th October 1999

A stable monomeric ruthenium(IV) octahedral complex is synthesized with 1,2-dicyanoethylene dithiolate(2−) (mnt^{2-}) as ligand and its ligand rearranged product obtained in solution is structurally characterized as a novel bis(1,2-dicyano-2-mercaptoethylene)sulfide(2−) ($mnts^{2-}$) coordinated ruthenium(II) compound.

Over thirty years ago there was a great deal of interest in the structural and electronic properties of metal complexes with dithiolate ligands.[1] An interest in the preparation of higher oxidation state ruthenium in a coordination environment composed exclusively of sulfur donor atoms has promoted a re-examination of the use of dithiolate ligands. Tris-dithiolate complexes exhibit a variety of different structural types and reactivities.[2] Trigonal prismatic coordination is commonly observed. Some studies of ruthenium(III) and (IV) 1,1-dithiolate[3] and thiolate[4] complexes have been reported but those with 1,2-dithiolate remain scant.[5] Interestingly, to date there is no report of a tris-dithiolate ruthenium(IV) complex despite the characterization of the corresponding species for iron(IV).[6] Indeed, there is no report of ruthenium(IV) in a coordination environment composed exclusively of sulfur donors.

A facile synthetic route has been developed for $[NEt_4]_3[Ru^{III}(mnt)_3]\cdot 2MeCN$ **1**. This tris-dithiolate complex has a geometry which is the closest approximation to an octahedral arrangement of this donor atom set reported to date.[2] $[Ru^{III}(mnt)_3]^{3-}$ is readily oxidized to the deep green compound, $[NEt_4]_2[Ru^{IV}(mnt)_3]$ **2**, by addition of an equivalent amount of an oxidizing agent such as I_2, H_2O_2 or $[NH_4]_2[Ce(NO_3)_6]$.† $[Ru^{III}(mnt)_3]^{2-}$ is the first structurally characterized all sulfur coordinated ruthenium(IV) complex. This species also has an octahedral arrangement of donor atoms. $[Ru^{III}(mnt)_3]^{2-}$ decomposes in the presence of light to the compound $[NEt_4]_2[Ru^{II}(mnts)_2]\cdot 0.5H_2O$ **3**, containing a novel tridentate ligand, bis(1,2-dicyano-2-mercaptoethylene)sulfide(2−) ($mnts^{2-}$).

The X-ray structure‡ of $[Ru^{III}(mnt)_3]^{3-}$ (Fig. 1) shows a C_3 axis of symmetry with the Ru located on this axis. The average twist angle[7] is 50.2° and the S–Ru–S *trans* angle is 172.2°, only 4.9° less than the value calculated for the 'octahedral limit' with the constrained ligand bite angle.[8] This is the smallest *trans* angle deviation for transition metal tris-dithiolate complex reported so far.[2] The crystal structure of $[Ru^{IV}(mnt)_3]^{2-}$ (Fig. 2) is more distorted than $[Ru^{III}(mnt)_3]^{3-}$ but again the ruthenium atom is ligated with six sulfur atoms. Two Ru–S distances for one ligand are shorter than the other four. The twist angle is 47.1° and the average S–Ru–S *trans* angle is 169.4°, 7.0° less than the calculated 'octahedral limit.' The *trans* angle deviation is close to that reported for the iron analogue.[6] The increase in the oxidation state of ruthenium between $[Ru^{III}(mnt)_3]^{3-}$ and $[Ru^{IV}(mnt)_3]^{2-}$ is not reflected by any substantial change in the average Ru–S distance. However, the C=C distance in the ligand is shorter in $[Ru^{IV}(mnt)_3]^{2-}$, an unexpected result since formal ligand oxidation involves C–S multiple bonding and would imply the opposite trend for the C=C distance.

Both of these complexes are paramagnetic. Magnetic moments of 1.69 and 2.84 μ_B for $[Ru^{III}(mnt)_3]^{3-}$ and $[Ru^{IV}(mnt)_3]^{2-}$, respectively, correspond to their octahedral low-spin configuration. $[Ru^{IV}(mnt)_3]^{2-}$ [$E°$(IV/III) = −0.70 V, (III/II) = −1.71 V *vs.* Fc^+/Fc in CH_2Cl_2, 0.1 M $NBu^t_4PF_6$, 25 °C] is highly susceptible to reducing agents such as PhSH and gives $[Ru^{III}(mnt)_3]^{3-}$ in good yield. In dilute solution, $[Ru^{IV}(mnt)_3]^{2-}$ is both light and air sensitive. In CH_2Cl_2 or acetone, the green solution of $[Ru^{IV}(mnt)_3]^{2-}$ turns brown on Hg irradiation for 3 h and this product undergoes further decomposition on standing for one day in the presence of air. A major decomposition product is the deep purple ruthenium(II) complex, $[Ru^{II}(mnts)_2]^{2-}$, coordinated with two tridentate sulfur ligands. The unique sulfur ligands have formed from two

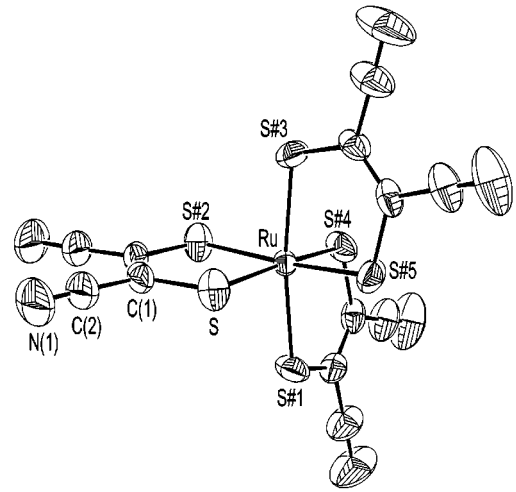

Fig. 1 Structure of the $[Ru(mnt)_3]^{3-}$ anion with 40% thermal ellipsoids and atomic labeling scheme. Selected bond lengths (Å) and angles (°): Ru–S 2.3468(8), S–C(1) 1.709(4), C(1)–C(1)#2 1.389(7), S–Ru–S#2 87.08(5), S–Ru-S#4 172.18(6).

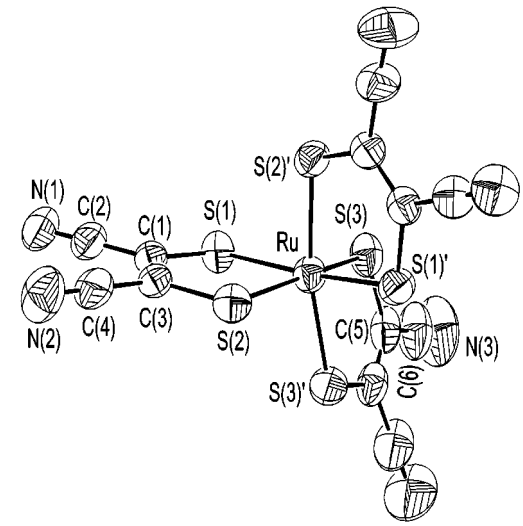

Fig. 2 Structure of the $[Ru(mnt)_3]^{2-}$ anion with 40% thermal ellipsoids and atomic labeling scheme. Selected bond lengths (Å) and angles (°): Ru–S(1) 2.3419(13), Ru–S(2) 2.3512(13), Ru–S(3) 2.3349(14), S(1)–C(1) 1.720(5), S(2)–C(3) 1.722(5), S(3)–C(5) 1.725(5), C(1)–C(3) 1.369(6), C(5)–C(5)#1 1.349(11), S(1)–Ru–S(2) 86.63(5), S(3)–Ru–S(3)#1 86.22(8), S(1)–Ru–S(1)#1 169.99(7).

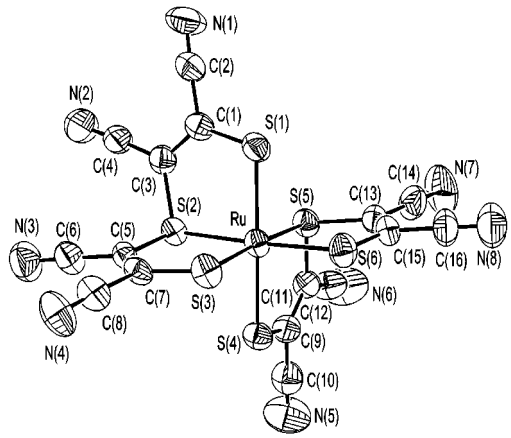

Fig. 3 Structure of the $[Ru(mnt)_2]^{2-}$ anion with 40% thermal ellipsoids and atomic labeling scheme. Selected bond lengths (Å) and angles (°): Ru–S(1) 2.341(2), Ru–S(2) 2.311(2), Ru–S(3) 2.329(2), Ru–S(4) 2.352(2), Ru–S(5) 2.318(2), Ru–S(6) 2.341(2), S(1)–C(1) 1.690(8), S(2)–C(3) 1.763(7), S(2)–C(5) 1.747(7), S(3)–C(7) 1.710(8), S(1)–Ru–S(4) 176.43(7), S(1)–Ru–S(2) 88.51(7), S(2)–Ru–S(3) 88.08(7), S(2)–Ru–S(5) 93.23(7).

mnt^{2-} ligands. Attempts to characterize the intermediate brown species structurally were unsuccessful but FAB MS data suggest an oligomeric species. It is conceivable that the complexes link by formation of disulfide bonds[9] and that the $mnts^{2-}$ ligand forms by subsequent elimination of sulfur. The structure of $[Ru^{II}(mnts)_2]^{2-}$ [$E°(III/II)$ = +0.42 V *vs.* Fc^+/Fc in CH_2Cl_2, 0.1 M $NBu^t_4PF_6$, 25 °C] is shown in Fig. 3. The trivalent sulfur atoms of the two ligands are *cis* to each other. The average Ru–S distance and S–Ru–S *trans* angle are 2.332(2) Å and 177°, respectively, with an octahedral arrangement of donors.

Notes and references

† *Syntheses*: compound **1**: a solution of $Na_2(mnt)$ (0.600 g, 3.23 mmol) in water is added to a stirred aqueous solution of $RuCl_3{\cdot}3H_2O$ (0.207 g, 1.0 mmol) and the mixture is warmed to 50 °C. Addition of NEt_4Br (0.735 g, 3.5 mmol) to the resultant red–brown solution gives **1** which is washed with cold water and propan-2-ol and recrystallized from MeCN–Pr^iOH to give dark brown crystalline compound, **1**, yield 0.5 g, (50%). Anal: calc. (found) for $C_{40}H_{66}N_{11}S_6Ru$: C, 48.31 (47.50); H, 6.68 (6.81); N, 15.49 (15.24); S, 19.34 (18.88)%. IR (KBr pellet, cm^{-1}): 2183vs [ν(CN)] UV–VIS [CH_2Cl_2, λ/nm (ε/M^{-1} cm^{-1})]: 327(19050), 405(14930), 500(sh).

Compound **2**: a solution of **1** (0.167 g, 0.1 mmol) in 10 mL acetone is oxidized with I_2 (0.0127 g, 0.05 mmol) in 5 mL CH_2Cl_2 under argon. The solvent is evaporated completely by the argon flow and the green product extracted with 5 mL CH_2Cl_2, filtered, and the microcrystals precipitated on addition of 10 mL of light petroleum (bp 35–60 °C), yield 0.15 g, 90%. The $AsPh_4^+$ salt of $[Ru(mnt)_3]^{2-}$ is prepared by metathesis of **2** with $AsPh_4Cl$. Anal: calc. (found) for $C_{60}H_{40}N_6S_6As_2Ru$: C, 55.93 (55.82); H, 3.12 (3.30); N, 6.52 (6.26); S, 14.93 (15.06)%. IR (KBr pellet, cm^{-1}): 2198vs [ν(CN)],UV-VIS [CH_2Cl_2, λ/nm (ε/M^{-1} cm^{-1})]: 376(11261), 649(3429), 681(3413).

Compound **3**; a solution of **2** (0.391 g, 0.5 mmol) in acetone (30 mL) is irradiated by a Hg-vapor lamp in a photochemical reactor for 3 h and then left in air for 1 day. The resulting solution is evaporated and the solid chromatographed on silica gel with CH_2Cl_2 as eluent. The purple product is recrystallized from Pr^iOH–light petroleum to give purple-red crystals, yield (25%). Anal: calc. (found) for $C_{32}H_{41}N_{10}S_6O_{0.5}Ru$: C, 44.42 (44.65); H, 4.77 (4.39); N, 16.18 (16.47); S, 22.23 (21.95)%. IR (KBr pellet, cm^{-1}): 2190vs, 2217w [ν(CN)] UV–VIS [CH_2Cl_2, λ/nm (ε/M^{-1} cm^{-1})]: 297(17550), 362(14676), 400(sh), 524(9642).

‡ All data were collected on an Enraf-Nonius CAD4 diffractometer at 293(2) K and the structures were solved by direct methods and refined by full-matrix least squares on F^2. Absorption correction based on ψ-scan was applied.

Crystal data: for $[NEt_4]_3[Ru(mnt)_3]{\cdot}2MeCN$: M = 994.47, hexagonal, space group $P\bar{6}2c$, a = b = 13.494(2), c = 16.834(2) Å, γ = 120°, U = 2654.6 (6) $Å^3$, Z = 2, D_c = 1.244 g cm^{-3}. Of a total of 1797 reflections collected, 916 were unique. R_1 = 0.0219 and wR_2 = 0.0568; largest peak, hole in the final difference map = 0.168, −0.235 e $Å^{-3}$.

For $[AsPh_4]_2[Ru(mnt)_3]$: M = 1288.25, orthorhombic, space group *Pbcn*, a = 20.399(2), b = 15.674(2), c = 18.020(2) Å, U = 5761.8(10) $Å^3$, Z = 4, D_c = 1.485 g cm^{-3}. Of a total of 5068 reflections collected, 2984 were unique. R_1 = 0.0471 and wR_2 = 0.0999; largest peak, hole in the final difference map = 0.283, −0.411 e $Å^{-3}$.

For $[NEt_4]_2[Ru^{II}(mnts)_2]{\cdot}0.5H_2O$: M = 867.20, monoclinic, space group $P2_1/c$, a = 13.182(2), b = 27.145(5), c = 12.767(3) Å, β = 111.319(10)°, U = 4255.6(14) $Å^3$, Z = 4, D_c = 1.353 g cm^{-3}. Of a total of 7790 reflections collected, 7448 were unique. R_1 = 0.0705 and wR_2 = 0.1907; largest peak, hole in the final difference map = 0.854, −0.679 e $Å^{-3}$. CCDC 182/1449. See http://www.rsc.org/suppdata/cc/1999/2349/ for crystallographic files in .cif format.

1 J. A. McCleverty, *Prog. Inorg. Chem.*, 1968, **10**, 49; D. Coucovanis, *Prog. Inorg. Chem.*, 1970, **11**, 233; R. Eisenberg, *Prog. Inorg. Chem.*, 1970, **12**, 295; D. Coucovanis, *Prog. Inorg. Chem.*, 1979, **26**, 301.

2 (*a*) D. Sellmann, A. C. Hennige and F. W. Heinemann, *Eur. J. Chem.*, 1998, 819; (*b*) M. Cowie and M. J. Bennett, *Inorg. Chem.*, 1976, **15**, 1595 and references cited therein; (*c*) M. Cowie and M. J. Bennett, *Inorg. Chem.*, 1976, **15**, 1584.

3 W. H. Leung, J. L. C. Chim, H. Hou, T. S. M. Hun, I. D. William and W. T. Wong, *Inorg. Chem.*, 1997, **36**, 4432; M. Kawano, H. Uemura, T. Watanabe and K. Matsumoto, *J. Am. Chem. Soc.*, 1993, **115**, 2068; D. J. Duffy and L. H. Pignolet, *Inorg. Chem.*, 1974, **13**, 2045, 2051; B. M. Mattson, J. R. Heiman and L. H. Pignolet, *Inorg. Chem.*, 1976, **15**, 564; K. W. Given, B. M. Mattson and L. H. Pignolet, *Inorg. Chem.*, 1976, **15**, 3153; B. M. Mattson and L. H. Pignolet, *Inorg. Chem.*, 1977, **16**, 489.

4 S. A. Koch and M. Millar, *J. Am. Chem. Soc.*, 1983, **105**, 3362; M. M. Millar, T. O'Sullivan, N. deVries and S. A. Koch, *J. Am. Chem. Soc.*, 1985 **107**, 3714; S. Soong, J. H. Hain, M. Millar and S. A. Koch, *Organometallics*, 1988, **7**, 556.

5 D. Sellmann, M. Geck, F. Knoch and M. Moll, *Inorg. Chim. Acta*, 1991, **186**, 187; R. DeSimone, *J. Am. Chem. Soc.*, 1973, **95**, 6238; J. Millar and A. L. Balch, *Inorg. Chem.*, 1971, **7**, 1410; L. H. Pignolet, R. A. Lewis and R. H. Holm, *J. Am. Chem. Soc.*, 1971, **93**, 360.

6 A. Sequeira and I. Bernal, *J. Cryst. Mol. Struct.*, 1973, **3**, 157; E. I. Steifel, L. E. Bennett, Z. Dori, T. H. Crawford, C. Simo and H. B. Gray, *Inorg. Chem.*, 1970, **9**, 281.

7 E. I. Stiefel and G. F. Brown, *Inorg. Chem.*, 1972, **11**, 434.

8 See the footnotes 30 and 40 of refs. 2(*b*) and (*c*), respectively. The limiting S–M–S *trans* angle can be calculated from the complement of the chelate bite angle. G. F. Brown and E. I. Stiefel, *Inorg. Chem.*, 1973, **12**, 1240.

9 H. E. Simmons, R. D. Vest, D. C. Blomstrom and T. L. Cairns, *J. Am. Chem. Soc.*, 1962, **84**, 4746.

Communication 9/05243G

Sterically induced transmutations in cobalt amine chemistry†

Rodney J. Geue,*[ab] C. Jin Qin,[a] Stephen F. Ralph,[a] Alan M. Sargeson,*[ab] Brian W. Skelton,[c] Allan H. White[c] and Anthony C. Willis[a]

[a] *Research School of Chemistry, The Australian National University, Canberra, ACT 0200, Australia*
[b] *Department of Chemistry, Faculty of Science, The Australian National University, Canberra, ACT 0200, Australia*
[c] *Department of Chemistry, University of Western Australia, Nedlands, WA 6907, Australia*

Received (in Cambridge, UK) 7th September 1999, Accepted 6th October 1999

Steric forces within a hexaaza bicyclic cobalt cage system cause chromophore expansions which bring about extraordinary transformations in the CoN_6 chemistry, leading to $Co^{III/II}N_6$ redox potentials close to +0.8 V (*vs.* SHE) and Co^{II} hexaamine complexes that are air and substitution stable.

Steric factors pervade chemistry and their capacity to affect isomerism, structure and reactivity in transition metal coordination chemistry is well known.[1] They have also dramatically influenced metal complex stabilities and electron transfer rates, especially for macrocyclic[2] and polycyclic cage[3] ligand systems. When the steric forces cooperate to change the intrinsic geometry or rigidity of a metal complex chromophore, its spectroscopic, redox and photophysical characteristics change in response to the new ligand field and potential energy (PE) surfaces. Recently, the incorporation of relatively high stability and stereorigidity factors with modified chromophore PE surfaces in sterically crowded, expanded cavity cage complexes has led to unusual ground and excited state properties for MN_6(M = Co^{III}, Rh^{III}, Pt^{IV}, Cr^{III}) amine type chromophores.[4]

In the pursuit of kinetically stable metal amine systems that radically transform MN_6 chemistry, a Co^{II} cage complex $[Co(Me_8tricosatrieneN_6)]^{3+}$ **1** ($Me_8tricosatrieneN_6$ = 1,5,5,9,13,13,20,20-octamethyl-3,7,11,15,18,22–hexaazabicyclo[7.7.7]tricosa-3,14,18-triene) was synthesized by an approach based on the $[Co(tame)_2]^{3+}$ {tame = ethylidynetris(methanamine)} template.[5a,c] A vigorously agitated mixture of $[Co(tame)_2]Cl_3$ (2 g) and $NaClO_4$ (9.4 g) in acetonitrile (50 ml) was treated with paraformaldehyde (5 equiv.), 2-methylpropanal (50 equiv.) and triethylamine (8 ml), quenched with HCl after stirring for 30 min at 20 °C, and chromatographed by cation exchange methods to give a bright crimson major product (15–20% yield), which was identified as the C_3 symmetric Co^{III} triimine ion **1** by its ^1H and ^{13}C NMR spectra,† and a single crystal X-ray analysis of its tetrachlorozincate salt.†‡ The cation structure has virtual C_3 symmetry in the crystal with equivalent imines as well as equivalent chiral nitrogen centres. Although the CoN_6 geometry in the structure is close to octahedral, the Co–N distances are remarkably long compared to those found in complexes with near optimal $Co^{III}N_6$ (amine, imine) dimensions.[3c,5] In particular, the average Co–N (endoimine) distance of 2.011 Å is 0.11 Å longer than the value of 1.90 Å for analogous bonds in relatively unstrained systems.[5] In spite of this exceptional expansion of the $Co^{III}N_6$ module, triimine **1** is stable to metal ion substitution and imine hydrolysis in aqueous solution from 6 M HCl to pH *ca.* 8 at 20 °C. This result contrasts with the relatively high lability found for most Co^{III} amines having mean Co–N distances ⩾2.00 Å,[3c] but is consistent with that observed for another expanded cavity cage complex[4a] with a mean§ Co^{III}–N (amine) distance of 2.023(±0.01) Å.

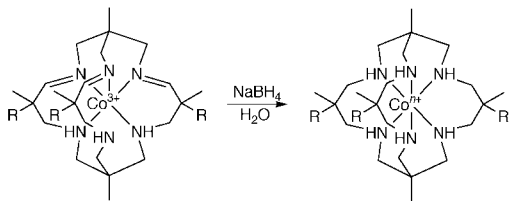

1 R = CH_3
2 R = H
3 R = CH_3, *n* = 2
4 R = H, *n* = 3

Scheme 1

The formal similarities between $[Co(Me_8tricosatrieneN_6)]^{3+}$ **1** and its homologue[4a] $[Co(Me_5tricosatrieneN_6)]^{3+}$ **2** are obvious, especially the identical bonding frameworks linking the nitrogen atoms of the chromophore. However, the apparent likeness between the two species is largely limited to their C_3 symmetry and solution stability (at pH ⩽ 8), and they exhibit important fundamental differences in their chromophore electron chemistry. The electronic spectrum of the octamethyl complex **1** (Cl_3 salt in H_2O) shows the first spin-allowed ligand field absorptions at λ_{max} (ε_{max}) 518 (150) and 367 (150), compared with 468 (107) and 343 nm (135 $dm^3\ mol^{-1}\ cm^{-1}$) for the corresponding bands of the pentamethyl homologue **2**,[4a] which by spectral comparison with analogous Co^{III} (amine, imine) systems[5] is thought to have a fairly optimal $Co^{III}N_6$ geometry. These results imply that the Co–N distances in **1** are much longer than those of **2**. The striking differences in the chromophore sizes and ligand field spectra of the two homologues are attributed to steric factors arising from the three additional methyl groups of $[Co(Me_8tricosatrieneN_6)]^{3+}$, which block the ligand conformation that is needed to form an optimal cavity size for Co^{III}. Reduction potentials (*vs.* SHE) of *E* +0.40 and −0.16 V for the $Co^{III/II}$ couples of **1** and **2** were determined using cyclic voltammetry in aqueous 0.1 M NaCl. It is likely that the expanded cavity of the conformation adopted by **1** to accommodate its extra methyl groups, is a good fit for Co^{II} and is probably also preferred by **2** in the Co^{II} state. This would imply that the 560 mV positive shift in the $Co^{III/II}$ potential for the larger cavity species **1** arises mainly from a destabilization of its Co^{III} state rather than a stabilization of Co^{II}. Furthermore, the difference in the $Co^{III}N_6$ sizes of **1** and **2** means that a substantial part of the destabilization energy is associated with the expansion of the chromophore.

More profound CoN_6 redox and spectral behaviour results when $[Co^{III}(Me_8tricosatrieneN_6)]^{3+}$ is reduced to the more sterically crowded saturated amine form $[Co^{II}(Me_8tricosaneN_6)]^{2+}$ **3**. These phenomena involve fundamental changes in the nature of CoN_6 (amine) chemistry and are not entirely understood at present. The Co^{II} complex **3** was first formed by stirring the trichloride salt of **1** with $NaBH_4$ (6 equiv.) in basic aqueous solution (pH 10) for 20 min at 20 °C and quenching with saturated $NaHCO_3$ solution (1 h), and then isolated as a *pink* dinitrate salt (95% yield), following cation-exchange chromatography using aqueous $LiNO_3$ as eluent and evaporation of the eluted complex solution. A *violet* tetrachlorozincate salt of **3** was also obtained by anion-exchange chromatography (Cl^- form) of the aqueous nitrate solution, addition of excess $ZnCl_2$ solution (pH 5) and concentration at 20 °C. All operations

† Electronic supplementary data (ESI) available: Cyclic voltammetry, NMR and crystallographic data. See http://www.rsc.org/suppdata/cc/1999/2351/

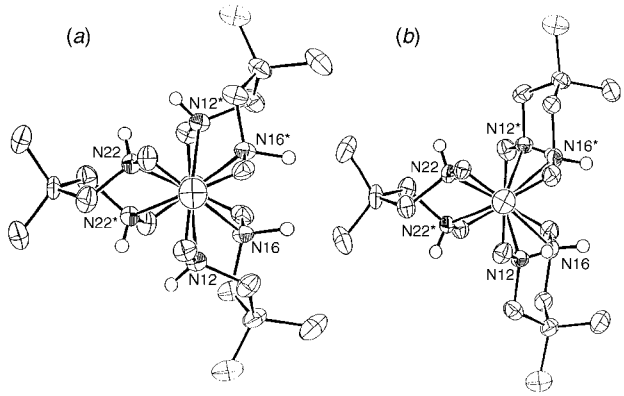

Fig. 1 The (*a*) $\Lambda(S_6)$ and (*b*) $\Lambda(S_4R_2)$ cations of **3** in its $(NO_3)_2{\cdot}H_2O$ and $ZnCl_4$ salts. Selected bond lengths (Å) and angles (°) for (*a*) (D_3 averaged§): Co–N 2.223 (±0.020); N(12)–Co–N(16) 86.3(±0.4), Co–N–C (cap) 114.1(±0.4). For (*b*) (C_2 independent): Co–N(12) 2.135(4), Co–N(16) 2.355(4), Co–N(22) 2.206(4); N(12)–Co–N(16) 82.2(2), N(22)–Co–N(22*) 88.8(2), Co–N(22)–C(21) 116.2(3), Co–N(12)–C(11) 117.0(3), Co–N(16)–C(15) 116.7(3).

were conducted in air and the $[Co^{II}(Me_8tricosaneN_6)]^{2+}$ ion was identified by elemental microanalysis (C, H, N, Cl, Co), ^{1}H NMR† and VIS-near IR electronic spectra, and the single crystal X-ray analyses of its $(NO_3)_2$ and $ZnCl_4$ salts.†‡ The synthesis and isolation of an *air and* relatively substitution stable Co^{II} hexaamine species is an unusual development that involves new CoN_6 redox chemistry.

The ^{1}H NMR spectrum† of $[Co^{II}(Me_8tricosaneN_6)]^{2+}$ in D_2O solution at 25°C is consistent with the presence of two main species that do not interconvert on the 300 MHz ^{1}H NMR timescale. The CH_2 and CH_3 proton resonances display paramagnetic broadening and upfield δ shifts within the range −10 to −50 ppm, and are clearly in accord with two dominant species averaging D_3 (6 signals) and C_2 (15 discrete signals) symmetry in D_2O. These two forms of **3** most likely correspond to diastereoisomers of the type $\Lambda(S_6)$ and $\Lambda(S_4R_2)$, and their enantiomers $\Delta(R_6)$ and $\Delta(R_4S_2)$, where *R* or *S* defines the configuration of each of the six chiral nitrogen centres and Λ or Δ the configuration about the metal ion. The Co^{II} system appears to be stable to net ligand dissociation in the presence of anions such as Cl^-, ClO_4^-, NO_3^-, SO_4^{2-}, $CH_3CO_2^-$ and CO_3^{2-} in a variety of solvents. However, the lability of individual Co^{II}–N bonds should facilitate interconversion between the diastereoisomers within minutes. Diagrams of the two distinct Co^{II} cations found in single crystals of the *pink* $(NO_3)_2$ and *violet* $ZnCl_4$ salts of **3** are shown in Fig. 1(*a*) and (*b*), viewed down their bridgehead axes. The crystal structures clearly reveal the virtual D_3 symmetry of the $\Lambda(S_6)$ cation (*a*) and the C_2 symmetry of the $\Lambda(S_4R_2)$ cation (*b*), consistent with their being the major components in solution. Mean Co^{II}–N distances are very similar for the $\Lambda(S_6)$(2.223 Å) and $\Lambda(S_4R_2)$(2.232 Å) structures, but the latter has two short (2.135(4) Å) and two very long (2.355(4) Å) bonds. Notably, the mean distances are 0.05–0.07 Å longer than those of 2.16–2.18 Å observed for other $Co^{II}N_6$(amine) structures[6] having nearly optimal $Co^{II}N_6$ sizes. It follows from the data that these two conformations of the free ligand would prefer a larger ion than Co^{II}. Overall, the implication is that strong steric influences in the $[Co(Me_8tricosaneN_6]^{n+}$ system stabilize larger cavity conformations, which markedly expand both $Co^{II}N_6$ and $Co^{III}N_6$ centres relative to those of the formally analogous $[Co(fac\text{-}Me_5tricosaneN_6)]^{n+}$ system,[4a] which has a C_3 tris-(chair) conformation in the Co^{III} complex (**4**) and probably also in the Co^{II} state.[4a] The structures also show sizeable $Co^{II}N_6$ twist distortions away from O_h geometry about the molecular bicyclic axes, with the average§ twist angles (ϕ)¶ being 46.0(±0.8)° for the $\Lambda(S_6)$ isomer (assuming D_3 symmetry), and 46.2 and 31.5° for the two independent angles of the C_2 symmetric $\Lambda(S_4R_2)$ form. However the distortions are decidedly less than that of $[Co^{II}(NH_3)_2sar)]^{4+}$ (sar = 3,6,10,13,16,19-hexaazabicyclo[6.6.6]icosane, apically substituted) in its $(NO_3)_4$ salt structure[6c] [ϕ 29.0(±0.9)°], which accommodates an optimal Co^{II}–N mean distance of 2.170(±0.021) Å.

The expanded $Co^{II}N_6$ cores of the $[Co^{II}(Me_8tricosaneN_6)]^{2+}$ components exert substantial influences on the positions of the main ligand field bands, in the visible and near-IR absorption spectrum of **3** in aqueous solution at 25 °C. These transitions, of origin $^4T_{1g}(F) \rightarrow {}^4T_{2g}$ and $^4T_{1g}(F) \rightarrow {}^4T_{1g}(P)$ at λ_{max} (ε) 1062 (4.8) and 498 nm (11.1 dm^3 mol^{-1} cm^{-1}), are red shifted by 150 and 35 nm (> 1500 cm^{-1}) from those of analogous cobalt(II) amine complexes[4a,6a] with relatively optimal chromophore dimensions. Although the binary composition of **3** may cause broadening, asymmetry and lower resolution, particularly for the lower intensity bands, its overall spectral profile remains similar to that of the smaller cavity analogues.[4a,6a]

Cyclic voltammetry of the $[Co^{II}(Me_8tricosaneN_6)]^{2+}$ system in aqueous 0.1 M KCl reveals unusual $Co^{III/II}$ redox behaviour. A complete interpretation requires more data for the isolated Co^{III} species,[7] but the general features account for the extraordinary air stability of the Co^{II} system, which is not oxidised by O_2 or H_2O_2. The voltammogram† is distinctly asymmetric, with the oxidation and main reduction wave peaks occurring at *ca*. +0.84 and +0.29 V(*vs*. SHE at 100 mV s^{-1}), and was reproduced using multiple and reverse scans and several different salts of **3**. The system is electrochemically irreversible but chemically reversible, and the main wave features are consistent with configurations of $[Co(Me_8tricosaneN_6)]^{3+/2+}$ that reduce at *ca*. 0.3 V and oxidise at *ca*. 0.8 V (*vs*. SHE). The system has not been completely unravelled yet but there are clearly at least two diastereoisomers of the Co^{II} complex involved, and recently a blue and an orange form of the Co^{III} complex have been characterized after coulometric oxidation (800 mV *vs*. SCE) of the Co^{II} form.[7] The Co^{III} forms appear to be conformationally interconvertible, both with D_3 symmetry and clearly very different ligand fields (λ_{max} for $^1A_{1g} \rightarrow {}^1T_{1g}$ *ca*. 600 and 480 nm.

The results in total show some astonishing changes in $Co^{II/III}$ amine spectroscopy and redox chemistry that are tied to dimensional changes in the $Co^{II/III}N_6$ chromophores, and clearly demonstrate the potential of sterically crowded expanded cavity cage systems in the development of new ML_6 chemistry.

Notes and references

‡ CCDC 182/1433. See http://www.rsc.org.suppdata/cc/1999/2351/ for crystallographic files in .cif format.

§ The number in parentheses defines the range of observed values.

¶ ϕ is defined by the torsion angles N···C_{quat}···C'_{quat}···N′ for $\Lambda(S_6)$ and N···C_{quat}···Co···N′ for $\Lambda(S_4R_2)$, with N,N′ in the same bridge.

1 D. A. Buckingham and A. M. Sargeson, *Top. Stereochem.*, 1971, **6**, 219; C. A. Tolman, *Chem. Rev.*, 1977, **77**, 313; A. M. Sargeson, *Pure Appl. Chem.*, 1978, **50**, 905.

2 L. F. Lindoy, *The Chemistry of Macrocyclic Ligand Complexes*, Cambridge UP, Cambridge, 1989.

3 (*a*) R. J. Geue, M. G. McCarthy and A. M. Sargeson, *J. Am. Chem. Soc.*, 1984, **106**, 8282; (*b*) R. J. Geue, A. J. Hendry and A. M. Sargeson, *J. Chem. Soc., Chem. Commun.*, 1989, 1646; (*c*) P. Hendry and A. Ludi, *Adv. Inorg. Chem.*, 1990, **35**, 117 and references therein.

4 (*a*) R. J. Geue, A. Höhn, S. F. Ralph, A. M. Sargeson and A. C. Willis, *J. Chem. Soc., Chem. Commun.*, 1994, 1513; (*b*) R. J. Geue, M. B. McDonnell, A. W. H. Mau, A. M. Sargeson and A. C. Willis, *J. Chem. Soc., Chem. Commun.*, 1994, 667; (*c*) K. N. Brown, R. J. Geue, T. W. Hambley, A. M. Sargeson and A. C. Willis, *Chem. Commun.*, 1996, 567; (*d*) K. N. Brown, PhD Thesis, Australian National University, 1994.

5 J. M. Harrowfield, A. M. Sargeson, J. Springborg, M. R. Snow and D. Taylor, *Inorg. Chem.*, 1983, **22**, 186.

6 (*a*) I. I. Creaser, R. J. Geue, J. M. Harrowfield, A. J. Herlt, A. M. Sargeson, M. R. Snow and J. Springborg, *J. Am. Chem. Soc.*, 1982, **104**, 6016; (*b*) S. Kummer and D. Babel, *Z. Naturforsch., Teil B*, 1984, **39**, 1118; (*c*) P. Comba, A. M. Sargeson, L. M. Engelhardt, J. M. Harrowfield, A. H. White, E. Horn and M. R. Snow, *Inorg. Chem.*, 1985, **24**, 2325.

7 C. J. Qin, PhD Thesis, Australian National University, 1997.

Communication 9/07237C

ChemComm

First bile acid-derived chiral dendritic species with nanometric dimensions

R. Balasubramanian, Photon Rao and U. Maitra*

Department of Organic Chemistry, Indian Institute of Science, Bangalore 560 012, India.
E-mail: maitra@orchem.iisc.ernet.in

Received (in Cambridge, UK) 9th September 1999, Accepted 12th October 1999

This paper describes the first synthesis of branched bile acid oligomers.

The chemistry of dendrimers has been a dominating theme in chemical sciences in recent years. Chiral dendritic species[1] also appeared in the chemical literature shortly after the first achiral version was reported.[2] Apart from their potential applications in asymmetric catalysis and chiral recognition,[3] chiral dendritic species have been of considerable interest because of a search towards *macromolecular asymmetry*.[4] A dendrimer possesses three distinct regions, *viz.* the core, the branching units and the end groups, and the incorporation of chirality in the dendrimer can in general be achieved by choosing one or more such components to be chiral.[1b] Molecules from the natural chiral pool, *e.g.* amino acids,[1a] nucleic acids,[5] sugars[6] and tartaric acid,[4e,f] have been employed to design chiral dendrimers. Bile acids, forming another class of the naturally occurring group of chiral molecules, have been extensively used in supramolecular chemistry including the synthesis of cyclic and linear polymers.[7] Bile acids (*e.g.* **1**–**3**) offer a carboxy group and multiple

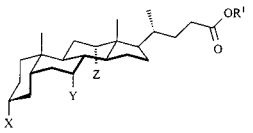

1 Lithocholic acid	X = OH, Y = Z = H, R^1 = H
2 Deoxycholic acid	X = Z = OH, Y = H, R^1 = H
3 Cholic acid	X = Y = Z = OH, R^1 = H
4 Deoxycholic acid, 3,12-diacetate	X = Z = OAc, Y = H, R^1 = H
5 1-Naphthylmethyl deoxycholate	X = Z = OH, Y = H, R^1 = 1-CH_2Np
6 Cholic acid, 3,7,12-triacetate	X = Y = Z = OAc, R^1 = H
7 1-Naphthylmethyl cholate	X = Y = Z = OH, R^1 = 1-CH_2Np

hydroxy groups (up to three) and are versatile AB_2 or AB_3 building blocks for dendritic construction. We report here the synthesis of the *first* bile acid-based chiral dendrons **8** and **9**, a heptamer and a nonamer, respectively. These relatively small oligomers of large chiral building blocks are of nanometric dimensions.

We adopted *Fréchet's* convergent strategy[8] to accomplish the synthesis of **8** and **9**. Orthogonal protection of deoxycholic acid **2** with acetate and 1-naphthylmethyl groups[9] generated steroids **4** (Ac_2O, Et_3N, DMAP, 92%) and **5** (1-naphthylmethyl chloride/DBU/DMF, 79%), respectively. In an analogous manner cholic acid **3** was converted to **6** (45%) and **7** (77%).

Steroid **4** was converted to the acid chloride, and reacted with **5**, (CaH_2, $BnEt_3N^+Cl^-$, toluene, reflux, 2 d) to generate trimer **10** (70%) which was characterized by IR, ^1H and ^{13}C NMR, UV, HPLC, elemental analysis and MALDI-TOF MS (Scheme 1). The deprotection of **10** to **11** (Pd/C, H_2), conversion to the acid chloride and subsequent reaction with **5** provided heptamer **8** in 75% yield.[10]

The use of cholic acid-based starting materials **6** and **7** led to an increase in the number of branching units, which allowed us to construct tetramer **12** in 69% yield. The deprotection of **12** to **13**, followed by its coupling with **5** generated nonamer **13** (35%).[10] One of the (many possible) conformations of **9** is shown in Fig. 1.

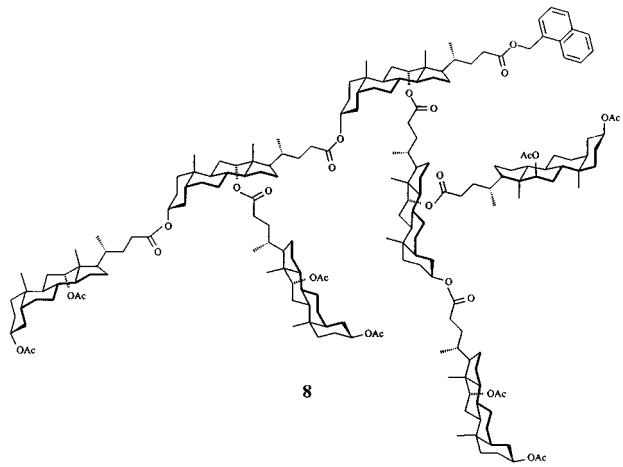

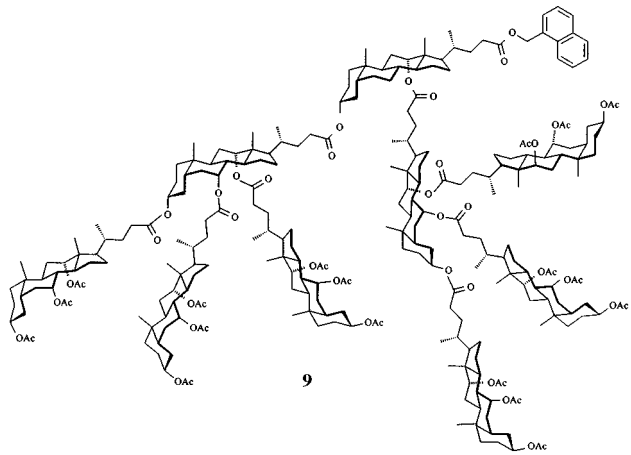

The mobility of these compounds on reversed-phase HPLC shows an interesting pattern (Table 1). With the increase in the oligomeric size, both the polarity (increased number of ester groups) and the lipophilicity (increased number of bile acid

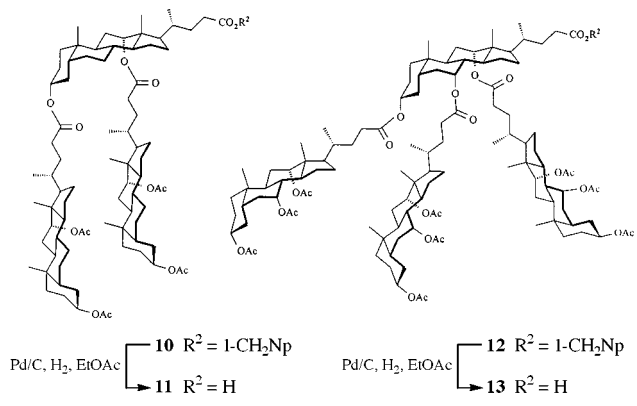

Scheme 1

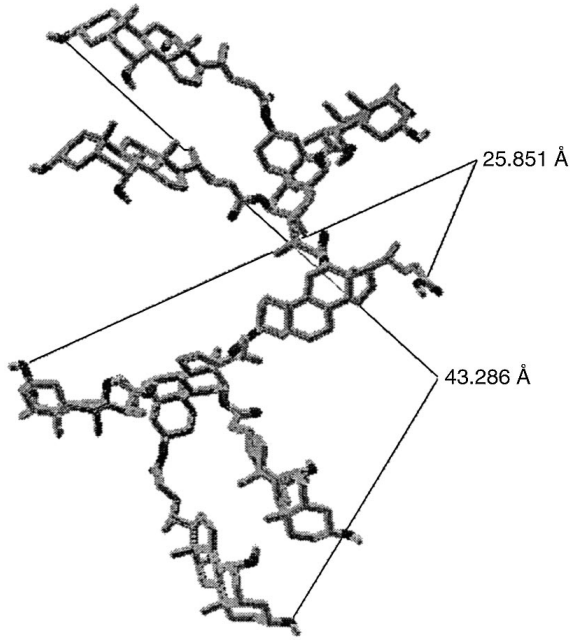

Fig. 1 Representation of one of the many possible conformations of **9**. The 'length' and the 'width' are indicated in Å.

Table 1 HPLC data on bile acid oligomers (25 cm C-18 column, 4.6 mm id)

Steroidal oligomers	Solvent system	Retention time/min
8 (7[a], 15[b])	30% THF–MeOH	14.5
9 (9, 27)	15% THF–MeOH	12.9
10 (3, 7)	15% THF–MeOH	17.1
12 (4, 13)	MeOH	13.8

[a] Number of bile acid moieties present. [b] Number of ester linkages.

units) increase. Experimentally, the order of elution (increasing retention time) on a C-18 column is: **12** < **9** < **10** < **8**. On silica gel TLC a different order is observed; the R_f values increase in the order: **9** < **12** < **8** < **10** (EtOAc–hexanes, 2 : 3 v/v).

The optical rotations of these dendrons are given in Table 2. The molar rotation values show a roughly linear relationship with the number of bile acid units in each dendron (or its molecular weight). This suggests the absence of chiral conformations and local micropolarity which might affect the optical rotation.

These bile acid-based dendrons are of considerable interest because of their shape and nanometric dimensions. The design of larger functionalized dendrimers using analogous repeating units is in progress in our laboratory.

Table 2 Molar and specific rotation values of dendrons in $CHCl_3$

Compound (MW)	Specific rotation	Molar rotation
8 (3116.4)	102.9	3207
9 (4413.9)	84.2	3717
10 (1450.0)	86.6	1256
11 (1309.9)	94.7	1240
12 (2098.8)	80.8	1696
13 (1958.6)	80.6	1579

Financial support from the Department of Science & Technology, New Delhi (grant # SP/S1/G-08/96), is gratefully acknowledged. We thank P. Balaram, R. Sudha and C. Das of the Molecular Biophysics Unit of this Institute for the MALDI-TOF MS, and S. Ghosh for his involvement in the synthesis and purification of **12**.

Notes and references

1 (*a*) The first report of a chiral dendrimer: R.G. Denkewalter, J. F. Kolc and W. J. Lukasavage, *U.S. Pat.* 4,410,688, 1979; (*b*) Review on chiral dendrimers: H. W. I. Peerlings and E. W. Meijer, *Chem. Eur. J.*, 1997, **3**, 1563; C. W. Thomas and Y. Tor, *Chirality*, 1998, **10**, 53; D. Seebach, P. B. Rheiner, G. Greiveldinger, T. Butz and H. Sellner, *Top. Curr. Chem.*, 1998, **197**, 125.

2 E. Buhleier, W. Wehner and F. Vögtle, *Synthesis*, 1978, 155.

3 D. A. Tomalia, A. M. Naylor and W. A. Goddard III, *Angew. Chem., Int. Ed. Engl.*, 1990, **29**, 138; D. A. Tomalia and H. D. Durst, *Top. Curr. Chem.*, 1993, **165**, 193; J. Issenberner, R. Moors and F. Vögtle, *Angew. Chem., Int. Ed. Engl.*, 1994, **33**, 2413; G. R. Newkome and C. N. Moorefield, *Dendrimers*, in *Comprehensive Supramolecular Chemistry*, ed. J. L. Atwood, J. E. D. Davies, D. D. MacNicol, F. Vögtle, J.-M. Lehn, Pergamon, Tarrytown, NY, 1996, vol. 10, p. 777; F. Zeng and S. C. Zimmerman, *Chem. Rev.*, 1997, **97**, 1681; D. K. Smith and F. Diederich, *Chem. Eur. J.*, 1998, **4**, 1353; M. Fischer and F. Vögtle, *Angew. Chem., Int. Ed.*, 1999, **38**, 884.

4 (*a*) G. R. Newkome, X. Lin and C. D. Weis, *Tetrahedron: Asymmetry*, 1991, **2**, 957; (*b*) D. Seebach, J.-M. Lapierre, K. Skobridis and G. Greiveldinger, *Angew. Chem., Int. Ed. Engl.*, 1994, **33**, 440; (*c*) P. Murer and D. Seebach, *Angew. Chem., Int. Ed. Engl.*, 1995, **34**, 2116; (*d*) J. F. G. A. Jansen, H. W. I. Peerlings and E. M. M. de Brabander–van den Berg, E. W. Meijer, *Angew. Chem., Int. Ed. Engl.*, 1995, **34**, 1206; (*e*) H.-F. Chow and C. C. Mak, *J. Chem., Soc., Perkin Trans. 1*, 1994, 2223; (*f*) H.-F. Chow and C. C. Mak, *Pure Appl. Chem.*, 1997, **69**, 483; (*g*) H.-T Chang, C.-T Chen, T. Kondo, G. Siuzdak and K. B. Sharpless, *Angew. Chem., Int. Ed. Engl.*, 1996, **35**, 182; (*h*) J. R. McElhanon and D. V. McGrath, *J. Am. Chem. Soc.*, 1998, **120**, 1647.

5 R. H. E. Hudson and M. J. Damha, *J. Am. Chem. Soc*, 1993, **115**, 2119.

6 K. Aoi, K. Itoh and M. Okada, *Macromolecules*, 1995, **28**, 5391.

7 U. Maitra and L. J. D'Souza, *J. Chem. Soc., Chem. Commun.*, 1994, 2793; U. Maitra, S. Balasubramanian, *J. Chem. Soc., Perkin Trans. 1*, 1995, 83; A. P. Davis, R. P. Bonar-law and J. K. M. Sanders, *Receptors Based on Cholic Acid*, in *Comprehensive Supramolecular Chemistry*, ed. J. L. Atwood, J. E. D. Davies, D. D. MacNicol, F. Vogtle and J-M. Lehn, Pergamon, Tarrytown, NY, 1996, vol. 4, p. 257; P. A. Brady, R. P. Bonar-law, S. J. Rowan, C. J. Suckling and J. K. M. Sanders, *Chem. Commun.*, 1996, 319; Y. Li and J.R. Dias, *Chem. Rev.*, 1997, **97**, 283; Y. H. Zhang, M. Akram, H. Y. Liu and X. X. Xhu, *Macromol. Chem. Phys.*, 1998, **199**, 1399.

8 C. J. Hawker and J. M. J. Fréchet, *J. Am. Chem. Soc.*, 1990, **112**, 7638.

9 The 1-naphthylmethyl group was employed for easier identification of the dendrons in the purification steps, and also in the analysis of the sample by UV and HPLC measurements.

10 The MALDI-TOF MS spectrum showed a peak for **8** at *m/z* 3143.0 [expected for $(M+Na)^+$ 3139.4] (Calc. for $C_{195}H_{292}O_{30}$: C, 75.15; H, 9.44%. Found: C, 75.33; H, 9.83%). For **9**, MALDI-TOF MS spectrum showed a peak for at *m/z* 4440.6 [expected for $(M+Na)^+$ = 4436.9] (Calc. for $C_{263}H_{388}O_{54}$: C, 71.57; H, 8.86. Found: C, 71.89; H, 9.26%).

Communication 9/07297G

ChemComm

Carbon nanocage structures formed by one-dimensional self-organization of gold nanoparticles

Takeo Oku* and Katsuaki Suganuma

Institute of Scientific and Industrial Research, Osaka University, Mihogaoka 8-1, Ibaraki, Osaka 567-0047, Japan. E-mail: Oku@sanken.osaka-u.ac.jp

Received (in Cambridge, UK) 15th July 1999, Accepted 25th October 1999

Carbon nanocapsules and nanotubes have been formed by one-dimensional self-organization of gold nanoparticles, caused by the adhesive force at the step edge of amorphous carbon thin films; the present result is expected to be a promising fabrication technique for self-assembling nanowires and cluster-protected quantum dots at scales beyond the limits of current photolithography.

The recent speed-up of ultra-large scale integrated circuits (ULSI) of semiconductor devices is highly dependent on the minimization of the design rule. New properties are also expected by formation of low dimensional arrays of quantum dots. The photolithography technique is used for the formation of these nanostructures, and ULSI with 0.07 μm rule will be produced in 2009.[1] However, the limit of the design rule is reported to be 0.05 μm (= 50 nm) using extreme ultraviolet lithography.[2] The establishment of nanostructure-formation technique by self-organization of nanoparticles[3–8] is worth investigation in order to overcome this lithography limit. However, self-organization has been of two- and three-dimensional type, whereas one-dimensional (1D) self-organization is required for the 'nanowiring' formation of the future ULSI devices.

The purpose of the present work is to form 1D carbon nanocage arrangements using self-organization of metal nanoparticles with a size below 10 nm. Gold colloids have been used for the formation of single electron transistors.[9,10] In the present work, gold (Au) nanoparticles were selected because of easy control of cluster size.[11] Fabrication of 1D Au nanodots and nanowires encapsulated in carbon nanocage structures was attempted by annealing the 1D self-organized nanoparticles on carbon thin films. In order to understand the self-organization mechanism, high-resolution electron microscopy (HREM)[12,13] was carried out. The present work gives a guideline for the design and synthesis of 1D self-organized nanostructures, which are expected for future nanoscale devices.

Au nanoparticles (ULVAC Ltd.) with a size of *ca.* 5 nm are selected in the present work for the 1D positioning. The surface of these nanoparticles was stabilized by α-terpineol ($C_{10}H_{18}O$) in toluene solution. The Au nanoparticle solution was dispersed on holey carbon grids with thickness *ca.* 15 nm (Oken Syoji. Co. Ltd.). After drying the specimens, they were loaded into the vacuum chamber and annealed at 400 °C for 30 min in a vacuum of *ca.* 7×10^{-4} Pa. HREM observations were performed with a 1250 kV electron microscope (ARM-1250) equipped with a top entry goniometer having a point-to-point resolution of 0.12 nm. To avoid sample damage by electron irradiation, the electron beam width for HREM observations was minimized by using a small spot size.

A low magnification image of as-prepared Au nanoparticles on amorphous carbon film is shown in Fig. 1(a). 1D ordering of Au nanoparticles with a size of 5 nm is observed over a length of 70 nm and a line profile of amorphous carbon across the row is shown. The image intensity of amorphous carbon at the lower side is 1.2 times stronger than that of the upper side as indicated by white lines in the inset to Fig. 1(a), which indicates that the step edge of the carbon thin films is *ca.* 3 nm (0.2×15 nm). The longest size of the 1D ordering was *ca.* 1.5 μm, which is dependent on the length of step edge of the carbon thin films. An enlarged HREM image of the self-organized Au nanoparticles is shown in Fig. 1(b). The image contrast of amorphous carbon in region A is brighter than that in region B, which also indicates the step edge of the carbon film as measured in Fig. 1(a). 1D positioning of Au nanoparticles with a width of *ca.* 15 nm is also observed in Fig. 1(c), which consists of two or three rows of Au nanoparticles. Reproducibility of the 1D self-organization was confirmed.

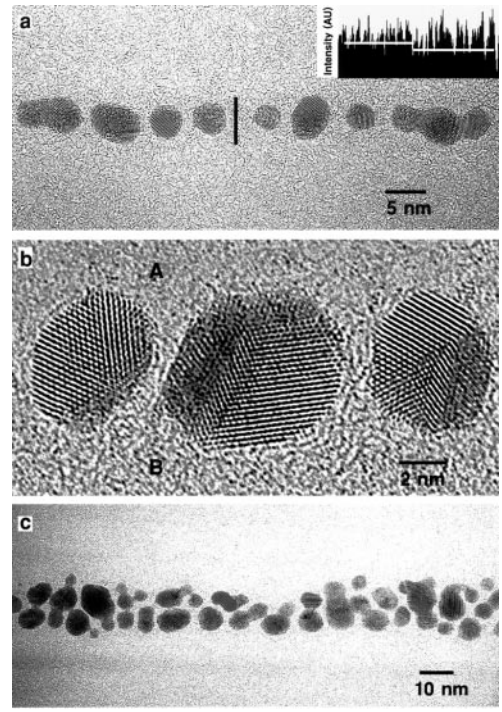

Fig. 1 (a) Low magnification image of 1D self-organized Au nanoparticles on amorphous carbon film with the intensity distribution across the interface indicated. (b) Enlarged HREM image of 1D self-organized Au nanoparticles. (c) 1D self-organization of Au nanoparticles with a width of *ca.* 15 nm.

Fig. 2 shows HREM images of annealed Au nanoparticles at 400 °C. Au nanoparticles encapsulated in carbon nanocapsules are observed in Fig. 2(a). At elevated temperatures, Au nanoparticles grow by coalescence, and the particle size is *ca.* 15 nm. The carbon nanocapsules are isolated owing to the surface diffusion of Au and C atoms and the surface tension of the nanoparticles. Amorphous carbon would be graphitized by the catalytic effect[14] of the active Au surface at low temperature of 400 °C compared to that of ordinary chemical formation of carbon nanocapsules.[15] An enlarged image of the Au nanoparticles encapsulated in carbon nanocapsules is shown in Fig. 2(b). All the Au nanoparticles are surrounded and isolated by double or triple graphite sheets, which would prevent the nanoparticles from growing and so acts as cluster protection. Au nanowires encapsulated in carbon nanotubes are often formed as shown in Fig. 2(c). An Au nanoparticle encapsulated in a

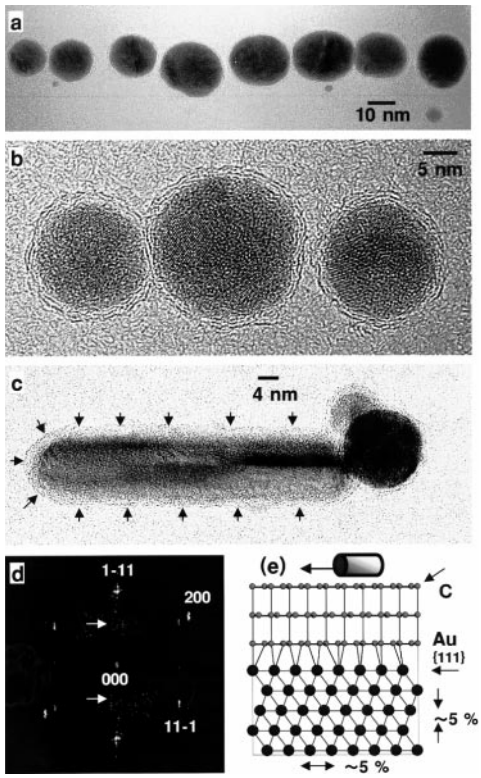

Fig. 2 (a) Low magnification image of annealed Au nanoparticles at 400 °C. (b) HREM image of Au nanoparticles encapsulated in carbon nanocapsules. (c) Au nanowire encapsulated in carbon nanotube. (d) Fourier transformed pattern of the nanotube. (e) Structural model of Au{111}/C{002} interface.

carbon nanocapsule is also observed at the tip of the nanotube. The one-dimensionality is retained after the coalescence of nanoparticles, which is a useful formation technique for protected nanowires. The maximum length of the continuous wire is *ca.* 100 nm, and the length is dependent on the nanoparticle distance. A Fourier transformed pattern of a circular cross-section of a cut Au nanotube is shown in Fig. 2(d). The diffractogram is indexed with the [011] incidence of Au. In the Fourier transform, lattice distortion is observed as indicated by the streaks of each reflection perpendicular to the growth direction of the nanowire. Some distortion is observed in all Au nanowires. The $1\bar{1}1$ reflection is expanded, which indicates reduction of lattice distance of Au{111}. The maximum difference between $1\bar{1}1$ and $11\bar{1}$ reflections is *ca.* 10%. Diffuse scattering of carbon 002 is observed as indicated by arrows, which is due to the carbon layers of the nanotube. A structure model of the $Au\{111\}/C\{002\}_{nanotube}$ interface is shown in Fig. 2(e). Lattice expansion and reduction are observed parallel and perpendicular to the growth axis, respectively. It is believed that the distortion of nanowire is due to the coalescence of nanoparticles along the growth direction at low temperatures. The maximum distortion is *ca.* 10%, which would indicate expansion and reduction of *ca.* 5%, respectively.

The formation of graphitic coatings around metal nanoparticles supported on amorphous-C films is often observed when subjected to high intensity electron beam irradiation.[16] However, a high intensity electron beam was not used here. As is evident in Fig. 1, which was obtained with a 1250 kV electron microscope, there are no graphite layers around the Au nanoparticles for the as-prepared samples. If the formation of the graphite layers around the nanoparticles is due to the effect of the electron beam, there should be carbon layers around the nanoparticles for the as-prepared samples. When a high intensity electron beam is used, an amorphous carbon matrix is also graphitized. However, an amorphous carbon matrix is observed around the carbon nanocapsules and nanotubes in Fig. 2. In addition, several micrographs for the as-prepared and annealed samples were taken under the same conditions in the present work, and formation of carbon layers around the nanoparticles was observed only for the annealed samples. These results indicate that the formation of these carbon nanocage structures is due to annealing, and that this method is effective for the homogeneous formation of carbon nanocage structures.

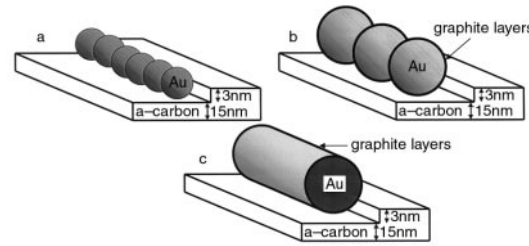

Fig. 3 Schematic illustration of (a) 1D self-organized Au nanoparticles, (b) carbon nanocapsules and (c) a carbon nanotube.

A schematic illustration of self-organized Au nanoparticles, carbon nanocapsules and a carbon nanotube is shown in Fig. 3. Adhesion due to the step edge and substrate is the main force leading to the 1D arrangement whereas 2D self-organization[6–8] of nanoparticles is due to inter-nanoparticle forces by ligands around particles. The present result indicates that the 1D arrangement is strongly dependent on the step edge of the substrate. The formation of carbon nanocapsules and nanotubes would depend on the distance between gold nanoparticles. For larger distances, carbon nanocapsules will be formed while for smaller distances, gold nanowires will be formed by the coalescence of gold nanoparticles. Although step edges are formed by a simple sample preparation technique in the present work, the step edge size can be controlled by ordinary lithography techniques such as use of an electron beam, and is expected to be a viable nanofabrication technique for future electronic devices.

We acknowledge Professors K. Hiraga and E. Aoyagi for allowing us to use the electron microscope. This work was partly supported by The Shinsedai Foundation, and Grant-in-Aid for Scientific Research, Ministry of Education, Science, Sports and Culture, Japan.

Notes and references

1 *National Technology Roadmap for Semiconductors*, The Semiconductor Industry Association, San Jose, CA, 1997.
2 J. E. Bjorkholm, J. Bokor, L. Eichner, R. R. Freeman, J. Gregus, T. E. Jewell, W. M. Mansfield, A. A. MacDowell, E. L. Raab, W. T. Silfvast, L. H. Szeto, D. M. Tennant, W. K. Waskiewicz, D. L. White, D. L. Windt and O. R. Wood II, *J. Vac. Sci. Technol. B*, 1990, **8**, 1509.
3 C. B. Murray, C. R. Kagan and M. G. Bawendi, *Science*, 1995, **270**, 1335.
4 C. A. Mirkin, R. L. Letsinger, R. C. Mucic and J. J. Storhoff, *Nature*, 1996, **382**, 607.
5 L. Motte, F. Billoudet, E. Lacaze, J. Douin and M. P. Pileni, *J. Phys. Chem. B*, 1997, **101**, 138.
6 Z. L. Wang, S. A. Harfenist, R. L. Whetten, J. Bentley and N. D. Evans, *J. Phys. Chem. B*, 1998, **102**, 3068.
7 C. J. Kiely, J. Fink, M. Brust, D. Bethell and D. J. Schiffrin, *Nature*, 1998, **396,** 444.
8 K. Pohl, M. C. Bartelt, J. de la Figuera, N. C. Barttelt, J. Hrbek and R. Q. Hwang, *Nature*, 1999, **397**, 238.
9 D. L. Klein, R. Roth, A. K. L. Lim, A. P. Alivisatos and P. L. McEuen, *Nature*, 1997, **389**, 699.
10 L. Feldheim and C. D. Keating, *Chem. Soc. Rev.*, 1998, **27**, 1.
11 G. Schmid, *Chem. Rev.*, 1992, **92**, 1709.
12 T. Oku and S. Nakajima, *Appl. Phys. Lett.*, 1999, **75**, 2226.
13 T. Oku and J.-O. Bovin, *Phil. Mag. A*, 1999, **79**, 821.
14 R. Lamber, N. Jaeger and G. Schulz-Ekloff, *Surf. Sci.*, 1988, **197**, 402.
15 T. Oku, K. Niihara and K. Suganuma, *J. Mater. Chem.*, 1998, **8**, 1323.
16 T. Oku, G. Schmid and K. Suganuma, *J. Mater. Chem.*, 1998, **8**, 2113.

Communication 9/05767F

ChemComm

A model for pathways of radical addition to fullerenes

Kevin M. Rogers and Patrick W. Fowler*

School of Chemistry, University of Exeter, Stocker Road, Exeter, UK EX4 4QD. E-mail: p.w.fowler@exeter.ac.uk

Received (in Cambridge, UK) 14th July 1999, Accepted 18th October 1999

A sequential π-electronic model that simulates addition of large radicals to fullerenes yields pathways to the experimental structures of $C_{60}X_6$ (X = Cl, Br) and $C_{70}Cl_{10}$ and predicts structures for $C_{60}X_{12}$ and $C_{60}X_{18}$.

The fullerenes behave as giant electron-deficient alkenes[1] and possess a rich addition chemistry. Derivatives in which the addends are halogen atoms were among the first to be fully characterised: $C_{60}Cl_6$,[2] $C_{60}Br_6$,[3] $C_{60}Br_8$[3] and $C_{70}Cl_{10}$[4] have all been synthesised and their structures identified. Analogous derivatives have been made by replacing some or all of the halogen addends with aryl[5] and allyl[6] groups. Six nitro groups add to C_{60} to give a derivative that is thought to be isostructural with $C_{60}Br_6$.[7] Direct alkylation, haloalkylation and arylation *via* radical species have also been studied.[8,9] Whilst benzylation of fullerenes, for example, clearly involves radical species, often leading to relatively stable radical products,[8,9] halogenation leads directly to products with even numbers of addends and stable electronic configurations. However, it is believed that addition of halogen atoms also occurs *via* a radical mechanism.[10]

The present communication describes a simple model based on topology alone that is designed to predict the most likely sites for addition of large radicals to an extended carbon π system. Application of the model to C_{60} and C_{70}, the two fullerenes for which data exist, generates addition pathways that lead to stable addend patterns isostructural with experimentally produced compounds. The potential for generalisation of the approach when new fullerenes become available in quantity is clear.

The model is based on Hückel molecular-orbital (HMO) theory, which is often used to provide simple qualitative π-electronic information of fullerenes. The background is given in many textbooks.[11] In the simplest ('topological') approximation, Coulomb integrals α are equal for all atoms, resonance integrals β are equal for all σ-bonded pairs and all more distant interactions are neglected. Diagonalisation of the adjacency matrix gives the dimensionless eigenvalues $\lambda = (\varepsilon - \alpha)/\beta$ (where ε is an orbital energy) and their corresponding eigenvectors. One useful feature of the Hückel model is that topological coordinates of the atoms of a fullerene can be generated from the eigenvectors of its adjacency matrix.[12] The model developed here generates several π-electronic properties of fullerenes from their Hückel eigenvectors.

One property readily derived from HMO eigenvectors is p_{rs}, the π *bond order* between two atoms r and s in an extended π system. It is a sum over the partial mobile bond orders contributed by all molecular orbitals [eqn. (1)],

$$p_{rs} = \sum_j n_j c_{jr} c_{js} \quad (1)$$

where c_{jr} is the coefficient of the p_π orbital of atom r in the jth molecular orbital and n_j is the *occupation number*.

The model applied here is based on two further properties. The first, *free-valence index*, was used in early work by Coulson and coworkers on radical addition to small unsaturated hydrocarbons.[13] The free-valence index F_r, defined by Coulson,[14] measures ease of attack by species, particularly free radicals, at an atom r in a conjugated π system [eqn. (2)].

$$F_r = N_{\max} - N_r \quad (2)$$

N_r is the sum of π bond orders over all bonds joining atom r to the remainder of the π system. $N_{\max}$ is the maximum value of this sum and depends on how many other sp^2 carbons are attached to the atom in question; $N_{\max}$ is $\sqrt{m}$ for an sp^2 carbon attached to m others.[15] The second property, *spin density*, $\rho_{(\pi)r}$, measures the amount of unpaired electron density on an atomic site of a molecule in an open-shell state [eqn. (3)],

$$\rho_{(\pi)r} = \sum_j v_j (c_{jr})^2 \quad (3)$$

where v_j is the *spin number* of the jth molecular orbital. In this model, empty and full (doubly occupied) orbitals have spin number zero and the spin number may be non-integral for a partially filled, degenerate HOMO.

The two properties are used in combination to create a model for simulation of free-radical attack, specified as follows. Assume that addends are attached to a fullerene framework sequentially, in a game with two rules. Attack of the first addend on the closed-shell molecule obeys *rule* (*i*): attach to a position of maximum free valence. This produces a radical product, which is attacked in the next addition, under *rule* (*ii*): attach to an available position of maximum spin density amongst all those that will quench the radical. If steric effects are ignored, all sites are 'available', but for a bulky addend such as Cl, Br or $PhCH_2$, neighbours of sp^3 sites can be taken to be unavailable unless their occupation becomes necessary for radical quenching. It turns out that in the examples investigated here, the position of maximum free valence is never adjacent to an sp^3 site [hence the omission of the term 'available' from rule (i)], although this may not be the case for other examples.

Addition to C_{60}: following rules (i) and (ii), addition to C_{60} occurs in a straight-forward sequence. After one addition, the site of maximum spin density is at the other end of the attacked formal double bond (hexagon–hexagon edge), but the preference for *non-adjacent* attack leads to attachment at the 1,4 position of a hexagon. Successive brominations continue to make 1,4 patterns, winding around a central pentagon [Fig. 1(*a*)]. By the addition of the fifth Br atom, the pentagon in question is isolated and is effectively a cyclopentadienyl radical in the Hückel model (although in more sophisticated theory, the radical moiety would interact weakly with the rest of the cage *via* homoconjugation[16]). The only way to quench the radical at the next step is by addition within the surrounded pentagon, giving the experimental $C_{60}X_6$ (X = Cl, Br) pattern with a single sp^3–sp^3 adjacency.[2,3] This addition sequence, summarised in Fig. 1(*a*), is compatible with more sophisticated calculations and the ESR measurements on known radical additions such as benzylation,[8] where the long lifetime of the intermediate allyl and cyclopentadienyl radicals makes direct observation possible. Such radical intermediates are stabilised by the hyperconjugation and steric protection provided by the bulky organic addends.[8,9] Neither of these features is provided by atomic halogen addends; hence any radical intermediate is susceptible to rapid further addition.

Extended application of the model to C_{60} leads to incorporation of two further sets of six addends, indicating possible stability for derivatives with 12 and 18 bulky ligands. The pattern of addition in both of these further sets is identical to the first, proceeding *via* allyl and cyclopentadienyl intermediates. However, isomers are possible owing to the number of possible locations of the addends in the central pentagons. Addition

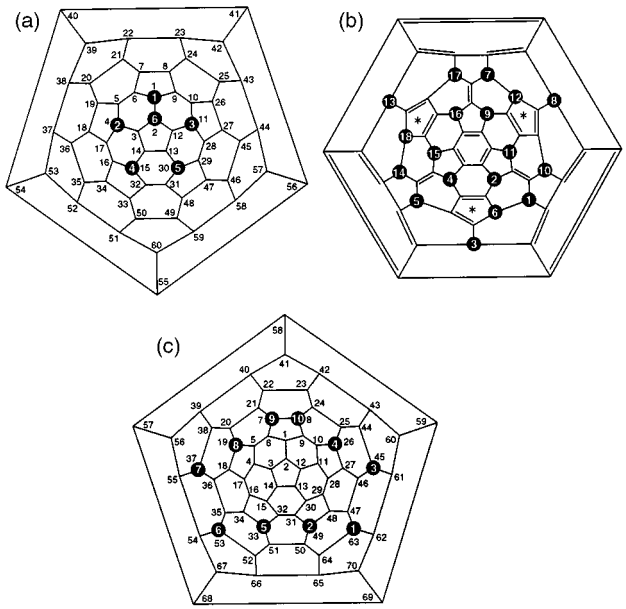

Fig. 1 Sequence of attack on C_{60} and C_{70} (in the IUPAC numbering scheme).[17] (a) The first six addends on C_{60} give the experimental structure $C_{60}X_6$ (X = Cl, Br).[2,3] (b) After 18 additions, the remaining six available sp^2 sites (outer hexagon of the Schlegel diagram) are part of an 18-atom aromatic π system. Isomers are possible since addends 6, 12 and 18 could be attached to any of the five sites in the pentagons marked with an asterisk. (c) The first ten addends on C_{70} give the experimental structure of $C_{70}Cl_{10}$.[4,18]

beyond 18 addends may be less favourable as the six remaining available (non-adjacent) sp^2 sites are part of a stable aromatic π system. The predicted order of attack by addends 7–12 and 13–18, leading to $C_{60}X_{12}$ and $C_{60}X_{18}$ respectively, is summarised in Fig. 1(*b*). Although not found for Br, these structures are plausible candidates for addition of, for example, X = Cl.

Addition to C_{70}: for C_{70} it is not necessary to invoke the bulk of the addend, as 1,4 addition is favoured electronically at every spin-quenching stage. Addition according to rules (i) and (ii) proceeds around the equator, forming a belt of 1,4 links across hexagons, which after the ninth addition can be spin-quenched by forming an sp^3–sp^3 adjacency. Addition at this position (8 in the IUPAC labelling[17]), which is the centre of maximum spin density, splits the π system into 28- and 32-atom components, each with a significant HOMO–LUMO gap. (The site that would be occupied under strict non-adjacent attack has a much lower spin density, 0.097 *cf.* 0.270.) Again, the result of alternate quenching of free valence and spin [Fig. 1(*c*)] is a known pattern, the experimental structure of $C_{70}Cl_{10}$.[4] At least within the small number of structures compatible with the ^{13}C NMR spectrum of the compound, this structure is also the one that is thermodynamically favoured over its competitors.[18]

The model presented here can be seen as essentially a kinetic one, since the rules choose the site most directly reactive towards an approaching radical, rather than necessarily the thermodynamically most stable product. The practice of predicting addition patterns by following sequences of thermodynamically stable species is common,[19] and has correctly predicted the structures of experimentally characterised derivatives. As the degree of addition to the cage increases, a combinatorially exploding number of thermodynamic calculations is needed to cover all possible patterns at each step. The model developed here is based on simple rules that lead directly from one pattern to the next in a deterministic sequence. Examples exist where semi-empirical thermodynamic energies predict no clear candidate for the most stable isomer, a case in point being $C_{60}Br_8$.[20] It is certain that in $C_{60}Br_6$ itself, some rearrangement must occur on further bromination, as its six bromine positions do not form a subset of those in either $C_{60}Br_8$ or $C_{60}Br_{24}$.[3] The present Br_6 pattern *may* in fact also be the thermodynamic result for $C_{60}Br_6$, but this is not established. A theoretical test would be a calculation of energies for all $C_{60}Br_6$ isomers. In this connection, it is worth noting that the experimental isomers of $C_{60}Br_6$ and $C_{70}Cl_{10}$ are selected uniquely from 418 470 and 19 835 545 518 possibilities[21] by the present, purely graph-theoretical model.

K. M. R. acknowledges EPSRC for financial support of this work, and both authors acknowledge the EU TMR network contracts FMRX-CT97-0126 and FMRX-CT98-0192.

Notes and references

1 P. J. Fagan, J. C. Calabrese and B. Malone, *Acc. Chem. Res.*, 1992, **25**, 134.
2 P. R. Birkett, A. G. Avent, A. D. Darwish, H. W. Kroto, R. Taylor and D. R. M. Walton, *J. Chem. Soc., Chem. Commun.*, 1993, 1230.
3 P. R. Birkett, P. B. Hitchcock, H. W. Kroto, R. Taylor and D. R. M. Walton, *Nature*, 1992, **357**, 479.
4 P. R. Birkett, A. G. Avent, A. D. Darwish, H. W. Kroto, R. Taylor and D. R. M. Walton, *J. Chem. Soc., Chem. Commun.*, 1995, 683.
5 P. R. Birkett, A. G. Avent, A. D. Darwish, I. Hahn, H. W. Kroto, G. J. Langley, J. O'Loughlin, R. Taylor and D. R. M. Walton, *J. Chem. Soc., Perkin Trans. 2*, 1997, 1121; A. G. Avent, P. R. Birkett, A. D. Darwish, H. W. Kroto, R. Taylor and D. R. M. Walton, *Tetrahedron*, 1996, **52**, 5235.
6 A. K. Abdul-Sada, A. G. Avent, P. R. Birkett, H. W. Kroto, R. Taylor and D. R. M. Walton, *J. Chem. Soc., Perkin Trans. 1*, 1998, 393.
7 V. Anantharaj, J. Bhonsle, T. Canteenwala and L. Y. Chiang, *J. Chem. Soc., Perkin Trans. 1*, 1999, 31.
8 P. J. Krusic, E. Wasserman, P. N. Keizer, J. R. Morton and K. F. Preston, *Science*, 1991, **254**, 1183; J. R. Morton, F. Negri and K. F. Preston, *Acc. Chem. Res.*, 1998, **31**, 63.
9 *The Chemistry of Fullerenes*, ed. R. Taylor, World Scientific, Singapore, 1995.
10 A. J. Adamson, J. H. Holloway, E. G. Hope and R. Taylor, *Fullerene Sci. Technol.*, 1997, **5**, 629.
11 A. Streitwieser, Jr., *Molecular Orbital Theory for Organic Chemists*, Wiley, New York, 1961; L. Salem, *The Molecular Orbital Theory of Conjugated Systems*, W. A. Benjamin, New York, 1966; P. W. Fowler and D. E. Manolopoulos, *An Atlas of Fullerenes*, Oxford University Press, Oxford, 1995.
12 D. E. Manolopoulos and P. W. Fowler, *J. Chem. Phys.*, 1992, **96**, 7603.
13 F. H. Burkitt, C. A. Coulson and H. C. Longuet-Higgins, *Trans. Faraday Soc.*, 1951, **47**, 553.
14 C. A. Coulson, *Faraday Discuss. Chem. Soc.*, 1947, **2**, 9.
15 W. E. Moffitt, as reported by C. A. Coulson, *J. Chim. Phys. Phys.-Chim. Biol.*, 1948, **45**, 243.
16 H. Iikura, S. Mori, M. Sawamura and E. Nakamura, *J. Org. Chem.*, 1997, **62**, 7912.
17 E. W. Godly and R. Taylor, *Pure Appl. Chem.*, 1997, **69**, 1411.
18 S. J. Austin, P. W. Fowler, J. P. B. Sandall, P. R. Birkett, A. G. Avent, A. D. Darwish, H. W. Kroto, R. Taylor and D. R. M. Walton, *J. Chem. Soc., Perkin Trans. 2*, 1995, 1027.
19 See, for example: B. W. Clare and D. L. Kepert, *J. Mol. Struct. (THEOCHEM)*, 1995, **340**, 125; 1995, **358**, 79; P. A. Cahill and C. M. Rohlfing, *Tetrahedron*, 1996, **52**, 5247.
20 J. B. Peel and R. G. Rothwell, *Aust. J. Chem.*, 1994, **47**, 131; P. W. Fowler and J. P. B. Sandall, *J. Chem. Soc., Perkin Trans. 2*, 1995, 1247.
21 K. Balasubramanian, *J. Phys. Chem.*, 1993, **97**, 6990.

Communication 9/05719F

ChemComm

Geometric requirements in the ferriin oxidation of benzylic 1,2-diols

John H. Penn,* Robert C. Plants and An Liu

Department of Chemistry, West Virginia University, Morgantown, WV 26506-6045, USA. E-mail: jpenn2@wvu.edu

Received (in Corvallis, OR, USA) 12th July 1999, Accepted 8th October 1999

The rates of ferriin [*i.e.* tris(1,10-phenanthroline)iron(III)] oxidation of *cis*- and *trans*-1,2-diphenylcyclohexane-1,2-diol have been found to be dramatically different; *cis*-1,2-diphenylcyclohexane-1,2-diol reacts a minimum of 10^4 times faster than the corresponding *trans*-isomer; implications for the oxidation of benzylic diols by ferriin are discussed.

The oxidative cleavage of 1,2-diols by a variety of reagents has been extensively studied.[1] The mechanisms are conventionally classified into several types.[1] In the first class of oxidative cleavage of *vic*-diols [eqn. (1)], a bidentate complex between

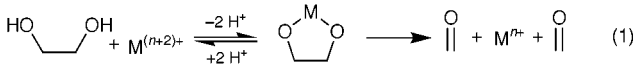

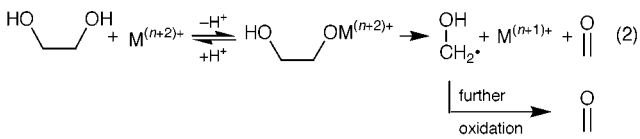

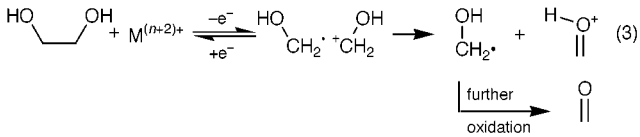

the oxidant and the glycol breaks down by an apparent six-electron process (two electrons to the oxidant).[1] The second general class of oxidative cleavage mechanisms of *vic*-diols [eqn. (2)] invokes a monodentate complex, which yields an intermediate radical *via* a one-electron process, followed by C–C fission and then further oxidation of the resulting radical.[1] A third general class of oxidative cleavage reactions for appropriately substituted *vic*-diols [eqn. (3)] is a single electron transfer to form a radical cation, that can subsequently undergo bond cleavage to form fragments similar to those formed in [eqn. (2)].[2,3]

In our laboratories, we hoped to use *vic*-diols that undergo cleavage by the general mechanism shown in [eqn. (3)] in order to determine fundamental reaction rate constants. Our initial studies demonstrated that ferriin readily oxidized tetraaryl-ethane-1,2-diols to the corresponding ketones [eqn. (4)].[4] By

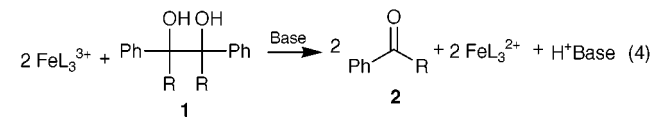

applying a mechanism in which a slow rate-determining outer-sphere electron transfer was followed by rapid bond cleavage {general mechanism of [eqn. (3)]}, we reported endergonic electron transfer rate constants that were faster than expected, based upon estimates of the solution phase oxidation potential.[5] As we have varied functionality in standard structure–reactivity probes in an attempt to understand this anomalously fast electron transfer rate, we have observed non-isosbestic point behavior during a kinetics experiment on appropriately substituted compounds. This has served as an indication that the reaction mechanism is more complex than originally thought.[6]

As part of our reinvestigation of this reaction mechanism, we have studied the geometric relationship of the hydroxy groups in this oxidation reaction. Our preliminary investigation of the reactivity differences exhibited by *dl*- and *meso*-1,2-diphenyl-ethane-1,2-diol indicated to us that steric requirements existed in this reaction and that the geometry of the reacting groups might be important. The free rotation of the central C–C bond in the *dl*- and *meso*-isomers of 1,2-diphenylethane-1,2-diol does not allow for a definitive analysis of the various intramolecular interactions, which may be responsible for the observed reactivity. In order to lock the geometry of all components in place, we chose to study *cis*- and *trans*-1,2-diphenylcyclohex-ane-1,2-diol. These compounds were synthesized based on Tomboulian's method.[7] In brief, *cis*-**3** was obtained from 1,4-dibenzoylbutane in a McMurry coupling reaction with $TiCl_3/LiAlH_4$ followed by OsO_4 oxidation to give the *cis*-1,2-diphenylcyclohexane-1,2-diol in 27% yield [mp 86.5–87.5 °C (lit.,[7] 86–87 °C)]. *trans*-1,2-Diphenylcyclohex-ane-1,2-diol was obtained from reaction of cyclohexane-1,2-dione with excess (3 equiv.) of PhLi at reflux in dry THF for 20 h, followed by appropriate work-up to yield the resultant white needle-like crystals, mp 122–123 °C (lit.,[7] 121–122 °C).

Quantitative analysis of the reaction of ferriin (10 mM) with *cis*- and *trans*-**3** (5 mM) in MeCN at room temperature was accomplished by reverse-phase HPLC on a C-18 column eluted with MeCN–H_2O, using methyl benzoate as an internal standard. A base (2,6-di-*tert*-butylpyridine) was added to avoid the possible carbocation-induced rearrangement product (*i.e.* the pinacol rearrangement). *cis*-**3** reacted quantitatively (mass balance = 98.9% at 34% conversion) to form the anticipated bond cleavage product (*i.e.* 1,4-dibenzoylbutane). The error limits for this determination are ±5%, which means that a small amount of the *trans*-1,2-diphenylcyclohexane-1,2-diol could have been formed in this reaction. The data were carefully analyzed for the appearance of the *trans*-1,2-diphenyl-1,2-cyclohexanediol. Since no *trans*-diol was observed and the appearance of 1,4-dibenzoylbutane was near quantitative, we conclude that the major reaction pathway (by a factor of $> 20:1$) is oxidative cleavage of the 1,2-diol C–C bond.

In contrast, the *trans*-1,2-diphenylcyclohexane-1,2-diol did not react within a time period of two days. In fact, we were unable to see a reaction under any conditions employed by us. Therefore, we were unable to confirm that the expected oxidation product arose from this reaction. Under controlled conditions where both *cis*-**3** and *trans*-**3** were reacted in the same solution, we were able to show that a minimum reactivity difference of 10^4 exists between these isomers. Thus, there is a significant reactivity difference between *cis*-**3** and *trans*-**3** for ferriin oxidation.

This extreme reactivity difference between the two isomers required an analysis of the possible conformations of *cis*- and *trans*-**3**. These conformations are shown in Fig. 1. For *cis*-**3**, both available ring-flipped conformations have one phenyl group in the axial conformation and one phenyl group in the equatorial conformation. Thus, the energetics of these two

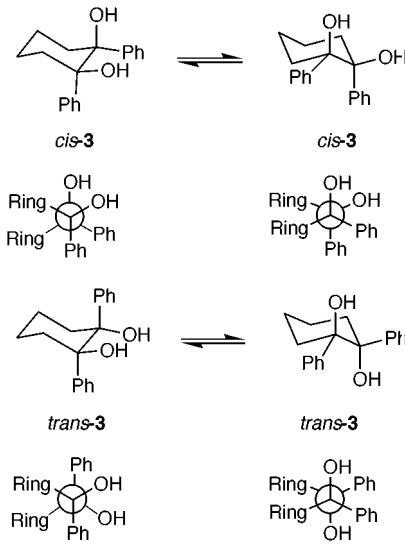

Fig. 1 Conformations of *cis*- and *trans*-1,2-diphenylcyclohexane-1,2-diol.

alternative conformations are equivalent. In contrast, *trans*-**3** does not have equivalent conformational energies. Since the phenyl group is larger than the hydroxy group,[8] one would anticipate that the conformation in which the phenyl groups are equatorial would be quite a bit more stable than the conformation in which the hydroxy groups are in the axial position. This conformational preference tends to 'lock' the cyclohexanediol into the conformation with both phenyl groups in the equatorial position in the same way that the *tert*-butyl group is said to 'lock' the conformation of substituted cyclohexanes. In this conformation, the hydroxy groups are in an *anti*-relationship to each other. This expectation is consistent with molecular mechanics calculations in which the energetic difference between the conformation in which the phenyl groups are axial and the conformation in which the phenyl groups are equatorial is 5.4 kcal mol^{-1}. From this relative arrangement of groups, we conclude that either *syn*-OH groups or an antiperiplanar phenyl–OH arrangement can lead to the observed bond cleavage reactions.

The results of this study have important implications for the ferriin oxidation of *vic*-diols. A simple outer-sphere electron transfer reaction, in which an electron is transferred from the electron donor to the ferriin molecule, cannot explain the observed reactivity differences. One would anticipate that the oxidation potentials of *cis*-**3** and *trans*-**3** would be identical, since *cis*- and *trans*-1,2-diphenylcyclohexane have identical photoelectron spectra (identical ionization potentials).[9] Our estimate of a minimum rate differential for these two compounds of 10^4 would be inconsistent with the energetic equivalence of these two reactions.

Alternatively, one could argue that electron transfer occurs in both species, but that *trans*-$\mathbf{3}^{\bullet+}$ is a stable species and does not lead ultimately to the dione, while *cis*-$\mathbf{3}^{\bullet+}$ is relatively unstable and reacts rapidly to form the dione. This argument is ruled out by two experimental results. First, there is no trace of *trans*-1,2-diphenylcyclohexane-1,2-diol in the reactions starting from the *cis*-1,2-diphenylcyclohexane-1,2-diol isomer. This argues against equilibration of *cis*-$\mathbf{3}^{\bullet+}$ and *trans*-$\mathbf{3}^{\bullet+}$. Further, preliminary experimental results in which *cis*-$\mathbf{3}^{\bullet+}$ and *trans*-$\mathbf{3}^{\bullet+}$ were generated by single electron transfer to excited state dicyanoanthracene showed similar non-reactivity for both the *cis*- and *trans*-isomers.

The reactivity differences between *cis*- and *trans*-**3** seem to preclude reaction through a general mechanism such as that shown by the general cleavage mechanism of eqn. (2). A mechanistic interpretation that there is a sufficient energetic difference for complexation of an equatorial OH group as compared to an axial OH group is, in principle, possible. Combined with evidence that the monomethyl ethers of both *meso*- and *dl*-1,2-diphenylethane-1,2-diol are unreactive in comparison[10] allows us to definitively rule out the general mechanism of eqn. (2), since two OH groups are required for the reaction.

To the best of our knowledge, such geometric requirements for the two hydroxy groups are unprecedented in the cleavage of *vic*-diols by one-electron oxidizing reagents [general oxidative cleavage mechanism shown in eqn. (2)]. We are continuing our efforts to fully understand the mechanism of this reaction in order to better understand the oxidation reaction mechanisms of one electron oxidants in reactions such as the Belousov–Zhabotinski (B–Z) reaction.[11,12]

The geometric requirements for the ferriin oxidation of aromatic 1,2-diols involve the orientation of the two OH groups in a *syn*-position or an anti-periplanar phenyl–OH arrangement. The differing reactivity of **3a** and **3b** with ferriin indicates a very unexpected and unusual non-outer sphere oxidation mechanism for this type of compound.

We gratefully acknowledge the financial support of the West Virginia University Department of Chemistry.

Notes and references

1 R. A. Sheldon and J. K. Kochi, *Metal-Catalyzed Oxidations of Organic Compounds*, Academic Press, New York, 1981.
2 L. W. Reichel, G. W. Griffin and A. J. Muller, *Can. J. Chem.*, 1984, **62**, 424.
3 H. F. Davis, P. K. Das, L. W. Reichel and G. W. Griffin, *J. Am. Chem. Soc.*, 1984, **106**, 6968.
4 J. H. Penn, D.-L. Deng and K.-J. Chai, *Tetrahedron Lett.*, 1988, **29**, 3635.
5 H. J. Penn, Z. Lin and D.-L. Deng, *J. Am. Chem. Soc.*, 1991, **113**, 1001.
6 J. H. Penn, A. Liu, S. Svarovsky and R. H. Simoyi, submitted.
7 P. J. Tomboulian, *J. Org. Chem.*, 1961, **26**, 2652.
8 E. L. Eliel and M. Manoharan, *J. Org. Chem.*, 1981, **46**, 1959.
9 S. Ruppel, PhD Thesis, Universitaet zu Koeln, 1995.
10 J. H. Penn, A. Liu, S. Svarovsky and R. H. Simoyi, manuscript in preparation.
11 Y.-C. Chou, H.-P. Lin, S. S. Sun and J. J. Jwo, *J. Phys. Chem.*, 1993, **97**, 8450.
12 J. Ungvarai, Z. Nagy-Ungvarai, J. Enderleihn and S. C. Mueller, *J. Chem. Soc., Faraday Trans.*, 1997, **93**, 69.

Communication 9/05728E

Melt supramolecular assembly of oligomers with regularly spaced, alternating hydrogen bonding and hydrophobic sites

Bryan Greener* and John Rose

Smith & Nephew Group Research Centre, York Science Park, Heslington, York, UK YO10 5DF. E-mail: bryan.greener@smith-nephew.com

Received (in Liverpool, UK) 18th August 1999, Accepted 18th October 1999

The melt condensation of 2,5-dihydroxybenzoic acid with dodecanedioyl dichloride resulted in oligomers with regularly spaced, multiple hydrogen bonding sites; fibres were drawn from melts at 150 °C.

Non-covalent interactions dominate the mechanisms of life. Hydrogen bonds and hydrophobic effects are frequently invoked to describe complex biochemical processes.[1] Much recent endeavour has been directed at the modelling of these exquisite interactions,[2] in the hope that such principles can be applied to industrial syntheses. It is striking that biochemical processes require the complementary interplay of both hydrophobic and hydrophilic interactions. This observation has provided inspiration in the fields of self assembly[3] and supramolecular polymer chemistry.[4] Attempts to create polymers linked only by non-covalent interactions (multiple hydrogen bonds) have achieved varying degrees of success.[4]

Replacing a single covalent bond with a non-covalent interaction of equivalent strength requires the interaction of multiple adjacent hydrogen bonding sites,[5] and it has been demonstrated that even the ordering of donor and acceptor groups at these sites can have a significant effect upon the overall interaction achieved.[6] Multiple adjacent sites have been realised, to date, by employing a limited range of nitrogen based donor/acceptor moieties.[4] To overcome the entropic barrier to the assembly of multiple non-covalent interactions systems reported thus far have clustered the interactive groups at terminal sites only,[5] thus limiting the number of hydrogen bonds that can be accommodated between adjacent molecules. With the aim of increasing the number of non-covalent interactions between adjacent molecules, here we report the synthesis and preliminary characterisation of biocompatible oligomers capable of multiple, multisite hydrogen bonding and hydrophobic interactions.[7]

The direct melt reaction of the aspirin metabolite and moth silk component,[8] 2,5-dihydroxybenzoic acid (gentisic acid) **G** with 1 equiv. of lauroyl chloride **L** produced 3-carboxy-4-hydroxyphenyl laurate **GL** in > 99% purity as determined by ^{1}H NMR spectroscopy. The specificity of this reaction was proposed to be due to the strong nucleophilicity of **G** in the 5-hydroxy position compared to the intramolecularly hydrogen bonded 2-hydroxy position. Furthermore, melt reactions involving *n* equiv. of **G** and $(n-1)$ equiv. of dodecanedioyl dichloride **D** produced a series of oligomers of average composition $\mathbf{G}_n\mathbf{D}_{n-1}$ (n = 2, 3, 4). While $\mathbf{G_2D_1}$ was a discrete compound, reaction products $\mathbf{G_3D_2}$ and $\mathbf{G_4D_3}$ were distributed over a narrow oligomeric range, as elucidated by electrospray MS and ^{1}H NMR spectroscopy. The three $\mathbf{G}_n\mathbf{D}_{n-1}$ oligomers were > 95% **G** capped (through the 5-hydroxy) as shown by ^{1}H and ^{13}C NMR spectroscopy. Reaction of 1 equiv. **G** with 1 equiv. of **D** produced **GD**, an oligomeric distribution centred around three of each subunit with random end-caps (**G** capping through the 5-hydroxy). For purposes of comparison, equivalent compounds were synthesised in an identical manner with methyl-2,5-dihydroxybenzoate **MeG** in the place of **G**; all lacked an intermolecular hydrogen bond donor.

All of the aforementioned compounds were fully soluble in THF, while only the **MeG**-based compounds were soluble in $CHCl_3$. Remarkably, **GD** dissolved a 40-fold molar excess of $CHCl_3$, resulting in liquification; phase separation occurred in the presence of excess $CHCl_3$. Comparison of the ^{13}C NMR spectra of **GD** in THF-d_8 and $CDCl_3$ showed a 5 ppm down-field shifting of inner-chain **G** carbonyl carbons (from δ_c 165.0 to 170.0) and a 1 ppm down-field shifting of terminal **G** carbonyl carbons (from δ_c 170.5 to 171.5) on moving from THF-d_8 to $CDCl_3$. This shifting was consistent with the **G** carbonyl oxygen acting as an intermolecular hydrogen bond acceptor site in terminal and inner-chain positions.[9] Infrared spectroscopic study of the oligomers was hampered by the intramolecular hydrogen bonding already present, however, **G** carbonyl absorbances (1700 cm^{-1}) were broadened due to multiple overlapping bands in contrast to the sharp discrete absorbance in **MeG**-based oligomers.

The melt behaviour of $\mathbf{G}_n\mathbf{D}_{n-1}$ oligomers was in sharp contrast to that of $\mathbf{MeG}_n\mathbf{D}_{n-1}$ oligomers in the respect that transparent, flexible, self-adherent fibres could be pulled from $\mathbf{G}_n\mathbf{D}_{n-1}$ compounds in the melt (150 °C) while $\mathbf{MeG}_n\mathbf{D}_{n-1}$ showed no such tendancy. Viscometric analysis of the oligomers was performed, in duplicate, at 150 °C and the resulting measured viscosities are shown in Table 1.[10] In general, the viscosity of **G**-based oligomers was an order of magnitude greater than that of the corresponding **MeG**-based oligomers. The significantly higher viscosities observed for **GD** than for $\mathbf{G}_n\mathbf{D}_{n-1}$ were due to a significantly broader oligomeric distribution in the former oligomers. These differences in physical properties can be attributed only to intermolecular hydrogen bonding interactions present in $\mathbf{G}_n\mathbf{D}_{n-1}$ but not $\mathbf{MeG}_n\mathbf{D}_{n-1}$.

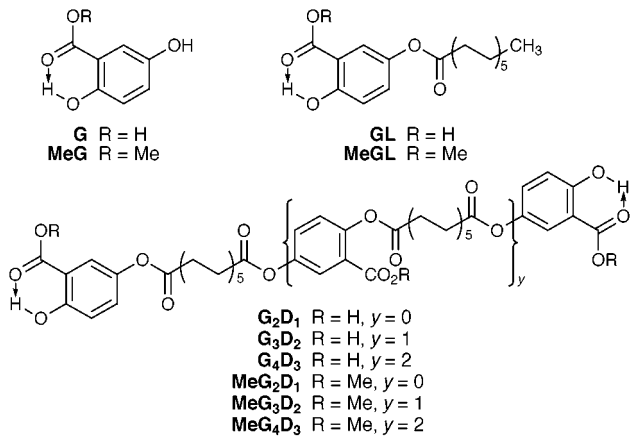

Table 1 Variation of viscosity in **G**- and **MeG**-based compounds

Oligomer	Viscosity/Pa s		Oligomer	Viscosity/Pa s	
MeGL	0.001	0.001	**GL**	0.007	0.009
$\mathbf{MeG_2D_1}$	0.007	0.010	$\mathbf{G_2D_1}$	0.148	0.066
$\mathbf{MeG_3D_2}$	0.022	0.017	$\mathbf{G_3D_2}$	0.346	0.319
$\mathbf{MeG_4D_3}$	0.030	0.017	$\mathbf{G_4D_3}$	0.820	0.771
MeGD	0.249	0.465	**GD**	2.909	3.399

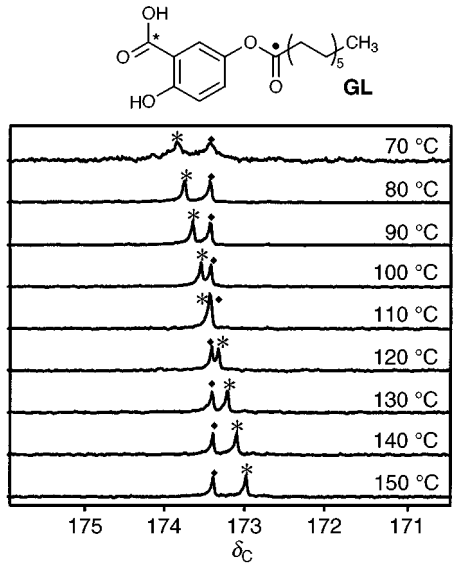

Fig. 1 ^{13}C NMR spectra (67 MHz) of neat **GL** recorded at various temperatures.

Further evidence of the intermolecular hydrogen bonding present in **GL**, in contrast to **MeGL**, was provided by a variable temperature ^{13}C NMR melt study. Neat samples of **GL** and **MeGL** were heated to temperatures in the range 70–150 °C. At each temperature the ^{13}C NMR spectrum of the sample was recorded. The result for **GL** is shown in Fig. 1. It can be seen that as the temperature was decreased the carboxylic carbonyl shifted to lower field, consistent with electronic donation to a hydrogen bond from the attached carbonyl oxygen.[9] No shifting was observed over this temperature range for **MeGL**.

The importance of hydrophobic interactions, between the alkyl chains of the oligomers, in producing the above physical effects was supported by the UV–VIS spectroscopic observations summarised in Fig. 2. It can be seen that λ_{max} did not vary widely for compounds with free 5-hydroxys, **G** and **MeG** (330–341 nm), or **MeGL** (315–318 nm), on going from THF solution to cast film (solid); 2-hydroxybenzoic acid (salicylic acid) **S** is also shown in Fig. 2 for comparison. The exception to

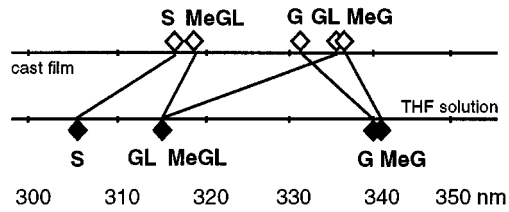

Fig. 2 Position of λ_{max} for **S**, **G**, **MeG**, **GL** and **MeGL** recorded as THF solutions and solid cast films on KBr.

this general rule was **GL**, which exhibited a 21 nm bathochromic shift on going from THF solution to cast film (solid), consistent with the effect of hydrogen bond formation in the solid state.[9] Extinction coefficients at these wavelengths were in the range 3700–7500 mol^{-1} dm^3 cm^{-1} for all compounds ($\pi\rightarrow\pi^*$ transition). In $\mathbf{G}_n\mathbf{D}_{n-1}$ and $\mathbf{MeG}_n\mathbf{D}_{n-1}$ oligomers a pair of absorbance bands were observed. The variation of these bands with formulation allowed us to deduce that the band at 313 nm was the result of a $\pi\rightarrow\pi^*$ transition in terminal **G** units (consistent with observations recorded in Fig. 2), while the band at 289 nm was the result of a $\pi\rightarrow\pi^*$ transition in inner chain **G** units.

We propose that the physical and spectroscopic observations reported herein can be accounted for by the hydrogen bonded aggregation of **G**-based subunits in a manner consistent with the previously reported crystal structure of **G**.[11] The hydrophobic compatibility of **D** with **D**, the hydrophilic, hydrogen bonded attraction of **G** with **G** and the mutual incompatibility of these two interactions promotes the hydrogen bonded aggregation of **G** moieties.

In conclusion, we have demonstrated the synthesis and preliminary characterisation of a new group of biocompatible supramolecular polymers. Further chemical and physical investigation of these systems is underway.

Notes and references

1 D. N. Silverman and S. Lindskog, *Acc. Chem. Res.*, 1988, **21**, 30.
2 B. Greener, M. H. Moore and P. H. Walton, *Chem. Commun.*, 1996, 27.
3 J. S. Moore, *Curr. Opin. Colloid Interface Sci.*, 1999, **4**, 108; N. Zimmerman, J. S. Moore and S. C. Zimmerman, *Chem. Ind.*, 1998, **15**, 604; R. B. Prince, T. Okada and J. S. Moore, *Angew. Chem., Int. Ed.*, 1999, **38**, 233.
4 R. P. Sijbesma, F. H. Beijer, L. Brunsveld, B. J. B. Folmer, J. H. K. K. Hirschberg, R. F. M. Lange, J. K. L. Lowe and E. W. Meijer, *Science*, 1997, **278**, 1601 and references cited therein.
5 B. J. B. Folmer, E. Cavini, R. P. Sijbesma and E. W. Meijer, *Chem. Commun.*, 1998, 1847; M. Kotera, J-M Lehn and J-P Vigneron, *J. Chem. Soc., Chem. Commun.*, 1994, 197.
6 T. J. Murray and S. C. Zimmerman, *J. Am. Chem. Soc.*, 1992, **114**, 4010.
7 Pat. Appl. 9917461.7
8 T. Ji, J. H. Hu, J. Wang, H. F. Guo, D. Z. Jin and J. T. Ju, *Sci. Chin., Ser. B*, 1993, **36**, 1046.
9 S. N. Vinogradov and R. H. Linnell, *Hydrogen Bonding*, Van Nostrand Reinhold, New York, 1971.
10 Samples were tested, in duplicate, on a Carrimed CSL500 constant stress rheometer, using a 4 cm diameter parallel plate and a 500 μm gap. Tests were carried out at 150 °C, except for $\mathbf{G_2D_1}$ which was tested at 170 °C as the material was solid at 150 °C.
11 M. Haisa, S. Kashino, S-I. Hanada, K. Tanaka, S. Okazaki and M. Shibagaki, *Acta Crystallogr., Sect. B*, 1982, **38**, 1480.

Communication 9/06756F

Synthetic, structural and theoretical studies on new aromatic 1,2,4-azadiphosphole ring systems: crystal and molecular structure of $P_2C_2Bu^t_2NPh$

F. Geoffrey N. Cloke,*[a] Peter B. Hitchcock,[a] John F. Nixon,*[a] D. James Wilson,[a] Frank Tabellion,[b] Uwe Fischbeck,[b] Fritz Preuss,*[b] Manfred Regitz*[b] and Laszlo Nyulászi*[c]

[a] *School of Chemistry, Physics and Environmental Science, University of Sussex, Brighton, Sussex, UK BN1 9QJ. E-mail: j.nixon@sussex.ac.uk*

[b] *Fachbereich Chemie der Universität Kaiserslautern, Erwin-Schroedinger Strasse, D-67663, Kaiserslautern, Germany*

[c] *Department of Inorganic Chemistry, Technical University of Budapest, H-1521 Budapest, Hungary*

Received (in Cambridge, UK) 17th September 1999, Accepted 13th October 1999

Two different synthetic routes to the new aromatic 1,2,4-azadiphosphole ring system $P_2C_2Bu^t_2NR$ (R = Pr^i, Pr, Ph, MeC_6H_4, Bu^tCH_2 and cyclohexyl) are presented and the planar structure of $P_2C_2Bu^t_2NPh$, established by a single crystal X-ray diffraction study, is in good agreement with theoretical calculations at the B3LYP/6-311G* level on the parent $P_2C_2H_2NH$ ring.

We recently described reactions of vanadium(V), titanium(IV) and zirconium(IV) imides with phosphaalkynes (RC≡P).[1,2] Thus, $Bu^tC{\equiv}P$ reacts with $VCl_3{=}NBu^t$ or its DME adduct to afford 2,4,6-tri-*tert*-butyl-1,3,5-triphosphabenzene or 3-aza-1,2,4,6-tetraphosphaquadricyclane, respectively.[1] Likewise one- and two-step [2 + 2] cycloaddition reactions of $Bu^tC{\equiv}P$ with $[Zr(\eta^5\text{-}C_5H_5)_2(NC_6H_3\text{-}2,6\text{-}Me_2)]$ and $[TiCl_2(NBu^t)(py)_3]$ gave the structurally characterised complexes $[Zr(\eta^5\text{-}C_5H_5)_2(PCBu^tNC_6H_3\text{-}2,6\text{-}Me_2)]$ and $[TiCl_2(P_2C_2Bu^t_2N\text{-}Bu^t)(py)]$.[2]

We now report that minor modification of the reactions described above leads to the formation of the first examples of the previously unknown aromatic 1,2,4-azadiphosphole ring systems $P_2C_2Bu^t_2NR$. Thus heating $[TiCl_2(NPh)(py)_3]$ with $Bu^tC{\equiv}P$ at 60 °C for 56 h gave $P_2C_2Bu^t_2NPh$ **1** (31%) as a white solid after sublimation.† The analogous $P_2C_2Bu^t_2N(p\text{-tolyl})$ **2** (30%), $P_2C_2Bu^t_2NEt$ **3** (15%) and $P_2C_2Bu^t_2NPr^i$ **4** (20%) were also made by a similar route using the appropriate titanium imide precursor.

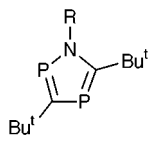

1 R = Ph
2 R = *p*-Tol
3 R = Et
4 R = Pr^i
5 R = Pr
6 R = CH_2Bu^t
7 R = Cy

In a related series of reactions, **4** was also obtained (67%) from the reaction of the vanadium imido complex $[VCl_3{=}NR]$ (R = Pr^i) with $Bu^tC{\equiv}P$ on warming the mixture from −78 °C to room temperature.‡

This route also afforded $P_2C_2Bu^t_2NPr$ **5** (55%), $P_2C_2Bu^t_2NCH_2Bu^t$ **6** (87%) and $P_2C_2Bu^t_2N$(cyclohexyl) **7** (61%). The $^{31}P\{^1H\}$ NMR spectra of all the 1,2,4-azadiphospholes **1**–**7** exhibited the characteristic AX pattern of lines whose chemical shifts, as expected, both lay in the unsaturated region.

The reaction mechanism of the vanadium imide reaction most likely involves the four-membered ring intermediate $[VCl_3(NR)P{=}CBu^t]$ (Scheme 1), which was characterised spectroscopically (R = Bu^t).§

The molecular structure of the phenyl-substituted 1,2,4-azadiphosphole **1** has been determined by a single crystal X-ray diffraction study (Fig. 1).¶ The ring is completely planar (Σ internal angles = 539.9°; Σ angles at N = 359.9° and the P(2)–N [1.715(6) Å], P(2)–C(1) [1.697(8) Å], P(1)–C(1) [1.746(8) Å], P(1)–C(2) [1.740(9) Å] and C(2)–N [1.366(10) Å] bond distances are all fully consistent with significant electron delocalisation.

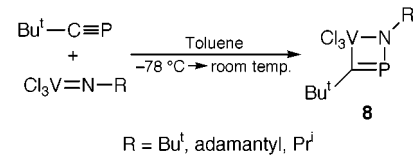

8

R = Bu^t, adamantyl, Pr^i

Scheme 1

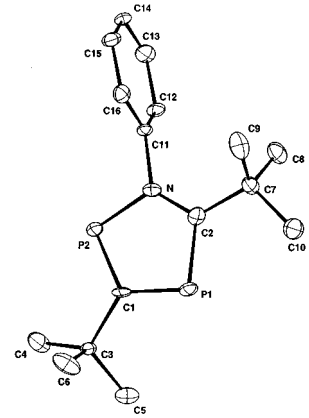

Fig. 1 Molecular structure of **1**.

The parent hydrogen-substituted derivative $P_2C_2H_2NH$ **9** has been calculated at the B3LYP/6-3111G* level of the theory.[3] The free azadiphosphole was a real minima on the potential

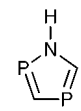

9

energy surface and the five-membered ring is perfectly planar. The calculated bond lengths and bond angles, which are in good agreement with those obtained from the X-ray diffraction study on **1**, are collected in Table 1. To characterise the aromaticity of the system several criteria were investigated. According to geometric BDSHRT[4] and Bird[5] indices (BI) and NICS[6] data the 1,2,4-aza-, 1,2,4-oxa- and 1,2,4-thia-diphosphole ring systems are somewhat less aromatic than the analogous organic rings furan, pyrrole and thiophene (see Table 2).

Table 1 Theoretical and observed bond length data and bond angles of azadiphospholes **9** and **1** (ring numbering as in Fig. 1)

	Calculated bond lengths for **9**/Å	Observed bond lengths for **1**/Å	Calculated bond angles for **9** (°)	Observed bond angles for **1** (°)
N–P2	1.725	1.715(6)	P2NC2 119.4	119.6(5)
P2–C1	1.709	1.697(8)	NC2P1 117.1	113.7(6)
C1–P1	1.764	1.746(8)	C2P1C1 92.2	95.8(4)
P1–C2	1.734	1.740(9)	P1C1P2 118.8	115.8(5)
C2–N	1.354	1.366(10)	C1P2N 92.5	95.0(4)

Table 2 BDSHRT, BI and NICS data for several unsaturated rings systems

Ring	BDSHRT	BI	NICS
1,2,4-Oxadiphosphole	46	37	−11.0
1,2,4-Aziadiphosphole	48	52	−12.8
1,2,4-Thiadiphosphole	53	56	−12.4
Furan	51	49	−12.3
Pyrrole	55	73	−14.7
Thiophene	57	68	−13.2

It is also interesting to compare NMR data for the 1,2,4-azadiphosphole rings with the isoelectronic series of 1,2,4-oxa-[7] and 1,2,4-thia-diphosphole[8] ring systems, $P_2C_2R'_2E$, (R′ = Bu^t, Mes; E = O, S).

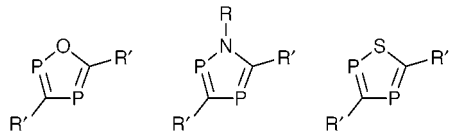

As the electronegativity of the heteroatom becomes smaller, the *difference* in chemical shifts of the two unsaturated P centres decreases significantly (161, 99 and 11 ppm respectively for E = O, NR and S). The magnitude of the $^2J_{(PP')}$ cross-ring coupling constants are also dependent on the nature of the heteroatom [17.5, (E = O) 34.9 (E = NR) and 49.9 Hz (E = S)].

We anticipate that, by analogy with other unsaturated polyphosphorus ring systems,[9] the new 1,2,4-azadiphosphole ring systems will have an interesting coordination chemistry, behaving as 2e, 4e or 6e donors towards suitable transition metal centres, and this aspect is currently under investigation.[10]

We thank the Alexander von Humboldt Foundation and OTKA T014555 for financial support (for L. N.) and the Royal Society for joint funding (for J. F. N. and L. N.).

Notes and references

† *Synthesis* of **1**: A high pressure ampoule was loaded with [Ti(NC$_6$H$_5$)Cl$_2$(py)$_3$], (0.400 g, 0.89 mmol), P≡CBu^t (0.027 g, 2.70 mmol) and toluene (25 ml). The reaction vessel was stoppered (Teflon stopcock) and heated with stirring at 60 °C for 56 h. The volatiles were removed *in vacuo* and the resulting brown residue was extracted with light petroleum (bp 40–60 °C) (20 ml). Volatiles were removed from the filtrate and the residue sublimed (70 °C, 10^{-5} mbar), yielding **1** as an off-white powder (0.08 g, 31%). Crystals suitable for X-ray analysis were grown by careful sublimation under static vacuum (10^{-2} mbar, 70 °C) (Found: C, 65.88; H, 8.20; N, 5.32. $C_{16}H_{23}NP_2$ requires: C, 65.97; H, 7.96; N, 4.81%). *Selected data* for δ_H(benzene-d_6, 295 K, 300.13 MHz) 7.1, 6.98 (m, 5H, C$_6$H$_5$), 1.64 [d, 9H, PC(C(CH$_3$)$_3$)P, $^4J_{(PH)}$ 1.3], 1.29 [d, 9H, PC(C(CH$_3$)$_3$N, $^4J_{(PH)}$ 1.93; δ_P(benzene-d_6, 295 K, 121.52 MHz) 262.6 (d, NPC, $^2J_{(PP)}$ 30.4, 156.3 (d, PCP, $^2J_{(PP)}$ 30.4; *m/z* (EI) 291 ([M]$^+$, 70%), 276 (M − Me]$^+$, 55). For δ_H(benzene-d_6, 295 K, 300.13 MHz) 7.34, 7.22 [(AB)$_2$, 4H, C$_6$H$_4$, $^3J_{(HH)}$ 7.88], 2.47 (s, 3H, CCH$_3$), 1.56 [d, 9H, PC(C(CH$_3$)$_3$)P, $^4J_{(HP)}$ 1.19], 1.37 [d, 9H, PC(C(CH$_3$)$_3$N, $^4J_{(HP)}$ 1.92]; δ_C(benzene-d_6, 295 K, 75.48 Hz) 204.3 (dd, PCP, $J_{(CP)}$ 57.9 Hz, $J_{(CP)}$ 62.7), 196.8 [dd, br, NCP, $J_{(PC)}$ 60.7, $^2J_{(PC)}$ unresolved), 140.5 [dd, *ipso*-NC$_6$H$_4$(CH$_3$), $^2J_{(CP)}$ 16.1], 138.7 [d, *p*-NC$_6$H$_4$(CH$_3$), $^5J_{(CP)}$ 2.1], 129.54 [d, *o*-NC$_6$H$_4$(CH$_3$), $^3J_{(PC)}$ 5.2], 128.83 [d, *m*-NC$_6$H$_4$(CH$_3$), $^4J_{(PC)}$ 1.2], 39.91 [dd, NC*C*(CH$_3$), $^2J_{(PC)}$ 14.95, $^4J_{(PC)}$ 3.1], 37.5 [dd, PC(*C*(CH$_3$)$_3$), $^2J_{(PC)}$ 16.77], 35.59 [dd, PC(C(*C*H$_3$)$_3$)P, $^3J_{(PC)}$ 8.12, 11.13], 33.41 [d, NCC(*C*H$_3$), $^3J_{(CP)}$ 13.14], 21.5 [C$_6$H$_4$(*C*H$_3$)]; δ_P(benzene-d_6, 295 K, 121.52 MHz) 262.5 [d, NP, $^2J_{(PP)}$ 29.2], 153.5 [d, NCP, $^2J_{(PP)}$ 29.2 *m/z* (EI) 305 ([-M]$^+$, 90%), 290 [M − Me]$^+$, 35), 234 ([M − Me − Bu^t], 30).

‡ *Synthesis* of **4**: To a solution of [VCl$_3$=NPr^i] (0.14 g, 0.63 mmol) in toluene (5 ml) was added, with stirring, Bu^{t}C≡P (0.06 g, 0.63 mmol) at −78 °C and the solution was warmed to room temperature. After 24 h the solvent was removed *in vacuo* and the residue dissolved in *n*-pentane and filtered through Celite. The product **4** was obtained (by distillation at 130 °C, 10^{-2} mbar) as a white solid (0.055 g, 67%); δ_H(benzene-d_6, 295 K, 300.13 MHz) 1.63 [dd, 9H, PC(C(CH$_3$)$_3$)P, $^4J_{(HP)}$ 1.8, 0.7], 1.39 [d, 9H, PC(C(CH$_3$)$_3$)N, $^4J_{(HP)}$ 2.2], 1.38 [d, 6H, $^3J_{(HH)}$ 6.6], 4.69 [dsep, 1H, $^3J_{(HH)}$ 6.6, $^3J_{(HP)}$ 2.7]; δ_C(benzene-d_6, 295 K, 75.48 MHz) 202.2 [dd, PCP, $J_{(CP)}$ 62.3, $J_{(CP)}$ 52.5], 193.8 (dd, NCP, $J_{(PC)}$ 59.8, $^2J_{(PC)}$ 3.7), 53.2 [dd, (CH) $^2J_{(PC)}$ 17.1, $^3J_{(PC)}$ 2.5], 38.2 [dd, NC*C*(CH$_3$), $^2J_{(PC)}$ 19.1, $^3J_{(PC)}$ 2.5], 37.4 [dd, PC(*C*(CH$_3$)$_3$), $^2J_{(PC)}$ 28.1, 17.3], 35.4 [dd, PC(C(*C*H$_3$)$_3$)P, $^3J_{(PC)}$ 8.6, 11.0], 32.0 [d, NCC(*C*H$_3$), $^3J_{(CP)}$ 13.4], 27.6 [d, (CH$_3$)$_2$, $^3J_{(CP)}$ 12.1]; δ_P(benzene-d_6, 295 K, 121.52 MHz) 247.3 (d, NP, $^2J_{(PP)}$ 34.9), 148.1 (d, NCP, $^2J_{(PP)}$ 34.9); *m/z* (EI) 275 ([M]$^+$, 29%), 242 ([M − Me]$^+$, 6), 200 ([M − Pr^{1}N]$^+$, 12), 186 (M − Pr^i − Me]$^+$, 7), 57 (Bu$^+$, 20), 43 (Pr$^+$, 11).

§ *Selected data* for δ_P(benzene-d_6, 81 MHz) −73.0 ($^2J_{(PV)}$ 30.3); δ_V 310.

¶ *Crystal data* for **1**: $C_{16}H_{23}NP_2$, M = 291.3, orthorhombic space group $Pna2_1$ (No. 33), a = 26.960(5), b = 5.916(2), c = 10.299(3) Å, U = 1642.6(8), Å^3, Z = 4, D_c = 1.18 Mg m^{-3}, crystal dimensions 0.1 × 0.1 × 0.05 mm, F(000) = 624, T = 173(2) K, Mo-Kα, radiation λ = 0.71073 Å Data were collected on an Enraf-Nonius CAD4 diffractometer. A total 1071 reflections were measured. $R1$ = 0.044 for 859 reflections with $I > 2\sigma(I)$, $wR2$ = 0.106 for all data. All non-H atoms were anisotropic. H atoms were included in riding mode with U_{iso}(H) equal to 1.2eq(C) or 1.5eq(C) for methyl groups. CCDC 182/1447. See http://www.rsc.org/suppdata/cc/1999/2363/ for crystallographic data in .cif format.

1 F. Tabellion, A. Nachbauer, S. Leininger, C. Peters, F. Preuss and M. Regitz, *Angew. Chem., Int. Ed.*, 1998, **37**, 1233.
2 F. G. N. Cloke, P. B. Hitchcock, J. F. Nixon, D. J. Wilson and P. Mountford, *Chem. Commun.*, 1999, 661.
3 Quantum-chemical calculations were carried out by using the GAUSSIAN 94 package and optimisation of the structures was first carried out at the B3LYP/3-21G(*) level. The stationary points obtained were then characterised by second derivative calculations as real minima. Further reoptimisation was carried out by using the 6-311G* basis. Gaussian 94, Revision B.2, M. J. Frisch, G. W. Trucks, H. B. Schlegel, P. M. W. Gill, B. G. Johnson, M. A. Robb, J. R. Cheeseman, T. Keith, G. A. Petersson, J. A. Montgomery, K. Raghavachari, M. A. Al-Laham, V. G. Zakrzewski, J. V. Ortiz, J. B. Foresman, J. Cioslowski, B. Stefanov, A. Nanayakkara, M. Challacombe, C. Y. Peng, P. Y. Ayala, W. Chen, M. W. Wong, J. L. Andres, E. S. Replogle, R. Gomperts, R. L. Martin, D. J. Fox, J. S. Binkley, D. J. Defrees, J. Baker, J. P. Stewart, M. Head-Gordon, C. Gonzalez and J. A. Pople, Gaussian Inc., Pittsburgh PA, 1995.
4 L. Nyulászi, P. Várnai and T. Veszprémi, *THEOCHEM*, 1995, 358.
5 C. W. Bird, *Tetrahedron*, 1985, **41**, 1409.
6 P. v. R. Schleyer, C. Maerker, A. Dransfeld, H.Jiao and N. J. R. v. E. J. Hommes, *J. Am. Chem. Soc.*, 1996, **118**, 6317.
7 A. Mack, U. Bergsträsser, G. J. Reiss and M. Regitz, *Eur. J. Org. Chem.*, 1999, 587.
8 R. Appel and R. Moers, *Angew. Chem., Int. Ed. Engl.*, 1986, **98**, 570; G. Märkl, W. Höbel, H. Kallmünser, U. L. Ziegler and B. Nuber, *Tetrahedron Lett.*, 1991, **33**, 4421; E. Lindner and T. Schlenker, *J. Organomet. Chem.*, 1994, **464**, C31; B. Burghardt, S. Krill, Y. Okano, W. Ando and M. Regitz, *Synlett*, 1991, **5**, 356.
9 K. B. Dillon, F. Mathey and J. F. Nixon, *Phosphorus: The Carbon Copy*, Wiley, Chichester, 1998 and references therein.
10 S. E. d'Arbeloff-Wilson, P. B. Hitchcock, M. J. Maah, J. F. Nixon and D. J. Wilson, unpublished results.

Communication 9/07550J

A new diastereoselective synthesis of a 1β-methylcarbapenem intermediate

Chang-Young Oh and Won-Hun Ham*

College of Pharmacy, SungKyunKwan University, Suwon 440-746, Korea. E-mail: whham@speed.skku.ac.kr

Received (in Cambridge, UK) 1st October 1999, Accepted 13th October 1999

A 1β-methylcarbapenem key intermediate is synthesized from methyl (*R*)-3-hydroxybutyrate *via* the diastereoselective alkylation and regioselective cuprate ring opening of a chiral epoxide which is readily prepared from Sharpless asymmetric epoxidation of the corresponding allylic alcohol.

The discovery that 1β-methylcarbapenem has potent and broad-spectrum antibacterial activitiy as well as enhanced metabolic and chemical stability[1] has prompted many synthetic organic chemists to develop efficient methods for the stereoselective synthesis of the key 1β-methyl intermediate **1**, and recent reviews describe impressive progress in this area.[2, 3]

Our approach to the enantioselective synthesis of **1** relies on regioselective ring opening of chiral epoxy alcohol **3**, which is readily available from Sharpless asymmetric epoxidation of the allylic alcohol (Scheme 1). This allylic alcohol **7**, containing two stereocenters which are requisite for key intermediate **1**, could be easily obtained from diastereoselective alkylation of methyl (*R*)-3-hydroxybutyrate **4** followed by a short transformation.

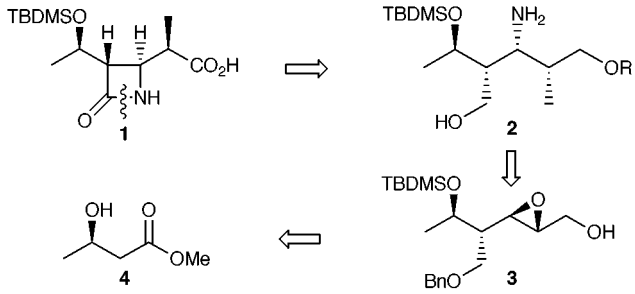

Scheme 1

Thus, methyl ester **4**, available in high enantiomeric purity, was converted into the allylic alcohol **7** as shown in Scheme 2. To this end, β-hydroxy ester **4** was alkylated with benzyloxymethyl chloride (BOMCl). Generally, alkylation of the dianions of such β-hydroxy esters has been shown to yield products of high diastereomeric excess with predictable stereoselectivity, but in this case alkylation with BOMCl afforded the benzyl ether with moderate stereoselectivity (*ca.* 10::1) and low conversion yield (*ca.* 50%).[4–6] Fortunately, there was a dramatic improvement both in conversion yield and diastereomeric ratio (70% and 35:1) when we added HMPA as an additive.[7] The secondary alcohol of the resulting benzyl ether **6** was protected as an TBDMS ether in high yield and the ester was subsequently reduced to the corresponding alcohol **6** with DIBAL-H at −78 °C. Swern oxidation of **6** afforded the aldehyde, which without purification was subjected to a Horner olefination with triethyl phosphonoacetate under the conditions developed by Masamune and Roush.[8] to give the α,β-unsaturated ester with complete *E*-selectivity. Reduction of the *E*-unsaturated ester using DIBAL-H at −78 °C produced the allylic alcohol **7**. The epoxidation of this allylic alcohol under Sharpless conditions employing D-(−)-diisopropyl tartrate as stereodirecting ligand gave rise to the epoxide **3** with excellent diastereoselectivity (15:1). The stage was now set to introduce the fourth chiral center in **3** and for this we made use of the ubiquitous high order cuprate protocol; the highly regioselective opening of the epoxide with $Me_2Cu(CN)Li_2$ gave the 1,3-diol. The primary hydroxy group of the resulting diol was selectively protected as a TBDMS ether to give **8**.

The conversion of **8** to **9** was accomplished by a four step sequence. Mesylation of the secondary alcohol followed by

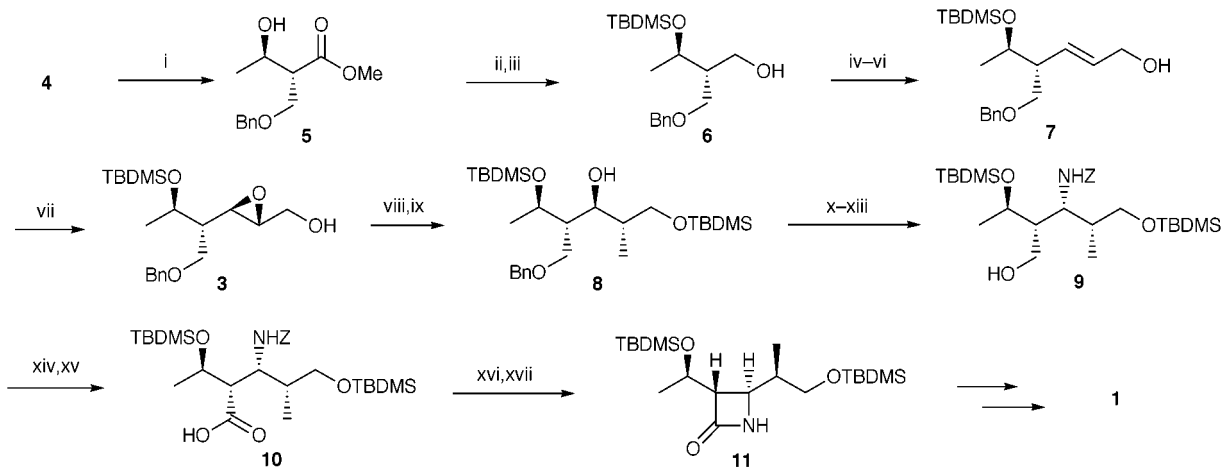

Scheme 2 *Reagents and conditions*: i, LDA (2 equiv.), BOMCl, HMPA, −78 °C, 70%; ii, TBDMSCl, imidazole, DMF, 90%; iii, DIBAL-H, Et_2O, −78 °C, 86%; iv, $(COCl)_2$, DMSO, Et_3N, CH_2Cl_2, −65 to −55 °C; v, $(MeO)_2POCH_2CO_2Me$, LiCl, Pr^i_2NEt, MeCN, 84% for 2 steps; vi, DIBAL-H, Et_2O, −78 °C, 95%; vii, $Ti(OPr^i)_4$, D-(−)-diisopropyl tartrate, Bu^tOOH, 76.5%; viii, $Me_2Cu(CN)Li_2$, Et_2O, −20 to 0 °C, 72.4%; ix, TBDMSCl, Et_3N, DMAP, CH_2Cl_2, 84.4%; x, MsCl, pyridine, 97.7%; xi, NaN_3, DMF, 76.4%; xii, $Pd(OH)_2$, H_2 (1 atm,), MeOH, EtOAc; xiii, $ClCO_2Bn$, $NaHCO_3$, Et_2O, 0 °C, 51% for 2 steps; xiv, $(COCl)_2$, DMSO, Et_3N, CH_2Cl_2, −65 to 55 °C; xv, $NaClO_2$, 2-methylbut-2-ene, NaH_2PO_4, H_2O, Bu^tOH, 71% for 2 steps; xvi, Pd-black, MeOH, H_2 (1 atm); xvii, $(PyS)_2$, PPh_3, MeCN, reflux, 79% for 2 steps.

sequential azide substitution, reduction of the corresponding azide under Pd/C and the protection of the amino group with $ClCO_2Bn$ afforded **9** in 41% overall yield in four steps. Unfortunately attempts, including Mitsunobu conditions, to directly convert the alcohol to amine stereospecifically were not successful. This result may be due to the steric hindrance present in **8**. Swern oxidation of **9** led to the β-amino aldehyde, which was further oxidized to the corresponding acid **10** with $NaClO_2$. Finally removal of the Z group by catalytic hydrogenation followed by cyclization using Ohno's conditions[9] furnished the known key intermediate **11**.[10–12] The physicochemical properties of **11** obtained by the present synthesis were in complete agreement with those reported in the literature {$[\alpha]_D^{27}$ −7.8755 (*c* 0.53, $CHCl_3$) [lit,[12] $[\alpha]_D^{22}$−7.8777 (*c* 1.03, $CHCl_3$)]}.

In summary, we report a new synthetic method for the 1β-methylcarbapenem key intermediate from commercially available methyl (*R*)-3-hydroxybutyrate **4**. The key features in this strategy are the diastereoselective alkylation of the dianion of the β-hydroxy ester, Sharpless asymmetric epoxidation and subsequent regioselective cuprate ring opening of the chiral epoxide.

The financial support provided by the GITP is gratefully acknowledged.

Notes and references

1 D. H. Shih, F. Baker, L. Cama and B. G. Christensen, *Heterocycles*, 1984, **21**, 29.
2 K. Kondo, M. Seki, T. Kuroda, T. Yamanaka and T. Iwasaki, *J. Org. Chem.*, 1997, **62**, 2877.
3 For a review, see: A. H. Berks, *Tetrahedron*, 1996, **52**, 331 and references cited therein.
4 S. Hatakeyama, N. Ochi, H. Numata and S. Takano, *J. Chem. Soc., Chem. Commun.*, 1988, 1202.
5 R. E. Ireland and R. B. Wardle, *J. Org. Chem.*, 1987, **52**, 1780.
6 O. Muraoka, N. Toyooka, Y. Oshima, N. Narita and T. Momose, *Heterocycles*, 1989, **29**, 269.
7 Details will be published in full elsewhere.
8 M. A. Blanchette, W. Choy, J. T. Davis, A. P. Essenfeld, S. Masamune, W. R. Roush and T. Sakai, *Tetrahedron Lett.*, 1984, **25**, 2183.
9 S. Kobayashi, T. Iimori, T. Izawa and M. Ohno, *J. Am. Chem. Soc.*, 1981, **103**, 2406.
10 A. Sasaki, H. Masumura, T. Yano, S. Takata and M. Sunagawa, *Chem. Pharm. Bull.*, 1992, **40**, 1098.
11 Y. Ito, Y. Kimura and S. Terashima, *Bull. Chem. Soc. Jpn.*, 1987, **60**, 3337.
12 N. Tsukada, T. Shimada, Y. S. Gyoung, N. Asao and Y. Yamamoto, *J. Org. Chem.*, 1995, **60**, 143.

Communication 9/07922J

ChemComm

Novel macrocycles with 1,1′-binaphthyl substituents for the recognition of saccharides

Oleksandr Rusin and Vladimír Král*

Department of Analytical Chemistry, Institute of Chemical Technology, Technická 5, 166 28 Prague 6, Czech Republic. E-mail: vladimir.kral@vscht.cz

Received (in Liverpool, UK) 6th May 1999, Accepted 18th October 1999

Novel saccharide-selective receptors 1 and 2 based on *a* porphyrin with 1,1′-binaphthyl substituents were synthesized and tested for binding of mono-, di- and tri-saccharides; *a* binding selectivity for di- and tri-saccharides was found.

Recent developments in the area of supramolecular chemistry have led to the study of carbohydrate complexation by artificial receptors.[1] The design of artificial receptors that bind selectively to sugars in aqueous or non-aqueous media is an important topic in bioorganic chemistry.[2] As a contribution to this effort we focused our attention on the preparation of a variety of macrocyclic derivatives with peripheral functionalities giving interesting recognition properties.[3–8]

Here we present the synthesis and basic properties of 1,1′-binaphthyl substituted porphyrins **1** and **2** designed as specific receptors for biologically important polyhydroxylic compounds. There are several host systems reported in the recent literature that utilized sterically organized receptors for recognition of biologically important substrates.[10–14] The design of receptors is based on multiple H-bonding, where receptor **1** is an H-bonding acceptor and receptor **2** is an H-bonding donor. The binding site of **2** contains eight acidic phenolic hydroxy groups that presumably can form hydrogen bonds with guests. The binding mode was proven by ^{1}H NMR, Raman and IR studies for methyl *O*-glucoside, where the 1,1′-binaphthyl subunit's interaction was clearly observed, indicating complex formation.[17] The synthesis of **1** (Scheme 1) was carried out according to the known methodology for the preparation of porphyrins (Rothemund protocol) by cyclotetramerization of protected 1,1′-binaphthyl-3-carbaldehyde with pyrrole.[1] TLC, HPLC and the photometric analysis of the reaction products was used to identify the major and minor porphyrinic components. The solvent was removed and the major product was isolated by column chromatography on silica gel with MeOH–CH_2Cl_2 (95 : 5) as eluent, characterized as the (*R,S*)-α,β,α,β-isomer and used for the complexation study. The structure was proved by ^{1}H NMR analysis, where characteristic signals for identical binaphthyls and singlet pyrrolic β-protons were observed, as described for the unsubstituted binaphthol–porphyrin derivative.[15] This product **1**, as a single atropoisomer, was collected in 4% yield. Product **2** was obtained by treatment of **1** with BBr_3 in dry CH_2Cl_2. The deprotected product was isolated in 80% yield.

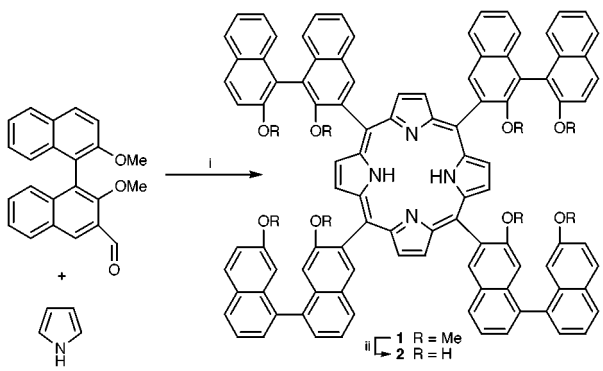

Scheme 1 *Reagents and conditions*: i, propionic acid, reflux, 4 h, then silica gel, CH_2Cl_2–MeOH (95 : 5), 4%; ii, BBr_3 (10 equiv.), CH_2Cl, 1 day, room temp., wash with H_2O, dry, isolate on reverse phase column, MeOH, 80%.

The binaphthylic subunits of macrocycles **1** and **2** contain peripheral methoxy or hydroxy groups. These groups play an essential role in the formation of complexes with saccharides. The two host binding pockets formed by the bulky aryl substituents were specifically designed for binding of di- and tri-saccharides in a similar way as in lectins. The effect of solvent was also important. Thus the host **1** is insoluble in water whereas **2** is soluble in H_2O–MeOH (5–10% MeOH, v/v) allowing determination of binding constants for saccharides. The binding constants for both hosts were determined in DMSO at room temperature by UV–VIS titration experiments. The change in the absorbance at 427 nm was observed upon addition of the saccharide species to the hosts **1** and **2**. In this media the receptor **1** (R = OMe) displays low binding affinity for unmodified saccharides (for octyl glucopyranoside and *p*-nitrophenyl galactopyranoside strong binding was observed). The methoxy groups of the binaphthylic subunits form weak hydrogen bonds with the guests.[17] However substrates such as α- or β-D-methylglucopyranose are able to interact better with this host than unsubstituted glucose, with a remarkable selectivity for the β-anomer (Table 1). Saccharide derivatives with octyl and *p*-nitrophenyl substituents, namely octyl α-D- and octyl β-D-glucopyranoside and -galactopyranoside showed selectivity for the α-anomer and more pronounced interaction. The decisive role in these host–guest interactions apparently belongs to the hydrophobic interactions between the alkyl (or aryl) chain of the substrates and the naphthyl rings of the host **1**. A different tendency was observed for the host **2**. The receptor **2** (R = OH) easily interacts with unmodificated saccharides in

Table 1 Association constants for binding of saccharide derivates with porphyrins **1** and **2** in DMSO (UV–VIS titration)[a]

	$K_a/10^2$ M^{-1}	
Saccharide	**1**	**2**
Octyl α-D-glucopyranoside	5.42	6.41
Octyl β-D-glucopyranoside	0.08	1.96
Methyl α-D-glucopyranose	< 0.08	0.72
Methyl β-D-glucopyranose	1.89	2.01
p-Nitrophenyl galacto-β-pyranoside	3.61	2.58

[a] The formation and UV–VIS estimation constants of sugar–receptor complexes. In a 1 cm square quartz cuvette was placed a 6.15×10^{-6} M solution of macrocycle **1** or **2** in DMSO or H_2O contained 5% of MeOH (v/v). A known amount of saccharide was added in increments (0–1000 equiv.). The absorbance changes were measured in maxima (room temperature), and data were then evaluated with the aid of the Benesi–Hildebrand equation. From the linear plot of $-1/A$ *vs.* 1/[saccharide], the intercept was estimated as K_a. Linear fits had a correlation coefficient of 0.95. The K_a was calculated for 1 : 1 complexes. The reproducibility of the K_a values was ±10% in triplicate runs.

Table 2 Association constants for complexation of host **2** with saccharides in DMSO and H_2O

	$K_a/10^2$ M^{-1}		
	Fluorescence	UV–VIS	
Saccharide	DMSO	DMSO	H_2O
D-glucose	0.42	1.16	0.60
D-Fructose	0.72	1.22	2.00
D-Galactose	0.32	1.14	0.92
D-Ribose	1.42	1.53	1.50
D-α-Lactose	27.60	28.00	2.55
D-β-Lactose	23.50	32.60	7.30
D-Trehalose	11.56	20.00	4.86
Maltotriose	6.28	9.50	8.77

water (with 5–10% MeOH) and DMSO and displays a significant preference for the di- and tri-saccharides over the monosaccharides. The results of the UV–VIS titration of **2** with different sugars are presented in Table 2. The tendency for preferable interaction of host **2** with di- and tri-saccharides was confirmed also by fluorescence spectroscopy (Table 2). Moreover, for monosaccharides, differences between pyranoses and furanoses were observed in both media (K_a see Table 2). Cooperation of several H-bonds in binding to particular saccharides led to higher values of binding constants. Introduction of the hydroxy groups into the porphyrin core often drastically changed their binding abilities for neutral guests.[16] The Job's plots for different series of the macrocycle–sugar interactions showed the initial formation of 1 : 1 host–guest type complexes, although in our observations, ditopic hosts **1** and **2** also formed other complexes at higher saccharide concentration. The sensitivity of **1** and **2** to the saccharides could be changed by incorporation of metal into the porphyrin core;[12] this work is now underway.

In conclusion, we have found that 1,1′-binaphthyl receptor **2** displayed effective complexation abilities for unmodificated saccharides, while **1** formed complexes with alkyl- or aryl-glycosides. The receptor **2** can serve as a successful model for efficient and selective di- and tri-saccharide binding in highly competitive media such as DMSO and H_2O, where sugar binding is easy monitored in the visible wavelength region. Due to the size of the host binaphthylic cavity above and below the porphyrin plane, trends towards stronger binding of oligosaccharides in comparison with monosaccharides were observed.

The study of the binding of saccharides with receptors based on phosphorylated analogues of compound **2** under physiological conditions is in progress.

Financial support from the Grant Agency of the Czech Republic (Grant No. 203/96/0740 and No. 203/97/1099), the Ministry of Education (grant No. VS 97135 and Project CEZ: J19/98:2234000008) and the Howard Hughes Medical Institute (74195-541101) is gratefully acknowledged.

Notes and references

1 *The Porphyrins*, ed. D. Dolphin, Academic Press, New York, 1978, vol. 1, pp. 85–100.
2 G. Deng, T. D. James and S. Shinkai, *J. Am. Chem. Soc.*, 1994, **116**, 4567.
3 S. Arimori, M. Takeushi and S. Shinkai, *Supramolecular Science*, 1998, vol. 5, **1**–**2**, 1.
4 V. Král and J. L. Sessler, *Tetrahedron*, 1995, **51**,539.
5 V. Král, A. Andrievsky and J. L. Sessler, *J. Chem. Soc., Chem. Commun.*, 1995, 2349.
6 J. L. Sessler, P. I. Sansom, V. Král, D. O'Connor and B. L. Iverson, *J. Am. Chem. Soc.*, 1996, **118**, 12322.
7 J. L. Sessler, A. Andrievsky, V. Král and V. Lynch, *J. Am. Chem. Soc.*, 1997, **119**, 9385.
8 P. A. Gale, J. L. Sessler and V. Král, *Chem. Commun.*, 1998, 1.
9 V. Král, H. Furuta, K. Shreder and V. Lynch, *J. Am. Chem. Soc.*, 1996, **118**, 1595.
10 P. Lustenberger, E. Martinborough, T. Mordasini Denti and F. Diederich, *J. Chem. Soc., Perkin Trans. 2*, 1998, 747.
11 V. Alcázar, J. R. Moran and F. Diederich, *Angew Chem., Int. Ed. Engl.*, 1992, **31**, 1521.
12 E. Martinborough, T. Mordasini Denti, P. P. Castro, T. B. Wymann, C. B. Knobler and F. Diederich, *Helv. Chim. Acta*, 1995, **78**, 1037.
13 S. Anderson, U. Neidlein, V. Gramlich and F. Diederich, *Angew Chem., Int. Ed. Engl.*, 1995, **34**,1596.
14 P. B. Savage and S. H. Gellman, *J. Am. Chem. Soc.*, 1993, **115**, 10448.
15 S. O'Malley and T. Kodadek, *J. Am. Chem. Soc.*, 1989, **111**, 9116.
16 K. Kano, Y. Tamiya, C. Otsuki, T. Shimomura, T. Ohno, O. Hayashida and Y. Murakami, *Supramol. Chem.*, 1993, **2**, 137.
17 *Selected data* for **1**: δ_H(300 MHz, $CDCl_3$) 9.15–8.61 (H, m, Ar), 8.18–7.26 (H, m, Ar), 4.01 (H, m, OCH_3), 2.65 (H, m, OCH_3), −2.41 (s, 2H, NH); *m/z* (FAB) 1560.5 (MH_2^+, 100%, calc. for $C_{108}H_{78}N_4O_8$: 1559.8). For **2**: *m/z* (FAB) 1448.5 (MH_2^+, 100%, calc. for $C_{108}H_{72}O_{16}$: 1447.5). All compounds gave satisfactory elemental analyses. Complexation studies revealed that receptor **1** forms weak H-bonded complexes, while receptor **2** on the other hand showed strong H-bonding donor ability. The complex of **2** with β-D-methylglucopyranose showed a downfield shift of 0.6 ppm with respect to free **2** in CD_3CN; IR showed the strong complexation of the phenolic OH (shift from 3060 to 3100 cm^{-1} and from 3300 to 3400 cm^{-1}) and Raman spectra also indicated the strong complexation (broadening and merging of the multiple peaks in the area of 1460–666 cm^{-1}).

Communication 9/03658J

Glaser coupling reaction in supercritical carbon dioxide

Jinheng Li and Huanfeng Jiang*

Guangzhou Institute of Chemistry, Chinese Academy of Sciences, PO Box 1122, Guangzhou 510650, China. E-mail: jhf@mail.gic.ac.cn

Received (in Cambridge, UK) 5th October 1999, Accepted 18th October 1999

It is demonstrated for the first time that Glaser coupling can be carried out smoothly in supercritical carbon dioxide using a solid base (NaOAc) instead of amines.

Considerable attention has recently been focused on using supercritical carbon dioxide ($scCO_2$) as a medium for organic reactions.[1–3] As a solvent the attractive physical and toxicological properties of $scCO_2$ have made it superior to conventional organic solvents with regard to environmental considerations.

Diacetylenes are central to many biological and polymer molecules.[4–8] Many of the most useful methods for the synthesis of diacetylenes[8–10] involve cupric salt promoted coupling reactions, Glaser first observed that terminal acetylenes underwent oxidative coupling to diacetylenes with CuCl in the presence of NH_4OH. Subsequent studies have shown that a variety of cupric salts or oxygen in the presence of cuprous salts can be employed. The oxidation has the further advantage of solvent versatility. Water, methanol, Methyl Cellosolve, acetone, pyridine, cyclohexylamine and toluene have all been used as solvents for the reaction with nearly equal success. Amines, most frequently pyridine and tetramethylenediamine, are required in almost all Cu^{II}-promoted Glaser coupling. However, amines often have unpleasant smells and flavors. The present study is the first demonstration that Glaser coupling can be carried out in the presence of $CuCl_2$ in $scCO_2$ using NaOAc instead of amines (Scheme 1).

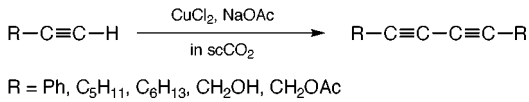

Scheme 1

Our investigation began with an effort to optimize reaction conditions for the oxidation coupling of terminal acetylenes using $CuCl_2$ and NaOAc. Phenylacetylene was chosen as a model substrate for the optimization process (entries 1–8, Table 1). The final optimized reaction conditions for Glaser coupling in $scCO_2$ consisted of $CuCl_2$ (2 mmol), NaOAc (2 mmol), MeOH (1 ml) and CO_2 (14 MPa) at 40 °C.† Other terminal acetylenes besides phenylacetylene were employed successfully using the optimized conditions (entries 9–12, Table 1).

The coupling reaction gave low conversion and yield in pure $scCO_2$ (entry 1, Table 1), in which $CuCl_2$ and NaOAc cannot dissolve (entries 1, 4 and 7, Table 2). It has been reported that some organic or inorganic compounds, so-called 'modifiers', can be added to the supercritical fluids to increase its solvent power.[11] Our results indeed show that the presence of MeOH remarkably enhanced the rate of the reaction (entries 1 and 6, Table 1). We further examined the solubility of different reagents in different solvents in $scCO_2$ and the results were summarized in Table 2. MeOH, as modifier or co-solvent, increased the solubility of $CuCl_2$ and NaOAc in $scCO_2$ (entries 3, 6 and 8, Table 2).[2,3,11,12] Increasing the amount of MeOH to 3 ml in the reaction, decreased the rate and the yield to a small extent. It is of interest to note that if only MeOH was used as solvent, both the rate and the yield decreased and the reaction was not clean (entry 2, Table 1). These results imply that $scCO_2$ and MeOH are of the same importance to the reaction. The low viscosity of $scCO_2$ allows the products (diacetylenes) to diffuse away from $CuCl_2$ and NaOAc, while the proper amounts of MeOH makes $CuCl_2$ and NaOAc partially dissolve in $scCO_2$, although excess MeOH may affect the diffusion of the products.

The pressure of CO_2 also affected the reaction rate to some extent. Our results indicate that a higher CO_2 pressure is preferable (entries 5 and 6, Table 1).

In earlier studies, when cupric chloride or cupric acetate was added as a promoter, an organic base (pyridine) was usually added to retain $CuCl_2$ or $Cu(OAc)_2$ in solution as complexes or solvates and to catch the acid liberated during the coupling reaction. In $scCO_2$, to our surprise, the coupling took place without base with higher conversion and yield than those in the presence of pyridine (entries 3 and 4, Table 1). When NaOAc

Table 1 Oxidation coupling of terminal acetylenes in $scCO_2$[a]

Run	Alkyne	Base	*t*/h	Conv. (%)[b]	Isolated yield (%)
1[c]	PhC≡CH	NaOAc	4	12	10
2[d]	PhC≡CH	NaOAc	4	81	39
3	PhC≡CH	none	4	63	50
4	PhC≡CH	pyridine	4	50	44
5[e]	PhC≡CH	NaOAc	4	99	98
6	PhC≡CH	NaOAc	3	100	100
7[f]	PhC≡CH	NaOAc	3	78	73
8[g]	PhC≡CH	NaOAc	3	98	96
9	$C_5H_{11}C{\equiv}CH$	NaOAc	4	100	95
10	$C_6H_{13}C{\equiv}CH$	NaOAc	5	100	92
11	$HC{\equiv}CCH_2OH$	NaOAc	4	100	71
12	$HC{\equiv}CCH_2OAc$	NaOAc	4	100	93

[a] Alkyne (1 mmol), $CuCl_2$ (2 mmol), base (2 mmol), MeOH (1 ml), P_{CO_2} = 14 MPa, 40 °C. [b] Determined by GC analysis. [c] Did not add MeOH. [d] Only used MeOH (10 ml) as solvent. [e] P_{CO_2} = 7.5 MPa. [f] Added 1 mmol of $CuCl_2$. [g] Added 3 ml of MeOH.

Table 2 Solubility of related reagents in different solvents[a]

Entry	Reagents[b]	Solvent	Solubility
1	$CuCl_2$	$scCO_2$	insoluble
2	$CuCl_2$	MeOH	soluble
3	$CuCl_2$	MeOH/$scCO_2$	partial
4	NOAc	$scCO_2$	insoluble
5	NOAc	MeOH	partial
6	NOAc	MeOH/$scCO_2$	partial
7	$CuCl_2$/NOAc	$scCO_2$	insoluble
8	$CuCl_2$/NOAc	MeOH/$scCO_2$	partial
9	$CuCl_2$/NOAc	MeOH[c]	soluble
10	Pyridine	$scCO_2$	soluble
11	$CuCl_2$/pyridine	MeOH	partial[d]

[a] The procedure for determining solubility in $scCO_2$: The desired amount of the related reagents was placed in a 25 ml stainless steel cell. The cell was sealed and filled with liquid carbon dioxide (14 MPa). The cell was then heated to 40 °C for the desired time and the solubility of the related reagents was monitored by viewing through a sapphire observation window. [b] Amounts of reagents: $CuCl_2$ = 269 mg, NaOAc = 164 mg, pyridine = 158 mg. Amounts of solvent: $scCO_2$ = 14 MPa, MeOH = 1 ml. [c] 10 ml. [d] The solubility of solid in this experiment is more than that of entry 8.

was added, the reaction gave a satisfactory result (entry 6, Table 1). It is clear that NaOAc is superior to pyridine in $scCO_2$. The results in Table 1 also show that a sufficient amount of cupric chloride is necessary for the Glaser coupling (entries 6 and 7, Table 1).

At least two reaction pathways had been proposed in earlier reports.[8a,d] One involves a radical mechanism and the other formation of a cupric complex. We used two radical traps (*N*-*tert*-butylbenzylideneamine *N*-oxide and 2-methyl-2-nitrosopropane) in the reaction, but we did not detect any radicals.

Base on the results shown in Tables 1 and 2, we could conclude several points. (i) In $scCO_2$, the presence of NaOAc plays an important role in enhancing the reaction rate. (ii) A sufficient amount of cupric chloride is necessary for the Glaser coupling. (iii) the low viscosity of $scCO_2$ favors the oxidation coupling reaction of terminal acetylenes. (iv) Addition of a correct amount of MeOH can increase the dissolution of $CuCl_2$, and enhance the rate of the reaction.

In summary, we have observed that Glaser coupling reactions can proceed smoothly in $scCO_2$ in good yields. Of particular note is the fact that this new Glaser coupling reaction is more environmentally friendly than the traditional reaction and shows potential utility in industry. The mechanism and applications of the reaction are currently under investigation in our laboratory.

We thank the National Natural Science Foundation of China for financial support (No. 29772036 and 29872039) and Dr Fanglü Huang for helpful discussion. We also thank Professor Buxing Han (Beijing Institute of Chemistry, Chinese Academy of Sciences) for providing the reaction cell.

Notes and references

† *Typical procedure*: To a mixture of $CuCl_2$ (2 mmol) and NaOAc (2 mmol) in an HF-25 autoclave, MeOH (1 ml) and alkyene (1 mmol) were added. Liquid CO_2 was then transferred into the autoclave to the desired pressure. The reaction mixture was stirred at 40 °C for 3–5 h. After the reaction, the CO_2 was vented and the surplus was extracted with Et_2O. The conversion was determined by GC using an internal standard. The product was then purified by preparative TLC on silica gel using light petroleum–EtOAc (10 : 1) as eluent.

1 P. G. Jessop, T. Ikariya and R. Noyori, *Chem. Rev.*, 1999, **99**, 475.
2 L. Jia, H. Jian and J. Li, *Green Chem*., 1999, 91.
3 L. Jia, H. Jiang and J. Li, *Chem. Commun.*, 1999, 985.
4 F. Bohlmann, F. T. Burkhart and C. Zero, *Naturally Occurring Acetylenes*, Academic Press, London and New York, 1973.
5 L. Hansen and P. M. Boll, *Phytochemistry*, 1986, **25**, 285.
6 Y. S. Kim, S. H. Jin, S. L. Kim and D. R. Hahn, *Arch. Pharm. Res.*, 1989, **12**, 207.
7 H. Matsunaga, M. Katano, H. Yamamoto, H. Fujito, M. Mori and K. Tukata, *Chem. Pharm. Bull.*, 1990, **38**, 3480.
8 Review: (*a*) R. A. Raphael, E. C. Taylor and H. Wynberg, *Advances in Organic Chemistry*, Mack Printing CO, Easton, PA, New York, 1963, vol. 4, pp. 225–328; (*b*) W. S. Trahanovsky, *Oxidation in Organic Chemistry*, Academic Press, New York and London, 1973, vol. 5-B, p. 1; (*c*) M. Hudlicky, *Oxidation in Organic Chemistry*, ACS Monograph 186, Washington DC, 1990, p. 58; (*d*) H. G. Viehe, *Chemistry of Acetylenes*, Marcel Dekker, New York, 1969, p. 597; (*e*) K. Sonogashira, in *Comprehensive Organic Synthesis*, ed. B. M. Trost and I. Fleming, Pergamon, Oxford, 1991, vol. 3, p. 551.
9 R. Rossi, A. Carpita and C. Bigelli, *Tetrahedron Lett.*, 1985, **26**, 523.
10 S. Kenkichi, T. Yasuo and H. Nobue, *Tetrahedron Lett.*, 1985, **26**, 523.
11 J. A. Darr and M. Poliakoff, *Chem. Rev.*, 1999, **99**, 495.
12 A. Francis, *J. Phys. Chem.*, 1954, **58**, 1099; J. B. Ellington, K. M. Park and J. F. Brennecke, *Ind. Eng. Chem. Res.*, 1994, **33**, 965.

Communication 9/08014G

Pyridine ring formation through the photoreaction of arenecarbothioamides with diene-conjugated carbonyl compounds†

Kazuaki Oda,* Rikiji Nakagami, Naozumi Nishizono and Minoru Machida

Faculty of Pharmaceutical Sciences, Health Sciences University of Hokkaido, Ishikari-Tobetsu, Hokkaido 061-0293, Japan. E-mail: k-oda@hoku-iryo-u.ac.jp

Received (in Cambridge, UK) 27th August 1999, Accepted 19th October 1999

Irradiation of arenecarbothioamides with hexa-2,4-dienal in benzene solution gives 2-arylpyridines in moderate yields.

Of all the naturally occurring heterocycles, the pyridine ring is one of the most well-known simple structures. Pyridine and fused-pyridine moieties are present in numerous natural products, such as the quinoline and isoquinoline alkaloids,[2] and have a vast range of potential biological activities. Therefore, many methods for pyridine ring formation have been reported.[3] In addition, in fields other than the biological one, synthetic methods for pyridine derivatives were also required and developed. Since di- and tri-heteroaromatic compounds[4] containing pyridine have received significant attention in the fields of electrical materials,[5] biologically active molecules,[6] chelating agents and metal–ligand chemistry,[7] the synthesis of arylpyridine derivatives has become increasingly important.

In the course of our systematic study of the photochemistry of the arenecarbothioamide–alkene system,[8] we found that photoreaction of arenecarbothioamides with 2-furylacrylaldehyde in benzene proceeds *via* key intermediate 4-aminobut-3-enal to give 2,3-diarylpyrrole derivatives.[9] From this pyrrole formation, utilization of a diene-conjugated carbonyl as a photochemical substrate for pyridine formation was suggested. Here we report a facile synthesis of 2-arylpyridines, 2,6-diarylpyridines and benzo-fused pyridines through the photoreaction of arenecarbothioamides with diene-conjugated carbonyl compounds.

Photoreaction of arenecarbothioamide **1** with hexa-2,4-dienal **2** was carried out in benzene using a high-pressure mercury lamp through a Pyrex filter under a nitrogen atmosphere. The results are listed in Table 1. Irradiation of benzenecarbothioamide **1a** with 0.5 equiv.[10] of **2** for 5 h exclusively gave 2-phenylpyridine **3a** (32%). Further, the photoreactions of a series of heteroaromatic thioamides **1b–f** with **2** were performed. As expected, the corresponding 2-arylpyridines **3b–f** were obtained in moderate yields.

In addition, preparation of 2,6-diarylpyridines was also examined. The photolysis of arenecarbothioamide **1** with

Table 1 Photoreaction of arenecarbothioamides **1** with hexa-2,4-dienal **2**

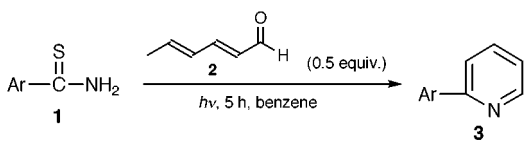

1	Ar		Yield (%)
1a	Ph	**3a**[a]	32
1b	3-pyridyl	**3b**[a]	34
1c	4-pyridyl	**3c**[a]	28
1d	2-furyl	**3d**[b]	35
1e	3-furyl	**3e**[b]	30
1f	2-thienyl	**3f**[c]	37

[a] See ref. 11. [b] See ref. 4. [c] See ref. 12.

† Photochemistry of the Nitrogen–Thiocarbonyl Systems. Part 34. For Part 33, see ref. 1.

Table 2 Photoreaction of arenecarbothioamides **1** with 1-arylhexa-2,4-dien-1-one **7**

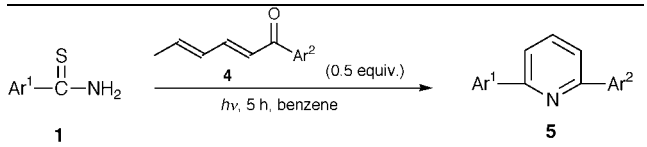

1	Ar[1]	4	Ar[2]		Yield (%)
1a	Ph	**4a**	Ph	**5a**[a]	32
1a	Ph	**4b**	3-pyridyl	**5b**	34
1a	Ph	**4c**	2-furyl	**5c**	28
1a	Ph	**4d**	2-thienyl	**5d**[b]	35
1d	2-furyl	**4c**	2-furyl	**5e**	30
1f	2-thienyl	**4d**	2-thienyl	**5f**[b]	37

[a] See ref. 13. [b] See ref. 14.

1-arylhexa-2,4-dien-1-one **4** was carried out under similar conditions to those described above. Similarly, the expected 2,6-diarylpyridines **5** were obtained in moderate yields (Table 2).

Next, as an extension of this reaction, photoreaction of **1a** with *o*-vinylbenzaldehyde **6** as the dienal equivalent was performed under similar conditions. Irradiation of **1a** with **6** for 5 h gave 4-methyl-3-phenylisoquinoline[15] **7** (28%) and (3-phenyl-4-isoquinolyl)methanethiol **8** (9%), accompanied by small amounts of **9** (Scheme 1).[16] Presumably, the isoquinoline **7** was derived from thiol derivative **8**. In fact, thiol **8** was easily converted to **7** by further irradiation.

From these experiments, the reaction seems to proceed in several steps involving initial thietane **10** formation between the thiocarbonyl and γ,δ-alkenyl moiety of **2**, leading to the key ω-aminodienal intermediate **12**,[17] which subsequently cyclizes to the pyridine derivatives **3** as shown in Scheme 2 (pathway A). However, no evidence is available at this time to suggest if this step is thermal or photochemical. In the case of *o*-vinylbenzaldehyde **6** as dienal analogue, formation of isoquinoline **7**

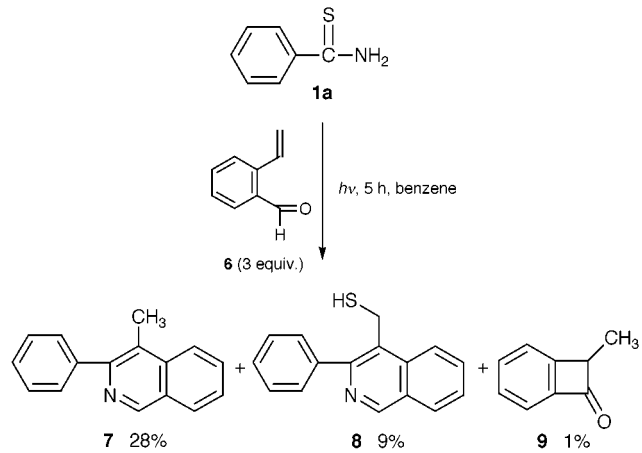

Scheme 1

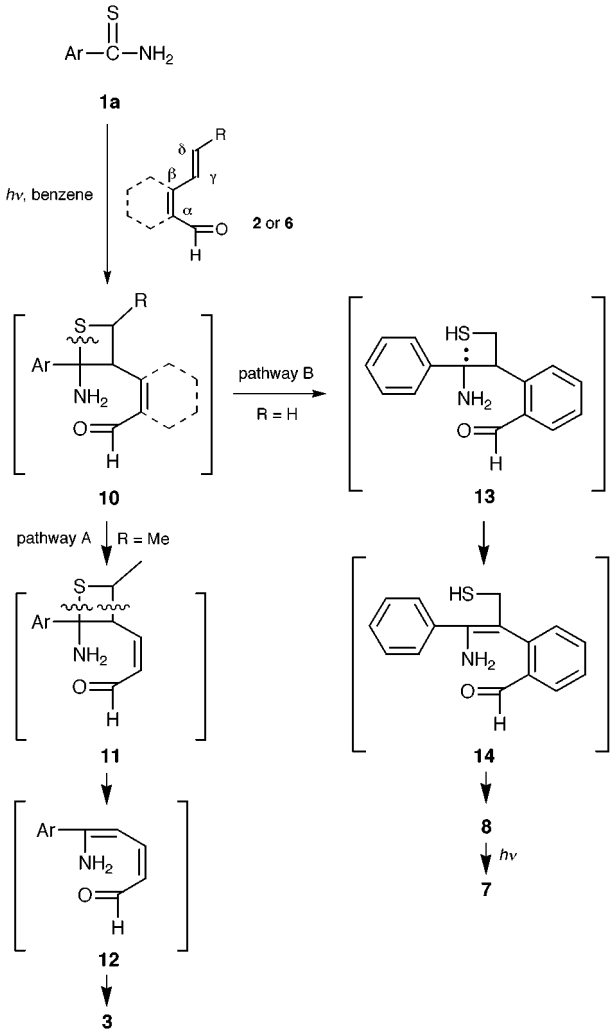

Scheme 2

seems to proceed *via* thiol **8** which arises from the initially formed thietane **10** followed by photochemical fission of the C–S bond of the thietane ring, and then subsequent cyclization (pathway B).

In this study, the new photochemical formation of pyridine promises to have broad applications for the synthesis of aryl- and heteroaryl-pyridines. In addition, it was shown that certain dienal species and their analogues are potentially useful building blocks in photosynthesis of nitrogen-containing heterocycles. A detailed study on further synthetic application and the reaction pathway of this reaction is in progress.

This work was supported in part by a Grant-in-Aid for High Technology Research Programs from the Ministry of Education, Science, Sports and Culture of Japan.

Notes and references

1 K. Oda, M. Sakai, K. Ohno and M. Machida, *Heterocycles*, 1999, **50**, 277.
2 F. S. Yates, in *Comprehensive Heterocyclic Chemistry*, ed. A. R. Katritzky and C. W. Rees, Pergamon, Oxford, 1984, vol. 2, p. 511.
3 H. Bönnemann and W. Brijoux, in *Advance in Heterocyclic Chemistry*, ed. A. R. Katritzky, Academic Press, San Diego, 1990, vol. 48, p. 177.
4 P. Ribereau and G. Queguiner, *Can. J. Chem*., 1983, **61**, 334 ; R. A. Jones and P. U. Civcir, *Tetrahedron*, 1997, **34**, 11529.
5 T. Kambara, K. Koshida, N. Sato, I. Kuwajima, K. Kubota and T. Yamamoto, *Chem. Lett*., 1992, 583.
6 K. V. Rao, K. Biemann and R. B. Woodward, *J. Am. Chem. Soc*., 1963, **85**, 2532.
7 T. Meyer, *Acc. Chem. Res*., 1989, **22**, 163.
8 K. Oda and M. Machida, *J. Chem. Soc., Chem. Commun*., 1994, 1477; K. Oda, H. Tsujita, K. Ohno and M. Machida, *J. Chem. Soc., Perkin Trans. 1*, 1995, 2931; K. Oda, R. Hiratsuka and M. Machida, *Heterocycles*, 1996, **43**, 463; K. Oda, M. Sakai and M. Machida, *Chem. Pharm. Bull*., 1997, **45**, 584; K. Oda, M. Sakai, H. Tsujita and M. Machida, *Synth. Commun*., 1997, **27**, 1183.
9 K. Oda, H. Tsujita, M. Sakai and M. Machida, *Chem. Pharm. Bull*., 1998, **46**, 1522.
10 To avoid formation of the photodimer of **2**, the molar ratio of **1a** and **2** was varied. As a result, the yield of **3a** increased to 32% using a ratio of 2 : 1.
11 C. J. Pouchert and J. R. Campbell, in *The Aldrich Library of NMR Spectra*, Aldrich Chemical Company, Wisconsin, 1974, vol. 9.
12 M. Tingoli, M. Tiecco, L. Testaferri, R. Andrenacci and R. Balducci, *J. Org. Chem*., 1993, **58**, 6097.
13 G. R. Newkome and D. L. Fishel, *J. Org. Chem*., 1972, **37**, 1329.
14 E. C. Constable, R. P. G. Henney and D. A. Tocher, *J. Chem. Soc., Dalton Trans*., 1992, 2467.
15 J. R. Brooks, D. N. Harcourt and R. D. Waigh, *J. Chem. Soc., Perkin Trans. 1*, 1973, 2588.
16 8-Methylbicyclo[4.2.0]octa-1(6),2,4-trien-7-one **9** was derived from **6** by intramolecular photocyclization. S. V. Kessar, A. K. S. Mankotia, J. C. Scaiano, M. Barra, J. Gebicki and K. Huben, *J. Am. Chem. Soc*., 1996, **118**, 4361.
17 J. Becher, *Synthesi*s, 1980, 589.

Communication 9/06965H

ChemComm

Simultaneous modification of mesopores and extraction of template molecules from MCM-41 with trialkylchlorosilanes

Valentyn Antochshuk and Mietek Jaroniec*

Department of Chemistry, Kent State University, Kent, Ohio 44242, USA. E-mail: jaroniec@columbo.kent.edu

Received (in Bloomington, IN, USA) 29th June 1999, Accepted 13th October 1999

The simultaneous removal of a surfactant template and attachment of trialkylsilyl groups has been successfully achieved by treating uncalcined MCM-41 with trialkylchlorosilanes, resulting in the synthesis of mesoporous hydrophobic materials of highly uniform pore structure.

The preparation of MCM-41 materials[1] usually includes a high temperature calcination step that in fact opens mesopores as well as resulting in structure shrinkage.[2] Functionalization with silanes is often employed to achieve materials with the desired surface properties for advanced adsorption and catalytic applications[3] and to increase their stability with respect to atmospheric humidity.[4] The main drawback of the conventional modification procedure[5] lies in the necessity for template removal prior to attachment of the ligands to the MCM-41 pore walls by either calcination (which leads to structure shrinkage) or solvent/HCl extraction. Another shortcoming of this conventional modification is the low bonding density of the resulting materials, especially when larger groups are attached. So far, only a few attempts at the modification of uncalcined MCM-41 materials have been reported.[6–8] The first two reports describe the modification of somewhat different materials, *i.e.* alkyltrimethylammonium–kanemite complexes[6] and MCM-48,[7] without providing clear information about the degree of surfactant removal and the structure of the bonded layer. Another report[8] deals with a stepwise post-synthesis silylation procedure, the first step of which was intended to modify only the external surface of MCM-41, whereas two additional subsequent steps were proposed to remove the template from the mesopores *via* HCl/ETOH extraction and to attach functional groups to their walls.

The current work shows that a one-step silylation of uncalcined MCM-41 materials leads not only to external surface modification, but also to the removal of the surfactant template from the mesopores and chemical modification of their walls. The proposed one-step treatment of uncalcined MCM-41 materials with trialkylchlorosilanes allows one to achieve several goals: (i) preparation of functionalized mesoporous materials with hydrophobic surfaces; (ii) removal of surfactant molecules from the mesopores; (iii) avoiding high temperature calcination or solvent extraction procedures; and (iv) avoiding structure shrinkage during the calcination process. Templating and charge balancing surfactant molecules, which interact with the silica surface *via* van der Waals and electrostatic forces, were replaced by more strongly (chemically) interacting groups, *e.g.* trialkylsilyl groups. The method reported here could be useful in the low temperature synthesis of catalytic materials and adsorbents with a high surface coverage of attached ligands (especially when larger silanes are used) and with a high degree of pore uniformity. The one-step procedure makes extraction or calcination of as-synthesized samples a redundant and superfluous step in the preparation of modified MCM materials.

The MCM-41 sample studied was prepared by a method involving post-synthesis hydrothermal restructuring.[9] Two unmodified samples were used: MCM-41U (uncalcined 'as prepared' mesoporous material) and MCM-41C (the same sample but calcined). Both samples were subjected to modification. The uncalcined material with template molecules inside the mesopores was functionalized in a one-step process that includes simultaneous trialkylsilanization and extraction of the template. Two modified samples were prepared: MCM-41UM and MCM-41UO, with attached trimethyl- and octyldimethylchlorosilyl groups, respectively. Calcined mesoporous material was modified with the trimethyl- and octyldimethyl-chlorosilanes using a conventional modification procedure,[10] and the resulting samples were designated as MCM-41CM and MCM-41CO, respectively.

In the proposed one-step modification procedure of uncalcined samples no additional pretreatment was performed. A typical synthesis (Scheme 1) included dispersion of the mesoporous material (about 0.2 g) in 10 ml of trialkylsilane, and refluxing the mixture for 36 h. Upon addition of *ca.* 5 ml of anhydrous pyridine to the mixture, it was refluxed for a further 18 h. After cooling, the modified mesoporous material was filtered off and washed several times with small portions of EtOH, EtOH–n-heptane and finally n-heptane to remove excess modifier and pyridine as well as possible products of hydrolysis. Finally, the modified mesoporous material was dried overnight in an oven at 95–100 °C under vacuum.

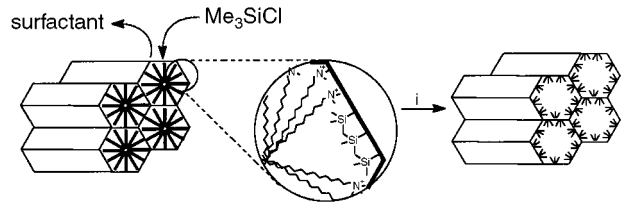

Scheme 1 *Reagents and conditions*: i, $ClSiMe_2CH_2R$ [R = H or $(CH_2)_6Me$], reflux, 36 h, then pyridine, reflux, 18 h.

Modification of the silica surface with alkylsilanes, *via* chemical bonding of alkylsilyl ligands to the surface, was proved by means of ^{13}C CP-MAS (chemical shifts in the interval between 0 and 40 ppm) and ^{29}Si NMR spectroscopy (decrease in the amount of Q^3 silanols with simultaneous increase of Q^4 siloxane sites at −99 and −108 ppm, and an additional signal at 12–15 ppm which corresponds to silane molecules attached to the surface in a monomeric fashion).[10] Elemental analysis showed the presence of bonded alkylsilyl groups (appropriate ratio C : H) and the successful removal of all surfactant molecules and pyridine (complete absence of nitrogen). The concentration of immobilized ligands is shown in Table 1. A much higher amount of attached octyldimethylsilyl

Table 1. Structural features of the 'parent' MCM-41 and materials functionalized with trialkylchlorosilanes

Sample	BET surface area/$m^2\ g^{-1}$	Mesopore volume/$cm^3\ g^{-1}$	Pore diameter (BJH)/nm	Amount of attached groups/mmol g^{-1} SiO_2
MCM-41U	~3	—	—	—
MCM-41C	915	1.06	5.65	—
MCM-41UM	540	0.69	5.25	2.81
MCM-41CM	570	0.65	4.95	2.76
MCM-41UO	385	0.38	4.20	2.83
MCM-41CO	395	0.39	4.10	2.15

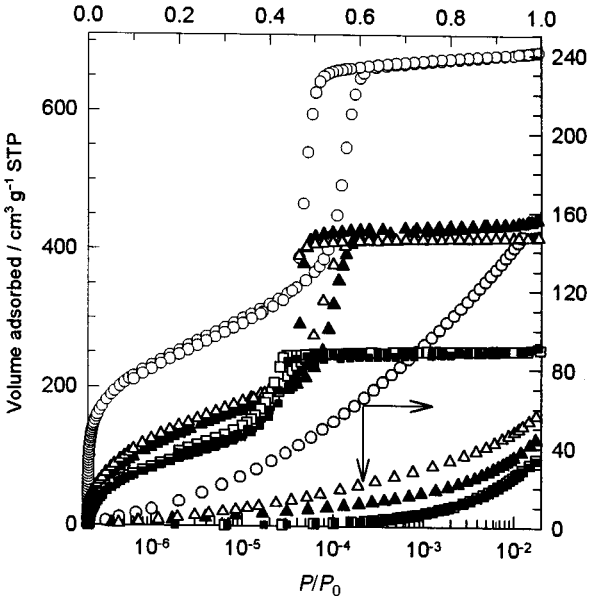

Fig. 1 Nitrogen adsorption isotherms and their low-pressure parts for (○) MCM-41C, (△) MCM-41CM, (▲) MCM-41UM, (□) MCM-41CO and (■) MCM-41UO.

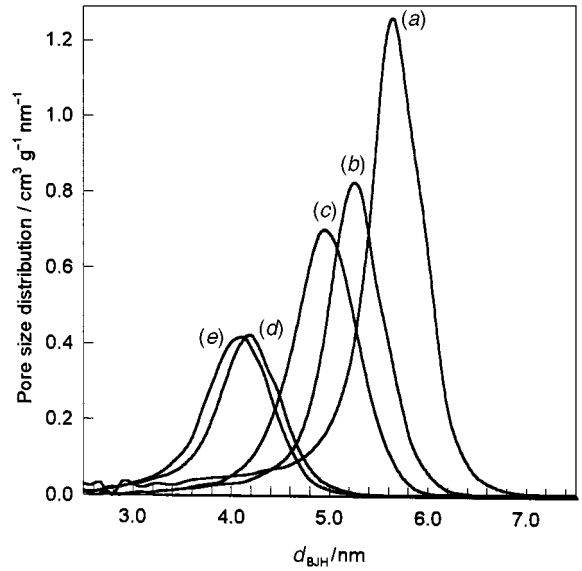

Fig. 2 Pore size distributions for (*a*) MCM-41C, (*b*) MCM-41UM, (*c*) MCM-41CM, (*d*) MCM-41UO and (*e*) MCM-41CO.

groups can be achieved in the one-step modification in comparison to the conventional procedure. The maximum number of attached groups in the one-step modification is probably limited by the size of the $SiMe_2CH_2R$ groups [where R = H or $(CH_2)_6Me$].

Adsorption studies showed opening of pores upon modification from completely filled (uncalcined as-prepared sample) to fully accessible pores of different diameter (modified samples). The pore diameter of the modified samples as well as the surface area and mesopore volume depend on the size of the attached ligands (see Table 1). Unmodified calcined sample MCM-41C has a very pronounced step in capillary condensation at $P/P_0 \sim 0.57$ (Fig. 1), which shifts gradually to lower pressure for modified samples. The size of the hysteresis loop decreases with increasing size of grafted ligands.

Thermogravimetric studies showed great similarity for the samples modified *via* the conventional and one-step procedures. A notable difference in the shape of the DTG curves for the samples with similar ligands is attributed to the presence of different conformations of the attached alkyl groups.[10] The pore diameters and pore size distributions for all samples were calculated from nitrogen adsorption data using the BJH method with the corrected form of the Kelvin equation (see Fig. 2).[11] The decrease in the pore size upon modification of the surface with trimethylchlorosilane is typically about 0.50 nm.[10,12] For the MCM-41CM and MCM-41UM samples there is a significant difference in the size of the mesopores, emphasizing the well-known effect of structure shrinkage upon calcination.[2] A similar tendency is observed for the MCM-41CO and MCM-41UO samples, but in this case the difference is smaller because of two competing factors: higher surface coverage (about 30%) and no shrinkage when uncalcined sample is used.

In conclusion, the MCM-41 mesoporous silicate can be functionalized *via* a one-step procedure using an uncalcined sample. Such a procedure greatly simplifies modification of MCM-41 and pore opening, and makes high temperature calcination or solvent extraction unnecessary. This has advantages such as higher surface coverage of grafted ligands and avoidance of the structure shrinkage. The current study shows that further investigation is needed to determine the detailed synthetic procedure required for selective polyfunctionalization of uncalcined MCM-41 or its complete modification with one reagent only.

We thank Dr A.Sayari for providing the MCM-41 sample. The donors of the Petroleum Research Fund administrated by the American Chemical Society are gratefully acknowledged for partial support of this research.

Notes and references

1 C. T. Kresge, M. E. Leonowicz, W. J. Roth, J. C. Vartuli and J. S. Beck, *Nature*, 1992, **359**, 710.
2 C.-Y. Chen, H.-X. Li and M.E. Davis, *Microporous Mat.*, 1993, **2**, 17.
3 X. Feng, G. E. Fryxell, L.-Q. Wang, A. Y. Kim, J. Liu and K. M. Kemner, *Science*, 1997, **276**, 923.
4 T. Tatsumi, K. A. Koyano, Y. Tanaka and S. Nakata, *Stud. Surf. Sci. Catal.*, 1998, **117**, 143.
5 K. Moller and T. Bein, *Stud. Surf. Sci. Catal.*, 1998, **117**, 53.
6 T. Yanagisawa, T. Shimizu, K. Kuroda and C. Kato, *Bull. Chem. Soc. Jpn.*, 1990, **63**, 1535.
7 J. C. Vartuli, K. D. Schmitt, C. T. Kresge, W. J. Roth, M. E. Leonowicz, S. B. McCullen, S. D. Hellring, J. S. Beck, J. L. Schlenker, D. H. Olson and E. W. Sheppard, *Chem. Mater.*, 1994, **6**, 2317.
8 M. Park and S. Komarneni, *Microporous Mesoporous Mater.*, 1998, **25**, 75.
9 A. Sayari, P. Liu, M. Kruk and M. Jaroniec, *Chem. Mater.*, 1997, **9**, 2499.
10 V. Antochshuk and M. Jaroniec, *J. Phys. Chem. B*, 1999, **103**, 6252.
11 M. Kruk, M. Jaroniec and A. Sayari, *Langmuir*, 1997, **13**, 6267.
12 C. P. Jaroniec, M. Kruk, M. Jaroniec and A. Sayari, *J. Phys. Chem. B*, 1998, **102**, 5503.

Communication 9/05242I

Iodine transfer cyclization mediated by DIBAL-H/THF

Arindam Chakraborty and Ilan Marek*

Department of Chemistry and Institute of Catalysis Science and Technology, Technion-Israel Institute of Technology, Technion City, Haifa 32000, Israel. E-mail: chilanm@tx.technion.ac.il

Received (in Cambridge, UK) 27th August 1999, Accepted 18th October 1999

The combination of DIBAL-H/THF in a 1:1 ratio offers a unique and useful protocol for iodine transfer cyclization *via* a radical pathway; different iodo acetals are employed to obtain the corresonding tetrahydrofuran derivatives in good to excellent yield.

The trialkyltin hydride mediated cyclization of hex-5-enyl and hex-5-ynyl halides (and related radical precursors) is one of the most powerful tools at the disposal of the synthetic chemist for the formation of carbocycles and heterocycles.[1] However, one of the inherent limitations of these tin hydride reagents is the formation of a carbon–hydrogen bond at the end of the sequence. Reagents that mediate the *non-reductive*[2] cyclization have been the focus of recent research and in this endeavour the photolytic ditin method has emerged as a remarkable general procedure due to its unique ability to promote atom transfer cyclizations[3] (or isomerizations)[4] in a *non-reductive* manner. Herein, we report our preliminary results in this area and specifically the use of DIBAL-H–THF (in a 1:1 ratio) as a reagent for iodine transfer cyclization.

During the course of a study aimed at the hydrometallation and carbometallation reactions of functionalized substrates,[5] we wanted to prepare a vinylaluminium derivative[6] in the presence of a sensitive acetal moiety and an sp^3 carbon–iodine bond. Earlier studies of Yamamoto *et al.*[7] revealed that DIBAL-H cleaves acetals regio- and stereo-selectively to the corresponding alcohols due to the complexation of one of the oxygen atoms of the acetal with the oxyphilic organoaluminium compound.[8] In order to overcome this cleavage it was necessary to decrease the Lewis acidity of the aluminium reagent. Accordingly, we felt that addition of 1 equiv. of THF per equiv. of DIBAL-H, as used by Zweifel for the hydroalumination reaction of propargylic THP ethers,[9] should prevent acetal cleavage. However, when we performed the reaction as per our plan, the chemical outcome was totally different and instead of the hydroalumination reaction, we observed an unexpected iodine transfer cyclization under mild conditions and in good overall yield, as described in Table 1.

Although radical processes are known in aluminium chemistry,[10] this type of iodine transfer cyclization[11] mediated by DIBAL-H has no precedent.[12] As expected for such isomerizations, we obtained two isomers for the vinyl iodides **1**, **2**, **3** and **5** in a 1:1 ratio; no trace of the β-fragmentation of the starting material into the propargylic alcohol or enol ether was observed. This behavior is characteristic of the generation of a radical since an organometallic is known to β-eliminate[13] faster than the carbocyclization reaction across a triple bond.[14] Moreover, when the reaction is performed in the presence of 40 mol% of Galvinoxyl or TEMPO, no iodine transfer is observed and only the starting material is recovered. The vinyl iodide **1** was also obtained in the same ratio and yield by isomerization following the photolytic ditin procedure.[3] It is interesting to note that variation of the concentration decreases the yield of **1**, and more specifically by changing the amount of THF with respect to DIBAL-H as described in Table 2.

The best result for cyclization was obtained using a stoichiometric ratio of DIBAL-H/THF (entries 1 and 5). In all examined cases, very little radical attack on the solvent is observed (less than 3%). Several other aluminium reagents were tested and we found that the dialkylaluminium hydrides was the best reagents for this isomerization (DIBAL-H, 80%), followed by trialkylaluminium derivatives (Me_3Al, 65%), alanate derivatives[15] [sodium bis(2-methoxyethoxy)aluminium hydride, known as Red-Al, 40%], dialkylaluminium halides (Et_2AlCl, 16%), and methylaluminoxane $[Al(CH_3)O]_n$ in only 7% yield; no isomerization was observed with activated aluminium oxide. Although the combination DIBAL-H/THF can be replaced by DIBAL-H/THP without any change in this overall isomerization, Et_3N as co-additive (instead of THF) did not lead to a good yield (26%).

Disubstituted alkynes (Table 1, entries 2 and 3) do undergo similar isomerization to provide both vinylic isomers of **2** and **3** in 1:1 ratio,whereas a secondary alkyl iodide (entry 4) gives the cyclic product as the *cis* isomer with a *Z*:*E* ratio of 13:1 in excellent yield.

Although it is tempting to speculate that the aluminium complex behaves in a similar fashion to BEt_3 in the presence of oxygen,[16] when we repeated the reaction in entry 1 (Table 1) either in a totally degassed THF and hexane solution or in the dark, we did not observe any change in the chemical outcome of this cyclization. Interestingly, during the formation of **4**, addition of benzaldehyde after the completion of the reaction yielded benzyl alcohol quantitatively, which emphasized the presence of the hydride in the reaction mixture even after the normal course of reaction.

To substantiate the generality of this newly found strategy, we examined the similar treatment of a substrate which did not have an acetal moiety. We were pleased to find that 1-iodohex-5-yne (entry 5, Table 1) produced the cyclic isomer as expected. When the alkyne is slightly activated as 6-iodo-1-trimethyl-

Table 1 Iodine transfer cyclization

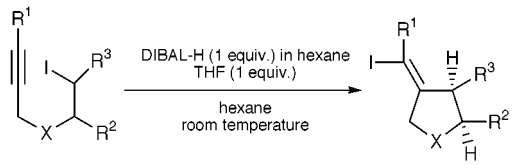

Entries	R^1	X	R^2	R^3	Product	Yield (%)[a]
1	H	O	OBu	H	**1**	80
2	Me	O	OBu	H	**2**	60
3	Et	O	OBu	H	**3**	60
4	H	O	$OCH_2CH_2CH_2$		**4**	90
5	H	CH_2	H	H	**5**	60

[a] Isolated yields after hydrolysis.

Table 2 Variation of the DIBAL-H:THF ratio for the formation of **1**

Entries	DIBAL-H:THF	Yield (%)[a]
1	1:1	80
2	1:2	50
3	1:5	42
4	2:1	0
5	3:3	94

[a] Isolated yields after hydrolysis.

silylhex-1-yne, the classical hydroalumination reaction occurs to give the vinyl silane after hydrolysis.

In conclusion, the use of the combination DIBAL-H/THF provides a new and efficient method for iodine transfer cyclization for the formation of five-membered rings.[17] Synthetic applications of the present methodology[18] and investigations to understand the mechanistic rationale of the reaction are now in progress in our laboratory.

I. M. is the Holder of the Lawrence G. Horowitz Career Development Chair, is a Ygal Alon fellow and Evelyn and Salman Grand Academic Lectureship-USA. This research was supported in part by The Israel Science Foundation founded by The Academy of Sciences and Humanities (No. 060-471) and by the fund for the promotion of research at the Technion. Acknowledgment is also made to the donors of The Petroleum Research Fund, administered by the ACS, for partial support of this research (PRF#33747-AC1). We thank also P. and E. Nathan Research Fund, N. Haar and R. Zinn Research Fund.

Notes and references

1 D. P. Curran, *Synthesis*, 1988, 417; B. Giese, *Radicals in Organic Synthesis: Formation of Carbon–Carbon Bonds*, Pergamon, Oxford, 1986; D. J. Hart, *Science*, 1984, **223**, 883.

2 D. P. Curran, E. Eichenberg, M. Collis, M. G. Roepel and G. Thoma, *J. Am. Chem. Soc.*, 1994, **116**, 4279; J. E. Forbes, R. N. Saicic and S. Z. Zard, *Tetrahedron*, 1999, **55**, 3791; J.-P. Vionnet, K. Schenik and P. Renaud, *Helv. Chim. Acta*, 1993, **76**, 2490; P. Dalko, *Tetrahedron*, 1995, **51**, 7579; W. A. Nugent and T. V. RajanBabu, *J. Am. Chem. Soc.*, 1998, **110**, 8561; G. A. Molander and L. S. Harring, *J. Org. Chem.*, 1990, **55**, 6171.

3 D. P. Curran, M. H. Chen and D. Kim, *J. Am. Chem. Soc.*, 1986, **108**, 2489; D. P. Curran, M. H. Chen and D. Kim, *J. Am. Chem. Soc.*, 1989, **111**, 6265; Y. Ichinose, S. I. Matsunaga, K. Fugami, K. Oshima and K. Utimoto, *Tetrahedron Lett.*, 1989, **30**, 3155.

4 J. Iqbal, B. Bhatia and N. K. Nayar, *Chem. Rev.*, 1994, **94**, 519.

5 I. Marek, *J. Chem. Soc., Perkin Trans. 1*, 1999, 535; I. Marek and J. F. Normant, *Carbometallation Reactions, Cross Coupling Reactions*, ed. P. J. Stang and F. Diederich, Wiley-VCH, Weinheim, 1998, p. 271.

6 G. Zweifel, *Org. React.*, 1984, **32**, 375.

7 A. Mori, K. Ishihara, I. Arai and H. Yamamoto, *Tetrahedron*, 1987, **43**, 755; K. Maruoka and H. Yamamoto, *Angew. Chem., Int. Ed. Engl.*, 1985, **24**, 668.

8 S. E. Denmark and T. M. Willson, *J. Am. Chem. Soc.*, 1989, **111**, 3475.

9 H. P. On, W. Lewis and G. Zweifel, *Synthesis*, 1981, 999.

10 K. Ziegler, F. Krupp and K. Zosel, *Angew. Chem.*, 1965, **67**, 425; J. J. Eisch and J. L. Considine, *J. Am. Chem. Soc.*, 1968, **90**, 6257.

11 Radical cyclizations mediated by organometallic derivatives were described in the literature but without any iodine transfer. H. Stadtmuller, A. Vaupel, C. E. Tucker, T. Studemann and P. Knochel, *Chem. Eur. J.*, 1996, **2**, 1204; J. Tang, H. Shinokubo and K. Oshima, *Synlett*, 1998, 1075; Y. Hayashi, H. Shinokubo and K. Oshima, *Tetrahedron Lett.*, 1998, **39**, 63; F. Villar and P. Renaud, *Tetrahedron Lett.*, 1998, **39**, 8655.

12 Palladium(0) promoted cyclizations of α-iodo carbonyl compounds also by an atom transfer mechanism: D. P. Curran and C. T. Chang, *Tetrahedron Lett.*,1990, **31**, 933.

13 W. F. Bailey and M. W. Carson, *J. Org. Chem.*, 1998, **63**, 361.

14 Moreover, the intramolecular addition of an organometallic across a triple bond is known to be a *syn* process. See ref. 5.

15 With Red-Al, the cyclic and linear reduced products are observed in 22 and 29% respectively.

16 C. Ollivier and P. Renaud, *Chem. Eur. J.*, 1999, **5**, 1468; D. P. Curran and J. Nanni, *Tetrahedron: Asymmetry*, 1996, **7**, 2417.

17 *Experimental procedure* for **4** (it is important to follow the order of addition of substrates for these experiments): Into a dry, argon-flushed flask kept under a static pressure of argon is placed a 1.0 molar solution of DIBAL-H (1.76 ml, 1.76 mmol) in hexane. To the cooled solution (0 °C) is added sequentially THF (127 mg, 1.76 mmol) and the iodide (467 mg, 1.76 mmol) in hexane (1 ml). The solution is stirred at 0 °C for 15 min and then allowed to attain room temperature and stirred overnight. The reaction mixture was then quenched with 1 M HCl, extracted with Et_2O and washed several times with water, dried ($MgSO_4$) and then the solvent was evaporated to provide the crude product. After purification by chromatography on silica gel (10% EtOAc in hexanes), 421 mg (90%) of the title compound was obtained.

18 All our attempts to form the six-membered ring as well as to promote the isomerization across a double bond failed.

Communication 9/06952F

Asymmetric amidation of saturated C–H bonds catalysed by chiral ruthenium and manganese porphyrins

Xiang-Ge Zhou, Xiao-Qi Yu, Jie-Sheng Huang and Chi-Ming Che*

Department of Chemistry, The University of Hong Kong, Pokfulam Road, Hong Kong. E-mail: cmche@hkucc.hku.hk

Received (in Cambridge, UK) 29th July 1999, Revised 2nd September 1999, Accepted 1st October 1999

Chiral ruthenium(II) and manganese(III) porphyrins catalyse the asymmetric amidation of saturated C–H bonds of ethylbenzene and ethylnaphthalenes to form the corresponding amides in up to 85% yield with 45–58% ee.

In the context of developing new protocols for asymmetric functionalisation of saturated C–H bonds, amidation *via* reactive metal–imido species is preferred over hydroxylation by reactive metal–oxo complexes because the latter usually suffers from further oxidation to give side products such as ketones. However, in contrast to the large number of investigations on the hydroxylation of saturated C–H bonds catalysed by both cytochrome P-450 and its chemical model systems such as iron and manganese porphyrins,[1] metalloporphyrin-catalysed amidations of saturated C–H bonds are rare.[2–6] Herein we describe the enantioselective amidation of saturated C–H bonds with chiral metalloporphyrin catalysts or directly by a chiral metal–imido complex (Scheme 1). Prior to this work, there was only one report on metal-mediated asymmetric amidation of saturated C–H bonds, with up to 31% ee obtained for indane,[7] despite the recent advances in metal-catalysed asymmetric aziridination of alkenes.[8]

The chiral porphyrin H_2Por* [Por* = 5,10,15,20-tetrakis(1,2,3,4,5,6,7,8-octahydro-1,4:5,8-dimethanoanthracen-9-yl)porphyrinato dianion] was synthesised by Halterman's method.[9] Its complexes with ruthenium(II) and manganese(III) ions, [Ru^{II}(Por*)(CO)(EtOH)] **1**[10] and [Mn^{III}(Por*)(OH)(MeOH)] **2**,[9,11] respectively, were prepared according to the published procedures. Both complexes were found to be effective catalysts for asymmetric amidation of saturated C–H bonds by PhI=NTs.† The results obtained for a series of substrates containing saturated C–H bonds, at a catalyst: PhI=NTs : substrate molar ratio of 1 : 100 : 500 with yields based on starting PhI=NTs, are summarised in Table 1. In each case, $TsNH_2$ was detected as a side product; the total yields of $TsNH_2$ and the amidation product were close to 100%. As can be seen from Table 1, both the yield and ee increase considerably with increasing temperature (entries 1–3; 4, 5; 8, 9), and less sterically demanding substrates could be amidated with higher ees. For example, the ee obtained for 2-ethylnaphthalene (48%, entry 13) is higher than that obtained for the more sterically demanding substrates 1-ethylnaphthalene (23%, entry 15) and indane (10%, entry 9). Mass balance studies were carried out in the case of ethylbenzene, which resulted in conversions of 14 (catalyst **1**) and 47% (actalyst **2**) for this substrate at a

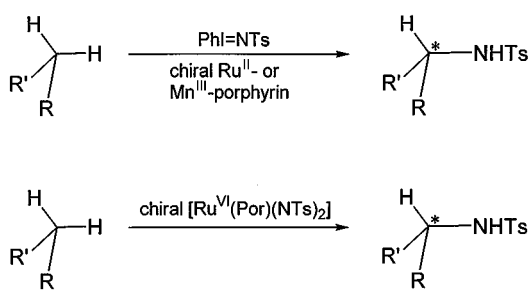

Scheme 1

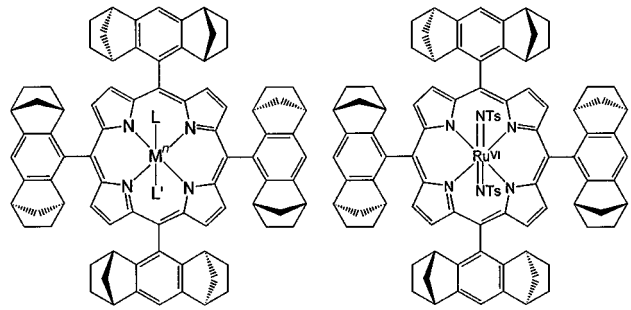

1 M = Ru, *n* = II, L = CO, L' = EtOH
2 M = Mn, *n* = III, L = HO^-, L' = MeOH

3

catalyst : ethylbenzene : PhI=NTs molar ratio of 1 : 75 : 150 (CH_2Cl_2, 40 °C, 2 h), with the yields of 1-tosylamino-1-phenylethane being 84 and 76%, respectively, based on the amount of ethylbenzene consumed.

Under the same conditions, the manganese catalyst **2** exclusively afforded the amidation product in a considerably higher yield (> 70% in all the cases except entries 4 and 16) than the ruthenium catalyst **1**. The highest yield obtained was 85% for 2-ethylnaphthalene (entry 14). Increasing the amount of **2** used considerably improved the yield but only slightly enhanced the chiral induction (entries 16 and 17). Interestingly, the manganese catalyst **2** also gave higher ees than the ruthenium catalyst **1**, except for tetrahydronaphthalene. The

Table 1 Asymmetric amidation of saturated C–H bonds by PhI=NTs catalysed by **1** and **2**[a]

Entry	R^1	R^2	Catalyst	Yield (%)[b]	Ee (%)[c]	*T*/°C
1	Ph	Me	**1**	16	34	0
2	Ph	Me	**1**	18	35	20
3	Ph	Me	**1**	23	43	40
4	Ph	Me	**2**	52	42	20
5	Ph	Me	**2**	72	45	40
6	*p*-$MeOC_6H_4$	Me	**1**	45	33	40
7	*p*-$MeOC_6H_4$	Me	**2**	82	47	40
8	1,2-$C_6H_4(CH_2)_2$		**1**	28	6	20
9	1,2-$C_6H_4(CH_2)_2$		**1**	34	10	40
10	1,2-$C_6H_4(CH_2)_2$		**2**	72	12	40
11	1,2-$C_6H_4(CH_2)_3$		**1**	47	31	40
12	1,2-$C_6H_4(CH_2)_3$		**2**	78	26	40
13	2-naphthyl	Me	**1**	45	48	40
14	2-naphthyl	Me	**2**	85	53	40
15	1-naphthyl	Me	**1**	24	23	40
16	1-naphthyl	Me	**2**	62	50	40
17[d]	1-naphthyl	Me	**2**	72	54	40

[a] Reaction conditions: PhI=NTs : substrate = 1 : 5 (molar ratio), CH_2Cl_2, 2 h (40 °C), 12 h (20 °C), 24 h (0 °C); 1 mol% catalyst (based on starting PhI=NTs). [b] Defined relative to starting PhI=NTs. [c] Determined by HPLC with chiral column. [d] 5 mol% catalyst (based on starting PhI=NTs) was used.

Table 2 Asymmetric amidation of saturated C–H bonds by complex **3**[a]

Entry	R^1	R^2	Yield (%)[b]	Ee (%)[c]	*T*/°C
1	Ph	Me	42	37	20
2	Ph	Me	54	43	40
3	*p*-$MeOC_6H_4$	Me	68	33	40
4	1,2-$C_6H_4(CH_2)_2$		70	15	40
4	1,2-$C_6H_4(CH_2)_3$		75	32	40
6	2-naphthyl	Me	78	58	40
7	1-naphthyl	Me	58	35	40

[a] Reaction conditions: CH_2Cl_2, 2 h (40 °C), 12 h (20 °C). [b] Defined relative to complex **3**. [c] Determined by HPLC with chiral column.

highest ee obtained in the catalytic amidations was 54% for 1-ethylnaphthalene (entry 17).

Efforts have been made to ascertain the active species in the ruthenium-catalysed amidation reactions. Treatment of complex **1** with 2 equiv. of PhI=NTs in CD_2Cl_2 at room temperature completely converted **1** into a bis(tosylimido)ruthenium(VI) complex, $[Ru^{VI}(Por^*)(NTs)_2]$ **3**, which was characterised by the following spectral methods. The ^1H NMR spectrum‡ of **3**, typical of a diamagnetic ruthenium porphyrin, shows *ortho*- and *meta*-proton resonances of axial tosyl groups, and the H_β resonances of the chiral porphyrinato ligand at δ 4.89, 6.19 and 8.76, respectively, with an integration ratio of 1 : 1 : 2. The UV–VIS spectrum of **3** exhibits Soret and β bands at 422 and 537 nm, respectively, both of which are red-shifted by *ca.* 8 nm when compared with the carbonyl complex **1**. All these spectral features strongly resemble those of $[Ru^{VI}(Por)(NTs)_2]$ (Por = achiral *meso*-tetraarylporphyrinato dianion).[6] Further, the positive ion electrospray mass spectrum of **3** shows a prominent cluster peak at *m/z* 1579.8 that can be attributed to the parent ion of **3**. Complex **3** constitutes the first example of a chiral imido metalloporphyrin, and, importantly, it was found to be reactive towards saturated C–H bonds, leading to an enantioselective insertion of the NTs group into these bonds.§ The results are listed in Table 2. Under identical conditions, the ees obtained for the stoichiometric amidation by complex **3** and for the catalytic amidation by **1**, except for substrates 1- and 2-ethylnaphthalene, are rather similar, suggesting that complex **3** likely functions as the active species responsible for the asymmetric amidation reactions. Notably, the amidation of 2-ethylnaphthalene by **3** gave 58% ee (entry 6), which represents the highest ee obtained in this work.

For the manganese catalysed reactions, we found that the positive ion electrospray mass spectrum of a reaction mixture of **2** and PhI=NTs in CH_2Cl_2 showed a prominent cluster peak at *m/z* 1569.1 ascribable to the fragment $[Mn(Por^*)(PhINTs)]^+$. This suggests the involvement of a manganese tosylamido reactive intermediate and suggests that different types of active species may be involved in the ruthenium and manganese catalyses. To probe the nature of the intermediates formed in the rate-limiting step during the amidation catalysed by **2**, we examined substitution effect by measuring the amidation rates (k_{rel}) of substituted ethylbenzenes *p*-YC_6H_4Et (Y = MeO, Me, F, Br) relative to that of ethylbenzene, which reveals that both electron-donating and -withdrawing substituents promote the amidation process. A dual-parameter (σ^+, $\sigma_{JJ}^\bullet$) fitting of log k_{rel}, as established by Jiang and co-workers,[12] through multiple regression gave rise to excellent linearity (Fig. 1), with ρ^+ and $\rho_{JJ}^\bullet$ values of −0.49 and 0.66, respectively, suggesting that the amidation reactions should proceed *via* a benzylic radical intermediate, which possibly resulted from H-atom abstraction from the substrates by the manganese tosylamido active intermediate.

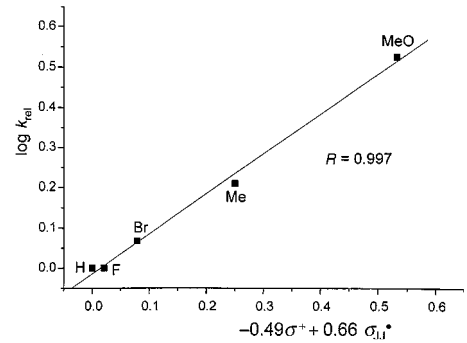

Fig. 1 Plot of log k_{rel} *vs.* (σ^+, $\sigma_{JJ}^\bullet$) for the amidation of substituted ethylbenzenes *p*-YC_6H_4Et (Y = MeO, Me, F, H, Br) by PhI=NTs catalysed by manganese catalyst **2**. The *R* value for the multiple regression is indicated.

We acknowledge support from the Hong Kong Research Grants Council and The University of Hong Kong.

Notes and references

† *General procedure* for the amidation reactions: To a Schlenk flask containing the complex (5 μmol) and molecular sieves (4 Å) (150 mg) was added a solution of substrate (2.5 mmol) in dry CH_2Cl_2 (5 ml) *via* syringe. The mixture was stirred for 10 min at room temperature under argon. PhI=NTs (0.5 mmol) was then added against a positive pressure of argon. The reaction was maintained at 40 °C for 2 h. After cooling, the molecular sieves were filtered off and washed with CH_2Cl_2. The filtrate and washings were evaporated to dryness and the organic product, purified by column chromatography, was identified by ^1H and ^{13}C NMR, and high-resolution MS, along with melting point.

‡ *Selected data* for **3**: δ_H(300 MHz, CD_2Cl_2) 8.76 (s, 8H), 7.37 (s, 4H), 6.19 (d, 4H), 4.89 (d, 4H), 3.54 (s, 8H), 2.69 (s, 8H), 1.97 (m, 8H), 1.84 (m, 14H), 1.34 (m, 24H), 1.07 (m, 8H).

§ The general procedure for the stoichiometric amidation of saturated C–H bonds by complex **3** is the same as that for the catalytic amidation by **1** and **2**, except that 0.25 mmol of **3**, formed *in situ* by treating **1** with 2 equiv. of PhI=NTs, was used instead of **1** and **2**, and no additional PhI=NTs was added.

1 A. Sorokin, A. Robert and B.Meunier, *J. Am. Chem. Soc.*, 1993, **115**, 7293 and references therein.
2 R. Breslow and S. H. Gellman, *J. Chem. Soc., Chem. Commun.*, 1982, 1400.
3 E. W. Svatis, J. H. Dawson, R. Breslow and S. H. Gellman, *J. Am. Chem. Soc.*, 1985, **107**, 6427.
4 J.-P. Mahy, G. Bedi, P. Battioni and D. Mansuy, *Tetrahedron Lett.*, 1988, 1927.
5 J.-P. Mahy, G. Bedi, P. Battioni and D. Mansuy, *New J. Chem.*, 1989, **13**, 651.
6 S.-M. Au, J.-S.Huang, W.-Y. Yu, W.-H. Fung and C.-M. Che, *J. Am. Chem. Soc.*, 1999, **121**, 9120.
7 I. Nägeli, C. Baud, G. Bernardinelli, Y. Jacquier, M. Moran and P. Müller, *Helv. Chim. Acta*, 1997, 1087.
8 See for example: K. J. O'Connor, S.-J. Wey and C. J. Burrows, *Tetrahedron Lett.*, 1992, **33**, 1001; D. A. Evans, M. M. Faul, M. T. Bilodeau, B. A. Anderson and D. M. Barnes, *J. Am. Chem. Soc.*, 1993, **115**, 5328; Z. Li, R. W. Quan and E. N. Jacobsen, *J. Am. Chem. Soc.*, 1995, **117**, 5889; H. Nishikori and T. Katsuki, *Tetrahedron Lett.*, 1996, **37**, 9245; S. Minakata, T. Ando, M. Nishimura, I. Ryu and M. Komatsu, *Angew. Chem., Int. Ed.*, 1998, **37**, 3392; J.-P. Simonato, J. Pécaut, W. R. Scheidt and J.-C. Marchon, *Chem. Commun.*, 1999, 989.
9 R. L. Halterman and S.-T. Jan, *J. Org. Chem.*, 1991, **30**, 5235.
10 T.-S. Lai, H.-L. Kwong, R. Zhang and C.-M. Che, *J. Chem. Soc., Dalton Trans.*, 1998, 3559; A. Berkessel and M. Frauenkron, *J. Chem. Soc., Perkin Trans. 1*, 1997, 2265.
11 T.-S. Lai, H.-L. Kwong, C.-M. Che and S.-M. Peng, *Chem. Commun.*, 1997, 2373.
12 X. Jiang, *Acc. Chem. Res.*, 1997, **30**, 283.

Communication 9/07653K

Synthesis of an anionic tridentate phosphinoborate and its reaction chemistry with Sn(II)

Alfred A. Barney, Alan F. Heyduk and Daniel G. Nocera*

Department of Chemistry, Massachusetts Institute of Technology, 6-335, 77 Massachusetts Avenue, Cambridge, MA 02139-4307, USA. E-mail: nocera@MIT.edu

Received (in Bloomington, IN, USA) 11th August 1999, Accepted 13th October 1999

Dichlorophenylborane reacts smoothly with [Li(tmen)][CH_2PPh_2] in THF to afford, in good yields, the Li(tmen)$^+$ salt of a novel monoanionic tridentate phosphinoborate, tris(diphenylphosphinomethyl)phenylborate; reaction of the ligand with $SnCl_2$ produces tris(diphenylphosphinomethyl) phenylboratotin(II) chloride, which may be dehalogenated to give the η^3 compound, {[PhB(CH_2PPh_2)$_3$]Sn}PF_6, tris(diphenylphosphinomethyl)-phenylboratotin(II) hexafluorophosphate.

By comparison to their neutral congeners,[1] tridentate anionic phosphines are rarely found within the coordination spheres of metal ions, emerging as viable ligands only recently in the preparation of water-soluble hydrogenation catalysts.[2] In these systems, an isolated anionic charge is introduced by sulfonylation of conventional phosphine ligands remote to the ligation site. With the desire of adding new, anionic six-electron donor ligands to the palette of coordination chemistry, we turned our attention to strategies that would permit the incorporation of a negative charge within the framework of a tridentate phosphine. As amply demonstrated in pyrazoylborate chemistry[3,4] and the recent synthesis of [PhB($CH_2SR)_3$]$^-$ by Riordan and coworkers,[5] the borate bridgehead provides both the desired negative charge and a scaffold to support three ligating arms with a hybridization that sustains a *fac* conformation about a metal center. We now report the synthesis and characterization of the novel anion, tris(diphenylphosphinomethyl)phenylborate **1**. The ligand features a negative charge proximate to a highly polarizable six-electron phosphine donor set. Within the context of hard/soft treatments of acid/base properties, **1** should exhibit a propensity to associate to soft metals. Along these lines, we initially elaborate the chemistry of **1** with tin(II), reporting the X-ray characterization of tris(diphenylphosphinomethyl)phenylboratotin(II) chloride **2** and its structural changes upon replacement of the coordinating chloride with an outer sphere anion PF_6.

Addition of diphenylphosphinomethide to dichlorophenylborane yields a borate salt, which subsequently undergoes substitution of its chlorides by two additional equivalents of diphenylphosphinomethide to provide the tris(diphenylphosphinomethyl)phenylborate ligand in good yields (Scheme 1).† Work up should follow immediately after the addition is completed, as prolonged reaction times lead to lower isolated yields. The crude compound is a pale yellow solid that can be recovered in a purified form from CH_2Cl_2. The phenyl and methylene resonances of the phosphinoborate anion are readily discerned in the ^{1}H NMR spectrum at δ 6.8–7.6 and 1.07, respectively, as are the methyl and ethylene protons of the Li(tmen)$^+$ cation at δ 2.18 and 2.30.

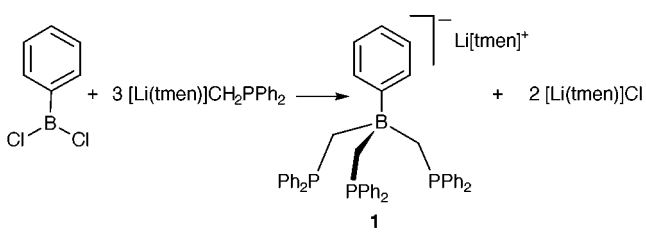

Scheme 1

Anion **1** reacts with $SnCl_2$ in CH_2Cl_2 to give [PhB($CH_2PPh_2)_3$]SnCl **2**, which was structurally characterized.‡ This is noteworthy in view of the small number of structurally characterized tin(II) phosphine complexes. The recent classification and analysis of structural data for > 500 tin coordination compounds[6] reveals *ca.* 200 to contain divalent tin. Of these, nitrogen and oxygen are the most common non-halogen atoms found to bond with Sn(II), with poly(pyrazolyl)borates figuring prominently within this classification.[7–9] However, structurally characterized monomeric compounds containing direct ligation of phosphorus to tin are few, and only a small number of these possess tin in its divalent oxidation state.[10–15] The solution of the single crystal X-ray structure of **2** now adds to this abbreviated list.

The most striking feature of the ORTEP diagram shown in Fig. 1 is that one of the phosphine arms of the ligand coordinates the metal center only weakly. The bond distance between Sn(1) and the two phosphorus atoms P(1) and P(3) are *d*[Sn(1)–P(3)] = 2.6746(14) Å and *d*[Sn(1)–P(1)] = 2.690(2) Å, respectively. These distances are slightly longer than those found in the limited data set for Sn–P bond lengths.[10,11,15–17] In contrast, the weakly bonded phosphorus, P(2), is situated far from the metal, *d*[Sn(1)–P(2)] = 3.036(2) Å, slightly beyond the standard covalent bonding distances for tin and phosphorus.[18] This coordination of **2** is distinguished from the analogous tin(II) pyrazoylborate complex insofar as the long Sn–N bond is well within the standard covalent bonding distance for a formal Sn–N bond. Nevertheless, the distorted trigonal bipyramidal coordination geometry about the metal, as is often observed for tin(II) pyrazolylborate complexes, is completed by a Sn(1)–

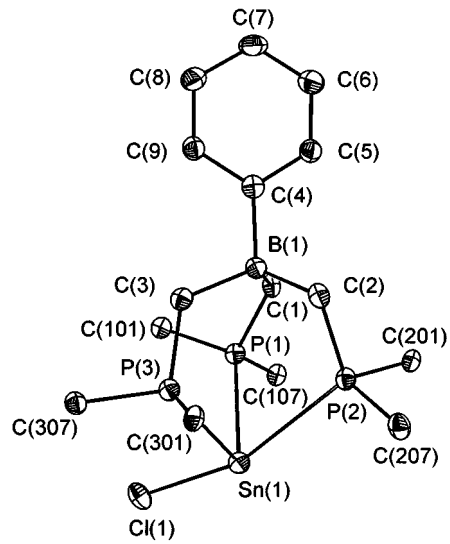

Fig. 1. ORTEP representation and labeling scheme of **2** with thermal ellipsoids drawn at the 35% probability level. Only the *ipso* carbons of the phenyl rings on phosphorus are shown for clarity.

Cl(1) bond, which is long at 2.599(2) Å, and the stereochemically active tin(II) lone pair. The intraligand P(1)–Sn(1)–P(3) bond angle of 81.76(4)° is markedly contracted relative to P–Sn–Cl angles of 87.57(4) and 95.18(5)°. Finally, the local geometry around the boron atom is approximately tetrahedral.

That all three phosphines are capable of bonding to the metal is revealed by the solution $^{31}P\{^{1}H\}$ NMR spectrum of **2**, which shows only a single broad peak, centered at δ −5.1. Similar results are observed for anionic bidentate phosphine[19] and poly(pyrazolyl)borate[7] complexes of tin(II) as well. With one coordination site of **2** occupied by chloride, the ligation of only two phosphines is consistent with the stereochemical influence exerted by the electron lone pair present on the tin(II) center. Accordingly, the removal of chloride from **2** would be expected to open a coordination site, thus allowing the dangling phosphine to strongly associate with the metal center. This contention is supported by the reaction chemistry of **2** with $TlPF_6$. Reaction of **2** with one equivalent of thallium hexafluorophosphate yields {[PhB(CH_2PPh_2)$_3$]Sn}PF_6 **3**. In contrast to **2**, the $^{31}P\{^{1}H\}$ NMR spectrum of **3** shows a single sharp resonance at δ +5.1 that is flanked by tin satellites. Coupling of three equivalent phosphorus atoms to ^{117}Sn (7.68%) and ^{119}Sn (8.59%) isotopes are clearly observed [$^{1}J(^{117/119}Sn–^{31}P)$ = 1330, 1270 Hz], consistent with the coordination of all three phosphines to the metal center.

Considering the rich coordination chemistry of the related tris(pyrazolyl)borate anion, a similarly diverse chemistry of **1** may be expected. The ligand is distinguished by its negative charge and ability of **1** to adopt four- and six-electron coordination modes about a highly polarizable metal center. The combination of these properties in a singular ligand system should find utility in the design of novel compounds and new metal-based catalytic schemes. Along these lines, the recent preparation of [PhB(CH_2PPh_2)$_3$](H)Ir(η^3-C_8H_{13}) and its reaction with H_2SiMes_2 to produce an iridium silylene[20] illustrates the unique reactivity engendered by this tridentate phosphinoborate ligand.

The National Science Foundation Grant CHE-9817851 provides generous support for this research. We thank Jonas C. Peters for useful discussions with regard to ligand design strategies.

Notes and references

† *Experimental procedures*: reactions were carried out under the nitrogen atmosphere of a dry box, which was capable of supporting a variety of standard synthetic methodologies. Solvents were freshly prepared for synthesis by their distillation from appropriate drying agents and by subsequently degassing prior to use. ^{1}H, ^{31}P and ^{11}B NMR spectra were recorded on Varian Unity 300 and Mercury 300 spectrometers. Chemical shifts for ^{1}H, ^{31}P, and ^{11}B NMR are reported in ppm *vs.* TMS, H_3PO_4 (85%) and BF_3•Et_2O, respectively.

1: [Li(tmen)]CH_2PPh_2[21] (3 g, 9.31 mmol), dissolved in 100 mL of THF, was added slowly with stirring over 1.5 h to a 25 mL THF solution of dichlorophenylborane (0.49 g, 3.1 mmol) maintained at 0 °C. The mixture was stirred an additional 30 min whereupon the solvent was removed *in vacuo* to leave an oily residue. The borate was dissolved in CH_2Cl_2 and the solution was filtered to remove LiCl. Solvent removal gave **1** as a microcrystalline solid and the product was dried *in vacuo* overnight (2.36 g, 82% yield). $C_{51}H_{57}BLiN_2P_3$; found: C, 75.5; H, 7.18; N, 3.66; P, 11.09; requires: C, 75.75; H, 7.10; N, 3.46; P, 11.49%. ^{1}H NMR (CD_3CN): δ 6.8–7.6 (m, 35H), 2.3 (s, 4H), 2.18 (s, 12H), 1.07 (br, 6H) $^{31}P\{^{1}H\}$ NMR: δ −10.2 [q, ^{2}J ($^{11}B–^{31}P$) 9.16 Hz], $^{11}B\{^{1}H\}$ NMR: δ −15.45 [q, ^{2}J ($^{31}P–^{11}B$) 9.16 Hz)].

2: a 50-mL CH_2Cl_2 solution of **1** (0.4 g, 0.5 mmol) was added to a mol equivalent of $SnCl_2$ (0.094 g) dissolved in 10 mL of CH_2Cl_2. The resulting solution was stirred overnight. A residue remained upon the vacuum evaporation of CH_2Cl_2. The product was extracted away from unreacted $SnCl_2$ with benzene, and the resulting solution was filtered and concentrated to a third of its original volume. Purified product was obtained by layering the benzene filtrate with an equal volume of pentane. Compound **2** formed over 2–3 days, after which the clear crystals were collected and dried (0.31 g, 74%). $C_{45}H_{41}BClP_3Sn$; found: C, 64.01; H, 5.03; P, 10.98; requires: C, 64.37; H, 4.92; P, 11.07%. ^{1}H NMR (C_6D_6): δ 6.7–7.8 (m, 35H), 1.9 (br, 6H); $^{31}P\{^{1}H\}$ NMR (C_6D_6): δ −5.1 (br); $^{11}B\{^{1}H\}$ NMR (C_6D_6): δ −13.23 (br).

3: the chloride ligand was removed from **2** by dissolving 0.25 g (0.30 mmol) of the compound in 50 mL of acetonitrile, followed by the addition of a mol equivalent (0.104 g) of $TlPF_6$. The reaction mixture was stirred overnight and then filtered to remove TlCl as a white solid. The filtrate was removed *in vacuo* to afford the product, which was dried *in vacuo* overnight (0.250 g, 89%). $C_{45}H_{41}BF_6P_4Sn$; found: C, 56.96; H, 4.55; P, 13.17; requires: C, 56.94; H, 4.35; P, 13.05%. ^{1}H NMR ($CDCl_3$), δ 6.7–7.8 (m, 35H), 1.9 (br, 6H); $^{31}P\{^{1}H\}$ NMR ($CDCl_3$), δ 5.1 [s, $^{1}J(^{117/119}Sn–^{31}P)$ 1331.8, 1272.8 Hz]; δ −142.9 [sept,$^{1}J(^{31}P–^{19}F)$ 708.42 Hz]; $^{11}B\{^{1}H\}$ NMR($CDCl_3$); δ –11.9 (br).

‡ *Crystal data* for **2**: $C_{45}H_{41}BClP_3Sn$, M = 839.64, monoclinic, space group $P2_1/c$, a = 12.099(4), b = 19.699(4), c = 17.215(6), β = 103.818(10)°, U = 3984(2) Å^3, Z = 4, D_c = 1.400 g cm^{-3}, T = 183(2) K, μ = 0.860 mm^{-1}, $wR2$ = 0.0992 (5698 independent reflections), $R1$ = 0.0408 [$I > 2\sigma(I)$]. CCDC 182/1450.

1 F. A. Cotton and B. Hong, *Prog. Inorg. Chem.*, 1992, **40**, 179.
2 C. Bianchini, P. Frediani and V. Sernau, *Organometallics*, 1995, **14**, 5458.
3 S. Trofimenko, *Acc. Chem. Res.*, 1971, **4**, 17.
4 S. Trofimenko, *Prog. Inorg. Chem.*, 1986, **34**, 115.
5 P. J. Schebler, C. G. Riordan, I. A. Guzei and A. L. Rheingold, *Inorg. Chem.*, 1998, **37**, 4754.
6 C. E. Holloway and M. Melnik, *Main Group Met. Chem.*, 1998, **21**, 371.
7 D. L. Reger, *Synth. Lett.*, 1992, 469.
8 D. L. Reger, S. J. Knox, M. F. Huff, A. L. Rheingold and B. S. Haggerty, *Inorg. Chem.*, 1991, **30**, 1754.
9 D. L. Reger, S. S. Mason, J. Takats, X W. Zhang, A. L. Rheingold and B. S. Haggerty, *Inorg. Chem.*, 1993, **32**, 4345.
10 H. H. Karsch, A. Appelt and G. Müller, *Organometallics*, 1986, **5**, 1664.
11 N. Froelich, P. B. Hitchcock, J. Hu, M. F. Lappert and J. R. Dilworth, *J. Chem. Soc., Dalton Trans.*, 1996, 1941.
12 U. Baumeister, H. Hartung, K. Jurkschat and A. Tzschach, *J. Organomet. Chem.*, 1986, **304**, 107.
13 A. L. Seligson and J. Arnold, *J. Am. Chem. Soc.*, 1993, **115**, 8214.
14 H. H. Karsch, A. Appelt and G. Müller, *Angew. Chem., Int. Ed. Engl.*, 1985, **24**, 402.
15 M. Westerhausen, M. M. Enzelberger and W. Schwarz, *J. Organomet. Chem.*, 1995, **491**, 83.
16 A. L. Balch and D. E. Oram, *Organometallics*, 1986, **5**, 2159.
17 M. Driess, S. Martin, K. Merz, V. Pintchouk, H. Pritzkow, H. Grützmacher and M. Kaupp, *Angew. Chem., Int. Ed. Engl.*, 1997, **36**, 1894.
18 A. H. Cowley, R. L. Geerts, C. M. Nunn and C. J. Carrano, *J. Organomet. Chem.*, 1988, **341**, C27.
19 P. G. Harrison, *Coord. Chem. Rev.*, 1990, **102**, 234.
20 J. C. Peters, J. D. Feldman and T. D. Tilley, *J. Am. Chem. Soc.*, in press.
21 N. E. Schore, L. S. Benner and B. E. Labelle, *Inorg. Chem.*, 1981, **20**, 3200.

Communication 9/06560A

The first chiral diimido chelate complexes of molybdenum and tungsten: transition metal diimido complexes on the way to asymmetric catalysis

Eike A. Kretzschmar, Jennifer Kipke and Jörg Sundermeyer*

Fachbereich Chemie, Philipps-Universität Marburg, D-35032 Marburg, Germany.
E-mail: jsu@chemie.uni-marburg.de

Received (in Basel, Switzerland) 13th September 1999, Accepted 25th October 1999

The first complexes [M(TADDAMINat)Cl_2(dme)] (M = Mo (2), W (4)) containing a chiral diimido ligand regime have been synthesized; 2 has been structurally characterized and used as catalyst for C–C and C–N bond formation reactions.

Transition metal imido complexes $[M^{VI}(NR)_2X_2]$ have attracted considerable attention as isolobal analogues of group 4 metallocene complexes $[cp_2M^{IV}X_2]$.[1] This may well make these diimido complexes, chelating ones in particular, promising alternatives to the well known,[2] highly efficient *ansa*-metallocenes for olefin polymerisation and other C–C or C–N coupling reactions.Although few applications of diimido complexes in catalysis are known,[3] no successful use in enantioselective transformations has been described so far.

Gibson *et al.* first reported chelating bis(arylimido) complexes, one of them revealing a solid state structure of C_2-symmetry.[4] However, this compound was found to be configurationally unstable in solution at room temperature. Here, we present the synthesis of the first chiral C_2-symmetric diimido complexes of molybdenum **2** and tungsten **4** derived from the enantiomerically pure chiral diamine **1**.

Our efforts towards the synthesis of chiral five-membered as well as seven-membered chelate complexes containing sp^2 carbon atoms in the ligand backbone failed, in accordance with the work of Siemeling *et al.*[5] In order to render the system more flexible we decided to use an entirely aliphatic backbone containing only sp^3 carbons in our chelate. The ligand TADDAMIN {(4*S*,5*S*)-2,2-dimethyl-α,α,α′,α′-tetraphenyl-1,3-dioxolan-4,5-dimethanamine} **1** reported by Seebach *et al.*[6] the amine derivative of the TADDOL family, which has proven its high efficiency in asymmetric synthesis,[7] looked very promising to us. Following the well established route for the synthesis of diimido complexes of the type $[Mo(NR)_2Cl_2(dme)]$ from Na_2MoO_4 in the presence of Me_3SiCl–Et_3N,[3] we obtained [Mo(TADDAMINat)Cl_2(dme)] **2** in 95% yield (Scheme 1).†

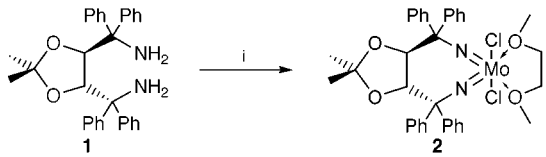

Scheme 1 Synthesis of molybdenum complex **2**. *Reagents and conditions*: i, Na_2MoO_4, **1**, Me_3SiCl, Et_3N, dme (Mo : **1** : Me_3SiCl : Et_3N = 1 : 1 : 20 : 20), 12 h, 85 °C.

Crystals of **2** suitable for X-ray structure determination‡ were grown from a saturated toluene solution. Each unit cell contains one solvent molecule (Fig. 1).

Group 6 metal complexes of the constraint-geometry [TADDAMINat]$^{4-}$ ligand type are isoelectronically related to the well known [TADDOLat]$^{2-}$ complexes of group 4 metals described by Seebach in ref. 9. Table 1 compares the most important structural features of the structurally characterized titanium TADDOLato complex **3**[10] with its isoelectronic TADDAMINato molybdenum counterpart **2**. Similar bonding distances and bond angles indicate comparable metal ligand π-bonding interactions and similar constraints within the isoelectronic TiO_2 and MoN_2 structural units.

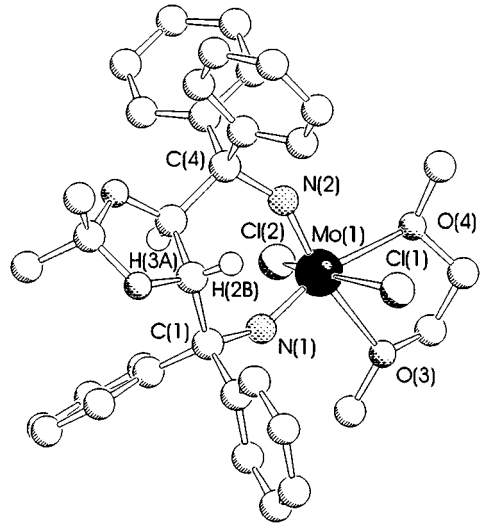

Fig. 1 The molecular structure of [Mo(TADDAMINat)Cl_2(dme)] **2** (toluene omitted for clarity). Selected bond lengths (pm) and angles (°): Mo–N(1) 173.7(2), Mo–N(2) 173.9(3), Mo–Cl(1) 240.7(1), Mo–Cl(2) 240.0(1), Mo–O(3) 236.6(2), Mo–O(4) 238.0(2), C(1)–N(1) 145.8(4), C(4)–N(2) 145.6(5); N(1)–Mo–N(2) 99.52(13), C(1)–N(1)–Mo 148.7(2), C(4)–N(2)–Mo 148.7(2), Cl(1)–Mo–Cl(2) 158.23(4), O(3)–Mo–O(4) 68.91(9).

Table 1 Comparison of bond lengths (Å) and angles (°) in the molybdenum complex **2** and the titanium complex **3**

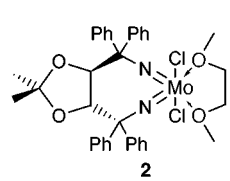

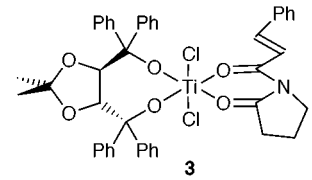

Mo≡N	1.74/1.74	Ti≡O	1.76/1.79
Mo—N—C	148.7/148.7	Ti—O—C	147.1/145.2
N—Mo—N	99.5	O—Ti—O	97.2

The analogous tungsten complex [W(TADDAMINat)-Cl_2(dme)] **4** was synthesized following a route used before in our group.[11] Reaction of WO_2Cl_2(dme), prepared *in situ* from $WOCl_4$,[12] with TADDAMIN **1** in the presence of Et_3N and TMSCl gave complex **4** as an off-white solid in 90% yield (Scheme 2).†

Since d^0 imido complexes are excellent Lewis acids, we were interested in the potential of enantiomerically pure **2** in various stereoselective reactions. Recently Leung *et al.* described the successful application of achiral group 6 organoimido com-

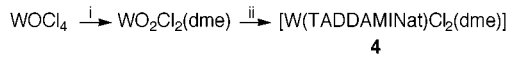

Scheme 2 Synthesis of tungsten complex **4**. *Reagents and conditions*: i, $WOCl_4$ (1 equiv.), $(Me_3Si)_2O$ (1 equiv.), dme, 0 °C followed by 3 h at 40 °C; ii, TMSCl (8 equiv.), Et_3N (5.6 equiv.), **1** (1 equiv.), dme, 6 d, 85 °C.

plexes in the ring opening of epoxides with $TMSN_3$.[13] Here we disclose our first results under non-optimized conditions,§ using **2** as catalyst for the kinetic resolution of racemic styrene oxide with $TMSN_3$ and the enantioselective trimethylsilylcyanation of benzaldehyde with TMSCN. Whereas the transformation of styrene oxide resulted in up to 30% ee at 100% conversion based on consumed $TMSN_3$ for the reaction of benzaldehyde with TMSCN 20% ee at 100% conversion could be obtained.[14]

As C_2-symmetric complexes of this type are of high interest for the stereoselective polymerisation of α-olefins, we currently are investigating their catalytic potential in this respect.

In conclusion, we present here the first chiral diimido complexes of molybdenum **2** and tungsten **4** and the application of **2** as a catalyst for enantioselective transformations using C–N and C–C bond forming reactions. Currently we are investigating modified ligand systems with sterically more demanding aryl substituents in order to further improve the stereodifferentiation using these complexes as a promising new class of chiral Lewis acid catalysts.

Financial support by Deutsche Forschungsgemeinschaft (SFB 260 Marburg), the Fonds der Chemischen Industrie, and the European Community (INTAS-96-I185) is gratefully acknowledged.

Notes and references

† *Selected spectroscopic data*. For **2**: ^{1}H NMR (300 MHz, $CDCl_3$, 298 K): δ 0.76 (s, 6H, CH_3), 3.72 and 3.89 (br s, 10H, CH_3, CH_2 dme),[a] 5.21 (s, 2H, CH), 7.20–7.54 (m, 20H, Ar-/Ar′-H). [a]Resolution at 223 K (400 MHz): δ 3.72 (d, 2H, CH_2), 3.81 (s, 6H, CH_3), 3.99 (d, 2H, CH_2). ^{13}C NMR ($CDCl_3$, 75 MHz, 298 K): δ 27.1 (q, CH_3), 62.6 (q, CH_3 dme), 71.0 (t, CH_2 dme), 80.0 (d, CH), 94.9, 107.7 (s, *C*Ph$_2$ and *C*Me$_2$), 127.4, 128.0, 128.2, 128.3, 130.7 (d, Ar-/Ar′-C), 141.7 (s, Ar-C$_{ipso}$), 142.7 (s, Ar-C′$_{ipso}$). MS (APCI positive, MeCN): 719 (M + 1). α_{298} = −207.2($CHCl_3$, c = 1 g 100 ml^{-1}, T = 298 K).

For **4**: ^{1}H NMR ($CDCl_3$, 300 MHz, 298 K): δ 0.69 (s, 6H, CH_3), 3.82 and 3.91 (br s, 10H, CH_2, CH_3 (dme)),[a] 5.05 (s, 2H, CH), 7.20–7.53 (m, 20H, aryl-H). [a]Resolution at 223 K (400 MHz): δ 3.79 (d, 2H, CH_2), 3.97 (s, 6H, CH_3), 4.03 (d, 2H, CH_2). ^{13}C NMR ($CDCl_3$, 75 MHz, 298 K): δ 27.1 (q, CH_3), 55.8 (q, CH_3 dme), 71.3 (t, CH_2 dme), 81.4 (d, CH), 90.3, 107.6 (s, *C*Ph$_2$ and *C*Me$_2$), 127.0, 127.1, 127.7, 128.1, 130.7 (d, Ar-/Ar′-C), 144.1 (s, Ar-C$_{ipso}$), 144.5 (s, Ar-C′$_{ipso}$).

‡ *Crystal data* for $C_{42}H_{46}Cl_2MoN_2O_4$ **2**: M = 809.65, monoclinic, space group $P2_1$ (no. 4), a = 1057.2(1), b = 1489.2(1), c = 1251.9(1) pm, β = 91.504(10), U = 1970.2(4) × 10^{-30} m^3, T = 223(2) K, Z = 2, μ(Mo-Kα) = 0.511 mm^{-1}, F(000) = 840, 6389 reflections measured, 6027 unique (R_{int} = 0.0205) which were used in all calculations. The final $wR(F_2)$ was 0.0838 and $R1$ = 0.0319 (all data). A colorless, irregular quadertype single crystal of **2** (dimensions 0.35 × 0.30 × 0.25 mm), recrystallized from toluene, was used. The structure was solved using direct methods and refined by full matrix least squares on F^2. CCDC 182/1455. See http://www.rsc.org/suppdata/cc/1999/2381/ for crystallographic files in .cif format.

§ *Conditions for catalytic epoxide ring opening reactions*: styrene oxide: $TMSN_3$: **2** = 2:1:0.01, 3 d room temp; *regioselectivity*: 1-trimethylsilyloxy-2-azido-2-phenyl ethane : 1-azido-2-phenyl-2-trimethylsiloxy ethane = 85:15 [c(**2**) = 6 mM]. *Conditions for catalytic trimethylsilylcyanation reaction*: benzaldehyde: TMSCN: **2** = 1:1:0.05, 3 d, −25 °C. Enantiomeric excess determined by chiral capillary GLC (CP-Chirasil-Dex CB).

1 P. W. Dyer, V. C. Gibson, J. A. K. Howard, B. Whittle and C. Wilson, *J. Chem. Soc., Chem. Commun.*, 1992, 1666; V. C. Gibson, *J. Chem. Soc., Dalton Trans.*, 1994, 1607.
2 H.-H. Brintzinger, D. Fischer, R. Müllhaupt, B. Rieger and R. Waymouth, *Angew. Chem., Int. Ed. Engl.*, 1995, **34**, 1143.
3 W.-H. Leung, M.-C. Wu, J. L. C. Chim, M.-T. Yu, H.-W. Hou, L.-L. Yeung, W.-T. Wong and Y. Wang, *J. Chem. Soc., Dalton Trans.*, 1997, 3525; W.-H. Leung, M.-T. Yu, M.-C. Wu and L.-L. Yeung, *Tetrahedron Lett.*, 1996, **37**, 891; M. P. Coles and V. C. Gibson, *Polym. Bull.*, 1994, **33**, 529; M. P. Coles, C. I. Dalby, V. C. Gibson, W. Clegg and M. R. J. Elsegood, *J. Chem. Soc., Chem. Commun.*, 1995, 1709; D. Jan, F. Simal, A. Demonceau, A. F. Noels, K. A. Rufanov, N. A. Ustynyuk and D. N. Gourevitch, *Tetrahedron Lett.*, 1999, **40**, 5695.
4 V. C. Gibson, C. Redshaw, W. Clegg, M. R. J. Elsegood, U. Siemeling and T. Türk, *J. Chem. Soc., Dalton Trans.*, 1996, 4513; C. Redshaw, V. C. Gibson, W. Clegg, A. J. Edwards and B. Miles, *J. Chem. Soc., Dalton Trans.*, 1997, 3343.
5 U. Siemeling, T. Türk, W. W. Schoeller, C. Redshaw and V. C. Gibson, *Inorg. Chem.*, 1998, **37**, 4738.
6 D. Seebach, A. K. Beck, M.Hayakawa, G. Jaeschke, F. N. M.Kuhnle, I. Nageli, A. B. Pinkerton, P. B. Rheiner, R. O. Duthaler, P. M. Rothe, W. Weigand, R. Wunsch, S. Dick, R. Nesper, M. Worle and V. Gramlich, *Bull. Soc. Chim. Fr.*, 1997, **134**, 315.
7 D. Seebach and A. K. Beck, *Chimia*, 1997, **51**, 293.
8 P. W. Dyer, V. C. Gibson, J. A. K. Howard, B. Whittle and C. Wilson, *J. Chem. Soc., Chem. Commun.*, 1992, 1666.
9 *Encyclopedia of Reagents for Organic Synthesis*, L. Paquett (ed. in chief), J. Wiley and Sons, Chichester, 1995, vol. 3, 2167.
10 K. V. Gothelf, R. G. Hazell and K. A. Jørgensen, *J. Am. Chem. Soc.*, 1995, **117**, 4435.
11 U. Radius, J. Sundermeyer and H. Pritzkow, *Chem. Ber.*, 1994, **127**, 1827.
12 V. C. Gibson, T. P. Kee and A. Shaw, *Polyhedron*, 1990, **9**, 2293.
13 W.-H. Leung, E. K. F. Chow, M.-C. Wu, P. W. Y. Kum and L.-L. Yeung, *Tetrahedron Lett.*, 1995, **36**, 107.
14 L. E. Martínez, J. L. Leighton, D. H. Carsten and E. N. Jacobson, *J. Am. Chem. Soc.*, 1995, **117**, 5897 and references therein; X.-B. Zhou, J.-S. Huang, P.-H. Ko, K.-K. Cheung and C.-M. Che, *J. Chem. Soc., Dalton Trans.*, 1999, 3303 and references therein.

Communication 9/07525I

ChemComm

Stabilization of a germanium–oxygen double bond: a theoretical study

Chiu-Ling Lin, Ming-Der Su* and San-Yan Chu*

Department of Chemistry, National Tsing Hua University, Hsinchu 30043, Taiwan, ROC.
E-mail: ggs@chu1.chem.nthu.edu.tw

Received (in Cambridge, UK) 22nd September 1999, Accepted 25th October 1999

Both B3LYP and CCSD(T) computational results suggest that fluorine substitution can dramatically stabilize $F_2Ge{=}O$, with respect to FGe–OF, both from a kinetic and from a thermodynamic viewpoint.

It is generally acknowledged that intermediates with germanium doubly bonded to other elements (such as oxygen, sulfur, nitrogen *etc.*) are very unstable.[1,2] Indeed, most of our experimental knowledge of multiply bonded germanium still comes from matrix isolation studies. Therefore, the study of compounds having multiple bonds to germanium has been one of the major challenges in main group chemistry.[3,4] For instance, the first evidence for compounds containing the Ge=O moiety was reported in 1971.[5] Since then several schemes for the synthesis of germanones have been devised. Nevertheless, up to now only indirect evidence was available to suggest their transient existence.[6–9] Moreover, according to our previous study,[10] three reaction pathways for the unimolecular decomposition of HXGe=O to HX and GeO exist. These are shown in Scheme 1. The theoretical findings suggest that the most favorable dissociation path is predicted to be the 1,2-H shift route, while the 1,2-X shift path has the highest energy requirement and therefore is the least energetically favorable path. It is these intriguing theoretical results that have inspired this study. If the 1,2-X shift is the most unfavorable mechanism for the unimolecular dissociation of HXGe=O, would it be possible to extend this to synthesize and isolate compounds containing the Ge=O double bond at room temperature? What interests us particularly is to explore the possibility of designing molecular systems where $X_2Ge{=}O$ is more stable than the isomeric XGe–OX, and where relatively large barriers separate the two isomers.

HXGeO ⟶ HX + GeO

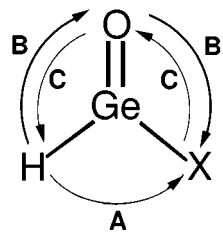

Path A:1,1-HX elimination
Path B:1,2-H shift (the most favorable)
Path C:1,2-X shift (the most unfavorable)
(X = H, F, Cl and Br)

Scheme 1

In view of the interest in isolating compounds containing a Ge=O double bond, we consider the possibility of stabilizing this moiety with various substituents. Here, we report a theoretical study concerning the effect of various substituents X (X = H, F, Cl, Br and Me) on the relative stability of $X_2Ge{=}O$ and XGe–OX isomers as well as on the transition states connecting them. See eqn. (1) in Table 1.

The geometries and energies of stationary points on the potential energy surface of eqn. (1) have been calculated using the non-localized density functional theory (DFT) in conjunction with the 6-311G* basis set, which is denoted as B3LYP/6-311G*.[11] All the stationary points have been positively identified as equilibrium structures [the number of imaginary frequency (NIMAG = 0) or transition states (NIMAG = 1)]. For better energetics, single-point calculations with B3LYP/6-311G* geometries were carried out at a higher level of theory which used coupled cluster single and double excitations including perturbative triple substitutions,[12] *i.e.* CCSD(T)/6-311++G**//B3LYP/6-311G* [hereafter designated CCSD(T)]. Unless otherwise noted, relative energies given in the text are those determined at CCSD(T) and include vibrational zero-point energy (ΔZPE) corrections determined at B3LYP/6-311G*.[13]

Some interesting points arising from the above calculations are as follows:

(1) Selected geometrical parameters of $X_2Ge{=}O$, XGe–OX, and the transition state for the reaction $X_2Ge{=}O \rightarrow$ XGe–OX [*i.e.* eqn. (1)] are listed in Table 1. It is apparent from Table 1 that halogen substitution (*i.e.* F, Cl and Br) strengthens the Ge=O double bond. In contrast, such substitutions seem to weaken the Ge–O single bond. On the other hand, methyl substitution appears to lengthen both Ge=O and Ge–O bonds slightly.

Table 1 Geometrical parameters of structures for eqn. (1) at the B3LYP/6-311G* level of theory (distances in Å, angles in degrees).

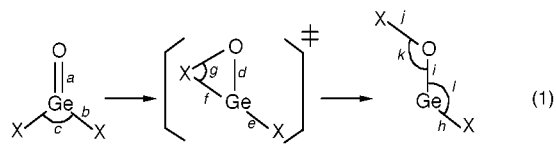

(1)

X	*a*	*b*	*c*	*d*	*e*	*f*	*g*	*h*	*i*	*j*	*k*	*l*
H	1.644	1.546	112.8	1.722	1.590	1.589	64.73	1.606	1.808	0.9642	112.8	92.63
Me	1.650	1.964	113.3	1.736	2.019	2.230	46.69	2.006	1.813	1.418	122.7	93.77
F	1.630	1.726	101.8	1.794	1.766	1.961	58.68	1.769	1.860	1.448	103.4	90.11
Cl	1.634	2.142	106.4	1.739	2.218	2.371	43.74	2.213	1.846	1.738	113.8	92.76
Br	1.638	2.300	108.4	1.727	2.386	2.506	41.01	2.373	1.836	1.875	114.9	93.43

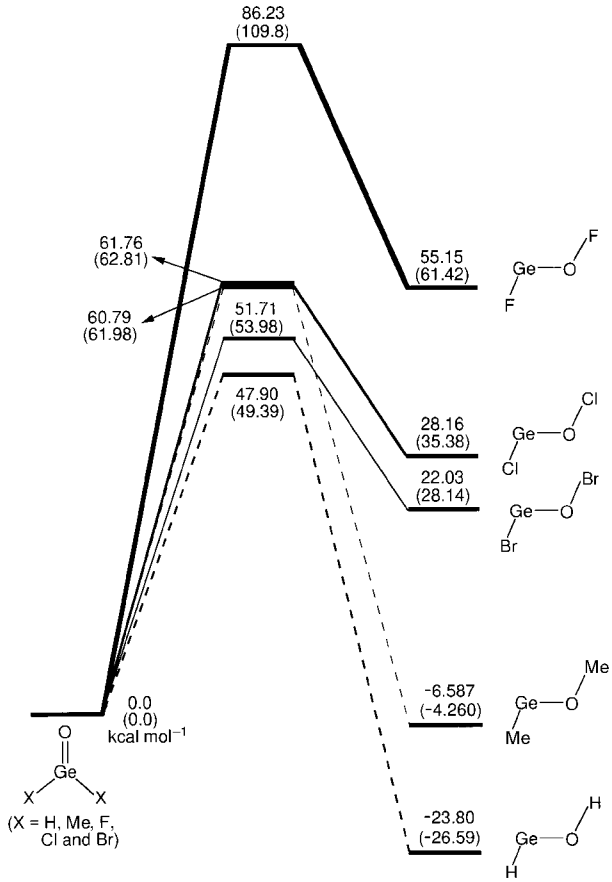

Scheme 2

(2) Scheme 2 shows the effects of various substitutions on the relative stabilities of $X_2Ge{=}O$ and XGe–OX at the B3LYP and CCSD(T) (in parentheses) levels of theory. It is worth noting that the relative stabilities of the doubly bonded and the *trans*-bent (singly bonded) species are dramatically reversed when hydrogens are replaced by electronegative substituents (such as F, Cl and Br). It is apparent from Scheme 2 that the energies of the XGe–OX molecules are much higher than those of the corresponding $X_2Ge{=}O$ by 61, 35 and 28 kcal mol^{-1} for X = F, Cl and Br, respectively. By contrast, the energies of HGe–OH and MeGe–OMe are below the energies of $H_2Ge{=}O$ and $Me_2Ge{=}O$ by 27 and 4.3 kcal mol^{-1}, respectively. Thus, the effect of dihalogen substitution is of special interest since it strongly stabilizes $X_2Ge{=}O$ relative to XGe–OX. In particular, our CCSD(T) results indicate that the endothermicity of eqn. (1) increases in the order X = Br (28 kcal mol^{-1}) < X = Cl (35 kcal mol^{-1}) < X = F (61 kcal mol^{-1}). It is therefore predicted that the more electronegative the halogen, the more stable the germanone ($X_2Ge{=}O$).

(3) The thermodynamic stability of $X_2Ge{=}O$ relative to XGe–OX may be understood in terms of the Ge–X *vs.* O–X bond energies.[14] That is to say, from eqn. (1) it is clear that a strong Ge–X bond and the weak O–X bond can overturn the large intrinsic preference of XGe–OX over $X_2Ge{=}O$.[15] Another surprising piece of evidence is that halogen substitution causes a shortening of the Ge=O double bond, as mentioned earlier. Therefore, it appears that halogen substitution strengthens the Ge=O double bond, particularly in the case of fluorine, assuming that bond energy–bond length relationships are valid. Furthermore, halogen substitution not only stabilizes the formal Ge=O double-bonded structure relative to XGe–OX, but it also raises the barrier to the $X_2Ge{=}O \rightarrow$ XGe–OX isomerizations, thus increasing the kinetic stability of the germanone molecules. For instance, as demonstrated in Scheme 2, the barrier for the isomerization of $X_2Ge{=}O$ to XGe–OX decreases in the order: X = F (110 kcal mol^{-1}) > X = Cl (63 kcal mol^{-1}) ≈ X = Me (62 kcal mol^{-1}) > X = Br (54 kcal mol^{-1}) > X = H (50 kcal mol^{-1}). In brief, fluorine is a particularly appealing possibility because of the strength of the Ge–F bonds.

(4) It should be pointed out that methyl substitution in eqn. (1) is predicted to be nearly thermoneutral, with an exothermicity of only 4.3 kcal mol^{-1}. Additionally, the barrier height for 1,2-CH_3 shift of $Me_2Ge{=}O$ is sizeable (63 kcal mol^{-1}), indicating that both $Me_2Ge{=}O$ and MeGe–OMe will have kinetic stability for such a migration reaction. This larger barrier ensures that, both isomers will be relatively stable kinetically if they were produced. Bulky substituents are generally expected to destabilize $X_2Ge{=}O$ relative to XGe–OX, owing to the steric effects.

In summary, the present work predicts that germanone $X_2Ge{=}O$ itself lies at the minimum of the potential energy surface and can be strongly stabilized in both a kinetic and a thermodynamic sense with a proper choice of substituents. For instance, the theoretical findings suggest that Ge=O double bonds can be synthesized as part of a stable compound by taking advantage of kinetic stabilization using bulky substituents as steric protection groups. Besides this, on the basis of the present theoretical results, we confidently predict that $F_2Ge{=}O$ should be very stable from both a thermodynamic and a kinetic viewpoint and should be easily observed experimentally.

We eagerly await experimental results to confirm our predictions.

We are grateful to the National Center for High-Performance Computing of Taiwan and the Computing Center at Tsing Hua University for generous amounts of computing time. We also thank the National Science Council of Taiwan for their financial support.

Notes and references

1 W. P. Neumann, *Chem. Rev*., 1991, **91**, 311.
2 P. Riviere, M. Riviere-Baudet, J. Satgé, in, *Comprehensive Organometalic Chemistry*, ed. E. W. Abel, F. G. A. Stone and G. Wilkinson, Pergamon, Oxford, UK, 1995, vol.2, ch 5.
3 W. J. Leigh, *Pure Appl. Chem*., 1999, **71**, 453; N. Tokitoh, *Pure Appl. Chem*., 1999, **71**, 495.
4 R. Okazaki, R. West, *Adv. Organomet. Chem*., 1996, **39**, 31.
5 M. Massol, D. Mesnard, J. Barrau and J. Stagé, *C. R. Hebd Seances Acad. Sci., Ser. C*, 1971, **272**, 2081.
6 J. Barrau, M. Bouchaut, A. Castel, A. Cazes, G. Dousse, H. Lavayssiere, P. Riviere and J. Stagé, *Synth. React. Inorg, Met.-Org. Chem*., 1979, **9**, 273.
7 J. Barrau, M. Bouchaut, H. Lavayssiere, G. Dousse and J. Stagé, *Helv. Chim. Acta*., 1979, **62**, 152.
8 P. Riviere, J. Stagé, A. Castel and A. Cazes, *J. Organomet. Chem*., 1979, **177**, 171.
9 R. Withnall and L. Andrews, *J. Phys. Chem*., 1990, **94**, 2351.
10 C.-L. Lin, M.-D. Su and S.-Y. Chu, *Chem. Phys*., in press and references therein.
11 A. D. Becke, *J. Chem. Phys. Rev. A*, 1988, **38**, 3098; C. Lee, W. Yang and R. G. Parr, *Phys. Rev. B: Condens. Matter*, 1988, **37**, 785; A. D. Becke, *J. Chem. Phys*., 1993, **98**, 5648.
12 J. A. Pople, M. Head-Gordon and K. Raghavachari, *J. Chem. Phys.*, 1987, **87**, 5968.
13 Gaussian 94: M. J. Frisch, G. W. Trucks, H. B. Schlegel, P. M. W. Gill, B. G. Johnson, M. A. Robb, J. R. Cheeseman, T. Keith, G. A. Petersson, J. A. Montgomery, K. Raghavachari, M. A. Al-Laham, V. G. Zakrzewski, J. V. Ortiz, J. B. Foresman, J. Cioslowski, B. B. Stefanov, A. Nanayakkara, M. Challacombe, C. Y. Peng, P. Y. Ayala, W. Chen, M. W. Wong, J. L. Andres, E. S. Replogle, R. Gomperts, R. L. Martin, D. J. Fox, J. S. Binkley, D. J. Defrees, J. Baker, J. P. Stewart, M. Head-Gordon, C. Gonzalez and J. A. Pople, Gaussian, Inc., Pittsburgh, PA, 1995
14 Bond dissociation energetics (kcal mol^{-1}): Ge–F 116, O–F 53, Ge–Cl‡ ≈ 103, O–Cl 65 , Ge–Br 61, O–Br 56, Ge–C 110, O–C 257, Ge–H ≤ 77, O–H 88. See: D. R. Lide and H. P. R. Frederikse, *CRC Handbook of Chemistry and Physics*, CRC Press, New York, 1998; pp. 9–107.
15 C. Trinquier, M. Pelissier, B. Saint-Roch and H. Lavayssiere, *J. Organomet. Chem*., 1981, **214**, 169; J. Kapp, M. Remko and P. v. R. Schleyer, *J. Am. Chem. Soc*., 1996, **118**, 5745.

Communication 9/07682D

Rhenacarborane complexes with nitrosyl and alkylidene ligands. Structures of the complexes [Re{=C(OMe)C_6H_4Me-4}(NO)(CO)(η^5-7,8-$C_2B_9H_{11}$)] and [Re(NO)(CNBu^t){η^5,σ-7-C=N(H)Bu^t-7,8-$C_2B_9H_{10}$}]

Dianne D. Ellis, Paul A. Jelliss and F. Gordon A. Stone*

Department of Chemistry and Biochemistry, Baylor University, Waco, Texas 76798-7348 USA. E-mail: gordon_stone@baylor.edu

Received (in Bloomington, IN, USA) 3rd September 1999, Accepted 15th October 1999

The first examples of rhenacarborane complexes with nitrosyl ligands have been prepared and used to synthesise alkylidene(nitrosyl)rhenacarboranes and a novel complex in which a conjoined carboranyl–iminium group is bound to rhenium both through the η^5-C_2B_3 face of the cage and the iminium carbon atom.

Because of their high compatibility with other groups when ligating metal centres the cyclopentadienide anion and its derivatives rank among the most important ligands in organo-transition metal chemistry.[1] Formally isolobal with $[C_5H_5]^-$ the dicarbollide dianion [*nido*-7,8-$C_2B_9H_{11}]^{2-}$ and its C-substituted derivatives have been known to form metal complexes for over 30 years.[2] However, the chemistry of these species is much less extensive than that of their cyclopentadienide analogs.[3] Herein we report the first rhenacarborane carbonyl nitrosyl compound, a useful synthon for preparing other species including the first isolable complexes with alkylidene groups ligating a metal centre in an M(η^5-7,8-R_2-7,8-$C_2B_9H_9$) (R = H, alkyl, aryl) group (Scheme 1).

Treatment of Cs[Re(CO)$_3$(η^5-7,8-$C_2B_9H_{11}$)] **1**[4] in tetrahydrofuran (THF) with [NO][BF_4] gave the stable complex [Re(NO)(CO)$_2$(η^5-7,8-$C_2B_9H_{11}$)] **2a** in high yield.† A range of complexes **2b**–**2h** have been synthesized from **2a** by substitution of one or both CO ligands. In a typical reaction **2a** reacts with excess CNBu^t in THF to give yellow crystals of [Re(NO)(CNBu^t)$_2$(η^5-7,8-$C_2B_9H_{11}$)] **2g**.†

Compound **2a** was treated initially with LiPh or Li[C_6H_4Me-4] and then with [Me_3O][BF_4]. Column chromatography on silica gel of the resulting mixture gave the alkylidene complexes [Re{=C(OMe)R}(NO)(CO)(η^5-7,8-$C_2B_9H_{11}$)] (R = Ph **3a**, C_6H_4Me-4 **3b**), respectively. The $^{13}C\{^1H\}$ NMR spectrum† of **3b** displays a diagnostic resonance for the alkylidene carbon nucleus at δ 295.1 to be compared with the NMR signal for this nucleus at δ 289.2 in the isolobal cation [Re{=*C*(OMe)C_6H_4Me-4}(NO)(CO)(η-C_5H_5)]$^+$.[5] The appearance in the ^1H and $^{13}C\{^1H\}$ NMR spectra of **3b** of only one signal for the OMe group indicated that only one enantiomeric pair of molecules was formed. An X-ray crystal structure analysis‡ established the structure (Fig. 1) and showed that the OMe and NO groups are transoid to one another [ϕ(NReC(9)O(4)) 163.5°]. The Re–C(9) bond distance [2.052(9) Å] is similar to that found [1.949(6) Å] for the alkylidene ligand in [Re(=CHPh)(NO)(PPh_3)(η-C_5H_5)][PF_6].[6] We have previously observed that when alkylidene ligands are exopolyhedral substituents on a tungsten centre in a *closo*-3,1,2-WC_2B_9 tungstacarborane complex they undergo rapid and irreversible hydroboration by an adjacent B–H bond in the cage $\overline{CCBBB}$ coordinating face.[7] Thus the formation and isolation of the complexes **3** was perhaps unexpected in icosahedral metallacarborane chemistry. Grimes and coworkers[8] have recently isolated the first transition metal alkylidene complex incorporating a sub-icosahedral metallacarborane, *viz*. [RuCo{=C(OMe)Ph}(CO)$_2$(η-C_5Me_5)(η^5-2,3-Et_2-5-Cl-2,3-$C_2B_3H_2$)]. This molecule comprises a ruthenium dicarbonyl phenylmethoxyalkylidene fragment pentacoordinated by the C_2B_3 face of a *nido*-cobaltacarborane ligand.

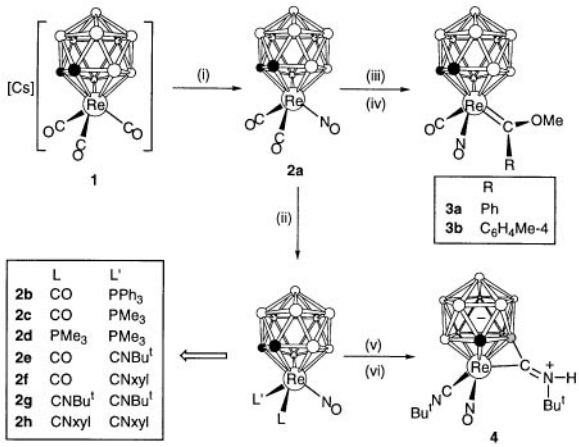

Scheme 1 *Reagetns and conditions*: i, [NO][BF_4], THF, −80 °C; ii, L/L′, THF, reflux; iii, LiR, Et_2O, −80 °C; iv, [Me_3O][BF_4], −50 °C; v, L = L′ = CNBu^t; LiPh, Et_2O, −50 °C; vi, HBF_4·OEt_2, −80 °C. Key: ○ = BH, ● = CH, ◎ = C, xyl = $C_6H_3Me_2$-2,6.

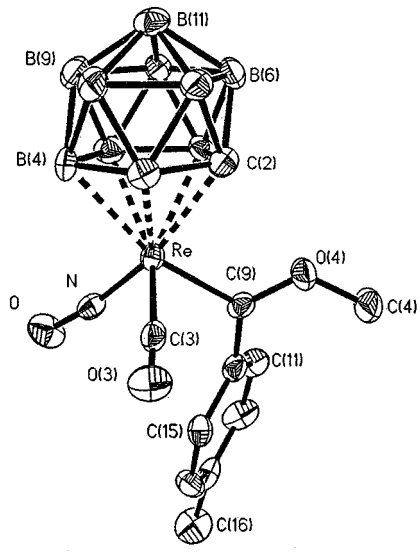

Fig. 1 Molecular structure of **3b** (thermal ellipsoids with 40% probability). Selected distances (Å) and angles (°): Re–N 1.768(8), Re–C(3) 1.963(10), Re–C(9) 2.052(9), N–O 1.188(9), C(3)–O(3) 1.130(11), C(9)–O(4) 1.321(11); N–Re–C(3) 92.7(3), N–Re–C(9) 93.4(4), C(3)–Re–C(9) 88.7(4), O–N–Re 172.0(7), O(3)–C(3)–Re 175.4(9), O(4)–C(9)–Re 117.2(6), C(9)–O(4)–C(4) 124.3(8), C(10)–C(9)–Re 124.4(7).

Reaction of LiPh with the bis(isonitrile)nitrosyl compound **2g** followed by addition of HBF_4·Et_2O affords the novel complex [Re(NO)(CNBu^t){η^5,σ-7-C=N(H)Bu^t-7,8-$C_2B_9H_{10}$}] **4**. Evidently the lithium reagent deprotonates one of the CH groups of the carborane cage to give an intermediate which on

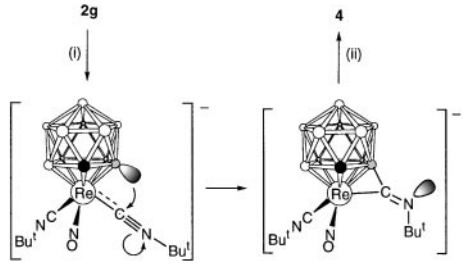

Scheme 2 *Reagents and conditions*: i, LiPh, Et_2O, −50 °C; ii, $HBF_4{\cdot}OEt_2$, −80 °C. Key: ○ = BH, ● = CH, ◍ = C.

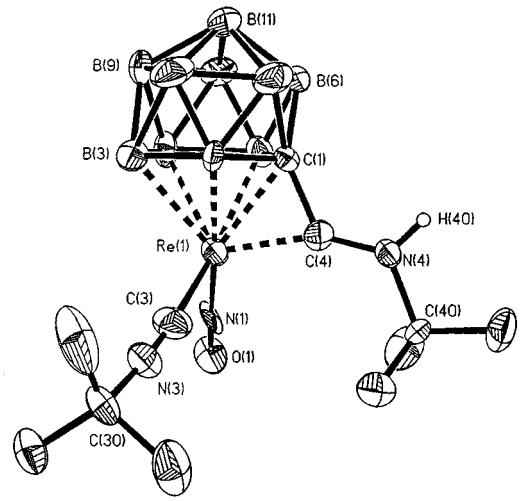

Fig. 2 Molecular structure of one of the independent molecules found in the asymmetric unit of **4** (thermal ellipsoids with 40% probability). Selected distances (Å) and angles (°): Re(1)–N(1) 1.769(11), Re(1)–C(4) 2.000(13), Re(1)–C(3) 2.02(2), C(1)–C(4) 1.49(2), N(1)–O(1) 1.206(12), C(3)–N(3) 1.14(2), C(4)–N(4) 1.29(2); N(1)–Re(1)–C(4) 111.9(5), N(1)–Re(1)–C(3) 93.0(5), C(4)–Re(1)–C(3) 101.3(5), O(1)–N(1)–Re(1) 174.1(11), N(3)–C(3)–Re(1) 173.3(14), C(3)–N(3)–C(30) 175(2), N(4)–C(4)–C(1) 127.6(12), N(4)–C(4)–Re(1) 154.7(11), C(1)–C(4)–Re(1) 76.2(7), C(4)–N(4)–C(40) 124.3(11).

protonation yields **4** (Scheme 2), formulated as a charge-compensated species. The structure was established by X-ray diffraction‡ (Fig. 2). Atom C(4) bridges the Re–C(1) connectivity [C(1)–C(4) 1.49(2), Re(1)–C(4) 2.000(13) Å]. Although the C(4)–N(4) distance [1.29(2) Å] is longer than C(3)–N(3) [1.14(2) Å] in the ligated isonitrile molecule it is somewhat shorter than that expected (1.34 Å) for a C=N double bond.[9] The NH proton is recognisable in the ^{1}H NMR spectrum† as a broad signal at δ 8.93, while in the ^{13}C{^{1}H} NMR spectrum the iminium carbon atom, which is both bound to the cage carbon vertex and to the rhenium centre (δ 218.8), can be readily distinguished from the ligating carbon atom of the classical isonitrile ligand (δ 137.7). The formation of **4** appears to be regioselective, since only one of several possible diastereomeric pairs of enantiomers was isolated. This may in part be due to the directive influence of the NO ligand and further studies with these complexes are in progress to examine this effect.

We thank the Robert A. Welch Foundation for support (Grant AA-1201).

Notes and references

† **2a**: Bright yellow microcrystals; yield 89%. Anal. Calc. for $C_4H_{11}B_9NO_3Re$: C, 11.9; H, 2.7; N, 3.5. Found: C, 12.4; H, 3.0; N, 3.3%; IR (CH_2Cl_2): ν_{max}(CO) 2093, 2034 cm^{-1}, ν_{max}(NO) 1776 cm^{-1}; ^{1}H NMR (360.13 MHz, CD_2Cl_2) δ 3.64 (s br, 2H, CH); ^{13}C{^{1}H} NMR (90.56 MHz, CD_2Cl_2) δ 187.4 (s, CO), 43.8 (s br, CH); ^{11}B{^{1}H} NMR (115.55 MHz, CD_2Cl_2) δ 1.7 (s, 1 B), −3.9 (s, 3 B), −11.4 (s, 2 B), −16.6 (s, 3 B).

2g: Yellow microcrystals; yield 67%. Anal. Calc. for $C_{12}H_{29}B_9N_3ORe$: C, 28.0; H, 5.7; N, 8.2. Found: C, 28.2; H, 5.8; N, 8.1%; IR (CH_2Cl_2): ν_{max}(NC) 2174, 2137 cm^{-1}, ν_{max}(NO) 1721 cm^{-1}; ^{1}H NMR (360.13 MHz, CD_2Cl_2) δ 3.11 (s br, 2H, CH), 1.58 (s, 18H, CMe_3); ^{13}C{^{1}H} NMR (90.56 MHz, CD_2Cl_2) δ 135.8 (s br, CN), 59.9 (s, *C*Me$_3$), 39.9 (s br, CH), 31.1 (s, C*Me*$_3$). ^{11}B{^{1}H} NMR (115.55 MHz, CD_2Cl_2) δ −4.2 (s, 1 B), −4.8 (s, 1 B), −7.3 (s, 2 B), −11.4 (s, 2 B), −19.6 (s, 3 B).

3b: Yellow microcrystals; yield 20% (unoptimised). Anal. Calc. for $C_{12}H_{21}B_9NO_3Re$: C, 28.2; H, 4.1; N, 2.7. Found: C, 28.4; H, 4.0; N, 2.7%; IR (CH_2Cl_2): ν_{max}(CO) 2029 cm^{-1}, ν_{max}(NO) 1750 cm^{-1}; ^{1}H NMR (360.13 MHz, CD_2Cl_2) δ 7.34, 7.39 [AB, 4H, C_6H_4, *J*(AB) 8 Hz], 4.53 (s, 3H, OMe), 3.05, 3.32 (s × 2, 2H, CH), 2.43 (s, 3H, Me-4); ^{13}C{^{1}H} NMR (90.56 MHz, CD_2Cl_2) δ 295.1 (s, =C), 195.9 (s, CO), 147.6, 145.4, 130.0, 127.0 (s × 4, C_6H_4), 69.7 (s, OMe), 45.3, 44.4 (s br × 2, CH), 21.8 (s, Me-4); ^{11}B{^{1}H} NMR (115.55 MHz, CD_2Cl_2) δ −2.4 (s, 1 B), −3.2 (s, 1 B), −5.4 (s, 2 B), −11.8 (s vbr, 2 B), −17.1 (s vbr, 2 B), −18.4 (s, 1 B).

4: Yellow microcrystals; yield 50%. Anal. Calc. for $C_{12}H_{29}B_9N_3ORe$: C, 28.0; H, 5.7; N, 8.2. Found: C, 28.0; H, 5.7; N, 8.2%; IR (CH_2Cl_2): ν_{max}(NC) 2147, 1587 cm^{-1}, ν_{max}(NO) 1667 cm^{-1}; ^{1}H NMR (360.13 MHz, CD_2Cl_2) δ 8.93 (s br, 1H, NH), 1.59 (s br, 1H, CH), 1.50, 1.51 (s × 2, 18 H, CMe_3); ^{13}C{^{1}H} NMR (90.56 MHz, CD_2Cl_2) δ 218.8 (s, C*C*=N), 137.7 (s br, *C*NBu^t), 59.7, 58.2 (s × 2, *C*Me$_3$), 57.7 (s br, *C*C=N), 35.7 (s br, CH), 31.1, 28.8 (s × 2, C*Me*$_3$); ^{11}B{^{1}H} NMR (115.55 MHz, CD_2Cl_2) δ 0.5 (s, 1 B), −1.4 (s, 1 B), −9.2 (s, 1 B), −12.4 (s, 2 B), −14.8 (s, 1 B), −17.2 (s, 1 B), −21.8 (s, 1 B), −29.4 (s, 1 B).

‡ *Crystal data*: Enraf-Nonius CAD4 diffractometer, Mo-Kα radiation (λ = 0.71073 Å), graphite-monochromated, Lorenz polarization and empirical absorption corrections. The structures were solved by direct methods and refined with the full-matrix, least-squares method on F^2 (SHELXL). **3b**: Crystals from CH_2Cl_2–toluene at −20 °C, $C_{12}H_{21}B_9NO_3Re$, 510.79, triclinic, space group $P\bar{1}$ (no. 2), a = 6.977(3), b = 10.9320(11), c = 12.6768(8) Å, α = 96.151(7), β = 99.368(14), γ = 95.04(2)°, Z = 2, U = 943.1(4) Å^3, μ(Mo-Kα) = 6.5 mm^{-1}, T = 293(2) K, ω scan mode, 3583 reflections measured, 3288 were unique (R_{int} = 0.0321) and 2769 observed [$I > 2\sigma(I)$], R_1 = 0.0429, wR_2 = 0.0919 [for 2769 reflections with $I > 2\sigma(I)$], R_1 = 0.0573, wR_2 = 0.0981 (for all 3288 data). **4**: crystals from CH_2Cl_2–light petroleum, $C_{12}H_{29}B_9N_3ORe$, 514.87, monoclinic, space group $P2_1/n$ (no. 14), a = 18.636(3), b = 11.757(2), c = 21.299(6) Å, β = 109.11(2)°, Z = 8, U = 4410(2) Å^3, μ(Mo-Kα) = 5.5 mm^{-1}, T = 293(2) K, ω–2θ scan mode, 5667 reflections measured, 5302 were unique (R_{int} = 0.0516) and 3797 observed [$I > 2\sigma(I)$], R_1 = 0.0512, wR_2 = 0.0889 [for 3797 reflections with $I > 2\sigma(I)$], R_1 = 0.0863, wR_2 = 0.0991 (for all 5302 data). CCDC 182/1453. See http://www.rsc.org/suppdata/cc/1999/2385/ for crystallographic files in .cif format.

1 C. Janiak and H. Schumann, *Adv. Organomet. Chem.*, 1991, **33**, 291.
2 M. F. Hawthorne, D. C. Young, T. D. Andrews, D. V. Howe, R. L. Pilling, A. D. Pitts, M. Reintjes, L. F. Warren and P. A. Wegner, *J. Am. Chem. Soc.*, 1968, **90**, 879.
3 R. N. Grimes, in *Comprehensive Organometallic Chemistry II*, ed. E. W. Abel, F. G. A. Stone and G. Wilkinson, Pergamon Press, Oxford, 1995; vol. 1 (ed. C. E. Housecroft), ch. 9, p. 399.
4 M. F. Hawthorne and T. D. Andrews, *J. Am. Chem. Soc.*, 1965, **87**, 2496; A. Zalkin, T. E. Hopkins and D. H. Templeton, *Inorg. Chem.*, 1966, **5**, 1189.
5 J. B. Sheridan, J. R. Johnson, B. M. Handwerker and G. L. Geoffroy, *Organometallics*, 1988, **7**, 2404.
6 W. A. Kiel, G.-Y. Lin, A. G. Constable, F. B. McCormick, C. E. Strouse, O. Eisenstein and J. A. Gladysz, *J. Am. Chem. Soc.*, 1982, **104**, 4865.
7 S. A. Brew and F. G. A. Stone, *Adv. Organomet. Chem.*, 1993, **35**, 135.
8 K. E. Stockman, M. Sabat, M. G. Finn and R. N. Grimes, *J. Am. Chem. Soc.*, 1992, **114**, 8733.
9 F. H. Allen, O. Kennard, D. G. Watson, L. Brammer, A. G. Orpen and R. Taylor, *J. Chem. Soc., Perkin Trans. 2*, 1987, S1.

Communication 9/07144J

ChemComm

Bi-edge condensation of imido–rhodium clusters leading to novel planar hexametallic structures

Cristina Tejel, Marta Bordonaba, Miguel A. Ciriano,* Fernando J. Lahoz and Luis A. Oro*

Departamento de Química Inorgánica, Instituto de Ciencia de Materiales de Aragón, Universidad de Zaragoza-C.S.I.C., Facultad de Ciencias, E-50009-Zaragoza, Spain.
E-mail: mciriano@posta.unizar.es; oro@posta.unizar.es

Received (in Basel, Switzerland) 20th September 1999, Accepted 25th October 1999

Oxidation of $[N(PPh_3)_2][Rh_3(\mu\text{-}NC_6H_4Me\text{-}p)_2(CO)_6]$ with $[FeCp_2]PF_6$ gives the novel hexarhodium compound $[\{Rh_3(\mu\text{-}NC_6H_4Me\text{-}p)_2(CO)_6\}_2]$, containing three nearly co-planar condensed metallic cycles forming a doubly-spiked square, by dimersisation of the trinuclear imidocomplex through the formation of unsupported metal–metal bonds.

Very recently we have reported a straightforward approach to tetrametallic rhodium and iridium chains by partial oxidation of appropriate dinuclear complexes.[1] After the electron abstraction, the hypothetical intermediate cations $[M^IM^{II}]^+$ promote a 'linear condensation' leading to an unsupported metal–metal bond between the two pairs of metal centres [Scheme 1(a)]. In a formal sense, the formation of this interdimer M–M bond could be related to simple C–C bond formation, assuming the similarity of the intermediate species $[M^IM^{II}]^+$ with organic radicals, for which coupling leading to dimerisation is a well known reaction. Looking for a similar condensation of triangular complexes induced by chemical oxidation one might expect doubly-spiked tetranuclear chains if a 'vertex-condensation' were operative [Scheme 1(b)]. However, other condensation schemes such as a 'bi-edge-condensation' would lead to a tetrametallic cycle [Scheme 1(c)].

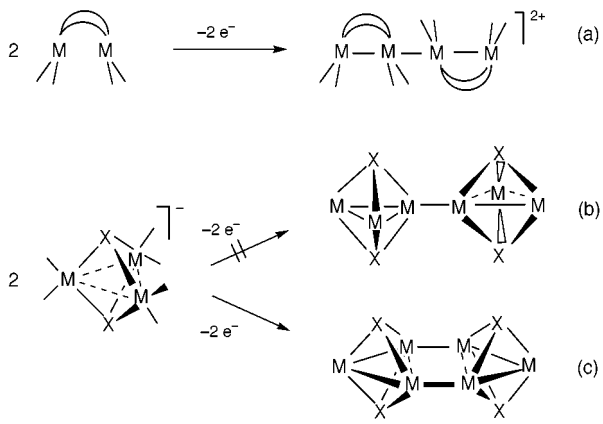

Scheme 1 Possible pathways for the formation of metal chains and cycles. M = metal, X = capping ligand (NR).

We have recently reported the first tri- and tetra-nuclear organoimido rhodium clusters.[2] In the search to develop this chemistry, and looking for higher nuclearity imido clusters, we have turned our attention to the 'active M–M edge' of the trinuclear organoimido anion $[Rh_3(\mu\text{-}NC_6H_4Me\text{-}p)_2(CO)_6]^-$. As the previously isolated salt[3] of this anion contains the redox active cation $[Rh(CO)(dppm)_2]^+$, we first prepared the new yellow compound $PPN[Rh_3(\mu\text{-}NC_6H_4Me\text{-}p)_2(CO)_6]$ **1** by reacting $[Rh_4(\mu\text{-}NC_6H_4Me\text{-}p)_2(CO)_7(cod)]_4$ with 2 mol equiv. of $[N(PPh_3)_2]Cl$ in dichloromethane and crystallization from diethyl ether.[5]

Oxidation of **1** in $CDCl_3$ with $[FeCp_2]PF_6$ (1:1 molar ratio) gives, immediately and quantitatively, an EPR silent emerald-green solution of $[\{Rh_3(\mu\text{-}NC_6H_4Me\text{-}p)_2(CO)_6\}_2]$ **2**. The ^1H NMR spectrum is quite surprising because it shows only two new singlets, one for the aromatic protons, which are isochronous, and the other for the methyl groups. More informative is the $^{13}C\{^1H\}$ NMR spectrum, showing two carbonyl resonances (1:2 ratio) and four resonances corresponding to equivalent *p*-tolylimido ligands, which indicates that the trimetallic core capped by two *p*-tolylimido ligands is maintained in the new compound. Moreover, the resonances for *ipso*- and *ortho*-C appear as quartets by coupling with three rhodium atoms ($^3J_{RhC}$ 1.3 Hz). This green solution is obtained in a preparative scale in a similar way in dichloromethane. Red–green microcrystals of **2**[6] are isolated in high yield (> 75%) after evaporation of the solution to dryness, removal of $[FeCp_2]$ by washing the residue with hexane followed by extraction with diethyl ether {to remove $[N(PPh_3)_2]PF_6$}, and layering the extract with hexanes.

The molecular structure of **2**, determined by single crystal X-ray diffraction,[7] reveals a hexanuclear metallic core. Thus, the novel organimido rhodium cluster $[\{Rh_3(\mu\text{-}NC_6H_4Me\text{-}p)_2(CO)_6\}_2]$ **2** consists of an almost planar tetrarhodium square with two opposite spiked edges generating a tricyclic hexametallic arrangement (Fig. 1) while four *p*-tolylimido ligands cap either side of the two metal triangles. Electron counting for **2** gives 94 valence electrons, *i.e.* two electrons less than the expected value (96 ve) for a cyclic hexametallic cluster, and two electrons over the expected counting for a doubly-spiked tetrametallic square (92 ve). The extra electron pair may be the cause of the long Rh–Rh separations for the edges connecting the fused cycles [Rh(1)···Rh(2) 3.1127(10) Å] when compared with the short Rh–Rh distances [2.7188(10) and 2.7048(9) Å] within the triangles, and the unsupported Rh–Rh bonds [Rh(1)–Rh(2′) 2.9921(9) Å] in the central square.

The formation of **2** from $[Rh_3(\mu\text{-}NC_6H_4Me\text{-}p)_2(CO)_6]^-$ can be envisaged as a one-electron oxidation reaction leading to the neutral radical complex $[Rh_3(\mu\text{-}NC_6H_4Me\text{-}p)_2(CO)_6]^{\cdot}$, which dimerises through the formation of two new unsupported Rh–Rh bonds. Accordingly, cyclic voltammetry measurements on **1** show an irreversible one-electron oxidation process at 0.57 V *vs.* SCE in CH_2Cl_2. However, a close inspection of this wave at fast scan rates (> 1 V s^{-1}) shows the observation of a very small reduction wave, which disappears at moderate scan rates, in accordance with a EC_{irrev} mechanism. In this case the C_{irrev} reaction ought to be the dimerisation process.

Furthermore, it is noteworthy that the major tendency of complex **1** is to undergo M–M coupling rather than C–C bond formation upon oxidation. Oxidative C–C coupling through the *para* carbon of the phenyl group in dinuclear rhodium phenyl imido/amido complexes has been reported by Sharp and coworkers,[8] and interpreted assuming that the proposed radical should be centred in the phenyl group. In our case, complex **1** shows a tunable donicity, *i.e.* it is able to coordinate metal fragments at the arene ring or at one rhodium–rhodium edge,[9] and therefore both processes, C–C coupling involving the phenyl group, and M–M coupling involving the Rh–Rh edge could *a priori* be possible. Most probably, the unpaired electron

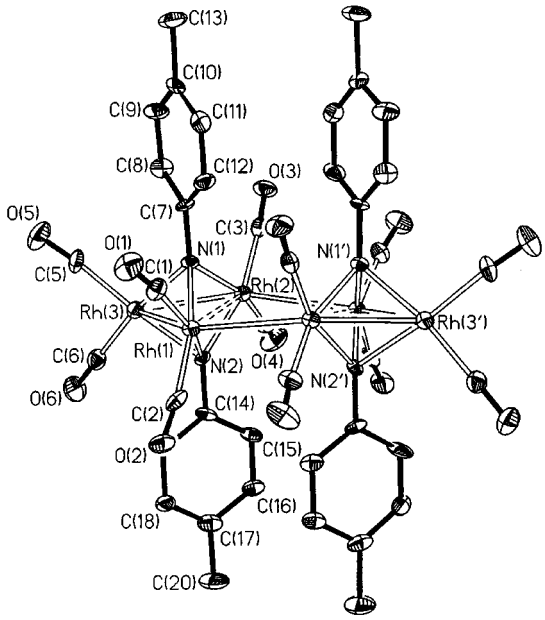

Fig. 1 Molecular diagram of $[\{Rh_3(\mu\text{-}NC_6H_4Me\text{-}p)_2(CO)_6\}_2]$ **2**; the molecule has internal crystallographic twofold symmetry. Selected bond interatomic distances (Å) and angles (°): Rh(1)–Rh(3) 2.7188(10), Rh(1)–Rh(2′) 2.9921(9), Rh(2)–Rh(3) 2.7048(9), Rh(1)···Rh(2) 3.1127(10), Rh(1)–N(1) 2.028(6), Rh(1)–N(2) 2.069(6), Rh(2)–N(1) 2.081(6), Rh(2)–N(2) 2.041(6), Rh(3)–N(1) 2.051(7), Rh(3)–N(2) 2.063(6); Rh(2)···Rh(1)–Rh(3) 54.77(2), Rh(2)···Rh(1)–Rh(2′) 88.43(3), Rh(2′)–Rh(1)–Rh(3) 142.98(3), Rh(1)···Rh(2)–Rh(3) 55.19(2), Rh(1)···Rh(2)–Rh(1′) 90.38(3), Rh(1′)–Rh(2)–Rh(3) 144.83(3), Rh(1)–Rh(3)–Rh(2) 70.05(3), Rh(1)–N(1)–Rh(2) 98.5(3), Rh(1)–N(1)–Rh(3) 83.6(2), Rh(2)–N(1)–Rh(3) 81.8(2), Rh(1)–N(2)–Rh(2) 98.5(3), Rh(1)–N(2)–Rh(3) 82.3(2), Rh(2)–N(2)–Rh(3) 82.5(2) (primed atoms are related to their unprimed equivalent by the symmetry transformation: $y - 1, 1 + x, -z$).

in the proposed neutral radical $[Rh_3(\mu\text{-}NC_6H_4Me\text{-}p)_2(CO)_6]^{\cdot}$ is delocalized in the trimetallic core. This interpretation provides a facile explanation for the formation of the hexametallic cluster by fusion of the two edges from two trimetallic triangles leading to **2**, in which the metals present formal fractional oxidation states.

The condensation reactions induced by oxidation [Scheme 1(a) and (c)] operate selectively depending on the structure of the starting materials and products, *i.e.* tetrametallic chains ('linear condensation') result from dinuclear complexes and tetrarhodium cycles ('bi-edge condensation') from a trinuclear complex. The origin of the selectivity is probably related to the presence of the third metallic centre, which plays a non-innocent role, since the metal–metal edge in the trinuclear complexes is more accessible for a close approach of a substrate to both metals than in a dinuclear species, thus allowing the formation of the tetrametallic cycle for the former whilst vertex condensation is preferred for the latter.

The result of an electron transfer reaction on a cluster is, in general, quite unpredictable. Fragmentation, isomerisation, rearrangement and distortion of clusters are common outcomes from cluster redox reactions in addition to well documented cases where the electron loss/addition processes proceeds cleanly with M–M bond formation/cleavage.[10,11]

Clusters with fixed capping groups based on group 15 elements are versatile in undergoing oxidation and/or reduction reactions.[12] However, to the best of our knowledge, a dimerisation of clusters induced by oxidation, such as shown here, is unusual. Moreover, the chemical oxidation of polynuclear compounds of low-valent electron-rich metals with capping groups in which metal–metal bonds are not evident represents a significant challenge for the creation of higher nuclearity species by methods other than redox-condensation using mononuclear metal fragments.

The generous financial support from DGES (Projects PB95-221-C1 and PB94-1186) and a fellowship (to M. B.) are gratefully acknowledged. We also thank Dr E. Gutierrez Puebla (ICMM-CSIC) for facilities and infrastructure to carry out X-ray data collection.

Notes and references

1 C. Tejel, M. A. Ciriano and L. A. Oro, *Chem. Eur. J.*, 1999, **5**, 1131; C. Tejel, M. A. Ciriano, J. A. López, F. J. Lahoz and L. A. Oro, *Angew. Chem., Int. Ed.*, 1998, **37**, 1542; M. A. Ciriano, S. Sebastián, L. A. Oro, A. Tiripicchio, M. Tiripicchio-Camellini and F. H. Lahoz, *Angew. Chem., Int. Ed. Engl.*, 1988, **27**, 402.

2 C. Tejel, Y.-M. Shi, M. A. Ciriano, A. J. Edwards, F. J. Lahoz and L. A. Oro, *Angew. Chem., Int. Ed. Engl.*, 1996, **35**, 633.

3 C. Tejel, Y.-M. Shi, M. A. Ciriano, A. J. Edwards, F. J. Lahoz, J. Modrego and L. A. Oro, *J. Am. Chem. Soc.*, 1997, **119**, 6678.

4 C. Tejel, Y.-M. Shi, M. A. Ciriano, A. J. Edwards, F. J. Lahoz and L. A. Oro, *Angew. Chem., Int. Ed. Engl.*, 1996, **35**, 1516.

5 The analytical data for **1** (Anal. Calc. for $C_{56}H_{44}N_3O_6P_2Rh_3$: C, 54.88; H, 3.62; N, 3.43. Found: C, 55.12; H, 3.71; N, 3.28%) are in accord with the proposed formulation, and the spectroscopic data are essentially identical to those described for the anion in $[Rh(CO)(dppm)_2][Rh_3(\mu\text{-}NC_6H_4Me\text{-}p)_2(CO)_6]$.

6 IR (CH_2Cl_2, cm^{-1}): ν(CO)/cm^{-1} 2062s, 2046s, 2021m, 2002m. ^1H NMR (300 MHz, $CDCl_3$, room temp.): δ 6.316 (s, 4H), 2.039 (s, 3H). $^{13}C\{^1H\}$ NMR (75 MHz, $CDCl_3$, room temp.): δ 187.5 (d, J_{RhC} 63 Hz, 8C, CO), 187.4 (d, J_{RhC} 75 Hz, 4C, CO), 164.8 (m, *ipso*-C), 135.1(*p*-C), 127.3(*m*-C), 120.4(q, J_{RhC} 1.3 Hz, *o*-C), 20.5(Me).

7 *Crystal data* for **2**: $C_{40}H_{28}N_4O_{12}Rh_6$, M = 1374.12, tetragonal, space group $P4_32_12$, a = 12.1187(8), c = 29.753(3) Å, V = 4369.7(6) Å^3, Z = 4, D_c = 2.089 g cm^{-3}, μ = 2.278 mm^{-1}. Crystal dimensions 0.09 × 0.07 × 0.02 mm. Bruker SMART CCD diffractometer, T = 153(1)K, Mo-Kα radiation (λ = 0.71073 Å). A complete hemisphere of data was scanned on ω (0.30° per frame) with a run time of 20 s. Absorption corrections were applied using SADABS. From 15970 reflections measured, 5400 were unique (R_{int} = 0.1223). The structure was solved by direct methods (SHELXS-97) and refined by full matrix least-squares on F^2 (SHELXL-97). Only half of the hexanuclear complex is crystallographically independent: 285 parameters; R = 0.0619 (3329 reflections with, $F \geqslant 4\sigma F_o$), $wR2$ = 0.0722 and S = 0.959. Absolute structure checked with Flack parameter, x = −0.11(6). CCDC 182/1461. See http://www.rsc.org/suppdata/cc/1999/2387/ for crystallographic files in .cif format.

8 Y.-W. Ge, Y. Ye and P. R. Sharp, *J. Am. Chem. Soc.*, 1994, **116**, 8384.

9 L. A. Oro, M. A. Ciriano, C. Tejel, Y.-M. Shi and J. Modrego, *Metal Clusters in Chemistry*, ed. P. Braunstein, L. A. Oro and P. Raithby, Wiley–VCH, Weinheim, 1999, ch. 1.20, p. 381.

10 N. G. Connelly and W. E. Geiger, *Adv. Organomet. Chem.*, 1985, **24**, 87.

11 D. Astruc, *Electron Transfer and Radical Processes in Transition Metal Chemistry*, Wiley–VCH, New York, 1995.

12 K. H. Withmire, *Adv. Organomet. Chem.*, 1998, **42**, 2.

Communication 9/07853C

Clathrate formation between halogenated species

A. Noman M. M. Rahman, Roger Bishop,* Donald C. Craig and Marcia L. Scudder

School of Chemistry, The University of New South Wales, Sydney 2052, Australia. E-mail: r.bishop@unsw.edu.au

Received (in Cambridge, UK) 10th September 1999, Accepted 19th October 1999

Analysis of X-ray crystallographic data reveals how the *exo,exo*-dibromodiquinoline derivative 4 encloses small halogenated guests as clathrate structures.

Clathrate compounds can result where molecules of a pure compound are unable to achieve efficient crystal packing by themselves.[1] This provides a strong driving force for inclusion of suitable guests but makes the design of new lattice inclusion systems a considerable synthetic challenge.[2]

Reaction of racemic bicyclo[3.3.0]octane-2,6-dione **1** and *o*-aminobenzaldehyde **2** gives the Friedländer condensation[3] product **3**† (Scheme 1). Molecules of this diquinoline derivative pack together efficiently in the solid phase and so exhibit no inclusion properties. Benzylic bromination of **3** affords the racemic dibromide **4**† which, in marked contrast, is an efficient host molecule. This change in behaviour was anticipated since its C_2 symmetry provides a favourable scissor topology[4] and since the *exo*-bromine sensor groups[4] destabilise potential aryl offset face–face attractions[5] and provide additional modes for intermolecular packing.[6]

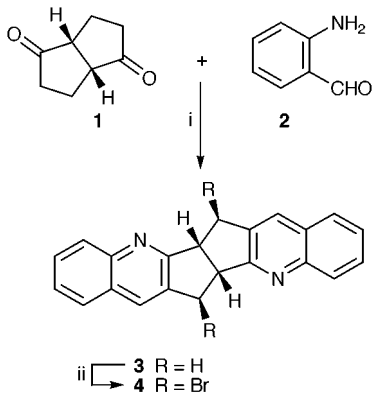

Scheme 1 *Reagents and conditions*: i, NaOH, H_2O, MeOH, 75%; ii, NBS, CCl_4, 78%.

Crystallisation of **4** from $MeCCl_3$ gave crystals of **4**·$(MeCCl_3)_{0.5}$ whose structure‡ in space group *C*2/*c* was determined by single crystal X-ray determination. Pairs of host molecules, related by a two-fold axis, enclose each disordered guest within a molecular pen of nearly square cross-section where the aromatic faces of **4** act as the surrounding fences (Fig. 1). If these host pairs were covalently linked at the corners of this structure the result would be a cyclophane[7] but, in fact, there is not even significant intermolecular attraction. Although pens thus only result from the net outcome of all lattice attractions (see Table 1) in the clathrate it is convenient to retain this term as a descriptor. There is a planar array of pens (Fig. 2) all constructed using the same enantiomer of **4**, and the slightly offset adjacent layers of pens are built from the second enantiomer.

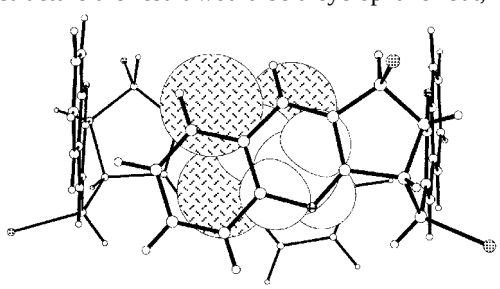

Fig. 1 Side view of the square molecular pen of **4**·$(MeCCl_3)_{0.5}$ showing the two host molecules (framework representation) acting as fences enclosing a $MeCCl_3$ guest (space-filling representation). The guest chlorine atoms are indicated by cross-hatching.

Table 1 Potential and actual supramolecular synthons operating in the clathrate structure **4**·$(MeCCl_3)_{0.5}$

Supramolecular synthon	Partners	Atoms involved	Distances/Å
Aryl offset face–face[a]	Host–host[b]	Ar···Ar	3.55
Aryl edge–face[a]	Host–host	Ar-*H*···*Ar*	Not present
Aryl C–H···N dimer[c]	Host–host[d]	*C*–H···*N*	3.38
(centrosymmetric)		C–*H*···*N*	2.47
Interhalogen[e]	Host–host[b]	Br···Br	3.69
Interhalogen[e]	Host–guest	Br···Cl	Not present
Aryl-halogen[f]	Host–guest[b]	Ar···Cl[g]	3.48, 3.77, 3.81, 3.98[h]
Aryl-alkyl[c]	Host–guest[b]	*Ar*···H_3C[g]	3.65, 3.66
Interhalogen[e]	Guest–guest	Cl···Cl	Not present

[a] Ref. 10. [b] Within layers. [c] Ref. 5. [d] Between layers. [e] Ref. 11. [f] Ref. 12. [g] Aromatic ring centroids used. [h] Values under 4.00 Å only.

Comparatively strong intermolecular forces (such as hydroxy group hydrogen bonding) are not used in the design of host **4**. Instead, a number of relatively weak interactions such as aryl offset face–face, aryl edge–face, aryl C–H···N dimer, aryl–halogen and interhalogen attractions are available for potential combinations of **4** and $MeCCl_3$. Since it is the best overall combination of these synthons[6] (along with size, shape and conformational factors) which determines the structure, some of

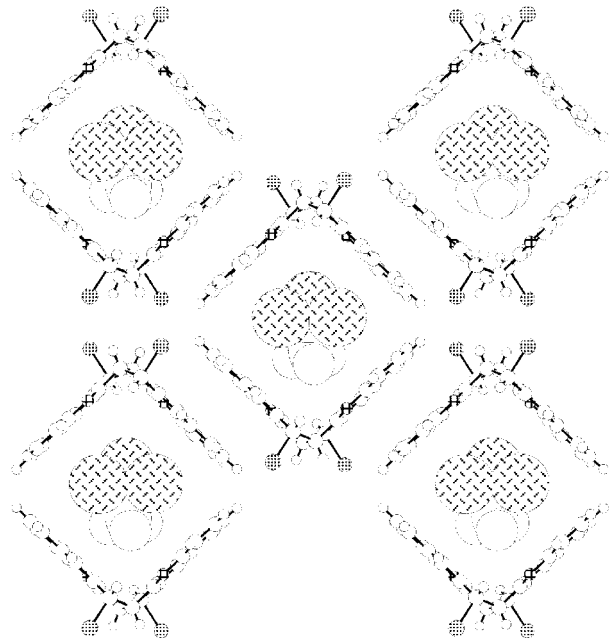

Fig. 2 Top view of part of a layer of the square molecular pens in **4**·$(MeCCl_3)_{0.5}$ showing how these are arranged in regular rows. The host bromine atoms are stippled and guest chlorine atoms cross-hatched. $MeCCl_3$ guests are shown in just one of their disorder positions.

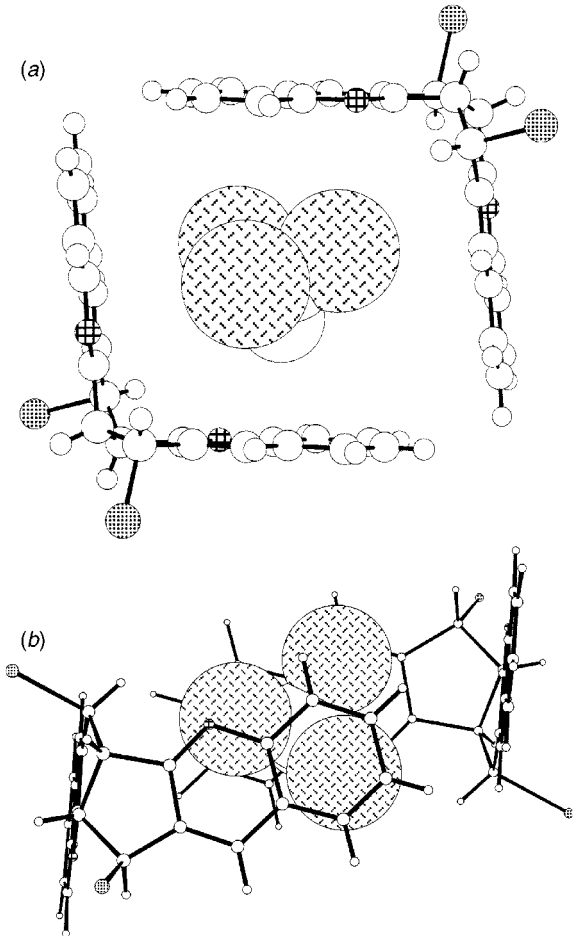

Fig. 3 (*a*) One of the two types of parallelogram-shaped molecular pens present in the clathrate structure **4**·$(CHCl_3)_{0.5}$. (*b*) Side view of the inclusion compound showing its overall parallelepiped geometry.

these turn out not to be used in **4**·$(MeCCl_3)_{0.5}$ while others (including the aryl C–H···N dimer[5]) do play a major role (Table 1).

The central bicyclic ring of the host molecule potentially allows considerable conformational mobility since, for example, the much flatter bis(*N*-oxide) derivative of **3**† has an angle of 133.4° between the normals to the two aromatic planes. It is significant that the two aromatic faces of **4** are almost orthogonal in the $MeCCl_3$ compound (97.7°). This allows maximisation of aryl–halogen and aryl–alkyl interactions between the π-deficient quinoline host and the nearly spherical electron-rich guest. Hence host **4** exhibits molecular tweezer characteristics[8,9] whereby two host molecules wrap around each $MeCCl_3$ guest.

The detailed energetic interplay changes with differing guests. Crystals of **4**·$(CHCl_3)_{0.5}$ were obtained from $CHCl_3$ solution. This structure‡ is more complex, but pairs of host molecules still enclose disordered guests in the same manner despite the changes in guest and space group ($P2_1/c$). Each molecular pen is now centrosymmetric and there are two crystallographically distinct pens (A and B) present in the lattice (angles 97.6 and 100.8° respectively). Both have a more parallelogram-like cross-section than previously (Fig. 3) and they stack alternately (-A-B-A-B-A-). Where these stacks abut, however, there is no layer formation. The pens are not parallel to each other along the stacks, but rather tilt somewhat back and forth.

The same types of intermolecular attractions operate in this second clathrate, but with different geometries. Unexpectedly, although the versatile aryl C–H···N dimer still operates between opposite enantiomers of **4**, this time it is non-centrosymmetric with two distinct *C*–H···*N* distances (3.45 and 3.49 Å). This is the first reported example of such behaviour for this motif.[5]

These preliminary results reveal the dibromide **4** to be an unusual new lattice inclusion host. The interplay of host–guest attractions results in molecular enclosure tailored to the requirements of the particular guest. The further inclusion behaviour of this host compound is under active investigation.

We gratefully acknowledge financial support from the Australian Research Council.

Notes and references

† The structures of all new compounds are based on IR, MS, ^{1}H and ^{13}C NMR spectroscopy and single crystal X-ray structural determinations.

‡ *Crystal data* for **4**·$MeCCl_3$: $C_{22}H_{14}Br_2N_2\cdot(C_2H_3Cl_3)_{0.5}$, M = 532.9, monoclinic, a = 17.006(9), b = 18.764(4), c = 13.421(7) Å, β = 92.05(3)°, U = 4280(3) Å^3, T = 294(1) K, space group $C2/c$ (no. 15), monochromated Mo-Kα radiation, λ = 0.7107 Å, Z = 8, D_c = 1.65 Mg m^{-3}, μ(Mo-Kα) = 39.5 cm^{-1}, 3761 reflections measured, 1519 unique (R_{int} = 0.056) which were used in all calculations. The final R was 0.059, and $wR(F)$ 0.069 (observed data). For **4**·$CHCl_3$: $C_{22}H_{14}Br_2N_2\cdot(CHCl_3)_{0.5}$, M = 525.9, monoclinic, a = 14.832(7), b = 16.754(5), c = 18.084(9) Å, β = 110.80(2)°, U = 4201(3) Å^3, T = 294(1) K, space group $P2_1/c$ (no. 14), monochromated Cu-Kα radiation, λ = 1.5418 Å, Z = 8, D_c = 1.66 Mg m^{-3}, μ(CuKα) = 68.2 cm^{-1}, 7879 reflections measured, 4503 unique (R_{int} = 0.027) which were used in all calculations. The final R was 0.051, and $wR(F)$ 0.071 (observed data). Both structures were determined by direct phasing (SIR92) and Fourier methods. CCDC 182/1452. See http://www.rsc.org.suppdata/cc/1999/2389/ for crystallographic data in .cif format.

1 *Inclusion Compounds*, ed. J. L. Atwood, J. E. D. Davies and D. D. MacNicol, Academic Press, London, 1984, vols. 1–3; Oxford University Press, Oxford, 1991, vols. 4 and 5.
2 R. Bishop, *Chem. Soc. Rev.*, 1996, **25**, 311.
3 C. C. Cheng and S. J. Yan, *Org. React.*, 1982, **28**, 37.
4 E. Weber, in *Inclusion Compounds*, ed. J. L. Atwood, J. E. D. Davies and D. D. MacNicol, Oxford University Press, Oxford, 1991, vol. 4, ch. 5, pp. 188–262.
5 C. E. Marjo, M. L. Scudder, D. C. Craig and R. Bishop, *J. Chem. Soc., Perkin Trans. 2*, 1997, 2099.
6 G. R. Desiraju, *Angew. Chem., Int. Ed. Engl.*, 1995, **34**, 2311.
7 For a discussion of cyclophanes enclosing neutral guests see: K. Odashima and K. Koga, in *Comprehensive Supramolecular Chemistry*, ed. F. Vögtle, Pergamon, Oxford, 1996, vol. 2, ch. 5, pp. 143–194.
8 J. Rebek, Jr., *Angew. Chem., Int. Ed. Engl.*, 1990, **29**, 245.
9 C. S. Wilcox, L. M. Green and V. Lynch, *J. Am. Chem. Soc.*, 1987, **109**, 1865.
10 G. R. Desiraju and A. Gavezzotti, *J. Chem. Soc., Chem. Commun.*, 1989, 621.
11 J. A. R. P. Sarma and G. R. Desiraju, *Acc. Chem. Res.*, 1986, **19**, 222.
12 N. W. Thomas and G. R. Desiraju, *Chem. Phys. Lett.*, 1984, **110**, 99.

Communication 9/07357D

ChemComm

Highly efficient, thermally and chemically stable nonlinear optical chromophores based on the α-perfluoroaryldicyanovinyl electron acceptors

Xiaoming Wu,† Jianyao Wu, Yunqi Liu and Alex K-Y. Jen*‡

Department of Chemistry, Northeastern University, Boston, MA 02115, USA. E-mail: ajen@lynx.dac.neu.edu

Received (in Cambridge, UK) 5th October 1999, Accepted 20th October 1999

A series of highly efficient, chemically and thermally stable (> 310 °C) nonlinear optical chromophores were prepared through the replacement of the most reactive CN group in tricyanovinylthiophene derivatives with perfluoroaryl units.

In practice, polymer based electro-optic (E-O) devices require that nonlinear optical (NLO) polymers possess excellent E-O properties. The large E-O coefficient (r_{33}) of a polymer is generally realized by aligning the dipole moment (μ) of efficient NLO chromophores with a high external electric field at a temperature above the glass-transition temperature (T_g) of the polymer.[1] Therefore, chromophores with large molecular nonlinearity (β) are crucial to the advancement of NLO polymers, and have drawn interest in their theory-guided design and state-of-the-art synthesis.[2] Among them, a series of highly polarizable chromophores based on tricyanovinyl-substituted heteroaromatic chromophores have demonstrated very large $\beta\mu$ values.[3] Although poled E-O polymers with these chromophores incorporated either as a guest in a host polymer or as a side-chain polymer have exhibited large electro-optic coefficients (r_{33}), there are several deficiencies associated with these materials [Fig. 1(*a*)]. For instance, the α-position of the tricyanovinyl acceptor is very susceptible to attack from nucleophiles, which may easily diminish the nonlinearity of the chromophores.[4] On the other hand, the flat structures of these charge-transfer chromophores have a strong tendency to form aggregates in a polymer matrix due to intermolecular electrostatic interactions.[5] This results in lower poling efficiency and a higher light-scattering optical loss. To overcome these problems, a strategy was designed to replace the α-CN with a bulky and electron-deficient moiety which is also inherently not a good leaving group. Here, the tetrafluoropyridyldicyanovinyl (TFPD) and the heptafluorotolyldicyanovinyl (HFTD) acceptors were adapted to improve the efficiency and chemical and thermal stability of NLO chromophores. As shown in the Fig. 1(*b*), the perfluoroaryl group blocks the α-position, prevents attack from amine nucleophiles[4] and greatly improves the chemical stability of the derived chromophores. In addition, due to their electron-deficient characteristics, these perfluoroaryl groups will enhance the strength of the dicyanovinyl acceptor, and subsequently increase the β of the chromophores.[6a] Furthermore, from simple MOPAC molecular modeling, the perfluoroaryl group is twisted out of the main conjugation plane due to steric hindrance. The 3-D structure may help to prevent intermolecular electrostatic interactions among the chromophores, which in turn may enhance the poling efficiency and decrease the scattering-induced optical loss.[6]

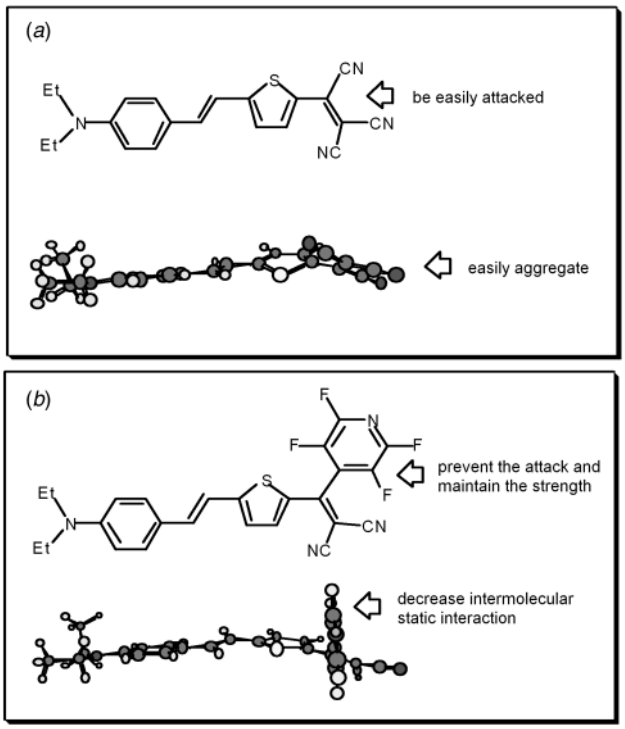

Fig. 1 Simple MOPAC modeling: (*a*) tricyanovinyl chromophore **1**; (*b*) α-perfluropyridyldicyanovinyl chromophore **1a**.

The general synthetic route for the α-perfluoroaryldicyanovinyl-containing chromophores is shown in Scheme 1. Tetrafluoropyridyllithium was prepared by the lithiation of tetrafluoropyridine with BuLi at −70 °C. Heptafluorotolyllithium was generated by the lithium–halogen exchange reaction of the heptafluoro-*p*-tolyl bromide with 2 equiv. of Bu^{t}Li at −78 °C. To the prepared perfluoroaryllithium solutions in THF at −70 °C, tricyanovinyl chromophores were added neat in one portion and the reaction mixtures were stirred at −70 °C for 1 h then warmed slowly to room temperature to give compounds **1a**–**3a** and **1b**–**3b** after purification by silica gel chromatography. All of the compounds were fully characterized by ^{1}H NMR and elemental analysis.

The chemical stability of the chromophores to a nucleophile was tested in a $CHCl_3$ solution that was saturated with a large excess of Et_2NH. The UV–VIS absorption spectra of these perfluoroaryldicyanovinyl containing chromophores showed excellent chemical stability in a nucleophilic environment (Fig. 2), unlike their tricyanovinyl analog which was almost instantaneously decolored.

The charge-transfer (CT) properties, electrochemical properties and intrinsic thermal stabilities of these chromophores are shown in Table 1. These perfluoroaryldicyanovinyl-containing chromophores have a blue-shifted CT band when compared to their corresponding tricyanovinyl counterparts. For instance, the λ_{max} valves of **1a** and **1b** in dioxane are located at 595 and 590 nm, respectively, while **1** is at 640 nm. The further deviation of the absorption band from the operating wavelengths of the lasers for telecommunication may help to decrease the absorption optical loss. However, the blue-shifted λ_{max} valves of both chromophores also indicated a decrease in strength of the new electron acceptors. This notion was supported by electrochemical measurements using cyclic voltammetry (CV).[7] The new chromophores **1a** and **1b** both

† Current address: Brewer Science, Inc., 2401 Brewer Drive, Rolla, MO 65401, USA.
‡ Present address: Department of Materials Science and Engineering, University of Washington, Seattle, WA 98195-2120, USA.

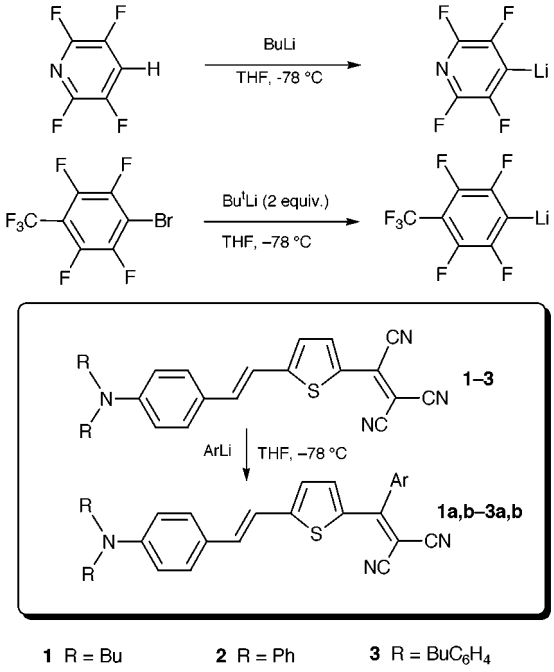

Scheme 1

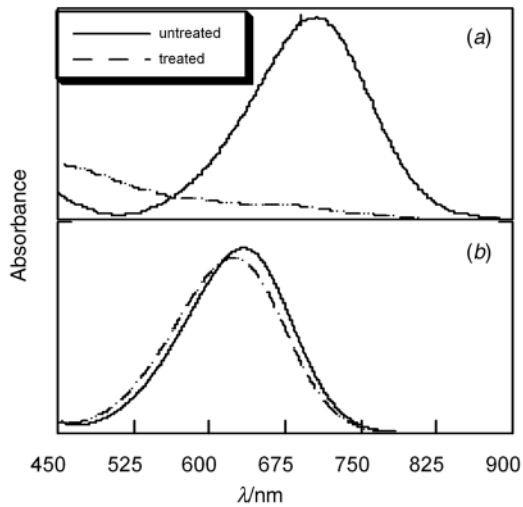

Fig. 2 Testing of the chemical stability of chromophores: a dilute solution of chromophore in $CHCl_3$ was treated with Et_2NH: (*a*) tricyanovinyl chromophore **1**; (*b*) α-perfluropyridyldicyanovinyl chromophore **1a**.

possess higher reduction potentials, at −1.02 and −1.04 V, respectively, when compared to −0.80 V for the parent compound **1**.

Thermal stability measurements using sealed pan differential scanning calorimetry (DSC) revealed that these chromophores possess excellent thermal stabilities (310–390 °C) which are much higher than that of **1** (240 °C).

Optical and E-O studies were performed on the polymers (guest–host) in which chromophores **1a** and **1b** (25 wt%) were formulated into polyquinoline (PQ-100). Optical quality thin films were spin-coated onto glass slides and indium-tin-oxide (ITO) glass substrates using a 12% w/w solution of the resin in cyclopentanone. These films were heated at 85 °C *in vacuo* for 24 h and then briefly baked on a hot stage (160 °C) under nitrogen for 20 min to remove the residual solvent. The dipole alignment of the chromophores was achieved by poling with a high electric field of 1.0 MV cm^{-1} at 200 °C. The r_{33} values of NLO polyquinoline films of **1a** and **1b** were 16 and 14 pm V^{-1} at 1.3 μm. The slight decrease in the E-O coefficients when compared to **1** may be attributed to several factors, such as the lower number density of **1a** and **1b** because of the higher molecular weights of these compounds, and the weaker electron-withdrawing ability of perfluoroaryldicyanovinyl.

Table 1 Properties of chromophores

	λ_{max}/nm[a]	E^0_{Red}/V[b]	E^0_{Ox}/V[b]	T_d/°C[c]
1	640	−0.80	0.56	240
2	601	N/A	N/A	315
3	625	N/A	N/A	315
1a	595	−1.02	0.52	320
2a	554	−0.98	0.73	390
3a	577	−1.01	0.61	360
1b	591	−1.04	0.56	310
2b	553	−1.03	0.72	340
3b	573	−1.04	0.61	370

[a] In a dilute dioxane solution. [b] In a $ClCH_2CH_2Cl$ solution of Bu_3NPF_6 (0.1 M), *vs.* Ag^+/Ag. [c] Sealed-pan DSC measurement in N_2, 20 °C min^{-1}.

The optical loss of the NLO polymer films (< 2 dB cm^{-1} measured at 1.3 μm) is much less than 6.0 dB cm^{-1} for a similar film containing a tricyanovinyl-substituted chromophore.[8] This supports our hypothesis that the 3-D structure of these perfluoroaryldicyanovinyl groups will prevent chromophores from forming aggregates.

In summary, a series of highly efficient, chemically and thermally stable (> 310 °C) nonlinear optical chromophores were prepared through the replacement of the most reactive CN group in tricyanovinylthiophene derivatives with perfluoroaryl units. The incorporation of these chromophores into high temperature polyquinoline demonstrated both high E-O properties and low optical loss.

We acknowledge the financial support from the Air Force Office of Scientific Research (AFOSR) under grant F49620-97-1-0240 and the Office of Naval Research (ONR) through MURI Center CAMP.

Notes and references

1 D. M. Burland, R. D. Miller and G. A. Walsh, *Chem. Rev.*, 1994, **94**, 31; *Nonlinear Optical Properties of Organic Molecules and Crystals*, ed. D. S. Chemela and J. Zyss, Academic Press, New York, 1987.
2 L. R. Dalton, A. W. Harper, R. Ghosn, W. H. Steier, M. Ziar, H. Fetterman, Y. Shi, R. V. Mustwcich, A. K.-Y. Jen and K. Shen, *J. Chem. Mater.*, 1995, **7**, 1060; S. R. Marder, B. Kippelen, A. K-Y. Jen and N. Peyghambarian, *Nature*, 1997, **388**, 845.
3 V. P. Rao, A. K.-Y. Jen, K. Y. Wong and K. J. Drost, *J. Chem. Soc., Chem. Commun.*, 1993, 1118; C-F. Shu, W. J. Tsai, J-Y. Chen, A. K-Y. Jen, Y. Zhang and T-A. Chen, *Chem. Commun.*, 1996, 2279.
4 V. P. Rao, A. K-Y. Jen and Y. Cai, *Chem. Commun.*, 1996, 1237.
5 A. W. Harper, J. Zhu, M. He, L. R. Dalton, A. M. Garner and W. H. Steier, *Mater. Res. Soc. Symp. Proc.*, 1998, **488**, 199.
6 (*a*) X. Wu, J. Wu, Y. Q. Liu and A. K-Y. Jen, *J. Am. Chem. Soc.*, 1999, **121**, 472; (*b*) C. Zhang, A. S. Ren, F. Wang, J. Zhu and L. R. Dalton, *Chem. Mater.*, 1999, **11**, 1966.
7 The CV measurements were carried out in a chromophore solution (1.0 mg in 10 ml of CH_2ClCH_2Cl) in the presence of Bu_3NPF_6 (0.1 M) at room temperature. Platinum, platinum gauze, and Ag/Ag^+ were used as the working electrode, counter electrode, and reference electrode respectively in a conventional three-electrode cell.
8 The optical loss was determined by the prism-coupled streak method on a slab waveguide.

Communication 9/08007D

A novel imidazolate-bridged copper–zinc heterodinuclear complex as a Cu, Zn–SOD active site model

Hideki Ohtsu,[a]† Yuichi Shimazaki,[a] Akira Odani[a] and Osamu Yamauchi*[ab]

[a] *Department of Chemistry, Graduate School of Science, Nagoya University, Chikusa-ku, Nagoya 464-8602, Japan. E-mail: b42215a@nucc.cc.nagoya-u.ac.jp*

[b] *Research Center for Materials Science, Nagoya University, Chikusa-ku, Nagoya 464-8602, Japan.*

Received (in Cambridge, UK) 2nd August 1999, Accepted 25th October 1999

A novel imidazolate-bridged Cu(II)–Zn(II) heterodinuclear complex of an imidazole derivative containing two metal-binding groups has been synthesized, and its structure and properties have been clarified.

Copper–zinc superoxide dismutase (Cu, Zn-SOD) contains an imidazolate-bridged Cu–Zn heterodinuclear metal center in its active site.[1–3] This enzyme catalyzes the dismutation of highly toxic superoxide anion produced as a byproduct to dioxygen and hydrogen peroxide in a sequence of dispersion-controlled reactions.[4] Since the enzyme structure was determined by X-ray analysis,[1] the unique active site structure attracted much attention, and a number of imidazolate-bridged complexes, such as the Cu(II)-Cu(II) homodinuclear complexes by Lippard *et al.*,[5] have been reported as mimics of the metal site and provided valuable insights into the structure and properties of the SOD active site. In contrast to this, only a few imidazolate-bridged Cu(II)–Zn(II) heterodinuclear model complexes have so far been reported.[6] Because such model complexes are often constructed by self-assembly of one or two complex units by incorporating a bridging imidazolate ring, the labile nature of Cu(II) and Zn(II) complexes and dissociation of self-assembled structures made it difficult to study in detail their structures in solution and SOD functions. We here report the first imidazolate-bridged Cu(II)–Zn(II) heterodinuclear complex derived from a new imidazole derivative, Hbdpi {Hbdpi = 4,5-bis[di(2-

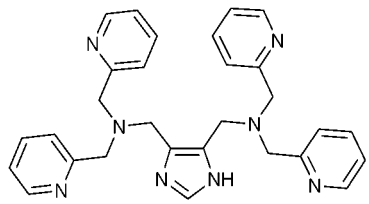

Hbdpi

pyridylmethyl)aminomethyl]imidazole}, which has two sets of 3N donor groups tethered to the 4 and 5 positions of the bridging imidazole ring.

Hbdpi was prepared from imidazole-4,5-dialdehyde[7] and bis(2-pyridylmethyl)amine by reductive aminomethylation using sodium cyanoborohydride in methanol, and was characterized by ^{1}H and ^{13}C NMR.‡ The heterodinuclear Cu(II)–Zn(II) complex of bdpi, $[CuZn(bdpi)(MeCN)_2](ClO_4)_3{\cdot}2MeCN$ **1**, was obtained as crystals by mixing Hbdpi and equimolar amounts of Cu(II) and Zn(II) in methanol and subsequent addition of triethylamine, and the composition of the dried sample of **1** was determined by elemental analysis, ICP, and ESI-mass spectral measurements. The corresponding Cu(II)–Cu(II) homodinuclear complex, $[Cu_2(bdpi)(MeCN)_2](ClO_4)_3{\cdot}2H_2O$ **2** was prepared in a similar manner using two equivalents of Cu(II).

The molecular structure of complex **1** was determined by X-ray analysis§ and is depicted in Fig. 1. As expected, the complex has an imidazolate-bridged dinuclear structure. In line with the previous observation,[6d] the copper and zinc sites are very similar to each other and indistinguishable, because the complex has a C_{2v}-like axis and both metal sites are statistically disordered. The metal ions are both in an approximately trigonal bipyramidal geometry with four nitrogen atoms of bdpi and a nitrogen atom of the solvent MeCN coordinated. The coordination site occupied by MeCN may be susceptible to ligand substitution, providing a possible binding site for substrate superoxide. The Cu(II)–Zn(II) distance of 6.197(2) Å in **1** is the same as that of native Cu, Zn–SOD (6.2 Å).[1]

The electronic spectrum of an acetonitrile solution of **1** (1 mM) showed two broad d–d bands at 645 and 880 nm (ε = 60 and 220 M^{-1} cm^{-1}, respectively). This spectrum is very close to that of $[Cu(tpa)Cl]PF_6$ [tpa = tris(2-pyridylmethyl)amine], indicating a trigonal bipyramidal structure at the copper site.[8] In addition, it exhibited an imidazolate-to-Cu(II) charge transfer (CT) band at 320 nm (ε = 1500 M^{-1} cm^{-1}). The intensities of the d–d and CT bands for **1** were half as strong as those observed for **2** at 645, 880 and 320 nm (ε = 110, 420 and 3000 M^{-1} cm^{-1}, respectively). The EPR spectrum of a solution of **1** (0.5 mM) in 1 : 1 MeCN–MeOH at 77 K ($g_{//}$ = 2.10, $g_{\perp}$ = 2.24 and $|A_{\perp}|$ = 12.0 mT) showed a line shape characteristic of mononuclear trigonal bipyramidal Cu(II) complexes,[9] but was very different from that of **2** having a single symmetrical derivative (g = 2.13**)**, which is similar to the spectrum of the imidazolate-bridged Cu(II)-glycylglycinate complex[10] and other imidazolate-bridged Cu(II)–Cu(II) dinuclear complexes.[11] These results as well as the ESI-mass spectrum in MeCN demonstrate that **1** in solution retains its imidazolate-bridged

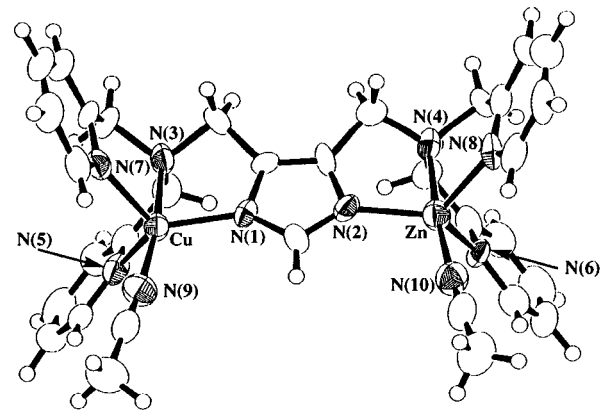

Fig. 1 X-Ray structure of complex **1** (perchlorate ions and the MeCN molecule of crystallization are omitted for clarity, and the Cu and Zn sites were so assigned that smaller R and R_w values could be obtained). Selected bonds (Å) and angles (°): Cu(1)–N(1) 2.001(7), Cu(1)–N(3) 2.104(7), Cu(1)–N(5) 2.074(7), Cu(1)–N(7) 2.105(8), Cu(1)–N((9) 2.004(9), Zn(1)–N(2) 2.005(7), Zn(1)–N(4) 2.112(7), Zn(1)–N(6) 2.076(8), Zn(1)–N(8) 2.084(7), Zn(1)–N(10) 2.023(10), N(1)–Cu–N(3) 82.5(3), N(1)–Cu(1)–N(5) 122.5(3), N(1)–Cu(1)–N(7) 118.3(3), N(3)–Cu(1)–N(9) 172.9(3), N(2)–Zn(1)–N(4) 83.0(3), N(2)–Zn(1)–N(6) 120.3(3), N(2)–Zn(1)–N(8) 120.1(3), N(4)–Zn(1)–N(10) 174.8(3).

† Present address: Department of Material and Life Science, Graduate School of Engineering, Osaka University, Suita, Osaka 565-0871, Japan.

Cu(II)–Zn(II) heterodinuclear structure and is not a 1:1 mixture of Cu(II)–Cu(II) (**2**) and Zn(II)–Zn(II) complexes. Whereas the cyclic voltammogram of **2** in MeCN exhibited two reversible redox waves at $E_{1/2}$ −0.09 and +0.19 V (*vs*. NHE), **1** showed only one reversible Cu(I)/Cu(II) redox couple at $E_{1/2}$ +0.19 V (*vs*. NHE), confirming that it has one copper ion site in the molecule. In this connection, an imidazolate-bridged asymmetric dinuclear Cu(II) complex showed one broad peak in the anodic and the cathodic wave,[12] and several mononuclear trigonal bipyramidal Cu(II) complexes of tripodal ligands containing pyridine and imidazole donors have been reported to have $E_{1/2}$ values between −0.187 and −0.290 V *vs*. NHE.[13] The positive shift of the $E_{1/2}$ values of **1** as compared with other mononuclear Cu(II) complexes may therefore be attributed to the electronic effect of the imidazolate-bound Zn(II), which could be an important factor for the efficient catalytic reaction of Cu, Zn–SOD. The SOD activities of **1** and **2** have been investigated by the cytochrome *c* assay[14] using the xanthine oxidase reaction as the source of superoxide. The IC_{50} values for **1** and **2** were determined to be 0.24 and 0.32 μM [*vs*. Cu(II) ion], respectively, which are higher than the value reported for native Cu, Zn–SOD (0.04 μM)[15] but comparable with the values of some structurally established model complexes.[6d,12,15] In addition, the IC_{50} value for $[Cu(tpa)(MeCN)](ClO_4)_2$ was determined to be 1.4 μM. The difference in IC_{50} among **1**, **2** and $[Cu(tpa)(MeCN)](ClO_4)_2$ may be ascribed to the imidazolate-bridge and zinc ion. The effect of zinc ion was recently reported for a Cu–Zn heterodinuclear complex prepared *in situ*, which was not structurally established.[16]

In conclusion, the new imidazole derivative containing two metal-binding groups incorporated Cu(II) and Zn(II) to form a heterodinuclear SOD model complex which was stable in solution, and the SOD activity measurements exhibited the effects of the imidazolate bridge and zinc ion on the SOD activity. Studies on the details of the SOD function and mechanism are now under way.

We are grateful to Prof. Wasuke Mori, Kanagawa University, for measurements of the magnetic susceptibility, Professor Hiromu Sakurai, Kyoto Pharmaceutical University, for measurements of the SOD activity and Sachiyo Nomura, Institute for Molecular Science, for ICP measurements. This work was supported by Grants-in-Aid for Scientific Research to A. O. (No. 07CE2003(COE)) and O. Y. (Nos. 09304062 and 09045032) from the Ministry of Education, Science, Sports and Culture of Japan, to which our thanks are due.

Notes and references

‡ *Experimental:* imidazole-4,5-dialdehyde (1.0 g, 8 mmol) was dissolved in methanol (100 ml), to which bis(2-pyridylmethyl)amine (3.2 g, 16 mmol) and a small amount of acetic acid were added. Sodium cyanotrihydroborate (1.0 g, 15.5 mmol) was then added dropwise to the mixture, and after the resulting solution had been stirred for three days at room temperature, it was acidified with concentrated HCl and concentrated almost to dryness under reduced pressure. The residue was dissolved in a saturated aqueous solution of Na_2CO_3 (50 ml) and extracted with three 50 ml portions of $CHCl_3$. The combined extracts were dried over Na_2SO_4 and after removal of the solvent gave a brown oily product, which was purified by silica gel column chromatography with $CHCl_3$–MeOH as eluent to give Hbdpi (3.16 g, 80.0%); ^{1}H NMR ($CDCl_3$, 400 MHz) δ 3.65 (s, 4H), 3.75 (s, 8H), 7.12 (m, 4H), 7.47 (dt, 4H), 7.61 (td, 4H), 7.66 (s, 1H), 8.51 (dq, 4H). ^{13}C NMR ($CDCl_3$; 100 MHz) δ 48.2 (CH_2), 59.2 (CH_2), 121.7 (Py), 122.0 (Im), 123.2 (Py), 133.8 (Im), 136.2 (Py), 148.4 (Py), 158.9 (Py). Complex **1** was prepared by mixing Hbdpi (0.50 g, 1.0 mmol) with a MeOH solution of $Cu(ClO_4)_2{\cdot}6H_2O$ (0.370 g, 1.0 mmol) and $Zn(ClO_4)_2{\cdot}6H_2O$ (0.372 g, 1.0 mmol) and adding NEt_3 (138.6 μl, 1.0 mmol). After filtration, the filtrate was allowed to evaporate slowly in the open air to give $[CuZn(bdpi)(MeCN)_2](ClO_4)_3{\cdot}2MeCN$ **1** as green crystals in 67.0% yield. Elemental analysis and ICP measurement were performed for the dried sample which lost the coordinated MeCN. The ratio of Cu(II) to Zn(II) was determined by ICP (SEIKODENKO SPS-700) with the use of the standard solutions (1000 ppm) of Cu(II) and Zn(II) obtained from Nacalai Tesque. Anal. Calc. for $[CuZn(bdpi)](ClO_4)_3{\cdot}0.25MeCN{\cdot}3H_2O$ ($C_{29.5}H_{35.75}N_{8.25}Cl_3O_{15}CuZn$): C, 36.11; H, 3.67; N, 11.78; Cu, 6.48; Zn, 6.66. Found: C, 35.88; H, 3.56; N, 11.77; Cu, 6.46; Zn, 6.65%. ESI-mass (MeCN): *m/z* 816 [$(M - ClO_4)^+$]. $[Cu_2(bdpi)(MeCN)_2](ClO_4)_3{\cdot}2H_2O$ **2** was prepared in a similar manner by using Hbdpi and 2 equiv. of $Cu(ClO_4)_2{\cdot}6H_2O$. Elemental analysis and ICP measurement were performed for the dried sample. Anal. Calc. for $[Cu_2(bdpi)](ClO_4)_3{\cdot}MeCN$ ($C_{31}H_{32}N_9O_{12}Cl_3Cu_2$): C, 38.94; H, 3.37; N, 13.18; Cu, 13.29. Found: C, 38.95; H, 3.32; N, 13.35; Cu, 13.27%. Effective magnetic moment μ_{eff} = 3.46 μ_B (300 K).

§ *Crystal data:* **1** (green): $[CuZn(bdpi)(MeCN)_2](ClO_4)_3{\cdot}2MeCN$, $C_{37}H_{41}N_{12}O_{13}Cl_3CuZn$, M = 1083.09, triclinic, space group $P\bar{1}$, a = 14.447(1), b = 14.561(1), c = 12.214(1) Å, α = 108.002(7), β = 106.920(7), γ = 89.069(7)°, V = 2330.3(4) Å^3, Z = 2, D_c = 1.508 g cm^{-3}, 5067 reflections collected, 4821 independent reflections, 3209 reflections used, 596 variables, R = 0.076, R_w = 0.110 [$I > 2.00\sigma(I)$]. The crystal was poorly diffracting. Rigaku AFC-5R four-circle automated diffractometer with graphite monochromated Cu-Kα radiation, λ = 1.54178 Å, and rotating anode generator. The structures were solved by the heavy-atom method and refined anisotropically for non-hydrogen atoms by full-matrix least-squares calculations. Hydrogen atoms for the structure were located from difference Fourier maps, and their parameters were isotropically refined. All the calculations were performed by using the teXsan crystallographic software package from the Molecular Structure Corporation. CCDC 182/1462. See http://www.rsc.org./suppdata/cc/1999/2393/ for crystallographic files in .cif format.

1 J. S. Richardson, K. A. Thomas, B. H. Rubin and D. C. Richardson, *Proc. Natl. Acad. Sci. USA.*, 1975, **72**, 1349; J. A. Tainer, E. D. Getzoff, K. M. Beem, J. S. Richardson and D. C. Richardson, *J. Mol. Biol.*, 1982, **160**, 181.
2 J. A. Tainer, E. D. Getzoff, J. S. Richardson and D. C. Richardson, *Nature*, 1983, **306**, 284.
3 I. Bertini, L. Banci and M. Piccioli, *Coord. Chem. Rev.*, 1990, **100**, 67; J. S. Valentine, *Met. Ions Biol. Syst*., 1999, **36**, 125.
4 I. Fridovich, *Annu. Rev. Biochem*., 1995, **64**, 97.
5 G. Kolks, C. R. Frihart, H. N. Rabinowitz and S. J. Lippard, *J. Am. Chem. Soc*., 1976, **98**, 5720; C.-L. O'Young, J. C. Dewan, H. R. Lilienthal and S. J. Lippard, *J. Am. Chem. Soc*., 1978, **100**, 7291; P. K. Coughlin, J. C. Dewan, S. J. Lippard, E. Watanabe and J.-M. Lehn, *J. Am. Chem. Soc*., 1979, **101**, 265; G. Kolks, C. R. Frihart, P. K. Coughlin and S. J. Lippard, *Inorg. Chem*. 1981, **20**, 2933; P. K. Coughlin, A. E. Martin, J. C. Dewan, E. Watanabe, J. E. Bulkowski, J.-M. Lehn and S. J. Lippard, *Inorg. Chem.*, 1984, **23**, 1004; P. K. Coughlin and S. J. Lippard, *Inorg. Chem.*, 1984, **23**, 1446.
6 (a) M. Sato, S. Nagae, M. Uehara and J. Nakaya, *J. Chem. Soc., Chem. Commun*., 1984, 1661; (b) Q. Lu, Q. H. Luo, A. B. Dai, Z. Y. Zhou and G. Z. Hu, *J. Chem. Soc., Chem. Commun*., 1990, 1429; (c) M. Zongwan, C. Dong, T. Wenxia, Y. Kaibei and L. Li, *Polyhedron*, 1992, **11**, 191; (d) J.-L. Pierre, P. Chautemps, S. Refaif, C. Beguin, A. E. Marzouki, G. Serratrice, E. Saint-Aman and P. Rey, *J. Am. Chem. Soc*., 1995, **117**, 1965; (e) Z.-W. Mao, M.-Q. Chen, X.-S. Tan, J. Liu and W.-X. Tang, *Inorg. Chem*., 1995, **34**, 2889.
7 H. Schubert and W. D. Rudorf, *Z. Chem.*, 1971, **11**, 175.
8 K. D. Karlin, J. C. Hayes, S. Juen, J. P. Hutchinson and J. Zubieta, *Inorg. Chem*., 1982, **21** 4106.
9 M. Duggan, N. Ray, B. Hathaway, G. Tomlinson, P. Brint and K. Pelin, *J. Chem. Soc., Dalton Trans*., 1980, 1342.
10 Y. Nakao, W. Mori, T. Sakurai and A. Nakahara, *Inorg. Chim. Acta*, 1981, **55**, 103.
11 M. S. Haddad and D. N. Hendrickson, *Inorg. Chem*., 1978, **17**, 2622.
12 G. Tabbi, W. L. Driessen, J. Reedijk, R. P. Bonomo, N. Veldman and A. L. Spek, *Inorg Chem*., 1997, **36**, 1168.
13 K. J. Oberhausen, R. J. O'Brien, J. F. Richardson and R. M. Buchanan, *Inorg. Chim. Acta*, 1990, **173**, 145.
14 C. Beauchamp and I. Fridovich, *Anal. Biochem.*, 1971, **44**, 276. Superoxide anion was generated *in situ* by the xanthine–xanthine oxidase system and detected spectrophotometrically by ferricytochrome *c* reduction. The SOD activity was assayed in a γ-collidine buffer (50 mM, pH 7.77, 25.0 °C) containing 10 μM ferricytochrome *c*, 50 μM xanthine and an appropriate amount of xanthine oxidase to cause a change of absorbance (ΔA_{550} = 0.025 min^{-1}). The IC_{50} value is defined as the 50% inhibition concentration of cytochrome *c* reduction. The inhibitory effect of Cu(II) ion and its complexes used in this study on xanthine oxidase was checked prior to the assay by using the absorbance at the 295 nm peak due to uric acid at pH 7.77 (N. Cotell, J. L. Bernier, J. P. Henichart, J. P. Catteau, E. Gaydou and J. C. Wallet, *Free Rad. Biol. Med*., 1992, **13**, 221; W. S. Chang, Y. J. Lee, F. J. Lu and H. C. Chiang, *Anticancer Res*., 1993, **13**, 2165). They did not show any inhibitory effect under the experimental conditions used.
15 U. Weser, L. M. Schubotz and E. Lengfelder, *J. Mol. Catal.*, 1981, **13**, 249.
16 S. Kawabata, T. Soma and K. Ichikawa, *Chem. Lett.*, 1997, 1199.

Communication 9/06226B

ChemComm

Selective control of sensitivity to imidazole derivatives of interference-based biosensors by use of a phase transition gel

Tetsu Tatsuma, Hiroshi Mori and Akira Fujishima

Department of Applied Chemistry, Faculty of Engineering, University of Tokyo, Hongo, Bunkyo-ku, Tokyo 113-8656, Japan. E-mail: akira_fu@fchem.chem.t.u.-tokyo.ac.jp

Received (in Cambridge, UK) 14th September 1999, Accepted 25th October 1999

Sensitivity to histidine of an interference-based biosensor coated with a phase transition gel is controlled by swelling and shrinking the gel, while that to imidazole is not changed significantly.

Interference-based biosensors are used for the detection and determination of inhibitors for biocatalysts including enzymes.[1] Inhibitors for enzymes are generally toxic and interference-based biosensors are more sensitive to a large number of toxic inhibitors. However, such sensors are essentially unselective to a specific inhibitor. For example, a sensor based on cytochrome oxidase is sensitive to cyanide, azide and H_2S[2] while a biosensor based on heme peptide (HP) is also sensitive to some inhibitors including imidazole and histidine.[3,4]

If one wishes to determine two inhibitors at the same time, two independent pieces of information have to be acquired. In response to this, an electrochemical/piezoelectric dual response biosensor was developed by modifying an electrode of a quartz crystal resonator with HP.[5] In this case, a decrease in the catalytic activity of HP (for H_2O_2 reduction) and an increase in the mass of the bound inhibitor are measured on the basis of the catalytic current and the resonance frequency, respectively. This dual transduction system is, however, not simple since both electrochemical and piezoelectric equipment must be employed. An alternative way to obtain two independent kinds of information is the use of a sensor array with some different biocatalysts. However, a two-channel electrochemical set-up and two different, but similar biocatalysts are necessary.

In the present work, a single interference-based biosensor is coated with a gel that exhibits a volume phase transition.[6] Permeability of the gel to substances can be controlled by changing an environmental factor, such as temperature. As the gel is shrunk, the permeability to some substances may be lowered, due chiefly to the reduced pore size of the polymer network. In this case, the suppression of the permeability to a large molecule should be more significant than that to a small molecule. On the basis of this effect, we intended to selectively control the sensitivity of the interference-based biosensor to inhibitors (Fig. 1). As a result, we are able to acquire two independent pieces of information, one from the sensor in the swollen state and the other from the sensor in the shrunken state.

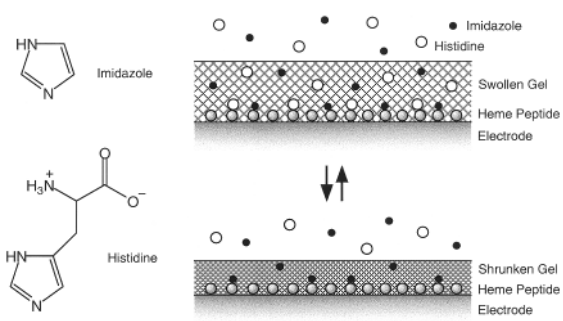

Fig. 1 Schematic depiction for the selective control of sensitivity to imidazole and histidine by shrinking and swelling the gel coated on a heme peptide-modified electrode.

This technique should also be important for the control of the apparent activity and selectivity of biocatalysts. Phase transition gels have been used to control the apparent activity of an enzyme immobilized in or on the gel.[7–14] However, to the best of our knowledge, the selective control of the apparent activity (equivalent to the sensitivity of a sensor) has not, as yet, been reported.

An indium tin oxide (ITO)-coated glass plate (area *ca.* 0.25 cm^2) was treated with a 10% toluene solution of (3-aminopropyl)triethoxysilane to introduce the amino group onto the electrode surface. The electrode was then treated with pH 7.4 phosphate buffer (0.0667 M) containing 1 g L^{-1} heme undecapeptide (HP, Sigma) and 20 mM 1-ethyl-3-(3-dimethylaminopropyl)carbodiimide so as to immobilize HP covalently to the electrode surface *via* amide bonding. The HP electrode thus obtained was further coated with a phase transition gel to obtain a gel–HP electrode. A 10 μL aliquot of a freshly prepared aqueous solution containing 700 mM *N*-isopropylacrylamide (NIPA), 7 mM *N*,*N*′-methylenebisacrylamide as a cross-linking agent, 0.087 mM $(NH_4)_2S_2O_8$ as a polymerization initiator, and 39 mM *N*,*N*,*N*′,*N*′-tetramethylethylenediamine as a reaction accelerator was applied to the electrode surface and was left for 5 h to obtain a gel. The gel–HP electrode thus obtained was then rinsed thoroughly with water (< 30 °C). The gel exhibited a volume phase transition at *ca.* 33 °C. It is known that NIPA-based gels are swollen at lower temperatures and shrunken at higher temperatures.[7,8,11,14] In the swollen state, the thickness of the present gel was *ca.* 1 mm while in the shrunken state, the gel was *ca.* an order of magnitude thinner.

Electrochemical measurements were performed at 25 °C (swollen gel) or 45 °C (shrunken gel) with a potentiostat LC-4C (BAS). Reference and counter electrodes were Ag/AgCl/NaCl(sat.) and a platinum wire, respectively while the electrolyte solution was 0.0133 M phosphate buffer, pH 7.4. The working electrode was polarized at +150 mV *vs.* Ag/AgCl, and a hydrogen peroxide solution was added to the electrolyte (final concentration, 10 μM), followed by the addition of an inhibitor (imidazole or histidine).

First an HP electrode not coated with the gel, was investigated. In response to the addition of hydrogen peroxide, a cathodic current was observed (1.6 nA at 25 °C and 3.9 nA at 45 °C). This is based on the electron transfer from the ITO electrode to compounds **I** and **II** of HP (oxidized forms) [eqns. (1)–(3)]

$$\text{Ferric HP} + H_2O_2 \rightarrow \text{Compound } \mathbf{I} + H_2O \quad (1)$$

$$\text{Compound } \mathbf{I} + H^+ + e^- \rightarrow \text{Compound } \mathbf{II} \quad (2)$$

$$\text{Compound } \mathbf{II} + H^+ + e^- \rightarrow \text{Ferric HP} + H_2O \quad (3)$$

Addition of imidazole or histidine suppressed the cathodic current since imidazole and histidine coordinate to the vacant coordination site of HP at which hydrogen peroxide reacts. These results have already been reported and exploited for the determination of imidazole derivatives.[3–5]

In the present paper, the response R is defined by eqn. (4)

$$R = 1 - (i/i_0) \quad (4)$$

where i_0 is the cathodic current observed after the addition of H_2O_2 (10 μM) and i is the current measured after addition of an

inhibitor (imidazole or histidine) (background current subtracted from both of the currents). In other words, the response *R* is the degree of interference. Even though the measurements were carried out at both 25 and 45 °C, relationships between the response to the inhibitor and the inhibitor concentration (Fig. 2) were similar for the HP electrode without the gel.

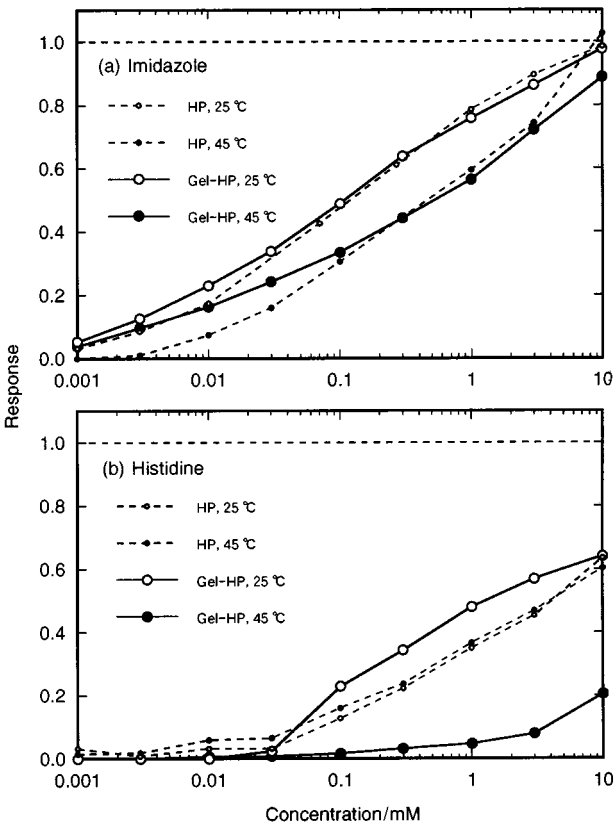

Fig. 2 Responses of the HP and gel–HP electrodes to imidazole (a) and histidine (b) at 25 °C (swollen gel) and 45 °C (shrunken gel) as a function of their concentrations.

The HP electrode coated with the phase transition gel, the gel–HP electrode, was then examined. At 25 °C, when the gel is swollen, the responses to both imidazole and histidine were almost the same as those obtained from the HP electrode without gel [Fig. 2(a) and (b)]. At 45 °C, where the gel is shrunk, while the responses of the gel–HP electrode to imidazole were similar to those of the HP electrode [Fig. 2(a)], the gel–HP electrode exhibited significantly smaller responses to histidine at 45 °C than did the HP electrode [Fig. 2(b)]. This temperature-dependent behavior was reversible for the gel–HP electrode. Additionally, the presence of both analytes (imidazole or histidine) did not interfere in the determination of each. At 45 °C, addition of histidine (final concentration, 1 mM) to 3 mM imidazole led only to a slight increase in the response, as expected from Fig. 2.

Thus, the sensitivity of the gel–HP electrode to histidine was lowered by shrinking the gel without significant changes of the sensitivity of imidazole. In other words, two independent responses can be acquired in the swollen and shrunken states. The concentration of histidine in the shrunken gel is lower than that in the solution by more than one order of magnitude. There are two possible reasons for this selective control of the sensitivity: (i) histidine (M = 155) is larger than imidazole (M = 68) so that the former permeates less effectively into the fine polymer network of the shrunken gel; and (ii) histidine, which has one positive and one negative charge at pH 7.4, should be more hydrophilic than imidazole, and hence would permeate less efficiently into the shrunken gel, which is relatively hydrophobic. In future work, we will examine the possibility of the determination of two interferants in one solution on the basis of the two responses obtained at swollen and shrunken states. Additionally, not only the size and hydrophilic/hydrophobic effects, but also electrostatic and some other effects will be exploited for the selective control of sensitivity of biosensors.

This work was supported in part by a Grant-in-Aid for Scientific Research on Priority Areas (No. 404, Molecular Synchronization for Design of New Material Systems) (No. 11167215 for T. T.) and a Grant-in-Aid for Encouragement of Young Scientists (No. 11750709 for T. T.) both from the Ministry of Education, Science, Sports and Culture of Japan.

Notes and references

1 F. Scheller and F. Schubert, *Biosensors*, Elsevier, Amsterdam, 1992.
2 W. J. Albery, A. E. G. Cass, B. P. Mangold and Z. X. Shu, *Biosens. Bioelectron.*, 1990, **5**, 397.
3 T. Tatsuma and T. Watanabe, *Anal. Chem.*, 1991, **63**,1580.
4 T. Tatsuma and T. Watanabe, *Anal. Chem.*, 1992, **64**, 143.
5 T. Tatsuma and D. A. Buttry, *Anal. Chem.*, 1997, **69**, 887.
6 T. Tanaka, *Sci. Am.*, 1981, **244**, 124.
7 L. C. Dong and A. S. Hoffman, *J. Controlled Release*, 1986, **4**, 223.
8 T. G. Park and A. S. Hoffman, *J. Biomed. Mater. Res.*, 1990, **24**, 21.
9 H. Kitano, C. Yan and K. Nakamura, *Makromol. Chem.*, 1991, **192**, 2915.
10 E. Kokufuta, O. Ogane, H. Ichijo, S. Watanabe and O. Hirasa, *J. Chem. Soc., Chem. Commun.*, 1992, 416.
11 T. Shiroya, N. Tamura, M. Yasui, K. Fujimoto and H. Kawaguchi, *Colloids Surf. B: Biointerf.*, 1995, **4**, 267.
12 T. Shiroya, M. Yasui, K. Fujimoto and H. Kawaguchi, *Colloids Surf. B: Biointerf.*, 1995, **4**, 275.
13 M. Yasui, T. Shiroya, K. Fujimoto and H. Kawaguchi, *Colloids Surf. B: Biointerf.*, 1997, **8**, 311.
14 T. Tatsuma, Y. Watanabe and N. Oyama, *Electrochem. Solid-State Lett.*, 1998, **1**, 136.

Communication 9/07436H

ChemComm

Fluoride ion-initiated α-fluorovinylation of carbonyl compounds with α-fluorovinyldiphenylmethylsilane

Takeshi Hanamoto,* Shigeo Harada, Keiko Shindo and Michio Kondo

Department of Chemistry and Applied Chemistry, Saga University, Honjyo-machi 1, Saga 840-8502, Japan. E-mail: hanamoto@cc.saga-u.ac.jp

Received (in Cambridge, UK) 4th October 1999, Accepted 20th October 1999

α-Fluorovinyldiphenylmethylsilane was synthesized in one step from 1,1-difluoroethylene; the TBAF-initiated reaction of the silane with carbonyl compounds smoothly proceeded to give the corresponding α-fluoroallylic alcohols in good yields.

Fluorinated allylic alcohols have recently received much attention due to their versatility as building blocks for complex structures.[1] These alcohols should be accessible from carbonyl compounds by fluorovinylation in a straightforward way. Although the di- or tri-fluorovinylation of carbonyl compounds to afford the corresponding fluorinated allylic alcohols has been reported,[2] to the best of our knowledge, no monofluorovinylation as the simplest case has been reported so far. The reason seems to be the lack of the generation of the monofluorovinylanion species.[3] We have considered the title compound as a promising candidate for a monofluorovinylation reagent which would generate the monofluorovinyl anion species by action of the fluoride source.[4] This report describes the first preparation and reactions of the α-fluorovinyldiphenylmethylsilane **2** as a useful reagent for introducing a monofluoroethylene moiety into carbonyl compounds.[5]

Our synthetic route for the preparation of α-fluorovinyldiphenylmethylsilane is depicted in Scheme 1. Since we have recently reported the convenient preparation of α-fluorovinyldiphenylphosphine from 1,1-difluoroethylene **1**,[6] this method was applied to the preparation of the silane. As expected, the reaction of diphenylmethylsilyllithium[7] and 1,1-difluoroethylene in THF at −78 °C proceeded smoothly to give the desired product in 56% yield *in one step*.† We believe that the key to this reaction is use of chlorodiphenylmethylsilane instead of chlorophenyldimethylsilane. When the latter was employed under similar reaction conditions, the yield of the corresponding α-fluorovinylphenyldimethylsilane was low and the contaminant 1,2-diphenyl-1,1,2,2-tetramethyldisilane could not be separated from the desired α-fluorovinylphenyldimethylsilane.

We have examined the use of α-fluorovinyldiphenylmethylsilane as a potential reagent for introducing an α-fluorovinyl group into various carbonyl compounds. The reaction of a slight excess of α-fluorovinyldiphenylmethylsilane (1.2 equiv.) and benzaldehyde in the presence of a catalytic amount of TBAF (1 M THF solution, 10 mol%) in THF gave the desired product in 34% yield. Increasing the amount of catalyst (30 mol%) did not significantly improve the yield (39%). Based on TLC analysis of the reaction mixture, we observed that the α-fluorovinyldiphenylmethylsilane was completely consumed although the benzaldehyde still remained. This finding may be explained as follows: the generated α-fluorovinylanion species decomposed to the vinylcarbene or abstracted a proton from the reaction medium due to its modest reactivity prior to its addition to benzaldehyde. On the basis of this idea, increasing the amount of the silane gave better results (1.5 equiv., 42%; 2.0 equiv., 61%). The reaction was applied to the silane and various carbonyl compounds under optimized conditions. These results are shown in Table 1. Although ketones afforded the adducts in low yields, probably due to their steric hindrance, aldehydes gave the adducts in fairly good yields. It is noteworthy that the reaction proceeded under mild conditions in contrast to the reaction of difluorovinyllithium.[8] Attempts to improve the ketone adducts at an elevated reaction temperature (55 °C) resulted in formation of a complex mixture of products.

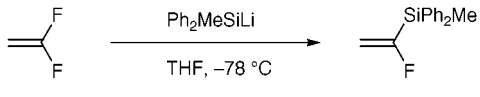

1 **2** (56%)

Scheme 1

Table 1 Reaction of α-fluorovinyldiphenylmethylsilane with various carbonyl compounds

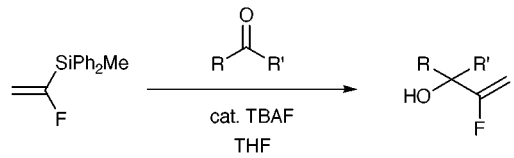

Entry	R	R′	Yield (%)[a]
1	Ph	H	61
2	4-$MeOC_6H_4$	H	77
3	4-PhC_6H_4	H	61
4	2-Naphthyl	H	65
5[b]	(*E*)-PhCH=CH	H	60
6[c]	$CH_3(CH_2)_9$	H	50
7	$PhCH_2CH_2$	Me	18
8	Ph	Me	13

[a] Isolated yield. [b] TBAF (20 mol%) was used. [c] TBAF was added to the reaction mixture at −70 °C.

A typical experimental procedure (Table 1, entry 2) is as follows: TBAF (1 M THF solution, 40.3 μl, 0.04 mmol, 10 mol%) was added to a mixture of α-fluorovinyldiphenylmethylsilane (97.7 mg, 0.40 mmol) and 4-methoxybenzaldehyde (24.5 μl, 0.20 mmol) dissolved in THF (1 ml) at 0 °C. The resulting mixture was stirred for 1 h at 0 °C and for 16 h at room temperature. After the usual workup, column chromatography (silica gel, hexane–EtOAc = 9:1) of the residue afforded 28.5 mg of 2-fluoro-1-(4′-methoxyphenyl)-2-propen-1-ol (77% yield).‡

In conclusion, we have demonstrated the first preparation of α-fluorovinyldiphenylmethylsilane from 1,1-difluoroethylene in one step. The generated α-fluorovinyl anion species derived from the silane by action of TBAF reacted with various carbonyl compounds to give the corresponding α-fluoroallylic alcohols in good yields. Further studies on its synthetic utility are now in progress in our laboratory.

Notes and references

† *Preparation* of **2**: To a solution of lithium wire (0.14 g, 20 mmol) in 10 ml of THF was added a catalytic amount of iodine and chlorodiphenylmethylsilane (1.03 ml, 5 mmol) at room temperature under argon. The solution was

irradiated with ultrasound for 30 min and a black–green color developed. After stirring for an additional 16 h, the solution was cooled to −78 °C. At this temperature, argon was replaced with 1,1-difluoroethylene (balloon). The mixture was stirred at −78 °C for 30 min, gradually warmed to 0 °C, and carefully quenched with saturated aqueous NH_4Cl. After the usual workup, the residue was chromatographed on silica gel (hexane as an eluent) to give the desired product (683 mg, 56%): ν_{max}(neat)/cm^{-1} 3071, 3050, 2963, 1620, 1429, 1256, 1160, 1115, 910, 881, 793, 729 and 698; δ_H($CDCl_3$) 0.72 (3H, s), 4.86 (1H, dd, *J* 3.4, 61.5), 5.48 (1H, dd, *J* 3.4, 32.7), 7.34–7.66 (10H, m); *m*/*z* 242 (0.7%, M$^+$), 201 (100), 197 (59), 181 (58), 179 (26), 164 (31), 149 (31), 139 (82), 105 (21), 91 (28) (calcd. for $C_{15}H_{15}FSi$: C, 74.34; H, 6.24. Found: C, 74.43; H, 6.25%).

‡ *Selected data* for 2-fluoro-1-(4′-methoxyphenyl)prop-2-en-1-ol: ν_{max}(neat)/cm^{-1} 3415, 2840, 1678, 1612, 1586, 1513, 1466, 1305, 1251, 1176, 1033, 942, 831 and 778; δ_H($CDCl_3$) 2.19 (1H, d, *J* 4.9), 3.81 (3H, s), 4.67 (1H, dd, *J* 2.9, 48.8), 4.76 (1H, dd, *J* 2.9, 17.3), 5.17 (1H, dd, *J* 4.9, 8.8), 6.91 (2H, d, *J* 8.8), 7.36 (2H, d, *J* 8.8); *m*/*z* 182 (24, M$^+$), 121 (100), 120 (30), 109 (98), 108 (38), 101 (35), 77 (81), 51 (35); (calcd. for $C_{10}H_{11}FO_2$: C, 65.92; H, 6.09. Found: C, 65.72; H, 6.21%).

1 T. Allmendinger, C. Angst and H. Karfunkel, *J. Fluorine Chem*., 1995, **72**, 247.

2 D. J. Burton, Z-Y. Yang and P. A. Morken, *Tetrahedron*, 1994, **50**, 2993.

3 The synthesis of α-fluorovinyltributyltin has been reported. However, no reaction with carbonyl compounds has been reported. D. P. Matthews, P. P. Waid, J. S. Sabol and J. R. McCarthy, *Tetrahedron Lett*., 1994, **35**, 5177.

4 A use of a similar methodology has been reported. M. Fujita, M. Obayashi and T. Hiyama, *Tetrahedron*, 1988, **44**, 4135; G. K. S. Prakash, R. Krishnamurti and G. A. Olah, *J. Am. Chem. Soc*., 1989, **111**, 393.

5 Alternative methods to prepare α-fluoroallylic alcohols have been reported. T. Ernet and G. Haufe, *Synthesis*, 1997, 953; T. Dubuffet, C. Bidon, P. Martinet, R. Sauvêtre, and J.-F. Normant, *J. Organomet. Chem*., 1990, **393**, 161.

6 T. Hanamoto, Y. Kiguchi, K. Shindo, M. Matsuoka and M. Kondo, *Chem. Commun*, 1999, 151.

7 We modified the preparation of the phenyldimethylsilyllithium reagent. I. Fleming, R. S. Roberts and S. C. Smith, *J. Chem. Soc., Perkin Trans. 1*, 1998, 1209.

8 S. A. Fontana, C. R. Davis, Y.-B. He and D. J. Burton, *Tetrahedron*, 1996, **52**, 37.

Communication 9/07978E

Effective signal control (off-on-off action) by metal ionic inputs on a new chromoionophore-based calix[4]crown

Yuji Kubo,*[ab] Satoru Obara[b] and Sumio Tokita[b]

[a] *PRESTO, Japan Science and Technology Corporation (JST)*
[b] *Department of Applied Chemistry, Faculty of Engineering, Saitama University, 255 Shimo-ohkubo, Urawa, Saitama 338-8570, Japan. E-mail: yuji@apc.saitama-u.ac.jp*

Received (in Cambridge, UK) 5th October 1999, Accepted 25th October 1999

A new chromoionophore-based calix[4]crown 1 possessing an effective 'off-on-off' signalling for metal cationic inputs has been developed, the controllable signal function of which may not only be welcome for molecular information processing but also contribute to the design of new sensory materials.

The design and construction of devices miniaturized to the molecular level would not only contribute to the development of nanotechnology, but would also be of scientific interest.[1] Such progress may have important implications for biomimetic engineering.[2] Ionically-controlled optical signalling is a particularly attractive approach to switchable molecular devices for the use in information processing. In order to achieve such processing, effective ionic signal control is no doubt of importance. So far, de Silva *et al*. have reported pioneering work on developing molecular logic devices based on photo-induced electron transfer (PET) characteristics.[3] In many instances, it is of particular interest that a tailored PET system possessing two different proton binding sites forms a pH-dependant 'off-on-off' photoionic switch[4] that is a molecular emulator of an electronic device. However, the more intricate switches have only dealt with the simplest ion: H^+.[5] 'Off-on-off' switchable systems induced by ionic guests other than H^+ are as yet unknown. Thus, as an alternative approach, we have found it worthwhile to design a simplified receptor system based on competitive cation-induced 'off-on-off' colorimetric signal control:[6] it is in principle required that this system should show a colorimetric effect ('off-on' step) with the first ion, and then, if the second ion can not only bind to the system with greater affinity than the first but also induce no colorimetric effect, the second ion would release the first ion efficiently to bring about an active 'on-off' signal switch. Here we report that calix[4]crown-5[7] **1** does in fact serve as such a photoionic system.

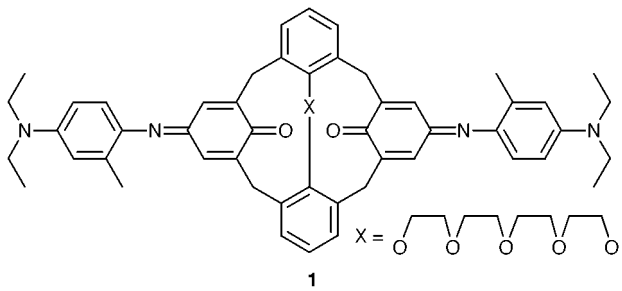

1

The system **1** contains paired indoaniline chromophores that allow a color change to be induced when a cation becomes encapsulated within the cavity. A critical design feature of this system is the use of the crown-strapped cavity. This means that an alkali metal ion can be bound with high affinity, as it is known that calix[4]crown-5 derivatives possess high K^+ selectivity.[8] However, it occurred to us that the carbonyl groups of the chromophores, being more polar donor groups than the ethers, strongly favor Ca^{2+} over either Na^+ or K^+.[9] Indeed, we reported that a bis(ethyl acetate)-derived calix[4]arene–indoaniline conjugate efficiently encapsulated Ca^{2+} with a remarkable bathochromic absorbance shift, making it of potential use as an optical sensor for Ca^{2+} detection.[10] Taken together, if an alkali metal ion such as K^+, which is bound by the macroring crown oxygens, forms a more favorable complex with **1** than Ca^{2+}, the Ca^{2+}-induced signal response could be efficiently switched off by the cation. As a consequence, it is expected that system **1** will define a rather unique chromogenic system capable of effective 'off-on-off' signal control. As detailed below, this does indeed occur.

System **1**† was synthesized from calix[4]arene[11] *via* a set of straightforward steps involving a Williamson synthesis with 3,6,9-trioxaundecane-1,11-diyl ditosylate in the presence of a base, and condensation with 2-amino-5-(diethylamino)toluene monohydrochloride under alkaline conditions in the presence of $KMnO_4$. Based on our previous work,[10] system **1** was expected to complex Ca^{2+} with high efficiency within its cavity. Indeed, an EtOH solution of **1** showed a remarkable bathochromic shift ($\Delta\lambda$ = 112 nm) and an increase in absorption intensity upon addition of Ca^{2+}, resulting in an immediate color change from blue to green. At a [Ca^{2+}] to [**1**] ratio of 1.5:1, a new absorption band at 734 nm was observed ('off-on' switch; Fig. 1). Independent Job plot analysis[11] was consistent with the formation of a 1:1 stoichiometric complex. This then allowed an association constant (K_a) of 1.8×10^6 M^{-1} to be calculated using a nonlinear least-squares curve fitting procedure. The Ca^{2+}-induced colorimetric effect is mainly attributed to efficient ion–dipole interactions between the encapsulated Ca^{2+} and the quinone carbonyl groups of the indoaniline chromophores. In contrast, upon interaction with K^+ under similar conditions, no evidence of significant interaction between this cation and the chromophores was obtained. However, of particular interest is

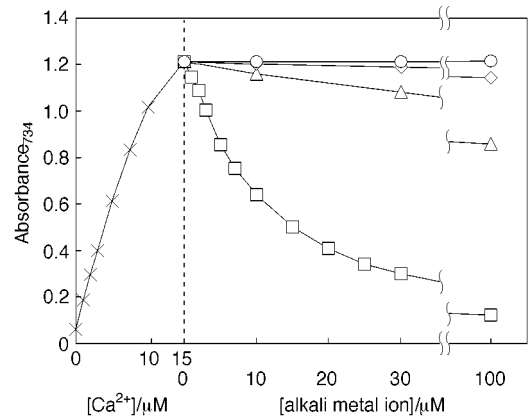

Fig. 1 Absorption intensity change at 734 nm induced by Ca^{2+} addition and subsequent alkali metal ion additions: (○) Ca^{2+}-**1** plus Li^+, (Δ) Ca^{2+}–**1** plus Na^+, (□) Ca^{2+}-**1** plus K^+ and (◇) Ca^{2+}–**1** plus Cs^+. These data were collected in EtOH at 25 °C where the concentration of receptor **1** is 10 μM.

that a competitive titration, involving adding K^+ to a solution of **1** (10 μM) and 1.5 equiv. of Ca^{2+}, exhibited significant reversed spectral changes ('on-off' switch; Fig. 1); when adding 2 equiv. of K^+ to the solution, *ca*. 70% of the absorption intensity at 734 nm was apparently diminished. This phenomenon was readily detected visually, being clearly consistent with the encapsulated Ca^{2+} being released from **1** in an almost stoichiometric reversible and competitive fashion as K^+ was added.‡

Semi-quantitative assessment of the competitive complexation process came from FAB mass spectrometric analyses. The formation of a 1 : 1 complex between **1** and Ca^{2+} was confirmed by monitoring the peaks at *m/z* 970 ($[M+Ca]^+$) and 1027 ($[M - H + Ca + SCN]^+$) using a *m*-nitrobenzyl alcohol matrix. Upon adding K^+ to the **1**–Ca^{2+} complex, the peak due to the Ca^{2+} complex was almost completely suppressed, whereas a new peak signal at *m/z* 968 ($[M-H + K]^+$) could be detected. These results are consistent with those obtained from the UV–Vis titrations and thus strongly support the notion that reversible competitive complexation takes place between Ca^{2+} and K^+ in the case of receptor **1**. We were interested to know whether or not the effective 'on-off' switch obtained in **1** can be induced by only K^+. Thus, we tested alkali metal ions other than K^+. As depicted in Fig. 1, the Ca^{2+}-induced signal was barely influenced by Li^+, Na^+ and Cs^+. The association constants (K_a) for the complexation of the alkali metal ions to **1** were calculated using a mathematical method that may be applied to competition experiments[13] and **1** was found to have peak affinity with K^+ ($K_a = 7.2 \times 10^6\ M^{-1}$); the selectivity of K^+ over Ca^{2+} was 4.0. As K^+ induced almost no color change, and can switch off the Ca^{2+}-induced optical signal with high selectivity over other alkali metal ions, an effective 'off-on-off' switch for system **1** could be achieved by making use of the combination of Ca^{2+} and K^+.

NMR studies were carried out in an effort to understand the detail of the substrate–receptor interactions. Although the ^1H NMR spectra showed that both the Ca^{2+} and K^+ complexes in CD_3OD adopt cone conformations, the binding modes are slightly different, as inferred from 2D COSY and NOESY experiments.§ These different modes in the cavity might suggest that the guest Ca^{2+} is bound by the more polar carbonyl groups of the indoanilines to induce the drastic color change, whereas K^+ interacts with the convergent crown oxygens to switch off the Ca^{2+}-induced signal more efficiently than other alkali metal ions.

In conclusion, the results described here lead us to suggest a new approach to the generation of photochemical 'off-on-off' switching systems. On a different level, the selective 'on-off' switching step described herein could prove useful in terms of generating a molecular sensor in analytical chemistry.[14] We feel that such possibilities warrant future exploration.

This work was partly supported by TORAY Award in Synthetic Organic Chemistry, Japan.

Notes and references

† *Selected data* for **1**: δ_H(400 MHz, DMSO-d_6, 373 K) 1.16 (t, *J* 7.0, 12H), 2.26 (s 6H), 3.19–3.31 (br d, 4H), 3.40 (q, *J* 6.9, 8H), 3.51–3.99 (m, 20H), 6.57–6.84 (m, 12H), 7.08 (2H, s) and 7.14 (2H, s); *m/z* (FAB) 930 $[M]^+$ (Calc. for $C_{58}H_{66}N_4O_7{\cdot}0.5H_2O$: C, 74.10; H, 7.18; N, 5.96. Found: C,73.92; H, 7.22; N, 6.28%); λ_{max}(EtOH)/nm (ε_{max}/dm^3 mol^{-1} cm^{-1}) 622 (47000).

‡ The Ca^{2+}-induced absorption intensity at 734 nm ('on' state) was scarcely influenced by adding 100 μM of H^+.

§ This work will be reported elsewhere.

1 *Molecular Electronic Devices*, ed. F. L. Carter, R. E. Siatkowski and H. Wohltjen, Elsevier, Amsterdam, 1988; *Nanotechology*, ed. B. C. Crandall and J. Lewis, MIT Press, Cambridge, MA, 1992; L. Fabbrizzi and A. Poggi, *Chem. Soc. Rev.*, 1995, 197; V. Balzani and F. Scandola, in *Comprehensive Supramolecular Chemistry, Vol. 10*, ed. D. N. Reinhoudt, Pergamon, Oxford, 1996, pp. 687–746.

2 K. E. Drexler, *Namosystems: Molecular Machinary, Manufacturing, and Computation*, Wiley, New York, 1992.

3 A. P. de Silva, H. Q. N. Gunaratne, T. Gunnlaugsson, A. J. M. Huxley, C. P. McCoy, J. T. Rademacher and T. E. Rice, in *Advances in Supramolecular Chemistry, Vol. 4*, ed. G. W. Gokel, JAI Press, Greenwich, 1997, pp. 1–53.

4 A. P. de Silva, H. Q. N. Gunaratne and C. P. McCoy, *Chem. Commun.*, 1996, 2399; S. A. de Silva, A. Zavaleta, D. E. Baron, O. Allam, E. V. Isidor, N. Kashimura and J. M. Percarpio, *Tetrahedron Lett.*, 1997, **38**, 2237.

5 For another example of pH-dependent 'off-on-off' control, see: F. Barigelletti, L. Flamigni, M. Guardigli, J.-P. Sauvage, J.-P. Collin and A. Sour, *Chem. Commun.*, 1996, 1329.

6 For an example of a colorimetric logic gate system, see: M. Inouye, K. Akamatsu and H. Nakazumi, *J. Am. Chem. Soc.*, 1997, **119**, 9160.

7 A review of calixarene chemistry, see: C. D. Gutsche, in *Calixarenes Revisited, Monographs in Supramolecular Chemistry*, ed. J. F. Stoddart, The Royal Society of Chemistry, Cambridge, 1998.

8 E. Ghidini, F. Ugozzoli, R. Ungaro, S. Harkema, A. A. El-Fadl and D. N. Reinhoudt, *J. Am. Chem. Soc.*, 1990, **112**, 6979; P. D. Beer, Z. Chen, M. G. B. Drew and P. A. Gale, *J. Chem. Soc., Chem. Commun.*, 1994, 2207; A. Casnati, A. Pochini, R. Ungaro, C. Bocchi, F. Ugozzoli, R. J. M. Egberink, H. Struijk, R. Lugtenberg, F. de Jong and D. N. Reinhoubt, *Chem. Eur. J.*, 1996, **2**, 436.

9 V. J. Gatto and G. W. Gokel, *J. Am. Chem. Soc.*, 1984, **106**, 8240.

10 Y. Kubo, S. Hamaguchi, A. Niimi, K. Yoshida and S. Tokita, *J. Chem,. Soc., Chem. Commun.*, 1993, 305; Y. Kubo, S. Tokita, Y. Kojima, Y. T. Osano and T. Matsuzaki, *J. Org. Chem.*, 1996, **61**, 3758.

11 C. D. Gutsche and L.-G. Lin, *Tetrahedron*, 1986, **42**, 1633.

12 P. Job, *Ann. Chim. Ser.*, 1928, **9**, 113.

13 K. A. Conners, in *Binding Constants, The Measurement of Molecular Complex Stability*, Wiley, New York, 1987.

14 T. Hayashita and M. Takagi, in *Comprehensive Supramolecular Chemistry, Vol. 1*, ed G. W. Gokel, Pergamon, Oxford, 1996, pp. 635–669; D. Diamond and M. A. McKervey, *Chem. Soc. Rev.*, 1996, 15; A. W. Czarnik and J. Yoon, in *Perspectives in Supramolecular Chemistry, Vol. 4*, ed. D. N. Reinhoudt, Wiley, New York, 1999, pp. 177–191. For recent interesting reports of colorimetric replacement assays, see: K. Niikura, A. P. Bisson and E. V. Anslyn, *J. Chem. Soc., Perkin Trans. 2*, 1999, 1111; P. A. Gale, L. J. Twyman, C. I. Handlin and J. L. Sessler, *Chem. Commun.*, 1999, 1851.

Communication 9/08001E

ChemComm

General acid catalysed hydrolysis of β-sultams involves nucleophilic catalysis

Nicholas J. Baxter, Andrew P. Laws, Laurent J. H. Rigoreau and Michael I. Page*

Department of Chemical and Biological Sciences, University of Huddersfield, Huddersfield, UK HD1 3DH. E-mail: m.i.page@hud.ac.uk

Received (in Cambridge, UK) 15th September 1999, Accepted 13th October 1999

The hydrolysis of the four-membered ring sulfonamide *N*-benzyl β-sultam is catalysed by carboxylic acids, which is attributed to specific acid–nucleophilic catalysis with the intermediate formation of a mixed anhydride which can be trapped with aniline.

Contrary to intuition, the four-membered monocyclic β-lactams are not significantly more reactive than their acyclic amide analogues. For example, the second-order rate constant for the alkaline hydrolysis of *N*,*N*-dimethylacetamide is only three times greater than that of *N*-methyl β-lactam.[1] By contrast, β-sultams undergo alkaline hydrolysis at least 10^8-fold faster than an analogous acyclic sulfonamide.[2] It is normally difficult to study the mechanism of reactions of sulfonamides because of their intrinsic stability,[3] despite their inherent interest as potential therapeutic agents.[4] The four-membered β-sultams therefore offer the opportunity to readily investigate sulfonyl transfer reactions.

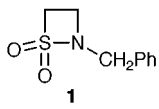

1

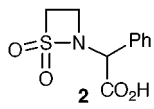

2

The rate of hydrolysis of *N*-benzyl β-sultam **1** was measured by monitoring changes in its UV spectrum at 225–235 nm in a range of carboxylate buffers under pseudo-first-order conditions. At a constant pH, ionic strength [I = 1.0 M (KCl)] and at 30 °C, the observed first-order rate constants increase linearly with increasing concentrations of buffer, indicative of buffer catalysis. Plots of k_{obs} against the total buffer concentration yield slopes (k_{cat}) which give the total contribution to the rate law by both the concentration of the undissociated carboxylic acid and the carboxylate anion. The intercepts of these buffer plots (k_{int}) correspond to the calculated observed first-order rate constants for the specific acid catalysed hydrolysis based on the second-order rate constant (k_{H^+} = 1.52 M^{-1} s^{-1}) obtained from reactions studied in solutions of hydrochloric acid. For each series of buffers, a plot of k_{cat} against α, the fraction of the buffer present as the free base, gives intercepts, when α = 0 and 1.0, of k_{HA} and k_{A^-}, respectively, the individual second-order rate constants for catalysis by the acidic and basic buffer components. The values of k_{A^-} were indistinguishable from zero. The rate law for the hydrolysis of *N*-benzyl β-sultam in carboxylate buffers is thus given by eqn. (1).

$$k_{obs} = k_H[H^+] + k_{HA}[HA] \quad (1)$$

The values of the second-order rate constants k_{HA} are given in Table 1, from which it can be seen that they increase with decreasing pK_a of the carboxylic acid buffer. The observation of general acid catalysed hydrolysis is in contrast to the general base catalysis seen with the buffer catalysed hydrolysis of β-lactams of penicillins.[5] Although catalysis by acidic species other than the protonated solvent is usually referred to as 'general acid catalysis', mechanistically the reaction may proceed *via* different but kinetically equivalent processes. Mechanistic general acid catalysed hydrolysis could involve nucleophilic attack by water which is concerted with the protonation of the β-sultam by the undissociated carboxylic acid. Interestingly, there is no evidence of intramolecular general acid catalysis in the hydrolysis of *N*-carboxy(phenyl)-methyl β-sultam **2**. Alternatively, a specific acid–general based catalysed pathway could involve pre-equilibrium protonation of the β-sultam nitrogen, followed by the general base catalysed attack by water, the nucleophilicity of which is enhanced as a result of proton abstraction by the carboxylate anion.

Table 1 Second-order rate constants for the carboxylic acid catalysed hydrolysis of *N*-benzyl β-sultam at 30 °C [I = 1.0 M (KCl)]

Carboxylic acid	pK_a	k_{HA}/M^{-1} s^{-1}
$ClCH_2CO_2H$	2.70	7.61×10^{-2}
$MeOCH_2CO_2H$	3.38	2.95×10^{-2}
HCO_2H	3.67	7.53×10^{-2}
CH_3CO_2H	4.57	4.14×10^{-3}

The third and probable mechanism of buffer catalysis involved specific acid–nucleophilic catalysis (Scheme 1). The β-sultam undergoes reversible protonation, probably on nitrogen, followed by direct nucleophilic attack of the carboxylate anion to form a mixed acid anhydride intermediate which is subsequently hydrolysed. Nucleophilic catalysis in the carboxylate buffer hydrolysis of β-sultams was confirmed by trapping the mixed acid anhydride intermediate with aniline to give acetanilide. A series of high performance liquid chromatograms were obtained by injecting samples of acetate buffer (0.2 M, pH 4.83) containing aniline (0.50 M) with and without added *N*-benzyl β-sultam. In the presence of the β-sultam, a peak with a retention time corresponding to that of acetanilide was observed, whereas in the absence of the β-sultam no acetanilide is produced. These observations provide the most conclusive evidence that the carboxylate buffer catalysed hydrolysis of β-sultams is due to specific acid–nucleophilic catalysis.

The hydrolysis of *N*-benzyl β-sultam in acetate buffers showed unusual behaviour because the kinetics showed biphasic behaviour; an initial exponential burst of UV absorbance was followed by a much slower first order reaction. This was only observed for acetate buffers and the catalytic rate constants were obtained from the initial rates. The biphasic kinetics observed in the acetate buffer hydrolysis of *N*-benzyl β-sultam may be attributed to the accumulation and subsequent hydrolysis of the anhydride intermediate. The rate of decomposition of the intermediates derived from the 2-chloroacetate, 2-methoxyacetate and formate anions are greater than those for their formation because of the high nucleofugacity of these anions.

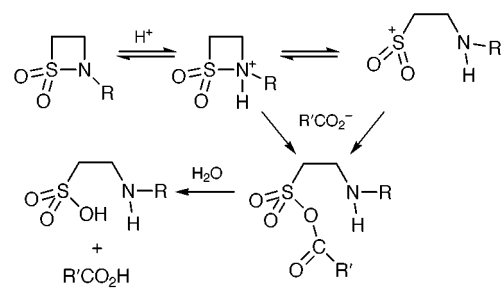

Scheme 1

As a result, the intermediates decompose faster than they are formed and normal first-order kinetics are observed.

There is convincing evidence that the protonation of sulfonamide occurs on nitrogen[6] and the general acid-catalysed hydrolysis of the β-sultam could occur by a unimolecular A-1 type process with the carboxylate anion trapping the reversibly formed electron-deficient sulfonylium ion (Scheme 1). The evidence for such a mechanism in the hydrolysis of five-membered γ-sultams is ambiguous, although most of it is consistent with a bimolecular mechanism.[7] Unimolecular ring opening has been suggested for the acid-catalysed hydrolysis of both β-lactams[8] and β-phospholactams.[9]

The Brønsted plot (not shown) for the carboxylic acid catalysed hydrolysis of *N*-benzyl β-sultam gives a good correlation between the values of log k_{HA} and the pK_a for 2-chloroacetic, 2-methoxyacetic and acetic acids with a slope of −0.67. This corresponds to a β_{nuc} of 0.33 for the specific acid–nucleophilic mechanism, indicative of an early transition state in which there has been a small amount of neutralisation of the negative charge on the carboxylate anion. Formic acid shows a positive derivation from this line which is again indicative of a nucleophilic pathway for catalysis.

The solvent isotope effect k_{H_2O}/k_{D_2O} of 1.57 for the chloroacetate buffer hydrolysis of *N*-benzyl β-sultam is compatible with the specific acid–nucleophilic process, as is the observed entropy of activation of −148 J K^{-1} mol^{-1} for the chloroacetic acid catalysed hydrolysis.

Notes and references

1 A. P. Laws, J. R. Stone and M. I. Page, *J. Chem. Soc., Chem. Commun.*, 1994, 1223.
2 N. J. Baxter, A. P. Laws, L. Rigoreau and M. I. Page, *J. Chem. Soc., Perkin Trans. 2*, 1996, 2245.
3 H. Maskill, *Chem. Soc. Rev.*, 1989, **18**, 123; A. J. Buglass and J. G. Tillett, *The Chemistry of Sulphonic Acids, Esters and their Derivatives*, ed. S. Patai and Z. Rappoport, Wiley, Chichester, UK, 1991, ch. 19.
4 W. J. Moree, A. Schouten, J. R. Kroon and R. M. V. Liskamp, *Int. J. Pept. Protein Res.*, 1995, **45**, 501.
5 A. M. Davis, P. Proctor and M. I. Page, *J. Chem. Soc., Perkin Trans. 2*, 1991, 1213.
6 R. G. Laughlin, *J. Am. Chem. Soc.*, 1967, **89**, 4268; F. M. Menger and L. Mandell, *J. Am. Chem. Soc.*, 1967, **89**, 4424.
7 Y. Bekdemir, J. G. Tillett and R. I. Zalewski, *J. Chem. Soc., Perkin Trans. 2*, 1993, 1643; D. Klamann and G. Hofbauer, *Liebigs Ann. Chem.*, 1953, **581**, 182; D. Klamann and E. Fabienka, *Chem. Ber.*, 1959, 712; W. F. Erman and J. C. Kretschmar, *J. Am. Chem. Soc.*, 1961, **83**, 4841.
8 P. Proctor, N. P. Gensmantel and M. I. Page, *J. Chem. Soc., Perkin Trans. 2*, 1982, 1185.
9 M. I. Page, A. P. Laws, M. J. Slater and J. R. Stone, *Pure Appl. Chem.*, 1995, **67**, 711.

Communication 9/07501A

Structure and bonding in the d^4/d^3 alkyne redox pairs $[WX(CO)(MeC{\equiv}CMe)Tp']^z$ (X = F, Cl, Br and I; z = 0 and 1): halide stabilisation of electron deficient metal alkyne complexes

Ian M. Bartlett,[a] Susannah Carlton,[a] Neil G. Connelly,*[a] David J. Harding,[a] Owen D. Hayward,[a] A. Guy Orpen,*[a] Christopher D. Ray[a] and Philip H. Rieger*[b]

[a] *School of Chemistry, University of Bristol, Bristol BS8 1TS, UK. E-mail: Neil.Connelly@bristol.ac.uk*
[b] *Department of Chemistry, Brown University, Rhode Island, RI 02912, USA*

Received (in Basel, Switzerland) 28th September 1999, Accepted 25th October 1999

X-Ray structural and EPR spectroscopic studies of the redox-related pairs $[WX(CO)(MeC{\equiv}CMe)Tp']^z$ (X = F, Cl, Br and I; z = 0 and 1) [Tp′ = hydrotris(3,5-dimethylpyrazolyl)borate] are consistent with the HOMO of the d^4 (z = 0) species being π-bonding with respect to the W–CO bond, π-antibonding with respect to the W–X bond, and δ-bonding with respect to the W–alkyne bond.

We have recently shown[1] that the oxidation of $[Cr(CO)_2(\eta\text{-}PhC{\equiv}CPh)(\eta\text{-}C_6HMe_5)]$ (d^6) to $[Cr(CO)_2(\eta\text{-}PhC{\equiv}CPh)(\eta\text{-}C_6HMe_5)][PF_6]$ (d^5), and of $[Mo(CO)_2(\eta\text{-}PhC{\equiv}CPh)Tp']$ (d^5) to $[Mo(CO)_2(\eta\text{-}PhC{\equiv}CPh)Tp'][PF_6]$ (d^4) is accompanied by structural changes consistent with stepwise removal of two electrons from the antibonding M–alkyne π⊥ orbital (of the d^6 alkyne complex). In this series, the alkyne effectively acts as an electron-sink. We now describe an unexpected and remarkable extension of this work wherein the d^4 complexes $[WX(CO)(MeC{\equiv}CMe)Tp']$ (X = F, Cl, Br and I) undergo one-electron *oxidation* affording isolable d^3 complexes $[WX(CO)(MeC{\equiv}CMe)Tp'][BF_4]$. The halide both influences the ease of oxidation and allows stabilisation of the resulting electron deficient d^3 metal alkyne complexes.

Treatment of $[W(CO)_2(MeC{\equiv}CMe)Tp'][BF_4]$ with $[NBu^n_4]X$ (X = F, Br or I) or $[N(PPh_3)_2]Cl$ in CH_2Cl_2 gives the neutral complexes $[WX(CO)(MeC{\equiv}CMe)Tp']$ **1** (X = F, Cl, Br or I[2])† in 40–60% yield. Each complex undergoes reversible one-electron oxidation, at a Pt electrode in CH_2Cl_2, followed by a second, irreversible, oxidation process at a more positive potential (Table 1). The potential for the first oxidation step, $E°'_1$′, becomes more positive and ν(CO) *increases* in energy in the order X = F < Cl < Br < I (Table 1), manifestations of the 'inverse halide order'[3] where the complex of the most electronegative halogen (X = F) has the most electron rich metal centre.

Treatment of **1** with $[Fe(\eta\text{-}C_5H_4COMe)Cp][BF_4]$ in CH_2Cl_2 gives 40–70% yields of the paramagnetic salts $[WX(CO)(MeC{\equiv}CMe)Tp'][BF_4]$ ($\mathbf{1}^+[BF_4]^-$)† which show ν(CO) shifted to very much higher energy, by 160 (X = I) to 189 cm^{-1} (X = F). In addition, the order ν(CO) = F ≈ I < Br < Cl is now more nearly that expected on the basis of inductive effects due to halogen electronegativities (except for F).

The d^3 cations in CH_2Cl_2–thf (1:2) show well resolved EPR spectra; parameters are given in Table 1 and the spectra of $\mathbf{1}^+$ (X = F), at 300 and 77 K are shown in Fig. 1. The isotropic metal coupling, $<A^W>$, decreases in the order F > Cl > Br suggesting a smaller metal contribution and larger participation of the halogens in the HOMO of **1** on descending the halogen group. The increase in $<g>$ in the series F to I suggests a smaller metal contribution and a larger heavy halogen participation in the LUMO as well.[4]

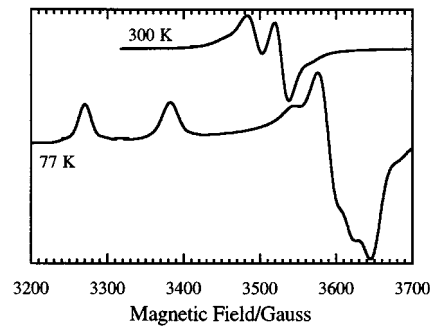

Fig. 1 EPR spectra of $[WF(CO)(MeC{\equiv}CMe)Tp']^+$ at 300 and 77 K in CH_2Cl_2–thf (1:2).

Table 1 Spectroscopic and electrochemical data for $[WX(CO)(MeC{\equiv}CMe)Tp']^z$

X	z	Electron configuration	ν(CO)/cm^{-1} (in CH_2Cl_2)	$E°'_1$/V[a]	$<g>$[b]	$<A^W>$, $<A^X>$[b,c]
F	0	d^4	1876	0.30 (1.48)		61.4, 31.3
	1	d^3	2065		1.924[d]	
Cl	0	d^4	1896	0.45 (1.63)		51.7,–
	1	d^3	2076		1.936[e]	
Br	0	d^4	1899	0.46 (1.60)		49.6, 16.1
	1	d^3	2074		1.957[f]	
I	0	d^4	1904	0.47 (1.57)		< 100, 22.8
	1	d^3	2064		2.002[g]	

[a] Potentials are relative to the saturated calomel electrode. Oxidation peak potential, at a scan rate of 200 mV s^{-1}, for the second, irreversible, oxidation process in parentheses. Under the experimental conditions, $E°'$ for the one-electron oxidation of $[Fe(\eta\text{-}C_5H_4COMe)_2]$ is 0.97 V. [b] Isotropic EPR parameters for d^3 complexes in CH_2Cl_2–thf (1:2) at 300 K. [c] All hyperfine coupling constants in units of 10^{-4} cm^{-1}. [d] 77 K: g_1 = 2.031, g_2 = 1.875, g_3 = 1.858, A_1^W = 40, A_2^W = 70, A_3^W = 72, A_1^F = 106, A_2^F = 22, A_3^F = 18. [e] 77 K: g_1 = 2.035, g_2 = 1.905, g_3 = 1.868, A_2^W = 83. [f] 77 K: g_1 = 2.036, g_2 = 1.954, g_3 = 1.874, A_1^{Br} = 60, A_3^{Br} = 52. [g] 77 K: g_1 = 2.050, A_1^W = 30, A_1^I = 79.

Single crystal X-ray diffraction studies‡ on the two redox pairs $[WX(CO)(MeC{\equiv}CMe)Tp']^z$ (X = Cl and Br, z = 0 and 1) show the structural effects of oxidation. The gross structures of the four complexes are generally similar; that of $[WCl(CO)(MeC{\equiv}CMe)Tp']$ **1** (X = Cl) is shown in Fig. 2 as a representative example. In each case the alkyne is aligned approximately parallel to the W–CO bond. However, there are significant changes in metal–ligand bond lengths on oxidation (Table 2). Thus, for both pairs there is a significant shortening of the W–X bond (by *ca.* 0.09 Å), and a considerable lengthening of the W–C(O) bond [by 0.15–0.17 Å. consistent with the very large increase in ν(CO)]. In contrast to the shortening of the $M–C_{alkyne}$ bonds in the d^6/d^5 and d^5/d^4 pairs noted above (*ca.* 0.10–0.11 Å on oxidation), there is a very small lengthening of the $W–C_{alkyne}$ bonds (average *ca.* 0.02 Å) on oxidation of **1**.

The structural changes are consistent with the HOMO of **1** being largely d_{yz} in character but π-antibonding with respect to the W–X bond, π-bonding with respect to the W–C(O) bond, and weakly δ-bonding with respect to the W–alkyne bond (see

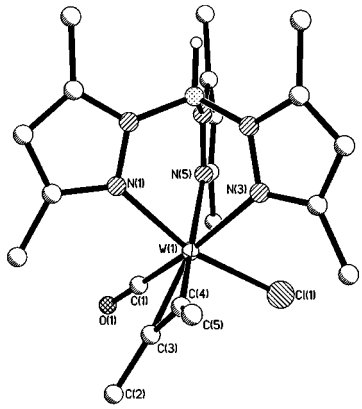

Fig. 2 Structure of [WCl(CO)(MeC≡CMe)Tp′] (hydrogen atoms omitted for clarity); important bond lengths are given in Table 2.

Table 2 Important bond lengths (Å) for [WX(CO)(MeC≡CMe)Tp′]^z

X	z	Electron configuration	W–C_{alkyne}	W–X	W–C(O)	C–O	W–N (av.)
Cl	0	d^4	2.050(6) 2.002(6)	2.429(1)	1.941(6)	1.174(6)	2.223(8)
Cl	1[a]	d^3	2.067(3) 2.035(3)	2.343(1)	2.087(3)	1.114(4)	2.179(3)
Br	0	d^4	2.053(7) 2.010(7)	2.595(1)	1.941(7)	1.164(8)	2.235(9)
Br	1[a]	d^3	2.076(4) 2.027(4)	2.503(1)	2.118(5)	1.080(5)	2.184(6)

[a] As the $[BF_4]^-$ salt.

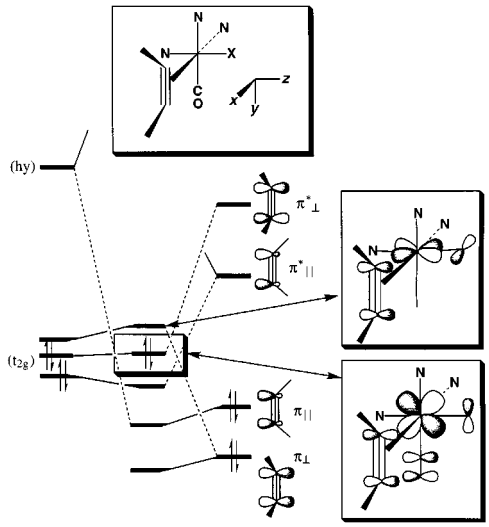

Fig. 3 Schematic diagram of the orbital interactions in d^4 [WX(CO)(MeC≡CMe)Tp′] (hy = σ-hybrid orbital).

Fig. 3). This pattern of interactions, and the magnitude of the orbital contributions to the SOMO suggested by the EPR parameters, are reproduced by EHMO calculations on **1**.

As noted above, the variations in both $E°'_1$′ and ν(CO) indicate an 'inverse halide order' for the set of complexes **1**; X = F < Cl < Br < I. The sequence of ν(CO) for **1** (Table 1) indicates strongest M–C bonding in **1** (X = F) and weakest in **1** (X = I) and by implication greatest metal π-donor ability (or electron releasing ability) in **1** (X = F). The ν(CO) data show a decreasing sensitivity of the carbonyl ligand in **1** to the effect of oxidation, in the order F > Cl > Br > I. The implication is that the contribution of the carbonyl ligand to the HOMO of **1** is greatest for X = F and least in X = I. This trend is also reproduced in EHMO calculations which show that more electronegative halogens make contributions preferentially to the lower energy molecular orbitals.

The inverse halide order has been noticed previously during electrochemical studies[5,6] or organometal halide complexes, and attributed to variation in either X-to-M p_π–d_π[7] or M-to-X d_π–d_π[3,6] donation. In most previous studies, the absence of data on the fluoride complex has hindered distinction between these two possibilities. For **1**, it is clear that the inverse halide order also encompasses the fluoride member of the series yet M–F d_π–d_π overlap is impossible. A recent study[7] revealed an inverse halide order for the series $[FeX(dppe)(\eta\text{-}C_5Me_5)]^z$ (z = 0 and 1; X = F to I) where changes in bond dissociation energies (from electrochemical studies) showed that the HOMO/SOMO is significantly M–X bonding. This, is clearly different from **1** where oxidation is accompanied by W–X bond shortening, indicating that the HOMO is W–X antibonding (at least for X = Cl and Br). The π-donation of the halides is apparently the key to their ability to stabilise electron deficient species such as $\mathbf{1}^+$. The EHMO-computed halogen atomic orbital participation in the HOMO of **1** rises in the sequence F < Cl < Br < I while the metal contribution falls monotonically.

We thank the EPSRC for Studentships (to D. J. H. and O. D. H.) and the University of Bristol for a Postgraduate Scholarship (to I. M. B.).

Notes and references

† All new complexes had satisfactory elemental analyses (C, H and N). Complexes [WX(CO)(MeC≡CMe)Tp′]. X = F: blue–purple crystals, yield 60%; X = Cl: royal blue crystals, yield 48%; X = Br: blue crystals, yield 43%; X = I: blue–green crystals, yield 60%. Complexes [WX(CO)(MeC≡CMe)Tp′][BF_4]. X = F: green–brown crystals, yield 38%; X = Cl: dark green crystals, yield 41%; X = Br: dark green crystals, yield 47%; X = I: purple crystals, yield 69%.

‡ X-Ray data were collected on a Bruker SMART diffractometer at 173 K for θ < 27.5° with $\bar{\lambda}$ = 0.71073 Å. The structures were solved by direct methods and refined by least squares against all F^2 values with $F^2 > 3\sigma(F^2)$ corrected for absorption.

Crystal data: [WCl(CO)(MeC≡CMe)Tp′] (from diethyl ether–*n*-hexane): $C_{20}H_{28}BClN_6OW$, M = 598.59, monoclinic, space group *Cc* (no. 9), a = 18.243(4), b = 10.094(2), c = 14.012(2) Å, β = 116.552(3)°, V = 2308.1(7) Å^3, Z = 4, μ = 5.14 mm^{-1}, $R1$ = 0.0265. [WCl(CO)(MeC≡CMe)Tp′][BF_4] (from CH_2Cl_2–*n*-hexane): $C_{20}H_{28}B_2ClF_4N_6OW$, M = 685.40, triclinic, space group $P\bar{1}$ (no. 2). a = 8.1371(10), b = 11.7697(25), c = 13.3634(15) Å, α = 87.723(7), β = 84.451(12), γ = 85.235(12)°, V = 1268.8(3) Å^3, Z = 2, μ = 4.71 mm^{-1}, $R1$ = 0.0199.

[WBr(CO)(MeC≡CMe)Tp′]·$CHCl_3$·0.75C_6H_{14} (from $CHCl_3$–*n*-hexane): $C_{25.5}H_{29}BBrCl_3N_6OW$, M = 816.7, triclinic, space group $P\bar{1}$ (no. 2), a = 10.297(3), b = 11.663(2), c = 13.935(2) Å, α = 88.34(1), β = 70.03(2), γ = 78.05(1)°, V = 1537.2(5) Å^3, Z = 2, μ = 0.57 mm^{-1}, $R1$ = 0.0363.

[WBr(CO)(MeC≡CMe)Tp′][BF_4] (from CH_2Cl_2–*n*-hexane): $C_{20}H_{28}B_2BrF_4N_6OW$, M = 729.86, triclinic, space group $P\bar{1}$ (no. 2), a = 8.1498(15), b = 11.8631(19), c = 13.4742(14) Å, α = 89.028(10), β = 85.677(7), γ = 85.247(11)°, V = 1294.5(3) Å^3, Z = 2, μ = 6.06 mm^{-1}, F(000) = 706, $R1$ = 0.0293. CCDC 182/1456. See http://www.rsc.org/suppdata/cc/1999/2403/ for crystallographic files in .cif format.

1 I. M. Bartlett, N. G. Connelly, A. G. Orpen, M. J. Quayle and J. C. Rankin, *Chem. Commun.*, 1996, 2583.
2 S. G. Feng, C. C. Philipp, A. S. Gamble, P. S. White and J. L. Templeton, *Organometallics*, 1991, **10**, 3504.
3 T. C. Zietlow, M. D. Hopkins and H. B. Gray, *J. Am. Chem. Soc.*, 1986, **108**, 8266.
4 C. Balagopalakrishna, J. T. Kimbrough and T. D. Westmoreland, *Inorg. Chem.*, 1996, **35**, 7758.
5 P. M. Treichel, K. P. Wagner and H. J. Mueh, *J. Organomet. Chem.*, 1975, **86**, C13; M. Bochmann, M. Green, H. P. Kirsch and F. G. A. Stone, *J. Chem. Soc., Dalton Trans.*, 1977, 714.
6 Y. Y. Lau, W. W. Huckabee and S. L. Gipson, *Inorg. Chim. Acta*, 1990, **172**, 41.
7 M. Tilset, J.-R. Hamon and P. Hamon, *Chem. Commun.*, 1998, 765.

Communication 9/07912B

Transition metal Kinamycin model as a DNA photocleaver for hypoxic environments: bis(9-diazo-4,5-diazafluorene)copper(II) nitrate†

Hilary J. Eppley,[a] Susan M. Lato,[a] Andrew D. Ellington[b] and Jeffrey M. Zaleski*[a]

[a] *Department of Chemistry and Biochemistry, Indiana University, Bloomington, IN 47405, USA. E-mail: zaleski@indiana.edu*

[b] *Department of Molecular Biology, University of Texas, Austin, TX 78712, USA*

Received (in Bloomington, IN, USA) 19th August 1999, Accepted 13th October 1999

Bis(9-diazo-4,5-diazafluorene)copper(II) nitrate is an effective DNA photocleaving agent under anaerobic conditions using visible light and represents a potential model for the action of Kinamycin antitumor antibiotics.

The natural product antitumor antibiotic Kinamycin C **1**,[1,2] was recently found to contain a reactive terminal diazo group that is thought to be responsible for the DNA cleaving activity of the

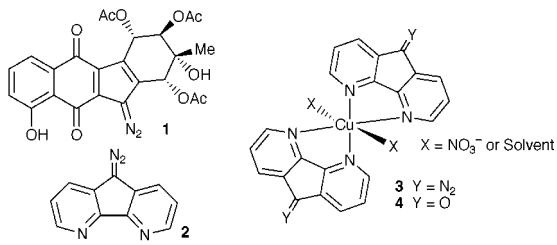

molecule. Although very little is known about the details of Kinamycin's antibiotic activity, the thermal and photochemical reactivity of organic diazo compounds has been long established.[3] Recently, organic chemists have sought to mimic the function of Kinamycin C using simple synthetic diazo analogs, while monitoring biological activity through DNA cleavage assays.[4,5] Although functional, these agents are typically activated through long thermal incubations or UV photolyses, conditions that are less than ideal for medicinal uses.

In addition to their photochemical lability, the thermal decomposition of diazo groups is known to be accelerated by both oxidizing[6,7] and reducing[8] agents. Addition of Cu^{II} salts has been shown to significantly increase the thermal DNA cleaving ability of synthetic diazo compounds.[7] Notably, Kinamycin C contains a redox-active quinone unit in close proximity to the diazo group, suggesting that the antibiotic may use this functionality as an *intramolecular* redox switch to promote N_2 release. To this end, we sought to investigate the effect of binding a redox active transition metal to a diazo-containing ligand on the reactivity and DNA-photocleaving properties of the resulting complex. Ligand **2** was chosen for our initial studies because it is a simple nitrogen chelate containing an exocyclic diazo group that would direct a highly reactive carbene or radical intermediate toward potential substrates.

Compound **2** was synthesized from 4,5-diazafluorenone, using modified literature procedures.[9] The copper(II) complex **3** was synthesized by adding methanolic $Cu(NO_3)_2{\cdot}2.5H_2O$ to a solution of ligand in a 1 : 2 ratio. The full solution and solid-state characterization, as well as the X-ray crystallographic analysis, of the complex are reported elsewhere.[10]† Compound **4**, the ketonic diazo precursor complex, was prepared in an analogous manner and used as a control for DNA cleavage studies.

The effectiveness of DNA cleavage was assessed under rigorously anaerobic conditions by comparison of supercoiled (form I) DNA to the circular relaxed (form II) and linear (form III) DNA. As seen in Fig. 1(*a*), control photoreactions with DNA alone (lane 3) or 200 μM **4** (lane 4) and dark control reactions with 200 or 100 μM **3** (lane 5, 6) resulted in little or no DNA cleavage. In contrast, photoreactions of **3** using visible wavelength light resulted in significant production of linear and nicked DNA depending on the concentrations of **3** used. At a concentration of 200 μM (lane 7), no distinct bands are observable because the plasmid has been degraded into many minor fragments, resulting only in a faint streak on the gel. At concentrations of 100 (lane 8), 50 (lane 9) and 25 μM (lane 10), significant amounts of linear and nicked DNA are visible. Even at concentrations as low as 12.5 μM (lane 11), approximately half of the supercoiled plasmid has been converted to the nicked form. Discernable photocleavage by **3** is also observed at concentrations of 12.5 μM when wavelengths longer than 590 nm are used over 12 h (lane 12).‡

A comparison of efficiency between 2 equiv. of **2** and 1 equiv. of **3** was made because it is possible that both ligands of the Cu^{II} complex could react with DNA substrate. Significantly less cleavage was detected in the case of **2** alone [Fig. 1(*b*), lanes 3, 5, 7] relative to **3** (lanes 4, 6, 8) at one half the concentration, respectively. Close inspection of both gels in Fig. 1 reveals that the migration of the linear DNA product is slightly retarded relative to that of the linearized control, suggesting that the 4,5-diazafluorene moiety may be covalently bound to the DNA strand following photolysis. Evidence for alkylation of DNA by radical intermediates is well-established in the literature.[11]

In an effort to gain chemical insight into the reactivity of **3**, photolysis reactions were performed in aqueous solution in the absence and presence of calf thymus DNA and buffer. Anaerobic photolysis of **3** at $\lambda \geqslant 455$ nm in unbuffered water

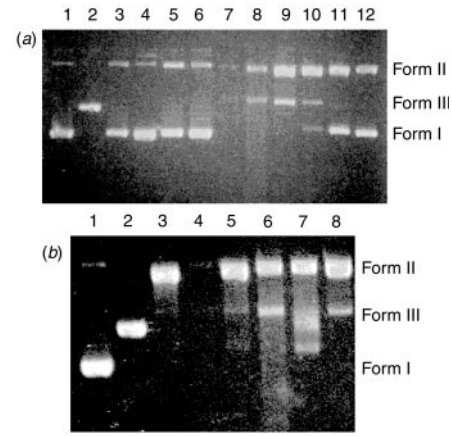

Fig. 1 Agarose gel electrophoresis of the photocleavage reaction of plasmid pUC118 (3162 bp) by **3** and related control compounds. Reactions were performed air-tight Pyrex conical vials with 50 μM bp in 10 mM Tris acetate pH 7.6 buffer at $\lambda \geqslant 455$ nm, t = 1 h, T = 20 °C unless otherwise noted. (*a*) Lane 1: pUC118 control. Lane 2: linearized pUC118 (EcoR1 digest). Lane 3: pUC118. Lane 4: 200 μM **4**. Lane 5: 200 μM **3** control. Lane 6: 100μM **3** control. Lane 7: 200 μM **3**. Lane 8: 100 μM **3**. Lane 9: 50 μM. Lane 10: 25 μM **3**. Lane 11: 12.5 μM **3**. Lane 12: 12.5 μM **3**, λ > 590 nm. (*b*) Lane 1: pUC118 control. Lane 2: linearized pUC118 (EcoR1 digest). Lane 3: 400 μM **2**. Lane 4: 200 μM **3**. Lane 5: 200 μM **2**. Lane 6: 100 μM **3**. Lane 7: 100 μM **2**. Lane 8: 50 μM **3**.

† Experimental and spectral data for this communication are available from the RSC web site, see http://www.rsc.org/suppdata/cc/1999/2405/

results in the formation of new absorption feature at λ_{max} ~ 590 nm [Fig. 2(*a*), inset]. In the presence of O_2 this transition bleaches due to reaction of Cu^I with O_2 yielding reactive oxygen species (•OH or O_2^-) which oxidize the ligand generating a new absorption feature at 415 nm. Interestingly, the absorption band at 415 nm also appears in the photolysis of **2** under anaerobic buffered conditions, ruling out assignment of this feature as a Cu^{II} ligand-to-metal charge transfer transition and suggesting that it may arise from a conjugated organic species such as a dimerization product.§ Photodimerization and thermal dimerization of carbene intermediates to form ketazine and bifluorenylidene species have been documented for **2** and the related 9-diazofluorene derivatives in the presence of bulky or unreactive solvents.[3,12] However, since the absorption feature is also observed upon anaerobic photolysis of **3** and subsequent O_2 oxidation in unbuffered aqueous solution, the growth of the feature at 415 nm likely arises from oxidation of the ligand *via* either hydroxyl radicals from Cu^I/O_2 reactivity, or carboxy radicals generated by H-atom abstraction from buffer in the absence of O_2. Both of these reactive species are capable of addition reactions with aromatic frameworks to yield hydroxylated, ketonized or carboxylated ligand products.[3,7,13,14] In fact, one of the organic products detected upon extraction with $CHCl_3$ is the 4,5-diazafluorenone (λ_{max} = 390 nm). Further oxidation of this species yields the 4,5-diazafluorene-3,9-dione which has an absorption maximum at 414 nm.[13]

Anaerobic photolysis of **3** in 10 mM Tris acetate buffer at $\lambda \geqslant 455$ nm shows clean conversion to photoproduct during the first 40 min, resulting in the formation of the absorption feature at 415 nm and a broad transition at lower energies (λ_{max} ~ 590 nm). This profile indicates partial conversion to a Cu^I species and formation of oxidized ligand product [Fig. 2(*a*)].† Photolysis of **3** in the presence of calf thymus DNA (0.33 mM in bp) under identical conditions is shown in Fig. 2(*b*). The optical spectrum indicates a significantly different product distribution relative to reaction without DNA substrate. Of note is the diminished growth of the band at 415 nm indicating that the photolysis intermediate of **3** is predominantly reacting with the CT DNA substrate rather than forming dimerization products or generating potent radical oxidants. Neither simple H-atom abstraction from the deoxyribose ring nor phosphonation of diazofluorene[15] would yield products exhibiting the strong absorption band at 415 nm. Also, the prominent growth of the Cu^I band at low energy is not evident in the reaction with DNA, demonstrating that any Cu^I formed is also reoxidized in the acetate/DNA environment.

We are currently investigating the differences in reactivity of **2** and **3** toward DNA substrates. One plausible mechanism involves the binding of the copper dication to the negatively charged DNA backbone. Although the crystal structure shows two asymmetrically bound ligands and two nitrates bound tightly to the complex, conductivity studies indicate that the nitrate anions dissociate to form a 2:1 electrolyte in aqueous solution creating a labile site that permits the DNA substrate to bind to the Cu center. The mechanism for photoactivated DNA cleavage by **3** is intriguing in that excitation at 455 nm would be expected to lead directly to decomposition and N_2 release *via* the ligand centered n $\rightarrow \pi^*$ state localized on the diazo group. However, detection of photoreduced Cu^I suggests that metal–ligand redox chemistry may also play a role in activation of the diazo unit, possibly generating a diazonium cation prior to N_2 release. This is indeed supported by precedence for electrooxidative[6,7] and bimolecular photooxidative N_2 release.[16] Electrochemical studies of **3** in DMSO show a chemically reversible Cu^{2+}/Cu^+ couple at +0.094 V *vs*. SCE, while parallel studies of **2** exhibit an irreversible oxidation at +1.3 V corresponding to N_2 release.[8] From these values a Cu^+–$L^{\cdot+}$ ligand radical state would lie in the vicinity of +1.2 V above the ground state and would be accessible *via* $\lambda \geqslant 455$ nm excitation. The ability of transition metal diazo compounds to employ an additional unimolecular photoredox pathway to release N_2 and form ligand-bound, DNA-damaging radical intermediates suggests that the quinone subunit of Kinamycin C may indeed be serving as a redox source in a parallel N_2-releasing mechanism.

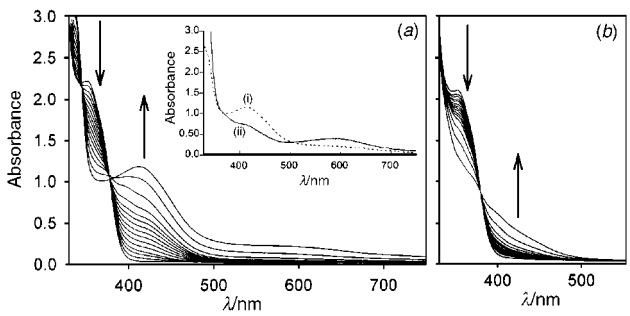

Fig. 2 Evolution of the electronic absorption spectra upon anaerobic photolyses of **3** (0.33 mM, $\lambda \geqslant 455$ nm) in the absence (*a*) and the presence (*b*) of CT DNA (0.33 mM in bp) in Tris acetate buffer (pH 7.6). Times shown are 0, 1, 2, 3, 4, 5, 6, 7, 8, 9, 10, 12, 16, 24 and 40 min. The spectra obtained upon anaerobic photolysis of **3** in unbuffered aqueous solution (i) prior to and (ii) following exposure to O_2 are given in the inset.

Complexes such as **3** represent the first of a new class of potent transition metal diazo DNA photocleavers that may be activated using visible light under hypoxic conditions. The ability to employ metal–ligand photoredox chemistry *via* visible region excitation may allow compounds based on this photo-triggering unit to find potential applications in structural biology and the growing field of photomedicine.

The support of the American Cancer Society (RPG-99-156-01-C) and the Donors of the Petroleum Research Fund (PRF #33340-G4), administered by the American Chemical Society, is gratefully acknowledged. H. J. E. thanks the Helen Hay Whitney Foundation for a postdoctoral fellowship.

Notes and references

‡ Control experiments involving photolysis of the plasmid DNA alone at $\lambda \geqslant 590$ nm for 12 h yielded only slight nicking, comparable to that observed in Fig. 1(*a*), lane 3, confirming the activity of **3** at these wavelengths.

§ 9,9′-Bi(4,5-diazafluorenylidene) has been prepared recently and also shows a distinct band at 417 nm in CH_2Cl_2. Photolysis of **4**, the 4,5-diazafluorenone analog, resulted in no change in the absorption spectrum over a period of 3 h, indicating that the observed reactivity is derived from the diazo unit. Loss of the diazo group on photolysis in **3** has been unequivocally confirmed by N_2 bubble formation and disappearance of the asymmetric diazo stretch in the IR at 2080 cm^{-1} (ref. 10).

¶ Photolysis studies show that DNA cleavage does indeed occur under aerobic conditions as well.

1 S. Mithani, G. Weeratunga, N. J. Taylor and G. I. Dmitrienko, *J. Am. Chem. Soc.*, 1994, **116**, 2209.
2 S. J. Gould, N. Tamayo, C. R. Melville and M. C. Cone, *J. Am. Chem. Soc.*, 1994, **116**, 2207.
3 M. Regitz and G. Maas, *Diazo Compounds: Properties and Synthesis*, Academic Press, Orlando, 1986.
4 B. G. Maiya, C. V. Ramana, S. Arounaguiri and M. Nagarajan, *Bioorg. Med. Chem. Lett.*, 1997, **7**, 2141.
5 K. Nakantani, S. Maekawa, K. Tanabe and I. Saito, *J. Am. Chem. Soc.*, 1995, **117**, 10635.
6 V. D. Parker and D. Bethell, *J. Am. Chem. Soc.*, 1987, **109**, 5066.
7 D. P. Arya and D. J. Jabaratnan, *J. Org. Chem.*, 1995, **60**, 3268.
8 D. Bethell and V. D. Parker, *J. Am. Chem. Soc.*, 1986, **108**, 7194.
9 N. Koga, Y. Ishimaru and H. Iwamura, *Angew. Chem., Int. Ed. Engl.*, 1996, **35**, 755.
10 H. J. Eppley, J. C. Huffman and J. M. Zaleski, in preparation.
11 S. J. Hawthorne, M. Pagano, P. Harriott, D. W. Halton and B. Walker, *Anal. Biochem.*, 1998, **261**, 131.
12 A. A. Abdel-Wahab, M. T. Ismail, O. S. Mohamed, H. Durr and Y. Ma, *Liebigs Ann./Recl.*, 1997, 1611.
13 P. N. W. Baxter, J. A. Conner, J. D. Wallis, D. C. Povey and A. K. Powell, *J. Chem. Soc., Perkin Trans. 1*, 1992, **13**, 1601.
14 J. Fossey, D. Lefort and J. Sorba, *Free Radicals in Organic Chemistry*, Wiley, New York, 1995.
15 J. S. Wieczorek, B. Boduszek and R. Gancarz, *J. Prakt. Chem.*, 1984, **326**, 349.
16 D. G. Stoub and J. L. Goodman, *J. Am. Chem. Soc.*, 1997, **119**, 11110.

Communication 9/06764G

First heterogenisation of Rh–MeDuPHOS by occlusion in PDMS (polydimethylsiloxane) membranes

Ivo Vankelecom,*[a] Adi Wolfson,[b] Shimona Geresh,[b] Miron Landau,[b] Moshe Gottlieb[b] and Moti Hershkovitz[b]

[a] *Centre for Surface Chemistry and Catalysis, Faculty of Agricultural and Applied Biological Sciences, Katholieke Universiteit Leuven, Kardinaal Mercierlaan 92, 3001 Leuven, Belgium. E-mail: ivo.vankelecom@agr.kuleuven.ac.be*

[b] *Blechner Center, Chemical Engineering Department, Ben-Gurion University of the Negev, PO Box 653, Beer-Sheva, Israel*

Received (in Cambridge, UK) 6th September 1999, Accepted 26th October 1999

The first heterogeneous system of Rh–MeDuPHOS, obtained by occlusion of the complex in a PDMS membrane, is reported and tested in the hydrogenation of methylacetoacetate (MAA).

Asymmetric synthesis with homogeneous chiral complexes is one of the best methods to prepare enantiopure compounds.[1] In 1991, Burk developed a set of new chiral biphosphine ligands referred to as DuPHOS [1,2-bis(phospholano)benzene] and BPE [1,2-bis(phospholano)ethane],[2] both commercially available nowadays. The Rh and Ru complexes of these ligands were found to be extremely effective in the enantioselective hydrogenation of a vast array of unsaturated substrates.[3–8] All reactions are characterized by high convenience, selectivity, catalytic productivity and activity, adaptability and durability. A major class of these substrates form the β-ketoesters. Their reduction was recently reviewed by Klabunovskii and Sheldon.[9] The authors stated that chiral metal complexes constitute the most elegant and efficient way to asymmetric hydrogenation with the broadest scope, but that facilitation of their recycling by immobilizing them, still remained an important future challenge.

We report here the first heterogenisation of Rh–MeDuPHOS, chosen as a typical representative of the class of catalysts reported by Burk *et al.*[2–8] Immobilisation was realized by occluding the catalyst in a polydimethylsiloxane membrane. This easy approach to heterogenisation was earlier applied already for several transition metal complexes.[10–12] The hydrogenation of MAA was selected as a test reaction (Scheme 1). A PDMS solution was prepared by mixing 0.075 g of crosslinker [tetrakis-(dimethylsiloxy)silane, United Chemical Technologies], 22 μl of Pt catalyst [*cis*-dichlorobis(diethyl sulfide)platinum(II), Aldrich, applied as a 2 wt% solution in toluene], 2.25 g of the vinyldimethyl terminated silicone polymer (M_n = 5350 with a polydispersity = 2.27, obtained after stripping the polymer under vacuum till constant weight, United Chemical Technologies), and 0.465 g of the silica (Hi-sil 233, pretreated at 120 °C, PPG Industries) in 11.5 g of dichloromethane (Fig. 1). The catalyst was prepared by dissolving the Rh salt [bis(cycloocta-1,5-diene)rhodium(I) trifluoromethanesulfonate, 99%, Strem] and the ligand {(−)-1,2-bis[(2*R*,5*R*)-2,5-dimethylphospholano]benzene, 99%, Strem} separately in methanol (Fig. 2). An amount of 0.0397 g of Rh salt and 0.0264 g of ligand were dissolved in 2.1 and 0.7 g of methanol, respectively. The ligand solution was then added dropwise to the Rh salt solution under constant stirring. Further stirring for 15 min turned the yellow solution into dark orange. A portion of 0.174 g of this solution, corresponding to 5 μmol

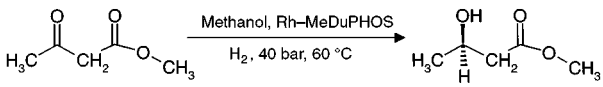

Scheme 1 Asymmetric hydrogenation of MAA.

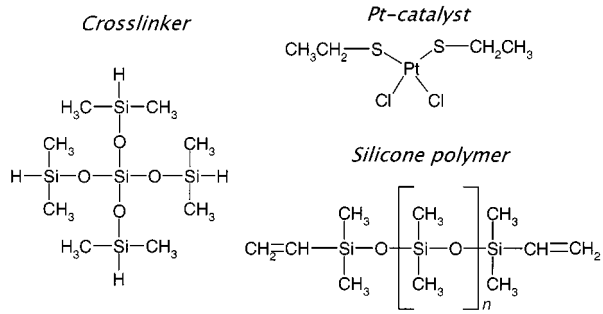

Fig. 1 PDMS constituents.

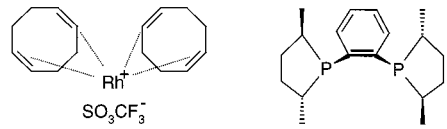

Fig. 2 Rh salt and ligand for Rh–MeDUPHOS synthesis.

of the Rh complex, was poured in a Petri dish and after removal of the methanol, 1.5 g of the PDMS solution was added. After complete dissolution of the complex in this mixture, the solvent was allowed to evaporate. Approximately 3 h later, the curing of the PDMS was finished and the resulting membrane was stored under nitrogen prior to use in the reactor. A typical TEM image of such a composite membrane is shown in Fig. 3, proving the good dispersion of the silica particles in the membrane matrix. A 20 ml reactor with magnetic stirring was used in which the membrane was clamped between two porous stainless steel disks. A volume of 18 ml of methanol was added to the reactor, together with 2 g of MAA. Reaction took place at 60 °C at a pressure of 40 bar during 24 h for the membrane reaction and 2 h for the homogeneous reference reaction. The reaction mixture was analysed with gas chromatography (Chiraldex G-TA column, Astec).

A homogeneous reaction (Table 1) was performed in order to test the activity of the prepared catalyst and its ability to reduce MAA. Even though attempts to utilize Rh–MeDuPHOS in enantioselective ketone hydrogenations were reported to be unavailing[5] and in spite of the fact that Burk *et al.* found other DuPHOS and BPE related catalysts performing better than Ru-BINAP,[3,4] we found for Rh–MeDuPHOS an activity in the MAA hydrogenation at 60 °C that was even superior to that of Ru–BINAP, a catalyst commonly used for this reaction.[9,13,14] The membrane occluded catalyst (membrane thickness 452 μm) was first tested in ethylene glycol (EG), the solvent preferentially used for the analogous Ru–BINAP/PDMS system.[15] The activity of the catalyst was lower than in the homogeneous reaction but remained constant in a second run, in which the same enantioselectivity was maintained. No reactivity was

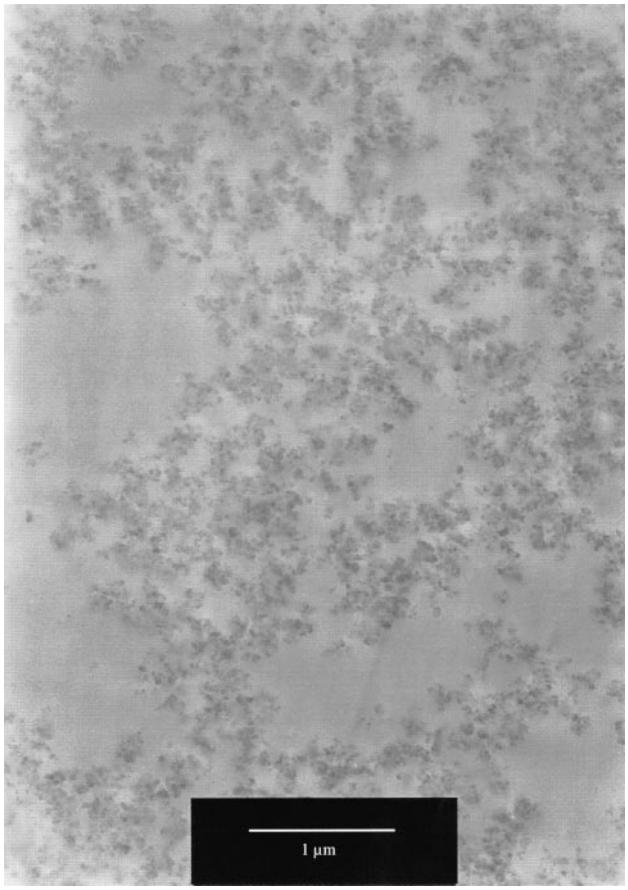

Fig. 3 TEM photograph of a PDMS membrane containing 10 wt% silica.

Table 1 Turnover frequency and enantioselectivity in the hydrogenation of MAA. (H = homogeneous reaction; 1 = first membrane reaction; 2 = second membrane reaction). All reaction selectivities were 100%. Reaction time: 2 h (for homogeneous reactions) or 24 h (for heterogeneous reactions)

Catalyst	Solvent	TOF/h^{-1}	ee(%)
Rh–MeDuPHOS (H)	MeOH	482	99
Ru–BINAP (H)	MeOH	135	90
Rh–MeDuPHOS/PDMS (1)	EG	7	93
Rh–MeDuPHOS/PDMS (2)	EG	7	93
Rh–MeDuPHOS/PDMS (1)	MeOH	28	90
Rh–MeDuPHOS/PDMS (2)	MeOH	28	90

found when only the reaction mixture from the first membrane catalysed reaction was used in another run after adding new substrate to the reactor. This proved that the reported system was a truly heterogeneous version of the catalyst. By performing the reaction in methanol, the membrane activity (thickness 578 μm) could be increased fourfold, while leaving enantioselectivity quasi-unaffected. Exactly the same results were found in a second run. This is remarkable because methanol is a good solvent for the catalyst and it was found earlier that the use of such solvents generally causes leaching of the catalyst from PDMS membranes.[11] Also the mixture of this reaction proved to be completely inactive in a subsequent run with new substrate added. The absence of Rh in all reaction mixtures was also confirmed subsequently with ICP-MS.

The reported heterogenisation allows facile recycling of this versatile catalyst and should enable the development of continuous processes. Experiments to improve the activity of the reported membrane system by optimizing the membrane properties and to expand it further to other reactions and catalysts of this class are planned. In particular, the complete absence of leaching in methanol opens interesting perspectives in this respect.

I. V. thanks the Fund of Scientific Research (F.W.O.) for a grant as a Post-Doctoral Researcher.

Notes and references

1 R. A. Sheldon, *Chirotechnology*, Marcel Dekker Inc., New York, 1993.
2 M. J. Burk, *J. Am. Chem. Soc*., 1991, **113**, 8518.
3 M. J. Burk, T. G. P. Harper and C. S. Kalberg, *J. Am. Chem. Soc*., 1995, **117**, 4423.
4 M. J. Burk, M. F. Gross, T. G. P. Harper, C. S. Kalberg, J. R. Lee and J. P. Martinez, *Pure Appl. Chem.*, 1996, **68**, 37.
5 M. J. Burk, *Proceedings from Chiral Europe*, France, October 1998, p. 1.
6 M. J. Burk, M. F. Gross and J. P. Martinez, *J. Am. Chem. Soc*., 1995, **117**, 9375.
7 M. J. Burk and J. E. Feaster, *Tetrahedron Lett.*, 1992, **33**, 2099.
8 M. J. Burk, J. E. Feaster, W. A. Nugent and R. L. Harlow, *J. Am. Chem. Soc*., 1993, **115**, 10 125.
9 E. I. Klabunovskii and R. A. Sheldon, *Cattech*, December 1997, 153.
10 I. F. J. Vankelecom, K. Vercruysse, P. Neys, D. Tas, K. B. M. Janssen, P.-P. Knops-Gerrits and P. A. Jacobs, *Top. Catal.*, Special Issue on Fine Chemicals Catalysis, 1998, **5**(1–4), 125.
11 I. F. J. Vankelecom and P. A. Jacobs, *Catal. Today*, in press.
12 R. F. Parton, I. F. J. Vankelecom, D. Tas, K. Janssen, P.-P. Knops-Gerrits and P. A. Jacobs, *J. Mol. Catal*., 1996, **113**, 283.
13 M. Kitamura, M. Tokunaga, T. Ohkuma and R. Noyori, *Tetrahedron Lett.*, **32**, 4163.
14 R. Noyori and H. Takaya, *Acc. Chem. Res*., 1991, **23**, 345.
15 I. F. J. Vankelecom, D. Tas, R. F. Parton, V. Van de Vyver and P. A. Jacobs, *Angew. Chem., Int. Ed. Engl*., 1996, **35**, 1346.

Communication 9/07187C

ChemComm

Confinement of dimeric sulfuric acid in a self-assembled molecular capsule: $[(H_2SO_4)_2\subset(\text{calix[5]arenesulfonic acid})_2]$

Michaele J. Hardie, Mohamed Makha and Colin L. Raston

Department of Chemistry, Monash University, Clayton, Melbourne, Victoria, 3168, Australia.
E-mail: c.raston@sci.monash.edu.au

Received (in Columbia, MO, USA) 14th September 1999, Accepted 7th October1999

Self-assembled molecular capsules are formed on crystallisation of calix[5]arenesulfonic acid resulting from treating calix[5]arene with sulfuric acid; the calix[5]arenesulfonic acid molecules dimerise *via* hydrogen bonding through the sulfonic acid groups, shrouding two hydrogen-bonded sulfuric acid molecules as the supermolecule $[(H_2SO_4)_2]\subset\{(\text{calix[5]arenesulfonic acid})_2]$.

Highly charged water soluble sulfonated calix[4,5,6,8]arenes form a diverse range of complexes and structural types depending on the counter ion/degree of protonation.[1–13] We recently showed that *p*-sulfonatocalix[4]arenes form superanions or ionic capsules in water at low pH in which two calixarenes shroud an 18-crown-6 molecule bearing sodium and two *trans*-water molecules, or a tetra-protonated cyclam molecule, the counter ions being chromium(III) oligomeric species.[12,13] This work relates to a surge in contemporary studies on the formation of self-assembled molecular capsules using hydrogen bonding,[14–18] and the formation of other ionic capsules held together by coordination interactions.[19,20] In general, molecular/ionic capsules are of interest in building large polyhedral structures similar to those in biological systems, trapping and stabilising molecules, and for novel functions such as drug delivery, separation problems and chemical transformations.[14–20]

We now report the synthesis and structural characterisation of a molecular capsule comprised of two calix[5]arenesulfonic acid molecules which encapsulate two sulfuric acid molecules as a hitherto unknown hydrogen bonded dimer. Treatment of calix[5]arene† with sulfuric acid then cooling the brown solution to –15 °C for several weeks gave the corresponding *para*-substituted penta-sulfonic acid isolated as a mixed sulfuric acid/water adduct, (calix[5]arenesulfonic acid)-$(H_2SO_4)_4(H_2O)_{1.5}$ **1** (Scheme 1). The composition of the material was established from single crystal X-ray diffraction data collected at 123(1) K.[24] The samples appeared uniform but attempts to isolate the crystals were compounded by the extremely fragile, hygroscopic and indeed deliquescent nature of the material on removal from the mother liquor. The decomposed material can be converted to the corresponding sodium salt, as a derivative of compound **1** (yield 50%). NMR studies to ascertain the formation of the capsules in DMSO-d_6 and other solvents were inconclusive. While sulfuric acid is the reagent of choice for sulfonating calixarenes,[1–13] the formation of a sulfuric acid adduct of a calixarene, indeed a host–guest complex, is without precedence.

Details of the structure of **1** are shown in Fig. 1.‡ The compound crystallises in space group $P\bar{1}$ with one supermolecule or molecular capsule, $[(H_2SO_4)_2\subset(\text{calix[5]arenesulfonic acid})_2]$, in the unit cell and thus the capsules lie on inversion centres. In addition to the capsule the unit cell contains six sulfuric acid molecules, disordered over several positions with partial occupancies, and three water molecules of crystallisation, also disordered. The capsules and solvent molecules form a 1D hydrogen bonded network. In contrast the two symmetry equivalent encapsulated sulfuric acid molecules are fully occupied. The S–O bond lengths indicate that S–OH/S=O disorder is likely for the encapsulated sulfuric acids, with one S=O and one S–OH linkage clearly identifiable and the remaining S–O bonds similar within estimated standard deviations. There are several salient features of the capsule. The calixarenes are in the cone conformation, although two of the phenol groups disposed in the 1,3 positions in the calixarene ring are noticeably more tilted away from the principle axis of the calixarene than the other phenolic groups. The tilt angles relative to the plane defined by the five phenolic O-centres are sequentially 150.8, 113.0, 148.7, 125.5 and 123.7° (tilt angle defined as angle from arene centroid to centroid of O_5 plane at the phenolic oxygen). The most tilted phenol group is hydrogen bonded to a sulfuric acid molecule in the cavity of the calixarene, with an O··O separation of 2.92 Å. While the precision of the structure precluded location of the hydrogen atoms, the O··O distances in general are indicative of hydrogen bonding interactions.

Other features of the capsule are that it is flattened in the direction of the principle axes of the calixarenes, and that the calixarenes are slipped relative to each other (Fig. 1). This gives

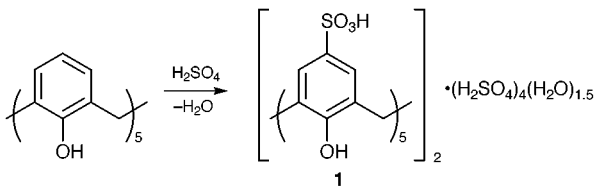

1

Scheme 1

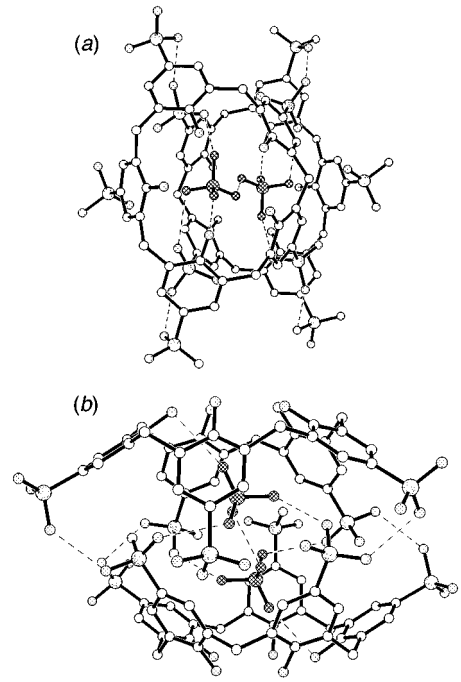

Fig. 1 Projections of the molecular capsule $[(H_2SO_4)_2\subset(\text{calix[5]arenesulfonic acid})_2]$ in the structure of **1** showing (*a*) the alignment of the calixarenes and sulfuric acid molecules in the capsule involving hydrogen bonding, and (*b*) the flattening of the molecular capsule. Hydrogen bonds are shown as dashed lines and the sulfuric acid molecules are cross-hatched.

a snug fit of the sulfuric acid dimer in the capsule, with one sulfuric acid molecule in each of the cavities of the calixarenes, and hydrogen bonding of the sulfonic acid groups of one calixarene with the other. There are four such inter-calixarene (intracapsule) hydrogen bonds (Fig. 1) at O··O separations of 2.62 and 2.64 Å, with inter-digitation of some of the sulfonic acid groups of one calixarene with those of the other calixarene. The binding of the sulfuric acid molecules is driven by four hydrogen bonding interactions per molecule, one for each of the oxygen centres of each sulfuric acid molecule. The oxygen centre residing deepest in the cavity has a hydrogen bond to one of the phenolic O-centres which is skewed furthest from the average cone conformation. Two others are to sulfonic groups of the other calixarene, at 2.39 and 2.79 Å, and this also is a manifestation of the flattened nature of the capsule. The other hydrogen bond involves an oxygen atom of its centrosymmetric related sulfuric acid molecule at an O··O distance of 2.63 Å.

The single hydrogen bond linking the sulfuric acid dimer is particular noteworthy in the context of the structure of crystalline sulfuric acid. Here there is a continuous two-dimensional puckered sheet-like array of acid molecules held together by hydrogen bonding interactions such that each oxygen in the tetrahedral arrangement of O-atoms around each sulfur forms a single hydrogen bond to another sulfuric acid molecule (O··O separation 2.62 Å).[21] Thus the present structure has two adjacent sulfuric acid molecules interacting with each other through vertices of the tetrahedra analogous to the continuous structure of sulfuric acid itself. Furthermore the S–O··O angles are similar (109.9 *cf.* 120.4° in **1**). This is also the type of hydrogen bonding in the few sulfuric acid adducts which have been structurally authenticated.[22] Alternative hydrogen bonding modes are possible including face-to-face linking of the tetrahedra. Effectively we have stabilised a dimer of a similar spatial arrangement as two adjacent sulfuric acid molecules in the continuous structure.

The structure of compound **1** is notably different from that of the corresponding Na salt where the calixarenes do not form molecular capsules.[3,9] This is in direct contrast to the only other structurally authenticated calixarenesulfonic acid, {calix[6]arenesulfonic acid}.23H_2O, which is isostructural with its corresponding Na salt, and has the calix[6]arene in a double partial cone conformation, effectively excluding the possibility of capsule formation.[23]

The results herein extend the range of molecular capsules which can be assembled using the principles of supramolecular chemistry, from the initial studies on calix[4]arene[12,13] to the larger calix[5]arene. Success here suggests that a range of species may be encapsulated, depending on interaction complementarity between the molecules and with calixarenes and between the calixarenes. It is likely that the larger calix[5]arene has greater flexibility, able to form a flattened, slipped structure, as in **1**, or an expanded structure able to encapsulate larger molecules, beyond the crown ether in the above calix[4]arene studies.[12,13]

Support of this research from the Australian Research Council is gratefully acknowledged.

Notes and references

† *Synthesis:* *p-tert*-Butylcalix[5]arene was prepared by the literature method (ref. 24) and debutylated by standard procedures (ref. 25). Calix[5]arene (0.25 g, 0.47 mmol) was treated with 98% sulfuric acid (3 ml) at 80 °C for 10 h, and the resulting brown solution cooled then stored at –15 °C for several weeks, whereupon colourless crystals of deliquescent (calix[5]arenesulfonic)(H_2SO_4)$_4$(H_2O)$_{1.5}$ deposited which proved difficult to isolate in an analytically pure form. δ_H(DMSO-d_6) 7.15 (s, ArH), 6.22 (s, broad, COH/SOH, shifts downfield with increasing [H_2SO_4]), 3.85 (s, $ArCH_2Ar$). For H_2SO_4: δ_H(DMSO-d_6) 12.32 (s, SOH).

‡ *Crystal data* for **1**: A prismatic crystal of dimensions 0.25 × 0.20 × 0.15 mm was mounted on a glass capillary under oil and quickly placed under a stream of cold nitrogen. The crystal lost clarity during mounting, indicating a degree of deterioration. X-Ray data were collected at 123(1) K on an Enraf-Nonius KappaCCD single crystal diffractometer with Mo-Kα radiation (λ = 0.71073 Å). Data was corrected for Lorentzian and polarisation effects, but not absorption. The structure was solved by direct methods with SHELXS-97 and refined by full-matrix least-squares on F^2 using SHELXL-97. (Calix[5]arenesulfonic acid)(H_2SO_4)$_4$(H_2O)$_{1.5}$: $C_{35}H_{49}O_{37.5}S_9$, M_r = 1358.28 g mol^{-1}, triclinic, space group $P\bar{1}$, a = 11.7770(3), b = 15.9118(4), c = 16.0580(4) Å, α = 105.459(1), β = 90.871(1), γ = 105.767(1)°, U = 2778.68(12) Å^3, Z = 2, ρ_{calc} = 1.623 g cm^{-1}, μ = 0.464 mm^{-1}, 2.6 < 2θ < 55.0, 57663 reflections measured, 12660 unique reflections (R_{int} = 0.073), 7156 observed [($I > 2\sigma(I)$], 846 parameters, 2 restraints, R_1 = 0.1267 (observed data), wR_2 = 0.4012 (all data), S = 1.384. C–H hydrogen atoms of the calixarene were fixed at geometrically estimated positions with a riding refinement. A number of the sulfuric acid molecules and the waters were disordered and given partial occupancies. Two disordered sulfuric acid groups were modelled with restrained S–O bond lengths. CCDC 182/1459. See http://www.rsc.org/suppdata/cc/1999/2409/ for crystallographic data in .cif format.

1 C. D. Gutsche, *Calixarenes Revisited*, Royal Society of Chemistry, Cambridge, 1998; V. Bohmer, *Angew. Chem., Int. Ed. Engl.*, 1995, **34**, 713.
2 J. L. Atwood, G. W. Orr, K. D. Robinson and F. Hamada, *Supramol. Chem.*, 1993, **2**, 309.
3 J. W. Steed, C. P. Johnson, C. L. Barnes, R. K. Juneja, J. L. Atwood, S. Reilly, R. L. Hollis, P. H. Smith and D. L. Clark, *J. Am. Chem. Soc.*, 1995, **117**, 11 426.
4 A. W. Coleman, S. G. Bott, S. D. Morley, C. M. Means, K. D. Robinson, H. Zhang and J. L. Atwood, *Angew. Chem., Int. Ed. Engl.*, 1988, **27**, 1361.
5 J. L. Atwood, A. W. Coleman, H. Zhang and S. G. Bott, *J. Inclusion Phenom.*, 1989, **7**, 203.
6 J. L. Atwood, F. Hamada, K. D. Robinson, G. W. Orr and R. L. Vincent, *Nature*, 1991, **349**, 683.
7 S. Shinkai, H. Koreishi, K. Ueda, T. Arimura and O. Manabe, *J. Am. Chem. Soc.*, 1987, **109**, 6371.
8 S. Shinkai, Y. Shiramama, H. Satoh, O. Manaba, T. Arimura, K. Fujimoto and T. Matsuda, *J. Chem. Soc., Perkin Trans. 2*, 1989, 1167.
9 C. P. Johnson, J. L. Atwood, J. W. Steed, C. B. Bauer and R. D. Rogers, *Inorg. Chem.*, 1996, **26**, 2602.
10 A. T. Yordanov, O. A. Ganshow, M. W. Brechbiel, L. M. Rogers and R. D. Rogers, *Polyhedron*, 1999, **18**, 1055 and references therein.
11 A. Drljaca, M. J. Hardie, J. C. Johnson, C. L. Raston and H. R. Webb, *Chem. Commun*., 1999, 1135.
12 A. Drljaca, M. J. Hardie, C. L. Raston and L. Spiccia, *Chem. Eur. J*., 1999, **5**, 2295.
13 S. Airey, A. Drljaca, M. J. Hardie and C. L. Raston, *Chem. Commun*., 1999, 1137.
14 T. Heinz, D. M. Rudkevich and J. Rebek, *Nature*, 1998, **394**, 764; J. Rebek, *Acc. Chem. Res.*, 1999, **32**, 278 and references therein.
15 L. R. MacGillivray and J. L. Atwood, *Nature*, 1997, **389**, 469; L. R. MacGillivray and J. L. Atwood, *Angew. Chem., Int. Ed*., 1999, **38**, 1019.
16 O. Mogek, M. Pons, V. Bohmer and W. Vogt, *J. Am. Chem. Soc.*, 1997, **119**, 5706.
17 K. Nakamura, C. Sheu, A. E. Keating, K. N. Houk, J. C. Sherman, R. G. Chapman and W. L. Jorgensen, *J. Am. Chem. Soc.*, 1997, **119**, 4321.
18 K. Murayama and K. Aoki, *Chem. Commun.*, 1998, 607.
19 T. Kusukawa and M. Fujita, *J. Am. Chem. Soc*., 1999, **121**, 1397; N. Takeda, K. Umemoto, K. Yamaguchi and M. Fujita, *Nature*, 1999, **398**, 794; B. Olenyuk, J. A. Whiteford, A. Fechtenkotter and P. J. Stang, *Nature*, 1999, **398**, 796 and references therein.
20 A. Ikeda, M. Yoshimura, H. Udzu, C. Fukuhara and S. Shinkai, *J. Am. Chem. Soc*., 1999, **121**, 4296.
21 P. Y. Pu and T. C. W. Mak, *J. Cryst. Mol. Struct.*, 1978, **8**, 193; A. R. Moodenbaugh, J. E. Hartt, J. J. Hurst, R. W. Youngblood, D. E. Cox and B. C. Frazer, *Phys. Rev.*, 1983, **B28**, 3501.
22 O. Hassel and C. H. R. Romming, *Acta Chem. Scand*., 1960, **14**, 398; M. M. Ilczyszyn, A. J. Barnes, A. Pietraszko and H. Ratajczak, *J. Mol. Struct*., 1995, **354**, 109; P. Prusiner and M. Sundaralingam, *Acta Crystallogr.*, 1972, **B28**, 2142; C. C. Calabrese and K. H. Gardner, *Acta Crystallogr*., 1985, **C41**, 389.
23 J. L. Atwood, D. L. Clark, R. K. Juneja, G. W. Orr, K. D. Robinson and R. L. Vincent, *J. Am. Chem. Soc*., 1992, **114**, 7558.
24 D. R. Stewart and C. D. Gutsche, *Org. Prep. Proced. Int.*, 1993, **25**, 137.
25 V. Bocchi, F. A. Pochini, R. Ungaro and G. D. Andretti, *Tetrahedron Lett.*, 1982, **38**, 373.

Communication 9/07469D

^{1}H NMR of $C_{61}H_2^{6-}$: the aromatic character of C_{60} upon reduction—a view from the bridge of $C_{61}H_2$

Tamar Sternfeld,[a] Fred Wudl,[b] Kees Hummelen,[b] Amir Weitz,[b] Robert C. Haddon[c] and Mordecai Rabinovitz*[a]

[a] *Department of Organic Chemistry, The Hebrew University of Jerusalem, Givat Ram, Jerusalem, 91904 Israel. E-mail: mordecai@vms.huji.ac.il*

[b] *Exotic Materials Institute, Department of Chemistry and Biochemistry, University of California, Los Angeles, CA 90095, USA*

[c] *Department of Chemistry, University of Kentucky, Lexington, Kentucky 40506, USA.*

Received (in Cambridge, UK) 20th September 1999, Accepted 27th October 1999

The ^{1}H NMR spectrum of the fulleroid $C_{61}H_2^{6-}$ consists two high field doublets, providing experimental evidence for diamagnetic five-membered rings in C_{60}^{6-}.

Aromaticity, one of the most important and interesting concepts of organic chemistry, has undergone certain modifications since the original proposition by Hückel in 1931.[1] The theory was then devoted to single π-conjugated ring systems, later expanded to polycyclic molecules[2] and recently to non-planar molecules.[3]

The discovery of fullerenes[4] offers a new challenge in the field of aromaticity as the fullerenes are not only conjugated systems but are also spherical and therefore, no borderlines exist and numerous Kekulé structures can be assigned.[5] In the quest to understand the nature of the electronic structure of fullerenes their reduction is a method of choice as these molecules are capable of accepting a high number of electrons with only small changes in their rigid skeleton.

For the most abundant fullerene C_{60}, calculations,[6] as well as experimental data,[6b,7] demonstrate only a modest aromatic character. Calculations also indicate that the lowest unoccupied molecular orbital (LUMO) of C_{60} is low-lying and triply degenerate, and hence is capable of accepting six electrons,[6a,8] which is confirmed by the presence of six reduction waves in its cyclic voltometry.[9]

The magnetic ring current susceptibility of C_{60}^{6-} is expected to be very high[6a] in contrast to C_{60}, as was recently shown experimentally.[10] This is corroborated by calculations showing that the ring current of C_{60} is a result of two contributions, the diamagnetic six-membered rings (6-MRs) and the paramagnetic five-membered rings (5-MRs). These two opposite contributions cancel each other in C_{60}, leading to a low magnetic susceptibility. Moreover, calculations predict that in C_{60}^{6-} the 5-MRs will be diamagnetic, which should cause a high diamagnetic ring current in the entire system.[11]

An accepted method of studying local ring currents in polycyclic arrays is by attaching a methylene bridge, where the protons of the bridge are located above the centers of the ring, and their chemical shifts can probe the magnetic character of each ring.[2]

By the addition of CH_2N_2 to C_{60} two methylene adduct isomers of $C_{61}H_2$ were prepared.[12] The two protons of the methylene can be located either both above two 6-MRs (**1**) or one above a 6-MR (H^a) and the other one above a 5-MR (H^b) (**2**). In isomer **2**, the two different protons can serve as external and localized probes for the two rings types. The ^{1}H NMR spectrum of **2** consists of two doublets, at δ 2.84 and 6.35, which are ascribed to H^a and H^b, respectively.[12a] Therefore, it can be deduced that the 6-MR is diamagnetic, and the 5-MR is paramagnetic, as predicted by calculations.[11]

Here we report the reduction of **2** to a hexaanion and the characterization of the anion by NMR.[13] The reduction was carried out, in a 5 mm NMR tube equipped with a reduction chamber on top, in THF-d_8, with excess lithium metal and in the presence of corannulene (**3**). Lithium metal reduction of fullerenes requires extreme conditions, including the use of an ultrasonic bath. However, it has previously been reported that polycyclic molecules and especially **3** could serve as 'electron shuttles' which transport electrons in etheral solution to fullerenes, and thus enable the reduction of the insoluble C_{60} under mild conditions.[10] The solution was brought into contact with the lithium metal by repeatedly inverting the tube, and formation of the anion was detected by ^{1}H, ^{13}C and ^{7}Li NMR spectroscopy.

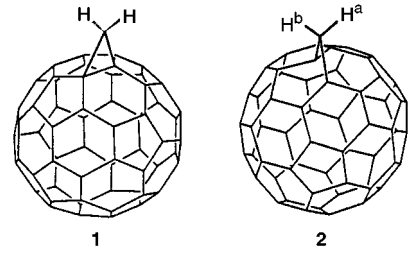

1 **2**

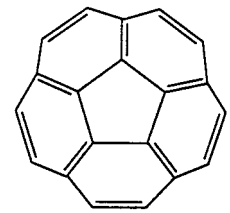

3

The ^{1}H NMR spectrum of the anion (Table 1) shows two doublets at δ 1.34 and 2.74 (J = 8.93 Hz). The $\Delta\delta$ between these two peaks is significantly smaller than the difference between the peaks of the neutral molecule [$\Delta\delta$(**2**) = 3.51 ppm compared with $\Delta\delta$(**2**$^{6-}$) = 1.4 ppm].[12a] The small $\Delta\delta$ of **2**$^{6-}$ suggests a similar magnetic environment for the two protons, in contrast to the neutral molecule, and moreover, the two protons of **2**$^{6-}$ are shielded. Since they are located above the centers of the rings, it confirms that these two rings are both diamagnetic, and thus the 5-MR is forced to become diamagnetic.

The ^{13}C NMR spectrum of **2**$^{6-}$ shows an NMR band at δ 37.08 assigned to the methylene carbon, and the fullerene

Table 1 Proton and carbon chemical shifts

	δ_C	δ_H	Ref.
C_{60}	142.68		16
C_{60}^{6-}	156.7		14
$C_{61}H_2$ (**2**)	38.4 (CH_2), 135.15–149.25	2.84, 6.35	12(*a*)
$C_6H_2^{6-}$ (**2**$^{6-}$)	37.08 (CH_2), 138.07–164.68	1.34, 2.74	

skeleton NMR bands appear in the region δ 138.07–164.68. The ^{7}Li NMR spectrum shows an absorption at δ 1.93 (200 K, relative to 1 M LiCl in D_2O at 298 K). Comparison of these chemical shifts to those of C_{60}^{6-} (δ_C 156.7 and δ_{Li} 1.6)[14] shows two phenomena: (i) the reduction of **2** leads to a hexaanion, as does C_{60};[6a,8,9] (ii) the character of $\mathbf{2}^{6-}$ is 'fullerene like' and has a similar charge distribution and aromaticity to C_{60}^{6-}.

Charging of $C_{61}H_2$ not only sheds light on the magnetic properties of its hexaanion, but it also contributes to the understanding of the nature of the building blocks of C_{60} itself. These results are in a good agreement with calculation,[11] and with ^{3}He chemical shift measurement[15] of He@C_{60} and He@C_{60}^{6-} that have been previously reported.[10] While the ^{3}He served as an endohedral probe of the bulk magnetic properties, the protons in **2** serve as external and localized probes. Therefore, it can be concluded that the extra electrons of C_{60}^{6-} convert 5-MRs from paramagnetic building blocks ('anti-aromatic') to components having diamagnetic nature ('aromatic'). The change of the ring current in the 5-MRs on the one hand, and the similarity of the aromatic 6-MRs in the neutral and the charged species on the other, demonstrates and rationalizes the highly aromatic character of C_{60}^{6-}.

We thank the Research and Development Authority of the Hebrew University of Jerusalem for financial support.

Notes and references

1 E. Hückel, *Z. Phys.*, 1931, **70**, 204; E. Hückel, *Z. Phys.*, 1931, **72**, 310.

2 V. I. Minkin, N. M. Glukhovteen and B. Ya. Simkin, *Aromaticity and Antiaromatcity: Electronic and Structural Aspects*, Wiley, New York, 1994.

3 R. C. Haddon, *J. Am. Chem. Soc.*, 1987, **109**, 1676.

4 H. W. Kroto, J. R. Heath, C. S. O'Brien, R. F. Curl and R. E. Smalley, *Nature*, 1985, **318**, 162; H. W. Kroto, A. W. Allaf and S. P. Balm, *Chem. Rev.*, 1991, **91**, 1213.

5 D. J. Klein, T. G. Schmalz, G. E. Hite and W. A. Seitz, *J. Am. Chem. Soc.*, 1986, **108**, 1301.

6 (*a*) V. Elser and R. C. Haddon, *Nature*, 1987, **325**, 792; (*b*) R. C. Haddon, L. F. Schneemeyer, J. V. Waszczak, S. H. Glarum, R. Tycko, G. Dabbagh, A. R. Kortan, A. J. Muller, A. M. Mujsce, M. J. Rosseinsky, S. M. Zahurak, A. V. Makhija, F. A. Thiel, K. Raghavachari, E. Cockayne and V. Elser, *Nature*, 1991, **350**, 46; (*c*) R. S. Ruoff, D. Beach, J. Cuomo, T. McGuire, R. L. Whetten and F. Diederich, *J. Phys. Chem.*, 1991, **95**, 3457; (*d*) A. P. Ramirez, R. C. Haddon, O. Zhou, R. M. Fleming, J. Zhang, S. M. McClure and R. E. Smalley, *Science*, 1994, **265**, 84.

7 For example: R. Taylor and D. R. M. Walton, *Nature*, 1993, **363**, 685; J. M. Hawkins, A. Meyer, T. A. Lewis, S. Loren and F. J. Hollander, *Science*, 1991, **252**, 313.

8 P. W. Fowler and J. Woolrich, *Chem. Phys. Lett.*, 1986, **127**, 78; A. J. Stone and D. I. Wales, *Chem. Phys. Lett.*, 1986, **128**, 501.

9 F. Zhou, C. Jehoulet and A. J. Bard, *J. Am. Chem. Soc.*, 1992, **114**, 11 004; Q. Xie, E. Pérez-Cordero and L. Echegoyen, *J. Am. Chem. Soc.*, 1992, **114**, 3978; Y. Ohsawa and T. Saji, *J. Chem. Soc., Chem. Commun.*, 1992, 781.

10 E. Shabtai, A. Weitz, R. C. Haddon, R. E. Hoffman, M. Rabinovitz, A. Khong, R. J. Cross, M. Saunders, P. C. Cheng and L. T. Scott, *J. Am. Chem. Soc.*, 1998, **120**, 6389.

11 A. Pasquarello, M. Schlüter and R. C. Haddon, *Science*, 1992, **257**, 1660; M. Pasquarello, M. Schlüter and R. C. Haddon, *Phys. Rev. A*, 1993, **47**, 1783; R. C. Haddon, *Science*, 1993, **261**, 1545.

12 (*a*) T. Suzuki, Q. Li, K. C. Khemani and F. Wudl, *J. Am. Chem. Soc.*, 1992, **114**, 7301; (*b*) A. B. Smith, III, R. M. Strongin, L. Brard, G. T. Furst, W. J. Romanow, K. G. Owens and R. C. King, *J. Am. Chem. Soc.*, 1993, **115**, 5829.

13 A justification for using the fulleroid **2** as an analogous system to C_{60} is based on the small change of the ^{3}He chemical shift between ^{3}He@C_{60} and ^{3}He@$C_{61}H_2$, which is evidence that both have the same bulk magnetic properties and there is no perturbation of the C_{60} π-system in $C_{61}H_2$ (see ref. 15).

14 J. W. Bausch, G. K. S. Parakash and G. A. Olah, *J. Am. Chem. Soc.*, 1991, **113**, 3205.

15 M. Saunders, R. J. Cross, H. A. Jiménez-Vázquez, R. Shimshi and A. Khong, *Science*, 1996, **271**, 1693; M. Saunders, H. A. Jiménez-Vázquez, B. W. Bangerter and R. J. Cross, *J. Am. Chem. Soc.*, 1994, **116**, 3621; M. Saunders, H. A. Jiménez-Vázquez, R. J. Cross, S. Mroczkowski, D. I. Freedberg and F. A. L. Anet, *Nature*, 1994, **367**, 256.

16 R. Taylor, J. P. Hare, A. K. Abdul-Sada and H. W. Kroto, *J. Chem. Soc., Chem. Commun.*, 1990, 1423.

Communication 9/07604B

A cylindrical cavity with two different hydrogen-binding boundaries: the calix[4]arene skeleton screwed onto the *meso*-positions of the calix[4]pyrrole†

Lucia Bonomo,[a] Euro Solari,[a] Gülsen Toraman,[a] Rosario Scopelliti,[a] Mario Latronico[b] and Carlo Floriani*[a]

[a] *Institut de Chimie Minérale et Analytique, BCH, Université de Lausanne, CH-1015 Lausanne, Switzerland. E-mail: carlo.floriani@icma.unil.ch*

[b] *Dipartimento di Ingegneria e Fisica dell'Ambiente, Università della Basilicata, I-85100 Potenza, Italy*

Received (in Cambridge, UK) 17th September 1999, Accepted 20th October 1999

The acid-catalyzed condensation of pyrrole with *p*- or *m*-hydroxyacetophenone led to the formation of *meso*-tetramethyltetrakis(hydroxyphenyl)calix[4]pyrroles occurring in three isomeric forms, with the cone conformer displaying topologically variable multi-site or multi-point surfaces for binding neutral or anionic substrates.

There has been a recent explosive development in the realm of molecular recognition of polar, and often uncharged, multifunctional organic molecules in which multi-point hydrogen bonds provide stabilization.[1–3] Multi-point hydrogen bonding molecules are appropriate devices for the maintenance of the function and structure of complex biomolecules.[4] Many of them are bifunctional molecules, *i.e.* amino acids[5a] and steroids,[5b,3c] all requiring bifunctional hosts which have two chemically different binding areas. The present report deals with the discovery of a class of compounds particularly appropriate to play a role in multi-point or multi-site host–guest interactions. An important factor in any artificial receptor is simplicity of synthesis, and this is the case reported here. The general synthetic procedure is shown in Scheme 1. The acid-catalyzed condensation of pyrrole with *p*- or *m*-hydroxyacetophenones led to the formation of the expected *meso*-octaalkylporphyrinogen derivatives[6,7] **1**‡ and **2**,† occurring in three isomeric forms (the cone **a**, the partial cone **b** and the 1,2 alternate conformation **c**) in a 7:2:1 ratio.

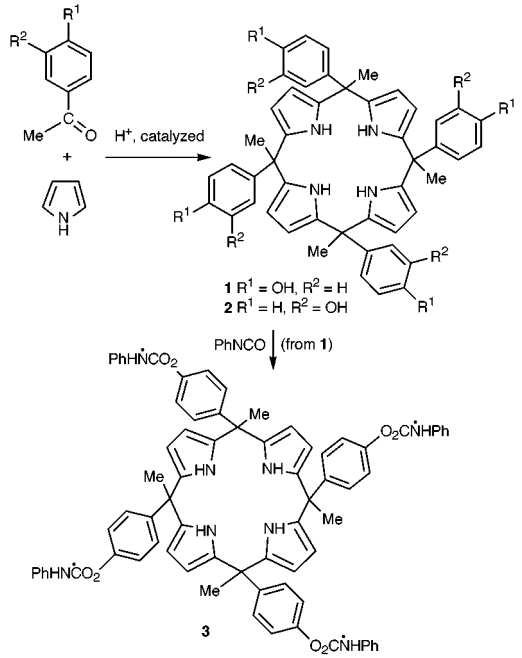

Scheme 1

The separation of the three isomers was performed either by crystallization or chromatography.†‡ The identification of the three isomers is conveniently made by ^{1}H NMR spectroscopy. Compound **1** in its cone conformation **a** is associated into dimers or trimers, the molecular complexity being determined by the guest molecule.[1–3,8] In the presence of hydrogen-binding substrates such as DMF or acetic acid, the isomer **1a** is assembled into closed two-basket cavity dimers,[1] **1a**·DMF (Fig. 1),§ or into cyclic trimeric units, **1a**·AcOH (Fig. 2),§ displaying C_3 symmetry. The trimeric cavity hosts nine molecules of AcOH, three of them being associated to the porphyrinogen moieties while the other six establish an intermolecular hydrogen bonding network with other trimers.

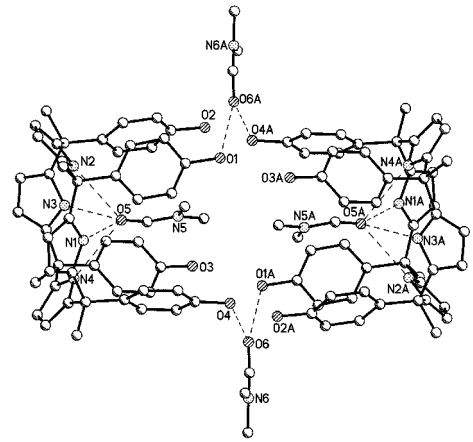

Fig. 1 A plot of **1a**·DMF linked into pairs by hydrogen bonds. Selected bond distances (Å) and angles (°): N–H···O [H···O$_{av}$ = 2.15, N···O$_{av}$ = 3.013(7), N-H···O$_{av}$ = 170.0]. Letter *A* denotes the symmetry transformation −*x*, −*y*, −*z*.¶

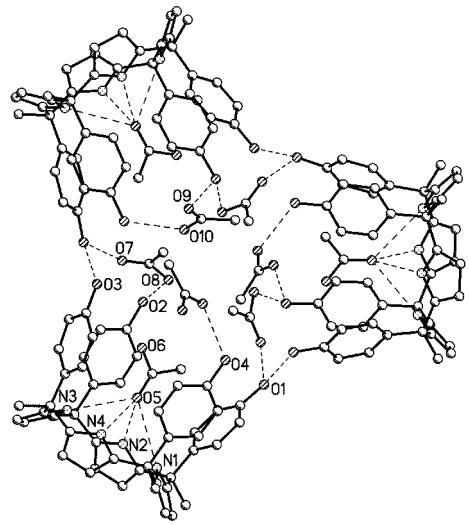

Fig. 2 A plot of **1a**·AcOH associated into trimers by hydrogen bonds and viewed down the three-fold axis. Selected bond distances (Å) and angles (°): N–H···O [H···O$_{av}$ = 2.26, N···O$_{av}$ = 3.140(5), N–H···O$_{av}$ = 174.0].¶

† Details of the synthesis and characterisation of **1**–**3** are available from the RSC web site, see http://www.rsc.org/suppdata/cc/1999/2413/

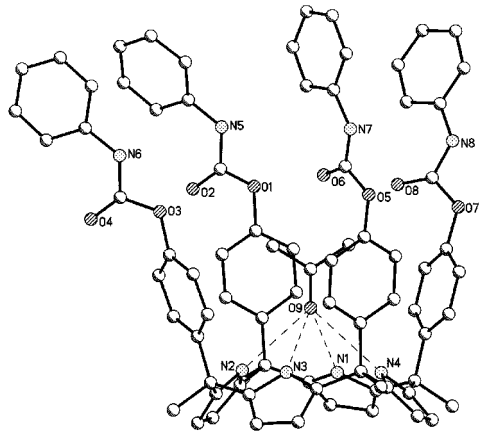

Fig. 3 A plot of **3** showing the interaction with the inner acetone. Selected bond distances (Å) and angles (°): N–H···O [H···O$_{av}$ = 2.26, N···O$_{av}$ = 3.12(1), N–H···O$_{av}$ = 168.1].¶

Therefore the overall structure of **1a**·AcOH is a tridimensional cylindrical cavity. Compound **1a** has been converted into the corresponding *N*-phenylcarbamate **3**,† which was crystallized from acetone (Fig. 3).§ The structure of **3** shows the same conformation of the monomeric unit in **1**. The guest molecules, except those bonded to the porphyrinogen moiety,[9] are loosely bonded and easily lost on gentle heating *in vacuo* or in solution, as shown by the ^{1}H NMR spectra.

Unlike other attempts,[10] our approach maintained in **1**–**3** both the OH and NH surfaces associated with the cone conformation of calix[4]arene and calix[4]pyrrole, thus, depending on the tunable spacer, being appropriate hosts of functionalizable molecules.

The overall structures of **1**–**3** deserve some additional comments concerning the calix[4]arene fragment, since the calix[4]pyrrole moieties are structurally very close to that of the well known *meso*-octaalkylporphyrinogens.[7] In our case, we are dealing in fact with an upside down flexible calix[4] unit cavity, the connectivity between the phenol groups being assured through the *p*-carbons of the phenyl substituent rather than through the *o*-carbons. In the three compounds the most significant structural parameters related to the monomeric building block are very close: (*i*) the planarity of the N_4 and O_4 set of atoms; (*ii*) the distance between the two parallel O_4 and N_4 planes [5.482(4), **1a**·DMF; 5.492(7), **1a**·AcOH; 5.53(2) Å, **3**]; (*iii*) the size of the slightly elliptical cavity, which can be roughly estimated from the opposite oxygen's distance [9.915(7) and 8.14(1), **1a**·DMF; 10.146(5) and 8.435(6), **1a**·AcOH; 10.478(9) and 8.19(1) Å, **3**]. The general synthesis outlined in Scheme 1, with an appropriate choice of acetophenone derivatives and the various conformations associated both with the porphyrinogen and the calix[4]arene moieties, will allow us to obtain topologically variable (tubes, cylinders *etc.*) multi-site or multi-point surfaces for binding neutral or anionic substrates.

We thank the FNS Grant No. 20-53336.98) and COST D9 for financial support.

Notes and references

‡ *Synthesis* of **1**: MeOH (10 ml) was added to a solution of *p*-hydroxyacetophenone (80.0 g, 588 mmol) and pyrrole (40 cm^3, 588 mmol) in MeOH (200 cm^3). The reaction was refluxed for 3 h and then quenched with water (700 cm^3). A yellow solid precipitated, which was collected and dissolved in Et_2O (400 cm^3). A black residue was filtered off and the solution was evaporated to dryness to give a light pink powder, which was dried *in vacuo* (10^{-7} Mbar) at 90 °C for 24 h (65.3 g, 60%). The ^{1}H NMR spectrum of this powder showed a mixture of the three isomers **1a**–**c** in a 7:2:1 ratio. Each isomer was isolated by flash chromatography (CH_2Cl_2–*n*-hexane–MeOH, 8:1.4:0.6). All the fractions were dried *in vacuo* (10^{-7} Mbar) at 90 °C for 24 h. The third fraction [R_f = 0.193 (UV)] contained the major isomer **1a**: δ_H (acetone-d_6, 400 MHz, 298 K) 8.74 (s br, 4H, NH),8.15(s br, 4H, OH), 6.76 (d, *J* 8.8, 8H, ArH), 6.65 (d, *J* 8.8, 8H, ArH), 5.94 (d, *J* 2.45, 8H, C_4H_2N), 1.8 (s, 12H, CH_3). The major isomer **1a** (30.0 g) was also isolated by crystallization of the isomeric mixture from AcOH (19.4 g, 59%); δ_H(THF-d_8, 200 MHz, 298 K) 8.35 (s br, 4H, NH), 6.90 (d, *J* 8.8, 8H, ArH), 6.56 (d, *J* 8.8, 8H, ArH), 5.63 (d, *J* 2.45, 8H, C_4H_2N), 1.88 (s, 12H, CH_3 overlapping with s, 3H, CH_3COOH). Acetic acid elimination from **1a**·AcOH was carried out by azeotropic distillation with Bu_2O. Crystals suitable for X-ray diffraction, grown from a THF–AcOH solution, contain AcOH in a **1a**:AcOH = 1:3 molar ratio. Crystals of **1a**·DMF suitable for X-ray analysis and containing DMF in a **1a**: DMF = 1:3 molar ratio were obtained from a DMF–THF solution of the isomeric mixture; δ_H(THF-d_8, 200 MHz, 298 K) 9.14 (s br, 4H, NH), 8.12 (s br, 3H, CHO), 6.69 (d, *J* 8.8, 8H, ArH), 6.48 (d, *J* 8.8, 8H, ArH), 5.90 (d, *J* 2.6, 8H, C_4H_2N),2.70 (s br, 18H, CH_3), 1.75 (s, 12H, CH_3); (THF-d_8, 200 MHz, 330 K) 9.12 (s br, 4H, NH), 7.91 (s br, 3H, CHO), 6.70 (d, *J* 8.8, 8H, ArH), 6.48 (d, *J* 8.8, 8H, ArH), 5.90 (d, *J* 2.6, 8H, C_4H_2N), 2.60 (s, 12H, CH_3), 2.25 (s br, 6H, CH_3), 1.76 (s, 12H, CH_3).

§ *Crystal data* for **1a**·DMF: $C_{48}H_{44}N_4O_4{\cdot}C_4H_8O{\cdot}3C_3H_7NO$, *M* = 1032.26, monoclinic, space group $P2_1/c$, *a* = 10.960(2), *b* = 21.081(4), *c* = 24.039(5) Å, β = 90.42(3)°, *V* = 5554.0(19) Å^3, *Z* = 4, D_{calc} = 1.235 g cm^{-3}, *F*(000) = 2208, λ(Mo-Kα) = 0.71070 Å, μ(Mo-Kα) = 0.082 mm^{-1}; crystal dimensions 0.20 × 0.13 × 0.10. Diffraction data were collected on a mar345 Imaging Plate at 143 K. For 3355 observed reflections [$I > 2\sigma(I)$] and 686 parameters, the conventional *R* is 0.0942 (*wR2* = 0.2662 for 6736 independent reflections). For **1a**·AcOH: $C_{48}H_{44}N_4O_4{\cdot}C_4H_8O{\cdot}3C_2H_4O_2$, *M* = 993.13, trigonal, space group $P3_2$, *a* = 20.054(5), *b* = 20.054(5), *c* = 11.079(3) Å, *V* = 3858.6(17) Å^3, *Z* = 3, D_{calc} = 1.282 g cm^{-3}, *F*(000) = 1584, λ(Mo-Kα) = 0.71070 Å, μ(Mo-Kα) = 0.089 mm^{-1}; crystal dimensions 0.25 × 0.23 × 0.22. Diffraction data were collected on a mar345 Imaging Plate at 143 K. For 4394 observed reflections [$I > 2\sigma(I)$] and 659 parameters, the conventional *R* is 0.0459 (*wR2* = 0.1105 for 5796 independent reflections). For **3**: $C_{76}H_{64}N_8O_8{\cdot}5C_3H_6O$, *M* = 1507.74, monoclinic, space group $P2_1/c$, *a* = 11.3580(19), *b* = 19.927(3), *c* = 35.860(4) Å, β = 94.400(12)°, *V* = 8093(2) Å^3, *Z* = 4, D_{calc} = 1.238 g cm^{-3}, *F*(000) = 3200, λ(Mo-Kα) = 0.71070 Å, μ(Mo-Kα) = 0.083 mm^{-1}; crystal dimensions 0.17 × 0.13 × 0.06. Diffraction data were collected on a KUMA CCD at 143 K. For 4534 observed reflections [$I > 2\sigma(I)$] and 1009 parameters, the conventional *R* is 0.1119 (*wR2* = 0.3308 for 9923 independent reflections). CCDC 182/1457.

¶ Hydrogens and some solvent molecules have been omitted for clarity, while labels have been used only for oxygen and nitrogen atoms.

1 J. Rebek, Jr., *Chem. Soc. Rev.*, 1996, 255; M. M. Conn and J. Rebek, Jr., *Chem. Rev.*, 1997, **97**, 1647; T. Martín, U. Obst and J. Rebek, Jr., *Science*, 1998, **281**, 1842; C. A. Schalley, R. K. Castellano, M. S. Brody, D. M. Rudkevich, G. Siuzdak and J. Rebek, Jr., *J. Am. Chem. Soc.*, 1999, **121**, 4568 and references therein.

2 J.-M. Lehn, *Supramolecular Chemistry, Concepts and Perspectives*, VCH, Weinheim, 1995; G. S. Hanan, D. Volkmer, U. S. Schubert, J.-M. Lehn, G. Baum and D. Fenske, *Angew. Chem., Int. Ed. Engl.*, 1997, **36**, 1842; J. L. Atwood and L. R. MacGillivray, *Nature*, 1997, **389**, 469.

3 (*a*) K. A. Jolliffe, P. Timmerman and D. N. Reinhoudt, *Angew. Chem., Int. Ed.*, 1999, **38**, 933 and references therein; (*b*) W. T. S. Huck, R. Hulst, P. Timmerman, F. C. J. M.Van Veggel and D. N. Reinhoudt, *Angew. Chem., Int. Ed. Engl.*, 1997, **36**, 1006; (*c*) I. Higler, P. Timmerman, W. Verboom and D. N. Reinhoudt, *J. Org. Chem.*, 1996, **61**, 5920; (*d*) P. Timmerman, R. H. Vreekamp, R. Hulst, W. Verboom, D. N. Reinhoudt, K. Rissanen, K. A. Udachin and J. Ripmeester, *Chem. Eur. J.*, 1997, **3**, 1823.

4 Y. Aoyama, in *Advances in Supramolecular Chemistry*, ed. G. W. Gokel, JAI Press, Greenwich, CT, 1992, vol. 2, pp. 65–92; A. D. Hamilton, in *Advances in Supramolecular Chemistry*, ed. G. W. Gokel, JAI Press, Greenwich, CT, 1990, vol. 1; pp. 1–64.

5 (*a*) R. E. Babine and S. L. Bender, *Chem. Rev.*, 1997, **97**, 1359; (*b*) P. Wallimann, T. Marti, A. Fürer and F. Diederich, *Chem. Rev.*, 1997, **97**, 1567.

6 A. Baeyer, *Chem. Ber.*,1886, **19**, 2184.

7 C. Floriani, *Chem. Commun.*, 1996, 1257 and references therein; C. Floriani, *Pure Appl. Chem.*, 1996, **68**, 1 and references therein.

8 O. Mogck, E. F. Paulus, V. Böhmer, I. Thondorf and W. Vogt, *Chem. Commun.*, 1996, 2533; J. J. González, P. Prados and J. de Mendoza, *Angew. Chem., Int. Ed.*, 1999, **38**, 525.

9 P. A. Gale, J. L. Sessler and V. Král, *Chem. Commun.*, 1998, 1;W. E. Allen, P. A. Gale, C. T. Brown, V. M. Lynch and J. L. Sessler, *J. Am. Chem. Soc.*, 1996, **118**, 12 471; P. A. Gale, J. L. Sessler, V. Král and V. Lynch, *J. Am. Chem. Soc.*, 1996, **118**, 5140; J. L. Sessler, A. Andrievsky, P. A. Gale and V. Lynch, *Angew. Chem., Int. Ed. Engl.*, 1996, **35**, 2782.

10 P. A. Gale, J. L. Sessler, V. Lynch and P. I. Sansom, *Tetrahedron Lett.*, 1996, **37**, 7881; P. A. Gale, J. W. Genge, V. Král, M. A. McKervey, J. L. Sessler and A.Walker, *Tetrahedron Lett.*, 1997, **38**, 8443.

11 For the structural parameters, see the Captions of the Figures in the supplementary data (see note †).

Communication 9/07563A

ChemComm

Dendrimers based on cyclophosphazene units and containing chiral ferrocenyl ligands for asymmetric catalysis†

Raoul Schneider, Christoph Köllner, Immo Weber and Antonio Togni*

Laboratory of Inorganic Chemistry, Swiss Federal Institute of Technology, ETH Zentrum, CH-8092 Zürich, Switzerland. E mail: togni@inorg.chem.ethz.ch

Received (in Basel, Switzerland) 29th September 1999, Accepted 26th October 1999

A simple and efficient synthesis and characterization of a series of first generation dendrimers based on cyclophosphazene cores and containing up to 16 peripheral chiral ferrocenyl ligands is described.

Dendrimers,[1] highly branched three-dimensional monodisperse macromolecules, are in principle useful for applications in catalysis, but have still rarely been prepared for this purpose.[2] As an interface between heterogeneous and homogeneous catalysis, such catalysts react in homogeneous solution but may be recycled by means of nanofiltration.[3] We have previously shown that chiral ferrocenyl ligands may be successfully applied to a variety of asymmetric catalytic reactions,[4] and that these ligands could be conveniently functionalised with a view to attaching them to the periphery of dendrimers by a convergent approach.[5] It has been found that such macromolecules, when used in catalytic reactions, do not show relevant differences in terms of stereoselectivity and catalytic activity, as compared to their monomeric congeners and are completely recovered by nanofiltration.[5]

In continuation of our studies, we aimed to improve and simplify the preparation of our dendritic ligands. We report now an efficient three-step synthesis of a new family of dendrimers containing up to 16 chiral ferrocenyl ligand units with PP or PN chelating systems. The synthesis starts from compounds of type **1** and utilises cyclotriphosphazene or tetraphosphazene units as dendrimer cores. Although the N_3P_3 fragment has been used previously in pioneering work by Majoral and co-workers,[1g,h] the next larger oligomeric N_4P_4 phosphazene ring[6] has not been exploited before in dendrimer chemistry. The precursors $N_3P_3Cl_6$ and $N_4P_4Cl_8$ offer more branching points, as compared to more commonly used internal fragments, such as trisubstituted benzenes, or tetrasubstituted adamantanes, implying that, for an equal number of synthetic steps, dendrimers containing a higher number of peripheral units may be obtained. Furthermore, because of the higher internal branching, dendritic particles approaching a spherical shape may be obtained with a lower number of generations.

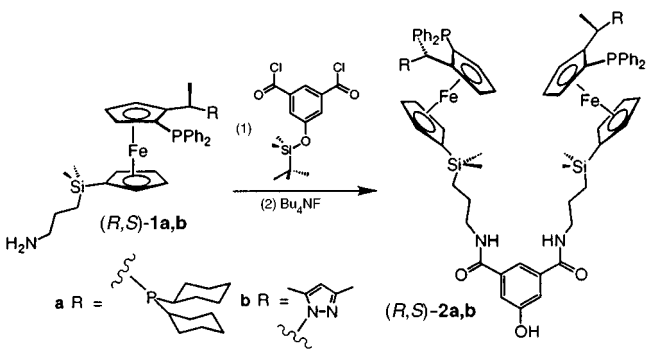

Scheme 1

Thus, the synthesis of the first-generation dendrimers **$G_1$12PN**, **$G_1$12PP** and **$G_1$16PP**, containing 12, 12 and 16 ferrocenyl groups, respectively, was achieved from intermediates **2** (Scheme 1), obtained by reacting **1** with 5-(*tert*-butyldimethylsiloxy)isophthaloyl dichloride followed by deprotection with Bu_4NF. A slight excess of the sodium salt of **2** was allowed to react in dioxane with $N_3P_3Cl_6$ and $N_4P_4Cl_8$, respectively, affording the desired compounds as orange powders in good yields after purification by column chromatography (Scheme 2).

All new multiple ferrocenyl ligands were characterised by NMR (^{1}H, ^{13}C and ^{31}P) and mass spectroscopy.† As expected, the ^{31}P NMR spectra of the products show one singlet for the cyclophosphazene phosphorus atoms, indicating full substitution of the central core [Fig. 1(*a*)]. The peripheral phosphorus atoms in **$G_1$12PN** display a singlet, whereas **$G_1$12PP** and **$G_1$16PP** each show one pair of doublets with a typical long range $^4J_{PP}$ coupling constant of *ca*. 40 Hz, indicating the equivalence of the ferrocenyl units. The new dendrimers were also characterised by MALDI-TOF mass spectroscopy and in all cases the molecular peak could be detected. Several in-source fragmentations at *m/z* values in good agreement with the calculated ones were observed.† Furthermore, addition of 16 equiv. of $[Rh(COD)_2]BF_4$ to **$G_1$16PP**, for example, led to the corresponding monodisperse species containing 16 equivalent and non-interacting Rh complexes, as indicated by the ABX-spin system in the ^{31}P NMR spectrum of Fig. 1(*b*), displaying $^2J_{PP}$ and $^1J_{PRh}$ coupling constants of 30 and 142 Hz. Preliminary experiments with **$G_1$12PP** and **$G_1$16PP** in the Rh-catalysed hydrogenation of dimethyl itaconate, under the conditions

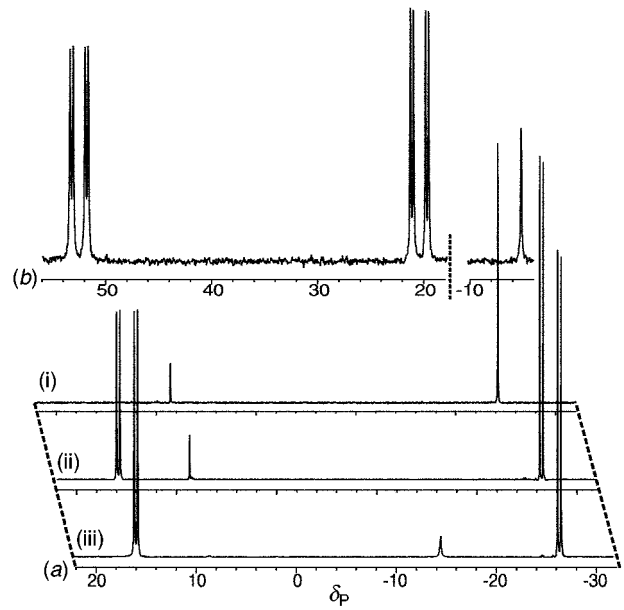

Fig. 1 ^{31}P NMR (101.202 MHz, $CDCl_3$) spectra of G1-dendrimers: (*a*) (i) **$G_1$12PN**, (ii) **$G_1$12PP** and (iii) **$G_1$16PP** and (*b*) **$G_1$16PP** + 16 equiv. of $[Rh(COD)_2]BF_4$.

† Experimental and spectral data for (*R,S*)-**2b**, **$G_1$12PN**, **$G_1$12PP** and **$G_1$16PP** are available from the RSC web site, see http://www.rsc.org/suppdata/cc/1999/2415/

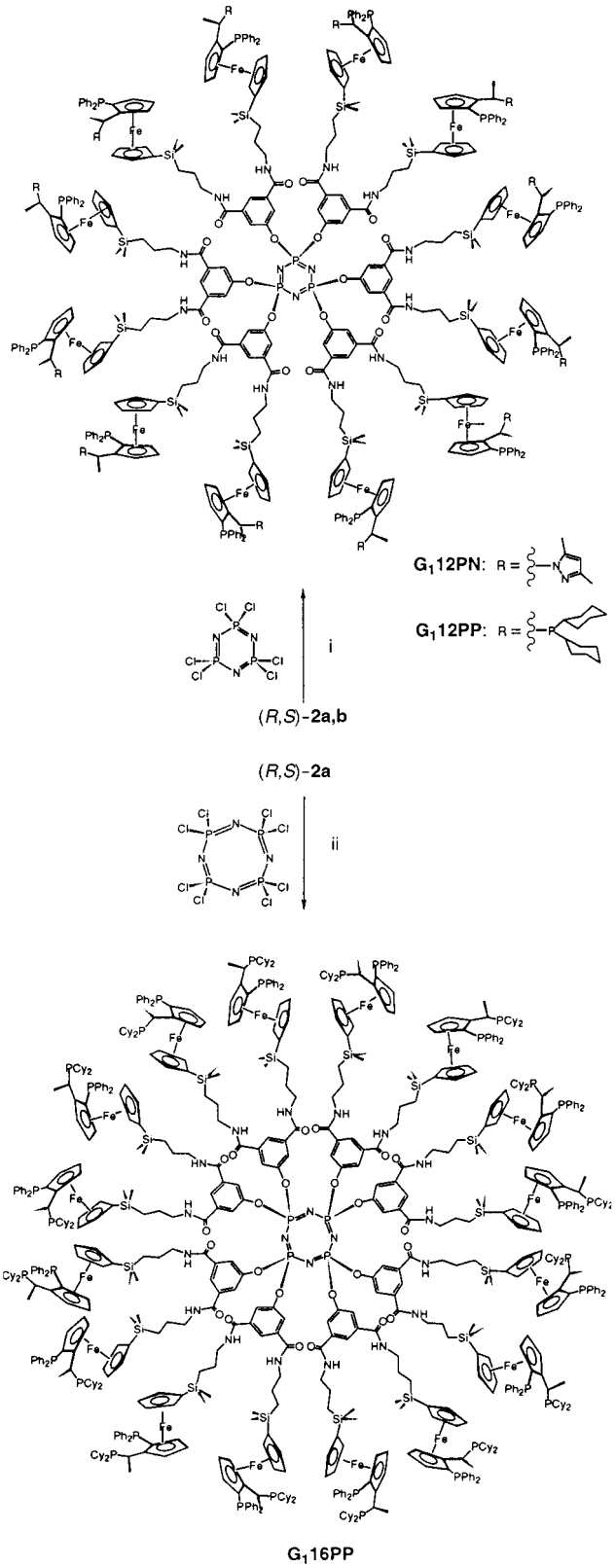

Scheme 2 *Reagents and conditions*: i, Na, MeOH–1,4-dioxane, 60 °C, 1 h, then $N_3P_3Cl_6$, 1,4-dioxane, 16 h (**$G_1$12PN**: 54%, **$G_1$12PP**: 64,5%); ii, Na, MeOH–1,4-dioxane, 60 °C, 1 h, then $N_4P_4Cl_8$, dioxane, 16 h, 83%.

previously reported,[5] afforded the product in *ca*. 98% ee. This indicates that the dendritic structure of the catalyst, as compared to its monomeric version, is not significantly detrimental to enantioselectivity, at least up to the size of **$G_1$16PP**.

We are currently exploiting cyclophosphazenes for the preparation of dendrimers of higher generations, as well as using such dendrimers as catalysts in a continuous asymmetric hydrogenation process. The results of such investigations shall be disclosed in due course.

We are grateful to Walter Amrein (Laboratory of Organic Chemistry, ETH-Zürich) for measuring MALDI-TOF mass spectra.

Notes and references

† *Selected data* for **$G_1$12PN**: δ_H(250 MHZ, $CDCl_3$)7.93 (s, 36H, C_6H_3), 7.61 (s, 12H, C_6H_3), 7.48 (m, 24 Ph-H), 7.33 (m, 36 Ph-H), 7.02 (m, 36 Ph-H), 6.70 (m, 36H, 24 Ph-H and 12 NH), 5.56 (dq, 12H, 12 C*H*MeN), 5.05 (s, 12 Pz-H), 4.72 (m, 12 Cp-H), 4.36 (m, 12 Cp-H), 4.26 (m, 12 Cp-H), 4.12 (m, 12 Cp-H), 4.04 (m, 12 Cp-H), 3.73 (m, 12 Cp-H), 3.60 (m, 12 Cp-H), 3.21 (m, 24H, 12 CH_2NH), 2.11 (s, 36H, 12 Pz C^5-*Me*), 1.94 (s, 36H, 12 Pz C^3-*Me*), 1.78 (d, 36H, 12 CH*Me*N), 1.43 (m, 24H 12 $CH_2CH_2CH_2$), 0.49 (m, 24H, 12 CH_2Si), 0.12 (s, 36H, 36H of 12 $SiMe_2$), 0.01 (s, 36H, 36H of 12 $SiMe_2$); δ_c(62.86 MHz, $CDCl_3$) 165.7 (C=O), 150.1 (Ar C of C_6H_3), 146.7 (PzC^5), 138.4–127.0 (PPh_2, PzC^3, Ar C of C_6H_3), 123.0 and 121.7 (Ar C of C_6H_3), 101.1 (Pz CH), 94.0 (d, Cp C), 75.2 (d, Cp C), 74.6–70.1 (Cp CH and Cp C), 51.7 (d, *C*HMeN), 43.4 (CH_2N), 24.0 ($CH_2CH_2CH_2$), 20.6 (CH*Me*N), 14.0 (CH_2Si), 13.6 (Pz C^3-*Me*), 11.3 (d, Pz C^5-*Me*), −2.4 ($SiMe_2$), −2.5 ($SiMe_2$); $d3_p$(101.202 MHz, $CDCl_3$) 8.5 (s, Pz), −24.2 (d, PPh_2); *m/z* (MALDI) 8321 ($[M + Na]^+$), 7948 ($[M - \{C_5H_3(PPh_2)(CH(Me)C_5H_7N_2\}]^+$), 6991 ($[M - \{$**2b**$\}]^+$), 6616 ($[6991 - \{C_5H_3(PPh_2)(CH(Me)C_5H_7N_2\}]^+$), 5662 ($[M - \{2 \times$**2b**$\}]^+$), 5291 ($5662 - \{C_5H_3(PPh_2)(CH(Me)C_5H_7N_2\}]^+$).

1 For reviews, see, *e.g.*: (*a*) G. R. Newkome, E. He and C. H. Moorefield, *Chem. Rev.*, 1999, **99**, 1689; (*b*) J.-P. Majoral and A.-M. Caminade, *Chem. Rev.*, 1999, **99**, 845; (*c*) A. W. Bosman, H. M. Janssen and E. W. Meijer, *Chem. Rev.*, 1999, **99**, 1665; (*d*) A. Archut and F. Vögtle, *Chem. Soc. Rev.*, 1998, **27**, 233; (*e*) M. Fischer and F. Vögtle, *Angew. Chem., Int. Ed.*, 1999, **38**, 885; (*f*) M. A. Hearshaw and J. R. Moss, *Chem. Commun.*, 1999, 1. For the synthesis of dendrimers incorporating phosphorus, see: (*g*) C. Galliot, D. Prévoté, A.-M. Caminade and J.-P. Majoral, *J. Am. Chem. Soc.*, 1995, **117**, 5470; (*h*) M. Slany, M. Bardají, M.-J. Casanove, A.-M. Caminade, J.-P. Majoral and B. Chaudret, *J. Am. Chem. Soc.*, 1995, **117**, 9764.

2 P. B. Rheiner, H. Sellner and D. Seebach, *Helv. Chim. Acta*, 1997, **80**, 2027; C. Bolm, N. Derrien and A. Seger, *Synlett*, 1996, 387; H. Brunner, *J. Organomet. Chem.*, 1995, **500**, 39; M. T. Reetz, G. Lohmer and R. Schwickardi, *Angew. Chem., Int. Ed. Engl.*, 1997, **36**, 1526; G. E. Oosterom, R. J. van Haaren, J. N. H. Reek, P. C. J. Kamer and P. W. N. M. van Leeuwen, *Chem. Commun.*, 1999, 1119; H. P. Dijkstra, P. Steenwinkel, D. M. Grove, M. Lutz, A. L. Spek and G. van Koten, *Angew. Chem., Int. Ed.*, 1999, **38**, 2186; J. W. J. Knapen, A. W. van der Made, J. C. de Wilde, P. W. N. M. van Leeuwen, P. Wijkens, D. M. Grove and G. van Koten, *Nature*, 1994, **372**, 659.

3 U. Kragl and C. Dreisbach, *Angew. Chem., Int. Ed. Engl.*, 1996, **35**, 642; D. de Groot, E. B. Eggeling, J. C. de Wilde, H. Kooijmann, R. J. van Haaren, A. W. van der Made, A. L. Spek, D. Vogt, J. N. H. Reek, P. C. J. Kamer and P. W. N. M. van Leeuwen, *Chem. Commun.*, 1999, 1623; N. J. Hovestad, E. B. Eggeling, H. J. Heidbüchel, J. T. B. H. Jastrzebski, U. Kragl, W. Keim, D. Vogt and G. van Koten, *Angew. Chem., Int. Ed.*, 1999, **38**, 1655.

4 See, *e.g.* A. Togni, in *Metallocenes. Synthesis, Reactivity, Applications*, ed. A. Togni and R.L. Halterman, Wiley-VCH, Weinheim, 1998, vol. 2, pp. 685–721 and references cited therein.

5 C. Köllner, B. Pugin and A. Togni, *J. Am. Chem. Soc.*, 1998, **120**, 10 274.

6 C. W. Allen, *Chem. Rev.*, 1991, **91**, 119; H. R. Allcock, D. C. Ngo, M. Parvez and K. Visscher, *J. Chem. Soc., Dalton Trans.*, 1992, 1687; L. G. Lund, N. L. Paddock, J. E. Proctor and H. T. Searle, *J. Chem. Soc.*, 1960, 2542.

Communication 9/07931I

New π-extended organic donor containing a stable TEMPO radical as a candidate for conducting magnetic multifunctional materials

Hideki Fujiwara* and Hayao Kobayashi

Institute for Molecular Science, Myodaiji, Okazaki 444-8585, Japan. E-mail: fuji@ims.ac.jp

Received (in Cambridge, UK) 10th September 1999, Accepted 20th October 1999

A novel organic electron donor containing a stable TEMPO radical (TEMPOET) was synthesized and its magnetic and electrochemical properties were investigated; furthermore, the crystal structure and physical properties of the $Au(CN)_2^-$ salt of TEMPOET were clarified.

Organic molecular magnetism has become a very active field of research since the discovery of the first pure organic ferromagnet, *p*-nitrophenyl nitronyl nitroxide (β-NPNN), in 1991 and the subsequent development of several ferromagnets based on aminoxyl radicals.[1,2] On the other hand, recent studies on molecular conductors and superconductors containing magnetic transition metal anions, such as the $(ET)_2[(H_2O)Fe(C_2O_4)_3]$•PhCN salt, a series of λ-$(BETS)_2Fe_xGa_{1-x}Cl_4$ alloy salts and the κ-$(BETS)_2FeBr_4$ salt[3] [where ET is bis(ethylenedithio)-TTF and BETS is bis(ethylenedithio)tetraselenafulvalene], have stimulated interest in the interplay between conductivity and magnetism in the search for new organic conductors. Among them, several donors containing a stable aminoxyl radical have been prepared by several research groups for the development of novel organic conducting magnetic multifunctional materials and organic ferromagnetic metals.[4,5] However, no highly conducting salt has been obtained from these donors so far. From the view point of the realization of metallic conductivity, we designed a molecular structure as the fusion of a stable TEMPO radical moiety to a DTET-TTF skeleton, which is a promising building block for realizing stable metallic behavior, as reported in the cases of MeDTET

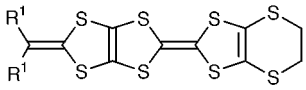

R^1 = Me, MeDTET
$2R^1$ = –$(CH_2)_4$–, CPDTET

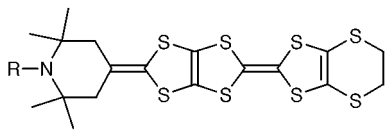

1 R = O•; TEMPOET
2 R = H

and CPDTET salts.[6,7] Here we present the synthesis, structure and physical properties of novel organic donor TEMPOET **1**. Furthermore, we report here the structure and physical properties of its $Au(CN)_2^-$ salt as the first X-ray structure analysis of a cation radical salt based on a TEMPO radical-containing donor.

TEMPOET **1** was synthesized as shown in Scheme 1. Thus, the ketone **5** was obtained in 52% yield by the Wittig–Horner reaction of **4**[8] and 4-oxo-TEMPO **3**. It was then reacted with thione **6** by a cross-coupling reaction. TEMPOET was obtained as air-stable microcrystals in 45% yield.†

As shown in Fig. 1, TEMPOET presents four waves at +0.56, +0.88, +1.17 and +1.77 V *vs.* Ag/AgCl, the first and third ones are slightly reversible, the second one is completely reversible and the fourth one irreversible. The first oxidation potential, +0.56 V, is almost the same as that of ET (+0.53 V). On the other hand, the corresponding piperidine analogue **2** showed

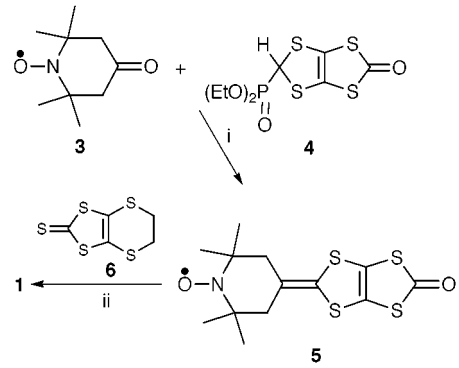

Scheme 1 *Reagents and conditions*: i, 0.5 M LDA (1.1 equiv.), THF, −78 °C, 15 min; ii, $P(OEt)_3$ (100 equiv.), 75 °C, 45 min.

three redox waves. Comparing the redox potentials of **1** to those of **2**, three (+0.56, +0.88 and +1.77 V) of the four potentials of **1** are almost equivalent to the three potentials of **2** (+0.55, +0.87 and +1.74 V). Therefore, the oxidation of the TEMPO radical part is considered to occur at the third oxidation process (+1.17 V), suggesting the possibility of the formation of the cation radical salts with an active TEMPO radical spin. However, the almost complete loss of reversibility of the first redox wave of **1** might indicate the existence of some further reaction in the reductive process of the cation radical state of **1** dissimilar to the case of **2**. The static magnetic susceptibility measurement of **1** showed a paramagnetic value (χ_{rt} = 1.25 × 10^{-3} emu mol^{-1}) corresponding to one S = 1/2 spin per molecule and a Curie–Weiss temperature dependence (θ = −1.00 K).

The $Au(CN)_2^-$ salt of **1** was electrochemically prepared in 1,2-dichloroethane. An X-ray structure analysis revealed that the D:A ratio of this salt is 2:3 and each TEMPOET has +1.5 valence.‡ The N–O bond length of the TEMPO radical part is 1.42(1) Å and is a little longer than that of the reported neutral TEMPO radicals (1.27–1.30 Å).[9] When a TEMPO radical is oxidized, the N–O bond length becomes shorter than the neutral one because of N^+=O double bond formation, as in the case of TEMPO•$TCNQF_4$ complex [1.195(5) Å].[10] Furthermore, judging from the bent form of the N–O bond from the C–N–C plane

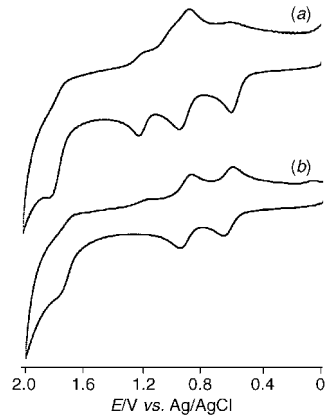

Fig. 1 Cyclic voltammograms of (*a*) **1** and (*b*) **2** in PhCN (scan rate 50 mV s^{-1}).

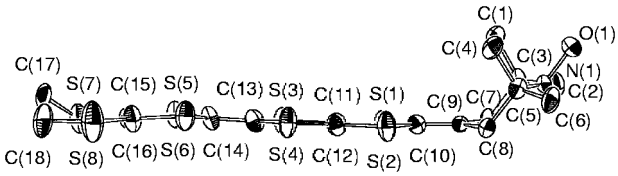

Fig. 2 Structure of the donor molecule in the $(\mathbf{1})_2[Au(CN)_2]_3$ salt.

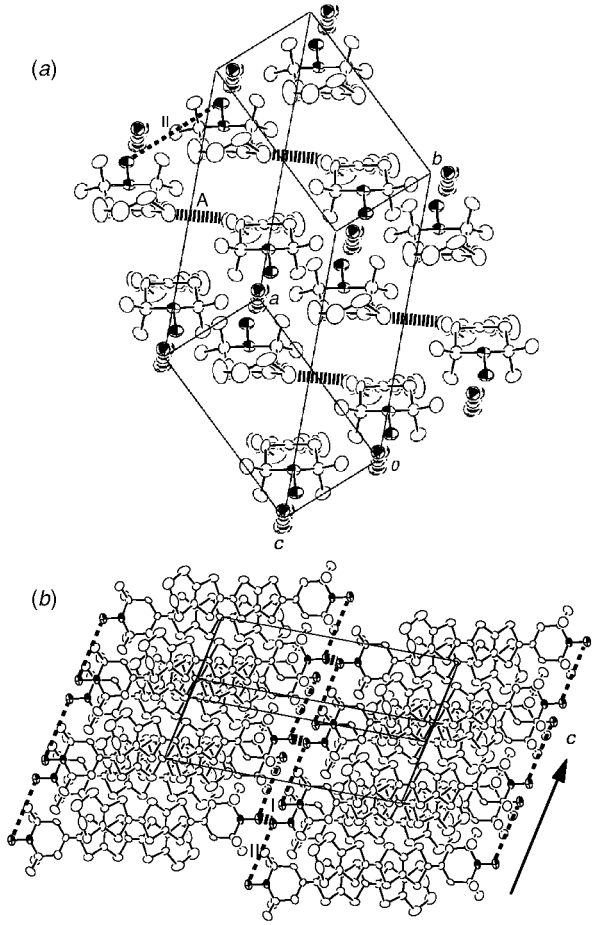

Fig. 3 Crystal structure of $(\mathbf{1})_2[Au(CN)_2]_3$ salt viewed (*a*) along the molecular long axis and (*b*) perpendicular to the molecular planes. S–S contacts: A S(1)–S(7) 3.624(5), S(3)–S(5) 3.658(5) and S(3)–S(7) 3.529(5) Å. O–O distances: I 3.24 and II 7.43 Å.

and the redox behavior of this donor discussed above, we think that the TEMPO radical part is not oxidized in this $Au(CN)_2^-$ salt. The framework of TEMPOET is almost flat except for the chair-formed TEMPO part, suggesting the oxidation of the donor part (Fig. 2). One of the $Au(CN)_2^-$ anions exists between the donor dimers, indicating no overlap of π-orbitals between dimers in the donor stack [Fig. 3(*a*)]. The dimers array along the *c*-axis with an offset of the molecular long axis (4.84 Å) and form sheet-like structure [Fig. 3(*b*)]. There is one very short O··O contact [3.24(2) Å] between the donor sheets. The room temperature electrical conductivity of this salt is low, with a value of about 10^{-3} S cm^{-1}, due to the highly oxidized state and undesirable stacking of donors. The temperature dependence of the resistivity produces semiconducting behaviour with an activation energy of 0.20 eV. The measurement of the magnetic susceptibility of this salt showed a much smaller room temperature value (9.6×10^{-4} emu mol^{-1} for a 2:3 salt) than the expected high value from the coexistence of two TEMPO radical spins and one cation radical spin in the $(\mathbf{1})_2[Au(CN)_2]_3$ salt. This result suggests the existence of intramolecular spin singlet formation and/or intermolecular strong antiferromagnetic spin configuration, which may be derived from the strong spin–spin interaction *via* the very short O–O distances between donor sheets (I). Furthermore the χT value decreases monotonically with decreasing temperature, as shown in Fig. 4. The

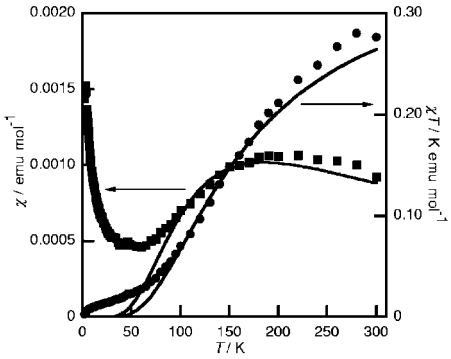

Fig. 4 χ-T (■) and χT–T (●) plots for the $(\mathbf{1})_2[Au(CN)_2]_3$ salt. Solid lines are calculated on the basis of a Bleaney–Bowers expression.

temperature dependence of the magnetic susceptibility is roughly fitted to a Bleaney–Bowers expression[11] and the singlet–triplet gap is estimated to large, with a value of $-2J$ = 206 cm^{-1}, except for the lower temperature region probably due to a small amount of paramagnetic impurities and lattice defects. This result suggests the strong antiferromagnetic interaction between two spins and an almost singlet ground state.

Notes and references

† *Selected data* for **1**: mp 206–207 °C (decomp.); *m/z* (70 eV, EI) 523 (100%) [M$^+$ + 1], 525 (24) [$C_{18}H_{20}NOS_8$ (522.84): calc. C, 41.35; H, 3.86; N, 2.68. Found: C, 41.27; H, 3.71; N, 2.64%]; EPR (benzene) g = 2.0061, a_N = 15.1 G.

‡ *Crystal data* for $\mathbf{1}_2[Au(CN)_2]_3$: $C_{21}H_{20}S_8N_4Au_{1.5}O$, M = 896.34, triclinic, space group $P\bar{1}$, a = 11.047(3), b = 18.643(7), c = 7.433(2) Å, α = 90.94(3), β = 100.51(2), γ= 74.04(2)°, U = 1446.2(8) Å^3, T = 293 K, Z = 2, μ (Mo-Kα) = 8.237 mm^{-1}, 6561 reflections measured, 6259 independent (R_{int} = 0.040). The final R and R_w were 0.046 and 0.047 (3413 reflections [$I > 3.0\sigma(I)$]). One of the $Au(CN)_2^-$ anions is disordered over an inversion centre. CCDC 182/158. See http://www.rsc.org/suppdata/cc/1999/2417/ for crystallographic data in .cif format.

1 M. Kinoshita, P. Turek, M. Tamura, Y. Nozawa, D. Shiomi, Y. Nakazawa, M. Ishikawa, M. Takahashi, K. Awaga, T. Inabe and Y. Maruyama, *Chem. Lett.*, 1991, 1225; R. Chiarelli, M. A. Novak, R. Rassat and J. L. Tholence, *Nature*, 1993, **363**, 147; T. Nogami, K. Tomioka, T. Ishida, H. Yoshikawa, M. Yasui, F. Iwasaki, H. Iwamura, N. Takeda and M. Ishikawa, *Chem. Lett.*, 1994, 29.

2 H. Iwamura, *Adv. Phys. Org. Chem.*, 1990, **26**, 179; K. Togashi, R. Imachi, K. Tomioka, H. Tsuboi, T. Ishida, T. Nogami, N. Takeda and M. Ishikawa, *Bull. Chem. Soc. Jpn.*, 1996, **69**, 2821.

3 A. W. Graham, M. Kurmoo and P. Day, *J. Chem. Soc., Chem. Commun.*, 1995, 2061; H. Kobayashi, A. Sato, E. Arai, H. Akutsu, A. Kobayashi and P. Cassoux, *J. Am. Chem. Soc.*, 1997, **119**, 12 392; E. Ojima, H. Fujiwara, K. Kato, H. Kobayashi, H. Tanaka, A. Kobayashi, M. Tokumoto and P. Cassoux, *J. Am. Chem. Soc.*, 1999, **121**, 5581.

4 K. Yamaguchi, H. Namimoto, T. Fueno, T. Nogami and Y. Shirota, *Chem. Phys. Lett.*, 1990, **166**, 408.

5 T. Sugano, T. Fukasaka and M. Kinoshita, *Synth. Met.*, 1991, **41**–**43**, 3281; T. Sugimoto, S. Yamaga, M. Nakai, K. Ohmori, M. Tsujii, H. Nakatsuji and N. Hosoito, *Chem. Lett.*, 1993, 1361; S. Nakatsuji and H. Anzai, *J. Mater. Chem.*, 1997, **7**, 2161; R. Kumai, A. Izuoka and T. Sugawara, *Mol. Cryst. Liq. Cryst.*, 1993, **232**, 151.

6 Y. Misaki, H. Nishikawa, H. Fujiwara, K. Kawakami, T. Yamabe, H. Yamochi and G. Saito, *J. Chem. Soc., Chem. Commun.*, 1992, 1408; Y. Misaki, H. Nishikawa, H. Fujiwara, T. Yamabe, T. Mori, H. Mori and S. Tanaka, *Synth. Met.*, 1995, **70**, 1151.

7 H. Fujiwara, Y. Misaki, M. Taniguchi, T. Yamabe, T. Kawamoto, T. Mori, H. Mori and S. Tanaka, *J. Mater. Chem.*, 1998, **8**, 1711.

8 Y. Misaki, T. Ohta, N. Higuchi, H. Fujiwara, T. Yamabe, T. Mori, H. Mori and S. Tanaka, *J. Mater. Chem.*, 1995, **5**, 1571.

9 R. N. Shibaeva, *Zh. Strukt. Khim*, 1975, **16**, 330.

10 S. Nakatsuji, A. Takai, K. Nishikawa, Y. Morimoto, N. Yasuoka, K. Suzuki, T. Enoki and H. Anzai, *Chem. Commun.*, 1997, 275.

11 B. Bleaney and K. D. Bowers, *Proc. R. Soc. London, Ser. A*, 1952, **214**, 451; for example, F. L. de Panthou, D. Luneau, J. Laugier and P. Rey, *J. Am. Chem. Soc.*, 1993, **115**, 9095.

Communication 9/07363I

Dramatic effect of the porphyrinic metal on the conformation of a two-ring threaded system

Myriam Linke, Jean-Claude Chambron,* Valérie Heitz and Jean-Pierre Sauvage*

Laboratoire de Chimie Organo-Minérale, U.M.R. 7513 au C.N.R.S.,Université Louis Pasteur, Institut Le Bel, 4, rue Blaise Pascal, 67000 Strasbourg, France. E-mail: sauvage@chimie.u-strasbg.fr

Received (in Basel, Switzerland) 6th September 1999, Accepted 25th October 1999

Porphyrin homodimers have been assembled by transition-metal-directed threading of porphyrin-incorporating macrocycles onto a rigid-rod bis-chelate, and the relative orientations of the porphyrins shown to be controlled by the nature of the metal that they contain.

Assemblies of naturally-occurring porphyrins or analogues held by noncovalent interactions are important components of photosynthetic systems, as light antennas, energy funnels, and electron transfer chains.[1] These facts, recently highlighted by beautiful X-ray crystal structures,[2] have stimulated the design and synthesis of multifarious porphyrin aggregates mainly based on coordination bonds, some of them showing relevant electron transfer properties.[3] In particular, the preparation and study of simple dimers of stacked porphyrins is highly significant,[4] as far as mimicking the unusual spectroscopic properties of the Special Pair of bacterial reaction centers is concerned.[5]

We have recently described the efficient assembly of porphyrin dimers by the transition-metal-controlled *threading* of macrocycles bearing *pendant* porphyrins and incorporating a 2,9-diphenyl-1,10-phenanthroline (dpp) chelate onto molecular threads containing two such dpp fragments.[6] Here we show that when a rod-like, phenanthroline-based bis-chelate and macrocycles *incorporating* metalloporphyrins in their backbone are used, the relative orientations of the porphyrins can be controlled by the nature of the metal that they contain.†

The bis-phenanthroline rigid-rod molecule **4** and the dpp-based macrocycles **9** and **10** incorporating a Zn^{II} and a Au^{III} porphyrin, respectively, as well as their precursors, are represented below. Suzuki coupling of 3-bromophenanthroline **1**[7] and diboronic acid **2**[8] in stoichiometric amounts [$Pd(PPh_3)_4$, aq. Na_2CO_3, EtOH–$PhCH_3$, reflux] afforded bis-phenanthroline **3** in 55% yield after chromatography.[9] This compound was further reacted with lithioanisole (3 equiv.) in THF at −5 °C.[10] After hydrolysis, MnO_2 aromatization and chromatographic separation from substitution isomers and homologues, bis-phenanthroline **4** was isolated in 32% yield. Direct precursors of macrocycle **8**, which incorporates a free-base porphyrin, are the phenanthroline derivative **5** and porphyrin **7**. This latter compound was obtained in quantitative yield by treatment of porphyrin **6**[11] with an excess of BBr_3 in CH_2Cl_2 at −78 °C. High-dilution condensation of **5** and **7** in DMF at 55 °C containing Cs_2CO_3 (5 equiv.) provided **8** in 28% yield after chromatography.[12] Insertion of Zn^{II} was carried out by reaction with $Zn(OAc)_2{\cdot}2H_2O$ (1 equiv.) in a 2:1 refluxing mixture of $CHCl_3$ and CH_3OH, to produce the Zn^{II} porphyrin-incorporating macrocycle **9** in 85% yield. The preparation of the Au^{III} porphyrin-incorporating macrocycle **10**, which could not be obtained by direct metallation of **8**, has been described elsewhere.[11]

Copper(I)-directed threading of either macrocycle **9** or **10** onto bis-phenanthroline rod **4** was carried out as follows (Scheme 1).[6,10] Equimolar amounts of $Cu(CH_3CN)_4{\cdot}PF_6$ in CH_3CN and the desired macrocycle in CH_2Cl_2 were combined under argon. Compound **4** (0.5 equiv.) in CH_2Cl_2 was subsequently transferred to the reaction mixture. After removal of the solvents under reduced pressure, the crude material was flash-chromatographed on silica gel, affording the threaded assembly. The Zn^{II} porphyrin dimer **11** was obtained in 85% yield and its Au^{III} porphyrin analogue **12** in 50% yield. Since the threading experiments proceeded more or less quantitatively, these isolated yields show that partial dethreading takes place during chromatographic purification, especially in the case of the Au^{III}porphyrin dimer **12**.

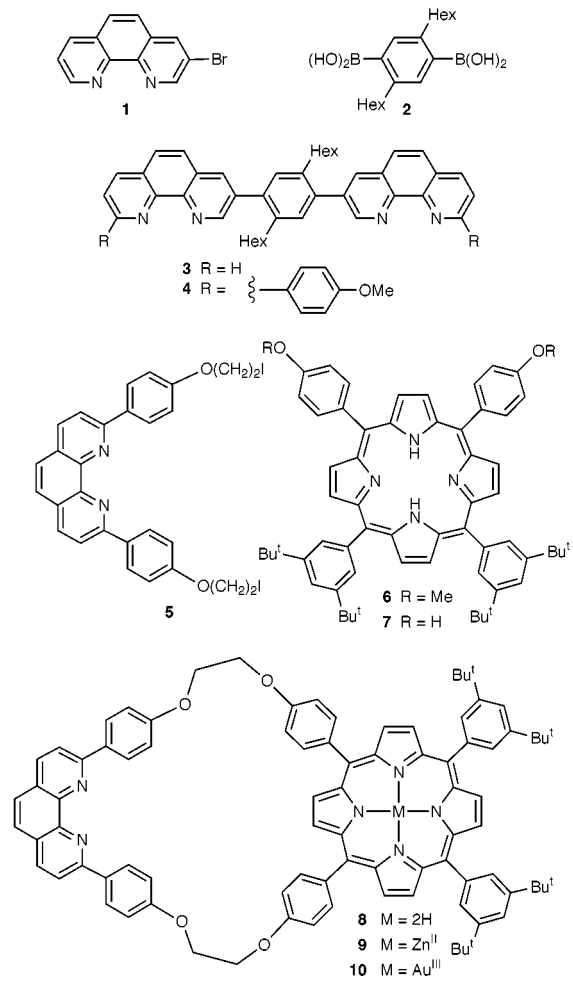

Diagnostic of macrocycle threading onto bis-phenanthroline **4** are the large upfield shifts of protons *m′* of **4** both for **11** (−1.28 ppm) and **12** (−0.98 ppm), due to ring current effects of the phenanthroline fragment included in the macrocycles on the anisyl extremities of **4**.[13] Methyl protons of these groups are also affected, albeit to a lesser extent. As expected, threading also breaks off the symmetry plane of the macrocycle, which contains the C_2 symmetry axis. The largest resulting splittings are observed for **11**. *o″* and *m″* protons of the porphyrins produce two pairs of signals, indicating that the rotation of the

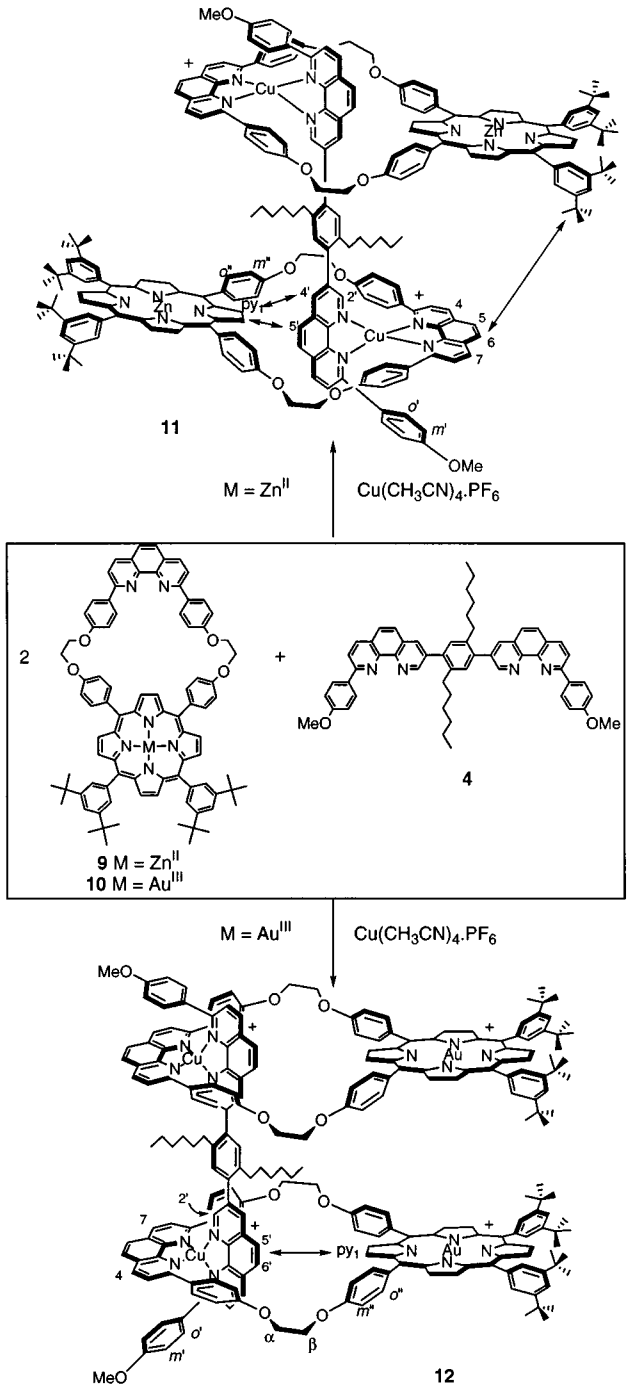

Scheme 1 Cu^{I}-directed threading of macrocycle **9** or **10** onto bisphenanthroline **4**. Protons highlighted in the text are indicated, as well as intercomponent NOE effects.

corresponding phenylene groups is slow on the NMR timescale, and α and β protons of **11** clearly form two sets of diastereotopic pairs of atoms.

Despite these common features, the ^{1}H NMR spectra of the threaded complexes **11** and **12** showed dramatic differences, which could not be attributed solely to the different nature of the metal cation of the porphyrins. Upon threading, protons 2′ of **4** and (4,7) of the macrocycles are −2.54 and −0.59 ppm more shielded, respectively, when **11** is compared to **12**. 2D ^{1}H NMR ROESY experiments on **11** showed a remarkable intercomponent NOE crosspeak between the Zn^{II} porphyrin Bu^{t} groups and the pair (5,6) of protons of the phenanthroline fragment belonging to a different macrocycle, that was absent in the case of **12**. For the latter, a symmetrical correlation between py_1 of the Au^{III} porphyrins and the pairs (5′,6′) of protons of **4** could be observed, which, in the case of **11**, involved protons 4′ and 5′ instead.

All of these data suggest that, in the threaded system **11**, the Zn^{II} porphyrin components are roughly antiparallel, as shown in Scheme 1, each being tilted towards the phenanthroline chelate of the macrocycle maybe thanks to attractive interactions between the electron-rich Zn^{II} porphyrin of one macrocycle and the electron-deficient Cu^{I}-complexed phenanthroline included in the other macrocycle. The significant differences in the ^{1}H NMR spectra of **11** and **12** suggest that the Au^{III} porphyrin dimer has a conformation dramatically different from that of the Zn^{II} porphyrin dimer. The Au^{III} porphyrins being cationic, they are no longer able to stack with the Cu^{I}-complexed phenanthrolines, due to electrostatic repulsion. A likely conformation would be that represented in Scheme 1, in which the two Au^{III} porphyrins are roughly parallel. In conclusion, the threaded complexes **11** and **12** represent new members of the family of porphyrin dimers assembled with coordination bonds. The present study also shows that, by modifying the nature of the central metal in threaded porphyrin-containing systems, dramatic geometrical changes are induced.

We warmly thank J.-D. Sauer for the 400 MHz NMR spectra and R. Huber for the FAB mass spectra. We are grateful to P. Staub for the preparation of 3-bromophenanthroline. M. L. thanks the Ministère de l'Enseignement Supérieur et de la Recherche for a fellowship.

Notes and references

† All of the new compounds were characterized by ^{1}H NMR and mass spectrometry or elemental analysis, and the data are in agreement with the structures.

1 J. Deisenhofer and H. Michel, *Angew. Chem., Int. Ed. Engl.*, 1989, **28**, 829; R. Huber, *Angew. Chem., Int. Ed. Engl.*, 1989, **28**, 848; W. Kühlbrandt, *Nature*, 1995, **374**, 497; T. Pullerits and V. Sundström, *Acc. Chem. Res.*, 1996, **29**, 381.
2 J. Deisenhofer, O. Epp, K. Miki, R. Huber and H. Michel, *J. Mol. Biol.*, 1984, **180**, 385; J. P. Allen, G. Feher, T. O. Yeates, H. Komiya and D. C. Rees, *Proc. Natl. Acad. Sci. U.S.A.*, 1987, **84**, 5730.
3 A. M. Brun, S. J. Atherton, A. Harriman, V. Heitz and J.-P. Sauvage, *J. Am. Chem. Soc.*, 1992, **114**, 4632; A. Harriman, F. Odobel and J.-P. Sauvage, *J. Am. Chem. Soc.*, 1995, **117**, 9461; A. V. Chernook, A. M. Shulga, E. I. Zenkevich, U. Rempel and C. von Borczyskowski, *Ber. Bunsenges. Phys. Chem.*, 1996, **100**, 2065; C. A. Hunter and R. K. Hyde, *Angew. Chem., Int. Ed. Engl.*, 1996, **35**, 1936; R. V. Slone and J. T. Hupp, *Inorg. Chem.*, 1997, **36**, 5422.
4 M. R. Wasielewski, U. H. Smith, B. T. Cope and J. J. Katz, *J. Am. Chem. Soc.*, 1977, **99**, 4172; Y. Kobuke and H. Miyaji, *J. Am. Chem. Soc.*, 1994, **116**, 4111; R. T. Stibrany, J. Vasudevan, S. Knapp, J. A. Potenza, T. Emge and H. J. Schugar, *J. Am. Chem. Soc.*, 1996, **118**, 3980.
5 W. W. Parson and A. Warshel, *J. Am. Chem. Soc.*, 1987, **109**, 6153; J. R. Reimers and N. S. Hush, *Chem. Phys.*, 1995, **197**, 323.
6 D. B. Amabilino, C. O. Dietrich-Buchecker and J.-P. Sauvage, *J. Am. Chem. Soc.*, 1996, **118**, 3285.
7 Y. Saitoh, T. Koizumi, K. Osakada and T. Yamamoto, *Can. J. Chem.*, 1997, **75**, 1336.
8 M. Rehahn, A. D. Schlüter and G. Wegner, *Makromol. Chem.*, 1990, **191**, 1991.
9 P. Galda and M. Rehahn, *Synthesis*, 1996, 614.
10 J.-C. Chambron, C. Dietrich-Buchecker, J.-F. Nierengarten, J.-P. Sauvage, N. Solladié, A.-M. Albrecht-Gary and M. Meyer, *New J. Chem.*, 1995, **19**, 409.
11 M. Linke, J.-C. Chambron, V. Heitz, J.-P. Sauvage and V. Semetey, *Chem. Commun.*, 1998, 2469.
12. C. O. Dietrich-Buchecker and J.-P. Sauvage, *Tetrahedron*, 1990, **46**, 503; D. B. Amabilino and J.-P. Sauvage, *New J. Chem.*, 1998, **22**, 395.
13 C. O. Dietrich-Buchecker, P. A. Marnot, J.-P. Sauvage, J.-P. Kintzinger and P. Maltèse, *Nouv. J. Chim.*, 1984, **8**, 573.

Communication 9/07284E

ChemComm

Synthesis and structure of $Li_2Al_3(HO_3PMe)_2(O_3PMe)_4Cl{\cdot}7H_2O$, an ionic, layered lithium aluminium methylphosphonate

Gary B. Hix,*† David S. Wragg, Ivor Bull, Russell E. Morris and Paul A. Wright

Department of Chemistry, University of St. Andrews, St. Andrews, Fife, UK KY16 9ST. E-mail: gbh1@st-and.ac.uk

Received (in Cambridge, UK) 20th September 1999, Accepted 20th October 1999

A new layered mixed metal methylphosphonate, which contains interlayer chloride anions, has been prepared by contacting an LDH with molten methylphosphonic acid, and its structure solved using microcrystal X-ray diffraction at a synchrotron source.

It is only recently that aluminium phosphonates have been reported in the literature.[1–8] The breakthrough was made by Maeda *et al.*, who reported the synthesis of two crystalline microporous aluminium methylphosphonates, AlMePO-β[1,2,4,7] and AlMePO-α.[3] Subsequently, two layered methylphosphonates,[7,8] several phenyl phosphonates[6,9] and a carboxymethylphosphonate[10] have been reported.

A previous attempt at using layered double hydroxides (LDHs) in the preparation of mixed metal phosphonates by Vichi and Alves[11] succeeded in introducing both phenyl- and carboxyethylphosphonate groups. The crystal structures of the materials formed were not solved, however, and there was no evidence that the anion initially present in the LDH remained in the products after intercalation of the phosphonate groups.

The overwhelming majority of aluminium phosphonates are formed by hydrothermal syntheses,[1–7,9,10] with only a few examples prepared by other methods (*e.g.* refluxing[6,9] or contacting an aluminium source with a molten phosphonic acid[8]). The title compound was synthesised by grinding the layered double hydroxide, $LiAl_2(OH)_6Cl{\cdot}H_2O$[12] with methylphosphonic acid (such that the Al:P ratio in the reaction mixture was 1 : 3·5). The mixture was placed in a sealed glass tube and heated at 110 °C (the melting point of methylphosphonic acid is 104 °C) for 5 days. Products were recovered, washed with distilled water and dried in air at 60 °C.

Inspection of the recovered sample under a microscope revealed the presence of small crystals amongst a polycrystalline phase. One of these crystals was removed from the sample and used in a single crystal determination of the structure.

The crystals were too small (max. size 20 × 20 × 10 μm) for single crystal X-ray data collection using a standard laboratory four-circle diffractometer, so diffraction data were collected at low temperature (150 K) using a Bruker AXS SMART CCD area-detector diffractometer on the high-flux single-crystal diffraction station 9.8 at CCLRC Daresbury Laboratory Synchrotron Radiation Source, Cheshire, UK.

As a result of the single crystal structure determination,† the material was found to possess a stoichiometry of $Li_2Al_3(HO_3PMe)_2(O_3PMe)_4Cl{\cdot}7H_2O$. It is believed that this is the first example of a layered phosphonate, which is charged and contains interlayer anions. Comparison of a calculated powder XRD pattern with that obtained from the bulk product shows that the bulk contains a quantity of $Al(HO_3PMe)(O_3PMe){\cdot}H_2O$ as an impurity phase.[8] This necessarily means that an accurate analysis of the composition of the material by conventional methods (*e.g.* XRF, chemical analysis) is not possible.

Single crystal structure determination† revealed that the material is layered, with the lamellae stacking in the (100) direction (Fig. 1). All three of the Al atoms in the structure are octahedrally coordinated by oxygen. The six phosphonate groups possess tetrahedral coordination about the P atom. Two of the phosphonate groups, however, are monoanionic, $[HO_3PMe]^-$, whilst the other four are di-anionic, $[O_3PMe]^{2-}$. The layers are made up from corner sharing of the equatorial positions of the Al octahedra with the four dianionic phosphonate groups. The P–C bonds of these four methylphosphonate groups are oriented perpendicular to the plane of the layers (Fig. 2).

The axial positions of the octahedral Al coordination sphere are occupied by water molecules, or oxygens shared with the two remaining protonated methylphosphonate groups. One Al

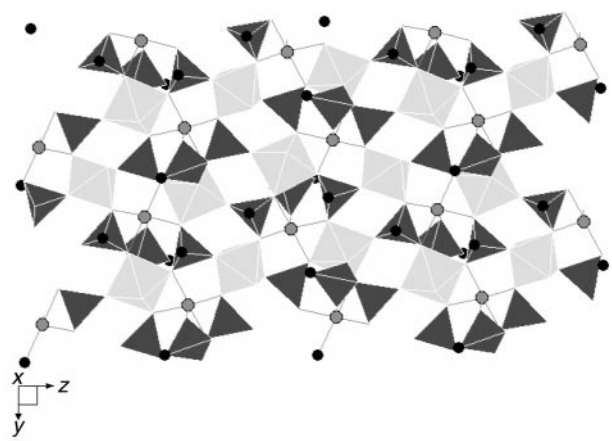

Fig. 1 A view of the layers along the (100) direction. The CPO_3 tetrahedra and the AlO_6 octahedra are shown as dark grey and light grey polyhedra respectively. Carbon atoms are shown as small black circles and lithium atoms as small grey circles. The interlayer water molecules and chlorine atoms are omitted for clarity.

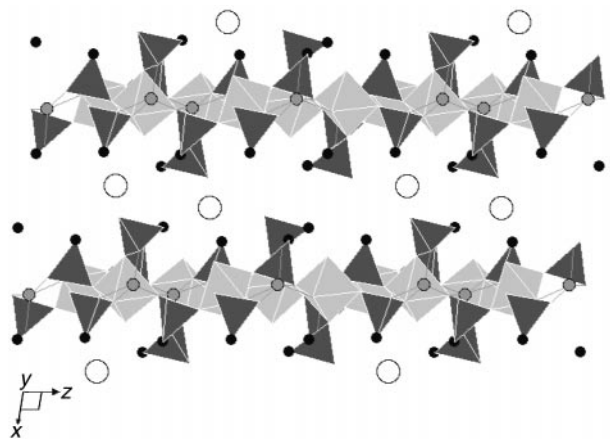

Fig. 2 Polyhedral view along the (010) direction showing the lamellae separated by interlayer chloride anions, and the different orientations adopted by the methylphosphonate groups. The CPO_3 tetrahedra and the AlO_6 octahedra are shown as dark grey and light grey polyhedra respectively. Carbon atoms are shown as small black circles, chlorine atoms as large white circles, and lithium atoms as small grey circles. The interlayer water molecules have been omitted for clarity.

† Present address: School of Chemistry, Hawthorn Building, De Montfort University, The Gateway, Leicester, UK LE1 9BH. E-mail: ghix@dmu.ac.uk

atom is coordinated by two water molecules in axial positions, whilst the other two have only one coordinated water molecule. The remaining axial positions of these two octahedra are occupied by an O from a methylphosphonate. The P–C bonds of those phosphonate groups attached to the axial positions of the Al atoms, are oriented parallel to the direction of the layers (Fig. 2). This has also been observed in another aluminium methylphosphonate, which we reported previously.[8]

The Li atoms are situated inside six-membered rings within the layers. The Li atom is coordinated by five oxygen atoms (Fig. 3), in a distorted square pyramidal environment. The axial oxygen atom is attached to the phosphonate group which is also attached to the axial position of one of the Al atoms. Bond valence calculations (using the method of Brown and Altermatt)[13] yielded values of 1.000 and 1.045 for the two Li ions, hence showing that the Li cations are in good coordination spheres.

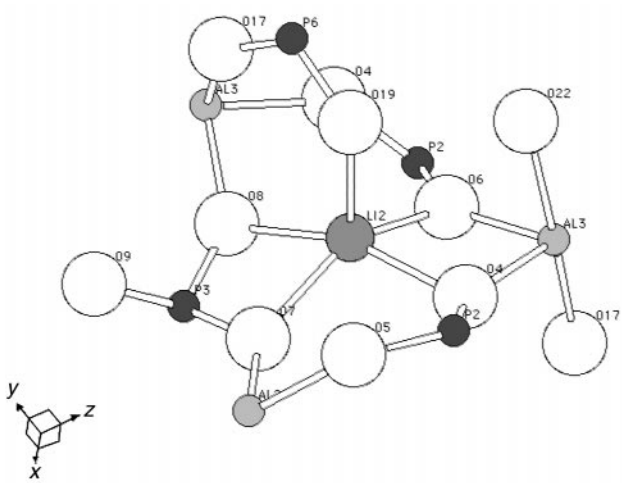

Fig. 3 Representation of the coordination about the Li ions, showing the phosphonate group bridging the Al and Li atoms.

The chloride anions are located in the interlayer region along with the three remaining water molecules. Hydrogen bonding between the interlayer species and the water molecules coordinated to the Al atoms hold the layers together.

TG experiments, carried out upon a sample of the crystals separated manually from the reaction product, show stepwise mass losses upon heating. The loss of water beginning around 90 °C and ending around 350 °C is complex, but peaks in the derivative of the weight loss curve indicating that the losses are centred at 162 and 296 °C. This can be rationalised by considering that the lower temperature event is the loss of the three water molecules in the interlayer region, and the higher temperature event is the loss of the two water molecules coordinated to each of the Al atoms. There is then a further exothermic weight loss at 550 °C of *ca*. 7.8 mass%, which is associated with decomposition of the methyl groups. The final mass loss is centred at 1100 °C and corresponds to removal of P_2O_5 from the material to leave a mixture of $AlPO_4$, Li_2O and LiCl (as shown by XRD).

The authors would like to thank Dr David Taylor and Dr Simon Teat of the SRS for their help in the X-ray data collection and the EPSRC for funding. R.E.M. would like to thank the Royal Society for provision of a Personal Research Fellowship.

Notes and references

† *Crystal data* for $Li_2Al_3(HO_3PMe)_2(O_3PMe)_4Cl{\cdot}7H_2O$: M_w = 822.40, monoclinic, space group $P2_1$ (no. 4), a = 10.1220(3), b = 9.4659(2), c = 15.7849(1) Å, β = 95.805(1)°, U = 1504.66(2) Å^3, T = 150 K, D_c = 1.82 g cm^{-3}, Z = 2, λ = 0.6894 Å, μ = 0.611 mm^{-1}, 15374 reflections measured, 8145 reflections unique, 7936 reflections observed (R_{int} = 0.0874) which were used in all calculations. The final $wR(F^2_{all\ data})$ was 0.138 and $R(F_{all\ data})$ was 0.055. The crystal structure was solved using direct methods and refined by full-matrix least squares on F^2. The positions of the Li atoms were refined isotropically. Corrections were made for synchrotron beam intensity decay as part of the standard interframe scaling procedure.

CCDC 182/1451. See http://www.rsc.org/suppdata/cc/1999/2421/ for crystallographic files in .cif format.

1 K. Maeda, J. Akimoto, Y. Kiyozumi and F. Mizukami, *Angew. Chem., Int. Ed. Engl.*, 1994, **33**, 2335.
2 K. Maeda, J. Akimoto, Y. Kiyozumi and F. Mizukami, *J. Chem. Soc., Chem. Commun.*, 1995, 1033.
3 K. Maeda, J. Akimoto, Y. Kiyozumi and F. Mizukami, *Angew. Chem., Int. Ed. Engl.*, 1995, **34**, 1199.
4 K. Maeda, J. Akimoto, Y. Kiyozumi and F. Mizukami, *Stud. Surf. Sci Catal.*, 1997, **105**, 197.
5 L.-J. Sawers, V. J. Carter, A. R. Armstrong, P. G. Bruce, P. A. Wright and B. E. Gore, *J. Chem. Soc., Dalton Trans.*, 1996, 3159.
6 L. Raki and C. Detellier, *Chem. Commun.*, 1996, 2475.
7 V. J. Carter, P. A. Wright, J. D. Gale, R. E. Morris, E. Sastre and J. Perez-Pariente, *J. Mater. Chem.*, 1997, **7**, 2287.
8 G. B. Hix, V. J. Carter, D. S. Wragg, R. E. Morris and P. A. Wright, *J. Mater. Chem.*, 1999, **9**, 179.
9 A. Cabeza, M. A. G. Aranda, S. Bruque, D. M. Poojary, A. Clearfield and J. Sanz, *Inorg. Chem.*, 1998, **37**, 4168.
10 G. B. Hix, D. S. Wragg, P. A. Wright and R. E. Morris, *J. Chem. Soc., Dalton Trans.*, 1998, 3359.
11 F. M. Vichi and O. L. Alves, *J. Mater. Chem.*, 1997, **7**, 1631.
12 A. V. Besserguenev, A. M. Fogg, R. J. Francis, S. J. Price, D. O'Hare, V. P. Isupov and B. P. Tolochko, *Chem. Mater.*, 1997, **9**, 241.
13 I. D. Brown and D. Altermatt, *Acta Crystallogr., Sect. B.*, 1985, **41**, 244.

Communication 9/07599B

Facile synthesis and conformation of 3′-*O*,4′-*C*-methyleneribonucleosides

Satoshi Obika, Ken-ichiro Morio, Yoshiyuki Hari and Takeshi Imanishi*

Graduate School of Pharmaceutical Sciences, Osaka University, 1-6 Yamadaoka, Suita, Osaka 565-0871, Japan. E-mail: imanishi@phs.osaka-u.ac.jp

Received (in Cambridge, UK) 7th September 1999, Accepted 26th October 1999

Bicyclic nucleoside analogues, 3′-*O*,4′-*C*-methyleneribonucleosides 1, including thymine, cytosine, adenine and guanine nucleobases, were conveniently synthesized from D-glucose, and the ribofuranose ring of 1 was found to exist predominantly in a *S*-conformation by means of ^{1}H NMR and X-ray analysis.

In recent studies aimed at developing an effective antisense molecule, numerous oligonucleotide analogues have been synthesized with various chemical modifications of the phosphodiester backbone, sugar moiety and/or nucleobase region.[1] In these attempts, the oligonucleotide analogues containing 'non-genetic' 2′,5′-phosphodiester linkages (2′,5′-linked oligonucleotides) were found to be favorable as antisense molecules because of their RNA selective hybridization ability and

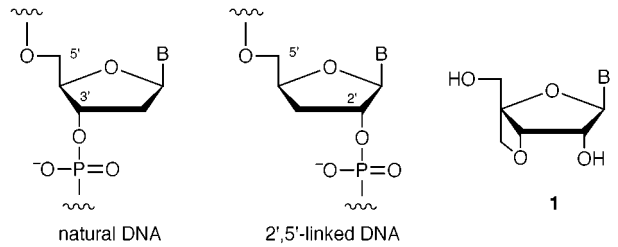

enzymatic stability.[2] Furthermore, 2-5A (2′,5′-linked oligoadenylate 5′-triphosphate) is well-known to have an important role in the interferon-mediated antiviral system in living cells,[3] and intensive studies on various 2-5A analogues have been reported.[4] However, there is only limited information available on the relationship between the sugar conformation in 2′,5′-linked oligonucleotides and their attractive properties, such as hybridization ability and antiviral activity.[5]

From the consideration that the restriction of sugar puckering in nucleosides to a proper conformation would serve as an advantageous strategy to develop a desired antisense (antigene) molecule,[6,7] we have recently accomplished the synthesis of conformationally restricted nucleoside analogues, 3′-*O*,4′-*C*-methylene-uridine and -cytidine **1** (B = U and C) by using uridine as a starting material,[8] and also demonstrated interesting properties of the 2′,5′-linked oligonucleotide analogues containing **1** (B = U and T), *e.g.* RNA selective hybridization abilities.[9]

Unfortunately, the synthetic route of **1** was not practical for purine analogues. We now report a novel and practical synthetic route to **1** bearing various nucleobases, exemplfied by synthesis of all four nucleoside analogues **1** (B = T, C^{Bz}, A^{Bz} and G^{iBu}), and also discuss their conformation.

After several attempts,† the synthesis of the target compounds **1** was performed by a coupling reaction of a 1-*O*-acetylribofuranose derivative with silylated nucleobases and a subsequent oxetane ring formation, as shown in Scheme 1. A stereoselective silylation of the diastereotopic hydroxy groups in 3-*O*-benzyl-4-hydroxymethyl-1,2-*O*-isopropylidene-α-D-ribofuranose **2**[10] gave the desired compound **3** (67%). The stereochemistry at C4 in **3** was confirmed by means of NOE measurements. A *p*-tolylsulfonylation of **3** afforded the tosylate **4** (97%), which was converted to diacetate **5** (86%) by treatment with AcOH and Ac_2O in the presence of a catalytic amount of H_2SO_4. Debenzylation and subsequant acetylation of the 3-hydroxy group in **5** gave the triacetate **6** (91%). The reaction of **6** with *O*,*O*′-bis(trimethylsilyl)thymine (T·2TMS) under Vorbrüggen's conditions[11] afforded only the β-anomer of

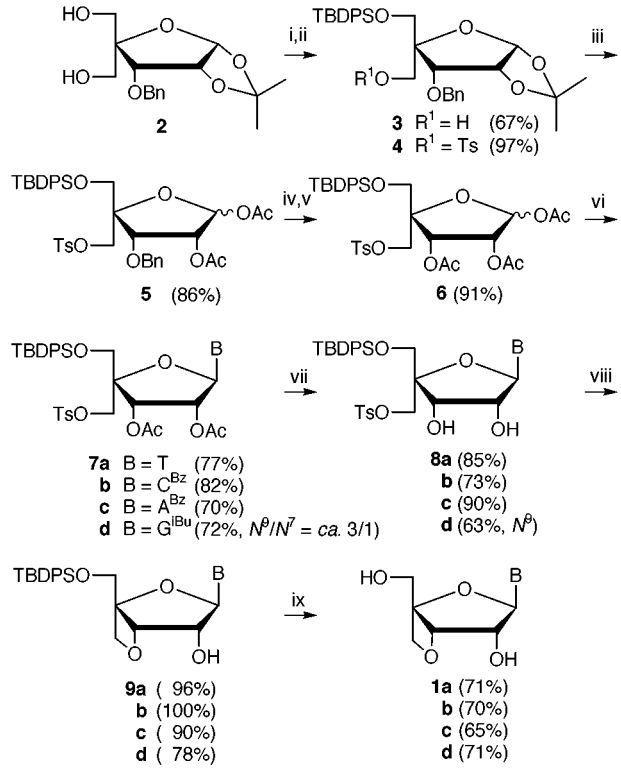

Scheme 1 *Reagents and conditions*: i, TBDPSCl, Et_3N, CH_2Cl_2, room temp., 14 h; ii, TsCl, Et_3N, DMAP, CH_2Cl_2, room temp., 16 h; iii, AcOH, Ac_2O, conc. H_2SO_4, room temp., 30 min; iv, 10% Pd-C/H_2, Et-OAc–$CHCl_3$, room temp., 17 h; v, Ac_2O, Py, room temp., 20 h; vi, sililated base, TMSOTf, $CH_2CH_2Cl_2$, reflux, 8–18 h; vii, K_2CO_3, room temp., 15 min; viii, NaHMDS, THF, room temp., 1h; ix, TBAF, THF, room temp., 15 min.

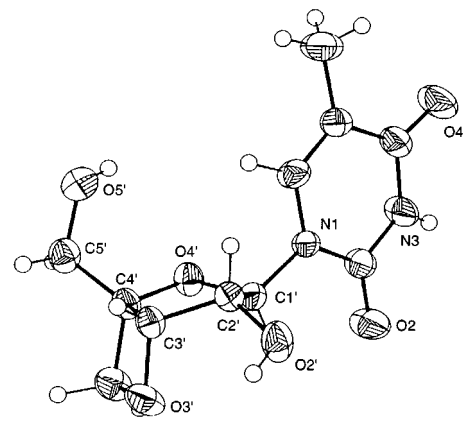

Fig. 1 ORTEP drawing of **1a**.

thymidine derivative **7a** (77%). The triacetate **6** was also coupled with silylated N^4-benzoylcytosine (C^{Bz}·2TMS), N^6-benzoyladenine (A^{Bz}·2TMS) and N^2-isobutyrylguanine (G^{iBu}·3TMS) to give the corresponding β-nucleoside derivatives **7b** (82%), **7c** (70%) and **7d** (72%),‡ respectively. Methanolysis of **7** gave diols **8** (63–90%) and then oxetane ring formation from **8** was accomplished on treatment with sodium hexamethyldisilazide in THF at room temperature, yielding only the corresponding 3′-*O*,4′-*C*-methyleneribonucleoside derivatives **9** (78–100%). The desired products **1** were obtained (65–71%) by removal of a TBDPS group in **9**. We have, thus, achieved a facile synthesis of 3′-*O*,4′-*C*-methyleneribonucleosides **1** in good yield.§

The conformational analysis of the obtained 3′-*O*,4′-*C*-methyleneribonucleosides **1** was carried out by means of ^{1}H NMR and X-ray crystallographic data. Namely, all of the bicyclic nucleoside analogues **1** show a relatively large $J_{1'2'}$ value (7.3–7.6 Hz in CD_3OD), which means that these nucleoside analogues have predominantly the *S*-conformation (*S*% = 91–96%),¶ regardless of the type of the nucleobase. Furthermore, an X-ray crystallographic analysis of **1a** shows that the sugar pucker pseudorotation phase angle (*P*) is 136.2° and the maximum out-of-plane pucker (ν_{max}) is 32.3°, characteristic of the C1′-*exo*-C2′-*endo* form (*S*-conformation) of sugar puckering.‖

It is noteworthy and very interesting that the expressed *S*-preference of the nucleoside analogues **1** is vastly different from conformational analysis of other nucleosides possessing a 2′-OH group, *e.g.* uridine (*S*% = 52%),[8] cytidine (*S*% = 26%),[8] 3′-deoxyuridine (*S*% = 3%)[8,12] and 3′-deoxycytidine (*S*% = 0%).[8,13]

Further studies on these bicyclic nucleosides are now in progress.

A part of this work was supported by a Grant-in-Aid for Scientific Research (B), No. 09557201, from the Japan Society for the Promotion of Science. We are also grateful to the Takeda Science Foundation for financial support.

Notes and references

† As an altanative route for the synthesis of **1**, we briefly tried a coupling reaction of the oxetane derivative **10** with silylated thymine, resulting in exclusive C–O bond fission of the oxetane ring to afford only **11**.

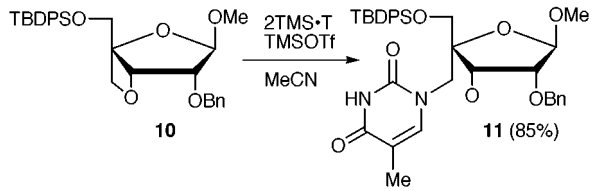

‡ Guanosine derivative **7d** was obtained as a mixture of N^9 and N^7 regioisomers (72%, N^9/N^7 = *ca.* 1/3) which was directly converted to **8d** without separation. The N^9 and N^7 isomers of **8d** were obtained in 63 and 18% yield, respectively, after silica gel chromatography. The stereochemistry of each isomer **8d** was determined by comparison of their ^{1}H and ^{13}C NMR data.

§ *Selected data* for **1a**: mp 119–120 °C (AcOEt); $[\alpha]_D^{25}$ −63.1 (*c* 0.44, MeOH); ν_{max}(KBr)/cm^{-1} 4016, 3451, 1723; $\delta_H(CD_3OD)$ 1.89 (3H, s), 3.75, 3.83 (2H, AB, *J* 12), 4.14 (1H, d, *J* 8), 4.51, 4.83 (2H, AB, *J* 8), 5.05 (1H, d, *J* 5), 6.42 (1H, d, *J* 8), 7.52 (1H, s); *m/z* (FAB) 277 (M+Li$^+$) (calc. for $C_{11}H_{14}N_2O_6$·H_2O: C, 45.83; H, 5.59; N, 9.72. *Found*: C, 45.81; H, 5.51; N, 9.71%).

¶ The percentage of *S*-conformation (*S*%) is calculated from the equation: *S*% = 100($J_{1'2'}$ − 1)/6.9. See ref. 8 and 14.

‖ *Crystal data* for **1a**: $C_{11}H_{14}N_2O_6$·H_2O, *M* = 288.26, colourless plate, 0.30 × 0.20 × 0.10 mm, orthorhombic, $P2_12_12_1$, *a* = 8.6242(10), *b* = 20.6008(8), *c* = 7.2767(11) Å, *V* = 1292.8(3) Å^3, *T* = 283 K, *Z* = 4, μ (Cu–Kα) = 1.54 mm^{-1}, 1177 reflections measured, 1155 independent reflections, 1037 reflections observed, *R* = 0.0397, R_w = 0.0984. CCDC 182/1463. See http://www.rsc.org/suppdata/cc/1999/2423/ for crystallographic data in .cif format.

1 E. Uhlmann and A. Peyman, *Chem. Rev*., 1990, **90**, 543; S. L. Beaucage and R. P. Iyer, *Tetrahedron*, 1993, **49**, 6123; J. F. Milligan, M. D. Matteucci and J. C. Martin, *J. Med. Chem*., 1993, **36,** 1923; N. T. Thuong and C. Hélène, *Angew. Chem., Int. Ed. Engl.*, 1993, **32**, 666.
2 H. Hashimoto and C. Switzer, *J. Am. Chem. Soc.*, 1992, **114**, 6255; J. P. Dougherty, C. J. Rizzo and R. Breslow, *J. Am. Chem. Soc*., 1992, **114**, 6254; P. A. Giannaris and M. J. Damha, *Nucleic Acids Res.*, 1993, **21**, 4742; R. Alul and G. D. Hoke, *Antisense Res. Dev.*, 1995, **5**, 3; T. P. Prakash, K.-E. Jung and C. Switzer, *Chem. Commun.*, 1996, 1793; T. L. Sheppard and R. Breslow, *J. Am. Chem. Soc*., 1996, **118**, 9810; E. R. Kandimalla, A. Manning, Q. Zhao, D. R. Shaw, R. A. Byrn, V. Sasisekharan and S. Agrawal, *Nucleic Acids Res.*, 1997, **25**, 370.
3 H. C. Schröder, R. J. Suhadolnik, W. Pfleiderer, R. Charubala and W. E. G. Müller, *Int. J. Biochem.*, 1992, **24**, 55.
4 M. Wasner, R. J. Suhadolnik, S. E. Horvath, M. E. Adelson, N. Kon, M.-X. Guan, E. E. Henderson and W. Pfleiderer, *Helv. Chim. Acta*, 1997, **80**, 1061; E. I. Kvasyuk, T. I. Kulak, O. V. Tkachenko, S. L. Sentyureva, I. A. Mikhailopulo, R. J. Suhadolnik, E. E. Henderson, S. E. Horvath, M.-X. Guan and W. Pfleiderer, *Helv. Chim. Acta.*, 1998, **81**, 1278.
5 V. Lalitha and N. Yathindra, *Curr. Sci.*, 1995, **68**, 68; H. Robinson, K.-E. Jung, C. Switzer and A. H.-J. Wang, *J. Am. Chem. Soc*., 1995, **117**, 837; J. Doornbos, J. A. J den Hartog, J. H. van Boom and C. Altona, *Eur. J. Biochem.*, 1981, **116**, 403; J. Doornbos, R. Charubala, W. Pfleiderer and C. Altona, *Nucleic Acids Res.*, 1983, **11**, 4569.
6 P. Herdewijn, *Liebigs Ann. Chem.*, 1996, 1337; E. T. Kool, *Chem. Rev.*, 1997, **97**, 1473.
7 S. Obika, D. Nanbu, Y. Hari, K. Morio, Y. In, T. Ishida and T.Imanishi, *Tetrahedron Lett.*, 1997, **38,** 8735; S. Obika, D. Nanbu, Y. Hari, J. Andoh, K. Morio, T. Doi and T. Imanishi, *Tetrahedron Lett.*, 1998, **39**, 5401; S. K. Singh, P. Nielsen, A. A. Koshkin and J. Wengel, *Chem. Commun.*, 1998, 455; A. A. Koshkin, S. K. Singh, P. Nielsen, V. K. Rajwanshi, R. Kumar, M. Meldgaard, C. E. Olsen and J. Wengel, *Tetrahedron*, 1998, **54**, 3607; S. K. Singh and J. Wengel, *Chem. Commun.*, 1998, 1247; A. A. Koshkin, P. Nielsen, M. Meldgaard, V. K. Rajwanshi, S. K. Singh and J. Wengel, *J. Am. Chem. Soc.*, 1998, **120**, 13 252.
8 S. Obika, K. Morio, D. Nanbu and T. Imanishi, *Chem. Commun.*, 1997, 1643.
9 S. Obika, K. Morio, Y. Hari and T. Imanishi, *Bioorg. Med. Chem. Lett.*, 1999, **9**, 515.
10 R. D. Youssefyeh, J. P. H. Verheyden and J. G. Moffatt, *J. Org. Chem.*, 1979, **44**, 1301.
11 H. Vorbrüggen, K. Krolikiewiczz and B. Bennua, *Chem. Ber.*, 1981, **114**, 1234; H. Vorbrüggen and G. Höfle, *Chem. Ber.*, 1981, **114**, 1256.
12 Measured in $(CD_3)_2SO$: T.-S. Lin, J.-H. Yang, M.-C. Liu, Z.-Y. Shen, Y.-C. Cheng, W. H. Prusoff, G. I. Birnbaum, J. Giziewicz, I. Ghazzouli, V. Brankovan, J.-S. Feng and G.-D. Hsiung, *J. Med. Chem.*, 1991, **34**, 693.
13 T. L. Sheppard, A. T. Rosenblatt and R. Breslow, *J. Org. Chem*., 1994, **59**, 7243.
14 C. Altona and M. Sundaralingam, *J. Am. Chem. Soc.*, 1973, **95**, 2333; C. Altona, *Recl. Trav. Chim. Pays-Bas*, 1982, **101**, 413; F. A. A. M. de Leeuw and C. Altona, *J. Chem. Soc., Perkin Trans. 2*, 1982, 375.

Communication 9/07218G

The change in the X-ray dipole moment as a quantitative measure of the polarizing effect of the molecular environment: application to a complex of *p*-amino-*p′*-nitrobiphenyl with triphenylphosphine oxide

Yuegang Zhang and Philip Coppens*

Department of Chemistry, State University of New York at Buffalo, Buffalo, New York, 14260-3000, USA. E-mail: coppens@acsu.buffalo.edu

Received (in Columbia, MO, USA) 14th September 1999, Accepted 13th October 1999

The X-ray determined dipole moment has been used to assess the strength of the electrostatic interactions in a new complex of *p*-amino-*p'*-nitrobiphenyl, which is a suitable candidate for photo-crystallographic studies of transient species.

Prior to photo-crystallographic studies of light-induced excited molecular states, suitable candidates for such time-resolved studies must be identified.[1,2] A relatively long-lived triplet excited state of *p*-amino-*p′*-nitrobiphenyl (PANB) has been reported to exist at room temperature in solution.[3] PANB is a typical donor–acceptor molecule; upon excitation an intramolecular charge transfer occurs from the amine donor to the nitro acceptor group.[4] Correspondingly, fluorescence and time-resolved microwave measurements indicate a large increase in dipole moment (by more than 20 D) when the molecule is excited.[5] In order to increase the conversion percentage of excited state molecules upon irradiation, and/or reduce the number of photons to be absorbed by the crystal, it is highly desirable to dilute the photoactive species with photo-inert spacer molecules. In a previous study, the β-cyclodextrin complex of PANB was found to show disorder in the guest molecules, and thus to be less suitable for photo-crystallographic studies.[3]

We report here on the 90 K structure and charge density of a fully-ordered mixed crystal of PANB. We use the molecular dipole moment as determined from the X-ray diffraction data as a measure of the strength of the electrostatic forces acting on the host molecule. This analysis is based on the extensive evidence indicating a pronounced enhancement of the electrostatic moments of polar molecules in crystals.[6–8] The enhancement is directly dependent on the molecular environment, and it thus varies with crystal composition and molecular packing.

Triphenylphosphine oxide (TPPO) is a strong hydrogen acceptor. It has been shown to form high quality crystals with molecules containing donor hydrogen atoms, like the amino hydrogens of PANB.[9] As the TPPO molecule does not absorb above 300 nm,[10] its absorption does not interfere with the charge-transfer absorption of PANB, which peaks at 400 nm,[11] an essential condition for a photo-inert 'spacer' molecule. X-Ray data on a specimen grown by slow evaporation[12] were collected on a Bruker SMART 1K CCD diffractometer at 90(1) K.[13]

Hydrogen bonding between the NH_2 groups and the oxygen atoms of TPPO (Fig. 1) leads to a synthon consisting of four molecules (two each of TPPO and PANB), which is the basic unit in the crystal.[14] The square arrangement of hydrogen bonded atoms is similar to that in TPPO tetrachloropyrocatechol monohydrate, in which water molecules of crystallization are the hydrogen donors.[15] A comparable arrangement is found in bis(triphenylphosphine oxide) tris(toluene-*p*-sulfonamide) where the two P=O groups are bridged by three sets of hydrogen bonds, donated by NH_2 groups.[16] Unlike in neat PANB, the nitro groups in PANB/TPPO are involved only in weak O···H–C interactions.[17] The crystals are fully ordered and do not contain solvent molecules.

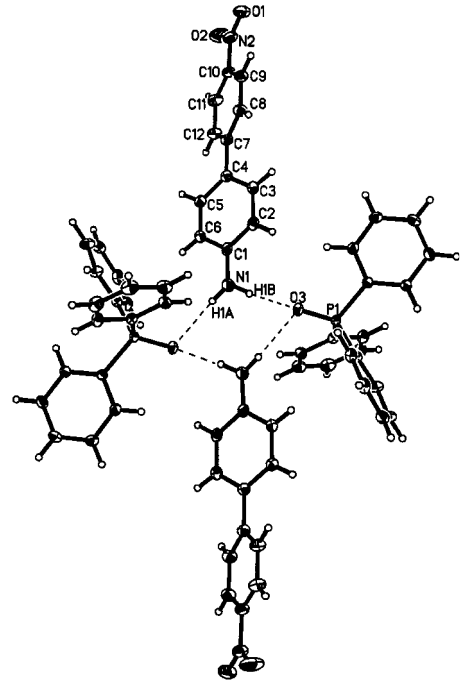

Fig. 1 Illustration of the basic packing motif in the PANB/TPPO crystal.

In the neat crystal the biphenyl group adopts a close to planar conformation (see Fig. 2),[18,19] though calculations[20] indicate the isolated molecule to be twisted by 43.3°, similar to what is found for gas-phase biphenyl.[21,22] In the current structure the inter-ring twist angle is 30.27(3)° (Fig. 2), compared with values of 40.6(2) and 42.0(1)° at 20 K for the two independent molecules in the less constraining environment of β-cyclodextrin. The concentration of PANB in PANB/TPPO is 2.64 M compared with 6.56 M in the neat crystal.

In general the dipole moment of a molecule in a polar crystal is enhanced relative to that of the isolated molecule in the gas phase. The increase in dipole moment is a quantitative measure of the polarizing field exerted on the molecules by the crystal matrix. While the isolated molecule value is calculated as 9.12 D for the configuration of the PANB molecule as observed in the neat crystal, and as 8.17 D for the twisted optimized geometry,[20] the value derived by topological analysis of the theoretical density for the periodic crystal is 23.0 D.[8] This

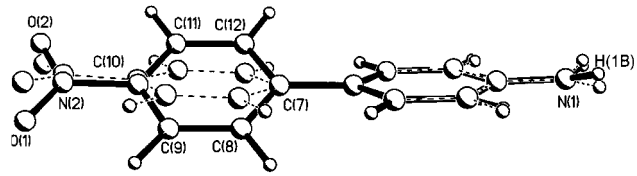

Fig. 2 The molecular structure of PANB in the TPPO complex (twisted), compared with the almost planar conformation in the neat crystal.

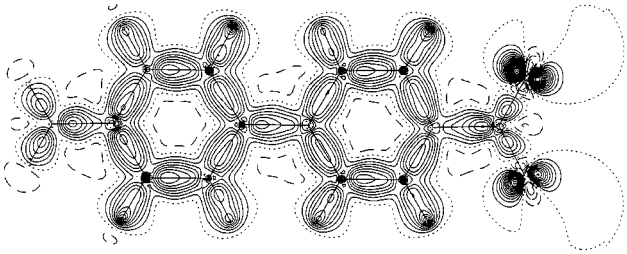

Fig. 3 Deformation density map of PANB in the PANB/TPPO crystal as calculated from the aspherical atom multipole refinement results. For illustration purposes, the two phenyl rings of the non-planar molecule have been rotated into the plane of the paper. Contours at 0.1 eÅ^{-3}. Positive contours: full lines; zero contour: dotted; negative contours: broken.

compares with an experimental X-ray result of *ca*. 40 D.[8,19] An aspherical atom refinement[23,24] of the current data shows the molecular dipole moment in the mixed crystal to be 16.8(1.6) D, much in excess of the isolated molecule values, but significantly below that in neat PANB (the static deformation density map in the least square planes of the two phenyl rings is shown in Fig. 3). The neat crystal contains sheets of parallel molecules, leading to parallel and anti-parallel (between sheets) alignment of the dipole moments such as to maximize electrostatic interactions. By comparison, the electrostatic interactions are significantly reduced in PANB/TPPO, in agreement with the relatively weak interactions of the nitro group in the complex. Since the molecular dipole moment can now be routinely obtained from good quality X-ray data, it provides a readily accessible measure of the electrostatic interactions in a crystal.

In summary, the PANB/TPPO mixed crystal is a candidate for excited state diffraction studies, given the absence of disorder and undesirable spectral overlap, and the reduced concentration of the active species. Both the experimental dipole moment and the inter-ring twist angle are intermediate between those of the isolated molecule and the neat PANB crystal. The X-ray dipole moment can be used to characterize related solids, and provides insight into factors relevant to crystal engineering.

Support of this work by the National Science Foundation (CHE9615586) and the Petroleum Research Fund of the American Chemical Society (PRF32638AC3) is gratefully acknowledged. All theoretical calculations were carried out on the SGI Origin-2000 supercomputer at the Center for Computational Research at SUNY/Buffalo, which is supported by a grant (DBI9871132) from the National Science Foundation.

Notes and references

1 P. Coppens, D.V. Fomitchev, M. D. Carducci and K. Culp, *J. Chem. Soc., Dalton Trans.*, 1998, 865.
2 Y. Zhang, G. Wu, B. R. Wenner, F. V. Bright and P. Coppens, *Cryst. Eng.*, 1999, **2**, 1.
3 T. J. Brett, S. Liu, P. Coppens and J. J. Stezowski, *Chem. Commun.*, 1999, 551.
4 P. Piotrowiak, R. Kobetic, T. R. Schatz and G. Strati, *J. Phys. Chem.*, 1995, **99**, 2250.
5 J. Czekalla, W. Liptay and K. O. Meyer, *Ber. Bunsen-Ges. Phys. Chem.*, 1963, **67**, 465; M. N. Paddon-Row, A. M. Oliver, J. W. Warman, K. J. Smit, M. P. de Haas, H. Oevering and J. W. Verhoeven, *J. Phys. Chem.*, 1988, **92**, 6958.
6 C. Gatti, V. R. Saunders and C. Roetti, *J. Chem. Phys.*, 1994, **101**, 10 686.
7 S. T. Howard, M. B. Hursthouse, C. W. Lehmann, P. R. Mallinson and C. S. Frampton, *J. Chem. Phys.*, 1992, **97**, 2962.
8 Yu. A. Abramov, A. V. Volkov and P. Coppens, *Chem. Phys. Lett.*, 1999, **311**, 81.
9 M. C. Etter and P. W. Baures, *J. Am. Chem. Soc.*, 1988, **110**, 639.
10 SADTLER standard UV spectrum, 1962, NO. 4852UV.
11 K. A. Al-Hassan and M. A. El-Bayoumi, *Chem. Phys. Lett.*, 1987, **138**, 594.
12 Crystals of PANB/TPPO were grown by slow evaporation (four days) from an acetone solution of PANB (TCI America) and excess TPPO (Aldrich). Large transparent specimens of up to 0.5 × 1.0 × 1.0 cm^3 were obtained, with an orange red color less intense than that of pure PANB. ^{1}H NMR indicated a 1:1 ratio of the two components.
13 *Crystal data* for $(C_{18}H_{15}OP)(C_{12}H_{10}N_2O_2)$: M = 492.49, triclinic, a = 9.2719(8), b = 10.4330(10), c = 14.4569(11) Å, α = 106.122(4), β = 107.714(5), γ = 94.691(4)°, U = 1258.47(19) Å^3, T = 90(1) K, space group $P\bar{1}$ (no. 2), Z = 2, D_c = 1.300 g cm^{-3}, crystal size 0.13 × 0.25 × 0.25 mm^3, μ(Mo-Kα) = 0.144 mm^{-1}, 89125 reflections, 13140 unique reflections (R_{int} = 0.0421), $2\theta_{max}$ = 105.54°, GOF = 0.865, $R(F)$ = 0.033, for 9163 reflections with $F_o > 4\,\sigma(F_o)$, $Rw(F^2)$ = 0.084 for all reflections, 426 parameters. Data were collected by the oscillation method on a Bruker SMART 1K CCD diffractometer. Reflections were integrated by the SAINT program and scaled by SORTAV. The structure was solved by direct methods with XS in SHELXTL (SHELXTL NT Version 5.10, G. M. Sheldrick, Program for the Refinement of Crystal Structures, University of Göttingen, Germany, 1997), and refined with XL. All the non-hydrogen atoms were refined anisotropically. Positions of hydrogen atoms were located from the difference Fourier map and refined isotropically, each with its own isotropic temperature parameters. No constraint was applied in the refinement. CCDC 182/1464. See http://www.rsc.org.suppdata/cc/1999/2425/ for crystallographic data in .cif format.
14 N1···O3^{I} = 3.055(1) Å, ∠N1–H1A···O3^{I} = 146.6(1.2)°, (I = 1+x, y, 1 + z); N1···O3^{II} = 2.931(1) Å, ∠N1–H1B···O3^{II} = 176.0(1.3)°, (II = 2 − x, −y, 1 − z).
15 M. Y. Antipin, A. I. Akhmedov, Y. T. Struchkov, E. I. Matrosov and M. I. Kabachnik, *Zh. Strukt. Khim*., 1983, **24**, 86.
16 G. Ferguson and C. Glidewell, *J. Chem. Soc., Perkins Trans. 2*, 1988, 2129.
17 C15···O2^{III} = 3.447(1) Å, ∠C15–H15···O2^{III} = 167.4(1.0)°, (III = 1 + x, y, z).
18 E. M. Graham, V. M. Miskowski, J. W. Perry, D. R. Coulter, A. E. Stiegman, W. P. Schaefer and R. E. Marsh, *J. Am. Chem. Soc.*, 1989, **111**, 8771.
19 A. V. Volkov, G. Wu and P. Coppens, *J. Synchrotron Radiat.*, 1999, **6**, 1007.
20 HF, 6311G** basis set, Jaguar 3.5, Schrödinger, Inc. Portland, OR, 1998.
21 O. Bastiansen, *Acta Chem. Scand.*, 1949, **3**, 408.
22 C. P. Brock and R. P. Minton, *J. Am. Chem. Soc*.. 1989, **111**, 4586.
23 T. Koritsanszky, S. Howard, T. Richter, Z. Su, P. R. Mallinson, N. K. Hansen, *XD-A Computer Program Package for Multipole Refinement and Analysis of Electron Densities from Diffraction Data*, Free University Berlin, Germany, 1995.
24 X–H distances taken from *International Tables for Crystallography, Vol. C*, were used for all C–H and N–H bonds. The κ′ restricted multipole model (KRMM)[8] was applied, $R(F)$ = 0.019, $Rw(F^2)$ = 0.041.

Communication 9/07473B

Bispyrene based chiroptical molecular redox switch

Christian Westermeier, Hans-Christoph Gallmeier, Markus Komma and Jörg Daub*

Institut für Organische Chemie der Universität Regensburg, Universitätsstraße 31, D-93040 Regensburg, Germany. E-mail: joerg.daub@chemie.uni-regensburg.de

Received (in Cambridge, UK) 14th September 1999, Accepted 28th October 1999

The chiral *trans*-cyclohexanediol bispyrene esters (1*R*,2*R*)-1a and (1*S*,2*S*)-1b are reversibly reduced to the corresponding bisradical anions $1a^{2-}$ and $1b^{2-}$ which show strong absorption bands at 510 nm exhibiting exciton-split circular dichroism (CD) with opposite signs, whereas the radical anions of the bisamides 2a and 2b failed to show split CD signals.

Molecular switches are intensively studied due to their potential applications in molecular devices and optical data storage systems.[1] In this context, much attention has been given to photochemically and electrochemically induced switching processes (photochromic and electrochromic compounds) which lead to significant optical spectra changes. Pyrene derivatives are one of the well-exploited probes for the design of fluorescent molecular switches due to their monomer–excimer emission characteristics.[2] Surprisingly, pyrene based chiroptical molecular redox switches have not received any attention. However, the use of chiroptical molecular switches based on photochromic chiral ethenes has been demonstrated recently by Feringa and co-workers.[3] Circular dichroism spectroelectrochemistry (CD spectroelectrochemistry) is a recent technique that we have introduced to study molecular switches.[4,5] Here the characteristic optical absorption and reversible redox behaviour of pyrene are integrated with the optical activity of *trans*-cyclohexanediol for the design of novel redox active chiroptical molecular switches. The redox switching between the neutral and radical ion states is monitored by both UV–VIS–NIR and circular dichroism (CD) spectroelectrochemical methods.

The requirements for the design of an efficient chiroptical molecular redoxswitch are: (i) stability of the optical active forms, (ii) chemical reversibility of the redox processes, (iii) high sensitivity of the chiroptical response and (iv) potential application in multimode switching. During the process of screening several systems we found that pyrene functionalized *trans*-1,2-substituted cyclohexanes appear to be excellent candidates for chiroptical redox switching due to intramolecular exciton coupling which leads to split CD.[6] Bis-esters **1a**,**b** and bis-amides **2a**,**b** were synthesized in the optically active forms (1*R*,2*R*)-**1a** [mp 208 °C, $[\alpha]_D^{20}$ 115.0, (*c* 0.42 in CH_2Cl_2)] and (1*S*,2*S*)-**1b** [mp 208 °C, $[\alpha]_D^{20}$ −111.6 (*c* 0.40 in CH_2Cl_2)], and (1*R*,2*R*)-**2a** [mp 379–380 °C, $[\alpha]_D^{20}$ 114.3 (*c* 0.01 in THF)] and (1*S*,2*S*)-**2b** (mp 379–380 °C, $[\alpha]_D^{20}$ −111.4 (*c* 0.012 in THF)], starting from the corresponding optically active *trans*-cyclohexane-1,2-diols and *trans*-1,2-diaminocylohexanes respectively. Compounds **1a** and **1b** show reversible reduction (Fig. 1) to the bis-radical anions in a 'one-wave-two-electron transfer' cyclic voltammogram [$E_{1/2}$(reduction) = −2120 mV (*vs.* Fc^+/Fc)] leading to the appearance of an intense absorption at 510 nm [Fig. 2(*a*)]. Formation of radical anions of both pyrene units was established by comparison with the cyclic voltammetric data of analogous model compounds.[7] Obviously, the two redox active pyrene groups in **1a** and **1b** are weakly coupled in the ground state and can be classified as Robin/Day class I systems. The stationary absorption and CD spectra of the *R*,*R* isomer **1a** are illustrated in Fig. 2. The CD spectra of **1a** and **1b** show the expected mirror-image features. CD spectroelectrochemistry of **1a** on reduction leads to a split CD with a positive sign at 504 nm [Fig. 1(*c*)]. The band formation is reversible and the process can be repeated continously. Compound (*S*,*S*)-**1b**

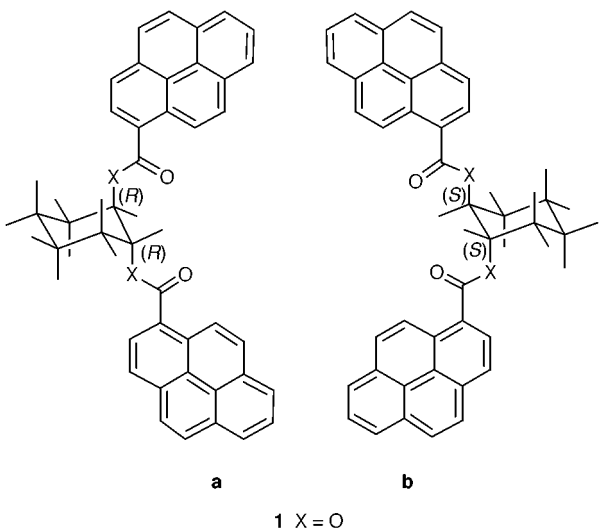

1 X = O
2 X = NH

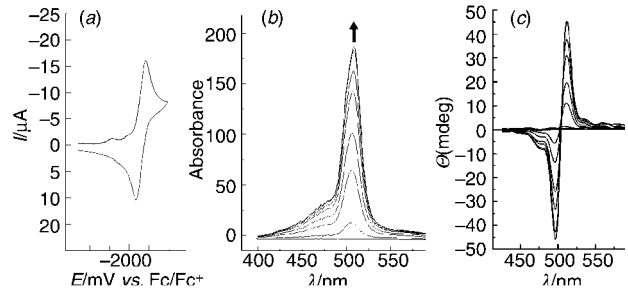

Fig. 1 (*a*) Cyclic voltammogramm of **1a** ⇄ $\mathbf{1a^{2-}}$, and (*b*) UV–VIS–NIR spectroelectrochemistry and (*c*) CD spectroelectrochemistry of **1a** ⇄ $\mathbf{1a^{2-}}$ obtained by scanning over the reduction wave at $E_{1/2}$ = −2120 mV (*vs.* Fc^+/Fc in THF, ν = 250 mV s^{-1}).

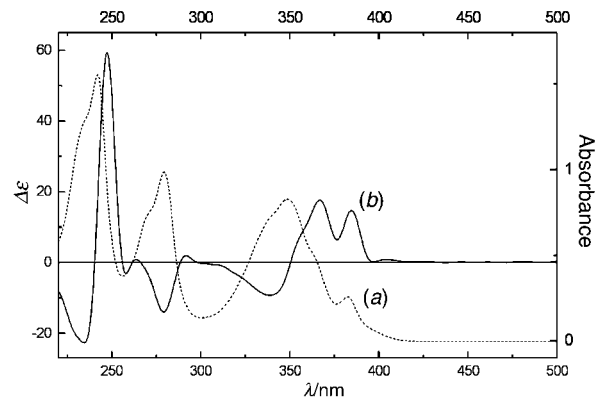

Fig. 2 (*a*) UV–VIS absorption and (*b*) CD spectra of (*R*,*R*)-**1a** (c = 10^{-5} mol dm^{-3} in THF).

behaves identically with a negative sign for the couplet at 504 nm.

It is also interesting to briefly refer on the fluorescence spectra of **1a** and **1b** since these compounds may be of interest for fluorescence-detected circular dichroism[6c] and circularly polarized luminescence. Bis-esters **1a** and **1b** show the typical pyrene emissions at 387, 409 and 432 nm and in addition an excimer emission at 517 nm ($c = 10^{-6}$ mol l^{-1}). The excimer emission depends strongly on concentration, which is characteristic of the intermolecular association of the pyrene moieties. At 10^{-4} mol l^{-1} a three-fold increase in the intensity of the excimer emission is observed.

We also investigated the redox switching behaviour of bis-amids (1*R*,2*R*)-**2a** and (1*S*,2*S*)-**2b**. Both bis-amides **2a** and **2b** are reversibly reduced to their radical anions ($E_{1/2} = -2420$ mV *vs*. Fc/Fc^+) leading to an absorption for the pyrene radical anion at 510 nm. The chiroptical behaviour of **1** and **2** is however different. Even though the neutral compounds **2a** and **2b** showed the expected mirror-image CD spectra, reduction to the radical anions does not lead to a split-CD signal around 500 nm. On reoxidation, the original CD spectrum is restored. Even though at this point the exact reason for this observation is not clear, we assume that proton transfer from the amide linkage at the radical anion stage or possible hydrogen bonding inhibits the appearance of a CD couplet.

In summary, we found that C_2-symmetric pyrene conjugated cyclohexanes **1** are well-suited as reversible chiroptical redox switches, which behave differently from bisamides **2a** and **2b**. The circular dichroism spectroelectrochemical method has been successfully employed for the monitoring of the switching behaviour. Work to apply compounds **1a** and **1b** as probes for molecular sensing is in progress. Also investigations to correlate the sign of the Cotton effects with the molecular structure of the pyrene-linked cyclohexanes are under way.

C. W. and M. K. are grateful to the Stiftung Stipendien-Fonds des Verbands der Chemischen Industrie, Frankfurt for doctoral fellowships. The authors thank Dr A. Ajayaghosh for stimulating comments, Mrs M. Lutz for synthetic work and Professor O. S. Wolfbeis for making the spectropolarimeter available.

Notes and references

1 J.-M. Lehn, *Supramolecular Chemistry*, VCH, Weinheim, 1995; *Molecular Electronics*, ed. J. Jortner and M. Ratner, Blackwell, Oxford, 1997; A. P. de Silva, H. Q. N. Gunaratne, T. Gunnlaugsson, A. J. M. Huxley, C. P. McCoy, J. T. Rademacher and T. E. Rice, *Chem. Rev.*, 1997, **97**, 1515.

2 T. Jin, K. Ichikawa and T. Koyama, *J. Chem. Soc., Chem. Commun.*, 1992, 499; T. Saika, T. Iyoda, K. Honda and T. Shimidzu, *J. Chem. Soc., Chem. Commun.*, 1992, 591; A. Knorr and J. Daub, *Angew. Chem., Int. Ed. Engl.*, 1995, **34**, 2664.

3 B. L. Feringa, N. P. M. Huck and A. M. Schoevaars, *Adv. Mater.*, 1996, **8**, 681.

4 J. Daub, I. Aurbach and J. Salbeck, *Angew. Chem., Int. Ed. Engl.*, 1988, **27**, 291; *Angew. Chem.*, 1988, **100**, 278; J. Salbeck, I. Aurbach and J. Daub, *Dechema Monographien*, 1989, **112**, 117; M. Porsch, G. Sigl-Seifert and J. Daub, *Adv. Mater.*, 1997, **9**, 635; For a recent application of CD spectroelectrochemistry, see: Y. J. Lu, Y. C. Zhu, G. J. Cheng and S. J. Dong, *Electroanalysis*, 1999, **11**, 601.

5 The spectroelectrochemical cell has been described: J. Salbeck, *Anal. Chem.*, 1993, **65**, 2169; CD spectra were recorded on a JASCO J-710 spectropolarimeter.

6 (*a*) N. Harada and K. Nakanishi, *Circular Dichroic Spectroscopy*, University Science Books, Oxford University Press, 1983; (*b*) K. Nakanishi and N. Berova, in *Circular Dichroism, Principles and Applications*, ed. K. Nakanishi, N. Berova and R. W. Woody, VCH, New York, 1994, ch. 13, pp. 361–398; (*c*) T. Nehira, C. P. Parish, S. Jockusch, N. J. Turro, K. Nakanishi and N. Berova, *J. Am. Chem. Soc.*, 1999, **121**, 8681.

7 A. Knorr, PhD thesis, Universität Regensburg, 1995. Pyrene radical anion has a characteristic and strong absorption at 488 nm under the same experimental conditions.

Communication 9/07454F

Unambiguous characterisation of dienylimines as intermediates in Fischer indolisation of *o*-substituted *N*-trifluoroacetyl enehydrazines

Okiko Miyata, Yasuo Kimura and Takeaki Naito*

Kobe Pharmaceutical University, Motoyamakita, Higashinada, Kobe 658-8558, Japan.
E-mail: taknaito@kobepharma-u.ac.jp

Received (in Cambridge, UK) 17th September 1999, Accepted 1st November 1999

Thermal cyclisation of *o*-substituted *N*-trifluoroacetyl enehydrazines was systematically investigated and found to proceed *via* dienylimine intermediates, which were unambiguously characterised by X-ray and spectral analysis.

The Fischer indole synthesis provides a versatile and convergent route to a wide variety of indoles.[1] Although today the key step in Fischer indolisation is regarded as a [3,3]-sigmatropic rearrangement of the enehydrazines, which is related to the Cope and Claisen rearrangements,[1,2] there have been only a few reports on the isolation and characterisation of the dearomatised dienylimine (**1** or **2**) intermediates because of

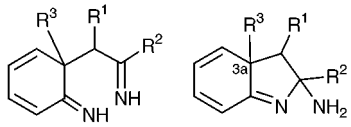

1 **2**

their instability. To the best of our knowledge, there has been only one paper[3] pertaining to the isolation of a pure dienylimine having a methyl group at the 3a-position in which the relative configurations at the 2-, 3- and 3a-positions remain to be established.

During the course of our investigation on reactivity of *N*-trifluoroacetyl enamine moieties,[4] we investigated the thermal cyclisation of *o*-substituted *N*-trifluoroacetyl enehydrazines under mild conditions and succeeded in the isolation and structure determination of the dienylimine intermediates in the Fischer indolisation. *o*-Substituted hydrazones are generally known to react more sluggishly than the *m*- and *p*-substituted analogs and sometimes give low yields of the desired indoles accompanied with side reactions.[1]

We first examined the thermal cyclisation of *N*-trifluoroacetyl enehydrazine **3a** having an *o*-methoxy group (Table 1). Previously, characterisation[1,5] of the dienylimine intermediate with a methoxy group had been attempted but found to be unsuccessful. A solution of **3a** in THF was heated at 65 °C for 10 h to give a mixture of indoline **4a** and two dienylimines **6a** in 63 and 36% yields, respectively (entry 1). Furthermore, **6a** was easily separated into two diastereomers, *cis-syn*-**6a** and *cis-anti*-**6a**, in a 5 : 1 ratio. The stereostructure of *cis-syn*-**6a** was established unambiguously by single-crystal X-ray analysis[6] (Fig. 1) and then the relative configuration of the isomeric *cis-anti*-**6a** was deduced from comparison of its ^{1}H and ^{13}C NMR spectra with those of *cis-syn*-**6a**. Therefore, we have now succeeded in the isolation and structure determination of the dienylimine intermediate in the Fischer indolisation of the *o*-methoxy enehydrazine. Additionally, the *cis-syn*-isomer was obtained as the major product.

Interestingly, the polarity of the organic solvent used influences both the product ratio of **4a** and **6a** and the reaction time (entries 2–4). In MeCN, the reaction proceeded smoothly to give a 1 : 1 mixture of **4a** and **6a** in 98% yield (entry 3). On the other hand, in non-polar hexane, **4a** was obtained as the major product in 75% yield, although prolonged reaction time was required for complete consumption of **3a** (entry 4). Heating the indoline **4a** in xylene at 138 °C afforded the corresponding indole **5a** in quantitative yield as a result of the elimination of

Table 1 Thermal cyclisation of *N*-trifluoroacetyl enehydrazines **3**

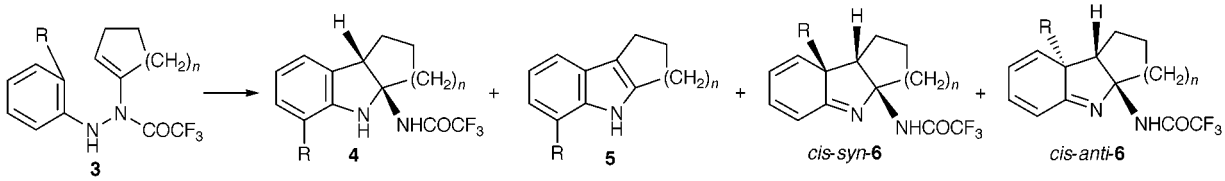

				Conditions			Yield (%)			
Entry	Substrate	R	*n*	Solvent	*T*/°C	*t*/h	Total	**4**	**5**	**6** (*cis-syn* : *cis-anti*)
1	**3a**	MeO	1	THF	65	10	99	63	—	36 (5 : 1)
2	**3a**	MeO	1	PhMe	90	7	98	69	—	29 (4 : 1)
3	**3a**	MeO	1	MeCN	80	5	98	51	—	47 (5 : 1)
4	**3a**	MeO	1	hexane	80	22	99	75	—	24 (4 : 1)
5	**3b**	MeO	2	PhMe	90	10	84	—	75	9 (2 : 1)
6	**3b**	MeO	2	MeCN	80	10	73	—	54	19 (2 : 1)
7	**3c**	Me	1	PhMe	90	8	74	14	42	18 (14 : 1)
8	**3c**	Me	1	MeCN	110	8	99	30	37	32 (7 : 1)
9	**3d**	Me	2	PhMe	110	10	78	—	71	7 (7 : 1)
10	**3d**	Me	2	MeCN	110	10	87	—	76	11 (6 : 1)
11	**3e**	Cl	1	PhMe	90	15	74	70	4	—
12	**3f**	NO_2	1	PhMe	110	29	31 (85)[a]	31 (85)[a]	—	—

[a] Yields in parentheses are for the recovered starting material.

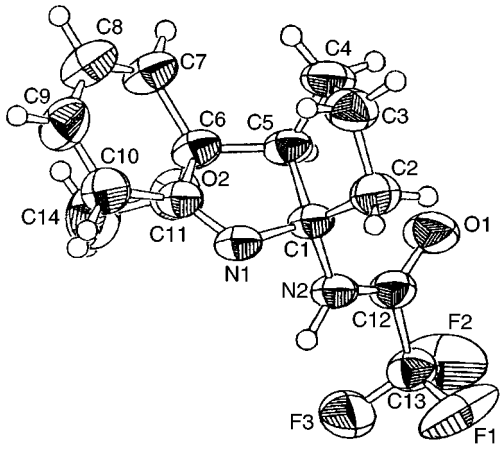

Fig. 1 ORTEP drawing of the molecule *cis-syn*-**6a** at the 50% probability level. The structure depicted is one of the independent molecules with the major component of the disordered CF_3 group.

trifluoroacetamide. Under the same conditions, both *cis-syn*-**6a** and *cis-anti*-**6a** were converted into indole **7**. Reaction of cyclohexene hydrazines **3b** proceeded slowly under similar mild conditions to give 7-methoxyindole **5b** as the major product with no detection of indoline **4b** (entries 5 and 6).

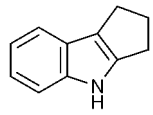

7

It is well-known that Fischer indolisation of (2-methoxyphenyl)hydrazone gives 7-methoxyindole as a minor product and the abnormal 6-substituted indole as a major product, respectively. [1,7,8] On the other hand, our results indicate that the indolisation reaction of **3** proceeds preferentially at the unsubstituted position to give 7-methoxyindole as the major product. Consequently, the thermal cyclisation of **3** has provided a practical synthetic method for the 7-oxygenated indoles, which are known to be potential intermediates for the synthesis of biologically active compounds.

Next, we turned our attention to the corresponding *o*-methyl *N*-trifluoroacetyl enehydrazines **3c**,**d**. Reaction of **3d** proceeded smoothly at a high temperature (110 °C) to give **5d** with moderate regioselectivity, while **3c** afforded a mixture of **4c**, **5c**, *cis-syn*-**6c** and *cis-anti*-**6c** (entries 7, 8, 9 and 10). The *cis-syn* and *cis anti*-dienylimines **6c**,**d** were obtained as minor products. Their stereostructures were deduced from comparisons of their ^{1}H and ^{13}C NMR spectra with those of *cis-syn*-**6a**,**b** and *cis-anti*-**6a**,**b**. Brown [9] has reported that attempts to isolate a tricyclic dienylimine having a methyl group were unsuccessful. Therefore, our result is the first example of the isolation and structure determination of the tricyclic dienylimine with a methyl group.

When an electron-withdrawing group such as a chlorine or nitro group was present in the *o*-position, the indolisation occurred regioselectively at the unsubstituted position to give 7-substituted products (entries 11 and 12).

Finally, the isolation and structure determination of the dienylimines intermediates in the Fischer indolisation of *o*-methoxy and *o*-methyl enehydrazines provides good evidence for the postulated reaction mechanism, including a stereochemical rationalisation, particularly for the [3,3]-sigmatropic rearrangement step.

This work was supported in part by a Grant-in-Aid for Scientific Research (No. 09672293) from the Ministry of Education, Science, Sports and Culture, Japan and a research grant from the Science Research Promotion Fund of the Japan Private School Promotion Foundation. We thank Dr K. Aoe (Analytical Research Laboratory, Tanabe Seiyaku) for the X-ray crystallographic structure determination of **6a**.

Notes and references

1 Reviews of Fischer indole synthesis: B. Robinson, *Chem. Rev*., 1963, **63**, 373; B. Robinson, *Chem. Rev*., 1969, **69**, 227; B. Robinson, *The Fischer Indole Synthesis*, Wiley, New York, 1982; D. L. Hughes, *Org. Prep. Proced. Int*., 1993, **25**, 609.

2 K. Bast, T. Durst, R. Huisgen, K. Lindner and R. Temme, *Tetrahedron*, 1998, **54**, 3745.

3 G. S. Bajwa and R. K. Brown, *Can. J. Chem*., 1969, **47**, 785.

4 Recently we found a novel synthetic route for indoles (or indolines) *via* thermal cyclisation of *N*-trifluoroacetyl enehydrazines. O. Miyata. Y. Kimura, K. Muroya, H. Hiramatsu and T. Naito, *Tetrahedron Lett.*, 1999, **40**, 3601.

5 C. S. Barnes, K. H. Pausacker and C. I. Schubert, *J. Chem. Soc*., 1949, 1381.

6 The crystal contains two independent molecules in the asymmetric unit. Both molecules have disordered CF_3 groups with occupancy factor of 0.67/0.33 and 0.81/0.19, respectively and one of the molecules has additional disorder at the fused cyclopentane (C_{17}-C_{18}) with occupancy factors of 0.56 and 0.44. *Crystal data* for *cis-syn*-**6a**: $C_{14}H_{15}F_3N_2O_2$, mp 140–141 °C, triclinic, $P\bar{1}$, a = 11.277(2), b = 12.015(2), c = 11.056(2) Å, α = 97.87 (1), β = 94.66(2), γ = 71.73(1)°, V = 1408.1(4) Å^3, Z = 4, μ = 1.056 mm^{-1}, D_c = 1.416 mg m^{-3}, F_{000} = 624, T = 293 K. Final R value was 0.0684 for 4788 reflections. CCDC 182/1467. See http://www.rsc.org/suppdata/cc/1999/2429/ for crystallographic data in .cif format.

7 H. Ishii, *Acc. Chem. Res*., 1981, **14**, 275.

8 Y. Murakami, H. Yokoo, Y. Yokoyama and T. Watanabe, *Chem. Pharm. Bull.*, 1999, **47**, 791.

9 G. S. Bajwa and R. K. Brown, *Can. J. Chem.*, 1970, **48**, 2293.

Communication 9/07539I

Synthesis of 'crushed fullerene' $C_{60}H_{30}$

Berta Gómez-Lor,[ab] Óscar de Frutos,[a] and Antonio M. Echavarren*[a]

[a] *Departamento de Química Orgánica, Universidad Autónoma de Madrid, Cantoblanco, 28049 Madrid, Spain. E-mail: anton.echavarren@uam.es*

[b] *Instituto de Ciencia de Materiales de Madrid, CSIC, Cantoblanco, 28049 Madrid, Spain.*

Received (in Cambridge, UK) 31st August 1999, Accepted 22nd October 1999

The synthesis of benzo[1,2-*e*:3,4-*e′*:5,6-*e″*]tribenzo[*l*:*l′*:*l″*]-triacephenanthrylene ($C_{60}H_{30}$) has been accomplished by a triple palladium-catalysed arylation of a *syn*-trialkylated truxene.

Part of the recent outburst in the chemistry of bowl-shaped polycyclic aromatic hydrocarbons (polyarenes)[1,2] concerns their potential use as starting materials for the development of syntheses of fullerenes as alternatives to those based on the vaporisation of graphite.[2–4] Indeed, fullerenes have been formed pyrolytically in low yield from aromatic hydrocarbons such as naphthalene and corannulene.[2] Additionally, the development of practical syntheses of functionalised bowl-shaped polyarenes should allow for the construction of fullerene-like molecular cages with polycyclic aromatic substructures. Progress towards the synthesis of giant polyarenes is also of interest in the area of materials science.[5]

We have recently completed a synthesis of polyarene **1**, benzo[1,2-*e*:3,4-*e′*:5,6-*e″*]triacephenanthrylene,[6] using the palladium-catalysed intramolecular arylation reaction that we previously applied for the preparation of benzo[*e*]acephenanthrylenes and related polycyclic aromatic hydrocarbons.[7] The synthesis of **1** was carried out by the intramolecular arylation of *syn*-trialkylated truxene[8] **2** by using $Pd(OAc)_2$ as the catalyst at 130 °C in DMF (Scheme 1), while cyclisation of the *anti*-isomer of **2** had to be performed at 150 °C under otherwise identical conditions.[6]

We decided to apply this approach for the synthesis of the higher analogue **3**, benzo[1,2-*e*:3,4-*e′*:5,6-*e′*]tribenzo[*l*:*l′*:*l″*]-triacephenanthrylene. Polyarene **3** contains a decacyclene core (highlighted in boldface in **3″**) fused with three naphthyl units and possesses half of the rings of C_{60} as shown in the Schlegel diagram **3′**.

The alkylation of the lithium trianion of truxene with 2-bromomethylnaphthalene gave selectively the *anti*-isomer of **4**. Initial isomerisation to the more stable *syn*-isomer **4** failed under the standard conditions (heating with KOBu^t in Bu^{t}OH)[6] due to the insolubility of the *anti*-isomer. However, simple addition of a small amount of CH_2Cl_2 as co-solvent allowed for the almost quantitative conversion of the *anti*-isomer into **4** (75% overall yield). The preparation of the required starting material for the palladium-catalysed arylation was carried out by the alkylation of the lithium trianion of truxene with

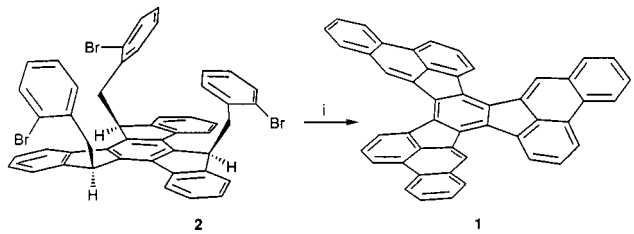

2 1

Scheme 1 *Reagents and conditions*: i, $Pd(OAc)_2$, $BnMe_3NBr$, K_2CO_3, DMF, 130 °C, 71%.

† The EI mass spectrum of **1** is available as supplementary data, see http://www.rsc.org/suppdata/cc/1999/2431/

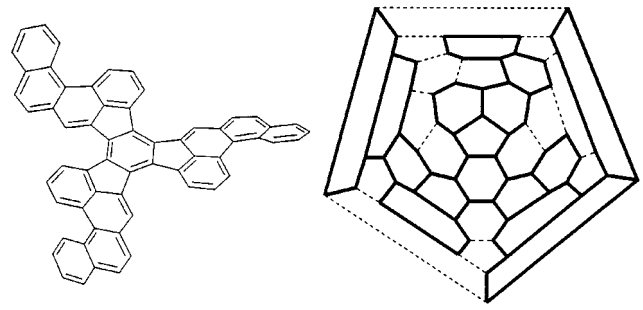

3 3'

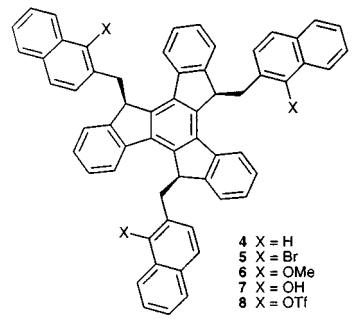

4 X = H
5 X = Br
6 X = OMe
7 X = OH
8 X = OTf

1-bromo-2-bromomethylnaphthalene[9] to give the *anti*-stereoisomer of **5** as the major compound, which was isomerised with KOBu^t in Bu^{t}OH under refluxing conditions to give *syn*-5,10,15-tris(1-bromo-2-naphthylmethyl)truxene **5** (62%). Similarly, **6** was obtained by using 2-bromomethyl-1-methoxynaphthalene[10] as the electrophile in the alkylation reaction, followed by base-catalysed isomerization (85% overall yield). Demethylation of **6** with BBr_3 in CH_2Cl_2 at −78 °C afforded trisnaphthol **7** (83%), which was treated with Tf_2O and 2,6-lutidine in CH_2Cl_2 (−30 to 0 °C) to give tris(triflate) **8** (52%).[11]

Treatment of **5** with $Pd(OAc)_2$ (10–20 mol%) in the presence of $BnMe_3NBr$ and K_2CO_3 or NaOAc in DMF or DMA at 110–160 °C gave complex reaction mixtures of insoluble materials. However, use of higher amounts of $Pd(OAc)_2$ (100 mol%, 0.3 equiv.) led to cleaner reaction mixtures from which **3** could be isolated in 42% yield.[12]‡ Treatment of tris(triflate) **8** in the presence of $Pd(PPh_3)_2Cl_2$ (150 mol%) and excess NaOPiv in DMA (120 °C, 26 h) also led to **3**, albeit in lower yield (11%).[13]

Polyarene **3** is a highly insoluble substance and its ^{1}H NMR could only be determined in 1,1,2,2-tetrachloroethane-d_2 at 130 °C. The EI-MS of **3** was very revealing since it showed the molecular ion at *m/z* 750 as the base peak along with characteristic M^{2+} and M^{3+} peaks at 375 and 248, respectively (Fig. 1). Additionally, peaks corresponding to loss of two (*m/z* 748, 6%), four (*m/z* 746, 4%), and six hydrogens (*m/z* 744, 2%) were clearly observed in the EI-MS. No $C_{60}^{+\cdot}$ (*m/z* 720) was observed in the mass spectrum. Polyarene **1** showed a similar EI mass spectrum to that of **3** under identical conditions, with

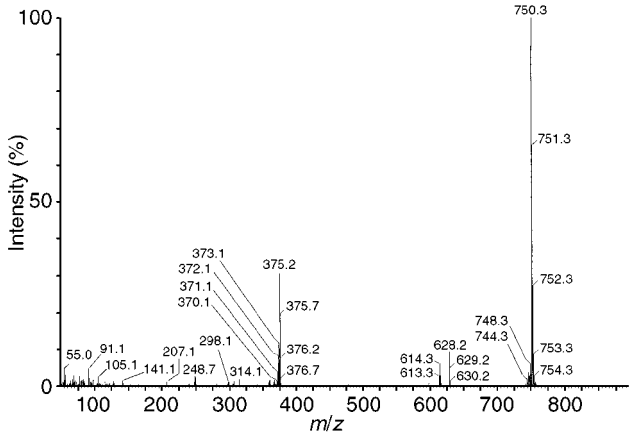

Fig. 1 EI-MS (probe temperature: 600 °C, ion source: 300 °C, 90 eV) of **3**.

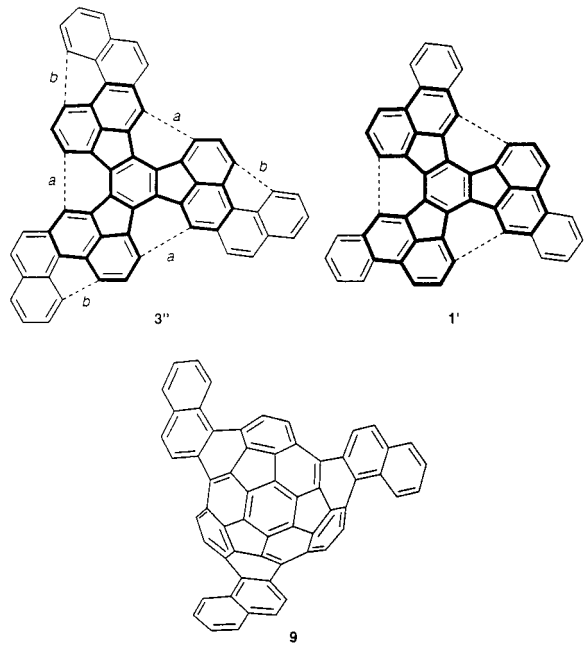

dehydrogenations presumably corresponding to that shown in **1′**.[14] This result suggests that under the conditions of the EI spectrum, **3** suffers the cyclodehydrogenations labelled *a* (**3″**).

The synthesis of **3** from **5** highlights the synthetic utility of the intramolecular C–H activation through aryl–palladium complexes.[15] Now readily available polyarene **3** could serve as the starting material for the preparation of **9** ($C_{60}H_{24}$) by a triple cyclodehydrogenation analogous to that recently carried out on decacyclene by Scott to form the fullerene fragment $C_{36}H_{12}$.[16] Additionally, bowl-shaped open fullerene **9** could be a direct precursor of C_{60} by a cascade of cyclodehydrogenation reactions.[3] Efforts along these lines are in progress.

We are grateful to the *DGES* (Project PB97-0002) for support of this research and to the *MEC* for a postdoctoral contract to B. G.-L. We acknowledge Johnson Matthey plc for a generous loan of $PdCl_2$ and Dr Maite Alonso (SIdI-UAM) for her skilled MS determinations.

Notes and references

‡ *Synthesis* of **3**: A mixture of **5** (150 mg, 0.15 mmol), $Pd(OAc)_2$ (34 mg, 0.15 mmol), $BnMe_3NBr$ (69 mg, 0.3 mmol) and K_2CO_3 (207 mg, 1.5 mmol) in DMA (8 ml) was stirred at 140 °C for 36 h. The mixture was cooled to 23 °C and the solid was filtered off and washed with CH_2Cl_2 and acetone. The solid was suspended in aqueous NaCN and stirred for 1 h. The solid was filtered off and washed with water and acetone to give **3** as a clear brown powder (47 mg, 42%): mp > 300 °C; δ_H(1,1,2,2-tetrachloroethane-d_2, 130 °C, 300 MHz) 9.26–9.01 (m, 12 H), 8.13–8.02 (m, 12 H), 7.80–7.69 (m, 6 H); *m/z* (EI) (probe temperature: 600°C, ion source: 300 °C, 90 eV) *m/z* 750 (M^+, 100%), 748 ($M^+ -2$, 6), 746 ($M^+ -4$, 4%), 744 ($M^+ -6$, 2%), 375 (M^{2+}, 30%), 248 (M^{3+}, 2%).

1 R. Faust, *Angew. Chem., Int. Ed. Engl.*, 1995, **34**, 1429; P. W. Rabideau and A. Sygula, *Acc. Chem. Res.*, 1996, **29**, 235; L. T. Scott, *Pure Appl. Chem.*, 1996, **68**, 291; L. T. Scott, *Pure Appl. Chem.*, 1996, **68**, 291; Y. Rubin, *Chem. Eur. J.*, 1997, **3**, 1009; G. Mehta and H. S. P. Rao, *Tetrahedron*, 1998, **54**, 13 325; L. T. Scott, H. E. Bronstein, D. V. Preda, R. B. M. Ansems, M. S. Bratcher and S. Hagen, *Pure Appl. Chem.*, 1999, **71**, 209.

2 C. Crowley, H. W. Kroto, R. Taylor, D. R. M. Walton, M. S. Bratcher, P.-C. Cheng and L. S. Scott, *Tetrahedron Lett.*, 1995, **36**, 9215; C. Crowley, R. Taylor, H. W. Kroto, D. R. M. Walton, P.-C. Cheng and L. S. Scott, *Synth. Met.*, 1996, **77**, 17; R. Taylor, G. J. Langley, H. W. Kroto and D. R. M. Walton, *Nature*, 1993, **366**, 728.

3 M. J. Plater, *J. Chem. Soc., Perkin Trans. 1*, 1997, 2897; F. Diederich and Y. Rubin, *Angew. Chem., Int. Ed. Engl.*, 1992, **31**, 1101.

4 Observation of $C_{60}^{+\cdot}$ in the MS of cyclic polyines: Y. Tobe, N. Nakagawa, K. Naemura, T. Wakabayashi, T. Shida and Y. Achiba, *J. Am. Chem. Soc.*, 1998, **120**, 4544; Y. Rubin, T. Parker, S. J. Pastor, S. Jalisatgi, C. Boulle and C. L. Wilkins, *Angew. Chem., Int. Ed.*, 1998, **37**, 1226. For a brief review: R. Faust, *Angew. Chem., Int. Ed.*, 1998, **37**, 2825. Fullerenes have also been observed in the MS of products obtained by the glow discharge of $CHCl_3$ vapor: S. Y. Xie, R. B. Huang, L.-H. Chen, W.-J. Huang and L. S. Zheng, *Chem. Commun.*, 1998, 2045.

5 M. Müller, C. Kübel and K. Müller, *Chem. Eur. J.*, 1998, **4**, 2099.

6 Ó. de Frutos, B. Gómez-Lor, T. Granier, M. A. Monge, E. Gutiérrez-Puebla and A. M. Echavarren, *Angew. Chem., Int. Ed.*, 1999, **38**, 204.

7 J. J. González, N. García, B. Gómez-Lor and A. M. Echavarren, *J. Org. Chem.*, 1997, **62**, 1286.

8 Truxene (10,15-dihydro-5*H*-diindeno[1,2-*a*;1′,2′-*c*]fluorene) was prepared from indan-1-one: E. V. Dehmlow and T. Kelle, *Synth. Commun.*, 1997, **27**, 2021.

9 M. S. Newman and S. I. Kosak, *J. Org. Chem.*, 1949, **14**, 375.

10 S. Kuwahara, A. Nemoto and A. Hiramatsu, *Agric. Biol. Chem.*, 1991, **55**, 2909.

11 Compounds were characterised by ^{1}H and ^{13}C NMR, EI or FAB MS and elemental analysis. Additionally, the configuration of **6** was confirmed by X-ray diffraction. The ^{1}H NMR spectra of **4**–**8** in $CDCl_3$ are concentration-dependent due to association (ref. 6).

12 Key to the isolation of **3** is the ready elimination of Pd^{II} by an aqueous solution of NaCN: B. L. Shaw, S. D. Perera and E. A. Staley, *Chem. Commun.*, 1998, 1361.

13 Palladium-catalysed arylation of triflates: J. E. Rice, Z.-W. Cai, Z.-M. He and E. La Voie, *J. Org. Chem.*, 1995, **60**, 8101 and references therein.

14 *Selected data* for **1**: *m/z* (EI) (probe temperature: 600 °C, ion source: 300 °C, 90 eV) *m/z* 600 (M^+, 100%), 598 ($M^+ -2$, 18%), 596 ($M^+ -4$, 4), 594 ($M^+ -6$, 3), 300 (M^{2+}, 29%), 200 (M^{3+}, 2).

15 A recent review: G. Dyker, *Angew. Chem., Int. Ed.*, 1999, **38**, 1698.

16 L. T. Scott, M. S. Bratcher and S. Hagen, *J. Am. Chem. Soc.*, 1996, **118**, 8743; S. Attar, D. M. Forkey, M. M. Olmstead and A. L. Balch, *Chem. Commun.*, 1998, 1255.

Communication 9/06990I

The first Diels–Alder reaction of a 9,10-bis(1,3-dithiol-2-ylidene)-9,10-dihydroanthracene derivative: synthesis and crystal structure of a novel donor–π–anthraquinone diad

Christian A. Christensen,[a] Martin R. Bryce,*[a] Andrei S. Batsanov,[a] Judith A. K. Howard,[a] Jan O. Jeppesen[b] and Jan Becher[b]

[a] *Department of Chemistry, University of Durham, Durham, UK DH1 3LE. E-mail: m.r.bryce@durham.ac.uk*
[b] *Department of Chemistry, Odense University, Campusvej 55, DK 5230 Odense M, Denmark*

Received (in Cambridge, UK) 27th September 1999, Accepted 20th October 1999

An exocyclic diene derivative of 9,10-bis(1,3-dithiol-2-ylidene)-9,10-dihydroanthracene undergoes Diels–Alder reaction with naphthoquinone to provide the D–π–A diad 10.

Derivatives of the π-electron donor **1** are emerging as versatile components of organic conductors,[1] nonlinear optical materials,[2] multi-stage redox assemblies[3] and cyclophanes.[4] System **1**

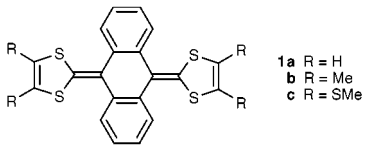

offers a unique combination of redox and structural properties, *viz.* a quasi-reversible two-electron oxidation process to yield a thermodynamically stable dication [E^{ox} +0.30 to +0.40 V (*vs.* Ag/AgCl)].[5] The neutral molecule adopts a saddle-shape; on oxidation the anthracene ring becomes aromatic and planar, with the 1,3-dithiolium cations almost orthogonal to this plane.[1b,5d]

We are developing methodology for the synthesis of new derivatives of **1**.[6] Herein we describe the first Diels–Alder reaction involving system **1**, *viz*. the reaction of the transient exocyclic diene derivative **9** with naphthoquinone to afford the aromatised adduct **10**. This study is timely in the light of interest in the Diels–Alder trapping of diene derivatives of tetrathiafulvalene[7] and 1,3-dithiole-2-one systems.[8]

Bis(chloromethyl) compound **8** is the precursor to our target diene **9** (Scheme 1). Hexylsulfanyl substituents enhance the solubility. The bis-DPTBS protected diol **2**[9] was methylated with MeOTf to afford the unstable salt **3** which was sufficiently pure for immediate reaction with the anion of anthrone, which gave ketone derivative **4** (70% yield from **2**). Horner–Wadsworth–Emmons olefination with the anion of reagent **5**[10] gave compound **6** (77% yield), which yielded the diol derivative **7** (88% yield). Reaction of a concentrated solution of diol **7** and PPh_3 in a mixture of CCl_4 and MeCN at 90 °C[11] gave the stable bis(chloromethyl) derivative **8** in 45% yield ($SOCl_2$ in CCl_4 at 20 °C gave only 10% of **8**). A mixture of **8**, KI, 18-crown-6 and 1,4-naphthoquinone was heated in toluene for 5 h, whereupon 2,3-dichloro-5,6-dicyanoquinone (DDQ) was added. After further heating the aromatised adduct **10**† was isolated (63% yield from **8**).

The good stability of the dichloro compound **8** contrasts with the attempted preparation of the bis(bromomethyl) derivative of **7** using conditions described[7c,9] for other 4,5-bis(bromomethyl)-1,3-dithiole systems. Reaction of diol **7** with CBr_4 and PPh_3 in THF at 0 °C gave a complex mixture of products (TLC analysis) from which the bis(bromomethyl) derivative (if present) could not be isolated; instead, the formyl derivative **14**† was obtained. The yield of **14** was optimised (61%) by using a dilute solution of **7** and CBr_4 and PPh_3 (3.0 equiv.). Formyl derivatives as byproducts during the synthesis of related

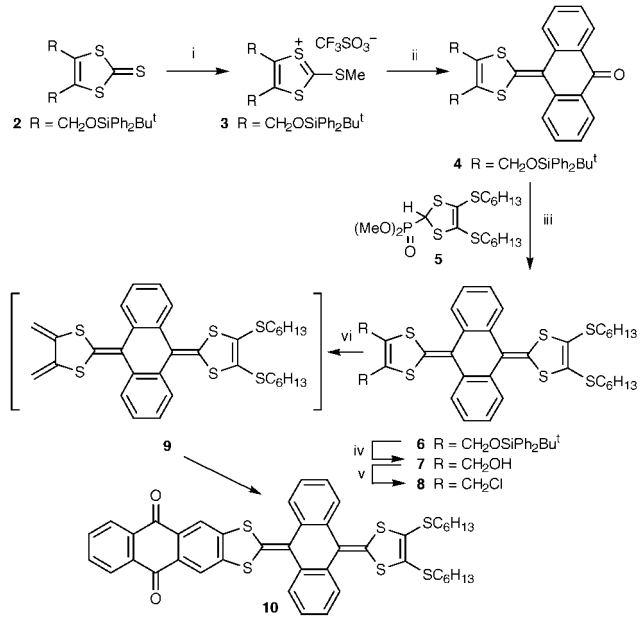

Scheme 1 *Reagents and conditions*: i, MeOTf, CH_2Cl_2, 20 °C, 1 h; ii, anthrone, pyridine–AcOH, 55 °C, 3 h, then 120 °C, 3 h; iii, **5**, LDA, −78 °C, 2 h, then add **4**, THF, −78 °C to 20 °C, 12 h; iv, Bu_4NF, THF, 20 °C, 1.5 h; v, PPh_3 (3.0 equiv.), CCl_4, (excess), MeCN, reflux, 1 h; vi, KI (3 equiv.), 18-crown-6 (3 equiv.), 1,4-naphthoquinone (4 equiv.), PhMe, 90 °C, 5 h, then DDQ (4 equiv.), 90 °C, 4 h.

4,5-bis(bromomethyl)-1,3-dithiole systems has been noted previously,[12] but no mechanism for their formation has been published.[13] A possible route is shown in Scheme 2. Loss of bromide from intermediate **11** would give **12** and hence the intermediate **13**, which could undergo an oxy-Cope type rearrangement to give **14**.

The structures of compounds **10** and **14** (Fig. 1 and 2) were confirmed by X-ray crystal structure analysis.‡ The asymmetric

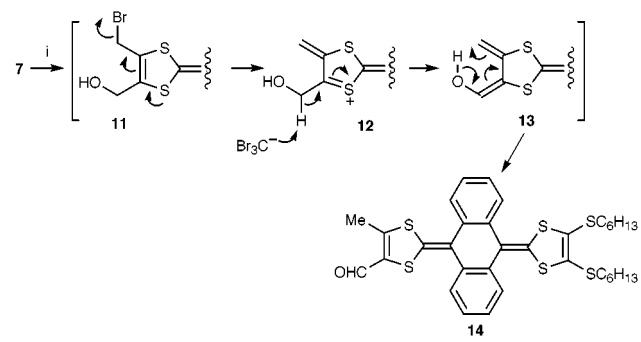

Scheme 2 *Reagents and conditions*: i, PPh_3 (3.0 equiv.), CBr_4 (3.0 equiv.), CH_2Cl_2, 20 °C, 16 h.

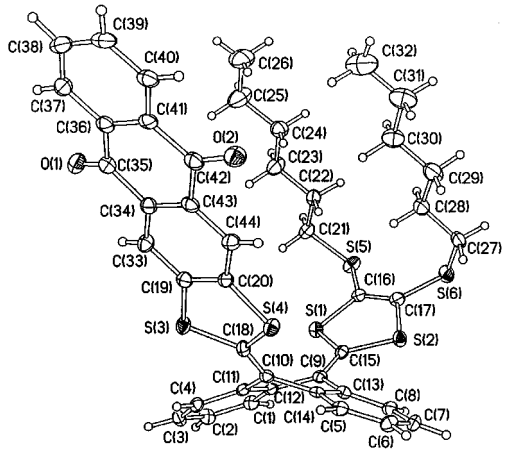

Fig. 1 Molecular structure of **10**.

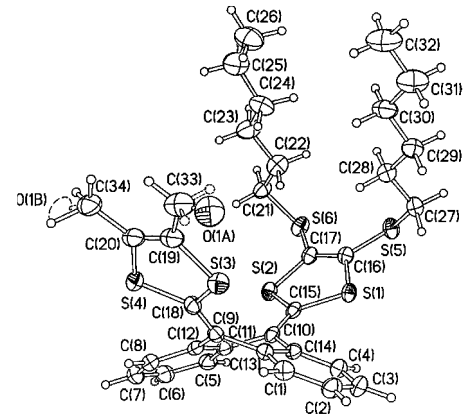

Fig. 2 Molecular structure of **14**; CH_3 and CHO substituents are evenly distributed between C(19) and C(20).

unit in the crystal of **10** contains only one independent molecule, while that of **14** comprises two molecules of similar but non-identical conformations; in one molecule, one of the *n*-hexyl chains is disordered. The anthracenediylidene system is folded along the C(9)···(10) vector by *ca.* 39° in **10** and 41° in **14** and both dithiole rings are folded inward along the S···S vectors (by 8–14°). The anthracenediylidenebis(dithiole) system is U-shaped, with an acute angle between the S(1)C(16)C(17)S(2) and S(3)C(19)C(20)S(4) planes: 83° in **10**, 82° in **14**.

The *n*-hexyl chains adopting all-*trans* conformations lie parallel to the nearly planar anthraquinone (**10**) or formylthiole (**14**) system. Such parallelism particularly highlights the packing motif characteristic for 'molecular saddles': namely, a pseudo-dimer of mutually engulfing molecules, symmetrically related *via* an inversion centre.[6b]

Cyclic voltammetry shows a quasi-reversible two-electron oxidation wave at E^{ox} +0.64 V (**10**) and E^{ox} +0.54 V (**14**). Additionally for **10** a quasi-reversible reduction wave of the AQ moiety is observed at E^{red} −0.95 V [CV data were recorded *vs.* Ag/AgCl, electrolyte $Bu_4N^+ClO_4^-$ (0.1 M), CH_2Cl_2, 20 °C, scan rate 100 mV s^{-1}].

The UV–VIS spectrum of compound **10** displays two bands characteristic of system **1**[5d,6] at 348 and 428 nm: no absorption was observed at longer wavelengths where intramolecular charge-transfer (ICT) bands would be expected. Studies aimed at photoinducing ICT in system **10**, and increasing the acceptor strength of the AQ moiety,[14] are in progress.

We thank the EPSRC and the Danish Research Academy for funding.

Notes and references

† *Selected data* for **10**: shining black crystals, mp 229–230 °C (from CH_2Cl_2–hexane); $\delta_H(CDCl_3)$ 8.30–8.25 (m, 2H), 8.07 (s, 2H), 7.80–7.77 (m, 2H), 7.73–7.68 (m, 2H), 7.65–7.60 (m, 2H), 7.40–7.35 (m, 4H), 2.82–2.72 (m, 4H), 1.64–1.52 (m, 4H), 1.38–1.22 (m, 12H), 0.83 (t, 6H, *J* 6.8); $\lambda_{max}(CH_2Cl_2)$/nm (lg ε) 348 (4.58), 428 (4.53). For **14**: orange prisms, mp 178–179 °C (from CH_2Cl_2–hexane); $\delta_H(CDCl_3)$ 9.70 (s, 1H), 7.65–7.56 (m, 4H), 7.33–7.30 (m, 4H), 2.84–2.74 (m, 4H), 2.43 (s, 3H), 1.63–1.53 (m, 4H), 1.40–1.25 (m, 12H), 0.87 (t, 6H, *J* 6.4).

‡ *Crystal data* for **10**: $C_{44}H_{40}O_2S_6$, M = 793.1, T = 120 K, triclinic, space group $P\bar{1}$ (No. 2), a = 9.925(2), b = 12.940(3), c = 15.319(5) Å, α = 94.16(1), β = 94.13(1), γ = 99.06(1)°, U = 1930.8(9) Å^3, Z = 2, D_c = 1.36 g cm^{-3}, 13240 reflections (6762 unique), R = 0.039 [4525 data, $I > 2\sigma(I)$], $wR(F^2)$ = 0.086. For **14**: $C_{34}H_{38}OS_6$, M = 655.0, T = 120 K, triclinic, space group $P\bar{1}$ (No. 2), a = 15.208(3), b = 16.298(3), c = 16.510(3) Å, α = 111.95(1), β = 95.52(1), γ = 113.86(1)°, U = 3320(1) Å^3, Z = 4, D_c = 1.31 g cm^{-3}, 25912 reflections (12113 unique), R = 0.042 [8781 data, $I > 2\sigma(I)$], $wR(F^2)$ = 0.096 (Mo-Kα radiation). CCDC 182/1460. See http://www.rsc.org/suppdata/cc/1999/2433/ for crystallographic data in .cif format.

1 (*a*) Y. Yamashita, Y. Kobayashi and T. Miyashi, *Angew. Chem., Int. Ed. Engl.*, 1989, **28**, 1052; (*b*) M. R. Bryce, A. J. Moore, M. Hasan, G. J. Ashwell, A. T. Fraser, W. Clegg, M. B. Hursthouse and A. I. Karaulov, *Angew. Chem., Int. Ed. Engl.*, 1990, **29**, 1450; (*c*) S. Triki, L. Ouahab, D. Lorcy and A. Robert, *Acta Crystallogr., Sect . C*, 1993, **49**, 1189; (*d*) Y. Yamashita and M. Tomura, *J. Mater. Chem.*, 1998, **8**, 1933.

2 M. A. Herranz, N. Martín, L. Sánchez, J. Garín, J. Orduna, R. Alcalá, B. Villacampa and C. Sánchez, *Tetrahedron*, 1998, **54**, 11 651.

3 G. J. Marshallsay and M. R. Bryce, *J. Org. Chem.*, 1994, **59**, 6847; N. Martín, I. Pérez, L. Sánchez and C. Seoane, *J. Org. Chem.*, 1997, **62**, 870; N. Martín, I. Pérez, L. Sánchez and C. Seoane, *J. Org. Chem.*, 1997, **62**, 5690.

4 T. Finn, M. R. Bryce, A. S. Batsanov and J. A. K. Howard, *Chem. Commun.*, 1999, 1835.

5 (*a*) A. J. Moore and M. R. Bryce, *J. Chem. Soc., Perkin Trans. 1*, 1991, 157; (*b*) M. R. Bryce, M. A. Coffin, M. B. Hursthouse, A. I. Karaulov, K. Müllen and H. Scheich, *Tetrahedron Lett.*, 1991, **32**, 6029 ; (*c*) N. Martín, L. Sánchez, C. Seoane, E. Ortí, P. M. Viruela and R. Viruela, *J. Org. Chem.*, 1998, **63**, 1268; (*d*) A. S. Batsanov, M. R. Bryce, M. A. Coffin, A. Green, R. E. Hester, J. A. K. Howard, I. K. Lednev, N. Martín, A. J. Moore, J. N. Moore, E. Ortí, L. Sánchez, M. Savíron, P. M. Viruela, R. Viruela and T.-Q. Ye, *Chem. Eur. J.*, 1998, **4,** 2580.

6 (*a*) M. R. Bryce, T. Finn and A. J. Moore, *Tetrahedron Lett.*, 1999, **40**, 3221; (*b*) M. R. Bryce, T. Finn, A. J. Moore, A. S. Batsanov and J. A. K. Howard, *Eur. J. Org. Chem.*, 1999, in the press.

7 (*a*) J. Llacay, M. Mas, E. Molins, J. Veciana, D. Powell and C. Rovira, *Chem. Commun.*, 1997, 659; (*b*) J. Llacay, J. Veciana, J. Vidal-Gancedo, J. L. Bourdelande, R. Gonzalez-Moreno and C. Rovira, *J. Org. Chem.*, 1998, **63**, 5201; (*c*) P. Hudhomme, S. G. Liu, D. Kreher, M. Cariou and A. Gorgues, *Tetrahedron Lett.*, 1999, **40**, 2927.

8 C. Boulle, O. Desmars, N. Gautier, P. Hudhomme, M. Cariou and A. Gorgues, *Chem. Commun.*, 1998, 2197.

9 J. O. Jeppesen, K. Takimiya, N. Thorup and J. Becher, *Synthesis*, 1999, 803.

10 Reagent **5** was prepared from zinc bis[2-thioxo-1,3-dithiole-4,5-bis-(thiolate)] (C. Wang, A. S. Batsanov, M. R. Bryce and J. A. K. Howard, *Synthesis*, 1998, 1615) by the same methods used previously for close analogues [ref. 5(*a*)].

11 R. Appel, *Angew. Chem., Int. Ed. Engl.*, 1975, **14**, 801.

12 R. M. Renner and G. R. Burns, *Tetrahedron Lett.*, 1994, **35**, 269; Similar reactions afford 4-formyl-5-methyl-4′,5′-bis(methylsulfanyl)TTF and 4,5-bis(2-cyanoethylsulfanyl)-4′-formyl-5-methyl-TTF (*ca.* 40% yields) (J. O. Jeppesen and J. Becher, unpublished results). The former reaction was also observed (25% yield) by P. Blanchard, PhD Thesis, Université de Nantes, 1994. A very different mechanism from Scheme 2 was postulated.

13 Other workers have observed the formation of bis(oxydimethylene)-TTF when chlorinating tetrakis(hydroxymethyl)-TTF [ref. 7(*c*) and S. Hsu and L. Chiang, *Synth. Met.*, 1988, **27**, B651].

14 N. Martín, J. L. Segura and C. Seoane, *J. Mater. Chem.*, 1997, **7**, 1161.

Communication 9/07768E

Designer cyclopalladated-amine catalysts for the asymmetric Claisen rearrangement

Pak-Hing Leung,*[a] Khim-Hui Ng,[a] Yongxin Li,[a] Andrew J. P. White[b] and David J. Williams[b]

[a] *Department of Chemistry, National University of Singapore, Kent Ridge, Singapore 119260. E-mail: chmlph@nus.edu.sg*

[b] *Department of Chemistry, Imperial College, London, UK SW7 2AY*

Received (in Cambridge, UK) 20th September 1999, Accepted 2nd November 1999

The novel ortho-metallated complex (*R*,*R*)-di-μ-chlorobis{9-[(1-dimethylamino)ethyl]-10-phenanthrenyl-*C*,*N*}dipalladium has been prepared and found to be a significantly better catalyst than its phenyl and naphthylamine analogues for the asymmetric Claisen rearrangement of a non-activated allyl imidate.

Over the past decade, chiral cyclopalladated-amine complexes have contributed significantly to many aspects of synthetic stereochemistry.[1] They have been frequently used as efficient resolving agents for chiral ligands, clear and reliable references for the NMR assignment of unknown absolute stereochemistry in solution, sensitive chiral shift reagents for the determination of optical purities, activators for the asymmetric carbon–carbon bond formation and as chiral templates for the synthesis of functionalized P-chiral phosphines. Surprisingly, these easily accessible square-planar organometallic complexes have not been used in any catalytic asymmetric transformations. Here, we present the systematic application of three analogous cyclopalladated-amine complexes **1**–**3** for the asymmetric Claisen rearrangement. Similar to the Diels–Alder reaction, Claisen rearrangement is an efficient and elegant method for asymmetric carbon–carbon bond formation.[2]

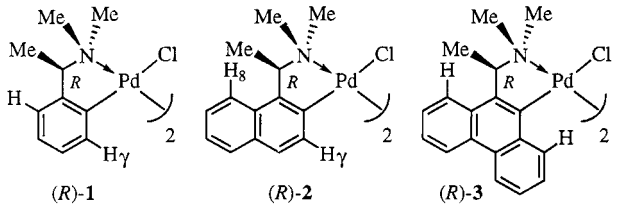

Both enantiomeric forms of complexes **1** and **2** are well documented. The optically active forms of the new phenanthrylamine ligand for complex **3** were obtained by optical resolution using *O*,*O*′-dibenzoyltartaric acid as the resolving agent. Thus, both the (*R*)-(+)- and (*S*)-(−)-forms of α-(9-phenanthryl)ethylamine were obtained as white solids in 60–70% yields, mp 79–81 °C, $[\alpha]_D$ ±44.0 (*c* = 0.5, CH_2Cl_2). The ortho-metallated complex (*R*)-**3** was prepared from the (*R*)-(+)-phenanthrylamine and $[Pd(MeCN)_4](ClO_4)_2$ in the presence of Et_3N followed by the treatment with an excess of NH_4Cl. The dimeric complex was obtained as pale yellow needles (60%), $[\alpha)_D$ −393 (*c* = 0.6, CH_2Cl_2). However, single crystals of (*R*)-**3** that are suitable for structural analysis could not be produced. In an effort to determine the absolute stereochemistry of the phenanthrylamine ligand, (*R*)-**3** was converted quantitatively to the perchlorate salt (*R*)-**4** by treatment of the dimeric complex with silver perchlorate in acetonitrile, $[\alpha]_D$ −198 (*c* = 0.5, CH_2Cl_2). X-Ray structural analysis of the highly crystalline cationic complex (*R*)-**4** was achieved (Fig. 1).† Similar to that observed in (*R*)-**2**,[1] the X-ray analysis of the phenanthrylamine complex reveals that the methyl group at the *R*-chiral carbon centre is located at the axial position. The geometry at palladium is distorted square planar with *cis* angles ranging between

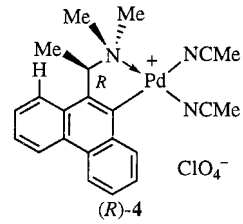

80.2(2) and 96.4(2)°, the most acute being associated with the five-membered chelate ring which has a distinctly folded conformation with C(14) and C(15) lying 0.61 and 1.04 Å respectively out of the coordination plane. The palladium coordination distances are unexceptional, though the Pd–N bond *trans* to carbon is significantly longer than those *trans* to nitrogen. The phenanthrylene ring has a slightly twisted conformation, with deviations from planarity of up to 0.07 Å; the palladium atom lies 0.35 Å from this plane.

To compare the efficiency of the three analogous complexes on the Claisen rearrangement, an electronically non-activated allyl imidate was selected (Scheme 1). All the rearrangement processes were carried out at the optimum temperature of 20 °C in the presence of a palladium catalyst (10 mol%). Interestingly, while all three dimeric catalysts gave the corresponding amide efficiently, the cationic complex (*R*)-**4** could not catalyse the rearrangement. Apparently an electronically neutral Pd(II) species is required for this catalytic process. Furthermore, in

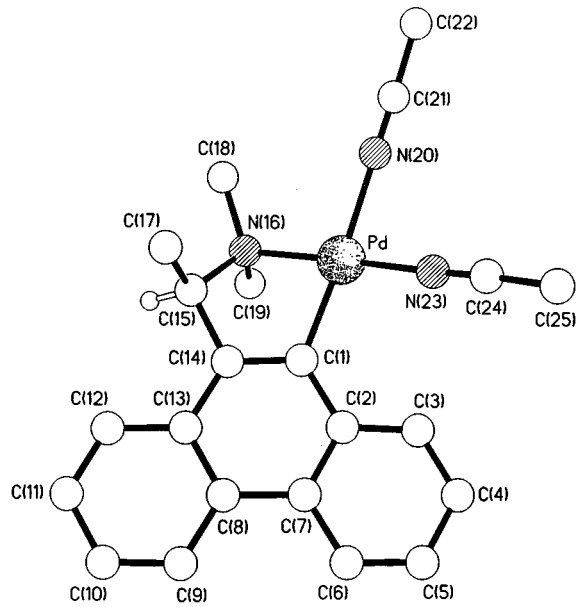

Fig. 1 Molecular structure and absolute stereochemistry of the complex cation (*R*)-**4**. Selected bond lengths (Å) and angles (°); Pd–C(1) 2.000(4), Pd–N(16) 2.062(4), Pd–N(20) 2.126(5), Pd–N(23) 2.023(4); C(1)–Pd–N(16) 80.2(2), C(1)–Pd–N(20) 176.2(2), C(1)–Pd–N(23) 96.3(2), N(16)–Pd–N(20) 96.4(2), N(16)–Pd–N(23) 172.0(2), N(20)–Pd–N(23) 86.9(2).

terms of stereoselectivities, it is obvious that (*R*)-**3** is the best asymmetric catalyst among the three studied. When benzene was used as the solvent, (*R*)-**3** produced the chiral amide with 79% ee.‡ Under the same reaction conditions, however, only 4% ee could be achieved by both (*R*)-**1** and (*R*)-**2**. These catalytic results are indeed in agreement with our expectations, based on the well established stereoelectronic features of complexes **1** and **2**. The five-membered organometallic ring in complex (*R*)-**1** is stereochemically non-rigid and the chiral chelate adopts both the δ and λ conformations in the solid state and these ring chiralities are inter-convertable in solution. In complex (*R*)-**2**, however, there is a strong steric inter-locking force operating between the methyl group at the chiral carbon centre and the neighbouring H(8) of the naphthylenyl ring.[1,3] Thus the δ conformation is secured in the skew organometallic ring in (*R*)-**2** and cannot be inverted into the λ form, even at elevated temperatures. Thus the stereochemistry of the naphthylamine moiety is expected to be transmit *via* the prochiral NMe groups and the H_γ proton onto the neighbouring coordination sites without any fluctuation. The X-ray analysis of (*R*)-**4** and the 2D ^{1}H ROSEY NMR studies of (*R*)-**3** and (*R*)-**4** in $CDCl_3$ confirmed that similar stereochemical inter-locking forces are operating within the palladium–phenanthrylamine chelates. In terms of electronic directing effects, it is well established that in both (*R*)-**1** and (*R*)-**2**, the Pd–Cl bonds which are located *trans* to the π-accepting aromatic carbon are stable and inert.[1,4] In contrast, the Pd–Cl bonds that are *trans* to the σ-donating nitrogen are kinetically labile. As the donor atoms in all three complexes are similar, we therefore expect that the Pd–Cl bonds in (*R*)-**3** to exhibit similar kinetic stabilities as their counterparts in (*R*)-**1** and (*R*)-**2**. Undoubtedly the labile chloro ligands in these chiral complexes provide the catalytic sites for the asymmetric Claisen rearrangements. It is noted that the stereochemical environment of the catalytic sites in (*R*)-**1** and (*R*)-**2** are controlled only by the projecting H_γ protons. However, the influence exerted by these H_γ protons is less than that of the extended aromatic ring in (*R*)-**3** as the protons are small and further away from the site. Currently we are investigating the absolute stereochemistry of the Claisen rearrangement products. In addition synthesis of analogous optically active chrysenylamine complexes and further studies of the asymmetric Claisen rearrangements involving activated allyl imidates are currently in progress.

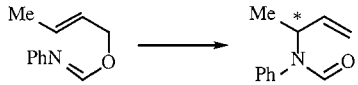

Catalyst	Solvent	*T*/°C	Enantiomer	ee(%)
(*R*)-**1**	CH_2Cl_2	20	(−)	10
(*R*)-**2**	CH_2Cl_2	20	(−)	13
(*R*)-**3**	CH_2Cl_2	20	(−)	67
(*R*)-**4**	CH_2Cl_2	20	NR	—
(*R*)-**1**	C_6H_6	20	(−)	4
(*R*)-**2**	C_6H_6	20	(+)	4
(*R*)-**3**	C_6H_6	20	(−)	79
(*R*)-**4**	C_6H_6	20	NR	–

Scheme 1 NR = no reaction.

We are grateful to the National University of Singapore for support of this research (Grant No. RP960675) and research scholarships to K.-H. N. and L. Y. S.

Notes and references

† *Crystal data* for (*R*)-**4**: $C_{22}H_{24}N_3O_4ClPd\cdot0.25H_2O$, M = 540.8, monoclinic, space group $P2_1$ (no. 4), a = 12.399(2), b = 7.601(1), c = 13.098(1) Å, β = 108.60(1)°, V = 1169.8(2) Å^3, Z = 2, D_c = 1.535 g cm^{-3}, μ(Mo-Kα) = 9.41 cm^{-1}, F(000) = 549. A pale yellow prism with dimensions 0.61 × 0.39 × 0.21 mm was used for diffraction studies. A total of 2879 independent reflections were measured on a Siemens P4/PC diffractometer with Mo-Kα radiation (graphite monochromator) using ω-scans. All the non-hydrogen atoms were refined anisotropically. Full-matrix least-squares refinement based on F^2 with absorption corrected data gave R_1 = 0.032, wR_2 = 0.077. The absolute stereochemistry was determined unambiguously by a combination of *R*-factor tests (R_1^+ = 0.0269, R_1^- = 0.0327) and by use of the Flack parameter [x^+ = −0.01(3), x^- = +0.99(3)] using a data set collected on the same crystal with Cu-Kα radiation (with the exception of those associated with the chirality assignment, the data and derived parameters given are for the Mo-Kα data set as it has a higher data to parameter ratio). CCDC 182/1470. See http://www.rsc.org/suppdata/cc/1999/2435/ for crystallographic files in .cif format.

‡ Determined by HPLC using a perfunctionalized cyclodextrin column eluted with 2% Pr^{i}OH–*n*-hexane.[5]

1 S. B. Wild, *Coord. Chem. Rev.*, 1997, **166**, 291; N. W. Alcock, D. I. Hulmes and J. M. Brown, *J. Chem. Soc., Chem. Commun.*, 1995, 395; V. V. Dunina, E. B. Golovan, N. S. Gulyukina and A. V. Buyevich, *Tetrahedron: Asymmetry*, 1995, **6**, 2371; J. Spencer and M. Pfeffer, *Tetrahedron: Asymmetry*, 1995, **6**, 419; W. McFarlane, J. D. Swarbrick and J. L. Bookham, *J. Chem. Soc., Dalton Trans.*, 1998, 3233; G. Zhao, Q. G. Wang and T. C. W. Mak, *J. Organomet. Chem.*, 1999, **574**, 311; Y. C. Song, J. J. Vittal, S. H. Chan and P. H. Leung, *Organometallics*, 1999, **18**, 650.

2 B. Bosnich, *Asymmetric Catalysis*, Martinus, Dordrecht, 1986; H. Ito and T. Taguchi, *Chem. Soc. Rev.*, 1999, **28**, 43; S. Saito and H. Yamamoto, *Chem. Commun.*, 1997, 1585; F. Cohen and L. E. Overman, *Tetrahedron: Asymmetry*, 1998, **9**, 3213.

3 S. Y. M. Chooi, M. K. Tan, P. H. Leung and K. F. Mok, *Inorg. Chem.*, 1994, **33**, 3096.

4 B. H. Aw, T. S. A. Hor, S. Selvaratnam, K. F. Mok, A. J. P. White, D. J. Williams, N. H. Rees, W. McFarlane and P. H. Leung, *Inorg. Chem.*, 1997, **36**, 2138.

5 L. F. Zhang, Y. C. Wong, L. Chen, C. B. Ching and S. C. Ng, *Tetrahedron Lett.*, 1999, **40**, 1815.

Communication 9/07617D

ChemComm

Intramolecular cyclization of 1-nitroalkenyl radicals generated by one-electron oxidation of *aci*-nitro anions with CAN: stereoselective formation of 3,4-functionalized tetrahydrofurans

Anne-Catherine Durand, Estelle Dumez, Jean Rodriguez and Jean-Pierre Dulcère

RéSo, Réactivité en Synthèse organique, UMR 6516, Faculté des Sciences et Techniques de St Jérôme, Boîte D 12, Av. Esc. Normandie-Niemen, F-13397, Marseille Cedex 20, France. E-mail: jean-pierre.dulcere@reso.u-3mrs.fr

Received (in Liverpool, UK) 28th September 1999, Accepted 28th October 1999

Upon one-electron oxidation by ammonium hexanitratocerate(IV) (CAN), *aci*-nitro anions 3a-d resulting from oxa-Michael addition of allylic alcohol to α,β-disubstituted nitroalkenes 1a-d undergo stereoselective radical cyclization into 3-nitro-4-nitrooxymethyltetrahydrofurans 6a-d and 3-nitro-4-hydroxymethyltetrahydrofurans 7,8a-d.

One-electron oxidation of carbanions is one of the simplest methods for generation of carbon-centered radicals. However, so-generated radicals usually afford self-condensation products,[1] and intermolecular[2] carbon–carbon bond forming reactions have only occasionally been disclosed in the literature.

Recently, ammonium hexanitratocerate(IV) (CAN) was found to be an efficient one-electron oxidant of *aci*-nitro anions to provide 1-nitroalkyl radicals which add intermolecularly to electron-rich olefins;[3] moreover, secondary 1-nitroalkenyl radicals undergo intramolecular cyclization to afford isoxazoles, provided the olefinic moiety is appropriately substituted.[4]

The failure of tertiary α-nitroalkyl radicals to cyclise, except in particular cases in which the yields of cyclized products are not satisfactory,[5] prompted us to study the reactivity of readily available α-substituted β-allyloxynitronates **3** upon oxidation with CAN.

α-Substituted β-allyloxy nitro compounds **2a**–**d**, obtained in 85–90% yield by oxa-Michael addition of allylic alcohol[6] to nitroalkenes **1a**–**d**, were reacted with NaH to afford *aci*-nitro anions **3a-d** (Scheme 1); addition of **3a**–**d** to a solution of CAN (3 equiv.) in THF at −78 °C generated radical anion intermediates **4** resulting in the stereoselective formation of *exo* nitronitrates **6a-d**† (45–60%) along with nitro alcohols **7,8a**–**d** (5–8%, **7**:**8** = 5:1).‡§ Alternatively, the same product mixture could be obtained directly from **1a-d**, in a one-pot process. According to previous reports,[4,5] reduction by solvent of alkyl radicals **5** resulting from direct 5-*exo* cyclization was not observed; indeed, a further transformation occurs, and the transformation into nitronitrates **6** which constitute the major products of the reaction could be related to a ligand transfer reaction in the presence of CAN.[7]

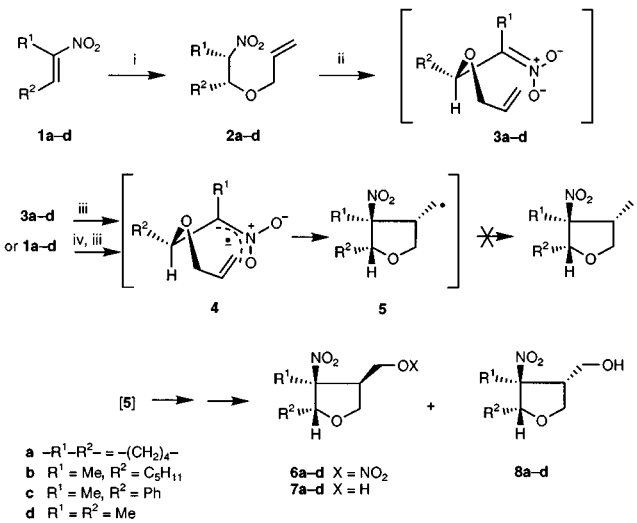

Scheme 1 *Reagents and conditions*: i, Bu^{t}OK (1.5 equiv.), Bu^{t}OH–benzene (0.5:1), then allylic alcohol, then H$^+$, 85–90%; ii, Na, H, THF; iii, CAN, THF, −78 °C, then 0.1 M $Na_2S_2O_3$, 45–60%; iv, NaH, THF, then allylic alcohol, 60% (**6a**), 58% (**6b**), 52% (**6c**), 45% (**6d**), 6% [(**7** + **8**)**a**], 7% [(**7** + **8**)**b**], 8% [(**7** + **8**)**c**], 5% [(**7** + **8**)**d**].

The relative *cis* stereochemistry for R^1 and R^2 in acyclic compounds **6**–**8** arises from favored conformation **B** required by allylic 1,3-strain (Scheme 2) during the intramolecular *C*-alkylation; [8] the Beckwith transition state model[9] invoked to account for these selective transformations has previously been proposed for radical cyclisations of α-nitroalkyl radicals.[10]

Moreover, the isolation of *endo* nitro alcohols **8** as minor products indicates that the observed stereochemistry is also consistent with a reversible tandem cyclisation,¶ leading to a persistent *cis*-fused bicyclic nitroxyl radical **9**-*exo*,‖ which could act as a driving force for this stereoselective cyclisation to occur; oxidation of nitroxyl radical **9** with a second molecule of CAN affords cation **10** which is then neutralized by ligand exchange with CAN[7] (Scheme 2).

Selective formation of bicyclo compound **6a** is well-interpreted by using the '*cis*-decalin' model for cyclization of cyclohexyl radicals (Scheme 3).[11] This model predicts that *exo* product should result from conformation **C** in which the allyloxy substituent is axial, while cyclisation of **D**, with an equatorial substituent, should provide *endo* product. Indeed NMR data of 1-nitro-2-dimethylallyloxycyclohexane **2e** indicates that, even at room temperature, only the conformation with an axial dimethylallyloxy group is observed**†† (Scheme

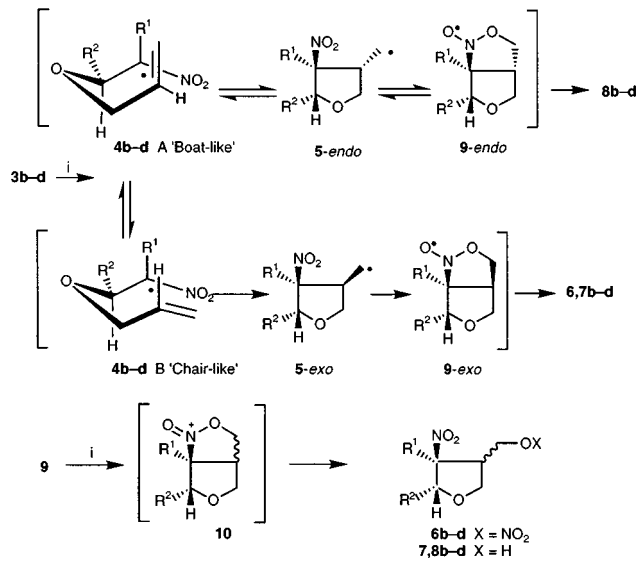

Scheme 2 *Reagents and conditions*: i, CAN, THF, −78 °C.

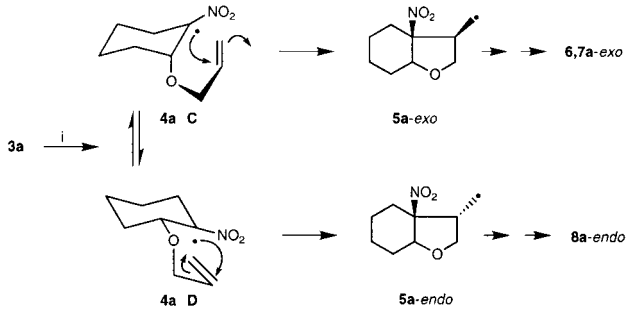

Scheme 3 *Reagents and conditions*: i, CAN, THF, −78 °C.

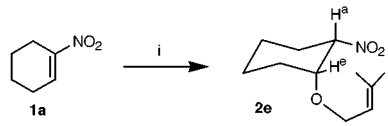

Scheme 4 *Reagents and conditions*: i, NaH, THF, then 3-methylbut-2-en-1-ol, then H^+, 12%.

4); this fact could argue for the high selectivities obtained at low temperature.

Therefore, although an intramolecular [3+2][12] cycloaddition of radical **4** could account for a totally stereoselective formation of *exo*-nitronitrates **6** through the bicyclic intermediate **9**-*exo* (Scheme 2), the proposal of a prior 5-*exo*-*trig* radical cyclization is better supported by the selectivities obtained in these transformations.

Solvolytic decomposition of nitrate esters in alkaline solution[13] accounts for the formation of nitro alcohols **7**-**8**; the isolation of *endo* nitro alcohol **8** as a minor compound could argue for the initial formation of *endo* nitro nitrate, transformation of which into **8** is quantitative under the reaction conditions, while the major *exo* nitro nitrate **6** is only partially converted into *exo* alcohol **7** (Scheme 5); indeed, when pure **6a** was reacted with NaH in 0.1 M $Na_2S_2O_3$ for 48 h, pure **7a** was isolated in 28% yield,‡‡ along with some remaining **6a**, while **8a** could not be detected by NMR. Thereby, the apparent total *exo* selectivity observed in the formation of nitro nitrates **6** should arise from the total transformation of the minor *endo* diastereomer into alcohol **8**.

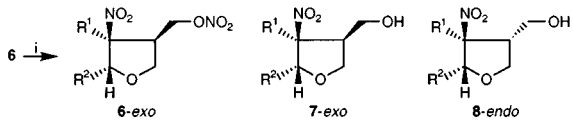

Scheme 5 *Reagents and conditions*: i, NaH, THF.

In conclusion, although it has been previously believed that cyclization of α-nitroalkenyl radicals for synthetic purposes could only be useful if groups more nucleophilic than unactivated alkenes are present,[14] our results show that, in turn, α-nitroalkenyl radicals generated by one-electron oxidation of *aci*-nitro anions with CAN lead stereoselectively to bifunctionalized tetrahydrofurans bearing three contiguous stereogenic centers. Moreover, the scope of subsequent conversions of the nitro and nitrate ester groups[15] should expand the utility of this new strategy in organic synthesis.

We are grateful to Professor M. Bertrand and Dr R. Faure (Marseille), Professor W. Dolbier Jr (Gainesville) and Professor D. P. Curran (Pittsburg) for useful suggestions.

Notes and references

† *Selected data* for **6a**: υ/cm^{-1} 2945, 2903, 1639, 1540, 1282, 861; δ_H(400 MHz, $CDCl_3$) 1.30 (m, 1H), 1.42 (m, 1H), 1.51 (m, 2H), 1.82 (m, 2H), 1.95 (ddd, *J* 14.6, 10.9, 3.7, 1H), 2.50 (dt, *J* 14.6, 3.7, 1H), 2.75 (quin, *J* 7.9, 1H), 3.8 (dd, *J* 9.5, 6.4, 1H), 4.25 (dd, *J* 9.5, 8.3, 1H), 4.42 (dd, *J* 11.1, 7.7, 1H), 4.49 (t, *J* 4.5, 1H); δ_C(100 MHz, $CDCl_3$) 19.6, 21.2, 26.4, 30.9, 32.6, 44.4, 68.6, 71.0, 77.7, 92.7.

‡ *Selected data* for **7a**: υ/cm^{-1} 3427, 2941, 2868, 1538, 1055; δ_H(400 MHz, $CDCl_3$) 1.40 (m, 4H), 1.72 (m, 2H), 1.92 (m, 1H), 2.48 (m, 1H), 2.52 (quin, *J* 5.8, 1H), 3.64 (t, *J* 5.7, 2H), 3.84 (dd, *J* 9.3, 5.8, 1H), 4.18 (dd, *J* 9.2, 8.3, 1H), 4.50 (td, *J* 3.7, 1.0, 1H); δ_C(100 MHz, $CDCl_3$) 19.5, 21.4, 26.1, 33.5, 49.6, 61.5, 68.6, 79.4, 92.4.

§ *Selected data* for **8a**: δ_H(400 MHz, $CDCl_3$) 1.42 (m, 4H), 1.51 (m, 2H), 1.82 (m, 1H), 2,40 (m, 1H), 2.50 (m, 1H), 3.65 (m, 2H), 3.90 (dd, *J* 11.1, 7.9, 1H), 4.22 (dd, *J* 9.6, 9, 1H), 4.44 (t, br, *J* 3.3, 1H); δ_C(100 MHz, $CDCl_3$) 19.1, 21.0, 25.6, 26.1, 50.8, 60.0, 68.1, 79.4, 92.4.

¶ Although alkyl-substituted radicals undergo exothermic cyclizations which are not reversible, Julia and co-workers showed that cyclizations could be reversible in the presence of radical-stabilizing groups (ref. 16).

‖ The transient formation of cyclic nitroxide to account for a similar transformation of an *aci*-nitro anion of a norbornene derivative upon oxidation with $K_3Fe(CN)_6$ was previously reported (ref. 14).

** The low yield obtained in the preparation of **2e** (12%) resulted from a retro-Michael reaction, facilitated by the *trans* diaxial position of acidic hydrogen and the dimethylallyloxy substituent; attemps to generate the radical by oxidation of **3e** with CAN met with failure.

†† Assignement of the *axial* position for the dimethylallyloxy group resulted from an ^1H–^{13}C correlation experiment.

‡‡ Nevertheless, nitrate esters are easily transformed into the corresponding alcohols according to a known procedure (ref. 17).

1 H. J. Schäfer, *Angew. Chem., Int. Ed. Engl.*, 1981, **20**, 911; H. G. Thomas, M. Streukens and R. Peek, *Tetrahedron Lett*., 1978, 45; J. L. Morgat and R. Pallaud, *C. R. Acad Sci*., 1965, **260**, 5579.
2 H. Schäfer and H. Küntzel, *Tetrahedron Lett.*, 1970, 3333; P. Renaud and M. A. Fox, *J. Org. Chem*., 1988, **53**, 3745; K. Narasaka, K. Iwakura and T. Okauchi, *Chem. Lett.*, 1991, 423; A. S. Kende, K. Koch and C. A. Smith, *J. Am. Chem. Soc*., 1988, **110**, 2210; T. Cohen, K. McNamara, M. A. Kuzemko, K. Ramig, J. J. Landi, Jr. and Y. Dong, *Tetrahedron*, 1993, **49**, 7931.
3 N. Arai and K. Narasaka, *Chem. Lett*., 1995, 987.
4 N. Arai and K. Narasaka, *Bull. Chem. Soc. Jpn*., 1997, **70**, 2525.
5 W. R. Bowman, D. S. Brown, C. A. Burns and D. Crosby, *J. Chem. Soc., Perkin Trans. 1*, 1994, 2083; W. R. Bowman, D. Crosby and P. J. Westlake, *J. Chem. Soc., Perkin Trans. 2*, 1991, 73.
6 N. Ono, H. Miyake, A. Kamimura, I. Hamamoto, R. Tamura and A. Kaji, *Tetrahedron*, 1985, **41**, 4013; J. L. Duffy, J. A. Kurth and M. J. Kurth, *Tetrahedron Lett*., 1993, **34**, 1259.
7 T. L. Ho, *Synthesis*, 1973, 347; C. A. Horiuchi, Y. Nishio, D. Gong, T. Fujisaki and S. Kiji, *Chem. Lett.*, 1991, 607; S. Hanessian and R. Léger, *J. Am. Chem. Soc*., 1992, **114**, 3115.
8 E. Dumez, J. Rodriguez and J.-P. Dulcère, *Chem. Commun*., 1997, 1831; J.-P. Dulcère and E. Dumez, *Chem. Commun*., 1997, 971.
9 A. L. Beckwith, C. J. Easton, T. Lawrence and A. K. Serelis, *Aust. J. Chem*., 1983, **36**, 545; A. L. Beckwith and A. K. Serelis, *J. Chem. Soc., Chem. Commun.*, 1980, 484
10 W. R. Bowman and S. W. Jackson, *Tetrahedron*, 1990, **46**, 7313.
11 T. V. RajanBabu, *Acc. Chem. Res*., 1991, **24**, 139; D. P. Curran, N. A. Porter and B. Giese, *Stereochemistry of Radical Reactions*, VCH, New York, 1996, p. 58.
12 S. E. Denmark, Y-C. Moon and C. B. W. Senanayake, *J. Am. Chem. Soc*., 1990, **112**, 311; P. Armstrong, R. Grigg, F. Heaney, S. Surendrakumar and W. J. Warnock, *Tetrahedron*, 1991, **47**, 4495.
13 D. C. J. Wu, C. J. Cheer, R. P. Panzica and E. Abushanab, *J. Org. Chem.*, 1982, **47**, 2661; J. W. Baker and D. M. Easty, *J. Chem. Soc*., 1952, 1193; G. R. J. Thatcher and H. Weldon, *Chem. Soc. Rev.*, 1998, **27**, 331.
14 W. R. Bowman, D. S. Brown, C. A. Burns and D. Crosby, *J. Chem. Soc., Perkin Trans. 1*, 1993, 2099.
15 D. Seebach, E. W. Colvin, F. Lehr and T. Weller, *Chimia*, 1979, **33**, 1; J. P. Adams and D. S. Box, *Contemp. Org. Synth*., 1997, 415; J. P. Adams and D. S. Box, *J. Chem. Soc., Perkin Trans. 1*, 1999, 749; G. Rosini and R. Ballini, *Synthesis*, 1988, 833; T. Shono, M. Chuankamnerdkarn, H. Maekawa, M. Ishifune and S. Kashimura, *Synthesis*, 1994, 895.
16 M. Julia, M. Maumy and L. Mion, *Bull. Soc. Chim. Fr*., 1967, 2641; M. Julia and M. Maumy, *Bull. Soc. Chim. Fr*., 1969, 2427.
17 R. T. Merrow, S. J. Cristol and W. V. Dolah, *J. Am. Chem. Soc*., 1953, **75**, 4259.

Communication 9/07842H

Cyclization reactions of vicinal dianions with 1,2-dielectrophiles: synthesis and properties of the first 2,3-diiminothietanes†

Peter Langer*[a] and Manfred Döring[b]

[a] *Institut für Organische Chemie der Georg-August-Universität Göttingen, Tammannstrasse 2, 37077 Göttingen, Germany. E-mail: planger@uni-goettingen.de*

[b] *Institut für Anorganische und Analytische Chemie der Universität Jena, August-Bebel-Strasse 2, 07743 Jena, Germany*

Received (in Cambridge, UK) 25th August 1999, Accepted 14th October 1999

Reaction of dilithiated ethyl thioglycolate with bis(imidoyl chloride)s of oxalic acid afforded the first 2,3-diiminothietanes, which underwent ring expansion reactions upon treatment with ethyl thioglycolate or dimethyl acetylenedicarboxylate.

Four-membered ring lactams and lactones represent pharmacologically important compounds which, due to their ring strain, readily undergo ring-expansion or -opening reactions.[1] To the best of our knowledge, azetidine-2,3-diones represent the only known heterocycles which combine the biologically significant structural features of a four-membered ring and a 1,2-dione subunit.[2] Due to their high reactivity, oxetanes and thietanes containing a 1,2-dione subunit are unknown to date. However, a few examples of the corresponding heterocyclic 1,2-diimines have been reported.[3,4] We envisaged that reaction of 1,2-dianions with oxalic acid dielectrophiles could provide a convenient synthesis of four-membered ring heterocycles containing a 1,2-dione or related subunit. Much to our surprise, until recently cyclization reactions of oxalic acid dielectrophiles with 1,1-, 1,2-, 1,3- or 1,4-dianions had not been reported.[5] This is presumably due to the fact that these reactions can suffer from several drawbacks, such as overaddition of the nucleophile, expulsion of CO or decomposition. We have recently shown that bis(imidoyl chloride)s of oxalic acid [$Cl_2C_2(NR)_2$] represent useful C_2 building blocks in cyclization reactions with 1,3-dianions.[6] Herein we report that bis(imidoyl chloride)s can be cyclized with 1,2-dianions equally successfully. To the best of our knowledge, these transformations represent the first examples of cyclization reactions of 1,2-dianions with 1,2-dielectrophiles to date.[7]

Our first aim was the preparation of 2,3-diiminothietanes by reaction of dilithiated thiols with bis(imidoyl chloride)s.[4,8] Unfortunately, treatment of bis(imidoyl chloride) **2a** with the dianion of BnSH **1b**[9a] gave a complex reaction mixture from which the cyclic disulfide **3** was isolated in low yield (Scheme 1). Formation of **3** can be explained by initial condensation of **2a** with 2 equiv. of **1b** and subsequent oxidative cyclization. The yield of **3** could be improved by the use of 2 rather than only 1 equiv. of the dianion. However, a change of the reaction conditions (slow addition of the dianion to **2a**) and of the work-up procedure (filtration under inert conditions rather than aqueous work-up) did not provide the desired product **4**. Similar disappointing results were obtained when the dianion of prop-2-enethiol was employed.

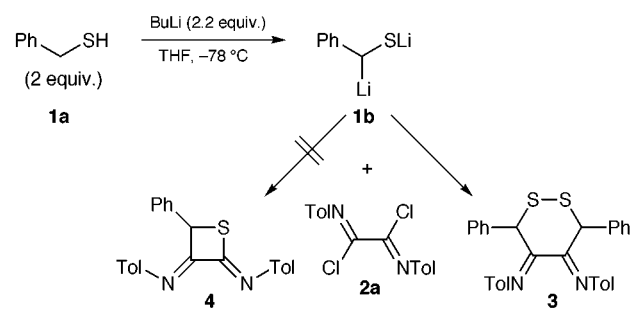

Scheme 1

Much to our satisfaction, reaction of bis(imidoyl chloride) **2a** with the dianion of ethyl thioglycolate **5b**[9b] afforded the 2,3-diiminothietane **6a** in 30% yield (Scheme 2).‡ Thietane **6a** could be readily isolated by chromatography as it represented the only Et_2O-soluble product formed in the reaction. In contrast, reaction of **5b** with oxalyl chloride or diethyl oxalate gave polymeric material under a variety of conditions. In contrast to the open-chained derivative Me(PhHN)C=CH-CO_2Et, thietane **6a** adopted a 3-iminopropionate- rather than a 3-aminocrotonate structure, presumably for electronic reasons. Variable temperature ^{1}H NMR ($CDCl_3$) showed that 2,3-diiminothietane **6a** represented a structurally mobile compound due to *E*/*Z* isomerization of the imino group at C-3.§

Interestingly, treatment of bis(imidoyl chloride)s **2b**,**c** with the dianion **5b** resulted in formation of the 1,2-dithioles **7b** and **7c** in 41 and 40% yields, respectively (Scheme 2).[10] The formation of the dithioles **7** can be explained by initial cyclization to give the 2,3-diiminothietanes **6**, subsequent ring opening, addition of a second equivalent of the dianion, cyclization and expulsion of EtOAc.

In order to elucidate the mechanism of the conversion of 2,3-diiminothietanes **6** into the bisthioles **7**, cycloaddition reactions of **6a** were studied. When a toluene solution of thietane **6a** and dimethyl acetylenedicarboxylate (DMAD) was stirred at 80 °C for 12 h, the yellow coloured thioimino ether **9** was isolated in 64% yield (Scheme 3). The formation of cycloadduct **9** can be explained by initial ring-opening of thietane **6a** to give the 1,4-zwitterionic intermediate **8** and subsequent regioselective cyclization of the latter with DMAD.¶ Bisthiole **7a** was isolated in 58% yield when a toluene

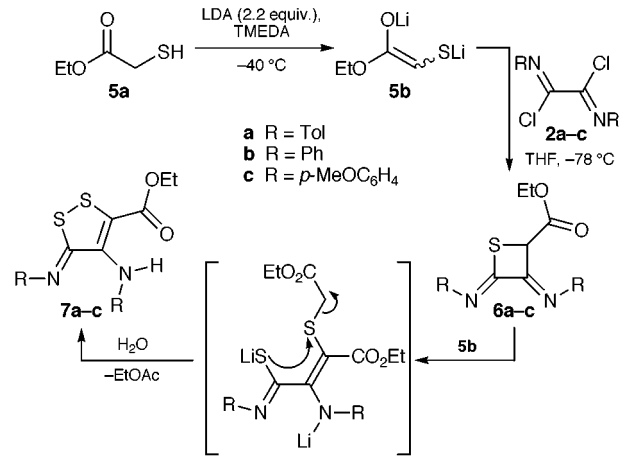

Scheme 2

† Dedicated to Professor A. Zeeck on the occasion of his 60th birthday.

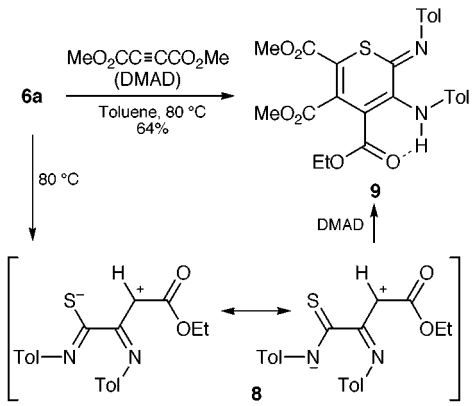

Scheme 3

solution of **6a** and of ethyl thioglycolate **5a** was stirred for 12 h at 80 °C. This experiment suggested that intermediate **8** was not only involved in the formation of the cycloadduct **9** but also in the conversion of the 2,3-diiminothietanes **6a**–**c** into the bisthioles **7a**–**c**.

The influence of the heteroatoms of the 1,2-dianion on the regiochemistry of cyclization was next studied. No cyclization could be induced in the reaction of bis(imidoyl chloride) **2a** with the dianion of ethyl lactate, presumably due to the lower nucleophilicity of the oxygen relative to the sulfur atom. In contrast, reaction of **2a**,**b** with the dianion of ethyl hippurate **10**[11] afforded the 6-imino-6*H*-1,3-oxazines **11a**,**b** by regioselective cyclization *via* the carbon and the oxygen atom of the dianion (Scheme 4). The regioselectivity of this reaction, which was carried out under kinetic conditions, can be explained by the higher electron density at the oxygen rather than at the nitrogen atom of the dianion or, alternatively, by initial formation of a four-membered ring and subsequent ring expansion. Similar to bisthioles **7a**–**c**, oxazines **11a**,**b** represent masked 1,2,3,4-tetracarbonyl systems containing strong intramolecular hydrogen bonds (N–H···O).

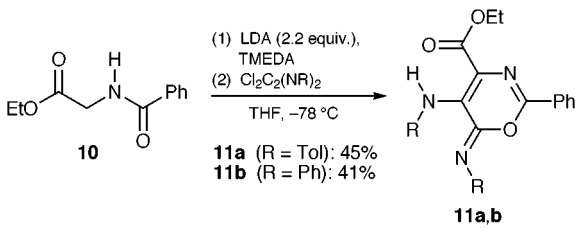

Scheme 4

P. L. thanks Professor A. de Meijere for his support. Financial support from the Fonds der Chemischen Industrie (scholarship and funds for P. L.) is gratefully acknowledged.

Notes and references

‡ *Preparation* of **6a**: A THF solution of LDA (2.5 equiv.) was prepared by addition of BuLi (9.4 ml, 1.6 M solution in hexane) to a THF solution (15 ml) of diisopropylamine (2.1 ml) at 0 °C. To this solution TMEDA (2.3 ml) and ethyl thioglycolate (0.54 ml) were added at −40 °C. The deep yellow solution was stirred at 0 °C for 2 h and subsequently transferred to a THF solution (80 ml) of **2a** (1.8 g) at −78 °C. The temperature was allowed to rise to ambient and the mixture was stirred for 2 h at 20 °C. The solvent was removed *in vacuo* and the residue was purified by chromatography (silica gel, Et_2O–light petroleum = 1 : 10 → 1 : 3) to give 634 mg (30%) of a yellow solid, mp 110 °C (decomp.); δ_H($CDCl_3$, 200 MHz) 0.98 (t, *J* 7, 3 H, CH_2CH_3), 2.32, 2.34 (s, 6 H, Tol-CH_3), 4.94 (m, 2 H, CH_2CH_3), 5.33 (s, 1 H, $CHCO_2Et$), 6.95–7.25 (m, 8 H, Tol); δ_C($CDCl_3$, 50 MHz) 13.62 (CH_2CH_3), 21.01, 21.18 (Tol-CH_3), 54.47 (CH, $CHCO_2Et$), 62.21 (CH_2CH_3), 121.44, 122.37, 129.75, 129.99 (CH, Tol), 136.66, 137.34 (C, Tol-C to CH_3), 142.95, 143.25 (C, Tol-C to N), 157.00 (C, CHCNTol), 158.99 (C, SCNTol), 167.39 (C, CO_2Et); ν_{max}(KBr)/cm^{-1} 2980 (w), 1738 (s), 1655 (m), 1641 (m), 1505 (s), 1268 (s), 1235 (m), 1125 (m), 1030 (m), 823 (m); *m*/*z* (CI, H_2O) 353 (M^+ + 1), 236 (M^+ + 1 − TolN=C), 203 (M^+ + 1 − TolN=C=S) (Calc. for $C_{20}H_{20}N_2O_2S$: C, 68.16; H, 5.72; N, 7.94. Found: C, 68.51; H, 5.79; N, 8.07%).

§ From 90 to 60 °C the ^1H NMR spectra exhibited only one set of signals. By cooling, broadening of the signals and coalescence (60 °C) were observed giving rise to two signals each for the CH, CH_2 and CH_3 group with the integration ratio 1 : 5. Singlets were detected for the CH groups and multiplets were detected for the CH_2 groups, both for the major and the minor component. The free energy of activation of this process ($\Delta G^‡$ = 74.0 kJ mol^{-1}) lies in the range of typical activation barriers for *E*/*Z* isomerizations of imines.

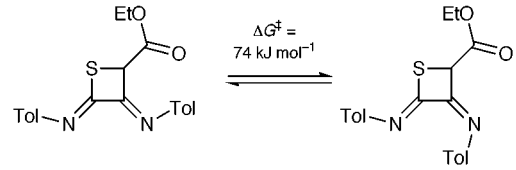

¶ To the best of our knowledge, open-chained 1,4-zwitterions related to **8** have not been reported so far. In contrast, 1,3-zwitterions have been previously discussed as intermediates in the chemistry of thietanes, see refs. 4(*a*) and 8(*c*). The mass spectrum of **6a** exhibited characteristic fragment peaks (loss of electroneutral TolN=C=S) which independently supported the existence of intermediate **8**. Cleavage of the carbon–sulfur bond of a 2-iminothietane has been observed during the thermal rearrangement of the latter to an α,β-unsaturated thioamide, see ref. 8(*b*).

1 J. A. Pono and S. L. Schreiber, in *Comprehensive Organic Synthesis*, ed. B. M. Trost, Pergamon, Oxford, 1991, vol. 5, p. 151; J. Mattay, R. Conrads and R. Hoffmann, in *Houben-Weyl*, ed. G. Helmchen, R. W. Hoffmann, J. Mulzer and E. Schaumann, 4th edn., Thieme, Stuttgart, 1995, vol. E21c, p. 3133.
2 L. A. Paquette, R. R. Rothhaar, M. Isaac, L. M. Rogers and R. D. Rogers, *J. Org. Chem.*, 1998, **63**, 5463; J. D. Buynak, H. B. Borate, G. W. Lamb, D. D. Khasnis, C. Husting, H. Isom and U. Siriwardane, *J. Org. Chem.*, 1993, **58**, 1325.
3 Only a single report related to the synthesis of 2,3-diiminooxetanes has appeared: H.-J. Kabbe, *Angew. Chem.*, 1968, **80**, 406; *Angew. Chem., Int. Ed. Engl.*, 1968, **7**, 389.
4 For the preparation of a triiminothietane, see: (*a*) G. L'abbé and L. Huybrechts, *J. Chem. Soc., Chem. Commun.*, 1979, 161; for the preparation of a 2,4-diiminothietane, see (*b*) G. L'abbé and J.-P. Dekerk, *Tetrahedron Lett.*, 1979, 3213; (*c*) H. J. Bestmann, *Angew. Chem.*, 1977, **89**, 370; *Angew. Chem., Int. Ed. Engl.*, 1977, **16**, 358.
5 P. Langer and M. Stoll, *Angew. Chem.*, 1999, **111**, 1919; *Angew. Chem., Int. Ed.*, 1999, **38**, 1803.
6 P. Langer, M. Döring, H. Görls and R. Beckert, *Liebigs Ann./Recl.*, 1997, 2553; P. Langer and M. Döring, *Synlett*, 1998, 396; P. Langer and M. Döring, *Synlett*, 1998, 399; P. Langer, J. Wuckelt, M. Döring and R. Beckert, *Eur. J. Org. Chem.*, 1998, 1467.
7 For reactions of 1,2-dianions with 1,3-dielectrophiles, see: K. G. Bilyard, P. J. Garratt, R. Hunter and E. Lete, *J. Org. Chem.*, 1982, **47**, 4731; for the preparation of β-lactams by reaction of 1,3-amide dianions with CH_2I_2, see: K. Hirai and Y. Iwano, *Tetrahedron Lett.*, 1979, 2031.
8 Only a few 2-iminothietanes have been prepared so far: (*a*) A. Dondoni, A. Batagha, P. Giorgianni, G. Gilli and M. Sacerdoti, *J. Chem. Soc., Chem. Commun.*, 1977, 43; (*b*) J. Mulzer and T. Kerkmann, *Angew. Chem.*, 1980, **92**, 470; *Angew. Chem., Int. Ed. Engl.*, 1980, **19**, 466; (*c*) E. Schaumann, M. Möller and G. Adiwidjaja, *Chem. Ber.*, 1988, **121**, 689; (*d*) M. Sakamoto, T. Ishida, T. Fujita and S. Watanabe, *J. Org. Chem.*, 1992, **57**, 2419.
9 (*a*) K. H. Geiß, D. Seebach and B. Seuring, *Chem. Ber.*, 1977, **110**, 1833; (*b*) K. Tanaka, N. Yamagishi, R. Tanikaga and A. Kaji, *Chem. Lett.*, 1977, 471.
10 Heterocyclic bisthioles are present in natural products, for example in the antibiotic thiolutine: H.-D. Stachel and K. Zeiler, *Liebigs Ann.*, 1995, 2011.
11 A. P. Krapcho and E. A. Dundulis, *Tetrahedron Lett.*, 1976, 2205.

Communication 9/06913E

ChemComm
FEATURE ARTICLE

Iridium PCP pincer complexes: highly active and robust catalysts for novel homogeneous aliphatic dehydrogenations

Craig M. Jensen

Department of Chemistry, University of Hawaii, Honolulu, HI 96822, USA. E-mail: jensen@gold.chem.hawaii.edu

Received (in Cambridge, UK) 5th May 1999, Accepted 17th August 1999

The PCP pincer complexes, $IrH_2\{C_6H_3(CH_2PR_2)_2\text{-}2,6\}$ (R = Bu^t, Pr^i) are extraordinarily active and robust catalysts for aliphatic dehydrogenation reactions. Their application to alkane dehydrogenation has resulted in the first efficient catalytic systems for homogeneous thermochemical alkane dehydrogenation without the use of a sacrificial hydrogen acceptor and for dehydrogenation of *n*-alkanes to α-olefins. The pincer catalysts also effect other aliphatic dehydrogenations which had not previously been accomplished *via* homogeneous catalysis including the conversion of cycloalkanes to arenes, ethylbenzene to styrene and tetrahydrofuran to furan. All of these catalytic reactions are inhibited by even traces of nitrogen. This is apparently due to the formation of the remarkably stable dinitrogen complexes: $[Ir\{C_6H_3(CH_2PR_2)_2\text{-}2,6\}]_2(\mu\text{-}N_2)$. Mechanistic studies have indicated that the high activity of the pincer catalysts may be in part due to 'agostic promotion' by phosphino aliphatic groups.

Introduction

The selective functionalization of aliphatic groups is one of the great unsolved problems of organic chemistry. The quest for methods to effect this type of transformation continues to entice chemical researchers through economic incentives and intellectual challenge. One of the most commercially tantalizing possibilities is the production of major organic feedstocks such as terminal alkenes (α-olefins) through regioselective aliphatic dehydrogenation reactions. Two decades ago, Crabtree *et al.* first reported the stoichiometric dehydrogenation of alkanes to alkenes by soluble transition metal complexes.[1] This was followed by the 1983 discovery by Baudry *et al.* of the first homogeneous catalyst for the transfer dehydrogenation of alkanes to alkenes.[2] A variety of other complexes were found during the next 12 years that operate in systems that are driven by the hydrogen transfer from alkanes to hydrogen acceptors (transfer-dehydrogenation),[3–9] photoirradiation,[5,10] and the thermal evolution of hydrogen.[11,12] The systems generally suffered from very slow reaction rates and rapid catalyst decomposition.[1–5,8,11,12] The first efficient thermochemical system for the transfer dehydrogenation of alkanes was achieved by Goldman and coworkers in 1991 using $Rh(CO)Cl(PMe_3)_2$ as catalyst under a hydrogen atmosphere.[6] Unfortunately, this system also catalyzes a 4–20 fold excess of direct (non-transfer) hydrogenation of the sacrificial alkene. It was subsequently found that closely related rhodium arsine[7] and phosphine enolate[9] complexes function as efficient catalysts under similar conditions. Notably the excess of acceptor which is consumed is significantly reduced when the reaction is catalyzed by arsine complexes.[7] While the state of the art of homogeneous alkane dehydrogenation catalysts had continuously advanced, it was apparent that the development of practical systems awaited the discovery of catalysts with greatly improved thermal stability and enhanced reactivity with alkane C–H bonds.

Hydrido complexes containing a tridentate monoanionic aryl bis(phosphino), 'PCP pincer' ligand were first prepared by Moulton and Shaw.[13] The complexes $IrClH\{C_6H_3(CH_2PBu^t_2)_2\text{-}2,6\}$ **1a** and $RhClH\{C_6H_3(CH_2PBu^t_2)_2\text{-}2,6\}$ **1b**, were found to possess unusually high thermal stabilities and sublime at 180–200 and 245–350 °C, respectively, without decomposition.[13] In 1979, it was observed that the intermediate resulting from the dehydrochlorination of **1b** with $NaN(SiMe_3)_2$, reacted readily with pentane, octane and cyclohexane to produce hydride complexes.[14,15] Thus it seemed that '$M\{C_6H_3(CH_2PBu^t_2)_2\text{-}2,6\}$' (M = Ir, Rh) might have the right combination of thermal stability and high reactivity with aliphatic C–H bonds to function as practical alkane dehydrogenation catalysts. Unfortunately, '$Rh\{C_6H_3(CH_2PBu^t_2)_2\text{-}2,6\}$' has proven to be too unstable to isolate. Attempts to utilize the complex for the catalytic transfer dehydrogenation of alkanes upon *in situ* generation from **1b** were also unsuccessful. Thus we considered alternative methods of generating a PCP pincer catalyst.

A number of dihydrido iridium bis(phosphine) complexes had been found to be catalysts for alkane dehydrogenation.[3–5,8,11] Therefore, we reasoned that the dihydrido PCP pincer complexes $MH_2\{C_6H_3(CH_2PBu^t_2)_2\text{-}2,6\}$, (M = Ir, **2a**; Rh, **2b**) were logical catalyst candidates. As we began our exploration of the pincer catalyst in the spring of 1996, we were unaware that the groups of Goldman[16] and Leitner[17] had independently identified rhodium complexes containing very similar chelating phosphine ligands as likely candidates for advanced alkane dehydrogenation catalysts and were embarking on similar studies.

Synthesis and characterization of dihydrido pincer complexes

The dihydrido complex **2a** had not previously been synthesized and isolated. A species previously generated *in situ* and identified as **2a**[18] is actually the tetrahydride complex, $IrH_4\{C_6H_3(CH_2PBu^t_2)_2\text{-}2,6\}$, **3a**. We have found methods whereby the dihydride complexes can be prepared and isolated in > 85% yield.[19] The iridium complex **2a** was synthesized by the two step procedure seen in Scheme 1. This reaction

Craig M. Jensen is a Professor of Chemistry at the University of Hawaii. He was born and raised in Wenatchee, Washington, USA. His undergraduate education began at the University of Washington and was completed, after a sabbatical in the Aleutian Islands, at the University of California at Santa Barbara. He obtained his PhD at the University of California at Los Angeles under the supervision of Professor H. D. Kaesz. Following a postdoctoral appointment at the University of California at San Diego, he joined the faculty at UH in 1986. In addition to pincer catalysts, his research group is developing advanced hydrogen storage materials.

sequence had previously been developed by Kaska and coworkers for the preparation of $IrH_2\{HC(C_2H_4PBu^t_2)_2\}$ from $IrClH\{HC(C_2H_4PBu^t_2)_2\}$.[20] In the first step of this procedure, the hydrido chloride complex **1a** is converted to the white tetrahydride complex **3a** through reaction with $LiBEt_3H$ under an atmosphere of H_2. Following isolation and recrystallization of **3a**, the brown dihydrido complex, **2a** is obtained quantitatively upon heating finely powdered **3** at 130 °C *in vacuo*.

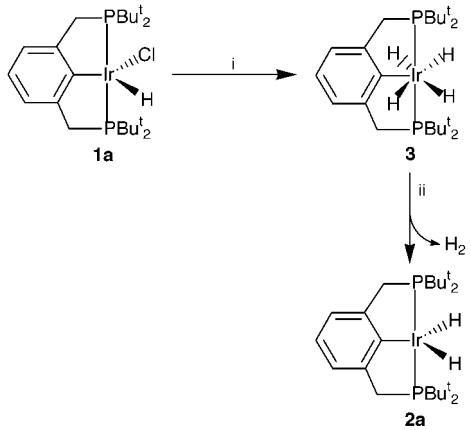

Scheme 1 *Reagents and conditions*: i, $LiEt_3BH$ (1 M in THF) 1 equiv., 1 atm H_2, 25 °C, pentane; ii, 3×10^{-3} torr, 130 °C, 24 h.

An X-ray structure determination was carried out on a single crystal of **2a** in order to verify the structural composition.[19] A diagram of the determined molecular structure is presented in Fig. 1. This depiction underscores how the rigid coordination

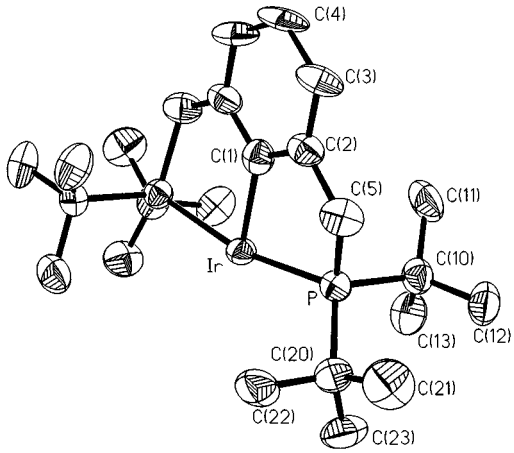

Fig. 1 Projection of $IrH_2\{C_6H_3(CH_2PBu^t_2)_2$-2,6} **2a** with the thermal ellipsoids at 50% probability. Selected bond distances (Å) and angles (°): Ir–C(1) 2.12(1), Ir–P 2.308(2), P–Ir–C(1) 82.41(6), P–Ir–P(a) 164.8(1).

framework of the PCP pincer ligand effectively restricts the access of the metal center to the P–C and C–C bonds of the ligand thus rendering the complex to be sufficiently robust to withstand high temperatures.

The synthesis of **2b** is not complicated by the formation of a tetrahydride. Thus the rhodium PCP dihydride can be prepared directly from the hydrido chloro complex. It was initially obtained among the products resulting from the treatment of **1b** with either $NaN(SiMe_3)_2$ or KH under an atmosphere of hydrogen.[15] A much cleaner reaction occurs with $LiBEt_3H$ under an atmosphere of H_2 and purified **2b** can be isolated upon recrystallization.[21]

Dehydrogenation of alkanes to alkenes

Cyclooctane

The enthalpy of dehydrogenation of cyclooctane is 23.3 kcal mol^{-1}, 5–7 kcal mol^{-1} lower than for most alkanes. This 'best case' substrate has been the conventional starting point for most studies of homogeneous catalysts for the dehydrogenation of alkanes. As mentioned above, a sacrificial hydrogen acceptor is generally required in thermochemical catalytic systems. Crabtree *et al.* found *tert*-butylethylene (tbe) to be a particularly effective acceptor in their early studies[1] and its use in these systems has become standard.

Our initial attempts to utilize the di- and tetra-hydrido pincer complexes as catalysts for the generic cyclooctane–tbe system were unsuccessful. No catalytic activity was observed when the complexes were used either directly upon generation *in situ* or in crude unpurified form. The key to the discovery of the extraordinary catalytic activity of both **2a**[19] and **3a**[21] was the recrystallization of the complexes from pentane to remove borate impurities introduced during its generation from $LiBEt_3H$. At 150 °C the dehydrogenation of cyclooctane by **2a** proceeds at a rate of 82 turnovers h^{-1} while a rate of 12 turnovers min^{-1} is observed at 200 °C. Appreciable activity (20.5 turnovers h^{-1}) is observed as low as 100 °C. Furthermore, no significant decomposition of the catalyst occurs within the time required for the complete consumption of the hydrogen acceptor. The long term maintenance of catalyst integrity contrasts with the short, *ca.* 12 h half lives which had typically been found for alkane dehydrogenation catalysts.

Prior to our studies of the pincer catalysts, only rhodium complexes had been found to exhibit high activity as alkane dehydrogenation catalysts.[6,7,9,10] Thus it is surprising that **2b** shows only very low catalytic activity. For example, a rate of only 0.8 turnovers h^{-1} was observed for the dehydrogenation of cyclooctane by **2b** at 200 °C.[21] *Ab initio* calculations have shown[22] that addition of H_2 to $Rh(PH_3)_2Ph$ is $\geqslant$ 20 kcal mol^{-1} less favorable than addition to $Ir(PH_3)_2Ph$, $Rh(PH_3)_2Cl$ or $Ir(PH_3)_2H$.[23] This suggests that addition of closely related C–H bonds to rhodium PCP pincer complexes may also be unfavorable thus accounting for the low observed catalytic activity. In support of this hypothesis, Milstein *et. al.* have recently found the alkyl rhodium pincer complexes $RhR\{C_6H_3(CH_2P^tBu_2)_2$-2,6}I (R = Pr^i, Pr^n, Et) to be exceptionally stable against intermolecular addition of the β-C–H bonds of the alkyl ligands.[24]

Nitrogen and alkene inhibition

The catalytic activity of the pincer complexes is suppressed by N_2. In order to achieve the maximum catalytic rates, reaction mixtures must be freeze–pump–thaw degassed prior to heating to remove any vestiges of N_2. This unusual N_2 inhibition of the catalytic activity is due to the formation of the surprisingly stable dinitrogen complex, $[Ir\{C_6H_3(CH_2PBu^t_2)_2$-2,6}$]_2(\mu$-$N_2)$ **4**.[25] The complex was isolated by treating a cyclohexane solution **2a** with a 15 fold excess of tbe under 1 atm of nitrogen at 80 °C. The dinitrogen complex is produced in nearly quantitative yield within 1 h. The formation of **4** is evidently initiated by the reaction of nitrogen with the intermediate resulting upon the dehydrogenation of **2a** by tbe as nearly one equivalent of *tert*-butylethane is produced in the reaction.

The molecular structure of **4** was elucidated through a single crystal X-ray structure determination[25] and is depicted in Fig. 2. The dihedral angle between the planes defined by Ir(1), P(11), P(12) and Ir(2), P(21), P(22) is 89.5°. This nearly perpendicular arrangement results in the encapsulation of the nitrogen ligand and is apparently responsible for the surprising stability of **4** and the pronounced inhibiting effect of nitrogen on the catalytic reactions.

The dehydrogenation activity of **2a** is inhibited by high concentrations of alkene. Thus the loading of hydrogen acceptor in the reaction mixture is restricted. For example, diminished rates of catalysis are found in solutions containing > 300 : 1 ratio of tbe to catalyst. In order to achieve high turnover numbers, a limited amount of tbe must be periodically added to reaction

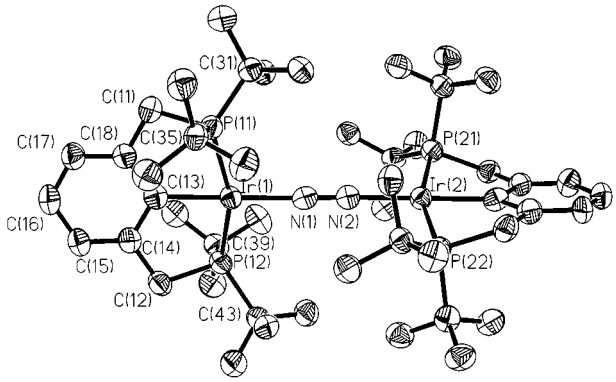

Fig. 2 Projection of [Ir{$C_6H_3(CH_2PBu^t_2)_2$-2,6}]$_2$(μ-N_2) **4** with the thermal ellipsoids at 25% probability. Selected bond distances (Å) and angles (°): Ir(1)–C(13), 2.053(12), Ir(1)–P(11) 2.312(3), Ir(1)–N(1) 2.007(11), N(1)–N(2) 1.176(13), C(13)–Ir(1)–P(11) 78.6(3), P(11)–Ir(1)–P(12) 160.22(10), Ir(1)–N(1)–N(2) 178.7(9).

mixtures. Following incremental additions of tbe, the dehydrogenation of cyclooctane is observed to again proceed at a rate of 12 turnovers min^{-1}.[21]

At higher concentrations, the cyclooctene product inhibits the catalyst and only *ca*. 10% of the cyclooctane can be dehydrogenated. Overcoming this problem of product inhibition is one of the major challenges to be met in the development of synthetically useful methods based on pincer complex catalyzed dehydrogenation reactions.

Linear alkanes

Terminal alkenes (α-olefins) are a major feedstock for the production of plastics, detergents and lubricants. Their production through the selective dehydrogenation of linear alkanes would be an attractive alternative to the present commercial processes based on hydrogen, ethylene and trialkylaluminium catalysts.[26] Several studies of alkane activation by rhodium and iridium complexes have shown that oxidative addition of primary C–H bonds is kinetically preferred despite their greater bond strength.[27] Thus it is plausible that a kinetically controlled, catalytic system based on rhodium or iridium complexes could be developed for the regioselective dehydrogenation of *n*-alkanes to terminal alkenes. An early study by Felkin *et al.* found that $IrH_5(PPr^i_3)_2$ catalyzes the transfer dehydrogenation of *n*-hexane to hex-1-ene with >90% selectivity.[3] However, only 0.3 catalytic turnovers were achieved owing to the low activity and stability of the catalyst. Other catalytic systems were found to have higher activity with *n*-alkanes but the observed product distributions were essentially thermodynamically controlled and contained little or no terminal alkene.[6,7,10] The hope of developing a system which capitalized on the kinetic preference of iridium and rhodium complexes for the activation of the terminal C–H bonds of alkanes was raised by the discovery that $RhCl(CO)(PMe_3)_2$ catalyzed a photochemical system for the efficient, regioselective carbonylation of the terminal position of *n*-alkanes.[28] In view of the high activity found for **2a** in our studies with cyclooctane, it seemed possible that its application to the dehydrogenation of *n*-alkanes might lead to the selective production of the kinetically preferred terminal alkenes.

Our initial studies of the dehydrogenation of *n*-octane with the pincer catalyst **2a** indicated that the reaction was highly selective for internal octenes over oct-1-ene.[29] However, a study of product distribution *vs*. time at 150 °C revealed a more complicated situation.[30] The data presented in Fig. 3 clearly illustrates the high kinetic selectivity of the reaction for oct-1-ene. To our knowledge this is the first catalytic system for the efficient and selective dehydrogenation of linear alkanes to terminal alkenes. It can also be seen that **2a** also functions less efficiently as an alkene isomerization catalyst. While the net

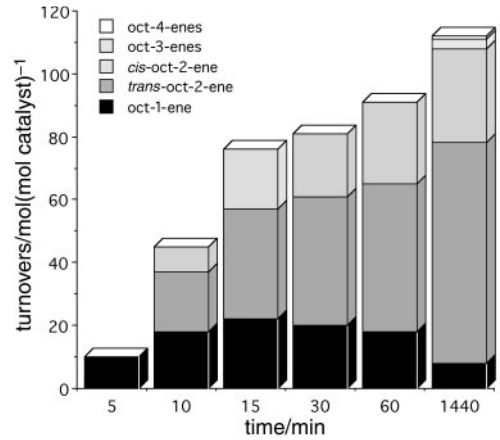

Fig. 3 Distributions of octenes produced at various times from the transfer dehydrogenation of *n*-octane catalyzed by **2a** at 150 °C.

production of octenes begins to level off within the first hour due to octene inhibition of the dehydrogenation reaction, the distribution of octenes continues to slowly shift towards the internal isomers. Although the practical utility of this system is limited by the secondary alkene isomerization reaction, modification of the system may permit production of high yields of terminal alkenes. For example, Goldman and coworkers have found that the rate of the isomerization reaction is sensitive to the steric bulk of hydrogen acceptor. Using the combination of dec-1-ene as hydrogen acceptor and **2a** as catalyst for the transfer dehydrogenation of *n*-octane, a 68% selectivity for oct-1-ene after 143 total turnovers is observed before its level begins to decline due to secondary isomerization.[30]

Acceptorless dehydrogenation of alkanes to alkenes

Both economical and environmental considerations preclude systems requiring a sacrificial hydrogen acceptor from consideration for the commercial production of alkenes. Thus there is great interest in the development of 'acceptorless' systems in which alkanes are transformed to alkenes upon the direct elimination of H_2. In 1990 Fujii and Saito reported the first thermochemical homogeneous catalytic systems for acceptorless dehydrogenation of alkanes.[11] In order to circumvent unfavorable equilibrium constraints, hydrogen was evolved from the refluxing systems *via* a continuous purge with an inert gas. Other systems for acceptorless alkane dehydrogenation were developed using this approach but suffered from the usual problems of very low catalytic activities (<2 turnovers h^{-1}) and catalyst instability.[11,12]

The iridium PCP pincer complexes have been found to be much more efficient catalysts for acceptorless dehydrogenation.[22,31] As a result of their high activity and long term stability at very high temperatures, the turnover numbers which can be achieved in continuously purged, open reflux systems are increased by two orders of magnitude. Recently, Liu and Goldman observed turnover numbers approaching 1000 for the acceptorless dehydrogenation of cyclodecane in experiments employing $IrH_2\{C_6H_3(CH_2PPr^i_2)_2$-2,6} **6**, the isopropyl analog of **2a,** as catalyst.[31]

Mechanistic studies

The overall mechanism of the transfer dehydrogenation of alkanes by **2a** is largely unexplored. However, the initial process in the catalytic sequence is undoubtedly the dehydrogenation of the dihydride by the hydrogen acceptor to produce the key intermediate '$Ir\{C_6H_3(CH_2PBu^t_2)_2$-2,6}'. This reaction occurs cleanly at 25 °C and has been studied in detail.[25] The dehydrogenation of **2a** in neat tbe at 25 °C gives a stoichiometric amount of *tert*-butylethane (tba) within 1 h. As seen in Scheme 2, experiments in neat $H_2C{=}CDCMe_3$ produce ex-

clusively β labeled tba. We also observed that no deuterium is scrambled into **2a** during the course of the dehydrogenation reaction. These findings lead to the conclusion that hydride migration to coordinated tbe is irreversible.

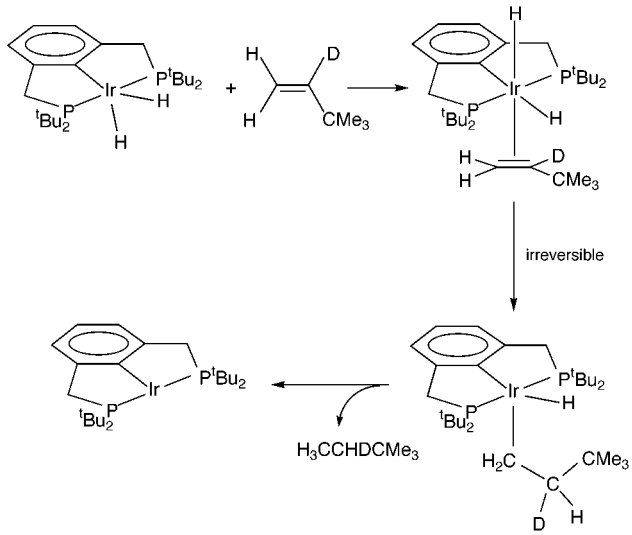

Scheme 2 Mechanism of the dehydrogenation of **2a** by $H_2C=CDCMe_3$.

Results of studies of dehydrogenation of **2a** contrast with those of our earlier study with the chloro complex $IrClH_2(P\text{-}Pr^i_3)_2$ **5**.[8] While coordination of tbe and subsequent hydride migration are also facile with **5**, the reductive elimination of tba from the resulting alkyl hydride complex requires the addition of an alkane and heating to 150 °C. The high barrier to elimination of tba in the case of **5** renders the hydride migration step reversible as demonstrated by the transfer of deuterium from $IrClD_2(PPr^i_3)_2$ (**5**-d_2) to the β position of tbe.

It is possible that an agostic interaction with a methyl C–H bond of a *tert*-butyl methyl group triggers tba elimination from the pincer complex. This hypothesis is supported by the observation of deuterium scrambling in the dideuterio complex, **2a**-d_2. The exchange between the deuteride and the methyl hydrogens of the *tert*-butyl methyl groups of the pincer ligand was apparent within 2 h of dissolving **2a**-d_2 in cyclohexane at 25 °C. In contrast, heating the dideuterio complex, **5**-d_2 in toluene solution at 150 °C for 24 h does not result in transfer of the deuterium label to isopropyl methyl groups of phosphine ligands.[32] The ability of the phosphine alkyl groups of **2a** to interact with the iridium center may eliminate the requirement of alkane association for tba elimination found for **5**.[8] Thus 'agostic promotion' by the pendent *tert*-butyl methyl groups may partially account for **2a** having much higher activity for the catalytic transfer dehydrogenation of alkanes than **5**.

The complex which is produced upon the dehydrogenation of **2a** has been characterized by ^1H and ^{31}P NMR spectroscopy. These data confirm the presence of the pincer ligand and absence of hydride ligands. However, it remains questionable whether the product is the 14-electron species $Ir\{C_6H_3(CH_2P\text{-}Bu^t_2)_2\text{-}2,6\}$ as the spectroscopic data do not preclude the possibilities of highly fluxional agostic interactions with phosphine alkyl groups or the presence of tbe and/or solvent ligands which undergo rapid exchange with the bulk solution. As found for the rhodium analog, '$Ir\{C_6H_3(CH_2PBu^t_2)_2\text{-}2,6\}$' is highly reactive and all attempts to isolate it as a crystalline solid gave rise to a complicated mixture of unidentified products. Similar, highly reactive intermediates have recently been reported to result from the dehydrogenation of $IrFH_2(P\text{-}Bu^t_2Ph)_2$ by ethylene.[33] The '$Ir\{C_6H_3(CH_2PBu^t_2)_2\text{-}2,6\}$' intermediate reacts instantaneously at room temperature with N_2 to form the dinitrogen complex **4** and is trapped with ethylene by the formation of the stable complex $Ir(C_2H_4)\{C_6H_3(CH_2P\text{-}Bu^t_2)_2\text{-}2,6\}$.[30] Similar reactivity has been found for the analogous rhodium complexes $Rh\{C_6H_3(CH_2PBu^t_2)_2\text{-}2,6\}$[12] and $Rh\{CH(CH_2CH_2PBu_2)_2\text{-}2,6\}$.[34] Thus the nitrogen and alkene inhibition of the pincer catalytic dehydrogenation reactions apparently arise through this intermediate. The surprisingly low alkene affinity, which has been ascribed to crowding in the coordination sphere of the metal, accounts for the occurrence of catalytic inhibition only at high alkene concentrations.

The alkane dehydrogenation side of the catalytic cycle can be envisioned to proceed *via* a reversal of the mechanism for the hydrogenation of tbe: alkane substrate C–H oxidative addition, β-hydride elimination from the resulting alkyl group and dissociation of the product alkene to regenerate **2b**. This mechanism is complicated in the case of linear alkanes by the secondary catalytic alkene isomerization reaction. As seen in Scheme 3, the dissociation of terminal alkenes from the metal center is apparently much faster than hydride migration to the α-carbon of the coordinated alkene to produce a secondary alkyl group. This kinetic preference for the production of terminal alkenes can be ascribed to the pronounced steric constraints conferred by the pincer ligand. Goldman[30] has pointed out that the partitioning of the dehydrogenation/isomerization catalytic pathways can be viewed simply as a competition between the initial terminal alkene product and the sacrificial acceptor alkene for coordination to the dihydrido complex. This hypothesis accounts for the high concentrations of terminal alkenes which are obtained early in the dehydrogenation reaction when dec-1-ene is used as an acceptor in place of the sterically encumbered tbe.[30] The terminal alkenes do, however, eventually reassociate and follow the thermodynamically mandated isomerization pathway. The steric control of the kinetics of the isomerization process is further evidenced by the observation that the subsequent isomerization of alk-2-enes to further internalized alkenes occurs at much slower rates than the initial 1–2 isomerization.

The dehydrogenation of the dihydrido complexes in the absence of a hydrogen acceptor must occur by the direct reductive elimination of H_2 as seen in Scheme 3. Unlike the reaction with sacrificial alkenes which occurs at room temperature, the direct reductive elimination of H_2 occurs only at elevated temperatures. The sizable increase in the barrier to entering the dehydrogenation pathway results in the predominance of the isomerization pathway and thus precludes the possibility of production of significant concentrations of terminal alkenes. Even at very short reaction times, only traces of terminal alkenes are found when the catalytic dehydrogenation of linear alkanes are carried out in open reflux systems.

Dehydrogenation of cycloalkanes to arenes

The dehydrogenation of alkanes through catalytic reforming is the leading commercial method of producing arenes.[35] Platinum (often with a rhenium promoter) on alumina catalysts employed in this reaction require temperatures of 450 to 550 °C.[35] It is anticipated that homogeneous systems for the dehydrogenation of cycloalkanes to arenes would operate under milder conditions and give improved product selectivities. However, prior to our development of the pincer catalysts, only a few examples of such systems had been discovered.[36–41] Pioneering studies by Shilov and coworkers showed that K_2PtCl_4 catalyzes the reaction of H_2PtCl_6 with cycloalkanes to produce a mixture of arenes, alcohols and chlorinated species at 100–120 °C in aqueous trifluroacetic acid.[36] $Pd(OCOCF_3)_2$ has been reported to catalyze the dehydrogenation of cyclohexene to benzene[37] but reacts with cyclohexane only stoichiometrically in the presence of CF_3CO_2H to produce benzene.[38] $Ru(styrene)_2(PPh_3)_2$, $[Ir(cod)(PPh_3)_2]^+$, and $[Ir(cod)\{P(C_6H_4F\text{-}p)_3\}_2]^+$ catalyze the dehydrogenation of cyclohexene to benzene but are unreactive with cyclohexane[39] while $PdSO_4$ in the presence of

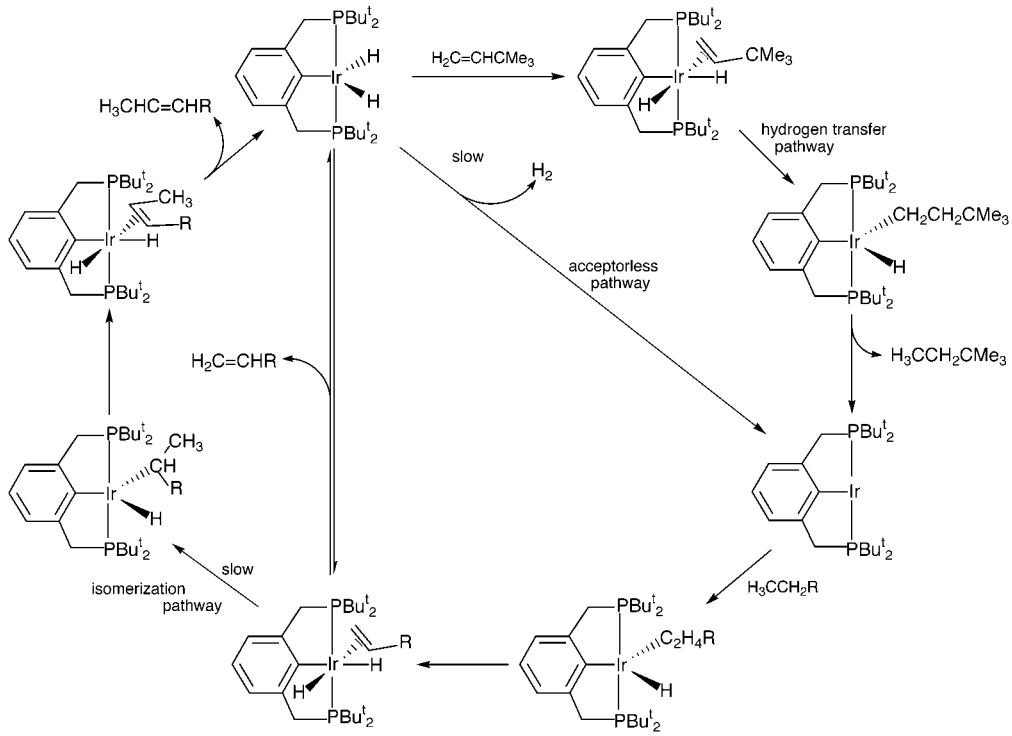

Scheme 3 Proposed mechanism for the catalytic dehydrogenation of linear alkanes by **2a**.

H_2SO_4 effects only the stoichiometric conversion of cyclohexane to benzene.[40] Crabtree *et al.* found an oxidative addition type system in which $IrH_2\{OC(O)CF_3\}(PPr^i_3)_2$ effects the dehydrogenation of alkanes to arenes at 150 °C in the presence of the hydrogen acceptor, tbe.[41] This system fails to turnover catalytically because hydrogenolysis of the phosphine P–C bonds occurs at the temperatures of 135 °C or above that are required for the release of the arenes from the intermediate complexes. Thus the development of a homogeneous system which was completely catalytic in precious metal awaited the development of catalysts such as the PCP pincer complexes that did not decompose at temperatures required to achieve arene elimination.

We have found **2a** will catalyze the transfer dehydrogenation of the six membered aliphatic ring of cyclohexane, methylcyclohexane, and decalin at temperatures as low as 150 °C.[19] The distribution of products arising after 1 h at 200 °C from solutions of the cycloalkanes containing equal loadings of the catalyst and tbe are given in Table 1. These data show that the initial dehydrogenation of cycloalkanes to cycloalkenes is much faster than the subsequent dehydrogenation of the cycloalkenes to arenes. It can also be seen that dehydrogenation reactions are sensitive to the stringent steric constraints at the iridium center. These conclusions are reinforced by the observation that the conversion of significant amounts of decalin to naphthalene occurs only after 72 h at 200 °C.

As mentioned previously, the dehydrogenation activity of **2b** is inhibited at tbe : catalyst ratios of $> 350:1$. Thus, high turnover numbers can be achieved only through periodic incremental additions of tbe. After about 10% of the saturated substrate has been consumed, product inhibition occurs and there is virtually no net increase in the amount of hydrogen that can be transferred to tbe. However, as is the case with linear alkanes, the complex also catalyzes secondary hydrogen transfer reactions. The dehydrogenation of methylcyclohexane at 200 °C provides an excellent example of this reactivity. As seen in Fig. 4, very little additional hydrogen elimination from the substrate occurs between 1 and 24 h of reaction. However, during this period the catalytic system remains active for the conversion of 2- and 3-methylcyclohexene to the thermodynamically preferred products, 1-methylcyclohexene and toluene. A similar time dependent shift in the product distribution toward the ternary alkene was observed in the dehydrogenation of methylcyclohexane to methylcyclohexenes by IrH_5-$(PPr^i_3)_2$.[4] However, the further dehydrogenation of methylcyclohexenes to toluene does not occur in this catalytic system.

Table 1 Product distributions [mol(mol **2a**)$^{-1}$] resulting after 1 h at 200 °C from the transfer dehydrogenation of various substrates using **2a** (5 μM) as catalyst and tbe as hydrogen acceptor

Substrate	Products (mol/mol catalyst)
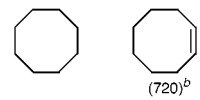	(720)[b]
	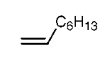 (8) 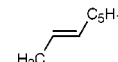 (47) 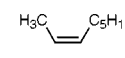 (26)
	 (86)  (77)
	 (41)  (20)  (8) 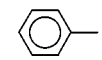 (11)
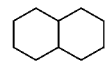	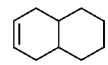 (69) 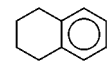 (16) 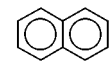 (26)
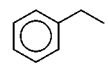	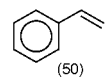 (50)
	 (86) (6) (53)

[a] In all cases, the quantified amounts of dehydrogenated C–C bonds and *tert*-butylethane balance within 5%. [b] Accomplished through incremental addition of tbe.

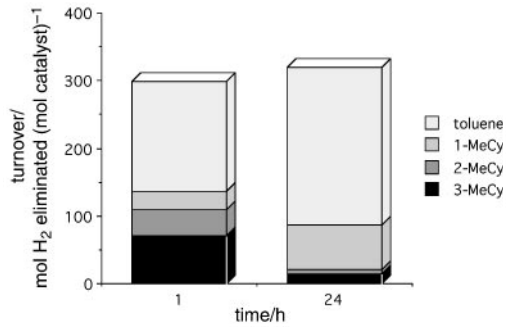

Fig. 4 Comparison of the product distributions obtained from transfer dehydrogenation of methylcyclohexane catalyzed by **2a** after 1 and 24 h of reaction at 200 °C.

Aliphatic dehydrogenation in the presence of functional groups

The catalytic dehydrogenation of aliphatic C–H bonds in the presence of functional groups is of major industrial importance. For example, the direct dehydrogenation of ethylbenzene accounts for 85% of the commercial production of styrene.[42] The reaction is carried out commercially at *ca.* 620 °C in the vapor phase over catalysts which primarily consist of iron oxide and potassium salt promoters.[42] Recently there has been considerable interest in the development of higher activity dehydrogenation catalysts which are also more selective for styrene over the degradation products, benzene and carbon.[42]

Our finding that **2a** remains catalytically active in the presence of relatively high concentrations of arenes suggested its application to the aliphatic dehydrogenation of alkyl benzenes. As seen in Table 1, **2a** will catalyze the transfer dehydrogenation of ethylbenzene to styrene.[43] However, the production of styrene ceases after only 50 turnovers. Thus it appears that the catalytic activity is inhibited by styrene at concentrations that are much lower than those observed for unfunctionalized alkenes. However, the observation of this catalytic activity was significant as it represented the first example of a homogeneous catalytic system for aliphatic dehydrogenation of a substrate containing an aromatic functionalization.

We have also investigated the reactivity of **1** with saturated ethers[43] and alcohols.[44] Surprisingly, the catalyst is not deactivated by either class of functionality. As seen in Table 1, the cyclic ether tetrahydrofuran (thf) is transfer dehydrogenated to a mixture of dihydrofurans and furan. However, pronounced product inhibition limits the reaction to < 200 turnovers. The dehydrogenation of alcohols is much more efficient and up to 80% conversion to products can be achieved. However, dehydrogenation of the aliphatic groups does not occur. Instead, much more pedestrian dehydrogenation of the alcohol functionality occurs to produce aldehydes from terminal alcohols and ketones from the internal alcohols.

Conclusions

Dihydrido iridium PCP pincer complexes have been found to be extraordinarily active and robust catalysts for aliphatic dehydrogenation reactions. This unique reactivity can be ascribed to the PCP pincer ligand which introduces a remarkable balance of electronic and steric effects such that the metal center is reactive with aliphatic C–H bonds but at the same time can not access the P–C and C–C bonds of the ligand. The resulting combination of high thermal stability and reactivity with aliphatic C–H bonds can be used to great advantage. The unusual high thermal stability of the pincer catalysts results in a two orders of magnitude improvement in the efficiency of homogeneous thermochemical systems for the dehydrogenation of alkanes without a sacrificial hydrogen acceptor. The unprecedented high reactivity of the pincer catalysts provides the basis for the first catalytic system of any kind for the selective dehydrogenation of linear alkanes to α-olefins. The combination of the pincer catalysts' high reactivity and stability has opened the door to other aliphatic dehydrogenations which had not previously been accomplished *via* homogeneous catalysis including the conversion of cycloalkanes to arenes, ethylbenzene to styrene and tetrahydrofuran to furan. These reactions represent major steps toward the development of viable methods for the selective functionalization of aliphatic groups. However, none are of practical value owing to the problems of product inhibition and/or requirement of sacrificial acceptors. Mechanistic studies have revealed the sources of these limitations and suggest possible designs for advanced catalysts. Modified PCP pincer complexes may well provide a means for the commercial production of commodity chemicals from alkanes and other abundant organic resources through catalytic aliphatic dehydrogenation reactions.

Acknowledgments

This article is dedicated to Professor Herbert D. Kaesz on the occasion of his 65th birthday. I wish to thank my collaborators and coworkers whose names appear in the list of references for their dedicated efforts and invaluable contributions to this work. The ongoing open exchange of preliminary results and ideas with Professor Alan S. Goldman of Rutgers University is gratefully acknowledged. This relationship has greatly aided our progress and enhanced the pleasure of exploring PCP pincer catalysis. I also thank Dr David Milstein of the Weizmann Institute of Science for sharing results prior to publication. Finally I thank Professor William Kaska (University of California at Santa Barbara) for my introduction to hydrido rhodium and iridium PCP pincer complexes. The financial support of this research was provided by the U.S. Department of Energy Hydrogen Program.

Notes and references

1 R. H. Crabtree, J. M. Mihelcic and J. M. Quirk, *J. Am. Chem. Soc.*, 1979, **101**, 7738.
2 D. Baudry, M. Ephritikhine, H. Felkin and R. Holmes-Smith, *J. Chem. Soc., Chem. Commun.*, 1983, 788.
3 H. Felkin, T. Fillebeen-Khan, R. Holmes-Smith and J. Zakrzewski, *Tetrahedron Lett.*, 1984, **25**, 1279.
4 (4) H. Felkin, T. Fillebeen-Khan, R. Holmes-Smith and Y. Lin, *Tetrahedron Lett.*, 1985, **26**, 1999.
5 M. W. Burk, R. H. Crabtree and D. V. McGrath, *J. Chem. Soc. Chem. Commun.*, 1985 1829; M. W. Burk and R. H. Crabtree, *J. Am. Chem. Soc.*, 1987, **109**, 8025.
6 J. A. Maguire and A. S. Goldman, *J. Am. Chem. Soc.*, 1991, **113**, 6706; J. A. Maguire, A. Petrillo and A. S. Goldman, *J. Am. Chem. Soc.*, 1992, **114**, 9492.
7 J. A. Miller and L. K. Knox, *J. Chem. Soc., Chem. Commun.*, 1994, 1449.
8 J. Belli and C. M. Jensen, *Organometallics*, 1996, **15**, 1532.
9 P. Braustein, Y. Chauvin, J. Nahring, A DeCian, J. Fischer, A. Tiripicchio and F. Ugozzoli, *Organometallics*, 1996, **15**, 5551.
10 K. Nomura and Y. Saito, *J. Chem. Soc., Chem. Commun.*, 1988, 161; K. Nomura and Y. Saito, *J. Mol. Catal.*, 1989, **54,** 57; T. Sakakura, T. Sodeyama and M. Tanaka, *New J. Chem.*, 1989, **13**, 737; J. A. Maguire, W. T. Boese and A. S. Goldman, *J. Am. Chem. Soc.*, 1989, **111**, 7088; T. Sakakura, T. Sodeyama, F. Abe and M. Tanaka, *Chem. Lett.*, 1991, 297.
11 T. Fujii and Y. Saito, *J. Chem. Soc., Chem. Commun.*, 1990, 757; T. Fujii, Y. Higashino and Y. Saito, *J. Chem. Soc., Dalton Trans.*, 1993, 517.
12 T. Aoki and R. H. Crabtree, *Organometallics*, 1993, **12**, 294
13 C. J. Moulton and B. L. Shaw, *J. Chem. Soc., Dalton Trans.*, 1976, 1020.
14 C. M. Jensen, S. Nemeh and W. C. Kaska: presented at the 1980 Biennial Inorganic Chemistry Symposium, Guelph, Ontario, Canada, June 1980.
15 S. Nemeh, C. Jensen, E. Binamira-Soriaga and W. C. Kaska, *Organometallics*, 1983, **2**, 1442 and references therein.
16 K. Wang, M. E. Goldman, T. J. Emge and A. S. Goldman, *J. Organomet. Chem.*, 1996, **518**, 55.

17 W. Leitner and C. Six, *Chem. Ber./Recueil*, 1997, **130**, 555.
18 S. Nemeh, Ph.D. Thesis, University of California at Santa Barbara, 1986.
19 M. Gupta, C. Hagen, W. C. Kaska, R. E. Cramer and C. M. Jensen, *J. Am. Chem. Soc.*, 1997, **119**, 840.
20 M. A. McLoughlin, R. J. Flesher, W. C. Kaska and H. A. Mayer, *Organometallics*, 1994, **13**, 3816.
21 M. Gupta, C. Hagen, W. C. Kaska, R. Flesher and C. M. Jensen, *Chem. Commun.*, 1996, 2083.
22 W-W. Xu, G. P. Rosini, M. Gupta, C. M. Jensen, W. C. Kaska, K. Krough-Jespersen and A. S. Goldman, *Chem. Commun.*, 1997, 2273.
23 T. R. Cundrai, *J. Am. Chem. Soc.*, 1994, **116**, 340.
24 M. E. van der Boom, C. L. Higgitt and D. Milstein, *Organometallics*, 1999, **18**, 2413.
25 D. W. Lee, W. C. Kaska and C. M. Jensen, *Organometallics*, 1998, **17**, 1.
26 A. Behr, in *Ullmann's Encyclopedia of Industrial Chemistry*, ed. B. Elvers, S. Hawkins and W. Russey, VCH Verlagsgesellschaft, Weinheim, 5th edn., 1994, pp. 242–249.
27 A. H. Janowicz and R. G. Bergman, *J. Am. Chem. Soc.*, 1983, **105**, 3929; W. D. Jones and F. J. Feher, *Organometallics*, 1983, **2**, 562; R. A. Periana and R. G. Bergman, *Organometallics*, 1984, **3**, 508; M. V. Baker and L. D. Field, *J. Am. Chem. Soc.*, 1987, **109**, 2825; W. D. Jones and E. T. Hessell, *J. Am. Chem. Soc.*, 1993, **115**, 554; T. G. P. Harper, P. J. Desrosiers and T. C. Flood, *Organometallics*, 1990, **9**, 2523.
28 T. Sakakura, T. Sodeyama, K. Sasaki, K. Wada and M. Tanaka, *J. Am. Chem. Soc.*, 1990, **112**, 7221; G. P. Rosini, K. Zhu and A. S. Goldman, *J. Organomet. Chem.*, 1995, **504**, 115.
29 C. Hagen, M. Gupta, W. C. Kaska and C. M. Jensen, paper INOR 221, presented at the 213th American Chemical Society National Meeting, San Francisco, CA, April 13, 1997.
30 F. Liu, E. B. Pak, B. Singh, C. M. Jensen and A. S. Goldman, *J. Am. Chem. Soc.*, 1999, **121**, 4086.
31 F. Liu and A. S. Goldman, *Chem. Commun.*, 1999, 655.
32 J. Belli, Ph.D. Thesis, University of Hawaii, 1999.
33 A. C. Cooper, K. Folting, J. C. Huffman and K. C. Caulton, *Organometallics*, 1997, **16**, 505.
34 A. Vigalok, Y. Ben-David and D. Milstein, *Organometallics*, 1996, **15**, 1839.
35 P. Wiseman, *Petrochemicals*, Ellis Horwood, Chichester, England, 1986, pp 90–91.
36 N. F. Gol'dshleger, V. V. Es'kova, A. E. Shilov and A. A. Shteinman, *Russ. J. Phys. Chem.*, 1972, **46**, 785. A. E. Shilov, *Activation of Saturated Hydrocarbons by Transition Metal Complexes*, Reidel, Dorrecht, Holland, 1984, pp 164-165.
37 B. M. Trost and P. J. Metzner, *J. Am. Chem. Soc.*, 1980, **102**, 3572.
38 N. F. Goldshleger, M. L. Khidekel, A. E. Shilov and A. A. Shteinman, *Kinet. Katal.*, 1974, **15**, 261.
39 B. N. Chaudret, D. J. Cole-Hamilton and G. Wilkinson, *Acta Chem. Scand., Ser. A.*, 1978, **32**, 763.
40 E. S. Rudakov, V. V. Zamashchikov, N. P. Belyaeva and R. I. Rudakova, *Zh. Fiz. Khim.*, 1973, **47**, 2732.
41 R. H. Crabtree, C. P. Parnell and R. J. Uriarte, *Organometallics*, 1987, **6**, 696.
42 D. H. James and W. M. Castor, in *Ullmann's Encyclopedia of Industrial Chemistry*, ed. B. Elvers, S. Hawkins and W. Russey, VCH Verlagsgesellschaft, Weinheim, 5th edn., 1994, p. 332.
43 M. Gupta, W. C. Kaska and C. M. Jensen, *Chem. Commun.*, 1997, 461.
44 R. Redon, D. Morales-Morales and C. M. Jensen, unpublished work.

Paper 9/03573G

[1 + 4]-Cycloaddition of a stable silylene to 2,4,6-tri-*tert*-butyl-1,3,5-triphosphabenzene

Scott B. Clendenning, Barbara Gehrhus,* Peter B. Hitchcock and John F. Nixon*

The School of Chemistry, Physics and Environmental Science, University of Sussex, Brighton, UK BN1 9QJ. E-mail: J.Nixon@sussex.ac.uk

Received (in Cambridge, UK) 25th October 1999, Accepted 29th October 1999

The stable bis(amino)silylene Si[(NCH$_2$Bu^t)$_2$C$_6$H$_4$-1,2] 1 undergoes [1 + 4]-cycloaddition with 2,4,6-tri-*tert*-butyl-1,3,5-triphosphabenzene 2 to afford compound 3: the molecular structure of 3 is supported by NMR spectroscopic data and confirmed by a single crystal X-ray diffraction study.

Addition reactions of transient as well as stable silylenes to CX (X = N or O) multiple bonds have been well documented in recent years.[1–8] Little is known, however, about the reactions of R_2Si: species with CP multiple bonds.[9] So far, it has been shown that R_2Si: (R = Bu^t) gives a phosphasilirene[10] in a [1 + 2]-cycloaddition with the CP triple bond of a phosphaalkyne; with R_2Si: (R = mesityl), the initially formed three-membered ring undergoes subsequent insertion of another R_2Si: moiety to afford a phosphadisilacyclobutene.[11] In our studies on the reactions of the stable silylene Si[(NCH$_2$Bu^t)$_2$C$_6$H$_4$-1,2] **1** we became interested in the reaction of **1** with 2,4,6-tri-*tert*-butyl-1,3,5-triphosphabenzene **2**. The latter has only recently been synthesised by metal-induced cyclotrimerisation of the phosphaalkyne Bu^{t}CP[12,13] and although its structure and PE spectrum have been reported,[14] its chemistry has not been studied in depth. Binger and coworkers[15] have described the synthesis of tetraphosphabarrelene and semibulvalene derivatives by addition of different phosphaalkynes to **2**. The former products resulted from a conventional [4 + 2]-cycloaddition reaction and the latter most likely from nucleophilic attack at one of the ring C atoms, followed by ring closure.

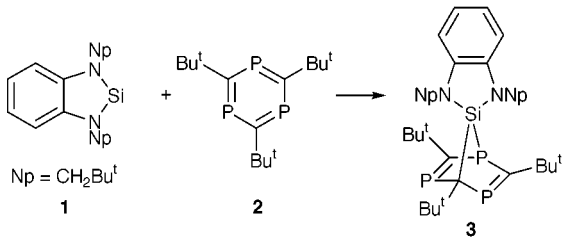

Scheme 1

We found that treatment of the silylene **1** with triphosphabenzene **2** in benzene at room temperature afforded, after evaporation of the solvent, an orange solid which was recrystallised from toluene–hexane at −25 °C to yield the [1 + 4]-cycloaddition product **3** (pale orange crystals, mp 224–225 °C, yield 66%) (Scheme 1). Compound **3** was characterised by analytical and spectroscopic techniques,† and its structure was confirmed by a single crystal X-ray diffraction study.‡

The ^{31}P, ^{29}Si, ^{13}C and ^{1}H NMR spectroscopic data are in agreement with the proposed [1 + 4]-cycloaddition product. The ^{31}P{^{1}H} NMR spectrum exhibits the expected doublet and triplet consistent with a plane of symmetry bisecting both the triphosphabenzene and silylene moieties. The doublet at δ 320.4 is characteristic of an unsaturated P environment, while the triplet at δ −63.8 is typical of a saturated P centre. These values are similar to those of δ 324.1 and −87.0 reported recently for the tetraphosphabarrelene.[14] The ^{29}Si chemical shift of δ 3.8 is consistent with a tetravalent Si centre and the $^1J_{SiP}$ coupling of 7.1 Hz to the bridgehead P lies within the expected range.

The structure of **3** (Fig. 1) clearly reveals it to be the [1 + 4]-cycloaddition product of the silylene across the triphosphabenzene ring; the P=C bond distances of 1.68 Å and the longer P–C bond distances of 1.85 Å to the bridgehead atoms are appropriate for this formulation.

Compound **3** did not react further with **1**, using an excess of the silylene, even on heating up to 80 °C in a sealed NMR spectral tube. It was not possible to extend the reaction of **2** to the higher group 14 metal analogues of the silylene. Thus, no reaction was observed on treatment of M[(NCH$_2$Bu^t)$_2$C$_6$H$_4$-1,2] (M = Ge, Sn or Pb) with **2**, even at higher temperatures. The reactions of **2** with carbenes are currently under investigation and follow significantly different reaction pathways than that observed with the silylene.

We thank NSERC of Canada for a scholarship (for S. B. C.) and the EPSRC for a Fellowship for B. G. (with M. F. Lappert), an Advanced Fellowship (for B. G. from 1/1/2000) and for their continuing support (to J. F. N.) for phosphaorganometallic chemistry.

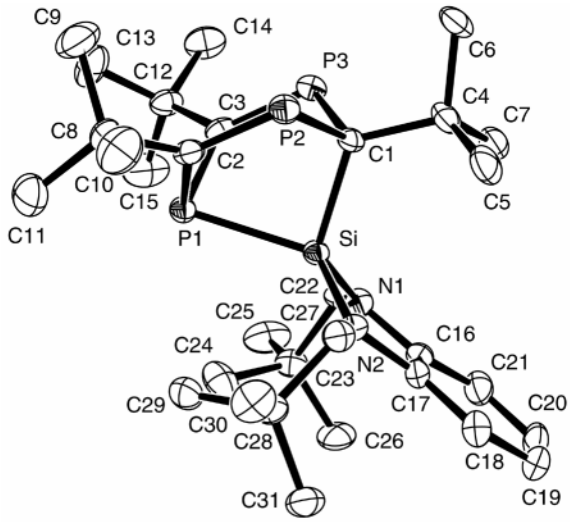

Fig. 1 Molecular structure of **3**. Selected bond lengths (Å) and angles (°): Si–N(2) 1.736(3), Si–N(1) 1.738(3), Si–C(1) 1.935(3), Si–P(1) 2.289(2), P(1)–C(2) 1.850(4), P(1)–C(3) 1.857(4), P(2)–C(2) 1.685(4), P(2)–C(1) 1.858(4), P(3)–C(3) 1.680(4), P(3)–C(1) 1.853(4), N(1)–C(16) 1.408(5), N(2)–C(17) 1.417(5); N(2)–Si–N(1) 91.71(14), C(1)–Si–P(1) 90.27(11), C(2)–P(1)–C(3) 98.67(16), C(2)–P(2)–C(1) 102.67(16), C(3)–P(3)–C(1) 102.00(17).

Notes and references

† *Selected spectroscopic data* for **3**: ^{1}H NMR (300 MHz, C$_6$D$_6$): δ 0.95 (s, 18H), 1.38 (s, 9H), 1.55 (s, 18H), 3.23 (AB-type, 4H), 6.63–6.69 (m, 2H) and 6.73–6.79 (m, 2H). ^{13}C{^{1}H} NMR (75.48 MHz, C$_6$D$_6$): δ 29.5 [C(*C*H$_3$)$_3$, d, ^5J(^{13}C, ^{31}P) 2.7 Hz], 33.8 [C(*C*H$_3$)$_3$, t, ^3J(^{13}C, ^{31}P) 9.2 Hz], 34.5 [C(*C*H$_3$)$_3$, dd, ^3J(^{13}C, ^{31}P) 14.0, 7.0 Hz], 35.4 [*C*(CH$_3$)$_3$, d, ^4J(^{13}C, ^{31}P)

0.4 Hz], 36.9 [$C(CH_3)_3$, t, $^2J(^{13}C, ^{31}P)$ 16.2 Hz], 43.3–43.9 [$C(CH_3)_3$, m, $^2J(^{13}C, ^{31}P)$ 10.7 Hz], 54.1 (CH_2, s), 103.1 [CSi, td, $^1J(^{13}C, ^{31}P)$ 64.8, $^3J(^{13}C, ^{31}P)$ 8.4 Hz], 111.6, 118.4 and 138.1 (phenyl) and 218.3 (P=C, m). $^{31}P\{^1H\}$ NMR (121.49 MHz, C_6D_6): δ −63.8 [t, $^2J(^{31}P, ^{31}P)$ 30.7 Hz] and 320.4 [d, $^2J(^{31}P, ^{31}P)$ 30.7 Hz]. $^{29}Si\{^1H\}$ NMR (99.33 MHz, C_6D_6): δ 3.8 [d, $^1J(^{29}Si, ^{31}P)$ 7.1 Hz]. MS: *m/z* 574 (M^+).

‡ *Crystal data for* **3**: $C_{31}H_{53}N_2P_3Si$, M = 574.75, specimen 0.3 × 0.3 × 0.2 mm, triclinic, space group $P\bar{1}$ (no. 2), a = 11.0632(18), b = 11.090(5), c = 15.682(7) Å, α = 77.81(4), β = 76.87(3), γ = 62.15(3)°, U = 1644.4(11) Å^3, Z = 2, μ = 0.24 mm^{-1}, T = 173(2) K, 5781 unique reflections collected, $R1$ = 0.054 for 4575 reflections with $I > 2\sigma(I)$, $wR2$ = 0.136 for all reflections. Data collection CAD4, full-matrix least-squares refinement on F^2, SHELXL-97. CCDC 182/1468. See http://www.rsc.org/suppdata/cc/1999/2451/ for crystallographic files in .cif format.

1 M. Weidenbruch, *Coord. Chem. Rev.*, 1994, **130**, 275.
2 J. Belzner, H. Ihmels, L. Pauletto and M. Noltemeyer, *J. Org. Chem.*, 1996, **61**, 3315.
3 J. Belzner, H. Ihmels and M. Noltemeyer, *Tetrahedron Lett.*, 1995, **36**, 8187.
4 P. Jutzi, D. Eikenberg, B. Neumann and H. G. Stammler, *Organometallics*, 1996, **15**, 3659.
5 P. Jutzi, D. Eikenberg, E. A. Bunte, A. Möhrke, B. Neumann and H. G. Stammler, *Organometallics*, 1996, **15**, 1930.
6 B. Gehrhus, P. B. Hitchcock and M. F. Lappert, *Organometallics*, 1997, **16**, 4861.
7 B. Gehrhus, P. B. Hitchcock and M. F. Lappert, *Organometallics*, 1998, **17**, 1378.
8 B. Gehrhus and M. F. Lappert, *Polyhedron*, 1998, **17**, 999.
9 K. B. Dillon, F. Mathey and J. F. Nixon, *Phosphorus: The Carbon Copy*, John Wiley, Chichester, 1998, and references therein.
10 A. Schafer, M. Weidenbruch, W. Saak and S. Pohl, *Angew. Chem., Int. Ed. Engl.*, 1987, **26**, 776.
11 M. Weidenbruch, S. Olthoff, K. Peters and H. G. von Schnering, *Chem. Commun.*, 1997, 1433.
12 P. Binger, S. Leininger, J. Stannek, B. Gabor, R. Mynott, J. Bruckmann and C. Krüger, *Angew. Chem., Int. Ed. Engl.*, 1995, **34**, 2227.
13 F. Tabellion, A. Nachbauer, S. Leininger, C. Peters, F. Preuss and M. Regitz, *Angew. Chem., Int. Ed.*, 1998, **37**, 1233.
14 R. Gleiter, H. Lange, B. Binger, J. Stanneck, C. Kruger, J. Bruckmann, U. Zenneck and S. Kummer, *Eur. J. Inorg. Chem.*, 1998, 1619.
15 P. Binger, S. Stutzmann, J. Bruckmann, C. Krüger, J. Grobe, D. LeVan and T. Pohlmeyer, *Eur. J. Inorg. Chem.*, 1998, 2071.

Communication 9/08483E

ChemComm

Shape selectivity in the adsorption of propane/propene on the all-silica DD3R

W. Zhu,* F. Kapteijn and J. A. Moulijn

Industrial Catalysis, DelftChemTech, Delft University of Technology, Julianalaan 136 2628 BL Delft, The Netherlands. E-mail: W.Zhu@tnw.tudelft.nl

Received (in Cambridge, UK) 9th August 1999, Accepted 1st November 1999

High adsorption selectivity for propene suggests that the all-silica DD3R might be effective as an adsorbent for the separation or purification of propene and propane mixtures.

Cryogenic distillation has been the dominant technology utilized for propane/propene separations for many years. Although traditional distillation is reliable and essentially unchallenged in this application, the necessary low temperatures and high pressures make it an energy-intensive separation scheme because of the small difference in their relative volatilities.[1]

A process configuration based on a hybrid adsorption/distillation system has been proposed to be an attractive commercial arrangement.[2] In order to achieve this objective, it is of utmost importance to find an effective adsorbent. Commercial zeolites (13X, 5A and 4A) and some Ag^+-substituted resins and $CuCl/\gamma$-Al_2O_3 have been investigated.[3–6] Such adsorbents show high selectivity for propene over propane.

Regeneration of zeolite-based adsorbents is difficult in applied vacuum swing adsorption (VAS) processes at temperatures as low as 298 K.[6] Increasing the operating temperature can improve this, but high temperatures can lead to propene oligomerization and possibly cracking owing to catalytic action of these materials, eventually blocking the adsorbents. In addition, these hydrophilic zeolites are sensitive to moisture.[2] Separations by adsorption *via* π-complexation are susceptible to deactivation by feed contaminants.[1]

Here, we demonstrate the selective adsorption of propene/propane on the all-silica DD3R, a highly hydrophobic and inert adsorbent, which is stable up to high temperatures.

Deca-dodecasil 3R (DD3R) is a member of the clathrasil family possessing topologically different frameworks. Gies[7] did pioneering work on the synthesis of the clathrasil DD3R. An optimum procedure for the clathrasil DD3R crystallization that ensures the phase purity of DD3R has been developed for scale-up by Den Exter *et al.*[8] The accessible pore space consists of 19-hedron cavities, connected *via* windows consisting of eight oxygen anions. Each cavity is connected to three other cavities in a hexagonal planar arrangement.[9]

The all-silica DD3R crystals had been synthesized in-house.[8] The template inside the clathrasil DD3R crystals was removed by calcination at 973 K for 6 h. The apparent density of the all-silica DD3R was 1.714 g cm^{-3} and the adsorption of N_2 indicated an accessible microporous void volume of 0.15 cm^3 g^{-1}. The crystal size was in the range of 5–10 μm as determined by SEM.

A Rupprecht & Patashnick TEOM 1500 mass analyzer with 100 mg sample size was used in an experimental set-up designed for measurement of equilibrium and transient adsorption on microporous materials.[10]

Prior to the experiments the crystals were outgassed in a helium flow of 200 cm^3 min^{-1} at 573 K for 24 h in order to remove adsorbed impurities. Helium was obtained as an ultra-high purity gas (> 99.999%). Propane and propene were 3.5 grade (> 99.95%).

The difference in the adsorption behavior between propane and propene is shown in Fig 1. The mass uptake for propane is much lower than that for propene under the same conditions. Fig. 1 also shows the mass uptake of binary mixture of propane and propene, which is the same as that of propene at the same partial pressure. This indicates that the presence of propane hardly affects the adsorption of propene.

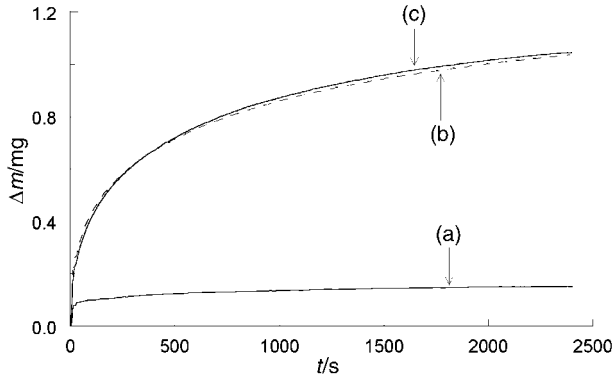

Fig. 1 Mass uptakes of single components, propane and propene, and their mixture in flowing He at a total pressure of 101.3 kPa and 373 K. A sample of 48.7 mg of the all-silica-DD3R was used in the TEOM. (a) propane (25 kPa), (b) propene (25 kPa) and (c) propane (25 kPa)–propene (25 kPa).

The critical diameter of propene (see Table 1) is significantly smaller than the free cross diameter of the 8-ring window (0.45 nm) and their molecules can enter into the 19-hedron cavities. However, the critical diameter of propane is close to 0.45 nm, so it can be expected that propane molecules are restricted from entering the 19-hedron cavities. The results shown in Fig. 1 indicate that the 8-ring window cavities are accessible to propene, while they exclude propane molecules. The small amount adsorbed for propane is attributed to adsorption at the external surface of the DD3R crystals.

Table 1 Characteristic diameters of the adsorbate molecules studied

Adsorbate	σ_s[a]/nm	σ_C[b]/nm
Propane	0.280	0.446
Propene	0.265	0.431

[a] Structural diameter defined as the diameter of the smallest cylinder that can be drawn around the molecule in its most favorable conformation through the centers of the extreme binding atoms.[11] [b] Critical diameter calculated by the summation of the structural diameter and the effective van der Waals radii of two extreme hydrogen atoms.

It takes a long time for the uptake of propene to reach the equilibrium state. This phenomenon can be interpreted in terms of the accessibility of the cavities to the adsorbate molecules. The orientation of the molecules to enter the 8-ring window and to move to the next cavity will play a role. Such a diffusion resistance can be improved by increasing the operating temperature.

The isotherms of propene on the all-silica DD3R at a temperature between 303 and 473 K are shown in Fig. 2 where closed symbols represent desorption. The isotherms were reversible over the complete pressure range investigated, resulting in the overlay of the adsorption and desorption

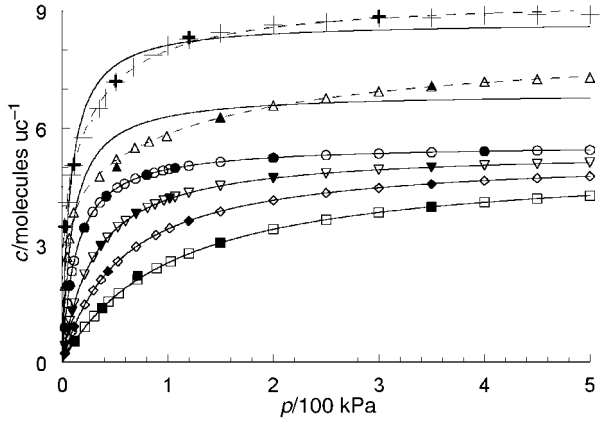

Fig. 2 Isotherms of propene on the all-silica DD3R. Open symbols adsorption data and closed symbols desorption data, solid lines Langmuir isotherm model fits and dashed lines dual-site Langmuir isotherm model fits; (+) 303 K, (▲) 338 K, (●) 373 K, (▼) 408 K,(◆) 438 K, (■) 473 K.

isotherms in Fig. 2. The isotherm data of propene are well described by the Langmuir model at high temperatures. However, deviations from the Langmuir model have been observed at 303 and 338 K and the higher-pressure range, at which the amount adsorbed exceeds six molecules per unit cell, corresponding to one molecule per cavity. These deviations from the Langmuir model are attributed to interactions between adsorbates as the number of molecules sitting inside the 19-hedron cavity exceeds one. The isotherm data at 303 and 338 K are better fitted by the dual-site Langmuir model (DSL). This DSL model takes into account implicitly interactions between adsorbates, which give rise to a pseudo-second adsorption site.

Various experimental results reveal high selectivity for propene on the all-silica DD3R. This adsorbent does not show any catalytic activity to hydrocarbons over a wide range of temperature. Furthermore, water hardly adsorbs on this material. In conclusion, the all-silica DD3R is an effective shape-selective adsorbent for the separation or purification of propane–propene mixtures. Its potential application in separation is being further investigated.

The authors are indebted to Dr J. C. Jansen for supplying the sample of the all-silica DD3R and to Mr J. H. ter Horst for preparing the graphical abstract.

Notes and references

1 D. J. Safarik and R. B. Eldridge, *Ind. Eng. Chem. Res.*, 1998, **37**, 2571.
2 R. B. Eldridge, *Ind. Eng. Chem. Res.*, 1993, **32**, 2208.
3 F. A. Da Siva and A. E. Rodrigues, *Ind. Eng. Chem. Res.*, 1999, **38**, 2051.
4 R. T. Yang and E. S. Kikkinides, *AIChE J.*, 1995, **41**, 509.
5 Z. B. Wu, S. S. Han, S. H. Cho, J. N. Kim, K. T. Chue and R. T. Yang, *Ind. Eng. Chem. Res.*, 1997, **36**, 2749.
6 S. U. Rege, J. Padin and R. T. Yang, *AIChE J.*, 1998, **44**, 799.
7 H. Gies, *J. Inclusion Phenom.*, 1984, **2**, 275.
8 M. J. Den Exter, J. C. Jansen, H. Van Bekkum and A. Zikanova, *Zeolites*,1997, **19**, 353.
9 H. Gies, *Z. Kristallogr.*, 1986, **175**, 93.
10 W. Zhu, J. M. Van de Graaf, L. J. P. Van den Broeke, F. Kapteijn and J. A. Moulijn, *Ind. Eng. Chem. Res.*, 1998, **37**, 1934.
11 R. M. Ruthven, R. I. Derrah, and K. F. Loughlin, *Can. J. Chem.*, 1973, **51**, 3514.

Communication 9/06465F

Reactivity of acryloyl chloride towards the anion $[Cp_2(CO)_4Mo_2(\mu\text{-}PPhH)]^-$; synthesis of an unusual phosphaalkene

John E. Davies, Martin J. Mays,* Paul R. Raithby and Anthony D. Woods

Department of Chemistry, Lensfield Road, Cambridge, UK CB2 1EW. E-mail: mjm14@cus.cam.ac.uk

Received (in Basel, Switzerland) 25th September 1999, Accepted 1st November 1999

Deprotonation of the complex $[Cp_2(CO)_4Mo_2(\mu\text{-}PPhH)(\mu\text{-}H)]$ by Bu^{t}Li at −78 °C and subsequent addition of acryloyl chloride affords the metallophosphaalkene complex $[Cp_2(CO)_4Mo_2(\eta^1\text{-}\eta^2\text{-}PhP{=}CHMe)]$ in high yield; the complex exhibits *cis*/*trans* isomerism, both isomers having been crystallographically characterised.

Metallophosphaalkenes have been shown to be important synthons in the preparation of phosphorus-functionalised heterocycles owing to the highly polar P=C moiety present in such complexes.[1,2] A high yield route to the previously unknown dinuclear Group 6 metallophosphaalkenes is now described.

We have previously demonstrated that the anion obtained from deprotonation of $[Cp_2(CO)_4Mo_2(\mu\text{-}Ph_2)(\mu\text{-}H)]$ with Bu^{t}Li at −78 °C reacts with ECl_3 to give $[Cp_2(CO)_4Mo_2(\mu\text{-}\eta^2\text{-}PE)]$ (E = P, As, Sb)[3] and with organometallic halides to give $[Cp_2(CO)_4Mo_2\{\mu\text{-}P(R)ML_n\}(\mu\text{-}H)]$ [ML_n = $W(CO)_3Cp$, $Fe(CO)_2Cp$, $Mn(CO)_5$].[4,5] We now report that reaction of $[Cp_2(CO)_4Mo_2(\mu\text{-}PPhH)(\mu\text{-}H)]$ **1** with Bu^{t}Li and acryloyl chloride leads to the unusual metallophosphaalkene *trans*-$[Cp_2(CO)_4Mo_2(\eta^1\text{-}\eta^2\text{-}PhP{=}CHMe)]$ **2** in high (70–80%) yield rather than to the formation of a complex containing an acyl-substituted bridging phosphido group as would have been predicted on the basis of earlier work.[4] Previously only mononuclear Group 6 metal complexes containing phosphaalkenes have been characterised; these involve coordination of the ligand *via* the phosphorus atom only.[6] To the authors' knowledge there exists only one other group of complexes containing a phosphaalkene bonding in an η^1–η^2 fashion to a bimetallic fragment. These were formed in low yield by the reaction of $[Cp_2(CO)_2(\mu\text{-}CO)Fe_2(\mu\text{-}CSMe)]^+$ with $HP(SiMe_3)_2$.[7]

A possible reaction pathway for the formation of *trans*-$[Cp_2(CO)_4Mo_2(\eta^1\text{-}\eta^2\text{-}PhP{=}CHMe)]$ **2** is shown in Scheme 1. It is proposed that electrophilic attack of the acryloyl chloride on deprotonated **1** to give intermediate **A** is followed by deinsertion of CO to give **B** and reductive elimination to give **C**. A 1,3 hydrogen shift within the bridging ligand then leads to **2**. This reaction sequence is supported by the isolation and structural characterisation of $[Cp_2(CO)_4(\eta^1\text{-}\eta^2\text{-}Ph_2PCH{=}CH_2)]$ **4**, an analogue of intermediate **C**. Complex **4** is obtained by treatment of deprotonated $[Cp_2(CO)_4Mo_2(\mu\text{-}PPh_2)(\mu\text{-}H)]$ with acryloyl chloride. Presumably the final [1,3] sigmatropic shift which converts intermediate **C** into the metallophosphaalkene **2** is precluded in **4** by the absence in $[Cp_2(CO)_4Mo_2(\mu\text{-}PPh_2)]^-$ of a hydrogen atom on the bridging phosphido group. The vinyl phosphine moiety present in **4** acts as an η^1–η^2 4-electron ligand; such a mode of coordination has only previously been reported in Fe_3 and Ru_5 clusters as the result of alkyne insertion into a P–M bond.[8,9]

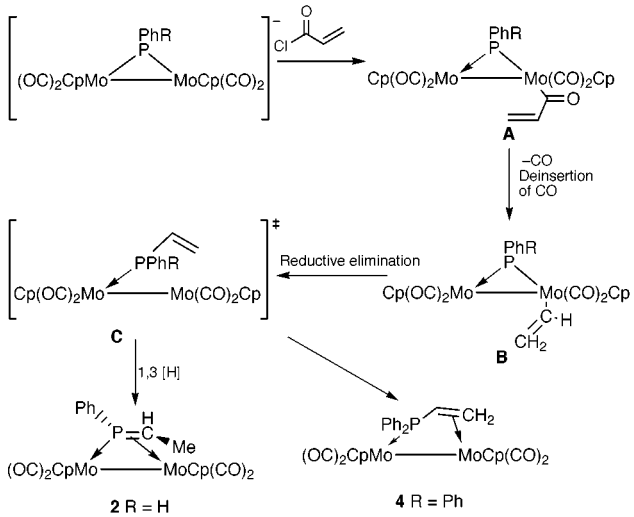

Scheme 1 Possible reaction pathway for formation of **2** and **4**.

Thermolysis of the *trans* isomer **2** leads to the formation of *cis*-$[Cp_2(CO)_4Mo_2(\eta^1\text{-}\eta^2\text{-}PhP{=}CHMe)]$ **3**, in which the methyl group of the phosphaalkene now lies *cis* to the PPh group and points towards a cyclopentadienyl ring.† Presumably thermolysis of **2** overcomes the barrier to rotation of the P=CHMe moiety to yield **3** as the thermodynamically favoured product.

The structures of **2** and **3** have been determined by X-ray diffraction analysis, confirming the *trans* and *cis* assignments (Fig. 1). The two molecules exhibit several significant differences.‡

Thus complex **3** shows a significantly shorter Mo–Mo bond length of 3.220(1) Å as compared to 3.240(1) Å in **2** and the P–Mo separations are both significantly shorter in the former

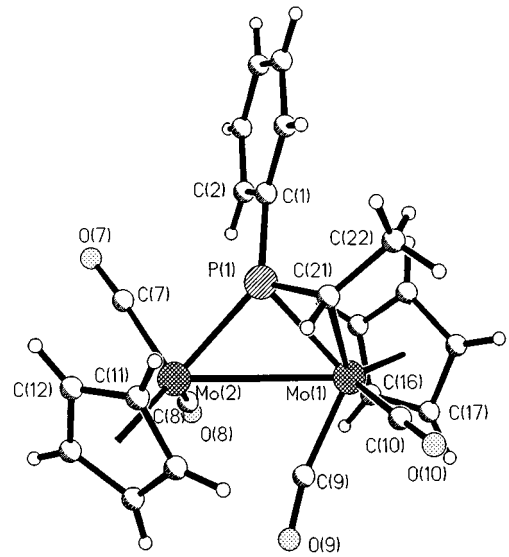

Fig. 1 Molecular structure of **2** and **3**. Selected bond lengths (Å) and angles (°): **2**: Mo(1)–Mo(2) 3.240(1), Mo(1)–P(1) 2.435(2), Mo(1)–C(21) 2.382(7), Mo(2)–P(1) 2.346(2), P(1)–C(21) 1.754(7); C(1)–P(1)–C(21) 107.3(4), P(1)–C(21)–C(22) 121.2(6), P(1)–C(21)–Mo(1) 70.3(2), P(1)–C(21)–Mo(2) 121.0(3), P(1)–Mo(1)–Mo(2) 46.19(5), C(21)–Mo(1)–Mo(2) 77.46(5), Mo(1)–C(9)–O(9) 166.6(6). **3**: Mo(1)–Mo(2) 3.220(1), Mo(1)–C(21) 2.392(3), Mo(1)–P(1) 2.418(1), Mo(2)–P(1) 2.334(1), P(1)–C(21) 1.749(3); C(1)–P(1)–C(21) 114.6(2), P(1)–C(21)–C(22) 127.4(3), P(1)–C(21)–Mo(1) 69.5(1), P(1)–Mo(1)–Mo(2) 46.27(2), C(21)–Mo(1)–Mo(2) 74.96(8), Mo(1)–C(9)–O(9) 167.2(3).

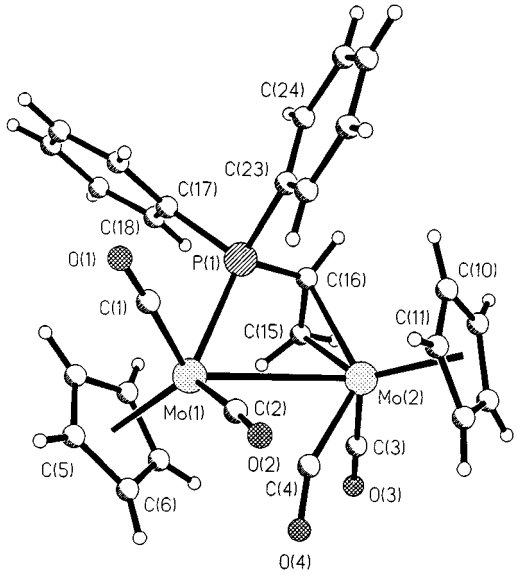

Fig. 2 Molecular structure of **4**. Selected bond lengths (Å) and angles (°): Mo(1)–Mo(2) 3.288(1), Mo(1)–P(1) 2.408(1), Mo(2)–C(16) 2.295(3), Mo(2)–C(15) 2.339(3), C(16)–C(15) 1.409(4); C(23)–P(1)–C(16) 101.9(2), P(1)–C(16)–Mo(2) 97.3(2), C(15)–C(16)–Mo(2) 74.0(2), Mo(1)–Mo(2)–C(16) 74.6(2).

complex (see Figs. 1 and 2). The P(1)–C(21)–C(22) bond angle increases from 121.2(6) to 127.4(3) on conversion of **2** to **3**.

The P=C bond lengths of 1.754(7) and 1.749(3) Å for **2** and **3**, respectively, are significantly shorter than the 1.812(9) Å recorded by Weber *et al.* for their related complex [Cp_2-$(CO)_2Fe_2\{\eta^1$–η^2-$(Cp(CO)_2Fe)P{=}CHSMe\}$].[7] However, they do fall within the range recorded by Williams *et al.* for their series of cluster-stabilised phosphaalkenes.[10] Both **2** and **3** contain a semi-bridging carbonyl group linking to the second molybdenum atom.

The molecular structure of **4** shows a Mo–Mo bond length of 3.288(1) Å, which is slightly longer than that present in **2** and **3** (Fig. 2). The C(15)–C(16) bond length of 1.409(4) Å is typical of that in other complexes containing a η^1–η^2 vinyl phosphine.[11,12]

The ^{1}H NMR spectra of **2** and **3** highlight the different environments of the vinylic proton. In **2** the proton resonates as a doublet of quartets at δ 4.14, whereas the analogous resonance in **3** occurs as a broad peak at δ 1.48; this latter value is in good agreement with that recorded by Weber *et al.* for their compound.[7]

Bimetallic Group 6 metal complexes coordinated to phosphaalkenes have not been reported previously, and an η^1–η^2 bonding mode for a phosphaalkenes is extremely rare. Additionally, the described method represents the first high yield route to metallophosphaalkenes that contain no other heteroatom substituents.

We thank the EPSRC for a quota award to A. D. W. and ICI for a CASE award to A. D. W. EPSRC support for the purchase of the Nonius Kappa CCD diffractometer is also gratefully acknowledged.

Notes and references

† *Selected spectroscopic data*: [IR (ν_{CO}/cm^{-1}) measured in hexane; ^{1}H NMR and ^{31}P {^{1}H} NMR spectra were recorded in $CDCl_3$ solution relative to TMS and 85% H_3PO_4(aq) respectively, with upfield shifts negative; *J* in Hz].

For **2**: ν_{CO} 1955m, 1927.6vs, 1822s, 1851m; NMR: ^{1}H δ 7.8–7.3 (m, 5H, Ph), 5.24 (s, 5H, Cp), 4.82 (s, 5H, Cp), 4.14 (dq, $^2J_{PH}$ 14.1, $^3J_{HH}$ 7.1, 1H, P=CH), 1.42 (dd, $^3J_{PH}$ 17.82, $^3J_{HH}$ 7.1, 3H, P=CCH_3); ^{31}P{^{1}H}, δ 158.32; ^{13}C, δ 242.31 (d, $^2J_{PC}$ 22.96, Mo–CO), 235.32 (d, $^2J_{PC}$ 7.55, Mo–CO), 230.02 (s, Mo–CO), 141.03–128.27 (m, PPh), 92.90 (s, Cp), 91.39 (s, Cp), 42.29 (d, $^1J_{PC}$ 12.4, P=C), 18.62 (d, $^2J_{PC}$ 7.23, P=CCH_3) FAB MS: *m*/*z* 572 (M^+), 544 (M^+ − CO); $C_{22}H_{19}MoO_4P$ requires C, 46.34; H, 3.36; P 5.43. Found: C, 46.21; H, 3.38; P 5.42%.

For **3**: ν_{CO} 1951m, 1921vs, 1880s, 1847m; NMR: ^{1}H, δ 7.69–7.45 (m, 5H, Ph), 5.04 (s, 5H, Cp), 5.03 (s, 5H, Cp), 1.80 (dd, $^3J_{PH}$ 13.03, $^3J_{HH}$ 7.04, 3H, P=CCH_3), 1.48 (dq, $^2J_{PH}$ 20.84, $^3J_{HH}$ 7.04, 1H, P=CH); ^{31}P{^{1}H}, δ 164.81; ^{13}C, δ 229.71 (Mo–CO), 134.88–128.54 (m, phenyl region), 93.17 (s, Cp), 91.39 (s, Cp), 49.14 (d, $^1J_{PC}$ 22.82, P=C), 24.05 (d, $^2J_{PC}$ 12.68, P=C*C*H_3); FAB MS: *m*/*z* 572 (M^+), 544 (M^+ − CO). $C_{22}H_{19}MoO_4P$ requires C, 46.34; H, 3.36; P, 5.43. Found: C, 46.10; H, 3.29; P, 5.42%.

For **4**: ν_{CO} 1938m, 1888vs, 1868s; NMR: ^{1}H, δ 7.79–7.17 (m, 10H, Ph), 4.75 (s, Cp), 4.72 (s, Cp), 3.32 (ddd, $^2J_{PH}$ 29.2, $^3J_{HH}$ 9.1, $^3J_{HH}$ 2.3, 1H, $Ph_2PCH{=}CH_2$), 1.96 (ddd, $^3J_{PH}$ 21.8, $^3J_{HH}$ 12.4, $^3J_{HH}$ 2.3, 1H, *cis*-$Ph_2PCH{=}CHH$), 1.61 (ddd, $^3J_{HH}$ 12.4, $^3J_{HH}$ 9.1, $^3J_{PH}$ 2.1, 1H, *trans*-$CH{=}CHH$); ^{31}P{^{1}H}, δ 35.93; ^{13}C, δ 238 (CO), 228 (CO), 137.37–128.10 (m, phenyl groups), 91.71 (s, Cp), 91.16 (s, Cp), 50.84 (d, $^2J_{PC}$ 14.17, $Ph_2PC{=}C$), 10.64 (d, $^1J_{PC}$ 41.70, $Ph_2PC{=}C$); FAB MS: *m*/*z* 650 (M^+). $C_{28}H_{23}Mo_2O_4P$ requires C, 52.03; H, 3.59; P 4.79. Found: C, 52.29; H, 3.66; P, 4.68%.

‡ *Crystal data*: Data in common: graphite monochromated Mo-Kα radiation; λ = 0.71069; data collected at 180(2) K using an Oxford Cryostream cooling apparatus. Solution by direct methods (SIR 9)[13] and subsequent Fourier syntheses, anisotropic full-matrix least-squares refinement on F^2 (SHELXL 93),[14] hydrogen atoms included using a riding model.

2: *trans*-$C_{22}H_{19}Mo_2O_4P$, M = 570.22, red plate, 0.20 × 0.15 × 0.10 mm, monoclinic, space group $P2_1/n$, a = 8.278(3), b = 14.908(6), c = 16.694(6) Å, β = 92.97(3)°, U = 2057.4(13) Å^3, Z = 4, D_c = 1.841 Mg m^{-3}, μ(Mo-Kα) = 1.323 mm^{-1}, F(000) = 1128, 5467 reflections measured using ω-2θ method on a Rigaku AFC7R diffractometer, 3631 unique (R_{int} = 0.059) used in all calculations. Data collection range 2.69 < θ < 25.03. R_1 = 0.0538, wR_2 = 0.1540 for 2960 observed reflections [I > 2σ(I)] and 262 parameters.

3: *cis*-$C_{22}H_{19}Mo_2O_4P$, M = 570.22, red plate, 0.15 × 0.12 × 0.12 mm, orthorhombic, space group $P2_12_12_1$, a = 9.615(3), b = 14.568(4), c = 15.191(3) Å, U = 2127.8(1) Å^3, Z = 4, D_c = 1.780 Mg m^{-3}, μ(Mo-Kα) = 1.279 mm^{-1}, F(000) = 1128. 8608 reflections measured on a Nonius Kappa CCD diffractometer, 4896 unique (R_{int} = 0.0031). Data collection range 1.94 < θ < 27.48. R_1 = 0.025, wR_2 = 0.0735 for 4648 observed reflections [I > 2σ(I)] and 263 parameters.

4: $C_{28}H_{23}Mo_2O_4P$, M = 646.31, red plate, 0.10 × 0.05 × 0.03 mm, triclinic, space group $P\bar{1}$, a = 8.304(1), b = 9.978(1), c = 16.024(1) Å, α = 94.19(1), β = 102.92(1), γ = 106.26(1)°, U = 1229.2(2) Å^3, Z = 4, D_c = 1.746 Mg m^{-3}, μ(Mo-Kα) = 1.119 mm^{-1}, F(000) = 644, 8421 reflections measured on a Nonius Kappa CCD diffractometer, 5589 unique (R_{int} = 0.037). Data collection range 1.32 < θ < 27.46. R_1 = 0.0398, wR_2 = 0.0732 for 5582 observed reflections [I > 2σ(I)] and 316 parameters.

CCDC 182/1469. See http://www.rsc.org/suppdata/cc/1999/2455/ for crystallographic files in .cif format.

1 R. Appel, in *Multiple Bonds and Low Coordination in Phosphorus Chemistry*, M. Regitz and O. J. Scherer, Thieme, Stuttgart, 1990 and references therein; J. F. Nixon, *Chem. Rev.*, 1988, **88**, 1327.
2 L. Weber, O. Kaminski, H.-G. Stammler, B. Neumann and V. D. Romanenko, *Z. Naturforsch., Teil B*, 1993, **48**, 1784.
3 J. E. Davies, L. C. Kerr, M. J. Mays, P. R. Raithby, P. K. Tompkin and A. D. Woods, *Angew. Chem., Int. Ed. Engl.*, 1998, **37**, 1428.
4 J. E. Davies, M. J. Mays, E. J. Pook, P. R. Raithby and P. K. Tompkin, *J. Chem. Soc., Dalton Trans.*, 1997, 3283.
5 P. K. Tompkin, PhD Dissertation, University of Cambridge, 1997.
6 D. Gudat, E. Niecke, W. Malisch, U. Hofmockel, S. Quashie, A. H. Cowley, A. M. Arif, B. Krebs and M. Dartmann, *J. Chem. Soc., Chem. Commun.*, 1985, 1687; S. Holand, C. Charrier, F. Mathey, J. Fischer and A. Mitschler, *J. Am. Chem. Soc.*, 1984, **106**, 826; D. Gudat, E. Niecke, B. Krebs and M. Dartmann, *Chimia*, 1985, **39**, 277; L. Weber, *Angew. Chem. Chem., Int. Ed. Engl.*, 1996, **35**, 271.
7 L. Weber, I. Schumann, H.-G. Stammler and B. Neumann, *Organometallics*, 1995, **14**, 1626.
8 K. Knoll, G. Huttner, L. Zsolani and O. Orami, *Angew. Chem., Int. Ed. Engl.*, 1986, **25**, 1119.
9 C. J. Adams, M. I. Bruce, B. W. Skelton and A. H. White, *J. Organomet. Chem.*, 1996, **506**, 191.
10 G. D. Williams, G. L. Geoffrey, R. R. Whittle and A. L. Rheingold, *J. Am. Chem. Soc.*, 1985, **107**, 729.
11 J. Lunniss, S. A. MacLaughlin, N. J. Taylor, A. J. Carty and E. Sappa, *Organometallics*, 1985, **4**, 2066.
12 D. Buchholz, G. Huttner and L. Zsolani, *J. Organomet. Chem.*, 1990, **381**, 97.
13 A. Altomare, G. Cascarano, C. Giacavazzo, A. Guagliardi, M. C. Byrla, G. Polidori and M. Camalli, *J. Appl. Crystallogr.*, 1994, **27**, 435.
14 G. M. Sheldrick, SHELXL 93, University of Göttingen, 1993.

Communication 9/07915G

ChemComm

Dinuclear complexes as connectors for carboxylates. Self-assembly of a molecular box

Richard P. Bonar-Law,* Thomas D. McGrath, Nirmal Singh, Jamie F. Bickley and Alexander Steiner

Department of Chemistry, University of Liverpool, Liverpool, UK L69 7ZD. E-mail: bonarlaw@liv.ac.uk

Received (in Cambridge, UK) 5th August 1999, Accepted 8th October 1999

A dinuclear complex derived from dirhodium(II) tetraacetate has been used as a corner unit for the synthesis of metallomacrocyles, including a square box with aromatic side walls.

Metal complexes are versatile building blocks in supramolecular chemistry.[1] Apart from the range of geometries available, coordination chemistry is well suited to self-assembly[2] since metal–ligand bonds are often formed cleanly and reversibly. Recent examples include one-pot syntheses of macrocycles from square-planar Pt and Pd complexes and polydentate nitrogen ligands.[3] These and related macrocylces are of particlar interest in having internal cavities large enough to accommodate other molecules.[1–3] Although metallomacrocycles are being prepared from an increasing variety of metals and ligands,[4] metal–amine coordination remains the dominant structural motif.[5] It occurred to us that a common functional group which has not been exploited for metalloassembly in solution is carboxylic acid/carboxylate.[6] One reason for this may be that two carboxylates rarely coordinate to a single metal atom in a predictable, symmetrical fashion.[7] In this respect dinuclear complexes such as $Rh_2(OAc)_4$ **1** seemed promising, since acids can be joined in well defined orientations, either in

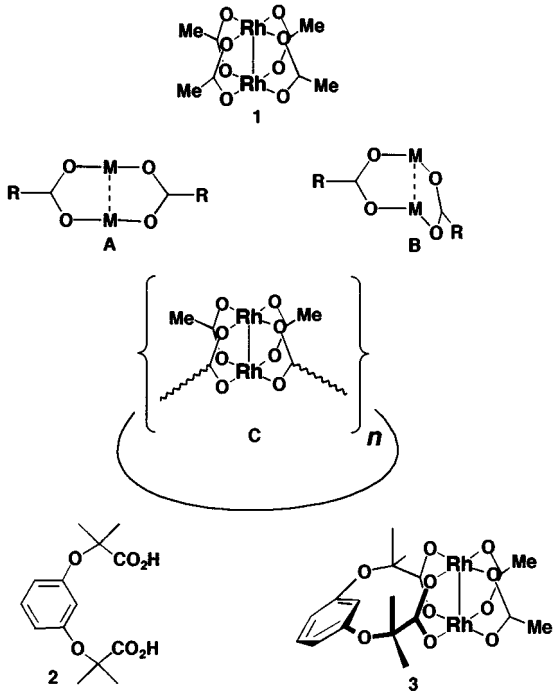

a linear fashion, **A** (an analogue of the classical hydrogen bonded dimer) or at right-angles, **B**. Anticipating that cyclic species would have interesting properties, our initial goal was to exploit geometry **B** to connect dicarboxylic acids at right angles to give macrocycles, **C**. At the outset of our work, two small cyclic 'dimers-of-dimers' had been structurally characterised, $[Mo_2\{O_2C(CH_2)_2CO_2\}(MeCN)_6]_2[BF_4]_4$[8a] and $[Ru_2\{O_2C(CH_2)_3CO_2\}(CO)_4(PBu_3)_2]_2$.[8a] Several linear or polymeric species based on Mo_2, W_2, Ru_2 or Cu_2 cores have also been prepared recently.[9] We chose to concentrate on dirhodium compounds[10] because they are neutral, diamagnetic, kinetically stable with respect to carboxylate exchange at room temperature,[11] and most importantly for practical applications, not appreciably air or water sensitive. A very recent report[12] by Cotton and Murillo *et al.* on diacid-linked Rh_2 and Mo_2 macrocycles with formamidinate ligands $[M_2(O_2C–R–CO_2)(ArNCHNAr)_2]_n$ prompts the communication of our efforts.

The first step was to reduce the possibility of uncontrolled polymerisation by blocking substitution of a pair of *cis*-acetates in **1**. We elected to retain the basic tetracarboxylate structure, and designed dicarboxylic acid **2** to act as a substitution-inert corner ligand.[13] Heating **1** with 1 equivalent of **2** in hot *N*,*N*-dimethylaniline provided diacetate **3** in 60% yield with liberation of acetic acid, along with roughly equal amounts of unreacted **1** and a complex in which all the acetates had been replaced by two molecules of **2**. The choice of solvent was important—a polar coordinating solvent was found to be necessary to keep reactants and intermediates in solution. Heating **3** with an excess of benzoic acid displaced only the acetate groups, demonstrating the kinetic stability of the chelating dicarboxylate. In the solid state structure of **3**·2(4-*tert*-butylpyridine) (Fig. 1),† the phenyl ring of the dicarboxylate is strongly tilted, although in solution the geminal methyl groups of **3** (with or without axial ligands) appear as a sharp singlet in ^{1}H NMR spectra at room temperature, suggesting that the chelate ring is flexible.

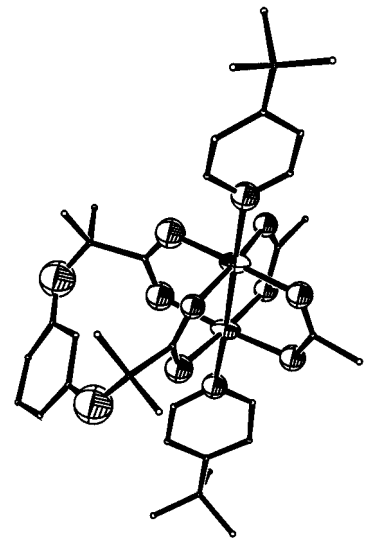

Fig. 1 Crystal structure of **3**·2(4-*tert*-butylpyridine).

Heating **3** with 1.1 equivalents of benzene-1,4-dicarboxylic acid in *N*,*N*-dimethylaniline produced a cyclic tetramer **4** in 80% yield after chromatography. The structure of **4**·8(4-*tert*-butylpyridine)·2(hexane) (Fig. 2)† shows a box 1.1 nm wide (measured between adjacent Rh_2 centres) with one pair of chelates pointing up and the other down. Like **3**, this asymmetry

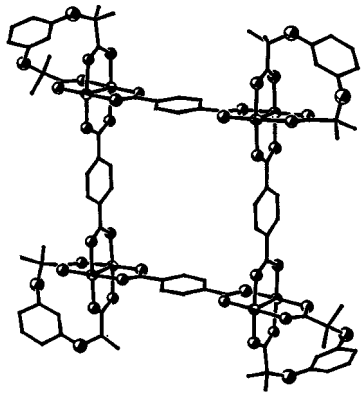

Fig. 2 Crystal structure of **4**·8(4-*tert*-butylpyridine)·2(hexane). The 4-*tert*-butylpyridine ligands and solvent molecules have been removed for clarity.

in the solid state is not evident in solution by ^{1}H NMR. In the crystal the boxes pack in two-dimensional layers, with hexane molecules between adjacent boxes, and nothing inside the macrocycles. The layers are held apart by axial pyridine ligands. The assembly of **4** was shown to be reversible: addition of excess acetic acid to the reaction mixture regenerated starting complex **3**, and subsequent heating to evaporate excess acid reformed **4**. The yield of **4** was insensitive to reactant concentration and **4** was still the main product with excess diacid, consistent with assembly under thermodynamic control.

Cyclocondensation of **3** with rigid diacids appears to be fairly general. Crystalline macrocyles have been obtained from benzene-1,3-dicarboxylic acid, naphthalene-1,4-dicarboxylic acid, naphthalene-2,6-dicarboxylic acid, biphenyl-4,4′-dicarboxylic acid and adamantane-1,3-dicarboxylic acid, among others. A characteristic feature of these species is aggregation in non-polar solvents. ^{1}H NMR spectra in chloroform are broad, but sharp in the presence of polar additives (methanol, acetone, pyridine) which can coordinate to the Lewis acidic metal centres. Monomeric dinuclear carboxylates are known to associate in the solid state *via* intermolecular metal–oxygen coordination;[14] this effect may be amplified in cyclic arrays to the extent that it becomes observable in solution.

In summary, a simple strategy for connecting carboxylic acids at right angles has been developed, illustrated by the synthesis of air- and water-stable metallomacrocyles. We are currently extending the synthetic studies, and plan to investigate the physical properties of these macrocycles, in particular inclusion chemistry and further supramolecular assembly.

We acknowledge financial support from the EPSRC, and thank Johnson Matthey PLC for generous loans of rhodium.

Notes and references

† Data were collected on a Stoe-IPDS diffractometer using graphite monochromated Mo-Kα radiation (λ = 0.71073), T = 293 K, full-matrix least squares refinements on F^2 using all data (G. M. Sheldrick, SHELX97, Crystal structure determination program, Göttingen, 1997). Non-hydrogen atoms were refined anisotropically except the methyl groups of 4-*tert*-butylpyridine ligands in **3** and all atom positions of 4-*tert*-butylpyridine ligands and the crystallographically independent hexane molecule in **4**. Hydrogen positions were set geometrically. The structure of **3** is twinned both racemically and across a pseudo mirror along c (Flack parameter = 0.42(12)). Crystals of **4** were weakly diffracting leading to poorly defined bond lengths and angles.

Crystal data: for **3**·2(4-*tert*-butylpyridine): $C_{36}H_{48}N_2O_{10}Rh_2$, M = 874.58, rhombohedral, space group $R\bar{3}$, a = 31.600(4), c = 12.700(3), U = 10983(3) Å^3, Z = 9, μ(Mo-Kα) = 0.720 mm^{-1}, 19768 reflections collected 6376 unique (R_{int} = 0.0331), $R1$ = 0.047 ($F > 4\sigma F$), $wR2$ = 0.1422 (all data). For **4**·8(4-*tert*-butylpyridine)·hexane, red plates from dichloromethane–hexane: $C_{160}H_{184}N_8O_{40}Rh_8\cdot 2(C_6H_{14})$, M = 3855.20, triclinic, space group $P\bar{1}$, a = 13.485(2), b = 19.834(3), c = 23.522(5), α = 69.66(2), β = 75.12(2), γ = 83.331(19)°, U = 5698.5(18) Å^3, Z = 1, μ(Mo-Kα) = 0.553 mm^{-1}, 31008 reflections collected, 14177 unique (R_{int} = 0.178), $R1$ = 0.056 ($F > 4\sigma F$), $wR2$ = 0.168 (all data).

CCDC 182/1442. See http://www.rsc.org/suppdata/cc/1999/2457/ for crystallographic files in .cif format.

1 C. J. Jones, *Chem. Soc. Rev.*, 1998, **27**, 289; *Comprehensive Supramolecular Chemistry*, ed. J. L. Atwood, J. E. D. Davies, D. D. MacNicol and F. Vögtle, Pergamon, Oxford, 1996, vol. 9, in particular ch. 2, 5, 6 and 7.

2 D. Philp and J. F. Stoddart, *Angew. Chem., Int. Ed. Engl.*, 1996, **35**, 1155.

3 M. Fujita, *Chem. Soc. Rev.*, 1998, **27**, 417; B. Olenyuk, A. Fechtenkotter and P. J. Stang, *J. Chem. Soc., Dalton Trans.*, 1998, 1707.

4 X. Sun, D. W. Johnson, D. L. Calder, R. E. Powers, K. N. Raymond and E. H. Wong, *Angew. Chem., Int. Ed.*, 1999, **38**, 1303; M. Albrecht, M. Schneider and H. Röttele, *Angew. Chem., Int. Ed.*, 1999, **38**, 557; R. W. Saalfrank, N. Low, B. Demleitner, D. Stalke and M. Teichert, *Chem. Eur. J.*, 1998, **4**, 1305; A.-K. Duhme, S. C. Davies and D. L. Hughes, *Inorg. Chem.*, 1998, **37**, 5380; D. J. McCord, J. H. Small, J. Greaves, Q. N. Van, A. J. Shaka, E. B. Fleisher and K. J. Shea, *J. Am. Chem. Soc.*, 1998, **120**, 9763; F. S. McQuillan, T. E. Berridge, H. Chen, T. A. Hamor and C. J. Jones, *Inorg. Chem.*, 1998, **37**, 4959; Y. Zhang, S. Wang, G. D. Enright and S. R. Breeze, *J. Am. Chem. Soc.*, 1998, **120**, 9398; J. R. Farrell, C. A. Mirkin, L. M. Liable-Sands and A. L. Rheingold, *J. Am. Chem. Soc.*, 1998, **120**, 11834; P. Jacopozzi and E. Dalcanale, *Angew. Chem., Int. Ed. Engl.*, 1997, **36**, 613; S. Mann, G. Huttner, L. Zsolnai and K. Heinze, *Angew. Chem., Int. Ed. Engl.*, 1996, **35**, 2808.

5 A. M. Garcia, F. J. Romero-Saluero, D. M. Bassani, J.-M. Lehn, G. Baum and D. Fenske, *Chem. Eur. J.*, 1999, **5**, 1803; S.-G. Roh, K.-M. Park, G. J. Park, S. Sakamoto, K. Yamaguchi and K. Kim, *Angew. Chem., Int. Ed.*, 1999, **38**, 638; R.-D. Schneback, E. Freisinger and B. Lippert, *Angew. Chem., Int. Ed.*, 1999, **38**, 168; S. Roche, C. Haslam, H. Adams, S. L. Heath and J. A. Thomas, *Chem. Commun.*, 1998, 1681; K. D. Benkstein, J. T. Hupp and C. L. Stern, *J. Am. Chem. Soc.*, 1998, **120**, 12982; J. R. Hall, S. L. Loeb, G. K. H. Shimizu and G. P. A. Yap, *Angew. Chem., Int. Ed.*, 1998, **37**, 121; A. C. Try, M. M. Harding, D. G. Hamilton and J. K. M. Sanders, *Chem. Commun.*, 1998, 723; K.-S. Jeong, Y. L. Cho, J. U. Song, H.-Y. Chang and M.-G. Choi, *J. Am. Chem. Soc.*, 1998, **120**, 10982; C. M. Hartshorn and P. J. Steel, *Chem. Commun.*, 1997, 541; H. Chen, S. Ogo and R. H. Fish, *J. Am. Chem. Soc.*, 1996, **118**, 4993; X. Chi, A. J. Guerin, R. A. Haycock, C. A. Hunter and L. D. Sarson, *J. Chem. Soc., Chem. Commun.*, 1995, 2567.

6 For hydrogen bonded assembly of acids see *e.g.* G. R. Desiraju, *Chem. Commun.*, 1997, 1475; S. C. Zimmerman, F. W. Zeng, D. E. C. Reichert and S. V. Kolotuchin, *Science*, 1996, **271**, 1095.

7 C. Oldham, in *Comprehensive Coordination Chemistry*, ed. G. Wilkinson, R. D. Gillard and J. A. McCleverty, Pergamon, Oxford, 1987, vol. 2, p. 435.

8 (*a*) E. Whelan, M. Devereux, M. McCann and V. McKee, *Chem. Commun.*, 1997, 427; (*b*) M. Bianchi, G. Menchi, P. Frediani, F. Piacenti, A. Scrivanti and U. Matteoli, *J. Mol. Catal.*, 1989, **50**, 277.

9 F. A. Cotton, C. Lin and C. A. Murillo, *J. Chem. Soc., Dalton Trans.*, 1998, 3151; S. Takamizawa, W. Mori, M. Furihata, S. Takeda and K. Yamaguchi, *Inorg. Chim. Acta*, 1998, **283**, 268; W. Mori, F. Inoue, K. Yoshida, H. Nakayama, S. Takamizawa and M. Kishita, *Chem. Lett.*, 1997, 1219; R. H. Cayton, M. H. Chisholm, J. C. Huffman and E. B. Lobkovsky, *J. Am. Chem. Soc.*, 1991, **113**, 8709.

10 F. A. Cotton and R. A. Walton, *Multiple Bonds Between Metal Atoms*, Clarendon Press, Oxford, 1993, p. 431; F. H. Jardine and P. S. Sheridan, in *Comprehensive Coordination Chemistry*, Pergamon, Oxford, 1987, vol. 4, p. 933.

11 J. M. Casas, R. H. Clayton and M. H. Chisholm, *Inorg. Chem.*, 1991, **230**, 358.

12 F. A. Cotton, L. M. Daniels, C. Li and C. A. Murillo, *J. Am. Chem. Soc.*, 1999, **121**, 4538.

13 Diacid **2** was prepared by alkylation of resorcinol with ethyl bromoisobutyrate followed by ester hydrolysis. For other chelating diacids see *e.g.* J. F. Gallagher, G. Ferguson and A. J. McAlees, *Acta. Crystallogr., Sect. C*, 1997, **53**, 576; D. F. Taber, R. P. Meagley, J. P. Louey and A. L. Rheingold, *Inorg. Chem. Acta*, 1995, **239**, 25.

14 D. V. Baxter, R. H. Cayton, M. H. Chisholm, J. C. Huffman, E. F. Putilina, S. L. Tagg, J. L. Wesemann, J. W. Zwanziger and F. D. Darrington, *J. Am. Chem. Soc.*, 1994, **116**, 4551 and references therein.

Communication 9/06415J

Synthesis of zeolite EMT with a novel route promoted by surfactants and its benefit in catalytic performance

Jianwei Sun, Mingxing Sun, Cong Nie and Quanzhi Li*

Department of Chemistry, Fudan University, Shanghai 200433, P.R. China. E-mail: qzli@fudan.edu.cn

Received (in Cambridge, UK) 24th August 1999, Accepted 15th October 1999

Zeolite EMT with small crystal size, which was catalytically active in the alkylation of isobutane with butenes, was synthesized *via* a novel route promoted by surfactants with a low molar ratio of 18-crown-6 to Al_2O_3 and a short crystallization time.

Zeolite EMT, which is constructed by the linkage of sodalite cages through double six-rings, is the hexagonal analogue of faujasites. The two dimensional direct channel system with 12-ring aperture in EMT is unique and of great interest in catalysis and adsorption.[1–4] Pure EMT was first synthesized by Delprato and coworkers[5] using 1,4,7,10,13,16-hexaoxacyclooctadecane (18-crown-6) as template, which plays a key structure-directing role, in the form of the $[Na\text{-}18\text{-}crown\text{-}6]^+$ complex, during crystallization. In a traditional synthetic system, not all the 18-crown-6 molecules can participate in the templating effect because the molar ratio of 18-crown-6 to Al_2O_3 needed is higher than 0.7.[5–10] Although the ratio can be decreased to 0.4–0.5 with a low content of water,[11–12] the starting hydrogels are not easy to work with. It is well known that the solvent plays a vital role during crystallization of zeolites and other microporous materials. One of the most effective synthetic strategies is the introduction of surfactant to the solvent because it can help to change the properties of the solvent greatly. del Val *et al.*[13] demonstrated that a cationic surfactant favors the replacement of P by Si in the VPI-5 framework. Franco *et al.*[14] found that a cationic surfactant also leads to deep changes in crystal morphology, *etc.* However, these authors did not focus on the effect of surfactant on the improvement of structure-directing efficiency. Here we report a novel synthetic route to produce the EMT phase promoted by surfactant and explain its effect in detail. In addition, the catalytic properties of H-EMT were also explored for the alkylation of isobutane with butenes.

In our study, the surfactants used were dodecylbenzyldimethylammonium chloride (DBDMACl), sodium lauryl sulfate (SLS), dioctadecyldimethylammonium chloride (DODMACl), alkyl glycoside (AG, $C_{12–14}$) and polyoxyethylene (15) ether lauric monoethanolamide (POE (15) LMEA). The reaction mixture was obtained by dissolving one of the surfactants, sodium aluminate (43 wt% Al_2O_3), sodium hydroxide (96 wt%) and 18-crown-6 (99 wt%) in distilled water in turn. Finally, colloidal silica (25 wt% SiO_2, < 0.5 wt% Na_2O) was added to the mixture dropwise with stirring. The resulting hydrogel was continuously stirred for 2 h, and aged for one day at room temperature without agitation. The molar composition of the hydrogel was as follows: 10 SiO_2: 1 Al_2O_3: 2.2 Na_2O: x 18-crown-6: y surfactant: 160 H_2O. The crystallization was carried out in a PTFE-lined stainless-steel autoclave at 373 K for 3–30 days. The solid obtained was filtered off, washed thoroughly with distilled water and then dried at 353 K overnight. In order to remove the organic molecules, the as-synthesized EMT was calcined at 523 K for 2 h followed at 773 K for 5 h in air. The H-EMT was prepared by ion exchange with 2 M NH_4NO_3 solutions at 353 K (three times for 3 h each) and the following calcination at 813 K for 7 h in air.

Fig. 1 shows the XRD patterns of the products synthesized by using the surfactant alkyl glycoside (AG) with different ratios of 18-crown-6 to Al_2O_3 (x) and crystallization time (t). When x = 0.37 and t = 3 d, the three characteristic peaks of the EMT phase in the 2θ region 5–7°, which are indexed as 100, 002 and 101 reflections, can be observed. It indicates that there is a significant amount of EMT in the product, but some amorphous substance still exists [Fig. 1(a)]. The pure EMT can be obtained when t is increased to 5 d [Fig. 1(b)]. This result means that the structure-directing efficiency of 18-crown-6 molecules is improved by adding surfactant to the starting hydrogels. It was also found that the intergrowth of EMT and FAU, deduced from the increased intensity of the central peak in the 5–7° 2θ region, was produced when x was further decreased to 0.19 even if t was long enough [Fig. 1(c)]. The SEM photograph reveals that EMT crystals synthesized in the presence of AG are hexagonal plates with an average size below 2 μm [Fig. 2(a)], smaller than those synthesized without surfactant [Fig. 2(b)]. Different categories of surfactant have also been used to synthesize EMT in a more efficient manner (Table 1). This demonstrates that, no matter what kind of surfactant is used, the EMT phase can be

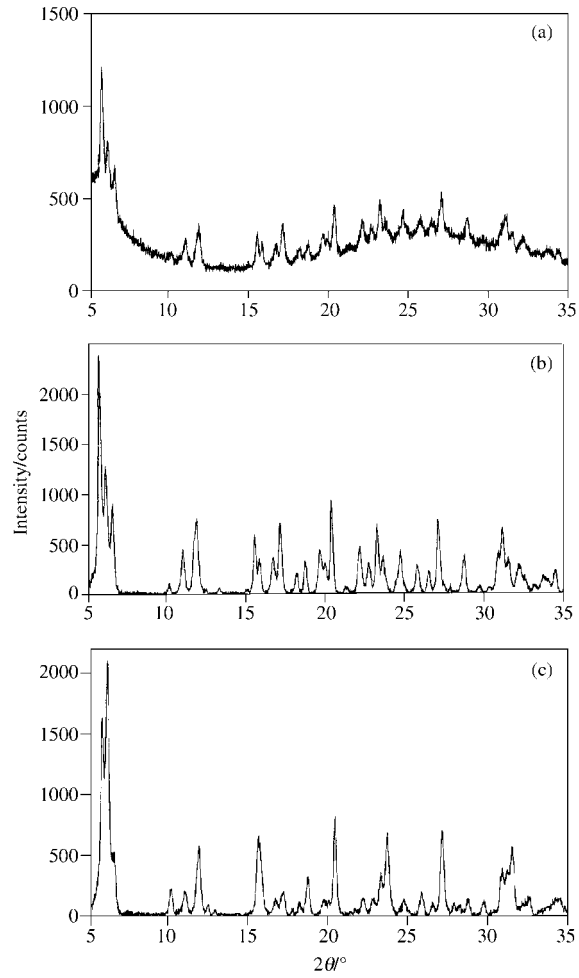

Fig. 1 Powder X-ray diffraction patterns of the as-synthesized products prepared using the surfactant AG. (a) x = 0.37, y = 0.043, t = 3 d; (b) x = 0.37, y = 0.043, t = 5 d and (c) x = 0.19, y = 0.042, t = 30 d.

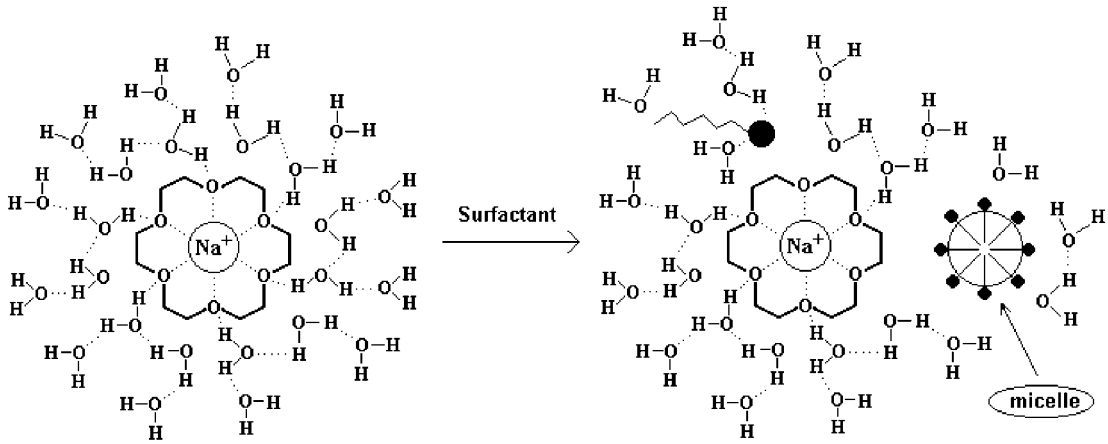

Scheme 1 Representation of the interactions between the [Na-18-crown-6]$^+$ complex, added surfactant and water solvent. (Dotted lines indicate hydrogen bonds or dipole–ion interactions.)

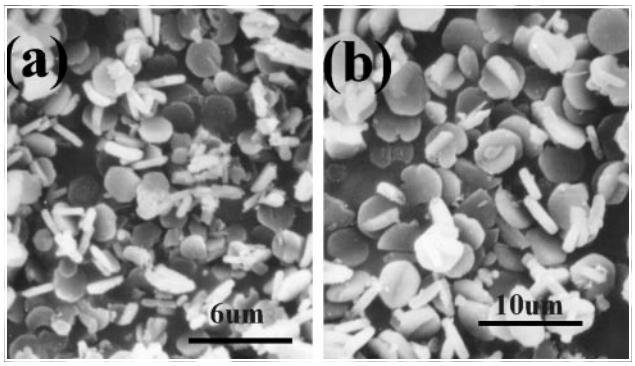

Fig. 2 SEM images of as-synthesized EMT prepared (a) with the surfactant AG (x = 0.36, y = 0.043, t = 30 d) and (b) without surfactant (x = 0.68, y = 0, t = 30 d).

Table 1 Synthesis of zeolite EMT using surfactants other than AG at x = 0.36 and t = 6 d

Surfactant	y	Product
Cationic		
DBDMACl	0.047	Amorphous
	0.102	EMT
DODMACl	0.035	EMT + Amorphous
	0.061	EMT
Anionic		
SLS	0.051	EMT
Nonionic		
POE (15) LMEA	0.017	EMT + Amorphous
	0.040	EMT

synthesized at low x and t values when the ratio of surfactant to Al_2O_3 (y) exceeds a certain level, which varies according to the surfactant.

Comparison of the ^{13}C CP MAS NMR spectra and the DTA curves of EMT synthesized with or without surfactant reveals that the surfactant molecules do not enter the channels or cages of EMT. Therefore, the surfactant must play an auxiliary role during crystallization, instead of a structure-directing role. In a synthetic system, the interaction between structure-directing agent and solvent would occur, but must not be so strong as to prevent the framework-forming species from interacting with the structure-directing molecules to form the zeolite phase.[15] In the starting hydrogel for producing EMT without surfactant, there is a balance of interactions between the water solvent, framework species and the [Na-18-crown-6]$^+$ complex. When surfactant is added to the hydrogel, the balance is upset due to the interactions between the surfactant and solvent and/or other dissolved species. Although this process is very complicated, it is clear that the interaction between the [Na-18-crown-6]$^+$ complex and the water solvent is weakened because of the interaction of surfactant with water (Scheme 1). As a result, it becomes more favorable for 18-crown-6 molecules to access the framework-forming species and direct the formation of the crystal nucleus and the following growth. On the other hand, the surface tension of the water solvent is decreased in the presence of surfactant, *i.e.* the interface energy between the newly-formed EMT phase and the solvent would be lowered, helping to shorten the crystallization time and reduce the particle size of EMT crystals produced.

For the alkylation of isobutane with butenes, the catalytic properties of H-EMT prepared by our method with AG were compared with those of H-EMT synthesized without surfactant under the same reaction conditions. It was found that the former is more selective for the main products, trimethylpentanes (TMPs), than the latter. It shows that the diffusion of bulky TMPs in small crystals is beneficial because the catalytic reaction takes place in the pores of EMT.

In conclusion, we have demonstrated a novel route to synthesize zeolite EMT by using surfactants at a low molar ratio of 18-crown-6 to Al_2O_3 and a short crystallization time. The average crystal size of the product is less than that of EMT synthesized without surfactant, which is more favorable for the alkylation of isobutane with butenes. Our route can be expanded to synthesize other types of zeolite in order to improve the templating effect, a study which is underway in our laboratory.

Financial support from the National Natural Science Foundation of China is gratefully acknowledged (Grant No. 29733070).

Notes and references

1 J. A. Martens and P. A. Jacobs, *J. Mol. Catal.*, 1993, **78**, L47.
2 M. Stöcker, H. Mostad and T. Rørvik, *Catal. Lett.*, 1994, **28,** 203.
3 S. Morin, A. Berreghis, P. Ayrault, N. S. Gnep and M. Guisnet, *J. Chem. Soc., Faraday Trans.*, 1997, **93**, 3269.
4 F. Eder and J. A. Lercher, *Zeolites*, 1997, **18**, 75.
5 F. Delprato, L. Delmotte, J. L. Guth and L. Huve, *Zeolites*, 1990, **10**, 546.
6 F. Dougnier, J. Patarin, J. L. Guth and D. Anglerot, *Zeolites*, 1992, **12**, 160.
7 E. J. P. Feijen, K. D. Vadder, M. H. Bosschaerts, J. L. Lievens, J. A. Martens, P. J. Grobet and P. A. Jacobs, *J. Am. Chem. Soc.*, 1994, **116**, 2950.
8 C. Wu and K. Chao, *J. Chem. Soc., Faraday Trans.*, 1995, **91**, 167.
9 U. Lohse, I. Pitsch, E. Schreier, B. Parlitz and K. H. Schnabel, *Appl. Catal. A.*, 1995, **129**, 189.
10 E. J. P. Feijen, B. Matthijs, P. J. Grobet, J. A. Martens and P. A. Jacobs, *Stud. Surf. Sci. Catal.*, 1997, **105**, 165.
11 T. Chatelain, J. Patarin, M. Soulard and J. L. Guth, *Zeolites*, 1995, **15**, 90.
12 T. Chatelain, J. Patarin, E. Brendlé, F. Dougnier, J. L. Guth and P. Schulz, *Stud. Surf. Sci. Catal.*, 1997, **105**, 173.
13 S. del Val, T. Blasco, E. Sastre and J. Perez-Pariente, *J. Chem. Soc., Chem. Commun.*, 1995, 731.
14 M. J. Franco, A. Mifsud and J. Perez-Pariente, *Zeolites*, 1995, **15**, 117.
15 R. E. Morris and S. J. Weigel, *Chem. Soc. Rev.*, 1997, **26**, 309.

Communication 9/06867H

Getting the right answer to a key question concerning molecular wires

F. Albert Cotton,*[a] Lee M. Daniels,[a] Carlos A. Murillo*[a,b] and Xiaoping Wang[a]

[a] *Laboratory for Molecular Structure and Bonding and Department of Chemistry, Texas A&M University, PO Box 30012, College Station, TX 77842-3012, USA. E-mail: cotton@TAMU.edu*

[b] *Department of Chemistry, Universidad de Costa Rica, Ciudad Universitaria, Costa Rica. E-mail: murillo@TAMU.edu*

Received (in Bloomington, IN, USA) 18th August 1999, Accepted 13th September 1999

It is shown that the $Cr_5(tpda)_4Cl_2$ molecule has alternating long and short (Cr···Cr) contacts in three compounds, including one in which an evenly spaced chain was recently claimed.

Recently, growing attention has been focused in this laboratory[1] and elsewhere[2] on *molecular compounds*[3] having linear chains of metal atoms in which there are—or may be—bonding contacts between some or all adjacent metal atoms. Even for the simplest case of only two metal atoms[4] the question of metal–metal bonding has been, and in some cases still is, problematical. Even more challenging problems arise with the more recently discovered compounds in which there are three[1a–f,2a–e] or more[1d,2f–h] metal atoms, that is with the *molecular wire* molecules, as we call them.

It is, of course, self-evident that here, as anywhere else in chemistry, a true understanding of electronic structures is possible only when the correct molecular structures are known. Thus, while it is obviously important to pursue the chemistry necessary to make molecular wire molecules, we assert that 'the key question concerning molecular wire molecules' is: how are the metal atoms spaced along the chain direction? This is a more subtle question than might have been expected.

Even for only three metal atoms, there are two possibilities, symmetrical and unsymmetrical:

M—M—M

M—M·····M

For compounds with a $Co_3(dpa)_4^{2+}$ core,† both of these structures occur and, indeed, as we recently showed,[5] the 'same' molecule, $Co_3(dpa)_4Cl_2$, may give a mixture of two types of crystals from the same solution (in which there are only symmetrical molecules[6]), one type containing symmetrical molecules and the other unsymmetrical molecules. We have also shown that there is a similar situation with $Cr_3(dpa)_4^{2+}$ species.[7]

For five metal atoms, at least three possible arrangements may be considered:

(a) M—M—M—M—M

(b) M—M·····M—M·····M

(c) M—M·····M·····M—M

We have reported the first preparation and structural characterization of the $Cr_5(tpda)_4Cl_2$ molecule,[8] and the chain of five Cr atoms was shown to have alternating Cr to Cr distances, as in pattern (b) above. Thus, to a rough approximation, there are two Cr–Cr quadruple bonds and one isolated Cr^{II} atom at the end, the latter accounting for the magnetic moment of 4.2 μ_B. We may also recall that the compound $[Cr_4(DpyF)_4Cl_2][PF_6]_2$† has the Cr atoms grouped into two Cr_2 quadruple bonds.[1d]

A recent publication[9] claims to have obtained the $Cr_5(tpda)_4Cl_2$ molecule in arrangement (a), that is, with a more or less evenly spaced arrangement of the five metal atoms. This paper also gives a lengthy discussion of the electronic structure of such an evenly-spaced Cr_5 chain. If this structure were correct it would implicate a duality of structure in Cr_5^{10+} chains similar to that for Co_3^{6+} chains, that is, sometimes evenly spaced and sometimes with alternating short and long distances.

In fact, however, this structure is incorrect and only the (b) type structure is found in each of three different crystalline forms of the $Cr_5(tpda)_4Cl_2$ molecule, namely, the one we reported,[8] the one which has just been reported in ref. 9,[9]‡ and a third‡ one that we have also characterized. The key results for all three are collected in Table 1. There is no doubt that the $Cr_5(tpda)_4Cl_2$ molecule consistently has a structure with alternating Cr–Cr distances, Cr≡Cr···C≡Cr···Cr, and the claim made[9] for evenly spaced metal atoms is erroneous.

The mistake made in the previous report of the $Cr_5(tpda)_4Cl_2$•$2Et_2O$•$4CHCl_3$ structure is obvious in Fig. 1 of ref. 9. The displacement ellipsoids of two of the inner Cr atoms look like rugby balls or American footballs. This is because at each of these positions (as well as the other three) there are two Cr atoms owing to an end-to-end disorder of the molecules:

Cr≡Cr·····Cr≡Cr·····Cr

Cr·····Cr≡Cr·····Cr≡Cr

On the other hand, when this structure is refined correctly,‡ with disordered alternately-spaced Cr_5 chains, all thermal displace-

Table 1 Cr–Cr distances (Å) in three crystal forms of $Cr_5(tpda)_4Cl_2$, M

	Cr(1)–Cr(2)	Cr(2)–Cr(3)	Cr(3)–Cr(4)	Cr(4)–Cr(5)
M·CH_2Cl_2[8]	2.578(7)	1.901(6)	2.587(6)	2.031(6)
M·$2Et_2O$·$4CHCl_3$	2.598(3)	1.872(2)	2.609(2)	1.963(3)
M·Et_2O	2.661(3)	1.862(3)	2.644(3)	1.931(3)

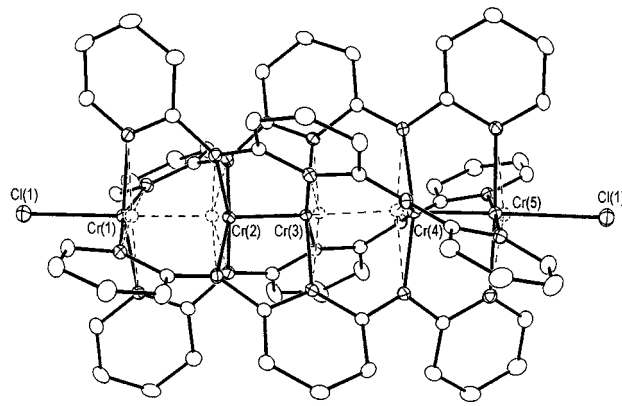

Fig. 1 The $Cr_5(tpda)_4Cl_2$ molecule as it is found in the compound $Cr_5(tpda)_4Cl_2$•$2Et_2O$•$4CHCl_3$. The four alternating Cr–Cr distances are listed in Table 1. Atoms are shown as their thermal displacement ellipsoids at the 30% probability level.

ment ellipsoids behave properly, as shown in Fig. 1, and the residuals are reduced. In the other two crystalline forms the same disorder exists and we took account of it in each of our refinements.

There was another problem with the previously reported structure. The electronic structure analysis[9] thereof led to a prediction of two unpaired electrons. This cannot be reconciled with an observed effective magnetic moment of 4.2 μ_B. This value is consistent with the correct structure, as we previously pointed out.[8] The lengthy molecular orbital analysis of the erroneous structure is also invalid.

Based on the results reported here, we would venture to say that a Cr_7 molecule of this ilk would also be expected to have strongly alternating Cr–Cr distances. However a recent report[10] shows a structure with approximately even spacing and pronounced prolate shapes for the Cr atom thermal ellipsoids.

We thank the National Science Foundation for support.

Notes and references

† dpa is the anion of di(2-pyridyl)amine; tpda is the dianion of tripyridyldiamine; DpyF is the di(2-pyridyl)formamidinate anion.

‡ *Crystal data*: $Cr_5(tpda)_4Cl_2{\cdot}2Et_2O{\cdot}4CHCl_3$. For the correct solution of this structure: formula $C_{72}H_{68}Cl_{14}Cr_5N_{20}O_2$; M_w = 2001.76, monoclinic, space group $C2/c$, T = 213 K, a = 28.417(1), b = 13.9755(2), c = 24.8327(7) Å, β = 122.780(3)°, V = 8291.6(4) Å^3, Z = 4, μ = 1.144 mm^{-1}, 22906 reflections collected, 7260 independent, R_{int} = 0.059, final residuals $R1$ = 0.047, $wR2$ = 0.102 [$I > 2\sigma(I)$]; $R1$ = 0.056, $wR2$ = 0.111 (all data).

$Cr_5(tpda)_4Cl_2{\cdot}Et_2O$. Formula $C_{64}H_{54}Cl_2Cr_5N_{20}O$; M_w = 1450.17; tetragonal, space group $I4/m$, T = 213 K, a = 10.7234(7), c = 26.663(4) Å, V = 3066.0(5) Å^3, Z = 2, μ = 1.008 mm^{-1}, 9543 reflections collected, 1892 independent, R_{int} = 0.051, final residuals $R1$ = 0.060, $wR2$ = 0.144 [$I > 2\sigma(I)$]; $R1$ = 0.074, $wR2$ = 0.164 (all data). The complex and the included solvent in this structure are quite disordered in the high-symmetry space group $I4/m$; the disorder persists even when the structure is refined in a lower symmetry group. CCDC 182/1424. See http://www.rsc.org/suppdata/cc/1999/2461/ for crystallographic files in .cif format.

1 (*a*) F. A. Cotton, L. M. Daniels, and G. T. Jordan IV, *Chem. Commun*., 1997, 421; (*b*) F. A. Cotton, L. M. Daniels, C. A. Murillo and I. Pascual, *J. Am. Chem. Soc*., 1997, **119**, 10 223; (*c*) F. A. Cotton, L. M. Daniels, G. T. Jordan IV and C. A. Murillo, *J. Am. Chem. Soc*., 1997, **119**, 10 377; (*d*) F. A. Cotton, L. M. Daniels, C. A. Murillo and X. Wang, *Chem. Commun*., 1998, 39; (*e*) F. A. Cotton, L. M. Daniels, C. A. Murillo and I. Pascual, *Inorg. Chem. Commun.*, 1998, **1**, 1; (*f*) R. Clérac, F. A. Cotton, K. R. Dunbar, C. A. Murillo, I. Pascual and X. Wang, *Inorg. Chem*., 1999, **38**, 2655.

2 (*a*) L.-P. Wu, P. Field, T. Morrissey, C. Murphy, P. Nagle, B. Hathaway, C. Simmons and P. Thornton, *J. Chem. Soc., Dalton Trans*., 1990, 3835; (*b*) G. J. Pyrka, M. El-Mekki and A. A. Pinkerton, *J. Chem. Soc., Chem. Commun*., 1991, 84. (*c*) S. Aduldecha and B. Hathaway, *J. Chem. Soc., Dalton Trans*., 1991, 993; (*d*) E.-C. Yang, M.-C. Cheng, M.-S. Tsai and S.-M. Peng, *J. Chem. Soc., Chem. Commun*., 1994, 2377; (*e*) J.-T. Sheu, C.-C. Lin, I. Chao, C.-C. Wang and S.-M. Peng, *Chem. Commun*., 1996, 315; (*f*) S.-J. Shieh, C.-C. Chou, G.-H. Lee, C.-C. Wang and S.-M. Peng, *Angew. Chem.*, 1997, **109**, 57; (*g*) C.-C. Wang, W.-C. Lo, C.-C. Chou, G.-H. Lee, J.-M. Chen and S.-M. Peng, *Inorg. Chem*., 1998, **37**, 4059; (*h*) S.-Y. Lai, T.-W. Lin, Y.-H. Chen, C.-C. Wang, G.-H. Lee, M.-H. Yang, M.-K. Leung and S.-M. Peng, *J. Am. Chem. Soc*., 1999, **121**, 250; (*i*) M.-M. Rohmer and M. Bénard, *J. Am. Chem. Soc*., 1998, **120**, 9372.

3 The term *molecular compounds* is emphasized because it distinguishes the discrete molecules we are interested in from a host of previously known substances in which linear chains of metal atoms arise *in the solid state only* by stacking of flat molecules (*e.g.* $K_2Pt(CN)_4Br_{0.3}$ or $Pt(NH_3)_4PtCl_4$) or by formation of μ-X bridged chains of octahedra (*e.g.* $NbCl_4$).

4 F. A. Cotton and R. A. Walton, *Multiple Bonds between Metal Atoms*, Oxford University Press, Oxford, UK, 2nd edn., 1992.

5 F. A. Cotton, C. A. Murillo and X. Wang, *J. Chem. Soc., Dalton Trans*., 1999, 3327.

6 F. A. Cotton, C. A. Murillo and X. Wang, *Inorg. Chem*., in press.

7 R. Clérac, F. A. Cotton, L. M. Daniels, K. R. Dunbar, C. A. Murillo and I. Pascual, *Inorg. Chem*., submitted.

8 F. A. Cotton, L. M. Daniels, T. Lu, C. A. Murillo and X. Wang, *J. Chem. Soc., Dalton Trans*., 1999, 517.

9 H.-C. Chang, J.-T. Li, C.-C. Wang, T.-W. Lin, H.-C. Lee, G.-H. Lee and S.-M. Peng, *Eur. J. Inorg. Chem*., 1999, 1243.

10 Y. H.-Chen, C.-C. Lee, C.-C. Wang, G.-H. Lee, S. Y. Lai, F.-Y. Li, C.-Y. Mou and S.-M. Peng, *Chem. Commun*., 1999, 1667.

Communication 9/06727B

ChemComm

Extension of the Karplus relationship to vicinal coupling within the P–Ru–S–H moiety of the H_2S complexes *cis*-$RuX_2(P–N)(PPh_3)(SH_2)$ {X = Cl, Br; P–N = [*o*-(*N*,*N*-dimethylamino)phenyl]diphenylphosphine}

Erin S. F. Ma, Steven J. Rettig† and Brian R. James*

Department of Chemistry, University of British Columbia, Vancouver, British Columbia, V6T 1Z1, Canada. E-mail: brj@chem.ubc.ca

Received (in Bloomington, IN, USA) 10th September 1999, Accepted 28th October 1999

The Ru(II)–H_2S complexes *cis*-$RuX_2(P–N)(PPh_3)(SH_2)$ {X = Cl, Br; P–N = [*o*-(*N*,*N*-dimethylamino)phenyl]diphenylphosphine} are characterised crystallographically and by $^{31}P\{^1H\}$, ^1H and $^1H\{^{31}P\}$ NMR spectroscopies; the ^1H NMR spectra at −50 °C show three-bond coupling of only one H-atom of the coordinated H_2S to the P-atom of the P–N ligand, and this represents an extension of the Karplus relationship to vicinal coupling within a P–Ru–S–H system.

The reactions of H_2S with transition metal complexes are beginning to be explored, the systems having relevance in the biological sulfur cycle, in the formation of ores, in hydrodesulfurisation (HDS) catalysis, and in conversion of H_2S to H_2 and elemental sulfur (or organosulfur compounds).[1]

We recently reported the second structurally characterised transition metal–H_2S complex *cis*-$RuCl_2(P–N)\{P(C_6H_4Me\text{-}p)_3\}(SH_2)$ **1** {P–N = [*o*-(*N*,*N*-dimethylamino)phenyl]diphenylphosphine}, formed under ambient conditions from the reaction of the five-coordinate complex $RuCl_2(P–N)\{P(C_6H_4Me\text{-}p)_3\}$ with H_2S; unfortunately, although the formulation was unambiguous, only one H atom of the coordinated H_2S was located in the X-ray analysis.[2] We present here the X-ray structures of *cis*-$RuX_2(P–N)(PPh_3)(SH_2)$, (X = Cl **2** or Br **3**), where both H atoms of the H_2S are isotropically refined.

† Deceased October 27, 1998.

The yellow complex **2** was prepared by adding 1 atm H_2S to $RuCl_2(P–N)(PPh_3)$, formed *in situ* from $RuCl_2(PPh_3)_3$ (200 mg, 0.21 mmol) and P–N (64 mg, 0.21 mmol) in acetone (10 mL) at 50 °C.[3] This solution was stirred for 8 h at room temperature, and the resulting precipitate of **2**·Me_2CO was collected and dried *in vacuo* for 1 h (yield: 140 mg, 80%). Complex **3**·Me_2CO was prepared similarly in 72% yield using $RuBr_2(P–N)(PPh_3)$ (100 mg, 0.12 mmol) as precursor, this being isolated in 50% yield from a stirred suspension containing an excess of NaBr (1.14 g, 11 mmol), $RuCl_2(PPh_3)_3$ (420 mg, 0.44 mmol) and P–N (136 mg, 0.44 mmol) in acetone (10 mL).

Crystals of **2**·Me_2CO and **3**·C_6H_6 were obtained from saturated acetone and C_6H_6 solutions of the respective complexes left standing under 1 atm H_2S. The ORTEP plots of **2** and **3** (Fig. 1)‡ reveal pseudo-octahedral geometries with *cis* X-atoms, the coordinated H_2S ligand being *cis* to both P-atoms, and the PPh_3 ligand and the –NMe_2 being mutually *trans*. With the exception of the larger Ru–X bonds in **3**, the geometries of **1**–**3** are very similar. The S–H bond lengths (1.20, 1.30 Å in **2**, and 1.25, 1.34 Å in **3**) are generally shorter than those of gaseous H_2S (1.33 Å),[4] but other weak interactions are present and may play a role in stabilising the coordinated H_2S: H-bonding is observed within H(2)···Cl(2) (2.69 Å) and H(1)···Br(1) (2.85 Å), and both H atoms of the H_2S in **2** and **3** point towards phenyl planes. The shortest phenyl···SH distances are 2.80 Å [H(1)···C(9)] and 2.97 Å [H(2)···C(21)] within **2**, and 2.52 Å [H(1)···C(20), phenyl from P–N] and 2.59 Å

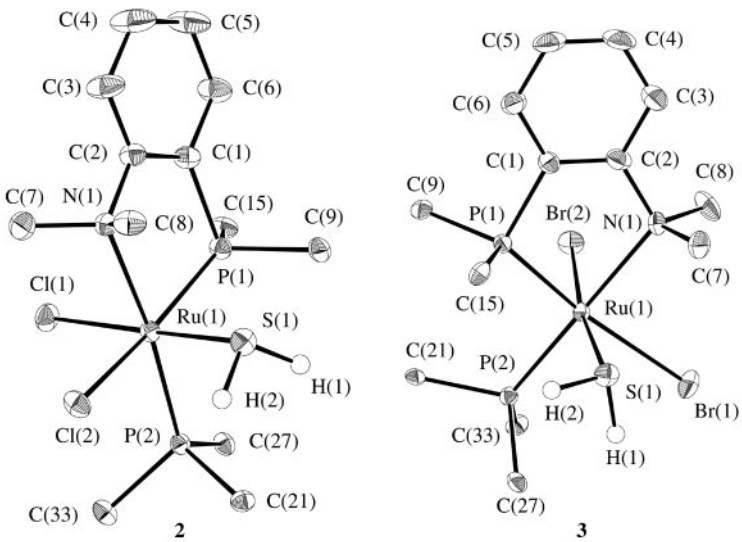

Fig. 1 The ORTEP plots of **2** and **3**. Thermal ellipsoids for non-hydrogen atoms are drawn at 33% probability (some phenyl carbons have been omitted for clarity). Selected bond lengths (Å) and angles (°): for **2**: S(1)–H(1) 1.20(3), S(1)–H(2) 1.30(3), Ru(1)–S(1) 2.3503(3), Ru(1)–P(1) 2.2712(6), Ru(1)–P(2) 2.3110(7), Ru(1)–N(1) 2.338(2), Ru(1)–Cl(1) 2.4238(6), Ru(1)–Cl(2) 2.4721(5); H(1)–S(1)–H(2) 102(2), Ru(1)–S(1)–H(1) 111(1), Ru(1)–S(1)–H(2) 103(1), Cl(1)–Ru(1)–S(1) 175.18(2), Cl(2)–Ru(1)–S(1) 82.63(2), S(1)–Ru(1)–P(1) 90.54(2), S(1)–Ru(1)–P(2) 93.76(2), S(1)–Ru(1)–N(1) 89.18(5). For **3**: S(1)–H(1) 1.25(7), S(1)–H(2) 1.34(6), Ru(1)–S(1) 2.333(1), Ru(1)–P(1) 2.262(1), Ru(1)–P(2) 2.301(1), Ru(1)–N(1) 2.372(3), Ru(1)–Br(1) 2.6343(5), Ru(1)–Br(2) 2.5540(4); H(1)–S(1)–H(2) 98(4), Ru(1)–S(1)–H(1) 101(3), Ru(1)–S(1)–H(2) 115(2), Br(1)–Ru(1)–S(1) 79.77(3), Br(2)–Ru(1)–S(1) 172.31(3), S(1)–Ru(1)–P(1) 93.87(4), S(1)–Ru(1)–P(2) 93.48(4), S(1)–Ru(1)–N(1) 89.43(9).

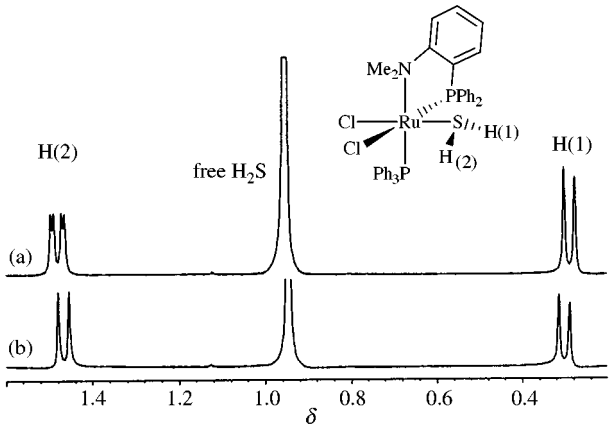

Fig. 2 (a) ^{1}H NMR spectrum (500 MHz) of **2** in CD_2Cl_2 at −50 °C (under 1 atm H_2S) and (b) the corresponding $^1H\{^{31}P\}$ NMR spectrum.

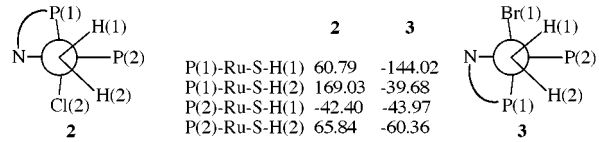

	2	**3**
P(1)-Ru-S-H(1)	60.79	-144.02
P(1)-Ru-S-H(2)	169.03	-39.68
P(2)-Ru-S-H(1)	-42.40	-43.97
P(2)-Ru-S-H(2)	65.84	-60.36

Fig. 3 End-on view of the solid state structures of **2** and **3**, with dihedral angles corresponding to P–Ru–S and Ru-S–H planes.

[H(2)···C(28)] within **3** (Fig. 1); related phenyl···mercapto proton interactions have been detected, for example, in $(PhMe_2P)_3Ru(\mu\text{-}SH)_3Ru(SH)(PMe_2Ph)_2$,[5] and implicated in HDS mechanisms.[6]

The $^{31}P\{^1H\}$ NMR spectra (200 MHz, 20 °C) of **2** and **3** in CD_2Cl_2 under 1 atm H_2S§ give AX patterns at δ 49.81 (*P*–N) and 43.30 (*P*Ph_3) ($^2J_{PP}$ 28.78 Hz) and δ 53.41 (*P*–N) and 44.36 (*P*Ph_3) ($^2J_{PP}$ 29.20 Hz), respectively, the coupling constants being characteristic of *cis*-P atoms.[3] Equivalent ^{1}H signals for the Ru–SH_2 resonances of **2** in solution are seen at 20 °C as a broad peak at δ *ca.* 1.0, but at −50 °C in CD_2Cl_2 (500 MHz) this peak is resolved into a doublet at δ 0.30 [H(1)] and doublet of doublets at δ 1.49 [H(2)], when the solution structure approaches that in the solid state [Fig. 2(a)]. The assignments for H(1) and H(2) are based on the observed H-bonding which would deshield the H(2) relative to H(1). The data show that H(1) and H(2) are mutually coupled ($^2J_{HH}$ = 12.3 Hz), while H(2) is coupled to a P-atom ($^3J_{HP}$ 3.50 Hz) and H(1) is not; the $^1H\{^{31}P\}$ NMR spectrum [Fig. 2(b)] shows the H(2) multiplet reduced to a doublet, and by selective ^{31}P decoupling, it was determined that H(2) is coupled to the P-atom of the P–N ligand.

The findings conform nicely to the Karplus relationship, which was initially established for vicinal coupling of protons (^3J, *H*–C–C–*H*),[7] and has been extended to *P*–C–C–*H*, *P*–O–C–*H* and *P*–S–C–*H* systems.[8] For our Ru–H_2S systems, the dihedral angles for P–Ru–S–H can be visualised by an end-on view of the Ru–S bond shown in Fig. 3. The absolute dihedral angles (ϕ) for non-coupling P and H atoms in **2** are 60.79, 42.40 and 65.84°, and these correspond to P(1)–H(1), P(2)–H(1) and P(2)–H(2) interactions, respectively, where orbital overlaps are negligible. For P(1)–H(2), ϕ is 169.03° where the $^3J_{HP}$ coupling is observed, consistent with Karplus curves that give maximum coupling when ϕ = 180°; the P(1)–Ru–S–H(2) arrangement likely results from interactions of H(2) with Cl(2) and a phenyl group of PPh_3.

Similar findings were obtained for **3**; at −50 °C H(2) appears as a doublet at δ_H 0.48 while H(1), which is H-bonded to Br(1), appears as a doublet of doublets at δ_H 1.23 ($^2J_{HH}$ 12.2, $^3J_{HP}$ 4.3 Hz). Decoupling experiments again show that H(1) is coupled to P(1), where ϕ = 144.02° (Fig. 3). The equivalence of the proton signals of the coordinated H_2S at 20 °C (for **2** and **3**) does not result from exchange with free H_2S,§ and presumably involves inversion at the S atom.

The NMR coupling through a metal centre described should be of quite general application, and provides a further structural probe for any *A*–metal–X–*B*-type system, where A and B are NMR-active nuclei, and X is an appropriate donor atom. To our knowledge, there is no corresponding example involving coordinated water.

We thank the NSERC of Canada for financial support, Johnson Matthey Ltd. and Colonial Metals Inc. for the loan of Ru, and Dr N. Burlinson of this department for assistance with the low-temperature NMR experiments.

Notes and references

‡ Crystallographic data for both structures were collected on a Rigaku/ADSC CCD area detector with graphite monochromated Mo-Kα radiation (λ = 0.71069 Å) at 180 K, solved by heavy-atom Patterson methods and expanded using Fourier techniques with the teXsan crystallographic software package of Molecular Structure Corporation. The non-hydrogen atoms were refined anisotropically; the S–H hydrogens were refined isotropically, the rest were fixed in calculated positions with C–H = 0.98 Å.

Crystal data: for $C_{41}H_{43}Cl_2NOP_2RuS$ **2**·Me_2CO: M = 831.78, yellow–brown prisms, crystal size 0.28 × 0.30 × 0.38 mm, monoclinic, space group $P2_1/n$ (no. 14), a = 14.843(2), b = 16.0292(9), c = 16.0099(8) Å, β = 95.286(2)°, V = 3792.8(5) Å^3, Z = 4, D_c = 1.46 g cm^{-3}, F(000) = 1712, μ(Mo-Kα) = 7.27 cm^{-1}, 33910 total reflections, 9547 unique (R_{int} = 0.041), 6176 observed [$I > 3\sigma(I)$], $R(R_w)$ = 0.028(0.025).

For $C_{44}H_{43}Br_2NP_2RuS$ **3**·C_6H_6: M = 940.72, orange prisms, crystal size 0.15 × 0.20 × 0.25 mm, monoclinic, space group $P2_1$ (no. 4), a = 9.667(1), b = 18.976(2), c = 11.6270(4) Å, β = 110.3292(7)°, V = 2000.0(3) Å^3, Z = 2, D_c = 1.56 g cm^{-3}, F(000) = 948, μ(Mo-Kα) = 25.61 cm^{-1}, 18513 total reflections, 5234 unique (R_{int} = 0.031), 8318 observed [$I > 3\sigma(I)$], $R(R_w)$ = 0.059(0.074). CCDC 182/1473.

§ 1 atm H_2S ensures complete formation of **2** and **3** within equilibria with the respective five-coordinate precursors;[2] the same NMR signals (together with those of the precursors)[3] are observed for solutions of the complexes in the absence of added H_2S.

1 B. R. James, *Pure Appl. Chem.*, 1997, **69**, 2213 and references therein; T. Y. H. Wong, B. R. James, P. C. Wong and K. A. R. Mitchell, *J. Mol. Catal. A: Chem.*, 1999, **139**, 159 and references therein.
2 D. C. Mudalige, E. S. Ma, S. J. Rettig, B. R. James and W. R. Cullen, *Inorg. Chem.*, 1997, **36**, 5426.
3 D. C. Mudalige, S. J. Rettig, B. R. James and W. R. Cullen, *J. Chem. Soc., Chem. Commun.*, 1993, 830.
4 T. H. Edwards, N. K. Moncur and L. E. Snyder, *J. Chem. Phys.*, 1967, **46**, 2139; I. G. Csizmadia, in *The Chemistry of the Thiol Group, Part I*, ed. S. Patai, John Wiley & Sons, Toronto, 1974, p. 7.
5 K. Osakada, T. Yamamoto and A. Yamamoto, *Inorg. Chim. Acta*, 1985, **105**, L9.
6 R. Angelici, *Acc. Chem. Res.*, 1988, **21**, 387.
7 M. Karplus, *J. Chem. Phys.*, 1959, **30**, 11; *J. Am. Chem. Soc.*, 1963, **85**, 2870.
8 W. G. Bentrude and W. N. Setzer, in *Phosphorus-31 NMR Spectroscopy in Stereochemical Analysis*, ed. J. G. Verkade and L. D. Quin, VCH Publishers, Inc., Deerfield Beach, FL, 1987, p. 365.

Communication 9/07360D

ChemComm

Carbohydrates from glycerol: an enzymatic four-step, one-pot synthesis

Rob Schoevaart, Fred van Rantwijk and Roger A. Sheldon*

Laboratory of Organic Chemistry and Catalysis, Delft University of Technology, Julianalaan 136, 2628 BL Delft, The Netherlands. E-mail: r.a.sheldon@tnw.tudelft.nl

Received (in Cambridge, UK) 30th September 1999, Accepted 1st November 1999

A novel one-pot procedure, involving a cascade of four enzymatic steps, for the synthesis of carbohydrates from glycerol and an aldehyde is reported.

Dihydroxyacetone phosphate (DHAP)-dependent aldolases catalyze the highly stereoselective synthesis of a wide variety of natural and non-natural carbohydrates[1–3] *via* the aldol reaction of DHAP with an aldehyde acceptor. C–C bond formation can produce four different stereoisomers and it is possible, by an appropriate choice of aldolase, to selectively produce any one of the four possible stereoisomers. For example, the fructose-1,6-bisphosphate aldolase[4] (FruA) used in this study produces an aldol adduct with 3*S*,4*R* stereochemistry. Chemical methods for preparing DHAP are circuitous and/or require expensive reagents.[5] Known enzymatic methods require the use of expensive enzymes (kinases) and regeneration of ATP.[6,7] We reasoned that the use of a phosphatase[8,9] as the phosphorylation catalyst would enable the use of inexpensive inorganic pyrophosphate as the phosphate source.

Our synthetic scheme embodies a cascade of four enzymatic steps: kinetically controlled phosphorylation of glycerol by inorganic pyrophosphate, glycerol phosphate oxidase (GPO)-catalysed aerobic oxidation of L-glycerol-3-phosphate to DHAP coupled with catalase mediated decomposition of hydrogen peroxide,[10] aldol reaction of DHAP with an aldehyde acceptor[11] and, finally, enzymatic dephosphorylation of the aldol adduct (see Scheme 1). The key to its success depends on the judicious use of pH control to switch the activities of the various enzymes on and off during the cascade.†

The phosphatase of choice was phytase[12] from *Aspergillus ficuum*, which is a cheap and readily available industrial enzyme. Its production of DL-glycerol-3-phosphate is pH dependent with a very broad optimum. For quick analysis L-glycerol-3-phosphate is detected by oxidation to DHAP and subsequent coupled assay[13] (equal amounts of the D-isomer are assumed to be formed). At pH 2 phosphorylation [glycerol > 10% (v/v)] was substantial and it decreased above pH 4 to become zero at pH 7. The yield of glycerol-3-phosphate (at pH 4) increased with increasing glycerol concentration, presumably because the competing hydrolysis of pyrophosphate and glycerol-3-phosphate is suppressed at low water concentrations. At 95% glycerol 75 mM L-glycerol-3-phosphate (corresponding to the theoretical yield of 50%) was formed according to the assay, after 24 h reaction time. ^{31}P NMR analysis confirmed that under these conditions the conversion of pyrophosphate into DL-glycerol-3-phosphate was 100%. Glycerol-2-phosphate was absent in the reaction mixture, demonstrating that phytase is completely regiospecific.

The concentration of glycerol was adjusted to 55%, because the activity of glycerol phosphate oxidase (GPO) is low in 95% glycerol. Moreover, the pH was increased to pH 7.5, which corresponds with the optimum of GPO and catalase (and that of the aldolase as well) and renders the phytase inactive, thus preventing undesirable hydrolysis. After quantitative oxidation of L-glycerol-3-phosphate to DHAP, fructose-1,6-bisphosphate aldolase (FruA) from *Staphylococcus carnosus* and butanal[14,15] were added to start the aldol addition (78% conversion after 4 h). Lowering the pH to 4 initiated the dephosphorylation of the butanal–DHAP adduct, affording 5-deoxy-5-ethyl-D-xylulose[14] in 57% yield from L-glycerol-3-phosphate. The addition of extra phosphatase for removal of the phosphate group was not necessary since phytase was still present and active.

The combination of four different enzymes and four enzymatic transformations in one pot provides an attractive procedure for performing aldol reactions with DHAP aldolases starting from the cheap, readily available glycerol and pyrophosphate. Combined with the broad substrate specificity of DHAP aldolases towards acceptor substrates, a wide variety of carbohydrates is readily accessible using this method.

Generous gifts of enzymes by Roche Diagnostics (Penzberg, Germany) are gratefully acknowledged. This work was financially supported by the Innovation Oriented Program Catalysis (IOP-catalysis).

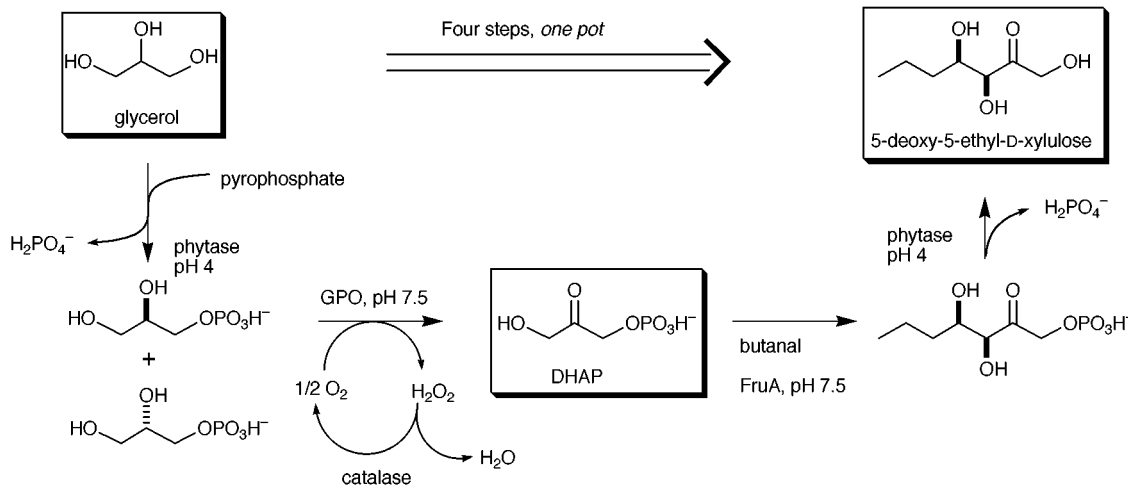

Scheme 1

Notes and references

† Optimal conditions (per ml): phosphorylation was carried out in 95% glycerol with 150 mM pyrophosphate and 1 mg phytase at pH 4.0. After shaking at 37 °C for 24 h the pH was adjusted to 7.5 and the glycerol concentration was reduced to 55% by dilution. GPO (5 units) and catalase (50 units) were added and oxygen was applied for 3 h at room temperature. Then the mixture was shaken for 4 h with FruA (1.25 units) and butanal (100 mM). Lowering the pH to 4, stirring overnight and extraction with EtOAc afforded 5-deoxy-5-ethyl-D-xylulose (57% from L-glycerol-3-phosphate).

1 P. G. Wang, W. Fitz and C.-H. Wong, *CHEMTECH*, 1995 (April), 22.
2 H. J. M. Gijsen, L. Qiao, W. Fitz and C.-H. Wong, *Chem. Rev.*, 1996, **91**, 443.
3 W.-D. Fessner and C. Walter, *Angew. Chem., Int. Ed. Engl.*, 1992, **31**, 614.
4 H. Brockamp and M. Kula, *Appl. Microbiol. Biotechnol.*, 1990, **34**, 287.
5 S.-H. Jung, J.-H. Jeong, P. Miller and C.-H Wong, *J. Org. Chem.*, 1994, **59**, 7182.
6 C.-H. Wong and G. M. Whitesides, *J. Org. Chem.*, 1983, **48**, 3493.
7 D. C. Crans and G. M. Whitesides, *J. Am. Chem. Soc*., 1985, **107**, 7019.
8 A. Pradines, A. Klaébé, J. Périé, F. Paul and P. Monsan, *Tetrahedron*, 1988, **44**, 6386.
9 A. Pradines, A. Klaébé, J. Périé, F. Paul and P. Monsan, *Enzyme Microb. Technol.*, 1991, **13**, 19.
10 W.-D. Fessner and G. Sinerius, *Angew. Chem., Int. Ed. Engl.*, 1994, **33**, 209.
11 Oxidation and aldol reaction can be conducted *in situ*, see ref. 10.
12 J. Dvorakova, *Folia Microbiol. (Prague)*, 1998, **43**, 323.
13 H. U. Bergmeyer, *Methods of Enzymatic Analysis*, Verlag Chemie, Mannheim, 1984, vol. IV, pp. 342–350.
14 R. Schoevaart, F. van Rantwijk and R. A. Sheldon, *Tetrahedron: Asymmetry*, 1999, **10**, 705.
15 Butanal was used as acceptor because we had already fully characterized the corresponding final product, 5-deoxy-5-ethyl-D-xylulose. (ref. 14).

Communication 9/07874F

ChemComm

Exergonic fragmentations in photogenerated zwitterions

Przemyslaw Maslak* and Jennifer M. McGuinn

Department of Chemistry, The Pennsylvania State University, University Park, PA, USA. E-mail: pm@chem.psu.edu

Received (in Corvallis, OR, USA) 8th October 1999, Accepted 25th October 1999

The competition between the fluorescent back-electron transfer and the exergonic fragmentation of radical anions in photogenerated intramolecular zwitterions showed that the rate of fragmentation followed the driving force of the reaction, with the notable exception of the most exergonic case.

Mesolytic cleavages[1] provide an excellent opportunity to experimentally investigate the functional dependence of the reaction rate (kinetics) on the driving force (thermodynamics) for an elementary reaction. Several theoretical and experimental studies have shown[2] that quadratic (Marcus-type) free-energy relationships may account for the main features of such fragmentation reactions. Indeed, in many instances the cleavage may be viewed as a dissociative intramolecular electron transfer, and analyzed in similar terms.[2]

To date, most of the fragmentation data have been obtained in the endergonic (or weakly exergonic) region. However, to better define the curvature of the free-energy function for the cleavage and to probe for the existence of an inverted region (similar to that found in electron-transfer reactions), data in the highly exergonic region are required. To probe such a regime, high-energy radical ions have to be generated rapidly, and once generated, they should be able to undergo fragmentation of a homolytically weak bond, giving a stable ionic fragment.[3]

Based on work of Singer[4] *et al.*, we have designed an experimental system (Scheme 1) wherein the radical ion pairs (zwitterions) are generated by an intramolecular electron-transfer from the excited state of the aminophenyl moiety to the naphthyl ring bearing a suitable leaving group in a benzylic position. The fluorescent back-electron transfer within the zwitterion competes with the fragmentation of the benzylic bond in the naphthyl radical anion, providing a sensitive handle on the dynamics of the system.

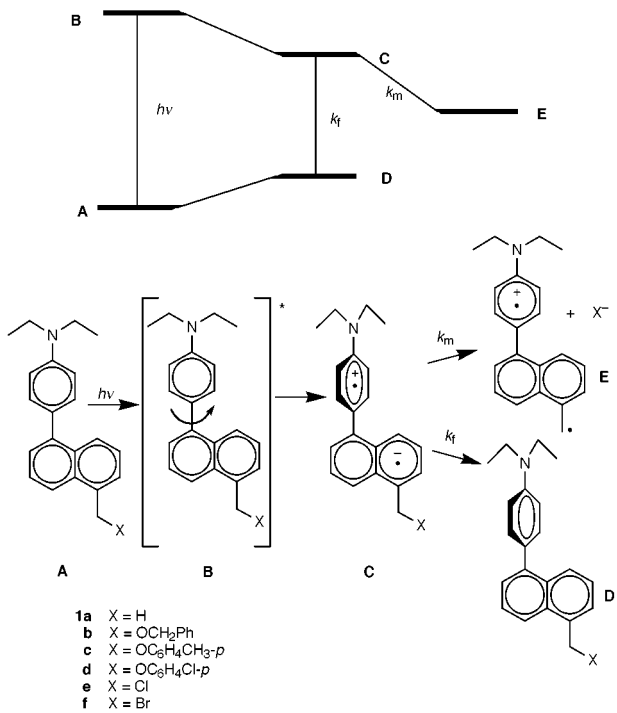

Scheme 1

UV–Visible spectra of all compounds[5] in MeCN were very similar, with the low-energy absorption band maxima at 325–330 nm. These bands was red-shifted (*ca.* 15 nm) and significantly more intense than the corresponding band of 4-bromo-*N*,*N*-diethylaniline, suggesting some charge-transfer nature of the transition (**A** → **B**). The degree of twist between the phenyl and the naphthyl moieties in **A** in solution is unknown and, therefore, the extent of the electronic coupling between the donor (aminophenyl) and the acceptor (naphthyl) could not be easily determined. The energy separation between the ground state (**A**) and the Franck–Condon state (**B**) is *ca.* 87 kcal mol^{-1}.

All compounds showed fluorescence with λ_{max} around 475 nm (**1a** has λ_{max} of 454 nm). All the fluorescence bands had identical shapes (widths) when recorded on the energy scale, but their intensity varied strongly with the nature of the substituent X (Fig. 1). The fluorescence corresponds[4] to the transition from the zwitterionic state (**C**) to the neutral state **D** (wherein the twist and solvation status is that of **C**, rather than that of the fully relaxed **A**). It is believed[4] that degree of twisting in **C** should approach 90°, but is probably somewhat less, leading to only a partial electron transfer between the donor and acceptor moieties.[6] The energy separation between **C** and **D** is *ca.* 60 kcal mol^{-1} (68 kcal mol for **1a**).

The oxidation potential of the donor part is 0.74 V *vs.* SCE, and the reduction potential of the acceptor component is −2.38 V *vs.* SCE.[7] The difference (3.12 eV) corresponds to the energy separation between the neutral state (**A**) and the zwitterionic state (**C**), assuming that the coulombic interactions (in MeCN) between the cation and the anion and the electronic coupling between them[4,6] (which depends on the twist angle) are relatively small. This approximation suggests that **B** → **C** and **D** → **A** relaxation processes (solvent and internal) correspond to *ca.* 15 and 12 kcal mol^{-1}, respectively (Scheme 1).

In the zwitterion **C** bearing a potential leaving group (**1b**–**f**) the unimolecular fragmentation reaction (k_m) of the naphthyl-centered radical anion (mesolysis) competes with the fluorescent decay (k_f). Such an additional reaction leads to a non-radiative depletion of **C**, and to the apparent change in the fluorescent life-time and the quantum yield as compared to that of the non-reactive model **1a** (Fig. 1).

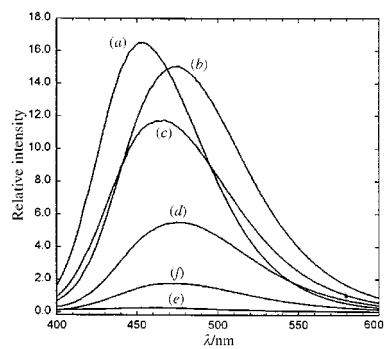

Fig. 1 Steady-state fluorescence spectra of (*a*) **1a**, (*b*) **1b**, (*c*) **1c**, (*d*) **1d** and (*e*) **1e** recorded in acetonitrile under identical experimental conditions.

Table 1 Thermodynamic and kinetic data for mesolytic fragmentation

Compound	ΔG_h(C–X)[a]/ kcal mol^{-1}	E^{ox} (X^-)[b]/ V *vs.* SCE	ΔG_m[c]/ kcal mol^{-1}	Φ_{rel}[d]	k_m[e]/s^{-1}
1a	77	−0.12	25	1.00	—
1b	70	0.77	−3	0.83	3.6×10^7
1c	51	0.28	−10	0.71	7.2×10^7
1d	51	0.38	−13	0.34	3.4×10^8
1e	65	1.62	−27	0.02	8.6×10^9
1f	53	1.28	−31	0.10	1.6×10^9

[a] Free energy of homolysis of the benzylic bond in the neutral molecule, from ref. 10. [b] Oxidation potential of the anion formed in the cleavage, from ref. 11 and 12. [c] Free energy of the mesolysis as calculated from the formula in the text. [d] Relative quantum yields for fluorescence determined in deoxygenated MeCN under argon, under identical experimental conditions for all the compounds. [e] The rate constant for radical anion fragmentation calculated as described in ref. 8.

Using the relative quantum yield data, and the fluorescence lifetime of the model compound (**1a**), values for the rate of the mesolysis (k_m) can be determined for each of the reactive compounds[8] (**1b–f**). In general, the lower the relative quantum yield for fluorescence, the faster the rate of mesolysis. The results of such calculations are collected in Table 1.

The thermodynamics of mesolytic cleavage was calculated on the basis of a simple thermodynamic cycle (Table 1).[1a,9] The free energy of mesolysis (ΔG_m) is a function of the free energy of homolysis (ΔG_h) of the scissile bond in the radical ion precursor, and the difference (ΔE) in the redox potentials of the radical ion and the ionic fragments produced. Specifically, in this case ΔE is the difference between the oxidation potential of the anion formed [$E^{ox}(X^-/X^{\cdot})$] and the reduction potential of the radical anion precursor (the reduction potential of the naphthyl moiety E^{red} = −2.38 V *vs.* SCE). Thus, $\Delta G_m = \Delta G_h - 23.06\ (E^{ox} - E^{red})$. The homolytic bond free energies are available from the literature.[10] The oxidation potentials of various ions can be obtained from thermodynamic cycles[11] or from direct measurements.[12]

The obtained data clearly show that the fragmentation rate of the radical anion correlates with the driving force for the reactions. In general, the more exergonic the reaction, the faster the cleavage of the radical anion, with the notable exception of the bromide **1f**. In this case the fragmentation reaction is five times slower than that of the less exergonic chloride (**1e**).

The sub-nanosecond lifetimes observed for these cleavage reactions are in general agreement with the reaction rates observed for other radical anion fragmentations with similar driving forces,[2b,d,13] and are, perhaps, only slightly slower than what would be expected for such exergonic processes based on other literature data.[2,13] This observation suggests that the electronic coupling does not drastically diminish the electron density in the naphthyl radical anions with the radical cation moiety in the zwitterion.[6]

The molecules studied here provide rates for the most exergonic mesolytic fragmentations studied so far. In this context, the inversion in the free-energy profile that is observed for the bromide (**1f**) suggests a possible existence of an inverted region analogous to that observed in electron-transfer reactions.[14] To the best of our knowledge this would be the first example of a reaction where bonds are broken (or made) showing such a behavior. More data are necessary before any firm conclusions can be reached, but the position of the inversion point on the free-energy plot suggests that these reactions have rather small intrinsic barriers.

According to the classical Marcus formulation,[15] the top of the parabola in the (log *k*) *vs.* ΔG plot should be located at the ΔG value equal to four times the intrinsic barrier (with the negative sign). In our case the maximum rate *at best* can be halfway between the ΔG_m values for the chloride and the bromide. Such simplified analysis suggests that the intrinsic barrier for the mesolytic cleavages of this type of radical anions is *ca.* 7 kcal mol^{-1} or less. This estimate is in very good agreement with previous observations,[2b,d,13] where the intrinsic barrier was postulated to be between 8–4 kcal mol^{-1}.

The observation of a possible inversion point on the free-energy function also suggests that the maximum rate for the cleavage reaction of radical anions is up to two magnitudes lower than what would be expected from transition state theory with a transmission coefficient of unity. Such a result would suggest that the electronic coupling between the π-system bearing the unpaired electron and the σ* orbital of the scissile bond is not very strong.

We thank the NSF and PRF for support of this research.

Notes and references

1 Mesolysis is defined as a unimolecular fragmentation of a radical ion into a radical and ion. See: (*a*) P. Maslak and J. N. Narvaez, *Angew. Chem., Int. Ed. Engl.*, 1990, **29**, 283; (*b*) P. Müller, *Pure Appl. Chem.*, 1994, 1077.

2 (*a*) J.-M. Savéant, *J. Phys. Chem.*, 1994, **98**, 3716; (*b*) P. Maslak, T. M. Vallombroso, W. H. Chapman Jr. and J. N. Narvaez, *Angew. Chem., Int. Ed. Engl.*, 1994, **33**, 73; (*c*) A. Anne, S. Fraoua, J. Moiroux and J.-M. Savéant, *J. Am. Chem. Soc.*, 1996, **118**, 3938; (*d*) M. L. Andersen, W. Long and D. D. M. Wayner, *J. Am .Chem. Soc.*, 1997, **119**, 6590.

3 For a review see: P. Maslak, *Top. Curr. Chem.*, 1993, **168**, 1.

4 J. C.-C. Tseng, S. Huang and L. A. Singer, *Chem. Phys. Lett.*, 1988, **153**, 401; J. C.-C. Tseng and L. A. Singer, *J. Phys. Chem.*, 1989, **93**, 7092; M. J. Foley and L. A. Singer, *J. Phys. Chem.*, 1994, **98**, 6430.

5 The reactive compounds for these studies were prepared from **1b**. Both **1a** and **1b** were synthesised following the literature procedure (ref. 4). All compounds were stable for several weeks at −10 °C under argon in the dark. Each compound was prepared and studied independently at least twice.

6 The electronic coupling between the radical cation and the radical anion in **C** (if the twist angle is less than 90°) would lead to a shift of electron density from the radical anion moiety to the radical cation site, diminishing the degree of electron transfer, and affecting somewhat the thermodynamic calculations presented here.

7 The reversible redox potentials were obtained using cyclic voltammetry on **1a**.

8 Quantum yield of the model compound (**1a**) is $Q^\circ = k_f/(k_f + k_{other})$, where k_{other} includes all non-radiative decay paths of **C**. Quantum yield of the reactive compounds (**1b–f**) is $Q = k_f/(k_f + k_{other} + k_m)$, and therefore, $k_m = (Q^\circ/Q - 1)\tau^\circ$, where τ° is the fluorescent life-time of the model [$\tau^\circ = 1/(k_f + k_{other})$ determined by time-resolved fluorescence to be 5.6 ns.

9 D. D. M. Wayner and V. D. Parker, *Acc. Chem. Res.*. 1993, **26**, 287.

10 S. W. Benson, *Thermochemical Kinetics*, Wiley, New York, 1976; S. W. Benson, F. R. Cruickshank, D. M. Golden, G. R. Haugen, H. E. O'Neal, A. S. Rodgers, R. Shaw and R. Walsh, *Chem. Rev.*, 1969, **69**, 279; S. E. Stein, *Structure and Properties*, National Institute of Standards and Technology, Standard Reference Data Program, Gaithersburg, 1994.

11 The data for halogen ions (and H^-) are based on the gas phase ionization potentials, hydration energies, and solvation energies for transfer from water to MeCN, and are adjusted for the reference electrode used here (SCE): R. G. Pearson, *J. Am. Chem. Soc.*, 1986, **108**, 6109; Y. Marcus, *Pure Appl. Chem.*, 1985, **57**, 1103.

12 P. Hapiot, J. Pinson and N. Yousfi, *New J. Chem.*, 1992, **16**, 877; E. M. Arnett, K. Amarnath, N. G. Harvey and S. Venimadhavan, *J. Am. Chem. Soc.*, 1990, **112**, 7346; F. G. Bordwell and J.-P. Cheng, *J. Am. Chem. Soc.*, 1991, **113**, 1736; F. G. Bordwell, X.-M. Zhang, A. V. Satish and J.-P. Cheng, *J. Am. Chem. Soc.*, 1994, **116**, 6605; J. Lind, X. Shen, T. E. Eriksen and G. Merenyi, *J. Am. Chem. Soc.*, 1990, **112**, 479; G. Merenyi, J. Lind and M. Jonsson, *J. Am. Chem. Soc.*, 1993, **115**, 4945.

13 P. Maslak, J. Kula and J. E. Chateauneuf, *J. Am. Chem. Soc.*, 1991, **113**, 2304.

14 See for example: P. F. Barbara, T, J. Meyer and M. A. Ratner, *J. Am. Chem. Soc.*, 1996, **100**, 13 148.

15 R. A. Marcus, *Discuss. Faraday Soc.*, 1960, **29**, 21; R. Marcus, *Annu. Rev. Phys. Chem.*, 1964, **15**, 155; R. Marcus and N. Sutin, *Biochim. Biophys. Acta*, 1985, **811**, 265.

Communication 9/08152F

Novel chlorin–diene building block by enyne metathesis: synthesis of chlorin–fullerene dyads

Gang Zheng,[a] Thomas J. Dougherty[a] and Ravindra K. Pandey*[ab]

[a] *Chemistry Division, Photodynamic Therapy Center, Roswell Park Cancer Institute, Buffalo, NY, 14263, USA. E-mail: rpandey@sc3103.med.buffalo.edu*

[b] *Department of Nuclear Medicine, Roswell Park Cancer Institute, Buffalo, NY, 14263, USA*

Received (in Corvallis, OR, USA) 23rd August 1999, Accepted 25th October 1999

The first example demonstrating the utility of enyne metathesis in preparing a chlorin–diene system as a novel and versatile building block is discussed; Diels–Alder reaction [4 + 2] of the diene with fullerene (C_{60}) produced the chlorin–fullerene dyad, a new artificial photosynthetic model; compared to the non-fullerene analogs, the corresponding free base and Zn^{II} chlorin–C_{60} dyads showed a remarkable decrease in their fluorescence intensity, indicating a rapid quenching of the chlorin excited singlet state by the fullerene moiety.

Fullerene C_{60} is one of the most widely studied molecules of the decade.[1] It has been reported as a promising new building block acting as an acceptor in artificial photosynthetic models,[2] and several porphyrin–C_{60} systems have been studied for this purpose.[3] It has been shown that C_{60} acts as an effective primary electron acceptor in a carotene–porphyrin–fullerene triad system, generating long-lived charge separated states with reasonable quantum yields.[4] Recent work by Imahori *et al.* on a C_{60}-linked Zn^{II} porphyrin system demonstrate that photoinduced electron transfer rates depend on the nature of linkages between the two chromophores.[5]

Natural chlorin pigments stand in marked contrast to symmetric porphyrin pigments due to substantially stabilized S_1 energies, a strong Qy absorption band, and unique redox reactivities. As a result, work is underway in our and various other laboratories to construct chlorin and bacteriochlorin based dimers with variable geometry and distances between the chromophores.[6] In certain fullerene-based electron and energy transfer (ET) models it has been suggested that large and spherical acceptors like C_{60} could show peculiar ET dynamics different from those shown by smaller counterparts such as benzoquinone and pyromellitic diimides, as well as by large π acceptors such as porphyrins and polycondensed aromatic compounds.[5] We believe that the synthesis of such chlorin–fullerene dyads with various spacers should provide valuable information for a deeper understanding of electron-transfer in photosynthetic reaction centers.

As a part of our research program to establish new methodologies for preparing such systems, the metathesis reaction caught our attention because of its unique ability to form C–C bonds. In recent years the applications of this approach have dramatically increased due to the availability of well-defined catalysts, in particular, Grubbs' catalyst $Cl_2(PCy_3)_2Ru{=}CHPh$ (Cy = cyclohexyl).[7] However, olefin metathesis has rarely been used in porphyrin chemistry. The only applications reported are those in which ligand metathesis has been used for preparing metalloporphyrins.[8]

Recently, Mori and co-workers reported a novel 1,3-diene synthesis from alkynes and ethylene by ruthenium-catalyzed enyne metathesis.[9] We thought it worthwhile to extend this methodology to the preparation of chlorin–fullerene conjugates *via* a sequence of enyne metathesis and Diels–Alder reactions.

For our studies, purpurin-18 methyl ester **1** was used as a starting material.[10] As shown in Scheme 1, reaction of **1** with propargylamine in toluene at 80 °C for 6 h produced propargylimide derivative **2** in 80% yield, which was used as a substrate for enyne metathesis. Treatment of the CH_2Cl_2 solution of **2** with Grubbs' catalyst (10 mol%) under ethylene gas atmosphere for 48 h at room temperature afforded the desired chlorin–diene building block **3** in 40% yield (on the basis of the starting material recovered, the yield was 100%). The structures of the intermediate chlorins **2** and **3** were confirmed by ^1H NMR and FAB mass spectometry analyses [*m/z* 616.7 and 644.6 (M + 1) respectively, exact mass calculated for compound **3** ($C_{39}H_{41}N_5O_4$): 643.3158, found: 644.3150 (M + 1)]. On comparing the resonances observed for **2** and **3**, the *N*-CH_2 protons which appeared as a singlet in diene **3** (δ 5.31, 2H) were observed as a multiplet (δ 5.29, 2H) in propargylimide **2** due to long range coupling with the acetylene proton.

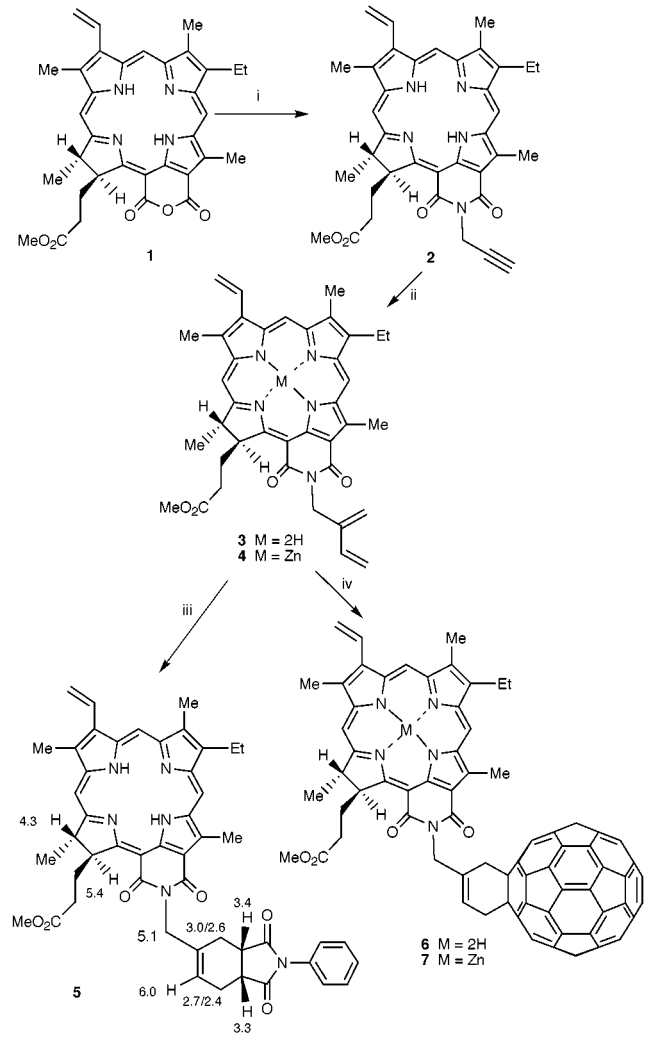

Scheme 1 *Reagents and conditions*: i, $NH_2CH_2C{\equiv}CH$, toluene, 80 °C, 6 h; ii, Grubbs's catalyst, $CH_2{=}CH_2$, CH_2Cl_2, 48 h; iii, *N*-phenylaleimide, toluene, reflux, 1 h; iv, C_{60}, toluene, reflux, 2 h.

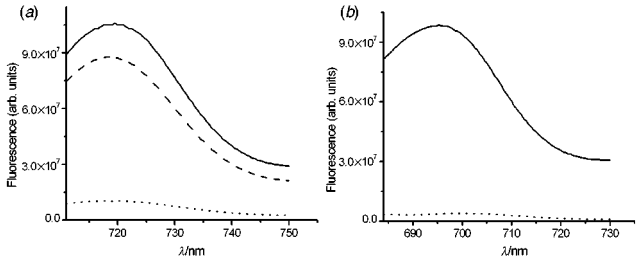

Fig. 1 (*a*) Fluorescence spectra of chlorin **3** (—), chlorin–maleimide **5** (- - -) and chlorin–C_{60} **6** (···) at 5 μmol l^{-1}. (*b*) Fluorescence spectra of Zn^{II} chlorin **4** (—) and Zn^{II} chlorin–C_{60} **7** (···) at 5 μmol l^{-1}.

To establish the reaction conditions needed to obtain chlorin–fullerene dyads, model studies were initially performed by using *N*-phenylmaleimide as dienophile, which is known to have similar reactivity to the fullerene C_{60} system.[11] As expected, reaction of free base chlorin **3** with *N*-phenylmaleimide in toluene for 1 h at 120 °C produced the corresponding Diels–Alder adduct **5** as a diastereomeric mixture (1 : 1) in 60% yield. Structural identification of **5** was performed by NMR and mass spectrometry analyses. In the ^{1}H NMR spectrum, the equal splitting of the CO_2CH_3 protons (17-$CH_2CH_2CO_2CH_3$) clearly indicated the presence of a diastereomeric mixture. Extensive spin-decoupling experiments further enabled us to assign the resonances and the coupling constants attributed to the respective protons. The chemical shift assignments of selected protons for the chlorin–*N*-phenylmalemide conjugate are shown in Scheme 1.

The reaction conditions established for the preparation of the model chlorin conjugate were then followed for the construction of the desired chlorin–fullerene conjugate. The Diels–Alder reaction of diene **3** with fullerene in refluxing toluene for 2 h afforded the chlorin–fullerene dyad **6** in 30% yield. The structure of **6** was confirmed by NMR and mass spectrometry analyses [exact mass calculated for $C_{99}H_{41}N_5O_4$: 1363.3158, found 1364.3160 (M + 1)]. In the ^{1}H NMR spectrum, the resonances of the newly formed cyclohexene ring system were observed at δ 3.98 (d, J = 5.5 Hz, 2H), 4.33 (m, 1H) and 7.22 (t, J = 5.5 Hz, 1H). The signals for the cyclohexene CH_2 (δ 4.3, see Scheme 1) and *N*-CH_2 protons appeared as multiplets, each integrating for two protons.

In our attempts to determine the effects of metallochlorins on energy/electron transfer (ET), dyad **6** was converted into the related Zn^{II} complex **7** (λ_{max} 684 nm**)** in quantitative yield following the standard methodology. The fluorescence spectra of the dyads **5**–**7** were compared with the free base diene **3** and the related Zn^{II}–**4** in CH_2Cl_2 by exciting their corresponding long wavelength absorptions (Qy band).[12] As can be seen from Fig. 1, conversion of diene **3** into the related *N*-phenylmaleimide adduct **5** had a limited effect on its fluorescence intensity. In contrast, dyads **6** and the Zn^{II} analog **7** containing the fullerene moieties showed a remarkable decrease in fluorescence, indicating a rapid quenching of the chlorin excited singlet state by C_{60}. The electronic absorption spectra of diene **3** and dyad **6** in CH_2Cl_2 and benzene indicate insignificant electronic interactions between the chromophores in the ground state. Detailed photophysical studies, such as fluorescence lifetime measurements, time-resolved transient absorption spectroscopy and the estimation of energy levels of these newly synthesized compounds, are underway. In order to determine the linkage dependence of photoinduced charge separation (CS) and subsequent charge recombination (CR), the synthesis of a series of chlorin– and bacteriochlorin–fullerene dyads with various spacers of fixed distances and geometry is currently in progress.

In conclusion, we have developed a new approach for the preparation of a versatile chlorin–diene building block **3** *via* ruthenium-catalyzed enyne metathesis. The utility of this highly reactive diene has been demonstrated by preparing new chlorin–fullerene dyads by following the [4 + 2] cycloaddition approach. The novel chlorin–diene building block has great potential for preparing not only promising models for photosynthetic reaction centers, but also for constructing a wide variety of porphyrin-based compounds of other biological significance.

The authors thank Dr S. Dutta, Molecular and Cellular Biophysics, RPCI, Buffalo, for mass spectrometry analyses. Partial support of the NMR facility by the NIH (grant CA-16056) is also acknowledged.

Notes and references

1 K. M. Kadish and R. S. Ruoff, *Fullerenes, The Electrochemical Society, NJ*, 1995; A. Hirsch, *The Chemistry of Fullerenes*, 1994, Georg Thieme Verlag, Stuttgart, 1994.
2 S. Fukuzumi, I. Nakanishi, T. Suenobu and K. M. Kadish, *J. Am. Chem. Soc.*, 1999, **121**, 3468; D. Guldi, G. Torres-Garcia and J. Mattay, *J. Phys. Chem. A.*, 1998, **102**, 9679.
3 For recent examples see: P. Cheng, S. R. Wilson and D. I. Schuster, *Chem. Commun.*, 1999, 89; T. Da Ros, M. Prato, D. Guldi, E. Alessio, M. Ruzzi and L. Pasimeni, *Chem. Commun.*, 1999, 635; D. Gust, T. A. Moore and A. L. Moore, *Pure Appl. Chem.*, 1998, **70**, 2189; K. Tamaki, H. Imahori, Y. Nishimura, I, Yamazaki, A. Shimomura, T. Okada and Y. Sakata, *Chem. Lett.*, 1999, 227; J.-P. Bourgeois, F. Diederich, L. Echegoyen and J.-F. Nierengarten, *Helv. Chim. Acta*, 1998, **81**, 1835.
4 P. Liddell, D. Kuciauskas, J. Sumida, B. Nash, D. Nguyen, A. Moore, T. Moore and D. Gust, *J. Am. Chem. Soc.*, 1997, **119**, 1400.
5 H. Imahori, K. Hagiwara, A. Masanori, T. Akiyama, S. Taniguchi, T. Okada, M. Shirakawa and Y. Sakata, *J. Am. Chem. Soc.*, 1996, **118**, 11771.
6 G. Zheng, J. L. Alderfer, M. O. Senge, M. Shibata and R. K. Pandey, *J. Org. Chem.*, 1998, **63**, 6435; J. Jaquinod, M. O. Senge, R. K. Pandey, T. P. Forsyth and K. M. Smith, *Angew. Chem., Int. Ed. Engl.*, 1996, **35**, 1840; G. Zheng, R. K. Pandey, T. P. Forsyth, A. N. Kozyrev, T. J. Dougherty and K. M. Smith, *Tetrahedron Lett.*, 1997, **38**, 2409; A. Osuka, S. Marumo, Y. Wada, I. Yamazki, T. Yamazki, Y. Shirakawa and Y. Nishimura, *Bull. Chem. Soc. Jpn.*, 1995, **68**, 2909.
7 R. H. Grubbs and S. Chang, *Tetrahedron*, 1998, **54**, 4413.
8 D. S. Bohle, C. H. Hung and B. D. Smith, *Inorg. Chem.*, 1998, **37**, 5798.
9 A. Kinoshita, N, Sakakibara and M. Mori, *Tetrahedron*, 1999, **55**, 8155.
10 P. H. Hynninen, in *Chlorophylls*, ed. H. Scheer, CRC Press, Boca Raton, Florida, 1991, p. 146.
11 S. R. Wilson and Q. Lu, *Tetrahedron Lett.*, 1993, **34**, 8043.
12 Excitation wavelengths: chlorin **3**, 707 nm; Zn^{II} chlorin **4**, 680 nm; chlorin–maleimide **5**, 707 nm; chlorin–C_{60} **6**, 710 nm and Zn^{II} chlorin–C_{60} **7**, 683 nm. Compared to diene **3**, the fluorescence of dyad **6** in CH_2Cl_2 and benzene solution was quenched by 88 and 63%, respectively, indicating a significant interaction between the chlorin and fullerene moieties.

Communication 9/06889I

ChemComm

Electrochemical polymerization of a bis(thienyl)bithiazole osmium complex

Brian J. MacLean and Peter G. Pickup*

Department of Chemistry, Memorial University of Newfoundland, St. John's, Newfoundland, Canada A1B 3X7. E-mail: ppickup@morgan.ucs.mun.ca

Received (in Columbia, MO, USA) 27th July 1999, Accepted 1st November 1999

A novel and easily n-doped conjugated metallopolymer has been prepared by the electrochemical polymerization of Os(bpy)$_2$[5,5′-bis(2-thienyl)-2,2′-bithiazole]$^{2+}$.

2,2′-Bithiazole is an attractive component for conjugated metallopolymers[1] because of its structural similarity to bithiophene and high π-electron density relative to bipyridine. Thus, unlike (bi)pyridine containing polymers, bithiazole based materials can be stable when p-doped and can exhibit relatively high conductivities.[2–5] An appealing approach to well defined bithiazole based metallopolymers is *via* the electrochemical polymerization of complexes of bis(thienyl)bithiazoles such as **1**. However, we have found that such complexes {Os(bpy)$_2$L^{2+}

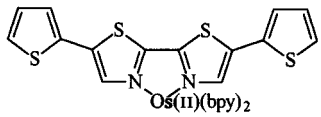

1

and Ru(bpy)$_2$L^{2+}, where bpy = 2,2′-bipyridine and L = 5,5′-bis(2-thienyl)-2,2′-bithiazole (bthbthz), 5,5′[bis(2-thienyl)-4,4′-dimethyl-2,2′-bithiazole, or 5,5′-bis[2-(3-methoxythienyl)]-4,4′-dimethyl-2,2′-bithiazole} can not be polymerized under conventional conditions. Zhu and Swager have found that complexes of the analogous bipyridine ligand, 5,5′-bis(2-thienyl)-2,2′-bipyridine, are also resistant to electrochemical polymerization.[6,7] These authors circumvented the problem by extending the terminal thiophenes to bithiophenes, which gave polymerizable complexes.

The reason for the failure of complexes with single thiophene rings on the ligand to polymerize appears to be due to instability of the bithiophene linkages that are formed at the high potentials needed to drive the polymerization. As can be seen in Fig. 1, the oxidation of the bthbthz ligand of **1**,† does not begin until *ca.* +1.55 V *vs.* SSCE (E_{pa} = 1.68 V). This wave decreases rapidly with cycling (not shown), indicating that a passivating film is produced on the electrode. Interestingly, the Os(III/II) wave remains unchanged with extensive cycling, indicating that the passive layer contains electroactive Os centres. Indeed, a small Os(III/II) wave can still be seen when a passivated electrode is transferred to a blank electrolyte. Although the Os centres in the passivating layer can mediate the electrochemistry of Os(II) in solution, their redox potential is not high enough to mediate the oxidation/polymerization of the bthbthz ligand.

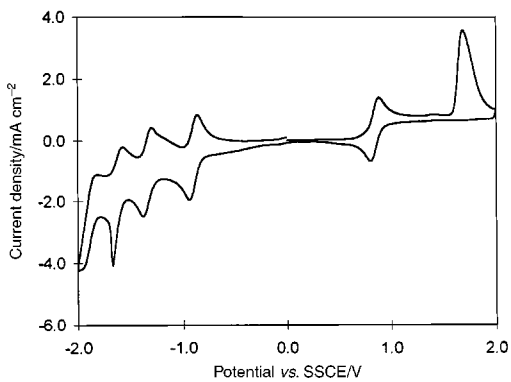

Fig. 1 Cyclic voltammetry (100 mV s^{-1}) of **1** in acetonitrile containing 0.1 mol dm^{-3} NEt$_4$ClO$_4$.

Reasoning that the passivating nature of the film formed by **1** was due to nucleophilic attack of residual water‡ on oxidized segments of the bithiophene-bithiazole backbone,[8] we added $BF_3{\cdot}OEt_2$ (Aldrich) to the acetonitrile–0.1 mol dm^{-3} NEt$_4$ClO$_4$ electrolyte solution. This reagent has been reported to be an excellent solvent system for the electrochemical synthesis of polythiophene.[9] The rationale for its use here is the deactivation of residual water by complexation with the BF_3. As shown in Fig. 2, compound **1** undergoes facile and sustained electrochemical polymerization in the $BF_3{\cdot}OEt_2$ containing electrolyte when the potential is cycled into the ligand oxidation wave at *ca.* 1.65 V. The Os(III/II) wave at a formal potential ($E^{\circ\prime}$) of +0.85 V increases monotonically with cycling of the potential into the ligand oxidation wave, and new waves appear in the region between the Os and ligand waves. The number, positions, and intensities of these new waves are somewhat variable. They are in the expected potential region for oxidation and re-reduction of a conjugated polymer backbone formed from polymerization of the bthbthz ligand at the 5-positions of the thiophene end groups, and therefore provide evidence that the complex polymerizes in this way. A deep red–purple film was observed on the electrode following the cyclic voltammetry shown in Fig. 2.

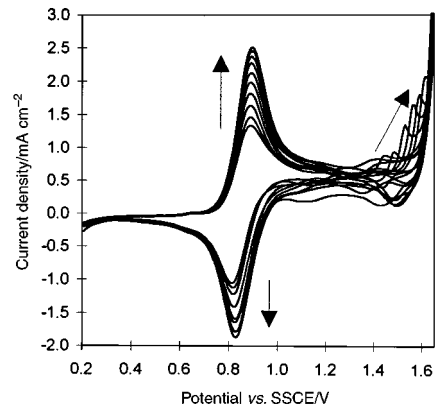

Fig. 2 Cyclic voltammetry (100 mV s^{-1}) of **1** in acetonitrile containing 0.1 mol dm^{-3} NEt$_4$ClO$_4$ and 0.45 mol dm^{-3} $BF_3{\cdot}OEt_2$. Arrows indicate changes with cycling.

Fig. 3 shows cyclic voltammograms of a poly-**1** coated electrode in the absence of **1** in solution. A reversible Os(III/II) wave appears at $E^{\circ\prime}$ = 0.865 V and a series of reduction waves are seen in the region −0.5 to −2.0 V. Based on the first three redox potentials for reduction of Os(bpy)$_3^{2+}$ (−1.26, −1.45 and −1.76 V[10]), which are for ligand based reductions,[10] the most positive reduction wave ($E^{\circ\prime}$ = −0.79 V) can be assigned to n-doping of the polymer backbone, while those at $E^{\circ\prime}$ = −1.62 and −1.85 V can be assigned to bpy based reductions. The mild potential and reversibility of the polymer based reduction, and the good stability of the n-doped form (indicated by the lack of significant decay of peak heights on multiple scans), open up the possibility of applications in molecular electronics and the

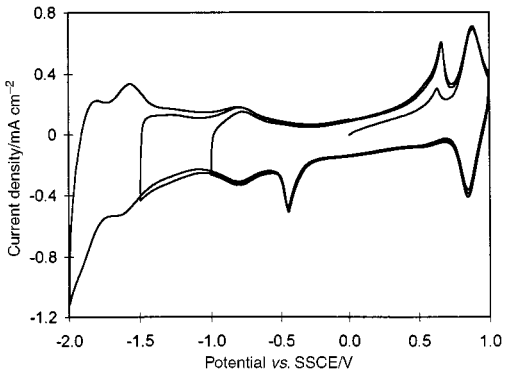

Fig. 3 Cyclic voltammetry (100 mV s^{-1}) of a poly-**1** coated Pt electrode in acetonitrile containing 0.1 mol dm^{-3} NEt_4ClO_4. Three consecutive scans to increasingly negative potentials are shown.

catalysis of reduction processes. The pre-peaks observed before the Os oxidation wave and the first reduction wave are typical of redox polymers based on bipyridine complexes.[11]

The Os(III/II) wave of poly-**1** is stable to multiple cycles extending down to −2.0 V, but decays rapidly when the potential is cycled to +2.0 V. Although no well defined polymer oxidation wave has been observed, it would appear that the polymer backbone is unstable to oxidation. Since the film remains visible on the electrode, the loss of the Os based electrochemistry implies that it is mediated by the polymer backbone. Since the backbone is not electroactive in the region of the Os(III/II) wave, electron transfer between Os sites presumably occurs *via* a superexchange interaction through the backbone.[1] Electron transport studies aimed at confirming these proposals, and establishing the influence of the metal (Os *vs.* Ru) and substituents on the polymer backbone are in progress. These studies can be expected to produce valuable guidance for the development of molecular electronics and electrocatalytic systems based on conjugated metallopolymers.

This work was supported by the Natural Sciences and Engineering Research Council of Canada and Memorial University.

Notes and references

† **1** was prepared by the reaction of $Os(bpy)_2Cl_2$[12] with 5,5′-bis(2-thienyl)-2,2′-bithiazole[3] at reflux in 70% aqueous ethanol. It was precipitated as the perchlorate salt and purified on a Sephadex LH-20/MeOH column.
‡ Acetonitrile was dried by distillation from CaH_2 immediately before use and NEt_4ClO_4 was dried at 120 °C under vacuum.

1 P. G. Pickup, *J. Mater. Chem.*, 1999, **8**, 1641.
2 I. H. Jenkins and P. G. Pickup, *Macromolecules*, 1993, **26**, 4450.
3 M. O. Wolf and M. S. Wrighton, *Chem. Mater.*, 1994, **6**, 1526.
4 T. Maruyama, H. Suganuma and T. Yamamoto, *Synth. Met.*, 1995, **74**, 183.
5 T. Yamamoto, H. Suganuma, T. Maruyama and K. Kubota, *J. Chem. Soc., Chem. Commun.*, 1995, 1613.
6 S. S. Zhu and T. M. Swager, *Adv. Mater.*, 1996, **8**, 497.
7 S. S. Zhu and T. M. Swager, *J. Am. Chem. Soc.*, 1997, **119**, 12 568.
8 A. A. Pud, *Synth. Met.*, 1994, **66**, 1.
9 C. Li, G. Q. Shi, G. Xue, S. Jin, B. Yu and S. J. Yang, *J. Polym. Sci: Part B: Polym. Phys.*, 1995, **33**, 2199.
10 H. D. Abruna, *J. Electroanal. Chem.*, 1984, **175**, 321.
11 P. Denisevich, H. D. Abruna, C. R. Leidner, T. J. Meyer and R. W. Murray, *Inorg. Chem.*, 1982, **21**, 2153.
12 D. A. Buckingham, F. P. Dwyer, H. A. Goodwin and A. M. Sargeson, *Aust. J. Chem.*, 1964, **17**, 325.

Communication 9/06102I

Nickel mediated sulfur–selenium and sulfur–sulfur bond formation

Chia-Huei Lai, Joseph H. Reibenspies and Marcetta Y. Darensbourg*

Department of Chemistry, Texas A&M University, College Station, Texas 77843, USA.
E-mail: marcetta@mail.chem.tamu.edu

Received (in Bloomington, IN, USA) 18th May 1999, Revised manuscript received 4th August 1999, Accepted 22nd October 1999

Electrophilic addition of the PhSeCl to a nickel dithiolate yields *S,S′*-bis(phenylselenenyl-*N,N′*-bis(mercaptoethyl)-1,5-diazacyclooctane nickel(II) dichloride and a dimeric, intermolecular bis-disulfide which results from ligand oxidation.

To extend the well known S-based nucleophilicity of [*N,N′*-bis(mercaptoethyl)-1,5-diazacyclooctane]nickel(II), (bme–daco)Ni or **Ni-1**,[1] especially with regard to developing reactive ligand functionalities, we explored the reactivity of **Ni-1** with PhSeCl, Scheme 1. The desired nickel-bound selenosulfide **1**, a moiety which should be capable of subsequent oxidative addition to low-valent metals and thus of potential usefulness to the preparation of heterobimetallics, was obtained (Scheme 1). In addition the intermolecular bis-disulfide of H_2bme–daco **2** was also isolated and characterized. The latter represents the product of ligand oxidation proposed in one-electron oxidative processes of **Ni-1**,[2] concomitantly releasing Ni^{2+} which is rapidly scavenged by **Ni-1**, producing the stable trimetallic species. Its existence supports our supposition that the monomeric intramolecular disulfide of the bme–daco ligand is sterically prohibited, accounting for much of the well behaved S-oxygenation chemistry displayed by the ligand.[3]

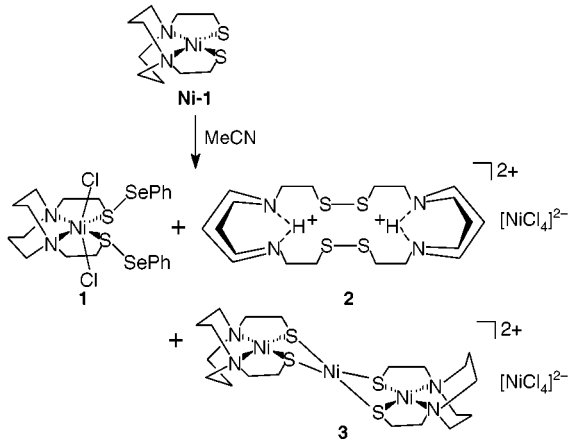

Scheme 1 Synthetic scheme of the reaction of **Ni-1** and PhSeCl.

Compound **1** is, to our knowledge, the only example of a structurally characterized mixed RS–SeR′ ligand which is S-bound to a transition metal. Our literature and data base searches find only one other structurally characterized mixed dichalcogenide, a low yield byproduct of an organometallic reaction which is Se-bound, (PhS*Se*Ph)$Cr(CO)_5$.[4] An interesting bioinorganic reaction of selenocysteine–S-dithiolene coupling at the molybdenum site of *Desulfovibrio desulfuricans* ATCC 27774 formate dehydrogenase (FDH) has implied both Se and S binding at Mo.[5] The following report is a designed mixed dichalcogenide synthesis, doubtlessly made possible by the well known ability of nickel to facilitate the nucleophilicity of thiolate-S as well as to bind charge-neutralized sulfur, stabilizing the RS–SeR′ toward disproportionation.

On mixing MeCN solutions of orange PhSeCl with purple **Ni-1**, two different precipitates developed; a major component was green and the minor, dark red–brown.[6] The mixture was separated by extraction with CH_2Cl_2 into which the former dissolved. The latter dark solid **3** was identified as a salt of a trimetallic cation[2] (Scheme 1). The green material crystallized in two forms, compounds **1** and **2**, which were characterized by X-ray crystallography. When dissolved in MeOH under Ar, the isolated and purified compound **1**, rapidly disproportionated, producing a mixture of **2**, **3** and diphenyl diselenide (as determined by ^{1}H NMR).

The molecular structures of **1** and **2** are shown in Figs. 1 and 2. Complex **1** contains a pseudo-octahedral nickel in $N_2S_2Cl_2$ coordination; the average deviation in the NiN_2S_2 best plane is 0.096 Å. The axial chlorides are bent away from the daco framework with a Cl–Ni–Cl angle of 159.07(14)°. As is usual for six-coordinate Ni complexes containing the diazacyclooctane moiety,[7] the fused nickel diazacyclohexane rings adopt chair/chair configurations with the pendant ethylene linkages (NCH_2CH_2S) staggered with respect to each other, across the N_2S_2Ni plane.

Another open, N_2S_2 tetradentate, six-coordinate complex based on **Ni-1**,[8] the dibenzyl dibromide complex **4**, is compared to that of **1** in Table 1. Notably, in compound **4** the benzyl groups are on the same side of the N_2S_2 planes, while the phenylselenolate groups of complex **1** are in *transoid* positions. For both complexes the S–Ni–S angles are *ca*. 10° greater than that of the parent **Ni-1**, corresponding to larger S···S distances (as contrasted to 3.04 Å in **Ni-1**).[7a] The Se–S_{av} distance of 2.202(4) Å agrees well with that of Se-bound $(CO)_5Cr$(PhS-*Se*Ph) ([Se–S = 2.226(6) Å][4] and the sum of covalent radii of 2.21 Å for a Se–S single bond.[9] The Ph(PhSe)*S*→Ni dative bond presumably relaxes the typical 90° torsion angle in REE′R dichalcogenides which minimizes lone-pair repulsion. In fact the C–S–Se–CPh torsion angles are 73 and 82°.

A combination of solution conductivity and electrochemical measurements, when compared with previous detailed studies

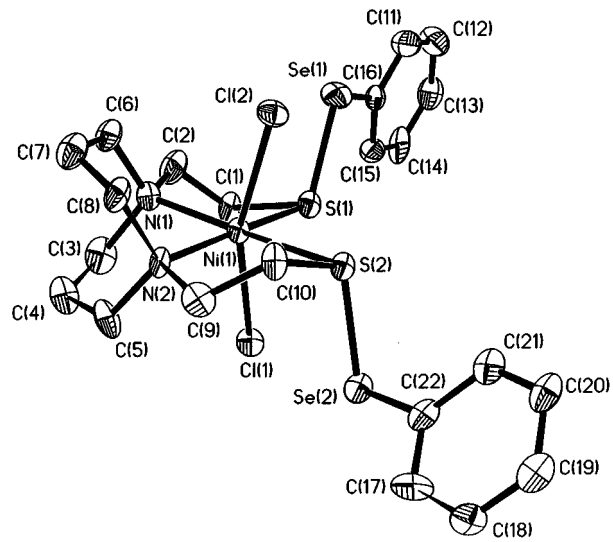

Fig. 1 ORTEP drawing (50% probability ellipsoids) of complex **1**. Metric data are given in Table 1.

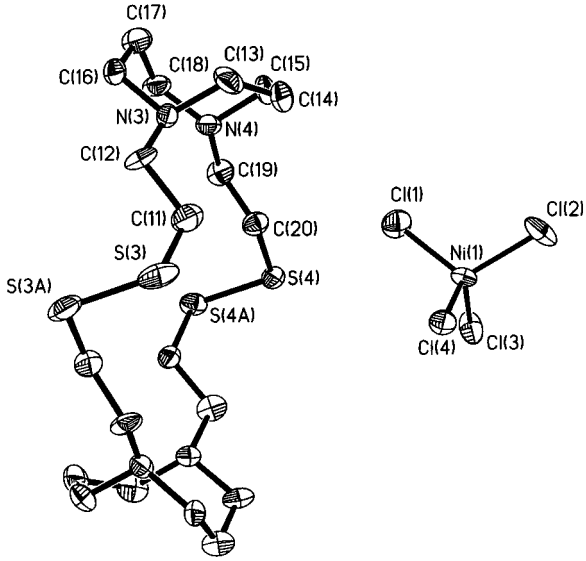

Fig. 2 ORTEP drawing (50% probability ellipsoids) of complex **2**. Selected distances (Å) and angles (°): S(3)–S(3A) 2.048(7), S(3)–C(11) 1.786(13), S(4)–S(4A) 2.023(6), S(4)–C(20) 1.845(11), av. Ni–Cl 2.272(4); av. Cl–Ni–Cl 107.1(2), C(11)–S(3)–S(3A) 104.0(4), C(20)–S(4)–S(4A) 102.7(4).

Table 1 Metrical structural data and electrochemical data

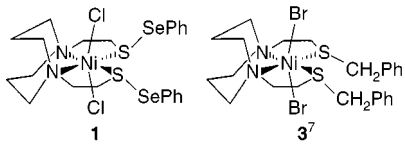

1 **3**[7]

Ni–S_{av}/Å	2.560(4)	2.493(1)
Ni–N_{av}/Å	2.120(11)	2.118(3)
S··S/Å	3.95	3.767
X–Ni–X/°	159.07(14)	162.01(2)
S–Ni–S/°	100.91(12)	98.14(3)
Ni–S–Se(C)$_{av}$/°	109.71(13)	114.91(14)
Reduction potential ($Ni^{II/I}$)/V	−0.38, −0.86	−0.67

of analogues of compound **4** and similar derivatives,[7,8,10] led to the conclusion expressed in Scheme 2. The $Ni^{II/I}$ couple at −0.38 V is the most positive observed thus far in a wide range of **Ni-1** thioether dicationic derivatives suggesting that the addition of two $SePh^+$ groups to the thiolate S achieves a charge neutralization better than that of any carbon-based electrophile. The selenosulfide derivative is less stable to reduction, consistent with weaker S–Se bonds at reduced nickel as compared to S–C bonds.[11] It is also consistent with the observed loss of the Se–S interaction in the reduction of the Mo^{VI}-selenosulfide site of FDH_H.[5] A complicated anodic region of the cyclic voltammogram was not resolved as to ligand or metal-based oxidation.[10,12]

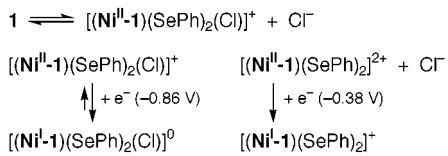

Scheme 2 The combined results of solution conductivity measurements and electrochemical studies.

The intermolecular disulfide **2** crystallizes in a dicationic protonated form, with $NiCl_4^{2-}$ as counter ion. The bisdisulfide attains a cage conformation (C_2 symmetry) with a typical disulfide S–S average distance (2.04 Å) and a large cross cage S(3)··S(4) distance of 7.207 Å. A similar bisdisulfide was isolated as a byproduct of a N_2S_2 ligating reaction of $VOCl_2(thf)_2$.[13] The H-bonding interaction linking the two N atoms significantly shortens the N··N distance to 2.633 Å, in contrast to **Ni-1**, 2.783 Å.

We gratefully acknowledge financial support from the National Science Foundation (CHE-9812355 for this work, and CHE 85-13273 for the X-ray diffractometer and crystallographic computing system, and CHE-8912763 for the EPR spectrometer) and contributions from the R. A. Welch Foundation. We thank Dr Guang Ming Li for ^{77}Se NMR spectra measurements.

Notes and references

† *Syntheses*: **1** and **2**: At 0 °C, 2 equiv. of PhSeCl (0.150 g, 0.8 mmol) added to a 15 mL CH_3CN solution of **Ni-1** (0.116 g, 4.0 mmol) produced a green precipitate and a red–brown solid. The resulting mixture was stirred for 30 min, and the solvent was removed *in vacuo*. Extraction of the residue with 20 mL of CH_2Cl_2 gave a deep green solution. Slow evaporation yielded dark green crystals of **1** and blue–green crystals of **2** in 55 and 3% yield, respectively. **1**: Anal. Calc. (Found) for $C_{22}H_{30}N_2S_2NiCl_2Se_2$: C, 39.20 (39.90); H, 4.49 (4.59); N, 4.16 (4.19)%. UV–VIS(MeOH) λ_{max}/nm (ε/M^{-1} cm^{-1}): 236(3232), 270(937), 316 (272), 338 (145). MS: +ESI; *m*/*z* (% intensity); 639 (20), 545 (29), 547 (29), 447 (9), 290 (10). ^{77}Se NMR (CH_2Cl_2): δ −372. **2**: Anal. Calc. (Found) for $C_{20}H_{42}N_4S_4NiCl_4$: C, 36.00 (36.08); H, 6.34 (5.98)%. MS: +ESI; m/z (% intensity); 594 (6), 466 (49), 250 (21), 233 (96), 146 (100).

‡ *Crystal data*: **1**: $C_{22}H_{30}N_2S_2NiCl_2Se_2$, M = 674.13, triclinic, space group $P\bar{1}$, a = 7.714(2), b = 8.031(3), c = 22.728(7) Å, α = 81.31, β = 85.50, γ = 65.610(10)°, U = 1267.4(7) Å^3, Z = 2, D_c = 1.766 g cm^{-3}. X-Ray crystallographic data were obtained on a Siemens R3m/V single crystal X-ray diffractometer using Mo-Kα (λ = 0.71073 Å) radiation and equipped with a Siemens LT-2 cryostat. A single crystal was mounted on a glass fiber with epoxy cement at 193(2) K. Structures were solved by direct methods. The elbow carbons C4, C7, C9 and C10 were found to be disordered and were modelled accordingly. Anisotropic refinement for all non-hydrogen atoms was by full-matrix least squares with R = 0.0861 and R_w = 0.2187.

2: $C_{20}H_{42}Cl_4N_4NiS_4$, M = 667.33, orthorhombic, space group *Fdd2*, a = 27.396(6), b = 18.885(4), c = 22.838(5) Å, U = 11816(4) Å^3, Z = 16, D_c = 1.501 g cm^{-3}. X-Ray crystallographic data were obtained on a Siemens R3m/V single crystal X-ray diffractometer using Cu-Kα (λ = 1.54178 Å) radiation and equipped with a Siemens LT-2 cryostat. The structures were solved by direct methods. Anisotropic refinement for all non-hydrogen atoms was by full-matrix least squares with R = 0.0569 and R_w = 0.1461. A single crystal was mounted on a glass fiber with epoxy cement at room temperature. CCDC 182/1466.

1 H_2bme–daco = *N*,*N*′-bis(mercaptoethyl)-1,5-diazacyclooctane; D. K. Mills, J. H. Reibenspies and M. Y. Darensbourg, *Inorg. Chem*., 1990, **29**, 4364.
2 P. J. Farmer, T Solouki, D. K. Mills, T. Soma, D. H. Russell, J. H. Reibenspies and M. Y. Darensbourg, *J. Am. Chem. Soc*., 1992, **114**, 4601.
3 C. A. Crapperhaus and M. Y. Darensbourg, *Acc. Chem. Res*., 1998, **31**, 451.
4 D. Neugebauer and U. Schubert, *J. Organomet. Chem*., 1983, **256**, 43.
5 G. N. George, C. Costa, J. J. G. Moura and I. Moura, *J. Am. Chem. Soc*., 1999, **121**, 2625.
6 The dark red–brown precipitate was characterized by spectroscopy as bis{*N*,*N*′-bis(mercaptoethyl)-1,5-diazacyclooctane]nickel(II)}nickel(II) tetrachloronickelate: UV–VIS(MeOH): λ_{max}/nm (ε/M^{-1} cm^{-1}): 408 (3033), 486 (1316), 548 (850). Anal. Calc. (Found) for $C_{20}H_{40}N_4S_4Ni_4Cl_4$: C, 28.55 (29.55); H, 4.79 (4.63)%. MS: +ESI; *m*/*z* (% intensity) 319 (85), 70 (100), 42 (82), 23 (39).
7 (*a*) M. Y. Darensbourg, I. Font, D. K. Mills, M. Pala and J. H. Reibenspies, *Inorg. Chem*., 1992, **31**, 4965; (*b*) D. C. Goodman, T. Tuntulani, P. J. Farmer, M. Y. Darensbourg and J. H. Reibenspies, *Angew. Chem., Int. Ed. Engl*., 1993, **32**, 116.
8 R. M. Buonomo, J. H. Reibenspies and M. Y. Darensbourg, *Chem. Ber*., 1996, **129**, 779.
9 N. J. Brondmo, S. Esperas and S. Husebye, *Acta Chem. Scand., Ser. A*, 1975, **29**, 93.
10 P. J. Farmer, J. H. Reibenspies, P. A. Lindahl and M. Y. Darensbourg, *J. Am. Chem. Soc*., 1993, **115**, 4665.
11 T. L. Cottrell, *The Strengths of Chemical Bonds*, Academic Press Inc. Publishers, New York, 1958.
12 M. Kumar, R. O. Day, G. J. Colpas and M. J. Maroney. *J. Am. Chem. Soc*., 1989, **111**, 5974.
13 W. Tsagkalidis, D. Rodewald and D. Rehder, *Inorg. Chem*., 1995, **34**, 1943.

Communication 9/03973B

ChemComm

Cyclic metallopeptides, cyclo[Gly-L-Cys(terpyPt^{II})]$_n$Cl$_n$†

Kentaro Tanaka,[a]‡ Kazuki Shigemori[b] and Mitsuhiko Shionoya*[a]‡

[a] *Coordination Chemistry Laboratories, Institute for Molecular Science, Myodaiji, Okazaki 444-8585, Japan*
[b] *Graduate University for Advanced Studies, Myodaiji, Okazaki 444-8585, Japan*

Received (in Columbia, MO, USA) 28th July 1999, Accepted 27th October 1999

An efficient strategy for the liquid-phase synthesis of cyclic metallopeptides, cyclo[Gly-L-Cys(terpyPt^{II})]$_n$Cl$_n$ (n = 3, 4), has been developed, which could provide a powerful tool for arraying metal centers on cyclopeptide frameworks.

Cyclopeptides are a class of compounds with biological activity[1] and great potential as functional molecules.[2] The development of strategies for functionalizing cyclopeptides is a fundamental challenge in the emerging field of *de novo* protein design. One of the most exciting recent advances in this field is the development of a wide range of structural and functional capabilities for self-assembling nanotubes made from cyclic D,L-α-peptides and from cyclic β-peptides.[3] As another advantageous tool for the functionalization of peptides, metal binding sites have been engineered into peptides and proteins using the side chains of naturally occurring amino acids or unnatural metal binding sites incorporated at the residues, for model studies of protein folding and enzymes, biosensors and molecular architectures.[4] Our approach is based on the use of amino acids containing a metal coordinating site (*e.g.* the thiol group of Cys)§ as the components of cyclopeptides for constructing cyclopeptide–metal complex conjugates. Herein we describe an efficient strategy for the liquid-phase synthesis of cyclopeptides having a repeating Gly-L-Cys(terpyPt^{II}) sequence, cyclo[Gly-L-Cys(terpyPt^{II})]$_n$Cl$_n$, **2** (n = 3) and **3** (n = 4).§ Interest in the incorporation of a terpyPt^{II} complex onto L-Cys was initially aroused by its binding to DNA and antitumor properties.[5] In these peptides, positively charged Pt^{II} complexes are designed to align on the periphery of the macrocyclic peptide scaffold. We have found that these cyclic metallopeptides provide a novel structural motif in the receptor site for anionic guest molecules.

The synthetic route for the cyclopeptides is shown in Scheme 1. The linear peptides, H$_2$(Gly-L-Cys)$_n$OH·(CF$_3$CO$_2$) (n = 3 and 4), were prepared on a peptide synthesizer using standard Fmoc chemistry. Treatment of these peptides with 1.2n equiv. of [(terpyPt^{II})Cl]Cl·2H$_2$O in H$_2$O at room temperature afforded H$_2$[Gly-L-Cys(terpyPt^{II})]$_n$OH·(CF$_3$CO$_2$)$_{n+1}$ **1a** (n = 3) and **1b** (n = 4), in 88 and 97% yields, respectively, after purification by RP-HPLC [eluent: H$_2$O–MeCN (7:3) containing 0.1% TFA].§ The resulting linear peptides, **1a** and **1b**, were cyclized at a concentration of *ca.* 0.50 mM in H$_2$O–MeCN (7:3) at 25 °C for 48 and 72 h, respectively, in the presence of excess HOBt and EDC.§ Cyclo[Gly-L-Cys(terpyPt^{II})]$_n$Cl$_n$, **2** (n = 3) and **3** (n = 4) were obtained as red precipitates in 58% yield in both cases.[6,7] The products were highly pure even in the crude form. Whereas the ^{1}H NMR spectral patterns for the linear **1a** and **1b** were highly complicated, those for the cyclopeptides **2** and **3** were much more symmetrical and only one set of signals corresponding to a Gly-L-Cys(terpyPt^{II}) moiety was observed in each case. The electrostatic repulsion that would occur intramolecularly between the positively charged Pt^{II} complexes may complicate the solvent-dependent prefolding of the linear starting peptides, and at the same time may facilitate the intramolecular cyclization. Although the ESI MS data showed *m/z* 587 for both **2** and **3**, the rings of the cyclopeptides were clearly shown to be 18- and 24-membered, respectively, from the numbers of split lines observed in the high-resolution

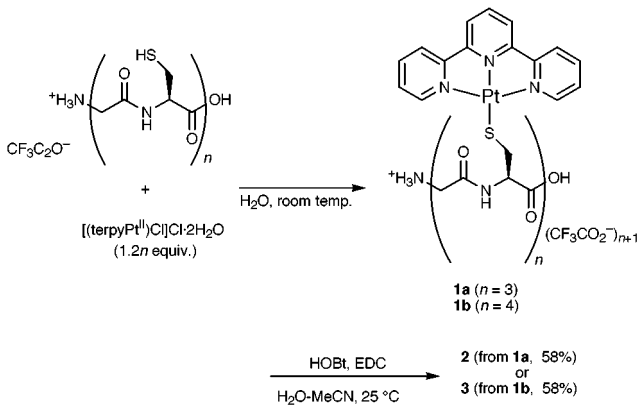

Scheme 1

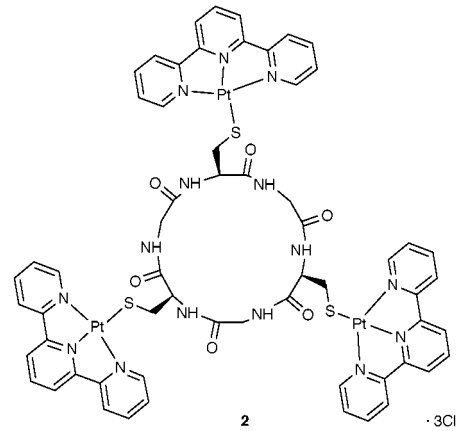

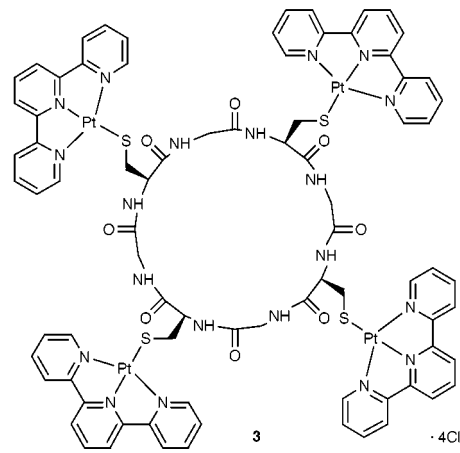

† Experimental and spectral data for **1a**,**b**, **2** and **3** are available from the RSC web site, see http://www.rsc.org/suppdata/cc/1999/2475/

‡ Present address: Department of Chemistry, School of Science, the University of Tokyo, Hongo, Bunkyo-ku, Tokyo 113-0033, Japan. E-mail: shionoya@chem.s.u-tokyo.ac.jp

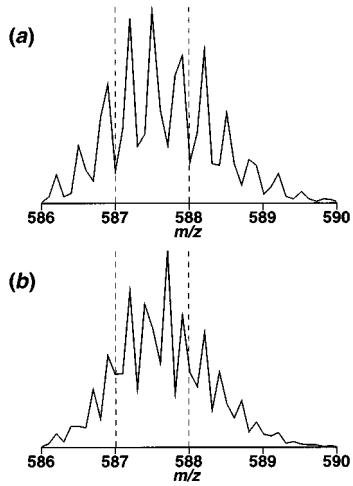

Fig. 1 High resolution ESI mass spectra for (*a*) **2** and (*b*) **3**.

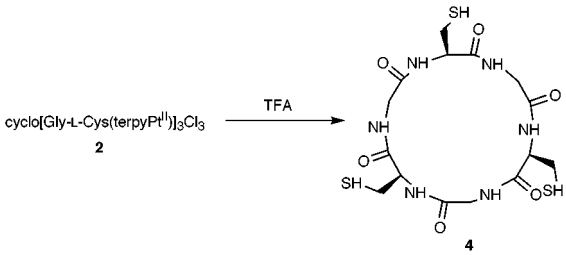

Scheme 2

spectra (Fig. 1). To the best of our knowledge, this is the first example providing an efficient strategy for the liquid-phase synthesis of cyclic metallopeptides from linear peptides bearing functional metal complexes.

The terpyPt^{II} complex moieties of **2** were readily removed by treatment with TFA to afford the corresponding cyclopeptide, cyclo[Gly-L-Cys]$_3$ **4**, as indicated by its ESI MS data (*m/z* 479 [M − H$^+$]$^-$) (Scheme 2). Consequently, terpyrPt^{II} complexes can be regarded as both protecting and promoting groups for peptide cyclization.

These cyclic metallopeptides were found to act as positively charged anion receptors.[8] In these receptors, coulombic interactions were expected primarily to contribute to the attractive force for anion binding. We have examined the binding of cyclohexapeptide **2** to benzenetricarboxylate anions (1,2,3-, 1,2,4- and 1,3,5-tricarboxylates).[9] It was clearly demonstrated from its ^{1}H NMR studies that the cyclohexapeptide **2** selectively separated benzene-1,3,5-tricarboxylate from an equimolar mixture of the three tricarboxylates to form a 1 : 1 ternary complex in neutral water at room temperature.

We have demonstrated an efficient strategy for the liquid-phase synthesis of cyclopeptides containing a repeating Gly-L-Cys(terpyPt^{II}) sequence. These results raise the intriguing possibility that this strategy will provide a powerful tool for arraying metal centers on cyclopeptide frameworks, which could lead to structural as well as functional control of multinuclear metal complexes.

Support from Monbusho (Grant-in-Aids for Scientific Research on Priority Areas, No. 10149101 'Metal-assisted Complexes', No. 08249103 'Biometalics', and No. 706 'Dynamic Control of Stereochemistry') is gratefully acknowledged.

Notes and references

§ Abbreviations used: Gly, glycine; Cys, cystein; Fmoc, fluoren-9-ylmethoxycarbonyl; RP-HPLC, reverse-phase high performance liquid chromatography; HOBt, 1-hydroxy-1*H*-benzotriazole monohydrate; EDC, *N*-ethyl-*N*′-[3-(dimethylamino)propyl]carbodiimide hydrochloride; ESI MS, electrospray ionization mass spectrometry.

1 R. Haubner, D. Finsinger and H. Kessler, *Angew. Chem., Int. Ed. Engl.*, 1997, **36**, 1374.
2 W. F. DeGrado, *Adv. Protein Chem.*, 1988, **39**, 51; J. S. Richardson and D. C. Richardson, *Trends Biochem. Sci.*, 1989, **14**, 304.
3 M. R. Ghadiri, J. R. Granja, R. A. Milligan, D. E. McRee and N. Khazanovich, *Nature*, 1993, **366**, 324; M. R. Ghadiri, J. R. Granja and L. Buehler, *Nature*, 1994, **369**, 301; H. S. Kim, J. Hartgerink and M. R. Ghadiri, *J. Am. Chem. Soc.*, 1998, **120**, 4417.
4 For recent examples, see M. R. Ghadiri and C. Choi, *J. Am. Chem. Soc.*, 1990, **112**, 1630; F. Ruan, Y. Chen and J. Hopkins, *J. Am. Chem. Soc.*, 1990, **112**, 9403; M. Lieberman and T. Sasaki, *J. Am. Chem. Soc.*, 1991, **113**, 2533; C. A. Kim and J. M. Berg, *Nature*, 1993, **362**, 267; D. E. Robertson, R. S. Farid, C. C. Moser, J. L. Urbauer, S. E. Mulholland, R. Pidikiti, J. D. Lear, A. J. Wand, W. F. DeGrado and P. L. Dutton, *Nature*, 1994, **368**, 425; J. Schneider and J. W. Kelly, *J. Am. Chem. Soc.*, 1995, **117**, 2533; R. P. Cheng, S. L. Fisher and B. Imperiali, *J. Am. Chem. Soc.*, 1996, **118**, 11349; W. D. Kohn, C. M. Kay, B. D. Sykes and R. S. Hodges, *J. Am. Chem. Soc.*, 1998, **120**, 1124.
5 S. J. Lippard, *Acc. Chem. Res.*, 1978, **11**, 211.
6 These metallopeptides were characterized by ^{1}H NMR, ESI MS and elemental analyses.
7 In the case with n = 2, the intermolecular coupling predominantly occurred to produce the linear octapeptide and then cyclooctapeptide **3** as the main product. The isolation of the desired cyclotetrapeptide as the minor product was not successful.
8 *Comprehensive Supramolecular Chemistry*, ed. J. L. Atwood, J. E. D. Davies, D. D. MacNicol, F. Vogtle, J.-M. Lehn and G. W. Gokel, Elsevier Science, Oxford, 1996, vol. 1.
9 The binding constants could not be determined accurately due to the low solubility of the complex with carboxylate anions in general solvents.

Communication 9/06144D

ChemComm

Diffusion coefficients of zirconocene–borate ion pairs studied by pulsed field-gradient NMR—evidence for ion quadruples in benzene solutions

Stefan Beck,† Armin Geyer* and Hans-Herbert Brintzinger

Fakultät für Chemie, Universität Konstanz, D-78457 Konstanz, Germany. E-mail: Hans.Brintzinger@uni-konstanz.de

Received (in Oxford, UK) 11th October 1999, Accepted 5th November 1999

Diffusion coefficients for ion pairs containing zirconocene cations and fluorinated tetraphenyl- or methyltriphenylborate anions in benzene solutions are substantially smaller than those expected for monomeric species and indicate that ion quadruples are present in these solutions.

Electron deficient metallocene alkyl cations of group 4 metals, in combination with weakly coordinating anions are considered to be reactive species in homogeneous olefin polymerization catalysis.[1] Particularly well defined in this regard, in several instances even by solid-state structures,[2,3a] are zirconocene ion pairs which contain the fluorinated borate anions $B(C_6F_5)_4^-$ or $MeB(C_6F_5)_3^-$; these are obtained by reaction of a dimethyl zirconocene complex with a triorganylammonium or triphenylcarbenium salt of $B(C_6F_5)_4^-$ or with $B(C_6F_5)_3$, respectively.[4] The binding of the anion to the cationic center in these contact-ion pairs is of importance for the activity of a catalyst system, since the anion A^- has to be displaced by the olefin substrate to initiate the catalytic cycle. Exchange of these anions between zirconocene coordination sites as well as their displacement by entities such as a Lewis base, $AlMe_3$ or another dimethyl zirconocene complex have been studied in considerable detail.[1–3] Rather little is known, however, about the structures of these ion pairs in solution, especially with regard to the extent to which they form dissociated, associated or aggregated ion pairs in the non-polar solvents commonly used for homogeneous olefin polymerizations. In order to clarify this point, we have determined the size of these catalytically active species in solution by measuring their translational diffusion coefficients D_t by NMR methods.

The LED (longitudinal eddy current delay) experiment measures the intensity of a spin–echo amplitude as a consequence of the change in spatial position of a molecule during the time interval between two pulsed field gradients.[5] The changing signal intensity (I) with incremented gradient strength G is related to the translational diffusion coefficient D_t by the Stejskal–Tanner equation $I = I_0\exp\{-(\gamma\delta G)^2\,[\Delta - (\delta/3)]\,D_t\}$,[6] where γ is the gyromagnetic ratio, δ the gradient duration and Δ the interval between the pulsed field gradients. The method works also for complexes and salts.[7] For approximatively spherical particles which are significantly larger than the solvent molecules, the Stokes–Einstein equation $D_t = kT/(6\pi\eta r)$, where k = Boltzmann constant, T = absolute temperature and η = viscosity of the solvent, is used to relate the translational self-diffusion coefficient D_t to the radius r of the dissolved particle. For molecules with van der Waals radii $r_W <$ 5 Å, the Stokes–Einstein factor of 6 has to be changed to a value of 4.[8] We find this so-called perfect slip condition to hold for dilute benzene solutions of the bis(cyclopentadienyl) dimethylzirconium compounds shown in Scheme 1 (Table 1). The diffusion coefficients of these neutral, monomeric zirconocene complexes decrease linearly with increasing molecular size: The inverse diffusion coefficients of these species correlate with their calculated van der Waal's radii r_W with deviations of $< 10\%$ (Fig. 1).

Rather unexpected results, however, pertain to a number of ion pairs derived from compounds **1** and **5**: While the D_t value obtained for the methylborate ion pair **5A** deviates only slightly from the calibration provided by compounds **1**–**5**, the experimentally determined D_t value of ion pair **1A** amounts to only *ca.* 80% of the expected value. These deviations from expectation are even more pronounced for the ion pairs **1B** and **5B**, which contain the more weakly coordinating $B(C_6F_5)_4^-$ anion and are, hence, presumably more polar. The D_t value obtained for ion pair **1B** in particular (5.1×10^{-10} m^2 s^{-1}), yields an apparent particle volume of 1260 Å^3, which corresponds to just twice the expected volume of this ion pair.

Even though a number of caveats have to be heeded—a pronounced anisotropic molecular shape, a change from perfect slip (SE factor 4) to perfect stick conditions (SE factor 6) or an increased solvent shell might contribute to the observed decrease of D_t—we propose that ion pair **1B** is present in these solutions predominantly in form of its dimer, *i.e.* of an ion quadruple (Scheme 2). This contention is supported by the observation that **1B** has practically the same diffusion coefficient as the related ion pair $[(C_5H_5)_2ZrMe(\mu\text{-}Me)MeZr(C_5H_5)_2]^+\,B(C_6F_5)_4^-$ **1C**, for which a binuclear structure has been independently established.[3a,9]

From the theory of ion solutions in organic solvents it is indeed to be expected that ion quadruples are present in benzene solutions of ion pairs such as **1B** at the concentrations considered here,[10] which are close to the limiting concentrations at which these ion pairs begin to form separate phases. In accord with these theoretical considerations, the degrees of ion quadruple formation, indicated by the deviations of D_t from the values expected for monomeric species, are higher for the more polar ion pairs **1B** and **5B** than for the presumably partly covalent ion pairs **1A** and **5A** and higher for ion pairs **1A** and **1B**, which contain the rather small $(C_5H_5)_2ZrMe^+$ cation, than for their more voluminous analogues **5A** and **5B**, respectively.

More detailed data on degrees of aggregation and their dependence on the nature of the zirconocene cation and its counter anion will clearly be needed for a full description of

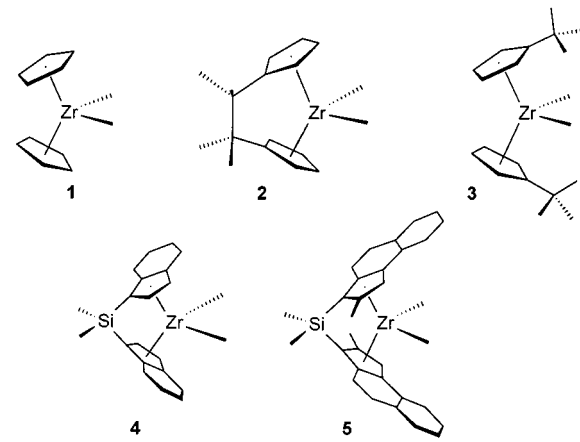

Scheme 1

† Present address: School of Chemistry, University of Leeds, Leeds, UK LS2 9JT.

Table 1 Diffusion coefficients D_t, measured for the neutral dimethyl zirconocene compounds **1**–**5** and for the ion pairs **1A**–**C** and **5A**, **B** in C_6D_6 solution at 300 K, and van der Waals radii r_W and molecular volumes V_W of these zirconocene complexes

Zirconocene complex [a]	10^{10} D_t[b]/m^2 s^{-1}	r_W[c]/Å	V_W[c]/Å^3
1 $(C_5H_5)_2ZrMe_2$	14.9	3.6	196
2 $Me_4C_2(C_5H_4)_2ZrMe_2$	13.4	4.1	290
3 $(C_5H_4Bu^t)_2ZrMe_2$	12.0	4.3	335
4 *rac*-$Me_2Si(ind)_2ZrMe_2$	11.5	4.4	354
5 *rac*-Me_2Si(2-Me-benz[*e*]ind)$_2ZrMe_2$	10.1	4.9	481
1A $[(C_5H_5)_2ZrMe^+\cdots MeB(C_6F_5)_3^-]$	8.1	5.0	513
1B $[(C_5H_5)_2ZrMe^+\cdots B(C_6F_5)_4^-]$	5.1	5.2	593
1C $[\{(C_5H_5)_2ZrMe\}_2(\mu\text{-}Me)^+]$ $B(C_6F_5)_4^-$	4.9	5.7	789
5A [*rac*-Me_2Si(2-Me-benz[*e*]ind)$_2ZrMe^+\cdots MeB(C_6F_5)_3^-$]	8.2	5.7	797
5B [*rac*-Me_2Si(2-Me-benz[*e*]ind)$_2ZrMe^+\cdots B(C_6F_5)_4^-$]	6.1	5.9	877

[a] Zirconocene concentrations (mmol dm^{-3}): **1**, 1–20; **2**–**5**, 1; **1A**, 4.7; **1B**, 1.6; **1C**, 2; **5A**, 4; **5B**, 2. [b] Measured on a Bruker DRX 600 spectrometer with a BGU II gradient unit using ten different gradient strengths (5–50 G cm^{-1}) of 1 ms duration, with diffusion times Δ of 0.5 s (32 scans) and relaxation delays of 20 s. Integrals and peak intensities were quantified with the Bruker T1/T2 software package. Independent D_t values, determined for individual NMR signals of each complex, gave the average values listed with mean deviations of $< 5\%$. [c] Calculated from molecular hard-sphere volume increments: D. Ben-Amotz and K. G. Willis, *J. Phys. Chem.*, 1993, **97**, 7736.

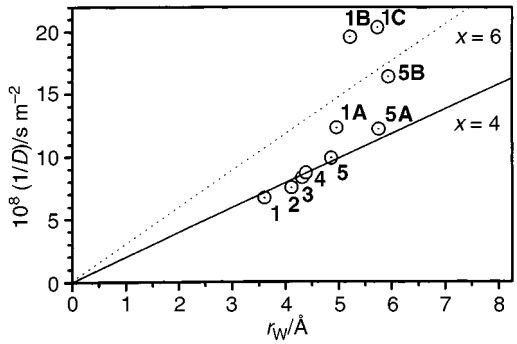

Fig. 1 Reciprocal diffusion coefficients, $1/D_t$, and van der Waals radii, r_W, for the neutral zirconocene complexes **1**–**5**, for the ion pairs $[(C_5H_5)_2ZrMe^+\cdots MeB(C_6F_5)_3^-]$ **1A**, $[(C_5H_5)_2ZrMe^+\cdots B(C_6F_5)_4^-]$ **1B**, [*rac*-Me_2Si(2-Me-benz[*e*]ind)$_2ZrMe^+\cdots MeB(C_6F_5)_3^-$] **5A** and [*rac*-$Me_2Si$(2-Me-benz-[*e*]ind)$_2ZrMe^+\cdots B(C_6F_5)_4^-$] **5B**, and for the dinuclear complex $[\{(C_5H_5)_2ZrMe\}_2(\mu\text{-}Me)^+]B(C_6F_5)_4^-$ **1C**.

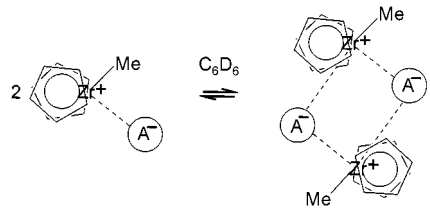

Scheme 2

reaction systems of this type. From the data presented here it is already clear, however, that the hitherto entirely neglected formation of ion quadruples will have to be taken into account for an analysis of exchange reactions between anions and other ligands in zirconocene-based catalyst systems.

Financial support of this work by BASF AG, BMBF and by funds of the University of Konstanz is gratefully acknowledged.

Notes and references

1 M. Bochmann, *J. Chem. Soc., Dalton Trans.*, 1996, 255 and references therein.
2 X. Yang, C. L. Stern and T. J. Marks, *J. Am. Chem. Soc.*, 1994, **116**, 10 015; P. A. Deck, C. L. Beswick and T. J. Marks, *J. Am. Chem. Soc.*, 1998, **120**, 1772; L. Luo and T. J. Marks, *Top. Catal.*, 1999, **7**, 97 and references therein.
3 (*a*) S. Beck, M. H. Prosenc, H. H. Brintzinger, R. Goretzki, N. Herfert and G. Fink, *J. Mol. Catal., A: Chem.*, 1996, **111**, 67; (*b*) S. Beck, M. H. Prosenc and H. H. Brintzinger, *J. Mol. Catal. A: Chem.*, 1997, **128**, 41.
4 G. G. Hlatky, H. W. Turner and R. R. Eckman, *J. Am. Chem. Soc.*,1989, **111**, 2728; J. A. Ewen and M. J. Elder, *Makromol. Chem., Macromol. Symp.*, 1993, **66**, 179; J. C. Chien, W. M. Tsai and M. D. Rausch, *J. Am. Chem. Soc.*, 1991, **113**, 8570.
5 S. J. Gibbs and C. S. Johnson, Jr., *J. Magn. Reson.*, 1991, **93**, 395; K. F. Morris and C. S. Johnson, Jr., *J. Am. Chem. Soc.*, 1993, **115**, 4291.
6 E. O. Stejskal and J. E. Tanner, *J. Chem. Phys.*, 1965, **42**, 288.
7 A. Mayzel and Y. Cohen, *J. Chem. Soc., Chem. Commun.*, 1994, 1901; R. E. Hoffman, E. Shabtai, M. Rabinovitz, V. S. Iyer, K. Müllen, A. K. Rai, E. Bayrd and L. T. Scott, *J. Chem. Soc., Perkin Trans. 2*, 1998, 1659.
8 R. A. Robinson and R. H. Stokes, *Elektrolyte Solutions*, Butterworth, London, 2nd edn. revised, 1970; J. T. Edwards, *J. Chem. Educ.*, 1970, **47**, 261; M. Ue, *J. Electrochem. Soc.*, 1994, **141**, 3336.
9 M. Bochmann and S. J. Lancaster, *J. Organomet. Chem.*, 1992, **434**, C1; *Angew. Chem., Int. Ed. Engl.*, 1994, **33**, 1634; Y.-X. Chen. C. L. Stern, S. Yang and T. J. Marks, *J. Am. Chem. Soc.*, 1996, **118**, 12 451; I. Tritto, R. Donetti, M. C. Sacchi, P. Locatelli and G. Zannoni, *Macromolecules*, 1997, **30**, 1247.
10 C. A. Kraus, *J. Chem. Phys.*, 1956, **60**, 129; J. E. Gordon, *The Organic Chemistry of Electrolyte Solutions*, Wiley, New York, 1975, p. 371.

Communication 9/08203D

Anodic and cathodic electrografting of alkynes on porous silicon†

Edward G. Robins, Michael P. Stewart and Jillian M. Buriak*

Department of Chemistry, Purdue University, West Lafayette, IN 47907-1393 USA. E-mail: buriak@purdue.edu

Received (in Bloomington, IN, USA) 18th August 1999, Accepted 25th October 1999

A versatile electrochemical grafting reaction connects conjugated molecules to porous silicon surfaces with either a positive or negative bias.

Porous silicon, an interconnected network of silicon nanowires and nanocrystallites,[1] is terminated by metastable silicon–hydride groups (Si–H_x) and Si–Si bonds. There are now a number of techniques utilized for chemical modification of these species on the surface of porous silicon.[2–6] Using the Si surface as a semiconducting electrode, several workers have reported electrochemical Si–C bond formation by direct grafting, an approach with few parallels to soluble, molecular silane chemistry.[7–9] Herein we report a system for electrochemically grafting terminal alkynes to porous silicon which gives two distinct surface derivatizations, depending on the polarity of the surface bias. *Cathodic* electrografting (CEG) directly attaches alkynes to the surface, whereas *anodic* electrografting (AEG) yields an alkyl surface.

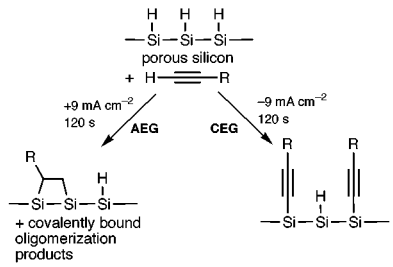

FTIR analysis of phenylacetylene CEG (surface **1**, Fig. SM3†) reveals Si–H_x stretches which are broadened and decreased in integrated intensity compared to unmodified porous silicon. The absence of a ν(≡CH) mode around 3300 cm^{-1} and an observed sharp silylated alkyne ν(C≡C) at 2159 cm^{-1} is consistent with a Si–alkynyl surface and not simple physisorption. For instance, the ν(C≡C) of 1-phenyl-2-(trimethylsilyl)acetylene appears at 2160 cm^{-1} while that of phenylacetylene is observed at 2110 cm^{-1}. Similarly, CEG of dodec-1-yne (surface **2**, Fig. SM1†) shows a ν(C≡C) at 2176 cm^{-1}, which is identical to the silylated molecular analogue 1-trimethylsilyldodec-1-yne at 2176 cm^{-1}; underivitized dodec-1-yne appears at 2120 cm^{-1}. Fig. 1(*a*) shows the pentynyl terminated surface (surface **3**) with the ν(C≡C) at 2179 cm^{-1}. This surface was hydroborated with a 0.5 M THF solution of disiamylborane[10] to verify the presence of the silylated triple bond. The appearance of a broad band at 1580 cm^{-1} and the concomitant consumption of the ν(C≡C) is indicative of a silylated, borylated double bond, which was verified by hydroboration of 1-trimethylsilyldodec-1-yne and subsequent FTIR analysis [ν(C=C) at 1584 cm^{-1}].

Covalent electrografting of alkynes also appears to occur when an anodic potential is applied, although AEG surfaces show complete reduction of all unsaturated bonds. The C≡C triple bond is not observed, with only a weak vibration corresponding to a hydrosilylated double bond mode (1600 cm^{-1}) in the FTIR spectra. In contrast to CEG, AEG of dodec-1-yne [surface **8**, Fig. 1(*b*)] has features relating only to aliphatic C–H bonds. In the spectrum of phenylacetylene AEG (surface **9**, Fig. SM8†), ring breathing modes at 1599, 1493 and 1446 cm^{-1} compare closely with polystyrene films and differ from those observed for the conjugated CEG surface **1** at 1596, 1489 and 1443 cm^{-1}. Boiling of the surfaces functionalized through AEG for 30 min in $CHCl_3$ results in no change in the FTIR spectrum, suggesting covalent bonding as opposed to physisorption. Based on the coincidence of the ring modes and the saturation of the C≡C bonds, we conclude that doubly hydrosilylated (bis-silylation) or possibly oligomeric material decorates the porous silicon surface (*vide infra*).

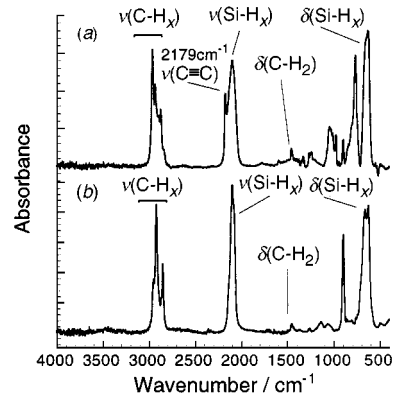

Fig. 1 Transmission FTIR of derivatized porous silicon: (*a*) CEG of pent-1-yne (surface **3**). (*b*) AEG of dodec-1-yne (surface **8**).

Photoluminescence (PL) spectra of CEG samples show varying intensities depending on the surface type (Fig. 2). Surfaces **2**–**4** (alkynyl groups) retain between *ca.* 5–15% of the light emission, with a small red shift of *ca.* 10 nm relative to freshly prepared porous silicon (λ_{max} = 663 nm). The phenethynyl surface **1** and other arynyl terminated surfaces (surfaces **5** and **6**) show no light emission whatsoever, as has been observed by Song and Sailor previously.[5a] Similarly, diphenylphosphinoethynyl surface **7** exhibits complete PL quenching as well. AEG samples have more intense PL, with *ca.*

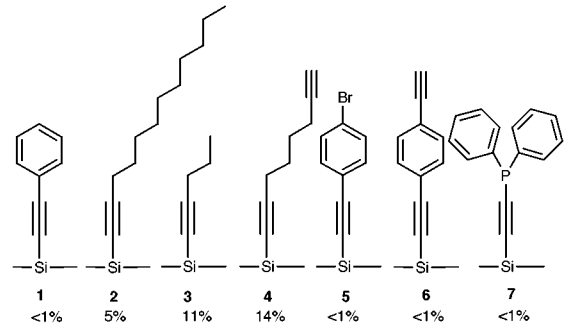

Fig. 2 Representative surfaces prepared by CEG of alkynes to porous silicon. The bold numbers refer to the numbering system in the text, and the % values represent the % photoluminescence (PL) remaining after functionalization through CEG.

† Electronic supplementary information (ESI) available. Further details concerning preparation of porous silicon and CEG, PL studies, and FTIR spectra for all surfaces reported here (**1**–**10**) and for the product of hydroboration of 1-trimethylsilyldodec-1-yne (http://www.rsc.org/suppdata/cc/1999/2479/

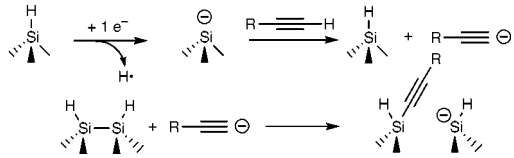

Fig. 3 Proposed mechanism for the CEG of alkynes to porous silicon. Cathodic reduction of a surface Si–H group forms the active silyl anion which initiates the reaction.

20% remaining for the alkyl protected surface **9** as compared to the freshly etched hydride terminated surface.

Stability tests using boiling aqueous NaOH solution (pH 10) demonstrate the chemical resistance of AEG and CEG samples compared to unfunctionalized porous silicon. Unmodified surfaces are destroyed under such conditions in *ca.* 180 s,[3c] whilst the CEG functionalized samples remain essentially unchanged after 10 min except for an increase in the ν(Si–O) mode at 1050 cm^{-1}. Extended treatment with ethanolic HF solution also results in no change in FTIR spectra. The combined stability with respect to both HF and alkaline treatment is known only for Si systems with covalently attached organic layers.[2b–d,11]

We believe the CEG reaction proceeds *via* a silyl anion intermediate formed by reduction of surface Si–H bonds in a space charge layer (Fig. 3) to yield either H$^{\bullet}$ or, 1/2 H_2. The silyl anion species has been previously inferred for the mechanism of alkyl halide grafting.[8,12] The subsequent *in situ* generation of a carbanion from deprotonation of the weakly acidic alkyne leads directly to nucleophilic Si–Si bond attack, as observed by previous workers.[5,6,8] The silyl anion is quenched in the presence of a proton source (0.1 M HCl in diethyl ether), leading to no incorporation of alkyne. Other weakly acidic moieties can be grafted *via* this CEG reaction, such as dodecane-1-thiol (surface **10**, Fig. SM11†), presumably through a similar deprotonation step and subsequent attack of Si–Si bonds by an RS^- species. Minor incorporation of butyl groups (2956, 2923 and 2872 cm^{-1}), which may be due to tenacious physisorption or electrochemical decomposition of the NBu_4PF_6 electrolyte,[13] is observed in all CEG reactions. The butyl groups are not removed after 30 min in boiling chloroform.

Given the observations noted in FTIR of surfaces **8** and **9** (*vide supra*), it is likely that a surface-initiated cationic hydrosilylation mechanism[12,14] is responsible for the Si–C bond formation in AEG reactions (Fig. 4). Positive charges are stabilized in the depletion layer at the semiconductor–electrolyte interface,[15] which are attacked by alkyne monomers. This can then be the starting point for a successive hydrosilylation or cationic polymerization reaction.[16]

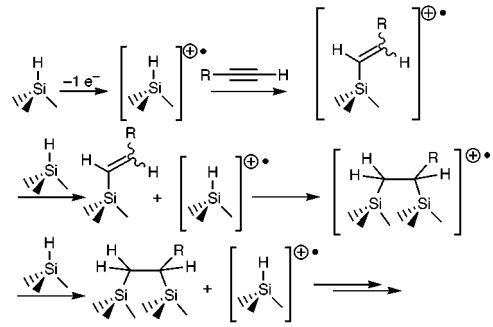

Fig. 4 Proposed mechanism for the AEG of alkynes to porous silicon. Anodic oxidation of a surface Si–H group results in formation of the active cationic silyl species.

In conclusion, a technique in which alkylation and alkynylation of porous silicon surfaces can be accomplished through CEG and AEG is reported. Future work concerns the further elucidation of the mechanisms *via* investigations using new electrolyte systems and alkynes, and the application of new experimental apparatus.

We gratefully acknowledge financial support from the National Science Foundation for a Career Award, the Camille and Henry Dreyfus Foundation, Inc., for a New Faculty Award to J. M. B., the Link Foundation for a pre-doctoral energy fellowship to M. P. S., and Purdue University and the Purdue Research Foundation.

Notes and references

1 A. G. Cullis, L. T. Canham and P. D. J. Calcott, *J. Appl. Phys.*, 1997, **82**, 909.
2 For reviews of chemistry on porous silicon see the following and references therein: (*a*) *Properties of Porous Silicon*, ed. L. T. Canham, INSPEC, London, 1997; (*b*) M. J. Sailor and E. J. Lee, *Adv. Mater.*, 1997, **9**, 783; (*c*) J. M. Buriak, *Adv. Mater.*, 1999, **11**, 265; (*d*) J. M. Buriak, *Chem. Commun.*, 1999, 1051.
3 (*a*) J. M. Buriak and M. J. Allen, *J. Am. Chem. Soc.*, 1998, **120**, 1339; (*b*) M. P. Stewart and J. M. Buriak, *Angew. Chem., Int. Ed.*, 1998, **37**, 3257; (*c*) J. M. Buriak, M. P. Stewart, T. W. Geders, M. J. Allen, H. C. Choi, J. Smith, D. Raftery and L. T. Canham, *J. Am. Chem. Soc.*, in press.
4 J. E. Bateman, R. D. Eagling, D. R. Worrall, B. R. Horrocks and A. Houlton, *Angew. Chem., Int. Ed.*, 1998, **37**, 2683.
5 (*a*) J. H. Song and M. J. Sailor, *J. Am. Chem. Soc.*, 1998, **120**, 2376; (*b*) J. H. Song and M. J. Sailor, *Inorg. Chem.*, 1999, **38**, 1498.
6 N. Y. Kim and P. E. Laibinis, *J. Am. Chem. Soc.*, 1998, **120**, 4516.
7 C. Vieillard, M. Warntjes, F. Ozanam and J.-N. Chazalviel, *Proc. Electrochem. Soc.*, 1996, **95**, 250; F. Ozanam, C. Vieillard, M. Warntjes, T. Dubois, M. Pauly and J.-N. Chazalviel, *Can. J. Chem. Eng.*, 1998, **76**, 1020.
8 C. Gurtner, A. W. Wun and M. J. Sailor, *Angew. Chem., Int. Ed.*, 1999, **38**, 1966.
9 C. H. de Villeneuve, J. Pinson, M. C. Bernard and P. Allongue, *J. Phys. Chem. B*, 1997, **101**, 2415; C. H. de Villeneuve, J. Pinson, F. Ozanam, J.-N. Chazalviel and P. Allongue, *Mater. Res. Soc. Symp. Proc.*, 1997, **451**, 185.
10 H. C. Brown, *Organic Syntheses via Boranes*, John Wiley and Sons, New York, 1975, p. 100.
11 M. R. Linford, P. Fenter, P. M. Eisenberger and C. E. D. Chidsey, *J. Am. Chem. Soc.*, 1995, **117**, 3145.
12 V. V. Jouikov, *Russ. Chem. Rev.*, 1997, **66**, 509; V. Jouikov and G. Salaheev, *Electrochim. Acta*, 1996, **41**, 2623; A. Kunai, O. Ohnishi, T. Sakurai and M. Ishikawa, *Chem. Lett.*, 1995, 1051.
13 C. A. Ferreira, S. Aeiyach, M. Delamar and P. C. Lacaze, *Surf. Interface Anal.*, 1993, **20**, 749.
14 A. A. Khapicheva, N. T. Berberova, E. S. Klimov and O. Yu Okhlobystin, *Zh. Obsch. Khim.*, 1985, **55**, 1533; O. Yu Okhlobystin and N. T. Berberova, *Dokl. Akad. Nauk. SSSR*, 1993, **332**, 599.
15 N. Sato, *Electrochemistry at Metal And Semiconductor Electrodes*, Elsevier, Amsterdam, 1998.
16 *Cationic Polymerization*, ed. R. Faust and T. D. Shaffer, American Chemical Society, Washington DC, 1997, vol. 665.

Communication 9/06726D

Molecular imprinting with an organometallic transition state analogue

Kurt Polborn and Kay Severin*

Institut für Anorganische Chemie, Ludwig-Maximilians-Universität, D-81377 München, Germany. E-mail: kse@cup.uni-muenchen.de

Received (in Basel, Switzerland) 3rd October 1999, Accepted 3rd November 1999

The microenvironment, and thus the activity and selectivity of an immobilised ruthenium catalyst, was modified in a controlled way using a transition state analogue as the catalyst precursor in combination with an imprinting technique.

Molecular recognition between enzymes and substrates, as well as subsequent catalytic transformation, is largely controlled by precisely positioned functional groups within cavities formed by the protein. The implementation of such cavities into artificial, biomimetic catalysts is one of the major challenges in this field. Current approaches are often based on organic host molecules (*e.g.* cyclodextrins) covalently attached to catalytically active groups but the synthetic effort required for the construction of such systems is generally substantial.[1] Alternatively, materials with cavities of molecular dimensions can be obtained by imprinting techniques.[2] Here, polymeric materials are generated in the presence of template molecules, removal of which creates cavities with complementary shapes. Several groups have tried to utilise this technology for the synthesis of catalytically active polymers using transition state analogues as templates but the observed activities were generally modest.[2] Recently, a very nice example of a synthetic esterase which shows a rate enhancement of 10^2 was reported by Wulff *et al.*[3] Nevertheless these values are several orders of magnitude lower than those observed for natural enzymes. Our goal is to produce *highly active* and *selective* enzyme mimics by combining the power of organometallic catalysts with the methodology of molecular imprinting.[4] Preliminary results are reported below.

The transfer hydrogenation of aromatic ketones catalysed by ruthenium half-sandwich complexes has recently received much attention since with certain chiral amine-based ligands excellent enantioselectivities were obtained.[5] In these reactions propan-2-ol or formic acid serves as the hydrogen source (Scheme 1). In accordance with all experimental results a six-membered cyclic transition structure **A** was suggested for transformations of this kind.[5b] To imitate this structure with a coordinatively fixed pseudo-substrate we propose phosphinato complexes of the general formula **B** as organometallic transition state analogues (TSA). Our strategy for using such a TSA for the generation of an immobilised catalyst with a form-selective cavity in proximity to the catalytic centre is summarised in Scheme 2. A ruthenium complex **1** with a styrene side chain is synthesised from $[(\eta^6\text{-cymene})RuCl_2]_2$ and the respective amine ligand[6] in the presence of NaOMe (Ru:ligand:base = 1:2:2). The chloride ligand is then substituted with a diphenylphosphinato ligand to give complex **2** in good yield. The anticipated structure with a monodentate phosphinato ligand which shows a hydrogen bond to the amine group of the coligand was confirmed by the results of a single crystal X-ray analysis (Fig. 1).† To the best of our knowledge this complex represents the first structurally characterised organometallic TSA.[7] Complex **2** is copolymerised with ethylene glycol dimethacrylate (Ru:EGDMA = 1:99) in the presence of a porogen (chloroform) to give the highly crosslinked jet porous polymer **3**.[8] To initiate the reaction we employed 2,2′-azobis(4-methoxy-2,4-dimethylvaleronitrile) (V-70) which allows the polymerisation to be carried out under very mild conditions.[9]

The polymer was ground and wet-sieved to obtain uniform particle sizes of between 25 and 100 μm. The phosphinato ligand was selectively cleaved off using a solution of $BnNEt_3Cl$ in methanol (0.1 M) to give polymer **4** containing a ruthenium chloro complex.[10] The polymer was finally washed with methanol and dried *in vacuo*. To determine the influence of the cavity generated this way we made the polymer **5** using complex **1** instead of the TSA **2** following an otherwise identical protocol.

When tested for their ability to catalyse the reduction of benzophenone both polymers displayed a high activity indicating good incorporation and accessibility of the ruthenium

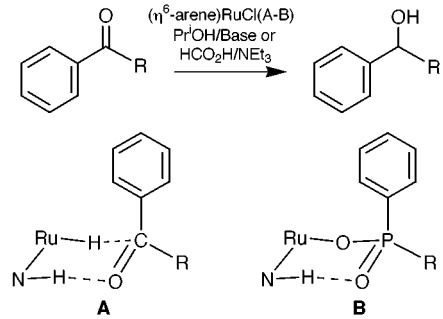

Scheme 1 Transfer hydrogenation of aromatic ketones catalysed by ruthenium half-sandwich complexes (A–B represents an anionic chelate ligand). The proposed transition structure **A** is mimicked by the phosphinato complex **B**.

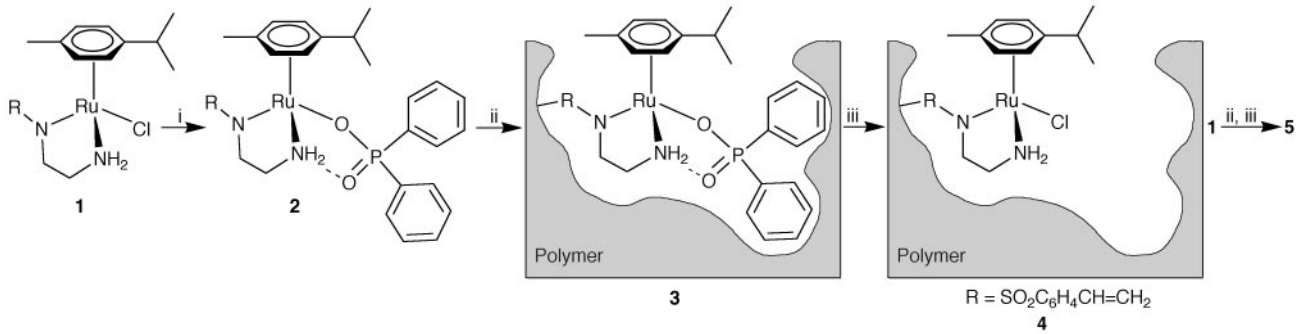

Scheme 2 *Reagents and conditions*: i, AgO_2PPh_2, CH_2Cl_2, room temp., 96 h; ii, EGDMA, $CHCl_3$ (Ru:$CHCl_3$:EGDMA = 1:100:99), V-70 (1.5%), 35 °C, 20 h; then 65 °C, 4 h; iii, $[BnNEt_3]Cl$ in MeOH (0.1 M).

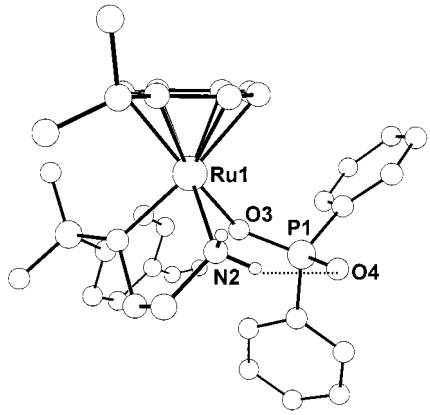

Fig. 1 The molecular structure of **2** in the crystal (most hydrogen atoms are omitted for clarity). Selected bond distances (Å) and angles (°): Ru(1)–N(2) 2.135(3), Ru(1)–O(3) 2.155(3), P(1)–O(4) 1.499(3), P(1)–O(3) 1.518(3), N(2)–O(4) 2.972(3); N(2)–Ru(1)–O(3) 82.81(12), O(4)–P(1)–O(3) 116.5(2), P(1)–O(3)–Ru(1) 131.9(2).

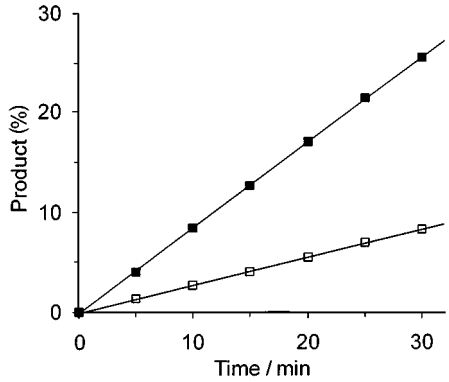

Fig. 2 Product formation as a function of time for reactions carried out at 70 °C with 500 μl of azeotropic HCO_2H/NEt_3, 500 μl of MeCN, 100 μmol of benzophenone and 1 μmol of catalyst **4** (■) or catalyst **5** (□), respectively. To calculate the amount of catalyst, a quantitative incorporation of complex **1** and **2** into the polymer was assumed. Every 5 min a sample of 100 μl was removed from the reaction vessel, quenched with $MeCN/MeCO_2H$ (3:1), filtered and analysed by capillary GC. The data represent averaged values from two independent experiments; the errors are < 0.2 %.

complexes. To quantify the activity the initial turnover frequencies (TOF) were determined. The experiments revealed that the molecularly imprinted polymer (MIP) **4** was significantly more active than polymer **5** [TOF(**4**) = 51.4 h^{-1}, TOF(**5**) = 16.5 h^{-1}, Fig. 2]. The rate enhancement of greater than a factor of three is remarkable considering that both polymers contain the same amount of ruthenium complexes having an identical first coordination sphere.

The MIP-catalyst **4** was also expected to display an increased selectivity for benzophenone, the substrate which was imitated during the polymerisation process by the pseudo-substrate diphenylphosphinate. We therefore performed a series of competition experiments with equimolar amounts of benzophenone and a cosubstrate, chosen to differ in size, shape and reactivity. The selectivity was determined comparing the initial rates of product formation (Table 1). In all cases catalyst **4** showed a substantially higher specificity for benzophenone than the control catalyst **5**. The relative increase in selectivity was slightly larger for aliphatic ketones (entries 1–3) as compared to aromatic ketones (entries 4–6).

These results show that the activity and selectivity of an immobilised catalyst can be enhanced using organometallic TSAs as templates in combination with an imprinting technique. Currently we are trying to apply this methodology to other catalytic transformations including enantioselective reactions. Further results will be reported in due course.

Table 1 Substrate-selectivity of the MIP-catalyst **4** and the control polymer **5**

		Selectivity[b]	
Entry[a]	Cosubstrate	**4**	**5**
1	2-Norbornanone	4.3	2.2
2	2-Adamantanone	4.9	2.5
3	Cyclohexyl methyl ketone	14.2	7.4
4	Acetophenone	2.8	1.8
5	α-Tetralone	3.8	2.2
6	Phenyl isopropyl ketone	20.6	13.8

[a] The reactions were carried out with 50 μmol of benzophenone, 50 μmol of the cosubstrate and 1 μmol of the respective catalyst. [b] The selectivity was calculated by dividing the initial rate of diphenylmethanol formation by the initial rate of product formation for the reduction of the cosubstrate. For norborneol the sum of isomers was used.

K. S. thanks Professor Dr W. Beck for his generous support and B. Grosch and E. Karaghiosoff for technical assistance. Financial funding from the Bayerischer Habilitations-Förderpreis (K. S.) is gratefully acknowledged.

Notes and references

† *Crystal data* for $C_{32}H_{37}N_2O_4PS \cdot 0.5CH_3OH$ **2**: M = 693.76, triclinic, space group $P\bar{1}$, a = 10.387(2), b = 11.762(5), c = 14.362(2) Å, α = 88.05(3), β = 81.10(2), γ = 73.33(3)°, U = 1660.6(8) Å^3, Z = 2, μ = 0.622 mm^{-1}, T = 298 K, 5196 independent reflections, 5439 collected (R_{int} 0.0221). Final R indices [$I > 2\sigma(I)$] R_1 0.0471, wR_2 0.1233. The vinyl group was disordered and two independent positions for the two C-atoms were refined. CCDC 182/1474. See http://www.rsc.org/suppdata/cc/1999/2481/ for crystallographic files in .cif format.

1 A. J. Kirby, *Angew. Chem.*, 1996, **108**, 770; *Angew. Chem., Int. Ed. Engl.*, 1996, **35**, 707; J. K. M. Sanders, *Chem. Eur. J.*, 1998, **4**, 1378; Y. Murakami, J. Kikuchi, Y. Hisaeda and O. Hayashida, *Chem. Rev.*, 1996, **96**, 721.
2 K. Haupt and K. Mosbach, *Trends Biotech.*, 1998, **16**, 468; G. Wulff, *Angew. Chem.*, 1995, **107**, 1958; *Angew. Chem., Int. Ed. Engl.*, 1995, **34**, 1812.
3 G. Wulff, T. Groß and R. Schönfeld, *Angew. Chem.*, 1997, **109**, 2050; *Angew. Chem., Int. Ed. Engl.*, 1997, **36**, 1962.
4 A similar concept was recently proposed by Gagné and coworkers but so far only preliminary results have been presented: B. P. Santora, A. O. Larsen and M. R. Gagné, *Organometallics*, 1998, **17**, 3138.
5 (*a*) M. J. Palmera and M. Wills, *Tetrahedron: Asymmetry*, 1999, **10**, 2045; (*b*) R. Noyori and S. Hashiguchi, *Acc. Chem. Res.*, 1997, **30**, 97.
6 The ligand was prepared by reaction of *p*-styrenesulfonyl chloride with ethylenediamine in dichloromethane. Complexes **1** and **2**, as well as the ligand, were characterised by ^1H, ^{13}C NMR and elemental analysis.
7 For the production of Diels–Alder catalytic antibodies a cyclopentadienyl iron complex was used as a haptenic group: J. T. Yli-Kauhaluoma, J. A. Ashley, C.-H. Lo, L. Tucker, M. M. Wolfe and K. D. Janda, *J. Am. Chem. Soc.*, 1995, **117**, 7041.
8 The morphology of EGDMA polymers in the presence of various porogens was investigated in detail: B. Sellergren and K. J. Shea, *J. Chromatogr.*, 1993, **635**, 31.
9 So far, 2,2′-azobis(4-methoxy-2,4-dimethylvaleronitrile) has rarely been used as the thermal initiator in molecular imprinting studies although low polymerisation temperatures are generally advantageous.
10 NMR experiments have shown that addition of $[BnNEt_3]Cl$ to a solution of **2** in MeOH leads to a quantitative exchange of the phosphinato ligand.

Communication 9/08047C

Group 5 transition metal imido complexes with dianionic guanidinate ligands displaying extended interactions

Natesan Thirupathi, Glenn P. A. Yap and Darrin S. Richeson*

Department of Chemistry, University of Ottawa, Ottawa, ON, K1N 6N5. Canada.
E-mail: darrin@science.uottawa.ca

Received (in Bloomington, IN, USA) 27th August 1999, Accepted 15th October 1999

***N,N′,N″*–tri(isopropyl)guanidinate complexes of M(v) (M = Nb, Ta) bearing imido ligands represent unique examples of monoanionic and dianionic guanidinate complexes of these metals; single crystal X-ray analyses for two of the latter species, {[μ-(NPr^i)$_3$C]$_2$TaMe(NPr^i)}(Mg$_2$Cl$_2$)·4C$_6$D$_6$ and {(μ-η^2:η^2 (Pr^{i}N)$_3$C)Ta(NPr^i)Cl}$_2$, exhibit unusual bonding modes involving all of the nitrogen centers of the ligand.**

Guanidinate anions have received surprisingly limited attention as supporting ligands for metal complexes in comparison with isoelectronic amidinate species.[1] This omission is particularly conspicuous with electrophilic main group and early transition metals where amidinate complexes have displayed an exceptionally rich and varied organometallic and inorganic chemistry.[2,3] Guanidinates should certainly possess the same versatility and flexibility in coordination properties that have been exhibited by amidinates. Moreover, the presence of a third nitrogen center, which can bear either one or two organic substituents provides an additional coordination site within the ligand and the added capability of yielding dianionic species. This aspect offers bonding motifs that are not possible for the related amidinate systems.

Employing *N,N′,N″*-trialkylguanidines as ligands requires the development of fundamental ideas regarding the introduction of guanidinate anions and dianions into a metal coordination sphere, the definition of features that favor different binding modes of the ligand, and investigation of the general reactivity characteristics of these complexes. Reported preparative routes to trialkylguanidiante complexes include the elimination of HX (X = Cl, Br) from halo metal complexes,[4] elimination of H_2 from metal hydrides,[5] elimination of alkane from a metal alkyl,[6] and elimination of amine from a metal amido complex.[7,8] Examples of a dianionic guanidinate complexes include [(OC)$_3$Fe{μ-η^2(RN)$_2$CNR}Fe(CO)$_3$] (R = Pr^i or Cy),[9] (cod)Pt[C(NPh)$_3$][10] and the main group species, Li$_2$[C(NPh)$_3$],[11] Li$_2$[C(NBu^t)$_3$],[12] and Sb[(Pr^{i}N)$_2$CNHPr^i][(Pr^{i}N)$_3$C].[8] We wish to expand upon the procedures for introducing guanidinate ligands and to find general methods for the generation of dianionic guanidinate ligands.

The room temp. reaction of MCl_5 (M = Ta, Nb) with *N,N′,N″*-tri(isopropyl)guanidine lead to direct formation of MCl(NPr^i)[(NPr^i)$_2$C(NHPr^i)]$_2$ (M = Ta **1**; M = Nb **2**) after separation of guanidinium hydrochloride from the reaction mixture [eqn. (1)].† Reproducible yields in the range 30–40%

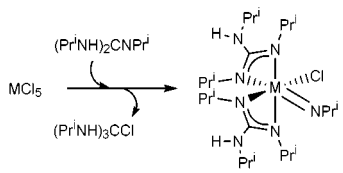

(1)

can be obtained from this procedure using spectroscopically (^{1}H, ^{13}C NMR) and analytically pure tri(isopropyl)guanidine. On the basis of these observations it seems clear that the imido function must arise from cleavage of the parent guanidine, the mechanism of this transformation is currently under investigation.[13,14] In contrast, reaction of M(NMe$_2$)$_5$ with guanidine yields only [(Pr^{i}N)$_3$C]M(NMe$_2$)$_3$ a species which possessed a single dianionic guanidinate ligand.[8]

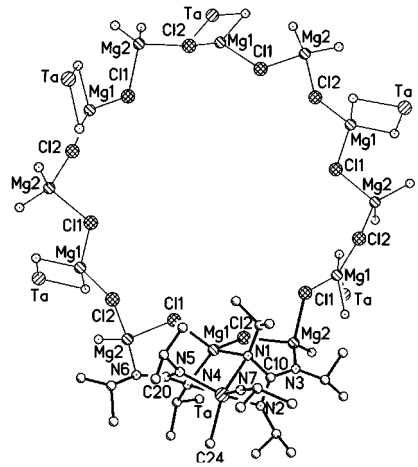

Fig. 1 Molecular structure of **3** showing a labeled asymmetric unit and the aggregation described in the text. Within the asymmetric unit, hydrogen atoms and benzene molecules of crystallization have been omitted for clarity. All atoms atoms have been refined anisotropically.

With only one equivalent of MeMgX (X = Cl, Br), complex **1** only undergoes halogen exchange. However, employing two equivalents or more readily generated alkyl complex **3**.[15] Owing to the likelihood that our synthetic procedure had generated a dianionic guanidinate ligand we performed an X-ray analysis of **3** with the results shown in Fig. 1.‡ Complex **3** exhibits a Ta center in a pseudo-octahedral environment with two dianionic chelating bidentate guanidinate ligands, one Me group and an imido function. The two guanidinate ligands span axial/equatorial sites and the bonding features within the {[(NPr^i)$_3$C]$_2$TaMe(NPr^i)}$^{2-}$ fragment are reminiscent of the reported bis(amidinate)Nb(O)Cl and the bis(guanidinate) complexes **1** and **2**.†[16] Charge balance for this fragment and completion of the asymmetric unit is provided by an (Mg$_2$Cl$_2$)$^{2+}$ cation which is coordinated to the guanidinate ligands.

Both guanidinate ligands form planar cycles with the Ta(v) center and exhibit similar bonding parameters. Within the guanidinate CN_3 cores the central C is planar as are the N atoms [N(2), N(5)] that coordinate exclusively to Ta. The C=N bond appears to be localized between these three coordinate N atoms with the longest C–N bonds observed for the four coordinate N centers [N(1), N(4)] which interact with one of the Mg^{2+} cations. The isopropyl imido linkage is similar to that observed in **1** and **2** and in **4** reported below. The *trans* influence of the imido ligand is manifest in the elongation of Ta–N(4) bond relative to Ta–N(1) [2.486(7) *cf.* 2.365(7) Å].

The two Mg centers within the asymmetric unit possess different coordination environments with Mg(1) being coordinated to the two *cis*-oriented N atoms [N(1), N(4)], and to Cl(1) and Cl(2) to give a pseudo-tetrahedral coordination sphere while Mg(2) is coordinated only to N(6) and Cl(1) within the asymmetric unit. Bridging interactions of Mg(2) to N(3) and

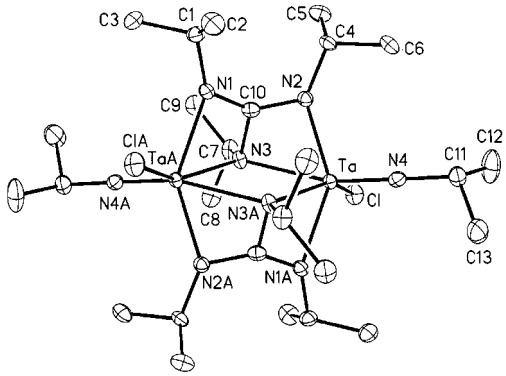

Fig. 2 Molecular structure of **4**. Hydrogen atoms have been omitted for clarity.

Cl(2) of an adjacent unit complete the coordination sphere of this center and result in a supramolecular aggregation of these subunits. This assemblage of complexes propagated through the bridging interactions of Mg(2) generates a macrocyclic ring of six subunits with a diameter of 12.1 Å which is colinear with a crystallographic 6 axis as shown in Fig. 1. The void space left in the center of this cyclic arrangement is occupied in this case with four benzene molecules of crystallization.

The ^{1}H and ^{13}C NMR spectra of **3** provide a probe of the solution behavior of this species. Based on the similarity of these spectra to those of complexes **1** and **2**, it appears that the intermolecular interactions exhibited by the observed static structure of **3** are not maintained in solution.

Reaction of metal halides with a lithium guanidinate, Li{(Pr^iN)$_2$CN(H)Pr^i}, offers an alternative metathetical route for introduction of guanidinate anions. From the reaction between *in situ* generated monolithium guanidinate and $TaCl_5$, complex **4** was isolated.† The complexity of the NMR spectra for this reproducibly obtained product prompted us to investigate **4** by X-ray crystallography. The results are summarized in Fig. 2.‡

Complex **4** is a dinuclear species possessing two bridging dianionic tri(isopropyl)guanidinate ligands each exhibiting a previously unknown chelating bridging coordination mode in which two of the nitrogen atoms [N(1), N(2)] bond to one Ta center and the third [N(3)] bridges the two metal centers. The coordination geometry of each Ta center can be described as distorted octahedral with the overall geometry of **4** being an edge-sharing bioctahedral polyhedron. An inversion center relates the two halves of the molecule. The individual Ta centers are in geometries reminiscent of the other bis(guanidinate) complexes reported herein. For example, within the asymmetric unit the metrical parameters of the guanidinate ligand are similar to those observed in **3**, *i.e.* the ligand spans axial equatorial sites with a bite angle [N(2)–Ta–N(3)] of 60.83(16)º. The central C atom of the guanidinate CN_3 core is planar. Furthermore N(1) and N(2) exhibit very similar geometric parameters and are nearly planar [Σ N(1) = Σ N(2) = 357º]. In contrast, the bridging N atom [N(3)] is distorted tetrahedral with the six defining angles ranging from 81.7(3) to 125.5(3)º (av. = 107º). The C=N double bond of the dianionic ligand appears to be delocalized between C(10)–N(1) and C(10)–N(2) as reflected by bond distances. As in **1**–**3**, the Ta coordination sphere is completed by an isopropyl imido function and a chloride ligand [Cl(1)] remaining from the starting material.

The mechanism of formation for **4** is still under scrutiny. Attempts to employ the dianionic form of tri(isopropyl)guanidinate, in what would appear to be a more direct pathway to **4**, also yield **4** but in a lower yield.

In the case of **4**, both ^{1}H and ^{13}C NMR data confirm that the observed structure remains intact upon dissolution in organic solvents. For example each of the isopropyl CH_3 signals appears as a distinct doublet. While the isopropyl(imido) function appears to exhibit equivalent methyl groups in the ^{1}H NMR, these CH_3 groups are distinguishable in the ^{13}C NMR spectra.

Our continuing efforts are directed toward the further development of these complexes and of guanidinate ligands with the specific goals of understanding the details that dictate the formation of mono- *vs.* dianionic ligands. Furthermore, we are interested in understanding the features that govern the intra- and inter-molecular interactions exhibited by these ligands.

This work was supported by the Natural Sciences and Engineering Research Council of Canada (NSERC).

Notes and references

† Complexes **1–4** have been fully characterized by ^{1}H and ^{13}C NMR spectroscopy and by elemental analysis. In addition, single crystal X-ray diffraction studies have been performed on **1** and **2** and will be reported in the full paper.

‡ *Crystal data*: for $C_{40.50}H_{68.50}Cl_2Mg_2N_7Ta$ **3**: M = 953.99, rhombohedral, space group $R\bar{3}$, a = 37.664(2), b = 37.664(2), c = 18.532(1) Å, U = 22768(2) Å^3, T = 203(2) K, Z = 18, μ(Mo-Kα) = 2.335 mm^{-1}, reflections measured 60471, 5423 unique (R_{int} = 0.1911) which were used in all calculations. Final R indices [$I > 2\sigma(I)$] $R1$ = 0.0478 $wR2$ = 0.1138.

For $C_{26}H_{56}Cl_2N_8Ta_2$ **4**: M = 913.59, monoclinic, space group $P2_1/n$, a = 11.420(1), b = 10.220(1), c = 14.876(2) Å, β = 100.098(2)º, U = 1709.5(3) Å^3, T = 293(2) K, Z = 2, μ(Mo-Kα) = 6.581 mm^{-1}, reflections measured 13443, 4108 unique (R_{int} = 0.0695) which were used in all calculations. Final R indices [$I > 2\sigma(I)$] $R1$ = 0.0326 $wR2$ = 0.0647.

The structures were solved using direct methods and refined by full-matrix least squares on F^2. CCDC 182/1454.

1 For recent reviews of amidinate complexes see: J. Barker and M. Kilner, *Coord. Chem. Rev.*, 1994, **133**, 219; F. T. Edelmann, *Coord. Chem. Rev.*, 1994, **137**, 403.

2 C. E. Radzewich, M. P. Coles and R. F. Jordan, *J. Am. Chem. Soc.*, 1998, **120**, 9384; R. Gomez, R. Duchateau, A. N. Chernega, J. H. Teuben, F. T. Edelmann and M. L. H. Green, *J. Organomet. Chem.*, 1995, **491**, 153; J. C. Flores, J. C. W. Chien and M. D. Rausch, *Organometallics*, 1995, **14**, 1827; J. R. Hagadorn and J. Arnold, *J. Chem. Soc., Dalton Trans.*, 1997, 3087; D. Herskovics-Korine and M. Eisen, *J. Organomet. Chem.*, 1995, **503**, 307; A. Littke, N. Sleiman, C. Bensimon, D. S. Richeson, G. P. A. Yap and S. Brown, *Organometallics*, 1998, **17**, 446; S. Foley, G. P. A. Yap and D. S. Richeson, *Organometallics* in press.

3 J. Barker, N. C. Blacker, P. R. Phillips, N. W. Alcock, W. Errington and M. G. H Wallbridge, *J. Chem. Soc., Dalton Trans.*, 1996, 431; A. Ochi, H. K. Bowen and W. E. Rhine, *Mater. Res. Symp. Proc.*, 1988, **121**, 663.

4 J. R. da S. Maia, P. A. Gazard, M. Kilner, A. S. Batsanova and J. A. K Howard, *J. Chem. Soc., Dalton Trans.*, 1997, 4625; P. J. Bailey, L. A. Mitchell and S. Parsons, *J. Chem. Soc., Dalton Trans.*, 1996, 2839.

5 S. D. Robinson and A. Sahajpal, *J. Chem. Soc., Dalton Trans.*, 1997, 3349.

6 R. Snaith, K. Wade and B. K. Wyatt, *J. Chem. Soc. A.*, 1970, 380.

7 P. J. Bailey, R. O. Gould, C. N. Harmer, S. Pace, A. Steiner and D. S. Wright, *Chem. Commun.*, 1997, 1161.

8 M. K. T. Tin, G. P. A. Yap and D. S. Richeson, *Inorg. Chem.*, 1999, **38**, 998; M. K. T. Tin, N. Thirupathi, G. P. A. Yap and D. S. Richeson, *J. Chem. Soc., Dalton Trans.*, 1999, 2947.

9 N. J. Bremer, A. B. Cutcliffe, M. F. Farona and W. G. Kofron, *J. Chem. Soc. (A)*, 1971, 3264; N. J. Bremer, A. B. Cutcliffe and M. F. Farona, *Chem. Commun.*, 1970, 932.

10 M. B. Dinger and W. Henderson, *Chem. Commun.*, 1996, 211.

11 P. J. Bailey, A. J. Blake, M. Kryszczuk, S. Parsons and D. Reed, *J. Chem. Soc., Chem. Commun.*, 1995, 1647.

12 T. Chivers, M. Parvez and G. Schatte, *J. Organomet. Chem.*, 1998, **550**, 213.

13 The effects of varying the reaction conditions on the yield of **1** and **2** will be reported in the full paper. Our best yields have been obtained using a ratio of tri(isopropyl)guanidine:MCl_5 of 4:1. Carbodiimide has not been isolated from the reaction mixture.

14 S. W. Krska, R. L. Zuckerman and R. G. Bergman, *J. Am. Chem. Soc.*, 1998, **120**, 11 828.

15 A. N. Chernega, M. L. H. Green and A. G. Suárez, *J. Chem. Soc., Dalton Trans.*, 1993, 3031.

16 P. J. Stewart, A. J. Blake and P. Mountford, *Inorg. Chem.*, 1997, **36**, 1982.

Communication 9/06976C

ChemComm

Direct synthesis of acetylene from methane by direct current pulse discharge

Shigeru Kado,* Yasushi Sekine and Kaoru Fujimoto

Department of Applied Chemistry, School of Engineering, The University of Tokyo, Hongo, Bunkyo-ku, Tokyo 113-8656, Japan. E-mail: tt97208@mail.ecc.u-tokyo.ac.jp

Received (in Cambridge, UK) 25th September 1999, Accepted 1st November 1999

In non-catalytic direct conversion of methane to acetylene by using direct current pulse discharge under conditions of ambient temperature and atmospheric pressure, the selectivity of acetylene from methane was >95% at methane conversion ranging from 16 to 52%; coexisting oxygen was very effective in removing deposited carbon and stabilized the state of discharge.

Methane, which is a major constituent of natural gas, is so stable that high reaction temperatures such as 1273 K or higher are required for its pyrolysis to ethylene or acetylene.[1] Although high reaction temperature is favorable for high conversion, higher temperature promotes the consecutive decomposition of the products to carbon.[1,2] Recently, direct conversion of methane to higher hydrocarbons using plasma technology has been studied to improve the selectivity and yield of the desired products.[3–8] For example, in microwave plasma reaction, acetylene was produced with a selectivity of >90% from methane at as low a reaction pressure as 4.5 kPa.[6] The plasma catalytic conversion of methane by using dc corona discharge was also found to produce acetylene with high selectivity and yield under atmospheric pressure in the temperature range 343–773 K. The nature of the catalyst surface in contact with the plasma was very important for homogeneous activation of methane and NaY zeolite gave the highest yields of C_2 hydrocarbons. The highest yield of C_2 hydrocarbons (32%) was obtained in a hydrogen-containing plasma at a flow rate of 10 cm^3 min^{-1}.[7] In this study, dc pulse discharge was applied to non-catalytic direct conversion of methane at ambient temperature and under atmospheric pressure to prepare C_2 hydrocarbons selectively, with high methane conversion.

A flow type reaction apparatus which was composed of a Pyrex glass tube of 4.0 mm internal diameter was used as the reactor. Reactant gas which was premixed at a given ratio was fed at a constant flow rate. Stainless steel electrodes of 2 mm diameter were inserted from each end of the reactor as shown in Fig. 1 and the distance between the electrodes was 1.5 mm. A dc pulse discharge was initiated by supplying a negative high voltage with a dc power generator. The wave signal was observed by a digital oscilloscope and the pulse duration was *ca.* 10 ms. All the reactions were conducted at atmospheric pressure and ambient temperature without any catalyst and all products were analyzed by gas chromatography. Product selectivity was defined as follows; selectivity (%) = yield of the product (Carbon mmol)/sum of all the products (Carbon mmol) × 100.

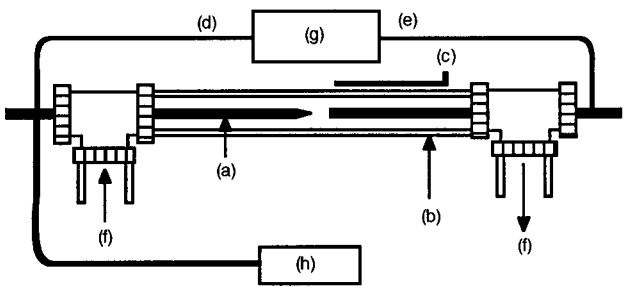

Fig. 1 Schematic diagram of the reactor. (a) 2.0 mm diameter stainless steel electrode, (b) 4.6 mm internal diameter quartz tube, (c) thermocouple, (d) negative high voltage, (e) ground, (f) direction of the flow gas, (g) direct current high voltage power supply, (h) digital oscilloscope.

Upon dc pulse discharge, methane was activated readily to form acetylene with a selectivity of >90% in the absence of catalyst. Fig. 2 shows methane conversion, yield of C_2 hydrocarbons and selectivity of acetylene, ethylene and ethane *vs.* supplied power. While methane conversion increased up to 52% by the increasing power supply, acetylene selectivity was very stable at *ca.* 95%. Applying a discharge for methane activation thus led to the selective formation of acetylene with high C_2 yield and stable selectivity, not observed in conventional homogenous gas phase reactions. Other hydrocarbon products such as prop-1-yne and buta-1,3-diyne were at <1%. Some carbon deposition occurred on both electrodes and the reactor wall during the reaction and eventually resulted in unstable discharge and sometimes in cessation.

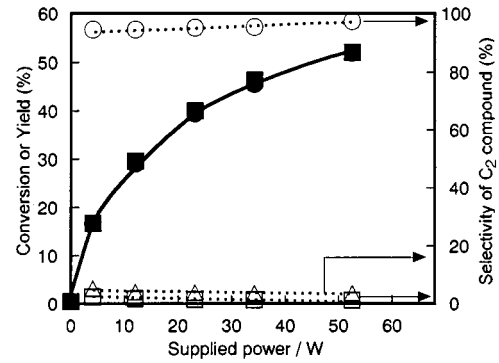

Fig. 2 Effect of supplied power on conversion and selectivity. Reaction conditions: pure methane, 10 cm^3 min^{-1} (NTP) flow rate, ambient temperature, 0.1 MPa, 1.5 mm electrode distance, (■) methane conv., (●) C_2 yield, (○) acetylene selectivity, (△) ethylene selectivity, (□) ethane selectivity.

In order to prevent carbon deposition during discharge, O_2 and Ar were added to give a resultant feed gas composition CH_4–O_2–Ar = 5 : 1 : 4. Reaction results under a flow of 10 cm^3 min^{-1} at normal temperature and pressure (NTP) and 25 W power supply are given in Table 1. Carbon monoxide was produced as well as carbon dioxide (selectivity <1% to CO_2), in addition to C_2 compounds. Comparing results with those of the reaction with pure methane, there was little difference in C_2 yield, which indicates that the increased methane conversion was essentially due to the carbon monoxide formed. Additionally, the composition of C_2 compounds was not much affected. In the reaction using pure methane, the C_2 yield was 40.6% and the amount of acetylene in the C_2 products was 94.4%, while the reaction in the presence of O_2 gave 91% acetylene selectivity in terms of non-CO/CO_2 carbon products with yields of C_2 compounds and CO of 38 and 20%, respectively. These results suggest that the precursor of the deposited carbon is converted to carbon monoxide by reaction with oxygen. Also the reaction in the presence of O_2 led to stable discharge.

The effect of total flow rate (from 3 to 225 cm^3 min^{-1} in the presence of O_2) with a supplied power of *ca.* 25 W is also shown in Table 1. Methane and oxygen conversion was remarkably

Table 1 Effect of coexisting oxygen and total flow rate[a]

Feed gas	Flow rate (NTP)/ $cm^3\ min^{-1}$	Conv. (%)		Yield (%)		Selectivity (%)	
		CH_4	O_2	C_2	CO	C_2H_2	CO
CH_4	10	40.6	—	39.9	—	94.4	—
CH_4–O_2–Ar (5:1:4)	3	83.9	100.0	49.6	33.8	56.2	40.3
CH_4–O_2–Ar (5:1:4)	10	58.9	69.9	38.1	20.2	58.9	33.8
CH_4–O_2–Ar (5:1:4)	225	6.8	9.7	4.9	1.9	62.3	27.9

[a] *Reaction conditions*: ambient temperature, 0.1 MPa, 1.5 mm electrode distance, 25 W supplied power.

affected by the total flow rate. At 3 $cm^3\ min^{-1}$ total flow rate, oxygen conversion reached 100% and methane conversion was 84%. On the other hand, the selectivity towards acetylene was scarcely affected while the C_2 yield increased to *ca*. 50%. The selectivity to carbon monoxide increased slightly as the total flow rate was decreased. If carbon monoxide was formed by a chain reaction, its selectivity should increase more drastically with decreasing flow rate. Thus, the behavior of carbon monoxide selectivity to the total flow rate indicated that carbon monoxide formation was separate from C_2 compound formation and derived from a coke precursor.

We also attempted to stabilize the discharge by using hydrogen as the coexisting gas, since using oxygen caused the formation of carbon monoxide which decreased the selectivity to C_2 compounds. The reaction results were much the same as for pure methane, and H_2 did not stabilize discharge as well as O_2. However, dilution of methane by hydrogen such that $CH_4:H_2 = 1:4$ was effective for stabilization of the discharge.

Table 2 shows methane conversion, C_2 yield and selectivities to each C_2 compound at various H_2 concentrations from 0 to 90%. Up to 50% hydrogen concentration, a marked effect of H_2 was not observed. However as the hydrogen concentration was increased, methane conversion and C_2 yield increased from 44% (pure methane) to 57% ($CH_4:H_2 = 1:2$). At 80% hydrogen concentration, methane conversion and acetylene selectivity decreased slightly, and selectivity towards ethane and ethylene increased. At conditions of > 80% hydrogen concentration, the excessive concentration of hydrogen interfered with electron attack on methane, leading to drastic reduction in methane conversion and to an increase in ethane selectivity.

Table 2 Effect of hydrogen concentration on conversion and selectivity[a]

H_2 concentration (%)	CH_4 conv. (%)	C_2 yield (%)	Selectivity (%)		
			C_2H_6	C_2H_4	C_2H_2
0	44.3	44.2	0.6	2.8	94.6
50	46.3	46.2	1.1	4.4	94.2
67	57.4	57.1	1.2	5.7	92.7
80	47.0	46.6	2.9	8.1	88.2
90	11.8	11.4	17.7	15.2	63.7

[a] *Reaction conditions*: 10 $cm^3\ min^{-1}$ (NTP) flow rate, ambient temperature, 0.1 MPa, 1.5 mm electrode distance, 4 mA dc.

In conclusion, when a dc pulse discharge was applied for methane activation, acetylene was produced directly and selectively. Oxygen removed deposited carbon by oxidation to form carbon monoxide, and stabilized the state of discharge. Dilution of methane with hydrogen up to 80% also stabilized the state of discharge without changing the product selectivity. We assume that the formation of acetylene is *via* dimerisation of CH radicals which form by dc discharge, and that the high selectivity to acetylene is a characteristic feature of short range pulse discharge.

Notes and references

1 F. G. Billaud, F. Baronnet and C. P. Gueret, *Ind. Eng. Chem. Res*., 1993, **32**, 1549.
2 A. Holmen, O. Olsvik and O. A. Rokstad, *Fuel Process. Technol*., 1995, **42**, 249.
3 M. S. Ioffe, S. D. Pollington and J. K. S. Wan, *J. Catal*., 1995, **151**, 349.
4 C. Liu, A. Marafee, B. Hill, G. Xu, R. Mallinson and L. Lobban, *Ind. Eng. Chem. Res*., 1996, **35**, 3295.
5 A. Marafee, C. Liu, G. Xu, R. Mallinson and L. Lobban, *Ind. Eng. Chem. Res*., 1997, **36**, 632.
6 K. Onoe, A. Fujie, T. Yamaguchi and Y. Hatano, *Fuel*, 1997, **76**, 281.
7 C. Liu, R. Mallinson and L. Lobban, *J. Catal*., 1998, **179**, 326.
8 K. Thanyachotpaiboon, S. Chavadej, T. A. Caldwell, L. L. Lobban and R. G. Mallinson, *AIChE J*., 1998, **44**, 2252.

Communication 9/06914C

Elucidation of acceptor–acceptor interactions in a Ru(II) supramolecular photosynthetic model complex†

Stefan H. Bossmann,*[a] M. Francesca Ottaviani,[b] Dietmar van Loyen,[c] Heinz Dürr[c] and Claudia Turro*[d]

[a] *Lehrstuhl für Umweltmesstechnik, Universität Karlsruhe, 76128 Karlsruhe, Germany*
[b] *Department of Chemistry, University of Florence, 50121 Florence, Italy*
[c] *Fachbereich 11.2, Organische Chemie, Universität Saarbrücken, 66041 Saarbrücken, Germany*
[d] *Department of Chemistry, Ohio State University, Columbus, OH 43210, USA. E-mail: turro@chemistry.ohio_state.edu*

Received (in Columbia, MO, USA) 7th June 1999, Accepted 7th October 1999

The interaction between the two viologen acceptors in a TEMPO-labeled Ru(II) bisviologen photosynthetic model system assembly has been investigated using EPR spectroscopy; the results are consistent with no viologen–viologen spin exchange in water at temperatures above 5 °C, although upon crystallization (≤2 °C) strong spin exchange is observed; the strong spin exchange interaction results in a single broad line at temperatures below 1 °C, unlike the three broad lines measured for free TEMPO upon solvent freezing; this evidence for the TEMPO-labeled complex indicates that there is no interaction of the two viologen acceptors in the supramolecular Ru(II) bis-viologen structure in solution, thus making it indeed a viable model for the photosynthetic reaction center.

A remarkable feature of the photosynthetic reaction center (RC) lies in its utilization of only one of the two nearly identical electron transfer (ET) pathways available from the excited state of the special pair to the Q_A and Q_B quinone acceptors.[1] A large number of covalently linked diads and triads of varying geometry and rigidity possessing excited state electron donors and electron acceptors have been explored as RC model assemblies.[2] These systems are generally aimed at solar energy conversion, and are therefore designed to attain a long lifetime of the charge separated state formed upon photoexcitation. Such *D–A, *D–A_1–A_2, and D–*D–A (*D = photoexcited donor, D = donor, A, A_1, A_2 = acceptors) structures are schematically shown in Fig. 1(a),[3] where in many cases *D is a Ru(II) diimine complex.[4] Although these supramolecular donor/acceptor systems have proven useful in the investigation of long-lived charge separation, only a few can be utilized in the modeling of the dual ET pathways found in the reaction center.[5] Such systems possess two chemically identical acceptors tethered to the donor, A–*D–A [Fig. 1(b)], thus providing a bifurcated pathway for the photoinduced electron transfer. One previously reported A–*D–A supramolecular assembly is of particular importance owing to the similarity in the spatial arrangement of the donor and acceptors compared to that in the RC. This system is of the type $[Ru^{II}(dmbpy)_2(di\text{-}V^{2+}\text{-}bpy)]^{4+}$ (dmbpy = 4,4′-dimethyl-2,2′-bipyridine), where the structure of ligand di-V^{2+}-bpy in the complex is shown in Fig. 2(a) and possesses two linked 4,4′-dialkyl viologens.[6] A crucial criteria for the investigation of the charge transfer processes in this supramolecular complex is the assessment of the interaction between the two viologens, since a RC model system should not possess electron exchange between the two acceptors.

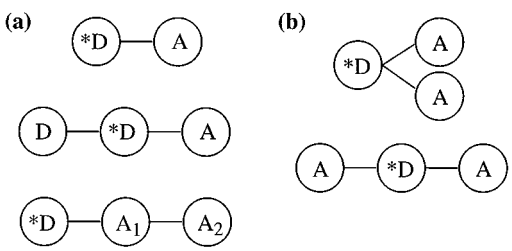

Fig. 1 Schematic representation of donor/acceptor (D/A) asseblies aimed at (a) long charge-separated states and (b) bifurcated ET pathway.

To investigate the interaction between the two viologens in the $[Ru^{II}(dmbpy)_2(di\text{-}V^{2+}\text{-}bpy)]^{4+}$ complex we have synthesized the Ru(II) complex with a bis-TEMPO (TEMPO = 2,2′,6,6′-tetramethylpiperidine *N*-oxide) labeled ligand, di-(TEMPO-V^{2+})-bpy, shown in Fig. 2(b). The CW-EPR spectral features of the nitroxide radical in each TEMPO moiety are highly sensitive to dynamics, motion and distance from other radicals. This work presents EPR evidence against the interaction of the two acceptors in the $[Ru^{II}(dmbpy)_2(di\text{-}V^{2+}\text{-}bpy)]^{6+}$ model complex.

The synthesis and characterization of [Ru(dmbpy)(di-TEMPO)-V^{2+})-bipy)]$^{6+}$ is given as ESI data.† Elemental analysis is consistent with the expected structure. Transient absorption measurements were conducted on an instrumental setup previously described.[7] The EPR instrument has been previously reported.[8]

As expected from the molar absorption coefficients of the Ru(II)–diimine MLCT (metal-to-ligand charge transfer) transitions and the TEMPO absorption in the visible region, the electronic absorption spectrum of the $[Ru^{II}(dmbpy)_2(di\text{-}(TEMPO\text{-}V^{2+})\text{-}bpy)]^{6+}$ complex is nearly identical to that of

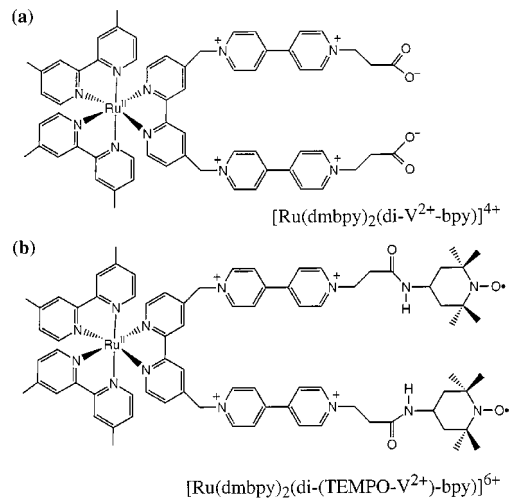

Fig. 2 Molecular structures of the photosynthetic model complex (a) $[Ru^{II}(dmbpy)_2(di\text{-}V^{2+}\text{-}bpy)]^{6+}$ and (b) the bis-TEMPO labeled analog $[Ru^{II}(dmbpy)_2(di\text{-}(TEMPO\text{-}V^{2+})\text{-}bpy)]^{6+}$.

† Electronic supplementary information (ESI) available: synthesis and characterization of $[Ru(dmbpy)_2(di\text{-}(TEMPO\text{-}V^{2+})\text{-}bipy)]^{6+}$, electrospray MS, HPLC, redox potentials and molecular model. See http://www.rsc.org/suppdata/cc/1999/2487/

Table 1 Comparison of the EPR fit parameters for doubly- and singly-TEMPO labeled complexes at 25 °C†

	τ_c/ps	g_{xx}	g_{yy}	g_{zz}	A_{xx}/G	A_{yy}/G	A_{zz}/G
$[Ru^{II}(phen)_2(TEMPO\text{-}phen)]^{2+}$ [a]	80	2.0097	2.0063	2.0035	6.8	7.5	37.3
$[Ru^{II}(dmbpy)_2(di\text{-}(TEMPO\text{-}V^{2+})\text{-}bpy)]^{6+}$	50	2.0090	2.0060	2.0030	7.0	7.0	36.5

[a] TEMPO-phen = 4-$(CH)_2OC(O)$N-(TEMPO)-1,10-phenanthroline, data from ref. 6.

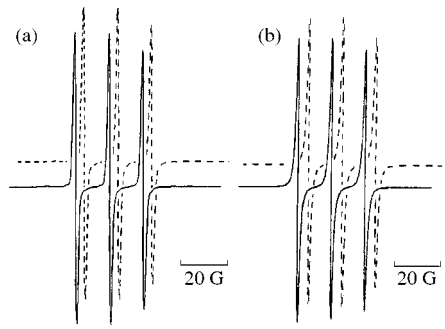

Fig. 3 EPR spectra (——) of 1×10^{-4} M $[Ru^{II}(dmbpy)_2(di\text{-}(TEMPO\text{-}V^{2+})\text{-}bpy)]^{6+}$ in water at (a) 30 and (b) 5 °C, with their respective computed spectra (– – – –).

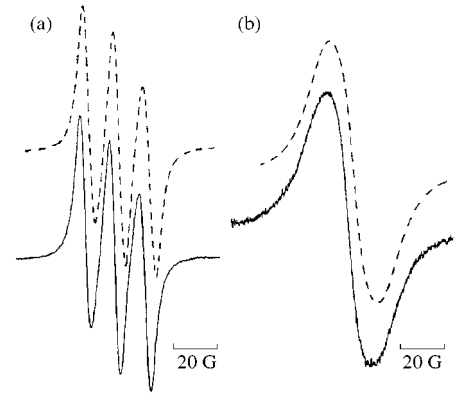

Fig. 4 EPR spectra (——) of 1×10^{-4} M $[Ru^{II}(dmbpy)_2(di\text{-}(TEMPO\text{-}V^{2+})\text{-}bpy)]^{6+}$ in water at (a) 1 and (b) −3 °C, with their respective computed spectra (– – – –).

$[Ru^{II}(dmbpy)_2(di\text{-}V^{2+}\text{-}bpy)]^{4+}$. Both complexes are non-emissive in deoxygenated aqueous solution and possess similar excited state charge transfer characteristics. In the model complex $[Ru^{II}(dmbpy)_2(di\text{-}V^{2+}\text{-}bpy)]^{4+}$, visible excitation leads to fast ET from the Ru(II) metal center to one of the viologens with risetime of *ca.* 1–2 ps (λ_{exc} = 450 nm, FWHM *ca.* 200 fs).[9] A typical lifetime of the charge separated state, τ_{CS}, of *ca.* 250 ± 20 ns was determined from fits of the monoexponential decay of photoexcited solutions of 5.0×10^{-5} M $[Ru^{II}(dmbpy)_2(di\text{-}V^{2+}\text{-}bpy)]^{4+}$ (λ_{exc} = 532 nm, FWHM *ca.* 4 ns), where the transient absorption of $MV^{\cdot+}$ was monitored at 610 nm. To ensure that the TEMPO-labeling of the complex did not lead to different ET dynamics, the same experiments were performed on $[Ru^{II}(dmbpy)_2(di\text{-}(TEMPO\text{-}V^{2+})\text{-}bpy)]^{6+}$, which indicate that within experimental error the risetime and lifetime of the charge separated state are identical. Furthermore, reduction of the TEMPO radicals in $[Ru^{II}(dmbpy)_2(di\text{-}(TEMPO\text{-}V^{2+})\text{-}bpy)]^{6+}$ complexes was not observed by UV-VIS absorption and HPLC measurements.

Solution CW-EPR measurements of $[Ru^{II}(dmbpy)_2(di\text{-}(TEMPO\text{-}V^{2+})\text{-}bpy)]^{6+}$ in water were conducted at temperatures ranging from 5 to 30 °C. Selected spectra (5 and 30 °C) are shown in Fig. 3 along with the simulation traces for each experiment.† Throughout this temperature range no spectral broadening was observed at low concentration (< 1 mM), indicative of no interaction between the two TEMPO units within each complex. The solution spectra collected for 1.0×10^{-4} M $[Ru^{II}(dmbpy)_2(di\text{-}(TEMPO\text{-}V^{2+})\text{-}bpy)]^{6+}$ are similar to those measured for singly TEMPO-labeled Ru(II) complexes. The correlation time for motion, *g*-values, and isotropic hyperfine coupling constants for $[Ru^{II}(dmbpy)_2(di\text{-}(TEMPO\text{-}V^{2+})\text{-}bpy)]^{6+}$ and a related singly labeled Ru(II) complex are listed in Table 1 from which it is clear that all the parameters for both the singly- and doubly-TEMPO labeled complexes are nearly identical, indicating that the presence of the second TEMPO in the molecule does not affect the motion or magnetic features. In addition, for $[Ru^{II}(dmbpy)_2(di\text{-}(TEMPO\text{-}V^{2+})\text{-}bpy)]^{6+}$ the correlation time for motion, τ_c, increases as the temperature is lowered, consistent with slower motion at lower temperatures.

Cooling the sample below 2 °C results in the formation of red crystals, prior to solvent freezing at *ca.* 0 °C. The EPR spectra of $[Ru^{II}(dmbpy)_2(di\text{-}(TEMPO\text{-}V^{2+})\text{-}bpy)]^{6+}$ at 1 °C and −3 °C are shown in Fig. 4. For free TEMPO and most of its derivatives, lowering the temperature below the freezing of the solvent point results in broadening of all three individual lines without the occurrence of exchange broadening, which appears as a single broad line.[10] The observed spectra shown in Fig. 4 are consistent with increased exchange frequency, W_{ex}, as the temperature is lowered with W_{ex} values of 1.0×10^8 and 2.7×10^8 s^{-1} at 1 and −3 °C, respectively. The increased spin exchange between the two viologen units of $[Ru^{II}(dmbpy)_2(di\text{-}(TEMPO\text{-}V^{2+})\text{-}bpy)]^{6+}$ is only observed upon the formation of crystals (below 2 °C), but not when free in solution. It may be concluded from these observations that only in the crystalline form are the two viologen chains able to interact with each other or with TEMPO units of neighboring complexes within the close-packed lattice.

This work was partially supported by a NATO Collaborative Research Grant (CRG 971178), by a National Science Foundation (CHE-9733000) and the Petroleum Research Fund (31878-G4) grants to C. T., and a German Research Foundation grant (DFG-BO 1060/III) to S. H. B.

Notes and references

1 L. L. Laporte, V. Palaniappan, D. G. Davis, C. Kirmaier, C. C. Schenck, D. Holten and D. F. Bocian, *J. Phys. Chem.*, 1996, **100**, 17 696.
2 *Molecular and Supramolecular Photochemistry, Vol. 2: Organic and Inorganic Photochemistry*, ed. V. Ramamurthy and K. S. Schanze, Marcel Dekker, New York, 1998.
3 N. Liang, J. R. Miller and G. L. Closs, *J. Am. Chem. Soc.*, 1990, **112**, 5353.
4 A. Juris, V. Balzani, F. Barigelletti, S. Campagna, P. Belser and A. von Zelewsky, *Coord. Chem. Rev.*, 1988, **84**, 85.
5 M. Seiler, H. Dürr, I. Willner, E. Joselevich, A. Doron and J. F. Stoddart, *J. Am. Chem. Soc.*, 1994, **116**, 3399.
6 D. v. Loyen, Doctoral Thesis, University of Saarland, 1999; M. Seiler and H. Dürr, *Liebigs Annalen-Organic and Bioorganic Chemistry*, 1995, 407.
7 Y.-Z. Hu, D. v. Loyen, O. Schwarz, S. H. Bossmann, H. Dürr, V. Huch and M. Veith, *J. Am. Chem. Soc.*, 1998, **120**, 5822.
8 M. F. Ottaviani, C. Turro, N. J. Turro, S. H. Bossmann and D. A. Tomalia, *J. Phys. Chem.*, 1996, **100**, 13 667.
9 D. v. Loyen, G. d. Belder, G. Schweitzer, F. C. DeSchryver and H. Dürr, *J. Phys. Chem. A*, 1999, submitted.
10 *Spin Labeling. Theory and Applications*, ed. L. J. Berliner, Academic Press, New York, 1976, vol 1; 1979, vol. 2.

Communication 9/04525B

ChemComm

Synthesis and characterisation of a framework microporous stannosilicate

Z. Lin, J. Rocha* and A. Valente

Department of Chemistry, University of Aveiro, 3810 Aveiro, Portugal. E-mail: ROCHA@DQ.UA.PT

Received (in Cambridge, UK) 11th October 1999, Accepted 5th November 1999

The synthesis and structural characterisation of AV-6, a microporous framework stannosilicate with the structure of the mineral umbite, are reported.

Presently, the synthesis of inorganic microporous framework solids possessing structures which consist of interlinked octahedra and tetrahedra is raising considerable interest. We have been particularly concerned with the chemistry of microporous titanium silicates containing tetracoordinated Si^{4+} and Ti^{4+} usually in octahedral coordination.[1,2]

Several minerals containing SnO_6 and SiO_4 polyhedra are known and a few (dense) stannosilicate phases have been crystallised from high-temperature conditions.[3] Two microporous and a layered stannosilicate have been reported by Corcoran and Vaughan.[3] Subsequently, Dyer and Jáfar reported the synthesis of a third microporous stannosilicate.[4] The structure of all these materials is, however, unknown. Here, we report the synthesis of a synthetic stannosilicate (AV-6, Aveiro microporous solid no. 6) which possesses the structure of the rare mineral umbite ($K_2ZrSi_3O_9{\cdot}H_2O$).[2,5]

In a typical AV-6 synthesis an alkaline solution was prepared by dissolving 3.47 g of precipitated silica (BDH), 7.60 g KOH (85%, Aldrich) and 2.45 g KF (Aldrich) in 17.33 g H_2O. 5.84 g $SnCl_4{\cdot}5H_2O$ (98%, Riedel-deHaën) were added to the alkaline solution and stirred thoroughly. This gel, with a molar composition 4.82 K_2O:3.54 SiO_2:1.00 SnO_2:64 H_2O, was transferred to a Teflon-lined autoclave and treated at 230 °C for three days under autogenous pressure without agitation. The crystalline product was filtered off, washed at room temperature with distilled water and dried at 70 °C overnight, the final product being an off-white microcrystalline powder (crystallite size 0.2–0.3 μm). Chemical analysis (EDS) gave Si/Sn and K/Sn molar ratios of 2.8–3.1 (different crystal clusters) and 2.0–2.1, respectively.

AV-6 samples were characterised by chemical analysis (EDS), powder X-ray diffraction (XRD), scanning electron microscopy (SEM), ^{29}Si and ^{119}Sn solid state NMR spectroscopy, thermogravimetry and adsorption measurements (water and nitrogen).

In the structure of umbite and AV-6 (Fig. 1) the M octahedra $(Zr,Sn)O_6$, and the T tetrahedra, SiO_4, form a three-dimensional MT-condensed framework.[5] The M octahedra are coordinated by six T. In addition to the M–O–T bonds these tetrahedra also form T–O–T links with each other. Among all the known silicates and their T analogues, the umbite structure seems to be the first to display such a MT-condensed framework.

Fig. 2 shows the experimental and simulated powder XRD patterns of AV-6. The unit cell parameters have been calculated assuming an orthorhombic unit cell, space group $P2_12_12_1$ with cell dimensions a = 10.103, b = 13.132, c = 7.154 Å, and are similar to those reported for synthetic umbite with some Ti for Zr substitution (Zr/Ti = 0.5) (a = 10.063, b = 13.135, c = 7.139 Å).[2] Powder XRD shows that the framework of AV-6 is stable up to *ca.* 700 °C.

The AV-6 ^{29}Si solid-state NMR spectrum with magic-angle spinning (MAS) (Fig. 3) displays three sharp peaks at δ −84.6, −85.5 and −86.7 in 0.74:1:0.98 intensity ratios. Previously reported framework stannosilicates give resonances in the range δ −78 to −92.[3,4] The crystal structure of umbite indicates the presence of three unique Si sites with equal populations.[5] The

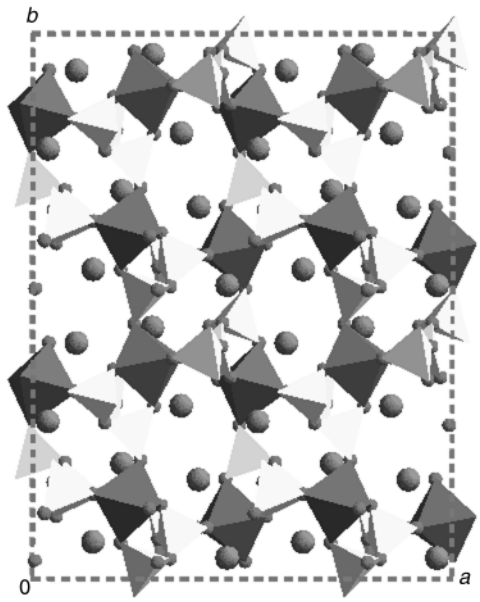

Fig. 1 Polyhedral representations of the umbite (and AV-6) structure viewed along [001]. For clarity, the water molecules are omitted.

fact that the relative population of one of the Si sites in AV-6 is slightly smaller than unity is, at present, not entirely understood. The use of NMR relaxation delays from 30 s up to 180 s did not show any difference in the relative intensities of the peaks. The ^{29}Si MAS spectrum recorded with cross-polarisation and the MAS spectrum are similar, showing only slight differences in peak intensities. Moreover, samples from different syntheses always displayed the same type of spectrum.

The ^{119}Sn MAS MNR spectrum of AV-6 (not shown) displays a single peak at δ − 709 (relative to tetramethyltin) with a full-width at half-maximum of 200 Hz. The framework stannosilicates reported by Corcoran and Vaughan which contain octahedral Sn(IV) give ^{119}Sn MAS MNR signals at δ *ca.* −706 and −708.[3]

The total AV-6 mass loss (ascertained by thermogravimetry) between 30 and 650 °C is *ca.* 5.3% while in synthetic umbite

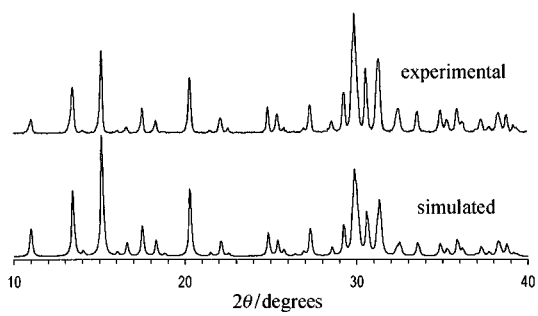

Fig. 2 Experimental and simulated powder XRD patterns of AV-6.

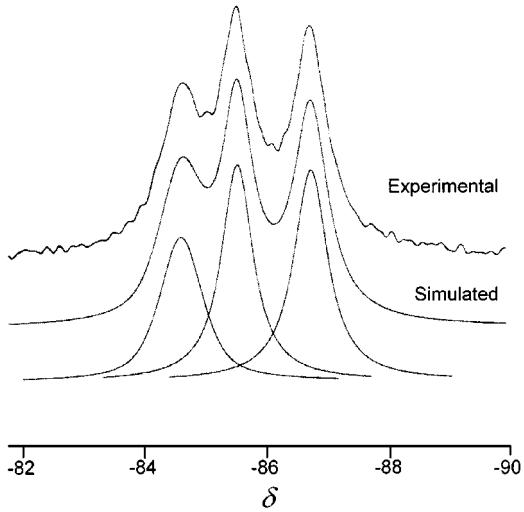

Fig. 3 Experimental and simulated ^{29}Si MAS NMR spectra of AV-6 recorded at 79.5 MHz on a Bruker MSL 400P. Chemical shifts are quoted in ppm from $SiMe_4$.

(AM-2) it is *ca*. 5.0%. This water loss is reversible. It was not possible to record a nitrogen adsorption isotherm of AV-6 probably because its pores are small. The water isotherms are of type I with maximum uptakes of *ca.* 3.34 mmol g^{-1} at P/P_0 = 0.4.

In conclusion, we report the successful synthesis and structural characterisation of AV-6, a stannosilicate which possesses the structure of the rare mineral umbite. This is the first report of a framework microporous stannosilicate with a known structure.

This work was supported by PRAXIS XXI and FEDER.

Notes and references

1 M. W. Anderson, O. Terasaki, T. Ohsuna, A. Philippou, S. P. Mackay, A. Ferreira, J. Rocha and S. Lidin, *Nature*, 1994, **367**, 347.
2 Z. Lin, J. Rocha, P. Brandão, A. Ferreira, A. P. Esculcas, J. D. Pedrosa de Jesus, A. Philippou and M. W. Anderson, *J. Phys. Chem. B*, 1997, **101**, 7114.
3 E. W. Corcoran, Jr. and D. E. W. Vaughan, *Solid State Ionics*, 1989, **32**/**33**, 423.
4 A. Dyer and J. J. Jáfar, *J. Chem. Soc., Dalton Trans.*, 1990, 3239.
5 G. D. Ilyushin, *Inorg. Mater.*, 1993, **29**, 853.

Communication 9/08128C

ChemComm

A new Na^+ sensor based on intramolecular fluorescence energy transfer derived from calix[4]arene

Takashi Jin

Section of Intelligent Materials and Devices, Research Institute for Electronic Science, Hokkaido University, Sapporo 060-0812, Japan. E-mail: jin@imd.es.hokudai.ac.jp

Received (in Liverpool, UK) 14th September 1999, Accepted 1st November 1999

A new calix[4]arene having pyrene (as a donor) and anthroyloxy (as an acceptor) moieties at the lower rim has been synthesized as a fluorescent Na^+ sensor based on intramolecular energy transfer.

Calixarenes have been shown to be useful building blocks in the design of fluorescent ion sensors for detecting metal ions and anions.[1–8] There are several designs of calixarene-based fluorescent ion sensor in which ion complexation can be monitored by intramolecular pyrene excimer formation,[1,2] intramolecular fluorescence quenching[3] and photoinduced electron transfer.[6–8] The objective of this work is to apply fluorescence energy transfer to the metal ion sensing system based on calixarenes. An advantage of the metal ion sensing system using fluorescence energy transfer is that a variety of fluorophore pairs can be chosen for the design of fluorescent ion sensors. Herein we report a new Na^+ sensor, based on intramolecular fluorescence energy transfer, derived from calix[4]arene.

Fluorescence energy transfer is the transfer of the excited state energy from a donor (d) to an acceptor (a). This transfer occurs as a result of transition dipole–dipole interactions between a d–a pair.[9] Thus, if a d–a pair is introduced to the appropriate sites of ionophoric calixarenes,[10] it is expected that the ion complexed by the calixarenes can be monitored by the change in the yield of fluorescence energy transfer between the d–a pair. In view of this, we have introduced pyrene (as a donor) and anthroyloxy (as an acceptor) moieties to the terminal positions of the ion binding sites (RCO-)[10] of ionophoric calix[4]arenes.

Fluorescent calix[4]arene **3** was prepared in three steps from the parent calix[4]arene. *p-tert*-Butylcalix[4]arene was dialkylated using 2 equiv. ethyl bromoacetate and 2 equiv. of K_2CO_3 in THF. The remaining two phenolic groups were functionalized firstly with 1.5 equiv. 1-pyrenemethyl iodoacetate and 2 equiv. K_2CO_3, and then with 1.5 equiv. *p*-(9-anthroyloxy)phenacyl bromide and 2 equiv. K_2CO_3 in THF. Mono-fluorophore calix[4]arenes **1** and **2** were prepared by the reaction of the tris-ethoxycarbonylmethyl ether[11] of *p-tert*-butylcalix[4]arene with the fluorescent reagents described above. All compounds were identified by ^1H NMR and field desorption mass spectroscopy.† The ^1H NMR measurements of the $ArCH_2Ar$ protons confirmed that the calixarenes **1**–**3** have rigid cone conformations in $CDCl_3$ solution.

Energy transfer from a donor to an acceptor depends on the extent of overlap of the fluorescence spectrum of the donor and the absorption spectrum of the acceptor.[9] Fig. 1 shows the fluorescence spectrum of **1** and the absorption spectrum of **2** in THF. The fluorescence spectrum of **1** is characterized by the pyrene monomer emission (*ca.* 385 nm). The absorption spectrum of **2** results from the absorption of the anthroyloxy group (λ_{max} 363 nm). Thus, the overlap between the emission of **1** and the absorption of **2** suggests that intramolecular fluorescence energy transfer from the pyrene to the anthroyloxy group can take place in **3**.

To verify the intramolecular energy transfer from the pyrene to the anthroyloxy group in **3**, we measured the fluorescence spectra of **1**, **2** and **3** at identical concentrations of 5.0 μmol

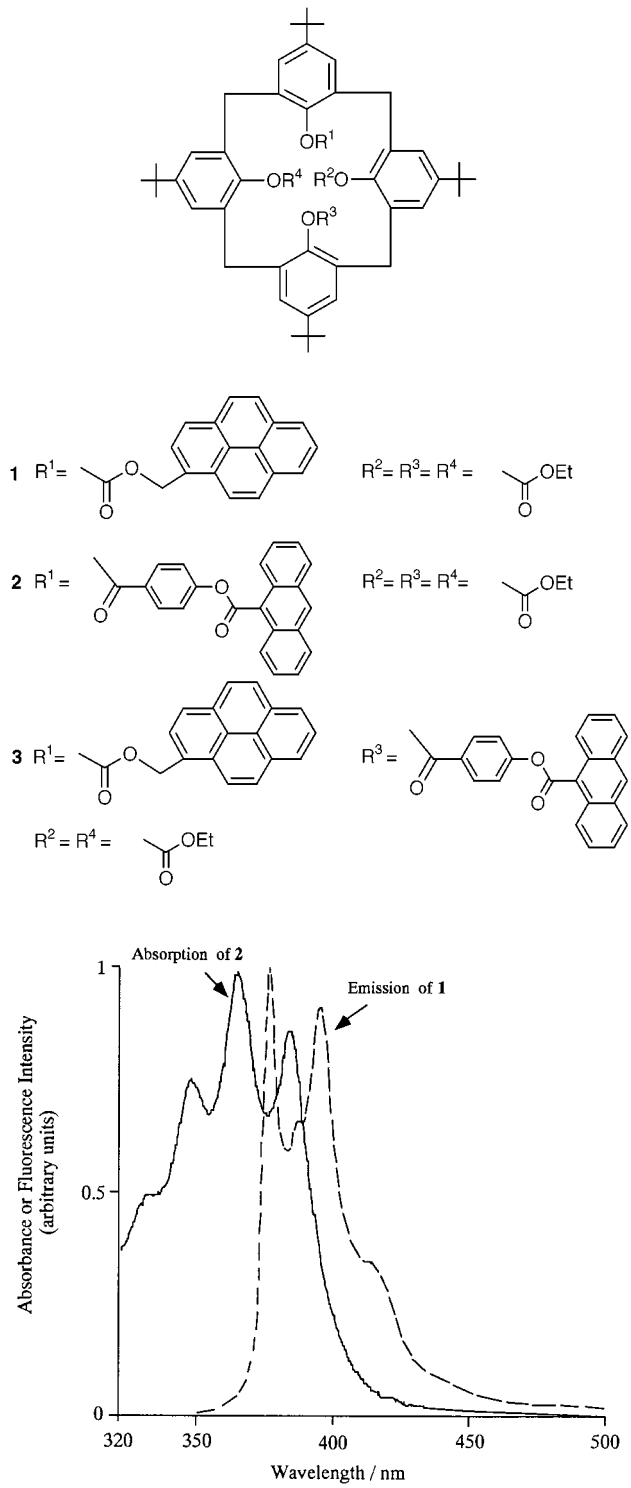

Fig. 1 Spectral overlap between the fluorescence spectrum of **1** and the absorption spectrum of **2**.

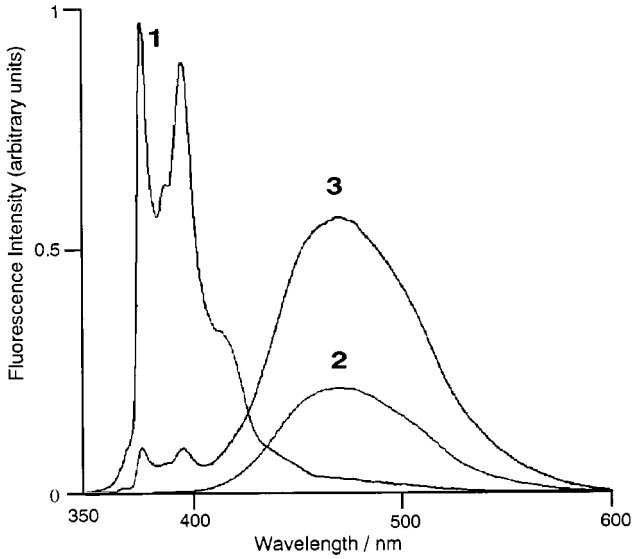

Fig. 2 Fluorescence spectra (ex. 330 nm) of **1**, **2** and **3** in THF at 25 °C.

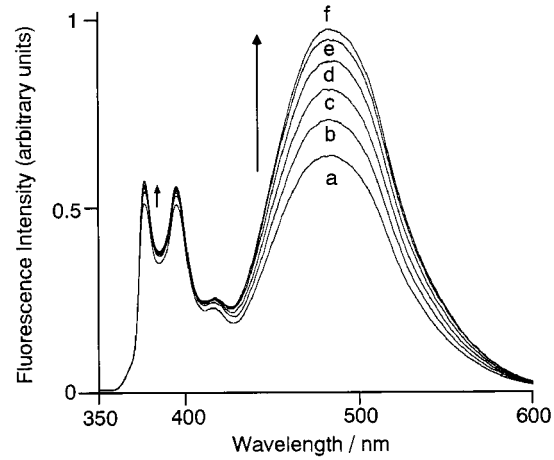

Fig. 3 Na^+ titration of the fluorescence spectra of **3** (5.0 μmol dm^{-3}) in MeOH–THF (15:1 v/v) at 25 °C: a, [NaSCN] = 0; b, [NaSCN] = 5.8; c, [NaSCN] = 17.4; d, [NaSCN] = 46.3; e, [NaSCN] = 104; f, [NaSCN] = 218 μmol dm^{-3}.

dm^{-3} (Fig. 2). At this concentration, **1** shows only the pyrene monomer emission; the intermolecular excimer emission is negligible. The fluorescence spectrum of **2** shows a broad, structureless band (λ_{max} 480 nm), which does not have an anthracene monomer-like structure.[12] It is well known that the 9-anthroyloxy group affords a large Stokes' shift of the broad emission which is a consequence of an excited-state rotation of the carboxyl group into the plane of the anthracene ring.[12] If energy transfer takes place in **3**, the emission of the anthroyloxy group (as an acceptor) should be enhanced compared with that of **2**, and the emission of the pyrene monomer (as a donor) should be depressed compared with that of **1**. As expected, the emission intensity of the anthroyloxy group of **3** increased by a factor of *ca.* 2.5 compared with **2**, while the emission intensity of the pyrene monomer of **3** decreased by a factor of *ca.* 10 compared with that of **1**. It should be noted that the emission of the anthroyloxy group of **3** has its maximum at the same wavelength (λ_{max} 480 nm) as that due to this group in **2**. This provides evidence that the anthroyloxy group is not forming an intramolecular exciplex with the pyrene in **3**.

The effects of addition of NaSCN to **1** and **2** were first examined in MeOH–THF (15:1 v/v) solution. The emissions of **1** and **2** were only slightly affected by the presence of Na^+ ions. The emission of the pyrene monomer of **1** (5.0 μmol dm^{-3}) at 385 nm was enhanced by a factor of 8% in the presence of excess amounts of NaSCN (454 μmol dm^{-3}). In the case of **2** (5.0 μmol dm^{-3}), the emission of the anthroyloxy group at 480 nm was depressed by a factor of 3% under the same NaSCN concentration. The fluorescence responses of these calix[4]arenes toward Na^+ ions are very poor and they have no potential as Na^+ sensors. In contrast, the fluorescence spectra of **3** showed a significant change in the presence of Na^+ and K^+ ions. Fig. 3 shows Na^+ titrations of the fluorescence spectra of **3** in MeOH–THF (15:1 v/v). When NaSCN was added to the solution of **3**, the fluorescence intensity of the anthroyloxy group increased significantly compared with that of the pyrene monomer. Such a fluorescence change was also observed in the case of KSCN. In contrast, the addition of other alkali metal ions such as Li^+, Rb^+ and Cs^+ did not cause fluorescence changes at concentrations as high as 50 mmol dm^{-3}. From the Na^+ titration data, the dissociation constant of the Na^+–**3** complex was determined to be 15 μmol dm^{-3}.‡ The Na^+/K^+ selectivity evaluated from the dissociation constants was found to be *ca.* 59. For Li^+, Rb^+ and Cs^+, the affinities were too low to be determined accurately and the dissociation constants were estimated to be greater than 100 mmol dm^{-3}.

In conclusion, we have synthesized a first example of a Na^+ sensor based on fluorescence energy transfer. The next step of this investigation will be the synthesis of a fluorescent calix[4]arene-based Na^+ sensor which can be excited by visible light along the same design principles. From the standpoint of the practical application of fluorescent ion sensors, the visible-light excitation is desirable to avoid a breaching of fluorescent dyes introduced to sensor compounds. We believe that a variety of donor–acceptor fluorophore pairs can be used for the design of calixarene sensors based on fluorescence energy transfer.

We thank Mr E. Yamada for the measurement of ^1H NMR spectra.

Notes and references

† *Selected data* for **3**: ^1H NMR (400 MHz, $CDCl_3$), δ 0.98 (s, 18H, CMe_3), 1.08 (t, 6H, CH_2CH_3), 1.17 and 1.19 (s, 9H, CMe_3), 3.14, 3.26, 4.85 and 5.02 (d, 2H, $ArCH_2Ar$, *J* 13.0 Hz), 4.05 (m, 4H, CH_2CH_3), 4.73 (s, 4H, OCH_2O), 5.09 (s, 2H, OCH_2OCH_2Py), 5.83 (s, 2H, CH_2COPh), 5.87 (s, 2H, CH_2Py), 6.62 and 6.69 (d, 2H each, ArH, *J* 2.4 Hz), 6.86 and 6.95 (s, 2H, ArH), 7.45–8.62 (m, 18H, anthracene and pyrene); field desorption mass spectrum, *m/z* 1431 (M^+).

‡ Since the absorption spectrum of **3** did not change upon addition of Na^+ and K^+ ions, a simple relationship between the intensity change (ΔF) in the anthroyloxy emission after complexation with metal ions and the concentration ([M^+]) of the metal ion can be derived as follows: $1/\Delta F = c + cK_d/[M^+]$, where K_d and *c* represent the dissociation constants of the metal ion complexes and a constant including terms of the quantum yields of free and complexing species, respectively.

1 T. Jin, PhD Thesis, Hokkaido University, 1990, p. 89; T. Jin, K. Ichikawa and T. Koyama, *J. Chem. Soc., Chem. Commun.*, 1992, 499.
2 I. Aoki, H. Kawabata, K. Nakashima and S. Shinkai, *J. Chem. Soc., Chem. Commun.*, 1991, 1771.
3 I. Aoki, T. Sakaki and S. Shinkai, *J. Chem. Soc., Chem. Commun.*, 1992, 730.
4 C. Pérez-Jiménez, S. J. Harris and D. Diamond, *J. Chem. Soc., Chem. Commun.*, 1993, 480.
5 F. Unob, Z. Asfari and J. Vicens, *Tetrahedron Lett.*, 1998, **39**, 2951.
6 H.-F. Ji, G. M. Brown and R. Dabestani, *Chem. Commun.*, 1999, 609.
7 I. Larey, F. O'Reilly, J.-L. Habib Jiawan, J.-Ph. Soumillion and B. Valeur, *Chem. Commun.*, 1999, 795.
8 P. D. Beer, V. Timoshenko, M. Maestri, P. Passaniti and V. Balzani, *Chem. Commun.*, 1999, 1755.
9 J. R. Lakowicz, *Principles of Fluorescence Spectroscopy*, Plenum, New York, 1983.
10 A. Arduini, A. Pochini, S. Reverberi, R. Ungaro, G. D. Andreetti and F. Ugozzoli, *Tetrahedron*, 1986, **42**, 2089; F. Arnaud-Neu, E. M. Collins, M. Deasy, G. Ferguson, S. J. Harris, B. Kaitner, A. J. Lough, M. A. McKervey, E. Marques, B. L. Ruhl, M. J. Schwing-Weill and E. M. Seward, *J. Am. Chem. Soc.*, 1989, **111**, 8681; T. Jin and K. Ichikawa, *J. Phys. Chem.*, 1991, **95**, 2601.
11 K. Iwamoto and S. Shinkai, *J. Org. Chem.*, 1992, **57**, 7066.
12 T. C. Werner and D. M. Hercules, *J. Phys. Chem.*, 1969, **73**, 2005; T. C. Werner and R. M. Hoffman, *J. Phys. Chem.*, 1973, **77**, 1611; T. C. Werner, T. Matthews and B. Soller, *J. Phys. Chem.*, 1976, **80**, 533; M. N. Berberan-Santos, M. J. E. Prieto and A. G. Szabo, *J. Phys. Chem.*, 1991, **95**, 5471.

Communication 9/07457K

ChemComm

Control of single crystal structure and liquid crystal phase behaviour *via* arene–perfluoroarene interactions†

Chaoyang Dai,[a] Paul Nguyen,[a] Todd B. Marder,*[ab] Andrew J. Scott,[c] William Clegg[c] and Christopher Viney[de]

[a] *Department of Chemistry, University of Waterloo, Waterloo, Ontario, Canada N2L 3G1*
[b] *Department of Chemistry, University of Durham, Durham, UK DH1 3LE. E-mail: todd.marder@durham.ac.uk*
[c] *Department of Chemistry, University of Newcastle upon Tyne, Newcastle upon Tyne, UK NE1 7RU*
[d] *Department of Materials, University of Oxford, Oxford, UK OX1 3PH*
[e] *Department of Chemistry, Heriot-Watt University, Edinburgh, UK EH14 4AS*

Received (in Cambridge, UK) 30th July 1999, Accepted 4th November 1999

In contrast to the solid-state structures of the individual compounds, arene-perfluoroarene face-to-face stacking and C–H···F–C in-plane interactions dominate the solid-state structure of 1:1 co-crystals of 1,4-bis(phenylethynyl)-tetrafluorobenzene 1b and 1,4-bis(pentafluorophenylethynyl)-benzene 1c, with this supramolecular aggregation leading to the stabilisation of a nematic liquid crystalline phase.

Non-covalent interactions between aromatic units play a significant role in determining the structures and properties of molecular assemblies in biology, chemistry and materials science.[1] In the past ten years, arene–arene interactions have been employed widely in supramolecular chemistry[2] and are critical to the packing of organic molecules in crystals and in crystal engineering for the design of functional materials.[3] The stability and phase behaviour of many liquid crystals have also been reported to arise from such interactions.[4] Arene–perfluoroarene interactions are a special case which have been studied extensively since 1960 when Patrick and Prosser reported[5] that benzene (mp 5.5 °C) and hexafluorobenzene (mp 4 °C) form a 1:1 complex with a melting point of 24 °C. Although the exact nature of these face-to-face interactions is still a subject of study, they may be dominated by electrostatic forces and the large but opposite in sign quadrupole moments of C_6H_6 and C_6F_6.[6] While our work was in progress, Coates and Grubbs *et al.* reported the use of arene–perfluoroarene interactions in buta-1,3-diynes and stilbene derivatives to induce crystal packing suitable for topochemical polymerisation or dimerisation in the solid-state.[7] Herein, we present our results on the liquid crystal (LC) phase behaviour of a series of 1,4-bis(phenylethynyl)benzenes containing 0, 4, 10 or 14 fluorine atoms, namely 1,4-bis(phenylethynyl)benzene **1a**, 1,4-bis(phenylethynyl)tetrafluorobenzene **1b**, 1,4-bis(pentafluorophenylethynyl)benzene **1c** and 1,4-bis(pentafluorophenylethynyl)tetrafluorobenzene **1d**, and the single crystal structure and LC properties of 1:1 co-crystals‡ of **1b**·**1c**. These compounds were prepared by Pd/Cu catalysed cross-coupling reactions of appropriate terminal alkynes and iodoarenes as part of a larger study in our laboratories on the structure, linear and non-linear optical properties, and LC phase behaviour of conjugated rigid-rod systems.[8]

In contrast to the single crystal structures of **1a**–**d**, in which there is no evidence of any type of arene–arene interaction, 1:1 co-crystals‡ of **1b**·**1c** show two such interactions (Fig. 1). Thus, there is clear π-stacking of *all* arene and perfluoroarene moieties along the *b* axis [Fig. 1(*c*)] with the lateral slippage typical of such systems being about one C–C bond length [Fig. 1(*a*)]. As all molecules lie on inversion centres, the stacking is regular rather than alternating (*i.e.* the spacing between all molecules along *b* is equal). The perpendicular separation between mean planes in a stack is 3.337 Å. The intermolecular C–H···F–C interactions[7] shown dashed in Fig. 1(*b*) are 2.500–2.574 Å§ (sum of van der Waals radii = 2.67 Å) with C–F···H and C–H···F angles of 120–160°, the molecules thereby forming sheets which are very close to planar. We have not yet been able to grow single co-crystals of **1a**·**1d** suitable for X-ray diffraction; the sample discussed below was prepared by dissolving equimolar quantities of the two components in $CHCl_3$ and removing the solvent *in vacuo*.

Table 1 lists the axial ratio and the phase transitions detected on heating for compounds **1a**–**d**, and for the two mixed formulations. Surprisingly, molecules with an axial ratio as low as 4.1 (or 4.0 in the case of one of the co-crystals) are capable of forming liquid crystalline phases. Furthermore, the co-crystallized materials exhibit a greater liquid crystalline range and a higher temperature to obtain a fully isotropic fluid,

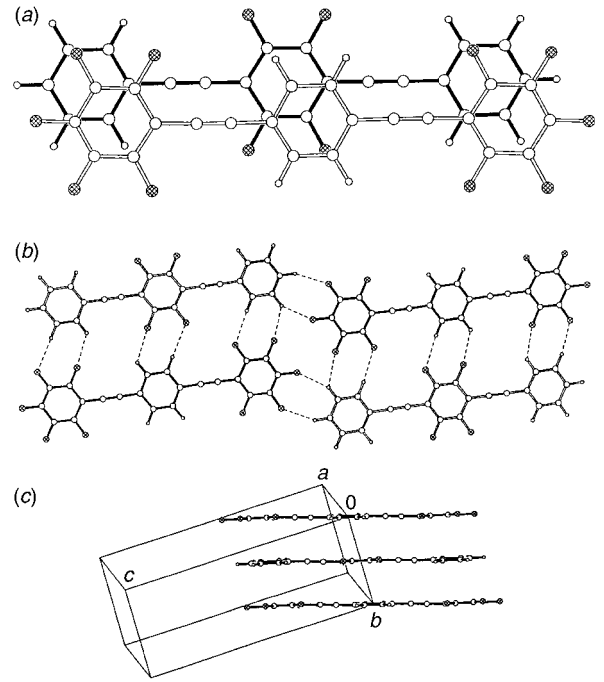

Fig. 1(*a*) Overlap diagram viewed perpendicular to the central C_6 ring of the two molecules in **1b**·**1c**, drawn in parallel projection without perspective, **1b** with solid bonds and **1c** with hollow bonds. Distances between ring centroids in adjacent molecules are 3.770 Å (central rings) and 3.750 and 3.789 Å (outer rings) with these inter-centroid vectors inclined on average 25.7° to the plane normals. Twists about the C–C≡C–C linkage in **1b**·**1c** are only 3.9° (**1b**) and 3.0° (**1c**) whereas in crystals of the individual components **1b** and **1c** these angles are 16.7 and 9.7° respectively. (*b*) A view showing the 'in-plane' intermolecular H···F contacts of 2.500–2.574 Å. (*c*) A packing diagram showing the stacking along the *b* axis.

† Preliminary results were presented at the NATO ASI Summer School on 'Crystal Engineering: The Design and Application of Functional Solids', Digby, Nova Scotia, September 1996, the RSC Dalton Division Symposium on 'Molecules to Materials', London, March 1998, and the 1998 National Congress of the RSC, Durham, April 1998.

Table 1 Axial ratio (*L/D*) and phase transitions[a]

Compound	*L/D*	Transitions on heating/°C
PhC≡CC$_6$H$_4$C≡CPh **1a**	4.45	K 181.7 I (I 164.3 N 159.5 K on cooling)
PhC≡CC$_6$F$_4$C≡CPh **1b**	3.98	K 182.5 I
C$_6$F$_5$C≡CC$_6$H$_4$C≡CC$_6$F$_5$ **1c**	4.10	K 196.5 N/I[b]
C$_6$F$_5$C≡CC$_6$F$_4$C≡CC$_6$F$_5$ **1d**	4.10	K 226.1 I
Co-crystal (1:1) of **1b·1c**	—	K 189.3 N 199.0 I
Two-component system (*ca.* 1:1) of **1a·1d**	—	K 178.5 S_B 196.2 bi N/I[c] 231.5 I

[a] Transition temperatures were determined by DSC and phases were assigned on the basis of the textures observed by transmitted polarised light microscopy. [b] N/I denotes that the nematic phase exists over a very narrow temperature range, and is observed only transiently by microscopy. The crystal-to-nematic and nematic-to-isotropic transition temperatures lie unresolvably close together. A single DSC endotherm is observed, and its onset temperature is quoted. [c] bi N/I denotes that the sample forms a two-phase (biphasic) mixture of both nematic and isotropic material. The subsequent clearing point refers to the nematic regions only.

compared to either of their respective constituents. These results are interesting for three reasons.

First, it is well known[9] that mixing two mesogenic species can lead to a reduction in melting point and so expand the temperature range of liquid crystallinity exhibited by either constituent; often a simple eutectic phase diagram is obtained. Here, however, we have two cases where liquid crystallinity is promoted by mixing compounds that, on their own, show no or only transient tendency to form a LC phase when heated. Also, as noted, it is not just the melting point that is lowered; the clearing points of these mixtures are raised above the temperature needed to render the respective constituents isotropic. Both observations suggest the possibility of intermolecular association in the liquid crystalline phase.

Second, it has been demonstrated previously for unsubstituted tolan oligomers, which have an approximately uniform charge distribution along the length of each molecule, that an axial ratio of 4.45 is barely sufficient to stabilize liquid crystallinity at ambient pressure.[10] The monotropically nematic compound **1a** illustrates this point. When molecules lack the necessary shape anisotropy, they can nevertheless form a liquid crystalline phase if there are sufficiently strong and anisotropic 'soft' interactions between them.[11] In some systems, intermolecular attractions can lead to the assembly of supramolecular aggregates[12] which then promote liquid crystalline order. For example, strong hydrogen bonding between benzoic acids and pyridines can lead to the formation of supramolecular mesogenic structures.[13] Our results suggest that aggregation may play a role in the present case, but that it is probably not due to strong hydrogen bonding.

Third, the fully fluorinated compound **1d** does not exhibit liquid crystallinity, but **1c**, which has the same axial ratio but contains both fluorinated and non-fluorinated phenyl residues, is transiently nematic. We also note that the liquid crystalline two-component systems contain both fluorinated and non-fluorinated phenyls. These observations suggest that arene–perfluoroarene stacking interactions, as observed in the solid-state for **1b·1c**, are the cause of the proposed aggregation in the LC phases.[14] The fact that nematic phases are formed, requiring rod-like or nearly rod-like structures, suggests that it is unlikely that large flat sheets persist at the temperatures of the phase transitions that we observe. Thus, although C–H···F–C interactions in two dimensions may play a role in LC phase behaviour, a one dimensional model based on face-to-face quadrupolar interactions between fluoroarene and arene units is preferred at this time.

Studies examining the phase behaviour of a full range of compositions of these compounds are in progress.

T. B. M. acknowledges support from NSERC of Canada, the University of Durham, the University of Newcastle upon Tyne for a Senior Visiting Research Fellowship, and the NSERC/Royal Society (London) Bilateral Exchange Program, P. N. thanks NSERC for a Postgraduate Scholarship, A. J. S. thanks the EPSRC for a studentship, W. C. thanks the EPSRC for an equipment grant, and C. V. thanks the University of Oxford and Heriot-Watt University for financial support.

Notes and references

‡ Co-crystals of ***1b*·1c** suitable for X-ray diffraction were grown by dissolving solid samples of **1b** (70 mg, 0.2 mmol) and **1c** (92 mg, 0.2 mmol) in hot $CHCl_3$ (5 ml). Colourless needles were collected after cooling to ambient temperature. GC/MS analysis showed that these crystals contained **1b** and **1c** in a 1:1 ratio (calc. for $C_{44}H_{14}F_{14}$: C, 65.53; H, 1.41; F, 32.56. Found: C, 65.36; H, 1.75; F, 32.89%). *Crystal data* for **1b·1c**: $C_{22}H_{10}F_4{\cdot}C_{22}H_4F_{10}$, M = 808.55, triclinic, space group, $P\bar{1}$ a = 6.0932(7), b = 7.5393(9), c = 19.114(2) Å, α = 96.044(3), β = 99.102(3), γ = 96.538(3)°, U = 854.54(17) Å^3, Z = 1, D_c = 1.571 g cm^{-3}, μ(Mo-Kα) = 0.145mm^{-1}, T = 160(2) K, crystal size = 0.62 × 0.18 × 0.02 mm. Full-matrix least-squares refinement on F^2 (G. M. Sheldrick, SHELXTL manual, Bruker AXS Inc., Madison, WI, USA, 1994, version 5) anisotropic displacements for all non-H atoms and isotropic for H (263 parameters) using 2918 unique data (4436 total collected; R_{int} = 0.0449) from a Bruker AXS SMART CCD diffractometer (θ < 25.00°) gave $R1$ [$I > 2\sigma(I)$] = 0.0685, $wR2$ (all data) = 0.1661. Residual electron density within ± 0.30 e Å^{-3}. CCDC 182/1475. See http://www.rsc.org/suppdata/cc/1999/2493/ for crystallographic data in .cif format.

§ All C–H bonds have been extended to the expected internuclear separation of 1.08 Å for all geometry calculations in this paper.

1 C. A. Hunter, *Angew. Chem., Int. Ed. Engl.*, 1993, **32**, 1584; *Chem. Soc. Rev.*, 1994, **23**, 101.
2 P. R. Ashton, J. Huff, S. Menzer, I. W. Parsons, J. A. Preece, J. F. Stoddart, M. S. Tolly, A. J. P. White and D. J. Williams, *Chem. Eur. J.*, 1996, **2**, 31; K. Ochai, Y. Mazaki, S. Nashikiori, K. Kobayashi and S. Hayashi, *J. Chem. Soc., Perkin Trans. 2*, 1996, 1139; D. G. Hamilton, J. K. M. Sanders, J. E. Davies, W. Clegg and S. Treat, *Chem. Commun.*, 1997, 897; J. E. Kickham, S. J. Loeb and S. L. Murphy, *Chem. Eur. J.*, 1997, **3**, 1203.
3 G. R. Desiraju, *Crystal Engineering: The Design of Organic Solids*, Elsevier, New York, 1989; *Chem. Commun.*, 1997, 1475.
4 D. Adam, P. Schuhmaker, J. Simmerer, L. Häussling, K. Slemensmeyer, K. H. Etzbach, H. Ringsdorf and D. Haarer, *Nature*, 1994, **371**, 141; J. Zhang and J. S. Moore, *J. Am. Chem. Soc.*, 1994, **116**, 2655; K. M. Lee, C. K. Lee and I. J. B. Lin, *Angew. Chem., Int. Ed. Engl.*, 1997, **36**, 1850.
5 C. R. Patrick and G. S. Prosser, *Nature*, 1960, **187**, 1021. For a recent theoretical study see: A.P. West Jr., S. Mecozzi and D. Dougherty, *J. Phys. Org. Chem.*, 1997, **10**, 347.
6 J. H. Williams, *Acc. Chem. Res.*, 1993, **26**, 593.
7 G. W. Coates, A. R. Dunn, L. M. Henling, D. A. Dougherty and R. H. Grubbs, *Angew. Chem., Int. Ed. Engl.*, 1997, **36**, 248; G. W. Coates, A. R. Dunn, L. M. Henling, J. W. Ziller, E. B. Lobkovsky and R. H. Grubbs, *J. Am. Chem. Soc.*, 1998, **120**, 3641. See also: M. L. Renak, G. P. Bartholemew, S. Wang, P. J. Ricatto, R. J. Lachicotte and G. C. Bazan, *J. Am. Chem. Soc.*, 1999, **121**, 7787.
8 P. Nguyen, Z. Yuan, L. Agocs, G. Lesley and T. B. Marder, *Inorg. Chim. Acta*, 1994, **220**, 289; P. Nguyen, G. Lesley, C. Dai, N. J. Taylor, T. B. Marder, C. Viney, I. Ledoux and J. Zyss, in *Applications of Organometallic Chemistry in the Preparation and Processing of Advanced Materials*, ed. J. F. Harrod and R. M. Laine, Kluwer, Dordrecht, 1995, p. 333; M. S. Khan, A. K. Kakkar, N. J. Long, J. Lewis, P. Raithby, P. Nguyen, T. B. Marder, F. Wittmann and R. H. Friend, *J. Mater. Chem.*, 1994, **4**, 1227; P. Nguyen, G. Lesley, T. B. Marder, I. Ledoux and J. Zyss, *Chem. Mater.*, 1997, **9**, 406 and references therein.
9 *Liquid Crystals—Applications and Uses*, ed. B. Bahadur, World Scientific, Singapore, 1990, vol. 1.
10 R. J. Twieg, V. Chu, C. Nguyen, C. Dannels and C. Viney, *Liq. Cryst.*, 1996, **20**, 287.
11 W. Maier and A. Saupe, *Z. Naturforsch., Teil A*, 1959, **14**, 882.
12 C. T. Imrie, *Trends Polym. Sci.*, 1997, **3**, 22; C. Viney, *Supramol. Sci.*, 1997, **4**, 75; A. E. Huber and C. Viney, *Phys. Rev. Lett.*, 1998, **80**, 623.
13 T. Kato, Y. Kubota, M. Nakano and T. Uryu, *Chem. Lett.*, 1995, 1127; H. Kihara, T. Kato, T. Uryu, S. Ujiie, U. Kumar, J. M. J. Fréchet, D. W. Bruce and D. J. Price, *Liq. Cryst.*, 1996, **21**, 25.
14 After our paper was submitted, Grubbs *et al*. reported the use of arene–perfluoroarene interactions to stabilise discotic LC phases: M. Weck, A. R. Dunn, K. Matsumoto, G. W. Coates, E. B. Lobkovsky and R. H. Grubbs, *Angew. Chem., Int. Ed.*, 1999, **38**, 2741.

Communication 9/06199A

ChemComm

7-Oxabicyclo[2.2.1]heptadiene derivatives: reactivity towards Brønsted acids

Alain Maggiani, Arlette Tubul and Pierre Brun*

Laboratoire de Synthèse Organique Sélective, GCOPL, ESA 6114, Université de la Méditerranée, Faculté des Sciences de Luminy, 163 Avenue de Luminy, case 901, F-13288 Marseille Cedex 9, France.
E-mail: brun@chimlum.univ-mrs.fr

Received (in Liverpool, UK) 22nd October 1999, Accepted 4th November 1999

7-Oxabicyclo[2.2.1]heptadiene derivatives can be converted to phenols, fulvenes and/or the products from a retro-Diels–Alder-like reaction by treatment with Brønsted acids; the outcome of the reaction depends on the experimental conditions and the nature of the Brønsted acid used.

During the course of our investigations we have synthesised a large variety of arylphenols. These compounds are easily obtained *via* Diels–Alder reaction between arylfurans and dimethyl acetylenedicarboxylate (DMAD).[1] However, in most cases a mixture of the phenolic and the oxabicyclic derivatives is obtained. The proportions of the two species depend on the nature and the position of the substituent on the phenyl group. 7-Oxabicyclo[2.2.1]heptadiene derivatives are often used in organic synthesis as synthons for natural product elaboration.[2,3] We have shown previously that dimethyl 1-aryl-7-oxabicyclo-[2.2.1]heptadiene-2,3-dicarboxylates **1** can be converted to phenols **2** or to 6-hydroxyfulvenes **3** by reaction with Lewis acids.[4] Depending on the acid used, **2** or **3** can be formed in a totally selective and quantitative way (Scheme 1). Never in the past have such high yields and such a selectivity been described.[5–8] We report here the results obtained when **1** is reacted with Brønsted acids.

As with Lewis acids, depending on the nature of the Brønsted acid, phenols **2** and/or hydroxyfulvenes **3** are formed. However, another reaction was observed: a retro-Diels–Alder like reaction (retro-DA) leading to **4** and DMAD **5** (Scheme 2).

Our results are reported in Table 1. These results were obtained using 1-(2-chlorophenyl)-7-oxabicyclo[2.2.1]hepta-diene-2,3-dicarboxylate as a model compound, but similar results were observed with **1** for R = *p*-nitro or *p*-acyl.

In the presence of gaseous HCl or with glacial AcOH (entries 4, 6–9) the retro-DA reaction is totally regioselective and is the only process observed. In AcOH, the conversion rate increases with the temperature. However, the retro-DA reaction is not a purely thermal one, as exemplified by the absence of conversion when **1** is heated at reflux in a $CHCl_3$–CCl_4 mixture (entry 10).

When mineral aqueous acids are used (HCl or H_2SO_4) the results depend on the experimental conditions and particularly on the solvent and temperature (entries 1–3, 5). In Et_2O, at room temperature, only the phenol **2** is formed. In CH_2Cl_2, with H_2SO_4, only tars are formed starting from compound **1**. With aqueous HCl, under heating, the reaction is not selective and the

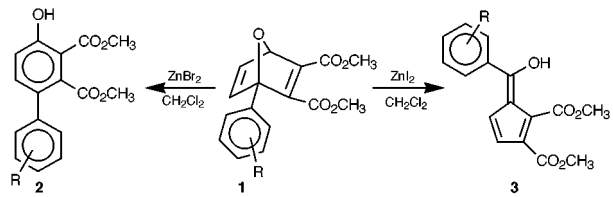

Scheme 1

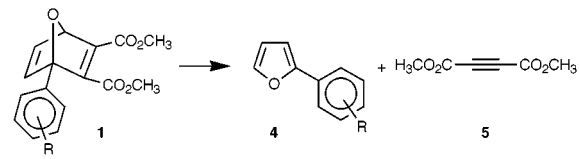

Scheme 2

Table 1 Influence of the Brønsted acids nature on the behaviour of **1**[a]

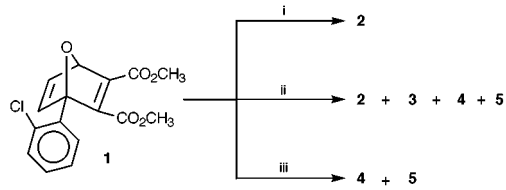

Entry	Acid	Solvent	*T*/°C	*t*/h	Yield (%)[b] 1	2	3	4 + 5
1	HCl (aq.)	CH_2Cl_2	55	24		44–37	6–0	50–63
2	HCl (aq.)	CH_2Cl_2	reflux	24	9	8	72	11
3	HCl (aq.)	Et_2O	25	24	11	89		
4[c]	HCl (g)	CH_2Cl_2	25	48				100
5	H_2SO_4	Et_2O	25	24	5	95		
6	AcOH	—	25	48	100			
7	AcOH	—	60	48	40			60
8	AcOH	—	90	48	25			75
9	AcOH	—	reflux	48	18			82
10	None	$CHCl_3$–CCl_4	reflux	48	100			

[a] *Reagents and conditions*: i, aq. HCl or H_2SO_4, Et_2O, room temp.; ii, aq. HCl, CH_2Cl_2, reflux; iii, anhydrous HCl, Et_2O or CH_2Cl_2, room temp. (or AcOH, reflux.) [b] The indicated yields are based on pure isolate compounds. [c] Ref. 9.

retro-DA process is observed along with the formation of **2** and **3**. The ratio of the different compounds depends on the temperature, and the yield of the retro-DA reaction increases with the temperature (entries 1, 2) while the yield of fulvene **3** decreases. It must be noted that the formation of the fulvene **3** and the retro-DA reaction are totally regioselective processes: only the 6-hydroxyfulven **3** and the 2-arylfurane **4** are formed, without any traces of another regioisomers.

With Lewis acids, **2** and **3** can be obtained selectively as unique compounds. Similarly with gaseous HCl or AcOH, the retro-DA-like reaction is the only one observed. Although we have no evidence for the mechanism of that reaction, we have observed, by thin layer chromatography, that an intermediate compound is formed during the reaction with gaseous HCl. This compound could not be isolated as it is rapidly converted to arylfuran and DMAD. This suggest that the retro-DA-like process could occur by chlorination (or acetoxylation in the case of AcOH) of the starting compound followed by subsequent rearrangements.

Our results show the great reactivity of 7-oxabicyclo-[2.2.1]heptadiene derivatives towards Brønsted acids. This was also demonstrated with Lewis acids. However, although with Lewis acids it is possible to synthesise phenols and/or 6-hydroxyfulvenes, we have shown that with Brønsted acids it is also possible to observe a quantitative and totally regioselective retro-Diels–Alder like reaction in AcOH or with gaseous HCl. Although, in our case, the retro-DA products are the same as the ones used for preparing the starting compound **1**, our observations may be applied to other 7-oxabicyclo-[2.2.1]heptadiene derivatives and thus could be very useful, as interest in retro-Diels–Alder reactions as a tool in organic synthesis is increasing.[10]

Notes and references

1 A. Maggiani, A. Tubul and P. Brun, *Synthesis*, 1997, 631.
2 R. D. Little and G. N. Muller, *J. Am. Chem. Soc.*, 1981, **103**, 2744.
3 R. D. Little, G. L. Caroll and J. L. Petersen, *J. Am. Chem. Soc.*, 1983, **105**, 928.
4 A. Maggiani, A Tubul and P. Brun, *Tetrahedron Lett.*, 1998, **39**, 4485.
5 P. Vogel, B. Willhalm and H. Prinzbach, *Helv. Chim. Acta*, 1969, **52**, 584.
6 D. S. Stusche and H. Prinzbach, *Chem. Ber.*, 1973, **106**, 3817.
7 A. Bruggink, H. Hogeveenh and T. B. Middlekoop, *Tetrahedron Lett.*, 1972, 4961.
8 R. K. Bansal, A. W. McCulloch, P. W. Rasmussen and A. G. McInnes, *Can. J. Chem.*, 1975, **53**, 138.
9 *General procedure* for the retro-DA reaction induced by anhydrous HCl: a stirred solution of the oxabicyclic derivative **1** in CH_2Cl_2 (0.5 ml per 0.1 mmol of substrate) was saturated with anhydrous HCl (between 1.5 and 2 h). The solution was stirred at room temperature for 48 h. The solution was washed with water to neutrality. The organic layer was dried over $MgSO_4$ and then concentrated under vacuum. The crude product was purified by flash chromatography (eluent: hexane–Et_2O).
10 R. Bloch and G. Mandville, *Novel strategies for the use of retro-Diels–Alder reactions in stereoselective synthesis*, in *Recent research developments in organic chemistry*, ed. S. G. Pandalai, TRN, Trivadrum, India, 1998, vol. 2, pp. 411-452.

Communication 9/08451G

ChemComm

Synthesis and photochromic properties of helically locked 1,2-dithienylethenes

Liviu Dinescu and Zhi Yuan Wang*

Department of Chemistry, Carleton University, 1125 Colonel By Drive, Ottawa, Ontario, Canada K1S 5B6. E-mail: wangw@ccs.carleton.ca

Received (in Corvallis, OR, USA) 17th August 1999, Accepted 2nd November 1999

The synthesis of a new family of 1,2-diarylethenes, helically locked 1,2-dithienylethenes, is reported, along with their photochromic properties in solution and as polymeric films.

In recent years a considerable effort has been made towards 1,2-diarylethenes, a class of photochromic compounds known to undergo a reversible ring closing and opening upon irradiation at two different wavelengths. Properties such as thermal stability in isomeric forms, easy preparation and good resistance to repetitive photoisomerization cycles make diarylethenes potential materials for optical data storage.[1] In order to avoid a competing *trans–cis* photoisomerization, the aryl moieties are bound to the double bond of a cycloalkene.[2] To date, all the reported photochromic 1,2-diarylethenes have a five-membered cycloalkene, which can be considered as derivatives of maleic anhydride, maleimide and perfluorocyclopentene. Recently, Feringa *et al.* succeeded in synthesizing a series of 1,2-dithienylethenes based on the cyclopentene moiety and showed that one compound was suitable for multiple photoisomerization cycles.[2]

One of features of known 1,2-dithienylethenes is that the aryl rings are able to rotate around the alkene–aryl single bond. As a result, the molecules are distributed between two equally populated conformational states resulting from the parallel and antiparallel orientations of the aryl rings.[3] According to the Woodward–Hoffman rule, photocyclization of a hexa-1,3,5-triene system is allowed only in conrotatory mode. In addition to this, the photocyclization reaction of 1,2-diarylethylenes is restricted to proceed only for molecules that are in the antiparallel orientation (Scheme 1). ^{1}H NMR studies have shown that the full interconversion of the two conformers occurs at temperatures exceeding 40 °C, which is above the temperature limit ideal for most practical applications.[3] Hence, it would be of fundamental interest to design and study a rigid dithienylethene system, in which the two thiophene rings are 'frozen' or locked in an antiparallel orientation suitable for efficient cyclization. Such a system can be realized by connecting the R^1 and R^2 groups of the 1,2-dithienylethenes shown in Scheme 1. Herein we report a new class of photochromic compounds: helical 1,2-dithienylethenes **1a**,**b** (Scheme 2) that are built on the rigid frame of $\Delta^{4a(b)}$-dodecahydrophenanthrene. The multi-ring locked structure and the overlapping methyl substituents give rise to a molecular helicity in these compounds, which allows the thiophene rings to adopt an almost an antiparallel orientation. The increase in the molecular rigidity might also provide a stabilizing effect on the isomers **2a**,**b**.

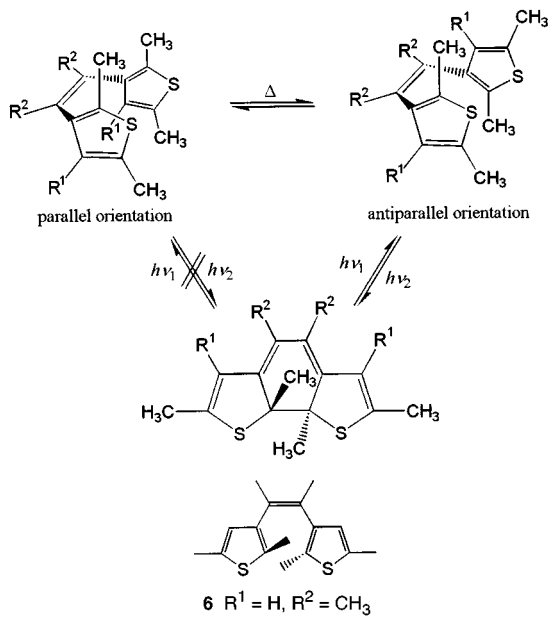

Scheme 1

As shown in Scheme 2, our synthetic approach to these compounds began with commercially available 2,5-dimethylthiophene (Aldrich), which was converted into cyclic ketone **3** using a known method.[4] The McMurry–Mukaiyama coupling[5] of **3** with $TiCl_4$ and Zn in THF gave pinacol **4** in 95% yield. Without further purification, pinacol **4** was dehydrated using $POCl_3$ in pyridine to give the diene **5** in 84% yield. The subsequent steps involved the Diels-Alder reactions of **5** with maleic anhydride or *N*-ethylmaleimide to produce the racemic *endo* adducts **1a**,**b**.

Molecular mechanics calculations indicated that dithienylethenes **1a**,**b** are highly unsymmetrical. Due to the *cis*-fusion of the anhydride and imide moieties, the preferred conformations of **1a**,**b** do not exhibit any C_2 and mirror symmetry elements, as evidenced by the NMR spectral data of **1a**,**b**.[6] The NOESY and COSY NMR data recorded for **1b** were consistent with an *endo* configuration.[7]

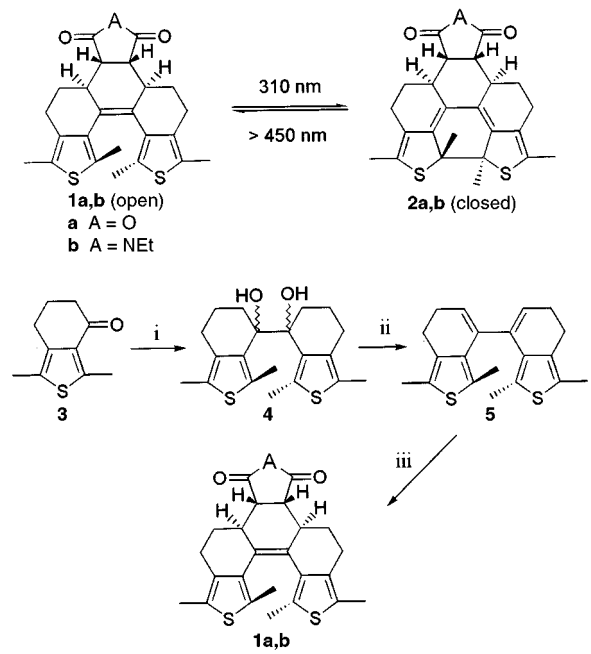

Scheme 2 *Reagents and conditions*: i, $TiCl_4$, Zn, THF, 25 °C; ii, $POCl_3$, pyridine, 120 °C; iii, dienophile, xylene, reflux.

At first, the photocyclization of dithienylethenes **1** was examined in solution (Scheme 2). Solutions of **1a** and **1b** in oxygen-free benzene (1×10^{-4} M) were irradiated at wavelengths corresponding to the absorption bands of the open (λ = 310 nm) and closed isomers (λ > 450 nm). Upon irradiation with UV light (λ = 310 nm, Hg medium pressure lamp), the solutions turned from clear to yellow, as illustrated by the absorption change shown in Fig. 1(*a*). Alternatively, irradiation of the yellow solutions with white light (tungsten lamp) caused the decoloration of the solutions as the closed isomers **2a**,**b** were converted back to **1a**,**b**. The thermal stability of the closed isomers was found to be comparable with that of the closed isomer derived from *cis*-2,3-bis(2,5-dimethyl-3-thienyl)but-2-ene (**6**, R^1 = H, R^2 = CH_3, Scheme 1), a non-helical analogue reported by Irie.[8] A deoxygenated solution of **2b** in benzene was kept at 60 °C for 15 h and no visible change in the UV–VIS absorption spectrum was found.

Previous experiments conducted with diarylethenes in the crystalline state have shown that the photochemical ring closing proceeded reversibly and unrestricted.[9] Thus, it was useful to monitor the photochromic behavior of diarylethenes **1a** and **1b** in an amorphous polymeric film. A polycarbonate film containing **1a** or **1b** was irradiated at 310 and > 450 nm, respectively. The photocyclization proceeded readily at ambient temperature, as evidenced by the absorption maximum (λ = 450 nm) of the closed isomer [Fig. 1(*b*)]. Similar to the results of the solution experiment, irradiation of the polycarbonate film containing **2a** or **2b** with white light led to the recovery of **1a** or **1b**, respectively. Therefore, in contrast to some non-helical 1,2-dithienylethenes,[10] the complete switch between **1** and **2** in solution and in the solid polymer film can conceivably be attributed to molecular rigidity (*i.e.* locked rings) and helical conformation (*i.e.* antiparallel orientation) of compound **1**.

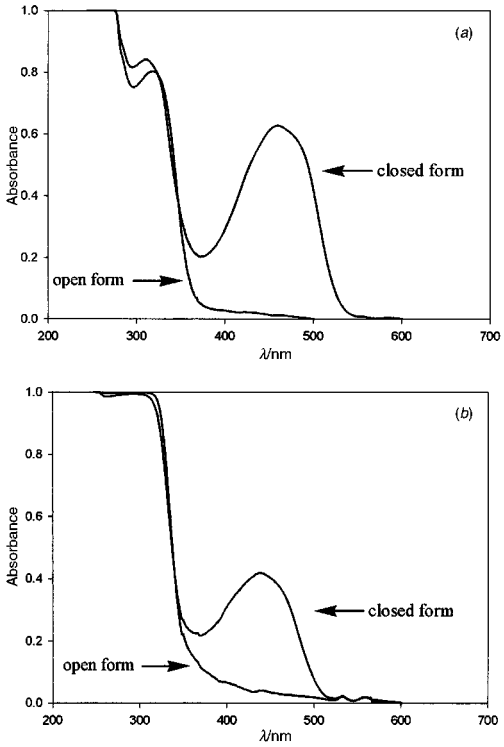

Fig. 1 UV–Visible absorption spectra of (*a*) **1b** in benzene (1×10^{-4} M) in the dark and after irradiation at 310 nm; (*b*) **1b** in polycarbonate film (6.8×10^{-2} mg per mg polymer) in the dark and after irradiation at 310 nm.

The fatigue resistance properties can be determined by the number of colour change cycles over which the color intensity of the photochromic medium decreases to 80% of that of the first cycle.[3] Accordingly, it was found that the fatigue resistance for dithienylethenes **1a**,**b** in benzene in air is about four cycles. A similar cycle number was recorded for **6** (Scheme 1),[8] which has a similar chromophore core (absorption peak corresponding to the closed isomer is 431 nm in benzene). When oxygen was removed from the benzene solution, more than ten switching cycles could be easily achieved without a noticeable decrease in the photochromic intensity.

In conclusion, we have demonstrated a new series of 1,2-dithienylethenes that display distinct photochroism at 310 and 450 nm at ambient temperatures.

The Natural Sciences and Engineering Research Council financially supported this work.

Notes and references

1 M. Irie and K. Uchida, *Bull. Chem. Soc. Jpn.*, 1998, **71**, 985.
2 N. L. Lucas, J. Van Esch, M. R. Kellog and B. L. Feringa, *Chem. Commun.*, 1998, 2313.
3 K. Uchida, Y. Nakayama and M. Irie, *Bull. Chem. Soc. Jpn.*, 1990, **63**, 1311.
4 N. P. Buu-Hoi, N. Hoan and N. H. Khoi, *Recl. Trav. Chim. Pays-Bas*, 1950, **69**, 1053.
5 T. Mukaiyama, T. Sato and J. Hanna, *Chem. Lett.*, 1973, 1041.
6 *Selected data* for **1a**: δ_H(400 MHz, $CDCl_3$) 1.36 (s, 3H), 1.37 (s, 3H), 1.75–1.90 (m, 2H), 2.04–2.15 (m, 2H), 2.22 (s, 6H) 2.44 (dt, *J* = 14.0, 3.2, 1H), 2.63 (dd, *J* 8.4, 2.8, 2H), 2.73–2.86 (m, 3H), 3.38–3.47 (m, 2H). For **1b**: δ_H(400 MHz, $CDCl_3$) 1.22 (t, *J* 7.2, 3H), 1.23–1.33 (m, 1H), 1.44 (s, 3H), 1.53 (s, 3H), 1.52–1.60 (m, 1H), 2.22 (q, *J* 13.5, 2H), 2.32 (s, 3H), 2.33 (s, 3H), 2.50–2.55 (m, 1H), 2.61–2.86 (m, 6H), 2.95–3.00 (m, 1H), 3.61 (q, *J* 7.2, 2H).
7 F. Fringuelli and A. Taticchi, in *Dienes in the Diels–Alder Reaction*, Wiley, New York, 1990.
8 M. Irie and M. Mohri, *J. Org. Chem.*, 1988, **53**, 803.
9 M. Irie, K. Uchida, T. Eriguchi and H. Tsuzuki, *Chem. Lett.*, 1995, 899; M. Irie, T. Lifka and K. Uchida, *Mol. Cryst. Liq. Cryst.*, 1997, **297**, 81.
10 M. Irie, K. Sakemura, M. Okinaka and K. Ukida, *J. Org. Chem.*, 1995, **60**, 8305.

Communication 9/06680B

Catalytic dehydrogenation of a mixture of C_{10}–C_{14} *n*-paraffins to linear C_{10}–C_{14} monolefins in a supercritical phase

Wei Wei, Yuhan Sun* and Bing Zhong

State Key Laboratory of Coal Conversion, Institute of Coal Chemistry, Chinese Academy of Sciences, Taiyuan 030001, P.R. China. E-mail: sklcc@public.ty.sx.cu

Received (in Cambridge, UK) 16th August 1999, Accepted 10th November 1999

The catalytic dehydrogenation of a mixture of C_{10}–C_{14} *n*-paraffins (*n*-alkanes) to linear C_{10}-C_{14} monolefins (alkenes) over a commercial Pt-Sn/γ-Al_2O_3 catalyst was observed to be two to three times higher in a supercritical phase of the reactant themselves than in the gas phase; this indicated that the thermodynamic equilibrium was strongly shifted under supercritical conditions.

The preparation of linear C_{10}-C_{14} monolefins (alkenes) from a mixture of C_{10}–C_{14} *n*-paraffins (alkanes) by catalytic dehydrogenation is an important process in the production of synthetic detergents and surface-active agents.[1] Because of equilibrium limitations and deep dehydrogenation of monolefins, the present industrial process at most reaches *ca.* 12% conversion with 92% selectivity. Neither conversion nor selectivity have been significantly enhanced although the catalysts used have been highly improved. A new technique is thus required to improve the process.

Supercritical fluids (SCFs), which are fluids above their critical temperatures and pressures, have been used for extraction and separation since their discovery 170 years ago by Baron Charles Cagniard de la Tour.[2] In recent years, much interest has been generated in supercritical reactions[3] and some comprehensive reviews appeared.[4,5] Generally, supercritical fluids not only enhance the reaction rate, but also shift chemical equilibria, and hence significantly improve the performance of heterogeneous catalysis as a result of the enhancement of the physicochemical properties of the fluid near the critical state.[6,7] The supercritical catalytic dehydrogenation of a mixture of C_{10}–C_{14} *n*-paraffins to a mixture of linear C_{10}-C_{14} monolefins was thus investigated for improvement in conversion and selectivity.[8]

The feedstock composition of the C_{10}–C_{14} *n*-paraffin mixture is given in Table 1. The dehydrogenation of C_{10}–C_{14} *n*-paraffins to linear C_{10}–C_{14} monolefins was carried out over commercial Pt-Sn/γ-Al_2O_3 catalyst (DEH-7 supplied by UOP) at supercritical conditions for the C_{10}–C_{14} *n*–paraffin mixture in a downflow fixed bed reactor with inner diameter of 1.4 cm. The products were determined by the UOP analysis methods in which the conversion is represented by bromine value, the diolefin content by diolefin number, and the aromatics were determined by UV spectrometry.[9] Typical data are shown in Fig. 1 and Table 2.

Table 1 Feedstock composition of the *n*-C_{10}–C_{14} paraffin mixture

Component	C_{10}	C_{11}	C_{12}	C_{13}	C_{14}
Composition (wt%)	8.76	32.42	36.12	22.45	0.23

Fig. 1 indicated that the pressure strongly influenced the performance of the reactions. When the reaction pressure was below the critical pressure (region A) of the reactant, the reaction conversion was low. At reaction pressures of > 2.5 MPa (region C), the conversion of the reactants was slightly higher than the calculated equilibrium conversions, which might be due to the higher solubility of the products in the higher density supercritical phase relative to the gas phase. Only when both the pressure and temperature of the reaction system approached critical conditions for the C_{10}–C_{14} *n*-paraffin mixture, was conversion greatly increased and highly exceeded the equilibrium conversion. This fact indicated that the equilibrium is strongly shifted under supercritical conditions for the reactants, which might be due to either the high solubility of the products in supercritical fluids[10] or quick desorption of monolefins from the catalyst surface.[11,12] Table 2 shows that the diolefin content in the supercritical phase was relatively lower than that in the gas phase, and aromatics were scarcely observed in the supercritical phase (*cf.* 0.9–1.5% in the gas phase). These results can be attributed to the fast desorption of the main products (*i.e.* monolefins) from the surface of the catalyst, which prevents deep dehydrogenation of the main products to diolefins and aromatics,[11] so leading to a high selectivity of linear C_{10}–C_{14} monolefins (> 98%).

Unlike the present industrial processes in which a large amount of hydrogen is used (typically mol ratio H_2 : alkanes =

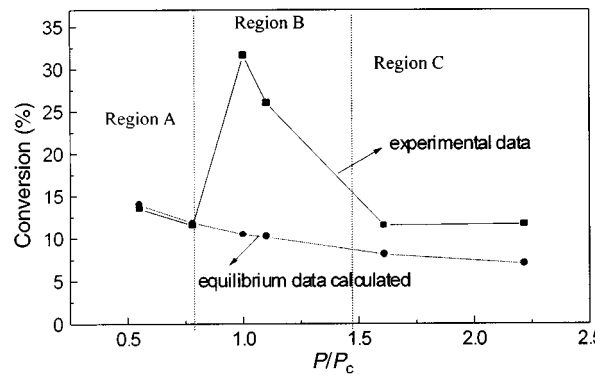

Fig. 1 Comparison of the experimental data with the equilibrium conversion calculated at different P/P_c values in the absence of hydrogen at 713 K.

Table 2 The dehydrogenation of a mixture of C_{10}–C_{14} *n*-paraffins in supercritical (SC) and gas phases (GP)

	T/K	LHSV[a]/h^{-1}	*p*/MPa	H_2 : HC[b] (mol ratio)	Monolefin (wt%)	Diolefin (wt%)	Aromatics (wt%)
GP	725–738	28–32	0.1–0.4	8 : 1	8.0–12.0	0.20–0.50	0.9–1.5
SC	673–743	32	1.7–2.1	0 : 1	13.5–30.7	0.21–0.33	0
SC	673–743	32	3.5–4.4	1 : 1	8.6–20.4	0.11–0.21	0

[a] Liquid hour space velocity. [b] HC = Alkanes.

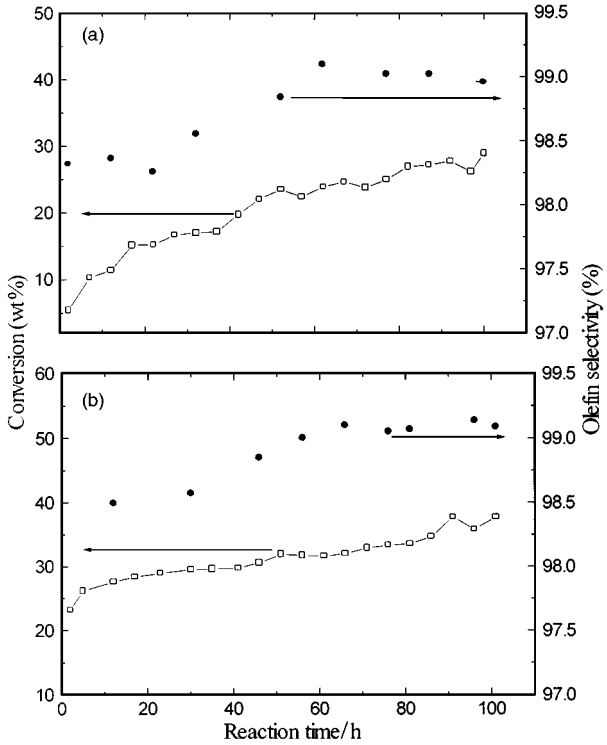

Fig. 2 Variation of conversion and selectivity with reaction time in the supercritical phase of the reactant. (a) mol ratio H_2:alkanes = 1:1, 4.0 MPa, 723 K, LHSV = 32 h^{-1}; (b) mol ratio H_2:alkanes = 0:1, 2.0 MPa, 723 K, LHSV = 32 h^{-1}.

8:1) to avoid severe coke formation, supercritical dehydrogenation could be carried out without hydrogen (see Table 2 and Fig. 2). Fig. 2 indicates that both the activity and the selectivity scarcely decreased over 100 h in the absence of hydrogen in the supercritical phase of a mixture of C_{10}–C_{14} *n*-paraffins. Moreover, TG–DTA illustrated a reduction of coke formation over the catalysts used in the supercritical phase. This is as expected if the formation of carbonaceous species on the surface of the catalyst is suppressed by supercritical fluids.[13,14] Indeed, a partial pressure of hydrogen was detrimental on the performance of the supercritical phase, possibly owing to a change of supercritical conditions in the presence of hydrogen. The mechanism of the process is currently under investigation.

The above results indicate that reaction in a supercritical phase leads to a substantial improvement in both conversion and selectivity as well as the reduction of coke formation in the catalytic dehydrogenation of a mixture of C_{10}–C_{14} *n*-paraffins to linear C_{10}–C_{14} monolefins.

Financial support from the National Natural Science Foundation of China is highly acknowledged.

Notes and references

1 D. J. Ward and V. B. Vora, *US Pat.*, 4393259, 1982; V. B. Vora and D. L. Elling, *US Pat.*, 4761509, 1987; T. Imai, *US Pat.*, 4762960, 1988.
2 G. M. Destraction and G. Wilke, *Extraction with Supercritical Gases*, Verlag Chemie, Weinheim, 1979.
3 K. P Johnston and J. M. Penninger, *Supercritical Fluid Science and Technology*, ACS Symp. Ser. 406, American Chemical Society, Washington, DC, 1989.
4 H. Tiltscher, H. Wolf and J. Schelchshorn, *Angew. Chem., Int. Ed. Engl.*, 1981, **20**, 892.
5 P. E. Savage, S. Gopalan, T. I. Mizan, C. J. Martino and E. E. Brock, *AICHE J.*, 1995, **41**, 1723.
6 A. Eckert, B. L. Knuston and P. G. Debenedetti, *Nature*, 1996, **383**, 26.
7 L. Fan, I. Nakamura, S. Ishida and K. Fujimoto, *Ind. Eng. Chem. Res.*, 1997, **36**, 1458.
8 B. Zhong, Y. Sun and W. Wei, *Chin. Pat.*, 98104545.6, 1998.
9 Y. Sun, P. Wu, M. Wei and X. Wang, *China Surfactant Deter. Cosmt.*, 1987, **2**, 7.
10 K. Yokota and K. Fujimoto, *Ind. Eng. Chem. Res.*, 1991, **30**, 95.
11 X. G. Zhang, S. Peng, B. Zhong and Y. W. Li, *J. Fuel Chem. Technol.*, 1998, **49**, 6.
12 C. S. Tan and D. C. Liou. *Ind. Eng. Chem. Res.*, 1988, **27**, 988.
13 H. Tiltscher and H. Hofmann, *Chem. Eng. Sci.*, 1987, **42**, 959.
14 M. G. Süer, Z. Dardas, Y. H. Ma and W. R. Moser, *J. Catal.*, 1996, **162**, 320.

Communication 9/06617I

Through-space ^{13}C–^{19}F coupling can reveal conformations of modified BODIPY dyes†

Jiong Chen, Joe Reibenspies, Agnes Derecskei-Kovacs and Kevin Burgess*

Department of Chemistry, Texas A & M University, PO Box 30012, College Station, TX 77842-3012, USA. E-mail: burgess@chemvx.tamu.edu

Received (in Corvallis, OR, USA) 13th September 1999, Accepted 27th October 1999

The fact that only compounds 1a, 1b and 2a in the series 1–3 show long-range ^{13}C–^{19}F coupling can be used to draw conclusions regarding the structures of these molecules.

Through-space coupling between carbon and fluorine atoms that are forced together through geometric constraints is a well-known phenomenon,[1–3] but it is not often used as a tool to gauge molecular conformations.[4–6] Here we describe such an application as applied to 3,5-diaryl-4,4-difluoro-4-bora-3a,4a-diaza-*s*-indacene (BODIPY®) dyes **1**–**3**.[7]

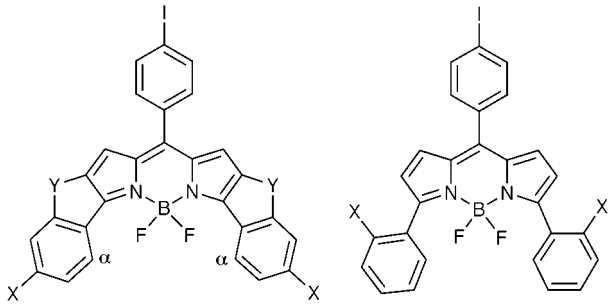

1a X = OMe, Y = CH_2CH_2
b X = H, Y = CH_2CH_2
2a X = H, Y = S
b X = H, Y = O

3a X = H
b X = OMe

Briefly, the circumstances that led to this study were as follows. Our group is attempting to prepare new fluorescent dyes for biotechnological applications.[8,9] An important part of these studies is to refine the fluorescence properties of the target dyes by relating them to molecular structure. As part of our investigations to determine molecular structure we observed that a through-space ^{13}C–^{19}F coupling[10] is observed only for compounds **1a**, **1b** and **2a** in this series, and this parameter can be correlated with their molecular conformation. These compounds show a triplet in their $^{13}C\{^1H\}$ spectra (**1a** δ 130.1, t, J = 11.0 Hz; **1b** δ 128.4, t, J = 11.2; **2a** δ = 126.7, t, J = 5.2 Hz). APT and HETCOR experiments[11] established that the carbons responsible for these triplets were the ones marked **α** (henceforth referred to as C^α). A combination of two decoupling experiments was performed on **1a** to prove that this splitting was due to coupling with the two fluorine atoms. First, a ^{13}C NMR spectrum was recorded without any decoupling, and the C^α appeared as a doublet of triplets (J = 164 and 11 Hz). A proton-coupled, fluorine-decoupled ^{13}C NMR spectrum of the same sample was then recorded, and the carbon of interest appeared as a doublet (J = 164 Hz). These experiments indicate that the triplet arises from coupling of the C^α to the two fluorine atoms.

A comparison of spectral data for compounds **1** and **2** is shown in Table 1. The ^{19}F and ^{11}B NMR chemical shifts for these dyes decrease in the order **1** > **2a** > **2b**, and the same trend was also observed in the ^1H NMR spectra of these materials. The observed C–F coupling constants in this series decrease in the same order. These observations imply that the factors that govern the ^{19}F chemical shifts also impact C–F coupling constants in this series.

Table 1 Selected spectroscopic data for **1**–**2**

	Chemical shift (δ/ppm)[a]		
Compound	^1H[b]	^{19}F[c]	^{11}B[d]
1a	8.78	−137.5	9.29
1b	8.82	−137.3	3.98
2a[e]	8.75	−147.0	—
2b	8.24	−150.6	0.41

[a] In $CDCl_3$. [b] For C^α–*H* or the corresponding C–*H*, at 300 MHz relative to a deuterium lock. [c] At 282 MHz relative to $CFCl_3$ as external reference. [d] At 64 MHz relative to $BF_3{\cdot}OEt_2$ as external reference. [e] ^{11}B NMR data could not be obtained for this compound since it is relatively insoluble in the common organic solvents used for NMR studies.

It is unlikely that C^α is coupled to the fluorine atoms *via* covalent bonds in the aromatic system, for several reasons. First, if it were to occur, the observed value of 11 Hz would be an exceptionally large *J*-parameter for a five-bond coupling. Second, other carbons in compounds **1** and **2a** would most probably be affected in the same way if that coupling mechanism was operative, especially those that are less than five bonds away. Finally, similar five-bond coupling might then also be observed for compound **2b** and **3**, but they were not.

A single crystal, X-ray diffraction analysis was performed on compound **1a** to gain more insight into the nature of the C^α–F interactions.‡ Molecule **1a** crystallizes in a bow-shaped conformation making the two fluorine atoms inequivalent (even though they are equivalent in the ambient solution phase ^{19}F NMR spectrum of this compound, Fig. 1). Moreover, there are four C^α–F distances since the BF_2 entity does not reside at a

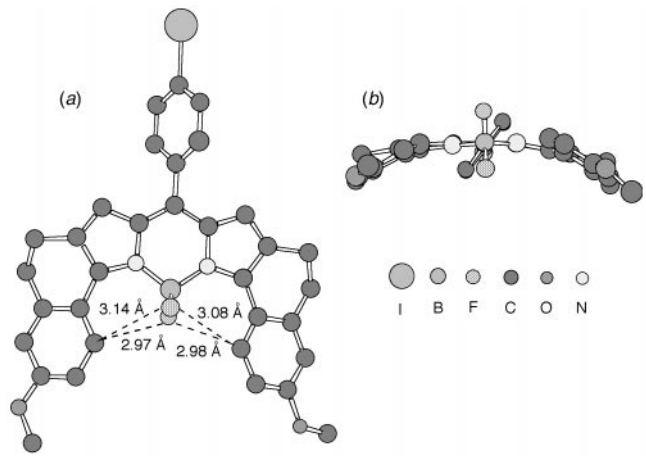

Fig. 1 Chem3D representations of **1a** from X-ray crystallographic data: (*a*) top view showing C^α–F distances; (*b*) side view illustrating curvature of the molecule.

† Spectral data for **1a,b** and **2a,b** and colour versions of Fig. 1 and 2 are available from the RSC web site, see http://www.rsc.org/suppdata/cc/1999/2501/

position that is exactly equidistant to both aromatic rings in the crystal structure. The four C^{α}–F distances are similar; they vary between 2.97(1) and 3.14(1) Å, and average to 3.04(8) Å. More variance was observed for the C^{α}–*H*··*F* distances. Electron density maps were used to locate the protons in this molecule, and their positions were refined (though of course, not to the same degree of accuracy as the heavier atoms). Nevertheless, the shorter C^{α}–*H*··*F* distance is no less than 2.29(1) Å, the longer one is no more than 2.75(1) Å, and the average value was measured as 2.5(2) Å. Comparison of the average C–F distance {3.04(8) Å} with the sum of the van der Waals radii for carbon and fluorine (3.19 Å)[12] implies that an interaction between these atoms is likely. Similarly, the average C^{α}–*H*··*F* distance {2.5(2) Å} is less than the sum of the van der Waals radii for hydrogen and fluorine (2.62 Å).

It appeared from the solid state structural analyses, outlined above, that the C^{α}–F interaction observed in the ^{13}C NMR spectra of compounds **1** is due to a close interaction of these atoms, through space. Crystallographic data was not obtained for compounds **2**, but a series of calculations was performed to establish why the interaction was observed for **2a** but not **2b**. Briefly, these were performed in the Cerius2 collection of programs (Molecular Simulations, Inc.). Preliminary optimizations were performed *via* molecular mechanics using the Universal Force Field (designed to accommodate all the atoms in the periodic table).[13–15] Final geometry optimizations were obtained at the semi-empirical level using the AM1 method within MOPAC.[16,17] Throughout these calculations, the iodine atoms in the real molecules were substituted by chlorine atoms in the virtual compounds.

Calculations on the Cl-for-I analog of compound **1a** gave a minimized structure obtained having the same curved conformation observed from the X-ray diffraction study (Fig. 1). Moreover, all the bond parameters were similar (data not shown). This result indicated that the AM1 calculations were reliable for this molecular type.

Simulated structures of the Cl-for-I analogs of compounds **2** are shown in Fig. 2. Comparison of Fig. 1 and 2 shows that the latter are essentially planar: they do not have the bow-shaped structure that compound **1a** has. Distances between the F- and C^{α}-atoms increase in the order **1a** < **2a** < **2b**. They are no longer within the sum of the van der Waals radii for carbon and fluorine for compound **2b**.

These structural studies clarify why the trend on the F-to-C^{α} coupling constants should be as observed. The ethylene bridges of compound **1a** force the benzene rings inwards towards the fluorine atoms, giving an exceptionally close interaction between the C^{α} and F atoms. Conversely, the S and O atoms in compounds **2** pull the benzene rings outward, giving a relatively open structure. However, this effect is less important for **2a** than for **2b** for two related reasons that expand the five-membered rings containing the sulfur atoms. First, the atomic size of sulfur is greater than that of oxygen. Second, C–S bond lengths are longer than for C–O bonds (typically 1.75 Å for sp^2 C–S bond *vs*. 1.34 Å for sp^2 C–O bond).

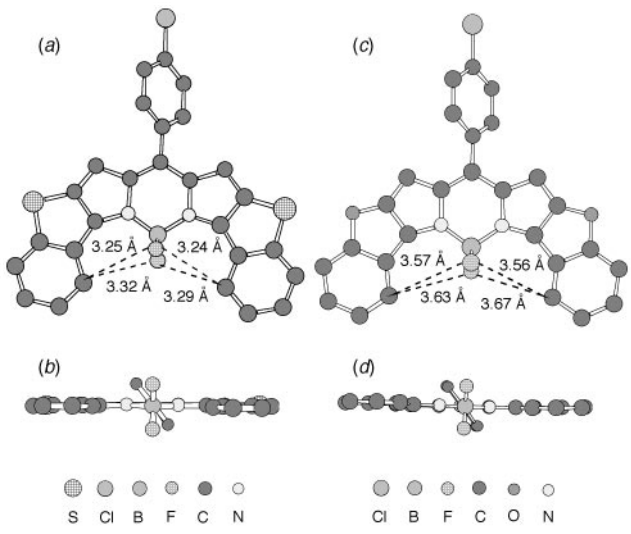

Fig. 2 Chem3D representations of the Cl-for-I analogs from AM1 calculations: (*a*) top view of **2a** showing C^{α}–F distances; (*b*) side view of **2a**; (*c*) top view of **2b** showing C^{α}–F distances; (*d*) side view of **2b**.

It is surprising that couplings between the C^{α}–*H*··*F* atoms were not observed for compounds **1** and **2a**. It appears that the C^{α}–*H*··*F* coupling is too small to be observed conveniently in the proton NMR spectra of these compounds. However, the C^{α}–H resonance for compound **1a** was broader than other aromatic protons in this molecule (2.7 Hz at half-peak-height) and sharpened in a $^1H\{^{19}F\}$ experiment (2.1 Hz at half-peak-height).

There are two possible rationales for the coupling observed between the C^{α}–F atoms in compounds **1** and **2a**. One is a thermodynamically favorable H-bonding interaction between the aromatic hydrogen and the fluorine atoms. Similar interactions have been proposed before.[18–20] However, we believe that the coupling is really a consequence of crowding within the bay area that contains the BF_2 entity in these molecules. Whatever the origin of these effects, it's clear from the data presented here that they can be used as a tool to access molecular structure.

We thank Ben Lane for running the ^{11}B NMR spectra for this study, and Steve Silber for assistance with the decoupled NMR spectra. Financial support for this work was provided by the NIH (HG01745) and The Robert A. Welch Foundation.

Notes and references

‡ *Crystal data* for **1a**: $C_{34}H_{28}BCl_2F_2IN_2O_2$, M = 743.19, a = 17.646(3), b = 11.457(3), c = 15.829(4) Å, β = 104.90(2)°, U = 3093(1) A^3, T = 193(2) K, space group $P2_1/c$ (No. 14), Z = 4, μ(Mo-Ka) = 1.256 mm^{-1}, 5576 absorption correct reflections measured, 5538 unique (*R*int = 0.0419) which were used in calculations. The final *R*(F) and *wR*(F^2) were 0.0880 and 0.1749 respectively (all data). CH_2Cl_2 was modeled as disordered. CCDC 182/1472.

1 R. H. Contreras, C. G. Giribet, M. A. Natiello, J. Pérez, I. D. Rae and J. A. Weigold, *Aust. J. Chem.*, 1985, **38**, 1779.
2 L. C. Hsee and D. J. Sardella, *Magn. Reson. Chem.*, 1990, **28**, 688.
3 L. Shimoni, H. L. Carrell, J. P. Glusker and M. M. Coombs, *J. Am. Chem. Soc.*, 1994, **116**, 8162.
4 P. Szczecinski and J. Zachara, *J. Organomet. Chem.*, 1993, **447**, 241.
5 T. Miyake and Y. Koyama, *Carbohydr. Res.*, 1994, **258**, 11.
6 K. Matsubara, A. Oba and Y. Usui, *Magn. Reson. Chem.*, 1998, **36**, 761.
7 A preparation of **3** was reported in ref. 8 and syntheses of **1** and **2** will be reported elsewhere.
8 L. H. Thoresen, H. Kim, M. B. Welch, A. Burghart and K. Burgess, *Synlett*, 1998, 1276.
9 H. Kim, A. Burghart, M. B. Welch, J. Reibenspies and K. Burgess, *Chem. Commun.*, 1999, 1889.
10 F. B. Mallory and C. W. Mallory, *Coupling Through Space in Organic Chemistry*, in *Encyclopedia of Nuclear Magnetic Resonance*, Wiley, New York, 1996.
11 A. E. Derome, *Modern NMR Techniques for Chemistry Research*, Permagon, Oxford, 1987.
12 A. Bondi, *Phys. Chem.*, 1964, **68**, 441.
13 A. K. Rappe, C. J. Casewit, K. S. Colwell, W. A. Goddard-III and W. M. Skiff, *J. Am. Chem. Soc.*, 1992, **114**, 10 024.
14 L. A. Castonguay and A. K. Rappe, *J. Am. Chem. Soc.*, 1992, **114**, 5832.
15 A. K. Rappe, K. S. Colwell and C. J. Casewit, *Inorg. Chem.*, 1993, **32**, 3438.
16 M. J. S. Dewar, E. G. Zoebisch, E. F. Healy and J. J. P. Stewart, *J. Am. Chem. Soc.*, 1985, **107**, 3902.
17 M. J. S. Dewar, C. Jie and E. G. Zoebisch, *Organometallics*, 1988, **7**, 513.
18 E. J. Corey, J. J. Rohde, A. Fischer and M. D. Azimioara, *Tetrahedron Lett.*, 1997, **38**, 33.
19 T. Steiner, *Chem. Commun.*, 1997, 727.
20 A. Mele, B. Vergani, F. Viani, S. V. Meille, A. Farina and P. Bravo, *Eur. J. Org. Chem.*, 1999, 187.
21 F. H. Allen and O. Kennard, *Chem. Des. Automat. News*, 1993, **8**, 31.

Communication 9/07559C

ChemComm

One step synthesis of [7]metacyclophanediyne complexes from bis(propargyldicobalt) dication equivalents

Richard Guo and James R. Green*

Chemistry and Biochemistry, School of Physical Sciences, University of Windsor, Windsor, Ontario, Canada N9B 3P4. E-mail: jgreen@uwindsor.ca

Received (in Covallis, OR, USA) 1st October 1999, Accepted 4th November 1999

The $BF_3{\cdot}OEt_2$ mediated addition reactions of electron-rich arenes to 1,3-dialkoxyhepta-2,5-diyne(dodecacarbonyl)-tetracobalt complex 1 directly afford [7]metacyclophanediyne(dodecacarbonyl)tetracobalt complexes.

The chemistry of small cyclophanes has been the focus of much attention, due to their structural and electronic properties, and their ability to include either metal ions or neutral or charged organic molecules.[1–3] Syntheses of these classes of compounds, however, are rarely straightforward. Access to the smaller [*n*]metacyclophanes ($n \leqslant 8$), for example, is most often accomplished by rearrangement of propellanes or spirocycloalkadienones, intramolecular Diels–Alder reactions of dienynes, or extrusion reactions of sulfoxides.[1,2] Direct intermolecular cycloaddition approaches towards these systems have not been efficient ones.[4]

The use of hexacarbonyldicobalt alkyne complexes has become important in organic synthesis.[5–7] Among the noteworthy features of these complexes is their ability to serve as protected versions of alkynes that would be severely or prohibitively strained.[8] This property has seen application as a tactic in the chemistry of cyclohexynes and cycloheptynes,[9] Bergman cyclization precursors,[10] and other polyacetylenic macrocycles.[11]

We have begun a program on the investigation of the chemistry of dodecacarbonyltetracobalt complexes of hepta-2,5-diynyl 1,7-diethers **1** and closely related compounds as latent 1,4-diynes, dienes, or enynes, based on the known ability of hexacarbonyldicobalt complexes of propargyl alcohols and their derivatives to form cations readily.[5] The diether complex **1** underwent ready reaction with electron-rich arenes in the presence of $BF_3{\cdot}OEt_2$, but did not stop cleanly at the monoarylation products. When **1** was subjected to equimolar amounts of $BF_3{\cdot}OEt_2$ and 1,3,5-trimethoxybenzene at 0 °C (at 10^{-2} M each in CH_2Cl_2), only a 24% yield of **2** could be isolated. The predominant product (26%) proved to be [7]metacyclophanediyne complex **3a**, stemming from two substitution reactions by trimethoxybenzene on **1**. The yields of **3a** realized could be improved considerably by increasing the amounts of both $BF_3{\cdot}OEt_2$ and trimethoxybenzene to 2 equiv; **3a** was then obtained in 92% yield after 5 h at 0 °C.†

Other electron-rich benzenes also gave [7]metacyclophanediyne complexes under analogous conditions (Table 1). 1,2,3-Trimethoxybenzene gave **3b** in a more modest yield (34%), while 1,3-dimethoxybenzene gave two separable cyclophanes, **3c** and **3d**, in 78% combined yield (63% **3c** + 15% **3d**). Among heterocycles tested, furan gave [7](2,5)furanocyclophane complex **3e** in 30% yield. Pyrrole, unlike the other electron rich arenes, afforded monocondensation product **4** as the only tractable product in 51% yield. Subsequent addition of **4** to excess $BF_3{\cdot}OEt_2$ (4 equiv.) at 0 °C in CH_2Cl_2 (24 h, 10^{-2}M) then gave [7](2,5)pyrrolophane **3f** in 40% yield. Thiophene proved insufficiently reactive to give any condensation product with **1**. Conducting the reactions at lower concentration (10^{-3} M) increased the necessary reaction time considerably (3 d at 0 °C), but gave some improvement in the yields of **3c** (68% **3c** + 15% **3d**) and **3e** (43%). The yield of **3b** was actually inferior (19%) at the lower concentration.

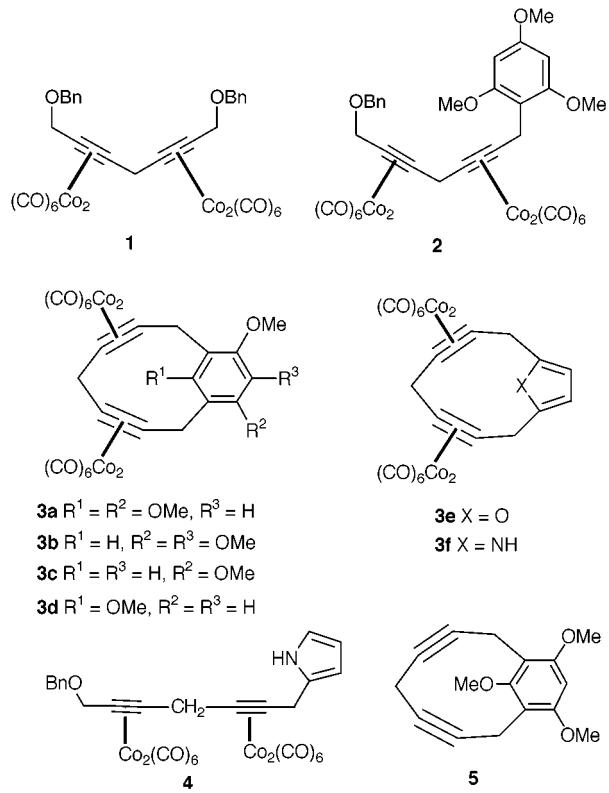

The ^{1}H NMR spectra of these [7]metacyclophanediyne complexes possessed characteristics that fell into two distinctly different groups. Those which contained a methoxy function between the two termini of the bridge (**3a** and **3d**) revealed highly diastereotopic methylene groups; the bispropargylic methylene function of **3a**, for example, gave resonances at δ 4.99 and 4.31, whereas the benzylic methylene function gave resonances at δ 4.34 and 4.09. The other cyclophanediyne complexes (**3b**, **3c**, **3e**, **3f**) showed methylene groups whose protons were isochronous.

The number of alkyne containing cyclophanes is relatively modest,[11,12] and dominated by cases where the alkyne function serves simply as a spacer,[13] but there is much interest in the demonstrated coordinating ability of the alkyne function of

Table 1 Additions between diyne complexes **1** or **4** with arenes

Diyne	Nucleophile	Product (% yield)
1	1,3,5-trimethoxybenzene	**3a** (92)
1	1,2,3-trimethoxybenzene	**3b** (34)
1	1,3-dimethoxybenzene[a]	**3c** (68)
		3d (15)
1	Furan[a]	**3e** (43)
1	Pyrrole	**4** (51)
4	—	**3f** (40)

[a] Conducted at [**1**] = 10^{-3} M.

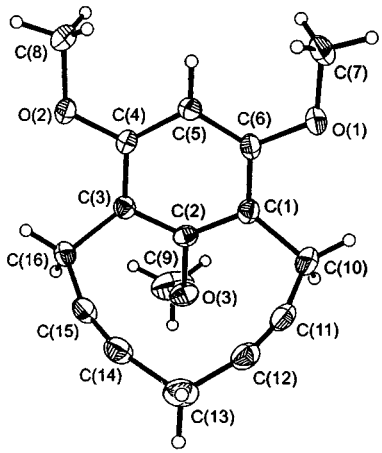

Fig. 1 ORTEP drawing of **5** (30% probability). H atoms not shown. Selected bond lengths (Å) and angles (°): C(1)–C(2) 1.398(3), C(14)–C(15) 1.186(3), C(13)–C(14)–C(15) 164.0(2), C(14)–C(15)–C(16) 162.9(2), C(12)–C(14) 106.1(2), C(2)–C(3)–C(16) 117.2(2).

cyclic polyynes.[14] As a result, we deemed it of interest to determine whether or not decomplexation of **3** could be accomplished. In fact, attempted removal of the hexacarbonyldicobalt units from **3a** by the usual reagents [Me_3NO, $(NH_4)_2Ce(NO_3)_6$, $CuCl_2$, $FeCl_3$] resulted in complete destruction of the cyclophanediyne unit. On the other hand, stirring complex **3a** in a pyridine–Et_2O solvent mixture (1:1, in air) over a 10 d period resulted in the formation of **5** in 56% yield. The ^{1}H NMR spectrum of **5** also showed the presence of diastereotopic methylene groups; the resonances for the benzylic hydrogen atoms appeared at δ 3.48 and 3.41, while the bispropargylic hydrogen atoms gave resonances at δ 2.92 and 2.61. Compound **5** gave crystals suitable for X-ray diffraction, which revealed the structure represented in Fig. 1.‡ It is apparent that there is strain in this molecule, which is reflected in several ways. Among the most notable of these are the bond angles at the alkynyl carbon atoms, which have been bent to 164 (at C-11 and C-15) and 163° (at C-12 and C-14). The arene ring also shows these effects, as the benzylic carbon atoms are pulled out of the plane of the C-1, C-3, C-4, C-6 arene ring carbons by 32.9° (β), and the benzene ring itself deviates slightly from planar at both C-2 (α = 11.2°) and at C-5 (γ = 5.5°) (Fig. 2). Nevertheless, compound **5** has good thermal stability. The structural data also suggest strongly that the diastereotopic methylene groups in **3a**, **3d** and **5** are consequences of the ring inversion represented in Fig. 2 at the slow exchange limit (Fig. 2, shown for **5**). The singlets observed for **3b**, **3c**, **3e** and **3f** stem from molecules at the fast exchange limit of the analogous inversion process.[15]

The [7]metacyclophanediyne **5** is the smallest [*n*]metacyclophane containing a triple bond reported to date. Nevertheless, a small number of reported metacyclophanes have larger deformation angles (α, β, γ),[16] and a number alkynes with smaller bond angles also exist.[17] These data suggest that smaller alkyne containing [*n*]metacyclophanes may be accessible.

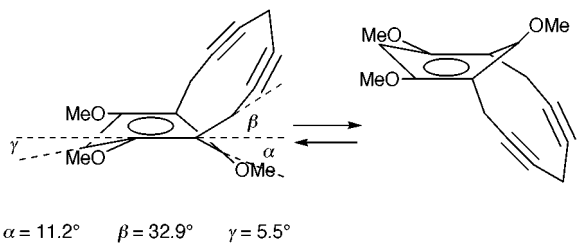

Fig. 2 Distortion angles and fluxional process for **5**.

We are grateful to NSERC (Canada) for support of this research. We wish to thank Professor Doug Stephan and Professor Stephen Loeb (WINMOL) for the crystallographic structural work on **5**.

Notes and references

† The use of the theoretically required 1 equiv. of 1,3,5-trimethoxybenzene with 2 equiv. of BF_3-OEt_2 afforded **3a** in 86% yield.

‡ *Crystal data* for **5**: $C_{16}H_{16}O_3$, with Mo-Kα radiation, M = 256.30, triclinic, a = 7.836(3), b = 7.925(4), c = 11.378(7) Å, α = 101.66(4), β = 98.03(3), γ = 95.35(5)°, U = 679.8(6) Å^3, T = 293 K, space group P1, Z = 2, D_c = 1.252 Mg m^{-3}, μ = 0.086 mm^{-1}, θ range 1.85–25.0°. GOF on F^2 1.003 for 2338 unique observed data on 172 parameters, R_1 = 0.0476, wR_2 = 0.1355. CCDC 182/1476. See http://www.rsc.org/suppdata/cc/1999/2503/ for crystallographic data in .cif format.

1 *Cyclophanes*, ed. P. M. Klein and S. M. Rosen, Academic Press, New York, 1983, vol. 1 and 2; F. Diederich, *Cyclophanes*, Royal Society of Chemistry, Cambridge, 1991.
2 V. V. Kane, W. H. de Wolf and F. Bickelhaupt, *Tetrahedron*, 1994, **50**, 4575; Y. Tobe, *Top. Curr. Chem.*, 1994, **172**, 1.
3 J. Schulz and F. Vögtle, *Top. Curr. Chem.*, 1994, **172**, 41.
4 For an exception in [8]paracyclophane chemistry, see T. Tsuji, T. Shibata, Y. Hienuki and S. Nishida, *J. Am. Chem. Soc.*, 1978, **100**, 1806.
5 M. J. Went, *Adv. Organomet. Chem.*, 1997, **41**, 69
6 A. J. M.Caffyn and K. M. Nicholas, in *Comprehensive Organometallic Chemistry II*, ed. E. W. Abel, F. G. A. Stone and G. Wilkinson, vol. ed. L. S. Hegedus, Pergamon, Oxford, 1995, vol. 12, ch. 7.1; K. M. Nicholas, *Acc. Chem. Res.*, 1987, **20**, 207.
7 N. E. Schore, in *Comprehensive Organometallic Chemistry II*, ed. E. W. Abel, F. G. A. Stone and G. Wilkinson, vol. ed. L. S. Hegedus, Pergamon, Oxford, 1995, vol. 12, ch. 7.2; N. E. Schore, *Org. React.*, 1991, **40**, 1. N. E. Schore, in *Comprehensive Organic Synthesis*, ed. B. M. Trost, vol. ed. L. A. Paquette, Pergamon, Oxford, 1991, vol. 5, ch. 9.1; N. E. Schore, *Chem. Rev.*, 1988, **88**, 1081.
8 W. M. Jones and J. Klosin, *Adv. Organomet. Chem.*, 1998, **42**, 147.
9 M. M. Patel and J. R. Green, *Chem. Commun.*, 1999, 509; S. L. Schreiber, M. T. Klimas and T. Sammakia, *J. Am. Chem. Soc.*, 1986, **108**, 3128; T. Nakamura, T. Matsui, K. Tanino and I. Kuwajima, *J. Org. Chem.*, 1997, **62**, 3032; N. E. Schore and S. D. Najdi, *J. Org. Chem.*, 1987, **52**, 5296; C. Yenjai and M. Isobe, *Tetrahedron*, 1998, **54**, 2509 and references therein; N. Iwasawa and H. Satoh, *J. Am. Chem. Soc.*, 1999, **121**, 7951.
10 P. Magnus, *Tetrahedron*, 1994, **50**, 1397; M. E. Maier, *Synlett*, 1995, 13; J. W. Grissom, G. U. Gunawardena, D. Klingberg and D. Huang, *Tetrahedron*, 1996, **52**, 6453.
11 M. M. Haley and B. L. Langsdorf, *Chem. Commun.*, 1997, 1121.
12 G. J. Bodwell, T. J. Houghton and D. Miller, *Tetrahedron Lett.*, 1998, **39**, 2231; T. Kawase, N. Ueda and M. Oda, *Tetrahedron Lett.*, 1997, **38**, 6681 and references therein; H. Ueda, C. Katayama and J. Tanaka, *Bull. Chem. Soc. Jpn.*, 1981, **54**, 891 and references therein; H. Hopf, P. G. Jones, P. Bubenitschek and C. Werner, *Angew. Chem.*, 1995, **107**, 2592, *Angew. Chem., Int. Ed. Engl.*, 1995, **34**, 2367.
13 D. O'Krongly, S. R. Denmeade, M. Y. Chang and R. Breslow, *J. Am. Chem. Soc.*, 1985, **107**, 5544.
14 T. Nishinaga, T. Kawamura and K. Komatsu, *Chem. Commun.*, 1998, 2263; J. D. Ferrara, A. Djebli, C. Tessier-Youngs and W. J. Youngs, *J. Am. Chem. Soc.*, 1988, **110**, 647; D. Solooki, J. D. Bradshaw, C. A. Tessier and W. J. Youngs, *Organometallics*, 1994, **13**, 451; D. Zhang, D. B. McConville, J. M. Hrabusa III, C. A. Tessier and W. J. Youngs, *J. Am. Chem. Soc.*, 1998, **120**, 3506.
15 For a discussion of conformational properties of cyclophanes, see R. H. Mitchell, in *Cyclophanes*, ed. P. M. Klein and S. M. Rosen, Academic Press, New York, 1983, vol. 1, ch. 4.
16 J. L. Pierre, P. Baret, P. Chautemps and M. Armand, *J. Am. Chem. Soc.*, 1981, **103**, 2986.
17 A. Krebs and J. Wilke, *Top. Curr. Chem.*, 1983, **109**, 189; H. Meier, *Adv. Strain Org. Chem.*, 1991, **1**, 215.

Communication 9/07991B

ChemComm

Unusual formation of a hex-3-ene-1,5-diyne-3-yl ligand from a buta-1,3-diyne in the $Cp^*_2TiCl_2$–Mg system

Paul-Michael Pellny,[a] Frank G. Kirchbauer,[a] Vladimir V. Burlakov,[a] Anke Spannenberg,[a] Karel Mach[b] and Uwe Rosenthal*[a]

[a] *Institut für Organische Katalyseforschung an der Universität Rostock, Buchbinderstr. 5 - 6, D-18055 Rostock, Germany. E-mail: Uwe.Rosenthal@ifok.uni-rostock.de*

[b] *J. Heyrovský Institute of Physical Chemistry, Academy of Sciences of the Czech Republic, Dolejškova 3, 182 23 Prague 8, Czech Republic*

Received (in Cambridge, UK) 20th August 1999, Accepted 10th November 1999

The reaction of $[Cp^*_2TiCl_2]$ with equimolar amounts of magnesium in the presence of $Me_3SiC{\equiv}C–C{\equiv}CSiMe_3$ yields the first early transition metal η^3-enyne complex $[Cp^*_2Ti\{\eta^3\text{-}Me_3SiC_3{=}C(C{\equiv}CSiMe_3)SiMe_3\}]$ 1 which is suggested to be an intermediate in early transition metal catalysed oligomerization reactions of alk-1-ynes.

Some years ago we found that $Me_3SiC{\equiv}C–C{\equiv}CSiMe_3$ is cleaved[1a] by the $[Cp_2TiCl_2]$–Mg system in THF to give the dimeric titanium(III) complex $[\{Cp_2Ti(C{\equiv}CSiMe_3)\}_2]$,[1] and, that in the presence of the $[Cp^*_2TiCl_2]$–Mg system with an excess of Mg, the paramagnetic $[\{Cp^*_2Ti(C{\equiv}CSiMe_3)_2\}\{MgCl(THF)\}]$ tweezer-type compound was obtained.[2a] We have also described that when the diacetylide $[Cp^*_2Ti(C{\equiv}CSiMe_3)_2]$ is irradiated by UV light it undergoes the reverse reaction, with a coupling of the acetylides to give the titanacyclopropene complex $[Cp^*_2Ti(\eta^2\text{-}Me_3SiC_2–C{\equiv}CSiMe_3)]$.[3a] This complex also forms from the above mentioned reduction of $[Cp^*_2TiCl_2]$ in the presence of $Me_3SiC{\equiv}C–C{\equiv}CSiMe_3$ with an equimolar amount of Mg.[3b]

Here, we report the synthesis and the structure of the paramagnetic d^1 complex $[Cp^*_2Ti\{\eta^3\text{-}Me_3SiC_3{=}C(C{\equiv}CSiMe_3)SiMe_3\}]$ **1** which arises from the $[Cp^*_2TiCl_2]$–Mg–$Me_3SiC{\equiv}C–C{\equiv}CSiMe_3$ system using the molar ratios indicated in eqn. (1).

(1)

1

Compound **1** is thus the third product, in addition to the above-mentioned titanacyclopropene and the tweezer complex, which has been obtained from this system under different stoichiometric conditions. The structure of the paramagnetic complex **1** was verified by elemental analysis, EPR, IR‡ and crystallography.

An X-ray crystal structure analysis of **1**§ (Fig. 1) revealed that a bent permethyltitanocene binds an unusual carbyl, 1,4,6-tris-(trimethylsilyl)hex-3-ene-1,5-diyne-3-yl, in an η^3-mode. The Ti–C2, Ti–C3 and C2–C3 distances are consistent with a η^2-bonded triple bond and the Ti–C1 distance with a Ti–C σ bond. The alkenyl double bond is slightly elongated and the remote triple bond does not differ from the analogous bond in $[Cp^*_2Ti(\eta^2\text{-}Me_3SiC_2–C{\equiv}CSiMe_3)]$.[3a] The entire ligand moiety is nearly planar with the sums of the valence angles around the atoms C1 and C18 both being 360° and the silylalkynyl group is almost linear. The bite angle Cp1–Ti–Cp2 of nearly 140° (Cp = centroid of cyclopentadienyl ring) and the dihedral angle between the least-squares planes of the cyclopentadienyl rings of *ca*. 41° do not indicate a significant steric hindrance imposed by the hex-3-ene-1,5-diyne-3-yl ligand.

The solution EPR spectrum of **1** consists of a single line at $g = 1.991$ ($\Delta H = 1.7$ G). The absence of low-intensity satellites due to the interaction of d^1 electron with ^{49}Ti and ^{47}Ti isotopes (I_N = 7/2 and 5/2, respectively) indicates that the unpaired electron is largely delocalized over the hex-3-ene-1,5-diyne-3-yl ligand. EPR measurements of the reacting mixtures showed the following succession of formed paramagnetic species: $[Cp^*_2TiCl]$, $[\{Cp^*_2Ti(C{\equiv}CSiMe_3)_2\}\{MgCl(THF)\}]$ and **1**.

Similar 1,4-substituted η^3-butenyne ligands coordinated to transition metals are known for *e.g.* Ru,[4a–d] Os,[4e] W[4f] and Fe,[4g,h] and their molecular parameters are essentially similar to those of the hex-3-ene-1,5-diyne-3-yl ligand in **1**. However, none of the known η^3-butenyne complexes is paramagnetic. Thus, compound **1** is the first early transition metal η^3-enyne complex and also the first paramagnetic complex of this type. While the above η^3-butenyne complexes are in many cases suggested to be intermediates in the catalysed dimerisations of alk-1-ynes, in early transition metal-based systems such intermediates like **1** have not yet been observed.[2b,5] Additionally, no such complex has been formed previously by cleavage of the central C–C single bond in a 1,3-butadiyne unit and coupling of the formed acetylide fragment with another buta-1,3-diyne.

The mechanism for the formation of complex **1** is yet not clear. On the basis of the starting materials $\{[Cp^*_2TiCl_2]$, Mg, $Me_3SiC{\equiv}C–C{\equiv}CSiMe_3\}$, the intermediacy of $[Cp^*_2TiCl]$ and

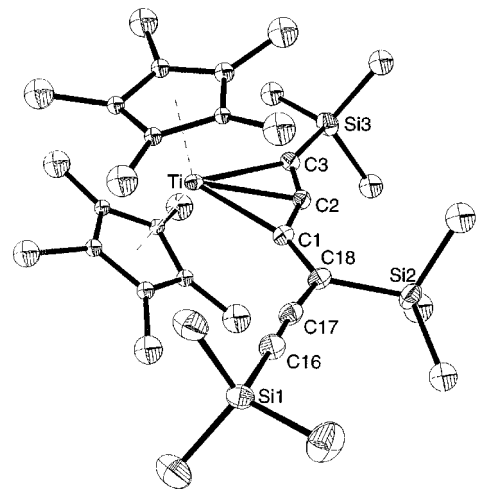

Fig. 1 Crystal structure of **1** with 30% probability level thermal ellipsoids. Hydrogen atoms and disordered groups are omitted for clarity. Selected bond lengths (Å) and angles (°): Ti–C2 2.302(4), Ti–C3 2.471(4), C2–C3 1.250(5), Ti–Cl 2.234(4), C1–C2 1.386(5), C1–C18 1.362(5), C16–C17 1.211(5), C17–C18 1.429(5); Si1–C16–C17 177.3(4), C16–C17–C18 173.2(4).

isolated products of this system {[{$Cp^*_2Ti(C{\equiv}CSiMe_3)_2$}{MgCl(THF)}], [$Cp^*_2Ti(\eta^2\text{-}Me_3SiC_2{-}C{\equiv}CSiMe_3)$] as well as other compounds which can reasonably be expected in the reaction mixture {*e.g.* [$Cp^*_2Ti(C{\equiv}CSiMe_3)_2$], [$Cp^*_2Ti(C{\equiv}CSiMe_3)$] and [$Mg(C{\equiv}CSiMe_3)Cl(THF)_n$] a variety of reaction pathways are possible.

In analogous zirconocene chemistry, Negishi and coworkers showed that [Cp_2ZrCl_2] reacts with 3 equiv. of the acetylides LiC≡CR to yield, after hydrolysis, the enynes RCH=CH–C≡CR.[6] The mechanism of their formation suggested the presence of the 'ate' intermediates [{$Cp_2Zr(C{\equiv}CR)_3$}Li] and [{$Cp_2Zr(C{\equiv}CR)(\eta^2\text{-}RC_2{-}C{\equiv}CR)$}Li] which, however, were not isolated. Very recently this mechanism has been supported by Choukroun and Cassoux who succeeded in isolating and determining the crystal structure of the 'ate' complex [{$Cp_2Zr(C{\equiv}CPh)(\eta^2\text{-}PhC_2{-}C{\equiv}CPh)$}Li], generated from the reaction of [Cp_2ZrCl_2] with 3 equiv. of LiC≡CR.[7]

By taking into account these results one could assume that the isolated products, the titanacyclopropene [$Cp^*_2Ti(\eta^2\text{-}Me_3SiC_2{-}C{\equiv}CSiMe_3)$][3] or, alternatively, the tweezer compound [{$Cp^*_2Ti(C{\equiv}CSiMe_3)_2$}{MgCl(THF)}],[2] react with [$Cp^*_2Ti{-}C{\equiv}CSiMe_3$] or [$ClMg{-}C{\equiv}CSiMe_3$], resulting in the 'ate' complex [$Cp^*_2Ti(C{\equiv}CSiMe_3)(\eta^2\text{-}Me_3SiC_2{-}C{\equiv}CSiMe_3)]^-[Y]^+$ {$[Y]^+ = [Cp^*_2Ti]^+$ or $[MgCl]^+$}, both being similar to what has been discussed by Negishi and coworkers as non-isolable intermediates and to species which have recently been characterized by Choukroun and Cassoux. Since titanium is much less electropositive than zirconium and provides a considerably smaller coordination sphere, the diyne is inserted into the Ti–C acetylide bond (inter- or intra-molecularly) and complex **1** is formed.

Notes and references

† *General procedure* for the preparation of **1**: a suspension of [$Cp^*_2TiCl_2$] (792 mg, 2.04 mmol), Mg (48 mg, 1.97 mmol) and bis(trimethylsilyl)buta-1,3-diyne (593 mg, 3.05 mmol) in thf (10 mL) was stirred under argon for 5 days at 60 °C. The solution changed to dark-brown and all magnesium was dissolved. After filtration and standing at −78 °C for one day brown crystals formed which were separated and dried in vacuum to give 560 mg (46%) of **1**: mp 202–203 °C (decomp.). *m/z* 610 (M^+).

‡ *Spectral data* for **1**: EPR (THF, 220 °C): g = 1.991, ΔH = 1.7 G; IR(Nujol)/cm^{-1}: 2109 ν(C≡C) (uncoordinated triple bond), 1868 cm^{-1} ν(C≡C) (coordinated triple bond). Anal. $C_{35}H_{57}Si_3Ti$ (M = 610.0): calc.: C, 68.92; H, 9.42. Found: C, 68.71; H, 9.32%.

§ *X-Ray structure analysis* of **1**: STOE-IPDS diffractometer, graphite monochromated Mo-Kα radiation, solution of structures by direct methods (SHELXS-86: G. M. Sheldrick, *Acta. Crystallogr., Sect. A*, 1990, **46**, 467), refinement with full-matrix least-square techniques against F^2 (SHELXL-93: G. M. Sheldrick, University of Göttingen, Germany, 1993), triclinic, space group $P\bar{1}$; a = 10.034(2), b = 11.487(2), c = 16.326(3) Å, α = 98.92(3), β = 92.62(3), γ = 90.55(3)°, V = 1856.8(6) $Å^3$, Z = 2, D_c = 1.091 g cm^{-3}; 5556 reflections measured, 5556 were independent of symmetry and 4084 were observed [$I > 2\sigma(I)$], R = 0.060, wR^2 (all data) = 0.161, 326 parameters. All atoms of the Cp* groups and the methyl groups at Si2 and Si3 are disordered. The atoms of the disordered fragments were refined isotropically. All other non-hydrogen atoms were refined anisotropically. Hydrogen atoms were inserted in calculated positions and refined riding with the corresponding atom. CCDC 182/1480. See http://www.rsc.org.suppdata/cc/1999/2505/ for crystallographic data in .cif format.

1 (*a*) U. Rosenthal and H. Görls, *J. Organomet. Chem.*, 1992, **439**, C36; (*b*) G. L. Wood, C. B. Knobler and M. F. Hawthorne, *Inorg. Chem.*, 1989, **28**, 382.

2 (*a*) S. I. Troyanov, V. Varga and K. Mach, *Organometallics*, 1993, **12**, 2820; (*b*) V. Varga, L. Petrusová, J. Cejka and K. Mach, *J. Organomet. Chem.*, 1997, **53**2, 251.

3 (*a*) F. G. Kirchbauer, Ph.D. Thesis, University of Rostock, 1999; (*b*) P.-M. Pellny, F. G. Kirchbauer, V. V. Burlakov, W. Baumann, A. Spannenberg and U. Rosenthal, *J. Am. Chem. Soc.*, 1999, **121**, 8313.

4 (*a*) C. Bianchini, P. Innocenti, M. Peruzzini, A. Romerosa and F. Zanobini, *Organometallics*, 1996, **15**, 272; (*b*) C. Bianchini, M. Peruzzini, F. Zanobini, P. Frediani and A. Albinati, *J. Am. Chem. Soc.*, 1991, **113**, 5453; (*c*) G. Jia, A. L. Rheingold and D. W. Meek, *Organometallics*, 1989, **8**, 1379; (*d*) D. C. Liles and P. F. M. Verhoeven, *J. Organomet. Chem.*, 1996, **522**, 33; (*e*) J. Gotzig, H. Otto and H. Werner, *J. Organomet. Chem.*, 1985, **287**, 247; (*f*) A. K. McMullen, J. P. Selegue and J.-G. Wang, *Organometallics*, 1991, **10**, 3421; (*g*) M. Akita, S. Sugimoto, M. Terada and Y. Moro-oka, *J. Organomet. Chem.*, 1993, **447**, 103; (*h*) D. L. Hughes, M. Jimenez-Tenorio, G. J. Leigh and A. T. Rowley, *J. Chem. Soc., Dalton Trans.*, 1993, 3151 and references therein.

5 (*a*) M. Horáček, I. Císařová, J. Čejka, J. Karban, L. Petrusová, and K. Mach, *J. Organomet. Chem.*, 1999, **577**, 103; (*b*) H. Akita, H. Yasuda and A. Nakamura, *Bull. Chem. Soc. Jpn.*, 1984, **57**, 480; (*c*) A. D. Horton, *J. Chem. Soc., Chem. Commun.*, 1992, 185; (*d*) M. Yoshida and R. F. Jordan, *Organometallics*, 1997, **16**, 4508; (*e*) V. Varga, L. Petrusová, J. Čejka, V. Hanuš and K. Mach, *J. Organomet. Chem.*, 1996, **509**, 235; (*f*) P. Štěpnička, R. Gyepes, I. Císařová, M. Horáček, J. Kubišta and K. Mach, *Organometallics*, 1999, **18**, 4869.

6 K. Takagi, C. J. Rousset and E. Negishi, *J. Am. Chem. Soc.*, 1991, **113**, 1440.

7 R. Choukroun and P. Cassoux, *Acc. Chem. Res.*, 1999, **32**, 494.

Commnication 9/06777I

A remarkably stable copper(I) ethylene complex: synthesis, spectroscopy and structure

Bernd F. Straub, Frank Eisenträger and Peter Hofmann*

Organisch-Chemisches Institut der Universität Heidelberg, Im Neuenheimer Feld 270, D-69120 Heidelberg, Germany. E-mail: ph@phindigo.oci.uni-heidelberg.de

Received (in Basel, Switzerland) 29th September 1999, Accepted 9th November 1999

The novel copper(I) ethylene complex [$Bu^t_2P(NSiMe_3)_2$-κ^2N]Cu(η^2-C_2H_4) and its norbornene analogue have been synthesized and characterized and their solid state structures determined.

Copper(I) olefin complexes play an important role in biochemistry and modern organic chemistry. Copper-catalyzed addition of carbanions to α,β-unsaturated carbonyls and copper-catalyzed cyclopropanation of alkenes by α-carbonyl diazoalkanes involve copper olefin complexes as catalytically active species or resting states.[1–4] Ethylene, the smallest plant hormone, binds tightly to the copper receptor site ETR 1,[5,6] participating in a variety of stress responses and developmental processes.[7] Thompson *et al.* synthesized and characterized the first stable copper(I) ethylene complex, [HB(3,5-Me_2-1,2-$HC_3N_2)_3$-κ^3N]Cu(η^2-C_2H_4), in 1983.[8] Nevertheless, the stability of the ethylene/receptor complex is much higher than that of any reported artificial copper ethylene complex.[5,6,9]

Owing to the notorious lability of ethylene coordination in known copper(I) complexes, only one extrapolated ^{13}C NMR chemical shift relative to free ethylene ($\Delta\delta$ = 31.1)[10] and no $^1J_{CH}$ coupling constant for copper(I) coordinated ethylene could be determined. Obviously, such data are highly relevant for an understanding of the copper(I)–ethylene bond.

Here, we report a remarkably stable copper(I) ethylene complex **1**, which is easily accessible by utilizing a tailor-made sterically demanding and electron-rich iminophosphanamide, first described by Scherer and Schieder more than 30 years ago,[11] as a co-ligand, generated by *in situ* deprotonation (Scheme 1).[12]

The stability of **1** in the solid state and in solution is unprecedented. Colorless crystals of **1** can be dried at 10^{-3} mbar at ambient temperature without decomposition. Complex **1** melts at 108 °C to a colorless liquid which only slowly decomposes at that temperature. Protonated **1** could be observed in the gas phase (CI + MS, 2-methylpropane). No free ethylene is detected by ^1H NMR spectroscopy upon dissolving **1** in C_6D_6, $CDCl_3$ or toluene-d_8 in an argon atmosphere. The presence of additional ethylene leads to separate broad signals of free and of coordinated C_2H_4, indicating associative olefin exchange.

The C–C distance of ethylene in **1** is 1.362(6) Å, which does not differ significantly from the corresponding distance in free ethylene [1.3369(16) Å].[13] The sp^2-character of the C_2H_4 carbons is in accordance with a $^1J_{CH}$ coupling constant of 158 Hz, which is even larger than in free ethylene (156 Hz).[14]

The ^1H NMR resonance of the ethylene protons at δ 3.48 (C_6D_6, 298 K; for free ethylene δ 5.24 under the same conditions) is shifted by 0.5 ppm to higher field than the most upfield copper(I) ethylene signal (δ 4.0) reported so far.[15] The ^{13}C NMR signal is detected at δ 73.0 with an upfield shift of 50 ppm compared to free ethylene. Lower temperatures and aromatic solvents lead to an upfield shift of the ethylene protons (δ 3.35, toluene-d_8, 233 K; δ 3.63, $CDCl_3$, 223 K).

The norbornene complex [$Bu^t_2P(NSiMe_3)_2$-κ^2N]Cu(η^2-C_7H_{10}) **2** could be obtained in a similar way.† Its solid state geometry, structurally analogous to **1**, is shown in Fig. 2.

Unlike **1**, complex **2** allows determination of the rotational barrier of the olefin ligand as $\Delta G^{\ddagger}$ = 41.5 ± 2.0 kJ mol^{-1} (VT $^{13}C\{^1H\}$NMR) through coalescence of the signals of both the diastereotopic $C(CH_3)_3$ and $C(CH_3)_3$ carbons.

The high basicity of the anionic iminophosphanamide σ- and π-donor ligand and the small bite angle N–Cu–N of 77.80(9)° in the four-membered neutral chelate ring system seem to be responsible for the unprecedented stability and unusual spectral properties of **1**. The high HOMO and the low LUMO energy of a d^{10}-ML_2 fragment with a small bite angle[16] lead to increased π-back bonding towards the olefin and a strong olefin-to-metal dative bond, thus causing an increased ethylene ligand dissociation energy compared to other neutral and, even more so, cationic copper(I) units. Formation of stable dinuclear olefin-free copper(I) complexes with nearly linear N–Cu–N fragments and concomitant weak d^{10}–d^{10} interaction as known from other systems[8] is hampered by the sterically demanding iminophosphanimide ligand system with its $SiMe_3$ groups bent towards the olefin side (P–N–Si ≈ 150°).

Complex **1** catalyzes cyclopropanation of styrene with α-carbonyl diazoalkanes at room temperature. The extremely high

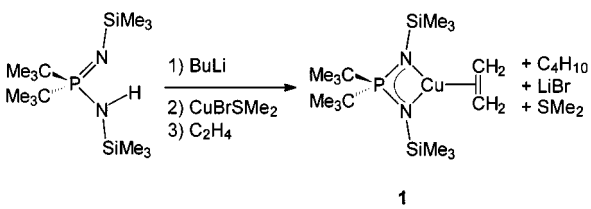

1

Scheme 1 Synthesis of **1**†

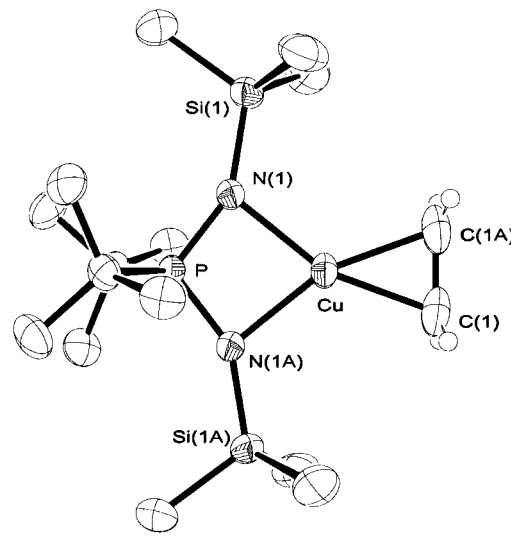

Fig. 1 ORTEP diagram of the solid state structure of **1**.‡ Hydrogen atoms of the methyl groups are omitted for clarity. Selected bond lengths (Å) and angles (°): P–N(1) 1.6013(16), Si(1)–N(1) 1.7055(17), Cu–N(1) 2.0140(16), Cu–C(1) 1.987(3), C(1)–C(1A) 1.362(6); P–N(1)–Si(1) 151.35(11), N(1)–P–N(1A) 104.33(12), P–N(1)–Cu 88.93(8), N(1)–Cu–N(1A) 77.80(9).

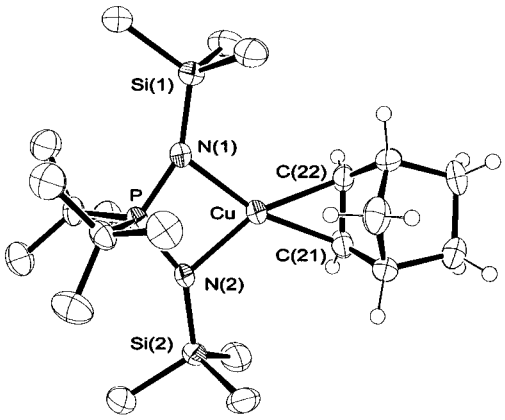

Fig. 2 ORTEP diagram of the solid state structure of **2**.‡ Hydrogen atoms of the methyl groups are omitted for clarity. Average values of the three independent molecules with assumed C_s-symmetry in the asymmetric unit (standard deviation) are quoted. Selected bond lengths (Å) and angles (°): P–N(1) 1.599(5), Si(1)–N(1) 1.704(9), Cu–N(1) 2.031(7), Cu–C(2) 2.026(23), C(21)–C(22) 1.377(20); P–N(1)–Si(1) 149.4(1.5), N(1)–P–N(2) 104.7(3), P–N(1)–Cu 89.0(4), N(1)–Cu–N(2) 77.1(1).

solubility of **1** even in alkanes and its NMR active nuclei (^{1}H, ^{13}C, ^{29}Si and especially ^{31}P) now offer an ideal chance to investigate mechanistic aspects of organometallic copper(I) chemistry, especially of copper(I)-catalyzed cyclopropanation.

Support of this work by a PhD stipend of the Fonds der Chemischen Industrie for B. F. S. is gratefully acknowledged.

Notes and references

† *Synthesis* of **1**: 13 ml 1.6 M Bu^{n}Li in hexane (21 mmol) were added to 5.78 g (18.0 mmol) Bu$^t_2$P[N(SiMe$_3$)]NH(SiMe$_3$)[11] in 20 ml of hexane under an argon atmosphere, and the solution was refluxed for 1 min,[12] then added to a suspension of 4.97 g (24 mmol) CuBrSMe$_2$ in 20 ml of hexane at −78 °C and stirred while warming to ambient temperature. Ethylene (99.7%) was bubbled into the black suspension for 2 min. The suspension was filtered through Celite under an ethylene atmosphere. From the slightly yellow solution crude **1** was crystallized at −78 °C. Recrystallization yielded 3.21 g (7.8 mmol, 43.4%) of **1**; crystallization from the collected organic phases yielded another batch of 2.80 g (6.6 mmol, 36.7%) (purity >97% **1**). Colorless crystals, mp 108 °C (slow gas evolution and decomp. of the colorless liquid); IR (KBr/cm^{-1}): ν 1516 (C=C); ^{1}H NMR (298 K, C_6D_6, 300.13 MHz): δ 3.48 (s + sat, $^1J_{CH}$ 158 Hz, CH_2; 4H), 1.21 [d + sat, $^3J_{PH}$ 14 Hz, $^1J_{CH}$ 126.5 Hz, C(CH$_3$)$_3$; 18H], 0.21 [s + sat, $^1J_{CH}$ 117 Hz, Si(CH$_3$)$_3$; 18H]; ^{13}C NMR (gated decoupling) (298 K, C_6D_6, 75.47 MHz): δ 73.0 (t, $^1J_{CH}$ 158 Hz, $^2J_{CH}$ 4 Hz, CH_2), 37.2 [ddez, $^1J_{CP}$ 64 Hz, $^2J_{CH}$ 4 Hz, *C*(CH$_3$)$_3$], 28.2 [q sept d, $^1J_{CH}$ 126.5 Hz, $^3J_{CH}$ 5.1 Hz, $^2J_{CP}$ 2.6 Hz, C(*C*H$_3$)$_3$], 5.6 [q'oct' + sat, $^1J_{CSi}$ 57 Hz, $^3J_{CH} \approx 2$ Hz $\approx {}^3J_{PC}$, Si(CH$_3$)$_3$]; ^{29}Si{^{1}H} NMR (DEPT) (298 K, C_6D_6, 59.63 MHz): δ −14.2 (d + sat, $^2J_{PSi}$ 14.8 Hz, $^1J_{CSi}$ 57 Hz); ^{31}P{^{1}H} NMR (298 K, C_6D_6, 121.50 MHz): δ 61.2 (s + sat, $^1J_{CP}$ 64 Hz, $^2J_{PSi}$ 14.8 Hz); CI-MS (%): *m/z* 764.3 ($L_2Cu_2^+$) (77), 687.3 ($L_2Cu - CH_3 + H^+$) (57), 629.3 ($L_2Cu^+ - CH_3 - C_4H_9$) (75.1), 411.2 ($M + H^+$) (2.1), 395.2 ($M^+ - CH_3$) (16), 383.2 ($LCu + H^+$) (35), 321.2 ($LH + H^+$) (100); elemental analysis for $C_{16}H_{40}N_2CuPSi_2$; calc: C, 46.74; H, 9.80; N, 6.81; P, 7.53; found: C, 46.38; H 10.04; N, 6.89; P, 7.24%.

Spectroscopy of **2**: ^{1}H NMR (298 K, C_6D_6, 300.13 MHz): δ 4.16 (s + sat, $^1J_{CH}$ 164 Hz, =CH; 2H), 2.96 (br. s, CH, 2H), 1.38 (dt, $^2J_{HH}$ 9.5 Hz, $^3J_{HH}$ 1.8 Hz, *syn*-C*H*H; 1H), 1.24 [d, $^3J_{PH}$ 14 Hz, C(C*H*$_3$)$_3$; 18H], 1.22 (dd, J_{HH} 2 and 13 Hz, *exo*-C*H*H; 2H), 0.74 (dd, J_{HH} 2.3 and 7.7 Hz, *endo*-CH*H*; 2H), 0.68 (dt, $^2J_{HH}$ 9.5 Hz, $^3J_{HH}$ 1.4 Hz, *anti*-CH*H*; 1H), 0.36 [s, Si(CH$_3$)$_3$; 18H]; ^{13}C{^{1}H} NMR (298 K, C_6D_6, 75.47 MHz): δ 93.1 (s, =CH), 43.7 (s, CH), 42.9 (s, CH_2), 37.7 [d, $^1J_{CP}$ 64 Hz, *C*(CH$_3$)$_3$], 28.2 [d, $^2J_{CP}$ 2.4 Hz, C(*C*H$_3$)$_3$], 25.5 (s, CH_2CH_2), 5.8 [d, $^3J_{PC}$ 2 Hz, Si(CH$_3$)$_3$]; ^{29}Si{^{1}H} NMR (DEPT) (298 K, C_6D_6, 59.63 MHz): δ −14.8 (d, $^2J_{PSi}$ 15 Hz); ^{31}P{^{1}H} NMR (298 K, C_6D_6, 121.50 MHz): δ 60.1 (s + sat, $^1J_{CP}$ 65 Hz, $^2J_{PSi}$ 15 Hz); VT ^{13}C{^{1}H} NMR (toluene-d$_8$, 75.47 MHz): *C*(CH$_3$)$_3$, T_c = 197.5 ± 4.0 K, k_c = 42 Hz; C(*C*H$_3$)$_3$, T_c = 200.5 ± 4.0 K, k_c = 68 Hz; temperature calibration by external MeOH. Addition of norbornene has no effect on the coalescence temperatures, ruling out associative mechanisms for the observed degenerate rearrangement.

‡ Data were collected on a Bruker SMART CCD instrument and the structure solutions were performed using SHELXTL V5.10,[17] respectively. Intensities were corrected for Lorentz and polarization effects, an empirical absorption correction was applied using SADABS[18] based on the Laue symmetry of the reciprocal space.

Crystal data: **1**: $C_{16}H_{40}CuN_2PSi_2$, M = 411.19, monoclinic, space group *C*2/*c*, a = 11.6400(2), b = 15.9236(3), c = 12.6352(2) Å, β = 95.949(1)°, V = 2329.33(7) Å^3, Z = 4, half a molecule per asymmetric unit, μ = 1.11 mm^{-1}, 8508 reflections measured at −73 °C, 2002 independent reflections (R_{int} = 0.0239), 1679 reflections observed [$I > 2\sigma(I)$], final agreement factors for 115 parameters: $R1$ = 0.027, $wR2$ = 0.064 (observed reflections) and $R1$ = 0.037, $wR2$ = 0.068 (all data).

2: $C_{21}H_{46}CuN_2PSi_2$, M = 477.29, monoclinic, space group $P2_1/n$, a = 10.2429(2), b = 42.4725(1), c = 18.6134(4) Å, β = 98.442(1)°, V = 8009.9(3) Å^3, Z = 12, three independent molecules per asymmetric unit, μ = 0.98 mm^{-1}, 59684 reflections measured at −73 °C, 13850 independent reflections (R_{int} = 0.1098), 7346 reflections observed [$I > 2\sigma(I)$], final agreement for 790 parameters: $R1$ = 0.078, $wR2$ = 0.159 (observed reflections), and $R1$ = 0.167, $wR2$ = 0.195 (all data).

CCDC 182/1478. See http://www.rsc.org/suppdata/cc/1999/2507/ for crystallographic files in .cif format.

1 G. Hallnemo, T. Olsson and C. Ullenius, *J. Organomet. Chem.*, 1985, **282**, 133.
2 S. Mori and E. Nakamura, *Chem. Eur. J.*, 1999, **5**, 1534 and references therein.
3 M. Mar Díaz-Requejo, M. C. Nicasio and P. J. Pérez, *Organometallics*, 1998, **17**, 3051.
4 M. Mar Díaz-Requejo, T. Belderrain, M. C. Nicasio, F. Prieto and P. J. Pérez, *Organometallics*, 1999, **18**, 2601.
5 G. E. Schaller and A. B. Bleecker, *Science*, 1995, **270**, 1809.
6 F. I. Rodríguez, J. J. Esch, A. E. Hall, B. M. Binder, G. E. Schaller and A. B. Bleecker, *Science*, 1999, **283**, 996.
7 J. R. Ecker, *Science*, 1995, **268**, 667 and references therein.
8 J. S. Thompson, R. L. Harlow and J. F. Whitney, *J. Am. Chem. Soc.*, 1983, **105**, 3522.
9 M. Munakata, S. Kitagawa, S. Kosome and A. Asahara, *Inorg. Chem.*, 1986, **25**, 2622.
10 A. Borg, T. Lindblom and R. Vestin, *Acta. Chem. Scand., Ser. A*, 1975, **29**, 475.
11 O. J. Scherer and G. Schieder, *Chem. Ber.*, 1968, **101**, 4184.
12 W. Wolfsberger and W. Hager, *Z. Anorg. Allg. Chem.*, 1977, **433**, 247.
13 L. S. Bartell, E. A. Roth, C. D. Hollowell, K. Kuchitsu and J. E. Young, Jr., *J. Chem. Phys.*, 1965, **42**, 2683.
14 H. Friebolin, *Basic One- and Two-dimensional NMR spectroscopy*, VCH, Cambridge, 1992.
15 W. Kläui, B. Lenders, B. Hessner and K. Evertz, *Organometallics*, 1988, **7**, 1357.
16 P. Hofmann, H. Heiß and G. Müller, *Z. Naturforsch., Teil B*, 1987, **42**, 395.
17 G. M. Sheldrick, Bruker Analytical X-Ray-Division, Madison, WI, 1997.
18 G. M. Sheldrick, 1996, unpublished work, based on the method described in: R. H. Blessing, *Acta Crystallogr., Sect. A*, 1995, **51**, 33.

Communication 9/07928I

Solid-phase synthesis of a putative heptapeptide intermediate in vancomycin biosynthesis

Ernst Freund and John A. Robinson*

Institute of Organic Chemistry, University of Zurich, Winterthurerstrasse 190, 8057 Zurich, Switzerland. E-mail: robinson@oci.unizh.ch

Received (in Liverpool, UK) 1st October 1999, Accepted 1st November 1999

The solid-phase synthesis was completed of the heptapeptide D-Leu-D-Tyr-L-Asn-Hpg-Hpg-L-Tyr-Dhpg, a putative intermediate in vancomycin biosynthesis, where Dhpg = (*S*)-3,5-dihydroxyphenylglycine and Hpg = (*R*)-4-hydroxyphenylglycine, using 2-chlorotrityl resin, benzyl side-chain protecting groups for the aromatic residues, and Alloc chemistry for chain elongation; the heptapeptide was obtained in 16% yield with the correct relative and absolute configuration.

Important progress has been made recently in elucidating the biosynthetic pathway to glycopeptide antibiotics of the vancomycin family. The nucleotide sequence of a gene cluster from the chloroeremomycin-producing microorganism revealed a large number of open reading frames encoding putative peptide synthetases, halogenases, hydroxylases and P450-like cytochromes, amongst many others.[1,2] Similar genes have also been cloned and sequenced from the balhimycin producer,[3] and disruption of a P450-like gene in this organism has provided the first confirmation of its role in the biosynthesis of the glycopeptide antibiotic, as well as indicating a likely role in a phenol coupling reaction.[4] Presently, however, the sequence of steps in glycopeptide antibiotic biosynthesis is largely unknown. Since most, if not all, the biosynthetic genes are now available for study, progress in this area should be facilitated by access to putative biosynthetic intermediates. We report here a convenient solid-phase synthesis of the heptapeptide **1**, which

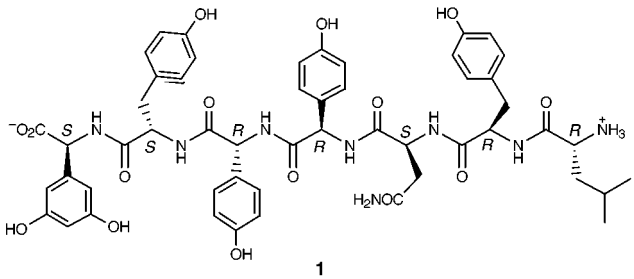

1

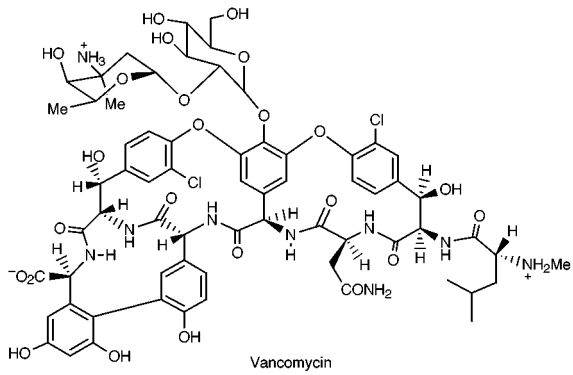

Vancomycin

may be considered[5] a possible product of the vancomycin peptide synthetase, and hence a potential substrate of downstream enzymes such as the halogenases, hydroxylases, or those catalyzing phenol coupling reactions.

A major concern in planning the solid-phase synthesis of **1** was the sensitivity of several amino acids to epimerization during chain assembly and/or subsequent deprotection steps, when using standard Fmoc or tBoc chemistry. We chose, therefore, to investigate Alloc chemistry for chain elongation, since deprotection of the N-terminus at each step of chain assembly can be performed under almost neutral conditions.[6] The amino acids (*R*)-4-hydroxyphenylglycine (Hpg) and (*S*)-3,5-dihydroxyphenylglycine (Dhpg) were synthesized by standard methods,[5] and protected on N^{α} with the Alloc group, and in the aromatic side chains with benzyl ethers. For the synthesis of **1**, (*S*)-Alloc-Dhpg$(OBn)_2$-OH was first coupled to 2-chlorotrityl chloride resin[7] in CH_2Cl_2 with NMM† as base. The peptide chain was then elaborated using for each coupling HATU/HOAt (4 equiv.) and the required amino acid derivative (4 equiv.) in DMF. For Alloc removal,[8] $Pd(PPh_3)_4$ and $PhSiH_3$ were used, as outlined in Scheme 1.

Upon completion of the solid-phase synthesis, the protected heptapeptide was first cleaved from the resin, and the N-terminal Boc and side-chain protecting groups were then

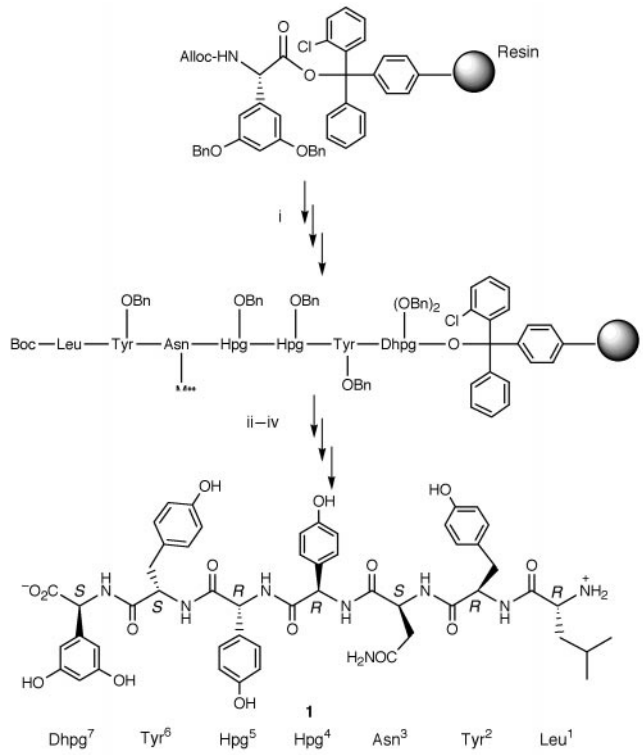

Scheme 1 *Reagents and conditions*: i, for coupling (*R*)-Alloc-Hpg(OBn)-OH, (*R*)- and (*S*)-Alloc-Tyr(OBn)-OH, L-Alloc-Asn(Mtt)-OH, or D-Boc-Leu-OH (4 equiv.), HATU and HOAt (each 4 equiv.), NMM, DMF, and for Alloc deprotection $Pd(PPh_3)_4$ (0.5 equiv.) and $PhSiH_3$ (30 equiv.) in CH_2Cl_2; ii, CF_3CH_2OH–AcOH–CH_2Cl_2 (1 : 1 : 3); iii, TFA–CH_2Cl_2 (1 : 1) + 5% Pr^i_3SiH, 0 °C, 2 h; iv, TFA, thioanisole (3 : 1), 20 °C, 3 h.

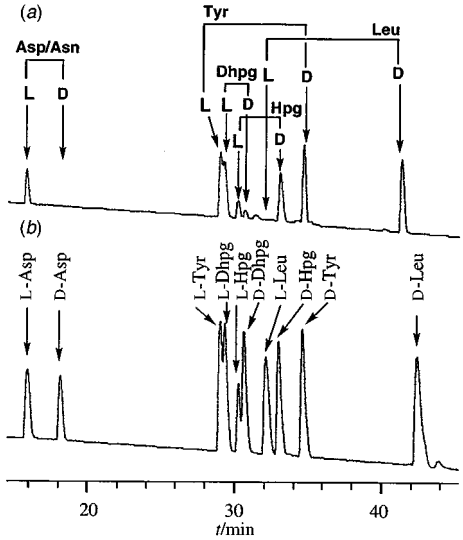

Fig. 1 HPLC chromatograms (Waters C_{18} column, 5 μm, 100 Å, 3.9 × 100 mm, flow rate: 1 ml min^{-1}, gradient, 5–100% MeCN in 0.1 M ammonium acetate buffer pH 7.4, over 130 min) showing (*a*) derivatives formed by reaction of *N*α-(2,4-dinitro-5-fluorophenyl)-L-valinamide with the amino acid hydrolysate of peptide **1** (the identities of the peaks are indicated) and (*b*) the standards prepared by reacting each optically pure amino acid with the same reagent (the identity of each peak was confirmed by MS and ^{1}H NMR spectroscopy).

removed in two steps (Scheme 1). Analysis of the crude product by HPLC revealed three main products in a ratio of *ca.* 6:2:1. The predominant product was identified by spectroscopic data as the required heptapeptide,‡ which was isolated by preparative HPLC (Vydac C_{18} 218TP1010, 10 μm, 300 Å, 10 × 250 mm, flow rate: 5 ml min^{-1}, gradient 10–40% MeCN in water + 0.1% TFA over 25 min) in *ca.* 16% overall yield. Due to difficulty in their purification, the minor products were not investigated in detail, although their mass spectra indicated the same mass as for **1**. Model studies (not described here) indicated that in particular the Hpg residues are susceptible to partial epimerization during the solid-phase synthesis.

In order to prove that the main product of the synthesis has the desired configuration, it was hydrolysed with 6 M HCl at 115 °C, under Ar, in the presence of phenol. The amino acids were immediately reacted with the modified Marfey's reagent *N*α-(2,4-dinitro-5-fluorophenyl)-L-valinamide[9] and analyzed by HPLC. Conditions were used that allowed the resolution on a C_{18} reversed phase column of a mixture of D- and L-Asp, D- and L-Tyr, D- and L-Leu, D- and L-Hpg and D- and L-Dhpg (see Fig. 1), each as a derivative with the modified chiral Marfey's reagent. In this way, the amino acid hydrolysate was seen to consist of L-Asp and D-Leu, of D- and L-Tyr, and predominantly of L- (rather than D-) Dhpg and D- (rather than L-) Hpg. This corresponds to the expected constitution of the heptapeptide **1**.

The solid-phase synthesis reported here allows the convenient preparation of **1** in multi-milligram amounts, as required for enzymatic studies of vancomycin biosynthesis. The method also appears amenable to parallel synthesis methods, that might allow the production of small combinatorial libraries of related peptides as tools to study the substrate specificities of these enzymes.

The authors thank the Swiss National Science Foundation for financial support.

Notes and references

† Abbreviations: HATU, *O*-(7-azabenzotriazol-1-yl)-*N*,*N*,*N*′,*N*′-tetramethyluronium hexafluorophosphate; HOAt, 1-hydroxy-7-azabenzotriazole; Mtt, 4-methyltrityl; NMM, *N*-methylmorpholine.

‡ *Spectral data* for **1**: *m/z* (ESI) 1035.5 $[M + H]^+$, 538 $[M + H + K]^{2+}$, 518.5 $[M + 2H]^{2+}$; $\delta_H CD_3OD–H_2O$ 1:1, *ca.* pH 5; 600 MHz; internal TSP δ = 0; with presaturation of the water resonance; 300 K) 8.82 (weak br s, HN Tyr^2), 8.29 (d, HN Hpg^4), 8.21 (d, HN Hpg^5), 8.16 (d, HN Asn^3), 8.15 (d, HN Tyr^6), 8.10 (d, HN Dhpg^7), 7.36 (s, HD^E Asn^3), 7.24 (d, H2,6 Hpg^4), 7.00 (d, H2,6 Tyr^2), 6.97 (d, H2,6 Hpg^5), 6.83 (d, H3,5 Hpg^4), 6.78 (d, H3,5 Tyr^2), 6.76 (d, H2,6 Tyr^6), 6.74 (d, H3,5 Hpg^5), 6.64 (s, HD^Z Asn^3), 6.55 (d, H3,5 Tyr^6), 6.48 (d, H2,6 Dhpg^7), 6.27 (t, H4 Dhpg^7), 5.50 (d, HA Hpg^4), 5.28 (d, HA Hpg^5), 5.02 (d, HA Dhpg^7), 4.67 (m, HA Asn^3), 4.61 (m, HA Tyr^6), 4.29 (m, HA Tyr^2), 3.87 (t, HA Leu^1), 2.97 (dd, HB2 Tyr^6), 2.94 (dd, HB2 Tyr^2), 2.88 (dd, HB1 Tyr^2), 2.70 (dd, HB1 Tyr^6), 2.51 (dd, HB2 Asn^3), 2.47 (dd, HB1 Asn^3), 1.50 (m, HG Leu^1), 1.45 (m, HB Leu^1), 0.85 (d, HD2 Leu^1), 0.81 (d, HD1 Leu^1). The assignments were made by 2D TOCSY, DQF-COSY and NOESY experiments. The connectivity within each spin system was confirmed by intra-residue *J* couplings and NOEs, and the amino acid sequence by inter-residue $d_{\alpha N}$ (*i*, *i* + 1) NOEs.

1 A. M. A. vanWageningen, P. N. Kirkpatrick, D. H. Williams, B. R. Harris, J. K. Kershaw, N. J. Lennard, M. Jones, S. J. M. Jones and P. J. Solenberg, *Chem. Biol.*, 1998, **5**, 155.
2 P. J. Solenberg, P. Matsushima, D. R. Stack, S. C. Wilkie, R. C. Thompson and R. H. Baltz, *Chem. Biol.*, 1997, **4**, 195.
3 S. Pelzer, R. Sussmuth, D. Heckmann, J. Recktenwald, P. Huber, G. Jung and W. Wohlleben, *Antimicrob. Agents Chemother.*, 1999, **43**, 1565.
4 R. D. Sussmuth, S. Pelzer, G. Nicholson, T. Walk, W. Wohlleben and G. Jung, *Angew. Chem., Int. Ed.*, 1999, **38**, 1976.
5 K. C. Nicolaou, C. N. C. Boddy, S. Bräse and N. Winssinger, *Angew. Chem., Int. Ed.*, 1999, **38**, 2096.
6 For a review, see F. Guibé, *Tetrahedron*, 1998, **54**, 2967.
7 K. Barlos, O. Chatzi, D. Gatos and G. Stavropoulos, *Int. J. Pept. Protein Res.*, 1991, **37**, 513.
8 N. Thieriet, J. Alsina, E. Giralt, F. Guibé and F. Albericio, *Tetrahedron Lett.*, 1997, **38**, 7275.
9 H. Brückner and C. Keller-Hoehl, *Chromatographia*, 1990, **30**, 621.

Communication 9/08058I

ChemComm

Carbonylation of methanol in supercritical CO_2 catalysed by a supported rhodium complex

Rebecca J. Sowden, Murielle F. Sellin, Nicola De Blasio and David J. Cole-Hamilton*

School of Chemistry, University of St. Andrews, St. Andrews, Fife, Scotland, UK KY16 9ST. E-mail: djc@st-and.ac.uk

Received (in Basel, Switzerland) 16th August 1999, Accepted 27th October 1999

A rhodium complex supported on polyvinylpyrrolidone catalyses the carbonylation of methanol to methyl ethanoate and ethanoic acid in supercritical CO_2 at rates up to *ca.* 50% those in liquid solution but with minimal catalyst leaching.

The rhodium catalysed carbonylation of methanol is an important commercial application of homogeneous catalysis in which the product can be separated from the catalyst by distillation.[1] Since this separation is carried out separately from the reaction, not all of the catalyst can be employed in the desired reaction at any one time.[1] There is, therefore, an interest in developing truly continuous processes.

One possibility would be to use a supported catalyst and to flow the reagents over it. However, in the liquid phase, catalyst leaching from the support is always a problem, although a demonstration reactor has been commissioned in which the catalyst is $[RhI_2(CO)_2]^-$ attached to an ion exchange resin. Catalyst does leach, but the dissolved catalyst is collected on a downstream bed of the resin which is recycled to the reactor.[2]

We have recently reported studies of a catalyst consisting of $[RhI_2(CO)_2]^-$ supported on polyvinylpyrrolidone (PVP).[3,4] In the liquid phase, we showed that the rate constant for the homogeneous reaction was only 2.2 times that for the heterogeneous reaction but that significant leaching of Rh occurs.[3] In the gas phase, after activation, stable activity was observed over long periods, there was no leaching, but the overall methanol consumption rate is low because of the low concentration of methanol that can be attained in the gas phase.[4]

We reasoned that supercritical CO_2 might be an ideal vector for this reaction since it dissolves large quantities of methanol and methyl iodide, is totally miscible with CO, has gas-like diffusion properties and is a poor solvent for ionic species such as $[RhI_2(CO)_2]^-$ so that leaching should be minimised. We now report preliminary results from a study of this system.

Rhodium supported on PVP was prepared as described previously[3] and tested for its activity in the bulk liquid phase. The result (Table 1, run A1) is broadly consistent with our previous results, as is the extent of rhodium leaching.[3]

The catalysts were then used for reactions in $scCO_2$. The catalyst was loaded into an autoclave with a sapphire bottom (for observation purposes). Degassed methanol and MeI were injected into the autoclave against a stream of CO_2, the autoclave sealed, pressurised to 40 bar with CO and then CO_2 added from a cooled head HPLC pump. The amount of CO_2 was varied to control the final reaction pressure which was achieved at the reaction temperature (150 °C). Observation of the catalyst shows that it changes from red to pale yellow at the onset of the reaction as indicated by a decrease in the slope of the *p vs. T* curve, which occurred between 100 and 140 °C. At the end of the reaction, the autoclave was cooled to 0 °C then to −80 °C and vented. The liquid product was removed for analysis and the autoclave recharged with methanol, MeI, CO and CO_2. We have shown, through observations on mixtures of CO_2, MeI, methanol and CO, in the absence of the catalyst, that the mixture with the same composition as that used for experiments B and C is monophasic above 130 °C. Replacing the methanol in this mixture with ethanoic acid raises the temperature at which it becomes monophasic to 150 °C, whilst a mixture in which the methanol is replaced by methyl acetate, (1.2 cm^3), ethanoic acid (0.4 cm^3) and water (0.4 cm^3) also becomes monophasic at 150 °C.

The results of a series of runs using the same sample of catalyst are shown in Table 1 (B1–6) and Fig. 1. The rate of methanol carbonylation was *ca.* 23% that in liquid methanol, despite the fact that the concentrations of methanol and iodomethane were reduced by a factor of *ca.* 25.† Interestingly, and reproducibly, the rate increased for the second run (58% of the rate in the liquid phase) and then levelled off at a lower level for subsequent runs, despite the fact that significant amounts of Rh were leached from the support. Run B6 was carried out in the absence of added MeI; carbonylation activity was still observed at a rate similar to that observed in the previous reaction (B5). In other experiments, we have shown that the activity drops off on subsequent runs in the absence of MeI and that, if MeI is omitted from the first run in a series, no activity is observed. These results suggest that the catalyst support takes up MeI and that the rate increases as the MeI content reaches saturation either because the concentration of MeI in the supercritical phase is increased, or because the rhodium on the surface reacts with surface bound MeI (see below). When MeI is omitted from the reaction mixture, the MeI adsorbed in the surface is then used, before or after desorption, as the promoter. (Fig. 2).

In experiments B1–6, the liquid products spend significant amounts of time (up to 4 h) on the catalyst during the cooling

Table 1 Yields of carbonylation products and extent of rhodium leaching during the carbonylation of methanol catalysed by a supported rhodium catalyst under various conditions[a]

Run	MeI added/ cm^3	MeOAc yield (%)	HOAc yield (%)	Turnover frequency[b]/ h^{-1}	Rh leached (%)
A1[c]	0.8	2.6	50.4	870	52.2
B1	0.3	17.0	2.2	197	12.2[d]
B2	0.3	42.2	6.9	504	11.3[d]
B3	0.3	22.8	3.4	269	6.8[d]
B4	0.3	27.0	5.6	335	3.9[d]
B5	0.3	24.5	10.5	361	12.1[d]
B6	0	33.5	4.2	383	12.4[d]
C1	0.3	20.8	1.1	178	< 0.08[e]
C2	0.3	37.5	1.3	315	0.08
C3	0.3	30.1	4.8	283	< 0.15[e]
C4	0.3	21.8	3.5	205	< 0.3[e]
C5	0.3	28.4	2.7	252	< 0.3[e]

[a] Catalyst was rhodium on polyvinylpyrrolidone (0.17 g; B, 0.82% Rh; C, 1.04% Rh); MeOH (1.5 cm^3, 1.8 cm^3 if no MeI added); CO (40 bar at ambient temperature); $CO_{2(l)}$ (12 cm^3, 12.7 g); 150 °C; p_{150} = 200 bar, 3 h. In repetitive experiments, we have found the reproducibility is ±10%; [b] Mol of product (mol of Rh)$^{-1}$ h^{-1}. [c] Liquid phase reaction: catalyst (0.17 g, 0.82% Rh); MeOH (4.2 cm^3); CO (40 bar at ambient temperature), 150 °C, 5 h. [d] From analysis of the solution recovered after each run. Analysis of the solid catalyst after the six runs indicated 39.2% of the rhodium had leached. This is less than the total of the solution figures because some of the solution and hence part of the leached rhodium remained in the autoclave after removing the condensed liquid by syringe at the end of each run. Yields of HOAc and MeOAc might be slightly overestimated for runs B2–B6 as a result of this. [e] From analysis of the solution collected in the second autoclave, detection limits for the particular experiment are shown; these correspond to < 0.3 ppm in the analyte.

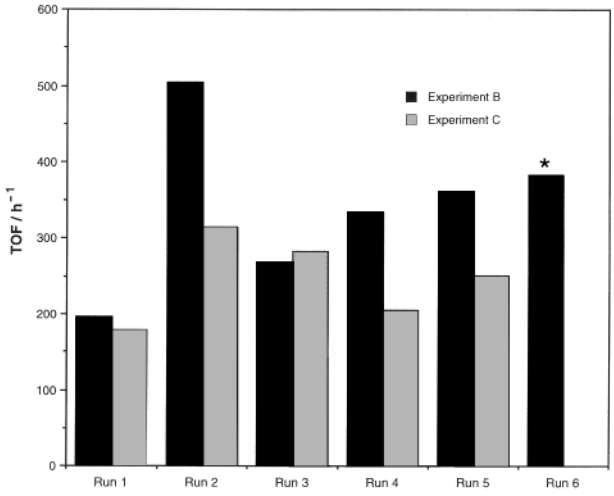

Fig. 1 Plot of turnover frequency/h^{-1} for repetitive catalytic reactions. The same catalyst was reused for all runs in a series, but different samples were used for runs B and C. For runs B, the products were condensed onto the catalyst and removed by syringe; for runs C, the products were flushed from the autoclave using $scCO_2$. The asterisk means that iodomethane was not added for this run.

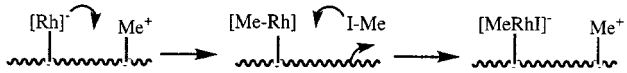

Fig. 2 Possible mechanism of reaction of the catalyst with surface bound methyl groups and remethylation of the surface.

and venting process and we surmised that the observed catalyst leaching might occur during this period of contact between the catalyst and the liquid products. To investigate the leaching under supercritical conditions, we carried out the reaction in the same way except that at the end of the reaction the stirrer was stopped and, in a process similar to that introduced by Leitner and co-workers[5] for the separation of products from homogeneous catalysts after reactions in $scCO_2$, fresh $scCO_2$ was passed into the bottom of the autoclave at the reaction temperature and pressure to flush the product solution into a second autoclave held at 40 bar and −80 °C. During this process, the CO_2 and CO were vented through an ethanol trap. The catalyst remaining in the first autoclave was reused five times (Table 1, Fig. 1, runs C1–5). The liquid product collected in the second autoclave (up to 1.2 cm^3) was analysed for the organic products by GLC and for rhodium content by atomic absorption. This series of experiments was carried out with a slightly higher catalyst loading than that for experiments B1–5, so the apparent yields are lower.‡ These lower apparent yields may arise because some solution was always left on the catalyst in the B series of experiments because the product solution was removed by syringe. This means that the starting solution for all the B series experiments, except B1, contained some product. In the C series experiments, all the product apart from that adsorbed on the support (see below) was removed by the venting process.

None of the solutions recovered after the supercritical venting process (series C) contained detectable rhodium (< 0.3% of Rh charged), apart from C2, which contained 0.08% of the rhodium charged,§ suggesting that leaching has been minimised. To confirm this, we analysed the catalyst before and after use (Table 2). The mass of the catalyst recovered was higher than that loaded, and the total rhodium content had dropped slightly (12%, although the precision of the analyses is such that this may not be significant) (see Table 2), confirming that rhodium leaching is greatly reduced when the reaction is carried out and the products are recovered in the supercritical phase.

In order to understand the increase in weight of the catalyst, we heated a sample of the recovered catalyst to constant weight in a closed system and analysed the gas phase. MeI and $MeCO_2H$ were detected by GLC and the weight loss was 22%,

Table 2 Analysis of supported catalyst used in experiments C1–5 after various treatments

	Mass of catalyst/mg	Rh content (%)	Total Rh (10^{-5} mol)
Charged[a]	170	1.04	1.7 ± 0.1
Recovered[b]	205	0.74	1.5 ± 0.1
Heated[c]	27		
Recovered[d]	21		
Expected[e]	22.4		

[a] To the reactor at the start of the series C experiments. [b] From the reactor after experiment C5. [c] Sample of catalyst taken for heating to 200 °C. [d] After heating to 200 °C, MeI and $MeCO_2H$ were released; weight loss by TGA = 13.7%. [e] If all the mass gained during the catalytic experiment were from adsorption of MeI and $MeCO_2H$.

cf. 17% if all the weight gained during the catalysis were lost. In a similar experiment carried out using thermal gravimetric analysis (TGA), the weight loss in a transient process starting at 33 °C and complete by 70 °C was 13.7%. TGA was also carried out on samples of the catalyst support washed with MeI and with ethanoic acid separately. For MeI, the transient process had an onset temperature of *ca.* 30 °C and was complete at 99 °C, whilst for ethanoic acid, onset was at 22 °C and the loss was complete at 70 °C. In all the TGA experiments, substantial further weight loss occurred above 250 °C, probably from decomposition of the polymer support. The observation that MeI is held on the catalyst (even after storing for several days) supports our suggestion[4] that it interacts with the support.

The rates obtained in the supercritical experiments are of the same order of magnitude as those obtained in the liquid phase reactions, despite the lower concentrations of methanol and MeI in the supercritical reactions. Turnover frequencies in the gas phase reactions are comparable with those obtained in the supercritical phase (up to 595 h^{-1}, at 190 °C in the gas phase compared with up to 504 h^{-1} at 150 °C for the supercritical phase reactions). However, the gas phase reactions were carried out at a higher temperature, and the concentration of methanol achievable is very much less (1 cm^3 in 9.8 dm^3, as opposed to 1.5 cm^3 in 50 cm^3 for the supercritical reactions). Rhodium leaching is a severe problem for the bulk liquid phase reactions,[3] but is very much reduced for the reactions carried out in the supercritical or gas[4] phases.

We conclude that methanol carbonylation in the supercritical phase has the potential to overcome the problems of liquid phase (catalyst leaching) and gas phase (low methanol throughput) reactions using the same supported catalyst.

We thank the EEC for a Fellowship (M. F. S.) and support under a TMR programme and for support under the ERASMUS programme (N. De B).

Notes and references

† The supercritical reactor has a volume of 50 cm^3, whilst the liquid phase reactions were carried out in a liquid volume of 5 cm^3.

‡ Using this catalyst for an experiment under the conditions of experiment B1, we obtained a turnover frequency of 176 ± 13 h^{-1}, within experimental error the same as that obtained with the batch of catalyst used for the B experiments (197 ± 20 h^{-1}).

§ In this experiment, all of the recovered solution was used for the atomic absorption analysis, improving the detection limit for this analysis. The amount detected is at this detection limit (0.5 ppm in the analysed sample).

1 M. J. Howard, M. D. Jones, M. S. Roberts and S. A. Taylor, *Catal. Today*, 1993, **18**, 325.
2 H. Sugiyama, F. Uemura, N. Yoneda, T. Minami, T. Maejima and K. Hamato, *Jpn. Pat.*, 1997, 235250; *Chem. Abstr.*, 1997, **127**, 279841j.
3 N. De Blasio, M. R. Wright, E. Tempesti, C. Mazzocchia and D. J. Cole-Hamilton, *J. Organomet. Chem.*, 1998, **551**, 229.
4 N. De Blasio, E. Tempesti, A. Khaddouri, C. Mazzocchia and D. J. Cole-Hamilton, *J. Catal.*, 1998, **176**, 253.
5 S. Kainz, A. Brinkman, W. Leitner and A. Pfaltz, *J. Am. Chem. Soc.*, 1999, **121**, 6421 and references therein.

Communication 9/06653E

ChemComm

Controlled partial hydrolysis of spherosilicate frameworks: syntheses of *endo*-[$(Me_3SiO)_6Si_6O_7(OH)_4$] and *endo*-[$(Me_3SiO)_6Si_6O_7\{OSiMe_2(CH{=}CH_2)\}_4$] from [$(Me_3SiO)_6Si_6O_9$]

Frank J. Feher,* Raquel Terroba and Ren-Zhi Jin

Department of Chemistry, University of California, Irvine, CA 92697-2025, USA. E-mail: fjfeher@uci.edu

Received (in Bloomington, IN, USA) 10th September 1999, Accepted 3rd November 1999

Readily available $(RMe_2SiO)_6Si_6O_9$ (3 R = Me, 5 R = CH=CH_2); reacts cleanly with aqueous NEt_4OH in THF to afford *endo*-C_{2h}-$(RMe_2SiO)_6Si_6O_7(OH)_4$ (7 R = Me, 9 R = CH=CH_2); exhaustive silylation of 7 with $(CH_2{=}CH)Me_2SiCl/NEt_3$ affords *endo*-C_{2h}-$(Me_3SiO)_6Si_6O_7[OSiMe_2(CH{=}CH_2)]_4$ (10).

Discrete polyhedral clusters containing silicon and oxygen are attractive building blocks for the preparation of Si/O/M frameworks, inorganic solids and hybrid inorganic–organic materials.[1–10] Two broad families of polyhedral Si/O clusters exist: (1) polyhedral silsesquioxanes (*e.g.* **1** and **2**), which are

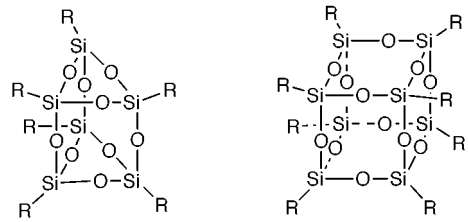

1 R = c-C_6H_{11}
3 R = $OSiMe_3$
5 R = $OSiMe_2(CH{=}CH_2)$

2 R = c-C_6H_{11}
4 R = $OSiMe_3$

usually obtained from hydrolytic condensation reactions of trifunctional organosilicon monomers ($RSiX_3$);[11] and (2) spherosilicates (*e.g.* **3** and **4**), which are most often prepared by silylation of silicate solutions.[12–15] Both families have enormous potential as precursors to advanced materials if cost-effective methods can be devised to produce appropriately functionalized Si/O frameworks on a large scale.

Over the past three years, we have developed highly selective methods for effecting the partial hydrolysis of fully condensed polyhedral silsesquioxanes with structures **1** and **2**.[16–20] These methods provide access to a variety of functionalized silsesquioxanes, but they are generally not useful for the modification of spherosilicates. Here, we report the first highly selective procedure for effecting partial hydrolysis of a spherosilicate framework. This procedure produces a C_{2h}-symmetric tetrasilanol *via* base-catalyzed hydrolysis of both Si_3O_3 rings in [$(Me_3SiO)_6Si_6O_9$] **3**, which is readily available from $Si(OEt)_4$, NEt_4OH and Me_3SiCl.[14,15] Subsequent reaction of this tetrasilanol with $(CH_2{=}CH)Me_2SiCl$ affords the corresponding tetrasilylated product. Implications of these results for the development of incompletely condensed Si/O frameworks as precursors to hybrid inorganic–organic materials[1] and as ligands for transition-metal catalysts[3,21–23] are discussed.

The reaction of **3** with 35% aqueous NEt_4OH in THF occurs rapidly upon mixing at −40 to −25 °C to produce a new silicate cluster in quantitative NMR yield.† As illustrated in Fig. 1 (top spectrum), this cluster exhibits two sets of ^{29}Si NMR resonances with relative integrated intensities of 2:1. One set appears at δ *ca.*12 and is assignable to TMSO (*i.e.*, 'M') groups. The second set of ^{29}Si resonances appears at δ *ca.* −100 to −110 and is assignable to framework silicate (*i.e.* 'Q') groups in two different environments. The smaller resonance at δ −109.27 is characteristic of ^{29}Si nuclei in fully condensed spherosilicates with relatively unstrained Si_nO_n rings. (For comparison, the ^{29}Si NMR resonance for **4** is at δ −108.95.[24]) The larger resonance at δ −100.12 is slightly upfield from the resonance for **3** (δ −99.31) and *ca.* 10 ppm downfield from the resonance for **4**. Although this resonance is in the range expected for fully condensed spherosilicates with Si_3O_3 rings, it is also consistent with $(SiO)_3Si(OH)$ groups in relatively unstrained Si_nO_n rings.[25–27] On the basis of these data—as well as ^1H and ^{13}C NMR data, electrospray mass spectrometry data† and structure/^{29}Si chemical shift correlations observed for structurally similar cyclohexyl-substituted silsesquioxanes (*i.e.* **1**, **2** and **6**)[20]—the product obtained from the reaction of **3** with NEt_4OH must be a C_{2h}-symmetric tetrasilanol derived from cleavage of both Si_3O_3 rings. Structures **7** and **8** are equally consistent with most of our data, but structure **7** is much more likely for two reasons: (1) the ^1H NMR chemical shift for the SiOH groups is strongly deshielded (*ca.* 7 ppm), consistent with extensive intramolecular hydrogen bonding,[20,28,29] and (2) the NEt_4OH-catalyzed hydrolysis of Si–O–Si linkages in both **1** and **2** are known to proceed with complete retention of stereochemistry at Si.[19,20] A structurally similar tetrasilanol (*i.e.* **9**) is also obtained from the reaction of **5** with aqueous NEt_4OH.

Tetrasilanols **7** and **9** are stable at 25 °C and soluble in many common organic solvents, including hydrocarbons, diethyl ether, chlorocarbons and acetone. They are also soluble in most of the polar solvents used as nonsolvents for the crystallization of polyhedral silsesquioxanes and spherosilicates (*e.g.* MeCN and MeOH). Both **7** and **9** separate from solution as colorless waxes rather than microcrystalline solids. Neither compound has been successfully crystallized, but it is clear from Fig. 1 (as well as ^1H and ^{13}C NMR spectra of crude reaction mixtures) that the crude product obtained after an aqueous work-up is quite pure.

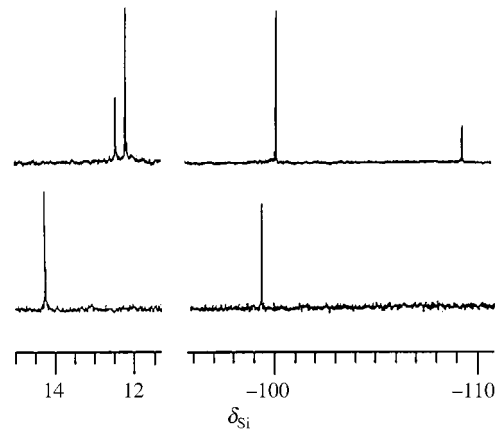

Fig. 1 ^{29}Si {^1H} NMR (99.3 MHz, $CDCl_3$, 25 °C) spectra from the reaction of $(Me_3SiO)_6Si_6O_9$ **3** with 35% aqueous NEt_4OH in THF at −40 to −25 °C. The lower spectrum is for pure **3**. The upper spectrum is for crude *endo*-C_{2h}-$(Me_3SiO)_6Si_6O_7(OH)_4$ **7** obtained after an aqueous work-up.

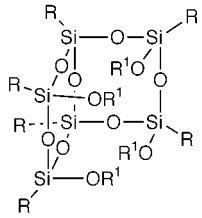

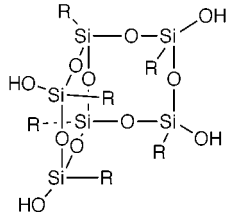

	R′	R
6	H	c-C_6H_{11}
7	H	$OSiMe_3$
9	H	$OSiMe_2(CH{=}CH_2)$
10	$OSiMe_2(CH{=}CH_2)$	$OSiMe_3$

8 R = $OSiMe_3$

Although the chemistry of C_{2h}-symmetric $R_6Si_6O_7(OH)_4$ frameworks[20,28,29] is largely undeveloped, these tetrasilanols offer interesting possibilities as building blocks for more elaborate Si/O and Si/O/M frameworks. For example, the reaction of **7** with $(CH_2{=}CH)Me_2SiCl$ and NEt_3 produces **10** in essentially quantitative yield after an aqueous work-up.‡ This compound is also obtained as a highly soluble waxy solid that resists crystallization. As expected, both ^{29}Si NMR resonances for the framework silicate groups appear at δ *ca.* −110 and the diastereotopic Me groups on the four chemically equivalent $(CH_2{=}CH)Me_2SiO$ groups appear as two resonances with equal intensities in both the ^{1}H and ^{13}C NMR spectra.

The results described here represent an important advance in the chemistry of spherosilicates, and they have major implications for many emerging applications for discrete Si/O clusters. From the standpoint of developing cost-effective methods for producing functionalized Si/O frameworks for use in hybrid inorganic–organic materials and incompletely condensed Si/O frameworks for use as ligands for transition metal catalysts, the ability to produce appropriately functionalized compounds from spherosilicates is attractive because many spherosilicates—including **3** and **4**—can be obtained in high yield from either silica or $Si(OEt)_4$. More importantly, the recognition that **3** can be partially hydrolyzed in high yield at high conversion offers a strategy for preparing functionalized spherosilicates that does not rely on inherently unselective pendant group modifications. If similarly selective methods can be devised for effecting partial hydrolysis of other spherosilicates (*e.g.* **4**), many of the applications being developed for polyhedral silsesquioxanes with one or two well defined functional groups can be extended to spherosilicates.

These studies were supported by Hybrid Plastics (Fountain Valley, CA) under an Advanced Technologies Program grant from the National Institute of Standards and Technology and the Air Force Research Laboratory (Edwards AFB).

Notes and references

† *Reaction* of **3** with NEt_4OH: aqueous NEt_4OH (35%, 82.3 μL, 0.20 mmol) was added to a solution of **3** (170 mg, 0.20 mmol) in THF (4 mL) at −40 °C. The resulting mixture was stirred between −40 and −25 °C for 40 min then neutralized with dilute aqueous HCl. Extraction with Et_2O, washing with brine, drying over $MgSO_4$ and evaporation of the volatiles gave **7** (175 mg, 99%) as a waxy colorless solid. ^{1}H NMR (500 MHz, $CDCl_3$, 25 °C) δ 6.53 (br s, 4H), 0.14 (s, 54H). ^{13}C{^{1}H} NMR (125.8 MHz, $CDCl_3$, 25 °C) δ 1.24, 1.28 (1:2). ^{29}Si{^{1}H} NMR (99.3 MHz, $CDCl_3$, 25 °C) δ 12.44, 12.19 (2:4 for $SiMe_3$), −100.12 (4 Si, O_3SiOH), −109.27 (2 Si, O_4Si). MS (ESI, 100% MeOH): *m/z* 905.4 ($[M + Na]^+$, 100%); 921.3 ($[M + K]^+$, 12%).

‡ *Reaction* of **7** with $(CH_2{=}CH)Me_2SiCl$: a solution of **3** (175 mg, 0.20 mmol) in Et_2O was added to a solution of $(CH_2{=}CH)Me_2SiCl$ (122 μL, 0.88 mmol) and NEt_3 (139 μL, 1.00 mmol) in Et_2O solution (5 mL). The mixture was stirred at room temp. for 4 h and then concentrated under reduced pressure. Extraction of the residue with hexane, filtration and evaporation under high vacuum gave spectroscopically pure **10** (226 mg, 92%) as a waxy white solid. ^{1}H NMR (500 MHz, $CDCl_3$, 25 °C) δ 0.13 (s, 54H), 0.14 (s, 12H), 0.18 (s, 12H), 5.75 (dd, ^2J 20, ^3J 4 Hz, 4H), 5.93 (dd, ^3J 15, ^3J 4 Hz, 4H), 6.13 (dd, ^2J 20, ^3J 15 Hz, 4H). ^{13}C{^{1}H} NMR (125.8 MHz, $CDCl_3$, 25 °C) δ 0.11, 1.52 (1:1 for $SiMe_aMe_b$), 1.62 ($SiMe_3$), 132.00 (SiCH), 138.79 (=CH_2). ^{29}Si NMR (99.3 MHz, $CDCl_3$, 25 °C) δ 11.24, 10.17 (1:2 for $SiMe_3$), −1.35 [$SiMe_2(CH{=}CH_2)$], −108.31 [4 Si, $O_3SiOSiMe_2(CH{=}CH_2)$], −108.70 (2 Si, O_4Si). MS (ESI, 100% MeOH): *m/z* 1241.6 ($[M + Na]^+$, 100% for [M + 2]); 1257.5 ($[M + K]^+$, 8% for [M + 2]). Anal. Calc. (found) for $C_{34}H_{90}O_{17}Si_{16}$: C, 33.46 (33.26); H, 7.43 (7.40)%.

1 J. J. Schwab and J. D. Lichtenhan, *Appl. Organomet. Chem.*, 1998, **12**, 707.
2 E. G. Shocky, A. G. Bolf, P. F. Jones, J. J. Schwab, K. P. Chaffee, T. S. Haddad and J. D. Lichtenhan, *Appl. Organomet. Chem.*, 1999, **13**, 311.
3 F. J. Feher and T. A. Budzichowski, *Polyhedron*, 1995, **14**, 3239.
4 P. G. Harrison, *J. Organomet. Chem.*, 1997, **542**, 141.
5 I. Hasegawa, *Trends Organomet. Chem.*, 1994, **1**, 131.
6 P. C. Cagle, W. G. Klemperer and C. A. Simmons, *Mater. Res. Soc. Symp. Proc.*, 1990, **180**, 29.
7 A. Sellinger and R. M. Laine, *Chem. Mater.*, 1996, **8**, 1592.
8 C. Zhang and R. M. Laine, *J. Organomet. Chem.*, 1996, **521**, 199.
9 C. Zhang, F. Babonneau, C. Bonhomme, R. M. Laine, C. L. Soles, H. A. Hristo and A. F. Yee, *J. Am. Chem. Soc.*, 1998, **120**, 8380.
10 H. C. L. Abbenhuis, H. W. G. van Herwijnen and R. A. van Santen, *Chem. Commun.*, 1996, 1941.
11 M. G. Voronkov and V. Lavrent'ev, *Top. Curr. Chem.*, 1982, **102**, 199.
12 D. Hoebbel and W. Wieker, *Z. Anorg. Allg. Chem.*, 1971, **384**, 43.
13 P. A. Agaskar, *Colloids. Surf.*, 1992, **63**, 131.
14 R. Weidner, N. Zeller, B. Deubzer and V. Frey, *US Pat.*, 5 047 492, 1991.
15 P. G. Harrison, R. Kannengiesser and C. J. Hall, *Main Group Met. Chem.*, 1997, **20**, 137.
16 F. J. Feher, D. Soulivong and A. E. Eklund, *Chem. Commun.*, 1998, 399.
17 F. J. Feher, D. Soulivong and G. T. Lewis, *J. Am. Chem. Soc.*, 1997, **119**, 11 323.
18 F. J. Feher, D. Soulivong and F. Nguyen, *Chem. Commun.*, 1998, 1279.
19 F. J. Feher, R. Terroba and J. W. Ziller, *Chem. Commun.*, 1999, 2309.
20 F. J. Feher, R. Terroba and J. W. Ziller, *Chem. Commun.*, 1999, 2153.
21 M. Crocker, R. H. M. Herold and A. G. Orpen, *Chem. Commun.*, 1997, 2411.
22 H. C. L. Abbenhuis, S. Krijnen and R. A. van Santen, *Chem. Commun.*, 1997, 331.
23 T. Maschmeyer, M. C. Klunduk, C. M. Martin, D. S. Shepard, J. M. Thomas and B. F. G. Johnson, *Chem. Commun.*, 1997, 1847.
24 I. Hasegawa, M. Ishida and S. Motojima, *Synth. React. Inorg. Met.-Org. Chem.*, 1994, **24**, 1099.
25 R. K. Harris, C. T. G. Knight and W. E. Hull, *J. Am. Chem. Soc.*, 1981, **103**, 1577.
26 I. Hasegawa and S. Motojima, *J. Organomet. Chem.*, 1992, **441**, 373.
27 W. G. Klemperer, V. V. Mainz and D. M. Millar, *Mater. Res. Soc. Symp. Proc.*, 1986, **73**, 3.
28 F. J. Feher, T. A. Budzichowski, R. L. Blanski, K. J. Weller and J. W. Ziller, *Organometallics*, 1991, **10**, 2526.
29 T. W. Hambley, T. Maschmeyer and A. F. Masters, *Appl. Organomet. Chem.*, 1992, **6**, 253.

Communication 9/07419H

ChemComm

CAN induced double ether ring formation: synthesis of *trans*- and *cis*-fused tricyclic ethers from 3-oxabicyclo[3.1.0]hexyl sulfides

Yoshiji Takemoto,*[a] Syun-ichirou Furuse,[b] Hiroki Hayase,[b] Tomoki Echigo,[b] Chuzo Iwata,[b] Tetsuaki Tanaka[b] and Toshiro Ibuka[a]

[a] *Graduate School of Pharmaceutical Sciences, Kyoto University, Sakyo-ku, Kyoto 606-8501, Japan. E-mail: takemoto@pharm.kyoto-u.ac.jp*

[b] *Graduate School of Pharmaceutical Sciences, Osaka University, 1-6 Yamada-oka, Suita, Osaka 565-0871, Japan*

Received (in Cambridge, UK) 8th October 1999, Accepted 11th November 1999

CAN oxidation of 3-oxabicyclo[3.1.0]hexy sulfides 4 and 5 possessing two hydroxy groups in the C-2 and C-4 side chains promoted a double ether ring formation along with a cleavage of the most substituted cyclopropyl bond to give tricyclic ketal adducts 8 and 10, which were converted to *trans*- and *cis*-fused tricyclic ethers 9 and 11 with high or moderate stereoselectivity by a TMSOTf-mediated trialkylsilane reduction.

Recently, a number of biologically active polyether toxins, such as the brevetoxins, ciguatoxins and halichondrins, have been isolated from marine organisms. The structural complexity and biological activities of these molecules have attracted the attention of synthetic chemists, and many new methods for the synthesis of cyclic ethers have been developed over the last few years.[1] Because these natural products have a unique ladder-like polycyclic molecular framework consisting of contiguous *trans*- and/or *cis*-fused polyether rings ranging in size from five- to nine-membered rings, several new synthetic methods have been aimed at the rapid construction of bi-, tri- and tetra-cyclic systems, including iterative strategies.[2]

We have already reported that the ceric(IV) ammonium nitrate (CAN) oxidation of cyclopropyl sulfides bearing a hydroxy group in a side chain promotes a S_N2-type nucleophilic substitution by the hydroxy group along with cleavage of the more substituted cyclopropyl carbon–carbon bond, giving rise to tetrahydrofuran and tetrahydropyran rings with perfect regio- and stereo-selectivity.[3] Our own interest in cyclic ether synthesis has recently been directed to a tandem synthesis of the polycyclic systems, using CAN induced double ether ring formation (**3** → **2**) and a Lewis acid-mediated trialkylsilane reduction (**2** → **1**), as shown in Scheme 1. We now report a stereoselective formation of the *trans*- and *cis*-fused tricyclic ether ring systems **1** containing five- and six-membered rings starting from 2α,4α- and 2β,4β-disubstituted 3-oxabicyclo-[3.1.0]hexyl sulfides **3**.

The several model compounds **4a**–**c** and **5b**–**c**, which possess different stereochemistry at C-2 and C-4, were synthesized to examine the applicability of the CAN-induced double ether ring formation (Table 1). Upon treatment of **4b** with CAN (8 equiv.) in dry MeOH in the presence of MS 3A at room temperature,[3] the *trans*-fused 6-6-5 tricyclic ketal **8b**† was obtained in 68% yield, and no other stereoisomers were detected (entry 2). Similarly, **4c** readily cyclized to the *cis*-fused 6-6-5 tricyclic ketal **8c**‡ in 62% yield under the same conditions (entry 3). In contrast to the *cis*-2,4-disubstituted diols **4b** and **4c**, the *trans*-2,4-disubstituted adduct **4a** gave no cyclized adducts. Indeed, only the bicyclic ketals **6** and **7** which were generated by an intermolecular nucleophilic substitution of a nitrate or methoxy group, were produced in 24 and 25% yields, respectively (entry 1). Although the different reactivity of **4a** compared with **4b** and **4c** is not clear at this stage, it is assumed that, in the case of **4a**, solvent and nitrate were introduced predominantly because the hydroxy group of the C-4 side chain, which is oriented axially in a preferred conformation (A), cannot attack the cyclopropyl carbon (C-5) from the proper back-side direction. In any event, these results demonstrate that the oxidative nucleophilic substitution by a hydroxy group to the cyclopropyl sulfides always occurs with perfect regio- and stereo-selectivity and that the sterically defined alignment of the nucleophile and fissile cyclopropyl bond is important for the ether ring formation.

Furthermore, both of the 6-6-5 triyclic ketals **8b** and **8c** were easily converted into the corresponding 6-6-5 tricyclic ethers **9b** and **9c** in good yields by known methods.[4] Specifically, the treatment of **8b** and **8c** with TMSOTf and Et_3SiH in CH_2Cl_2 at −78 °C resulted in stereoselective reduction, giving rise to the *trans-syn-cis*- and *cis-syn-cis*-fused 6-6-5 tricyclic products **9b**† and **9c**‡ as single isomers, respectively (entries 2 and 3). Finally, this method was applied to **5b** and **5c**, which possess two three-carbon side chains, with the aim of constructing a 6-6-6 tricyclic system. The same treatment of *cis*-2,4-disubstituted diols **5b** and **5c** as for **4a**–**c** gave the desired *trans-syn-trans*- and *cis-syn-trans*-fused 6-6-6 tricyclic ethers **11A**/**11B**[5] and **11C**† as the only products, respectively (entries 4 and 5).‡

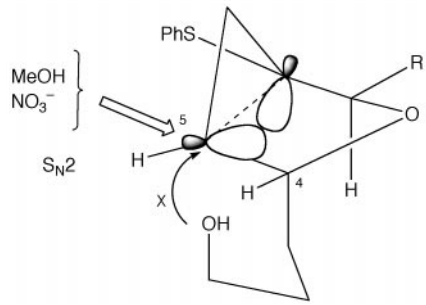

Fig. 1 Intermolecular nucleophilic ring-opening of **4a**.

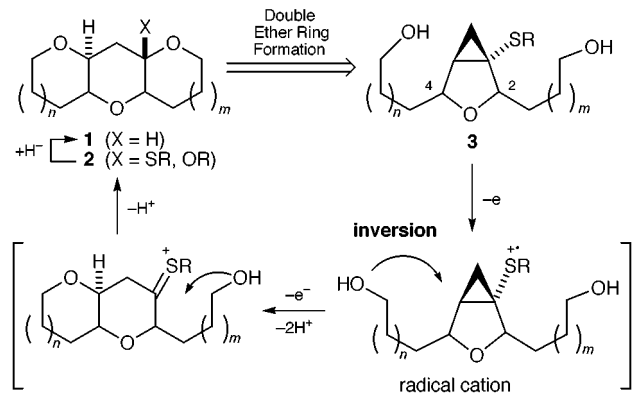

Scheme 1

Table 1 Tricyclic ether formation from bicyclic sulfides **4a**,**b** and **5b**,**c**

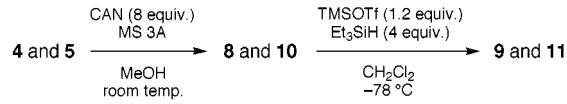

Entry	Substrate	Cyclic acetals (% yield)	Cyclic ethers (% yield)
1	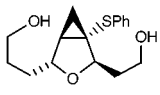 **4a**	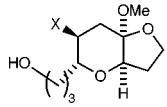 **6** X = OMe (24) **7** X = ONO_2 (25)	–
2	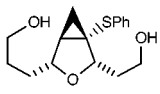 **4b**	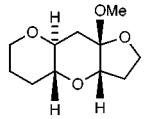 **8b** (68)	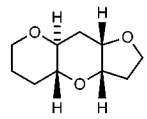 **9b** (68)
3	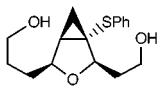 **4c**	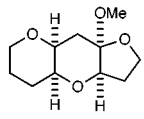 **8c** (62)	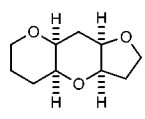 **9c** (67)
4	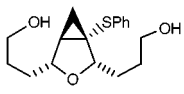 **5b**	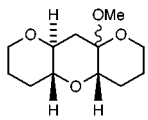 **10A/10B**[a] (60)	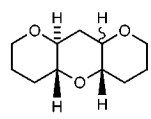 **11A** (α-H) **11B** (β-H) (79)[b]
5	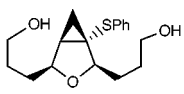 **5c**	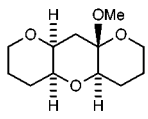 **10C** (70)	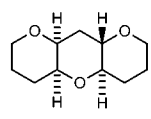 **11C** (88)

[a] **10A**:**10B** = 3:1. The ratio was calculated from isolated yields, but their stereochemistry could not be determined. [b] **11A**:**11B** = 3:1. The ratio was deduced from ^{1}H NMR analysis.

Since these tricyclic ether ring systems are frequently encountered constituents in polycyclic natural toxins, this method should be a versatile tool for the asymmetric synthesis of these biologically active natural products. More efficient synthesis of the starting bicyclic sulfides and further application to more advanced chiral fragments are under way in these laboratories.

This study was supported in part by a Grant-in-Aid for Scientific Research from the Ministry of Education, Science, Sports and Culture, Japan.

Notes and references

† Stereochemical assignments of these compounds were confirmed by NOE studies.

‡ Because the same treatment of the diastereomerically pure product **10A** also provided **11A** and **11B** with the same ratio (**11A**:**11B** = *ca.* 3:1), it appears that the stereochemistry of these diastereomers has no effect on the silane reduction.

1 Review: E. Alvarez, M. Candenas, R. Pérez, J. L. Ravelo and J. D. Martín, *Chem. Rev.*, 1995, **95**, 1953 and references cited therein; N. Hiro, H. Matsukura, G. Matsuo and T. Nakata, *Tetrahedron Lett.*, 1999, **40**, 2811; M. Sasaki, T. Noguchi and K. Tachibana, *Tetrahedron Lett.*, 1999, **40**, 1337; K. Fujiwara, K. Saka, D. Takaoka and A. Murai, *Synlett*, 1999, 1037; J. L. Bowman and F. E. McDonald, *J. Org. Chem.*, 1998, **63**, 3680; T. Oishi, Y. Nagumo and M. Hirama, *Chem. Commun.*, 1998, 1041; J. S. Clark and J. G. Kettle, *Tetrahedron Lett.*, 1997, **38**, 123; K. C. Nicolaou, M. H. D. Postema and C. F. Claiborne, *J. Am. Chem. Soc.*, 1996, **118**, 1565; S. D. Rychnovsky and V. H. Dahanukar, *J. Org. Chem.*, 1996, **61**, 7648; M. Isobe, S. Hosokawa and K. Kira, *Chem. Lett.*, 1996, 473; I. Kadota, P. Jung-Youl, N. Koumura, G. Pollaud, Y. Matsukawa and Y. Yamamoto, *Tetrahedron Lett.*, 1995, **36**, 5777.

2 Y. Mori, K. Yaegashi and H. Furukawa, *Tetrahedron Lett.*, 1999, **40**, 7239; P. A. Evans, J. D. Roseman and L. T. Garber, *J. Org. Chem.*, 1996, **61**, 4880; N. Hayashi, K. Fujisawa and A. Murai, *Tetrahedron Lett.*, 1996, **37**, 6173; J. L. Ravelo, A. Regueiro, E, Rodríguez, J. de Vera and J. D. Martín, *Tetrahedron Lett.*, 1996, **37**, 2869.

3 Y. Takemoto, T. Ibuka, H. Hayase, A. Iwanaga, S. Yamagata, C. Iwata and T. Tanaka, *Tetrahedron Lett.*, 1998, **39**, 7545; Y. Takemoto, T. Ohra, H. Koike, S. Furuse, C. Iwata and H. Ohishi, *J. Org. Chem.*, 1994, **59**, 4727; Y. Takemoto, T. Ohra, S. Furuse, H. Koike and C. Iwata, *J. Chem. Soc., Chem. Commun.*, 1994, 1529.

4 K. C. Nicolaou, C.-K. Hwang and D. A. Nugiel, *J. Am. Chem. Soc.*, 1989, **111**, 4136; R. Noyori, S. Murata and M. Suzuki, *Tetrahedron*, 1981, **37**, 3899.

5 An authentic sample of **11B** was described in the following paper: E. Alvarez, R. Pérez, M. Rico, R. M. Rodríguez and D. Martín, *J. Org. Chem.*, 1996, **61**, 3003.

Communication 9/08088K

Synthesis and first application of a new family of monophosphine ferrocene ligands (MOPF)

Henriette L. Pedersen and Mogens Johannsen*

Department of Organic Chemistry, Technical University of Denmark, Building 201, DK-2800 Lyngby, Denmark. E-mail: okmj@pop.dtu.dk

Received (in Liverpool, UK) 9th November 1999, Accepted 11th November 1999

A new family of monophosphine ferrocene ligands (MOPF) has been synthesised in two steps from an optically pure ferrocenyl sulfoxide and the first preliminary studies employing these ligands in asymmetric hydrosilylation of styrene are presented.

During the last decades only very few efficient chiral monophosphine ligands have been developed, in which the only Lewis base is the phosphorus atom. The fact that bisphosphine ligands form more rigid and stable complexes with metals, as compared to those with monophosphines, has probably stimulated the more abundant research in the former type. However, recently it has become increasingly clear that there is a need for efficient chiral monophosphine ligands for use in those reactions where the usual C_2-symmetric bisphosphines (*e.g.* BINAP) fail.[1]

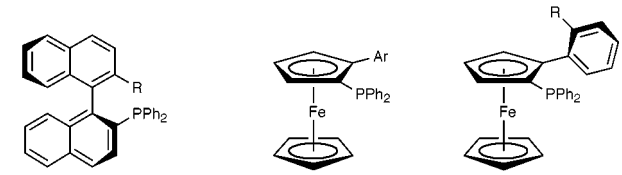

1 (*S*)-H-MOP R = H, (*S*)-MeO-MOP R = OMe

2 (*S*)-aryl-**MO**no**P**hosphino**F**errocene [(*S*)-MOPF]]

(*S*)-**2a** R = H, (*S*)-**2b** R = OMe

One of the few efficient types of monophosphine ligands discovered to date is Hayashi's MOP ligands **1**.[1a,2] Here we disclose a new family of arylMOnoPhosphinoFerrocene ligands **2** (herafter abbreviated MOPF), which show some resemblance to the MOP ligands, but are simpler to modify in a rational manner.[3]

We also present the first catalytic reactions employing these new ligands. In terms of enantioselectivity, the results are very encouraging and we believe that they can be further improved by simple variation of the aryl unit.

During the initial phase of this project we searched for a simple procedure to obtain a suitable building block for this new family of ligands. Recently, great progress has been achieved within the field of Directed *ortho*-Metallation (D*o*M) of ferrocenes.[4] However, the enantioselective *ortho*-lithiation of *e.g.* diphenylphosphinoferrocene, which in principle would allow us to synthesise these ligands in a single step, has met with only limited success.[5] On the other hand, Kagan *et al.*[4a,6] and Robinson *et al.*[4b] have recently described highly selective *ortho*-lithiation procedures of optically pure ferrocenyl sulfoxides. As the sulfoxide can be removed from the ferrocene by treatment with Bu^{t}Li we chose this compound as a starting material for the synthesis of the MOPF ligands. The synthesis of the first two members of the MOPF family is shown in Scheme 1. After diastereoselective *ortho*-lithiation of the sulfoxide (*S*)-**3**[4a] and lithium–zinc exchange, the aryl scaffold is introduced by a Negishi coupling giving **4**. The selective removal of the sulfoxide is accomplished with Bu^{t}Li and the lithiated ferrocene is then captured with $ClPPh_2$ giving the ligands (*S*)-**2a,b**.

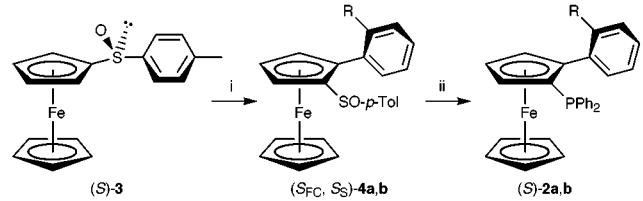

(*S*)-**3** (S_{FC}, S_S)-**4a,b** (*S*)-**2a,b**

Scheme 1 *Reagents and conditions*: i, LDA (1.2 equiv.), THF, −78 °C, 20 min, then $ZnCl_2$ (1 equiv.) −78 °C, 1 h, then Pd_2dba_3 (2 mol%), $P(fur)_3$ (8 mol%), aryl iodide, (1.5 equiv.), (R = H) room temp., 96 h, 67%, (R = OMe) reflux, 72 h, 54%; ii, (2 equiv.) Bu^{t}Li, THF, −78 °C, 5 min; then $ClPPh_2$, (3.5 equiv.) room temp., 3 h, (R = H) 67%, (R = OMe) 76%.

The potential and efficiency of the MOPF ligands is exemplified in the asymmetric hydrosilylation of styrene.[7] This transformation belongs to the class of reactions where *e.g.* BINAP gives only poor results.[1a] However, using the most simple phenyl-MOPF ligand **2a** the reaction proceeds nicely with up to 70% ee (Table 1, entries 1 and 2). Introducing a simple methoxy substituent on the aryl group interferes slightly with the selectivity of the reaction and it is observed that the addition of benzene as solvent improves the enantioselectivity from 60 to 64% (entries 3 and 4). Currently, we have no information on the catalytically active species in this reaction, but it is noteworthy that a similar but more pronounced behaviour has been observed in the hydrosilylation of styrene using H-MOP (91% ee) and MeO-MOP (14% ee) as ligands.[8] Moreover the sense of induction in the reactions using the (*S*)-MOPF or the (*S*)-H-MOP ligands is the same. The rationalisation of these observations, however, must await further study.

In summary, a short and efficient synthesis of two members of a novel family of monodentate phosphine ferrocene ligands (MOPF) has been carried out. The simple procedure developed paves the way for the preparation of an array of structurally varied aryl-MOPF ligands. The preliminary catalytic reactions employing these ligands have given encouraging results and we

Table 1 Enantioselective hydrosilylation of styrene using MOPF ligands 2a,b.[9]

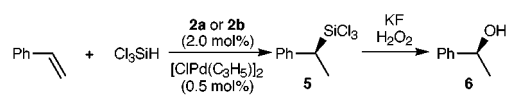

Entry	Ligand	*t*/h	*T*/°C	Yield of **5** (%)[a]	Ee of **6** (%)[bc]
1	**2a**	24	room temp.	66	70 (*S*)
2	**2a**	36	room temp.	73	70 (*S*)
3	**2b**	36	room temp.	49	60 (*S*)
4	**2b**	72	room temp.	41[d]	64 (*S*)[e]

[a] Isolated yield after destillation or flash chromatography. [b] Ee determined by HPLC on a DAICEL OD-H column. [c] Absolute configuration determined by optical rotation [see ref. 2(*b*)]. [d] Yield of **6** based on styrene. [e] Benzene added as solvent.

are pursuing the synthesis of a range of new aryl-MOPF as well as alkyl-MOPF family members in order to find even better ligands.[10]

Leo Pharmaceutical Products, the Technical University of Denmark and the Danish Ministry of Education are gratefully acknowledged for funding.

Notes and references

1 For some examples where monophosphine ligands or ligands with a phosphine and a hemilabile coordinating group are superior to the usual bisphosphines, see *e.g.*: (*a*) Asymmetric hydrosilylation: Y. Uozumi and T. Hayashi, *J. Am. Chem. Soc.*, 1991, **113**, 9887; (*b*) Asymmetric hydrovinylation: T. V. RajanBabu, N. Nomura, J. Jin, B. Radetich, H. Park and M. Nandi, *Chem. Eur. J.*, 1999, **5**, 1963; (*c*) Asymmetric Grignard cross-coupling: T. Hayashi, K. Hayashizaki, T. Kiyoi and Y. Ito, *J. Am. Chem. Soc.*, 1988, **110**, 8153.

2 For the synthesis and application of MOP and other monophosphine ligands see *e.g.*: (*a*) Y. Uozumi, A. Tanahashi, S.-Y. Lee and T. Hayashi, *J. Org. Chem.*, 1993, **58**, 1945; (*b*) K. Kitayama, Y. Uozumi and T. Hayashi, *J. Chem. Soc., Chem. Commun.*, 1995, 1533; (*c*) H. Tye, D. Smyth, C. Eldred and M. Wills, *Chem. Commun.*, 1997, 1053; (*d*) C. D. Graf, C. Malan, K. Harms and P. Knochel, *J. Org. Chem.*, 1999, **64**, 5581; (*e*) G. Zhu, Z. Chen, Q. Jiang, D. Xiao, P. Cao and X. Zhang, *J. Am. Chem. Soc.*, 1997, **119**, 3836; (*f*) B. L. Feringa, M. Pineschi, L. A. Arnold, R. Imbos and A. H. M. de Vries, *Angew. Chem., Int. Ed. Engl.*, 1997, **36**, 2620; (*g*) B. Bartels and G. Helmchen, *Chem. Commun.*, 1999, 741.

3 The MOPF ligands are structurally different from known ferrocene monophosphines which have a methylene spacer group next to the phosphine. See *e.g.* T. Hayashi, in *Ferrocenes*, ed. A. Togni and T. Hayashi, VCH, Weinheim, 1995, p. 118.

4 (*a*) O. Riant, G. Argourch, D. Guillaneux, O. Samuel and H. B. Kagan, *J. Org. Chem.*, 1998, **63**, 3511; (*b*) D. H. Hua, N. M. Lagneau, Y. Chen, P. M. Robben, G. Clapham and P. D. Robinson, *J. Org. Chem.*, 1996, **61**, 4508; (*c*) M. Tsukazaki, M. Tinkl, A. Roglans, B. J. Chapell, N. J. Taylor and V. Snieckus, *J. Am. Chem. Soc.*, 1996, **118**, 685; (*d*) For references prior to 1996 see: A. Togni, *Angew. Chem.*, 1996, **108**, 1581.

5 D. Price and N. S. Simpkins, *Tetrahedron Lett.*, 1995, **36**, 6135.

6 F. Rebière, O. Riant, L. Richard and H. B. Kagan, *Angew. Chem.*, 1993, **105**, 644.

7 For other asymmetric hydrosilylation reactions of styrene see *e.g.*: G. Bringmann, A. Wuzik, M. Breuning, P. Henschel, K. Peters and E.-M. Peters, *Tetrahedron: Asymmetry*, 1999, **10**, 3025; G. Pioda and A. Togni, *Tetrahedron: Asymmetry*, 1999, **9**, 3903; T. Okada, T. Morimoto and K. Achiwa, *Chem. Lett.*, 1990, 999.

8 This selectivity has been shown to be substrate dependent. MeO-MOP generally gave better results than H-MOP using non-styrene-type substrates such as *e.g.* oct-1-ene (up to 96% ee) [ref. 2(*b*)]. We are currently investigating the MOPF ligands to see whether they display similar behaviour.

9 *A representative hydrosilylation–oxidation procedure*: To a flame dried Schlenk tube was added $[ClPd(C_3H_5)]_2$ (6.2 mg, 0.017 mmol) and **2b** (30 mg, 0.067 mmol) under N_2. The solids were dried on the vacuum line for 1 h before styrene (0.378 ml, 3.3 mmol) and 2 ml of benzene were added *via* syringe. After another 30 min the silane (0.404 ml, 4 mmol) was added *via* syringe and the solution was left with stirring for 72 h. An aliquot of the reaction was used for NMR and it showed that the reaction was completed. The crude reaction mixture was slowly added to a suspension of KF (3.9 g, 67 mmol) in 30 ml of MeOH and the resulting solution was stirred for 30 min. The solvent was evaporated *in vacuo* and the resulting solid was suspended in 40 ml of DMF. Finally 4 ml H_2O_2 (35%) was added at room temperature and the reaction was heated to 60 °C for 1 h before quenching with 30 ml saturated $Na_2S_2O_3$ (aq). After aqueous workup and extraction the product was purified by flash column chromatography (15% EtOAc in pentane) giving **6** as a colorless oil in 41% yield (167 mg) and 64% ee detected by HLPC using a Chiralcel OD-H column (10% Pr^iOH–90% hexane, 0.5 ml min^{-1}). $[\alpha]_D^{rt}$ –36 (*c* 1.065, $CHCl_3$). Spectroscopic data were in accordance with those from a commercial sample.

10 During the course of our investigation we became aware of a paper from another group synthesising related benzene chromium tricarbonyl complexes. This prompted us to report our findings at this early stage. See: S. C. Nelson and M. A. Hilfiker, *Org. Lett.*, 1999, **1**, 1379.

Communication 9/08921G

ChemComm

Intramolecular Diels–Alder reaction in 1-oxaspiro[2.5]octa-5,7-dien-4-one and sigmatropic shifts in excited states: novel route to sterpuranes and linear triquinanes: formal total synthesis of (±)-coriolin

Vishwakarma Singh* and S. Q. Alam

Department of Chemistry, Indian Institute of Technology Bombay, Powai Mumbai 400 076, India. E-mail: vks.ether.chem.iitb.ernet.in

Received (in Cambridge, UK) 13th October 1999, Accepted 9th November 1999

A novel, stereoselective synthesis of sterpuranes and coriolin *via* modulation of the photochemical reactivity of a tricyclic system having a β,γ-enone chromophore, which was assembled *via* intramolecular $\pi^{4s} + \pi^{2s}$ cycloaddition of 1-oxaspiro[2.5]octa-5,7-dien-4-ones, is presented.

The fungal metabolites **1**–**3** and coriolin **4** are natural products of the sterpurane[1] and triquinane[2] families of sesquiterpenes, respectively, which are biogenetically derived from humulene

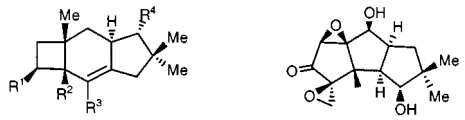

cyclization cascades.[1f] Coriolin[3] and other triquinanes have witnessed a high level of sustained interest which has led to the development of several new and elegant methods for the construction of tricyclopentanoids.[3–5] However, sterpuranes have elicited only modest interest[6] despite their unique structure, which contains a cyclobutane ring fused to a hydrindane system, and their role in silver leaf disease[1] and phytotoxicity.[6e] There are only a few methods for the synthesis of sterpuranes and most of these generate the carbocyclic framework in an iterative fashion wherein the cyclobutane ring is formed *via* intermolecular $\pi^{2s} + \pi^{2s}$ photocycloaddition.[6b–f] The elegant routes devised by Okamura[6g] and Krause,[6h] although efficiently generating the framework, begin with a precursor containing a cyclobutane ring. In continuation[7] of our efforts to develop new methods for the synthesis of natural products derived from humulene cyclization cascades, we contemplated a novel and general strategy to create the tricyclic sterpurane framework in a single stereoselective sequence which does not rely upon $\pi^{2s} + \pi^{2s}$ photocycloaddition for the formation of the cyclobutane ring. Remarkably, this strategy also provides a new route to linearly fused triquinanes from the same precursor *via* modulation of the chemical reactivity in the excited state.

The cornerstone of our strategy is the recognition of the structural and functional relationship between the sterpurane framework and the tricyclic system **6** containing a β,γ-enone chromophore. It was envisaged that a 1,3-acyl shift[8] in **6** upon singlet excitation would readily furnish the sterpurane framework **5** in such a fashion as to create all three rings in the correct relative stereochemical orientation and the double bond at the desired position, in a single step (Scheme 1). It was further thought that the key tricyclic precursor **6** might be synthesized *via* intramolecular $\pi^{4s} + \pi^{2s}$ cycloaddition of 1-oxaspiro-[2.5]octa-5,7-dien-4-ones of type **8** and further manipulation of the resulting adduct. In addition, we also visualized that triplet sensitized 1,2-migration[8,9] of the acyl group in **6** would lead to the tetracyclic system **7** (Scheme 1), which upon cleavage of the

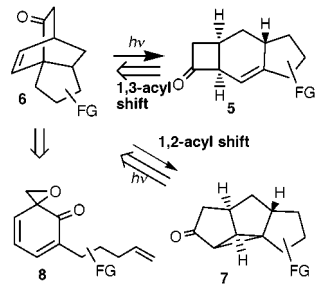

Scheme 1

cyclopropane ring might lead to linearly fused *cis*:*anti*:*cis*-:triquinanes. We report herein our exploratory results leading to a novel and general entry to sterpuranes and a formal total synthesis of coriolin from a common precursor.

Towards our objective, the key precursor **10** was prepared from aldehyde **9a**, which was obtained from alcohol **9b**.[10] Thus, the addition of Grignard reagent prepared from 4-bromobutene to aldehyde **9a** and subsequent oxidation of the resulting alcohol, followed by alkylation and removal of the acetonide protection, readily furnished the desired precursor **10**. Oxidation of **10** with $NaIO_4$ in MeCN–H_2O at 0 °C smoothly furnished the adduct **12** (Scheme 2) in excellent yield (71%). The adduct **12** is formed as a result of *in situ* generation of **11** during the oxidation and subsequent intramolecular Diels–Alder reaction. The structure and stereochemistry of the adduct were deduced from its high field ^{1}H NMR, COSY and NOE spectra. † The orientation of the oxirane ring is suggested on the basis of the general tendency of cyclohexa-2,4-dienones during addition.[7,11] It should be mentioned that there are only a few

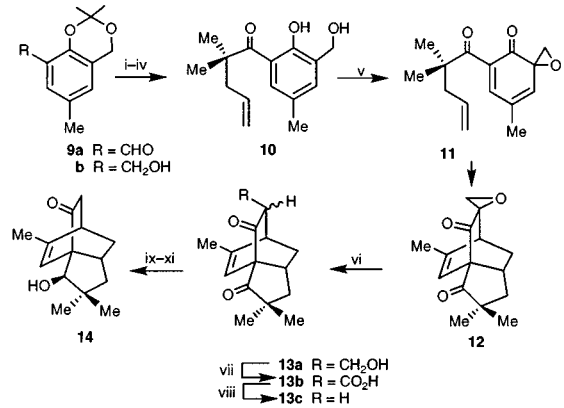

Scheme 2 *Reagents and conditions*: i, Mg, 4-bromobutene, THF, 85%; ii, PDC, CH_2Cl_2, 87%; iii, NaH, THF, MeI, 93%; iv, $HClO_4$, MeOH–H_2O, 81%; v, $NaIO_4$ MeCN–H_2O, 71%; vi, Zn, NH_4Cl, MeOH–H_2O, 78%; vii, Jones oxidation, 90%; viii, THF–H_2O, Δ, 71%; ix, ethylene glycol, benzene, TsOH, quant.; x, $NaBH_4$, THF–MeOH–H_2O, 85%; xi, HCl, acetone–water, 86%.

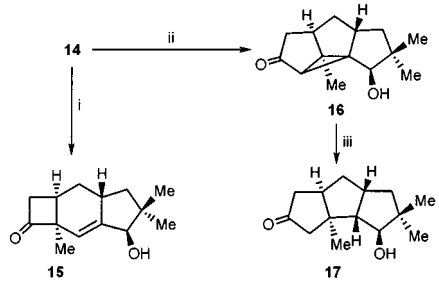

Scheme 3 *Reagents and conditions*: i, *hν*, benzene, 0.5 h, 55%; ii, *hν*, acetone, 1 h, 78%; iii, Bu_3SnH, AIBN, benzene, Δ, 5 h, 70%.

methods[12] for the preparation of bicyclo[2.2.2]octenones of type **12** annulated through bridgeheads.

The reduction of **12** with zinc and NH_4Cl in aqueous MeOH gave the β-keto alcohol **13a** [as a *syn*:*anti* mixture, ^{1}H NMR (300 MHz)] which was oxidized with Jones' reagent, and the resulting β-keto acid **13b** was subjected to decarboxylation to furnish the tricyclic system **13c** in good yield. Protection of the carbonyl group at the ethano bridge as a ketal and subsequent reduction of the resulting keto ketal with $NaBH_4$ in THF–MeOH–H_2O followed by deprotection of the ketal group efficiently gave the desired chromophoric system **14**. The stereochemical orientation of the hydroxy group is suggested from the down field signal of the C*H*OH proton (δ 4.06, br s) which was further confirmed *via* its transformation to the known triquinane **17** (*vide infra*).

Towards the synthesis of sterpuranes, a solution of **14** in dry benzene was irradiated with a mercury vapour lamp (125 W, Applied Photophysics) for about 30 min, upon which a clean reaction occurred (TLC, IR). Removal of the solvent followed by chromatography gave the tricyclic compound **15** in good yield (55%)‡ as a result of 1,3-acyl shift (Scheme 3). The structure of the photo-product **15** was clearly revealed from its spectral data.§

On the other hand, the triplet sensitized irradiation of **14** in acetone (sensitizer as well as solvent) in a Pyrex immersion well under nitrogen furnished the tetracyclic compound **16** in good isolated yield (78%) [83% conversion, unchanged starting material was recovered] whose structure was deduced from spectral data¶ and comparison with the spectral features of its precursor.[13] Cleavage of the peripheral cyclopropane bond with Bu_3SnH–AIBN[14] in refluxing benzene gave triquinane **17** (mp 117–118 °C) (Scheme 3), which has already been elaborated to coriolin.[15] The physical and spectral characteristics of **17** compared well with the reported data.[15] Thus, the formal synthesis of coriolin was complete.

In summary, we have described a novel and stereoselective method for the synthesis of sterpuranes which has wide synthetic potential, and a formal total synthesis of (±)-coriolin employing the intramolecular $\pi^{4s} + \pi^{2s}$ cycloaddition of 1-oxaspiro[2.5]octa-5,7-dien-4-one and sigmatropic shifts in excited states. This method, in turn, also provides a new and efficient avenue to annulated bicyclo[2.2.2]octenones of type **12**–**14** which are not readily accessible otherwise.

We thank RSIC, I.I.T. Bombay, for the use of high field NMR and mass spectral facilities. Financial support from BRNS is gratefully acknowledged. S.Q. Alam is grateful to I.I.T. Bombay for a Teaching Assistantship.

Notes and references

†All the compounds were thoroughly characterised with the help of spectral and analytical data. *Selected data* for adduct **12**: mp 66 °C; ν_{max}(KBr)/cm^{-1} 1755, 1716; δ_H(300 MHz, $CDCl_3$) 5.41 (br s, 1H), 3.16 (part of an AB system, J_{AB} ~7, 1H), 2.84 (part of AB system, J_{AB} ~7, 1H), 2.75 (m, 1H), 2.47–2.38 (complex m, 1H), 2.34 (m, 1H), 2.02 (dd, J_1 ~ 12, J_2 ~ 6.5, 1H), 1.94 (d with str, J ~ 2 , allylic coupling, 3H), 1.50 (superimposed dd, J_1 = J_2 = ~12 , 1H), 1.32 (ddd, J_1 ~ 12, J_2 ~ 7.5 , J_3 ~ 1.7, 1H), 1.14 (s, 3H), 1.09 (s, 3H,); δ_C(75 MHz, $CDCl_3$) 214.72 (CO), 197.55 (CO), 148.03, 118.25, 65.61, 56.87, 51.38, 48.24, 44.84, 42.39, 37.07, 27.81, 25.25, 23.92, 20.16; *m/z* 246 (M^+).

‡ All yields refer to isolated yields. Some unchanged starting material was recovered (~ 65% conversion).

§ *Selected data* for **15**: ν_{max}(film)/cm^{-1}: 3427,1773; δ_H(300 MHz, $CDCl_3$) 5.54 (br s, 1H), 3.99 (br m, 1H), 3.0 (d, of part of an AB system, J_1 18, J_2 9, 1H), 2.77 (d of part of an AB System, J_1 18, J_2 7, 1H), 2.55 (m, 1H), 2.37 (m, 1H), 2.0–1.92 (complex m, 2H), 1.60 (br d, J ~ 6, 1H, O-H), 1.29 (s, 3H, CH_3), 1.20 (dd, J_1 12, J_2 9, 1H, CH_2), 1.07 (dd, J_1 12, J_2 ~ 5, 1H, CH_2), 1.0 (s, 6H); δ_C(50 MHz, $CDCl_3$–CCl_4) 209.9, 150.5, 124.1, 82.5, 64.0, 46.14, 43.4, 41.3, 31.9, 31.5, 28.0, 27.8, 21.5, 21.1; *m/z* 220 (M^+).

¶ *Selected data* for **16**: mp 136–138 °C; ν_{max}(KBr)/cm^{-1} 3395, 1691; δ_H(300 MHz, $CDCl_3$) 3.42 (br d, 1H), 2.70-2.45 (m, 3H), 2.7 (s,1H), 1.95 (dd, J_1 12, J_2 9, 1H), 1.86-1.68 (m, 3H),1.40 (s, 4H, CH_3 and OH), 1.29 (dd, J_1 12, J_2 ~7, 1H), 1.08 (s, 3H), 1.02 (s, 3H); δ_C(75 MHz, $CDCl_3$) 215.25, 79.08, 56.53, 46.81, 46.56, 46.28, 46.23, 46.14, 45.43, 44.06, 42.10, 26.69, 21.98, 14.51; *(m/z* 220(M^+).

1 Isolation of **1**–**3**: (*a*) W. A. Ayer and M. H. Saeedi-Ghomi, *Can. J. Chem*., 1981, **59**, 2536; (*b*) O. Sterner, T. Anke, W. S. Sheldrick and W. Steglich, *Tetrahedron*, 1990, **46**, 2389; (*c*) J.-L. Xie, L.-P. Li and Z.-Q. Dai, *J. Org. Chem.*, 1992, **57**, 2313. Isolation of other sterpuranes: (*d*) C. Abell and A. P. Leech, *Tetrahedron Lett*., 1987, **28**, 4887; (*e*) G. Cimino, A. D. Giulio, S. D. Rosa and S. D. Stefano, *Tetrahedron*, 1989, **45**, 6479; (*f*) W. A. Ayer and L. M. Browne, *Tetrahedron*, 1981, **37**, 2199.

2 T. Takeuchi, H. Iinuma, J. Iwanaga, S. Takahashi, T. Takita and H. Umezawa, *J. Antibiot*., 1969, **22**, 215; S. Takahashi, H. Naganawa, H. Iinuma, T. Takita, K. Maeda and H. Umezawa, *Tetrahedron Lett*., 1971, 1955.

3 K. Domon, K. Masuya, K. Tanino and I. Kuwajima, *Tetrahedron Lett*., 1997, **38**, 465; V. Singh and B. Samanta, *Tetrahedron Lett*., 1999, **40**, 383; H. Mizuno, K. Domon, K. Masuya, K. Tanino and I. Kuwajima, *J. Org. Chem.*, 1999, **64**, 2648. For other references on synthesis of coriolin see ref. 4(*a*).

4 (*a*) For excellent review on polyquinane natural products: G. Mehta and A. Srikrishna, *Chem. Rev*., 1997, **97**, 671 and references cited therein; (*b*) R. D. Little, *Chem. Rev*., 1996, **96**, 93; (*c*) V. Singh and B. Thomas, *Tetrahedron*, 1998, **54**, 3647; (*c*) L. A. Paquette, *Top. Curr. Chem*., 1984, **119**, 1.

5 K. Masuya, K. Domon, K. Tanino and I. Kuwajima, *J. Am. Chem. Soc*., 1998, **120**, 1724; M. Lautens and J. Blackwell, *Synthesis*, 1998, 537; V. Krishnamurthy and V. H. Rawal, *J. Braz. Chem. Soc*., 1998, **9**, 341.

6 (*a*) Y. Murata, T. Ohtsuka, H. Shirahama and T. Matsumoto, *Tetrahedron Lett*., 1981, **22**, 4313; (*b*) L. Moens, M. M. Baizer and R. D. Little, *J. Org. Chem*., 1986, **51**, 4497; (*c*) L. A. Paquette, H.-S. Lin, B. P. Gunn and M. J. Coghlan, *J. Am. Chem. Soc*., 1988, **110**, 5818; (*d*) S.-K. Zhao and P. Helquist, *J. Org. Chem*., 1990, **55**, 5820; (*e*) G. M. Strunz, R. Bethell, M. T. Dumas and N. Boyonoski, *Can. J. Chem*., 1997, **75**, 742; (*f*) O. J. Birkenes, T. V. Hansen, S. M'dachi, L. Skattebol and Y. Stenstrom, *Acta. Chem. Scand*., 1998, **52**, 806; (*g*) R. A. Gibbs, K. Bartels, R. W. K. Lee and W. H. Okamura, *J. Am. Chem. Soc*., 1989, **111**, 3717; (*h*) N. Krause, *Liebigs Ann. Chem*., 1993, 521; (*i*) A. Arnone, C. D. Gregorio, G. Nasini and O. V. D. Pava, *J. Chem. Soc., Perkin Trans. 1*, 1997, 1523.

7 V. Singh, *Acc. Chem. Res*., 1999, **32**, 324.

8 D. I. Schuster, in *Rearrangement in Ground and Excited States*, ed. P. deMayo, Academic Press, New York, 1980, vol. **3**; V. Singh and M. Porinchu, *Tetrahedron*, 1996, **52**, 7087.

9 H. E. Zimmerman and D. Armesto, *Chem. Rev*., 1996, **96**, 3065.

10 K. Tsubaki, T. Otsubo, K. Tanaka, K. Fuji and T. Kinoshita, *J. Org. Chem*., 1998, **63**, 3260.

11 E. Adler and K. Holmberg, *Acta. Chem. Scand*., 1974, **28B**, 465; V. Singh, A. V. Bedekar and M. R. Caira, *J. Chem. Res*. (*S*), 1995, 452.

12 M. Demuth and W. Hinsken, *Angew. Chem., Int. Ed. Engl*., 1985, **24**, 973; J.-T Hwang and C.-C. Liao, *Tetrahedron. Lett*., 1991, **32**, 6583.

13 For synthesis of tetracyclic systems of type 16 by *meta*-photocycloaddition, P. A. Wender and J. J. Howbert, *Tetrahedron Lett*., 1982, **23**, 3983.

14 E. J. Enholm and Z.J. Jia, *J. Org. Chem*., 1997, **62**, 174.

15 R. L. Funk, G. L. Bolton, J. U. Daggett, M. M. Hansen and L. H. M. Horcher, *Tetrahedron*, 1985, **41**, 3479; L. V. Hijfte, R. D. Little, J. L. Petersen and K. D. Moeller, *J. Org. Chem*., 1987, **52**, 4647.

Communication 9/08223I

New bipyridyl ligands bearing azo- and imino-linked chromophores. Synthesis and nonlinear optical studies of related dipolar zinc complexes†

Adam Hilton,[a] Thierry Renouard,[a] Olivier Maury,[a] Hubert Le Bozec,*[a] Isabelle Ledoux[b] and Joseph Zyss[b]

[a] *Laboratoire de Chimie de Coordination et Catalyse, UMR 6509 CNRS-Université Rennes 1, Campus de Beaulieu, 35042 Rennes cedex, France. E-mail: lebozec@univ-rennes1.fr*

[b] *Laboratoire de Physique Quantique Moléculaire, ENS Cachan, 61 avenue du président Wilson, 94235 Cachan, France*

Received (in Cambridge, UK) 8th October 1999, Accepted 10th November 1999

The synthesis and optical properties of 4,4′-bis(dialkylaminophenylazo)-2,2′-bipyridine and 4,4′-bis(dialkylaminophenylimino)-2,2′-bipyridine ligands are described; the corresponding dipolar bipyridyl zinc dichloride complexes have been prepared and their second order nonlinear optical properties determined by electric field-induced second harmonic generation (EFISH) at 1.34 μm.

Poled polymers containing second order nonlinear (NLO) molecules are particularly promising for electrooptic device applications. Usually, dipolar chromophores have to be aligned by using electric field poling near the glass transition temperature (T_g) of the polymer.[1] Besides this approach, which requires high temperature treatment, new mild optical poling techniques have been developed recently. The so-called 'photo-assisted electrical' poling[2] and the 'all optical' poling[3] can be used at room temperature for the macroscopic noncentrosymmetric organisation of dipolar and octupolar chromophores, respectively. These methods require the presence of chromophores featuring a photoisomerisable moiety and use the 'flexibility' of the molecule to break the centrosymmetry of the material.

We have previously reported that metalloorganic complexes containing π-donor substituted 4,4′-alkenyl-2,2′-bipyridyl ligands[4] such as **a** and **b** (Scheme 1), show large dipolar or octupolar microscopic nonlinearities.[5] As the C=C double bond is known to be poorly photoisomerisable as compared, for example, to the N=N double bond,[6] we sought to design new potentially photoisomerisable bipyridines by introducing nitrogen atoms into the transmitter. Herein we report the synthesis and characterisation of new bipyridines bearing azo- as well as imino-linked donor groups. We also describe the preparation of the corresponding dipolar zinc(II) complexes; the influence of the nature of the π-bridge on the linear and nonlinear properties of these complexes is also reported.

The synthesis of the azo-containing bipyridyl ligand **c** was readily accomplished in two steps from 4,4′-dinitro-2,2′-bipyridine-1,1′-dioxide[7] [Scheme 1, eqn. (1)]: 4,4′-diamino-2,2′-bipyridine was first prepared in quantitative yield by using hydrazine hydrate in the presence of Pd/C.[8] This mild and efficient method contrasts favourably with the well-known but poorly yielding (20%) procedure using Fe/AcOH as the reducing agent.[9] Finally, the diazotation of 4,4′-diamino-2,2′-bipyridine with sodium nitrite and subsequent coupling with *N*,*N*-dibutylaniline afforded derivative **c**, which was isolated (yield 25%) as dark red microcrystals after chromatographic workup. Imino-containing bipyridine **d** was synthesised in excellent yield (95%) by a Schiff base condensation reaction between *N*,*N*-diethyl-1,4-phenylenediamine and 4,4′-diformyl-2,2′-bipyridine[10] [Scheme 1, eqn. (2)]. Attempts to isolate the 'reverse' imino-bipyridine from the reaction of 4,4′-diamino-2,2′-bipyridine and diethylaminobenzaldehyde failed, confirming the already observed deactivation of the amino and carbonyl functions in the presence of acceptor and donor groups, respectively.[11] Ligands **c** and **d** were characterised by ^{1}H NMR and high resolution mass spectrometry. Their optical spectra and those of the related aminostyryl derivatives **a** and **b** are displayed in Fig. 1. Most importantly, a large bathochromic shift of the ICT band is observed on exchanging the C=C bond for an N=N ($\Delta\lambda_{max}$ = 71 nm) or N=C ($\Delta\lambda_{max}$ = 36 nm) bond. This effect has been already described for other chromophores: Ulman *et al.*[12] reported a bathochromic shift of 40 nm between 4-dimethylamino-4′-dimethylsulfonylazobenzene and the corresponding stilbene derivative, while Whitall *et al.* described a 20 nm shift between an imino-benzene and the corresponding stilbene ruthenium complex.[11a] In the latter case the shift was accompanied by a strong decrease of the molar extinction coefficient ε, an hypsochromic effect which is not observed in our case.

Tetrahedral zinc complexes **1a**–**d** (Scheme 2) were readily prepared upon room temperature treatment of the ligands **a**–**d** with $ZnCl_2$ in dichloromethane.[5a] In their UV-vis spectra (Fig. 1, Table 1), a red-shift of the intense ILCT (intraligand charge-transfer) band is observed ($\Delta\lambda_{max}$ = 45–60 nm), as expected from the inductive acceptor strength of the Lewis acid.[13] As in the free ligand, λ_{max} is sensitive to the nature of the X=Y transmitter and follows the order N=N > N=C > C=C.

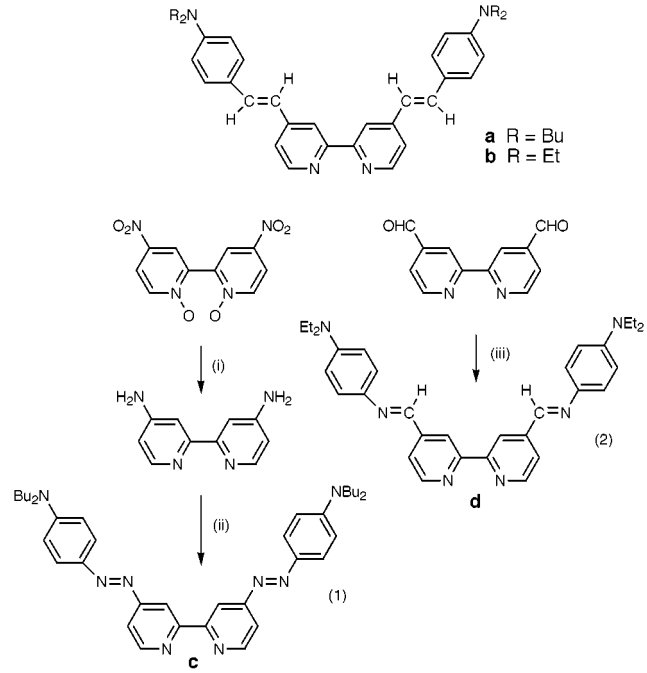

Scheme 1 (i) Pd/C (10%), $N_2H_4{\cdot}H_2O$, EtOH, reflux, 8 h, 100%; (ii) $NaNO_2$, $Bu_2NC_6H_5$ in THF, 0–5 °C, 2 h, 25%; (iii) $Et_2NC_6H_4NH_2$, $MgSO_4$, THF, reflux, 12 h, 95%.

† Electronic supplementary information (ESI) available: experimental procedures and spectroscopic data. See http://www.rsc.org/suppdata/cc/1999/2521/

Table 1 Linear and nonlinear data for the free ligands and their $ZnCl_2$ complexes

Ligand	λ_{max}[a]/nm	ε/mol^{-1} cm^{-1}	Complex	λ_{max}[a]/nm	ε/mol^{-1} cm^{-1}	$\mu\beta$[b]/10^{-48} esu[c]	$\mu\beta_0$[b]/10^{-48} esu[c]
a	397	57000	**1a**	455	62000	1420	660
b	401	65000	**1b**	459	62000	1830	850
c	471	63000	**1c**	516	63000	2160	700
d	433	52000	**1d**	491	55000	1610	620

[a] Solution in CH_2Cl_2. [b] Solution in $CHCl_3$; the precision of the measurement is about 10%. [c] Correlation between esu and SI units: β(SI) = 4.172 × 10^{-10} β (esu).

The molecular hyperpolarisabilities $\mu\beta$ of **1a**–**d** were measured in chloroform using electric field-induced second harmonic generation (EFISH) at 1340 nm, and the nonresonant $\mu\beta_0$ values were calculated using the two-level model (Table 1).[14] The results show that these complexes have good nonlinear optical activities, which are sensitive to the nature of both the transmitter and donor groups. For a given bridge, such as in **1a** and **1b**, dibutylaminophenyl is more efficient than the diethylaminophenyl group, a variation already observed for octupolar complexes.[5d] For a given donor, a slight increase in $\mu\beta$ is also observed on replacing CH by N. However, comparison of the zero-frequency $\mu\beta_0$ values reveals that the increase in nonlinearity seems to be mainly due to resonant enhancement.

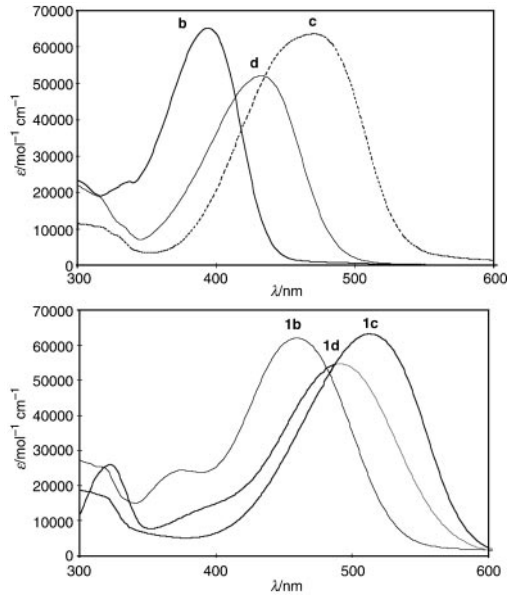

Fig. 1 UV-Vis spectra of the free bipyridine ligands (top) and related complexes (bottom).

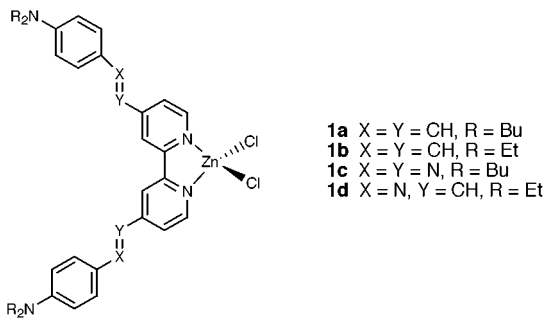

Scheme 2 (L-L)$ZnCl_2$ complexes.

In conclusion we have described the synthesis of new bipyridyl ligands bearing imino and azo substituents. The NLO activity of the chromophore **1c**, which contains the most suitable photoisomerisable azo ligand, can be favourably compared with that of the prototypical azo dye DR1 (λ_{max} = 480 nm, $\mu\beta_0$ = 450 × 10^{-48} esu).[15] Research is now in progress to study the photoassisted electrical poling of such dipoles in polymer films. Finally, these ligands provide access to D_3 octupolar complexes which will be promising candidates for the 'all optical' poling method.

We thank the CNRS (Programme Matériaux), the CNET and the Conseil Régional de Bretagne for financial support.

Notes and references

1 T. J. Marks and M. A. Ratner, *Angew. Chem., Int. Ed. Engl.*, 1995, **34**, 155 and references therein.
2 Z. Sekkat and M. Dumont, *Mol. Cryst. Liq. Cryst. Sci. Technol., Sect B*, 1992, **2**, 359; R. Loucif-Saibi, K. Nakatani, J. A. Delaire, M. Dumont and Z. Sekkat, *Chem. Mater.*, 1993, **5**, 229.
3 J. M. Nunzi, F. Charra, C. Fiorini and J. Zyss, *Chem. Phys. Lett.*, 1994, **219**, 349.
4 A. Juris, S. Campagna, I. Bidd, J. M. Lehn and R. Ziessel, *Inorg. Chem.*, 1988, **27**, 4007; M. Bourgault, T. Renouard, B. Lognoné, C. Mountassir and H. Le Bozec, *Can. J. Chem.*, 1997, **75**, 318.
5 For dipolar molecules see: (*a*) M. Bourgault, K. Baum, H. Le Bozec, G. Pucetti, I. Ledoux and J. Zyss, *New J. Chem.*, 1998, 517. For octupolar molecules see: (*b*) C. Dhenaut, I. Ledoux, I. D. W. Samuel, J. Zyss, M. Bourgault and H. Le Bozec, *Nature*, 1995, **374**, 339; (*c*) T. Renouard, H. Le Bozec, I. Ledoux and J. Zyss, *Chem. Commun.*, 1999, 871. For a review see: (*d*) H. Le Bozec and T. Renouard, *Eur. J. Inorg. Chem.*, in press.
6 V. Wing-Wah Yam, V. Chor-Yue Lau and L. X. Wu, *J. Chem. Soc., Dalton Trans.*, 1998, 1461.
7 P. Wehman, G. C. Dol, E. R. Morrman, P. C. J. Kamer and P. W. N. M. van Leeuwen, *Organometallics*, 1994, **13**, 4856. **CAUTION!** During a nitration reaction, a strong explosion occurred.
8 H. Camren, M.-Y. Chang, L. Zen and E. McGuire, *Synth. Commun.*, 1996, **26**, 1247.
9 G. Maerker and F. H. Case, *J. Am. Chem. Soc.*, 1958, **80**, 2745.
10 P. Dupau, T. Renouard and H. Le Bozec, *Tetrahedron Lett.*, 1996, **37**, 7503.
11 (*a*) I. R. Whittall, M. G. Humphrey, A. Persoons and S. Houbrechts, *Organometallics*, 1996, **15**, 1935; (*b*) S. S. P. Chou, D. J. Sun, H. C. Lin and P. K. Yang, *Chem. Commun.*, 1996, 1045.
12 A. Ulman, C. S. Willand, W. Köhler, D. R. Robello, Q. J. Williams and L. Handley, *J. Am. Chem. Soc.*, 1990, **112**, 7083.
13 D. R. Kanis, P. G. Lacroix, M. A. Ratner and T. J. Marks, *J. Am. Chem. Soc.*, 1994, **116**, 10 089.
14 J. L. Oudar, *J. Chem. Phys.*, 1977, **67**, 446; I. Ledoux and J. Zyss, *Chem. Phys.*, 1982, **63**, 203.
15 C. W. Dirk, H. E. Katz, M. L. Schilling and L. A. King, *Chem. Mater.*, 1990, **2**, 700.

Communication 9/08197F

First asymmetric desymmetrisation of a centrosymmetric molecule: CBS reduction of a 2-pyridone [4 + 4]-photodimer derivative

Alan C. Spivey,*[a] Benjamin I. Andrews,[a] Alan D. Brown[b] and Christopher S. Frampton[c]

[a] *Department of Chemistry, University of Sheffield, Brook Hill, Sheffield, UK S3 7HF. E-mail: a.c.spivey@sheffield.ac.uk*
[b] *Pfizer Central Research, Sandwich, Kent, UK CT13 9NJ*
[c] *Roche Discovery Welwyn, 40 Broadwater Road, Welwyn Garden City, Hertfordshire, UK AL7 3AY*

Received (in Liverpool, UK) 6th October 1999, Accepted 25th October 1999

The *B*-Me-(*S*)-CBS catalysed borane reduction of centrosymmetric bis-*N*-Boc tetrahydro photodimer 3 has been achieved with virtually complete enantiotopic group selectivity (>97% ee) and in good yield (76%).

The exploitation of latent molecular symmetry to expedite synthesis is an attractive strategy in organic chemistry.[1] An exemplary tactic in this regard is the asymmetric desymmetrisation of *meso* intermediates,[2,3] *i.e.* compounds containing more than one stereocentre but which are achiral by virtue of overall molecular symmetry. This approach can provide access to enantiomerically pure compounds, often with a high degree of molecular complexity, in relatively few synthetic steps. The enantiotopic group differentiation can be achieved by either enzymatic[4] or synthetic[5] means.

However, to the best of our knowledge, this strategy has only been employed with *meso* compounds containing a mirror plane. We were intrigued by the possibility of asymmetric desymmetrisation of *meso* compounds containing a centre of symmetry, *i.e.* centrosymmetric compounds. Of particular interest to us was the prospect of desymmetrising centrosymmetric [4 + 4]-photodimer derivatives of 2-pyridone[6] as the key step in a conceptually new route to functionalised amino acids. Here we describe enantiotopic amide carbonyl group differentiation using 'chiral' hydride (Scheme 1).

Despite the plethora of literature pertaining to asymmetric carbonyl reduction by chiral hydride reagents,[7] the only work reported on amidic compounds has been the desymmetrisation of *meso* imides.[8] For example, Speckamp has described the catalytic asymmetric reduction of cyclic *meso* imides using the Corey–Bakshi–Shibata (CBS) method in 68–94% ee.[8]

For the CBS reduction of [4 + 4]-photodimers of 2-pyridone to be successful, we anticipated that 'activation' of the amide carbonyl groups towards reduction would be necessary and envisaged that *N*-Boc derivatisation would serve this purpose.[9] Furthermore, we decided to work initially on a saturated tetrahydro photodimer derivative so as to allow the optimisation of the CBS reduction without the potential complications of competing hydroboration.[10]

Irradiation (350 nm) of an aqueous solution of 2-pyridone **1** (20 g in 50 ml) in a Rayonet reactor over 5 days caused [4 + 4]-photodimer **2** to precipitate from solution as white crystals (10.4 g, 52%).[11] Treatment with BuLi/Boc_2O in THF gave the bis-*N*-Boc derivative, and subsequent bis-hydrogenation using Adams' catalyst[11] furnished the bis-*N*-Boc tetrahydro photodimer **3** in excellent yield (Scheme 2).

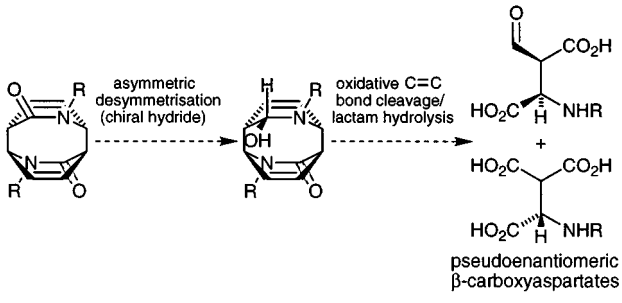

Scheme 1

Uncatalysed reaction of the bis-*N*-Boc tetrahydro photodimer **3** with $BH_3{\cdot}SMe_2$ was found to be slow, affording the racemic monolactamol† (±)-**4** in 16% yield after 22 h (entry 1, Table 1). Examination of the single crystal X-ray structure of this racemic monolactamol (±)-**4**‡ revealed it to have been formed by 'axial' attack of hydride at C3§ (this was expected as 'equatorial' attack of hydride at C3 is blocked by the C9, C10 ethylene bridge).

Using *B*-Me-(*S*)-CBS·BH_3 complex synthesised from (*S*)-proline,[12]¶ a systematic investigation of the asymmetric reduction of bis-*N*-Boc tetrahydro photodimer **3** was undertaken (Table 1).

Initial attempts at the asymmetric reduction in CH_2Cl_2 gave poor conversions and moderate ees, presumably due to the low catalyst loading and competing uncatalysed reduction by excess $BH_3{\cdot}SMe_2$ (entries 2, 3). A stoichiometric amount of catalyst and a 1:1 ratio of catalyst to borane gave significantly improved yields and ees (entries 4–6). Finally, performing the reaction at higher concentrations in $CHCl_3$ allowed for sub-stoichiometric amounts of catalyst to be used, producing the bis-*N*-Boc

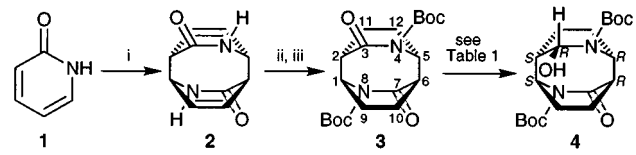

Scheme 2 *Reagents and conditions*: i, hν = 350 nm, H_2O (52%); ii, BuLi (2.5 equiv.), Boc_2O (4 equiv.), THF (98%); iii, H_2 (3 bar), PtO_2 (0.2 equiv.), EtOAc (100%).

Table 1 Optimisation of the *B*-Me-(*S*)-CBS·BH_3 catalysed asymmetric reduction of bis-*N*-Boc tetrahydro photodimer **3**

					Monolactamol **4**	
Entry[a]	*B*-Me-(*S*)-CBS·BH_3/ equiv.	$BH_3{\cdot}SMe_2$/ equiv.	*t*/h	Solvent (ml)	Yield[b] (%)	Ee[c] (%)
1	0	1.2	22	CH_2Cl_2 (10)	16	0
2	0.2	1.2	22	CH_2Cl_2 (10)	34	66
3	0.2	1.2	6	CH_2Cl_2 (10)	16	64
4	1	1	6	CH_2Cl_2 (10)	41	86
5	1	1	14	CH_2Cl_2 (10)	57	94
6	1	1	14	$CHCl_3$ (5)	63	96
7	0.5	0.5	14	$CHCl_3$ (2)	49	97
8	0.5	0.5	22	$CHCl_3$ (1)	76	97

[a] All reactions were performed on a 100 mg scale. [b] Isolated yield after column chromatography; the mass balance consists of photodimer **3** and lesser amounts of over-reduced products. [c] Determined by chiral HPLC [Column: Chiralcel OD (25 × 0.46 cm), eluting with 99.2:0.8 hexane–Pr^iOH, 1.0 ml min^{-1}, 40 °C, UV detection at 225 nm].

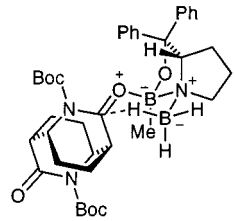

Fig. 1 Predicted transition state for the *B*-Me-(*S*)-CBS·BH_3 reduction of the bis-*N*-Boc tetrahydro-dimer **3** (NB. the larger *N*-Boc substituent is oriented equatorially and the smaller alkyl substituent is oriented axially in the chair transition state).

tetrahydro monolactamol in 76% yield and 97% ee (entries 7 and 8).

Based on the model proposed by Corey,[10] and corroborated by Speckamp for his imide reductions,[8] we predicted that the *B*-Me-(*S*)-CBS catalyst would deliver hydride selectively to the *Si*-face of the photodimer (Fig. 1).

To confirm this prediction we grew X-ray quality crystals of the enantiomerically pure monolactamol (+)-**4** {from entry 8, $[\alpha]_D$ +8.0, $[\alpha]_{365}$ +90.2 (*c* 0.5 $CHCl_3$)} and performed a single crystal X-ray structure determination using Cu-Kα irradiation.‖ This established the absolute configuration of monolactamol (+)-**4** as being (1*S*,2*S*,3*R*,5*R*,6*R*) as expected (Fig. 2, and as depicted in Scheme 2).

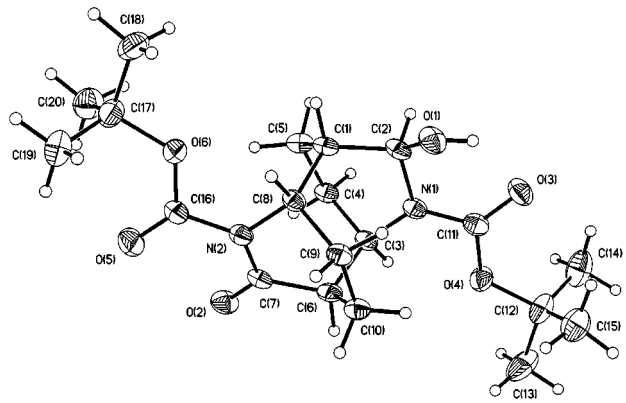

Fig. 2 ORTEP (50% probability ellipsoids) of the enantiomerically pure monolactamol (+)-**4**.‖

In conclusion, we have demonstrated that *B*-Me-(*S*)-CBS catalysed borane reduction of a bis-*N*-Boc tetrahydro photodimer can be achieved with virtually complete enantiotopic group selectivity (97% ee) and in good yield (76%). This provides efficient access to an enantiomerically pure product containing five chiral centres and represents the first asymmetric desymmetrisation of a centrosymmetric compound. It is also the first example of the asymmetric reduction of a *meso* diamide, and as such represents a significant extension of the scope and versatility of the CBS reduction process.

We are currently investigating the utility of related asymmetric desymmetrisations of unsaturated and more highly functionalised [4 + 4]-photodimer derivatives of 2-pyridone for the preparation of enantiomerically pure β-carboxyaspartic acid derivatives.

We thank the EPSRC and Pfizer for provision of a CASE studentship, and also the Nuffield Foundation and The Royal Society Equipment Fund for financial support of this work.

Notes and references

† We use the term lactamol in preference to cyclic hemiaminal (*cf.* lactone → lactol *vs.* lactam → lactamol).

‡ The single crystal X-ray structure for racemic monolactamol (±)-**4** is topologically superimposable on that of the enantiomerically pure compound (+)-**4**.‖

§ 'Axial' attack refers to the trajectory of hydride attack which results in an axial hydrogen in the 'double boat' structure of the photodimer product.

¶ The quality of the catalyst was confirmed by performing the asymmetric reduction of acetophenone to (*R*)-1-phenylethan-1-ol (ref. 13) in quantative yield and 95% ee using *B*-Me-(*S*)-CBS·BH_3 (0.1 equiv.), BH_3·SMe_2 (1.2 equiv.), CH_2Cl_2, room temp., 1 h.

‖ *Crystal data* for (+)-**4**: $C_{20}H_{32}N_2O_6$, M_r = 396.48, Rigaku AFC7R diffractometer, crystal dimensions 0.30 × 0.35 × 0.40 mm, T = 123(1) K, monoclinic, space group $P2_1$, a = 633.2(4), b = 2600.0(4), c = 672.0(3) pm, β = 112.63(4) °, V = 1.0211(8) nm^3, Z = 2, $\rho_{calc.}$ = 1.289 Mg m^{-3}, Cu-Kα radiation, (λ = 1.54178 Å), μ = 0.781 mm^{-1}, θ = 3.40–67.45°. 4008 reflections collected, 3589 were unique including one set of Bijvoet opposites (+h, +k, ±l and −h, −k, ±l) (R_{int} = 0.0140). Data were corrected for absorption by the method of ψ-scans, T_{min} and T_{max} = 0.916 and 0.999, repectively. Refinement by full-matrix least-squares on F^2, 295 refined parameters, 1 restraint gave R_1 = 0.0418, wR^2 = 0.1177 and GOF = 1.009 based on all 3589 data, absolute structure parameter = 0.14(19), residual density –0.22 and +0.19 e $Å^{-3}$. The structure was solved and refined using the SHELXTL suite of programs. All hydrogen atoms with the exception of the hydroxy, H(1B), were placed in geometric position, (U_{iso} freely refined). The hydroxy hydrogen was located in a difference map and its positional parameters and U_{iso} freely refined. CCDC 182/1471. See http://www.rsc.org/suppdata/cc/1999/2523/ for crystallographic data in .cif format.

1 *Symmetry: A Basis for Synthesis Design*, ed. T.-L. Ho, Wiley, New York, 1995.
2 M. C. Willis, *J. Chem. Soc., Perkin Trans. 1*, 1999, 1765.
3 S. R. Magnuson, *Tetrahedron*, 1995, **51**, 2167; C. S. Poss and S. L. Schreiber, *Acc. Chem. Res.*, 1994, **27**, 9.
4 F. Theil, *Chem. Rev.*, 1995, **95**, 2203.
5 M. Maier, *Group Selective Reactions*, in *Organic Synthesis Highlights II*, ed. H. Waldmann, VCH, Weinheim, 1995, p. 203.
6 S. McN. Sieburth and N. T. Cunard, *Tetrahedron*, 1996, **52**, 6251.
7 S. Itsuno, *Org. React.*, 1998, **52**, 395.
8 M. Ostendorf, R. Romagnoli, I. C. Pereiro, E. C. Roos, M. J. Moolenaar, W. N. Speckamp and H. Hiemstra, *Tetrahedron: Asymmetry*, 1997, **8**, 1773 and references therein.
9 R. K. Dieter and R. R. Sharma, *J. Org. Chem.*, 1996, **61**, 4180 and references therein.
10 E. J. Corey and C. J. Helal, *Angew. Chem., Int. Ed.*, 1998, **37**, 1986.
11 L. A. Paquette and G. Slomp, *J. Am. Chem. Soc.*, 1963, **85**, 765; E. C. Taylor and R. O. Kan, *J. Am. Chem. Soc.*, 1963, **85**, 776.
12 L. C. Xavier, J. J. Mohan, D. J. Mathre, A. S. Thompson, J. D. Carroll, E. G. Corley and R. Desmond, *Org. Synth.*, 1996, **74**, 50.
13 E. J. Corey, R. K. Bakshi and S. Shibata, *J. Am. Chem. Soc.*, 1987, **109**, 5551.

Communication 9/08059G

ChemComm

Selective binding of substrates using sodium salts of linked C_3 symmetric aryl oxides

Maarten B. Dinger and Michael J. Scott*

Department of Chemistry, University of Florida, PO Box 117200, Gainesville, FL 32611-7200, USA. E-mail: mjscott@chem.ufl.edu

Received (in Columbia, MO, USA) 14th September 1999, Accepted 3rd November 1999

Tris(3,5-dialkyl-2-hydroxyphenyl)methanes (*tert*-butyl, *tert*-pentyl) react with three equivalents of sodium hydride to give hexanuclear dimers; these bulky aggregates have six well-defined coordination 'pockets' which demonstrate selectivity toward a variety of ketones.

The design of molecules for the selective recognition of substrates has been an extremely active and growing area of research over the last number of years.[1] The utility of metal coordination chemistry, particularly aluminium, in a steric environment to give Lewis acidic selective reagents is clear, and a considerable body of work, largely pioneered Yamamoto,[2] regarding their use for a wide range of selective organic functional group transformations has been published.[3] Less developed work, using lithium phenolates[4] and zirconium naptholates,[5] amongst others, towards similar purposes have also been reported.

During our investigations[6] of the alkali metal salts of tris(3,5-dialkyl-2-hydroxyphenyl)methanes **1**,[7] it was clear from X-ray structure determinations that the sodium salts **2** are hexanuclear aggregates, with six coordinated solvent molecules (THF) residing in identical binding sites; somewhat surprisingly, this Na_6O_6 core had been structurally characterized only once previously.[8] From an examination of the structures, it was evident that the solvate molecules binding the metal atoms reside in a sterically crowded environment, offering the opportunity to prepare metal clusters capable of facilitating selective binding of a range of substrates. Herein we communicate our findings regarding these novel systems.

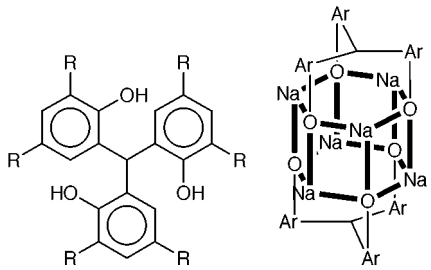

The reaction of tris(3,5-di-*tert*-butyl-2-hydroxyphenyl)methane **1a** with sodium hydride in Et_2O generates the dimeric, hexanuclear sodium salt **2a** in almost quantitative yield (^{1}H NMR).† When the bulkier tris(3,5-di-*tert*-pentyl-2-hydroxyphenyl)methane **1b** is used, refluxing THF is required for cluster formation. Examination of the crystal structures of the THF adducts of **2a** and **2b** reveals the solvent molecules reside in 'pockets' created by the aromatic rings and their aliphatic substituents. Complete removal of the coordinated solvent molecules can be readily achieved by evacuation with gentle warming.

The electrophilic nature of the coordinatively unsaturated sodiums is witnessed by their propensity to interact with very poor donor molecules. The solid state structure of the CH_2Cl_2 adduct of **2b** (Fig. 1)‡ reveals that all six sodium atoms are associated by a solvent molecule with an Na···Cl distance of 2.891(1) Å. Furthermore, the aromatic rings are canted slightly to allow for weak *ipso*-interactions with the sodiums [Na···C(3) 2.771(3) Å]. The sodium atoms clearly adopt extremely distorted tetrahedral geometries, exemplified with a minimum angle for O(1′)–Na–O(1) of only 93.21(7)°. When crystallized solely from Et_2O,[6] the cluster is forced to distort even more dramatically to allow for the binding of Et_2O molecules to only two of the six sodium atoms, and in the absence of a donor molecule, the average distance of the remaining four metal centers to the *ipso*-carbon of the aryl ring decreases to 2.676(5) Å.

Accordingly, addition of 6 equiv. of a variety of oxygen donor substances of suitable size and shape (THF, acetone, benzaldehyde, acetophenone, *trans*-cinnamaldehyde or cyclohexyl methyl ketone) to **2a** in Et_2O readily yields the corresponding adducts.§ In contrast, bulkier substrates, such as 2,5-dimethyltetrahydrofuran and 2,2,4,4-tetramethylpentan-3-one, fail to bind. Aromatic substrates immediately impart a color change upon coordination to **2a** or **2b**, with a distinctive absorption maxima evident in the visible region, providing a convenient avenue to rapidly screen binding affinities of new substrates. Et_2O and α,α,α-trimethylacetophenone bind only very poorly, and are readily displaced upon addition of more suitable molecules. Thus, addition of an equimolar mix of α,α,α-trimethylacetophenone and acetophenone to **2a** allows for complete separation of the two ketones by evaporation of the

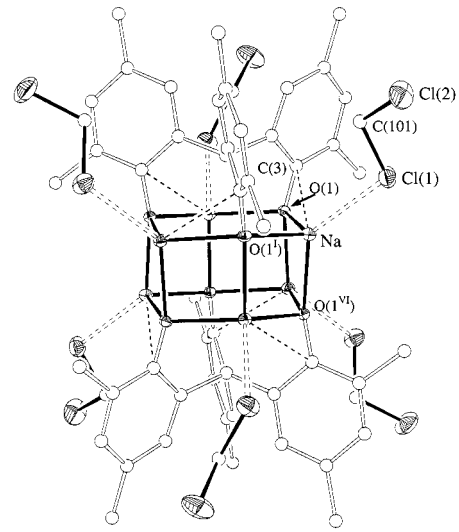

Fig. 1 Structure of **2b**·8.6CH_2Cl_2 (30% probability ellipsoids for Na, O and Cl). The molecule crystallizes on an S_6 symmetry position. Selected bond lengths (Å) and angles (°): Na···Cl(1) 2.89(1); Na···C(3) 2.771(3); Na–O(1) 2.326(2); Na–O(1) 2.280(2); Na–O(1^{VI}) 2.246(2); O(1)–Na–O(1^I) 112.88(9); O(1)–Na–O(1^{VI}) 93.21(7); O(1^I)–Na–O(1^{VI}) 94.47(7); O(1)–Na–Cl(1) 118.92(6); O(1^I)–Na–Cl(1) 103.91(6); O(1^{VI})–Na–Cl(1) 131.19(6)°. *tert*-Pentyl groups, hydrogen atoms, and additional CH_2Cl_2 solvate molecules have been omitted for clarity.

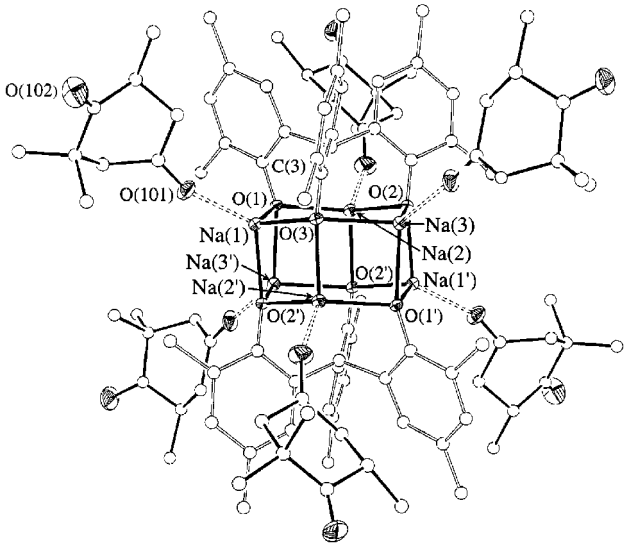

Fig. 2 Structure of **2b**·$6C_9H_{14}O_2$·$0.4Et_2O$ (30% probability ellipsoids for Na and O). Selected bond lengths (Å) and angles (°): Na(1)···O(101) 2.257(3); Na(1)–O(1) 2.362(2); Na(1)–O(3) 2.297(2); Na(1)–O(2′) 2.272(2); Na(1)···C(3) 2.748(3); O(1)–Na(1)–O(3) 116.82(8); O(1)–Na(1)–O(2′) 93.49(7); O(3)–Na(1)–O(2′) 96.27(8); O(1)–Na(1)–O(101) 116.67(9); O(3)–Na(1)–O(101) 109.54(9); O(2′)–Na(1)–O(101) 122.15(9). The *tert*-pentyl groups, hydrogen atoms and Et_2O solvate have been omitted for clarity.

solvent, and subsequent washing of the residue with pentane, in which the acetophenone adduct of **2a** is insoluble. In solution, ^{1}H NMR investigations demonstrate that only acetophenone binds in this mixture and a spectrum identical to an authentic sample of **2a**·$6C_8H_8O$ is observed.

Commercial 2,6-dimethylcyclohexanone is a thermodynamic mixture of isomers,[9] which we determined by GC to be in the ratio of 81:19 for *cis*:*trans*. When this ketone is added to **2a** so that at least 6 equiv. of the *trans* isomer are present, following workup, GC and NMR analyses reveals that the ratio of isomers now clearly favors the *trans* by 1:5. This selectivity further highlights the relative rigidity and discrete size of the 'pockets', since the two isomers differ only subtly in size and shape. To demonstrate the utility of this separation, 6 equiv. of 2,4-dinitrophenylhydrazine were added to the dimethylcyclohexanone coordinated cluster, and after work-up and recrystallization, exclusively the *trans*-isomer of the corresponding hydrazone was obtained in 73% yield.

Finally, when 2,2,6-trimethylcyclohexane-1,4-dione, a diketone that features both sterically and non-sterically crowded carbonyl functionalities, is added to **2b**, only the non-bulky end was found to bind the sodium metal (Fig. 2).¶ The ketone is obviously a much better donor than CH_2Cl_2 and maintains an average Na···O=C contact of 2.271(3) Å, a distance indistinguishable from the sodium–aryl oxide bonds. Despite the superior donor abilities of the carbonyl moiety in comparison to CH_2Cl_2, the Na–*ipso*-carbon interactions persist in this complex, with an average length of 2.749(3) Å. This system demonstrates the possibility for sterically protecting multifunctional group containing compounds, with the more reactive groups rendered inert, whilst chemistry at the less reactive sites is undertaken. The present compound, unfortunately, is only sparingly soluble, hindering reactivity studies.

In summary, we have synthesized coordinatively unsaturated sodium salts of bulky triaryloxymethanes, wherein the vacant coordination sites reside in discretely sized 'pockets'. The compounds have been successfully used to selectively bind only molecules that possess a size and shape compatible with the 'pocket'. In addition to simple chemical separations, this selectivity may have utility for the protection of reactive functional groups in chemical reactions.

We thank the University of Florida, the National Science Foundation (CAREER Award 9874966) and the donors of the American Chemical Society Petroleum Research Fund for funding this research. Support from the Research Corporation is also gratefully acknowledged.

Notes and references

† *General procedure* for synthesis of **2a**: Tris(3,5-di-*tert*-butyl-2-hydroxyphenyl)methane was dissolved in anhydrous Et_2O (20 ml) and dry NaH (0.03 g, excess) added. The resulting mixture was stirred at room temperature for 17 h. The excess NaH was filtered off, to leave a solution of **2a**, which was sufficiently pure for further reactions. **2b**: Tris(3,5-di-*tert*-pentyl-2-hydroxyphenyl)methane was dissolved in THF (15 ml), and excess NaH added. The milky solution was refluxed under nitrogen for 1 h. The solvent was evaporated under vacuum, and the resulting dry residue was heated to 60 °C under vacuum for 3 h, to remove coordinated THF. The residue was dissolved in Et_2O, and the excess NaH filtered off, leaving a solution of **2b** which was sufficiently pure for further reactions.

‡ *Crystal data* for **2b**·$8.6CH_2Cl_2$: $C_{106.6}H_{163.2}O_6Na_6Cl_{17.2}$, M = 2288.45, a = 14.423(2) , c = 50.468(8) Å, V = 9092(2) Å^3, rhombohedral, space group $R\bar{3}$ Z = 3, T = 173 K, final $R1$ = 0.0681 [for 3138 data $I \geq 2\sigma(I)$], $wR2$ = 0.1928 (all 3568 reflections), GoF (on F^2) = 1.098.

§ General procedure for synthesis of adducts: To an Et_2O solution of crude **2a** or **2b** was added 6 equiv. of aldehyde or ketone. The Et_2O was then slowly allowed to evaporate under a dry atmosphere, to give a crystalline residue. The crystals were then thoroughly washed with pentane producing the corresponding adduct.

¶ *Crystal data* for **2b**·$6C_9H_{14}O_2$·$0.4Et_2O$: $C_{153.6}H_{234}O_{18.4}Na_6$, M = 2519.13, a = 19.911(1), b = 15.528(1), c = 24.873(2) Å, β = 91.051(1)°, V = 7688.8(9) Å^3, monoclinic, space group $P2_1/n$, Z = 2, T = 173 K, final $R1$ = 0.0746 [for 9656 data $I \geq 2\sigma(I)$], $wR2$ = 0.2395 (all 15676 reflections), GoF (on F^2) = 1.029. Both structures were solved using the direct methods option of SHELXS. Full-matrix least-squares refinements based on F^2 were subsequently performed using SHELXL-97. (ref. 10). All non-hydrogen atoms, with the exception of a disordered CH_2Cl_2 in **2b**·$8.6CH_2Cl_2$ and a disordered Et_2O molecule in **2b**·$6C_9H_{14}O_2$·$0.4Et_2O$, were assigned anisotropic temperature factors, with corresponding hydrogen atoms included in calculated positions. CCDC 182/1479. See http://www.rsc.org/suppdata/cc/1999/2525/ for crystallographic data in .cif format.

1 Special thematic issue on molecular recognition, *Chem. Rev.*, 1997, **97**, 1231.
2 S. Saito and H. Yamamoto, *Chem. Commun.*, 1997, 1585 and references therein.
3 M. D. Healy, M. B. Power and A. R. Barron, *Coord. Chem. Rev.*, 1994, **130**, 63; A. Marx and H. Yamamoto, *Syn. Lett.*, 1999, 584 and references therein; T. Ooi, Y. Kondo and K. Maruoka, *Angew. Chem., Int. Ed.*, 1998, **37**, 3039.
4 L. M. Baigrie, H. R. Seiklay and T. T. Tidwell, *J. Am. Chem. Soc.*, 1985, **107**, 5391.
5 H. Ishitani, M. Ueno and S. Kobayashi, *J. Am. Chem. Soc*., 1997, **119**, 7153.
6 M. B. Dinger and M. J. Scott, manuscript in preparation.
7 The tris(3,5-dialkyl-2-hydroxyphenyl)methane ligands have also been utilized for the preparation of extended structures and the synthesis of the platforms will be reported elsewhere. M. B. Dinger and M. J. Scott, submitted for publication.
8 S. Schutte, U. K Lingebiel and D. Schmidt-Base, *Z. Naturforsch., Teil. B*, 1993, **48**, 263.
9 T. D. J. D'Silva and H J. Ringold, *Tetrahedron Lett*., 1967, 1505.
10 G. M. Sheldrick, SHELX, programs for crystal structure determination, University of Göttingen, 1997.

Communication 9/07476G

A β-galactoside phosphoramide mustard prodrug for use in conjunction with gene-directed enzyme prodrug therapy

Ajit K. Ghosh, Saeed Khan and David Farquhar*

Department of Experimental Therapeutics, The University of Texas M. D. Anderson Cancer Center, Houston, Texas 77030, USA. E-mail: dfarquha@mdanderson.org

Received (in Corvallis, OR, USA) 22nd September 1999, Accepted 2nd November 1999

4-(β-D-Galactopyranosyl)benzyl *N,N,N′,N′*-tetrakis(2-chloroethyl)phosphorodiamidate 1 was facilely biotransformed to the alkylating antitumor agent, *N,N,N′,N′*-tetrakis(2-chloroethyl) phosphorodiamidic acid, 4, when incubated with *E. coli* β-galactosidase, and therefore has potential for use in conjunction with gene-directed enzyme prodrug therapy.

Gene-directed enzyme prodrug therapy (GDEPT) has found increasing application in cancer therapy. In this approach, a foreign gene is introduced into the target tumor, usually with the aid of a viral or liposomal vector.[1–3] When the gene is expressed, it encodes for an enzyme that can convert a nontoxic prodrug to a cytotoxic product. Most GDEPT approaches reported to date have used ganciclovir and fluorocytosine as prodrugs, with HSV thymidine kinase (HSV tk-) and cytosine deaminase (CD), respectively, as the activating enzymes. Although promising results have been described with both prodrug/enzyme combinations, a limitation of HSV tk- and CD as drug-activating enzymes is that they only accept as substrates compounds that closely resemble the natural substrates. In an effort to broaden the scope of the GDEPT approach, we investigated the potential of *E. coli* β-galactosidase as a drug-activating enzyme. Because of its permissive nature, β-galactosidase can cleave a wide structural variety of β-galactosides. Here we describe the preparation of 4-(β-D-galactopyranosyl)benzyl-*N,N,N′,N′*-tetrakis(2-chloroethyl) phosphorodiamidate **1**, a prodrug of the antitumor alkylating phosphoramide mustard *N,N,N′,N′*-tetrakis(2-chloroethyl)phosphorodiamidic acid, **4**.

The anticipated mechanism of activation of **1** is shown in Scheme 1. Under neutral aqueous conditions, the prodrug is expected to be stable and non-reactive. In the presence of β-galactosidase, however, it should be cleaved to the corresponding phenol **2**. This intermediate should undergo spontaneous 1,6-elimination to release the cytotoxic mustard **4** and quinone methide **3**. The latter should have only a transient existence before being converted to 4-hydroxybenzyl alcohol **5**.

Compound **1** was prepared as shown in Scheme **2**. 2,3,4,6-Tetra-*O*-acetyl-α-D-galactopyranosyl bromide **6** was reacted with 4-hydroxybenzaldehyde **7** in the presence of freshly prepared anhydrous Ag_2O (2 equiv.) in MeCN at room

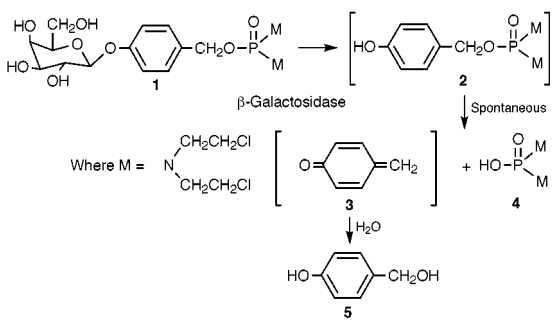

Scheme 1

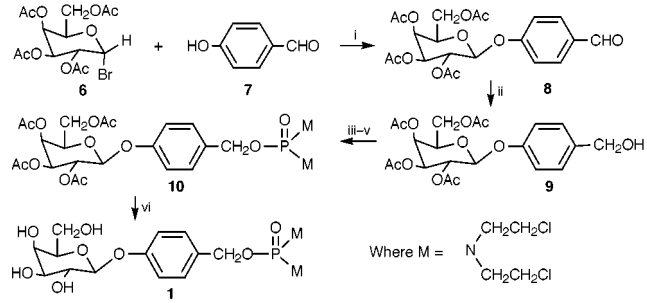

Scheme 2 *Reagents and conditions*: i, Ag_2O, MeCN; ii, $NaBH_4$, $CHCl_3$–Pr^iOH; iii, PCl_3, Et_3N; iv, $HN(CH_2CH_2Cl)_2$; v, *tert*-butyl hydroperoxide; vi, NaOMe, MeOH.

temperature for 8 h to give **8** (73% yield). Reduction of **8** with $NaBH_4$ in anhydrous $CHCl_3$–Pr^iOH (4 : 1) gave the corresponding benzyl alcohol **9** in 72% yield. Compound **9** was reacted successively with PCl_3 (1 equiv.) and bis(2-chloroethyl)amine (2 equiv.), and the intermediate phosphoramidite was oxidized *in situ* with *tert*-butyl hydroperoxide to afford **10**† as a white solid (47% yield) after purification over silica gel. Compound **10** was converted to the free galactoside **1**‡ in 87% yield by treatment with NaOMe in anhydrous MeOH.

The stability and enzyme activation of 1 was then investigated. A solution of **1** (10^{-4} M) in 0.05 M phosphate buffer, pH 7.4, was incubated at 37 °C in the absence or presence of *E. coli* β-galactosidase (2 units per μmole of **1**). At selected time intervals, 100 μl aliquots were withdrawn and analyzed by HPLC.§ In the absence of enzyme, the peak intensity of **1** decreased with a half life of 9.4 h. In presence of enzyme, the half-life was reduced to 7.6 min. A new peak, chromatographically identical to 4-hydroxybenzyl alcohol, appeared soon after incubation started and progressively increased with time. Since the phosphoramide mustard **4**, does not contain a strong chromophore, it was not evident in the reaction mixture using a UV detector. To establish the formation of **4**, the incubation mixture was further analyzed by LC/MS.¶ The peak suspected to be 4-hydroxybenzyl alcohol gave rise to a molecular ion of mass 107. This is consistent with the hydroxytropylium ion formed by rearrangement of the 4-hydroxybenzyl cation ion derived from **7**. Another peak, not evident when the mixture was analyzed using a UV detector, gave rise to a four-chlorine molecular ion cluster with *m/z* 345 characteristic of the free mustard **4**. These findings strongly support the rationale inherent in the design of **1**. Biological studies of this compound are in progress and will be reported in the future.

In summary, 4-(β-D-galactopyranosyl)benzyloxy *N,N,N′,N′*-tetrakis(2-chloroethyl) phosphorodiamidate **1** was prepared and shown to be converted to the free phosphoramide **4** in the presence of β-galactosidase. Compounds such as **1** might have good potential in conjunction with GDEPT to increase antitumor selectivity in cancer chemotherapy. The synthesis of other β-galactoside anticancer prodrugs are in progress.

This research was supported by NIH grant CA 71527.

Notes and references

† Satisfactory elemental analyses were obtained for the new compounds. *Selected data* for **10**: R_f 0.3 (3:2 EtOAc–hexane); mp 118 °C; $\delta_H(CDCl_3)$ 7.33 (2H, d, ArH), 7.01 (2H, d, ArH), 5.48 (1H, H-2), 5.46 (1H, m, H-4), 5.11 (1H, H-3), 5.06 (1H, H-1), 5.01 (2H, d, CH_2OP), 4.0–4.30 (3H, m, H-5 and CH_2OAc), 3.54–3.67 (8H, m, 4 × NCH_2), 3.30–3.44 (8H, m, 4 × CH_2Cl), 2.19 (3H, s, $OCOCH_3$), 2.07 (6H, br s, 2 × $OCOCH_3$), 2.03 (3 H, s, $OCOCH_3$).

‡ *Selected data* for **1**: R_f 0.46 (15:85, MeOH–$CHCl_3$); mp 130–131 °C; δ_H(acetone-d_6) 7.39 (2H, d, ArH), 7.07 (2H, d, ArH), 5.01 (2H, d, CH_2OP), 4.92 (1H, d, anomeric proton), 3.96–3.90 (1H, m), 3.87–3.60 (13H, m), 3.55–3.35 (8H, m, 4 × CH_2Cl); $\delta_C(CD_3OD)$ 159.58 (Ar-C4), 131.2 (Ar-C1), 130.9 (Ar-C2), 118 (Ar-C3), 102.8 (anomeric carbon), 76.9, 74.8, 72.2, 70.2 (C2, C3, C4 and C5 but don't know which is which), 68.7 (benzylic carbon), 62.4 (C6), 50.4 (N-C), 43.0 (C-Cl).

§ HPLC conditions: A C-18 reverse phase column (Phenomenex, 150 × 3.90 mm) was used. The mobile phase was MeCN–0.05 M phosphate buffer, pH 7.0 (35:65) with a flow rate of 1.0 ml min^{-1}. A variable wavelength UV detector, set at 260 nm with 0.01 AUFS sensitivity (Waters Model 484) was used and quantitated electronically as a function of time using an NEC Pinwriter P6200 integrator. The half-life were calculated by linear least-squares regression analysis of the pseudo-first-order reactions. The retention time for **1** and 4-hydroxy benzyl alcohol were 5.7 and 1.8 min respectively. Two units of β-galactosidase per μmol of **1** were used. *E. coli* β-galactosidase was purchased from Sigma Chemical Company (Cat. No. G-2513).

¶ A Zorbax C18 (1 X 150) reverse phase column was used. The mobile phase was 60:40 water–MeCN containing 0.1 % (v/v) formic acid, at a flow rate of 0.1 ml min^{-1}.

1 A. A. Gutierrez, N. R. Lemoine and K. Sikora, *Lancet*, 1992, **339**, 715.
2 C. A. Mullen. *Pharmacol. Ther.*, 1994, **63**, 199.
3 T. A. Connors, *Gene Ther.*, 1995, **2**, 702.

Communication 9/07719G

Stereoselective synthesis of chiral coordination polymers with partial control of the rigid main chain topology

Jianbo Chen and Frederick M. MacDonnell*

Department of Chemistry and Biochemistry, University of Texas at Arlington, Arlington, TX 76019, USA. E-mail: macdonn@uta.edu

Received (in Bloomington, IN, USA) 12th August 1999, Accepted 3rd November 1999

The condensation polymerization between the appropriate enantiomers of [Ru(1,10-phenanthroline-5,6-dione)$_2$(bpy)]$^{2+}$ 1 and [Ru(1,10-phenanthroline-5,6-diamine)$_2$(bpy)]$^{2+}$ 2 in *meta*-cresol gave the homochiral coordination polymers Δ-3 and Λ-3 as well as the *meso* polymer, ΔΛ-3, which exhibit rigid, ribbon-like structures with different main chain topologies.

Ruthenium(II) polypyridine complexes have been incorporated into oligomers, dendrimers and polymers because they combine considerable thermal and chemical stability with advantageous catalytic, luminescent and redox properties.[1] Recently, through the work of the groups of Lehn[2] and Tor[3] and ourselves,[4] it has been shown that substitutionally inert, enantiopure derivatives of [Ru(bpy)$_3$]$^{2+}$ and]Ru(phen)$_3$]$^{2+}$ are robust chiral synthons for the synthesis of oligomeric and dendritic polynuclear assemblies. The use of enantiopure monomers permits stereospecific synthesis of a particular diastereomer (in most cases) and allows detailed study of the properties and topology of individual isomers.[5]

Rehahn and coworkers have shown that coordination polymers of the type [Ru(bpy)(tpphz)]$_n^{2n+}$ (tpphz = tetrapyrido[3,2-*a*:2′,3′-c:3″,2″,-h:2‴,3‴-j]phenazine) can be synthesized with P_n ranging from 11 to 30.[6] These polymers have a conformationally rigid main chain and high overall charge, yet remain readily soluble and easily characterized by NMR. Owing to the synthetic approach, however, the absolute stereochemistry at each ruthenium site is random which also significantly affects the main-chain topology.

We have developed a stereospecific syntheses of this polymer as shown in Scheme 1. Chiral monomers Δ-**1**[PF$_6$]$_2$ and Λ-**1**[PF$_6$]$_2$ are prepared from oxidation of Δ- and Λ-[Ru(phen)$_2$(bpy)][PF$_6$]$_2$, respectively, and are converted to Δ-**2**[PF$_6$]$_2$ and Λ-**2**[PF$_6$]$_2$,† as described for related compounds in the literature.[7] By using comonomers, it is possible to prepare three isomeric condensation polymers:‡ the enantiomorphic homochiral polymers Λ-**3** and Δ-**3** and the alternating Δ–Λ 'copolymer', ΔΛ-**3**, which is a *meso* structure. This, to the best of our knowledge, is the first example of a soluble, chiral coordination polymer in which the chirality is centered at the metal sites.§

The absorption and ^{1}H NMR spectra for all three isomers are indistinguishable and match that observed for polymer assembled from racemic monomers. All three are also luminescent at room temperature in MeCN with an emission maximum (λ_{em} = 675 nm) comparable to related multinuclear compounds.[8] Rehahn and coworkers had noted that the presence of diastereomers in their 'racemic' polymers apparently did not complicate the NMR spectrum, presumably owing to the large distance (12.7 Å) between stereocenters.[6] Our results here and with dendritic assemblies bridged by tpphz ligands confirm this hypothesis. End-group analysis of the ^{1}H NMR spectrum give a minimum P_n of 13–15 for all three isomers of **3** which corresponds to M_n of *ca.* 12 000–14 000 (as the PF_6^- salt). *meta*-Cresol was the only solvent that gave a reasonable degree of polymerization with common solvents (H_2O, MeCN, EtOH) yielding only oligomers (P_n = 3–5). Similar solvent effects had been reported in the synthesis of organic ladder polymers.[8]

The stereochemistry of the monomers is retained despite the harsh polymerization conditions, as determined by CD. The CD of the polymers, Δ-**3**, Λ-**3** and ΔΛ-**3**, are displayed in Fig. 1 where the $\Delta\varepsilon$ is reported on a per mole repeating unit. As found with related tpphz bridged dimers, tetramers, hexamers and decamers,[4] the chromophores are not significantly electronically coupled and the CD intensity in the visible region is close to that calculated on a per chromophore basis. The enantiomorphic Δ-**3** and Λ-**3** exhibit strong Cotton effects and show the expected mirror image relationship. The ΔΛ-**3** (*meso*) polymer is achiral and not expected to show any CD however a small Cotton effect is observed. We have observed a side reaction in our studies of related ruthenium dimers, tetramers, hexamers and decamers[4] which is most likely responsible for the observed CD. Coordinated phendione can undergo a two electron–two proton reduction with coordinated phendiamine to yield a coordinated catechol and phendiimine, respectively. The phendiimine is able to further react with coordinated phendiamine to form a tpphz bridge with expulsion of NH_3. The net

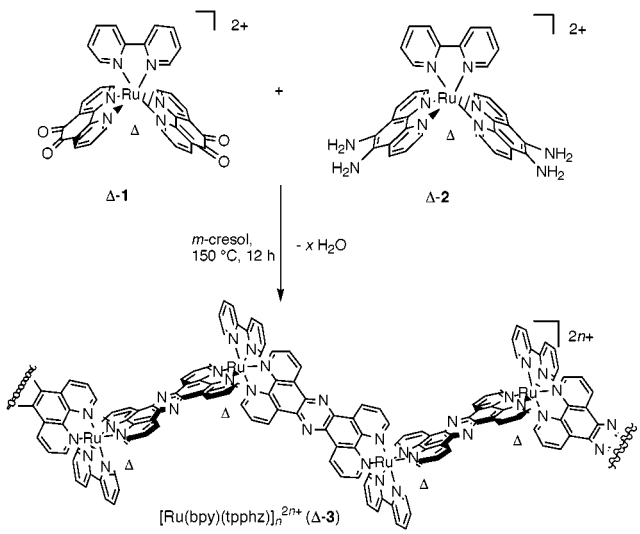

Scheme 1 *Reagents and conditions: meta*-cresol, 150 °C, 12 h, N_2 atm.

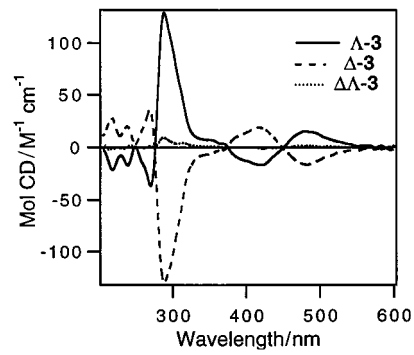

Fig. 1 CD of Λ-**3**, Δ-**3** and ΔΛ(*meso*)-**3** in MeCN.

result here would be the occasional incorporation (*ca.* 7%) of adjacent monomers **2** into the polymer and formation of chain terminating catechol species. Several lines of evidence support this. The sign of the CD found in the *meso* polymer always corresponds to the sign of the **2** monomer used in the reaction. Ammonia, in the form of ammonium ion, is observed to appear in the NMR of model complexes prepared from monomers in a NMR tube experiment in CD_3CN. Oligomers of **3** can be formed upon reaction of **2** with *para*-tetrachloroquinone. It is also possible that the observed CD is due to end-group effects, however, we note that the redox reaction described above would likely enrich the end-groups with the catechol terminated product which would likely give a CD of the opposite sign.

Rehahn and coworkers observed that the topology of the rigid, ribbon-like main chain will be dependent on the absolute configuration of the individual ruthenium centers.[6] In our system it is possible to control this variable, however, this alone does not permit complete topochemical control of the resulting polymer chain. Four 'locked' torsional isomers are possible for this polymer, two for the *meso* and two for the homochiral structures. Every four-metal unit can exhibit a form of *syn* and *anti* stereochemistry of which the torsional angle (Θ for Ru_1–Ru_2–Ru_3–Ru_4) is dependent on the chirality of the individual metal centers. Newman projections for the *meso* (Fig. 2, left) and homochiral (Fig. 2, right) polymers viewed down the Ru_2–Ru_3 axis (with the intervening tpphz parallel with the horizontal axis) show the orientation of the remaining chelate rings (bpy or bridging tpphz) on the front and back rutheniums. If the polymer chain is oriented such that the link to the front Ru_1 comes in at the b quadrant, we can denote each isomer by which quadrants the entering (Ru_1–Ru_2: dark arrow) and leaving (Ru_3–Ru_4: gray arrow) tpphz ligands are in (quadrants labeled in Fig. 2). For the *meso* polymer, only the *syn*-(b,b)-isomer and the *anti*-(b,d)-isomer are allowed, which have torsional angles (Θ) of 0 and 180°, respectively. The descriptors, *syn* and *anti*, are determined relative to the horizontal tpphz plane. Importantly, the homochiral polymers have different torsional angles for the *syn*-(b,a)-isomer (Θ = 72°) and *anti*-(b,c)-isomer (Θ = 108°) which will dramatically affect the overall main chain configuration. The torsional angles were determined from molecular modeling of related dendrimer systems in conjunction with crystallographic data for Λ-$[Ru(phen)_3][PF_6]_2$[10] and the dimer ΔΛ-$[(bpy)_2Ru(tpphz)Ru(bpy)_2][NO_3]_4$.[11]

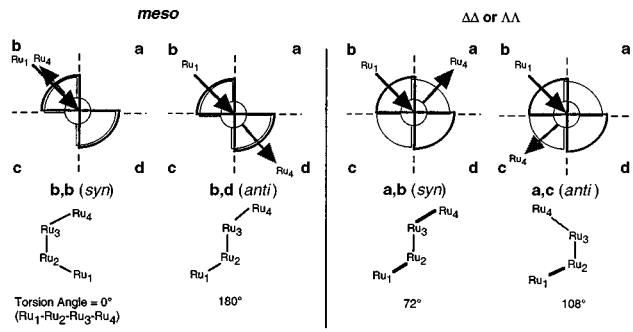

Fig. 2 Newman projections and torsional angle data for the various torsional isomers of the polymer **3**.

From the above considerations, we can predict that the *meso* polymer has a zigzag structure containing only b,b and b,d-isomers (excepting redox related defects as described above) and therefore a structure in which all the Ru atoms are approximately coplanar. On the other hand, the homochiral polymers will form random coil structures owing to the presence of only b,c- and b,a-isomers. Currently, the use of enantiopure monomers only permits partial control of the main chain topology, however steric bulk has been used with some success to favor the more expanded chain structures (in racemic polymers)[6c] and may be useful here to further direct the stereochemical outcome of this reaction.

In conclusion, we have developed a new route to coordination polymers containing chiral ruthenium trisdiimine complexes in the main chain backbone which we can use to partially control the topology of the rigid polymer main-chain. Together these results show that it is possible to exert considerable control over both the local and global polymer stereochemistry. Ultimately materials such as these may be useful in a variety of chiral technologies including chiral sensing, catalysis and separations.

We thank the Robert A. Welch Foundation (Grant Y-1301) for financial support and the National Science Foundation (CHE-9601771) for the purchase of a 500 MHz NMR spectrometer.

Notes and references

† The enantiomers of **1** and **2** were characterized by ^1H and ^{13}C NMR, elemental analyses, UV–VIS and CD spectroscopy. CD (Λ-**1**) [λ_{max}/nm ($\Delta\varepsilon$/M^{-1} cm^{-1})]: 242 (−39.8), 260 (+45.5), 283 (−39.0), 307 (+128), 328(sh) (+12.4), 350 (−9.05), 411 (−30.6), 461 (+12.5), 507(sh) (+8.23). CD (Λ-**2**) [λ_{max}/nm ($\Delta\varepsilon$/M^{-1} cm^{-1})]: 236 (−12.7), 259 (+8.48), 268(sh) (+7.20), 283 (−14.3), 307 (+87.2), 350 (−2.29), 418 (−16.2), 483 (+11.5).

‡ Polymers Λ-**3**, Δ-**3** and ΔΛ-**3** were characterized by ^1H and ^{13}C NMR, elemental analyses, UV–VIS and CD spectroscopy. Typical yield was 65%.

§ A coordination polymer is defined as requiring coordinate bonds to form the polymer main chain.[11] Several examples of chiral complexes coordinated to a organic polymer chain or metallation of a chiral main-chain are known.[3a,13] Non-racemic helical coil oligomers and polymers have also been reported.[14]

1 V. Balzani, A. Juris, M. Venturi, S. Campagna and S. Serroni, *Chem. Rev.*, 1996, **96**, 759; G. R. Newkome, E. He and C. N. Moorefield, *Chem. Rev.*, 1999, **99**, 1689.
2 K. Wärnmark, J. A. Thomas, O. Heyke and J.-M. Lehn, *Chem. Commun.*, 1996, 701.
3 (*a*) E. C. Glazer and Y. Tor, *Polym. Prepr.*, 1999, **40**, 513; (*b*) D. Tzalis and Y. Tor, *Chem. Commun.*, 1996, 1043; (*c*) D. Tzalis and Y. Tor, *J. Am. Chem. Soc.*, 1997, **119**, 852.
4 F. M. MacDonnell, M.-J. Kim and S. Bodige, *Coord. Chem. Rev.*, 1999, **185–186**, 535; S. Bodige, A. S. Torres, D. J. Maloney, D. Tate, A. Walker, G. Kinsel and F. M. MacDonnell, *J. Am. Chem. Soc.*, 1997, **117**, 10 364; S. Campagna, S. Serroni, S. Bodige and F. M. MacDonnell, 1999, **38**, 692; M.-J. Kim, F. M. MacDonnell, M. E. Gimon-Kinsel, T. DuBois, N. Asgharian and J. C. Griener, *Angew. Chem., Int. Ed.*, in press.
5 F. R. Keene, *Coord. Chem. Rev.*, 1997, **166**, 121.
6 (*a*) R. Knapp, A. Schott and M. Rehahn, *Macromolecules*, 1996, **29**, 478; (*b*) S. Kelch and M. Rehahn, *Macromolecules*, 1997, **30**, 6185; (*c*) S. Kelch and M. Rehahn, *Macromolecules*, 1998, **31**, 4102.
7 R. D. Gillard and R. E. E. Hill, *J. Chem. Soc., Dalton. Trans.*, 1974, 1217; A. S. Torres, D. J. Maloney, D. Tate and F. M. MacDonnell, *Inorg. Chim. Acta*, 1999, **293**, 37; S. Bodige and F. M. MacDonnell, *Tetrahedron Lett.*, 1997, **38**, 8159.
8 J. Bolger, A. Gourdon, E. Ishow and J.-P. Launay, *Inorg. Chem.*, 1996, **35**, 2937.
9 K. Imai, M. Kurihara, L. Mathias, J. Wittman, W. B. Alston and J. K. Stille, *Macromolecules*, 1973, **6**, 158.
10 D. J. Maloney and F. M. MacDonnell, *Acta Crystallogr, Sect. C*, 1997, **53**, 705.
11 J. Bolger, A. Gourdon, E. Ishow and J.-P. Launay, *J. Chem. Soc., Chem. Commun.*, 1995, 1799.
12 R. D. Archer, *Coord. Chem. Rev.*, 1993, **128**, 49.
13 L. Pu, *Chem. Rev.*, 1998, **98**, 2405.
14 Y. Dai, T. J. Katz and D. A. Nichols, *Angew. Chem., Intl. Ed. Engl.*, 1996, **35**, 2109; T. J. Katz, A. Sudhakar, M. F. Teasley, A. M. Gilbert, W. E. Geiger, M. P. Robben, M. Wuensch and M. D. Ward, *J. Am. Chem. Soc.*, 1993, **115**, 3812.

Communication 9/06645D

ChemComm

The synthesis and single crystal structure of an amino acid intercalated layered niobium phosphate: $[(NbOPO_4)_4{\bullet}(H_3NCH_2CO_2H)_2][H_2PO_4][OH, F]$

Xiqu Wang, Lumei Liu, Heidi Cheng and Allan J. Jacobson*

Department of Chemistry and Materials Research Science and Engineering Center, University of Houston, Houston, Texas 77204-5641, USA. E-mail: ajjacob@uh.edu

Received (in Bloomington, IN, USA) 7th September 1999, Accepted 3rd November 1999

Niobium phosphate containing interlayer glycinium phosphate has been synthesized hydrothermally and its structure determined from single crystal X-ray diffraction data.

The structure of anhydrous niobium phosphate $NbOPO_4$ contains layers of NbO_6 distorted octahedra connected in their equatorial planes by PO_4 tetrahedra *via* sharing of corners.[1] Adjacent layers are connected through corner-sharing the remaining unshared oxygen atoms in the NbO_6 octahedra. Niobium phosphate forms a series of hydrates with composition $NbOPO_4{\bullet}nH_2O$ that have been characterized by powder diffraction and infrared spectroscopy.[2–5] No single crystal structural data are available but the hydrates most probably contain layers similar to those found in the anhydrous phase with the bridging oxygen atoms replaced by H_2O molecules to give layers of composition $NbO(H_2O)PO_4$. The presence of the interlayer coordinated water molecules permits intercalation of various types of amines and alcohols between the formally electroneutral layers. The coordination intercalation chemistry is similar to that first observed in $VOPO_4{\bullet}2H_2O$.[4,6] The niobium phosphate layers are stable at high temperature, with respect to radiation damage and in most organic environments. Consequently they are suitable hosts for building composite materials.[7]

We are interested in direct incorporation of organic templates into layered compounds by using hydrothermal synthesis. Here, we report an unusual compound resulting from these studies, $[(NbOPO_4)_4{\bullet}(H_3NCH_2CO_2H)_2][H_2PO_4][OH,F]$ **1** and, to the best of our knowledge, the first single crystal structure of a $NbOPO_4$ intercalation compound.

In a typical synthesis of compound **1**, a solution was prepared by dissolving 0.1 g glycine, 0.12 ml phosphoric acid and 28 mg NH_4HF_2 in 2.1 ml H_2O. The solution (pH = 2.5) was then sealed together with 20 mg niobium metal in a Teflon bag in air. The bag was subsequently sealed in a steel reaction vessel filled with water to about 60% volume, and heated at 165 ºC for 38 h. After cooling to room temperature for 3 h, the products were filtered off, washed with water, and dried in air. Colorless square-like plates of **1** with rather uniform sizes of *ca.* 0.1 × 0.1 × 0.01 mm were recovered together with residual niobium metal. The solution pH was 2.7 at the end of the reaction. Incorporation of glycine into the structure was confirmed by the crystal structure refinement† and the IR spectrum.‡

The crystal structure of **1** consists of $NbOPO_4$ layers bridged by the carboxylic groups of the glycinium $H_3NCH_2CO_2H$ cations with H_2PO_4, F and OH anions located in the interlayer spaces. The layers are structurally equivalent to those of $NbOPO_4$, and are formed from alternating NbO_6 octahedra and PO_4 tetrahedra interconnected through Nb–O–P bonds. The four equatorial oxygen atoms of each NbO_6 octahedron with Nb–O bond lengths of 2.028–2.033 Å are shared by four phosphate tetrahedra. The two apical positions of the NbO_6 octahedron are completed by a terminal Nb=O bond of 1.708 and a weak Nb–O bond (2.219 Å) to an oxygen atom of the interlayer glycinium cation (Fig. 1). The layers are parallel to the (100) plane and stacked in ABAB… sequences. Neighboring layers are shifted relative to each other along [010] by exactly 0.5*b* and along [001] by *ca.* 0.43*c*. The shifts are

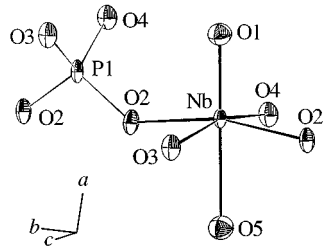

Fig. 1 Coordination environments of the Nb and P atoms in the layers. Thermal ellipsoids are drawn at the 50% probability level. Bond lengths (Å): Nb–O(1) 1.708(5), Nb–O(4) 2.028(4), Nb–O(2) 2.029(3)(×2), Nb–O(3) 2.033(4), Nb–O(5) 2.219(5), P(1)–O(4) 1.535(4), P(1)–O(3) 1.536(4), P(1)–O(2) 1.539(3)(×2).

required by the glycinium cations that bridge neighboring layers through Nb–O–C–O–Nb bonds (Fig. 2). While the oxygen atoms of the glycinium cations are ordered, the C–C–N chain is disordered randomly over four symmetry equivalent positions inside the large interlayer cavities. Although the two oxygen atoms of the carboxyl group are symmetry equivalent, there are two C–O bond lengths, 1.35 and 1.41 Å. The latter corresponds to C–OH–Nb bonds and confirms the protonation of the glycine molecule as expected from the highly acidic synthesis conditions. Because of the C–O–Nb bonding, the C–O distances are longer than those typically found in isolated glycine molecules. The charge balancing $(H_2PO_4)^-$ anions are disordered and were located from difference maps, but not unambiguously, at two

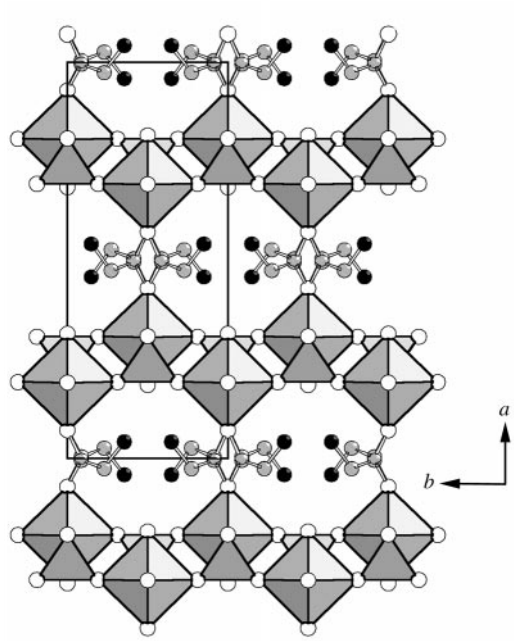

Fig. 2 Projection of the structure along [001]. Open, hatched and solid circles represent O, C and N atoms, respectively. The $H_3NCH_2CO_2H$ cations are disordered randomly over four orientations. The disordered interlayer anions are omitted for clarity.

non-equivalent positions in the interlayer cavities. Both positions can be included in the refinements as rigid groups with a fixed occupancy of 6.3% in agreement with the electron microprobe analysis§ that gave the atomic ratios: Nb : P : F = 4 : 5.0 : 0.4. The charge balancing F^- and probably also OH^- anions could not be located because of electron density overlapping caused by the disorder. Thermogravimetric analysis measured in air up to 900 ºC shows two continuous weight loss stages separated by *ca.* 300 ºC. The total observed weight loss of 17.8% agrees well with the given formula assuming the residue to be $Nb_4P_5O_{22.3}F_{0.4}$ (calc. 17.7%).

The structure of **1** is closely related to the structure model proposed for $NaNb_2(OH)_2(PO_4)_3 \cdot nH_2O$ based on powder X-ray diffraction data. In the model, neighboring niobyl phosphate layers are bridged by PO_4 tetrahedra.[6] There are several precedents for $NbOPO_4$ intercalation compounds in which the layers are bridged by anionic groups. $(VOSO_4)_2 \cdot H_2SO_4$ is generally considered to be the archetype but there are several other examples.[8,9] Compound **1** is unusual because the bridging carboxylate group is cationic and consequently the interlayer charge is compensated for by interlayer anions. All of the other examples in this family contain interlayer cations. $[(NbOPO_4)_4 \cdot (H_3NCH_2CO_2H)_2][H_2PO_4][OH,F]$ is a rare example of a layered inorganic anion exchanger and is analogous to the hydrotalcites.

In summary, we have synthesized single crystals of a novel layered niobium phosphate containing glycinium cross-linking adjacent $NbOPO_4$ layers. Our preliminary data also show that layered niobium phosphates incorporating other organic species can also be obtained in single crystal form through hydrothermal reactions.

We thank the National Science Foundation (DMR9214804), the R. A. Welch Foundation for financial support. This work made use of MRSEC/TCSUH Shared Experimental Facilities supported by the National Science Foundation under Award Number DMR-9632667 and the Texas Center for Superconductivity at the University of Houston.

Notes and references

† *Crystal data*: $C_4N_2H_{14.6}O_{28.6}F_{0.4}Nb_4P_5$, M = 1082.3, crystal system: monoclinic, space group $C2/m$, a = 17.020(2), b = 6.4973(7), c = 6.4992(7) Å, β = 109.304(2)º, V = 678.3(1) Å^3, Z = 1, T = 223 K, μ = 1.99 mm^{-1}, $R(F)$ = 0.036. Measured/independent reflections: 2117/850, R_{int} = 0.033, refined variables: 74. CCDC 182/1477. See http://www.rsc.org/suppdata/cc/1999/2531/ for crystallographic files in .cif format.

‡ IR data (cm^{-1}): 3464m, 3217m, 1618m, 1501m, 1468m, 1416m, 1352w, 1115s, 1015vs, 692m, 581w, 525m, 463w. The peaks between 1352 and 1618 cm^{-1} are characteristic of amino acetic acid.

§ Electron microprobe analysis was carried out with a JEOL 8600 electron microprobe operating at 15 keV with a 10 μm beam diameter and a beam current of 30 nA.

1 J. M. Longo and P. Kierkegaard, *Acta Chem. Scand*., 1966, **20,** 72.
2 N. G. Chernorukov, N. P. Egorov and I. R. Mochalova, *Russ. J. Inorg. Chem.*, 1978, **23**, 1627.
3 G. I. Deulin, R. B. Dushin and V. N. Krylov, *Russ. J. Inorg. Chem.*, 1979, **24**, 1291.
4 K. Beneke and G. Lagaly, *Inorg. Chem.*, 1983, **22**, 1503.
5 S. Bruque, M. Martinez-Lara, L. Moreno-Real, A. Jimenez-Lopez, B. Casal, E. Ruiz-Hitzky and J. Sanz, *Inorg. Chem.*, 1987, **26**, 847.
6 N. Kinomura and N. Kumada, *Inorg. Chem*., 1990, **29**, 5217.
7 Y. K. Shin, and D. Nocera, *J. Am. Chem. Soc*., 1992, **114**, 1265.
8 W. T. A. Harrison, K. Hsu and A. J. Jacobson, *Chem. Mater*., 1995, **7**, 2004.
9 M. Tachez and F. Theobald, *Acta Crystallogr., Sect. B*, 1981, **37,** 1978.

Communication 9/07293D

Selective extraction of strontium with supercritical fluid carbon dioxide

Chien M. Wai,*[a] Yurii Kulyako,[b] Hwa-Kwang Yak,[a] Xiaoyuan Chen[a] and Suh-Jane Lee[a]

[a] *Department of Chemistry, University of Idaho, Moscow, ID 83844, USA. E-mail: cwai@uidaho.edu*
[b] *Vernadsky Institute of Geochemistry and Analytical Chemistry, Russian Academy of Sciences, Moscow, Russia*

Received (in Columbia, MO, USA) 3rd June 1999, Accepted 9th November 1999

Strontium (Sr^{2+}) can be selectively extracted from aqueous solutions into supercritical fluid CO_2 at 60 °C and 100 atm with dicyclohexano-18-crown-6 (DC18C6) using $CF_3(CF_2)_6CO_2^-$ ($PFOA^-$) or $CF_3(CF_2)_6CF_2SO_3^-$ ($PFOSA^-$) as a counter anion; at a mole ratio of Sr^{2+} : DC18C6 : $PFOA^-$ = 1:10:50, the extraction of Sr (5.6×10^{-5} M) from water at pH 3 is near quantitative whereas Ca^{2+} and Mg^{2+} at equal concentration are only extracted to a level of 7 and 1%, respectively; $PFOSA^-$ is an effective counter anion for selective extraction of Sr^{2+} from 1.3 M HNO_3 with DC18C6 in supercritical CO_2.

Research in selective transport of metal ions in supercritical (sc)-CO_2 is of considerable current interest because of its potential applications in a variety of chemical processes which may be carried out in this environmentally friendly solvent.[1,2] Selective extraction of alkali metal and alkaline earth metal ions from aqueous solutions to organic solvents with crown ethers is well established in the literature. Extraction of these hard metal ions with crown ethers in $scCO_2$ is expected to be difficult because of limited solubilities of the resulting metal complexes in CO_2.[3] It is known that fluorinated metal chelates are CO_2-philic.[4] Thus, fluorination of ligands is one method of increasing solubility of metal complexes in CO_2. This approach requires the design and synthesis of specific fluorinated macrocyclic compounds. Another method is to extract crown ether-metal complexes as ion-pairs into $scCO_2$ utilizing fluorinated counteranions. We report for the first time the successful extraction of Sr^{2+} from aqueous media into $scCO_2$ utilizing a macrocyclic compound and a fluorinated counter anion.

It is known that 18-membered crown ethers with cavity diameters in the range 2.6–2.8 Å are the most suitable hosts for Sr^{2+} (2.2 Å).[5] For example, ^{90}Sr can be selectively extracted from nitric acid solutions with dicyclohexano-18-crown-6 (DC18C6) dissolved in a paraffinic or halogenated solvent, where nitrate serves as the counter anion.[6] This macrocyclic system is currently being evaluated for removing ^{90}Sr ($t_{\frac{1}{2}}$ = 30 years), a major uranium fission product, from the high level acidic nuclear wastes stored at the Idaho DOE site. However, disposal of organic liquid wastes generated from any solvent extraction process is a problem of environmental concern today because of changing government regulations. Supercritical fluid extraction provides several advantages over conventional solvent extraction including minimization of waste generation, allowing rapid separation of extracted metal complexes, and enhancement of transport speed due to high diffusivity of the supercritical fluid.

The high-pressure apparatus for supercritical fluid extraction of aqueous systems has been described previously.[7] A measured amount of DC18C6 and a fluorinated counter anion, both dissolved in chloroform, was loaded into a 10 mL stainless steel extraction vessel and evaporated to dryness on a water bath at 60 °C with flowing nitrogen gas. 5 mL of an aqueous solution containing a mixture of Sr^{2+}, Ca^{2+} and Mg^{2+} at 5.6×10^{-5} M each were then added to the vessel. The vessel was pressurized with CO_2 and heated to the desired temperature. After 20 min of static extraction, the exit valve was opened and the system was flushed with $scCO_2$ for 20 min. The aqueous solution before and after extraction was analyzed by an ICP/AES instrument for metal contents.

DC18C6 is quite soluble in $scCO_2$, with a solubility estimated to be $> 10^{-2}$ mol L^{-1} at 60 °C and 100 atm, according to our experiments. Direct extraction of Sr^{2+} (5.6×10^{-5} M) with an excess of DC18C6 (5.4×10^{-4} M) in supercritical CO_2 showed virtually no detectable extraction of Sr^{2+} from water (Table 1) or from a 1.3 M nitric acid solution (Table 2). With the addition of a fluorinated carboxylic acid such as pentadecafluoro-*n*-octanoic acid (HPFOA), extraction of Sr^{2+} from water with DC18C6 in $scCO_2$ became significant. The pH of water in equilibrium with $scCO_2$ under the experimental conditions should be *ca*. 2.9 according to a previous study.[8] Because of the inductive effect of the fluorinated group in HPFOA, the pK_a value of this perfluorinated acid is *ca.* 1. Therefore, HPFOA is expected to exist as the anionic form $PFOA^-$ under the specified experimental conditions of this water/$scCO_2$ system. With a concentration of $Sr^{2+} = 5.6 \times 10^{-5}$ M and a mol ratio of Sr^{2+}: DC18C6 : $PFOA^-$ = 1 : 5 : 10, *ca.* 36% of the Sr^{2+} was removed from the water after 20 min of static extraction

Table 1 Extraction of Sr^{2+}, Ca^{2+} and Mg^{2+} from water by sc fluid CO_2 containing DC18C6 and perfluorinated counter anion $PFOA^-$ or $PFOSA^-$ at 60 °C and 100 atm[a]

Mol ratio			Extraction (%)		
Sr^{2+} : DC18C6 : HPFOA			Sr^{2+}	Ca^{2+}	Mg^{2+}
1	10	0	1	0	0
1	0	10	4 ± 1	1 ± 1	1 ± 1
1	5	10	36 ± 2	1 ± 1	1 ± 1
1	10	10	52 ± 2	2 ± 1	1 ± 1
1	10	50	98 ± 2	7 ± 2	2 ± 1
		NEt_4PFOSA			
1	0	10	12 ± 2	6 ± 2	2 ± 1
1	5	10	98 ± 2	45 ± 4	2 ± 1
1	10	10	99 ± 1	66 ± 5	2 ± 1
		KPFOSA			
1	10	10	97 ± 2	8 ± 2	2 ± 1

[a] The aqueous solution contained a mixture of Sr^{2+}, Ca^{2+} and Mg^{2+} with a concentration of 5.6×10^{-5} M each; pH of water under equilibrium with $scCO_2$ = 2.9; 20 min static followed by 20 min dynamic flushing at a flow rate of 2 mL min^{-1}. HPFOA = $CF_3(CF_2)_6CO_2H$; NEt_4PFOSA = $NEt_4[CF_3(CF_2)_6CF_2SO_3]$; KPFOSA = $CF_3(CF_2)_6CF_2SO_3K$.

Table 2 Extraction of Sr^{2+}, Ca^{2+} and Mg^{2+} from 1.3 M HNO_3 by $scCO_2$ containing DC18C6 and HPFOA or PFOSA salt at 35 °C and 200 atm[a]

Mol ratio			Extraction (%)		
Sr^{2+} : DC18C6 : HPFOA			Sr^{2+}	Ca^{2+}	Mg^{2+}
1	10	0	1	0	0
1	10	50	18 ± 2	2 ± 1	1 ± 1
		KPFOSA			
1	10	50	60 ± 3	8 ± 2	2 ± 1
1	20	50	76 ± 3	8 ± 2	1 ± 1
		NEt_4PFOSA			
1	10	50	61 ± 3	7 ± 2	2 ± 1

[a] The acid solution contained a mixture of Sr^{2+}, Ca^{2+} and Mg^{2+} with a concentration of 5.6×10^{-5} M each; 20 min static followed by 20 min dynamic flushing at a flow rate of 2 mL min^{-1}.

followed by 20 min of dynamic flushing at 60 °C and 100 atm. The percentage extraction of Ca^{2+} and Mg^{2+} (at equal concentration as Sr^{2+}) under the same conditions was negligible (3% or less). By doubling the concentration of DC18C6 (*i.e.* at a mol ratio of Sr^{2+}: DC18C6 : $PFOA^-$ = 1:10:10), *ca.* 52% of the Sr^{2+} in the water phase was removed at 60 °C and 100 atm. Assuming the percentage Sr extraction from water represents equilibrium partition, we may estimate the distribution coefficient D_{Sr} (concentration of Sr in the CO_2 phase over that in the aqueous phase) from the extraction data using the relationship $D_{Sr} = (C_i - C_f)/C_f$, where C_i and C_f are the concentration of Sr in water before and after the extraction, respectively. The D_{Sr} value appears to double (from 0.56 to 1.08) when the Sr^{2+}: DC18C6 : $PFOA^-$ ratio is increased from 1:5:10 to 1:10:10, suggesting the stoichiometry of Sr to DC18C6 in the complex is most likely 1:1. In the absence of DC18C6, extraction of Sr^{2+} was negligible at 60 °C and 100 atm (Sr^{2+}: $PFOA^-$ = 1:10). Pressure has a minor effect on Sr^{2+} extraction. At 60 °C and 300 atm, the percentage extraction of Sr^{2+} was increased to 58% at a mol ratio of Sr^{2+}: DC18C6: $PFOA^-$ = 1:10:10.

The extraction of Sr^{2+} showed a strong dependence on $PFOA^-$ concentration. With a mol ratio of Sr^{2+}: DC18C6:$PFOA^-$ = 1:10:50, nearly quantitative extraction (98%) of Sr^{2+} from water into $scCO_2$ was observed at 60 °C and 100 atm. Under these conditions, Ca^{2+} and Mg^{2+} were extracted at 7 and 1%, respectively. Selective transport of Sr^{2+} in the presence of Ca^{2+} and Mg^{2+} from an aqueous solution to the $scCO_2$ phase apparently can be achieved using DC18C6 and $PFOA^-$ according to the results shown in Table 1. Based on the extraction data, we also estimated the variation of D_{Sr} with respect to the HPFOA concentration. Values of D_{Sr} increase from 1.1 to *ca.* 49 when the concentration of the HPFOA is increased by a factor of five. This suggests that the Sr^{2+}–crown complex extracted into the supercritical fluid probably involves 2 $PFOA^-$. Accurate measurement of *D* values in supercritical fluids requires a different experimental design. The preliminary results obtained from this supercritical fluid extraction study appear consistent with the charge neutralization requirement and the general concept of crown ether extraction.

The rate of extraction of Sr^{2+} from aqueous phase into $scCO_2$ with DC18C6 and HPFOA is reasonably fast. At 60 °C, 100 atm and with a Sr^{2+}: DC18C6:$PFOA^-$ ratio of 1:10:10 in water, the supercritical fluid extraction of Sr was found to be 11, 49, 52 and 51, for 5, 11, 19 and 30 min of static extraction, respectively. The dynamic flushing time for these experiments was fixed at 20 min. Under the specified experimental conditions, 20 min of static extraction appear sufficient to reach equilibrium.

When perfluoro-1-octanesulfonic acid tetraethylammonium salt, NEt_4 PFOSA, was used instead of HPFOA, the extraction efficiency for Sr^{2+} from water became higher but the selectivity for Sr^{2+} over Ca^{2+} and Mg^{2+} was reduced. At a Sr^{2+}: DC18C6:NEt_4PFOSA ratio of 1:10:10, the percentage extraction of Sr^{2+}, Ca^{2+} and Mg^{2+} were 99, 66, and 2%, respectively. If the potassium salt KPFOSA was used in the extraction instead of the NEt_4^+ salt, selective extraction of Sr^{2+} was observed. For KPFOSA, the extraction of Sr^{2+}, Ca^{2+} and Mg^{2+} were 97, 8 and 2%, respectively (Table 1). The cause of the unusual Ca^{2+} extraction from water with NEt_4PFOSA and DC18C6 in supercritical CO_2 is not known.

Selective extraction of Sr^{2+} by $scCO_2$ with DC18C6 and a fluorinated counter anion was also observed in 1.3 M HNO_3 (Table 2). The extraction of Sr^{2+} in the acid solution with a Sr^{2+}:DC18C6:KPFOSA ratio of 1:10:50 was 60% whereas Ca^{2+} and Mg^{2+} were extracted at a level of *ca.* 8 and 2%, respectively. The extraction efficiency of Sr^{2+} increased to 76% when the crown ether concentration was doubled (Table 2). NEt_4PFOSA did not show unusual Ca^{2+} extraction from the acid solution when it was used with DC18C6 in $scCO_2$. The fluorinated carboxylic acid HPFOA is less effective than the fluorinated sulfonic acid for Sr^{2+} extraction in the acid solution. In general, a high selectivity of extracting Sr^{2+} over Ca^{2+} and Mg^{2+} was observed in all the acid solution experiments. It should be pointed out that the high level acidic nuclear wastes stored at the Idaho DOE site is in 1.3 M HNO_3.

The experimental results obtained from this study suggest that Sr^{2+} in water or in 1.3 M nitric acid can be selectively extracted as ion-pairs with DC18C6 and a fluorinated counter anion in supercritical fluid CO_2. Utilizing the same principle of synergism, other alkali metal and alkaline earth metal ions probably can also be extracted in supercritical CO_2 with proper selection of macrocyclic hosts and perfluorinated counter anions. The possibility of extracting and transporting alkali metals and alkaline earth metals selectively in supercritical CO_2 suggests a number of potential applications including removal of major fission products ^{137}Cs and ^{90}Sr from aqueous or acidic nuclear wastes and phase transfer catalysis for specific reactions in supercritical CO_2.

The authors wish to express their gratitude to the DOE-EMSP Program and to NRC-Nuclear Waste Management Program for financial support.

Notes and references

1 C. M. Wai, F. Hunt, M. Ji and X. Chen, *J. Chem. Educ*., 1998, **75**, 1641.
2 N. G. Smart, C. L. Phelps and C. M. Wai, *Chem. Br*., 1998, **34**(**8**), 34.
3 N. G. Smart, T. E. Carleson, T. Kast, A. A. Clifford, M. D. Burford and C. M. Wai, *Talanta*, 1997, **44**, 137.
4 K. E. Laintz, C. M. Wai, C. R. Yonker and R. D. Smith, *J. Supercrit. Fluids*, 1991, **4**, 194.
5 E. Blasius, W. Klein and U. J. Schoeon, *J. Radioanal. Nucl. Chem*., 1985, **89**, 389.
6 B. S. Mohite and S. M. Khopkar, *Anal. Chem*., 1987, **59**, 1200.
7 Y. Lin, N. G. Smart and C. M. Wai, *Environ. Sci. Technol*., 1995, **29**, 2706.
8 K. L. Toews, R. M. Shroll, C. M. Wai and N. G. Smart, *Anal. Chem*., 1995, **67**, 4040.

Communication 9/04527I

Oxy-Cope rearrangements of fluorinated divinylcyclohexanols: a modular method for the construction of selectively fluorinated cyclic ketones

Gianluca Dimartino,[a] Thomas Gelbrich,[b] Michael B. Hursthouse,[b] Mark E. Light,[b] Jonathan M. Percy*[a] and Neil S. Spencer[a]

[a] *School of Chemistry, University of Birmingham, Edgbaston, Birmingham, UK B15 2TT. E-mail: jmpercy@chemistry.bham.ac.uk*

[b] *EPSRC National X-Ray Crystallography Service, Department of Chemistry, University of Southampton, Highfield, Southampton, UK SO17 1BJ*

Received (in Liverpool, UK) 25th October 1999, Accepted 10th November 1999

Oxy-Cope rearrangements of fluorinated divinylcyclohexanols afford access to cyclodecenones containing from two to five fluorine atoms.

The oxy-Cope rearrangement has become a tool of awesome transformative power;[1,2] ring systems can be constructed and interconverted with ease, opening routes to highly complex and densely functionalised polycyclic molecular architecture. However, oxy-Cope rearrangements of fluorinated substrates have remained uncharted territory.[3] The effect of fluorine atom substituents upon the thermodynamic parameters of simple Cope rearrangement systems is well known, thanks to the extensive and rigorous efforts of Dolbier.[4] Terminal fluorine atom substituents lower the enthalpy of activation, while the entropy of activation usually increases; overall, the rearrangement reaction in which the CF_2 centre rehybridises from sp^2 to sp^3 is favoured.

Cyclic (especially medium to large ring) difluoro ketones have a relatively unexplored chemistry because there are few rational routes for their synthesis. More highly fluorinated cyclic ketones show interesting keto/enol tautomerisation[5] behaviour that is quite different from that of acylic congeners,[6] an important class of compounds with well-defined and useful hydration behaviour.[7] Routes to conformationally-restricted difluoro ketones may therefore be of interest and there is also potential for novel transannular interactions and reactions.[8] We therefore decided to examine the oxy-Cope rearrangement as a possible novel strategy for the construction of medium to large rings with controllable patterns of selective fluorination.

We chose the divinyl cyclohexanol/cyclodecenone system, studied originally by Marvell and Whalley,[9] as our starting point and followed their synthetic strategy. Cyclohexene oxide was opened with metallated fluoroalkenes **1a**,[10a] **1b**[10b] and **1c**[10c] to afford alcohols **2a–c** in 69, 64 and 76% isolated yields. Swern oxidation of each followed to afford the corresponding ketones **3a** (83%), **3b** (52%) and **3c** (72%). We were happy to note that these β,γ-unsaturated species, which are presumably destabilised by the vinylic CF_2 centre, did not isomerise and could be purified by column chromatography (Scheme 1).

Next, we added vinylmetals, with the intention of demonstrating that a degree of flexibility was possible in precursor construction. Vinyllithium reacted smoothly with **3a** and **3c** to afford dienols **4a** and **4c** in 78 and 68% yields respectively. When the metallated fluoroalkene derived from HFC-134a **1c** was added to **3a**, a mixture of diastereoisomeric dienols **5a** with distinct ^{19}F NMR spectra were obtained (2.3:1 mixture, 57%). Finally lithiodihydropyran was added to **3a–c** to afford **6a–c**, completing a preliminary range of representative species. The three latter dienols in particular could not be purified because of decomposition during column chromatography, but crude material could be obtained directly from the addition reaction with satisfactory ^1H and ^{19}F NMR spectra. In general, we were not able to free any of the preceding dienols completely from trace amounts of hydrocarbon impurities so they were taken on without being characterised fully.

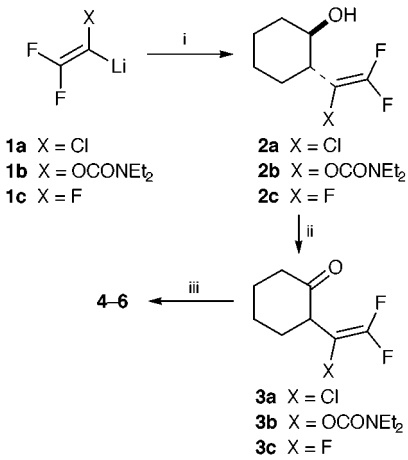

Scheme 1 *Reagents and conditions*: i, cyclohexene oxide, $BF_3{\cdot}OEt_2$, THF, −78 °C; ii, DMSO, $(COCl)_2$, −78 °C, then Et_3N; iii, alkenylmetal, THF, −78 °C (see text).

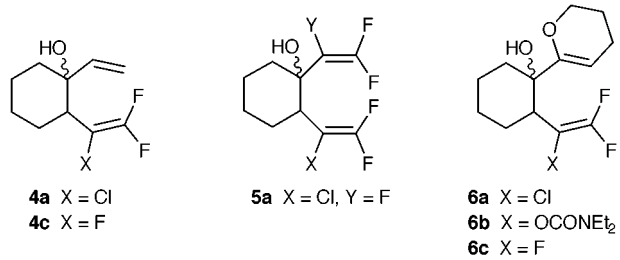

We chose to investigate the neutral oxy-Cope in anticipation of problems arising from the high nucleophilicity of potassium alkoxides and enolates, the potential for fluoride ion loss, and the known high electrophilicity of perhaloalkenes. The rearrangements were initiated by heating small samples of the dienols in dry xylene in sealed (Ace) tubes at progressively higher temperatures until appropriate ^{19}F NMR spectral changes were observed, or ^1H NMR changes in the case of **10**. No attempt was made at this stage to measure rate constants or determine activation parameters but we did run a number of substrates at 150 °C to allow some qualitative comparisons to be made (Table 1) with **10**.

Substrates **4a**, **5a** and **6a** all reacted smoothly at 150 °C in short reaction times; however, **10** failed to react at all in one week at that temperature and only underwent a slow conversion at 225 °C in xylene. Of the three series of compounds, the chlorinated congeners appeared to be more reactive than the fluorinated or oxygenated counterparts.[11] The relatively low temperatures of the rearrangements are most encouraging and suggest that a rather general method of fluoro ketone synthesis may be available.[12] Structural assignment was made by ^1H

Table 1 Rearrangement conditions and outcomes for fluorinated dienols

Dienol	T^a/°C	t^b/h	Product	Yield[c] (%)
4a	125	8	**7a**	67
4a	150	3	**7a**	58
4c	125	46	**7c**	72
5a	150	1.75	**8a**	73
6a	150	3	**9a**	65
6b	155	9	**9b**	62
6c	140	17	**9c**	84
10	150	168	**11**	—
10	225	24	**11**	49

[a] Reactions in sealed tubes in xylene. [b] Time for complete consumption of starting dienol by NMR. [c] Isolated yield.

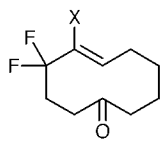

7a X = Cl
7c X = F

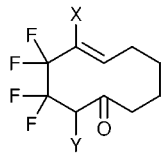

8a X = Cl, Y = F

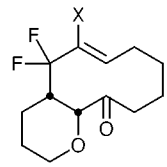

9a X = Cl
9b X = OCONEt$_2$
9c X = F

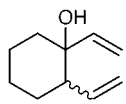

10

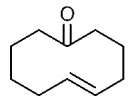

11

NMR COSY and GOESY experiments.[13] By ^{19}F NMR, we were able to detect only products with a single double bond configuration, assumed *trans* with respect to the mutual location of the ring bonds. Unambiguous proof of alkene configuration was then obtained in the case of **9a** when single crystals[14] were grown and subjected to analysis by X-ray diffraction (Fig. 1). Also, the $^3J_{H\text{-}F}$ couplings across the alkene bond in **7c** (33.7 Hz) and **9c** (32.4 Hz) were entirely consistent with this arrangement.

We have therefore shown that oxy-Cope systems can be assembled rapidly, and that fluorinated cyclodecenones and more complex species can be developed from simple fluoroalkene building blocks. Work to define the scope and kinetic parameters of oxy-Cope rearrangement systems that contain fluorinated vinylic components is in progress.

Fig. 1 The molecular structure of **9a**. The *cis*-ring junction and *trans*-ring bonds can be seen clearly.

We thank the Engineering and Physical Sciences Research Council of Great Britain for a Project Studentship (to G. D.) under the ROPA Scheme.

Notes and references

1 C. J. Roxburgh, *Tetrahedron*, 1995, **51**, 9767.
2 L. A. Paquette, *Tetrahedron*, 1997, **53**, 13 971.
3 For reviews of [3,3]-rearrangements of fluorinated substrates, see: S. T. Purrington and S. C. Weeks, *J. Fluorine Chem.*, 1992, **56**, 165; V. G. Andreev and A. F. Kolomiets, A. F. *Usp. Khim.*, 1993, **62**, 594. Rearrangements in the context of fluorinated building block chemistry are discussed in: J. M. Percy, *Top. Curr. Chem*., 1997, **193**, 131; J. M. Percy and M. E. Prime, *J. Fluorine Chem*., 1999, in the press.
4 W. R. Dolbier and K. W. Palmer, *J. Am. Chem. Soc.*, 1993, **115**, 9349.
5 P. E. Lindner and D. M. Lemal, *J. Org. Chem.*, 1996, **61**, 5109; P. E. Lindner, R. A. Correa, J. Gino and D. M. Lemal, *J. Am. Chem. Soc.*, 1996, **118**, 2556.
6 P. E. Lindner and D. M. Lemal, *J. Am. Chem. Soc.*, 1997, **119**, 3259.
7 D. Schirlin, J. M. Rondeau, B. Podlogar, C. Tardif, C. Tarnus, V. Vandorsselaer and R. Farr, *ACS Symp. Ser.*, 1996, **639**, 169; H. L. Sham, *ACS Symp. Ser.*, 1996, **639**, 184.
8 D. Colclough, J. B. White, W. B. Smith and Y. L. Chu, *J. Org. Chem.*, 1993, **58**, 6303; Y. L. Chu, D. Colclough, D. Hotchkin, M. Tuazon and J. B. White, *Tetrahedron*, 1997, **53**, 14 235.
9 E. N. Marvell and W. Whalley, *Tetrahedron Lett.*, 1970, 509.
10 (*a*) J. M. Bainbridge, S. J. Brown, P. N. Ewing, R. R. Gibson and J. M. Percy, *J. Chem. Soc., Perkin Trans. 1*, 1998, 2541; (*b*) J. A. Howarth, W. M. Owton, J. M. Percy and M. H. Rock, *Tetrahedron*, 1995, **51**, 10289; (*c*) J. Burdon, P. L. Coe, I. B. Haslock and R. L. Powell, *Chem. Commun.*, 1996, 49.
11 N. Y. Jing and D. M. Lemal, *J. Am. Chem. Soc.*, 1993, **115**, 8481. In a study of a Cope rearrangement of a perfluorinated hexadiene, the substitution of a chlorine atom for a fluorine atom was reported to exert only a minimal effect upon rearrangement rate and outcome. Products of biradical pathways reported by these authors were not detected in our study.
12 *Selected data* for **9c:** colourless rhombi, mp 94 °C; (Found: C, 59.68; H, 6.61. Calc. for $C_{13}H_{17}F_3O_2$: C, 59.54; H, 6.49%); δ_H(300 MHz, $CDCl_3$) 5.32 (dddd, ^3J 32.4, J 11.4, J 6.3, J 3.0, 1H), 4.16 (dd, ^2J 11.4, J 5.5, 1H), 3.72 (t, J 3.4, 1H), 3.48 (ddt, ^2J 11.4, J 13.0, J 3.1, 1H), 3.10 (dd, J 19.1, J 10.5, 1H), 2.88 (dddd, ^3J 31.6, J 10.8, ^3J 5.5, J 2.9, 1H), 2.38–2.30 (m, 2H), 2.19–2.05 (m, 3H), 2.04–1.95 (m, 1H), 1.86 (dtd, J 16.8, 10.9, 5.5, 1H), 1.73 (ddt, J 19.8, ^2J 14.3, J 5.5, 1H), 1.63–1.55 (m, 1H), 1.40 (d, ^2J 14.3, 1H), 1.31 (q, J 14.0, 1H); δ_F (282 MHz, $CDCl_3$) −101.9 (dd, ^2J 255.6, ^3J 26.7, 1F), −109.5 (dd, ^2J 255.6, ^3J 31.7, 1F), −124.8 (t, ^3J 31.2, 1F); $^{13}\delta_C$ (75 MHz, $CDCl_3$) 207.5, 150.5 (ddd, ^2J 260.5, ^2J 38.4, ^2J 27.7), 117.6 (ddd, ^1J 244.7, ^1J 252.1, ^2J 37.9), 113.0, 83.2, 69.5, 40.9 (dd, ^2J 27.1, ^2J 21.5), 38.5, 29.1, 28.5, 23.1, 22.0, 20.5; ν_{max}/cm^{-1} 1711.9; m/z (CI) 280 ($M+NH_4^+$).
13 J. Stonehouse, P. Adell, J. Keeler and A. J. Shaka, *J. Am. Chem. Soc.*, 1994, **116**, 6037.
14 *Crystal data* for **9a**: $C_{13}H_{17}ClF_2O_2$, M = 278.7, triclinic, a = 8.0670(2), b = 8.3194(3), c = 10.5779(3) Å, U = 633.65(3) Å^3, T = 150(2) K, space group $P\bar{1}$, Z = 2, μ(Mo-K$_\alpha$) 0.318 mm^{-1}, 10852 reflections measured, 2555 unique (R_{int} = 0.0441) which were used in all calculations. The final $wR(F^2)$ was 0.0718 (all data). CCDC 182/1482. See http://www.rsc.org/suppdata/cc/1999/2535/ for crystallographic data in .cif format.

Communication 9/08450I

Asymmetric synthesis of 2,3-disubstituted oxepanes *via* acetalization–cyclization of an enantioenriched functionalized allylsilane with aldehydes

Michinori Suginome, Taisuke Iwanami and Yoshihiko Ito*

Department of Synthetic Chemistry and Biological Chemistry, Graduate School of Engineering, Kyoto University, Kyoto 606-8501, Japan. E-mail: yoshi@sbchem.kyoto-u.ac.jp

Received (in Cambridge, UK) 28th October 1999, Accepted 12th November 1999

According to the protocol for the acetalization–intramolecular allylsilane cyclization, a new enantioenriched allylsilane, (*R*)-(*E*)-7-(dimethylphenylsilyl)undec-5-en-1-ol, in the presence of a variety of aldehydes provided enantioenriched *trans*-2,3-disubstituted oxepanes stereoselectively.

Allylsilanes bearing hydroxylated alkyl groups have been utilized for the efficient synthesis of cyclic ethers *via* an acetal formation with aldehydes, followed by an intramolecular cyclization of the allylsilane with an oxonium ion generated from the acetal in the presence of an acid catalyst.[1,2] Moreover, an asymmetric version of the acetalization–intramolecular allylsilane cyclization (AIAC) protocol was recently established by us with use of enantioenriched allylsilanes, which were synthesized *via* a highly stereoselective intramolecular bis-silylation of enantioenriched allylic alcohols.[3] Although the AIAC protocol was successfully applied to the stereoselective synthesis of five- and six-membered cyclic ethers, attempt at the seven-membered ring formation has never been reported. In the light of the synthetic importance of the oxepane derivatives, it is highly desirable to develop a new methodology for the stereoselective construction of oxepanes. Herein, we report stereoselective synthesis of enantioenriched seven-membered cyclic ethers through the AIAC protocol by use of a new enantioenriched allylsilane **1**, which was readily available from δ-valerolactone in a multigram scale.[4]

Reaction of δ-valerolactone with 1-lithiohex-1-yne followed by THP protection (THP = tetrahydropyranyl) of the resulting hydroxy group provided the ynone **2** (Scheme 1). Ruthenium-catalyzed enantioselective reduction of the carbonyl group afforded the propargyl alcohol **3** with high optical purity.[5] After the conversion of **3** to the corresponding allylic alcohol **4**, the enantiomeric excess was determined to be 97.1%. Compound **4** was then subjected to our protocol for the synthesis of enantioenriched allylsilanes.[6] The palladium-catalyzed intramolecular bis-silylation of the disilanyl ether **5** and subsequent treatment with BuLi followed by THP deprotection with PPTS afforded the enantioenriched allylsilane (*R*)-**1** with a hydroxybutyl chain.[7] The enantiomeric purity of 96.3% ee was confirmed by chiral HPLC analysis after the appropriate derivatization.[3] Note that the procedure was efficient enough to enable us to prepare (*R*)-**1** on a 10 g scale without difficulty.

With the enantioenriched allylsilane (*R*)-**1** in hand, the AIAC reaction with acetaldehyde was examined in the presence of TMSOTf (2 equiv.). Under essentially the same conditions that we reported previously for the six-membered ring formation, the cyclization took place to give the seven-membered cyclic ether **6a** in 63% yield (Table 1, entry 1).

It is noteworthy that only the *trans*-2,3-disubstituted seven-membered ring ether with *E* olefin geometry was selectively produced.[8] The enantiomeric excess of **6a** was determined to be not less than 92%; finding the chiral GC or HPLC conditions for the complete separation of the enantiomers **6a** proved difficult. Also, the cyclizations with some aliphatic aldehydes proceeded with a good level of chirality transfer (> 96%) (entries 2–4).[9,10] As observed for the reaction of acetaldehyde, only the *trans*-*E*-oxepanes **6b**–**d** were selectively obtained in the cyclization. The amount of the TMSOTf could be reduced to 1.1 equiv. without a decrease in the yield or stereoselectivity (entry 3).

Reaction with benzaldehyde also proceeded in good yield with high stereoselectivity (entry 5). A trace amount (2%) of *cis*-oxepane was detected by ^{1}H NMR, however, the enantiomeric excess of the *trans*-oxepane **6e** was found to be 95.6%. This high stereoselectivity in the seven-membered ring formation with benzaldehyde is in sharp contrast with the correspond-

Table 1 Synthesis of enantioenriched 2,3-disubstituted oxepanes through cyclization of (*R*)-**1** (96.3% ee) with aldehydes[a]

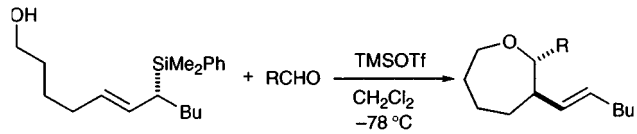

(*R*)-**1** (96.3% ee) **6**

Entry	R	Product (% yield)[b]	*trans*:*cis*[c]	*E*:*Z*[c]	Ee (%)[d]	Stereo conservation (%)[e]
1	Me	**6a** (63)	> 99:1	> 99:1	92[f]	96
2	*n*-Hex	**6b** (71)	> 99:1	> 99:1	93.6	97
3[g]	Pr^i	**6c** (94)	> 99:1	> 99:1	92.5	96
4	Bu^t	**6d** (71)	> 99:1	> 99:1	93.9	98
5	Ph	**6e** (82)	50:1	> 99:1	95.6	99
6	*p*-MeC$_6$H$_4$	**6f** (70)	40:1	> 99:1	93.3	97
7	*p*-NO$_2$C$_6$H$_4$	**6g** (74)	20:1	> 99:1	90.9	94

[a] The reactions were carried out at −78 °C in CH_2Cl_2 for 2 h in the presence of TMSOTf (2.0 equiv.) unless otherwise noted. [b] Isolated yields. [c] Determined by ^{1}H NMR. [d] Determined by chiral HPLC unless otherwise noted (ref. 9). [e] (Ee of the product **6**)/[ee of (*R*)-**1**]. [f] Determined by chiral GC (Chrompack Cyclodextrine-β-236M-19) with incomplete separation of signals for enantiomers. [g] Use of 1.1 equiv. of TMSOTf.

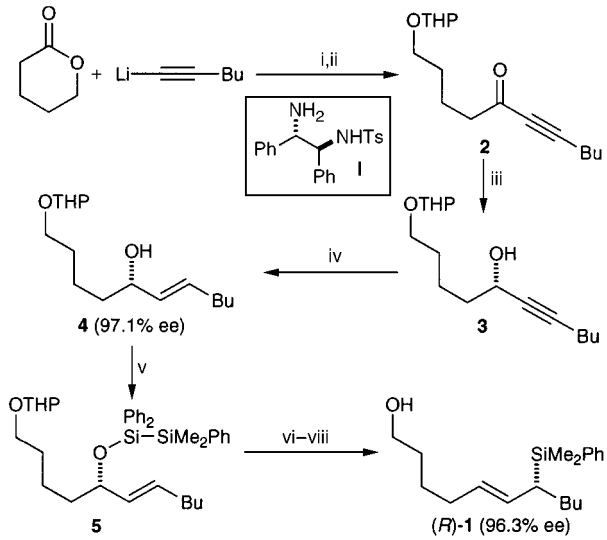

Scheme 1 *Reagents and conditions*: i, THF, 0 °C; ii, DHP, TsOH, CH_2Cl_2, room temp.; iii, **I**, $[RuCl_2(p\text{-cymene})]_2$ (cat), KOH, Pr^iOH, room temp., 41% for 3 steps; iv, Red-Al, THF, 0 °C to reflux, 95%; v, $ClPh_2SiSiMe_2Ph$, Et_3N, DMAP (cat), THF, room temp., 87%; vi, $Pd(acac)_2$, $Bu^tCH_2CMe_2NC$, toluene, reflux; vii, BuLi, THF, 0 °C; viii, PPTS, EtOH, 60 °C, 72% for 3 steps.

ing non-stereoselective six-membered ring formation, where all four possible diastereomers were formed. Reaction of **1** with *p*-tolualdehyde also gave *trans*-*E*-oxepane **6f** stereoselectively (entry 6). Interestingly, benzaldehydes bearing electron-donating or -withdrawing substituents at the *p*-positions presented contrasting results in the reactions with **1**. Thus, *p*-nitrobenzaldehyde successfully afforded the corresponding oxepane **6g** of 91% ee with slightly lower diastereoselectivity (entry 7), while no reaction occurred with *p*-anisaldehyde.

In summary, a new and highly stereoselective synthesis of oxepanes has been developed on the basis of the stereoselective preparation of the enantioenriched allylsilane. The success in the practical synthesis of **1** may lead to the synthesis of related functionalized allylsilanes, which can be used as enantioenriched building blocks in organic synthesis.

We thank the Ministry of Education, Science, Sports, and Culture, Japan for a Grant-in-Aid for Scientific Research (11650873).

Notes and references

1 For the five-membered ring formation, see: P. Mohr, *Tetrahedron Lett.*, 1993, **34**, 6251; T. Oriyama, A. Ishiwata, T. Sano, T. Matsuda, M. Takahashi and K. Koga, *Tetrahedron Lett.*, 1995, **36**, 5581; T. Sano and T. Oriyama, *Synlett*, 1997, 716.

2 For the six-membered ring formation, see: I. E. Markó and A. Mekhalfia, *Tetrahedron Lett.*, 1992, **33**, 1799; I. E. Markó and D. J. Bayston, *Tetrahedron*, 1994, **50**, 7141; I. E. Markó, M. Bailey, F. Murphy, J. P. Declercq, B. Tinant, J. Feneau-Dupont, A. Krief and W. Dumont, *Synlett*, 1995, 123.

3 M. Suginome, T. Iwanami and Y. Ito, *J. Org. Chem.*, 1998, **63**, 6096.

4 For a review of the reactions of chiral allylsilanes, see: C. E. Masse and J. S. Panek, *Chem. Rev.*, 1995, **95**, 1293.

5 K. Matsumura, S. Hashiguchi, T. Ikariya and R. Noyori, *J. Am. Chem. Soc.*, 1997, **119**, 8738; K.-J. Haack, S. Hashiguchi, A. Fujii, T. Ikariya and R. Noyori, *Angew. Chem., Int. Ed. Engl.*, 1997, **36**, 285. The absolute configuration (*S*) of **3** was assigned by an analogy with these reports.

6 M. Suginome, A. Matsumoto and Y. Ito, *J. Am. Chem. Soc.*, 1996, **118**, 3061; M. Suginome, T. Iwanami, A. Matsumoto and Y. Ito, *Tetrahedron: Asymmetry*, 1997, **8**, 859.

7 The absolute configuration (*R*) was assigned by analogy with previous reports. See ref. 5 and 6. *Selected data* for (*R*)-**1**: $\delta_H(CDCl_3)$ 0.24 (s, 3H), 0.25 (s, 3H), 0.82 (t, *J* 6.9, 3H), 1.04–1.68 (m, 13H), 1.97–2.05 (m, 2H), 3.62 (t, *J* 6.6, 2H), 5.10–5.25 (m, 2H), 7.31–7.37 (m, 3H), 7.43–7.51 (m, 2H); $\delta_C(CDCl_3)$ −5.1, −4.5, 13.9, 22.3, 26.0, 28.5, 31.4, 32.4, 32.5, 62.9, 127.6, 128.5, 128.8, 131.5, 134.1, 138.4; ν_{max}(neat)/cm^{-1} 3356, 2968, 2940, 2864, 1432, 1250, 1114 (calc. for $C_{19}H_{32}OSi$ 304.2222, found 304.2221); $[\alpha]_D^{20}$ −8.38 (*c* 3.1, benzene).

8 The *trans* stereochemistry in the seven-membered ring was determined on the basis of the ^1H NMR coupling constant between the 2- and 3-protons in the ring. Compound **6a** exhibited a coupling constant of 9.6 Hz, whereas that for *trans*- and *cis*-2-(phenylsulfonylmethyl)-3-(phenylmethyl)oxepane were reported as 8.5 and 2.6 Hz, respectively. See: P. L. López-Tudanca, K. Jones and P. Brownbridge, *Tetrahedron Lett.*, 1991, **32**, 2261.

9 The enantiomeric excesses of **6**, except for **6a**, were determined after derivatization to the corresponding 2-substituted 3-oxepanecarboxylic acid by RuO_2-catalyzed oxidative C=C bond cleavage in the presence of $NaIO_4$ (CCl_4, MeCN, H_2O). The 3,5-dinitrophenylanilides were subjected to chiral HPLC with Sumichiral OA columns indicated below [compound, column, solvent (a ratio of hexanes–1,2-dichloroethane–ethanol)]: (**6b**, OA-4400, 50:15:1); (**6c**, OA-4500 × 3, 15:15:1); (**6d**, OA-4400, 15:5:1); (**6e**, OA-4900, 15:5:1); (**6f**, OA-4500, 15:5:1); (**6g**, OA-4600, 15:5:1). The absolute configurations were assigned by analogy with the stereochemical outcome for the six-membered ring formation reported previously. See ref. 3.

10 The slight decrease in the enantiomeric excesses may be attributed to a minor contribution of '*syn* attack' of the electrophiles on the allylsilane moieties during the cyclization in addition to the normal '*anti* attack'. For a discussion on the '*anti*' *vs.* '*syn*' attack in the reaction of allylsilanes with electrohiles, see: M. J. C. Bucke, I. Fleming and S. Gil, *Tetrahedron Lett.*, 1992, **33**, 4479.

Communication 9/08603J

Periodic mesoporous organosilicas, PMOs: fusion of organic and inorganic chemistry *'inside'* the channel walls of hexagonal mesoporous silica

Chiaki Yoshina-Ishii, Tewodros Asefa, Neil Coombs, Mark J. MacLachlan and Geoffrey A. Ozin*

Materials Chemistry Research Group, University of Toronto, Department of Chemistry, 80 St. George Street, Toronto, Ontario, M5S 3H6, Canada. E-mail: gozin@alchemy.chem.utoronto.ca

Received (in Cambridge, UK) 14th October 1999, Accepted 19th November 1999

Synthesis and characterization of new periodic mesoporous organosilicas, PMOs, containing benzene and thiophene groups 'within' the channel walls, is presented.

Since the first report of surfactant-templated mesoporous silica by Kresge *et al.*,[1] the area of periodic mesoporous materials has exploded. This is due to the promising properties and applications of materials with ordered arrangements of pores in a new length scale in chemistry, including size exclusion chemistry and chromatography, catalysis, sensors and host materials for polymers, organic and inorganic substances.[2,3]

Recently, a new class of materials, periodic mesoporous organosilicas (PMOs), have been reported.[4–7] These materials are unique compared to first generation periodic mesoporous silica materials since the channel walls contain both organic and inorganic substances. This marriage of organic chemistry with inorganic materials chemistry offers fascinating new possibilities and applications. Some important advantages of integrated organic–inorganic channel walls (smart channels) that were not possible with first generation materials include the following. (i) Organic moieties are homogeneously dispersed *'inside'* the channel walls with a maximum loading of 100%, not achievable with organics 'hanging' in the channels with a maximum loading before collapse of 25%. (ii) Bridge bonded organics *'inside'* the channel walls do not block the pores from chemistry. (iii) 'Soft' organics *'integrated within'* the channel walls should impart interesting mechanical properties to the 'hard' inorganics not seen before. (iv) The organic precursors are easily varied to produce a wide range of materials with potentially interesting electronic, optical, charge-transport and magnetic properties.

The preparation of these materials involves the catalyzed hydrolysis of bis(trialkoxysilyl) organic precursors in the presence of a surfactant template. The presence of the organic moiety greatly influences the nature of the hydrolysis reaction and a number of new factors become important in the synthesis of these materials. Most notably, we were concerned with the stability of the Si–C bond under the hydrolysis conditions and the degree of order in the resulting product. Certain materials, such as the bis-silylated ethylene, methylene and ethane precursors show great stability to strongly acidic or basic conditions. This is confirmed by ^{29}Si NMR, which shows virtually no cleavage even under harsh conditions.[7] In more complicated bridging organic precursors, however, aqueous hydrolysis often results in significant cleavage, as well as a decrease in the degree of order in the material.

The synthesis of the precursors utilized bis-metallated organic intermediates, which reacted with chlorotriethoxysilane prepared from the partial alcoholysis of silicon tetrachloride.[8] Precursors that we synthesized include 1,4-bis(triethoxysilyl)benzene **1**,[9] 2,5-bis(triethoxysilyl)thiophene **2**,[9] 1,1′-bis-(triethoxysilyl)ferrocene **3**,[10,11] bis(triethoxysilyl)bithiophene **4**,[9] and bis(triethoxysilyl)acetylene **5** (Fig. 1).[12] Thiophene and ferrocene PMOs may have interesting electrochemical applications. PMOs with unsaturated organic groups such as benzene offer the possibility of 'chemistry *of* the channels', or act as '*ligand* channels' for metal complexes and organometallics in catalytic applications.

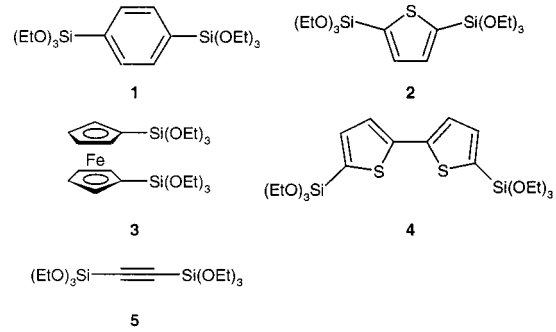

Fig. 1 Structures of the PMO precursors.

When the strongly basic conditions utilized for the synthesis of ethylene-bridged mesoporous silica[4] were applied to the benzene **1** and thiophene **2** precursors, white powders were obtained almost immediately [1.0 Si : 114 H_2O : 15.0 NH_3 (aq) (35 wt%) : 0.12 CTABr]. The powders were aged at 80 °C for two days. ^{29}Si CP MAS NMR showed that almost all the organic moieties had been cleaved from the silica. When a similar experiment was performed under acidic conditions using the thiophene precursor, ^{29}Si CP MAS NMR showed characteristic signals attributed to $Si(OSi)_4$ (Q_4 δ −112), $(HO)Si(OSi)_3$ (Q_3 δ −103) and $(HO)_2Si(OSi)_2$ (Q_2 δ −92), which clearly indicate that a proportion of the Si–C bonds had been cleaved, as well as signals which showed the presence of the organic moieties; $CSi(OSi)_3$ (T_3 δ −84), $CSi(OSi)_2(OH)$ (T_2 δ −76) and $CSi(OSi)(OH)_2$ (T_1 δ −66) [Fig. 2(a)]. ^{13}C CP MAS NMR showed that indeed the benzene and thiophene organic moieties were intact. The PXRD pattern showed very good structural order in the hexagonal phase. Most of the surfactant template could be removed by extracting into an MeOH–HCl mixture at room temp. for 2–3 days and the structural integrity of the material was maintained, as shown by PXRD and TEM studies.

To decrease the amount of cleavage of Si–C bonds in the benzene and thiophene PMOs, a decreased concentration of acid was used to catalyze the hydrolysis, as well as allowing the

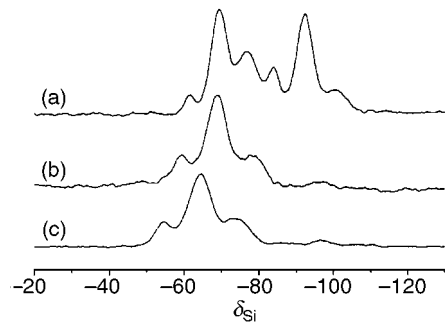

Fig. 2 ^{29}Si CP MAS NMR spectra of periodic organosilica materials. Thiophene bridged PMO prepared in (a) strong acid and (b) under the optimized procedure. (c) Benzene bridged PMO prepared under the optimized procedure.

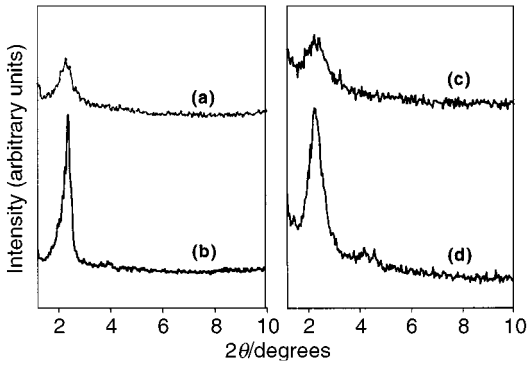

Fig. 3 PXRD of periodic mesoporous organosilica materials with a comparable degree of Si–C bond cleavage. Benzene bridged PMO prepared in (a) dilute acid and (b) under the optimized procedure. Thiophene bridged PMO prepared in (c) dilute acid and (d) under the optimized procedure.

powder to age at room temp. instead of 80 °C. NMR studies confirmed that under milder conditions, the amount of cleavage decreased. However, PXRD indicated that the degree of order of the material was diminishing with decreased acid concentration [Fig. 3(a,c)]. This is presumably due to the decreased charge concentration on the silicate species. This reduces the coulombic attraction between surfactant and silicate species that contributes to the 'surfactant templating' mechanism.[13] Also, under very dilute acidic conditions, the yield of the powder product decreased considerably as did the degree of polymerization as observed by ^{29}Si NMR. This decreased yield may be due to the formation of low molecular weight soluble silicates.

To obtain a satisfactorily ordered PMO containing benzene or thiophene in an aqueous synthesis medium, a different approach to hydrolytic polycondensation needed to be considered. The following procedure for the bis-silylated thiophene PMO gives a satisfactory sample and is representative of the approach. Cetylpyridinium chloride (CPCl) followed by 2,5-bis(triethoxysilyl)thiophene was added to an acidic aqueous solution and stirred moderately at room temp. briefly. After the resulting mixture was neutralized with portionwise addition of solid $NaHCO_3$, NH_4F (0.1 mol%) was added and the slurry allowed to stand at room temp. for two days.[14] After filtering and washing with copious amounts of water, a white powder was obtained. The material thus obtained showed only a small amount of Si–C bond cleavage [Fig. 2(b,c)] and the PXRD showed a good hexagonal mesoporous organosilica (100) reflection [Fig. 3(b,d)]. TEM also showed the presence of the expected crystalline mesoporosity (Fig. 4).[15,16] NMR did not show the presence of triethoxysilyl moieties, suggesting the hydrolysis is essentially complete.

The other precursors proved to be more challenging. For example, the bis(triethoxysilyl)ferrocene precursor **3** showed partial cleavage of the Si–C bond and a lower degree of order.

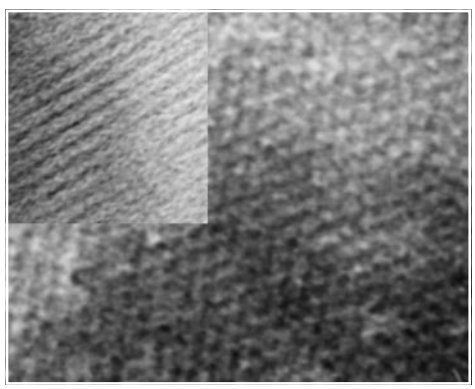

Fig. 4 TEM of hexagonal mesoporous benzene silica. Images perpendicular and parallel (inset) to the channel axis confirm the hexagonal structure of the PMO. Extensive TEM lattice imaging studies of large areas of the sample show that the PMO phase always dominates over any amorphous organosilicate xerogel phase.

NMR studies showed that a significant amount of ferrocene remained intact in the silica framework, and thus shows promise for further study. The acetylene precursor **4** had a particularly labile Si–C bond and was difficult to control under aqueous conditions. The attempt to place the bithiophene moiety **5** within the walls of the channels resulted in a material with poorer order.

The preparation of various hybrid 'organic–inorganic' walled periodic mesoporous silicas is currently being optimized.

PMOs with organic functionality *'inside'* the channel walls are a new class of materials with much promise for a wide variety of applications. PMOs are distinct from organosilica xerogels that have been previously reported. Organosilica xerogels have a *'random distribution of polydispersed mesopores'*. This is to be contrasted with PMOs that have *'crystalline mesoporosity'* and *'Angstrom precise pore dimensions'*, both considered necessary prerequisites for size selective applications.

This work was supported by the National Sciences and Engineering Research Council of Canada (NSERC). We thank NSERC for a post-graduate scholarship (M. J. M., 1995–99) and an undergraduate summer research scholarship (C. Y.-I., 1999).

Notes and references

1 C. T. Kresge, M. E. Leonowicz, W. J. Roth, J. C. Vartuli and J. S. Beck, *Nature*, 1992, **359**, 710.
2 K. Moller and T. Bein, *Chem. Mater.*, 1998, **10**, 2950.
3 G. A. Ozin, E. Chomski, D. Khushalani and M. J. MacLachlan, *Curr. Opin. Colloid Interface Sci.*, 1998, **3**, 181.
4 T. Asefa, M. J. MacLachlan, N. Coombs and G. A Ozin, *Nature*, 1999, submitted.
5 S. Inagaki, S. Guan, Y. Fukushima, T. Ohsuna and O. Terasaki, *J. Am. Chem. Soc.*, 1999, **121**, 9611.
6 B. J. Melde, B. T. Holland, C. F. Blanford and A. Stein, *Chem. Mater.*, 1999, **11**, 3302.
7 Ö. Dag, C. Yoshina-Ishii, T. Asefa, M. J. MacLachlan, H. Grondey and G. A. Ozin, *Adv. Mater.*, 1999, submitted.
8 D. F. Peppard, W. G. Brown and W. C. Johnson, *J. Am. Chem. Soc.*, 1946, **68**, 70.
9 R. J. P. Corriu, J. J. E. Moreau, P. Thepot and M. W. C. Man, *Chem. Mater.*, 1992, **4**, 1217.
10 G. Cerveau, C. Chuit, E. Colomer, R. J. P. Corriu and C. Reyé, *Organometallics*, 1990, **9**, 2415.
11 M. S. Wrighton, M. C. Palazzotto, A. B. Bocarsly, J. M. Bolts, A. B. Fischer and L. Nadjo, *J. Am. Chem. Soc.*, 1978, **100**, 7264.
12 R. J. P. Corriu, J. J. E. Moreau, P. Thepot, M. W. C. Man, C. Chorro, J.-P. Lère-Porte and J.-L. Sauvajol, *Chem. Mater.*, 1994, **6**, 640.
13 For a recent review, see: J. Y. Ying, C. P. Mehnert and M. S. Wong, *Angew. Chem., Int. Ed.*, 1999, **38**, 56.
14 The following procedure for the synthesis of mesoporous benzenesilica is representative: bis(triethoxysilyl)benzene (0.96 g, 2.4 mmol) was added to a homogeneous solution of water (4.88 g, 0.27 mol), HCl (36%, 0.81 g, 8.1 mmol), and CPCl (0.11 g, 0.3 mmol) at *ca.* 32 °C, and the solution was stirred moderately for 15 min. The resulting mixture was neutralized with portionwise addition of $NaHCO_3$ prior to adding NH_4F (0.1 mg, 2.7 μmol) and aging at room temp. for two days. The powder was filtered and washed with copious amounts of water.
15 The possibility that a mixture of amorphous organosilica and periodic mesoporous organosilica resulting from hydrolytic cleavage of the Si–C bond could give rise to the observed PXRD and NMR was addressed by examining large areas of the powder by TEM. The results of an extensive TEM study show that the PMO phase dominates over any amorphous organosilicate xerogel phase. Therefore the PMOs are responsible for both the solid state NMR and PXRD data reported here. Polarisation optical microscopy and micro-Raman spectroscopy confirm this proposal and show bridge bonded organics homogeneously dispersed throughout the PMO.[7]
16 Surfactant-free mesoporous benzenesilica shows a Type IV nitrogen adsorption isotherm at 77 K. Calculated BET suface area = 1365 m^2 g^{-1}, pore volume = 0.67 cm^3 g^{-1}, pore diameter = 2 nm, which together with PXRD–TEM d_{100} = 3.8–3.2 nm provides a channel wall thickness ≈ 2 nm.

Communication 9/08252B

Reductive coupling of alkynes to give ruthenium and osmium clusters of the type $[M_3(1,3\text{-diene})(\mu_3\text{-X})(CO)_8]$ containing $\mu\text{-}\eta^2,\eta^2$- or η^4-1,3-diene

Shahbano Ali,[a] Antony J. Deeming,*[a] Graeme Hogarth,*[a] Nikesh A. Mehta[a] and Jonathan W. Steed[b]

[a] *Department of Chemistry, University College London, 20 Gordon Street, London, UK WC1H 0AJ. E-mail: a.j.deeming@ucl.ac.uk and g.hogarth@ucl.ac.uk*

[b] *Department of Chemistry, King's College London, Strand, London, UK WC2R 2LS*

Received (in Basel, Switzerland) 29th October 1999, Accepted 12th November 1999

Replacement of a CO ligand by MeCN in the capped clusters $[M_3(\mu\text{-H})_2(\mu_3\text{-X})(CO)_9]$ (M = Ru, X = $NSO_2C_6H_4Me$-4 or M = Os, X = S) allows reductive coupling of alkynes (RC≡CH, R = H or Ph) to give regioselectively the 1,3-diene clusters $[M_3(C_4H_4R_2)(\mu_3\text{-X})(CO)_8]$, with the diene $\mu\text{-}\eta^2,\eta^2$-coordinated for ruthenium and η^4 for osmium.

Hydrido clusters usually react with alkynes to give $\mu\text{-}\sigma,\eta^2$-alkenyl containing clusters.[1–3] Dihydrido clusters either give hydrido–alkenyl compounds[1,2] or exceptionally dialkenyl compounds by double insertion.[3] Two organyl ligands formed by double insertion could couple to give new organic ligands. More commonly both hydride ligands are delivered to the same organic function leading to simple hydrogenation, for example alkyne to alkene. We now report 1,3-diene-containing clusters formed by double insertion of alkyne into M–H bonds, followed by alkenyl–alkenyl coupling. Reductive coupling of alkynes to give 1,3-dienes is not very common[4] and an alkenyl–alkenyl coupling mechanism has not been established previously, although alkenyl coupling with other organic ligands has been implicated in Fischer–Tropsch synthesis.[5] Our approach was to displace CO by more labile MeCN in strongly capped Os_3 and Ru_3 clusters with two basal hydrido bridges, thereby creating a reactive basal plane of metal atoms within a robust cluster.

The cluster $[Ru_3(\mu\text{-H})_2(\mu_3\text{-NR})(CO)_9]$ (R = $SO_2C_6H_4Me$-4) **1**[6] was treated with $Me_3NO{\cdot}2H_2O$ and MeCN to form $[Ru_3(\mu\text{-H})_2(\mu_3\text{-NR})(CO)_8(MeCN)]$ **2** with the MeCN ligand *cis* to the capping atom N; two sharp hydride ^{1}H NMR doublets observed at −25 °C are exchange-broadened at 20 °C. Treatment of **2** with $Bu^tC{\equiv}CH$ gives the mono-insertion product $[Ru_3(\mu\text{-H})(\mu\text{-}trans\text{-CH=CHBu}^t)(\mu_3\text{-NR})(CO)_8]$ **3**† reversibly. Compound **3** liberates $Bu^tCH{=}CH_2$ and $[Ru_3(\mu_3\text{-NR})(CO)_{10}]$ on treatment with CO at room temperature. In contrast, the less bulky alkynes RC≡CH (R = Ph or H) both react with **2** to give mixtures from which we could isolate two compounds, $[Ru_3(\mu\text{-}\eta^2,\eta^2\text{-}C_4H_4R_2)(\mu_3\text{-NR})(CO)_9]$ **4** (R = H) (7%) and **5** (R = Ph) (17%).

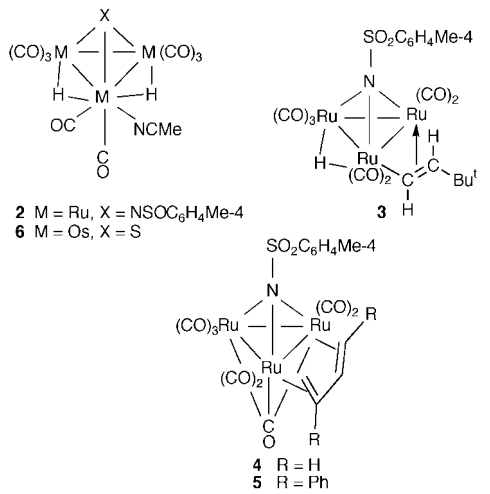

2 M = Ru, X = $NSOC_6H_4Me$-4
6 M = Os, X = S

3

4 R = H
5 R = Ph

Spectra† show that **4** and **5** are very similar and ^{1}H NMR spectra for **5** confirm head-to-tail coupling of phenylacetylene to give the *trans*-1,3-diphenylbutadiene ligand. The single-crystal structure of **4** (Fig. 1)‡ shows the presence of μ_3-NR, μ_3-CO and $\mu\text{-}\eta^2,\eta^2$-*s*-*cis*-butadiene. While $\mu\text{-}\eta^2,\eta^2$-*s*-*cis*-1,3-diene is known in several cases,[7] $\mu\text{-}\eta^2,\eta^2$-*s*-*trans*-butadiene,[8] $\mu\text{-}\eta^1,\eta^3$-*s*-*cis*-butadiene[9] and $\mu\text{-}\eta^1,\eta^4$-*s*-*cis*-1,3-diene[10] are also known. The cluster $[Os_3(CO)_{10}(\mu\text{-}C_4H_6)]$ contains $\mu\text{-}\eta^2,\eta^2$-*s*-*trans*-butadiene.[11]

Intermediate alkenyl complexes were not observed in the formation of **4** and **5**, although the formation of **3** suggests that they are involved. The Os analogue of **2** only reacts with alkynes to give clusters related to **3**, without diene formation. However, the cluster $[Os_3(\mu\text{-H})_2(\mu_3\text{-S})(CO)_8(MeCN)]$ **6**, formed as for **2**, was treated with PhC≡CH in refluxing THF for 24 h to give various insertion products: $[Os_3(\mu\text{-H})(\mu\text{-PhC=CH}_2)(\mu_3\text{-S})(CO)_8]$ **7** (23%), $[Os_3(\mu\text{-H})(\mu\text{-CH=CHPh})(\mu_3\text{-S})(CO)_8]$ **8** (11%), $[Os_3(\mu\text{-PhC}_2H_2)_2(\mu_3\text{-S})(CO)_7]$ **9** (17%) and $[Os_3(\eta^4\text{-PhCH=CHCPh=CH}_2)(\mu_3\text{-S})(CO)_8]$ **10** (12%). The isomeric mono-insertion products **7** and **8** were shown by ^{1}H NMR to be non-interconverting regioisomers. The di-insertion product **9** exists as a mixture of isomers (^{1}H NMR evidence) with both $CPh{=}CH_2$ and CH=CHPh ligands present. The 1,3-diphenylbutadiene complex **10** from treatment of **6** with PhC≡CH is also formed by treating the dialkenyl cluster **9** with CO. ^{1}H NMR data for **10** confirm head-to-tail alkyne coupling but there are very different chemical shifts for the four vinylic hydrogen atoms in **10** compared with those for **5** (δ 1.55, 2.43, 3.58 and 6.79 for **10** *cf.* δ 2.98, 4.72, 5.53 and 5.82 for **5**).

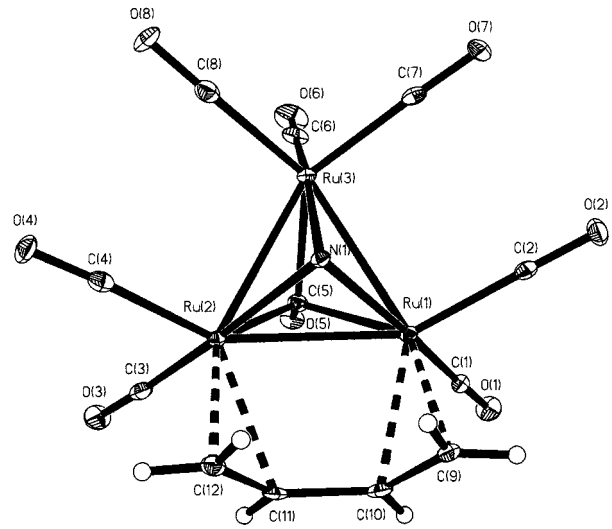

Fig. 1 Thermal ellipsoid drawing (30% probability) of $[Ru_3(\mu\text{-}\eta^2,\eta^2\text{-}C_4H_6)(\mu_3\text{-}NSO_2C_6H_4Me\text{-}4)(CO)_8]$ **4** with the tosyl group omitted. Selected lengths (Å) and angles (°): Ru(1)–Ru(2) 2.7560(3), Ru(1)–Ru(3) 2.7416(4), Ru(2)–Ru(3) 2.7554(3), Ru(1)–C(9) 2.258(3), Ru(1)–C(10) 2.304(3), Ru(2)–C(11) 2.338(3), Ru(2)–C(12) 2.246(3), C(9)–C(10) 1.393(5), C(10)–C(11) 1.461(4), C(11)–C(12) 1.393(5); C(9)–C(10)–C(11) 127.5(3), C(10)–C(11)–C(12) 127.6(3).

Furthermore there is no IR evidence for μ_3-CO in **10**. A single-crystal structure determination (Fig. 2)‡ confirms that **10** has a different structure from that of **4** or **5**. Indeed there is no μ_3-CO in **10**, but instead the two CO ligands at Os(1) are semibridging to Os(2) and Os(3) respectively. More importantly the 1,3-diene is η^4-co-ordinated to Os(1) rather than bridging as in **4**.

The formation of 1,3-diene-containing clusters from simple alkynes is unique. The mono-insertion compounds $[M_3(\mu\text{-H})(\mu\text{-alkenyl})(\mu_3\text{-X})(CO)_8]$ appear to be more reactive towards further alkyne insertion into the second M–H bond than towards reductive elimination of alkene. This almost certainly results from the ligands being along separate M–M edges and indicates that hydrogenation reactions induced by clusters could be very different from those catalysed by mononuclear compounds. The formation of μ-η^2,η^2-diene for Ru and η^4-diene for Os may reflect different alkenyl–alkenyl coupling mechanisms. We are attempting to establish the structures of the isomeric dialkenyl compounds and the geometric details of the alkenyl–alkenyl coupling.

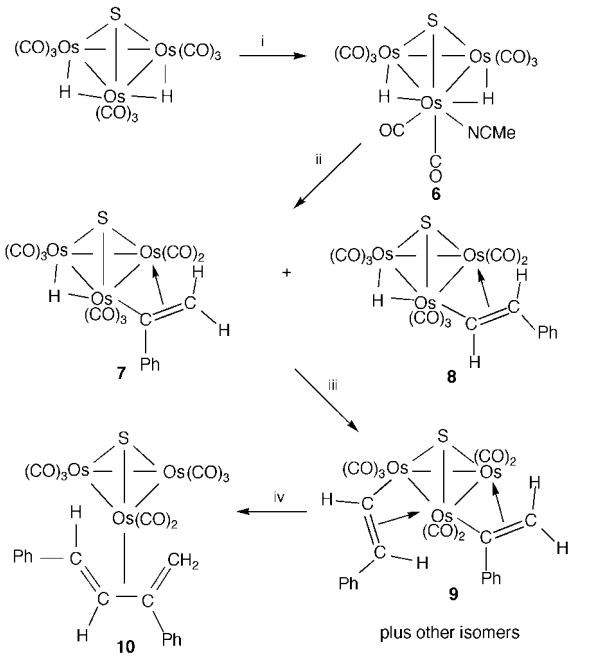

Scheme 1 *Reagents and conditions*: i, $Me_3NO{\cdot}2H_2O$, MeCN, CH_2Cl_2, 293 K, 30 min; ii, PhC_2H, THF, 293 K, 24 h; iii, PhC_2H; iv, CO.

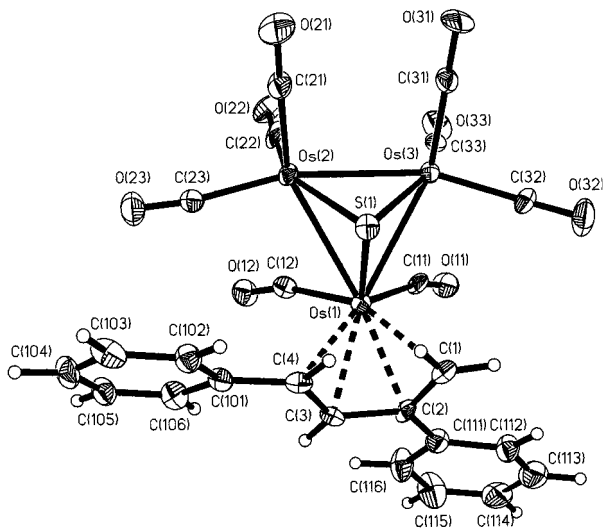

Fig. 2 Thermal ellipsoid drawing (30% probability) of $[Os_3(\eta^4\text{-}PhCH{=}CHCPh{=}CH_2)(\mu_3\text{-}S)(CO)_8]$ **10**. Selected lengths (Å) and angles (°): Os(1)–Os(2) 2.8696(12), Os(1)–Os(3) 2.8524(10), Os(2)–Os(3) 2.7339(9), Os(1)–C(1) 2.214(13), Os(1)–C(2) 2.252(12), Os(1)–C(3) 2.252(12), Os(1)–C(4) 2.267(12), C(1)–C(2) 1.40(2), C(2)–C(3) 1.44(2), C(3)–C(4) 1.46(2); C(1)–C(2)–C(3) 116.9(12), C(2)–C(3)–C(4) 118.0(12).

Notes and references

† *Selected spectroscopic data* (IR for light petroleum solutions, ^{1}H NMR in $CDCl_3$, 400 MHz, 25 °C, unless stated otherwise; aryl and tosyl signals omitted). **2**: ν(CO)/cm^{-1} (CH_2Cl_2) 2092m, 2065s, 2057s, 2013s, br; ^{1}H NMR (−25 °C, 500 MHz): δ −22.37 (d, *J* 2.5 Hz), −16.63 (d, *J* 2.5 Hz), 2.32 (s, MeCN); **3**: ν(CO)/cm^{-1} (CH_2Cl_2) 2105m, 2074s, 2040s, 1984m; ^{1}H NMR (300 MHz) δ −13.64 (s), 1.22 (s, Bu^t), 6.17 (d, *J* 12.2 Hz, CH=C*H*Bu^t), 9.82 (d, *J* 12.2 Hz, C*H*=CHBu^t); **4**: ν(CO)/cm^{-1} 2093s, 2054s, 2044s, 2029m, 2019m, 2006m, 1990w, 1758w, br; ^{1}H NMR (300 MHz) AA′BB′CC′ spectrum for C_4H_6: δ 2.91 (d, *J* 13.4 Hz), 3.98 (d, *J* 9.5 Hz), 4.58 (m); **5**: ν(CO)/cm^{-1} 2090s, 2083m (sh), 2053s, 2043s, 2027m, 2018m, 2010m, 2004w, 1997w, 1990w, 1960w, 1948w 1752m, br; ^{1}H NMR (300 MHz) δ 2.98 (d, *J* 1.0 Hz), 4.72 (s), 5.53 (d, *J* 13.5 Hz), 5.82 (dd, *J* 1.5, 13.4 Hz); **6**: ν(CO)/cm^{-1} (CH_2Cl_2) 2121w, 2085m, 2049s, 1996s, br; ^{1}H NMR δ −24.69 (s), −19.65 (d, *J* 1.2 Hz), 2.54 (s, MeCN); **7**: ν(CO)/cm^{-1} 2097m, 2063s, 2037s, 2022m, 2013s, 2000m, 1990w, 1980m; ^{1}H NMR δ −13.52 (s), 4.29 (d, *J* 1.4 Hz), 4.59 (d, *J* 1.4 Hz); **8**: ν(CO)/cm^{-1} 2099m, 2067s, 2035s, 2022m (sh), 2017s, 2004w, 1992w, 1978m; ^{1}H NMR δ −14.07 (s), 5.91 (d, *J* 11.6 Hz, CH=C*H*Ph), 9.46 (d, *J* 11.6 Hz, C*H*=CHPh); **9**: ν(CO)/cm^{-1} 2077m, 2044s, 2026, 2013s, 2009s, 1980ms, 1969w; **10**: ν(CO)/cm^{-1} 2082m, 2049s, 2025m, 2006s, 1996m, 1979m, 1963w, 1918w; ^{1}H NMR δ 1.55 (d, *J* 3.5 Hz), 2.43 (d, *J* 3.4 Hz), 3.58, (d, *J* 9.1 Hz), 6.79 (d, *J* 9.0 Hz).

‡ *Crystal data*: for **4**: $C_{19}H_{13}NO_{10}Ru_3S$, *M* = 750.57, orthorhombic, space group *Pbc*2$_1$, *a* = 10.3720(2), *b* = 13.5883(2), *c* = 16.0282(3) Å, *V* = 2258.98(7) Å^3, *Z* = 4, D_c = 2.207 g cm^{-3}, λ(Mo-*K*α) = 0.71073 Å, μ = 2.129 mm^{-1}, *F*(000) = 1448. 4203 independent reflections were measured in the θ range 3.80–26.00° for a yellow crystal in an oil droplet solidifed at *T* = 100(2) K. 309 parameters were refined to give *R* (all data) = 0.0180 and *wR*2 (all data) = 0.0456. The Nonius 'Collect' program was used for indexing and data collection. The structure was solved by direct methods and refined (SHELXL-97) with all non-hydrogen atoms anisotropic and with hydrogen atoms included using a riding model.

For **10**: $C_{24}H_{14}O_8Os_3S$, *M* = 1033.01, triclinic, space group $P\bar{1}$, *a* = 9.406(2), *b* = 10.615(2), *c* = 13.885(3) Å, α = 91.58(3), β = 108.82(3),γ = 104.51(3)°, *V* = 1261.4(5) Å^3, *Z* = 2, D_c = 2.720 g cm^{-3}, λ(Mo-*K*α) = 0.71073 Å, μ = 15.201 mm^{-1}, *F*(000) = 932. 4421 independent reflections were measured at room temperature in the θ range 2.65–25.05°. 325 parameters were refined to give *R* (all data) = 0.0564 and *wR*2 (all data) = 0.1453. The structure was solved by direct methods and refined (SHELXL-97) with all non-hydrogen atoms anisotropic and with hydrogen atoms included using a riding model. CCDC 182/1484. See http://www.rsc.org/suppdata/cc/1999/2541/ for crystallographic files in .cif format.

1 A. J. Deeming, S. Hasso and M. Underhill, *J. Organomet. Chem*., 1974, **80**, C53; *J. Chem. Soc., Dalton Trans*., 1975, 1614.
2 S. C. Brown and J. Evans, *J. Chem. Soc., Dalton Trans*., 1982, 1049; D. H. Hamilton and J. R. Shapley, *Organometallics*, 1998, **17**, 3087; M. Koike, D. H. Hamilton, S. R. Wilson and J. R. Shapley, *Organometallics*, 1996, **15**, 4930.
3 H. Chen, B. F. G. Johnson, J. Lewis and P. R. Raithby, *J. Organomet. Chem*., 1989, **376**, C7.
4 N. Satyanarayana and M. Periasamy, *Tetrahedron Lett*., 1986, **27**, 6253; S. A. Rao and M. Periasamy, *J. Chem. Soc., Chem. Commun*., 1987, 495; I. Ryu, N. Kusumato, A. Ogawa, N. Kambe and N. Sonoda, *Organometallics*, 1989, **8**, 2279; M. I. Bruce, G. A. Koutsantonis, E. R. T. Tiekink and B. K. Nicholson, *J. Organomet. Chem*., 1991, **420**, 271; K. Tani, K. Ueda, K. Arimitsu, T. Yamagata and Y. Kataoka, *J. Organomet. Chem*., 1998, **560**, 253.
5 P. M. Maitlis, H. C. Long, R. Quyoum, M. L. Turner and Z.-Q. Wang, *Chem. Commun*., 1996, 1.
6 Prepared by reaction of $[Ru_3(CO)_{12}]$ with 4-$MeC_6H_4SO_2NH_2$.
7 Y. Kaneko, T. Suzuki and K. Isobe, *Organometallics*, 1998, **17**, 996; J. A. King, Jr and K. P. C. Vollhardt, *Organometallics*, 1983, **2**, 684.
8 V. C. Adams, J. A. J. Jarvis, B. T. Kilbourn and P. G. Owston, *Chem. Commun*., 1971, 467; T. Murahashi, N. Kanehisa, Y. Kai, T. Otani and H. Kurosawa, *Chem. Commun*., 1996, 825.
9 A. Scholz, A. Smola, J. Scholz, J. Loebel, H. Schumann and K.-H. Thiele, *Angew. Chem., Int. Ed. Engl*., 1991, **30**, 435.
10 J. T. Barry, J. C. Bollinger, M. H. Chisholm, K. C. Glasgow, J. C. Huffman, E. A. Lucas, E. B. Lubkovsky and W. E. Streib, *Organometallics*, 1999, **18**, 2300.
11 M. Tachikawa, J. R. Shapley, R. C. Haltiwanger and C. G. Pierpont, *J. Am. Chem. Soc*., 1976, **98**, 4651.

Communication 9/08706K

Coordination modes of 2-(indenyl)phenoxide ligation at early d-block metal centers

Matthew G. Thorn,[a] Phillip E. Fanwick,[a] Robert W. Chesnut*[b] and Ian P. Rothwell*[a]

[a] *1393 Brown Building, Department of Chemistry, Purdue University, West Lafayette, IN 47907-1393, USA. E-mail: rothwell@purdue.edu*

[b] *Department of Chemistry, Eastern Illinois University, 600 Lincoln Avenue, IL 61920, USA*

Received (in Bloomington, IN, USA) 6th August 1999, Accepted 22nd October 1999

Three distinct bonding modes for the ligand 2-(indenyl)-4,6-di-*tert*-butylphenoxide at early d-block metal centers have been identified

The use of constrained geometry cyclopentadienyl ligation has had a considerable impact on early transition metal chemistry in recent years.[1] As part of our work on novel *ortho*-substituted aryloxide ligation[2] we have synthesized the compound 2-(inden-3-yl)-4,6-di-*tert*-butylphenol **1** (Scheme 1).[3] Unlike previously reported ligands of this type, chelation of **1** to a metal center *via* deprotonation will generate an inherently chiral environment. Here we report on our initial forays into the chemistry of this ligand, which demonstrate three distinct bonding modes to transition metal centers.

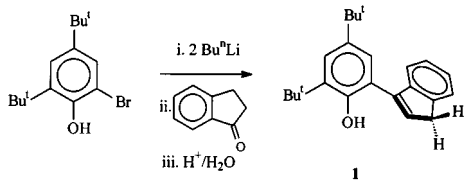

Scheme 1

Compound **1** is obtained in gram quantities *via* the synthetic route shown in Scheme 1. When **1** is added to the compound [$CpTiCl_3$] in the presence of excess pyridine the simple aryloxide [$Cp_2Ti(OC_6H_2Bu^t_2$-4,6-Ind-2)Cl_2] **2** is obtained.† The solid state structure of **2** (Fig. 1) shows the *ortho*-inden-3-yl group to be unbound with a Ti–O–C angle of 158.7(1)°.‡ Surprisingly, addition of LiMe to **2** produces the corresponding dimethyl derivative **3** (Scheme 2) with no deprotonation of the inden-3-yl ligand being observed. At ambient temperatures the potentially diastereotopic methylene protons in the *ortho*-inden-3-yl groups of both **1** and **2** appear as broad singlets in the ^{1}H NMR spectra owing to inden-3-yl rotation on the NMR timescale. At lower temperatures these signals broaden and resolve into the AB pattern expected for the static structure. Similarly both Ti–*Me* groups in **3** appear as one broad singlet in

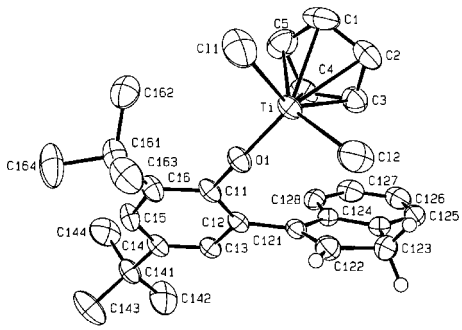

Fig. 1 Molecular structure of **2** showing the atomic numbering scheme. Selected interatomic distances (Å) and angles (°): Ti–O(1) 1.785(2), Ti–Cl(1) 2.2581(8), Ti–Cl(2) 2.2554(8); Cl–Ti–Cl 100.24(4), Cp–Ti–O(1) 118.1(1), Ti–O(1)–C(11) 158.7(1).

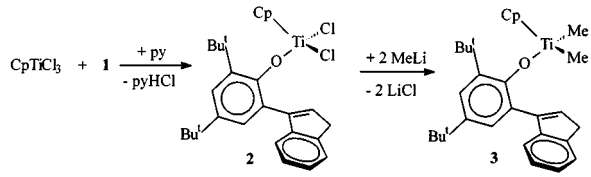

Scheme 2

both the ^{1}H and ^{13}C NMR spectra at ambient temperatures but appear as two well resolved resonances at lower temperatures. Variable temperature NMR studies of **2** and **3** in toluene-d_8 allow the barrier to inden-3-yl rotation (enantiomer interconversion) to be estimated at 13.9(5) kcal mol^{-1} (at 20 °C) and 13.4(5) kcal mol^{-1} (at −5 °C), respectively. These barriers are significantly lower than that measured for corresponding 2-(1-naphthyl)phenoxides.[2c]

Addition of **1** to the zirconium precursor [$Zr(NMe_2)_4$][4] leads to the complex [$Zr\{(OC_6H_3Bu^t_2$-4,6-(η^5-Ind)$\}_2$] **4**. In solution **4** is shown by NMR to exist as a mixture of two isomers (Scheme 3). Recrystallization from benzene–pentane generates crystals of **4a** shown (Fig. 2) to contain a crystallographic C_2 axis of symmetry. It can be seen that in the solid state both indenyl rings are η^5-bound to the same zirconium metal center, Zr–O–C angle = 128.4(2)°. In $CDCl_3$ solution **4a** undergoes slow (days at room temperature) conversion to a 50 : 50 mixture of **4a** : **4b**. In both **4a** and **4b** the aryloxide groups are equivalent (NMR) ruling out their formulation as the two alternative isomers **4c** and **4d** that contain no symmetry elements (Scheme 3).

Treatment of the compound [$Ta(NMe_2)_5$][5] with **1** initially produces the substitution compound **5** (Scheme 4) with elimination of one equivalent of $HNMe_2$. Upon theromolysis

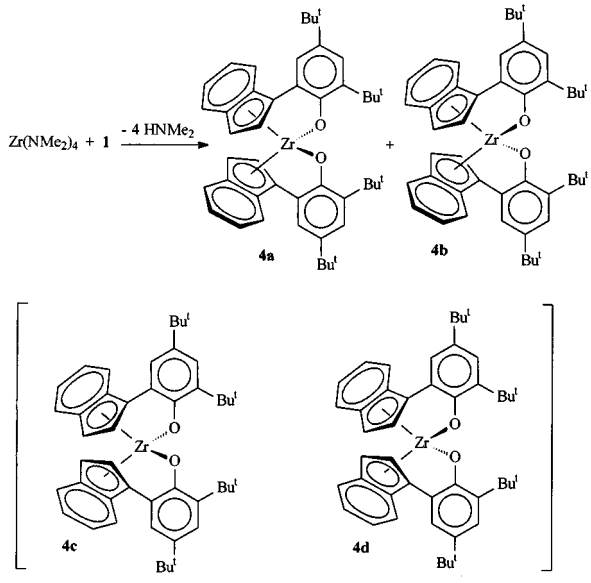

Scheme 3

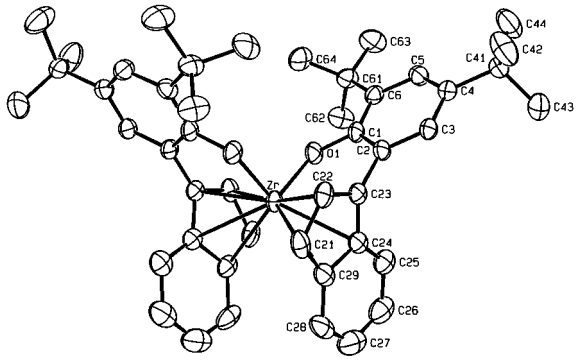

Fig. 2 Molecular structure of **4a** showing the atomic numbering scheme. Selected interatomic distances (Å) and angles (°): Zr–O(1) 2.015(2), Zr–C(23) 2.487(3), Zr–C(22) 2.500(3), Zr–C(21) 2.532(3), Zr–C(24) 2.568(3), Zr–C(29) 2.640(3), O(1)–Zr-O(1) 97.6(1), Zr–O(1)–C(1) 128.4(2).

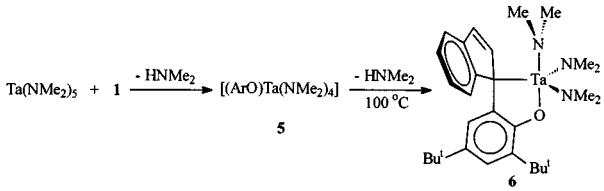

Scheme 4

(100 °C) in C_6D_6, a further equivalent of $HNMe_2$ is lost from **5** with formation of **6** (Scheme 4). The solid state structure of **6** (Fig. 3) shows the ligand to be chelated to the metal *via* an η^1-indenyl interaction, Ta–O–C angle = 122.7(6)°. The metal is attached to the *ipso* carbon atom yielding a five-membered metallacycle ring. The coordination environment about the Ta metal center in **6** is best described as tbp, with an axial oxygen atom. In the ambient temperature ^{1}H NMR spectrum of **6** a single broad resonance is observed for the Ta–N*Me*$_2$ protons. At lower temperatures this signal splits out into four singlets in the ratio of 2:2:1:1. We interpret the two larger signals as being due to the two, non-equivalent equatorial Ta–NMe_2 groups undergoing rapid rotation. The remaining signals are due to the unique axial Ta–NMe_2 group that is undergoing restricted rotation on the NMR timescale. Presumably the higher barrier to rotation of the axial group is due to the presence of the η^1-indenyl ring (Fig. 3).

We thank the National Science Foundation (Grant CHE-9700269) for financial support of this research.

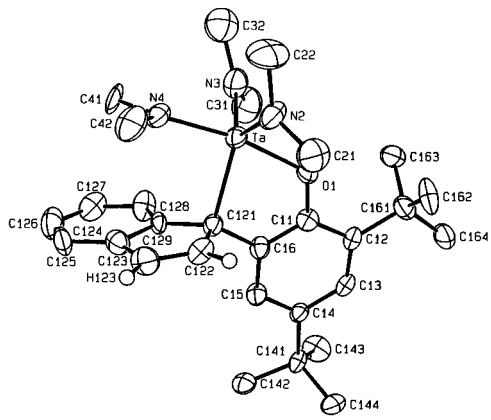

Fig. 3 Molecular structure of **6** showing the atomic numbering scheme. Selected interatomic distances (Å) and angles (°): Ta–N(2) 1.95(1), Ta–N(3) 1.95(1), Ta–N(4) 2.005(8), Ta–C(121) 2.285(9), Ta–O(1) 2.025(7); O(1)–Ta–N(4) 169.9(3), O(1)–Ta–N(2) 90.8(3), O(1)–Ta–N(3) 93.8(4), O(1)–Ta–C(121) 75.4(3), N(2)–Ta–N(3) 117.6(5), N(2)–Ta–N(4) 92.8(4), N(3)–Ta–N(4) 92.9(4), C(121)–Ta–N(2) 123.6(4), C(121)–Ta–N(3) 117.7(4), C(121)–Ta–N(4) 94.7(3), Ta–O(1)–C(11) 122.7(6).

Notes and references

† Spectral data obtained in C_6D_6 at 30 °C unless otherwise stated. ^{1}H NMR: **1**: ($CDCl_3$) δ 7.27–7.67 (aromatics); 6.78 (t, ^3J 2.1 Hz, CH); 5.68 (s, OH); 3.69 (d, ^3J 1.6 Hz, CH_2); 1.57 (s), 1.44 [s, $C(CH_3)_3$]. **2**: δ 7.13–7.61 (aromatics); 6.61 (t, CH); 5.81 (s, C_5H_5); 3.36 (br, CH_2); 1.61 (s), 1.28 [s, $C(CH_3)_3$]. (C_7D_8, −30 °C): δ 6.72–7.58 (aromatics); 6.60 (br, CH); 5.67 (s, C_5H_5); 3.48 (d), 3.12 (d, ^2J 23.8 Hz, CH_2); 1.58 (s), 1.25 [s, $C(CH_3)_3$]. **3**: δ 7.57 (d), 7.33 (d, ^{4}J 2.4 Hz, *m*C_6H_2); 7.04-7.55 (other aromatics); 6.29 (t, CH); 5.59 (s, C_5H_5); 3.05 (d, CH_2); 1.60 (s), 1.28 [s, $C(CH_3)_3$]; 0.64 (br, TiMe). (C_7D_8, −45 °C): δ 6.97–7.61 (aromatics); 6.31 (d, CH); 5.50 (s, C_5H_5); 2.99 (AB, CH_2); 1.64 (s), 1.30 [s, $C(CH_3)_3$]; 0.76 (s), 0.65 (s, TiMe). **4**: δ 6.79-7.40 (aromatics); 6.18 (d), 6.12 (d), 5.19 (d, η^5-C_5H_2); 1.36 (s), 1.29 (s), 1.29 (s), 1.24 [s, $C(CH_3)_3$]. ($CDCl_3$): δ 6.89–7.48 (aromatics); 6.89 (d), 6.75 (d), 6.62 (d), 5.42 (d, η^5-C_5H_2); 1.31 (s), 1.30 (s), 1.19 (s), 1.05 [s, $C(CH_3)_3$]. **5**: δ 7.17–7.73 (aromatics); 6.60 (t, CH); 3.48 (br, CH_2); 3.15 (s, NMe_2); 1.70 (s), 1.37 [s, $C(CH_3)_3$]. **6**: δ 7.58 (d), 7.51 (d), 7.28 (t), 7.05 (t, C_6H_4); 7.43 (d), 6.76 (d, *m*-H); 7.10 (d), 6.62 (d, C_5H_2); 2.76 (br, NMe_2); 1.74 (s), 1.15 [s, $C(CH_3)_3$]. (C_7D_8, 40 °C): δ 7.56 (d), 7.49 (d), 7.25 (t), 7.05 (t, C_6H_4); 7.39 (d), 6.69 [d, ^4J 1.7 Hz, *m*-H); 7.09 (d), 6.64 (d, C_5H_2); 2.87 (s, NMe_2); 1.73 (s), 1.21 [s, $C(CH_3)_3$]. (C_7D_8, −30 °C): δ 6.59-7.63 (aromatics); 2.98 (br), 2.43 (br), 1.92 (br, NMe_2); 1.79 (s), 1.18 [s, $C(CH_3)_3$]. (C_7D_8, −55 °C): δ 6.57–7.64 (aromatics); 3.00 (s, 6H), 2.86 (s, 6H), 2.36 (s, 3H), 1.88(s, 3H, NMe_2); 1.81 (s), 1.17 [s, $C(CH_3)_3$]. Selected ^{13}C NMR, **1**: ($CDCl_3$): δ 149.3 (OC); 144.4, 144.2, 141.7, 141.5, 135.3, 132.7, 126.5, 125.5, 124.1, 123.9, 123.8, 121.2, 120.9 (unsaturated C); 38.7 (CH_2); 35.1, 34.3 [$C(CH_3)_3$]; 31.7, 29.7 [$C(CH_3)_3$]. **2**: δ 165.5 (TiOC); 121.0 (C_5H_5); 38.7 (CH_2); 35.9, 34.7 [$C(CH_3)_3$]; 31.5, 30.6 [$C(CH_3)_3$]. **3**: δ 161.7 (TiOC); 114.3 (C_5H_5); 57.7 (br, TiMe); 38.4 (CH_2); 35.7, 34.5 [$C(CH_3)_3$]; 31.7, 30.5 [$C(CH_3)_3$]. (C_7D_8, −45 °C): δ 161.6 (TiO*C*); 114.3 (C_5H_5); 58.8, 56.8 (TiMe); 38.3 (CH_2); 35.8, 34.6 [$C(CH_3)_3$]; 31.7, 30.3 [$C(CH_3)_3$]. **4**: δ 172.2, 171.5 (ZrOC); 115.5, 97.0, 96.9 (η^5-C_5H_2); 35.1, 34.5, 34.4 [$C(CH_3)_3$]; 31.9, 29.6 [$C(CH_3)_3$]. ($CDCl_3$, 30 °C): δ 171.5, 170.9 (ZrOC); 115.2, 99.9, 96.6, 96.4 (η^5-C_5H_2); 34.7, 34.3, 34.2, 34.1 [$C(CH_3)_3$]; 31.8, 31.8, 30.2, 29.2 [$C(CH_3)_3$]. **5**: δ 157.2 (TaOC); 47.1 (NMe_2); 39.1 (CH_2); 35.8, 34.5 [$C(CH_3)_3$]; 31.8, 30.3 [$C(CH_3)_3$]. **6**: δ 163.0 (TaOC); 103.4 (TaC); 44.5 (NMe_2); 35.1, 34.5 [$C(CH_3)_3$]; 32.0, 30.4 [$C(CH_3)_3$].

‡ *Crystallographic data*: for **2** at 203 K: $TiOCl_2C_{31}H_{35}$, M = 542.43, space group $P2_1/n$ (no. 14), a = 12.2422(4), b = 12.6093(4), c = 18.9505(6) Å, β = 102.517(2)°, V = 2855.8(3) Å^3, D_c = 1.262 g cm^{-3}, Z = 4. Of the 5004 unique reflections collected ($8.00 \leqslant 2\theta \leqslant 60.94°$) with Mo-$K_\alpha$ (λ = 0.71073 Å), the 4070 with $F_o^2 > 2\sigma(F_o^2)$ were used in the final least-squares refinement to yield $R(F_o)$ = 0.045 and $R_w(F_o^2)$ = 0.111; for **4a** at 203 K: $ZrO_2C_{52}H_{58}$, M = 806.26, space group $C2/c$ (No. 15), a = 14.3043(4), b = 10.7900(5), c = 28.522(1) Å, β = 97.875(3)°, V = 4360.7(5) Å^3, D_c = 1.228 g cm^{-3}, Z = 4. Of the 4399 unique reflections collected ($8.00 \leqslant 2\theta \leqslant 52.73°$) with Mo-$K_\alpha$ (λ = 0.71073 Å), 3651 with $F_o^2 > 2\sigma(F_o^2)$ were used in the final least-squares refinement to yield $R(F_o)$ = 0.055 and $R_w(F_o^2)$ = 0.132; for **5** at 203 K: $TaON_3C_{29}H_{44}$, M = 631.64, space group $P\bar{1}$ (no. 2), a = 9.6679(5), b = 12.1261(6), c = 13.9575(4) Å, α = 86.118(3), β = 72.704(3), γ = 67.257(2)°, V = 1438.8(2) Å^3, D_c = 1.458 g cm^{-3}, Z = 2. Of the 5428 unique reflections collected ($8.00 \leqslant 2\theta \leqslant 52.75°$) with Mo-$K_\alpha$ (λ = 0.71073 Å), 5011 with $F_o^2 > 2\sigma(F_o^2)$ were used in the final least-squares refinement to yield $R(F_o)$ = 0.061 and $R_w(F_o^2)$ = 0.153. Atom C(32) was refined isotropically. CCDC 182/1465.

1 G. J. P.Britovsek, V. C. Gibson and D. F. Wass, *Angew. Chem., Int. Ed.*, 1999, **38**, 428 and references therein; M.Bochmann, *J. Chem. Soc., Dalton Trans.*, 1996, 255; H.-H. Brintzinger, D. Fischer, R. Mülhaupt, B. Rieger and R. M. Waymouth, *Angew. Chem., Int. Ed. Engl.*, 1995, **34**, 1143; P. C. Möhring and N. J. Coville, *J. Organomet. Chem.*, 1994, **479**, 1; W. Kaminsky, K. Kulper and H. H. Brintzinger, *Angew. Chem., Int. Ed. Engl.*, 1985, **24**, 507.

2 (*a*) J. S. Vilardo, M. A. Lockwood, L. G. Hanson, J. R. Clark, B. C. Parkin, P. E. Fanwick and I. P. Rothwell, *J. Chem. Soc., Dalton Trans.*, 1997, 3353; (*b*) J. S. Vilardo, M. G. Thorn, , P. E. Fanwick and I. P. Rothwell, *Chem. Commun.*, 1998, 2425; (*c*) M. G. Thorn, J. S. Vilardo, P. E. Fanwick and I. P. Rothwell, *Chem. Commun.*, 1998, 2427.

3 For related ligands, see: (*a*) Y.-X. Chen, P.-F. Fu, C. L. Stern and T. J. Marks, *Organometallics*, 1997, **16**, 5958; (*b*) K. Kawai, T. Kitahara and T. Fujita, (Mitsui Petrochemical Ind, Japan), Jpn. Kokai Tokkyo Koho JP08,325,283, 1996 (*Chem. Abstr.* 1996, **126**, 172048h).

4 G. M. Diamond, R. F. Jordan and J. L. Petersen, *J. Am. Chem. Soc.*, 1996, **118**, 8024.

5 P. N. Riley, J. R. Parker, P. E. Fanwick and I. P. Rothwell, *Organometallics*, 1999, **18**, 3579.

Communication 9/06443E

ChemComm

A highly efficient synthesis of triisopropylsilyldifluorobromopropyne yields a versatile *gem*-difluoromethylene building block

ZhiGang Wang and Gerald B. Hammond*

Department of Chemistry and Biochemistry, The University of Massachusetts Dartmouth, North Dartmouth, Massachusetts 02747, USA. E-mail: ghammond@umassd.edu

Received (in Corvallis, OR, USA) 23rd September 1999, Accepted 8th November 1999

Triisopropylsilyldifluorobromopropyne, readily prepared in excellent yield from the reaction of lithium triisopropylsilylacetylide with CF_2Br_2, provides a convenient entry into a functionalized CF_2 synthon.

The *gem*-difluoromethylene unit is a key structural motif in many fluorine containing compounds of biological and pharmaceutical significance. For this reason, it is an important synthetic target.[1] Two complementary approaches to such important unit exist. These are (i) substitution of a carbonyl or an active methylene group by fluorine;[2] and (ii) use of small *gem*-difluoromethylene-containing building blocks.[3] When it comes to fluorinate complex molecules, the latter approach is preferred because of the reactivity, thermal instability, hazards and cost associated with electrophilic and nucleophilic fluorinating agents. The two most frequently used *gem*-difluoromethylene synthons, $(EtO)_2P(O)CF_2Br$ and $EtOC(O)CF_2Br$, were developed in the late 70s and early 80s by Burton[4] and Fried,[5] respectively. Stimulated by our earlier work in the synthesis of fluorinated phosphonates,[6] we sought a new generation of difluorinated building blocks from inexpensive industrial fluorine feedstock such as CF_2Br_2 (not included in the list of CFCs to be phased out). Our initial target, triisopropylsilyldifluoropropyne **1** (Fig 1), is a highly functionalized three-carbon backbone that contains a propargyl silane moiety. This feature should facilitate multiple synthetic conversions containing the *gem*-difluoromethylene unit.

A literature search revealed that difluoropropargyl substrates, without exception, have been prepared in disappointingly low yields.[7] The low yields obtained have probably contributed to the lack of use of the difluoropropargyl building block in the literature. To our satisfaction, **1** was very efficiently assembled in one step (92% GC-MS, 81% isolated) by the reaction of CF_2Br_2 with lithium triisopropylsilylacetylide. This reaction has been carried out on 5, 16 and 50 g scales and the results have shown excellent reproducibility.[8] We attributed the success of this reaction to the presence of the TIPS group, which possesses remarkably different properties compared to other alkylsilyl groups.[9] Chiefly, the presence of TIPS enhances the stability of the triisopropylsilyldifluoropropyne anion intermediate.[10] Although the reaction mechanism is still unclear, our experimental observation of a typical 5–10 min induction period supports the difluorocarbene based ionic chain path proposed by Wakselman and co-workers.[7a] With a highly efficient preparation of **1** in hand, we explored the synthesis of various *gem*-difluoromethylene-containing compounds. Preliminary results, summarized in Scheme 1,[11] unveiled a highly versatile building block.

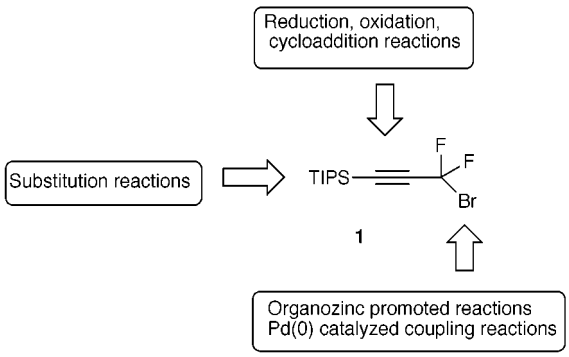

Fig. 1 Building block potential of **1**.

Reduction with $LiAlH_4$ gave allene **2**, whereas nucleophilic substitution with $MP(O)(OEt)_2$ afforded difluoropropyne **3** and difluoropropargyl phosphonate **4**, although the latter was obtained in low yield. Because compound **4** is a potential precursor for isosteric and isoelectronic phosphate mimics of enzyme inhibitors,[12] an optimization of this reaction is in progress. Using ultrasound, **1** reacted rapidly with zinc dust yielding the alkynyl organozinc reagent **5** *in situ*. This organozinc intermediate is a useful synthetic building block as can be seen in the Reformatsky-type reactions shown at the bottom of Scheme 1. Addition of Zn to **1** produced dimer **6** in nearly quantitative yield. Compound **6** is a potential intermediate in the synthesis of CF_2CF_2-containing bioactive molecules.[13] If **5** is quenched with powdered iodine, it produces difluoroiodopropyne **7**, another important *gem*-difluoromethylene synthon.[14] Addition of *trans*-cinnamaldehyde to **5** afforded difluoro alcohol **8** in 70% yield. When needed, the TIPS-protecting group can be easily removed, as demonstrated by the conversion of **8** to **9** under mild conditions, and in excellent yield. The latter result will allow an easy entry to the preparation of propargylic, and possibly allylic, α,α-difluorocarbonyl compounds, after oxidation of the alcohol and hydrogenation of the triple bond.

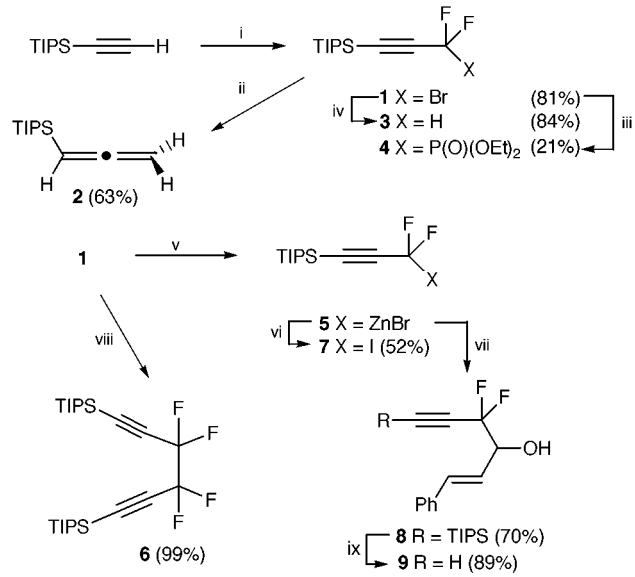

Scheme 1 *Reagents and conditions*: i, BuLi, CF_2Br_2, THF, −20 °C to room temp.; ii, $LiAlH_4$ (0.6 equiv.), THF, −80 °C; iii, NaN $(TMS)_2$, $HP(O)(OEt)_2$ (1.0 equiv.), THF, −10 °C; iv, $HP(O)(OEt)_2$, BuLi (1.5 equiv.), −10 °C; v, Zn (1.2 equiv.),THF, room temp., ultrasound; vi, I_2 (1 equiv.), 0 °C; vii, *trans*-cinnamaldehyde, 20 h, room temp.; viii, **1** (1.0 equiv.), Zn (2.0 equiv.), room temp.; ix, TBAF (1.0 equiv., 1 M in THF), −80 °C.

Other synthetic modifications of **1** and the preparation of a monofluorinated counterpart to **1** are under investigation.

The generous support of the National Science Foundation (CHE-9711062), Petroleum Research Fund (PRF#32595-B1) and the Camille and Henry Dreyfus Foundation (TH-96-012) is gratefully appreciated.

Notes and references

1 For a recent leading reference see: K. Uneyama, G. Mizutani, K. Maeda and T. Kato, *J. Org. Chem.*, 1999, **64**, 6717. For a recent review see: M. J. Tozer and T. F. Herpin, *Tetrahedron*, 1996, **52**, 8619.

2 *Organo-Fluorine Compounds*, ed. B. Baasner, H. Hagemann and J. C. Tatlow, Thieme, Stuttgart, 1999, vol. E 10 a.

3 For an updated compilation of references see: J. M. Percy, *Top. Curr. Chem.*, 1997, **193**, 131.

4 D. J. Burton and R. M. Flynn, *J. Fluorine Chem.*, 1977, **10**, 329. For recent reviews, see: D. J. Burton and L. Lu, *Top. Curr. Chem.*, 1997, **193**, 45; D. J. Burton, Z. Y. Yang and W. M. Qiu, *Chem. Rev.*, 1996, **96**, 1641.

5 E. A. Hallinan and J. Fried, *Tetrahedron Lett.*, 1984, **25**, 2301. Also: T. Taguchi, O. Kitagawa, Y. Suda, S. Ohkawa, A. Hashimoto, Y. Iitaka and Y. Kobayashi, *Tetrahedron Lett.*, 1988, **29**, 5291 and references therein; S. Mcharek, S. Sibille, J. Y. Nedelec and J. Perichon, *J. Organomet. Chem.*, 1991, **401**, 211; J. M. Altenburger and D. Schirlin, *Tetrahedron Lett.*, 1991, **32**, 7255; J. M. Andres, M. A. Martinez, R. Pedrosa and A. Perez-Encabo, *Synthesis*, 1996, 1070.

6 F. Benayoud, D. J. deMendonca, C. A. Digits, G. A. Moniz, T. C. Sanders and G. B. Hammond, *J. Org. Chem.*, 1996, **61**, 5159; F. Benayoud and G. B. Hammond, *Chem. Commun.*, 1996, 1447.

7 (*a*) I. Rico, D. Cantauzene and C. Wakselman, *J. Chem. Soc., Perkin. Trans. 2*, 1982, 1063; (*b*) P. Y. Kwok, F. W. Muellner, C. K. Chen and J. Fried, *J. Am. Chem. Soc.*, 1987, **109**, 3684; (*c*) Y. Hanzawa, K. Inazawa, A. Kon, H. Aoki and Y. Kobayashi, *Tetrahedron Lett.*, 1987, **28**, 659.

8 Under Ar atmosphere, a solution of triisopropylsilylacetylene (36 g, 0.2 mol) in THF (300 ml) was cooled to −20 °C. BuLi (125 ml, 1.6 M solution in hexane) was added *via* syringe and the resulting solution was stirred for 30 min before CF_2Br_2 (62 g, 1.5 equiv.) was added. The solution was allowed to warm to room temperature and stirred for 9 h. After solvent removal, NH_4Cl (120 ml) was added and the oily layer was extracted with Et_2O (3 × 100 ml). Standard work-up gave the crude product as a viscous orange oil (92% yield by GC−MS) which was purified by distillation (bp 51–52 °C/0.1 mmHg) to yield **1** (49.9 g, 81%); δ_H(300 MHz, $CDCl_3$) 1.11 (s, TIPS protons); δ_C(75 MHz, $CDCl_3$) 100.61 (t, $^1J_{CF}$ 290), 97.16 (t, $^2J_{CF}$ 36.5), 95.1 (t, $^3J_{CF}$ 4.7), 18.01, 11.28; δ_F −32.60 (s, 2F); *m/z* (GC-MS) 312 (M^+ + 1, 4), 310 (M^+ − 1, 4), 269 (14), 267 (14), 143 (27), 77 (100) (calc. for $C_{12}H_{21}SiF_2Br$: C, 46.33; H, 6.75. Found: C, 46.91; H, 6.83%). The triisopropylsilylacetylene starting material, purchased from GFS Co., contained diisopropylpropenylsilylacetylene (11%) and diisopropylpropylsilylacetylene (14%). Fractional distillation did not remove these impurities. The GC-MS analysis of **1** shows all three components were alkylated and their ratios perfectly match that of the starting material. The calculated C% and H% were based on the formula of triisopropylsilyldifluorobromopropyne. If the two impurities are removed from the calculation, the values found for C% and H% are 46.84 and 6.67%, respectively.

9 For a recent review of the TIPS group in organic chemistry see: C. Rücker, *Chem. Rev.*, 1995, **95**, 1009.

10 Similarly, whereas ynolates lack convenient methods for their generation a lithium silylynolate has been used in ketenylation reactions: H. Kai, K. Iwamoto, N. Chatani and S. Murai, *J. Am. Chem. Soc.*, 1996, **118**, 7634.

11 *Selected data* for **2**: δ_H(300 MHz, $CDCl_3$) 1.06 (s, TIPS protons), 4.81 (t, 1H, $^4J_{HH}$ 7.23), 4.30 (d, 2H, $^4J_{HH}$ 7.23); *m/z* (GC-MS) 196 (M^+), 157, 153, 125, 97, 83, 67. For **3**: δ_H(300 MHz, $CDCl_3$) 1.09 (s, TIPS protons), 6.17 (t, $^2J_{HF}$ 54.8); δ_F −105.49 (s); *m/z* (GC-MS) 232 (M^+), 189, 161, 133, 105, 81, 77. For **4**: δ_H(300 MHz, $CDCl_3$) 1.11 (s, 21H, TIPS protons), 1.39 (t, 6H, $^3J_{HH}$ 7.00), 4.32 (m, 4H); δ_F −96.79 (d, $^2J_{PF}$ 109.01); δ_P 4.23 (t, $^2J_{PF}$ 109.10); *m/z* (GC-MS) 325 (M^+ − 43), 297, 269, 153, 109, 81. For **6**: δ_H(300 MHz, $CDCl_3$) 1.10 (s, TIPS protons); δ_F −99.01 (s, 4F); *m/z* (GC-MS) 462 (M^+), 377, 307, 239, 183, 115, 77. For **7**: δ_H(300 MHz, $CDCl_3$) 1.11 (s, TIPS protons); δ_F −28.13 (s); *m/z* (GC-MS) 315 (M^+ − 43), 265, 237, 189, 165, 119, 105, 77. For **8**: δ_H(300 MHz, $CDCl_3$) 7.41–7.26 (m, 5H), 6.82 (d, 1H, $^3J_{HH}$ 15.9), 6.26 (dd, 1H, $^3J_{HH}$ 15.9, $^3J_{HH}$ 6.2), 4.55 (m, 1H, CHOH), 2.05 (s, 1H, OH), 1.06 (s, 21 H, TIPS protons); δ_F −94.3 (d, 1F, $^2J_{FF}$ 274), −96.7 (d, 1F, $^2J_{FF}$ 274). For **9**: δ_H(300 MHz, $CDCl_3$) 7.45–7.30 (m, 5H), 6.85 (dd, 1H, $^4J_{HH}$ 0.9, $^3J_{HH}$ 15.9), 6.24 (dd, 1H, $^3J_{HH}$ 15.9, $^3J_{HH}$ 6.3), 4.55 (m, 1H, CHOH), 2.85 (t, 1H, $^3J_{HF}$ 5.0), 2.04 (s, 1 H); δ_F −95.9 (d, 1F, $^2J_{FF}$ 277), −96.9 (d, 1F, $^2J_{FF}$ 277); *m/z* (GC-MS) 206 (M^+, 5),170 (3), 159 (2), 133 (100), 115 (30), 77 (26), 55 (46).

12 The major by-product is **3**, an indication that, compared to the bromide, the triisopropylsilyldifluoropropyne anion is a better leaving group. For a leading reference on fluorinated phosphate mimics, see: D. O'Hagan and H. S. Rzepa, *Chem. Commun.*, 1997, 645.

13 W. C. Sun, C. S. Ng and G. D. Prestwich, *J. Org. Chem.*, 1992, **57**, 132.

14 We have also prepared **8** in 73% yield by the reaction of lithium triisopropylsilylacetylide with CF_2I_2. However, the prohibitive cost of commercial CF_2I_2 will most likely limit its use in large-scale synthesis.

Communication 9/07784G

A curiously short carbon–carbon double bond?

Jack D. Dunitz

Organic Chemistry Laboratory, Swiss Federal Institute of Technology, ETH-Zentrum, CH-8092 Zurich, Switzerland. E-mail: dunitz@org.chem.ethz.ch

Received (in Corvallis, OR, USA) 20th September 1999, Accepted 9th November 1999

The discrepancy between the 'curiously short' carbon–carbon double bond distance in 3-ethynylcyclopropene, as measured experimentally by X-ray analysis [1.255(2) Å], compared with the value derived from high level *ab initio* calculations (*ca.* 1.28 Å), is largely due to neglect of corrections for molecular motion in the crystal.

The carbon–carbon double bond length in 3-ethynylcyclopropene has been described as 'curiously short' because the value 1.255(2) Å estimated from a low-temperature (120 K) X-ray crystallographic study was 'the shortest C=C double bond known in any hydrocarbon' and markedly shorter than that obtained from high-level theoretical calculations, *ca.* 1.28 Å.[1] On the basis of further, more extensive calculations, Wesolowski *et al.*[2] confirmed the validity of the discrepancy, obtaining values between 1.269 and 1.323 Å for the double bond length at different levels of theory. This apparent discordance between computational theory and experimental measurement has attracted considerable attention[3] but it probably has a simple explanation.

In 1956 Cruickshank[4] noted that rotational oscillations of molecules in crystals cause the apparent atomic positions to be slightly displaced from the true positions towards the rotation axis. This is because X-ray analysis locates the centroids of atomic distributions that are undergoing vibrations, and separations computed from these positions cannot be interpreted directly as interatomic distances.[5] Crystal structure analysis provides not only mean atomic positions but also anisotropic displacement parameters (ADPs or U_{ij} tensor components) from which principal axes and eigenvalues of the molecular libration tensor $\boldsymbol{L}$ and of the translation tensor $\boldsymbol{T}$ can be estimated together with components of a tensor $\boldsymbol{S}$ that allows for the quadratic correlation between librational and translational motion.[6,7] From the principal axis directions and mean-square librational amplitudes (eigenvectors and eigenvalues of $\boldsymbol{L}$) approximate corrections for the shrinkage effect of the librational motion can be applied. Such corrections can easily amount to 0.025 Å.[4] In the work described in ref. 1 these corrections were not applied.

There is a problem. The ***TLS*** analysis can be applied only to the ADPs of the heavy atoms, here carbon. Because of the low X-ray scattering power of hydrogen atoms, their motions are usually approximated by isotropic displacement parameters and their contributions to the ***TLS*** analysis need to be omitted. If the five carbon atoms in the C_5H_4 molecule were exactly coplanar, the least-squares fitting of the experimental U_{ij} tensor components to the components of $\boldsymbol{L}$ would lead to a singular matrix. Indeed, the five atoms are not coplanar, but the maximum deviation from the best plane is only 0.58 Å. Moreover, as Professor H. B. Bürgi has informed us, a singular matrix also results from the condition that the atoms in the molecule lie on two mutually perpendicular lines,[8] a condition that is closely satisfied in the carbon skeleton of the C_5H_4 molecule. In addition, with only $5 \times 6 = 30$ 'observables' to be fitted to 20 tensor components, any estimate of $\boldsymbol{L}$ and hence of the shrinkage corrections must necessarily be imprecise. Nevertheless, in keeping with the low melting point (179 K), the U_{ij} values obtained in the X-ray analysis at 120 K[9] are comparable to those obtained in many room temperature analyses and are indicative of possibly large librational motions of the molecules.

Analysis of the experimental ADPs of 3-ethynylcyclopropene with the computer program THMA[10] leads to a mean-square librational amplitude of 150 deg^2 about an axis nearly orthogonal (71°) to the double bond. The resulting correction to the double bond distance is +0.022 Å, leading to a corrected bond distance of 1.278 Å, much closer to the theoretical estimates. Because of problems mentioned above, the ***TLS*** analysis cannot be expected to yield an accurate correction for the effect of molecular libration. Indeed, correlation coefficients among tensor components are close to unity, in accord with the expected near singularity in the least-squares matrix. However, even if the values of $\boldsymbol{T}$, $\boldsymbol{L}$ and $\boldsymbol{S}$ given by the analysis are not uniquely determined, they represent a possible assignment among the various molecular motions that fits the experimental U_{ij} values and is also physically reasonable. Thus, the THMA analysis indicates that neglect of thermal motion is the main source of the discrepancy between the X-ray distance and the theoretical estimates.[11]

It cannot be stressed too strongly that molecular dimensions obtained by X-ray crystal structure analysis in general may be considerably in error unless corrected for the effect of molecular libration. This is apart from and in addition to any error introduced because of the inadequacy of the free-atom scattering factors for low-order reflections.

I am grateful to Professor Roland Boese for kindly providing the atomic coordinates and U_{ij} values, and for his continued interest, and to Dr W. Bernd Schweizer for running the THMA program.

Notes and references

1 K. M. Baldridge, B. Biggs, D. Bläser, R. Boese, R. D. Gilbertson, M. M. Haley, A. H. Maulitz and J. S. Siegel, *Chem. Commun.*, 1998, 1137.
2 S. S. Wesolowski, J. M. Gonzales, P. v. R. Schleyer and H. F. Schaefer III, *Chem. Commun.*, 1999, 439.
3 D. Bradley, *Chem. Br.*, June 1999, p. 16.
4 D. W. J. Cruickshank, *Acta Crystallogr.*, 1956, **9**, 757.
5 R. Busing and H. A. Levy, *Acta Crystallogr.*, 1964, **17**, 142.
6 J. D. Dunitz, V. Schomaker and K. N. Trueblood, *J. Phys. Chem.*, 1988, **92**, 856.
7 This discussion applies to rigid-body molecular motions. Complications arising from internal molecular motions are discussed by V. Schomaker and K. N. Trueblood, *Acta Crystallogr.*, 1998, **B54**, 505, but do not affect us here.
8 H.-B. Bürgi, personal communication.
9 We thank Professor Roland Boese for kindly making these available to us.
10 A FORTRAN program by the late Professor K. N. Trueblood for analysis of ADPs; available from Dr W. B. Schweizer, Organic Chemistry Laboratory, ETH-Zentrum, 8092 Zurich, Switzerland (schweizer@org.chem.ethz.ch) or Professor E. M. Maverick, Chemistry Department, UCLA, Los Angeles CA 90024, USA (maverick@chem.ucla.edu).
11 The ***TLS*** analysis leads to positive corrections to all the carbon–carbon bond distances in the molecule. Indeed, on the basis of Fig. 1 of ref. 2, the uncorrected experimental bond lengths all tend to be shorter than the best theoretical estimates.

Communication 9/07593C

Design, synthesis and self-association behavior of water soluble self complementary facial amphiphiles

Lyle Isaacs,*[a] Dariusz Witt[b]† and James C. Fettinger[a]

[a] *Department of Chemistry and Biochemistry, University of Maryland, College Park, MD 20742, USA. E-mail: li8@umail.umd.edu*

[b] *Chemical Faculty, Technical University of Gdansk, Narutowicza St. 11/12, 80-952 Gdansk, Poland*

Received (in Corvallis, OR, USA) 14th September 1999, Accepted 30th October 1999

Self-complementary facially amphiphilic derivatives of glycoluril are useful building blocks for hydrophobic self-assembly in water; we describe the design, synthesis and characterization of six dimeric self-assembled structures with values of K_S up to 1840 M^{-1} in pD 7.4 buffered D_2O.

Nature employs the hydrophobically driven self-assembly of amphiphilic molecules such as phospholipids, polypeptides and oligonucleotides to form functional structures like cell membranes, α-helical coiled coils that regulate transcription, DNA and viral capsids.[1] Ultimately, chemists would like to prepare synthetic structures that are as structurally and functionally complex as these natural systems. In efforts toward this goal some chemists have focused on the preparation of amphiphiles with novel geometries and studied their aggregation behavior in water.[2] Others are trying to deduce the rules governing the use of highly directional interactions like hydrogen bonds and metal–ligand interactions in non-polar solvents ($CHCl_3$).[3] The use of the hydrophobic effect to form designed self-assembled structures in water has received less attention.‡ Here we describe our initial efforts toward the use of self-complementary facial amphiphiles **1**–**6** as building blocks for self-assembly in water. Our goal is to develop the hydrophobic effect as a strong, directional, and predictable non-covalent interaction in water much as hydrogen bonds are now used routinely in chloroform.

Our design of **1**–**6** was based on the observation of Nolte that water soluble glycoluril derivative **7** aggregated in water to give cigar shaped aggregates with dimensions on the order of 1 μM. This result was attributed to the interaction of the water solubilizing groups with the hydrophobic cavity of another molecule of **7**.[4] We reasoned that if we replaced the hydrophobic aromatic solubilizing groups with strictly hydrophilic carboxylate groups, we would be able to eliminate their secondary hydrophobic interactions and form well-defined dimeric structures. We decided, therefore, to use derivatives of glycoluril as building blocks for our studies since: (i) well-established synthetic precedents were available, (ii) we could impart solubility in neutral water by attaching carboxylates or ammonium groups to the convex face of the molecule, and (iii) the glycoluril subunits lead to curvature that creates a cleft-like geometry that allows dimerization.[5,6]

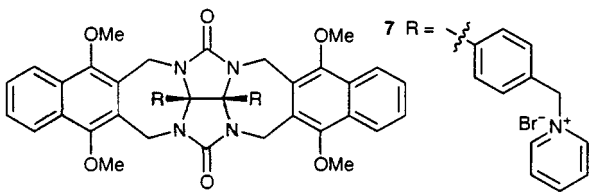

Scheme 1 outlines the synthetic procedures used to prepare **1**—**6**.[4–6]§ The self-complementary facial amphiphiles **1**–**6** all have good solubility in pD 7.4 buffered D_2O (> 5 mM). We synthesized **1** and **2** to allow us to test the influence of the charge on the convex face of the molecule on its self-association constant (K_S). Compounds **3**–**6** were synthesized in order to assess the influence of methoxy substituents on K_S and to investigate possible orientational preferences in **3**·**3** and **4**·**4**.

We obtained single crystals of **15** by slow evaporation of a benzene solution. Fig. 1 shows an ORTEP plot of the structure of **15** in the crystal.¶ The important features of this structure are: (i) the disposition of the ethyl ester groups on a single face of the molecule (facially amphiphilic), (ii) the formation of a hydrophobic cleft, at least in the solid state, due to the *anti* conformation of the xylylene units with respect to the ethoxycarbonyl substituents on the convex face,[7] and (iii) the distance between the centers of the phenyl rings of 6.35 Å is suitable for the complexation of an aromatic ring. The solvating benzene ring partially fills the cleft of **15** by interacting with the xylylene wall in an edge-to-face type manner (Fig. 1).

We performed dilution experiments to investigate the self-association behavior of **1**–**6**[8] In these experiments, ^1H NMR spectra were obtained at a series of concentrations and changes

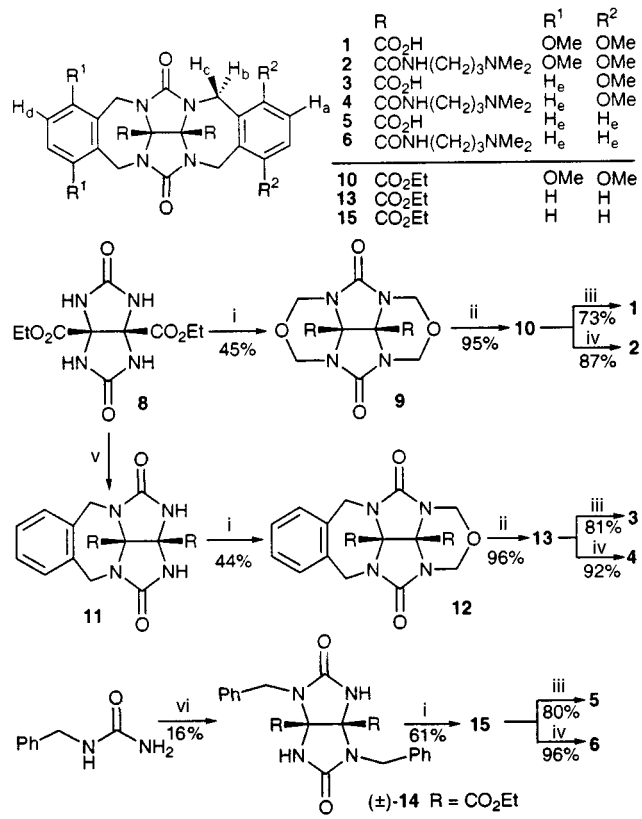

Scheme 1 *Reagents and conditions*: i, TFA, $(CH_2O)_n$, reflux; ii, TFA, Ac_2O, $C_6H_4(OMe)_2$, reflux; iii, MeOH, H_2O, LiOH, 60–65 °C; iv, $H_2N(CH_2)_3NMe_2$, 70–90 °C; v, DMSO, Bu^tOK, $C_6H_4(CH_2Cl)_2$; vi, PhH, TFA, $(EtO_2CCO)_2$, reflux.

† On sabbatical leave from the Technical University of Gdansk.

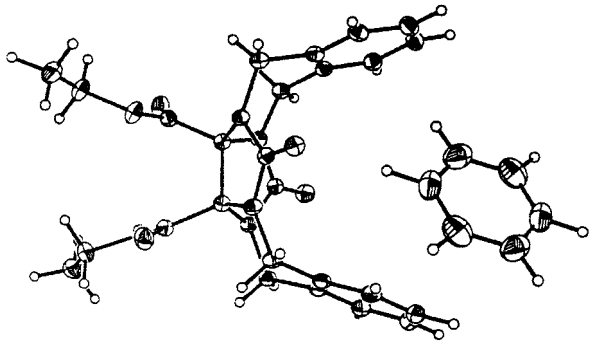

Fig. 1 Crystal structure of **15**·$(C_6H_6)_{0.25}$ with 30% probability ellipsoids.

that occurred in the chemical shifts of the different protons were monitored. The shifts in the ^{1}H NMR resonances were then fitted to the theoretical equation governing self-association of two molecules.[8]‖ For example, when the concentration of **2** is 0.2 mM, the resonance for H_a (Scheme 1) is broadened and appears at δ 6.45, which is close to the chemical shift observed for this proton in $CDCl_3$ (δ 6.73). At a concentration of 5 mM, H_a resonates at δ 5.78, indicating more extensive dimerization at that concentration. The upfield direction of this shift suggests that the H_a protons are proximal to an aromatic ring in the complex. In these experiments, we observe a single broadened resonance for each set of protons in the monomer and the dimer. This observation indicates that the monomer and dimer are in the fast exchange regime on the NMR time scale.

Table 1 summarizes the results of our studies. The values of K_S reported are the results of duplicate dilution experiments at a series of at least seven different concentrations and are averaged over all of the protons undergoing significant complexation induced shifts (> 0.1 ppm). Evaluation of each of these different protons gave similar values of K_S. Based on the values of K_S and $\Delta\delta$ we are able to draw the following conclusions. First, in all three cases—compare **1** with **2**, **3** with **4**, and **5** with **6**—the carboxylic acid and the amine derivatives have approximately equal self-association constants. This result indicates that the charged groups on the convex face of the amphiphile are merely solubilizing groups and do not alter the dimerization process. Second, compounds with greater numbers of methoxy substituents have higher self-association constants. Compounds **5** and **6** undergo no concentration dependant changes in chemical shift up to 5 mM, indicating that self-association does not occur at these concentrations. We rationalize the differences in K_S by the increase in the amount of hydrophobic surface area in **1** and **2**.[9] Third, we suggest that dimers **3**·**3** and **4**·**4** are oriented such that each dimethoxyphenyl ring is complexed in the cavity of the second molecule. We base this suggestion** on the higher values of $\Delta\delta$ for H_a and lower values of $\Delta\delta$ for H_d or **3** and **4** when compared to the $\Delta\delta$ for H_a of **1** and **2** (Table 1). Those protons that are complexed within the hydrophobic cavity experience the anisotropic effect of two phenyl rings, whereas those that are on the outside of the cavity only feel the effect of one phenyl ring. This type of selectivity could allow the orientation of several components in larger self-assembled structures.

We have shown that facially amphiphilic derivatives of glycoluril containing water solubilizing carboxylate or ammonium groups can be used as a platform for the study of hydrophobic self-assembly in water. Self-complementary facial amphiphiles **1**–**4** self-associate in aqueous solution to give dimers. The self-association constant and the orientation of the molecules in the dimeric complex are influenced by the number of methoxy groups in the monomer. Ongoing investigations are directed toward the design and synthesis of compounds with more solubilizing groups and larger amounts of hydrophobic surface area that dimerize with higher values of K_S and reduced exchange rates, as well as the covalent connection of several molecules of **6** to allow for self-assembly rather than simple dimerization.

Table 1 Thermodynamic data and induced chemical shift changes for the self-association of **1**–**6**

Compound	K_S[a]/M^{-1}	$\Delta\delta$[b] H_a	H_d	H_e	$\Delta G°$/ kcal mol^{-1}
1	1840	1.22	[c]		−4.5
2	1530	1.41	[c]		−4.3
3	140	1.48	0.61	0.12	−2.9
4	130	1.79	0.73	0.37	−2.9
5	[d]	[d]	[cd]	[d]	[d]
6	[d]	[d]	[cd]	[d]	[d]

[a] The error in the determination of K_S is ≈15%; the corresponding error in $\Delta G°$ is ≈0.1 kcal mol^{-1}. All dilution experiments were performed in 100 mM phosphate buffered D_2O (pD = 7.4) at 25 °C. [b] Based on the calculated values of the chemical shift for the dimer and the monomer. [c] H_a and H_d are symmetry equivalent. [d] The observed changes in chemical shift up to 5 mM are negligible.

We thank the University of Maryland and the donors of the Petroleum Research Fund (PRF 33946-G4) for financial support of this work.

Notes and references

‡ The 1 : 1 host–guest properties of water-soluble cyclodextrins, calixarenes and cyclophanes are well known.

§ New compounds were characterised by ^{1}H NMR, ^{13}C NMR, IR, MS, melting point and HR-MS or elemental analysis.

¶ *Crystal data* for **15**: $[C_{26}H_{26}N_4O_6][C_6H_6]_{0.25}$, M = 510.04, monoclinic, a = 17.973(2), b = 14.284(3), c = 19.986(4) Å, β = 106.050(11)°, V = 4931.1(14) Å^3, T = 173(2) K, space group $P2_1/c$, Z = 8, D_X = 1.374 g cm^{-3}, μ(Mo-Kα) = 0.098 mm^{-1}, F(000) = 2148, $R(F)$ = 7.22%, $wR(F^2)$ = 14.55% for all 11315 independent reflections. CCDC 182/1481. See http://www.rsc.org/suppdata/cc/1999/2549/ for crystallographic data in .cif format.

‖ Vapor pressure osmometry measurements are in good agreement with a monomer–dimer equilibrium.

** The ROESY spectrum of **4** does not allow us to make firm conclusions regarding the detailed geometry of **4**·**4**.

1 W. Blokziji and J. B. F. N. Engberts, *Angew. Chem., Int. Ed. Engl.*, 1993, **32**, 1545; C. Tanford, *The Hydrophobic Effect*, 2nd edn., Wiley, New York, 1980; F. Diederich, *Angew. Chem., Int. Ed. Engl.*, 1988, **27**, 362; A. Lupas, *Trends Biochem. Sci.*, 1996, **21**, 375.

2 D. T. McQuade, D. G. Barrett, J. M. Desper, R. K. Hayashi and S. H. Gellman, *J. Am. Chem. Soc.*, 1995, **117**, 4862; Y. Cheng, D. M. Ho, C. R. Gottleib, D. Kahne and M. A. Bruck, *J. Am. Chem. Soc.*, 1992, **114**, 7319; S. Shawaphun, V. Janout and S. L. Regen, *J. Am. Chem.Soc.*, 1999, **121**, 5860; F. M. Menger and C. A. Littau, *J. Am. Chem. Soc.*, 1993, **115**, 10 083; J. Q. Nguyen and B. L. Iverson, *J. Am. Chem. Soc.*, 1999, **121**, 2639.

3 J.-M. Lehn, *Supramolecular Chemistry: Concepts and Perspectives*, VCH, New York, 1995; G. M. Whitesides, J. P. Mathias and C. T. Seto, *Science*, 1991, **254**, 1312; D. Philp and J. F. Stoddart, *Angew. Chem., Int. Ed. Engl.*, 1996, **35**, 1154; P. J. Stang and B. Olenyuk, *Acc. Chem. Res.*, 1997, **30**, 502.

4 J. N. H. Reek, A. Kros and R. J. M. Nolte, *Chem. Commun.*, 1996, 245; J. A. A. W. Elemans, R. de Gelder, A. E. Rowan and R. J. M. Nolte, *Chem. Commun.*, 1998, 1553.

5 R. P. Sijbesma and R. J. M. Nolte, *Recl. Trav. Chim. Pays-Bas*, 1993, **112**, 643; H. J. H. Fenton, *J. Chem. Soc.*, 1895, **67**, 48.

6 N. Branda, R. M. Grotzfeld, C. Valdés and J. Rebek, Jr., *J. Am. Chem. Soc.*, 1995, **117**, 85.

7 J. N. H. Reek, J. Elemans and R. J. M. Nolte, *J. Org. Chem.*, 1997, **62**, 2234.

8 K. A. Connors, *Binding Constants*, Wiley, New York, 1987.

9 B. R. Peterson, P. Wallimann, D. R. Carcanague and F. Diederich, *Tetrahedron*, 1995, **51**, 401; K. A. Sharp, A. Nicholls, R. F. Fine and B. Honig, *Science*, 1991, **252**, 106.

Communication 9/07474K

ChemComm

Preparation of an amine *N*-oxide on solid phase: an efficient promoter of the Pauson–Khand reaction

William J. Kerr,*[a] David M. Lindsay[a] and Stephen P. Watson[b]

[a] *Department of Pure and Applied Chemistry, University of Strathclyde, 295 Cathedral Street, Glasgow, Scotland, UK G1 1XL. E-mail: w.kerr@strath.ac.uk*

[a] *GlaxoWellcome, Medicines Research Centre, Gunnels Wood Road, Stevenage, UK SG1 2NY*

Received (in Liverpool, UK) 14th October 1999, Accepted 8th November 1999

A novel, recyclable polymer-supported amine *N*-oxide has been prepared and shown to be a good promoter of the Pauson–Khand reaction under mild conditions, affording good to excellent yields of cyclopentenones.

The field of solid phase chemistry, as applied to organic synthesis, has grown exponentially in recent years.[1] Immobilising either reagents or substrates on a polymeric support provides two complementary methods which both offer significant advantages over traditional solution phase methods. The use of polymer supported reagents[2] affords a clean approach to solution phase chemistry, whereby a reagent may be removed by filtration, aiding facile product purification. Alternatively, by establishing the substrate molecule on solid phase, excess reagents may be used to drive the reaction to completion, with the work-up procedures remaining as simple washing and filtration steps. Furthermore, this approach is highly compatible with the preparation of combinatorial libraries.

In recent years, the preparation of libraries of small organic molecules on solid phase has emerged as a powerful strategy in the drug discovery process.[3] However, these combinatorial methods are not only limited to drug discovery; recently they have also been applied to the discovery of novel compounds for a variety of purposes, most notably in the search for new asymmetric catalysts and reagents.[4] In this regard, based on our drive to further develop our chiral *N*-oxide mediated asymmetric versions[5] of the Pauson–Khand (P–K) reaction,[6] we envisioned that preparing an amine *N*-oxide on solid phase would provide a convenient polymer-supported promoter for this cobalt-mediated annulation process. More importantly, a controlled and adaptable synthetic strategy, which allowed for the incorporation of functional diversity, would also permit the preparation of libraries of chiral amine *N*-oxides. In turn, these mild oxidants could be used to further refine our methodology for inducing asymmetry in the P–K cyclisation process. Herein, we report our initial studies in this area, specifically, the preparation of an amine *N*-oxide on solid phase, and demonstrate the efficiency of this species as the first such supported promoter of the P–K reaction.

To initiate our studies, we needed to develop a flexible synthesis of solid supported tertiary amines and the corresponding *N*-oxides. We chose to generate tertiary amines *via* reductive amination of solid supported aldehydes which are, in turn, attached to the support *via* an acid labile, carboxylic acid releasing linker. Thus, ArgoGel-NH_2[7] was functionalised with the hydroxymethylphenoxyacetic acid linker in a two step process, followed by attachment of 4-formylbenzoic acid to the linker *via* standard esterification conditions (Scheme 1) to give **1**.

The supported aldehyde **1** was then aminated with morpholine, catalysed by acetic acid, and the intermediate reduced with acetoxyborohydride to give the tertiary amine (Scheme 2). At this stage, following TFA cleavage from the support, the amine product was analysed by NMR; clean reductive amination had occurred under the reaction conditions shown. It should also be noted that, in the initial amination stage, the use of less equivalents of amine, more acid, or shorter reaction times all ultimately led to large quantities of by-products derived from carbonyl reduction.

The supported amine was then oxidised using the *N*-sulfonyl oxaziridine reported by Davis,[8] cleanly furnishing the desired *N*-oxide **2** (Scheme 2). Following cleavage of the *N*-oxide from a known amount of resin the overall yield for this five step process was calculated† to be 51%.‡

Having established a flexible approach to the solid phase *N*-oxide **2**, its use as a promoter in the P–K reaction was then evaluated by reacting a series of cobalt complexes with norbornene. To our delight, all reactions were complete in under 30 min at room temperature, cleanly affording cyclopentenones **3** in good to excellent yields (Table 1).§ Additionally, a significant practical advantage over the more traditional P–K protocols was found in that, on reaction work-up, the oxidised cobalt residues remained bound to the resin, allowing the cyclopentenone products to be isolated in > 95% purity simply by filtration and removal of the solvent *in vacuo*. In due course, a variety of alkene substrates were also examined. These reactions also proceeded rapidly and in good yield (Table 2) with even the normally less reactive alkenes, 2,5-dihydrofuran

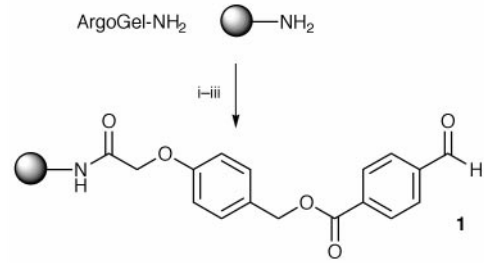

Scheme 1 *Reagents and conditions*: i, 4-formylphenoxyacetic acid, HATU, Pr^i_2NEt, DMF, room temp., 2 h; ii, Bu_4NBH_4, CH_2Cl_2, room temp., 16 h; iii, 4-formylbenzoic acid, diisopropylcarbodiimide, DMAP, DMF, room temp., 16 h.

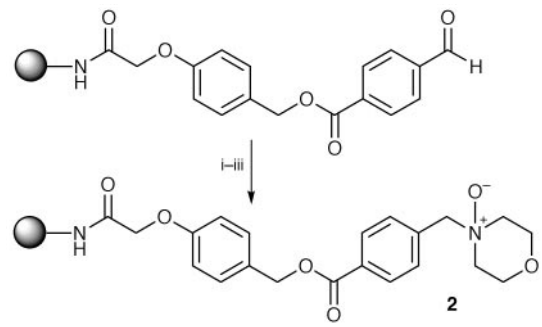

Scheme 2 *Reagents and conditions*: i, morpholine (10 equiv.), AcOH (1 equiv.), CH_2Cl_2, room temp., 7 h; ii, Bu_4NBH_4 (10 equiv.), AcOH (20 equiv.), CH_2Cl_2, room temp., 16 h; iii, *N*-(phenylsulfonyl)phenyloxaziridine (4 equiv.), CH_2Cl_2, room temp., 3 h.

Table 1 Solid phase *N*-oxide promoted P-K reactions

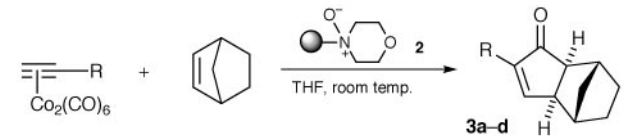

R	*t*/min	Product	Yield (%)
$Me_2(OH)C$	30	**3a**	91
Ph	15	**3b**	99
Me_3Si	15	**3c**	59
Bu^t	30	**3d**	74

Table 2 P–K reactions with a selection of alkenes

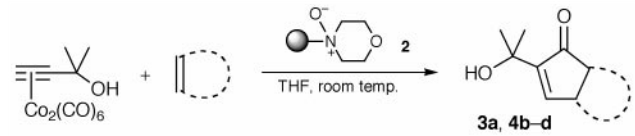

Alkene	*t*/min	Product	Yield (%)
Norbornene	30	**3a**	91
Norbornadiene	30	**4b**	95
2,5-Dihydrofuran	30	**4c**	79
Cyclopentene	30	**4d**	51

and cyclopentene, efficiently affording the desired products **4c** and **4d.**¶

In all cases, the bound cobalt residues could be subsequently removed from the resin by washing with a 2:1 mixture of THF and 1 M HCl, the amine then being regenerated from its hydrochloride salt by washing with a 10% solution of Pr^i_2NEt in DMF. This facile recovery of the amine opens up the possibility for recycling the polymer supported *N*-oxide by simply re-treating the resin with the Davis reagent. Indeed, this was shown to be the case. As illustrated by the reaction between the dimethylpropargyl alcohol complex and norbornene with recycled supported *N*-oxide **2**, the excellent yield and short reaction time is maintained through five cycles, demonstrating the durability of the tethered amine (Table 3).

In conclusion, we have achieved the synthesis of an amine *N*-oxide on solid phase and found it to be a highly efficient and re-usable promoter of the Pauson–Khand reaction, affording cyclopentenones in high purity without the need for column chromatography. Furthermore, due to the nature of the synthetic route, this methodology allows for a diverse set of *N*-oxides to be leveraged on solid phase. The application of this methodology to the preparation of a library of chiral *N*-oxides and the use of other resins, to allow higher loading for the polymer supported reagent, is currently under investigation and will be reported in due course.

We thank Glaxo Wellcome and the EPSRC for generous support (Industrial CASE Award, D. M. L.). We also thank the

Table 3 P–K reactions using recycled *N*-oxide

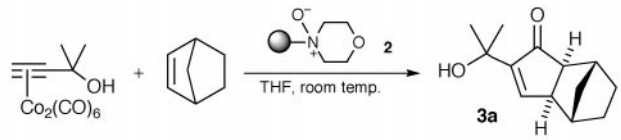

Run	1	2	3	4	5
t/min	30	30	30	30	30
Yield (%)	91	72	77	74	86

EPSRC Mass Spectrometry Service, University of Wales, Swansea, for analyses.

Notes and references

† The cleaved *N*-oxide was analysed by ^{1}H NMR using *p*-nitrophenol as an internal standard.

‡ To the best of our knowledge, only one other polymeric *N*-oxide, poly(vinylpyridine *N*-oxide), has been described. Besides practical concerns, this material has the disadvantage of being less adaptable and, in turn, less utilisable as a basis for the generation of a library of supported *N*-oxides (ref. 9).

§ Representative experimental procedure: Amine *N*-oxide resin **2** (1.12 g, 0.447 mmol) was swelled in THF (15 ml) for 10 min. Norbornene (35 mg, 0.372 mmol) and hexacarbonyl(2-methylbut-3-yn-2-ol)dicobalt (24.3 mg, 0.066 mmol) were added sequentially and the reaction shaken at room temperature for 30 min. The solvent was drained and the resin washed with THF (10 × 2 ml) and CH_2Cl_2 (10 × 2 ml). The combined filtrates were then evaporated *in vacuo* to afford **3a** as a white crystalline solid (12.3 mg, 91% yield). The product was >95% pure as indicated by ^{1}H NMR analysis.

¶ Cyclopentenones **4c** and **4d** required purification by column chromatography.

1 J. S. Früchtel and G. Jung, *Angew. Chem., Int. Ed. Engl.*, 1996, **35**, 17.
2 For reviews, see D. C. Bailey and S. H. Langer, *Chem. Rev.*, 1981, **81**, 109; A. Akelah and D. C. Sherrington, *Chem. Rev.*, 1981, **81**, 557.
3 F. Balkenhohl, C. von dem Bussche-Hünnefeld, A. Lansky and C. Zechel, *Angew. Chem., Int. Ed. Engl.*, 1996, **35**, 2288.
4 See, for example, A. M. Porte, J. Reibenspies and K. Burgess, *J. Am. Chem. Soc.*, 1998, **120,** 9180; M. S. Sigman and E. N. Jacobsen, *J. Am. Chem. Soc.*, 1998, **120,** 4901; H. B. Kagan, *J. Organomet. Chem.*, 1998, **567,** 3; B. M. Cole, K. D. Shimizu, C. A. Krueger, J. P. A. Harrity, M. L. Snapper and A. H. Hoveyda, *Angew. Chem., Int. Ed. Engl.*, 1996, **35**, 1668; G. Liu and J. A. Ellman, *J. Org. Chem.*, 1995, **60**, 7712.
5 W. J. Kerr, G. G. Kirk and D. Middlemiss, *Synlett*, 1995, 1085; see also A. M. Hay, W. J. Kerr, G. G. Kirk and D. Middlemiss, *Organometallics*, 1995, **14**, 4986; W. J. Kerr, G. G. Kirk and D. Middlemiss, *J. Organomet. Chem.*, 1996, **519**, 93.
6 For a review see O. Geis and H.-G. Schmalz, *Angew. Chem., Int. Ed.*, 1998, **37**, 911.
7 Argonaut Technologies, St Jakob-Strasse 148, PO Box 43, 4132 Muttenz 2, Switzerland.
8 F. A. Davis, S. Chattopadhyay, J. C. Towson, S. Lal and T. Reddy, *J. Org. Chem.*, 1988, **53**, 2087.
9 B. Tamami and N. Goudarzian, *Eur. Polym. J.*, 1992, **28**, 1035.

Communication 9/08267K

Typeset and printed by Black Bear Press Limited, Cambridge, England